

Annual Cumulated Index

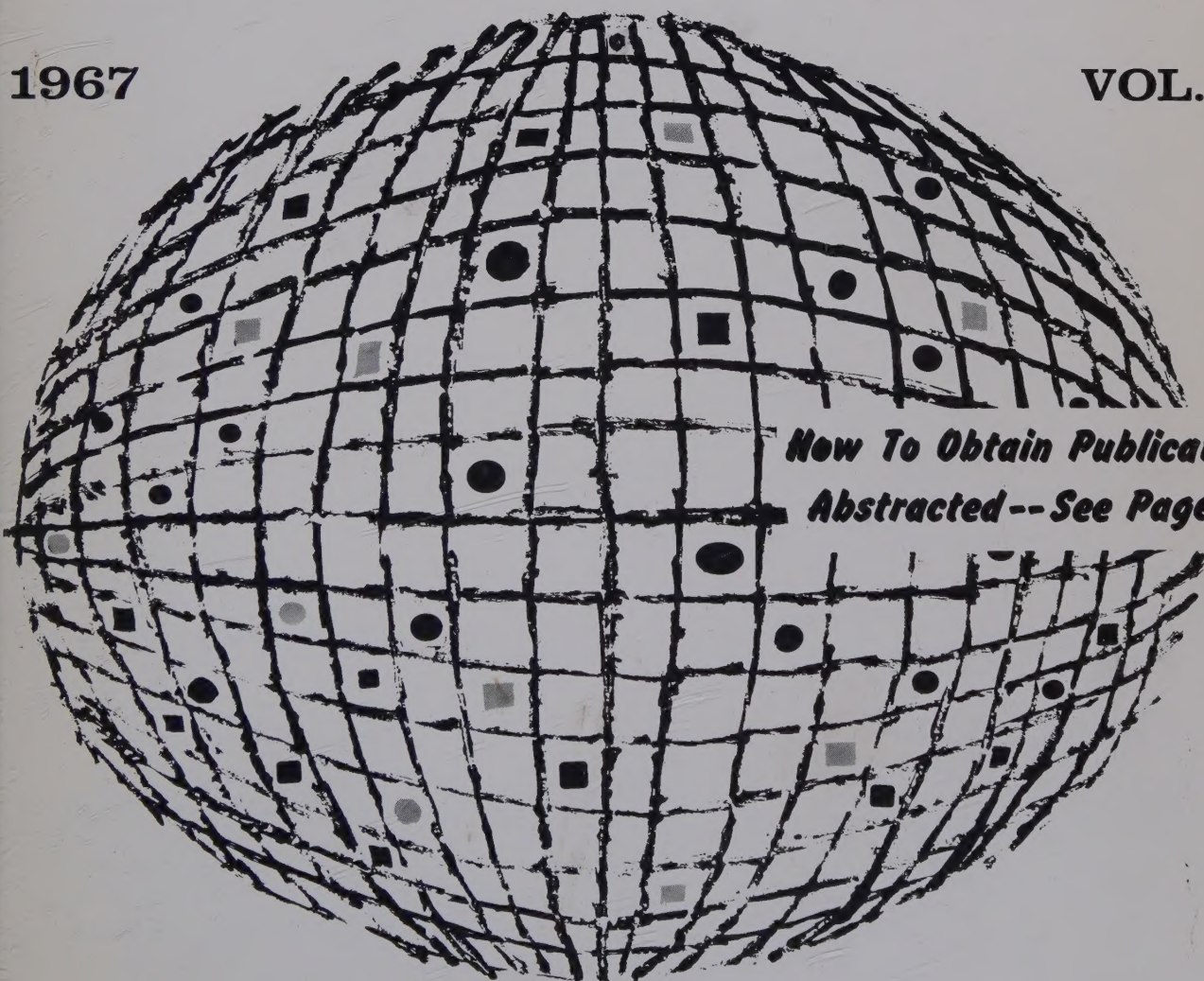
ACCESSION NOS. A67-10001 to A67-43116

INTERNATIONAL AEROSPACE ABSTRACTS

PART 1, PERIODICALS SCANNED, SUBJECT INDEX, A - L

1967

VOL. 7



*How To Obtain Publications
Abstracted--See Page IV*

PUBLISHED BY THE TECHNICAL INFORMATION SERVICE
AMERICAN INSTITUTE OF AERONAUTICS AND ASTRONAUTICS

INTERNATIONAL AEROSPACE ABSTRACTS

Prepared and published by the TECHNICAL INFORMATION SERVICE,
AMERICAN INSTITUTE OF AERONAUTICS AND ASTRONAUTICS, INC., under
NATIONAL AERONAUTICS AND SPACE ADMINISTRATION

Contract No. NSR 33-003-009

TL
500
I57
vol. 7
index
pt. 1
NIC

ANNUAL CUMULATED INDEX

PART 1 PERIODICALS SCANNED, SUBJECT INDEX, A - L

VOLUME 7 JANUARY-DECEMBER 1967

ACCESSION NUMBERS A67-10001 to A67-43116

INTERNATIONAL AEROSPACE ABSTRACTS is published semimonthly by the Technical Information Service, American Institute of Aeronautics and Astronautics, Inc., at Phillipsburg, N. J.
Editorial and Subscription Offices: 750 Third Avenue, New York, N. Y. 10017
Telephone: 212 TN-7-8300 TWX: 212 867-7265

SUBSCRIPTION INFORMATION.

Semimonthly issues: United States and Possessions, 1 year, \$25 postpaid; Foreign Countries, 1 year, \$33 postpaid.

Cumulated Index Volumes: United States and Possessions, 1 year, \$25 postpaid; Foreign Countries, 1 year, \$33 postpaid.

Second-class postage paid at Phillipsburg, N. J.

Copyright © 1967 by the American Institute of Aeronautics and Astronautics, Inc.

CONTENTS

Pages

PART 1

INTRODUCTION	iii	
HOW TO OBTAIN PUBLICATIONS ABSTRACTED	iv	
CROSS REFERENCES	iv	
LIST OF PERIODICALS SCANNED	v	— xxi
SUBJECT INDEX, A - L	A1	— A894

PART 2

INTRODUCTION	iii	
HOW TO OBTAIN PUBLICATIONS ABSTRACTED	iv	
CROSS REFERENCES	iv	
SUBJECT INDEX, M - Z	A895	— A1871

PART 3

INTRODUCTION	iii	
HOW TO OBTAIN PUBLICATIONS ABSTRACTED	iv	
PERSONAL AUTHOR INDEX	B1	— B728
CONTRACT NUMBER INDEX	C1	— C69
MEETING PAPER AND REPORT NO. INDEX	D1	— D29
ACCESSION NUMBER INDEX	E1	— E148

STAFF, AIAA Administrator—Technical Information Programs, ROBERT R. DEXTER

STAFF, TECHNICAL INFORMATION SERVICE Director, JOHN J. GLENNON • Associate Director—
Administrative, THOMAS J. MESKEL • Associate Director—Technical, IRENE W. BOGOLUBSKY •
Manager—Information Systems, WILLIAM T. MORRIS, JR. • Index Editor, MILDRED C. OGDEN •
Supervisor—Abstracting Department, DAVID A. HOWELL • Chief Librarian, PATRICIA M. MARSHALL

Printed by Sheridan Printing Company, Inc.
Phillipsburg, N. J.

INTRODUCTION

1127-19

INTERNATIONAL AEROSPACE ABSTRACTS (IAA) is an abstracting and indexing service covering the world's published literature in the field of aeronautics and space science and technology. IAA is issued semimonthly, on the 1st and 15th of each month.

Coverage of Published Literature

The following types of publications are covered in IAA:

- Periodicals (including government-sponsored journals) and books.
- Meeting papers and conference proceedings issued by professional societies and academic organizations.
- Translations of journals and journal articles.

Coverage of Reports ("Unpublished" Literature)

Abstracts and indexes of report literature are issued in SCIENTIFIC AND TECHNICAL AEROSPACE REPORTS (STAR), which is published by the Scientific and Technical Information Division, National Aeronautics and Space Administration.

By special arrangement between NASA and the American Institute of Aeronautics and Astronautics, IAA is issued in coordination with the twice-monthly schedule of STAR, which appears on the 8th and 23rd of each month.

IAA and STAR utilize both identical subject categories and indexes, which are described below.

Thus the two services provide comprehensive access to the national and international unclassified report and published literature of current significance to aerospace science and technology.

Arrangement of the Semimonthly Issues

IAA is arranged in two major sections:

- (1) Abstracts Section. This section contains complete bibliographic citations with informative abstracts, arranged by appropriate subject categories to facilitate scanning. The subject categories are numbered from 01 to 34, and the scope of each category is outlined in the Table of Contents and again at the beginning of each category in the Abstracts Section. Each abstract is prefixed by the IAA accession number.
- (2) Index Section. Four indexes are contained in this section: Subject, Personal Author, Meeting Paper and Report Number, and Accession Number. Each index is prefaced by explanatory notes to guide the user to the desired abstract.

Cumulated Indexes

Cumulated indexes are prepared and issued promptly at the end of each quarter year, with the 4th quarterly being the Annual Index.

Each cumulated index contains the following sections: A—Subject Index, B—Personal Author Index, C—Contract Number Index, D—Meeting Paper and Report Number Index, and E—Accession Number Index.

Guide to the Subject Indexes

A GUIDE TO THE SUBJECT INDEXES FOR STAR has been issued by the Scientific and Technical Information Division of NASA. This publication contains an alphabetic listing of the subject headings and cross-references used in both STAR and IAA indexes, which use the same subject terminology.

Subscribers to the IAA Cumulated Indexes may obtain copies of the guide by writing to the AIAA Technical Information Service, 750 Third Avenue, New York, N.Y. 10017.

Information regarding SCIENTIFIC AND TECHNICAL AEROSPACE REPORTS and the availability of INTERNATIONAL AEROSPACE ABSTRACTS to organizations having contractual arrangements with NASA may be obtained from the following address:

National Aeronautics and Space Administration
Scientific and Technical Information Division
Attention: Code USS-A
Washington, D. C. 20546

how to obtain publications abstracted

All publications abstracted are available from the AIAA Technical Information Service.

Address all inquiries and requests to:

TECHNICAL INFORMATION SERVICE
AMERICAN INSTITUTE OF AERONAUTICS
AND ASTRONAUTICS, INC.
750 Third Avenue, New York, N. Y. 10017

Telephone: 212 TN-7-8300

TWX: 212 867-7265

Document services are provided as follows:

- Paper copies of accessions announced in *IAA* and of other published articles in the TIS library are available at \$3.00 per document, regardless of the number of pages.
- Paper copies of accessions announced in *Scientific and Technical Aerospace Reports (STAR)* and of similar unpublished reports in the TIS library are available at the rate of \$0.25 per page, minimum order \$3.00.
- Microfiche of documents announced in *IAA* are available at the rate of \$0.50 per microfiche on demand. Documents available in this manner are identified by the symbol # following the accession number in the Abstracts Section and in the Meeting Paper and Report Number and the Accession Number Indexes.
- Minimum air-mail postage to foreign countries is \$1.00.

A number of publications, because of their special characteristics, are available only for reference in the library.

PLEASE REFER TO THE ACCESSION NUMBER WHEN REQUESTING PUBLICATIONS.

NOTE: The AIAA does not sell the publications abstracted except those issued by AIAA.

CROSS REFERENCES

The subject index includes two types of cross references to aid the user of the index in locating the material being sought:

1. "SEE" references (S) direct the user to alternate headings under which material on the subject will be found, for example:

COLUMBIUM
S NIOBIUM

2. "SEE ALSO" references (SA) refer the user to additional headings in the same subject area, for example

LUMINESCENCE
SA ELECTROLUMINESCENCE

The periodicals listed in this section were scanned for material to be announced in *International Aerospace Abstracts* in 1967. The periodicals were received regularly throughout the year in all but a few instances. In the case of titles preceded by an asterisk, only the articles abstracted in *International Aerospace Abstracts* are available. All abstracted articles can be obtained from the AIAA Technical Information Service (see page iv).

BM — Bimonthly

BW — Biweekly

Irreg. — Irregular

M — Monthly

Q — Quarterly

SA — Semiannual

SM — Semimonthly

W — Weekly

A

Académie des Sciences (Paris), Comptes Rendus, Série A — Sciences Mathématiques, Série B — Sciences Physiques (formerly *Académie des Sciences /Paris/, Comptes Rendus*). Académie des Sciences; Gauthier-Villars & Cie, Paris. W

Académie des Sciences (Paris), Comptes Rendus, Série C — Sciences Chimiques (formerly *Académie des Sciences /Paris/, Comptes Rendus*). Académie des Sciences; Gauthier-Villars & Cie, Paris. W

Académie des Sciences (Paris), Comptes Rendus, Série D — Sciences Naturelles. Académie des Sciences; Gauthier-Villars & Cie, Paris. W

Académie Polonaise des Sciences, Bulletin, Série des Sciences Mathématiques, Astronomiques et Physiques. Académie Polonaise des Sciences; Polish Scientific Press, Warsaw. M

Académie Polonaise des Sciences, Bulletin, Série des Sciences Techniques. Académie Polonaise des Sciences; Polish Scientific Press, Warsaw. M

Académie Royale de Belgique, Classe des Sciences, Bulletin. Académie Royale de Belgique; Office International de Librairie, Brussels. M

Academy of Sciences, USSR, Bulletin, Physical Series (*Akademiia Nauk SSSR, Izvestiia, Serii Fizicheskaiia*). Columbia Technical Translations, White Plains, N. Y. M

Academy of Sciences, USSR, Izvestiya, Atmospheric and Oceanic Physics (*Akademiia Nauk SSSR, Izvestiia, Fizika Atmosfery i Okeana*). American Geophysical Union, Washington, D. C. M

Accademia Nazionale dei Lincei, Atti, Rendiconti — Classe di Scienze Fisiche, Matematiche e Naturali. Accademia Nazionale dei Lincei, Rome. M

ACM, Communications. Association for Computing Machinery, New York. M

Acoustical Society of America, Journal. Acoustical Society of America, New York. M

Acta Astronomica. Warsaw. Q

**Acta Crystallographica*. International Union of Crystallography, Copenhagen. M

Acta Electronica Sinica. The Chinese Society of Electronics, Peking. Q

Acta Geophysica Polonica. Polska Akademia Nauk; Panstwowe Wydawnictwo Naukowe, Warsaw. Q

Acta Geophysica Sinica. Chinese Geophysical Society, Peking. Q

Acta Mathematica. Hungarian Academy of Sciences, Budapest. Irreg.

Acta Mechanica. Springer Verlag, Vienna. Q

Acta Mechanica Sinica. Chinese Society of Mechanics, Peking. Q

Acta Metallurgica. Pergamon Press, Ltd., Oxford. M

Acta Physica. Academiae Scientiarum Hungaricae, Budapest. Q

Acta Physica Austriaca. Österreichische Akademie der Wissenschaften; Springer Verlag, Vienna. Q

Acta Physica Polonica. Polska Akademia Nauk, Instytut Fizyki and Polskie Towarzystwo Fizyczne, Warsaw. M

Acta Physica Sinica. Chinese Physical Society, Peking. M

Acta Polytechnica Scandinavica, Mathematics and Computing Machinery Series. Scandinavian Council for Applied Research, Stockholm. Irreg.

Acta Polytechnica Scandinavica, Physics Including Nuclearonics Series. Scandinavian Council for Applied Research, Stockholm. Irreg.

**Acta Psychologica*. North Holland Publishing Co., Amsterdam. Irreg.

**Acta Radiologica — Therapy, Physics, Biology*. Radiological Societies of Denmark, Finland, Norway and Sweden, Stockholm. SA

Acta Technica. Hungarian Academy of Sciences, Budapest. M

Acta Technica ČSAV. Československá Akademie Věd, Prague. BM

Acustica. S. Hirzel Verlag KG, Stuttgart. BM

Advanced Energy Conversion. Pergamon Press, Ltd., Oxford. Q

Advances in Physics. Taylor & Francis, Ltd., London. Q

Aero-Revue. Aero-Club der Schweiz, Zurich. M

Aeronautical Quarterly. Royal Aeronautical Society, London. Q

Aeronautical Society of India, Journal. Aeronautical Society of India, New Delhi. Q

INTERNATIONAL AEROSPACE ABSTRACTS

- Aeroplane.* Temple Press, Ltd., London. W
- Aerospace Medicine.* Aerospace Medical Association, Washington, D. C. M
- L'Aerotecnica.* Associazione Italiana di Aerotecnica, Rome. BM
- AIAA Journal.* American Institute of Aeronautics and Astronautics, Inc., New York. M
- AIAA Student Journal.* American Institute of Aeronautics and Astronautics, Inc., New York. Q
- A.I.Ch.E. Journal.* American Institute of Chemical Engineers, New York. BM
- AIMS, Transactions.* American Institute of Mining, Metallurgical and Petroleum Engineers, New York. BM
- Air-Espace Techniques* (formerly *Air Techniques*). Boulogne, France. BM
- Air et Cosmos.* Paris. W
- Air Line Pilot.* Air Line Pilots Association/International, Chicago. M
- Air Techniques* (see *Air-Espace Techniques*).
- Aircraft Engineering.* Bunhill Publications, Ltd., London. M
- Akademiia Nauk Armianskoi SSR, Doklady.* Akademiia Nauk Armianskoi SSR, Yerevan. 10 issues per year
- Akademiia Nauk Armianskoi SSR, Izvestiia, Fizika.* Akademiia Nauk Armianskoi SSR, Yerevan. BM
- Akademiia Nauk Armianskoi SSR, Izvestiia, Matematika.* Akademiia Nauk Armianskoi SSR, Yerevan. BM
- Akademiia Nauk Armianskoi SSR, Izvestiia, Mekhanika.* Akademiia Nauk Armianskoi SSR, Yerevan. BM
- Akademiia Nauk Armianskoi SSR, Izvestiia, Nauki o Zemle.* Akademiia Nauk Armianskoi SSR, Yerevan. BM
- Akademiia Nauk Armianskoi SSR, Izvestiia, Seriiia Tekhnicheskikh Nauk.* Akademiia Nauk Armianskoi SSR, Yerevan. 10 issues per year
- Akademiia Nauk Azerbaidzhanskoi SSR, Doklady.* Akademiia Nauk Azerbaidzhanskoi SSR, Baku. M
- Akademiia Nauk Azerbaidzhanskoi SSR, Izvestiia, Seriiia Fiziko-Tekhnicheskikh i Matematicheskikh Nauk.* Akademiia Nauk Azerbaidzhanskoi SSR, Baku. BM
- Akademiia Nauk BSSR, Doklady.* Akademiia Nauk Belorusskoi SSR, Minsk. M
- Akademiia Nauk Gruzinskoi SSR, Soobshcheniia.* Akademiia Nauk Gruzinskoi SSR, Tiflis. M
- Akademiia Nauk Kazakhskoi SSR, Izvestiia, Seriiia Fiziko-Matematicheskaiia.* Akademiia Nauk Kazakhskoi SSR, Alma Ata. BM
- Akademiia Nauk Kazakhskoi SSR, Vestnik.* Akademiia Nauk Kazakhskoi SSR, Alma Ata. M
- Akademiia Nauk Latviiskoi SSR, Izvestiia.* Akademiia Nauk Latviiskoi SSR, Riga. M
- Akademiia Nauk Latviiskoi SSR, Izvestiia, Seriiia Fizicheskikh i Tekhnicheskikh Nauk.* Akademiia Nauk Latviiskoi SSR, Riga. BM
- Akademiia Nauk SSSR, Doklady.* Akademiia Nauk SSSR, Moscow. 36 issues per year
- Akademiia Nauk SSSR, Izvestiia, Energetika i Transport.* Akademiia Nauk SSSR, Moscow. BM
- Akademiia Nauk SSSR, Izvestiia, Fizika Atmosfery i Okeana.* Akademiia Nauk SSSR, Moscow. M
- Akademiia Nauk SSSR, Izvestiia, Fizika Zemli.* Akademiia Nauk SSSR, Moscow. M
- Akademiia Nauk SSSR, Izvestiia, Mekhanika (see Akademiia Nauk SSSR, Izvestiia, Mekhanika Zhidkosti i Gaza).*
- Akademiia Nauk SSSR, Izvestiia, Mekhanika Zhidkosti i Gaza* (formerly *Akademiia Nauk SSSR, Izvestiia, Mekhanika*). Akademiia Nauk SSSR, Moscow. BM
- Akademiia Nauk SSSR, Izvestiia, Metally.* Akademiia Nauk SSSR, Moscow. BM
- Akademiia Nauk SSSR, Izvestiia, Seriiia Biologicheskaiia.* Akademiia Nauk SSSR, Moscow. BM
- Akademiia Nauk SSSR, Izvestiia, Seriiia Fizicheskaiia.* Akademiia Nauk SSSR, Moscow. M
- Akademiia Nauk SSSR, Izvestiia, Seriiia Matematicheskaiia.* Akademiia Nauk SSSR, Moscow. BM
- Akademiia Nauk SSSR, Izvestiia, Tekhnicheskaiia Kibernetika.* Akademiia Nauk SSSR, Moscow. BM
- Akademiia Nauk SSSR, Sibirskoe Otdelenie, Izvestiia, Seriiia Tekhnicheskikh Nauk.* Akademiia Nauk SSSR, Sibirskoe Otdelenie, Novosibirsk. 3 issues per year
- Akademiia Nauk SSSR, Vestnik.* Akademiia Nauk SSSR, Moscow. M
- Akademiia Nauk SSSR, Zhurnal Eksperimental'noi i Teoreticheskoi Fiziki* (see *Zhurnal Eksperimental'noi i Teoreticheskoi Fiziki*).
- Akademiia Nauk Turkmenskoi SSR, Izvestiia, Seriiia Fiziko-Tekhnicheskikh, Khimicheskikh i Geologicheskikh Nauk.* Akademiia Nauk Turkmenskoi SSR, Ashkhabad. BM
- Akademiia Nauk Ukrains'koi RSR, Dopovidi, Seriiia A — Fiziko-Tekhnichni i Matematichni Nauki.* Akademiia Nauk Ukrains'koi RSR; Naukova Dumka, Kiev. M
- Akademiia Nauk Ukrains'koi RSR, Dopovidi, Seriiia B — Geologiiia, Geofizika, Khimiiia i Biologiiia.* Akademiia Nauk Ukrains'koi RSR; Naukova Dumka, Kiev. M
- Akademiia Nauk Uzbekskoi SSR, Doklady.* Akademiia Nauk Uzbekskoi SSR, Tashkent. M
- Akademiia Nauk Uzbekskoi SSR, Izvestiia, Seriiia Fiziko-Matematicheskikh Nauk.* Akademiia Nauk Uzbekskoi SSR, Tashkent. BM
- Akademiia Nauk Uzbekskoi SSR, Izvestiia, Seriiia Tekhnicheskikh Nauk.* Akademiia Nauk Uzbekskoi SSR, Tashkent. BM
- Akademiia Navuk BSSR, Vetsi, Seryia Fizika-Tekhnichnykh Navuk.* Akademiia Navuk Belaruskai SSR, Minsk. Q
- Akusticheskii Zhurnal.* Akademiia Nauk SSSR, Moscow. Q
- Alata Internazionale.* Etas Kompass, Milan. M
- Alta Frequenza.* Associazione Elettrotecnica Italiana, Milan. M
- Aluminium.* Aluminium-Zentrale e.V.; Aluminium-Verlag GmbH, Düsseldorf. M
- American Ceramic Society, Bulletin.* American Ceramic Society, Inc., Columbus, Ohio. M
- American Ceramic Society, Journal.* American Ceramic Society, Inc., Columbus, Ohio. M
- American Chemical Society, Journal.* American Chemical Society, Washington, D.C. SM
- American Helicopter Society, Journal.* American Helicopter Society, Inc., New York. Q

- American Industrial Hygiene Association, Journal.* American Industrial Hygiene Association, Cincinnati. BM
- **American Journal of Cardiology.* R. H. Donnelley Corp., New York. M
- **American Journal of Economics and Sociology.* New York. Q
- American Journal of Physics.* American Institute of Physics, Inc., New York. M
- **American Journal of Physiology.* American Physiological Society, Washington, D.C. M
- **American Mathematical Monthly.* Mathematical Association of America, University of Buffalo, Buffalo. 10 issues per year
- **American Mathematical Society, Bulletin.* American Mathematical Society, Providence, R.I. BM
- **American Mathematical Society, Transactions.* American Mathematical Society, Providence. M
- **American Medical Association, Journal.* American Medical Association, Chicago. W
- American Meteorological Society, Bulletin.* American Meteorological Society, Boston. M
- **American Mineralogist.* Mineralogical Society of America c/o U.S. Geological Survey, Washington, D.C. BM
- American Museum Novitates.* American Museum of Natural History, New York.
- **American Philosophical Society, Proceedings.* American Philosophical Society, Philadelphia. BM
- American Society of Civil Engineers, Aero-Space Transport Division, Journal.* American Society of Civil Engineers, New York. Q
- American Society of Civil Engineers, Engineering Mechanics Division, Journal.* American Society of Civil Engineers, New York. BM
- American Society of Civil Engineers, Structural Division, Journal.* American Society of Civil Engineers, New York. BM
- **American Statistical Association, Journal.* American Statistical Association, Washington, D.C. Q
- **Anaesthetist.* Deutsche Gesellschaft für Anaesthesie und Wiederbelebung; Österreichische und Schweizerische Gesellschaft für Anaesthesiologie; Springer Verlag, Berlin. M
- **Analytical Biochemistry.* Academic Press, Inc., New York. M
- Analytical Chemistry.* American Chemical Society, Washington, D.C. M
- **Anesthesiology.* American Society of Anesthesiologists; J. B. Lippincott Co., Philadelphia. BM
- Ankara, Université, Faculté des Sciences, Communications, Série A — Mathématiques, Physique et Astronomie.* Ankara University, Ankara, Turkey.
- Annalen der Physik.* Johann Ambrosius Barth Verlag, Leipzig. Irreg.
- Annales d'Astrophysique.* Centre National de la Recherche Scientifique, Paris. BM
- Annales de Géophysique.* Centre National de la Recherche Scientifique, Paris. Q
- Annales de Physique.* Centre National de la Recherche Scientifique; Bd. Masson & Cie, Paris. BM
- Annales de Radioélectricité.* Groupe de la Compagnie Générale de Télégraphie sans Fil, Paris. Q
- Annales des Télécommunications.* Centre National d'Etudes des Télécommunications, Issy-les-Moulineaux (Seine), France. BM
- Annali di Geofisica.* Istituto Nazionale de Geofisica, Rome. Q
- **Annals of Mathematical Statistics.* Illinois, University, Urbana, Ill. BM
- Annals of Occupational Hygiene.* Pergamon Press, Ltd., Oxford. Q
- Annals of Physics.* Academic Press, Inc., New York. M
- Annals of the International Geophysical Year.* Pergamon Press, Ltd., Oxford. Irreg.
- APL Technical Digest.* Johns Hopkins University, Silver Spring, Md. BM
- Aplikace Matematiky.* Československá Akademie Věd, Matematický Ústav, Prague. BM
- Applied Materials Research.* Plenum Publishing Corp., New York. Q
- Applied Mechanics Reviews.* American Society of Mechanical Engineers, New York. M
- **Applied Microbiology.* American Society for Microbiology, Baltimore. BM
- Applied Optics.* Optical Society of America, Inc., Washington, D.C. M
- Applied Physics Letters.* American Institute of Physics, Inc., New York. SM
- Applied Polymer Symposia.* John Wiley & Sons, Inc., New York. Irreg.
- Applied Scientific Research.* Martinus Nijhoff, The Hague. Irreg.
- Applied Spectroscopy.* Society for Applied Spectroscopy, Boston College, Mass.; American Institute of Physics, Inc., New York. BM
- Archiv der elektrischen Übertragung.* S. Hirzel Verlag, KG, Stuttgart. M
- Archiv für Elektrotechnik.* Springer Verlag, Berlin. Irreg.
- Archiv für Meteorologie, Geophysik und Bioklimatologie, Serie A — Meteorologie und Geophysik.* Springer Verlag, Vienna. Irreg.
- Archiv für Meteorologie, Geophysik und Bioklimatologie, Serie B - Allgemeine und biologische Klimatologie.* Springer Verlag, Vienna. Irreg.
- Archiv für technisches Messen und industrielle Messtechnik.* R. Oldenbourg Verlag, Munich. M
- Archive for Rational Mechanics and Analysis.* Springer Verlag, Berlin. Irreg.
- Archives des Sciences.* Société des Physique et d'Histoire Naturelle de Genève, Geneva. 3 issues per year
- **Archives of Biochemistry and Biophysics.* Academic Press, Inc., New York. M
- **Archives of Pathology.* American Society for Experimental Pathology; American Medical Association, Chicago. M
- Archiwum Automatyki i Telemekhaniki.* Akademia Nauk, Instytut Automatyki; Panstwowe Wydawnictwo Naukowe, Warsaw. Q
- Archiwum Budowy Maszyn.* Polska Akademia Nauk, Komitet Budowy Maszyn, Warsaw. Q
- Archiwum Elektrotechniki.* Wydawnictwo Polskiej Akademii Nauk, Warsaw. Q
- Archiwum Mechaniki Stosowanej.* Académie Polonaise des Sciences, Warsaw. BM

INTERNATIONAL AEROSPACE ABSTRACTS

- Arkiv för Astronomi.* Kungliga Svenska Vetenskapsakademien; Almqvist & Wiksells Boktryckeri AB, Stockholm. Irreg.
- Arkiv för Fysik.* Kungliga Svenska Vetenskapsakademien; Almqvist & Wiksells Boktryckeri AB, Stockholm. Irreg.
- Arkiv för Geofysik.* Kungliga Svenska Vetenskapsakademien; Almqvist & Wiksells Boktryckeri AB, Stockholm. Irreg.
- Artificial Satellites.* Polish Academy of Sciences, Warsaw. Q
- ASHRAE Journal.* American Society of Heating, Refrigerating and Air-Conditioning Engineers, Inc., New York. M
- ASLE Transactions.* American Society of Lubrication Engineers; Academic Press, New York. Q
- ASM Transactions Quarterly.* American Society for Metals, Metals Park, Ohio. Q
- ASME Transactions, Series A - Journal of Engineering for Power.* American Society of Mechanical Engineers, New York. Q
- ASME Transactions, Series B - Journal of Engineering for Industry.* American Society of Mechanical Engineers, New York. Q
- ASME Transactions, Series C - Journal of Heat Transfer.* American Society of Mechanical Engineers, New York. Q
- ASME Transactions, Series D - Journal of Basic Engineering.* American Society of Mechanical Engineers, New York. Q
- ASME Transactions, Series E - Journal of Applied Mechanics.* American Society of Mechanical Engineers, New York. Q
- ASME Transactions, Series F - Journal of Lubrication Technology.* American Society of Mechanical Engineers, New York. Q
- Association for Computing Machinery, Journal.* Association for Computing Machinery, New York. Q
- Astrofizika.* Akademiia Nauk Armianskoi SSR, Yerevan. Q
- Astronautica Acta.* International Academy of Astronautics, International Astronautical Federation; Pergamon Press, Ltd., Oxford. BM
- Astronautics and Aeronautics.* American Institute of Aeronautics and Astronautics, Inc., New York. M
- Astronautik.* Hermann Oberth-Gesellschaft, Hannover. BM
- L'Astronautique.* Société Française d'Astronautique, Paris. Q
- Astronautyka.* Polskie Towarzystwo Astronautyczne, Warsaw. Q
- Astronomical Institutes of Czechoslovakia, Bulletin.* Czechoslovak Academy of Sciences, Prague. BM
- Astronomical Institutes of the Netherlands, Bulletin.* Astronomical Institutes of the Netherlands; North-Holland Publishing Co., Amsterdam. Q
- Astronomical Institutes of the Netherlands, Bulletin, Supplement Series.* Astronomical Institutes of the Netherlands; North-Holland Publishing Co., Amsterdam. Irreg.
- Astronomical Journal.* American Astronomical Society, Evanston, Ill. M
- Astronomical Society of Japan, Publications.* Astronomical Society of Japan, Tokyo. Q
- Astronomical Society of the Pacific, Publications.* Astronomical Society of the Pacific, San Francisco. BM
- Astronomicheskii Vestnik.* Vsesoiuznoe Astronomo-Geodezicheskoe Obshchestvo; Izdatel'stvo Nauka, Moscow. Q
- Astronomicheskii Zhurnal.* Akademiia Nauk SSSR, Moscow. BM
- L'Astronomie.* Société Astronomique de France, Paris. M
- Astronomie und Raumfahrt.* Deutsche Astronautische Gesellschaft, Berlin. 5 issues per year
- Astronomische Gesellschaft, Mitteilungen.* Astronomische Gesellschaft, Hamburg. Biennial.
- Astronomische Nachrichten.* Akademie Verlag GmbH, Berlin. Irreg.
- Astrophysica Norvegica.* Oslo, University, Institute of Theoretical Astrophysics; Norske Videnskaps-Akademi i Oslo, Oslo. Irreg.
- Astrophysical Journal.* University of Chicago Press, Chicago. 8 issues per year
- Astrophysical Journal Supplement Series.* University of Chicago Press, Chicago. Irreg.
- Astrophysics (Astrofizika).* The Faraday Press, Inc., New York. Q
- Atomic Energy Review.* International Atomic Energy Agency, Vienna. Q
- *Australian Journal of Chemistry.* Commonwealth Scientific and Industrial Research Organization, Melbourne. M
- Australian Journal of Physics.* Commonwealth Scientific and Industrial Research Organization, Melbourne. BM
- Australian Mathematical Society, Journal.* Australian Mathematical Society; P. Noordhoff N. V., Groningen, Netherlands. Q
- Automation and Remote Control (Avtomatika i Telemekhanika).* Instrument Society of America, Pittsburgh, Pa. M
- Automatisme.* Association Française de Régulation et d'Automatisme, Paris. M
- Automatizace.* Czechoslovak Scientific Society, Special Group for Automation, Prague. M
- Aviatsionnaia Tekhnika.* Ministerstvo Vysshego i Srednego Spetsial'nogo Obrazovaniia SSSR; Kazanskii Aviatsionnyi Institut, Kazan. Q
- Avtomatika.* Akademiia Nauk Ukrainskoi SSR, Kiev. BM
- Avtomatika i Telemekhanika.* Akademiia Nauk SSSR, Moscow. M

B

- Babeş-Bolyai, Universitas, Studia, Series Mathematica-Physica.* Babeş-Bolyai, Universitas, Cluj, Rumania. SA
- Battelle Technical Review.* Battelle Memorial Institute, Columbus, Ohio. M
- Beiträge aus der Plasmaphysik.* Deutsche Akademie der Wissenschaften, Berlin. BM
- Beiträge zur Physik der Atmosphäre.* Akademische Verlagsgesellschaft, mbH, Frankfurt/Main. Q
- Bell Laboratories Record.* Bell Telephone Laboratories, Inc., New York. M

- Bell System Technical Journal*. American Telephone and Telegraph Co., New York. 10 issues per year
- Bildmessung und Luftbildwesen*. Herbert Wichmann Verlag, Karlsruhe. Q
- **Biochemical and Biophysical Research Communications*. Academic Press, Inc., New York. SM
- **Biochemistry*. American Chemical Society, Washington, D.C. M
- **Biochimica et Biophysica Acta*. Elsevier Publishing Co., Amsterdam. W
- **Biophysical Journal*. Biophysical Society, New York. BM
- **Biotechnology and Bioengineering*. Interscience Publishers, New York. Q
- B'lgarska Akademiia na Naukite, Izvestiia na Geofizichnii Institut*. B'lgarska Akademiia na Naukite, Sofia. Irreg.
- Bolgarskaia Akademiia Nauk, Doklady*. Bolgarskaia Akademiia Nauk, Sofia. M
- Bölkow-WMD/SIAT Report*. Bölkow-WMD/SIAT-Firmengruppe, Munich.
- Bollettino di Geofisica Teorica ed Applicata*. Osservatorio Geofisico Sperimentale, Trieste. Q
- Bristol Siddeley Journal*. Bristol Siddeley Engines, Ltd., London. Q
- British Astronomical Association, Journal*. British Astronomical Association, Hounslow West, Middx., England. 8 issues per year
- British Journal of Applied Physics*. Institute of Physics and The Physical Society, London. M
- British Welding Journal*. Institute of Welding and The British Welding Research Association, London. M
- Brno, Vysoké Učení Technické, Sborník*. Polytechnical Institute, Brno. M
- Brüel and Kjaer Technical Review*. B & K Instruments, Inc., Cleveland, Ohio.
- Bulletin Astronomique*. Centre National de la Recherche Scientifique, Service des Publications; Gauthier-Villars & Cie, Paris. Irreg.
- Bulletin d'Informations Scientifiques et Techniques*. Dunod Editeur, Paris. M
- **Bulletin Volcanologique*. Union Géodésique et Géophysique Internationale, Brussels.
- **Business and Government Review*. Missouri, University, B & PA Research Center, Columbia, Mo.

C

- Cambridge Philosophical Society, Proceedings*. Cambridge University Press, London. Q
- Canada, National Research Council, Division of Mechanical Engineering and National Aeronautical Establishment, Quarterly Bulletin*. National Research Council of Canada, Ottawa. Q
- Canadian Aeronautics and Space Journal*. Canadian Aeronautics and Space Institute, Ottawa. M
- **Canadian Journal of Chemistry*. National Research Council of Canada, Ottawa. SM
- Canadian Journal of Physics*. National Research Council of Canada, Ottawa. M
- **Canadian Journal of Psychology*. Canadian Psychological Association, Toronto. Q

- Canadian Metallurgical Quarterly*. Canadian Institute of Mining and Metallurgy, Dept. of Mines and Technical Surveys, Ottawa, Canada. Q
- Canadian Operational Research Society, Journal*. Canadian Operational Research Society, Ottawa. 3 issues per year
- **Carbon*. Pergamon Press, Ltd., London. Q
- Československý Časopis pro Fysiku*. Československá Akademie Věd, Prague. BM
- Challenge*. General Electric Co., Missile and Space Div., Philadelphia. Q
- Chalmers Tekniska Högskolas Handlingar*. Chalmers Tekniska Högskola, Göteborg, Sweden. Irreg.
- Chartered Mechanical Engineer*. Institution of Mechanical Engineers, London. M
- Chemia Stosowana, Seria B*. Polish Academy of Sciences, Warsaw. Q
- Chemical Engineering Progress*. American Institute of Chemical Engineers, New York. M
- Chemical Engineering Progress, Symposium Series*. American Institute of Chemical Engineers, New York. M
- Chemical Physics Letters*. North-Holland Publishing Co., Amsterdam. M
- **Chemical Reviews*. American Chemical Society, Washington, D.C. BM
- **Chemical Society of Japan, Bulletin*. Chemical Society of Japan, Tokyo. M
- Chinese Journal of Physics/Peking/ (Acta Physica Sinica)*. American Institute of Physics, Inc., New York. M
- Chinese Mathematics (Acta Mathematica Sinica)*. American Mathematical Society, Providence. Q
- Ciel et Terre*. Société Belge d'Astronomie, de Météorologie et de Physique du Globe, Brussels. BM
- **Circulation*. American Heart Association, New York. M
- **Circulation Research*. American Heart Association, New York. M
- Cobalt*. Centre d'Information du Cobalt, Brussels. Q
- Collins Signal*. Collins Radio Co., Dallas. Q
- Combustion, Explosion, and Shock Waves (Fizika Goreniia i Vzryva)*. The Faraday Press, Inc., New York. Q
- Combustion and Flame*. Combustion Institute; Butterworth & Co., Ltd., London. Q
- Communications on Pure and Applied Mathematics*. New York University, Institute of Mathematical Sciences; Interscience Publishers, New York. Q
- Component Technology*. The Plessey Co., Ltd., Ilford, Essex, England. Q
- Computer Journal*. British Computer Society, London. Q
- **Confinia Neurologica*. S. Karger AG, Basel. BM
- Contamination Control*. American Association for Contamination Control; Blackwell Publishing Co., Inc., Los Angeles. M
- Contemporary Physics*. Taylor and Francis, Ltd., London. BM
- Control*. Morgan Brothers (Publishers), Ltd., London. Q
- Control Engineering*. McGraw-Hill Publishing Co., Inc., New York. M
- The Controller*. International Federation of Air Traffic Controllers' Association, East Twickenham, Middx.,

INTERNATIONAL AEROSPACE ABSTRACTS

- England; Verlag W. Kramer & Co., Frankfurt/Main. Q
- Convair Traveler*. General Dynamics Corporation, Convair Division, San Diego. BM
- Coopération Méditerranéenne pour l'Energie Solaire, Bulletin*. Coopération Méditerranéenne pour l'Energie Solaire (COMPLES), Madrid. SA
- Corrosion*. National Association of Corrosion Engineers, Houston. M
- Cosmic Research (Kosmicheskie Issledovaniia)*. Consultants Bureau Enterprises, Inc., New York. BM
- COSPAR Information Bulletin*. COSPAR Secretariat, Paris. Irreg.
- **Cryogenic Technology*. Cryogenic Society of America, Los Angeles. BM
- **Cryogenics*. Heywood-Temple Publications, London. BM
- **Crystal Growth*. Pergamon Press, Ltd., Oxford.
- Current Science*. Current Science Association, Bangalore, India. SM
- **Currents in Modern Biology*. North-Holland Publishing Co., Amsterdam.
- Cybernetics (Kibernetika)*. The Faraday Press, Inc., New York. BM
- Czechoslovak Journal of Physics, Series B*. Czechoslovak Academy of Sciences, Prague. M

D

- Defectoscopy (Defektoskopiia)*. Consultants Bureau Enterprises, Inc., New York. BM
- **Deutsche Keramische Gesellschaft, Berichte*. Deutsche Keramische Gesellschaft, Bad Honnef/Rh. M
- Deutscher Aerokurier*. Deutscher Aero-Club, E.V., Frankfurt/Main. M
- **DFL-Mitteilungen*. Deutsche Forschungsanstalt für Luft- und Raumfahrt, Stuttgart. Irreg.
- DGRR, Mitteilungen*. Deutsche Gesellschaft für Raketentechnik und Raumfahrt, Munich. Q
- Differential Equations (Differentsial'nye Uravneniia)*. The Faraday Press, New York. M
- Differentsial'nye Uravneniia*. Izdatel'stvo Nauka i Tekhnika, Minsk. M
- Doc-Air-Espace*. Service de Documentation Scientifique et Technique de l'Armement, Paris. BM
- **Duke Mathematical Journal*. Duke University Press, Durham, N.C. Q
- DVL-Nachrichten*. Deutsche Versuchsanstalt für Luft- und Raumfahrt e.V., Porz-Wahn, West Germany. Irreg.

E

- Earth and Planetary Science Letters*. North-Holland Publishing Co., Amsterdam. BM
- EEE — The Magazine of Circuit Design Engineering*. Mactier Publishing Corporation, New York. M
- Eesti NSV Teaduste Akadeemia, Toimetised, Füüsika-Matemaatika- ja Tehnikateaduste Seeria*. Tallinn. Q

- Electrical Communication*. International Telephone and Telegraph Corp., New York. Q
- Electrical Engineering in Japan (Denki Gakkai Zasshi)*. Institute of Electrical and Electronics Engineers, Inc., New York.
- Electro-Technology*. Conover-Mast Technical Publications Corp., New York. M
- **Electrochemical Society, Journal*. Electrochemical Society, Inc., New York. M
- **Electrochemical Technology*. Electrochemical Society, Inc., New York. BM
- Electromechanical Design*. Electromechanical Design, Brookline, Mass. M
- Electron (Sao Paulo)*. Sao Paulo, Brazil.
- Electronic Applications*. N. V. Philips' Gloeilampenfabrieken, Eindhoven. Q
- Electronic Communicator*. Horizon House, Dedham, Mass. BM
- Electronic Design*. Hayden Publishing Co., Inc., New York. BW
- Electronic Engineer*. Chilton Co., Philadelphia. M
- Electronic Engineering*. Morgan Brothers, Ltd., London. M
- Electronic Packaging and Production*. Milton S. Kiver Publications, Inc., Chicago. M
- Electronics*. McGraw-Hill Publishing Co., Inc., New York. BW
- Electronics and Communications in Japan*. Institute of Electrical and Electronics Engineers, Inc., New York. M
- Electronics and Power*. Institution of Electrical Engineers, London. M
- Electronics Letters*. Institution of Electrical Engineers, London. M
- Electronique*. Editions PEPTA, Paris. M
- Elektromekhanika*. Ministerstvo Vysshego i Srednego Spetsial'nogo Obrazovaniia SSSR, Novocherkassk. M
- Elektronik*. Teknisk Forlag A/S, Copenhagen. M
- Elektronische Datenverarbeitung*. Friedr. Vieweg & Sohn, Braunschweig. BM
- Elektronische Rechenanlagen*. Verein deutscher Ingenieure, Nachrichtentechnische Gesellschaft, Munich. BM
- Elektrosviaz'*. Ministerstvo Sviazi SSSR, Moscow. M
- Elektrotechnický Obzor*. State Central Technical Library, Prague. M
- Endeavour*. Imperial Chemical Industries, London. Q
- **Endocrinology*. Endocrine Society, Philadelphia. M
- Energomashinostroenie*. Gosudarstvennyi Komitet Tiazhelogo, Energeticheskogo i Transportnogo Mashinostroeniia pri Gosplane SSSR, Leningrad. M
- The Engineer*. Morgan Brothers (Publishers), Ltd., London. W
- Engineering*. Engineering, Ltd., London. W
- Engineering Bulletin*. Motorola, Inc., Military Electronics Div., Scottsdale, Ariz. Irreg.
- Engineering Cybernetics (Akademiia Nauk SSSR, Izvestiia, Tekhnicheskaiia Kibernetika)*. Institute of Electrical and Electronics Engineers, Inc., New York. BM
- Engineering Journal*. Engineering Institute of Canada, Montreal. M
- English Electric Journal*. English Electric Co., Ltd., Stafford, England. BM

- Entropie*. Editions Bartheye & Cie, Paris. BM
- Environmental Engineering*. Society of Environmental Engineers; Kenneth Mason Publications, Ltd., London. BM
- Environmental Quarterly*. Environmental Publications, Inc., Little Neck, N.Y. Q
- **Enzymologia*. The Hague. Irreg.
- Ericsson Technics*. Telefonaktiebolaget LM Ericsson, Stockholm. SA
- Esso Air World*. Esso International, Inc., New York. BM
- Evaluation Engineering*. A. Verner Nelson Associates, Chicago. BM
- **Excerpta Medica International Congress Series*. Excerpta Medica Foundation, Amsterdam. M
- Experimental Mechanics*. Society for Experimental Stress Analysis, Westport, Conn. M
- **Experimental Neurology*. Academic Press, Inc., New York. BM
- Explosifs*. Association des Fabricants Belges d'Explosifs et de Recherches Scientifiques; Editions Science et Technique, Brussels. Q
- Explosivstoffe*. Erwin Barth Verlag KG, Mannheim, Germany. M

F

- **Federation Proceedings*. Federation of American Societies for Experimental Biology, Washington, D.C. Q
- Finommechanika*. Budapest. M
- Fizika*. Ministerstvo Vysshogo i Srednego Spetsial'nogo Obrazovaniia SSSR; Tomskii Universitet, Tomsk. BM
- Fizika Gorenii i Vzryva*. Akademiia Nauk SSSR, Sibirskoe Otdelenie; Izdatel'stvo Nauka, Novosibirsk. Q
- Fizika i Tekhnika Poluprovodnikov*. Akademiia Nauk SSSR; Izdatel'stvo Nauka, Leningrad. M
- Fizika Metallov i Metallovedenie*. Akademiia Nauk SSSR, Sverdlovsk. M
- Fizika Tverdogo Tela*. Akademiia Nauk SSSR, Moscow. M
- Flight International*. Iliffe Transport Publications, Ltd., London. W
- Flug-Revue*. Vereinigte Motor-Verlage GmbH, Stuttgart. M
- Flugwelt*. Krausskopf-Flugwelt-Verlag GmbH, Mainz. M
- Forces Aériennes Françaises*. Comité d'Etudes Aéronautiques Militaires, Paris. M
- Forschung im Ingenieurwesen*. VDI-Verlag GmbH, Düsseldorf. BM
- **Fortschritte der Mineralogie*. Deutsche mineralogische Gesellschaft; Schweizerbart'sche Verlagsbuchhandlung, Stuttgart.
- France, Ministère de l'Air, Publications Scientifiques et Techniques*. Service de Documentation Scientifique et Technique de l'Armement, Paris. Irreg.
- France, Ministère de l'Air, Publications Scientifiques et Techniques, Notes Techniques*. Service de Documentation Scientifique et Technique de l'Armement, Paris. Irreg.

- Franklin Institute, Journal*. Franklin Institute, Philadelphia. M
- Frequency*. Frequency, Inc., Brookline, Mass. BM
- Frequenz*. Fachverlag Schiele und Schön, Berlin. M
- Fujitsu Scientific and Technical Journal*. Fujitsu, Ltd., Kanagawa, Japan. SA
- Fyzikálny Časopis*. Slovenska Akademia Vied, Bratislava. Q

G

- G. E. C. Journal of Science and Technology*. General Electric Co., Ltd., London. 3 issues per year
- Geliotekhnika*. Akademiia Nauk Uzbekskoi SSR, Tashkent. BM
- General Motors Engineering Journal*. General Motors Corp., Warren, Mich. Q
- Genève, Société de Physique et d'Histoire Naturelle, Compte Rendu des Séances*. Genève, Société de Physique et d'Histoire Naturelle, Geneva. 3 issues per year
- Geochimica et Cosmochimica Acta*. Pergamon Press, Ltd., Oxford. M
- Geodesy and Aerophotography (Geodeziia i Aerofotos'emka)*. American Geophysical Union, Washington, D. C. BM
- **Geodetic Society of Japan, Journal*. Chiba, Japan. Irreg.
- Geodeziia i Aerofotos'emka*. Moskovskii Institut Inzhenerov Geodezii, Aerofotos'emki i Kartografi, Moscow. BM
- Geodeziia i Kartografiia*. Gosudarstvennyi Geologicheskii Komitet SSSR, Moscow. M
- Geodezja i Kartografia*. Polska Akademia Nauk, Komitet Geodezji; Państwowe Wydawnictwo Naukowe, Warsaw. Q
- Geofisica e Meteorologia*. Società Italiana di Geofisica e Meteorologia, Genoa. BM
- Geofysikální Sborník*. Československá Akademie Věd, Geofysikální Ustav, Prague. Annual
- Geofysiske Publikasjoner (Geophysica Norvegica)*. Norske Videnskaps-Akademi, Oslo. Irreg.
- **Geologiska Föreningens i Stockholm Förhandlingar*. Stockholm. Q
- Geomagnetism and Aeronomy (Geomagnetizm i Aeronomiia)*. American Geophysical Union, Washington, D.C. BM
- Geomagnetizm i Aeronomiia*. Akademiia Nauk SSSR, Moscow. BM
- Geophysical Journal*. Royal Astronomical Society, London. M
- Gerlands Beiträge zur Geophysik*. Akademische Verlagsgesellschaft Geest & Portig, KG, Leipzig. BM
- Glavnaia Geofizicheskaiia Observatoriia imeni A. I. Voeikova, Trudy*. Glavnoe Upravlenie Gidrometeorologicheskoi Sluzhby pri Sovete Ministrov SSSR, Leningrad.

H

- Hawker Siddeley Review*. The Hawker Siddeley Group, London. Q
- Helvetica Physica Acta*. Societas Physicae Helveticae, Basel. BM

- High Temperature (Teplofizika Vysokikh Temperatur).* Consultants Bureau Enterprises, Inc., New York. BM
- Hiroshima University, Journal of Science, Series A - II.* Hiroshima University, Hiroshima. SA
- Hochfrequenztechnik und Elektroakustik.* Akademische Verlagsgesellschaft Geest & Portig, KG, Leipzig. BM
- Hovering Craft and Hydrofoil.* Kalerghi Publications, London. M
- Human Factors.* Pergamon Press, Ltd., Oxford. BM
- Hydraulics and Pneumatics.* Industrial Publishing Corp., Cleveland. M

I

- Iasi, Institutul Politehnic, Buletinul.* Iasi, Institutul Politehnic, Iasi, Rumania. Q
- IBM Journal of Research and Development.* International Business Machines Corp., New York. BM
- IBM Systems Journal.* International Business Machines Corp., New York. Q
- Icarus.* Academic Press, Inc., New York. BM
- I & EC — Industrial and Engineering Chemistry.* American Chemical Society, Washington, D.C. M
- I & EC — Industrial and Engineering Chemistry, Fundamentals.* American Chemical Society, Washington, D. C. Q
- I & EC — Industrial and Engineering Chemistry, Process Design and Development.* American Chemical Society, Washington, D. C. Q
- I & EC — Industrial and Engineering Chemistry, Product Research and Development.* American Chemical Society, Washington, D. C. Q
- IEEE, Proceedings.* Institute of Electrical and Electronics Engineers, Inc., New York. M
- IEEE Journal of Quantum Electronics.* Institute of Electrical and Electronics Engineers, Inc., New York. M
- IEEE Journal of Solid-State Circuits.* Institute of Electrical and Electronics Engineers, Inc., New York. Q
- IEEE Spectrum.* Institute of Electrical and Electronics Engineers, Inc., New York. M
- IEEE Transactions on Aerospace and Electronic Systems.* Institute of Electrical and Electronics Engineers, Inc., New York. BM
- IEEE Transactions on Antennas and Propagation.* Institute of Electrical and Electronics Engineers, Inc., New York. BM
- IEEE Transactions on Automatic Control.* Institute of Electrical and Electronics Engineers, Inc., New York. Q
- IEEE Transactions on Bio-Medical Engineering.* Institute of Electrical and Electronics Engineers, Inc., New York. Q
- IEEE Transactions on Broadcasting.* Institute of Electrical and Electronics Engineers, Inc., New York. Q
- IEEE Transactions on Circuit Theory.* Institute of Electrical and Electronics Engineers, Inc., New York. Q
- IEEE Transactions on Communication Technology.* Institute of Electrical and Electronics Engineers, Inc., New York. Q
- IEEE Transactions on Education.* Institute of Electrical and Electronics Engineers, Inc., New York. Q
- IEEE Transactions on Electrical Insulation.* Institute of Electrical and Electronics Engineers, Inc., New York. Irreg.
- IEEE Transactions on Electromagnetic Compatibility.* Institute of Electrical and Electronics Engineers, Inc., New York. Q
- IEEE Transactions on Electron Devices.* Institute of Electrical and Electronics Engineers, Inc., New York. M
- IEEE Transactions on Electronic Computers.* Institute of Electrical and Electronics Engineers, Inc., New York. BM
- IEEE Transactions on Engineering Management.* Institute of Electrical and Electronics Engineers, Inc., New York. Q
- IEEE Transactions on Engineering Writing and Speech.* Institute of Electrical and Electronics Engineers, Inc., New York. Irreg.
- IEEE Transactions on Human Factors in Electronics.* Institute of Electrical and Electronics Engineers, Inc., New York. Irreg.
- IEEE Transactions on Industrial Electronics and Control Instrumentation.* Institute of Electrical and Electronics Engineers, Inc., New York. Irreg.
- IEEE Transactions on Information Theory.* Institute of Electrical and Electronics Engineers, Inc., New York. Q
- IEEE Transactions on Instrumentation and Measurement.* Institute of Electrical and Electronics Engineers, Inc., New York. Q
- IEEE Transactions on Magnetics.* Institute of Electrical and Electronics Engineers, Inc., New York. Q
- IEEE Transactions on Microwave Theory and Techniques.* Institute of Electrical and Electronics Engineers, Inc., New York. BM
- IEEE Transactions on Nuclear Science.* Institute of Electrical and Electronics Engineers, Inc., New York. BM
- IEEE Transactions on Parts, Materials and Packaging.* Institute of Electrical and Electronics Engineers, Inc., New York. Q
- IEEE Transactions on Reliability.* Institute of Electrical and Electronics Engineers, Inc., New York. Irreg.
- IEEE Transactions on Sonics and Ultrasonics.* Institute of Electrical and Electronics Engineers, Inc., New York. Irreg.
- IEEE Transactions on Systems Science and Cybernetics.* Institute of Electrical and Electronics Engineers, Inc., New York. Irreg.
- IEEE Transactions on Vehicular Communications.* Institute of Electrical and Electronics Engineers, Inc., New York. Irreg.
- *Illinois Journal of Mathematics.* University of Illinois Press, Urbana, Ill. Q
- *Illinois State Academy of Science, Transactions.* Illinois State Museum, Springfield, Ill. Q
- Indian Academy of Sciences, Proceedings, Section A.* Indian Academy of Sciences, Bangalore. M
- Indian Institute of Science, Journal.* Indian Institute of Science, Bangalore. Q
- Indian Journal of Mathematics.* Allahabad Mathematical Society, Allahabad. SA

- Indian Journal of Meteorology and Geophysics.* India Meteorological Department, Delhi. Q
- Indian Journal of Pure and Applied Physics.* Council of Scientific and Industrial Research, New Delhi. M
- Indian Journal of Technology.* Council of Scientific and Industrial Research, New Delhi. M
- Industrial Electronics.* Iliffe Electrical Publications, Ltd., London. M
- Industrial Laboratory (Zavodskaia Laboratoriia).* Instrument Society of America, Pittsburgh. M
- Industrial Quality Control.* American Society for Quality Control, Inc., Milwaukee. M
- Industrial Research.* Industrial Research, Inc., Beverly Shores, Ind. M
- Information and Control.* Academic Press, Inc., New York. BM
- Information Display.* Information Display Publications, Inc., Los Angeles. BM
- Infrared Physics.* Pergamon Press, Ltd., Oxford. Q
- Ingeniería Aeronáutica y Astronáutica.* Asociación de Ingenieros Aeronáuticos, Madrid. BM
- Ingenieur-Archiv.* Springer Verlag, Berlin. Irreg.
- **Inorganic Chemistry.* American Chemical Society, Washington, D. C. M
- Institut Français du Pétrole, Revue.* Editions Technip, Paris. M
- Institut Royal Météorologique de Belgique, Publications, Série B.* Institut Royal Météorologique de Belgique, Brussels. Irreg.
- Institute of Mathematics and Its Applications, Journal.* Academic Press, Ltd., London. Q
- Institute of Navigation, Journal.* Institute of Navigation, London. Q
- Institute of Physical and Chemical Research, Scientific Papers.* Tokyo Rikagaku Kenkyusho, Tokyo. Q
- **Institute of Statistical Mathematics, Annals.* Institute of Statistical Mathematics; Japan Publications Trading Co., Tokyo. 3 issues per year
- Institution of Electrical Engineers, Proceedings.* Institution of Electrical Engineers, London. M
- **Institution of Engineers (Australia), Mechanical and Chemical Engineering Transactions.* Commonwealth Scientific and Industrial Research Organization, Melbourne.
- Institution of Engineers (India), Journal, Electronics and Telecommunication Engineering Division.* The Institution of Engineers, Calcutta. 3 issues per year
- Institution of Engineers (India), Journal, Mechanical Engineering Division.* Institution of Engineers, Calcutta. BM
- Institution of Mechanical Engineers, Proceedings.* Institution of Mechanical Engineers, London. Irreg.
- Institution of Radio and Electronics Engineers (Australia), Proceedings.* Institution of Radio and Electronics Engineers, Sydney. M
- **Institution of Telecommunication Engineers, Journal.* Institution of Telecommunication Engineers, New Delhi. M
- Instituto de Matemática, Astronomía y Física, Boletín.* Córdoba, Universidad Nacional, Córdoba, Argentina. SA
- Instrument Practice.* United Trade Press, Ltd., London. M
- Instrumentation Technology.* Instrument Society of America, Pittsburgh. M
- Instruments and Control Systems.* Instruments Publishing Co., Inc., Pittsburgh. M
- Instruments and Experimental Techniques (Pribery i Tekhnika Eksperimental).* Instrument Society of America, Pittsburgh. BM
- Instytut Lotnictwa, Prace.* Instytut Lotnictwa, Warsaw. Irreg.
- Instytut Maszyn Przepływowych, Prace.* Polska Akademia Nauk, Instytut Maszyn Przepływowych, Gdansk.
- Interavia.* Interavia S. A., Geneva. M
- Inter-Electronique.* Editions LEPS, Paris. M
- International Chemical Engineering.* American Institute of Chemical Engineers, New York. Q
- International Journal of Control, First Series.* Taylor and Francis, Ltd., London. M
- International Journal of Electronics, First Series.* Taylor and Francis, Ltd., London. M
- International Journal of Engineering Science.* Pergamon Press, Ltd., Oxford. BM
- International Journal of Fracture Mechanics.* P. Noordhoff, Ltd., Groningen, Netherlands. Q
- International Journal of Heat and Mass Transfer.* Pergamon Press, Ltd., Oxford. M
- International Journal of Mechanical Sciences.* Pergamon Press, Ltd., Oxford. M
- International Journal of Non-Linear Mechanics.* Pergamon Press, Ltd., Oxford. Q
- International Journal of Powder Metallurgy.* American Powder Metallurgy Institute, New York. Q
- International Journal of Solids and Structures.* Pergamon Press, Ltd., Oxford. Q
- International Science and Technology.* Conover-Mast Publications, Inc., New York. M
- Internationale elektronische Rundschau.* Verlag für Radio-Foto-Kinotechnik GmbH, Berlin. M
- **Internationale Zeitschrift für angewandte Physiologie einschliesslich Arbeitsphysiologie.* Springer Verlag, Berlin. 3 issues per year
- **Investigative Urology.* Williams & Wilkins Co., Baltimore. BM
- Inzhenerno-Fizicheskii Zhurnal.* Akademiia Nauk BSSR, Minsk. M
- Inzhenernyi Zhurnal - Mekhanika Tverdogo Tela.* Akademiia Nauk SSSR, Moscow. BM
- **Irish Astronomical Journal.* Irish Astronomical Society, Armagh, Northern Ireland. M
- ISA Transactions.* Instrument Society of America, Pittsburgh. Q
- Ishikawajima-Harima Engineering Review.* Ishikawajima-Harima Heavy Industries Co., Ltd., Tokyo. BM
- Israel Journal of Mathematics.* Weizmann Science Press of Israel, Jerusalem. Q
- Israel Journal of Technology.* Weizmann Science Press of Israel, Jerusalem. Q

J

- Japan Institute of Metals, Transactions.* Japan Institute of Metals, Sendai. Q
- Japan Society for Aeronautical and Space Sciences, Journal.* Japan Society for Aeronautical and Space Sciences, Tokyo. M

INTERNATIONAL AEROSPACE ABSTRACTS

- Japan Society for Aeronautical and Space Sciences, Transactions.* Japan Society for Aeronautical and Space Sciences, Tokyo. M
- Japan Society of Lubrication Engineers, Journal.* Japan Society of Lubrication Engineers, Tokyo. M
- Japanese Journal of Applied Physics.* Physical Society of Japan and Japan Society of Applied Physics, Tokyo. M
- Jemná Mechanika a Optika.* Ministerstvo Těžkého Průmyslu; Státní Nakladatelství Technické Literatury, Prague. M
- JETP Letters (ZHETF Pis'ma v Redaktsiiu).* American Institute of Physics, Inc., New York. SM
- Journal d'Analyse Mathématique.* Jerusalem Academic Press, Ltd., Jerusalem.
- Journal de Mathématiques Pures et Appliquées.* Gauthier-Villars & Cie, Paris. Q
- Journal de Mécanique.* Gauthier-Villars & Cie, Paris. M
- Journal de Physique.* Société Française de Physique, Paris. M
- Journal of Air Law and Commerce.* Southern Methodist University, School of Law, Dallas. Q
- Journal of Aircraft.* American Institute of Aeronautics and Astronautics, Inc., New York. BM
- Journal of Applied Mechanics and Technical Physics (PMTF - Zhurnal Prikladnoi Mekhaniki i Tekhnicheskoi Fiziki).* The Faraday Press, Inc., New York. BM
- Journal of Applied Meteorology.* American Meteorological Society, Boston. Q
- Journal of Applied Physics.* American Institute of Physics, Inc., New York. M
- **Journal of Applied Physiology.* American Physiological Society, Washington, D.C. BM
- **Journal of Applied Polymer Science.* Interscience Publishers, New York. BM
- Journal of Atmospheric and Terrestrial Physics.* Pergamon Press, Ltd., Oxford. M
- **Journal of Bacteriology.* American Society of Microbiology, Baltimore.
- **Journal of Biological Chemistry.* American Society of Biological Chemists, Baltimore. M
- **Journal of Bone and Joint Surgery.* American Orthopaedic Association, Boston. 8 issues per year
- Journal of Chemical Physics.* American Institute of Physics, Inc., New York. SM
- **Journal of Clinical Investigation.* American Society for Clinical Investigation, Inc., Boston. M
- **Journal of Comparative and Physiological Psychology.* American Psychological Association, Inc., Washington, D.C. BM
- Journal of Composite Materials.* Technomic Publishing Co., Inc., Stamford, Conn. Q
- Journal of Computational Physics.* Academic Press, Inc., New York. Q
- Journal of Computer and System Sciences.* Academic Press, Inc., New York. Q
- Journal of Differential Equations.* Academic Press, Inc., New York. Q
- Journal of Engineering Mathematics.* P. Noordhoff, Ltd., Groningen. Q
- Journal of Engineering Physics (Inzhenerno-Fizicheskii Zhurnal).* The Faraday Press, Inc., New York. M
- Journal of Engineering Psychology.* Elias Publications, Washington, D. C. Q
- Journal of Environmental Sciences.* Institute of Environmental Sciences, Mt. Prospect, Ill. BM
- **Journal of Experimental Psychology.* American Psychological Association, Washington, D.C. M
- Journal of Fluid Mechanics.* Cambridge University Press, London. M
- **Journal of General Microbiology.* Society for General Microbiology; Cambridge University Press, London. M
- **Journal of Geomagnetism and Geoelectricity.* Kyoto University, Geophysical Institute, Kyoto, Japan. Q
- Journal of Geophysical Research.* American Geophysical Union, Washington, D. C. SM
- **Journal of Inorganic and Nuclear Chemistry.* Pergamon Press, Ltd., Oxford. M
- **Journal of Laboratory and Clinical Medicine.* Central Society for Clinical Research, St. Louis. M
- **Journal of Laryngology and Otology.* Headley Bros., London. M
- Journal of Materials.* American Society for Testing and Materials, Philadelphia. Q
- Journal of Materials Science.* Chapman & Hall, Ltd., London. Q
- Journal of Mathematical Analysis and Applications.* Academic Press, Inc., New York. BM
- Journal of Mathematical Physics.* American Institute of Physics, Inc., New York. M
- Journal of Mathematics and Mechanics.* Indiana University, Graduate Institute for Mathematics and Mechanics, Bloomington; Technology Press, Cambridge, Mass. BM
- Journal of Mathematics and Physics.* Massachusetts Institute of Technology, Cambridge, Mass. Q
- Journal of Mechanical Engineering Science.* Institution of Mechanical Engineers, London. Q
- Journal of Metals.* American Institute of Mining, Metallurgical and Petroleum Engineers, Inc., New York. M
- Journal of Microwave Power.* International Microwave Power Institute, Vancouver. Q
- Journal of Nuclear Energy, Part C - Plasma Physics, Accelerators, Thermonuclear Research (see Plasma Physics).*
- **Journal of Organic Chemistry.* American Chemical Society, Washington, D.C. M
- **Journal of Pharmacology and Experimental Therapeutics.* American Society for Pharmacology and Experimental Therapeutics, Inc.; Williams and Wilkins Co., Baltimore. M
- Journal of Photographic Science.* Royal Photographic Society of Great Britain, London. BM
- Journal of Physical Chemistry.* American Chemical Society, Washington, D. C. M
- **Journal of Physics and Chemistry of Solids.* Pergamon Press, Ltd., Oxford. M
- Journal of Plasma Physics.* Cambridge University Press, London. Q
- **Journal of Polymer Science, Part B — Polymer Letters.* Interscience Publishers, Inc., New York. M
- **Journal of Polymer Science, Part C — Polymer Symposia.* Interscience Publishers, Inc., New York. M
- **Journal of Quantitative Spectroscopy and Radiative Transfer.* Pergamon Press, Ltd., Oxford. Q

- Journal of Research, Section A – Physics and Chemistry.* National Bureau of Standards; Supt. of Documents, Washington, D. C. BM
- Journal of Research, Section B – Mathematics and Mathematical Physics.* National Bureau of Standards; Supt. of Documents, Washington, D. C. Q
- Journal of Research, Section C – Engineering and Instrumentation.* National Bureau of Standards; Supt. of Documents, Washington, D. C. Q
- Journal of Scientific and Industrial Research.* Council of Scientific and Industrial Research, New Delhi. M
- Journal of Scientific Instruments.* Institute of Physics and The Physical Society, London. M
- Journal of Sound and Vibration.* Academic Press, Inc., New York. Q
- Journal of Spacecraft and Rockets.* American Institute of Aeronautics and Astronautics, Inc., New York. BM
- Journal of Strain Analysis.* Institution of Mechanical Engineers, London. Q
- **Journal of Surgical Research.* W. B. Saunders Co., Philadelphia. M
- Journal of Technology.* Bengal Engineering College, Howrah, India. SA
- Journal of the Astronautical Sciences.* American Astronautical Society, Inc., Baltimore. BM
- Journal of the Atmospheric Sciences.* American Meteorological Society, Boston. BM
- Journal of the Less-Common Metals.* Elsevier Publishing Co., Amsterdam. M
- Journal of the Mechanics and Physics of Solids.* Pergamon Press, Ltd., Oxford. BM
- Journal of Vacuum Science and Technology.* American Institute of Physics, Inc., New York. BM
- JSME, Bulletin.* Japan Society of Mechanical Engineers, Tokyo. Q

K

- Kakioka Magnetic Observatory, Memoirs.* Kakioka Magnetic Observatory, Kakioka, Japan.
- Khimii i Tekhnologiiia Topliv i Masel.* Ministerstvo Neftpererabatyvaiushchei i Neftekhimicheskoi Promyshlennosti SSSR, Akademiia Nauk SSSR, and Nauchno-Tekhnicheskoe Obshchestvo Neftianoi i Gazovoi Promyshlennosti, Moscow. M
- Kibernetika.* Akademiia Nauk Ukrainskoi SSR; Naukova Dumka, Kiev. BM
- Kinetika i Kataliz.* Akademiia Nauk SSSR, Sibirskoe Otdelenie, Novosibirsk. BM
- **Kolloid-Zeitschrift und Zeitschrift für Polymere.* Dr. Dietrich Steinkopff Verlag, Darmstadt, Germany. M
- Koninklijke Nederlandse Akademie van Wetenschappen, Proceedings, Series B - Physical Sciences.* North-Holland Publishing Co., Amsterdam. 5 issues per year
- Kosmicheskaiia Biologiia i Meditsina.* Ministerstvo Zdravookhraneniia SSSR; Izdatel'stvo Meditsina, Moscow. BM
- Kosmicheskii Issledovaniia.* Akademiia Nauk SSSR, Moscow. BM
- Kovové Materiály.* Slovak Academy of Science, Prague. BM
- Kristallografiia.* Akademiia Nauk SSSR, Moscow. BM

- **Kybernetik.* Springer Verlag, Berlin. Annual
- Kybernetika.* State Technical Library, Prague.
- Kyoto University, Faculty of Engineering, Memoirs.* Kyoto University, Faculty of Engineering, Kyoto, Japan. Q
- Kyushu University, Research Institute for Applied Mechanics, Reports.* Kyushu University, Fukuoka. Irreg.

L

- **Laboratory Investigation.* International Academy of Pathology, New York. M
- **Language and Speech.* Robert Draper, Ltd., Teddington, Middx., England. Q
- Laser Focus.* International Data Publishing Co., Newtonville, Mass. M
- Lasers.* PML Banque Européenne d'Informations, Paris. BM
- Leningradskii Universitet, Vestnik, Serii Matematiki, Mekhaniki i Astronomii.* Leningradskii Universitet, Leningrad. Q
- Lietuvos Fizikos Rinkiny.* Akademiia Nauk Litovskoi SSR, Vilnius. Q
- **Life Sciences.* Pergamon Press, Ltd., Oxford. BW
- Light Metals (Tokyo).* Japan Institute of Metals, Tokyo. BM
- **Lipids.* American Oil Chemists' Society, Chicago. BM
- Lockheed Georgia Quarterly.* Lockheed-Georgia Co., Marietta, Ga. Q
- Lockheed Horizons.* Lockheed-California Co., Burbank, Calif. Q
- Lockheed Service Digest.* Lockheed-California Co., Burbank, Calif. BM
- Lubrication.* Texaco, Inc., New York. M
- Lubrication Engineering.* American Society of Lubrication Engineers, Park Ridge, Ill. M
- Luftfahrt-Forschungsberichte.* Verein deutscher Ingenieure, Düsseldorf. Irreg.
- Luftfahrt-Zubehör.* Luftfahrtverlag Walter Zuerl, Steinbach/Wörthsee, Germany. M
- Luftfahrttechnik Raumfahrttechnik.* Verlag Deutscher Ingenieure, Düsseldorf. M

M

- Machine Design.* Penton Publishing Co., Cleveland. BW
- Machinery and Production Engineering.* Machinery Publishing Co., Ltd., London. W
- Magnetohydrodynamics (Magnitnaia Gidrodinamika).* The Faraday Press, Inc., New York. Q
- Magnitnaia Gidrodinamika.* Akademiia Nauk Latvinskoi SSR, Riga. Q
- Marconi Review.* Marconi Co., Ltd., Chelmsford, Essex., England. Q
- Matematicheskii Institut imeni V. A. Steklova, Trudy.* Akademiia Nauk SSSR, Moscow. Irreg.
- Matematicheskii Sbornik.* Izdatel'stvo Nauka, Moscow. M
- Matematicko-Fyzikálny Časopis.* Slovenská Akadémia Vied, Bratislava. Q

Matematika. Kazanskii Gosudarstvennyi Universitet, Kazan. BM

Materials Evaluation. Society for Nondestructive Testing, Evanston. M

Materials Protection. National Association of Corrosion Engineers, Inc., Houston. M

Materials Research and Standards. American Society for Testing and Materials, Philadelphia. M

Materials Science and Engineering. Elsevier Publishing Co., Amsterdam. BM

Mathematica. Societatea de Științe Matematice și Fizice, Filiala Cluj, Cluj, Rumania. SA

**Mathematics Magazine*. Mathematical Association of America, University of Buffalo, Buffalo. BM

Mathematics of Computation. American Mathematical Society, Providence. Q

Mathematika. University College, Dept. of Mathematics, London. SA

**Mathematische Annalen*. Springer Verlag, Berlin.

Max-Planck-Institut für Aeronomie, Mitteilungen. Springer Verlag, Berlin. Irreg.

Meccanica. Italian Association of Theoretical and Applied Mechanics; Tamburini Editore, Milan. Q

Mechanical Engineering. American Society of Mechanical Engineers, New York. M

Mechanika Teoretyczna i Stosowana. Polskie Towarzystwo Mechaniki Teoretycznej i Stosowanej; Państwowe Wydawnictwo Naukowe, Warsaw. Q

Mekhanika Polimerov. Akademiia Nauk Latviiskoi SSR, Riga. BM

Mérés és Automatika. Budapest. M

Metal Progress. American Society for Metals, Metals Park, Ohio. M

Metal Science and Heat Treatment (Metallovedenie i Termicheskaiia Obrabotka Metallov). Consultants Bureau Enterprises, Inc., New York. BM

Metallovedenie i Termicheskaiia Obrabotka Metallov. Ministerstvo Tiazhelogo Mashinostroeniia and Tsentral'nyi Nauchno-Issledovatel'skii Institut Tekhnologii i Mashinostroeniia, Moscow.

Metals Engineering Quarterly. American Society for Metals, Metals Park, Ohio. Q

**Meteoritics*. Meteoritical Society, New Haven, Conn.; c/o Gerald L. Rowland, Long Beach City College, Long Beach, Calif. Irreg.

Meteorological Magazine. Meteorological Office; Her Majesty's Stationery Office, London. M

**Meteorological Society of Japan, Journal*. Japan Publications Trading Co., Tokyo. BM

Meteorologische Rundschau. Springer Verlag, Berlin. BM

Microelectronics and Reliability. Pergamon Press, Ltd., Oxford. Q

Microwave Journal. Horizon House, Inc., Dedham, Mass. M

Microwaves. Hayden Microwaves Corp., New York. M

Missili e Spazio. Associazione Italiana Razzi, Rome. BM

Mitsubishi Denki Laboratory Reports. Mitsubishi Electric Corp., Central Research Laboratories, Minami Shimizu, Amagasaki, Hyogo Prefecture, Japan. Q

Molecular Crystals. Gordon & Breach Science Publishers, Inc., New York. Q

**Monatshefte für Mathematik*. Springer Verlag, Vienna. 5 issues per year

Monthly Weather Review. U.S. Weather Bureau, Washington, D. C. M

Moskovskii Universitet, Vestnik, Serii I – Matematika, Mekhanika. Moskovskii Universitet, Moscow. BM

Moskovskii Universitet, Vestnik, Serii III – Fizika, Astronomiia. Moskovskii Universitet, Moscow. BM

Motorola Monitor. Motorola Semiconductor Products, Inc., Phoenix. BM

**Multivariate Behavioral Research*. Society of Multivariate Experimental Psychology; Texas Christian University, Fort Worth. Q

N

Nachrichtentechnische Zeitschrift. Nachrichtentechnische Gesellschaft; Friedr. Vieweg & Sohn, Braunschweig. M

Nagoya University, Faculty of Engineering, Memoirs. Nagoya University, Nagoya, Japan. Irreg.

Nagoya University, Institute of Plasma Physics, Annual Review. Nagoya University, Nagoya. Annual

Nagoya University, Research Institute of Atmospheric Proceedings. Nagoya University, Nagoya. Irreg.

**National Academy of Sciences, Proceedings*. National Academy of Sciences, Washington, D.C. M

National Institute of Sciences of India, Proceedings. National Institute of Sciences of India, New Delhi. BM

Nature. Macmillan & Co., Ltd., London. W

**Naturwissenschaftliche Rundschau*. Wissenschaftliche Verlagsgesellschaft mbH, Stuttgart. M

Naval Research Logistics Quarterly. U. S. Navy, Office of Naval Research; Supt. of Documents, Washington, D. C. Q

Navigation. Institute of Navigation, Washington, D. C. Q

Navigation (Paris). Institut Français de Navigation, Paris. Q

NEC Research and Development. Nippon Electric Co., Ltd., Tokyo. SA

**New Scientist*. London. Irreg.

New York Academy of Sciences, Annals. New York Academy of Sciences, New York. Irreg.

Nihon University, Research Institute of Technology, Journal. Nihon University, Tokyo. Irreg.

Nordrhein-Westfalen, Forschungsberichte. Westdeutscher Verlag, Cologne. Irreg.

**Norelco Reporter*. Philips Electronic Instruments, Mount Vernon, N.Y. Q

NTZ-Communications Journal. Friedr. Vieweg & Sohn, GmbH, Braunschweig. BM

Nuclear Applications. American Nuclear Society, Inc., Hinsdale, Ill. BM

Nuclear Engineering and Design (formerly Nuclear Structural Engineering). North-Holland Publishing Co., Amsterdam. BM

Nuclear Fusion. International Atomic Energy Agency, Vienna. Q

**Nuclear Instruments and Methods*. North-Holland Publishing Co., Amsterdam. M

**Nuclear Physics*. North-Holland Publishing Co., Amsterdam. BW

- **Nuclear Science and Engineering*. American Nuclear Society, Inc., Hinsdale, Ill. M
Nukleonika (Warsaw). Polska Akademia Nauk; Państwowe Wydawnictwo Naukowe, Warsaw. M
Numerische Mathematik. Springer Verlag, Berlin. Irreg.
Nuovo Cimento. Società Italiana di Fisica, Bologna. SM
Nuovo Cimento, Supplemento. Società Italiana di Fisica, Bologna. Irreg.

O

- Observatorio de Madrid, Boletín Astronómico*. Instituto Geografico y Catastral, Madrid.
The Observatory. Royal Greenwich Observatory, Hailsham, Sussex, England. BM
**Oklahoma Academy of Science, Proceedings*.
L'Onde Electrique. Société Française des Electroniciens et des Radioélectriciens, Paris. M
ONERA, TP. Office National d'Etudes et de Recherches Aérospatiales, Chatillon-sous-Bagneux (Seine), France. Irreg.
Operations Research. Operations Research Society of America, Baltimore. BM
Optica Acta. Taylor & Francis, Ltd., London. Q
Optical Society of America, Journal. Optical Society of America, Inc., Washington, D. C. M
Optical Spectra. Optical Publishing Co., Inc., Pittsfield, Mass. Q
Optics and Spectroscopy (Optika i Spektroskopiia). Optical Society of America, Inc., Washington, D. C. M
Optika i Spektroskopiia. Akademiia Nauk SSSR, Leningrad. M
**Organizational Behavior and Human Performance*. Academic Press, Inc., New York.
Osaka Prefecture, University, Bulletin, Series A - Engineering and Natural Sciences. Osaka Prefecture, University, Osaka. Irreg.
Osaka University, Technology Reports. Osaka University, Osaka. SA
Österreichische Akademie der Wissenschaften, Mathematisch-naturwissenschaftliche Klasse, Sitzungsberichte, Abteilung 2. Österreichische Akademie der Wissenschaften, Vienna. 10 issues per year

P

- Pacific Journal of Mathematics*. Berkeley, Calif. Q
Papers in Meteorology and Geophysics. Meteorological Research Institute, Tokyo. SA
**Patent, Trademark, and Copyright Journal of Research and Education*. Patent, Trademark and Copyright Research Institute, George Washington University, Washington, D.C. 5 issues per year
**Perception and Psychophysics*. Psychonomic Press, Goleta, Calif. M
**Perceptual and Motor Skills*. Southern Universities Press, Missoula, Mont. BM
Periodica Polytechnica, Electrical Engineering Series. Budapest, Polytechnical University, Budapest. Q
Periodica Polytechnica, Engineering Series. Budapest, Polytechnical University, Budapest. Q

- Philips Research Reports*. N. V. Philips' Gloeilampenfabrieken, Eindhoven. BM
Philips Research Reports Supplements. N. V. Philips' Gloeilampenfabrieken, Research Laboratories, Eindhoven. Irreg.
Philips Technical Review. N. V. Philips' Gloeilampenfabrieken, Research Laboratories, Eindhoven. M
Philips Telecommunication Review. N. V. Philips' Telecommunicatie Industrie, Hilversum. Q
Philosophical Magazine, 8th Series. Taylor and Francis, Ltd., London. M
Photogrammetria. Elsevier Publishing Co., Amsterdam. BM
Photogrammetric Engineering. American Society of Photogrammetry, Falls Church, Va. BM
Photographic Applications in Science and Technology. Photographic Applications in Science and Technology, Inc., New York. Q
Photographic Science and Engineering. Society of Photographic Scientists and Engineers, Washington, D. C. BM
Physica. Martinus Nijhoff, The Hague. M
Physica Status Solidi. Akademie Verlag GmbH, Berlin. M
Physical Review, 2nd Series. American Institute of Physics, Inc., New York. SM
Physical Review Letters. American Institute of Physics, Inc., New York. SM
Physical Society, Proceedings. Institute of Physics and The Physical Society, London. M
Physical Society of Japan, Journal. Physical Society of Japan, Tokyo. M
**Physics Letters*. North-Holland Publishing Co., Amsterdam. 4 issues per mo.
Physics of Fluids. American Institute of Physics, Inc., New York. M
Physics of Metals and Metallography (Fizika Metallov i Metallovedenie). Pergamon Press, Ltd., Oxford. M
Physics Today. American Institute of Physics, Inc., New York. M
**Physiologia Plantarum*. Scandinavian Society for Plant Physiology, Copenhagen. Q
Pisa, Scuola Normale Superiore, Annali, Scienze Fisiche e Matematiche. Pisa, Scuola Normale Superiore, Pisa. Q
Planetary and Space Science. Pergamon Press, Ltd., Oxford. M
**Plant Physiology*. American Society of Plant Physiology, Washington, D. C. BM
Plasma Physics (formerly *Journal of Nuclear Energy, Part C - Plasma Physics, Accelerators, Thermonuclear Research*). Pergamon Press, Ltd., Oxford. BM
PMM - Journal of Applied Mathematics and Mechanics (Prikladnaia Matematika i Mekhanika). Pergamon Press, Ltd., Oxford. BM
PMTF - Zhurnal Prikladnoi Mekhaniki i Tekhnicheskoi Fiziki. Akademiia Nauk SSSR, Sibirskoe Otdelenie, Novosibirsk. BM
Point to Point Telecommunications. Marconi Co., Ltd., Communications Division, Chelmsford, England. 3 issues per year
Pokroky Matematiky, Fysiky a Astronomie. Československá Akademie Věd, Prague. BM

INTERNATIONAL AEROSPACE ABSTRACTS

- Pomiary, Automatyka, Kontrola.* Naczelna Organizacja Techniczna, Warsaw. M
- Poroshkovaia Metallurgiiia.* Akademiia Nauk Ukrainskoi SSR, Kiev. BM
- Postępy Astronomii.* Obserwatorium Astronomiczne Politechniki, Warsaw. Q
- Postępy Fizyki.* Polskie Towarzystwo Fizyczne, Warsaw. BM
- Powder Technology.* Elsevier Publishing Co., Amsterdam. BM
- Priborostroenie.* Leningradskii Institut Tochnoi Mekhaniki i Optiki, Leningrad. BM
- Pribory i Tekhnika Eksperimenta.* Akademiia Nauk SSSR, Moscow. BM
- Prikladnaia Matematika i Mekhanika.* Akademiia Nauk SSSR, Otdelenie Tekhnicheskikh Nauk, Institut Mekhaniki, Moscow. BM
- Prikladnaia Mekhanika.* Akademiia Nauk Ukrainskoi SSR, Otdelenie Matematiki, Mekhaniki i Kibernetiki, Kiev. M
- Problemy Peredachi Informatsii.* Akademiia Nauk SSSR; Izdatel'stvo Nauka, Moscow. Q
- Proceedings of Vibration Problems.* Polish Academy of Sciences, Warsaw. Q
- Progress of Theoretical Physics.* Research Institute for Fundamental Physics and the Physical Society of Japan; Kyoto University, Kyoto, Japan. M
- Progress of Theoretical Physics, Supplement.* Research Institute for Fundamental Physics and the Physical Society of Japan; Kyoto University, Kyoto, Japan. BM
- Protection of Metals (Zashchita Metallov).* Scientific Information Consultants, Ltd., London. BM
- *Protoplasma.* Springer Verlag, Vienna. Irreg.
- Przegląd Elektroniki.* Polska Akademia Nauk, Komitet Elektroniki i Telekomunikacji and Stowarzyszenie Elektrykow Polskich, Sekcja Elektroniki i Telekomunikacji, Warsaw. M
- Przegląd Geodezyjny.* Warsaw. M
- *Psychonomic Science.* Goleta, Calif. M
- Pure and Applied Geophysics.* Birkhauser Verlag, Basel. 3 issues per year
- Pyrodynamics.* Gordon & Breach Science Publishers, Inc., New York. Q

Q

- Quarterly Journal of Mechanics and Applied Mathematics.* Oxford University Press, London. Q
- Quarterly of Applied Mathematics.* Brown University, Providence. Q

R

- *Radiation Research.* Academic Press, Inc., New York.
- *Radiation Research Supplement.* Academic Press, Inc., New York.
- Radio and Electronic Engineer.* British Institute of Radio Engineers, London. M
- Radio Engineering and Electronic Physics (Radiotekhnika i Elektronika).* Institute of Electrical and Electronics Engineers, Inc., New York. M

- Radio Research Laboratories, Journal.* Ministry of Posts and Telecommunications, Radio Research Laboratories, Tokyo. BM
- Radio Research Laboratories, Review.* Radio Research Laboratories, Ministry of Posts and Telecommunications, Tokyo. BM
- Radio Science.* Environmental Science Services Administration; Supt. of Documents, Washington, D.C. M
- Radioelektronika (formerly Radiotekhnika /Kiev/).* Ministerstvo Vysshogo Obrazovaniia, Kiev. M
- Radiofizika.* Gor'kovskii Universitet, Gorki. BM
- Radiotekhnika.* Nauchno-Tekhnicheskoe Obshchestvo Radiotekhniki i Elektrosviazi, Moscow. BM
- Radiotekhnika (Kiev) (see Radioelektronika).*
- Radiotekhnika i Elektronika.* Akademiia Nauk SSSR, Moscow. M
- Raumfahrtforschung.* Deutsche Gesellschaft für Raketentechnik und Raumfahrt, e.V., Stuttgart. Q
- RCA Review.* RCA Laboratories, Princeton, N. J. Q
- La Recherche Aéronautique.* Office National d'Etudes et de Recherches Aéronautiques, Chatillon-sous-Bagneux (Seine), France. BM
- La Recherche Spatiale.* Centre National d'Etudes Spatiales; Dunod Editeur, Paris. M
- *Regelungstechnik.* Verlag R. Oldenburg, Munich. M
- Report of Ionosphere and Space Research in Japan.* Science Council of Japan, Ionosphere Research Committee, Tokyo. Q
- Research/Development.* F. D. Thompson Publications, Inc., New York. M
- Research Institute for Applied Mechanics, Reports (see Kyushu University, Research Institute for Applied Mechanics, Reports).*
- Respiration Physiology.* North-Holland Publishing Co., Amsterdam. Q
- *Review of Economics and Statistics.* Harvard University Press, Cambridge, Mass. Q
- Review of Scientific Instruments.* American Institute of Physics, Inc., New York. M
- Reviews of Geophysics.* American Geophysical Union, Washington, D. C. Q
- Reviews of Modern Physics.* American Institute of Physics, Inc., New York. Q
- Revista de Aeronáutica y Astronáutica.* Ministerio del Aire, Madrid. M
- Revista Transporturilor.* Asociația Științifică a Inginerilor și Tehnicienilor din Republicii Populare Române, Bucharest. M
- Revue de Médecine Aéronautique (see Revue de Médecine Aéronautique et Spatiale).*
- Revue de Médecine Aéronautique et Spatiale.* Société Française de Physiologie et de Médecine Aéronautique et Cosmonautique; Masson et Cie., Paris. Q
- Revue de Métallurgie.* Paris. M
- Revue de Physique Appliquée.* Société Française de Physique, Centre National de la Recherche Scientifique, Paris. Q
- Revue d'Optique.* Institut d'Optique Théorique et Appliquée, Paris. M
- Revue Française d'Astronautique.* Société Française d'Astronautique, Paris. BM
- Revue Française de Droit Aérien.* Association d'Etudes et de Documentation de Droit Aérien, Paris. Q

S

- Revue Française de Mécanique.* Société Française des Mécaniciens, Paris. Q
- Revue Générale de l'Air et de l'Espace.* Editions Internationales, Paris. Q
- Revue Générale de l'Electricité.* Comité Electrotechnique Français et de l'Union Technique de l'Electricité, Paris. M
- Revue Générale de Thermique.* Institut Français des Combustibles et de l'Energie and Société Française des Thermiciens, Paris. M
- Revue mble.* Société Anonyme MBLE, Brussels. Q
- Revue Roumaine de Mathématiques Pures et Appliquées.* Académie de la République Populaire Roumaine, Bucharest. 10 issues per year
- Revue Roumaine des Sciences Techniques, Série de Mécanique Appliquée.* Académie de la République Populaire Roumaine, Bucharest. BM
- Revue Technique CECLES.* Gauthier-Villars & Cie, Paris. Q
- Revue Technique CFTH - HB.* Compagnie Française Thomson-Houston, Groupe Electronique, Paris. 3 issues per year
- **Rheologica Acta.* Dr. Dietrich Steinkopff Verlag, Darmstadt, Germany. Irreg.
- Ricerca Scientifica.* Consiglio Nazionale delle Ricerche, Rome. M
- Rivista Aeronautica.* Ministero Difesa Aeronautica, Rome. M
- Rivista di Ingegneria.* Milan. M
- Rivista di Medicina Aeronautica e Spaziale.* Rome. Q
- Rivista di Meteorologia Aeronautica.* Servizio Meteorologico d'Aeronautica, Rome. Q
- Roma, Università, Scuola d'Ingegneria Aerospaziale, Centro Ricerche Aerospaziali, Atti.* Roma, Università, Rome. Irreg.
- Royal Aeronautical Society, Journal.* Royal Aeronautical Society, London. M
- Royal Astronomical Society, Memoirs.* Royal Astronomical Society, London. BM
- Royal Astronomical Society, Monthly Notices.* Royal Astronomical Society, London. M
- **Royal Astronomical Society of Canada, Journal.* Royal Astronomical Society of Canada, Toronto. BM
- Royal Meteorological Society, Quarterly Journal.* Royal Meteorological Society, London. Q
- Royal Society (Edinburgh), Proceedings, Section A.* Royal Society of Edinburgh, Edinburgh. Irreg.
- Royal Society (London), Philosophical Transactions, Series A.* Royal Society, London. Irreg.
- Royal Society (London), Proceedings, Series A.* Royal Society, London. Irreg.
- Rozprawy Inżynierskie.* Polska Akademia Nauk, Instytut Podstawowych Problemów Techniki, Warsaw. Q
- **Rubber and Plastics Age.* Rubber and Technical Press, Ltd., London. M
- Ruimtevaart.* Nederlandse Vereniging voor Ruimtevaart, The Hague. Q
- Russian Journal of Physical Chemistry (Zhurnal Fizicheskoi Khimii).* Chemical Society, London. M
- Russian Mathematical Surveys (Uspekhi Matematicheskikh Nauk).* London Mathematical Society; Macmillan & Co., Ltd., London. BM
- **Schweizerische Bauzeitung.* W. Jegher & A. Ostertag, Zurich. W
- Science.* American Association for the Advancement of Science, Washington, D. C. W
- Science Journal.* Associated Iliffe Press, Ltd., London. M
- Science Progress.* Science Progress, London. Q
- Sciences et Industries Spatiales.* SADESI - Société Anonyme d'Editions Scientifiques et Industrielles, Geneva. BM
- Scientific American.* Scientific American, Inc., New York. M
- Semiconductor Products and Solid State Technology.* Cowan Publishing Corp., New York. M
- Shell Aviation News.* Shell Oil Co., London. M
- SIAM Journal on Applied Mathematics.* Society for Industrial and Applied Mathematics, Philadelphia. BM
- SIAM Journal on Control.* Society for Industrial and Applied Mathematics, Philadelphia. Q
- SIAM Journal on Numerical Analysis.* Society for Industrial and Applied Mathematics, Philadelphia. Q
- SIAM Review.* Society for Industrial and Applied Mathematics, Philadelphia. Q
- Siberian Mathematical Journal (Sibirskii Matematicheskii Zhurnal).* Consultants Bureau Enterprises, Inc., New York. BM
- Sibirskii Matematicheskii Zhurnal.* Akademiia Nauk SSSR, Sibirskoe Otdelenie, Novosibirsk. BM
- Siemens Review.* Siemens und Halske AG, Siemens-Schuckertwerke AG, Erlangen. M
- Signal.* Armed Forces Communications and Electronics Association, Washington, D. C. M
- Simulation.* Simulation Councils, Inc., La Jolla, Calif. M
- Sky and Telescope.* Harvard College Observatory, Cambridge, Mass. M
- Slaboproudý Obzor.* Státní Nakladatelství Technické Literatury, Prague. M
- SMPTE, Journal.* Society of Motion Picture and Television Engineers, Inc., New York. M
- **Society for Experimental Biology and Medicine, Proceedings.* Society for Experimental Biology and Medicine, New York. 11 issues per year
- Society of Experimental Test Pilots, Technical Review.* Society of Experimental Test Pilots, Lancaster, Calif. Q
- Society of Instrument Technology, Transactions.* Society of Instrument Technology, London. Q
- **Society of Rheology, Transactions.* American Institute of Physics, Inc., New York. SA
- Solar Energy.* Solar Energy Society, Arizona State University, Tempe. Q
- Solar Physics.* D. Reidel Publishing Co., Dordrecht, Netherlands. Q
- Solid-State Electronics.* Pergamon Press, Ltd., Oxford. M
- Sound and Vibration.* Acoustical Publications, Inc., Cleveland, Ohio. M
- Soviet Astronomy (Astronomicheskii Zhurnal).* American Institute of Physics, Inc., New York. BM

- Soviet Engineering Journal (Inzhenernyi Zhurnal)*. The Faraday Press, Inc., New York. BM
- Soviet Materials Science (Fiziko-Khimicheskaya Mekhanika Materialov)*. The Faraday Press, Inc., New York. BM
- Soviet Mathematics (Akademiia Nauk SSSR, Doklady)*. American Mathematical Society, Providence, R. I. BM
- Soviet Physics - Acoustics (Akusticheskii Zhurnal)*. American Institute of Physics, Inc., New York. Q
- Soviet Physics - Crystallography (Kristallografiia)*. American Institute of Physics, Inc., New York. BM
- Soviet Physics - Doklady (Akademiia Nauk SSSR, Doklady)*. American Institute of Physics, Inc., New York. M
- Soviet Physics - JETP (Zhurnal Eksperimental'noi i Teoreticheskoi Fiziki)*. American Institute of Physics, Inc., New York. M
- Soviet Physics - Semiconductors (Fizika i Tekhnika Poluprovodnikov)*. American Institute of Physics, Inc., New York. M
- Soviet Physics - Solid State (Fizika Tverdogo Tela)*. American Institute of Physics, Inc., New York. M
- Soviet Physics - Technical Physics (Zhurnal Tekhnicheskoi Fiziki)*. American Institute of Physics, Inc., New York. M
- Soviet Physics - Uspekhi (Uspekhi Fizicheskikh Nauk)*. American Institute of Physics, Inc., New York. BM
- Soviet Physics Journal (Fizika)*. The Faraday Press, Inc., New York. BM
- Soviet Powder Metallurgy and Metal Ceramics (Poroshkovaia Metallurgiiia)*. Consultants Bureau Enterprises, Inc., New York. M
- Soviet Radio Engineering (Radiotekhnika /Kiev/)*. The Faraday Press, Inc., New York. BM
- Soviet Radiophysics (Radiofizika)*. The Faraday Press, Inc., New York. BM
- Space/Aeronautics*. Conover-Mast Publications, Inc., New York. M
- Space Science Reviews*. D. Reidel Publishing Co., Dordrecht, Netherlands. 9 issues per year
- Spaceflight*. British Interplanetary Society, London. BM
- SPARMO Bulletin*. Solid Particles and Radiation Monitoring Organization, Meudon, France. Q
- SPE Journal*. Society of Plastics Engineers, Inc., Stamford, Conn. M
- Sperry Engineering Review*. Sperry Gyroscope Co., Great Neck, N.Y. Q
- SPIE Journal*. Society of Photo-Optical Instrumentation Engineers, Redondo Beach, Calif. BM
- Sterne und Weltraum*. Verlag Bibliographisches Institut AG, Mannheim. M
- Strain*. British Society for Strain Measurement, London. Q
- Studia Geophysica et Geodaetica*. Czechoslovak Academy of Sciences; Artia, Prague. Q
- Studia Scientiarum Mathematicarum Hungarica*. Hungarian Academy of Sciences, Budapest. SA
- Studii și Cercetări Matematice*. Academia Republicii Populare Române, Institutul de Matematica, Bucharest. 10 issues per year
- Surface Science*. North-Holland Publishing Co., Amsterdam. Q
- Tech Air*. Society of Licensed Aircraft Engineers and Technologists, Kingston-upon-Thames, England. M
- Technika Lotnicza i Astronautyczna*. Stowarzyszenie Inżynierów i Mechaników Polskich, Sekcja Lotnicza, Warsaw. M
- Technique et Science Aéronautiques et Spatiales*. Association Française des Ingénieurs et Techniciens de l'Aéronautique et de l'Espace, Paris. BM
- Tecnica Italiana*. Trieste. M
- Teknisk Tidskrift*. Svenska Teknologföreningen, Stockholm. W
- Telecommunications and Radio Engineering. Part I - Telecommunications, Part 2 - Radio Engineering. (Elektrosviaz', Radiotekhnika)*. Institute of Electrical and Electronics Engineers, Inc., New York. M
- Telefunken-Zeitung*. Telefunken AG, Berlin. Irreg.
- Telemetry Journal*. International Foundation for Telemetry, Los Angeles. BM
- Tellus*. Svenska Geofysiska Föreningen, Stockholm. Q
- Teoriia Veroiatnostei i ee Primeneniia*. Akademiia Nauk SSSR, Moscow. Q
- Teplofizika Vysokikh Temperatur*. Akademiia Nauk SSSR, Moscow. BM
- *Tetrahedron Letters*. Pergamon Press, Ltd., Oxford. SM
- Theory of Probability and its Applications (Teoriia Veroiatnostei i ee Primeneniia)*. Society for Industrial and Applied Mathematics, Philadelphia. Q
- Thin Solid Films*. Elsevier Publishing Co., Amsterdam. BM
- TNB General Precision Aerospace*. General Precision, Inc., Aerospace Group, Little Falls, N.J. Q
- *TNO-Nieuws*. Central Laboratorium TNO, Delft. M
- Tohoku University, Research Institute for Strength and Fracture of Materials, Reports*. Tohoku University, Sendai.
- Tohoku University, Science Reports, Series 5 - Geophysics*. Tohoku University, Sendai. 3 issues per year
- Tokyo, University, Faculty of Engineering, Journal, Series B*. Tokyo, University, Faculty of Engineering, Tokyo. Irreg.
- Tokyo, University, Institute of Space and Aeronautical Science, Bulletin*. Tokyo, University, Institute of Space and Aeronautical Science, Tokyo. Q
- Tokyo, University, Institute of Space and Aeronautical Science, Report*. Tokyo, University, Institute of Space and Aeronautical Science, Tokyo. Q
- Tokyo, University, Tokyo Astronomical Observatory, Annals, Second Series*. Tokyo, University, Tokyo Astronomical Observatory, Tokyo. Q
- Tokyo Astronomical Observatory, Tokyo Astronomical Bulletin, Second Series*. Tokyo, University, Tokyo Astronomical Observatory, Tokyo. Q
- Tool and Manufacturing Engineer*. American Society of Tool and Manufacturing Engineers, Dearborn, Mich. M
- *Torino, Accademia delle Scienze, Classe di Scienze Fisiche, Matematiche e Naturali, Memorie*. Torino, Accademia delle Scienze, Turin. Irreg.
- Toshiba Review*. Tokyo Shibaura Electric Co., Ltd., Tokyo. Q

Trend in Engineering. Washington, University, Engineering Experiment Station, Seattle. Q
TRW Space Log. TRW Systems, Redondo Beach, Calif. Q

Tsvetnaia Metallurgii. Ministerstvo Vysshego i Srednego Spetsial'nogo Obrazovaniia; Severokavkazskii Gornometallurgicheskii Institut, Ordzhonikidze. M

U

Ukrains'kii Fizichnii Zhurnal. Akademiia Nauk Ukrain'skoi RSR, Kiev. M

Ukrainskii Matematicheskii Zhurnal. Akademiia Nauk Ukrainskoi SSR, Kiev. BM

Ultrasonics. Iliffe Industrial Publications, Ltd., London. Q

Unione Matematica Italiana, Bollettino. Nicola Zanichelli Editore, Bologna. Q

Urania (Madrid). Sociedad Astronomica de España y America, Barcelona; Union Nacional de Astronomia y Ciencias Afines, Madrid. SA

Uspekhi Fizicheskikh Nauk. Akademiia Nauk SSSR, Moscow. M

Uspekhi Matematicheskikh Nauk. Akademiia Nauk SSSR and Moskovskoe Matematicheskoe Obshchestvo, Moscow. BM

V

**VDI-Berichte.* Verein deutscher Ingenieure; VDI-Verlag GmbH, Düsseldorf. Irreg.

VDI-Forschungsheft. VDI-Verlag GmbH, Düsseldorf. BM

VDI Zeitschrift. VDI-Verlag GmbH, Düsseldorf. 36 issues per year

Verti-Flite. American Helicopter Society, Inc., New York. M

Vertical World. Press-Tech, Inc., Evanston, Ill. M

Le Vide. Société Française des Ingénieurs et Techniciens du Vide, Nogent-sur-Marne (Seine), France. BM

Vilnius, Astronomijos Observatorijos, Biuletėnis. Vilnius Astronomical Observatory, Vilnius, Lithuania.

**Vision Research.* Pergamon Press, Ltd., Oxford. BM

W

Wear. Elsevier Publishing Co., Amsterdam. BM

Wehr und Wirtschaft. Gross-Talmon Verlag, Munich. M

Welding Journal. American Welding Society, New York. M

Welding Research Council Bulletin. Welding Research Council, New York. 8 issues per year

Weltraumfahrt Raketentechnik. Umschau-Verlag Frankfurt/Main. BM

Westinghouse Engineer. Westinghouse Electric Corp., Pittsburgh. BM

Wireless World. Iliffe Electrical Publications, Ltd., London. M

Wissenschaftliche Zeitschrift. Dresden, Technische Universität, Dresden. BM

World Aerospace Systems. Hanover Press, Ltd., London. M

Y

Yamagata University, Bulletin (Engineering). Yamagata University, Yamagata, Japan.

Z

Zashchita Metallov. Akademiia Nauk SSSR, Gosudarstvennyi Komitet Khimicheskoi Promyshlennosti pri Gosplane SSSR, Moscow. BM

Zeitschrift für angewandte Mathematik und Mechanik. Akademie-Verlag GmbH, Berlin. M

Zeitschrift für angewandte Mathematik und Physik. Birkhäuser Verlag, Basel. BM

Zeitschrift für angewandte Physik. Springer Verlag, Berlin. BM

Zeitschrift für Astrophysik. Springer Verlag, Berlin. Irreg.

Zeitschrift für Flugwissenschaften. Wissenschaftliche Gesellschaft für Luft- und Raumfahrt, e.V., and Deutsche Gesellschaft für Flugwissenschaften, e.V.; Friedr. Vieweg & Sohn, Braunschweig. M

Zeitschrift für Geophysik. Deutsche geophysikalische Gesellschaft, Hamburg; Physica-Verlag, Würzburg. BM

Zeitschrift für Instrumentenkunde. Wissenschaftliche und technische Geräte und Messwesen; Friedr. Vieweg & Sohn, Braunschweig. M

Zeitschrift für Luftrecht und Weltraumrechtsfragen. Köln, Universität, Institut für Luftrecht und Weltraumrechtsfragen; Carl Heymanns Verlag, KG, Cologne. Q

Zeitschrift für Metallkunde. Deutsche Gesellschaft für Metallkunde, e.V.; Riederer-Verlag GmbH, Stuttgart. M

Zeitschrift für Meteorologie. Akademie-Verlag GmbH, Berlin. M

Zeitschrift für Naturforschung, Ausgabe A. Verlag der Zeitschrift für Naturforschung, Tübingen. M

Zeitschrift für Physik. Deutsche physikalische Gesellschaft; Springer Verlag, Berlin. Irreg.

Zeitschrift für Vermessungswesen. Deutscher Verein für Vermessungswesen; Verlag Konrad Wittwer, Stuttgart. M

**Zeitschrift für Wahrscheinlichkeitstheorie und verwandte Gebiete.* Springer Verlag, Berlin.

ZHETF Pis'ma v Redaktsiiu. Akademiia Nauk SSSR, Moscow. SM

Zhurnal Eksperimental'noi i Teoreticheskoi Fiziki. Akademiia Nauk SSSR, Moscow. M

Zhurnal Nauchnoi i Prikladnoi Fotografii i Kinematografii. Akademiia Nauk SSSR, Moscow. BM

Zhurnal Tekhnicheskoi Fiziki. Akademiia Nauk SSSR, Moscow. M

Zhurnal Vychislitel'noi Matematiki i Matematicheskoi Fiziki. Akademiia Nauk SSSR, Moscow. BM

Zprava VZLÚ. Výzkumný a Zkušební Letecký Ústav, Prague. Irreg.

Zpravodaj VZLÚ. Výzkumný a Zkušební Letecký Ústav, Prague. BM

LIST OF SUBJECT HEADINGS OF
PUBLICATIONS

A Notation of Content, rather than the title of the publication, appears under each subject heading; it is listed under several subject headings which provide multiple access to the subject content of each accession. The IAA accession number is located under and to the right of the Notation of Content. It is preceded by numbers identifying the issue and page of International Aerospace Abstracts where the abstract is located.

To illustrate:

Issue Number	Page Number	Accession Number
01	p0007	A67-11162

A

A STAR

Energetic nuclear bombardment effects on stellar surface element abundance calculated with statistical theory in A magnetic variable star abundance anomaly 24 p4228 A67-42263

A-7 AIRCRAFT

Single point charger design for A-7A aircraft fluid power accumulators 02 p0182 A67-11843
Extension fittings for A-7A bomber having hydraulic system with no flexible hose 09 p1442 A67-21659
Hydraulic tubing permanent joints, made by induction-brazing method, for installation on A-7A Corsair II aircraft 17 p2801 A67-32007
A-7A aircraft maintenance guarantee and role of training 18 p2987 A67-34681

A-11

S ECHO I SATELLITE

A-11 AIRCRAFT

S YF-12 AIRCRAFT

A-12 S ECHO II SATELLITE

AAP
S APOLLO APPLICATIONS PROGRAM
/AAP/

ABDOMEN

SA DIGESTIVE SYSTEM

SA INTESTINE

Value of routine abdominal X-ray during aeromedical evaluation, noting number and significance of abnormalities detected 10 p1601 A67-23828

Abdominal blood flow changes in anesthetized dogs during transverse acceleration 23 p3950 A67-41535

ABERRATION

SA REFRACTION

Beryllium as substrate for mirrors of catadioptric lenses, noting strain-induced aberration 03 p0470 A67-14391

Diffraction based criteria use for image quality in automatic optical design, reviewing aberration tolerance theory 06 p1030 A67-17573
Telescope optics techniques for

compensation for lateral color aberration arising from atmospheric refraction, using modified Schupmann medial telescope 06 p1033 A67-18535

Self-focusing processes of laser pulses in dissipative medium, analyzing temporal nonlinear aberrations connected with thermal effects 10 p1664 A67-23332

Afocal field corrector for astronomical telescopes with paraboloidal mirrors 17 p2862 A67-33296

Spatial amplitude of field of ideally parallel laser beam focused by optical systems with spherical aberration 18 p3061 A67-34439

Optical glass selection for design of double-lens objective for IR region of spectrum, considering aberrations 20 p3451 A67-37157

ABIOTIC GENESIS

SA BIOGENESIS

Prebiotic synthesis of monocarboxylic acids suggested from mixture of methane and water exposed to semicorona discharge 19 p3181 A67-35882

ABLATING MATERIAL

SA NONABLATING MATERIAL

SA PYROLYTIC MATERIAL

Two superlight ablative compositions /SLA-741 and SLA-561/ developed for Mars Lander thermal protection, examining superiority to conventional low density charring ablators [SAE PAPER 660654] 01 p0103 A67-10614

Thermocouple errors resulting from heat conduction along thermocouple wire embedded in low conductivity ablative material indicate helicoil wire for optimum design 01 p0071 A67-11104

Calorimeter for measuring heat flux to ablating surface, noting theory of device 01 p0071 A67-11106

Oxidation and ablation characteristics of tantalum in hyperthermal arc tunnel filled with oxygen-nitrogen mixtures 01 p0102 A67-11153

Weight and cost comparative analysis of ablative and combined ablative/radiative heat shields for SV-5 and SV-32 lifting reentry vehicles [AIAA PAPER 66-990] 02 p0333 A67-12301

Ablative materials for thermal protection and minimum mass transfer of aircraft flying at hypersonic speeds [DVL-603] 03 p0532 A67-13026

Uncertainties in thermophysical properties of char-forming ablatives in intense convective and radiative heat transfer environments and effect on mathematical and physics models [AIAA PAPER 65-639] 03 p0534 A67-13059

Plasma arc tunnel tests show thermochemical heat of ablation of magnesia strongly dependent on stagnation enthalpy [AIAA PAPER 65-641] 03 p0449 A67-13061

Boron nitride fibers in composites for aerospace application, discussing fabrication, ablative properties, etc 03 p0452 A67-13409

Transient behavior of charring ablator under various thermal environments by finite difference method 04 p0723 A67-14847

Noncontour transpiration cooled heat shield for possible application to hypersonic atmospheric flight 04 p0725 A67-15435

Boundary layer cooling by spattering of ablating liquid films [ASME PAPER 66-WA/HT-5] 04 p0726 A67-15445

Ablative materials for thermal insulation of space vehicles, considering tungsten, tantalum, niobium, etc, as backing metals 04 p0726 A67-15536

Feasibility of making continuous measurements of ablation of spacecraft heat shield by use of radioisotopes embedded in

heat shield 05 p0841 A67-16529

Solid particle drag, convective heat transfer and ablation effects on structure of normal shock wave in nonreacting mixture of gas and ablating dust, using Runge-Kutta integration 08 p1427 A67-21120

Ablative properties of nylon-phenolic materials used in fabrication of composite heat shield with low residual stresses 09 p1523 A67-22506

Reentry vehicle heatshield materials including graphite, ablative reinforced plastics, etc 10 p1672 A67-23721

Ablative material performance under high shear reentry condition, noting hyperthermal test of cones and wedges for heat shield design 10 p1734 A67-23722

Refractory and ablating polymeric reentry heat shield materials evaluated under high radiant fluxes, measuring surface temperature, recession rate, flux emittance, etc refractory and ablating polymeric reentry heat 11 p1811 A67-24054

Visible and near IR spectral reflectance and emittance at high temperature of ablation chars, carbon and graphite [AIAA PAPER 67-326] 12 p2037 A67-26040

Ablative behavior of low and high density phenolic nylon in diffusion controlled surface combustion regime [AIAA PAPER 67-328] 12 p2038 A67-26042

Ablation study scheme enabling determination, for given environment and material, of ablation starting time and temperature distribution within mass of material 13 p2222 A67-26596

Nozzle ablations studied based on chemical mechanism, discussing pure on reinforced phenolic resin 14 p2404 A67-27896

Weight and cost comparative analysis of ablative and combined ablative/radiative heat shields for SV-5 and SV-32 lifting reentry vehicles [AIAA PAPER 66-990] 15 p2584 A67-29421

Photographic spectra of ablating plastics in thermodynamic environments related to species and temperatures in boundary layers [AIAA PAPER 66-132] 15 p2582 A67-30206

Ablation heat protection system materials performance in hypersonic regime, discussing potential solutions to shielding during atmospheric entry 16 p2778 A67-30722

Experiments on oxidation kinetics of refractory metals in undissociated and partly dissociated oxygen-chlorine mixtures 17 p2971 A67-33021

M-1 injector baffles, ablative chamber and start system design and development, using subscale testing [AIAA PAPER 67-461] 18 p2988 A67-33932

Stagnation ablation of blunt body hypersonic reentry with nonreacting gas, deriving laminar flow equations 20 p3356 A67-36509

Ablative material application to Apollo spacecraft for heat shielding using air injection guns 20 p3454 A67-36590

Ablation characteristics investigated using plasma jet wind tunnel, discussing effective heat of ablation and free stream stagnation enthalpy 20 p3544 A67-36640

Thermal protection technique using resin fiber ablative materials for use on reentry bodies during ascent, emphasizing nozzle 21 p3731 A67-38377

Tensile strength of charred ablation material under rapid heating conditions tested using plasma arc flow and miniaturized specimen 21 p3650 A67-38874

Precursor IR resonance radiation from hypervelocity ablating vehicles observed and related to photon absorption and water vapor presence in air 22 p3917 A67-39712

Ablators for severe reentry environments

evaluated from modifications of reference model constructed of epoxy resin with silica fiber and phenolic filler 22 p3826 A67-39887
Calorimeter for measuring heat flux to ablating surface, noting theory of device 24 p4155 A67-42289

ABLATING NOSE CONE

Geometric body profiles assumed by sphere and initially pointed cone during processes of ablation and shearing analyzed and combined to apply to sphere cones [AIAA PAPER 66-992] 03 p0353 A67-14145

Convective and radiative heat transfer to entry vehicles protected by ablation heat shield, obtaining absorption coefficients [AIAA PAPER 67-327] 12 p2038 A67-26041

Nose bluntness effect on hypersonic unsteady aerodynamics of ablating flared or conical slender reentry vehicles 15 p2416 A67-29442

Heat and mass transfer conditions in ablation of shear thinning and thickening fluids investigated at stagnation point [ASME PAPER 67-HT-78] 20 p3551 A67-36756

High temperature materials assessed for properties needed for aerospace applications including metals, alloys, refractory fasteners, aluminate coats, ablative insulation and ceramic compositions 22 p3824 A67-40333

ABLATION

SA AERODYNAMIC HEATING

Classical meteoric ablation theory generalized to include thermal radiation, conduction and meteoroid heat capacity in causing fragmentation 01 p0147 A67-10357

Materials for ablative cooling processes for rocket engines, noting structure and properties of porous and solid materials 02 p0306 A67-12791

Maximum temperature profile in phenolic resin-siliceous fiber heat shields on ICBM and Mercury spacecraft [AIAA PAPER 65-638] 03 p0533 A67-13058

Mars atmospheric composition and laminar convective heating and ablation studied to predict performance of heat protection systems during entry 06 p1119 A67-18849

Black Brant sounding rocket fin design, discussing flight characteristics, engine selection criteria and stability parameters 08 p1416 A67-20532

Ablation rate of hybrid rocket solid propellants in two-dimensional engine simulated chamber 08 p1373 A67-20804

Normalization technique for analysis of heat transfer, considering thermal entrance length, ablation and tektite problems 10 p1732 A67-22931

Superlight ablative systems for Mars Lander thermal protection 10 p1672 A67-23724

Low density shear resistant ablators for lifting reentry vehicles 10 p1672 A67-23725

Thermal and ablative lag induced by periodic heat input to oscillating flat plate in high velocity flow, showing crossover from dynamically stabilizing to destabilizing condition as oscillation frequency increases [AIAA PAPER 67-336] 12 p2039 A67-28050

Ablation of low melting models on ballistic facility, giving ballistic trajectory optimum conditions and ablation parameters calculation method 16 p2593 A67-31134

Frothing-sloughing ablation concept explains density variations of cometary meteors obtained from photographic and radar observations 17 p2943 A67-32541

Time lag effect on dynamic stability determined, using wind tunnel tests with 10 degree cone as test body simulating ablation process by gas injection into boundary layer [AIAA PAPER 66-757] 17 p2792 A67-33004

Microsphere ablation in free-flight range observed by laser photography, giving shadowgraphs with density contour map 19 p3346 A67-35757

Black Brant sounding rocket fin design, discussing flight characteristics, engine selection criteria and stability parameters 21 p3712 A67-37807

Superlight ablative systems for Mars Lander thermal protection 22 p3826 A67-40088

ABORT APPARATUS

Aircrew safety emphasizing prior to abort aspects in detection of catastrophic failure and initiation of abort sequence [AIAA PAPER 67-934] 24 p4245 A67-43024

ABORT TRAJECTORY

Abort velocity requirements for three-burn transfer maneuver out of lunar polar orbit

[AAS PAPER 66-133] 07 p1255 A67-19992

ABRASION

Airabrasion technique to improve Gunn oscillator performance using epitaxial GaAs, considering diode shape and contact structure 10 p1616 A67-23536

ABRASIVE

S CORUNDUM
S DIAMOND
S QUARTZ

ABSORBER

SA NEUTRON ABSORBER
SA SHOCK ABSORBER
SA SOLAR ABSORBER
SA VIBRATION ABSORBER

Curvature effect on reflection coefficient of layered absorbers, examining backscattering from coated cylinder and sphere 03 p0370 A67-13852

Spherical concentric geometry for designing absorber materials for application to curved surfaces determined by specular radar cross section 03 p0371 A67-13863

Extension of paper on saturable absorber giant pulse lasers to include effects of finite absorber lifetime on pulse parameters, noting pump role 06 p1011 A67-18148

Formation of short ruby laser light pulse and repetition frequency control using mode locking with saturable absorbers 23 p4015 A67-41036

ABSORPTION

SA ATMOSPHERIC ABSORPTION
SA AUROREAL ABSORPTION
SA ELECTROMAGNETIC ABSORPTION
SA ENERGY ABSORPTION
SA IONOSPHERIC ABSORPTION
SA LIGHT ABSORPTION
SA MAGNETIC ABSORPTION
SA MOLECULAR ABSORPTION
SA OPTICAL ABSORPTION
SA PHOTON ABSORPTION
SA POLAR CAP ABSORPTION
SA RADIATION ABSORPTION
SA RADIO SIGNAL ABSORPTION
SA THERMAL ABSORPTION
SA X-RAY ABSORPTION

Induced absorption in far IR by impurities and defects of single crystal of potassium bromide 09 p1557 A67-22571

Relationship between absorption of hydrogen fluoride by lined filter papers and exposure dosages investigated under controlled conditions of various factors 16 p2875 A67-31211

ABSORPTION BAND

SA SCHUMANN-RUNGE BAND SYSTEM

Electroabsorption measurements on rutile in clarifying band structure and dichroic nature at absorption edge 01 p0131 A67-10339

Spontaneous-emission probability and absolute intensity for IR absorption band of nitrous oxide 03 p0467 A67-12854

Cyclotron absorption in n type lead telluride with wide range of carrier concentrations, showing increase in transverse effective mass and decrease in anisotropic mass ratio 03 p0493 A67-13352

Width of spectral absorption line of water vapor at lambda equals 0.92 mm measured with aid of monochromatic radiation source and radiometer with thermal indicator 05 p0781 A67-16342

Saturated absorption of color centers in glass self-Q-switched pulses, as in glass codoped with uranyl oxide and Nd ions 05 p0822 A67-16878

Hydrogen atom excitation by Lyman alpha radiation absorption in electric field 05 p0848 A67-16795

Forbidden absorption bands of carbon monoxide in vacuum UV region, noting rotational and vibrational constants and perturbations 05 p0848 A67-16847

Annealing behavior and uniaxial stress response of radiation induced defects in Si causing 1.8, 3.3 and 3.9 micron IR absorption bands examined via EPR studies 05 p0870 A67-17194

Fundamental absorption band structure of mixed KCl and KBr single crystals 05 p0872 A67-17493

Absorption measurements of 139-Gc microwaves for very high purity mercury telluride, deducing electron effective mass 06 p1047 A67-17653

Quantitative intensity of weak carbon dioxide triad in 1 micron spectral region obtained, using pressure broadening techniques 06 p1031 A67-17870

Exponent in expression relating nuclear interaction cross section to atomic weight of absorber determined from absorption path of nuclear active particles of cosmic radiation 06 p1078 A67-18795

Interband electron absorption and dispersion during one-and two-photon processes in semiconductors subjected to electromagnetic field, noting laser applications 06 p1054 A67-18798

Local mode absorption bands for Al impurities in InSb and for P impurities in GaAs at various temperatures, using grating spectroscopy 06 p1059 A67-18910

IR transmission measurements in single crystal thin film semiconductors, observing absorption band near plasma frequency 06 p1071 A67-18992

IR absorption in high purity boron films, showing absence of absorption peaks at 2-15 microns 09 p1533 A67-22132

Self-broadening coefficients of spectral lines of absorbing atmospheric gases measured in comparison with line broadening effects of nitrogen 10 p1678 A67-22715

Aerobee rocket sounding of far UV spectra of six stars in Orion, extrapolating mass ejection from resonance absorption lines 11 p1861 A67-24488

Multiple scattering and finite detector bandwidth effects on shape of absorption features in atmospheric scattering 11 p1862 A67-24502

IR absorption measurements of Li localized vibrational modes in Li and Te doped GaAs 17 p2922 A67-33066

X-ray K spectra of phosphorus absorption and emission in indium, gallium and boron phosphide semiconductors and red phosphorus 18 p3095 A67-33440

Exponent in expression relating nuclear interaction cross section to atomic weight of absorber determined from absorption path of nuclear active particles of cosmic radiation 18 p3116 A67-34414

Interband electron absorption and dispersion during one-and two-photon processes in semiconductors subjected to electromagnetic field, noting laser applications 18 p3102 A67-34417

Spectral transmittance of mixture of carbon monoxide and nitrous oxide for overlapping absorption bands 19 p3266 A67-35696

Luminescence from ruthenium complexes, investigating charge-transfer absorption bands 19 p3181 A67-35880

Far UV interstellar absorption lines evaluated for main-sequence B stars 19 p3330 A67-36075

Molybdenum interband transitions noting low energy optical property anomalies and origin of two absorption bands 20 p3466 A67-36865

Radiative heat transfer in nonisothermal nongray gas model, measuring absorption and emission in carbon dioxide and water gases [ASME PAPER 66-WA/HT-25] 20 p3555 A67-37607

Charge compensation defects influence on UV excitation spectrum of rare earth doped crystals fluorescence 22 p3856 A67-39384

U-B and B-V color indices, total absorption, color excesses and reddening lines for hot black bodies, with energy curve corrections for absorption line effects 22 p3883 A67-39768

Conductivity and IR absorption spectra of organic semiconductors in polycrystalline, melt and liquid states 22 p3861 A67-39922

Attenuation of plane sinusoidal acoustic waves due to electromagnetic radiative properties of carbon dioxide and water vapor bands 22 p3829 A67-40232

Radiation measurement from satellite, discussing observation of ozone absorption band 24 p4181 A67-42397

ABSORPTION COEFFICIENT

Green function method applied to calculating resonance absorption of electromagnetic radiation for interlevel transitions in thin film 01 p0127 A67-10072

Atmospheric radio wave absorption coefficient and altitude determined and linked to effects of colliding paramagnetic oxygen molecules 01 p0022 A67-10391

X-ray irradiation effect on electrophysical properties of n-and p-type germanium, determining absorption

coefficient 01 p0136 A67-11044
Far IR absorption and dielectric constant of liquid water 01 p0115 A67-11082
Optical absorption edge in cadmium telluride, noting impurity bands and dependence on energy and temperature 02 p0281 A67-11492
Electromagnetic radiation absorption coefficient of atmospheric water vapor in long-wave portion of submillimeter range 02 p0190 A67-11568
Limb intensity profiles at center of hydrogen alpha calculated for several simple models of absorption coefficient at line center, showing abrupt changes in gradient 02 p0323 A67-11693
Solar autolization line profiles for Al I in rocket UV spectrum 02 p0323 A67-11699
Electric conductivity due to tunnel effect in aluminum-alumina-silver sandwich structures, determining potential barrier in alumina and absorption coefficient of hot electrons 02 p0295 A67-11762
Experimental setup for determining acoustic parameters of solids as media for ultrasound propagation 02 p0241 A67-11851
Optical constants of silver solid solutions with gold addition, noting dependence of refractive index, absorption coefficient and conduction electrons on impurity concentration 02 p0255 A67-11870
Ruby laser with liquid filter, considering relation between filter efficiency and absorption curve parameters when acting as Q-factor modulator 02 p0252 A67-12423
Induced absorption coefficients in atmosphere model measured for calculation of Venus lower atmosphere properties from radio observations 03 p0394 A67-12949
Polarized radiation measurements of far IR absorption coefficient and refractive indices in lithium niobium 03 p0496 A67-13571
Pressure induced monochromatic translational absorption coefficients for homopolar and nonpolar gases and gas mixtures, with application to molecular hydrogen 03 p0515 A67-14323
Donor electron IR absorption coefficients in semiconductors in 3-10 micron range used to study wavelength dependence 04 p0674 A67-14608
X-ray anomalous transmission used in analysis of gallium arsenide crystal perfection with various dislocation densities, determining ratios of anomalous absorption coefficient 04 p0674 A67-14620
Radiant energy transfer in absorbing medium with constant absorption coefficient 04 p0722 A67-14714
Nongray radiation effects on laminar boundary layer of absorbing gas over flat plate at low Eckert numbers [ASME PAPER 66-WA/HT-35] 04 p0724 A67-15428
Performance of GaAs semiconductor laser with resonator, noting dependence of forbidden zone width and absorption coefficient on free carrier concentration and incident photon energy 04 p0634 A67-15759
Atmospheric radio wave absorption at wavelengths ranging from 1.36 to 3.0 mm, determining absorption coefficients of molecular oxygen and water 05 p0761 A67-16343
Oscillation in CdS crystal by ruby laser induced two-photon excitation, noting proportionality of absorption coefficient to light beam intensity 05 p0821 A67-16667
Semiconductor lasers noting strong field behavior and absorption coefficient for saturation 05 p0821 A67-16672
Damage in glass induced by linear absorption of laser radiation 05 p0824 A67-16794
Fluorescence decay time of NO, determining transition moment 05 p0848 A67-16837
Velocity and temperature profiles of optically thick planar Couette flow, obtaining heat transfer rates for Rosseland mean absorption coefficient variation with temperature 05 p0793 A67-17343
Microradiowave absorption in air by water vapor dimers 06 p0963 A67-18206
Low accuracy of interferometric measurement of coefficient of ultrasound absorption in gas 06 p1004 A67-18395
Photolization and absorption coefficients of nitric oxide gas measured, using vacuum UV monochromator 06 p1037 A67-18573

Far IR resonant absorption in n-type silicon analyzed, considering donor-pair conduction dominant 06 p1068 A67-18974
Criteria for accuracy of line intensity and mean absorption coefficient measurements 07 p1185 A67-19404
Barometric coefficient for neutron monitor noting long term and altitude dependence 07 p1188 A67-19954
Light scattering influence on effective value of extinction coefficient considered as function of optical parameters of medium and of angular characteristics of source and receiver 07 p1221 A67-20007
Semiconducting compounds for thin film photovoltaic devices using GaAs crystals, considering absorption coefficient 08 p1284 A67-20725
Absorption coefficient of water vapor in relative windows of transparency for millimeter and submillimeter radio waves 08 p1294 A67-20817
Dielectric relaxation of gases and sharp rise in microwave absorption coefficient in Cytherean atmosphere 08 p1401 A67-21372
Virtual heights and absorption of radio waves in ionosphere, discussing methods of computation 09 p1484 A67-22441
Wave equation solution yielding steady absorption coefficient for laser diode 09 p1516 A67-22663
Photolization yield and absorption coefficient of nitric oxide at various wavelengths in 580-1350 angstrom region, using H sub 2 emission sources 10 p1681 A67-22738
Photon absorption coefficients measured in active and passive regions of electron-beam-pumped semiconductor laser 10 p1664 A67-22909
High power operation of semiconductor lasers, noting differential equation of field distribution along junction 10 p1665 A67-23519
Frequency temperature dependence of longitudinal and transverse hypersonic wave absorption coefficients in quartz and artificial ruby crystal 10 p1693 A67-23582
Multiquantum electron transfers within conductivity band of semiconductors accompanied by emission or absorption of acoustic phonon, calculating absorption coefficient of electromagnetic emission 10 p1695 A67-23658
Mass of shaped charge accelerator generated fragments determined via high speed flash X-ray photography of projectiles in flight 11 p1790 A67-24448
Convective and radiative heat transfer to entry vehicles protected by ablation heat shield, obtaining absorption coefficients [AIAA PAPER 67-327] 12 p2038 A67-26041
Structure of X-ray K absorption edge of iron in Fe compounds, noting nature of chemical bond and structure of electron energy spectrum 12 p1957 A67-26109
Prediction of total emissivity of nitrogen-broadened and self-broadened hot water vapor 13 p2155 A67-26493
Absorption intensity in ionospheric sporadic E layer 14 p2308 A67-27935
Reflection coefficient and separation of real and imaginary parts of optical index in nonmetal band-to-band transition model semiconductor 14 p2364 A67-27956
Velocity distribution function of gas measured with laser, noting relation to frequency variation of absorption coefficient across spectral line 14 p2317 A67-28194
Atmosphere model for pure helium star including only helium I and II transitions and electron scattering in calculating opacity 14 p2387 A67-28578
Optical absorption coefficient due to conduction electrons in nondegenerate semiconductors derived using Plakida method, noting light scattering 14 p2372 A67-28808
Spectral distribution of absorption coefficient in polycrystalline films of cadmium sulfide over wide temperature range 14 p2372 A67-28852
Effect of semiconductor glass shield temperature on absorption coefficient, output energy, pulse duration and energy and peak power of ruby laser 14 p2332 A67-28857
Method for complete observation of magnetic field structure in sunspots 14 p2390 A67-28942

Optical constants of ionic crystals at low temperatures determined from reflection spectra, noting correlation between absorption coefficient, magnitude and phonon difference processes 14 p2374 A67-28986
Ultrasonic measurement of temperature dependence of longitudinal sound absorption coefficient for main crystallographic directions in superconducting indium 14 p2375 A67-29070
Dependence of angular dimensions of discrete cosmic radio emission source on radiation flux density and frequency 15 p2549 A67-29140
Emission power of air measured by determining charged particle distribution behind spark discharge generating shock wave in plasma 15 p2530 A67-29861
Relation between steady state behavior of regenerative traveling wave laser and linear constant damping in medium 15 p2454 A67-30076
Mean absorption coefficient for optically thin plasma derived taking into account radiative losses, noting electron and ion temperature ratios 16 p2706 A67-30459
Structure of strong shock wave studied for simple models of nongray radiative transfer 16 p2658 A67-30938
Magnesium oxide and lithium fluoride in far UV, noting refractive and absorption indices 16 p2734 A67-31881
Altitude of lower boundary of ionosphere determined by electron density profile, considering absorption coefficient and magnetolonic signal components 16 p2669 A67-31906
Transmission coefficient associated with internal reflection from absorbing surface layer derived from reflection coefficient, noting relation to absorption 17 p2883 A67-32204
Kronig-Penney model for electron potential in crystal adapted to semiconductor, discussing cubic lattice 17 p2914 A67-32386
Thin airfoils in radiation gas dynamics, formulating linearized theory for plane steady motion via Fourier transform and obtaining solution for absorption coefficient 17 p2791 A67-32556
Upper limits on liquid water content in Venus atmosphere 17 p2945 A67-32652
X-ray absorption in chromium in chromium silicon after thermal processing at high temperatures 17 p2921 A67-32893
Microradiowave absorption in air by water vapor dimers 17 p2817 A67-33219
Multiquantum electron transfers within conductivity band of semiconductors accompanied by emission or absorption of acoustic phonon, calculating absorption coefficient of electromagnetic emission 17 p2924 A67-33339
Numerical solution of electromagnetic wave equations for semiconductor junction laser using McWhorter model 18 p3060 A67-34019
Lunar surface absorption coefficient in IR range, discussing limb-darkening, reflectivity, subsolar point temperature, radiation, spectral properties, etc 18 p3122 A67-34139
Free carrier absorption coefficients in 6H and 15R silicon carbide, showing probable ellipsoids of revolution 18 p3102 A67-34279
HF backscattering from absorbing infinite strip with arbitrary face impedances 18 p3005 A67-34730
Cadmium telluride electrical light absorption oscillations noting comparisons between experiment and theory, electric field, temperature range, etc 19 p3301 A67-34772
Absorption coefficients of radiation by water vapor and aerosols determined from atmospheric counter radiation 19 p3251 A67-34858
Temperature distribution in vortex cooled hydrogen arc obtained by emission and absorption coefficients in plasma source 19 p3279 A67-35142
Impurity effect on optical properties of interstellar graphite particles, examining wavelength dependence of absorption coefficient and refractive index of coals 19 p3323 A67-35423
Effect of semiconductor glass shield temperature on absorption coefficient, output energy, pulse duration and energy and peak power of ruby

laser 19 p3242 A67-36108
 Mean absorption coefficients for IR radiation of gases expressed as functions of gas spectroscopic and thermodynamic properties [ASME PAPER 67-HT-10] 20 p3545 A67-36708
 Absorption coefficient of radiative transfer equation and high temperature air opacity 20 p3485 A67-36930
 Volumetric absorption coefficient effect on Rosseland equilibrium radiative heat transfer and temperature profiles in optically thick fluid flowing past flat plate 20 p3553 A67-36936
 Germanium and cadmium telluride edge absorption, noting lattice imperfections causing absorption coefficient increase in indirect transition region 20 p3511 A67-37143
 Bouger law applicability for describing narrow collimated light beams attenuation in scattering media in terms of optical thickness 20 p3462 A67-37666
 Electron temperature of shock-heated argon plasma determined by measuring microwave noise radiation and absorption 21 p3660 A67-37741
 Optical system performance and atmosphere attenuation, analyzing absorption and scattering phenomena in terms of weather conditions 22 p3828 A67-39612
 Kinetic theory of electromagnetic propagation through magnetoactive plasma, determining reflection, transmission and absorption coefficients and plasma field configuration 22 p3761 A67-39758
 Radiating hydrogen two-dimensional equilibrium flow with variable absorption coefficient in axisymmetric nozzle analyzed in presence of gray radiation, examining transfer equation in diffusive approximation 22 p3785 A67-40013
 Electromagnetic propagation in plasma layer in magnetic field, determining absorption coefficient 22 p3762 A67-40123
 Atmospheric absorption of carbon dioxide laser radiation calculation from laboratory absorption coefficient measurements, discussing effects on power transmission and communications 22 p3816 A67-40237
 Integrated intensities for thermal radiation heat transfer in nongray nonscattering gas approximated, deriving effective absorption coefficient 22 p3920 A67-40442
 Emissivity expressions and absorption coefficients developed for plasma particles interacting with electromagnetic field and at equilibrium 22 p3854 A67-40527
 Symmetry of phonons and rules of corresponding selection for IR absorption and Raman diffusion for two phonons 23 p4026 A67-40689
 Faraday rotation in YIG studied from measurements at He-Ne laser wavelengths for applications to materials design 23 p4041 A67-41184
 Schottky photodiode narrow spectral response in Spicer absorption diffusion model shown to exist only in rapidly changing absorption coefficient region 23 p3981 A67-41272
 Absorption times for gases injected into mammalian eye anterior chamber 23 p3950 A67-41536
 Microwave production of plasma in trap at electron cyclotron resonance, investigating absorption and density 23 p4035 A67-41684
 Regenerable sorbent /GAT-O-SORB/ in granular form for carbon dioxide removal from air, discussing design and performance tests of laboratory prototype [SAE PAPER 670844] 24 p4115 A67-41997
 Electromagnetic wave absorption and transformation in resonant layer of nonuniform plasma at oblique incidence 24 p4119 A67-42071
 Absorption characteristics for laser power stabilization using Rayleigh active material 24 p4187 A67-42360
 Monograph on absorption and laser radiation covering absorption coefficients, high altitude gas concentration, low extinction coefficient measurements, molecular resonance absorption, etc 24 p4168 A67-42412
 Actinometric measurements from aircraft of short wave radiation fluxes and radiation balance, determining absorption coefficient for clouds and true albedo 24 p4182 A67-42882
 Dependence of angular dimensions of discrete cosmic radio emission source on

radiation flux density and frequency 24 p4222 A67-43063
 Laser-irradiated plasma theoretical study indicating absorption enhancement in external magnetic field 24 p4199 A67-43104
ABSORPTION CROSS SECTION
 Limiting behavior of absorption cross sections of negative hydrogen ion 01 p0116 A67-10359
 Sudden cosmic noise absorption and X-ray flares noting peak, nature of decay and theoretical and experimental values [RASSA PAPER 1-10-139] 03 p0373 A67-14247
 Scattering amplitude for multipole mixtures in Mossbauer effect determined, from which can be derived absorption cross section and complex refractive index 04 p0660 A67-14758
 Radiometer data analysis results concerning cosmic ray event of April 18, 1965 04 p0693 A67-14973
 Radar observations of Venus at 3.8 cm noting low value of cross section, echo spectrum, polarization characteristics, absorption cross section and atmospheric attenuation 05 p0889 A67-16298
 Continuous absorption cross section of argon from measurements of continuous emission of arc plasma in visible UV regions of spectrum and from temperature determination 05 p0854 A67-16988
 Continuous absorber effect on spectral line reversal gas phase temperature measurement [AIAA PAPER 67-108] 06 p1004 A67-18503
 Absorption wavelengths of QSOs, noting relatively large red shifts 09 p1567 A67-22243
 Beam wavelength and laser intensity effect on attenuation in carbon disulfide induced by ruby laser indicate two-photon absorption 10 p1687 A67-23776
 Anomalous IR attenuation in fast neutron irradiated GaAs and CdTe arises through scattering and absorption by highly conducting spike zones 11 p1850 A67-24910
 Laser transition absorption cross section at room temperature for neodymium ion in yttrium-aluminum garnet determined by two methods 14 p2331 A67-28713
 Photoadsorption of X-rays by interstellar gas using photoionization cross sections, showing neon K edge as distinctive feature of spectrum 17 p2937 A67-32752
 Saturable organic dye absorber giant pulse lasers in limit of large absorber cross section, normalized initial inversion and relaxation time 17 p2869 A67-33055
 Scattering theory for parameterization of absorption cross sections and refractivity for autoionizing spectral lines 18 p3082 A67-33878
 Electron-atom collision cross-section in afterglow of pulsed cesium plasma as function of electron cyclotron absorption resonance and electron temperatures 19 p3271 A67-35076
 Attenuation cross section at Lyman alpha for Xe deviation from Beer law indicating diatomic Xe molecule formation 20 p3491 A67-37688
 Electronic transitions optical saturations in polyatomic organic molecules with high intensity laser radiation, discussing relation to bleaching of dyes 22 p3817 A67-40487
ABSORPTION SPECTRUM
 Optical and magneto-optical phenomena in CdSnAs sub 2, discussing reflection and absorption spectrum, optical activity, double refraction, dielectric constant, etc 01 p0128 A67-10094
 Absorption spectrum of condensed oxygen in 1.26 to 0.3 micron region 01 p0116 A67-10509
 Shock tube measurement of dissociation energy of NH radical in reflected shocks through nitrogen-hydrogen-krypton and ammonia-krypton mixtures 01 p0117 A67-10787
 Hall effect and fine structure of X-ray fluorescence and absorption K spectrum of vanadium in silicides 01 p0101 A67-10935
 Absorption spectra models analyzed for use in IR radiation propagation in atmosphere 01 p0109 A67-11043
 Optical transmittance of fused silica at elevated temperatures, showing shift in UV to IR absorption with increasing temperature 01 p0138 A67-11074
 Four-linked rare earth chelate with sodium ion obtained with benzoylacetone and europium, analyzing molecular and ionic transitions by absorption and emission

spectra 02 p0251 A67-11518
 Tropospheric pressure-altitude data by satellite radiometric topography mapping, using oxygen absorption band centered at 5 mm 02 p0262 A67-12367
 Rotational intensity distribution of vacuum UV absorption spectrum bands of carbon monoxide arising through mixing of D state with neighboring states 02 p0269 A67-12450
 Optical absorption spectra of hexagonal red HgS single crystals at self-absorption edge at temperatures from 20.4 to 310 degrees K 02 p0300 A67-12476
 Temperature dependence of spectral distribution of radiation, excitation and quantum output of green luminescence of cadmium sulfide films 03 p0433 A67-12889
 Volume density of heat sources in ruby laser rod by numerical integration of pumping and absorption spectra 03 p0434 A67-13117
 Paraformaldehyde hypothesis of IR spectrum of Saturn ring 03 p0509 A67-13167
 Autoionization effects in UV absorption spectra of hot atomic gases 03 p0471 A67-13222
 Autoionization states and resonances in absorption spectra of rare gases 03 p0471 A67-13223
 Electron spin resonance absorption spectrum of Pt in YAG at low temperatures, noting ionic orientation 03 p0492 A67-13326
 Hertzian relaxation spectra of MOS structures showing existence of two absorption regions 03 p0493 A67-13453
 Absorption spectrum of activated nitrogen produced by microwave discharge in 600-1100 angstrom region [AFCLR-67-0109] 03 p0473 A67-13520
 Crystal absorption and lamp emission spectra for CW pumping of Nd-doped YAG by water-cooled Kr arcs 03 p0437 A67-13576
 Hydrodynamics of lower solar photosphere, examining connection between small-scale oscillatory Doppler shifts and exponentially decaying continuum 03 p0511 A67-13650
 Spectrographic observation of quasi-stellar and Haro-Luyten objects, noting hydrogen absorption spectra and emission wavelengths 03 p0511 A67-13652
 Multiparametric diagnostic technique for optically dense plasma 03 p0486 A67-14187
 Solar chromospheric structure noting network pattern of absorption in He 10830 angstrom region 03 p0514 A67-14312
 Adenine and guanine amounts in DNA determined spectrophotometrically by dialysis of DNA 04 p0564 A67-14406
 Horizon studies for monochromatic radiation following Lambert-Beer law of transmission, noting Chapman theory on exponential distribution of atmospheric constituent of absorption 04 p0613 A67-14697
 Excitonic effects in interband absorption of semiconductors noting electron-hole interaction, Coulomb interaction energy maxima and minima and scattering cross sections 04 p0676 A67-14926
 Absorption spectra of Te, Sn, Pb, PbTe and SnTe at various energy ranges, noting role of wave functions involved in absorption by d-electrons 04 p0681 A67-15295
 Self-absorption of radiation in high temperature plasma jet of hydrogen, argon and nitrogen 05 p0851 A67-16522
 Optically pumped ruby noting absorption and emission spectrum, transition stages and phonon terminated amplification 05 p0820 A67-16658
 Laser emission at 1.06 microns from ytterbium-neodymium glass, noting linearity of energy transfer with Yb concentration 05 p0820 A67-16664
 Structure function of interstellar absorption, noting spatial and frequency distribution of dust concentrated in clouds 05 p0897 A67-16774
 Calcium fluoride-cerium fluoride with neodymium additions as active medium for lasers, discussing absorption and luminescence spectra and induced radiation 05 p0825 A67-16922
 Effect of local states in forbidden band on electron processes in n-GaP crystals, diagramming absorption and photoluminescence excitation spectra 05 p0868 A67-17063
 X-ray emission and absorption spectra, electron structure and properties of metallic compounds of titanium 05 p0831 A67-17484

K-absorption spectrum of Ni as function of concentration of alloying elements and arrangement of atoms of alloying elements into Ni crystal lattice 06 p1017 A67-17952

Two-photon absorption spectrum of single crystal CdS, using polarized light and precise geometry 06 p1011 A67-18209

Optical properties of interstellar grains, noting complex index of refraction as function of wavelength 06 p1087 A67-18410

Two-phonon IR absorption and Raman scattering spectra to provide information about phonon spectra of crystals and phonon-electron interaction in filled valence bands 06 p1059 A67-18907

Lattice IR reflection and transmission spectra and Raman spectrum of monocrystalline and hot pressed pellets of ZnSe 06 p1059 A67-18909

Anomalous temperature dependence of IR absorption in p-type germanium attributed to phonon induced effects 06 p1060 A67-18913

Exciton and oscillatory magnetoabsorption spectra in layer type semiconductors in high magnetic fields 06 p1060 A67-18917

Absorption spectra and photoluminescence in n- and p-type GaAs before and after neutron and electron irradiation 06 p1062 A67-18933

Interband magnetoabsorption of InSb, noting anomalies caused by enhanced polaron self-energy effects 06 p1066 A67-18956

Concentration effect on light absorption and dispersion by impurity centers in case of weak electron-phonon coupling 07 p1233 A67-19648

Crab Nebula X-ray spectrum from balloon observations, noting importance of correction for escaped iodine K component 07 p1251 A67-19944

Wave interaction in saturable absorbers, noting hole burning in dye switched ruby laser 07 p1234 A67-20094

Radiation from equilibrium air over large temperature and density range 08 p1426 A67-20583

Uranus and Neptune spectral absorptions compared with laboratory spectra obtained with very long optical paths indicate methane role in planetary absorption 08 p1397 A67-21213

Red shift relationship with ionization potential for absorption lines in quasi-stellar object 3C 191 08 p1400 A67-21251

Paramagnetic resonance absorption spectrum of cerium in yttrium-gallium-garnet host crystal 08 p1371 A67-21312

Simultaneous recordings of cosmic noise absorption and VLF chorus, noting correlation from riometer recordings 08 p1327 A67-21374

Stimulated emission, absorption spectra and luminescence of neodymium-activated YAG crystals in pulsed laser 09 p1513 A67-22068

IR spectra of low temperature stars of type M, N/R/ and S, as well as NML objects in Cygnus and Taurus, noting atmospheric differences 09 p1566 A67-22224

Red shift and absorption line of PKS 0237-23 09 p1567 A67-22242

Collision induced far IR absorption in rare gas mixtures with emission spectrum calculation 09 p1535 A67-22382

Abnormal low helium abundance in atmospheres of old halo B star based on weak absorption lines in helium spectra 09 p1568 A67-22438

Calorimetric measurement of source and broadband spectral absorptances of spacecraft thermal control coatings during exposure to UV in vacuum 09 p1534 A67-22452

Near IR atmospheric absorption over 25-km horizontal path at sea level 10 p1629 A67-22744

Emission and absorption bands in K spectral region of titanium, using single setup 10 p1668 A67-23093

IR spectroscopy of absorption and emission in hydrogen-fluorine flames for more data on high temperature spectral properties of HF 10 p1697 A67-23134

Coincidences in measured positions of absorption lines in spectra of quasi-stellar objects 11 p1862 A67-24507

Absorption spectra and luminescence of p-type copper diffusion doped Ga-As crystals, noting appearance of temperature dependent

narrow spectral lines 12 p1984 A67-25522

Optical and paramagnetic resonance of ytterbium ions in calcium fluoride, obtaining correlation between site geometry and optical absorption 12 p1984 A67-25843

Reflectance, transmittance and absorbance of muscovite type mica as function of thickness measured, using prism and grating spectrophotometers [AIAA PAPER 67-288] 12 p1958 A67-26005

P- and n-type silicon spectral emissivity measured at several temperatures and wavelengths for carrier concentrations and direct current resistivities [AIAA PAPER 67-302] 12 p1958 A67-26017

High energy particle and electromagnetic space radiation effects on thermal control coating, noting spectral absorbance for various conditions [AIAA PAPER 67-339] 12 p1959 A67-26053

Thermal control coating spectral sensitivity to UV induced degradation, noting rapidly increasing damage as incident radiation wavelength decreases [AIAA PAPER 67-340] 12 p1959 A67-26054

Submillimeter-wave measurements for water-vapor detection from jet aircraft flying in stratosphere 13 p2114 A67-26795

Electronic absorption spectrum observed during cyanogen azide flash photolysis 13 p2177 A67-26988

Emission intensity and spatial distribution of fluorescence measured for transitions in He, noting resonance radiation absorption effect on 5016 angstrom light spread 14 p2317 A67-28196

Calcium fluoride-cerium fluoride with neodymium additions as active medium for lasers, discussing absorption and luminescence spectra and induced radiation 14 p2330 A67-28262

Gas laser radiation applied to light transmittance measurement of heavily doped gallium arsenide in absorption region by free carriers 14 p2368 A67-28528

Absolute oscillator strengths of three titanium resonance lines from absorption measurements in atomic beam 14 p2351 A67-28581

Far IR absorption spectra of chromium and titanium ions in aluminum oxide crystal, indicating Jahn-Teller effect reduction of trigonal field and spin-orbit coupling 14 p2370 A67-28714

Attenuation cross section and refractive index using collision theory, calculating resonance profiles of autoionizing lines based on scattering theory 14 p2351 A67-28811

Red shifts from absorption line spectra of quasi-stellar objects, discussing energy generation mechanism 14 p2390 A67-28851

Spectral distribution of absorption coefficient in polycrystalline films of cadmium sulfide over wide temperature range 14 p2372 A67-28852

Biological macromolecule detection using thiacarbocyanine dye and observation of absorption spectra changes 15 p2426 A67-29115

Coherent resonant absorption and emission in IR and visible spectrum, discussing Lorentz oscillator and Dicke spin model of radiating molecule 15 p2519 A67-29190

Lanthanum chromite activation energy determination from electrical resistivity and Hall coefficient variation as function of temperature and IR absorption spectrum 15 p2535 A67-29478

Effect of local states in forbidden band on electron processes in n-GaP crystals, diagramming absorption and photoluminescence excitation spectra 15 p2538 A67-29794

ZnS two-photon absorption spectrum to establish two-photon pumping capabilities of semiconducting crystals 15 p2500 A67-29816

Mixed crystals with fluoride base, investigating spectrum and time behavior of laser emission for operation below room temperature 16 p2725 A67-30809

Flow field and heat transfer in radiating stagnation-point shock layer of atmospheric-entry vehicles 16 p2591 A67-30940

Vacuum deposited amorphous and semicrystalline gallium phosphide film properties analyzed by electron diffraction 16 p2729 A67-31065

Pulsations in cosmic noise absorption of auroral zone, noting magnitude, shape and form of occurrence 17 p2841 A67-32213

Rydberg series in extreme UV observed in absorption spectrum of helium-nitrogen discharges and active nitrogen [AFRCL-66-835] 17 p2888 A67-32629

Relation between molecular structure of In and Sb semiconductor compounds and fine structure of X-ray absorption spectra 18 p3095 A67-33441

InSb-InAs solid solution thin films absorption spectra, noting band structure, temperature change and Hall EMF reduction 18 p3096 A67-33450

Absorption spectra and luminescence of p-type copper diffusion doped Ga-As crystals, noting appearance of temperature dependent narrow spectral lines 18 p3103 A67-34453

Mercury-argon low pressure discharge initiation stressing positive column establishment, examining breakdown effects by spectrographic techniques 19 p3272 A67-35088

Interstellar material, emphasizing chemical characterization of dust by absorption spectroscopy 19 p3323 A67-35331

Absorption lines in quasi-stellar source analysis to obtain estimates of either particle density in absorbing region or distance between continuum source and absorber 19 p3330 A67-36082

Absorption spectra, spectral dependence of luminescence quantum output, glow curves and radiation spectra of color centers in ruby crystal 20 p3506 A67-36223

Cesium uranyl nitrate crystal near-visible absorption spectrum at 20 degrees K cesium uranyl nitrate crystal near-visible absorption spectrum at 20 degrees K 20 p3506 A67-36229

Molecular oxygen absorption line equivalent widths measurement at 5 mm wavelength obtained from model atmosphere to determine earth atmospheric temperature 20 p3427 A67-36370

Radiative heat flux for free burning methanol and acetone flames of arbitrary size and geometry predicted, using transport equation [ASME PAPER 67-HT-47] 20 p3547 A67-36729

Laboratory investigation of laser emission line absorption by atmospheric gases in vacuum multiple-pass cell, obtaining data free of aerosol scattering 20 p3386 A67-37606

Impurity crystal-field spectra in II-VI and III-V compound semiconductors used to predict unexplored systems spectra impurity crystal-field spectra in II-VI and III-V compound semiconductors used to predict 21 p3682 A67-38388

Atmospheric long range spectral transmissivity measured by single beam photometer with recording potentiometer added to reduce beam noise 21 p3627 A67-38431

Phonon spectrum of neodymium trichloride crystal lattice determined from polarized vibronic transition spectra and Zeeman effect of trivalent Pr and Nd impurity ions 22 p3840 A67-39434

Absorption spectra of rare earth trichlorides with trivalent Pr, observing vibronic transitions noting assignments of phonon branches 22 p3840 A67-39435

Second order absorption spectra of symmetric cyanine dyes in methanol solution using spectrophotometer 22 p3757 A67-39444

Ammonium perchlorate deflagration studied by flash pyrolysis and kinetic spectroscopy noting radical concentrations 22 p3867 A67-39639

Reflectivity spectra of YIG and YGG crystals, observing YTG structure attributed to charge transfer enhanced crystal field transitions reflectivity spectra of YIG and YGG crystals, observing YIG structure attributed to charge 22 p3863 A67-40238

Externally adjustable pressure regulation of Fabry-Perot interferometer, using device to measure cesium vapor spectral absorption in D-I line 22 p3810 A67-40522

Spectroscopic properties of mixed complexes with two different ligand groups surrounding lanthanide ion, discussing energy transfer and absorption 23 p3971 A67-40747

Gas laser radiation applied to light transmittance measurement of heavily doped gallium arsenide in absorption region by free carriers 23 p4039 A67-40935

Spectral dependence of enhanced quantum efficiency and overlap integrals in InSb semiconductors, calculating impact ionization and hot electrons

thermalization 23 p4040 A67-41061
K-line spectra from sunspots, discussing
K-3 absorption line 23 p4067 A67-41241
presence
IR absorption spectrum of n-GaAs noting
free carrier contribution due to phonons and
ionized impurities 23 p4042 A67-41293
scattering
Thermally activated inert gas ion injection
into tungsten and gold to correlate energies
associated with peaks in desorption
spectrum 23 p4030 A67-41357
Absorption spectra of quasi-stellar objects
/QSO/, suggesting origin in galaxies through
which light passes on way to
earth 23 p4069 A67-41442
Spectral response of p-n semiconductor
heterojunction, considering absorption
effects and photocurrent
loss 24 p4202 A67-41981
Fluoride crystals for laser applications,
discussing crystal absorption
spectrum 24 p4166 A67-41983
Spectrofluorimetric studies on active site
of alpha-chymotrypsin using anthraniloyl as
chromophore 24 p4119 A67-42665

ABSORPTIVE INDEX

Absorptivity standard instrument to
investigate solar absorptance of four
surfaces used for spacecraft temperature
control for Mariner IV on Mars mission
[AIAA PAPER 65-650] 03 p0448 A67-13055
Geometric analysis of refractive index,
absorption index and polarization
characteristics of ionospheric radio
waves 08 p1295 A67-21168
Transmission of artificial quartz at room
temperature, obtaining optical constants in
far IR region 09 p1553 A67-21917
Transmission of artificial quartz at room
temperature, obtaining optical constants in
far IR region 14 p2365 A67-28246
Absorptance and emittance of metal
surfaces determined via cyclic incident
radiation, noting error computation and
method accuracy 19 p3346 A67-35742
Tellurium nonlinear optical properties
including absorption and refraction indices,
discussing second harmonic radiation
generation 20 p3507 A67-36324
Molecular sieves as casings filler for
semiconductor devices, discussing
stabilization of electrical parameters and
absorptive capacity of synthetic
zeolites 23 p4042 A67-41274
Absorptivity of medium, obtaining results
for spectral quantities referred to given
radiation frequency 23 p4083 A67-41288

AC

S ALTERNATING CURRENT /AC/

ACCELERATION

SA ANGULAR ACCELERATION
SA DECELERATION
SA IMPACT ACCELERATION
SA MAGNETOHYDRODYNAMIC
ACCELERATION
SA PARTICLE ACCELERATION
SA PHYSIOLOGICAL ACCELERATION
SA PLASMA ACCELERATION
Exhaust processes of gases at high initial
pressure from tubes, when flow is initiated
by acceleration of solid
body 02 p0235 A67-12788
Ripples in acceleration potential affect ion
beam of electrostatic propulsion system by
superimposing AC potential of 50 cps of
variable amplitude on constant acceleration
potential 02 p0306 A67-12790
Apparent mass increase of sphere
accelerated from rest and before boundary
layer separation in cylinders of oil or water
[ASME PAPER 66-WA/UNT-6] 04 p0601 A67-14483
Rising blue shift induced by acceleration
in relativistically expanding objects and
significance for intensity variations in
quasars 05 p0898 A67-16926
Pitching effect on aircraft gravity center
during passage through gust, noting
autopilot effect on tail
assembly 09 p1440 A67-22473
Time and distance measurement of freely
falling body to determine acceleration due
to gravity 10 p1857 A67-23317
Freely precessible gyroscope viscous fluid
nutational damping response to translational
and vibration accelerations near critical
frequencies 12 p1942 A67-25679
Parameters determining magnitude of

acceleration effect on burning rate increase
of aluminized and nonaluminized composite
solid propellants 15 p2581 A67-29991
Metalized and nonmetalized composite
solid propellant burning rates, analyzing
effects of acceleration, noting agglomeration
and nonnormal conditions
[AIAA PAPER 67-470] 18 p3157 A67-33940
Very high satellite air drag acceleration
studied by University of London
Observatory, discussing solar radiation
pressure acceleration 18 p3042 A67-34257
Coherent acceleration and velocity
observation in real time /CAVORT/ analog
radar signal processor for matched filtering
pulse trains from radial accelerated
targets 21 p3586 A67-38953
Measured acceleration time histories
analyzed for automatic handling of recorded
data, discussing advantage of amplitude
distribution method 23 p3986 A67-40719
Definition, terminology and classification
of experimental
accelerations 23 p3961 A67-40765
Constant acceleration flows applied to
high speed fixed geometry guns using H
propellant in constant projectile acceleration
problem 23 p3992 A67-41716

ACCELERATION PROTECTION

Drugs for protection and stimulation of
biological functions of spacecrews, noting
experimental results on transverse-
acceleration resistance of
animals 20 p3367 A67-36254

ACCELERATION STRESS

SA G FORCE

SA PHYSIOLOGICAL ACCELERATION

Space flight acceleration, vibration and
ionizing radiation effects on body functions,
oxidizing metabolism of central nervous
system and fission processes of hemopoietic
tissues 01 p0015 A67-10336
Cumulative and adaptive effects in animals
subjected to single and repeated transverse
g forces 02 p0188 A67-12328
Oxygen balance of organism during
prolonged accelerations, noting disturbed gas
exchange between alveoles and
capillaries 02 p0188 A67-12329
Combined linear and vibratory
accelerations effects on human body
dynamics and pilot performance
capabilities 02 p0189 A67-12409
Physical fitness of man with respect to
manual labor, oxygen deficiency and
acceleration 03 p0364 A67-13924
Human body response to acceleration
according to various models
[ASME PAPER 66-WA/BHF-13] 04 p0564 A67-15402

High gradient acceleration effect on
human renal clearances of free water and
creatinine following moderate water
load 05 p0756 A67-16288

Acceleration effect on rate of urine flow
and urinary excretion of sodium, potassium
and total solute in
rabbits 07 p1134 A67-19861

Statistical analysis of heart rates of Navy
carrier pilots during bombing attacks
compared with those for launch and
landing 09 p1455 A67-21718

Large deformations of zero moment
orthotropic shells of revolution under action
of inertial loads caused by centrifugal
acceleration of shells 12 p2028 A67-25629

Intracranial pressure measurements and
electroplethysmographic examination of
blood content in dog cranial cavity for
transverse acceleration up to 40
g 13 p2057 A67-26456

Remote aftereffect on hemopoietic tissue
of mice under simultaneous irradiation and
acceleration, using both X-rays and
protons 13 p2057 A67-26458

Space physiology acceleration problems
including engineering aspects of impact
absorption 13 p2059 A67-26760

Periodic prolonged low-intensity
acceleration stress provided by short radius
centrifuge in baboons 13 p2059 A67-26917

Chronic acceleration and acute Co 60
whole body irradiation effects on rats,
discussing weight to
ratio 15 p2427 A67-29268

Simulated acceleration and dynamic
pressure environments generated by space
vehicle flight ranging from weightlessness to
impact from ground landing
[AIAA PAPER 67-279] 15 p2465 A67-29425

Physiological reactions of man to effect of

overload during space flight compared to
results of laboratory /centrifuge/
tests 16 p2610 A67-30752

Cumulative effect of impact acceleration
on physiological functions of rats, studying
particularly lung lesions 16 p2612 A67-30904

Oxygen metabolism changes in muscular
and brain tissues of animals exposed to
prolonged transverse accelerations,
examining oxygen consumption and body
temperature 16 p2612 A67-30905

Exposure to acceleration and prolonged
confinement in bed studied for effects on
functional state of human
stomach 16 p2613 A67-30911

Water-salt metabolism changes during
prolonged confinement in bed following
exposure to acceleration indicating
dehydration and
decalcification 16 p2613 A67-30916

Acceleration stress effects on pilot
performance and dynamic
response 17 p2808 A67-33176

Soviet monograph on problem of
acceleration in aviation
medicine 20 p3375 A67-37466

Wheel acceleration influence on landing
gear operation at touchdown, noting effect
on shock absorption system and elastic
deformation of supporting
legs 21 p3566 A67-37949

Failure mechanisms in semiconductor
components under thermomechanical and
electrical stresses for D2 satellite
application 21 p3601 A67-38061

Performance of electromechanical pressure
transducers tested environmentally for static
and dynamic temperature, steady
acceleration and vibrational
acceleration 22 p3809 A67-40464

Survival times of rats studied from
positive and negative acceleration test
exposure in special
centrifuge 22 p3753 A67-40540

Bibliography dealing with vibration,
acceleration and ionizing radiation on
vestibular apparatus, noting lack of
information 23 p3943 A67-40764

General and cerebral hemodynamics and
functions of central nervous system during
positive and negative
accelerations 23 p3943 A67-40766

Brain tissue respiratory processes of
rabbits subjected to hypergravity and acute
hypoxia noting no significant difference
between experimental and control
animals 23 p3943 A67-40770

Transverse accelerations remote
aftereffect on conditioned alimentary
reflexes of rats, discussing prolonged
depression of higher nervous
activity 23 p3943 A67-40771

Combined effect of acceleration and
ionizing radiations on conditioned reflexes
of rats noting alleviation on radiation
leukopenia 23 p3943 A67-40772

Precentrifugation effect on radiation
reactions of vestibular analyzer in guinea
pigs, establishing substantial spontaneous
electric activity stimulation in hind legs,
extensor muscles 23 p3944 A67-40773

Cardiovascular acceleration-stress reactions
during G acceleration of dogs, noting blood
pressure, blood velocity and pressure
waves 23 p3951 A67-41551

Human circulatory response to sinusoidal
gravitational stimulus via Rotational Flight
Simulator /RFS/, discussing heart rate
variation 23 p3951 A67-41561

Hematological criteria of chronic
acceleration stress and
adaptation 23 p3953 A67-41587

Renin secretion measurement for human
adaptation to circulatory stress from G
acceleration, discussing high plasma renin
levels during acceleration 23 p3956 A67-41634

Oxygen role in cardiac rate in squirrel
monkeys during acceleration stress on
centrifuge 23 p3956 A67-41635

Centrifuge tests with squirrel monkeys for
pharmacologically denervated primate heart
response to acceleration
stresses 23 p3957 A67-41636

Color photographic study of blackout
during radial acceleration on human
centrifuge, presenting evidence confirming
central retinal arterial
collapse 23 p3957 A67-41638

Fluorescence angiography technique to
study human centrifugal acceleration effects
on retinal circulation during

blackout 23 p3957 A67-41639
Arterial oxygen tension during acceleration recorded on anesthetized greyhounds using microelectrode and physiological gas analyzer 23 p3958 A67-41653
Reactivity of animals to caffeine and strychnine during transverse acceleration aftereffects 24 p4111 A67-41850
Preirradiated organism reaction to space flight acceleration studied in determination of admissible ionizing radiation dose 24 p4113 A67-42393

ACCELERATION TOLERANCE

Prolonged centrifugal acceleration effect on gas exchange and resistance to hypoxia in rats 01 p0016 A67-11425
Human body response to stationary and nonstationary vibration [ASME PAPER 66-WA/BHF-15] 04 p0564 A67-15937

Biochemical measures made as part of habituation experiment in which four subjects were exposed to rotation for 6 days 05 p0754 A67-16277

Cupular function of man under acceleration, noting electroencephalographic results on caloric nystagmus under 1.2, 3 and 4 g and postrotational nystagmus 05 p0756 A67-16324

Motion reproduction, analyzing control systems, dynamic fidelity, voltage command, etc [AIAA PAPER 67-252] 07 p1166 A67-20070

Backward, forward and transverse acceleration effects on cardiopulmonary systems of men and dogs 10 p1599 A67-23810
Muller maneuver /forced inhalation with closed glottis/ improves tolerance to negative G 12 p1901 A67-25172

Nervous reflex mechanisms of hemodynamic shift control during rapidly and slowly increasing acceleration 13 p2058 A67-26757

Maximal intensity inflight stress effects on human tolerance investigated, noting deceleration experiments 14 p2257 A67-28218
Prolonged acceleration effect on human organism tested using retinal blood circulation observations 16 p2610 A67-30755

Mouse, rat and dog organism reaction to ionizing radiation, vibration and acceleration 16 p2611 A67-30765

Acceleration problems in astronautics noting axis determination and effect on human body 20 p3371 A67-36822

Motion reproduction, analyzing control systems, dynamic fidelity, voltage command, etc 21 p3608 A67-38540

Rats exposed to repeated radial acceleration studied for central nervous system adaptation and survival rates noting better adaptability of newborns 22 p3753 A67-40541

Laser gyro development and application noting advantages in cooling, power, starting time and acceleration influence 23 p3999 A67-40916

Physiological response and acceleration tolerance in dynamic simulation via human centrifuge, noting symptoms occurrence frequency 23 p3953 A67-41590

Human response to low intensity long duration transverse acceleration, discussing increase in splanchnic blood flow during centrifugation and orthostatic intolerance 23 p3958 A67-41652

Peripheral venous renin levels changes used to evaluate angiotensin system response to acceleration 23 p3960 A67-41700

Reactivity of animals to caffeine and strychnine during transverse acceleration aftereffects 24 p4111 A67-41850

Motion coordination under conditions of intermittent acceleration and weightlessness during parabolic aircraft flight 24 p4112 A67-41858

Electric stimulus effect on vestibular apparatus responses to acceleration increasing or decreasing reactions depending on applied voltage polarity 24 p4112 A67-41859

ACCELERATOR

SA BETATRON
SA COAXIAL ACCELERATOR
SA DECELERATOR
SA ELECTRON ACCELERATOR
SA HALL ACCELERATOR
SA HYPERVELOCITY ACCELERATOR
SA LINEAR ACCELERATOR
SA PARTICLE ACCELERATOR
SA PLASMA ACCELERATOR

SA VAN DE GRAAFF ACCELERATOR

Conducting gas flow in jet in front of electromagnetic accelerator nozzle exit region analyzed, giving jet shape and parameter distribution 11 p1842 A67-24951

High performance aerodynamic impulse facility with shock tunnel, expansion tube and accelerator for high velocity and high Reynolds number 21 p3605 A67-37768

Convective electric arc stability and slanting in thermionic rail accelerator [AIAA PAPER 67-674] 21 p3671 A67-38707

Conventional and composite grid designs tested with low voltage Kaufman thruster [AIAA PAPER 67-680] 21 p3692 A67-38711

ACCELEROMETER

SA INERTIAL ACCELEROMETER

SA STRAIN GAUGE ACCELEROMETER
Temperature control and complex heat path designs inertial components, platforms and strap-down guidance systems, considering floated gyros and accelerometers 02 p0241 A67-11789

Miniaturized high shock package utilizing FM-modulated 19.8 megacycle transmitter and piezoresistive accelerometer for measuring deceleration profiles 02 p0242 A67-12011

Accelerometer frequency response and quadratic lag function amplitude response curves and relation to resonant frequency 04 p0627 A67-15792

Absolute angular velocity measurement with aid of linear accelerometers on body of aircraft 06 p1028 A67-18179

Upper atmospheric density, pressure and temperature profile obtained from drag acceleration measurements on falling sphere 07 p1181 A67-19938

Mechanical shock filter for isolating accelerometer during high g-level shock testing 11 p1799 A67-24824

Accelerometer use for operational load measurements in aircraft, emphasizing automatic counting technique 11 p1880 A67-25059

Accelerometer mountings evaluated covering attachment, calibration, resonance frequencies, tension-compression, bending, shear interface and cantilever effect 12 p1942 A67-25680

Piezoelectric type accelerometer transverse sensitivity ratio /TSR/, discussing measurements of vibrations and rotations 12 p1943 A67-25703

Instrumentation for ballistic pendulum shock accelerometer calibrator provides readout and display of peak amplitudes 12 p1943 A67-25708

Electromagnetic element /Vectorsyn/ for improving mass element restraint and support for three-axes acceleration measurement system 12 p1947 A67-26123

Piezoelectric accelerometer capacitance measurement and computation involved in conversion of accelerometer voltage sensitivity from one external circuit capacitance to another 12 p1947 A67-26186

Inertial navigation system with damping of oscillations for enhancement of stability of stationary platform 13 p2118 A67-26375

Errors of real accelerometer and instability of rotation effect on accuracy of angular velocity measurements of aircraft motion 16 p2670 A67-30466

Guidance and control technology examining inertial guidance systems, Apollo space system, gyros, accelerometers and computers 16 p2699 A67-30650

Vehicle angular velocity determined, using configurations with only linear accelerometers and no gyroscopes for inertial navigation systems 16 p2675 A67-31266

Digital accelerometer converts data into pulse format without analog-digital conversion, noting bias stability determination by crystal characteristics 17 p2855 A67-32438

Miniature electrostatic accelerometer featuring suspension and force rebalance systems, discussing performance, applications and accuracy acceleration measurement 17 p2858 A67-32484

Aircraft mounted recording accelerometers for excessive turbulence compared with direct turbulence measurement 17 p2798 A67-32700

Accelerometer using interference fringes of Fabry-Perot system for measurement of

small vibratory disturbances 20 p3444 A67-36520

Gyrotach accelerometer errors in measuring object angular velocity and acceleration relative to one axis, deriving differential equations of motion 20 p3451 A67-37155

Calibration of shock accelerometers, discussing velocity change and impact force methods with specific examples of systems in use 23 p4003 A67-41335

Test accelerometer comparison calibrations via vibration standards, discussing sensitivity, relative motion and error analysis 23 p4003 A67-41336

Comparison calibration techniques for vibration transducers using quartz accelerometer 23 p4003 A67-41337

IC emitter follower line driver with input filtering for PWM signal conditioning, solving onboard high impedance problems in drop tests with piezoelectric accelerometer 23 p4005 A67-41372

Controlled transient signal distortion by shock monitoring instrumentation circuits using piezoelectric accelerometers 23 p4007 A67-41382

Differential piezoelectric accelerometer charge system for monitoring in-flight jet engine vibrations 23 p4007 A67-41384

ACCIDENT INVESTIGATION

SA AIRCRAFT ACCIDENT INVESTIGATION

SA AUTOMOBILE ACCIDENT

SA SEAT BELT

Vertebral lesion in fighter pilot following landing accident 04 p0561 A67-14632
Human error causes, accidents and effects of fatigue, microsleep and flicker fusion frequency 07 p1137 A67-20229

ACCIDENT PREVENTION

SAE Stapp Car Crash Conference, Holloman AFB, New Mexico, November 1966 08 p1288 A67-20609

Fuel system design criteria, discussing ways of reducing postcrash fires in aircraft 08 p1279 A67-20610

Vertebral fractures in pilots from helicopter accidents in dorso-lumbar junction of spinal column 12 p1902 A67-25170

Evaluation facility for rotor containment/control devices [SAE PAPER 670332] 12 p1925 A67-25873

Safety in business aircraft operations based on available statistics noting need for thorough pilot training 14 p2245 A67-28320

Bird hazard to aircraft at Auckland International Airport, examining geographical features, history, species, daily movement patterns and seasonal abundances 15 p2419 A67-29672

Aircraft accident prevention dynamics and data recording role noting repetitive causal factors, limitations and information loss 17 p2796 A67-32218

Electrical detonator characteristics and safety precautions in handling and use, noting untimely functioning and misfiring as causes of accidents 17 p2927 A67-33093

Incident/accident information exchange system for hazard information flow to safety teams 18 p3163 A67-34692

Skidding accident reduction investigated for runway and highway safety noting worn tires, smooth surface texture, locked wheels and pilot technique 19 p3173 A67-35930

Medicolegal problems in aircraft flight accidents and traumatic mechanisms 21 p3575 A67-38508

Air Force accident history noting importance of maintenance/material area 22 p3754 A67-39598

Aeromedical examiner relationship to accident prevention, discussing standardization of psychological approach 23 p3963 A67-41539

Human Error Research and Analysis Program /HERAP/ for man-machine system, investigating pilot error and performance and aircraft accident prevention [AIAA PAPER 67-848] 24 p4117 A67-42984

ACCIDENT PRONESS

Middle aged pilot medical fitness for flying, noting age-accident statistics, changes in skill, performance, senses and responses 22 p3756 A67-40535

ACCLIMATIZATION

SA ADAPTATION

SA ALTITUDE ACCLIMATIZATION

SA COLD ACCLIMATIZATION

SA ENVIRONMENTAL SCIENCE

SA HEAT ACCLIMATIZATION

- SA HEAT TOLERANCE
SA HUMAN TOLERANCE
Cardiac changes under hypoxia, experimental morphological study 13 p2058 A67-26756
- ACCOMMODATION**
S VISUAL ACCOMMODATION
ACCOMMODATION COEFFICIENT
SA THERMAL ACCOMMODATION COEFFICIENT
Revision of Levin average value of accommodation coefficient K for iron meteoric bodies 13 p2198 A67-26572
Momentum transfer of positively ionized nitrogen molecule incident on copper target, measuring accommodation coefficient with torsion balance, 13 p2098 A67-26945
Momentum accommodation coefficients of variable angle of incidence of monochromatic argon molecular beams 13 p2098 A67-26946
Normal and tangential momentum accommodation coefficients in low density facility 13 p2098 A67-26947
Surface interaction of free molecular flows or molecular beams, considering state variables in highly rarefied gas in Maxwellian equilibrium, stagnation temperature, etc 13 p2159 A67-27299
Probe for measuring energy transfer between satellite surface and upper atmosphere 16 p2670 A67-30646
Measuring methods for high energy molecules accommodation coefficients, determining dependence on energy, incidence angle, surface nature and outgassing 20 p3489 A67-36939
Atoms interaction with solid body surface, noting pair interaction law effect on characteristic energy accommodation coefficient and motion equation solution 24 p4190 A67-41938
- ACETATE**
Catalytic effect of thermal polyanhydro-alpha-amino acids on hydrolysis of p-nitrophenylacetate, noting role of histidine residues 13 p2065 A67-26732
- ACETAZOLAMIDE**
Acetazolamide effects in aiding altitude accommodation, examining action on blood and cerebrospinal fluid 23 p3951 A67-41566
- ACETIC ACID**
Catalytic decarboxylation of oxaloacetic acid into pyruvic acid by thermally prepared poly-alpha-amino acids 13 p2065 A67-26589
- ACETONE**
SA ACETYLACETONE
Stimulated Brillouin scattering in shock-compressed acetone 01 p0116 A67-10338
- ACETONITRILE**
Temperature dependence and reaction energetics of free radical addition of trifluoroacetonitrile to ethylene 09 p1459 A67-22364
Free radical addition of perfluoroacetonitrile to vinyl fluoride, noting formation of one isomeric compound 09 p1459 A67-22365
Laser activity from terbium trifluoroacetylacetonate in p-dioxane and acetonitrile at room temperature 11 p1803 A67-24833
- ACETYLACETONE**
Laser activity from terbium trifluoroacetylacetonate in p-dioxane and acetonitrile at room temperature 11 p1803 A67-24833
- ACETYLATION**
Acetylative capacity and lipid metabolic changes and readjustment to normality in rats in oxygen-rich environment 14 p2256 A67-28588
- ACETYLCHOLINE**
Exclusion effect of afferent signalization on tonic function of iliotibial muscle in frogs exposed to acetylcholine 24 p4112 A67-41852
- ACETYLENE**
Hydrocarbon flame ionization, discussing second process occurring in flames with acetylene and related unsaturated compounds 04 p0719 A67-14488
Gaseous mixture theory in calculating transport coefficients of combustion product plasma of oxygen and acetylene 06 p1119 A67-18723
Temperature characteristics, electric conductivity, electrode drop and heat loss of acetylene combustion gas mixed with seed material and nitrogen used as MHD fluid 09 p1580 A67-22151

ACHONDRITE

- Thermoluminescence of achondrite meteorites on lunar surface based on rate of temperature rise of lunar terminator 01 p0146 A67-10249
Bununu meteorite /pyroxene-plagioclase achondrite/ composition and structure 09 p1564 A67-21736
Isotopic composition of krypton in high and low calcium achondrites, noting measurement results 09 p1569 A67-22685
Enstatite characteristics in enstatite achondrite meteorites, discussing mineralogy and composition 13 p2200 A67-27236
Chemical analyses of stony meteorite and iron meteorite with silicate inclusions 16 p2751 A67-31456
Iodine, uranium and tellurium abundances in various achondrites, chondrites and mesosiderites from neutron activation analysis 24 p4233 A67-42616
Achondrites and mesosiderites containing brecciated structures indicate magnetic differentiation, recrystallization, refragmentation and ejection from parent body 24 p4233 A67-42619
- ACID**
SA ACETIC ACID
SA AMINO ACID
SA ASPARTIC ACID
SA BORIC ACID
SA BUTYRIC ACID
SA CARBOXYLIC ACID
SA CYTIDYLIC ACID
SA DEOXYRIBONUCLEIC ACID /DNA/
SA DICARBOXYLIC ACID
SA FATTY ACID
SA HYDROCHLORIC ACID
SA HYDROFLUORIC ACID
SA NITRIC ACID
SA NUCLEIC ACID
SA PERCHLORIC ACID
SA PHOSPHORIC ACID
SA PYRUVIC ACID
SA RIBONUCLEIC ACID /RNA/
SA SULFURIC ACID
IR spectra of gaseous, solid and matrix-isolated HNCS and DNCS, studying frequency shift, bending modes, fundamental vibrations, gas phase, etc 19 p3181 A67-35016
- ACID-BASE BALANCE**
SA PH FACTOR
Acid-base relation of blood and cerebrospinal fluid with respect to respiratory regulation studied in man at high altitude 17 p2806 A67-32333
- ACOUSTIC ATTENUATION**
Sound propagation in streaming air within tubes having changes of cross section and flow losses, discussing reflection coefficient dependence on flow velocity 01 p0114 A67-10819
Amplitude dependent attenuation in normal and superconducting lead for ultrasonic determination of superconducting energy gap 01 p0135 A67-10916
Ultrasonic attenuation of alkali halide crystals in 120 to 180 degrees K range, noting thermal annealing of dislocation pinning centers 02 p0298 A67-11888
Absorption dependence of ultrasonic waves in superconductors on amplitude of sound wave due to temperature 03 p0492 A67-13325
Acoustic wave energy absorption by superconductors in intermediate state 03 p0502 A67-14377
Vannier-Mott excitons effect on ultrasound absorption in piezoelectric semiconductors 04 p0678 A67-15134
Aluminum powder damping of HF instability in solid propellant combustion in vortex burner 06 p1115 A67-18307
Low accuracy of interferometric measurement of coefficient of ultrasound absorption in gas 06 p1004 A67-18395
Resonators use for higher sound attenuation in waveguide with sound absorbing cladding 06 p1032 A67-18397
Ultrasonic wave absorption in GaAs and GaSb compounds at temperatures from 95 to 300 degrees K 06 p1051 A67-18399
Changes in ultrasonic attenuation of superconducting niobium at low magnetic fields, considering effects of low critical field impurity phases 06 p1053 A67-18757
Subscale cold-flow rocket motor model used to determine effect of purely geometric variables on acoustic performance leading to axial mode combustion instability 06 p1075 A67-18853

- Ruby laser-induced effect of pulsed pressure on KDP crystal surface and thermal bulk effect on excitation of ultrasonic oscillation in crystal 08 p1337 A67-20417
Temperature dependence of relaxation-type ultrasound attenuation maxima in plastic deformation of molybdenum and niobium single crystals 08 p1367 A67-20419
Working principle of echo suppressor used in telephone link with high propagation time based on selective attenuation by frequency and time divisions 11 p1754 A67-24651
Vannier-Mott excitons effect on ultrasound absorption in piezoelectric semiconductors 12 p1978 A67-25158
Hypersonic sound velocity dispersion in liquids of low viscosity analyzed using Mandelstam-Brillouin components 12 p1967 A67-26133
Book on ultrasonic wave absorption and dispersion in gases, liquids and solids, discussing physical mechanisms involved in sound absorption 12 p1967 A67-26157
Longitudinal acoustic wave attenuation in superconducting aluminum measured, verifying acoustic attenuation predictions 14 p2373 A67-28858
Propagation of shear acoustic waves traveling parallel to magnetic field along symmetry direction in metal crystal 16 p2731 A67-31446
Temperature and frequency effects on amplitude-independent longitudinal ultrasonic attenuation in superconducting lead 19 p3304 A67-35536
Ultrasonic attenuation measurements at high magnetic fields in mixed state for clean and dirty limits 20 p3483 A67-36205
Longitudinal ultrasound attenuation in polycrystalline superconducting mercury at 9.3 GHz, studying temperature dependence 20 p3514 A67-37568
Viscoelastic theory solving Lighthill paradox by accounting for acoustic energy damping in fine grained isotropic turbulence 21 p3610 A67-37759
Aluminum powder damping of HF instability in solid propellant combustion in vortex burner 21 p3732 A67-38860
[AIAA PAPER 67-104]
Ultrasonic wave absorption in high purity gallium single crystals in magnetic field, observing large magnitude geometric oscillations at cryogenic temperature 22 p3859 A67-39653
Magnetoacoustic attenuation in metals with Fermi surface, open orbits and magnetic breakdown calculated by solving Boltzmann equation via path-integral method generalization 22 p3861 A67-39995
Attenuation of plane sinusoidal acoustic waves due to electromagnetic radiative properties of carbon dioxide and water vapor bands 22 p3829 A67-40232
Frequency dependence of attenuation coefficient for longitudinal ultrasonic waves in InSb over range 50 to 210 MHz for temperatures between 200 and 600 degrees K 24 p4202 A67-41980
- ACOUSTIC COMBUSTION**
S COMBUSTION INSTABILITY
ACOUSTIC DUCT
Aerodynamic forces of harmonically oscillating cylindrical duct with supersonic internal flow within framework of potential flow theory 20 p3357 A67-37003
- ACOUSTIC EXCITATION**
Simultaneous excitation of electron plasma and ion-acoustic oscillations, using single electromagnetic wave for plasma oscillation generation 01 p0125 A67-10913
Wideband multipoint real time device automatically calculating correlation functions of acoustic signals 04 p0620 A67-14890
Hypersonic excitations due to Brillouin scattering for case with Stokes feedback, deriving quantum equation of motion for creation of laser and Stokes modes and coupled acoustic mode 05 p0823 A67-16683
Acoustic field of random pressure pulsations into half-space behind infinite plate with arbitrary number of layers 05 p0846 A67-16708
Electron-piezoelectric interaction giving rise to currents responsible for acoustoelectric effects, gain and nonlinear mixing 06 p1050 A67-18140
Scattering in semiconductors, calculating collision term in Boltzmann equation for

acoustic modes and differential collision operator for isotropic part of distribution function 07 p1237 A67-20180

Pressure calibration methods for testing response of microphones in difficult conditions of temperature, pressure and frequency 09 p1484 A67-21938

Excitation of electroacoustic lateral waves in compressible plasma by nonelectromagnetic source 10 p1683 A67-22865

Finite element approach for determining rms deflections and stresses in randomly acoustically excited complex aerospace elastic structures 10 p1724 A67-23710

Free vibration and resonance of vibrating plate interacting with sound waves in surrounding air 11 p1874 A67-24228

Alkali metal plasma generator design and performance, noting characteristics of LF wave propagation parallel to magnetic field 11 p1837 A67-24396

Ion-acoustic wave excitation by vertical density gradients, noting effect of resulting instability on ionospheric fine structure 11 p1786 A67-24398

Connection between sub-ELF ionospheric emissions at night and high negative ion concentration, noting ion-acoustic wave excitation 11 p1787 A67-24399

Acoustic field of random pressure pulsations into half-space behind infinite plate with arbitrary number of layers 11 p1820 A67-24930

Vibration qualification of fly-away umbilical by induced acoustic excitation testing method in Apollo project 12 p1924 A67-25714

Spin wave interaction in YIG with acoustic, magnetoplastic and relaxation oscillations excited by laser and microwave 12 p1953 A67-25749

Characteristics of sound formation in turbulent flow and mechanism of flow energy conversion into sound 14 p2305 A67-28519

Acoustic radiation of panels excited by random pressure fluctuation of turbulent boundary layer investigated, showing agreement with experiment 15 p2574 A67-29770

Microwave sound generation by transient heating of material surface with laser pulses 20 p3457 A67-36386

ACOUSTIC FATIGUE

Optimum telemetry system characteristics for shock, vibration and acoustic measurements and data bandwidth sufficiency 02 p0196 A67-12009

Acoustic fatigue tests of aircraft components, determining sound field and stresses using actual jet engine or simulation 03 p0521 A67-13021

Proactive inhibition, redundancy and limited channel capacity under acoustic stress 24 p4116 A67-42701

ACOUSTIC GENERATOR

Experimental setup for determining acoustic parameters of solids as media for ultrasound propagation 02 p0241 A67-11851

Generators of sonic and ultrasonic frequencies using thyristors 05 p0773 A67-16458

Artificial pseudorandom binary noise generation for flight testing and aircraft control systems and correlation function and frequency spectra of noise 08 p1279 A67-21005

Strong traveling transverse acoustic modes generated by rotating gas jet in cylindrical cavity 23 p3993 A67-41763

ACOUSTIC IMPEDANCE

Gaseous composition of unknown planetary atmosphere determined, using acoustic experiment combined with pressure and temperature data 03 p0509 A67-13215

Nonlinear resistance of multiple resonator arrays at incident sound high pressure levels 19 p3311 A67-34963

Pressure dependent surface reaction effects on acoustic response of composite solid propellants studied for various coatings 19 p3309 A67-35010

External ear replica for acoustical testing noting sensing element, ear canal and eardrum impedance 21 p3577 A67-38148

ACOUSTIC INSTABILITY

S COMBUSTION INSTABILITY

ACOUSTIC RADIATION

Lethal effects of high intensity airborne sound and ultrasound and irradiation time

on Bacillus Subtilis for applications to spacecraft sterilization 01 p0016 A67-10881

Flame noise in spherical volume of combustible gas confined within soap bubble and spark ignited, noting relation between radiated sound and flame movement and combustion 01 p0168 A67-11290

Retarded time integral expression rearrangement for study radiation from dipole distribution in inhomogeneous convective motion 01 p0115 A67-11305

Correlation between free IR and acoustic signals produced during optical measuring of heat 04 p0619 A67-14545

Heat flow meter with short response time, measuring influence of acoustic field on forced convection 05 p0790 A67-16034

Sound field of vibrating circular plates and membranes 05 p0924 A67-17283

Minimum structural response and acoustic radiation for panel excited by turbulent boundary layer [AIAA PAPER 67-12] 06 p0985 A67-18256

Acoustic waveform procession to auditory centers of brain, discussing transformations used by animals 09 p1454 A67-21686

Characteristics of sound formation in turbulent flow and mechanism of flow energy conversion into sound 14 p2305 A67-28519

Acoustic radiation of panels excited by random pressure fluctuation of turbulent boundary layer investigated, showing agreement with experiment 15 p2574 A67-29770

Thermal conductivity variation of double-base solid propellants under acoustic irradiation compared with polymethyl methacrylate 15 p2545 A67-30199

Acoustic hologram formation retaining holographic properties of Leith-Upatneiks holograms 17 p2860 A67-32625

Nonlinear resistance of multiple resonator arrays at incident sound high pressure levels 19 p3311 A67-34963

Infrasonic wave anisotropic radiation from moving auroras analyzed using shock wave model, discussing sound propagation and ray tracing 24 p4147 A67-41882

ACOUSTIC SCATTERING

Stimulated Brillouin scattering in shock-compressed acetone 01 p0116 A67-10338

Disturbance current created by acoustic wave propagating in partially ionized gas 05 p0855 A67-17050

Acoustic waves omnidirectional scattering by rough imperfectly reflecting surfaces analyzed using physical optics method 10 p1680 A67-23314

Scattering of plane monochromatic sound wave by semilinear elastic pipe in moving medium, emphasizing axisymmetric oscillations 10 p1680 A67-23644

Electrical properties of degenerate intrinsic semiconductor noting spherical energy surfaces, parabolic density of states, acoustic phonon scattering, etc 15 p2535 A67-29487

Ion-acoustic interaction in weakly turbulent plasma deriving time variation of plasmon number 16 p2715 A67-31046

Scattering of plane monochromatic sound wave by semilinear elastic pipe in moving medium, emphasizing axisymmetric oscillations 18 p3080 A67-34413

Acoustic radio signal backscattering producing rippled signals, showing activity with broad ripple spectrum 19 p3185 A67-36018

Scattering amplitude of frequency spectrum components of isolated exponential acoustic pulse incident on hard sphere 21 p3657 A67-38057

Integral equation for asymptotic expansions of plane electromagnetic and acoustic fields diffracted by convex surfaces of variable curvature 22 p3836 A67-39389

IR absorption spectrum of n-GaAs noting free carrier contribution due to phonons and ionized impurities 23 p4042 A67-41293

ACOUSTIC SIMULATION

Noise and pressure measurement in difficult conditions of vibrations and temperature for use in pressure-transducer design of jet and rocket systems 09 p1497 A67-21939

Acoustical and aerodynamic characteristics of full scale axial flow air compressor simulation in Freon closed loop system operation

[ASME PAPER 67-GT-27] 11 p1742 A67-24806

Reverberation chamber for high intensity acoustic testing of specimen subjected to directionally predetermined spectral distribution of acoustic energy field 12 p1924 A67-25712

Engine generated and in-flight noise environment problems of space vehicles analyzed, using theoretical methods and scale model wind tunnel tests 13 p2212 A67-27216

Vibro-acoustic test system for simulation of Saturn V dynamic launch environment on major space vehicle structures, discussing design and operation characteristics 17 p2832 A67-32005

Image reconstruction from coarsely sampled acoustical hologram made from ordinary microphone waves 19 p3233 A67-36104

Antenna array simulator using acoustic waves in water to simulate electromagnetic propagation 20 p3397 A67-36580

ACOUSTIC STABILITY

Approximate calculation of local characteristics of sound waves into liquid and gaseous media 05 p0846 A67-16707

Influence of relative thickness of elastic case on acoustic stability of radial modes in solid propellant rockets [AIAA PAPER 66-473] 07 p1240 A67-19370

Approximate calculation of local characteristics of turbulence developing during intense injection of sound waves into liquid and gaseous media 11 p1820 A67-24929

T-burner technique for determining acoustic pressure-and velocity-coupled responses of solid propellants 12 p1988 A67-25910

Oscillation spectrum of weakly ionized plasma current flowing normal to applied magnetic field discussed and analyzed in linear approximation using MHD model 16 p2712 A67-30546

Steady state solutions for system of partial differential equations with two independent variables describing small perturbations of transonic gas flow near transition point 22 p3844 A67-39391

One-component nonviscous nonheatconducting perfect gas in container with gaseous adsorption at boundary, noting acoustic oscillation instability for certain frequency disturbances 22 p3836 A67-39719

ACOUSTIC STREAMING

Sound and vibration effects on convective heat transfer rates 12 p2039 A67-26167

Acoustic characteristics of jet determined, using Lighthill equation for free turbulent jet when components of flow fluctuation rate, turbulent vortex volume and turbulent fluctuation frequency are known 14 p2302 A67-28301

ACOUSTIC VELOCITY

Free stream turbulence effects on boundary layer transition, discussing acoustical disturbance as source of velocity fluctuations 05 p0794 A67-17364

Antenna impedance dependence on excitation of acoustic waves by biconical dipoles encased in dielectric sphere immersed in warm plasma 11 p1769 A67-25030

Fundamental relations for normal shock wave behavior in compressible fluid for classical and hydromagnetic cases 15 p2473 A67-30226

Debye-Sears effect in one-dimensional Fresnel zone plate moving at acoustic velocity causes scanning of focal spots 22 p3835 A67-39242

ACOUSTIC VIBRATION

Flame study of turbulence effects induced by sonic or ultrasonic vibration on combustion of liquid hydrocarbon jet 01 p0167 A67-10942

Hybrid CDC 3200 digital computer acquisition of response data from acoustic and high force vibration tests 01 p0029 A67-11025

Flame noise in spherical volume of combustible gas confined within soap bubble and spark ignited, noting relation between radiated sound and flame movement and combustion 01 p0168 A67-11290

Interaction of transverse distributed surface vibration with adjacent laminar flow, superimposing oscillatory pressure and velocity field developed in boundary layer fluid over idealized steady fluid flow 10 p1623 A67-22861

Negative ions in night ionosphere,

discussing sub-ELF emission and excitation of ion acoustic oscillations in plasma by electron drifts 11 p1784 A67-23933
Flow induced vibration and noise in tube bank heat exchangers due to Karman vortex streets analyzed, noting shedding frequency, lift, etc
[ASME PAPER 67-VIBR-48]

Erratic vibration peaks, recognized as variable acoustic resonance, during tests of jet engine compressors
[ASME PAPER 67-VIBR-57]

High volume data processing techniques applied to Ranger acoustic testing 12 p1924 A67-25713

Liquid scintillation counting method with sonic oscillations, noting decreased preparation time and increased counting efficiency 14 p2260 A67-28477

Rocket nozzle effect on acoustic losses from model motor chambers oscillating in first longitudinal mode 15 p2546 A67-29992

Cellular flame under constant volume bomb conditions, demonstrating vibratory combustion over range of gas compositions and characteristic initial pressures 17 p2974 A67-33143

High speed liquid jet in standing acoustic field with velocity vector transverse to jet axis, testing injector orifice diameter, viscosity, etc
[AIAA PAPER 67-473]

Diagnostic methods of rotating bearing defects, describing types of bearings, oils and equipment used in tests 19 p3235 A67-34888

Acoustic vibrations during solid-fuel combustion, studying acoustic energy increase rate and development 20 p3551 A67-36817

Acoustic vibration effect on heterogeneous mass transfer at sphere surface in high Prandtl number liquids 20 p3554 A67-37068

One-component nonviscous nonheatconducting perfect gas in container with gaseous adsorption at boundary, noting acoustic oscillation instability for certain frequency disturbances 22 p3836 A67-39719

Diagnostic system for jet engine malfunctions detection using digital computer sonic vibration analysis
[SAE PAPER 670871]

Internal combustion engine vibration signals application to automatic fault diagnosis, discussing engine instrumentation and signal analysis 24 p4207 A67-42008

Aircraft cabin noise due to fuselage vibration reduced, using mechanical impedance
[SAE PAPER 670873]

24 p4248 A67-42010

ACOUSTICS

SA HYDROACOUSTICS

SA NOISE

SA PSYCHOACOUSTICS

Absorption of electromagnetic energy in gases in centimeter range waves measured, using optical-acoustic method of signal changes 03 p0418 A67-12895

Absorption of electromagnetic energy in gases in centimeter range waves measured, using optical-acoustic method of signal changes 06 p1006 A67-18772

Phonons and hypersound - Conference, University of Grenoble, March-April 1966 14 p2373 A67-28980

Acoustic problems from SST and multimillion pound thrust launch vehicles studied at Eastern Test Range, using Launch Acoustics Measuring System /LAMS/ 20 p3415 A67-36593

ACQUISITION

S DATA ACQUISITION

S TARGET ACQUISITION

ACRYLATE

Organic glass disintegration induced by pulsed laser beams 02 p0257 A67-12241

ACTH

S ADRENOCORTICOTROPIN /ACTH/

ACTINOMETRY

Industrial F 115 photocompensation amplifiers for recording integral and reflected radiation aboard aircraft 01 p0062 A67-10127

Thermophile radiation receiver utilizing detector comprised of fuel cells in series studied for application to actinometry 21 p3628 A67-38530

Actinometric measurements from aircraft

of short wave radiation fluxes and radiation balance, determining absorption coefficient for clouds and true albedo 24 p4182 A67-42882

ACTIVATION

S NEUTRON ACTIVATION

ACTIVATION /BIOL/

S STIMULATION

ACTIVATION ANALYSIS

S NEUTRON ACTIVATION

ACTIVATION ENERGY

Interdiffusion of niobium and molybdenum over 1400-2300 degrees C range using diffusion couples, determining activation energy values 01 p0100 A67-10767

Carbon diffusion in refractory metals with bcc lattice at temperatures of 1100 to 1600 degrees C, considering activation energy and frequency factor 01 p0101 A67-10937

Rate controlling mechanism during yielding and flow of alpha-titanium below 0.4 times melting point 03 p0441 A67-13258

Current voltage characteristics of Cd-GaSe-Bi diode structure, rectification coefficient, activation energy and photocurrent spectral distribution 04 p0678 A67-14930

Uniaxial compression effect on two jump conductivity processes occurring in p-type silicon 04 p0679 A67-15145

Activation energy of high temperature internal friction for Cu, Al, Fe, Mo, W, Pb, Cd, Ni and Zn 04 p0640 A67-15978

Titanium oxidation characteristics, determining activation energy of scale formation, oxygen absorption of base metal and total oxygen absorption 05 p0829 A67-16759

Yield point and strain aging in tantalum, identifying interstitial atom in electron-beam melted tantalum after incremental plastic deformation 06 p1015 A67-17896

Annealing of fast neutron damage in impurity conducting n-type Ge, noting small activation energy in resistivity below 10 degrees K 06 p1050 A67-18146

Thermally activated motion of screw dislocations in bcc metals 07 p1209 A67-19640

Strain rate dependence of critical shear stress in cadmium single crystals used in activation energy determination 07 p1234 A67-20109

Second order strain accumulation in aluminum in reversed cyclic torsion at elevated temperatures 09 p1517 A67-21753

Relation in silicon between annealing rates, residual damage and defect concentrations, noting link to activation energy increase 09 p1557 A67-22420

Temperature dependence of Hall coefficient of tellurium doped GaAs ternary compound, noting activation energy parameter 10 p1694 A67-23656

Temperature, strain rate and purity effects on alpha-titanium deformation yield and flow stresses, ascertaining thermal activation rate controlling mechanism 11 p1807 A67-24567

Chemical impurities and native defects observed in GaAs using photoluminescence at 20 degrees K, noting role of optical activation energy 11 p1848 A67-24742

C domain wall motion in barium titanate crystals is dependent on A domains and activation fields throughout whole crystal 11 p1849 A67-24900

High resistivity cadmium selenide vacuum deposited films dielectric constant and electronic properties measured for different parameters 11 p1851 A67-25032

Stress rupture and creep behavior in binary and ternary vanadium alloys including tensile strength and activation energy, noting titanium role 12 p1954 A67-25140

Uniaxial compression effect on two jump conductivity processes occurring in p-type silicon 12 p1979 A67-25168

AC conductivity of glass semiconductor measured over various frequency and temperature ranges, noting activation energy 12 p1980 A67-25181

Reversed speed effect and grain boundary diffusion as explanations of discrepancy of activation energy values for strain aging under fatigue or simple stress conditions 12 p2013 A67-25284

Crack propagation kinetics by thermal fluctuation induction, considering endurance and breakdown of metallic and semimetallic materials 12 p2029 A67-25666

Temperature dependence of yield point of crystals described in terms of thermally

activated motion of dislocations in external forces field 13 p2131 A67-26449

Activation energy and volume of prismatic slip in beryllium 13 p2138 A67-27115

Polycrystalline beryllium creep at high temperature 13 p2139 A67-27122

Formation of hydride zinc film on titanium activated for deposition of galvanic coating 14 p2336 A67-27868

Activation energy of molecular relaxation processes in terms of areas under loss factor and reciprocal temperature curves 14 p2259 A67-28299

Tungsten powder compacts impregnation technique by metallic halides solutions, obtaining even distribution of metal 14 p2338 A67-28614

Lanthanum chromite activation energy determination from electrical resistivity and Hall coefficient variation as function of temperature and IR absorption spectrum 15 p2535 A67-29478

Decomposition and stability of diphenylamine compounds in nitrocellulose powder, determining activation energies 15 p2543 A67-29889

Activation energies of nucleation of crack and dislocation loops in crystals, noting crack propagation theories and temperature effect 16 p2772 A67-31303

Tritium diffusion from iron meteorite shortly after fall established by artificial proton irradiation 17 p2942 A67-32357

Impurity effect on annealing behavior of irradiated silicon studied via isothermal annealing of minority carrier lifetime 17 p2921 A67-33051

Production modes, physical deactivation with related electronic energy transfer and chemical reactions of D oxygen atoms, noting significance for upper atmosphere 17 p2809 A67-33203

Temperature dependence of Hall coefficient of tellurium doped GaAs ternary compound, noting activation energy parameter 17 p2923 A67-33337

Rate constants and activation energy in bimolecular transfer reactions for halogen atoms 18 p3154 A67-33835

Gas phase reactions of hydrazine with nitrogen dioxide, nitric oxide and oxygen, determining reaction rates, activation energy and order 18 p3109 A67-33837

Changes in experimental relationship between preexponential factor in diffusion equation and activation energy for solid solutions 19 p3243 A67-34928

Factors involved in initiation of reaction in cobalt /III/ amine azides, discussing thermal decomposition, activation energy, etc
[CI PAPER 67-15]

Surface ionization of atoms and molecules on nonmetals, determining work functions and activation energies for dissociation 19 p3264 A67-35083

Dynamic microstrain of niobium, considering purity and temperature effects, obtaining activation energy band spectrum 20 p3469 A67-37385

Grain boundary diffusion coefficients in tungsten at high temperatures, obtaining activation energy equation 20 p3470 A67-37388

Donor surface states and bulk acceptor traps in silicon on sapphire films due to activation of absorbed impurities 21 p3677 A67-38012

Chemical diffusion coefficients and heats of activation in nickel-aluminum intermetallic phases and solid solution calculated from layer growth experiments 21 p3645 A67-38775

TiC and ZrC powder properties after sintering investigated for linear growth rates vs temperature, obtaining sintering activation energy values 22 p3820 A67-39564

Carbon diffusion in refractory metals with bcc lattice at temperatures of 1100 to 1600 degrees C, considering activation energy and frequency factor 22 p3820 A67-39791

Flame activation energy and combustion process order based on homogeneous reactor model for mean temperature coefficient determination 23 p4082 A67-41141

Semiconducting diamonds photoconductive response measured noting correlation with activation energy 23 p4044 A67-41454

Gallium oxide desorption rate and activation energy after O adsorption on GaAs /111/ surface 23 p4045 A67-41464

ACTIVITY

S AURORAL ACTIVITY
S CATALYTIC ACTIVITY
S ENZYME ACTIVITY
S SOLAR ACTIVITY
ACTIVITY /BIOL/
SA CATALYTIC ACTIVITY
Modification of rat sensitivity to rotation through vestibular end organ damage or previous vestibular experience, studying activity changes 20 p3371 A67-36818

ACTIVITY CYCLE /BIOL/

S BIOLOGICAL RHYTHM

ACTUATOR

SA CARTRIDGE ACTUATED DEVICE
SA HYDRAULIC ACTUATOR
SA PROPELLANT ACTUATED DEVICE
SA SERVOACTUATOR
SA SERVOMECHANISM
Communications satellite orientation with respect to earth, using structure mounted electromagnetic actuator coils 05 p0905 A67-16831

Aircraft autopilot actuators move control surfaces in response to electric signals and include facilities for performing full automatic landing 05 p0754 A67-17048
Jaeger electromagnetic powder coupler characteristics and space application 07 p1131 A67-19525

Moving coil and variable air gap electromagnetic actuators, discussing characteristics and applications 14 p2247 A67-28266

Piezoelectric transducer electromechanical properties compared to electromagnet actuator, noting fluid control applications 14 p2248 A67-28267

High speed fluidic logic circuitry for pneumatic stepping motor 14 p2251 A67-28351
Time optimal control of system with multiple control inputs and bounded phase coordinates for design of autopilot for booster 16 p2762 A67-31643

Synthesis and design of on-line self-organizing control of multiple goal, multiple actuator systems 16 p2648 A67-31654

Adaptive controller synthesis for unstable mechanical system driven by bang-bang actuator adaptive controller synthesis for unstable mechanical system driven by bang-bang actuator 16 p2648 A67-31656

Fluidic actuator for direct digital control, converting computer information into mechanical motion 23 p3942 A67-41710

SST variable sweep wing actuation system and pivot bearing reliability [SAE PAPER 670884] 24 p4098 A67-42018

ACTUATOR DISK

Compressible nonswirling rotational flows through ducts with varying hub radii 09 p1489 A67-22161

ADAPTATION

SA ACCLIMATIZATION
SA DARK ADAPTION
SA DESERT ADAPTION
SA LIGHT ADAPTION
SA RETINAL ADAPTION

Biochemical measures made as part of habituation experiment in which four subjects were exposed to rotation for 6 days 05 p0754 A67-16277

Acetylative capacity and lipid metabolic changes and readjustment to normality in rats in oxygen-rich environment 14 p2256 A67-28588

Electrochemical generator concept noting compactness, adaptability, methods of adding active agents, evacuation of reaction products and decarbonation 14 p2253 A67-29020

Dog adaptation to increased carbon dioxide levels in normoxic environment, noting effects on arterial pH and bicarbonate level 23 p3950 A67-41537

ADAPTIVE CONTROL

Tabular adaptive predictive model for trajectory following control of nonlinear plant with switched two-level input 02 p0225 A67-12136

Adaptive visual signal preprocessor with quantized weights 02 p0207 A67-12140

Pattern recognition systems with fixed linear structure changing to nonlinear as result of repetitive generation and selection of relations among input measurements 02 p0208 A67-12141

Adaptive control by predictive identification and optimization in terms of time response 02 p0225 A67-12142

On-line estimation of states and

parameters for noisy discrete nonlinear dynamic system 02 p0226 A67-12153

Sequential suboptimal adaptive control of nonlinear systems, considering generation of optimum closed-loop control for startup dynamics of nuclear reactor 02 p0226 A67-12156

Path adaptive guidance modes for Saturn space vehicle, particularly Iterative Guidance Mode 02 p0264 A67-12318

Dispersion method of spontaneous subdivision of image space into compact sets /images/ 03 p0374 A67-13081

Adaptive utilization of communication satellite systems optimizing dynamic traffic handling of combined ground and satellite communications complex, noting network configurations 06 p0959 A67-17670

Communications satellite system efficiency enhanced by using automatic adaptive voice multiplexer in ground terminal equipment 06 p0960 A67-17676

Adaptive model reference systems without extremum search procedures 07 p1160 A67-19198

Search limit cycle frequency and magnitude in single dimensional optimizing systems with nonlinear function modeling of performance measurement process 07 p1161 A67-19206

Sensitivity models in terms of influence of time variation in given part on behavior of whole system 08 p1309 A67-20325

Adaptive power conditioning for optimal power transfer from solar cell array to load regardless of environment, impedance or volt-ampere characteristics 08 p1284 A67-20651

Self-optimizing and adaptive control systems achieved by feedback action or performance index optimization 08 p1312 A67-20753

Adaptive data compression systems of predictor-comparator type 12 p1907 A67-25992

Optimal statistical adaptive model used in defining characteristics of control plants 15 p2461 A67-30321

Parameter estimation representing differential equation coefficient of controlled system for quick-response adaptive identification 15 p2464 A67-30338

Adjustment uniqueness in defining dynamic characteristics with help of self-adjusting model 15 p2464 A67-30339

Adaptation technique for on-line steady-state optimizing control using updated control algorithm 16 p2648 A67-31655

Adaptive controller synthesis for unstable mechanical system driven by bang-bang actuator adaptive controller synthesis for unstable mechanical system driven by bang-bang actuator 16 p2648 A67-31656

Radar system using real-time on-line computer applied to adaptive control of beam direction and transmitter modulation 17 p2816 A67-32790

Adaptive unknown-waveform pulse signal detector algorithm construction method 20 p3384 A67-37333

Adaptive processes of human operator during control tasks involving sudden change of controlled plant dynamics 21 p3576 A67-37948

Steady state plant performance optimization for unknown dynamic characteristics, determining periodic input signal 21 p3603 A67-38439

Rapid parameter identification system for linear time-invariant plant with only input and output measurable 21 p3604 A67-38887

Open loop adaptive optimal control, calculating plant dynamic sensitivity coefficients for unknown disturbances, using digital computer on feedback path 22 p3776 A67-39411

Learning control systems, discussing adaptive time, searching, strategy, teaching, association, principle and behavior 22 p3776 A67-39412

ADAPTIVE CONTROL SYSTEM

SA SELF-ADAPTIVE SYSTEM

Lapuvov method application to adaptive loop redesign, using differential equations for model system errors coupled with squares of parameter differences 01 p0045 A67-11202

Direct approach to model referenced adaptive control systems using state space methods, showing simplicity in implementing adaptation equations 02 p0225 A67-12135

Automatic threshold control formulation

and probability distribution of adaptive detection mode for matched and mismatched clutter model 02 p0203 A67-12139

Choosing coefficients of prefiltering, series and feedback compensators for given time response specifications despite plant parameter variations 02 p0225 A67-12143

Adaptive machine using weighted matrix structure in generating decision space for fault detection or process control signals 02 p0243 A67-12144

Nonscanning adaptive automatic control system for plant with variable amplification factor 03 p0394 A67-14062

Adaptive flight control using parameter tracking mechanism functioning with any type of disturbance as input, for adjustment of control system parameters [ASME PAPER 66-WA/AUT-22] 04 p0552 A67-15393

Adaptive decoding technique for analyzing information-carrying signals in order to control signal to noise ratio during transmission time of single compound signal 05 p0768 A67-17401

Noise suppression on adaptive identification control systems, using series model 06 p0978 A67-18560

Model reference adaptive systems having linear processes and models of same form and order synthesized by Liapunov second method 07 p1160 A67-19196

Stability of model reference control systems determined by direct Liapunov method 07 p1160 A67-19197

Control of adaptive systems using sensitivity coefficients and logic circuits 08 p1308 A67-20318

Iterative algorithm for increasing stability of adaptive control systems 08 p1308 A67-20319

Adaptation scheme applied to pitch axis control system of supersonic aircraft, using stability analysis for system design 09 p1440 A67-22387

State space methods approach to model referenced adaptive control systems design using differential equations 11 p1771 A67-24894

Reduction of order technique pertaining to plant and reference model in controller design for linear plants transfer functions with zeros and slowly varying parameters 11 p1771 A67-24895

Adaptive feedback paths of adaptive aircraft control system in small signal stability analysis 11 p1772 A67-25081

Characterization and equivalent model construction technique for class of nonlinear systems mathematically described, constructing zero memory systems and systems with memory 12 p1919 A67-25285

Stability analysis of adaptive aircraft control system with random disturbance 13 p2088 A67-27241

Nonscanning adaptive automatic control system for plant with variable amplification factor 13 p2089 A67-27711

Digital computer application to direct control of system dynamics and implementation of adaptive/ learning loop 15 p2441 A67-30266

Predictive identification and fast moving target recognition technique for adaptive control and tracking systems 15 p2463 A67-30330

Systems with asymmetric nonlinearities analyzed and synthesized by setting up mathematical model applicable to control and adaptive systems 15 p2463 A67-30333

Process identification with use of search controlled adaptive model 15 p2464 A67-30334

Experimental identification of systems by adapting parallel model 15 p2464 A67-30336

Similarities between model-reference adaptive control systems and parameter identification by adjustable models 15 p2464 A67-30337

Suboptimal, adaptive solutions to sampled data problem for quadratic performance index minimization by obtaining control law and sampling scheme 16 p2649 A67-31660

Time optimal adaptive control system synthesis using off-line memorization with simple on-line calculations to determine control signal 16 p2650 A67-31672

Identification of continuous, nonlinear, time-dependent, single-input single-output systems represented by Volterra functional series model and stochastic

approximation 16 p2653 A67-31694
 Parallel electro-optical technique for implementing linear threshold adaptive networks 17 p2860 A67-32616
 Nonlinear decision surfaces determined by pattern-recognizing adaptive threshold device via generation of polynomial discriminant functions and computer programs 18 p3006 A67-34064
 Synthesis of closed loop system consisting of pitch control adaptive autopilot for changing flight conditions, using transient characteristics 18 p3075 A67-34282
 Bang-bang control using adaptive-predictive model applied to least-square error trajectory control of settling-time nonlinear systems 19 p3199 A67-34784
 Adaptive control systems for stabilizing structural bending modes of Saturn V launch vehicle [AIAA PAPER 67-591] 19 p3336 A67-35987
 Equations of motion of continuous single loop adaptive control system with scan modulated parameters, noting stability analysis method 20 p3408 A67-37044
 Design of adaptive systems with forced oscillations, using correlation and filter methods 20 p3410 A67-37228
 Book on optimal adaptive control systems, detailing material on game theory for use in control system design 21 p3603 A67-38266
 Transmission buffer overflow prevention in telemetry data compressors using adaptive queueing control system 21 p3586 A67-38956
 Adaptive terminal guidance scheme for circular orbit rendezvous to provide near optimal trajectory 22 p3832 A67-39964
 Book on adaptive control and optimization techniques covering basic mathematics, computer methods, differential equations, time domain, etc 24 p4133 A67-41793
 Time optimal adaptive control system synthesized via adaptive switching hypersurface and function generator/off-line memorization and on-line interpolation/ 24 p4134 A67-42177
 Synthesis of self-adaptive systems with variable structure, obtaining relationships between systems dynamics and characteristics of logical control law 24 p4137 A67-42699

ADAPTIVE FILTER

Kalman filter estimation of covariance parameters of linear system subjected to Gaussian driving functions 02 p0227 A67-12157
 Semiadaptive ancillary numerical filters for use in best estimate of trajectory computation, noting development of optimal differentiator for scalar function semiadaptive ancillary numerical filters for use 08 p1298 A67-20663
 Simulation results of adaptive tracking filter application to stabilization of structural bending modes of SI-B launch vehicle 13 p2212 A67-26818
 Human controller as adaptive low pass filter to track signal contaminated with noise 18 p2994 A67-34340
 Approximate investigation of standard model reference adaptive systems with random input effects based on filtering properties of automatic control systems 23 p3985 A67-41675

ADDITIVE

SA ANTIOXIDANT

SA PROPELLANT ADDITIVE

Oxygen as steady state electronegative additive in cesium thermionic converter shown to improve performance without surface corrosion 09 p1450 A67-22355
 Effect of additives on hydrazine nitrogen trioxide droplet flame structure and burning rate [AIAA PAPER 67-482] 18 p3158 A67-33951
 Influence of palladium additives and sintering temperature on tungsten molding noting shrinkage, density, microhardness, durability and microstructure 20 p3466 A67-36910
 Additive elements studied for influence on morphology, nature and hot plasticity of sulfides in austenitic stainless steels 21 p3646 A67-39077

ADENINE

Adenine and guanine amounts in DNA determined spectrophotometrically by dialysis of DNA 04 p0564 A67-14406

ADENOSINE TRIPHOSPHATE /ATP/

Autotrophic and heterotrophic carbon

dioxide fixation regulation in Hydrogenomonas, discussing two Calvin cycle enzymes 20 p3370 A67-36797

ADHESION

SA BONDING

Friction and adhesion coefficients of copper on copper measured in vacuum at temperatures ranging from minus 270 to 1000 degrees F and in controlled pressures of dry air [ASME PAPER 66-LUB-3] 03 p0431 A67-13754

Rotational motion of rigid sphere about z axis in elastic medium taking into account surface adhesion 07 p1223 A67-19219

Nature of forces causing adhesion of coatings produced by plasma jet sputtering techniques 07 p1190 A67-19304

Sessile drop technique to study effect of atmosphere and alloy additions of Ti and Cr on surface tension and contact angle of N on sapphire substrated at 1500 degrees C 08 p1343 A67-21543

Thin film adhesion to substrate, considering effect of interposed thin film 09 p1503 A67-22100

Microstructural study of adhesive behavior of powdered bakelite in intergrain pores of carbon-graphite compacts in terms of capillary attraction forces 11 p1810 A67-23900

Space environmental effects on filled elastomers, nylon parachute material and adhesion of metals 15 p2506 A67-29540

Metallic adhesion between Mo-Mo and Ti-Ti couples, showing contact resistance useful in determining contamination at conducting interface 17 p2871 A67-32465

Properties of adhesive bonding compared with spot welding and riveting in aircraft industry 19 p3236 A67-35821

Coanda effect shown to be caused by periodic system of vortices arising from nozzle edges 20 p3421 A67-36811

Adhesive qualities of lunar soil simulated by rock comminuted in ultrahigh vacuum 24 p4227 A67-42034

ADHESIVE

SA BINDER

Ultrasonic phase sensitive test procedure for adhesive bonded structures 04 p0622 A67-15265

Adhesive types and characteristics suitable for aluminum bonding 06 p1020 A67-18062

Cold hardened metal adhesive /Agomet E/, discussing polymerization, pot time, setting and temperature 07 p1193 A67-20291

Resistance spot-welded adhesive bonds between aluminum alloy components, using thermosetting film 09 p1502 A67-21688

Structural adhesives bonding - Symposium, Stevens Institute of Technology, Hoboken, September 1965 09 p1521 A67-22499

Criterion characterizing adhesive joints in structural bonding of military materiel 09 p1522 A67-22500

Design of three types of bonded metal-to-metal joints, discussing advantages of theoretical over empirical methods 09 p1576 A67-22501

Load carrying capability of adhesive bonded studs, analyzing resin systems and flexible linears 09 p1507 A67-22502

Shear strength of various joint designs measured, using steel adherends and rubbery adhesives to isolate factors affecting shear stress 09 p1577 A67-22503

Stresses in ordinary lap joint compared to variable adhesive joint 09 p1577 A67-22504

Creep measurement associated with adhesive bonding of aircraft structures, particularly creep of metal-metal lap joints and bonded sandwich structures creep measurement associated with adhesive bonding 09 p1522 A67-22505

Adhesive bonded honeycomb horizontal stabilizers, considering strength, aerodynamics, cost, endurance and serviceability 09 p1577 A67-22508

Adhesive-honeycomb relationship including filleting effect on honeycomb properties, compression properties, stresses at fillet, etc 09 p1577 A67-22509

Fatigue life on 727 aircraft structure improved through room temperature curing of adhesive film 09 p1577 A67-22510

Bonding of rigid insulation to case of solid propellant rocket motor, considering fabrication, operation and storage requirements 09 p1578 A67-22512

Medium temperature curing general

purpose structural adhesive system for use on helicopter 09 p1523 A67-22515

Graphite fibers as internal electrical resistance heat source for curing structural adhesives demonstrated in lap shears, larger area and sandwich construction 09 p1507 A67-22516

Polybenzimidazole /PBI/ structural adhesives for bonding stainless steel, beryllium and titanium alloys 09 p1523 A67-22517

Mechanical properties of polybenzimidazole resin show suitability for metal-to-metal and sandwich composite adhesives and high and cryogenic temperatures 09 p1523 A67-22518

Surface preparation for aluminum and bond strength dependence on cure temperature, humidity and impurities 09 p1507 A67-22519

Metal surface preparation by mechanical and chemical processing for adhesive bonding 09 p1507 A67-22520

Durability of adhesive lap-shear joints with sustained stress, describing portable jig 09 p1578 A67-22522

Structural adhesives for fabricating large one-piece hemispherical bulkheads, noting effect of radiation and high vacuum 09 p1578 A67-22523

Adhesive systems for substructure bonding to solid ablators and to honeycomb operating in extreme environments 09 p1578 A67-22524

Epoxy adhesive properties dependence on application variables according to test methods of MIL-A-8623 adhesive specification 09 p1523 A67-22525

Ultrasonic nondestructive inspection of adhesively bonded components, discussing pulse echo reflection, pulsed through transmission and sweep frequency coupling methods and scanning equipment 09 p1507 A67-22526

Quality control system for adhesive bonding using Fokker bond tester ultrasonic resonance instrument 09 p1508 A67-22527

Adhesives development, discussing chemically and mechanically blocked reactant system and water based, hot melt, oil absorbent, heat resistant and low temperature adhesives 09 p1523 A67-22529

Adhesive properties testing and damping behavior of thin viscoelastic material under different cyclic loadings [ASME PAPER 67-VIBR-25] 11 p1872 A67-24183

Book on adhesive bonding Alcoa aluminum covering techniques, applications including aircraft and military uses, classifications, etc 13 p2143 A67-27177

Treatise on adhesion and adhesives, Volume 1, Theory 14 p2340 A67-27793

Adhesive bonding techniques for aluminum, advantages, drawbacks, joint design and surface treatment before bonding 14 p2323 A67-27820

Adhesives for nuclear powered spacecraft tested for pressure, temperature and radiation effects 15 p2508 A67-29560

Adhesives for aircrafts and spacecrafts considering high temperature resistivity, waterproofing and brittleness 16 p2683 A67-31788

Glued metal joints properties analyzed from test results by method using theory of probability and statistical sample 21 p3716 A67-37950

Adhesives for bonding overlay materials to substrates for high speed hydrofoils, describing water tunnel and rotating arm tests 21 p3632 A67-38131

Adhesives to bond metal linings to filament-wound cryogenic pressure vessels evaluated by test series simulating fabrication and service conditions 23 p4010 A67-41347

Adhesive system for structural bonding of fiberglass reinforced polyester to itself and to metal 24 p4175 A67-42421

ADIABAT

One-dimensional adiabatic equilibration of plate with starting temperature compared with nonadiabatic equilibration and exoatmospheric cooling of cylindrical metallic and plastic shells 08 p1429 A67-21527

ADIABATIC EQUATION

Plasma density dependence of adiabatic motion of plasmoids in longitudinal magnetic field 01 p0122 A67-10351

Unsteady adiabatic centrally symmetric radial flow of ideal fluid in general theory

- of relativity 01 p0114 A67-10987
Plane adiabatic flow of ideal gas behind separated shock wave for uniform supersonic symmetrical flow past smooth profile 03 p0349 A67-12873
Adiabatic invariant analysis of charged particle motion in model magnetosphere 08 p1378 A67-21474
Plasma density dependence of adiabatic motion of plasmoids in longitudinal magnetic field 11 p1844 A67-25024
Time dependent large scale electric potential field effect on motion of geomagnetically trapped particles 12 p1997 A67-25809
Formulas for potential temperatures derived from thermodynamic principles, considering four stages of reversible adiabatic transformation of humid air 17 p2844 A67-32566
Oscillator analysis for particular class of adiabatic invariants 18 p3117 A67-33686
Dynamic equations for adiabatic changes of state for mixtures of partially ionized gases with chemical reactions 19 p3286 A67-35348
Classification of small amplitude waves, surfaces of weak discontinuity and shock waves in ideal MHD medium obeying adiabatic state equation 19 p3294 A67-35409
Radial adiabatic motion of spheres of uniform density and isotropic pressure in general relativity, giving bounce occurrence conditions 20 p3486 A67-37273
Reversible betatron acceleration mechanism during geomagnetic storm 20 p3434 A67-37425
Theta pinch plasma sheath and fields time development for relaxing radial electric field 21 p3662 A67-37754
Variations in parameters of magnetized plasmoids interacting in nonuniform fields determined by magnetic and electric probes 23 p4035 A67-41685
Adiabatic constant formula which holds for ideal and real gas derived, noting application of thermodynamics and gas dynamics formulas to real gas 24 p4256 A67-42592
- ADIPOSE TISSUE**
Nonphosphorylating respiration of mitochondria from brown adipose tissue of rats, providing example of electron transport 02 p0185 A67-12527
- ADMITTANCE**
S ELECTRIC IMPEDANCE
- ADRENAL GLAND**
Central nervous system, adenohypophysis and adrenal glands relation in oxygen deficiency 20 p3369 A67-36669
Adrenal gland reaction to different pressure breathing types by urine analysis 22 p3752 A67-40538
Rat adrenal gland responses to increased oxygen tension at ambient temperature, noting oxygen critical threshold partial pressure affecting survival time 23 p3950 A67-41538
- ADRENAL METABOLISM**
Adrenal corticosterone concentration changes in response to various doses of ACTH and time pattern of changes in hypophysectomized rats 04 p0560 A67-14525
Adrenal cortical activity changes correlated with pathological emotional states 06 p0952 A67-17848
Circadian rhythms detection, estimating parameters by cosinor procedure for temporal morphology aspects evaluation 14 p2255 A67-28480
- ADRENOCORTICOTROPIN /ACTH/**
Adrenal corticosterone concentration changes in response to various doses of ACTH and time pattern of changes in hypophysectomized rats 04 p0560 A67-14525
- ADSORPTION**
Nitrogen adsorption at room temperature on atomically clean polycrystalline rhenium, noting dependence of sticking coefficient upon surface coverage and temperature 02 p0257 A67-12728
Heats of adsorption of hydrogen and oxygen on semiconductors of zinc blende type calculated, using Clausius-Clapeyron and Bering-Serpinskii equations 03 p0496 A67-13646
Oxygen adsorption on tungsten crystal face studied by back-reflection low energy electron diffraction 03 p0447 A67-13647
Forces holding hydroxyl ions to surfaces of MgO particles 04 p0642 A67-15087
Low pressure physical adsorption and electron microscope study of surface of annealed pyrolytic graphite, using flash filament technique 06 p1020 A67-17988
Interaction energy of single atom adsorption at any point on single crystal planes of bcc structure, using Lennard-Jones potential 08 p1355 A67-20719
Temperature control and thermal coupling of cesium adsorption porous tungsten, charcoal and graphite reservoirs 09 p1450 A67-22350
Surface parameter measurements of stannic oxide in powder, ceramic and gel forms by nitrogen adsorption techniques 10 p1603 A67-23398
Adsorptive interaction of oxygen with tungsten surface 15 p2434 A67-30100
Surface leakage current and reverse current flow in silicon p-n junction diode affected by positive ion bombardment and oxygen adsorption 17 p2911 A67-32202
Adsorption of oxygen upon clean nickel surface and beginning of oxidation 19 p3244 A67-34937
Adsorption of oxygen on tungsten surface, discussing electron diffraction 19 p3246 A67-35786
Electron emission and adsorption of potassium on tungsten single crystal faces, noting work function values 20 p3504 A67-36165
Adsorption effect of various metals on electrical conductivity and Hall effect of thin nickel films 20 p3504 A67-36166
One-component nonviscous nonheatconducting perfect gas in container with gaseous adsorption at boundary, noting acoustic oscillation instability for certain frequency disturbances 22 p3836 A67-39719
Adsorbed ions and organic molecules effect on mobility of half-loops dislocation introduced by indenter into MgO surfaces 23 p4035 A67-40655
Isobars of adsorption of Ce on faces of W crystal measured for adsorption heat dependence on atom surface density 23 p4042 A67-41298
Gallium oxide desorption rate and activation energy after O adsorption on GaAs /111/ surface 23 p4045 A67-41464
Electron beam retarding potential method to measure work function changes resulting from Cs, oxygen and hydrogen adsorption on /110/ Ta single crystal 24 p4201 A67-41892
Dynamic mass transfer equation for design parameters of regenerable absorption beds for carbon dioxide removal in spacecraft life support system [SAE PAPER 670842] 24 p4115 A67-41996
Benzene and related molecules adsorption on uniform graphite surfaces investigated for lateral interaction and localization of lattice sites 24 p4118 A67-42195
Adsorption equilibrium data obtained at high pressure for methane and propane on silica gel using radioactive tracer pulsing 24 p4118 A67-42584
Steel dislocation structure under adsorption fatigue investigated by electron microscope, discussing surface active medium effect 24 p4174 A67-42724
- ADVANCED TECHNOLOGY SATELLITE S APPLICATIONS TECHNOLOGY SATELLITE /ATS/**
- ADVECTION**
SA CONVECTION
Second order accurate approximation to advection terms in hydrodynamics equations noting aliasing effects, amplitude and phase errors and stability criterion 23 p4024 A67-40994
- AE-A S EXPLORER XVII SATELLITE**
- AERIAL PHOTOGRAPHY**
SA PHOTOGRAMMETRY
Remote sensing techniques and data evaluation and processing in geography 01 p0058 A67-10308
Multispectral photography in gathering data on static physical and man-made elements of urban environment 01 p0058 A67-10309
IR imagery and concurrent aerial photography in depicting Arctic terrain features and conditions during daylight 01 p0058 A67-10312
Nautical chart information extracted from hyperaltitude color photographs obtained on Gemini orbital flights IV, V and VII 01 p0059 A67-10322
Terrain information from high altitude side-looking radar imagery of Arctic area 01 p0059 A67-10328
IR imagery application in locating anomalously hot earth in Yellowstone National Park 01 p0059 A67-10332
Conditional angular elements in external orientation of aerial photographs determined by orientating right photograph with baseline 01 p0068 A67-10855
Optimization of size of film negative for aerial cameras on grounds of economic efficiency 02 p0240 A67-11532
Interpretation of built-up areas in cities and industrial sites from aerial photographs 02 p0240 A67-11533
Updating application of aerial photographs to scale of map based on radio altimeter data 03 p0419 A67-13262
Airborne astronomical photography affected by instrument structural design, vibration, aircraft stability, image stabilization, navigation, observation time, boundary layer effect and viewing port [SMPT PREPRINT 100-9] 03 p0423 A67-13803
High resolution aerial photography, examining systems and techniques evolved over last two decades reaching level of 100 lines/mm [SMPT PREPRINT 100-10] 03 p0423 A67-13804
Autopilot programmer design for automatic guidance in approach and stabilization along course of aerial photography aircraft 03 p0465 A67-14284
Aerial photograph interpretation of landscape in terms of tone, texture and stereo effect 04 p0619 A67-14529
Aerial photograph physics in correct and faulty colors, discussing recognition of relation between landscape and photographic density 05 p0804 A67-16064
Frame camera for high speed aerial photography, discussing interlacing with advances in other areas 05 p0806 A67-16700
Photogrammetric refraction in high altitude surveying for isothermal atmosphere and for atmospheric polytropic through altitude of 11 km 05 p0808 A67-17033
Aerial photography processing problems using SD-3 and USD-1 stereographs 05 p0809 A67-17549
Aerial photographic techniques and equipment, noting use in reconnaissance and mapping 06 p1000 A67-17583
Photogrammetric network for large-area phototriangulation using star-tracking airborne cameras, discussing theoretical and technical aspects 06 p0994 A67-17716
Low resolution side-looking radar application for geological studies, noting advantage over small scale aerial photography 06 p0994 A67-17833
Angular distribution of reflected cloud and radiation fields according to IL-18 aircraft data of 1964 07 p1220 A67-19452
Automatic system for classifying and delineating terrain features in aerial photography, using general purpose computer 07 p1187 A67-19744
High resolution aerial photography, detailing photographic films, optical design, camera systems and methods of system analysis 08 p1330 A67-20645
Roughness data and statistical analysis of off-runway landing areas in Canada, using aerial photography for profile measurement 10 p1622 A67-23388
Goniometric measurement accuracy of aerial camera photogrammetric distortion 11 p1793 A67-24864
IR imagery from remote sensing, use in agriculture and forestry [AIAA PAPER 67-281] 12 p1967 A67-26000
Systematic local errors in radio leveling of aircraft for different scales and tracks, using aerial camera 13 p2118 A67-26462
Tilt angles for photographs of physically and geographically diverse terrains taken with different types of gyrostabilized aerial cameras 13 p2118 A67-26463
Errors, due to inaccurate tentative aerial observations, in determination of identification points for vertical aerial photography 13 p2118 A67-26464
Conditional angular elements in external orientation of aerial photographs determined by orientating right photograph with baseline 14 p2317 A67-28244
Soviet papers on photogrammetric

processing and interpretation of aerial photographs 14 p2318 A67-28370

Formulas for correcting errors in aerial-photograph and planar-model coordinates due to atmospheric refraction and earth curvature 14 p2318 A67-28371

Aerial and space photography for forestry 14 p2321 A67-28827

Electro-optical rectifier, types of materials generated, operational capability and lunar and aerial photographic application 14 p2321 A67-28828

Automatic exposure of longitudinal overlapping of aerial photographs solved by autonomous radio-navigation systems 15 p2485 A67-29137

Sensors and sensor control devices for use in high speed low altitude reconnaissance aircraft 15 p2485 A67-29162

Three-photo orientation solution to analytic aerotriangulation problem, investigating mathematical concepts and computer programming methods 15 p2486 A67-29298

Military surveillance satellite for high resolution photography noting design, application and projected performance 15 p2564 A67-29400

Parallelism between edges of aerial photographs and line of flight achieved by automatic rotation methods 16 p2671 A67-31031

Airborne camera system for high altitude photography of rocket and spacecraft vehicle launchings describing development 16 p2679 A67-31800

Aerial electronic photomapping and geodetic surveying system describing track-keeping navigation and verticality measuring 16 p2679 A67-31801

Airborne photographic systems defining performance criteria for quantitative analysis and application of transfer functions for evaluation 16 p2680 A67-31804

Airborne imagery screening using automatic target recognition device 17 p2859 A67-32509

Airborne astronomical photography affected by instrument structural design, vibration, aircraft stability, image stabilization, navigation, observation time, boundary layer effect and viewing port 18 p3044 A67-33575

Photography from aircraft of cloud-like objects in vicinity of libration points L4 and L5 of earth-moon system 19 p3251 A67-34953

Photogrammetric refraction in high altitude surveying for isothermal atmosphere and for atmospheric polytropic through altitude of 11 km 21 p3627 A67-38265

Aerial color photography advantages over black and white, discussing exposure, processing and viewing 22 p3797 A67-39450

Camera for multispectral color aerial photography noting four-band interpretation on companion viewer and application to target acquisition problems 22 p3797 A67-39451

Image shear analysis utilizing conventional coordinate and projective transformations performed on computer 24 p4157 A67-42603

Clouds over equatorial and tropical Pacific investigated by comparing photographs from Tiros satellites and jet aircraft 24 p4181 A67-42667

AERIAL RECONNAISSANCE

Radar imagery compilation of vegetation maps, noting extent of capabilities and results obtained 01 p0059 A67-10329

Radar backscatter return interpretation in identifying terrain phenomena and composition 01 p0059 A67-10330

Spectral polarimetry signature of terrestrial and planetary materials through remote sensing 01 p0059 A67-10331

Manned orbiting laboratories for surveying natural resources using advanced remote sensing techniques 08 p1325 A67-21072

Surveying earth resources from high flying aircraft and earth orbiting satellites 10 p1735 A67-23688

Radar, IR and laser sensors production trends for airborne reconnaissance 15 p2485 A67-29163

Analytical reduction of panoramic and strip photography to equivalent frame photography 15 p2486 A67-29299

Performance of fiber-optics coupled cascade image intensifier systems from standpoint of overall system noise, resolution, gain, contrast degradation and

information rate capability 17 p2859 A67-32504

Millimeter wave passive radiometry noting design, capability, detectability and aerial reconnaissance 17 p2814 A67-32521

Image motion compensation tracking study for earth reconnaissance from space, investigating computer and manual tracking modes, control dynamics and gain and magnification 18 p2993 A67-34337

AEROBEE ROCKET

Location of X-ray source Sco X-1 determined by instrumented payload flown on stabilized Aerobee rocket 02 p0308 A67-11771

Ionospheric electron density profile determined by local measurements of VLF fields radiated by ground emitter 03 p0413 A67-13531

Aerobee rockets measurement of sodium dayglow suggest equilibrium between sodium atoms and distribution of dust particles 07 p1180 A67-19917

Aerobee 350 sounding rocket for scientific use in heavy payload to moderate altitude performance region 08 p1404 A67-20496

Gyroless Solar Pointing Aerobee Rocket Control System /SPARCS/ using no inertial platform and having solid state circuitry 08 p1409 A67-20540

Mobile Aerobee Launch Facility /MALF/, noting applications to space science 08 p1314 A67-20544

IR observations in one to seven micron region using astronomical telescope on Aerobee rocket above atmosphere 08 p1397 A67-21185

Aerobee rocket instrumentation for solar spectroscopy in soft X-ray region 10 p1712 A67-23804

Aerobee 350 sounding rocket for scientific use in heavy payload to moderate altitude performance region 22 p3904 A67-40090

Gyroless Solar Pointing Aerobee Rocket Control System /SPARCS/ using no inertial platform and having solid state circuitry 24 p4242 A67-42905

AERODYNAMIC BALANCE

Lift curve slope and aerodynamic center for variable sweep wing configurations estimated using semiempirical technique [AIAA PAPER 67-135] 06 p0939 A67-18315

Balancing operations for rocket vehicles and payloads, defining terms, establishing relation between static and dynamic imbalance and flight vehicle motions, etc 08 p1408 A67-20535

Roll-rate reversal dispersion effects of ballistic reentry body due to mass and aerodynamic asymmetries 22 p3742 A67-40117

Commercial aircraft balance and weight measurement using on-board system, discussing wind load, runway tilt, hard landings and extreme temperature variation effects 23 p4007 A67-41386

AERODYNAMIC CHARACTERISTICS

SA LATERAL STABILITY AND CONTROL

SA LONGITUDINAL STABILITY AND CONTROL

SA STATIC AERODYNAMIC CHARACTERISTICS

Soviet book on aircraft building and air fleet equipment, Number 6 02 p0339 A67-12436

Air cushion vehicle design, calculating annular nozzle, air channel optimum parameters, power capacity, aerodynamic characteristics, etc 02 p0179 A67-12437

Aerodynamic characteristics calculation for wing-fuselage assembly in supersonic flow 02 p0180 A67-12793

Pivot center position effect on aerodynamic characteristics of variable sweepback wings during rotation 03 p0351 A67-12994

Subsonic and supersonic parachutes for soft landing on Mars, discussing aerodynamic coefficients, descent rate, dynamic stability, inflation, porosity and wind effects, etc 04 p0551 A67-14574

Characteristic dimension selection for optimum supersonic heat transfer in axisymmetric body of prescribed shape 04 p0546 A67-14794

Viscous and bluntness induced pressures for flat plates, wedges, cylinders and cones at Mach 41 [AIAA PAPER 65-399] 04 p0546 A67-14815

Helicopters, Design and Engineering, Book 1, Aerodynamics 04 p0551 A67-15266

Aerodynamic characteristics of pneumatic elements with jet propulsion and Coanda effect 05 p0791 A67-18378

Oscillations of staggered plate cascade in plane subsonic gas flow, showing fluid compressibility effect on aerodynamic characteristics 06 p0935 A67-17729

Aerodynamic characteristics of wings of complex planform at subsonic velocities, calculating flows past wings at moderate angles of attack 06 p0935 A67-17730

Reentry trim angle of attack and lift-drag ratios from Gemini flights compared to wind tunnel data for aerodynamic studies [AIAA PAPER 67-166] 06 p0939 A67-18295

Aerodynamic performance characteristics of three entry vehicles designed for maximum L/D ratio of three and two at Mach 19 and Reynolds number 3,200,000 tested in 22-inch Langley helium tunnel [AIAA PAPER 67-138] 06 p0940 A67-18439

Aerodynamic characteristics of Mars probe/lander configurations consisting of blunted cone, shell and spherical segment analyzed at various Mach numbers on ballistic range [AIAA PAPER 67-167] 06 p0941 A67-18482

Ballute aerodynamic characteristics in 0.1 to 10-Mach number region for various applications [AIAA PAPER 67-228] 06 p0942 A67-18518

Simulated high altitude hypersonic cold wall testing of lifting bodies, measuring lift, drag and static pitching moment 06 p0943 A67-18847

Aerodynamic characteristics of rough cylinders, noting effect on head drag coefficient and Reynolds number 07 p1126 A67-19323

Aerodynamic effect of volume addition to high lift to drag wing-body ratio at Mach 6 07 p1126 A67-19382

Three-dimensional plane shock wave intersection in space, noting parameter range for which two solutions exist 07 p1169 A67-20036

Aerodynamic characteristics /pressure distribution and wave drag/ or polygonal wings of symmetrical thickness in supersonic flow 07 p1127 A67-20209

Aerodynamic characteristics of flared bodies noting geometry, Reynolds number and boundary layer state effects on stability 08 p1275 A67-20499

High altitude supersonic isokinetic filter paper sampler for ALARR rocket, examining subsonic 3-D stagnation flow diffuser 08 p1276 A67-20500

Aerodynamic characteristics of forced lead-lag rotor system, noting parameters of horizontal force, rolling and/or pitching moments 09 p1437 A67-21741

Three-dimensional flutter calculations verification by wind tunnel results, using flexible supersonic aircraft planform model of determined characteristics to control calculations 10 p1622 A67-22882

Effect on stage characteristics of axial compressor of design procedure used for slightly elongated vanes 10 p1697 A67-23021

Computer calculation of induced circulations and influence coefficients for turbine blades with arbitrary profiles and oscillation shift 10 p1591 A67-23044

Rogallo wing aerodynamic characteristics compared for various wing configurations and Mach numbers for possible application to spacecraft recovery 11 p1869 A67-24093

Bell X-22A VTOL research vehicle, assessing mechanical and aerodynamic characteristics, variable stability and control system, etc 11 p1743 A67-24097

Aerodynamic boundary layer control by blowing, considering problems of lift increase, airfoil properties, etc 11 p1741 A67-24101

Aerodynamic characteristics of wedge wings determined for hypersonic viscous flow 11 p1742 A67-24347

Forward facing jets effect on blunt configurations aerodynamic characteristics from wind tunnel tests at Mach 6, emphasizing drag increase 11 p1742 A67-24354

Aeroelastic characteristics of stowed rotor system evaluated, considering aerodynamic excitations in forward flight, wind tunnel tests, etc 11 p1744 A67-24590

Aerodynamic characteristics of thin airfoil of small camber in nonuniform flow 11 p1742 A67-24658

Semiempirical method for predicting

aerodynamic interference of circular jet exhausting at right angles from wing, showing effect on lift 11 p1742 A67-24659

Acoustical and aerodynamic characteristics of full scale axial flow air compressor simulation in Freon closed loop system operation [ASME PAPER 67-GT-27] 11 p1742 A67-24806

Simulated high speed aerodynamic testing methods, factors complicating prediction of actual aerodynamics and various tunnels used 11 p1774 A67-25012

Null-yaw and fixed direction multihole probes for aerodynamic measurements, describing calibration charts and error sources 12 p1940 A67-25352

Aerodynamic development of configuration and control system of Gulfstream II business jet, discussing wing optimization, engine characteristics, etc 12 p1894 A67-25497

Cessna tandem twin aerodynamics noting propeller slipstream variation effects, comparing front and rear engine operation [SAE PAPER 670243] 12 p1894 A67-25498

Aerodynamic factors effect on airframe design and power plant selection for medium Mach twin turboprop business aircraft [SAE PAPER 670244] 12 p1894 A67-25499

Lift and drag of trapezoidal wing models in blown flow near free surface studied for sweepback angle effect on aerodynamic characteristics 13 p2093 A67-26595

Vortex breakdown effects on lift, drag and pitching moment coefficients of slender sharp-edged delta wings with different aspect ratios 13 p2050 A67-27194

Aerodynamic damping and frequency drift of turbomachine blades, discussing wind tunnel testing results for various geometric configurations 13 p2051 A67-27205

Aerodynamic characteristics of sphere and blunt cone in highly rarefied gas flow, noting molecular collision effect 13 p2052 A67-27620

Oscillation of rod in gas stream investigated for nonlinear factor effect on oscillations 14 p2243 A67-28639

Intake aerodynamics of upper wing surface studied with two-dimensional potential flow models and suction models, considering inlet problems 14 p2243 A67-28702

Designing propeller blades with maximum aerodynamic efficiency by vortex theory, considering engine power, propeller diameter, forward velocity, etc 15 p2417 A67-30079

Firing range for investigating Reynolds number effect on flow around bodies having complex design at transonic and supersonic velocities 16 p2655 A67-31116

Photographic recording by shadow method for alignment of optical equipment in firing range used to determine aerodynamic characteristics of various missiles 16 p2674 A67-31117

Aerodynamic investigation of spherical chambers, determining swirling velocity, tangential velocity and regions of air suction 16 p2594 A67-31209

Radio telemetry system for aerodynamic data acquisition from free-flight models in supersonic wind tunnels 16 p2675 A67-31259

Dynamic response of sailplanes to elevator control in longitudinal maneuvers, discussing load factors and tail loads as function of aerodynamic and inertial parameters 16 p2597 A67-31786

Reentry trim angle of attack and lift-drag ratios from Gemini flights compared to wind tunnel data for aerodynamic studies [AIAA PAPER 67-166] 17 p2789 A67-32061

Cross sectional variation effects on velocity potential evaluated using slender body theory 17 p2789 A67-32067

Vortex wake and aerodynamic load distribution of slender rectangular wings 17 p2790 A67-32215

Rarefied gas supersonic flows studied in wind tunnel for aerothermal/aerodynamic characteristics 17 p2790 A67-32231

Book on aerodynamic and aerothermal experiments on circular cylinders at angle of attack in supersonic flow 17 p2790 A67-32379

Aerodynamic deceleration system for target drone recovery with reduced impact damage, discussing design improvements 17 p2797 A67-32573

Concepts of wind drift and lateral

maneuver applied in flight mechanics 17 p2798 A67-32591

Flapped finite-span wing lift, center-of-pressure and hinge moment moving near solid wall determined as functions of flap length, rotation angle, etc 17 p2792 A67-32902

Thin slightly curved profiles positioned at small angle of attack in subsonic gas flow and developing harmonic random vibrations studied for aerodynamic interference 17 p2792 A67-32903

Wing flap aerodynamic performance as affected by wing flap surface cavities, noting usefulness in flow stabilization at high pressure gradient 17 p2792 A67-32904

Wing profile effect on thin wing aerodynamic characteristics approaching screen in incompressible fluid potential flow 18 p2981 A67-33412

Supersonic aircraft nozzle system aerodynamic performance at subsonic speeds [AIAA PAPER 67-452] 18 p2983 A67-33926

Aerodynamic characteristics of wing profile employing boundary layer control by blowing with controllable jet 18 p2984 A67-34202

Aerodynamic characteristics of Mars probe/lander configurations consisting of blunt cone, shell and spherical segment analyzed at various Mach numbers on ballistic range [AIAA PAPER 67-167] 19 p3169 A67-34816

Ballute aerodynamic characteristics in 0.1 to 10-Mach number region for various applications [AIAA PAPER 67-228] 19 p3169 A67-34817

Aerodynamic characteristics of wakes behind hypervelocity bodies [AIAA PAPER 66-53] 19 p3171 A67-35741

Multiple scaling for analyzing flight vehicle performance and dynamic behavior [AIAA PAPER 67-560] 19 p3335 A67-35957

Flare and landing performance of glide vehicles with low lift-drag ratio, noting aerodynamic characteristics effect [AIAA PAPER 67-575] 19 p3335 A67-35970

Lift penetration and growth effects on space vehicle response based on slender body theory 19 p3337 A67-35999

Aerodynamic forces and pressure on wing model for Carafoli type MHT-C-04-04-10 profile characteristics, discussing applications to blade rotors 20 p3355 A67-36193

Aerodynamic characteristics of polygonal wings with diamond-shaped profile in supersonic flow 20 p3355 A67-36194

Aircraft dynamics, Volume I, covering aircraft configuration, design problems, atmospheric properties, hydrodynamics, gasdynamics, boundary layer theory, etc 20 p3355 A67-36199

Subsonic and supersonic parachutes for soft landing on Mars, discussing aerodynamic coefficients, descent rate, dynamic stability, inflation, porosity and wind effects, etc 20 p3356 A67-36408

Aerodynamic characteristics of helicopter main rotor during steep descent, using ring vortices method 20 p3356 A67-36443

50 degree semivertex angle sphere-cone Voyager configuration wind tunnel tested in dry nitrogen for aerodynamic characteristics, pressure and heat transfer distribution 20 p3356 A67-36562

Aerodynamic interference effect with jet lift V/STOL aircraft under static and forward-speed conditions, stressing adverse flow 20 p3357 A67-36952

Soviet papers on aerodynamic characteristics of blade compressors and jet engines 20 p3358 A67-37078

Aerodynamic characteristics of plane compressor cascades with high subsonic flow analyzed, noting application in determining flow deflection angle and pressure loss coefficient 20 p3358 A67-37079

Geometric parameters effect on aerodynamic characteristics of plane compressor cascade with high subsonic flow 20 p3358 A67-37080

Book on thin wing and aerodynamic characteristics in subsonic gas flow 20 p3359 A67-37206

Surface pressure distribution on tubelattice cluster with transverse gas flow to determine aerodynamic characteristics 20 p3359 A67-37306

High altitude supersonic isokinetic filter paper sampler for ALARR rocket, examining subsonic 3-D stagnation flow

diffuser 21 p3563 A67-37803

Soviet book on aerodynamics, flight dynamics, flight vehicle structural design and mechanical and control considerations for various aircraft 21 p3566 A67-37833

Unsteady cascade flow and blade oscillation in axial condenser as aerodynamic boundary value problem 21 p3564 A67-37892

Electromechanical simulator of wing flutter with aileron under flight conditions 22 p3912 A67-39779

V-shaped wings with plane slides and sharp edges investigated for aerodynamic properties, deriving equations for flow parameters at Mach 6 22 p3741 A67-40016

Sound and white noise effects on turbulent jet aerodynamic characteristics studied at several Reynolds numbers 22 p3785 A67-40019

Multiple reflection of molecules effect on nonconvex wing aerodynamic characteristics for finite Mach number lateral free molecular flow 22 p3741 A67-40022

Handley Page Jetstream turboprop aircraft basic design requirements, emphasizing aerodynamic design philosophy 22 p3746 A67-40129

Spherical entry vehicle used to define planetary atmosphere structure and composition from dynamic response during entry, discussing aerodynamic characteristics 22 p3907 A67-40177

Wind tunnel hypersonic flow visualizations under low flow density conditions, comparing schlieren and phase-contrast methods 23 p3985 A67-40568

Blade airfoil sections two-dimensional aerodynamic characteristics studied in wind tunnel for aerodynamic optimization calculation of helicopter rotors 23 p3927 A67-40576

Hovercraft research noting internal and external aerodynamics, test techniques and instrumentation requirements 23 p3934 A67-41167

Airfoil and profiles theories emphasizing boundary layer theory, lift augmentation and wing aerodynamics 23 p3930 A67-41305

Ground proximity effect on aerodynamic characteristics of slender wings by extension of slender body theory, solving potential function equation 23 p3930 A67-41310

DC-9 wing and high lift system aerodynamic design and development, discussing STOL field length design goals and flight test results [SAE PAPER 670846] 24 p4093 A67-41999

Variable sweep pivoted wing fighter aircraft structural and aerodynamic design considerations, noting journal bearing endurance and aircraft fatigue life [SAE PAPER 670881] 24 p4094 A67-42015

Drag problems of Belfast aircraft solved by modifications developed in wind tunnel program 24 p4092 A67-42443

Large plane changes by synergetic maneuver with drag cancelled by thrust, noting reduced efficiency due to high altitude L/D decay 24 p4242 A67-42911

Flared afterbody aerodynamic characteristic predictions for aircraft stability at high Mach numbers, discussing turbulent separation 24 p4093 A67-42924

AERODYNAMIC COEFFICIENT

SA LIFT COEFFICIENT

Aerodynamic coefficients of finite wing with built-in lifting fans, noting additional lift and drag due to supercirculation at trailing end 01 p0006 A67-10769

Hypersonic aerodynamic coefficients for bodies of revolution in yaw 02 p0179 A67-12314

Aerodynamic qualities of flexible wings noting performance, lift drag ratio, application to powered aircraft and cargo gliders 03 p0359 A67-12993

Aerodynamic coefficients of symmetrical wing profiles and fuselages in rarefied gas calculated for free molecular flow 04 p0547 A67-14992

Statistical linearization of nonlinear aerodynamic coefficient of angle-of-attack moment of aircraft 04 p0549 A67-15884

Spin calculations corroborating vertical wind tunnel tests on delta wing aircraft, noting aerodynamic parameters [ONERA-TP-388] 05 p0751 A67-16477

Aerodynamic coefficients effects on aeroelastic instability predictions for aircraft with autopilot [ONERA-TP-418] 05 p0751 A67-16483

Forced oscillation method measurement of aerodynamic coefficient of hypersonic blowdown wind tunnel 05 p0788 A67-16764

Steady and unsteady aerodynamic coefficients determined by free flight analysis of trajectory and attitude variations in supersonic wind tunnel 05 p0748 A67-16765

Aerodynamic stability coefficients determined from sounding rocket flight data, using computer program for numerically integrating six degrees of freedom motion equations 08 p1407 A67-20517

Closed form solution for gliding lateral turn at constant height over flat earth of unpowered vehicle, using linearized aerodynamic coefficients 09 p1441 A67-22488

Inviscid flow characterized by annular elliptical region between shock wave and ducted body calculated by integral relation method, noting contraction coefficient values 10 p1591 A67-23045

Thesa nose cones in supersonic flight, calculating aerodynamic coefficients from trajectory and flight phases 13 p2051 A67-27291

Hermetically sealed ballistic facility design and operating principles, for testing at various Mach and Reynolds numbers to calculate aerodynamic coefficients and flow geometry 16 p2655 A67-31115

Aerodynamic effects of supersonic combustion studied in wind tunnels 18 p3154 A67-33829

Aerodynamic coefficients for bodies in free molecule flow determination method by generalized force coefficient equation 22 p3743 A67-40174

Measuring device for aerodynamic coefficients during wind tunnel tests by forced oscillation method 23 p3986 A67-40570

Aerodynamic power and moment coefficients of space-transport configurations for hypersonic reentry and trajectory calculations 23 p3931 A67-41399

AERODYNAMIC DRAG

S DRAG

AERODYNAMIC FORCE

Moment of aerodynamic resistance calculated for gyromotors operating in H and He, examining laminar flow near rotor 01 p0064 A67-10418

Combined effect of aerodynamic and gravity torques on stability of motion of passive satellites investigated by Liapunov direct method 04 p0704 A67-14827

Aerodynamic penetration and radius in drag and lift during atmospheric entry process 06 p1094 A67-18003

Unsteady aerodynamic forces on thin wing oscillating in transonic flow, discussing acoustic ray paths and signal transmission times [AIAA PAPER 67-16] 06 p0943 A67-18841

Variable aerodynamic forces in turbine grid during passage of nonstationary gas flow 07 p1125 A67-19135

Thrust vector control by supersonic splitline gimbaled nozzle, considering linear aerodynamics to understand magnitude of spring rate torque 07 p1126 A67-19378

Unsteady aerodynamic field with application to panel flutter in low supersonic flow 08 p1418 A67-20606

Aerodynamic forces on flexible plate embedded in right half-space undergoing arbitrary temporal and spatial motion 08 p1424 A67-21433

Solar environment and aerodynamic drag effect on deflection of structural booms in space [AIAA PAPER 66-502] 08 p1413 A67-21512

Aerodynamic problem of steady potential flow and added mass in unsteady motion of idealized hemispherical parachute 09 p1438 A67-22485

Lamellar homogeneous jet layer deformation under aerodynamic forces acting in incompressible flow 09 p1439 A67-22578

Aerodynamic flow field past cascade of plane thin turbine blades subjected to small random vibrations [ONERA-TP-412] 09 p1439 A67-22588

Unsteady aerodynamic forces and dynamic response of flexible aircraft structure to continuous turbulence in supersonic flight 10 p1595 A67-23736

Total aerodynamic forces and moments of free flying body in wind tunnel determined from accelerations measured and telemetered by onboard instruments

[AIAA PAPER 66-775] 11 p1773 A67-24349

Aerodynamic theory of blade vibration, discussing compressibility effect, stalling and design 12 p2014 A67-25412

Transient buffet loads on wings due to gust or maneuver 13 p2215 A67-26533

Optimum utilization of aerodynamic forces in aircraft maneuvers 13 p2213 A67-27326

Supersonic boom, discussing aerodynamic field of aircraft, sonic ray characteristics and noise suppression 16 p2589 A67-30832

Aerodynamic suckdown results obtained in investigation of VTOL ground-proximity effects 17 p2791 A67-32588

Low density wind tunnel enabling simulation of aerodynamic flows at high altitudes with rarefied air 17 p2835 A67-33132

Aerodynamic characteristics of wing profile employing boundary layer control by blowing with controllable jet 18 p2984 A67-34202

Aerodynamic forces pressure center on profile in plane rectilinear blade cascade 19 p3169 A67-34884

Unsteady aerodynamic forces due to gusts on supersonic bodies of revolution 19 p3172 A67-36001

Aerodynamic forces of harmonically oscillating cylindrical duct with supersonic internal flow within framework of potential flow theory 20 p3357 A67-37003

High performance aerodynamic impulse facility with shock tunnel, expansion tube and accelerator for high velocity and high Reynolds number environment 21 p3605 A67-37768

Glider towing cable configuration taking into account aerodynamic drag forces, using digital computer for numerical calculations and integrations 22 p3745 A67-39551

Safety device to prevent overloading of models and sensitive wire strain gauge balance by aerodynamic forces during starting and switching off in wind tunnel 22 p3780 A67-39756

Aerodynamic damping of turbine buckets and compressor blades noting flutter and frequency shift 23 p3927 A67-40669

Light gas gun model launching technique with advantages of aerodynamic and mechanical methods of sabot stripping 23 p3988 A67-41751

Orbit-and sun-oriented solar cell concepts compared, discussing aerodynamic drag penalties 24 p4105 A67-42517

Tektite classification by type based on external form, attributing surface sculpturing of type B to aerodynamic and not chemical processes 24 p4235 A67-42639

Earth and planetary atmosphere entry problems for blunt nosed slender vehicles noting aerodynamics, stability, heating, ablation and interaction of effects [AIAA PAPER 67-803] 24 p4243 A67-42963

AERODYNAMIC HEAT TRANSFER

Aerodynamic behavior and heat transfer of electric arc in air stream and transverse magnetic field 06 p1042 A67-18306

Eckert reference temperature yields approximations for heat transfer, skin friction and recovery temperature in high speed laminar diatomic nitrogen and carbon dioxide boundary layers 11 p1883 A67-24576

Equilibrium radiative transport properties of high temperature air coupled with aerodynamic flow field generated by planetary reentry vehicles 16 p2589 A67-30721

Aerodynamic behavior and heat transfer of electric arc in air stream and transverse magnetic field [AIAA PAPER 67-98] 23 p4035 A67-41724

AERODYNAMIC HEATING

Aerodynamic heating from turbulent boundary layer to swept surface symmetrical to surface line dividing flow obtained from momentum and energy integral equations 04 p0549 A67-15825

Thermal design of Isis A spacecraft, noting possibility of passive thermal control and computer programmed multinode heat balance analysis 05 p0904 A67-18294

Gap size effect on pressure and aerodynamic heating over flap of blunt delta wing in hypersonic flow [AIAA PAPER 66-408] 05 p0749 A67-17220

Critical heating conditions in hypersonic glider reentry 06 p1113 A67-17981

Hypersonic aerodynamics and heating of blunt body at high and low Reynolds numbers 06 p0937 A67-17982

Digital computer analysis of mission

parameters governing spacecraft thermal characteristics including ablation effects, radioisotope generator systems, etc 06 p0966 A67-18417

Reynolds number scaling theory for hypersonic ablation, deriving heat and mass transfer relationship [AIAA PAPER 67-155] 06 p1117 A67-18478

Heating restraints effect on aeroglide and aerocruise synergetic maneuver performance investigated for high lift-drag ratio vehicle [AIAA PAPER 67-169] 06 p1097 A67-18483

Asymptotic calorimetry, developing general relationship between temperature and unperturbed heat transfer coefficient for steady state nonisothermal heating 10 p1656 A67-23139

Instrumenting techniques for models under aerodynamic transient heating 11 p1793 A67-24826

Angular errors in antennas with aerodynamic radome heating due to temperature variability 13 p2080 A67-27034

Launcher for research and development on aerodynamic reentry 15 p2564 A67-29094

Aerodynamic heating through turbulent boundary layer of flat plate determined using Ferrari formula 15 p2415 A67-29328

Hypersonic trim angle of attack of lifting entry vehicles, correlating stagnation point values obtained from heat shield ablation and pressure distribution measurements 15 p2417 A67-29447

Ground simulation of Concorde aerodynamic heating effects by blowing air through ducts built over specimen surface 15 p2465 A67-29501

Aerodynamic heating about vehicle entering atmosphere for corridor and guidance requirements analyzed on basis of Newton two-body problem 15 p2417 A67-30046

Theoretical and experimental work in flow field analysis has enhanced ability to predict aerodynamic heating in atmospheric entry 16 p2760 A67-30720

Hypersonic reentry heating problems due to kinetic energy of space vehicle at reentry at orbital and escape velocity 17 p2970 A67-32828

Potential advantages of hypersonic vehicles compatible with missions combining more than one cruise-flight regime, discussing gas dynamic heating for propulsion [SAE PAPER 670354] 17 p2798 A67-32994

Antenna radome subjected to aerodynamic heating investigated for effects on radar system operational range, analyzing antenna noise 18 p2999 A67-33510

Vapor pressure of natural tektite melts at high temperatures determined by boiling point technique, applied to aerodynamic analysis 18 p3134 A67-34495

Heating restraints effect on aeroglide and aerocruise synergetic maneuver performance investigated for high lift-drag ratio vehicle [AIAA PAPER 67-169] 19 p3332 A67-34831

Aerodynamic, thermodynamic, heat shield and structural design aspects of ballistic vehicle entering planetary atmosphere 19 p3332 A67-35315

Ablation characteristics investigated using plasma jet wind tunnel, discussing effective heat of ablation and free stream stagnation enthalpy 20 p3544 A67-36640

Bluntness influence on nose cone heating in laminar flow in supersonic flight investigated to determine optimum design of rocket or space vehicle nose 20 p3359 A67-37165

Refractory metals in aerospace applications, considering aerodynamic heating, melting resistance, liquid-metal corrosion, electrical superconductors, etc 20 p3469 A67-37342

Thermal protection methods for structures subject to aerodynamic heating, discussing heat dissipation methods and thermophysical materials 23 p4082 A67-41042

Event recorder for in-flight measurements of missile heat-shield ablation 23 p4006 A67-41377

Laser macrophotography for size distribution of particulate debris dispersed from ablating zirconium alloy specimen in hyperthermal wind tunnel ablation testing 23 p4006 A67-41380

Tektite classification by type based on external form, attributing surface sculpturing of type B to aerodynamic and

- not chemical processes 24 p4235 A67-42639
- AERODYNAMIC LIFT**
- SA LIFT**
- AERODYNAMIC LOAD**
- SA GUST LOAD**
- Computational model for predicting unsteady aerodynamic loads of rotor blades divided into spanwise segments 04 p0545 A67-14490
- Energy method analysis of flutter instabilities in turbojet engine rotors caused by interaction between unsteady air loading and coupled vibration modes [ASME PAPER 66-WA/GT-6] 04 p0713 A67-15384
- Erosion destruction mechanism in polycrystalline graphite, noting effect of gas flow over surfaces, flow pulsation frequency and generated aerodynamic loads 04 p0642 A67-15761
- Book on aeroelastic static phenomena covering aerodynamic load characteristics, elastic deformation, drag effect on lift distribution, etc 05 p0924 A67-17227
- Noise and loading actions on helicopters, V/STOL aircraft and ground effect machines Symposium, University of Southampton, August-September 1965 06 p0945 A67-17905
- Periodic aerodynamic loading prediction for helicopters and VTOL aircraft 06 p0945 A67-17908
- Periodic aerodynamic loading of helicopter rotor blades approximated by principles of potential flow aerodynamics 06 p0937 A67-17914
- Aeroelastic response problem of rotating wings in steady state flight solved by numerical method 06 p1099 A67-17917
- Control surface instabilities of lifting body configurations at very high speeds and with separated flows analyzed by wind tunnel tests for unsteady control surface load problems [AIAA PAPER 67-15] 07 p1258 A67-19430
- Air loads on sounding rocket from distributed aerodynamics and pressure differential 08 p1276 A67-20501
- Aeroelastic vehicle body loads computed by coupled system of digital computer programs 08 p1405 A67-20505
- Air launched sounding rockets design, development and testing noting aerodynamic loading and surface, propulsion unit, cost effectiveness, etc 08 p1407 A67-20518
- Design procedure for slender multistage fast-burning rockets, noting modified flexural behavior and aerodynamic load 08 p1416 A67-20529
- Supersonic flutter characteristics of thin cantilever plate surfaces with low aspect ratio 08 p1416 A67-20530
- Complex velocity and circulation around thin wing 09 p1439 A67-22564
- Loads on bodies in wakes resulting from crossflow at submerged body or from wake translation over submerged body, noting dynamic instability 11 p1742 A67-24350
- Rotor blade stall, comparing power, flapping motion blade bending and vibratory hub shears for illustration [AHS PAPER 101] 16 p2595 A67-31818
- Aerodynamic loads and aeroelastic divergence characteristics on stopped rotor blades in flight [AHS PAPER 104] 16 p2595 A67-31821
- Radiation pattern changes for helicopter antenna located in rotor blade as result of flight dynamics [AHS PAPER 109] 16 p2597 A67-31825
- Suppression of oscillatory vertical force transmission from helicopter rotor to driving shaft using higher harmonic pitch angle inputs [AHS PAPER 129] 16 p2777 A67-31843
- Effect of rotor control feedback loads of two-bladed rotor system on helicopter fuselage vibrations [AHS PAPER 133] 16 p2777 A67-31847
- Energy method analysis of flutter instabilities in turbojet engine rotors caused by interaction between unsteady air loading and coupled vibration modes [ASME PAPER 66-WA/GT-6] 18 p3115 A67-34130
- Supersonic flutter characteristics of thin cantilever plate surfaces with low aspect ratio 19 p3343 A67-35775
- Air loads on sounding rocket from distributed aerodynamics and pressure differential 21 p3563 A67-37795
- Structural elastic deformations effect on aerodynamic steering loads of glider, examining lift changes caused by wing geometry variations 23 p3933 A67-40640
- Aerodynamic requirements for hovercraft and radial flow fans by adapting blade loading criteria for axial compressors 23 p3931 A67-41331
- Dynamic longitudinal stability of rigid glider towed by rigid aircraft with elastic cable subjected to aerodynamic loads, deriving motion differential equations 23 p3935 A67-41418
- Glider takeoff using tow winch, emphasizing flight path and aerodynamic loads and forces 24 p4093 A67-41917
- AERODYNAMIC NOISE**
- Similarity laws for jet noise and shear flow instability as suggested by experiments 10 p1628 A67-23830
- Engine generated and in-flight noise environment problems of space vehicles analyzed, using theoretical methods and scale model wind tunnel tests 13 p2212 A67-27216
- Characteristics of sound formation in turbulent flow and mechanism of flow energy conversion into sound 14 p2305 A67-28519
- Commercial aircraft noise system solution, considering engines, nacelles, operational procedures and airport options [AIAA PAPER 67-761] 23 p3933 A67-40992
- AERODYNAMIC STABILITY**
- Aerodynamics of sounding rockets, discussing stabilization by fins, conical flares, etc [ONERA-TP-441] 08 p1275 A67-20498
- Extra-atmospheric coning motions of Tomahawk sounding rocket caused by dynamic instability after motor burnout 08 p1405 A67-20502
- Ascending spherical balloon motion reduced by flight Reynolds number reduction from supercritical to subcritical values 08 p1278 A67-21529
- Stability of bilaterally symmetrical object towed in air along straight line, obtaining characteristic equation as test for lateral or longitudinal stability 11 p1743 A67-24309
- Low speed aerodynamic static stability of winged and wingless reentry configurations 14 p2239 A67-27796
- Lapunov functional for aeroelastic divergence noting application to partial differential equations 15 p2575 A67-30021
- Stall flutter instability of helicopter rotor blades analysis based on unsteady aerodynamic data [AHS PAPER 130] 16 p2777 A67-31844
- Limit of circulatory lift on wings with finite span, deriving lift and drag for flat and rolled up vortex sheets 17 p2789 A67-32035
- Flight control system of Saturn V launch vehicle, discussing attitude/attitude-rate scheme, gain required and stability achieved 19 p3331 A67-34808
- Lateral-directional flying qualities for power landing approach simulated, studying roll effects and damping [AIAA PAPER 67-577] 19 p3175 A67-35972
- Digital computer control system for aerodynamically unstable vehicles 20 p3534 A67-37257
- Compressor blade flutter stability in separating flow with external perturbations analyzed, using digital computer 20 p3517 A67-37488
- Potential linear theory applied to oscillatory profiles moving at uniform velocity inside ideal fluid 20 p3424 A67-37593
- Equilibrium stability of rigid rotor in aerodynamic bearings, determining lubricant effect on journal 22 p3811 A67-39316
- All-weather flight requirements of VTOL aircraft, suggesting artificial stabilization by automatic control system [AIAA PAPER 67-798] 24 p4096 A67-42959
- AERODYNAMIC VEHICLE**
- Open jet wind tunnel testing of Meteor sailplane, examining aerodynamic merging of wings, fuselage and cockpit 01 p0006 A67-10970
- Nose selection and vehicle motion dynamics for second stage of two-stage sounding rocket system, discussing nose shapes effect on altitude performance, overall vehicle stability, bending moments, etc 08 p1406 A67-20513
- High performance aerodynamic vehicle design noting configuration variables, optimum performance parameters, vehicle force characteristics, optimization of hypersonic aircraft performance, etc [AIAA PAPER 66-486] 13 p2054 A67-27584
- Digital computer control system for aerodynamically unstable vehicles 20 p3534 A67-37257
- AERODYNAMICS**
- SA FLUID MECHANICS**
- SA GAS DYNAMICS**
- SA ROTOR AERODYNAMICS**
- Aerodynamics of nacelle used in selection and integration of exhaust systems producing highest thrust-minus drag cruise performance [SAE PAPER 660734] 01 p0140 A67-10634
- Aerodynamic deceleration systems, discussing basic materials and fabrication techniques of BALLUTE program [AIAA PAPER 66-988] 02 p0181 A67-12299
- Analytic processes for evaluation of supersonic aerodynamics of configuration treating drag, wing design, warp, interference and sidewash [AIAA PAPER 65-717] 03 p0354 A67-12914
- Aerodynamics of slender wings executing simple harmonic oscillations and having leading edge separation 03 p0352 A67-13894
- Aerodynamic problems of turbomachinery, investigating effect of geometry and aerodynamic cascade parameters on flow deflection, static pressure difference and flow losses 04 p0547 A67-14985
- Moving and stationary fluid type facilities to simulate aerodynamics of charged particles in ionosphere 04 p0595 A67-14991
- Book on aerogas dynamics in relation to rocket and aviation technology including shock waves, rarefaction flow, heat transfer, skin friction, etc 05 p0747 A67-16173
- Aerodynamic problems due to air intake and exhaust nozzles effect on propulsion of hypersonic aircraft [ONERA-TP-416] 05 p0748 A67-16481
- Book on principles of ideal fluid aerodynamics covering vector algebra and calculus, Euler equations, steady and unsteady acyclic motion, complex variable, lift, etc 05 p0793 A67-17151
- Applied mathematics of space program fluid mechanics and aerodynamics 06 p0983 A67-17783
- Aerodynamic and structural data on supersonic decelerators, determining problem areas and voids [AIAA PAPER 67-201] 06 p0948 A67-18301
- Soviet papers on hydroaeromechanics including turbulent flow of conducting fluid, heat transfer, temperature stress in plates, etc 07 p1125 A67-19320
- Experimental aerodynamics, Volume 2, covering simulation, transonic, supersonic and hypersonic domains 09 p1437 A67-22215
- Low density shear resistant abators for lifting reentry vehicles 10 p1872 A67-23725
- Thermodynamics and fluid mechanics - Conference, Liverpool, April 1968 12 p1927 A67-25345
- Approach navigation accuracy and entry corridors for aerodynamic braking at Mars and Venus 13 p2212 A67-26837
- Linear aerodynamic theory of rotor blades for predicting lift distribution, considering wake vortex sheet distortion 13 p2051 A67-27589
- Aerodynamics survey emphasizing supersonic speed problems 14 p2239 A67-27874
- Soviet book on pilotless aircraft and missiles covering jet engine design, automatic control, radio engineering and aircraft aerodynamics 15 p2564 A67-29242
- Carrousel magnetoaerodynamic generator, defining equations governing development of electric and thermodynamic properties of plasma 16 p2608 A67-30599
- Dynamic response of sailplanes to longitudinal maneuvers based on steady lift coefficients on wing and tails 16 p2596 A67-31465
- Hydroaerodynamics of carrying surfaces - Conference, Kiev, October 1965 17 p2792 A67-32901
- Northrop program for V/STOL aircraft including systems studies, propulsion, aerodynamics, flight control technology, performance characteristics and operation and testing northrop program for V/STOL aircraft including 18 p2987 A67-34708
- Holographic moire patterns as white light viewing technique for aerodynamic flow

visualization 19 p3232 A67-35699
 Soviet book on aerodynamic flow calculations of axial flow turbines with subsonic and transonic blade cascade design method 21 p3565 A67-38766
 Fan-in-wing aerodynamics evaluated for datum inlet with circular arc lips with and without vanes
 [AIAA PAPER 67-746] 23 p3928 A67-40980
 Aerodynamic phenomena in stellar atmospheres - Conference, Nice, France, September 1965 23 p4067 A67-41275
 Wissenschaftliche Gesellschaft für Luft- und Raumfahrt, Annual Reports 1966 23 p3929 A67-41304

AEROELASTICITY

SA PANEL FLUTTER
 SA WING LOADING

Aerodynamic coefficients effects on aeroelastic instability predictions for aircraft with autopilot
 [ONERA-TP-418] 05 p0751 A67-16483

Book on aeroelastic static phenomena covering aerodynamic load characteristics, elastic deformation, drag effect on lift distribution, etc 05 p0924 A67-17227

Aeroelastic response problem of rotating wings in steady state flight solved by numerical method 06 p1099 A67-17917

Design procedure for slender multistage fast-burning rockets, noting modified flexural behavior and aerodynamic load 08 p1416 A67-20529

Nike-Tomahawk rocket aeroelastic behavior, noting occurrence of large extra-atmospheric coning angles 08 p1416 A67-20534

Direct measurement of aeroelastic parameters of aircraft wings, using dynamically similar models fitted on auxiliary rocket devices 09 p1576 A67-22462

Dynamic stability of structures, discussing parametric resonance, impulsive loading, circulatory loads, aeroelastic and buckling problems 14 p2396 A67-28079

Liapunov functional for aeroelastic divergence noting application to partial differential equations 15 p2575 A67-30021

Powered flight rotor instabilities using analysis of second-order flap-lag coupling effects of torsionally rigid blades 16 p2595 A67-30927

Static structural strengths, aeroelasticity and flutter problems for glider performance 16 p2776 A67-31466

Aeroelastic stability of two-dimensional flat panels in subsonic and transonic flow, noting flutter and divergence 16 p2776 A67-31545

Aerodynamic loads and aeroelastic divergence characteristics on stopped rotor blades in flight 16 p2595 A67-31821

[AHS PAPER 104] 16 p2595 A67-31821

Aeroelastic phenomena in aircraft stability, control and airframe vibration characteristics, describing testing methods 23 p4077 A67-41046

Nike-Tomahawk rocket aeroelastic behavior, noting occurrence of large extra-atmospheric coning angles 24 p4242 A67-42912

AEROGYRO HELICOPTER

S XH-51 HELICOPTER

AEROLOGY

Aircraft bumpiness conditions in free atmosphere relation to turbulence and other aerological data 02 p0263 A67-12647

Argentina 1964-1965 IQSY program emphasizing aerology, solar radiation, ozone concentration, geomagnetism, etc 19 p3224 A67-35499

AEROMAGNETO FLUTTER

Aeromagnetic flutter of walls of plane infinite channel with ionized gas flow 03 p0524 A67-13503

Aeromagneto flutter of plane duct of finite length 13 p2218 A67-26805

AERONAUTICAL ENGINEERING

Future prospects of aeronautical construction in Europe 01 p0168 A67-10264

Fluid dynamics, structures and operations research and development at Netherlands National Aerospace Laboratory 02 p0231 A67-12640

Future prospects of aeronautical construction in Europe 03 p0537 A67-12966

Cutting and milling processes in aeronautical industry, effect on costs and production rates 03 p0427 A67-13024

Aircraft research and testing - Conference, Prague, November 1966 09 p1440 A67-22470

Designing propeller blades with maximum aerodynamic efficiency by vortex theory,

considering engine power, propeller diameter, forward velocity, etc 15 p2417 A67-30079

Absolute and relative vibration measurement in aeronautical engineering, describing sensing units for vibration amplitude, rate and acceleration determinations 22 p3798 A67-39545

AERONAUTICS

Yearbook of European Aeronautical Congress, Munich, September 1965 03 p0354 A67-12965

Advancement in aeronautics and contribution of Royal Aeronautical Society 03 p0538 A67-14380

Aeronautical research in U.K. by government establishments, industry and universities 03 p0362 A67-14381

Light aviation, problems, prospects and performance 04 p0739 A67-14434

Progress in aeronautical sciences, Volume 8 10 p1589 A67-22870

Aviation and astronautics - Conference, Tel-Aviv and Haifa, February 1967 11 p1777 A67-24212

Aeronautical research in India, precision instrumentation design and production development, facilities, rocket launching station, etc 11 p1885 A67-24653

Soviet book on aeronautical meteorology covering wind and cloud effects on takeoff, landing and supersonic flying in storms and jet stream layers 18 p3074 A67-33676

Aviation and transportation system - Progress, profits and public interest - Conference, Hartford, December 1966, Panel 2, Aviation and technological progress 19 p3347 A67-34970

General aviation problems, discussing shortage of landing facilities and inadequacy of federal planning 19 p3348 A67-34973

Aviation and transportation system - Progress, profits and public interest - Conference, Hartford, December 1966, Panel 4, Aviation and public policy 19 p3348 A67-34975

Future improvements in aeronautical field covering noise control, centralization, TV communication, ultimate speed, sonic boom and nuclear cargo aircraft 22 p3746 A67-39846

AERONOMY

Atmospheric number density measured by attenuation of solar X-rays monitored when satellite passes from darkness to sunlight 11 p1857 A67-24605

Variations of ionizing radiation of E layer, eliminating aeronomical effects by considering seasonal variations of ionization index 13 p2191 A67-26767

Synoptical and monitoring projects for solar activity, interplanetary space, magnetosphere, ionosphere, aeronomy, etc 19 p3223 A67-35475

AEROSOL

SA ATOMIZATION

Experimental verification of Shifrin-Perelman method of determining spectrum of dispersed atmospheric aerosol particles from spectral transmittance 01 p0108 A67-10130

Rapid method of calculating effective spectral parameters of aerosol dimensions 01 p0108 A67-10132

Aerosol measurements using light scattering from searchlight probing, noting attenuation coefficient as function of altitude [AFCL-67-0003] 02 p0238 A67-12048

Idealized steady motion of aerosol particles and inertial deposition theory 03 p0404 A67-13836

Atmospheric chemistry, circulation and aerosols - International Symposium, Vlsby, Sweden, August 1965 03 p0414 A67-14085

Direct solar radiation up to 30 km and stratification of attenuation components in stratosphere, noting aerosol extinction properties in free atmosphere 07 p1170 A67-19390

Aerosol particle velocity measurement using optical compensation and photoelectric particle counter 08 p1428 A67-21422

Effect of gravitational changes on aerosol deposition in lungs of man, noting particle size and alveolar region 09 p1452 A67-21724

Photometric measurements of eclipses of artificial solar satellite 1960 Eta 2 at sunrise and sunset in Lyman alpha and violet spectral range 10 p1706 A67-23221

Geophysical rocket determination of aerosol scattering coefficient variation from

brightness values at 70-450 km heights 10 p1641 A67-23240

Hydrodynamic drawing together problem for aerosol particles oscillating in sonic field at small Reynolds numbers, showing optimal field frequency-approach velocity correspondence 10 p1627 A67-23643

Theory of nephelometric method for measuring transparency and structure of atmospheric aerosols 13 p2151 A67-26685

Idealized steady motion of aerosol particles and inertial deposition theory 13 p2107 A67-27712

Atmospheric aerosol internal changes, studying atmospheric transparency for direct solar radiation 18 p3073 A67-33562

Satellite technique for sounding atmospheric optical properties and height distribution of ozone and aerosols 18 p3040 A67-33853

Hydrodynamic drawing together problem for aerosol particles oscillating in sonic field at small Reynolds numbers, showing optimal field frequency-approach velocity correspondence 18 p3029 A67-34412

Stratospheric aerosol concentrations observed by optical radar echoes compared with expected return from molecular atmosphere to obtain vertical profile 18 p3042 A67-34493

Absorption coefficients of radiation by water vapor and aerosols determined from atmospheric counter radiation 19 p3251 A67-34858

Optical system for computer counting and analyzing aerosol particles on photofilm 19 p3227 A67-34861

Vertical distribution of diffuse sky light in stratosphere determined by rocket measurements, noting intensity peak in aerosol layer 19 p3221 A67-35273

On-the-ground optical determination method of stratospheric aerosol particle numbers and sizes from ruby laser radiation measurement scattering 19 p3225 A67-35531

70 to 450 km altitude atmospheric brightness at 5300 angstrom measured by rocket noting importance of aerosol component 21 p3623 A67-39043

AEROSPACE MEDICINE

SA BIOASTRONAUTICS

SA BIOSIMULATION

Statistical guidelines for flight surgeon remotely monitoring body fluids of astronauts, determining when subject undergoes changes in serum values 01 p0015 A67-10951

Statistical evaluation of changes in serum potassium, sodium and chlorides for aerospace flights 01 p0015 A67-10952

Medical investigation of 1964/1965 fatal aircraft accidents in Southwestern U.S., noting combined effects of drugs, fatigue, alcohol and hypoxia 01 p0017 A67-10961

Biomedical data from U.S. manned space flight experience including cardiovascular and central nervous systems, blood composition changes, etc 01 p0016 A67-11394

Pharmacology in prolonged space flight noting increasing resistance of organism to extremal flight factors, use of pharmaceuticals during flight, etc 02 p0185 A67-12320

Physiological telemetry application in long space flights for medical examination and control during space flight 02 p0187 A67-12323

Vestibular tests of caloric irrigations and mild angular accelerations of semicircular canals of professional figure skaters 03 p0364 A67-14288

Medical, design and operational aspects of quality requirements for reliability of manned space environment simulation chambers 05 p0788 A67-16621

Dental aspects of manned spaceflight, discussing preventive measures 06 p0954 A67-19030

Experimental program for orbiting biomedical/behavioral laboratory, discussing functions 08 p1287 A67-21069

Manned orbital laboratory for biological research, discussing experimental possibilities and requirements on spacecraft 08 p1287 A67-21070

Medical observations of astronauts on Voskhod and Voskhod II 08 p1288 A67-21111

Book on positive pressure breathing as means for acceptable arterial oxygen tension at altitudes above 40,000 ft and effects of raised intrapulmonary

pressure 08 p1288 A67-21500
Genetic studies in space, discussing free balloon, rocket and satellite experiments with microorganisms, plants and animals 09 p1453 A67-21901
Value of routine abdominal X-ray during aeromedical evaluation, noting number and significance of abnormalities detected 10 p1601 A67-23828
Vertebral fractures in pilots from helicopter accidents in dorso-lumbar junction of spinal column 12 p1902 A67-25170
Muller maneuver /forced inhalation with closed glottis/ improves tolerance to negative G 12 p1901 A67-25172
Flight activities of Russian cosmonauts in assessment of medical preparedness for orbital flight 12 p1902 A67-25653
Weightlessness and manned space flight medical data to date 12 p1902 A67-25727
Space flight to Mars, discussing medical problems originating from changing gravitational fields, meteorite dangers, radiation and psychological considerations 13 p2061 A67-26338
Soviet space psychophysiology, discussing cosmonaut selection and medical control 13 p2058 A67-26751
Spacecraft life support systems should ensure radiation protection, food, power supply, waste removal, etc 13 p2061 A67-26753
Medical testing, research and control during manned space flights, discussing diagnostic algorithms for onboard computer and frequency of data collection 13 p2062 A67-26762
EEG data from Astronaut Borman on Gemini flight GT-7 13 p2062 A67-26919
Human transfer function problem and compensatory tracking, analyzing variance and determining average rate of stick motion as underlying variable 13 p2063 A67-26923
Aeromedical problems associated with surgical procedures for relief of otosclerosis 13 p2060 A67-26928
Medical data on in-flight and postflight physiological performance to determine man's qualifications for long duration space flights 13 p2060 A67-27214
Medical factors involving ATC information displays 13 p2064 A67-27564
Enzyme activity in erythrocytes when MICORENE is used to prevent death from high altitude hypoxia 14 p2254 A67-28212
Human body resistance limit for ejection through aircraft canopy 14 p2257 A67-28215
Rate measurements determination and evaluation in analysis of space medical data 15 p2431 A67-29293
Long term biomedical monitoring of human heart rate through lithium chloride impregnated balsa electrodes, noting space flight application 15 p2431 A67-29918
Electrocardiogram amplifier-transmitter designed for long term heart rate monitoring on unrestrained subjects in orbiting laboratories 15 p2431 A67-29919
Special preprocessing circuit for cardiac beat recognition discriminates against noise artifacts in electrocardiogram 15 p2432 A67-29920
Digital cardiometer design noting binary counter, clock, operation cycle, etc 15 p2432 A67-29921
Hemodynamic modifications produced by orthostatism noting changes in cardiac frequency, arterial pressure and central blood volume produced 16 p2618 A67-30754
Prolonged acceleration effect on human organism tested using retinal blood circulation observations 16 p2610 A67-30755
Physiological limits of adaptation of eye with respect to body noting increase of pressure in ophthalmic artery under different conditions of hypoxia 16 p2611 A67-30757
Weightlessness effect on human cardiovascular system noting mechanical forces, amount of work done to overcome hydrostatic pressure, etc 16 p2612 A67-30773
Operational efficiency of astronauts evaluated on basis of Voskhod I and II flights, discussing manual operation, EVA memory efficiency, etc 16 p2618 A67-30780
Cosmic radiation protection during manned space flight, considering use of radiation warning devices and protective drugs 16 p2612 A67-30901
Automation problems in space-flight

operative medical control, giving equations of changes in physiological indices 16 p2618 A67-30902
Sleep characteristics during simulated space flight noting influence of noise, angular accelerations and isolation 16 p2613 A67-30913
Pilot self-medication causes and dangers, classifying dangerous drugs and studying effects on pilot performance 16 p2614 A67-31474
Medicophysiological aspects of NASA program stressing cardiovascular, muscular and osseous problems 16 p2614 A67-31538
Manning of space environment simulators, emphasizing integration of physical facility requirements and operation procedure to provide safety 17 p2807 A67-31960
Psychomotor adaptation to flight evaluated clinically, describing anxiety and other aviator symptoms in aerospace 17 p2806 A67-31964
Aortic insufficiency in flying personnel, discussing case histories and cardiovascular system 17 p2806 A67-31965
Biotelemetry improvements in manned space flights, emphasizing bit rate reduction required for electrocardiogram data transmission to earth 17 p2807 A67-32900
Pilot medical examination frequency and effect on safety 18 p2992 A67-34722
Gemini program study to provide safe and biologically sound method of man qualifying for space exploration 19 p3177 A67-35208
Space research activities in Czechoslovakia, discussing satellite observation, aerospace medicine, solar physics, etc 19 p3320 A67-35282
Rumanian space research in meteorology, fluid mechanics, space medicine, etc 19 p3321 A67-35305
Space environment utilization for biological and medical research, physiological studies and therapeutic purposes, discussing orbital hospital and ambulance launch vehicle 19 p3181 A67-35653
Drugs for protection and stimulation of biological functions of spacecrews, noting experimental results on transverse-acceleration resistance of animals 20 p3387 A67-36254
Human experiments to study somnolent and precollapoid /collapoid/ states when falling asleep and during prolonged standing tests 20 p3368 A67-36268
Soviet monograph on problem of acceleration in aviation medicine 20 p3375 A67-37466
Vasopressin-aldosterone interrelation in diuresis and antidiuresis to explain body fluid weight loss in astronauts during space travel 21 p3574 A67-38082
Medicolegal problems in aircraft flight accidents and traumatic mechanisms 21 p3575 A67-38508
Book on aviation and space medicine problems 22 p3752 A67-40532
Radioactive isotopes for aviation and space medicine, treating hemodynamic phenomena, metabolism, cytophysiological investigations and fluids distribution in organism 22 p3756 A67-40547
Soviet papers on certain problems of space neurophysiology 23 p3942 A67-40763
Manned space flight predicted exposure effects vs actual medical findings 23 p3945 A67-41067
Aerospace Medical Association Conference, Washington, D.C., April 1967 23 p3946 A67-41534
Aeromedical examiner relationship to accident prevention, discussing standardization of psychological approach 23 p3963 A67-41539
Aeromedical incidents among Canadian Air Force pilots, using mailed questionnaire 23 p3963 A67-41540
In-flight aeromedical monitoring of cardiorespiratory response of naval pilots during aircraft carrier combat operations, discussing physiological effects determination 23 p3963 A67-41541
Terminology, pathophysiology, treatment, prevention and clinical aspects of altitude decompression sickness 23 p3950 A67-41545
Bioastronautics Laboratory Research Tool /BIO-ALERT/ as automatic biomedical monitoring system composed of digital computer, analog-digital converters and input-outputs 23 p3964 A67-41548

Earth organism behavior under artificial gravity, proposing long term orbital experiments 23 p3950 A67-41549
High performance aircraft flight effect on blood glucose in fasting subjects noting no hypoglycemia tendency 23 p3950 A67-41550
Emergency dental kit for prolonged space flight, discussing filler materials 23 p3965 A67-41564
Medical support for SR-71 aircraft crew members, describing crew selection, flight preparation and medical examinations 23 p3966 A67-41600
Treatment of psychiatric diseases in ground staff and aircrew, discussing psychopharmacology in aeronautical medicine 23 p3967 A67-41603
Psychosomatic symptoms in student naval aviators 23 p3955 A67-41624
Sensory deprivation in space medicine, discussing irritation spectrum leading to pathological changes in psychic processes of test subjects 24 p4111 A67-41842
Cosmonaut physiological reactions during simulated space environment exposure outside Voskhod II spacecraft 24 p4113 A67-42054
Orbital research hospital design for utilizing zero and low gravity therapeutic value in treating physiological conditions [AIAA PAPER 67-833] 24 p4243 A67-42976
AEROSPACE SYSTEM
Potential payoffs of using high modulus filament reinforced composite materials in aerospace systems applications discussed in light of development programs 03 p0443 A67-13414
Interface management of aerospace systems noting associated disciplines, documentation, contractor interrelationships and procuring agencies [AAS PAPER 66-159] 08 p1430 A67-20976
RCA papers on systems support and aerospace systems 08 p1303 A67-21056
Integrated circuit in optimal design of aerospace systems, discussing potential low cost and use in computer analyses of circuits 08 p1303 A67-21060
Interface management of aerospace systems noting associated disciplines, documentation, contractor interrelationships and procuring agencies [AAS PAPER 66-159] 13 p2233 A67-27556
Aerospace systems - SAE Conference, Los Angeles, June 1967 17 p2798 A67-31967
Reliability studies for optimization of aerospace systems and military engineering design and manufacture 18 p3053 A67-33637
Operational system for handling and processing aerospace-system human-factors task data in government/contractor environment 18 p2994 A67-34343
Incident/accident information exchange system for hazard information flow to safety teams 18 p3163 A67-34692
Potable water quality control and standards for aerospace systems 21 p3576 A67-38071
Chemical, physical, microbiological and radiological standards of aerospace system water potability 23 p3968 A67-41620
Digital computer system for testing complex aerospace subsystems 24 p4126 A67-42932
Aerospace system power conditioning design optimization, treating efficiency, regulation, EMI, BITE, primary power, size, weight, radiation hardening and cost [AIAA PAPER 67-985] 24 p4110 A67-43057
AEROSPACE TECHNOLOGY
Production program and MAC operational experience of C-141A jet cargo transport [AIAA PAPER 66-791] 01 p0009 A67-10534
High strength magnesium casting alloys for aerospace applications, based on heat treatment involving internal precipitation of hydride [SAE PAPER 660856] 01 p0094 A67-10815
Concorde SST aircraft, discussing airframe, engine, ancillary power plant, afterburner, etc 01 p0081 A67-11253
Role of large solid propellant rocket motor in U.S. space program noting design, technology, testing, cost, thrust-vector control systems, etc 01 p0142 A67-11447
Radiolabelled isotopes for aerospace - symposium, Dayton, February 1966, Part 1, Advances and techniques 02 p0243 A67-12207
Space technology utilization in detection and prevention of cardiovascular disease, discussing instrumentation for monitoring

- microcirculatory system
[AIAA PAPER 66-951] 02 p0187 A67-12285
- Reinforced pyrolyzed plastic composites for aerospace applications, noting high temperature stability and ease of utilization 03 p0443 A67-13415
- Attachment concepts and problems in fibrous composite aerospace structures 03 p0523 A67-13444
- Design evolution studies defining technological, operational and cost characteristics for reusable aerospace passenger transport 03 p0519 A67-13791
- Glass in refractive space optics, discussing UV solarization and athermalization [SMPT PREPRINT 100-34] 03 p0469 A67-13808
- Aerospace technology information transfer to biology and medicine
[AIAA PAPER 66-952] 03 p0366 A67-14023
- Economic and technological analysis of jet transport and cargo aircraft relation to future air traffic problems
[AIAA PAPER 66-820] 03 p0538 A67-14134
- Design techniques for advanced flight structures providing statistical assessment of environmental loads, forecasts of high performance material response and higher reliability design criteria 04 p0707 A67-14423
- Analytical, test and coordinative methods in reliability problems in aerospace systems 04 p0627 A67-14579
- Ring laser inertial sensor for aerospace systems obtaining high accuracy angular resolution and mechanical simplicity 04 p0625 A67-15665
- Aerodynamic characteristics of pneumatic elements with jet propulsion and Coanda effect 05 p0791 A67-16378
- Radioisotopes for aerospace - Symposium, Dayton, February 1966, Part 2, Systems and applications 05 p0840 A67-16526
- Space technology influence on general progress of technology and effects on standard of living and economy 05 p0930 A67-17539
- Dual-purpose passenger/cargo aircraft noting design, passenger interior system, cargo handling system, compatibility, comparisons, etc 06 p0946 A67-18005
- German contribution to space flight and aerospace technology in international community 07 p1269 A67-19567
- Aerospace castings from light ternary Mg-Li-Si alloy, discussing fabrication development 07 p1193 A67-20254
- New aerospace-related technology in nonaerospace applications, noting NASA and petroleum industry 07 p1269 A67-20263
- Polar properties of fiberglass fabric laminates effect on strength for aerospace applications 08 p1345 A67-20431
- IEEE Aerospace Computer Symposium, Santa Monica, October 1966 08 p1296 A67-20624
- Aerospace and electronic systems - IEEE Convention, Washington, D.C., October 1966 08 p1290 A67-20646
- Static and transient strain measurement in aerospace structural materials using extensometer and compressive test jig, determining Young modulus, creep rate, etc 08 p1420 A67-20907
- Aerospace and electronic systems - Convention, Los Angeles, February 1967 09 p1466 A67-21674
- Design, production and experience of bonded structures in Europe for aerospace applications 09 p1577 A67-22511
- New steels for aerospace tooling, properties and applications 10 p1668 A67-23011
- Procedures for aircraft and spacecraft contractual arrangements to procure reliable systems, considering costs, qualification tests, etc 10 p1660 A67-23430
- Solid state diffusion bonding effect on structural design 10 p1662 A67-23733
- Cold starting and service test evaluation of SAE 10W30 aircraft engine oil [SAE PAPER 670249] 11 p1811 A67-23982
- Aerospace computer hardware, discussing general purpose requirement on basis of various computer designs 11 p1755 A67-24247
- Computer application to aerospace missions, discussing operation and equipment parameters, reliability, man-machine interaction, etc 11 p1756 A67-24248
- Man-Computer Graphics /MCG/ allows operator control through oscilloscope via light sensitive pen 11 p1756 A67-24251
- Cutting tool and cutting fluid evaluation, economic considerations for aerospace manufacturing [ASTME PAPER WES-7-27] 11 p1798 A67-24256
- Productibility of aerospace products with regard to machinability of aluminum alloy [ASTME PAPER WES-7-29] 11 p1798 A67-24257
- Aeronautical research in India, precision instrumentation design and production development, facilities, rocket launching station, etc 11 p1885 A67-24653
- Contaminant control in oxygen for breathing in aviation solved by gas chromatography 12 p1902 A67-25173
- Electronic and ultrasonic principles defining pulse-echo high resolution and application to electronic and electroacoustic circuitry for testing aerospace structures 12 p1948 A67-25218
- Future Air Force requirements for base metal forms and metal-working techniques including hot strength alloy forgings, fine wire, etc 12 p1948 A67-25286
- Airborne weather radar for general aviation aircraft, considering transmitter power, wavelength, target area, reflectivity characteristics, installation limitations, etc [SAE PAPER 670252] 12 p1905 A67-25503
- Space activities effect on International Civil Aviation Organization including navigational problems, aircraft communication, meteorological data and technological advances 12 p2043 A67-26151
- Be use in aerospace structure, gas turbines and aircraft brake disks 13 p2138 A67-27118
- Structural evaluation of sheet beryllum fabricated by three different methods 13 p2140 A67-27136
- Space propulsion technology and mission capabilities in fiscal year 2001 13 p2189 A67-27502
- Materials, space vehicle structures and reentry research and development 13 p2213 A67-27503
- U.S. overall economic outlook in light of space technology and systems to year 2001 13 p2231 A67-27511
- Future industrial automation prediction based on present knowledge 13 p2231 A67-27514
- Gear materials and lubrication methods to satisfy high speed and temperature requirements in aerospace applications 14 p2334 A67-27791
- Aluminum, Volume 2, Design and application 14 p2322 A67-27811
- Aluminum and aluminum alloys in aircraft and aerospace industry 14 p2323 A67-27817
- Space flight technology developments, particularly for booster rockets and space vehicles 14 p2393 A67-27873
- Communication satellite technology development depends on compatibility with deep-sea cables, channel demands and reflector technology 14 p2270 A67-28584
- Demand, applications and technology for future satellite communications covering transoceanic and military telecommunication, TV network, weather data, etc 14 p2274 A67-28912
- Pyrotechnic actuation, discussing parameters, equipment and performance of explosive devices 15 p2543 A67-29304
- Vapor cured resins for aerospace applications 15 p2506 A67-29544
- Space technology - Conference, Palo Alto, May 1967 15 p2565 A67-29828
- European aerospace transporter, and fundamental concepts and development 15 p2556 A67-29838
- Trends in technology for reusable launch vehicles 15 p2569 A67-29854
- Spacecraft landing systems technology, materials and hardware, model impact testing and para-sail landing rocket program 15 p2570 A67-29856
- NASA applications technology stressing stabilization and pointing systems, data retrieval, etc [AAS PAPER 67-77] 15 p2557 A67-29944
- Communication technology role in commercial utilization of space, considering spectrum utilization, economic benefits and satellite programs [AAS PAPER 67-78] 15 p2437 A67-29945
- Business, government and possible home applications /including mail and education/ for electronic communications via satellites, discussing legal implications [AAS PAPER 67-91] 15 p2437 A67-29952
- Management control system for technical, production, financial and contractual management of large scale or technical industry programs [AAS PAPER 67-153] 15 p2583 A67-29969
- Support requirements for future manned space programs [AAS PAPER 67-56] 15 p2562 A67-30120
- Aerospace electrical and electronic equipment reliability requirements with reference to technology of miniature electrical connection devices 15 p2454 A67-30230
- Environmental adjustment factors for operating and nonoperating failure rates 15 p2495 A67-30417
- Rocket fuel production possibilities on moon surface and other planets for planetary explorations 16 p2655 A67-31008
- Adhesives for aircrafts and spacecrafts considering high temperature resistivity, waterproofing and brittleness 16 p2683 A67-31788
- Production, handling and shipping of elemental fluorine, noting materials, health and safety precautions, aerospace applications and toxicity effects 16 p2734 A67-31811
- Weldable tube fittings, welding equipment and inspection methods for connecting tubing in aircraft and aerospace hydraulic systems 17 p2864 A67-32008
- Aerospace electronics - Conference, Dayton, May 1967 17 p2855 A67-32467
- Aerospace industry quality control requirements and specification, noting small business role 17 p2974 A67-32818
- Hybrid simulators used for aerospace and military programs consisting of analog computers, digital computers and interface units for handling data flow 18 p3019 A67-33635
- Classical heterogeneous combustion and aerospace research, discussing multiple factor approach and mass transfer operations 18 p3150 A67-33801
- M-1 engine system technology items noting thrust chamber assembly, gas generator, fuel turbopump, etc [AIAA PAPER 67-520] 18 p3115 A67-33983
- Design and construction of equipment for oxygen, nitrogen and hydrogen determination in aerospace materials [ONERA-TP-466] 18 p2998 A67-34461
- Maintainability technology and controls developed during F-111 design 18 p2986 A67-34663
- Problem of manufacturing space vehicles with rigidly controlled cleanliness and biological contamination for missions to other planets 18 p2995 A67-34677
- Ground technology program for nuclear rocket development, discussing NERVA and KIWI programs 18 p3077 A67-34706
- Fabrication, structure, possible failure and testing of coated refractory metals in applications for space technology 19 p3245 A67-34959
- Aviation and transportation system - Progress, profits and public interest - Conference, Hartford, December 1966, Panel 2, Aviation and technological progress 19 p3347 A67-34970
- Lubricant requirements for aircraft parts noting high and low temperature, radiation conditions, lubrication capability limits, etc 19 p3246 A67-34983
- Swiss space research programs noting experiments, technology, etc 19 p3321 A67-35301
- U.S. space research program /1966/, national organization, international participation, space vehicle research and experiments related to future programs 19 p3322 A67-35307
- International Telecommunications Satellite Consortium /INTELSAT/ organization 19 p3349 A67-35640
- Man capability to operate in cislunar space and lunar surface through Apollo program, discussing practical applications 19 p3326 A67-35644
- Influence of navigational requirements and technology on design of navigation-satellite system 19 p3256 A67-35682
- Book on star trackers and systems design including technology, use for navigation and guidance, reference frames, error sources,

atmospheric effects, etc 20 p3481 A67-36136
 Development of Indian sources of aerospace metals evaluated, noting availability, potential, priority of materials and research facilities 20 p3464 A67-36187
 Dynamic and static gas bearings uses and properties compared with fluid bearings, considering advantages for space applications 20 p3453 A67-36410
 Synthetics in aircraft and rocket construction, recommending 20 p3473 A67-36453
 Duropastics 20 p3473 A67-36453
 Aerospace instrumentation - Conference, Cranfield, Beds., England, March 1966, Volume 4 20 p3441 A67-36457
 Changing role of technical writers and editors during next decade 20 p3556 A67-36587
 Aerospace technology and hardware transference to commercial and architectural testing, noting application to flow measurements, hydraulic acoustics and helium leak detection 20 p3416 A67-36698
 Activity of Satellite Servo System and Electronic Division of San Giorgio in aerospace field 20 p3400 A67-37163
 Space activity and research in industry noting European participation, international cooperation /ELDO program/ and research organizations 20 p3556 A67-37164
 Refractory metals in aerospace applications, considering aerodynamic heating, melting resistance, liquid-metal corrosion, electrical superconductors, etc 20 p3469 A67-37342
 Materials in airlift technology noting adaptation of titanium and beryllium 20 p3471 A67-37533
 Space program in 1970s, discussing solar system exploration, investigation of universe, practical applications of space and development of technology [AIAA PAPER 67-626] 20 p3530 A67-37613
 Lessons from spacecraft industry experiences in 1960s and trends for 1970s, discussing subsystem performance experience, data acquisition, contracting, reliability, etc [AIAA PAPER 67-639] 20 p3557 A67-37622
 Chemistry and technology of explosives, Volume 3, covering rocket propellants, mining explosives and smokeless powder manufacture 21 p3688 A67-37900
 Heat treatment practices for precipitation hardening steels noting use in missile and aerospace applications 21 p3634 A67-38178
 Packaging of IC core memory for aerospace use, discussing design and production of boards 21 p3595 A67-38338
 Production process of hermetically sealed electronic package for aerospace use 21 p3595 A67-38340
 High temperature technology - Conference, Pacific Grove, California, September 1967 21 p3578 A67-38390
 Book on astronautics covering rocket theory, celestial mechanics and space problems 21 p3703 A67-38434
 Soviet book on microminiaturized aerospace digital computers noting production problems, reliability, electronics, storage units and foreign computers 21 p3588 A67-38765
 Developments in optics and applications in industry - Conference, Sussex, April 1967 22 p3836 A67-39328
 Book on reusable protective packaging of military, electronic and aerospace instruments and systems 22 p3771 A67-39832
 Slurry coating applied to aerospace refractory metal component for oxidation protection [ASM PAPER C6-1.5] 23 p4020 A67-41407
 Supersonic civil aircraft, considering journey time, safety and operating economy 24 p4093 A67-41886
 Soviet studies of Ni- and Fe-based heat resistant aging alloys and aircraft gas turbine technology 24 p4169 A67-41919
 Threaded fasteners for application to aerospace structures noting preload, torque and lubrication 24 p4160 A67-42080
 Aircraft fasteners, airline operation and maintenance requirements and improvement of standardization 24 p4161 A67-42082
 Technical feasibility of rocket propellant combinations involving metal combustion and chemical heating of excess H 24 p4206 A67-42403
 Apollo historical perspectives, background to U.S. man on moon decision in mid-1961,

rocket booster development and space mobility [AIAA PAPER 67-839] 24 p4259 A67-42978
 Stabilization and control techniques for future unmanned commercial space vehicles, emphasizing application of projected technological advances in instrumentation [AIAA PAPER 67-878] 24 p4244 A67-42997
 Costs and savings of computer graphics systems used for preparing and maintaining aerospace engineering drawings [AIAA PAPER 67-899] 24 p4127 A67-43008
 Integrated Life Support System program contributions to aerospace technology [AIAA PAPER 67-924] 24 p4117 A67-43020
 Comparative projections of helicopters, compound helicopters and tilting propeller low-disk-loading VTOL aircraft for civil applications 24 p4097 A67-43029
 Cryogenic liquid propellant rocket engine technology and design [AIAA PAPER 67-978] 24 p4208 A67-43053
AEROSPACE VEHICLE
 Effects of subsonic, supersonic, hypersonic and orbital environments on structures [SAE PAPER 660671] 01 p0160 A67-10578
 Rational mechanics principles of inertial navigation and relation to gravitational field structure in vicinity of maneuvering vehicle [ONERA-TP-352] 01 p0110 A67-11088
 Thin shells and stability in aerospace structures [AIAA PAPER 66-1022] 03 p0529 A67-14154
 Aerospace vehicle simulation concept defined, examining relation to major problem areas of checkout 03 p0399 A67-14210
 Arnold Engineering Development Center, discussing aircraft and space vehicle environmental simulation and testing 05 p0788 A67-16619
 Onboard digital computer navigation, guidance and control of reentry and aerospace vehicles 06 p1028 A67-17922
 Linear and nonlinear attitude control law synthesis for spinning aerospace vehicles, including analog simulation for control designs based on frequency symmetry 07 p1257 A67-19359
 Thin shells and stability in aerospace structures [AIAA PAPER 66-1022] 10 p1715 A67-22767
 Rules for comparing designs of aerospace transporters and selecting optimum configuration, based on overall cost criterion 10 p1713 A67-23482
 Optimal control of maneuver induced vibration in flexible aerospace vehicles 10 p1714 A67-23754
 Dynamic stability problems in actual structures in vehicle design 14 p2397 A67-28084
 French concept for aerospace transporter capable of horizontal takeoff from existing major airstrips 15 p2568 A67-29842
 Digital computer program FORTRAN coded, analyzing electric power distribution system of aerospace vehicle 17 p2804 A67-32511
 Composite material with titanium strength-weight ratio and aluminum safety for aerospace vehicle construction [ASTM PAPER 15] 18 p3067 A67-34576
 Composite propulsion systems for aerospace missions, considering Mach range, specific impulse, oxygen source, design characteristics, capabilities and limitations 22 p3868 A67-39890
 Missiles and aerospace vehicles sciences - AAS Conference, Huntsville, Alabama, December 1966, Volume 1 22 p3900 A67-39926
 Missiles and aerospace vehicles sciences - Conference, Huntsville, Alabama, December 1966, Volume 2 22 p3904 A67-40134
 Optimal control of maneuver induced vibration in flexible aerospace vehicles 23 p4071 A67-41725
 Impact of future aeronautical vehicles on development test facility planning [AIAA PAPER 67-780] 24 p4139 A67-42947
AEROSPACEPLANE
 Aerospacecraft, reusable self-contained man-rated vehicle, noting economy, propulsion system and possible configurations 06 p1098 A67-19022
AEROTHERMOCHEMISTRY
 Turbulence in free shear layer in mixing region of circular jet, comparing statistical characteristics of mathematical and physical models [AIAA PAPER 65-805] 01 p0054 A67-11164

Aerothermochemical analysis of solid propellant combustion 04 p0722 A67-14824
 Perfect gases reacting mixture flows formulated for system of differential equations 06 p0955 A67-18114
 Aerothermochemical eddy diffusion model for predicting rapid wake ionization decay behind hypersonic slender clean cone obtained in free flight ballistic range [AIAA PAPER 67-21] 06 p0938 A67-18257
 Optical radiation emission from rocket exhaust plumes, noting dependence on aerothermochemical properties, considering radiative transfer 18 p3152 A67-33821
 Aerothermochemistry of high temperature multicomponent reactive systems, examining thermodynamic and transport characteristics and ionized and dissociated working fluid processes 22 p3921 A67-40447
AEROTHERMODYNAMICS
SA AERODYNAMIC HEATING
 By-pass propulsion systems development for V/STOL transports including aerothermodynamic aspects [AIAA PAPER 64-606] 03 p0502 A67-12902
 Aerothermodynamic testing of heat protective systems in arc tunnel 15 p2466 A67-29538
 Formula for thrust derived from thermodynamic steady flow energy equations 15 p2472 A67-29673
 Aerothermodynamics for Apollo spacecraft design and results of flight tests 16 p2781 A67-30935
 Rarefied gas supersonic flows studied in wind tunnel for aerothermal/aerodynamic characteristics 17 p2790 A67-32231
 Book on aerodynamic and aerothermal experiments on circular cylinders at angle of attack in supersonic flow 17 p2790 A67-32379
 Equations of one-dimensional aerothermodynamic flow of dissociating gas 20 p3420 A67-36599
 Spherical entry vehicle used to define planetary atmosphere structure and composition from dynamic response during entry, discussing aerodynamic characteristics 22 p3907 A67-40177
AEROTHERMOELASTICITY
S AERODYNAMIC HEATING
AFRICA
SA NORTH AFRICA
 Mean monthly winds at low level calculated for equatorial station in East Africa, noting monsoon patterns and jet streams 06 p1025 A67-18024
 South African space research, describing ground-based observations and tracking stations 19 p3321 A67-35304
AFTERBODY
S CYLINDRICAL AFTERBODY
AFTERBURNER
S GAS TURBINE
AFTERGLOW
SA HELIUM AFTERGLOW
SA OXYGEN AFTERGLOW
SA PHOSPHORESCENCE
SA VEGARD-KAPLAN BAND
 Afterglow decay of number density and electron temperature of plasma with rare collisions between electrons and molecules 03 p0487 A67-14343
 Nitrogen atoms recombination in fast flow system using photometry, determining atom concentration, noting nitrogen afterglow intensity 06 p0956 A67-18760
 Time dependence of electron density in afterglow of electrodeless discharge in hydrogen plasma measured, using microwave interferometer 07 p1229 A67-19682
 Recombination instability in plasma if temperature dependence is strong 15 p2522 A67-29208
 Electron thermal diffusivity in room temperature neon afterglow plasma measured using Tonks-Dattner resonance, noting independence of electron density 15 p2532 A67-30381
 Attachment and detachment processes effect on plasma quenching by electronegative gases, showing usefulness of steady state nitrogen afterglow flow system 16 p2720 A67-31238
 Lifetime and diffusion coefficient of lowest excited state of molecular nitrogen from intensity decay measurements of Vegard-Kaplan band 17 p2889 A67-33243
 Afterglows from atmospheric nuclear detonations related to natural airglow and aurora 18 p3036 A67-33604
 Optical IR characteristics of long-time

- afterglow from high altitude nuclear detonations 18 p3036 A67-33605
- Atomic collision processes in ionized gases, studying ambipolar diffusion, electron attachment, electron-ion recombination and Penning ionization by afterglow technique 19 p3264 A67-35070
- Electron-temperature dependence of electron collision frequency in afterglow plasma 21 p3667 A67-38414
- Relaxation times of carbon dioxide vibrational levels and afterglow pulsed gain for nonflowing gas laser amplifiers 22 p3814 A67-39354
- Optical instrumentation for auroral and afterglow studies with applications of grating spectroscopic systems, monochromators, interferometers and photometers 23 p3996 A67-41256
- AGC**
- S AUTOMATIC GAIN CONTROL /AGC/**
- AGE FACTOR**
- Direct observation on precipitation and aging behavior in Cu-Ti alloys by transmission electron microscopy 11 p1809 A67-24948
- Cosmological model covering early and late stages, presenting period time when matter density equaled radiation density 17 p2947 A67-32759
- Middle aged pilot medical fitness for flying, noting age-accident statistics, changes in skill, performance, senses and responses 22 p3756 A67-40535
- Age limitations of flying personnel taking into account physical condition and professional capabilities 22 p3756 A67-40542
- Rentgenographic kymography in evaluating cardiovascular apparatus in middle aged pilots 22 p3753 A67-40543
- Laboratory psychophysiological efficiency in flying personnel of various ages covering pursuit reaction tests, serial motor activity and optico-acoustic signal analysis 22 p3753 A67-40544
- AGE HARDENING**
- SA PRECIPITATION HARDENING**
- Strain aging of ordered alloys at temperatures above and below critical point, discussing yield point and hardening factor 01 p0101 A67-10938
- Internal friction in 18 percent Ni maraging steel noting rapid dislocation recovery, independence of temperature and age hardening characteristics 05 p0828 A67-16468
- Effects of cold work by rolling and by shock waves on precipitation hardening in Al-6 percent Cu alloy 08 p1343 A67-21544
- Beryllium alloys age hardening noting increase in flow stress with time 13 p2138 A67-27104
- Age hardenable low-expansion alloy for cryogenic service 13 p2142 A67-27675
- Thermal processing of precipitation-hardenable aluminum alloys, noting changes in structural and mechanical properties 14 p2335 A67-27804
- Reversible contribution to flow stress in Ni-Al alloy analyzed by temperature change as function of tensile strain and precipitation hardening 18 p3065 A67-34363
- Thermal and thermomechanical treatments effect on structure and mechanical properties of Fe-Ni-base alloy with Al and Ti additions 19 p3247 A67-35834
- Chondrites solidification age measured via rubidium-strontium pairs in component minerals, using phase separation method 21 p3702 A67-38125
- Qualitative and quantitative variation in alloy phase composition with temperature and age hardening length, studying structural diagram 22 p3818 A67-39321
- Aging of iron-nickel-titanium alloys during heating in reverse martensitic alpha to gamma transformation process, investigating phase parameter changes 22 p3820 A67-39824
- AGENA ROCKET**
- SA ATLAS AGENA LAUNCH VEHICLE**
- Computer program for automated design of hyperstatic truss structures under resonant frequency used in multisatellite Agena launcher 03 p0526 A67-13968
- Flexibility required to establish systems facility necessary to support Agena vehicle during development, testing and activation phases 04 p0600 A67-15781
- Hypergolic propellant ignition experience during Project Sure Fire of Gemini program [AIAA PAPER 67-259] 07 p1241 A67-20046
- Permanent joints for Agena pressure systems, discussing retention of pressurized gases in connector tubing system 17 p2801 A67-31984
- AGING**
- SA CURING**
- SA STORAGE**
- SA STRAIN AGING**
- Modulated structure of aged Ni-Al alloys, including electron micrograph and phase diagram studies of particle growth kinetics 01 p0092 A67-10056
- Aging of Ni containing maraging steel and related alloys analyzed by electrical resistivity, X-ray diffraction and hardness measurements, noting nature of Co-Mo interaction 03 p0440 A67-13250
- Ozone determination by electrochemical and colorimetric methods compared for effects of sensor cell aging 03 p0413 A67-13931
- Plastic deformation and aging effect on kinetics of beta phase decay, dispersion and alpha phase distribution of TC8 by optical and electron microscopy and measurements of hardness and mechanical properties in tension 04 p0640 A67-15976
- Precipitation effect of dispersed calcium titanate-rich phase on shape, organization and thickness of ferroelectric domains in barium titanate 06 p1020 A67-18047
- Hydrogen effect on processes occurring in alloy VT3-1 during aging shown to increase beta phase 07 p1200 A67-19247
- Hardness variation of alloys of system Al-Cu-Cd-Mn-Li as function of composition and aging conditions 07 p1201 A67-19252
- Structure of system Ti-Mo-Cr-Fe-Al alloys when quenched from beta region, noting maximum hardness at aging temperatures 07 p1205 A67-19272
- Aluminum alloy with various metal additions analyzed for aging, using electron microscope 08 p1342 A67-20806
- Electrical resistance changes in quaternary alloy during simultaneous occurrence of phase solution coalescence and silicon spheroidization, noting effects of aging and various metal additions 08 p1342 A67-20807
- Aging effect on structure of cobalt alloys annealed at 1200 degrees C suggests formation of lamellar regions 08 p1342 A67-20812
- Hypersthene chondrite origin and history studied using noble gas content and shock and reheating by X-ray diffraction 11 p1865 A67-24602
- Aging kinetics and lattice defects in Al-Zn and Al-Zn-Mg alloys 11 p1809 A67-24947
- Martensitically hardened high strength stainless steel, physical properties, heat treatment effects, etc 11 p1810 A67-25103
- Effect of small cold deformation preceding aging in nickel maraging steel 13 p2132 A67-26575
- Beryllium aging kinetics when having different purities 13 p2136 A67-27105
- Barium titanate polycrystal dielectric constant aging, discussing 90 degree splitting in domain structure 14 p2364 A67-28228
- Current gain and collector-base saturation current and breakdown voltage in aged silicon transistors 15 p2453 A67-30064
- Structures from two-step aging of aluminum-magnesium-silicon alloy, discussing effect on needle precipitation 18 p3065 A67-34362
- Optimum aging temperatures obtained from electric resistance of beryllium alloys containing chromium and zirconium 19 p3245 A67-35472
- Aging effect on structure and properties of complex alloyed heat resistant steel 24 p4173 A67-42190
- AGRICULTURE**
- IR imagery from remote sensing, use in agriculture and forestry [AIAA PAPER 67-281] 12 p1967 A67-26000
- Economic benefits from space systems used to survey food producing areas and weather 19 p3350 A67-35850
- Multispectral remote sensing techniques for agricultural surveys from orbiting satellites, discussing in-flight signal processing 22 p3806 A67-40387
- Multichannel image data handling and processing system using multispectral analysis for remote agricultural sensing and surveying from aerospace platforms 24 p4157 A67-42435
- Automatic crop surveys contribution to agricultural technology in developed and underdeveloped countries [AIAA PAPER 67-766] 24 p4258 A67-42935
- AILERON**
- SA ELEVON**
- SA SPOILER-SLOT AILERON**
- Electromechanical simulator of wing flutter with aileron under flight conditions 22 p3912 A67-39779
- AIR**
- SA ALVEOLAR AIR**
- SA ATMOSPHERE**
- SA COMPRESSED AIR**
- SA HIGH TEMPERATURE AIR**
- SA SECONDARY AIR**
- SA UPPER AIR**
- Density dependence of refractive index of air and phase and group refractive index as function of pressure, temperature and composition 05 p0838 A67-16783
- Approximation equations of thermodynamic data of air-carbon plasma with arbitrary carbon content in atomic region 10 p1732 A67-22919
- Region of air with slight variation in refractive index from surrounding air recorded by holographic technique 15 p2488 A67-29725
- Emissive power of air measured by determining charged particle distribution behind spark discharge generating shock wave in plasma 15 p2530 A67-29861
- Electrodeless annular discharges in argon and air 17 p2897 A67-32174
- Turbulent thermal convection properties measured in air between constant temperature horizontal plates, discussing structure 17 p2968 A67-32281
- Hydrogen-air reaction kinetics analyzed using standing wave normal shock, noting wall effects, ignition delay and recombination [AIAA PAPER 67-479] 18 p3157 A67-33948
- Air ionization behind shock wave front, estimating free electron concentration, ionization time and collision frequency 19 p3293 A67-35401
- AIR BREATHING ENGINE**
- Effects of improved refractory blade materials and internal cooling on inlet temperatures, design and performance of air breathing engines at supersonic speeds [AIAA PAPER 65-743] 03 p0502 A67-12904
- Propulsion system development for very high speed winged vehicles application 03 p0505 A67-14382
- Structural design problems of hypersonic air vehicles with air breathing propulsion, discussing relation to future hypersonic commercial air transport 03 p0362 A67-14383
- Supersonic combustion air breathing engines as propulsion systems for hypersonic vehicles [AIAA PAPER 66-826] 04 p0688 A67-14624
- Ground test facilities for aircraft air breathing propulsion system development 08 p1315 A67-21063
- Air breathing rocket using external combustor formed by two short annuli 08 p1376 A67-21284
- Thrust deflection in hypersonic air breathing vehicles, noting increased cruise range and effects of gross thrust/ram drag ratio 09 p1441 A67-22497
- Launch vehicle development in reusable and airbreathing configurations 09 p1572 A67-22674
- Hypersonic air breathing engine, specifically scramjet, noting vehicle design, combustion system, nozzle, friction, etc 10 p1697 A67-22873
- Air breathing reusable rocket launchers for European development, comparing ramrocket and turboramjet propulsion 15 p2568 A67-29844
- Steepest-ascent optimization program developed for flight path of current vehicles, particularly supersonic transport vehicles 19 p3257 A67-35958
- Book on production of boranes and related research for high energy fuels for air breathing engines 23 p4047 A67-41443
- Sub-, super- and hypersonic air breathing engines, examining developments on ground test and simulation facilities [AIAA PAPER 67-779] 24 p4206 A67-42946
- AIR CARGO HANDLING**
- Dual-purpose passenger/cargo aircraft noting design, passenger interior system, cargo handling system, compatibility, comparisons, etc 06 p0946 A67-18005
- Air conditioning and refrigeration in air

- cargo industry 06 p0981 A67-18566
Philadelphia International Airport facility planning based on forecasts, population and business growth, economic factors and historic trends 21 p3734 A67-38805
Master plan for Philadelphia International Airport to accommodate increased air travel, cargo and jet aircraft 21 p3608 A67-38806
- AIR CONDITIONING**
SA COOLING SYSTEM
Air conditioning and refrigeration in air cargo industry 06 p0981 A67-18566
Air conditioning system of P-3 aircraft, noting redesign to include auxiliary power unit for functioning during ground operation 20 p3363 A67-36512
Environmental control for high performance military aircraft covering air conditioning, temperature and pressure control and oxygen supply systems 21 p3572 A67-39130
- AIR CONDUCTIVITY**
Impedance errors of coaxial air transmission lines and mechanical and electrical characteristics of Preciflex connectors 02 p0213 A67-11648
- AIR COOLING**
Air-cooled rotor and guide vanes of turbojet engine 06 p1073 A67-17607
Perforated plenum technique for direct forced air cooling of electronic equipment inside rack enclosure 08 p1303 A67-21061
Testing of transpiration air cooled turbine, discussing blade fabrication [ASME PAPER 67-GT-29] 11 p1854 A67-24807
High temperature long life turbine design, noting role of air cooling of critical parts [SAE PAPER 670345] 12 p1990 A67-25880
Estimation of mean overheating of casing and heated space inside air cooled electronic device 16 p2778 A67-30470
High temperature operation of air-cooled turbine blades and vanes 18 p3115 A67-34377
Gas turbine cooling, discussing high temperature problems, solutions and benefits of air cooled blades and vanes 20 p3517 A67-37168
Optimum relative angular velocity selected for cooled high temperature gas turbine stages, discussing blade mean cooling depth and cooling heat 22 p3870 A67-40456
- AIR CURRENT**
SA EKMAN LAYER
SA TURBULENT AIR CURRENT
SA VERTICAL AIR CURRENT
Calculating shock wave separation and relaxation velocities for supersonic airflow past sphere 03 p0349 A67-12863
- AIR CUSHION VEHICLE**
SA GROUND EFFECT MACHINE
Peripheral jet air cushion vehicle circular platform design, discussing dimensionless design parameter determination from operating height, translational speed and weight 22 p3745 A67-39726
Steady tunnel operation effects on tracked hovercraft air cushion performance, discussing tunnel entrance problems 22 p3746 A67-40067
Hovercraft research noting internal and external aerodynamics, test techniques and instrumentation requirements 23 p3934 A67-41167
- AIR DEFENSE SYSTEM**
Binomial probability distribution applied to air battle analysis, discussing fire doctrines, attrition rates, weapon design classes and limitations of approach [AIAA PAPER 66-781] 01 p0169 A67-10527
Data utilization in Air Defense Command /ADC/ weapon systems management 13 p2233 A67-27560
Eldorado low altitude detection and short reaction time defense system, examining Doppler effect and Mirador pulse radar 17 p2816 A67-32751
- AIR DUCT**
Dust remover using paper filters and wind tunnel with turbulence in cylindrical duct used for pressure determination 16 p2657 A67-30867
Experimental duct for plane deformation of homogeneous turbulence, measuring mean velocities in axis and symmetry plane 20 p3420 A67-36393
Forces on spheres inside diffusers noting instability onset 23 p3932 A67-41734
- AIR FILTER**
Air-oil separator for aircraft hydraulic system stops nose wheel shimmying, based on lowering pressure principle and using filter screen barrier 24 p4099 A67-42427
- AIR INLET**
Method for matching jet engine intake and ejector pumping characteristics to evaluate static and in-flight performance of air-augmented nozzles, considering external aerodynamics influence [AIAA PAPER 65-596] 03 p0350 A67-12903
Hydrogen-LOX rocket booster engines 03 p0504 A67-13873
Feasibility of effective aerodynamic round-lip inlet for supersonic aircraft takeoff and low speed flight 09 p1438 A67-22495
Supersonic inlets for jet aircraft, discussing positioning of terminal shock at intake for most efficient engine performance 15 p2415 A67-29303
Boundary layer effect on mass flow parameter and ram efficiency of submerged intakes 20 p3360 A67-37490
Engine air intake design and development for Concorde aircraft, discussing design constraints [AIAA PAPER 67-752] 23 p4048 A67-40986
- AIR JET**
Atmospheric jet streams in tropical latitudes, discussing velocities, seasonal variations, etc 04 p0652 A67-15474
Radial momentum equation of flow outward from axisymmetric turbulent wall air jet impinging on solid surface 05 p0792 A67-16819
Initial turbulence effect on characteristics of axisymmetric submerged air jets, using thermo-anemometer to measure averaged velocity and mean quadratic longitudinal pulsation rate component 11 p1779 A67-24320
Electric field intensity distribution over length of plasmatron arc stabilized by longitudinal vortex air flow 11 p1843 A67-24972
Air gauge circuit analysis extended to fluidic restrictor circuits and complex resistor circuits, using Bernoulli and continuity equations 14 p2252 A67-28353
Reattachment of two-dimensional compressible air jets to planes, discussing pressure maximum and inlet Mach numbers 22 p3786 A67-40068
Flame stabilization mechanism of homogeneous combustible fluid flow using air jets through peripheral slits to join main flow producing gasdynamic screens 22 p3921 A67-40455
Soviet papers on turbulent jets of air, plasma and real gas 23 p3988 A67-40727
Fluidic digital component design utilizing wave phenomena produced by two interacting low entropy pneumatic jets, discussing nozzle geometry and fluidic oscillators 23 p3936 A67-41421
- AIR LAUNCH**
Air launched sounding rockets design, development and testing noting aerodynamic loading and surface, propulsion unit, cost effectiveness, etc 08 p1407 A67-20518
Launching and ballistic flight of Rubis IV rocket, discussing scientific preparation and payload testing 24 p4241 A67-42573
- AIR MASS**
Air mass measurement during turbulent axial flow towards surface of rotating disk, noting entrainment rates for high and low Reynolds numbers 09 p1437 A67-22159
- AIR NAVIGATION**
SA ALL-WEATHER AIR NAVIGATION
SA TACTICAL AIR NAVIGATION
/TACAN/
Navigation of SST with respect to optimum trajectory, flight system and traffic control 13 p2153 A67-26710
Air navigation, classical methods, instrumentation and air traffic control 15 p2513 A67-29092
FAA navigation improvement program, discussing approach and landing, short and long distance navigation and performance assurance 15 p2514 A67-29738
Long distance air navigation aids, stressing supersonic flight safety requirements 16 p2701 A67-31248
Soviet book on flight vehicle navigation accuracy and reliability 17 p2881 A67-31933
Systems recommended to meet area navigation requirements, considering pictorial display/ course line computer /PD/CLD/ application 17 p2881 A67-32391
Optimum mixer-filter for aircraft navigation systems consisting of inertial platform aided by Doppler and/or Loran designed, using Kalman filtering 17 p2825 A67-32525
Soviet book on aircraft navigation covering theory, earth shape, map use, coordinate systems, instrumentation and aeronautical astronomy 19 p3254 A67-34894
Worldwide navigation satellite system in next decade, studying economical, organizational, technological, operational and safety aspects 19 p3255 A67-35658
Aircraft position determination and surveillance requirements for ATC 19 p3256 A67-35860
Air traffic control, navigation techniques, requirements and equipment for general aviation to end of century 19 p3256 A67-35861
Long and short range air navigation trends, discussing digital computer application, collision prevention and landing systems 19 p3256 A67-35864
- AIR POLLUTION**
Air monitoring instruments used in detection and control of air pollution 01 p0050 A67-11037
Stallwood jet and DC arc in analysis of air contamination in inert gases 05 p0758 A67-16368
Radioactive clathrate technique to detect reactive gaseous contaminants in atmosphere in parts per million range 05 p0843 A67-16550
Mass spectrometric investigations of interaction of atmospheric ions with molecules of rocket gas release 10 p1640 A67-23215
Materials evaluation and selection for compatibility with manned spacecraft environment 15 p2507 A67-29551
Searchlight brightness measurements for vertical turbidity layer of troposphere using computing scattering functions 19 p3225 A67-35532
Atmospheric turbulence and diffusion, detailing turbulent energy and thermal variance budgets measurements, parallel plate convection, air pollution, etc 20 p3480 A67-36898
Contaminant control in space cabins by systematic screening of materials and supplies used, noting significance of test temperature 21 p3577 A67-38077
Advanced meteorological satellite objectives, discussing storm warnings, weather forecasting and atmospheric pollution 24 p4240 A67-42392
- AIR PURIFICATION**
SA CARBON DIOXIDE REMOVAL
Multifunctional chemical compounds development for use as air revitalization materials 16 p2618 A67-30778
Physicochemical techniques for gas separation emphasizing pulsed gas chromatography for carbon dioxide removal in spacecraft 23 p3964 A67-41555
Regenerable sorbent /GAT-O-SORB/ in granular form for carbon dioxide removal from air, discussing design and performance tests of laboratory prototype [SAE PAPER 670844] 24 p4115 A67-41997
- AIR SAMPLING**
High altitude supersonic isokinetic filter paper sampler for ALARR rocket, examining subsonic 3-D stagnation flow diffuser 08 p1276 A67-20500
Space-time wind variability for forecasting from near ground surface sampling for unguided rocket impact prediction 17 p2880 A67-32551
High altitude supersonic isokinetic filter paper sampler for ALARR rocket, examining subsonic 3-D stagnation flow diffuser 21 p3563 A67-37803
- AIR SPEED**
Variable-stability feedback control low range air speed system for X-22A aircraft 01 p0073 A67-11121
Helicopter and VTOL vehicle low air speed measuring techniques and devices including pitot-static tube, hot-wire anemometer, sphere sensor and exotic techniques 01 p0073 A67-11122
Coupling between neutral air motion and plasma transport in model F-2 layer, noting nonlinear diffusion equation, velocity profiles, etc 17 p2852 A67-33241
- AIR TO AIR MISSILE**
First order linear differential equation describing line-of-sight system of air-to-air missiles in two-dimensional case 02 p0265 A67-12731

AIR TO SURFACE MISSILE

In-flight transfer, fine and maneuver alignment of air to surface missile guidance system 17 p2881 A67-32487

Optimal terminal guidance law for linearized equations of air-to-surface missile 19 p3258 A67-35975

AGM-69A program-management system using CRT display for PERT/Time and Cost Control data translation [AIAA PAPER 67-920] 24 p4260 A67-43019

AIR TRAFFIC

Total systems concept utilizing aerospace planning and preliminary design techniques as solution to future megalopolis airport requirements [AIAA PAPER 66-944] 02 p0230 A67-12279

Airline strategy for domination of Northeast Corridor despite improvements in high speed ground transportation [AIAA PAPER 66-942] 03 p0361 A67-14021

Air cargo transport from 1960 to 1970, discussing new methods of traffic promotion [AIAA PAPER 66-1018] 03 p0361 A67-14024

Economic and technological analysis of jet transport and cargo aircraft relation to future air traffic problems [AIAA PAPER 66-820] 03 p0538 A67-14134

Airline viewpoint on air traveler handling and airport problems and effects of new jet aircraft [AIAA PAPER 66-845] 04 p0595 A67-14978

Genoa airport construction problems on land reclaimed from sea 05 p0789 A67-17100

Long-haul intercontinental air transportation, discussing passenger and cargo traffic increases and airport and airway crowding [AIAA PAPER 66-1017] 06 p0946 A67-17980

Computer /third level/ airline industry development [SAE PAPER 670241] 13 p2054 A67-27295

Supersonic transport size determination for competitive operation in air traffic market using traffic volume, aircraft type and flight frequency forecasts [SAE PAPER 670371] 18 p2985 A67-33569

Clear air turbulence /CAT/ evaluated to alleviate effects on air traffic, noting forecasting techniques and in-flight and ground-based remote detectors 19 p3254 A67-35931

Master plan for Philadelphia International Airport to accommodate increased air travel, cargo and jet aircraft 21 p3608 A67-38806

Thunderstorms endanger air traffic and travel, considering turbulence, ice formation, hail and lightning 23 p4025 A67-41303

Highway, ramp, terminal, runway and approach congestion problems for airports, suggesting separated general aviation airports and runways to alleviate big jet airports [AIAA PAPER 67-871] 24 p4139 A67-42992

AIR TRAFFIC CONTROL

SA LANDING AID

Satellite relay techniques providing paths for aircraft-ground communication over ocean used in ATC, noting repeater electronics 01 p0021 A67-10207

Analog and digital wideband radar transmission and application to air traffic control 01 p0021 A67-10213

Atlanta advanced radar traffic control system with automatic alphanumeric field installation system and computerized program for controlling aircraft approach 01 p0110 A67-10666

Ground-Air-Ground /G/A/G/ communication channels analyzed in air traffic control 02 p0283 A67-12125

Operation of VTOL aircraft in vicinity of airport including safety, noise and air traffic control factors 03 p0357 A67-12974

Position finding techniques based on precise observations of satellite orbits for ATC purposes 03 p0465 A67-13025

Weather information interpretation and utilization for air traffic control 04 p0650 A67-14688

Evaluation of tracking performance of various systems for airspace management using concept of real and apparent tracks, considering turn-following tracking 04 p0654 A67-15059

Tracking in air traffic control environment, noting differences with military environment and cooperative tracking methods 04 p0654 A67-15060

Terminal configuration with alphanumeric display and center-metrex equipment for

automation implementation in radar tracking data for expanding ATC 04 p0654 A67-15061

ARSR Weather Surveillance System design, operation and performance 07 p1142 A67-19542

SRT Daylight Display System for ATC in which radar video signals are passed through data processor 07 p1221 A67-19543

Cardiovascular health of air traffic controllers age-matched with noncontrollers 07 p1134 A67-19859

Fundamentals of technology and operation of SST aircraft for commercial aviation 07 p1131 A67-20292

ATC automation, discussing first stage implementation called NAS En Route Stage A, Center Computer Complex and computer programming 08 p1315 A67-20678

Digital data processing, transfer and display equipment applied to ATC terminal operations, using surveillance radars and radar beacons 08 p1351 A67-20677

FAA simulation systems for air traffic control noting computer simulated radar target generation, display equipment, etc 08 p1315 A67-20678

Radar applications to ATC, pictorial display and role of paper flight strip, present and future 09 p1484 A67-21678

Program for satellite supported air traffic control 09 p1528 A67-21679

Air traffic control systems engineering and design - Conference, London, March 1967 09 p1527 A67-22628

Omega navigation system composed of eight transmitters will give worldwide coverage on frequencies 10.2 kc and 13.6 kc 09 p1527 A67-22627

Direct view storage tubes for radar displays 09 p1528 A67-22628

Flight testing of radio navigation aids for civil aviation noting techniques, teleroscope and typical test 09 p1528 A67-22629

Short range radar with 1 m resolution for FM-CW technique for vehicle guidance in fog, describing equipment 09 p1528 A67-22630

Computerized decision making for air traffic control 09 p1528 A67-22631

Digital radar simulator capable of displaying 40 aircraft for air traffic control 09 p1528 A67-22632

VHF and UHF radio/telephone communication channels for air traffic control 09 p1465 A67-22633

Scan-converted bright displays for air traffic control systems 09 p1528 A67-22635

Automatic tracking in aircraft identification and updating of flight prediction parameters for air traffic control 09 p1529 A67-22636

Air-to-ground asynchronous digital communications system with premium error detection for air traffic control 09 p1529 A67-22639

High resolution 12 inch radar/synthetic display for air traffic control centers 09 p1465 A67-22640

Transoceanic aircraft control and communication via satellite 09 p1466 A67-22641

Flight trial determination of range and reliability of LF ground-to-air data link for air traffic control 09 p1529 A67-22642

Visual presentation of data required for ATC task, noting possible traffic display and attributes 09 p1529 A67-22646

Navigation aids for ATC, discussing ground reference aids in terms of accuracy 09 p1530 A67-22649

Automation role in air traffic control, discussing flight route planning 09 p1530 A67-22651

Seastations in conjunction with submarine cables for aviation communication, navigation and air traffic control 09 p1530 A67-22652

Mathematical formulae for yielding storage requirement and work loadings to provide requirement to computer designer for traffic conditions in controlled area 09 p1531 A67-22654

Flexible flight plan processing system with high continuity of service, using differing degrees of redundancy and having comprehensive system monitoring and control facilities 09 p1531 A67-22658

Secondary surveillance radar /SSR/ as principal sensor in future air traffic control service 09 p1466 A67-22657

TACAN off-track airborne navigation computer and suitable indicator provide

nonradial straight course as aid to ATC 09 p1531 A67-22658

Airport traffic control tower instrument panel displaying continuously telemetered data on current weather conditions of runway complex 10 p1656 A67-23087

Costs involved in delays occasioned by either ATC or airport acceptance rate for New York-Boston-Washington complex [SAE PAPER 670264] 11 p1884 A67-23987

FAA development program for air traffic control, navigation and landing aids and airport capacity [SAE PAPER 670265] 11 p1885 A67-23988

Video mapping technique making possible radar moving target indication for permanent echoes only 12 p1909 A67-25128

Air traffic control systems analyzed by simulation techniques 12 p1964 A67-25229

Air traffic control radar beacon system with automatic altitude reporting system [SAE PAPER 670256] 12 p1941 A67-25506

Positive control system for placing aircraft under precisely described flight path [SAE PAPER 670340] 12 p1895 A67-25878

Computer processed air traffic control, automatic weather data collection and forecasting 13 p2153 A67-26665

Navigation of SST with respect to optimum trajectory, flight system and traffic control 13 p2153 A67-26710

Supersonic aircraft effect on air traffic control facility, radar and landing aids 13 p2154 A67-26712

Second order personality factor analysis applied to air traffic control specialists 13 p2063 A67-26929

Human factors in air traffic control displays 13 p2064 A67-27563

Medical factors involving ATC information displays 13 p2064 A67-27564

Air traffic control system, discussing effect on business aircraft operations 14 p2347 A67-28317

Air navigation, classical methods, instrumentation and air traffic control 15 p2513 A67-29092

FAA navigation improvement program, discussing approach and landing, short and long distance navigation and performance assurance 15 p2514 A67-29738

Data acquisition, processing and display in computer based ATC system using radar with automatic position-reporting data link 15 p2515 A67-29941

Air traffic control simulation, describing functions to be fulfilled and system requirements for EUROCONTROL 15 p2441 A67-30184

Air traffic control operations forecasting, stressing proposed STOL and VTOL port [AIAA PAPER 67-398] 15 p2515 A67-30365

Satellite relay to provide communication paths for aircraft-ground communication over ocean, considering system design for ATC using reflex repeater 16 p2629 A67-31530

Computerized mathematical procedures application in advanced large-scale automated systems 16 p2634 A67-31568

Statistical analysis of observed relationship between independent air traffic and resultant communication channel loading parameters 17 p2810 A67-32110

Australian ATC radar network describing long range surveillance and control of neighboring airport 17 p2834 A67-32749

Solutions for aviation crisis of congestion, delays and noise, including problems anticipated with jumbo and SST jets 19 p3207 A67-34968

Air traffic control delays, terminal congestion and inadequate ground transportation facilities effect on regional airline operation 19 p3348 A67-34972

Future traffic control system for ensuring flight safety and automatic functioning by automatic radar observation and aircraft-movements control 19 p3255 A67-35806

Techniques and methods of automation in air-traffic control, discussing reliability, operation time reduction, etc 19 p3255 A67-35808

Aircraft position determination and surveillance requirements for ATC 19 p3256 A67-35860

Air traffic control, navigation techniques, requirements and equipment for general aviation to end of century 19 p3256 A67-35861

Navigational requirements of V/STOL

- aircraft in high density urban areas 19 p3256 A67-35863
- Air traffic control /ATC/ in 1970s, discussing airports, electronic facilities and collision avoidance 20 p3482 A67-37441
- Modernizing air traffic control, governmental procedures, airports and support facilities to accommodate Boeing 747 and supersonic transports 20 p3418 A67-37442
- Provision of additional metropolitan airport facilities to accommodate supersonic transportation noting noise abatement, traffic growth and off-airport processing 20 p3556 A67-37444
- Floating airports proposed as solution to short haul air traffic problems in New York 20 p3418 A67-37445
- Smaller airports to support small jet feeder line service noting need for expansion and integration of airports with urban centers 22 p3744 A67-39378
- Long range supersonic cruising aircraft research and design techniques, methods and approaches for optimizing efficiency, drag and ATC [AIAA PAPER 67-748] 23 p3987 A67-40982
- Operational error analysis program /OEAP/ use with multiprocessing in air traffic control application 23 p3976 A67-41059
- Application of IBM 9020 multiprocessing system to air traffic control 23 p3976 A67-41060
- Johnson touch display for updating flight data combining visual display and keyboard functions 24 p4152 A67-41780
- Reliability and safety for STOL aircraft and low airspeed operation, discussing automatic flight control system, air traffic control, etc [AIAA PAPER 67-797] 24 p4095 A67-42958
- Communication constraint in ATC system modeled with Markov chain, noting data collection and reduction and data link utilization [AIAA PAPER 67-868] 24 p4124 A67-42991
- AIR TRANSPORTATION**
- SA CIVIL AVIATION**
- SA SUPERSONIC TRANSPORT**
- Long-period trend in global air transport rates and effect of volume of operations on accident rates statistically analyzed [AIAA PAPER 66-805] 01 p0009 A67-10036
- VTOL and STOL aircraft applications, Boston to Washington [AIAA PAPER 66-964] 02 p0182 A67-12638
- Future short haul air transportation in northeast corridor of U.S., considering conventional, STOL and VTOL air transport systems 03 p0538 A67-13783
- Capabilities of passenger aircraft for short-range operations, noting design and economic suitability [AIAA PAPER 66-945] 03 p0361 A67-14022
- West German wartime military air transport requirements regarding fleet size and composition 04 p0551 A67-14566
- Helicopter capabilities in solving interurban mass transport problems, particularly cost and time considerations [SAE PAPER 660336] 04 p0552 A67-15611
- Coordination of marine and air transportation, complementary aspects and necessity for government subsidy of shipping 05 p0920 A67-16603
- Aircraft engine design and economic pressures effect on development 06 p0949 A67-18735
- Air transport effect on Italian balance of payments 08 p1429 A67-20767
- Competition and integration between maritime and air transport 08 p1429 A67-20770
- Aeronautical telecommunications in air transport for transmission and reception of signals, written messages, sounds and images 08 p1294 A67-20784
- Air freight transport development by Alitalia, noting Flumicino terminal 08 p1429 A67-20785
- International factors in German air transport, noting progress due to limiting differences between domestic and foreign air carriers 12 p2040 A67-25490
- International factors in air transport under treaty establishing European Economic Community [SAE PAPER 670231] 12 p2040 A67-25491
- Three STOL commercial transports performance and cost compared with conventional transports 12 p1894 A67-25492
- Book on air transport economics in supersonic era covering air cargo operational problems, mechanical loading, VTOL transport operation, etc 13 p2052 A67-26256
- Long period trend in global air transport rates and effect of volume of operations on accident rates statistically analyzed 13 p2052 A67-26422
- VTOL short-haul transportation design requirements and configuration 13 p2053 A67-27067
- Computer /third level/ airline industry development [SAE PAPER 670241] 13 p2054 A67-27295
- Disease vector transport by aircraft as international health hazard 15 p2429 A67-29284
- Air breathing reusable rocket launchers for European development, comparing ramrocket and turboramjet propulsion 15 p2568 A67-29844
- Navigation satellites of next decade, discussing services for air and sea intercontinental transportation vehicles [AAS PAPER 67-101] 15 p2570 A67-29956
- Local transportation in commercial space operations, extravehicular activity evolution and space environment characteristics utilization [AAS PAPER 67-116] 15 p2432 A67-29963
- Evolutionary concept for mass transportation system [AIAA PAPER 67-381] 15 p2420 A67-30351
- Commercial rotor VTOL for economic intercity transportation, discussing time-frame and design requirements and analyzing improvement factors [AIAA PAPER 67-410] 15 p2422 A67-30377
- Plaggio-Douglas PD-808, Italian executive jet emphasizing safety [AGARDOGRAPH 95] 15 p2422 A67-30399
- Four engine STOL aircraft for short distance hauls, noting fuselage and wing design 16 p2595 A67-30601
- British air transportation, discussing 1946 Bermuda Pact, government control and role of private enterprise 17 p2974 A67-32124
- Capabilities of passenger aircraft for short range operations, noting design and economic suitability [AIAA PAPER 66-945] 17 p2797 A67-32583
- Operating economics in short-haul air transports noting advantages of conversion to turbine powered equipment [SAE PAPER 670357] 17 p2975 A67-32996
- Aircraft fuselage design noting planning philosophy, parameters, future problems and considerations [SAE PAPER 670370] 18 p2985 A67-33568
- Aviation and transportation system, Progress, profits and public interest - Conference, Hartford, December 1966, Panel I 19 p3347 A67-34967
- Close coordination of aviation with other transportation facilities, considering airport/heliport planning within city planning, high speed train competition, highways congestion, etc 19 p3347 A67-34969
- Aviation and transportation system - Progress, profits and public interest - Conference, Hartford, December 1966, Panel 2, Aviation and technological progress 19 p3347 A67-34970
- Short haul air transportation potentials and problems, considering legislative, administrative and financial aspects of implementation and planning 19 p3347 A67-34971
- Airspace and ground environment systems approach to air transportation planning 19 p3348 A67-34974
- Aviation and transportation system - Progress, profits and public interest - Conference, Hartford, December 1966, Panel 4, Aviation and public policy 19 p3348 A67-34975
- Airlines and airport owners problems, particularly introduction of superjets, competition, V/STOL aircraft, etc 19 p3348 A67-34976
- Air transportation opportunities for development and elimination of subsidy through strengthening of smaller carriers 19 p3348 A67-34977
- Potential capital and profits growth in air transportation, discussing government, management and industry 19 p3348 A67-34978
- Airlines and governmental regulatory agencies controlling competition, new entry and rate policies relationship, examining all-cargo carrier and passenger trunk line 19 p3349 A67-34980
- Short-haul aircraft operations spectrum, discussing intercity, feeder, social services, etc 19 p3349 A67-35064
- German Institute for Air and Space Travel, 1966 Annual Report 20 p3418 A67-37313
- Planned introduction of Boeing 747 into airline service noting advances in technology for passenger comfort, cargo handling and rate reduction 20 p3361 A67-37443
- Minimizing time for deployment of infantry force by airlift analyzed by computer procedures based on loading, effectiveness and productivity 20 p3361 A67-37529
- Three STOL commercial transports performance and cost compared with conventional transports 20 p3362 A67-37530
- Rotary wing role in short haul intercity transportation, comparing V/STOL and STOL advantages over fixed wing aircraft, noting need for compound helicopter 21 p3734 A67-38013
- Philadelphia air transportation, discussing runway construction program, passenger terminal, automated cargo handling, etc 21 p3608 A67-38804
- Smaller airports to support small jet feeder line service noting need for expansion and integration of airports with urban centers 22 p3744 A67-39378
- Airport requirements for V/STOL and short haul air transportation, stressing need for solution of noise problem 22 p3779 A67-39381
- Automatic navigation trends, discussing cost effectiveness, transportation objectives and application rate 22 p3831 A67-39465
- Commercial V/STOL operating characteristics in Northeast Corridor, discussing commuter design and cost analyses [AIAA PAPER 67-769] 24 p4095 A67-42937
- Hot cycle rotor/wing aircraft for high speed city-center transportation, estimating cost and performance [AIAA PAPER 67-770] 24 p4095 A67-42938
- Conceptual aircraft suitability for short haul transportation systems, discussing operation, design, noise factors, flight profiles and V/STOL certification rules [AIAA PAPER 67-771] 24 p4095 A67-42939
- STOL and VTOL takeoff and landing areas, discussing urban and suburban air transportation and operational weather requirements [AIAA PAPER 67-795] 24 p4258 A67-42956
- V/STOL aircraft scheduling for passenger demand and equipment mix, optimizing airline earnings with mathematical programming model [AIAA PAPER 67-801] 24 p4259 A67-42961
- Traffic prediction for high speed aircraft and surface vehicles and VTOL aircraft city-center to city-center transportation [AIAA PAPER 67-802] 24 p4259 A67-42962
- Commuter airline planning using systems analysis to examine technical, managerial, legal and economic aspects [AIAA PAPER 67-843] 24 p4259 A67-42981
- Short haul VTOL air transportation airport-community noise problem, examining propulsion systems and site planning [AIAA PAPER 67-867] 24 p4096 A67-42990
- Elevated vertiport and stolport configurations and design, investigating flight operations, supporting services and legal aspects [AIAA PAPER 67-891] 24 p4140 A67-43003
- Comparative projections of helicopters, compound helicopters and tilting propotor low-disk-loading VTOL aircraft for civil applications 24 p4097 A67-43029
- Rotor VTOL aircraft for future transport noting rotor systems for low downwash velocity, minimum noise and low fuel consumption [AIAA PAPER 67-940] 24 p4097 A67-43030
- V/STOL and STOL concepts as applied to short haul transportation [AIAA PAPER 67-941] 24 p4097 A67-43031
- V/STOL airbus transportation system schedules, travel times and fares for Northeast Corridor generated by computer method [AIAA PAPER 67-972] 24 p4127 A67-43049
- AIRBORNE EQUIPMENT**
- Environmental corrections for airborne IR radiation thermometer 01 p0063 A67-10313
- Airborne double bolometer technique for deriving atmospheric water vapor profiles by solving radiative transfer

equations 01 p0108 A67-10315
 Anisotropy of reflected solar radiation from various surfaces as measured with aircraft-mounted radiometer 01 p0146 A67-10318
 Tunable airborne L-band radiometer designed to provide reliable operation over long period of time with minimum of operator adjustment 01 p0063 A67-10323
 Airborne surface temperature measurement relating surface appearances to radiation parameters 01 p0063 A67-10327
 L-3 rocket observation of proton and electron fluxes at high altitudes, using solid state detectors 01 p0144 A67-10564
 Self-contained semiautomatic and automatic onboard checkout systems for aircraft [SAE PAPER 660701] 01 p0010 A67-10595
 Semiautomatic test equipment for airborne electronics equipment for reducing checkout time [SAE PAPER 660704] 01 p0049 A67-10597
 Computer-controlled data system with remote checkout capability for airborne electronic system 01 p0030 A67-11030
 Rotating vane electric field meter system flown on Nike-Cajun sounding rocket to determine electrostatic potential on vehicle throughout flight 01 p0074 A67-11126
 All-solid state airborne low level PAM multichannel that employs N-channel FETs for all analog switching functions of system 02 p0216 A67-12013
 Liquid nitrogen cooled rocketborne telescope, measuring IR signals from diffuse and discrete astronomical sources 02 p0243 A67-12047
 Physical and functional characteristics of contoured amplifying semiconductor radiation detectors for use in missile and satellite instrumentation 02 p0244 A67-12211
 Onboard equipment designed for transport aircraft landings with visibilities less than 200 ft and runways less than 2800 ft, having all devices duplicated 03 p0464 A67-13001
 Integrated air-ground problem of flight data acquisition 03 p0374 A67-13379
 Airborne astronomical photography affected by instrument structural design, vibration, aircraft stability, image stabilization, navigation, observation time, boundary layer effect and viewing port [SMPTE PREPRINT 100-9] 03 p0423 A67-13803
 Future onboard checkout systems including integrated onboard checkout, in-flight maintenance, onboard checkout modes and onboard/ground checkout 03 p0398 A67-14202
 Evaluation of automatic test equipment for airborne weapon systems from standpoint of effect on readiness of weapon system 03 p0399 A67-14206
 S-, Se- or Te-based nonoxide chalcogenide glassy systems for airborne IR optical equipment materials 03 p0456 A67-14390
 Linear and nonlinear three-dimensional longitudinal stability coefficients from free flight measurements aboard missiles 04 p0703 A67-14553
 Design and instrumentation of Rubis research rocket payload for analysis of geomagnetic and electric fields 04 p0703 A67-14565
 Medical research in glider plane noting airborne electrocardiograph 04 p0563 A67-14630
 Radar and airborne instrumentation sampling of atmosphere, noting linked mode or one-one comparison between returned radar signal and meteorological probe 04 p0570 A67-14685
 Side-looking airborne radar in which long antenna mounted along side of aircraft faces at right angles to flight path 04 p0573 A67-15039
 Airborne Early Warning /AEW/ system designed to provide low altitude coverage in detection of enemy aircraft 04 p0573 A67-15040
 Airborne Doppler navigation techniques and configurations 04 p0653 A67-15041
 Gyro-stabilized platform operating mode and stabilization, for use in aircraft as onboard position reference system 04 p0624 A67-15537
 Telemetry systems, discussing PAM/FM/FM system, airborne equipment parts, ground support system and electronic

testing procedures 04 p0577 A67-15728
 Electro-optical imaging systems used in military aerial TV display, emphasizing variables involved in viewing related to visual interpretation 05 p0757 A67-16309
 Thermoelectric /Peltier/ refrigeration technique for cooling complex electronic equipment in avionics weapon systems line replaceable units 05 p0754 A67-17454
 Packaging failures in reentry/recoverable aerospace equipment due to design deficiencies in parts, materials and/or processes associated with physical hardware 05 p0779 A67-17468
 Data processing and control by spaceborne computer on instrumentation satellite used for analyzing space scientific properties, noting factors influencing system design 05 p0768 A67-17516
 Inertial navigation equipment applied to meteorological research, using aircraft for vertical gust measurement 06 p1002 A67-18025
 Absolute angular velocity measurement with aid of linear accelerometers on body of aircraft 06 p1028 A67-18179
 Design and instrumentation of Rubis research rocket payload for analysis of geomagnetic and electric fields 07 p1258 A67-19572
 Airborne photoelectric device for registration of cloud drops 07 p1189 A67-20009
 Nortronics NDC-1051 computer design and performance for military airborne applications 08 p1296 A67-20625
 Random access storage of program for airborne digital computer system 08 p1297 A67-20628
 Software generation for airborne digital computer systems 08 p1297 A67-20630
 Airborne environment, compatibility and memory for airborne software 08 p1297 A67-20631
 AVNI low cost IC airborne digital inertial navigation system with analog input and display, using MOS LSI techniques 08 p1297 A67-20633
 Power supply design for avionics digital computer systems 08 p1286 A67-21031
 Preflight and operational status test set /PTS/ for radiation testing of electronic equipment on military aircraft 08 p1303 A67-21059
 IR observations in one to seven micron region using astronomical telescope on Aerobee rocket above atmosphere 08 p1397 A67-21185
 Airborne guidance computations using prescribed-H-method, representing two-body motion in inertial space, presenting equations for target hitting, circular orbit, etc 08 p1352 A67-21532
 TV camera to be used by Apollo astronauts noting integrated circuits, optical system, light intensifier, etc 09 p1499 A67-22175
 Spectrum of quiet sun between 30 and 128 angstroms analyzed in November 1965, using rocketborne grating monochromator with Gelger detector 09 p1566 A67-22232
 Omnigraph airborne navigation equipment with small digital computer and closed loop display 09 p1526 A67-22389
 TACAN off-track airborne navigation computer and suitable indicator provide nonradial straight course as aid to ATC 09 p1531 A67-22658
 Maksutov-Cassegrain type telescope for rocket mounting, design and performance 10 p1654 A67-22751
 Multipurpose satellite computer for data processing 10 p1608 A67-22974
 Spacecraft instrumentation, discussing selection criteria for signal conditioning, transducer sensors, photographic equipment, etc 10 p1655 A67-23000
 Planar packaging concepts for avionics equipment systems and circuit boards developed from extensive use of microcircuits and thin film circuits [SAE PAPER 670251] 11 p1758 A67-23984
 Aerospace computer hardware, discussing general purpose requirement on basis of various computer designs 11 p1755 A67-24247
 Aircraft UHF radio system for distance measurements between airplane and two ground stations, noting onboard antenna 11 p1793 A67-24863
 Multifunction airborne radar instruments, discussing air to air, air to ground, shared

aperture and combined systems, spoiled beam technique for ground mapping, etc 11 p1754 A67-25007
 Packaging integrated circuit airborne tape control unit 12 p1911 A67-25273
 Airborne weather radar for general aviation aircraft, considering transmitter power, wavelength, target area, reflectivity characteristics, installation limitations, etc [SAE PAPER 670252] 12 p1905 A67-25503
 Field testing of self-powered recorder for vibration data in environmental studies 12 p1942 A67-25682
 Recoil proton detectors used for rocket measurements of fast neutron intensity above Fort Churchill, Canada, during 1964 and 1965 12 p1998 A67-25828
 Digitized spark chamber for gamma ray and charged particle experiments on balloons and satellites noting construction, performance characteristics and results 12 p1944 A67-25854
 Directional neutron detector using liquid scintillator for low mev energy range for rocket and satellite experiments 12 p1945 A67-25860
 Vertical gust components in altocumulus clouds measured by airborne instruments 13 p2152 A67-26741
 Medical testing, research and control during manned space flights, discussing diagnostic algorithms for onboard computer and frequency of data collection 13 p2062 A67-26762
 Automatic radiosonde data processing system providing azimuth and elevation angles, temperature, humidity, etc 13 p2069 A67-27019
 Avionics system development for V/STOL tactical aircraft, emphasizing onboard electrical system 13 p2053 A67-27222
 Primary cosmic ray intensity and structure of air showers at high altitudes investigated by aircraft, balloons and sounding rockets 13 p2193 A67-27247
 Electron precipitation in conjugate regions of auroral zone latitudes examined via X-ray measurements with balloon-borne instrumentation 13 p2115 A67-27255
 Airborne radio telemetry equipment transmitting in-flight data to ground station for monitoring and analysis, using frequency- and time-division multiplexing 14 p2261 A67-28038
 Aircraft engine parameter control by onboard recording instruments 14 p2315 A67-28059
 General purpose digital computer for airborne and spaceborne guidance and navigation systems 14 p2275 A67-28684
 Inertial navigation system and onboard navigation course computer evaluated, noting performance data and circular error 15 p2515 A67-29742
 Onboard data systems selection and design and relation to ground networks [AAS PAPER 67-54] 15 p2440 A67-30118
 Saphir g space vehicle guidance systems consisting of inertial center and computer 16 p2701 A67-30800
 New navigation system/ADVANCE/ consisting of two-degrees-of-freedom gyro and accelerometer noting UTM grid-zone distribution system 16 p2701 A67-30928
 Digital onboard checkout system for SST and other commercial/military aircrafts to discover in-flight malfunctions digital onboard checkout system for SST and other commercial/military aircraft to discover in-flight 16 p2596 A67-31493
 Airborne photo-optical instrumentation - Conference, Cocoa Beach, Florida, February 1967 16 p2678 A67-31791
 Computer program for optimizing performance of high resolution airborne photo-optical recording system using modulation transfer function analysis 16 p2678 A67-31792
 Airborne long focal length photographic system environmental effects studied with Cassegrainian type Maksutov telescope 16 p2678 A67-31793
 Airborne photographic instrumentation system for photometric observation of total solar eclipse, noting automatic tracking system 16 p2678 A67-31794
 Airborne Astrographic Camera System using meteor orbit theory to observe reentry trajectory discussing data reduction theory and photo-optical instrumentation 16 p2679 A67-31795

Airborne ground profiler using CW and pulsed lasers range finders discussing performance 18 p2679 A67-31798

Airborne optical satellite tracking, discussing accuracy limitations and comparing to ground stations 18 p2630 A67-31799

Airborne camera system for high altitude photography of rocket and spacecraft vehicle launchings describing development 16 p2679 A67-31800

Airborne photographic systems defining performance criteria for quantitative analysis and application of transfer functions for evaluation 16 p2680 A67-31804

Attenuation rates at vlf from aircraft measurements presented as curves of dominant waveguide mode vs. geomagnetic bearing of propagation path 18 p2631 A67-31854

Airborne field strength measurements in NPM antipode region noting variation with inverse square root of distance over sections of antipodal area 16 p2631 A67-31855

Computer simulation model for cost effectiveness of built-in test equipment /BITE/ in airborne radar systems 17 p2833 A67-32491

Airborne low light level TV facility for reconnaissance, target recognition and acquisition, evaluating five sensor combinations 17 p2803 A67-32505

Low light level TV as aid to nighttime air rescue, describing ionoscope and image orthicon of camera system 17 p2859 A67-32506

Airborne analyzer and digital recording system to assess, diagnose and predict turbojet engine health on immediate and long term basis [SAE PAPER 670359] 17 p2861 A67-32998

Airborne astronomical photography affected by instrument structural design, vibration, aircraft stability, image stabilization, navigation, observation time, boundary layer effect and viewing port 18 p3044 A67-33575

Transfer function use in outgoing IF radiation temperature measurement of vertical profile over Caspian Sea by airborne modulation radiometer 18 p3040 A67-34001

Dual-antenna AMTI radar ground clutter cancellation and signal enhancement 18 p3001 A67-34117

IR spectrophotometer developed for airborne study of spectral energy distribution in atmospheric self-radiation 19 p3227 A67-34859

Solar X-ray spectra below 25 angstroms from crystal spectrometer mounted on solar pointer flown on satellite 19 p3318 A67-35198

Digital computing complex optimum configuration for future aircraft, discussing computer role 19 p3186 A67-35311

Air traffic control, navigation techniques, requirements and equipment for general aviation to end of century 19 p3256 A67-35881

Onboard computer equations for rocket vehicle guidance to elliptical orbit, discussing iteration absence from computations and digital simulation results [AIAA PAPER 67-821] 19 p3260 A67-36010

Spacecraft computers role on advanced manned missions 20 p3391 A67-36549

Self-contained and vehicle integrated onboard checkout systems, considering controller-evaluator and sensors 20 p3449 A67-36979

Onboard Checkout System /OCS/ design, considering system selection techniques, design development, equipment, etc, with orientation on OCS design by NASA/MS 20 p3417 A67-36988

Digital computers for built-in self-test in airborne weapon system, with examples of mechanized tests from F-106/MA-1 system 20 p3392 A67-36989

Inertial guidance system in ELDO-A satellite launch vehicle performance assessed using onboard computer 20 p3481 A67-37167

Concorde fire protection system based on Firewire Triple FD equipment, discussing extinguishant toxicity, low vapor pressure, etc 20 p3364 A67-37245

Spacecraft computer managed laboratory /CML/ for flexible decision making in space missions of 1970s [AIAA PAPER 67-643] 20 p3393 A67-37624

Onboard receiver-decoder control unit for ESRO I and II consisting essentially of four-

state signal corresponding to time modulated pulses 21 p3581 A67-38201

Traveling wave tube as hyperfrequency amplifier onboard satellites for reliable space communications 21 p3592 A67-38212

Onboard and ground radio-engineering system for stratospheric transport balloon noting telemetering, remote control and localization functions integrated in system 21 p3581 A67-38213

Measuring assembly containing logarithmic-response electrometric amplifiers for sounding rockets 21 p3592 A67-38222

Packaging design of modular power supplies for airborne computers 21 p3596 A67-38341

Airborne precipitation collector, determining washed out radioactive particles from air between cloud base and surface by comparing surface and airborne samples 21 p3628 A67-38583

Electrometer and varactor devices for onboard low current measurements in space probes 21 p3599 A67-38634

High reliability PCM digital telemetry system for onboard data transmission of analog and digital signals 21 p3583 A67-38635

Magnetic deviation ion mass spectrometer for ionospheric rocket probes, noting onboard application 21 p3628 A67-38657

Junction field effect transistors for onboard satellite equipment, noting resistance to ionizing radiation 21 p3600 A67-38659

Solar proton and alpha radiation flux and spectral distribution measuring device on satellite HEOS A 21 p3629 A67-38665

Radar type instrument for measuring reflection coefficients of planetary surfaces from unmanned spacecraft 22 p3795 A67-39159

Digital temperature compensation and statistical filtering procedures for fast reaction alignment of inertial navigators 22 p3831 A67-39886

Airborne measurement of microwave emission from earth surface and atmosphere for potential application of radiometry to weather satellite reconnaissance 22 p3806 A67-40361

Airborne multiple scan interferometry for low temperature IR emission spectral distribution of minerals 22 p3807 A67-40368

Compact air-to-ground laser rangefinder onboard helicopter nose section 23 p3999 A67-41028

Germ sampling at high altitudes using hydroaeroscopes attached to conventional aircraft 23 p3963 A67-41072

Auroral zone phenomena analyzed using rocketborne counters 23 p3997 A67-41333

Wavelengths and intensities of IR coronal lines of silicon and magnesium ions from airborne total solar eclipse observations 24 p4224 A67-41822

Earth science and resource studies with orbiting imaging radars onboard space vehicles [AIAA PAPER 67-767] 24 p4258 A67-42936

Onboard computer-based checkout simulator system to assist astronauts in monitoring data requirements of future space programs [AIAA PAPER 67-951] 24 p4127 A67-43035

Onboard checkout system /OCS/ impact on space station program [AIAA PAPER 67-953] 24 p4245 A67-43037

AIRBORNE INFECTION

Space cabin environmental changes studied for susceptibility of mice to viral infection 21 p3574 A67-38080

AIRBORNE RANGE AND ORBIT DETERMINATION /AROD/

Position fix and range data techniques for preliminary orbit determination for lunar satellites, using least squares method for data smoothing 22 p3879 A67-39310

AIRCRAFT

SA A-7 AIRCRAFT

SA AEROSPACEPLANE

SA ANTISUBMARINE WARFARE AIRCRAFT

SA ANTONOV AN-24 AIRCRAFT

SA ATTACK AIRCRAFT

SA AUTOGYRO

SA AVRO WHITWORTH HS-748 AIRCRAFT

SA B-52 AIRCRAFT

SA BAC 111 AIRCRAFT

SA BALLOON

SA BLACKBURN B-103 AIRCRAFT

SA BOEING 2707 AIRCRAFT

SA BOEING 727 AIRCRAFT

SA BOEING 737 AIRCRAFT

SA BOEING 747 AIRCRAFT

SA BOMBER AIRCRAFT

SA C-5 AIRCRAFT

SA C-141 AIRCRAFT

SA CANADAIIR CL-84 AIRCRAFT

SA CESSNA 336 AIRCRAFT

SA COMMERCIAL AIRCRAFT

SA CONCORDE AIRCRAFT

SA CONVAIR CV-990 AIRCRAFT

SA DASSAULT MYSTERE XX AIRCRAFT

SA DE HAVILLAND DH-121 AIRCRAFT

SA DOUGLAS DC-9 AIRCRAFT

SA DRONE

SA EXECUTIVE AIRCRAFT

SA F-4 AIRCRAFT

SA F-5 AIRCRAFT

SA F-106 AIRCRAFT

SA F-111 AIRCRAFT

SA FAN-IN-WING AIRCRAFT

SA FIAT G-91 AIRCRAFT

SA FIAT G-222 AIRCRAFT

SA FIGHTER AIRCRAFT

SA FIXED-WING AIRCRAFT

SA FOKKER F-28 AIRCRAFT

SA GLIDER

SA GROUND EFFECT MACHINE

SA HAMBURGER HFB 320 AIRCRAFT

SA HANDLEY PAGE H.P. 137 AIRCRAFT

SA HELICOPTER

SA HUNTER F-2 AIRCRAFT

SA HYDROPLANE

SA HYPERSONIC AIRCRAFT

SA ILYUSHIN IL-18 AIRCRAFT

SA INTERCEPTOR

SA JET AIRCRAFT

SA JINDIVIK TARGET AIRCRAFT

SA LIGHT AIRCRAFT

SA LOCKHEED L-500 AIRCRAFT

SA MANNED AIRCRAFT

SA MILITARY AIRCRAFT

SA MITSUBISHI MU-2 AIRCRAFT

SA NUCLEAR AIRCRAFT

SA OV-10 AIRCRAFT

SA P-3 AIRCRAFT

SA PIAGGIO-DOUGLAS PD-808 AIRCRAFT

SA PILOTED AIRCRAFT

SA PRIVATE AIRCRAFT

SA RECONNAISSANCE AIRCRAFT

SA RESEARCH AIRCRAFT

SA ROTARY WING AIRCRAFT

SA SAAB 37 AIRCRAFT

SA SAILPLANE

SA SEAPLANE

SA SHORT SC-5 AIRCRAFT

SA STOL AIRCRAFT

SA SUBSONIC AIRCRAFT

SA SUD VJ-101 AIRCRAFT

SA SUPERSONIC AIRCRAFT

SA TERRAIN FOLLOWING AIRCRAFT

SA TILT-WING AIRCRAFT

SA TRAINING AIRCRAFT

SA TRANSALL C-160 AIRCRAFT

SA TRANSONIC AIRCRAFT

SA TRANSPORT AIRCRAFT

SA TURBOFAN AIRCRAFT

SA TURBOJET AIRCRAFT

SA TURBOPROP AIRCRAFT

SA UTILITY AIRCRAFT

SA V/STOL AIRCRAFT

SA VTO FIGHTER AIRCRAFT

SA VTOL AIRCRAFT

SA X-15 AIRCRAFT

SA X-22 AIRCRAFT

SA XB-70 AIRCRAFT

SA XC-142 AIRCRAFT

SA XV-4 AIRCRAFT

SA YF-12 AIRCRAFT

Parameters to be calculated in checking airport possibilities for accommodating IL-18 aircraft, considering maximum takeoff weight 03 p0360 A67-13780

Book on variational problems in flight dynamics of winged aircraft and space vehicles 04 p0705 A67-15007

Experimental aerodynamics, Volume 2, covering simulation, transonic, supersonic and hypersonic domains 09 p1437 A67-22215

AIRCRAFT ACCIDENT

Flight safety improvement in design and maintenance procedure brought about by jet transport accident investigation data [AIAA PAPER 66-809] 01 p0008 A67-10035

Long-period trend in global air transport rates and effect of volume of operations on accident rates statistically analyzed

[AIAA PAPER 66-805] 01 p0009 A67-10036
Pilots and passengers protection and
escape from aircraft after
accident 03 p0361 A67-14096
Dynamics of commercial aircraft seats
with viscous dampers and elastic couplings
during crash landing
[ASME PAPER 66-WA/SAF-1]

04 p0551 A67-15329
Carrier landing improvements in Fresnel
lens optical landing system, emphasizing
compensated-meatball stabilization
[AIAA PAPER 65-791] 09 p1441 A67-22494
Flight safety improvement in design and
maintenance procedure brought about by jet
transport accident investigation data
[AIAA PAPER 66-809] 10 p1595 A67-23550
Admiralty principles extended to
occurrences involving aircraft flight over
navigable water 12 p2040 A67-25486
Long period trend in global air transport
rates and effect of volume of operations on
accident rates statistically analyzed 13 p2052 A67-26422

Air safety statistics analysis based on set
of intrinsic accident rates in takeoff, cruise
and landing 17 p2797 A67-32580
Air collision statistics, discussing air
collision avoidance system 19 p3173 A67-35865
Cost effectiveness of digital and voice
accident recorders in small fighter and
military aircraft for low level missions,
reconnaissance, flight testing and
training 21 p3631 A67-39129

Air Force accident history noting
importance of maintenance/material
area 22 p3754 A67-39598
Aircraft/bird collision noting dispersion,
flock detection and windshield
protection 23 p3934 A67-41070

Aeromedical examiner relationship to
accident prevention, discussing
standardization of psychological
approach 23 p3963 A67-41539

Decompression tests, evaluating hazards of
ejections and fatal injuries following window
failure in small pressurized
aircraft 23 p3965 A67-41575

Night and day carrier landing pilot
performance, noting altitude position
estimation inaccuracy as contribution to
higher accident rate 23 p3968 A67-41618

Relation of time between flights to
accident potential of
pilots 23 p3970 A67-41696

Air Force undershoot and overshoot
experience examined to establish relative
frequency, historical trend, associated
variables and human
factors 23 p3970 A67-41701

AIRCRAFT ACCIDENT INVESTIGATION

Commercial aircraft accident causes,
emphasizing accidents occurring during
approach and landing
[AIAA PAPER 66-804] 01 p0008 A67-10030

Flight recorder may aid aircraft accident
investigation by furnishing data from which
energy analyses, flight tracks and profiles
can be made
[AIAA PAPER 66-810] 01 p0008 A67-10033

Medical investigation of 1964/1965 fatal
aircraft accidents in Southwestern U.S.,
noting combined effects of drugs, fatigue,
alcohol and hypoxia 01 p0017 A67-10961

Statistical analysis of aircraft accidents
from 1938 to present 06 p0949 A67-18746

Gastrointestinal symptoms and drug use as
possible contributing causes of fatal crash of
race pilot 09 p1456 A67-21734

Accident recording system for Concorde
and protection from moisture, shock, fire
and rough seas 12 p1939 A67-25231

Postmortem determination of pilot
psychological state during aircraft collisions
by examining sugar content of dead
bodies 14 p2255 A67-28226

X-ray examination of arms of pilots killed
in aircraft collisions, determining from bone
injuries degree of control before
collision 14 p2255 A67-28227

Safety in business aircraft operations
based on available statistics noting need for
thorough pilot training 14 p2245 A67-28320

Soft gravel and aerated concrete material
of various sizes tested to safely decelerate
aircraft overshooting runway during takeoff
and landing 14 p2246 A67-28817

Flight recorder system designed to satisfy
present and future mandatory requirements
in accident recording and to provide
economic solution to limited maintenance

recording 15 p2487 A67-29510
Computer model of aircraft accident
investigator, discussing generation and
testing of kinematic hypotheses on basis of
programmed empirical data 15 p2420 A67-29896

Flight recorder may aid aircraft accident
investigation by furnishing data from which
energy analyses, flight tracks and profiles
can be made
[AIAA PAPER 66-810] 17 p2796 A67-32216

Aircraft accident prevention dynamics and
data recording role noting repetitive causal
factors, limitations and information
loss 17 p2796 A67-32218

General aviation accident investigation
from medical and operational standpoint,
concluding pilots poor judgement was cause
of accident 18 p2996 A67-34724

Medicolegal problems in aircraft flight
accidents and traumatic
mechanisms 21 p3575 A67-38508

Injury and fatality analysis in survival
study of commercial jet aircraft /Boeing
727/ landing accident with subsequent
interior fire 23 p3969 A67-41650

Death and survival during water
immersion in plane crashes near Cape Cod
and Hamilton Bay 23 p3970 A67-41707

Human factors in fatal and nonfatal
general aviation accidents, discussing cause
of death and relationship of experience,
occupation and alcohol 23 p3971 A67-41708

Human Error Research and Analysis
Program /HERAP/ for man-machine system,
investigating pilot error and performance
and aircraft accident prevention
[AIAA PAPER 67-848] 24 p4117 A67-42984

AIRCRAFT ANTENNA

High temperature resistant materials for
antennas on reentry and high performance
aircraft 01 p0103 A67-10620

Test program on air-to-air propagation
between two jet aircraft at high altitude and
path lengths up to maximum radio line-of-
sight, considering antenna gain and
multipath fading 02 p0202 A67-12122

Antenna design and measurement
technology in antenna laboratory as applied
to aircraft antennas, considering types and
configurations 03 p0383 A67-13795

Aerodiscane antenna design and electric
characteristics 03 p0384 A67-13829

Flush cavity VOR antenna for DC-9
aircraft permitting omnidirectional radiation
pattern characteristics 04 p0590 A67-15906

AIRCRAFT BASE

Temperatures on hot days at Vandenberg
AFB 13 p2152 A67-26845

AIRCRAFT BRAKE

SA WHEEL BRAKE

Magnetic autogeneration for decelerating
and cooling effects on aircraft entering
dense atmospheric layer 04 p0684 A67-14791

Dual circuit hydraulic powered brake
control system for effective short landing of
F-111 aircraft 05 p0753 A67-16164

Resistance of aviation hydraulic fluids,
mineral, snuffer, phosphate ester, siloxane
and chlorosilicone to wheel brake fires,
evaluating lab test techniques and simulation
testing 09 p1521 A67-22250

Be use in aerospace structure, gas
turbines and aircraft brake
disks 13 p2138 A67-27118

Aircraft wheel and brake designs
especially for 63 Series of DC-8 noting
materials, properties, construction, etc
[AIAA PAPER 67-404] 15 p2421 A67-30371

AIRCRAFT BREATHING APPARATUS

Human respiratory system impedance
simulator for dynamic testing of aircraft
breathing equipment to detect possible
instabilities 24 p4114 A67-41782

AIRCRAFT CABIN

SA CABIN ATMOSPHERE

SA PRESSURIZED CABIN

Aircraft cabin fire tests to determine if
filling cabin with high expansion foam could
keep temperature within survival limits
while controlling combustion
products 02 p0181 A67-12232

Ozone concentration in commercial jet
aircraft measured for possible seasonal and
meteorological correlation 06 p0947 A67-18008

Human tolerance to changes in aircraft
cabin pressurization 10 p1602 A67-23825

Small pressurized cabin design for light
commercial aircraft including safe life vs
fail-safe approaches, fatigue strength testing,
etc

[SAE PAPER 670259] 12 p2016 A67-25508

Pressurization of Mooney M22 aircraft by
low cost exhaust-driven turbosupercharger
based on diesel automotive unit
[SAE PAPER 670267] 12 p1899 A67-25511

SST air inlet control system, considering
maintainability, impact on cockpit
procedures and component reliability effect
on dispatch reliability
[SAE PAPER 670325] 12 p1895 A67-25869

Cockpit noise levels of various airline
aircraft noting propeller
effect 23 p3964 A67-41556

Aircraft cockpit and surface temperatures
after solar radiation exposure in desert,
showing inadequacies of meteorological data
for thermal stress
predictions 23 p3935 A67-41593

AIRCRAFT CARRIER

Carrier Onboard Delivery aircraft,
discussing cost effectiveness by reduced
delivery time of critical spare parts
[AIAA PAPER 66-790] 01 p0009 A67-10533

All-weather carrier landing system using
precision tracking radar and microelectronic
data link aboard carrier 01 p0026 A67-10969

Boundary layer control systems on
Buccaneer S. Mk 1 and S. Mk 2 carrier-based
strike aircraft 03 p0353 A67-12846

Boundary layer control system of
Buccaneer carrier based combat aircraft for
producing high lift coefficient at relatively
low speed 04 p0552 A67-15541

Digital computer driven display system of
electronic data and semiautomatic film
plotters for rapid evaluation of aircraft
carrier landing
parameters 07 p1164 A67-19623

Carrier landing improvements in Fresnel
lens optical landing system, emphasizing
compensated-meatball stabilization
[AIAA PAPER 65-791] 09 p1441 A67-22494

High speed linear bearing to take launch
uploads in aircraft-launching steam
catapult 12 p1948 A67-25328

Strong forward flow of engine exhaust gas
in blast deflection flow field of twin jet F-
111B 17 p2797 A67-32568

Carrier Onboard Delivery aircraft,
discussing cost effectiveness by reduced
deliver time of critical spare
parts 17 p2797 A67-32572

Criteria for determination of minimum
usable approach speed for landing of carrier
based aircraft
[AIAA PAPER 67-578] 19 p3175 A67-35973

Visual aspects of carrier landing,
discussing research program to evaluate
pilot ability to make critical visual
judgments 22 p3755 A67-39847

In-flight aeromedical monitoring of
cardiorespiratory response of naval pilots
during aircraft carrier combat operations,
discussing physiological effects
determination 23 p3963 A67-41541

Night and day carrier landing pilot
performance, noting altitude position
estimation inaccuracy as contribution to
higher accident rate 23 p3968 A67-41618

AIRCRAFT COMMUNICATION

Aircraft-to-ground communications using
Applications Technology Satellite B as
repeater in VHF COM
band 01 p0024 A67-10665

Test program on air-to-air propagation
between two jet aircraft at high altitude and
path lengths up to maximum radio line-of-
sight, considering antenna gain and
multipath fading 02 p0202 A67-12122

Communication relay to aircraft by
satellite, discussing wave propagation
characteristics, standing wave pattern, signal
fading rates, etc 02 p0205 A67-12306

Fading and multipath propagation
mechanism for communication links
involving satellites and aircraft with antenna
beams, assuming fading models and
estimating margins required for FSK
teletype transmission 06 p0960 A67-17673

Sea station and satellite for long range
communication with
aircraft 08 p1294 A67-20778

Seastations in conjunction with submarine
cables for aviation communication,
navigation and air traffic
control 09 p1530 A67-22652

Push-pull electrostatic loudspeaker for
aircraft cockpit, helmet and ear-insert
communication 11 p1767 A67-24702

Space activities effect on International
Civil Aviation Organization including

navigation problems, aircraft communication, meteorological data and technological advances 12 p2043 A67-26151
Automatic satellite navigation and communication system for aircraft and ships using cooperating ground stations 16 p2700 A67-30695
V/STOL all-weather operation developments noting navigation and communications, operations under icing and noise problems [SAE PAPER 670348] 17 p2798 A67-32990
Ground-based radio aids to navigation as represented by existing major systems 19 p3255 A67-35857
Radio interior communication /RADIC/ system used in Apollo program, discussing future capabilities and advantages 20 p3380 A67-36559
Active VHF translation repeater onboard ATS-1 for aircraft communication systems 20 p3381 A67-36591

AIRCRAFT CONFIGURATION

Analytic processes for evaluation of supersonic aerodynamics of configuration treating drag, wing design, warp, interference and sidewash [AIAA PAPER 65-717] 03 p0354 A67-12914
Three-dimensional flow separation over structures with various geometric configurations, calculating limiting streamlines for subsonic laminar boundary layer conditions 05 p0747 A67-16293
Joint NASA-USAF lifting body flight test program and M2/F2, HL-10 and SV-5P research vehicles 06 p0947 A67-18197
VTOL test bed for ground effects test, noting environmental characteristics, configuration dependence of lift and hot gas ingestion [AIAA PAPER 67-181] 06 p0980 A67-18297
Flat G91Y and G222 aircraft at Second International Aeronautical Exhibition, Turin, noting performance, physical characteristics and component parts 09 p1439 A67-22092
Aerodynamic boundary layer control by blowing, considering problems of lift increase, airfoil properties, etc 11 p1741 A67-24101
Aerodynamic development of configuration and control system of Gulfstream II business jet, discussing wing optimization, engine characteristics, etc 12 p1894 A67-25497
Vortex flow about wings, fins and fuselages of slender aircraft and missiles analyzed using small water tunnel 15 p2465 A67-29399
Hueycobra helicopter design and configuration noting maneuverability range, endurance, crew protection, weapons system, etc [AHS PAPER 113] 16 p2598 A67-31829
Integration of propulsion system into airframe of hypersonic cruise aircraft, discussing configurations, cooling and supersonic combustion 17 p2796 A67-32475
Span loading on wing of complete aircraft configuration determined, using segmented wing in wind tunnel test technique and least squares method [AIAA PAPER 66-768] 17 p2834 A67-32576
Circulation control rotor blades of circular or elliptical cross section for helicopters, VTOL and STOL and possible application to aircraft 18 p2987 A67-34707
Aircraft dynamics, Volume I, covering aircraft configuration, design problems, atmospheric properties, hydrodynamics, gasdynamics, boundary layer theory, etc 20 p3355 A67-36199
Aircraft terminal apron design, considering passenger convenience, variations in aircraft configuration and changes in aircraft mix and loading facilities 22 p3779 A67-39379
Glider towing cable configuration taking into account aerodynamic drag forces, using digital computer for numerical calculations and integrations 22 p3745 A67-39551
Honeycomb sandwich structures for aircraft and missile construction, discussing panel configurations 23 p4077 A67-41047
High lift characteristics of various aircraft configurations in wind tunnel model using different leading and trailing edge lift augmentation devices 23 p3934 A67-41309
VTOL aircraft configurations features and characteristics including helicopter, compound, composite, tilt-wing, lift-fan, lift/cruise and lift engine [SAE PAPER 670686] 24 p4093 A67-41987

AIRCRAFT CONSTRUCTION

SA WOOD AIRCRAFT CONSTRUCTION
Fabrication methods for aircraft, rockets and space vehicles including adhesives, sandwich and laminated structures, plastic fiberglass forms and explosion forming 01 p0078 A67-10304
Basic surface curves derived and defined by aircraft manufacturer for engineering, tooling and manufacturing airframe [SAE PAPER 660353] 01 p0078 A67-10567
Materials for structural usage in high altitude/ high temperature supersonic transports, comparing aluminum, titanium, etc, alloys for mechanical and physical properties [SAE PAPER 660665] 01 p0094 A67-10573
Soviet book on aircraft building and air fleet equipment, Number 6 02 p0339 A67-12436
Wheel trimming quality effect on thread grinding temperature for aircraft materials 03 p0428 A67-13196
Maraging, 15CDV6 and 40CDV20 steel for missile and aircraft construction 05 p0830 A67-17269
Antonov An-24V Soviet high wing monoplane and use of electrical spot welding and metal bonding in construction 06 p0944 A67-17597
Soviet papers on structure and properties of aviation steels and alloys 07 p1198 A67-19238
Book on aircraft materials strength calculations including load determination, heating problems, creep and fatigue strength, etc 07 p1128 A67-19578
Fatigue life on 727 aircraft structure improved through room temperature curing of adhesive film 09 p1577 A67-22510
Concorde structural development noting effects of temperature on fatigue and creep strength of aluminum alloys [AIAA PAPER 67-402] 15 p2578 A67-30369
Evaluating, reporting and improving on quality performance of suppliers and subcontractors of helicopter construction firm 15 p2584 A67-30404
Book on matrix methods of structural analysis emphasizing force and displacement methods, noting civil and aircraft construction applications 16 p2787 A67-31253
Computer program for design and routing of external plumbing of aircraft gas turbine engines 17 p2928 A67-32006
Aircraft AC electrical systems using changeover contactors and rapid fault clearance, discussing reliability and maintenance 20 p3382 A67-36316
Soviet papers on aircraft construction and techniques used by Air Force covering stress, loading, stability, etc 21 p3567 A67-38040
Loading frequency influence on endurance characteristics of V95 aluminum alloy notched for stress concentration 21 p3644 A67-38051
Soviet papers on aircraft construction and techniques used by Air Force covering theory, engines, design, manufacture and operation 21 p3568 A67-38901
Block diagram, schematic circuit and amplitude and frequency characteristics of wideband transistorized amplifier for studying high speed aircraft industrial processes 21 p3600 A67-38918
Aircraft circuit and installation requirements referring to short time characteristics of cables and effect on circuit protection, coordination and weight saving 21 p3572 A67-39072
Design, performance and development of aircraft wiring cables noting need for high temperature operation 21 p3572 A67-39073
Aircraft construction techniques for terminating cables by pressure type connections, examining design factors 21 p3572 A67-39074
Programmer for operational strength tests during aircraft construction 22 p3912 A67-39755
Plastics in aircraft and rocket parts construction noting silicon oils and solid polysiloxanes, discussing temperature resistance and rubber-elastic properties 23 p4021 A67-41400

AIRCRAFT CONTROL

Hoverbug VTOL twin-jet flying simulator operational experience and management and construction techniques [AIAA PAPER 66-799] 01 p0009 A67-10537

Control power usage for typical flight maneuvering in hover determined from flight test data of VJ-101 aircraft and of hover-rig with similar thrust-geometry and mass distribution [AIAA PAPER 66-816] 01 p0010 A67-10538
Flight performance and low speed behavior of V/STOL aircraft, noting correlation between thrust angle and aircraft attitude 02 p0180 A67-11524
Airplane longitudinal controllability criteria for range of small deviations from reference conditions of steady straight and level flight 02 p0182 A67-12733
Experimental fixed and moving-base flight simulator investigation of generalized aircraft longitudinal pilot induced oscillations [AIAA PAPER 65-793] 03 p0365 A67-12913
Sensitivity analysis of VTOL aircraft control in vertical-horizontal transition 03 p0358 A67-12982
Control method excluding static and dynamic stability aspects of aircraft from guidance problem 03 p0464 A67-13003
Comparative stability and control considerations for fixed wing and rotating wing aircraft 06 p0944 A67-17628
Doetsch deflection calibration device for aircraft control surfaces 06 p0950 A67-18022
Aircraft sizing methodology and hover control comparative analysis on V/STOL fighter-bomber using lift plus lift cruise propulsion [AIAA PAPER 67-133] 06 p0948 A67-18358
Adaptive functions of man in vehicle control systems 07 p1221 A67-19194
Extraterritorial extent of powers of aircraft commander for maintaining safety and order on board 07 p1269 A67-19519
Aircraft hollow control rods with threaded joints noting compression and testing 07 p1192 A67-19753
Handling and operation of XB-70A aircraft at Mach 3 speed noting folding wing tips, variable-geometry air inlet duct, etc 07 p1129 A67-19910
Aircraft position determined, using angle indications provided by vertical and directional gyro 07 p1189 A67-20151
Laws for aircraft control in terrain-following and formation-flight modes of operation, applying solution of Euler-Poisson equation 08 p1351 A67-20700
Artificial pseudorandom binary noise generation for flight testing and aircraft control systems and correlation function and frequency spectra of noise generators 08 p1279 A67-21005
Adaptation scheme applied to pitch axis control system of supersonic aircraft, using stability analysis for system design 09 p1440 A67-22387
Missile and aircraft control systems design, discussing root locus and stability curve methods for solving characteristic equation 09 p1483 A67-22489
Longitudinal perturbed motion of aircraft with free-floating canard, obtaining differential equation corresponding to characteristic equation 10 p1595 A67-23606
Aircraft DC electronic controls and generators for voltage regulation and system protection [SAE PAPER 670250] 11 p1745 A67-23983
Bell X-22A VTOL research vehicle, assessing mechanical and aerodynamic characteristics, variable stability and control system, etc 11 p1743 A67-24097
Aircraft control system of subsonic airplanes operated over wide speed ranges, noting flight test results 11 p1744 A67-24578
Adaptive feedback paths of adaptive aircraft control system in small signal stability analysis 11 p1772 A67-25081
Supersonic combat biplane airframe, power plant, fuel, control and escape system, instrumentation and weapons system 13 p2052 A67-26420
Turbulent atmosphere load effect on gliders noting influence of piloting techniques 13 p2052 A67-26484
Handling criteria for basic stability and control characteristics of slender wing and V/STOL aircraft 13 p2053 A67-27192
Stability analysis of adaptive aircraft control system with random disturbance 13 p2088 A67-27241
Optimum utilization of aerodynamic forces in aircraft maneuvers 13 p2213 A67-27326
Pilot techniques for determining aircraft

longitudinal short period dynamics /natural frequency and damping ratio/ for standard analysis 14 p2244 A67-27741

Aircraft engine parameter control by onboard recording 14 p2315 A67-28059

Stabilization gyros used for monitoring and detecting performance of avionics inertial navigation system, considering failure modes and effects 17 p2881 A67-32488

Compressed-air control system for lift capacity and maneuverability increment of Buccaneer type aircraft during landing and takeoff 19 p3173 A67-35876

Aircraft performance, stability and control characteristics in nonsteady flight with high accuracy instrumentation system 20 p3442 A67-36466

Minimum time-of-flight aircraft trajectory between two points, with account of earth sphericity 20 p3481 A67-37202

Complex multi-aircraft control systems with hierarchical control structure with imposed universal optimality criterion 20 p3411 A67-37373

Aircraft flight dynamics optimized in angle of attack by variational calculus, analyzing control system 20 p3361 A67-37377

Adaptive processes of human operator during control tasks involving sudden change of controlled plant dynamics 21 p3576 A67-37948

Control power usage for typical flight maneuvering in hover determined from flight test data of VJ-101 aircraft and of hover-rig with similar thrust-geometry and mass distribution 21 p3568 A67-38541

Jindivik Mk 103A jet propelled target drone ground and flight control systems stressing climb, cruise, approach and descent commands 21 p3570 A67-39131

Flight control system for future large aircraft, obtaining structural fatigue reduction, better handling and smoother ride 21 p3570 A67-39133

Spoilers for aircraft steering, discussing wind tunnel tests, banking moment and spoiler-slat allorion 22 p3739 A67-39535

Inverted pendulum and VTOL control experiments with and without motion cues, discussing various motion effects 22 p3755 A67-40087

Longitudinal stability and control wind tunnel results, considering swept and variable geometry wing aircraft during deep stall conditions 23 p3932 A67-40567

Structural elastic deformations effect on aerodynamic steering loads of glider, examining lift changes caused by wing geometry variations 23 p3933 A67-40640

Aeroelastic phenomena in aircraft stability, control and airframe vibration characteristics, describing testing methods 23 p4077 A67-41046

Flash blindness, recovery time and aircraft control loss studied in flight simulator 23 p3966 A67-41580

Automatic test equipment for checkout and fault finding on Saab 37 Viggen 24 p4137 A67-41898

AIRCRAFT DESIGN
SA HELICOPTER DESIGN

Optimum design safety for VTOL aircraft, noting noise and vibration elimination [AIAA PAPER 66-813] 01 p0008 A67-10031

Optimization of aircraft design for counter-insurgency /COIN/ operations using digital computers and wind tunnel tests, considering cost effectiveness [AIAA PAPER 66-779] 01 p0009 A67-10526

ASL 70-mm photoelectronic system in studying approach and landing parameters for aircraft design and testing 01 p0075 A67-11133

Design and construction of Franco-British Concorde SST, examining cabin, noise problem, production and tests 02 p0180 A67-12040

Fuselage optimization for short haul transport aircraft 02 p0181 A67-12199

Boeing model 747 aircraft /large capacity subsonic transport/ engine aerodynamics and design objectives [AIAA PAPER 66-821] 02 p0181 A67-12248

Aircraft structural design criteria and analysis methods, noting procedures which result in discrepancies between design loadings and actual flight test results [AIAA PAPER 66-881] 02 p0339 A67-12263

Objection to marine propeller application to VTOL aircraft 02 p0182 A67-12427

DC-9 aerodynamic design features and control systems [AIAA PAPER 65-738] 03 p0354 A67-12905

Aerodynamic design of Boeing 737 covering data of analytical studies, wind tunnel and flight tests, aerodynamic parameters and drag, flap system size, efficiency, wing geometry and handling qualities [AIAA PAPER 65-739] 03 p0354 A67-12906

Deep-stall characteristics of T-tailed aircraft configurations and recovery procedures, noting parameters of pitch-up, angle of attack, etc [AIAA PAPER 66-13] 03 p0350 A67-12912

Short-haul aircraft design for low direct operating costs, noting wings 03 p0357 A67-12968

Design principles for sailplane with glide ratio of 100 03 p0358 A67-12976

Lift-drag ratio, specific impulse, aspect ratio and weight of payload and power plant considered for STOL aircraft 03 p0358 A67-12980

Heligyro configuration in autogyro, helicopter and VTOL aircraft 03 p0359 A67-12987

C-5A aircraft design load criteria for landing gear of large aircraft that must operate from semimproved airfields [AIAA PAPER 65-711] 03 p0360 A67-13781

Manned hypersonic vehicle /MHV/ design, considering performance, shape, size, propulsion, etc 03 p0360 A67-13792

Supersonic transport design using double delta wing planform 03 p0360 A67-13918

Capabilities of passenger aircraft for short-range operations, noting design and economic suitability [AIAA PAPER 66-945] 03 p0361 A67-14022

Supersonic transport design using double delta wing planform 03 p0362 A67-14299

Vertical takeoff technology effect on aircraft design noting flexibility, reliability, decreased takeoff distance, etc 04 p0550 A67-14410

Design techniques for advanced flight structures providing statistical assessment of environmental loads, forecasts of high performance material response and higher reliability design criteria 04 p0707 A67-14423

Human engineering aspects of design of future military high performance aircraft, noting automatic control and display system requirements 04 p0562 A67-14535

Variable-sweep aircraft developments, design and problems [AIAA PAPER 66-983] 04 p0551 A67-14663

Simulation system and hovering vehicle prototype design for use in development of VTOL aircraft 04 p0600 A67-15540

Similarity constant variation method of aircraft design 04 p0552 A67-15892

V/STOL aircraft design evolution, discussing propeller and jet engine configuration, control surfaces and jets for attitude control 05 p0751 A67-16382

Variable geometry SST project and expected support program 05 p0752 A67-16753

Nondestructive test development to meet inspection requirements of advanced aircraft design, discussing titanium fusion and resistance spot welds and adhesive bonding honeycomb components 05 p0808 A67-17087

Man-computer graphics for computer aided design 05 p0768 A67-17514

Dual-purpose passenger/cargo aircraft noting design, passenger interior system, cargo handling system, compatibility, comparisons, etc 06 p0946 A67-18005

Flight testing Lear Jet Models XXIII, XXIV and XXV noting flutter, redundancy, hydroplaning, etc [AIAA PAPER 67-263] 07 p1130 A67-20086

VTOL capability in military and civil aircraft, discussing Italian and German efforts 07 p1130 A67-20122

Spin conditions for aircraft with nose-and tail-heavy longitudinal moment 07 p1130 A67-20148

VTOL technique and advanced aircraft design 07 p1130 A67-20220

Light aircraft design using fiberglass reinforced plastic primary structure for fibrous composite airframe 08 p1414 A67-20429

Aerodynamic design of Boeing 737 covering data of analytical studies, wind tunnel and flight tests, aerodynamic parameters and drag, flap system size, efficiency, wing geometry and handling qualities [AIAA PAPER 65-739] 08 p1279 A67-21043

Spin characteristic of fighter type aircraft investigated by using Kerr criteria, noting yawing velocity and recovery 09 p1439 A67-21836

Center of gravity in aircraft design and effects on performance 09 p1441 A67-22670

Aerodynamic design of swept wing-fuselage combination for cruising at transonic and supersonic speeds, noting pressure distribution role 10 p1589 A67-22872

Action of concentrated loads in plane problem of mechanics of deformable solids 10 p1715 A67-22921

Flexible sailplane designs allowing for towing cable analyzed with analog computer for gust loading 10 p1593 A67-23015

Reducing stress levels on crack propagation growth rate investigated for aircraft design problems 11 p1804 A67-24037

British aircraft one-eleven 500 series, detailing stretched version, flight tests to begin in August 1967 with aerodynamic prototype 11 p1743 A67-24039

Arava light twin-turboprop STOL transport aircraft operating from short rough airfield, noting wind tunnel results 11 p1743 A67-24213

Hypersonic transport design, considering payload vs range and weight and power plant, aerodynamic, structural and flight profile problems 11 p1744 A67-24579

Nondestructive testing in aircraft industry evaluated, considering role in aircraft structural design, crack detection, etc 11 p1799 A67-24654

V/STOL aircraft gas turbine systems, discussing propulsion system configurations applied to fighter, fighter attack and transport cargo aircraft [ASME PAPER 67-GT-48] 11 p1744 A67-24809

Simple and stress corrosion problems in aircraft design emphasizing protection of joints 12 p1954 A67-25127

Aerodynamic factors effect on airframe design and power plant selection for medium Mach twin turboprop business aircraft [SAE PAPER 670244] 12 p1894 A67-25499

Supersonic business jet designs, unswept trapezoidal wing model and delta wing model [SAE PAPER 670246] 12 p1895 A67-25501

Flutter characteristics of slab tail or stabilator installation, discussing prevention and design [SAE PAPER 670260] 12 p1895 A67-25509

Boeing SST inlet, control and power system development, discussing test program, design objectives and cost [SAE PAPER 670318] 12 p1990 A67-25886

DC-8 61, 62, 63 development, design and engineering 13 p2053 A67-26907

VTOL short-haul transportation design requirements and configuration characteristics 13 p2053 A67-27067

High performance aerodynamic vehicle design noting configuration variables, optimum performance parameters, vehicle force characteristics, optimization of hypersonic aircraft performance, etc [AIAA PAPER 66-486] 13 p2054 A67-27584

Liquid hydrogen for SST fuel compared with hydrocarbons, considering range, payload, weight, drag, engine design, storage and safety 13 p2186 A67-27635

F-111 crew escape module design and performance 14 p2244 A67-27739

Yak 40, Soviet three-engine jet airliner, for operation off short natural-surface airfields 14 p2245 A67-27893

Stress-strain problems in design load of commercial aircraft, noting role of frequency distribution curves 14 p2245 A67-28060

Magnification problems facing aircraft designers analyzed by computerized iterative procedures 14 p2245 A67-28062

Civilian aircraft electrical equipment design and construction including Caravelle and Concorde 14 p2252 A67-28568

Soviet book on pilotless aircraft and missiles covering jet engine design, automatic control, radio engineering and aircraft aerodynamics 15 p2564 A67-29242

Strike aircraft design noting weapons compatibility, use of analytical and scale testing techniques, etc 15 p2418 A67-29396

Influence of weapons on basic line, avionics, flight controls and handling

- qualities of future aircraft 15 p2418 A67-29397
- Optimum design safety for VTOL aircraft, noting noise and vibration elimination [AIAA PAPER 66-813] 15 p2419 A67-29411
- Book on aircraft design covering turboprop, subsonic turbojet, supersonic and water-based aircraft, missiles, helicopters, etc 15 p2419 A67-29417
- Hawker Siddeley 748 design noting utilization rates, maintenance costs and indefinite fatigue life 15 p2419 A67-29509
- Four combat aircraft designs /tailless delta, swept wing, variable geometry and VTO aircraft/ using same bypass engines /Pratt Whitney-SNECMA TF-306s/ 15 p2419 A67-29670
- Nondestructive determination of stress distribution in three-layer tempered glass aircraft windshield by scattered-light photoelastic method 15 p2575 A67-30033
- Jaguar, Franco-British military aircraft designed for combat training and tactical support during 1970s 15 p2420 A67-30127
- Boeing 727 QC aircraft development, manufacture, design objectives, cargo pallet system, seat pallet system, etc [AIAA PAPER 67-395] 15 p2421 A67-30362
- Boeing 747 characteristics for passenger and cargo service noting economic gain, operational performance, control cabin, engine, etc [AIAA PAPER 67-397] 15 p2421 A67-30364
- Automatic all-weather landing system design having integration of autopilot and flight director [AIAA PAPER 67-406] 15 p2516 A67-30373
- DC-9 environmental control design and first year service experiences [AIAA PAPER 67-407] 15 p2423 A67-30374
- Bell Model 266 composite VTOL aircraft, discussing tilting rotor principle for conversion from helicopter to aircraft 18 p2595 A67-30495
- Four engine STOL aircraft for short distance hauls, noting fuselage and wing design 16 p2595 A67-30601
- Wing pivoting design for supersonic aircraft adaptability to different flight conditions, noting experiments with F 111 16 p2590 A67-30839
- Transparent plastic materials for aircraft application, noting glass developments and thermal stress conditions 16 p2694 A67-30980
- Short-haul airliner /Fokker F-28 Fellowship/, noting moderate size, twin bypass engines, high speed, landing field requirements, etc 16 p2596 A67-31012
- Competition aspects of United States supersonic transport, discussing various aircraft designs 16 p2596 A67-31246
- Fokker F-28 Fellowship conceived as jet contemporary of turboprop Fokker Friendship, noting structural and operational details 18 p2597 A67-31561
- Concorde SST third and fourth flying prototypes described, discussing structural design, power plant, control systems, landing gear, etc 16 p2597 A67-31785
- Lighter-than-air, nuclear-powered dirigible described giving details on capacity, safety and mode of propulsion 16 p2597 A67-31787
- Composite aircraft performance potential, with helicopter comparison with compound-type aircraft, noting range, speed, weight, productivity, etc [AHS PAPER 110] 16 p2597 A67-31826
- Compound aircraft flying quality improvement methods, noting VTOL characteristic and high speed as compared to pure helicopters [AHS PAPER 111] 16 p2598 A67-31827
- Aircraft flotation requirements, emphasizing surface strength reduction 17 p2832 A67-31986
- Controls Development /CODE/ program for proving design validity of B2707 SST flight control and hydraulic systems prior to flight 17 p2795 A67-32004
- Tactical aircraft survivability in North and South Vietnam, discussing missile and interceptor ineffectiveness and limited-war considerations for aircraft 17 p2796 A67-32434
- Computer program for synthesizing and analyzing performance of preliminary designs of hypervelocity cruise vehicles 17 p2819 A67-32474
- Aircraft electric power systems and future use of solid state high power devices, integrated microcircuits and solid rotor generator 17 p2804 A67-32512
- Solid state switching applied to aircraft electric systems noting design, performance and contactless switching concept 17 p2825 A67-32513
- Capabilities of passenger aircraft for short range operations, noting design and economic suitability [AIAA PAPER 66-945] 17 p2797 A67-32583
- Aircraft fuselage design noting planning philosophy, parameters, future problems and considerations [SAE PAPER 670370] 18 p2985 A67-33568
- Supersonic transport size determination for competitive operation in air traffic market using traffic volume, aircraft type and flight frequency forecasts [SAE PAPER 670371] 18 p2985 A67-33569
- German SIAT 223 Flamingo sports, trainer and cross-country aircraft, noting design, components and tabulated technical data 18 p2985 A67-33641
- Exhaust gas recirculation for VTOL aircraft [AIAA PAPER 67-439] 18 p2985 A67-33916
- Hawker Siddeley 748 short-to-medium range civil transport aircraft design features including take off/landing field length, pressurized cabin, engines, payload, etc 18 p2986 A67-34074
- A-300 Airbus, economic subsonic passenger transport for short and medium ranges 18 p2986 A67-34075
- Structural design for gust loads on USAF aircraft based on continuous turbulence and failure probabilities 18 p2986 A67-34653
- Maintainability technology and controls developed during F-111 design 18 p2986 A67-34663
- A-7A aircraft maintenance guarantee and role of training 18 p2987 A67-34681
- Soviet collection of articles on aircraft engine strength and dynamics 19 p3234 A67-34870
- German VJ101C VTOL fighter aircraft design and testing, with description of engines and telemetric testing 19 p3173 A67-35522
- AH-56A weapons system design approach, detailing avionics subsystem 19 p3196 A67-35866
- IR technology influence on military aircraft design 19 p3173 A67-35932
- Hypervelocity vehicle volume decreasing method by applying dual-fuel concept [AIAA PAPER 67-559] 19 p3174 A67-35956
- Aircraft dynamics, Volume I, covering aircraft configuration, design problems, atmospheric properties, hydrodynamics, gasdynamics, boundary layer theory, etc 20 p3355 A67-36199
- Performance requirements and design aspects of variable sweep aircraft, examining swing pivot systems 20 p3361 A67-36498
- Supersonic transport variable sweep wing design, showing root glove and Mach number effects on aerodynamic center of strike aircraft 20 p3361 A67-36499
- Transall C 160 aircraft wings, fuselage, tail surfaces, landing gear and power units 20 p3361 A67-36633
- Aircraft fuselage shapes analysis for drag reduction and maximum useful space based on streamlined bodies found in nature 20 p3375 A67-36887
- Aircraft design by statistical methods, presenting samples for interceptor fighter, shorthaul jet and light twin-engine cargo aircraft 20 p3361 A67-37170
- Aircraft design automation using computer techniques by linking geometrical concepts to design parameters 20 p3455 A67-37246
- Commercial aircraft planning and design, considering technology, market environment and manufacturers desires and capabilities 20 p3556 A67-37446
- Aircraft structural design criteria and analysis methods, noting procedures which result in discrepancies between design loadings and actual flight test results 21 p3568 A67-38537
- Boeing model 747 aircraft /large capacity subsonic transport/ engine aerodynamics and design objectives 21 p3568 A67-38542
- Peripheral jet air cushion vehicle circular platform design, discussing dimensionless design parameter determination from operating height, translational speed and weight 22 p3745 A67-39726
- Boeing SST competition, cost, operation, design, airport noise and sonic boom 22 p3746 A67-39882
- Hatfield V/STOL tunnel design problems and tunnel model test results 22 p3780 A67-40063
- Handley Page Jetstream turboprop aircraft basic design requirements, emphasizing aerodynamic design philosophy 22 p3746 A67-40129
- Handley Page Jetstream load carrying structural design, materials employed and structural test program 22 p3746 A67-40130
- Computer aided techniques applied to structural analysis of aircraft noting design problems in aluminum fatigue life, unclad alloys, insulation and composite structures 22 p3915 A67-40331
- Cost Analysis Model - Parametric /CAMP/ computer method of estimating hardware and logistics life cycle costs for air vehicles in design stage 23 p4085 A67-40589
- Long range supersonic cruising aircraft research and design techniques, methods and approaches for optimizing efficiency, drag and ATC [AIAA PAPER 67-748] 23 p3987 A67-40982
- VFW/Flat joint project to develop single-seater fighter/reconnaissance aircraft noting structural design, power source and liftoff weight 23 p3934 A67-41255
- Wissenschaftliche Gesellschaft für Luft- und Raumfahrt, Annual Reports 1966 23 p3929 A67-41304
- Design characteristics of various SST, discussing Mach numbers and wing configuration 23 p3935 A67-41398
- Crack propagation rate and residual static strength of fatigue cracked Ti and steel cylinders for SST design data 24 p4247 A67-41943
- Short haul military requirements /1970-1980/, considering assault and logistic airlifts supporting ground forces and V/STOL aircraft [SAE PAPER 670827] 24 p4093 A67-41992
- DC-9 wing and high lift system aerodynamic design and development, discussing STOL field length design goals and flight test results [SAE PAPER 670846] 24 p4093 A67-41999
- Design and flying qualities of variable geometry aircraft, discussing wing pivot location and longitudinal stability characteristics [SAE PAPER 670879] 24 p4094 A67-42013
- Variable sweep wing aerodynamic problems in subsonic, supersonic and hypersonic aircraft design [SAE PAPER 670880] 24 p4094 A67-42014
- Variable sweep pivoted wing fighter aircraft structural and aerodynamic design considerations, noting journal bearing endurance and aircraft fatigue life [SAE PAPER 670881] 24 p4094 A67-42015
- Variable sweep wing aircraft mechanical design, control and actuation equipment and wing mounted system interconnects [SAE PAPER 670882] 24 p4094 A67-42016
- Wing pivot joint and actuation system configurations for SST variable geometry design [SAE PAPER 670883] 24 p4160 A67-42017
- Development, design and production phases of Canadair CL-215 water bomber and potential variants [SAE PAPER 670902] 24 p4094 A67-42020
- Design methods to combat fatigue effects on economics of civil aircraft, discussing structural weight role, maintenance, inspection, etc 24 p4250 A67-42441
- Fall-safe design, nondestructive testing and inspection facilities at design stage for aircraft structures 24 p4250 A67-42442
- Drag problems of Belfast aircraft solved by modifications developed in wind tunnel program 24 p4092 A67-42443
- Commercial V/STOL operating characteristics in Northeast Corridor, discussing commuter design and cost analyses [AIAA PAPER 67-769] 24 p4095 A67-42937
- Aircraft fuselages, wings, fillets, ducts and other free form surfaces defined using man-machine graphical interaction with computer [AIAA PAPER 67-895] 24 p4126 A67-43004
- Man-computer system for aircraft design and manufacture emphasizing graphic and analytical routines [AIAA PAPER 67-898] 24 p4127 A67-43007
- V/stol concepts for short haul commercial aircraft compared for gross weight, operating cost, gust sensitivity and noise

levels
[AIAA PAPER 67-938] 24 p4096 A67-43028
Emergency oxygen supply systems for aircraft, discussing simplicity, standardization, safety, reliability and maintenance
[AIAA PAPER 67-965] 24 p4110 A67-43043
Commercial VTOL transport compared with conventional aircraft and ground transportation, discussing design and operating costs
[AIAA PAPER 67-970] 24 p4097 A67-43048

AIRCRAFT DETECTION
SA RADAR AIRCRAFT DETECTOR
Ground monitoring system for ILS localizer signals reflected from landing aircraft 06 p0957 A67-17578
Blind height effect in radar measurements of aircraft cruising speed treated by repetition frequency 07 p1139 A67-19228
Control systems functions and programming approaches, Volume B, covering electronic data processing, factory automation and computer center administration 13 p2153 A67-26664
Aircraft detection and in-flight tracking by real time computers, assessing role in missile and satellite tracking 13 p2153 A67-26666
Problems involved in ditching business aircraft on ocean and subsequent recovery 14 p2245 A67-28319
Probability of overlapping intercept by system of random intercepts and application to detection of flying objects in cloudy skies 20 p3477 A67-37036
Devices to help pilot detection of aircraft evaluated for systematic relationship between detection functions under fixated conditions and in visual search 22 p3755 A67-39848

AIRCRAFT ENGINE
SA GAS TURBINE
SA JET ENGINE
SA TURBOCHARGER
Nonlinearities such as limitation of linear characteristics, dead band, hysteresis, etc, in aircraft gas turbine control system 01 p0011 A67-10167
Mathematical model for determining optimal maximum operating times for aircraft engines, using discrete failure rate to determine cost 01 p0141 A67-11340
By-pass propulsion systems development for V/STOL transports including aerothermodynamic aspects
[AIAA PAPER 64-606] 03 p0502 A67-12902
Comparison of piston engine with turbojet engine noting power-weight ratio, specific fuel consumption, performance characteristics, etc 03 p0502 A67-13005
Supercharging turbojet engine for light aircraft compared to piston and turbojet engines 03 p0502 A67-13006
General and mechanical property requirements for metal matrix composite materials used for aircraft gas turbine compressor blades 03 p0443 A67-13418
Soviet book on strength and dynamics of aircraft engines 03 p0526 A67-14068
VTOL power plant design noting jet deflection, lift fans, RB-162 engine, etc 04 p0687 A67-14435
Aircraft piston engine components reliability characteristics determined from defect data survey, using statistics 04 p0691 A67-15902
Aircraft engine design and economic pressures effect on development 06 p0949 A67-18735
Ground test facilities for aircraft air breathing propulsion system development 08 p1315 A67-21063
Load, vibration, temperature, surface oxides, etc, effect on wear resistance of materials for aircraft gas turbine engines 09 p1506 A67-22194
XV-4B vertical lift aircraft with lift engines noting stability, control, structural design, flight control system, etc 09 p1439 A67-22284
Temperature distribution in tail pipe of M 701 engine, based on differences between readings obtained from onboard thermocouples 09 p1560 A67-22463
Inductive sensor development for measurement of pressure, airspeed, altitude and acceleration during aircraft testing 09 p1501 A67-22465

Aircraft engine service life and reliability during series production, analyzing failure of parts 09 p1560 A67-22476
Precision rolling for fabrication of small gas turbine compressor blades for use in aircraft and stationary engines
[SAE PAPER 670095] 09 p1508 A67-22538
Aircraft gas turbine and fuel control design to meet engine requirement in broad environmental challenges
[SAE PAPER 670140] 09 p1560 A67-22541
Business jet aircraft engine design for increased service life, detailing turbine nozzles, bearings, rotors, etc
[SAE PAPER 670234] 11 p1851 A67-23981
Aircraft engine development and economic efficiency, discussing need for new fuels for rocket engines 11 p1853 A67-24630
High pressure hot gas solid propellant cartridge starter for aircraft turbine engine [ASME PAPER 67-GT-21] 11 p1854 A67-24803
Dynamic vibration in aircraft power plant components, noting responsiveness of parts and fatigue life evaluation
[SAE PAPER 670237] 12 p1989 A67-25495
Two-stroke cycle light aircraft engine with respect to competitive power plants 12 p1989 A67-25496
Lubricants for utility aircraft piston engines, cost, availability, compatibility, etc [SAE PAPER 670248] 12 p1989 A67-25502
Glass fiber reinforced composite materials for aircraft engine, discussing construction of bearing and compressor casings [SAE PAPER 670333] 12 p1958 A67-25874
Materials requirements for aircraft turbojet and ramjet engines 13 p2187 A67-26694
Mach 2 plus Olympus 593 turbojet power plant for Anglo-French SST, analyzing fuel system, lubrication and cooling on test run 13 p2187 A67-26701
Hydraulic, pneumatic and electric circuits for twin loop engine control system of Olympus 593 in Concorde SST 13 p2187 A67-26702
Aircraft engine reliability, considering local surface stresses, engine component distortion under load, vibration problems and material variability 13 p2188 A67-27000
Digital computer used for on-line control of jet engine 13 p2074 A67-27190
Technical, economic and operation criteria for airlines when switching from conventional engines to turboprops or turbojets 14 p2409 A67-28499
Fuel injection system used on aircraft engines noting system layout, advantages and disadvantages, fuel corrosion, etc 14 p2377 A67-28500
Test procedure and apparatus for evaluating oxidation-corrosion characteristics of aircraft gas turbine engine lubricants at high temperature 14 p2326 A67-28794
Reinforced plastics composites for jet lift engines 15 p2508 A67-29671
JT9D turbofan engine for Boeing 747 commercial transport aircraft, analyzing design and performance potentials [AIAA PAPER 67-374] 15 p2548 A67-30346
Rolls-Royce three-shaft turbofan engine vibration, number of parts and maintainability [AIAA PAPER 67-375] 15 p2548 A67-30347
Concorde SST third and fourth flying prototypes described, discussing structural design, power plant, control systems, landing gear, etc 16 p2597 A67-31785
Axial gear differential /AGD/ design and selection for constant speed AC generator drive for aircraft engines 17 p2800 A67-31976
Computer program for design and routing of external plumbing of aircraft gas turbine engines 17 p2928 A67-32006
Engine development and manufacture in Sweden 17 p2928 A67-32123
Film cooling theory applied to aircraft gas turbine chambers shows slot geometry effect as negligible 17 p2967 A67-32126
Book on design and structural strength of aircraft gas turbine engines covering inlet and exhaust systems, compressors, combustion chambers, rotors, etc 17 p2928 A67-32564
Engine nacelle location, size and shape effects on drag due to wing thickness and drag due to lift 17 p2791 A67-32567
[AIAA PAPER 68-665]
Design criteria and configuration for long-life aircraft gas turbines [SAE PAPER 670344] 17 p2929 A67-32988

Unscheduled civil aircraft power plant diagnostic removals evaluated by metal detection, performance deterioration, vibration, oil consumption and nonoperational categories [SAE PAPER 670358] 17 p2930 A67-32997
Data selection, collecting and processing for automatic performance recording and monitoring of aircraft gas turbine engine, considering hardware and software [SAE PAPER 670360] 17 p2835 A67-32999
Diagnostic devices for sensing performance deterioration and mechanical malfunctions in supersonic aircraft engines [SAE PAPER 670363] 17 p2930 A67-33000
Color contrast penetration method for crack detection in aircraft engines and motor car parts 18 p3045 A67-33739
Temperature measurement for aircraft gas-turbine engine development 18 p3157 A67-33898
Soviet collection of articles on aircraft engine strength and dynamics 19 p3234 A67-34870
Periodic stress and heating during creep, studying deformation adaptability of material for conditions experienced by aircraft engine components 19 p3338 A67-34885
Gasoline-injection system for aircraft engines noting construction details, economics, advantages, etc 19 p3312 A67-36052
Superalloys for SST engine, discussing materials properties, structures, turbine disk production, welding, alloy design, coating-base metal interactions, etc 20 p3469 A67-37358
Soviet papers on vibrations and strength of aircraft engine components 21 p3726 A67-38830
Reliability in aircraft engines from start of assembly to completion and delivery 22 p3867 A67-39285
Aircraft engine turbine structure effect on blade tip clearance, analyzing clearance variations as function of rotor angular velocity 22 p3868 A67-39548
Unscheduled civil aircraft power plant diagnostic removals evaluated by metal detection, performance deterioration, vibration, oil consumption and nonoperational categories [SAE PAPER 670358] 23 p4048 A67-40866
PT6 series of small shaft turboprop engines for STOL aircraft and high speed surface vehicles noting performance and environmental tolerance improvements [AIAA PAPER 67-744] 23 p4048 A67-40978
Soviet studies of Ni- and Fe-based heat resistant aging alloys and aircraft gas turbine technology 24 p4169 A67-41919
SST engines design, combustion and thrust augmentation systems, engine controls and complications facing users [SAE PAPER 670865] 24 p4207 A67-42005
Fastener applications for gas turbine engines noting materials selection and design 24 p4160 A67-42079

AIRCRAFT EXHAUST
Fuel additives investigated for jet engine exhaust smoke elimination [SAE PAPER 670866] 24 p4206 A67-42006

AIRCRAFT FUEL
High temperature stability of SST turbine fuel samples from refineries and airports [SAE PAPER 660710] 01 p0139 A67-10624
Fuel requirements for high altitude high-Mach number aircraft noting thermal stability, autooxidation, self-ignition, specific heat, etc [DVL-599] 03 p0502 A67-13015
Technical characteristics of Peschanyi Island oil and feasibility study of technological process for aviation oil production 04 p0627 A67-14742
Emulsified fuel effect on gas turbine combustors, noting good operation in low altitude flight but inhibited combustion at start and at high altitudes [SAE PAPER 670366] 12 p1987 A67-25884
Aviation fuels and requirements that refineries must meet 13 p2185 A67-28862
Liquid hydrogen for SST fuel compared with hydrocarbons, considering range, payload, weight, drag, engine design, storage and safety 13 p2186 A67-27635
Future supersonic and hypersonic aircraft horizontal liquid hydrogen fuel tank requirements, discussing insulation optimization using variable thickness 13 p2054 A67-27657

Aircraft fuel explosion problem, analyzing mechanism of lightning-induced explosions and discussing protection methods 16 p2597 A67-31810

Fuel emulsions for helicopters to minimize hazards associated with liquid fuel, discussing composition, stability, corrosion and flow properties [SAE PAPER 670364] 17 p2927 A67-33001

Generation and loading of triple point hydrogen for high performance aircraft, boosters and spacecraft [AIAA PAPER 67-468] 18 p3110 A67-33938

Parametric analysis on hydrogen-fueled hypersonic aircraft for long range passenger transport missions and launch vehicle missions, noting propulsion system-airframe interactions [AIAA PAPER 67-493] 18 p2985 A67-33957

Gelled, emulsified and otherwise thickened fuels for aircraft fire safety, discussing requirements and engine operation [AIAA PAPER 67-503] 18 p3110 A67-33967

Fuel requirements for Concorde SST stressing flame luminosity, radiant heat, spontaneous ignition, fuel viscosity and density 18 p3110 A67-34533

Aircraft fuel tank pressurization, discussing pressure supply sources and control system, tank venting, system integration and equipment used 21 p3571 A67-38104

SST aircraft influence on fuel quality requirements, considering use of liquefied gaseous hydrocarbon fuels 21 p3688 A67-38192

AIRCRAFT FUEL SYSTEM

Aircraft fuel tank pressurization and venting systems, evaluating refueling, defueling, inerting systems, recuperators and system integration 04 p0554 A67-14883

Mathematical model of aircraft nucleonic fuel gauging facility system allowing performance evaluation and optimization by computer techniques 05 p0842 A67-16542

Test rig for fuel system in Concord aircraft noting construction, control system, equipment, installation and operation 10 p1623 A67-23548

Aircraft fuel gauging systems noting float type and reliability defects [SAE PAPER 670263] 11 p1789 A67-23986

Concorde aircraft fuel, discussing fuel transfer, problem of boiling, in-flight environment simulation, payload/mass ratio, etc 16 p2734 A67-31809

Apron underground fueling systems, using experience in aircraft fueling to justify reduction or elimination of hydrant servicer vehicles 22 p3779 A67-39380

Microbial contamination of jet aircraft fuel systems [SAE PAPER 670869] 24 p4206 A67-42007

AIRCRAFT GUIDANCE

Navigational satellite in aiding ships and aircraft in positioning, meteorology, communications, search and rescue, etc 01 p0111 A67-11390

Monograph on system philosophy of automatic learning systems in application to autopilots, discussing man-aircraft system cybernetics, human behavior, environmental effects, etc 02 p0186 A67-12084

Control method excluding static and dynamic stability aspects of aircraft from guidance problem 03 p0464 A67-13003

Autopilot programmer design for automatic guidance in approach and stabilization along course of aerial photography aircraft 03 p0465 A67-14284

Aircraft radio guidance system combining ILS and precision approach radar 04 p0653 A67-15042

Automatic star trackers for long range aircraft navigation, discussing instrumentation methods and use of pulse code modulation for sensor design 04 p0655 A67-15661

Astronomical Guidance System for Air Navigation which detects altitude and azimuth errors resulting from precomputed and preadjusted deviations 04 p0655 A67-15666

Cruise error analysis for strapdown inertial navigation system with pulse torqued instruments in presence of small amplitude oscillations 06 p0947 A67-18007

Evaluation of minimum-time courses for aircraft and inherent error 07 p1222 A67-19680

Omnigraph airborne navigation equipment

with small digital computer and closed loop display 09 p1528 A67-22389

Omega receiver navigation set for high performance aircraft lane-position resolution 09 p1528 A67-22391

Aircraft inertial navigator performance estimation techniques 09 p1528 A67-22392

En-route guidance system using ILS localizer techniques for both en-route navigation and landing 09 p1528 A67-22634

High integrity guidance for approach and landing, noting VHF ILS system and downwind antenna system 09 p1529 A67-22638

Doppler radar and Doppler navigation system capabilities, applications, cost and reliability for supersonic and subsonic aircraft [SAE PAPER 670328] 12 p1964 A67-25870

Proposed worldwide navigation, communication and traffic control system for all weather to guide aircraft and vessels, locate distressed vehicles and direct rescue operations at sea [AAS PAPER 67-102] 15 p2515 A67-29957

Observed nonstationarity of low frequency radar echo envelope correlation with aircraft motion relative to receiver 16 p2625 A67-31273

Switching surface construction using one to one correspondence between points in controllability region and points on surface of nth order system 20 p3410 A67-37230

Aircraft tracking problems in airport approach zone solved using cameras, descriptive geometry and vector computations 21 p3568 A67-38809

AIRCRAFT HAZARD

Radioactive contamination of high flying aircraft, discussing empirical observations and possible decontamination procedure 05 p0751 A67-16300

Soviet book on aeronautical meteorology noting atmospheric conditions, clouds, ice formation, flight data utilization, Soviet Civil Aviation services, etc 07 p1220 A67-19579

Fuel system design criteria, discussing ways of reducing postcrash fires in aircraft 08 p1279 A67-20610

Lightning strikes on aircraft in flight from 1949 to 1966 12 p1896 A67-26170

Disease vector transport by aircraft as international health hazard 15 p2429 A67-29284

Bird hazard to aircraft at Auckland International Airport, examining geographical features, history, species, daily movement patterns and seasonal abundances 15 p2419 A67-29672

Tactical aircraft survivability in North and South Vietnam, discussing missile and interceptor ineffectiveness and limited-war considerations for aircraft 17 p2796 A67-32434

AIRCRAFT HYDRAULIC SYSTEM

Pump loop testing and operational evaluation of SST hydraulic fluids [SAE PAPER 660664] 01 p0103 A67-10572

Single point charger design for A-7A aircraft fluid power accumulators 02 p0182 A67-11843

Simplified neutron activation technique for analyzing metallic wear from aircraft hydraulic systems, computing activities of desired radiolotopes by cookbook procedure 02 p0249 A67-12221

Fatigue testing facility for tubings in aviation hydraulic systems 02 p0231 A67-12447

Effect of internal fluid pressure and installation inaccuracies on fatigue resistance of line connections for aircraft hydraulic and gas systems 02 p0184 A67-12448

Cavitation erosion in Hawker Siddeley Trident hydraulic system and steps to find solution 05 p0753 A67-16748

Cost and power requirements influence on aircraft hydraulic pump design 05 p0753 A67-16751

Aircraft equipment retrieval after long term storage for periods of up to 23 years under jungle, desert and arctic environment, discussing sealing and hydraulic systems [AIAA PAPER 67-185] 06 p0951 A67-18487

Exothermically brazed tubing joints for XB-70 hydraulic system 07 p1190 A67-19212

Leaks in hydraulic system of Hawker Siddeley Trident jet transport due to cavitation erosion 07 p1132 A67-20149

Extension fittings for A-7A bomber having hydraulic system with no flexible hose 09 p1442 A67-21659

Management of aircraft hydraulic vacuum, deicing system and pneumatic

components 09 p1581 A67-22127

BAC 111 hydraulic system, discussing service experience, reliability, maintenance, performance characteristics, etc 09 p1444 A67-22128

Hydraulic system of Boeing 737 jet transport, noting flight safety and system reliability throughout design 09 p1444 A67-22129

C-5A hydraulic system design for high power and capacity application, noting landing gear and ramps 09 p1444 A67-22130

Aircraft hydraulic systems contamination by particles from wear or external sources 09 p1445 A67-22131

Closed compartment fire-resistance test for hydraulic fluids leaking near heated aircraft skin with or without electric arcing 09 p1521 A67-22245

Fire hazard testing of hydraulic fluids, coolants and lubricants in aircraft with reference to SST hot wing compartment conditions 09 p1521 A67-22246

Spontaneous ignition temperature of flammable fluid in facsimile high speed aircraft hydraulic system 09 p1521 A67-22249

Resistance of aviation hydraulic fluids, mineral, snuffer, phosphate ester, siloxane and chlorosilicone to wheel brake fires, evaluating lab test techniques and simulation testing 09 p1521 A67-22250

Design problems for hydraulic loading circuit with random variation of loading with time 09 p1451 A67-22472

Jet aircraft lubrication oil application and degradation factors 10 p1597 A67-23411

C-5A flight control system, examining subsystems, handling qualities, hydraulic power distribution and mechanical failures 17 p2794 A67-31997

Controls Development /CODE/ program for proving design validity of B2707 SST flight control and hydraulic systems prior to flight 17 p2795 A67-32004

Hydraulic tubing permanent joints, made by induction-brazing method, for installation on A-7A Corsair II aircraft 17 p2801 A67-32007

Weldable tube fittings, welding equipment and inspection methods for connecting tubing in aircraft and aerospace hydraulic systems 17 p2864 A67-32008

Hydraulic design of Japan YS-11 twin turboprop transport aircraft, noting component accessibility and ground service simplification 19 p3175 A67-34787

Fokker F-28 aircraft systems fuel system, auxiliary power unit, hydraulics, flight controls, pressurization and electrical systems and avionics 19 p3176 A67-35559

Improved filtration techniques for aircraft hydraulic systems, noting high pressure filter unit using paper-based element for ground service 20 p3418 A67-37169

Air-oil separator for aircraft hydraulic system stops nose wheel shimmying, based on lowering pressure principle and using filter screen barrier 24 p4099 A67-42427

Filters in commercial aircraft hydraulic systems, discussing cleaning methods including ultrasonics 24 p4109 A67-42710

AIRCRAFT INDUSTRY

Future prospects of aeronautical construction in Europe 01 p0168 A67-10264

System effectiveness critical activities covering reliability, maintainability, quality, design guides, etc, for aerospace industry 01 p0170 A67-11333

Future prospects of aeronautical construction in Europe 03 p0537 A67-12966

Book on thermal effects and cutting machinability of aircraft materials 03 p0427 A67-13190

Thermal field of cutting area of aircraft structural material analyzed, using differential equations of thermoconductivity 03 p0427 A67-13191

V/STOL military transports purchase decisions based on analyses of operational employment, engineering design and economic utility 04 p0551 A67-14803

Measuring and calculating methods in testing of aircraft - Conference, Prague, April 1966 09 p1500 A67-22453

Design, production and experience of bonded structures in Europe for aerospace applications 09 p1577 A67-22511

Nondestructive testing in aircraft industry evaluated, considering role in aircraft structural design, crack detection, etc 11 p1799 A67-24654

Management methods in military equipment development to be used with aircraft 11 p1885 A67-24655
Aerospace company management characteristics and problems 12 p2041 A67-25742
DC-8 61, 62, 63 development, design and engineering 13 p2053 A67-26907
Use of computer in aircraft design problems 13 p2074 A67-27191
Aluminum and aluminum alloys in aircraft and aerospace industry 14 p2323 A67-27817
Behavior study of titanium alloys of interest to aeronautics industry, stressing creep resistance 14 p2338 A67-28628
Analysis of management methods applicable to aerospace industry, considering introduction of integrated information systems 15 p2583 A67-29669
Transparent plastic materials for aircraft application, noting glass developments and thermal stress conditions 16 p2694 A67-30980
Fusion-and resistance-welding techniques used in aircraft industry, discussing tungsten-arc and electron-beam welding principles 18 p3053 A67-33431
Air traffic control delays, terminal congestion and inadequate ground transportation facilities effect on regional airline operation 19 p3348 A67-34972
Aviation and transportation system - Progress, profits and public interest - Conference, Hartford, December 1966, Panel 4, Aviation and public policy 19 p3348 A67-34975
Potential capital and profits growth in air transportation, discussing government, management and industry 19 p3348 A67-34978
Properties of adhesive bonding compared with spot welding and riveting in aircraft industry 19 p3336 A67-35821
Space activity and research in industry noting European participation, international cooperation /ELDO program/ and research organizations 20 p3556 A67-37184
Planned introduction of Boeing 747 into airline service noting advances in technology for passenger comfort, cargo handling and rate reduction 20 p3361 A67-37443
Commercial aircraft planning and design, considering technology, market environment and manufacturers desires and capabilities 20 p3556 A67-37446
Block diagram, schematic circuit and amplitude and frequency characteristics of wideband transistorized amplifier for studying high speed aircraft industrial processes 21 p3600 A67-38918
Technological and economic factors affecting airline progress, discussing fares, traffic, SST and terminal areas 22 p3922 A67-40062
Cost comparisons between UK aircraft industry and competing industries elsewhere 22 p3922 A67-40065

AIRCRAFT INSTRUMENTATION

SA ALTIMETER
SA APPROACH AND LANDING INSTRUMENT
SA FLIGHT INSTRUMENT
SA FLIGHT LOAD RECORDER
SA GAUGE
SA LANDING AID
SA POSITION INDICATOR

Implementation of air data computers with solid state transducing and computing techniques 01 p0029 A67-10667
Mark XII and XIV microcircuit computers for real-time navigational computation on military and civil aircraft 01 p0029 A67-10668
Miniaturized magnetic-type mass spectrometer for multigas analysis in high performance aircraft 01 p0068 A67-10957
Mobile model test rigs and model instrumentation for CL-84 V/STOL aircraft 01 p0073 A67-11120
Triplex flight control system for VTOL aircraft noting new servomotor, simple mechanical construction and increased reliability 02 p0284 A67-12206
Terrain relief appearance on aircraft radar determined from radar parallax and shadow parallax 02 p0239 A67-12539
Aerospace Instrumentation - ISA National Symposium, Los Angeles, October 1965 03 p0395 A67-13377
Short wave and very short wave direction finding from aircraft 03 p0465 A67-13394
Cardan error of directional gyro on rocking base, with application to

aircraft 03 p0425 A67-14281
Medical research in glider plane noting airborne electrocardiograph 04 p0563 A67-14630
Electronic display in flight instrumentation, with reference to integrated flight system, qualitative and quantitative displays and qualitative-quantitative combinations 06 p1000 A67-17598
November 12, 1966 total eclipse observation from aircraft flying in moon shadow, describing instrumentation and results 06 p1004 A67-18383
Pilot-aircraft compatibility in landing approach 07 p1136 A67-19888
Aerial barometric altitude measurement improvement and residual error reduction 07 p1190 A67-20289
Aircraft sensor systems, discussing recording and evaluation tasks and performance characteristics 09 p1501 A67-22454
Aircraft instrumentation for oceanographic measurement platform including radiation thermometer, wave meter and expendable bathythermograph [AIAA PAPER 66-695] 09 p1441 A67-22498
Aircraft UHF radio system for distance measurements between airplane and two ground stations, noting onboard antenna 11 p1793 A67-24863
Multifunction airborne radar instruments, discussing air to air, air to ground, shared aperture and combined systems, spoiled beam technique for ground mapping, etc 11 p1754 A67-25007
Accelerometer use for operational load measurements in aircraft, emphasizing automatic counting 11 p1880 A67-25059
Airborne weather radar for general aviation aircraft, considering transmitter power, wavelength, target area, reflectivity characteristics, installation limitations, etc [SAE PAPER 670252] 12 p1905 A67-25503
Electronics package for category II qualified jet business aircraft and function of system components [SAE PAPER 670254] 12 p1941 A67-25504
Instrumentation and fuel systems for turbocharged and/or pressurized aircraft, discussing vapor lock problem, hydrocarbon fuels and vapor pressure equipment [SAE PAPER 670282] 12 p1899 A67-25510
Medical/human factors affecting pilots during atmospheric turbulence 13 p2064 A67-27262
Aircraft engine parameter control by onboard recording 14 p2315 A67-28059
Required safety standards for selection of commuter airlines and contracted flying 14 p2245 A67-28318
Panel layout for rectilinear instruments 14 p2257 A67-28661
Sensors and sensor control devices for use in high speed low altitude reconnaissance aircraft 15 p2485 A67-29162
Aircraft flow meters for simultaneous rate and volume measurements, examining equations of motion 16 p2871 A67-31006
Method to extend operation range of FM altimeters, with block diagram of proposed system 16 p2876 A67-31274
Sensor and calibration techniques for measurement of infrasonic and gravity waves noting error control and possible applications 16 p2877 A67-31430
Calibration system for PRESS optical aircraft program utilizing portable collimators 16 p2879 A67-31796
Avionics equipment development for Cayuse helicopter, discussing design with respect to weight, size, maintainability and other logistical considerations [AHS PAPER 105] 16 p2680 A67-31822
Aircraft mounted recording accelerometers for excessive turbulence compared with direct turbulence measurement 17 p2798 A67-32700
Flight instrumentation aiming at improving safety of approach and landing of commercial aircraft [SAE PAPER 670327] 17 p2860 A67-32983
Noise discrimination microphones in aircraft, discussing performance characteristics, design, construction, applications, clarity, size, etc 18 p2994 A67-34399
Digital computing complex optimum configuration for future aircraft, discussing

computer role 19 p3186 A67-35311
Data processing using digital computer, multiplexing and analog-to-digital conversion equipment for flight control and evaluation 20 p3390 A67-36465
Performance characteristics of XB-70 flight test data acquisition system 20 p3442 A67-36467
Visual display for aircraft, presenting simplest visual picture compatible with current pilot task 20 p3375 A67-36873
Design and operation of various recording instruments /speedobarographs/ for simultaneous measurements of aircraft altitude and speed 22 p3798 A67-39550
Handley Page Jetstream aircraft major systems, auxiliary equipment and instrumentation 22 p3748 A67-40132
Light Observation Helicopter Avionics Package /LOHAP/, designed for OH-6A Cayuse helicopter, providing communications and navigational capabilities 23 p3980 A67-40927
Alkaline concentrator appears superior to acid and solid units for possible onboard generation of oxygen 23 p3963 A67-41543
Installation problems of head-up displays in commercial aircraft 24 p4152 A67-41886
Actinometric measurements from aircraft of short wave radiation fluxes and radiation balance, determining absorption coefficient for clouds and true albedo 24 p4182 A67-42882

AIRCRAFT LANDING

Parameters to be calculated in checking airport possibilities for accommodating IL-18 aircraft, considering maximum takeoff weight 03 p0360 A67-13780
Dynamics of commercial aircraft seats with viscous dampers and elastic couplings during crash landing [ASME PAPER 66-WA/SAF-1] 04 p0551 A67-15329
Low clouds effect on ILS jet landing at Bombay airport during monsoon season, noting airfield climatology data 05 p0838 A67-16711
Buckling isolator system for carrier aircraft landing and catapult shock environment allowing use of available clearance for dynamic deflection 05 p0814 A67-17459
Airport lighting for category II landings with aid of all-weather landing systems by following ICAO guidelines, noting threshold markings, runway lights, etc 07 p1167 A67-20150
Correlation between heart rate, landing error and field of view for binocular and monocular sphere of vision of jet pilots 09 p1455 A67-21717
Carrier-landing improvements in Fresnel lens optical landing system, emphasizing compensated-meatball stabilization [AIAA PAPER 65-791] 09 p1441 A67-22494
Ground integrity monitor for category III ILS for use with automatically landing aircraft 09 p1529 A67-22644
OV-10A aircraft testing in landing and takeoff from fields, jungle clearings and primitive roadways 10 p1594 A67-23391
Measurement of torsional fatigue loads on aircraft undercarriage under service conditions 11 p1880 A67-25057
Instrumentation development making it possible to land safely under poor visibility conditions, goal being zero-zero landing 14 p2347 A67-28990
Airplane automatic-flare system actuating flaps and elevators as lift and moment controllers 15 p2418 A67-29313
All-weather landing for civilian aircraft, discussing equipment, terminology used and low visibility flight simulation 17 p2795 A67-32122
Defogging procedure for all-weather aircraft landing, with operational results 18 p3021 A67-34608
Microwave direction-finding receiver with digital output for blind aircraft landing and navigational uses 19 p3254 A67-35551
Instrument-landing system including microwave apparatus 19 p3255 A67-35807
All-weather landing examined in terms of operational techniques and design criteria for airline performance and safety [AIAA PAPER 67-572] 19 p3258 A67-35968
Flare and landing performance of glide vehicles with low lift-drag ratio, noting aerodynamic characteristics effect [AIAA PAPER 67-575] 19 p3335 A67-35970

Criteria for determination of minimum usable approach speed for landing of carrier based aircraft
[AIAA PAPER 67-578] 19 p3175 A67-35973
Bad weather landing of VTOL aircraft noting landing profiles, meteorological parameters and control system 20 p3361 A67-36455
Visibility in warm fog produced in cloud chamber by seeding with sodium chloride particles, with application for aircraft landing clearance 22 p3828 A67-39338
Pilot and automatic control function coordination in piloting and landing aircraft, discussing precision problems, safety and development of new processes 22 p3831 A67-39750
Visual aspects of carrier landing, discussing research program to evaluate pilot ability to make critical visual judgments 22 p3755 A67-39847
Night and day carrier landing pilot performance, noting altitude position estimation inaccuracy as contribution to higher accident rate 23 p3968 A67-41618
Air Force undershoot and overshoot experience examined to establish relative frequency, historical trend, associated variables and human factors 23 p3970 A67-41701

AIRCRAFT MAINTENANCE

State-of-the-art trainers for military applications, airborne trainers, aerospace ground equipment, aircraft weapons control system trainer and ground crew training devices 01 p0049 A67-10532
T-38 pilot trainer with mandatory stability control characteristics to meet current supersonic aircraft requirements [AIAA PAPER 66-798] 01 p0009 A67-10536
Aerospace ground equipment requirement determination prior to aircraft flight test and operational use [SAE PAPER 660700] 01 p0049 A67-10594
Self-contained semiautomatic and automatic onboard checkout systems for aircraft [SAE PAPER 660701] 01 p0010 A67-10595
Optimized distribution of personnel reduction in naval overhaul and repair activities with minimum reduction in readiness 01 p0016 A67-10932
Corrosion control requirements of P-3 Orion aircraft, including six steps to corrosion control and remedial measures 01 p0011 A67-11012
Reliability and maintainability requirements and electronic systems division /AFSC/ application 01 p0042 A67-11368
Distribution of maintenance manhour intervals for tasks on military aircraft compared with logarithmic normal distribution, presenting histograms and cumulative distributions 01 p0171 A67-11382
Accomplishments and costs of airline flight recording for aircraft maintenance 03 p0420 A67-13380
SST servicing and maintenance characteristics and suitability of existing and planned airports 03 p0360 A67-13919
Long-haul transport aircraft structural considerations and effect on operating empty weight and on airframe maintenance [AIAA PAPER 66-882] 03 p0361 A67-14019
Proposed system for maintaining helicopters in close-order formation during inclement weather and/or night operations 05 p0839 A67-16531
Aircraft exfoliation corrosion, discussing methods for prevention in fastener holes 07 p1210 A67-20087
Structural predictions of mean times between failures through maintenance activity for aircraft power systems 09 p1580 A67-22287
Integral fuel tank maintenance, summarizing tank-sealant repair data 09 p1442 A67-22678
Lockheed C-5 quantitative maintainability program and application to air vehicle utilization and cost effectiveness 11 p1745 A67-24939
Electronic package design for rugged military field service 12 p1911 A67-25268
Nondestructive testing techniques for turbojet engines noting advantage of planned inspection [SAE PAPER 670339] 12 p1950 A67-25876
Systems and techniques in aircraft maintenance to meet problems of parts reliability, longevity and shop cost

[SAE PAPER 670338] 12 p1895 A67-25877
Aircraft technician training levels, methods and equipment analysis indicating need for specialty training equipment development 13 p2091 A67-27266
Estimating maintenance man-hours per flight hour for business turbojet airplanes [SAE PAPER 670228] 13 p2053 A67-27294
Required safety standards for selection of commuter airlines and contracted flying 14 p2245 A67-28318
Data reduction with maintenance recording system onboard BAC 111 aircraft, noting use of automatic mode initiation logic, data compression, etc [AIAA PAPER 67-377] 15 p2420 A67-30348
Multiparameter recording on DC-9 jet aircraft for advancing maintenance techniques, discussing use in engine, fire warning and air conditioning systems performance [AIAA PAPER 67-378] 15 p2420 A67-30349
Aircraft radiography for turbojet engine integrity and serviceability determination [AIAA PAPER 67-380] 15 p2494 A67-30350
Gulfstream II maintainability program, examining support department responsibility, insurance and material support [AIAA PAPER 67-383] 15 p2421 A67-30352
Trace /tape controlled recording automatic checkout equipment/ system design to accommodate aircraft ground support task 16 p2635 A67-30834
Battery charger system for aircraft application noting nickel-cadmium battery, logic circuitry, wide environmental operation conditions, etc 17 p2804 A67-32515
Boeing SST maintenance requirements considered in terms of aircraft characteristics, economics, facilities, operations, etc [SAE PAPER 670373] 17 p2798 A67-33003
Maintainability technology and controls developed during F-111 design 18 p2986 A67-34663
A-7A aircraft maintenance guarantee and role of training 18 p2987 A67-34681
Fokker F-28 aircraft features for minimum turnaround time, noting self-sufficiency provided by auxiliary power unit 19 p3173 A67-35558
Gate arrival terminal design for Kansas City MCI airport noting loading positions, maintenance hangars, service roads, post office, etc 22 p3779 A67-39375
Book on inspection, construction, operation, maintenance and repair of aircraft and aerospace vehicles including metal, steel frames, wood structures and high temperature structural material 22 p3811 A67-39441
Air Force accident history noting importance of maintenance/material area 22 p3754 A67-39598
Null-field static dischargers location and maintenance on Convair 880/880M and 990 aircraft 22 p3745 A67-39733
Logistics simulation modeling for optimizing spares mix needed for maintenance of airborne systems at minimum cost 23 p4085 A67-40590
Wing pivot joint and actuation system configurations for SST variable geometry design [SAE PAPER 670883] 24 p4160 A67-42017
Aircraft fasteners, airline operation and maintenance requirements and improvement of standardization 24 p4161 A67-42082
Maintenance schedule for small commercial aircraft fleet, periodic inspection check principles and engine reliability program 24 p4094 A67-42277
VTOL aircraft operational expense estimation using standard method, measuring maintenance costs in various planning stages and in operation [AIAA PAPER 67-828] 24 p4096 A67-42974
Time factor in onboard checkout and in-flight maintenance of manned spacecraft, discussing mission events and man-machine interaction [AIAA PAPER 67-950] 24 p4245 A67-43034
Emergency oxygen supply systems for aircraft, discussing simplicity, standardization, safety, reliability and maintenance [AIAA PAPER 67-965] 24 p4110 A67-43043

AIRCRAFT MODEL
Automatic three-dimensional model measuring machine using data programming for aircraft contour

measurement 05 p0811 A67-17047
Three-dimensional flutter calculations verification by wind tunnel results, using flexible supersonic aircraft planform model of determined characteristics to control calculations 10 p1622 A67-22882
Construction and operational possibilities of gimbal mounted servo-controlled aircraft model for optical simulation of flight mechanical motions 18 p3019 A67-33458
Exhaust gas recirculation for VTOL aircraft [AIAA PAPER 67-439] 18 p2985 A67-33916
V/STOL aircraft model wind tunnel tests on wing and propellers, describing strain gauge balances 22 p3745 A67-39728
Safety device to prevent overloading of models and sensitive wire strain gauge balance by aerodynamic forces during starting and switching off in wind tunnel 22 p3780 A67-39756
Aircraft flutter characteristics calculated from electromechanical analog using elastic mass vibration model and analog computer 22 p3746 A67-40451

AIRCRAFT MULTIPURPOSE TEST EQUIPMENT /AMTIDE/
Automatic testing and fault-isolation capabilities in advanced avionics systems 01 p0034 A67-10272
Avionic computer testing and fault-locator of weapons systems and system control 01 p0034 A67-10273

AIRCRAFT NOISE
Public airport noise problem, examining extent to which constitutional-taking theory has been usual ground for damage suits 01 p0170 A67-10929
Measurement and control of corona-generated noise in aircraft, noting charge rate during takeoff via potential gradient method 02 p0190 A67-11501
Jet aircraft noise alleviation problems near national airports noting noise limits fixations, engine noise reduction, steeper takeoff and landings, etc [AIAA PAPER 66-909] 02 p0181 A67-12274
VTOL jet transport noise effect on surrounding habitants and guidelines for airport design 03 p0357 A67-12973
Aircraft noise characteristics and relationship to Lockheed SST design 03 p0360 A67-13920
Near field and far field sonic boom signature of supersonic transport, noting structural response 03 p0360 A67-13921
Interactions among technical, economic and political aspects of aircraft noise problem, examining relation between thrust and jet engine noise 03 p0539 A67-14384
Aircraft noise measurement evaluation and control, discussing monitoring and mapping 04 p0551 A67-14591
Large scale experiment on aircraft noise involving 148 subjects listening to sounds of aircraft flying overhead 04 p0552 A67-15576
Global examination of growth of aircraft noise nuisance in vicinity of airports, determining index of community nuisance 05 p0751 A67-16385
Government agencies activity in dealing with alleviation of aircraft noise 05 p0929 A67-16386
Aircraft noise control at international airports with special reference to Heathrow 05 p0752 A67-17101
Electromagnetic noise effect on aircraft examined, using fuselage mounted monitoring antennas 05 p0768 A67-17533
Noise and loading actions on helicopters, V/STOL aircraft and ground effect machines - Symposium, University of Southampton, August-September 1965 06 p0945 A67-17905
Lifting rotor-propeller noise prediction for military helicopters and V/STOL aircraft in forward flight 06 p0945 A67-17909
Helicopter blade slap noise as induced by blade passing through tip vortex shed by another blade 06 p0946 A67-17910
Hingeless-rotor structural loads and dynamics research 06 p1099 A67-17911
External noise characteristics of lifting systems for VTOL aircraft 06 p0946 A67-17912
Hovercraft noise problem compared with surface transport, noting siting of terminals and noise reduction techniques 06 p0946 A67-17915
Helicopter rotor noise prediction and investigation using three-bladed Wessex rotor mounted on whirl

- tower 08 p1278 A67-20478
 Jet engine noise sources, discussing noise radiation patterns, penalties for improved specific fuel consumption, etc 09 p1559 A67-21701
 Global examination of growth of aircraft noise nuisance in vicinity of airports, determining index of community nuisance 09 p1439 A67-21702
 Aircraft noise characteristics and relationship to Lockheed SST design 09 p1439 A67-21703
 Acoustic noise and control - Conference, London, January 1967 09 p1532 A67-21937
 Human response to comparative sounds from aircraft and objective measurement of reference sound, determining acceptable noise levels 09 p1456 A67-21940
 Automatic aircraft-noise monitoring equipment at Frankfurt airport to measure noise levels during takeoff and maintain them within regulations 09 p1484 A67-21941
 Methods to minimize sonic boom ground exposure, considering aircraft design and maneuverability as function of altitude 09 p1439 A67-21942
 Cabin noise in aircraft, discussing measurement techniques for sonic boom, shock wave intensity, etc 09 p1440 A67-22467
 Lower bounds for sonic boom intensity from slender aircraft flying straight and level at supersonic speeds 10 p1594 A67-23470
 Near field and far field sonic boom signature of supersonic transport, noting structural response 11 p1743 A67-24038
 Aircraft noise monitoring system for Zurich airport 13 p2052 A67-26535
 Aircraft noise and siting of major airport 13 p2089 A67-26536
 Aircraft noise acceptability criteria noting political-legal aspects 13 p2053 A67-26537
 Aircraft noise regulation at Kennedy International Airport 13 p2053 A67-26538
 Research approaches to alleviation of airport community noise 13 p2053 A67-26539
 Program for perceived noise levels reduction on ground of turbofan-powered commercial transport by acoustically absorptive lining of ducts [AIAA PAPER 66-389] 15 p2548 A67-30357
 Cabin noise reduction in DC-9 by tuned vibration absorbers attached to engine support structure [AIAA PAPER 67-401] 15 p2421 A67-30368
 Subjective/objective measurement types required for systematic aircraft noise regulation around airports, based on maximum permissible noise exposure criterion 17 p2795 A67-32121
 Added narrow band noises and tones influence on subjective response to shaped white noise 17 p2795 A67-32125
 Solutions for aviation crisis of congestion, delays and noise, including problems anticipated with jumbo and SST jets 19 p3207 A67-34968
 Noise reduction in residential areas near landing strips using Tu-124 aircraft studded with suggested takeoff and landing piloting techniques 21 p3569 A67-38928
 Sonic boom and subsonic aircraft noise test results 21 p3569 A67-39118
 Prospects for lower noise levels of current and future aircraft, considering noise reduction at source /engine/ and greater separation distance from affected community 23 p3933 A67-40725
 Civil high speed intercity VTOL aircraft using fan lift engines, discussing noise, installation, aerodynamics and thrust deflection [AIAA PAPER 67-745] 23 p4048 A67-40979
 SST fleet size, flight time, station stop time, seat mile costs, fuel consumption, noise and sonic boom problems affecting airline economics [AIAA PAPER 67-749] 23 p3933 A67-40983
 Commercial aircraft noise system solution, considering engines, nacelles, operational procedures and airport options [AIAA PAPER 67-761] 23 p3933 A67-40992
 Perceived noise level measurement procedure applied to aircraft noise exposure using Kryter techniques 23 p4027 A67-41143
 Aircraft auxiliary power unit noise control, considering acoustical materials and installation techniques 23 p3935 A67-41144
 Aircraft flyover noise recording system, considering calibration, weather tape recording and synchronization system equipment 23 p3999 A67-41145
 Cockpit noise levels of various airline aircraft noting propeller effect 23 p3964 A67-41556
 Aircraft cabin noise due to fuselage vibration reduced, using mechanical impedance [SAE PAPER 670873] 24 p4248 A67-42010
 Short haul VTOL air transportation airport-community noise problem, examining propulsion systems and site planning [AIAA PAPER 67-867] 24 p4096 A67-42990
 Rotor VTOL aircraft for future transport noting rotor systems for low downwash velocity, minimum noise and low fuel consumption [AIAA PAPER 67-940] 24 p4097 A67-43030
AIRCRAFT PART
 High by-pass fan engine installation in subsonic transport in terms of configuration, environmental severity, structures and systems [SAE PAPER 660737] 01 p0140 A67-10636
 Replacement policies for aircraft and missile parts that fail according to normal log-normal or Weibull continuous probability distribution 01 p0083 A67-11339
 Acoustic fatigue tests of aircraft components, determining sound field and stresses using actual jet engine or simulation 03 p0521 A67-13021
 Compression, shear and bending strengths of tubular synthetic products as materials for aircraft structural component 04 p0715 A67-15539
 Rivet type aircraft fasteners 05 p0810 A67-16232
 Molded aircraft wheels of epoxy resin reinforced with noncontinuous glass filaments 06 p1007 A67-18026
 Wall thickening of aircraft structural components by compression of blanks to produce counter force 07 p1191 A67-19749
 Aircraft hollow control rods with threaded joints noting compression and testing 07 p1192 A67-19753
 Glass fiber reinforced parts for Boeing 737 noting fabrication, properties and applications 07 p1193 A67-20252
 Extension fittings for A-7A bomber having hydraulic system with no flexible hose 09 p1442 A67-21659
 Interferoscope used in testing large glass panels for aircraft camera windows 10 p1652 A67-22701
 Aviation avionics microelectronic devices stressing reliability, maintenance, circuitry, etc [SAE PAPER 670253] 11 p1758 A67-23985
 Aircraft fuel gauging systems noting float type and reliability defects [SAE PAPER 670263] 11 p1789 A67-23986
 Threaded fastener reliability factors noting mechanical testing 11 p1795 A67-24040
 Aircraft alternator test drives and specification requirements 13 p2081 A67-27238
 Giant forging press for aircraft and aerospace components 21 p3634 A67-38198
 Aircraft pipeline flanges manufacture by compression permit direct connection of sections into single main 21 p3637 A67-38924
 Aircraft skin friction balance components for hostile environments noting system design 22 p3795 A67-39188
 Plastics in aircraft and rocket parts construction noting silicon oils and solid polysiloxanes, discussing temperature resistance and rubber-elastic properties 23 p4021 A67-41400
AIRCRAFT PERFORMANCE
 European airline depreciation practice and suggested modification 01 p0168 A67-10269
 VTOL aircraft static and dynamic performance measurement technology, analyzing application of data processing methods 03 p0418 A67-12983
 Category II Systems Evaluation Test of C-141A aircraft 07 p1129 A67-19616
 VTOL/STOL aircraft evaluation via performance characteristics 07 p1130 A67-20219
 Computing methods and techniques in aircraft testing, discussing measurements, application of mathematical statistics, etc 09 p1469 A67-22455
 V/STOL theory for equilibrium level flight, evaluating optimum performance over complete velocity spectrum 09 p1441 A67-22487
 Longitudinal stability of rigid glider in towed flight, calculating lift coefficients for various rope-plane configurations 09 p1441 A67-22607
 Aircraft control system of subsonic airplanes operated over wide speed ranges, noting flight test results 11 p1744 A67-24578
 Military aircraft characteristics and performance evaluation 11 p1885 A67-25102
 Jaguar, Franco-British military aircraft designed for combat training and tactical support during 1970s 15 p2420 A67-30127
 Boeing 747 characteristics for passenger and cargo service noting economic gain, operational performance, control cabin, engine, etc [AIAA PAPER 67-397] 15 p2421 A67-30364
 Initial VGH data on small turbojet operations in commercial transport service relating to accelerations, airspeed operating practices and unusual events [AIAA PAPER 67-408] 15 p2421 A67-30375
 Design requirements of commercial supersonic aircraft engines [AIAA PAPER 67-376] 15 p2549 A67-30423
 Numerical characteristics of random functions applied to aircraft load evaluation 16 p2596 A67-31152
 Static structural strengths, aeroelasticity and flutter problems for glider performance 16 p2776 A67-31466
 Composite aircraft performance potential, with helicopter comparison with compound-type aircraft, noting range, speed, weight, productivity, etc [AHS PAPER 110] 16 p2597 A67-31826
 Compound aircraft flying quality improvement methods, noting VTOL characteristic and high speed as compared to pure helicopters [AHS PAPER 111] 16 p2598 A67-31827
 Optimum speed capability evaluation of aerial weapons system in relation to value and cost, noting aircraft performance characteristics 16 p2783 A67-31830
 Unscheduled civil aircraft power plant diagnostic removals evaluated by metal detection, performance deterioration, vibration, oil consumption and nonoperational categories [SAE PAPER 670358] 17 p2930 A67-32997
 Atmospheric condition effects on SST aircraft, noting Concorde performance data analysis results 19 p3173 A67-35309
 Multiple scaling for analyzing flight vehicle performance and dynamic behavior [AIAA PAPER 67-560] 19 p3335 A67-35957
 Aircraft performance, stability and control characteristics in nonsteady flight with high accuracy instrumentation system 20 p3442 A67-36466
 Optimal airline aircraft selection, discussing cost efficiency factors 22 p3922 A67-39537
 Unscheduled civil aircraft power plant diagnostic removals evaluated by metal detection, performance deterioration, vibration, oil consumption and nonoperational categories [SAE PAPER 670358] 23 p4048 A67-40866
 US SST airframe prototype, surveying hardware developments, flight control, pivoting system, landing performance and pilot cabin [AIAA PAPER 67-750] 23 p3933 A67-40984
 Performance and design parameters for VTOL fighter aircraft engine and wings, stressing takeoff weight factor 23 p3935 A67-41316
 Low altitude flight load spectra for light aircraft 24 p4094 A67-42755
AIRCRAFT POWER SOURCE
 Optimization of power plant of short range aircraft accounting for high by-pass ratios 04 p0687 A67-14530
 Power plants for electric equipment in aircraft 06 p0950 A67-18117
 Power plants for electric equipment in aircraft 08 p1286 A67-20905
 Structural predictions of mean times between failures through maintenance activity for aircraft power systems 09 p1560 A67-22287
 Electric power generating equipment for aircraft noting brushless rectifier AC generator, solid rotor AC generator and brushless DC generator 09 p1451 A67-22666
 Orion P-3 electrical power system changes effect on weapons system, noting power distribution and generation systems 09 p1452 A67-22677

Pneumatic starting systems for gas turbine engines including energy sources, system components and arrangements
 [ASME PAPER 67-GT-15] 11 p1854 A67-24800

Supersonic combat biplane airframe, power plant, fuel, control and escape system, instrumentation and weapons
 system 13 p2052 A67-26420

Lighter-than-air, nuclear-powered dirigible described giving details on capacity, safety and mode of propulsion 16 p2597 A67-31787

Structural design, analysis and tests pertaining to hot cycle rotor system used on XV-9A aircraft
 [AHS PAPER 121] 16 p2598 A67-31836

Noise control of aircraft auxiliary power units, noting installation of special acoustic materials 17 p2800 A67-31977

Shaft power from conventional two-spool turbofan engines for composite aircraft applications
 [SAE PAPER 670352] 17 p2929 A67-32992

Nuclear propulsion for aircraft, discussing reactor compactness and shielding techniques
 [AIAA PAPER 67-508] 18 p3076 A67-33972

Advanced high Mach number aircraft secondary power system requirements, discussing high pressure hydraulic systems and complex pneumatic positioning control systems 22 p3749 A67-40341

Aircraft and missile electric/hydraulic power supplies, describing turboalternator performance, design and applications 24 p4107 A67-42532

Aerospace system power conditioning design optimization, treating efficiency, regulation, EMI, BITE, primary power, size, weight, radiation hardening and cost
 [AIAA PAPER 67-985] 24 p4110 A67-43057

AIRCRAFT PRODUCTION
 SA EQUIPMENT SPECIFICATIONS
 Aircraft research and testing - Conference, Prague, November 1966 09 p1440 A67-22470

Book on aircraft design covering turboprop, subsonic turbojet, supersonic and water-based aircraft, missiles, helicopters, etc 15 p2419 A67-29417

Analysis of management methods applicable to aerospace industry, considering introduction of integrated information systems 15 p2583 A67-29669

Cost of titanium, steel and aluminum alloys in high performance aircraft production
 [AIAA PAPER 67-400] 15 p2505 A67-30367

Computerized system for calculating spares quantities and providing overall adequacy within monetary, weight or volume constraint 23 p4085 A67-40583

Development, design and production phases of Canadair CL-215 water bomber and potential variants
 [SAE PAPER 670902] 24 p4094 A67-42020

AIRCRAFT RELIABILITY
 SA AIRWORTHINESS REQUIREMENT
 SA COMPONENT RELIABILITY
 SA STRUCTURAL RELIABILITY
 Reliability improvement effect on cost in tactical aircraft, examining obsolescence, risk factor determination, etc 01 p0170 A67-11350

Powered flying control systems developments, considering reliability and autostabilization 05 p0753 A67-16750

Quality control and internal combustion aircraft engine reliability from mechanical engineering viewpoint 05 p0812 A67-17243

Category II Systems Evaluation Test of C-141A aircraft 07 p1129 A67-19616

Optimizing reliability level in conceptual phase system to ultimately yield operational systems of desired capability, illustrating with C-130/C-141 transport aircraft study 09 p1582 A67-22293

Aircraft reliability as function of fatigue life of welded joints noting static strength variation, S-N curve and multiple safety factor 09 p1506 A67-22471

Aircraft flight and ground strain measurements for static strength clearance and fatigue life assessment, noting structural integrity evaluation 11 p1880 A67-25058

Airline operation, reliability, personnel and training techniques
 [SAE PAPER 670343] 12 p2041 A67-25879

Hawker Siddeley 748 design noting utilization rates, maintenance costs and indefinite fatigue life 15 p2419 A67-29509

Design requirements of commercial

supersonic aircraft engines
 [AIAA PAPER 67-376] 15 p2549 A67-30423

Manual altitude and attitude control effects on short-period handling quality requirements 19 p3175 A67-35974

Automatic test equipment /ATE/ to ensure aircraft availability noting operation, circuitry, computer methods, etc 21 p3609 A67-39132

Air Force accident history noting importance of maintenance/material area 22 p3754 A67-39598

Logistics simulation modeling for optimizing spares mix needed for maintenance of airborne systems at minimum cost 23 p4085 A67-40590

Maintenance schedule for small commercial aircraft fleet, periodic inspection check principles and engine reliability program 24 p4094 A67-42277

Conceptual aircraft suitability for short haul transportation systems, discussing operation, design, noise factors, flight profiles and V/STOL certification rules
 [AIAA PAPER 67-771] 24 p4095 A67-42939

Reliability and safety for STOL aircraft and low airspeed operation, discussing automatic flight control system, air traffic control, etc
 [AIAA PAPER 67-797] 24 p4095 A67-42958

AIRCRAFT SAFETY
 Optimum design safety for VTOL aircraft, noting noise and vibration elimination
 [AIAA PAPER 66-813] 01 p0008 A67-10031

Pilot training, regulation, instrumentation and airspace environment changes for increased safety
 [AIAA PAPER 66-812] 01 p0008 A67-10032

Bird impact hazard to aircraft simulated with hens propelled against windshields and metal targets 01 p0049 A67-10539

Aviation fuel static electricity elimination by Shell additive ASA-3 05 p0872 A67-16234

Semipermanent repellant for aircraft windshields to overcome effect of visual errors caused by rain on windshields 08 p1279 A67-21042

Developments in fire detection equipment noting continuous wire, armored wire and surveillance detectors 09 p1439 A67-21704

Closed compartment fire-resistance test for hydraulic fluids leaking near heated aircraft skin with or without electric arcing 09 p1521 A67-22245

Fire hazard testing of hydraulic fluids, coolants and lubricants in aircraft with reference to SST hot wing compartment conditions 09 p1521 A67-22246

Flight load maneuver data for fatigue evaluation of F-4 series aircraft 10 p1594 A67-23435

Aircraft flight and ground strain measurements for static strength clearance and fatigue life assessment, noting structural integrity evaluation 11 p1880 A67-25058

Executive aircraft structure safe-life fatigue analysis and tests
 [SAE PAPER 670257] 12 p2016 A67-25507

Small pressurized cabin design for light commercial aircraft including safe life vs fail-safe approaches, fatigue strength testing, etc 12 p2016 A67-25508

Positive control system for placing aircraft under precisely described flight path
 [SAE PAPER 670340] 12 p1895 A67-25878

Airline flight testing problems, discussing aircraft availability, equipment competency, crew proficiency, safety, economy, etc 13 p2052 A67-26424

Air traffic control system, discussing effect on business aircraft operations 14 p2347 A67-28317

Possible decompression effects in supersonic transport cabin in terms of biomedical considerations for passenger safety 14 p2258 A67-28866

Soft gravel and aerated concrete material of various sizes tested to safely decelerate aircraft overshooting runway during takeoff and landing 14 p2246 A67-28817

Optimum design safety for VTOL aircraft, noting noise and vibration elimination
 [AIAA PAPER 66-813] 15 p2419 A67-29411

Radar display layout for aircraft safety consisting of digital computer and CRT 15 p2468 A67-30129

Plaggio-Douglas PD-808, Italian executive jet emphasizing safety
 [AGARDOGRAPH 95] 15 p2422 A67-30399

Long distance air navigation aids, stressing supersonic flight safety requirements 16 p2701 A67-31248

Contaminant concentration in liquid breathing oxygen of aircraft converter determined by gas chromatography 16 p2619 A67-31475

Lighter-than-air, nuclear-powered dirigible described giving details on capacity, safety and mode of propulsion 16 p2597 A67-31787

Aircraft fuel explosion problem, analyzing mechanism of lightning-induced explosions and discussing protection methods 16 p2597 A67-31810

Evolution and future objectives of ejection-seat escape systems design, noting characteristics and deficiencies in conventional ejection seats 17 p2795 A67-32002

All-weather landing for civilian aircraft, discussing equipment, terminology used and low visibility flight simulation 17 p2795 A67-32122

Air safety statistics analysis based on set of intrinsic accident rates in takeoff, cruise and landing 17 p2797 A67-32580

Space vehicle checkout procedure application to near-future transport aircraft, noting NASA sponsored advances
 [SAE PAPER 670337] 17 p2835 A67-32987

Failure safety design of rotary wing aircraft, emphasizing airline type operation
 [SAE PAPER 670349] 17 p2798 A67-32991

Fuel emulsions for helicopters to minimize hazards associated with liquid fuel, discussing composition, stability, corrosion and flow properties
 [SAE PAPER 670364] 17 p2927 A67-33001

Gelled, emulsified and otherwise thickened fuels for aircraft fire safety, discussing requirements and engine operation
 [AIAA PAPER 67-503] 18 p3110 A67-33967

Aircraft front windshields, discussing thermal stability, clear vision maintenance, bird impact, atmospheric pressure effect, cabin pressure changes and tensile strength 18 p2986 A67-34099

AH-56A /AAFSS/ safety engineering, failure effects method, Army role, etc 18 p2987 A67-34690

Air collision statistics, discussing air collision avoidance system 19 p3173 A67-35865

Skidding accident reduction investigated for runway and highway safety noting worn tires, smooth surface texture, locked wheels and pilot technique 19 p3173 A67-35930

All-weather landing examined in terms of operational techniques and design criteria for airline performance and safety
 [AIAA PAPER 67-572] 19 p3258 A67-35968

Radar and aircraft simultaneous clear air turbulence /CAT/ observations 20 p3481 A67-36996

Concorde fire protection system based on Firewire Triple FD equipment, discussing extinguishant toxicity, low vapor pressure, etc 20 p3364 A67-37245

Pilot and automatic control function coordination in piloting and landing aircraft, discussing precision problems, safety and development of new processes 22 p3831 A67-39750

Bird strike data on piston engine transport horizontal stabilizers summarized by bird weight, impact velocity, target-station distance and simulated and test load 22 p3746 A67-39845

Light effects and aircraft safety studied for lightning strikes, noting temporary blindness and slowing of psychomotor reactions 23 p3945 A67-41069

Mathematical technique to determine probabilities associated with critical system performance capability measured under varying human and environmental conditions 23 p3964 A67-41547

Decompression tests, evaluating hazards of ejections and fatal injuries following window failure in small pressurized aircraft 23 p3965 A67-41575

Polyimide passenger smoke hood for protection from smoke, toxic gases and flame inhalation 23 p3968 A67-41623

Decompression tests for potential hazards of ejection or fatal head injuries in small pressurized aircraft 23 p3970 A67-41693

System-safety mathematical model for commercial jet airplanes using fault-tree modeling technique
 [AIAA PAPER 67-910] 24 p4096 A67-43017

AIRCRAFT SPECIFICATION

C-141A cargo aircraft structural analysis, discussing design, load and gust criteria, flight and static test programs, vibration and noise control
[SAE PAPER 660669] 01 p0010 A67-10576

C-141A cargo aircraft structural analysis, discussing design, load and gust criteria, flight and static test programs, vibration and noise control
[SAE PAPER 660669] 07 p1131 A67-20232

Fokker F-28 Fellowship conceived as jet contemporary of turboprop Fokker Friendship, noting structural and operational details
16 p2597 A67-31561

Inference of vehicle and atmosphere parameters from free flight motion measurements using iterative calculations of parameter values
19 p3337 A67-35996

AIRCRAFT STABILITY

Low level turbulence effects on structure of large logistic aircraft
[SAE PAPER 660670] 01 p0160 A67-10577

Dynamic stability tests of aircraft mockups in transonic and supersonic flows, using free-oscillation method
[ONERA-TP-390] 01 p0011 A67-11093

B-52 structural response to random turbulence with various stability augmentation systems, noting rigid body motions, normal vibration modes and control surface rotations
[AIAA PAPER 66-998] 02 p0181 A67-12302

Aircraft bumpiness conditions in free atmosphere relation to turbulence and other aerological data
02 p0263 A67-12647

Deep-stall characteristics of T-tailed aircraft configurations and recovery procedures, noting parameters of pitch-up, angle of attack, etc
[AIAA PAPER 66-13] 03 p0350 A67-12912

Load factor estimation for flights in turbulent conditions by replacing exact transfer function with equivalent statistical model
03 p0351 A67-12997

Constant component of Cardan error of directional gyro subject to regular rocking
03 p0425 A67-14282

Motion equation and measurement of angles of aircraft closely approaching vertical plane, using new coordinate system
04 p0704 A67-14776

Aerodynamic coefficients effects on aeroelastic instability predictions for aircraft with autopilot
[ONERA-TP-418] 05 p0751 A67-16483

Jet engine gyroscopic moments effect on coupling of longitudinal and transverse motions of aircraft
06 p0944 A67-17624

Air density gradient effect on longitudinal aircraft motion
06 p0944 A67-17625

Comparative stability and control considerations for fixed wing and rotating wing aircraft
06 p0944 A67-17628

Flapping motions of helicopters in control axes system
06 p0935 A67-17629

Tilt rotor VTOL aircraft stability, discussing results of wind tunnel tests on rotor-pylon behavior at different velocities
[AIAA PAPER 67-17] 06 p0948 A67-18254

General lateral stability and control equations for steep gradient aircraft in terms of equivalent aircraft in level flight without inertial cross coupling
06 p0949 A67-18597

Book on flight characteristics, static stability, equations of motion, excitation and response
06 p0949 A67-18725

Self-adaptive system employing quick identification of parameters of aircraft short period pitch transfer function
07 p1128 A67-19199

Longitudinal stability of L-29 aircraft, comparing measurement results from independent experiments
09 p1440 A67-22469

Least squares methods for calculating stability derivatives of aircraft from unsteady flight data
09 p1438 A67-22474

Motion equations used in determining lateral stability and control derivatives for STOL aircraft
10 p1595 A67-23551

Flutter characteristics of slab tail or stabilator installation, discussing prevention and design
[SAE PAPER 670260] 12 p1895 A67-25509

Aircraft handling qualities research with variable static stability aircraft used as in-flight simulator
[SAE PAPER 670261] 13 p2054 A67-27296

Aerodynamics survey emphasizing supersonic speed

problems
14 p2239 A67-27874

Pilot training for future commercial transports, noting flight simulation devices for safety and economic factors
[AIAA PAPER 67-388] 15 p2432 A67-30356

Errors of real accelerometer and instability of rotation effect on accuracy of angular velocity measurements of aircraft motion
16 p2670 A67-30466

Aircraft flutter testing using free-air turbulence as exciter
16 p2764 A67-30861

Longitudinal static stability margin of glider for small lift coefficients showing effect of torsional deformation
16 p2596 A67-31001

XC-142A flight control and stability augmentation systems
17 p2794 A67-31996

Optimal control for aircraft gust alleviation using frequency domain theory and short period mode approximation
17 p2795 A67-32036

Lateral-directional stability equations for aircraft with nonzero product of inertial flying along steep flight path gradient
17 p2796 A67-32219

Jet VTOL aircraft problems, considering vertical thrust/aircraft weight, thrust application to aircraft gravity center, stability in hovering, thrust exertion, etc
17 p2796 A67-32392

Minimax fuel requirement of aircraft angular stabilization for undetermined inertial moment probability distribution
19 p3202 A67-35887

Soviet papers on aircraft construction and techniques used by Air Force covering stress, loading, stability, etc
21 p3567 A67-38040

Aircraft autopilot system in longitudinal flight stabilization regime, using synthesis method based on time characteristics
22 p3831 A67-39609

Longitudinal stability and control wind tunnel results, considering swept and variable geometry wing aircraft during deep stall conditions
23 p3932 A67-40567

Aeroelastic phenomena in aircraft stability, control and airframe vibration characteristics, describing testing methods
23 p4077 A67-41046

Buffet limit for aircraft wings in transonic region based on boundary layer theory, determining transonic pressure distribution and separation points
23 p3931 A67-41311

Flared afterbody aerodynamic characteristic predictions for aircraft stability at high Mach numbers, discussing turbulent separation
24 p4093 A67-42924

AIRCRAFT STRUCTURE

SA AIRFRAME

Computer algorithm for framework diagram in synthesizing thin walled shells strengthened by ribs
02 p0340 A67-12443

Synthetic spherulites in plastic foam and synthetic tube segments in honeycomb form as fillers in sandwich construction
03 p0521 A67-13022

Long-haul transport aircraft structural considerations and effect on operating empty weight and on airframe maintenance
[AIAA PAPER 66-882] 03 p0361 A67-14019

Straining equipment for testing aircraft structures
04 p0708 A67-14584

Book on methods of determining temperature fields in thin walled elements characteristic of structure of flight vehicles and engines
04 p0723 A67-15010

Aircraft skin panel fatigue failure under hypersonic conditions, noting effect of natural vibration frequency and axisymmetric oscillations
05 p0918 A67-16229

Global method application to vibration problems, discussing present trends in experimental methods
[ONERA-TP-405] 05 p0919 A67-16478

Maximum slope method for obtaining natural frequency and damping ratio of highly damped second order systems from time history data
06 p1100 A67-18012

Wall thickening of aircraft structural components by compression of blanks to produce counter force
07 p1191 A67-19749

Filamentary reinforced resin matrix composite materials for high specific strength and specific modulus necessary for aircraft structures
08 p1333 A67-20359

Reinforced plastic facings as sandwich materials instead of metal skins noting cost effectiveness, weight efficiency and layup times
08 p1414 A67-20430

Direct measurement of aeroelastic

parameters of aircraft wings, using dynamically similar models fitted on auxiliary rocket devices
09 p1576 A67-22462

Creep measurement associated with adhesive bonding of aircraft structures, particularly creep of metal-metal lap joints and bonded sandwich structures creep measurement associated with adhesive bonding
09 p1522 A67-22505

Adhesive bonded honeycomb horizontal stabilizers, considering strength, aerodynamics, cost, endurance and serviceability
09 p1577 A67-22508

Adhesive-honeycomb relationship including filletting effect on honeycomb properties, compression properties, stresses at fillet, etc
09 p1577 A67-22509

Structural fatigue in aircraft - ASTM Symposium, Seattle, October-November 1965
10 p1594 A67-23429

Structurally significant material properties effect on reliability of aircraft structures regarding unserviceability, ultimate load failure, etc, stressing stochastic concepts in strength analysis
10 p1718 A67-23433

Random-loading fatigue crack growth behavior of airframe aluminum and titanium alloys under sinusoidal, narrow band and broad band random loading
10 p1669 A67-23434

Scatter factor for fatigue life of aluminum aircraft structures subjected to identical loading histories
10 p1594 A67-23436

Principle of maximum entropy and application in reliability estimation of aircraft structures
10 p1726 A67-23730

Unsteady aerodynamic forces and dynamic response of flexible aircraft structure to continuous turbulence in supersonic flight
10 p1595 A67-23736

Approximate formulae for transient temperature prediction due to kinetic heating in aircraft type structures
11 p1883 A67-24661

Supersonic combat biplane airframe, power plant, fuel, control and escape system, instrumentation and weapons system
13 p2052 A67-26420

Doping of aircraft and rockets
13 p2124 A67-27500

Concorde SST third and fourth flying prototypes described, discussing structural design, power plant, control systems, landing gear, etc
16 p2597 A67-31785

Structural design, analysis and tests pertaining to hot cycle rotor system used on XV-9A aircraft
[AHS PAPER 121] 16 p2598 A67-31836

Aircraft flotation on bare soil, discussing approaches for improvement, test results on tires, deflection magnitude, etc
17 p2793 A67-31987

C-5A landing gear, discussing design and evolution of requirements such as kneeling, steering, weight and flotation
17 p2794 A67-31988

Parametric analysis on hydrogen-fueled hypersonic aircraft for long range passenger transport missions and launch vehicle missions, noting propulsion system-airframe interactions
[AIAA PAPER 67-493] 18 p2985 A67-33957

Aircraft structural form optimized through changes in geometry
20 p3542 A67-37531

Titanium alloy resistivity and aircraft structure role as current return and electromagnetic shield, discussing greater use of wire for susceptible circuits to achieve EMC
20 p3405 A67-37643

Soviet book on aerodynamics, flight dynamics, flight vehicle structural design and mechanical and control considerations for various aircraft
21 p3566 A67-37833

Machines and machining technology for materials used in Mach-3 aircraft structures, discussing cutting fluids, cutter and best metal removal rate
21 p3631 A67-38014

Soviet papers on aircraft construction and techniques used by Air Force covering stress, loading, stability, etc
21 p3567 A67-38040

Aircraft empty weight equations as function of takeoff weight, using mathematical statistics
21 p3567 A67-38041

Laterally flattened cylindrical shells under internal pressure representing aircraft sections strength analyzed, deriving formulas for stress-strain distribution
21 p3724 A67-38784

Low pressure diffusion welding and brazing process producing joints with

mechanical properties close to titanium 6Al-4V 22 p3811 A67-39446

Reinforced plastic materials for light aircraft wing structures, calculating torque strength 22 p3912 A67-39729

High structural efficiency of aircraft materials emphasizing fatigue characteristics, fracture toughness and corrosion resistance 22 p3823 A67-40332

Materials selection for external structures of transport aircraft flying at Mach 3 speeds, noting characteristics of maraging steels 23 p4019 A67-41045

Honeycomb sandwich structures for aircraft and missile construction, discussing panel configurations 23 p4077 A67-41047

Ultrasonic monitoring technique for fatigue damage and crack formation and propagation in aircraft structures [AIAA PAPER 87-793] 24 p4251 A67-42954

AIRCRAFT TIRE

Roll fatigue tests of forged ZK60A-T5 magnesium and 2014-T6 aluminum wheels 10 p1661 A67-23439

Critical rolling speed of aircraft tires calculated and experimentally verified 16 p2596 A67-31002

Jet aircraft tire testing machine simulating taxiing, takeoff and landing loads 16 p2656 A67-31914

Aircraft flotation on bare soil, discussing approaches for improvement, test results on tires, deflection magnitude, etc 17 p2793 A67-31987

Landing gear for operating off rough terrain and unprepared airstrips in OV-10A Bronco aircraft for counter insurgency 17 p2794 A67-31989

AIRCRAFT WAKE

Vortex wake and aerodynamic load distribution of slender rectangular wings 17 p2790 A67-32215

AIRCREW

Airline flight testing problems, discussing aircraft availability, equipment competency, crew proficiency, safety, economy, etc 13 p2052 A67-26424

F-111 crew escape module design and performance 14 p2244 A67-27739

System engineering approach to commercial aircraft crew requirements [AIAA PAPER 87-399] 15 p2433 A67-30366

EEG finding in aircrew personnel to obtain information about 14 and 6 per second positive spiking phenomenon 21 p3574 A67-38085

Altitude chamber studies of passively pressurizing partial pressure suit for possible use by SST crew 23 p3969 A67-41647

Subjective effects of fatigue on aircrew expressed in work cycle terms from data of continuing daily activity log 23 p3959 A67-41663

Aircrew safety emphasizing prior to abort aspects in detection of catastrophic failure and initiation of abort sequence [AIAA PAPER 87-934] 24 p4245 A67-43024

AIRFIELD SURFACE MOVEMENT

Concrete pavement performance at ten civil airports, examining durability of surfaces, jointing subbase thickness and maintenance 02 p0229 A67-11841

AIRFLOW

Sound propagation in streaming air within tubes having changes of cross section and flow losses, discussing reflection coefficient dependence on flow velocity 01 p0114 A67-10819

Turbulent annular airflows in turbulent film lubrication of high speed bearings [ASME PAPER 66-LUB-14] 03 p0403 A67-13755

Transient air flow rates into gas turbine metered, using two critical flow circular arc venturi 03 p0421 A67-13770

Airflow instability with square edge circular orifice, discussing hysteresis effect on discharge coefficient 04 p0601 A67-14487

Convective heat transfer in accelerated heated air flows through cooled conical supersonic nozzles of three different configurations 04 p0723 A67-14837

Low speed cascade tunnel experiments for improvement of airflow and testing techniques, noting porous sidewall suction effect on axial velocity changes [ASME PAPER 66-WA/GT-7] 04 p0548 A67-15385

Airflow in small wind tunnel with roughened heat transfer surface, using flow visualization techniques 04 p0727 A67-15801

Gas dynamics and geometry in mixing zone of Freon 12, air and helium jets in wake air flow, determining effect of jet velocity, gas density, etc 06 p0982 A67-17743

Asymptotic method for solution of boundary layer equations for generalized three-dimensional flow of dissociated air at chemical equilibrium near stagnation point 06 p0984 A67-18113

Film cooling by helium secondary flow injection into incompressible low speed airflow in turbulent boundary layer above flat plate 06 p1116 A67-18385

Human perception of airflow resistance and perception thresholds under various conditions 07 p1133 A67-19478

Spread of turbulent plane jet issuing into parallel moving air stream, noting Reynolds number variation 08 p1321 A67-20713

Book on airflow measurement techniques and flow meters 08 p1321 A67-20759

Electric conductivity and kinetic energy in seeded and unseeded airflow MHD experiments in hypersonic shock tunnels for aerospace applications 09 p1542 A67-21809

Airflow characteristics and heat transfer in right angle water-jacketed bend, measuring boundary layer profile at midbend 09 p1487 A67-21831

Airflow past wing profile with leading edge slot blowing foreign gases, noting schlieren photographs of flow patterns and concentration distribution measurement 10 p1589 A67-22724

Cooling and heating effectiveness of plane surface in turbulent air flow by injection of air film, noting temperature effect 11 p1881 A67-23898

Dust content of air flow created by piston engine Mi-1 and Mi-4 helicopters in landing and takeoff 11 p1744 A67-24530

Hydrodynamic boundary layer velocity profile on disks in transverse airflow analyzed theoretically and by wind tunnel tests 12 p1891 A67-25318

Two-dimensional nonsteady airflow in shaped duct prediction, using numerical method 12 p1928 A67-25357

Probability distribution of square of vertical wind velocity difference during unstable stratification 12 p1963 A67-25484

Inverse heat transfer problem in air flow past cylinder, calculating heat transfer coefficient and scaling functions 13 p2224 A67-27053

Model of inviscid, incompressible and variable density airflow in long channel over mountain treated mathematically 14 p2346 A67-28004

Wind tunnel heat transfer measurements from circular cylinders to transverse air flow, noting recovery factor as function of Knudsen number 14 p2405 A67-28178

Aircraft flow meters for simultaneous rate and volume measurements, examining equations of motion 16 p2671 A67-31006

Unsteady heat transfer in tube during heat-flux fluctuations 17 p2967 A67-32130

Low speed cascade tunnel experiments for improvement of airflow and testing techniques, noting porous sidewall suction effect on axial velocity changes [ASME PAPER 66-WA/GT-7] 18 p2983 A67-34131

Summit areas of severe storms, measuring stratospheric-tropospheric interchange, air flow and hydrometeors 19 p3252 A67-35057

Heat transfer coefficients from supersonic wind tunnel airflow through grid with rectangular bars [ASME PAPER 87-HT-74] 20 p3550 A67-36754

Heated thin film anemometer used to measure fluctuating velocity in airflow, noting relation of dynamic sensitivity to static calibration 20 p3447 A67-36846

Airflow velocity measurement device in cylindrical or rectangular tubes at low gas pressures 20 p3451 A67-37300

Analog computer method application for determining critical frequency and critical flutter speed of wing having torsional bending vibrations in 21 p3718 A67-37992

Convective heat transfer between tube and airflow in tube for pulsating flow with pressure fluctuation frequency deviating from resonant frequency 23 p4082 A67-41285

AIRFOIL

SA HYDROFOIL

SA SUPERSONIC AIRFOIL

SA THIN AIRFOIL

Nonlinear two-dimensional unsteady potential flow around arbitrarily shaped airfoil in inviscid and incompressible fluid, considering method of calculating pressure, forces and moments 02 p0178 A67-12291

Fuselage interference effect on annular airfoils determined by measuring lift and drag of model aircraft equipped with annular wing for each semispan and empennage 03 p0352 A67-13313

Theoretical derivation of modification of shape of given airfoil which reduces moment values and sustains original lift 04 p0545 A67-14411

Oscillations of staggered plate cascade in plane subsonic gas flow, showing fluid compressibility effect on aerodynamic characteristics 06 p0935 A67-17729

Subsonic drag rise for airfoil determined by limit line analysis in hodograph plane [AIAA PAPER 67-4] 06 p0938 A67-18248

Velocity distribution for low drag airfoil with little tendency toward separation of turbulent boundary layer 08 p1275 A67-20407

Effect of straightening section of airfoil contour on local supersonic flow, noting deformation of sonic line or characteristics 09 p1438 A67-22217

Wafer thin button size sensor for differential pressure measurement across airfoils 11 p1795 A67-25061

Tandem cascade of airfoils slow speed performance flow characteristics 12 p1891 A67-25349

Subsonic drag rise for airfoil determined by limit line analysis in hodograph plane [AIAA PAPER 67-4] 13 p2051 A67-27599

Lighthill uniformization technique applied to singular perturbation problems using Lagrange expansion 14 p2346 A67-29059

Interference of open and closed wind tunnels with ground board calculated and results applied to airfoils 16 p2590 A67-30854

Retractable airfoil and hinged cowl modifications of supersonic inlet to reduce drag below choking point for subsonic operations 17 p2791 A67-32575

Airfoil unsteady motion problem near screen in incompressible fluid with given horizontal/ vertical velocity 18 p2981 A67-33410

Effect of straightening section of airfoil contour on local supersonic flow, noting deformation of sonic line or characteristics 18 p2982 A67-33756

Three-dimensional vortex flow inverse problem through axial fan solved using isolated airfoil method 19 p3171 A67-35723

Unsteady airfoil stall noting frequency effects on velocity distribution and angle of attack for oscillating pitch 21 p3565 A67-38547

Two-dimensional incompressible flow near airfoil trailing edge treated by inviscid flow model, with constant vorticity inducing velocity field causing flow retardation 23 p3928 A67-41245

AIRFOIL CHARACTERISTICS

Aerodynamic boundary layer control by blowing, considering problems of lift increase, airfoil properties, etc 11 p1741 A67-24101

Fully stalled airfoil steady state pitching oscillations in one degree of freedom, deriving torsional flutter equation [ASME PAPER 67-VIBR-12] 11 p1872 A67-24172

High lift techniques for STOL aircraft compared based on maximum lift coefficient, noting airfoil stall characteristics and flow separation delay devices [SAE PAPER 870245] 12 p1894 A67-25500

Para-Poil models tested in wind tunnel and free flight for flight capability, L/D ratios, deployment, control and maneuverability, etc 14 p2246 A67-29054

Powder-metallurgical methods using mechanical filing, isostatic pressing and high vacuum-high temperature sintering for fabrication of airfoil turbine-blade blocks 17 p2865 A67-32821

Soviet book on high velocity hydrodynamics including airfoil motion at distances from screen, hodograph method in MGD, drag coefficient determination, etc 18 p3021 A67-33409

Flexure-torsion cascade flutter of airfoils with two degrees of translational and torsional vibration freedom 22 p3914 A67-40040

Airfoil and profiles theories emphasizing boundary layer theory, lift augmentation and wing aerodynamics 23 p3930 A67-41305

Aircraft wing drag noting relation between Mach number, thickness chord ratio, aspect ratio, airfoil shape and wing configuration 23 p3930 A67-41306

Hypersonic aerodynamics, discussing tunnel testing, inviscid flows, airfoil shapes, real gas effect, shock wave theory and boundary layers 23 p3930 A67-41307

High speed computer graphic techniques for airfoil sections characteristics in two-dimensional compressible flow [SAE PAPER 670845] 24 p4091 A67-41998

AIRFOIL PROFILE

Flow of compressible fluids past straight cascades of arbitrary airfoils using Kármán-Tsien method, obtaining velocity distribution around airfoil through continuity equation 02 p0177 A67-11470

Plane adiabatic flow of ideal gas behind separated shock wave for uniform supersonic symmetrical flow past smooth profile 03 p0349 A67-12873

Subsonic compressible flow around profile obtained by conformal transformation, reducing to Dirichlet problem 05 p0749 A67-16845

Integral representation for transonic flow about thick airfoils obtained from equations for two-dimensional inviscid flow and locally surface-orthogonal shock waves [AIAA PAPER 67-3] 06 p0939 A67-18331

Magnification in profile drag of airfoil due to effect of pressure gradients on boundary layer downstream of isolated roughness element 06 p0990 A67-18748

Computer calculation of induced circulations and influence coefficients for turbine blades with arbitrary profiles and oscillation shift 10 p1591 A67-23044

Aerodynamic characteristics of thin airfoil of small camber in nonuniform flow 11 p1742 A67-24658

Auxiliary singularity-carrier-curve theorems derived for blade profile design calculations 12 p1893 A67-25970

Separated compression shock circulation in front of wedge profiles at high Mach numbers 13 p2049 A67-26640

Nonlinear differential equation for shock wave of several circular arc airfoils integrated to give shock wave location 14 p2239 A67-27797

Thin slightly curved profiles positioned at small angle of attack in subsonic gas flow and developing harmonic random vibrations studied for aerodynamic interference 17 p2792 A67-32903

Profile velocity distribution and shape determinations for flow around thin profile with jet flap 19 p3172 A67-35819

Flow pattern at low Reynolds numbers about airfoil cascade illustrated by hydrogen bubble flow-visualization technique 20 p3359 A67-37483

Optimum design of ring airfoil device for maintaining pressure recovery efficiency of conical diffuser 22 p3743 A67-40168

Blade airfoil sections two-dimensional aerodynamic characteristics studied in wind tunnel for aerodynamic optimization calculation of helicopter rotors 23 p3927 A67-40576

Airfoil and profiles theories emphasizing boundary layer theory, lift augmentation and wing aerodynamics 23 p3930 A67-41305

AIRFOIL SECTION

Ventilated airfoil sections characteristics in free jet 05 p0793 A67-17321

Three-dimensional flow in axial fan, consisting of rotor only, having finite number of blades, by method of isolated airfoil of finite span 19 p3171 A67-35712

AIRFOIL THICKNESS

Transonic airfoil problem solved via differentiation of airfoil thickness ratio by infinitesimal perturbation method [AIAA PAPER 66-90] 08 p1276 A67-20563

AIRFRAME

SA FUSELAGE

SA LANDING GEAR

SA TAIL

Static and fracture tests with C-160 /Transall/ transport 01 p0048 A67-10212

Gust reduction equations governing numerical procedure for transforming to inertial frame continuous records of air turbulence velocity via matrix methods [AIAA PAPER 66-967] 02 p0246 A67-12290

Rocket cost dependence on weight and airframe resistance studied for design problem solutions 14 p2245 A67-28638

Integration of propulsion system into airframe of hypersonic cruise aircraft, discussing configurations, cooling and supersonic combustion 17 p2796 A67-32475

AIRFRAME MATERIAL

Basic surface curves derived and defined by aircraft manufacturer for engineering, tooling and manufacturing airframe [SAE PAPER 660353] 01 p0078 A67-10567

Titanium fabrication techniques for XB-70 and space booster [SAE PAPER 660650] 01 p0079 A67-10611

Correlation between increased performance demands and cost of lightweight airframe structures [SAE PAPER 660674] 04 p0716 A67-15783

Newer titanium alloys compared with present production alloys from closed die forgings in typical airframe and engine configuration 06 p1017 A67-17999

Airframe heat protection for high performance sounding rockets, using plasma jet testing for leading edge design selection 08 p1425 A67-20528

Creep properties of sheet materials in SST environment for selection of optimal airframe materials 22 p3818 A67-39225

Book on inspection, construction, operation, maintenance and repair of aircraft and aerospace vehicles including metal, steel frames, wood structures and high temperature structural material 22 p3811 A67-39441

Materials selection for external structures of transport aircraft flying at Mach 3 speeds, noting characteristics of maraging steels 23 p4019 A67-41045

Airframe heat protection for high performance sounding rockets, using plasma jet testing for leading edge design selection 24 p4256 A67-42914

AIRGLOW

SA ATMOSPHERIC EMISSION

SA AURORA

SA SKY BRIGHTNESS

Magnetic storm enhancement of 5577 angstrom airglow emission intensity [AFCLR-66-866] 03 p0505 A67-12836

Cameras used in auroral and airglow experiments including SP3 spectrophotometer, three-channel photometer and all-sky camera 03 p0419 A67-13376

Probability distribution of square of vertical wind velocity difference during unstable stratification 03 p0463 A67-14228

Day and night airglow measurements by K and L rockets 05 p0798 A67-16863

Emitting height of night airglow determined by rocketborne photoelectric equipment 05 p0798 A67-16865

Doppler profiles of nocturnal green line /5577 angstroms/ nonthermal emission resulting from molecular oxygen ion dissociative recombination [AFCLR-67-0443] 05 p0803 A67-17411

Vibrational and rotational temperature at altitudes between 50 to 250 km determined from analysis of airglow in OH bands, using Fastie-Ebert spectrometer 07 p1172 A67-19562

Brightness variations of oxygen in day and twilight airglow observed by balloon-borne instruments 07 p1173 A67-19663

Aerobee rockets measurement of sodium dayglow suggest equilibrium between sodium atoms and distribution of dust particles 07 p1180 A67-19917

Airglow resonant emission transfer in Doppler incoherent scattering medium with respect to optically thick atmosphere 10 p1634 A67-23050

Large amplitude variations of intensity of oxygen emission in night airglow and structure of lower

thermosphere 10 p1634 A67-23051

Brightness of night glow measured in several spectral ranges by Cosmos 92 satellite-installed colorimeter 10 p1647 A67-23276

Airglow lines measured through photometers on OGO-II satellite, noting nadir and zenith airglow 10 p1660 A67-23278

Nocturnal decline of ionospheric airglow 6300 angstrom line intensity due to diatomic oxygen ion-electron recombination 10 p1649 A67-23294

Diurnal and latitudinal variations in 5577 angstrom zenith nightglow intensity

compared with 6300 angstrom calibrations 10 p1650 A67-23337

Rocketborne photometer data analysis of night sky airglow and spectrum in 6300 angstrom region 11 p1786 A67-24072

Spectroscopic twilight airglow measurements for upper atmosphere interpreted using rocket flight data 11 p1786 A67-24263

Airglow and enhanced electromagnetic radiation in southern radiation anomaly observed with scintillation crystal during aircraft flight 12 p1996 A67-25775

Spatial inhomogeneities in green line of atomic oxygen, using electrophotometry during airglow 13 p2111 A67-26567

Photoelectric scanning observations of night airglow for two spectral lines of OI 14 p2306 A67-27788

Nightglow continuum 14 p2313 A67-28576

Intensity and polarization of hydrogen Lyman alpha lines in day airglow as function of altitude for principal far UV emission 14 p2314 A67-28849

Characteristic enhancement of forbidden doublet in nitrogen excitation observed in night airglow during traveling ionospheric F region perturbation 15 p2474 A67-29479

Nightglow measurements noting intensity relation to spread-F and sporadic E [AGARDOGRAPH 95] 15 p2485 A67-30308

Correlation of monthly and nightly green line 5577 Angstroms /OI/ airglow intensity with sunspot number and 10.7 cm flux 16 p2749 A67-31404

Upper atmospheric nightglow emission intensity measured finding continuous excitation of oxygen atoms as energy reservoir 16 p2670 A67-31918

Soviet book on polar auroras and night airglow 17 p2848 A67-32951

Drift azimuths, sizes and displacements of spatial inhomogeneities in oxygen atom emission at 5577 angstroms during night airglow 17 p2848 A67-32952

Night airglow brightness spatial distribution observed by photoelectric photometry in 5893 angstrom band, including isophotes charts and emission-inhomogeneity drift histogram 17 p2848 A67-32953

H-alpha diurnal and seasonal intensity variations in geocorona indicating hydrogen content build-up during night 17 p2851 A67-33202

Aurora and airglow - NATO Conference, Keele University, England, August 1966 18 p3031 A67-33578

Aurora Borealis and airglow history, discussing sunspot cycle influence, theories concerning origin, etc 18 p3032 A67-33579

Auroras and airglows in relation to ionospheric phenomena 18 p3033 A67-33584

Dayglow emissions observation by ground-based instruments indicate atmospheric response to concurrent input of solar energy 18 p3033 A67-33586

Chemical reactions fluorescent and resonant scattering, electron impact and photodissociation from sunlight upon atmosphere 18 p3036 A67-33602

Afterglows from atmospheric nuclear detonations related to natural airglow and aurora 18 p3036 A67-33604

Nightglow emission structure and variation at airglow equator, discussing predawn and storm effects, intensity variations with solar cycle, OH bands, etc 18 p3036 A67-33607

Airglow emission analysis from low altitude observations, discussing temporal and spatial variations 18 p3037 A67-33608

Bates theory of atomic oxygen excitation in upper atmosphere as cause of F layer nightglow emissions 18 p3038 A67-33616

Ionospheric electron temperature incoherent backscatter measurements confirming predawn enhancement of 6300 angstroms airglow 18 p3039 A67-33624

Airglow and auroral phenomena, discussing ideal coordinate system, electric fields, morphology, solar wind-magnetosphere interactions, and particle precipitation 18 p3039 A67-33625

Height profile of atomic oxygen 6300 angstrom emission in night airglow determined by rocket photography 19 p3215 A67-35177

Rocket observations of visible and UV dayglow including emission rates and electron density and

- temperature 19 p3221 A67-35277
Hydrogen and hydroxyl emissions in 19 p3223 A67-35483
Airglow measurement apparatus and procedure at Tehran 19 p3224 A67-35488
Fabry-Perot interferometer with magnetostrictive scanning and SNR improves system for solar physics and airglow observations 20 p3440 A67-36360
Fabry-Perot spectrometer applied to upper atmospheric emission measurements of airglow and aurora 20 p3440 A67-36362
Nitrogen and oxygen dayglow emissions observed during total solar eclipse of May 1965, studying emission/continuum intensity ratio 20 p3427 A67-36368
Night airglow research during IQSY noting correlation of low activity with sunspot minimum 20 p3430 A67-36905
OH Meinel band, nitrogen dioxide continuum and O I S to I D transitions maxima altitudes in midlatitude night airglow emissions from rocket radiometer measurements 23 p3995 A67-40613
- AIRLINE**
European airline depreciation practice and suggested modification 01 p0168 A67-10269
Airline safety rules formulation, considering future aircraft capacities. [AIAA PAPER 66-844] 03 p0360 A67-14015
Airline strategy for domination of Northeast Corridor despite improvements in high speed ground transportation [AIAA PAPER 66-942] 03 p0361 A67-14021
Airline viewpoint on air traveler handling and airport problems and effects of new jet aircraft [AIAA PAPER 66-845] 04 p0595 A67-14978
Service abandonment aspects of movement against subsidization of airways by CAB 05 p0929 A67-16770
Systems and techniques in aircraft maintenance to meet problems of parts reliability, longevity and shop cost [SAE PAPER 670338] 12 p1895 A67-25877
Airline operation, reliability, personnel and training techniques [SAE PAPER 670343] 12 p2041 A67-25879
Airline flight testing problems, discussing aircraft availability, equipment competency, crew proficiency, safety, economy, etc 13 p2052 A67-26424
Technical, economic and operation criteria for airlines when switching from conventional engines to turboprops or turbojets 14 p2409 A67-28499
Earth orbital transportation, proposing airline type system and composite nuclear-airbreathing engines for reusability with minimum refurbishment [AAS PAPER 67-84] 15 p2546 A67-29950
Commercial airline equipment selection, schedule simulation, routing and fleet planning [AIAA PAPER 67-392] 15 p2421 A67-30360
Inertial systems application to airline operation, discussing data insertion, power supply integrity, alignment display, dynamic testing, etc [AIAA PAPER 67-396] 15 p2515 A67-30363
Airline terminal building concept to provide practical approach to terminal complex design [SAE PAPER 670320] 17 p2835 A67-32981
Air traffic control delays, terminal congestion and inadequate ground transportation facilities effect on regional airline operation 19 p3348 A67-34972
Airlines and airport owners problems, particularly introduction of superjets, competition, V/STOL aircraft, etc 19 p3348 A67-34976
Air transportation opportunities for development and elimination of subsidy through strengthening of smaller carriers 19 p3348 A67-34977
Economic trends interrelationship with future investment climate for airline securities 19 p3349 A67-34979
Airlines and governmental regulatory agencies controlling competition, new entry and rate policies relationship, examining all-cargo carrier and passenger trunk line 19 p3349 A67-34980
All-weather landing examined in terms of operational techniques and design criteria for airline performance and safety [AIAA PAPER 67-572] 19 p3258 A67-35968
Legal and financial problems in obtaining airline tickets for third persons 20 p3555 A67-36300
- V/STOL aircraft scheduling for passenger demand and equipment mix, optimizing airline earnings with mathematical programming model [AIAA PAPER 67-801] 24 p4259 A67-42961
V/STOL airline economics simulated with computerized dynamic programming model [AIAA PAPER 67-841] 24 p4096 A67-42979
Commuter airline planning using systems analysis to examine technical, managerial, legal and economic aspects [AIAA PAPER 67-843] 24 p4259 A67-42981
- AIRPORT**
SA HELIPORT
SA LANDING AID
Public airport noise problem, examining extent to which constitutional-taking theory has been usual ground for damage suits 01 p0170 A67-10929
STOL aircraft characteristics compared with VTOL aircraft and helicopter, noting airport layout 03 p0357 A67-12969
VTOL jet transport noise effect on surrounding habitants and guidelines for airport design 03 p0357 A67-12973
Operation of VTOL aircraft in vicinity of airport including safety, noise and air traffic control factors 03 p0357 A67-12974
Passenger volume handled and area accommodated by commercial airports in West Germany 03 p0538 A67-12978
C-5A aircraft design load criteria for landing gear of large aircraft that must operate from semimproved airfields [AIAA PAPER 65-711] 03 p0360 A67-13781
SST servicing and maintenance characteristics and suitability of existing and planned airports 03 p0360 A67-13919
Airline viewpoint on air traveler handling and airport problems and effects of new jet aircraft [AIAA PAPER 66-845] 04 p0595 A67-14978
Low clouds effect on ILS jet landing at Bombay airport during monsoon season, noting airfield climatology 05 p0838 A67-16711
Aircraft noise control at international airports with special reference to Heathrow 05 p0752 A67-17101
Multiple-access worldwide satellite communication system for aircraft terminals with limited antenna gain and transmitter power 06 p0960 A67-17674
Airport traffic control tower instrument panel displaying continuously telemetered data on current weather conditions of runway complex 10 p1656 A67-23087
Recording telethermometer for use at airports, noting performance characteristics including unattended reliability, rapid response time, etc 10 p1656 A67-23088
Airport accessibility, discussing rail extensions to airports, bus lanes and bus-rail vehicles [SAE PAPER 670322] 12 p1925 A67-25868
Aircraft noise monitoring system for Zurich airport 13 p2052 A67-26535
Aircraft noise and siting of major airport 13 p2089 A67-26536
Aircraft noise regulation at Kennedy International Airport 13 p2053 A67-26538
Research approaches to alleviation of airport community noise 13 p2053 A67-26539
Bird hazard to aircraft at Auckland International Airport, examining geographical features, history, species, daily movement patterns and seasonal abundances 15 p2419 A67-29672
Public and private financing of vertiports /VTOL aircraft terminals/ for intercity service, investigating financial self-supporting possibilities [AIAA PAPER 67-829] 24 p4259 A67-42975
- AIRPORT LIGHT**
Airport lighting for category II landings with aid of all-weather landing systems by following ICAO guidelines, noting threshold markings, runway lights, etc 07 p1167 A67-20150
Ground requirements for instrument landing systems noting approach lighting, runway marking, taxi guidance and blind navigation [AIAA PAPER 67-756] 23 p3933 A67-40989
- AIRPORT PLANNING**
Concrete pavement performance at ten civil airports, examining durability of surfaces, jointing subbase thickness and maintenance 02 p0229 A67-11841
Optimum passenger handling in long haul air transportation for various airport facilities [AIAA PAPER 66-843] 02 p0181 A67-12257
Total systems concept utilizing aerospace planning and preliminary design techniques as solution to future megalopolis airport requirements [AIAA PAPER 66-944] 02 p0230 A67-12279
Parameters to be calculated in checking airport possibilities for accommodating IL-18 aircraft, considering maximum takeoff weight 03 p0360 A67-13780
Genoa airport construction problems on land reclaimed from sea 05 p0789 A67-17100
STOL and VTOL aircraft performance and cost for intercity travel, discussing airport network 08 p1279 A67-20782
Costs involved in delays occasioned by either ATC or airport acceptance rate for New York-Boston-Washington complex [SAE PAPER 670264] 11 p1884 A67-23987
FAA development program for air traffic control, navigation and landing aids and airport capacity [SAE PAPER 670265] 11 p1885 A67-23988
Soft gravel and aerated concrete material of various sizes tested to safely decelerate aircraft overshooting runway during takeoff and landing 14 p2246 A67-28817
Airport requirements for Boeing model 747, including description of necessary modification of terminal facilities and ground equipment [AIAA PAPER 67-384] 15 p2468 A67-30353
Economic factors controlling development of high capacity supersonic transport aircraft 16 p2782 A67-30838
Aircraft flotation requirements, emphasizing surface strength reduction 17 p2832 A67-31986
Airport terminal planning for Tampa eliminating long walk, using circular multistory structure with handling equipment for passengers and baggage [SAE PAPER 670319] 17 p2835 A67-32980
Airline terminal building concept to provide practical approach to terminal complex design [SAE PAPER 670320] 17 p2835 A67-32981
Airport economics application to new airports, considering social implications, cost, profit and land value [SAE PAPER 670356] 17 p2974 A67-32995
Solutions for aviation crisis of congestion, delays and noise, including problems anticipated with jumbo and SST jets 19 p3207 A67-34968
Close coordination of aviation with other transportation facilities, considering airport/heliport planning within city planning, high speed train competition, highways congestion, etc 19 p3347 A67-34969
Air traffic control delays, terminal congestion and inadequate ground transportation facilities effect on regional airline operation 19 p3348 A67-34972
Airlines and airport owners problems, particularly introduction of superjets, competition, V/STOL aircraft, etc 19 p3348 A67-34976
Air traffic control /ATC/ in 1970s, discussing airports, electronic facilities and collision avoidance 20 p3482 A67-37441
Modernizing air traffic control, governmental procedures, airports and support facilities to accommodate Boeing 747 and supersonic transports 20 p3418 A67-37442
Provision of additional metropolitan airport facilities to accommodate supersonic transportation noting noise abatement, traffic growth and off-airport processing 20 p3556 A67-37444
Floating airports proposed as solution to short haul air traffic problems in New York 20 p3418 A67-37445
Philadelphia International Airport facility planning based on forecasts, population and business growth, economic factors and historic trends 21 p3734 A67-38805
Master plan for Philadelphia International Airport to accommodate increased air travel, cargo and jet aircraft 21 p3608 A67-38806
Airport wheel hub terminal circumscribed by two satellite buildings noting passenger vehicular access, pedestrian movement, aircraft servicing, etc 21 p3608 A67-38807
Airport terminal facilities - Conference, Houston, April 1967 22 p3778 A67-39373
Houston Intercontinental airport planning and development for supersonic jet, superjet and SST aircraft 22 p3779 A67-39374

Gate arrival terminal design for Kansas City MCI airport noting loading positions, maintenance hangars, service roads, post office, etc 22 p3779 A67-39375

Air terminal complex at Pittsburgh noting construction and expansion proposed under master plan 22 p3779 A67-39376

Development of major air terminal buildings at Canadian airports by maximum operational capacity, land availability, noise contours and capital investment 22 p3779 A67-39377

Smaller airports to support small jet feeder line service noting need for expansion and integration of airports with urban centers 22 p3744 A67-39378

Aircraft terminal apron design, considering passenger convenience, variations in aircraft configuration and changes in aircraft mix and loading facilities 22 p3779 A67-39379

Apron underground fueling systems, using experience in aircraft fueling to justify reduction or elimination of hydrant service vehicles 22 p3779 A67-39380

Airport requirements for V/STOL and short haul air transportation, stressing need for solution of noise problem 22 p3779 A67-39381

Problems of handling people on future giant aircraft noting reservations, ticketing, boarding procedures and baggage-handling functions 22 p3780 A67-39382

Airport planning in 1970s noting environment compatibility, crosswind tolerance, passenger volume, automobile parking and metropolitan access [AIAA PAPER 67-760] 23 p3987 A67-40991

Commuter airline planning using systems analysis to examine technical, managerial, legal and economic aspects [AIAA PAPER 67-843] 24 p4259 A67-42981

Short haul VTOL air transportation airport-community noise problem, examining propulsion systems and site planning [AIAA PAPER 67-867] 24 p4096 A67-42990

Highway, ramp, terminal, runway and approach congestion problems for airports, suggesting separated general aviation airports and runways to alleviate big jet airports [AIAA PAPER 67-871] 24 p4139 A67-42992

AIRPORT SURFACE DETECTION

EQUIPMENT /ASDE/

Aircraft noise measurement evaluation and control, discussing monitoring and mapping 04 p0551 A67-14591

Automatic aircraft-noise monitoring equipment at Frankfurt airport to measure noise levels during takeoff and maintain them within regulations 09 p1484 A67-21941

AIRWORTHINESS REQUIREMENT

Stalling in swept wing jet aircraft with reference to satisfying airworthiness regulations and aerodynamic problems 03 p0362 A67-14300

Dynamic response of sailplanes to elevator control in longitudinal maneuvers, discussing load factors and tail loads as function of aerodynamic and inertial parameters 16 p2597 A67-31786

Gliders examined from construction standpoint including damage tolerance, airworthiness, radiation, operational loads and repairability 20 p3360 A67-36454

Factors for SST safety and airworthiness requirements, discussing environment, engineering level, learning and flying quality [AIAA PAPER 67-751] 23 p3933 A67-40985

AIRYS STRESS FUNCTION

SA POISSON RATIO

Thermal stresses in isotropic circular cylinder under temperature distribution effect, reducing problem to solution of boundary value in form of Airy stress function 01 p0159 A67-10278

Stress function boundary conditions along perfectly free edges of membrane-like disks and shells loaded by optionally distributed forces 11 p1881 A67-25096

Stress concentrations around shaped holes in plates under uniform tension, deriving formulas by perturbation method 15 p2577 A67-30268

ALBEDO

SA COSMIC RAY ALBEDO

SA EARTH ALBEDO

Reflective properties of natural surfaces, noting dependence on surface properties of total reflected energy, spectral distribution, polarization degree of radiation, etc [AIAA PAPER 65-665] 03 p0411 A67-13045

Differential energy spectra and fluxes of charged splash and reentrant albedo proton measurement of cosmic radiation in various energy ranges 08 p1377 A67-21467

Aircraft measurements of clouds in spectral range from 8 to 12 microns, determining albedo for stratified clouds 18 p3073 A67-33559

ALCOHOL

SA CHOLESTEROL

SA ETHYL ALCOHOL

SA METHYL ALCOHOL

Esterification of secondary alcohols, using amino acids 06 p0956 A67-18576

Mass spectra of amino ketones and amino alcohols and related substances 09 p1458 A67-22057

ALDEHYDE

SA FORMALDEHYDE

Flash pyrolytic technique applied to McFayden-Stevens reaction for various simple aliphatic aldehydes 04 p0565 A67-14524

ALFVEN WAVE

SA MAGNETOHYDRODYNAMICS

Cerenkov and cyclotron absorption of Alfven and fast magnetoacoustic waves in plasma with gas-kinetic pressure in quasi-linear approximation 01 p0124 A67-10747

MHD wave generation in sunspots, examining depth of solar magnetic layer that affects magnetic convection 01 p0151 A67-11283

Alfven standing wave generation by current injection and/or electromagnetic induction in conducting liquid 02 p0272 A67-11520

Nonlinear hydromagnetic wave propagation in inviscid conducting compressible fluid 03 p0480 A67-13726

Propagation of nonaxisymmetric Alfven waves in linear discharge tube filled with nonuniform plasma 03 p0485 A67-14045

Alfven wave in outward corona as natural explanation of fast drift bursts 04 p0691 A67-14485

Induction drag of long cylindrical satellites and Alfven waves emitted from them, determining potential and current distribution and effect on energy loss [AIAA PAPER 66-478] 04 p0704 A67-14829

Alfven velocity distribution in magnetosphere to understand nature of geomagnetic micropulsation 05 p0795 A67-16062

Drift waves in finite pressure plasma, noting oscillation caused instabilities induced by Alfven type and slow magnetoacoustic wave interaction 05 p0852 A67-16693

Oblong shape and Alfven waves of looped expanding coronal prominence 06 p1078 A67-18157

Transverse diffusion of particle perpendicular to magnetic field by assembly of random Alfven waves explains increase in electric field energy 11 p1840 A67-24753

Magnetofluid dynamics - AIAA Selected Reprint Series, Volume II 11 p1841 A67-24946

Parametric resonance excitation of Alfven waves by small LF modulation of DC magnetic field imposed on ideal MHD plasma 11 p1844 A67-25062

Hydromagnetic wave propagation and energy transfer in stratified isothermal plasma embedded in parallel uniform gravity and magnetic fields 11 p1868 A67-25083

Cerenkov and cyclotron absorption of Alfven and fast magnetoacoustic waves in plasma with gas-kinetic pressure in quasi-linear approximation 13 p2166 A67-26776

Alfven wave propagation in viscous incompressible infinitely conductive fluid under effect of gradually varying magnetic field 13 p2170 A67-27363

Electromagnetic wave propagation characteristics in solid plasmas without magnetic induction, showing dynamic Hall effect 14 p2366 A67-28473

Radiants associated with some, magnetosonic and Alfven waves and definition in terms of distribution of delta operator of infinitesimal discontinuity 14 p2359 A67-28511

Drift waves in finite pressure plasma, noting oscillation caused instabilities induced by Alfven type and slow magnetoacoustic wave interaction 15 p2530 A67-29864

Oblong shape and Alfven waves of looped expanding coronal prominence 16 p2737 A67-30501

Charged particles with Alfven velocities distribution in magnetosphere analyzed

based on cold plasma density, emphasizing data of OGO A 17 p2899 A67-32256

Collisionless shock waves in plasmas with high beta parameter, discussing Alfven wave turbulence, firehose instability, dissipation and structure 17 p2901 A67-32528

Hydromagnetic wave propagation in collisionless plasma based on Vlasov equation, finding Alfven, magnetoacoustic and nonoscillating waves 17 p2902 A67-32673

Magnetosonic resonances location in exosphere, showing diagram of Alfven velocity profile 18 p3042 A67-34389

Alfven and magnetosonic wave generation and propagation in magnetosphere, detailing azimuth number approaching infinity 18 p3042 A67-34391

Torsional Alfven waves attenuation in decaying hydrogenous plasma 19 p3290 A67-35377

Super-Alfvenic counterpart of transient sub-Alfvenic aligned-fields flow past airfoil 19 p3170 A67-35538

Model of nonradiative energy transport in sunspots, in which Alfven waves generated in convectively unstable layer propagate upward into overlying stable layer 19 p3330 A67-36079

MHD instability of sub-Alfven equations for zonal flow outside diurnally oscillating boundary layer of precessing spheroid 20 p3494 A67-36147

Alfven waves in ionized plasma of finite electrical conductivity, giving equations for semiphenomenological model 20 p3496 A67-36271

Highly asymmetric equation for MHD resonance of guided poloidal mode solved using dipole coordinates 20 p3502 A67-37427

Proton mechanism of escape from earth magnetic field, analyzing charged particle in Alfven wave field 20 p3520 A67-37667

Rotation effect on growth of discontinuity across Alfven wavefront, solving differential equations 21 p3662 A67-37761

Alfven velocity distributions in magnetosphere used to understand nature of geomagnetic micropulsation 21 p3616 A67-37849

Wave kinetics of free Alfven oscillations using Lagrange function of collisionless plasma, calculating energy growth rate and relaxation times 21 p3667 A67-38372

Decay instability of steady state waves in plasma, considering Alfven wave 21 p3674 A67-38803

Alfven standing wave formation due to interaction of magnetosphere with geomagnetic pulsation 21 p3621 A67-39023

Alfven, fast and slow magnetoacoustic and entropy hydromagnetic wave propagation in anisotropic collisionless magnetoplasma 22 p3843 A67-39268

Magnetic shear effects on density gradient drift instabilities in plasma with plasma pressure to magnetic pressure ratio larger than electron-ion mass ratio 22 p3845 A67-39463

Geomagnetic perturbation data from high altitude nuclear weapon detonations, deriving theoretical model based upon MHD resonance, noting Alfven wave behavior 22 p3792 A67-39932

ALGAE

SA CHLORELLA

Oxygen, carbohydrates, proteins, etc, produced by unicellular algae through photosynthesis, finding optimum efficiency of process 02 p0186 A67-11861

Mixed cultures of Chlorella pyrenoidosa TX 71105 and various bacteria and use in closed systems for support of man 10 p1598 A67-23626

Chromatographic accumulation of primary and secondary carotenoids in Spongiolochloris typica over 8-week period 14 p2254 A67-28065

Continuous synchronous culture of photosynthetic microorganism Chlorella cultivated in illuminated and dark stirred tanks 19 p3177 A67-34913

Chlorella and Scenedesmus unicellular algae mixture tested for biological protein value in humans for possible food source 19 p3179 A67-35228

Biological life support system for regenerating closed atmosphere by photosynthesis, using gas exchange between man and microalgae 19 p3180 A67-35236

Secretory activity of algal Chlorella cells effect on buffering characteristics of Tris or sodium citrate-citric acid suspending

- fluid 21 p3573 A67-37729
Survival of desert algae at extremely low temperatures and diurnal freeze thaw cycles 23 p3945 A67-41346
Unicellular algae continuous culture as autotrophic component of closed ecological system, discussing stabilization of biomass concentration to provide oxygen requirement 24 p4114 A67-41844
Biological regeneration of enclosed atmosphere with algae photosynthesis noting effect of diet change 24 p4114 A67-41845
Biological value of algal and soya proteins on four generations of white rats 24 p4111 A67-41847
- ALGEBRA**
SA BOOLEAN ALGEBRA
SA DIFFERENTIAL ALGEBRA
SA MATRIX ALGEBRA
Analog computer solution of simultaneous systems of linear algebraic equations, based on modified Gauss-Zeidel method 01 p0105 A67-10542
Transonic plane gas flow equations with algebraic self-similar solutions used for analysis of flow in various nozzles 02 p0178 A67-11951
Acceleration of iteration process convergence when dividing polynomial by quadratic trinomial, approximating curves for remainder coefficients by straight lines 06 p0125 A67-18557
Tame subsets of spheres in Euclidean-3 space, showing tameness of closed subset F of 2-sphere S 07 p1215 A67-19507
Computer manipulative algebra programs for Fourier series 08 p1299 A67-21260
Analytic formulas for locating real and complex roots of polynomial equations up to and including seventh degree 08 p1350 A67-21536
Root squaring and subresultant /RSSR/ routine as root finder for polynomial equations with real coefficients 09 p1468 A67-22050
Existence and preservation of algebraic sign in Green function for two-point boundary value problem 11 p1813 A67-24519
Nonuniform distributed network problems solved by Lie algebras 12 p1919 A67-25979
Transonic plane gas flow equations with algebraic self-similar solutions used for analysis of flow in various nozzles 17 p2841 A67-33268
Linear algebra describing equilibrium chemical systems and complex chemical mixtures, discussing hydrogen-fluorine coupling reaction at elevated temperatures 18 p2997 A67-34124
Natural torsional vibration frequency calculation method, with frequency as algebraic equations with real roots, discussing example problems 19 p3341 A67-35711
- ALGORITHM**
Stochastic approximation theory to obtain algorithms for recovery of functions, using noisy measurements taken at randomly selected points 01 p0028 A67-10450
Algorithm based on penalty functions to determine hyperplane used as iterative solution for separating convex sets 01 p0028 A67-10495
Algorithm based on affine transformation of plane figures used to compare images of written letters of alphabet 01 p0028 A67-10541
Numerical trajectory optimization method based on indirect and direct approaches for computer of limited memory 01 p0046 A67-11205
Evaluation of redundancy reduction algorithms to facilitate comparison in terms of performance by computer simulation, using real and synthesized data 02 p0197 A67-12015
Continuous linear programming problems with time delays in constraints, noting construction of solutions to dual problem from solution to primal problem 02 p0207 A67-12059
Abstraction problem in pattern classification, using algorithms with convergence properties 02 p0208 A67-12173
Iterative realization of pattern recognition networks consisting of multilayer of linear threshold elements 02 p0208 A67-12174
Algorithm for approximate solution of Wiener-Hopf integral equation 02 p0209 A67-12175
Variant of averaging functional errors method in solving linear integral boundary value equations 03 p0457 A67-13116
Algorithm for directed random search for minimum of function of n-variables 03 p0374 A67-13182
Equivalence relations for optimal control problems classification and algorithm construction 03 p0391 A67-13266
Unsolvability of recognition of linear context-free language, searching for algorithm and generalizing to metalinear languages 03 p0375 A67-13562
Automated learning methods used to design fault diagnosis procedures 03 p0400 A67-14217
Algorithm for statistical solution of radiant flux distribution in solar receivers with paraboloidal collectors 04 p0553 A67-14666
Algorithms in ZAM-2 computer program to calculate recording error parameters of linear scale measuring device 04 p0621 A67-14918
Optimal multichannel nonlinear filtering problem of minimum variance estimation of state of n-dimensional nonlinear system subject to stochastic disturbance 04 p0592 A67-15084
Test system for static tests on combinative unit for comparing two quantities given in binary code 05 p0768 A67-16265
Numerical algorithm for supersonic gas flow past blunt bodies with shock wave separation, using Dorodnitsyn method of integral correlation 05 p0791 A67-16374
Numerical method for calculation of finite amplitude orographic disturbances by using finite difference algorithm 05 p0837 A67-16484
Jordan form matrix algorithm of Wasow for reducing systems of first order ordinary differential equations with turning point 05 p0835 A67-16779
Nekrasov method application to construction of algorithm for small solutions to nonlinear integral equations, using recursion techniques 05 p0836 A67-17488
Algorithm for locating ambiguous lobes in radiation pattern of large circular array 05 p0781 A67-17535
Approximation techniques generating algorithm for iteratively solving sequential optimization of nonlinear control systems 06 p0974 A67-17930
Algorithm encountered while solving trajectory optimization problems, discussing variational concepts, indirect, gradient, second variation and generalized Newton-Raphson methods 06 p1082 A67-17932
Matrix error analysis compared to algorithm optimization problems of numerical analysis 06 p1024 A67-18475
Time optimal search algorithms in pulsed extremal control systems with inertial or transport delays for case with known time constants and delay time 06 p0978 A67-18794
Nonlinear self-adjusting system with linear prediction analyzed by digital computer 07 p1160 A67-19200
Iterative algorithm for increasing stability of adaptive control systems 08 p1308 A67-20319
Algorithms for dichotomous representation of macrocircuits, considering computer programs and establishment of flow graphs 08 p1299 A67-20326
Algorithm determining negative resistance intervals in parametric amplifier 08 p1299 A67-20334
Conjugate gradient minimization method in function space 08 p1310 A67-20337
Experiment selection process for specific flights in Apollo applications program /AAP/, using algorithms [AAS PAPER 66-142] 08 p1411 A67-20967
Van der Monde systems and numerical differentiation based on Neville formula 08 p1349 A67-21194
Algorithm for analyzing general electric circuits with lumped parameters in transient state by automatic digital computer 09 p1469 A67-22440
Rapid and accurate ray tracing algorithm for horizontally stratified atmosphere, using effective earth-radius technique 09 p1464 A67-22450
Learning machines used for classifying measurement data of objects representable as points in n-dimensional space after training by forced learning 10 p1654 A67-22757
Algorithm based on penalty functions to determine hyperplane used as iterative solution for separating convex sets 10 p1608 A67-23617
IBM System/360 Model 91 systems design using decomposition algorithm and three-cycle multiplication 11 p1755 A67-23948
High speed floating-point algorithm of IBM System/360 Model 91 for exploiting multiple execution units 11 p1755 A67-23950
Positional coordinates of spacecraft determined by algorithm, using distance from three predetermined points as found by rangefinders 11 p1816 A67-24083
Algorithms for operator partitioning method in reducing shell equations solution to calculation of solid intersecting rod systems 12 p2026 A67-25617
Computer-aided layout of minitask artwork 12 p1950 A67-26130
Numerical method for calculation of finite amplitude orographic disturbances by using finite difference algorithm 13 p2150 A67-26340
Simultaneous stability and quality control of pulse regulation, discussing computation of sum of squares of difference 13 p2086 A67-26474
Matrix algorithm for calculating mean square error for synthesis of optimum control systems 13 p2087 A67-26612
General algorithm for solving atmospheric optics problem applicable to short wave radiation transfers of atmospheres with various light scattering, using Monte Carlo method 13 p2151 A67-26684
Two LMS algorithms related to steepest descent method, obtaining generalized theorems 13 p2147 A67-27173
Ordinary and time lag root locus diagram generating algorithm for adaptation to programming on digital computer 13 p2074 A67-27223
Zeros of polynomials with real or complex coefficients determined, using steepest descent method in convergent procedure 13 p2148 A67-27496
Experiment selection process for specific flights in Apollo applications program /AAP/, using algorithms [AAS PAPER 66-142] 13 p2214 A67-27548
Algorithm construction for processing of telemetry data in determination of space vehicle trajectories, applying dynamic filtering method 14 p2382 A67-27853
Theory of nonself-adjoint ordinary second order differential operators, discussing solution algorithms 14 p2343 A67-28478
Cross section central line algorithm developed and applied to torsional problems of rods with polyconal cross section 14 p2401 A67-28739
All-pass networks design method using algorithm and computer program for communications system application 14 p2274 A67-28914
Step-by-step self-adaptive algorithm for selective systems with automatic control 15 p2455 A67-29123
Computational errors in generation of direction cosine matrix in strapdown system 15 p2515 A67-29741
Modular distance measurement using geometric model for electronic continuous wave distance measuring equipment 15 p2511 A67-29893
Large scale integration of arithmetic functions utilizing picosecond circuits, noting ease of fabrication, flexibility and module multipliers 15 p2452 A67-29936
Backward and forward algorithms of dynamic programming for time dependent systems, noting advantages of forward algorithm for optimization of system 15 p2440 A67-30157
Algorithm for statistical estimation of nonlinear function of signal containing noise 16 p2643 A67-30921
Random signal treatment by Monte Carlo method for cutting tool applications 16 p2643 A67-30922
Linear programming algorithm for optimizing channel assignments in satellite communication systems 17 p2810 A67-32111
Linear programming algorithm for optimizing life support systems of space vehicles in terms of minimum weight/efficiency ratio 17 p2807 A67-32254
Solving general integer programs,

investigating cutting methods, rounding algorithm, branch and bound method and partition method 17 p2819 A67-32427

Algorithm for constructing state equations corresponding to linear time varying system of differential equations 17 p2829 A67-32627

Geometrical and equilibrium equations derived for circular plates, introducing Lagrange type coordinate as independent variable 17 p2961 A67-32807

Perceptron system for correcting average line position of open loop portion of control system, discussing pole interaction and self-organization 17 p2830 A67-33098

Algorithms for dichotomous representation of macrocircuits, considering computer programs and establishment of flow graphs 18 p3005 A67-33498

Synthesis of time optimal control for discrete plants described by difference equations, deriving algorithm defining surface in phase space of variables 18 p3017 A67-33872

Algorithm for Fredholm type integral equation solution incorporating successive approximations, kernel replacement by degenerate kernel, averaging functional corrections and band methods 18 p3071 A67-34167

Lunar forced physical librations calculation improved by using digital computer programmed to generate iterative solutions 18 p3129 A67-34307

Algorithm for construction of discrete approximations to linear differential expressions in terms of ordinates 18 p3072 A67-34394

Time optimal search algorithms in pulsed extremal control systems with inertial or transport delays for case with known time constants and delay time 18 p3018 A67-34459

Algorithm for computing matrix Riccati equation solution in optimization problems 19 p3249 A67-34781

Internal states minimization of sequential machines by developing algorithm 19 p3200 A67-34844

Chebyshev approximation principle applied to electronics problems, giving algorithm 19 p3201 A67-34909

Identification problem solution by gradient and Newtonian methods, using algorithm simplified by sensitivity function 19 p3205 A67-35914

Functional analysis applied to optimum control by reduction of variational problem to finite dimensional analysis and calculation of algorithms for use with digital computer 20 p3477 A67-37034

Dynamic programming for optimal algorithm for extremal control in presence of noise at system input and output 20 p3408 A67-37072

Modulo control algorithms application in circuit for finding residues 20 p3392 A67-37153

Optimal control theory for linear distributed parameter systems, presenting solution algorithms and computational results for several problems 20 p3411 A67-37321

Adaptive unknown-waveform pulse signal detector algorithm construction method 20 p3384 A67-37333

Numerical methods for linear optimal control problems, noting applicability of algorithms to certain nonlinear problems 20 p3411 A67-37375

Sequential decoding algorithm with memoryless channel, obtaining lower bound to distribution of computation and limiting factor [JPL-TR-32-1121] 20 p3412 A67-37494

Digital switching functions and pattern recognition realization through computer-programable algorithm for designing feed-forward threshold logic nets 21 p3588 A67-38182

General algorithm for solving atmospheric optics problem applicable to short wave radiation transfers of atmospheres with various light scattering, using Monte Carlo method 21 p3618 A67-38428

Algorithm for selecting optimum parameters for mathematical programming problem in thin walled systems, noting stress-strain state characteristics 21 p3728 A67-38904

Discrete method extension for bending stability problem in sectorial plates, obtaining algorithm for solutions of

boundary conditions and external loads 21 p3729 A67-38907

Strapped-down inertial navigation computational problems solved by Euler parameter algorithms require less computer time 21 p3656 A67-38951

Stochastic optimal control algorithm for pursuit process in problem of encounter of two cosmic objects 22 p3878 A67-39183

Triaxial orbital orientation control algorithm for space vehicle with incomplete angular position information 22 p3899 A67-39191

Optimal algorithm for single parameter linear and nonlinear correction of interplanetary flight, noting application to space vehicle approach to designated planet 22 p3830 A67-39193

Algorithm for piecewise smooth point-to-point mapping of straight line onto straight line to determine various motions 22 p3777 A67-39778

Threshold discrimination for two unknown a priori probability signals against noise background, using stochastic approximation in algorithm 24 p4134 A67-41795

Algorithm for processing primary motor characteristics of human motions on digital computer 24 p4114 A67-41857

Approximate solution to irregular waveguides with impedance boundary conditions based on amplitude of normal wave propagation 24 p4120 A67-42159

Random Gaussian signal with unknown mean value reception using adaptive systems 24 p4120 A67-42224

Dynamic programming, deriving successive sweep method for optimal control problems, discussing discrete algorithm for numerical problems 24 p4136 A67-42694

Pattern recognition model as self-learning algorithm noting Nagy and Shelton scheme 24 p4137 A67-42821

Ad hoc exact solution techniques for nonlinear partial differential equations noting physical applications 24 p4180 A67-43085

ALIGNMENT
SA FIELD-ALIGNED IRREGULARITY /FAI/
Calculation of scale functions of alignment nomogram as applied to sets of functions 01 p0104 A67-10279

Time optimum control of alignment process for gyrocompasses 07 p1186 A67-19629

In-flight transfer, fine and maneuver alignment of air to surface missile guidance system 17 p2881 A67-32487

Stationary or long range space vehicle transmitting antennas remote alignment technique using received signal AM 18 p3016 A67-34596

Digital temperature compensation and statistical filtering procedures for fast reaction alignment of inertial navigators 22 p3831 A67-39886

ALIPHATIC COMPOUND
S ORGANIC COMPOUND
KALKI
Physicochemical processes in thin evaporated films studied in terms of emf of galvanic cell with film acting as electrode 02 p0290 A67-11735

Alkali ion scattering coefficient from tungsten single crystals surface and dependence on incidence angle 06 p1036 A67-18424

General relations for amplification and oscillation development in optically pumped alkali vapor maser derived and applied to rubidium 85 15 p2501 A67-30095

KALKI HALIDE
Kinetics of stored energy buildup in alkali halide crystals after proton irradiation, noting dependence on lattice energy of crystal 01 p0136 A67-11050

Ultrasonic attenuation of alkali halide crystals in 120 to 180 degrees K range, noting thermal annealing of dislocation pinning centers 02 p0298 A67-11888

Disintegration of alkali halide single crystals, polymers and glasses under laser radiation, noting parameters of disintegration region 03 p0439 A67-14367

L-and K-band absorption due to optical transitions starting from ground state of F center in alkali halide 05 p0864 A67-16801

Single crystal film structure of fcc metals evaporated in ultrahigh vacuum onto alkali

halide surfaces cleaved in air and in situ 09 p1552 A67-21677

Molecular beam electric resonance /MBER/ spectrometer for hyperfine structure of rubidium 11 p1821 A67-23968

fluoride 11 p1821 A67-23968

Doped alkali-halogen-crystal color center origin and transformation at liquid N temperature using ruby laser, noting temporary bleaching 12 p1951 A67-25204

Radiation-induced electroconductivity and secondary emission in alkali halide single crystals under positive ion bombardment 13 p2177 A67-27073

Energy distribution of electrons emitted from alkali halide films on Mo substrates during positive helium and argon ion bombardment 13 p2177 A67-27073

Thermionic properties, surface ionization, atomic and ionic sublimation of Re, Mo, Ta and W 19 p3264 A67-35082

Surface ionization of atoms and molecules on nonmetals, determining work function and activation energies for dissociation 19 p3264 A67-35082

IR absorption in alkali-halide crystals containing molecular ion impurities caused by intralattice vibrations 20 p3511 A67-37140

Experimental determination of compression and rarefaction shock waves structure causing high pressure phase formation and decay in potassium halides 23 p3989 A67-40909

Two-photon absorption in alkali halide crystal via gas laser noting F center formation 24 p4187 A67-42361

KALKI METAL
SA CESIUM
SA LITHIUM
SA POTASSIUM
SA RUBIDIUM
SA SODIUM
Fabrication of columbium alloy liquid metal loop to study boiling and condensing characteristics of Na and K up to 1000 degrees F with gas tungsten arc welding in helium atmosphere 01 p0080 A67-10945

Density of liquid alkali metals in generalized equation obtained by method of thermodynamic similarity 04 p0640 A67-15596

Cross sections for charge transfer between alkali-metal ions and cesium atoms determined as function of primary ion beam energy, noting structure consisting of oscillations 04 p0661 A67-15766

Unfamiliar metals properties and potentialities from viewpoint of metallurgist 05 p0830 A67-17088

Differential Stark effect in second excited state of alkali metal atoms described, using electric field level crossing spectroscopy 06 p1035 A67-17830

Hugoniot equation of state of alkali metals, using technique based on isentropic sound speed measurement at room temperature 06 p1032 A67-18141

Diagnostic measurements in alkali plasma Hall accelerator /alpha/ including azimuth and axial velocity components, energy flux, total beam power, etc [AIAA PAPER 67-46] 06 p1042 A67-18493

Sharp line emission spectra due to alkali metal doping in ZnO crystals at low temperatures 06 p1060 A67-18914

Li, Na, K, Rb and Cs vacuum tests as coolants and working fluids in high temperature compact space power plant 07 p1223 A67-19464

Three-photon ionization transition rates for alkali atoms, using quantum defect Coulomb functions to evaluate perturbation formula 07 p1195 A67-19496

Dimensionality of superconductivity in alkali-metal-graphite lamellar compounds 07 p1236 A67-20138

Oscillator strength of atomic and ionic lines, normalization of NBS gf values and solar abundances of alkali metals 07 p1256 A67-20167

Syringe injection system for seeding plasma with Na-K alloy in study of MHD power generation and propulsion 08 p1279 A67-20377

Charge exchange of protons in alkali metal vapors with formation of highly excited hydrogen atoms, noting cross section, reaction mechanism, etc 08 p1358 A67-20855

Molecular association in Na, K and Cs vapors, noting existence of dimer and tetramer molecules 08 p1355 A67-21033

Measurements of conductivity, electron

density and ionization rate of cesium in argon on alkali shock tube, describing MHD generator wind tunnel experiment 09 p1540 A67-21789

Temperature dependence of saturated vapor pressure of sodium and potassium 09 p1579 A67-21857

Electric propulsion for space exploration, discussing testing results on Rankine cycle power system [AIAA PAPER 66-890] 09 p1559 A67-21870

Flute instability in mirror confined plasmas assuming particle drift under external forces 11 p1830 A67-24004

Magnetic field curvature effects on low temperature alkali metal plasma column stability 11 p1830 A67-24007

Plasma stability, discussing flute and Kadomtsev instabilities and possibility of anomalous diffusion for confined steady state 11 p1831 A67-24011

Effective cross sections of excitation of lower energy levels during electron collisions in alkaline metals, noting dependence of various levels on quantum number and atomic number 11 p1822 A67-24018

Equilibrium and stability of K plasma with internal E field normal to confining magnetic field, noting wave propagation at ion momentum velocity 11 p1833 A67-24369

Alkali metal plasma generator design and performance, noting characteristics of LF wave propagation parallel to magnetic field 11 p1837 A67-24396

Electron cyclotron resonance heating of alkali plasmas by electromagnet resonant absorption 11 p1838 A67-24407

Porous W-Ta emitters as ion source for production of quiescent alkali plasmas of improved symmetry, reproducibility and uniformity 11 p1838 A67-24411

Thermal accommodation coefficient measurements with rare gases and metals and alkali metal sets 13 p2223 A67-26942

Thermally ionized low density alkali-metal plasma for simulating controlled fusion processes, noting high particle losses and instability 14 p2362 A67-29038

Cavitation damage in alkali metal pumps, noting damage resistance and material properties for application in space power systems 15 p2494 A67-30151

Atmospheric pressure discharges in inert gases seeded with alkali metal vapor, noting transition to low voltage high current discharge 16 p2709 A67-30513

Polyatomic gaseous impurity effect on electric conductivity of alkaline plasma from axial field and electron temperature measurements 16 p2710 A67-30520

Alkali metal vapor and inert gas mixtures with alkali seeding radiation properties, noting nonequilibrium argon-krypton plasma parameter determination in electrical discharge 16 p2710 A67-30522

Physical properties of binary pulsed discharge plasma in helium and argon seeded with Cs and K 16 p2711 A67-30525

Hydrogen solubility in eutectic sodium-potassium mixture, noting usefulness as nuclear reactor coolants, and dependence on pressure and temperature variations 16 p2619 A67-30620

Density of lithium, sodium and potassium up to 1600 degrees C, using pycnometer method, showing dependence of density on temperature 16 p2692 A67-31773

Electric propulsion for space exploration, discussing testing results on Rankine cycle power system [AIAA PAPER 66-890] 17 p2928 A67-32051

Ionization of low temperature supersonic plasma jets, noting kinetics of elementary processes, gas dynamic parameters and effects of combustion and alkali metal admixtures 17 p2896 A67-32170

Optically pumped alkali metal vapors orientation checking by light pulse method, noting relaxation curve 17 p2869 A67-32811

Existence in alkali-metal-seeded rare gases of mode of nonequilibrium electric discharge with constricted positive column 17 p2910 A67-33385

Twilight observations for 80-100 km region, noting orthohelium measurements for solar radiation and dust and alkali-metal concentrations for D-region ionic constitution 18 p3035 A67-33601

Ionization and recombination processes of

alkali metal ions in hydrogen-oxygen-nitrogen flames with hydrocarbon additives 18 p3107 A67-33806

Excitation and radiation of OH molecules and alkali metals in low pressure flames and rocket exhausts 18 p3152 A67-33819

Alkaline-metal-plasma machine design, studying operating modes with electric probes 18 p3091 A67-34631

Alkali-metal magnetoplasma properties related to enhanced diffusion, showing relationship to beam-plasma interaction 19 p3287 A67-35360

Plasma wave propagation dispersion in sodium and potassium at cryogenic temperature using Landau-Fermi liquid theory 20 p3514 A67-37570

Energy level behavior of metastable alkali atoms against autoionization and radiative decay 20 p3492 A67-37691

Alkali plasma Hall accelerator /ALPHA/ thruster performance, discussing acceleration mechanisms and correlating data [AIAA PAPER 67-687] 21 p3692 A67-38718

Cycle and separator efficiencies and specific radiator area compared for liquid alkali metal-lithium MHD power generators 21 p3572 A67-38864

Electron impact ionization cross sections and rate coefficients for atoms and ions of Hg, rare gas and alkali metal groups 21 p3660 A67-39098

Pseudopotential-structure factor relation for small wave vector applied to liquid alkali metal electric resistivities and temperatures 21 p3686 A67-39102

Plasma and sheath characteristics computation for alkali plasma devices involving contact ionization for ion production [AIAA PAPER 67-691] 22 p3868 A67-39843

Optically pumped vapor rotatory power as optical pumping experiment monitoring technique, discussing specific rotatory power and refractive index dependence on light frequency 22 p3816 A67-40320

Na and K introduced into Si by diffusion from thin layer of alkali metal and during electrolysis of molten alkali halogenides 23 p4037 A67-40721

Electron-electron interaction effect on Li soft X-ray emission spectrum, liquid metal optical absorption and alkali metal dielectric response 23 p4037 A67-40760

Na-acenaphthene reaction temperature dependence, studying optical density, precipitation, ion pair formation, coupling constants and hyperfine structure [JPL-TR-32-1144] 24 p4118 A67-42326

Real gases examined for application as working fluid in Brayton cycle power plant, considering radiator area reduction to Rankine cycle 24 p4102 A67-42488

Alkali, alkaline earth and rare earth elements distribution in chondrite component minerals 24 p4236 A67-42646

Alkali metal Rankine cycle space power system component and systems design 24 p4186 A67-42887

ALKALINE EARTH METAL

SA BARIUM

SA BERYLLIUM

SA CALCIUM

SA MAGNESIUM

SA STRONTIUM

Electronic band structure calculations phase of Ca, Sr and Ba over wide range of atomic volumes under pressure electronic band structure calculations for fcc phase of Ca, Sr and Ba over wide range of 10 p1682 A67-23399

Superconducting transition temperatures and low field magnetization of ceramic mixed Ba, Sr and Ca-Sr titanates, showing particle nature of 19 p3302 A67-35037

Average dwell times and velocities of Ba, Sr, Li, Ti, Sn, Bi, Be, Zn, and Hg in argon plasma 19 p3281 A67-35155

Electron paramagnetic resonance of trivalent rare earth-monovalent alkaline earth ion pairs in calcium fluoride 21 p3676 A67-37815

Alkali, alkaline earth and rare earth elements distribution in chondrite component minerals 24 p4236 A67-42646

ALKALINE EARTH OXIDE

S BERYLLIUM OXIDE

S CALCIUM OXIDE

S MAGNESIUM OXIDE

ALKALOID

SA STRYCHNINE

Structures and stereochemistry of clivonine and clivimine analyzed through mass spectroscopy and nuclear magnetic resonance 09 p1458 A67-22059

ALKANE

Gas chromatographic and mass spectrometric analysis of chlamydospores of Ustilago maydis, U. nuda and Sphacelotheca reiliana for hydrocarbon content 03 p0363 A67-13594

Frequency shift and absorption bands in IR spectra of some alpha,omega-dinitroxy alkanes 05 p0758 A67-16367

Pitzer acentric factor relationship to Morse intermolecular potential function appears to hold only for normal fluids 07 p1138 A67-20193

ALKYNE

Stereospecific addition of organophosphides to terminal alkynes 04 p0565 A67-14522

Photochemical study of propyne with 2062-A iodine line 24 p4118 A67-42327

ALL-SKY PHOTOGRAPHY

Cameras used in auroral and airglow experiments including SP3 spectrophotometer, three-channel photometer and all-sky camera 03 p0419 A67-13376

All-sky camera data used to construct isoauroral diagrams for IQSY period describing incidence of auroral forms and behavior pattern 22 p3791 A67-39806

Azimuths of extended auroral features measured on all-sky photography during IQSY, discussing arc alignments and auroral oval 22 p3791 A67-39807

ALL-WEATHER AIR NAVIGATION

All-weather carrier landing system using precision tracking radar and microelectronic data link aboard carrier 01 p0026 A67-10969

All-weather landing system for C-141 jet cargo transport using vertical navigation computer for military operations 03 p0464 A67-12907

Onboard equipment designed for transport aircraft landings with visibilities less than 200 ft and runways less than 2600 ft, having all devices duplicated 03 p0464 A67-13001

Proposed system for maintaining helicopters in close-order formation during inclement weather and/or night operations 05 p0839 A67-16531

All-weather satellite navigation system using AN/SRN-9 Doppler data equipment 05 p0839 A67-17389

ILS equipment for category III all-weather landing 07 p1222 A67-19671

STAN 37-38-39, designed to meet operational requirements of category III all-weather landings and providing ground beacon requirements of ILS systems 09 p1529 A67-22645

Automatic all-weather landing system design having integration of autopilot and flight director [AIAA PAPER 67-406] 15 p2516 A67-30373

C-141A engineering development test program, discussing flight, accelerated service and all-weather testing [AIAA PAPER 67-409] 15 p2422 A67-30376

All-weather landing for civilian aircraft, discussing equipment, terminology used and low visibility flight simulation 17 p2795 A67-32122

V/STOL all-weather operation developments noting navigation and communications, operations under icing and noise problems [SAE PAPER 670348] 17 p2798 A67-32990

Defogging procedure for all-weather aircraft landing, with operational results 18 p3021 A67-34608

All-weather landing examined in terms of operational techniques and design criteria for airline performance and safety [AIAA PAPER 67-572] 19 p3258 A67-35968

Ground requirements for instrument landing systems noting approach lighting, runway marking, taxi guidance and blind navigation [AIAA PAPER 67-756] 23 p3933 A67-40989

Automatic landing system introduction for civil transport aircraft noting certification program and requirements and development of operable system [AIAA PAPER 67-757] 23 p4025 A67-40990

V/STOL all-weather guidance system developments and flight experimentation,

discussing enroute navigation compatibility and terminal area operations
[AIAA PAPER 67-796] 24 p4183 A67-42957

All-weather flight requirements of VTOL aircraft, suggesting artificial stabilization by automatic control system
[AIAA PAPER 67-798] 24 p4096 A67-42959

ALLOY

SA ALUMINUM ALLOY
SA ANTIMONY ALLOY
SA BERYLLIUM ALLOY
SA BINARY ALLOY
SA BISMUTH ALLOY
SA BORON ALLOY
SA CADMIUM ALLOY
SA CHROMIUM ALLOY
SA COBALT ALLOY
SA COPPER ALLOY
SA EUTECTIC ALLOY
SA GALLIUM ALLOY
SA GERMANIUM ALLOY
SA GOLD ALLOY
SA HASTELLOY
SA HIGH STRENGTH ALLOY
SA HIGH TEMPERATURE ALLOY
SA INDIUM ALLOY
SA IRON ALLOY
SA LEAD ALLOY
SA MAGNESIUM ALLOY
SA MANGANESE ALLOY
SA MOLYBDENUM ALLOY
SA NICKEL ALLOY
SA NIMONIC ALLOY
SA NIOBIUM ALLOY
SA PALLADIUM ALLOY
SA PERMALLOY
SA PLATINUM ALLOY
SA POTASSIUM ALLOY
SA RARE EARTH ALLOY
SA REFRACTORY ALLOY
SA RHENIUM ALLOY
SA SILICON ALLOY
SA SILVER ALLOY
SA SODIUM ALLOY
SA TANTALUM ALLOY
SA TELLURIUM ALLOY
SA THORIUM ALLOY
SA TIN ALLOY
SA TITANIUM ALLOY
SA TUNGSTEN ALLOY
SA VANADIUM ALLOY
SA WROUGHT ALLOY
SA YTTRIUM ALLOY
SA ZINC ALLOY
SA ZIRCONIUM ALLOY

Electron-based superconductivity mechanism involving two overlapping conduction bands in alloys 01 p0127 A67-10062

High temperature electrical material evaluation for Rankine cycle [SAE PAPER 660662] 01 p0094 A67-10571

Substrate temperature effect on structure of evaporated alloy thin films 02 p0287 A67-11716

Initial saturation voltage effects in alloy-type transistors at high injection levels 02 p0215 A67-11977

Maximum limiting value of uniform deformation of metals and alloys by stretching, deriving hyperbola tangent to true-stress curve 02 p0341 A67-12676

Aging of Ni containing maraging steel and related alloys analyzed by electrical resistivity, X-ray diffraction and hardness measurements, noting nature of Co-Mo interaction 03 p0440 A67-13250

Spin-lattice relaxation time of dirty type II superconductor alloys in mixed state in almost upper critical field 03 p0493 A67-13472

Fatigue mechanisms for fcc metals and alloys, reviewing research on crack initiation and propagation 03 p0447 A67-13800

Evaporation process and pore development in alloy samples under tensile stresses 03 p0424 A67-14058

Electron energy spectrum for alloyed semiconductors, determining state densities via Thomas-Fermi statistical method 04 p0681 A67-15296

Inverse Hall effect of noble metals alloyed with B-group metals as affected by residual resistivity and phonon scattering 04 p0682 A67-15465

Book on structure of metallic alloy including phase diagram of vanadium-gallium system 05 p0827 A67-16325

Short and long range redistribution of solute in weld fusion zones of alloy systems through data from electron microprobe analyses 05 p0811 A67-16830

Microstructure and mechanical properties as functions of degree of deformation of pressed rods of Tsm2A alloy at 1300 degrees C 05 p0832 A67-17509

Transmission electron microscopy study of phase transformations of Ti-8Al-1Mo-1V alloy 06 p1014 A67-17804

Plane strain fracture toughness, strain instability, slow crack growth and different modes of cracking in metal alloys 06 p1014 A67-17806

Refractory metals and metal alloys analyzed regarding electron work function and threshold temperature for surface ionization in all-metal guard ring diode with directly heated wire 06 p1035 A67-18137

[AIAA PAPER 66-223] 06 p1035 A67-18137

Soviet papers on structure and properties of aviation steels and alloys 07 p1198 A67-19238

Cooling rate from homogenization temperature effect on structure and properties of forged alloy KhN77TiU 07 p1199 A67-19241

Phase and structural transformations in metals and alloys studied with aid of exoelectronic emission 07 p1201 A67-19257

Structure of system Ti-Mo-Cr-Fe-Al alloys when quenched from beta region, noting maximum hardness at aging temperatures 07 p1205 A67-19272

Alloying effect on elastic modulus, strength and plasticity of titanium in temperature range from - 196 to 800 degrees 07 p1206 A67-19280

Structure of rolling texture of bcc metals and alloys under various external deformation conditions 07 p1210 A67-20107

Mechanical properties of alloys in descriptive approach, noting data on precipitation hardening, plastic strain and creep 07 p1211 A67-20176

Aluminum alloy with various metal additions analyzed for aging, using electron microscope 08 p1342 A67-20806

Electrical resistance changes in quaternary alloy during simultaneous occurrence of phase solution coalescence and silicon spheroidization, noting effects of aging and various metal additions 08 p1342 A67-20807

Metal working problems involving sheet metal, powder metallurgy, extrusion, nondestructive testing and concerning high strength, refractory and superalloys [SAE PAPER 670098] 09 p1509 A67-22540

Book on superconductivity of metals and alloys including fundamental properties, condensed state, analysis of Landau-Ginsburg equations, magnetic field effects, etc 10 p1690 A67-23160

Refractory materials for hypersonic vehicle leading edges 10 p1670 A67-23723

Hot corrosion of aircraft gas turbine alloys operating in marine environment reproduced in laboratory test, analyzing nature of attack 11 p1804 A67-23918

Dispersed-phase alloy production noting structure types, deformation and fracture behavior at various temperatures 11 p1807 A67-24636

Various factors affecting hardening of KhN35VTiU/E1787/ alloy 12 p1955 A67-25367

Low temperature mechanical properties of E1827 alloy investigated under static uniaxial elongation, noting ultimate strength increases with decreasing temperature 12 p1955 A67-25370

Alloy 718 composition, microstructure and heat treatment behavior correlated with mechanical properties, noting strengthening and oxidation resistance [ASME PAPER 67-MET-5] 12 p1956 A67-25949

Metallic element concentrations in metals studied using atomic absorption spectrophotometry, noting chemical and bulk effect interferences 12 p1947 A67-26127

Book on stress corrosion of metals covering mechanisms, resistance techniques and tests 13 p2141 A67-27174

Book on high temperature oxidation of metals and alloys, fundamental aspects and reaction mechanisms 13 p2141 A67-27176

Metal-semiconductor electric contacts for GaAs bulk effect device noting uniformity, linearity, usefulness, adaptability, etc 13 p2183 A67-27567

Age hardenable low-expansion alloy for cryogenic service 13 p2142 A67-27675

Radiation effects on shear strength of several alloys at liquid hydrogen

environment 13 p2143 A67-27678

Aluminum welding techniques, evaluating various filler alloys and forms for welding ease and efficiency 14 p2323 A67-27819

Amplitude dependence of energy dissipation due to internal friction in metals and alloys of various lattice types under near-resonance loading vibrations 15 p2504 A67-29970

Book on mechanical properties of ordered alloys including formation of superlattices 15 p2504 A67-30028

Cost of titanium, steel and aluminum alloys in high performance aircraft production [AIAA PAPER 67-400] 15 p2505 A67-30367

Zr-Nb alloy structure effect on critical superconductivity parameters determined, using electron microscopy of thin films 17 p2916 A67-32721

Structural characteristics of Ni-Mo alloys analyzed using electron microscopy and X-ray diffraction scattering 17 p2872 A67-32723

Soviet book on study of defects of crystalline structure of metals and alloys including X-ray analysis of aluminum single crystals, radiation effects on niobium, etc 17 p2874 A67-32894

Alloys for failure-safe structures tested, determining fracture toughness, fatigue strength and stress-corrosion cracking resistance 17 p2875 A67-33048

Magnetization measurements in applied magnetic fields at cryogenic temperatures of dirty type II superconducting transition metal alloys 17 p2925 A67-33375

Yielding effects in stress corrosion cracking in susceptible alloys 18 p3063 A67-33487

Vacancy source and sink effect on behavior of nonequilibrium concentration of vacancies in diffusion region during creep process 18 p3141 A67-33768

Hydrogen effect on stability of beta phase in alloy VT15 18 p3065 A67-34291

Liquid-zone melting process for preparing alloy bars with variable compositions 18 p3065 A67-34294

Short time tensile and long time creep-rupture properties of HF and HH iron-chromium-nickel alloys at high temperatures [ASTM PAPER 52] 18 p3068 A67-34582

Diffusion saturation methods of alloy surfaces by metals and metalloids classified by physicochemical characteristics of active phase of diffusing element 19 p3242 A67-34916

Collection of papers of high purity metals and alloys, discussing properties fabrication and testing 19 p3243 A67-34923

Microstructure and mechanical properties as functions of degree of deformation of pressed rods of Tsm2A alloy at 1300 degrees C 21 p3644 A67-38037

Qualitative and quantitative variation in alloy phase composition with temperature and age hardening length, studying structural diagram 22 p3818 A67-39321

Carbon thermodynamic activity in molybdenum carbide alloyed with small additions of Fe, Ni and Ti 24 p4171 A67-41962

Aging effect on structure and properties of complex alloyed heat resistant steel 24 p4173 A67-42190

ALOUETTE I SATELLITE

Solar radiation field interaction with flexible antenna as possible explanation of anomalous rapid spin decay of satellites [AIAA PAPER 67-39] 06 p1096 A67-18350

Plasma ringing phenomena stimulated by Alouette I and other ionospheric probes at upper hybrid frequency and cyclotron frequency harmonics in near zero group velocity regions 07 p1179 A67-19916

Contour maps of percentage occurrence of earth echoes observed on Alouette I ionograms, noting noise level 17 p2852 A67-33236

Ionospheric refractive irregularities and traveling disturbances from Alouette I satellite data, calculating electron density profiles using lamination method 23 p3994 A67-40780

ALOUETTE HELICOPTER

S SUD-AVIATION SA 330 HELICOPTER

ALOUETTE SATELLITE

Topside ionosphere over American continents, noting electron density and scale height distribution [RASSA PAPER 1-10-132] 03 p0417 A67-14243

Oblique z-mode echoes in topside ionosphere between plasma and upper hybrid frequencies 04 p0614 A67-14956

Electron number density determined using interference pattern recorded by satellite ionograms at high latitudes 06 p0996 A67-18568

Field aligned electron concentration profiles of equatorial anomaly, using parametric description for theoretical results 06 p0997 A67-18697

Early results from topside sounder experiments in Alouette II satellite, presenting ionograms, plasma spike, electron number density and scale height 10 p1649 A67-23302

Ion composition and natural electromagnetic emissions of VLF phenomena observed by Alouette I and II 10 p1649 A67-23303

Geomagnetic field measurements in Brazilian magnetic anomaly, using Alouette topside sounder satellite 12 p1933 A67-25777

Electrostatic waves in LF noise bands as cause of diffuse traces observed by Louette satellite ionospheric probe electrostatic waves in LF noise bands as cause of diffuse traces observed by Alouette satellite 14 p2312 A67-28518

Topside ionospheric swept-frequency pulsed sounder onboard Alouette 2 satellite, discussing transmitter power, large range receiver and antenna array 21 p3583 A67-38636

ALPHA DECAY

Semiconductor surface barrier Si n-type detector yielding fast resolution curve in alpha-gamma radiation coincidence experiment 01 p0066 A67-10657

Time resolved spectroscopic measurements of intensity and Stark width during decay of hydrogen plasma produced by ruby laser, determining electron density and temperature decay 05 p0852 A67-16653

ALPHA RADIATION

SA LYMAN ALPHA RADIATION

Semiconductor device measuring pulsed nanosecond currents produced in detectors by alpha particles 01 p0065 A67-10651

High temperature operation of diamond counters for nuclear particles 01 p0068 A67-10927

Operational alpha counting characteristics for point plane counter in air working in corona streamer mode 02 p0241 A67-11680

Solar cosmic ray generation, discussing proton energy spectrum analysis and wave propagation in interplanetary space 02 p0310 A67-12572

Proton and alpha particle effects on thermal properties of spacecraft and solar concentrator coating of anodic-coated aluminum, zinc oxide/ potassium silicate, etc [AIAA PAPER 65-649] 03 p0448 A67-13054

Nuclear emulsion measurements of primary cosmic ray alpha particle flux over Hyderabad during high solar activity in 11-year cycle 03 p0506 A67-13720

Lunar surface chemical analysis using interaction of monoenergetic alpha particles with matter [JPL-TR-32-1065] 05 p0805 A67-16463

Lunar surface chemical composition analysis by Surveyor-borne instrument based on alpha interaction with matter [JPL-TR-32-1090] 08 p1411 A67-20946

CdTe properties evaluated through pulse height response of surface barrier devices to monoenergetic alpha particles normally incident to surface 08 p1356 A67-21308

Plasma characteristics of partially dissociated and ionized air due to alpha emissions from radioisotope surface material 09 p1543 A67-21819

Energy spectrum of primary cosmic ray alpha particles measured by nuclear photographic emulsion, estimating geomagnetic cut-off energies 09 p1562 A67-22418

Alpha particle irradiation effect at liquid-helium temperature on transition temperature of superconductive tin, indium and thallium foils 17 p2926 A67-33405

Electron mobility and trapping time in semi-insulating cadmium telluride through observing transient response to alpha particles 19 p3308 A67-36101

Differential cross sections for inelastic large angle alpha particle scattering from unnatural parity states in Mg showing diffraction pattern 20 p3488 A67-36931

Alpha particle proton ratio of geomagnetic field from data from charged-particle telescope on OGO 1

satellite 20 p3519 A67-37412

Peak energy dependence on atomic number in inelastic alpha particle scattering at 24.8 Mev by Ni 58, Cu, Ag, Ta and Au 21 p3659 A67-38401

Differential cross sections for elastic scattering of alpha particles by oxygen, giving angular distributions and resonances 21 p3659 A67-38517

Differential cross sections of elastic scattering of alpha particles by oxygen, measuring angular distributions 21 p3659 A67-38518

Silicon semiconductor alpha particle detector for spectrometry, noting radiation resistance for low energy proton bombardment 21 p3628 A67-38596

Solar proton and alpha radiation flux and spectral distribution measuring device on satellite HEOS A 21 p3629 A67-38665

Back collection of charge due to ionizing alpha or beta particles by silicon p-n junction detector with space charge width less than range 22 p3797 A67-39345

Satellite and ground based measurements of incident proton neutral hydrogen flux and Balmer alpha optical emission in auroral hydrogen arc 23 p3995 A67-40803

Abundance anomalies in stellar surface layers by proton and alpha particle bombardment caused nucleus breakdown and buildup to lower and higher mass numbers respectively 24 p4228 A67-42264

Angular distributions of elastic and inelastic alpha scattering from tellurium isotopes using Lewis cyclotron 24 p4192 A67-42732

ALTERNATING CURRENT /AC/

SA DIRECT CURRENT /DC/

AC measurements on hard superconductors exposed to magnetic field, obtaining critical surface current and density from voltage-time curves 03 p0487 A67-12809

Field intensity probe measurements of potential distribution and I-V characteristics in AC arc plasma 03 p0475 A67-13087

Temperature fluctuation in AC heated filaments and magnitude and phase of harmonic components of temperature 04 p0723 A67-15117

Flux jumps in hard superconductor AC and DC magnetic fields 04 p0682 A67-15328

Large signal AC field effect measurements on A and B real surfaces of InSb exposed to different ambients 05 p0862 A67-16604

AC power generation by linear channel liquid metal MHD inductive generator 05 p0754 A67-17348

Measuring apparatus for scalar and tensor plasma conductivity in AC MHD generators and accelerators 09 p1538 A67-21775

AC conductivity of glass semiconductor measured over various frequency and temperature ranges, noting activation energy 12 p1980 A67-25181

Response of superconducting sheath state of lead-indium in AC and DC magnetic fields studied, noting transition changes response of superconducting sheath state of lead-indium in AC and DC magnetic fields studied, 12 p1985 A67-25847

Temperature dependence of small signal AC field effect kinetics in silicon within 170-300 K, considering majority carriers and one energy level theory 13 p2176 A67-26708

DC and AC parameters of germanium tunnel diodes in 3 to 5 millamp range measured by ammeter dC and AC parameters of germanium tunnel diodes in 3 to 5 millamp range measured by ammeter 15 p2449 A67-29807

Simultaneous AC and DC in ring-shaped hard superconductors, confirming critical AC and superimposed DC existence 18 p3098 A67-33521

Experimental data applicability for DC arcs in construction of AC plasmotrons 18 p3088 A67-34058

Electric field of AC solenoid of finite length in Hall conducting medium 18 p2990 A67-34500

Power semiconductor devices, emphasizing thyristors and silicon rectifier diodes applications 20 p3397 A67-36643

Continuous DC EMF in semiconductor with symmetrical nonlinear conductivity analyzed in variable AC waveguide magnetic

field 20 p3513 A67-37449

Silicon AC strain gauges performance investigated by employing oriented p-Si crystals operating in static and dynamic modes 22 p3798 A67-39569

Modulated signal nonlinear distortions from AC system resulting from system components nonlinearities 22 p3763 A67-40478

Constant voltage steps of AC Josephson effect observed in drop-form junctions exposed to radiation 24 p4200 A67-41864

Equivalent circuit to study AC posistor temperature characteristics and determine active and reactive components of net resistance 24 p4130 A67-42253

ALTERNATING CURRENT GENERATOR

Electric power generating equipment for aircraft noting brushless rectifier AC generator, solid rotor AC generator and brushless DC generator 09 p1451 A67-22666

Axial gear differential /AGD/ design and selection for constant speed AC generator drive for aircraft engines 17 p2800 A67-31976

Weak DC signals conversion into electric pulses by magnetic semiconductor pulse width modulator using AC generator 17 p2823 A67-32224

Synchronous and asynchronous idealized induction alternating current MGD generators 17 p2803 A67-32340

AC motor design for operation in He in cryogenic to room temperature range, noting performance parameters and design considerations [AIAA PAPER 67-456] 18 p2988 A67-33930

MHD jet converter research, reviewing basic equations, AC/DC generators and thermodynamic/ electric problems 19 p3268 A67-35062

ALTIMETER

SA RADAR ALTIMETER

SA RADIO ALTIMETER

All-weather pulsed X-ray instrument for altitude measurement and terrain identification 05 p0806 A67-16528

Aerial barometric altitude measurement improvement and residual error reduction 07 p1190 A67-20289

Tester to check altimeter of Apollo lunar module 14 p2318 A67-28291

Altimeter using pulse repetition frequency /PRF/ tracking design with solid state X-band frequency source 17 p2859 A67-32522

Design and operation of various recording instruments /speedobarographs/ for simultaneous measurements of aircraft altitude and speed 22 p3798 A67-39550

ALTITUDE

SA FLIGHT ALTITUDE

SA HIGH ALTITUDE

SA LOW ALTITUDE

SA SIMULATED ALTITUDE

Altitude of lower boundary of ionosphere determined by electron density profile, considering absorption coefficient and magnetotonic signal components 16 p2669 A67-31906

ALTITUDE ACCLIMATIZATION

Hematocrit ratio in affecting survival and acclimatization of dogs at high altitude 07 p1135 A67-19862

Acetazolamide effects in aiding altitude accommodation, examining action on blood and cerebrospinal fluid 23 p3951 A67-41566

ALTITUDE CONTROL

Altitude control for VTOL aircraft facilitates control of hovering flight, noting construction, operation principles and performance 03 p0363 A67-12981

Altitude control system with optimized guidance device which reduces flight altitude of guided low trajectory missiles over sea surface 04 p0652 A67-14562

Air traffic control radar beacon system with automatic altitude reporting system [SAE PAPER 670256] 12 p1941 A67-25506

Lunar terrain uncertainties effect on trajectory optimization using Kalman filter during lunar landing powered descent [AIAA PAPER 67-543] 19 p3256 A67-35942

Manual altitude and attitude control effects on short-period handling quality requirements 19 p3175 A67-35974

Pilot performance in simulator training during acute hypoxia noting effect on altitude, engine power and directional control 20 p3374 A67-36264

ALTITUDE SICKNESS

Symptomatic responses of eight college females to high altitude exposure include headaches, drowsiness, fatigue and

insomnia 03 p0365 A67-14298
Bilateral conjunctival hyperemia attributed to cardio-hemo-respiratory
decompression 04 p0561 A67-14628
Metabolic cerebellum changes under nonlethal hypoxia, noting system compensation during symptomatic stages and destruction of Purkinje cells at critical stages 04 p0561 A67-14629
Altitude dysbarism treatment with high pressure oxygen, reporting three cases 05 p0756 A67-16291
Pathogenesis of focal neurological dysbarism in pilots during altitude decompression sickness 10 p1600 A67-23827
Terminology, pathophysiology, treatment, prevention and clinical aspects of altitude decompression sickness 23 p3950 A67-41545
Seven year follow-up X-ray survey for bone changes in low pressure chamber operators to determine long term effects of altitude decompression sickness 23 p3957 A67-41641

ALTITUDE SIMULATION

High altitude test stands of DVL rocket test range at Lampoldshausen, planning considerations and preliminary results from altitude simulation
[DVL-604] 03 p0394 A67-13029
Simulated high altitude effects on emphysematous blebs and bullae under reduced ambient barometric pressure 03 p0365 A67-14297
Upper atmospheric oxygen atom concentration profiles obtained via wind tunnel simulation of NO releases
[AFCRIL-67-0053] 04 p0615 A67-14971
Physiological effects of high altitude flights on human organism 12 p1903 A67-26164
Rats exposed to simulated altitude studied for acute changes in iodine metabolism, noting dichotomy between thyroidal iodine uptake and secretion rates 15 p2428 A67-29279
Von Karman gas dynamics counterflow facility for simulating model high velocities and altitudes of reentry conditions 16 p2655 A67-31261
Electrodeless slip-type MHD steady state acceleration of subsonic and supersonic high density gas flows for simulating reentry speeds and altitudes 21 p3607 A67-37778
Arterial and venous blood of brain and mixed venous blood of heart measured in dogs exposed to simulated altitude, noting body deoxygenation 24 p4111 A67-41851
White Sands Test Facility /WSTF/ constructed by NASA for hot firing tests of lunar module at simulated altitude 24 p4138 A67-42031

ALTITUDE TEST

SA HIGH ALTITUDE TESTING
Wind tunnel ejector and hot water supply for ramjet power plant attitude test stand, noting synchronization of ejector with test section 17 p2834 A67-32817
Altitude chamber studies of passively pressurizing partial pressure suit for possible use by SST crew 23 p3969 A67-41647
Brightness thresholds and reading ability tests evaluated for male subjects under varied simulated conditions of altitude and oxygen breathing 23 p3959 A67-41694

ALTITUDE TOLERANCE

Metabolic reaction of deer mice to temperature and altitude, analyzing various enzyme systems 04 p0561 A67-14593
GHOST balloon experiments, determining life, stability and clustering characteristics at several altitudes 07 p1219 A67-19065
Oxygen consumption and phosphorylation processes relation studied in rats for high altitude stability 20 p3367 A67-36259

ALU

SA ARITHMETIC AND LOGIC UNIT /ALU/

ALUMINATE

Relative enthalpy and thermodynamic properties of beryllium aluminate from room temperature to melting point 15 p2508 A67-29764

ALUMINIZATION

Electron beam process for vapor plating aluminum on beryllium for welding 11 p1798 A67-24264
Coating of titanium with aluminum and silicon by immersion of titanium samples in molten aluminum or in aluminum/silicon melts 12 p1955 A67-25360
Parameters determining magnitude of

acceleration effect on burning rate increase of aluminized and nonaluminized composite solid propellants 15 p2581 A67-29991

ALUMINUM

SA POWDERED ALUMINUM

Surface charge after annealing of aluminum-silicon dioxide-silicon structures in inert atmospheres, analyzing effect of applied electric field 01 p0032 A67-10004
Tenfold increase in fatigue life of 1100 aluminum in reverse bending at vacuum level below 10-2 torr due to retardation of crack propagation phase of fatigue process 01 p0092 A67-10053
Second phase interface influence on work-hardening behavior of aluminum-5 atomic percent silver alloy, examining substructure development and flow stress behavior 01 p0092 A67-10055
Amplitude-dependent internal friction and defect structures measured in aluminum excited longitudinally by mechanical resonator 01 p0067 A67-10842
Amplitude-dependent internal friction and defect structures in pure aluminum measured by bridge-circuit method for difference temperatures 01 p0100 A67-10843
Amplitude-dependent internal friction and defect structures in pure aluminum from bridge-circuit measurements performed by combined kHz-mHz method 01 p0101 A67-10844
Amplitude-dependent internal friction and defect structures in aluminum, measuring critical alternating shearing stress by bridge-circuit method 01 p0101 A67-10845
Effects of aluminum electrode and hydrogen atom on MOS structure during annealing 01 p0137 A67-11069
Capacitance and optical thickness of fatty acid monolayers sandwiched between Al-films 02 p0290 A67-11732
Angular distribution of secondary electrons emitted at reverse side of aluminum films 02 p0290 A67-11734
Boron fiber-reinforced aluminum composites fabrication by plasma spraying and tensile testing 03 p0444 A67-13431
Effect of beryllium, boron, titanium, etc. additions on recovery and recrystallization processes in pure aluminum, using differential calorimetric techniques 04 p0637 A67-14910
Substructure of aluminum monocrystals in relation to silicon content 05 p0827 A67-16075
Shearing stress induced shock wave propagation in annealed aluminum under biaxial plastic prestresses
[ASME PAPER 66-WA/APM-3] 05 p0909 A67-16143
Titanium surface alloying in aluminum melts at temperatures from 700 to 1000 degrees C 05 p0828 A67-16328
Differential cross sections corresponding to excitation of seven states of residual nucleus in Al-Mg reaction at 20.9 Mev 05 p0849 A67-17381
Metallographic, X-ray and electron microscope studies of dislocation substructure and fatigue life extension in bending-fatigued Al and Ag crystals 06 p1013 A67-17798
Adhesive types and characteristics suitable for aluminum bonding 06 p1020 A67-18062
Aluminum powder damping of HF instability in solid propellant combustion in vortex burner 06 p1115 A67-18307
Crack growth rate and measurements of temperature effect on low pressure fatigue of Al 06 p1019 A67-18561
Second order strain accumulation in aluminum in reversed cyclic torsion at elevated temperatures 09 p1517 A67-21753
Single stage bonding of tapered aluminum honeycomb panels employing wrap-around skins and nonperforated core 09 p1507 A67-22507
Surface preparation for aluminum and bond strength dependence on cure temperature, humidity and impurities 09 p1507 A67-22519
Temperature dependence of magnetization and resistivity in SHF magnesium-aluminum ferrite 10 p1688 A67-22830
Operational economy of dip brazing method of joining aluminum and reliability of ultrasonic printout procedures for inspection of assemblies 10 p1660 A67-23007
Vitreous silica and molten Al reaction, penetration rate of Al, reaction rate and effect of Bi and Sb on rates by lamellar

compound formation 10 p1669 A67-23381
Scatter factor for fatigue life of aluminum aircraft structures subjected to identical loading histories 10 p1594 A67-23436
Thermal properties and environmental stability of barrier layer anodized aluminum surfaces in space, noting emittance and absorption values 10 p1671 A67-23744
Cut-off turning test on 40 mm Al bar, effect of mineral oil and kerosene on cutting depth and speed and of feed on tangential force and chip size 11 p1809 A67-24945
Solar wind trapping in solids using ion bombardment of aluminum foils at various energies and temperatures 11 p1825 A67-25079
Hot pressing technique for aluminum sheet and stainless steel wire to produce composite high tensile strength plate 12 p1954 A67-25289
Low solar absorption surface coatings of aluminum, silver and silica with controlled emittance for spacecraft thermal control [AIAA PAPER 67-343] 12 p1959 A67-26057
Creep rupture, fatigue strength and brittle-ductile transition of aluminum as affected by nuclear radiation 13 p2133 A67-27090
Book on adhesive bonding Alcoa aluminum covering techniques, applications including aircraft and military uses, classifications, etc 13 p2143 A67-27177
Statistical analysis of aluminum welds tested at cryogenic temperatures 13 p2124 A67-27674
Aluminum, Volume 1, Properties, physical metallurgy and phase diagrams 14 p2334 A67-27801
Aluminum, Volume 2, Design and application 14 p2322 A67-27811
Aluminum and aluminum alloys properties for service at cryogenic temperatures 14 p2323 A67-27816
Aluminum and aluminum alloys in aircraft and aerospace industry 14 p2323 A67-27817
Aluminum, Volume 3, Fabrication and finishing 14 p2323 A67-27818
Aluminum welding techniques, evaluating various filler alloys and forms for welding ease and efficiency 14 p2323 A67-27819
Adhesive bonding techniques for aluminum, advantages, drawbacks, joint design and surface treatment before bonding 14 p2323 A67-27820
Aluminum pretreating and finishing agents noting cleaning, etching, roughening and coatings 14 p2324 A67-27821
Mono- and polycrystalline samples of Al and Cu bombardment by argon ions in presence of oxygen and by oxygen and nitrogen ions under vacuum 14 p2351 A67-28513
Longitudinal acoustic wave attenuation in superconducting aluminum measured, verifying acoustic attenuation predictions 14 p2373 A67-28858
Perpendicular critical magnetic fields of superconducting aluminum, tin and gallium small grained films examined for superconducting transition temperature enhancement 14 p2373 A67-28860
Temperature homogenization effect on structure of industrial aluminum, determining mechanical properties dependency on Fe/Si ratio 15 p2504 A67-29975
Aluminum renewal from titanium electrolytes by reacting electrolyte melt at high temperature 16 p2687 A67-30843
Low strain rate and temperature effects on crack initiation and growth, recovery and boundary migration for Al and Al alloy 16 p2689 A67-31368
Microstructure stability of aluminum reinforced with Al-Ni whiskers, noting tensile strength and mechanical property dependence on temperature 16 p2690 A67-31372
Aluminum content effect on stress-rupture properties of chromium-molybdenum-vanadium steel, noting notch sensitivity and ductility 16 p2693 A67-31869
Aluminum particle combustion in solid rocket grains, noting drop formation mechanism and droplet combustion analysis [ONERA-TP-486] 17 p2926 A67-32697
X-ray spectral analysis of bent aluminum single crystals with crystallographic plane parallel to reflecting surface of crystal 17 p2874 A67-32895

- Aluminum welded joints investigated by radiographic and metallographic methods for bubbles and cracks 18 p3053 A67-33743
- Ignition and combustion characteristics of single aluminum and beryllium particles burning in gaseous environment, discussing oxides role 18 p3149 A67-33796
- Flow stress of aluminum related to strain, strain rate and temperature, discussing compression testing machine and results 18 p3064 A67-34078
- Iron-chromium-bauxite cermets preparation and properties 18 p3065 A67-34260
- Sapphire whisker reinforced aluminum composites fabrication and evaluation [ASTM PAPER 2] 18 p3070 A67-34568
- Aluminum-boron composites stress-strain behavior, considering synergism increasing over rule of mixtures 18 p3067 A67-34572
- Mechanical behavior of fiber-reinforced aluminum and effect on engineering application [ASTM PAPER 10] 18 p3070 A67-34575
- Resonance absorption and zero-field nuclear spin relaxation in normal and superconducting aluminum, studying phase change 19 p3303 A67-35044
- Strain rate history effects on strain hardening curve for aluminum described by state equation 19 p3245 A67-35448
- Aluminum powder damping of HF instability in solid propellant combustion in vortex burner [AIAA PAPER 67-104] 21 p3732 A67-38860
- Al impurity redistribution near Si semiconductor surface subjected to high temperature oxidation 22 p3857 A67-39502
- Low temperature transient creep behavior of polycrystalline aluminum investigated experimentally for recovery of surface layer stress 22 p3821 A67-40054
- ALUMINUM ALLOY**
- Modulated structure of aged Ni-Al alloys, including electron micrograph and phase diagram studies of particle growth kinetics 01 p0092 A67-10056
- Tensile deformation behavior of commercial aluminum-5 percent magnesium alloy, correlating uneven yielding regions with occurrence of markings on specimen surface 01 p0093 A67-10060
- Principle magnetic properties of series of anisotropic alloys of Alnico type with 38 percent cobalt and coercive forces in excess of 2000 oe 01 p0093 A67-10518
- Experimental determination of column initial deflection and load eccentricity in aluminum alloy indicate minor magnitude of load eccentricity 01 p0160 A67-10561
- Mechanical property data on Lockalloy /62 Be, 38 Al/ and comparison with other lightweight structural metals [SAE PAPER 660652] 01 p0094 A67-10613
- Arc radiation and selective solute vaporization from arc spot region of weld pool used to explain formation of overlap segregation in aluminum alloy weldments 01 p0080 A67-10947
- Maximum alloying temperature and cooling rate of p-n junctions effect on volt-ampere characteristics of silicon diode and minority carrier lifetime 01 p0039 A67-11053
- Cutting temperature and heat distribution in cutting tool and blank in superhigh speed cutting process for deformable aluminum alloys 03 p0428 A67-13197
- Residual stress effect on stress-strain curve of uniaxial composite consisting of stainless steel wire and aluminum alloy matrix 03 p0444 A67-13432
- Boron filaments for reinforcement of aluminum alloys used in turbomachinery 03 p0444 A67-13436
- Aluminum alloy composite bulkhead fabrication under tensile stress with improved bonding uniformity 03 p0430 A67-13556
- Deformation and diffusion bonding of Al, Ti and stainless steel alloys, discussing surface condition, time, temperature, cold work, heat treatment and intermediate materials 03 p0430 A67-13692
- Crack propagation in heat-affected zone during HF AC current gas-tungsten arc welding of Al alloy test plate 03 p0430 A67-13693
- Niobium-aluminum alloys elasticity, shear cubic compressibility moduli, Poisson ratio, characteristic temperature and crystal lattice structure 04 p0635 A67-14431
- Oxidation of Al-2 percent aluminum oxide SAP type alloy foil heated in situ and observed by hot stage transmission microscopy, electron diffraction and motion picture microscopy 04 p0635 A67-14513
- Mean tensile strength of aluminum alloys using torsion tests determined at high strain levels and compared with extrusion tests values 04 p0636 A67-14907
- Momentum transfer during impact, penetration depth, crater form and mass loss at various velocities, using spherical aluminum projectiles and aluminum targets 04 p0710 A67-15005
- Cracking during welding of aluminum alloy noting effect of strain, maximum temperature and cooling rate [ASME PAPER 66-WA/MET-5] 04 p0639 A67-15341
- Fatigue crack propagation rates for aluminum cantilever beams in reversed bending under two-level constant amplitude and random excitation, noting stress cycle effect [ASME PAPER 66-WA/MET-3] 04 p0639 A67-15343
- Mean strain cumulative damage and effect in low cycle fatigue of 2024-T351 aluminum alloy, covering strain cycling, fatigue life, residual ductility, etc [ASME PAPER 65-WA/MET-5] 05 p0827 A67-16214
- Two oxidation mechanisms for Ti-Al alloys based on increased diffusion rate and decreased oxidation rate 05 p0829 A67-16492
- Separation of load eccentricity and initial deviation determined through column compressive tests, using aluminum alloy bars and strain gauges 05 p0919 A67-16588
- Low endurance fatigue of aluminum alloy and stainless steel in plane bending at ambient and elevated temperatures 05 p0920 A67-16810
- Eddy current conductivity technique for monitor of heat effects in nondestructive testing of 2014 Al alloy weldments 05 p0813 A67-17260
- Electron microscopy analysis of dissolved hydrogen induced fracture in room temperature cantilever bend fatigue testing of dispersion strengthened aluminum-aluminum oxide alloy 06 p1013 A67-17796
- Oxide dispersion hardening of intermetallic NiAl and FeAl compounds for improved high temperature strength 06 p1014 A67-17803
- Manganese aluminide precipitation effect on primary recrystallization in metal systems, indicating softening processes in metals 06 p1015 A67-17810
- Diffusion welding of aluminum alloys and austenitic stainless steel tubular joints 07 p1190 A67-19214
- Phase composition and structure of alloys in aluminum corner of system Al-Cu-Cd-Mn with constant manganese concentration of 0.7 percent at 500 degrees C 07 p1201 A67-19251
- Hardness variation of alloys of system Al-Cu-Cd-Mn-Li as function of composition and aging conditions 07 p1201 A67-19252
- Mechanical properties of alloys of systems Al-Zn-Li and Al-Zn-Li-Mg 07 p1201 A67-19253
- Small additions of refractory elements effect on structure and properties of sheets of Al-Zn-Mg alloy in various states 07 p1201 A67-19254
- Small additions of refractory elements effect on structure and properties of aluminum alloy castings containing Zn and Mg 07 p1201 A67-19255
- Oxygen effect on mechanical property and heat resistance of alloys AT3 and AT8 07 p1205 A67-19276
- Static and fatigue properties of repair welded aluminum and magnesium premium quality castings 08 p1333 A67-20360
- Corrosive media effects on fatigue strength and endurance limits of three Al alloys used in aircraft components 08 p1341 A67-20598
- Surface oxide films and lifetime of vacancies in thin crystals analyzed for pure aluminum and dilute aluminum alloys 08 p1369 A67-20794
- Electrical resistance and weight increase measurements in aluminum and Al-Mg alloys, noting relation between oxidation rate and Mg content during annealing 08 p1341 A67-20796
- Aluminum alloy with various metal additions analyzed for aging, using electron microscope 08 p1342 A67-20806
- Kinetics of two-phase decomposition of solid solution of magnesium-aluminum alloy using X-ray analysis, noting grain orientation and size 08 p1342 A67-20810
- Test method for aluminum and titanium alloys, estimating tendency toward brittle failure and recording kinetics of crack formation 08 p1342 A67-21176
- Alloying effect on aluminum K and iron L X-ray emission spectra in Al-Fe binary system 08 p1343 A67-21304
- Axially loaded cylindrical structures analyzed for optimum weight construction consistent with cost constraint, emphasizing beryllium-aluminum alloys 08 p1424 A67-21521
- Effects of cold work by rolling and by shock waves on precipitation hardening in Al-6 percent Cu alloy 08 p1343 A67-21544
- Resistance spot-welded adhesive bonds between aluminum alloy components, using thermosetting film adhesive 09 p1502 A67-21688
- Postquenching deformation effect on mechanical properties and creep resistance of aluminum alloys [ONERA-TP-423] 09 p1519 A67-22156
- X-ray diffraction residual stress measurements in aluminum alloy [SAE PAPER 670153] 09 p1509 A67-22543
- Column compressive tests of aluminum alloy bars, determining load eccentricity and initial straightness deviation 10 p1715 A67-22826
- Stress corrosion resistance of explosively deformed high strength steels and aluminum alloy [ASTME PAPER WES-7-63] 10 p1667 A67-23009
- Elastoplastic properties of copper, aluminum alloys and brass under explosive load, noting increased temperature effect on elastoplastic wave parameters 10 p1668 A67-23092
- Random-loading fatigue crack growth behavior of airframe aluminum and titanium alloys under sinusoidal, narrow band and broad band random loading 10 p1669 A67-23434
- Bending fatigue tests of unmachined, mechanically machined and chemically machined panels of aluminum and titanium alloys 10 p1669 A67-23437
- Roll fatigue tests of forged ZK60A-T5 magnesium and 2014-T6 aluminum wheels 10 p1661 A67-23439
- Optical absorption of Al and some Al-Mg alloys in region from 0.7 to 2.0 ev investigated by conventional polarimetric reflection technique 10 p1696 A67-23773
- Reducing stress levels on crack propagation growth rate investigated for aircraft design problems 11 p1804 A67-24037
- Tensile strength retaining characteristics of aluminum alloys determined after varied soaking periods at various elevated temperatures 11 p1805 A67-24271
- Microwave surface absorption in static magnetic field affects surface resistance of superconducting alloys 11 p1846 A67-24584
- Aging kinetics and lattice defects in Al-Zn and Al-Zn-Mg alloys 11 p1809 A67-24947
- Low endurance fatigue analysis for steel and Al alloy under cyclic torsion with controlled shear strain amplitude 12 p2016 A67-25425
- Fracture toughness of 7075-T6 and -T651 sheet, plate and multilayered adhesive bonded panels, showing independence of thickness and number of layers [ASME PAPER 67-MET-4] 12 p1956 A67-25948
- Dent effect on buckling strength of aluminum alloy tubular columns subjected to axial compression [ASME PAPER 67-MET-12] 12 p2030 A67-25951
- Stress concentration factor role in evaluating notch toughness of aluminum alloy 13 p2220 A67-27185
- Stability of titanium-aluminum alloys during oxidation in air 13 p2142 A67-27287
- Notch toughness of some aluminum alloy castings at cryogenic temperatures 13 p2221 A67-27672
- Test program of Al-Zn-Mg alloy /AZ5G/ to determine strength, fracture toughness, weldability and physical properties for cryogenic application 13 p2142 A67-27673
- Aluminum alloy systems physical and

structural characteristics and phase diagrams 14 p2334 A67-27802

Microstructure of aluminum alloys analyzed for composition, fabrication and thermal treatment, using electron microscopy 14 p2334 A67-27803

Thermal processing of precipitation-hardenable aluminum alloys, noting changes in structural and mechanical properties 14 p2335 A67-27804

Alloying elements and impurities effects on aluminum-alloy systems properties including neutron absorption, temperature changes, electric conductivity, etc 14 p2335 A67-27805

Stress corrosion resistance and control for aluminum alloys, noting types, causes and methods 14 p2335 A67-27806

Commercial aluminum casting alloys physical and mechanical properties 14 p2335 A67-27807

Commercial aluminum wrought alloys properties, describing temper designation and heat and nonheat treatment classification 14 A67-27808

Aluminum powders and aluminum powder metallurgy products properties, discussing powder and particle applications in metallurgy 14 p2335 A67-27809

Phase equilibrium diagrams of Al alloy systems, designating solid phases by chemical symbols and allotropic or polymorphic forms by prefixing Greek letters 14 p2335 A67-27810

Aluminum, Volume 2, Design and application 14 p2322 A67-27811

Commercial forms of aluminum alloys, production, applications and marketing 14 p2336 A67-27812

Design factors for aluminum castings 14 p2323 A67-27813

Aluminum impact extrusion process design 14 p2323 A67-27814

Aluminum alloy forgings design 14 p2323 A67-27815

Aluminum and aluminum alloys properties for service at cryogenic temperatures 14 p2323 A67-27816

Aluminum and aluminum alloys in aircraft and aerospace industry 14 p2323 A67-27817

Transmission electron microscopy of interfacial areas in metal-matrix composites 14 p2336 A67-28096

Tensile creep behavior of thick walled aluminum titanium alloy cylinders under internal pressure at high temperature 14 p2339 A67-29001

Creep behavior of materials in nuclear reactors, gas turbines and electric power plants, noting aluminum alloy and high temperature material fatigue 15 p2502 A67-29506

Welding characteristics of aluminum alloys, noting influence of quenching temperature, quenching process delay and cooling velocity on weld tensile strength 15 p2503 A67-29781

Concorde structural development noting effects of temperature on fatigue and creep strength of aluminum alloys [AIAA PAPER 67-402] 15 p2578 A67-30369

Crack resistance properties of high strength aluminum alloys, noting test results on fracture toughness enhancement 16 p2688 A67-31308

Ultrahigh vacuum and air fatigue testing of aluminum alloy observing corrosion process influence on mechanism by latter 16 p2689 A67-31369

Cumulative fatigue at root of circular notch of coupon type aluminum alloy specimens subjected to low cycle compression-tension strains 17 p2957 A67-32028

Fatigue properties of explosively formed parts tested by repeated axial loading and results compared with statically formed specimens 17 p2871 A67-32433

Recovery Stage III in neutron irradiated Al-Cu alloy, discussing vacancies and interstitials 17 p2873 A67-32743

Mechanical properties of welded junctions of rolled sheets of aluminum alloys at room and cryogenic temperatures 17 p2873 A67-32769

Two oxidation mechanisms for Ti-Al alloys based on increased diffusion rate and decreased oxidation rate 17 p2875 A67-33175

Book on machining Alcoa aluminum covering Al alloys properties, requirements for machine tools, cutting conditions and

compounds, finishing operations, etc 18 p3053 A67-33771

Aluminum alloy examined for dislocation arrangements and susceptibility to intergranular stress corrosion cracking, using electron microscopy 18 p3063 A67-34000

Strength characteristics of single crystals of nickel aluminide /gamma phase/, discussing temperature and orientation dependence of work hardening 18 p3064 A67-34079

Semimonocoque aluminum alloy glider design features, recommending integral construction with metal bonding or combination metal bonding and riveting 18 p3054 A67-34374

Fiber orientation and morphology effect on anisotropic tensile behavior of Al-Ni whisker reinforced aluminum, studying solidification rate, etc 18 p3067 A67-34569

[ASTM PAPER 3] 18 p3067 A67-34569

Strain distribution in aluminum filament reinforced metal, investigating matrix plastic behavior and residual stresses, etc [ASTM PAPER 8] 18 p3067 A67-34573

Correlations between elastic limit, tensile strength and elongation in foundry aluminum alloys used in control reliability 20 p3465 A67-36479

Maximum strengths of aluminum alloy and metal columns under parameter variation, using mathematical model 20 p3538 A67-36780

Nickel aluminide structure, examining arrangement of Ti, Cr and W in lattice via X-ray spectroscopy 20 p3467 A67-37116

Ti-Al alloys ordering transformation studied by electron microscopy and electron and X-ray diffraction, showing existence of three phase fields 20 p3470 A67-37386

Structural changes due to fatigue in cladding layer of alloy D16AT studied by X-ray diffraction 21 p3642 A67-37826

Aluminum alloy creep rates with changing temperature and stresses in hollow sphere, using time dependent viscosity coefficient 21 p3643 A67-38019

Loading frequency influence on endurance characteristics of V95 aluminum alloy notched for stress concentration 21 p3644 A67-38051

Dilute magnesium addition effect on growth and shrinkage of dislocation loops in aluminum studied by isothermal annealing of thin foils 21 p3644 A67-38088

Alnico alloys containing Ti studied for columnar crystal growth, noting Ti content influence on crystal structure formation 21 p3645 A67-38376

Plastic deformation of single-crystal Ni-Al investigated for temperature, orientation and strain-rate dependence of tensile flow 21 p3645 A67-38774

Chemical diffusion coefficients and heats of activation in nickel-aluminum intermetallic phases and solid solution calculated from layer growth experiments 21 p3645 A67-38775

Mean stress level effect on corrosion fatigue strength of aluminum clad D16AT alloy sheet under asymmetric loads 21 p3646 A67-39008

Variable loading effect on durability of D16T aluminum alloy exposed to continuous action of corrosive medium 21 p3642 A67-39009

Initial tension and compression effects on fatigue strength of aluminum alloy structures during plastic cold working 22 p3911 A67-39549

Destructive and nondestructive testing of thickness of oxide coatings on Al and Al alloys 22 p3798 A67-39552

Cyclic stress-strain in annealed and cold worked fcc polycrystalline metals and alloys studied for hardening and softening by transmission electron microscopy 22 p3821 A67-40033

Aluminum magnesium alloys prepared by powder metallurgy and hot extrusion evaluated for tension, compression, impact, fatigue and creep 22 p3821 A67-40053

Distribution function of durability in light structural alloys based on mass fatigue tests analyzed for influence of scale factor and stress concentration 22 p3915 A67-40301

Spontaneous inflammability temperatures of Al, Mg and Al-Mg alloy powders measured noting moisture effect 22 p3919 A67-40325

Chemical milling of aluminum alloy parts by dimensional etching, discussing protective

coatings 23 p4009 A67-4064

Aluminum-magnesium alloy dislocation networks structure and formation investigated by thin foil technique after rapid solidification 23 p4017 A67-40665

Random load fatigue life and reliability via fail-safe structural model, obtaining statistical distribution of 2024-T4 aluminum alloy bending strength 23 p4076 A67-4073

Dislocation of aluminum during creep investigated for change in block structure 23 p4020 A67-41301

Tensile properties and notch toughness of aluminum alloy sheet and welded joints evaluated at room and subzero temperatures 23 p4020 A67-41344

Temperature dependence of elastic constants of 1060 and 6061-T6 aluminum using ultrasonic pulse echo method estimating high pressure state equation 23 p4021 A67-41465

Weldability of Al when used in low temperature container construction noting shielding with rare gases 24 p4159 A67-41839

Edge effects in tunneling characteristics of thin film aluminum diodes in superconducting state, showing anomalies associated with quasi-particle tunneling through film edges 24 p4128 A67-41866

Deformable aluminum alloys low temperature mechanical properties 24 p4170 A67-41923

Transmission electron microscopy for microstructure observations at growing fatigue crack tips in aluminum alloys, discussing plastic dislocation morphology and density 24 p4170 A67-41947

High strength aluminum alloy panel resistance to fatigue crack propagation, discussing axial load fatigue machine 24 p4170 A67-41948

Tensile to shear transition behavior of fatigue crack fronts during cycling of sheet materials, noting correlation of shear with crack stress intensities 24 p4170 A67-41950

Fatigue microcrack and macrocrack propagation in aluminum alloys, discussing continuum mechanics approach 24 p4248 A67-41952

Fatigue crack propagation in aluminum alloy studied for influence of maximum stress, stress range and sequence of load application 24 p4171 A67-41954

Quenched structures and precipitation in Al-Cu alloys with and without traces of Cd studied electromicroscopically, showing possible CD stabilizing effect 24 p4173 A67-42166

Aluminum alloy sheet welds with high silicon and magnesium content analyzed for tensile properties and fracture toughness 24 p4161 A67-42330

Torsion creep theory for circular and noncircular tubes using Bredt equation, measuring anisotropy in tubes, calculating torsion stresses 24 p4250 A67-42381

ALUMINUM ANTIMONIDE

Band structure of GaAs, GaP, InP and AlSb obtained by k.p method 06 p1058 A67-18904

Superconductivity of metallic aluminum antimonide and comparison of results with measurements on InSb and GaSb 07 p1238 A67-20279

ALUMINUM CARBIDE

Aluminum and tungsten carbides formed from metal powders mixed with acetylene black and exposed to explosive shock 03 p0440 A67-12927

ALUMINUM COMPOUND

SA ORGANIC ALUMINUM COMPOUND

Deformation properties of polycrystalline and single crystal specimens of intermetallic compound N1Al studied as function of testing temperature and composition 01 p0092 A67-10059

Chemiluminescent gas phase reactions involving electronically excited oxygen molecules trimethylaluminum and diborane near 3 millitorr 01 p0019 A67-11007

Energies of combustion of aluminum diboride and alpha aluminum dodecaboride measured in bomb calorimeter using fluorine oxidant 22 p3758 A67-39766

ALUMINUM FLUORIDE

Aluminum fluoride effect on propagative ignition of fuel oxidant mixtures and on combustion between aluminum and oxygen 07 p1238 A67-19070

Enthalpy measurement of anhydrous crystalline aluminum trifluoride with ice

calorimeter and drop method obtaining thermodynamic properties 16 p2620 A67-31761

ALUMINUM NITRIDE

Synthesis conditions for materials of B-Al-N system determined by sintering mixtures of BN plus Al and AlN plus B powder in nitrogen atmosphere 03 p0456 A67-13544

AlN single crystal thermostable semiconductor optical/electrical properties, measuring space-charge-limited current and photocurrent 21 p3684 A67-38522

Epitaxial growth of aluminum nitride on silicon carbide studied for influence of substrate temperature on perfection of crystal deposit 23 p4037 A67-40722

ALUMINUM OXIDE

Stress required for brittle fracture of alumina at room temperature based on theory of dislocation movement of cracks 01 p0092 A67-10054

Electric conductivity due to tunnel effect in aluminum-alumina-silver sandwich structures, determining potential barrier in alumina and absorption coefficient of hot electrons 02 p0295 A67-11762

Solar absorptance and thermal emittance of aluminum coated with vacuum deposited films of aluminum oxide of various thicknesses [AIAA PAPER 65-656] 03 p0448 A67-13036

Sliding friction characteristics in vacuum of single and polycrystalline aluminum oxide in contact and with various metals 03 p0428 A67-13231

Photoelectron emission from aluminum-aluminum oxide-gold film system with electric field in dielectric 03 p0492 A67-13295

Mechanical characterization and structural perfection of alpha aluminum oxide wool whiskers in diameter range of 0.6 to 4.0 microns 03 p0449 A67-13307

Coatings of nickel, chromium and Cu on SiC and aluminum oxide whiskers by electroforming and metallizing, using electron microscope techniques 03 p0444 A67-13434

Thermal conductivity and degree of blackness of aluminum oxide coatings at high temperatures, using argon plasma jets 03 p0536 A67-13608

Oxidation of Al-2 percent aluminum oxide SAP type alloy foil heated in situ and observed by hot stage transmission microscopy, electron diffraction and motion picture micrography 04 p0635 A67-14513

Photoelectron emission from aluminum-aluminum oxide-gold film system with electric field in dielectric 04 p0674 A67-14720

High grade oxide ceramics for making dielectrically transparent insulating structures in microwave power tube 04 p0641 A67-14856

Electron beam float-zone melting process applied to dielectric compound aluminum trioxide to obtain sapphire crystals 04 p0628 A67-15320

Aluminum oxide hygrometer performance obtained from balloon flight tests 05 p0808 A67-17307

Electron microscopy analysis of dissolved hydrogen induced fracture in room temperature cantilever bend fatigue testing of dispersion strengthened aluminum-aluminum oxide alloy 06 p1013 A67-17796

Factors affecting strength of whisker reinforced metals noting characteristics [ASME PAPER 66-MD-8] 06 p1015 A67-17835

Upper atmospheric temperature measurement by analysis of AIO spectra 08 p1327 A67-21370

Structure and mechanical properties of extruded Ni-Al-oxide cermet materials, noting high compression strength 09 p1517 A67-21876

Tensile strength and cross sectional area measurement of aluminum oxide whiskers 10 p1669 A67-23326

Friction and wear properties of various alumina bearings for use in gas lubricated gyros 10 p1673 A67-23747

Composite structure of glass with crystalline aluminum oxide and zirconium oxide inclusions tested for strength and elastic properties 11 p1811 A67-24642

Hardening and softening of nickel-alumina alloys 12 p1955 A67-25365

Microwave power coupling from waveguide to helicon mode in doped indium antimonide by placing aluminum oxide cones on semiconductor surface 12 p1986 A67-26160

Aluminum oxide whiskers structure and

properties 13 p2141 A67-27186

Far IR absorption spectra of chromium and titanium ions in aluminum oxide crystal, indicating Jahn-Teller effect reduction of trigonal field and spin-orbit coupling 14 p2370 A67-28714

Sapphire whisker strength coated with thin metal film determined at room and elevated temperatures 16 p2694 A67-31522

Formation and degradation mechanisms of aluminate coatings on Ni-base superalloys, discussing experimental procedures 16 p2693 A67-31871

Dispersed aluminum oxides effect on size of nickel grains in sintered or extruded nickel-aluminum oxide cermets, studying compressive strength dependence 17 p2871 A67-31924

Thermal conductivity and degree of blackness of aluminum oxide coatings at high temperatures, using argon plasma jets 18 p3161 A67-34473

Mesosphere winds and turbulence observed by forming aluminum oxide smoke trails 18 p3043 A67-34496

Interaction between environment, oxide layer and surface slip formation in aluminum during cyclic bending 19 p3247 A67-35788

Sliding friction characteristics in vacuum of single and polycrystalline aluminum oxide in contact and with various metals 19 p3237 A67-35838

Aluminum corrosion behavior stressing surface oxide film condition 20 p3465 A67-36635

Oxidation mechanisms for nickel-aluminum alloys studied for effects of temperature and alloy composition 21 p3645 A67-38773

Ti additive effect on aluminum oxide particle growth in Ni matrix from 1000 to 1350 degrees C 24 p4171 A67-41959

ALUMINUM 26

Zodiacal dust explained by radioactive Al 26 deposited in marine sediments and brought by micrometeorites exposed to solar protons 15 p2553 A67-29157

Al 26 content of stony meteorites by coincidence spectrometry noting cosmic ray exposure ages for eight meteorites 24 p4234 A67-42630

ALVEOLAR AIR

Effect of gravitational changes on aerosol deposition in lungs of man, noting particle size and alveolar region 09 p1452 A67-21724

Reaction time during voluntarily controlled alveolar hyperventilation used to study effects on psychomotor performance of aircrew 09 p1453 A67-21728

Bronchial tube diameter makes possible alveolar ventilation with minimum metabolism or entropy production in musculature 09 p1454 A67-21986

Theoretical lung with equal ventilation-perfusion ratio used to study determinants in inert gas elimination 21 p3575 A67-38515

Ventilation-perfusion inequality effects studied in inert gas elimination from lungs 21 p3575 A67-38516

AMBIPOLAR DIFFUSION

Ambipolar diffusion theory for describing diffusion of nonuniformities in ionosphere including F region 07 p1230 A67-19717

Ambipolar diffusion and drift of plasma of added carriers in semiconductor in presence of magnetic field 08 p1369 A67-20900

Sounding rocket-released artificial strontium and barium ion cloud motion in upper atmosphere, based on equations of ambipolar diffusion 10 p1644 A67-23254

Ambipolar diffusion of plasma cloud imbedded in ionized gas with homogeneous magnetic field, assuming electric current is not vanishing 10 p1648 A67-23293

Properties of partially ionized Ar computed via Chapman-Enskog-Burnett expressions noting ambipolar diffusion coefficient, electron-atom momentum, electrical and thermal conductivity, etc 11 p1775 A67-23865

Plasma thermoconductivity in general force fields, showing validity of Meador-Staton results in case of ambipolar diffusion and nonuniform total pressure 11 p1827 A67-23884

Behavior of nighttime equatorial F-2 layer under ambipolar diffusion and electrodynamic drift 11 p1784 A67-23935

Motion and dispersion of inhomogeneity in unbounded plasma in magnetic and electric fields 14 p2359 A67-28504

Magnetoplasma diffusion equation of F-2

layer allowing electric currents and temperature variations, noting transverse drift of field 16 p2666 A67-31402

Bohm criterion of boundary layer stability related to ambipolar sound generation in positive column plasma discharge, deriving plasma density ambipolar potential distribution 17 p2905 A67-32972

Ambipolar potential-enhanced loss in magnetic trap reduced by potential difference in magnetic mirror throats dividing field 17 p2909 A67-33116

Surface recombination velocities relationship in depletion, inversion and accumulation surface layers of p-type silicon, using ambipolar carrier transport formulation 18 p3104 A67-34593

Atomic collision processes in ionized gases, studying ambipolar diffusion, electron attachment, electron-ion recombination and Penning ionization by afterglow technique 19 p3264 A67-35070

AMIDE

SA ACETAZOLAMIDE

SA FORMAMIDE

SA POLYAMIDE

Pituitary enzymes hydrolyzing aminoacyl arylamides and relation to peptidases 01 p0015 A67-10488

AMINE

SA AMPHETAMINE

SA CATECHOLAMINE

SA DIPHENYLAMINE

SA FLUOROAMINE

Color phenomena on moon 08 p1396 A67-21165

Mass spectra of amino ketones and amino alcohols and related substances 09 p1458 A67-22057

Factors involved in initiation of reaction in cobalt /III/ amine azides, discussing thermal decomposition, activation energy, etc [CI PAPER 67-15] 19 p3309 A67-35009

Amine-tin antioxidant systems for aliphatic hydrocarbons and related alkyl substituted fluids 20 p3474 A67-37594

X-ray analysis of hydrate of diethylamine three-dimensional crystal structure, determining bond distances and angles 22 p3757 A67-39634

AMINO ACID

SA ADENINE

SA ASPARTIC ACID

SA GLYCINE

SA PROTEIN

Mass spectrometric determination of amino acid sequence from oligopeptides 04 p0566 A67-15613

Esterification of secondary alcohols, using amino acids 06 p0956 A67-18576

Beta hydroxyvaline synthesis, resolution and configuration 07 p1137 A67-20014

Pyrrolic compound formation by UV irradiation of delta-aminoolevulinic acid 08 p1290 A67-21254

Hydrolysis of phthalamide ring with carboxylate group linked through alkyl group as anionic intramolecular catalyst 10 p1602 A67-23159

Protein synthesis reduced and turnover stimulated by valine in P saccharophila in nongratiuitous inducing conditions 13 p2058 A67-26584

Catalytic decarboxylation of oxaloacetic acid into pyruvic acid by thermally prepared poly-alpha-amino acids 13 p2065 A67-26589

Catalytic effect of thermal polyanhydro-alpha-amino acids on hydrolysis of p-nitrophenylacetate, noting role of histidine residues 13 p2065 A67-26732

Inactivation of thermal catalytically active polyanhydro-alpha-amino acids by heating in buffered solution, noting hydrolysis of cyclic imide bonds 13 p2065 A67-26733

Tissue protein synthesis in hypodynamic rats studied with aid of carbon 14 and sulfur 35 tagged amino acids 13 p2059 A67-26759

Free radical formation in amino acids exposed to thermal hydrogen atoms 13 p2065 A67-26869

Pasteur Probe, assay of asymmetry of D, L amino acids in detection of Martian life 15 p2433 A67-29116

Amino acid formation by formamide thermal decomposition, noting support for hydrogen cyanide oligomerization hypothesis 20 p3376 A67-36700

Alpha aminonitriles formation by electric discharge through anhydrous methane and ammonia mixture, showing hydrolysis to

amino acid as possible bearing on chemical evolution 20 p3369 A67-36764

Organic phosphate shown as inhibitory factor from B. stearothermophilus for attachment of amino acids to transfer RNA 20 p3370 A67-36798

Sterically controlled synthesis of optically active alpha-amino acids from alpha-keto acids: by reductive amination 20 p3376 A67-36874

Carbonyl compounds reaction with N-salicylidene-glycinatoaquocopper (II)/syntheses of beta-hydroxy alpha-amino acid from glycine 20 p3376 A67-36877

Simultaneous copolymerization of Leuchs anhydrides of 18 amino acids common to protein, discussing nutritional significance 20 p3377 A67-37397

Gas chromatography parameters of fluoro derivatives of amino acids compared for use in packed columns or sensitivity evaluation 21 p3578 A67-38764

Hydrazine effects on free amino acid concentrations of plasma and urine in dogs 23 p3952 A67-41570

Molecular weight and amino acid composition of chromatum ferredoxin 24 p4113 A67-42653

Optically active alpha amino acids synthesized from alpha keto acids by hydrogenolytic asymmetric transamination 24 p4119 A67-42703

AMMONIA

SA LIQUID AMMONIA

Frequency stability of double beam ammonia laser with thermostatic quartz resonators on 3-2 line 01 p0088 A67-10247

Gaseous ammonia composite solid propellant ignition upon contact with oxidizing vapors such as perchloric acid vapor 06 p1073 A67-18869

Color phenomena on moon 08 p1396 A67-21165

Fluctuation measurements in amplitude of oscillation of ammonia beam maser 09 p1513 A67-22043

Measurements of induction period, ammonia consumption rate after induction and radiation from electronically excited OH radicals in ammonia-oxygen reaction 18 p3155 A67-33836

Reaction zones of ammonia-oxygen and hydrazine decomposition flames, measuring temperature and concentration profiles 18 p3155 A67-33838

Ignition energy, quenching distance, flame stability and gas turbine burner performance of ammonia-air mixture 18 p3109 A67-33843

Ammonia-air combustion, flame speed needed to obtain optimum performance 18 p3110 A67-33844

Midband saturation characteristics of ammonia maser amplifier and variation of maser bandwidth with gain 20 p3458 A67-36431

Ammonia inversion transition hyperfine structure for nitrogen 14 and 15 nuclear masses measured with two-cavity maser spectrometer 20 p3462 A67-37565

UV absorption of ammonia at high temperatures behind shock waves, discussing NH radical formation from shock tube ammonia decomposition 22 p3756 A67-39442

AMMONIUM CHLORIDE

Gaseous ternary diffusion instabilities observed by ammonium chloride smoke technique, studying pressure and composition effects 22 p3917 A67-39713

AMMONIUM COMPOUND

High intensity triboluminescence in europium tetrakis /dibenzoylmethide/-triethylammonium crystals under mechanical impact 01 p0019 A67-10897

Raman effect in solutions of potassium, sodium and ammonium dichromate and potassium dichromate single crystal 19 p3240 A67-35421

Pulsed propulsive performance of low thrust subliming solid ammonium carbamate reaction jet, discussing transient response, apparatus, techniques, etc 21 p3697 A67-39152

AMMONIUM NITRATE

Double- and multiple-based nitrate propellants and gunpowders with tabulated characteristics analyzed, particularly nitrocellulose-nitroglycerin, diglycol-dinitrate, nitroguanidine and ammonium nitrate compounds 13 p2185 A67-26337

AMMONIUM PERCHLORATE

Comparison of decomposition rate for pure ammonium perchlorate, chlorate ion doped

ammonium perchlorate and X-rayed ammonium perchlorate at 236 degrees C 04 p0687 A67-14635

Combustion characteristics and ballistic performance of dual layer propellant grains using polybutadiene/potassium perchlorate and polyurethane/ammonium perchlorate for end-burning type rocket motor 05 p0872 A67-16589

Catalyzed thermal decomposition of ammonium perchlorate 05 p0759 A67-17374

Surface temperature of deflagrating ammonium perchlorate crystals calculated from crystal phase transition thickness [AIAA PAPER 67-68] 06 p1073 A67-18469

Ammonium perchlorate composite propellant deflagration studied by two burner analogs [AIAA PAPER 67-101] 06 p1073 A67-18472

Erosive burning of ammonium perchlorate solid propellants for combustion in turbulent boundary layer determined, using flat plate heat transfer correlation 07 p1238 A67-19069

Thermal stability of ammonium perchlorate-lithium perchlorate mixture, noting explosion above 280 degrees C for various compositions 07 p1239 A67-19078

Temperature coefficient of combustion rate for mixtures of ammonium perchlorate with various hydrocarbons 07 p1267 A67-19311

Mechanism of decomposition of ammonium perchlorate in accord with experimental fact 10 p1697 A67-23157

Enthalpy changes in ammonium perchlorate during linear heating, noting crystal structure transformation and subsequent decomposition 14 p2376 A67-28903

High density moisture-proof noncrystalline family of gas generator propellants, surveying burning rates, physical properties and application 15 p2544 A67-29980

Kinetics and energetics of condensed phase thermal decomposition reactions of ammonium perchlorate composite propellants analyzed, using differential scanning calorimetry 15 p2544 A67-29989

Combustion characteristics of crystalline oxidizers noting materials used, experiments performed and results 15 p2581 A67-29990

Sound velocities in granular ammonium perchlorate and potassium chloride, discussing chemical reaction of shocks 16 p2734 A67-31521

Vaporization by dissociation of amine-type perchlorates revealed by infrared spectroscopy, proving role of proton transfer reaction in perchlorates thermal decomposition 16 p2619 A67-31536

Ammonium perchlorate solid propellant ignition characteristics recording preignition surface exotherms 17 p2927 A67-33027

Cadmium compounds catalytic effect on ammonium perchlorate decomposition rate and ignition temperature 18 p3107 A67-33810

Composite ammonium perchlorate propellant temperature profile beneath burning surface, discussing main decomposition energy, heat sources, etc composite ammonium perchlorate propellant 18 p3107 A67-33811

Combustion mechanism of ammonium perchlorate propellants, discussing gasification, decomposition, pressures, binders, burning rates, temperatures, etc 18 p3108 A67-33812

Effect of copper chromite, carbon and other potential catalysts on thermal decomposition and ignition of ammonium perchlorate 18 p3108 A67-33813

Deflagration of ammonium perchlorate studied using cleaved sections of large single crystals grown from water solution, discussing burning rate and combustion zone 18 p3108 A67-33814

Condensed phase thermal decomposition of ammonium perchlorate, studying pressure and additives effect on kinetics 19 p3309 A67-35003

Electric conductivity variation with temperature for solid ammonium perchlorate, determining energy barrier and enthalpy of lattice defect formation and migration 20 p3377 A67-37134

Surface temperature of deflagrating ammonium perchlorate crystals calculated from crystal phase transition thickness [AIAA PAPER 67-68] 21 p3688 A67-38859

Ammonium perchlorate deflagration studied by flash pyrolysis and kinetic spectroscopy noting radical

concentrations 22 p3867 A67-3963

High density moisture-proof noncrystalline family of gas generator propellant: surveying burning rates, physical properties and application 24 p4207 A67-4292

AMMONIUM PHOSPHATE

UV radiation generation from output of Nd glass laser by frequency doubling in ammonium dihydrogen phosphate crystals 06 p1011 A67-18711

AMPHETAMINE

Individual caged mice susceptibility found greater than groups to toxic effect of amphetamine [AFOSR-66-1883] 19 p3178 A67-35888

AMPLIFICATION

S FLUID AMPLIFICATION

S SOUND AMPLIFICATION

AMPLIFICATION FACTOR

Combined automatic control systems with automatic adjustment of amplification coefficient of disturbance controller for error reduction 01 p0044 A67-10244

Variation of antenna amplification ratio with distance as function of phase error as antenna aperture with exciter off-focus as error source 01 p0035 A67-10393

Weimer triode with contact rectifier for use as component of microminiature radio circuits, noting effect of contact rectification on current-voltage characteristics and amplifying power of such triodes 01 p0035 A67-10394

Amplification factor of circular polarization antennas calculated by mirror image method 02 p0209 A67-11503

Frequency dependences of amplification index of linear amplifier at 3.39 micron wavelength for various excitation levels 02 p0191 A67-11578

Spectral density measurement of relative fluctuations of current amplification factor common-base transistor circuit 02 p0213 A67-11646

Automatic adjustment of amplification factor of control systems in response to perturbation 03 p0389 A67-13080

Power gain of submillimeter wave in traveling wave amplifier with periodic delay line structure 03 p0380 A67-13557

Nonscanning adaptive automatic control system for plant with variable amplification factor 03 p0394 A67-14062

Instability of amplification factor and stability of transmission coefficient of multistage transistorized amplifier without feedback 05 p0772 A67-16454

Dual control of plant with random amplification factor as Bayesian problem 06 p0976 A67-18408

Small signal nonlinear amplitude distortion and phase shift measurement in TWT 07 p1151 A67-19427

Partial amplification factors of multistage cascade amplifier to determine transmission coefficient of follower 08 p1305 A67-21278

Criterion for spatial amplification or nontransmittance using double Laplace transforms in light of complex values of wave vector 09 p1463 A67-21992

Static current amplification factor of transistor dependence on operating conditions in switching circuits 13 p2075 A67-26347

Nonscanning adaptive automatic control system for plant with variable amplification factor 13 p2089 A67-27711

Magnification problems facing aircraft designers analyzed by computerized iterative procedures 14 p2245 A67-28062

Amplification factor of circular polarization antennas calculated by mirror image method 14 p2283 A67-28069

Flutter amplitude of stressed panels analyzed in terms of amplification ratios 14 p2399 A67-28139

Resistive transistor stage with feedback, deriving input-output impedances, amplification factors, conductance and resistance 14 p2283 A67-28276

Transistorized resonant cascade amplifier with added active resistance for amplifier stability improvement 14 p2283 A67-28277

Laser emission under external signal, analyzing competition between amplification mode and parasitic generation arising at resonant frequency, noting signal role 15 p2498 A67-29469

Amplification factor of air-cushion vehicles and its physical significance for bell-and-peripheral-jet concepts 16 p2596 A67-31444

Amplification of traveling-wave tube calculated to determine effect of continuous current interception along delay system 16 p2640 A67-31506

Traveling wave amplification by interaction of drifting carriers in semiconductors with external slow wave circuit 17 p2826 A67-32656

Symmetrical traveling-wave antenna design with given sidelobe level and amplification factor, determining coupling coefficient and maximum utilization 18 p3011 A67-34178

Tunnel diode amplifier with single circuit, stability analysis and calculation of circuit parameters 18 p3011 A67-34179

Saturation current measurement in diffusion transistors by method yielding current amplification factors and voltage dependence of emitter current 19 p3197 A67-35726

Dispersion equations for two types of transverse interaction tubes analyzed numerically in presence of strong space charge 19 p3198 A67-36022

Holography by amplitude division, eliminating destructive interference by using optical prism 20 p3435 A67-36200

Equations of motion of continuous single loop adaptive control system with scan modulated parameters, noting stability analysis method 20 p3408 A67-37044

Amplification factor stabilization or variance of transistorized radio astronomy receivers, discussing circuit diagram, performance and reliability 20 p3403 A67-37517

Reflected wave amplitude dependence on degree of inhomogeneity of medium 21 p3580 A67-38112

Necessary and sufficient conditions for linear system response to input vector with limited amplitude and slope, noting singular case existence 21 p3603 A67-38175

Laser emission under external signal, analyzing competition between amplification mode and parasitic generation arising at resonant frequency, noting signal role 21 p3641 A67-38550

Neodymium-glass laser amplifier gain saturation investigation using laser driving signal, discussing Schulz-DuBois steady state theory and inversion density 22 p3813 A67-39349

Coherent Raman amplification dynamics, considering pump depletion and coupling saturation and stimulated Raman scattering by polarization waves 22 p3816 A67-40318

Odd value correlation coefficient and wave amplitude fluctuation effects on mean radiation pattern and antenna amplification losses 23 p3977 A67-40599

Steady state vertical displacements at surface of elastic half-space due to Rayleigh waves from sonic boom, obtaining shock amplification factors 23 p4074 A67-40632

Antenna linear array design with limited amplitude tapering, showing desirable pattern characteristics in partially uniform array 23 p3978 A67-40827

Pulse regenerative amplification in Q-switched argon-ion laser during buildup time to saturation 23 p4014 A67-41030

AMPLIFIER

SA BEAM-PLASMA AMPLIFIER

SA BISTABLE AMPLIFIER

SA BROADBAND AMPLIFIER

SA CHOPPER

SA CROSSED FIELD AMPLIFIER

SA CURRENT AMPLIFIER

SA DIFFERENTIAL AMPLIFIER

SA ELECTRON MULTIPLIER

SA ELECTRONIC AMPLIFIER

SA FEEDBACK AMPLIFIER

SA FLUID AMPLIFIER

SA FLUID JET AMPLIFIER

SA FREQUENCY AMPLIFIER

SA JET AMPLIFIER

SA KLYSTRON

SA LASER

SA LIGHT AMPLIFIER

SA LIMITER AMPLIFIER

SA MAGNETIC AMPLIFIER

SA MAGNETOSTATIC AMPLIFIER

SA MASER

SA OPTICAL AMPLIFIER

SA PARAMAGNETIC AMPLIFIER

SA PARAMETRIC AMPLIFIER

SA PHOTOMULTIPLIER

SA PHOTOTUBE

SA PREAMPLIFIER

SA PUSH-PULL AMPLIFIER

SA QUANTUM AMPLIFIER

SA SERVOAMPLIFIER

SA TRANSFORMER

SA TRANSISTOR AMPLIFIER

SA TRAVELING WAVE AMPLIFIER

SA VOLTAGE AMPLIFIER

Ultralow-noise tunable S-band amplifier using TWM as second stage 01 p0034 A67-10106

Noise factor of linear receiving systems in quantum and classical regions, noting role of dual push-pull amplifier and frequency converter 01 p0022 A67-10393

Circuit design measuring travel time required by low energy particle of varying mass 01 p0066 A67-10654

Accuracy of DC amplifiers solving linear differential equations with constant coefficients, examining effect of drift and grid currents 01 p0031 A67-11264

High performance LF wideband discriminators with negative voltage feedback 01 p0040 A67-11316

Bulk GaAs Gunn effect oscillators and amplifiers and electron transfer between high mobility and low mobility conduction bands 02 p0218 A67-12099

Gallium arsenide negative conductance amplifiers used in calculation of negative mobility 02 p0221 A67-12512

Klystron amplifier performance, noting increased efficiency by using double interaction in output 02 p0222 A67-12531

Tunnel-diode amplifier sensitivity gain due to negative resistance variation 03 p0382 A67-13668

Synthesis method for immittance matrix with grounded unity gain amplifier /GUGA/ as only active element 03 p0393 A67-13979

RC active circuit under effect of amplifier finite input impedance, nonzero output impedance and nonzero source impedance 05 p0785 A67-17299

Direct-to-home TV broadcasting satellite system for upper UHF, describing stabilization, thermal control, antenna, power amplifier, etc 06 p1094 A67-17689

Direct-to-home TV broadcasting satellite system for upper UHF, describing stabilization, thermal control, antenna, power amplifier, etc 06 p0964 A67-18414

Resonance cascade amplifier using additional AC resistance resulting in gain increase without band pass increase 06 p0972 A67-18900

Output signal of switched amplifier with arbitrary input signal analyzed, using Fourier series 07 p1154 A67-19656

Temperature effect on microwave-gain characteristics of bulk GaAs amplifier, interpreting results in terms of changing carrier concentration 10 p1612 A67-23371

Klystron amplifier performance, noting increased efficiency by using double interaction in output 14 p2279 A67-28008

Midband saturation characteristics of ammonia maser amplifier and variation of maser bandwidth with gain 20 p3458 A67-36431

Protective devices in electrodynamic vibration exciters, examining design, operational principles and possible cause of failures 22 p3781 A67-40403

AMPLIFIER DESIGN

Pump noise contribution to total noise of LF parametric converter, analyzing effect of magnitude of bridge out-of-balance voltage 01 p0032 A67-10002

Stabilization scheme for certain active networks, examining compensated one-port Y in simple amplifier connection 01 p0033 A67-10015

Industrial F 115 photocompensation amplifiers for recording integral and reflected radiation aboard aircraft 01 p0062 A67-10127

Intermediate frequency logarithmic amplifier using twin-gain stages and transistors and avoiding successive detection principle and video delay line 01 p0025 A67-10814

Receiver design for LF time signals on kilometric waves 02 p0190 A67-11481

Power amplifier used in electrodynamic shakers for transforming electrical into mechanical vibrations, examining range,

deformations, humming and impedance 03 p0363 A67-13398

MOS-FET amplifier RC network design 03 p0382 A67-13670

Paraelectrics as prospective materials for UHF amplifiers with very low noise level 03 p0382 A67-13711

Book on network theory of negative-resistance tunnel diode linear and nonlinear sinusoidal circuits and application to amplifiers 03 p0383 A67-13817

Transistor hybrid equivalent circuit of large amplitude sinusoidal voltage used in design of LC oscillators, power amplifiers, etc 03 p0387 A67-13998

Self-activating microwave cold cathode crossed field amplifiers for modulation circuits in complex radar systems 03 p0387 A67-14121

Very high input impedance direct current chopper amplifier using field effect transistor characterized by very low gate leakage current and capacitance 03 p0389 A67-14378

Ferromagnetic magnetostatic amplifier using various types of oscillations for pumping and signal amplification 04 p0583 A67-15168

Wide temperature and parameter range transistor amplifier stage stabilization circuit design based on linear approximation of characteristics in terms of H parameters for CE circuit 04 p0586 A67-15669

Book on transistor IF amplifier design for radio, television and radar receivers 05 p0769 A67-16071

Amplitude characteristic in transistorized selective logarithmic amplifier with video output, discussing circuitry of proposed multistage amplifier 05 p0773 A67-16459

Ultrahigh input impedance for measuring electrical activity of biological cell 05 p0773 A67-16512

Amplifier using electro-optic junction modulator combined with photodetector, showing gain at microwave frequencies 05 p0774 A67-16822

Quantum paramagnetic traveling wave amplifier using rutile with admixture of chromium and combined with magnet with superconducting coil 05 p0825 A67-17161

Automatic phase control /APC/ loop for stabilization of phase shift in RF amplifier 05 p0778 A67-17395

S-band parametric amplifier pumped at J-band using balanced idler circuit with two varactor diodes incorporated in one encapsulation 06 p0966 A67-17580

Logarithmic amplifier design at UHF frequencies starting from linear amplifier, using successive detection method 06 p0967 A67-17811

Transistorized wideband and pulse type amplifiers for nanosecond frequency range 06 p0970 A67-18191

RF amplifier circuit diagrams, obtaining logarithmic amplitude characteristic by switching nonlinear elements to plate or cathode circuits 06 p0972 A67-18899

Operational amplifier using monolithic integrated circuit noting calculation, layout and topological integration 08 p1302 A67-20920

Chopper circuit theory and design methods with DC amplifier comparison 08 p1302 A67-20991

Ultralow-noise two-channel tunable cascade amplifier system using upconverter and traveling wave maser 08 p1304 A67-21222

Low temperature components for data processing, low noise amplifiers and microwave technology, noting superconductor elements like cryotron 09 p1463 A67-21760

Small signal thin beam theory application to design of amplifiers, noting electronic gain as function of various parameters 09 p1478 A67-22261

Maser for traveling waves over large cm wave band used as low noise amplifier 09 p1482 A67-22481

Continuous magnetic field satisfies conditions of stability, size, orientation, uniformity and controllability of maser type amplifier employing superconductor winding 09 p1516 A67-22482

Amplifying elements ensuring required dynamic properties of resolving amplifier without calculating entire amplifier circuitry 10 p1611 A67-22983

Compact nonresonant five-pass carbon

dioxide laser amplifier structure giving small signal gains 11 p1800 A67-24245

Reflection amplifier design for use in tunnel diode UHF radio 11 p1766 A67-24689

repeater 11 p1766 A67-24689

Power gain sensitivity of transistors with conjugate matched two-port amplifier 12 p1910 A67-25260

Parametric amplifier varactor characteristics, construction methods and qualities for hyperfrequency low noise parametric amplification 12 p1913 A67-25299

Logarithmic amplifier designs based on follower type circuits 12 p1915 A67-25858

VHF transistor, attempting design of 60 MHz passband amplifier 13 p2077 A67-26653

Distributed tunnel diode amplifier design noting magnitude of attenuation by shunt for LF and HF [AFOSR-67-1406] 13 p2079 A67-26876

HF transistorized pulse amplifier with rise of 1 nsec and output voltages of more than 4 v designed for trigger pulses and traveling wave oscilloscope 13 p2082 A67-27400

Liquid helium traveling wave maser amplifier for low noise ground station satellite communication 14 p2329 A67-27777

receiver 14 p2329 A67-27777

Cooling system for maser amplifier for ground station satellite communication 14 p2277 A67-27778

Microelectronic technique application to active filter design, noting monolithic realization of operational amplifier 14 p2280 A67-28017

Proportional momentum beam deflection fluid amplifier design 14 p2249 A67-28327

Impact stage of impacting jet amplifiers studied by interposing disk between two opposing coaxial jets, obtaining pressure gain 14 p2250 A67-28332

Signal-source noise mismatch and alignment in linear triode amplifier networks 14 p2289 A67-28864

Tunnel diode logarithmic amplifier circuit design using thin film passive components and tiny inductors 15 p2442 A67-29166

Microelectronic amplifiers, emphasizing reliability improvement and decreased sensitivity to parameter changes 15 p2443 A67-29239

Ferromagnetic magnetostatic amplifier using various types of oscillations for pumping and signal amplification 15 p2443 A67-29354

Two-port network design applied to FET in common source and common gate amplifier configuration 15 p2451 A67-29917

Low noise amplifier specifications for communication satellite earth station 16 p2635 A67-30473

Active filter design employing impedance converters, amplifiers and gyrators, providing equations for component values 17 p2824 A67-32394

Electrical design, mechanical fabrication and performance data of integrated broadband balanced transistor amplifier 17 p2825 A67-32599

Low noise transistorized amplifier at 408 MHz for synthesis radiotelescope 17 p2827 A67-32785

Monolithic operational amplifiers with simplified frequency-compensated network using minimum stages and integrated circuit components 17 p2828 A67-32899

Tunnel diode amplifier with single circuit, stability analysis and calculation of circuit parameters 18 p3011 A67-34179

Design, operation, characteristics and applications of carbon dioxide lasers with DC excitation and fixed mirrors 18 p3061 A67-34350

Linear microcircuits evaluation and application covering offset voltage and current, noise properties, input impedance, etc 18 p3013 A67-34548

Bipolar and field effect transistor combinations for high gain amplifiers, discussing various circuitries 19 p3191 A67-34943

MOS and silicon transistors for design of logarithmic amplifiers for space instrumentation 19 p3194 A67-35463

Design and characteristics/gain, noise factor and bandwidth of parametric amplifier 19 p3194 A67-35548

Lower frequency pumped parametric amplifier with three idler frequencies 19 p3195 A67-35626

Stability criterion for bandpass tunnel

diode amplifier, determining limitations on diode series inductance as function of negative resistance 19 p3196 A67-35662

Input-to-output amplitude and phase modulation characteristics derived for multicavity klystron amplifiers 19 p3197 A67-35809

Momentum amplifier based on primary, secondary and control jet momentum flux interaction 20 p3362 A67-36120

Transistor admittance parameters for mathematical model formulation representing small signal operations, for wideband transistor amplifier design 20 p3394 A67-36236

Design and stability of wideband tunnel diode amplifiers for microwave radiolink receivers 20 p3395 A67-36248

Cut-off amplifiers in frequency stabilization klystron designed to cut off only HF wave applied to discriminator 20 p3396 A67-36327

Microwave amplifier using varactor diode with coaxial signal, lumped element idler and waveguide pump circuit for broadband radio link at 20 db 20 p3401 A67-37357

Short tube orifices, confined turbulent jets, jet-wall and jet-receiver interactions and characteristics of diffusion process for design of fluid amplifiers 20 p3365 A67-37361

Ionospheric ion and electron densities by Langmuir probes, stressing solid state logarithmic amplifier for spatial electrometry 21 p3592 A67-38223

Choke-coupled magnetic amplifiers and amplifiers with rotational magnetization, considering multicycle and single-cycle amplification 21 p3593 A67-38290

500 to 1000 MHz ultrahigh RF hybrid amplifier fabricated with microelectronic multilayer thin film technique, noting performance of components 21 p3596 A67-38342

Low noise temperature traveling wave maser preamplifier for microwave reception, discussing design, applications and specific electron gain 21 p3641 A67-38640

Block diagram, schematic circuit and amplitude and frequency characteristics of wideband transistorized amplifier for studying high speed aircraft industrial processes 21 p3600 A67-38918

Magnetron type microwave amplifier gain increase, discussing electron beam interaction region M-type device gain calculations 22 p3770 A67-39654

Nonreciprocal parametric amplifier obtained by using parametric elements in frequency inverting case without unigude or circulator 22 p3771 A67-39838

Solid state linear digital amplifier with external modulation using high operating efficiency of transistors as saturated switching elements 22 p3771 A67-39841

Design and performance of high gain amplifier consisting of cadmium sulfide single crystal and thin film transducers 23 p3977 A67-40690

Varactor inductance effects on design varactor tuned circuits above 50 MHz 23 p3982 A67-41504

Moderate bandwidth tunnel diode amplifier using directional filter as bandpass structure 24 p4131 A67-42445

AMPLITUDE

SA PULSE AMPLITUDE

SA PULSE WIDTH AMPLITUDE

CONVERTER

SA SCATTERING AMPLITUDE

Sum signal of output of system consisting of two detuned resonators and two amplitude detectors used for automatic measurement of signal frequencies 01 p0022 A67-10413

Amplitude and frequency characteristics of hydrogen-atom beam maser 02 p0251 A67-11574

Estimated amplitude of echo-signal for uniform, Rayleigh and a priori distribution of probability density of noise amplitudes 02 p0194 A67-11976

Absorption dependence of ultrasonic waves in superconductors on amplitude of sound wave due to temperature 03 p0492 A67-13325

Phase locked laser loop for amplitude and phase measuring device for coherent optical wave fronts 04 p0632 A67-15076

Accelerometer frequency response and quadratic lag function amplitude response curves and relation to resonant

frequency 04 p0627 A67-15792

Electronic analog detection and separation of oscillations slightly differing in amplitude 06 p1109 A67-18667

Amplitude and polarization of radio pulse from extensive cosmic ray air shower indicating geomagnetic deflection mechanism of emission 18 p3116 A67-34196

Construction and uniqueness of time optimal control of multidimensional linear system with constraints on control signal amplitudes and rates 18 p3017 A67-34280

AMPLITUDE DISTRIBUTION ANALYZER

Circuit design measuring travel time required by low energy particle of varying mass 01 p0066 A67-10654

Synthesis and sidelobe reduction of unequally spaced antenna arrays with uniform or stepped amplitude distribution, achieving desirable radiation characteristics 02 p0217 A67-12095

Amplitude distributions of solar photospheric fluctuations 10 p1711 A67-23795

Radiation pattern of irregular antennas, using digital computer and superimposition of components to determine composite pattern 12 p1915 A67-25974

Crossing rates of atmospheric radio noise in high range of threshold field strength measured and compared with integrated field strength 14 p2306 A67-27881

Amplitude distributions of refractive index differences showing spikes superimposed on variations continuum due to water vapor clustering 21 p3617 A67-38187

Measured acceleration time histories analyzed for automatic handling of recorded data, discussing advantage of amplitude distribution method 23 p3986 A67-40719

Diurnal variation in cosmic ray anisotropy from observations during solar activity minimum, giving amplitudes and phases distribution 23 p4058 A67-41122

Differentiation between true variation amplitude and statistical instrument error, deriving diurnal variation amplitude and phase distribution expressions 23 p4059 A67-41131

Self-gravitating isothermal nonrotating gas layer stability, discussing amplitude density distributions in space 24 p4225 A67-41826

Oscillating circuits with nonlinear active elements amplitude and phase frequency characteristics graphically plotted, noting effects on frequency devices 24 p4136 A67-42191

AMPLITUDE MODULATION

Nonlinear distortion of envelope of amplitude modulated signal in selective HF channel 01 p0020 A67-10200

Book on statistical communications theory, digital communications, AM and FM CW communications, binary communications and noise 01 p0021 A67-10306

Counting errors and amplitude spectra distortion in detectors for statistical characteristics of information contained in signals 01 p0066 A67-10653

Switching and dynamic characteristics of germanium peak diodes used as AM devices 02 p0210 A67-11531

Microwave direction-finding systems based on amplitude comparison for use with pulse or continuous wave signals, noting switching system 02 p0198 A67-12067

Statistical distribution of AM laser signal envelope upon passage through turbulent atmosphere 03 p0438 A67-13988

Book on circuitry for RF, AM and FM electronic communication systems 03 p0388 A67-14272

Optimum AM reception in presence of interference signal and fluctuating noise 04 p0568 A67-14451

Fluctuation characteristics and spectrum of monochromatic radio waves when propagating in interplanetary medium 04 p0575 A67-15163

Resonant frequency change of oscillatory circuit due to nonlinear capacitance of semiconductor diode used as amplitude detector 04 p0586 A67-15677

Electronic testing of transmitters and receivers noting AM and FM systems sensitivity, noise figures and image rejection 04 p0590 A67-15727

Oscillation amplitude modulation in ammonia beam maser oscillator with single cavity followed by two cavities in cascade 05 p0817 A67-16636

Phase separation and synchronization

during separation of AM signals with overlapping frequency 05 p0764 A67-16903

Pulse interference inhibition in AM signals reception by nonlinear negative feedback loop in HF cascades of receiving device 05 p0785 A67-17471

Time structure and amplitude self-modulation of emission from GaAs injection laser observed, using electron-optical converter 06 p1009 A67-17756

Alternating method of measuring Hall constant by modulation of voltage amplitude on arbitrarily shaped plates 06 p1005 A67-18727

Method for receiving radio signals against background of strong amplitude-modulated noise signal 06 p0965 A67-18898

Spectrum of AM sequences of video pulse packages 07 p1140 A67-19233

Transformation of spectrum of AM periodic sequence of video pulse by inertial detector 07 p1140 A67-19234

Transmission methods, analyzing noise threshold, signal bunching, etc 07 p1141 A67-19339

Kerr cell properties noting four-electrode cell giving frequency shift of 60 mc for laser beam 07 p1142 A67-19552

Threshold value lowering in synchronous demodulation, determining output SNR as function of input SNR 08 p1294 A67-20771

Effect of tunnel diode amplifier V-I characteristics on cross modulation products in electromagnetic spectrum 09 p1557 A67-22266

System characteristics of tunnel diode amplifiers, discussing noise figure, intermodulation, AM-PM conversion, etc 09 p1481 A67-22479

Ultrarapid AM of hyperfrequency mm wave in waveguide 09 p1465 A67-22568

Parameters of simultaneous amplitude phase modulation of periodic cosmic ray variations obtained from satellite observations 10 p1698 A67-22779

AC background in phase of output oscillation of multistage frequency multipliers attributed to presence of HF harmonics in automatic bias circuit 10 p1613 A67-23448

Amplitude and frequency fluctuations in flicker noise region of transistorized quartz oscillator 13 p2075 A67-26395

Spread spectrum for amplitude modulated transmitters and receivers 13 p2066 A67-26405

Optimum AM reception in presence of interference signal and fluctuating noise 15 p2435 A67-29288

Fluctuation characteristics and spectrum of monochromatic radio waves when propagating in interplanetary medium 15 p2435 A67-29350

Frequency dependence of radio star scintillations 15 p2555 A67-29621

Tunnel current modulation by acoustic wave in superconductors 15 p2537 A67-29708

Possible directional pattern forms obtainable for single-ring circular arrays, using Fourier harmonic analysis technique 15 p2454 A67-30138

Phase separation and synchronization during separation of AM signals with overlapping frequency spectra 16 p2622 A67-30879

Cosmic ray variations methodology, considering solar system geometry, interstellar cosmic ray gradient, phase and amplitude modulation, etc 17 p2934 A67-32103

Simultaneous amplitude and phase modulation of periodic cosmic ray variations by using two frequencies 17 p2934 A67-32106

Automatic AM control noting proportionate variation of carrier level to signal volume 18 p2998 A67-33502

Amplitude modulation using varicaps and p-n junction in transistorized transmitter, analyzing HF oscillator 18 p2999 A67-33507

Woodward ambiguity function extended to broadband signals including Doppler distortions of modulation function 18 p3001 A67-34114

Stationary or long range space vehicle transmitting antennas remote alignment technique using received signal AM 18 p3016 A67-34596

Noise wave amplitude reduction method by suitable initial wind field adaptation to pressure field studied for applications to divergent barotropic

model 19 p3253 A67-35530

Input-to-output amplitude and phase modulation characteristics derived for multicavity klystron 19 p3197 A67-35809

Estimation of fluctuation sensitivity of measuring radio receiver modulated by intermediate frequency amplifier 19 p3198 A67-36016

Small correlated amplitude and frequency fluctuations of stochastically-modulated radio waves 19 p3241 A67-36025

Electric vector expression of amplitude-modulated electromagnetic wave propagating in nonlinear dispersive medium 20 p3499 A67-36992

Traveling wave maser saturation and signal distortion, determining magnetic moment 21 p3642 A67-38813

Laser radiation photon number and amplitude fluctuations quantum mechanical calculation by deriving two coupled equations 22 p3815 A67-39784

Optical mixing of two low level signals in atomic states of He-Ne laser noting amplitude modulation of visible laser output 23 p4012 A67-40891

True and false sidereal diurnal cosmic ray variation, examining modulating effects leading to false variations 23 p4058 A67-41128

Sidereal diurnal cosmic ray variation caused by modulation in solar system, discussing variations in coordinate systems 23 p4059 A67-41129

Tunnel current modulation by acoustic wave in superconductors 24 p4200 A67-41778

Parameters of simultaneous amplitude phase modulation of periodic cosmic ray variations obtained from satellite observations 24 p4209 A67-42115

Noise immunity in binary detection and temporal shift measurement of pseudorandom amplitude keyed echo signal in multichannel system 24 p4120 A67-42233

Millisecond bursts in radio emission from Jupiter not imposed by interplanetary scintillation but by amplitude or frequency variation in source 24 p4231 A67-42452

AMPLITUDE PROBABILITY ANALYZER

Linear amplitude characteristics in synthesis of instrumental servosystems with saturated components such as amplifiers 11 p1794 A67-25040

Hybrid computer calculation of instantaneous and peak amplitude probability distribution of random signal 15 p2440 A67-29774

AN-24 AIRCRAFT

S ANTONOV AN-24 AIRCRAFT

ANALOG COMPUTER

SA DIGITAL COMPUTER

SA HYBRID COMPUTER

Analog computer solution of simultaneous systems of linear algebraic equations, based on modified Gauss-Zeidel method 01 p0105 A67-10542

Analog computer ionization recombination parameters and balance equation of charged particles in F-2 layer 02 p0236 A67-11659

Nonconservative oscillatory systems studied for stability and frequency characteristics, using analog computer and equation transformation 02 p0227 A67-12420

Linear equations solving methods on analog computers where system parameters are reproduced, using potentiometers and admittances 02 p0209 A67-12683

Analog computer solution to autonomous systems with one degree of freedom capable of self-excited oscillation or excited by external periodic force 02 p0209 A67-12712

Instrument, force and motion servos in cockpit simulation in large aerospace flight simulators, using DC analog voltages 03 p0395 A67-13386

Analog circuits for statistical correlation in time measurements, with application to subsonic and supersonic flow turbulence 04 p0620 A67-14889

Analog computer design noting operation principles, application to guidance problems and testing and troubleshooting methods 04 p0579 A67-15737

Simulation of controlled diffusion-type Markov processes applied to two stochastic equations related to problem of misadjustment on analog computer 05 p0768 A67-16263

Method of approximating functions with aid of orthonormal systems and single channel optimization, using analog

computer 05 p0768 A67-16264

Analog/hybrid computer design, noting inclusion of solid state and integrated circuits for reliability cost reduction and speed 05 p0769 A67-17519

Optimum guidance law simulation by analog computer using logic controlled analog, spatial analog and trajectory riding techniques 06 p1028 A67-17614

Electric analog and mechanical model used to investigate single particle impact dampers 07 p1262 A67-19410

Flow around variable profile in analog study of Laplacian field according to Dirichlet data 07 p1128 A67-20225

Operational and circuit features of laboratory device built to simulate dynamic electrical output characteristics of programmable solar array in orbital flight 08 p1315 A67-20660

Repetitive analog computer for Monte Carlo method solution of linear stochastic programming problems 08 p1299 A67-21198

Stress-strain diagrams under dynamic conditions obtained by processing strain gauge data, using analog computer 09 p1492 A67-21560

Functional converters of magnetic type for mathematical operations with analog computers 09 p1498 A67-22032

Fourier series and integrals in analog, digital and hybrid computation 09 p1470 A67-22667

Analog computer applied to solve two-point boundary value problem for fourth order optimal control problem with applied Pontryagin maximum principle 11 p1771 A67-24893

Special purpose analog computer for analyzing wideband signals in two parts of network, with automatically plotting and coupling factor as function of frequency 13 p2089 A67-26410

Analog computer application in linear, nonlinear and time-varying systems 13 p2072 A67-26995

Correlation method for generating sensitivity coefficients of dynamic system on high speed iterative analog computer 13 p2073 A67-27061

Dynamic errors in electronic analog computers, noting expressions for shift in characteristic roots of equations under solution 13 p2073 A67-27064

Electrodynamically coupled system consisting of RCL circuit, transformer and mechanical system analyzed by mathematical analogy and analog computer 15 p2440 A67-30081

Process identification by cyclic parameter adjustment with automatic iteration, using analog and hybrid computers 15 p2465 A67-30342

Statistical probability distribution for determining systematic errors of potentiometer multiplier by Monte Carlo method /static testing/ 16 p2633 A67-30464

Statistical methods and application to treatment of information in space domain, noting correlation functions 16 p2633 A67-30671

Analog computer method for approximation of real functions, discussing applications and limitations 16 p2634 A67-30831

Analog computer ionization recombination parameters and balance equation of charged particles in F-2 layer 16 p2665 A67-31074

Analog computer use in design of automatic steering control system of Apollo station ships for precision geographical track-keeping 16 p2701 A67-31659

Mathematical programming on analog computers solved by saddle point and extremum methods, using differential equations 17 p2817 A67-32225

Book on control systems and linear vibrational mechanical systems emphasizing use of analog and digital computers, frequency response, complex plane and root locus plots, FORTRAN method, etc 17 p2822 A67-33133

Soviet book on high velocity hydrodynamics including airfoil motion at distances from screen, hodograph method in MGD, drag coefficient determination, etc 18 p3021 A67-33409

Construction and operational possibilities of gimbal mounted servo-controlled aircraft model for optical simulation of flight mechanical motions 18 p3019 A67-33458

Digital and analog computers evolution, discussing microelectronics, speed, accuracy, bulk and human brain 18 p3010 A67-33551

Complex partial differential equations solutions by channel analog memory used with analog computer 19 p3186 A67-34966

Dynamic identification of loop system consisting of square-law operator, with behavior function of input signal and initial conditions 19 p3206 A67-35916

Analog computer solution of linear algebraic equations system modified to eliminate negative coefficients, guaranteeing computational system stability 19 p3187 A67-36032

Computer principles-equipment and programming for instrumentation systems, comparing digital computers with analog computers 20 p3390 A67-36463

High chamber-pressure propulsion systems and components captive testing, describing ground support system analysis, design and mechanisms 20 p3414 A67-36534

Noise rejecting algorithms for ODE solutions with computer, using redundancy, placement of control and feedback techniques 20 p3392 A67-37224

Flow velocity calculation by analog computer, discussing Laplace equation role 20 p3424 A67-37302

Soviet book on electronic and semiconductor devices of servosystems, examining theoretical principles, computational methods, design principles, analog and digital computers, etc 20 p3406 A67-37700

Analog and digital computer methods for research and development of fluidic circuit components, discussing scaling effects 21 p3612 A67-38106

Rocket control using analog computers, determining thrust vectors for trajectory 21 p3655 A67-38208

Book on simulation of mechanical systems giving analytical, graphic and analog computer methods 21 p3588 A67-38252

Operational analysis and DC design of Esaki diode pair bistable circuit used in high speed counting network performed by analog computer simulation 21 p3604 A67-38603

Repetitive analog computer for Monte Carlo method solution of linear stochastic programming problems 22 p3764 A67-39865

MOSFET integrated circuits for use in analog computers noting simplicity and switching qualities for control of hybrid devices 22 p3775 A67-40465

Circuit for plotting extremal values of cycle during analog computer simulation 23 p3976 A67-41339

Algebraic and transcendental equations solutions using analog computer model described by differential equations, noting Liapunov stability theorem and asymptotic equilibrium 23 p3976 A67-41392

Stability boundaries of double-dead-time model describing chugging in liquid bipropellant rocket engine 24 p4207 A67-42689

ANALOG DATA

Bias and variability errors in analog data reduction equipment [SAE PAPER 660716] 01 p0028 A67-10605

Analog device for measuring coefficient of space-time signal correlations and applications to statistical mechanics of turbulent fluids and random noise 01 p0054 A67-11090

DATA CORE, integrated launch area telemetry data system using high speed digital computers and analog or digital display 03 p0375 A67-13382

Tensile analog data reduction technique for determination of principal stress differences history at points of two nonhomogeneous photoviscoelastic models 05 p0921 A67-16826

HF analog microcircuits in sensors for information transmission systems, noting problems of precision and high power 05 p0776 A67-17039

Data compression for analog signal transmission with smaller bandwidth requirement obtained from reduced signal redundancy and simulation of techniques 14 p2275 A67-28683

PCM coder, programmer and analog switch of D-2 satellite, including systems characteristics and diagrams 21 p3599 A67-38647

Analog treatment of digital telemetering signals using a priori information about transmission, noting Q-factor, storage and use of existing emissions 21 p3584 A67-38660

Analog and digital data processes for interplanetary photoscience with reference to Mariner Mars flyby mission, discussing telemetric transmission and SNR [IEEE PAPER 19-TP-66-1134] 23 p3998 A67-40740

Logarithmic nature of I-V characteristics of silicon junction diodes for design of analog multiplier with differential operational amplifier 24 p4131 A67-42478

ANALOG SIMULATION

Extension of manual control to liquid rocket engine necessary to enable pilot to save primary mission or to change to planned secondary mission 04 p0703 A67-14426

Dynamic characteristics of distributed elastic structures in passive analog simulation, noting plate loading [AIAA PAPER 67-40] 06 p1102 A67-18334

Linear and nonlinear attitude control law synthesis for spinning aerospace vehicles, including analog simulation for control designs based on frequency symmetry 07 p1257 A67-19359

Electric analog simulation of periodic nonuniform heat transfer mechanism in film boiling from coated plate 08 p1427 A67-21321

Dynamic simulation of linear differential equations 09 p1469 A67-22620

Parametric coupling analyzed in electrical RLC circuit coupled with mechanical system through nonlinear inductance [ASME PAPER 67-VIBR-30] 11 p1797 A67-24188

Electrothermal analogies for heat transfer simulation by equivalent electrical circuits 11 p1884 A67-25047

Simulation of dynamic performance of pneumatic rebound-nozzle signal converters by analog computer 13 p2056 A67-27240

Design and optimal performance considerations on application of derived rate increment feedback to satellite attitude control systems in limit cycle and acquisition systems 13 p2212 A67-27297

Closed loop simulation of movement of center of gravity and optimum guidance laws for space vehicles by analog computer techniques 16 p2700 A67-30662

Elimination of electrical transients in high performance sleeve induction motors for missile guidance control systems 16 p2609 A67-31664

Hover augmentation system /HAS/ design for analog computer helicopter simulation and flight control 17 p2797 A67-32574

M-1 Engine Thrust Chamber Assembly test facilities and analog computer simulation during checkout [AIAA PAPER 67-455] 18 p3019 A67-33929

Optimal discrete filter corresponding to given analog filter for minimum mean square error 19 p3199 A67-34782

Project 666a Automatic Terrain Following Program and Automatic Flight Control System /AFCS/, with digital and analog simulation and test results 19 p3174 A67-35965

Analog translational trajectory program replacing digital program for orbiting and reentry vehicles 19 p3190 A67-36070

Analog simulation of differential equation system for Cardan-suspended gyro, considering dry friction, support and aircraft motion 20 p3454 A67-36954

Weierstrass canonical product analog for integral functions of many complex variables, discussing existence problems and canonical function construction 22 p3827 A67-39215

Magnus version of first harmonic approximation method for nonlinear systems engineering, using analog computer simulation for accuracy examination 22 p3776 A67-39327

General three-terminal p-n-p-n triode turn-on criterion equation derived and simplified for practical external-circuit arrangements 22 p3770 A67-39731

Lunar missions evaluated for scientific effectiveness via use of earth analogs assuming hypothetical terrestrial objectives parallel to lunar program 22 p3887 A67-40142

Ground based simulation program for EVA evaluation including center of mass and inertia products of model

astronaut 22 p3780 A67-40153

Up-rated Saturn I first stage propulsion system dynamic characteristics simulated by analog computer 22 p3869 A67-40169

Analog simulation of electromagnetic radiation from antenna of revolution in vacuum and plasma via networks, discussing rocket nose cone shapes 23 p3977 A67-40578

ANALOG-TO-DIGITAL CONVERTER

SA DIGITAL-TO-ANALOG CONVERTER

Multichannel Data Logging System for recording short-term simultaneous analog data from 25 to 100 parallel input channels 01 p0076 A67-11142

Logarithmic conversion of input-signal amplitudes into pulse numbers, using oscillatory circuit 02 p0221 A67-12419

Analysis technique for determining analog-to-digital converter time aperture error, taking into account nonlinear A-D conversion process 04 p0578 A67-14867

Quantum size in analog-to-digital conversion and effect on quantization noise in output of moving target indicator /MTI/ radar processors 04 p0570 A67-14873

Harmonic analysis of accuracy of reproduction in digital form of operators selecting period of time quantization, duration of analog-to-digital conversion, etc 05 p0781 A67-16258

Synthesis of capacitive converters of angular displacements into digital code 06 p1003 A67-18175

Analog circuit for presenting fixed pulse output corresponding to each cardiac cycle of given electrocardiogram and highly unresponsive to noise interference 09 p1455 A67-21715

Data handling systems, describing apparatus for processing of analog time varying signals in computer 09 p1501 A67-22466

Radar scan-antenna angle transmission over DC voltage in binary form for digital computer or display 11 p1760 A67-24269

Ten-channel tunnel diode analog-to-digital converter 12 p1909 A67-25856

Encoding and decoding techniques using integrated circuits and applicable to binary digitizing of electrical analog information 13 p2072 A67-26412

Open loop and feedback analog-to-digital conversion techniques, discussing conversion time, aperture and complexity 14 p2276 A67-28771

Statistical methods and application to treatment of information in space domain, noting correlation functions 16 p2633 A67-30671

Analog-to-digital conversion method for measuring weak currents, giving diagram of measuring circuit 16 p2635 A67-30672

Analog-to-code converter using negative resistance of unijunction transistor, noting construction and results 16 p2636 A67-30900

Semiconductor negative resistance devices to achieve analog to digital conversion 20 p3390 A67-36252

Data processing using digital computer, multiplexing and analog-to-digital conversion equipment for flight control and evaluation 20 p3390 A67-36465

Voltage comparator with high speed analog-to-digital converter and tunnel diode circuit 20 p3398 A67-36771

Instrumentation for observing limb darkening of solar continuum during annular eclipse of May 1966 20 p3529 A67-37502

Bioastronautics Laboratory Research Tool /BIO-ALERT/ as automatic biomedical monitoring system composed of digital computer, analog-digital converters and input-outputs 23 p3964 A67-41548

ANALYSIS

S CHEMICAL ANALYSIS

S CREEP ANALYSIS

S CRITICAL PATH ANALYSIS

S DATA ANALYSIS

S DIFFERENTIAL THERMAL ANALYSIS

/DTA/

S DIMENSIONAL ANALYSIS

S FACTOR ANALYSIS

S FLUTTER ANALYSIS

S FOURIER ANALYSIS

S FREQUENCY ANALYSIS

S FUNCTIONAL ANALYSIS

S HARMONIC ANALYSIS

S MATRIX ANALYSIS

S MICROANALYSIS

S NETWORK ANALYSIS

S NUMERICAL ANALYSIS

S PREFLIGHT ANALYSIS
 S QUALITATIVE ANALYSIS
 S QUANTITATIVE ANALYSIS
 S REGRESSION ANALYSIS
 S SENSOR FOR AIRBORNE TERRAIN ANALYSIS /SATAN/
 S SEQUENTIAL ANALYSIS
 S SIGNAL ANALYSIS
 S SPECTRAL ANALYSIS
 S STATISTICAL ANALYSIS
 S STRESS ANALYSIS
 S SYSTEMS ANALYSIS
 S TENSOR ANALYSIS
 S TRAJECTORY ANALYSIS
 S VECTOR ANALYSIS
 S WEIGHT ANALYSIS
 S X-RAY ANALYSIS
ANALYTIC FUNCTION
 SA CAUCHY-RIEMANN EQUATION
 SA COMPLEX VARIABLE
 SA POWER SERIES
 Stable convexity criteria of region in one-sheeted conformal mapping 01 p0104 A67-10287
 Partial fraction expansion in derivation of inverse Laplace transform of rational function with complex and/or repeated poles 01 p0104 A67-10479
 Identity of uniqueness and convergence constants of interpolation problems, discussing Abel-Goncharov function 02 p0258 A67-11624
 Stress functional properties of plastic materials, discussing analyticity and continuity in terms of tensor analysis 02 p0336 A67-11630
 Analytical and p-analytical functions of complex variable used to solve three-dimensional axisymmetric problems in elasticity theory 02 p0338 A67-11967
 Complex roots of dispersion relations involving transcendental analytic functions 03 p0486 A67-14056
 Linear continuous operators in analytic space exchangeable with differential operators 04 p0646 A67-15261
 Walsh approximation problem, establishing properties and uniqueness of analytic function 05 p0835 A67-17001
 Criterion of completeness of system of polynomials in singly connected space 05 p0836 A67-17118
 Inversion formula for principal integral representation of class of P-analytic functions applicable to axisymmetrical problems of elastic bodies 05 p0923 A67-17185
 Possio integral equation kernel derived in analytical form for wing flow 06 p0935 A67-17623
 Linear supersonic conical flow past lower surface of triangular wing, obtaining homogeneous boundary value problem for analytical function of complex variable 06 p0936 A67-17739
 Polynomials orthogonal with respect to contours, examining analytic function representation via Fourier series expansion of such polynomials 06 p1025 A67-18695
 Necessary and sufficient set conditions for continuous function analytic within internal points of set to permit smooth approximation by means of rational fractions 07 p1212 A67-19137
 Fourier convergence of analytic functions 07 p1215 A67-19474
 Analytic properties of solutions to generalized axisymmetric Schroedinger equation 08 p1346 A67-20355
 Soviet book on boundary value problems for analytic functions as applied to integral equations with Cauchy and Hilbert kernels 08 p1347 A67-20760
 Fourier integral and series approach to semiinfinite strip subject to general symmetrical tractions along three edges 08 p1422 A67-20978
 Numerical quadrature methods of Romberg, Chebyshev and Monte Carlo, noting analytic function and program for machine evaluation 09 p1468 A67-22047
 Extensions of Nevanlinna 2-constant theorem for harmonic function on disk and Hadamard 3-circle 10 p1673 A67-22965
 Gamma function concept for varying difference interval and complex argument 11 p1812 A67-23966
 Two-dimensional problem of thermoelasticity solved using analytic functions 11 p1879 A67-24885

Linearized Crocco equation for zero pressure gradient and constant viscosity density product applied to boundary layer problem 12 p1929 A67-25907
 Unified method of numerical quadrature for integrands of certain complex analytic functions, obtaining asymptotic expansion of error functional 13 p2145 A67-26734
 Analytic power series solution of nonrelativistic Schroedinger equation for two-electron atom, assuming fixed nucleus and singlet and triplet S states 15 p2520 A67-30158
 Rapidly converging analytic solution by integral series of nonrelativistic Schroedinger equation for He atom 15 p2520 A67-30159
 Tension equations for oval thin walled cylinders reinforced with lateral rigid ribs noting wall strength, complex bending moment computation, etc 15 p2577 A67-30185
 Optimal scanning problem variant with simple analytical solution, determining cessation moment 15 p2459 A67-30227
 Mixed boundary value problem for x-analytic function solved through Fredholm integral equation of second kind 17 p2879 A67-32872
 Zero-moment stressed state in shells of revolution under concentrated loading described by p-analytic functions 17 p2962 A67-32875
 Analytical and p-analytical functions of complex variable used to solve three-dimensional axisymmetric problems in elasticity theory 17 p2966 A67-33284
 Book on variational principles of mechanics covering basic concepts, calculus of variation, equations of motion, etc 18 p3079 A67-34100
 Potential fields representation for electrostatic image tubes with curved cathodes, using analytic functions 19 p3194 A67-35544
 Circumferentially symmetrical stressed state of half-space determined using Polozhyi formulas in axisymmetric elasticity theory and p-analytic functions 20 p3538 A67-36918
 Infinitesimal deflections of positively Gaussian curved surfaces solved by application of /p, q/ analytic functions after affine transformation 21 p3715 A67-37903
 Solution for boundary value problems in elasticity theory for ellipsoid of revolution and cavity with surface loading, determining coefficients in closed form 21 p3718 A67-37984
 Analytical solution to cosmological model containing radiation and matter assuming spatial homogeneity and isotropy, stress-energy and adiabatic expansion 21 p3711 A67-39121
 Analytic and harmonic transformations applied to Faber series summation, harmonic function approximation and logarithmic potential approximation 23 p4023 A67-40923
ANALYTIC GEOMETRY
 SA CONE
 SA CYLINDER
 SA ELLIPSE
 SA PARABOLA
 Soviet monograph on geometry of earth ellipsoid describing analytic geometry methods for solving geodetic problems on spheroid surface 21 p3616 A67-37965
 Determination of coordinates from satellite observations noting triangulation method and optical technique 23 p3994 A67-40700
ANALYTICAL CHEMISTRY
 SA QUALITATIVE ANALYSIS
 SA QUANTITATIVE ANALYSIS
 Calorimetric, titrimetric and gravimetric methods for determination of hexogen-octogen mixtures 05 p0872 A67-17153
 Rapid micro dry combustion determination of carbon, hydrogen and nitrogen in high explosives 05 p0759 A67-17154
 Hydrogen peroxide oxidation and ozonolysis of polymer type material in coal, kerosene and Orguella 08 p1289 A67-21174
 High resolution gas chromatography combined with mass spectrometry applied to analysis of pyrolysis products of isoprene from 300 to 1000 degrees C 10 p1602 A67-22947
ANALYZER
 SA AMPLITUDE DISTRIBUTION
 ANALYZER

SA AMPLITUDE PROBABILITY ANALYZER
 SA DIFFERENTIAL ANALYZER
 SA GAS ANALYZER
 SA INDICATOR
 SA SIGNAL ANALYZER
 Bias and variability errors in analog data reduction equipment 01 p0028 A67-10605
 Digital to analog pulser system for integral and differential testing pulse height analyzers [JPL-TR-32-1049] 18 p3049 A67-34485
 Pulsed ion flow energy and mass spectra analyzer suitable for 1 to 3 msec duration and time variation over 10 msec 24 p4158 A67-42741
ANATOMY
 S BRAIN
 S GLAND
 S INTESTINE
 S LIVER
ANCHORED INTERPLANETARY MONITORING PLATFORM
 S EXPLORER XXXIII SATELLITE
ANECHOIC CHAMBER
 SA ECHO
 Transition zone anechoic chambers for field checkout, production and radiation testing of microwave antennas 03 p0397 A67-14102
 Conducting loop resonant size determination and geometrical shape effect on resonant size in anechoic chamber experiment 16 p2639 A67-31356
 Anechoic chamber characteristics, noting indoor antenna pattern measurements and transmission attenuation variations 16 p2640 A67-31364
ANELASTICITY
 S INTERNAL FRICTION
ANEMOMETER
 SA HOT-WIRE ANEMOMETER
 SA SONIC ANEMOMETER
 Two-component drag force anemometer design and performance, noting method for wind bearing and velocity measurements 05 p0808 A67-17308
 Space-time correlation measurements in fluctuating turbulent wakes behind projectiles [AIAA PAPER 67-19] 06 p0940 A67-18434
 Motor driven cup anemometer and freely rotating cup anemometer in free and artificial flows 06 p1006 A67-18836
 Low density air flow measured by anemometer with pulsed ion generation in air stream 10 p1658 A67-23787
 Mechanically and electrically simple cup-type anemometer developed with starting speed of 6 cm/sec and linear response 21 p3628 A67-38581
ANESTHETICS
 Neurophysiology of anesthesia 15 p2429 A67-29294
ANGLE
 S ELEVATION ANGLE
 S LOOK ANGLE
 S PHASE ANGLE
 S REENTRY ANGLE
 S SWEEPBACK ANGLE
ANGLE OF ATTACK
 SA ZERO ANGLE OF ATTACK
 Supersonic jet from finite length nozzle in supersonic stream at angle of attack, analyzing flow characteristics by using linearized theory 02 p0177 A67-11523
 Angle of attack measurements of hypersonic reentry vehicle derived from flight test pressure data 02 p0178 A67-11942
 Hypersonic flow past lower surface of slender delta wing for wide-range of angle of attack, determining velocity component, pressure and density distribution 03 p0350 A67-12874
 Plane transonic gas flow past symmetrical convex profile at zero angle of attack along axis of channel with parallel walls 03 p0352 A67-13620
 Equivalency coefficient dependence on angle of attack, Mach number and angle of incidence for subsonic and supersonic gas flow past plate grid 03 p0353 A67-14082
 Mass transfer measurements of paradichloro benzene cylinders at various turbulent intensities and angles of attack, showing free flow turbulence effect on local mass transfer coefficient 04 p0548 A67-15493
 Tip bluntness, surface roughness and angle of attack effects on laminar boundary layer for 10 degree cone, measuring heat transfer

and detecting transition 04 p0549 A67-15823
 Statistical linearization of nonlinear aerodynamic coefficient of angle-of-attack moment of aircraft 04 p0549 A67-15884
 Aerodynamic characteristics of wings of complex planform at subsonic velocities, calculating flows past wings at moderate angles of attack 06 p0935 A67-17730
 Laminar boundary layer on ellipsoids of revolution situated at zero angle of attack in supersonic flow of perfect gas 06 p0936 A67-17740
 Maximum slope method for obtaining natural frequency and damping ratio of highly damped second order systems from time history data 06 p1100 A67-18012
 Reentry trim angle of attack and lift-drag ratios from Gemini flights compared to wind tunnel data for aerodynamic studies [AIAA PAPER 67-166] 06 p0939 A67-18295
 Steady roll resonance accompanied by large amplification of nonrolling trim angle, considering compound asymmetry such as lateral center of gravity offset [AIAA PAPER 67-137] 06 p1097 A67-18504
 Dynamic flight characteristics of spin-stabilized sounding rockets during passage through atmosphere, emphasizing roll resonance and motions leading to roll lock-in and angle of attack 08 p1407 A67-20514
 Closed form solution for gliding lateral turn at constant height over flat earth of unpowered vehicle, using linearized aerodynamic coefficients 09 p1441 A67-22488
 Lamellar homogeneous jet layer deformation under aerodynamic forces acting in incompressible flow 09 p1439 A67-22578
 Inviscid conical flow around pointed cone at angle of attack transformed into hyperbolic flow 10 p1592 A67-23136
 Supersonic delta wing problem, discussing new approach in determining flow parameters 10 p1593 A67-23687
 Boundary layer transition displacement as function of nose bluntness, angle of attack and boundary layer cooling of half-angle cone [AIAA PAPER 66-495] 12 p1893 A67-25903
 Total equilibrium shock layer radiation data for Martian entry body shapes at various angles of attack extrapolated to trajectory condition [AIAA PAPER 67-324] 12 p1894 A67-26039
 Partial differential equations for three-dimensional inviscid flow solved for flow field over blunt body shapes at various angles of attack, for application to Apollo spacecraft [AIAA PAPER 66-413] 14 p2240 A67-28110
 Hypersonic trim angle of attack of lifting entry vehicles, correlating stagnation point values obtained from heat shield ablation and pressure distribution measurements 15 p2417 A67-29447
 Numerical solution for angle-of-attack distribution, downwash and motion of high-speed helicopter rotor 16 p2590 A67-30930
 Reentry trim angle of attack and lift-drag ratios from Gemini flights compared to wind tunnel data for aerodynamic studies [AIAA PAPER 67-166] 17 p2789 A67-32061
 Book on aerodynamic and aerothermal experiments on circular cylinders at angle of attack in supersonic flow 17 p2790 A67-32379
 Convection coefficient distribution in supersonic flow, noting wind tunnel measurement results at Mach 3.3 and at various angles of attack 17 p2791 A67-32702
 Thin slightly curved profiles positioned at small angle of attack in subsonic gas flow and developing harmonic random vibrations studied for aerodynamic interference 17 p2792 A67-32903
 Electric vortex-field integrator using aluminum foil sheet and external field to simulate circular flow about wing profile at various angles of attack 17 p2834 A67-32905
 Supersonic flow past windward side of delta wings with angles of attack from 0 to 80 degrees, verifying experimental and theoretical values 18 p2984 A67-34208
 Supersonic fluid flow past elliptical and circular conical bodies at large angles of attack, using straight line method 18 p2984 A67-34211
 Supersonic flow past smooth body with internal duct incident at angle of attack 18 p2984 A67-34212
 Pressure-distribution estimation over entire forward face of blunt body at angle of attack 19 p3169 A67-34833

Wind penetration effects on flight simulations evaluated in frequency domain by solution of theoretical transfer function, showing relationship to angle of attack [AIAA PAPER 67-609] 19 p3208 A67-36000
 Plane compressor and guide vane cascades design, deriving relations for angle of attack, angle of lag, etc 20 p3358 A67-37081
 Aircraft flight dynamics optimized in angle of attack by variational calculus, analyzing control system 20 p3361 A67-37377
 Stretched sail behavior in sonic, supersonic and hypersonic flows, discussing profile dependence on angle of attack and free-stream Mach number 21 p3563 A67-37889
 Supersonic delta wing problem, discussing new approach in determining flow parameters 21 p3564 A67-38288
 Unsteady airfoil stall noting frequency effects on velocity distribution and angle of attack for oscillating pitch 21 p3565 A67-38547
 Lift reduction and increase of helicopter maximum speed by controlling optimum angle of attack of rotor blades over surface of revolution 22 p3744 A67-39548
 Laminar heat transfer computing method for spherically blunted cone at angle of attack requiring small numerical calculations 22 p3740 A67-39937
 Drag coefficients used to evaluate normal force and pitching moment characteristics of revolving body at angle of attack 22 p3740 A67-39943
 Angle of attack determination from rotational body rates, formulating ordinary differential equations 22 p3741 A67-40093
 Flow past disk at angle to stream with marked periodic motions caused by vortex ring shedding increasing with angle of incidence 23 p3990 A67-41171
 Incidence angle effects on wall heat flux in symmetry plane of cone of revolution in hypersonic regime, discussing wall pressure measurements 24 p4092 A67-42660
 Dynamic flight characteristics of spin-stabilized sounding rockets during passage through atmosphere, emphasizing roll resonance and motions leading to roll lock-in and angle of attack 24 p4242 A67-42917
ANGULAR ACCELERATION
 HF electromagnetic angular displacement signal generator for use in gyro guidance systems 02 p0220 A67-12224
 Operator reorientation of attitude of simulated remote maneuvering unit (RMU) using on-off acceleration command control system 02 p0186 A67-12230
 Angular acceleration sensor for control system stabilization using MHD principles, obtaining transfer function 08 p1331 A67-20697
 Stimulus thresholds for perception of angular acceleration in man 15 p2427 A67-29267
 Visual arousal interaction and specificity of nystagmic habituation 17 p2805 A67-31958
 Variable turbine geometry in gas turbine engines, discussing part power fuel consumption, acceleration characteristics, etc [AIAA PAPER 67-417] 18 p3111 A67-33904
 Hydraulic angular acceleration sensor motion equation obtained by kinetostatic method 22 p3809 A67-40477
 Rats exposed to repeated radial acceleration studied for central nervous system adaptation and survival rates noting better adaptability of newborns 22 p3753 A67-40541
 Time dependent gravitational constant theory, studying earth rotation secular acceleration 24 p4229 A67-42321

ANGULAR CORRELATION

Independent control of angular location of independent zeros of directional pattern for linear array 11 p1762 A67-24290
 Angular correlation in helium atom with electron-electron interaction 13 p2161 A67-27182
 Perturbation factors in angular correlation function for multidomain ferromagnetic materials determined taking into account magnetic field fluctuations 14 p2371 A67-28728
 Angular spread of backscattered spread-F echoes compared with that associated with normal F region returns [AGARDOGRAPH 95] 15 p2480 A67-30278
 Correlation coefficient dependence on angular dispersion and ratio between antenna directivity and width of energy

spectrum of waves scattered by troposphere 22 p3759 A67-39433
ANGULAR DISTRIBUTION
 Mie scattering and plane wave diffraction theory for small angle light dispersion from sphere 01 p0112 A67-10131
 Absolute intensity and angular distribution of microwaves scattered from oscillating plasma column, noting diffraction patterns and frequency shifts 01 p0027 A67-11325
 Angular dimensions of radio sources from interplanetary flickering in radio emission intensity used to study structure of sun supercorona at large distances 02 p0322 A67-11684
 Angular distribution of secondary electrons emitted at reverse side of aluminum films 02 p0290 A67-11734
 Electron angular distribution in copper and gold thin films attributed to individual close interaction scattering phenomena 02 p0297 A67-11834
 Statistical analysis of cosmic ray particle elastic scattering, noting isotropic nature of angular distribution 02 p0315 A67-12750
 Integral energy spectra and angular distribution of muons, comparing computational and experimental data 02 p0317 A67-12773
 Spatial and angular particle distributions in muon-generated electron photon cascade, using spark chamber muon detectors 02 p0317 A67-12774
 Red shift of magnetic zenith hydrogen line profiles and role of injection pitch-angle distribution of auroral protons 03 p0409 A67-12943
 Angle-of-arrival measurements over troposcatter path by simultaneous reception in angle diversity, using antenna beams 05 p0760 A67-15998
 Local variations in spacing and orientation of lattice plane in silicon single crystal, measuring angular positions of diffraction peak - by double crystal spectrometer 05 p0866 A67-16977
 Charged particle distribution in wake of fast moving body in rarefied plasma 05 p0855 A67-17123
 Asymmetrical angular elastic scattering distribution of electrons on helium atoms, using Monte Carlo method 06 p1034 A67-17648
 Angular distribution of intensity and phase of electromagnetic wave scattered by cylindrical plasma column 06 p1041 A67-18138
 Radioactive tracer technique for measurement of yield and angular distribution of molybdenum sputtered by cesium ion beam 06 p1036 A67-18139
 Energy and angular distributions of neutral atoms and charge-exchange ions from mercury electron bombardment thruster, determining particle effluxes [AIAA PAPER 67-82] 06 p1075 A67-18498
 Gas transport cross sections, angular distribution of elastic scattering of colliding gas particles and transport equation degeneration 07 p1225 A67-19129
 Angular distribution of fast hydrogen atoms from exothermic reaction measured for various proton energies and scattering angles 07 p1225 A67-19495
 Cesium vapor flow from orifices and tubes into vacuum analyzed, noting dependence of angular distribution and center line intensity on Knudsen numbers 08 p1324 A67-21495
 Properties of solar cosmic rays causing polar cap absorption measured with satellites 10 p1700 A67-23188
 Discovery of or setting upper limit to strength of features of small angular size when studying isotropy of cosmic background radiation 11 p1857 A67-25000
 Visible and near IR spectral reflectance and emittance at high temperature of ablation chars, carbon and graphite [AIAA PAPER 67-326] 12 p2037 A67-26040
 X-ray source in Crab Nebula size and position, showing visible light distribution having common center within 15-inch precision of measurement and finite angular extent 13 p2189 A67-26263
 Gas atom scattering from solid surface, analyses and comparisons 13 p2097 A67-26937
 Angular distribution of earth outgoing thermal radiation in IR region measured by geophysical rocket 14 p2306 A67-27860
 Angular, spectral and geographical distributions of outgoing fluxes of thermal radiation and earth albedo measured, using

Cosmos satellite 14 p2306 A67-27861
 Large scale nonrandom angular
 distribution of faint radio sources from drift
 records 14 p2383 A67-27958
 Measurement of angular spectrum of radio
 waves from sources outside solar
 system 14 p2386 A67-28445
 Angular diameter of scintillating source 3C
 279 determined from fluctuation spectrum
 width 14 p2389 A67-28843
 Dependence of angular dimensions of
 discrete cosmic radio emission source on
 radiation flux density and
 frequency 15 p2549 A67-29140
 Cross section and angular scattering law
 for Venus and Mercury from delay and
 Doppler frequency shift radar echo
 measurements 15 p2556 A67-29870
 Numerical solution for angle-of-attack
 distribution, downwash and motion of high-
 speed helicopter rotor 16 p2590 A67-30930
 Yield and angular distribution of cesium
 ion-sputtered copper, noting dependence on
 angle of incidence, target temperature and
 energy 16 p2728 A67-31056
 Polarization and angle of arrival
 fluctuations for plane wave propagated
 through turbulent
 medium 16 p2625 A67-31344
 Microwave emission intensity from InSb,
 examining dependence on angle between DC
 electric and magnetic
 fields 17 p2914 A67-32615
 Weak radio sources of small angular size
 studied by lunar occultation technique, using
 steerable telescope 17 p2943 A67-32634
 Upper limit data about reported very low
 temperature distributed-source microwave
 background radiation and small-scale angular
 distribution 17 p2945 A67-32653
 Inelastic differential scattering cross
 sections and angular distribution of Ni first-
 excited-state protons determined by
 distorted wave calculation 17 p2888 A67-32733
 Energy spectrum and pitch-angle
 distribution of protons in auroras based on
 H-beta line profiles 17 p2938 A67-32962
 External corrective system significantly
 decreased angular radiation divergence of
 single pulse laser, determining effect on
 focal spacing of corrective
 lens 18 p3061 A67-34042
 Angular distribution of products in
 electron impact dissociation of hydrogen
 molecule calculated following Born
 approximation for scattering
 amplitude 20 p3487 A67-36231
 Angular divergence of gas-laser radiation
 as function of output power, analyzing
 interaction of angular
 modes 20 p3459 A67-36689
 Differential cross sections for inelastic
 large angle alpha particle scattering from
 unnatural parity states in Mg showing
 diffraction pattern 20 p3488 A67-36931
 Probability distribution errors effect in
 linear and planar impulse orbital transfers,
 considering angular orientation and
 impulsive velocity 20 p3527 A67-37259
 Gas transport cross sections, angular
 distribution of elastic scattering of colliding
 gas particles and transport equation
 degeneration 21 p3659 A67-38172
 Angular divergence of solid state laser
 radiation for case of variable resonator and
 pump parameters 21 p3640 A67-38367
 Charged particle distribution in wake of
 fast moving body in rarefied
 plasma 21 p3668 A67-38466
 Differential cross sections for elastic
 scattering of alpha particles by oxygen,
 giving angular distributions and
 resonances 21 p3659 A67-38517
 Differential cross sections of elastic
 scattering of alpha particles by oxygen,
 measuring angular
 distributions 21 p3659 A67-38518
 Doubly differential cross section for
 ejected secondary electrons energy and
 angular distribution calculated from He by
 fast protons 22 p3839 A67-39201
 Statistical analysis of cosmic ray particle
 elastic scattering, noting isotropic nature of
 angular distribution 22 p3841 A67-40252
 Integral energy spectra and angular
 distribution of muons, comparing
 computational and experimental
 data 22 p3877 A67-40275
 Spatial and angular particle distributions
 in muon-generated electron photon cascade,

using spark chamber muon
 detectors 22 p3877 A67-40276
 Microwave background radiation angular
 distribution anisotropy lower limit estimated
 from perturbations of cosmological
 model 22 p3892 A67-40498
 Light gas escape flux from atmosphere
 velocity and angular distributions near
 critical level using Monte Carlo
 analysis 24 p4224 A67-41823
 Rocket measurements in auroral zone,
 considering proton and electron intensities,
 energy spectra and angular
 distribution 24 p4209 A67-42262
 Angular distributions of elastic and
 inelastic alpha scattering from tellurium
 isotopes using Lewis
 cyclotron 24 p4192 A67-42732
 Shower particles angular distribution
 investigated using Wilson cloud chamber,
 obtaining agreement with results by
 kinematic methods 24 p4217 A67-42828
 Secondary particles angular distribution in
 showers studied with cloud chamber,
 ionization calorimeter and counters to
 identify particles causing shower asymmetry
 and symmetry 24 p4217 A67-42829
 Charged particles zenithal angular
 distributions determined by photorecordings
 for mean energies of 60
 GeV 24 p4217 A67-42831
 Asymmetry in angular distribution of
 secondary particles in cosmic ray
 showers 24 p4218 A67-42838
 Positive rho meson and doubly positive
 nucleon-pion resonance generation in 2.34
 GeV/c 24 p4193 A67-42856
 Expressions for angular distribution
 function of electrons at various depths in
 cascade showers with given primary particle
 energy 24 p4221 A67-42872
 Equilibrium angular distribution function
 computer calculations for cascade particle
 numbers in iron and lead reveal dependence
 on primary particle
 energy 24 p4221 A67-42873
 High energy cosmic ray muon integral
 angular and integral spectrum below earth
 surface 24 p4222 A67-42877
 Dependence of angular dimensions of
 discrete cosmic radio emission source on
 radiation flux density and
 frequency 24 p4222 A67-43063
ANGULAR MOMENTUM
SA QUANTUM NUMBER
 Mean powers of r, sum rule and improved
 transition integrals computed for effective
 quantum number range up to 8.5, using
 Coulomb approximation wave
 functions 01 p0112 A67-10142
 Motion laws for variable mass system,
 discussing versions of law and problem of
 angular momentum 01 p0113 A67-10507
 Spin conditions for aircraft with nose-and
 tail-heavy longitudinal
 moment 07 p1130 A67-20148
 Evolution of low mass stars, differences
 between solar system planets and black
 dwarfs and rotational angular momentum of
 G, K and M dwarfs 08 p1398 A67-21217
 Northern Hemispheric mean meridional
 circulation determined, using angular
 momentum and continuity
 equations 09 p1490 A67-21549
 Contact binaries origin and evolution,
 discussing orbital angular momentum
 dissipation through mass ejection along
 magnetic lines of force 09 p1568 A67-22367
 Absolute angular momentum of outflow
 winds and radar targets in hurricanes and
 typhoons 10 p1676 A67-22813
 Parametrization of reduced problem of
 stationary axially symmetric gravity
 fields 11 p1819 A67-24597
 Planetary system abundance for stellar
 system mass near solar mass determined
 from mass/angular momentum
 diagram 11 p1865 A67-24610
 Steady state model of solar wind flow in
 equatorial plane solved for radial and
 azimuthal motions, taking into account
 pressure gradient, magnetic field and
 gravitational effects 12 p2010 A67-26241
 Angular momentum considerations for
 stability of satellites with moving inner
 masses 13 p2211 A67-26623
 Meridional and vertical wind components
 analyzed for angular momentum, balance,
 heat influx and internal
 friction 13 p2113 A67-26678
 Integrals of motion in three-dimensional

restricted three-body problem as
 generalizations of angular
 momentum 13 p2205 A67-27480
 Geostrophic wind angular momentum
 transport at 500 mb in Northern
 Hemisphere, using zonal harmonic analysis,
 noting quasi-biennial
 cycle 15 p2512 A67-29201
 Rotational analysis theorem concerning
 earth satellite motion about angular-
 momentum vector with respect to inertial
 reference frame 15 p2519 A67-30209
 Gas flow through annular duct of constant
 cross section analyzed in terms of
 conservation of energy, mass and angular
 momentum laws 16 p2593 A67-31153
 Super-Alfvénic point or distance of
 effective corotation for loss of angular
 momentum in solar wind
 plasma 17 p2945 A67-32644
 Angular momentum and vibrational energy
 transfer between nearly colliding
 stars 21 p3700 A67-37732
 Electromagnetic interactions in hyperfine
 structure of vibrational and rotational states
 in rubidium and potassium isotopes/
 fluorides, using electric resonance
 method 22 p3839 A67-39203
 Fragmentation and excess angular
 momentum problems in star formation
 theories, examining relevance to simplifying
 assumptions and physical
 situation 22 p3895 A67-40517
 Angular momentum densities of planet-
 satellite systems, discussing earth-moon
 system and origin of celestial
 bodies 23 p4066 A67-41009
 Angular momentum density vs mass log-
 log plot extended from planetary mass range
 to asteroids, noting support for constant
 period law 23 p4066 A67-41010
 Gravitational torque mechanism for radial
 outward angular momentum transport in
 solar nebula 24 p4223 A67-41790
 Book on nonlinear theory of thin shells
 covering deformation and stress state,
 surface kinetics, momentum conservation,
 etc 24 p4246 A67-41800
 Optimum stabilization system for manned
 space station with asymptotic damping of
 initial angular momentum 24 p4240 A67-42088
 Fission hypothesis of lunar origin,
 reviewing energy, dynamics, angular
 momentum, geology and physical
 properties 24 p4230 A67-42323
ANGULAR MOTION
 Integrated Trajectory System, measuring
 spatial positions, velocities, accelerations and
 scalar and vector miss distances for
 targets 04 p0654 A67-15045
 Action-angle coordinates for particle
 motion in magnetic mirror
 systems 10 p1684 A67-22901
 Angular stabilization of flight vehicle by
 introduction of cubic terms of variable
 parameters into control
 law 10 p1678 A67-23319
 Stability in whirl theory, considering
 internal damping role on motion of elastic
 shaft 11 p1798 A67-24316
 Four-plate compensators of Jamin and
 Lowe type for interferometers, emphasizing
 linear dependence of phase difference on
 dispersion and rotation
 angle 14 p2315 A67-28074
 Rotational motions of second order
 autonomous systems, proposing determining
 algorithm 17 p2885 A67-32883
 Determination of Love number of earth
 from variations of orbital inclinations of
 satellites 18 p3041 A67-34250
 Minimax fuel requirement of aircraft
 angular stabilization for undetermined
 inertial moment probability
 distribution 19 p3202 A67-35887
 Motion equations of spin-stabilized rocket
 under thrust with jet damping, variable
 mass and momentum effects and all angular
 disturbances 19 p3334 A67-35938
 Motion simulator with spherical self-
 regulating gas bearing for testing attitude
 control, analyzing turbine and tilting
 momentum 22 p3778 A67-39165
 Triaxial orbital orientation control
 algorithm for space vehicle with incomplete
 angular position
 information 22 p3899 A67-39191
 Static reaction of radial gas dynamic
 bearing to journal axis angular displacement
 determined by splicing asymptotic solutions
 for low and high pressure

levels 22 p3810 A67-39232
 Strapdown system application studies related to surface to surface missile, considering angular vibration environment and constant rates about output and spin axes of gyro 22 p3833 A67-40186

ANGULAR VELOCITY
 Tachometer measuring angular velocity from time of definite number of rotations, noting diagram of basic circuit 01 p0062 A67-10164
 Graphic solution of Lambert time of flight equation for spacecraft correctional maneuvers with respect to initial velocity 01 p0152 A67-11399
 Nonideal clock model of georotational velocity irregularities derived from astronomical observations 02 p0236 A67-11512
 Ring laser rotation sensing system, evaluating accuracy limit for minimized inaccuracy of known sources of error 03 p0438 A67-13992
 Stability of motion of gyro suspension, noting gyrohorizon compass operation for constant suspension point and angular velocities 03 p0424 A67-14158
 Ring laser inertial sensor for aerospace systems obtaining high accuracy angular resolution and mechanical simplicity 04 p0625 A67-15665
 Brightness angular velocity and geometry of moving object relationship to camera parameter to determine exposure and focal length and contrast for optimum recording 05 p0808 A67-17032
 Rotational speed of upper atmosphere obtained by measuring changes in orbital inclinations of satellites or movements of vapor trails 06 p0993 A67-17564
 Absolute angular velocity measurement with aid of linear accelerometers on body of aircraft 06 p1028 A67-18179
 Euler angles sets, particularly right-handed coordinate systems and positive rotations, with solutions for angular velocities 06 p1032 A67-18527
 Rotational speed of upper atmosphere determined from satellite measurements 10 p1652 A67-23493
 Motion of arbitrary gyrostabilizer in central Newtonian force field, applying Liapunov stability conditions for regular precession 11 p1791 A67-24683
 General solution for motion equation of rotating shaft with changing angular velocity, noting transition through critical speed 12 p1949 A67-25408
 Nonrelativistic theory of rotating configurations in terms of gravitational potential, center mass density and variable angular velocity 14 p2382 A67-27833
 Time dependent viscous flow between two rotating spheres analyzed by extension of numerical methods 14 p2296 A67-27905
 Rigid lifting body movement transfer function derived from translational and angular velocity components transfer functions 14 p2393 A67-28061
 Pneumatic angular rate sensor performance characteristics, solving boundary layer equations for radial flow 14 p2318 A67-28340
 Fluoric pressure, temperature and angular rate sensors for military and commercial applications [ASME PAPER 67-DE-12] 14 p2252 A67-28869
 Flexural wave velocity-amplitude relation indicates possibility of stationary waves for fixed ratio of wave amplitude and spinning membrane angular velocity 14 p2403 A67-29016
 Subjective responses to oscillation in yaw 15 p2427 A67-29269
 Errors of real accelerometer and instability of rotation effect on accuracy of angular velocity measurements of aircraft motion 16 p2670 A67-30466
 Stability of prismatic shaft rotating with constant angular velocity as function of mass and setting point of rotating mass 16 p2766 A67-31151
 Microscopic interpretation of generalized Helmholtz equation, considering particle in charged gas in adiabatic flow as rotating cylinder model 16 p2720 A67-31245
 Vehicle angular velocity determined, using configurations with only linear accelerometers and no gyroscopes for inertial navigation systems 16 p2675 A67-31266
 Expression analytically representing

progressive and long-term variations of earth rotation velocity 16 p2667 A67-31442
 Rotational time scale and analytical representation by single formula for earth rotation variation 16 p2750 A67-31443
 Surface stress effect on oblateness of sun and surface stress distribution, noting latitude dependence of angular velocity 17 p2940 A67-32207
 Rotation and heating of planet Mercury, examining insolation and surface temperatures from coupling of orbital and rotational periods 17 p2940 A67-32210
 Rotational velocity of neutral hydrogen subsystem in outer regions of Galaxy outside galactic plane 17 p2950 A67-33163
 Circular disk error magnitude determination by measuring rear-wall echo with angular probe 18 p3044 A67-33736
 Cassini second and third laws are independent of first law 18 p3128 A67-34303
 Radio interferometry method using precision clocks for earth rotation period measurement 18 p3043 A67-34528
 Disk structural characteristics influence on rotors critical angular velocity 19 p3235 A67-34881
 Upper atmosphere rotational speed determined by analyzing changes in satellites orbital inclinations 19 p3216 A67-35182
 Jupiter Great Red Spot and three white ovals show correlation between oval rotational velocity and longitudinal distance from Red Spot 20 p3527 A67-37400
 Rotating observer relative to inertial observer in relativity 20 p3486 A67-37501
 Stress distribution in homogeneous isotropic body under finite elastic deformation rotating with constant angular velocity 20 p3542 A67-37680
 Brightness angular velocity and geometry of moving object relationship to camera parameter to determine exposure and focal length and contrast for optimum recording 21 p3627 A67-38264
 Upper atmosphere angular velocity determined from changes in satellite orbital inclinations, noting increase with height 21 p3619 A67-38512
 Satellite attitude stabilization using gimbaled star trackers, analyzing satellite and star tracker motion in terms of angular velocity 22 p3830 A67-39170
 Aircraft engine turbine structure effect on blade tip clearance, analyzing clearance variations as function of rotor angular velocity 22 p3868 A67-39546
 Angle of attack determination from rotational body rates, formulating ordinary differential equations 22 p3741 A67-40093
 Forced convective heat transfer in straight pipe rotating around parallel axis with large angular velocity 22 p3920 A67-40419
 Optimum relative angular velocity selected for cooled high temperature gas turbine stages, discussing blade mean cooling depth and cooling heat 22 p3870 A67-40456
 Gyroscopic large drift angles effect on aperiodic transition condition of four-gyro vertical, deriving precession equations for system 22 p3810 A67-40482
 Involuntary vestibularly driven head movements in man during rotational simulation 23 p3959 A67-41659
 Turbojet engine gasdynamic parameters dependence on reduced rotational velocity for in-flight characteristics determination, assuming variable compression and critical pressure ratio 24 p4207 A67-41916
 Inertial navigation system operation errors on moving power plant due to inaccurate initial data feeding into computer 24 p4182 A67-42300
 Earth rotation variation in historical time using day length, eclipses and earth angular velocity 24 p4151 A67-42317

ANHYDRIDE
 Carbonaceous fiber yarn reinforcements in epoxy-anhydride binder, noting moisture adsorption degradation of interlaminar shear values 03 p0452 A67-13405
 Charge transfer energies of pyromellitic dianhydride and mellitic trianhydride with aromatic hydrocarbon donors 04 p0567 A67-15952
 Crystallization of boric anhydride obtained only through maintaining high water content in reactive agent during thermal treatment 13 p2143 A67-26812
 Enthalpy measurement of anhydrous

crystalline aluminum trifluoride with ice calorimeter and drop method obtaining thermodynamic properties 16 p2620 A67-31761
 Simultaneous copolymerization of Leuchs anhydrides of 18 amino acids common to protein, discussing nutritional significance 20 p3377 A67-37397

ANIMAL STUDY
 SA BIRD
 SA CAT
 SA DOG
 SA FISH
 SA GUINEA PIG
 SA MAMMAL
 SA METAZOAN
 SA MONKEY
 SA ORGANISM
 SA RABBIT
 SA RAT
 Extraction method for renin from rats with bioassay simplified by using microphonic method after injecting renin extract into tail vein 01 p0015 A67-10412
 Long-term biomedical instrumentation in Air Force space program 01 p0017 A67-11029
 Prolonged centrifugal acceleration effect on gas exchange and resistance to hypoxia in rats 01 p0016 A67-11425
 Cumulative and adaptive effects in animals subjected to single and repeated transverse g forces 02 p0188 A67-12328
 Oxygen balance of organism during prolonged accelerations, noting disturbed gas exchange between alveoles and capillaries 02 p0188 A67-12329
 Nonphosphorylating respiration of mitochondria from brown adipose tissue of rats, providing example of electron transport 02 p0185 A67-12527
 Animal study showing aversiveness of simulated gravity and importance of separating rotation effects from effects of G forces 02 p0189 A67-12633
 Radar observation of insects in free flight, noting backscatter and velocity measurement results [AFCLR-67-0127] 03 p0371 A67-13916
 Weightlessness effect on level of vigilance of cats and rats launched in rockets, examining electrical activity of cerebral cortex 03 p0364 A67-13927
 Telemetering and programming equipment used by CERMA in nose cones of rockets containing cats and rats in state of weightlessness 03 p0366 A67-13928
 Anesthetized rabbits exposed to high explosive air shock waves in shock tube, examining changes of elastic properties of lungs of rabbits 03 p0364 A67-14292
 Vestibular section of labyrinth contribution to postrotational changes in level of adrenalin and noradrenalin content in some tissues of white rats 03 p0365 A67-14330
 Effects of 1, 1, 3-tricyano-2-aminopropene /TCAP/ on incorporation of protein and nucleic acid precursors into frog nervous system in vitro 04 p0560 A67-14408
 Glycogen accumulation in monkey and cat brain exposed to proton irradiation, discussing astrocytes function in carbohydrate metabolism 04 p0560 A67-14489
 Adrenal corticosterone concentration changes in response to various doses of ACTH and time pattern of changes in hypophysectomized rats 04 p0560 A67-14525
 Responses of lateral geniculate nucleus of monkey to light increment and decrement and encoding of brightness 04 p0561 A67-14592
 Metabolic reaction of deer mice to temperature and altitude, analyzing various enzyme systems 04 p0561 A67-14593
 Mammalian neuron networks for visual pattern recognition, noting equivalence of processing by memory neurons with matrix multiplication 04 p0563 A67-14798
 Radar probe of clear atmosphere confirming detectability of birds, insects and irregularities in clear air refractivity 04 p0650 A67-15172
 Low pressure environmental chamber for estimation of gas exchange ratio during exposure of animals under controlled conditions [ASME PAPER 66-WA/HT-52] 04 p0599 A67-15438
 Individual phospholipids in hemispheres of rat brains and rate of turnover of phosphate groups during oxygen deprivation 04 p0562 A67-15548

High magnetic fields effect on cardiac activity in spontaneously excited isolated turtle heart by simultaneous and separate electrical and mechanical measurement 05 p0755 A67-16282

Long term effects of oxygen environment on rat colony at 210 mm Hg absolute showed no significant physiological changes and no difficulty in readaptation 05 p0755 A67-16285

Visual acuity decrement from laser lesion in fovea of stump tail macaque monkeys 05 p0756 A67-16287

Spontaneous discharges from single units in cochlear nucleus after destruction of cochlea, noting results of animal study 06 p0952 A67-17847

Cannulation of renal capsular lymphatics in anesthetized dogs, testing if lymph fluid can serve to assess tissue oxidation 06 p0952 A67-17853

Roentgen radiation effect on glycogen metabolism of rat brain 07 p1133 A67-19468

Acceleration effect on rate of urine flow and urinary excretion of sodium, potassium and total solute in rabbits 07 p1134 A67-19861

Hematocrit ratio in affecting survival and acclimatization of dogs at high altitude 07 p1135 A67-19862

Impact tests on animals at velocity changes suggestive of automobile crash conditions, confirming effect of isovolumetric containment of torso on increased survival limits 08 p1289 A67-20612

Acoustic waveform procession to auditory centers of brain, discussing transformations used by animals 09 p1454 A67-21686

Cardiovascular deconditioning caused by microcirculatory changes which reduce proprioceptor sensory input of unanesthetized rat 09 p1452 A67-21714

Vibration tolerance of rats previously irradiated by X-rays and hypothetical mechanisms of stress involved 09 p1452 A67-21719

Mice inoculated with tetanus exposed to high pressure oxygen /OHP/ under immediate and delayed administration 09 p1453 A67-21727

Immediate and subsequent effects of brain damage in rats, using closed field intelligence tests 09 p1454 A67-22058

Blockage of electrically evoked pupilodilation in cat by irradiating hypothalamus with cyclotron-accelerated alpha particles 10 p1598 A67-23394

Changes in reproduction and growth of mice and rats under chronic centrifugation at various g force conditions 10 p1598 A67-23416

Absolute threshold of cat optic nerves determined by inspection of poststimulus time histograms, computed from responses of identical flashes of white light 10 p1598 A67-23581

Surgical technique for implanting and maintaining arterial and venous catheters in monkeys 10 p1601 A67-23627

Backward, forward and transverse acceleration effects on cardiopulmonary systems of men and dogs 10 p1599 A67-23810

Monomethylhydrazine effect on methemoglobin production in vitro and in vivo 10 p1599 A67-23812

Phagocytic activity and hepatic function following localized proton radiation to liver, discussing results of experiments performed on white rats 10 p1599 A67-23814

Dog study on microwave radiation and effect on response to X-ray irradiation 10 p1599 A67-23815

Graded dose gamma radiation effect on monkeys, noting change in number of white blood cells and occurrence of gastrointestinal disturbances 10 p1599 A67-23816

Hepatic effects of breathing pure oxygen for eight months upon rats, dogs and monkeys 10 p1600 A67-23818

Changes produced in urinary sodium, potassium, and calcium excretion in mice exposed to homogeneous magnetic field 10 p1600 A67-23819

Pressure changes in cerebrospinal fluid in rhesus monkey cranial cavity with applied forces at abdominal wall 10 p1600 A67-23821

Dog experiments, determining microwave radiation effects on physiological response 10 p1600 A67-23824

Reinforcing effect of informative stimulus that is not positive discriminative

stimulus 11 p1748 A67-25065

Effects of radiation protective pharmacocochemical agents /cystamine, serotonin AET, strychnine, etc/ on animals subjected to centrifugation, for application to astronauts 12 p1902 A67-25654

Intracranial pressure measurements and electroplethysmographic examination of blood content in dog cranial cavity for transverse acceleration up to 40 g 13 p2057 A67-26456

Minimal value of artificial gravity for normal electroactivity of skeletal muscles determined for otherwise weightless condition 13 p2057 A67-26457

Remote aftereffect on hemopoietic tissue of mice under simultaneous irradiation and acceleration, using both X-rays and protons 13 p2057 A67-26458

Biological clocks and cycles in man, lower animals and plants, discussing circadian rhythms 13 p2058 A67-26607

Cardiac changes under hypoxia, experimental morphological study 13 p2058 A67-26756

Nervous reflex mechanisms of hemodynamic shift control during rapidly and slowly increasing acceleration 13 p2058 A67-26757

Vestibular stimulation effect on activity of neurons of optical cortex of curarized cats under vertical acceleration 13 p2058 A67-26758

Tissue protein synthesis in hypodynamic rats studied with aid of carbon 14 and sulfur 35 tagged amino acids 13 p2059 A67-26759

Fourth-week syndrome in addition to normal medullary syndrome in DBA/2J mouse strain response to acute ionizing lethal irradiation 13 p2059 A67-26868

Periodic prolonged low-intensity acceleration stress provided by short radius centrifuge in baboons 13 p2059 A67-26917

Lung, liver, kidney and heart pathology of dogs, monkeys, rats and mice exposed for 2 to 13 weeks to pure oxygen atmosphere at reduced pressure 13 p2059 A67-26918

Physiological effects in baboon of prolonged decompressions simulating loss of cabin pressure 13 p2060 A67-26924

Effects of long term repeated short treatments of mice with hyperbaric oxygen on organ and body weights and hematologic and histologic development 13 p2060 A67-26926

Rhesus monkeys liver damage after irradiation by penetrating protons 14 p2254 A67-28064

Emergency recompression procedures during space flight studied by exposure of chimpanzees to near vacuum 14 p2257 A67-28219

Acetylative capacity and lipid metabolic changes and readjustment to normality in rats in oxygen-rich environment 14 p2256 A67-28588

Analysis of brain wave records from Gemini flight GT-VII by computations to be used in 30-day primate flight 15 p2425 A67-29104

Chronic acceleration and acute Co 60 whole body irradiation effects on rats, discussing weight to mass ratio 15 p2427 A67-29268

Cardiovascular changes at onset of whole body, X-axis sinusoidal vibration in anesthetized mongrel dogs and unsedated humans 15 p2428 A67-29272

Blood pressure changes and pulmonary edema in rat associated with hyperbaric oxygen 15 p2428 A67-29275

Proliferative pulmonary lesions in monkeys exposed to high concentrations of oxygen at 600 to 760 mm Hg pressure 15 p2428 A67-29276

Rats exposed to simulated altitude studied for acute changes in iodine metabolism, noting dichotomy between thyroidal iodine uptake and secretion rates 15 p2428 A67-29279

Prolonged recording from single vestibular units in frog during plane and space flight, significance and technique 15 p2430 A67-29281

Neurophysiology of anesthesia 15 p2429 A67-29294

Mouse, rat and dog organism reaction to ionizing radiation, vibration and acceleration 16 p2611 A67-30765

Effectiveness of therapeutic modalities upon mongrel dogs subjected to dysbarism

by overcompression-decompression 16 p2611 A67-30770

Heat emission and equilibrium temperature of homothermal organism calculated using factors of surrounding medium 16 p2617 A67-30772

Cumulative effect of impact acceleration on physiological functions of rats, studying particularly lung lesions 16 p2612 A67-30904

Oxygen metabolism changes in muscular and brain tissues of animals exposed to prolonged transverse accelerations, examining oxygen consumption and body temperature 16 p2612 A67-30905

Hypoxia effect on cellular and humoral immunity of mice to bacterial infection 16 p2612 A67-30906

Physiological reaction of human body to applied stimuli, developing method evaluating metabolism 16 p2612 A67-30907

Biological value of plant proteins for closed life-support system, studying diet effects on rats 16 p2612 A67-30908

Physiological regeneration on cornea epithelium and intestines exposed to fractional irradiation with fission neutrons, studying mitotic index and chromosome aberrations content 16 p2613 A67-30909

Acute hyperbaric oxygenation histological effects on pulmonary circulation of rabbits 16 p2614 A67-31473

Depressurization behavior of human organism, noting endurance as flight duration and altitude function, and von Beckh chimpanzee absolute-vacuum experiments 16 p2615 A67-31766

Photo-optical instrumentation for biosatellite 30-day orbiting primate mission discussing adverse environmental effects and other constraints regarding requirements 16 p2680 A67-31806

Relationship between oxygen tension and radiosensitivity in complex biological system 17 p2806 A67-31962

Reflected light microscope for viewing unstained brain and ganglion cells 18 p2991 A67-34530

Active parotin preparation to lower serum calcium levels, Ca excretion and possibly prevent decalcification, for applicability to potential system engineering 18 p2991 A67-34712

Cortical electroencephalographic activity /EEG/ relation to behavioral changes in chimpanzee following rapid decompression to near vacuum 18 p2991 A67-34713

Hydrazine effect, alone and with nicotinic acid, on oxygen consumption, respiratory quotient, carbohydrate pool and heat losses in rats studied using gradient calorimeter 18 p2992 A67-34714

Stereoisomers of sulfur containing amino acids effect on local skin protection in X-irradiated mice 18 p2992 A67-34716

Pure oxygen effect on activity of lysosomal aryl sulfatase in brain, liver and liver tissue homogenates from rats 18 p2992 A67-34719

Monkey psychomotor reactions during ballistic flight investigated noting alertness reduction during weightlessness 19 p3178 A67-35241

Automatic life-support system tried on leeches for space applications 19 p3180 A67-35248

Monkey psychomotor reactions during ballistic flight, noting alertness reduction during weightlessness 19 p3181 A67-35466

Individual caged mice susceptibility found greater than groups to toxic effect of d-amphetamine [AFOSR-66-1883] 19 p3178 A67-35885

Aminasine injection and electrolysis effects on formatio reticularis of animals after exposure to hypoxia 20 p3367 A67-36255

Spermatogenesis condition of experimental dogs after 22-day space flight and reproduction function in first offspring generation 20 p3367 A67-36257

Animal study for motor reflexes under simulated weightlessness and during gravitational pulses 20 p3367 A67-36258

Oxygen consumption and phosphorylation processes relation studied in rats for high altitude stability 20 p3367 A67-36259

Hypokinesia effects on nitrogen metabolism of rats 20 p3368 A67-36261

Micrometazoa as model systems for studying physiology of memory at cellular level, examining habituation and maze behavior 20 p3369 A67-36657

Modification of rat sensitivity to rotation through vestibular end organ damage or previous vestibular experience, studying activity changes 20 p3371 A67-36818

Gravity effect on liver regeneration in rats measured by mitotic count 20 p3372 A67-36963

Gas laser IR radiation hazards to eyes tested on rabbits indicates irreversible changes in cornea leading to impaired vision 20 p3375 A67-37276

Anatomical locus of behavior reinforcement, discussing survival mechanism development in animals and humans 20 p3373 A67-37432

Improved response acquisition in deep hypothermia adapted rats 20 p3373 A67-37433

Quantification of response suppression in conditioned anxiety training with fixed duration preaversive stimulus /CS/ 20 p3373 A67-37577

Ability of hypothermia-adapted rats to learn and perform at low body temperature 20 p3373 A67-37669

Glands in two sea snakes located in oral area compared, identified and proved not to be salt glands 21 p3573 A67-37898

Comparative pathology of animals continuously exposed to varied concentrations of carbon tetrachloride vapor in altitude chamber 21 p3573 A67-38070

Scuba diving relation to development of aviator decompression sickness, investigating decompression time before flying 21 p3574 A67-38078

Permeation of neon, nitrogen and sulfur hexafluoride through living tissue in rats, using subcutaneous gas pockets as decompression sickness bubbles model 21 p3574 A67-38079

Space cabin environmental changes studied for susceptibility of mice to viral infection 21 p3574 A67-38080

Vasopressin-aldoosterone interrelation in diuresis and antidiuresis to explain body fluid weight loss in astronauts during space travel 21 p3574 A67-38082

Traumatic sickness in dogs due to high gravity impact noting enzymatic activity changes and immunizing reaction 21 p3575 A67-38509

Nucleic acid metabolism in Chinese hamster fibroblasts grown in vitro noting effects of concentrations of sodium azide 21 p3575 A67-38798

Hemodynamic responses of conscious dogs exposed to various centrifugation levels and back angles to determine optimum angle for positioning astronauts 22 p3750 A67-39593

Trauma in lateral impact at high entrance velocity compared with rearward and forward facing body orientations of baboons when restrained by lap belt only 22 p3750 A67-39594

Rapid decompression effect on lymph pressure of dog, discussing immediate and delayed rise phases 22 p3751 A67-39600

Lung changes resulting from prolonged exposure to 100 percent oxygen at 550 mm Hg suggest media erosion and evidence of hypertrophy and hyperplasia 22 p3751 A67-39601

Pulmonary isotopic scanning technique in dog to assess embolism before and after lethal decompression 22 p3751 A67-39602

Chimpanzee mesenteric artery blood flow for various activities during 24 hr period monitored by radio telemetry 22 p3751 A67-39603

Survival times of rats studied from positive and negative acceleration test exposure in special centrifuge 22 p3753 A67-40540

Rats exposed to repeated radial acceleration studied for central nervous system adaptation and survival rates noting better adaptability of newborns 22 p3753 A67-40541

Toxicity of radioprotective amino ethyl isothiorium bromide from animal studies noting hazardous effects in human organism 22 p3753 A67-40546

Gamma irradiation effect on spinal cord timed differently, considering time factor in reactions of nervous system in guinea pigs 23 p3943 A67-40767

Functional relation between oxidation, metabolism, blood flow volume rate and brain temperature in rats exposed to vibration, noting temperature decrease and blood supply and oxygen consumption

stimulation 23 p3943 A67-40769

Brain tissue respiratory processes of rabbits subjected to hypergravity and acute hypoxia noting no significant difference between experimental and control animals 23 p3943 A67-40770

Transverse accelerations remote aftereffect on conditioned alimentary reflexes of rats, discussing prolonged depression of higher nervous activity 23 p3943 A67-40771

Combined effect of acceleration and ionizing radiations on conditioned reflexes of rats noting alleviation on radiation leukopenia 23 p3943 A67-40772

Precentrifugation effect on radiation reactions of vestibular analyzer in guinea pigs, establishing substantial spontaneous electric activity stimulation in hind legs extensor muscles 23 p3944 A67-40773

RNA fractions base composition and labelling kinetics in presence and absence of actinomycin for rapidly labelled RNA in rabbit bone marrow rich in erythroid cells 23 p3944 A67-40801

Metabolic depression in animals exposed to air after living in helium-oxygen environment, suggesting denitrogenation period effect 23 p3944 A67-40823

Potential contamination of equipment by primate passenger during 30-day earth orbit, studying skin, body particulate matter and indigenous microflora 23 p3944 A67-40856

Hepatic hemorrhagic lesions produced by 32 and 55 Mev proton radiation in rhesus monkeys 23 p3944 A67-41017

Multiplace metabolimeter closed circuit system with servo-driven volume meter for animal oxygen consumption in gaseous artificial environments 23 p3999 A67-41088

Abdominal blood flow changes in anesthetized dogs during transverse acceleration 23 p3950 A67-41535

Dog adaptation to increased carbon dioxide levels in normoxic environment, noting effects on arterial pH and bicarbonate level 23 p3950 A67-41537

Rat adrenal gland responses to increased oxygen tension at ambient temperature, noting oxygen critical threshold partial pressure affecting survival time 23 p3950 A67-41538

Earth organism behavior under artificial gravity, proposing long term orbital experiments 23 p3950 A67-41549

Cardiovascular acceleration-stress reactions during G acceleration of dogs, noting blood pressure, blood velocity and pressure waves 23 p3951 A67-41551

Canine cardiac displacement and cardiovascular dynamic response during abrupt deceleration impact, discussing traumatic ruptures and pressure effects 23 p3951 A67-41552

Circadian oscillations of deep body temperature and heart rate in ambulatory primate in controlled environment 23 p3951 A67-41554

Vitamins A and E deficiency effects on rats exposed to pure oxygen noting less weight gain and growth 23 p3952 A67-41568

Hydrazine effects on free amino acid concentrations of plasma and urine in dogs 23 p3952 A67-41570

Anesthetized dogs subjected to near vacuum condition before and after clinical death, comparing data of venous and arterial pressure 23 p3952 A67-41572

Reactions of animals exposed to pure oxygen space cabin atmosphere for 235 days, noting no systematic toxicity 23 p3952 A67-41574

Semicircular canal physiological response in cats recorded for case of parallel swing rotation, noting mechanical excitation mode of canal 23 p3952 A67-41576

Hematological criteria of chronic acceleration stress and adaptation 23 p3953 A67-41587

Hypoxia stimulated pulmonary arterial pressure increase in dog and baboon noting hemodynamic effects 23 p3953 A67-41588

Animal study of body volume increase and pressure changes causing lungs and thorax expansion during decompression to near vacuum 23 p3954 A67-41594

Animal study of irreversible trauma in lateral impact when restrained only by aircraft lap seat belt 23 p3954 A67-41595

Intracranial pressure in Macaca speciosa monkeys during controlled abrupt linear

deceleration 23 p3954 A67-41596

Toxic metabolic effects of MMH, discussing methemoglobinemia as indicator of exposure dosage in animal study 23 p3955 A67-41602

Energy transfer effects on pathophysiological responses of guinea pigs and bradycardia response in monkeys under minus G impact 23 p3955 A67-41610

acceleration 23 p3955 A67-41610

Pharmacological alterations of vibration tolerance 23 p3955 A67-41613

Oxygen toxicity relation to nutrition, hormonal secretion and age factors, discussing experiments on rats 23 p3956 A67-41632

Decerebrate cat experiments for semicircular canal response to rotational stimulation 23 p3956 A67-41633

Oxygen role in cardiac rate in squirrel monkeys during acceleration stress on centrifuge 23 p3956 A67-41635

Centrifuge tests with squirrel monkeys for pharmacologically denervated primate heart response to acceleration stresses 23 p3957 A67-41636

Acute and chronic cellular level effects of low energy proton irradiation in rat skin 23 p3957 A67-41644

Pathological effects, including carcinogenesis following proton whole body irradiation in rats 23 p3958 A67-41645

Sulphydrylamine drugs effect for protection in rats exposed to high, low, sublethal, lethal and supralethal dose of X and gamma radiation 23 p3958 A67-41648

Lung changes relation to fatal outcome of 100 percent oxygen exposure 23 p3958 A67-41649

Arterial oxygen tension during acceleration recorded on anesthetized greyhounds using microelectrode and physiological gas analyzer 23 p3958 A67-41653

Increased oxygen tension causing increased free radical flux in rat kidney tissue akin to ionizing radiation exposure 23 p3958 A67-41654

High venous pressures during exposure of dogs to near-vacuum conditions 23 p3960 A67-41699

Tissue oxygenation during hemorrhage in dogs at 1 and 3 atm oxygen, noting oxygen at high pressure /OHP/ does not prevent stagnant hypoxia [SAM-TR-66-258] 24 p4111 A67-41802

Biological value of algal and soya proteins on four generations of white rats 24 p4111 A67-41847

Rats resistance and reactivity in hypothermal state to very low atmospheric pressure by hypercapnia-hypoxia exposure 24 p4111 A67-41849

Reactivity of animals to caffeine and strychnine during transverse acceleration aftereffects 24 p4111 A67-41850

Arterial and venous blood of brain and mixed venous blood of heart measured in dogs exposed to simulated altitude, noting body deoxygenation 24 p4111 A67-41851

Exclusion effect of afferent signalization on tonic function of iliotibial muscle in frogs exposed to acetylcholine 24 p4112 A67-41852

Histochemical investigation of effect of hypothermia and hypobiosis on activity of oxidizing tissue enzymes of carbohydrate, amino acid, nucleotide and aliphatic metabolism of rats 24 p4112 A67-41853

Rats exposed to different hyperoxic atmospheres for 20 days studied for toxic lipids formation 24 p4112 A67-41854

Space genetics, discussing space environment exposure of experimental animals as cause of mutations, hereditary damage, etc 24 p4113 A67-42053

Polydipsia elicited by synergistic action of saccharin and glucose solution 24 p4113 A67-42099

Visually controlled placing response tests for kittens reared without sight of limbs 24 p4113 A67-42221

Preirradiated organism reaction to space flight acceleration studied in determination of admissible ionizing radiation dose 24 p4113 A67-42393

ANION

SA ANODE

SA CATION

Mass spectrometric investigation of composition of negative ion sputtering products of solid metal surfaces under

cesium ion bombardment 06 p1036 A67-18425
 Single- and double-quantum
 photodetachment of negative ions, giving
 cross sections for electron elastic
 scattering 07 p1225 A67-19494
 Cross sections for photodetachment of
 electron from negative atomic oxygen
 ion 07 p1225 A67-19497
 Potentials of zero charge of gold, silver
 and mercury electrodes as affected by
 cations and respective metal ion
 interaction 11 p1749 A67-23920
 Dispersion relation for LF oscillations in
 plasma with negative ions derived in three-
 fluid approximation 11 p1834 A67-24375
 Chemical effects in X-ray spectra and
 inner shell photoelectron spectra of sulfur-
 and chlorine-oxygen anions and molecular
 orbital method 18 p2998 A67-34520
 Thermally ionized cesium plasma produced
 containing negative Cl
 ions 19 p3272 A67-35084
 Negative ion accumulation in HF resonant
 discharges at low pressure and plasmoid
 formation 19 p3275 A67-35112
 Two-ion D region model for polar cap
 absorption events 20 p3426 A67-36302
 N-vinyl carbazole reactions with anionic
 initiators, discussing radical anion and
 polymer formation and ESR spectra
 [JPL-TR-32-1126] 24 p4118 A67-42601

ANISOTROPIC FLUID
 Radiation in Lorentzian moving anisotropic
 plasma 01 p0123 A67-10442
 Continuum with director and constitutive
 equations for anisotropic fluids, obtaining
 solutions for simple shear, Poiseuille and
 Couette flows 01 p0053 A67-10849
 Infinite cylindrical antenna insulated from
 surrounding uniaxially anisotropic plasma by
 concentric cylindrical sheath of free
 space 03 p0384 A67-13849
 Idempotent method solution of transport
 equations for radiative heat transfer in
 nonisothermal anisotropic scattering medium
 between two parallel plates
 [ASME PAPER 66-WA/HT-28] 04 p0725 A67-15441
 Nonlinear medium anisotropy and
 saturation effects on orientation of
 polarization ellipse of gas laser
 mode 06 p1010 A67-17823
 Optimum MHD generators using
 anisotropic plasma, discussing conducting-gas
 MHD flow, Hall effect, ion slip effect,
 etc 06 p0950 A67-18089
 Steady flow of anisotropic conducting
 medium in half-space under influence of
 magnetic field 07 p1230 A67-20033
 Approximate mode decomposition for
 treating boundary value problems for
 uniform compressible anisotropic
 plasma 11 p1753 A67-24307
 Steady flow of anisotropically conducting
 fluid in plane or annular channel of MHD
 generator with nonequilibrium plasma at
 small Reynolds numbers 16 p2600 A67-30541
 HF magnetic fields for plasma sheath with
 perpendicularly superimposed static
 magnetic field and resonance excitation of
 electron cyclotron waves 19 p3276 A67-35117
 Wave propagation in anisotropic plasma in
 presence of electron density irregularities,
 noting Faraday effect 19 p3184 A67-35825
 Biorthogonality relation derived between
 eigenfunctions of operator representing
 linearized anisotropic multilayer warm
 plasma and eigenfunctions of adjoint
 operator 20 p3503 A67-37711
 Perturbation method using stream
 function for investigating anisotropic wave
 propagation describable by hyperbolic
 differential equations 21 p3611 A67-37891

ANISOTROPIC MATERIAL
 Skin effect association with anisotropy of
 medium in solid mechanics, analyzing
 surface instability, internal buckling and
 surface wave propagation 01 p0113 A67-10406
 Principle magnetic properties of series of
 anisotropic alloys of Alnico type with 38
 percent cobalt and coercive forces in excess
 of 2000 oe 01 p0093 A67-10518
 Bounds for overall elastic moduli of solid
 composite materials with uniform phases
 that may be arbitrarily
 anisotropic 02 p0337 A67-11795
 Anisotropy effect of continuous filament
 composites on material strength, noting
 dependency on test specimen configuration
 in evaluation of mechanical
 properties 03 p0523 A67-13446

Anisotropic medium capacitance
 calculation, using method based on point-
 charge field behavior analysis in isotropic
 medium, for biconical
 antenna 03 p0371 A67-13866
 Longitudinal magnetoresistance anisotropy
 and Hall coefficient anisotropy in p-type
 indium antimonide, noting similarities with
 galvanomagnetic anisotropy of p-type
 germanium 04 p0674 A67-14609
 Courant-Hilbert ray theory and Thomas
 singular surfaces theory of wave propagation
 in anisotropic homogeneous linearly elastic
 medium, based on growth
 equation 04 p0657 A67-15083
 Optimum thin wall pressure vessels of
 anisotropic materials of monolithic and
 filamentary construction
 [ASME PAPER 66-APM-BB] 04 p0717 A67-15915
 Stressed state of anisotropic half-plane
 weakened by finite number of elliptical
 holes with centers on straight line
 perpendicular to boundary of
 half-plane 05 p0907 A67-16018
 Anisotropy effect on strength of unwoven
 glass fiber reinforced plastic, ascertaining
 nature of stressed state arising at high
 temperature 05 p0912 A67-16183
 Orientation effects in mechanical behavior
 of anisotropic structural materials - Astm
 Symposium, Seattle, October-November
 1965 06 p1107 A67-18653
 Electric conduction models for biological
 tissues as anisotropic
 medium 08 p1288 A67-20602
 Elastic interaction between dislocation
 loops and straight dislocations in orthotropic
 anisotropic materials analyzed for various
 graphite configurations 08 p1346 A67-20797
 Collective energy losses by plasmas in
 crystals caused by excitation of volume or
 surface plasmons 08 p1369 A67-20828
 Restrictions on relaxation moduli of
 anisotropic linear viscoelastic
 solid 08 p1419 A67-20880
 Craggs propagating crack model for
 isotropic solid extended for general elastic
 anisotropy, obtaining propagation theory
 under tensile or shear
 stress 08 p1421 A67-20952
 Stimulated Raman effects in anisotropic
 crystal potassium dihydrogen phosphate with
 Stokes generations 11 p1800 A67-24243
 Current distribution and input admittance
 of infinitely long cylindrical antenna driven
 by slice generator and immersed in
 anisotropic plasma 11 p1761 A67-24284
 Plane electromagnetic wave diffraction by
 conducting half-plane embedded in uniaxial
 anisotropic medium 11 p1753 A67-24315
 Properties of anisotropic continuous media
 with energy and stresses depending on
 deformation tensor gradients and other
 tensor magnitudes 11 p1876 A67-24676
 Reflection and transmission of
 electromagnetic waves at interface between
 stationary isotropic medium and moving
 anisotropic medium 11 p1820 A67-24919
 Generalized hypoelasticity theory includes
 theory of anisotropic elasticity as special
 case and thermal effects 12 p2032 A67-26169
 Mechanical properties of beryllium with
 emphasis on influence of anisotropy in
 forming and grain size in powder
 metallurgy 13 p2140 A67-27134
 Steady state wave propagation in
 homogeneous anisotropic media studied from
 near field behavior of
 matrix 13 p2158 A67-27179
 Elastic moduli of composite materials with
 anisotropic filaments 14 p2398 A67-28101
 Anisotropy in tunneling density of states
 in pure type II superconductors, examining
 ideal case of perfectly specular boundary
 scattering at tunneling
 junction 14 p2365 A67-28294
 Asymptotic solution of oblique waves in
 inhomogeneous vertically magnetized
 plasma 14 p2361 A67-28922
 Electromagnetic wave diffraction by
 infinite set of parallel metallic plates,
 obtaining exact solution by Wiener-Hopf
 technique 15 p2435 A67-29191
 Anisotropic macroscopically neutral plasma
 excitations by arbitrary current described by
 potentials, noting electroacoustic wave
 propagation 15 p2527 A67-29482
 Interaction of incident H-wave with
 infinite conducting cylinder coated with
 inhomogeneous and anisotropic plasma

sheath, noting far field pattern of scattered
 field 16 p2626 A67-31350
 Uniqueness theorem for general linear
 anisotropic time-variable viscoelastic body
 under boundary conditions, using Laplace
 transformation 17 p2964 A67-33135
 Steady state wave propagation in
 homogeneous anisotropic media governed by
 symmetric hyperbolic partial differential
 equations 18 p3077 A67-33429
 Anisotropic composites viscoelastic
 analysis applied to orthotropic cylinder
 pressurization, glass fiber cooling and
 relaxation shear moduli
 problems 20 p3474 A67-37267
 Reciprocal theorem in linearized theory of
 couple stresses for perfectly elastic
 nonhomogeneous anisotropic
 materials 20 p3540 A67-37281
 Nonlinear elastic anisotropic wedge
 deformation for short time loading moment
 applied to apex, approximating stress
 function 20 p3542 A67-37660
 Fields with boundaries radiated by electric
 or magnetic current phased-line
 distributions, interpreting field constituents
 as geometric-optical and diffracted
 contributions 20 p3388 A67-37702
 Electromagnetic point source in presence
 of planar interface between two anisotropic
 media, obtaining far fields through Fourier
 integral and ray optical
 calculation 20 p3388 A67-37703
 Anisotropy due to molecular structure
 orientation in vitreous inorganic glass fibers,
 noting phase equilibrium
 relation 21 p3648 A67-37880
 Hooke law type anisotropic fiberglass
 reinforced plastic, discussing elastic
 deformation and brittle fracture, using
 revised Mises ellipse
 equation 21 p3649 A67-37907
 Plastic deformation theory applicable
 range for case of linear anisotropic
 consolidating medium 21 p3720 A67-38298
 Alfven, fast and slow magnetoacoustic and
 entropy hydromagnetic wave propagation in
 anisotropic collisionless
 magnetoplasma 22 p3843 A67-39268
 Synchrotron radiation intensity of
 relativistic electron moving in anisotropic
 medium 22 p3851 A67-39735
 Anisotropic energy gap measurements in
 niobium single crystals by
 tunneling 22 p3865 A67-40440
 Flexible anisotropic ferrite magnets
 preparation, noting influence of binder in
 orientation of crystals 23 p4041 A67-41183
 Light propagation in electrically and
 magnetically anisotropic medium and
 diffraction by birefringent cylinder using
 coupled integrodifferential
 equations 24 p4119 A67-41889
 Maxwell equations solved for Gaussian
 beam form in anisotropic medium, discussing
 laser applications 24 p4167 A67-42092
 Demagnetizing fields in thin magnetic
 films, considering saturation, film thickness
 and anisotropy 24 p4204 A67-42338
 Electromagnetic wave diffraction in
 magnetoactive plasma by conducting wedge
 using Laplace integral in rotating reference
 frame 24 p4123 A67-42706

ANISOTROPIC PLATE
 Stress distribution in elastic anisotropic
 plate with row of elliptical holes reinforced
 by elastic rings 01 p0158 A67-10221
 Boundary bending conditions for
 anisotropic plates with free, hinged or
 rigidly clamped edge 03 p0531 A67-14200
 Tension of homogeneous anisotropic
 elastic semiminfinite plate with rigid stiffener
 attached on segment of straight
 boundary 05 p0910 A67-16150
 Linear theory of homogeneous anisotropic
 elastic shells and plates without considering
 Love-Kirchhoff
 assumptions 05 p0921 A67-16883
 Transverse elastic impact of isotropic
 sphere against thin rectangular anisotropic
 plate 05 p0922 A67-17174
 Bending equations for thin elastic
 anisotropic plates, using Goldenveizer
 method 06 p1106 A67-18630
 Polynomial solutions for differential
 equations describing thermoelastic
 equilibrium of thin anisotropic
 plates 10 p1718 A67-23405
 Bending under transverse load of isotropic
 plate with elastic base, using Ambartsumian
 theory of anisotropic

plates 11 p1878 A67-24857
 Plane stress state near circular hole in infinite anisotropic plate of rigid-plastic nonhardening material 11 p1879 A67-24882
 Iteration solution for system of equations for nonlinear deflection and stability of anisotropic plates 13 p2217 A67-26632
 Differential equations and potential for simply supported anisotropic sandwich plate under compression and shear stresses above buckling limit 19 p3341 A67-35575
 Anisotropic plate with two elliptical holes studied for stresses under edge load by solving linear algebraic equations infinite system 22 p3910 A67-39452

ANISOTROPIC SHELL
 Solutions to equations of multilayer anisotropic shells represented in terms of resolving function for high order equation 01 p0162 A67-10985
 Plastic analysis of rib reinforced cylindrical shells using strain mapping method for Tresca yield conditions [ASME PAPER 66-WA/APM-14] 04 p0713 A67-15406
 Linear theory of homogeneous anisotropic elastic shells and plates without considering Love-Kirchhoff assumptions 05 p0921 A67-16883
 Yield surfaces for nonhomogeneous anisotropic shells of revolution under rotationally symmetric conditions of loading and support 10 p1719 A67-23544
 Asymptotic integration of elasticity theory equations and analysis of stressed state of anisotropic shell 11 p1871 A67-24160
 Stress-strain condition in thin walled shells having anisotropic moduli with one end clamped and torsion applied at other end 11 p1878 A67-24860
 Stability of inhomogeneous anisotropic cylindrical shells containing elastic cores under pressure, axial load and torsion 14 p2399 A67-28119
 First order finite difference numerical analysis of thin elastic orthotropic and inhomogeneous cylindrical shells with small deformations from external forces 15 p2574 A67-29471

ANISOTROPY
SA CRYSTAL STRUCTURE
SA PLASTIC ANISOTROPY
 Horizontal drift and anisotropy in F-1 region during geomagnetically active and quiet conditions 01 p0057 A67-10117
 Anisotropy of Hall effect dependence on field and temperature in dysprosium crystal 01 p0133 A67-10743
 Elastic interaction energies between edge and screw dislocations and tetragonal defects in anisotropic NaCl lattice 02 p0298 A67-11885
 Anisotropy of thermal expansion and microstructural changes due to thermal stresses 03 p0446 A67-13564
 V-I tunneling characteristics and energy gap anisotropy of Pb-Bi superconducting alloy, discussing mean free path 03 p0501 A67-14341
 Dielectric permittivity of barium titanate monocrystals with anisotropic stratified domain structure 04 p0678 A67-15131
 Magnetic field finiteness effect on effectiveness of gyrotronic plasma waveguide excitation by coaxial line of force 04 p0665 A67-15165
 Phenomenological theory of longitudinal Hall effect in cubic crystals, assuming anisotropic dispersion law and tensorial relaxation time 04 p0681 A67-15291
 Anisotropy in stellar diurnal cosmic ray variations in Northern and Southern Hemispheres, noting distributions of stellar and antistellar vectors 05 p0881 A67-16120
 Anisotropic semiconductor in hot electron theory, deriving volt-ampere characteristics 05 p0867 A67-17053
 Anisotropic elastic constants and strength characteristics of fiberglass reinforced plastics during shear 06 p1020 A67-18099
 Tunneling measurements of energy gap anisotropy in thick and thin superconducting films of Al, Pb, In and Sn 06 p1052 A67-18571
 Effective triaxial anisotropy in exchange-coupled composite three-layered uniaxial ferromagnetic thin films 07 p1231 A67-19488
 Superconducting energy-gap parameter anisotropy effect on critical field in presence of nonmagnetic impurities 07 p1235 A67-20132

Anisotropy and temperature dependence of upper critical field of type II superconductor single crystals with cubic structure 07 p1236 A67-20136
 Anisotropy of energy gap in superconducting Pb analyzed using superconductive tunneling 07 p1236 A67-20137
 Reverse magnetization and energy of anisotropy of single crystal ferromagnetic films 08 p1368 A67-20607
 Electromagnetic-wave radiation peculiarities in homogeneous anisotropic dispersive magnetic plasma 08 p1294 A67-20821
 Magnetosonic wave effect on anisotropic relativistic plasma component, obtaining cosmic ray plasma instability when wave frequencies are less than electron cyclotron frequency 09 p1546 A67-22230
 Pioneer VI detector to measure degree of anisotropy of cosmic radiation at various energy ranges 09 p1500 A67-22427
 Landau-Ginzburg theory extended to anisotropic superconducting energy gap, considering diffuse and specular boundary scattering 10 p1687 A67-22759
 Anisotropic cosmological solution with energy density determined only by neutrinos moving along one axis, noting expansion 10 p1708 A67-23334
 Anisotropic vector functions of vector argument connected with crystal symmetry 11 p1812 A67-24148
 Dielectric permittivity of barium titanate monocrystals with anisotropic stratified domain structure 12 p1978 A67-25155
 Current carrier concentration distribution in semiconductor with intrinsic anisotropy created by strong electric field 13 p2173 A67-26362
 Anisotropy in thin dielectric films of tantalum and titanium anodic oxide from various measurements explained by transistor-like model 13 p2175 A67-26655
 Anisotropy of Hall effect dependence on field and temperature in dysprosium crystal 13 p2176 A67-26772
 Magnetic field finiteness effect on effectiveness of gyrotronic plasma waveguide excitation by coaxial line of force 15 p2526 A67-29352
 Anisotropic semiconductor in hot electron theory, deriving volt-ampere characteristics 15 p2538 A67-29784
 Magnetic susceptibilities and anisotropies of manganous acetate tetrahydrate crystal measured at various temperatures 15 p2540 A67-30091
 Fields generated by infinitesimal, arbitrarily oriented, electric-dipole source located in isotropic medium bounded by parallel plane-stratified, anisotropic media 16 p2632 A67-31858
 Temperature dependence of Josephson critical current in superconductor model having anisotropic energy gap 17 p2915 A67-32719
 Differential transport equation system in n-dimensional anisotropic space solved using matrices, discussing heat conduction equations 17 p2972 A67-33070
 Cosmic radiation anisotropy variation with time and direction described on intensity contour map, noting application for neutron monitors data reduction 17 p2938 A67-33209
 Polarization properties of single mode operating gas laser in small axial magnetic field with initial cavity anisotropy 17 p2870 A67-33368
 Knoop hardness anisotropy in unalloyed titanium and iodide titanium sheets, discussing orientation, hardness variations, rolling, cross section planes and indentation [ASTM PAPER 53] 18 p3068 A67-34583
 Silicon doped YIG containing iron ions, studying loss mechanism, low temperature anisotropy, annealing and rotational hysteresis 18 p3105 A67-34629
 Anisotropy of electron energy distribution measurement in electron cyclotron-resonance plasma using diamagnetic loop 18 p3093 A67-34756
 Time dependency, anisotropy degree and spectral composition of cosmic radiation generated during July 1966 solar flares as observed by Pioneer VI 19 p3314 A67-35270
 Galactic anisotropies observation, giving procedure for detecting periodicities and data on sidereal daily variation amplitude 19 p3315 A67-35484
 Mode-matching technique for bifurcated

anisotropic waveguide, discussing Bresler biorthogonality relationships to derive anisotropic guide mode equations 20 p3407 A67-37712
 Standard equation method for normal incidence of plane monochromatic electromagnetic wave propagation in inhomogeneous anisotropic medium 21 p3579 A67-38111
 Current carrier concentration distribution in semiconductor with intrinsic anisotropy created by strong electric field 21 p3680 A67-38319
 Stress determination in elastic plate with remanent elasticity and cylindrical anisotropy, using integral-operational method 21 p3723 A67-38555
 Cosmic ray diurnal anisotropy component annual means variation with two solar cycles 23 p4051 A67-40817
 Solar activity cycle effect on cosmic ray anisotropy diurnal variation 23 p4057 A67-41120
 Cosmic ray anisotropy in solar system, considering diurnal variation in terms of anisotropic diffusion 23 p4058 A67-41121
 Diurnal variation in cosmic ray anisotropy from observations during solar activity minimum, giving amplitudes and phases distribution 23 p4058 A67-41122
 Anisotropy in stellar diurnal cosmic ray variations in Northern and Southern Hemispheres, noting distributions of stellar and antistellar vectors 24 p4214 A67-42796

ANNA SATELLITE
 Electron cloud-like distribution in ionosphere shown from phase measurements of 162 and 324 mc emissions of Transit and Anna satellites [RASSA PAPER 1-10-135] 03 p0417 A67-14246
 ANNA satellite geodesy experiments emphasizing operation of strobe light 07 p1176 A67-19766
 U.S. Navy Doppler geodetic Tranet system configuration and operation, discussing tropospheric and ionospheric refraction, timing and frequency errors 18 p3003 A67-34241

ANNEALING
 Surface charge after annealing of aluminum-silicon dioxide-silicon structures in inert atmospheres, analyzing effect of applied electric field 01 p0032 A67-10004
 Stacking faults in steam-oxidized silicon wafers annealed in vacuum at 800, 1000 and 1200 degrees C observed by chemical etching and transmission electron microscopy 01 p0126 A67-10052
 X-ray diffraction-Fourier series analysis and electron microscopy analysis of annealing effects on structural properties of cold worked dispersion-strengthened alloys 01 p0097 A67-10698
 Effects of aluminum electrode and hydrogen atom on MOS structure during annealing 01 p0137 A67-11069
 Quantitative in situ X-ray diffractometer investigations of evaporated metal films and after annealing treatments ranging up to 370 degrees C 02 p0287 A67-11713
 Ultrasonic attenuation of alkali halide crystals in 120 to 180 degrees K range, noting thermal annealing of dislocation pinning centers 02 p0298 A67-11888
 Kinetics of degassing of tantalum-nitrogen solid solutions by annealing in high vacuum at various high temperatures 04 p0637 A67-14909
 Various combinations of preanneal and diffusion anneal conditions used in experiments for determining environmental effects on diffusion of Ta 182 in bcc titanium 04 p0637 A67-14937
 Annealing effect on texture of titanium alloys with electrodeposited chromium and nickel 04 p0637 A67-14944
 Annealing production of acceptor defect centers in indium antimonide single crystal 04 p0683 A67-15651
 Transient annealing following pulsed neutron exposure in silicon transistors and solar cells as function of temperature and injection level 04 p0684 A67-15693
 Phase diagram of vanadium-gallium system by differential thermal analysis of thirty-five 10-g V-Ga alloy samples prepared in arc oven 05 p0827 A67-16326
 Superlattice formation and lattice spacing changes in copper-gold alloys annealed for various periods 05 p0862 A67-16506
 Defects in silicon p-n solar cells with Li

diffused N region produced by electron irradiation and spontaneously annealed at room temperature interpreted as Li ions 05 p0870 A67-17273

Cold plastic deformation, rolling direction and annealing temperature effect on mechanical properties of sheet niobium at room and high temperature 05 p0831 A67-17504

Plasticity of cast molybdenum improved by vacuum-annealing at temperatures from 900 to 1200 degrees C 05 p0832 A67-17511

Transmission electron microscopy analysis of microstructural phase properties of Ti-8Al-1V-1Mo alloy after duplex and mill annealing treatments 06 p1013 A67-17797

Annealing of neutron irradiation induced changes in impurity conduction in Sb-doped Ge 06 p1068 A67-18969

Steady states in annealing of niobium and tantalum in oxygen atmosphere, noting relation of pressure to temperature 07 p1210 A67-20110

Niobium and tantalum purification from interstitial impurities by high vacuum annealing, noting effect on electric resistivity 07 p1210 A67-20112

Annealing of proton radiation damage in silicon solar cells 07 p1237 A67-20143

Electrical resistance and weight increase measurements in aluminum and Al-Mg alloys, noting relation between oxidation rate and Mg content during annealing 08 p1341 A67-20796

Relation in silicon between annealing rates, residual damage and defect concentrations, noting link to activation energy increase 09 p1557 A67-22420

DNA-agar annealing of residual DNA after degradation by ionizing radiation 11 p1746 A67-23919

X-ray analysis of lattice strain and crystallite size changes in tungsten carbide compressed at high pressure, noting annealing effect 11 p1809 A67-24949

Annealing effect on damping rods for magnetic field stabilized satellites 12 p2011 A67-25212

Recovery of deformed copper-palladium and gold-palladium alloys by isothermal and isochronal annealing, noting vacancy and interstitial migration 13 p2133 A67-27007

Recrystallization of Ge and Si thin films and structural changes due to electron bombardment and thermal annealing 13 p2177 A67-27071

Internal friction in nickel chromium alloys heated to annealing temperature, noting 530 and 800 degree peaks and origin of latter 14 p2338 A67-28675

Ti-Zr-C and Ti-Hf-C alloy X-ray and microstructural studies noting homogenizing, annealing, quenching and phase equilibria 15 p2505 A67-30388

Heat treating effects on titanium alloy properties, discussing ductility and strength annealing, etc 16 p2681 A67-30486

Niobium alloys under annealing and aging analyzed, noting formation of oxide, nitride and carbide phases followed by coagulation and brittleness 16 p2687 A67-30844

Deformation effects on thermal conductivity, microhardness, and thermal EMF of annealed bismuth telluride bars 16 p2730 A67-31160

Effects of electric fields and configurations on thermal annealing and radiation hardening of MOSFETs 17 p2916 A67-32835

Impurity effect on annealing behavior of irradiated silicon studied via isothermal annealing of minority carrier lifetime 17 p2921 A67-33051

Silicon doped YIG containing iron ions, studying loss mechanism, low temperature anisotropy, annealing and rotational hysteresis 18 p3105 A67-34629

Au and P doped n-type Si, noting formation of p-type surface layer of increasing thickness when heat treated 19 p3299 A67-34761

Indium-antimony alloy thin film preparation by vacuum evaporation, noting effect of heating and annealing on electrical resistivity 19 p3305 A67-35609

Silicon transistors transient defect annealing from pulsed particle irradiation, stressing time factors 19 p3305 A67-35667

Isochronal annealing of short-circuit current of electron irradiated silicon solar cells 19 p3305 A67-35668

Isochronal annealing of proton-irradiated silicon solar cells studied in vacuum over various temperature ranges 19 p3305 A67-35669

Annealing under continuous irradiation in p-on-n silicon solar cells with lithium diffused in N region 19 p3306 A67-35671

Conductivity profiles investigated as function of ion energy, total flux and annealing schedule, when implanting boron into silicon 19 p3307 A67-35812

Thermal annealing of silicon solar cells with direct solar heating or electric storage methods to avoid radiation damage 20 p3364 A67-37129

Characteristics of niobium annealed at 2000 C, describing texture development and crystal perfection variation with annealing time 20 p3470 A67-37391

Cold plastic deformation, rolling direction and annealing temperature effect on mechanical properties of sheet niobium at room and high temperature 21 p3644 A67-38032

Plasticity of cast molybdenum improved by vacuum-annealing at temperatures from 900 to 1200 degrees C 21 p3644 A67-38039

Dilute magnesium addition effect on growth and shrinkage of dislocation loops in aluminum studied by isothermal annealing of thin foils 21 p3644 A67-38088

Molybdenum heat resistance improvement after structural polygonization by deformation and annealing, describing durability dependence on treatment conditions 22 p3819 A67-39324

Softening and incipient recrystallization temperature of deformed niobium during annealing measured by X-ray analysis and mechanical properties examination 22 p3823 A67-40326

Machining advantages and economy of annealed steels over maraged steels 23 p4010 A67-41352

Li behavior in self-healing radiation resistant Si solar cells 23 p3941 A67-41522

Spontaneous annealing models of lithium-diffused Si solar cells, discussing defect compensation and metastable defect formation 23 p3941 A67-41523

Li doped Si solar cell, studying irradiation damage, recovery effect, carrier removal, time dependency and annealing 23 p4047 A67-41525

Li doped Si solar cell radiation resistance to high energy electrons, noting fabrication methods and annealing behavior differences 23 p3941 A67-41527

Li doped p-plus/n solar cells optimum design and radiation resistance, noting concentration and room temperature annealing conditions 23 p3942 A67-41528

Alloying effect on diffusion thermopower in relation to Fermi surface variations in dilute silver-gold alloys [JPL-TR-32-1095] 24 p4200 A67-41840

ANNUAL VARIATION

Annual variation of quiet sun radio emission during solar cycle, noting daily mean values of flux at different frequencies 03 p0513 A67-14005

Possible annual variation of gravitational constant shown to eliminate systematic errors noted in redeterminations of gravitational constant 09 p1492 A67-22616

Semiannual variations of magnetic activity 10 p1630 A67-22796

Seasonal and annual variations of electron density in ionospheric F layer interpreted as changes in production rate and ionization loss caused by atmospheric composition variations from neutral atmosphere 10 p1647 A67-23274

26 month oscillation in zonal wind and temperature in equatorial atmosphere 13 p2150 A67-26440

Diurnal, annual and seasonal variations of high altitude turbulent motions in upper atmosphere through observation of meteor trails by coherent pulse method 13 p2110 A67-26506

Temperature and wind fields in stratosphere obtained with rocket probes, noting diurnal and annual temperature variation differences for heights beyond 35 km 13 p2113 A67-26679

Biennial variations of zonal atmospheric circulation at equatorial latitudes analyzed using hydrothermodynamics 13 p2150 A67-26680

Quasi-biennial cycles in cosmic ray

intensity 15 p2549 A67-29203

Annual cosmic ray variations and changes in cosmic radiation intensity as function of earth heliolatitude 15 p2550 A67-30012

Diurnal and annual variations of occurrence frequency and dispersion of whistlers during IGY and IQSY 15 p2478 A67-30068

Diurnal, annual, latitudinal and sunspot cycle-influenced variations of spread-F intensity at very high latitudes [AGARDOGRAPH 95] 15 p2481 A67-30281

Diurnal variation of hard component near minimum solar activity, emphasizing temperature effects 17 p2932 A67-32080

IQSY electrophotometric and spectrometric measurements of annual and nighttime variations in rotational temperatures and integral intensity of hydroxyl emission bands 17 p2849 A67-32957

Hydrogen distribution in upper atmosphere and geocorona, relating H-alpha emission increase to solar activity decrease 17 p2849 A67-32961

Mesosphere and lower thermosphere density variations related to solar cycle obtained, using rocket grenades 19 p3219 A67-35231

Solar gravitational effect on earth seismic activity, showing relation between annual variations and earth-sun radius 19 p3221 A67-35430

Iranian ionospheric observations, giving monthly median values of vertical-incidence data and critical frequency graphs 19 p3224 A67-35489

Quasi-biennial oscillation in ozone in northern Hemisphere harmonically analyzed 19 p3225 A67-35921

Annual and diurnal variations of geomagnetic anomaly in Australasian Zone during sunspot minimum, stressing role in transequatorial propagation of VHF radio signals 22 p3759 A67-39473

Cosmic ray yearly variation during solar activity cycle, discussing flare and acceleration mechanisms, stable coronal condensation and sunspot magnetic field 22 p3874 A67-40045

Solar active formations relation to annual cosmic ray variations, discussing spot group, chromospheric flares and calcium flocculi area distributions 23 p4059 A67-41132

Semiannual variations of magnetic activity 24 p4149 A67-42132

ANNULAR FLOW

Azimuthal current effect on electrical efficiency of MHD vortex generator 01 p0120 A67-10174

MHD rotation of conducting viscoplastic fluid between two coaxial cylinders in crossed fields 01 p0120 A67-10180

Stability of inviscid flows of perfectly conducting fluid between two concentric circular cylinders with axial volume current distribution 03 p0403 A67-13732

Turbulent annular airflows in turbulent film lubrication of high speed bearings [ASME PAPER 66-LUB-14] 03 p0403 A67-13755

Effects of horizontal shear and aspect ratio change on baroclinic instability in rotating annulus heated differentially 03 p0463 A67-13932

Temperature and stress distributions in annulus partially filled with cold fluid 03 p0531 A67-14363

Quantity of separated liquid deposited on wall of rectangular channel from turbulent air-water dispersed annular flow, calculating liquid flow rate 04 p0602 A67-14641

Motion induced by electric and magnetic fields on initially static fluid between two concentric tubes [ASME PAPER 66-WA/FE-35] 04 p0668 A67-15366

Tests for measuring heat-transfer coefficients in horizontal annulus filled with gas and visualization of flow 04 p0732 A67-15829

Lie series formalism applied to solution of Bessel equation describing behavior of laminary oscillating MHD fluid 05 p0854 A67-16989

Hydromagnetic stability of dissipative flow between rotating permeable cylinders 06 p1040 A67-18129

Dimensional analysis of turbulent MHD flow in interspace between two coaxial cylinders in rotating circular magnetic field and similarity criteria for EM power

- losses 06 p1042 A67-18548
Film boiling of saturated nitrogen flowing upward in vertical heated tube, noting annular-flow regime change to vapor matrix [ASME PAPER 65WA/HT-26]
- Axisymmetric thermal convection in rotating fluid annulus for various Peclet numbers, obtaining mean thermal structure and heat transfer 08 p1323 A67-21387
Electric arc model in longitudinal gas flow through annular gap between rod cathode and cylindrical anode 09 p1546 A67-22314
Vortex stabilized electrodeless annular discharge in argon at atmospheric pressure, describing experimental equipment, procedure and results 09 p1547 A67-22319
Convective heat transfer in fluid between concentric cylinders with inner heated cylinder rotating and outer cooled cylinder stationary 20 p3543 A67-36422
Turbulent fluid flow velocity and temperature fields in annular and plane gaps calculated by integral approximation for turbulent viscosity and heat conduction coefficients 24 p4142 A67-42213
Incompressible viscous fluid rotary turbulent flow microstructure between rotating cylinders, analyzing centrifugal force effects on turbulent heat transfer processes 24 p4142 A67-42214
Temperature distribution in homogeneous eccentric annular layer with constant internal heat generation 24 p4254 A67-42286
- ANNULAR JET**
Interaction between two rectangular parallel jets analyzed using heat conduction theory 07 p1167 A67-19151
- ANNULAR NOZZLE**
Air cushion vehicle design, calculating annular nozzle, air channel optimum parameters, power capacity, aerodynamic characteristics, etc 02 p0179 A67-12437
Correlation of local heat transfer and friction coefficients for subsonic turbulent flow of air through high temperature annulus 06 p1117 A67-18386
Approximate analysis of subsonic compressible flow in annular nozzle of short duct fan engines and inner wall curvature effect on pressure distributions 06 p0944 A67-18871
Local heat transfer in water flow in horizontal annular tube, estimating local longitudinal and circumferential variations in Nusselt number at tube wall as function of Reynolds and Rayleigh numbers 11 p1881 A67-24025
Turbofan jet propulsion system reversed-thrust, discussing momentum net change, external drags, clamshell and annular targets and cascade reversers [AIAA PAPER 67-418] 18 p2982 A67-33905
- ANNULAR PLATE**
Stress concentration in annular rotor with notch /or crack/ on inner surface, using integral equation 01 p0159 A67-10276
Simplified equations for equilibrium problem in large deflection theory for thin annular plates 08 p1414 A67-20348
Scalar wave equation of annular membrane for origin symmetric motion and arbitrary initial and boundary conditions 08 p1415 A67-20476
Inviscid flow characterized by annular elliptical region between shock wave and ducted body calculated by integral relation method, noting contraction coefficient values 10 p1591 A67-23045
Electrical simulation of finite difference calculations of problems of bending and natural oscillations of circular, annular and sector plates 12 p2032 A67-25968
Differential equations for stressed thin orthotropic plates of variable thickness derived and solved in cylindrical coordinates 20 p3539 A67-36919
- ANODE**
SA ANION
SA CATHODE
Design method for electron gun with specified anode shape 07 p1154 A67-19655
Anodic behavior of GaAs single crystals at increased current densities in alkaline and acidic solutions, discussing etch tunnels 11 p1848 A67-24743
Formation of hydride zinc film on titanium activated for deposition of galvanic coating 14 p2336 A67-27868
Anode emission influence on thermionic diode energy converter maximum efficiency 14 p2247 A67-28033
Water cooled copper anode operation compared to porous graphite transpiration cooled annular anode to study energy transfer in wall stabilized cascaded arc 19 p3279 A67-35141
Hollow anode glow discharge noting motion of ions and electrons in beam configuration 19 p3195 A67-35598
Anode heat transfer in MPD arc, discussing configurations and thrusters [AIAA PAPER 67-673] 21 p3691 A67-38706
- ANOMALY**
SA GEOMAGNETIC ANOMALY
SA MAGNETIC ANOMALY
Anomalous photocurrent generation in transistors, noting carrier generation and transport processes 04 p0685 A67-15696
Anomalous photovoltaic effect in semiconductor Ge, Si, CdTe and GaAs thin films due to photodiffusion and microtransitions 04 p0685 A67-15758
Anomalous transport phenomena in ring discharge studied for instability and losses due to noise, using mc RF oscillator [AROD-6398-2] 11 p1831 A67-24010
Revised ionization-equilibrium equation to obtain criterion for presence of winter anomaly in E layer 14 p2307 A67-27912
Diamant launcher transmitter characteristics noting anomalies during first two firings 21 p3581 A67-38226
- ANOXIA**
Potato radiation resistivity improvement in conditions of anoxia 13 p2058 A67-26755
- ANTARCTICA**
Effects of AZA and PCA on radio wave propagation in Antarctic, noting reliability and radiation power requirements 07 p1143 A67-19692
Cosmic ray nucleonic component in Antarctic zone measured by neutron monitor, standardized and related to solar activity 10 p1699 A67-22862
Ionospheric measurements at Antarctic station in south radiation anomaly region showing precipitated electron flux associated with ionospheric disturbances 12 p1934 A67-25778
Diurnal, seasonal and geographic variations of frequency of spread-F occurrence over Antarctica [AGARDOGRAPH 95] 15 p2481 A67-30282
Evidence regarding possibility of midwinter stratospheric warmings in Southern Hemisphere 17 p2880 A67-32553
Surface air radioactivity and ozone measurements in Antarctica reveal fission product yearly oscillation 20 p3429 A67-36871
- ANTARES MISSILE**
Antares triaxial tracking camera noting mounting, electronic and optical systems and performance techniques 19 p3229 A67-35267
- ANTENNA**
SA AIRCRAFT ANTENNA
SA CASSEGRAIN ANTENNA
SA DIPOLE ANTENNA
SA DIRECTIONAL ANTENNA
SA HELICAL ANTENNA
SA HORN ANTENNA
SA LENS ANTENNA
SA LOG PERIODIC ANTENNA
SA LOG SPIRAL ANTENNA
SA LOOP ANTENNA
SA MICROWAVE ANTENNA
SA MISSILE ANTENNA
SA MONOPULSE ANTENNA
SA OMNIDIRECTIONAL ANTENNA
SA RADAR ANTENNA
SA RADIO ANTENNA
SA RHOMBIC ANTENNA
SA SELF-ERECTING ANTENNA
SA SHUNT
SA SLOT ANTENNA
SA SLOTTED ANTENNA
SA SPIRAL ANTENNA
SA STEERABLE ANTENNA
SA TRACKING ANTENNA
SA TURNSTILE ANTENNA
SA WAVEGUIDE ANTENNA
SA YAGI ANTENNA
Signal excitation in negatively charged antenna rod in effect of unfocused laser beam 01 p0091 A67-10835
Resolving power of circular-aperture antenna affected by plane turbulent layer between antenna and point of observation 02 p0210 A67-11570
Imperfectly conducting cylindrical transmitting antenna design, examining contribution by ohmic resistance to distribution of current and impedance 02 p0210 A67-11590
Complex wave number, current distribution, admittance and radiating efficiency of cylindrical antennas made of imperfect conductors evaluated numerically 02 p0210 A67-11591
Large multiplate steerable-beam antenna built by using independent reflectors that redirect energy from desired direction to focus 02 p0210 A67-11592
Interstices in multiplate antennas, determining gap and shadowing losses, receiving cross section variations and radiation pattern 02 p0210 A67-11593
Driving-point impedance and current for long resonant cylindrical antennas 02 p0212 A67-11605
Shaped-beam pattern attitude-stabilized satellite communications antenna as improvement over conventional horn antenna 02 p0212 A67-11606
Flexible antenna effect on stability of spin-stabilized satellite in viscous damped oscillator model 02 p0330 A67-11927
Large monolithic radome antenna fabrication 02 p0215 A67-11980
Optimum control of antenna pointing direction and space vehicle height subject to random disturbance 02 p0219 A67-12147
Dynamics of spin-stabilized satellite with nonrigid extendible antennas, noting effects of terrestrial magnetic and gravitational field 02 p0333 A67-12309
Statistical analysis of sidelobe region of offset-feed parabolic reflector antenna 03 p0382 A67-13673
Book on antennas covering electromagnetic waves, transmission line, radiators, arrays, etc 03 p0382 A67-13713
Transmission line antenna tunable over greater than octave bandwidth 03 p0384 A67-13847
Impedance of finite insulated cylindrical antenna in cold plasma with longitudinal magnetic field 03 p0385 A67-13850
Scatterers identification by measuring separations between antenna grating lobes, signal direction and difference in levels of maxima and minima 03 p0370 A67-13856
Antenna aperture size effect on tropospheric phase-of-arrival fluctuations determined by theoretical considerations of atmospheric turbulence 03 p0385 A67-13864
Erectable antenna design for S-band communications between lunar surface and earth during lunar stay portion of Apollo mission 04 p0569 A67-14501
Transmitter modulation choice for nonconventional radar system, taking into account scanning antenna modulation effects 04 p0572 A67-15029
Monte Carlo technique in predicting antenna performance 05 p0775 A67-16969
Implementation of electronically despun satellite antenna system, considering limits of impracticability because of excessive weight, control power, etc [AIAA PAPER 66-325] 06 p0967 A67-17686
Input resistance of short filamental antenna in warm plasma according to kinetic theory and hydrodynamic equations 07 p1151 A67-19445
Field strength measurements in multipath field using linear and circular probing 07 p1142 A67-19448
Digital, matrix and intermediate frequency scanning 07 p1152 A67-19547
Time vs space in antenna theory and frequency variation 07 p1152 A67-19548
Phase variation dependence at receiver output on polarization of wave incident on antenna of phase measuring system 07 p1144 A67-19694
Impedance test performed with plane dielectric antenna of various configurations 07 p1158 A67-20295
Millimeter wave satellite communications, considering propagation, orbital and system design parameters, antenna pointing and satellite and ground equipment 08 p1292 A67-20671
Antennas for HF radio communications integrated with shipboard structures 08 p1301 A67-20772
Adaptive antenna for ground reception of wideband RF signals in space communications systems 08 p1301 A67-20776
Inertial forces on straight light appendage used as antenna on artificial satellite 08 p1410 A67-20786

- Radio telescope antenna phase errors due to structural rigidity and fabrication accuracy 08 p1306 A67-21346
- Fluctuating effective gain of rocket telemetry links determined from signal strength data of Black Brant sounding rockets 09 p1463 A67-21829
- Admittance of circumferential gap in infinite cylindrical antenna covered by set of coaxial dielectric or plasma layers, noting excited metal cylinder 09 p1481 A67-22447
- Impedance of strip antenna embedded in dielectric layer overlain by cold plasma, considering reflection coefficient and static magnetic field effect 11 p1763 A67-24305
- Antenna in interplanetary plasma, noting fluctuation noise in exosphere and radiation impedance when exposed to solar wind 14 p2279 A67-27856
- Noncircular and asymmetrical aperture radio telescopes, considering cylindrical paraboloid, Pulkova and Kraus type Nancy telescopes 14 p2284 A67-28431
- Spherical reflector radio telescope design, performance and application, describing parameters of Tokyo, Lockheed, Nancy and Arecibo 14 p2284 A67-28432
- Stability in electronic equipment 14 p2285 A67-28438
- Radio telescope antenna phase errors due to structural rigidity and fabrication accuracy 17 p2822 A67-31942
- Central station construction for German ground-station system for research satellites 18 p3021 A67-34607
- Motion rate of pendulum with two antennas moving in electromagnetic field with standing wave measured by correlation meter 21 p3631 A67-39115
- Weather effects on exposed and enclosed earth based satellite communications antenna systems, discussing performance characteristics under various meteorological conditions 22 p3763 A67-40408
- Cylindrical antenna admittance taking into account antenna to coaxial line junction geometry, using magnetic current mathematical model 23 p3980 A67-41205
- Electrically thick cylindrical antenna driven by delta function generator, discussing numerical solutions to two different mathematical models 23 p3980 A67-41206
- Shielding factors for electrostatic aerials 24 p4129 A67-41973
- ANTENNA ARRAY**
- SA LINEAR ARRAY**
- Gain optimization for antenna arrays for determination of maximum expected gain and required excitations when finding random errors in amplitudes and phases of excitations 01 p0032 A67-10005
- Optimization of directive gain and SNR of arbitrary antenna array with or without constraint on array Q-factor 01 p0035 A67-10431
- Currents in elements of linear uniformly spaced antenna array when mutual impedance between neighboring elements is taken into account 01 p0041 A67-11326
- Planar slot array with four independent beams, discussing special design problems and effect of dimensional tolerances on port isolation 02 p0211 A67-11594
- Directive gain and impedance calculated for ring array of antennas that concentrate radiated power in plane of ring and are omnidirectional 02 p0211 A67-11595
- Computer program for optimizing network components and evaluation of improvement of planar array match by compensation through contiguous element coupling 02 p0211 A67-11597
- Nonuniformly spaced planar arrays in which elements are located on lattice derivable from conformal mapping of uniform lattice 02 p0211 A67-11599
- Multielement scanning feed system for parabolic cylindrical antenna by controlling phase and amplitude of signal radiating from each element 02 p0211 A67-11600
- Variational expression for dominant mode coupling coefficients between elements of infinite array 02 p0212 A67-11604
- Approximation theory of optimum performance of nonuniformly spaced arrays 02 p0212 A67-11613
- Modal analysis of mutual coupling effects of triangular grid array of waveguide radiators having nonzero wall thickness 02 p0212 A67-11614
- Radiation pattern and standing wave ratio for antenna system consisting of paraboloidal cylindrical reflector and frequency-independent feed 02 p0213 A67-11644
- Mills cross arrays applied to radar systems, especially when target signals vary and great angular accuracy is needed 02 p0216 A67-12068
- Elevation angle of arrival of ionospherically propagated HF radio signals determined with circular antenna arrays 02 p0217 A67-12088
- Synthesis and sidelobe reduction, of unequally spaced antenna arrays with uniform or stepped amplitude distribution, achieving desirable radiation characteristics 02 p0217 A67-12095
- Spaced antenna technique for determining drift and anisotropy of equatorial E and F region irregularities 03 p0407 A67-12833
- Arbitrary reflector array of Van Atta type analyzed for dipole elements 03 p0384 A67-13845
- Grating-lobe series for impedance variation with phasing in infinite planar array of elements with periodic spacing 03 p0384 A67-13848
- VHF antenna proposed as working gain standard, determining antenna gain by two identical antenna method 03 p0385 A67-13859
- Amplitudes and phases of element weighting factors in linear processor determined in order to maximize SNR of array receiving random signal in noisy environment 03 p0385 A67-13860
- Signal distortion introduced by series-fed array compensated in presence of noise by prefilter and postfilter 04 p0570 A67-14874
- Electronic scanning of antenna beams, reducing feed complexity of large phased array by grouping of elements, tapering and array thinning 04 p0581 A67-15050
- Fast switching microwave phase shifters for high power array radars, describing drive control techniques 04 p0581 A67-15053
- Statistical parameters of linear antenna arrays after removal of emitters 04 p0583 A67-15149
- Mean and mean square directivity factor of antenna array in presence of phase and amplitude distortions 04 p0583 A67-15164
- Stationary antenna arrays for target detection and tracking noting radiation patterns, radar systems, etc 04 p0654 A67-15538
- Simultaneous radiation of center-fed slotted rectangular waveguide array antenna for monopulse tracking radar 04 p0590 A67-15905
- Statistical characteristics of radiation pattern of antenna array with randomly positioned radiators determined from density distribution of radiators 05 p0775 A67-16963
- Multielement antenna scanning grid-phasing method having random function distribution at aperture 05 p0776 A67-17159
- Synphase antenna with broadband active reflector 05 p0778 A67-17394
- Electromagnetic noise effect on aircraft examined, using fuselage mounted monitoring antennas 05 p0768 A67-17533
- Radio pulses from air shower detection, noting correlation between shower arrival direction and antenna pattern and shower size and pulse frequency 06 p1078 A67-17554
- Angular resolving power limitations for linear arrays of equispaced elements receiving EM or acoustic waves, in cases of mechanical rotation and electron beam scanning 06 p0966 A67-17576
- Electronically despun switched antenna using variable phase shifters to control phase of incident power to circular array of elements 06 p0967 A67-17684
- Electronic self-steering techniques applied to satellite communications system with high gain antennas, noting transdirective array and self-phasing array [AIAA PAPER 66-326] 06 p0967 A67-17690
- Lightweight vertical multiwire antennas for HF range, describing construction and performance 06 p0973 A67-19050
- Finite scattering matrix for plane wave excited infinite array in relating array number and active element properties 07 p1151 A67-19442
- Microwave scanning antennas, Volume 3, Array systems 07 p1151 A67-19544
- Feeding and phase scanning in various antenna arrays 07 p1152 A67-19545
- Self-phased arrays and remote phase synchronization techniques 07 p1152 A67-19549
- Microwave scanning antennas, Volume 2, Array theory and practice 07 p1154 A67-19780
- Properties of antenna systems composed of individual arrays noting effect of spatial distribution, orientation, etc 07 p1154 A67-19781
- Properties of real radiators and effects of mutual coupling between pairs noting impedance, pattern and polarization characteristics 07 p1154 A67-19782
- Behavior of infinite arrays including radiation pattern approach yielding expressions for gain and periodic structure approach yielding input impedance variation with scan angle 07 p1154 A67-19783
- Phase compensation technique for signals received at widely spaced antennas and processed at central location 07 p1155 A67-19876
- Angular resolution of plane circular array with multiple targets 07 p1145 A67-19881
- Antenna systems and equipment providing ICAO Category I-III performance for ILS, analyzing configurations for localizer, markers, etc, calculating glide slope course bends 08 p1351 A67-20696
- Power pattern synthesized as product of two individual patterns produced from single linear array, obtaining formula for array element weighting coefficients 09 p1470 A67-21590
- Gaussian errors effects on antenna pattern of any array of elements, describing errors in terms of rms amplitude and phase errors at each element 09 p1470 A67-21591
- Eagle antenna parameters for planar and three-dimensional beam rocking 09 p1472 A67-21956
- Direction finding errors of method of instantaneous amplitude comparison in elliptically polarized antenna arrays 09 p1473 A67-21960
- Illinois 400-ft radio telescope with compromised branching system and traveling wave system as transmission line 09 p1486 A67-22443
- Basic design differences illustrating paraboloidal reflector variations, noting factors contributing to or detracting from antenna efficiency 10 p1613 A67-23413
- Spaced antenna reception by quadratic addition of signals providing efficient operation at various statistical characteristics of radio channel 10 p1607 A67-23447
- Steady state dynamic properties of large spinning net-like antenna suitable for radio signal reception from space 10 p1727 A67-23753
- Field statistics of linear in-phase antenna array in presence of periodically correlated phase errors 11 p1757 A67-23912
- Phased array antenna impedance matched for all scan angles assuming connecting circuits are lossless 11 p1758 A67-23975
- Amplitude control of wind induced oscillation in antenna system through cross section shape [ASME PAPER 67-VIBR-39] 11 p1777 A67-24194
- Planar antenna array with randomly spaced elements experimentally investigated, using holey plate technique 11 p1761 A67-24282
- Stabilized cross correlation radiometer for use at decametric wavelength, using two feedback loops controlling four noise diodes 11 p1762 A67-24288
- Transmission line approach for determining input admittance of slotted antenna array covered by dielectric sheet 11 p1762 A67-24293
- Simulator measurements of active impedance of phased array antenna element at two different scan angles by single element in waveguide 11 p1763 A67-24299
- Atmospheric distortion effect on signal reception by large dimensional antennas, obtaining numerical estimates for various parameters 11 p1753 A67-24439
- Antenna aperture and array effect on characteristics and performance of radio direction finder 11 p1794 A67-25005
- Parametric double pumping mixer of down converter type for multiple-beam low noise receiving antenna 12 p1913 A67-25302
- Gain bandwidth relations in H-plane array

of log periodic dipole elements 12 p1914 A67-25426

Book on radioastronomical methods of antenna measurements covering physics of extraterrestrial sources and receiving equipment characteristics 12 p1915 A67-25842

Determinants of electronically steerable antenna arrays 12 p1917 A67-26158

Design of broadband steerable Wullenweber antenna arrays allowing HF element rings to be within LF rings 13 p2074 A67-26257

U.S. communication satellites design and transmission, including antenna types offering interference-free reception 13 p2066 A67-26334

Apollo spacecraft-earth two-way communications provided by vehicle-mounted variable gain antenna array, automatically tracking ground-transmitted signals 13 p2068 A67-26802

Two-mirror antenna with automatic phase error control, noting experimental model correlation 13 p2080 A67-27024

Range characteristics of antenna arrays composed of identical transmitters located along circumferential arc and producing pencil beam 13 p2080 A67-27027

Rectangular guide receiver passband, estimating boundary effect, noting data characterizing interrelation of arrayed transmitters 13 p2069 A67-27032

Interconnection of transmitters with no noninteracting elements reduces input traveling wave ratio of antenna arrays with power supply systems 13 p2080 A67-27033

Discrete recording of radiation patterns of antenna arrays 13 p2080 A67-27035

Three-dimensional multielement transponder array designed to give directional replies toward source of interrogating signals 13 p2071 A67-27404

Maximization of directive gain for circular and elliptical arrays 13 p2082 A67-27406

Phased-array microwave antenna system for scanning simultaneous targets whose distance and direction are changing rapidly 13 p2083 A67-27566

Induced impedance dependence on scanning angle and array parameters calculated, analyzing edge effects 14 p2279 A67-28005

Earth rotation synthesis using arrays of small antennas for better low declination sensitivity 14 p2284 A67-28434

Optimum spacing arrangement for 1100101 array of four antennas in straight line with spectral sensitivity in switched and unswitched cases 14 p2284 A67-28435

Y-shape, T-shape and hollow circle arrays, considering u-v plane coverage, number of antenna elements, etc 14 p2285 A67-28436

Large apertures and arrays for radio telescopes 14 p2285 A67-28449

Signal processing in antennas with coupling elements between circuit and space fields 14 p2285 A67-28450

Method of radiation pattern synthesis for equally and unequally spaced arrays 14 p2285 A67-28451

VHF antenna array, electronically despun, designed for spin-stabilized synchronous-altitude communications 14 p2288 A67-28693

Directivity factor of linear antenna array with Chebyshev radiation 14 p2289 A67-28862

RCA papers on defense electronic products including search radar, superconductor devices, data and spacecraft communications, speech recognition 14 p2274 A67-28910

Spacecraft high aperture efficiency small scan communication antenna, noting radar installation 14 p2289 A67-28911

Statistical parameters of linear antenna arrays after removal of emitters 15 p2443 A67-29336

Mean and mean square directivity factor of antenna array in presence of phase and amplitude distortions 15 p2443 A67-29351

Phase lock techniques applied to microwave antenna arrays noting problems, advantages, properties, etc 15 p2451 A67-29922

Omnidirectional radiation pattern for S-band telemetry on rockets more than 1/2 ft in diameter by small electrical separation of antennas 15 p2454 A67-30116

[AAS PAPER 67-51] Possible directional pattern forms

obtainable for single-ring circular arrays, using Fourier harmonic analysis 15 p2454 A67-30138

Deflections and stresses of paraboloidal shells of revolutions under gravity loads for applications to paraboloidal reflector antenna construction 16 p2763 A67-30678

Signal phase acquisition techniques for arrays of large aperture steerable antennas discussing SNR role 16 p2638 A67-31264

Gain maximization for arbitrary antenna arrays with excitation amplitude and phase and element positions are subjected to random errors 16 p2638 A67-31336

Hemisphere coverage by n planar phased arrays arranged in pyramids or pyramidal frustra solved by transformations leading to analytical solution 16 p2638 A67-31337

Necessity of incremental phase shift during IF time delay steering of antenna array main beam 16 p2639 A67-31354

Correcting feed for Arecibo Ionospheric Observatory reflector noting antenna gain 16 p2639 A67-31359

Variation of radiation pattern of array of two traveling-wave V-antennas and use as spacecraft antenna 16 p2639 A67-31360

Concentric ring array application to space tapering of planar arrays, noting obtainable frequency ranges and scan angles 16 p2640 A67-31526

Digital pulse compression radar receiver with digital-pulse compression advantages and disadvantages, noting target acquisition, range tracking and antenna scanning system 16 p2630 A67-31738

Systematic boresight and off-boresight tracking errors in planar monopulse phased rectangular arrays produced by analog phase shifters with nonlinear transfer characteristics 17 p2825 A67-32617

East-west parabolic reflector array for design of high resolution multielement interferometer for solar noise observations 17 p2864 A67-33402

Current distribution and element spacings for beam efficiency and gain optimization of antenna array 18 p3012 A67-34429

Lagrange interpolation pattern synthesis technique using moment criterion for optimum pattern approximation by nonuniform antenna array 18 p3012 A67-34430

Radant, integrated radome antenna system incorporating three trapezoidal-tooth log periodic radiating elements 18 p3016 A67-34598

Antenna array simulator using acoustic waves in water to simulate electromagnetic propagation 20 p3397 A67-36580

Eagle antenna parameters for planar and three-dimensional beam rocking 20 p3400 A67-37186

Direction finding errors of method of instantaneous amplitude comparison in elliptically polarized antenna arrays 20 p3400 A67-37190

Chilbolton 25 m steerable antenna for radio wave propagation research 20 p3400 A67-37203

Soviet papers on wideband cross-shaped radio telescope and radio astronomy studies 20 p3402 A67-37504

Spaced antenna array radiation pattern frequency control analyzed for relationship between arrival angle and heterodyne frequency 20 p3402 A67-37506

Multiply-tuned antenna array operating over certain frequency range through electric beam shifting 20 p3403 A67-37507

Remote preamplifiers in multielement antenna arrays of radio telescopes operating at meter wavelengths, noting noise temperature effect 20 p3403 A67-37508

Correlation type arrays resolving power noting role of averaging processes 20 p3403 A67-37509

Multielement correlation type arrays response to several point sources studied by extending spectral method 20 p3403 A67-37510

Despun antenna system for satellite stabilized by rotation around axis perpendicular to orbital plane 21 p3591 A67-38204

Telemetering antenna of instrument container of D-1 satellites 21 p3592 A67-38218

Antenna array radiation pattern in isotropic linear medium by radiation pattern synthesis in moving medium 21 p3598 A67-38607

Receiving system for telemetering with

orientable antenna error-measuring signal receiver and servo loops 21 p3599 A67-38645

High gain directional antenna networks for space communications 21 p3600 A67-38670

Field statistics of linear in-phase antenna array in presence of periodically correlated phase errors 21 p3600 A67-38940

Synthesis of nonuniformly spaced antenna arrays using lambda functions to reduce space factor and prescribed radiation pattern 21 p3602 A67-39071

Active impedance and current distribution in infinite, planar and collinear arrays of cylindrical antennas, deriving Fourier series for antenna current 22 p3769 A67-39629

Distributed power generation for radar and communications covering cost comparisons, antenna subsystems and reliability of solid state devices 22 p3761 A67-39861

S-band rectangular digital phase shifter combining advantages of waveguide design with compactness of strip transmission line structure 22 p3773 A67-39909

Parallel plate antenna for LF transmission and reception in conducting medium 22 p3773 A67-40307

Designs and performance of communications satellites, discussing long life, cooling, efficiency, larger future satellites, antennas and arrays 22 p3763 A67-40337

Radome antenna systems design utilizing dielectric structure applicable in aircraft, spacecraft and missile systems 22 p3775 A67-40468

Omnidirectional double slot array of thin X-band rectangular waveguides, noting design for slot conductance and power handling capacity 23 p3977 A67-40699

Very large array /VLA/ of radio telescopes designed based on Ryle aperture synthesis principle, consisting of parabolic antennas and used for radio maps 23 p3978 A67-40798

Radiation from infinite aperiodic array of parallel plate waveguides, using Wiener-Hopf technique for edge effect evaluation 23 p3978 A67-40825

Antenna linear array design with limited amplitude tapering, showing desirable pattern characteristics in partially uniform array 23 p3978 A67-40827

Radio telescope design, considering sensitivity and resolving power, discussing classical optics and multiplicative antenna based telescope 23 p3980 A67-41081

Two-antenna interferometer baseline observations and scanning interferometer characteristics, determining source coordinate, and solar radiation center 24 p4129 A67-42227

Array antenna directive pattern scanning utilizing difference in phase lead between heterodyne and converted signals at feeder 24 p4130 A67-42234

ANTENNA COUPLER

SA ELECTROMAGNETISM

SA ENERGY TRANSFER

SA IMPEDANCE MATCHING

SA TRANSMISSION LINE

Variational expression for dominant mode coupling coefficients between elements of infinite array 02 p0212 A67-11604

Experimental aperture-to-medium coupling loss between one and two large antennas 02 p0213 A67-11620

Discrepancies between Boithias and other theories on troposcatter antenna-to-medium coupling loss, showing graph of path gain loss 02 p0213 A67-11621

TE mode-selective coaxial directional coupler with coaxial primary line and rectangular waveguide as secondary line 02 p0214 A67-11650

Generalized method of calculating multielement antenna and feeder system 10 p1611 A67-22981

Triode version of active LF directional coupler compared to passive coupler 13 p2081 A67-27198

External mutual coupling of rectangular waveguide-slot emitters, deriving coefficient of reflection 17 p2826 A67-32683

Squinted, sum and difference radiation patterns interrelationships for amplitude monopulse antennas with impedance mismatch and mutual coupling between feeds 19 p3197 A67-35824

Electromagnetic interference reduction between antennas on space

vehicles 20 p3405 A67-37642
 Scattering matrix method, determining power transfer between closely coupled antennas in complex environment 20 p3405 A67-37644
 Transient response and current distribution of thin vertical antenna coupled to pulse generator by electric network, determining radiation field 21 p3590 A67-38117
 Coupler type bend for double layer pillbox antennas, discussing measurements for performance characteristics 21 p3597 A67-38565

ANTENNA FIELD
 Variation of antenna amplification ratio with distance as function of phase error at antenna aperture with exciter off-focus as error source 01 p0035 A67-10392
 Broadside log-periodic antenna, noting lab dimensions of models, power patterns and input impedance 01 p0036 A67-10472
 Taylor line source distributions as reference set of antenna transfer functions 01 p0023 A67-10481
 Fill factor of radar beams reflected from meteorological targets of various forms derived, taking antenna radiation pattern into account 01 p0025 A67-10790
 Ultrashort antenna with conical spiral, noting effect of negative reactance component of impedance [ONERA-TP-373] 01 p0039 A67-10948
 Amplification factor of circular polarization antennas calculated by mirror image method 02 p0209 A67-11505
 Asymmetrically truncated parabolic antenna in three-dimensional problem, noting effect of shifting 02 p0209 A67-11506
 Statistical communication theory of antenna response to complex partially polarized nonisotropic random radio wave processes 02 p0191 A67-11588
 Null-free antenna radiation pattern shown to contain all axial ratios of elliptical polarization 02 p0211 A67-11598
 Choke slots or corrugated structure in walls of horn antenna for reducing sidelobe and backlobe level by controlling illumination of E-plane edge 02 p0211 A67-11601
 Radiation patterns and impedance plots of sleeve antenna over band with frequency ratio of 4 to 1 02 p0212 A67-11607
 Point boundary value matching method calculation of current distribution in thin linear antenna 02 p0212 A67-11610
 Symmetrical radiation feed patterns which are consequence of specified form of hybrid mode fields as disclosed by focal plane analysis 02 p0213 A67-11615
 Linearly polarized horn antenna with same power pattern in all planes through axis made from synthetic material for which boundary conditions on E and H planes are same 02 p0213 A67-11616
 Low noise receivers to achieve high sensitivity and accurate cross correlation measurement of antenna patterns, using radio star sources 02 p0213 A67-11617
 Forced convection effects on VHF CW and X-band antenna voltage breakdowns in wind tunnel experiments, using cold nonconducting gas 02 p0213 A67-11647
 Lambda 1 distribution in circular aperture energizer for low noise parabolic antennas 02 p0214 A67-11796
 Polarization pattern dependence on phase-amplitude distribution of field at microwave antenna aperture 02 p0214 A67-11905
 Spatial radiation patterns of curved high-directivity antenna array as function of amplitude distribution and directivity 02 p0214 A67-11906
 Cross polarized component of radiation from spherical antenna produced by anisotropic plasma sheath 02 p0220 A67-12193
 High resolution LF observations of time stationary discrete sources and background continuum distribution, using two satellites in interferometric mode [AIAA PAPER 66-886] 02 p0221 A67-12265
 Communication relay to aircraft by satellite, discussing wave propagation characteristics, standing wave pattern, signal fading rates, etc 02 p0205 A67-12306
 Flying target detection and tracking with fixed antennas having radiation pattern scanning and multibeam characteristics 02 p0205 A67-12730

Asymptotic evaluation for k approaching infinity of antenna field emerging from currents induced on surface of reflector with incident spherical wave 02 p0223 A67-12796
 Stationary phase technique synthesis of continuous linear antenna and integral equation for determining radiation pattern 03 p0378 A67-13284
 Vector potential representation of planar logarithmic spiral antenna field 03 p0378 A67-13285
 Antenna design and measurement technology in antenna laboratory as applied to aircraft antennas, considering types and configurations 03 p0383 A67-13795
 Aerodisc antenna design and electric characteristics 03 p0384 A67-13829
 Stored energy of planar aperture radiating into lossless homogeneous medium 03 p0384 A67-13843
 Grating-lobe series for impedance variation with phasing in infinite planar array of elements with periodic spacing 03 p0384 A67-13848
 Impedance of finite insulated antenna in cold plasma with perpendicular magnetic field 03 p0385 A67-13851
 Fields of horizontal dipole over stratified anisotropic half-space 03 p0370 A67-13858
 Anisotropic medium capacitance calculation, using method based on point-charge field behavior analysis in isotropic medium, for biconical antenna 03 p0371 A67-13866
 Equivalent linear antenna substitution for antenna with plane aperture in statistical analysis of antennas 03 p0386 A67-13958
 Telemetry design factors, discussing interference problems, antenna design, oscillator stability, preamplifiers, etc 03 p0372 A67-14120
 Beam scanning and beam forming techniques for phased-array radar, noting frequency and phase scan methods 04 p0596 A67-15049
 Antenna with limited excited region, discussing emitter design with prescribed radiation pattern and near field behavior 04 p0583 A67-15148
 Elliptically polarized wave reception by antenna, itself elliptically polarized, for use in interferometry problems, noting relation to complex vector 04 p0658 A67-15626
 Antenna feed eliminating compromise between antenna illumination and spillover efficiencies by placing dielectric guiding structures between primary feed and reflector 04 p0590 A67-15903
 Fourier transform synthesis of aperture distributions producing sector beam patterns 04 p0590 A67-15907
 Rotating interferometer measuring spread and coherence ratio of scattered radio wave 05 p0760 A67-15997
 Angle-of-arrival measurements over troposcatter path by simultaneous reception in angle diversity, using antenna beams 05 p0760 A67-15998
 Radiation resistance and modes of oriented electric dipole in loss-free magnetoplasma 05 p0853 A67-16848
 Antenna synthesis for wide band radiation reception using Fredholm integral equation 05 p0774 A67-16912
 Radiation pattern of linear nonequidistant antenna array 05 p0775 A67-16964
 Tuning of lens and mirror antennas with circularly polarized radiation 05 p0766 A67-17239
 Factors governing amplitudes of reradiated signals from tall obstacles distorting VHF and UHF transmission 05 p0766 A67-17296
 Large ground antenna performance with solar noise jamming 05 p0780 A67-17524
 Algorithm for locating ambiguous lobes in radiation pattern of large circular array 05 p0781 A67-17535
 Simple secondary radar antenna with fan-shaped beam for monopulse operation 06 p0967 A67-17616
 Fading and multipath propagation mechanism for communication links involving satellites and aircraft with antenna beams, assuming fading models and estimating margins required for FSK teletype transmission 06 p0960 A67-17673
 Equations and curves defining pattern loss for fan-and pencil-beam arrays, discussing radar efficiency factor 06 p0968 A67-17964
 Cloud melting zone, noting increased

antenna temperature for radiation trapping between cloud layer and ground [AIAA PAPER 67-188] 06 p1026 A67-18491
 Optical systems and holography in reconstruction of SHF antenna radiation patterns from field measurements in Fresnel zone 07 p1183 A67-19143
 Thin plasma effect on admittance of aperture antenna in infinite conducting plane for various modes 07 p1151 A67-19447
 Frequency and phase scanning for pencil-shaped beam antenna 07 p1152 A67-19546
 Directional radiation pattern for circular arc antenna, using three-step method in which current distribution is treated as truncated Fourier series 07 p1152 A67-19550
 Distribution function of modulus of directivity characteristic of antenna grid shown as modified Rayleigh distribution 07 p1143 A67-19596
 Control of polarization of radiation field of waveguide-slot antenna emitter 07 p1153 A67-19598
 Radiation enhancement and resonance scattering due to plasma sheath between spherical antenna and surrounding plasma layer 07 p1153 A67-19611
 Far field localizer and glide path monitoring for ILS installations, noting spaced antennas system and receiver for detection of radio interference 07 p1222 A67-19653
 Antenna orientation effect on polarization components of radio waves reflected from ionosphere, noting occurrence and properties of magnetotonic component of polarization 07 p1173 A67-19690
 Radar antenna synthesis for optimum and suboptimum filtering of spatial signals according to mean square error minimization 07 p1158 A67-20238
 Radio telescope antenna gain losses due to surface irregularity atmospheric scattering and absorption 07 p1158 A67-20241
 Radiation coupling of helical antenna, noting impedance measurement methods 07 p1158 A67-20294
 Higher order waveguide mode radiation incorporated antenna feed systems for performance improvement, evaluating S-and C-band dual frequency Cassegrain feed 08 p1300 A67-20681
 Transient condition effects on radiation resistance and expansion in linear antennas 08 p1302 A67-20826
 Cross-polarization radiation of axisymmetric mirror antennas 08 p1305 A67-21277
 Wideband feed with electrical scanning of radiation pattern for cross shaped radio telescope 08 p1306 A67-21341
 Sidelobes and amplification factors of narrow beam parabolic antennas in near zone 08 p1306 A67-21348
 Electromagnetic wavefront perturbations from plane wave propagation resolved into random tilt and residual phase perturbation 09 p1461 A67-21596
 Spatial coherence measurement in 3.2 mm horizontal transmission, considering amplitude and phase fluctuations received in two spaced antennas 09 p1461 A67-21599
 Average far field intensity patterns of antennas calculated for quasi-monochromatic space-time stationary signals 09 p1470 A67-21607
 Average power patterns for various values of rms phase difference for points separated by aperture radius in turbulent atmosphere 09 p1462 A67-21610
 Effective field for microwave breakdown for gas in external DC magnetic field and electric field valid for any stationary random signal 09 p1462 A67-21646
 Antenna height protection against microwave diffraction fading determined, using digital computer to evaluate residue series for grazing conditions 09 p1464 A67-22444
 Current, input impedance and far field pattern of cylindrical antenna with tapered resistive loading 09 p1481 A67-22446
 Spectral densities of electromagnetic fields of thermal radiation in magnetoplasma as related to radiation resistance of immersed antenna 09 p1464 A67-22448
 Boundary value solutions for current density and radiation patterns in spiral excited sheath antennas in terms of Hankel function 09 p1482 A67-22696
 Asymmetrically fed linear antenna loaded

with loading impedance analyzed in terms of two coexistent current distributions 10 p1609 A67-22774

Antenna temperature in wings of line centered at 61.1506 GHz, comparing experimental and theoretical values on atmospheric oxygen 10 p1632 A67-22857

Reduction in directivity and increase in main lobe width of linear antenna due to turbulent troposphere 10 p1607 A67-23442

Wideband and optimum antennas, using Lepidopter antenna as example 10 p1613 A67-23506

Doppler phenomena arising in rotation of system of electromagnetic wave emitters and reflectors 11 p1750 A67-23908

Effect of finite aperture dimension of antenna in vertical plane on conditions of ultrashort wave propagation within limits of direct visibility 11 p1757 A67-23916

Fourier transform for exact solution of current distribution and input admittance of infinite cylindrical dielectric-coated antenna 11 p1757 A67-23972

Distribution formula for unloaded prolate spheroidal receiving and scattering antenna 11 p1758 A67-23974

Time varying electromagnetic field pattern of prolate spheroid antenna with rotationally symmetric current distribution motion pictures generated by 11 p1758 A67-24115

Polarization characteristics of antenna measured, using stereographic projections of polarization sphere and various graphical methods 11 p1761 A67-24279

Feed system design for spherical reflector illumination specifying required field distribution and primary gain 11 p1761 A67-24281

Traveling wave V antenna, discussing parameter variation effect on radiation patterns 11 p1761 A67-24283

Time behavior of radiation field of infinite cylindrical antenna upon DC voltage pulse at input 11 p1762 A67-24292

Measurement and theory of two modes in antenna apertures of magnitudes one to two wavelengths, obtaining field distribution 11 p1763 A67-24295

Correction for gain computations based on pattern integration during translational motion of antenna 11 p1763 A67-24297

Far field radiation patterns of Advanced Antenna System presented by Surveyor I on lunar surface [JPL-TR-32-1079] 11 p1763 A67-24298

Systematic design of matrix network, consisting of hybrids with phase delays in interconnecting lines, used for antenna beam steering 11 p1763 A67-24300

Line source antenna radiation pattern computed from complex voltage patterns measured at various range lengths in near field 11 p1763 A67-24301

Nonreciprocal characteristics of long distance HF ionospheric propagation path interpreted as interaction of waves with transmitting and receiving antennas 11 p1754 A67-24718

High directional gap antenna, considering radiation sources of equal energy located on concentric rings 12 p1914 A67-25311

Radiation pattern of irregular antennas, using digital computer and superimposition of components to determine composite pattern 12 p1915 A67-25974

RF sources imbedded in ionized plasma noting developments since 1963 12 p1908 A67-26162

Computer calculation of noise temperature of high gain antennas, noting application to design and analysis of paraboloidal and Cassegrain systems 12 p1917 A67-26195

Axial mode helical antenna radiation and impedance improvement by using tapered feeds and terminations 13 p2076 A67-26514

Stability analysis of computer controlled linear hydraulic antenna control system 13 p2088 A67-26996

Directivity factor of convex SHF pencil-beam antennas with given magnetic currents, noting planar cophased aperture 13 p2080 A67-27025

Calculation of dimensions of effective radiation regions for conical spiral antennas 13 p2080 A67-27030

Angular errors in antennas with aerodynamic radome heating due to temperature variability 13 p2080 A67-27034

Discrete recording of radiation patterns of

antenna arrays 13 p2080 A67-27035

Radiation field of monopole antenna hinged on spherical conducting support calculated with Green function technique 13 p2081 A67-27200

HF power from transmitters in drop capsules of tube used for weightlessness experiments, utilizing Goubau transmission line to guide signals toward receiver 14 p2279 A67-27897

Amplification factor of circular polarization antennas calculated by mirror image method 14 p2283 A67-28069

Asymmetrically truncated parabolic antenna in three-dimensional problem, noting effect of shifting radiator 14 p2283 A67-28070

Synthesis of field distribution over aperture of antenna radiating maximum portion of power into given solid space angle 14 p2283 A67-28274

Integral expression derived for current distribution on infinite antenna aligned with magnetic field immersed in plasma, using generalized eigenfunctions 14 p2284 A67-28378

Diversity distances and loss in path antenna gain, noting association with beam width 14 p2264 A67-28399

Large parabolic radio astronomy antennas, discussing design and performance of current and next generation dishes 14 p2284 A67-28430

One-and two-dimensional antenna synthesis for instruments of large resolving power and effective collecting area 14 p2284 A67-28433

Signal processing in antennas with coupling elements between circuit and space fields 14 p2285 A67-28450

Behavior of RF sources embedded in plasma, determining antenna properties by configuration, current distribution and surrounding sheath properties 14 p2359 A67-28464

Large antenna radiation from radio astronomy Explorer satellite determined on basis of antenna current distribution 14 p2286 A67-28507

RF design of communication satellite earth stations, discussing receiving, sensitivity parameters, etc 14 p2273 A67-28798

Millimeter wave attenuation measurement in rain using low height antennas 14 p2274 A67-28923

Antenna with limited excitation region, discussing emitter design with prescribed radiation pattern and near field behavior 15 p2443 A67-29335

Cassegrain monopulse feed system using end-fire polyrod radiators 15 p2451 A67-29925

Fat cylindrical antenna admittance measured noting behavior similar to that of thin antenna admittances 15 p2454 A67-30137

Lambda functions describe antenna/diffraction patterns, showing familiar patterns from linear, rectangular and circular apertures 16 p2635 A67-30474

French interferometer for satellite tracking featuring antennas with single radiating element covering all useful space 16 p2621 A67-30681

Antenna synthesis for wide band radiation reception using Fredholm integral equation 16 p2636 A67-30889

Resistive antenna receiving properties determined via transmitting antenna driving-point impedance and short circuit current 16 p2638 A67-31338

Angle diversity performance of wire-grid lens antenna determined using statistical analysis 16 p2639 A67-31361

Anechoic chamber characteristics, noting indoor antenna pattern measurements and transmission attenuation variations 16 p2640 A67-31364

Diffraction coefficients in Keller theory extended to near-field and shadow-boundary regions of edge, introducing two correction factors 16 p2627 A67-31365

Polarization characteristics of radio emission from rough lunar surface, analyzing averaging effects of antenna radiation pattern and surface roughness 16 p2628 A67-31495

Wideband feed with electrical scanning of radiation pattern for cross shaped radio telescope 17 p2822 A67-31937

Sidelobes and amplification factors of narrow beam parabolic antennas in near zone 17 p2822 A67-31944

Variationally computed antenna impedances and accuracy of resulting current distributions 17 p2824 A67-32301

Radiation from dielectric antenna, noting erroneous radiation formula applications 17 p2824 A67-32308

Modes of boresight shift in conical-scan and sequential-lobing types of amplitude sensitive angle-tracking antennas 17 p2814 A67-32523

External noise levels effect on angular accuracy of tracking radar pencil-beam antennas, emphasizing radome noise and dielectric coating characteristics 17 p2826 A67-32685

Optical systems and holography in reconstruction of SHF antenna radiation patterns from field measurements in Fresnel zone 17 p2861 A67-33222

Antenna characteristics of Dwingeloo radio telescope, determining directivity, response pattern, ohmic loss, etc 18 p3008 A67-33433

Antenna radome subjected to aerodynamic heating investigated for effects on radar system operational range, analyzing antenna noise 18 p2999 A67-33510

Soviet book on digital processing of radar information covering signal processing, algorithms, discretization, etc 18 p3006 A67-33717

Symmetrical traveling-wave antenna design with given sidelobe level and amplification factor, determining coupling coefficient and maximum utilization 18 p3011 A67-34178

Equivalent circuit of two-port antennae with application to magic-T systems 18 p3013 A67-34527

Plasma layer effect on antenna performance from wind tunnel studies, discussing antenna transmission and breakdown in plasma jet flow 18 p3004 A67-34645

Directional maximum gain of antennas with discrete propagation elements 20 p3398 A67-36775

Cassegrain antenna beam-pointing accuracy, analyzing reflector beam deviation and feed displacement effects 20 p3398 A67-36819

Current distribution coefficients determination and antenna impedances 20 p3400 A67-37219

Distribution function of modulus of directivity characteristic of antenna grid shown as modified Rayleigh distribution 20 p3384 A67-37335

Control of polarization of radiation field of waveguide-slot antenna emitter 20 p3401 A67-37337

Electromagnetic interference reduction between antennas on space vehicles 20 p3405 A67-37642

Aperture antennas near field radiation patterns calculated by computer program based on semisimulated method 20 p3405 A67-37645

Radiation of monofrequency antenna in compressible magnetoplasma expressing far field as sum of modal plane waves 20 p3388 A67-37701

Approximate method for calculating electromagnetic field structure of vertical antenna 21 p3590 A67-38118

Despun antenna design, functioning and performance for communications satellites, discussing pattern, scanning and phase shifters 21 p3591 A67-38205

Gemini spacecraft antennas performance during reentry into ionized medium, discussing electron concentration profiles, nonearth atmosphere extrapolation and antenna breakdown effect 21 p3591 A67-38210

Principles, design and operation of synthetic plasma source for studying space vehicle antennas over wide frequency band 21 p3664 A67-38214

Meander-line antenna operated under backfire conditions studied for electrical performance and radiation properties 21 p3597 A67-38397

Atmospheric inhomogeneities effect on large antenna directive gain, noting dependence on length and wave field 21 p3600 A67-38812

Doppler phenomena arising in rotation of system of electromagnetic wave emitters and reflectors 21 p3585 A67-38936

Effect of finite aperture dimension of antenna in vertical plane on conditions of ultrashort wave propagation within limits of

direct visibility 21 p3600 A67-38944
 Radiation pattern lobing structure
 elimination for recessed annular slot in
 coated metal cylinder 22 p3767 A67-39274
 Radiation pattern of linear antenna
 erected over tapered ground screen, noting
 system surface impedance
 variation 22 p3760 A67-39628
 Radiation pattern of dielectric antenna
 using integral equations, noting differences
 between real antenna and idealized linear
 traveling wave antenna 22 p3770 A67-39656
 Random error effect on directional gain of
 sectional parabolic antenna with automatic
 phasing, setting sections effectively by three
 control points method 22 p3770 A67-39657
 Emission of axisymmetric parabolic
 antenna with antiphase field distribution at
 aperture, calculating radiation pattern of
 principal and cross polarization components
 of field 22 p3770 A67-39658
 Phase distribution in antenna aperture for
 small displacement of antenna feed from
 focal point calculated on basis of theorem
 proved 22 p3762 A67-39870
 Pencil-beam antenna with field
 distribution fluctuation determined for
 resolving power by mean square measuring
 of radiation pattern, detailing parabolic
 reflectors with rough
 surfaces 22 p3763 A67-40125
 MF surface wave launching over earth,
 considering field strength at ground for
 given radiated power 22 p3763 A67-40315
 Odd value correlation coefficient and wave
 amplitude fluctuation effects on mean
 radiation pattern and antenna amplification
 losses 23 p3977 A67-40599
 Antenna immersed in plasma problem
 solved using electromagnetic radiation in
 ionized medium principles 23 p3978 A67-40707
 Nonreflecting resistive loaded dipole
 antenna with step function internal
 impedance, measuring current amplitude,
 input admittance and radiation field
 pattern 23 p3978 A67-40826
 Electromagnetic field components of
 vertical and horizontal dipole antennas in
 quasi-near range 23 p3979 A67-40828
 Bifilar complementary loaded helical
 antenna, determining radiation patterns,
 near field amplitudes and phase
 velocities 23 p3979 A67-40834
 Asymptotic expansion of radiating antenna
 field in penumbra region 23 p3973 A67-40836
 Finite ground plane influence on raised
 electric dipole far field radiation
 pattern 23 p3980 A67-41202
 Currents in load impedance of
 transmission lines near cylindrical scatterer
 noting antenna field
 equations 23 p3981 A67-41209
 Field of loop antenna with arbitrary
 current distribution located inside cylinder
 with arbitrary dielectric constant studied for
 effects on radiation
 pattern 23 p3982 A67-41666
 Cloud melting zone, noting increased
 antenna temperature for radiation trapping
 between cloud layer and ground
 [AIAA PAPER 67-188] 23 p4025 A67-41747
 Equilateral triangular stepped helical
 aerial observed characteristics including
 impedance variation, radiation patterns, axial
 ratio and velocity factor 24 p4128 A67-41970
 Mixed problems of antenna synthesis,
 solving approximately specified amplitude
 and phase radiation patterns and given
 antenna current amplitude or
 phase 24 p4129 A67-42228
 Errors in measuring scattering patterns of
 arbitrary body in Fresnel region due to
 body/antenna finite distances and
 directivities 24 p4120 A67-42229
 Strongly enhanced radiation from antenna
 surrounded by dielectric layer and plasma
 sheath, noting resonance at given operating
 frequency for certain plasma
 densities 24 p4121 A67-42266
 Linear and planar phased array antennas
 investigated for radiation impedance as
 function of scan variable 24 p4130 A67-42339
 Proton gyrofrequency effect on antenna
 resonance at electron plasma frequency
 using Alouette II satellite 24 p4125 A67-43111

ANTHRACENE
 Nature of excited state resulting from
 two-quantum absorption associated with
 fluorescence in anthracene produced by
 ruby laser 05 p0814 A67-16130

ANTHROPOMETRY
 SA BODY MEASUREMENT /BIOL/
 SA BODY SIZE /BIOL/
 SA BODY VOLUME /BIOL/
 SA HUMAN ENGINEERING
 SA ORGAN WEIGHT
 Measurement of dimensions and inertial
 properties of 50th percentile anthropometric
 dummy 08 p1289 A67-20611
 Ground based simulation program for EVA
 evaluation including center of mass and
 inertia products of model
 astronaut 22 p3780 A67-40153

ANTI-AIRCRAFT MISSILE
 Cost and effectiveness of surveillance
 device for anti-aircraft weapon
 system 03 p0538 A67-13695

ANTIBACTERIALS
 Lethal effect of high intensity sonic and
 ultrasonic waves on spores of *Bacillus*
subtilis var. *niger* ATCC
 9372 04 p0562 A67-14520

ANTICONVULSANT
 S ACETAZOLAMIDE

ANTICYCLONE
 S CYCLONE

ANTIFERROELECTRICITY
 Electric field forced ferroelectric-
 antiferroelectric state transitions in
 transducers 03 p0426 A67-14301
 Energy densities of polar and antipolar
 arrays in barium titanate including nonlinear
 oxygen polarizability 21 p3683 A67-38406

ANTIFERROMAGNETISM
 SA FERROMAGNETISM
 SA HYSTERESIS
 Entanglement effect of plasma and
 magnetic branches of oscillations in
 antiferromagnetic semiconductors on LF
 expanding plasma waves in strong electric
 fields 04 p0678 A67-15133
 Spectral analysis of interacting
 electromagnetic, plasma and spin waves in
 antiferromagnetic semiconductors and metals
 with easy-axis and plane type
 anisotropy 09 p1555 A67-22073
 Entanglement effect of plasma and
 magnetic branches of oscillations in
 antiferromagnetic semiconductors on LF
 expanding plasma waves in strong electric
 fields 12 p1978 A67-25157
 Magnetic ordering effect on electrical
 properties of antiferromagnetic
 semiconductor MnTe indicate temperature
 anomaly above 440 degrees
 K 12 p1982 A67-25326
 Rubidium nickel trifluoride transparent
 single crystal magnetic and optical
 properties analyzed, concluding compound is
 antiferromagnetic 12 p1984 A67-25747
 Simple metal spin-density-wave state
 analyzed using electron-electron exchange
 interaction 12 p1985 A67-25849
 Spin-density waves effect on electronic
 properties and Fermi surface of
 antiferromagnetic metals 21 p3676 A67-37817
 Conduction electron ground state and
 anomalous magnetic moment in
 antiferromagnetic semiconductor, considering
 magnetic polaron 22 p3857 A67-39462
 Structural studies of FeNi-FeNiMn type
 thin films with ferro-antiferromagnetic
 coupling by Lorentz electron
 microscopy 24 p4206 A67-43109

ANTIGRAVITY
 Temporary irritation by anti-g and change
 in vestibular motor reflex action under
 laboratory conditions 14 p2257 A67-28224
 Gravitation and antigravitation, with
 relativity review, noting gravitational energy
 field 16 p2703 A67-31764

ANTIMATTER
 Antimatter in meteors from interpretation
 of mean gamma radiation intensity
 measurements 04 p0698 A67-14940
 Tunguska meteorite composition,
 evaluating validity of theory attributing
 nucleon-antinucleon annihilation to
 antimatter composition 04 p0701 A67-15546
 Comets hypothesized to consist of
 antimatter originating from parts of galaxy
 consisting entirely of
 antimatter 07 p1247 A67-19098
 Antimatter and
 cosmology 11 p1858 A67-23994
 Energy spectrum and production rates for
 secondary antiprotons from inelastic
 collisions of high energy galactic cosmic
 radiation with interstellar gas
 nuclei 19 p3316 A67-36098
 Possibility of antimatter meteor reaching

earth surface on basis of collision theory
 between matter and
 antimatter 22 p3882 A67-39589
 Experimental facilities to test antimatter
 hypothesis of comets and meteoric
 swarms 23 p4069 A67-41689
 Statistical significance of mathematical and
 logical foundations of information processing
 method applied to meteor
 stream 23 p4070 A67-41690

ANTIMONIDE
 SA ALUMINUM ANTIMONIDE
 SA CADMIUM ANTIMONIDE
 SA GALLIUM ANTIMONIDE
 SA INDIUM ANTIMONIDE
 SA ZINC ANTIMONIDE
 Band-to-band radiative recombination in
 compounds of gallium and indium with
 phosphorus, arsenic and
 antimony 12 p1979 A67-25177

ANTIMONY
 Directional correlation of first forbidden
 beta group and gamma ray in decay of
 antimony at four beta
 energies 02 p0269 A67-11863
 Diffusion of antimony and indium in
 germanium in range from 700 to 855 degrees
 C, taking into account effect of internal
 electric field 03 p0489 A67-13149
 Specific radioactivity of Sb-124 and effect
 on diffusion of antimony in Sb-doped n-type
 Ge single crystals and Ga-doped p-type Ge
 single crystals 03 p0500 A67-14067
 Antimony diffusion into germanium using
 vacuum furnace, giving graphs with variation
 of antimony concentration and depth of
 diffused p-n junction 05 p0869 A67-17089
 Band structure of Bi-Sb alloy system,
 using Shubnikov-de Haas technique with
 supplemental transport
 measurements 06 p1070 A67-18983
 Diffusion of antimony and indium in
 germanium in range from 700 to 855 degrees
 C, taking into account effect of internal
 electric field 10 p1690 A67-23098
 Galvanomagnetic properties of single
 crystal antimony as function of temperature,
 deriving carrier mobilities and densities,
 detailing nature of Fermi
 surface 14 p2364 A67-28105
 Thermomagnetic oscillation effect in
 arsenic, bismuth and antimony using
 cryostat, noting field strength
 variation 17 p2912 A67-32267
 Accelerated antimony diffusion in
 germanium due to excess vacancies from
 proton irradiation, determining migration
 energy and diffusion length of
 vacancies 17 p2919 A67-32862
 Fe rods in Fe-Sb matrix eutectic system,
 measuring rod diameter and Fe volume
 fraction effects on magnetic
 properties 23 p4039 A67-40884
 Antimony abundance in meteorites,
 tektites and terrestrial rock by neutron
 activation analysis 24 p4236 A67-42647

ANTIMONY ALLOY
 SA ANTIMONIDE
 Transverse magnetic field effect on
 thermoelectric properties of n-type
 polycrystals of bismuth-antimony alloys
 containing 0, 5, 12 and 19 percent antimony
 in bismuth
 [ASME PAPER 66-WA/ENER-4] 04 p0682 A67-15368
 Structural defects of reciprocally oriented
 polycrystalline bismuth-antimony films
 analyzed by moire
 method 20 p3510 A67-36813

ANTIMONY COMPOUND
 Interferometric technique for measuring
 thickness and optical constant of thin
 antimony trisulfide films 02 p0288 A67-11721
 Stripe pattern characteristic of voltage-
 controlled negative resistance and LF
 electric oscillation observed in SbSI due to
 diffraction effect 04 p0674 A67-14619
 Optical method observations of phase
 transition of ferroelectric monocrystal
 SbSI 06 p1047 A67-17758
 Temperature dependence of complex
 permittivity and spontaneous polarization of
 SbSI single-crystal whiskers in phase
 transformation region 15 p2537 A67-29707
 Photo-induced microwave response of SbSI
 crystals to variations in reflection
 coefficient indicates photodiodelectric
 effect 17 p2915 A67-32675
 SbS recombination center concentration,
 hole capture cross sections and trap energy
 levels 22 p3846 A67-39503

Temperature dependence of complex permittivity and spontaneous polarization of SbSI single-crystal whiskers in phase transformation region 24 p4199 A67-41777

ANTINEUTRINO

Solar neutrino-electron interaction and use of boron-cycle solar neutrino fluxes to determine existence of neutrino and antineutrino scattering

effects 02 p0317 A67-12776
Solar neutrino-electron interaction and use of boron-cycle solar neutrino fluxes to determine existence of neutrino and antineutrino scattering effects 22 p3877 A67-40278

ANTIOXIDANT

Amine-tin antioxidant systems for aliphatic hydrocarbons and related alkyl substituted fluids 20 p3474 A67-37594

ANTIPARTICLE**SA ANTINEUTRINO**

Eigenstates of particle mixing matrices and relation to physical antiparticles 16 p2705 A67-31565

Antiproton production by primary cosmic ray collisions with atmospheric nuclei compared with interstellar gas 21 p3620 A67-38843

ANTISUBMARINE WARFARE AIRCRAFT**SA SHIN MEIWA UF-XS AIRCRAFT**

Tilt and vertical float program of Naval Air Systems Command comprising four studies covering factors involved in any open ocean aircraft 03 p0354 A67-12901

UF-XS Japanese STOL seaplane used to investigate slow speed flying quality and hydrodynamic characteristics of PX-S aircraft 14 p2245 A67-27743

ANTONOV AN-24 AIRCRAFT

Antonov An-24V Soviet high wing monoplane and use of electrical spot welding and metal bonding in construction 06 p0944 A67-17597

ANXIETY

Quantification of response suppression in conditioned anxiety training with fixed duration preaversive stimulus

/CS/ 20 p3373 A67-37577
Correlation of airsickness in early flight training with subjective anxiety 21 p3575 A67-38086

Airsickness early in flight training indicates high levels of anxiety and attrition potentials and poor prognosis 23 p3963 A67-41544

APERIODIC FUNCTION

Radiation from infinite aperiodic array of parallel plate waveguides, using Wiener-Hopf technique for edge effect evaluation 23 p3978 A67-40825

APERTURE

Choke slots or corrugated structure in walls of horn antenna for reducing sidelobe and backlobe level by controlling illumination of E-plane edge 02 p0211 A67-11601

Step procedure for synthesizing circular aperture patterns 02 p0212 A67-11609

Plane problems of moment theory of elasticity for plane weakened by finite number of circular apertures, obtaining uniqueness of solutions 02 p0338 A67-11954

Aperture admittance, material loading and higher order modes effect on rectangular cavity slot antenna design 02 p0218 A67-12098

Stored energy of planar aperture radiating into lossless homogeneous medium 03 p0384 A67-13843

Equivalent linear antenna substitution for antenna with plane aperture in statistical analysis of antennas 03 p0386 A67-13958

Transmission coefficient for passage of electromagnetic wave through circular aperture in plane diaphragm 04 p0577 A67-15657

Angular power pattern for circular aperture receiving plane wave perturbed by passage through turbulent atmosphere 06 p1033 A67-18538

Electromagnetic diffraction at aperture, comparing three theories for case of partial polarized incident field 06 p1033 A67-18541

Relationship between statistics of log amplitude and irradiance fluctuations due to atmospheric turbulence used to estimate effect of aperture in collecting scintillating light 10 p1603 A67-22711

Effect of finite aperture dimension of antenna in vertical plane on conditions of ultrashort wave propagation within limits of direct visibility 11 p1757 A67-23916

Optimum antenna aperture distribution for finite line source and desired radiation pattern with given superdirective ratio upper boundary 11 p1768 A67-24943

Irregular fields effect on aperture reception characteristics 13 p2071 A67-27402

Diffraction field parts of slit aperture formed by two nonplanar screens satisfy variational principle 14 p2261 A67-28106

Synthesis of field distribution over aperture of antenna radiating maximum portion of power into given solid space angle 14 p2283 A67-28274

Design, principles and applications of optical stellar interferometer, gratings, aperture synthesis and pencil beam telescopes 14 p2284 A67-28429

Noncircular and asymmetrical aperture radio telescopes, considering cylindrical paraboloid, Pulkova and Kraus type Nancy telescopes 14 p2284 A67-28431

Earth atmosphere effect on propagation of radio waves from space, image formation, phase stability, technical problems and multiaperture instruments 14 p2285 A67-28437

Two-dimensional aperture synthesis in lunar CW radar astronomy, showing measurement possibility for Fourier transform components of sky brightness distribution 14 p2385 A67-28442

Large apertures and arrays for radio telescopes 14 p2285 A67-28449

Effect of random amplitude errors of continuous apertures on radiation pattern and gain 16 p2627 A67-31353

Nagelberg formula locating Fresnel region phase center of aperture antennas examined by calculating phase patterns of radiation field 16 p2639 A67-31357

Dependence of focusing property of aperture on coherence length of illuminating field in Fresnel diffraction from aperture 16 p2639 A67-31358

Plane problems of moment theory of elasticity for plane weakened by finite number of circular apertures, obtaining uniqueness of solutions 17 p2966 A67-33271

Pulsed-discharge-current interruption in constricting aperture by pinch effect, loss of ions, gas heating and oscillation generation 19 p3278 A67-35127

Aperture antennas near field radiation patterns calculated by computer program based on semisimulated method 20 p3405 A67-37645

Effect of finite aperture dimension of antenna in vertical plane on conditions of ultrashort wave propagation within limits of direct visibility 21 p3600 A67-38944

Irradiance due to square array of circular apertures from scalar Fresnel-Kirchhoff diffraction theory, giving plots of Fresnel diffraction patterns 22 p3835 A67-39235

Sidelobe reduction by stepping E-plane field distribution on rectangular horn antenna aperture, finding values of geometrical parameters 22 p3767 A67-39273

Phase distribution in antenna aperture for small displacement of antenna feed from focal point calculated on basis of theorem proved 22 p3762 A67-39870

Multimode monopulse feed system optimum aperture distribution determination, obtaining maximum rate of signal change on axis 22 p3763 A67-40313

Aperture usage for random optical communication channel through turbulent atmosphere 24 p4124 A67-42814

APOGEE
Flight trajectories having apogees unaffected by geomagnetic field, giving numerical solution, discussing radial propagation laws 17 p2941 A67-33239

APOLLO APPLICATIONS PROGRAM /AAP/
Apollo Applications Program objectives, discussing revisitation and reuse of hardware left in orbit, in-flight maintenance for long duration space missions, etc 18 p2994 A67-34657

Pointing control system /PCS/ for Apollo Telescope Mount /ATM/ for solar observations [AIAA PAPER 67-534] 19 p3334 A67-35936

Spacecraft ephemeris, orbit compatibility and scheduling in AAP mission experiments 22 p3885 A67-39959

Gemini program engineering aspects compared to Gemini/Mercury, discussing basic design rules adopted and Apollo Applications Project objectives 22 p3904 A67-40064

Equipment integration for Apollo Application Program /AAP/ physiological experiments, discussing design and dimensions [AIAA PAPER 67-846] 24 p4117 A67-42982

Manned orbiting space station operation in association with unmanned observatory, comparing gimbal mounted, free floating, tethered and firmly fixed modes [AIAA PAPER 67-926] 24 p4245 A67-43022

APOLLO PROJECT
SA LUNAR EXPLORATION SYSTEM FOR APOLLO /LESA/

SA LUNAR LAUNCH

SA LUNAR MOBILE LABORATORY /MOLAB/

U.S. Saturn/Apollo moon program, considering Saturn V booster, Apollo spacecraft and Lunar Excursion Module 01 p0154 A67-11001

Methods, schedules and cost of applying computer technology to circuit design, including Apollo and LEM programs 01 p0031 A67-11335

Apollo launch data telemetry system development from inception through planning and into final hardware implementation 02 p0195 A67-11997

Apollo X-ray astronomy experiment, noting instrumentation techniques employed and advantages [AIAA PAPER 66-888] 02 p0246 A67-12267

Thermal control subsystem for Apollo lunar surface experiments package, noting construction and operation principles 02 p0184 A67-12357

Apollo thermal control systems and concepts, discussing self-shadowing 02 p0334 A67-12390

Nondestructive testing /NDT/ of materials, components and systems for Saturn-Apollo program 02 p0250 A67-12631

Ames emissivity experiment on OSO-II to measure thermal radiation properties of temperature control coatings exposed to space environment [AIAA PAPER 65-651] 03 p0448 A67-13056

Integration, testing and launching of flight hardware for Apollo/Saturn V space vehicle at Kennedy Space Center [AIAA PAPER 66-837] 03 p0397 A67-14126

Maintainability efforts in support of Acceptance Checkout Equipment/Apollo-Spacecraft /ACE-S/C/ program 03 p0398 A67-14205

Factory-to-launch sequences of checkout in Saturn/Apollo program, examining present and planned levels of automation 03 p0399 A67-14207

Local scientific survey module /LSSM/, small lunar vehicle designed to provide two astronauts with transportation and portable scientific lab on lunar surface 03 p0400 A67-14308

Erectable antenna design for S-band communications between lunar surface and earth during lunar stay portion of Apollo mission 04 p0569 A67-14501

X-band Cassegrainian tracking antenna for space rendezvous position and rate information for navigation and guidance computations 04 p0569 A67-14502

Vibration testing facilities for Apollo Saturn V launch vehicle, noting structural assemblies under dynamic testing 05 p0786 A67-16156

NASA Apollo-Saturn V Moon Project crawlerway construction for lunar launch complex 05 p0788 A67-16615

Chemical propellants in Apollo program, noting Saturn launch vehicle and spacecraft propulsion 05 p0874 A67-17016

Metrology requirements for Apollo project, noting control and measuring equipment and calibration procedures 05 p0814 A67-17263

Apollo computer design mechanical packaging, implementing heat and vibration model to conduct thermal vibration and sealing tests 05 p0814 A67-17460

Apollo TV scan conversion, discussing equipment and performance 06 p0964 A67-18413

Transient heat transfer analysis of Apollo Service Module [AIAA PAPER 67-157] 06 p1118 A67-18506

Apollo manned lunar landings, system hardware, operational problems and development of lunar surface experiments package /ALSEP/ [AIAA PAPER 67-116] 07 p1163 A67-19438

Functions of Lunar Receiving Laboratory including lunar samples distribution to scientists, quarantine, storage, contamination, etc 07 p1164 A67-20021

Hybrid simulation for design of Apollo guidance navigation and control system [AIAA PAPER 67-233] 07 p1222 A67-20042

Manual thrust vector control development for Apollo Command and Service Module Stabilization and Control System [AIAA PAPER 67-243] 07 p1260 A67-20043

Free flying lunar landing research vehicle tested for more than two years and used in lunar landing simulations supporting Apollo project [AIAA PAPER 67-238] 07 p1129 A67-20044

Apollo command and -service modules simulation [AIAA PAPER 67-231] 07 p1260 A67-20050

Apollo engineering simulation activity, particularly analog-digital real time hybrid simulation for guidance and control [AIAA PAPER 67-230] 07 p1164 A67-20055

Apollo external visual simulation display systems, discussing optical methods applied during navigation, guidance and control tests [AIAA PAPER 67-253] 07 p1189 A67-20085

Automatic checkout system /ACS/ and digital guidance programs for titan III and Apollo automatic checkout system /ACS/ and digital guidance programs for Titan III and Apollo 08 p1297 A67-20632

Experiment selection process for specific flights in Apollo applications program /AAP/, using algorithms [AAS PAPER 66-142] 08 p1411 A67-20967

Saturn S-IVB Apollo systems application to planetary exploration, using extension of technology and hardware for lunar exploration 08 p1411 A67-21074

Apollo Extension System for lunar surface missions, discussing extension of mission time by unmanned LEM laboratory 08 p1316 A67-21083

Scientific objectives for Lunar Exploration Systems for Apollo, noting compatibility with geoscience operation and radiation investigation 08 p1393 A67-21090

Manned lunar exploration systems for Saturn-Apollo 08 p1393 A67-21091

Gemini ground support system extension to cover Apollo program, stressing launch complex, deep space tracking, S-band linkage, communications satellite, etc 08 p1317 A67-21281

Cargo delivery to lunar surface using Apollo hardware and Saturn V 09 p1486 A67-22403

Manned planetary exploration, Mercury and Gemini flight programs and projected goals of Apollo Applications Program 12 p2002 A67-25233

Evolutionary manned interplanetary exploration program with modular elements used for flyby, orbital capture and Mars landing, noting influence of Apollo program 13 p2199 A67-26827

Lunar scientific exploration requirements in post-Apollo period, discussing lunar and earth geophysics 13 p2199 A67-27212

Apollo mission constraint deviations required to permit landing anywhere on moon and to extend lunar stay time 13 p2199 A67-27215

Experiment selection process for specific flights in Apollo applications program /AAP/, using algorithms [AAS PAPER 66-142] 13 p2214 A67-27548

Management scheme for Apollo program 13 p2233 A67-27553

Computer controlled dynamic test facility to provide data on flight characteristics of Apollo-Saturn V launch vehicle by measuring vibration amplitudes 14 p2293 A67-28593

NASA STADAN and Apollo network antenna systems, analyzing tracking antenna systems, command systems and operational problems 14 p2287 A67-28681

Lunar module onboard guidance equipment design, noting operational strategies, control systems, etc 15 p2514 A67-29601

Apollo/Saturn V vehicle launching site, assembly building and lunar flight 15 p2569 A67-29849

NASA space applications and future possibilities noting ATS-I satellite for cloud photography, omnidirectional aircraft antennas and Apollo Applications Program [AAS PAPER 67-89] 15 p2583 A67-29951

Apollo manned space flight program

including mission profile, spacecraft and constituent systems 16 p2756 A67-30626

Gemini-Apollo capability, Apollo application and proposed earth-orbital experiments, describing typical missions with illustrative experimental payloads 16 p2756 A67-30627

Ground installations for development, qualification and checkout testing of Apollo space vehicle 16 p2854 A67-30676

Laser radar selenodesy for ground control selection of Apollo landing sites 16 p2623 A67-30982

Analog computer use in design of automatic steering control system of Apollo station ships for precision geographical track-keeping 16 p2701 A67-31659

Cryogenic fluid storage subsystems for Gemini program, noting more advanced designs for Apollo, Lunar Module, Biosatellite, Manned Orbiting Laboratory, etc 17 p2954 A67-32013

Vacuum-ignition phenomena in Apollo rocket engine when oriented in upward-firing attitude 18 p3114 A67-33977

[AIAA PAPER 67-514] Apollo ranging code with phase locked loop for bit synchronization, plotting SNR vs error probability and acquisition time 18 p3000 A67-34102

Control integration for lunar mapping 18 p3131 A67-34321

Apollo lunar landing mission noting lunar geodetic, cartographic and topographic information deficiencies and correction programs 18 p3132 A67-34329

Thin film hybrid subaudio active filter design and fabrication, discussing power consumption, circuit breadboard performance, etc 18 p3015 A67-34559

Apollo Applications Program objectives, discussing revisitation and reuse of hardware left in orbit, in-flight maintenance for long duration space missions, etc 18 p2994 A67-34657

Reliability prediction, modeling and analysis activities in Apollo program 18 p3139 A67-34697

Apollo mission launch noise and physiological effects on crew 18 p2996 A67-34718

Australian space research, discussing support to Apollo and U.S. manned space flight programs, ionospheric observations, satellite information, etc 19 p3320 A67-35286

Operational capabilities of Saturn-Apollo space vehicle, discussing lunar missions 19 p3333 A67-35643

Man capability to operate in cislunar space and lunar surface through Apollo program, discussing practical applications 19 p3326 A67-35644

Collection, processing and return to earth of lunar specimens as part of Apollo program 19 p3328 A67-35929

Apollo Manned Spacecraft Program systems design requirements, emphasizing instrumentation system and Phase I spacecraft 20 p3443 A67-36469

Orpheus program for space flight safety using lifeboat rescue of astronauts on Apollo and other manned missions 20 p3532 A67-36572

Apollo Range Instrumentation Aircraft /ARIA/ deployment model to determine flight plans for support of translunar injection phase of Apollo mission 20 p3361 A67-36600

Liquid rocket propellants use in U.S. space program, particularly Apollo project, discussing future trends 20 p3515 A67-36880

Apollo program automatic checkout equipment, examining computer controlled checkout concept for Apollo spacecraft 20 p3417 A67-36974

Apollo-Saturn program automatic checkout systems, discussing ground support equipment facility automation, computer software and checkout technique applications to nuclear electronic systems 20 p3533 A67-36977

Lunar mission simulators for Saturn-Apollo project noting optimal computer approach on flexibility, accuracy, cost, etc 20 p3418 A67-37482

Apollo command module communication and data system design, discussing environmental and reliability requirements 21 p3584 A67-38668

Mission planning for post-Apollo period including selection of lunar landing sites and

definition of preferred scientific activity 22 p3888 A67-40144

Apollo Crawler System analyzed by computer simulation for dynamic interactions of transporter and umbilical tower 22 p3782 A67-40466

Maintainability problems analyzed noting Apollo/ Saturn program 23 p4070 A67-40581

Systems planning for transportation of large launch vehicles and spacecraft noting land transporter and seagoing barge used for Apollo booster 23 p4070 A67-40584

Tracking ground station on Ascension Island to relay communication with Apollo spacecraft via INTELSAT II 23 p3986 A67-40706

Writing and use of ground checkout procedures in Apollo program using computer-assisted editing, publishing and information retrieval 23 p3976 A67-41055

Apollo fuel cell power system transient temperature and voltage response characteristics predicted by analytic model 24 p4106 A67-42523

Apollo historical perspectives, background to U.S. man on moon decision in mid-1961, rocket booster development and space mobility [AIAA PAPER 67-839] 24 p4259 A67-42978

Manned spacecraft recovery safety noting operational testing of postlanding systems, recovery support and retrieval procedures for Apollo [AIAA PAPER 67-852] 24 p4243 A67-42985

Apollo manned Lunar Module /LM/ earth orbital development missions, reviewing key subsystems and technical problems [AIAA PAPER 67-863] 24 p4244 A67-42987

Lunar exploration planning methodology for after post-Apollo landing based on equipment evolution [AIAA PAPER 67-865] 24 p4238 A67-42988

APOLLO SPACECRAFT

SA COMMAND MODULE

SA LUNAR EXCURSION MODULE

SA SERVICE MODULE

U.S. Saturn/Apollo moon program, considering Saturn V booster, Apollo spacecraft and Lunar Excursion Module 01 p0154 A67-11001

Apollo Guidance and Navigation System positioning by electrically torquing gyros, discussing error sources 01 p0073 A67-11115

Mechanical impact attenuation system for Apollo spacecraft provides stable land landing platform, noting deployed heat shields, extended legs, pneumatic bags, etc [AIAA PAPER 66-989] 02 p0333 A67-12300

Apollo lunar surface experiments package /ALSEP/ of scientific instruments and supporting subsystems [AIAA PAPER 66-919] 03 p0397 A67-14133

Apollo guidance and navigation by computer holding fixed program with diverse and flexible applications 05 p0809 A67-17550

Model tests for determination of structural response of Apollo Command Module to water impact 07 p1257 A67-19368

Man-machine simulations for Apollo navigation, guidance and control system [AIAA PAPER 67-242] 07 p1136 A67-20063

Apollo spacecraft hybrid real time flight simulation ensuring 40 msec sampling interval [AIAA PAPER 67-255] 07 p1166 A67-20071

Apollo spacecraft, discussing performance of Command and Service Module with typical payloads 08 p1412 A67-21077

Base-mounted landing rocket system for Apollo type vehicle evaluated for heat-shield water pressure, ground effect, vehicle dynamics, etc 08 p1413 A67-21515

Design, tests, operation and limitations of Apollo man-rated environmental control system simulation chamber 11 p1748 A67-24340

Scan converter for Apollo TV performing time base conversion with destructive readout storage element and flicker correction with magnetic disk [SMPTE PAPER 101-53] 12 p1904 A67-25468

Vibration qualification of fly-away umbilical by induced acoustic excitation testing method in Apollo project 12 p1924 A67-25714

Vibration response of Apollo shell structures to acoustic and aerodynamic noise 12 p2012 A67-25728

Apollo spacecraft-earth two-way

communications provided by vehicle-mounted variable gain antenna array, automatically tracking ground-transmitted signals 13 p2068 A67-26802

Partial differential equations for three-dimensional inviscid flow solved for flow field over blunt body shapes at various angles of attack, for application to Apollo spacecraft [AIAA PAPER 66-413] 14 p2240 A67-28110

Landing radar system for Apollo lunar module using three-beam Doppler velocity sensor and single-beam altimeter 14 p2318 A67-28290

Tester to check altimeter of Apollo lunar module 14 p2318 A67-28291

Explosive-actuated cutting mechanism for severing electrical service lines connecting Apollo command module to service module and lunar module to spacecraft-LM adapter [ASME PAPER 67-DE-33] 14 p2394 A67-28874

Cartridge-actuated thruster system design for jettisoning Apollo spacecraft heat shield for recovery system deployment [ASME PAPER 67-DE-34] 14 p2394 A67-28875

Mechanical impact attenuation system for Apollo spacecraft provides stable land landing platform, noting deployed heat shields, extended legs, pneumatic bags, etc [AIAA PAPER 66-989] 15 p2564 A67-29423

Aerothermodynamics for Apollo spacecraft design and results of flight tests 16 p2761 A67-30935

Medicophysiological aspects of NASA program stressing cardiovascular, muscular and osseous problems 16 p2614 A67-31538

Hardware characteristics of control moment gyro /CMG/, determining nonlinearity effects on performance by simulation 17 p2853 A67-31995

Fluid dynamics effect on spontaneous pressure spikes in Apollo SPS thrust chamber, noting increased combustion instability, occurrence and mechanism of pops, etc [AIAA PAPER 67-513] 18 p3114 A67-33976

Operational computerized system for automatic surveillance of reliability and maintainability of spacecraft hardware 18 p3021 A67-34701

Design, construction and procedure changes in Apollo following fire of January 1967 19 p3334 A67-35928

Apollo gyro reliability covering Guidance, Navigation and Control systems, stressing failure mode prediction 19 p3259 A67-35984

Vapor phase decontamination for removing residual hypergolic propellants in Apollo propulsion system 20 p3516 A67-36578

Ablative material application to Apollo spacecraft for heat shielding using air injection guns 20 p3454 A67-36590

Electromagnetic compatibility operational problems aboard Apollo spacecraft tracking ship 20 p3387 A67-37641

Apollo lunar landing mission strategy development concerning guidance, control and landing and propulsion systems 22 p3897 A67-39166

Automatic control of Block II Apollo ECS space radiator system, deriving linearized control equations for subsystem 22 p3916 A67-39174

Man-machine design for Apollo spacecraft navigation, guidance and control systems 22 p3830 A67-39180

Fire in Apollo 204 spacecraft noting alterations in oxygen and electrical systems, escape hatch, materials and communications 22 p3900 A67-39888

Information Service, computerized storage and retrieval system for Apollo spacecraft parts, materials and processes 22 p3765 A67-39951

Saturn V launch vehicle and Apollo spacecraft hardware systems applied to unmanned exploration of Jupiter 22 p3887 A67-40138

Program for preventing earth environment biological contamination by lunar material 23 p3961 A67-40845

Apollo spacecraft H-O chemical to electric energy converting fuel cell performance degradation resulting from O electrode contamination due to inert diluent impurities in O supply 24 p4106 A67-42525

APPARATUS

S ABORT APPARATUS
S AIRCRAFT BREATHING APPARATUS
S DISTILLATION APPARATUS
S HYPERSONIC TEST APPARATUS

S INSTRUMENT
S LABORATORY APPARATUS
S LOADING APPARATUS
S MEASURING APPARATUS
S MICROWAVE APPARATUS
S NONELECTRONIC APPARATUS
S OXYGEN APPARATUS
S PENDULUM APPARATUS
S PHOTOELECTRIC APPARATUS
S PHOTOGRAPHIC APPARATUS
S PRESSURE APPARATUS
S SPRAYING APPARATUS
S TIMING APPARATUS
S VAPOR PRESSURE APPARATUS
S VESTIBULAR APPARATUS
S WIND TUNNEL APPARATUS

APPLICATIONS TECHNOLOGY SATELLITE /ATS/
Aircraft-to-ground communications using Applications Technology Satellite B as repeater in VHF COM band 01 p0024 A67-10665

Fluxgate magnetometer onboard applications technology satellite for measuring MHD wave propagation within magnetosphere 04 p0626 A67-15723

Automatic real time data acquisition and processing for ATS communications experiments 08 p1298 A67-20669

Cloud photographs obtained on board ATS-I satellite with camera equipped with reflecting telescope show feasibility of short-lived weather systems from synchronous altitude 10 p1657 A67-23367

Preflight testing of ATS-1 Thermal Coatings Experiment /TCE/, discussing cup designs, sensor and cup calibrations, etc [AIAA PAPER 67-333] 12 p2038 A67-26047

French installations for space research, describing laboratory work and industrial investments for satellite launching 14 p2320 A67-28606

NASA space applications and future possibilities noting ATS-I satellite for cloud photography, omnidirectional aircraft antennas and Apollo Applications Program [AAS PAPER 67-89] 15 p2583 A67-29951

Applications Technology Satellite /ATS/ emphasizing communications facilities, repeater, antenna array, etc 16 p2760 A67-30694

Electrostatic ion engine timetable, noting contact ion and electron bombardment engines and application to NASA Applications Technology Satellite series 17 p2928 A67-32435

Environmental Measurements Experiment /EME/ package for applications technology satellites 19 p3226 A67-34788

Practical space applications - Conference, San Diego, February 1966 19 p3326 A67-35634

Application satellite program, discussing meteorological and communications satellites, noting ESSA 1, Syncom, etc 19 p3333 A67-35635

Attitude determination and hydrogen peroxide control system for spacecraft orientation in Syncom, Early Bird and ATS [AIAA PAPER 67-532] 19 p3334 A67-35934

Active VHF translation repeater onboard ATS-I for aircraft communication systems 20 p3381 A67-36591

Functional maser consisting of amplifier, low noise header and superconducting magnet for use in ATS satellite 20 p3459 A67-36595

ATS-I spin scan camera experiment for photographic recording of weather motions 20 p3446 A67-36610

Cold welding under flight conditions of ATS silver-plated beryllium copper damper boom, discussing ultrahigh vacuum equipment and test techniques 24 p4160 A67-42033

ATS-I spin scan camera experiment for photographic recording of weather motions 24 p4156 A67-42405

APPROACH AND LANDING
Commercial aircraft accident causes, emphasizing accidents occurring during approach and landing [AIAA PAPER 66-804] 01 p0008 A67-10030

ASL 70-mm photoelectric system in studying approach and landing parameters for aircraft design and testing 01 p0075 A67-11133

Simulator program which uses modified head-up display unit from British Buccaneer aircraft 04 p0653 A67-14882

Flexible wings for hypersonic vehicles allowing for safe controllable landings,

stressing leading edge parawing concept, flow visualization, lift-drag ratio, etc [AIAA PAPER 67-200] 07 p1258 A67-19440

Approaching and soft landing on planet surface in absence of atmosphere, finding optimum acceleration vector control as function of generalized parameters 09 p1571 A67-21889

En-route guidance system using ILS localizer techniques for both en-route navigation and landing 09 p1528 A67-22634

FAA navigation improvement program, discussing approach and landing, short and long distance navigation and performance assurance 15 p2514 A67-29738

Flight instrumentation aiming at improving safety of approach and landing of commercial aircraft [SAE PAPER 670327] 17 p2860 A67-32983

Air Force undershoot and overshoot experience examined to establish relative frequency, historical trend, associated variables and human factors 23 p3970 A67-41701

APPROACH AND LANDING INSTRUMENT
TALAR ground-to-aircraft microwave transmission landing approach system for use in conjunction with instrument landing system /ILS/ crosspointer indicator 06 p1028 A67-17721

Pilot-aircraft compatibility in landing approach 07 p1136 A67-19888

High integrity guidance for approach and landing, noting VHF ILS system and downwind antenna system 09 p1529 A67-22638

Electronics package for category II qualified jet business aircraft and function of system components [SAE PAPER 670254] 12 p1941 A67-25504

Instrument-landing displays evaluated in IFR landing approaches with helicopter, noting flight performance and pilot evaluation of display concepts [AHS PAPER 106] 16 p2680 A67-31823

Helicopter landing systems requirements, considering manual instrument approaches with guidance information from ground station including landing environment 23 p4026 A67-41500

APPROACH CONTROL
SA RADAR APPROACH CONTROL /RAPCON/
Effects of anthocyanin glucosides on night vision of airport approach controllers 04 p0561 A67-14633

Rocket control with limited-power engine when approaching target planet 14 p2394 A67-28640

Aircraft tracking problems in airport approach zone solved using cameras, descriptive geometry and vector computations 21 p3568 A67-38809

Manual steering problem and function of lunar module /LM/ manual hybrid guidance system, with automatic guidance system produced trajectory 22 p3898 A67-39176

Optimal algorithm for single parameter linear and nonlinear correction of interplanetary flight, noting application to space vehicle approach to designated planet 22 p3830 A67-39193

Ground requirements for instrument landing systems noting approach lighting, runway marking, taxi guidance and blind navigation [AIAA PAPER 67-756] 23 p3933 A67-40989

APPROXIMATION
S BORN APPROXIMATION
S BOUSSINESQ APPROXIMATION
S OSEEN APPROXIMATION
S PADE APPROXIMATION
S POHLHAUSEN SOLUTION
S QUADRATURE APPROXIMATION
S SOMMERFELD APPROXIMATION

APPROXIMATION METHOD
Quasi-one-dimensional approximation for MGD equations 01 p0118 A67-10047

Approximation method for deriving expressions for small angle polydispersed indicatrix of gamma distribution of particles in light field 01 p0107 A67-10125

Mean powers of r, sum rule and improved transition integrals computed for effective quantum number range up to 8.5, using Coulomb approximation wave functions 01 p0112 A67-10142

Anisotropies and harmonics of homogeneous Lorentz plasma under electric field, using approximation method 01 p0121 A67-10230

Successive approximations to determine

vector in theory of optimal control 01 p0043 A67-10236

Stochastic approximation theory to obtain algorithms for recovery of functions, using noisy measurements taken at randomly selected points 01 p0028 A67-10450

Evaluation of residue integral for finite number of poles in behavior function of control circuit 01 p0045 A67-10796

Successive approximation method of estimating effect of stratification and dynamic nonuniformity of crosswind on trajectory of circular turbulent jet 01 p0053 A67-10824

Constructive representation of zero classes of differentiated functions of many variables based on theory of approximations 01 p0106 A67-10902

Computation by approximate methods of stress resultants for shell of revolution under distributed externally applied load 01 p0164 A67-11185

Solution properties of linear difference equations approximating differential equations in nonoscillation interval 01 p0107 A67-11251

Approximate numerical solution used to calculate delay of z-directed magnetoelastic wave in yttrium iron garnet 01 p0138 A67-11321

Geometrical study of Picard method of successive approximations for solving first order differential equations 02 p0257 A67-11479

Approximate method for calculating parallel flow past slender bodies of noncircular cross section 02 p0177 A67-11517

Interplanetary trajectory correction via radial heliocentric velocity pulses, noting calculation by linear approximation 02 p0321 A67-11538

Continued fraction rational approximations to solution of second-order nonlinear equation, including Riccati equations treated by Merkes, Scott and Fair 02 p0258 A67-11558

Approximation theory of optimum performance of nonuniformly spaced arrays 02 p0212 A67-11613

Approximate solutions for integral equations with Hilbert kernel and degenerate nucleus 02 p0258 A67-11625

Quasi-Newton methods in nonlinear equation solving and unconstrained optimization 02 p0259 A67-11801

Kantorovich theorem, Goodman-Lance method and two-point boundary value problems, noting numerical results obtained on IBM 7094 computer 02 p0259 A67-11836

Jackson theorem on optimal approximations of periodic functions with r-th derivative belonging to metric generalized to case of Orlicz space 02 p0259 A67-11872

Radiant heating by inhomogeneous hot gases, determining spectral transmittances of inhomogeneous optical paths using Curtis-Godson approximation 02 p0342 A67-12050

Digital simulation results for random approximation solutions of binary signal detection problems 02 p0204 A67-12169

Algorithm for approximate solution of Wiener-Hopf integral equation 02 p0209 A67-12175

Near circular orbit of satellite in terrestrial gravitational field analyzed, using approximate solution of perturbed Kepler motion 02 p0327 A67-12373

Line profile in one-electron approximation compared with impact approximation 02 p0270 A67-12521

Existence and uniqueness theorem and upper and lower Chaplygin function approximations for solutions of Cauchy problem for quasi-linear first order PDE 03 p0456 A67-12884

Successive approximations for determining direct and backward wave in inhomogeneous medium and consequently reflection coefficient and total field 03 p0467 A67-12893

Harmonic approximation of infinite crystal dynamics problem, noting collisional case and action of external force on atoms 03 p0520 A67-12930

Aerodynamic forces of oscillating lifting surfaces of large aspect ratio in subsonic range investigated by approximation method 03 p0351 A67-12996

Approximation of variable time delays and design of constant and variable delay circuits, noting simulation of delays in automatic control systems by

computers 03 p0390 A67-13104

Critical load equations for plate weakened by sharp stress raisers extended to account for effect of arbitrarily oriented external forces 03 p0522 A67-13122

Exact and approximate solutions to Cauchy problem for nonlinear wave equation in affine connection field theory 03 p0457 A67-13171

Optimal approximations by trigonometric polynomials for classes of periodic functions belonging to Banach space 03 p0459 A67-13645

Exact monotonic and approximate oscillatory solutions of nonlinear differential equations of high order 03 p0460 A67-13656

Approximate method of computing attitude of sounding rockets from magnetometer data 03 p0519 A67-13782

Approximation method for computation of radiation patterns from circular apertures and reflectors by single integration at wide angles and large Fresnel numbers 03 p0384 A67-13844

Approximate solution to nonlinear differential Riccati equation, using Bessel function 03 p0460 A67-13879

Exact difference replacement for hyperbolic equation system where $n \times n$ symmetric matrices become coefficients of vectors in two-dimensional space 03 p0460 A67-13880

Thermally radiating and absorbing plane piston problem, obtaining zero order approximation in series expansion in density ratio across shock layer 03 p0405 A67-14029

Extreme value problem of constant type and extremal approximating operators with positive kernels 03 p0461 A67-14106

Continuous periodic function approximation by Fourier series 03 p0462 A67-14108

Error equations for Schuler vertical, estimating discrepancy between solutions for various changes in coefficients 03 p0465 A67-14160

Approximation method for calculating autocorrelation function of quantized noise 04 p0567 A67-14405

Successive approximation solution of initial value problem, noting convergence of sequence 04 p0642 A67-14481

Analytic approximation method for thermal convection at large Rayleigh numbers 04 p0721 A67-14649

Approximate relations for solution to equations of nonisothermal laminar boundary layer 04 p0722 A67-14711

Regular approximation of solutions for complex elliptic equations of any order 04 p0643 A67-14725

Nonlinear recognition procedures, discussing probability distribution approximation by orthogonal expansion and by-product of low order conditional probabilities 04 p0578 A67-14800

Variational approximation of normal velocity on oscillating wings including linear approximation, numerical integration and comparison to least squares method 04 p0547 A67-14842

Approximation of functions of many variables by Bernstein polynomials, using method based on conjugate operators 04 p0646 A67-15258

Approximation method for molecular integrals that depends on replacement of two-center charge distributions by single-center distributions, giving results in terms of Coulomb type integrals 04 p0566 A67-15547

Information theory assessment of optimizing criteria and approximation for steady state gain of optimum filter, based on Wiener type 04 p0586 A67-15639

Rational approximation of generalized Duffing equation, damped mass spring oscillator equation and generalized second order Riccati equation 04 p0647 A67-15660

Approximate solution of thermoconductivity equation for multilayer cylinder in constant-temperature medium 04 p0738 A67-15891

Approximation in sandwich plate analysis obtained by various methods 04 p0717 A67-15913

Boundary layer problem in approximate solution obtained from multiparameter treatment 04 p0610 A67-15922

Relation between cosmic ray cut-off rigidity and L parameter, solving approximately 7th degree algebraic

equation 05 p0880 A67-16113

Closed-loop automatic control system with unvalued substantially nonlinear element, using approximation of characteristics by Fourier series 05 p0781 A67-16254

Approximation method determining follow-up failure conditions for nonlinear automatic systems in presence of control and noise signals 05 p0781 A67-16255

Function approximation from finite number of arbitrary points, using iteration methods 05 p0833 A67-16260

Reliability of finite automata determined from analysis of elements capable of misalignment, input errors and structural design 05 p0782 A67-16261

Method of approximating functions with aid of orthonormal systems and single channel optimization, using analog computer 05 p0768 A67-16264

Approximation method of geometric optics in theory of electromagnetic waves in gyrotropic medium 05 p0762 A67-16347

First-kind operator equation solution by reduction to dual extremum problem, proving existence and convergence 05 p0834 A67-16375

Harmonic components of current of HF transistor under sinusoidal excitation, using piecewise parabolic approximation 05 p0772 A67-16456

Error estimation in linear matrix equation systems by rounding-off inaccuracies 05 p0834 A67-16721

Cylindrical electronic microwave tubes, deriving expressions for zero and first approximations of physical parameters 05 p0774 A67-16906

Temperature field of active medium of pulsed laser using variational methods, considering two approximate solutions 05 p0825 A67-16935

Walsh approximation problem, establishing properties and uniqueness of analytic function 05 p0835 A67-17001

Fourier series approximation of functions with structural properties differing with segments of domain of definition 05 p0836 A67-17107

Error estimate for approximate solution of linear parabolic equation using Kantorovich theorem on functional analysis in normalized space 05 p0836 A67-17108

Z component of geomagnetic field, determining parameters of sloping dipoles 05 p0802 A67-17149

Idealized radar range equation using narrow beam approximation of Probert-Jones 05 p0767 A67-17309

Approximation for low thrust trajectory without singularity at escape and having correct behavior up to and beyond escape, using motion equation 05 p0903 A67-17363

Boundary value problem solution via direct methods of approximate analysis 05 p0925 A67-17370

Rayleigh thermal instability in horizontal circular cylinder, discussing two approximate methods for calculating upper bounds to critical Rayleigh number 05 p0929 A67-17415

Stability of elastic plates of arbitrary shape treated approximately 05 p0925 A67-17476

Approximation of functions of several variables, using one-dimensional analogy to determine rapidity of convergence 06 p1022 A67-17566

Ochkur and Rudge approximation for exchange in electron-atom collisions adapted for atom-atom collisions 06 p1034 A67-17649

Successive approximations determining radiation pressure effect on and disturbing function of motion equations of artificial satellite 06 p1081 A67-17787

Two variable expansion procedure for approximate asymptotic solution to nonlinear differential equation 06 p1022 A67-17789

Self-focusing and self-trapping of intense light beams in nonlinear medium examined, using approximations of geometrical optics and accounting for diffraction effects 06 p1031 A67-17880

Kalman filter, modern version of Gaussian least squares method linear estimation of orbital elements of celestial body 06 p0974 A67-17926

Approximation techniques generating algorithm for iteratively solving sequential optimization of nonlinear control systems 06 p0974 A67-17930

Differential approximation applied to

radiative transfer in various geometric configurations 06 p1113 A67-18116

Piecewise linear approximation procedure for linearization of readings of nondifferential vibrating and string transducers 06 p1003 A67-18174

Model estimation programming to determine optimum design criteria for rocket propulsion system using estimating function, approximation solved by Lagrange method [AIAA PAPER 67-208] 06 p1024 A67-18330

Control system synthesis based on approximation principle using transfer function expansion in MacLaurin series 06 p0978 A67-18559

Transient stress-strain state of elastic system developing combination resonance analyzed, using approximate method 06 p1106 A67-18621

Boundary conditions for two-dimensional steady heat flow in rectangular region with temperature discontinuity at corners 06 p1119 A67-18650

Nonlinear problems of thin plate bending, using successive approximations method 06 p1108 A67-18661

Dynamic stress concentration for plate with square hole, using approximate method of boundary shape perturbation and conformal mapping 06 p1109 A67-18665

Successive approximations for determining direct and backward wave in inhomogeneous medium and consequently reflection coefficient and total field 06 p1034 A67-18771

Approximation method of determining statistical characteristics of phase coordinates of linear automatic control systems 06 p0978 A67-18792

Rational approximation method for calculating supersonic axisymmetric flow of perfect gas around given blunt body 06 p0943 A67-18846

Approximate solutions for uniform gas cloud expansion into vacuum with attention to inaccuracies 06 p0993 A67-18890

Necessary and sufficient set conditions for continuous function analytic within internal points of set to permit smooth approximation by means of rational fractions 07 p1212 A67-19137

Numerical solutions of nonlinear differential equations - Conference, U.S. Army Mathematics Research Center, Madison, May 1966 07 p1212 A67-19152

Error estimation for approximate solutions of differential equations, using functional analysis 07 p1213 A67-19153

Solution approximation for nonlinear parabolic PDEs, using linear combination of finite set of selected functions 07 p1213 A67-19159

Order of approximation of continuous functions through Hermite-Feier polynomial along entire axis 07 p1213 A67-19161

Approximate solution of temperature field of thin isotropic cylindrical shell heated by time dependent thermal fluxes from two ambient media 07 p1266 A67-19162

Approximate solutions for differential and integral equations in form of second order asymptotic polynomials 07 p1214 A67-19216

Approximate solution of integral equations with aid of least squares for steady motions of viscous incompressible fluid in rotating cylinder 07 p1168 A67-19217

Ultraconvergence of sequence of optimal approximation polynomials 07 p1216 A67-19583

Pulse distortion in ionospheric plasma, discussing reflection from layer via geometrical optics and quadratic approximation 07 p1143 A67-19594

Polonnikov generalization of Bode amplitude approximation technique to phase approximate evaluation 07 p1161 A67-19879

Approximate method for predicting lunar satellite lifetimes and application to lunar orbit mission analysis [AAS PAPER 66-130] 07 p1255 A67-19989

Coupled Green function equations for Helsenberg ferromagnet approximated via differential equations 07 p1237 A67-20141

Extended average energy approximation of first order perturbation wave function, proposing procedure for multidimensional problems 07 p1137 A67-20186

Combination into unified setting of various results for approximate solution of fixed point equation, using iterative process 07 p1218 A67-20212

Electromagnetic wave scattering by rough surface computed by approximate method 07 p1147 A67-20237

Remedies for deficiencies in approximations near transition point in asymptotic methods used for estimates of solutions to differential equations governing axisymmetric vibrations of thin elastic shells 08 p1414 A67-20346

Simultaneous approximation of function and derivatives, ensuring uniqueness by imposing linear conditions on coefficients of polynomials 08 p1347 A67-20368

Error in application of WKB method to linearized postburnout equation of motion of sounding rocket 08 p1406 A67-20510

Compatibility relations and generalized finite difference approximation for three-dimensional steady supersonic flow 08 p1320 A67-20566

Third order control system saturation, considering approximate solution to third order bang-bang system 08 p1312 A67-20722

Fourier integral and series approach to semilinear strip subject to general symmetrical tractions along three edges 08 p1422 A67-20978

Convergence rate of approximate Ritz and Bubnov-Galerkin method in application to equations having solutions in form of linear combination of functions 08 p1349 A67-21200

Approximate solution of some nonstationary boundary layer problems with allowance for magnetic field, discussing nonsteady flow of viscous incompressible electrically conducting fluid past flat plate 08 p1362 A67-21202

Rational iteration function with high order convergence for solving equations compared with other methods 08 p1349 A67-21258

Self-consistent field approximation to ion-beam-plasma boundary interaction noting effect on ion beam structure, boundary conditions and resulting current density 08 p1363 A67-21307

Approximation method for calculating self-ignition delay for monodisperse air-fuel mixtures 08 p1428 A67-21425

Normal approximation of error transition probability for correlation receiver preceded by wideband hard limiter 09 p1459 A67-21579

Approximation method to general solutions yielding coherence tensors of electromagnetic waves excited by source distribution with known coherence properties 09 p1462 A67-21606

Ordinary linear differential equations with variable coefficients solved by phase plane displacements 09 p1524 A67-21648

Large deflection of asymmetrically layered plate, using parametric expansion techniques to extract system of differential equations governing scaling of stresses and displacement component for boundary conditions 09 p1574 A67-21756

Stochastic approximation method for determining real number from observation of random variables 09 p1524 A67-21933

Approximation of zero of transcendental equation by iterative methods 09 p1468 A67-22049

Moments of output coordinates of nonlinear system determined by algorithm based on approximation method, applied to automatic control system 09 p1525 A67-22079

Nonlinear automatic system with logical device analyzed in presence of external action, obtaining harmonic linearization coefficients 09 p1482 A67-22080

Medium flow parameter measurement via stationary sensors for simulated test stages of axial compressor 09 p1438 A67-22456

First approximation for MHD nozzle flows with end effects 09 p1550 A67-22589

Hydrogen line profiles in model atmospheres using quasi-static approximation for electrons and ions 10 p1704 A67-22883

Solving quasi-linear automatic system with n degrees of freedom in cases of incommensurable frequencies by approximation method 10 p1673 A67-22935

Best Chebyshev approximation and approximation in Cartesian product space 10 p1674 A67-22966

Attenuation constant of model helix waveguide determined using approximate method, considering electromagnetic leakage due to wall irregularity 10 p1606 A67-23064

Modified differential approximation for external radiation sources in radiation gas dynamics 10 p1733 A67-23113

Approximate solution of heat transfer problems with phase change for time dependent surface 10 p1733 A67-23119

Reduction of PDE system of heat transfer, using Hermitian approximating polynomials to obtain solution to initial system 10 p1608 A67-23323

Analytic solution to blunt body problem in supersonic flow of ideal gas approximated, using power series [NOR REPORT 65-239] 10 p1593 A67-23454

Controllability of quasi-linear systems proved by Picard classical method of successive approximation 10 p1681 A67-23682

Radial distribution function differential equation solution studied numerically and analytically for plasma parameters, using closure approximation 11 p1826 A67-23871

Elastic wave diffraction around elliptical hole in thin plate, obtaining dynamic stress concentration coefficient through approximate solution 11 p1870 A67-23897

Polynomial approximation method for determining satellite orbits from large-time-interval trajectory measurements 11 p1858 A67-24066

Averaging method in nonlinear mechanics, discussing results of Bogolubov studies 11 p1818 A67-24089

Minimax problem for pursuit problem of two linearly controlled objects describable by identical differential equations 11 p1812 A67-24145

Boundary between applicability ranges of network and steepest descent methods in equation integration of Timoshenko theory in analysis of plate deformation 11 p1871 A67-24159

Approximation method calculation of propagation constants of dielectric loaded TE wire-grid leaky wave antenna for near endfire radiation 11 p1763 A67-24296

Stability of bilaterally symmetrical object towed in air along straight line, obtaining characteristic equation as test for lateral or longitudinal stability 11 p1743 A67-24309

Kantorovich method applied to approximate solution of nonlinear problems of heat conductivity theory of plate 11 p1883 A67-24323

Reentry guidance by threshold network storage of precomputed optimum commands, using analogy of surface approximation problem in N plus one-dimensional space [AIAA PAPER 66-52] 11 p1869 A67-24338

Dispersion relation for LF oscillations in plasma with negative ions derived in three-fluid approximation 11 p1834 A67-24375

WKB /Wentzel-Kramers-Brillouin/ approximation to solve linearized Vlasov equation for oscillations of inhomogeneous one-dimensional plasma 11 p1838 A67-24404

Expression for electron contribution to Stark broadening, using impact approximation with Lewis or Debye cut-offs 11 p1823 A67-24491

Formal expansion schemes in predicting statistical properties of turbulent flows at high Reynolds numbers 11 p1780 A67-24540

Hydrodynamic stability problems solved through approximate and numerical methods involving eigenvalue spectrum and Orr-Sommerfeld equation for parallel flow 11 p1781 A67-24552

Transfer process effect on stability of plane flame front, deriving revised approximate solution for large finite Reynolds numbers 11 p1883 A67-24672

Galerkin method applied to approximation of periodic solution of system of singular differential equations 11 p1819 A67-24762

Temperature profile of single stage axial flow turbine disk and blades determined by approximation method using impingement cooling [ASME PAPER 67-GT-14] 11 p1854 A67-24799

Single parameter apparatus for approximation of set of continuous functions 11 p1813 A67-24849

Approximation methods for multiply connected problems in two-dimensional theory of elasticity 11 p1878 A67-24875

Approximate solution using finite difference method of bending of rectangular plate beyond elastic limit 11 p1879 A67-24886

Eigenvalue scalar product solutions for closed loop time optimal control of linear systems 11 p1771 A67-24897

Modified collocation method for linear boundary value problem for

- integrodifferential equation, giving approximate solutions which converge to exact solution 11 p1814 A67-25048
- Semirelativistic approximation of matter-radiation interaction 12 p1966 A67-25146
- Approximation problem in curve gamma, which is continuous image of interval I 12 p1960 A67-25257
- Piezotransistor static characteristics approximated by exponential function of two variables 12 p1939 A67-25281
- Noise calculation in parametric amplifier using approximation method 12 p1913 A67-25300
- Boundary value problem solution by approximation method of Kupradze with differential operators and given and unknown functions 12 p1960 A67-25440
- Boundary value problem of smooth closed contour dividing plane in inward and outward region solved by successive approximations 12 p1961 A67-25442
- Approximate solution of Novozhilov equilibrium equation for noncircular cylindrical shells by small parameter method 12 p2019 A67-25562
- Approximate method for determining free oscillation frequencies of hinged rectangular plate with variable thickness 12 p2021 A67-25574
- Approximate solutions for boundary value problems of cylindrical shells of arbitrary geometry 12 p2021 A67-25576
- Approximate solution of equilibrium problem for shallow cylindrical shell of rational profile under pressure distribution from convex side 12 p2024 A67-25603
- Heat equation of thin closed cylindrical shell exact solution analyzed using least squares method 12 p2034 A67-25606
- Approximate method for calculating stagnation point laminar boundary layer equations taking into account chemical reactions in gas phase and surface of body 12 p1928 A67-25673
- Approximate method for solving bending problem of rectangular plates of nonuniform thickness under arbitrary external edge loading 12 p2031 A67-25962
- Decomposition of stress functional with respect to small parameter 12 p2032 A67-26103
- Generalized Bubnov-Galerkin-Kantorovich method for approximate solution of boundary value problem 12 p1962 A67-26106
- Parameters of supercompressed detonation wave in solid propellant system noting wavefront pressure, density and propagation rate dependence on displacement rate of interface 12 p1930 A67-26116
- Approximate technique using perturbation theory in analyzing microwave interaction with gyrotropic media 12 p1908 A67-26183
- Spanwise distribution of aerodynamic shear and bending-moment on cantilever tapered wings 13 p2215 A67-26485
- Surface temperature of one-dimensional homogeneous thermally isotropic body impervious to radiation 13 p2222 A67-26610
- Discrete rational approximation problem, procedure for solution 13 p2145 A67-26615
- Separated compression shock circulation in front of wedge profiles at high Mach numbers 13 p2049 A67-26640
- Unified theory of gas-solid energy transfer in perturbation approximation, examining physical principles 13 p2223 A67-26940
- Drag coefficient for cylinder rotating in rarefied gas, comparing numerical method and approximate analytical solution 13 p2101 A67-26963
- Accuracy of approximation solutions of Boltzmann equation for rarefied gas flow 13 p2104 A67-26979
- Unsteady thermoelastic stress calculation in plane wall 13 p2219 A67-27059
- Functional extremals approximation method applied to compressible subsonic fluid flows 13 p2050 A67-27148
- Variation diminishing spline approximation method of linear interpolation 13 p2147 A67-27468
- Convergence considerations on second order method of parabolic equations approximate solution 13 p2148 A67-27473
- Iterative numerical method for solving equations of single variable by using several approximations applied to parallel processing environment 13 p2148 A67-27487
- Approximate method for predicting lunar satellite lifetimes and application to lunar orbit mission analysis [AAS PAPER 66-130] 13 p2209 A67-27541
- Earth-moon and moon-earth trajectory parameters related to lunar orbit conditions for synthesizing lunar orbit trajectory 13 p2210 A67-27616
- Three-dimensional supersonic flow past pointed nonaxisymmetrical bodies characterized by great local surface curvature changes, using new approximation 13 p2051 A67-27617
- Regularization method for maximum height ascent of rocket uniformly approximating control function by gradient projection method 13 p2149 A67-27618
- Asymptotic form of uniform approximation of abstract functions by single family of linear integral operators occurring in Banach space topology 14 p2341 A67-27834
- Euler-Lambert equation for orbital transfer in Newtonian field solved by approximate method 14 p2383 A67-27865
- Continuum flow analysis for leading edge region of flat plate, using model based on hypersonic thin layer type of approximation 14 p2240 A67-28163
- Nonlinear inviscid transonic flow in throat of two-dimensional curved nozzle, using approximate method [ASME PAPER 67-FE-11] 14 p2242 A67-28360
- General formulation and solution methods of electromagnetic wave diffraction and scattering problems 14 p2268 A67-28448
- Infinite plate temperature field determined by approximate method when heat transfer coefficient is time dependent 14 p2407 A67-28647
- Flow rate and pressure coefficients approximate determination for surface of symmetrical hypersonic flow past circular cone 14 p2243 A67-28656
- Theorems derived from approximate methods of analysis applied to collocation, moment and Galerkin methods for solving linear integral and differential equations 14 p2344 A67-28671
- Steady state heat conduction approximation solution based on effective boundary conditions concept 14 p2408 A67-28805
- Collocation method applied to approximation solution of loaded integral equations 14 p2344 A67-28895
- Extension of Zygmund approximation series to two dimensions, noting periodic function role 14 p2345 A67-28938
- Generalization of two theorems proved by Freud /1966/ concerning rational approximation 14 p2345 A67-28939
- Strong approximation of continuously differentiated function by means of differentiated expressions of finite line matrix 14 p2345 A67-28940
- Approximate expression derivation for calculating propagation rate of strong shock wave in inhomogeneous cosmic medium 15 p2552 A67-29146
- Approximate model for simplification of linear dynamic system, neglecting effect of higher order time constants 15 p2457 A67-29370
- Stationary functionals construction for linear boundary value problem solution or solution derivatives at specified but arbitrary point 15 p2509 A67-29383
- Formula for pressure vs flow deflection at hypersonic speeds, useful in studies involving pressure on inclined surfaces 15 p2472 A67-29675
- Difficulties arising in applying Liapunov first method to solution of canonical systems and ways to overcome them 15 p2511 A67-29885
- Nonlinear differential equations of systems describable by state model solved by incremental linearization technique 15 p2458 A67-29908
- Matrix formulation and resultant approximations as approach to nonlinear chemical reaction rate equations 15 p2434 A67-30023
- Motion equations of heavy symmetrical gyroscope in gimbal suspension, noting integrals of second approximation 15 p2490 A67-30174
- Nonlinear nonconservative systems stability analysis by approximate method based on principle of energy conservation 15 p2519 A67-30194
- Electron temperature reduction possibility in individual valleys of multivalley semiconductors, based on energy-balance equation in electron-temperature approximation 15 p2542 A67-30246
- Control system identification and loop stability limit, noting dominant components of time functions and classification of substitute functions 15 p2461 A67-30317
- Control system identification for noise corrupted input/output data, using algorithmic approach and iteration procedure 15 p2461 A67-30320
- Thermal slip rate of gas near solid surface determined by measuring gas-flow distribution function according to Bhatnagar, Gross and Krook 15 p2582 A67-30390
- Striated layer flow of working fluid in duct of synchronous induction MGD generator studying stability by approximation 16 p2607 A67-30594
- Polynomial substitution formulas for complicated equations of multipoint boundary value and optimization problems in flight mechanics and astrodynamics 16 p2695 A67-30733
- Optimum performance of propulsion acceleration calculated by approximation method, noting earth-Mars transfer and Jupiter and Saturn missions 16 p2760 A67-30735
- Analog computer method for approximation of real functions, discussing applications and limitations 16 p2634 A67-30831
- Elastic deformation calculation using linear real tension-elongation law 16 p2764 A67-30855
- Cylindrical electronic microwave tubes, deriving expressions for zero and first approximations of physical parameters 16 p2636 A67-30883
- Motion in ternary stellar system consisting of central body and close and distant companions 16 p2746 A67-30956
- Fluctuating function method for approximate solution of boundary value problems for linear differential equations with reduced variational problems 16 p2696 A67-31013
- Approximate calculation of coefficients in equation for perturbed motion of rigid body containing liquid 16 p2765 A67-31051
- Stress-strain state determination of nonlinear plate with circular holes, deriving boundary conditions and basic equations 16 p2766 A67-31147
- Numerical approximation of evolution equation solution for linear and nonlinear operators by finite difference method 16 p2696 A67-31198
- One-dimensional charged particle flow in bounded system, particularly overlapping steady state zero-temperature flow approximation solutions, noting instabilities 16 p2704 A67-31233
- Successive approximation method for asymptotic solution of waves in inhomogeneous gyrotropic plasma 16 p2627 A67-31366
- Iterative solution methods for minimizing convex, differentiable function in Euclidean space 16 p2697 A67-31424
- Laminar flow of electrically-conducting fluid suddenly expanding in magnetic field calculated by approximate method 16 p2722 A67-31573
- Interplanetary trajectory correction via radial heliocentric velocity pulses, noting calculation by linear approximation 16 p2752 A67-31604
- Suboptimal control of large scale dynamic system consisting of two weakly coupled subsystems using aggregation 16 p2647 A67-31645
- Suboptimal control function sequence generation by combining approximation in control policy space with stability criteria from direct method of Liapunov 16 p2648 A67-31658
- Finite dimensional approximations of optimal nonlinear filters for class of large-noise, nonlinear, continuous-time problems 16 p2651 A67-31680
- Precomputed approximation to weighting matrix in extended Kalman filter for ballistic reentry vehicle trajectories estimation 16 p2651 A67-31682
- Identification of continuous, nonlinear, time-dependent, single-input single-output systems represented by Volterra functional series model and stochastic approximation 16 p2653 A67-31694

Approximation method for steady laminar flows of incompressible viscous fluid in curved pipes, obtaining flow rate 17 p2836 A67-32038

Response of one degree of freedom system with power law time dependent damping and restoring forces using WKBJ approximation 17 p2958 A67-32128

Radiation transport in spectral lines as photon absorptions and emissions, discussing contemporary theories, approximation methods and applications 17 p2893 A67-32143

Strain due to even pressure in oval or circular tubes, calculating deformations 17 p2958 A67-32259

Excitation and propagation of surface plasma waves along plasma column in noble gases, obtaining plasma dispersion curves 17 p2899 A67-32309

Asynchronous pulse modulation systems developed using step and linear segment approximations of message waveforms 17 p2812 A67-32318

Multidigit delta modulation system using individual optimized stages developed by successive approximation of message waveform 17 p2812 A67-32319

Flexural rigidity of plates reinforced by parallel stiffeners for direction normal to stiffener orientation determined together with stresses induced by bending moment 17 p2959 A67-32408

Mathematical methods of nonlinear programming, discussing convexity, quasi-convexity, gradient, Taylor series and quadratic approximations 17 p2818 A67-32425

Closed form regularized solutions in polar coordinates of two-body problem obtained and applied to restricted three-body problem 17 p2943 A67-32440

Variational principles and methods of approximation for nonself-adjoint and nonlinear systems 17 p2969 A67-32449

Maximum heating temperature of smallest particles of polydisperse material in two-phase flow by approximation method 17 p2970 A67-32462

Conservative series-parallel approximations to study systems models for reliability analysis and display 17 p2865 A67-32585

Simplification of linear equation of first kind with Tikhonov smoothing functionals 17 p2878 A67-32680

Boundary value problem of linear partial differential equation reduced to linear equation system with block-tridiagonal matrix by difference approximation 17 p2820 A67-32801

Galerkin method analysis of vibrations of clamped rectangular plates, using polynomial approximation 17 p2962 A67-32823

Single frequency vibrations of beams and girders solved by applying asymptotic methods 17 p2962 A67-32881

Approximate solution for hypersonic flow past unyawed cone by small disturbance stream function equation 17 p2793 A67-33024

Renormalizing approximate wave functions so that amplitude is correct by means of matrix, with applications to Born approximation 17 p2887 A67-33318

Quasi-one-dimensional approximation for MGD equations 17 p2910 A67-33325

Approximation solution of three-dimensional problems associated with slender wing motion in transonic gas flow with perturbations 18 p2981 A67-33535

Uniformly valid approximation of two-dimensional subsonic flow along thin airfoil with blunt elliptical shape 18 p2982 A67-33663

Superposition approximation for dense gases and liquids equilibrium theory, using phase-space distribution functions from maximization of information entropy 18 p3078 A67-33669

Temperature range approximation determination in unsteady thermal boundary layer formed in plane parallel flow around body, solving equation with boundary conditions 18 p3025 A67-33680

Successive approximation method analysis of flow around single barrier extending downstream and in direction of velocity at infinity upstream 18 p3025 A67-33682

Transition probabilities for molecular collision excitation by differential equation matrix, approximations, perturbation theory, etc 18 p3081 A67-33785

Band and total emissivities estimation procedures for polyatomic molecules,

discussing empirical emissivity charts and radiative exchange at local thermodynamic equilibrium 18 p3152 A67-33817

Algorithm for Fredholm type integral equation solution incorporating successive approximations, kernel replacement by degenerate kernel, averaging functional corrections and band methods 18 p3071 A67-34167

Turbulent boundary layer on plane catalytic plate in nonequilibrium dissociating gas calculated by successive approximation technique 18 p3027 A67-34204

Cup spring designing method, with generatrix curvature included in approximation, gives better characteristic curve and stresses 18 p3144 A67-34262

Algorithm for construction of discrete approximations to linear differential expressions in terms of ordinates 18 p3072 A67-34394

Rational approximations to incomplete elliptic integral of first and second kinds derived by main diagonal Padé approximations 18 p3072 A67-34397

Limiting values for remainder forms in Taylor series and error estimation procedures for power series approximations, including truncation error 18 p3072 A67-34398

Approximation method of determining statistical characteristics of phase coordinates of linear automatic control systems 18 p3018 A67-34457

Schottky approximate formula adaptation for abrupt junctions with asymmetric doping ratios 18 p3106 A67-34646

Time dependent expression for droplet-size distribution function of clouds undergoing forcible modification or natural evolution 19 p3251 A67-34862

Parametric expansions in linear theory of cylindrical shells noting loading and boundary conditions, approximation formation, fiber elongation, etc 19 p3339 A67-35054

Boundary value wave problem in elastoviscoplastic medium solved by approximate method using Courant concept 19 p3340 A67-35444

Approximation method for Einstein-Maxwell field equations successive solution applied to Weyl canonical problems and field equations for point particle 19 p3262 A67-35576

Solution to moment equations for near-equilibrium spherically-symmetric expanding flows by using Bernstein-Greene-Kruskal theory for Boltzmann equation 19 p3212 A67-35764

Underexpanded jet boundary streamline calculations by exact and approximate methods 19 p3171 A67-35768

Rectangular sandwich plates large deflection equations solved by successive approximation method 19 p3342 A67-35770

Validity range for weak turbulence theory in case of wave resonant interaction mechanism, treating Fokker-Planck and nonlinear optics approximations 19 p3298 A67-35792

Computer solution of optimal control problems by finite difference method 19 p3202 A67-35886

Approximate method of solving integral equations of local radiation characteristics applied to numerical solution of specific problems of radiative heat transfer 19 p3347 A67-35898

Hansen planetary theory representing position of disturbed planet as deviation in time and space from position of fictitious planet with Keplerian motion [AIAA PAPER 67-565] 19 p3328 A67-35961

Impact characterization and length, determining contact energy with Hertz equation and integrating nonlinear differential equation for system motion 20 p3483 A67-36195

Formulas describing hologram properties, considering emulsion thickness effect on recording and reconstruction 20 p3435 A67-36202

Nonlinear approximation of thin elastic plane plates noting influence of elastic medium and strain tensor deformations 20 p3535 A67-36279

Stream function of plane flow of incompressible viscous fluid around parabolic profile, using successive approximations method 20 p3420 A67-36394

Thin rectangular vortex wing in uniform

flow, solving nonlinear equations by successive approximations 20 p3356 A67-36439

Approximate solution for subsonic gas flow, deriving approximation for Chaplygin function for use in boundary value problems 20 p3356 A67-36442

Asymmetric stability loss of nonuniformly heated circular plate rib, determining elastic properties and critical temperature jump value 20 p3536 A67-36447

Shortest distance between two quasi-coplanar elliptical asteroid orbits, solving transcendental equations by consecutive approximation method 20 p3523 A67-36628

Radiant heat transfer computations from gray isothermal dispersions with isotropic scattering, using approximation methods and integrodifferential equation [ASME PAPER 67-HT-8] 20 p3544 A67-36706

Approximate solution to heat transfer coefficient on flat plate in linear shearing flow [ASME PAPER 67-HT-46] 20 p3547 A67-36728

Approximation integral method for solution of coupled equations of heat and mass transfer in porous medium, discussing nonlinear and linear problems 20 p3553 A67-36938

Time optimal feedback control using extension of Hermes approximation theorem 20 p3408 A67-37074

Necessary condition for optimal control in nonlinear automatic control system determined, using method of successive approximations 20 p3410 A67-37229

Pulse distortion in ionospheric plasma, discussing reflection from layer via geometrical optics and quadratic approximation 20 p3384 A67-37334

Approximate solutions for nonlinear differential equations to study periodic motions for analysis of pressure relief system 20 p3366 A67-37369

Rott approximate method applied to steady compressible laminar boundary layer on unyawed seminfinte solid circular cone with attached shock wave 20 p3360 A67-37595

Three-dimensional boundary layer for gas flow past generatrix of cylinder of arbitrary transverse cross section 20 p3360 A67-37658

Boundary value problem solution by approximation method of Kupradze with differential operators and given and unknown functions 20 p3479 A67-37723

Reynolds stress in turbulent flow dependence on mean velocity field determined by rational sequence of approximations 21 p3609 A67-37734

Papers on functional analysis covering approximation methods and Cauchy, Dirichlet and boundary value problems 21 p3651 A67-37832

Integration of Cauchy problem for class of nonlinear higher order partial differential equations 21 p3651 A67-37901

Successive approximation and Chebyshev uniform approximation method for solving Fredholm integral equation 21 p3651 A67-37904

Stress concentration near hole in large radius sphere solved by approximation method for Helmholtz equations in coordinated system 21 p3716 A67-37906

Hydrodynamic pressure on elastic cylindrical shell from acoustic shock wave, using higher order asymptotic approximations 21 p3717 A67-37973

Approximate method for calculating interaction between flow and soft spherical shell 21 p3717 A67-37976

Boundary value solutions by approximate method for variable thickness and rigidity shells using equilibrium equations 21 p3718 A67-37983

Combination paramagnetic resonance in mechanical system containing rotating body, giving procedure for approximate determination of oscillation amplitude and resonant zone boundaries 21 p3625 A67-37990

Nonlinear variational trial function for atomic hydrogen dynamic polarizability, discussing first order perturbed wave function and perturbation-variation method 21 p3659 A67-38004

Geometrical-optics approximation method for electromagnetic wave propagation in parametric medium 21 p3580 A67-38113

Approximate method for calculating electromagnetic field structure of vertical antenna 21 p3590 A67-38118

Approximate method for design of FM

systems using variable capacitance varactor diodes, noting time varying differential equation 21 p3593 A67-38234

Controllability of quasi-linear systems proved by Picard classical method of successive approximation 21 p3653 A67-38283

Helly problem of moment theory and optimum approximation of finite defect by subspace elements of continuous functions, examining uniqueness and existence 21 p3653 A67-38400

Convergence of perturbed Galerkin method to construct general theory of approximate methods for nonlinear equations 21 p3653 A67-38419

Z component of geomagnetic field, determining parameters of sloping dipoles 21 p3619 A67-38491

Polygonal approximation method for systems with nonlinear characteristics analyzed using continuous functions 21 p3657 A67-38551

Approximate method for electric propulsion missions analysis, determining system components effects on performance [AIAA PAPER 67-709] 21 p3693 A67-38736

Vibrations of turbine disks of variable thickness calculated by Ritz method, applying functions approximating actual thickness of disk 21 p3636 A67-38836

Discontinuous systems proved for stability and instability, using almost-reducible linear approximations 21 p3654 A67-38850

Plasticity stress-strain approximation for initial elastic behavior and incompressible state approach 21 p3728 A67-38880

Sample continuous second order martingale process, determining existence of limit of stochastic processes using approximation theorems 21 p3654 A67-38966

Curve approximation method applied to incompressible laminar boundary layer, comparing Head approximation method and exact solutions 21 p3615 A67-39081

Approximate method for evaluation of processing loss in delay line MTI receiver 22 p3758 A67-39211

Finite discontinuity jump conditions for plasma in strong magnetic field determined by approximation and Maxwell equation, noting possible application to satellite data 22 p3843 A67-39269

Approximate solution of elastic buckling of radially constrained circular ring under uniformly distributed loading 22 p3908 A67-39287

Approximate shell theory for unrestricted elastic deformation, discussing treatment of motion equations 22 p3909 A67-39293

Optimal control of quasi-linear system perturbed motion, developing approximation method 22 p3776 A67-39305

Magnus version of first harmonic approximation method for nonlinear systems engineering, using analog computer simulation for accuracy examination 22 p3776 A67-39327

Problem solving method based on averaging over periodic functions for steady waves in nonlinear one-dimensional distributed systems, deriving approximate equations 22 p3815 A67-39761

Approximation method for solution of Bellman equation in optimal control problems 22 p3777 A67-39828

Approximating method for predicting multiengine exhaust geometry and thermodynamic properties with single reference engine 22 p3902 A67-39940

Quasi-cylindrical approximation theory on swirling nozzle flow in relation to spin effect on rocket nozzle performance 22 p3742 A67-40118

Homogeneous and sandwich spherical caps axisymmetric vibration natural frequencies solved approximately, noting application to shallow and spherical shell problems 23 p4073 A67-40617

Approximation method for finite element bending analysis of variable structural plates, giving linear equations defining nodal values 23 p4073 A67-40627

Stiffness matrix for shallow rectangular shell element and application of finite element displacement method 23 p4073 A67-40628

Nonlinear system suboptimal feedback control technique based on method for determining approximate solutions for Hamilton-Jacobi-Bellman equation 23 p3983 A67-40645

Differential equations maximum parameter values for single mass nonlinear system passage through resonance point determined with approximate methods based on small parameter method 23 p4026 A67-40686

Approximate solution for turbulent jet expansion in opposite gas flow, discussing hydraulic drag coefficient formula derivation 23 p3989 A67-40731

Soviet book on approximate methods for boundary value problem solutions of ordinary and partial differential equations and certain integral equations 23 p4022 A67-40841

Analytic and harmonic transformations applied to Faber series summation, harmonic function approximation and logarithmic potential approximation 23 p4023 A67-40923

Averaging method for studying system oscillations over infinite time interval subject to pulsed action 23 p4027 A67-40925

Linear Boltzmann equation approximation by Fokker-Planck equation leading to logical inconsistency 23 p4029 A67-40963

Second order accurate approximation to advection terms in hydrodynamics equations noting aliasing effects, amplitude and phase errors and stability 23 p4024 A67-40994

Three-dimensional heat conduction, heat and mass transfer and thermoelasticity problems solved by approximate method using functional parameters 23 p4083 A67-41290

Technique for simulating stochastic approximation methods for selection of properties to ensure predetermined output signal characteristics 23 p3976 A67-41340

Correlation calculus applied in metrology, estimating correlation coefficient 23 p4008 A67-41397

Approximate investigation of standard model reference adaptive systems with random input effects based on filtering properties of automatic control systems 23 p3985 A67-41675

Imploding shocks and detonations propagation investigated by similarity solution extended to early imploding processes, using Oshima quasi-similar approximation 23 p3992 A67-41722

Approximate methods for solving heat transfer problems with phase change, considering applicability to Stefan problem 23 p4084 A67-41749

Orthogonal transformation of neighboring quantum states into classical two-component plasmas, using WKB approximation 24 p4195 A67-42107

Lower bounds for eigenvalues of differential linear elliptical operator using Rayleigh-Ritz approximation extension 24 p4177 A67-42154

Approximate solution to irregular waveguides with impedance boundary conditions based on amplitude of normal wave propagation 24 p4120 A67-42159

Turbulent fluid flow velocity and temperature fields in annular and plane gaps calculated by integral approximation for turbulent viscosity and heat conduction coefficients 24 p4142 A67-42213

Probability of signal detection and accuracy of measurement in fluctuating multichannel system parameters 24 p4120 A67-42223

Mixed problems of antenna synthesis, solving approximately specified amplitude and phase radiation patterns and given antenna current amplitude or phase 24 p4129 A67-42228

Relation between cosmic ray cut-off rigidity and L parameter, solving approximately 7th degree algebraic equation 24 p4214 A67-42789

High energy nucleon and pi-and K-mesons inelastic interaction cross sections from quasi-linear approximation of optical model 24 p4192 A67-42852

Book on stochastic approximation and nonlinear regression covering convergence, asymptotic methods, real time problem in presence of noise, etc 24 p4179 A67-42900

Approximate expression derivation for calculating propagation rate of strong shock wave in inhomogeneous cosmic medium 24 p4239 A67-43069

Improvement of understated eigenvalue approximations 24 p4179 A67-43079

Non-Newtonian elastoviscous channel flow between rigid boundaries solved by

asymptotic expansion in lubrication approximation 24 p4145 A67-43086

High order accurate difference methods in hydrodynamics 24 p4146 A67-43095

APTITUDE

S PERSONALITY

S PERSONNEL SELECTION

ARC

S AURORAL ARC

S CARBON ARC

S ELECTRIC ARC

S MAGNETIC ANNULAR ARC

S MERCURY ARC

S PLASMA ARC

ARC CHAMBER

Lanthanum germanide synthesis using arc furnace, noting chemical properties 13 p2131 A67-26470

ARC DISCHARGE

Rotating flame resulting from instability of inhomogeneous plasma produced by arc discharge in magnetic field approaching criticality 01 p0123 A67-10739

Effect of shifting radial electrical field sign on instability state of inhomogeneous plasma produced by arc discharge in equipotential volume 01 p0123 A67-10741

Energy transfer to anode, cathode and surroundings in high current argon arc 01 p0125 A67-10976

Oxidation and ablation characteristics of tantalum in hyperthermal arc tunnel filled with oxygen-nitrogen mixtures 01 p0102 A67-11153

Ion engine arcing frequency from micrometeoroid impact [AIAA PAPER 66-205] 02 p0302 A67-11936

Introductory text on electrical discharges in gases, emphasizing physical behavior of electrons and ions in ionized state 02 p0279 A67-12720

Vaporization rate and diffusion of Cu, Mg and Cr in arc discharge plasma determined from curves of spectral-line emission energies 02 p0279 A67-12743

Mean static current density over cross section of arc moving in slot chamber under action of external magnetic field effectively measured by probing technique 03 p0476 A67-13179

Emissive capacity of argon in direct current arc at high pressure and temperature, noting experimental setup and results 03 p0478 A67-13602

Thermal and nonthermal cosmic radio sources explained by short circuit breakdown of predischarged field initiated by breakdown to thermally ionized arc discharge 04 p0691 A67-14433

Thermal similarity theory in accounting for convective heat transfer in arc discharge 04 p0667 A67-15192

Gas temperature decay characteristics for interrupted high pressure arcs at various current intensities 05 p0850 A67-16068

Resistance of DC arc gap recovering freely after interruption instantaneously measured, using voltage and current probing techniques 05 p0850 A67-16069

Transition probabilities for S I multiplets measured from arc spectra running through sulphuryl chloride liquid vortex 06 p1038 A67-17656

Cylindrically symmetric dynamic wall-stabilized plasma arc theory, considering detailed structure of column 06 p1040 A67-18123

Aerodynamic behavior and heat transfer of electric arc in air stream and transverse magnetic field 06 p1042 A67-18306

Self-healing electric breakdown in MOS structures noting magnitude duration, temperature and propagation characteristics 07 p1157 A67-19904

Auxiliary arc electrodes for solution to cold boundary layer and cathode emissivity problems in MHD generators 09 p1444 A67-21822

Two-frequency correlation method for determining time dependent mean statistical voltage and current values for DC arc 09 p1547 A67-22323

Electron sources from arc discharge plasma in metal vapor, using copper and tin cathodes 09 p1548 A67-22327

Symptomatic behavior and anode regimes of arc for electric arc with superimposed subsonic flow of argon [AIAA PAPER 66-479] 10 p1685 A67-23123

Knudsen low voltage discharge with hot cathode, determining electron distribution,

velocity profiles, V-I characteristics, etc 11 p1831 A67-24020

Plasmatron jet with vortical air stabilization of arc, correlating jet structure with nozzle geometry and electrode polarity 11 p1832 A67-24027

Approximate similarity criterion for arc with self-adjusting length, burning in plasmatron with gas vortex stabilization, determined by shunting 11 p1843 A67-24969

Shunting process and associated fluctuations in plasmatron with vortex stabilized arc, noting anode spots 11 p1843 A67-24971

Steady state properties of spheroidally symmetric static arcs with only conduction losses 12 p1970 A67-25290

Behavior of high current arcs driven by strong external magnetic fields with respect to hypersonic flow generation by MHD forces 12 p1974 A67-25399

Plasma propagation theory of arc retrograde motion in transverse magnetic field 12 p1974 A67-25400

Cathode spot phenomena in pulsed vacuum arc utilized for electric microthrusters, testing cathode materials by mass and momentum transfer 12 p1989 A67-25403

Mathematical theories applicable to excitation and ionization of atoms in plasmas at thermal equilibrium, determining electron density and temperature 12 p1988 A67-25432

Axially flowing gas through arc discharge, examining effect on I-V characteristic and radial temperature distribution in arc column 12 p1975 A67-25751

Ionization dependence of Na, K, Ca, Mg, Al, Fe and Si on arc temperature, noting correlations between temperature and electron concentration independent of plasma composition 12 p1977 A67-26108

Soviet book on physical optics 12 p1967 A67-26131

Rotating flame resulting from instability of inhomogeneous plasma produced by arc discharge in magnetic field approaching criticality 13 p2166 A67-26768

Effect of shifting radial electrical field sign on instability state of inhomogeneous plasma produced by arc discharge in equipotential volume 13 p2166 A67-26770

Driver chamber for very high temperatures obtained with ceramic liner for arc driven shock tube, reducing contamination and cooling of driver gas 14 p2293 A67-28749

Electric discharge in vacuum consisting of two successive phases, arc formation characterized by X-ray emission and weak current and arc characterized by light emission 14 p2349 A67-28899

Generation of quiescent variable-parameter arc plasma in strong magnetic field 15 p2523 A67-29228

Plasma drift instability in discharge with oscillating electrons, measuring plasma vibration spectrum 15 p2528 A67-29711

Dispersion relations of moving striations in rare gases, noting wave nature and dependence on discharge current 15 p2472 A67-29733

Electrical characteristics of low current arc discharge in magnetic field determining effect of nonequilibrium plasma on conductivity 16 p2710 A67-30524

High power argon ion laser with wall stabilized arc discharge determining laser output 16 p2685 A67-30825

Cross sectional shape of magnetically balanced arc determined, noting elongation perpendicular to flow 17 p2906 A67-33033

Stabilized arc discharge characteristics using Elenbaas-Heller equation as basis for calculations 17 p2906 A67-33088

Instrument for generation of thermal plasmas in direct current-arc discharges and expansion to walls of coaxial corotating cylinder 17 p2835 A67-33389

Emissive capacity of argon in direct current arc at high pressure and temperature, noting experimental setup and results 18 p3090 A67-34467

Radial pressure distribution in hydrogen arc located in axial magnetic field using Saha equation, determining temperatures and electron densities 19 p3279 A67-35139

Retrograde motion of electric arc discharge at low pressure with transverse magnetic field, including cathode vaporization 19 p3281 A67-35153

Shock wave interaction with plasma arc discharge, investigating wave refraction, arc response to pressure and temperature pulses and aftershock flow field 19 p3294 A67-35407

Inhomogeneous plasma instability from low pressure arc discharge in magnetic field 20 p3498 A67-36683

Laser interferometric measurements of electron density in plasma arc discharge at atmospheric pressure 21 p3664 A67-38017

Apparatus for refractory single crystal fusion growth at high temperature using arc melting 21 p3636 A67-38769

Electrical and spectral investigation of pulsed high pressure arc produced by capacitor bank discharge in helium and hydrogen 22 p3845 A67-39426

Cesium plasma ionization in low voltage arc discharge, measuring electron ionization capacity, electron temperature and cesium ionization and excitation cross sections 22 p3847 A67-39510

Integrated transport cross sections obtained for nitrogen as function of temperature using gaskinetic formulas 22 p3841 A67-40050

Low pressure argon ion laser cold emission cathode, considering electron production by cathode sputtering owing to self-sustained arc discharge 22 p3817 A67-40413

Carbon and iron grain production in argon arc discharge studied for implications of light scattering in interstellar absorption 22 p3896 A67-40531

Discharge model for relative abundances of different ions extracted from Ar duoplasmatron from Langmuir probe measurements 23 p4033 A67-41190

Apparatus for plasma investigation of pulsed arc discharge in high pressure argon 23 p4035 A67-41686

Aerodynamic behavior and heat transfer of electric arc in air stream and transverse magnetic field 23 p4035 A67-41724

[AIAA PAPER 67-98] Ar produced in capillary arc discharge, studying charged particle density and electron temperature dependence on magnetic field intensity 24 p4196 A67-42244

Ar II population inversion of 4s and 4p states in stationary arc discharge, measuring ionic and atomic spectral line shift, widths and intensities and emission power 24 p4196 A67-42245

Net convective and radiative heat flow to electrodes of coaxial plasma generator may exceed heat flow from moving arc spot within arc burning region 24 p4098 A67-42250

V-I characteristics correlated with energy release from arc column, noting turbulent nature of heat transfer in arc with transverse blowing 24 p4255 A67-42589

ARC GENERATOR

Arc formation at metal surface in hydrogen plasma analyzed at various gas pressures, using Penning discharge, noting heat treatment effect on hydrogen 05 p0850 A67-16066

Vortex gas stabilization of arc and effect of current strength, flow rate and geometrical dimensions 09 p1547 A67-22320

Volt-ampere characteristics, generation and decay of interrupted and AC arcs in nitrogen, air, argon and carbon dioxide at zero gravity 14 p2354 A67-27760

ARC HEATING

Design features of high velocity test stand with arc heater and MHD accelerator 04 p0595 A67-14543

Mixing at constant section of two flows of different enthalpies, demonstrating phenomenon with arc type reheater 04 p0602 A67-14569

Aerodynamic detector measuring dynamic pressure distribution in laminar He jet heated by electric arc 05 p0850 A67-16035

Performance capability of transpiration cooled constricted arc heater, treating hydrogen 10 p1698 A67-23122

Arc rotation heat transfer effects in self-induced magnetic field plasma arc heaters used for aerodynamic tests 12 p2034 A67-25346

Boundary layer in nozzle of arc-heated wind tunnel, obtaining velocity, temperature and density profiles 14 p2299 A67-28171

Aerothermodynamic testing of heat protective systems in arc tunnel 15 p2466 A67-29538

Arc image ignition of solid propellants

compared to conductive ignition, outlining corrective steps and deriving ignition time delay 15 p2581 A67-29987

Arc burning mechanism of vortex-stabilized plasmatrons, noting effect of arc shunting on volt-ampere characteristics 17 p2897 A67-32171

Arc-image furnace for direct gas heating at high temperature by concentrated radiation studies and efficient cavity-type receiver development 17 p2834 A67-32696

Electrode heating of arc burning in moving plasma in vacuum, giving setup, heat emission diagrams, etc 17 p2907 A67-33091

Fractional excitation and ionization for argon beam extracted from arc-heated supersonic free jet, noting molecular ions and neutralization 18 p3082 A67-34028

Electric arcs in cross flow with variable magnetic field across electrode space 19 p3281 A67-35154

Radial temperature distribution in high power argon arcs measured at atmospheric pressure and 5 atm for currents ranging from 200 to 500 amp 22 p3853 A67-40049

ARC JET

Plasma propulsion devices and phenomena responsible for energy losses, considering plasma gun and MPD arc jet 01 p0141 A67-11388

Hydrogen arcjet plume spectroscopy, examining exhaust at various H mass flow rates 05 p0874 A67-17357

Critical mass flow rate existence for maximum thrust from MPD arc jet 06 p1075 A67-18866

Current density distribution in MPD arc jet exhaust measured, using Hall effect sensors 08 p1375 A67-20573

[AIAA PAPER 66-116] Acceleration of propellant in arcjet devices by thermal and self-magnetic forces, using various nozzle configurations 08 p1375 A67-20574

Lorenz, two-line and calorimetric methods for plasma jet temperature measurements 11 p1793 A67-24825

Arc jet exhaust velocity compared with propagation velocity of random light fluctuations 13 p2188 A67-26839

Local mass flux and local impact pressure measurement in arc jet exhaust flow fields 17 p2861 A67-33029

Probe for total enthalpy measurements in arc jet exhausts 17 p2971 A67-33030

Arc jet power efficiencies tested in insulated tank, comparing deuterium with hydrogen 21 p3691 A67-38710

[AIAA PAPER 67-677] Propellants and propellant mixtures effects on MPD arc jet performance in test for ions and neutrals mixture acceleration to high velocity 21 p3688 A67-38715

[AIAA PAPER 67-684] Steady flow ammonia MPD arc jet thruster propulsion performance, discussing test chamber pressure variation, thrust data and cooling systems 21 p3696 A67-38930

[AIAA PAPER 67-690] Fast response thin skinned calorimeters for high heat flux profiles of arc jet flows 23 p4006 A67-41381

ARC LAMP

Crystal absorption and lamp emission spectra for CW pumping of Nd-doped YAG by water-cooled Kr arcs 03 p0437 A67-13576

Plasma flows from normal and coaxial electrode contact points of arc and effect of external forces by schlieren photography 10 p1687 A67-23849

S-4A solar simulator consisting of hexagonal array of 19 interreflector modules 12 p1922 A67-25699

Copper anode lamp for solar simulation facilities, discussing effect on arc brightness and anode loading of magnetic fields, gas mixtures, pressure, etc 12 p1925 A67-25734

Iso-irradiance contours close to high pressure mercury arc lamp 12 p2037 A67-26030

[AIAA PAPER 67-315] Optical interferometer for refractive plasma diagnosis, noting Q-switched ruby laser and pulsed arc lamp 21 p3630 A67-38768

Field induced photoelectron emission /FPE/ from Si surface barrier diodes, discussing FPE measurement using xenon arc lamp and grating monochromator 23 p3980 A67-40890

ARC MELTING

Eliminating solidification cracks in arc-melted ingots of high strength crack-prone

Mo-TZC type alloy by capping with unalloyed molybdenum 02 p0248 A67-12704

Soviet monograph on vacuum arc melting of titanium alloy ingots noting crystallization process, structural changes and properties of end-products 03 p0447 A67-13925

ARC WELDING

SA PLASMA ARC WELDING

SA SPOT WELDING

Fabrication of columbium alloy liquid metal loop to study boiling and condensing characteristics of Na and K up to 1000 degrees F with gas tungsten arc welding in helium atmosphere 01 p0080 A67-10945

Transverse oscillated electron beam welding procedures of D6AC steel and mechanical properties—evaluation show comparable results to corresponding gas tungsten arc welds 01 p0080 A67-10946

Arc radiation and selective solute vaporization from arc spot region of weld pool used to explain formation of overlap segregation in aluminum alloy weldments 01 p0080 A67-10947

Computer welding skate for automatic gas tungsten-arc welding of contoured or double-contoured parts, providing control without touching work surface with transducers 01 p0081 A67-11040

Mississippi Test Facility gas metal-arc welding of T-1 steel critical high pressure piping systems for Saturn V launch vehicle 03 p0430 A67-13691

Crack propagation in heat-affected zone during HF AC current gas-tungsten arc welding of Al alloy test plate 03 p0430 A67-13693

Laser and electron beam welding techniques, noting weld joint characteristics and tungsten inert gas arc welding 10 p1660 A67-23008

Percussive arc mode welding applicability to delicate components and butt type joints 12 p1948 A67-25269

Pulsed inert gas metal-arc welding technique for titanium 721, investigating arc characteristics in argon, argon/helium and helium 12 p1950 A67-25738

Steel cryogenic vessel AC welding method using special emission coated electrodes nullifying arc blow effect 14 p2327 A67-28820

Weldability test method, developing rig which permits arc welding in argon atmosphere with TIG electrode 16 p2681 A67-30833

Fracture toughness and stress corrosion cracking of titanium alloy weldments indicating resistance differences between base metal and weldment 24 p4161 A67-42329

Radio noise data compared for transmission lines, automotive traffic and RF stabilized arc welders 24 p4123 A67-42718

ARCAS ROCKET

Inflatable parachute system developed for deceleration of ionospheric probe instrumentation descending after expulsion from rocket 03 p0359 A67-13369

ARCH

Dynamic snap-through of shallow arches under stochastically varying transverse loads 10 p1725 A67-23711

ARCTIC

IR imagery and concurrent aerial photography in depicting Arctic terrain features and conditions during daylight 01 p0058 A67-10312

Arctic upper atmosphere neutral gas composition and altitude distribution studied, using meteorological rockets 19 p3219 A67-35251

ARGENTINA

Solar eclipse study program in Argentina 07 p1260 A67-20226

Stratosphere and mesosphere wind and temperature measurements, noting additional cosmic radiation measurements during 1966 solar eclipse in Argentina 19 p3320 A67-35287

Argentina 1964-1965 IQSY program emphasizing aerology, solar radiation, ozone concentration, geomagnetism, etc 19 p3224 A67-35499

ARGO D-4 ROCKET

S JAVELIN ROCKET

ARGON

Numerical method to obtain emission coefficients from emitted spectral intensities for asymmetrical plasma sources such as atomic spectral argon line 01 p0115 A67-11073

Proposed modification of Wetzel model of direct ionization by primary continuum in light of recent steady state precursor

electron density measurements ahead of Ar shocks 01 p0118 A67-11193

Absolute direct excitation cross section from neutral ground state for upper levels of transition in argon 02 p0253 A67-12520

Diffusive separation of helium-argon mixtures in underexpanded free jets and normal shock waves studied by electron beam 02 p0234 A67-12543

Role of amplification due to impacts of second kind in emission of nitrogen and CO molecular bands in mixture of nitrogen-argon and CO-Ar in glow discharge 02 p0270 A67-12674

Twyman-Green arrangement of interferometer with narrow laser beam and twin photomultipliers, examining strong shocks in argon in 15.2 cm shock tube 02 p0247 A67-12688

Low energy electron diffraction techniques for niobium /110/ surface, noting argon ion bombardment 02 p0257 A67-12729

Low energy total and momentum-transfer scattering cross sections for electrons on He and Ar compared, using modified effective range formulas 03 p0471 A67-13319

Primordial argon and metamorphism of chondrites 05 p0886 A67-16025

Energetic and angular studies of argon deuteride and nitrogen deuteride positive ion formation using angular ion scattering apparatus 05 p0848 A67-16835

Atmospheric argon effect on hypersonic stagnation point convective heat transfer, using arc-heated shock tube simulating flight velocities up to 34,000 fps [AIAA PAPER 66-29] 05 p0928 A67-17337

Neutron exposure ages of meteorites, estimating amount of shielding which surrounds samples in space from Co-60 and Ar-39 activity data 06 p1082 A67-17871

Three-body collisional recombination coefficients calculated for cesium and argon atomic ions, assessing Gryzinski cross sections 06 p1036 A67-18151

Relative intensities and cascade transition ratio in CW Ar II laser near 4103.9 angstroms 07 p1195 A67-19560

First two terms of high temperature equation of state for argon 08 p1355 A67-21255

Concentration of cesium in argon-cesium flow determined by total radiation absorption in resonance line of cesium 09 p1538 A67-21778

Electron-ion recombination behind shock waves in argon containing dilute lean mixtures of hydrocarbons and oxygen 09 p1457 A67-22024

Charge exchange cross sections measurements for ion-molecule pairs of hydrogen, argon, krypton, helium and xenon 09 p1535 A67-22381

Momentum accommodation coefficients of variable angle of incidence of monochromatic argon molecular beams 13 p2098 A67-26946

Lobular scattering of 1 ev energy chopped argon beams from silver, mica and brass surfaces, noting distributions and contamination effects 13 p2099 A67-26950

Collisional parameters in kinetic model equations for binary gas mixtures, treating shock structure in weakly ionized argon 13 p2103 A67-26977

Temperature and transport properties of helium and argon at high temperatures from ultrasonic determination of sound velocity and sound absorption 15 p2580 A67-29882

Numerical calculations of parameters of steady state HF high pressure vortical discharge of argon in air 16 p2723 A67-31769

Radiation spectra of plasma jets from IR to UV, determining electron density and argon excitation temperature, noting bremsstrahlung 17 p2893 A67-32144

Electrodeless annular discharges in argon and air 17 p2897 A67-32174

Spark produced in cell containing argon when concentrating laser beam in small volume, calculating temperature distribution 17 p2869 A67-32804

Cross sections for electron capture by protons measured for various energies in nitrogen, argon and helium 17 p2889 A67-33227

Electron flow in low density argon gas diode analyzed by Monte Carlo method 18 p3091 A67-34641

Ionization mechanism of argon-permanent

gas mixture in radioionization detector used for gas chromatography 19 p3226 A67-34797

Volt-ampere characteristics of long free-burning convection-free DC and AC arcs in nitrogen, argon and carbon dioxide 19 p3280 A67-35149

Retrograde motion of electric arc discharge at low pressure with transverse magnetic field, including cathode vaporization 19 p3281 A67-35153

Electronic energy transfer between metastable argon and nitrogen molecule, noting rotational enhancement 20 p3487 A67-36228

Direct excitation in argon gas from metastable state to upper laser state compared with two-step excitation 20 p3460 A67-36860

Ion mobility and reactions in argon measured using Townsend and Tyndall techniques with mass analysis 20 p3492 A67-37690

Quadratic Stark effect in argon II calculated assuming LS coupling 21 p3659 A67-38408

Radial temperature distribution in high power argon arcs measured at atmospheric pressure and 5 atm for currents ranging from 200 to 500 amp 22 p3853 A67-40049

ARGON PLASMA

Effective electron scattering cross section in helium and argon plasma with cesium vapor admixture measured by Langmuir probe theory 01 p0119 A67-10134

Solderability of 15 CDV 6 25 mm thick steel using argon arc and electric arc, noting mechanical properties of resulting alloy 01 p0078 A67-10270

Spectrographic method for measurement of temperature in plasma jets at atmospheric pressure, using amplification of beta line of hydrogen 01 p0124 A67-10773

Energy transfer to anode, cathode and surroundings in high current argon arc 01 p0125 A67-10976

Forward and backward wave striations in constricted positive column of high pressure argon discharge 02 p0273 A67-12188

Self-locking modes in argon ion laser, observing subnanosecond pulsation of laser output with wideband photomultiplier 02 p0253 A67-12503

Emissive capacity of argon in direct current arc at high pressure and temperature, noting experimental setup and results 03 p0478 A67-13602

Electrical current passage across neutral or ionized argon flow in presence of accelerating or decelerating magnetic field 03 p0478 A67-13605

Nonequilibrium conductivity of argon-cesium plasma 03 p0478 A67-13614

Phenomena preceding shock waves in argon, evaluating electron density profile and UV brightness of plasma 03 p0483 A67-13885

Stability and steadiness of gas flow of argon plasma jet analyzed, using dual grating spectrograph 04 p0664 A67-14848

Temperature distribution in argon plasma jet with variable mass flow measured, using grating spectrometer [ASME PAPER 66-WA/HT-50] 04 p0669 A67-15434

Viscosity and thermoconductivity of partially ionized argon plasma at atmospheric pressure measured, using equilibrium plasma jet 05 p0851 A67-16508

Self-absorption of radiation in high temperature plasma jet of hydrogen, argon and nitrogen 05 p0851 A67-16522

CW argon ion laser scattering in argon plasma, noting resonance and correlation between data and plasma properties 05 p0820 A67-16685

Continuous absorption cross section of argon from measurements of continuous emission of arc plasma in visible UV regions of spectrum and from temperature determination 05 p0854 A67-16988

Plasma in Ar positive column DC discharge examined for wavelike perturbations about equilibrium, noting striation dispersion relation, density variations and electron temperature 05 p0857 A67-17427

Induction coupled argon plasma at atmospheric pressure, noting vortex stabilization on discharge 06 p1039 A67-18067

Particle concentration and luminescence intensity correlation with electron cyclotron

frequency in stationary SHF argon discharge in magnetic field 06 p1040 A67-18094

Charged particles for lasing, discussing manufacture of argon laser 07 p1194 A67-19083

Argon, helium and nitrogen high temperature plasma compositions used to calculate radial temperature distribution 07 p1229 A67-19566

Asymmetric broadening of H-beta Balmer line in hydrogen doped argon plasma arc 09 p1536 A67-21562

Supersonic flow velocity and density probe for direct measures of mass and momentum influx, noting solution of H-T diagram of argon and probe criteria 09 p1497 A67-21776

Argon-cesium plasma spectroscopy, describing equipment, ionization, conductivity, recombination, concentration, etc 09 p1538 A67-21779

Flow velocity, seeding ratio and electrical conductivity in seeded argon plasma, noting relation between plasma and MHD generator characteristics 09 p1539 A67-21780

Electrode conduction processes and segmented electrode-insulator ratio effects in MHD power generation experiments 09 p1539 A67-21785

Current-voltage characteristics of moving argon plasma, noting variation of plasma conductance with flush and filament electrodes 09 p1540 A67-21786

Action of strong transverse magnetic field on supersonic current of ionized argon 09 p1540 A67-21787

Shock tube studies of magnetically induced nonequilibrium ionization in potassium-seeded argon plasma, noting electrical conductivity, current density, wall potential, Soule dissipation and radiation loss 09 p1540 A67-21788

Measurements of conductivity, electron density and ionization rate of cesium in argon on alkali shock tube, describing MHD generator wind tunnel experiment 09 p1540 A67-21789

Relaxation process and magnitude of nonthermal ionization in MHD generator, describing experimental equipment and results in xenon and in argon 09 p1540 A67-21790

Microwave interferometer for measurement of effective recombination coefficient of decaying argon-cesium plasma with hot electrons at various argon pressures 09 p1542 A67-21817

Vortex stabilized electrodeless annular discharge in argon at atmospheric pressure, describing experimental equipment, procedure and results 09 p1547 A67-22319

Electron temperature higher than gas temperature in dense argon plasma in presence of electric field 09 p1547 A67-22325

Dynamic pressures in helium and argon plasma jets in ambient atmosphere measured with sensitive probes 09 p1549 A67-22554

Electron recombination in argon plasma at atmospheric pressure in vicinity of 10,000 degrees K 09 p1550 A67-22584

High resolution external probe for measuring electrical conductivity of argon plasma behind shock wave 10 p1684 A67-22963

Effect of varying magnetic field, vacuum and ion density at 27 MHz on properties of cylindrical argon plasma column, using capacitive and inductive coupling 10 p1686 A67-23504

Properties of partially ionized Ar computed via Chapman-Enskog-Burnett expressions noting ambipolar diffusion coefficient, electron-atom momentum, electrical and thermal conductivity, etc 11 p1775 A67-23865

Argon laser design for long life noting ion sputtering and gas clean-up 11 p1800 A67-24242

Ion radial drift velocity in argon ion laser discharge tube 11 p1803 A67-24931

Supersonic rarefied argon plasma jet, determining pressure distribution, electron concentration and temperature 11 p1842 A67-24963

Cesium seeded argon plasma at atmospheric pressure, noting electron heating effect on conductivity curve and applicability to MHD conversion 12 p1970 A67-25253

Ionization rate in helium, argon and xenon plasmas determined by microwave technique 12 p1970 A67-25291

RF electromagnetic fields to control state of flowing thermal plasma 12 p1975 A67-25921

Current voltage characteristics of argon cesium plasma in inductive hydrodynamic shock tube 14 p2354 A67-27761

Argon plasma thermal conductivity at atmospheric pressure and various temperatures determined in central zone of arc column 14 p2404 A67-28031

Argon plasma accelerator producing diamagnetic discharge measured along axis for plasma properties 14 p2362 A67-29046

Decrease in degree of ionization of shock-heated argon resulting from radiative emission 15 p2527 A67-29563

Viscosity and thermoconductivity values of partially ionized argon plasmas derived by investigating temperature decay and stream velocity distribution in argon plasma jet 15 p2531 A67-30203

Nonequilibrium tensor conductivity in argon-potassium plasma under MHD generator conditions 16 p2709 A67-30514

Alkali metal vapor and inert gas mixtures with alkali seeding radiation properties, noting nonequilibrium argon-krypton plasma parameter determination in electrical discharge 16 p2710 A67-30522

Weakly ionized argon plasma electrical conductivity in direct current arc determined, noting experimental equipment 16 p2710 A67-30523

Current distribution in Faraday MHD generator measured with potassium resonance lines 16 p2599 A67-30529

MHD power generation experiments with potassium seeded argon plasmas to study performance at Faraday and Hall parameters 16 p2601 A67-30554

Spectral linewidth and shift of Ti I lines produced by neutral argon atoms analyzed using high pressure arc as light source 16 p2703 A67-30665

Weldability test method, developing rig which permits arc welding in argon atmosphere with TIG electrode 16 p2681 A67-30833

Argon pulsed arcs produced at high pressures, considering emission absorption 16 p2717 A67-31184

Time-dependent mean-mass temperature of argon jet produced by arc plasmator with powdered metal carbides injected into jet calculated using heat transfer equations 16 p2721 A67-31393

Ionization outside equilibrium and relaxation of ionization in cesium seeded argon 17 p2894 A67-32152

Thermal conductivity coefficient experimentally determined for argon plasma at atmospheric pressure and temperatures from 10,000 to 13,000 degrees K 17 p2895 A67-32157

Composition, heat conduction and radiative energy transfer characteristics of hydrogen and argon plasmas produced by arc in cylindrical channel with cooled walls 17 p2897 A67-32172

Induced argon discharge shown to have shape of plasma filament, noting detachment from chamber walls 17 p2897 A67-32176

Voltage induced by magnetic field using shock tube with high velocity ionized argon flow 17 p2898 A67-32184

Hall field intensity and asymptotic electron temperature of ionized argon-cesium mixture flow in transverse magnetic field with subsonic velocity 17 p2900 A67-32338

Determination of electron density and temperature, gas temperature, atomic composition and flow velocity of high temperature gas stream 17 p2900 A67-32339

Line width vs optical thickness in pulsed argon-ion laser used to determine level population in plasma 17 p2887 A67-32452

Arc oscillation in argon in cross flow facility noting parameter ranges, electrode spacing effects, etc 17 p2906 A67-33037

Elliptical patterns on emission lines of argon plasma jets attributed to antihalation backing during hypersensitization of film 17 p2863 A67-33305

Argon plasma injection effect into low pressure coaxial magnetic field noting pressure, flow speed, electron temperature, etc 18 p3084 A67-33647

Fractional excitation and ionization for argon beam extracted from arc-heated supersonic free jet, noting molecular ions and neutralization 18 p3082 A67-34028

Shock wave argon ionization in constant magnetic field, showing attenuation decrease of microwave signal in plasma and modulus change curves 18 p3087 A67-34045

Buildup time for nonequilibrium argon ionization at inlet of MHD generator channel 18 p2989 A67-34048

High pressure vortical discharge in air and argon, solving differential equations for heat conduction and electromagnetic field by digital computer 18 p3088 A67-34062

Electron density radial distribution, neutral gas temperature and ionization-caused column contraction calculated for cylindrical discharge plasma in argon 18 p3089 A67-34298

Temperature and frequency response of argon arc continuum emission coefficient, explaining unexpected deviations 18 p3089 A67-34299

Emissive capacity of argon in direct current arc at high pressure and temperature, noting experimental setup and results 18 p3090 A67-34467

Electrical current passage across neutral or ionized argon flow in presence of accelerating or decelerating magnetic field 18 p3091 A67-34470

Nonequilibrium conductivity of argon-cesium plasma 18 p3091 A67-34479

Argon plasma radiation emission and absorption measurement, determining transition probabilities 18 p3091 A67-34732

Charge recombination coefficient of decaying He and Ar plasmas with Cs vapor additions at increased pressures 19 p3271 A67-35073

Argon plasma ionization by oscillator supplying power near electron cyclotron resonance, measuring density variation 19 p3276 A67-35116

Radial and axial temperature profiles of free-burning argon arc at various pressures, measuring continuum intensities [DVL-625] 19 p3278 A67-35135

High pressure, high power argon arc studied using cascade apparatus, showing spectral line absorption increases and temperature decreases with increasing pressure 19 p3278 A67-35136

Self-consistent model for cathode region of high pressure arc, showing application to 200 amp arc in argon and boundary condition matching 19 p3279 A67-35138

Energy balance of high current argon arc, showing main energy supply supported by cathodic plasma beam, measuring temperature decay and field 19 p3279 A67-35143

Energy balance of electric arcs in argon without and with superimposed gas flow investigated at various pressures [DVL-626] 19 p3280 A67-35146

Supersonic free plasma jet with axial current, solving MGD equations for structure modifications due to self-magnetic forces 19 p3288 A67-35363

Initial ionization processes in shock heated argon consisting of atom-atom collisions followed by electron-atom processes 19 p3293 A67-35397

Plasma-magnetic shock wave propagation in high pressure, partially ionized argon plasma 19 p3293 A67-35400

Faraday effect in microwave region used for electron density determination in argon and helium low pressure plasmas and comparison with cyclotron radiation data 19 p3297 A67-35592

Electronic relaxation of shock-heated nonequilibrium argon plasma flow in microscopic-macroscopic treatment 19 p3298 A67-35745

Major difficulties encountered in open and closed cycle MHD, particularly temperature resistance of heat exchanger 20 p3362 A67-36366

Quasi-CW oscillation at 4880 angstrom of wide-bore AR II ion laser by plasma inductive excitation 20 p3458 A67-36387

Temperature effect on seeding atom emission in argon plasma laminar jet 20 p3497 A67-36397

Argon arc plasma generator with film cooled anode for producing stable high temperature gas jet [ASME PAPER 67-HT-72] 20 p3498 A67-36752

Excitation temperature of low pressure magnetically confined argon plasma, using spectroscopic transition probability 20 p3499 A67-37028

Probe for measuring three directional components of argon plasma magnetic field inside theta pinch conical coil, noting vortex structures
[AIAA PAPER 67-659] 21 p3671 A67-38695

Energy transfer and electron conduction in nonequilibrium argon arc column at one atmosphere
[AIAA PAPER 67-693] 21 p3672 A67-38722

Axial electron density profile in weakly ionized seeded argon plasma expanding through supersonic nozzle determined experimentally using microwave interferometer
[AIAA PAPER 67-704] 21 p3672 A67-38731

Magnetic field effect on flow field and drag of blunt body in partially ionized argon plasma, obtaining electron density and temperature
[AIAA PAPER 67-729] 21 p3673 A67-38753

Flow velocity and magnetic field effects on characteristics of single controlled glow discharge in cesium seeded argon
21 p3674 A67-38888

Quasi-one-dimensional nonequilibrium argon plasma flow equation, discussing kinetic model with atom-atom and electron-atom impact ionization
22 p3850 A67-39708

Ar plasma refractive index measured at very high temperatures using gas laser
23 p4032 A67-40961

Discharge model for relative abundances of different ions extracted from Ar duoplasmatron from Langmuir probe measurements
23 p4033 A67-41190

Apparatus for plasma investigation of pulsed arc discharge in high pressure argon
23 p4035 A67-41686

Absolute measurement of Ar II transition probabilities using tungsten ribbon lamp as calibration standard
24 p4194 A67-41888

Spectral lines diagrammed for temperature distribution in Ar plasma arc channel transverse emission with axial flow of working fluid
24 p4196 A67-42219

Ar produced in capillary arc discharge, studying charged particle density and electron temperature dependence on magnetic field intensity
24 p4196 A67-42244

Ar II population inversion of 4s and 4p states in stationary arc discharge, measuring ionic and atomic spectral line shift, widths and intensities and emission power
24 p4196 A67-42245

Interferometer crossed with spectrograph used for electron concentration investigation in ionized argon behind shock waves propagating at high Mach numbers
24 p4197 A67-42358

Ar atomic beam produced by plasma burner measured for kinetic energy and Mach number
24 p4198 A67-42576

Measurement of time varying spectra of argon plasma in coaxial gun for two different gun geometries
24 p4198 A67-42730

Steady electric power from Cs seeded Ar plasma in nonequilibrium ionization flowing at high speed through magnetic field
24 p4109 A67-42895

ARGON 40

Spallation produced Ar 40 in iron meteorites for determining cosmic ray exposure ages from radiogenic Ar 40 content
02 p0326 A67-12308

ARIEL II SATELLITE

Problems of temperature data from Explorer and Ariel II satellites including magnetometer failure, poor conduction, paint degradation, etc
03 p0518 A67-13074

Micrometeorite flux through thin aluminum foil determined using Ariel II satellite
12 p2008 A67-25824

Penetration rates of thin aluminum foil sensors of Ariel II satellites compared with flux measured by microphone detectors in vicinity of earth
21 p3722 A67-38494

ARIEL SATELLITE

NASA FM telemetry system for data acquisition and processing from Ariel satellites including methods for storage, transmission, handling, etc
04 p0568 A67-14437

UK-3 satellite electrical design and ground checkout equipment
09 p1484 A67-21828

Solar cell system for UK-3 satellite, discussing design, material selection, development and fabrication
09 p1445 A67-22179

Solar simulation tests on UK-3 satellite, evaluating thermal environment and sorting out interface problems between spacecraft

and test chamber
09 p1486 A67-22434

Electronic systems in Ariel III satellite detailing power distribution, storage control, telecommand, telemetry and data handling
17 p2827 A67-32822

Ariel III satellite design, development, mechanisms, power supply and data handling systems
22 p3898 A67-39178

Ariel III satellite attitude determination using optical glint technique
24 p4240 A67-41877

ARITHMETIC

Minimization of number of arithmetical operations in matrix transformation process
04 p0644 A67-14729

Book on matrices for structural analysis, including elementary algebra and detailed arithmetic of matrix methods applied to structure theory
10 p1719 A67-23476

ARITHMETIC AND LOGIC UNIT /ALU/

Defining noise margins on noise immunity in binary electrological systems, discussing static /steady state/, with graphs for exemplary integrated logical units
09 p1469 A67-22097

AROD

S AIRBORNE RANGE AND ORBIT DETERMINATION /AROD/

AROMATIC COMPOUND

SA BENZENE

SA PHENOL

Electron affinity data for various pentacyclic aromatic hydrocarbons, predicting ionization potentials
01 p0019 A67-10882

Tetrafluoroditertiary arsine preparation and coordinating properties, noting effect from introduction of fluorine atoms
01 p0135 A67-10896

Polycyclic aromatic hydrocarbon distribution in Cold Bokkeveld and Orgueuil meteorites
02 p0320 A67-11476

Spin relaxation times of ground state of atomic cesium in aromatic gases measured using optical pumping, noting dependency on temperature
04 p0680 A67-14611

Charge transfer energies of pyromellitic dianhydride and mellitic trianhydride with aromatic hydrocarbon donors
04 p0567 A67-15952

Substituent effects on unimolecular ion decomposition reactions, noting role of Hammett equation and electron energies
06 p0954 A67-17568

Torsional creep and creep recovery behavior of amorphous 1, 3, 5-tri-alpha-naphthyl benzene close to or below glass transition temperature
06 p1019 A67-17827

Characteristic optical density and equilibrium of alkyl-sodium and aromatic hydrocarbons as function of temperature and wavelengths, correlating electron affinity with enthalpy values
09 p1458 A67-22214

High resolution gas chromatography combined with mass spectrometry applied to analysis of pyrolysis products of isoprene from 300 to 1000 degrees C.
10 p1802 A67-22947

Polycyclic aromatic hydrocarbons in soot of premixed acetylene-oxygen flames, discussing graphs of flame height vs mixture composition
10 p1602 A67-22960

Crystal growth, nucleation, supercooling, solidification, glass forming and kinetics of 1, 3, 5-tri-alpha-naphthylbenzene
17 p2809 A67-33255

Temperature resistant aromatic ordered copolyamide fibers, obtaining tensile properties and radiation resistance
21 p3647 A67-37871

High temperature properties of aromatic polyimide fibers, noting thermal and dimensional stability
21 p3648 A67-37874

Aromatic poly-1, 3, 4-oxadiazole fiber preparation noting thermostability, property retention at high temperature and resistance to hydrolytic degradation
21 p3648 A67-37877

Aromatic compounds in benzene eluate fractions from carbonaceous chondrites by high resolution capillary gas-liquid chromatography
24 p4236 A67-42640

ARRAY

S ANTENNA ARRAY

S LINEAR ARRAY

S PHASED ARRAY

S SYNTHETIC ARRAY

ARSENIC

Tetrafluoroditertiary arsine preparation and coordinating properties, noting effect from introduction of fluorine atoms
01 p0135 A67-10896

De Haas-van Alphen effect in arsenic, noting two kinds of oscillations /Fermi surface and thin cylindrical surface/ and doping effect
06 p1070 A67-18982

Hall effect measurement in single crystal of arsenic at liquid helium temperatures in magnetic fields noting quantum oscillations
16 p2727 A67-30820

Thermomagnetic oscillation effect in arsenic, bismuth and antimony using cryostat, noting field strength variation
17 p2912 A67-32267

Simultaneous diffusion of gallium and arsenic in silicon from gallium arsenide source, obtaining profiles at various temperatures
19 p3308 A67-36035

Arsenic evaporation from gallium arsenide experiment used to study volatile solid evaporation suppression
21 p3686 A67-39134

ARSENIC COMPOUND

Indium arsenic antimonide single crystals in p-n junction laser
01 p0087 A67-10087

Temperature dependence of electroconductivity of As-Su-Ge system in vitreous state
06 p1052 A67-18610

Electric conductivity of AsSeGe-AsSGe glasses
06 p1052 A67-18611

Impurity effects on electroconductivity of vitreous AsSe
06 p1053 A67-18612

Electric conductivity of vitreous As-Se semiconductor
06 p1053 A67-18614

Electric conductivity of vitreous As-S-Th
06 p1053 A67-18615

Fluctuation levels and induced photoconductivity in vitreous semiconductor thallium selenide and arsenic telluride mixture
09 p1553 A67-21969

Epitaxial gallium arsenide properties and preparation using arsenic trichloride
10 p1692 A67-23510

Fluctuation levels and induced photoconductivity in vitreous semiconductor thallium selenide and arsenic telluride mixture
17 p2923 A67-33306

Temperature effect on gold diffusion in crystalline and glassy cadmium germanium arsenide samples
19 p3301 A67-34776

ARSENIDE

SA GALLIUM ARSENIDE

SA INDIUM ARSENIDE

Semiconducting properties of platinum arsenide with pyrite-type crystal structure
03 p0488 A67-12926

Cadmium selenide arsenide single crystals obtained free of cracks, using synthesis method
06 p1048 A67-17840

Band-to-band radiative recombination in compounds of gallium and indium with phosphorus, arsenic and antimony
12 p1979 A67-25177

Cadmium selenide arsenide single crystals obtained free of cracks, using synthesis method
17 p2922 A67-33218

ARTERY

Chimpanzee mesenteric artery blood flow for various activities during 24 hr period monitored by radio telemetry
22 p3751 A67-39603

ARTHROPOD

S INSECT

S SPIDER

ARTIFICIAL CLOUD

Monograph on rocket experiments for studies of D region ion concentration and emission from released chemicals in twilight and aurora
03 p0412 A67-13366

Artificial sodium cloud in twilight produced by French rocket studied, using auroral spectrophotometer and cameras
03 p0412 A67-13370

Artificial cloud produced in twilight over Wallops Island by payload containing sodium azide and lithium azide
03 p0412 A67-13371

Emission from sodium trail released from rocketborne vaporizer in height range 85 to 165 km during aurora of brightness IBC II
03 p0412 A67-13372

Intensity of sodium D-lines and auroral nitrogen band produced by sodium trail in aurora measured by calibrated photometer
03 p0412 A67-13373

Rocket payload with weight of 9 lb for release of sodium and lithium in aurora for study of D-region ion concentration and emission
03 p0413 A67-13375

Upper atmospheric wind measurement by artificial cloud method which releases sodium at twilight and trimethyl aluminum at night
05 p0798 A67-16858

Upper atmospheric wind measurements derived from vapor trail

soundings 06 p1025 A67-17594
Motion equations for ionized irregularity of finite length applied to barium ion cloud, deriving expression for ionospheric electric field 08 p1326 A67-21357
Wind velocity, direction and diffusion coefficients determined with aid of artificial luminescent cloud 10 p1675 A67-22795
Sounding rocket-released artificial strontium and barium ion cloud motion in upper atmosphere, based on equations of ambipolar diffusion 10 p1644 A67-23254
Internal scale measurements of atmospheric turbulence in 80 to 100 km altitude using alkaline clouds produced by ejecting sodium metal and trimethyl aluminum from rocket 12 p1935 A67-25793
High intensity electric field used to freeze out large quantity of droplets from supercooled artificial fog 16 p2699 A67-31717
Motion of artificial high density ionization cloud released in ionosphere 17 p2844 A67-32545
Dynamical structure of lower ionosphere obtained by studying atomic structure of sodium clouds 18 p3033 A67-33589
Spectral data and energy level diagrams from magnetic and electric field passage through barium cloud 18 p3036 A67-33606
Passive electronics countermeasure device /chaff/ consisting of metal strips to produce radar echoes 18 p3001 A67-34118
Mobile laser transceiver for atmospheric targets detection, discussing real time technique for determining atmospheric function 23 p4014 A67-41022
Wind velocity, direction and diffusion coefficients determined with aid of artificial luminescent cloud 24 p4181 A67-42131
Medium range radio communication system using artificial ionosphere consisting of ion-electron cloud created by Cs-Al mixture explosion [AIAA PAPER 67-789] 24 p4152 A67-42952

ARTIFICIAL EAR
External ear replica for acoustical testing noting sensing element, ear canal and eardrum impedance 21 p3577 A67-38148

ARTIFICIAL GRAVITY
Rotating artificial gravity system for manned orbital vehicles and stations requiring no expenditure of propulsive mass to attain full vehicle rotation 05 p0906 A67-17203
Scaling equations for wind tunnel simulation of trajectory of jetisoned stores from aircraft 06 p0979 A67-18006
Changes in reproduction and growth of mice and rats under chronic centrifugation at various g force 10 p1598 A67-23416
Optimum three-dimensional ascent trajectories in model gravitational field using maximum principle 12 p2000 A67-25211
Minimal value of artificial gravity for normal electroactivity of skeletal muscles determined for otherwise weightless condition 13 p2057 A67-26457
Earth organism behavior under artificial gravity, proposing long term orbital experiments 23 p3950 A67-41549

ARTIFICIAL INTELLIGENCE
SA BIOSIMULATION
SA GAME THEORY
Anthropotechnique as scientific discipline, discussing environmental layout, adaptation of machine to man and limits of intelligent machine handling 04 p0562 A67-14539

ARTIFICIAL RADIATION BELT
Brazil geomagnetic anomaly and artificial radiation belt observations from Cosmos series satellites 12 p1996 A67-25773
Structure and decay of artificial radiation belt produced by high altitude nuclear explosion 17 p2936 A67-32534

ARTIFICIAL SATELLITE
S SATELLITE

ASBESTOS
Thermo-oxidative stability of polyphenylene resins in asbestos reinforced laminates 03 p0451 A67-13400
Asbestos reinforced plastics evaluated for physical and optical properties, thermal-vacuum and UV resistance 15 p2507 A67-29550
Reinforced plastics pressed sheet materials series based on chrysotile asbestos fibers and thermoplastic resin combinations or thermoplastic and thermosetting resins 24 p4176 A67-42423

ASCENT TRAJECTORY

Analytic solution in terms of modified Bessel functions of synergetic turn in exponential atmosphere, using spacecraft engines only for drag cancellation and orbit trimming [AIAA PAPER 66-487] 02 p0331 A67-11938
Ascent or descent from initially Keplerian orbit by constant low thrust analyzed by two-variable expansion procedure 04 p0704 A67-14828
Approximation for low thrust trajectory without singularity at escape and having correct behavior up to and beyond escape, using motion equation 05 p0903 A67-17363
Optimal guidance equations for ascent trajectories into circular orbits, developing feedback guidance loop for real onboard control system 06 p1029 A67-18495
Atmospheric density, winds and turbulence relative influence on Saturn V vehicle control system and structural bending moment response during Atlantic Missile Range ascent flight [AIAA PAPER 66-341] 07 p1257 A67-19372
Combination numerical-analytical approach to ascent trajectory optimization 07 p1253 A67-19971
Propellant cost optimization using minimum characteristic velocity solutions for extra-atmospheric part of rocket ascent trajectory, emphasizing final elliptical orbit of arbitrary orientation 10 p1704 A67-22877
Optimum three-dimensional ascent trajectories in model gravitational field using maximum principle 12 p2000 A67-25211
Combination numerical-analytical approach to ascent trajectory optimization [AAS PAPER 66-112] 13 p2208 A67-27528
Optimization of extra-atmospheric phase of orbital ascent by assumption of certain hypotheses concerning atmosphere transit cost and nonnegligible-aerodynamic atmosphere thickness 17 p2946 A67-32695
Ascent of satellite of variable mass from elliptic orbit along spiral trajectories by low thrust 17 p2948 A67-33022
Ascent and descent gravity turn trajectories of rocket in constant gravitational field, considering drag forces in motion equation [AIAA PAPER 67-596] 19 p3336 A67-35992
Thermal protection technique using resin fiber ablative materials for use on reentry bodies during ascent, emphasizing nozzle 21 p3731 A67-38377
Parachute descent training for USAF pilots using Para-Sail ascending parachute 23 p3967 A67-41609
Equations for spherical superpressure balloon vertical rise in calm air 24 p4095 A67-42927

ASDE

S AIRPORT SURFACE DETECTION EQUIPMENT /ASDE/

ASIA

S INDIA
S JAPAN
S U.S.S.R.

ASPARTIC ACID

Inactivation of thermal catalytically active polyanhydro-alpha-amino acids by heating in buffered solution, noting hydrolysis of cyclic imide bonds 13 p2065 A67-26733

ASPECT RATIO

Compressor cascades with different irregularities in forward flow, noting special case of low aspect ratio blades 02 p0179 A67-12439
Effects of horizontal shear and aspect ratio change on baroclinic instability in rotating annulus heated differentially 03 p0463 A67-13932
Forced-convective heat transfer in asymmetrically heated rectangular ducts as function of prandtl number, Reynolds number, aspect ratio and temperature difference 04 p0728 A67-15804
Finite difference solution of parabolic equation for laminar heat transfer in inlet of rectangular duct as function of wall temperature and Nusselt number for different aspect ratios 04 p0728 A67-15805
Inviscid flow method predicting nonlinear supersonic and hypersonic lift component of highly swept wings with low aspect ratio 06 p0937 A67-18013
Nonlinear singularities method for calculating velocity distribution over thick wing of finite aspect ratio situated at zero

angle of attack in incompressible frictionless potential flow 07 p1127 A67-19887
Aspect ratio effect on cascade performances, noting complex variation of boundary layer thickness and changes in axial velocity ratio 09 p1437 A67-21742
Fiber aspect ratio, residual stress state and geometry of multifiber arrays studied in terms of influence on local stress concentration and matrix reinforcement 10 p1671 A67-23705
Separation and nonseparation of skewed boundary layer, considering two-dimensional wing of finite aspect ratio at large angle of incidence 11 p1777 A67-24051
Vortex breakdown effects on lift, drag and pitching moment coefficients of slender sharp-edged delta wings with different aspect ratios 13 p2050 A67-27194
Fluid jet amplifier switching mechanism, discussing effect of aspect ratio and logic element with downstream control ports 14 p2248 A67-28268
Aspect ratio effect on noise in proportional fluid amplifiers 14 p2250 A67-28330
Incompressible fluid flow in convergent nozzle with finite aspect ratio, predicting offset on nozzle flow and jet reattachment 14 p2303 A67-28334
Attachment distance for two-dimensional jet shown unaffected by presence or absence of second sidewall and nozzle aspect ratio 14 p2303 A67-28339
Jet reattachment for inclined walls at low Reynolds numbers and moderate nozzle aspect ratios [ASME PAPER 67-FE-25] 14 p2305 A67-28369
Steady flow in rectangular cavity with driving motion by uniform translation of one wall 17 p2836 A67-32279
Analyses of small-and large-deflection problems of clamped skewed plates under uniform pressure 17 p2958 A67-32407
Two-dimensional steady flows of viscous fluid in external infinite region on basis of fourth order nonlinear Helmholtz equation in vortex terms 18 p2981 A67-33420
Nonlinear theory of lifting wing surface of arbitrary aspect ratio, deriving velocity potential, lift coefficient and induced drag 18 p2981 A67-33536
Critical Reynolds number of laminar-turbulent transition for Newtonian flow in rectangular ducts to verify minimum in curve as function of duct aspect ratio 19 p3210 A67-35616
Plane compressor cascades, comparing small and large aspect blades and studying aspect ratio effect 21 p3564 A67-38045
Maximum stresses with changes in Poisson ratio for thin parallelogramic panels with nonlinear behavior 22 p3911 A67-39666
Aircraft wing drag noting relation between Mach number, thickness chord ratio, aspect ratio, airfoil shape and wing configuration 23 p3930 A67-41306
Interfiber distance and temperature effects on critical aspect ratio in fiber composites obtained from modified pull-out test 24 p4173 A67-42474

ASPHALT
Aliphatic hydrocarbons isolated from Trinidad Lake asphalt by gas chromatography and mass spectrometry appear to be unlike hydrocarbons 24 p4149 A67-42100

ASTEROID
SA EROS ASTEROID
SA METEOR
Planetary proximity influence on motion of planetoid, with application to solar influence on Venus as studied by Mariner II 02 p0321 A67-11495
Meteorites from asteroids in hypothesis based on chemical composition, structure and gas absorption age 04 p0702 A67-15562
Asteroid /1685-Toro/ discovered in 1948 and observed again in 1956 and 1964, noting semimajor axis equal to 1.3677 AU and period of sidereal revolution equal to 584.2 days 04 p0702 A67-15607
Planned encounters with asteroids in manned missions to Mars for observational purposes, using computer program [AAS PAPER 66-124] 07 p1254 A67-19983
Asymmetric distribution of asteroids in heliocentric latitude and longitude 10 p1705 A67-22894
Planned encounters with asteroids in manned missions to Mars for observational

purposes, using computer program
[AAS PAPER 66-124] 13 p2209 A67-27537

Generalization of Oepik theory of planetary bodies collision to include case where orbits of both colliding bodies are ellipses 14 p2384 A67-28055

Corrections to equinox and equator of FK3 from meridian observations of Ceres, Pallas, Juno and Vesta 15 p2557 A67-29873

Commensurability cases of asteroid and Jupiter within framework of secular perturbation theory 15 p2559 A67-30038

Heliocentric orbits of former Jupiter satellites, relating direct or retrograde satellite to heliocentric semimajor axis as asteroid 17 p2946 A67-32754

Asteroid belt study with spin-stabilized flyby probes 19 p3322 A67-35317

Corrected orbital data for 60 minor planets, giving osculating elements for asteroids 20 p3522 A67-36618

Differential coefficients of asteroids Gerda, Flora and Juno in heliocentric coordinate system including Jupiter and Saturn perturbations 20 p3523 A67-36627

Shortest distance between two quasi-coplanar elliptical asteroid orbits, solving transcendental equations by consecutive approximation method 20 p3523 A67-36628

Spherical coordinates from integration of 20 asteroids differential motion equations including Jupiter, Saturn perturbation and orbital element determinations 20 p3523 A67-36629

Distribution asteroids in space studied by computer analysis from selected plots of orbital elements 20 p3524 A67-36654

Solar system resonances emphasizing nongravitational forces in resonance formation and asteroid collision formation of Kirkwood gaps 23 p4062 A67-40623

Angular momentum densities of planet-satellite systems, discussing earth-moon system and origin of celestial bodies 23 p4066 A67-41009

Angular momentum density vs mass log-log plot extended from planetary mass range to asteroids, noting support for constant period law 23 p4066 A67-41010

ASTRONOMICS

S ASTRONAUTICS

ASTROBIOLOGY

S BIOASTRONAUTICS

S EXTRATERRESTRIAL LIFE

ASTRODYNAMICS

Astrodynamic perturbation theory in which perturbed space-vehicle motion is described in terms of osculating hodograph applied to lunar landing
[AIAA PAPER 67-25] 06 p1085 A67-18304

Astrodynamics - IAF Conference, Athens, September, 1965, Volume 6 astrodynamics - IAF Conference, Athens, September 1965, Volume 6 16 p2742 A67-30723

Lunar structure from lunar moments of inertia, noting thick layer denser than lead near surface 17 p2947 A67-32757

Accurate geodetic altitude and sublatitude of low altitude space vehicle 22 p3879 A67-39312

Lunar origin and earth-moon system, discussing dynamical requirements based on secular variation of some parameters 24 p4230 A67-42322

Fission hypothesis of lunar origin, reviewing energy, dynamics, angular momentum, geology and physical properties 24 p4230 A67-42323

ASTROMETRY

Arguments supporting IAU Executive Committee refusal to recommend changes in conventional values of principal planetary masses 05 p0900 A67-17081

Lunar parallax determination by four methods 08 p1395 A67-21158

Apparent area as basis for solar flare importance, noting dependence on position 08 p1376 A67-21237

Book on space-time relations of stellar positions on celestial sphere, detailing long focus astrometry, emphasizing mathematical principles 13 p2199 A67-26933

Moon-earth distance and moon-earth system astrometric parameters by laser ranging, describing artificial light reflector design 23 p4066 A67-41037

ASTRON THERMONUCLEAR REACTOR

Negative-mass instability of cylindrical layer of relativistic electrons in geometrical configuration approximating Astron machine 12 p1970 A67-25254

ASTRONAUT

SA PILOT

Protective shielding for astronauts from ionizing radiation from solar and galactic cosmic rays and radiation belts 03 p0365 A67-13539

Effect of man walking inside or outside of satellite on attitude 05 p0906 A67-17205

Food quality design for Gemini and Apollo space programs 05 p0757 A67-17261

Manual calculation and navigation of spacecraft orbiting near planets 08 p1352 A67-21112

Effects of radiation protective pharmacological agents /cystamine, serotonin AET, strychnine, etc/ on animals subjected to centrifugation, for application to astronauts 12 p1902 A67-25654

Physiological/psychotechnical selection of French cosmonauts with reference to ballistic, orbital and space flight 19 p3179 A67-35066

ASTRONAUT LOCOMOTION

Information model for manual control of astronaut motion and space orientation in free space 02 p0188 A67-12330

Role, mobility, maneuvering, tools and techniques of future astronaut engaged in doing mechanical work 04 p0563 A67-14603

Reduced gravity, pressure suit and load effect on human self-locomotion on lunar surface
[ASME PAPER 66-WA/BHF-6] 04 p0564 A67-15400

Subgravity traction simulation experiments to determine effects on metabolic rates during walking on treadmill 05 p0755 A67-16280

System concepts, combinations and missions for lunar exploration using LEM 08 p1316 A67-21082

Manipulators for astronauts using anthropomorphic mechanical hands and arms controlled by bilateral servo system in exoskeletal master 11 p1749 A67-25011

Reduced gravity, pressure suit and load effect on human self-locomotion on lunar surface
[ASME PAPER 66-WA/BHF-6] 17 p2807 A67-32814

ASTRONAUT PERFORMANCE

SA PILOT PERFORMANCE

EEG of pilot during orbital flight on Gemini VII used to study sleep cycles 01 p0015 A67-10954

Upper torso exercises effect compared with torque maneuvers effect on oxygen metabolism under reduced gravity conditions 01 p0017 A67-10959

Requirements and alternate systems approaches for extravehicular operations in space
[AFAPL-CONF-67-8] 01 p0018 A67-11400

Physiological functions of cosmonauts during flight of Voskhod, discussing measurement results of ECG, EEG, dynamography, etc 02 p0185 A67-11545

Physiological measurements of Soviet cosmonauts in Voskhod spacecraft, noting human performance characteristics and detection techniques 02 p0185 A67-11546

Water-immersion weightlessness simulation to determine astronaut EVA capabilities and man-machine interfaces
[AIAA PAPER 66-903] 02 p0187 A67-12270

NASA research on visual problems of extended spaceflight 02 p0189 A67-12408

Model for social system for extended-duration spaceship crews subject to isolation, confinement and/or stress 03 p0366 A67-14293

Heat, noise, vibration and acceleration simulation to determine beneficial effects of boost and reentry stresses on humans 03 p0366 A67-14389

Physiological monitoring applied to man in space environment, emphasizing overall philosophy including need and results of monitoring
[AIAA PAPER 66-928] 04 p0563 A67-14625

Scheduling manned space flight missions 04 p0704 A67-14902

Gemini program evaluation, discussing information gained from experiments performed during flights
[AIAA PAPER 66-1027] 04 p0704 A67-14979

Ocular scattering in Gemini astronauts and imperceptibility of stars in daytime 06 p1089 A67-18647

Pre-and postflight medical examinations of Voskhod I cosmonauts 07 p1133 A67-19108

Lunar landing simulation data, noting pilot performance and manual control modes
[AIAA PAPER 67-241] 07 p1165 A67-20062

Astronaut performance evaluation in Lunar Module hover and landing, separation and docking simulation
[AIAA PAPER 67-249] 07 p1165 A67-20067

Manned vs unmanned space exploration, discussing increased mechanization of operation 08 p1392 A67-21067

Lunar ground data for interpretation of AES orbital experiments such as electromagnetic radiation monitoring, photographic data evaluation, spectrography, etc 08 p1392 A67-21078

Simulator studies of MOL tracking experiments 08 p1317 A67-21105

Medical observations of astronauts on Voskhod and Voskhod II 08 p1288 A67-21111

Psychology and space flight 09 p1454 A67-22056

Cardiovascular and respiratory reactions of cosmonauts during Voskhod II orbital flight 09 p1454 A67-22384

Visual observations of earth, sea and sky made by astronauts and cosmonauts during space flights 09 p1569 A67-22604

Variable-duty-cycle spacecraft power switching circuit design giving high efficiency crewman illumination control of reticle within optical alignment sight 10 p1597 A67-23308

Flight activities of Russian cosmonauts in assessment of medical preparedness for orbital flight 12 p1902 A67-25653

In-space visual environment simulation, discussing photometric and geometric requirements, solar illumination characteristics and effects on human performance 12 p1922 A67-25700

Prolonged weightlessness exposure and expected effects on man 12 p1902 A67-25725

Soviet space psychophysiology, discussing cosmonaut selection and medical control 13 p2058 A67-26751

Research astronaut selection 13 p2062 A67-26763

EEG data from Astronaut Borman on Gemini flight GT-7 13 p2062 A67-26919

EEG baselines covering wide range of states of wakefulness and sleep in astronaut candidates estimated by computation and pattern recognition techniques 13 p2062 A67-26921

Medical data on in-flight and postflight physiological performance to determine man's qualifications for long duration space flights 13 p2060 A67-27214

Life sciences in fiscal year 2001, advanced concepts with emphasis on neurophysiological and behavioral problems 13 p2061 A67-27505

Lowering of psychic tone, absentmindedness and vigilance decline during astronaut weightlessness on long space flights 15 p2425 A67-29103

Advanced vision research for extended space flight 15 p2430 A67-29274

Neutral buoyancy /water immersion/ technique for simulated space crewman performance, noting psychophysiological, man-machine and anthropomorphic parameters affecting space station design 15 p2431 A67-29282

Water-immersion weightlessness simulation to determine astronaut EVA capabilities and man-machine interfaces
[AIAA PAPER 66-903] 15 p2431 A67-29439

Belaev description of 17-orbit flight of Voskhod II including spacecraft design and control, life support system and walk-in-space 16 p2616 A67-30758

Electrophysiological tests performed onboard Voskhod I noting apparatus recording electroencephalograph, electrooculogram, dynamogram and motion coordination in writing of astronauts 16 p2616 A67-30760

Ionizing radiation dosimetry for space pilots on short-and long-term space flights 16 p2617 A67-30764

Operational efficiency of astronauts evaluated on basis of Voskhod I and II flights, discussing manual operation, EVA memory efficiency, etc 16 p2618 A67-30780

Human psychological reactions to space flight problems, investigating effects of weightlessness, immobility and confinement on cosmonaut health and ability 16 p2612 A67-30903

Physiological functions of cosmonauts

during flight of Voskhod, discussing measurement results of ECG, EEG, dynamography, etc 16 p2614 A67-31611

Physiological measurements of Soviet cosmonauts in Voskhod spacecraft, noting human performance characteristics and detection techniques 16 p2614 A67-31612

Lunar environment simulation test bed, noting lunar gravity effect on astronaut performance 17 p2832 A67-32003

Manual control stationkeeping simulation, studying tether visual rendezvous techniques and fuel economy [AIAA PAPER 67-617] 19 p3337 A67-36006

Examination of ability of man to determine drift angle of spacecraft with optical sight [AIAA PAPER 67-624] 19 p3337 A67-36013

Cosmonauts diets on short, intermediate and long space flights, with suggestions and concepts of onboard natural-food production 20 p3374 A67-36253

Mathematical models for retrieval systems for future extravehicular operations, discussing rotational and translational motion and constraint equations 22 p3753 A67-39157

Hemodynamic responses of conscious dogs exposed to various centrifugation levels and back angles to determine optimum angle for positioning astronauts 22 p3750 A67-39593

Lunar landing simulation data, noting pilot performance and manual control modes [AIAA PAPER 67-241] 22 p3780 A67-40100

Mission planning for post-Apollo period including selection of lunar landing sites and definition of preferred scientific activity 22 p3888 A67-40144

Ground based simulation program for EVA evaluation including center of mass and inertia products of model astronaut 22 p3780 A67-40153

Manned space flight predicted exposure effects vs actual medical findings 23 p3945 A67-41067

Vestibular organ acceleration while walking at lunar and earth gravity 23 p3953 A67-41584

Experiments for relief of astronauts from cardiovascular and respiratory distress during EVA 23 p3953 A67-41586

Conditioned falling reflex of analyzer systems effect on change of human posture and spatial position 24 p4114 A67-41848

Manned testing of EVA equipment in simulated space environment, emphasizing crewman ingress and egress and mission objectives 24 p4115 A67-42049

Cosmonaut physiological reactions during simulated space environment exposure outside Voskhod II spacecraft 24 p4113 A67-42054

Water immersion simulation, studying astronaut performance characteristics in Gemini and proposed Apollo missions [AIAA PAPER 67-773] 24 p4116 A67-42941

Lunar gravity, reduced pressure and suit encumbrance effects examined in lunar surface environment simulation test bed, assessing astronaut performance [AIAA PAPER 67-866] 24 p4117 A67-42989

Astronaut role in balanced in-flight testing for manned spacecraft [AIAA PAPER 67-949] 24 p4245 A67-43033

ASTRONAUT TRAINING

SA PILOT TRAINING

Space rescue capability and proposed concepts to achieve it [AIAA PAPER 66-905] 02 p0332 A67-12271

Medical tests of spacemen Beliaev and Lenov during training and orbital flight 11 p1748 A67-24080

Astronaut training techniques applicability to conventional aircraft pilots training, discussing instruction and high fidelity simulation devices 13 p2064 A67-27273

First walk in space from Voskhod II described by Leonov, noting importance of simulated training 16 p2616 A67-30759

Trends in digital flight simulation for training 17 p2833 A67-32489

Rescue teams for manned testing in environmental chamber for Gemini spacecraft noting personnel, chamber and personal equipment, test operations and rescue function and drill 17 p2807 A67-32598

Collection, processing and return to earth of lunar specimens as part of Apollo program 19 p3328 A67-35929

Weightlessness effect on human body noting brain hemodynamics, cardiovascular system, calcium metabolism, task

performance, etc 20 p3369 A67-36668

European approaches to physiological and psychotechnical selection and training of cosmonauts 20 p3375 A67-36925

Astronauts and astronaut support personnel training requirements 23 p3960 A67-40594

Aerospace nursing, present applications and future implications 23 p3968 A67-41622

ASTRONAUTICS

SA BIOASTRONAUTICS

SA SPACE NAVIGATION

Space research and astronautics, importance to science and European economy 01 p0168 A67-10268

Control system of ACIC augmented by 100 points, constructing corresponding contour map 02 p0319 A67-11457

Yearbook of European Aeronautical Congress, Munich, September 1965 03 p0354 A67-12965

Post Apollo space exploration - AAS Meeting, Chicago, May 1965 08 p1391 A67-21064

Aviation and astronautics - Conference, Tel-Aviv and Haifa, February 1967 11 p1777 A67-24212

Direct energy conversion techniques in generating electric power in space for future astronautic systems 14 p2253 A67-29044

Mathematical methods of celestial mechanics and astronautics - Conference, West Germany, March 1964 15 p2558 A67-30034

Error assessment in numerical integration for ordinary differential equations applied to many-body problem 15 p2512 A67-30053

Astronautics and Education, International Astronautical Congress, Athens September 1965, Volume Eight astronautics and education - IAF Conference, Athens, September 1965, Volume 8 16 p2781 A67-30783

Astronautics education for RAF and USAF officers 16 p2782 A67-30786

Book on astronautics covering rocket theory, celestial mechanics and space problems 21 p3703 A67-38434

ASTRONAVIGATION

S CELESTIAL NAVIGATION

ASTRONOMICAL COORDINATE

SA SOLAR LONGITUDE

SA SOLAR POSITION

Planetary proximity influence on motion of planetoid, with application to solar influence on Venus as studied by Mariner II 02 p0321 A67-11495

Identification of strong extragalactic radio sources in declination zone zero to minus 20 degrees 04 p0697 A67-14773

Book on moon covering motion of moon and dynamics of earth-moon system, internal constitution, topography, radiation and surface structure 06 p1087 A67-18428

Matrix techniques for finding geomagnetic field strength in solar ecliptic coordinate system 07 p1170 A67-19111

Near planet orbital navigation by astronauts, celestial surfaces of position combine to define unique three-dimensional position of observer 09 p1526 A67-22388

Corrections to station coordinates and nonzonal coefficients of geogravitational potential from Baker-Nunn observations by combined dynamical and geometrical method 10 p1636 A67-23179

Astronomic data error effect on position of reference surface trigonometric net with regard to earth axis of rotation 11 p1787 A67-24593

Comet P/Wolf I motion perturbations of six planets, searching ephemeris for perihelion in August 1967 11 p1868 A67-25085

Localization of radio source 3C 17 from moon occultations and identification with near galaxy 12 p2011 A67-26249

Satellite and astronomical refraction determined from formulas for air refractive index determination 13 p2199 A67-26854

Corrections to equinox and equator of FK3 from meridian observations of Ceres, Pallas, Juno and Vesta 15 p2557 A67-29873

Astronomical determination of position on moon 18 p3120 A67-33864

Ephemeris time corrections /1900-1966/ with respect to UT after revision of Brown lunar theory 22 p3881 A67-39516

Absolute coordinates of 910 lunar features determined by stereoscopic method 23 p4065 A67-41005

ASTRONOMICAL MAP

Lunar craters, quadrant IV, designation, diameter, position, central peak information, etc 01 p0152 A67-11331

Maps of 2-cm brightness distribution of various radio sources including Taurus and Orion 03 p0511 A67-13796

Micrometric measurement of absolute and relative heights of 163 unobtrusive points on lunar surface, comparing values of Maedler, Schmidt and U.S. Army Map Service 04 p0700 A67-15177

Lunar photography application to creation of selenographic coordinates enveloping near and far sides of moon 08 p1388 A67-21000

ASTRONOMICAL MODEL

Polarization measurements of distribution of ionized interstellar gas near galactic plane using two galactic region models 02 p0322 A67-11645

X-ray emission from old novae noting possibility that hot coronas may arise from vibration 02 p0308 A67-12032

Meteor sighting probability and problem of actual number of meteors 03 p0511 A67-13815

Nuclear physics of neutron emission in stellar interiors, reaction rates of neutron-producing processes evaluated with optical model of nucleus and uncertainties assessed 03 p0508 A67-14315

Possible models for X-ray source SCO-X-1, discussing conditions of gravitational confinement 04 p0694 A67-14484

Vector field C defined at each point of space-time when curvature is zero, leading to series of cosmological models that satisfy Hoyle relativistic equations 04 p0698 A67-14809

Meteorite size prior to entering atmosphere, noting radius and use of isotope activity nomogram 04 p0702 A67-15751

Homogeneous anisotropic cosmological model with magnetic field for solution of Einstein gravitational and Maxwell equations in space filled with ideal matter 04 p0702 A67-15984

Mach principle as consequence of de Sitter universe filled with Dirac dust 05 p0847 A67-16803

Dynamical model of steady state self-gravitating stellar system with finite total mass 05 p0897 A67-16804

Spoerer and Gleissberg laws for Babcock and Tuominen models of solar activity concerning migration in heliographic latitude of sunspot area and role of solar magnetic field 05 p0897 A67-16809

Mokhnach model explaining surface brightness distribution observed by miller in 1959 k comet 06 p1082 A67-17839

Observational distinction between ice and graphite models of interstellar grains 06 p1082 A67-17978

Comet model construction assuming rectangular coordinates system, noting particle motion initial velocity and repelling acceleration 06 p1084 A67-18205

Model atmospheres and astronomical and parallax refraction 07 p1174 A67-19716

Models of reflection nebulae light for single scattering, pure or modified by internal nebular extinction, on spherical grains imitating dielectric or metallic particles 11 p1861 A67-24487

CH molecule solar spectral observations interpreted using several upper photosphere models and assuming local thermodynamic equilibrium approximation 11 p1861 A67-24495

One-dimensional model of stellar system evolution, using computer to calculate minimum energy configuration 11 p1862 A67-24500

Brans-Dicke theory of gravitational scalar field effect on structure of neutron cold spherical stellar model analyzed and compared with relativity theory 11 p1864 A67-24596

Pulsating model of closed universe, noting ordinary matter time-dependent scalar field interaction and equation for nonvanishing pressure 11 p1868 A67-24867

Solar chromospheric model composed of four discrete groups of filaments 12 p2001 A67-25221

Hydrodynamic axial-symmetric model of plasma flow on sunward side of comet assuming cometary gas is ionized by solar UV radiation only 12 p1993 A67-25227

Pulsation properties of star models with

linear density distribution, considering radial, adiabatic contraction and dynamical stability 12 p2011 A67-26253

Solar wind structure model, proposing surface granularities correlation with modulation at source of 13 p2190 A67-26313

Solar corona broadening mechanism studied using microscopic model including kinetic equations, determining proton escape velocity from sun 13 p2194 A67-27340

Spectroscopic observation of sunspot structure, detailing sunspot model on basis of magnetic field and large scale motions interpretation 13 p2203 A67-27425

Hot and cold component model of sunspot umbrae derived from observation of continuous and line 13 p2203 A67-27427

Sunspot magnetic field affecting convective energy transport so that resulting pressure gradient together with gravity force balances magnetic field 13 p2204 A67-27436

Experiment to represent sunspot model having mechanism of natural turbulent convection of liquid mercury inhibited in presence of magnetic field 13 p2171 A67-27437

Sunspot structure, discussing photospheric model, magnetic field influence, MHD structure and energy balance, and photospheric and chromospheric parts 13 p2205 A67-27438

Discrete equilibrium temperatures of hypothetical planet with atmosphere and hydrosphere of one-component two-phase system under constant solar radiation 13 p2116 A67-27462

Ionization structure of elements H, He, C, N, O, Ne in planetary nebulae computed for theoretically determined electron temperature and electron density variation 14 p2382 A67-27847

Homogeneous anisotropic cosmological model with magnetic field for solution of Einstein gravitational equations and Maxwell equations in space filled with ideal matter 14 p2386 A67-28485

Geomagnetic pulsations and auroral activity, using magnetosphere simplified model 15 p2474 A67-29505

Hot model of universe supported by radioastronomical observations, estimating quark number density 15 p2555 A67-29640

Statistical correlation of latitude with time of maximum darkening of Mars dark areas, noting consistency of 2 models 16 p2749 A67-31401

Cosmological model for universe based on astronomical observations and validity of einstein theory and existing laws of physics 16 p2752 A67-31540

Nonrotating, hydrostatic models of geochemically likely planets calculated using solar elemental abundances and equations of state for cold materials 16 p2754 A67-31748

Model of dust distribution in interplanetary space accounting for solar effects 17 p2947 A67-32758

Cosmological model covering early and late stages, presenting period time when matter density equaled radiation 17 p2947 A67-32759

Isostatical equilibrium form of moon model having homogeneous semimolten core and homogeneous solid 17 p2949 A67-33123

Crust 17 p2949 A67-33123

Cosmic ray motion in interplanetary electromagnetic field for isotropic/anisotropic diffusion situations presented by convective diffusion models assuming spherical symmetry for solar cavity 17 p2938 A67-33188

Mokhnach model explaining surface brightness distribution observed by Miller in 1959 k comet 17 p2951 A67-33214

Comet model construction assuming rectangular coordinates system, noting particle motion initial velocity and repelling acceleration 17 p2951 A67-33215

Dome formation in corona around prominence during February 1961 eclipse, describing observed features and proposing three-dimensional model 17 p2953 A67-33399

Quantum cosmology, discussing continuous fluid models as representations of early dense universe 18 p3117 A67-33515

Trajectories of auroral charged particles accelerated in geomagnetic tail computed, using fields of magnetosphere reconnection

model 18 p3038 A67-33614

Auroral and polar magnetic substorms related to magnetic field lines reconnection in magnetosphere tail 18 p3117 A67-33615

Martian atmosphere circulation model from Mariner IV occultation experiment, studying lateral eddy viscosity, winds, surface temperature and stress 18 p3124 A67-34153

Gravitational instability of homogeneous anisotropic cosmological models 18 p3133 A67-34432

Superdense cosmical object model, discussing negative mass defect necessary for expansion to diffuse state 18 p3133 A67-34433

Quasar regarded as early stage in formation of system like galaxy nucleus, using model 19 p3317 A67-34950

Quiescent solar prominences general appearance described by theoretical model 19 p3324 A67-35436

Gravitational model for chromosphere flarelike brightenings following dispartitions brusques, examining prominence and chromospheric characteristics 19 p3324 A67-35437

Interplanetary magnetic field variation properties and effects on solar cosmic rays determined through Mariner II recordings employed to develop model 19 p3314 A67-35452

Electron component observation in studying solar modulation of galactic cosmic rays, discussing Parker model and Gloeckler-Jokipii model 19 p3315 A67-35496

Luminous and intergalactic matter, background radiation, radio sources, quasars, cosmic rays and other observational data relevant to cosmological models 19 p3327 A67-35870

Differentiation between gravitational and cosmological components of quasars red shift by observational means 20 p3521 A67-36295

Cosmic-ray electron spectrum in disk-halo galactic model, studying inconsistencies in Ramaty and Lingenfelter analysis 20 p3518 A67-36946

Quasars and radio galaxies characteristics contrasted, drawing conclusions about evolution using radio emission synchrotron hypothesis and consistent model 20 p3526 A67-37250

Critical comments on Shklovsky model for newly identified X-ray source Sco XR-1 20 p3527 A67-37394

Stable height to distance to supporting magnetic field origin ratio for prominences, noting agreement with Klippenhahn-Schlueter model 20 p3528 A67-37469

Steady state model of system consisting of solar corona and interplanetary plasma, noting plasma efflux from sun 20 p3529 A67-37520

Lunar surface materials choice narrowing method via albedo, color and polarization property examinations to find possible candidates for lunar surface model 21 p3701 A67-37897

Spherical symmetric problems in general relativity 21 p3707 A67-38962

Oblique rotator model for magnetic stars supported by variability, line width, variable polarization and stellar rotation data 21 p3708 A67-38984

Evidence for relationship between solar flares and magnetic fields explained by neutral point type model, considering smaller flares 21 p3699 A67-38988

Jupiter and Saturn models, giving planet constitution, heat balance and atmospheric composition 21 p3710 A67-39001

Analytical solution to cosmological model containing radiation and matter assuming spatial homogeneity and isotropy, stress-energy and adiabatic expansion 21 p3711 A67-39121

Empirical model of sunspot activity within solar cycle limits indicating separate consideration of magnetic field generation and spot formation 22 p3879 A67-39300

Tensor calculation of origin of local concentration of matter in universe model, considering effect of gravitational perturbations 22 p3880 A67-39314

Gravitational collapse model with pressure gradient and no energy flow, discussing spectral shift and mass radius relation 22 p3884 A67-39833

Microwave background radiation angular distribution anisotropy lower limit estimated from perturbations of cosmological model 22 p3892 A67-40498

Interstellar gas properties noting insufficient information for constructing models or drawing conclusions 22 p3894 A67-40512

Close binary protostellar system formation using model with stellar wind mass loss and primeval magnetic field 22 p3896 A67-40520

Spectral index dependence on flux density and cosmological red shift, considering model universes populated with radio sources 23 p4062 A67-40634

Free-free radiation absorption from discrete radio sources calculated for various isotropic world models as red shift, electron density and temperature function 23 p4063 A67-40777

Cosmic ray intensity from balloon sounding, discussing proton to He ratio behavior as time function within Parker solar modulation model 23 p4051 A67-40809

Apparent Jupiter rotation rate change from decimeter emission probability histograms shown to differ from dynamic radiation spectra 23 p4065 A67-41002

Moon moment of inertia calculated for model with homogeneous core and homogeneous mantle, varying mantle density, core density and core radius 23 p4066 A67-41011

Equations governing umbra structure of single spot integrated on spot axis, consistent model can be obtained only for narrow electron pressure range at surface 23 p4067 A67-41230

Effective temperature for late type stars with or without water vapor opacity calculated for several masses, determining convective energy transport efficiency 24 p4224 A67-41818

Streaming and spatial gradient equations of cosmic ray particles in interplanetary medium model, discussing Fokker-Planck equation and heliocentric field modulation 24 p4208 A67-41832

Incompatibility of microwave phase effects measurements in Mercury thermal emission with simple model for thermal behavior of planet surface 24 p4226 A67-41837

Bolometric magnitude, angular diameter and radiolux density of various world models and red shift values, calculating universe and horizon age 24 p4228 A67-42259

Radio evidence for two supernova remnants in Southern Milky Way and observations of shell type radio sources, considering shell model fitting problem 24 p4230 A67-42332

Friedman cosmological models describing spatially homogeneous and isotropic universe 24 p4231 A67-42454

ASTRONOMICAL OBSERVATORY

SA CELESTIAL OBSERVATION

SA OAO

SA SOLAR OBSERVATORY

Astronomical observatory construction on moon 03 p0513 A67-14098

Dynamical effect of explosive phenomena in comet Halley and nuclear rotation based on 1909.1911 observations 04 p0694 A67-14469

Lunar astronomical observatory, discussing telescopes and optical devices, instrumentation transportation to moon and expectations for astronomical information acquisition 04 p0597 A67-15067

Instrumentation and research potentialities of lunar radio astronomy observatory 04 p0598 A67-15069

OAO satellites for astronomical experiments, discussing planning and specific features 06 p1098 A67-19048

Residuals in right ascension and declination of Mars observations made with astrolabe in France 07 p1250 A67-19723

Radio observation of quasar CTA 102 at various frequencies from Arecibo for possible explanation of sinusoidal variation of flux density 08 p1397 A67-21186

Lunar photography by refractor and reflector telescopes at Pic du Midi Observatory 10 p1710 A67-23563

Meteorological observations of earth from lunar surface 12 p1920 A67-25648

Comparison of lunar surface photography from space probes and ground-based observatories 16 p2671 A67-30990

Spectra broadening mechanism on reflector of Vilnius

Observatory 18 p3044 A67-33659
 Artificial satellites tracking by
 Smithsonian Astrophysical Observatory,
 discussing station locations, instrumentation,
 operation modes, interface and
 selection 18 p3003 A67-34236
 Smithsonian Astrophysical Observatory
 Differential Orbit Improvement program for
 lunar orbits, with selenocentric reference
 system 18 p3132 A67-34327
 Geos satellite observational technique in
 France 19 p3182 A67-35237
 Two-mirror Nancay
 radiotelescope 19 p3193 A67-35462
 Minor planets position observations at
 Crimean Astrophysical Observatory during
 August and September 1964 20 p3522 A67-36620
 Minor planets position observations at
 Crimean Astrophysical Observatory from
 October 1964 through March 1965 20 p3522 A67-36621
 Astronomical research /1965/ noting New
 Zealand observatory, telescopes in Chile,
 Hawaii and China, solar activity, planet
 studies, etc 21 p3700 A67-37830
 Observatory building for ultrahigh energy
 cosmic ray and cascade phenomena /air
 showers/ observation, describing Fresnel
 lens system 22 p3873 A67-39973
 Geomagnetic crotchets of solar flares
 based on materials analysis recorded at
 Hurbanovo, discussing time factors and
 characteristics 23 p4049 A67-40670
 Latitude variation and motion of
 instantaneous pole from astronomical
 stations during IGY, using differential
 method for coordinate system 23 p3997 A67-41350
ASTRONOMICAL PHOTOGRAPHY
SA ELECTRONIC PHOTOGRAPHY
SA HELIOGRAPHY
SA LUNAR PHOTOGRAPHY
SA SATELLITE PHOTOGRAPHY
SA SPACE PHOTOGRAPHY
 Correlation function of stellar image
 fluctuations and pulsations due to earth
 atmospheric influences for two stars
 separated by small angular
 distances 02 p0325 A67-11984
 Twenty-eight blue and yellow photographs
 of comet Humason, tabulating exposure
 time 02 p0326 A67-12066
 Kilston and Barbon comets detection and
 observation history 03 p0511 A67-13653
 Airborne astronomical photography
 affected by instrument structural design,
 vibration, aircraft stability, image
 stabilization, navigation, observation time,
 boundary layer effect and viewing port
 [SMPTE PREPRINT 100-9] 03 p0423 A67-13803
 Physical parameters, absolute values and
 discovery dates of comets observed from
 1954 through 1960 05 p0886 A67-16030
 Comet Ikeya-Seki observations from Mauna
 Kea, Hawaii 05 p0896 A67-16719
 Solar eclipse of May 20, 1966, first and
 fourth contact times, sky brightness and
 temperature and photographic
 records 05 p0897 A67-16731
 Film cooling technique for color
 photographs of astronomical objects to
 diminish effects of reciprocity failure and
 increase light sensitivity 06 p1002 A67-17975
 Wide latitude low gamma Ilford Phenidone
 /POTA/ developer for astronomical and
 scientific photography 06 p1002 A67-17976
 Analysis of differences in number of
 sunspot groups between Greenwich and
 Zurich observations 06 p1083 A67-18066
 Bright meteoric orbits according to
 photographic observations at Dushanbe and
 Odessa 06 p1084 A67-18165
 November 12, 1966 total eclipse
 observation from aircraft flying in moon
 shadow, describing instrumentation and
 results 06 p1004 A67-18383
 High precision artificial satellites
 photography experiment to measure
 astronomical bearings 07 p1144 A67-19768
 Astrometric processing of synchronous
 photographic observations of Echo I
 satellite 07 p1144 A67-19769
 Solar corona observations of Surveyor I,
 discussing extent of measurable radiance
 and occurrence of streamer 08 p1386 A67-20943
 Coronal observations during solar eclipse
 in Bolivia, discussing equipment used and
 results 08 p1391 A67-21044

Space astronomy program development,
 discussing manned orbital observatory
 concept and instrumentation 08 p1392 A67-21071
 Multispectral photography for AES
 missions, describing lunar color studies
 [AFRL-66-796] 08 p1331 A67-21081
 Lunar photography by refractor and
 reflector telescopes at Pic du Midi
 Observatory 10 p1710 A67-23563
 Saturn edgewise rings rapid fading and
 brightness variation on disk 10 p1710 A67-23564
 Systematic errors in earthward coordinates
 of selenodetic points, noting results of
 triangulation 11 p1860 A67-24461
 Photographic meteor observations 1957-
 1961 at Kiev 13 p2196 A67-26495
 Meteor orbital elements according to
 photographic observations 13 p2196 A67-26496
 Drag effects on meteoric bodies studied
 by photographic observations 13 p2196 A67-26499
 Meteor particle density study based on
 photographic observations 13 p2197 A67-26501
 Rotational velocity of Venus spots based
 on sidereal rotation measurements 13 p2198 A67-26588
 Photographs of sunspots analyzed to
 obtain magnetic field strength data 14 p2384 A67-28076
 Monochromatic photographs through filters
 for observation of shading variation in
 intensity of solar emission between center
 and edge of solar disk 14 p2387 A67-28517
 Homogeneity of solar prominences studied
 photographically in monochromatic
 light 14 p2382 A67-28941
 Large scale structure of chromosphere
 examined using birefringent filter,
 comparing filtergrams with
 spectroheliograms of perturbed and active
 regions of solar disk 15 p2552 A67-29143
 Bright meteoric orbits according to
 photographic observations at Dushanbe and
 Odessa 16 p2741 A67-30509
 Number of rays and brightness of Comet
 Morehouse derived from photographs taken
 with Greenwich reflector 16 p2742 A67-30666
 Distribution of meteoritic matter in solar
 system determined, using radar observations
 and astronomical photography 17 p2941 A67-32321
 Processing results of meteor photographs
 using panchromatic films and program-
 controlled exposure time 17 p2942 A67-32328
 Difference between ephemeris and
 universal time based on observations of
 lunar occultations 17 p2950 A67-33129
 Airborne astronomical photography
 affected by instrument structural design,
 vibration, aircraft stability, image
 stabilization, navigation, observation time,
 boundary layer effect and viewing
 port 18 p3044 A67-33575
 Contribution of earth-made observations to
 direct planet exploration 18 p3121 A67-34136
 Martian atmosphere transparency and
 visibility of surface details in blue and UV
 light, showing dark and semitone areas
 intensity, etc 18 p3124 A67-34154
 UV radiation observed beyond atmosphere
 in winter Milky Way, noting nebula
 detection and photographic
 apparatus 18 p3125 A67-34190
 Criticism of classical theory of Mercury
 rotation period equal to revolution around
 sun 18 p3125 A67-34191
 Lunar profile deviations from circle
 determined from annular solar eclipses,
 discussing measurement techniques 18 p3130 A67-34314
 Palomar Schmidt telescope use as moon-
 star camera proved impractical 18 p3049 A67-34315
 Everhart comet and various minor planets
 positions through photographic observations
 at Tartu 20 p3522 A67-36622
 Various minor planets positions from
 photographic observations at Crimean
 Astrophysical Observatory 20 p3523 A67-36630
 Janus /Saturn tenth satellite/ discovery on
 December 15, 1966, noting orbit in ring
 plane and period 20 p3527 A67-37399
 Spatial filtering for altering relative
 harmonic coefficients in two-dimensional
 Fourier integral representation of
 astronomical photographs eliminates ringing
 effects 23 p3997 A67-40625
 Large scale structure of chromosphere
 examined using birefringent filter,

comparing filtergrams with
 spectroheliograms of perturbed and active
 regions of solar disk 24 p4239 A67-43066
ASTRONOMICAL PHOTOMETRY
 Optical identification of position of X-ray
 astronomical source Sco X-1, noting
 similarity of certain properties with old
 novae 02 p0324 A67-11772
 Photometric features of eastern and
 western limb zones of lunar surface
 compared with data on photometric
 mean 02 p0329 A67-12493
 Lunar disk color index derivation by
 applying method of photographic photometry
 in UV and IR spectral
 regions 02 p0329 A67-12493
 Directional absorptivity characteristics of
 conical cavities and use as thermal model
 for lunar meteor craters
 [AIAA PAPER 65-669] 03 p0508 A67-13049
 Zodiacal light and solar activity, examining
 results of visual observations and
 photometric measurements for correlation
 between phenomena 03 p0413 A67-13455
 Photometric cross section of nonradial
 coronal structure in 5303 angstrom line
 following proton flares with cosmic,
 subcosmic and corpuscular
 emissions 03 p0507 A67-13810
 Spinning-image coded X-ray star camera,
 based on image coding, permitting
 reconstruction of two-dimensional image
 [AIAA PAPER 66-850] 03 p0424 A67-14016
 Aurora photometry and stratospheric
 cosmic ray intensity, noting electron
 intrusion and correlation between aurora
 intensity and X-ray emission 05 p0879 A67-16102
 Comet photometry using revolving table to
 study brightness distribution in head and
 determine intrinsic brightness 05 p0888 A67-16200
 Photometry of comet Arend-Roland, 1956
 h, calculating brightness decrease along tail
 streams 05 p0888 A67-16201
 Soviet papers on problems of comet
 photometry 05 p0890 A67-16329
 Visual and photographic comet photometry
 problems, noting brightness estimates
 obtained by individual observers 05 p0890 A67-16330
 Visual techniques for measuring comet
 total brightness based on
 nonfocality 05 p0890 A67-16331
 Photographic comet photometry as
 technique for studying comet
 brightness 05 p0890 A67-16332
 Photographic technique for photometric
 comet observations, noting automatic
 polarograph and high transmission meniscus
 telescope 05 p0890 A67-16333
 Comet photometry for measuring weak
 fluxes of light produced by heavenly bodies,
 analyzing photoelectromultipliers 05 p0805 A67-16336
 Brightness and spatial luminosity
 distribution in comet heads analyzed for
 steady and variable emissive
 processes 05 p0891 A67-16339
 Difference of dynamic and photometric
 mass of meteors cannot be explained in
 terms of differences in constants of drag
 and light curve equations alone 05 p0897 A67-16806
 Photometric measurements of ash-moon,
 using large coronagraph 06 p1082 A67-18014
 Physical characteristics of comets, 1961-
 1965 06 p1083 A67-18163
 Photometric features of eastern and
 western limb zones of lunar surface
 compared with data on photometric
 mean 10 p1708 A67-23360
 Lunar disk color index derivation by
 applying method of photographic photometry
 in UV and IR spectral
 regions 10 p1708 A67-23361
 Intermediate band pass photometric
 system properties and reduction and
 calibration procedures 11 p1792 A67-24778
 Astronomical satellite for photoelectric
 spectrometry in UV region to measure stars
 of galactic clusters 12 p2002 A67-25460
 Number of fragments in meteor
 fragmentation 13 p2197 A67-26500
 Classification of slit spectrograms of 185
 bright stars in Morgan-Keenan
 system 14 p2387 A67-28560
 Design and operation of all-reflecting
 Schmidt camera 14 p2319 A67-28562
 Photoelectric two-cell polarimeter with
 rotating achromatic half-wave plane noting

wavelength restriction 14 p2319 A67-28563
 Nightglow continuum emission 14 p2313 A67-28576
 Photoelectric solar spectroscopy at Nice Observatory, discussing suitability of location and results 14 p2387 A67-28592
 OH emission in H II region W3, using improved equipment 14 p2389 A67-28845
 Spark chamber telescope observations on cosmic ray neutral primary sources 14 p2381 A67-28846
 Saturn photograph analysis discussing interpretation of thin line on edge of ring system 14 p2393 A67-29029
 Optical characteristics of cosmic and terrestrial surfaces, noting color distribution on moon, asteroids, stony meteorites, etc 15 p2516 A67-29152
 Spinning-image coded X-ray star camera, based on image coding, permitting reconstruction of two-dimensional image [AIAA PAPER 66-850] 15 p2486 A67-29440
 Interpretation of tests for randomness of lunar craters, noting clustering and alignment 15 p2554 A67-29458
 Multichannel photometer for space applications requiring low weight and power, no moving parts and high sensitivity divided in four electrically and optically distinct quadrants 15 p2491 A67-30433
 Physical characteristics of comets, 1961-1965 16 p2741 A67-30507
 Illumination impinging on geocentric satellite during eclipse by earth 16 p2761 A67-30958
 Proton-irradiation darkening of rock powders, noting contamination, temperature effects and applications to solar wind darkening of moon [JPL-TR-32-1130] 16 p2753 A67-31743
 Micrometric measurement of lengthening of horns of Venus crescent, phase and moment of dichotomy 17 p2942 A67-32329
 Comet Burnham C2 coma photometry, discussing error sources in isophotes and photometric scale and tabulating oval isophote size against axes mean ratio 17 p2943 A67-32442
 Very high optical resolution via lunar occultation noting experimental technique 17 p2945 A67-32646
 Experimental determination of orientation elements of FK3 catalog from short series of lunar observations 17 p2950 A67-33128
 Residuals and rms residuals of control measurements made by Manchester Lunar Group members, showing reduced heights not affected by personal errors 18 p3132 A67-34331
 Optical auroral pulsations in various frequency ranges analyzed using automatic zenith photometer 19 p3222 A67-35459
 Photometry and spectrophotometry of short-period variable stars 19 p3330 A67-36076
 Photometric data on Mars opposition effect /nonlinear brightness surge at zero alpha phase angle/ noting phase curve steepness 24 p4226 A67-41838
 Aurora photometry and stratospheric cosmic ray intensity, noting electron intrusion and correlation between aurora intensity and X-ray emission 24 p4213 A67-42778
 Optical characteristics of cosmic and terrestrial surfaces, noting color distribution on moon, asteroids, stony meteorites, etc 24 p4190 A67-43075
 Photometry of zodiacal light during IQSY, discussing extension to poles 24 p4152 A67-43114

ASTRONOMICAL SPECTRUM
 Thermoluminescence of achondrite meteorites on lunar surface based on rate of temperature rise of lunar terminator 01 p0146 A67-10249
 Possible correlation between color indices of quasi-stellar radio sources and red shift 02 p0323 A67-11697
 Water vapor lines in spectrum of Venus obtained by photoelectric scanning of spectrum 02 p0324 A67-11769
 Solar content of carbon isotope 13 obtained by examining solar atmosphere at center of disk 02 p0324 A67-11770
 Autoionization mechanism role in formation of astrophysical spectra 03 p0509 A67-13217
 Solar corona temperature measurements, noting discrepancy between results from

observations of forbidden emission lines and ionization balance 03 p0470 A67-13218
 Spectrographic observation of quasi-stellar and Haro-Luyten objects, noting hydrogen absorption spectra and emission wavelengths 03 p0511 A67-13652
 Extraterrestrial radiation source spectrum determined by comparing main beam and sidelobe signal power received on suitable bandwidth 03 p0371 A67-13946
 Hydrogen line intensity decrease in solar photosphere and chromosphere, noting agreement with Schroedinger equation results 03 p0512 A67-14004
 Mean values of methane wavelengths in Uranus spectrum measured for determination of atmospheric temperature 03 p0515 A67-14327
 Book on middle UV science and technology 04 p0612 A67-14690
 Astronomical UV radiation noting galactic composition and extragalactic systems, stellar emission and molecular and atomic H 04 p0696 A67-14700
 Molecular hydrogen features in spectra of Saturn and Uranus 04 p0696 A67-14738
 Spectral study of Jupiter, Saturn and rings of Saturn, determining methane concentration in cloud layers 04 p0701 A67-15557
 Halley comet head diameter change determined by converting propane and ethylene molecules in photon and corpuscular radiation field of sun 05 p0888 A67-16202
 Spectral indices of radio galaxies and quasi-stellar sources explained by relativistic electron injection into magnetic field by recurring blasts 05 p0891 A67-16400
 Variations in RF spectra of 3C 84, 3C 273, 3C 279 and other radio sources 05 p0891 A67-16401
 Photoelectric observation results of short period variable DQ Cephei star 05 p0891 A67-16405
 Photometry of integrated light of Venus, inferring presence of ice in atmosphere from halo effect of brightness dispersion 05 p0892 A67-16407
 Radio emission from Jupiter, Saturn and Mercury noting disk temperatures [AD-653438] 05 p0892 A67-16409
 X-rays from Coma cluster of galaxies, investigating origin by applying virial theorem 05 p0882 A67-16413
 Optical observation of brightest X-ray source in Scorpius, giving tabulated data as function of radius 05 p0892 A67-16414
 Correlation between position and red shift of quasars indicating anisotropic universe or galactic origin of quasars 05 p0898 A67-16887
 Chemical signatures from astronomical bodies, noting spectral results obtained from ground stations and orbiting spacecraft 06 p1092 A67-19014
 Uranus and Neptune spectral absorptions compared with laboratory spectra obtained with very long optical paths indicate methane role in planetary absorption 06 p1397 A67-21213
 Magnetic fields in solar corona, observing bursts with frequency splitting to determine correlation with plasma radiation theory 09 p1565 A67-21981
 Carbon dioxide study in Mercury atmosphere yields negative results from observations made with IR spectrometer and 61 inch reflector 09 p1565 A67-22016
 Absorption wavelengths of QSOs, noting relatively large red shifts 09 p1567 A67-22243
 Angular size of OH emission measured using high resolution interferometer 10 p1709 A67-23491
 Solar wind region magnitude, scattering transport path of particles and spectral variation of magnetic inhomogeneities analyzed on basis of 11-year cosmic ray cycle 11 p1855 A67-23930
 Aerobee rocket sounding of far UV spectra of six stars in Orion, extrapolating mass ejection from resonance absorption lines 11 p1861 A67-24488
 Coincidences in measured positions of absorption lines in spectra of quasi-stellar objects 11 p1862 A67-24507
 Fe IR line excitation in solar corona, noting abundance of iron relative to H and linear polarization of IR lines in coronal streamer 12 p2010 A67-26242
 Radial velocities and spectral types for 13

stars, listing photoelectric magnitudes and colors for six 14 p2387 A67-28565
 Decametric radio noise data from Jupiter apparitions /1960-1964/ 14 p2389 A67-28838
 Angular diameter of scintillating source 3C 279 determined from fluctuation spectrum width 14 p2389 A67-28843
 Red shift determinations for quasi-stellar radio sources using spectrographic techniques 14 p2389 A67-28844
 Spectral energy distribution of source 3C 446 between August 17 and December 12, 1966 14 p2389 A67-28850
 UBV values and red shifts of quasars interpreted within steady state and Friedman cosmological models 14 p2392 A67-28965
 Kinematic, spectroscopic and photometric data for pygmy stars /blue ultradwarfs/ 17 p2945 A67-32645
 Spectra broadening mechanism on reflector of Vilnius Observatory 18 p3044 A67-33659
 Planetary spectra improvement by Fourier spectroscopy, discussing modulation method reduction of atmospheric turbulence effects and fast transmission system 20 p3438 A67-36345
 Pressure scanned Fabry-Perot interferometer for twilight sky and zodiacal light observations 20 p3440 A67-36361
 Fabry-Perot spectrometer applied to upper atmospheric emission measurements of airglow and aurora 20 p3440 A67-36362
 Red shifts of radio galaxies observed spectroscopically with 120-inch telescope, using prime focus and image tube 20 p3527 A67-37392
 Galactic radio source W49 at 3.4 mm, showing no additional components in spectrum with turnover points at various frequency ranges 20 p3527 A67-37393
 U-B and B-V color indices, total absorption, color excesses and reddening lines for hot black bodies, with energy curve corrections for absorption line effects 22 p3883 A67-39768

ASTRONOMICAL TELESCOPE
 SA RADIO TELESCOPE
 Stellar differential chromatic refraction effects on guiding large-focal-length astronomical telescopes 02 p0325 A67-11983
 Programmed telescope control systems on equatorial mount 02 p0241 A67-11992
 Fluctuation of stellar images and analysis of systematic errors in guidance of telescope as result of atmospheric refraction and flexure of telescope 02 p0241 A67-11993
 Radio astronomical observation technique, eliminating tropospheric radiation noise fluctuation effects on telescope 02 p0198 A67-12033
 Liquid nitrogen cooled rocketborne telescope, measuring IR signals from diffuse and discrete astronomical sources 02 p0243 A67-12047
 LEM optical astronomy package /OAP/ containing astronomical telescope, spectrophotometer, data processing subsystem and other devices, for unmanned landing and life support 02 p0246 A67-12414
 Stellar diurnal variation determined during reduced solar activity from crossed-telescope and neutron monitor data 02 p0311 A67-12594
 Moon trajectory and rotation effects on lunar astronomical telescope 04 p0597 A67-15068
 Rotating shutter telescopic observation for optical measurement of faint meteor velocity 05 p0897 A67-16805
 Structure of lunar lithosphere using data from ground telescopes and Ranger photographs 06 p1092 A67-19004
 Optical problems when making IR astrophysical observations with balloon-borne telescope noting data documentation, focusing, image slicer, spectrometer, aberration correction, etc 07 p1184 A67-19388
 Balloon-borne telescope guidance by offset sun tracking 07 p1184 A67-19392
 Balloon-UV polarimetry using two different telescope-gondola systems 07 p1184 A67-19395
 Coronal observations during solar eclipse in Bolivia, discussing equipment used and results 08 p1391 A67-21044
 IR observations in one to seven micron region using astronomical telescope on Aerobee rocket above atmosphere 08 p1397 A67-21185

Far UV radiation flux measurement by satellite-borne telescopic stellar spectrophotometer 08 p1399 A67-21234
Maksutov-Cassegrain type telescope for rocket mounting, design and performance 10 p1654 A67-22751
Oscillating plateholder for determining instantaneous focal length of large telescopes 11 p1791 A67-24459
Center-to-limb variations for continuum, faint iron lines and core of strong Fraunhofer lines measured along polar and equatorial diameters of solar disk 11 p1861 A67-24492
Mean declinations correction for Talcott pairs of 191 stars from zenith telescope observations 11 p1868 A67-25088
Earth axis orbital path, using Horrebow-Talcott method for determination of polihody 13 p2110 A67-26465
Large telescopes with 100 m aperture with plastic foil or balloon lenses 13 p2121 A67-27359
Sunspot observation methods and techniques in white light, considering requirements, diffraction limitations on resolution, site selection and local seeing and telescope choice 13 p2202 A67-27421
Astronomical radio telescope control, noting altazimuth and equatorial modes of operation, overall accuracy, etc 15 p2492 A67-29532
Optical astronomy opportunities in cosmology, stressing need for additional telescopes located in Southern Hemisphere 15 p2563 A67-30393
Atmospheric trajectories of faint telescopic meteors observed by separate stations simultaneously and probability of plotting 16 p2751 A67-31461
Continuous monitoring and control of primary mirror figure of orbiting, diffraction limited astronomical telescope for optimum performance 16 p2680 A67-31802
Circuitry of transistorized azimuthal supertelescope designed for measurement of general ionization component of cosmic rays 17 p2854 A67-32097
Spherical and chromatic aberrations, astigmatism and field error of catadioptric telescope, determining resolving power with various methods 17 p2855 A67-32327
Weak radio sources of small angular size studied by lunar occultation technique, using steerable telescope 17 p2943 A67-32634
Motion of lunar images in focal plane of horizontal telescope without celostat arrangement 17 p2950 A67-33130
Afocal field corrector for astronomical telescopes with paraboloidal mirrors 17 p2862 A67-33296
Large orbiting astronomical telescope design, discussing minimum waver, high resolution image recording, compactness and thermal warpage 18 p3043 A67-33493
Interference and spectroscopic devices improving photographic detection of astronomical telescopes on ground and in space 18 p3048 A67-34189
Lunar research at Egyptian observatory at Kottamia 18 p3020 A67-34310
Palomar Schmidt telescope use as moon-star camera proved 18 p3049 A67-34315
Low pressure gas Cerenkov detector and spectrometer coupled into charged particle telescope for cosmic ray electron spectrum measurements, discussing efficiency and instrument calibration 20 p3452 A67-37566
Astronomical research /1965/ noting New Zealand observatory, telescopes in Chile, Hawaii and China, solar activity, planet studies, etc 21 p3700 A67-37830
Sidereal cosmic ray diurnal variations, taking into account data correction for barometric pressure and temperature effects 23 p4059 A67-41130
Solar prominence activation on March 25, 1967 observed with H-alpha visual patrol refracting telescope at Anacapri 23 p4060 A67-41234
Horizontal telescope used for solar corona photography during total eclipse /1966/, determining radii passing through solar magnetic poles 24 p4227 A67-42153

ASTRONOMICAL UNIT

Functional relation between mass, radius and angular velocity of earth, solar mass and corresponding lunar quantities shown via reciprocity principle 04 p0702 A67-15582
Masses of moon and Venus and

astronomical unit determined from Mariner II Doppler data, noting sources of error 05 p0895 A67-16575
Time delay measurements and radar echo determinations of planetary motions compared with IAU values 05 p0900 A67-17082
Astronomical unit determination by dynamical method 15 p2555 A67-29577
Atomic clock application for Universal Time determination, describing various corrective measures, atomic beam technique, etc 15 p2487 A67-29581
Planetary masses, radii and orbital element and astronomic unit determinations from radar time delay and Doppler shift measurements 15 p2556 A67-29871
Radar determinations of astronomical unit and orbits, radii and rotation vectors of inner planets, proposing general relativity radar test 18 p3123 A67-34145
Corrected derivation of earth-moon mass and various astronomical constants from Eros orbital motion 23 p4061 A67-40620
Numerical integration of Eros orbital motion normals, obtaining earth-moon mass and various astronomical constants 23 p4061 A67-40621

ASTRONOMY
SA INFRARED ASTRONOMY
SA RADAR ASTRONOMY
SA RADIO ASTRONOMY
SA SELENOLOGY
Selection and weighting of direct measurements, evaluating result of variational series by number x alone, using arithmetical mean and median 01 p0068 A67-10854
Stroke and Restrict method used in Fourier transform application to spectroscopy and astronomy and in obtaining holograms 01 p0069 A67-11008
Geological and astronomical research - Lunar International Laboratory Symposium, Athens, September 1965 04 p0596 A67-15062
Soviet papers on geophysics and astronomy 04 p0650 A67-15218
Communications of Lunar and Planetary Laboratory /University of Arizona/, Volume 4 /Numbers 64-69/ 05 p0896 A67-18716
IAU General Assembly, Hamburg, August-September 1964 05 p0899 A67-17068
Astronomical Society Conference, Göttingen, West Germany, September 1966 05 p0885 A67-17265
Soviet book on comets covering photometric and spectral studies, solar activity, structural elements, characteristics tables and bibliography 07 p1247 A67-19300
Solar and stellar systems orbit theory - IAU Symposium, Salonika, Greece, August 1964 08 p1379 A67-20380
Physics of moon and environment - Conference, London, June 1965 08 p1388 A67-21008
Neutrino theory and application to astronomy 09 p1563 A67-21651
Compiled data for Mars apparition in 1967 giving general visibility conditions, phases, seasons and positions of Mars and earth 10 p1710 A67-23562
Astronomical year-report, 1965, including bibliographies and works on instruments, position astronomy, interplanetary objects, quasars, etc 13 p2200 A67-27225
Astronomical data regarding longitude differences studied, deriving evening averages, time parameters, coefficients, etc, via Chebyshev approximation 14 p2384 A67-28075
Astronomical almanac 1967 covering chronology, solar and planetary data, time-signal transmission, etc 14 p2385 A67-28146
Selection and weighting of direct measurements, evaluating result of variational series by number x alone, using arithmetical mean and median 14 p2317 A67-28243
Space studies of Mars and Jupiter through cislunar and interplanetary rocket probes in near future [AAS PAPER 67-32] 15 p2562 A67-30105
Space research in Brazil, discussing rocket launching facility, meteorological experiments, X-ray astronomy, satellite observations, etc 19 p3320 A67-35285
Instrumentation for observing limb darkening of solar continuum during annular eclipse of May 1966 20 p3529 A67-37502
Astronomical research /1965/ noting New Zealand observatory, telescopes in Chile,

Hawaii and China, solar activity, planet studies, etc 21 p3700 A67-37830
U.S.S.R. astronomical almanac for 1970 21 p3703 A67-38200
Image tube properties in astronomical data acquisition, discussing photographic plate failure and various image intensifier applications 22 p3799 A67-39774
Advances in astronomy and astrophysics, Volume 5, covering zodiacal light, periodic oscillations, sunspot groups, etc 22 p3889 A67-40425
Book on universe covering development of astronomy from optical observation to radio, satellite and space probing investigations 24 p4223 A67-41783
Neutrino behavior in beta decay, proton-neutrino and proton-proton reactions, discussing astronomical implications of neutrino radiation 24 p4227 A67-42197

ASTROPHYSICS
Fundamental problems in cosmic radiation astrophysics 02 p0310 A67-12577
Atomic interactions and space physics - Symposium, Goddard Space Flight Center, Greenbelt, Maryland, August 1965 03 p0470 A67-13216
Kinetic plasma equations in form of Boltzmann equation or Fokker-Planck or Vlasov type of equations applied to astrophysics 03 p0481 A67-13736
Book on solar atmosphere with emphasis on chromospheric network and surface topography 03 p0515 A67-14331
Davis radiochemical experiment for detection of solar neutrinos and sampling techniques for detecting high energy atmospheric neutrinos 03 p0516 A67-14338
Partial fragmentation of pregalaxy in early phase of contraction with large internal velocity difference 04 p0697 A67-14806
Soviet papers on physics of comets and meteors 05 p0888 A67-16199
Symmetry of time axis and solar observations, offering counterworld alternative to Stannard 06 p1079 A67-17605
Large scale quasar clusters in inhomogeneous universe 07 p1250 A67-19665
Anisotropic distribution of quasars with large red shift as effect of observational selection 07 p1250 A67-19666
Stellar evolution model compared with observation to determine interior structure of real stars 08 p1387 A67-20982
Extended manned lunar surface operations in study of lunar origin and history with respect to solar system 09 p1588 A67-22408
Antimatter and cosmology 11 p1858 A67-23994
Albedo upper and lower fluctuation bounds determined by astrophysical comparison and three other methods 12 p2003 A67-25684
Zeeman effect in measuring magnetic fields of sun and stars, noting apparatus 12 p2010 A67-26235
Moon thermal history investigated using thermal model, comparing results with astrophysical and geological evidence including melting and fluid convection effects 14 p2390 A67-28888
Methods in computational physics, Volume 7, Astrophysics 14 p2392 A67-28992
Plasma dynamics - AIAA and Northwestern University Conference, Evanston, August 1965 14 p2361 A67-29034
Interaction between ion and electron waves in plasma 18 p3089 A67-34186
Bulgarian research in spectroscopy, solar system, ionosphere, gravitation equations, astrophysics, etc 19 p3320 A67-35283
U.S. space research program /1966/, national organization, international participation, space vehicle research and experiments related to future programs 19 p3322 A67-35307
Solar identifications for forbidden carbon I lines in solar spectrum 19 p3324 A67-35435
Advances in astronomy and astrophysics, Volume 5, covering zodiacal light, periodic oscillations, sunspot groups, etc 22 p3889 A67-40425
Cosmic ray physics - Conference, Alma-Ata, Kazakh SSR, October 1966 23 p4051 A67-41089
Solar neutrino astrophysics, universal neutrino sea, high energy neutrinos, neutrino detectors, stellar energy production, solar thermometry and gravitational constant time variation 23 p4056 A67-41111

Possible circular polarization of compact quasar radio and optical radiation, discussing astrophysical implications 24 p4226 A67-41884

Relativistic gravitational collapse, considering asymmetric nonrotating star collapse 24 p4226 A67-41885

ASYMPTOTIC FUNCTION

Oscillation formation by violation of sufficient conditions of asymptotic stability in linear system 01 p0047 A67-11215

Asymptotic stability of nonlinear systems, noting application to systems with control and Liapunov function 01 p0048 A67-11318

Singular perturbation theory of differential equations applied in control engineering, noting asymptotic expansion of solution 02 p0227 A67-12681

HF gaseous squeeze film bearing asymptotically analyzed by considering internal and edge regions separately [ASME PAPER 66-LUB-11] 03 p0431 A67-13760

Asymptotic rate of convergence of Gauss-Seidel type iterative processes for nonlinear difference equations 03 p0460 A67-13881

Asymptotic characteristic of eigenfunctions of two-dimensional scalar wave equation with boundary conditions at equidistant curves 04 p0570 A67-14743

Degeneration of solutions of well-posed systems of first order partial differential equations when particular parameter approaches zero 05 p0836 A67-17315

Asymptotic kinetic equation for inhomogeneous plasma compared to results for initial value problem and Bogoliubov method 06 p1042 A67-18572

Approximate solutions for differential and integral equations in form of second order asymptotic polynomials 07 p1214 A67-19216

MHD equations for spectral energy tensors of weak homogeneous magnetoturbulent field and derivation of asymptotic decay law by method of steepest descent 08 p1359 A67-21122

Stability analysis of symmetrically loaded thin walled spherical shell, noting construction of asymptotic expansion, error estimation and application of elasticity theory 11 p1871 A67-24152

Interpretation of results obtained by Liapunov method, using parallelepiped imbedded in region of asymptotic stability 12 p1919 A67-25912

Stability and asymptotic behavior of perturbed nonlinear systems of ordinary differential equations 12 p1961 A67-26060

Orbits in Copenhagen problem asymptotic at L4 and genealogy 13 p2205 A67-27481

Asymptotic form of uniform approximation of abstract functions by single family of linear integral operators occurring in Banach space topology 14 p2341 A67-27834

Asymptotic short wave flow equations simplified for various viscous heat conducting gas flows 14 p2295 A67-27838

Types of closed characteristics in bounded region of two-dimensional autonomous differential equation 16 p2695 A67-30856

Asymptotic stability criterion for autonomous feedback system with single odd monotonic nonlinearity, using functional analysis 16 p2646 A67-31639

Asymptotic stability of homogeneous system of partial differential equations in stratification wave theory, introducing source function for local plasma disturbance effect 17 p2907 A67-33101

Long time behavior of weakly interacting nonlinear waves, emphasizing mathematical features common to physical situations 18 p3079 A67-34002

Definition of asymptotic stability conditions and instability of zero solutions of differential equations 18 p3080 A67-34605

Asymptotic approximations for analysis of nonlinear resonant circuits through differential equations, assuming oscillation processes similar to harmonic system processes 20 p3409 A67-37113

Asymptotic series in theory of nonlinear systems of ordinary differential equations 20 p3479 A67-37718

Asymptotic behavior of solutions for nonlinear differential equations 20 p3479 A67-37720

Testing procedures for null hypothesis sensitive to ordered alternatives where at

least one inequality is strict 21 p3650 A67-37780

Asymptotic representations of Whittaker functions /with terms of standard equation coefficients equal/ applicable to wave propagation in inhomogeneous media 21 p3652 A67-38109

Positive linear second order differential equation solutions, with proof of general theorems about qualitative asymptotic behavior 21 p3652 A67-38195

Asymptotic formulas for propagating discontinuity diffusion in magnetoplasma, considering discontinuity shape, diffusion and lifetime 21 p3621 A67-39020

Dissociation and recombination of diatomic molecules by invert third bodies described by stochastic theory 22 p3756 A67-39386

Asymptotic solution for class of integral equations of first kind with application to contact problem of infinite elastic cylinder 22 p3909 A67-39400

Approximation method for solution of Bellman equation in optimal control problems 22 p3777 A67-39828

Field scattering by convex cylinders solved by asymptotes expressing reduced wave equations 23 p3972 A67-40751

Asymptotic expansion of radiating antenna field in penumbra region 23 p3973 A67-40836

Asymptotic perturbation of hypersonic flow over blunt slender cones and wedges showing oscillatory nature 23 p3931 A67-41665

Asymptotic solutions of eigenvalue problem with two transition points applied to Graetz problem involving heat transfer in fluid 23 p4083 A67-41668

Constant thickness elastic conical shells subject to lateral loads, deriving asymptotic solution 23 p4080 A67-41727

Bayes estimate of regression coefficients in cost function selection in presence of unsteady noise 24 p4134 A67-41796

Radiative heat transfer for light reflection and transmission by optically thick scatterers with three-term phase function, obtaining asymptotic formulas 24 p4147 A67-41820

First approximation analysis of rarefied hypersonic gas flow asymptotic properties near surface and front edge of thin plate, determining macroparameters 24 p4142 A67-42272

Uniformization of asymptotic expansions, constructing counterterms by nesting increasing number of extensions for both secular and singular perturbation terms 24 p4190 A67-43094

ASYMPTOTIC METHOD

Extension of Waltman theorems regarding oscillation and asymptotic behavior of solutions of nonlinear differential equation, proving solution existence for initial value problem 01 p0105 A67-10730

Asymptotic method of refining classical theory of bending and stretching of plates by construction of two-dimensional equations for processes involved 01 p0163 A67-10996

Boltzmann equations in kinetic theory of rarefied gas dynamics 01 p0054 A67-11092

Geometrical optics method modified for asymptotic solution to scalar wave equation for wave penetrating caustic surface 02 p0192 A67-11637

Asymptotic evaluation for k approaching infinity of antenna field emerging from currents induced on surface of reflector with incident spherical wave 02 p0223 A67-12796

Asymptotic form of correlation functions facilitated by use of Hamiltonian 03 p0458 A67-13342

Stability of forced oscillations described by second order nonlinear differential equation determined by Pinnl asymptotic method 03 p0530 A67-14177

Steady blunt body problem solution via time-dependent technique, performing computation in shock layer 04 p0546 A67-14818

Asymptotic method of synthesizing FM pulse signals from given autocorrelation function 04 p0575 A67-15160

Asymptotic flow theory laws of friction and heat transfer in turbulent boundary layer 04 p0610 A67-15838

Asymptotic directions of cosmic rays for Soviet cosmic ray stations 05 p0880 A67-16114

Evolution of nonlinear perturbations in

plasmas, noting physical meaning of self-similar solution based on Korteweg-de Vries equation 05 p0853 A67-16698

Matched asymptotic expansions method for perturbation problem of nearly equilibrium dissociating boundary layer flow 05 p0792 A67-16818

Error bounds for asymptotic solutions of differential equations, using Volterra equations for actual and formal solution vectors 06 p1021 A67-17565

Two variable expansion procedure for approximate asymptotic solution to nonlinear differential equation 06 p1022 A67-17789

Asymptotic method for solution of boundary layer equations for generalized three-dimensional flow of dissociated air at chemical equilibrium near stagnation point 06 p0984 A67-18113

Equation of cylindrical shell under cyclic loads, using asymptotic method 06 p1106 A67-18629

Asymptotic representation of integral operator used in describing time-varying load function in quasi-static and dynamic elastic heredity problems of creep materials 06 p1107 A67-18638

Graphical and analytical solutions to wave propagation in inhomogeneous media in conditions of wave number variations oscillating along coordinate 06 p1034 A67-18814

Asymptotic solution for oscillations of quasi-linear gyroscopic systems taking into account internal resonance 07 p1261 A67-19189

Free oscillation of thin elastic shell, using asymptotic method for integrating dynamic equations in classical linear theory 07 p1263 A67-20031

Space-time diffraction for asymptotic solution of Klein-Gordon dispersive hyperbolic equation in bounded domain 07 p1218 A67-20270

Remedies for deficiencies in approximations near transition point in asymptotic methods used for estimates of solutions to differential equations governing axisymmetric vibrations of thin elastic shells 08 p1414 A67-20346

Asymptotic and particular solutions of conical shells subjected to lateral normal loads, discussing membrane forces, bending effects and boundary conditions for moments and shearing force 09 p1573 A67-21754

Asymptotic behavior of laminar boundary layer, reducing system to heat equation, noting viscosity effects and uniqueness of homogeneous solution [ONERA-TP-458] 10 p1623 A67-22878

Sufficient conditions for asymptotic invariance of Bayes estimate of regression coefficient for nonstationary noise 10 p1619 A67-22952

Asymptotic exponential laws of contraction of plane and axisymmetric jets of weightless fluids, obtaining expressions for stream function and velocity component 10 p1624 A67-23039

Asymptotic properties of solutions to kinetic coefficient equation system, noting mass velocity dependence on time 10 p1625 A67-23042

Reynolds equation analysis for pressure distribution in gas bearing clearances by asymptotic solution 10 p1660 A67-23046

One-dimensional steady laminar premixed flame characterized by matched asymptotic expansions 10 p1733 A67-23145

Deflection of free three-layer strip under impact, determining displacement function and bending oscillations 10 p1721 A67-23610

Matched asymptotic expansion for singular pressure loading behavior for oscillating wings or control surface edges 10 p1593 A67-23712

Asymptotic solution of typical bay in hydrostatically loaded ring-reinforced noncircular cylinder of finite length 10 p1729 A67-23766

Asymptotic expansion procedure applied to Donnell equations for cylindrical shell, obtaining solution for interaction of infinite cylinder reinforced by radially loaded ring [ASME PAPER 66-WA/APM-27] 10 p1730 A67-23839

Asymptotic analysis of radiative Rayleigh problem in flow of compressible viscous heat-conducting radiating gray gas extended to high plate Mach

numbers 11 p1774 A67-23855
 Matched asymptotic expansions method for developing higher order approximations to structure of laminar detonation wave supported by irreversible unimolecular chemical reaction 11 p1749 A67-23858
 Matched asymptotic expansions for solution of singular perturbation problem of stresses and deformations in pressurized toroidal membrane 11 p1871 A67-24086
 Asymptotic integration of elasticity theory equations and analysis of stressed state of anisotropic shell 11 p1871 A67-24160
 Asymptotic calculation of effect of small tangential thrust on satellite motion problem solved for satellite orbit in first and second approximation 11 p1870 A67-24684
 Asymptotic method of integrating differential equations applied to analysis of axisymmetrical oscillations of thin elastic LF shells of revolution 12 p2027 A67-25624
 Asymptotic methods of obtaining refined solutions for zero moment equations of concentrated loads applied to shells with Gaussian curvature 12 p2028 A67-25630
 Asymptotic integration of elasticity theory equations applied to two-dimensional dynamic theory for cylindrical shells 12 p2029 A67-25636
 Asymptotic integration technique for small axisymmetrical oscillations of thin walled elastic shell of revolution for case of double reversal point 12 p2029 A67-25675
 Natural frequencies of free longitudinal oscillations of circular rod with random parameters determined by modified Krylov-Bogoliubov asymptotic method 12 p2031 A67-25957
 Navier-Stokes asymptotic solutions for large Reynolds number flows, emphasizing incompressible axial flow past seminfinitesimal cylinders 12 p1930 A67-26179
 Mixed problem for linear hyperbolic partial differential equation asymptotically represented and reduced to boundary value problem and Cauchy problem 13 p2144 A67-26377
 Asymptotic theory for near-continuum gas flows applied to BGKW equation, deriving slip coefficient 13 p2101 A67-26964
 Spherical supersonic source expansion of neutral disparate molecular weight binary gas mixture studied asymptotically as source Knudsen number tends to zero 13 p2104 A67-26984
 Mechanical quadrature theory and convergence problems 13 p2148 A67-27469
 Asymptotic form of correlation functions facilitated by use of Hamiltonian 13 p2149 A67-27713
 Stability and asymptotic behavior of dynamical systems defined by autonomous functional or partial differential equation and conditions for applying Liapunov theorem 14 p2342 A67-28081
 Asymptotic study of Markov stationary discrete time and finite number of states decision process 14 p2291 A67-28510
 Linearization of oscillation differential equations containing even nonlinearities, using asymptotic polynomials 14 p2344 A67-28810
 Asymptotic solution of oblique waves in inhomogeneous vertically magnetized plasma 14 p2361 A67-28922
 Asymptotic method of synthesizing FM pulse signals from given autocorrelation function 15 p2435 A67-29347
 Asymptotic method for solving equations of theory of elasticity and mathematical physics 15 p2574 A67-29691
 Evolution of nonlinear perturbations in plasmas, noting physical meaning of self-similar solution based on Korteweg-de Vries equation 15 p2530 A67-29869
 Nonlinear system analysis by subdividing total motion of system into fast and slow components, noting application to control systems 15 p2458 A67-29886
 Asymptotic calculation of satellite orbit evolution in noncentral gravitational field of earth 16 p2743 A67-30724
 Matched asymptotic expansions and patched conics used to simplify flyby interplanetary trajectories [AIAA PAPER 65-689] 16 p2743 A67-30728
 Integration of laminar boundary layer equations in compressible gas by asymptotic method, calculating friction and heat flux 16 p2660 A67-31135
 Mutual coupling between sectoral horns

side-by-side formulated in terms of rays, modes and mode caustics excited in each horn 16 p2639 A67-31355
 Successive approximation method for asymptotic solution of waves in inhomogeneous gyrotropic plasma 16 p2627 A67-31366
 Transformation of van der Pol equation into piecewise linear differential equation, determining periodic solution from asymptotic expansion 17 p2878 A67-32712
 Single frequency vibrations of beams and girders solved by applying asymptotic methods 17 p2962 A67-32881
 Rotational motions of second order autonomous systems, proposing determining algorithm 17 p2885 A67-32883
 Uniqueness theorem for general linear anisotropic time-variable viscoelastic body under boundary conditions, using Laplace transformation 17 p2964 A67-33135
 Averaging method extended to physical systems described by differential equations simultaneously dependent on almost periodic fast time and periodic slow time 17 p2885 A67-33140
 Sufficient conditions guaranteeing asymptotic stability of class of linear dynamic systems with bounded narrow band parametric excitation [ASME PAPER 67-APM-24] 17 p2830 A67-33152
 Elastic plates linear theories for micropolar and director displacements, deriving plate equations by asymptotic expansion method 17 p2966 A67-33349
 Iterative methods for integration of linear partial differential equations, determining relaxation factor 18 p3071 A67-33753
 Homogeneous MHD turbulence on large scale structure, finding asymptotic forms of velocity and magnetic field correlations 19 p3295 A67-35540
 Wave propagation in real gases, considering one-dimensional time-dependent disturbances seminfinitesimal in extent, emphasizing matched asymptotic expansion and coordinate stretching methods 19 p3212 A67-35798
 Matched asymptotic expansion method applied to hypervelocity flight trajectories, obtaining solutions to flight dynamic equations 19 p3336 A67-35994
 Steady two-dimensional laminar flow of incompressible viscous fluid, noting asymptotic convergence of velocity profile in Prandtl boundary layer 19 p3212 A67-36031
 Boundary value problem of oscillatory system with time lag quasi-linear partial differential equation 19 p3251 A67-36050
 Slightly resistive plasma stability analyzed by asymptotic methods, studying small perturbation growth rate 20 p3493 A67-36145
 Deflection of free three-layer strip under impact, determining displacement function bending oscillations 20 p3542 A67-37540
 Asymptotic solution to nonplanar earth-to-moon trajectories in restricted four-body problem 21 p3705 A67-38613
 Density, electric field and volt-ampere characteristics for spherical electrostatic Langmuir probe in collision plasma with weak ionization and recombination, using asymptotic method [AIAA PAPER 67-705] 21 p3672 A67-38732
 Electromagnetic waves passage through thin radio-transparent layer solved by asymptotic series 21 p3585 A67-38810
 Integral equation for asymptotic expansions of plane electromagnetic and acoustic fields diffracted by convex surfaces of variable curvature 22 p3836 A67-39389
 Asymptotic solution for electromagnetic field of electric dipole above stratified half-space 22 p3763 A67-40311
 Corrections for three results in asymptotic solution of nonideal Bose-Einstein particle system nonlinear integral equations 23 p4026 A67-40718
 Discretization error analyzed for accumulation during numerical solution of equations of orbital motion 23 p4023 A67-40864
 Revolving thin elastic shell free axisymmetric oscillation described by equation system derived by asymptotic integration technique with single reversal point 24 p4250 A67-42304
 Asymptotic method for solving differential equations, giving equilibrium composition of gaseous combustion

products 24 p4178 A67-42390
 Boundary layer theory in gas bearing lubrication problems, obtaining pressure asymptotic expansions for infinitely long slider squeeze-film bearing [ASME PAPER 67-LUB-7] 24 p4162 A67-42671
 Viscoelastic lubricant in squeeze film configuration for sphere impinging on lubricant covered plane, noting pressure peak sensitivity to viscoelastic constants [ASME PAPER 67-LUB-24] 24 p4164 A67-42682
 Asymptotic directions of cosmic rays for Soviet cosmic ray stations 24 p4214 A67-42790
 Asymptotic functional dependences and eigenvalues of guided wave modes in uniform and nonuniform structures deduced by ray-optical techniques 24 p4124 A67-42807
ATHENA ROCKET
 Relationship of management to reliability aspects during Athena program 18 p3138 A67-34651
ATLANTIC OCEAN
 Atmospheric ozone distribution, air flows and temperature at high altitudes in equatorial latitudes of Atlantic Ocean 05 p0799 A67-17026
ATLAS AGENA LAUNCH VEHICLE
 Oscillatory ground wind response of Atlas/Agena examined, using statistical theory of extreme values 06 p1104 A67-18492
 Shroud for Lunar Orbiter atop Atlas-Agena launch vehicle, noting structural alloys used 07 p1193 A67-20255
 Optimization of Atlas-Agena trajectories via steepest ascent computer program 15 p2514 A67-29602
 Comet missions, discussing spacecraft exploration criteria for short period and long period first-apparition comets 16 p2745 A67-30749
 Comet mission study using space probes boosted by Atlas Agena and Atlas Centaur launch vehicles for interception from 1967 to 1975 16 p2745 A67-30750
ATLAS CENTAUR LAUNCH VEHICLE
 Suitability of Saturn IB/Centaur and Atlas/Centaur launched solar-electric propulsion vehicles for performing 0.1-AU solar probe mission [AIAA PAPER 66-496] 11 p1852 A67-24343
 Comet mission study using space probes boosted by Atlas Agena and Atlas Centaur launch vehicles for interception from 1967 to 1975 16 p2745 A67-30750
ATLAS LAUNCH VEHICLE
 Test program to evaluate characteristics of existing Atlas engine boots in flight environment and provide parameters for design change [AIAA PAPER 67-277] 07 p1241 A67-20054
 Atlas booster materials compatibility with fluorine oxidizers 13 p2186 A67-27687
ATMOSPHERE
 SA AIR
 SA CABIN ATMOSPHERE
 SA EARTH ATMOSPHERE
 SA EXOSPHERE
 SA FREE ATMOSPHERE
 SA INERT ATMOSPHERE
 SA IONOSPHERE
 SA LOWER ATMOSPHERE
 SA LUNAR ATMOSPHERE
 SA MID-LATITUDE ATMOSPHERE
 SA NONGRAY ATMOSPHERE
 SA OZONOSPHERE
 SA PLANETARY ATMOSPHERE
 SA SOLAR ATMOSPHERE
 SA SPACE CABIN ATMOSPHERE
 SA STANDARD ATMOSPHERE
 SA STELLAR ATMOSPHERE
 SA STRATOSPHERE
 SA TROPOPAUSE
 SA TROPOSPHERE
 SA UPPER ATMOSPHERE
 Statistical problems in use of EM data for remote sensing of geological attributes of lithosphere-atmosphere interface 05 p0803 A67-17387
 Experimental Inter-American Meteorological Rocket Network /EXAMETNET/ for Southern Hemisphere research 08 p1350 A67-20549
 Auroral particle fluxes and effects from coordinated satellite, aircraft-and ground-based measurements 18 p3034 A67-33590
 Soviet collection of articles on atmospheric physics 19 p3213 A67-34850
ATMOSPHERE EXPLORER
S EXPLORER XVII SATELLITE

ATMOSPHERE EXPLORER-A

S EXPLORER XVII SATELLITE

ATMOSPHERE MODEL

F-2 layer ion-atom interchange coefficients, ion-neutral diffusion coefficient and flux of solar ionizing radiation, comparing ionospheric data 01 p0056 A67-10108
Experimental verification of calculation of short wave radiation fluxes in real atmosphere from model 01 p0108 A67-10128
Synthetic line profiles generated for variety of model atmospheres containing linear and quadratic velocity fields, used to analyze solar chromosphere 02 p0323 A67-11690
Radiative energy loss from solar chromosphere and corona estimated in order to identify mechanical energy input mechanism 02 p0323 A67-11692
Internal gravity-shear waves in troposphere for two-and three-layer model of air density and horizontal velocity, noting phase velocities 02 p0238 A67-12190
Amplitude of perturbations about each interface in internal gravity-shear waves in troposphere according to three-layer model 02 p0239 A67-12191
Leading particle model of formation of extensive air showers, showing determination of energy spectrum 02 p0319 A67-12785
Model for ionospheric drift measurements made by spaced receiver method when scattered wave has frequency above plasma frequency of scattering region 03 p0407 A67-12831
Induced absorption coefficients in atmosphere model measured for calculation of Venus lower atmosphere properties from radio observations 03 p0394 A67-12949
Two-dimensional dynamic model of diurnal variation of thermosphere 04 p0611 A67-14651
Laboratory experiments on atmospheric simulation, mainly rapidly rotating fluids, with limitation to incompressible fluids 04 p0613 A67-14802
Primitive earth atmosphere model suggesting that in early history of earth, reducing atmosphere could be stable against gravitational escape 04 p0701 A67-15545
Statistical method of calculation of atmospheric thermal, conservative and dynamic characteristics using measured ozone distribution 05 p0796 A67-16488
Geometric model of radiative atmospheric space used in research on mean radiation temperature of space by frigidometer 06 p1025 A67-17637
Physical model of turbulence used in developing forecasting scheme of clear air turbulence /CAT/ over mountains [AIAA PAPER 67-184] 06 p1026 A67-18298
Upper atmospheric formation of electron cloud produced by chemionization reactions of chemical release agents [AIAA PAPER 67-148] 06 p0995 A67-18360
Atomic and molecular processes in upper atmospheres of Venus, Mars and Jupiter investigated by atmospheric models, presenting solar-planetary relationship 06 p1087 A67-18429
Horizontal variability of properties of model thermosphere with seasonal changes 06 p0996 A67-18564
Upper atmospheric condition noting solar activity effect, synoptic meteorology, etc 06 p1027 A67-18607
Numerical integration of quasi-geostrophic atmospheric model with asymmetric zonal current 06 p0999 A67-18739
Model atmospheres and astronomical and parallax refraction 07 p1174 A67-19716
Characteristics of atmospheric convection, obtained by vertical and horizontal heat transport processes and represented by difference equation, used to derive analytical solution 09 p1491 A67-21553
High altitude atmospheric models, discussing Harris-Priester and Nicolet theories 10 p1640 A67-23217
Photometric measurements of eclipses of artificial solar satellite 1960 Eta 2 at sunrise and sunset in Lyman alpha and violet spectral range 10 p1706 A67-23221
Numerical modeling role in studies of general circulation of atmosphere 10 p1677 A67-23368
Line profiles and equivalent widths for diffuse reflection of sunlight from model planetary atmosphere calculations, using

invariant imbedding 10 p1710 A67-23635
Homogeneous solar photosphere and lower chromosphere model in hydrostatic and local thermodynamic equilibrium, reproducing continuous and line spectrum 11 p1858 A67-24112
Microwave spectral brightness measurements of Venus compared with several model atmospheres 11 p1865 A67-24601
Radar, radio astronomic and IR spectroscopic observations of Venus surface and atmosphere, examining general and surface data, chemical composition and atmospheric model construction 11 p1867 A67-24843
Magnetosphere phenomena investigated via atmosphere model to explain planetary nebulae and eruptive solar prominences 12 p1992 A67-25119
Magnetospheric model of Jupiter from numerical calculation of maximum number density of plasma 12 p2000 A67-25206
Martian atmosphere models with different composition, pressure and temperature 12 p2003 A67-25685
Japanese rocket observations of upper atmospheric wind and temperatures in relation to new Cira model atmosphere 12 p1937 A67-25841
Model for vertical eddy heat flux in stable atmosphere 13 p2149 A67-26275
Martian daytime atmosphere from zero to 50 km presenting spherical particle terminal velocities and possible sizes for observations, using Mariner IV occultation 13 p2195 A67-26316
Statistical method of calculation of atmospheric thermal, conservative and dynamic characteristics using measured ozone distribution 13 p2109 A67-26344
Statistical properties of phase and amplitude fluctuations during total reflection of waves from ionospheric layer 13 p2067 A67-26551
Transfer of large scale tropospheric perturbations into stratosphere analyzed using hydrodynamic model, noting role of atmospheric stratification, refractive index, etc 13 p2112 A67-26674
Photochemical reaction and turbulent diffusion effect studied using mesospheric model, establishing relation between composition and dynamic state 13 p2113 A67-26681
Atmospheric boundary layer dynamics models, similarity hypothesis and theories 13 p2151 A67-26687
Astronomical refraction in polytropic atmosphere adapted to automatic computers 13 p2152 A67-27484
Three-layer atmospheric model for use in two-dimensional diffusion equation for steady state conditions incorporating eddy diffusion of momentum 13 p2153 A67-27607
Model thermospheres, studying ducted traveling acoustic gravity waves originating in ionosphere 14 p2310 A67-28054
Atmosphere model for pure helium star including only helium I and II transitions and electron scattering in calculating opacity 14 p2387 A67-28578
Geopotential and wind field calculations for Northern Hemisphere using statistical models 14 p2346 A67-28764
Behavior at infinity of specific intensity in plane-parallel atmosphere 14 p2391 A67-28946
Model stellar atmosphere computations predict emergent radiation spectrum 14 p2392 A67-28993
Dayside distortion of geomagnetic field by solar wind beyond 3.5 earth radii measured and compared with three magnetosphere models 15 p2475 A67-29612
Randomly distributed initial energy input effect on unbounded rotating barotropic atmosphere, noting energy density function as initial condition 15 p2478 A67-30056
Sensible heat transfer influence on dynamic stability of harmonic perturbations superimposed on zonal current, using Lorentz two-level model 15 p2512 A67-30057
Negative ion density and composition in lower ionosphere 16 p2665 A67-31019
Multiple light scattering in inhomogeneous spherically symmetrical planetary atmosphere with exponentially varying attenuation coefficient 16 p2698 A67-31096
Two-layer model of Venusian atmosphere satisfying radioastronomic and radar self-radiation measurements 17 p2941 A67-32322

Mathematical model for global atmospheric circulation prediction and mean properties in terms of tensor algebra 17 p2843 A67-32466
Physical model of turbulence used in developing forecasting scheme of clear air turbulence /CAT/ over mountains 17 p2880 A67-32552
Distinction between macro-and microturbulence in solar photosphere studied from line profiles 17 p2944 A67-32641
Optimization of extra-atmospheric phase of orbital ascent by assumption of certain hypotheses concerning atmosphere transit cost and nonnegligible-aerodynamic atmosphere thickness 17 p2946 A67-32695
Carbon dioxide ions with electrons dissociative recombination measurements with microwave-afterglow differentially pumped quadrupole mass-spectrometer apparatus, noting Martian atmosphere model [SRCC-55] 17 p2888 A67-32826
Model for distribution of thermal plasma in magnetosphere of Jupiter under assumption of corotation with planet 17 p2951 A67-33196
Perspective and path length effects on determination of spatial distribution of auroral luminosity from optical observations 17 p2851 A67-33206
Hydrogen and helium lateral flow in collisionless exosphere calculated on model for various sinusoidal temperature and concentration variations over exobase surface 17 p2852 A67-33235
Coupling between neutral air motion and plasma transport in model F-2 layer, noting nonlinear diffusion equation, velocity profiles, etc 17 p2852 A67-33241
Atomic and molecular processes in Cytherean, Martian and Jovian upper atmospheres 18 p3124 A67-34158
Mars emission spectrum computed for two atmospheric models, presenting weighting functions for different wave numbers 18 p3125 A67-34159
Effective braking height /EBH/ for small interplanetary particles of cosmic velocity entering Martian upper atmosphere 18 p3135 A67-34541
Upper atmosphere density, temperature and variation determined from satellite drag data, proposing thermosphere model 19 p3214 A67-34931
Long term global integrations of primitive meteorological equations for free surface model, using spherical polar coordinates 19 p3252 A67-35058
Quasi-biennial zonal wind and temperature oscillation in stratosphere and mesosphere, discussing periodicity and oscillation model 19 p3220 A67-35272
Noise wave amplitude reduction method by suitable initial wind field adaptation to pressure field studied for applications to divergent barotropic model 19 p3253 A67-35530
Total atmospheric ozone from satellite measurements of solar UV reflected radiation determined, using atmospheric model with Rayleigh scattering 19 p3226 A67-35923
Bistatic radar cross section of coherent-dot radar angel in convective thermal model 20 p3480 A67-36286
Two-ion D region model for polar cap absorption events 20 p3426 A67-36302
Sodium cloud between 85 and 110 km shows turbulent phenomena stratification exists and disappears with upward propagation of movements due to energy decreases 20 p3427 A67-36367
Primitive-earth atmosphere models irradiated with UV light and ionizing radiation for primordial organic synthesis 20 p3369 A67-36656
Sudden commencement and initial phase of magnetic storm explained in terms of currents induced in ionosphere 20 p3434 A67-37422
Perturbation scheme deriving geomagnetic Euler potentials applied to magnetospheric model with solar wind effect 20 p3434 A67-37423
Equilibrium state for interstellar gas-magnetic field system as described by model 20 p3528 A67-37472
Photochemical reaction and turbulent diffusion effect studied using mesospheric model, establishing relation between composition and dynamic

state 21 p3618 A67-38426
 Atmospheric boundary layer dynamics models, similarity hypothesis and theories 21 p3654 A67-38429
 Unstable light scattering in atmospheric models studied in relation to medium optical properties, using phase shift measurement 21 p3627 A67-38448
 Rainfall associated with atmospheric convective activity estimated by radio ray attenuation model 21 p3582 A67-38577
 Smith gyrofrequency model for determination of vertical electron concentration distribution in magnetosphere, using whistling atmospherics data 21 p3621 A67-39022
 Two-dimensional diffusion model for gas propagation in lunar atmosphere, discussing contamination by lunar module exhaust gases and solar wind loss mechanism 22 p3883 A67-39817
 Long period surface gravity waves in atmosphere 22 p3792 A67-39974
 Venus radiation spectrum in mm range from Venus atmosphere models 22 p3886 A67-40120
 Atmosphere of Mars studied using three models generated to show high, mean and low density compositions to account for gravitational and magnetic fields 22 p3887 A67-40140
 Luminance of lunar surface site predicted by direct solar and earth reflected illumination together with local albedo variations 22 p3887 A67-40143
 Leading particle model of formation of extensive air showers, determining energy spectrum 22 p3878 A67-40287
 Giant and continuous pulsations and pulsation trains in geomagnetic field studied from six giant pulsation events in 1963, discussing Wilson model 23 p3994 A67-40694
 Cosmic ray propagation through atmosphere, developing model for elementary particles behavior 24 p4218 A67-42837

ATMOSPHERIC ABSORPTION

Atmospheric radio wave absorption coefficient and altitude determined and linked to effects of colliding paramagnetic oxygen molecules 01 p0022 A67-10391
 Electromagnetic radiation absorption coefficient of atmospheric water vapor in long-wave portion of submillimeter range 02 p0190 A67-11568
 Space communication maximum usable frequency and limitations imposed by atmospheric absorption 02 p0205 A67-12735
 Barometric coefficient of cosmic ray variations determined from observation of Forbush effects and cosmic ray flare effects 05 p0881 A67-16123
 Atmospheric radio wave absorption at wavelengths ranging from 1.36 to 3.0 mm, determining absorption coefficients of molecular oxygen and water vapor 05 p0761 A67-16343
 Microradiowave absorption in air by water vapor dimers 06 p0963 A67-18206
 Planetary atmospheric absorption spectroscopy employing split-trajectory dual flyby mode [AIAA PAPER 67-121] 06 p1085 A67-18311
 Extreme IR atmospheric absorption calculation shown in graphs and compared with available results in submillimeter and millimeter range 06 p0998 A67-18717
 Book on atmospheric absorption, diffusion and polarization of light and radioelectric radiation 06 p0998 A67-18718
 Radio telescope antenna gain losses due to surface irregularity atmospheric scattering and absorption 07 p1158 A67-20241
 Transition of extensive air showers in atmosphere with determination of lateral structure, mean free path and inelasticity 08 p1377 A67-21437
 Near IR atmospheric absorption over 25-km horizontal path at sea level 10 p1629 A67-22744
 Rapid and slow spreading absorption of cosmic rays over polar cap 10 p1699 A67-22790
 Atmospheric reaction with energetic particles and resultant production of atomic oxygen, atomic nitrogen and nitric oxide 10 p1637 A67-23191
 UV solar radiation absorption in upper atmosphere determined from measurement of photoelectron currents emitted by planar metallic orthogonal photocathodes onboard

Cosmos II satellite 10 p1647 A67-23282
 Absorption and brightness temperature variations of atmosphere on basis of statistical characteristics of vertical temperature and humidity structures 11 p1785 A67-23956
 Atmospheric absorption problem solution, using cavity maser operating at 4 mm wavelength 12 p1952 A67-25297
 Rayleigh scattering and Lambert ground reflection effect on solar energy absorbed by ozone in earth molecular atmosphere evaluated on basis of transfer equation 12 p1932 A67-25341
 Molecular oxygen densities in range 70-90 km determined by rocket measurements of atmospheric absorption of solar UV radiation in Southern Hemisphere 12 p1934 A67-25786
 Atmospheric long range spectral transmissivity measured by single beam photometer with recording potentiometer added to reduce beam noise 13 p2119 A67-26689
 Anomalous absorption and scattering in global and diffuse radiation measurements during cloudless summer days 13 p2113 A67-26739
 Energy absorption profile and ionization rates for electron beam dependence on beam energy, altitude and atmospheric layer thickness and mass 14 p2379 A67-27921
 Absorption law for weak lines in semiminfinite homogeneous scattering atmosphere for isotropic scattering 14 p2314 A67-28848
 Microradiowave absorption in air by water vapor dimers 17 p2817 A67-33219
 Solar X-ray measurement with satellite noting radio noise flux, absorption in atmosphere and optical density changes 17 p2939 A67-33242
 Microburst precipitation of energetic electrons into auroral zone 18 p3035 A67-33596
 Absorption by atmospheric oxygen and rain of mm waves, using device permitting continuous frequency variation 18 p3002 A67-34230
 Atmospheric heating due to radiative heat transfer of direct and earth-reflected solar rays calculated as function of moisture content 19 p3251 A67-34851
 Solar x-ray spectral intensity distribution using atmospheric extinction of solar radiation as measured by satellites 19 p3314 A67-35441
 Balloon-borne diffusing system designed to measure absorption of minor atmospheric constituents, as sun set and passed below horizon 19 p3232 A67-35697
 Atmospheric radiation absorption measurements by radio-astronomy methods at wavelengths from 1.8 to 0.87 mm 19 p3185 A67-36014
 Accurate determination of atmospheric gases spectral lines positions required for estimating atmospheric absorption coefficient of monochromatic laser radiation 20 p3462 A67-37559
 Laboratory investigation of laser emission line absorption by atmospheric gases in vacuum multiple-pass cell, obtaining data free of aerosol scattering 20 p3386 A67-37606
 Atmospheric absorption of gas laser radiation at two wavelengths noting dependence on gas pressure and amount of methane 20 p3463 A67-37668
 Atmospheric long range spectral transmissivity measured by single beam photometer with recording potentiometer added to reduce beam noise 21 p3627 A67-38431
 Atmospheric ground layer water vapor absorption of 183.31 GHz electromagnetic wave 22 p3759 A67-39506
 Atmospheric absorption of carbon dioxide laser radiation calculation from laboratory absorption coefficient measurements, discussing effects on power transmission and communications 22 p3816 A67-40237
 Earth atmosphere humidity profiles and cloud densities interpreted from 1 cm microwave absorption measurement, water vapor resonance and radiosonde measurement 22 p3806 A67-40359
 Radiometric determination of absorption by earth atmosphere and solar brightness temperature at 5.65 mm 22 p3897 A67-40560
 Atmospheric opacity and extraterrestrial radio source intensity related by improved

Taylor series technique using least squares method [JPL-TR-32-1115] 23 p4062 A67-40733
 Rapid and slow spreading absorption of cosmic rays over polar cap 24 p4209 A67-42126
 Monograph on absorption and laser radiation covering absorption coefficients, high altitude gas concentration, low extinction coefficient measurements, molecular resonance absorption, etc 24 p4168 A67-42412
 Absorption of black body radiation by horizontal atmospheric layer, deriving expression of integral coefficient of atmospheric transparency 24 p4255 A67-42599
 Barometric coefficient of cosmic ray variations determined from observation of Forbush effects and cosmic ray flare effects 24 p4214 A67-42799
ATMOSPHERIC ATTENUATION
 Night sky phenomena and atmospheric attenuation of light from Beta Canis Majoris photographed from Gemini IX 01 p0151 A67-10965
 Total atmospheric attenuation measurement at 3.2 Ghz due primarily to nonresonance absorption of molecular oxygen 02 p0237 A67-11855
 Boundaries and attenuating media effect on radiometric sounding of planetary atmospheres by remote sensing techniques 02 p0239 A67-12406
 Seasonal atmospheric attenuation measurements at 3.27 cm wavelength indicate twice as much vertical attenuation in winter as in summer [RASSA PAPER 1-10-142] 03 p0417 A67-14250
 Horizon studies for monochromatic radiation following Lambert-Beer law of transmission, noting Chapman theory on exponential distribution of atmospheric constituent of absorption 04 p0613 A67-14697
 Vertical intensity measurement of rigid gamma quanta at various atmospheric depths 05 p0879 A67-16098
 Radar observations of Venus at 3.8 cm noting low value of cross section, echo spectrum, polarization characteristics, absorption cross section and atmospheric attenuation 05 p0889 A67-16298
 Direct solar radiation up to 30 km and stratification of attenuation components in stratosphere, noting aerosol extinction properties in free atmosphere 07 p1170 A67-19390
 VLF transmission loss calculated from spectral components of atmospherics arriving from within adjustable azimuthal direction 09 p1464 A67-22442
 Plane shock formed by steepening of continuous wave into shock in atmosphere having exponentially decreasing density 10 p1624 A67-22969
 Hydromagnetic shock wave intensity decrease in nonuniform magnetosphere treated by Chisnell-Whitham method 10 p1634 A67-23053
 Atmospheric attenuation at millimeter wavelength measured noting correlation with weather conditions and solar flux effect 11 p1751 A67-23971
 Rain effects at random antenna elevation 11 p1753 A67-24303
 Thermal conduction and viscosity and energy propagation upward in atmospheric oscillation theory 13 p2114 A67-26742
 Seasonal variations and attenuation of ionospheric absorption, using A3 method 14 p2312 A67-28570
 Lower atmosphere nucleonic component measurement, noting attenuation coefficient dependence on atmospheric depth 17 p2842 A67-32364
 Measurement of solar extreme UV radiation atmospheric attenuation to establish daytime variations in upper-atmosphere composition 17 p2843 A67-32535
 Volume backscattering functions and optical extinction coefficients for visible and IR radiation and selected cloud models 17 p2817 A67-33293
 Transit drift-scan observations of radio sources using cornucopia horn reflector antenna 19 p3330 A67-36073
 Photographic techniques for atmospheric attenuation in air to ground visibility 20 p3441 A67-36399
 Optical system performance and atmosphere attenuation, analyzing absorption and scattering phenomena in terms of

weather conditions 22 p3828 A67-39612
Radiometric determination of absorption
by earth atmosphere and solar brightness
temperature at 5.65 mm 22 p3897 A67-40560
frequency 22 p3897 A67-40560
Stratospheric attenuation measurements in
near UV during rocket flight compared with
values computed for dust free
atmosphere 23 p3993 A67-40677
Atmospheric opacity and extraterrestrial
radio source intensity related by improved
Taylor series technique using least squares
method [JPL-TR-32-1115] 23 p4062 A67-40733
Solar radiant energy attenuation by
atmospheric ozone, deriving transmission
function relation to ozone content 24 p4181 A67-41915
Vertical intensity measurement of rigid
gamma quanta at various atmospheric
depths 24 p4213 A67-42774

ATMOSPHERIC CHEMISTRY

Atmospheric chemistry, circulation and
aerosols - International Symposium, Visby,
Sweden, August 1965 03 p0414 A67-14085
Chemical aspects of evolution of
terrestrial atmosphere, noting role of
photolysis in oxygen production 03 p0414 A67-14089
Atomic and molecular processes in upper
atmospheres of Venus, Mars and Jupiter
investigated by atmospheric models,
presenting solar-planetary
relationship 06 p1087 A67-18429
Oxygen photochemical equilibrium above
150 km, assuming dominant role of radiative
recombination above 120 km 07 p1178 A67-19814
Flowing afterglow reaction device for
measuring ionospheric ion-molecule
reactions 10 p1644 A67-23259
Average distribution and time variation of
ozone in stratosphere and mesosphere in
study of contribution of photochemical
reactions involving hydrogen 10 p1645 A67-23263
Book on ionospheric chemistry, noting
chemical and photochemical reactions above
60 km, and ionization processes 16 p2619 A67-31252
Ion-molecule chemistry of Jupiter upper
atmosphere, studying equilibrium and
nonequilibrium abundances of hydrocarbon
products due to UV radiation 18 p3135 A67-34540
Atmospheric corrosion resistance of
titanium alloys [ASTM PAPER 31] 18 p3068 A67-34579

ATMOSPHERIC CIRCULATION

SA WIND CIRCULATION

Solitary waves in compressible atmosphere
with arbitrary wind and density profiles,
obtaining solution for critical speed by
perturbation scheme 03 p0463 A67-14032
Atmospheric chemistry, circulation and
aerosols - International Symposium, Visby,
Sweden, August 1965 03 p0414 A67-14085
Radiant heat influx to free atmospheric
layers, atmospheric macrocirculation and
time-corresponding geopotential field
charts 03 p0463 A67-14226
Deep circulation in Venusian atmosphere
model opaque to solar and planetary
radiation but with differential
heating 03 p0514 A67-14310
Convective mechanism in clear air,
examining isolated plume by new model
which differs from similarity model 04 p0648 A67-14647
Soviet papers on planetary atmospheric
circulation and artificial earth
satellites 04 p0651 A67-15467
Structure of wind field in thermally
stratified atmosphere based on spectra of
horizontal wind speed fluctuations 05 p0837 A67-16485
Atmospheric ozone distribution, air flows
and temperature at high altitudes in
equatorial latitudes of Atlantic Ocean 05 p0799 A67-17026
Rocket sounding of stratospheric
circulation, noting relationship between
minima in westerly zonal flow of 45-55 km
stratopause layer and tropospheric cut-off
lows 05 p0838 A67-17306
Upper atmospheric wind measurements
derived from vapor trail soundings 06 p1025 A67-17594
Mean monthly winds at low level
calculated for equatorial station in East
Africa, noting monsoon patterns and jet

streams 06 p1025 A67-18024
Weather forecasting - Symposium, Vienna,
September 1965 06 p1026 A67-18598
Aerologic and synoptic weather
forecasting 06 p1026 A67-18599
Cyclogenetic processes from baroclinic
instability occurring in zonal and meridional
flow 06 p1027 A67-18602
Long range weather forecasting, discussing
synoptic, statistical and physical
approaches 06 p1027 A67-18604
Long range weather forecasting, discussing
necessity of nonadiabatic processes 06 p1027 A67-18605
Energy, time and physical morphology of
atmosphere, hydrosphere and lithosphere
surfaces 06 p1091 A67-18994
Large scale motions of atmosphere, noting
hydrostatic and geostrophic equilibrium 07 p1170 A67-19334
Vertical velocities in atmospheric front
motions, noting pressure and temperature
field distributions and application of
computer to solve obtained equations 07 p1219 A67-19356
Book on structure of stratosphere and
mesosphere noting rocket exploration
results, synoptic observations, solar control
over temperature variations, etc 07 p1172 A67-19603
Cyclotron resonance amplification of VLF
and ULF whistlers, evaluating power
transfer for various whistler distributions 07 p1179 A67-19915
Relationship between terrestrial and
Jovian atmospheric circulations due to solar
activity 08 p1398 A67-21215
Removal of incident wave spectrum by
background wind shears during atmospheric
gravity waves propagation to ionosphere
from lower regions 08 p1328 A67-21477
Thermal and momentum eddy diffusivities
computed from wind profile and turbulence
of rocket released chemical clouds 08 p1328 A67-21478
Northern Hemispheric mean meridional
circulation determined, using angular
momentum and continuity equations 09 p1490 A67-21549
Horizontal tropospheric probe using
constant altitude balloons 09 p1525 A67-22560
Orthogonal functions of time, describing
daily perturbations in 100 mb circulation
over eastern U.S. 09 p1562 A67-22684
Punch card deck for serially completed
upper wind observations as substitute for
map scaling 09 p1525 A67-22691
General atmospheric circulation for mean
state conditions, using synoptic charts 10 p1633 A67-22868
Meteorological rocket network
observations of complex circulation system
in middle and upper atmosphere 10 p1643 A67-23247
Wind shear theory of formation of
temperate zone blanketing sporadic E layers,
noting motion equation for ions in
ionospheric E region 10 p1644 A67-23258
Numerical modeling role in studies of
general circulation of atmosphere 10 p1677 A67-23368
Atmospheric circulation in weak easterly
region in troposphere over northwest Pacific
in summer 10 p1677 A67-23499
Diurnally oscillating component of
thermospheric east-west pressure
acceleration at equator, noting balancing
effect of viscous diffusion, ion distribution,
etc 11 p1785 A67-23939
Ionospheric electron density profile
measurement via radio wave interaction
technique, noting superiority of partial
reflection method 11 p1785 A67-23946
Atmospheric ozone data on basis of
meteorological observations and synoptic
maps on ship in Atlantic 11 p1785 A67-23958
Effect of macrometeorological conditions
and local peculiarities on lower atmospheric
temperature, humidity and wind distribution 11 p1815 A67-24326
Slice method forecasting of convective
cloud cover, rain showers and
hail 11 p1815 A67-24327
General atmospheric circulation,
observation methods and apparatus 11 p1815 A67-24328
Macroscopic neutral and ionized gas
motions in ionospheric D and E layer
interpreted from wind and radio wave
scattering measurements 11 p1787 A67-24595
Terrestrial rotation fluctuations and

volcanic activity analyzed, considering
existence of viscous and liquid masses at
interior of earth 11 p1788 A67-24780
Convection in cellular pattern of clouds in
atmosphere treated by classical
methods 12 p1932 A67-25191
Yellow-green luminosity accompanying
injection of triethylborane into upper
atmosphere 12 p1932 A67-25208
Radiant heat influx to free atmospheric
layers, atmospheric macrocirculation and
time-corresponding geopotential field
charts 12 p1963 A67-25482
Neutral upper atmosphere winds near
equator, discussing sodium vapor rocket
observation results 12 p1934 A67-25790
Circulation patterns in upper atmosphere,
using sounding rockets from Indian
equatorial station during monsoon and
winter periods 12 p1935 A67-25791
Structure of wind field in thermally
stratified atmosphere based on spectra of
horizontal wind speed fluctuations 13 p2150 A67-26341
26 month oscillation in zonal wind and
temperature in equatorial atmosphere 13 p2150 A67-26440
Meteor trains detection and study of
motions in upper atmosphere using Garchy
meteor radar with continuous wave 13 p2195 A67-26467
Meridional and vertical wind components
analyzed for angular momentum, balance,
heat influx and internal friction 13 p2113 A67-26678
Biennial variations of zonal atmospheric
circulation at equatorial latitudes analyzed
using hydrothermodynamics 13 p2150 A67-26680
Characteristic scales of thermal convection
in unstable atmosphere, discussing time
evolution of total kinetic energy and
lifetime for dry air case 13 p2116 A67-27460
Meteorological rocket measurement of
wind patterns noting velocities, turbulences,
stratospheric diffusion coefficients,
etc 13 p2117 A67-27611
Directional dependency of slow tail ELF
atmospheric waveforms, noting generation
by cloud to ground type lightning
discharges 14 p2312 A67-28571
Satellite tracking of ghost balloons used
for data collection on atmospheric
circulation in troposphere and stratosphere
[AAS PAPER 67-103] 15 p2420 A67-29958
Effect of ozone on mean meridional
circulation in upper atmosphere and
mesosphere 16 p2666 A67-31098
Monograph on upper atmosphere kinetics
noting Boltzmann equations, MHD processes,
thermal diffusion, etc 16 p2666 A67-31166
Effect of atmospheric parameter changes
on terrestrial surface, discussing Coriolis
forces, atmospheric circulation, etc 16 p2668 A67-31567
Mathematical model for global atmospheric
circulation prediction and mean properties
in terms of tensor algebra 17 p2843 A67-32466
Motion of artificial high density ionization
cloud released in ionosphere 17 p2844 A67-32545
Zonal and meridional distributions of 5-day
averaged outgoing long wave radiation and
relation to Northern Hemisphere
circulation 17 p2879 A67-32548
Strontium and Ba vapor releases in upper
atmosphere, testing yield of evaporated
metal for different chemical
reactions 17 p2851 A67-33194
Theory of available potential energy and
rate of change and variational approach to
atmospheric energetics 18 p3074 A67-34096
Biennial oscillations effect on spring wind
reversal in stratosphere and mesosphere,
showing transition date dependence on
geographical location and height 18 p3074 A67-34352
Tropospheric circulation observation
through FR-2 satellite project, discussing
instrumentation, ground stations, trajectory
analysis, etc 19 p3332 A67-35243
Seasonal variations in incidence of E-2
layer from 1960 through 1965 19 p3221 A67-35429
Stratospheric mean adiabatic vertical
motion and temporal correlations with
temperature, isobaric height, zonal/meridional wind and horizontal kinetic
energy computed based on seasonal
averages 19 p3224 A67-35529

Early autumn stratospheric circulation of Southern Hemisphere investigated by meteorological rocket observations 19 p3253 A67-35920

Ionspheric winds required to produce lunar daily geomagnetic variations deduced from atmospheric dynamo theory, estimating electric conductivity 20 p3425 A67-36281

Atmospheric energetics, discussing stratospheric-tropospheric energetics differences, atmospheric radiation balance distribution, meteorological satellite data, computer studies of atmospheric circulation, etc 20 p3429 A67-36895

Zonal winds studied by meridional sections from observations made during some months over several years 20 p3480 A67-36965

Latitude, altitude and local time variation of forces controlling 100 to 700 km atmospheric winds, noting effects on ionospheric phenomena 21 p3654 A67-37994

Mesoscale structure of atmospheric winds analyzed using data obtained from FPS-16 radar/Jimsphere precision wind measuring system 21 p3655 A67-38576

Photometric observation data on Jupiter atmospheric activity /1964-1965/ noting three-month periodic change 22 p3879 A67-39299

Large scale eddy terms for balancing mean meridional circulation in winter, discussing terms magnitudes in different latitudes 22 p3828 A67-39326

Nighttime variation of ionospheric winds over Barbados via luminous trails measurements, obtaining steady state components for seasonal variations 23 p3995 A67-40807

Inertial guidance technology for atmospheric motion measurements, discussing system limitations in accuracy and resolution 23 p4026 A67-41444

Objective criteria for irrotational flow in geostrophic, isobaric and thermal wind flow 24 p4180 A67-41788

Anabatic winds caused by solar heating of slope, investigating flow patterns useful for soaring purposes 24 p4181 A67-42022

Large scale atmospheric motions control, discussing weather control, long term effect and instability 24 p4182 A67-42756

ATMOSPHERIC COMPOSITION

Contribution of regular and irregular components to ionospheric instability 02 p0237 A67-11671

Aerosol measurements using light scattering from searchlight probing, noting attenuation coefficient as function of altitude [AFCRL-67-0003] 02 p0238 A67-12048

Gaseous composition of unknown planetary atmosphere determined, using acoustic experiment combined with pressure and temperature data 03 p0509 A67-13215

Carbon dioxide content in troposphere and lower stratosphere measured at various altitudes, showing seasonal variations 03 p0414 A67-14086

Time-dependent photochemical model for space-time variations of oxygen allotropes in 20 to 100 km layer 03 p0414 A67-14087

Radiation equilibria in UV light on air, oxygen, carbon dioxide, etc, analyzed by bromine lamp in connection with studies of planetary atmospheres 03 p0513 A67-14088

Vertical ozone distribution in atmosphere and transport processes, noting results of tracer experiments 03 p0414 A67-14090

Radio astronomical and satellite studies of atmosphere - USAF Symposium, Boston, October 1965 03 p0415 A67-14234

Doppler technique application to radar measurement of clear air target motion 04 p0569 A67-14684

Radar and airborne instrumentation sampling of atmosphere, noting linked mode or one-one comparison between returned radar signal and meteorological probe 04 p0570 A67-14685

Meteorological instrumentation for measuring physical characteristics of atmosphere 04 p0649 A67-14686

Atmospheric ozone in middle UV spectral region, noting vertical distribution, destruction by solar radiation, lifetime below layer in photochemical equilibrium, etc 04 p0612 A67-14694

Upper atmospheric oxygen atom concentration profiles obtained via wind tunnel simulation of NO releases [AFCRL-67-0053] 04 p0615 A67-14971

Photometry of integrated light of Venus, inferring presence of ice in atmosphere from halo effect of brightness dispersion 05 p0892 A67-16407

Effects of atmospheric composition and electric field on electron temperature 05 p0798 A67-16862

Upper atmospheric density and composition determined by means of solar radiation attenuation and day airglow fluorescence 05 p0798 A67-16864

Atmospheric ozone distribution, air flows and temperature at high altitudes in equatorial latitudes of Atlantic Ocean 05 p0799 A67-17026

Atmospheric argon effect on hypersonic stagnation point convective heat transfer, using arc-heated shock tube simulating flight velocities up to 34,000 fps [AIAA PAPER 66-29] 05 p0928 A67-17337

Atmospheric nitrogen contamination effect on tensile creep of chromium-tantalum alloys 06 p0108 A67-18369

North American ozonesonde network investigation of isentropic and vertical distribution of ozone mixing ratio in lower stratosphere in May 1963 06 p0996 A67-18446

Vertical distribution of neutral composition of atmosphere between 100 and 200 km, comparing mass spectrometer with optical measurement 07 p1169 A67-19097

Height dependence of albedo in earth upper atmosphere, calculating total quantity of neutral hydrogen in ionosphere 07 p1170 A67-19103

Statistical characteristics of atmospheric ozone distribution, determining autocorrelation and cross correlation functions, concentration and temperature profiles 07 p1170 A67-19357

Atmospheric mixing time and lifetime of atomic and molecular oxygen at high altitude, noting agreement with barometric distribution law, concentration pattern, etc 07 p1178 A67-19813

Estimation of ion formation rate at various altitudes in ionosphere and zenith angles during low and high solar activity periods 07 p1178 A67-19830

Atmospheric composition data from Explorer XVII satellite, obtaining expression for thermal diffusion factor of He 07 p1181 A67-19937

Thermodynamic equilibrium composition of Venus atmosphere computed from atomic composition deduced spectroscopically 07 p1256 A67-20022

Fractional volume abundance of atmospheric nitrous oxide, considering photodissociation, microbiological reactions and mixing 08 p1327 A67-21369

Rocketborne RF mass spectrometers use in study of atmospheric composition at high altitudes, discussing sampling 09 p1491 A67-21895

Efficiency of fibrous filters for radioactive particles and small ions increased, using greater flow rate 09 p1562 A67-22683

Self-broadening coefficients of spectral lines of absorbing atmospheric gases measured in comparison with line broadening effects of nitrogen 10 p1678 A67-22715

Vertical profile of concentration of atmospheric electron-ion gas flux under action of gravitational field 10 p1631 A67-22804

Atmospheric dust content estimation, using solar radiation depletion by particulate matter and separating attenuation by gases and water vapor 10 p1700 A67-23086

Rocket measurement of diurnal variation of ozone profiles above maximum concentration level 10 p1638 A67-23202

Seasonal-latitudinal variations in lower thermospheric density, temperature and composition 10 p1639 A67-23210

Neutral particle densities of nitrogen, molecular and atomic oxygen and argon in upper atmosphere, noting density profile irregularities, diffusive separation altitude, etc 10 p1639 A67-23213

Seasonal and annual variations of electron density in ionospheric F layer interpreted as changes in production rate and ionization loss caused by atmospheric composition variations from neutral atmosphere 10 p1647 A67-23274

Behavior of line source function of low density gas in presence of nonthermal velocity field, examining strong shock

situation and differential velocity via ordered velocity structure 11 p1861 A67-24489

Venus atmosphere spectra obtained by Michelson interferometer, finding HCl lines consistent with 2-mm Amagat of gas [JPL-TR-32-1106] 11 p1863 A67-24510

Vertical distribution of ozone over Tallahassee, noting maximum and minimum density altitudes, seasonal variations, etc 11 p1787 A67-24555

Radar, radio - astronomic and IR spectroscopic observations of Venus surface and atmosphere, examining general and surface data, chemical composition and atmospheric model construction 11 p1867 A67-24843

Martian atmosphere models with different composition, pressure and temperature 12 p2003 A67-25685

Upper atmospheric composition data compared, showing erroneous nature of Hinteregger and Pokhunkov measurements on oxygen-nitrogen ratio 12 p1934 A67-25789

Planetary atmospheric composition study under ambient conditions using instrument involving very high Q Fabry-Perot microwave cavities 12 p1946 A67-25986

Mars atmospheric composition determination by shock layer radiometry technique during probe experiment [AIAA PAPER 67-293] 12 p2009 A67-26009

Cross correlation /by superposed epoch method/ between upper atmospheric sodium and stratospheric warmings at high latitude 13 p2110 A67-26441

Photochemical reaction and turbulent diffusion effect studied using mesospheric model, establishing relation between composition and dynamic state 13 p2113 A67-26681

Methylene role in atmospheric tritiated methane, specifically nitric oxide interference 13 p2117 A67-27604

Liquid nuclei formation at condensation centers in atmosphere analyzed for various degrees of saturation 14 p2346 A67-27908

Vertical distribution of tropospheric and stratospheric ozone based on observations of U.S. ozonometric stations at various latitudes 14 p2308 A67-27927

Unlikelihood of obtaining useful information on atmospheric composition from indirect sensing of scale heights by satellites 14 p2310 A67-27959

Atmospheric fine structure deduced from radio observation and from turbulence theory 14 p2311 A67-28396

Ionospheric D layer structure and formation, considering free electron height variation and collision rate 14 p2311 A67-28406

Soviet atmospheric turbulence studies considering microstructure, wave propagation in turbulent atmosphere, turbulent exchange in atmospheric ground layers, etc 14 p2346 A67-28763

Radio probe to derive relations between ozone content of lower stratosphere and origin of air in layers 15 p2474 A67-29525

Electromagnetic probing by laser, determining number densities of water, carbon dioxide and oxygen constituents of atmosphere 15 p2500 A67-29911

Structure and composition of Jupiter atmosphere, noting laboratory and observational data supporting hypothesis of consistency with solar elements abundance 16 p2746 A67-30932

Contribution of regular and irregular components to ionospheric instability 16 p2665 A67-31086

Ozone generator and calibrator, noting design principles, operation performance and results 16 p2676 A67-31374

Atmospheric ozone vertical distribution, discussing optical measurement method 16 p2676 A67-31375

Atmospheric ozone concentration measurement using potassium iodide method 16 p2676 A67-31376

Atmospheric ozone vertical distribution, measurement, discussing equipment design and underlying principles of method 16 p2676 A67-31377

Solar UV spectrum interpretation taking into account dielectronic recombination processes in ionization equilibrium computation, obtaining spectral lines intensities, abundances and atmospheric structure indications 17 p2941 A67-32235

Noctiluculent cloud formation by agglomeration of oxygen/ozone molecules in mesosphere layers 17 p2879 A67-32323

Meteoritic satellites of earth, estimating capture region dimensions 17 p2941 A67-32324

Measurement of solar extreme UV radiation atmospheric attenuation to establish daytime variations in upper atmosphere composition 17 p2843 A67-32535

Upper limits on liquid water content in Venus atmosphere 17 p2945 A67-32652

Bimolecular and termolecular kinetic rate constants for reactions involving atmospheric neutral species 17 p2809 A67-33240

Atmospheric aerosol internal changes, studying atmospheric transparency for direct solar radiation 18 p3073 A67-33562

Electron precipitation data examined to determine whether electron behavior can be understood on basis of binary collisions with atmospheric constituents and guidance by geomagnetic field 18 p3035 A67-33599

Oxygenic concentrations in primitive earth atmosphere, discussing Martian atmosphere composition 18 p3041 A67-34095

Stratospheric aerosol concentrations observed by optical radar echoes compared with expected return from molecular atmosphere to obtain vertical profile 18 p3042 A67-34493

Atmospheric ozone content compared for discrepancies between theoretical and experimental results for vertical, latitudinal and seasonal variations 19 p3214 A67-34856

Soviet and foreign studies of atmospheric oxygen by optical and spectral methods 19 p3214 A67-34857

Electron density and temperature, solar UV radiation and upper atmosphere neutral components measured using rockets 19 p3218 A67-35215

Arctic upper atmosphere neutral gas composition and altitude distribution studied, using meteorological rockets 19 p3219 A67-35251

Lower thermosphere composition and mean molecular weight analyzed for diurnal and latitude effects, using mass spectrometric measurements 19 p3220 A67-35265

Total atmospheric ozone from satellite measurements of solar UV reflected radiation determined, using atmospheric model with Rayleigh scattering 19 p3226 A67-35923

Inference of vehicle and atmosphere parameters from free flight motion measurements using iterative calculations of parameter values 19 p3337 A67-35996

Metastable helium atom altitude distribution and 10830 angstrom radiation emission rate, discussing possible explanation of helium loss from atmosphere 20 p3427 A67-36310

Surface air radioactivity and ozone measurements in Antarctica reveal fission product yearly oscillation 20 p3429 A67-36871

Structure and composition of upper atmosphere above stratopause, discussing temperature, density and wind variations 20 p3430 A67-36904

Photochemical reaction and turbulent diffusion effect studied using mesospheric model, establishing relation between composition and dynamic state 21 p3618 A67-38426

Jupiter and Saturn models, giving planet constitution, heat balance and atmospheric composition 21 p3710 A67-39001

Thermal comfort zone test for helium-oxygen and nitrogen-oxygen atmospheric mixture for 18-day continuous manned run 22 p3754 A67-39599

Spherical entry vehicle used to define planetary atmosphere structure and composition from dynamic response during entry, discussing aerodynamic characteristics 22 p3907 A67-40177

Vertical distribution of thermal stability in lower stratosphere compared with atmospheric ozone from ozone and temperature soundings 22 p3829 A67-40471

Martian atmosphere component due to proton penetration into atmosphere from solar wind, suggesting radio occultation by Mars orbiter 23 p4063 A67-40799

Intensities of cosmic ray produced deuterium and tritium in atmosphere measured from high altitude balloons 23 p3995 A67-40811

Extraterrestrial life detection studied from knowledge of major and trace components of atmospheres 23 p3944 A67-40999

Light gas escape flux from atmosphere velocity and angular distributions near critical level using Monte Carlo analysis 24 p4224 A67-41823

Upper limit of carbon dioxide abundance in Mercury atmosphere 24 p4225 A67-41836

Vertical profile of concentration of atmospheric electron-ion gas flux under action of gravitational field 24 p4150 A67-42141

ATMOSPHERIC CONDITION EFFECT

SA WEATHER FORECASTING

Stellar interferometer at Narrabri, Australia, to determine angular diameters of approximately 50 bright stars 01 p0062 A67-10283

Resolution limit imposed by atmospheric turbulence on image of ground object obtained by long exposure photography from high altitudes 01 p0109 A67-11080

Strong fluctuations of light intensity during propagation in ground layer of atmosphere approximated by smooth perturbation method 02 p0236 A67-11640

Correlation function of stellar image fluctuations and pulsations due to earth atmospheric influences for two stars separated by small angular distances 02 p0325 A67-11984

Lower atmospheric layer and meteorological conditions effect on oscillations of image of artificial source of light 02 p0238 A67-11987

Mean quadratic amplitude of star image deviation from average position dependence on zenith distance studied from stellar observation 02 p0261 A67-11988

NASA research on visual problems of extended spaceflight 02 p0189 A67-12408

Low clouds effect on ILS jet landing at Bombay airport during monsoon season, noting airfield climatology data 05 p0838 A67-16711

Atmospheric effects on supersonic aircraft operations, particularly sporadic effects near ground and in free atmosphere, density variations, etc 07 p1219 A67-19066

Wind and temperature effects on transitory and cruise phases of supersonic flight 07 p1219 A67-19067

Atmospheric density, winds and turbulence relative influence on Saturn V vehicle control system and structural bending moment response during Atlantic Missile Range ascent flight [AIAA PAPER 66-341] 07 p1257 A67-19372

SST flight performance as affected by wind, temperature and radiation 07 p1129 A67-19679

High data rate laser communication system, discussing integration of laser and wideband modulator and experimental results under field conditions 08 p1292 A67-20672

Ionosphere-stratosphere coupling and effect of atmospheric seasonal variations on plasma behavior 10 p1645 A67-23266

Turbulent transfer in diabatic conditions, deriving formulas for wind and temperature profiles 10 p1677 A67-23574

Lightning strikes on aircraft in flight from 1949 to 1966 12 p1896 A67-26170

Theory of nephelometric method for measuring transparency and structure of atmospheric aerosols 13 p2151 A67-26685

Tropospheric condition effect on near-ground ultrashort wave radio signal field-amplitude fluctuation, determining space-time correlation dependencies by radar observation 13 p2067 A67-26688

Propagation effects on distance, arrival angle and Doppler effect measurements with reference to tropospheric influence 14 p2264 A67-28400

Quasi-biennial cycles in cosmic ray intensity 15 p2549 A67-29203

Relationship between absorption of hydrogen fluoride by limed filter papers and exposure dosages investigated under controlled conditions of various factors 16 p2675 A67-31211

Ferromagnetic dust concentration variations in upper atmosphere during meteor shower 16 p2668 A67-31707

Propagation loss dependence in laser ranging systems on meteorological visibility and target-receiver range, noting inverse-

square law confirmation 17 p2812 A67-32305

Atmospheric variations effects on cosmic radiation records from plastic scintillation monitors, calculating pressure coefficients 17 p2938 A67-32795

Atmospheric condition effects on SST aircraft, noting Concorde performance data analysis results 19 p3173 A67-35309

Tropospheric condition effect on near-ground ultrashort wave radio signal field-amplitude fluctuation, determining space-time correlation dependencies by radar observation 21 p3582 A67-38430

Atmospheric inhomogeneities effect on large antenna directive gain, noting dependence on length and wave field 21 p3600 A67-38812

Performance limits of laser rangefinder for design of all-weather terrestrial rangefinder, discussing echo signal, backscatter noise and TPG 23 p3999 A67-41040

Six-stage monogram for refraction of radio wave entering earth atmosphere in terms of meteorological conditions and wave elevation angle 23 p3975 A67-41212

Aircraft cockpit and surface temperatures after solar radiation exposure in desert, showing inadequacies of meteorological data for thermal stress predictions 23 p3935 A67-41593

Digital computer restoration of atmospherically degraded images, studying techniques and limitations of former and mechanisms of latter 24 p4157 A67-42436

ATMOSPHERIC CONDUCTIVITY

Atmospheric potential gradient near ground in polar region correlation with solar radio emission on 1000 mc 07 p1172 A67-19423

Polar magnetic substorms noting flux tube flow, proposing structure for substorm current system [JPL-TR-32-1094] 11 p1784 A67-23928

Atmospheric potential gradient relation to solar activity at earth surface in polar region 14 p2306 A67-27884

Thunderstorm electric circuit physics with atmospheric electric conductivity and variation with height, noting atmospheric electric fields and currents 18 p3074 A67-33996

Ionospheric winds required to produce lunar daily geomagnetic variations deduced from atmospheric dynamo theory, estimating electric conductivity 20 p3425 A67-36281

ATMOSPHERIC DENSITY

SA SPACE DENSITY

March 1964-March 1965 seasonal variations in density, pressure and temperature at Woomera, Australia, by falling sphere method 01 p0061 A67-11260

Motion of satellite inside resisting atmosphere 04 p0696 A67-14737

Gamma ray backscatter principles for measurement of atmospheric density, using test results from altitude chambers in balloon and sounding rocket payloads 05 p0840 A67-16527

Upper atmospheric density and composition determined by means of solar radiation attenuation and day airglow fluorescence 05 p0798 A67-16864

Phugoid trajectories of ballistic reentry of hypothetical glider into variable density atmosphere 05 p0847 A67-17009

Atmospheric effects on supersonic aircraft operations, particularly sporadic effects near ground and in free atmosphere, density variations, etc 07 p1219 A67-19066

Upper atmosphere temperature, pressure and density determined by photographic observations of meteors, based on calculating height of homogeneous atmosphere 07 p1174 A67-19708

Upper atmospheric density, pressure and temperature profile obtained from drag acceleration measurements on falling sphere 07 p1181 A67-19938

Graphical method predicting orbital lifetime of satellite, considering oblate earth effects and long period fluctuations in atmospheric density [AAS PAPER 66-96] 07 p1252 A67-19960

Upper atmosphere density determined from satellite braking 08 p1325 A67-21002

Solar cycle variations in atmospheric density deduced from meteor observations and rocket measurements in mesopause and thermosphere 10 p1638 A67-23204

Falling sphere measurements of

atmospheric density, noting temperature and density profiles, pressure distribution, etc 10 p1639 A67-23205

Mesosphere ice point temperature, atomic oxygen concentration and total density measurement with heat recorder 10 p1656 A67-23207

Shape and location of diurnal bulge in upper atmosphere, analyzing density and temperature distribution at high latitude from satellite drag data 10 p1639 A67-23208

Time delay between geomagnetic storm and corresponding maximum in atmospheric density obtained from satellite drag data 10 p1639 A67-23209

Seasonal-latitudinal variations in lower thermospheric density, temperature and composition 10 p1639 A67-23210

Latitudinal and seasonal variations in atmospheric densities during low solar activity obtained by inflatable air density satellites 10 p1639 A67-23211

Atmospheric density scale height and variation law at different heights obtained from San Marco satellite data 10 p1712 A67-23212

Upper atmosphere dynamics, noting role of horizontal and vertical winds in shifting density phase and amplitude and UV radiation as energy source 10 p1640 A67-23218

Effect of variation of vertical air density profile on relative optical air mass for ARDC standard model atmosphere 1959 compared with measurements 10 p1652 A67-23622

Satellite measurement of upper atmospheric density variations due to geomagnetic disturbances, correlating time delay with geographic latitude 11 p1783 A67-23922

Atmospheric density determination from drag of eleven low altitude satellites, discussing correlation with geomagnetic activity and daily periodicity 11 p1784 A67-23937

Atmospheric number density measured by attenuation of solar X-rays monitored when satellite passes from darkness to sunlight 11 p1857 A67-24605

Upper atmospheric density determination from data of satellite orbit evolution, noting effect of solar activity 12 p1932 A67-25533

Atmospheric density distribution at altitudes from 200 to 300 km based on Soviet satellite observations during minimum solar activity 12 p1934 A67-25788

Atmospheric density, temperature and pressure profiles obtained in Florida and New Mexico using rockets 12 p1937 A67-25837

Mars atmosphere and ionosphere analyzed by measuring effect on radio occultation of planet, determining shape, atmosphere density profile, diurnal variations, etc [JPL-TR-32-1157] 13 p2199 A67-26819

Approximate determination of satellite lifetime by nomogram constructed on basis of known upper atmosphere density data 13 p2213 A67-27324

Graphical method predicting orbital lifetime of satellite, considering oblate earth effects and long period fluctuations in atmospheric density [AAS PAPER 66-96] 13 p2208 A67-27520

Backscattered light intensity from laser beam for measuring atmospheric density variations, discussing optimization of sensitivity 13 p2072 A67-27609

Upper atmosphere densities and temperatures at 105-165 km from diffusion and spectral intensity of aluminum oxide trails 14 p2310 A67-28050

Computational method for high altitude atmosphere density, orbital elements, drag coefficients and potentials from satellite displacement and velocity measurements 15 p2562 A67-30069

San Marco project, joint effort of NASA and Italian Space Commission to launch satellite for atmospheric and ionospheric measurements 16 p2757 A67-30642

Probe for measuring energy transfer between satellite surface and upper atmosphere 16 p2670 A67-30646

Semiannual exospheric density variation confirmed by satellite orbit analysis 17 p2852 A67-33238

Artificial satellites lifetime in low altitude orbits, discussing atmospheric, geomagnetic, solar and lunar factors 18 p3136 A67-33550

Atmospheric density determination from satellite drag, noting effects of magnetic storms, diurnal and semiannual variations, solar activity, etc 18 p3041 A67-34253

Upper-atmosphere density determination methods, with comparison of orbital decay and instrument 18 p3041 A67-34254

Geomagnetic activity effect derived from Explorer IX drag data, with atmospheric temperature as geomagnetic storm intensity function and atmospheric density increase 18 p3042 A67-34255

Air drag effect on six Cosmos satellites orbits having low perigee, discussing diurnal air density variation at 280 km height 18 p3042 A67-34256

Phugoid trajectories of ballistic reentry of hypothetical glider into variable density atmosphere 18 p3079 A67-34272

Upper atmosphere density, temperature and variation determined from satellite drag data, proposing thermosphere model 19 p3214 A67-34931

Air density variations at heights near 150 km determined by analyzing satellite orbit changes, noting solar activity effect 19 p3215 A67-35181

Density, temperature, water vapor and atomic oxygen concentration in mesosphere measured by heat method 19 p3216 A67-35183

Exospheric density variation as related to solar activity determined from satellite orbits 19 p3217 A67-35211

Density, temperature and pressure profiles variations in upper atmosphere obtained from rocketborne experiments 19 p3218 A67-35219

Developments in upper atmosphere research noting atmospheric density, temperature, diurnal variations, solar and geomagnetic activity effects, etc 19 p3218 A67-35225

Diurnal atmospheric density bulge shifts observed by Explorer, showing latitudinal-seasonal variation in helium concentration 19 p3218 A67-35226

Mesosphere and lower thermosphere density variations related to solar cycle obtained, using rocket grenades 19 p3219 A67-35231

Upper atmosphere densities and scale heights from Soviet earth satellite drag data, noting diurnal variation 19 p3219 A67-35252

Air density variation at 220 km altitude shown due to increased solar activity, from satellite orbit observation 19 p3222 A67-35458

Upper atmospheric dynamics, considering day-night density and pressure variation, wind structure, gravity waves, etc 20 p3429 A67-36896

Structure and composition of upper atmosphere above stratopause, discussing temperature, density and wind variations 20 p3430 A67-36904

Probability characteristics of oscillating satellite motion, considering random parameter scatter and atmospheric density variations, with expectation obtained by numerical integration 20 p3485 A67-36922

Atmosphere of Mars studied using three models generated to show high, mean and low density compositions to account for gravitational and magnetic fields 22 p3887 A67-40140

Explorer 32 satellite atmospheric density experiment gas calibrations, comparing operation and pressure response of various ionization gauges 23 p4004 A67-41356

Mariner space vehicles design evolution noting contribution to future space flights through measurement of atmospheric density of Mars 24 p4241 A67-42399

ATMOSPHERIC DIFFUSION

Direct measurements of thoron from ground surface to height of 50 cm in atmosphere, describing turbulent diffusion of radioactive emanations from soil surface 02 p0237 A67-11853

Emission, collection and analysis of radioactive rare gas xenon 133 as atmospheric tracer whose inert characteristics allow diffusion processes to be followed 02 p0237 A67-11854

Turbulent diffusion in nonuniform stratification atmosphere, obtaining vertical concentration profile by random walk method [AFCL-66-836] 02 p0262 A67-12081

Project Prairie Grass diffusion experiments analyzed to determine Hay-Pasquill scale factor relating Lagrangian and

Eulerian turbulence scales 02 p0262 A67-12082

Hydrogen diffusion in earth upper atmosphere near critical level 04 p0612 A67-14654

Turbulent vertical diffusion in surface layer of atmosphere 04 p0652 A67-15568

Wind profile effect on turbulent diffusion for infinite linear source in surface layer of unstable stratified atmosphere 04 p0652 A67-15569

Cosmic ray variations classification and origin, taking into account possible interference between meteorological effects 05 p0877 A67-18082

Relative diffusion of liquid particles in turbulent flow with shear, deriving formulas 05 p0837 A67-16490

Book on atmospheric absorption, diffusion and polarization of light and radioelectric radiation 06 p0998 A67-18718

Diffusion and transport equation for turbulent atmosphere with variously heated air masses 06 p0999 A67-18740

Exhaust cloud diffusion from solid rocket motors correlated with measurable meteorological variables [AIAA PAPER 67-280] 07 p1221 A67-20084

Ionospheric diffusion spectra, obtaining information on neutral atmospheric winds and ionosphere dynamics 10 p1632 A67-22858

Average rate of eddy mixing obtained from some eddy transport problems in thermosphere, noting molecular diffusion 10 p1646 A67-23271

Nocturnal decline of ionospheric airglow 6300 angstrom line intensity due to diatomic oxygen ion-electron recombination 10 p1649 A67-23294

Three stages of solar cosmic rays entry into polar cap atmosphere due to differential arrival of solar electrons, protons and alpha particles 11 p1855 A67-23925

Relative diffusion of liquid particles in turbulent flow with shear, deriving formulas 13 p2093 A67-26345

Effective diffusion cross section for meteor atoms in atmosphere, using Thomas-Fermi-Dirac and dumbbell molecule models 13 p2111 A67-26553

Numerical integrations of equation for turbulent diffusion in atmosphere 13 p2152 A67-26863

Three-layer atmospheric model for use in two-dimensional diffusion equation for steady state conditions incorporating eddy diffusion of momentum 13 p2153 A67-27607

Method for complete observation of magnetic field structure in sunspots 14 p2390 A67-28942

Estimation of parameters of transverse diffusion in lowest atmospheric layer using Lagrange and Euler turbulence characteristics 16 p2698 A67-31095

Atmospheric turbulence and diffusion, detailing turbulent energy and thermal variance budgets measurements, parallel plate convection, air pollution, etc 20 p3480 A67-36898

Cosmic ray variations classification and origin taking into account possible interference between meteorological effects 24 p4212 A67-42758

ATMOSPHERIC ELECTRIC FIELD

Radiosonde for measurement of electric potential gradient in atmosphere at high altitudes 01 p0068 A67-10870

Charged particle motions calculated in model of earth magnetosphere including magnetic and electric field 03 p0410 A67-12953

Effects of atmospheric composition and electric field on electron temperature 05 p0798 A67-16862

Height profile of Sq current in ionosphere, showing dependence on electric field direction 05 p0799 A67-16872

Formative time lag for pulsed RF breakdown in dry air as function of gas pressure and power of slot antenna 07 p1153 A67-19607

Electric field measuring methods, showing Stark effect in rotational spectra of gases as most promising 08 p1311 A67-20652

Motion equations for ionized irregularity of finite length applied to barium ion cloud, deriving expression for ionospheric electric field 08 p1326 A67-21357

Vector electric field and particle intensity measurements from sounding rocket

launched into visible aurora 08 p1329 A67-21486

Ionization coefficients in helium over pressure range near to atmospheric show destruction of metastable states in gas accounts for dependence on electric field 10 p1681 A67-22962

Variations in position of mirror points of high energy electrons determined from Cosmos V satellite data 10 p1647 A67-23281

Relation between electron and proton distributions and existence of electric fields in magnetosphere 12 p1936 A67-25808

Lightning strikes on aircraft in flight from 1949 to 1966 12 p1896 A67-26170

Electrostatic, induction and radiation field effects of lightning discharge on intensity spectrum of atmospheric source 14 p2346 A67-27880

Coulomb interaction effect on time dependent variations of electron distributions in Van Allen belt, using kinetic equation 14 p2378 A67-27918

Numerical solutions to differential equations governing earth electric field near surface obtained by Runge-Kutta method 16 p2664 A67-30974

Thunderstorm electric circuit physics with atmospheric electric conductivity and variation with height, noting atmospheric electric fields and currents 18 p3074 A67-33996

Electric field measurements with isolated electrodes ejected near apex, finding continuous changes near 100 and 80 km 19 p3217 A67-35199

Atmospheric electric field as possible cause of radio pulses from extensive air showers 19 p3316 A67-35803

Diurnal variation investigated by rocket, discussing ionospheric electric currents and magnetosphere-ionosphere electric field 20 p3431 A67-36908

Ionospheric conductivities, electric currents and field height variations in equatorial electrojet region calculated from model, including solar activity 21 p3617 A67-38066

ATMOSPHERIC ELECTRICITY

SA LIGHTNING

Simplifying assumptions in theory of electrode effect 01 p0107 A67-10118

Weather satellite system determining worldwide occurrence and distributions of thunderstorms and associated atmospheric effects 02 p0262 A67-12399

Ionospheric properties and wave-electron interaction 03 p0405 A67-12801

Atmospheric charge density measurement by Faraday cage and Obolensky filter 05 p0803 A67-17384

Solar eclipse effect on atmospheric potential gradients analyzed, noting negativity and variation pattern with five peaks 10 p1651 A67-23347

Atmospheric electricity conditions at ground level independent from auroras and potential gradients 11 p1857 A67-25031

Main processes pertinent to convective storm development, with emphasis on structure and mechanics of storms already formed 18 p3074 A67-34094

Thermal tidal motions in lower ionosphere and differential charge mobility pictured as producing earth atmosphere electrical structure 19 p3220 A67-35255

Formation mechanism of luminous gas sphere /ionized vortex configuration/ due to atmospheric electrical discharge 21 p3655 A67-38902

Data analysis on electric potential gradient and air-to-earth current density 24 p4181 A67-41792

ATMOSPHERIC EMISSION

SA AIRGLOW

Balloon observation of thermal radio emission of molecular oxygen in terrestrial atmosphere 02 p0237 A67-11852

Current distribution in eddy configuration of atmospheric gas discharge, noting flow surface deformation rate and measurement techniques 02 p0180 A67-12441

Cameras used in auroral and airglow experiments including SP3 spectrophotometer, three-channel photometer and all-sky camera 03 p0419 A67-13376

Quantitative expression of technique for observing 5-mm self-emission from oxygen of earth atmosphere to obtain vertical sense [RASSA PAPER 1-10-144] 03 p0418 A67-14251

Radiation from flames and chemical perturbations of atmosphere, examining flame structure, irreversible processes, photoemissive events, etc 04 p0721 A67-14701

Molecular nitrogen ion emission in twilight, discussing intensities, rotational distribution, charge transfer zenith measurement and ion-atom interchange reaction 05 p0803 A67-17409

Radiation sources from high temperature equilibrium air noting measurements, equipment and results [AIAA PAPER 67-95] 06 p1114 A67-18279

Mechanism of enhancement of Li resonance line in twilight airglow due to upper atmospheric thermonuclear explosions 06 p0998 A67-18705

Temperature of atmospheric radio emission in decimeter range for elevation angles from 1/2 to 10 degrees 07 p1142 A67-19586

ULF radio emission of upper atmosphere and other related geophysical phenomena, analyzing hisses, choruses and contribution to earth radiation belt 08 p1324 A67-20862

Far UV rocket spectrophotometry of atmospheric phenomena such as airglow and auroras [JHU-TR-11] 10 p1653 A67-22739

Antenna temperature in wings of line centered at 61.1506 GHz, comparing experimental and theoretical values on atmospheric oxygen 10 p1632 A67-22857

Electron and ion emissions from hydrogen and helium UV glows in nighttime ionosphere 10 p1633 A67-23049

Airglow resonant emission transfer in Doppler incoherent scattering medium with respect to optically thick atmosphere 10 p1634 A67-23050

Large amplitude variations of intensity of oxygen emission in night airglow and structure of lower thermosphere 10 p1634 A67-23051

Space correlation of main emission lines for night sky emission spectra and altitude distribution of sodium luminescence 10 p1647 A67-23279

Atmospherics characteristics at source and propagation 14 p2265 A67-28412

IR radiation measurements by spectrometers flown on board stratospheric balloons, considering sky brightness, vertical distribution and thermal atmospheric emissions 14 p2313 A67-28768

Nightglow measurements noting intensity relation to spread-F and sporadic E [AGARDOGRAPH 95] 15 p2485 A67-30308

Emission time history for red 6300 angstrom atmospheric emission from atomic oxygen produced by nuclear explosion 16 p2664 A67-30978

IQSY and IGY comparison of night airglow OI latitude observations 16 p2667 A67-31517

Barometric and temperature coefficients determined from solar-diurnal, antisideral variation, atmospheric showers etc 16 p2741 A67-31900

Upper atmospheric nightglow emission intensity measured finding continuous excitation of oxygen atoms as energy reservoir 16 p2670 A67-31918

Photographic high atmosphere observations of hydroxyl and helium emission bands, determining solar UV radiation and electron flux 17 p2849 A67-32960

Worldwide morphology of atomic oxygen nightglows 18 p3032 A67-33580

Dayglow emissions observation by ground-based instruments indicate atmospheric response to concurrent input of solar energy 18 p3033 A67-33586

Chemical reactions fluorescent and resonant scattering, electron impact and photodissociation from sunlight upon atmosphere 18 p3036 A67-33602

Afterglows from atmospheric nuclear detonations related to natural airglow and aurora 18 p3036 A67-33604

Optical IR characteristics of long-time afterglow from high altitude nuclear detonations 18 p3036 A67-33605

Airglow emission analysis from low altitude observations, discussing temporal and spatial variations 18 p3037 A67-33608

Kinetic temperature measurements of 5577 angstrom line night airglow with Fabry-Perot interferometer, discussing nightly mean temperatures 18 p3037 A67-33609

Atmospheric emissions and electron and

proton precipitation latitude and diurnal variations measurements from satellite-borne photometric studies 18 p3039 A67-33623

Fabry-Perot spectrometer applied to upper atmospheric emission measurements of airglow and aurora 20 p3440 A67-36362

Temperature of atmospheric radio emission in decimeter range for elevation angles from 1/2 to 10 degrees 20 p3384 A67-37323

Hydrogen emission by sun offers no unique interpretation for Lyman alpha profile 21 p3700 A67-37733

Airborne measurement of microwave emission from earth surface and atmosphere for potential application of radiometry to weather satellite reconnaissance 22 p3806 A67-40361

Magnetospheric discrete VLF emissions, discussing gyroresonance extension, resonant electron and emission frequency 23 p3995 A67-40802

Ionospheric electron content and OI nightglow in Hawaii, discussing ionization density increases throughout bottomside F layer 24 p4147 A67-41878

High energy neutrino flux from atmosphere studied in South African gold mine using liquid scintillation detector 24 p4210 A67-42581

Fluctuation of Cerenkov glow in atmosphere caused by shower particles 24 p4220 A67-42868

ATMOSPHERIC ENERGETICS

Retrogression of nondiverging waves, noting phase velocity dependence on atmospheric stability 06 p1027 A67-18603

Upper atmosphere dynamics, noting role of horizontal and vertical winds in shifting density phase and amplitude and UV radiation as energy source 10 p1640 A67-23218

Millimeter waves in atmospheric research, discussing radar meteorology, radiometry, etc 13 p2072 A67-27493

Advances in geophysics, Volume 12, covering problems of earth crust and mantle, atmosphere interaction with sea surface, etc 18 p3040 A67-34092

Theory of available potential energy and rate of change and variational approach to atmospheric energetics 18 p3074 A67-34096

Potential energy flux across isobaric surfaces in atmosphere indicates flux direction dependent on correlation sign between temperature and vertical velocity at surfaces 19 p3224 A67-35526

ATMOSPHERIC ENTRY

Classical meteoric ablation theory generalized to include thermal radiation, conduction and meteoroid heat capacity in causing fragmentation 01 p0147 A67-10357

Aerodynamic, thermodynamic and structural design aspects of flight capsule entering low density Mars atmosphere from orbit 01 p0156 A67-11432

Positions of Echo satellites during reentry stage observed at Asiago in 1964 03 p0509 A67-13105

Friable structure of meteorites, examining disintegration under aerodynamic pressure in atmosphere 03 p0509 A67-13205

Control and stabilization of thrust producing final stages of recoverable space vehicles during atmospheric reentry 04 p0652 A67-14557

Fluid dynamic sources of radiation during atmospheric entry, considering equilibrium and nonequilibrium radiation, thermal radiation and relaxation processes in hypersonic flow 04 p0703 A67-14703

Meteorite size prior to entering atmosphere, noting radius and use of isotope activity nomogram 04 p0702 A67-15751

Differential equations and mathematical models for gas flows with chemical activity and radiative effects, particularly effects of reentry and propulsion 06 p0983 A67-17785

Mars atmospheric composition and laminar convective heating and ablation studied to predict performance of heat protection systems during entry 06 p1119 A67-18849

Inviscid equilibrium gas stability characteristics for pointed and spherically blunt bodies in unsteady supersonic flight in Mars atmosphere 07 p1258 A67-19380

Atmosphere entry, AIAA Selected Reprint Series, Volume 1 08 p1275 A67-20408

Flight dynamics of ballistic and lifting vehicle entries into planetary atmospheres of Mars, earth, Venus and

Jupiter 08 p1410 A67-20623
 Energy dissipation and other problems for alien planetary atmospheric entry at high speeds of interplanetary flight 08 p1394 A67-21155
 Free falling probe test during terminal descent for determining unknown planetary atmosphere profile from onboard measurements alone 10 p1629 A67-22768
 Disintegration of meteoric bodies in terrestrial atmosphere, disputing conclusion of Kramer 12 p2002 A67-25552
 Optimum entry vehicle design using aerobreaking for manned earth entry at hyperbolic speeds, examining blunted conic, biconic and tetrahedral configurations [AIAA PAPER 66-489] 15 p2564 A67-29422
 Theoretical and experimental work in flow field analysis has enhanced ability to predict aerodynamic heating in atmospheric entry 16 p2760 A67-30720
 Ablation heat protection system materials performance in hypersonic regime, discussing potential solutions to shielding during atmospheric entry 16 p2778 A67-30722
 Range of hypersonic gliders for various flight and reentry conditions, assuming small flight path angle and constant bank angle 16 p2595 A67-30963
 Atmospheric trajectories of faint telescopic meteors observed by separate stations simultaneously and probability of plotting 16 p2751 A67-31461
 Atmospheric properties at high temperature, discussing atmosphere radiation influence on flow around reentry device and radiative heat transfer 18 p3159 A67-34126
 Aerodynamic, thermodynamic, heat shield and structural design aspects of ballistic vehicle entering planetary atmosphere 19 p3332 A67-35315
 Multipurpose entry vehicle requirements for unmanned landings on bodies in solar system having tenuous atmospheres [AIAA PAPER 67-599] 19 p3336 A67-35995
 Thrust augmented maneuvering /TAM/ for lifting reentry vehicle compared with other glide vehicles using lift/drag ratio 20 p3533 A67-36584
 Electron beam probe for determination of local gas parameters in reentry simulation 20 p3445 A67-36588
 Basic shock layer radiation data obtained in shock tube and free-flight ballistic range facilities applicable to Venus or Mars atmosphere entry 21 p3563 A67-37788
 Gemini spacecraft antennas performance during reentry into ionized medium, discussing electron concentration profiles, nonearth atmosphere extrapolation and antenna breakdown effect 21 p3591 A67-38210
 Second order theory used to provide nearly exact solution for entry mechanics including solution of nonoscillating and oscillating trajectories [AIAA PAPER 66-488] 21 p3706 A67-38865
 Superorbital reentry environments, discussing materials, test environments and heat factors 22 p3919 A67-40383
 Earth and planetary atmosphere entry problems for blunt nosed slender vehicles noting aerodynamics, stability, heating, ablation and interaction of effects [AIAA PAPER 67-803] 24 p4243 A67-42963

ATMOSPHERIC HEAT BUDGET
 Mechanism regulating total amount of earth and Mars atmosphere transparent to visible and IR radiation 06 p0995 A67-18052
 IR flux for water vapor and flux divergence in atmosphere computed for rate of radiative cooling of atmosphere at coastal and continental stations 13 p2150 A67-26419
 Temperature profile in stratosphere, noting contribution to heat budget by turbulent thermoconductivity and UV radiation absorption in ozone layer 13 p2113 A67-26677
 Angular distribution of earth outgoing thermal radiation in IR region measured by geophysical rocket 14 p2306 A67-27860
 Atmospheric turbulence and diffusion, detailing turbulent energy and thermal variance budgets measurements, parallel plate convection, air pollution, etc 20 p3480 A67-36898

ATMOSPHERIC HEATING

Radiation effect on hydrodynamic shock wave parameter distribution for bodies entering dense atmospheric layers at supersonic velocities 07 p1125 A67-19110
 Satellite measurement of upper

atmospheric density variations due to geomagnetic disturbances, correlating time delay with geographic latitude 11 p1783 A67-23922
 Thermal behavior of vehicle entering earth atmosphere at velocities approaching 15 km/sec 13 p2224 A67-27325
 Atmospheric heating due to radiative heat transfer of direct and earth-reflected solar rays calculated as function of moisture content 19 p3251 A67-34851
 Radiative processes in lower stratosphere and average monthly heating rates over all latitudes due to direct and reflected solar short wave radiation 19 p3226 A67-35922
 Absorption 19 p3226 A67-35922
 Temperature and wind profiles in stratosphere and mesosphere during winter and summer determined by grenade soundings, noting diurnal variations 19 p3226 A67-35924
 Hot working effects in octahedrite parent gamma phase, discussing spinel twinning and polycrystal assembly of gamma phase before kamacite precipitation 24 p4232 A67-42609
 Iron meteorite with partially preserved fusion crust from atmospheric flight noting martensitic structures due to rapid cooling 24 p4232 A67-42611
 Hypersthene chondrite postformational history, discussing native copper and ilmenite content of Newmann lamellae and flowage 24 p4232 A67-42613

ATMOSPHERIC IMPURITY

Radioactive clathrate technique to detect reactive gaseous contaminants in atmosphere in parts per million range 05 p0843 A67-16550
 Selective imaging of objects in range using pulsed laser illuminator synchronized with Kerr cell camera, obtaining elimination of film exposure due to backscatter in turbid atmosphere 08 p1337 A67-20683
 Comparison of computed and experimental spectral transmissions through haze 13 p2152 A67-27357
 Volcanic and tectonic activity on Venus inferred from high surface temperature, considering possible effect on atmosphere obscuration 17 p2951 A67-33232
 Germ sampling at high altitudes using hydroaeroscopes attached to conventional aircraft 23 p3963 A67-41072

ATMOSPHERIC IONIZATION

Calorimetric measurement of ionization burst at 3200 m above sea level 02 p0315 A67-12758
 Ionization calorimeter determination of effective cross section of high energy primary cosmic ray proton inelastic interaction with atmospheric atomic particles 02 p0315 A67-12759
 Nucleon interaction generating high energy gamma rays, discussing photon and energy spectra of electron photon cascade, pion generation and gamma quantum detection in atmospheric nuclear interactions 02 p0316 A67-12763
 Ionization luminescence of air and possibilities of using it to record extensive air showers 02 p0318 A67-12781
 Air ionization rate behind high speed shock waves, determining electron density from IR emission 03 p0405 A67-14028
 Electron density profiles of Nike-Apache rocket observations of nitric oxide ionization by Lyman alpha radiation in E region at sunrise 03 p0415 A67-14114
 Atmospheric electrical conductivity of air at high temperatures 04 p0664 A67-14777
 Magnetic autogeneration for decelerating and cooling effects on aircraft entering dense atmospheric layer 04 p0664 A67-14791
 Vertical drift velocity of small scale ionization inhomogeneities in ionosphere, noting seasonal variation 05 p0802 A67-17146
 Chemical and photochemical reactions controlling ion composition of atmosphere between 150 and 300 km 07 p1170 A67-19100
 E layer ionization and characteristic number as affected by solar X radiation in 44-60 angstrom range 07 p1178 A67-19822
 Frequency correlation of ionospheric radio waves in inhomogeneous thin layer medium and effect of irregular horizontal ionization gradients 07 p1144 A67-19836
 Limiting daytime flux of ionization into protonosphere, obtaining expression for maximum upward flux supported by diffusion 07 p1180 A67-19918
 Effects of inhaled air ions on speed of response and attention level, heart and

respiration rate and transepithelial DC potential of men 09 p1452 A67-21720
 Maximum usable frequency for single discontinuity radio line calculated taking horizontal ionization gradients into account 10 p1604 A67-22794
 Vertically moving perturbations in nighttime ionosphere studied from vertical ionospheric sounding data, discussing type A4 which develops in F layer near maximum ionization 10 p1631 A67-22805
 Emission of bremsstrahlung X-rays caused by electrons precipitating isotropically into upper atmosphere 10 p1633 A67-23048
 Electron and ion emissions from hydrogen and helium UV glows in nighttime ionosphere 10 p1633 A67-23049
 Mass spectrometric investigations of interaction of atmospheric ions with molecules of rocket gas release 10 p1640 A67-23215
 Ion composition and effective recombination coefficient variation of ionosphere in study of X and UV radiation ionization of E layer 10 p1647 A67-23280
 Rocket probe measurements indicate existence of maximum ion concentration in stratosphere and lower ion concentration at equator than at midlatitudes 10 p1648 A67-23284
 Magnetosphere phenomena investigated via atmosphere model to explain planetary nebulas and eruptive solar prominences 12 p1992 A67-25119
 Cosmic radio wave absorption dependence on frequency and number of electron-ion collisions during atmospheric magnetic storms 12 p1933 A67-25548
 Rocket probe measurements indicate existence of maximum ion concentration in stratosphere and lower ion concentration at equator than at midlatitudes 12 p1933 A67-25650
 RF mass spectrometer with small dimensions and power requirements and high sensitivity designed for analysis of upper atmosphere ion and neutral composition 12 p1941 A67-25651
 Third Chapman-Enskog approximation to tensor electrical conductivity of partially ionized gas applied to two conductivity mixture rules for atmospheric cesium seeded argon 12 p1975 A67-25893
 Riometric data on ionospheric absorption applied to determination of dissociative recombination coefficient, noting atmospheric ionization by fragment gamma-radiation 14 p2306 A67-27858
 Ionospheric E region dynamical processes, discussing energy phenomena of planetary waves, tidal oscillations and gravity waves 14 p2311 A67-28408
 Statistics relating plasmopause position to three magnetic indices to clarify relationship between equatorial geocentric distance to plasmopause and worldwide magnetic activity level 15 p2477 A67-29627
 Field aligned structure of ionization associated with boundaries of spread-F at middle latitudes studied by combining topside and fast-sweeping ground-based ionograms [AGARDOGRAPH 95] 15 p2480 A67-30277
 Nonequilibrium air dissociation and ionization in stagnation region of blunt body investigated in merged layer regime 16 p2592 A67-30955
 Radar observation of meteor echoes in upper atmosphere, particularly deionization of processes in meteor trains 16 p2749 A67-31251
 Book on ionospheric chemistry, noting chemical and photochemical reactions above 60 km, and ionization processes 16 p2619 A67-31252
 Soviet book on meteors in earth atmosphere studied by radar discussing meteor trails, upper atmosphere winds, etc 16 p2754 A67-31866
 Nighttime profiles calculated with allowance for ionization beyond lower bound of frequency range of ionospheric station 16 p2669 A67-31896
 Day and night ion concentration as height function 17 p2842 A67-32258
 Electron impact excitation and ionization cross sections data of molecular nitrogen synthesized using modified Born approximation 20 p3489 A67-37418
 Inelastic electron impact cross sections for ionization and vibrational excitation of

- atmospheric molecular oxygen 20 p3489 A67-37419
- Vertical drift velocity of small scale ionization inhomogeneities in ionosphere, noting seasonal variation 21 p3619 A67-38488
- Calorimetric measurement of ionization burst at 3200 m above sea level 22 p3876 A67-40260
- Ionization calorimeter determination of effective cross section of high energy primary cosmic ray proton inelastic interaction with atmospheric atomic particles 22 p3876 A67-40261
- Nucleon interaction generating high energy gamma rays, discussing photon and energy spectra of electron photon cascade, pion generation and gamma quantum detection in atmospheric nuclear interactions 22 p3876 A67-40265
- Ionization luminescence of air and possibilities of using it to record extensive air showers 22 p3878 A67-40283
- Atmospheric ion mobility spectrograms measured with aspiration spectrometer 22 p3810 A67-40524
- Faraday rotation data from Explorer XXII, determining atmospheric electron content for magnetic field aligned ionization layer location and occurrence 23 p3996 A67-40818
- Ionospheric electron content and OI nightglow in Hawaii, discussing ionization density increases throughout bottomside F layer 24 p4147 A67-41878
- Maximum usable frequency for single discontinuity radio line calculated taking horizontal ionization gradients into account 24 p4120 A67-42130
- Vertically moving perturbations in nighttime ionosphere studied from vertical ionospheric sounding data, discussing type A4 which develops in F layer near maximum ionization 24 p4150 A67-42142
- ATMOSPHERIC MOISTURE**
- S HUMIDITY**
- ATMOSPHERIC NEUTRON FLUX**
- Book on natural neutron background of atmosphere and earth crust including effect of primary and secondary cosmic radiation, solar neutrons, presence in rocks, etc 01 p0143 A67-10042
- Detection of slow neutrons escaping from atmosphere by counters filled with boron fluoride onboard high altitude balloons 02 p0312 A67-12599
- Atmospheric slow neutron flux measurement in energy range from thermal to 100 ev carried out with sounding balloons from 1960 to 1962 05 p0885 A67-17140
- Cosmic ray neutron component intensity during magnetic perturbations, considering effect of magnetospheric deformation 10 p1699 A67-22781
- Temperature effect of cosmic ray neutron component 17 p2936 A67-32381
- Atmospheric slow neutron flux measurement in energy range from thermal to 100 ev carried out with sounding balloons from 1960 to 1962 21 p3698 A67-38482
- Indium activity measurements to determine epithermal neutron flux in atmospheric upper layers, giving results in terms of dependence on atmospheric depth 21 p3622 A67-39031
- Cosmic ray neutron component intensity during magnetic perturbations, considering effect of magnetospheric deformation 24 p4209 A67-42117
- ATMOSPHERIC NOISE**
- S ATMOSPHERICS**
- ATMOSPHERIC PRESSURE**
- SA BAROMETER**
- SA ISOBAR**
- March 1964-March 1965 seasonal variations in density, pressure and temperature at Woomera, Australia, by falling sphere method 01 p0061 A67-11280
- Quasi-stationary solar corpuscular fluxes, examining effect on atmospheric pressure in earth polar cap regions 01 p0061 A67-11279
- Distribution of solar-tropospheric disturbances over earth surface, based on simultaneous observations of 103 U.S.S.R. stations 01 p0061 A67-11280
- Seasonal changes in cosmic ray intensity including barometric effect in neutron component, effect of earth seasonal position, etc 02 p0307 A67-11665
- Tropospheric pressure-altitude data by satellite radiometric topography mapping, using oxygen absorption band centered at 5 mm 02 p0262 A67-12367
- Barometric pressure coefficient, correcting terrestrial neutron monitor intensities, dependency on magnitude variations related to changes of atmospheric water vapor content 03 p0505 A67-12958
- Dynamic pulmonary work of human males during muscular exertion at 2000 m and different barometric pressures 04 p0561 A67-14631
- Equatorial spread-F and tropical disturbances, supplying data on typhoon, geomagnetic activity and atmospheric pressure waves 04 p0612 A67-14653
- Nanosecond pulse microwave breakdown in air 04 p0657 A67-15120
- Daytime profile of electron density in C and D layers of ionosphere from measurements of surface ultralong wave fields and atmospheric pressure 05 p0801 A67-17131
- Barometric effect of cosmic rays with allowance for changes in D/R/ primary spectrum and cut-off 05 p0884 A67-17136
- Exploding wire phenomena in air at atmospheric and reduced pressures 05 p0847 A67-17317
- Molecular beam technique for mass spectrometric sampling of high temperature systems at high atmospheric pressure [AIAA PAPER 67-37] 06 p0956 A67-18305
- Photometric measurements on deviations from equilibrium state in burnt gases of laminar premixed shielded flames at atmospheric pressure [AIAA PAPER 67-9] 06 p1072 A67-18345
- Interdiurnal pressure variability as measure of kinetic energy of air masses 06 p1027 A67-18606
- Recombination rate increase in F region following magnetic activity due to passage of atmospheric wave 07 p1171 A67-19418
- Verbal communication intelligibility in man-rated altitude simulator with nitrogen or helium added to oxygen atmosphere 08 p1287 A67-20484
- Carbon dioxide abundance and surface pressure of Martian atmosphere, noting self-broadening correction 08 p1400 A67-21250
- V-I characteristics in flame by double probe method at atmospheric pressure 08 p1428 A67-21426
- Electron recombination in argon plasma at atmospheric pressure in vicinity of 10,000 degrees K 09 p1550 A67-22584
- Ionization coefficients in helium over pressure range near to atmospheric show destruction of metastable states in gas accounts for dependence on electric field 10 p1681 A67-22962
- Barometric pressure data analysis estimating autocovariance, using Fourier transform for spectral density calculation 11 p1816 A67-24840
- Diagnostic techniques for atmospheric pressure arc plasmas, noting that integrated current density measurements are consistent with measured total arc current 12 p1973 A67-25393
- Orographic factors effect on stratospheric pressure field, obtaining ascending vortical fluxes and heat input equations, discussing refractive index for atmospheric perturbations 13 p2112 A67-26672
- Sea-level pressure specification from 700-mb height by applying screening regression techniques to 17 years of synoptic data 13 p2114 A67-26740
- Solar activity cycle effect on northern hemisphere pressure field solar activity cycle effect on Northern Hemisphere pressure field 13 p2117 A67-27632
- Five-ball fatigue tester to investigate reduced pressure environment effect on rolling element fatigue life with polyphenyl ether [ASLE PREPRINT 67AM 8A-3] 14 p2326 A67-28795
- Nuclear explosion effects on atmospheric pressure, electron density, and F-2 layer height, noting dependence on time, season, etc 15 p2478 A67-30067
- Atmospheric pressure discharges in inert gases seeded with alkali metal vapor, noting transition to low voltage high current discharge 16 p2709 A67-30513
- Argon-potassium plasma electrical conductivity investigation showing that optimum increase in conductivity corresponds to optimum electrode length 16 p2602 A67-30560
- Seasonal changes in cosmic ray intensity including effect in neutron component, effect of earth seasonal position, etc 16 p2738 A67-31080
- Barometric correction in cosmic ray studies using partial barometric coefficient 17 p2934 A67-32105
- Hot flame gases ionization by electron reactions at atmospheric pressure 17 p2968 A67-32149
- Boiling process of binary mixtures examined by heat transfer mechanism at atmospheric pressure 17 p2969 A67-32458
- Deformations of earth crust produced by known forces of luni-solar and surface types 18 p3040 A67-34093
- Martian surface atmospheric pressure via photometric observations of Phobos eclipses 18 p3124 A67-34155
- Argon, deuterium and air ionization at atmospheric pressure and lower by focused ruby laser radiation, analyzing plasma spectrum 19 p3239 A67-35166
- Prognostic equation asymptotic solution for atmospheric pressure forecast 20 p3479 A67-36125
- Upper atmospheric dynamics, considering day-night density and pressure variation, wind structure, gravity waves, etc 20 p3429 A67-36896
- Atmospheric pressure at cloud top and hydrogen abundance in Jupiter atmosphere determined by analyzing methane spectral line widths 20 p3529 A67-37479
- Daytime profile of electron density in C and D layers of ionosphere from measurements of surface ultralong wave fields and atmospheric pressure profile 21 p3619 A67-38474
- Barometric effect of cosmic rays with allowance for changes in D/R/ primary spectrum and cut-off 21 p3698 A67-38479
- Radial temperature distribution in high power argon arcs measured at atmospheric pressure and 5 atm for currents ranging from 200 to 500 amp 22 p3853 A67-40049
- Sidereal cosmic ray diurnal variations, taking into account data correction for barometric pressure and temperature effects 23 p4059 A67-41130
- Space suit atmosphere physiological suitability for prolonged moderate work, studying blood-gas parameter changes 23 p3955 A67-41617
- Rats resistance and reactivity in hypothermal state to very low atmospheric pressure by hypercapnia-hypoxia exposure 24 p4111 A67-41849
- ATMOSPHERIC RADIATION**
- SA STRATOSPHERE RADIATION**
- Experimental verification of calculation of short wave radiation fluxes in real atmosphere from model 01 p0108 A67-10128
- Experimental verification of Shifrin-Perelman method of determining spectrum of dispersed atmospheric aerosol particles from spectral transmittance 01 p0108 A67-10130
- Absorption spectra models analyzed for use in IR radiation propagation in atmosphere 01 p0109 A67-11043
- Overlapping of bands of nitrogen oxide, CO and carbon dioxide in 4.5 micron region determined for inversion experiments 02 p0246 A67-12368
- Atmospheric showers and high energy nuclear-active particles 02 p0312 A67-12608
- Radiant equilibrium temperature of opaque absorbing body relation to radiative temperature variations of 02 p0343 A67-12646
- Latitude distribution of ozone at high altitudes, deduced from radiance of earth daylight atmosphere, measured with satellite-borne radiometer 03 p0410 A67-12948
- Fast neutron latitude variations in atmosphere during solar minimum measured by high-altitude balloons, noting neutron leakage into space 03 p0505 A67-12950
- Primary cosmic ray spectrum at high energies and spectra of gamma rays and muons in atmosphere 04 p0692 A67-14857
- Atmospheric cosmic ray fluxes measured on series of USAF jet aircraft flights [AFCLR-67-0099] 04 p0693 A67-14961
- Geometric model of radiative atmospheric space used in research on mean radiation temperature of space by frigorimeter 06 p1025 A67-17637
- Space nuclear radiation dose rates in earth

atmosphere with consideration of solar flare radiation variations 06 p1077 A67-18009

Radiosonde radiometer to measure long wave emission from earth and intervening atmosphere during night ascents 06 p1005 A67-18742

Radioactivity of Cosmos III satellite after U.S. thermonuclear explosion over Johnston Island 07 p1242 A67-19112

Balloon-borne Czerny-Turner grating spectrometer used to measure atmospheric transmittance in spectral regions between 2 and 14 μ 07 p1184 A67-19389

High altitude balloon-borne polarization measurements relevance in research program of radiation emerging from earth atmosphere 07 p1170 A67-19393

Soviet papers on optical radiation and ozonometric studies of atmosphere 07 p1219 A67-19451

Angular distribution of reflected cloud and radiation fields according to IL-18 aircraft data of 1964 07 p1220 A67-19452

Angular intensity distribution of short wave radiation measured by automatic stratospheric balloons 07 p1220 A67-19453

Actinometric radio probe measurement of effect of clouds on long wave radiation field and to locate upper cloud cover surface from vertical profile of radiative fluxes 07 p1220 A67-19454

Variations in long wave radiation field of free atmosphere within 7 to 10 hr time periods 07 p1220 A67-19455

Assessment of available methods for direct measurement of radiative heat influx in free atmosphere 07 p1172 A67-19458

Oxygen spectra in dayglow, twilight and during eclipse 07 p1173 A67-19662

Cosmos LXI spectrophotometric measurements of atmosphere-reflected UV radiation spectra 07 p1178 A67-19801

Vertical incidence CW Doppler phase path sounder spectral analysis of ionospheric motions and irregularities due to atmospheric wave propagation into ionosphere from below 07 p1182 A67-19952

Equilibrium air total radiation mechanism, vacuum UV radiation and relation to hypervelocity entry studied, using shock tube blunt model test flow [AIAA PAPER 66-103] 08 p1426 A67-20569

Radiation data measured by Tiros IV satellite for determination of global distribution of atmospheric water vapor 10 p1677 A67-23195

Heat radiative flux divergences and equilibrium temperature distribution with altitude calculated for heat regime modeling radiative transfer conditions in stratosphere and mesosphere 10 p1647 A67-23275

Cosmos 65 spectrophotometric measurements of atmosphere-reflected UV radiation spectra 10 p1647 A67-23277

Chemiluminescent radiation from interaction of nitric oxide with atmospheric ozone for PCA conditions [AFOSR-67-1379] 10 p1702 A67-23345

Spectrometry of primary and solar protons at Skogar-Iceland using apparatus consisting of scintillation and Cerenkov counters 12 p1991 A67-25114

Molecular, continuum and line radiation of planetary atmospheres, comparing molecular band structure models with spectral measurements of CN violet band [AIAA PAPER 67-323] 12 p2037 A67-26038

IR spectrum evaluation procedures and optical measurement as applied to atmosphere physics 14 p2311 A67-28401

Primary cosmic radiation and interaction in atmosphere studied during minimum solar activity by balloon flights to determine effect of latitude on secondary photons 15 p2550 A67-29533

Atmospheric radiation polarization characteristics, determining concentration and distribution of atmospheric scatterers 16 p2665 A67-30983

Atmospheric properties at high temperature, discussing atmosphere radiation influence on flow around reentry device and radiative heat transfer 18 p3159 A67-34126

Atmospheric radiation balance studies via daytime balloon measurements, obtaining vertical profile curves for albedos, total and reflected radiation, etc 19 p3214 A67-34853

Absorption coefficients of radiation by water vapor and aerosols determined from atmospheric counter 19 p3251 A67-34858

IR spectrophotometer developed for airborne study of spectral energy distribution in atmospheric self-radiation 19 p3227 A67-34859

Atmospheric spectra and related quantities calculated, obtaining radiation spectral distribution by radiative transfer equation, comparing results with other studies 19 p3220 A67-35260

Ionospheric and stratospheric UV radiation effects on survival of microorganisms 19 p3178 A67-35271

Atmospheric optics and radiation transfer covering sky brightness, solar insulation, earth radiance and albedo, etc 20 p3430 A67-36899

Auroral transition radiation calculated from electron impact 20 p3433 A67-37420

Earth upper atmosphere background radiance measured by UV radiometer carried on Air Force satellite 22 p3794 A67-40364

Balloon sounding data for atmospheric secondary and reentrant albedo proton intensity values, discussing empirical atmospheric secondary proton spectrum 23 p4051 A67-40810

Duhamel principle for internal radiation field in inhomogeneous finite atmosphere based on existence and uniqueness theorem for Milne integral equation 24 p4189 A67-42598

ATMOSPHERIC REFRACTION

SA LIGHT TRANSMISSION

Graphical calculation of wave refraction in dry atmosphere between 0.4 and 13 microns 01 p0108 A67-10129

Trajectories of electromagnetic rays across terrestrial atmosphere and computer program 01 p0028 A67-11419

Soviet papers on optical instability of earth atmosphere 02 p0261 A67-11982

Fluctuations of refraction index of surface layers of atmosphere observed directly in daytime and parameters of fluctuation distribution 02 p0325 A67-11985

Atmospheric agitation effect on image of extended celestial light sources, showing importance in long-range tropospheric propagation of ultrashort radio wave 02 p0325 A67-11986

Velocity aberration and atmospheric refraction pertaining to laser satellite communication experiments, obtaining equations for estimation of effects 02 p0198 A67-12054

Clear line-of-sight through atmosphere determined, using probability estimates [AFCLR-66-838] 02 p0262 A67-12080

Prediction of apparent elevation angle expected for object situated in troposphere at specified values of geometrical elevation angle height 02 p0199 A67-12083

Nonionized atmosphere effect on radial velocity measurement of satellite via Doppler-Fizeau method 03 p0369 A67-13530

Propagation of clear air radar echoes in nonionized media and use in determining planetary surface and atmospheric structure 05 p0760 A67-16009

Fluctuations of angle of incoming light waves from distributed source in atmosphere with turbulent pulsations of refractive index 05 p0761 A67-16346

Wavelength dependence of spectrum of laser beams traversing atmosphere 05 p0763 A67-16793

Photogrammetric refraction in high altitude surveying for isothermal atmosphere and for atmospheric polytropic through altitude of 11 km 05 p0808 A67-17033

Telescope optics techniques for compensation for lateral color aberration arising from atmospheric refraction, using modified Schupmann medial telescope 06 p1033 A67-18535

Model atmospheres and astronomical and parallax refraction 07 p1174 A67-19716

Rapid and accurate ray tracing algorithm for horizontally stratified atmosphere, using effective earth-radius technique 09 p1464 A67-22450

Radar echoes from cloud-free atmosphere caused by turbulent pulsations of microwave refractive index 10 p1677 A67-23500

Atmospheric distortion effect on signal reception by large dimensional antennas, obtaining numerical estimates for various parameters 11 p1753 A67-24439

Anisotropy of coarse ionospheric inhomogeneities determined from measurements of irregular radioastronomic

refraction 11 p1787 A67-2446

Gravitational wave propagation from upper to lower atmospheric layers analyzed taking into account reflection and refraction 13 p2112 A67-26677

Water-vapor rotational band transmission function calculations by atmospheric inhomogeneity approximate methods 13 p2151 A67-26688

Satellite and astronomical refraction: determined from formulas for air refractive index determination 13 p2199 A67-26855

Astronomical refraction in polytropic atmosphere adapted to automatic computers 13 p2152 A67-27441

Formulas for correcting errors in aerial photograph and planar-model coordinates due to atmospheric refraction and earth curvature 14 p2318 A67-28377

Atmospheric optics problems solved by Monte Carlo method, presenting results in tabular and graphical form 14 p2313 A67-28766

Laser measurements of long distance, using laser interferometers, modulated laser beams and laser radar 17 p2867 A67-32611

Satellite technique for sounding atmospheric optical properties and height distribution of ozone and aerosols 18 p3040 A67-33851

Orbit determination from Minitrack observations, discussing effects of ionospheric refraction, atmospheric drag and earth tesseral harmonics 18 p3126 A67-34244

Radio propagation of transmissions from stationary and near stationary satellites used to study anomalous atmospheric refraction at low angles of refraction 19 p3182 A67-35177

Photogrammetric refraction in high altitude surveying for isothermal atmosphere and for atmospheric polytropic through altitude of 11 km 21 p3627 A67-38263

Propagation anomalies of atmospheric acoustic signals of nuclear explosions due to nonlinearities and refraction effects 22 p3790 A67-39643

Design studies for reliable long range ground-to-air communication, noting line of sight propagation and HF propagation not involving ionospheric reflections 23 p3972 A67-40742

Optical measurement of atmospheric refractive index gradient showing approximate accuracy and simplicity for reasonably large gradients 24 p4188 A67-42093

ATMOSPHERIC SCATTERING

SA LIGHT SCATTERING

SA WAVE SCATTERING

Submillimeter wave scattering by fog, comparing experiments in clear atmosphere and dense fog 02 p0199 A67-12078

High Resolution spectrophotometric system for measuring atmospheric transmittance spectra 02 p0263 A67-12645

Model for ionospheric drift measurements made by spaced receiver method when scattered wave has frequency above plasma frequency of scattering region 03 p0407 A67-12831

Outward flux and intensity of scattered radiation for top of Rayleigh atmosphere lying above smooth water surface that reflects radiation according to Fresnel law [AIAA PAPER 65-664] 03 p0411 A67-13044

Laser backscatter signatures and transmissivity over horizontal and slant paths with respect to measuring extinction coefficients of scattering media 04 p0649 A67-14677

Tropospheric probe using vertically polarized signals scattered by clear air turbulence 04 p0649 A67-14683

Second order scattering effect on earth albedo calculations in middle UV, noting distribution functions and parameters used 04 p0613 A67-14696

Rotating interferometer measuring spread and coherence ratio of scattered radio wave 05 p0760 A67-15997

Multiple scattering effect on brightness of twilight sky, noting changes in spectral composition due to radiation absorbing effect of ozone and height variation of multiple layer 07 p1219 A67-19148

High altitude atmospheric scattering of intense light from ruby laser beam interpreted principally in terms of Rayleigh scattering from atmospheric molecules 07 p1171 A67-19419

Solar UV reflection and scattering from

- earth atmosphere, use in determining total concentration and vertical distribution of ozone 07 p1178 A67-19815
- Anisotropic nonconservative scattering in modified Schuster-Schwarzschild approximation and Venus cloud layer 08 p1385 A67-20931
- Daytime sky brightness relationship to atmospheric anisotropic light scattering 09 p1491 A67-21638
- Isotropic scattering of radiation in finite two-dimensional atmosphere using integral equation, solved by power series 09 p1532 A67-21662
- Greenhouse effect in semiinfinite scattering atmospheres, describing steady state distribution of thermal radiation 09 p1567 A67-22238
- Atmospheric scattering of solar flux in UV noting radiation transfer for airborne detector, air component absorption coefficient and spectra from rocket flight 10 p1629 A67-22736
- Multiple air scattering in mesosphere as function of zenith distance of sun and brightness of twilight sky 11 p1785 A67-23957
- Time course of blue-to-red light intensity ratio of visible solar spectrum during and after sunset 11 p1786 A67-24116
- Mutual coherence factor for plane electromagnetic wave propagating in stochastic locally homogeneous and isotropic medium of dielectric turbulence 11 p1818 A67-24415
- Multiple scattering and finite detector bandwidth effects on shape of absorption features in atmospheric scattering 11 p1862 A67-24502
- Microwave reflection from region with nonuniform hydrometeor for case where dimensions vary greatly and relation to wavelength is arbitrary 11 p1754 A67-24981
- Radar evidence for atmospheric dust layers around 80 km altitude 13 p2109 A67-26333
- Anomalous absorption and scattering in global and diffuse radiation measurements during cloudless summer days 13 p2113 A67-26739
- Solar radiation passage through earth atmosphere in triplet lines O I, considering molecular hydrogen absorption and brightness distribution of radiation 14 p2378 A67-27862
- Photometric theory of artificial satellite eclipse by earth with application to atmospheric study 16 p2745 A67-30746
- Radiative transfer for electron scattering atmosphere, obtaining eigenfunctions of transport equations 17 p2950 A67-33164
- Higher order atmospheric light scattering at zenith of twilight sky, tabulating ratio between higher order scattering and primary twilight intensity 18 p3040 A67-33631
- Rocketborne spectrograph measurement of UV reflectivity of Venus and Jupiter, noting atmospheric Rayleigh scattering effects 18 p3123 A67-34147
- Relation between surface pressure and atmospheric brightness in optically thin Rayleigh scattering atmosphere, considering application to Mars 18 p3134 A67-34536
- Laser and nonlaser light transmission through atmosphere, noting no difference in propagation 19 p3240 A67-35695
- 80 km atmospheric backscattering enhancement detected by optical radar 22 p3759 A67-39558
- Ozone parameters determination from measurements of radiation backscattered by earth atmosphere 22 p3794 A67-40365
- Soviet book on atmospheric visibility noting photometry, range, threshold, runway visual range, atmospheric transmittance and atmospheric boundary layer problems 23 p4024 A67-40600
- Light reflection and transmission by thick optical atmosphere according to phase function 24 p4147 A67-41819
- Radiative heat transfer for light reflection and transmission by optically thick scatterers with three-term phase function, obtaining asymptotic formulas 24 p4147 A67-41820
- Optical Raman scattering from atmospheric oxygen and nitrogen via pulsed nitrogen UV laser light source, discussing spectral analysis of air scattering 24 p4147 A67-41883
- Functional equations in internal radiation field in finite inhomogeneous isotropically scattering atmosphere, using invariant embedding and Duhamel principle 24 p4189 A67-42597
- Field strength data correlation with meteorological cyclonic parameters, noting possible prediction of scatter signal losses during frontal disturbances 24 p4124 A67-42823
- ATMOSPHERIC SHELL**
- Interaction between different layers of homosphere, discussing separating and null layers and vertical interaction 13 p2115 A67-26864
- ATMOSPHERIC STRATIFICATION**
- Radio wave reflection from ionosphere with perturbed electron density profile 02 p0192 A67-11618
- Turbulent diffusion in nonuniform stratification atmosphere, obtaining vertical concentration profile by random walk method [AFCLR-66-836] 02 p0262 A67-12081
- Thermal atmospheric sounding, discussing carbon dioxide transmission function parameters, water vapor and temperature effect 02 p0239 A67-12377
- Nonstationary models of cumuli and thermals in stratified atmosphere 02 p0262 A67-12641
- Probability distribution of square of vertical wind velocity difference during unstable stratification 03 p0463 A67-14228
- Ratio of Lagrange and Euler correlation scales determined from correlation of time fluctuation of transverse wind velocity and temperature variation 03 p0464 A67-14229
- Unstable modes of barotropic horizontally sheared zonal current in stratified atmosphere 04 p0611 A67-14650
- Wind profile effect on turbulent diffusion for infinite linear source in surface layer of unstable stratified atmosphere 04 p0652 A67-15569
- Ionospheric stratification and electron density distribution in F-1 layer by Serafimov method 04 p0618 A67-15572
- E layer stratification, fine structure and boundary accuracy in frequency measurements based on seasonal variations in solar activity 04 p0618 A67-15574
- Sporadic E layer stratification and morphology of M and N reflections produced by transparent and semitransparent E layer 05 p0799 A67-17029
- Criticism of photometric results of Ney and Pepin findings regarding link layer in terrestrial atmosphere 05 p0802 A67-17330
- Two-cell solution to vorticity equations in unstably stratified atmosphere 06 p1026 A67-18565
- Rocket measurements of small scale structure of ionization profile and wind speed fluctuations, propagation of gravity shock waves and stratification in upper atmosphere 08 p1325 A67-20986
- Cumulus convective cloud formation above isolated source of heat and water vapor 09 p1491 A67-21552
- Rapid and accurate ray tracing algorithm for horizontally stratified atmosphere, using effective earth-radius technique 09 p1464 A67-22450
- Distribution curves of ion density and condensation particle concentration in layers of atmosphere near sea level, noting criteria for instruments 10 p1657 A67-23695
- Probability distribution of square of vertical wind velocity difference during unstable stratification 12 p1963 A67-25484
- Ratio of Lagrange and Euler correlation scales determined from correlation of time fluctuation of transverse wind velocity and temperature variation 12 p1964 A67-25485
- Relation between diurnal, seasonal and cyclic variations of stratifications in E layer and fine structure of sporadic E layer and E-2 layer 13 p2110 A67-26550
- Soviet papers on physics of upper layers of atmosphere 13 p2111 A67-26667
- Gravitational wave propagation from upper to lower atmospheric layers analyzed taking into account reflection and refraction 13 p2112 A67-26673
- Transfer of large scale tropospheric perturbations into stratosphere analyzed using hydrodynamic model, noting role of atmospheric stratification, refractive index, etc 13 p2112 A67-26674
- Seasonal variations in high latitude stratosphere and mesosphere 13 p2113 A67-26675
- Water-vapor rotational band transmission function calculations by atmospheric inhomogeneity approximate methods 13 p2151 A67-26682
- Atmospheric boundary layer dynamics models, similarity hypothesis and theories 13 p2151 A67-26687
- Interaction between different layers of homosphere, discussing separating and null layers and vertical interaction 13 p2115 A67-26864
- Atmospheric wind effects on guided propagation of VLF infrasonic waves over long distances, including variable wind and temperature profiles 13 p2117 A67-27702
- Oblique incidence ionospheric reflections, from phase and amplitude variations of Loran-C pulse signals, noting lower ionosphere two-layer formation 16 p2632 A67-31862
- Charge transfer role in formation and maintenance of molecular and metal-ion layer in E region of ionosphere 19 p3217 A67-35204
- Vertical distribution of diffuse sky light in stratosphere determined by rocket measurements, noting intensity peak in aerosol layer 19 p3221 A67-35273
- Stratosphere and mesosphere wind and temperature measurements, noting additional cosmic radiation measurements during 1966 solar eclipse in Argentina 19 p3320 A67-35287
- Statistical properties of strong light intensity fluctuations propagating in ground layer of atmosphere investigated to measure frequency spectra 19 p3254 A67-36017
- Sodium cloud between 85 and 110 km shows turbulent phenomena stratification exists and disappears with upward propagation of movements due to energy decreases 20 p3427 A67-36367
- Ionospheric pulse absorption study of measurements taken in Bulgaria during solar eclipse of May 1966 21 p3616 A67-37995
- Atmospheric boundary layer dynamics models, similarity hypothesis and theories 21 p3654 A67-38429
- Long period surface gravity waves in atmosphere 22 p3792 A67-39974
- Solar hydrogen convection zone mean stratification derived from mixing length theory, discussing zone structure dependence on temperature and density dependence of opacity 23 p4068 A67-41278
- ATMOSPHERIC TEMPERATURE**
- SA IONOSPHERIC TEMPERATURE**
- Pilot experiment, recording simultaneously optical image position, atmospheric temperature fluctuations and wind direction 01 p0108 A67-10250
- March 1964-March 1965 seasonal variations in density, pressure and temperature at Woomera, Australia, by falling sphere method 01 p0061 A67-11260
- Atmospheric and surface temperature profile measurement using balloon mounted IR spectrometer 01 p0061 A67-11391
- Optimum averaging periods in measurements of wind velocity profile, temperature gradient, vertical thermal turbulent flow and atmospheric drag 02 p0263 A67-12644
- Radiant equilibrium temperature of opaque absorbing body relation to radiative temperature variations of air 02 p0343 A67-12646
- Total normal emittance of various oxidation-resistant materials to very high temperatures in air determined, using special apparatus [ATAA PAPER 65-655] 03 p0447 A67-13035
- Entropy defect and source function in gray atmosphere thermodynamics 03 p0537 A67-14314
- Mean values of methane wavelengths in Uranus spectrum measured for determination of atmospheric temperature 03 p0515 A67-14327
- Solar cycle effect on geomagnetic activity and temperature of near-earth tropospheric layer 04 p0616 A67-15227
- Temperature effect on diurnal variation of meson intensity at high latitudes, finding wave maximum amplitude in spring 05 p0796 A67-16117
- Atmospheric temperature and wind velocity in mesosphere measured by rocket grenade method 05 p0798 A67-16857
- Mesoscale temperature variability below

60,000 ft measured for calculation of supersonic aircraft fuel requirement 05 p0838 A67-17305

Density and temperature of upper atmosphere, satellite tracking, geodetic applications and long distance measurements, using laser output 06 p1008 A67-17591

Zonal harmonics investigation of mean temperature of stratospheric layers 06 p0996 A67-18447

Horizontal variability of properties of model thermosphere with seasonal changes 06 p0996 A67-18564

Electron-neutral particle collision and electron thermal conductivity effect on upper atmospheric electron and ion temperatures 06 p0998 A67-18702

Atmospheric temperature profile to 30 km determined by balloon-borne grating spectrometer of radiance of earth between 2100 and 2700 reciprocal cm [JPL-TR-32-1080] 07 p1171 A67-19394

Temperature of atmospheric radio emission in decimeter range for elevation angles from 1/2 to 10 degrees 07 p1142 A67-19586

Effect of thermal escape on neutral hydrogen density above 120 km 07 p1181 A67-19936

Upper atmospheric temperature measurement by analysis of AIO spectra 08 p1327 A67-21370

Vertical transport of latent and sensible heat of IR cooling and short wave heating 09 p1490 A67-21550

Optical effects of thermal structure in lower atmosphere 10 p1679 A67-22745

Heat transfer equations for rocketborne stratospheric temperature sensor in form of spherical bead thermistor and experimental analysis of physical, thermodynamic and electrical characteristics of rocketsonde [AIAA PAPER 66-385] 10 p1632 A67-22819

Hydrogen line profiles in model atmospheres using quasi-static approximation for electrons and ions 10 p1704 A67-22883

Upper atmospheric wind, temperature and pressure variations measured using grenade launched Skylark sounding rockets 10 p1638 A67-23199

Seasonal-latitudinal variations in lower thermospheric density, temperature and composition 10 p1639 A67-23210

Mass spectrometric measurements of upper atmosphere temperature 10 p1639 A67-23214

Absorption and brightness temperature variations of atmosphere on basis of statistical characteristics of vertical temperature and humidity structures 11 p1785 A67-23956

Atmospheric density, temperature and pressure profiles obtained in Florida and New Mexico using rockets 12 p1937 A67-25837

Atmospheric temperature, pressure, density and wind measurements between 30 and 80 km by Skylark rocket at Woomera, Australia 12 p1937 A67-25840

Model for vertical eddy heat flux in stable atmosphere 13 p2149 A67-26275

Cross correlation /by superposed epoch method/ between upper atmospheric sodium and stratospheric warmings at high latitude 13 p2110 A67-26441

Temperature determination in stratosphere via hydrodynamic equations taking into account energy inputs and atmospheric motion, suggesting existence of integral heat sources 13 p2113 A67-26676

Atmospheric warming over Central Europe related to low solar and magnetic activity 14 p2313 A67-28621

Temperature and humidity fields vertical structure determined under conditions of stratified cloudiness 14 p2346 A67-28765

Rocketsonde and radiosonde temperature comparisons and evaluation of computed rocketsonde pressure and density 14 p2347 A67-28885

Satellite drag analysis of atmospheric temperatures noting effects of UV, solar radiation and geomagnetic fluctuations 14 p2314 A67-29027

Error possibility in temperature measurements of 30-60 km region, noting solar irradiation effects on thermistor bead 15 p2474 A67-29202

Stratospheric temperatures in north and south polar regions shown to depend on

land mass temperatures 15 p2475 A67-29579

Ion temperature measurements in upper atmosphere to determine diurnal variation 16 p2666 A67-31416

Atmospheric temperature effect on latitudinal curve of cosmic ray intensity determined from radio probe observations 17 p2933 A67-32090

IQSY electrophotometric and spectrometric measurements of annual and nighttime variations in rotational temperatures and integral intensity of hydroxyl emission bands 17 p2849 A67-32957

Geomagnetic activity effect derived from Explorer IX drag data, with atmospheric temperature as geomagnetic storm intensity function and atmospheric density increase 18 p3042 A67-34255

Upper atmosphere density, temperature and variation determined from satellite drag data, proposing thermosphere model 19 p3214 A67-34931

Rocket observations of upper atmospheric winds, electron density, electron temperature, and neutral temperature in auroral region with Langmuir probes 19 p3214 A67-35169

Density, temperature, water vapor and atomic oxygen concentration in mesosphere measured by heat method 19 p3216 A67-35183

Density, temperature and pressure profiles variations in upper atmosphere obtained from rocketborne experiments 19 p3218 A67-35219

Developments in upper atmosphere research noting atmospheric density, temperature, diurnal variations, solar and geomagnetic activity effects, etc 19 p3218 A67-35225

Convection in atmosphere below cloud base considered from ground and aircraft observations 19 p3253 A67-35919

Molecular oxygen absorption line equivalent widths measurement at 5 mm wavelength obtained from model atmosphere to determine earth atmospheric temperature 20 p3427 A67-36370

Temperature of atmospheric radio emission in decimeter range for elevation angles from 1/2 to 10 degrees 20 p3384 A67-37323

Satellite-borne superheterodyne radiometer for measuring stratospheric temperature utilizing millimeter wave spectrum of molecular oxygen 21 p3584 A67-38669

Air temperature measurements at subsonic and supersonic flight speeds, discussing error sources and thermometer efficiency 22 p3797 A67-39542

Ground based atmospheric and ionospheric particle temperature measurements, examining methods and thermosphere heat sources 22 p3870 A67-39676

Jupiter environment, effects of huge mass, high rotation rate, temperature and dominant H and He atmosphere 22 p3887 A67-40141

Weighting function calculation for remote temperature sensing of terrestrial atmosphere using selective chopper radiometer 22 p3805 A67-40356

Planetary surface pressure and temperature of lower atmosphere determined from orbiting spacecraft with carbon dioxide laser 22 p3805 A67-40357

Atmospheric temperature profile to 75 km by remote sounding, using satellite measurement of molecular oxygen resonance line at 5 mm 22 p3806 A67-40360

Satellite Infrared Spectrometer /SIRS/ flown by balloon for cloud top and surface temperatures 22 p3829 A67-40370

Neutral atmospheric temperatures calculated from data provided by incoherent scatter soundings of ionosphere 22 p3794 A67-40474

Atmospheric temperature effect on cosmic ray hard component diurnal variation in high latitude regions, discussing anomalous diurnal variation 23 p4058 A67-41127

Temperature effect on diurnal variation of meson intensity at high latitudes, finding wave maximum amplitude in spring 24 p4152 A67-42793

ATMOSPHERIC TIDE

Atmospheric tides deduced from drifts of ionized meteor trains observed by Doppler shift of echoes 05 p0803 A67-17405

Eigenvalue and Hough functions for diurnal and semidiurnal components and

both symmetric and antisymmetric modes of atmospheric tides 10 p1634 A67-23051

Thermal oscillations of polar night stratosphere and upward propagation 10 p1643 A67-23244

Atmospheric tides, shorter period gravity waves and shear waves 10 p1643 A67-23244

Partial coherence functions to investigate contribution of solar radiation and gravitational tide in causing geomagnetic variations /ionospheric tides/ 11 p1785 A67-23934

Sporadic E backscatter noting two peaks in activity, motion, temporal component parameters and cause 13 p2107 A67-26306

Thermal tidal motions in lower ionosphere and differential charge mobility pictured as producing earth atmosphere electrical structure 19 p3220 A67-35255

Lunar semidiurnal air tide distribution and small lunar gravitational excitation noting lunar diurnal tide detectable only with wind data 22 p3882 A67-39551

ATMOSPHERIC TURBULENCE

SA CLEAR AIR TURBULENCE

Low level turbulence effects on structure of large logistic aircraft [SAE PAPER 660670] 01 p0160 A67-10577

Statistical and spectral density analyses of stationariness and behavior law of atmospheric turbulence 01 p0054 A67-11087

Fluctuations of refraction index of surface layers of atmosphere observed directly in daytime and parameters of fluctuation distribution 02 p0325 A67-11985

Atmospheric agitation effect on image of extended celestial light sources, showing importance in long-range tropospheric propagation of ultrashort radio wave 02 p0325 A67-11986

Atmospheric turbulence effect on quality of star images based on telescopic observations of stars shows pronounced correlation 02 p0261 A67-11989

Oscillations in turbulence angle in observations of quality of star images, considering role of synoptic front 02 p0261 A67-11990

Turbulent energy dissipation rates, eddy, fluxes of sensible heat, momentum and kinetic energy measured above nonhomogeneous surface 02 p0238 A67-12076

Project Prairie Grass diffusion experiments analyzed to determine Hay-Pasquill scale factor relating Lagrangian and Eulerian turbulence scales 02 p0262 A67-12082

B-52 structural response to random turbulence with various stability augmentation systems, noting rigid body motions, normal vibration modes and control surface rotations [AIAA PAPER 66-998] 02 p0181 A67-12302

Computer simulation for turbulence/upset studies on jet transports, emphasizing time dependency and nonlinear aerodynamics [AIAA PAPER 66-1002] 02 p0181 A67-12304

Aircraft bumpiness conditions in free atmosphere relation to turbulence and other aerological data 02 p0263 A67-12647

Load factor estimation for flights in turbulent conditions by replacing exact transfer function with equivalent statistical model 03 p0351 A67-12997

Antenna aperture size effect on tropospheric phase-of-arrival fluctuations determined by theoretical considerations of atmospheric turbulence 03 p0385 A67-13864

Energy spectrums, mean and eddy kinetic energies of atmosphere between surface and 50 km 03 p0463 A67-13930

Statistical distribution of AM laser signal envelope upon passage through turbulent atmosphere 03 p0438 A67-13988

Closed loop gust response control system, considering airframe loading, local accelerations, turbulence, structural mode, damping, etc [AIAA PAPER 66-997] 03 p0362 A67-14146

Power spectral density /PSD/ methods applied to prediction of aircraft responses to continuous turbulence [AIAA PAPER 66-1000] 03 p0362 A67-14147

Convective vortex over horizontal surface caused by nonuniform heating 04 p0612 A67-14652

Atmospheric turbulence compared with associated radar echoes, noting correlation coefficient for standard deviation of derived gust velocity with maximum radar reflectivity 04 p0649 A67-14687

Transfer functions and statistical properties of SST in atmospheric turbulence 04 p0620 A67-14893

Upper atmospheric measurements based on radiolocational observation of meteor trains 05 p0796 A67-16211

Rocket sounding of unpredictable geophysical disturbances, preparations, countdown procedure and difficulties encountered 05 p0904 A67-16295

Motion of cosmic radiation source effect on frequency spectrum of amplitude and phase fluctuations in turbulent atmosphere 05 p0761 A67-16344

Fluctuations of angle of incoming light waves from distributed source in atmosphere with turbulent pulsations of refractive index 05 p0761 A67-16346

Parameters of small scale turbulence in diabatic atmospheric surface layer, examining structure characteristics of temperature and vertical velocity field components 05 p0837 A67-16487

High altitude atmospheric turbulence effects on Reynolds number and vertical drift velocity gradients of M zone 05 p0799 A67-17030

Observational techniques and detection of solar turbulence by local Doppler shifts of Fraunhofer lines 05 p0899 A67-17069

Parametric fluctuations of spatially restricted light beam in turbulent atmosphere 05 p0766 A67-17229

Upper atmospheric turbulence and wind measurement by radio reflection from meteor tail 05 p0802 A67-17382

Laser applicability to line-of-sight atmospheric turbulence parameters 05 p0839 A67-17383

Air density gradient effect on longitudinal aircraft motion 06 p0944 A67-17625

Physical model of turbulence used in developing forecasting scheme of clear air turbulence /CAT/ over mountains [AIAA PAPER 67-184] 06 p1026 A67-18298

Atmospheric turbulence effects on statistical design and analysis of space vehicles [AIAA PAPER 67-134] 06 p1096 A67-18359

Multiple scattering of light in turbulent atmosphere noting relation to refraction index and power spectra, using Born series solution to wave equation 06 p1033 A67-18536

Log amplitude covariance for horizontal and nonhorizontal propagation path of plane wave through turbulent atmosphere, noting refractive index effect 06 p1033 A67-18537

Angular power pattern for circular aperture receiving plane wave perturbed by passage through turbulent atmosphere 06 p1033 A67-18538

Diffusion and transport equation for turbulent atmosphere with variously heated air masses 06 p0999 A67-18740

Atmospheric turbulence with attention to philosophy and measurement results 07 p1219 A67-19335

Soviet book on aeronautical meteorology noting atmospheric conditions, clouds, ice formation, flight data utilization, Soviet Civil Aviation services, etc 07 p1220 A67-19579

Signal to noise ratio of optical-heterodyne detection system as affected by atmospheric distortion of optical wave front 07 p1144 A67-19786

Internal turbulence scale for convection jets determined, using measurements of light intensity fluctuations 07 p1220 A67-20003

Doppler radar measurements of wind velocity horizontal components variation in rain and snow, calculating time correlation and structural functions for neutral and unstable stratifications 07 p1221 A67-20004

Cloudstreet formation by wind induced vorticity forces equal to buoyancy forces, noting Rayleigh number variation 08 p1350 A67-20951

Optimal gain settings for atmospheric turbulence in 407 atmosphere wind profiles [AIAA PAPER 66-484] 08 p1413 A67-21509

Spatial coherence measurement in 3.2 mm horizontal transmission, considering amplitude and phase fluctuations received in two spaced antennas 09 p1461 A67-21599

Average power patterns for various values of rms phase difference for points separated by aperture radius in turbulent atmosphere 09 p1462 A67-21610

Atmospheric turbulence determined from

coherence deterioration of laser beam 09 p1511 A67-21825

Clear air turbulence problems including forecasting inadequacy, detection device requirements, categories, etc 09 p1526 A67-22390

Relationship between statistics of log amplitude and irradiance fluctuations due to atmospheric turbulence used to estimate effect of aperture in collecting scintillating light 10 p1603 A67-22711

Covariance of log amplitude fluctuations for propagation of spherical wave in turbulent medium over horizontal path to obtain phase structure function 10 p1678 A67-22712

Optical effects of thermal structure in lower atmosphere 10 p1679 A67-22745

Upper air turbulence gusts, describing vertical component test method using F type radiosonde 10 p1676 A67-23085

Rocket observation of upper atmospheric winds noting wind shear, velocity, pressure, wind vector rotation, etc 10 p1638 A67-23198

Variation of inner scale of turbulence in upper atmosphere with height studied from density variations of alkaline clouds ejected by rockets 10 p1638 A67-23201

Lower thermospheric turbulence investigated for scale size, turbulent velocity spectra and energy dissipation rate 10 p1643 A67-23250

Reduction in directivity and increase in main lobe width of linear antenna due to turbulent troposphere 10 p1607 A67-23442

Turbulent transfer in diabatic conditions, deriving formulas for wind and temperature profiles 10 p1677 A67-23574

Unsteady aerodynamic forces and dynamic response of flexible aircraft structure to continuous turbulence in supersonic flight 10 p1595 A67-23736

Atmospheric turbulence statistical characteristics dependence on stratification and elevation from heat flux and wind friction stress 11 p1815 A67-23954

Spectral characteristics of turbulence in presence of mean velocity and temperature gradients 11 p1815 A67-23955

Laser beam modulation by atmospheric turbulence as function of receiving aperture size, range and atmospheric conditions 11 p1799 A67-24236

Restoration of digitized turbulence-degraded images by corrective processing of harmonic representation according to measured optical transfer function 11 p1789 A67-24414

Atmosphere effects on laser beam propagation noting diameter, intensity amplitude and power dependence on transmitter and receiver aperture dimensions 11 p1801 A67-24665

Electrostatic motor action in rotational momentum of tornado funnels, noting that driving power removal by electric discharge may cause dissipation 12 p1963 A67-25383

Nature of middle latitude ionospheric perturbations 12 p1932 A67-25543

Anomalous high diffusion coefficients determined from dispersion of chemical contaminant releases and long lasting meteor trails at various altitudes 12 p1935 A67-25792

Internal scale measurements of atmospheric turbulence in 80 to 100 km altitude using alkaline clouds produced by ejecting sodium metal and trimethyl aluminum from rocket 12 p1935 A67-25793

Vertical component of gusts in upper atmosphere estimated from rotation rate of ascending radioprobe fan 12 p1964 A67-26165

Spectrum and scales of upper atmospheric turbulence determined by photographic tracking 13 p2108 A67-26314

Parameters of small scale turbulence in diabatic atmospheric surface layer, examining structure characteristics of temperature and vertical velocity field components 13 p2150 A67-26343

Turbulent atmosphere load effect on gliders noting influence of piloting techniques 13 p2052 A67-26484

Diurnal, annual and seasonal variations of high altitude turbulent motions in upper atmosphere through observation of meteor trails by coherent pulse method 13 p2110 A67-26506

Orographic factors effect on stratospheric pressure field, obtaining ascending vortical fluxes and heat input equations, discussing

refractive index for atmospheric perturbations 13 p2112 A67-26672

Transfer of large scale tropospheric perturbations into stratosphere analyzed using hydrodynamic model, noting role of atmospheric stratification, refractive index, etc 13 p2112 A67-26674

Vertical gust components in altocumulus clouds measured by airborne instruments 13 p2152 A67-26741

Medical/human factors affecting pilots during atmospheric turbulence 13 p2064 A67-27262

Upper atmospheric turbulence velocity probability density investigated in 90 to 110 km region 14 p2346 A67-28058

Turbulent spectral density of radio refractive index in surface layer of atmosphere 14 p2262 A67-28379

Tropospheric turbulence and structure derived from phenomenon of electromagnetic wave propagation 14 p2264 A67-28397

Soviet atmospheric turbulence studies considering microstructure, wave propagation in turbulent atmosphere, turbulent exchange in atmospheric ground layers, etc 14 p2346 A67-28763

Microwaves and laser links for spacecraft-earth communications noting limitations by external noise effects, atmospheric turbulence, fabrication tolerances, etc 14 p2273 A67-28799

Compatibility of some spectral functions with Heisenberg theory in axisymmetric turbulence and in equilibrium range [ONERA-TP-461] 15 p2470 A67-29381

Aircraft flutter testing using free-air turbulence as exciter 16 p2764 A67-30861

Polarization and angle of arrival fluctuations for plane wave propagated through turbulent medium 16 p2625 A67-31344

Turbulence in upper atmosphere possibly due to density fluctuations accompanying internal gravity waves 17 p2843 A67-32538

Power spectral density /PSD/ methods applied to prediction of aircraft responses to continuous turbulence [AIAA PAPER 66-1000] 17 p2797 A67-32582

Aircraft mounted recording accelerometers for excessive turbulence compared with direct turbulence measurement 17 p2798 A67-32700

Simultaneous ejection of two vapor trails of different atomic mass, examining turbopause phenomena of atmospheric turbulence 17 p2853 A67-33254

Time resolved measurements of phase fluctuations of coherent beam at emergence from turbulent layer 17 p2817 A67-33304

Dynamical structure of lower ionosphere obtained by studying atomic structure of sodium clouds 18 p3033 A67-33589

Linear least squares filtering of distorted images, stressing turbulent atmosphere effect 18 p3047 A67-33882

Directional fluctuations in light waves propagating from edge of solar disk caused by atmospheric turbulence 18 p3080 A67-34436

Light intensity fluctuations along inclined inhomogeneous path with variable turbulence characteristics in lower atmospheric layer 18 p3080 A67-34437

Structural design for gust loads on USAF aircraft based on continuous turbulence and failure probabilities 18 p2986 A67-34653

Power spectra and dissipation rate for vertical velocity fluctuations measured with sonic anemometers 19 p3251 A67-35056

Summit areas of severe storms, measuring stratospheric-tropospheric interchange, air flow and hydrometeors 19 p3252 A67-35057

Temperature convection and vertical velocity fluctuations measured and compared with similarity theory of free convection and laboratory heated plates experiments 19 p3252 A67-35059

Soviet book on wave propagation in turbulent atmosphere covering geometric optics of electromagnetic and acoustic wave scattering and propagation, etc 19 p3182 A67-35206

Cyclogenesis due to baroclinic instability in zonal and meridional basic current showing relationship by superimposing perturbation 19 p3252 A67-35528

Lateral-directional flying qualities for power landing approach simulated, studying roll effects and damping

[AIAA PAPER 67-577] 19 p3175 A67-35972
Planetary spectra improvement by Fourier spectroscopy, discussing modulation method reduction of atmospheric turbulence effects and fast transmission system 20 p3438 A67-36345
Sodium cloud between 85 and 110 km shows turbulent phenomena stratification exists and disappears with upward propagation of movements due to energy decreases 20 p3427 A67-36367
Atmospheric turbulence and diffusion, detailing turbulent energy and thermal variance budgets measurements, parallel plate convection, air pollution, etc 20 p3480 A67-36898
Scintillation of ground-to-space laser beam through atmospheric turbulence 20 p3383 A67-37023
Maximum likelihood method used as criterion in processing optical images propagated through turbulent atmosphere 21 p3586 A67-38954
Vertical distribution of mechanical wave energy density in lower atmosphere and energy fraction escaping to high altitudes derived by integral transform methods 21 p3655 A67-39088
Atmospheric humidity effect on lower atmospheric layer turbulence above oceans, discussing velocity, temperature and humidity profile calculation formulas 22 p3828 A67-39220
Low altitude atmospheric turbulence analysis methods 22 p3828 A67-39665
Rapid temperature increase due to lower photosphere turbulence generation of mechanical waves, discussing gravity wave generation and acoustic noise 23 p4068 A67-41280
Statistical radiative transfer in turbulent atmosphere underlying region 23 p4068 A67-41281
Thunderstorms endanger air traffic and travel, considering turbulence, ice formation, hail and lightning 23 p4025 A67-41303
Length of supersonic core of axisymmetric jet exhausting into quiescent atmosphere 23 p3992 A67-41739
Mountain wave and air turbulence program using high altitude research aircraft measurements and stressing CAT 24 p4181 A67-42275
Barium fluoride film electric hygrometer element aging and possible causes of calibration drift with time in storage 24 p4156 A67-42380
Aperture usage for random optical communication channel through turbulent atmosphere 24 p4124 A67-42814

ATMOSPHERICS

SA STATIC ELECTRICITY
SA SUDDEN ENHANCEMENT OF ATMOSPHERICS /SEA/
SA WHISTLER
Characteristics of normal atmospherics, discussing VLF characteristics due to return strokes 01 p0109 A67-11228
Bit and message error rate dependence on variation of atmospheric noise statistical properties 02 p0203 A67-12165
Relation between sidelobe level and radar performance in clutter for nonresolvable difference between target and clutter Doppler 03 p0369 A67-13680
Theoretical curves for day and night time conditions for variation of peak frequency of radio atmospherics with distance computed from source spectrum and dominant propagation mode 03 p0415 A67-14117
Automatic radar system for low level target detection, obtaining Doppler resolution and eliminating fixed atmospheric noise 04 p0573 A67-15043
Sunrise effect on atmospheric radio noise intensity, directional variations and formation of D region 04 p0618 A67-15575
Scheme reducing decoding failures due to atmospheric noise in coherent-phase-shift-keyed data transmissions by ground wave 05 p0767 A67-17523
ELF and VLF wave propagation in earth-ionosphere waveguide at wide frequency range, giving amplitude spectra and mean phase velocity for day and night 06 p0994 A67-17970
VLF atmospherics noise level fluctuations, discussing daily variations as function of solar zenithal angles, sunrise and sunset and confusion of ionospheric propagation 07 p1171 A67-19422

VLF transmission loss calculated from spectral components of atmospherics arriving from within adjustable azimuthal direction 09 p1464 A67-22442
Long period fading of VLF atmospherics, attributing origin to ionospheric propagation characteristics induced by geomagnetic activity 11 p1785 A67-23947
Diurnal cyclic intensity variations of atmospheric radio noise at stations widely spaced over globe 13 p2111 A67-26571
Crossing rates of atmospheric radio noise in high range of threshold field strength measured and compared with integrated field strength 14 p2306 A67-27881
Higher harmonic components of tweeks as evidence of adequacy of waveguide mode theory of VLF propagation between earth and ionosphere 14 p2307 A67-27888
Whistler observations near Sofia and in Czechoslovakia 14 p2307 A67-27914
Radio whistlers occurrence relationship to solar and magnetic activities at various latitudes 14 p2265 A67-28413
VLF noise emissions originating in ionosphere and magnetosphere with reference to ground-based, rocket and satellite observations 14 p2265 A67-28414
Atmospheric noise properties possible influence on communication, measuring intensities and short term amplitude functions 14 p2266 A67-28416
Magnetic tape simultaneous recording of radio atmospherics from broadband receivers and from waveform photographs, computing Fourier phase and pulse amplitude spectra 16 p2629 A67-31508
Atmospheric modulation noise in optical heterodyne receiver, deriving signal power variance and mean-square frequency spread from propagation statistics for wave structure function 16 p2630 A67-31807
Atmospheric noise data for various frequencies and various latitudes and longitudes 16 p2632 A67-31861
Time statistics for reliable transmission of binary data in presence of atmospheric noise burst 17 p2811 A67-32113
Frequency amplitude spectra of atmospherics from multiple stroke lightning, showing shift to VLF 20 p3480 A67-36290
Smith gyrofrequency model for determination of vertical electron concentration distribution in magnetosphere, using whistling atmospherics data 21 p3821 A67-39022
Noise model for simulating tropospheric turbulence effects on radio guidance and tracking range and angular measurements for optimum filter synthesis 21 p3587 A67-39147
ELF waveforms spectral estimation at discrete frequencies of each polarity used for statistical comparison of mean spectra show normal distribution 22 p3789 A67-39474
Distant atmospherics waveform at night analyzed using digital computer for VLF phase spectra 24 p4149 A67-42068

ATOM

SA HELIUM ATOM
SA HYDROGEN ATOM
SA INTERSTITIAL ATOM
SA ION
SA METASTABLE ATOM
SA NITROGEN ATOM
SA OXYGEN ATOM
Methods for calculating interaction potentials of atoms, molecules and ions 03 p0473 A67-13613
Maxwellian and delta distribution models of reflected atoms in terms of mass, momentum and energy 05 p0749 A67-17109
Methods for calculating interaction potentials of atoms, molecules and ions 18 p3083 A67-34478
Linear/nonlinear molecule optical properties obtainable from light scattering in gas by strong optical field 20 p3488 A67-36437
ATOM CONCENTRATION
Three-body and wall recombination coefficients of atomic nitrogen, using electron spin resonance spectrometer for concentration measurements 01 p0117 A67-10883
Influence of polarized atoms diffusion on spatial distribution of optically oriented atoms 03 p0437 A67-13388
Chemiluminescence of upper atmospheric Ni and rocket probe measurement of Ni

atom concentration at night 07 p1182 A67-19951
Free sodium atom distribution in upper atmosphere related to diurnal and nocturnal variation 10 p1645 A67-23262
Radical concentrations and decays in lean hydrogen-nitrogen-oxygen flames 13 p2221 A67-26261
Chemiluminescent reactions of atomic oxygen with carbonyl sulfide and hydrogen sulfide in flow system as function of reaction time and reactant concentrations 14 p2260 A67-28781
Equilibrium deviation occurring in plasma with variable kinetic temperature due to radiation transport within plasma volume and outflow beyond limits of volume 16 p2723 A67-31767
Concentration ratios of cosmic ray-produced isotopes of helium, neon and argon measured and effective irradiation hardening parameter calculated 17 p2942 A67-32358
Helium and neon content and isotopic composition in iron meteorites, noting He 3 deficiency in hexahedrites due to tritium loss 17 p2942 A67-32359
Cesium vapor ionization on porous tungsten substrate creates gradients in surface atom concentrations diminishing ionization efficiency 20 p3487 A67-36170
Al impurity redistribution near Si semiconductor surface subjected to high temperature oxidation 22 p3857 A67-39502
Spectroscopic analysis of iron meteoroid radiation by emission growth curve method covering temperature factors and atom and electron concentrations 23 p4062 A67-40674
Li isotopic composition and abundance in chondrites and iron meteorites measured, noting implications for earth and meteoritic parent body formation 24 p4235 A67-42632
Stony meteorite Fe, Ni, Co, Ca, Cr and Mn concentration determined by X-ray fluorescence 24 p4235 A67-42638
ATOMIC BEAM
Amplitude and frequency characteristics of hydrogen-atom beam maser 02 p0251 A67-11574
High specific impulse thrust by sputter ejection of atoms from single crystals following ion bombardment, useful in space propulsion 02 p0306 A67-12716
Atomic beam source for metastable Ca atoms in measuring population numbers from absorption lines 09 p1534 A67-21564
Cesium plasma confinement time measured in Q device by observing plasma density decay after atomic beam shut off 11 p1835 A67-24385
Atomic beam resonance spectrophotometer used with solar telescope to observe solar line oscillation 11 p1861 A67-24494
Singly-ionized He measured for radiative lifetimes of various states using high energy atomic beam 13 p2160 A67-26880
Collimation of low density hypersonic jet from shock tube for atomic beam production, noting relation between beam intensity and velocity distribution 14 p2301 A67-28188
Absolute oscillator strengths of three titanium resonance lines from absorption measurements in atomic beam 14 p2351 A67-28581
Experimental determination of hydrogen atom beam density after focusing by hexapolar magnet 15 p2520 A67-29720
Atomic frequency standards, noting cesium and thallium atomic beam devices, H maser, rubidium gas cells, optical pumping, etc 17 p2860 A67-32601
Trapped plasma build-up in magnetic field by ionization of injected atomic beam, noting ionization cross section parameters 17 p2908 A67-33115
Thin self-supporting beryllium foils preparation for use as atomic and molecular ion beam targets 17 p2866 A67-33360
Resonance effect in low energy or low velocity Li-Hg total scattering cross section 18 p3082 A67-34031
Spectroscopic properties of ionic beam source, discussing particle densities, source purity, etc 19 p3231 A67-35682
Degree of ionization effect on yield of excited atoms from gas target 22 p3852 A67-39987
Ar atomic beam produced by plasma burner measured for kinetic energy and Mach number 24 p4198 A67-42576

ATOMIC CLOCK

Vertical hydrogen beam oscillator serving as atomic clock, noting design principle and operation 04 p0632 A67-14898

Radio measurement methods and standards, reviewing progress in atomic and quartz frequency standards, precision coaxial connectors, etc 05 p0804 A67-16008

Atomic clock design using beam method or optical pumping method to make transitions observable 07 p1186 A67-19527

Clock synchronization via communications satellite Relay II 09 p1494 A67-21617

Dual frequency VLF timing system for synchronization of remotely located clocks, noting WWVL radio carrier frequency, signal generator, etc 09 p1494 A67-21619

High stability clocks for trajectory measurement with oscillator, using atomic or molecular transitions [ONERA-TP-459] 10 p1655 A67-22880

Q parameter of hydrogen maser measurement by method of no clock structure modification and by inhomogeneous magnetic field method 11 p1802 A67-24754

Relativistic effect of atomic clocks, noting error- and magnitude increase with experiment duration 14 p2348 A67-27866

Global distribution of standard time by VLF for synchronization with microsecond accuracy 14 p2263 A67-28389

Trajectory systems, discussing atomic clock and laser based equipment design, operation and performance [ONERA-TP-446] 15 p2554 A67-29376

Atomic clock application for Universal Time determination, describing various corrective measures, atomic beam technique, etc 15 p2487 A67-29581

Atomic frequency standards based on rubidium gas cell approach, noting atomic clock types and applications 15 p2487 A67-29582

VLF worldwide comparison of atomic standards, noting statistical analysis of data and possible sources of error 16 p2632 A67-31860

Relative merits of atomic frequency standards, discussing limitations, future outlook and applications 17 p2860 A67-32602

Time signal transmission and reception, noting development of UHF spectroscopy and atomic frequency scales 18 p3004 A67-34400

Radio interferometry method using precision clocks for earth rotation period measurement 18 p3043 A67-34528

Upper limit of arc for hydroxyl /OH/ emission region associated with radio source W3, using Michelson interferometer consisting of two spaced radio telescope stations 20 p3523 A67-36648

Three geodetic measurement bases synchronized to within 100 microseconds by transporting atomic clock 23 p3997 A67-40573

Long term changes of earth RD length with respect to AD due to superposition of linear and alternating components 23 p3993 A67-40675

Irregular earth rotation velocity variation analyzed by comparing universal time with atomic time 24 p4150 A67-42312

ATOMIC COLLISION

SA MOLECULAR COLLISION

Impact expansions and interference patterns in atomic scattering theory for cases of forward scattering, backscatter, inversion problem and screened Coulomb potential approximation 01 p0112 A67-10143

Interaction between atoms of solid surface and gas phase, obtaining closed-form solution of motion equations 01 p0118 A67-11295

Interstellar molecule formation as result of chemical exchange reactions between atoms of interstellar gas and atoms chemically bound to interstellar grains 02 p0323 A67-11889

Ionization cross sections of neutral atoms caused by electron impact with Maxwellian velocity distribution 02 p0269 A67-12486

Role of amplification due to impacts of second kind in emission of nitrogen and CO molecular bands in mixture of nitrogen-argon and CO-Ar in glow discharge 02 p0270 A67-12674

Close-coupling calculation of resonant structure of scattering amplitude of excited-state atoms and molecules in continuum 03 p0471 A67-13221

Low energy electron-helium atom scattering, using formal optical potential in variational expression for scattering phase shifts 03 p0471 A67-13318

Electron scattering cross section of argon and atomic oxygen measured, using microwave interferometer for analysis of plasma produced in shock tube 03 p0472 A67-13320

Electron spectra in UV region noting excitation techniques, energy level mean lives and population distribution 03 p0472 A67-13324

Potassium atom reactive scattering from oriented methyl iodine molecules, determining variation of chemical reactivity over molecular surface 03 p0367 A67-13524

Hydrogen atom-molecule exchange reaction effect on transfer coefficients of dissociating mixture, noting anisotropy and collision integrals 03 p0473 A67-13608

Secondary scattering of low energy electrons by rows of atoms, obtaining diffraction pattern 03 p0496 A67-13648

Recoil ranges of products from reactions of Cu-65 with 11-35-mev He-3 ions 03 p0473 A67-13926

Effect of Doppler and impact line broadening of spectral characteristics of gas laser, noting standing monochromatic wave saturation 03 p0439 A67-14197

Charged particle collision as UV radiation source examined, using electron-excitation analytic cross section equations 04 p0660 A67-14698

Phase and amplitude fluctuation of gas and solid state lasers, accounting for noise caused by pumping, incoherent decay, lattice vibrations and atomic collisions 04 p0632 A67-14949

Ochkur and Rudge approximation for exchange in electron-atom collisions adapted for atom-atom collisions 06 p1034 A67-17649

Coherent radiation interaction with two-level atoms system in single mode approximation, obtaining equation for time dependent number of photon emission and absorption 06 p1012 A67-18804

Second virial coefficient for atomic gas with divergent potential energy curves 07 p1225 A67-19122

Interaction energy of single atom adsorption at any point on single crystal planes of bcc structure, using Lennard-Jones potential 08 p1355 A67-20719

Average diffusion cross section for elastic collisions of electrons with heavy particles, comparing calculated and measured values 09 p1534 A67-21864

Atomic collisions, excitation transfer processes and energy level transition probabilities in plasma of gas lasers 09 p1513 A67-22067

Modulated molecular beam apparatus with chopper used in conjunction with field emission microscope for studies of atomic interactions with surfaces 09 p1499 A67-22114

Ionization cross sections of neutral atoms caused by electron impact with Maxwellian velocity distribution 10 p1682 A67-23354

Excitation cross section of upper laser levels in ionized argon by electron collision with ground state neutral atoms measured, using incoherent light technique 10 p1665 A67-23382

Frequency redistribution function of noncoherently scattered radiation, noting effect on source functions of two-level atoms 11 p1823 A67-24490

Measuring atomic radiation and collision cross section coefficients of plasmas 11 p1839 A67-24551

Energy transfer during interaction of atoms with surface of ideal crystal in terms of classical mechanics 11 p1824 A67-24855

Three-dimensional hard spheres theory of gas atom scattering from solid surface noting velocity distribution, energy and momentum accommodation coefficients, etc 13 p2097 A67-26936

Gas atom scattering from solid surface, analyses and comparisons 13 p2097 A67-26937

Velocity dependence of total scattering cross sections for atom-atom collisions measured in high energy range 13 p2161 A67-27361

Autoionization effects accompanying impairment of forbidden intercombination transfer in plasma due to atom collision with plasma electron 13 p2171 A67-27626

Atomic collisions with negative ions,

deriving transition matrices for resonance reactions and scatterings to analyze rearrangement process of associative electron detachment 14 p2350 A67-28149

Effect of Doppler and impact line broadening of spectral characteristics of gas laser, noting standing monochromatic wave saturation 14 p2331 A67-28542

Asymptotic curve for single arbitrary reflection of atom from plane with weak surface roughness, calculating total momentum and energy fluxes 14 p2351 A67-28636

Nonstationary disturbance effect on electron producing bound s-state during slow collision of atoms 14 p2352 A67-29073

Particle energy distribution in low temperature nonequilibrium plasma in diffusion approximation description 16 p2720 A67-31386

Molecular nitrogen and oxygen ions colliding with atomic sodium examined in crossed-beam experiment for resonance charge transfers 16 p2705 A67-31758

Recharge cross section in collisions of slow atoms or ions involving interparticle transfer of one electron 16 p2705 A67-31781

Collision cross sections and energy scattering of atoms with slow electrons 17 p2893 A67-32137

Photoionization study of diatomic-ion formation in argon, krypton and xenon by collision process [AFRCL-66-785] 17 p2888 A67-32631

Coherent radiation interaction with two-level atoms system in single mode approximation, obtaining equation for time dependent number of photon emission and absorption 18 p3061 A67-34423

Hydrogen atom-molecule exchange reaction effect on transfer coefficients of dissociating mixture, noting anisotropy and collision integrals 18 p3083 A67-34471

Selective enhancement of molecular spectra of HD and diatomic deuterium in argon and krypton discharges 18 p3083 A67-34518

Counter traveling wave regime stability in ring gas laser, studying effects of atomic collisions, isotopic state and wave coupling 19 p3239 A67-34898

Interaction of three-dimensional model of gas with solid surface, discussing atomic velocity distribution from surface reflection, energy and momentum accommodation coefficients, etc 19 p3264 A67-34936

Atomic collision processes in ionized gases, studying ambipolar diffusion, electron attachment, electron-ion recombination and Penning ionization by afterglow technique 19 p3264 A67-35070

Initial ionization processes in shock heated argon consisting of atom-atom collisions followed by electron-atom processes 19 p3293 A67-35397

Electronic relaxation of shock-heated nonequilibrium argon plasma flow in microscopic-macroscopic treatment 19 p3298 A67-35745

Energy transfer during interaction of atoms with surface of ideal crystal in terms of classical mechanics 20 p3490 A67-37538

Temperature dependence of far IR collision-induced absorption as probe of rare gas mixtures interatomic potentials 20 p3490 A67-37567

Hyperfine splitting of spin interaction energy of two hydrogen atoms, determining eigenfunctions for effective Hamiltonian 21 p3658 A67-37814

Scaling law derived from small angle scattering theory, interpreting data in spectroscopic manner to deduce potentials and interactions between electronic states 22 p3839 A67-39205

Negative cyclotron resonance absorption due to electron elastic collisions with noble gas atoms, comparing results with kinetic plasma wave theory predictions 22 p3842 A67-40346

Optically pumped Rb in collisions with Kr inducing relaxation, noting two different correlation times due to kinetic collisions and metastable states present 23 p4012 A67-40792

Compound state resonances in atom/molecule collisions below first excitation threshold 23 p4029 A67-40959

Capture, ionization and ionization capture in collisions of protons with argon

- atoms 23 p4030 A67-41687
Optimization of high energy neutral particles source /Eolion/ measurements, noting application to atomic collisions problem 24 p4153 A67-41912
Atoms interaction with solid body surface, noting pair interaction law effect on characteristic energy accommodation coefficient and motion equation solution 24 p4190 A67-41938
Intermolecular forces theory, considering hydrogen atom interaction through Born-Oppenheimer approximation and variational calculations 24 p4191 A67-42666
[WIS-TCI-249] 24 p4191 A67-42666
Multiparticle mechanism of cosmic ray-atomic nuclei interactions assuming particle formation 24 p4218 A67-42842
Ionization cross section in slow atom collisions calculated by modified Franck-Condon principle 24 p4194 A67-42889
- ATOMIC ENERGY**
S NUCLEAR ENERGY
ATOMIC EXCITATION
Configurations of HF discharge plasma and dependence on gas pressure and annular electrode potential 01 p0122 A67-10348
Elementary processes in DC gas discharge plasma in helium, comparing measurements of population levels of excited states of atoms with calculated values 01 p0123 A67-10363
Inhomogeneity parameter for excited atom distributions and line width variations for dispersion contour of spectral line, noting dependency on frequency 01 p0125 A67-11045
Homogeneous transfer equation in line formation, noting correlation between thermalization length and line source function of two-level atom 02 p0266 A67-11698
Absolute excitation cross sections of helium levels colliding with low energy electrons 02 p0270 A67-12487
Electron excitation cross section of transitions between spin multiplets of ground state of neutral oxygen atom calculated, using continuous state Hartree-Fock formulation 03 p0472 A67-13322
CW He-Ne laser compared with mercury arc source, obtaining Raman spectra of carbon tetrachloride by three methods of excitation 03 p0438 A67-13912
Radial distribution of plasma formed in simple mirror machines by quantum effect field ionization of fast neutral atoms 04 p0671 A67-15644
Excited states in negative atomic oxygen ion, giving estimates of electron-atom interaction 04 p0661 A67-15764
Pulsed gas discharge lasers noting required energy level for maximum efficiency, experimental techniques and results 05 p0819 A67-16650
Elementary processes in DC gas discharge plasma in helium, comparing measurements of population levels of excited states of atoms with calculated values 06 p1038 A67-17621
Atomic energy levels in plasma, considering energy spectrum of hydrogen-like atom in plasma based on cut-off Coulomb potential model 06 p1039 A67-17881
Polarization and atom state distribution of excited atomic gas taking into account resonance excitation, using Boltzmann equation to determine line shape of electromagnetic wave absorption 06 p0991 A67-18799
Thermal excitation and de-excitation of alkali atoms in inert gas heat bath 07 p1265 A67-19075
Vainshtein method calculation of inelastic collision of electrons with atoms 07 p1225 A67-19207
Collisional excitation of Si ion from ground state to autoionization levels at coronal temperatures 07 p1256 A67-20168
Excitation cross section of states of Ne 2, Ar 2 and Kr 2 by electron collision 08 p1339 A67-21376
Excited atoms effect on nonequilibrium ionization of partially ionized plasma in direct energy conversion systems, using Klein effect 09 p1543 A67-21821
Calculation of effective excitation cross sections of hydrogen atoms for collisions with nitrogen molecules and hydrogen atoms 09 p1534 A67-21850
Collective oscillations of electron shells of atom, discussing energy, excitation and damping 09 p1534 A67-22004
Gas laser frequency and emitted power dependence on resonator 09 p1513 A67-22070
tuning 09 p1513 A67-22070
Flash spectroscopy apparatus with Q-switched ruby laser, discussing molecular electronic excitation 10 p1663 A67-22854
Spectrum of second order Raman lines in coupling of radiation and matter, using Green function 10 p1663 A67-22855
Absolute excitation cross sections of helium levels colliding with low energy electrons 10 p1682 A67-23355
Energetic metastable diatomic oxygen molecule excited by electron impact studied with high sensitivity molecular beam apparatus 10 p1682 A67-23386
Calculation of thermal excitation function and optimum temperature and pressure of atom and ion spectral line shift in two-component plasma 11 p1840 A67-24580
Auroral green lambda 5577 of oxygen atom analyzed from glow discharge emission, proposing excitation mechanism on basis of intensity variations 11 p1824 A67-24934
Configurations of HF discharge plasma and dependence on gas pressure and annular electrode potential 11 p1844 A67-25021
Rate equations for nonequilibrium excitation of neutral helium in plasmas of moderate density solved and compared with population densities 11 p1844 A67-25075
Absorption spectra and luminescence of p-type copper diffusion doped Ga-As crystals, noting appearance of temperature dependent narrow spectral lines 12 p1984 A67-25522
Density of energy levels in amorphous semiconductors induced by local fluctuations in atomic arrangement 13 p2172 A67-26353
Negative-ion gas laser with thermal excitation 13 p2125 A67-26386
Electron velocities distribution in plasma, studying boltzmann equation inelastic and superelastic collision operator, considering eigenfunctions and eigenvalues for electronic excitations and deexcitations 13 p2165 A67-26437
Position and width of lowest elastic scattering resonances in three-body atomic system, showing resonance shape dependence upon observation angle and angular resolution 14 p2351 A67-28152
Non-LTE line-transfer problem computational methods 14 p2351 A67-28994
Failure of conventional adiabatic criterion in case of excitation of helium atoms by helium ions 15 p2519 A67-29330
Characteristic enhancement of forbidden doublet in nitrogen excitation observed in night airglow during traveling ionospheric F region perturbation 15 p2474 A67-29479
Potentials occurring in excitation of highly ionized ions by electron impacts 15 p2520 A67-29527
Oscillations of confined cylindrical plasma with hot electron current, obtaining dispersion relation for large Debye radius 15 p2531 A67-30072
Semiconductor nonlinear polarizability at difference frequency calculated, considering exciton states alone and combined with band energy states 15 p2541 A67-30238
Plasma radiation analyzed by spectral line broadening theory as relaxation of excited atom, noting frequency dependent width and shift operators 15 p2532 A67-30380
Yield variation of excited hydrogen atoms formed by charge exchange with gas target thickness described by analytical model 16 p2714 A67-30874
Quasi-equilibrium number density of excited atoms and electronic transition rate in decaying optically-thick helium and hydrogen plasmas, considering Penning ionization 16 p2715 A67-31168
Transport coefficients calculated from adiabatic excitation transfer in atomic gases 16 p2661 A67-31222
Intrinsic optical excitation spectrum of crystalline solids for hole or electron localization, considering many-body relaxation effects influencing photoemission 16 p2732 A67-31698
Upper atmospheric nightglow emission intensity measured finding continuous excitation of oxygen atoms as energy reservoir 16 p2670 A67-31918
Probability of atomic excitation by electron bombardment 17 p2893 A67-32138
Bates theory of atomic oxygen excitation in upper atmosphere as cause of F layer nightglow emissions 18 p3038 A67-33616
Excitation and radiation of OH molecules and alkali metals in low pressure flames and rocket exhausts 18 p3152 A67-33819
Exact expression for line profile of stigmatic spectrograph without vignetting, noting results with foil-excited ions as light source 18 p3082 A67-33877
Radiation peak formation mechanism in spectral lines of nonequilibrium gas following passage of shock wave 18 p3083 A67-34060
Polarization and atom state distribution of excited atomic gas taking into account resonance excitation, using Boltzmann equation to determine line shape of electromagnetic wave absorption 18 p3029 A67-34418
Absorption spectra and luminescence of p-type copper diffusion doped Ga-As crystals, noting appearance of temperature dependent narrow spectral lines 18 p3103 A67-34453
Long range first order interaction between two excited hydrogen atoms yielding perturbation energy matrix, discussing diagonalization process 18 p3083 A67-34517
Secondary ionization processes in mercury vapor, calculating relative populations of excited and metastable atoms per ion pair 19 p3265 A67-35090
Excitation and ionization mechanisms in positive DC discharge columns in krypton and xenon 19 p3265 A67-35131
Multiple-photon ionization of atoms and molecules in strong varying electromagnetic field, measuring ionization probability dependence on field intensity 19 p3265 A67-35164
Ionizational relaxation and excitation behind shock waves, proposing solution for kinetic equation system 19 p3293 A67-35403
Excitation cross sections for protons incident on atomic hydrogen calculated by nonadiabatic method 20 p3491 A67-37686
S-matrix computations for quantum transitions, considering close coupling case of homonuclear diatomic molecular rotational excitation 21 p3659 A67-38005
Density of energy levels in amorphous semiconductors induced by local fluctuations in atomic arrangement 21 p3679 A67-38310
Zinc telluride laser generation by electron-beam excitation noting high threshold values 21 p3641 A67-38458
Negative-ion gas laser with thermal excitation 21 p3642 A67-38823
Excited nuclei electromagnetic de-excitation rate by inelastic scattering in stellar particles calculated as function of temperature, density, transition energy and multipole functions 21 p3660 A67-38846
Foil excitation technique used to measure 2p and 3p levels mean lifetime in He 2 cascading and agreement with theoretical value 22 p3840 A67-39206
Degree of ionization effect on yield of excited atoms from gas target 22 p3852 A67-39987
- ATOMIC EXPLOSION**
S NUCLEAR EXPLOSION
ATOMIC GAS
SA DIATOMIC GAS
SA MONATOMIC GAS
Autoionization effects in UV absorption spectra of hot atomic gases 03 p0471 A67-13222
Intergalactic atomic neutral hydrogen detection in emission in clusters of galaxy and in noncluster field 03 p0514 A67-14318
Polarization and atom state distribution of excited atomic gas taking into account resonance excitation, using Boltzmann equation to determine line shape of electromagnetic wave absorption 06 p0991 A67-18799
Second virial coefficient for atomic gas with divergent potential energy curves 07 p1225 A67-19122
Atmospheric mixing time and lifetime of atomic and molecular oxygen at high altitude, noting agreement with barometric distribution law, concentration pattern, etc 07 p1178 A67-19813
Continuous spectra of atomic gases and low temperature plasma, analyzing photoionization cross section and electron transitions in neutral atom field 10 p1682 A67-23067
Javelin rocket soundings with far UV scanning spectrometer, noting atomic hydrogen and oxygen

radiation 12 p1934 A67-25787
Atomic oxygen density profiles obtained from radiation intensity resulting from nitric oxide reaction 14 p2293 A67-28199
Transport coefficients calculated from adiabatic excitation transfer in atomic gases 16 p2661 A67-31222
Polarization and atom state distribution of excited atomic gas taking into account resonance excitation, using Boltzmann equation to determine line shape of electromagnetic wave absorption 18 p3029 A67-34418
Atomic Cs vapor experimental values for heat-transfer coefficient used to determine Cs atoms and molecules interaction potentials 24 p4253 A67-42211

ATOMIC PHYSICS

S NUCLEAR PHYSICS

ATOMIC RECOMBINATION

High resistivity silicon single crystals, discussing carrier lifetime, photoconductivity and recombination levels 02 p0297 A67-11832
Atomic interactions and space physics - Symposium, Goddard Space Flight Center, Greenbelt, Maryland, August 03 p0470 A67-13216
Nitrogen atoms recombination in fast flow system using photometry, determining atom concentration, noting nitrogen afterglow intensity 06 p0956 A67-18760
Oxygen atoms association and combination with nitrogen atoms, determining rate constants of reactions 06 p0956 A67-18761
Reaction rate kinetics of combination of H atoms with NO plus third body /M/ compared with H and O atoms plus M relative to argon 11 p1749 A67-24238
Motion and continuity equations for atomic and molecular oxygen density solved numerically as time dependent 16 p2664 A67-30975
Population of atomic levels by cascade, dielectric and three-body electronic recombination, discussing spontaneous transition, electron impact and RF spectra 17 p2947 A67-32762
Kinetics of coupled atomic recombination and vibrational de-excitation in continuously expanding gas flow 18 p3081 A67-33781
Mechanisms of atomic recombination at surfaces analyzed, considering behavior of insulators and semiconductor oxides 18 p2997 A67-33794
Atomic nitrogen-oxygen mixtures ion concentration enhancement in hydrocarbons presence, discussing atom recombination rate, etc 18 p3107 A67-33805

ATOMIC STRUCTURE

Nonlinear attenuation or gain characteristics of Doppler-broadened atomic resonance involving levels with small splittings, noting mode coupling of gas laser 01 p0087 A67-10152
Atomic planes and positions in bulk thinned specimens of crystalline Ge determined, using electron microscopy 03 p0501 A67-14345
Laser as source of optical Fourier analysis of atomic structure of crystals 05 p0824 A67-16921
Eigenvalues of five lowest lying states for three electron atomic systems obtained using conventional Rayleigh-Ritz variational method 07 p1226 A67-19500
Thermodynamic equilibrium composition of Venus atmosphere computed from atomic composition deduced 07 p1256 A67-20022
Electronic band structure calculations phase of Ca, Sr and Ba over wide range of atomic volumes under pressure electronic band structure calculations for fcc phase of Ca, Sr and Ba over wide range of 10 p1682 A67-23399
Lifetime of atomic state against decay induced by lepton coupling, estimating neutrino power radiation and astrophysical implications 11 p1821 A67-23959
Low temperature deposition of amorphous films of transition metals and alloys, noting atomic arrangement, comparing with case of metals condensed in crystalline state 12 p1982 A67-25451
Low temperature deuteron irradiation effect on type II superconductors noting atomic displacement, resistivity increase and transition temperature decrease 12 p1985 A67-25845
Mechanism for bounding quarks to atomic systems of low molecular

weight 13 p2109 A67-26330
Laser as source of optical Fourier transforms in analysis of atomic structure of crystals 14 p2330 A67-28261
Values of rigidity coefficient and space occupied by vacancy compared for deformed nickel samples 17 p2874 A67-32897
Dynamical structure of lower ionosphere obtained by studying atomic structure of sodium clouds 18 p3033 A67-33589
Integration scheme for variational r sub ij wave functions containing unlinked four-electron correlated terms for atoms up to neon 18 p3082 A67-34026
Distribution coefficients for impurities in gallium and indium arsenides as periodic function of atomic weight decreasing with increasing atomic number 18 p3102 A67-34289
Indium arsenide-tellurium ternary compounds chemical bond, microhardness and structure 20 p3506 A67-36226
Ground state hyperfine splitting of singly charged helium calculations by Zwanzger and Sternhelm evaluated by examining error corrections by Fortson et al 20 p3488 A67-36694
Molybdenum interband transitions noting low energy optical property anomalies and origin of two absorption bands 20 p3466 A67-36865
Book on plasticity theory and application to solidity, discussing inelastic deformation, crystal physics, atomic grid structure mechanics, etc 21 p3716 A67-37966
Quadratic Stark effect in argon II calculated assuming LS coupling 21 p3659 A67-38408

ATOMIZATION

SA AEROSOL

SA LIQUID ATOMIZATION

Flame-sprayed ceramic coating in space technology, examining solid atomization or Rokide process 06 p1021 A67-18764
Average heat of atomization in correlating composition and temperature limits of stability of NaCl type structure among IV-VI compound semiconductors 13 p2184 A67-27570

ATP

S ADENOSINE TRIPHOSPHATE /ATP/

ATS

S APPLICATIONS TECHNOLOGY

SATELLITE /ATS/

ATTACK AIRCRAFT

Flight and operational suitability testing of XC-142 V/STOL assault transport [AIAA PAPER 67-261] 07 p1130 A67-20074
Boundary layer control for improvement of lift at lower angles of attack by carrier-based supersonic aircraft [AIAA PAPER 65-751] 09 p1441 A67-22484
Design criteria for VTOL tactical aircraft power plant using turbojets for attack aircraft in support of land troops 23 p4049 A67-41044

ATTENUATION

S ABSORPTION

S ACOUSTIC ATTENUATION

S ATMOSPHERIC ATTENUATION

S FADING

S MICROWAVE ATTENUATION

S NOISE ATTENUATION

S RADAR ATTENUATION

S RADIO ATTENUATION

S SHOCK WAVE ATTENUATION

S WAVE ATTENUATION

ATTENUATION COEFFICIENT

Fringe effects in plane induction MHD machine compared for different methods of determination 01 p0012 A67-10191
Aerosol measurements using light scattering from searchlight probing, noting attenuation coefficient as function of altitude [AFRL-67-0003] 02 p0238 A67-12048
Amplifying elements ensuring required dynamic properties of resolving amplifier without calculating entire amplifier circuitry 10 p1611 A67-22983
Attenuation constant of model helix waveguide determined using approximate method, considering electromagnetic leakage due to wall irregularity 10 p1606 A67-23064
Anomalous IR attenuation in fast neutron irradiated GaAs and CdTe arises through scattering and absorption by highly conducting spike zones 11 p1850 A67-24910
Relation between attenuation coefficients of oriented and diffusive light fluxes in turbid media for arbitrary light scattering levels 13 p2151 A67-26686
Crossing rates of atmospheric radio noise

in high range of threshold field strength measured and compared with integrated field strength 14 p2306 A67-27881
Theory of pure type II superconductors in high magnetic fields, calculating ultrasonic attenuation coefficient 14 p2370 A67-28721
Attenuation cross section and refractive index using collision theory, calculating resonance profiles of autoionizing lines based on scattering theory 14 p2351 A67-28811
Acoustic wave attenuation coefficients for small gap superconductors, noting electromagnetic absorption and collisional drag as cause 16 p2729 A67-31059
Multiple light scattering in inhomogeneous spherically symmetrical planetary atmosphere with exponentially varying attenuation coefficient 16 p2698 A67-31096
Attenuation rates at vlf from aircraft measurements presented as curves of dominant waveguide mode vs. geomagnetic bearing of propagation path 16 p2631 A67-31854
Lower atmosphere nucleonic component measurement, noting attenuation coefficient dependence on atmospheric depth 17 p2842 A67-32364
E/k/-relation for complex insulator band structure, explaining polarity effect on tunneling through asymmetric barrier 20 p3508 A67-36425
Variation method of microwave diagnostics of homogeneous plasma based on attenuation coefficient measurements, determining collision frequency and plasma density 21 p3675 A67-39032
Acoustic ion waves phase velocity and attenuation constant measurements verify predicted dependence on ion mass, with attenuation due to ion-neutral collisions 21 p3675 A67-39054
Attenuation of continuous and pulsed laser emission studied for various thicknesses of artificial water fog 22 p3816 A67-39921
Stratospheric attenuation measurements in near UV during rocket flight compared with values computed for dust free atmosphere 23 p3993 A67-40677
Siegman maximum signal theorem for coherent scattering detection, estimating attenuation through scattering medium 23 p3973 A67-40835
Frequency dependence of attenuation coefficient for longitudinal ultrasonic waves in InSb over range 50 to 210 MHz for temperatures between 200 and 600 degrees K 24 p4202 A67-41980

ATTENUATOR
Microwave attenuation standard derived using waveguide below critical frequency as voltage divider to determine losses in components 13 p2067 A67-26488
RF attenuation measurement methods and standards 17 p2815 A67-32607

ATTITUDE
SA PITCH ATTITUDE
SA SATELLITE ATTITUDE
DISTURBANCE
SA YAW ATTITUDE
Steady and unsteady aerodynamic coefficients determined by free flight analysis of trajectory and attitude variations in supersonic wind tunnel 05 p0748 A67-16765

ATTITUDE CONTROL
SA FLIGHT CONTROL
SA HORIZON SENSING
SA REACTION JET ATTITUDE CONTROL TECHNIQUE
SA ROLL CONTROL
SA SATELLITE ATTITUDE CONTROL
Maneuvering propulsion problems for spacecraft attitude control 01 p0142 A67-11401
Spacecraft attitude control using rotation about single inertially fixed axis to change vehicle orientation 01 p0157 A67-11445
Inertia stabilized attitude control system for space vehicle, noting selection of compensating network parameters 02 p0331 A67-12160
Operator reorientation of attitude of simulated remote maneuvering unit /RMU/ using on-off acceleration command control system 02 p0186 A67-12230
Flywheel-augmented gravity gradient stabilization /FLAGGS/ 02 p0333 A67-12312
Influence on stability of masses which are in relative motion with respect to projectile determined, noting engine thrust effect on attitude control system

performance 03 p0517 A67-13027
 Low weather minima flight control system consisting of autopilot, flight system and gyromagnetic compass 03 p0466 A67-14385
 Optical system consisting of polarized laser beams for monitoring missile attitude during early launch phase 04 p0619 A67-14505
 Kaufman type electron bombardment ion source with 2.5 cm diameter for satellite low thrust attitude control system 04 p0554 A67-15018
 Ion thrust motors used to overcome solar-lunar attraction, earth triaxiality, solar pressure and other forces tending to perturb satellite orbit or modify orientation 04 p0705 A67-15027
 IR horizon sensor systems for spacecraft attitude determination, detailing field switched edge tracker 04 p0625 A67-15664
 ESRO II satellite project, describing systems and program management 05 p0905 A67-16728
 Stabilite system, three-axis attitude control system utilizing single reaction wheel 06 p1094 A67-17681
 Research and operational results obtained with nonaerodynamic variable stability flying platform for examining problem associated with lunar landing 06 p0948 A67-18202
 Structural compliance induced cross axis coupling effect on gimballing system stability of rocket engine two-axis attitude TVC system [AIAA PAPER 67-42] 06 p1097 A67-18448
 Diamant mechanical subsystems and programmer 07 p1258 A67-19524
 Time optimal position and velocity control of spinning vehicle with reaction jet [AAS PAPER 66-115] 07 p1259 A67-19974
 Free flying lunar landing research vehicle tested for more than two years and used in lunar landing simulations supporting Apollo project [AIAA PAPER 67-238] 07 p1129 A67-20044
 Flight attitude control problems of manned lunar landing vehicles emphasizing pitch control [AIAA PAPER 67-239] 07 p1129 A67-20045
 Controlled booster stage BER for sounding rockets to reduce dispersion of impact points at low acceleration [ONERA-TP-442] 08 p1404 A67-20495
 Spinning rocket attitude control technique including theory, system mechanization and performance 08 p1409 A67-20539
 Gyroless Solar Pointing Aerobee Rocket Control System /SPARCS/ using no inertial platform and having solid state circuitry 08 p1409 A67-20540
 Passive attitude control using gravity torques, solar torques and spin stabilization 08 p1410 A67-20622
 Thermal design of attitude translational control assembly /ACTA/ of lunar excursion module /LEM/ 08 p1303 A67-21062
 Two-impulse torquing scheme for reorienting spin axis of asymmetric spinning vehicle 08 p1413 A67-21510
 Ion thruster, including mercury feed system and shielded neutralizer, designed and tested for spacecraft station keeping and attitude control [AIAA PAPER 66-247] 10 p1698 A67-23120
 Simulation results of adaptive tracking filter application to stabilization of structural bending modes of SI-B launch vehicle 13 p2212 A67-26818
 Fluid flight control systems, discussing attitude and angular rate stabilization systems 14 p2248 A67-28273
 Remote maneuvering unit control during satellite inspection in simulated conditions 14 p2258 A67-28669
 Control moment gyro as attitude control actuator for spacecraft, noting advantages over other momentum transfer systems 15 p2486 A67-29307
 Attitude stabilization and control system for rotationally symmetric gyroscopic body with two degrees of freedom 15 p2490 A67-30156
 Rotating spacecraft attitude changes due to energy dissipation from angular deformation treated by modal method 15 p2572 A67-30201
 Development, design and test operation of attitude control system of space probe with mission duration of 7 minutes [ONERA-TP-271] 16 p2758 A67-30653
 Air-bearing facility for Lunar Orbiter attitude control system testing minimizing

external disturbances in platform, platform mass deflection and room thermal currents 16 p2655 A67-31260
 Second order discontinuous attitude control system using fixed impulse, determining average number of switchings before escape from vertical switch line 16 p2762 A67-31640
 Maintainability system operating parallel with cruise-mode spacecraft attitude-control system, noting application to Ranger III spacecraft 16 p2763 A67-31646
 Attitude control for orbiting astronomical observatories, noting system design and performance characteristics 16 p2763 A67-31689
 LEM-CSM analysis, elastic bending and propellant sloshing 17 p2955 A67-32478
 Design and performance characteristics of electrothermal microthruster systems for spacecraft functions [AIAA PAPER 67-423] 18 p2988 A67-33907
 Exhaust gases effect on satellites optical equipment calculated by determining propane attitude-control jet gas flow parameters 18 p3137 A67-34359
 Mathematical model of rigid, long space-body spinning at constant rate about symmetry axis for optimal attitude control calculations 19 p3331 A67-34777
 Flight control system of Saturn V launch vehicle, discussing attitude/rate scheme, gain required and stability achieved 19 p3331 A67-34808
 Pointing control system /PCS/ for Apollo Telescope Mount /ATM/ for solar observations [AIAA PAPER 67-534] 19 p3334 A67-35936
 Jet attitude control system analysis when subjected to external disturbing torques [AIAA PAPER 67-537] 19 p3174 A67-35939
 Singular optimal control and attitude problem in rocket guidance [AIAA PAPER 67-582] 19 p3258 A67-35977
 Controlled booster stage BER for sounding rockets to reduce dispersion of impact points at low acceleration 21 p3712 A67-37802
 Z-transform and W-transform theory applied to dynamic compensation of linear sampled data control systems for attitude control of large booster 21 p3713 A67-38027
 Thrust, power and performance requirements for synchronous satellite simulated for evaluating ion propulsion feasibility [AIAA PAPER 67-720] 21 p3694 A67-38746
 Motion simulator with spherical self-regulating gas bearing for testing attitude control, analyzing turbine and tilting momentum 22 p3778 A67-39165
 Europa I third stage attitude control system design, discussing various model configurations and overall simulation 22 p3897 A67-39171
 Acquisition phase of satellite with passive magnetic attitude stabilization, discussing programming difficulties and modified Rayleigh model for German 625A-1 satellite 22 p3898 A67-39173
 Quasi-optimum three-axis attitude control law for minimum time of rigid body, noting gyroscopic cross axis coupling 22 p3899 A67-39190
 Variational calculus for optimal attitude acquisition/stabilization controller synthesis for spinning and nonspinning space vehicles 22 p3904 A67-40105
 Orbital attitude reference system working model using strapped down principles and digital computer 22 p3907 A67-40187
 Cross coupling effects in strapdown orbital gyrocompass to determine attitude of vehicle with respect to planet-centered coordinate system 22 p3801 A67-40188
 Gyroless Solar Pointing Aerobee Rocket Control System /SPARCS/ using no inertial platform and having solid state circuitry 24 p4242 A67-42905
 Structural compliance induced cross axis coupling effect on gimballing system stability of rocket engine two-axis attitude TVC system [AIAA PAPER 67-42] 24 p4242 A67-42909
ATTITUDE GYRO
 Strap-down guidance systems using conventional inertial hardware, discussing computer function, computer selection and system errors 03 p0466 A67-13364
 Control moment gyro as attitude control actuator for spacecraft, noting advantages over other momentum transfer

systems 15 p2486 A67-29307
 Hardware characteristics of control moment gyro /CMG/, determining nonlinearity effects on performance by simulation 17 p2853 A67-31995
 Satellite orientation sensing and orbital gyrocompassing heading reference, examining effect of horizon sensor noise [AIAA PAPER 67-587] 19 p3258 A67-35983
 Control moment gyro /CMG/ and use in space-vehicle attitude-control system, emphasizing control laws [AIAA PAPER 67-589] 19 p3336 A67-35985
ATTITUDE INDICATOR
 Strap-down inertial navigation system compared with gimbaled system, noting methods of attitude reference and angular readout 01 p0110 A67-10489
 Approximate method of computing attitude of sounding rockets from magnetometer data 03 p0519 A67-13782
 Spacecraft attitude sensor types, principles and future development 03 p0465 A67-14100
 HF flight attitude indicator and forward and backward counting radio interferometer operating without rotating goniometer and phase locked oscillators 04 p0619 A67-14533
 Skylark rocket attitude in free space determined from solar and magnetic sensor data used in least squares method 08 p1406 A67-20508
 Attitude determination and hydrogen peroxide control system for spacecraft orientation in Syncom, Early Bird and ATS [AIAA PAPER 67-532] 19 p3334 A67-35934
 Examination of ability of man to determine drift angle of spacecraft with optical sight [AIAA PAPER 67-624] 19 p3337 A67-36013
ATTRITION
 Airlsickness early in flight training indicates high levels of anxiety and attrition potentials and poor prognosis 23 p3963 A67-41544
AUDIO EQUIPMENT
 Tape recorder for routine auditory screening of civil aviation personnel and criticism of whispered voice auditory test 18 p2993 A67-34725
 Electronic system for measuring operator information retrieval in bisensory configuration, using video-record radar set and playback 20 p3419 A67-37639
AUDIOFREQUENCY
SA SOUND WAVE
 Audio frequency proportional to rotation rate of reentrant laser cavity system derived from single output beam 01 p0091 A67-11322
 Theoretical curves for day and night time conditions for variation of peak frequency of radio atmospherics with distance computed from source spectrum and dominant propagation mode 03 p0415 A67-14117
 Direct digital display with high precision for audio frequencies 05 p0865 A67-16944
 Audiofrequency ILS /phase II/ used with VHF generator to check ILS instruments 11 p1745 A67-24554
 Monolithic circuits for RF communications systems 14 p2282 A67-28027
 Frequency modulated transmitter and receiver for audio high speed data transmission including discriminator for analyzing and distinguishing waveforms 20 p3379 A67-36247
AUDIOLOGY
 Tape recorder for routine auditory screening of civil aviation personnel and criticism of whispered voice auditory test 18 p2993 A67-34725
AUDITORY FATIGUE
 Central factor influence in pure tone induced auditory fatigue while performing threshold tracking or other mental activity 21 p3576 A67-39060
AUDITORY PERCEPTION
 Large scale experiment on aircraft noise involving 148 subjects listening to sounds of aircraft flying overhead 04 p0552 A67-15576
 Human response to comparative sounds from aircraft and objective measurement of reference sound, determining acceptable noise levels 09 p1456 A67-21940
 Signal duration effect on detection in presence of masking noise by human auditory system, using electric analogy for testing purposes 12 p1903 A67-26126
 Simultaneous primary and secondary voice message monitoring, discussing methods and experimental setup 15 p2431 A67-29895

Tape recorder for routine auditory screening of civil aviation personnel and criticism of whispered voice auditory test 18 p2993 A67-34725

Diffusion model of perceptual memory process when observer compares two consecutive stimuli, noting visual and auditory discrimination 21 p3576 A67-39097

Recall of two messages of equal word number presented with words of one message sequentially alternating with other 22 p3754 A67-39587

Speech audiometry for hearing loss examinations of middle aged pilots 22 p3753 A67-40545

Proactive inhibition, recency and limited channel capacity under acoustic stress 24 p4116 A67-42701

AUDITORY SIGNAL

S PSYCHOACOUSTICS

AUDITORY STIMULUS

SA NOISE

Model of speech perception against noise background, hypothesizing that acoustic stimuli are mapped in segments 05 p0763 A67-16706

Electric stimulation of crossed olivocochlear cats and effect on auditory nerve responses 08 p1287 A67-20483

Evoked brain response to clicks as measure of vigilance tested in work-rest schedule and pressure suit-sleep experiments on man 09 p1452 A67-21721

Sensory input overload effects on performance of civil aviation pilots during simulated instrument flights in Link AN 2550-1 trainer 09 p1455 A67-21726

Properties of favorable coding schemes, applying results to text transmission through auditory and tactile senses 12 p1907 A67-26081

Noise and vibration effect on human mental work capacity with increasing time limitation indicating efficiency reduction 16 p2614 A67-30917

Peripheral auditory system model relating all-or-none activity of nerve fibers to acoustic stimulation 17 p2806 A67-32044

Influence on hits and false alarms of response and signal events on preceding trial 20 p3372 A67-36962

AUDITORY TASK

Auditory vigilance task, assessing effects on performance of signal detection value, miss or false detection cost and set size from which signals were drawn 14 p2258 A67-28664

Diffusion model of perceptual memory process when observer compares two consecutive stimuli, noting visual and auditory discrimination 21 p3576 A67-39097

Speech audiometry for hearing loss examinations of middle aged pilots 22 p3753 A67-40545

AURORA

SA AIRGLOW

SA POLAR AURORA

SA RADIO AURORA

Auroral occurrence rate at zenith as function of latitude for magnetically quiet and magnetically disturbed periods 07 p1178 A67-19817

Physics of aurora as magnetospheric and cosmic phenomena 10 p1633 A67-22986

Flux, energy spectrum and angular anisotropy of auroral electrons analyzed from space vehicle 16 p2670 A67-30648

Aurora and airglow - NATO Conference, Keele University, England, August 1966 18 p3031 A67-33578

Airglow and auroral phenomena, discussing ideal coordinate system, electric fields, morphology, solar wind-magnetosphere interactions, and particle precipitation 18 p3039 A67-33625

AURORAL ABSORPTION

Rocket measurement of proton energy spectra and pitch angle distribution associated with auroral radio absorption, using solid state surface barrier detector 01 p0061 A67-11261

Effects of AZA and PCA on radio wave propagation in Antarctic, noting reliability and radiation power requirements 07 p1143 A67-19692

Radio wave absorption at high latitudes dependent on frequency, noting AZA and PCA are inversely proportional to powers of frequency 07 p1144 A67-19693

Auroral absorption of cosmic radio radiation recorded by shipboard station

drifting in North Geographic Pole region in winter 1963-64 07 p1178 A67-19824

Geomagnetic disturbance and correlation with PCA in auroral zone on February 10, 1958 08 p1329 A67-21539

Magnetospheric tail bursts of energetic electrons identified with auroral zone radiowave absorption 16 p2666 A67-31410

Short-period oscillations of auroral cosmic noise absorption 16 p2669 A67-31910

Radio wave absorption associated with auroras 18 p3038 A67-33619

High latitude disturbances influence on VLF propagation, showing high correlation with auroral absorption 18 p3004 A67-34426

Auroral absorption events, discussing bremsstrahlung X-rays spectrum, electron densities and temperatures measured with rockets 19 p3312 A67-35188

AURORAL ACTIVITY

Auroral region disturbances generating atmospheric waves in F layer that produce atmospheric mixing 01 p0056 A67-10112

Latitudinal effect and universal time effect on diurnal variations in auroral activity 02 p0236 A67-11664

Northern Hemisphere synoptic auroral charts on polar projection 02 p0238 A67-12035

Interchange of field lines between closed region of magnetosphere and open tail, explaining features of auroral breakup and geomagnetic bays 03 p0410 A67-12955

Geomagnetic and auroral storms provide information on interaction of solar plasma flows and magnetosphere 04 p0618 A67-15668

Nighttime magnetospheric auroral VLF hiss generation by suprathermal particle associated with coherent electron plasma radio emission 04 p0618 A67-15686

Auroral hydrogen emission measurements and indications of proton or electron excitations 05 p0797 A67-16851

Aurora and ring current theory confirming role of hydromagnetic plasma flow and frozen-in field lines in geomagnetic storms 06 p0995 A67-17973

Auroral radio blackout correlation with magnetic dip pole motion 07 p1173 A67-19669

Main phase of geomagnetic storms and magnetic and auroral substorms development by analyzing individual geomagnetic storms 07 p1183 A67-20016

Geomagnetic, auroral, ionospheric and cosmic ray perturbations interdependence and relationship with solar activity 07 p1183 A67-20174

Dayside geomagnetic field disturbances in auroral oval monitored by satellite in polar orbit at 1100 km 08 p1329 A67-21487

IGY and IQSY auroral observations at Murmansk of frequency of occurrence of polar auroras in years of solar activity maxima and minima 10 p1630 A67-22787

Auroral brightness variations related to magnetic field fluctuations, especially to pearl type fluctuations 10 p1632 A67-22811

East-West motion of auroras analyzed in Idaho using radar echoes, noting velocity, direction reversal, etc 10 p1651 A67-23344

Atmospheric electricity conditions at ground level independent from auroras and potential gradients 11 p1857 A67-25031

Correlated study of auroral luminosity at different wavelengths, auroral X-rays, geomagnetic micropulsation and ionosphere 12 p1937 A67-25834

Frequency spectrum of Pi 2 micropulsation activity and relation to planetary magnetic activity 13 p2109 A67-26327

Catalog of German polar aurora observations from 1882 to 1956 13 p2109 A67-26431

Coordinated experiments on auroras to understand particle-atmosphere interaction, emphasizing aircraft phase of measurement 13 p2115 A67-27256

Phase diagrams of elementary auroral disturbance and restoration on earth daylight side 14 p2309 A67-27941

Photometric auroral observations and geomagnetic field fluctuation magnetograms compared, noting relation between geomagnetic and auroral pulsations 14 p2309 A67-27944

Early appearance of active aurora during geomagnetic storm caused by westward traveling surges along expanded oval 14 p2313 A67-28575

Rocket soundings of electron angular distributions during auroral substorms,

noting effects of anisotropy, intensity variations, etc 15 p2473 A67-29187

Geomagnetic pulsations and auroral activity, using magnetosphere simplified model 15 p2474 A67-29505

Multichannel photometer for space applications requiring low weight and power, no moving parts and high sensitivity divided in four electrically and optically distinct quadrants 15 p2491 A67-30433

Latitudinal effect and universal time effect on diurnal variations in auroral activity 16 p2665 A67-31079

Auroral intensity ratio of green line of atomic oxygen and first negative band of nitrogen, showing rise in electron temperature above neutral particle temperature 16 p2666 A67-31413

Auroral arc orientations determination and attempt to verify ionospheric currents flow along auroral arc during display 16 p2667 A67-31511

Infrasonic waves from auroral and magnetic activity, origin in supersonic movement of large scale auroral forms 17 p2841 A67-32209

Magnetosphere and auroral phenomena including Van Allen radiation zones, satellite telemetry, solar wind fluctuations and cyclotron resonance 17 p2844 A67-32664

Pulsations in electron intensities in postbreakup aurora, noting possibility of distant processes affecting electrons 17 p2844 A67-32765

ULF radio emission properties determination and relation to other geophysical phenomena, noting experimental equipment and correlation with auroral activity 17 p2846 A67-32938

February 11, 1958 aurora observation during IGY, determining specific aurora features by all-sky camera and spectrographic techniques 17 p2849 A67-32964

Ashen light and magnetic field of Venus 17 p2948 A67-33096

Auroral particle precipitation, establishing latitude vs time pattern from gross statistical data on optical-and radio-auroral phenomena 17 p2850 A67-33191

Aurora Borealis and airglow history, discussing sunspot cycle influence, theories concerning origin, etc 18 p3032 A67-33579

Auroras and airglows in relation to ionospheric phenomena 18 p3033 A67-33584

Cinematographic observations of fast auroral variations 18 p3033 A67-33587

Auroral particle fluxes and effects from coordinated satellite-, aircraft- and ground-based measurements 18 p3034 A67-33590

Auroral oval between outer boundary of trapping region and ionosphere and dynamical and atomic interactions between magnetospheric plasma and neutral atmosphere 18 p3035 A67-33597

Static electric fields produced in magnetosphere and effects such as motion of visual and radio aurora and currents in ionosphere 18 p3035 A67-33600

Magnetic activity effect on position and characteristics of proton precipitation zone in aurora observed from Canada, noting temperatures and measurement method used 18 p3037 A67-33612

Balloon measurements of auroral X-rays, discussing flux and energy spectrum variations and bursts relation to magnetic storms 18 p3038 A67-33613

Auroral and polar magnetic substorms related to magnetic field lines reconnection in magnetosphere tail 18 p3117 A67-33615

Influence of aurora on radio wave propagation 18 p3038 A67-33617

Ionospheric observations of thick layer structure accompanying auroral activity, emphasizing ionization profiles, electric fields, aurora generation and global distribution 18 p3039 A67-33620

Polar auroral substorms, discussing mechanisms for dumping trapped particles 19 p3215 A67-35173

Optical auroral pulsations in various frequency ranges analyzed using automatic zenith photometer 19 p3222 A67-35459

IQSY program in U.S.S.R. /1964-1966/ including meteorology, aurora studies, solar activity, etc 19 p3223 A67-35482

Canadian program for IQSY including aurora studies, solar observation, space research, etc 19 p3224 A67-35498

Aurora events of July 1958 attributed to

solar flare from study of solar and geomagnetic data 19 p3225 A67-35618

Traveling-ionospheric disturbances observed at midlatitudes by backscattering technique, noting auroral zone and gravity waves role 20 p3425 A67-36280

Evening auroral activity characterized by westward traveling surges occurring not within auroral zone 20 p3426 A67-36291

VLF radio noise during auroral display studied by ground and rocketborne receivers, suggesting emissions triggered by high energy electron fluxes 20 p3428 A67-36374

Correlation of north-south component of telluric currents and brightness fluctuations in quiet form auroras 20 p3431 A67-36994

Auroral breakup relation to ring current interchange instability, studying dispersion relation effects 20 p3431 A67-37096

Irregular pulsations of diminishing periods /IPDP/, discussing cause and low energy electron flux variations 20 p3431 A67-37097

Auroral substorms, examining energy spectrum and flux of precipitating particles and morphology 20 p3431 A67-37100

Solar emissions and magnetic storms and auroras, discussing ring current, solar flux and Van Allen belt energetic particle density 21 p3620 A67-38978

Intense negative bays occurring inside evening and midnight sectors of auroral zone during polar magnetic substorms 22 p3789 A67-39477

Isolated irregularities in auroral ionosphere studied by analyzing radio signals from rockets and Beacon satellite 22 p3760 A67-39627

Auroras /ordinary and type with forbidden emission of atomic oxygen/, examining wind-aurora relation 22 p3790 A67-39675

All-sky camera data used to construct isoauroral diagrams for IQSY period describing incidence of auroral forms and behavior pattern 22 p3791 A67-39806

Azimuths of extended auroral features measured on all-sky photography during IQSY, discussing arc alignments and auroral oval 22 p3791 A67-39807

Polarizations of Pc 1 micropulsations intermittently recorded in Alaska with analysis of data for presence of right and left hand waves 22 p3793 A67-40078

Mean solar activity curves for 11-year and 80-year cycles from 1698 to 1964 reveal significant difference between two cycles 22 p3889 A67-40303

Auroral proton precipitation and hydrogen emissions 23 p3993 A67-40564

Optical instrumentation for auroral and afterglow studies with applications of grating spectroscopic systems, monochromators, interferometers and photometers 23 p3996 A67-41256

Auroral zone phenomena analyzed using rocketborne counters 23 p3997 A67-41333

IGY and IQSY auroral observations at Murmansk of frequency of occurrence of polar auroras in years of solar activity maxima and minima 24 p4149 A67-42123

Auroral brightness variations related to magnetic field fluctuations, especially to pearl type fluctuations 24 p4150 A67-42148

AURORAL ARC

Auroral arc orientations determination and attempt to verify ionospheric currents flow along auroral arc during display 16 p2667 A67-31511

Curves in polar plot representing auroral arcs over polar region organized in geomagnetic coordinate system and corrected by spherical harmonic terms 17 p2850 A67-33189

Statistical study of Carl Stormer height measurements of Aurora Borealis 18 p3033 A67-33588

Interpretation of multiple structure of auroral arc 18 p3035 A67-33598

Azimuths of extended auroral features measured on all-sky photography during IQSY, discussing arc alignments and auroral oval 22 p3791 A67-39807

Satellite and ground based measurements of incident proton neutral hydrogen flux and Balmer alpha optical emission in auroral hydrogen arc 23 p3995 A67-40803

AURORAL BOMBARDMENT

Auroral excitation of atomic oxygen forbidden lines, giving photon emission rate vs zenith angle 20 p3426 A67-36301

AURORAL ECHO

Oblique echo presence during winter nights on auroral and subauroral latitudes ionograms, analyzing electron number density of nighttime F region in midlatitude trough vicinity 03 p0409 A67-12947

Statistical analysis of auroral radar echoes reveals changes in shape of diurnal variation curve with level of magnetic disturbance and seasonal variation with peaks at equinoxes 03 p0513 A67-14112

Magnetospheric ion density measurement possibility from association of pulsating radio auroral echoes with sudden geomagnetic field fluctuations 14 p2313 A67-28574

Hydromagnetic mechanism explaining pulsating radio auroral echoes accompanying sudden commencements, considering Wentzel resonant interaction 17 p2845 A67-32766

Wavelength dependence and aspect sensitivity of radar auroral echoes show Booker field-aligned scattering model inadequate 20 p3433 A67-37411

Auroral ionization echoes observed simultaneously by separated VHF radar noting aspect sensitivity, time variation, correlation with visible aurora, etc 22 p3760 A67-39624

AURORAL ELECTROJET

Charge separation mechanism of auroral electrojets, noting enhanced ionospheric conductivity by electron bombardment 07 p1245 A67-19931

Polar magnetic substorms noting flux tube flow, proposing structure for substorm current system [JPL-TR-32-1094] 11 p1784 A67-23928

Frequency spectrum of Pi 2 micropulsation activity and relation to planetary magnetic activity 13 p2109 A67-26327

Origin of afternoon VHF radar echo from backscattering layer near auroral electrojet explained by plasma instability and perpendicular electric fields 16 p2627 A67-31407

Auroral oval between outer boundary of trapping region and ionosphere and dynamical and atomic interactions between magnetospheric plasma and neutral atmosphere 18 p3035 A67-33597

Intense negative bays occurring in auroral zone in early evening hours explained by westward extension of polar electrojet 20 p3426 A67-36285

Auroral zone diurnal tidal effect studied by high resolution spectrum analysis, noting large diurnal conductivity variation giving rise to lunar auroral electrojet 20 p3521 A67-36298

Pi micropulsation subtypes, one related to charged particles impulsive bursts from magnetospheric tail and another related to auroral electrojet 20 p3433 A67-37414

AURORAL EMISSION

Red shift of magnetic zenith hydrogen line profiles and role of injection pitch-angle distribution of auroral protons 03 p0409 A67-12943

Monograph on rocket experiments for studies of D region ion concentration and emission from released chemicals in twilight and aurora 03 p0412 A67-13366

Ion concentration in D region, describing wind tunnel experiments to determine electrode configuration for Gerdien condenser rocket probe 03 p0412 A67-13367

Emission from sodium trail released from rocketborne vaporizer in height range 85 to 165 km during aurora of brightness IBC II 03 p0412 A67-13372

Intensity of sodium D-lines and auroral nitrogen band produced by sodium trail in aurora measured by calibrated photometer 03 p0412 A67-13373

Artificial shock wave from TNT explosion in aurora, in attempt to determine effects on auroral emission and temperature 03 p0413 A67-13374

Rocket payload with weight of 9 lb for release of sodium and lithium in aurora for study of D-region ion concentration and emission 03 p0413 A67-13375

Cameras used in auroral and airglow experiments including SP3 spectrophotometer, three-channel photometer and all-sky camera 03 p0419 A67-13376

Solar radiation effect on planetary

atmosphere noting charged particle bombardment, dayglow phenomena, auroral emission, etc 04 p0696 A67-14699

Aurora photometry and stratospheric cosmic ray intensity, noting electron intrusion and correlation between aurora intensity and X-ray emission 05 p0879 A67-16102

Auroral hydrogen line emission quenching by collisional ionization 05 p0804 A67-17413

Pitch-angle distribution and differential energy spectrum of polar aurora protons penetrating earth 07 p1173 A67-19700

Vertical and horizontal variations of intensities of auroral OI and molecular nitrogen ion emissions 08 p1328 A67-21480

Strong geomagnetic disturbances distribution in space and time analyzed for correlation of magnetic activity with auroral brightness 10 p1632 A67-22809

Energy spectrum of primary electron flux and brightness of auroral light measured by rockets in active auroras used to derive electron production rate 10 p1650 A67-23306

Excitation and photon emission rates of auroral nitrogen first and second positive group 10 p1650 A67-23338

Auroral green lambda 5577 of oxygen atom analyzed from glow discharge emission, proposing excitation mechanism on basis of intensity variations 11 p1824 A67-24934

Channel multiplier instrument measuring low energy electron and proton auroral fluxes from polar orbiting satellites 12 p1944 A67-25855

Initial energy spectrum and flux of low energy protons responsible for luminescence of H in auroras 13 p2110 A67-26542

Spatial distribution of auroral radio signal reflection centers based on radar observations 13 p2111 A67-26566

Polar auroras statistically analyzed for relation between frequency of redness, solar activity and geomagnetic conditions 13 p2116 A67-27394

Magnetosphere rotation problem in presence of solar wind analyzed for auroral particle acceleration, noting perturbing field of induced electric current 14 p2307 A67-27917

Flux, energy spectrum and angular anisotropy of auroral electrons analyzed from space vehicle 16 p2670 A67-30648

Artificial red aurora created in southern conjugate region by atmospheric nuclear burst 16 p2664 A67-30977

Emission time history for red 6300 angstrom atmospheric emission from atomic oxygen produced by nuclear explosion 16 p2664 A67-30978

Volume emission profile vs height of positively ionized nitrogen molecule first negative band at 4278 angstroms 16 p2666 A67-31408

Drift azimuths, sizes and displacements of spatial inhomogeneities in oxygen atom emission at 5577 angstroms during night airglow 17 p2848 A67-32952

Vibrational temperature determined from relative populations of upper oscillation levels of auroras indicates latitude independence 17 p2849 A67-32963

Distribution of auroras during magnetically quiet and disturbed periods related to magnetosphere shape 17 p2849 A67-32965

Power spectrum of pulsating aurora measured at HF, noting relation to modulation mechanism in flux of primary particles 17 p2850 A67-33193

Perspective and path length effects on determination of spatial distribution of auroral luminosity from optical observations 17 p2851 A67-33206

Optical observations of daytime aurorae by means of atomic-oxygen-emission interferometry 17 p2852 A67-33212

Auroral radar echo association with aurora, noting connection with two-stream plasma instability 17 p2852 A67-33244

Auroral rocket measurements of electron densities, ionization rates, particle energy fluxes, energy spectra, pitch angle distribution, etc 18 p3034 A67-33592

Auroral position, motion and brightness measurements from high altitude nuclear tests in 1962 18 p3036 A67-33603

Afterglows from atmospheric nuclear detonations related to natural airglow and aurora 18 p3036 A67-33604

High latitude night sky emissions observed

by photographic spectrography, examining oxygen, nitrogen and hydrogen
 18 p3037 A67-33610
 VLF emission associated with aurora and particle precipitation, describing receiving equipment, types of emission and occurrence patterns
 18 p3039 A67-33621
 Enhanced VLF emissions near and south of auroral zone, discussing properties, geomagnetic disturbances, riometer absorption, time interval, polarity, etc
 18 p3039 A67-33622
 Rocket optical studies of daylight day-time auroras, discussing luminosity-height data of emission lines
 19 p3214 A67-35168
 Auroral transition radiation calculated from electron impact
 20 p3433 A67-37420
 Infrasonic wave anisotropic radiation from moving auroras analyzed using shock wave model, discussing sound propagation and ray tracing
 24 p4147 A67-41882
 Strong geomagnetic disturbances distribution and time analyzed for correlation of magnetic activity with auroral brightness
 24 p4150 A67-42146
 Auroral photometry and stratospheric cosmic ray intensity, noting electron intrusion and correlation between aurora intensity and X-ray
 24 p4213 A67-42778
AURORAL IONIZATION
 Dissociative recombination rate of auroral ionization
 02 p0236 A67-11661
 Magnetometer predictions of geomagnetic disturbances and intense sporadic E layer occurrences at various sunspot cycle times in auroral zone and effects on VHF absorption
 03 p0415 A67-14118
 Ionization structure of polar auroras from spatial distribution of radar-reflecting zones, taking into account magnetic field variations
 07 p1174 A67-19710
 High latitude increase in ionization of F layer correlating in space and time with auroral precipitation as shown by ionospheric electron number density data
 08 p1328 A67-21481
 Auroral brightness variations related to magnetic field fluctuations, especially to pearl type fluctuations
 10 p1632 A67-22811
 Electron and ion densities and temperatures measured by rockets in active auroras and correlated with directly measured ionizing flux
 10 p1650 A67-23307
 Dissociative recombination rate of auroral ionization
 16 p2665 A67-31076
 Spectrum and excitation mechanisms in aurora, discussing variations, excitation, ionization, hydrogen lines and temperature measurement
 18 p3032 A67-33582
 Auroral backscatter theory and relationship to instability concepts
 18 p3038 A67-33618
 Ionospheric observations of thick layer structure accompanying auroral activity, emphasizing ionization profiles, electric fields, aurora generation and global distribution
 18 p3039 A67-33620
 Auroral ionization echoes observed simultaneously by separated VHF radar noting aspect sensitivity, time variation, correlation with visible aurora, etc
 22 p3760 A67-39624
 Auroral brightness variations related to magnetic field fluctuations, especially to pearl type fluctuations
 24 p4150 A67-42148
AURORAL SPECTROSCOPY
 Rocket measurement of proton energy spectra and pitch angle distribution associated with auroral radio absorption, using solid state surface barrier detector
 01 p0061 A67-11261
 Auroral spectrograph data, 1959
 02 p0238 A67-12036
 Artificial sodium cloud in twilight produced by French rocket studied, using auroral spectrophotometer and cameras
 03 p0412 A67-13370
 Rocket measurement of secondary electron energy distribution in aurora, employing 180 degree electrostatic deflection analyzer
 03 p0418 A67-14357
 Image orthicon TV system and application to auroral observations, noting data acquisition mechanism
 06 p0993 A67-17563
 Electron flux measurement during visible aurora, using high resolution rocketborne spectrometer
 09 p1491 A67-20222
 Classification of auroras according to type and spectra variability, discussing mechanisms involved
 10 p1633 A67-22869

Auroral X radiation, measured by balloon-installed X-ray spectrometer incorporating scintillation counter with high speed analyzer, correlated with ionospheric radioelectric absorption and solar magnetic field variations
 10 p1702 A67-23304
 Diurnal variation of primary auroral electrons, average energy spectrum of 20-150 kev X-rays and time dependence of intensity and morphology
 10 p1702 A67-23305
 Satellite measurement of low energy electrons and protons in auroral regions, discussing use of instruments with variable energy electrostatic thresholds and postacceleration techniques
 12 p1944 A67-25851
 High luminosity spectrograph using inverse Wadsworth mounting constructed for recording auroral spectra in far UV
 14 p2315 A67-28157
 Energy spectrum and pitch-angle distribution of protons in auroras based on H-beta line profiles
 17 p2938 A67-32962
 Ionospheric observations of thick layer structure accompanying auroral activity, emphasizing ionization profiles, electric fields, aurora generation and global distribution
 18 p3039 A67-33620
 Fabry-Perot spectrometer applied to upper atmospheric emission measurements of airglow and aurora
 20 p3440 A67-36362
AURORAL TEMPERATURE
 Auroral intensity ratio of green line of atomic oxygen and first negative band of nitrogen, showing rise in electron temperature above neutral particle temperature
 16 p2666 A67-31413
 Vibrational temperature determined from relative populations of upper oscillation levels of auroras indicates latitude independence
 17 p2849 A67-32963
 Magnetic activity effect on position and characteristics of proton precipitation zone in aurora observed from Canada, noting temperatures and measurement method used
 18 p3037 A67-33612
AURORAL ZONE
 Position of oval zone of polar aurora on earth nocturnal side on magnetically quiet days
 02 p0236 A67-11663
 Transverse magnetic disturbances at high altitudes in auroral region observed with magnetically oriented satellite
 03 p0409 A67-12944
 400-kev electrons precipitation in auroral zone measured with solid state detector mounted on polar satellite
 03 p0410 A67-12952
 Characteristics of relativistic electron precipitation events in and near auroral zone during day and night
 03 p0410 A67-12957
 Latitudinal and diurnal variation of ionospheric electron content in auroral zone proximity
 [RASSA PAPER 1-10-126] 03 p0416 A67-14237
 Energetic electron precipitation and 5 to 40 second geomagnetic micropulsations relation to auroral substorms
 04 p0615 A67-14968
 Space and time characteristics of electron fluxes penetrating into terrestrial atmosphere in auroral zone, based on riometer measurements
 05 p0879 A67-16101
 Meteoritic dust particle effect on steady state distribution of electrons and ions in lower ionosphere, deriving expression for recombination coefficient from auroral radio absorption data
 06 p0995 A67-18074
 Stormer height measurements of aurora, analyzing height distribution at various geomagnetic latitudes, noting relation to solar activity
 06 p0997 A67-18694
 Corpuscular intrusions into earth magnetosphere involving entire auroral zone and occurring only on night side
 07 p1174 A67-19713
 Auroral zone position changes as function of magnetic activity and time of day
 07 p1178 A67-19816
 Diurnal and seasonal variations of sporadic layer in auroral zone
 07 p1178 A67-19823
 IMP-I satellite measurements of neutral sheet in geomagnetic tail noting dimensions, motion and parameters of sheet
 07 p1244 A67-19922
 Spatial and temporal characteristics of bremsstrahlung X-ray due to energetic electron precipitation in auroral zone, noting measurement techniques
 07 p1180 A67-19929
 Satellite measurement of low energy proton precipitation in auroral zone during

magnetically quiet period 07 p1245 A67-19930
 Criteria for determination of statistical aurora during IQSY, noting relation to magnetic activity
 07 p1180 A67-19932
 Ion temperature profiles obtained from satellite measurements of dawn-dusk auroral zone orbits
 08 p1329 A67-21482
 Vector electric field and particle intensity measurements from sounding rocket launched into visible aurora
 08 p1329 A67-21486
 Auroral oval properties from magnetic data, role in connecting visible auroras and related ionospheric disturbances to geophysical phenomena at high altitudes
 09 p1492 A67-22060
 Auroral zone irregularity correlated with perturbations in outer radiation belt, noting simultaneous displacement of boundary zone of perturbations
 10 p1699 A67-22784
 Boundary variations of auroral oval zones, noting dependence on magnetic perturbation intensity
 10 p1630 A67-22785
 Direct ionization and secondary excitation in proton auroras, noting magnitude of contribution by various processes
 11 p1784 A67-23927
 Balloon observations of large scale coherent pulsating electron precipitation events in auroral zone accompanied by geomagnetic continuous pulsations [AFOSR-67-1314]
 12 p1931 A67-25112
 Low energy proton precipitation measurements in austral and boreal auroral zones, using polar orbiting satellite
 12 p1937 A67-25813
 Molecular ion concentration around dawn-dusk auroral zone satellite orbit
 13 p2108 A67-26315
 Geomagnetic micropulsations and electron bremsstrahlung in northern auroral zone
 13 p2108 A67-26321
 Electron precipitation in conjugate regions of auroral zone latitudes examined via X-ray measurements with balloon-borne instrumentation
 13 p2115 A67-27255
 Auroral zone electron precipitation occurring in strong transient magnetic disturbances observed by bremsstrahlung
 14 p2310 A67-28056
 Early appearance of active aurora during geomagnetic storm caused by westward traveling surges along expanded oval
 14 p2313 A67-28575
 Recording and analysis of geomagnetic pulsations of auroral zone and comparison with bremsstrahlung measurement, using two-magnetometer arrangement
 15 p2474 A67-29524
 Statistics relating plasmopause position to three magnetic indices to clarify relationship between equatorial geocentric distance to plasmopause and worldwide magnetic activity level
 15 p2477 A67-29627
 Radio star Cassiopeia A scintillations and spread-F in auroral zone [AGARDOGRAPH 95]
 15 p2482 A67-30289
 Satellite scintillation in auroral zone depends on time of observation and on magnetic activity
 15 p2483 A67-30294
 Position of oval zone of polar aurora on earth nocturnal side on magnetically quiet days
 16 p2665 A67-31078
 Magnetospheric tail bursts of energetic electrons identified with auroral zone radiowave absorption
 16 p2666 A67-31410
 Pulsations in cosmic noise absorption of auroral zone, noting magnitude, shape and form of occurrence
 17 p2841 A67-32213
 Properties of slowly varying ionospheric absorption events in auroral zone analyzed using balloon soundings
 17 p2845 A67-32794
 Anomalous magnetic field charts for heights in ionosphere useful for studying auroras spatial distribution and sporadic E layer distribution
 17 p2847 A67-32948
 February 11, 1958 aurora observation during IGY, determining specific aurora features by all-sky camera and spectrographic techniques
 17 p2849 A67-32964
 Auroral belt dynamics including edge displacement rate, width, asymmetry of sides and relation to polar geomagnetic disturbances
 17 p2850 A67-33184
 Worldwide auroral morphology, discussing latitude and local time distribution and temporal variations
 18 p3032 A67-33581
 Geomagnetic time and latitude distribution of magnetic disturbances at auroral and polar cap latitudes
 18 p3032 A67-33583
 Statistical study of Carl Stormer height

measurements of Aurora
Borealis 18 p3033 A67-33588
Microburst precipitation of energetic
electrons into auroral
zone 18 p3035 A67-33596
Enhanced VLF emissions near and south
of auroral zone, discussing properties,
geomagnetic disturbances, riometer
absorption, time interval, polarity,
etc 18 p3039 A67-33622
Rocket observations of upper atmospheric
winds, electron density, electron
temperature, and neutral temperature in
auroral region with Langmuir
probes 19 p3214 A67-35169
Electron density and temperature
measurements using RF capacitance probe
and double Langmuir probe in auroral
zone 19 p3222 A67-35455
Classification of main data on morphology
and phenomenology of aurorae observed
visually and with all-sky cameras during
IGY 19 p3224 A67-35495
Intense negative bays occurring in auroral
zone in early evening hours explained by
westward extension of polar
electrojet 20 p3426 A67-36285
Evening auroral activity characterized by
westward travelling surges occurring not
within auroral zone
center 20 p3426 A67-36291
Abnormally early eastward auroral motion
appearance in evening and associated
magnetospheric plasma shell
motion 20 p3426 A67-36294
Auroral zone diurnal tidal effect studied
by high resolution spectrum analysis, noting
large diurnal conductivity variation giving
rise to lunar auroral
electrojet 20 p3521 A67-36298
Magnetic variations relationship to
magnetospheric perturbations, emphasizing
particle participation near auroral
zones 20 p3428 A67-36376
Particle trajectories for two model
configurations of electric and magnetic
fields in geomagnetic tail, noting application
to auroral acceleration 20 p3433 A67-37415
Evening sector polar magnetic substorm
disturbance field morphology in transition
region 21 p3616 A67-37998
F layer irregularities transverse scale
measurements by two-frequency scintillation-
ratio technique yielding 600-700 m scales in
auroral zone 22 p3789 A67-39470
Temporal periodicity of 10 cps observed in
flux of auroral electrons by rocketborne
radiation detectors 22 p3790 A67-39795
All-sky camera data used to construct
isauroral diagrams for IQSY period
describing incidence of auroral forms and
behavior pattern 22 p3791 A67-39806
Azimuths of extended auroral features
measured on all-sky photography during
IQSY, discussing arc alignments and auroral
oval 22 p3791 A67-39807
Auroral zone balloon measurement of 5
and 25 msec duration energetic electron
burst fluxes 22 p3873 A67-39821
Auroral zone irregularity correlated with
perturbations in outer radiation belt, noting
simultaneous displacement of boundary zone
of perturbations 24 p4209 A67-42120
Boundary variations of auroral oval zones,
noting dependence on magnetic perturbation
intensity 24 p4149 A67-42121
Rocket measurements in auroral zone,
considering proton and electron intensities,
energy spectra and angular
distribution 24 p4209 A67-42262
Space and time characteristics of electron
fluxes penetrating into terrestrial
atmosphere in auroral zone based on
riometer measurements 24 p4213 A67-42777

AUSTENITIC STEEL
SA MARTENSITIC STEEL
Stress-strain concentration in plates of
bilateral cut EI-437B heat resistant alloy and
EI-481 austenitic steel under rapid tensile
loading at high
temperature 03 p0529 A67-14084
Mechanical properties of Kh21GTAN5 steel
at liquid hydrogen
temperature 04 p0636 A67-14751
Stability of austenite in some Fe-Cr-Ni
alloys under low temperature
strain 04 p0636 A67-14753
Short-time tensile and long-time creep
rupture properties of HK-40 alloy and type
310 wrought stainless steel from room
temperature to 2000 degrees F

[ASME PAPER 66-WA/MET-2]
Quenching rate effect on athermal
stabilization of austenite
steel 06 p1014 A67-17801
Austenitic chrome-manganese steel
structure and properties as function of
nitrogen, molybdenum and
niobium 06 p1017 A67-18184
Carbide forming elements effect on
kinetics of isothermal transformation of
austenite and mechanical properties of
manganese-molybdenum
steel 07 p1199 A67-19239
Niobium effect on structure and
properties of chromium-manganese steels as
active nitride and carbide forming agent
increases deformation
resistance 08 p1343 A67-21206
Stress corrosion cracking of cold reduced
austenitic stainless steels noting effects of
marine atmosphere exposure, cold working,
welding, etc 11 p1807 A67-24586
Molybdenum and niobium effect on
structure and physical properties of
austenitic Cr-Mn steels with or without
nickel 12 p1955 A67-25439
Ductile failure initiation by fractured
carbides in austenitic stainless
steel 13 p2133 A67-27008
Alloying elements effect on austenite
hardening of high-nickel-content chromium-
nickel steels during cold plastic
deformation 13 p2142 A67-27285
Effect of thermomechanical treatments on
tensile properties of metastable austenitic
steels 16 p2693 A67-31872
Evaluation of plasticity, durability and
impact ductility of nonbrittle austenitic steel
during high and low
temperatures 17 p2873 A67-32767
Mechanical properties of Kh21GTAN5 steel
at liquid hydrogen
temperature 18 p3066 A67-34409
Stability of austenite in some Fe-Cr-Ni
alloys under low temperature
strain 18 p3066 A67-34411
Stress corrosion test method determined
from test program on precipitation
hardening semiaustenitic
steels 20 p3465 A67-36486
Additive elements studied for influence on
morphology, nature and hot plasticity of
sulfides in austenitic stainless
steels 21 p3646 A67-39077
Oxidation process and mechanical
properties of austenitic steels and alloys
under prolonged loading at high
temperatures, giving stress-durability
diagrams 22 p3819 A67-39322
Long term strength limit and fracture
propagation of AKN22 /Nimonic 80/ alloy
welds and AKN22-16/13 CrNi steel
composites welds 23 p4019 A67-41079
Rare earth metals effect on mechanical
properties of austenitic chromium steel at
high temperatures 24 p4169 A67-41920

AUSTRALIA
March 1964-March 1965 seasonal variations
in density, pressure and temperature at
Woomera, Australia, by falling sphere
method 01 p0061 A67-11260
Atmospheric temperature, pressure,
density and wind measurements between 30
and 80 km by Skylark rocket at Woomera,
Australia 12 p1937 A67-25840
Austrian ATC radar network describing
long range surveillance and control of
neighboring airport 17 p2834 A67-32749
Australian space research, discussing
support to Apollo and U.S. manned space
flight programs, ionospheric observations,
satellite information, etc 19 p3320 A67-35286

AUTOCALVE PROCESS
Heat sterilization of activated carbon at
135 degrees C for 24 hr or 165 degrees C
for 3 hr for application to
spacecraft 11 p1749 A67-24788

AUTOCORRELATION
Partial coherence theory to describe
Fourier /autocorrelation/ spectroscopy,
showing resolving power dependence upon
parameter of measuring instrument and
radiation 01 p0018 A67-10504
Autocorrelation function of radiation
electric field measurement from clipped
correlation function and spacing estimation
for optimally efficient SNR
determination 01 p0114 A67-10808
Terminology of phase-difference
modulated signal reception, noting coherent,

correlation and autocorrelation
methods 01 p0025 A67-10830
Mass distribution of meteoric bodies and
relation to autocorrelation function of
disintegrated planetary
surface 02 p0329 A67-12495
Incoherent scattering measurements of
ionospheric power spectrum and
autocorrelation function at geomagnetic
equator to determine electron and ion
temperatures, ion composition and ion
density 03 p0408 A67-12834
Approximation method for calculating
autocorrelation function of quantized
noise 04 p0567 A67-14405
Autocorrelation function in statistical
analysis of geomagnetic
activity 04 p0613 A67-14897
Asymptotic method of synthesizing FM
pulse signals from given autocorrelation
function 04 p0575 A67-15160
Line width of CW Ga-As lasers measured
using homodyne detection and
autocorrelation 05 p0821 A67-16670
Autocorrelation program for moving from
study arrangement to data band readable in
Fortran 06 p0965 A67-17587
Energetic particle scattering by laboratory
plasmas, deriving expressions for scattering
coefficients in terms of electric field
autocorrelation function 08 p1361 A67-21136
Pulse sequences with good autocorrelation
properties 10 p1608 A67-23330
Mass distribution of meteoric bodies and
relation to autocorrelation function of
disintegrated planetary
surface 10 p1709 A67-23363
Terminology of phase-difference
modulated signal reception noting coherent,
correlation and autocorrelation
methods 10 p1607 A67-23460
Random walks computer experiments on
ensembles of random binary homogeneous
velocity fields, using Eulerian and
Lagrangian statistics 11 p1756 A67-24542
Asymptotic method of synthesizing FM
pulse signals from given autocorrelation
function 15 p2435 A67-29347
Long term gyro drift rate evaluation
involving time series detrending and
autoregression, periodogram, autocorrelation,
spectral density and mathematical model
analysis 17 p2858 A67-32486
Autocorrelation functions for amplitude of
multiple echoes of fading radio signals
reflected from ionosphere 20 p3379 A67-36293
Nonstationary correlation analysis using
correlator in which bandwidths of two
filters resolve errors 20 p3484 A67-36695
Binary pulse compression codes generation
with low periodic
autocorrelation 20 p3386 A67-37493
Autocorrelation function of signal
scattered incoherently from ionosphere,
observing resonance at multiples of proton
gyroperiod 21 p3578 A67-37758
Time average of autocorrelation function
measured by CW radar illuminating moon
calculated without lunar surface properties
knowledge 21 p3703 A67-38189

AUTODYNE
Performance characteristics of tunnel
diode autodyne frequency
converters 05 p0774 A67-16917
Autodyne design and operational
principles for EPR in weak fields, using
coaxial resonator 11 p1793 A67-24865
Performance characteristics of tunnel
diode autodyne frequency
converters 16 p2636 A67-30894
Linear autodyne circuit allowing
sensitivity control irrespective of oscillation
level useful in NMR lines 19 p3202 A67-35791

AUTOGYRO
Heligyro configuration in autogyro,
helicopter and VTOL aircraft
design 03 p0359 A67-12987

AUTOTONIZATION
S SELF-IONIZATION
AUTOMATIC CONTROL
SA CYBERNETICS
SA SERVOCONTROL
Combined automatic control systems with
automatic adjustment of amplification
coefficient of disturbance controller for
error reduction 01 p0044 A67-10242
Model of retinal receptor incorporating
various feedback control processes
consistent with physiological and
psychological evidence 01 p0044 A67-10465
Periodic regimes in two-channel automatic

systems with nonlinear element in single channel part of loop, showing cross connections effect on
auto-oscillations 01 p0023 A67-10494
Method based on static characteristics for limit of saturation used to find relationships between voltages and currents in transformer in saturation
region 01 p0037 A67-10714
Oscillation formation by violation of sufficient conditions of asymptotic stability in linear system 01 p0047 A67-11215
Programmed telescope control systems on equatorial mount 02 p0241 A67-11992
Digital computer controlled telemetry ground station, examining six subsystems 02 p0229 A67-12002
Automatic threshold control formulation and probability distribution of adaptive detection mode for matched and mismatched clutter model 02 p0203 A67-12139
Dynamic behavior of electric angle drive unit in linear automatic control system, noting nonlinearities 02 p0227 A67-12197
Operation and control of satellite equipment, discussing automatic, semiautomatic, human and telefactor /man-extension system/ methods
[AIAA PAPER 66-918] 02 p0204 A67-12250
ELDO missile second stage automatic control system, noting programming control sequences, analysis of measurement results, etc 03 p0502 A67-12899
Automatic adjustment of amplification factor of control systems in response to perturbation 03 p0389 A67-13080
Synthesis of linear automatic control system with constant parameters for integral Q-factor, noting effect of small parameters on properties of optimum system 03 p0390 A67-13097
Solution of optimum filtering problems when input signals of automatic control system are described by different differential equations at successive time intervals 03 p0390 A67-13099
Approximation of variable time delays and design of constant and variable delay circuits, noting simulation of delays in automatic control systems by computers 03 p0390 A67-13104
Soviet book on theory of automatic control systems of regular linear, special linear and nonlinear types 03 p0390 A67-13108
Soviet papers on complex control systems 03 p0390 A67-13180
Invariance and sensitivity theories applied to automatic control system design 03 p0391 A67-13186
Invariant control device synthesis in multidimensional nonlinear automatic control systems 03 p0391 A67-13187
Necessary and sufficient conditions of invariance and autonomy of multidimensional nonlinear automatic control systems with right-hand discontinuities in describing differential equations 03 p0391 A67-13188
Invariance theory for automatically controlled underwater wings ensuring ship motion stability in perturbed medium 03 p0359 A67-13189
Complex testing method for two-stage rocket probe recovery system with aid of two successively opening parachutes 03 p0518 A67-13397
Linear nonstationary optimum filter discrimination and prediction in case of arbitrary additive noise 03 p0392 A67-13599
Nonscanning adaptive automatic control system for plant with variable amplification factor 03 p0394 A67-14062
Mean square error vs parameter curves determines applicability of perturbation method 04 p0591 A67-14421
Human engineering aspects of design of future military high performance aircraft, noting automatic control and display system requirements 04 p0562 A67-14535
Probability of tracking process for given level of fading in automatic control relay system 04 p0591 A67-14658
Optimization via information flow in system without memory, discussing ideal correction minimal and maximal error 04 p0592 A67-14904
Learning and self-learning in automatic control, noting quantitative aspects of information theory, solution algorithms and convergence criteria 04 p0592 A67-14905
Molten-Ti slag chlorination in automatic

optimization based on mathematical model 04 p0637 A67-14945
Real time evaluation of radar signals processed by digital detector used in automatic target tracking 04 p0574 A67-15058
Terminal configuration with alphanumeric display and center-metropex equipment for automation implementation in radar tracking data for expanding ATC 04 p0654 A67-15061
Closed-loop automatic control system with unvalued substantially nonlinear element, using approximation of characteristics by Fourier series 05 p0781 A67-16254
Approximation method determining follow-up failure conditions for nonlinear automatic systems in presence of control and noise signals 05 p0781 A67-16255
Automatic system auto-oscillations when transmission coefficient of nonlinear part of system depends on amplitude and frequency of input signal 05 p0782 A67-16323
Automatic checkout equipment for prelaunch use, describing packaging technique 05 p0789 A67-17461
Scheme for switching from automatic target search to range tracking, finding error distribution of backup system 05 p0787 A67-17473
Autonomy in multiply connected variable structure automatic control systems 05 p0786 A67-17542
Book on linear automatic control systems with varying parameters 06 p0973 A67-17714
Control law determination procedure for structural synthesis of combined automatic control systems for nonlinear plants 06 p0976 A67-18237
Inverse method of structural analysis of automatic control systems described by nonlinear differential motion equations 06 p0976 A67-18238
Automatic control system synthesis for fatigue testing of structural elements under random loads 06 p1101 A67-18239
Time constant determination for passive controlled plant with generalized nonlinear statistical characteristics, from response to sawtooth pulse probing 06 p0976 A67-18240
Dynamic characteristics of nonlinear automatically controlled plants 06 p0976 A67-18241
Matrix method determination of time response of time invariant linear systems to range of deterministic functions 06 p0976 A67-18402
Level quantization effect in statistical analysis of closed loop digital automatic systems 06 p0976 A67-18406
Dynamics of spherical gyroscope considered as automatic control system operating in presence of random perturbation 06 p1006 A67-18791
Approximation method of determining statistical characteristics of phase coordinates of linear automatic control systems 06 p0978 A67-18792
Self-adaptive control systems theory - IFAC Symposium, Teddington, Middx., England, September 1965 07 p1159 A67-19192
Classification of working fluids including applications in hydraulic control technology 07 p1212 A67-19733
Automatic system for classifying and delineating terrain features in aerial photography, using general purpose computer 07 p1187 A67-19744
Cost effectiveness of fully automatic checkout systems 07 p1269 A67-20078
[AIAA PAPER 67-269]
Inclusive classified bibliography pertaining to modeling human operator as element in automatic control system 07 p1137 A67-20173
Monostable fluidic amplifier with adjustable positive feedback /AF relay/ characteristics and application as oscillator, proximity switch, delay unit and in alarm annunciator systems 08 p1282 A67-20462
Spring controlled pneumatic switching units for switching machine operations and interlocking of machine controls 08 p1282 A67-20468
Insensitivity zone used for stabilizing nonlinear automatic control systems 08 p1313 A67-21323
Transient processes in linear automatic control systems dependent on parameters which appear when differential equations of analyzing system are transformed by Laplace-Karson method 08 p1313 A67-21324
Stability region for automatic nonlinear control systems unstable as

whole 09 p1532 A67-21913
Moments of output coordinates of nonlinear system determined by algorithm based on approximation method, applied to automatic control system 09 p1525 A67-22079
Nonlinear automatic system with logical device analyzed in presence of external action, obtaining harmonic linearization coefficients 09 p1482 A67-22080
Synthesis of control device for one class of nonlinear sampled data systems, obtaining processes with minimum control time 09 p1483 A67-22082
High temperature adsorption reservoir for automatic control of cesium pressure for use in thermionic converter 09 p1449 A67-22349
Caratheodory equivalent formulation relative to variational problem, showing role of min operator 09 p1483 A67-22596
Visual presentation of data required for ATC task, noting possible traffic display and attributes 09 p1529 A67-22646
Off-line autotracking evaluation system, discussing track initiation, following and termination 09 p1530 A67-22647
Prevention system of short circuit in vacuum chambers due to glow discharges 10 p1622 A67-23316
Stability of automatic control systems with nonlinearity and nonunique equilibrium state 10 p1619 A67-23318
Analytical design of controllers for linear autonomous systems of arbitrary order 10 p1619 A67-23320
Mechanical systems with automatic retardation /self-braking/ for application to brake mechanism and frictional transmission, analyzing Painleve paradoxes 10 p1680 A67-23607
Periodic regimes in two-channel automatic systems with nonlinear element in single channel part of loop, showing cross connections effect on auto-oscillations 10 p1608 A67-23616
Nomograms for analysis and synthesis of astatic automatic control systems 10 p1621 A67-23851
Graphs for frequency plot of closed loop automatic control system from phase amplitude of open loop and frequency relations between open and closed 10 p1621 A67-23852
Book on applied kinematics covering synthesis techniques for link-and-cam motion other than uniform rotation in high speed high performance automatic machines 11 p1795 A67-23921
Extension of Pontryagin maximum principle to variable control region, using Hamilton equation 11 p1812 A67-24208
Automatic optimization problem for linear Diophantine plant via analysis of discrete extremal problems 11 p1770 A67-24209
Nonlinear automatic control with random parameters, noting change of system operator as function of disturbances on system 11 p1770 A67-24211
Serial comparison technique for coding systems where weight of ascending bit is equal or greater than previous bit 11 p1756 A67-24266
Automatic height control test equipment for V/STOL aircraft, discussing experimental setup and performance 11 p1772 A67-24268
Solution of optimal control problems using hybrid computers 11 p1770 A67-24426
Multiposition grips for automatic mounting of metal or plastic specimens for low temperature mechanical tests 11 p1877 A67-24819
Inequality to derive error estimation of performance of automatic pulse servosystem inside interval of discreteness 11 p1772 A67-25039
NR fluidic elements for automatic control 12 p1896 A67-25104
Simulation of sampled data systems for pure servo delay by analog computer using potentiometer 12 p1919 A67-25203
Automatic photographic recording of laser output energy vs excitation energy obtained from fluorescence of ruby used to integrate laser light 12 p1952 A67-25333
Cyclic loading of thick tube with creep, plasticity and thermal effects 12 p2016 A67-25424
Automatic flight control development for general aviation, discussing fluidics, electropneumatic servoactuator and microelectronics
[SAE PAPER 670255] 12 p1895 A67-25505

Air traffic control radar beacon system with automatic altitude reporting system [SAE PAPER 870256] 12 p1941 A67-25506

Modified perceptron procedure for nonseparable cases, minimizing error probability and introducing reinforcement factors 12 p1961 A67-26064

Automatic production processes for semiconductors 12 p1951 A67-26224

Root trajectory theory use in automation schemes for analysis and synthesis of optimum control systems, outlining applications 13 p2085 A67-26394

Soviet book on pulsed self-adjusting and extremal automatic control systems covering theory and practice 13 p2086 A67-26459

Automatic cavity tuning of hydrogen masers to achieve frequency source of absolute accuracy over unlimited time periods 13 p2125 A67-26512

Control systems functions and programming approaches, Volume B, covering electronic data processing, factory automation and computer center administration 13 p2153 A67-26664

Satellite Telecommunications with Automatic Routing /STAR/ system composition and operation, detailing signal relaying procedure 13 p2067 A67-26717

Satellite Telecommunications with Automatic Routing /STAR/ system modulation techniques, channel capacity and Start-Stop /SS/ operation 13 p2067 A67-26718

Satellite Telecommunications with Automatic Routing /STAR/ system transmission system operation and modulation techniques 13 p2068 A67-26719

Alternative modulation techniques for Satellite Telecommunications with Automatic Routing, considering start-stop operation with PCM-FDM system 13 p2068 A67-26720

Satellite telecommunication with automatic routing noting switching concept and modulating methods 13 p2087 A67-26721

Satellite telecommunication with automatic routing noting switching 13 p2087 A67-26722

Automatic control systems classification for ordinary systems in relation to self-adaptive systems 13 p2088 A67-26800

Automatic pulse digital analyzer design to measure simultaneously all-pulse parameters used for control of closed loop systems 13 p2078 A67-26801

Stability analysis of computer controlled linear hydraulic antenna control system 13 p2088 A67-26996

Direct numerical method for finding optimal values of functionals and associated velocity fields in plastic limit analysis 13 p2219 A67-27153

Five classes of automated general purpose computer program for circuit design analysis 13 p2074 A67-27492

Optimal transients for third order system with stepwise external controls, determining switching surfaces 13 p2089 A67-27705

Nonscanning adaptive automatic control system for plant with variable amplification factor 13 p2089 A67-27711

Linear nonstationary optimum filter discrimination and prediction in case of arbitrary additive noise 14 p2290 A67-27845

Automatic pressure stepping control and recycling system for use with Fabry-Perot interferometer 14 p2315 A67-28158

Fluidic temperature sensor using frequency beating technique for generating analog pressure signal proportional to frequency differences 14 p2318 A67-28345

Automatic fluidic gain changer circuit for flight control systems counteracting Mach number and altitude pressure effects 14 p2251 A67-28352

Asymptotic study of Markov stationary discrete time and finite number of states decision process 14 p2291 A67-28510

Integral equations in automatic control theory, deriving theorem which leads to Popov frequency domain stability criterion 14 p2292 A67-28635

Smoke generator control and performance for flow visualization applications [JPL-TR-32-117] 14 p2293 A67-28751

Automatic positioning control and problems in normalizing programming codes used in numerical control 14 p2276 A67-28956

Hover augmentation system reducing VTOL pilot task in maintaining position by providing damping signals for automatic flight modes with accurate path control 14 p2246 A67-29082

Necessary and sufficient conditions for boundary of absolute stability domain of nonlinear automatic control systems 15 p2455 A67-29120

Step-by-step self-adaptive algorithm for selective systems with automatic control 15 p2455 A67-29123

Automatic exposure of longitudinal overlapping of aerial photographs solved by autonomous radio-navigation systems 15 p2485 A67-29137

Quantizer optimal design for closed-loop dynamic and open-loop static systems 15 p2456 A67-29364

Parameter stability regions with frequency response, noting interpretation for several parameters 15 p2457 A67-29366

Plotting inverse of transfer function, deriving equations for hodograph and for gain values which yield greater or equal damping ratios 15 p2457 A67-29372

Cross correlation bounds and positivity of nonlinear operators, examining criteria for positive composition 15 p2457 A67-29373

Two-person zero sum games with differential equation rules, noting location of optimal trajectories, separation properties, etc 15 p2509 A67-29404

Concorde automatic flight control system noting autostabilization, autopilot, electric trim, autothrottle, etc 15 p2419 A67-29508

Spatially distributed automatic control system used in plasma plant stabilization 15 p2530 A67-29724

Approximation of functions describing control loops output signals for various values of controller parameters 15 p2459 A67-30132

Air traffic control simulation, describing functions to be fulfilled and system requirements for EUROCONTROL 15 p2441 A67-30164

Identification in automatic control systems - Conference, Prague, June 1967, Part 1 15 p2459 A67-30309

Numerical techniques for process identification in automatic control systems, discussing methods such as autocorrelation, spectral density, differential approximation, etc 15 p2460 A67-30310

Parameter estimation in automatic control systems using statistical techniques such as likelihood, Markov and least square estimates 15 p2460 A67-30311

Statistical dispersion methods for identification of nonlinear controlled plants 15 p2462 A67-30324

Identification in automatic control systems - Conference, Prague, June 1967, Part 2 15 p2462 A67-30329

Parameter estimation representing differential equation coefficient of controlled system for quick-response adaptive identification 15 p2464 A67-30338

Rate variation of aerodynamic parameters of pitching equation for aircraft, identifying them with linear plant model for simulation studies 15 p2420 A67-30340

Process identification by cyclic parameter adjustment with automatic iteration, using analog and hybrid computers 15 p2465 A67-30342

Identification techniques with stochastic computers for advanced automatic control systems in form of learning machines 15 p2441 A67-30344

Book on modern control systems covering feedback control theory within framework of frequency and time domain analysis 16 p2643 A67-30621

Space vehicle automatic control considering order execution from guidance system and vehicle stabilization around its center of gravity 16 p2700 A67-30798

Trace /tape controlled recording automatic checkout equipment/ system design to accommodate aircraft ground support task 16 p2635 A67-30834

Automation problems in space-flight operative medical control, giving equations of changes in physiological indices 16 p2618 A67-30902

Effectiveness for automatic control systems estimated by comparing performance with ideally functioning systems 16 p2643 A67-30919

Nonlinear automatic control systems with random processes studied using orthogonal polynomials with Hermitian series expansion 16 p2643 A67-30924

Transient processes in nonlinear automatic

control systems 16 p2643 A67-30926

Parallelism between edges of aerial photographs and line of flight achieved by automatic rotation 16 p2671 A67-31031

Electronic equipment for generating delay times corresponding to missile velocity during optical recording by numerous sensors distributed along ballistic firing range 16 p2674 A67-31118

Realization of invariant multiloop control in case of near-critical and critical plant parameters 16 p2643 A67-31379

Automatic control - Conference, University of Pennsylvania, Philadelphia, June 1967 16 p2644 A67-31634

Behavior of high-order linear control systems analyzed using Liapunov second method, by finding low-order model with closely approximate response behavior of high order linear control systems analyzed, using Liapunov second method, 16 p2647 A67-31648

Component parameter identification, discussing techniques and applications 16 p2647 A67-31649

Synthesis and design of on-line self-organizing control of multiple goal, multiple actuator systems 16 p2648 A67-31654

Feedback from observations introduced into midcourse guidance correction program, showing optimal random feedback solution obtained for deterministic optimal feedback control problems 16 p2701 A67-31657

Analog computer use in design of automatic steering control system of Apollo station ships for precision geographical track-keeping 16 p2701 A67-31659

Applied synthesis technique using feedback and command controller elements for strongly interacting multivariable control systems, illustrated by flight control system design 16 p2649 A67-31661

Synthesis technique applying Liapunov theory for state vector tracking of nonlinear multivariable control systems illustrated by reactor control design 16 p2649 A67-31662

Describing functions for nonlinearity consisting of bang-bang with dead zone characteristic followed by linear integrator with constrained integration range 16 p2652 A67-31690

Automatic control systems, discussing open and closed loop control systems, mathematical model analysis and developments 17 p2830 A67-32788

Hydrodynamic equations for automatic control of speed and coordinates of craft with underwater foils moving on disturbed body of water 18 p3074 A67-33416

Learning in unknown stationary environment using stochastic approximation, discussing Bayesian interference, pattern recognition, automatic control and statistical communications 18 p3070 A67-33497

Automatic AM control noting proportionate variation of carrier level to signal volume 18 p2998 A67-33502

Automatic system auto-oscillations when transmission coefficient of nonlinear part of system depends on amplitude and frequency of input signal 18 p3017 A67-33875

Automatic control system for parameter evaluation, reducing stochastic errors by repeated measurements 18 p3017 A67-33991

Dynamics of spherical gyroscope considered as automatic control system operating in presence of random perturbation 18 p3049 A67-34456

Approximation method of determining statistical characteristics of phase coordinates of linear automatic control systems 18 p3018 A67-34457

Electronic circuit theoretical analysis noting nonlinear and qualitative processes 19 p3200 A67-34904

Stencil screening methods for printing integrated circuit patterns for resistors, capacitors, etc, discussing automation possibilities 19 p3192 A67-35026

Automatic high speed IC test equipment and procedure 19 p3192 A67-35027

Automatic life-support system tried on leeches for space applications 19 p3180 A67-35248

Future traffic control system for ensuring flight safety and automatic functioning by automatic radar observation and aircraft-movements control 19 p3255 A67-35806

Techniques and methods of automation in air-traffic control, discussing reliability,

operation time reduction, etc 19 p3255 A67-35808

Canonical form of filtering problems with solution identical to control problem 19 p3205 A67-35911

Feedback control system using pneumatic computing components and vibration isolators for automatic platform tilt stabilization, performance characteristics, etc [AIAA PAPER 67-548] 19 p3208 A67-35946

Reliability contribution of pilot using manual backup control for first stage of Saturn V tested using simulation [AIAA PAPER 67-554] 19 p3335 A67-35951

Project 666a Automatic Terrain Following Program and Automatic Flight Control System /AFCS/, with digital and analog simulation and test results 19 p3174 A67-35965

Automatic control systems general theory with distributed parameters and delay, proving existence and uniqueness of solutions of partial differential equations solutions 19 p3251 A67-36048

Synthesis of specific type of automatic microprogramming systems using complex microcommand signals conditioned by functional-blocks properties 19 p3190 A67-36094

Correlation position device for autonomous orbital navigation system 20 p3481 A67-36553

Digital computer test program for automatic checkout of Saturn launch vehicles allowing manual intervention 20 p3391 A67-36574

Man-machine graphical communication device for real time monitoring with automated checkout 20 p3446 A67-36589

Boundary value problem and singular integral equation applied to automatic control theory 20 p3475 A67-36652

Two-dimensional displays conversion to three-dimensional, using uniaxial crystals to vary optical path length and digital control with electro-optic polarization switches 20 p3447 A67-36806

Automatic electronic test and checkout techniques, automatic test equipment history and high points of 1957-1959 DOD symposia 20 p3416 A67-36970

Automatic test computer programming problems, discussing system planning, documentation, personnel, system compromises, etc 20 p3391 A67-36972

Apollo program automatic checkout equipment, examining computer controlled checkout concept for Apollo spacecraft 20 p3417 A67-36974

Automation techniques for stage checkout in Saturn program noting equipment, time factor, etc 20 p3417 A67-36975

Automatic test system employing optical and electrical input signals based on pattern recognition with CRT display 20 p3392 A67-36991

Input signal level for stability loss or self-oscillations automatic control in system, using analysis for nonlinear systems with forced vibrations 20 p3408 A67-37041

Device for automatic recording of laser emission and of energy of pumping pulse 20 p3460 A67-37149

Efficiency of using self-adjustment with respect to input signal in automatic control systems, estimating gain and stability 20 p3409 A67-37198

Necessary condition for optimal control in nonlinear automatic control system determined, using method of successive approximations 20 p3410 A67-37229

Stability of automatic systems for tracking point targets, noting nonlinear dependence of signals on channel mismatch and its limiting values 20 p3410 A67-37234

Nonstationary automatic control systems design by reaction quenching method 20 p3410 A67-37235

Digital computer control system for aerodynamically unstable vehicles 20 p3534 A67-37257

Nonlinear automatic control systems characteristics analyzed for various possible error accumulations 20 p3412 A67-37382

Automated system for growth and analysis of bacterial colonies using environmental chamber and computer controlled flying-spot scanner 20 p3453 A67-37598

Scientist role in automated laboratory for remote biological exploration of planets [AIAA PAPER 67-632] 20 p3375 A67-37615

Spacecraft computer managed laboratory

/CML/ for flexible decision making in space missions of 1970s 20 p3393 A67-37624

[AIAA PAPER 67-643] 20 p3393 A67-37624

Soviet book on information theory and application to problems in automatic monitoring and control 20 p3413 A67-37633

Synthesis procedure for linear automatic feedback control systems, examining time-domain response 20 p3413 A67-37679

Automatic apparatus for flooding or spraying test specimens with liquid corrosive media according to predetermined program 21 p3715 A67-37827

Book on optimal control theory covering Fourier and Laplace transforms, automatic control, mathematical theories, etc 21 p3602 A67-37829

Photoelectric device measuring cutting-tool temperature for automatic control of state of cutting edges 21 p3628 A67-38059

Industrial electronics measurement and control - Conference, Budapest, August 1967 21 p3591 A67-38157

Narrow and wide passband measurements of LRBA liquid propellant motors using test bench automatic measurement equipment 21 p3607 A67-38202

High performance automatic ground checkout system for boosters, noting rate improvement and error reduction 21 p3608 A67-38203

Set of states reachable in given time in control problem determined by heuristic and rigorous methods 21 p3603 A67-38441

Cesium bombardment ion engine performance, giving starting circuit and automatic discharge power control system [AIAA PAPER 67-666] 21 p3690 A67-38700

Mathematical programming problem for automating design of optimum thin walled systems, noting stress-strain state factors 21 p3728 A67-38903

Invariance principle proposed for controller analytical design for nonlinear invariant systems by reducing problem to quasi-linear problem 21 p3604 A67-39111

Automatic test equipment /ATE/ to ensure aircraft availability noting operation, circuitry, computer methods, etc 21 p3609 A67-39132

Controller design for booster gust alleviation, considering stochastic minimization problem solved by iteration yielding linear finite time controller with time-varying gains 22 p3897 A67-39162

Luna IX automatic station flight control complex, detailing communication, orientation and stabilization systems operation after separation from acceleration module 22 p3897 A67-39167

Automatic check system for investigation of dynamic characteristics of stabilization system for carrier and space vehicle, noting system reliability 22 p3830 A67-39172

Automatic control of Block II Apollo ECS space radiator system, deriving linearized control equations for subsystem 22 p3916 A67-39174

Two-channel control system for programmed roll of rapidly rotating carrier rocket, analyzing efficiency 22 p3898 A67-39175

Autonomous solution to orbital navigation problem yielding direct measure of orbital parameters 22 p3830 A67-39179

Flight control system for automatic interplanetary stations /AIS/, comparing Venera series orientation and correction system to Mariner 22 p3898 A67-39185

Automatic satellite-checkout system for use under simulated space environment and stress conditions 22 p3778 A67-39192

Two-beam capacitive converter for automatic systems reduced to synthesis of single beam converter 22 p3795 A67-39229

Automatic navigation trends, discussing cost effectiveness, transportation objectives and application rate 22 p3831 A67-39465

Photoelectric micrometer for automatic determination of meridian passage times, describing tracking servomechanism and collimation measurements device 22 p3881 A67-39515

Gas dynamic self-regulation of supersonic nozzle consisting of cylindrical channel with central body, measuring nozzle inlet and static pressures 22 p3868 A67-39544

Aircraft autopilot system in longitudinal flight stabilization regime, using synthesis method based on time

characteristics 22 p3831 A67-39609

Random error effect on directional gain of sectional parabolic antenna with automatic phasing, setting sections effectively by three control points method 22 p3770 A67-39657

Channel Evaluation and Call /CHEC/ system to improve air-ground-air communications by automatic selection of optimum channels 22 p3760 A67-39664

Pilot and automatic control function coordination in piloting and landing aircraft, discussing precision problems, safety and development of new processes 22 p3831 A67-39750

Equations for mode analysis in multichannel extremal control systems with harmonic probe signals, discussing synthesis of optimizers and phase shift automatic compensation 22 p3777 A67-39864

Vaporizing solid or liquid underlayers for transpiration cooling of reentry vehicles, discussing advantages, handling, storage and self-regulating system 22 p3901 A67-39934

Photoresistors thermal characteristics in automatic semiconductor control devices studied in steady and pulsed modes of operation, determining current-voltage characteristic and thermoresistance 22 p3801 A67-40214

Magnetolectric device development to measure and register weak signals in digital form in converters of automatic control systems 22 p3809 A67-40475

Nonlinear sampled data automatic control system optimization by statistical method 23 p3985 A67-41673

Approximate investigation of standard model reference adaptive systems with random input effects based on filtering properties of automatic control systems 23 p3985 A67-41675

Automatic test equipment for checkout and fault finding on Saab 37 Viggen 24 p4137 A67-41898

Nuclear subsystem controls and instrumentation for NERVA noting automatic startup, override, power and temperature controller testing 24 p4183 A67-42471

Spacecraft power conditioning reliability using standby redundancy at functional component level and performance monitoring automatic failure detector 24 p4108 A67-42539

Automatic systems optimization, adaptation and learning 24 p4136 A67-42697

Synthesis of self-adaptive systems with variable structure, obtaining relationships between systems dynamics and characteristics of logical control law 24 p4137 A67-42699

Synthesis of automatic systems optimum in mean noting difficulties arising from no restrictions on control law 24 p4137 A67-42722

All-weather flight requirements of VTOL aircraft, suggesting artificial stabilization by automatic control system [AIAA PAPER 67-798] 24 p4096 A67-42959

Automatic flight management of future high performance aircraft [AIAA PAPER 67-847] 24 p4183 A67-42983

AUTOMATIC DATA PROCESSING SYSTEM

Unidensity coherent light processing system /UNICON/ 01 p0030 A67-11034

Automatic radar system for low level target detection, obtaining Doppler resolution and eliminating fixed atmospheric noise 04 p0573 A67-15043

Group dynamics approach to resistance or counterpart of planning, conversion and management of automatic data processing systems design [ASME PAPER 66-WA/MBT-10] 04 p0740 A67-15334

Automatic telemetry checkout station for Saturn V systems using real time signal digitizer and general purpose computer 05 p0789 A67-17044

Automatic telemetry checkout station for Saturn V systems using real time signal digitizer and general purpose computer 06 p1089 A67-18861

Sensors of electromagnetic radiation in UV, visible and IR ranges, noting improvement through automatic data processing 06 p1006 A67-19013

IBM System/360 Model 91 machine organization alleviating disparity between storage time and circuit speed 11 p1755 A67-23949

High speed floating-point algorithm of IBM System/360 Model 91 for exploiting multiple execution units 11 p1755 A67-23950

Floating point execution unit of IBM System/360 Model 91, emphasizing design of instruction oriented units to reveal techniques employed to match burst instruction rate of one instruction per cycle 11 p1755 A67-23951

IBM System/360 Model 91 storage system design concepts 11 p1755 A67-23952

Versatile digital data handling system designed to accept and control output of space radiation scintillation spectrometer 12 p1909 A67-25864

Automatic multichannel system for data recording and processing obtained in studies of ionospheric structural inhomogeneities containing magnetic-tape memory and device for digital computer input 13 p2119 A67-26561

Aircraft detection and in-flight tracking by real time computers, assessing role in missile and satellite tracking 13 p2153 A67-26666

Automatic radiosonde data processing system providing azimuth and elevation angles, temperature, humidity, etc 13 p2069 A67-27019

Steady and dynamic loads on tandem rotor, controls and airframe flight tested with Army helicopter, using automatic data processing 13 p2054 A67-27596

Organizational techniques and trade-offs for low power operation in spaceborne data processing systems 17 p2820 A67-32503

Data selection, collecting and processing for automatic performance recording and monitoring of aircraft gas turbine engine, considering hardware and software [SAE PAPER 670360] 17 p2835 A67-32999

Operational computerized system for automatic surveillance of reliability and maintainability of spacecraft hardware 18 p3021 A67-34701

Learning threshold element circuit employing electrochemical controllable resistors as weight factors 22 p3809 A67-40480

Design characteristics of IBM 9020 system to provide automated aids for processing and updating flight information 23 p3976 A67-41057

Application of IBM 9020 multiprocessing system to air traffic control 23 p3976 A67-41060

Multichannel image data handling and processing system using multispectral analysis for remote agricultural sensing and surveying from aerospace platforms 24 p4157 A67-42435

Automatic crop surveys contribution to agricultural technology in developed and underdeveloped countries [AIAA PAPER 67-766] 24 p4258 A67-42935

AIDS data processing and analysis system for automated fault diagnosis and equipment trend prediction, describing methods applied to aircraft [AIAA PAPER 67-792] 24 p4126 A67-42953

AUTOMATIC DEPOSITION CONTROL

Automatic control of evaporation and deposition of thin films under vacuum 01 p0078 A67-10299

Automatic plating system insuring quality finishes by selectively phosphating or chromating parts after zinc plating 23 p4010 A67-41351

AUTOMATIC FREQUENCY CONTROL

Fluctuation noise effects on phase-locked automatic frequency control system obtained using Markov processes, determining phase difference probability density and statistical characteristics 01 p0037 A67-10713

Limiting SNR determines, for given initial detuning, probability close to unity of phase jumps in phase locked AFC system 03 p0380 A67-13580

Main properties of phase automatic frequency control, using standard signal as additional action on self-excited oscillator 05 p0764 A67-16904

Automatic phase control /APC/ loop for stabilization of phase shift in RF amplifier 05 p0778 A67-17395

He-Ne laser frequency stabilization using four automatic frequency control /AFC/ systems 06 p1010 A67-17965

Filtering properties of frequency-stability transport circuits of molecular beam generator, noting design considerations for

high efficiency 08 p1305 A67-21274

Lock-on band determination for inertial system of phase automatic frequency control in presence of fluctuation noises 11 p1750 A67-23910

Automatic frequency control for estimating random signal frequency when received against white noise background 13 p2069 A67-27037

Automatic frequency control circuit for SHF tunnel diode converter 13 p2069 A67-27043

Main properties of phase automatic frequency control, using standard signal as additional action on self-excited oscillator 16 p2823 A67-30880

Markov processes applied to synchronization failure in phase-lock AFC loop subjected to external fluctuations 18 p3000 A67-34086

Automatic frequency-control system using superconducting resonator and reflex klystron 19 p3192 A67-34984

Discriminator for fine automatic frequency control of reflex-klystron by error signal 19 p3228 A67-34991

Lock-on band determination for inertial system of phase automatic frequency control in presence of fluctuation noises 21 p3585 A67-38938

Systems with low noise factor and high selectivity tuned by varying pumping frequency 22 p3767 A67-39370

Phase locked automatic frequency control regulated phase distortion effects on radar signal mean peak power at matched receiver filter output 22 p3761 A67-39762

Magnetically tunable multisection bandpass filter in ferrite-loaded evanescent waveguide 22 p3772 A67-39907

Analysis of laser with selective resonator indicating stimulated emission basic characteristics determined by active medium band shape and Q-factor 23 p4013 A67-40907

Transmission behavior of double tuned band filters with frequency dependent feedback and stagger 24 p4129 A67-42206

AUTOMATIC GAIN CONTROL /AGC/

Tunable airborne L-band radiometer designed to provide reliable operation over long period of time with minimum of operator adjustment 01 p0063 A67-10323

Amplitude and phase direction-finding characteristics of monopulse automatic tracking system operating on sum-difference principle 02 p0214 A67-11904

Improved frequency stability and specific transistor characteristics of transistor oscillators with AGC 02 p0216 A67-11981

AGC and noise controlled dual-channel optimal ratio predetection combiners, examining design and performance by studying diversity combining techniques 02 p0198 A67-12025

Noise and signal fluctuation effects on angle tracking radar with amplitude comparison system 07 p1147 A67-20239

Automatic signal gain control system under constraints, determining time constants for signal filtering 13 p2088 A67-27041

Monolithic circuits for RF communications systems 14 p2282 A67-28027

Solid state pulsed carrier IF-AGC system design for microwave receivers noting input network, video circuit, AGC loop gain, etc 18 p3016 A67-34597

Postdetection maximal ratio diversity combiners, discussing signal to noise enhancement 20 p3397 A67-36583

AUTOMATIC LANDING SYSTEM

All-weather carrier landing system using precision tracking radar and microelectronic data link aboard carrier 01 p0026 A67-10969

All-weather landing system for C-141 jet cargo transport using vertical navigation computer for military operations 03 p0464 A67-12907

Automatic landing development in autopilot and autoflares for Trident aircraft 03 p0464 A67-13002

Autopilot requirements, particularly for VTOL aircraft and automatic instrument landing, noting introduction of redundant channels 03 p0464 A67-13004

Instrument landing system transmitter monitors for automatic blind landing, noting near field monitors and internal monitors 07 p1222 A67-19654

VHF ILS equipment achieves necessary instrumental accuracy for automatic landing operation 09 p1529 A67-22643

Ground integrity monitor for category III ILS for use with automatically landing aircraft 09 p1529 A67-22644

ILS as guidance component of all-weather automatic landing system, discussing operational need and specific vulnerabilities 13 p2154 A67-26985

Landing radar system for Apollo lunar module using three-beam Doppler velocity sensor and single-beam altimeter 14 p2318 A67-28290

Airplane automatic-flare system actuating flaps and elevators as lift and moment controllers 15 p2418 A67-29313

Automatic all-weather landing system design having integration of autopilot and flight director [AIAA PAPER 67-406] 15 p2516 A67-30373

Boeing 727 automatic flight control and landing system [AIAA PAPER 67-573] 19 p3258 A67-35969

All-weather landing systems for automatic and manual control, considering Category II and III operations 22 p3831 A67-39611

Automatic landing system introduction for civil transport aircraft noting certification program and requirements and development of operable system [AIAA PAPER 67-757] 23 p4025 A67-40990

AUTOMATIC PATTERN RECOGNITION

General purpose computer used in automatic photointerpretation process in relation to pattern recognition 05 p0768 A67-17513

Airborne imagery screening using automatic target recognition device 17 p2859 A67-32509

Fourier transform application to automatic pattern recognition, using photographic plate to record plane intensity distribution 22 p3764 A67-39331

AUTOMATIC PICTURE TRANSMISSION /APT/

Weather satellites, discussing photographic and radiation measuring equipment and automatic picture transmission 01 p0109 A67-10768

Stereo interpretation of Nimbus II automatic picture transmission photography for cloud patterns [AFRL-66-805] 02 p0241 A67-11970

Satellite photographs received from APT facility used in analysis of old occluded depression structure, deducing jet stream position and sea-ice presence 04 p0650 A67-14868

Electron beam evaporation of silicon dioxide producing storage layers for automatic picture transmission vidicon, analyzing causes of signal loss after short operating time in flight tubes 04 p0623 A67-15315

Tiros VIII, Nimbus I and II and Essa II weather satellites and radio reception of observational results by German meteorological service APT receiver stations 05 p0904 A67-16028

Graphical method by which small local users of meteorological satellite pictures can identify geographical position of features in image [AIAA PAPER 66-439] 07 p1184 A67-19373

Automatic electrostatic image orthicon camera with small weight, volume and input power, having full low-light level sensitivity capability 17 p2858 A67-32481

Australian space research, discussing support to Apollo and U.S. manned space flight programs, ionospheric observations, satellite information, etc 19 p3320 A67-35286

AUTOMATION

Physical phenomena and electrical effects of various bodies in creating new automation elements 07 p1159 A67-19185

Logic methods using conventional piston valves applied to general automation 08 p1282 A67-20470

ATC automation, discussing first stage implementation called NAS En Route Stage A, Center Computer Complex and computer programming 08 p1315 A67-20676

Cost- and labor-saving advantages of automatic and semiautomatic insertion of components in circuit board 08 p1335 A67-20748

Measuring technology and automation - Conference, Dusseldorf, October 1965 08 p1313 A67-21004

Automation role in air traffic control, discussing flight route 09 p1530 A67-22651

Future industrial automation prediction based on present knowledge 13 p2231 A67-27514

Computerized mathematical procedures application in advanced large-scale automated systems 16 p2634 A67-31568

Identification, optimization and stability of automatic systems - Conference, Slacay, France, May 1965 19 p3203 A67-35901

Automation in electronic test equipment - Conference, New York, August-September 1966, Volume 3, Built-in test and continuous monitoring 20 p3416 A67-36969

Automation in electronic test equipment - Conference, New York, August-September 1966, Volume 4, Built-in test and continuous monitoring 20 p3448 A67-36978

Automation in electronic test equipment - Conference, New York University, August-September 1966, Volume 5, Built-in test and continuous monitoring 20 p3417 A67-36987

Aircraft design automation using computer techniques by linking geometrical concepts to design parameters 20 p3455 A67-37246

AUTOMATON

SA FINITE-STATE MACHINE

Informal automaton simulating certain processes of information processing by human brain controlled by servosystems 03 p0365 A67-13084

Behavioral analysis of stochastic automata in random media, discussing automata design with quasi-linear behavior and expedient behavior 08 p1313 A67-21327

Automata Theory - Conference, Hanover, West Germany, October 19 p3201 A67-35604

Homomorphic decomposition set of state quantity of finite automation 19 p3202 A67-35605

K-multiple automata for language recognition or generation, discussing generalization from simple to multiple automata 19 p3202 A67-35607

Transfluxor as self-repair unit of redundant automata 20 p3454 A67-37038

Algorithm for processing primary motor characteristics of human motions on digital computer 24 p4114 A67-41857

AUTOMOBILE

Mineral insulated thermocouple applications in nuclear reactor, automobiles, steel, concrete, plastics, textiles, ceramics and heavy machinery 10 p1656 A67-23080

AUTOMOBILE ACCIDENT

SA SEAT BELT

SAE Stapp Car Crash Conference, Holloman AFB, New Mexico, November 1966 08 p1288 A67-20609

Skidding accident reduction investigated for runway and highway safety noting worn tires, smooth surface texture, locked wheels and pilot technique 19 p3173 A67-35930

AUTOMORPHISM

Duality principle for automorphic forms on semisimple Lie groups extended to include arbitrary topological unimodular groups 03 p0458 A67-13387

Ergodic theory of measurable partitions in Lebesgue space, extending Rokhlin-Sinai theory of increasing to flows generated by automorphism 04 p0644 A67-14756

AUTONOMIC NERVOUS SYSTEM

SA CENTRAL NERVOUS SYSTEM

Influence of different stresses on sugar content changes of blood and stabilization at another level as adaptation result of organism 14 p2255 A67-28221

Effects of breathing pure oxygen under pressure on autonomous regulatory systems / nervous, respiratory, circulatory/ of man 14 p2257 A67-28225

AUTOPILOT

Interceptor missile adaptive roll autopilot with new dither principle in simulated testing of stability 01 p0111 A67-11203

Monograph on system philosophy of automatic learning systems in application to autopilots, discussing man-aircraft system cybernetics, human behavior, environmental effects, etc 02 p0186 A67-12084

Autopilot requirements, particularly for VTOL aircraft and automatic instrument landing, noting introduction of redundant channels 03 p0464 A67-13004

Autopilot programmer design for automatic guidance in approach and stabilization along course of aerial

photography aircraft 03 p0465 A67-14284

Low weather minima flight control system consisting of autopilot, flight system and gyromagnetic compass 03 p0466 A67-14385

Aerodynamic coefficients effects on aeroelastic instability predictions for aircraft with autopilot [ONERA-TP-418] 05 p0751 A67-16483

Aircraft autopilot actuators move control surfaces in response to electric signals and include facilities for performing full automatic landing 05 p0754 A67-17048

Pitching effect on aircraft gravity center during passage through gust, noting autopilot effect on tail assembly 09 p1440 A67-22473

Missile and aircraft control systems design, discussing root locus and stability curve methods for solving characteristic equation 09 p1483 A67-22489

Conditional stability of class of controlled systems, noting aircraft controlled by autopilot 12 p1919 A67-26104

Automatic all-weather landing system design having integration of autopilot and flight director [AIAA PAPER 67-406] 15 p2516 A67-30373

Time optimal control of system with multiple control inputs and bounded phase coordinates for design of autopilot for booster 16 p2762 A67-31643

Synthesis of closed loop system consisting of pitch control adaptive autopilot for changing flight conditions, using transient characteristics 18 p3075 A67-34282

Aircraft autopilot system in longitudinal flight stabilization regime, using synthesis method based on time characteristics 22 p3831 A67-39609

Booster autopilot in bounded phase coordinates subject to disturbances, determining extremal control as function of time 22 p3833 A67-40149

AUTORADIOGRAPHY

Autoradiographs of metal diffusion in pyrolytic graphite 02 p0257 A67-11898

Correct method for affine transformation of model in processing of superwide angle photographs on 09 p1496 A67-21750

Chromium distribution in laser rubies with neutron activation 20 p3458 A67-36427

AUTOROTATION

Wind tunnel model for analysis of autorotating rotors for reentry space vehicles tested at transonic and supersonic regimes 09 p1440 A67-22285

Gas turbine auxiliary power unit design to provide boost to helicopter engine in powered and autorotational flight modes [AHS PAPER 116] 16 p2598 A67-31832

AUXILIARY POWER SOURCE

SA CHEMICAL AUXILIARY POWER SOURCE

SA NUCLEAR AUXILIARY POWER

HF design of DC-DC converters with low weight and high performance for spacecraft power systems 02 p0183 A67-12181

Electrical parameters of chemical current sources in determining capacitance by measuring emf, voltage and short circuit current 03 p0363 A67-13597

Electric propulsion role in auxiliary and primary spacecraft propulsion [AIAA PAPER 66-1025] 03 p0504 A67-14156

Space-power subsystems, evaluation of power sources 04 p0558 A67-15954

Design of solar cells as satellite power supply sources 04 p0558 A67-15956

Space energy supply plant with nuclear energy sources, noting transformer design 04 p0558 A67-15958

Radioisotope sources and nuclear reactors as energy sources for space vehicles 04 p0558 A67-15959

Radionuclide generators with thermoelectric transformer for space application 04 p0559 A67-15960

Thermoelectric generator design and development for space 04 p0559 A67-15961

VR 3, 5 DS cadmium-nickel sealed battery for space applications 07 p1131 A67-19528

Cadmium negative electrode mechanism, noting active material redistribution and anodic oxidation 09 p1445 A67-22176

Sealed Ni-Cd batteries with pocket plates and sintered plates, considering operational aspects 09 p1446 A67-22189

Mathematical model for predicting

temperature and life of silver-zinc battery system in spacecraft [AIAA PAPER 67-334] 12 p1901 A67-26048

Electrical parameters of chemical current sources in determining capacitance by measuring EMF, voltage and short circuit current 14 p2247 A67-27843

Radioisotope selection criteria for propulsion and auxiliary power generation in space 14 p2348 A67-27971

High density moisture-proof noncrystalline family of gas generator propellants, surveying burning rates, physical properties and application 15 p2544 A67-29980

Gas turbine auxiliary power unit design to provide boost to helicopter engine in powered and autorotational flight modes [AHS PAPER 116] 16 p2598 A67-31832

Noise control of aircraft auxiliary power units, noting installation of special acoustic materials 17 p2800 A67-31977

Primary electric propulsion application to satellite and other space missions, considering auxiliary systems and experimental thruster systems [AIAA PAPER 67-426] 18 p3112 A67-33910

Fokker F-28 aircraft features for minimum turnaround time, noting self-sufficiency provided by auxiliary power unit 19 p3173 A67-35558

Fokker F-28 aircraft systems fuel system, auxiliary power unit, hydraulics, flight controls, pressurization and electrical systems and avionics 19 p3176 A67-35559

Air conditioning system of P-3 aircraft, noting redesign to include auxiliary power unit for functioning during ground operation 20 p3363 A67-36512

Potassium Rankine cycle turboelectric space power system, emphasizing vapor fin type of condensing radiator 20 p3364 A67-37018

Thermionic conversion for space auxiliary power systems noting high reliability and longevity potential 20 p3364 A67-37019

Hydraulic power systems for V/STOL noting self-sufficiency on start-up and auxiliary power source 20 p3366 A67-37552

Aircraft auxiliary power unit noise control, considering acoustical materials and installation techniques 23 p3935 A67-41144

Orbit and sun-oriented solar cell concepts compared, discussing aerodynamic drag penalties 24 p4105 A67-42517

Methanol-air fuel cell development, discussing electrode performance, temperature effects and catalytic agents 24 p4106 A67-42520

Primary electric propulsion application to satellite and other space missions, considering auxiliary systems and experimental thruster systems [AIAA PAPER 67-426] 24 p4208 A67-42901

High density moisture-proof noncrystalline family of gas generator propellants, surveying burning rates, physical properties and application 24 p4207 A67-42921

AVALANCHE

SA ELECTRON AVALANCHE

Temperature dependence of optical phonon mean free paths and mean energy loss per collision predict avalanche multiplication and voltage breakdown of Si and Ge p-n junctions 01 p0132 A67-10374

Locked oscillation of silicon p-n junction avalanche diodes in 50 to 140 GHz range 01 p0035 A67-10438

Transition time dependence between avalanche and second breakdown on input power to p-n silicon junction, noting thermal effects in semiconductors 02 p0222 A67-12650

Silicon p-n junction avalanche breakdown voltages obtained from formula for ionization coefficient 05 p0869 A67-17090

Avalanche drift diode and application in microwave technology, analyzing dynamic negative resistance formation, volt-ampere characteristics and output power 06 p0970 A67-18169

Interaction between two high resistivity layers in Mn doped GaAs separated by region of bulk material 06 p1051 A67-18222

Avalanche multiplication in Ge and GaAs p-n junctions, comparing experimental and theoretical ionization rates, predicting voltage breakdown 06 p1085 A67-18954

Delay time of avalanche discharge in silicon p-n junction as function of overvoltage 07 p1238 A67-20256

Time dependence of avalanche in silicon

junctions including effects of different ionization rates and velocities of charge carriers 18 p3105 A67-34628
 Avalanche drift diode and application in microwave technology, analyzing dynamic negative resistance formation, volt-ampere characteristics and output power 20 p3404 A67-37592
 Avalanche breakdown voltage in Si planar p-n junctions studied for relation to impurity gradient 22 p3786 A67-39256
 Nuclear cascade avalanche absorption in Fe analyzed by ionization calorimeter 24 p4219 A67-42850

AVALANCHE RECTIFIER

Junction perfection in coherent microwave oscillation in avalanche p-n silicon diodes 01 p0036 A67-10449
 Microwave power generation by avalanche-transit time diodes, noting noise and excess heat problems 01 p0040 A67-11255
 Avalanche transit time diode, noting dynamic resistance mechanism of formation and linear and nonlinear diode behavior 04 p0583 A67-15154
 Localized breakdown in Ge mesa diodes due to inclusions 04 p0584 A67-15486
 Avalanche transistor properties in dynamical state derived from relation between current, collector voltage and concentrated load in base 06 p0970 A67-18186
 Avalanche breakdown voltages of diffused silicon p-n junction calculated, using impact ionization rates 09 p1556 A67-22205
 High efficiency pulsed gallium arsenide avalanche diode 11 p1767 A67-24722
 Pulsed power output for microwave GaAs oscillator biased into avalanche, with diodes grown by liquid phase epitaxy 15 p2442 A67-29172
 Current dependent modes in pulsed avalanche diodes 15 p2442 A67-29174
 Avalanche transit time diode, noting dynamic resistance mechanism of formation and linear and nonlinear diode behavior 15 p2443 A67-29341

AVIATION

S AERONAUTICS
 S CIVIL AVIATION
 S COMMERCIAL AVIATION
 S MILITARY AVIATION
 S PRIVATE AVIATION

AVIONICS

Avionics equipment development for Cayuse helicopter, discussing design with respect to weight, size, maintainability and other logistical considerations [AHS PAPER 105] 16 p2680 A67-31822
 Universal internal communications system /UICS/ for interconnecting avionic system components, using single coaxial cable and modules 17 p2813 A67-32472
 Stabilization gyros used for monitoring and detecting performance of avionic inertial navigation system, considering failure modes and effects 17 p2881 A67-32488
 Digital simulation role in advanced avionics system development such as air to air/air to ground weapon delivery, noting advantages, performance, etc 17 p2833 A67-32492
 Perturbing factors in avionics communications noting drawbacks and advantages of satellite utilization, possible commercial applications, etc 17 p2813 A67-32498
 F-111 MK 2 avionics system evaluation and parameter tradeoff considerations 17 p2819 A67-32499
 AH-56A weapons system design approach, detailing avionics subsystem 19 p3196 A67-35666
 Light Observation Helicopter Avionics Package /LOHAP/, designed for OH-6A Cayuse helicopter, providing communications and navigational capabilities 23 p3980 A67-40927

AVRO WHITWORTH HS-748 AIRCRAFT

Hawker Siddeley 748 design noting utilization rates, maintenance costs and indefinite fatigue life 15 p2419 A67-29509
 Hawker Siddeley 748 short-to-medium range civil transport aircraft design features including take off/landing field length, pressurized cabin, engines, payload, etc 18 p2986 A67-34074

AXIAL COMPRESSION

Elastic general instability of orthotropically stiffened cylinders under axial compression [ATAA PAPER 66-139] 01 p0163 A67-11154

Second order variation of system potential energy of axially compressed circular cylindrical shell with ring-stiffened edges evaluated for purely inextensional deformation 02 p0339 A67-12345
 Calculation of cylindrical minimum weight stringer shell in axial compression loading 02 p0340 A67-12662
 Modes effect on plastic buckling of compressed cylindrical shells, considering deformation theory vs incremental theory 04 p0710 A67-14852
 Buckling phenomena involving formation of indentation in thin circular cylindrical shells under axial compression 05 p0907 A67-16021
 Dynamic stability of coaxial cylindrical shells in nonuniform temperature field under uniformly distributed axial compression load 05 p0913 A67-16189
 Conical shell stability during axial compression and internal pressure under conditions of heating, noting reduction of critical load 05 p0913 A67-16192
 Cylindrical shell subjected simultaneously to axial compression and internal pressure 05 p0917 A67-16246
 Linear local buckling theory for finite length axially compressed circular cylinder and length effect on critical load 05 p0918 A67-16421
 Local buckling strength of high strength axially compressed maraging steel cylinders circumferentially prestressed with high strength epoxy-protected fiberglass filament windings 05 p0923 A67-17211
 Bending stresses in cylindrical shell with rigid circular inclusion examined under axial tension and internal pressure [AIAA PAPER 66-525] 05 p0924 A67-17351
 Shape of interaction curve for axial compression vs torsional buckling of conical shells 06 p1110 A67-18858
 Weight savings derived from use of contrasting ring, stringer and wall materials in J-stiffened axially compressed cylinders [AIAA PAPER 66-508] 08 p1424 A67-21522
 Prebuckling deformations, ring stiffeners and load eccentricity effect on buckling of stiffened cylinders 10 p1727 A67-23759
 Critical axial compression buckling loads of orthotropic cylinders having stiffening patterns analyzed, considering three instability failure modes 10 p1728 A67-23760
 Unified theory for bending and buckling of honeycomb type sandwich shell and linearized governing equations applied to axially compressed circular cylinder shells 10 p1728 A67-23761
 General solutions for linearized three-dimensional equations of elastic stability of medium compressed along one axis 11 p1870 A67-23896
 Closed cylindrical shell stability under combined bending and axial compression taking into account original arbitrary imperfection of shell form 12 p2020 A67-25567
 Propellant composition influence on finite-amplitude axial wave mode instability in solid propellant rockets [AIAA PAPER 66-600] 12 p1988 A67-25909
 Dent effect on buckling strength of aluminum alloy tubular columns subjected to axial compression [ASME PAPER 67-MET-12] 12 p2030 A67-25951
 Stability loss in steel cylindrical shells under axial compression for case of elastic and plastic strains 13 p2219 A67-26904
 Stress effect on minority carrier mobility and concentration in germanium and silicon p-n junctions under uniaxial compression 14 p2364 A67-27825
 Cylindrical elastic shell under axial compression studied for stability loss, considering large axial strains 14 p2401 A67-28737
 Stress-strain state of short cylindrical shell and square panel under axial compression hinged along edges 14 p2402 A67-28897
 Effect of single-axis compression on radiative impurity recombination in arsenic- and gadolinium-doped germanium 15 p2537 A67-29705
 Stiffener eccentricity effect on critical load in cylindrical shells under axial compression 17 p2961 A67-32775
 Axisymmetric plastic buckling of axially compressed cylindrical shells initiated under

increasing load 17 p2961 A67-32776
 Spectral and recombination radiation intensity changes from indium phosphide diode under different uniaxial compressions 18 p3100 A67-33718
 Threshold equilibrium of brittle plate with polygonal hole in biaxial tension-compression 19 p3343 A67-35845
 Buckling analysis of sandwich beams with elastic orthotropic cores under axial compression 20 p3537 A67-36641
 Shell of revolution stability under axial compressive loading with changes in curvature due to initial imperfections effects 21 p3719 A67-38053
 Eccentrically stiffened cylinders instability under axial compression, lateral or hydrostatic pressure and torsion 21 p3722 A67-38545
 Panel flutter analysis of hinged closed circular cylindrical shell in supersonic gas flow, considering axial compression and structural damping 21 p3725 A67-38788
 Two-layer circular cylindrical shell stability under axial compression with transverse displacements, analyzing axisymmetric deformation of longitudinal strip 21 p3725 A67-38793
 Axisymmetric creep in cylindrical shells, noting creep buckling collapse after high temperature compression loading 21 p3727 A67-38872
 Testing machine effect on buckling load of electroformed cylindrical shells under axial compression 22 p3909 A67-39291
 Curved plates tested under axial compression to prove curved plate buckling and postbuckling behavior formula, discussing stress distribution measurement 23 p4080 A67-41476
 Human spinal column stiffness under deflection rate /axial compression/ produced by impact 23 p3954 A67-41592
 Effect of single-axis compression on radiative impurity recombination in arsenic- and gadolinium-doped germanium 24 p4199 A67-41775
 Thin elastic shell neutral equilibrium under axial compression and hydrostatic pressure, obtaining parametric terms for expressions by using quadratic functional 24 p4249 A67-42303
 Long cylindrical two-layer shell critical asymmetric buckling time for steady creep due to external pressure and axial compression, applying variational principle 24 p4250 A67-42306

AXIAL COMPRESSOR

Axial compressor blade design for improvement of strength and vibration characteristics 01 p0006 A67-10545
 Streamline curvature computing procedures for turbomachinery and fluid flow problems, considering axisymmetric and nonaxisymmetric flow fields and compressible cascade flow [ASME PAPER 66-WA/GT-3] 04 p0607 A67-15358
 Cascade flow in axial transonic compressor, examining boundary layer separation condition 07 p1127 A67-20123
 Medium flow parameter measurement via stationary sensors for simulated test stages of axial compressor 09 p1438 A67-22456
 Effect on stage characteristics of axial compressor of design procedure used for slightly elongated vanes 10 p1697 A67-23021
 Impact and abrasion wear of axial and centrifugal helicopter compressor stages due to dust intake, showing direct proportionality to impact velocity and particle size 11 p1853 A67-24531
 Theory on secondary flows through axial compressor or turbine cascade 13 p2049 A67-26530
 End wall effects in axial compressors related to displacement thickness of boundary layer theory, using computer program [ASME PAPER 67-FE-16] 14 p2242 A67-28364
 Axial compressor blades considered as thin walled elastic shells studied for vibration forms, frequencies, stress distribution and blade geometry change effects 19 p3235 A67-34882
 Axial compressor inlet stator tests determining pressure loss relationship to geometric parameters 20 p3516 A67-37082
 Self-oscillations of axial compressor blades, taking into account variation in natural frequency of flexural vibrations

- between blades 21 p3727 A67-38835
Streamline curvature computing procedures for turbomachinery and fluid flow problems, considering axisymmetric and nonaxisymmetric flow fields and compressible cascade flow [ASME PAPER 66-WA/GT-3]
- Three-dimensional flow across supersonic single rotor axial compressor subsonic at rotor entry and exit 24 p4092 A67-42661
- ### AXIAL FLOW
- Axial flow dynamics of flexible slender cylindrical body immersed in fluid, emphasizing flow velocity, frictional forces, buckling and oscillatory instabilities 05 p0920 A67-16815
Three-dimensional flow in single stage axial flow fan rotor with prescribed and variable circulation along span 12 p1893 A67-25971
Navier-Stokes asymptotic solutions for large Reynolds number flows, emphasizing incompressible axial flow past semiinfinite circular cylinders 12 p1930 A67-26179
Interaction between buckling and flutter of circular cylindrical shell subjected to axial compression and placed in axial supersonic flow 14 p2398 A67-28092
Relativistic effects in HF plasma accelerators, noting decrease in transverse kinetic energy and axial velocity 15 p2527 A67-29475
Gas separation effects in Ranque-Hilsch vortex tube explained by dynamic model of axial flow 22 p3917 A67-39512
Spectral lines diagrammed for temperature distribution in Ar plasma arc channel transverse emission with axial flow of working fluid 24 p4196 A67-42219
Squeeze film journal bearing load support capability, noting axial pressure distribution in finite case is considerably greater than infinite case [ASME PAPER 67-LUB-14]
- 24 p4163 A67-42675
- ### AXIAL FLOW COMPRESSOR
- #### SA CENTRIFUGAL COMPRESSOR
- Circumferential asymmetry in axial flow compressors 01 p0008 A67-11272
Compressibility effect on characteristic curve of axial-flow compressor stage, using simplified assumptions and loss-free cascade flow 03 p0353 A67-14307
Noncavitating water flow tests of three loaded axial flow pump rotor blades [ASME PAPER 66-WA/FE-24]
- 04 p0607 A67-15354
Computer program for analysis of off-design performance characteristics of axial flow compressor [ASME PAPER 66-WA/GT-1]
- 04 p0548 A67-15357
Low speed cascade tunnel experiments for improvement of airflow and testing techniques, noting porous sidewall suction effect on axial velocity changes [ASME PAPER 66-WA/GT-7]
- 04 p0548 A67-15385
Prediction theory for effect of shear flows on outlet angle in axial compressor cascades, taking into account effects of secondary flow, Bernoulli surface rotation and spanwise flow displacement 04 p0548 A67-15387
Limitations on specific outputs and compression ratio per stage in supersonic compressors 05 p0874 A67-18746
Perturbation technique based on hydraulic analogy for estimating optimum efficiency and performance of axial flow compressor from description of geometry and aerodynamic environment 09 p1560 A67-22491
Acoustical and aerodynamic characteristics of full scale axial flow air compressor simulation in Freon closed loop system operation [ASME PAPER 67-GT-27]
- 11 p1742 A67-24806
Transonic axial flow compressor blade profile design, with incidence and deviation rules incorporating thickness and Mach number effects [ASME PAPER 67-GT-47]
- 11 p1742 A67-24808
Burst strength in high speed rotor in axial blower/gas turbine, noting effect of ductility and centrifugal force 17 p2961 A67-32688
Low speed cascade tunnel experiments for improvement of airflow and testing techniques, noting porous sidewall suction effect on axial velocity changes [ASME PAPER 66-WA/GT-7]
- 18 p2983 A67-34131
- Pressure drop increase in choke eliminates axial compressor stage discontinuity caused by disrupted flow formation 20 p3358 A67-37083
Stage operation compensation in multistage axial compressor during operating regimes variations along flow length 20 p3516 A67-37084
Boundary between stable operation of multistage axial flow compressor and rotational flow separation region, using variational condition 21 p3689 A67-38046
Boundary layer separation onset and propagation in axial flow compressor stages, discussing guide vane results 21 p3566 A67-38911
Onset delaying of rotating stall in axial flow compressors 22 p3744 A67-40563
Aerodynamic requirements for hovercraft and radial flow fans by adapting blade loading criteria for axial compressors 23 p3931 A67-41331
Computer program for analysis of off-design performance characteristics of axial flow compressor [ASME PAPER 66-WA/GT-1]
- 24 p4092 A67-42458
Noncavitating water flow tests of three loaded axial flow pump rotor blades [ASME PAPER 66-WA/FE-24]
- 24 p4143 A67-42465
- ### AXIAL FLOW TURBINE
- Velocity distributions at blade profiles in two-dimensional model of axial stage treated by numerical solution of Fredholm integral equations 01 p0006 A67-10525
Vibrational problems of rotor blades in axial turbomachinery [ASME PAPER 66-WA/GT-12]
- 04 p0712 A67-15362
Optimum geometrical parameters for diffuser of high pressure axial fan with straight blades 07 p1126 A67-19349
Temperature profile of single stage axial flow turbine disk and blades determined by approximation method using impingement cooling [ASME PAPER 67-GT-14]
- 11 p1854 A67-24799
Soviet book on aerodynamic flow calculations of axial flow turbines with subsonic and transonic blade cascade design method 21 p3565 A67-38766
- ### AXIAL LOAD
- Lateral motion of simply supported axially loaded viscoelastic column governed by system of linear ordinary differential equations with periodic coefficients 01 p0106 A67-10732
Ultimate bending moment capability of thin walled pressure stabilized cylinder with typical axial loads demonstrated to be 50 percent greater than bending moment at which compressive wrinkling occurs 03 p0522 A67-13230
Calculating combined radial and axial loads sustained by ball bearings in aircraft engines, turbine systems, propellers and other units 03 p0432 A67-14083
Thermophysical properties of glass-fiber reinforced plastics for selecting optimum structural patterns when under axisymmetrical load 04 p0708 A67-14787
Thin rod bending and twisting theory applied to critical speed of rotating shaft under axial loading and tangential torsion, using Galerkin approximation [ASME PAPER 66-WA/MD-1]
- 04 p0629 A67-15348
Elastic shells of revolution axisymmetrically loaded analyzed, using multisegment method for solution of boundary value problems governed by nonlinear differential equations [ASME PAPER 66-WA/APM-16]
- 04 p0713 A67-15407
Truncated conical shell stability under axial compression loads applied parallel to axis rather than along generatrix 08 p1105 A67-18593
Membrane solution of spirally corrugated shell under axial and torsional loading determined from thin shell bending equations 06 p1110 A67-18856
Imperfection sensitivity of eccentrically axial and ring stiffened cylindrical shells under axial compression and hydrostatic pressure 08 p1417 A67-20552
Cyclic torsion interaction with axial load, showing torsion angle larger than fatigue limit and applied tensile stress larger than Bauschinger yield 10 p1669 A67-23438
- Stress distribution prediction in multilayered circular cylinder subjected to combined bending and axial loading exhibiting multilinear stress-strain relationships 10 p1724 A67-23706
Deformation of laminated shell structures under axisymmetric loading, deriving differential equation by considering boundary conditions at both ends 10 p1731 A67-23846
Dynamic stability of pin-ended column under different types of random axial loading 14 p2397 A67-28091
Stabilizing effects of viscoelastic cores on response of long circular cylindrical shells subjected to time dependent axial loads 14 p2399 A67-28118
Axial load deformation of grains with end-face limitation used in solid propellant engines 14 p2377 A67-28651
Creep deformation of composite beam subjected to combined axial and bending loads 14 p2403 A67-29002
Column consisting of flexible and rigid section measured for buckling load, using Southwell method 14 p2404 A67-29057
High hydrostatic pressure effects on load cell using foil strain gauges and calibration for small uniaxial loads 17 p2855 A67-32393
Fatigue properties of explosively formed parts tested by repeated axial loading and results compared with statically formed specimens 17 p2871 A67-32433
Dynamic stability of homogeneous and inhomogeneous sandwich columns with pinned ends under pulsating periodic loads governed by Mathieu equation 17 p2963 A67-33036
Unidirectional fiber-reinforced composite under axial load, discussing power series along with point matching techniques for solving interface, matrix and filament stresses 20 p3474 A67-37268
Rotating bending fatigue limit and true stress/true strain parameters correlation for steels extended to axial load fatigue tests 21 p3719 A67-38132
U-shaped bellow fatigue strength under axial loading, discussing elastic and plastic fatigue tests using specially designed machine 22 p3913 A67-40037
High strength aluminum alloy panel resistance to fatigue crack propagation, discussing axial load fatigue machine 24 p4170 A67-41949
- ### AXIAL PUMP
- Noncavitating water flow tests of three loaded axial flow pump rotor blades [ASME PAPER 66-WA/FE-24]
- 04 p0607 A67-15354
Noncavitating water flow tests of three loaded axial flow pump rotor blades [ASME PAPER 66-WA/FE-24]
- 24 p4143 A67-42465
- ### AXIAL STRESS
- Statistical theory for strength of laminar composites used to optimize biaxial and multidirectional tensile strength properties of laminated materials 03 p0522 A67-13442
Dynamic response of cylindrical sandwich shell under axially symmetric moving ring load, considering steady state behavior 04 p0713 A67-15404
Reliable test method based on special strain gauge load transducer for embedment axial stress measurement in electronic modules 05 p0779 A67-17457
Monograph on creep and creep rupture as applied to aeronautics field noting problems in boundary and initial value, stability, stressed state, etc 07 p1264 A67-20301
Stress-dependence of Si p-n junctions with dense generation-recombination centers, showing that shifts in bias I-V characteristics are due to bandgap changes 09 p1553 A67-21947
Optimal control of elastic flight vehicles, describing axis oscillations by equations of beam with variable cross section 09 p1439 A67-22075
Short life fatigue failures in multiaxial stress-strain system 10 p1719 A67-23486
Influence of deep level impurities on uniaxial stress effect of Ge p-n junction 12 p1983 A67-25456
High pressure, uniaxial stress and temperature effects on GaAs electrical resistivity 13 p2180 A67-27159
Anisotropic circular cylindrical shell stability under linear axial stress and internal pressure 14 p2400 A67-28642

Intermediate principal stress effect on fatigue of thick wall steel tubes under triaxial stresses 15 p2573 A67-29402

Fatigue strength calculated using fracture criterion for multiaxial alternating stress and combined alternating bending and torsional stresses 17 p2960 A67-32632

Anisotropy of piezothermal EMF in Si and Ge under uniaxial stress 20 p3511 A67-37147

Axial shear wave radial propagation in nonhomogeneous elastic medium under axisymmetric loading solved by Laplace transform and characteristics method 21 p3719 A67-38146

Long cylindrical shell with externally loaded reinforcing ring, solving stress distributions and displacements 21 p3727 A67-38871

Permanent deformation and interaction effects of rigid plastic clamped beam with constraints against axial displacements and subjected to transverse impulsive loading 23 p4072 A67-40606

AXIS

S EARTH AXIS

S ROTOR AXIS

S TILTED PROPELLER AXIS

AXISYMMETRIC BODY

Plastic flow of axially symmetric notched bars pulled in tension, obtaining load factors 01 p0159 A67-10401

Characteristic dimension selection for optimum supersonic heat transfer in axisymmetric body of prescribed shape 04 p0546 A67-14794

Characteristic method analysis of linear system of dynamic cylindrical equation for axisymmetric motion, including rotary inertia and shear correction factor [AIAA PAPER 67-79] 06 p1104 A67-18497

Junction of several walls of revolution along parallel in axisymmetric vessel 06 p1105 A67-18588

Laminar, transitional and turbulent boundary layer flows with adverse pressure gradient on axisymmetric blunted conical flared body at Mach 10 06 p0943 A67-18844

[AIAA PAPER 66-493]

Deformed figures of Maclaurin spheroids from solving post-Newtonian hydrodynamic equations for uniformly rotating axisymmetric bodies 08 p1354 A67-21245

Boundary value problem for electrostatic field external to slender axisymmetric conductor 08 p1413 A67-21301

Magnetoaerodynamic flow relations for axisymmetric blunt bodies with shock layers in shifting equilibrium 10 p1591 A67-23114

Optimum stabilization problem for axisymmetric satellite, considering fuel consumption 12 p2011 A67-25639

Integration of boundary layer equations for axisymmetric body rotation in unbounded medium at rest 13 p2095 A67-26900

Optimum stabilization of axisymmetric satellite by system of n reactive jets 14 p2393 A67-27854

Gas dynamic functions for supersonic gas flow past axisymmetric bodies of various configurations 14 p2239 A67-27991

Unsteady aerodynamic forces due to gusts on supersonic bodies of revolution 19 p3172 A67-36001

Drag coefficients for random and planar tumbling satellites 21 p3563 A67-37809

Random thermoelastic stress concentration near edge of circular cylindrical shell determined using axisymmetric formulation 21 p3718 A67-37979

Boundary layer flow incident on smooth axisymmetric body in vicinity of critical point 21 p3613 A67-38422

Base pressure calculation of stepped axisymmetric body in supersonic flow based on turbulent mixing theory 22 p3740 A67-39944

Integral equation for discontinuous flows and free streamline solutions for axisymmetric bodies at zero and small angles of attack 22 p3743 A67-40166

Shock curvature and flow variable gradients at tip of pointed axisymmetric body in nonequilibrium flow, solving linear differential equations and singularity 23 p3928 A67-41176

Length of supersonic core of axisymmetric jet exhausting into quiescent atmosphere 23 p3992 A67-41739

AXISYMMETRIC DEFORMATION

Numerical solution of nonlinear

differential equations governing finite axisymmetric deformation of thin shells of revolution 01 p0164 A67-11176

Toroidal shell of circular cross section free of bending under uniform normal hydrostatic pressure 02 p0338 A67-11589

Stress-strain calculations for thin walled axisymmetric shells with arbitrarily shaped midplane based on second order theory 03 p0521 A67-13018

Axisymmetric modes of loss of stability of circular plates lying on elastic base in inhomogeneous stress field 03 p0529 A67-14163

Axisymmetric deformation of cylindrical shell reinforced by frames located at arbitrary distance from each other and having different geometrical and elastic characteristics 03 p0530 A67-14171

Tensile plastic instability in axisymmetric deformation of sheet metals 04 p0710 A67-14976

Steady state axisymmetric thermoelastic problems in bispherical coordinate system [ASME PAPER 66-WA/APM-12] 04 p0713 A67-15403

Shallow spherical shells with uniform and/or point loads in prebuckled or postbuckled configuration treated by approximate solution [ASME PAPER 66-WA/APM-21] 04 p0714 A67-15411

Integration of nonhomogeneous equations for axisymmetric bending of spherical shells by variation of parameters 04 p0717 A67-15887

Nonlinear equations for supercritical axisymmetric elastic deformation of circular cylindrical shell under longitudinal impact from rigid body 05 p0907 A67-18015

Spherical elastic inclusion in transversely isotropic material under axisymmetric torsion field 05 p0910 A67-18149

Axisymmetric deformation of shallow shells of revolution, noting membrane solutions 05 p0917 A67-18245

Axisymmetric bending of circular sandwich plates with lightweight compressible filler subject to special transverse or local loads 05 p0922 A67-17175

Small plastic deformation theory determination of elastoplastic stressed state of thin walled isotropic incompressible shell of revolution under axisymmetric power loads and nonuniform heating 05 p0922 A67-17177

Inversion formula for principal integral representation of class of P-analytic functions applicable to axisymmetrical problems of elastic bodies 05 p0923 A67-17185

Asymptotic solution to elasticity theory problem for hollow isotropic cylinder of finite dimensions and small thickness under axisymmetric load distributed over entire surface 06 p1100 A67-18033

Axisymmetric vibration modes of cylindrical-hemispherical membrane tank partly filled with liquid [AIAA PAPER 67-75] 06 p0988 A67-18273

Generalized Stodola iteration method for computer analysis of axisymmetric buckling of ring-stiffened orthotropic shells of revolution [AIAA PAPER 67-109] 06 p1103 A67-18339

First boundary value problem for general case of axisymmetric stressed state of body of revolution, using biharmonic solution of Love and Grodskii 07 p1264 A67-20037

Second order equations of motion for free axisymmetric deformation of thin spherical shells, discussing membrane and composite mode of solution 08 p1416 A67-20490

Axisymmetric crack formation problem in elastoplastic material including energy dissipation and face displacement calculations, noting agreement with Griffith theory 10 p1716 A67-22939

Finite element displacement method extended to bifurcation buckling of shells of revolution under axisymmetric loading 10 p1725 A67-23715

Exact solution of transverse shear deformation effect on axisymmetric large deflection of circular sandwich plates for different loading states and boundary conditions 10 p1728 A67-23762

Axisymmetric deformation of elastic slab with external crack interpreted as steady state problem of heat conduction 11 p1813 A67-24313

Nonlinear membrane theory for thin elastic inflatable shells during pressurization phase 11 p1875 A67-24432

Buckling test data for internal integral ring-stiffened aluminum cylinders under combinations of axisymmetrical axial load and external lateral pressure 11 p1875 A67-24611

Axisymmetric buckling of orthotropic circular plates with variable thickness in terms of lateral plate deflection and stress distribution 11 p1876 A67-24660

Thermoplasticity problem for circular cylindrical shell subjected to arbitrary axisymmetric heating and loading 12 p2023 A67-25593

Critical stresses of compressed three-layer cylindrical shell of asymmetrical structure in presence of variable temperature 12 p2026 A67-25614

Axisymmetrical deformation and static instability region of circular cylindrical shell under longitudinal compressive load 12 p2026 A67-25615

Rigid plastic cylindrical shell axisymmetrical deformations in terms of Tresca yield condition and gradient law when under load 12 p2026 A67-25618

Variational methods for calculating small axisymmetrical oscillations of conical shell of revolution partially filled with ideal incompressible fluid 12 p2028 A67-25633

Shallow conical shell stability acted upon by external hydrostatic pressure 12 p2028 A67-25635

Shells of revolution under axisymmetric loading analyzed within ideally plastic shell theory, examining mathematical difficulties of shell carrying capacity 12 p2029 A67-25637

Effect of axisymmetric impact against water on shallow clamped aluminum spherical shell-type caps 12 p2030 A67-25937

Axisymmetrical stability loss problem in thin walled cylindrical shell with continuous elastic filler 12 p2031 A67-25958

Axial load deformation of grains with end-face limitation used in solid propellant engines 14 p2377 A67-28651

Iterative solution through boundary value problem and integral equations for axisymmetric deformation of body remote from symmetry axis 17 p2962 A67-32874

Exact linear elastic analysis of end effect problems for isotropic cylinders 17 p2963 A67-33019

Monography on plastic axisymmetric collapse of ring stiffened cylindrical shells under external hydrostatic pressure 18 p3140 A67-33432

Evaluation of stored-energy function for elastomeric materials based on biaxial experiments [JPL-TR-32-1006] 18 p3145 A67-34486

Experimental duct for plane deformation of homogeneous turbulence, measuring mean velocities in axis and symmetry plane 20 p3420 A67-36393

Differential equation for axisymmetric deformation of thin circular cylindrical shell stiffened by circumferential rings and subjected to lateral and axial pressure 20 p3537 A67-36495

Circumferentially symmetrical stressed state of half-space determined using Polozhyl formulas in axisymmetric elasticity theory and p-analytic functions 20 p3538 A67-36918

Circular plate on nonlinearly elastic base with uniform load force at center, tangential force and contour moments for plate deflection 20 p3539 A67-36923

Linear equation for micropolar elastic solids deformation, including radial displacements with axial and radial symmetries 20 p3540 A67-37021

Flat plate bending and two-dimensional, axisymmetric and boundary value problems in elasticity theory investigated using Vlasov initial function method 21 p3725 A67-38792

Two-layer circular cylindrical shell stability under axial compression with transverse displacements, analyzing axisymmetric deformation of longitudinal strip 21 p3725 A67-38793

Aircraft pipeline flanges manufacture by compression permit direct connection of sections into single main 21 p3637 A67-38924

Stress-strain state of tubular blanks expanding under uniform distributed internal load 21 p3637 A67-38925

Finite difference method for

axisymmetrical and plane elasticity problems using high speed computer 22 p3908 A67-39290
Mode acceleration method for axisymmetric dynamic response due to time dependent loading in spherical and cylindrical shells 22 p3914 A67-40190
Thin toroidal elastoplastic shells of revolution loaded axisymmetrically, calculating force, moment, stress and strain interrelation for middle surface using complex representation 24 p4250 A67-42305

AXISYMMETRIC FLOW

Swirling axisymmetric radial jet flow of conducting fluid in presence of axial magnetic field, citing conditions for singularity in two-dimensional case 01 p0124 A67-10800
Turbulent mixing of axisymmetric jet of partially dissociated nitrogen with ambient air, establishing mixing and decay characteristics [AIAA PAPER 65-823] 01 p0055 A67-11171
Hydrodynamic tunnel wall effect on minimum cavitation number in axisymmetric cavitation flow around solids 02 p0232 A67-11631
Numerical solutions of equations of motion and energy for heating of non-Newtonian fluids in rectilinear axisymmetric laminar flow in circular tubes extended to case of cooling at constant tube-wall temperature 04 p0720 A67-14510
Streamline curvature computing procedures for turbomachinery and fluid flow problems, considering axisymmetric and nonaxisymmetric flow fields and compressible cascade flow [ASME PAPER 66-WA/GT-3] 04 p0607 A67-15358

Radial momentum equation of flow outward from axisymmetric turbulent wall air jet impinging on solid surface 05 p0792 A67-16819

Sixth order polynomial calculation of axisymmetric laminar boundary layer of incompressible fluid removed by suction and arbitrary velocity distribution 05 p0749 A67-17184

Wind tunnel results for expansion problem of two-dimensional and axisymmetric turbulent jets with zero excess impulse 06 p0982 A67-17742

Axisymmetric modes and frequency vibration of thin conical shells subjected to rapid surface heating 06 p1100 A67-18000

Rational approximation method for calculating supersonic axisymmetric flow of perfect gas around given blunt body 06 p0943 A67-18846

Hydraulic analogy applied to axisymmetric nonideal compressible gas systems, considering water table simulation of axisymmetric rocket nozzle 08 p1324 A67-21519

Axisymmetric vortex flow in neighborhood of point having sonic line orthogonal to velocity vector 10 p1624 A67-23034

Asymptotic exponential laws of contraction of plane and axisymmetric jets of weightless fluids, obtaining expressions for stream function and velocity component 10 p1624 A67-23039

Inviscid axisymmetric radiating flow over blunt body, analyzing paraboloidal shock wave thermal radiation effects on temperature, density, velocity, etc 10 p1592 A67-23453

Inviscid two-dimensional flow using extension of Hele-Shaw analogy, noting axisymmetric, compressible and MHD cases 10 p1627 A67-23554

Axisymmetric thermal convection flow in rotating fluid annulus 12 p1963 A67-25340

Axisymmetric supersonic jet injection from conical nozzle into supersonic wake flow or medium at rest 13 p2050 A67-26896

Subsonic-transonic drag of supersonic, two-dimensional and axisymmetric plug inlets 13 p2051 A67-27592

Three-dimensional supersonic flow past pointed nonaxisymmetrical bodies characterized by great local surface curvature changes, using new approximation 13 p2051 A67-27617

Averaged axisymmetric vortex flow of ideal incompressible fluid in turbine engine 14 p2296 A67-27986

Flow processes and static and dynamic performance characteristics of axisymmetric fluid jet modulator and single receiver-

diffuser studied experimentally 14 p2248 A67-28269
Simple impact position model for predicting subsonic mass flow for opposing axisymmetric jet 14 p2303 A67-28331
Weakly perturbed supersonic flows in presence of arbitrary number of nonequilibrium physicochemical processes 15 p2472 A67-29688
Linearized theory for unsteady flow about bodies of revolution in sonic stream 16 p2589 A67-30790
Elliptic nose shape bluntness effect on drag of bodies of revolution in axisymmetric subsonic flow 16 p2589 A67-30791
Vortex breakdown treated as failure of quasi-cylindrical approximation for viscous axisymmetric flow 16 p2658 A67-30948
Axisymmetric free turbulent jet flow with swirling vortex motion over wide range of swirl degree 17 p2838 A67-32417
Nonstationary plane and axisymmetric flows, discussing acoustic and Oswatitsch theories, velocity potentials, differential equations of motion, etc 17 p2839 A67-32713
Annular wing motion in compressible fluid axisymmetric flow, determining forces acting on wing cross section 18 p3022 A67-33411
Turbulent base pressure in supersonic axisymmetric flow behind blunt body [AIAA PAPER 67-446] 18 p3026 A67-33922
Axisymmetric flow equations for performance prediction of axial-flow turbomachines and stage design 20 p3355 A67-36186

Laminar boundary layer with heat transfer in liquids with variable fluid properties, including velocity and temperature profiles [ASME PAPER 67-HT-69] 20 p3550 A67-36749

Group properties of differential equations describing axisymmetric thin layer jet flow of ideal fluid propagating along surface of revolution 20 p3422 A67-37063

Exact solutions of incompressible Navier-Stokes equation for irrotational Beltrami nonconvective two-dimensional swirl and axially symmetric cross flows 21 p3609 A67-37737

Boundary value problems of wave propagation in plane, investigating coverage, source distribution and velocity perturbations 21 p3615 A67-39093

Boundary layer equation system for axial steady and unsteady flows past bodies of revolution 22 p3739 A67-39217

Rarefied gas axisymmetric stagnation point flow, clarifying relationship between continuum and Knudsen layer flow 22 p3784 A67-39836

Representation of characteristic surfaces of unsteady axisymmetric flow and steady three-dimensional supersonic flow by hyperbolic system of quasilinear differential equations 22 p3785 A67-40010

Haskell viscous flow equations describing very slow linearly viscous liquid with initially crater shaped surfaces solved and applied to lunar craters 23 p4065 A67-40998

Peristaltic viscous fluid motion through axisymmetric pipes and symmetrical channels produced by pressure gradients and cross section changes, using Stokes approximation 23 p3990 A67-41174

Inviscid steady axisymmetric flow inside closed annulus solution derived with extremal principle [ARL-66-0173] 24 p4140 A67-41807

Streamline curvature computing procedures for turbomachinery and fluid flow problems, considering axisymmetric and nonaxisymmetric flow fields and compressible cascade flow [ASME PAPER 66-WA/GT-3] 24 p4143 A67-42459

AXISYMMETRY

Energy functionals and universal integrals of motion for force field symmetric about axis of rotation 01 p0113 A67-10680

Analytic properties of solutions to generalized axisymmetric Schroedinger equation 08 p1346 A67-20355

Energy functionals and universal integrals of motion for force field symmetric about axis of rotation 11 p1821 A67-25069

AZIDE

SA SODIUM AZIDE

Artificial cloud produced in twilight over Wallops Island by payload containing sodium azide and lithium azide 03 p0412 A67-13371
Lead azide and pentaerythrite tetranitrate explosion triggered by laser

radiation 07 p1195 A67-19315
Electronic absorption spectrum observed during cyanogen azide flash photolysis 13 p2177 A67-26988
Factors involved in initiation of reaction in cobalt /III/ amine azides, discussing thermal decomposition, activation energy, etc [CI PAPER 67-15] 19 p3309 A67-35009

AZIMUTH

Azimuthal asymmetry in distribution of shower particles around shower axis, using Geiger-Muller counter telescopes 01 p0145 A67-11230

Precession theory of compensating gyroazimuth, discussing random disturbances reduction by introducing electric mismatch of both sensitive elements 16 p2670 A67-30467

Principal polarization radar cross sections as function of azimuth aspect angle for rectangular cylinder 19 p3183 A67-35518

AZINE

S PHENOTHIAZINE

AZO COMPOUND

Classification of 2-oxazolidones, examining preparation, physical chemistry, properties and polymerized derivatives 23 p3971 A67-41041

AZOLE

S IMIDAZOLE

S POLYBENZIMIDAZOLE

B

B-47 AIRCRAFT

Submillimeter-wave measurements for water-vapor detection from jet aircraft flying in stratosphere 13 p2114 A67-26795

B-52 AIRCRAFT

B-52 structural response to random turbulence with various stability augmentation systems, noting rigid body motions, normal vibration modes and control surface rotations [AIAA PAPER 66-998] 02 p0181 A67-12302

B-70 AIRCRAFT

S XB-70 AIRCRAFT

B STAR

Abnormal low helium abundance in atmospheres of old halo B star based on weak absorption lines in helium spectra 09 p1568 A67-22438

Total to selective interstellar absorption ratio, with improved values calculated for six-star group, considering spectral energy distribution and color excesses 22 p3883 A67-39767

U-B and B-V color indices, total absorption, color excesses and reddening lines for hot black bodies, with energy curve corrections for absorption line effects 22 p3883 A67-39768

O and B stars surveyed with 154 cm Catalina reflector show discrepancies from mean interstellar polarization-wavelength dependence near Orion 23 p4062 A67-40626

B-103 AIRCRAFT

S BLACKBURN B-103 AIRCRAFT

BAC 111 AIRCRAFT

Data reduction with maintenance recording system onboard BAC 111 aircraft, noting use of automatic mode initiation logic, data compression, etc [AIAA PAPER 67-377] 15 p2420 A67-30348

Plessey constant speed drive/starter /CSDS/ application to BAC 111 commercial transport, discussing dual role 17 p2800 A67-31975

BACILLUS

Sporulation mutations induced by heat in Bacillus subtilis 08 p1287 A67-20983

Organic phosphate shown as inhibitory factor from B. stearothermophilus for attachment of amino acids to transfer RNA 20 p3370 A67-36798

Oxidative phosphorylation effects on energy metabolism of Thiobacillus thioparus in cell-free system 20 p3371 A67-36927

Bacillus brevis var. G-B survival ratio dependence on space flight factors, noting no induction of dissociation products nor appearance of auxotrophic mutants 21 p3577 A67-38597

BACK INJURY

Vertebral fractures in pilots from helicopter accidents in dorso-lumbar junction of spinal column 12 p1902 A67-25170

BACKGROUND EFFECT

Wave propagation in random plasma

medium with inhomogeneous parabolic electron density profile background for ionospheric propagation applications 23 p3974 A67-41199

BACKGROUND NOISE

Noise limitations in obtaining three-dimensional images by holographic techniques, considering graininess of photographic emulsion 01 p0067 A67-10834
Background noise effect on low level light intensity measurement of microsecond transient discharge 02 p0243 A67-12185
Detectability criterion for signal received against random noise background 03 p0368 A67-13277

Attenuation of background noise and exterior static through use of low impedance links and use of light loading in transistorized assemblies 03 p0379 A67-13389
VHF antenna proposed as working gain standard, determining antenna gain by two-identical antenna method 03 p0385 A67-13859

Statistical theory for optimum direction-finding system for space-time signal processing against wideband fluctuation noise background 03 p0371 A67-13947
Model of speech perception against noise background, hypothesizing that acoustic stimuli are mapped in segments 05 p0763 A67-16706

Two-step procedure for high energy signal detection against noise background, based on statistical probability 05 p0765 A67-16954
Simultaneous estimate of delay time and drift of carrier frequency during nonoptimum reception against correlated noise background 05 p0766 A67-17166

Background noise produced by high energy radiation incident on photomultiplier tube, stressing differences between tubes in number of small pulses produced 10 p1618 A67-23809
LF noise fluctuation anomalies in narrow doped germanium p-n junctions at low temperatures 11 p1765 A67-24476

Automatic frequency control for estimating random signal frequency when received against white noise background 13 p2069 A67-27037
Radar antenna synthesis for maximum SNR and minimum error dispersion in target bearing, reducing problem to filter synthesis 13 p2069 A67-27039

Aperture efficiency of Parkes radio telescope reflector for decimeter and centimeter wavelengths obtained through celestial radio source 14 p2282 A67-28035
Rocket engine noise study in infrasonic range from launching pad ignition phase through flight phase, including ignition signals from upper stages 14 p2393 A67-28053

Cost function to evaluate quasi-optimal amplitude meter for signal with random initial phase on white noise background with random correlation function 16 p2623 A67-31015
Error probabilities of matched filter receiver operating in additive combination of impulsive and Gaussian noise 17 p2812 A67-32120

Threshold value of SNR of radar system in target detection against reflecting background, deriving block diagram consisting of linear group, detector and integrator 17 p2816 A67-32684
External noise levels effect on angular accuracy of tracking radar pencil-beam antennas, emphasizing radome noise and dielectric coating characteristics 17 p2826 A67-32685

Optimal signal selection on background of steady additive noise in realistic communications system 20 p3382 A67-36777
Optimum detection of Markov signals against noise background in case of discrete time 20 p3408 A67-37039

Optimal detection of signals by spatially distributed receiving system against random noise background, using space-time signal selection method 20 p3383 A67-37070
Fredholm equation solution and minlmax theory for p-dimensional vector signal detection against p-dimensional Gaussian noise background 22 p3762 A67-39876

N-type InSb microwave noise emission at low temperatures in low electric field regime, measuring magnetic field threshold and background continuum 22 p3864 A67-40345
Background noise measurement results using statistical model for vortex velocities, obtaining noise spectrum for type II superconductors 24 p4200 A67-41889

IR detectors analyzed for dependences of detectivities on temperature, noting noise role 24 p4201 A67-41907

Fundamental statistical oscillation characteristics expressions for quasi-harmonic self-excited oscillators with low noise and many degrees of freedom 24 p4129 A67-42225

Optimal reception of binary signals on background non-Gaussian noise determined by logarithm expansion for probability coefficient into Taylor series 24 p4122 A67-42377

Signal extraction and scattering of telluric currents studied for random sheets, semilinear medium and interface separating medium of different resistivities 24 p4152 A67-42885

BACKGROUND RADIATION

Radio sources and background radiation survey at 38 mc/s, presenting contour maps of brightness temperature and list of flux densities 01 p0151 A67-10966

Potential sensitivity of energy radiation detectors, examining measurement error causes for radiation power of natural and artificial sources 10 p1607 A67-23589

Cosmic microwave background measurements along celestial equator, using Dicke radiometer to study anisotropy of cosmic black body radiation 11 p1864 A67-24564

Discovery of or setting upper limit to strength of features of small angular size when studying isotropy of cosmic background radiation 11 p1857 A67-25000

Intergalactic radiation absorption and extragalactic sources contribution to LF background radiation 12 p1995 A67-25766

Solar gamma-ray flux in high energy region analyzed using OSO-I satellite 14 p2381 A67-28057

Excess cosmic microwave background temperature of 2 degrees K at 1.5 cm wavelength 15 p2551 A67-30161

Upper limit data about reported very low temperature distributed-source microwave background radiation and small-scale angular distribution 17 p2945 A67-32653

Energy spectrum of cosmic X-rays background component, proving experimentally rocketborne detector counting rate proportionality to field of view 19 p3314 A67-35278

Luminous and intergalactic matter, background radiation, radio sources, quasars, cosmic rays and other observational data relevant to cosmological models 19 p3327 A67-35870

Quasar sources studies set limits on possible density inhomogeneity magnitudes in universe by measuring cosmic microwave background isotropy and homogeneity 20 p3525 A67-36868

UV and X-ray background measurements by Venus 3 may lead to mean density estimation of matter in universe through determination of intergalactic medium density and thermal history 21 p3705 A67-38591

Earth upper atmosphere background radiance measured by UV radiometer carried on Air Force satellite 22 p3794 A67-40364

Microwave background radiation angular distribution anisotropy lower limit estimated from perturbations of cosmological model 22 p3892 A67-40498

Equivalent temperature of cosmic microwave background radiation at 3.2 cm wavelength, discussing Dicke type radiometer and error sources 23 p4063 A67-40922

Microwave background in steady state universe explained by starlight absorption and microwave reemission by interstellar dust, discussing young spiral galaxies 24 p4226 A67-41875

Radiation measurement from satellite, discussing observation of ozone absorption band 24 p4181 A67-42397

BACKSCATTER

Direct backscatter recordings from polar cap F-layer reflections used to predict communications 01 p0020 A67-10007

Impact expansions and interference patterns in atomic scattering theory for cases of forward scattering, backscatter, inversion problem and screened Coulomb potential approximation 01 p0112 A67-10143

Interdependent microwave radar-and radiometer-sensor measurements of backscatter and albedo characteristics of earth surface 01 p0021 A67-10333

Surface color explained using backscattering angle and diffraction properties of germanium films vacuum deposited onto heated substrate 01 p0138 A67-11076

Gaussian noise model of shadowing effect on wave backscatter from one-dimensional random rough surface 02 p0192 A67-11602

Electron number density profile measurements of moderate and heavy sporadic E over Arecibo by incoherent backscatter technique 03 p0409 A67-12946

Directional reflective coating consisting of cylindrical dielectric fibers oriented perpendicular to absorbing substrate [AIAA PAPER 65-671] 03 p0467 A67-13039

Curvature effect on reflection coefficient of layered absorbers, examining backscattering from coated cylinder and sphere 03 p0370 A67-13852

Raindrop and melting hailstone absorption, scattering and backscatter cross sections of millimeter waves in satellite communications and weather radars 04 p0577 A67-15685

Backscattering of centimeter waves from ruffled sea surface at small angles of slip 05 p0761 A67-16345

Gamma ray backscatter principles for measurement of atmospheric density, using test results from altitude chambers in balloon and sounding rocket payloads 05 p0840 A67-16527

All-weather pulsed X-ray instrument for altitude measurement and terrain identification 05 p0806 A67-16528

Terrain backscattering characteristics at low grazing angles for X-and S-band 05 p0768 A67-17527

Scatterometer measuring radar backscattering for prediction of terrain characteristics 08 p1293 A67-20682

Selective imaging of objects in range using pulsed laser illuminator synchronized with Kerr cell camera, obtaining elimination of film exposure due to backscatter in turbid atmosphere 08 p1337 A67-20683

Sporadic E backscatter noting two peaks in activity, motion, temporal component parameters and cause 13 p2107 A67-26306

Backscattered light intensity from laser beam for measuring atmospheric density variations, discussing optimization of sensitivity 13 p2072 A67-27609

Radar/backscatter/ cross section of wakes of vehicles in ionosphere, showing creation of mild electron depletion under broadside incidence conditions 14 p2261 A67-28125

Lunar radar echoes depolarization studied via lunar surface backscattering characteristics at 23 cm wavelength 14 p2261 A67-28374

Angular spread of backscattered spread-F echoes compared with that associated with normal F region returns [AGARDOGRAPH 95] 15 p2480 A67-30278

Origin of afternoon VHF radar echo from backscattering layer near auroral electrojet explained by plasma instability and perpendicular electric and magnetic fields 16 p2627 A67-31407

Conducting plate backscatter minimization method by load adjusting of loop in front of plate, noting experimental verification 17 p2815 A67-32622

Volume backscattering functions and optical extinction coefficients for visible and IR radiation and selected cloud models 17 p2817 A67-33293

Influence of aurora on radio wave propagation 18 p3038 A67-33617

Auroral backscatter theory and relationship to instability concepts 18 p3038 A67-33618

HF backscattering from absorbing infinite strip with arbitrary face impedances 18 p3005 A67-34730

Acoustic radio signal backscattering producing rippled signals, showing activity with broad ripple spectrum 19 p3185 A67-36018

Traveling-ionospheric disturbances observed at midlatitudes by backscattering technique, noting auroral zone and gravity waves role 20 p3425 A67-36280

80 km atmospheric backscattering enhancement detected by optical radar 22 p3759 A67-39558

Ozone parameters determination from measurements of radiation backscattered by earth atmosphere 22 p3794 A67-40365
 Atmospheric density, temperature and composition altitude variation measured by satellite observation of laser backscatter Raman component 22 p3806 A67-40366
 Electromagnetic backscatter from edge scattering centers found on cylinders and flat-backed cones, discussing hemispheric scattering 23 p3973 A67-40839
 Vector field theory of time dependent backscatter from distant slightly rough sphere for pulsed and sinusoidally steady state sources 23 p3974 A67-41200
BACKWARD WAVE
 Glow discharge positive column response to external perturbations, obtaining moving striations profile, structure and backward wave nature 19 p3273 A67-35094
 Backward waves effect on excitation of delay line by modulated electron beam with zero transit angle 22 p3767 A67-39422
BACKWARD WAVE OSCILLATOR
 Nonuniformity of mm wave detected by wideband frequency sweep control backward wave oscillator 16 p2643 A67-30896
 Crossed field cascade tubes as frequency oscillators and microwave generators, discussing improved performance and interaction efficiency of devices 22 p3775 A67-40559
BACTERIA
 SA BACILLUS
 SA HYDROGENOMONAS
 SA SPORE
 SA VIRUS
 Physical characteristics of residual DNA in bacterial cells after degradation due to ionizing radiation 06 p0953 A67-18774
 Enzymatic activity and inhibition, thermal stability and electrophoretic properties of induced and constitutive acid phosphatases of *Euglena gracilis* 10 p1598 A67-23397
 Protein synthesis reduced and turnover stimulated by valine in *P. saccharophila* in nongratuitous inducing conditions 13 p2058 A67-26584
 Ionizing radiation effect on bacterial cells noting inhibition due to generated hydrogen peroxide 13 p2059 A67-26867
 Bacteria survival and mutation in radiation environment on Voskhod I and II 14 p2254 A67-27864
 Mutagenic effects of primary cosmic radiation on bacteria 14 p2254 A67-28213
 Preservation of viable microbes in anabolism in potassium salts determined improbable by failure to grow bacteria 15 p2427 A67-29118
 Antimicrobial properties for various spacecraft materials, discussing impregnation methods for bactericides and two-stage sterilization 19 p3179 A67-35229
 Factors involved in use of thymine by uninfected cells in metabolism of *Escherichia coli* 20 p3370 A67-36799
 Automated system for growth and analysis of bacterial colonies using environmental chamber and computer controlled flying-spot scanner 20 p3453 A67-37598
 Microbe shock in human organism during prolonged space flight due to intestinal tract flora variation from food consumption lacking variety 22 p3750 A67-39334
 Molecular weight and amino acid composition of chromatium ferredoxin 24 p4113 A67-42653
BACTERIOLOGY
 Lethal effects of high intensity airborne sound and ultrasound and irradiation time on *Bacillus Subtilis* for applications to spacecraft sterilization 01 p0016 A67-10881
 Mixed cultures of *Chlorella pyrenoidosa* TX 71105 and various bacteria and use in closed systems for support of man 10 p1598 A67-23626
 Spacecraft habitability, discussing chemical and bacteriological changes, air contamination and biological compatibility for crew selection 13 p2061 A67-26754
 Low barometric pressure, high carbon dioxide concentration and water availability on simulated Mars environment related to survival and growth of *Bacillus cereus* 15 p2426 A67-29111
 Hypoxia effect on cellular and humoral immunity of mice to bacterial infection 16 p2612 A67-30906
 Survival and growth of *Bacillus cereus* and

B. subtilis in simulated Martian environment of diurnal temperature cycling and low moisture and oxygen level 20 p3372 A67-37160
 Isolation of *Acinetobacter anitratus* from subject and room area during spacecraft environmental tests 21 p3573 A67-38072
BACTERIOPHAGE
 Rapid assay for thymidylate synthetase as specific and sensitive measure of enzyme activity 14 p2260 A67-28479
 Lethal effect of solar UV radiations on dried Coliphage T-1 exposed to space at sounding rocket altitudes 19 p3177 A67-35184
 Alteration in pyrimidine metabolism occurring after infection of *E. coli* with T-even bacteriophage 20 p3370 A67-36795
BAFFLE
 Effect of several injector face baffle configurations on screech in 20,000-lb thrust hydrogen-oxygen rocket 04 p0691 A67-15987
 Damping of liquid oscillations in cylindrical tanks, determining rigid and flexible baffle loss coefficients, baffle efficiency and maximum bending stress [AIAA PAPER 66-97] 05 p0793 A67-17210
 Damping coefficients for rigid and flexible ring baffles for slosh suppression 15 p2470 A67-29438
 M-1 injector baffles, ablative chamber and start system design and development, using subscale testing [AIAA PAPER 67-461] 18 p2988 A67-33932
BAG
S CONTAINER
BALLOUT
 SA EJECTION
 SA PARACHUTING
 Optimal methods of escape from helicopter, examining rotor avoidance during ejection 14 p2256 A67-27745
 Ejection capability vs decision to eject 22 p3754 A67-39596
BAKER-NUNN CAMERA
 Standard earth geodetic coordinate system and Baker-Nunn camera station positions 01 p0056 A67-10038
 Corrections to Smithsonian astrophysical observing station coordinates and nonzonal harmonics from combination of dynamical and geometrical method 01 p0056 A67-10039
 NASA-sponsored satellite geodesy program using Baker-Nunn camera, noting station positions and gravitational potential determination 01 p0056 A67-10040
 Orbital elements determination from reduced Baker-Nunn observations of satellites, noting disturbance by resonance effects of earth gravitational potential sectorial and tesseral harmonics 05 p0763 A67-16562
 Tesseral harmonics of coordinates using Baker-Nunn data and geopotential and dynamical procedures, noting iterative cycle for correction determination 10 p1636 A67-23178
 Corrections to station coordinates and nonzonal coefficients of geogravitational potential from Baker-Nunn observations by combined dynamical and geometrical method 10 p1636 A67-23179
 Proposal for computation of unknown parts of gravitation field of earth from successive satellite passages 10 p1636 A67-23180
 Artificial satellites tracking by Smithsonian Astrophysical Observatory, discussing station locations, instrumentation, operation modes, interface and selection 18 p3003 A67-34236
 Low perigee satellite orbit determination by visual observation, comparing directional accuracy and orbital elements with Minitrack and Baker-Nunn 18 p3126 A67-34247
 Determination of Love number of earth from variations of orbital inclinations of satellites 18 p3041 A67-34250
 Optical data acquisition by NASA for National Geodetic Satellite Program flash photography 20 p3382 A67-36888
BALANCE
 S ACID-BASE BALANCE
 S AERODYNAMIC BALANCE
 S COMPENSATOR
 S HEAT BALANCE
 S MASS BALANCE
 S MICROBALANCE
 S STRAIN GAUGE BALANCE
 S WATER BALANCE
 S WIND TUNNEL BALANCE

BALANCE EQUATION
 SA MOTION EQUATION
 SA PRESSURE FIELD
 SA VORTICITY EQUATION
 Analog computer ionization recombination parameters and balance equation of charged particles in F-2 layer 02 p0236 A67-11659
 Energy balance equations including effects of heating by electron gas, cooling and energy coupling obtained for various ion species, assuming each ion gas has Maxwellian velocity 08 p1326 A67-21363
 Finite difference approximation of balance wind equation, discussing convergence of Liebmman relaxation process, Coriolls term and computer time 09 p1525 A67-21551
 Unbalance vibration of rotor analyzed for application to rotor bearing system with dynamic forces represented by spring and damping coefficients [ASME PAPER 67-VIBR-27] 11 p1796 A67-24185
 Wind and pressure fields diagnostic relations substituted for classical equation of stream function and solved as boundary value problem 13 p2149 A67-26273
 Analog computer ionization recombination parameters and balance equation of charged particles in F-2 layer 16 p2665 A67-31074
 Kinetic model of matter for energy momentum tensor of general relativity, noting freedom of divergence 17 p2883 A67-32360
 Buildup time for nonequilibrium argon ionization at inlet of MHD generator channel 18 p2989 A67-34048
BALANCED AMPLIFIER
 S PUSH-PULL AMPLIFIER
BALL BEARING
 Ball bearing lubrication with vapor from volatile organic compounds for wide temperature range and long-term operation 01 p0077 A67-10120
 Spring theory of ball bearing supporting rotor and role in vibration analysis of system 02 p0248 A67-11468
 Calculating combined radial and axial loads sustained by ball bearings in aircraft engines, turbine systems, propellers and other units 03 p0432 A67-14083
 Literature in 1965 on lubrication and bearings covering friction and wear, boundary, metal working, gear and spline lubrication, rolling element bearings, etc [ASME PAPER 66-WA/LUB-8] 04 p0629 A67-15349
 Model analysis of radial oscillations of shaft with pounding of ball bearings 05 p0812 A67-17236
 Motion equations for free vibrations of shaft mounted on ball bearings 07 p1191 A67-19355
 Ball bearing life operating in vacuum with molybdenum disulfide and oils as lubricant [ASLE PAPER 66AM 7A3] 08 p1335 A67-21036
 Loaded oil-lubricated steel ball bearings operating in vacuum and air investigated for electric current effect on damage [ASLE PREPRINT 67AM 1C-1] 14 p2325 A67-28783
 Materials rolling contact fatigue strength measured by tester intended to serve as screening device [ASME PAPER 67-LUBS-3] 16 p2676 A67-31381
 Gyromotor vibration level variation causes and ball rotation regimes permitting stabilization 18 p3047 A67-33994
 Unmanned spacecraft reliability, discussing design requirements, testing, lifetimes, performance and ball bearing failures 20 p3532 A67-36573
 Loaded oil-lubricated steel ball bearings operating in vacuum and air investigated for electric current effect on damage [ASLE PREPRINT 67AM 1C-1] 22 p3813 A67-40218
 High temperature lubricants for ball bearing applications, discussing bearing endurance and rolling-contact fatigue tests on synthetic paraffinic oil [ASME PAPER 67-LUB-21] 24 p4163 A67-42679
 Rolling element bearing fatigue life for cyclic race oscillation, analyzing variation with load, speed and oscillation amplitude via Weibull statistics [ASME PAPER 67-LUB-22]

- Chemical interactions in formation of oxidation resistant solid lubricant composites of tungsten diselenide-gallium alloys for use in ball bearing systems 24 p4163 A67-42680
[ASLE PAPER 67-LC-6] 24 p4164 A67-42745
- Optical elastohydrodynamic system for evaluation of lubricants using interference pattern obtained from metal ball rolling against plate glass
[ASLE PAPER 67-LC-12] 24 p4164 A67-42747
- ### BALLISTIC CAMERA
- U.S. Coast and Geodetic Survey satellite triangulation program based on optical tracking of passive satellites simultaneously from two or more mobile camera stations 07 p1176 A67-19764
- Position determination for mobile luminous objects in sky by triangulation, using ballistic photographic chambers in positions pinpointed by star sightings 07 p1188 A67-19770
- BMK ballistic camera with equatorial and azimuthal mount for stellar geodetic satellite tracking and punch card controlled mono- and stereocomparators 07 p1188 A67-19773
- Ballistic camera calibration method and triangulation of satellite position from camera observations 07 p1188 A67-19776
- Velocity measurement and image recording of freely moving objects during ballistic tests by electronic and photographic methods 16 p2674 A67-31126
- Photoelectric method measuring separation of head shock wave from supersonically-moving body, detailing equipment design and operation 16 p2674 A67-31128
- ### BALLISTIC MISSILE
- Photographic techniques developed for photographing ballistic missiles and associated explosive reactions, including shadowgraph and schlieren techniques [SMPT PREPRINT 100-59] 03 p0423 A67-13807
- Management of development, design, contracting, construction, checkout and acquisition in ballistic missile program 05 p0929 A67-16620
- Downrange radar and optical data reduction used for evaluation of ejection velocities of ballistic missile penetration aids at deployment
[AIAA PAPER 66-405] 05 p0902 A67-17209
- Simplified approach to predicting onset of spin-yaw instability of rapidly ascending rolling ballistic missile in absence of asymmetric forces 08 p1406 A67-20509
- Parameter management applied to roll rate control in ballistic missile target system /BMTS/ with fin incidence 08 p1407 A67-20516
- Operational phase of Minuteman program [AAS PAPER 66-162] 08 p1430 A67-20977
- Operational phase of Minuteman program [AAS PAPER 66-162] 13 p2233 A67-27557
- Inertial guidance system for ground-to-ground ballistic missiles or space vehicle launchers 16 p2700 A67-30799
- Parameter management applied to roll rate control in ballistic missile target system /BMTS/ with fin incidence 21 p3712 A67-37801
- Radio telemetry links perturbations during ballistic missile reentry due to plasma from kinetic heating 21 p3581 A67-38228
- Simplified approach to predicting onset of spin-yaw instability of rapidly ascending rolling ballistic missile in absence of asymmetric forces 22 p3904 A67-40103
- ### BALLISTIC RANGE
- Aerothermochemical eddy diffusion model for predicting rapid wake ionization decay behind hypersonic slender clean cone obtained in free flight ballistic range [AIAA PAPER 67-21] 06 p0938 A67-18257
- Aerodynamic characteristics of Mars probe/lander configurations consisting of blunted cone, shell and spherical segment analyzed at various Mach numbers on ballistic range
[AIAA PAPER 67-167] 06 p0941 A67-18482
- Nanosecond pulse light sources used in free flight hypersonics for ballistic range measurements, noting less photographic blurring of motion 06 p0981 A67-18881
- Statistical mechanics predictions of turbulent fluctuations in hypersonic wake from ballistic range experiments and theoretical stochastic model of gas particle motion [AIAA PAPER 67-22] 07 p1168 A67-19431
- Shock tube performance of Langmuir probe suitable for ballistic range applications, noting low pressure turbulent wakes 15 p2490 A67-30212
- Electronic equipment for generating delay times corresponding to missile velocity during optical recording by numerous sensors distributed along ballistic firing range 16 p2674 A67-31118
- Ballistic range blast-traversal testing technique using scale models containing fast response FM telemetry system modulated by capacitance type pressure transducer [AIAA PAPER 66-777] 17 p2832 A67-32063
- Time-resolved spectra for hypervelocity spheres and cones in free-flight ballistic range obtained by large aperture spectrograph and image converter 17 p2862 A67-33290
- Aerodynamic characteristics of Mars probe/lander configurations consisting of blunted cone, shell and spherical segment analyzed at various Mach numbers on ballistic range
[AIAA PAPER 67-167] 19 p3169 A67-34816
- Microsphere ablation in free-flight range observed by laser photography, giving shadowgraphs with density contour map 19 p3346 A67-35757
- ### BALLISTIC TRAJECTORY
- Compact flash X-ray systems for radiographic measurement of moving objects, radar ranging, atmospheric density, radiation effects, etc 02 p0245 A67-12215
- Phugoid trajectories of ballistic reentry of hypothetical glider into variable density atmosphere 05 p0847 A67-17009
- Complete error budget of ballistic flight orbit prediction including force model error effects
[AAS PAPER 66-106] 07 p1253 A67-19966
- Feasibility and design study of unguided solar orbital launch vehicle 08 p1404 A67-20493
- Photooptical system for determining velocity of projectile after target penetration 09 p1502 A67-22623
- Laser rangefinder limit for rocket, balloon or satellite trajectory, noting effects of various parameters related to source, receiver, etc 10 p1663 A67-22881
- Complete error budget of ballistic flight orbit prediction including force model error effects
[AAS PAPER 66-106] 13 p2208 A67-27524
- Real time meteorological system for ballistic high altitude multistage rocket trajectory, computation and prediction 13 p2091 A67-27610
- Drag coefficient of moving body during ballistic tests calculated from given space-time dependence 16 p2592 A67-31121
- Design and construction principles of radio telemetry recording systems for gasdynamic observations in ballistic testing 16 p2624 A67-31124
- Ablation of low melting models on ballistic facility, giving ballistic trajectory optimum conditions and ablation parameters calculation method 16 p2593 A67-31134
- Phugoid trajectories of ballistic reentry of hypothetical glider into variable density atmosphere 18 p3079 A67-34272
- Rocket launchings of French ballistic program, discussing trajectory study techniques 18 p3020 A67-34379
- Monkey psychomotor reactions during ballistic flight investigated noting alertness reduction during weightlessness 19 p3178 A67-35241
- Monkey psychomotor reactions during ballistic flight, noting alertness reduction during weightlessness 19 p3181 A67-35466
- Langvin similarity theorem applied to ballistic perturbation theory, deriving formulation containing temperature gradient, descent acceleration and kinetic height parameters 19 p3328 A67-35578
- Steering equation derived from dynamic equation of velocity gain, as function of booster state for rocket vehicle ballistic trajectory [AIAA PAPER 67-595] 19 p3259 A67-35991
- Terminal velocity theory of freely falling body with ballistic coefficient of 200 psf and altitude region between zero and 60,000 ft 21 p3656 A67-37811
- Steering equation derived from dynamic equation of velocity gain as function of booster state for rocket vehicle ballistic trajectory [AIAA PAPER 67-595] 24 p4182 A67-42910
- ### BALLISTIC VEHICLE
- Internal ballistic considerations in hybrid rocket design, noting throttling and regimes of operation involving effects of surface-or gas-phase reaction kinetics
[AIAA PAPER 66-628] 07 p1240 A67-19377
- Approximate formulas for determining speed reduction, maximum deceleration and orbit modifications for ballistic vehicle that grazes atmosphere 08 p1394 A67-21106
- Ballistic reentry vehicle recovery via low speed water impact or air snatch after vehicle has flown unperturbed trajectory down to altitude of maximum dynamic pressure 15 p2564 A67-29424
- Aerodynamic, thermodynamic, heat shield and structural design aspects of ballistic vehicle entering planetary atmosphere 19 p3332 A67-35315
- Crash and ballistic protection flight helmet with greater impact energy dissipating characteristics, noting laminated nylon fabric shell and polystyrene liner 21 p3577 A67-38075
- ### BALLISTICS
- #### SA INTERIOR BALLISTICS
- #### SA PENETRATION BALLISTICS
- Ballistic coefficients for power law body shapes compared with those for conical bodies having identical lengths, diameters and specific weights 05 p0750 A67-17360
- Supersonic liquid jets produced by ballistic extrusion with velocities of 4.58 km/sec 06 p0982 A67-17603
- Ballistic propellant combustion alteration and thermal effects due to dynamic spinning observed on solid propellant sounding rockets 08 p1408 A67-20522
- Linear relations between ballistic perturbation coefficients for main problem of external ballistics 13 p2211 A67-26705
- Ballistic aspects, structure and destructive power of Tungusk meteorite do not support thermal explosion hypothesis 15 p2558 A67-30010
- Hermetically sealed ballistic facility design and operating principles, for testing at various Mach and Reynolds numbers to calculate aerodynamic coefficients and flow geometry 16 p2655 A67-31115
- Pressure measurement at stagnation point of cylindrical missile with spherical nose cone during free flight in ballistic testing 16 p2593 A67-31123
- Ballistic aspects, structure and destructive power of Tungusk meteorite do not support thermal explosion hypothesis 20 p3530 A67-37534
- Dynamic ballistics of combustion termination by fluid injection in solid propellant motors, describing termination mechanisms 21 p3733 A67-38893
- Second order nonlinear differential equation derived for pressure-time curve required for ideal solid propellant rocket motor 24 p4208 A67-42923
- ### BALLOON
- #### SA HIGH ALTITUDE BALLOON PROGRAM
- #### SA METEOROLOGICAL BALLOON
- German lighter than air technical and economic travel problems of medium speed dirigibles using helium and nuclear power drives 22 p3745 A67-39751
- ### BALLOON FLIGHT
- Balloon launching problems at Port-aux-Francais 04 p0614 A67-14900
- Electron intensity measurement in primary cosmic radiation by high altitude balloons carrying telescope made of two plastic scintillation counters 05 p0878 A67-16097
- Aluminium oxide hygrometer performance obtained from balloon flight tests 05 p0808 A67-17307
- High altitude balloon flights with gamma ray spark chamber for search of cosmic gamma ray source in Cygnus 06 p1078 A67-18212
- Ascending spherical balloon motion reduced by flight Reynolds number reduction from supercritical to subcritical values 08 p1278 A67-21529
- Primary cosmic radiation and interaction in atmosphere studied during minimum solar activity by balloon flights to determine effect of latitude on secondary photons 15 p2550 A67-29533
- New lower upper limit on solar neutron flux at energies greater than 60 mev for

emission during quiet times 17 p2936 A67-32532

Balloon-borne Michelson interferometer for far IR solar spectrometry 20 p3438 A67-36344

Electron intensity measurement in primary cosmic radiation by high altitude balloons carrying telescope made of two plastic scintillation counters 24 p4213 A67-42773

Equations for spherical superpressure balloon vertical rise in calm air 24 p4095 A67-42927

BALLOON SOUNDING

High altitude balloon soundings, noting balloon construction parameters 01 p0010 A67-10934

Atmospheric and surface temperature profile measurement using balloon mounted IR spectrometer 01 p0061 A67-11391

Balloon observation of thermal radio emission of molecular oxygen in terrestrial atmosphere 02 p0237 A67-11852

Detection of slow neutrons escaping from atmosphere by counters filled with boron fluoride onboard high altitude balloons 02 p0312 A67-12599

Fast neutron latitude variations in atmosphere during solar minimum measured by high-altitude balloons, noting neutron leakage into space 03 p0505 A67-12950

Instrumental and observational aspects of balloon X-ray astronomy involving position, angular size, intensity and spectral measurements of X-ray sources [AIAA PAPER 66-1015] 03 p0514 A67-14151

Middle UV region of solar radiation, discussing rocket and balloon mounted spectrograph measurement results 04 p0695 A67-14691

Atmospheric ozone in middle UV spectral region, noting vertical distribution, destruction by solar radiation, lifetime below layer in photochemical equilibrium, etc 04 p0612 A67-14694

High-counting-rate particle detector for balloon sounding of atmospheric top 04 p0621 A67-14899

Cosmic radiation measurements in stratosphere from 39 sounding balloons 04 p0692 A67-14901

Energy spectrum of cosmic ray heavy nuclei, using stack of nuclear emulsions exposed during Quiet Sun on balloon flight 04 p0692 A67-14960

Isotropic component of cosmic X-rays at balloon altitude 04 p0693 A67-14963

Balloon observation of upper limits of solar gamma rays for spectral ranges 20-200 kev and 1-10 mev 04 p0693 A67-14974

Balloon payload orientation system for viewing fixed position on celestial sphere 05 p0805 A67-16465

Solar proton flux measurement with balloon-borne detectors in northern Scandinavia 05 p0882 A67-16740

GHOST balloon experiments, determining life, stability and clustering characteristics at several altitudes 07 p1219 A67-19065

Optical problems when making IR astrophysical observations with balloon-borne telescope noting data documentation, focusing, image slicer, spectrometer, aberration correction, etc 07 p1184 A67-19388

Balloon-borne Czerny-Turner grating spectrometer used to measure atmospheric transmittance in spectral regions between 2 and 14 μ 07 p1184 A67-19389

Balloon-borne high resolution Fourier interference spectrometers analyzed in terms of IR Michelson interferometer and near IR cats-eye interferometer [JPL-TR-32-1071] 07 p1184 A67-19391

Balloon-borne telescope guidance by offset sun tracking 07 p1184 A67-19392

Atmospheric temperature profile to 30 km determined by balloon-borne grating spectrometer of radiance of earth between 2100 and 2700 reciprocal cm [JPL-TR-32-1080] 07 p1171 A67-19394

Balloon-UV polarimetry using two different telescope-gondola systems 07 p1184 A67-19395

Balloon-borne sun seeker improvements through transistorized circuits and solid state switches 07 p1184 A67-19396

Azimuth stabilization of balloons, using frictionless bearing to decouple gondola 07 p1191 A67-19403

Angular intensity distribution of short wave radiation measured by automatic stratospheric balloons 07 p1220 A67-19453

Spatial and temporal characteristics of bremsstrahlung X-ray due to energetic electron precipitation in auroral zone, noting measurement techniques 07 p1180 A67-19929

Crab Nebula X-ray spectrum from balloon observations, noting importance of correction for escaped iodine K component 07 p1251 A67-19944

Low energy cosmic ray photons in atmosphere, noting X-ray generation by bremsstrahlung effect of electron component 08 p1377 A67-21466

Cosmic ray nuclei propagation in interstellar space and solar system examined from balloon, rocket and satellite soundings 08 p1378 A67-21473

Horizontal tropospheric probe using constant altitude balloons 09 p1525 A67-22560

Stratospheric free air turbulence detection from slant-range FPS-16 radar tracked Jimsphere balloons 10 p1676 A67-22815

Meteorological probes using GHOST balloons for wind measurements 10 p1594 A67-23197

Differential spectrum of cosmic protons at various latitudes and years surveyed by balloons 11 p1855 A67-23932

Primary cosmic radiation abundance measurements on iron and heavier nuclei, using Cerenkov counter on balloon flights 11 p1856 A67-24504

Digitized spark chamber for gamma ray and charged particle experiments on balloons and satellites noting construction, performance characteristics and results 12 p1944 A67-25854

Upper limits to hard X-ray flux from quiet sun analyzed by balloon-borne scintillation detector measuring celestial sources 13 p2189 A67-26302

Atmospheric electron energy spectrum in range 70-2000 mev measured, using scintillation telescope with gas Cerenkov detector and lead glass total energy spectrometer 15 p2475 A67-29615

Spectrometers, utilizing interference filter wedges, for field use, especially in hostile environments 15 p2491 A67-30430

Wind profile analysis from balloon sounding data, using Fourier series to filter out unwanted part of spectrum 16 p2668 A67-31742

Properties of slowly varying ionospheric absorption events in auroral zone analyzed using balloon soundings 17 p2845 A67-32794

Low energy H and He isotope detection in cosmic radiation at solar minima via balloon mounted scintillation counter 17 p2939 A67-33246

Far IR surveys of sky for thermal radiation from interstellar grains and other sources of far IR radiation, using balloon sounding 17 p2952 A67-33362

Balloon measurements of auroral X-rays, discussing flux and energy spectrum variations and bursts relation to magnetic storms 18 p3038 A67-33613

Atmospheric radiation balance studies via daytime balloon measurements, obtaining vertical profile curves for albedos, total and reflected radiation, etc 19 p3214 A67-34853

Absorption of total solar radiation using vertical profiles from balloon observations, estimating attenuation due to aerosols 19 p3214 A67-34854

Solar proton flux measurement by balloon on July 7, 1966 in northern Scandinavia, with differential proton flux calculated for several energies 19 p3312 A67-35175

Primary diffuse X-ray flux and spectrum found isotropic by balloon measurements made in three particular directions 19 p3313 A67-35244

Trajectory analysis of EOLE meteorological balloons flights in troposphere over Southern Hemisphere 19 p3332 A67-35276

Rocket and balloon studies of solar radiation, wind characteristics, equatorial electrojet and lower ionosphere electron density 19 p3223 A67-35474

Balloon-borne diffusing system designed to measure absorption of minor atmospheric constituents, as sun set and passed below horizon 19 p3322 A67-35697

Cosmic X-ray sources in 20-180 kev energy range detected in balloon flights, giving energy spectra 20 p3520 A67-37475

Onboard and ground radio-engineering system for stratospheric transport balloon noting telemetering, remote control and

localization functions integrated in system 21 p3581 A67-38213

Mesoscale structure of atmospheric winds analyzed using data obtained from FPS-16 radar/Jimsphere precision wind measuring system 21 p3655 A67-38576

Tethered sonde for micrometeorological soundings of lower atmosphere noting pressure transducer, servoswitching system, thermistor, hygistor, data acquisition, etc 21 p3628 A67-38582

Stabilized platform for stratospheric balloons for IR, UV and X-ray astronomy 22 p3830 A67-39184

Auroral zone balloon measurement of 5 and 25 msec duration energetic electron burst fluxes 22 p3873 A67-39821

Satellite Infrared Spectrometer /SIRS/ flown by balloon for cloud top and surface temperatures 22 p3829 A67-40370

Cosmic ray intensity from balloon sounding, discussing proton to He ratio behavior as time function within Parker solar modulation model 23 p4051 A67-40809

Balloon sounding data for atmospheric secondary and reentrant albedo proton intensity values, discussing empirical atmospheric secondary proton spectrum 23 p4051 A67-40810

Intensities of cosmic ray produced deuterium and tritium in atmosphere measured from high altitude balloons 23 p3995 A67-40811

Balloon-borne electronic system for heavy primary cosmic ray particle charge identification noting compactness, low power consumption and circuit design 23 p4009 A67-41479

Instrumental and observational aspects of balloon X-ray astronomy involving position, angular size, intensity and spectral measurements of X-ray sources [AIAA PAPER 66-1015] 23 p4070 A67-41711

Satellites and balloons for earth surface observation surveyed by types noting operations concerning geodesy, weather, oceanography, vegetation and wildlife 24 p4150 A67-42201

BALLUTE

SA DRAG DEVICE

SA PARACHUTE

Aerodynamic deceleration systems, discussing basic materials and fabrication techniques of BALLUTE program [AIAA PAPER 66-988] 02 p0181 A67-12299

Ballute aerodynamic characteristics in 0.1 to 10-Mach number region for various applications [AIAA PAPER 67-228] 06 p0942 A67-18518

Aerial delivery concepts including drag cones, lift platforms, gliding parachutes, ballute parachute, ultrafast-opening parachute, etc 17 p2796 A67-32519

Ballute aerodynamic characteristics in 0.1 to 10-Mach number region for various applications [AIAA PAPER 67-228] 19 p3169 A67-34817

BALMER SERIES

Radio telescope-spectrophotometric scanner investigation of continuous energy distribution of four quasars 08 p1398 A67-21230

Asymmetric broadening of H-beta Balmer line in hydrogen doped argon plasma arc 09 p1536 A67-21562

Satellite and ground based measurements of incident proton neutral hydrogen flux and Balmer alpha optical emission in auroral hydrogen arc 23 p3995 A67-40803

Decrement of Balmer line widths and H-alpha profiles when distributing fine components as function of radial velocity in optical prominences 24 p4232 A67-42595

BANACH SPACE

Kantorovich theorem, Goodman-Lance method and two-point boundary value problems, noting numerical results obtained on IBM 7094 computer 02 p0259 A67-11836

Optimal approximations by trigonometric polynomials for classes of periodic functions belonging to Banach space invariant 03 p0459 A67-13645

Abruptly varying random processes with determinate deflection, discussing phase space in form of Banach space 04 p0646 A67-15260

Stationary points of nonlinear maximum problems in Banach space B [DVL-642] 04 p0594 A67-15880

Lebesgue space in measure theory on Borel sets and Banach algebra over compact

semigroups 07 p1214 A67-19211
 Solvability of class of linear differential equations with polynomial coefficients 07 p1217 A67-20152
 Monograph on existence theorems for nonlinear equations, using functional analysis in Banach space 08 p1348 A67-21175
 Conditions required for Reynolds operator to be idempotent over Banach algebra 13 p2146 A67-27149
 Mysovskikh theorem concerning convergence of Newton method for finding zeros of nonlinear operators between Banach spaces 13 p2147 A67-27172
 Nonlinear programming in Banach space, considering saddle value problem 13 p2147 A67-27453
 Asymptotic form of uniform approximation of abstract functions by single family of linear integral operators occurring in Banach space topology 14 p2341 A67-27834
 Stationary Newton method for nonlinear functional equations in Banach spaces, formulating convergence conditions 16 p2697 A67-31332
 Homogeneous continuous Markov process without discontinuities of second kind and form of infinitesimal operator 17 p2878 A67-32735
 Real-valued function integration with respect to additive set function with real Banach space 17 p2879 A67-32810
 Kato perturbation theorems applied to ordinary differential equations in Banach space 20 p3478 A67-37575
 Extended dynamical systems in Banach space and use of invariance principle for stability theory of partial differential equations 24 p4178 A67-42652

BAND
 S ABSORPTION BAND
 S BLOCH BAND
 S CONDUCTION BAND
 S ENERGY BAND
 S FORBIDDEN BAND
 S FREQUENCY BAND
 S K-BAND
 S L-BAND
 S PHOTOLUMINESCENT BAND
 S SCHUMANN-RUNGE BAND SYSTEM
 S SLIP BAND
 S SPECTRAL BAND
 S SPIRAL BAND
 S SWAN BAND
 S VEGARD-KAPLAN BAND

BAND PASS FILTER
 Oscillating limiter effect on message modulation for band pass filter with flat amplitude and linear phase characteristics in input signal frequency range 01 p0025 A67-10859
 Shielded coupled strip transmission line with three center conductors, noting electrical behavior, cross section dimension evaluation from characteristic immittances, etc 02 p0193 A67-11777
 Two-frequency volume resonator with independent tuning within wide frequency band 02 p0214 A67-11911
 Ring trapped mode resonator for use in microwave filters, developing expressions for unloaded Q and resonant frequency in transverse electric mode 02 p0217 A67-12091
 Impulse and step responses of band stop equal element filters with varying degrees of dissipation calculated for transient responses of resonant circuits 02 p0220 A67-12177
 Quantum effects in noise-free communication channels with infinite and limited pass bands in channels with noise, in quantum counters and coherent amplifiers 03 p0368 A67-13140
 Power spectra analysis based on method of computing weighting sequence whose frequency characteristics approximate one-third octave filter and applying coefficients recursively to digitized data 03 p0375 A67-13563
 Lumped-constant filters whose bandpass depends only on one parameter of transmission coefficient, having lower bandpass for given transient process delay time 03 p0380 A67-13582
 Tuning techniques for waveguide band pass filters operating below cut-off frequency 03 p0387 A67-13994
 Solid organic filters using polymethyl siloxane resin as host material for 2000-3000 angstrom range 03 p0470 A67-14393
 Rayleigh distribution function of envelope

of signal/noise mixture in n parallel filter 04 p0568 A67-14453
 Digital computer-aided circuit sensitivity analysis using symbols, with example of band pass filter analysis 04 p0578 A67-15088
 Three-wire-line interdigital filters of Chebyshev and elliptic function characteristic for broad bandwidth 05 p0775 A67-16946
 Equivalent circuit synthesis for microwave band pass filter design consisting of interdigital or comb structure EM line-coupled resonators 07 p1149 A67-19132
 Waveguide resonant-iris bandpass filter with very wide passband and stopbands that provide transmission and attenuation characteristics for use with microwave generators 07 p1151 A67-19426
 Inductorless band pass filter to prove validity of hypothesis that all inductors in LC filter can be replaced by gyrator-capacitor equivalents 07 p1154 A67-19615
 Amplitude distortion as function of filter bandwidth for various generalized pulse shapes 07 p1157 A67-20090
 Direct-coupled confocal resonators used as band pass filters at mm wavelengths 08 p1305 A67-21229
 Phase frequency characteristics of two-and three-circuit band pass filters used in radio receiving devices 08 p1305 A67-21279
 Pulse compression parallel channel technique for evaluating channel filter characteristics effect on compressed pulse form 11 p1754 A67-24648
 Intermediate band pass photometric system properties and reduction and calibration procedures 11 p1792 A67-24778
 Output characteristic function for two-channel analog cross correlator with each channel input consisting of deterministic signal combined with stationary Gaussian noise 12 p1916 A67-26080
 Low pass high pass time-varying filter combination with stopband attenuation obtained by outphasing in quadrature-modulation arrangement 13 p2078 A67-26787
 Transmittance and reflectance measurements on wirecloth and metallic meshes using vacuum grating spectrometer for design of transmission band pass filter in far IR 13 p2121 A67-27354
 Statistics of fluctuation processes occurring at outputs of filter/discriminator/integrator system acted upon by wideband noise 14 p2283 A67-28279
 Design for active filters via eight-pin miniature component 14 p2283 A67-28288
 Rayleigh distribution function of envelope of signal/noise mixture in n parallel filter 15 p2435 A67-29290
 Design procedures for practical elliptic function filter with high selectivity in very compact configuration, noting bandpass and band-stop applications 15 p2444 A67-29453
 Cauer polynomials forming procedure suitable for synthesis of LC ladder filters without mutual coupling, giving design procedure of Cauer filter 15 p2452 A67-29935
 Resonant gate transistor used in integrated circuits as frequency selector element for tuning 16 p2642 A67-31724
 Active filter design employing impedance converters, amplifiers and gyrators, providing equations for component values 17 p2824 A67-32394
 Design criteria for narrow optical passband filters used in reception of nonparallel modulated monochromatic radiation 17 p2862 A67-33291
 Digital filters with ICs boost Q without inductors 18 p3012 A67-34490
 Resonant-transfer sampling technique stressing bandpass filtering design and time division multiplex 20 p3379 A67-36243
 Waveguide-below-cutoff bandpass filter theoretical design using equivalent circuit of filter to derive attenuation and bandpass properties 20 p3400 A67-37217
 Spectral irradiances determined by conventional prism monochromator and by system employing narrow bandpass interference filters 21 p3656 A67-37850
 Magnetically tunable multisection bandpass filter in ferrite-loaded evanescent waveguide 22 p3772 A67-39907
 Systematic design of TEM equal stub admittance filters on basis of insertion loss 22 p3773 A67-40061

Dissipation loss equation solved by graphic form for ripple values of Chebyshev band pass filters 22 p3774 A67-40344
 Two varactor diode bandpass filter for parametric amplifier, analyzing bandwidth vs gain 24 p4128 A67-41968
 Transmission behavior of double tuned band filters with frequency dependent feedback and stagger tuning 24 p4129 A67-42206
 Moderate bandwidth tunnel diode amplifier using directional filter as bandpass structure 24 p4131 A67-42445
 Low loss mechanically or magnetically tunable 1 to 12 GHz hybrid ferrimagnetic dielectric microwave bandpass filter with improved power handling 24 p4132 A67-42808

BANDWIDTH
 Power amplification/bandwidth product of active device as measure of rate at which power supply energy converts to signal energy, noting TWT role 01 p0032 A67-10011
 Signal-space quantization and bandwidth compression examined, using theory of mappings of signal spaces with Riemann matrices 01 p0027 A67-11239
 Radiation patterns and impedance plots of sleeve antenna over band with frequency ratio of 4 to 1 02 p0212 A67-11607
 Optimum telemetry system characteristics for shock, vibration and acoustic measurements and data bandwidth sufficiency 02 p0196 A67-12009
 Space bandwidth signal spectral analysis using multichannel optical system and two-dimensional optical system with increased frequency resolution 02 p0243 A67-12049
 Low noise parametric self-resonance amplifiers with bandwidths, discussing use of high diode Q-factor 02 p0220 A67-12204
 Bandwidth and distortion in pulse filters 03 p0389 A67-14303
 Unusual optical detection characteristics in multiplier phototube when monitoring circuit bandwidth is extended 05 p0807 A67-16791
 Width of i band of p-n nuclear emission detector during Li ion drift through doped Si semiconductor detector 05 p0872 A67-17500
 Simple diode parametric amplifier, discussing bandwidth and noise measurements and compensating circuits for gain-frequency response improvement 09 p1474 A67-22085
 Thermal and electrical properties and width of forbidden bands of PbTe and PbSe from 90 to 800 degrees K 12 p1986 A67-26094
 Triple-tuned broadband UHF junction circulator using lumped element technique 13 p2076 A67-26483
 Data compression for analog signal transmission with smaller bandwidth requirement obtained from reduced signal redundancy and simulation of techniques 14 p2275 A67-28683
 Spectral distribution of absorption coefficient in polycrystalline films of cadmium sulfide over wide temperature range 14 p2372 A67-28852
 Gain-bandwidth product of parametric reflection amplifiers with line-type resonators 15 p2454 A67-30145
 Maximum gravitational radiation detection range for binary stellar system analyzed by mechanically resonant antennas 15 p2563 A67-30162
 Wideband varactor upconverters for satellites use, emphasizing transmission characteristics and stability over wide temperature range 16 p2640 A67-31531
 Asynchronous pulse modulation systems developed using step and linear segment approximations of message waveforms 17 p2812 A67-32318
 Midband saturation characteristics of ammonia maser amplifier and variation of maser bandwidth with gain 20 p3458 A67-36431
 Bandwidths of reflex multicavity solid state masers containing active material in cavities 20 p3462 A67-37328
 Bandwidth restriction effect on SNR in NRZ signal from PCM transmission system 21 p3584 A67-38667
 Coded information transmission with reduced band emphasizing pulse prediction through redundancy, information quantity and delta signal 21 p3585 A67-38763
 Bandwidth reduction for holographic data transmission systems noting application to TV 22 p3796 A67-39260

Temperature dependence of ferromagnetic parallel resonance line width in Ni-Fe alloy films, stressing surface oxidation role 22 p3855 A67-39350

Short circuit photocurrent of avalanche photodiode, determining frequency response and multiplication effect on bandwidth 22 p3767 A67-39362

TV system resolution improvement without bandwidth increase, discussing accuracy of random alphabetic characters 23 p3975 A67-41282

Two varactor diode bandpass filter for parametric amplifier, analyzing bandwidth vs gain 24 p4128 A67-41968

Unilateral parametric amplifier using two varactor diode low pass filter with pumping phase difference, noting bandwidth and gain 24 p4128 A67-41969

Book on radar signals covering FM pulse compression signals, waveform, Doppler shift, time factor, etc 24 p4122 A67-42425

Channel bandwidth assignment determination using prescribed fraction of total radiated power of system contained in channel, discussing spectral distribution 24 p4123 A67-42714

Optical communications systems capable of microwave bandwidths evaluated experimentally and theoretically 24 p4123 A67-42805

Data handling capabilities of periodic time function for given bandwidth using Fourier series in sinusoidal spectrum 24 p4124 A67-42931

BANG-BANG CONTROL

Bang-bang control for feedback systems, applying computer to optimization of switching time from state to state of linear systems 05 p0784 A67-16854

Third order control system saturation, considering approximate solution to third order bang-bang system 08 p1312 A67-20722

Optimum transient response for bang-bang control system with finite time control activation 09 p1483 A67-22609

Quasi-linearization determination of optimum finite thrust and impulsive orbital transfers 10 p1706 A67-23130

Adaptive controller synthesis for unstable mechanical system driven by bang-bang actuator adaptive controller synthesis for unstable mechanical system driven by bang-bang actuator 16 p2648 A67-31656

Describing functions for nonlinearly consisting of bang-bang with dead zone characteristic followed by linear integrator with constrained integration range 16 p2652 A67-31690

Time optimal control for parabolic equations, proving bang-bang principle, smoothness, existence of minimum, etc 17 p2877 A67-32559

Bang-bang control using adaptive-predictive model applied to least-square error trajectory control of settling-time nonlinear systems 19 p3199 A67-34784

Single-axis time and fuel supoptimal /superior optimal/ control for spacecraft attitude control obtained via bang-bang manipulation of damping and jet commands 22 p3897 A67-39155

BAR

SA ELASTIC BAR

SA PRISMATIC BAR

Heat dissipation rate in straight bar of constant cross section generating heat internally, using Laplace transforms 01 p0166 A67-10551

Shape determination for uniform-strength clamped bar with constant dynamic stress distributions subjected to first order free vibrations 05 p0917 A67-16247

Plastic wave propagation in semiminfinite bar subjected to axially applied impact stress 20 p3536 A67-36416

BARBITURATE

S SECOBARBITAL

BARIUM

Optical properties of evaporated barium films investigated at various wavelengths, using ultrahigh vacuum reflectometer 03 p0499 A67-13909

Motion equations for ionized irregularity of finite length applied to barium ion cloud, deriving expression for ionospheric electric field 08 p1326 A67-21357

Sounding rocket-released artificial strontium and barium ion cloud motion in upper atmosphere, based on equations of ambipolar diffusion 10 p1644 A67-23254

Electronic band structure calculations phase of Ca, Sr and Ba over wide range of atomic volumes under pressure electronic band structure calculations for fcc phase of Ca, Sr and Ba over wide range of 10 p1682 A67-23399

Thermoelectronic properties of pure and barium-film coated face of tungsten single crystal thermoelectronic properties of pure and barium-film coated face of tungsten single crystal 10 p1694 A67-23646

Spectral data and energy level diagrams from magnetic and electric field passage through barium cloud 18 p3036 A67-33606

Fully ionized barium plasma column generating device, discussing spectroscopic measurements of ion motions, densities, temperatures and electron temperature 23 p4033 A67-41215

BARIUM COMPOUND

Dielectric properties of complete solid solutions with perovskite structures in barium titanate-barium stannate and barium titanate-barium ferrotantalate systems 07 p1231 A67-19489

Liquid scintillation counting method with sonic oscillations, noting decreased preparation time and increased counting efficiency 14 p2260 A67-28477

Interferometrically-measured ion temperatures compared to electron temperatures in pure barium and barium-cesium plasmas produced by contact ionization 16 p2720 A67-31243

Phonon annihilation during decay of two metastable fluorescent states of ionized Ba compound 24 p4205 A67-42737

BARIUM FLUORIDE

Sublimation and gaseous equilibria involving neodymium fluorides and barium fluorides 03 p0367 A67-13519

Self-lubricating properties of composites of porous nickel and nickel-chromium alloy impregnated with barium fluoride-calcium fluoride eutectic 08 p1335 A67-21035

Barium fluoride film electric hygrometer element aging and possible causes of calibration drift with time in storage 24 p4156 A67-42380

BARIUM TITANATE

Electron resonance and magnetic properties of solid solution in bismuth ferrite and barium titanate system, obtaining phase diagram 01 p0127 A67-10063

Mechanical pressure effect on polarization processes in barium titanate single crystals and barium titanate-zinc oxide solid solutions 03 p0489 A67-13145

Barium titanate single crystals at infrared frequencies investigated for polarization, effective permittivity and coercive field 03 p0497 A67-13697

Reversing permittivity of barium titanate single crystals measured, using lithium chloride solution for electrodes 03 p0497 A67-13698

Permittivity of barium titanate single crystals with laminar domain structure 03 p0497 A67-13699

Polarization and domain structure of barium titanate single crystals with double hysteresis loop 03 p0497 A67-13700

UHF dispersion in barium titanate ferroelectric crystals explained as microwave scattering 03 p0497 A67-13701

Slow polarization processes of barium titanate in weak field 03 p0497 A67-13702

Classification of ions capable of replacing Ti in barium titanate 03 p0497 A67-13703

Permittivity of barium titanate ferroceramic materials determined by various methods 03 p0498 A67-13705

Electromechanical hysteresis and relaxation effects in piezoelectric ceramics 03 p0498 A67-13706

Temperature autostabilization in barium and strontium titanate solid solutions during dielectric heating 03 p0498 A67-13707

Electric properties of thin ferroelectric films of barium titanate compound 03 p0498 A67-13708

Pyroelectrical effect in barium titanate ceramics used for weak thermal radiation recording 03 p0421 A67-13709

Temperature dependence of electroconductivity of pure barium titanate and Fe-and Co-doped barium titanate crystals 04 p0678 A67-15130

Dielectric permittivity of barium titanate

monocrystals with anisotropic stratified domain structure 04 p0678 A67-15131

Temperature dependence of dielectric constant and existence of microwave dispersion in barium titanate above Curie point 05 p0868 A67-17060

Precipitation effect of dispersed calcium titanate-rich phase on shape, organization and thickness of ferroelectric domains in barium titanate 06 p1020 A67-18047

Electron optical method for visualizing barrier layer concentrations in ceramic responsible for anomalous increase in resistivity observed in doped barium titanate 07 p1233 A67-19651

Crystal symmetry, optical properties and ferroelectric polarization of barium titanate single crystals 07 p1234 A67-20096

Semiconducting properties of ferroelectrics estimating free carrier densities in n and p regions and distributions over plate thickness semiconducting properties of ferroelectrics, estimating free carrier densities in n and p 08 p1367 A67-20314

Intracrystalline field and spontaneous polarization in barium titanate studied by EPR spectrum of Cd-3 ions 09 p1554 A67-21976

Ultrasonic flow meter for directly measuring average stream velocity using sing-around velocimeter with piezoelectric ceramics 10 p1656 A67-23079

C domain wall motion in barium titanate crystals is dependent on A domains and activation fields throughout whole crystal 11 p1849 A67-24900

Temperature dependence of electroconductivity of pure barium titanate and Fe-and Co-doped barium titanate crystals 12 p1978 A67-25154

Dielectric permittivity of barium titanate monocrystals with anisotropic stratified domain structure 12 p1978 A67-25155

Temperature dependence of electrical conductivity and Hall effect of barium-titanate crystals reduced by hydrogen, observing electron spin resonance and optical absorptions 14 p2363 A67-27824

Barium titanate polycrystal dielectric constant aging, discussing 90 degree splitting in domain structure 14 p2364 A67-28228

Temperature dependence of dielectric constant and existence of microwave dispersion in barium titanate above Curie point 15 p2538 A67-29791

Conductivity, Hall effect and Seebeck coefficient measurements on single domain crystals of barium titanate 16 p2729 A67-31060

Temperature dependence and order of magnitude of barium titanate and strontium titanate determined from three-phonon diffusion process 17 p2915 A67-32706

Intracrystalline field and spontaneous polarization in barium titanate studied by EPR spectrum of Cd-3 ions 17 p2923 A67-33313

Energy densities of polar and antipolar arrays in barium titanate including nonlinear oxygen polarizability 21 p3683 A67-38406

Hyperfine interaction between unpaired trapped electron and adjacent titanium 47 and 49 nuclei in F center ESR line in barium titanate 21 p3684 A67-38417

Ferroelectricity of barium titanate thin films noting dielectric, temperature, polarization and electric field variations 21 p3687 A67-39142

Electrical characteristics of thin triangular barium titanate crystals in strong electric fields 22 p3859 A67-39579

Time dependent relation between coloring and spontaneous conductivity increase in barium titanate single crystals by strong electric field 22 p3861 A67-39918

Raman scattering for overdamped soft optic vibrational mode in barium titanate, giving temperature dependence of Raman spectrum 23 p4038 A67-40796

Pyroelectric effect using single barium titanate crystals with liquid electrodes extending ferroelectric switching time measurements to low fields 24 p4203 A67-42090

Semiconducting mixed titanate superconducting transition observed at 0.5 degrees K ascribed to change in valley numbers in conduction band 24 p4205 A67-43099

BARKHAUSEN EFFECT

SA FERROMAGNETISM

Magnetic field variation indicator based on

Barkhausen effect 06 p1002 A67-17941

Magnetic field variation indicator based on

Barkhausen effect 18 p3046 A67-33777

BAROCLINIC WAVE

Effects of horizontal shear and aspect ratio change on baroclinic instability in rotating annulus heated differentially 03 p0463 A67-13932

Laboratory experiments on atmospheric simulation, mainly rapidly rotating fluids, with limitation to incompressible fluids 04 p0613 A67-14802

Cyclogenetic processes from baroclinic instability occurring in zonal and meridional flow 06 p1027 A67-18602

Retrosession of nondiverging waves, noting phase velocity dependence on atmospheric stability 06 p1027 A67-18603

Sensible heat transfer influence on dynamic stability of harmonic perturbations superimposed on zonal current, using Lorentz two-level model 15 p2512 A67-30057

Cyclogenesis due to baroclinic instability in zonal and meridional basic current showing relationship by superimposing perturbation 19 p3252 A67-35528

Stability of continuous baroclinic flow in zonal magnetic field examined for zonal-flow profile of hyperbolic tangent form 19 p3253 A67-35918

Baroclinic quasi-geostrophic prediction of geopotential field using two-parameter model 20 p3481 A67-37236

BAROMETER

Aerial barometric altitude measurement improvement and residual error reduction 07 p1190 A67-20289

Barometric sensors insensitive to high winds 17 p2860 A67-32816

BAROMETRIC PRESSURE

S ATMOSPHERIC PRESSURE

BAROTRAUMA

Barotrauma, circulatory constriction and other in-flight auditory troubles of civil aeronautical navigation personnel over 40 years old 14 p2257 A67-28214

BAROTROPIC FLOW

SA LEE WAVE

Unstable modes of barotropic horizontally sheared zonal current in stratified atmosphere 04 p0611 A67-14650

Earnshaw conjecture refuted for particle in three-dimensional lamellar motion 05 p0792 A67-16728

Randomly distributed initial energy input effect on unbounded rotating barotropic atmosphere, noting energy density function as initial condition 15 p2478 A67-30056

Noise wave amplitude reduction method by suitable initial wind field adaptation to pressure field studied for applications to divergent barotropic model 19 p3253 A67-35530

Nonlinear features of geostrophic adjustment in one-dimensional barotropic atmosphere number 19 p3253 A67-35917

Predictions from barotropic vorticity equation in spectral form analyzed for errors 21 p3654 A67-38575

Objective criteria for irrotational flow in geostrophic, isallobaric and thermal wind flow 24 p4180 A67-41788

BARREL

S CONTAINER

S LAUNCHING DEVICE

BARRIER LAYER

SA JUNCTION

Optical and electrical properties of barrier layers in Cu doped GaP, discussing intensity region of superlinearity dependence on temperature and IR light 03 p0491 A67-13202

First passage problems for lightly damped linear oscillator excited by white noise for two types of initial conditions and three types of barrier configurations 04 p0659 A67-15932

Wave diffraction in rectangular waveguides passing through double ribbon barriers 05 p0775 A67-16956

Change in basic barrier relation for heterojunction compared to homojunction of wide gap emitter injection laser 05 p0825 A67-17097

Electron optical method for visualizing barrier layer concentrations in ceramic responsible for anomalous increase in resistivity observed in doped barium titanate 07 p1233 A67-19651

Absolute value of photoconductivity in polycrystalline high resistivity CdS and CdSe SHF field and experimental determination of barrier amplification factor and intercrystalline barrier height 08 p1370 A67-20997

Pulsed sinusoidal bridge for simultaneous measurement of volt-capacitance and volt-ampere characteristics of relaxing p-n junction barriers 08 p1303 A67-20998

Capacitance of abrupt p-n heterojunctions and effects of interface states, noting capacitance-voltage characteristics 10 p1612 A67-23372

Barrier height between tungsten silicide films and n-type silicon base determined, using photoelectric response measurements 11 p1850 A67-24924

Design and fabrication of germanium Esaki diodes emphasizing development of planar process, using conventional oxide masking techniques 13 p2083 A67-27572

Localized uniaxial force effect on voltage-current relationship of gold-potassium tantalate Schottky barrier diodes, noting reversible changes 18 p2637 A67-31036

Semiconductor-metal potential barriers for semiconductor devices obtained by silicon dioxide and silicon local sputtering in argon discharge 17 p2916 A67-32809

Thin films deposited onto substrates cooled to low temperatures investigated for transition temperature in structures of superconductor-dielectric-superconductor 18 p3101 A67-33989

Basic operating-time contribution to pulse behavior of diffused transistor components, introducing system function for semiconductor barrier-layer component 19 p3195 A67-35580

E/k-relation for complex insulator band structure, explaining polarity effect on tunneling through asymmetric barrier 20 p3508 A67-36425

Diode volt-ampere characteristics, considering space charge in base barrier layer and rear contact oxide film, noting vertical section appearing on direct branch 21 p3593 A67-38291

Schottky tunneling measurements in GaAs with Au noting fine structure 22 p3861 A67-39996

Barrier system for oxidation resistant protective coating for high temperature protection of refractory coatings 23 p4018 A67-40900

Magnetic impurities in tunnel junction barriers investigated for effect on junction resistance 24 p4200 A67-41865

Different surface potential barrier models studied for T-F emission current density, energy distribution and Nottingham effect 24 p4201 A67-41893

Space charge effect on potential barrier in field emission, obtaining expression for work function increase using electrical image method 24 p4201 A67-41894

Phenomena between evaporated metal and semiconductor surface affecting potential barrier by metal electrons extraction potential and semiconductor fast state concentration 24 p4204 A67-42410

BARYON

SA MESON-BARYON RESONANCE

Elimination of certain contradictions in data concerning high energy cosmic rays explained by means of hypothesis of existence of passive S-state of baryon 02 p0316 A67-12766

Production of charged double pion in pi plus-proton scattering, noting isobar model failure to explain enhancement at 400 Mev 19 p3266 A67-36100

Elimination of certain contradictions in data concerning high energy cosmic rays explained by means of hypothesis of existence of passive S-state of baryon 22 p3877 A67-40268

BASE

S AIRCRAFT BASE

S ALKALI

S LUNAR BASE

BASE FLOW

Rutgers Axisymmetric Near-Wake Tunnel for testing turbulent supersonic base flow, temperatures and pressure distributions 02 p0230 A67-12361

Effects of fast expansion and consequent lip shock at shoulder of supersonic base or downstream-facing step, suggesting alleviation by shoulder

modification 10 p1592 A67-23156

Base bleed effects on flow behind two-dimensional model with blunt trailing edge, measuring base pressure, shedding frequency and vortex formation 21 p3566 A67-39078

Base flow characteristics and thermal environment of launch vehicles with strap-on solid rocket motors 22 p3902 A67-39939

BASE HEATING

Short duration technique providing simulation of thermodynamic properties and composition of exhaust products of liquid and solid propellant rocket engines [AIAA PAPER 66-760] 13 p2090 A67-26843

Nose bluntness and cone angle effects on base pressure and heating in laminar hypersonic flow regime, using free flight telemetry technique 21 p3565 A67-38882

BASE PRESSURE

Prediction of subsonic base drag of hypersonic reentry vehicles [AIAA PAPER 66-991] 03 p0353 A67-14144

Base pressure measurements on sharp and blunt 9 degree cones at Mach 3.50 to 9.20 04 p0547 A67-14851

Base pressure fluctuations behind cone in supersonic flow due to presence of stagnant zone with subsonic reverse flow in shape of annular vortex 06 p0936 A67-17735

Base pressure behind supersonic vehicle, calculating existence conditions for wake solutions and location of stable and unstable singularities [AIAA PAPER 67-60] 06 p0986 A67-18269

Variation problem solution in hypersonic gas dynamics, noting intake portion construction for body with minimum resistance for limited length and flat end 11 p1777 A67-24153

Ground effect of static circular peripheral jet, comparing derived relations between jet flow, base pressure and hover height with experimental model 15 p2415 A67-29262

Base pressure and geometry of separated region in boundary of supersonic accelerated flow analyzed and compared with Chapman-Korster model 16 p2592 A67-30951

Turbulent base pressure in supersonic axisymmetric flow behind blunt body [AIAA PAPER 67-446] 18 p3026 A67-33922

Base bleed and initial boundary layer thickness effects on base pressure variations, calculating combining parameter for vehicle performance evaluation 19 p3172 A67-35779

Modifying effect of base bleed investigated photographically for incompressible wake behind two-dimensional bluff body, estimating base pressure 20 p3421 A67-36844

Nose bluntness and cone angle effects on base pressure and heating in laminar hypersonic flow regime, using free flight telemetry technique 21 p3565 A67-38882

Base bleed effects on flow behind two-dimensional model with blunt trailing edge, measuring base pressure, shedding frequency and vortex formation 21 p3566 A67-39078

Base pressure measurements on elliptic cones in supersonic flow with turbulent boundary layer as function of geometry 21 p3566 A67-39083

Base pressure calculation of stepped axisymmetric body in supersonic flow based on turbulent mixing theory 22 p3740 A67-39944

Base pressure behind circular projection in Laval nozzles, measuring dependence on specific heat ratio at different Mach numbers by varying gas 22 p3741 A67-40021

Reynolds number effect on base pressure behind wedge in supersonic and hypersonic flow based on Chapman wake flow recompression model 23 p3930 A67-41308

BATHYTHERMOGRAPH

Aircraft instrumentation for oceanographic measurement platform including radiation thermometer, wave meter and expendable bathythermograph [AIAA PAPER 66-695] 09 p1441 A67-22498

BATTERY

SA DRY CELL BATTERY

SA ELECTRIC CELL

SA ELECTRODE

SA ELECTROLYTE

SA LECANCHE BATTERY

SA NICKEL-CADMIUM BATTERY

SA SILVER-CADMIUM BATTERY

- SA SILVER-ZINC BATTERY
SA STORAGE BATTERY
SA THERMAL BATTERY
SA ZINC-SILVER OXIDE BATTERY
Fuel cells and fuel batteries, investigating hydrogen, compromise fuels and hydrocarbons, studying reliability, working life and costs 04 p0556 A67-15549
Battery power supply for split-ring plasma arcs operating as P hypersonic propulsion tunnel heaters 04 p0556 A67-15638
Annex circuits for regulating electrolyte grade, cell temperature, reactant supply, fluid circulation and generated electricity of unit cells grouped in batteries 14 p2253 A67-29024
Battery charger system for aircraft application noting nickel-cadmium battery, logic circuitry, wide environmental operation conditions, etc 17 p2804 A67-32515
Solar cell/battery power systems for post-1975 satellites, discussing oriented thin film CdS solar cell array 24 p4105 A67-42515
Sealed heat sterilizable high impact resistant battery for space missions, grafting acrylic acid and polyethylene by irradiation for separator 24 p4106 A67-42521
- BAUXITE**
Iron-chromium-bauxite cermets preparation and properties 18 p3065 A67-34260
- BAYESIAN STATISTICS**
Dynamic programming recursive estimation of modal trajectory for nonlinear non-Gaussian noise and comparison with Bayesian estimation and case of Gaussian white noise 01 p0047 A67-11214
Bayesian statistics applicability to reliability estimation and decision-making 01 p0085 A67-11381
Bayesian statistics in dual control schemes for discrete-time noisy extremum systems 02 p0226 A67-12145
Reliability assessment technique, discussing application of Bayesian statistics 05 p0906 A67-17250
Probability estimation, discussing types, Bayesian method for binomial and multinomial distributions, sampling methods, etc 06 p1022 A67-17646
Sequential trajectory estimation improved by implementing simple running estimates of observation error variances [AIAA PAPER 67-89] 06 p1086 A67-18337
Dual control of plant with random amplification factor as Bayesian problem 06 p0976 A67-18408
Predicting structural reliability by recent developments in statistics, reliability, cost effectiveness analysis and decision theory [AIAA PAPER 66-503] 08 p1424 A67-21524
Troubleshooting problems in oscillator circuit solved via Bayesian computer program simulating critical behavior 09 p1456 A67-22369
Sufficient conditions for asymptotic invariance of Bayes estimate of regression coefficient for nonstationary noise 10 p1619 A67-22952
Nonlinear Bayes detector synthesized for Gaussian signal and noise fields using Wiener filters 12 p1919 A67-26087
Error probability for transmission of M orthogonal equally probable equal-energy signals over partially coherent channel 12 p1908 A67-26091
Book on optimization of stochastic systems noting probability distribution functions, random variables, Bayesian optimization convergence, linear and nonlinear system estimation, etc 15 p2459 A67-30024
Optimal statistical adaptive model used in defining characteristics of control plants 15 p2461 A67-30321
Learning in unknown stationary environment using stochastic approximation, discussing Bayesian interference, pattern recognition, automatic control and statistical communications 18 p3070 A67-33497
Risk assessment techniques for design, fabrication and testing of complex spacecraft noting component reliability, Bayesian statistics, Monte Carlo technique, etc 18 p3138 A67-34683
Reliability prediction with inadequate data in flight control systems, using nonelectric approach combining failure data with judgment 18 p3058 A67-34699
Sequential trajectory estimation improved by implementing simple running estimates of observation error variances [AIAA PAPER 67-89] 23 p4070 A67-41717
- Threshold discrimination for two unknown a priori probability signals against noise background, using stochastic approximation in algorithm 24 p4134 A67-41795
Bayes estimate of regression coefficients in cost function selection in presence of unsteady noise 24 p4134 A67-41796
- BCC**
S BODY CENTERED CUBIC /BCC/ CRYSTAL
- BE-B**
S EXPLORER XXII SATELLITE
- BEACON**
S RADAR BEACON
S RADIO BEACON
BEACON EXPLORER-B
S EXPLORER XXII SATELLITE
BEACON PROJECT
Air traffic control radar beacon system with automatic altitude reporting system [SAE PAPER 670256] 12 p1941 A67-25506
BEACON SATELLITE
Beacon satellite measurement of Faraday rotation and diurnal and seasonal variations of total electron content of ionosphere near Nairobi 03 p0406 A67-12825
Mean ionospheric height measurement from analysis of radio signals from beacon satellite 08 p1328 A67-21479
Ionospheric electron content variation across sunrise and sunset lines deduced from radio-beacon satellite transmissions 15 p2476 A67-29624
Short bursts of scintillation of satellite radio signals from S-66 satellite, discussing diurnal variation correlation with spread of occurrences 22 p3759 A67-39478
Isolated irregularities in auroral ionosphere studied by analyzing radio signals from rockets and Beacon satellite 22 p3760 A67-39627
Solar cell power systems design and control technique for use in satellite programs, specifically transit 3B and 4A, ionosphere Beacon satellite, etc 23 p3938 A67-41507
- BEAM**
S ATOMIC BEAM
S CANTILEVER BEAM
S CURVED BEAM
S ELECTRON BEAM
S GAMMA RAY BEAM
S I-BEAM
S ION BEAM
S MOLECULAR BEAM
S NEUTRAL BEAM
S OPTICAL BEAM SCANNING
S PARTICLE BEAM
S PHOTON BEAM
S PION BEAM
S PROTON BEAM
S RADAR BEAM
S RECTANGULAR BEAM
S STRUCTURAL BEAM
- BEAM COLUMN**
Self-focusing of laser beam in plasma, solving wave equation for slab and cylindrical beam configurations 02 p0252 A67-12089
Beam-column analysis by finite element method, establishing end load-deformation relationship via stiffness matrices 03 p0523 A67-13457
Dynamic stability of pin-ended column under different types of random axial loading 14 p2397 A67-28091
Column consisting of flexible and rigid section measured for buckling load, using Southwell method 14 p2404 A67-29057
Treating bending-torsion problem of straight beam using Trefftz definition of shear center 15 p2572 A67-29311
Dynamic stability of homogeneous and inhomogeneous sandwich columns with pinned ends under pulsating periodic loads governed by Mathieu equation 17 p2963 A67-33036
Dynamic stability of beam columns undergoing weakly nonlinear vibrations studied using Ritz-Galerkin procedure 19 p3342 A67-35758
Buckling of aging linearly viscoelastic beam columns with time variable mechanical properties, deriving integrodifferential equations and stability conditions 19 p3343 A67-35781
Structural analysis of welded joints in composite welded panels using beam column concepts 22 p3813 A67-40181
- BEAM CURRENT**
Currents caused by light pressure on metal surface and in flare plasma when laser beam hits surface 10 p1664 A67-23333
Control efficiency and perfect cut-off of beam current of controlled electron guns, noting focusing properties and variation in focusing with voltage 14 p2276 A67-27767
Amplification of traveling-wave tube calculated to determine effect of continuous current interception along delay system 16 p2640 A67-31506
Cathode study using electron images of recording storage tube cathodes 19 p3197 A67-35813
Microwave radiation from plasma beam interaction, measuring radiation intensity as function of discharge current 21 p3668 A67-38416
- BEAM-PLASMA AMPLIFIER**
Beam-plasma amplifier with input coupler as cavity and output coupling due to Cerenkov radiation 01 p0040 A67-11313
Monochromatic longitudinal wave amplification by charged particle beam in nonlinear plasma, noting amplitude dependence on coordinate 10 p1686 A67-23587
Microwave amplification when electron beam passes through cesium plasma, noting noise figure dependence on tube pressure 21 p3668 A67-38605
Harmonic generation and turbulence-like spectrum from pulsed HF beam-plasma interaction, tabulating harmonic wave properties 22 p3847 A67-39615
- BEAM SPLITTER**
Laser beam slitting hologram production technique using polarization controller and birefringent prism 17 p2864 A67-33359
- BEAM SWITCHING**
Generation of giant pulses of coherent radiation by rotating-mirror technique and by passive Q-switch using cryptocyanine 17 p2871 A67-33390
- BEAM WAVEGUIDE**
Modes of beam waveguide or beam waveguide resonator filled with axially magnetized plasma 02 p0213 A67-11619
Electromagnetic wave propagation along confocal lens line for variable refractive index of ambient medium 04 p0575 A67-15150
Optimum cavity beam hole diameter for traveling wave tube determined from beam parameters and slow wave structure parameters 04 p0583 A67-15153
Light beam deflection with low losses, using thermal gradient effects in gases 07 p1141 A67-19406
Material properties and capabilities of different types of optical waveguides including iterative electromagnetic wave beams, reflecting pipes, fiber guides, etc 12 p1906 A67-25976
Electromagnetic wave propagation along confocal lens line for variable refractive index of ambient medium 15 p2435 A67-29337
Optimum cavity beam hole diameter for traveling wave tube determined from beam parameters and slow wave structure parameters 15 p2443 A67-29340
Parabolic cylindrical reflector beam waveguide, discussing conduction and diffraction losses of TE and TM modes 21 p3583 A67-38608
Local reference beam principle for laser long distance hologram construction 24 p4158 A67-42819
- BEARING**
SA BALL BEARING
SA GAS BEARING
SA GAS LUBRICATED BEARING
SA JOURNAL BEARING
SA ROLLER BEARING
SA ROLLING CONTACT BEARING
SA THRUST BEARING
Liquid solid film lubrication of hydrodynamic bearings, including effects of solid particles in liquid base lubricant 01 p0077 A67-10122
Pressure distribution of porous self-lubricating bearing noting geometrical factors, dimensions, running speed, load, etc 01 p0079 A67-10708
Aerospace requirements for bearings and lubricants in natural environments 02 p0250 A67-12454
Monograph on higher modes of critical speed of shafts with elastic clamping moment at bearings 02 p0250 A67-12710
Machine design, capillary control selection, hydraulic circuitry and oil selection of two two-surface angular hydrostatic bearings used for azimuth turntable of radar antenna

pedestals 03 p0431 A67-13749
Turbulent annular airflows in turbulent film lubrication of high speed bearings [ASME PAPER 66-LUB-14]

Externally pressurized bearings treated as hydraulic closed loop servomechanism analyzed, using transfer functions [ASME PAPER 66-LUB-7]

Turbulent lubrication analysis in fluid film theory and turbulent shear flow, with application to bearings [ASME PAPER 66-LUB-12]

Stator whirl with rotors in bearing clearance noting jump and hysteresis phenomena [ASME PAPER 66-WA/MD-8]

MHD analysis of composite slider bearing using electroconductive lubricant such as liquid metal, in magnetic field perpendicular to bearing surface, for large and small Hartmann numbers [ASME PAPER 66-LUB-B]

Lubrication and bearing problems in space environment, noting molybdenum disulfide and silicones 05 p0811 A67-16932
Pivoted slider bearing under external magnetic field analyzed, considering pad surface curvature 05 p0811 A67-16981
Pressure distribution in externally pressurized bearings 06 p1007 A67-18060
Azimuth stabilization of balloons, using frictionless bearing to decouple gondola 07 p1191 A67-19403
Laser beam effect on hydrodynamic bearings, discussing microcracks and critical energy, explaining 08 p1337 A67-20840
SNAP-8 reactor oscillating bearings to provide low friction self-lubrication at 1150 degrees F [ASLE PAPER 66AM 7A1]

Rolling friction studies of intermetallic and zirconium oxide for control surface bearings for space reentry vehicle [ASLE PAPER 66AM 5D4]

Lab techniques for studying unusual bearing failures, noting damage from water contaminated lubricant, pitting, etc 09 p1506 A67-22195
Fluid film and rolling element bearings effect on turbomachinery rotor dynamics including critical speeds, imbalance response, instability, turbulence, etc [SAE PAPER 670059] 09 p1508 A67-22533
Nonlinear vibration damping functions for fluid film bearings [SAE PAPER 670061] 09 p1508 A67-22535
Mechanical difficulties in designing shaft, bearing and seal systems for three high speed turbine engines [SAE PAPER 670064] 09 p1560 A67-22537
Operating lifetime of porous bearings, discussing dependence on quality of impregnating lubricant 10 p1659 A67-22831
Time variability of bearing clearance due to temperature and pressure treated by iterative-numerical calculation 12 p1949 A67-25330
Alloys, cermet and ceramics used in bearing applications at 600 to 2000 degrees F, noting significance of oxides 14 p2324 A67-28001
Rotor bearing clearance effects on whirl of gimbal-mounted gyroscope 14 p2328 A67-29004
Air-bearing facility for Lunar Orbiter attitude control system testing minimizing external disturbances in platform, platform mass deflection and room thermal currents 16 p2655 A67-31260
Conducting Bingham plastic fluids considered as lubricants in rheostatic bearing in presence of constant magnetic field [ASME PAPER 67-LUBS-4]

Critical speed control by squeeze-film oil damper between two nonrotating parts in parallel with flexible bearing support, using mathematical model [SAE PAPER 670347] 17 p2865 A67-32989
Soviet book on dynamic effects of moving loads on beams supported by linear and nonlinear bearings and elastic

bases 18 p3140 A67-33661
Diagnostic methods of rotating bearing defects, describing types of bearings, oils and equipment used in tests 19 p3235 A67-34888
Plastic based bearings, discussing polymer chemistry, use of fillers, incorporation into matrices of various resins, etc 20 p3455 A67-37266
Optimal functional parameters of elastically damping turbine rotor bearing to determine critical velocities of shaft 21 p3695 A67-38832
Load carrying capacity of hydrostatic bearing having communicating chambers and operating with laminar flow of incompressible fluid, showing shaft vibration elimination 21 p3636 A67-38837
Synchronous motions in dynamic bearing system of nonlinear plants with one degree of freedom interacting through weak coupling 22 p3836 A67-39395
SST variable sweep wing actuation system and pivot bearing reliability [SAE PAPER 670884] 24 p4098 A67-42018

BED REST
Bed recumbency effect on ventilatory, metabolic and cardiac response to bicycle ergometer test, noting possible preventive effect of muscular exercises and venous occlusion 01 p0016 A67-10949
9-alpha-fluorohydrocortisone and venous occlusive cuffs effects on plasma volume and orthostatic tolerance following 28 to 78 days of bed rest 01 p0016 A67-10960
Objective statistical approach to tilt table data analysis using computer to define characteristics of cardiovascular deconditioning resulting from bed rest, water immersion and space flight 05 p0754 A67-16276
Absolute bed rest and recumbent exercise during bed rest effects on pulse rate response to submaximal work, cardiovascular functional capacity /maximal oxygen intake/, physical work capacity and orthostatic tolerance 05 p0755 A67-16283
Tilt table responses of human subjects improved by application of lower body negative pressure 05 p0755 A67-16286
Urinary loss of calcium, phosphorus, nitrogen, sodium and chloride in men under prolonged bed rest at ground level or at simulated altitudes [SAM-TR-66-296] 07 p1134 A67-19857
Plasma volume and extracellular fluid volume change associated with ten days bed recumbency 07 p1134 A67-19858
Tilt table response and blood volume changes in four males before and after 14-day bed rest 07 p1135 A67-19863
Weightlessness simulation by bed rest and water immersion, evaluating validity of protective measures, recovery time and tilt response 15 p2424 A67-29102
Exposure to acceleration and prolonged confinement in bed studied for effects on functional state of human stomach 16 p2613 A67-30915
Water-salt metabolism changes during prolonged confinement in bed following exposure to acceleration indicating dehydration and decalcification 16 p2613 A67-30916
Tilt table response and plasma volume changes in experimental subjects evaluated before and after short term periods of deconditioning 17 p2805 A67-31953
Extremity cuffs or leotards effect in preventing or controlling cardiovascular deconditioning of bed rest 18 p2992 A67-34715
Human brain hemodynamics during prolonged hypokinesia including orthostatic and bed-rest tests, using rheoencephalographic technique 20 p3368 A67-36266
Human acoustic analyzer functional state studied for hypokinesia effects 20 p3368 A67-36267
Inactivity and water immersion effects on fluid balance and tilt-table performance in dehydrated subjects, assessing vasopressin and positive pressure breathing effects 23 p3951 A67-41557
Autogenous and exogenous suggestion applied to changing of psychophysiological state of human organism after exposure to prolonged bed rest 24 p4112 A67-41855

BEEHIVE PROJECT
S PROPELLANT

BEHAVIOR
S CONDITIONED RESPONSE
S GROUP BEHAVIOR
S HUMAN BEHAVIOR
S LEARNING
S TRAINING

BELFAST AIRCRAFT
S SHORT SC-5 AIRCRAFT
BELL MILITARY AIRCRAFT
S X-22 AIRCRAFT

BELLOWS
Inertia effects of internal liquid column on vibration of thin walled pressurized elastic cylindrical bellows type container [AIAA PAPER 67-38] 06 p0986 A67-18262
Dynamic instability in undamped bellows face seals operating in cryogenic environment with torsional oscillation and diametrical rocking as primary motion [ASLE PAPER 66AM 2C2] 08 p1336 A67-21039
Rotating device for transmitting motion through walls of ultrahigh vacuum chambers, using circular motion of bellows envelope and internal gearing 17 p2863 A67-33358
U-shaped bellow fatigue strength under axial loading, discussing elastic and plastic fatigue tests using specially designed machine 22 p3913 A67-40037

BELTRAMI FLOW
Beltrami stress functions, presenting completeness proof 17 p2884 A67-32717
Exact solutions of incompressible Navier-Stokes equation for irrotational Beltrami nonconvective two-dimensional swirl and axially symmetric cross flows 21 p3609 A67-37737

BENDING
SA ELASTIC BENDING
Variational principles for plate bending problems not subjected to boundary conditions 01 p0162 A67-10850
Flexural wave propagation along beam with arbitrary periodic concentrated load 02 p0340 A67-12501
Orthogonal double series solutions of nonlinear deflections of thin rectangular plate 04 p0707 A67-14445
Integration of nonhomogeneous equations for axisymmetric bending of spherical shells by variation of parameters 04 p0717 A67-15887
Thin isotropic circular plate bending under eccentric moment load for clamped and simply supported cases 05 p0918 A67-16419
Stress distribution prediction in multilayered circular cylinder subjected to combined bending and axial loading exhibiting multilinear stress-strain relationships 10 p1724 A67-23706
Heat resistance, bending and tensile creep of multicomponent Ti alloys 12 p1955 A67-25366
Approximate method for solving bending problem of rectangular plates of nonuniform thickness under arbitrary external edge loading 12 p2031 A67-25962
Impact bending and tension processes using drop hammer technique evaluated with improved method using oscillography for high quality load-time measurements 13 p2215 A67-26391
Network method to derive differential difference equations for boundary condition of clamped and free edges and point supports of low aspect orthotropic wings network method to derive differential difference 21 p3724 A67-38782

BENDING DIAGRAM
Circular tube cross-sectional ovality in plastic bending 14 p2401 A67-28655
Analyses of small and large-deflection problems of clamped skewed plates under uniform pressure 17 p2958 A67-32407

BENDING FATIGUE
Tenfold increase in fatigue life of 1100 aluminum in reverse bending at vacuum level below 10-2 torr due to retardation of crack propagation phase of fatigue process 01 p0092 A67-10053
Crystal orientation of grains during fatigue and plastic deformation analyzed on copper using X-ray diffraction, noting crystal behavior 02 p0254 A67-11467
Indium antimonide specimens plastically bent to introduce excess of dislocations, examining dependence of lower yield stress for bending on direction of bend 03 p0498 A67-13870
Shearing stress failure theory for high

cycle fatigue employing rotating principal stress axes and nonsynchronous stresses [ASME PAPER 66-WA/MET-9]

04 p0712 A67-15374
Bending stresses in cylindrical shell with rigid circular inclusion examined under axial tension and internal pressure
[AIAA PAPER 66-525] 05 p0924 A67-17351
Bending strength of spur gear teeth calculating methods to optimize design for high speed, lightweight aircraft gearing [AHS PAPER 118] 16 p2684 A67-31834
Fatigue strength calculated using fracture criterion for multiaxial alternating stress and combined alternating bending and torsional stresses 17 p2960 A67-32632
Infinitely small bending deformations of convex surfaces with boundary condition of generalized slip, formulating boundary value problem for bending of surface 18 p3144 A67-34482
Structural section bending determined for fracturing tolerance 18 p3144 A67-34484
Bending strength dependence on porosity of sintered powdered glass beam 20 p3473 A67-36779
Rotating bending fatigue limit and true stress/true strain parameters correlation for steels extended to axial load fatigue tests 21 p3719 A67-38132
Random load fatigue life and reliability via fall-safe structural model, obtaining statistical distribution of 2024-T4 aluminum alloy bending strength 23 p4076 A67-40735
BENDING MOMENT
Shells of revolution analyzed under symmetric and antisymmetric loading by matrix displacement method 01 p0164 A67-11191
Monograph on higher modes of critical speed of shafts with elastic clamping moment at bearings 02 p0250 A67-12710
Ultimate bending moment capability of thin walled pressure stabilized cylinder with typical axial loads demonstrated to be 50 percent greater than bending moment at which compressive wrinkling occurs 03 p0522 A67-13230
Strength of cylindrical shells under local radial loads and circumferential bending moments conveyed by reinforcing elements 03 p0527 A67-14069
Tension and bending of two-layer rods under nonuniform heating and loading 03 p0527 A67-14071
Strains in twisted blades with rectilinear axes, examining general relations and parameters in postulated new theory 03 p0528 A67-14080
Torsional constraints in calculation of vibrational frequencies of compressor blade 03 p0528 A67-14081
In-flight bending moment and terminal drift minimization for flexible vehicle, applying two-point boundary value problem solution for optimum rigid body control system 04 p0706 A67-15422
Stress concentration in nonlinear creep of thin circular cylindrical shell loaded at one edge by symmetrical radial shear and bending moment 04 p0718 A67-15917
Bending of plates under moment induced and internal stresses 05 p0907 A67-16016
Bending of circular plate with two square holes under uniform load distribution around hole perimeters 05 p0916 A67-16225
Compression and tension of rod and plate with distribution of residual stresses such that deformation is partially plastic and elastic 06 p1107 A67-18633
Atmospheric density, winds and turbulence relative influence on Saturn V vehicle control system and structural bending moment response during Atlantic Missile Range ascent flight [AIAA PAPER 66-341] 07 p1257 A67-19372
Tensile and bending strengths as suitability criteria of pressworking of materials 07 p1192 A67-19755
Equilibrium and elastic properties of triangular and parallelogram bending elements for plate and shell networks, discussing transition element and matrix force methods 08 p1417 A67-20553
Asymptotic and particular solutions of conical shells subjected to lateral normal loads, discussing membrane forces, bending effects and boundary conditions for moments and shearing force 09 p1573 A67-21754
Deflection and bending moment coefficient

for clamped skew plate under uniform pressure obtained, using double series satisfying boundary conditions for differential equation 09 p1575 A67-22165
Bending of flexible tubes using variational calculus of Rayleigh-Ritz type 09 p1579 A67-22606
Helicopter rotor blade service life substantiation through tests with rotor excitation panels inducing blade bending moments 10 p1622 A67-23431
Bassall theory to calculate bending, twisting moments and shearing forces for thin elastic plates under transverse flexure for structural design application 10 p1720 A67-23569
Saturn IB flight test loads, comparing measured and calculated bending moment, noting launch time wind profile 10 p1713 A67-23734
Large deflections of beam loaded and supported at two points 11 p1871 A67-24088
Free oscillations of closed freely supported cylindrical shell of concentrated mass, determining frequency and bending moments 12 p2025 A67-25604
Approximate solution of creep and relaxation problem for plates and shells subject to bending moments and tensile forces 12 p2025 A67-25610
Elastoplastic equilibrium of rectangular compressible and incompressible plates under load concentrated near edge determined by elastic solutions and finite difference 12 p2031 A67-25960
Spanwise distribution of aerodynamic shear and bending-moment on cantilever tapered wings 13 p2215 A67-26485
Bent and twisted bars analysis using finite element method 14 p2399 A67-28133
Vlasov variational method applied to circular cylindrical shell design for local loading 14 p2400 A67-28643
Static deflection of parallelogram plates with clamped edges subjected to uniformly distributed pressure studied by energy method 15 p2573 A67-29312
Bending of circular and elliptical slabs clamped along contours under loads described by certain algebraic polynomials 15 p2573 A67-29465
Matrix method calculation for frequency, deformation, forces and moments of variable cross section in rotating turbine blade during natural bending oscillation 16 p2766 A67-31150
Creep effects in structures obtained by elastic solution applied to pressurized shells containing discontinuities 16 p2776 A67-31558
Flexural rigidity of plates reinforced by parallel stiffeners for direction normal to stiffener orientation determined together with stresses induced by bending moment 17 p2959 A67-32408
Large deflections of columns of variable flexural rigidity, assuming bending moment is proportional to curvature 17 p2963 A67-33020
Matrix method for calculating behavior of rod of constant cross section stressed by bending and stretching or compression loading 19 p3343 A67-35815
Stress concentration of plane curved beams with uniform cross section determined from photoelastic experiments 20 p3540 A67-37210
Tangential and normal tearing stresses distribution in adhesive joint under various loads and bending moment 21 p3716 A67-37909
I-beam ratio of depth to flange width for minimum weight obtained via modulus of rupture 21 p3722 A67-38548
Flexible ring reinforcing cylindrical shell under external load strength, considering ring cross-sectional shape change effect on bending moment 21 p3724 A67-38783
Ten thin walled cylindrical shells under internal load investigated for bending stability, comparing experimental and analytical results 21 p3724 A67-38785
Stress analysis for rib-reinforced cylindrical shell subjected to rapidly varying pressure, calculating deflections and bending moments 21 p3725 A67-38790
Displacement and stress distribution in shallow spherical shell under concentrated loads including normal force, tangential force and bending moment 21 p3730 A67-39087
Rectangular plate with clamped edges

studied for nonlinear cylindrical bending under uniform pressure 22 p3910 A67-39480
Bending of orthotropic strip to anticlastic surface by uniform moment, determining strain along neutral axis, bending moment and couple action 22 p3913 A67-40008
Approximation method for finite element bending analysis of variable structural plates, giving linear equations defining nodal values 23 p4073 A67-40627
Stresses, bending moments and displacements of variable rigidity toroidal shell in steady temperature field derived assuming independent thermal expansion coefficient and physical constants 23 p4075 A67-40680
BENDING THEORY
Quadrature solution method for bending of arbitrarily loaded thin slab whose circular edge is supported by elastic rod 01 p0158 A67-10223
Asymptotic method of refining classical theory of bending and stretching of plates by construction of two-dimensional equations for processes involved 01 p0163 A67-10996
Bending of orthotropic plates and beams supported by elastic layer under uniform transverse load, noting effect of length-width ratio change 03 p0520 A67-13017
Linear optimal control via root square locus to design simple effective structural bending control for four XB-70 coupled longitudinal bending modes [AIAA PAPER 66-970] 03 p0361 A67-14142
Boundary bending conditions for anisotropic plates with free, hinged or rigidly clamped edge 03 p0531 A67-14200
Bending of orthotropic sandwich plates in differential equation derived based on variational method 04 p0709 A67-14844
Metal addition effect on grain growth of matrix oxides, noting inhibitive results in most cases 04 p0642 A67-15086
Large elastoplastic deflection of simply supported plate subjected to uniform load, noting steel specimens 04 p0718 A67-15920
Finite difference equation for biharmonic equation of plane 05 p0833 A67-16032
Bending problem of isotropic shallow helical cantilever shell under distributed normal load 05 p0915 A67-16220
Bending of circular plate with two square holes under uniform load distribution around hole perimeters 05 p0916 A67-16225
Low endurance fatigue of aluminum alloy and stainless steel in plane bending at ambient and elevated temperatures 05 p0920 A67-16810
Axisymmetric bending of circular sandwich plates with lightweight compressible filler subject to special transverse or local loads 05 p0922 A67-17175
Validity of equations for bending, natural oscillations and stability of three-layer solid circular plate with rigid filling and asymmetric structure 06 p1106 A67-18628
Bending equations for thin elastic anisotropic plates, using Goldenveizer method 06 p1106 A67-18630
Rotation of thin walled elastoplastic tube of circular cross section after bending 06 p1107 A67-18635
Nonlinear problems of thin plate bending, using successive approximations method 06 p1108 A67-18661
Membrane solution of spirally corrugated shell under axial and torsional loading determined from thin shell bending equations 06 p1110 A67-18856
Governing equation for bending of multilayered sandwich elastic plates composed of n membranes developed by variational method 06 p1110 A67-18857
Heat resistance and fatigue strength of Ti alloys examined, using bending techniques 07 p1207 A67-19288
Nike-Tomahawk rocket aeroelastic behavior, noting occurrence of large extra-atmospheric coning angles 08 p1416 A67-20534
Stability of equilibrium of elastic systems under nonconservative load, discussing criteria of stability, modes of instability, follower force problems, etc 08 p1422 A67-21048
Mixed boundary value problem of flexure of elastic plate 08 p1422 A67-21201
Buckle pattern representation for isotropic cylinder rendering results of critical stress and role of buckle pattern upon ratio of critical stress 09 p1575 A67-22164
Bending of viscoelastic cylindrical shell

resting on viscoelastic base with monodirectional characteristic 10 p1717 A67-22945

Bending fatigue tests of unmachined, mechanically machined and chemically machined panels of aluminum and titanium alloys 10 p1669 A67-23437

Invariant stress and deformation functions for doubly curved shells, noting reduction of equilibrium equations and surface strain-displacement relations into compatibility equation 10 p1730 A67-23834

Computer program for solving bending of plates of any shape and with any variation in boundary conditions for static loading and transverse vibration 10 p1731 A67-23843

Bending theory for sandwich plates solved by Galerkin method assuming load distribution over upper and lower faces of plate 11 p1880 A67-25095

Closed cylindrical shell stability under combined bending and axial compression taking into account original arbitrary imperfection of shell form 12 p2020 A67-25567

Bending of three-layer plate freely supported along four edges in presence of variable surface heating 12 p2022 A67-25588

Stress-strain state of thin sandwich plate consisting of arbitrary number of elastic isotropic layers rigidly coupled to each other 12 p2024 A67-25602

Electrical simulation of finite difference calculations of problems of bending and natural oscillations of circular, annular and sector plates 12 p2032 A67-25968

Simulation results of adaptive tracking filter application to stabilization of structural bending modes of SI-B launch vehicle 13 p2212 A67-26818

Cylindrical bending of plate composed of strengthening and binding agents with different Youngs moduli 14 p2401 A67-28734

Creep deformation of composite beam subjected to combined axial and bending loads 14 p2403 A67-29002

Treating bending-torsion problem of straight beam using Trefftz definition of shear center 15 p2572 A67-29311

Linear theory of elastic Cosserat plate, noting bending theory which corresponds to bending of transversely isotropic three-dimensional plate 15 p2510 A67-29630

Displacement equations of prestressed thin bending-resistant shells 15 p2574 A67-29699

Numerical realization of partitioning method in case of rectangular plate bending with end loading, using bar scheme 15 p2576 A67-30180

Longitudinal bending and buckling of elastoplastic rods with allowance for creep 15 p2577 A67-30184

Refined plate bending theory taking into account edge effect 16 p2765 A67-31050

Torsion or coupled bending torsional wave theory for thin walled open section beams 17 p2959 A67-32413

Axisymmetric response of semilinearly truncated cone striking smooth rigid obstacle, determining early stages of motion 17 p2960 A67-32422

Nonlinear bending theory of sandwich plates with orthotropic layers 19 p3342 A67-35716

Thin walled structure bending in uniform temperature field, calculating stresses, deformations and creep 20 p3536 A67-36446

Hydraulic support system for free flight simulation with Saturn V-Apollo vehicle, discussing stability requirements, upper bounds of system design, conversion from nonlinear to linear model, 21 p3607 A67-37796

Pure plastic bending of sheet and strip at strains exceeding elastic limit analyzed by arbitrary stress-strain diagram 21 p3721 A67-38382

Transverse deflection of rectangular plate with bitrapezoidal cross section subjected to uniform longitudinal curvature, comparing theory with experiment 21 p3722 A67-38436

Strain energy method for analyzing large deflections of trapezoidal plates with constant thickness and rigidly clamped edges under uniformly distributed load 21 p3725 A67-38794

Thin plate idealization to Hrennikoff lattice model framework for linear stiffness method analysis 21 p3728 A67-38877

Discrete method extension for bending stability problem in sectorial plates,

obtaining algorithm for solutions of boundary conditions and external loads 21 p3729 A67-38907

Curvature for variable cross section beam bending with arbitrary transverse and longitudinal loads calculated by computer 22 p3915 A67-40449

Validity range of Flugge bending and Donnell theories established by comparing results with elasticity theory based results 23 p4074 A67-40630

Thin plate strong bending generalized and smooth solutions existence proved 23 p4076 A67-40716

Elastic bending of thin shells and plates perforated with holes in various arrays, calculating stress distribution and concentration 23 p4077 A67-40749

Thin boundary problems of bimaterial plates bonded along circular arcs behaving like crack imperfections under bending, using fracture mechanics to predict failure 23 p4078 A67-41164

Singular solutions for bending stresses in loaded infinite three-layer plate 23 p4079 A67-41415

Nike-Tomahawk rocket aeroelastic behavior, noting occurrence of large extra-atmospheric coning angles 24 p4242 A67-42912

BENDING VIBRATION

Eigenfrequencies of flexural vibrations of circular cylindrical shells calculated by various methods and compared with measured values 01 p0162 A67-10839

Matrix-Holzer method for predicting free vibration modes of clustered launch vehicles in bending applied to first eight modes of Saturn I model 02 p0337 A67-11931

Bending and torsion induced symmetric flutter of aircraft in supersonic flow 04 p0708 A67-14789

Distributed parameter transmission matrix analysis of bending vibrations of nonuniform elastic beam [SAE PAPER 660719] 04 p0716 A67-15782

Numerical analysis of constraint effects on trial function selection in variational calculus problem of pure torsional vibration of cantilever beam of thin walled open cross section 05 p0917 A67-16418

Bending torsional flutter of uniform swept wing with velocity component aerodynamic strip theory [AIAA PAPER 66-475] 06 p1110 A67-18860

Flexural-torsional vibration of rotating shaft with distributed parameters 07 p1264 A67-20104

Shear modulus determination from free flexural vibrations of sandwich beams with steel facing, using filled elastomer as core 09 p1574 A67-21838

Bending oscillations of hinged and clamped three-layer beams 09 p1575 A67-22219

Column compressive tests of aluminum alloy bars, determining load eccentricity and initial straightness deviation 10 p1715 A67-22826

Vibration characteristics of two-layered plates of arbitrary thickness and differing materials, noting coupling effect between flexure and extension 10 p1718 A67-23140

Flexural vibrations of plates studied by moire method for nodes, antinodes, local amplitude and phase distributions 12 p1966 A67-25293

Vibration characteristics of turbine and compressor blading under rotation 12 p2015 A67-25418

Natural frequencies of elastic toroids experimentally determined compared with theoretical results 13 p2219 A67-27091

Free vibrations of unsupported elliptical plates of lenticular section with flat or uniformly curved middle surfaces 16 p2764 A67-30841

Forced transverse vibrations of sandwich plates of symmetrical structure 16 p2776 A67-31547

Distributed parameter concepts of propagation, reflection and characteristic termination applied to dynamic analysis and control of bending vibration 16 p2776 A67-31686

Soviet book on unsteady oscillations of mechanical systems with any number of degrees of freedom 18 p3078 A67-33678

Bending oscillations of hinged and clamped three-layer beams 18 p3141 A67-33770

Free axisymmetric oscillations of

reinforced, closed, cylindrical circular shells, discussing natural frequencies and bending oscillations 19 p3338 A67-34877

Forced bending oscillations for three-layer cylindrical shell under pulsed internal pressure 19 p3338 A67-34878

IR spectra of gaseous, solid and matrix-isolated HNCS and DNCS, studying frequency shift, bending modes, fundamental vibrations, gas phase, etc 19 p3181 A67-35016

Adaptive control systems for stabilizing structural bending modes of Saturn V launch vehicle [AIAA PAPER 67-591] 19 p3336 A67-35987

Uniform cantilevered bar subject to eccentric compressive follower force, considering warping rigidity, bending-torsional flutter and stability 20 p3538 A67-36674

Elastic bending vibrations amplitude and frequency effects on current oscillations in CdS single crystals 20 p3514 A67-37463

Analog computer method application for determining critical frequency and critical flutter speed of wing having torsional bending vibrations in airflow 21 p3718 A67-37992

Harmonic oscillations and bending of elastic isotropic shells with variable curvature solved using Fourier transform 21 p3721 A67-38383

Method for finding bending vibration modes patterned on Holzer method for determining torsional vibration 21 p3728 A67-38881

Matrix displacement method for coupled bending-bending vibrations of pretwisted blading 23 p4078 A67-41329

BENZENE

SA CHLOROBENZENE

SA HEXAFLUOROBENZENE

Second harmonic generations and mixings of Raman lines produced in cyclohexane, acetone, benzene and carbon disulfide, photographing first order Stokes radiation 02 p0252 A67-12052

Laser beam effect on benzene and other organic compounds, noting formation of dark readily coagulating deposit 05 p0759 A67-17028

Initiation of explosive reaction in liquid mixture of tetranitromethane and benzene by methane-oxygen detonation 06 p1112 A67-17954

Crystal growth, nucleation, supercooling, solidification, glass forming and kinetics of 1, 3, 5-tri-alpha-naphthylbenzene 17 p2809 A67-33255

Benzene and related molecules adsorption on uniform graphite surfaces investigated for lateral interaction and localization of lattice sites 24 p4118 A67-42195

Aromatic compounds in benzene eluate fractions from carbonaceous chondrites by high resolution capillary gas-liquid chromatography 24 p4236 A67-42640

BERNOULLI EQUATION

Competing alternative pathways for formation of particular ion in mass spectra of substituted benzophenones 01 p0018 A67-10105

Free stream conditions approaching oscillating body in low speed wind tunnel, employing unsteady Bernoulli equation 03 p0352 A67-13899

Prediction theory for effect of shear flows on outlet angle in axial compressor cascades, taking into account effects of secondary flow, Bernoulli surface rotation and spanwise flow displacement 04 p0548 A67-15387

Tuned viscoelastic vibration dampers effect on responses of cantilever and clamped-clamped beams subject to Euler-Bernoulli beam equation, discussing loss factors based on transmissibility spectra 06 p1110 A67-18859

Air gauge circuit analysis extended to fluidic restrictor circuits and complex resistor circuits, using Bernoulli and continuity equations 14 p2252 A67-28353

Relativistic generalization of Bernoulli equation from three-dimensional vector analysis of acoustic and entropy waves 18 p3084 A67-33422

Motion equation of non-Newtonian fluids in initial section of cylindrical tube 18 p3024 A67-33539

Linearized system of water waves initial value problem, obtaining eigenvalue with parameter in boundary

condition 19 p3210 A67-35703
Closed form solution for two-dimensional reentry trajectories by transforming motion equations into Bernoulli with two arbitrary functions of inclination, considering constant gravitational field 22 p3881 A67-39526
Discharge line fluid conditions in cryogenic container with self-pressurized draining, using Bernoulli, continuity and general energy equations and fluid properties 22 p3784 A67-39968

BERNOULLI THEOREM

Quasi-invariance and ergodicity in binary sequence space with respect to discrete groups of Bernoulli schemes, noting finite entropy distance formulation of measure equivalence 14 p2343 A67-28502

BERYLLIUM

Room temperature microstrain behavior of zone-refined single crystal beryllium examined as function of prestrain 01 p0092 A67-10058

Beryllium rudder and structures for F-4C aircraft, discussing weight factor, analysis, design, fabrication, ground tests and fail-safe flight test programs 01 p0094 A67-10574 [SAE PAPER 660666]

Deformation processing of beryllium with respect to mechanical properties, economics and manufacturing considerations, examining production techniques 01 p0078 A67-10608 [SAE PAPER 660634]

Hot pressing of electrolytic grade CR beryllium, noting powder manufacturing process and quality control 01 p0099 A67-10707

Radial distribution analysis of films of Pb-12 percent Bi and beryllium in metastable phases prepared by low temperature condensation for electron diffraction tests 01 p0137 A67-11061

Beryllium wire reinforced epoxy-plastic composites in mechanical testing under various loadings 03 p0442 A67-13404

Brittle fracture of Be tube under differential thermal contraction-induced plastic strain 03 p0445 A67-13470

Beryllium as substrate for mirrors of catadioptric lenses, noting strain-induced aberration 03 p0470 A67-14391

Beryllium properties and treatment for use in manned space flight noting thermal stress resistance, toxicity, honeycomb structures, etc 04 p0635 A67-14563

Corrosive effects of chlorides in aqueous environment on pickled and anodized sheet beryllium 04 p0640 A67-15618

Grain oriented growth in beryllium condensates, discussing acicular structure of transverse sections of films 04 p0641 A67-15979

New metals replacing steels noting titanium, beryllium and niobium in French industry 06 p1017 A67-17994

Titanium alloy weld properties as affected by boron, beryllium and lanthanum additions 07 p1207 A67-19291

DC resistivity due to electron scattering from vacancy, octahedral and tetrahedral interstitials in beryllium computed by diffraction model concept of pseudopotentials in metal theory 07 p1209 A67-19643

Yielding phenomena in beryllium wire plastic composites, discussing static strength and moduli, failure modes and impact resistance 08 p1341 A67-20428

Synchro-turn system for precision machining of beryllium mirrors 10 p1659 A67-22988

High modulus high strength reinforcements incorporated in epoxy matrix plastic composites for aerospace structural use 10 p1671 A67-23704

Hydrostatic pressure effect on surface microstructure, dislocation substructure and stress-strain behavior of beryllium 11 p1805 A67-24110

Electron beam process for vapor plating aluminum on beryllium for welding 11 p1798 A67-24264

Beryllium single crystal dislocation and twinning induced by compression deformation 11 p1810 A67-25093

Diffusion saturation of industrial iron, molybdenum, Kh18N9T steel and ZhS6-K alloy with powdered beryllium mixture 12 p1955 A67-25369

Metallurgy of beryllium - Conference Grenoble, France, May 1965 metallurgy of beryllium - Conference, Grenoble, France,

May 1965

Beryllium and other hexagonal metals mechanical properties compared under neutron irradiation, elucidating causes of beryllium embrittlement 13 p2135 A67-27102

Hydrogen and nitrogen effect on ductility of beryllium purified by zone refining 13 p2136 A67-27103

Beryllium aging kinetics when having different purities 13 p2136 A67-27105

Electron microscope observations on matrix precipitation in beryllium 13 p2136 A67-27106

Beryllium oxidation in high temperature range 13 p2136 A67-27107

Beryllium corrosion in carbon dioxide under pressure at high temperatures 13 p2136 A67-27108

Dynamics of beryllium lattice noting dispersion curves of wave frequencies 13 p2137 A67-27109

Curves of fusion and alpha-beta transformation of beryllium as function of pressure 13 p2137 A67-27110

Plastic behavior of zone refined and prestrained beryllium single crystals 13 p2137 A67-27111

Carbon action effect on tensile deformation in single and polycrystalline beryllium in terms of solutionized and precipitated states 13 p2137 A67-27112

Ductility of beryllium samples subjected to compression at temperatures ranging from 300 to 600 degrees C, discussing slip effects 13 p2137 A67-27113

Activation energy and volume of prismatic slip in beryllium 13 p2138 A67-27115

Transmission electron microscopy of dislocation structure produced in beryllium by specific deformation 13 p2138 A67-27116

Electron microscope study of cold working and tempering of beryllium single crystals 13 p2138 A67-27117

Be use in aerospace structure, gas turbines and aircraft brake disks 13 p2138 A67-27118

Micro-yield stress determinations of cast and extruded beryllium as measure of dimensional stability 13 p2138 A67-27119

Beryllium brittleness, discussing effect of grain refinement and randomization on properties below 200 degrees C 13 p2138 A67-27120

Plastic deformation mechanisms of polycrystalline beryllium to analyze temperature dependence of critical shear in prismatic plane 13 p2138 A67-27121

Polycrystalline beryllium creep at high temperature 13 p2139 A67-27122

Plastic flow in beryllium under fluid pressure at room temperature 13 p2139 A67-27123

Beryllium deformation under hydrostatic pressure 13 p2139 A67-27124

High purity beryllium mechanical properties obtained by double electrolysis 13 p2139 A67-27126

Influence of grain-size purity relation beryllium fabrication and resulting mechanical properties 13 p2139 A67-27127

Activated sintering of beryllium 13 p2140 A67-27129

Gas pressure bonding for hot isostatic pressing of beryllium powder into complex shapes 13 p2123 A67-27131

Beryllium joints and structures tested for static and repeated loading fatigue at room and high temperatures 13 p2123 A67-27132

Machining damage in beryllium from single point turning and drilling 13 p2123 A67-27133

Mechanical properties of beryllium with emphasis on influence of anisotropy in forming and grain size in powder metallurgy 13 p2140 A67-27134

Statistical analysis of beryllium cross-rolled sheet, hot pressed block and ring rolled forgings 13 p2140 A67-27135

Structural evaluation of sheet beryllium fabricated by three different methods 13 p2140 A67-27136

Continuous total immersion stress corrosion testing of beryllium in synthetic sea water, discussing relationship between time-to-failure and tensile stress 14 p2336 A67-28147

Beryllium wire manufacture and uses, noting properties, drawing techniques, annealing effects, reinforcing filament use, etc 16 p2687 A67-30488

Thin self-supporting beryllium foils

preparation for use as atomic and molecular ion beam targets 17 p2866 A67-33360

Ignition and combustion characteristics of single aluminum and beryllium particles burning in gaseous environment, discussing oxides role 18 p3149 A67-33796

High temperature kinetics of bulk beryllium metal combustion in hydrogen-oxygen-water vapor system, studying flame environments, thermal balance, etc 18 p3151 A67-33809

Beryllium single crystal plasticity increased due to preprogrammed load 19 p3245 A67-35470

Beryllium corrosion occurrence, causes, effects, prevention and advantages over steel and aluminum 20 p3465 A67-36636

Materials in airlift technology noting adaptation of titanium and beryllium 20 p3471 A67-37533

Beryllium part fabrication by metal removal, discussing machining and surface treatment methods [SAE PAPER 670803] 24 p4159 A67-41990

Beryllium braze joining for light stiff components noting structural examples and fabrication techniques, with reference to Apollo SNAP-27 radiator housing [SAE PAPER 670805] 24 p4159 A67-41991

Electrolytic polishing technique for bright field etch of Be specimens 24 p4173 A67-42349

BERYLLIUM ALLOY

Mechanical property data on Lockalloy /62 Be, 38 Al/ and comparison with other lightweight structural metals [SAE PAPER 660652] 01 p0094 A67-10613

Satellite structure from Be-lockalloy, properties compared with Al and joining methods 07 p1192 A67-20251

Axially loaded cylindrical structures analyzed for optimum weight construction consistent with cost constraint, emphasizing beryllium-aluminum alloys 08 p1424 A67-21521

Polybenzimidazole /PBI/ structural adhesives for bonding stainless steel, beryllium and titanium alloys 09 p1523 A67-22517

Beryllium alloys age hardening noting increase in flow stress with time 13 p2136 A67-27104

Microstrain c-axis compression test on two Be-4.37 wt percent Cu crystals, detecting nonbasal pyramidal slip system and compression twinning 13 p2137 A67-27114

Properties of fabricated ingot beryllium sheet selectively alloyed with copper to obtain improved strength 13 p2139 A67-27125

Mechanical properties of beryllium-aluminum alloy sheet with improved fabricability 13 p2140 A67-27128

Microalloying beryllium for improved sintering characteristics and mechanical properties 13 p2140 A67-27130

Alloyed Ni-Be alloys properties, discussing influence of Mo, W, B, V and Co on heat resistance without impairing physical properties 15 p2504 A67-29974

Twinning of copper, silver, iron, and gold alloys of beryllium pressurized in solid medium noting structural changes 16 p2690 A67-31371

Abnormal X-ray interference pattern change during aging of nickel-beryllium alloys 19 p3245 A67-35471

Optimum aging temperatures obtained from electric resistance of beryllium alloys containing chromium and zirconium 19 p3245 A67-35472

BERYLLIUM CHLORIDE

Transpiration, torsion and gravimetric effusion experiments to obtain thermal functions and approximate composition of vapors over solid beryllium chloride 06 p1071 A67-17984

BERYLLIUM COMPOUND

Bonding mechanism between metals and ceramics, noting glass penetration theory 02 p0255 A67-12060

Stabilization of high temperature beryllium allotropes through transition element addition, noting appearance of superconductivity 10 p1688 A67-22890

Transition temperatures of Be compounds, noting evidence for strong coupling to Mo localized mode from observed isotope effect 11 p1846 A67-24582

Fracture concept for two-phase structures analyzed on basis of crack-tip displacement, discussing macro-and microstructural cases 14 p2400 A67-28424

Relative enthalpy and thermodynamic properties of beryllium aluminate from room temperature to melting point 15 p2508 A67-29764

BERYLLIUM HYDRIDE

Total energy of beryllium hydride molecule analyzed, using difference between SCF energies and single determinant wave function 20 p3377 A67-37139

Total energy of beryllium hydride molecule as sum of SCF, correlation and relativistic energy and SCF error by LCAO-MO method 24 p4118 A67-41926

BERYLLIUM OXIDE

Beryllium oxide occurrence, fabrication, properties and application 09 p1520 A67-22614

Metal-beryllium oxide bond for semiconductors noting mechanical and electrical strength, thermal conductivity and refractivity 10 p1696 A67-23691

Oxidation of Be thin films in oxygen and carbon dioxide, noting decomposition of Be-carbide and effects of heating by electron beam 13 p2132 A67-26998

BERYLLIUM POISONING

Beryllium component machine tool installations and operation, discussing contamination protective systems for toxic dust 23 p4009 A67-40687

BESSEL FUNCTION

Special functions for solving second-order or higher linear differential equations with variable coefficients in elasticity theory problems 01 p0158 A67-10215

Langmuir probe method, obtaining exact results for small amplitude plasma oscillations 01 p0123 A67-10461

Fundamental solutions to certain singular partial differential equations with constant coefficients, using Bessel iteration operator and Fourier-Bessel transforms 01 p0105 A67-10676

Infinitely divisible distributions of first passage times and hitting points in ordinary random walk solved by Bessel functions 01 p0106 A67-10735

Interaction between atoms of solid surface and gas phase, obtaining closed-form solution of motion 01 p0118 A67-11295

Rectilinear and smooth multiwave transition 02 p0215 A67-11914

Analytic solution in terms of modified Bessel functions of synergetic turn in exponential atmosphere, using spacecraft engines only for drag cancellation and orbit trimming [ATA PAPER 66-487] 02 p0331 A67-11938

Book on conductive heat transfer covering lumped, integral and differential formulations, two- and three-dimensional periodic functions, unsteady problems, Laplace transforms, etc 03 p0535 A67-13075

Approximate solution to nonlinear differential Riccati equation, using Bessel function 03 p0460 A67-13879

Output probability density distribution of stationary random noise containing regular signal components after mean squaring circuit 05 p0783 A67-16446

Lie series formalism applied to solution of Bessel equation describing behavior of laminary oscillating MHD fluid 05 p0854 A67-16989

Expansion of arbitrary function in terms of Bessel functions of complex index 06 p1024 A67-18555

Bessel function applications of two Sonin theorem formulations compared for range of applicability 07 p1215 A67-19472

Partial differential equations for displacement and stress functions of shallow shells expressed as Bessel functions 09 p1573 A67-21664

Critical volume of cylindrical reactors calculated using n-group diffusion theory 10 p1675 A67-23396

Temperature field of coaxial cylinders obtained as infinite series of Bessel and trigonometric functions 13 p2224 A67-27057

Nonaxisymmetric temperature fields for orthotropic hollow cylinder and sphere solved using Bessel functions, noting heat transfer between external and internal surfaces 15 p2579 A67-29697

Plane wave disturbances in infinite rotating collisionless system for wave vector normal to axis of rotation [AD-653420] 16 p2753 A67-31700

Transverse oscillations of elastic inhomogeneous rod with Young's modulus

varying along length; solved in Bessel functions infinite series 17 p2962 A67-32873

Computer program for heat transfer calculation by temperature distribution along wall surface, using Fourier-Bessel series to determine distribution coefficients 20 p3544 A67-36450

Long radio wave propagation in earth ionosphere waveguide channel, determining eigenvalues of boundary value problem from complex transcendental equation containing Bessel function 21 p3580 A67-38116

Expansion of arbitrary function in terms of Bessel functions of complex index 23 p4022 A67-40821

FM oscillations spectrum component amplitude formula for multiple frequency modulation using Bessel function 24 p4122 A67-42379

BETA RADIATION

SA LYMAN BETA RADIATION

Directional correlation of first forbidden beta group and gamma ray in decay of antimony at four beta energies 02 p0269 A67-11863

Radioisotope sources used for simulating space radiations, obtaining energy spectra by blending beta emitters 02 p0265 A67-12213

Corrosion detection of metal surface under protective coating, using beta radiation probe 02 p0245 A67-12218

Production of low energy cosmic ray electrons, investigating energy inputs to injected secondary electrons by possible low magnitude solar electric field and possible galactic Fermi acceleration 02 p0312 A67-12635

Simplified 180 degrees focusing beta-ray spectrometer, noting electron trajectory radius, shape of vacuum chamber walls, etc 05 p0806 A67-16500

Physical pattern of high altitude fission cloud and motion of gamma and beta fission fragments captured by geomagnetic field and observed by Cosmos satellite 07 p1242 A67-19102

Superconducting and superheated metastable state transition to normal state by beta irradiation 17 p2912 A67-32270

Superconducting magnet spectrometer using lithium drifted silicon detectors for measurement of electron spectra 20 p3444 A67-36523

Nilsson model used to derive expressions for nuclear matrix elements, considering forbidden beta decay of spheroidal-shaped nuclei 20 p3488 A67-36662

Approximate electron radial functions for uniformly charged nucleus /UCN/ used in analyzing boron 12 and nitrogen 12 beta decay spectra 20 p3488 A67-36915

Solar radio emission mechanism for spin transitions of neutron beta decay electrons in external magnetic field 20 p3520 A67-37522

Back collection of charge due to ionizing alpha or beta particles by silicon p-n junction detector with space charge width less than range 22 p3797 A67-39345

BETATRON

Reversible betatron acceleration mechanism during geomagnetic storm 20 p3434 A67-37425

BETHE-SALPETER EQUATION

S WAVE FUNCTION

BIBLIOGRAPHY

Bibliography of books and periodicals concerning heat transfer and related topics including applications, boundary layer, phase change, separated flow, etc 01 p0167 A67-10978

Bibliography of Russian works on heat transfer and related topics including heat conduction, thermodynamics, transfer processes involving phase and chemical conversion, etc 01 p0167 A67-10979

Bibliography on lasers covering modes, scattering mechanisms, quantum electrodynamics, matter-radiation interaction, plasma, holography and optics 06 p1010 A67-17890

Bibliography on cosmic rays for use as teaching aid for college physicists 07 p1242 A67-19622

Inclusive classified bibliography pertaining to modeling human operator as element in automatic control system 07 p1137 A67-20173

Bibliography and subject index to two-phase gas-liquid flow 07 p1269 A67-20300

Bibliography on lasers and laser

applications 09 p1511 A67-21713

Survey and bibliography of works on optimum control system design and statistical signal descriptions 09 p1483 A67-22386

ASTM 1964 references on fatigue 12 p2032 A67-26093

Astronomical year-report, 1965, including bibliographies and works on instruments, position astronomy, interplanetary objects, quasars, etc 13 p2200 A67-27225

Bibliography on electrical discharges in vacuum and properties of vacuum as electrical insulator 15 p2516 A67-29200

Heat transfer bibliography covering boundary layer, phase change, two-phase flow, channel flow, conduction, liquid metal, MHD, etc 17 p2969 A67-32450

Soviet heat transfer bibliography covering heat conduction, convective and radiative heat transfer, mass transfer, drying processes, high temperature, etc 18 p3160 A67-34166

Atmospheric optics and radiation transfer covering sky brightness, solar insulation, earth radiance and albedo, etc 20 p3430 A67-36899

Night airglow research during IQSY noting correlation of low activity with sunspot minimum 20 p3430 A67-36905

Laser bibliography V /July-December 1966/ covering giant-pulse techniques, Raman and Brillouin scattering, interaction effects, propagation, holography, etc laser bibliography V /July-December 1966/ 21 p3641 A67-38455

Book on laser systems covering quantum electronics, coherent radiation, modulation and spectral, distance, velocity and communication applications 22 p3814 A67-39445

Collected papers of Kapitza, Volume 3 covering low temperature production, stereoscopic films, liquid He, etc 24 p4188 A67-42294

BIHARMONIC EQUATION

SA ELASTICITY

Finite difference equation for biharmonic equation of plane 05 p0833 A67-16032

Solution to external biharmonic problem for simply connected region bounded by Liapunov curve given in form of Fourier series and applied to elasticity theory 05 p0908 A67-16041

General solution of two-dimensional linear elasticity problem in polar coordinates in term of stress function satisfying biharmonic equation 06 p1111 A67-18873

High accuracy alternating direction implicit difference schemes for biharmonic, heat conduction and Laplace equations 15 p2510 A67-29520

BINARY ALLOY

Equilibrium diagram of niobium-nickel system determined by thermal analysis, microscopical metallography and X-ray techniques 05 p0828 A67-16387

Superconductivity in aged Zr-Nb alloys, noting transition temperature increase of quenched alloy upon aging 05 p0828 A67-16469

Steady state kinetics and microstructures of simultaneous internal oxidation and external scale formation of Cb-Zr and Cb-Zr-Re alloys in pure oxygen at 1000 degrees C 05 p0828 A67-16471

Thermodynamic properties of binary Cu-Pt alloys determined, using Knudsen effusion technique 05 p0829 A67-16473

Superplastic effect in cr-30 at. pct Co alloy, noting low temperature bend ductility in quenched metastable single phased and near equilibrium conditions 05 p0829 A67-16474

High temperature cobalt iron alloy for square loop and power transformer applications 05 p0864 A67-16833

Magnetic properties of second kind superconductivity of indium-lead alloys as function of temperature down to 0.38 degrees K 05 p0864 A67-16893

Structure and mechanical properties of molybdenum-niobium system monocrystalline melts prepared by electron beam zonal melting 05 p0830 A67-17024

Band structure of Bi-Sb alloy system, using Shubnikov-de Haas technique with supplemental transport measurements 06 p1070 A67-18983

Mutual diffusion characteristics of titanium-tungsten mixtures at high

temperatures, noting discontinuity on concentration curve due to two-phase region presence 07 p1204 A67-19266

Phase diagram of titanium-rich alloys of system Ti-Al, measuring resistivity and hardness through X-ray diffraction, thermal analysis, etc 07 p1204 A67-19267

Heats of solution and formation of Ti-Al alloys in region of alpha-solid solution determined, using 07 p1204 A67-19268

Ni, Si and Nb effect on oxidation of binary alloys of titanium in air at high temperature, discussing heat resistance 07 p1205 A67-19275

Physical properties of quenched binary alloys of titanium 07 p1206 A67-19281

Rare earth metal/manganese alloys analyzed by amalgam 07 p1210 A67-20111

Scaling of binary titanium alloys in carbon dioxide at high temperatures using kinetic, metallographic and electron probe microanalysis [AAS PAPER 66-190] 08 p1341 A67-20763

Alloying effect on aluminum K and iron L X-ray emission spectra in Al-Fe binary system 08 p1343 A67-21304

Electrical characteristics of thin film nickel-chromium resistors dependency on variation in processing parameters including source and film composition, deposition rate, etc 09 p1555 A67-22103

Depressing effect of hafnium and zirconium on work function of tungsten, tantalum, niobium and 10 p1668 A67-23091

Shear modulus effect on stress distribution of planar array of screw dislocations near bimetallic welded half-planes interface 11 p1804 A67-24107

Co-Ni system heterodiffusion and interdiffusion coefficients variation with temperature and composition 11 p1808 A67-24772

Surface and volume diffusion in thin films of system Ag-Se investigated by electron diffraction and microscopic studies 12 p1979 A67-25179

Hardening and softening of nickel-alumina alloys 12 p1955 A67-25365

Properties of fabricated ingot beryllium sheet selectively alloyed with copper to obtain improved strength 13 p2139 A67-27125

Interaction between phases of nickel aluminum-nickel titanium pseudobinary system, determining concentration dependence of properties of system 13 p2142 A67-27286

Superconductivity of Nb₃-Al-Mo₃Al binary system 13 p2184 A67-27631

Structure and mechanical properties of molybdenum-niobium system monocrystalline melts prepared by electron beam zonal melting 14 p2338 A67-28491

Twinning of copper, silver, iron, and gold alloys of beryllium pressurized in solid medium noting structural changes 16 p2690 A67-31371

Hall angle of various superconducting niobium-tantalum alloys in mixed state, noting dependence on current and temperature 18 p3098 A67-33519

Reversible contribution to flow stress in Ni-Al alloy analyzed by temperature change as function of tensile strain and precipitation hardening 18 p3065 A67-34363

Field ion microscopy of Ni-Mo alloys 18 p3065 A67-34364

Scaling resistance of nickel and cobalt binary alloys investigated to determine heat resistance as function of composition 20 p3467 A67-37115

Ni-Fe-Mn alloy, Youngs modulus and magnetic saturation temperature dependence, noting order-disorder effects on Curie point 20 p3468 A67-37178

TiNi-TiFe system equilibrium diagram, studying melting points and heat treatment effects on microstructure 20 p3468 A67-37179

Compositional changes at alloy/oxide interface during protective oxidation calculated using finite difference method 20 p3468 A67-37247

Chromium activities in binary Cr-Ti solid solutions measured by Knudsen effusion technique, noting deviations from Raoult law and free energy calculation 20 p3469 A67-37384

Binary molybdenum-carbon system investigated using X-ray, metallographic,

thermoanalytical and melting-point techniques 20 p3470 A67-37389

Soviet book on physicochemical principles of semiconductor alloying covering chemical bonds, crystal structure, binary systems, etc 21 p3684 A67-38433

Superconductivity of Nb₃-Al-Mo₃Al binary system superconductivity of Nb₃-Al-Mo₃Al binary system 21 p3685 A67-38828

Powder X-ray structural analysis of compounds of Nb-Ni and Ta-Ni systems, establishing homogeneity region for NbNi 21 p3646 A67-38973

Surrounded atom model for thermodynamic enthalpy and entropy characteristics of mixing in liquid binary alloys 21 p3733 A67-39105

Closed form equation with variable segregation coefficient for single pass zone melting in binary alloy systems 22 p3856 A67-39368

Spin-disorder resistivity measurements in Gd-Yt alloys noting temperature and concentration effects 22 p3863 A67-40203

Cluster variation method based on W-shaped cluster in triangular lattice for lattice-gas liquid, phase-separating binary alloy and Ising model 23 p3971 A67-40969

Alloying effect on diffusion thermopower in relation to Fermi surface variations in dilute silver-gold alloys [JPL-TR-32-1095] 24 p4200 A67-41840

Interstitial solid solubility of N in Nb and Nb binary alloys containing Hf, Mo and W as function of pressure and temperature 24 p4172 A67-41976

Quenched structures and precipitation in Al-Cu alloys with and without traces of Cd studied electromicroscopically, showing possible CD stabilizing effect 24 p4173 A67-42166

Omega phase precipitation and superconducting critical transport currents in Ti-Nb wire samples 24 p4173 A67-42347

BINARY CODE

Ninety-eight-channel microelectronic PCM multiplexer-encoder design and development qualified to Apollo spacecraft environments 01 p0028 A67-10864

Multichannel Data Logging System for recording short-term simultaneous analog data from 25 to 100 parallel input channels 01 p0076 A67-11142

Probabilistic structure of and establishment time for group synchronization in time-division-multiplex /binary code/ transmission systems 01 p0027 A67-11238

Synthesis method for generating p-level pseudorandom signals derived from corresponding m-sequences, using standard binary logic elements 03 p0393 A67-13997

Chernoff bound and tilted distribution argument for obtaining error probability bounds for binary signaling on slowly fading Rician channel [JPL-TR-32-1051] 06 p0961 A67-17943

Optimal signal design for binary communications systems using sequential and nonsequential detection with feedback 06 p0962 A67-17944

Prefix coding of histograms for minimal storage 14 p2272 A67-28703

Coding for numerical data transmission over binary symmetric channel, discussing effectiveness of various error-correcting codes, taking average numerical error as fidelity criterion 15 p2439 A67-30387

Algorithm for converting binary code into uniform binary code with maximum predetermined number of zero symbols in any code combination 18 p2999 A67-33532

Binary pulse compression codes generation with low periodic autocorrelation 20 p3386 A67-37493

Binary symmetrical channel noise effect on PCM picture quality compared with white Gaussian noise effect in PAM system 20 p3386 A67-37496

Coded information transmission with reduced band emphasizing pulse prediction through redundancy, information quantity and delta signal 21 p3585 A67-38763

Noise immunity in binary detection and temporal shift measurement of pseudorandom amplitude keyed echo signal in multichannel system 24 p4120 A67-42233

Optimal reception of binary signals on background non-Gaussian noise determined by logarithm expansion for probability coefficient into Taylor series 24 p4122 A67-42377

Double signal modulation used to increase authenticity of information transmission in binary systems having resolving feedback 24 p4122 A67-42378

BINARY DATA

Book on statistical communications theory, digital communications, AM and FM CW communications, binary communications and noise 01 p0021 A67-10306

Statistical properties of input signals and effect on structure of optimal binary system of signal reception 01 p0024 A67-10722

PPM-frequency time hopping for multichannel communication system to transmit digital data over tropospheric scatter path 02 p0202 A67-12131

Error probability of binary receivers for digital transmission over radio channels characterized by specular and selective fading components 02 p0203 A67-12166

Digital simulation results for random approximation solutions of binary signal detection problems 02 p0204 A67-12169

Bias due to random bit errors that occur in PCM data during phases of operation of telemetry data processing system 07 p1145 A67-19874

Pure fluid four bit binary comparator design and construction 08 p1283 A67-20474

Radar scan-antenna angle transmission over DC voltage in binary form for digital computer or display 11 p1760 A67-24269

Encoding and decoding techniques using integrated circuits and applicable to binary digitizing of electrical analog information 13 p2072 A67-26412

Indeterminate recognition /game type/ and prediction systems 13 p2088 A67-27022

Invariant operating regime of optimum threshold receiver during binary signal reception 16 p2624 A67-31029

Time statistics for reliable transmission of binary data in presence of atmospheric noise burst 17 p2811 A67-32113

BINARY FLUID

Stability of motion of plane boundary interface between two different density coupled fluid jets analyzed to determine role of viscosity in drop formation 11 p1782 A67-24959

MHD power generation using bifluid liquid metal system /such as Li and Cs/ with two-phase generation 12 p1901 A67-25897

Pair correlations function in stable homogeneous plasma 13 p2164 A67-26295

Incompressible two-phase mixed flow through sharp edge orifice including shear force between phases 14 p2305 A67-29012

Cycle and separator efficiencies and specific radiator area compared for liquid alkali metal-lithium MHD power generators 21 p3572 A67-38864

Kinetic prediction theory for viscosity, thermal conductivity and diffusivity of binary liquid mixtures composed of molecules interacting with square-well potential 23 p4083 A67-41531

BINARY INTEGRATION

Binary detection probability for optical polarization modulation communication system using Gaussian approximation, noting signal to noise ratio 01 p0028 A67-10866

Moving-window detector for binary integration on quantized data, discussing possible application to multiple-range-element radar 12 p1916 A67-26079

Repeating incoherent pulsed signal detection problem in Gaussian noise studied by binary integration method assuming ideal control criteria 18 p2999 A67-33505

Generation of arbitrary binary sequence with integrated circuits, describing logic circuit by means of circuit algebra 21 p3590 A67-37946

BINARY MIXTURE

Shock wave structure in binary mixture, using Mott-Smith distribution postulating flow velocity and temperature of subsonic mode as position functions 02 p0234 A67-12542

Reflectance and emittance properties of binary coatings in sintered or compacted powder form in terms of properties of pure components [AIAA PAPER 65-870] 03 p0448 A67-13038

Nucleate boiling mechanism in superheated binary mixtures obtained from extension of theories of van Wijk, Vos and van Stralen by Scriven and Bruijn 04 p0720 A67-14637

Phenomenological theory of mass transfer

in binary systems near critical point applied to particular boundary value 04 p0727 A67-15683

Asymptotic solution method for frozen dissociated laminar boundary layer flow over flat plate surface with arbitrarily distributed catalytic 11 p1781 A67-24573

Binary van der Waals mixture near solution critical point, noting anomalous behavior of heat capacity, shear viscosity and bulk viscosity 11 p1884 A67-24990

Constitutive theory for fluid mixtures admitting diffusion and chemical interaction with heat conduction and plane wave propagation 11 p1783 A67-25001

Thermal conductivity of binary gas mixtures, estimating conductivity at high temperatures 12 p2033 A67-25217

Two component equivalent of two-stream distribution function solution to plane Couette flow, studying nonlinear effects 13 p2101 A67-26965

Spherical supersonic source expansion of neutral disparate molecular weight binary gas mixture studied asymptotically as source Knudsen number tends to zero 13 p2104 A67-26984

Turbulent mixing at interface of two different density media under influence of pressure gradient, considering diffusion 13 p2105 A67-27411

Stability of arbitrary one-dimensional hydrodynamical flow in quasi-isothermal case 13 p2105 A67-27413

True air life support system, describing concept for deriving fixed percentage binary gas from two steady state cryogenic liquids 13 p2064 A67-27638

Axial and radial velocity distributions in axisymmetric free jets of pure gases and binary gas mixtures, noting molecular beam production 14 p2301 A67-28183

Differential equations for heat and mass transfer in laminar boundary layer of binary gas mixture flow past porous wet flat plate 14 p2242 A67-28307

Boiling process of binary mixtures examined by heat transfer mechanism at atmospheric pressure 17 p2969 A67-32458

Viscosity of neon-nitrogen, helium-carbon dioxide and nitrogen-argon mixtures 18 p3161 A67-34522

Ti-C-N system studied for stoichiometric range and thermodynamics using gas equilibration techniques, measuring nitrogen/carbon activities 19 p3248 A67-34865

Generalized Mott-Smith functions for shock wave structure in binary mixtures, relative diffusion velocity obtained and compared with Diakov solution 20 p3421 A67-36678

Mass transfer cooling of carbon dioxide-nitrogen binary system in laminar boundary layer, stressing dissociation effect [ASME PAPER 67-HT-70] 20 p3550 A67-36750

Solution drops motion in diffusing binary gas mixture, analyzing velocity 20 p3421 A67-36812

Neutral carrier gas and slightly ionized plasma binary mixture model for nonhomogeneous seeding effects on rotating arc performance 21 p3674 A67-38885

Binary gas mixtures transport coefficients calculation, comparing experimental and theoretical values of viscosity and thermoconductivity dependent upon interaction between unlike molecules 21 p3733 A67-39064

Improvement of high performance liquid fuel rocket engine by optimization of liquid hydrogen /LOX/ propulsion mixtures 23 p4049 A67-41319

BINARY STAR

SA ECLIPSING BINARY STAR

Isotropic mass loss effect on binary star system orbital elements and period eccentricity relationship 08 p1380 A67-20385

Contact binaries origin and evolution, discussing orbital angular momentum dissipation through mass ejection along magnetic lines of force 09 p1568 A67-22367

Age and helium content correlations from recent mass determinations of two low mass binary star systems used in stellar evolution theory 11 p1858 A67-23996

Evolution in close binary star system through mass exchange leading to white dwarf with relatively unevolved companion 11 p1864 A67-24581

Planetary system abundance for stellar system mass near solar mass determined

from mass/angular momentum diagram 11 p1865 A67-24610

Maximum gravitational radiation detection range for binary stellar system analyzed by mechanically resonant antennas 15 p2563 A67-30162

Gravitation wave radiation rate from binary stars, using Brans-Dicke general relativity theory 21 p3706 A67-38842

Rotation and magnetic field effects on single and multiple stars 22 p3895 A67-40519

Close binary protostellar system formation using model with stellar wind mass loss and primeval magnetic field 22 p3896 A67-40520

Small stellar systems evolution, double star formation and bound subgroup occurrence after condensation from collapsed cloud calculated numerically 22 p3896 A67-40521

BINARY-TO-DECIMAL CONVERSION

Pure fluid binary to decimal converter using wall attachment OR/NOR elements 08 p1282 A67-20466

BINDER

SA ADHESIVE

SA PROPELLANT BINDER

Mechanical properties of continuous filament-graphite matrix composite in 0.50 inch diameter rod form, discussing limitation of binder phase and interface 03 p0453 A67-13412

Flexible anisotropic ferrite magnets preparation, noting influence of binder in orientation of crystals 23 p4041 A67-41183

BINDING ENERGY

Impurity band tails in degenerate semiconductors, showing relation between decay in density of states and screening density 06 p1061 A67-18923

Modulus of elasticity of metals and titanium alloys as function of electron structure and binding 07 p1206 A67-19279

Quantum limit galvanomagnetic phenomena in n-InSb 13 p2184 A67-27690

Chemical effects in X-ray spectra and inner shell photoelectron spectra of sulfur- and chlorine-oxygen anions and molecular orbital method 18 p2998 A67-34520

Interaction of two H atoms in ground states using Hirschfelder-Linnet wave function and Gaussian type 22 p3756 A67-39385

Bond formation effect on electron scattering cross sections for molecular H, N and O 23 p4029 A67-40966

Enthalpies of formation and bond energies of various fluorinated amines in gas state 23 p3971 A67-40975

MX solids refractory character correlation with volatility at triple point, calculating bond energy according to formation enthalpy equation 24 p4173 A67-42084

BINOCULAR VISION

Correlation between heart rate, landing error and field of view for binocular and monocular sphere of vision of jet pilots 09 p1455 A67-21717

BINOMIAL COEFFICIENT

Reliability analysis of active, standby and active-standby redundant system, discussing Poisson-binomial probability distribution function 13 p2123 A67-26828

BINOMIAL THEOREM

Binomial probability distribution applied to air battle analysis, discussing fire doctrines, attrition rates, weapon design classes and limitations of approach [AIAA PAPER 66-781] 01 p0169 A67-10527

Confidence limits for percentile analysis of guidance system errors 15 p2515 A67-29740

BIOASTRONAUTICS

SA AEROSPACE MEDICINE

Weightlessness effect on level of vigilance of cats and rats launched in rockets, examining electrical activity of cerebral cortex 03 p0364 A67-13927

Biological significance of space effort including colonization and adaptation of man to extraterrestrial habitats 06 p0954 A67-19040

Pre- and postflight medical examinations of Voskhod I cosmonauts 07 p1133 A67-19108

Comparative neurosciences research program suggestions 07 p1135 A67-19864

Genetic studies in space, discussing free balloon, rocket and satellite experiments with microorganisms, plants and animals 09 p1453 A67-21901

Radiation hazards and safety requirements

for lunar and Mars manned space flights, discussing radiosensitivity, restoration and permissible doses 13 p2059 A67-26761

Recessive lethals in X chromosome of drosophila and genetic shielding during flight of spaceship 13 p2060 A67-27337

Voskhod 13 p2060 A67-27337

Space flight effect on chromosomes of dry seed embryos, noting no significant change 13 p2061 A67-27344

Bioastronautics role in population explosion and technological evolution problems, noting biocybernetics, and aerospace systems 16 p2782 A67-30787

Cybernetics methods suited to complex systems associated with bioastronautics 16 p2618 A67-30788

Space environment factors effects on living organism including changing gravity, high vacuums and solar radiation 16 p2614 A67-31000

Automated biological laboratory /ABL/, comprehensive integrated system for detection of life on Mars 16 p2762 A67-31488

Automatic life-support system tried on leeches for space applications 19 p3180 A67-35248

Biostasis /suspended animation/ by frozen storage investigated for application to interstellar voyages, noting possible damage prevention during space trips 19 p3181 A67-35325

Monkey psychomotor reactions during ballistic flight, noting alertness reduction during weightlessness 19 p3181 A67-35466

Helium-oxygen environment relation to biological-thermal requirements of spacecrew 20 p3374 A67-36582

Space genetics, discussing space environment exposure of experimental animals as cause of mutations, hereditary damage, etc 24 p4113 A67-42053

BIOCHEMISTRY

SA PHYSIOCHEMISTRY

Gas chromatographic and mass spectrometric analysis of chlamydozoospores of *Ustilago maydis*, *U. nuda* and *Sphacelotheca reiliana* for hydrocarbon content 03 p0363 A67-13594

Cellular biochemical thermoregulation and organic mass changes in cold- and heat-acclimatized monkeys 04 p0560 A67-14582

Biochemical measures made as part of habituation experiment in which four subjects were exposed to rotation for 6 days 05 p0754 A67-16277

Deaggregation of chlorophyll by xanthophylls 09 p1454 A67-21990

Molecular sizes of diphosphopyridine nucleotide linked dehydrogenases of representative animal, plant and microbial species 11 p1750 A67-24784

Rapid assay for thymidylate synthetase as specific and sensitive measure of enzyme activity 14 p2280 A67-28479

Biological macromolecule detection using thiacarbocyanine dye and observation of absorption spectra changes 15 p2426 A67-29115

Biochemical reactions in human organism as indicator of cosmic ray variation, showing relationship between solar activity and erythrocytes in blood 17 p2934 A67-32099

Active parotin preparation to lower serum calcium levels, Ca excretion and possibly prevent decalcification, for applicability to potential system 18 p2991 A67-34712

BIOCONTROL SYSTEM

S RESPIRATORY SYSTEM

BIOCUORIER PROJECT

S LIFE SCIENCE

BIODYNAMICS

Air Force biodynamic research on injury due to impact during air crash or ejection 08 p1289 A67-20615

Simulated acceleration and dynamic pressure environments generated by space vehicle flight ranging from weightlessness to impact from ground landing [AIAA PAPER 67-279] 15 p2465 A67-29425

Prolonged confinement in small chambers effect on biodynamic processes of walking and other movements in special positions 16 p2813 A67-30914

BIOELECTRIC POTENTIAL

Effects of inhaled air ions on speed of response and attention level, heart and respiration rate and transepithelial DC potential of men 09 p1452 A67-21720

- Quasi-static potential distribution in inhomogeneous volume conductor analyzed using Green theorem 11 p1746 A67-23991
- Biopotential detection, recording and design noting electrocardiogram and electroencephalogram use to monitor weightlessness in manned space programs 17 p2807 A67-32666
- BIOELECTRICITY**
- Ultrahigh input impedance for measuring electrical activity of biological cell 05 p0773 A67-16512
- Minimal value of artificial gravity for normal electroactivity of skeletal muscles determined for otherwise weightless condition 13 p2057 A67-26457
- BIOENGINEERING**
- SA HUMAN ENGINEERING**
- Space technology utilization in detection and prevention of cardiovascular disease, discussing instrumentation for monitoring microcirculatory system [AIAA PAPER 66-951] 02 p0187 A67-12285
- Bioengineering and food processing - AICE Meeting, Minneapolis, September 05 p0757 A67-17155
- Electrical and electronics engineering - IEEE Conference, Jackson, Mississippi, April 1967 13 p2085 A67-26404
- Biological problems in prolonged space voyages including oxygen replacement, water supply and food 19 p3179 A67-35209
- Biomedical safety monitoring instrumentation for Lunar Module oxygen filled internal environment 23 p3969 A67-41640
- BIOGENESIS**
- SA AIOGENESIS**
- Nucleic acid molecule reproduction discussing probability of life development under favorable environmental circumstances 16 p2611 A67-30767
- Origin of life on earth, formation of nucleic acid molecules and metabolic mechanism 24 p4112 A67-42052
- Synthesis of biologically pertinent peptides under possible primordial conditions 24 p4118 A67-42606
- BIOGENY**
- Origin of round body structures in Orgueil meteorite 24 p4113 A67-42455
- BIOINSTRUMENTATION**
- Time division multiplexing system for LF bioelectric signals, noting operation parameters and modes 02 p0216 A67-12075
- Telemetry and programming equipment used by CERMA in nose cones of rockets containing cats and rats in state of weightlessness 03 p0366 A67-13928
- Human body as source of power for implanted electronic devices [AIAA PAPER 66-930] 03 p0366 A67-14137
- Mass spectrometer in physiological research or in medical monitoring 05 p0756 A67-16279
- Ultrahigh input impedance for measuring electrical activity of biological cell 05 p0773 A67-16512
- Cardiovascular changes due to orthostasis, evaluating influence of intravascular instrumentation on orthostatic tolerance of normal men 06 p0953 A67-18776
- Implant telemetry techniques and associated problems and potential of microelectronics 12 p1903 A67-26171
- Miniaturized multichannel multiplexed FM biotelemetry system designed to record physiological condition of pilot and test operational efficiency 14 p2256 A67-28210
- Biotelemetry improvements in manned space flights, emphasizing bit rate reduction required for electrocardiogram data transmission to earth 17 p2807 A67-32900
- BIOKINETIC THEORY**
- Prophylaxis for negative effect of hypokinesia on human cardiovascular system 13 p2059 A67-26764
- BIOLOGICAL CELL**
- SA CHROMOSOME**
- SA CYTOLOGY**
- SA ERYTHROCYTE**
- SA MITOCHONDRIA**
- SA NUCLEUS**
- Cellular biochemical thermoregulation and organic mass changes in cold and heat-acclimatized monkeys 04 p0560 A67-14582
- Cell survival rates and mutation development in *Chlorella vulgaris* plants carried by Cosmos 20 p3367 A67-36256
- Protoplast origin, discussing radiation effects on polymers, proteinoid properties and already synthesized polymer stability 24 p4113 A67-42656
- BIOLOGICAL EFFECT**
- SA PATHOLOGICAL EFFECT**
- SA PHYSIOLOGICAL RESPONSE**
- Optical activity in meteorite organic matter, recording observation of low amplitude 03 p0510 A67-13592
- Symptomatic responses of eight college females to high altitude exposure include headaches, drowsiness, fatigue and insomnia 03 p0365 A67-14298
- Fatigue failure induced by aging and disease of self-healing biological structure in mathematical model [ASME PAPER 66-WA/BHF-3] 04 p0564 A67-15399
- Inhibitory effect of light from cool white fluorescent lamps on growth of yeast, alga and protozoa 06 p0952 A67-17872
- Killing and mutagenic efficiencies of heavy ionizing particles in *Arabidopsis thaliana* 06 p0953 A67-18379
- Biological effect on mice of bombardment by protons of 120 Mev 07 p1133 A67-19114
- Biological effects of supersonic flight, discussing radiation at high altitudes and preventive measures 07 p1134 A67-19532
- Hazards of laser radiation, mechanisms, control and management 10 p1601 A67-23328
- Book on environmental biology covering effects of temperature, radiant energy, acceleration and gravity, etc 11 p1747 A67-24233
- Remote aftereffect on hemopoietic tissue of mice under simultaneous irradiation and acceleration, using both X-rays and protons 13 p2057 A67-26458
- Ionizing radiation effect on bacterial cells noting inhibition due to generated hydrogen peroxide 13 p2059 A67-26867
- Effects of long term repeated short treatments of mice with hyperbaric oxygen on organ and body weights and hematologic and histologic development 13 p2060 A67-26926
- Recessive lethals in X chromosome of drosophila and genetic shielding during flight of spaceship 13 p2060 A67-27337
- Voskhod 13 p2060 A67-27337
- Space flight effect on chromosomes of dry seed embryos, noting no significant change 13 p2061 A67-27344
- Mutagenic effects of primary cosmic radiation on bacteria 14 p2254 A67-28213
- Planetary quarantine constraints, noting prevention of Martian atmosphere contamination 15 p2424 A67-29098
- Prolonged recording from single vestibular units in frog during plane and space flight, significance and technique 15 p2430 A67-29281
- Biological value of plant proteins for closed life-support system, studying diet effects on rats 16 p2612 A67-30908
- Lethal effect of solar UV radiations on dried *Coliphage T-1* exposed to space at sounding rocket altitudes 19 p3177 A67-35184
- Drugs for protection and stimulation of biological functions of spacecrews, noting experimental results on transverse-acceleration resistance of animals 20 p3367 A67-36254
- Plasma volume, red blood cell mass and erythrocyte survival determination before and after space flight 20 p3372 A67-37429
- Biological effects of time-zone changes on circadian rhythms of urinary elimination of potassium and 17-hydroxycorticosteroids 22 p3751 A67-39606
- High performance aircraft flight effect on blood glucose in fasting subjects noting no hypoglycemia tendency 23 p3950 A67-41550
- Acute and chronic cellular level effects of low energy proton irradiation in rat skin 23 p3957 A67-41644
- Biological regeneration of enclosed atmosphere with algae photosynthesis noting effect of diet change 24 p4114 A67-41845
- Biological value of algal and soya proteins on four generations of white rats 24 p4111 A67-41847
- BIOLOGICAL MODEL**
- Physiological reaction of human body to applied stimuli, developing method evaluating metabolism 16 p2612 A67-30907
- Computer simulation of biological pattern generation processes 24 p4116 A67-42453
- Biochemical model for long term sequential memory in nervous system, introducing network serving as clock to maintain temporal order of stored events 24 p4116 A67-42698
- BIOLOGICAL RHYTHM**
- Phase shifts of human circadian system and performance deficit during periods of transition in north-south flight 05 p0756 A67-16289
- Biological clocks and cycles in man, lower animals and plants, discussing circadian rhythms 13 p2058 A67-26607
- Daily physiological rhythm changes associated with light intensity and color, noting body temperature oscillations vs light intensity, heart rate changes, etc 15 p2426 A67-29109
- Circadian clocks - Conference, Feldafing, West Germany, September 1964 20 p3370 A67-36805
- EEG and rhythmical tremor in outstretched upper extremities in man analyzed by autocorrelation and cross correlation 20 p3373 A67-37525
- BIOLOGY**
- SA BACTERIOLOGY**
- SA BOTANY**
- SA ECOLOGY**
- SA GENETICS**
- SA MEDICINE**
- SA MICROBIOLOGY**
- SA MORPHOLOGY**
- SA PHYSIOLOGY**
- SA PROTOBIOLOGY**
- SA RADIOBIOLOGY**
- Qualitative biological data conversion into pseudovariables permitting use of correlation analysis and prediction, considering occupation relation to cholesterol 01 p0017 A67-10956
- Long-term biomedical instrumentation in Air Force space program 01 p0017 A67-11029
- Manned orbital laboratory for biological research, discussing experimental possibilities and requirements on spacecraft 08 p1287 A67-21070
- Book on environmental biology covering effects of temperature, radiant energy, acceleration and gravity, etc 11 p1747 A67-24233
- Known and unknown principles of biological chronometry 11 p1747 A67-24937
- Biological and engineering problems in spacecraft sterilization, noting heat treatment 15 p2430 A67-29099
- Space environment utilization for biological and medical research, physiological studies and therapeutic purposes, discussing orbital hospital and ambulance launch vehicle 19 p3181 A67-35653
- Individual caged mice susceptibility found greater than groups to toxic effect of d-amphetamine [AFOSR-66-1883] 19 p3178 A67-35885
- Primitive-earth atmosphere models irradiated with UV light and ionizing radiation for primordial organic synthesis 20 p3369 A67-36656
- Scientist role in automated laboratory for remote biological exploration of planets [AIAA PAPER 67-632] 20 p3375 A67-37615
- BIOLUMINESCENCE**
- Manned spacecraft water supply microbial contamination detection using firefly bioluminescent reaction 23 p3968 A67-41627
- BIOMAGNETICS**
- High magnetic fields effect on cardiac activity in spontaneously excited isolated turtle heart by simultaneous and separate electrical and mechanical measurement 05 p0755 A67-16282
- BIOMECHANICS**
- Moments of inertia calculated for human body as whole and of certain parts in unsupported positions of weightlessness 02 p0187 A67-12325
- Relation between human mechanical impedance and coupling of human center of mass to environment, noting transfer function 09 p1456 A67-22370
- Wave dispersion phenomena in blood vessels analyzed as measures of cardiovascular parameters 11 p1748 A67-23990
- Book on environmental biology covering effects of temperature, radiant energy, acceleration and gravity, etc 11 p1747 A67-24233
- Algorithm for processing primary motor characteristics of human motions on digital computer 24 p4114 A67-41857

BIOMETRICS

S REGRESSION ANALYSIS

BIONICS

S CYBERNETICS

BIOPHYSICS

SA RADIOBIOLOGY

Book on environmental biology covering effects of temperature, radiant energy, acceleration and gravity, etc 11 p1747 A67-24233

Fluorimetric technique for phosphatase activity in soil based on beta-naphthol release from sodium-beta-naphthylphosphate 14 p2254 A67-28067

Cellular injury and resistance in freezing organisms - Conference, Sapporo, Japan, August 1966, Volume 2 20 p3367 A67-36141

BIOGENERATION

Electrolysis-Hydrogenomonas bacterial bioregenerative life support system for manned space flight of long duration 16 p2617 A67-30774

Gravity effect on liver regeneration in rats measured by mitotic count 20 p3372 A67-36963

BIOSATELLITE

Long-term biomedical instrumentation in Air Force space program 01 p0017 A67-11029

Hardware design and production problems in launch and at separation for minimizing earth bacteria biocontamination Martian lander 04 p0562 A67-14425

Biological satellite research, discussing radiation effects on living organism as measured by Cosmos 110 07 p1136 A67-19867

Thermodynamic system design in Biosatellite program noting mission and spacecraft 16 p2757 A67-30632

Photo-optical instrumentation for biosatellite 30-day orbiting primate mission discussing adverse environmental effects and other constraints regarding requirements 16 p2680 A67-31806

Biosatellite II, mission objectives and planned experiments 24 p4240 A67-41897

Environmental control and life support system design for NASA Biosatellite program, discussing experimental results [SAE PAPER 670839] 24 p4114 A67-41995

BIOSENSOR

S BIOINSTRUMENTATION

BIOSIMULATION

SA ARTIFICIAL INTELLIGENCE

Informal automaton simulating certain processes of information processing by human brain controlled by servosystems 03 p0365 A67-13084

Electric conduction models for biological tissues as anisotropic medium 08 p1288 A67-20602

Response of fungi to diurnal temperature extremes, describing soil, simulated Martian temperature regime and fungi growth 09 p1454 A67-21991

Metabolic rates during lunar gravity simulation 13 p2062 A67-26922

Mathematical model simulation of horseshoe crab eye lateral inhibition for nervous system pattern transformation, discussing human visual pattern recognition process 20 p3375 A67-37543

BIOTECHNOLOGY

Microbial cell population statistics and dynamics 05 p0757 A67-17156

Human factors and anthropotechnology in development of weapon systems 18 p2993 A67-33643

Human performance relation research relationship with aerospace mission oriented simulation studies, discussing methodological resolution and limitation 18 p2994 A67-34341

Oxygen concentration system for aviator breathing 18 p2995 A67-34717

Chlorella and Scenedesmus unicellular algae mixture tested for biological protein value in humans for possible food source 19 p3179 A67-35228

Soviet book on protective equipment for aviators and cosmonauts 21 p3576 A67-37934

Alkaline concentrator appears superior to acid and solid units for possible onboard generation of oxygen 23 p3963 A67-41543

Bioastronautics Laboratory Research Tool /BIO-ALERT/ as automatic biomedical monitoring system composed of digital computer, analog-digital converters and input-outputs 23 p3964 A67-41548

Human cardiac output estimated using impedance plethysmography, discussing simultaneous indicator dilution curves /Dye/ and impedance records

/Imp/ 23 p3951 A67-41563

Particle electrophoresis technique for rapid clinical microorganism identification in blood elements, noting applications in serum protein analysis and antigen antibody reaction quantitation 23 p3956 A67-41628

Reusable and disposable hydrosol filters tested with heavy bacterial suspension for ability to produce sterile filtrates 24 p4116 A67-42705

BIPROPELLANT

Temperature, valve and insulation criteria for designing low thrust subliming solid reaction systems 15 p2544 A67-29979

LF oscillations built up in bipropellant rocket engine equipped with pressurized feeding system 19 p3311 A67-35052

Injector inlet conditions effects on combustion delay time in liquid bipropellant rocket engine, noting propellant atomization and droplet vaporization 22 p3868 A67-40161

Space power system pulsed turbine concept using bipropellants, reviewing multistage and multiple pass reentry performance and operational characteristics 24 p4107 A67-42530

BIRD

Bird impact hazard to aircraft simulated with hens propelled against windshields and metal targets 01 p0049 A67-10539

Radar cross sections, tracks and fluctuation spectra of grackles, pigeons and English sparrows 04 p0569 A67-14679

Tracks of dot angels, insects and birds obtained by ultrasensitive multiwavelength radars 04 p0569 A67-14680

Bird strike hazard and ways to combat it 07 p1129 A67-19909

Bird hazard to aircraft at Auckland International Airport, examining geographical features, history, species, daily movement patterns and seasonal abundances 15 p2419 A67-29672

Bird strike data on piston engine transport horizontal stabilizers summarized by bird weight, impact velocity, target-station distance and simulated and test load 22 p3746 A67-39845

Aircraft/bird collision noting dispersion, flock detection and windshield protection 23 p3934 A67-41070

Bird strikes on high speed transport jet aircraft stabilizers 24 p4094 A67-42278

BIREFRINGENCE

Light modulation by large single crystal ZnS with negligible strain birefringence 01 p0138 A67-11330

Reflection and transmission of birefringent plates surrounded by semiminfinite birefringent media with incident waves having polarized electric fields 06 p1033 A67-18544

Plastic deformation of diamonds due to differences in initial defect distribution examined by birefringence, X-ray topography and electron microscopy 08 p1346 A67-20795

Photoelastic stress measurement techniques for birefringent high polymers extended to two- and three-dimensional linear viscoelasticity problems 08 p1420 A67-20887

Optical lossless double pass network synthesis techniques using birefringent crystals extended to complex and real transmittance amplitudes 11 p1818 A67-24418

Three-dimensional photoelasticity and determination of axes of birefringents and change in phase by scattering polarized light 13 p2219 A67-27092

Temperature measurement of ruby laser rods during pulsed pumping from birefringence dependence on temperature and resulting thermoelastic stresses 15 p2499 A67-29721

Equivalent transmission circuits for electromagnet propagation in birefringent media 18 p3002 A67-34226

Pump induced optical distortion in isotropic laser materials analyzed using Fermat principle, predicting ray refraction, beam divergence, etc 18 p3062 A67-34624

Birefringent properties of Voigt type viscoelastic medium and Noll hygrosteric material during stress relaxation 21 p3657 A67-38409

Strain birefringence around tektite surface notches, discussing specimen quenched in air stream from 1000 degrees C 21 p3704 A67-38506

Magnetically induced circular dichroism and birefringence in ICI electronic spectrum,

noting frequency dependence and molecular rotation effect 22 p3758 A67-39638

BIREFRINGENT COATING

Loss measurement for ruby laser resonant cavity, comparing thresholds for R sub 1 and R sub 2 line operation 05 p0819 A67-16655

BISMUTH

Radial distribution analysis of films of bismuth and gallium prepared by low temperature condensation for electron diffraction tests 01 p0137 A67-11060

Radial distribution analysis of films of Pb-12 percent Bi and beryllium in metastable phases prepared by low temperature condensation for electron diffraction tests 01 p0137 A67-11061

Quantum dimensional effects in bismuth films by tunnel spectroscopy, showing energy dependence of state density having form of step function 02 p0281 A67-11632

Resistivity, temperature coefficient of resistivity and Hall coefficient as function of bismuth film thickness, showing that size quantization of films leads to semiconductor metals 02 p0300 A67-12509

Oxidation of vacuum-deposited bismuth films, determining ionic and electronic transport numbers 06 p1013 A67-17659

Band structure of Bi-Sb alloy system, using Shubnikov-de Haas technique with supplemental transport measurements 06 p1070 A67-18983

Oscillatory magnetoresistance and Hall effect in single crystals of Sn-doped Bi to decrease Fermi energy 06 p1070 A67-18984

Resistivity, Hall coefficient and magnetoresistance of bismuth thin films at various temperatures, showing size dependence of effective mobilities of electrons and holes 06 p1070 A67-18985

De Haas-Shubnikov effect observation method and application to measurements on bismuth 07 p1155 A67-19891

Thermoelectric power of thin layers of bismuth in thermocouple with solid copper 12 p1978 A67-25151

Thermomagnetic oscillation effect in arsenic, bismuth and antimony using cryostat, noting field strength variation 17 p2912 A67-32267

Temperature and thickness effect on thermoelectric power by calibration curves of bismuth in thin layers, determining mean free path 18 p3102 A67-34188

Superconducting bismuth investigated using tunnel effect method to measure electron energy spectrum gap and phonon spectrum distribution 21 p3685 A67-38801

Bi and Ag nucleation on evaporated substrates studied as function of substrate temperature and impinging flux using electron microscopy 23 p4044 A67-41455

Change of conductivity with temperature measurements for stabilized amorphous bismuth films 24 p4200 A67-41866

BISMUTH ALLOY

Transverse magnetic field effect on thermoelectric properties of n-type polycrystals of bismuth-antimony alloys containing 0, 5, 12 and 19 percent antimony in bismuth [ASME PAPER 66-WA/ENER-4] 04 p0682 A67-15368

Superconducting indium-bismuth alloy films immersed in strong magnetic fields parallel and perpendicular to surface, studying film thickness effect by tunneling technique 14 p2371 A67-28723

Structural defects of reciprocally oriented polycrystalline bismuth-antimony films analyzed by moire method 20 p3510 A67-36813

Superconducting property of kappa phase in Bi-Sn alloy at high pressure, with determination of transition to superconducting state and temperature interval to keep stable state 22 p3857 A67-39460

BISMUTH COMPOUND

Electron resonance and magnetic properties of solid solution in bismuth ferrite and barium titanate system, obtaining phase diagram 01 p0127 A67-10063

Electron diffraction structural studies of lead bismuth selenide systems 01 p0136 A67-11009

Temperature dependence of elastic wave losses for bismuth germanium oxide, noting possible application for information storage VHF and microwave

- frequencies 02 p0300 A67-12507
Seebeck and Hall coefficients, electrical and thermal conductivity and figure of merit measured as function of dopant concentration of n-type CuBr doped bismuth antimonide telluride 03 p0501 A67-14350
Thermoelectric and galvanomagnetic measurements on p-type bismuth compound, explaining anomalous rise in Hall coefficient with temperature and effective mass ratios change 18 p3105 A67-34632
InBi single crystal electrophysical properties, giving temperature dependences 20 p3514 A67-37605
X-ray structural analysis of ferromagnetic/ferrimagnetic/ bismuth ferrite single crystal 21 p3685 A67-38967
Nondestructively optically read ferroelectric bismuth titanate single crystal memory device 22 p3767 A67-39261
- BISMUTH SULFIDE**
Optical transmission and transition in semiconductor single crystals of various unit cells, considering bismuth tellurium sulfide 02 p0289 A67-11725
- BISMUTH TELLURIDE**
Charged and neutral impurities effect on heat conductivity of bismuth telluride crystal lattice 01 p0127 A67-10073
Proton irradiation effect on Hall coefficient, resistivity and magnetoresistance of p-type bismuth telluride single crystals 02 p0298 A67-11882
Impurity microsegregation substructure in n-and p-type bismuth telluride crystals grown according to Bridgman method, measuring electrical properties, thermal emf, Hall constant, etc 05 p0861 A67-16498
Manufacturing process and life testing of bismuth telluride alloy based flat plate thermoelectric solar cells for near earth orbits 08 p1283 A67-20648
Schubnikow-De Haas oscillation analysis in n-type bismuth telluride indicates multivalley conduction band structure 14 p2369 A67-28596
Deformation effects on thermal conductivity, microhardness, and thermal EMF of annealed bismuth telluride bars 16 p2730 A67-31160
De Haas-van Alphen effect in bismuth telluride over range of carrier concentrations, noting existence of low mobility heavy mass band 17 p2912 A67-32268
Defects in single crystal foils of compound bismuth telluride caused by irradiation with protons 17 p2921 A67-33050
- BISTABLE AMPLIFIER**
Bidirectional counter and fluid state trigger element using high pressure recovery bistable amplifier with decoupled outputs 01 p0014 A67-11032
- BISTABLE CIRCUIT**
Bistable logic delay circuit using tunnel diodes in circuit branches, noting fast response time and numerical division capability 01 p0044 A67-10661
Impedance matching conditions, gain nonlinearity and bistable mode instability in solid state parametric frequency converters 03 p0381 A67-13637
Stability analysis of parametric phase-locked subharmonic tunnel diode oscillator circuits capable of bistable phase operation 07 p1153 A67-19610
Steady state and switching characteristics of OR/NOR and bistable wall attachment elements 08 p1280 A67-20438
Increasing effective sensitivity of bistable device using pulsed power 08 p1282 A67-20463
Fluid mechanical binary counter with bistable fluid elements 08 p1283 A67-20472
Monostable high speed pulse circuit using tunnel diode and transmission line, noting possibility of cascade connection without coupling elements between stages 10 p1609 A67-22773
Operational analysis and DC design of Esaki diode pair bistable circuit used in high speed counting network performed by analog computer simulation 21 p3604 A67-38603
- BIT SYNCHRONIZATION**
Probabilistic structure of and establishment time for group synchronization in time-division-multiplex /binary code/ transmission systems 01 p0027 A67-11238
Bit synchronization during transmission of heavily biased information on PCM data systems 06 p0963 A67-18110
- Apollo ranging code with phase locked loop for bit synchronization, plotting SNR vs error probability and acquisition time 18 p3000 A67-34102
- BUTIMINOUS MATERIAL**
Hydrogen peroxide oxidation and ozonolysis of polymer type material in coal, kerogen and Orgueil meteorite 08 p1289 A67-21174
- BLACK ARROW LAUNCH VEHICLE**
Three-stage Black Arrow satellite launcher, detailing guidance system used in first and second stages and system used to rotate third stage 03 p0519 A67-13929
Structural and systems design characteristics of British launch vehicle noting control and guidance system, flight development and test programs 19 p3333 A67-35841
Satellite programs for Black Arrow launch vehicle, discussing functions, tasks, tests, etc 19 p3333 A67-35842
- BLACK BODY RADIATION**
Cosmic ray electrons with energies above 12 gev, constructing differential energy spectrum for deduction of universal black body radiation 01 p0145 A67-10921
Black body spectral radiance calibration procedure incorporating Beckman IR-4 double-beam spectrophotometer with thermocouple, lead sulfide detector and two NBS-certified black bodies 01 p0069 A67-11023
Cosmic ray electron spectrum indicates universal 3 degrees K black body radiation confinement to galactic disk 04 p0692 A67-14948
Black body radiation equation approximating Planck equation in intermediate region with optical pyrometry application 05 p0807 A67-16788
Capture cross section of photons by zinc and mercury atoms in germanium determined from integral voltaic photosensitivity, using black body as radiation source 05 p0868 A67-17066
High energy primary electrons and universal body radiation 07 p1246 A67-20227
Thermal conductivity coefficient and integral hemispherical degree of blackness of niobium at temperatures above 1000 degrees C 09 p1517 A67-21856
Enhancement of fine detail in presence of large radiance differences, noting radiance profiles and moon radiance 10 p1653 A67-22746
Cosmic microwave background measurements along celestial equator, using Dicke radiometer to study anisotropy of cosmic black body radiation 11 p1864 A67-24564
Black body radiation deduced by analyzing spectrum of lightning in near IR at very high temperatures 11 p1816 A67-24755
Absolute emissivity calorimeter design for low temperature measurements above 60 degrees K using liquid helium as cryogenic fluid 13 p2122 A67-27661
Planetary radio emission measurements, noting no radio emission from Pluto 14 p2385 A67-28405
Capture cross section of photons by zinc and mercury atoms in germanium determined from integral voltaic photosensitivity, using black body as radiation source 15 p2538 A67-29797
Observational evidence disproving cosmological steady state theory in favor of expanding universe 15 p2562 A67-30082
Excess cosmic microwave background temperature of 2 degrees K at 1.5 cm wavelength 15 p2551 A67-30161
Radiative power of toothed surface when ambient medium is black body at zero temperature 16 p2778 A67-30714
Reduced blackness coefficients measured for coaxial system of tungsten-molybdenum surfaces by calorimetric method 16 p2780 A67-31778
Black body radiation, pressure and temperature dependences of equilibrium composition, enthalpy, specific heat and electron density of air-carbon plasmas 17 p2894 A67-32147
Upper limit data about reported very low temperature distributed-source microwave background radiation and small-scale angular distribution 17 p2945 A67-32653
Compact black body source utilizing thermoelectric heat pumping for uniform and stable temperature control 17 p2862 A67-33288
- Degree of blackness of normal black body radiation for various metals, studying temperature and kinetic relations and blackness of opaque oxide films 18 p3064 A67-34052
Emissivity and absorptivity of infinite length isothermal trapezoidal grooves with radiating gray walls 18 p3159 A67-34055
Spectral coefficients of blackness in materials with low thermoconductivity determined by measuring radiation intensity and solving equations derived from Planck and Kirchhoff laws 18 p3048 A67-34056
Local condensation in early stage of universe suggested from observation of spatial inhomogeneity of cosmic black-body radiation 19 p3312 A67-34893
U-B and B-V color indices, total absorption, color excesses and reddening lines for hot black bodies, with energy curve corrections for absorption line effects 22 p3883 A67-39768
Primary cosmic radiation electron component studies through differential energy spectrum observations, considering confinement regions and black body radiation at 3 degrees K 22 p3874 A67-40239
Coherent optics technology, presenting effective black body temperature of six radiation sources and output and pulse duration of four laser sources 22 p3817 A67-40351
Black body visible light at 2800 degrees K changed into energy distribution at 5500 degrees K via Fabry-Perot filter for white light standards for colorimetry 23 p3999 A67-41180
Radiometer using black plate with radiation toward night sky balanced by IR radiation transfer in vacuum system 24 p4152 A67-41787
Absorption of black body radiation by horizontal atmospheric layer, deriving expression of integral coefficient of atmospheric transparency 24 p4255 A67-42590
- BLACK BRANT III MISSILE**
Black Brant III sounding rocket analyzed via mathematical model to predict temperature distribution in ablation material 08 p1425 A67-20531
- BLACK BRANT V MISSILE**
Solid propellant motor design for Black Brant VB sounding rocket 08 p1375 A67-20519
- BLACK BRANT MISSILE**
Fin-flare combination for stabilizing upper stage of Black Brant IV two-stage sounding rocket 08 p1405 A67-20504
Black Brant sounding rocket fin design, discussing flight characteristics, engine selection criteria and stability parameters 08 p1416 A67-20532
Fluctuating effective gain of rocket telemetry links determined from signal strength data of Black Brant sounding rockets 09 p1463 A67-21829
Black Brant sounding rocket fin design, discussing flight characteristics, engine selection criteria and stability parameters 21 p3712 A67-37807
- BLACKBURN B-103 AIRCRAFT**
Boundary layer control systems on Buccaneer S. Mk 1 and S. Mk 2 carrier-based strike aircraft 03 p0353 A67-12846
Simulator program which uses modified head-up display unit from British Buccaneer aircraft 04 p0653 A67-14882
Boundary layer control system of Buccaneer carrier based combat aircraft for producing high lift coefficient at relatively low speed 04 p0552 A67-15541
Compressed-air control system for lift capacity and maneuverability increment of Buccaneer type aircraft during landing and takeoff 19 p3173 A67-35876
- BLACKOUT**
SA RADIO BLACKOUT
Blackout experimentation results, discussing centrifugation and ophthalmodynamometry blackout production and visual system effects 22 p3752 A67-39607
- BLADDER**
Multicycling metallic bladders for positive expulsion of cryogenic fluids stored in tanks [AIAA PAPER 67-444] 18 p3054 A67-33921
Polymeric materials in expulsion bladders for cryogenic liquids, describing fabrication, flexibility, permeability, storage, transfer, control factors, etc [AIAA PAPER 67-457] 18 p3069 A67-33931

BLADE

SA COMPRESSOR BLADE
SA IMPELLER BLADE
SA PROPELLER BLADE
SA ROTOR BLADE
SA STATOR BLADE
SA TURBINE BLADE
SA VANE

Photoelastic coating technique for measuring stress distribution in blades vibrating in resonant modes 12 p2014 A67-25415

Unsteady flow past blade cascade problem solved by splicing technique instead of conformal mapping 18 p2984 A67-34217

Aerodynamic forces pressure center on profile in plane rectilinear blade cascade 19 p3169 A67-34884

Aerodynamic requirements for hovercraft and radial flow fans by adapting blade loading criteria for axial compressors 23 p3931 A67-41331

BLASIUS EQUATION

Motion of two parts formed by rupture of gas-filled vessel in vacuo 16 p2761 A67-30745

BLAST

Mass effect on blast wave equations of shock generation by secondary injection of fluid into hypersonic flow 01 p0141 A67-11179

Prediction and scaling of reflected impulse from strong blast wave, with experimental correlation 06 p0984 A67-18059

Numerical calculations of blast waves by standard and Hartree techniques compared with analytical results and application of Richardson extrapolation method 10 p1625 A67-23110

Interaction of first and second shocks of blast-bow wave in double-driver shock tube, examining stagnation point pressure prediction methods 19 p3206 A67-34812

Diaphragm and piezoelectric pressure gauges for severe blast environment, discussing resonance, damping, heat shield and rise time 23 p4007 A67-41387

BLAST DEFLECTOR

Strong forward flow of engine exhaust gas in blast deflection flow field of twin jet F-111B 17 p2797 A67-32568

BLAST LOADING

Infinite series and finite difference solutions of elastic response of thin walled spherical shell to axisymmetric transient blast loading [ASME PAPER 66-APM-EE] 04 p0718 A67-15918

Explosive loading and structural response measurement techniques for predicting large elastic-plastic dynamic and permanent deformations of shells under dynamic loading conditions 07 p1262 A67-19411

BLEED-OFF

Effect of bleeding air behind compressor for VTOL stabilization on dynamic behavior of jet engine 03 p0503 A67-13009

BLIND LANDING

S INSTRUMENT LANDING SYSTEM

BLINDNESS

S FLASH BLINDNESS

S VISION

BLOCH BAND

Partial sum rules for transition and noble metals having resonant D state 07 p1238 A67-20216

Analytic properties of finite-band models in solids as generalization of Kohn procedure 15 p2534 A67-29324

BLOCH WALL

S FERROMAGNETISM

S MAGNETIC DOMAIN

BLOOD

Remote aftereffect on hemopoietic tissue of mice under simultaneous irradiation and acceleration, using both X-rays and protons 13 p2057 A67-26458

Acid-base relation of blood and cerebrospinal fluid with respect to respiratory regulation studied in man at high altitude 17 p2806 A67-32333

Trace contaminant experiment for studying effect of hyperoxic environment at high total pressure on human blood constituents 23 p3960 A67-41703

BLOOD CIRCULATION

SA BRAIN CIRCULATION

SA CAPILLARY CIRCULATION

SA CARDIORESPIRATORY SYSTEM

SA CARDIOVASCULAR SYSTEM

SA CIRCULATORY SYSTEM

SA CORONARY CIRCULATION

SA INTERCRANIAL CIRCULATION

SA OCULAR CIRCULATION

Tilt table responses of human subjects improved by application of lower body negative pressure 05 p0755 A67-16286

Wave dispersion phenomena in blood vessels analyzed as measures of cardiovascular parameters 11 p1748 A67-23990

Intracranial pressure measurements and electroplethysmographic examination of blood content in dog cranial cavity for transverse acceleration up to 40 g 13 p2057 A67-26456

Influence of different stresses on sugar content changes of blood and stabilization at another level as adaptation result of organism 14 p2255 A67-28221

Urinary output patterns relationship to arterial pressure, pulse rate and parameters of hemoconcentration in study of homeostatic circulation regulation during prolonged gravitational stress 15 p2428 A67-29273

Acute hyperbaric oxygenation histological effects on pulmonary circulation of rabbits 16 p2614 A67-31473

Effective viscosity of blood in circulation for large, intermediate and small vessels 18 p2990 A67-33511

Distribution of red blood corpuscles studied for complications arising from continued stays at high altitude 23 p3945 A67-41073

Color photographic study of blackout during radial acceleration on human centrifuge, presenting evidence confirming central retinal arterial collapse 23 p3957 A67-41638

Fluorescence angiography technique to study human centrifugal acceleration effects on retinal circulation during blackout 23 p3957 A67-41639

Human blood circulation times during weightlessness produced by parabolic flight 23 p3959 A67-41698

Arterial and venous blood of brain and mixed venous blood of heart measured in dogs exposed to simulated altitude, noting body deoxygenation 24 p4111 A67-41851

BLOOD COAGULATION

In-vivo inactivation of factor VII by hydrazine in ether anesthetized rats 07 p1134 A67-19856

BLOOD FLOW

Tilt table response and blood volume changes in four males before and after 14-day bed rest 07 p1135 A67-19863

Mechanism and pattern of human cerebrovascular regulation after rapid changes in blood carbon dioxide tension 11 p1746 A67-23989

Effective viscosity of blood in circulation for large, intermediate and small vessels 18 p2990 A67-33511

Carbon dioxide breathing effects on forearm blood vessels, discussing vascular resistance and carbon dioxide role in blood flow regulation 20 p3373 A67-37584

Chimpanzee mesenteric artery blood flow for various activities during 24 hr period monitored by radio telemetry 22 p3751 A67-39603

Functional relation between oxidation, metabolism, blood flow volume rate and brain temperature in rats exposed to vibration, noting temperature decrease and blood supply and oxygen consumption stimulation 23 p3943 A67-40769

Cerebral blood flow and metabolism during combined hypoxia and hypercapnia, noting cerebral vasodilatation effect 23 p3945 A67-41080

Abdominal blood flow changes in anesthetized dogs during transverse acceleration 23 p3950 A67-41535

Human response to low intensity long duration transverse acceleration, discussing increase in splanchnic blood flow during centrifugation and orthostatic intolerance 23 p3958 A67-41652

BLOOD GROUP

SA ERYTHROCYTE

SA LEUCOCYTE

SA PLATELET

Monomethylhydrazine effect on methemoglobin production in vitro and in vivo 10 p1599 A67-23812

BLOOD PLASMA

9-alphafluorohydrocortisone and venous occlusive cuffs effects on plasma volume and orthostatic tolerance following 28 to 78

days of bed rest 01 p0016 A67-10960

Plasma volume and extracellular fluid volume change associated with ten days bed recumbency 07 p1134 A67-19858

Plasma 17 hydroxycorticosteroids in healthy subjects after water immersion of 12 hr duration shows no stressful effect 15 p2427 A67-29270

Tilt table response and plasma volume changes in experimental subjects evaluated before and after short term periods of deconditioning 17 p2805 A67-31953

Plasma volume, red blood cell mass and erythrocyte survival determination before and after space flight 20 p3372 A67-37429

Hydrazine effects on free amino acid concentrations of plasma and urine in dogs 23 p3952 A67-41570

BLOOD PRESSURE

SA MANOMETER

SA TONOMETRY

Objective statistical approach to tilt table data analysis using computer to define characteristics of cardiovascular deconditioning resulting from bed rest, water immersion and space flight 05 p0754 A67-16276

Blood pressure response to carotid sinus pressure in normal and vasomotor instability subjects evaluated for personnel selection for flying training 05 p0756 A67-16290

Cumulative effects of venesection and lower body negative pressure on circulation 10 p1599 A67-23813

Blood pressure changes and pulmonary edema in rat associated with hyperbaric oxygen 15 p2428 A67-29275

Dynamics of pulse waves of intercranial pressure for transverse overloading accelerations 15 p2430 A67-30229

Human systolic and diastolic blood pressure measuring apparatus and method 23 p4008 A67-41424

Canine cardiac displacement and cardiovascular dynamic response during abrupt deceleration impact, discussing traumatic ruptures and pressure effects 23 p3951 A67-41552

Anesthetized dogs subjected to near vacuum condition before and after clinical death, comparing data of venous and arterial pressure 23 p3952 A67-41572

Hypoxia stimulated pulmonary arterial pressure increase in dog and baboon noting hemodynamic effects 23 p3953 A67-41588

High venous pressures during exposure of dogs to near-vacuum conditions 23 p3960 A67-41699

BLOWDOWN WIND TUNNEL

Pressure and stagnation temperature distribution in test chamber of blowdown hypersonic wind tunnel 01 p0049 A67-10558

Forced oscillation method measurement of aerodynamic coefficient of hypersonic blowdown wind tunnel 05 p0788 A67-16764

Blowdown wind tunnel for He-K MHD generator, considering magnetically induced ionization, conductivity, gas temperature, etc 12 p1898 A67-25389

Shock-on-shock effects explored in aerodynamic test facility combining blowdown wind tunnel and shock wave generator 13 p2091 A67-27490

AMICON 8000 kw plasma facility for simulating reentry environments for material and thermodynamic tests 20 p3415 A67-36551

BLOWER

S BELLOWS

S FAN

BLOWING

SA INJECTION

Leading edge blowing effects on pressure distribution of half-cone body with 75 degree sweep angle, obtaining normal and axial forces and pitching moments 02 p0178 A67-12225

Transient response of Couette shear flow to step function change in blowing velocity across channel 05 p0751 A67-17420

High lift coefficient production on helicopter rotor blades and application of circulation control by blowing 19 p3170 A67-35519

Laminar incompressible boundary layer on isothermal flat plate with strong blowing, comparing different solutions 19 p3211 A67-35754

Electric arc blowing in plasma of nonuniform conductivity and inclusion of effect in MHD flow 19 p3298 A67-35760

BLUE STREAK MISSILE

Data acquisition system for Blue Streak flight trials noting telemetry and radar and relation to trajectory, autopilot, structure, etc 04 p0568 A67-14438
Blue Streak launch vehicle control system, discussing destabilizing resonance effects, hydraulic system, propellant movement in tanks and testing 21 p3570 A67-38102

BLUFF BODY

Air velocity and temperature, stabilizer size and blockage effects on fresh mixture entrainment in recirculation zone of bluff body stabilized flames 02 p0342 A67-12029
Free streamline theory of two-dimensional separated potential flow past bluff body and formation of periodic vortex turbulent wake 02 p0178 A67-12233
Convective heat transfer from bluff bodies analyzed, particularly small electrically heated cylinders at low Reynolds numbers, noting correlation with Nusselt and Prandtl numbers 04 p0732 A67-15831
Elliptical wake formation behind sharp edged elliptical bodies, noting turbulent energy periodicity 08 p1277 A67-20710
Cylinders of rectangular section as aeroelastic nonlinear oscillators, theory of galloping oscillation and force measurements on stationary cylinder [ASME PAPER 67-VIBR-50]

11 p1777 A67-24200
Tailpipe length effect on flame stability in high velocity propane-air stream with bluff body or reverse jet flame holders [ASME PAPER 67-GT-4] 11 p1853 A67-24792
Channel blocking effect on motion of fluid in separation region behind bluff bodies 11 p1743 A67-24960
Two-dimensional flow past bluff body, comparing vortex street wake measurements to von Karman predictions 17 p2790 A67-32278
Wake from bluff bodies interaction with initially laminar boundary layer [AIAA PAPER 66-126] 17 p2793 A67-33005
Concentrated vortex model for Karman street in two-dimensional viscous incompressible laminar flow past bluff body 19 p3210 A67-35446
Hot-wire anemometer response in turbulent flow studied requires correction leading to constant results when applied to flat plate bluff body wakes normal to stream 19 p3230 A67-35523
Modifying effect of base bleed investigated photographically for incompressible wake behind two-dimensional bluff body, estimating base pressure 20 p3421 A67-36844

BLUNT BODY

Pressure and density of heat flux at surface of pointed or blunt nosed obstacle in divergent truncated cone of hypersonic nozzle 01 p0005 A67-10258
Hypersonic flow over blunt flat plate with surface mass transfer 01 p0007 A67-11180
Blunt cone laminar friction drag evaluated, using Reynolds analogy 01 p0007 A67-11181
Unsteady interaction between blunt bodies and shock wave, comparing reflected shock wave velocity decrease for plane spherically blunted cylinders 01 p0008 A67-11294
Convective and radiative heat transfer in shock layer of hypersonic blunt body, noting asymptotic behavior of Navier-Stokes equation and energy transfer 01 p0168 A67-11421
Shock tunnel study of effects of nose bluntness, angle of attack and boundary layer cooling on transition at Mach number 5.5 [AIAA PAPER 66-495] 02 p0177 A67-11514
Approximate determination of sonic line and pressure distribution on surface of blunt body in supersonic and hypersonic flows 02 p0178 A67-12042
Leading edge blowing effects on pressure distribution of half-cone body with 75 degree sweep angle, obtaining normal and axial forces and pitching moments 02 p0178 A67-12225
Diatomic gas flow past blunt bodies, noting effect of oscillation and dissociation relaxation on mean energy 02 p0180 A67-12465
Book on supersonic gas flow past blunt bodies under various conditions 03 p0349 A67-12851
Supersonic flow past blunt body with convex corner calculated to establish sonic

point on body 03 p0349 A67-12862
Laminar Prandtl boundary layer arising during steady flow past blunt cone at angle of attack studied by finite difference method 03 p0349 A67-12868
Prediction of subsonic base drag of hypersonic reentry vehicles [AIAA PAPER 66-991] 03 p0353 A67-14144
DVL free piston shock tunnel and measuring systems of three-component balance based on use of strain gauges 04 p0546 A67-14575
Hypersonic behavior of helium flow past highly blunt bodies, noting drag and shape of shock wave 04 p0546 A67-14779
Hypersonic helium flow past blunt cones compared with flow past sharp cones 04 p0546 A67-14781
Viscous and bluntness induced pressures for flat plates, wedges, cylinders and cones at Mach 41 [AIAA PAPER 65-399] 04 p0546 A67-14815
High resolution equilibrium radiation spectra for shock layer of blunt bodies at reentry velocities and radiative recombination of N and O ions [AIAA PAPER 66-104] 04 p0546 A67-14816
Steady blunt body problem solution via time-dependent technique, performing computation in shock layer 04 p0546 A67-14818
Base pressure measurements on sharp and blunt 9 degree cones at Mach 3.50 to 9.20 04 p0547 A67-14851
Effects of reentry vehicle physical characteristics and trajectory constraints on variation of velocity-atmospheric density ambient value function 04 p0706 A67-15244
Tip bluntness, surface roughness and angle of attack effects on laminar boundary layer for 10 degree cone, measuring heat transfer and detecting transition 04 p0549 A67-15823
Heat transfer tests of blunt nosed cone containing cylindrical protuberances tested in AEDC tunnel, including effects of local Mach number, Reynolds number and sweepback angle 04 p0549 A67-15832
Approximate method for measuring distance between head wave and tip of body in supersonic flow past blunt tip body 04 p0550 A67-15894
Numerical algorithm for supersonic gas flow past blunt bodies with shock wave separation, using Dorodnitsyn method of integral correlation 05 p0791 A67-16374
Existence and stability of uniform rotation of heavy blunt profile immersed in perfect incompressible irrotational fluid flow 05 p0792 A67-16595
Transport of vorticity and enthalpy in flow field in nose region of blunt body in viscous hypersonic flow 05 p0749 A67-16820
Gap size effect on pressure and aerodynamic heating over flap of blunt delta wing in hypersonic flow [AIAA PAPER 66-408] 05 p0749 A67-17220
Continuum viscous nonequilibrium flow partial differential equations in thin shock layer 05 p0750 A67-17335
Mass transfer perturbations about reversed flow profiles of Stewartson, noting computation of solutions to Falkner-Skan equation 05 p0794 A67-17369
Three-dimensional flow past blunt nosed cones 05 p0751 A67-17478
Hypersonic flow past sphere by relaxing gas with internal degrees of freedom in nonequilibrium 06 p0935 A67-17731
Explosion analogy in flows past slender blunt bodies, noting accuracy improvement by placing explosion center ahead of origin 06 p0936 A67-17732
Hypersonic laminar boundary layer on blunt cones, considering external flow vorticity caused by curved shock wave, calculating gas-enthalpy profile 06 p0936 A67-17734
Hypersonic aerodynamics and heating of blunt body at high and low Reynolds numbers 06 p0937 A67-17982
Schlieren techniques used in free flight range study of far wake of hypersonic cones [AIAA PAPER 67-31] 06 p0938 A67-18261
Laminar boundary layer separation and near wake flow for smooth blunt body at supersonic and hypersonic speeds [AIAA PAPER 67-62] 06 p0986 A67-18270
Radiation sources from high temperature equilibrium air noting measurements, equipment and results [AIAA PAPER 67-95] 06 p1114 A67-18279

Tests at Mach 8 on cone, analyzing effect of roughness elements and variable entropy on transition and heat transfer distribution [AIAA PAPER 67-132] 06 p0940 A67-18357
Time dependent computational method for three-dimensional blunt body flow fields traveling at supersonic speed including shock points, sphere cones and ellipsoid [AIAA PAPER 67-222] 06 p0941 A67-18461
Three-dimensional laminar boundary layer equations solved by finite difference methods for application to boundary layer flow on blunted cone, noting effect on crossflow [AIAA PAPER 67-159] 06 p0989 A67-18480
Aerodynamic characteristics of Mars probe/lander configurations consisting of blunted cone, shell and spherical segment analyzed at various Mach numbers on ballistic range [AIAA PAPER 67-167] 06 p0941 A67-18482
Rational approximation method for calculating supersonic axisymmetric flow of perfect gas around given blunt body 06 p0943 A67-18846
Aerodynamic characteristics of flared bodies noting geometry, Reynolds number and boundary layer state effects on stability 08 p1275 A67-20499
Design procedure for slender multistage fast-burning rockets, noting modified flexural behavior and aerodynamic load 08 p1416 A67-20529
Wakes behind axisymmetric blunt based bodies, noting similarity among wakes through measurements of velocity, turbulence and static pressure 08 p1277 A67-20706
Inviscid hypersonic flow over plane power law bodies where blast theory applies as first approximation, determining shape and pressure distribution 08 p1277 A67-20708
Mach number effect on hypersonic flow past delta wing with blunt edges at zero angle of attack 10 p1590 A67-23036
Symmetrical equilibrium flow past blunt body at superorbital reentry conditions calculated by integrating motion equations across shock layer 10 p1591 A67-23109
Magnetoaerodynamic flow relations for axisymmetric blunt bodies with shock layers in shifting equilibrium 10 p1591 A67-23114
Inviscid axisymmetric radiating flow over blunt body, analyzing paraboloidal shock wave thermal radiation effects on temperature, density, velocity, etc 10 p1592 A67-23453
Analytic solution to blunt body problem in supersonic flow of ideal gas approximated, using power series [NOR REPORT 65-239] 10 p1593 A67-23454
Steady hypersonic inviscid flow, including detached shock, around blunt body, using finite difference computations 10 p1593 A67-23633
Approximate iterative calculation of non-Newtonian supersonic gas flow past highly blunt bodies 11 p1741 A67-24156
Conditions at head shock wave in viscous hypersonic flow past blunt body for study of boundary layer separation 11 p1741 A67-24157
Forward facing jets effect on blunt configurations aerodynamic characteristics from wind tunnel tests at Mach 8, emphasizing drag increase 11 p1742 A67-24354
Radiometer system with photomultiplier tube for measuring absolute radiation from hypervelocity projectile flow fields 11 p1790 A67-24447
Approximate method for calculating stagnation point laminar boundary layer equations taking into account chemical reactions in gas phase and surface of body 12 p1928 A67-25673
Boundary layer transition displacement as function of nose bluntness, angle of attack and boundary layer cooling of half-angle cone [AIAA PAPER 66-495] 12 p1893 A67-25903
Singularities causing numerical instabilities used in steady gas dynamic Cauchy problem solution, exemplifying with supersonic blunt body 12 p1893 A67-25932
Hypersonic flow near stagnation point of blunt body taking radiation into account, noting large enthalpy and density gradients 13 p2050 A67-26897
Aerodynamic characteristics of sphere and blunt cone in highly rarefied gas flow, noting molecular collision effect 13 p2052 A67-27620

Asymptotic and numerical solutions of Goulard integrodifferential equation describing hypersonic flow near stagnation point past blunt bodies, allowing for radiative transfer effects 14 p2296 A67-27981

Two-dimensional self-similar problem for uniform penetration of plate into half-plane of perfect gas flow, determining flow pattern 14 p2239 A67-27982

Supersonic viscous flow near blunt body stagnation line, using Navier-Stokes equations 14 p2240 A67-27993

Laminar boundary layer separation and near wake flow for smooth blunt body at supersonic and hypersonic speeds [AIAA PAPER 67-62] 14 p2240 A67-28112

Heat transfer and skin friction increase for gas stream with liquid-droplet suspension flowing over blunt-nosed body near stagnation point 14 p2405 A67-28126

Parameter determination for flow field in space between shock wave of nonviscous supersonic gas flow and thin spherically blunt cone 14 p2243 A67-28659

Blunt nosed reentry vehicle model with skewed magnetic field investigated in magnetoaerodynamic flow for possible bow shock distortion 14 p2244 A67-29049

Axisymmetric blunt bodies shock standoff distances in hypersonic flow determined by numerical and analytic methods 14 p2244 A67-29056

Optimum entry vehicle design using aerobreaking for manned earth entry at hyperbolic speeds, examining blunted conic, biconic and tetrahedral configurations [AIAA PAPER 66-489] 15 p2564 A67-29422

Finite difference method for treating head-on axisymmetric interactions of blast wave and shock layer in nose region of high speed blunt body 15 p2416 A67-29432

Nose bluntness effect on hypersonic unsteady aerodynamics of ablating flared or conical slender reentry vehicles 15 p2416 A67-29442

Shock wave shapes around spherical and cylindrical-nosed bodies, assuming hyperbolic profile asymptotic to freestream Mach angle or attached shock angle 15 p2417 A67-29448

Elliptic nose shape bluntness effect on drag of bodies of revolution in axisymmetric subsonic flow 16 p2589 A67-30791

Nonequilibrium air dissociation and ionization in stagnation region of blunt body investigated in merged layer regime 16 p2592 A67-30955

Shock tube analysis of time dependent formation of supersonic flow near blunt bodies 16 p2592 A67-31102

Argon and nitrogen flows past sphere at low supersonic velocities analyzing formation of bow shock wave 16 p2592 A67-31103

Shadow method analysis of shock wave interaction with fixed bodies in shock tube at small and medium supersonic Mach numbers 16 p2673 A67-31105

Variable heat capacity of gas effects on supersonic flow past blunt body analyzed using dimensionless system of equations 16 p2592 A67-31113

Equations to investigate effect of simultaneous oscillation and dissociation relaxation on gas dynamic parameters of supersonic flow past blunt bodies 16 p2592 A67-31114

Shape dependence of detached shock wave in supersonic gas flow of blunt-nosed models on Mach number, heat capacity and bluntness ratio 16 p2593 A67-31131

Position determination of sonic points on head shock wave and blunt body surface in ballistics showing Mach number and gas type effects 16 p2593 A67-31132

Hypersonic magnetohydrodynamic flow over blunt bodies for small magnetic Reynolds number hypersonic magnetohydrodynamic flow over blunt bodies for small magnetic Reynolds number hypersonic magnetohydrodynamic flow over blunt 16 p2594 A67-31579

Integral relation method analysis of supersonic gas flow past blunt body of revolution 17 p2791 A67-32679

Schliren techniques used in free flight range study of far wake of hypersonic cones [AIAA PAPER 67-31] 17 p2793 A67-33006

Transport property difference effect on flow prediction of blunt body stagnation region heat transfer, noting laminar flow and compressible boundary layer equations 17 p2793 A67-33025

Lobb empirical relation applied to method for computing flow past blunt body when predicting sphere shock standoff distance 17 p2793 A67-33026

Uniformly valid approximation of two-dimensional subsonic flow along thin airfoil with blunt elliptical shape 18 p2982 A67-33663

Turbulent base pressure in supersonic axisymmetric flow behind blunt body [AIAA PAPER 67-446] 18 p3026 A67-33922

Shock and boundary layers about blunted two-dimensional slender bodies in hypersonic flow [AIAA PAPER 67-451] 18 p2982 A67-33925

Existence and stability of rectilinear translation motions of blunt body submerged in potential flow of incompressible fluid at rest at infinity 18 p3027 A67-34183

Mach and Reynolds numbers effect on rarefied supersonic gas flow pattern near forward stagnation point of blunt body, noting decrease in density 18 p3028 A67-34209

Three-dimensional hypersonic flow past blunt cones calculated by modified method of characteristics, taking into account physicochemical equilibrium conversions 18 p2984 A67-34213

Aerodynamic characteristics of Mars probe/lander configurations consisting of blunted cone, shell and spherical segment analyzed at various Mach numbers on ballistic range [AIAA PAPER 67-167] 19 p3169 A67-34816

Pressure-distribution estimation over entire forward face of blunt body at angle of attack 19 p3169 A67-34833

Time dependent computational method for three-dimensional blunt body flow fields traveling at supersonic speed including shock points, sphere cones and ellipsoid [AIAA PAPER 67-222] 19 p3171 A67-35736

Limits of application of binary scaling for hypersonic flight 19 p3212 A67-35769

Stagnation ablation of blunt body hypersonic reentry with nonreacting gas, deriving laminar flow equations 20 p3356 A67-36509

Bluntness influence on nose cone heating in laminar flow in supersonic flight investigated to determine optimum design of rocket or space vehicle nose 20 p3359 A67-37165

Characteristics method to determine radiative energy losses of supersonic gas flows past blunt cones 21 p3564 A67-38424

Magnetic field effect on flow field and drag of blunt body in partially ionized argon plasma, obtaining electron density and temperature [AIAA PAPER 67-729] 21 p3673 A67-38753

Supersonic blunt body problem noting sonic point singularity for reformulated integral relations 21 p3614 A67-38879

Nose bluntness and cone angle effects on base pressure and heating in laminar hypersonic flow regime, using free flight telemetry technique 21 p3565 A67-38882

Characteristic method computer program for calculating three-dimensional supersonic flow around blunt and pointed bodies of revolution in reasonable time 21 p3566 A67-38887

Roughness induced boundary layer transition in supersonic flow over blunt bodies 21 p3614 A67-38891

Radiative heat loss effect on steady axisymmetric hypersonic flow past blunt body using gray gas approximation, with numerical solution for stagnation region 22 p3739 A67-39530

Integral relations method for nonequilibrium hypersonic planetary entry, emphasizing flow fields and thermal environment determinations for blunt body vehicle configuration 22 p3740 A67-39936

Laminar heat transfer computing method for spherically blunted cone at angle of attack requiring small numerical calculations 22 p3740 A67-39937

Drag coefficients used to evaluate normal force and pitching moment characteristics of revolving body at angle of attack 22 p3740 A67-39943

Procedure for expanding parameter in asymptotic power series of any order to investigate viscous compressible supersonic gas flow past blunt body 22 p3740 A67-40014

Supersonic three-dimensional flow fields of inviscid nonconducting gas around delta

wing with blunted edges 22 p3741 A67-40025

Supersonic flow over flat and axisymmetric blunt bodies, discussing shock wave position, adiabatic index, surface pressure distribution and body geometric parameters 22 p3741 A67-40026

Dynamic destabilization for hypersonic flow around slender cone with severely blunt nose analyzed by blast wave analogy 22 p3742 A67-40109

Gas flow interaction with blunt body in transition flow regime between continuum and free molecule flow calculated using first collision model 22 p3743 A67-40175

Surface mass transfer effects on viscous hypersonic shock layer of blunt body including suction and injection of air into air 22 p3743 A67-40417

Asymptotic perturbation of hypersonic flow over blunt slender cones and wedges showing oscillatory nature 23 p3931 A67-41665

Chemiluminescent radiation from far wake of hypersonic spheres launched from light gas gun measured with filtered photomultiplier 23 p3931 A67-41712

Conformal mapping method for overcoming difficulties caused by limiting line in computing flow field about blunt body supporting paraboloidal shock wave 23 p3932 A67-41730

Chemical reaction effect on viscous boundary layer of hypersonic flow of reacting gas mixture past blunt body 24 p4091 A67-42270

BO-105 HELICOPTER

S BOLKOW BO-105 HELICOPTER

BODY

S AXISYMMETRIC BODY

S BLUFF BODY

S BLUNT BODY

S CELESTIAL BODY

S DUCTED BODY

S ELASTIC BODY

S FINNED BODY

S FLARED BODY

S FLEXIBLE BODY

S HEMISPHERE CYLINDER BODY

S HUMAN BODY

S INELASTIC BODY

S LENTICULAR BODY

S LIFTING BODY

S PYRAMIDAL BODY

S REENTRY BODY

S RIGID BODY

S ROTATING BODY

S SELF-LUMINOUS BODY

S SHROUDED BODY

S SLENDER BODY

S STREAMLINE BODY

S SUBMERGED BODY

S SYMMETRICAL BODY

S THIN BODY

S TOWED BODY

S TWO-DIMENSIONAL BODY

S WING BODY

BODY CENTERED CUBIC /BCC/ CRYSTAL

Carbon diffusion in refractory metals with bcc lattice at temperatures of 1100 to 1600 degrees C, considering activation energy and frequency factor 01 p0101 A67-10937

Various combinations of preanneal and diffusion anneal conditions used in experiments for determining environmental effects on diffusion of Ta 182 in bcc titanium 04 p0637 A67-14937

Thermally activated motion of screw dislocations in bcc metals 07 p1209 A67-19640

Dislocation theory of slip geometry and temperature dependence of flow stress in bcc metals 07 p1209 A67-19641

Structure of rolling texture of bcc metals and alloys under various external deformation conditions 07 p1210 A67-20107

Interaction energy of single atom adsorption at any point on single crystal planes of bcc structure, using Lennard-Jones potential 08 p1355 A67-20719

Theoretical strength with iron-nickel maraging steels 12 p1957 A67-26125

Temperature dependence of bcc metals elastic limit at low temperature, assuming sessile-dissociated screw dislocations formation during microdeformation, stressing stacking fault energy effect 13 p2130 A67-26438

Molybdenum polycrystal plastic strain rate in pre-yield region studied by successive stress relaxation method for dislocation density and mobility characteristics 14 p2337 A67-28230

Surface reactions and structure

determinations of oxides of niobium, tantalum and vanadium with /110/ surfaces from CO and oxygen

absorption 15 p2504 A67-29881

Pressurization produced free dislocations effect on yielding and fracture in bcc metals 18 p3063 A67-33484

Alloying effect on temperature and strain rate sensitivity of niobium-molybdenum bcc metal 19 p3246 A67-35730

Stacking faults in tungsten specimen heated rigidly for short time by electric discharge 20 p3464 A67-36225

Carbon diffusion in refractory metals with bcc lattice at temperatures of 1100 to 1600 degrees C, considering activation energy and frequency factor 22 p3820 A67-39791

Heterodiffusion of metallic impurities in body-centered phases of doped zirconium and titanium, determining diffusion coefficients via radioactive isotopes 22 p3820 A67-39823

Corrosion and hydrogen embrittlement resistant nickel stainless maraging steel with bcc martensite crystal structure for pressure vessel applications 24 p4161 A67-42328

BODY FLUID

SA CEREBROSPINAL FLUID

SA LYMPH

SA WATER

Estimation of changes in serum protein concentration under normal stress compared to human sera exposed to simulated altitude and aerospace flights 01 p0015 A67-10950

Statistical guidelines for flight surgeon remotely monitoring body fluids of astronauts, determining when subject undergoes changes in serum values 01 p0015 A67-10951

Statistical evaluation of changes in serum potassium, sodium and chlorides for aerospace flights 01 p0015 A67-10952

Tilt table responses of human subjects improved by application of lower body negative pressure 05 p0755 A67-16286

Plasma volume and extracellular fluid volume change associated with ten days bed recumbency 07 p1134 A67-19858

Pressure changes in cerebrospinal fluid in rhesus monkey cranial cavity with applied forces at abdominal wall 10 p1600 A67-23821

Vasopressin-aldoosterone interrelation in diuretics and antidiuretics to explain body fluid weight loss in astronauts during space travel 21 p3574 A67-38082

Na and water excretion, renal plasma flow and glomerular filtration rate lowered by lower body negative pressure /LBNP/, noting application to space flight weightlessness [SAM-TR-65-329] 24 p4110 A67-41801

BODY KINEMATICS

Aperiodic motion of two bodies of variable mass across canonical cross section, constructing osculating orbit and deriving equations for variation rate 04 p0700 A67-15202

Motion about fixed point of solid body with cavity filled with viscous incompressible fluid 06 p0991 A67-18810

Muscle system participation in bending and straightening of elbow joint muscle system participation in bending and straightening of elbow joint 07 p1133 A67-19346

Consistent difference equations for displacement components in thin elastic disk of variable thickness subjected to given body forces and edge tractions for various coordinate directions 09 p1573 A67-21755

Incompressible potential flow about arbitrary body shapes calculated, using singularity distribution over body surface computed as solution of integral equation 10 p1589 A67-22871

Complex measuring instrumentation effect upon tilt table response 10 p1602 A67-23823

Braking of bodies moving in rarefied plasma 12 p1892 A67-25536

Minimum-fuel transfers of moving body between infinitely close elliptical Keplerian orbits in central Newtonian field, considering propulsion system models 16 p2744 A67-30738

Surface temperatures of two rubbing bodies and heat partition between them determined numerically, using Fredholm integral equation solution 21 p3638 A67-39091

Trauma in lateral impact at high entrance velocity compared with rearward and forward facing body orientations of baboons

when restrained by lap belt only 22 p3750 A67-39594

BODY MEASUREMENT

SA ANTHROPOMETRY

Ballistic coefficients for power law body shapes compared with those for conical bodies having identical lengths, diameters and specific weights 05 p0750 A67-17360

Radio interferometric measurements of radio source diameters using 3074 km baseline 24 p4226 A67-41876

BODY MEASUREMENT /BIOL/

SA ANTHROPOMETRY

SA ELECTROCARDIOGRAPHY

SA ELECTROPLETHYSMOGRAPHY

Human body motions during load handling tasks for application in designing manipulators, walking machine and powered exoskeletons [ASME PAPER 66-WA/BHF-2] 04 p0563 A67-15398

BODY OF REVOLUTION

SA DISK

SA ELLIPSOID

SA HEMISPHERICAL SHELL

SA OGIVE

Steady motion stability of heavy homogeneous body of revolution on absolutely rough horizontal plane 01 p0115 A67-10992

Computation by approximate methods of stress resultants for shell of revolution under distributed externally applied load 01 p0164 A67-11185

Solutions for boundary value problems of potential theory and elasticity theory for single cavity hyperboloids of revolution 02 p0338 A67-11955

Body of revolution bounded by sphere rolling on stationary sphere with force function of applied forces dependent on only one coordinate 02 p0287 A67-11960

Local convection coefficient along windward line of axisymmetric obstacle in hypersonic flow with laminar boundary layer 02 p0178 A67-12061

Hypersonic aerodynamic coefficients for bodies of revolution in yaw 02 p0179 A67-12314

Turbulent boundary layer in subsonic or supersonic flow past pinched-waist bodies of revolution at various Mach numbers and pressure gradients 03 p0350 A67-12989

Yield surfaces for nonhomogeneous shells of revolution 03 p0523 A67-13501

Finite element method structural analysis of laminated orthotropic shell of revolution 03 p0524 A67-13787

Stability of transverse oscillation of thin finned elastic beam of revolution in gas flow acted upon by tracking force 03 p0520 A67-14172

Legendre series solution to contact problem of torsion of elongated ellipsoid of revolution under arbitrary torsional loading 03 p0530 A67-14199

Modification of Potter method of Gaussian elimination for solving eigenvalue problems of buckling and free vibrations of shells of revolution 04 p0656 A67-14839

Elastic shells of revolution axisymmetrically loaded analyzed, using multisegment method for solution of boundary value problems governed by nonlinear differential equations [ASME PAPER 66-WA/APM-16] 04 p0713 A67-15407

Skewed boundary layers over body of revolution rotating in axial stream 05 p0747 A67-16218

Soviet monograph on dynamics and durability of machines 05 p0915 A67-18219

Three-dimensional elastic problem of bodies of revolution, deriving Lamé and generalized Hooke equations in matrix form 05 p0916 A67-18226

Dynamic thermoelastic problem solution for body of revolution with cuts satisfying boundary conditions 05 p0810 A67-18228

Stressed state in rotationally symmetric shell assuming ideally rigid plastic, determining yield condition in terms of stress resultants 05 p0917 A67-18244

Axisymmetric deformation of shallow shells of revolution, noting membrane solutions 05 p0917 A67-18245

Reynolds number effect on surface pressure distributions and boundary layer velocity profiles on three-quarter power law bodies of revolution in hypersonic flow 05 p0747 A67-16431

Small plastic deformation theory determination of elastoplastic stressed state of thin walled isotropic incompressible shell of revolution under axisymmetric power loads and nonuniform heating 05 p0922 A67-17177

Supersonic flow past cone cylinder type body with circular grooves 05 p0751 A67-17480

Nonaxisymmetric nose section of bodies of revolution having minimum drag at high supersonic speed 06 p0936 A67-17737

Equilibrium shape of earth, discussing space science discoveries and hydrostatic flattening mechanism 06 p0994 A67-17767

Kollmann theory on critical rpm of hollow shells of revolution containing liquid, explaining unstable oscillations appearance in supercritical region 06 p1100 A67-17992

Inviscid flow method predicting nonlinear supersonic and hypersonic lift component of highly swept wings with low aspect ratio 06 p0937 A67-18013

Finite difference method stability analysis of deformed eccentrically stiffened shells of revolution, accounting for finite prebuckling rotations [AIAA PAPER 67-110] 06 p1101 A67-18285

Supersonic flow over axisymmetric bodies with continuous or discontinuous slope solved via parametric differentiation [AIAA PAPER 67-5] 06 p0939 A67-18303

Generalized Stodola iteration method for computer analysis of axisymmetric buckling of ring-stiffened orthotropic shells of revolution [AIAA PAPER 67-109] 06 p1103 A67-18339

Junction of several walls of revolution along parallel in axisymmetric vessel 06 p1105 A67-18588

Flow of thin layer of liquid on surface of rotating body of revolution in moving system of coordinates connected with body 06 p0991 A67-18817

First boundary value problem for general case of axisymmetric stressed state of body of revolution, using biharmonic solution of Love and Grodskii 07 p1264 A67-20037

Computer program for axisymmetric nonlinear behavior of stiffened elastic shells of revolution with variable thickness, calculating collapse pressures [AIAA PAPER 66-529] 08 p1417 A67-20558

Resonance oscillations and rotations in mechanical systems having n-dimensional quasi-static vector analyzed and applied to triaxial ellipsoid with unbalanced mass 10 p1680 A67-23409

Stress-strain state of elements of thin walled shells of revolution with hinged meridional edges under effect of force and thermal distributed load satisfying end conditions 10 p1720 A67-23601

Antisymmetric stress-strain state of thin walled isotropic and anisotropic sandwich shells of revolution with meridian of arbitrary shape for complex boundary conditions 10 p1720 A67-23603

Finite element displacement method extended to bifurcation buckling of shells of revolution under axisymmetric loading 10 p1725 A67-23715

Elastic-plastic analysis showing relationship between tangent modulus and initial strain methods 10 p1726 A67-23718

Boundary value problem solution governed by system of partial differential equations applied to analysis of curved thin walled shells of revolution 10 p1729 A67-23765

Linear motion equations including effects of transverse shear deformation and rotary inertia derived for thin elastic isotropic conical shells of revolution 10 p1729 A67-23767

Shells of revolution having arbitrary stiffness distribution of loads and temperatures 10 p1730 A67-23771

Nonlinear membrane equations for extremely thin shell of revolution of very deformable material, assuming large displacements, rotations and strains 10 p1730 A67-23836

Basic equations for shells with circular parallel sections including shells of revolution 10 p1731 A67-23844

Diffraction of plane electromagnetic wave from ideally conducting ellipsoid of revolution 11 p1751 A67-23915

Nonlinear membrane theory for thin elastic inflatable shells during pressurization phase 11 p1875 A67-24432

Integral equations of second boundary

value problem of equilibrium of elastic body of revolution, treating cylinder under pressure 11 p1878 A67-24877

Concentration of force and moments near circular holes in shells of revolution with large elastic displacements 11 p1878 A67-24879

Stress concentration near holes in perturbed shallow shells of revolution 11 p1878 A67-24880

Lower modes and frequencies of natural elastic oscillations of vessel formed by liquid-filled shell of revolution taking into account fluid surface wave and shell inertia 12 p2020 A67-25566

Dynamic problem of shell of revolution in axial rotation under action of plane compression wave 12 p2020 A67-25568

Locally loaded orthotropic shells of revolution under radial concentrated forces 12 p2021 A67-25575

Matrix integral equations to calculate critical stresses and natural frequencies of oscillation of thin walled isotropic shells of revolution 12 p2022 A67-25585

Natural oscillations of elastic truncated conical shells of revolution under composite static load 12 p2026 A67-25613

Asymptotic method of integrating differential equations applied to analysis of axisymmetrical oscillations of thin elastic LF shells of revolution 12 p2027 A67-25624

Natural oscillation frequency of multilayer shells of revolution with nonsymmetrical structure containing rigid filler and subjected to transverse load 12 p2027 A67-25626

Oscillation frequency and frequency density distribution equations derived for thin elastic shells of revolution clamped along two parallels, using differential equations 12 p2027 A67-25627

Large deformations of zero moment orthotropic shells of revolution under action of inertial loads caused by centrifugal acceleration of shells 12 p2028 A67-25629

Variational methods for calculating small axisymmetrical oscillations of conical shell of revolution partially filled with ideal incompressible fluid 12 p2028 A67-25633

Shells of revolution under axisymmetric loading analyzed within ideally plastic shell theory, examining mathematical difficulties of shell carrying capacity 12 p2029 A67-25637

Finite rotation of body due to revolutions of internal flywheels determined assuming total kinetic moment of system is zero 12 p1966 A67-25658

Asymptotic integration technique for small axisymmetrical oscillations of thin walled elastic shell of revolution for case of double reversal point 12 p2029 A67-25675

Reissner variational formulation of temperature distribution boundary value problem of axisymmetric thermal stresses in isotropic sandwich shells of revolution [AIAA PAPER 66-528] 12 p2030 A67-25917

Thesa nose cones in supersonic flight, calculating aerodynamic coefficients from trajectory and flight phases 13 p2051 A67-27291

Three-dimensional axisymmetrical boundary layer on spinning body of revolution in two-component fluid flow, discussing velocity distribution, drag and separation 14 p2295 A67-27835

Transonic gas flow past ducted bodies of revolution indicates shock wave asymptotic attenuation at infinity 14 p2296 A67-27969

Nonlinear dynamic response of thin walled shells of revolution 14 p2397 A67-28090

Testing conditions for near-wake study of solids of revolution in supersonic and hypersonic flow, using streamlined supports in magnetic suspension [ONERA-TP-454] 15 p2416 A67-29379

Interval size effect on minimum drag coefficients and optimum shapes of bodies of revolution determined from Newtonian impact theory 15 p2416 A67-29407

Flattening of ellipsoid of revolution considered as mathematical surface for solution of geodetic problems 15 p2477 A67-29744

Deflections and stresses of paraboloidal shells of revolutions under gravity loads for applications to paraboloidal reflector antenna construction 16 p2763 A67-30678

Linearized theory for unsteady flow about bodies of revolution in sonic stream 16 p2589 A67-30790

Elliptic nose shape bluntness effect on drag of bodies of revolution in axisymmetric subsonic flow 16 p2589 A67-30791

Shock-wave separation dependence on bluntness degree, Mach number and gas type during supersonic motion of ellipsoids of revolution 16 p2675 A67-31130

Double curvature influence on rigidity of shell of revolution analyzed for surface loading and cross sectional linear loading, using Fourier series 16 p2766 A67-31149

Pressure distribution and convective heat flux at slender bodies of revolution surface, considering sphericity influence of free hypersonic flow 16 p2594 A67-31468

Stationary flow in viscous fluid film on rotating body of revolution, using differential equations 17 p2836 A67-32261

Integral relation method analysis of supersonic gas flow past blunt body of revolution 17 p2791 A67-32679

Variational principle for determining fluid flow stability in differentially rotating self-gravitating stars and galaxies and for studying eigenfunctions properties 17 p2947 A67-32756

Zero-moment stressed state in shells of revolution under concentrated loading described by p-analytic functions 17 p2962 A67-32875

Finite difference method stability analysis of deformed eccentrically stiffened shells of revolution, accounting for finite prebuckling rotations [AIAA PAPER 67-110] 17 p2963 A67-33015

Shells of revolution with curved elements noting rigid body displacements in analysis by matrix displacement method 17 p2963 A67-33042

Solutions for boundary value problems of potential theory and elasticity theory for single cavity hyperboloids of revolution 17 p2966 A67-33272

Body of revolution bounded by sphere rolling on stationary sphere with force function of applied forces dependent on only one coordinate 17 p2886 A67-33277

Free carrier absorption coefficients in 6H and 15R silicon carbide, showing probable ellipsoids of revolution 18 p3102 A67-34279

Shells of revolution produced by fiber-wound distributing internal and boundary stresses uniformly over fiber contours 19 p3337 A67-34871

Fiber shells of revolution under compression loads analyzed for use in pressurized balloons 19 p3338 A67-34872

Quasi-static equilibrium of truncated conical shell of revolution discussed in terms of zero-moment theory, when under cyclic load 19 p3341 A67-35631

Laminar boundary layer for two-dimensional flow on bodies of revolution, noting suction velocity 19 p3210 A67-35721

Prestressed-shell buckling, using Budianski-Koiter tensor nonlinear equilibrium equations by numerical analysis 19 p3343 A67-35778

Dynamic stability analysis of bodies of revolution in supersonic flow, using characteristics method [AIAA PAPER 67-607] 19 p3172 A67-35998

Unsteady aerodynamic forces due to gusts on supersonic bodies of revolution 19 p3172 A67-36001

Stagnation ablation of blunt body hypersonic reentry with nonreacting gas, deriving laminar flow equations 20 p3356 A67-36509

Supersonic viscous gas flow around body of revolution involving perturbation damping, analyzing Navier-Stokes and heat transfer equations for flow chart 20 p3357 A67-36810

Group properties of differential equations describing axisymmetric thin layer jet flow of ideal fluid propagating along surface of revolution 20 p3422 A67-37063

Differential geometry and vector analysis used to design axisymmetric lens of arbitrary shape for observing phenomena in arbitrary flow field of revolution 21 p3610 A67-37810

Truncated elastic shell of revolution stability under tensile stress 21 p3718 A67-37978

Stress analysis of ribbed shell of revolution, noting case of open shell of zero Gaussian curvature with cyclic symmetrical stresses 21 p3718 A67-37980

Solution for boundary value problems in

elasticity theory for ellipsoid of revolution and cavity with surface loading, determining coefficients in closed form 21 p3718 A67-37984

Inversion formulas for parabolic functions solution to vibration equation in diffraction at paraboloid of revolution 21 p3652 A67-38110

Nonlinear equilibrium equation system derived for shells of revolution, considering shell stability 21 p3721 A67-38304

Boundary layer of chemically reacting unstable gas flow along generatrix of body of revolution 21 p3564 A67-38423

Characteristic method computer program for calculating three-dimensional supersonic flow around blunt and pointed bodies of revolution in reasonable time 21 p3566 A67-38887

Diffraction of plane electromagnetic wave from ideally conducting ellipsoid of revolution 21 p3586 A67-38943

Boundary layer equation system for axial steady and unsteady flows past bodies of revolution 22 p3739 A67-39217

Hypergeometric functions studied for solution of problems on elastic equilibrium of circular plates and shells of revolution 22 p3909 A67-39398

Ring finite element analysis for shells of revolution improved by extending polynomials representing displacements 22 p3911 A67-39499

Drag coefficients used to evaluate normal force and pitching moment characteristics of revolving body at angle of attack 22 p3740 A67-39943

Friction and heat flow resistances for three-dimensional compressible laminar gas boundary layer over ellipsoid of revolution at angle of attack 22 p3786 A67-40028

Reissner differential equation simplified for problems involving small strains in thin shells of revolution due to symmetrical deflections 23 p4073 A67-40612

Differential equations describing stressed state of revolving shell beyond elastic limit and solutions adaptable to computer programming 23 p4075 A67-40681

Solution for flow through circular array of blades contained between two surfaces of revolution separated by small variable distance obtained by Ackeret method 23 p3927 A67-40726

Electrostatic and magnetostatic potentials for slender bodies of revolution in axially symmetric external fields 23 p4026 A67-40753

Vector eigenfunctions solution of three-dimensional elastic theory problems, reviewing literature on bodies of revolution in various coordinates 24 p4248 A67-42101

Revolving thin elastic shell free axisymmetric oscillation described by equation system derived by asymptotic integration technique with single reversal point 24 p4250 A67-42304

Thin toroidal elastoplastic shells of revolution loaded axisymmetrically, calculating force, moment, stress and strain interrelation for middle surface using complex representation 24 p4250 A67-42305

Incidence angle effects on wall heat flux in symmetry plane of cone of revolution in hypersonic regime, discussing wall pressure measurements 24 p4092 A67-42660

BODY SIZE /BIOL/

Animal study of body volume increase and pressure changes causing lungs and thorax expansion during decompression to near vacuum 23 p3954 A67-41594

BODY SWAY TEST

Graphical demonstration of human reaction to shock or vibration input in horizontal plane to study physiological functions of equilibration 13 p2064 A67-27274

BODY TEMPERATURE

Evaluation of Einstein conclusion that moving body appears to be cool 03 p0466 A67-12847

Potential on hot body in plasma as function of surface temperature and plasma characteristics, considering case where photoemission is present 07 p1251 A67-19812

Temperature of moving body in relativistic frame of reference 10 p1680 A67-23497

Unsteady heat conduction and transfers by electrical simulation methods, determining temperature field in canonical metal bodies 17 p2973 A67-33082

Temperature field within multidimensional body in nonlinear heat conduction process in

terms of known temperature distribution along coordinates 24 p4254 A67-42254

BODY TEMPERATURE /BIOL/

SA HYPOTHERMIA

SA SKIN TEMPERATURE /BIOL/

Heat balance and ventilation of human body in pressure suit 09 p1455 A67-21731

Temporal characteristics of body temperature during high thermal stress, determining correlation between effective and rectal temperature 10 p1600 A67-23822

Circadian rhythms detection, estimating parameters by cosinor procedure for temporal morphology aspects 14 p2255 A67-28480

Daily physiological rhythm changes associated with light intensity and color, noting body temperature oscillations vs light intensity, heart rate changes, etc 15 p2426 A67-29109

Body temperature monitoring in external auditory meatus in pre-flight testing, showing correlation between sublingual and aural temperatures 18 p2995 A67-34709

Improved response acquisition in deep hypothermia adapted rats 20 p3373 A67-37433

Ability of hypothermia-adapted rats to learn and perform at low body temperature 20 p3373 A67-37669

Circadian oscillations of deep body temperature and heart rate in ambulatory primate in controlled environment 23 p3951 A67-41554

Telemetry system for measuring body temperature and heart rate for physiological evaluation of space suits 23 p3969 A67-41651

Water deficit effects on thermal sweating, noting extraneous effects due to higher body temperature and wet skin 24 p4110 A67-41781

Thermo-protective systems for ejected aircraft personnel noting cream product producing heat when dissolved in water [AIAA PAPER 67-967] 24 p4117 A67-43045

BODY TEMPERATURE REGULATION

Cellular biochemical thermoregulation and organic mass changes in cold- and heat-acclimatized monkeys 04 p0560 A67-14582

Conductive cooling method for pressure applications in body heat loss promotion at high exercise rate 23 p3964 A67-41558

Experiments on undercooling and overcooling with liquid cooling garments, noting correct cooling defined by narrow biothermal response band 23 p3970 A67-41655

BODY VOLUME /BIOL/

Leg volume changes in response to lower body negative pressure due to blood redistribution 23 p3955 A67-41619

BODY-WING COMBINATION

Normal force and pitching moment values for interference on body, wing and overall body-wing obtained, using pressure distribution integration 04 p0545 A67-14439

Velocity potential near disturbance boundary for steady supersonic flow past body-and-wing model 17 p2790 A67-32403

BOEING MILITARY AIRCRAFT

S B-52 AIRCRAFT

S CH-47 HELICOPTER

BOEING 7207 AIRCRAFT

Supersonic transport variable sweep wing design, showing root glove and Mach number effects on aerodynamic center of strike aircraft 20 p3361 A67-36499

BOEING 727 AIRCRAFT

Fatigue life on 727 aircraft structure improved through room temperature curing of adhesive film 09 p1577 A67-22510

Boeing 727 QC aircraft development, manufacture, design objectives, cargo pallet system, seat pallet system, etc [AIAA PAPER 67-395] 15 p2421 A67-30362

Boeing 727 automatic flight control and landing system [AIAA PAPER 67-573] 19 p3258 A67-35969

Injury and fatality analysis in survival study of commercial jet aircraft /Boeing 727/ landing accident with subsequent interior fire 23 p3969 A67-41650

BOEING 737 AIRCRAFT

Aerodynamic design of Boeing 737 covering data of analytical studies, wind tunnel and flight tests, aerodynamic parameters and drag, flap system size, efficiency, wing geometry and handling qualities [AIAA PAPER 65-739] 03 p0354 A67-12906

Aerodynamic design of Boeing 737 covering data of analytical studies, wind tunnel and flight tests, aerodynamic

parameters and drag, flap system size, efficiency, wing geometry and handling qualities [AIAA PAPER 65-739] 08 p1279 A67-21043

Hydraulic system of Boeing 737 jet transport, noting flight safety and system reliability throughout design 09 p1444 A67-22129

BOEING 747 AIRCRAFT

Boeing model 747 aircraft /large capacity subsonic transport/ engine aerodynamics and design objectives [AIAA PAPER 66-821] 02 p0181 A67-12248

JT9D turbofan engine for Boeing 747 commercial transport aircraft, analyzing design and performance potentials [AIAA PAPER 67-374] 15 p2548 A67-30346

Planning integration of Boeing 747 jet aircraft into commercial airline [AIAA PAPER 67-394] 15 p2421 A67-30361

Boeing 747 characteristics for passenger and cargo service noting economic gain, operational performance, control cabin, engine, etc [AIAA PAPER 67-397] 15 p2421 A67-30364

Modernizing air traffic control, governmental procedures, airports and support facilities to accommodate Boeing 747 and supersonic transports 20 p3418 A67-37442

Planned introduction of Boeing 747 into airline service noting advances in technology for passenger comfort, cargo handling and rate reduction 20 p3361 A67-37443

Boeing model 747 aircraft /large capacity subsonic transport/ engine aerodynamics and design objectives 21 p3568 A67-38542

BOGOLUBOV THEORY

Equations governing divergent many-body behavior within BBGKY hierarchy in Boltzmann approximation for cut-off potentials, noting nondivergent nature of solutions 01 p0118 A67-10915

Book on kinetic equations of gases and plasmas, with emphasis on theories which start from Liouville equation 04 p0660 A67-14581

Asymptotic kinetic equation for inhomogeneous plasma compared to results for initial value problem and Bogoliubov method 06 p1042 A67-18572

Relationships among Delaunay theory, Diliberto periodic surface theory and Krylov-Bogoliubov method of averaging in celestial mechanics 08 p1347 A67-20383

Radial distribution function differential equation solution studied numerically and analytically for plasma parameters, using closure approximation 11 p1826 A67-23871

Transport coefficients for dense gases via Bogoliubov theory of two-particle nonequilibrium distribution function 11 p1823 A67-24538

Solution to Bogoliubov differential equation for distribution functions of particle system by functional integration technique 12 p1962 A67-26174

Gas laser quantum theory, deriving motion equation for radiation-density matrix 14 p2332 A67-28716

Frequency shift associated with nonlinear extraordinary wave in cold plasma calculated using Bogoliubov method 15 p2524 A67-29230

Motion in ternary stellar system consisting of central body and close and distant companions 16 p2746 A67-30956

Bogoliubov existence theorem for one-dimensional integral manifold and two-dimensional local integral manifold extended to Hilbert space 17 p2879 A67-32879

Averaging method extended to physical systems described by differential equations simultaneously dependent on almost periodic fast time and periodic slow time 17 p2885 A67-33140

Continuous phase medium gas representation used to derive variational principles for Liouville, coupled Bogoliubov and kinetic equations 22 p3835 A67-39218

HF conductivity of partially ionized plasma in long wavelength limit, treating particle interactions by BBGKY and Boltzmann collision integral methods 23 p4031 A67-40888

BOILER

Boiler inlet impedance frequency response in single tube heat exchanger when pumped with oscillating flow 22 p3916 A67-39390

BOILER PLATE

Heat transfer data obtained from film boiling for four liquid compositions, using flat plate geometry 10 p1732 A67-22729

BOILING

SA EVAPORATION

SA FILM BOILING

SA NUCLEATE BOILING

SA VAPORIZATION

Stability of dry patches forming in thin liquid film flowing over heated surface, noting effects of vapor thrust and thermocapillarity 01 p0167 A67-10975

Density wave type flow oscillations in boiling Freon 11 examined, noting effects of partial evaporation superheat and liquid inlet temperature on stability [ASME PAPER 66-WA/HT-49] 04 p0725 A67-15433

Heat transfer - AICE International Conference, Chicago, August 1966, Volume 5, Flow boiling and radiation 04 p0736 A67-15859

Free convective heat transfer measurements of sodium boiling on surface of horizontal tube 04 p0736 A67-15860

Boiling Na free-and forced-convective heat transfer rates, surface temperature and pool-boiling heat-transfer coefficient measurements 04 p0737 A67-15861

Quasi-stationary heat transfer equations and maximum possible heat-transfer coefficient for solid surface moving in very fluid rotating boiling medium 06 p1118 A67-18549

Li, Na, K, Rb and Cs vacuum tests as coolants and working fluids in high temperature compact space power plant 07 p1223 A67-19464

Probability of effervescence of superheated liquids as function of temperature and pressure, analyzing N-pentane and hexane under isobaric heating and reduced pressure 09 p1580 A67-21907

Effect of underheating on development of boiling crisis in two-phase nonequilibrium flows 10 p1732 A67-23018

Saturn S-IB stage fuel system, studying LOX density fluctuations, heat transfer and boiling under various weather conditions 13 p2186 A67-27637

Liquid venting concept for zero gravity environment by suppressing vapor generation with open loop refrigeration, using extracted liquid as working fluid 13 p2056 A67-27639

Cooldown of shrouded spherical vessels in liquid nitrogen, determining smallest tank-shroud gap compatibility with rapid cooldown 13 p2229 A67-27666

Boiling process of binary mixtures examined by heat transfer mechanism at atmospheric pressure 17 p2969 A67-32458

Heat transfer analysis for cavitation and boiling, noting vapor bubble formation 17 p2970 A67-32463

Incipient boiling prediction extended from forced flow water to other fluids and natural flow conditions [ASME PAPER 67-HT-61] 20 p3549 A67-36743

BOLKOW BO-105 HELICOPTER

BO 105 light helicopter design and characteristics noting plastic rotor blades, fuselage semimonocoque construction, etc 18 p2985 A67-33642

BOLOMETER

Airborne double bolometer technique for deriving atmospheric water vapor profiles by solving radiative transfer equations 01 p0108 A67-10315

Miniature optically immersed thermistor bolometer arrays employed for earth atmospheric horizon scanning from orbiting vehicles 19 p3231 A67-35684

Metal bolometer impedance and noise generation, discussing Johnson and temperature fluctuation noises 22 p3797 A67-39343

BOLT

SA NUTS AND BOLTS

Statistical methods for evaluating displacement in increasing number of fasteners depending on nominal sizes and tolerances of fasteners and pairs of holes 02 p0336 A67-11776

BOLTZMANN DISTRIBUTION

Necessary conditions for equilibrium of Maxwell-Boltzmann distribution using analyticity of S-matrix 05 p0849 A67-17115

Small two-dimensional oscillations in XY plane for isothermal magnetosphere in uniform gravitational field, postulating Boltzmann equilibrium density distribution 07 p1173 A67-19699

Electric potential distribution in flame for

electronegative gas layer present between two electrodes 13 p2165 A67-26597

Factors affecting current methods of sizing Aitken nuclei 13 p2152 A67-26865
Equation describing electron transfer between semiconductor surface bands and space bands, applying Fermi concept 14 p2371 A67-28754

Diatomic gas vibrational relaxation by master equation analysis, discussing quasi-steady state vibrational population distribution and transition probability increases 18 p3081 A67-33782

Electrical conductivity of ionized plasma taking into account particle impenetrability, using Boltzmann and collision at distance integrals 24 p4198 A67-42662

BOLTZMANN EQUATION

SA CHAPMAN-ENSKOG METHOD

Variation of effective conductivity of thin metallic film with surface charge calculated by Boltzmann transport equation used with Fuchs-Sondheimer boundary conditions 01 p0130 A67-10204

Compressibility effects on rarefied gas flow in Rayleigh problem, using BGK model of Boltzmann equation 01 p0051 A67-10457

Boundary value problem solution for sound generated at oscillating wall, propagating into half-space, for linear Boltzmann equation with general cut-off molecular potential 01 p0114 A67-10736

Equations governing divergent many-body behavior within BBGKY hierarchy in Boltzmann approximation for cut-off potentials, noting nondivergent nature of solutions 01 p0118 A67-10915

Boltzmann equations in kinetic theory of rarefied gas dynamics [ONERA-TP-379] 01 p0054 A67-11092

Oscillatory semiconductor photoconductivity dependence on photon energy periodic in longitudinal-optical phonon energy treated by Boltzmann equation, noting elastic scattering 02 p0280 A67-11488

Structure of shock wave in monatomic gas analysis using orthogonal polynomial solution of Boltzmann equation, noting Mott-Smith distribution function 02 p0234 A67-12541

Diffusion phenomena in rarefied gases treated, using Boltzmann equation expanded in Sonine Legendre polynomials in velocity space 02 p0234 A67-12544

Exact solutions to kinetic moment equations of monatomic gas in absence of external forces to case of mixture of monatomic Maxwellian gases with external forces 03 p0401 A67-12869

Thermal creep in rarefied gas investigated using Boltzmann-Krook equation 03 p0402 A67-13359

Book on microwave breakdown in gases covering electron collisions, Boltzmann equation for ionized gas, breakdown in atmosphere, etc 03 p0369 A67-13559

Locally Maxwellian solution of Boltzmann kinetic equation 03 p0459 A67-13632

Instability of counterstreaming plasmas investigated by taking into account Coulomb collisions via Fokker-Planck coefficients in Boltzmann equation 04 p0662 A67-14519

Magnetic field effect on transport equation, presenting relationship between classical Boltzmann equation and corresponding quantum mechanical formalism 04 p0659 A67-15773

Boltzmann equation for cosmic ray particle motion in random magnetic field 05 p0878 A67-16094

Generalization of kinetic theory of gases, deriving Boltzmann kinetic equation for use in singly-partial distribution function 05 p0849 A67-17021

Diffusion-viscosity coupling in stationary flow of nitrous oxide-carbon dioxide mixture in case of Maxwellian intermolecular forces 05 p0794 A67-17380

Collisionless aspects of strong shock wave structure as approximated by Boltzmann equation examined, using orthogonal polynomial expansion technique in velocity space 05 p0794 A67-17421

Spherical electrostatic probe in stationary plasma analyzed based on kinetic theory using Krook type model for collision integral formulation 05 p0857 A67-17423

Closed form for perturbation terms of linear Boltzmann equation 05 p0847 A67-17438

Boltzmann equation applicability to flows satisfying condition of molecular chaos,

noting role of Knudsen layer 06 p1022 A67-17724

Polarization and atom state distribution of excited atomic gas taking into account resonance excitation, using Boltzmann equation to determine line shape of electromagnetic wave absorption 06 p0991 A67-18799

Boltzmann transfer equation consisting of DC electric field and two AC electric fields for nonlinear second harmonic generation and combination frequencies in homogeneous plasma 06 p1046 A67-18826

Boltzmann equation for GaAs, noting coupling constant scattering between low and high mass valleys 06 p1067 A67-18963

Hydrodynamic equations describing motion of electrons in weakly ionized plasma in external electric field derived from Boltzmann equation, using Chapman-Enskog method 07 p1228 A67-19503

Energy distribution function in cathode drop space of glow discharges in hydrogen derived by numerical integration of simplified Boltzmann equations 07 p1229 A67-19516

Drift velocity variation with electric field calculated in GaAs, using Boltzmann equation and incorporating additional scattering process 07 p1232 A67-19561

Boltzmann equation for rarefied gas flows between two parallel infinite plates for Maxwellian, hard sphere and BGK models 08 p1355 A67-21117

Discrete ordinate method for unsteady linearized Boltzmann Bhatnagar-Gross-Krook equation of rarefied gas flow 08 p1324 A67-21409

Nonsteady state processes in nonequilibrium plasma with local collisions, using Boltzmann kinetic equation for application in MHD generators 09 p1543 A67-21823

Ionosphere as binary two-temperature gas and transfer coefficients for elastic collisions based on Boltzmann equation 10 p1640 A67-23220

Possible initial perturbations development into galaxies with dissipative effects associated with transport processes treated via Boltzmann equation 11 p1867 A67-24838

Dynamical irreversible evolution of gas with short range repulsive forces, using n-particle distribution function with many-body interactions 11 p1824 A67-25077

Nonequilibrium process in one dimension in presence of constant and oscillating electric field, using distribution function 11 p1824 A67-25078

Plasma conductivity in external electric fields calculated by LF longitudinal oscillation, using Boltzmann equation 12 p1970 A67-25249

Rarefied gas flow between parallel plates based on discrete ordinate method 13 p2092 A67-26277

Electron velocities distribution in plasma, studying boltzmann equation inelastic and superelastic collision operator, considering eigenfunctions and eigenvalues for electronic excitations and deexcitations 13 p2165 A67-26437

Plasma-radiation interaction represented by Compton effect, utilizing Boltzmann term developed according to powers of perturbation caused by electron motion 13 p2165 A67-26598

Kinetic theory and rarefied gas dynamics, discussing and analyzing Boltzmann equation 13 p2099 A67-26951

Diffusion phenomena of increasing mean free path with altitude in rarefied gas analyzed, incorporating gravitational field effect in Boltzmann equations 13 p2099 A67-26952

Small parameter method for rarefied gas dynamics problems using Boltzmann equation solution and kinetic equations 13 p2099 A67-26953

Nonequilibrium processes, analyzing required number of additional conditions and region of applicability of most probable distribution function, noting relation to Boltzmann equation 13 p2100 A67-26954

Sound propagation in dilute monatomic gas confined in box and in unconfined rarefied monatomic gas assuming unidirectional perturbation of velocity distribution 13 p2100 A67-26955

Nonlinear heat transfer between parallel plates, using ellipsoidal statistical model of

Boltzmann equation 13 p2223 A67-26960

Discrete ordinate technique for nonlinear Boltzmann equation for hard sphere molecules, considering pseudoshock relaxation 13 p2102 A67-26973

Monte carlo evaluation of Boltzmann collision integral for translational relaxation and plane steady shock problems 13 p2103 A67-26974

Boltzmann equation and statistical properties for two-dimensional gas, analyzing integral iteration for shock wave flow 13 p2103 A67-26975

Shock wave structure according to Krook model and Boltzmann collision integral 13 p2103 A67-26978

Accuracy of approximation solutions of Boltzmann equation for rarefied gas flow 13 p2104 A67-26979

Boltzmann equation and deduced moment equations containing moments up to fourth order in arbitrary orthogonal curvilinear coordinates 14 p2297 A67-27998

Nonlinear harmonic generation in magnetoplasma using Boltzmann equation, noting sharp resonance peaks 14 p2358 A67-28236

Generalization of kinetic theory of gases, deriving Boltzmann kinetic equation for use in singly-partial distribution function 14 p2351 A67-28482

Boltzmann kinetic equation solution for completely ionized plasma in magnetic field 14 p2363 A67-29071

Coefficient for electron ion recombination during triple particle collision, using Boltzmann kinetic equations 14 p2363 A67-29077

Monograph on upper atmosphere kinetics noting Boltzmann equations, MHD processes, thermal diffusion, etc 16 p2666 A67-31166

Electron velocity distribution function obtained for partially ionized gas in weak, steady electric field by solving Boltzmann-Fokker-Planck equation 16 p2704 A67-31235

Plane wave propagation in kinetic theory, discussing Boltzmann equation use and asymptotic results beyond critical frequency 17 p2905 A67-32927

Plane wave propagation in kinetic theory, noting Boltzmann equation and kinetic model 17 p2885 A67-32928

Solution of linearized Boltzmann collision equation for ion motion through gas in inhomogeneous electric field, describing energy distribution functions for hydrogen ions 17 p2907 A67-33102

Book on plasma physics covering plasma clouds in electromagnetic force field, kinetic equations, Boltzmann equation, etc 18 p3089 A67-34370

Polarization and atom state distribution of excited atomic gas taking into account resonance excitation, using Boltzmann equation to determine line shape of electromagnetic wave absorption 18 p3029 A67-34418

Rarefied gas cylindrical Couette flow noting Knudsen number, Bhatnagar-Gross-Krook model for Boltzmann equation, transport integrodifferential equation, etc 18 p3029 A67-34738

Transport phenomena in electronic plasma as initial value problem noting distribution function relaxation 19 p3287 A67-35355

Relativistic Boltzmann collisionless equation solution in presence of certain external fields 19 p3266 A67-35710

Solution to moment equations for near-equilibrium spherically-symmetric expanding flows by using Bernstein-Greene-Kruskal theory for Boltzmann equation 19 p3212 A67-35764

Soviet book on rarefied gas dynamics involving methods and approaches for kinetic description of gas behavior, emphasizing Boltzmann equation 20 p3423 A67-37086

Electric conductivity of surface space charge layers in semiconductors, solving Boltzmann equation and determining current density and carrier mobility 20 p3511 A67-37144

Magnetic properties of relativistic equilibrium plasma in magnetic field studied in Boltzmann and quantum cases, using thermodynamic functions 20 p3502 A67-37557

Stagnation-point flow of rarefied gas, using linearized BGK model of Boltzmann equation with small Mach number 20 p3425 A67-37673

Steady state theory of low pressure

- plasma discharge column in axial magnetic field derived, using moments of Boltzmann equation 21 p3662 A67-37756
- Parametric excitation of electron plasma frequency derived using Boltzmann and Poisson equations 21 p3667 A67-38415
- BBGKY hierarchy description of plasmas, with application to ionized particle charge distribution in external electric field 21 p3675 A67-38932
- Shock structure in kinetic theory of gases, solving Krook model of Boltzmann equation with small perturbation technique 22 p3782 A67-39196
- Relaxation toward Maxwell distribution function of classical gas with initial nonequilibrium distribution function as velocity modulus function 22 p3782 A67-39406
- Kramers problem for rarefied gas flow, calculating slip coefficient for various collision frequency models, noting only slight model dependence 22 p3841 A67-39718
- Magnetoacoustic attenuation in metals with Fermi surface, open orbits and magnetic breakdown calculated by solving Boltzmann equation via path-integral method generalization 22 p3861 A67-39995
- HF conductivity of partially ionized plasma in long wavelength limit, treating particle interactions by BBGKY and Boltzmann collision integral methods 23 p4031 A67-40888
- Linear Boltzmann equation approximation by Fokker-Planck equation leading to logical inconsistency 23 p4029 A67-40963
- Integral equation derived from Boltzmann equation for one-dimensional radiative heat transfer in plane layers of gray media 24 p4252 A67-41934
- Free carrier effect on higher harmonic generation in semiconductors from nonlinear Boltzmann equation 24 p4202 A67-41985
- Boltzmann equation for cosmic ray particle motion in random magnetic field 24 p4213 A67-42770
- BOLTZMANN-VLASOV EQUATION**
- Alfvén waves in ionized plasma of finite electrical conductivity, giving equations for semiphenomenological model 20 p3496 A67-36271
- BOLZA PROBLEM**
- Necessary conditions from second variation, via transformed accessory minimum problem, for class of singular Bolza problems, including singular optimal control problems 04 p0594 A67-15879
- Newton-Raphson computational procedure for finding extremal control policies for nonlinear processes 15 p2456 A67-29363
- Trajectory optimization initial value problem, considering various conditions, methods of solution and reentry heating minimization 21 p3703 A67-38440
- BOMB**
- Mathematical model used to determine influence of nonlinear induced roll moment and yawing moment on dynamic stability of cruciform tailed bomb 15 p2416 A67-29428
- BOMBARDMENT**
- S AURORAL BOMBARDMENT
- S ELECTRON BOMBARDMENT
- S ION BOMBARDMENT
- S NEUTRON BOMBARDMENT
- BOMBER AIRCRAFT**
- Aircraft sizing methodology and hover control comparative analysis on V/STOL fighter-bomber using lift plus lift cruise propulsion [AIAA PAPER 67-133] 06 p0948 A67-18358
- Cardiorespiratory functioning in flight monitored on carrier pilots in combat 17 p2805 A67-31956
- Biochemical response pattern to combat flying stress of monitored carrier aircraft pilots 17 p2805 A67-31957
- Development, design and production phases of Canadair CL-215 water bomber and potential variants [SAE PAPER 670902] 24 p4094 A67-42020
- BONDING**
- SA ADHESION
- SA CERAMIC BONDING
- SA CHEMICAL BOND
- SA DIFFUSION BONDING
- SA JOINT
- SA METAL BONDING
- SA METAL-METAL BONDING
- SA MOLECULAR BONDING
- SA RESIN BONDING
- SA SOLDERING
- SA WELDING
- Sintered-metal friction materials from metallic and nonmetallic powders, noting composition 01 p0099 A67-10710
- Fatigue failure analysis in small metallurgically-bonded joints in very small electronic components, using statistical analysis of random forces and dynamic response of member 01 p0084 A67-11359
- Ultrasonic phase sensitive test procedure for adhesive bonded structures 04 p0622 A67-15265
- Nondestructive test development to meet inspection requirements of advanced aircraft design, discussing titanium fusion and resistance spot welds and adhesive bonding honeycomb components 05 p0808 A67-17087
- High density microelectronic circuitry, discussing interconnection through use of advanced materials and techniques 08 p1303 A67-21189
- Criterion characterizing adhesive joints in structural bonding of military materiel 09 p1522 A67-22500
- Load carrying capability of adhesive bonded studs, analyzing resin systems and flexible linears 09 p1507 A67-22502
- Ablative properties of nylon-phenolic materials used in fabrication of composite heat shield with low residual stresses 09 p1523 A67-22506
- Adhesive bonded honeycomb horizontal stabilizers, considering strength, aerodynamics, cost, endurance and serviceability 09 p1577 A67-22508
- Fatigue life on 727 aircraft structure improved through room temperature curing of adhesive film 09 p1577 A67-22510
- Bonding of rigid insulation to case of solid propellant rocket motor, considering fabrication, operation and storage requirements 09 p1578 A67-22512
- Medium temperature curing general purpose structural adhesive system for use on helicopter 09 p1523 A67-22515
- Ultrasonic inspecting technique for reinforced plastic components and adhesive bonds of solid propellant booster nozzles 10 p1659 A67-22930
- Electronic packaging technique in thin film technology using flip-chip bonding and MTFI techniques 12 p1910 A67-25264
- Testing instrument for determination of lead wire mechanical properties and bond strengths within semiconductor devices 12 p1911 A67-25270
- Bonding and packaging techniques in production of semiconductor integrated circuits, discussing chip, lead and thermopressure bonding methods 12 p1951 A67-26214
- Aluminum, Volume 3, Fabrication and finishing 14 p2323 A67-27818
- Photoelastic stress analysis on bonded interface of strip with different end configurations noting stress concentration, bonding problems, etc 16 p2764 A67-30933
- Flip-component technology discussing bonding of flip chips and face bonding of semiconductor devices 16 p2642 A67-31727
- Book on intermetallic compounds discussing bonding, crystal structure, microstructure, formation, stability, kinetics, transformations and properties 16 p2692 A67-31867
- Critical strain parameter concept for adhesive bond joints noting strength dependence on geometry and material elastic properties [SAE PAPER 670856] 24 p4160 A67-42003
- BONE**
- SA RIB
- Prolonged weightlessness exposure and expected effects on man 12 p1902 A67-25725
- Photon beam transmission measurement technique for determining bone mineral content in vivo 23 p3945 A67-41087
- Seven year follow-up X-ray survey for bone changes in low pressure chamber operators to determine long term effects of altitude decompression sickness 23 p3957 A67-41641
- BONE MARROW**
- RNA fractions base composition and labelling kinetics in presence and absence of actinomycin for rapidly labelled RNA in rabbit bone marrow rich in erythroid cells 23 p3944 A67-40801
- BOOLEAN ALGEBRA**
- Correspondence between logical relations of Boolean function implicants and numerical relations between identifiers 09 p1470 A67-22669
- Random pulse operation and random pulse machines structural requirements, with continuous variable dependent on certain sampling time 18 p3006 A67-34063
- BOOM**
- SA SONIC BOOM
- Solar environment and aerodynamic drag effect on deflection of structural booms in space [AIAA PAPER 66-502] 08 p1413 A67-21512
- BOOSTER**
- Design of gust alleviation controls for boost phase flight of missiles incorporating random winds, time-varying missile dynamics, control problem, etc [AIAA PAPER 66-969] 02 p0332 A67-12292
- Open and closed loop tools and techniques for guidance program validation and postvalidation operations 08 p1350 A67-20629
- Time optimal control of bounded phase coordinate process applied to unstable booster with actuator position and rate limits 12 p2012 A67-25911
- Satellite launch vehicle performance analysis based on velocity requirements and gravity and drag losses for applications to booster configurations 14 p2394 A67-28701
- Low cost rocket launch vehicles for various payload capacities 15 p2566 A67-29832
- Fixed wing reusable horizontal landing boosters, comparing weight, cost, technical difficulty and availability rate 15 p2567 A67-29836
- Reusable booster concept, economic justification, cost characteristics and management planning 15 p2569 A67-29850
- High energy liquid propellant boosters, noting design, performance characteristics and limitations 16 p2760 A67-30703
- Purification systems, filters and porous materials applications to liquids and gas systems associated with spacecraft, boosters and ground support equipment 21 p3570 A67-38103
- High performance automatic ground checkout system for boosters, noting rate improvement and error reduction 21 p3608 A67-38203
- BOOSTER RECOVERY**
- Post Apollo space flight technology, discussing recoverable and reusable booster rockets, spacecraft, life support systems, etc 08 p1391 A67-21065
- Reusable low weight hypersonic glider /space rotor/ for space vehicle reentry and recovery 15 p2568 A67-29845
- Titan IIIB launch vehicle spent stage I recovery experiment, evaluating feasibility of refurbishment and reuse 15 p2569 A67-29853
- Booster recovery systems development, payload and operational costs evaluated using postulated space program [AIAA PAPER 67-909] 24 p4245 A67-43016
- BOOSTER ROCKET**
- S ROCKET BOOSTER
- BORANE**
- SA DIBORANE
- Nuclear magnetic resonance and microwave spectra of some deuterio derivatives of 2, 4-dicarbadodecaborane/7/ [JPL-TR-32-1038] 01 p0019 A67-11146
- Yellow-green luminosity accompanying injection of triethylborane into upper atmosphere 12 p1932 A67-25208
- Book on production of boranes and related research for high energy fuels for air breathing engines 23 p4047 A67-41443
- BORATE**
- Vacuum deposition and mechanical properties of magnetic thin films of ferrite-borate mixtures 04 p0677 A67-15118
- Extreme pressure /EP/ films from lubricants containing borate esters, studying structure and mode of action 16 p2683 A67-31756
- BORIC ACID**
- Crystallization of boric anhydride obtained only through maintaining high water content in reactive agent during thermal treatment 13 p2143 A67-26812
- BORIC OXIDE**
- Properties of gallium arsenide crystals produced by pulling single crystals from melt of gallium arsenide covered by molten boric oxide 10 p1693 A67-23516
- BORIDE**
- SA DIBORIDE
- SA HEXABORIDE
- SA TITANIUM BORIDE

Formation conditions for yttrium boride-lanthanum boride solid solution by reduction of Y and La oxides in vacuum 01 p0138 A67-11244
X-ray study of lanthanum borides to verify existence of homogeneous compounds within large range of variations in composition 11 p1810 A67-23905
Methods of producing coatings based on metal-like high temperature materials 19 p3244 A67-34957
Energies of combustion of aluminum diboride and alpha aluminum dodecaboride measured in bomb calorimeter using fluorine oxidant 22 p3758 A67-39766

BORN APPROXIMATION

Born approximation theory of nonlinear scattering of microwaves from oscillating plasma column, noting diffraction patterns and frequency shifts 01 p0027 A67-11324
Multiple scattering of light in turbulent atmosphere noting relation to refraction index and power spectra, using Born series solution to wave equation 06 p1033 A67-18536
Absolute cross sections and isomeric yield ratios for d,p reactions up to 15 mev in various metals 14 p2350 A67-27790
Renormalizing approximate wave functions so that amplitude is correct by means of matrix, with applications to Born approximation 17 p2887 A67-33318
Friedel sum rule applied to semiconductors, discussing Born approximation role 18 p3104 A67-34591
Angular distribution of products in electron impact dissociation of hydrogen molecule calculated following Born approximation for scattering amplitude 20 p3487 A67-36231
Semiempirical electron impact cross sections for He from oscillator strengths, using Born approximation 20 p3489 A67-37416
Electron impact excitation and ionization cross sections data of molecular nitrogen synthesized using modified Born approximation 20 p3489 A67-37418
Quantum corrections to Maxwell plasma free energy in compensating electromagnetic field by method of displacements and collective variables for high temperatures 21 p3663 A67-37861
Doubly differential cross section for ejected secondary electrons energy and angular distribution calculated from He by fast protons bombardment 22 p3839 A67-39201
Integrals properties with respect to paraboloid and asymptotics of Born approximations in scattering theory for Schroedinger equation applied to parabola 22 p3835 A67-39307
Microwave scattering cross section for turbulent weakly ionized plasma column, noting square root of mean square plasma density fluctuation limit for Born approximation 22 p3850 A67-39722

BORN-INFELD THEORY

Relativistic electrodynamics of moving medium, discussing Maxwell-Minkowski equations, Born equations, field vector transformations, etc 09 p1533 A67-22449

BORON

Low energy electron diffraction study of interaction of thin deposit of amorphous boron with tungsten single crystal surfaces 01 p0093 A67-10205
Boron filaments for possible use as reinforcing phase in composite materials for aerospace structures 03 p0452 A67-13407
Surface treatment and interface stability of boron filaments reinforcing plastic composite materials 03 p0455 A67-13428
Compatibility and interaction characteristics of SiC and B fibers with metal matrices in composites prepared from powder metallurgy by hot pressing 03 p0444 A67-13430
Boron fiber-reinforced aluminum composites fabrication by plasma spraying and tensile testing 03 p0444 A67-13431
Boron filaments for reinforcement of aluminum alloys used in turbomachinery 03 p0444 A67-13436
Tensile test equipment and methods to determine modulus of elasticity and ultimate tensile strength of single boron filaments at room and elevated temperatures 03 p0455 A67-13445
Nondestructive test methods for monitoring service hardware during boron composite material development and

correlation with results of destructive tests 03 p0455 A67-13447
Fiber reinforced metals 03 p0456 A67-13893
Effect of beryllium, boron, titanium, etc, additions on recovery and recrystallization processes in pure aluminum, using differential calorimetric techniques 04 p0637 A67-14910
Combustion mechanism for boron-containing air-augmented propellant based on conductive, convective and radiant heat transfer between propellant and combustion products 04 p0687 A67-15814
Properties of pyrolytically produced boron fibers, noting strength decrease with temperature increase 06 p1016 A67-17903
Hexagonal indexing of tungsten boride phase in reaction of boron with tungsten core, obtaining X-ray powder diffraction pattern 06 p1016 A67-17904
Titanium alloy weld properties as affected by boron, beryllium and lanthanum additions 07 p1207 A67-19291
Filamentary reinforced resin matrix composite materials for high specific strength and specific modulus necessary for aircraft structures 08 p1333 A67-20359
Boron filament epoxy resin composites test program relative to mechanical design of reentry vehicle structure 08 p1345 A67-20424
Fabrication of complex hollow rib reinforced structures of wound boron filaments and anhydride cured epoxy resin for reentry vehicle application 08 p1345 A67-20435
Tape production process from noncontinuous boron fibers, noting mechanical properties and process parameters 08 p1335 A67-20911
Crystalline structure of amorphous boron fibers noting glass-like nature of fiber as exhibited by diffraction patterns 08 p1343 A67-21313
Laser transition in B 2, Br 2 and Sn in pulsed discharges of boron chloride, hydrogen bromide and stannic chloride respectively 08 p1339 A67-21379
IR absorption in high purity boron films, showing absence of absorption peaks at 2-15 microns 09 p1533 A67-22132
Continuous filament reinforcement data, analyzing boron and silicon carbide for metal matrix applications [ASTME PAPER WES-7-75] 10 p1668 A67-23010
Boron fiber reinforced epoxy matrix plastic composite for application to aircraft structures 10 p1723 A67-23697
Youngs modulus and shear modulus of inorganic filaments of tungsten and boron measured by oscillation 13 p2144 A67-27187
Polyhedral boundary precipitations of complex heat resistant nickel alloy in carbide phase caused by boron and cerium 14 p2338 A67-28674
Aluminum-boron composites stress-strain behavior, considering synergism increasing over rule of mixtures [ASTM PAPER 7] 18 p3067 A67-34572
Boron filaments mechanical properties and chemical compatibility compared with nickel and titanium matrices 19 p3245 A67-35728
Conductivity profiles investigated as function of ion energy, total flux and annealing schedule, when implanting boron into silicon 19 p3307 A67-35812
Approximate electron radial functions for uniformly charged nucleus/UCN/ used in analyzing boron 12 and nitrogen 12 beta decay spectra 20 p3488 A67-36915
Boron filament behavior in rotating-beam fatigue test 20 p3470 A67-37390
High tensile strength of composite amorphous boron filament, discussing Weibull relationship and measurements 23 p4018 A67-40787
Boron and graphite filament-resin composites tensile and interlaminar shear strengths and Al foil liner cyclic life in cryogenic pressure vessel tests 24 p4176 A67-42470

10 p1668 A67-23010

10 p1723 A67-23697

13 p2144 A67-27187

14 p2338 A67-28674

18 p3067 A67-34572

19 p3245 A67-35728

19 p3307 A67-35812

20 p3488 A67-36915

20 p3470 A67-37390

23 p4018 A67-40787

24 p4176 A67-42470

24 p4176 A67-42470

24 p4176 A67-42470

24 p4176 A67-42470

24 p4176 A67-42470

24 p4176 A67-42470

24 p4176 A67-42470

24 p4176 A67-42470

24 p4176 A67-42470

24 p4176 A67-42470

24 p4176 A67-42470

24 p4176 A67-42470

24 p4176 A67-42470

24 p4176 A67-42470

24 p4176 A67-42470

24 p4176 A67-42470

organoboranes 03 p0454 A67-13421
Solid solubility of boron in graphite as function of temperature and nature of solution from density and lattice constants 12 p1960 A67-26189

BORON COMPOUND

Hollow-rib reinforced structure design from boron filament reinforced epoxy resin, describing fabrication equipment, techniques and test results 03 p0429 A67-13417
Boron fibers and reinforced plastic composites, noting mechanical and physical properties, application, etc 06 p1021 A67-18855
Refractive index of amorphous boron films determined from interference of transmission curves 16 p2734 A67-31884

BORON FLUORIDE

Detection of slow neutrons escaping from atmosphere by counters filled with boron fluoride onboard high altitude balloons 02 p0312 A67-12599
Formation heat of boron trifluoride measured by elements direct combination in bomb calorimeter 16 p2620 A67-31762
Solar neutron observations with boron fluoride counter on OSO-1, discussing absence of diurnal variation 23 p4061 A67-41236

BORON HYDRIDE

Ti, Zr and La boride thin films by chemical conversion of thin films of these metals with gaseous boron hydrides 02 p0287 A67-11715
Cryogenic stability, kinetics and energetics of lower boron hydrides explored with negative results, using mass spectrometry 10 p1603 A67-23385

BORON NITRIDE

Antifrictional properties of mica and boron nitride for use instead of graphite as solid lubricant in cermet packing materials 01 p0081 A67-11246
Boron nitride fibers in composites for aerospace application, discussing fabrication, ablative properties, etc 03 p0452 A67-13409
Synthesis conditions for materials of B-Al-N system determined by sintering mixtures of BN plus Al and AlN plus B powder in nitrogen atmosphere 03 p0456 A67-13544
Chemical stability of silver graphite, molybdenum disulfide, zinc oxide, boron nitride, muscovite and phlogopite mica solid lubricants 10 p1659 A67-22829
Wear lifetimes for three greases thickened with submicron boron nitride powder [ASLE PREPRINT 67AM 2C-2] 14 p2325 A67-28785

14 p2325 A67-28785

17 p2866 A67-33169

19 p3247 A67-35850

21 p3649 A67-37886

21 p3649 A67-37886

21 p3649 A67-37886

21 p3649 A67-37886

21 p3649 A67-37886

21 p3649 A67-37886

21 p3649 A67-37886

21 p3649 A67-37886

21 p3649 A67-37886

21 p3649 A67-37886

21 p3649 A67-37886

21 p3649 A67-37886

21 p3649 A67-37886

21 p3649 A67-37886

21 p3649 A67-37886

21 p3649 A67-37886

21 p3649 A67-37886

21 p3649 A67-37886

21 p3649 A67-37886

21 p3649 A67-37886

21 p3649 A67-37886

BOSE GEOMETRY

Hydrodynamic approximation of Green function for superfluid Bose system 18 p3029 A67-34386

BOSON FIELD

Intermediate vector bosons as unobservable particles described by renormalizable Lagrangian in indefinite metric space 13 p2161 A67-27578

BOTANY

Prolonged Chlorella cultivation with recovery of medium without impairing production rate 24 p4114 A67-41846

BOUNDARY

S FLUID BOUNDARY

S FREE BOUNDARY

S GRAIN BOUNDARY

S INTERFACE

S JET BOUNDARY

BOUNDARY CONTRACTION METHOD

Fourier integral and series approach to semiinfinite strip subject to general symmetrical tractions along three edges 08 p1422 A67-20978

BOUNDARY LAYER

SA COMPRESSIBLE BOUNDARY LAYER

SA DRAG

SA HYPERSONIC BOUNDARY LAYER

SA LAMINAR BOUNDARY LAYER

SA THERMAL BOUNDARY LAYER

SA THREE-DIMENSIONAL BOUNDARY LAYER

SA TURBULENT BOUNDARY LAYER

MHD boundary layer development on accelerated body treated by reducing partial to ordinary differential equation, using stream function 01 p0121 A67-10190

Approximate solution of stationary boundary layer problems involving flow of viscous incompressible conducting fluid around flat plate in presence of magnetic field 01 p0123 A67-10540

Optimal subsonic flow diffusers based on Walz laminar and turbulent boundary layer theory 01 p0006 A67-10648

Interaction between boundary layer and external inviscid flow, noting unsteady motion of gas around infinite plate and steady flow around semiinfinite plate 01 p0053 A67-10983

Experimental study of turbulent transfer phenomena in isobaric mixing layer of supersonic flow containing preexisting boundary layer [ONERA-TP-327] 01 p0054 A67-11003

Mass transfer and first order boundary layer effects on sharp cone drag [AIAA PAPER 66-33] 01 p0007 A67-11161

Simultaneous effect of transverse curvature and fluid injection on boundary layer flow over parabola of revolution, obtaining iterative solution to differential equation 01 p0055 A67-11175

Hydrodynamic tunnel wall effect on minimum cavitation number in axisymmetric cavitation flow around solids 02 p0232 A67-11631

Boundary layer equations for nonstationary plane flow of viscous incompressible fluid 02 p0232 A67-11921

Solution to boundary layer equations for unsteady flow of viscous incompressible fluid under injection or suction 02 p0233 A67-11948

Steady state heat balance on opaque inner wall of enclosure 02 p0343 A67-12413

Shock wave attenuation due to boundary layer effect calculated from initial pressure conditions in shock tube 02 p0235 A67-12564

Convective heat transfer in radiating gas, examining boundary layer equations and boundary conditions involving luminescence 03 p0532 A67-12866

Exact solutions to equations for compressible boundary layer in case of power-law dependence of initial profile of stagnation enthalpy on stream function 03 p0400 A67-12867

Heat transfer and centrifugal force effects on hypersonic inlet boundary layer and pressure recovery [AIAA PAPER 65-605] 03 p0350 A67-12910

Boundary layer effect on lift and drag characteristics of hypersonic lifting bodies 03 p0351 A67-12991

Solutions of nonstationary equations of plane laminar MHD boundary layer, using transformation to specialized form of curvilinear coordinates 03 p0477 A67-13527

Asymptotic representation of solutions for boundary layers near weak shock waves in

conical flows 03 p0352 A67-13631

Free convective boundary layer flows of electrically conducting fluid in transverse magnetic field 03 p0481 A67-13734

Boundary layer phenomenon in nonlinear membrane theory, investigating problem of closing hole in membrane having John strain energy density 03 p0525 A67-13823

Uniform wall suction effect on inlet flow of porous cylindrical tube, noting laminar to turbulent transition 03 p0404 A67-13973

Shock tube flow nonuniformity analyzed where shock and contact surface have maximum separation, applying results to turbulent and laminar boundary layer for heat transfer studies 03 p0397 A67-14027

Boundary layer type theory for compressible half-jet with aligned magnetic field 03 p0483 A67-14033

Boundary bending conditions for anisotropic plates with free, hinged or rigidly clamped edge 03 p0531 A67-14200

Boundary layer measurements of friction losses due to finite thickness of leading edges of turbine blades 03 p0353 A67-14306

Two-dimensional convective motion in rectangular cavity with vertical sides maintained at different temperatures, analyzing heat transfer 04 p0719 A67-14460

Apparent mass increase of sphere accelerated from rest and before boundary layer separation in cylinders of oil or water [ASME PAPER 66-WA/UNT-6] 04 p0601 A67-14483

Composite heat transfer in moving gray medium, obtaining solution based on boundary layer equations 04 p0722 A67-14712

V-I characteristics of stagnation point electrodes in lightly ionized atmospheric pressure plasma, calculating electric resistance from conductivity measurements 04 p0664 A67-14821

Exponentially decaying solution of Hartree as limiting solution for Falkner-Skan equation 04 p0604 A67-14830

Boundary layer structure between rarefied plasma and magnetic field, detailing mathematical formulation in relativistic invariant form 04 p0665 A67-15179

Boundary layer cooling by spattering of ablating liquid films [ASME PAPER 66-WA/HT-5] 04 p0726 A67-15445

Boundary layer equations for pseudoplastic fluids solved for exact numerical solutions, specifically near stagnation point 04 p0609 A67-15599

Local details of influence of vertical sound field on heat transfer from circular cylinder determined, using schlieren system 04 p0733 A67-15845

Heat transfer to laminar flow of radiation absorbing-emitting fluid across isothermal plate 04 p0737 A67-15866

Boundary layer problem in approximate solution obtained from multiparameter treatment 04 p0610 A67-15922

Radiation effects on heat transfer and friction characteristics in natural and forced convection film boiling in boundary layer flows [ASME PAPER 66-WA/HT-6] 04 p0739 A67-15939

Skewed boundary layers over body of revolution rotating in axial stream 05 p0747 A67-16218

Stress concentration for steep spherical shell with arbitrary elliptic hole 05 p0916 A67-16223

Difference approximation with second order accuracy of numerical solution for parabolic type equations 05 p0834 A67-16372

Matched asymptotic expansions method for perturbation problem of nearly equilibrium dissociating boundary layer flow 05 p0792 A67-16818

Terminal shock-boundary layer interaction on slender cone-cylinder payloads at supersonic speeds and resulting flow separation [AIAA PAPER 66-471] 05 p0924 A67-17213

Ion density profiles in boundary layers associated with supersonic flow of shock heated air over flat plate measured by cylindrical and flush-mounted electrostatic probes [AIAA PAPER 66-159] 05 p0856 A67-17345

Hydromagnetic compressible boundary layer flow past flat plate analyzed via von Karman integral method 05 p0794 A67-17361

Unsteady circular motion of viscous fluid

with hollow vortex, showing motion vorticality in boundary layer region on free surface 06 p0982 A67-17728

Inflow boundary layer effect on secondary flow at blade tips of circular cascade of reaction turbine, considering tip and gap losses 06 p0937 A67-17991

Plasma half-space impedance for diffusive electron reflection from plasma vacuum boundary, noting damping decrement of surface electromagnetic wave, electric field Fourier components and absorption capacity 06 p1039 A67-18079

Asymptotic method for solution of boundary layer equations for generalized three-dimensional flow of dissociated air at chemical equilibrium near stagnation point 06 p0984 A67-18113

Compressibility effect on dual solutions recurrence in MGD boundary layer over flat plate 06 p1041 A67-18134

Free vortex decay above stationary boundary for varying viscosity, determining plate boundary layer solution for small nondimensional radial distances 06 p0985 A67-18135

Base pressure behind supersonic vehicle, calculating existence conditions for wake solutions and location of stable and unstable singularities [AIAA PAPER 67-60] 06 p0986 A67-18269

Boundary layer thickness in air measured in presence of sound field, determining flow velocity distribution in layer 06 p0988 A67-18400

Reynolds number scaling theory for hypersonic ablation, deriving heat and mass transfer relationship [AIAA PAPER 67-155] 06 p1117 A67-18478

Nonequilibrium boundary layer problem solution by direct treatment of two-point boundary value problem [AIAA PAPER 67-219] 06 p0990 A67-18515

Electrically conducting boundary layer flow past flat plate in TM field 06 p1043 A67-18677

Ordinary differential equation in boundary layer theory of reversed flow 06 p1025 A67-18730

Magnification in profile drag of airfoil due to effect of pressure gradients on boundary layer downstream of isolated roughness element 06 p0990 A67-18748

Boundary layer theory of heat exchange in vortex region of separated flow past cylinder 06 p1119 A67-18821

Three-dimensional boundary layer flow of incompressible second order viscous fluid near spinning cone 06 p0992 A67-18868

Constant pressure turbulent jet mixing between two compressible nonisoenergetic streams of identical composition with finite initial boundary layer effects 06 p0992 A67-18880

Near wake uniqueness and criticality condition in Crocco-Lees mixing theory, obtaining critical point from boundary layer equations of motion [AIAA PAPER 67-65] 07 p1168 A67-19433

Effect of fairing contraction into two-dimensional supersonic nozzle for wind tunnel, avoiding pressure gradients along walls unfavorable to boundary layer flow development 07 p1126 A67-19630

Wind profiles obtained from meteorological tower plotting wind velocity, normalized by value of friction velocity, as function of measurement heights 07 p1220 A67-20002

Velocity jump characteristics of boundary layer with gradient pressure for flows at inlet channel and in wake of symmetric and asymmetric bodies 07 p1169 A67-20223

Application limit of inviscid small perturbation theory to secondary flow in cascade, comparing experimental and calculated vortex strength 08 p1275 A67-20406

Surface pressure, heat transfer coefficient, wave structure and shock disturbances of inviscid supersonic flow field along corner of intersecting wedges [AIAA PAPER 66-128] 08 p1276 A67-20564

Integral method to study surface chemistry interaction due to combustion and attendant mass transfer on isothermal graphite cone in nonsimilar boundary layer flow 08 p1320 A67-20570

Flow field in turbulent far wake at high Mach and Reynolds numbers, obtaining solution of boundary layer

- equations 08 p1277 A67-20577
Boundary layer development in throat region of converging-diverging nozzle, obtaining self-consistent solutions 08 p1277 A67-20589
Curvature effect on heat transfer for turbulent flow in curved pipes under constant heat flux, considering boundary layer existence along wall 08 p1426 A67-20926
Film cooling data correlation using boundary layer model 08 p1427 A67-20930
Approximate solution of some nonstationary boundary layer problems with allowance for magnetic field, discussing nonsteady flow of viscous incompressible electrically conducting fluid past flat plate 08 p1362 A67-21202
Theory of electrostatic probes in high pressure plasma, discussing ionization and recombination phenomena, diffusion boundary layer, spherical probe, etc 09 p1539 A67-21784
MHD of flows with hot electrons in MHD ducts at low magnetic Reynolds numbers, emphasizing boundary layer and shock wave theory 09 p1541 A67-21797
Auxiliary arc electrodes for solution to cold boundary layer and cathode emissivity problems in MHD 09 p1444 A67-21822
Airflow characteristics and heat transfer in right angle water-jacketed bend, measuring boundary layer profile at midbend 09 p1487 A67-21831
Two-dimensional problem for layer with mixed boundary conditions, obtaining solutions for Fredholm integral equations and relations for temperature distribution 09 p1580 A67-21994
Laminar and turbulent flow and heat transfer in boundary layer on continuous moving surface 10 p1732 A67-22728
Three-dimensional flow in supersonic stream in symmetry plane of region of shock boundary layer interaction in front of obstacle mounted on plate, noting penetration in separation region 10 p1590 A67-23026
Friction and heat transfer across boundary layer in external flow with transverse inhomogeneity calculated by mean-mass values method 10 p1625 A67-23041
Finite difference scheme for solving set of Prandtl equations for nonstationary flow of viscous incompressible fluid 10 p1628 A67-23672
Boundary layer behavior in fully ionized two-temperature plasma 11 p1840 A67-24670
Plane viscous problem of gas motion through weak straight line discontinuity of acceleration, noting formation of boundary layer 11 p1742 A67-24687
Space charge and eddy currents in ionized gas flow in MHD channel determined, showing effect of cold electrode boundary layer on electrical performance 11 p1746 A67-24874
Hydrodynamic boundary layer velocity profile on disks in transverse airflow analyzed theoretically and by wind tunnel tests 12 p1891 A67-25318
Electric current conduction between cold electrodes in shock-ionized air plasmas, noting current-voltage characteristics in flow behind shock wave 12 p1974 A67-25401
Linearized Crocco equation for zero pressure gradient and constant viscosity density product applied to boundary layer problem 12 p1929 A67-25907
Boundary value problems solution for bodies with rapidly varying elastic properties using boundary layer type equations 12 p2032 A67-26107
Atmospheric boundary layer dynamics models, similarity hypothesis and theories 13 p2151 A67-26687
Study of transfers in mechanics of single-phase fluids, Volume 2, Boundary layer, experimental results 13 p2222 A67-26736
Displacement and momentum loss thickness in boundary layer of rough flat plate at low velocities as function of wall roughness, pressure gradient, etc 13 p2095 A67-26809
Boundary layer of principal region of turbulent nonisothermal plane-parallel jet of real gas 13 p2095 A67-26885
Integration of boundary layer equations for axisymmetric body rotation in unbounded medium at rest 13 p2095 A67-26900
Coupled nonlinear equations integration in boundary layer theory with specific reference to heat transfer near stagnation point in three-dimensional flow 13 p2224 A67-27463
Heat transfer calculation to turbine blading in cascade in presence of secondary flow, considering flow velocity estimation, blade boundary layer and related heat transfer properties 13 p2225 A67-27465
Wind tunnel tests of sonic boom phenomena, noting weak pressure field measurement, construction of extremely small models, boundary layer effects, etc [AIAA PAPER 66-765] 13 p2091 A67-27594
Stratification similitude laws for liquid hydrogen determined and extrapolated to full size tanks from small tank data 13 p2186 A67-27643
Three-dimensional axisymmetrical boundary layer on spinning body of revolution in two-component fluid flow, discussing velocity distribution, drag and separation 14 p2295 A67-27835
Gas flow at high speed out of solid or liquid surface accompanied by heat transfer investigated for boundary shock wave occurrence 14 p2296 A67-27906
Pressure driven flow at high Hartmann number along annular channel between nonconducting circular cylinders 14 p2355 A67-27907
Flow visualization, discussing schlieren process in light of Toepler, fine focusing, microscopic, phase contrast and field absorption processes 14 p2315 A67-27974
Boundary layer equations reduced to ordinary differential equations without using self-similarity assumptions, noting friction-drag and heat-transfer coefficient along MHD channel 14 p2356 A67-27978
Pneumatic angular rate sensor performance characteristics, solving boundary layer equations for radial flow 14 p2318 A67-28340
Planar incompressible free turbulent mixing with arbitrary velocity ratio and axial pressure gradient [ASME PAPER 67-FE-9] 14 p2304 A67-28359
End wall effects in axial compressors related to displacement thickness of boundary layer theory, using computer program [ASME PAPER 67-FE-16] 14 p2242 A67-28364
Aerodynamic heating through turbulent boundary layer of flat plate determined using Ferrari formula 15 p2415 A67-29328
Analytical method, based on polarography, for measuring concentration of class of polymers in dilute aqueous solutions 15 p2433 A67-29676
Optimal final value control theory, applying variational calculus and functional analysis to control function selection for dynamic systems 15 p2459 A67-30020
Numerical solution of boundary layer equations by finite difference integration 15 p2473 A67-30189
Photographic spectra of ablating plastics in thermodynamic environments related to species and temperatures in boundary layers [AIAA PAPER 66-132] 15 p2582 A67-30206
Boundary layer problem concerned with effects of radiation absorption and emission for flow of high speed gas over flat plate [AIAA PAPER 66-521] 15 p2473 A67-30207
Boundary layer equations similar solutions obtained for incompressible flow with external velocity and suction 16 p2657 A67-30613
Boundary layer effect on thrust of small rocket engines with high expansion ratio nozzles 16 p2736 A67-30706
Motion of two parts formed by rupture of gas-filled vessel in vacuo 16 p2761 A67-30745
Model for radial and axial structure of geophysical vortices involving Boussinesq boundary-layer equations similarity solution in point heat source 16 p2778 A67-30949
Shock tube analysis of time dependent formation of supersonic flow near blunt bodies 16 p2592 A67-31102
Argon and nitrogen shock wave damping along tube in absence of effects of oscillation excitation, gas dissociation, ionization and emission 16 p2659 A67-31104
Boundary layer theory applied to solution of problems of combined heat and mass transfer, using approximate single-parameter integral method 16 p2594 A67-31202
Electric conductivity of flowing plasma, discussing boundary layer problem when measuring with immersed electrodes 17 p2900 A67-32343
Electrodeless device for currentless plasmoid generation noting flowing plasma conductivity, boundary layer phenomena and potential distribution 17 p2900 A67-32344
Nozzle and membrane effects on shock wave intensity in tube, showing graphically Mach number dependence upon initial pressure 17 p2837 A67-32345
Boundary layer effect on primary wave propagation and gas states behind reflected wave in shock tube with nozzle 17 p2837 A67-32346
MHD boundary layer theory principles, demonstrating similarity solutions existing in incompressible fluid 17 p2901 A67-32348
Heat transfer bibliography covering boundary layer, phase change, two-phase flow, channel flow, conduction, liquid metal, MHD, etc 17 p2969 A67-32450
Time lag effect on dynamic stability determined, using wind tunnel tests with 10 degree cone as test body simulating ablation process by gas injection into boundary layer [AIAA PAPER 66-757] 17 p2792 A67-33004
Gas ejection and boat-tailing effect on cylindrical afterbody in supersonic flow 17 p2793 A67-33041
Static/time-discrete/ electrical integrators for solution of boundary layer equations 17 p2821 A67-33080
Separation and stall of impulsively started elliptic cylinder including interactions between boundary layer and outer flow [ASME PAPER 67-APM-31] 17 p2840 A67-33157
Solution to boundary layer equations for unsteady flow of viscous incompressible fluid under injection or suction 17 p2840 A67-33265
Speed deficits of oxyacetylene detonation waves passing through MHD channel in electromagnetic field explained by Hall effects altering boundary layer 18 p3086 A67-33825
Stable deflection of homogeneous plasma stream by linearly increasing transverse magnetic field, neglecting particle collisions 18 p3087 A67-34036
Leakage current on insulating walls in MHD channel calculations, evaluating variable electrical conductivity in plasma boundary layer plasma boundary layer leakage current on insulating walls in MHD 18 p3088 A67-34061
Parameters of viscous supersonic compressible gas flow past corner, giving smooth coupling conditions for Navier-Stokes and boundary layer solutions 18 p3027 A67-34205
Various boundary layer parameters and transducer shape effect on Measurement error of random pressure field by finite size transducer 19 p3228 A67-34964
Boundary layer structure between rarefied plasma and magnetic field solved in relativistic-invariant form 19 p3288 A67-35369
Turbulent velocity fluctuations dynamics in and outside viscous sublayer examined by linearizing motion equation around known mean velocity profile 19 p3209 A67-35414
Flat plate continuum Langmuir probe ion density measurements, analyzing boundary layer and sheath of supersonic flow behind shock wave 19 p3296 A67-35590
Simultaneous heat and mass transfer in laminar free convection boundary layer at vertical surface with moving interface 19 p3346 A67-35613
Base bleed and initial boundary layer thickness effects on base pressure variations, calculating combining parameter for vehicle performance evaluation 19 p3172 A67-35779
Steady two-dimensional laminar flow of incompressible viscous fluid, noting asymptotic convergence of velocity profile in Prandtl boundary layer 19 p3212 A67-36031
Conductance and capacitance measurements on grain boundaries in p-type indium antimonide 20 p3504 A67-36173
Aircraft dynamics, Volume I, covering aircraft configuration, design problems, atmospheric properties, hydrodynamics, gasdynamics, boundary layer theory, etc 20 p3355 A67-36199
Revised London theory of superconductivity destruction by current, using numerical methods for optimum phase-

- boundary configuration 20 p3505 A67-36208
Optical system using moiré patterns to measure refractive index gradients in boundary layer, showing relation to temperature and density gradient [ASME PAPER 67-HT-3] 20 p3447 A67-36702
Thermal boundary layer theory for steady cellular convection in viscous rotating flow 20 p3553 A67-36937
Effect of energy redistribution between ion and electron components of plasma flow in nonuniform magnetic field, deriving relativistic and polarization corrections to classical theory 20 p3500 A67-37050
Stress field on epitaxial dislocation line in weakly alloyed titanium, calculating energy of phase boundary and contribution of latter to plastic deformation 20 p3467 A67-37117
Plane and axisymmetrical boundary layer characteristics computation, estimating transition region length 20 p3424 A67-37344
Boundary layer effect on mass flow parameter and ram efficiency of submerged intakes 20 p3360 A67-37490
Soviet book on boundary layer of non-Newtonian fluids covering hydrodynamics, heat transfer and mass transfer 20 p3424 A67-37546
Approximate solutions of Prandtl boundary layer problem for incompressible laminar flow derived, using Nagumo-Westphal theorem on parabolic differential operators 21 p3563 A67-37888
MHD channel wall boundary layer equations for low temperature plasma, determining friction and heat transfer coefficients and leakage current 21 p3665 A67-38241
Velocity profiles of boundary layer of conducting fluid rotating over stationary dielectric disk of infinite radius in magnetic field 21 p3665 A67-38246
Finite difference scheme for solving set of Prandtl equations for nonstationary flow of viscous incompressible fluid 21 p3612 A67-38273
Boundary layer of chemically reacting unstable gas flow along generatrix of body of revolution 21 p3564 A67-38423
Atmospheric boundary layer dynamics models, similarity hypothesis and theories 21 p3654 A67-38429
Current distribution and electron temperature profiles in nonequilibrium crossed field devices, considering nonuniformities, thermal diffusion, boundary layers and finite reaction rates effects [AIAA PAPER 67-715] 21 p3673 A67-38741
Insulator boundary layers in supersonic MGD channel noting heat transfer rate, current density, stagnation, pressure distribution and skin friction [AIAA PAPER 67-717] 21 p3673 A67-38743
Electromagnetic waves passage through thin radio-transparent layer solved by asymptotic series 21 p3585 A67-38810
Upstream influence ahead of weak uniformly moving shock or expansion wave incident on plane wall boundary layer 21 p3615 A67-39089
Position of real singular point of solution function of differential equation of Prandtl boundary layer theory 21 p3615 A67-39096
Transverse field growth studied for generation of magnetic field in boundary layer by currents along magnetopause produced by tangential solar wind 22 p3871 A67-39801
Vaporizing solid or liquid underlayers for transpiration cooling of reentry vehicles, discussing advantages, handling, storage and self-regulating system 22 p3901 A67-39934
Hypersonic boundary layer of sharp cone, considering boundary layer interaction with outer viscous flow 22 p3741 A67-40027
Shadow photography study of underexpanded nozzle ejected supersonic turbulent jet off-design behavior, discussing static pressure distribution, boundary layer and Mach number effect 23 p3928 A67-40732
Momentum equation integration to determine two mixing parallel subsonic streams interface 23 p3991 A67-41667
Nonequilibrium boundary layer problem solution by direct treatment of two-point boundary value problem [AIAA PAPER 67-219] 23 p3991 A67-41715
Shock waves and boundary layer structure near tip of slender cone in rarefied hypersonic flow, discussing surface pressure peaks 23 p3932 A67-41762
Papers on fluid mechanics and singular perturbations including Navier-Stokes equations, boundary layer theory, etc 24 p4141 A67-42167
Prandtl equation system for two-dimensional incompressible flows expanded to construct solutions for three-dimensional unsteady flows by straight lines method 24 p4177 A67-42200
Chemical reaction effect on viscous boundary layer of hypersonic flow of reacting gas mixture past blunt body 24 p4091 A67-42270
Cascade particles interaction functions with substance determined by inverse problem method 24 p4221 A67-42875
Flared afterbody aerodynamic characteristic predictions for aircraft stability at high Mach numbers, discussing turbulent separation 24 p4093 A67-42924
BOUNDARY LAYER COMBUSTION
SA REGRESSION
Turbulent velocity fluctuation field in isothermal boundary layer with homogeneous injection and combustion [AIAA PAPER 65-820] 01 p0054 A67-11169
Aerodynamics of diffuse combustion in laminar boundary layer of two plane-parallel accompanying flows, emphasizing flame structure 06 p1112 A67-17961
Convective laminar heat transfer to hypersonic vehicle, deriving similarity relations between stagnation temperature profile and mass fractions of chemical species 09 p1579 A67-21699
Propulsion-oriented subsonic boundary layer combustion research, discussing turbulent and diffusion-limited conditions, radiant heat transfer, chemical kinetics and transient phenomena 18 p3150 A67-33800
Boundary layer combustion in hybrid rockets from simplified model comprising convective transport and chemical kinetic factors, analyzing fuel regression rate [AIAA PAPER 67-471] 18 p3157 A67-33941
Transient nature of heterogeneous boundary layer chemical reaction at stagnation point studied analytically, deriving stability conditions 19 p3211 A67-35740
BOUNDARY LAYER CONTROL
SA FLUTTER
SA POROUS BOUNDARY LAYER CONTROL
Boundary layer flow having periodically distributed suction over permeable surface 01 p0052 A67-10794
Boundary layer control systems on Buccaneer S. Mk 1 and S. Mk 2 carrier-based strike aircraft 03 p0353 A67-12846
Boundary layer control system of Buccaneer carrier based combat aircraft for producing high lift coefficient at relatively low speed 04 p0552 A67-15541
Shock wave attenuation in shock tube in Mach 4 to 7 range, noting equipment used and results 05 p0791 A67-18433
Steady free convection in porous medium heated from below and accounting for end effects and mass discharge 06 p1113 A67-18127
Boundary layer suction in two-component fluid flow around plate solved by method of partial averaging 06 p0985 A67-18204
Flight experiments to assess stalling behavior and handling problems arising in design, maintenance and operation of suction wing for high lift [AIAA PAPER 65-750] 09 p1441 A67-22483
Boundary layer control for improvement of lift at lower angles of attack by carrier-based supersonic aircraft [AIAA PAPER 65-751] 09 p1441 A67-22484
Lift gain of flapped wing through use of wing-slot suction of friction layer near knee of flap 10 p1590 A67-22917
Lateral efflux from flow along wall into suction slot computed by conformal mapping contraction coefficient 10 p1627 A67-23559
Aerodynamic boundary layer control by blowing, considering problems of lift increase, airfoil properties, etc 11 p1741 A67-24101
Fluid dynamics and chemical phenomena near injector exit of idealized supersonic combustion burner, noting parameters of ignition delay length [AIAA PAPER 67-496] 18 p3158 A67-33960
Aerodynamic characteristics of wing profile employing boundary layer control by blowing with controllable jet 18 p2984 A67-34202
Air suction effect on moment characteristics of cranked slender profile, determining boundary layer control 21 p3564 A67-38043
Boundary layer control by suction at trailing edge to reduce profile drag of helicopter rotor blades 22 p3742 A67-40133
Airfoil and profiles theories emphasizing boundary layer theory, lift augmentation and wing aerodynamics 23 p3930 A67-41305
BOUNDARY LAYER FLOW
Statical electrointegrator for numerical solution of boundary layer theory problems for incompressible fluid and compressible gas 04 p0603 A67-14642
Convective heat transfer in accelerated heated air flows through cooled conical supersonic nozzles of three different configurations 04 p0723 A67-14837
Book on quantitative relationships for non-Newtonian systems, considering classification and fluid behavior of materials with anomalous flow properties 08 p1322 A67-21268
Core and boundary layer flows in large scale MHD generator, noting viscous friction and heat transfer at walls 09 p1442 A67-21793
Boundary layer at electrode and center of flow of plane MHD generator calculated numerically by one-dimensional theory for subsonic and supersonic velocities 09 p1443 A67-21808
Transverse fluid flow stability between permeable boundaries for case with exact solution of perturbation spectrum 10 p1628 A67-23675
Asymptotic analysis of radiative Rayleigh problem in flow of compressible viscous heat-conducting radiating gray gas extended to high plate Mach numbers 11 p1774 A67-23855
Thermal differential method of determining critical points in flow past projection in pipe 11 p1741 A67-24032
Turbulence research applicability to solution of internal flow problems 11 p1776 A67-24046
Optimum geometry for rectilinear diffuser with rectangular, conical or annular cross section noting flow regime, performance characteristics and boundary layer effect 11 p1741 A67-24050
Magnetofluid dynamics - AIAA Selected Reprint Series, Volume II 11 p1841 A67-24946
Free turbulent shear flows and bound turbulent shear layer flows 12 p1928 A67-25355
Vortical interaction between free jet boundary layer and outer flow in separation area of hypersonic gas flow past body 12 p1892 A67-25671
Solutions to Falkner-Skan equation, making similarity solutions for pressure gradient parameter physically acceptable 12 p1893 A67-25935
Existence, uniqueness, stability and approximation of solutions of Prandtl system for nonstationary boundary layer 13 p2093 A67-26603
Existence of three-dimensional solution of boundary layer equations of viscous incompressible flow in neighborhood of stagnation point 13 p2050 A67-26912
Thermal boundary layer equation reduced to ordinary differential equation for flat plate with given heat conductivity 13 p2224 A67-27048
Flow and heat transfer in viscous fluid layer expanding over rotating disk, calculating energy and motion equations 13 p2224 A67-27050
Viscous fluid flow stability in boundary layer on plate, applying perturbation method, calculating critical values of modified Reynolds numbers 13 p2105 A67-27051
Similarity solutions for two-dimensional unsteady compressible boundary layer equations using group theoretic methods 14 p2297 A67-28135
Boundary layer in nozzle of arc-heated wind tunnel, obtaining velocity, temperature and density profiles 14 p2299 A67-28171
Similarity solution to laminar boundary layer heat transfer from monatomic gas to cooled wall with no applied electric or magnetic fields [JPL-TR-32-1143] 15 p2523 A67-29219
Solution of nonlinear flow problems through parametric

- differentiation 15 p2469 A67-29221
- MHD boundary layer flow past semiminfinite plate, applying fluctuating magnetic field to plate 15 p2510 A67-29631
- Aerodynamic heat flux measurements in frozen boundary layer flows taken in hyperthermal wind tunnel, considering surface catalytic effects 15 p2468 A67-30154
- Generalized streamline hypothesis for turbulent boundary layer flow with spatial variation of viscosity 15 p2473 A67-30210
- Hypersonic weak and strong interaction theory for case of uniform flow past flat plate, discussing boundary layer characteristics 15 p2473 A67-30220
- Three-dimensional turbulent boundary layer flow over infinite swept wing calculated using entrainment and momentum integral equations 16 p2657 A67-30617
- Theory and supporting experimental results on application of small heated film for skin friction measurements in laminar and turbulent boundary layers 16 p2659 A67-30950
- Turbulent boundary layer with large acceleration parameter studied for flow and heat transfer coefficient [JPL-TR-32-1119] 16 p2659 A67-30953
- Shock tunnel experiments with hypersonic turbulent boundary layer flow over flat plates with blunt and sharp leading edges and wall of expansion nozzle 16 p2659 A67-30954
- Boundary layer in low speed flow over dispersively coupled system of acoustic resonators, noting excitation by flexible wall of oscillations 16 p2660 A67-31214
- Curved mixing layer measured for probability density of turbulent velocities at several positions in curved mixing layer 16 p2660 A67-31219
- Hydrodynamic stability problems solutions by numerical methods of Orr-Sommerfeld equations 16 p2661 A67-31419
- Mhd boundary layer at various reynolds numbers and magnetic reynolds number conditions mhd boundary layer at various Reynolds numbers and magnetic Reynolds number conditions mhd boundary layer at various Reynolds numbers 16 p2722 A67-31569
- Solution of MHD boundary layers with magnetic field as exponential function of x coordinate, extended to transverse magnetic fields 16 p2722 A67-31570
- Conrad-type probe used to determine, in boundary layer of flattened ellipsoid, mean velocity of flow 16 p2663 A67-31711
- Difference method of solving boundary layer equation for laminar suction boundary layer using Crocco form 17 p2790 A67-32260
- Flow behavior recognition techniques using changes in boundary layer velocity diagram to predict flow separation 17 p2792 A67-32908
- Incompressible fluid flow past semiminfinite flat plate during ejection of another fluid from plane surface into main flow solved using motion equations 18 p3025 A67-33571
- Differential and boundary layer equations for free convection flow along vertical hot wall, investigating existence question 18 p3027 A67-34009
- Turbulent boundary layer in liquid hydrogen tank, determining attachment point, velocity and temperature profiles 19 p3310 A67-34810
- Day-and nighttime electron and ion density profiles in lower ionosphere deduced from blunt probe theory and measurements 19 p3218 A67-35213
- Transition in oscillating boundary layer flows studied for various parameters effect 19 p3209 A67-35413
- Longitudinal surface curvature effects on steady, two-dimensional incompressible laminar boundary layers, noting partial differential equations, computer solution, velocity profile, etc 19 p3209 A67-35415
- Temperature distribution within two-dimensional thermal boundary layer due to flow of second order fluid past flat plate 19 p3210 A67-35447
- Flow of incompressible viscous fluid past plane body, when flow boundary layer detaches from body producing aerodynamic wake 19 p3171 A67-35632
- Binary laminar boundary layer equations with second order transverse curvature for hypersonic flow with mass injection of foreign gases into air 19 p3211 A67-35737
- Incompressible turbulent boundary layers with arbitrary pressure gradients and divergent or convergent cross flows predicted by effective viscosity hypothesis 19 p3211 A67-35738
- Mixing-length velocity profile in boundary layers with transpiration, discussing Tennekes theory and turbulent kinetic energy change rate 19 p3211 A67-35752
- Underexpanded jet boundary streamline calculations by exact and approximate methods 19 p3171 A67-35768
- Temperature dependent viscosity effects on heat transfer and drag on wedge-shaped body, calculating boundary layers on surface 20 p3421 A67-36824
- Thermally induced boundary layer flows in isothermal rigid body rotation 20 p3421 A67-36843
- Laminar compressible plane stationary boundary layer flow described by differential equations, including momentum and energy equations 20 p3424 A67-37280
- Boundary layer theory applied to laminar flow with chemical reaction, considering coolant blown through porous wall and wall reaction with laminar boundary layer 20 p3424 A67-37345
- Viscoelastic flow, examining boundary layer approximation for flat plate with zero angle of incidence 20 p3424 A67-37503
- Velocity field in axisymmetric boundary layer described by nonlinear partial differential equations 20 p3425 A67-37677
- Transverse fluid flow stability between permeable boundaries for case with exact solution of perturbation spectrum 21 p3612 A67-38276
- Boundary layer flow incident on smooth axisymmetric body in vicinity of critical point 21 p3613 A67-38422
- Parallel conducting flow along insulating pipe under applied magnetic field, elucidating singularities of Hartmann boundary layers 21 p3668 A67-38495
- Viscous dissipation effect on heat transfer rates for laminar boundary layer flow of gray gas across flat plate 21 p3732 A67-38878
- Curve approximation method applied to incompressible laminar boundary layer, comparing Head approximation method and exact solutions 21 p3615 A67-39081
- MGD boundary layer flow for thermally conducting flat plate, deriving equations for any heat transfer condition 21 p3675 A67-39090
- Boundary layer equation system for axial steady and unsteady flows past bodies of revolution 22 p3739 A67-39217
- Momentum, heat and magnetic field diffusion in viscous, thermal and magnetic boundary layers of different thicknesses in MHD fluid 22 p3850 A67-39721
- Laminar boundary layer gas flows over slender bodies with massive blowing, discussing integral method solution and theoretical model including pressure effect 22 p3739 A67-39935
- Integral relations method for nonequilibrium hypersonic planetary entry, emphasizing flow fields and thermal environment determinations for blunt body vehicle configuration 22 p3740 A67-39936
- Incompressible laminar boundary layer flow on semiminfinite flat plate with impulsive motion solved using Meksyn steady pressure gradient boundary layer method 22 p3786 A67-40039
- Surface mass transfer effects on viscous hypersonic shock layer of blunt body including suction and injection of air into air 22 p3743 A67-40417
- Electromagnetic forces effects on steady rotating motions of conducting viscous incompressible fluids via adjustable local boundary layer first order approximation 23 p4031 A67-40604
- Longitudinal wall curvature effect on boundary layer flow stability and generalization of Rayleigh theorems for nonviscous instability 23 p3992 A67-41733
- Two-phase flow equations for turbulent boundary layer flows, considering solid particle effects 23 p3993 A67-41748
- Boundary layer equation solution with constant pressure gradient restriction, discussing singularities nature 24 p4142 A67-42171
- Heat and mass transfer processes in reacting laminar boundary layer flow with steady high speed gas flow 24 p4143 A67-42284
- Mass efflux of Poiseuille flow over naturally permeable wall, discussing boundary layer effect 24 p4144 A67-42571
- Boundary layer theory in gas bearing lubrication problems, obtaining pressure asymptotic expansions for infinitely long slider squeeze-film bearing [ASME PAPER 67-LUB-7] 24 p4162 A67-42671
- Two-and three-dimensional laminar viscous boundary layer flow nonlinear partial differential equations solved analytically, studying difference equation substitution 24 p4145 A67-43087
- BOUNDARY LAYER NOISE**
- Linear correlation-detection transducer arrays for directional noise field signals, giving N-element coherent detector performance in propagating and turbulent boundary layer 22 p3801 A67-40233
- BOUNDARY LAYER SEPARATION**
- SA LAMINAR BOUNDARY LAYER SEPARATION**
- Instability and transition to turbulence in separated shear layer produced by laminar boundary layer separation from rearward-facing step, noting periodic spanwise structure 02 p0232 A67-11563
- Shear layer and internal flow arising from turbulent boundary layer separation and heat transfer over cavity 02 p0179 A67-12344
- Integral relations method applied to separation of laminar boundary layer on cooled hypersonic reentry body 02 p0179 A67-12348
- Nonstationary flow of gas in transverse magnetic field, noting electric conductivity dependence on compressibility and temperature 04 p0665 A67-15178
- Step-induced separation of low speed turbulent boundary layer in incompressible flow 06 p0985 A67-18132
- Laminar boundary layer separation and near wake flow for smooth blunt body at supersonic and hypersonic speeds [AIAA PAPER 67-62] 06 p0986 A67-18270
- Flow field model for laminar hypersonic near-wake in inviscid expansion, viscous sublayer and recirculating flow [AIAA PAPER 67-63] 06 p0940 A67-18353
- Supersonic laminar two-dimensional boundary layer separation in compression corner with and without cooling [AIAA PAPER 67-191] 06 p0940 A67-18361
- Suction requirements for elimination of turbulent boundary layer separation in adverse pressure gradient, based on mixing rate hypothesis and von Karman momentum integral [AIAA PAPER 67-197] 06 p0988 A67-18442
- Two-dimensional adiabatic laminar separated regions in supersonic flow, examining effects of blowing and suction at wall [AIAA PAPER 67-192] 06 p0988 A67-18459
- Taylor series expansion of stream function, pressure and temperature about separation or reattachment points used to calculate incompressible closed streamline flows of unknown shape [AIAA PAPER 67-64] 06 p0989 A67-18468
- Laminar, transitional and turbulent boundary layer flows with adverse pressure gradient on axisymmetric blunted conical flared body at Mach 10 [AIAA PAPER 66-493] 06 p0943 A67-18844
- Incipient separation prediction in shock boundary layer interactions 06 p0992 A67-18874
- Laminar boundary layer separation length data in hypersonic flow show strong Mach number dependence 06 p0992 A67-18878
- Cascade flow in axial transonic compressor, examining boundary layer separation condition 07 p1127 A67-20123
- Switching of supersonic gas jets in convergent-divergent duct by atmospheric venting, using phenomena of boundary layer separation 08 p1279 A67-20436
- Jet deviation by curved convex wall and Reynolds number explained as effect of boundary layer separation 08 p1320 A67-20450
- Internal flow analysis noting interaction with wall, frictional effects, boundaries and method of analysis 11 p1776 A67-24042
- Turbulent boundary layer on smooth flat wall, measuring skin friction, turbulence intensity, shearing stress, transverse integral scale, etc 11 p1776 A67-24045
- Separation and nonseparation of skewed boundary layer, considering two-dimensional

wing of finite aspect ratio at large angle of incidence 11 p1777 A67-24051

Conditions at head shock wave in viscous hypersonic flow past blunt body for study of boundary layer separation 11 p1741 A67-24157

Solutions to Falkner-Skan equation, making similarity solutions for pressure gradient parameter physically acceptable 12 p1893 A67-25935

Laminar boundary layer separation and near wake flow for smooth blunt body at supersonic and hypersonic speeds [AIAA PAPER 67-62] 14 p2240 A67-28112

Numerical analysis of boundary layer separation effect on evolution of wake, noting sensitivity to initial velocity profile 14 p2297 A67-28129

Mixing function parameter behavior in boundary layer separations by Crocco-Lees method, noting linearized Glick differential equations 17 p2840 A67-33031

Slip flow of incompressible viscous fluid past permeable infinite plate during fluid seepage into main homogeneous outer flow 18 p3023 A67-33419

Flow pattern at low Reynolds numbers about airfoil cascade illustrated by hydrogen bubble flow-visualization technique 20 p3359 A67-37483

Interaction between plane electromagnetic wave and separating boundary, considering electric field with component normal to boundary 21 p3581 A67-38292

Boundary layer separation onset and propagation in axial flow compressor stages, discussing guide vane results 21 p3566 A67-38911

Two-dimensional adiabatic laminar separated regions in supersonic flow, examining effects of blowing and suction at wall [AIAA PAPER 67-192] 22 p3786 A67-40096

Mean flow and motion turbulence characteristics after separation from conical afterbody for various initial boundary layer thickness and convergence angles 23 p3927 A67-40631

Buffet limit for aircraft wings in transonic region based on boundary layer theory, determining transonic pressure distribution and separation points 23 p3931 A67-41311

Perturbation solution to one-dimensional nonadiabatic temperature distribution behind detached shocks taking into account absorption effects 23 p3992 A67-41738

Shock refraction effects due to velocity and temperature gradients in rocket nozzles investigated by studying leading shock in two-dimensional secondary fluid injection 23 p3992 A67-41740

Hydrodynamic separation using compatibility conditions for Prandtl steady boundary layer equations at zero skin friction point 24 p4142 A67-42172

BOUNDARY LAYER STABILITY

Self-preserving flow in turbulent boundary layer passing over surfaces with different roughness 02 p0232 A67-11561

Total pressure losses in hypersonic wind tunnel with Eiffel chamber, calculating coefficient of pressure recovery 04 p0546 A67-14780

Characteristics of atmospheric convection, obtained by vertical and horizontal heat transport processes and represented by difference equation, used to derive analytical solution 09 p1491 A67-21553

Aspect ratio effect on cascade performances, noting complex variation of boundary layer thickness and changes in axial velocity ratio 09 p1437 A67-21742

Pressure gradients effects on boundary layers grown on wall of wind tunnel, obtaining equilibrium boundary layers of Clauser type 09 p1489 A67-22415

Rotating Ekman boundary layer stability and transition for two-dimensional roll vortices superimposed upon basic boundary layer flow 11 p1781 A67-24543

Behavior of solution of system of equations for unsteady boundary layer of two-dimensional liquid as time approaches infinity 11 p1782 A67-24669

Instabilities of Ekman layer measured using hot-wire anemometers 15 p2471 A67-29655

Bohm criterion of boundary layer stability related to ambipolar sound generation in positive column plasma discharge, deriving plasma density ambipolar potential distribution 17 p2905 A67-32972

Laminar boundary layer flow of water over flat plates, noting heat transfer effects on velocity profile stability [ASME PAPER 67-HT-41] 20 p3547 A67-38725

Numerical solution of compressible boundary layer stability equations including perpendicular flow velocity component terms 21 p3814 A67-38854

Inviscid instability of cylindrical two-dimensional free boundary layer vortex flow, using approximation by axisymmetrical vortex model 23 p3990 A67-41169

Laminar boundary layer subject to local three-dimensional disturbance, studying growth, flow field and transition to turbulence 23 p3991 A67-41175

Influence of sweptback wing leading edge geometry on boundary layer instability using supersonic flat plates 23 p3928 A67-41247

BOUNDARY LAYER TRANSITION

SA TURBULENCE

Shock tunnel study of effects of nose bluntness, angle of attack and boundary layer cooling on transition at Mach number 5.5 [AIAA PAPER 66-495] 02 p0177 A67-11514

Helium 2 film free convection heat transfer, discussing mathematical analysis for vertical flat plate and horizontal circular cylinder [ASME PAPER 65-WA/HT-10] 03 p0536 A67-14007

Geometric body profiles assumed by sphere and initially pointed cone during processes of ablation and shearing analyzed and combined to apply to sphere cones [AIAA PAPER 66-992] 03 p0353 A67-14145

Transitional immersed cylinder heat transfer measurements used in conjunction with theory of boundary layer transition to determine free-stream turbulence intensity 04 p0601 A67-14508

Pressure variational law effect along boundary layer of flat plate on formation of turbulent spots measured via hot-wire technique 04 p0602 A67-14598

Controlled three-dimensional roughness effect on hypersonic laminar boundary layer transition [AIAA PAPER 66-28] 04 p0547 A67-14819

Variation of transition Reynolds number with wall to recovery temperature ratio at hypersonic speeds, comparing transition measurements with and without Pitot tube 04 p0604 A67-14836

Tip bluntness, surface roughness and angle of attack effects on laminar boundary layer for 10 degree cone, measuring heat transfer and detecting transition 04 p0549 A67-15823

Free stream turbulence effects on boundary layer transition, discussing acoustical disturbance as source of velocity fluctuations 05 p0794 A67-17364

Hot-wire anemometer measurements of transition in incompressible wake of cone at low Reynolds number 05 p0751 A67-17439

Wind tunnel study of boundary layer transition structure on ogive nose cylinders aligned parallel to flow [AIAA PAPER 67-129] 06 p0939 A67-18314

Boundary layer transition measurements of contoured nozzle flow at hypersonic Mach numbers 08 p1320 A67-20584

Turbulent spots and wall roughness effects in shock tube boundary layer transition, noting stable region behind shock 08 p1322 A67-21382

Rotating Ekman boundary layer stability and transition for two-dimensional roll vortices superimposed upon basic boundary layer flow 11 p1781 A67-24543

Boundary layer transition displacement as function of nose bluntness, angle of attack and boundary layer cooling of half-angle cone [AIAA PAPER 66-495] 12 p1893 A67-25903

Transition sticking in wake of slender hypersonic cone as Reynolds number increases 12 p1893 A67-25927

Shape effects on hypersonic slender body wake geometry and transition distance 13 p2050 A67-26832

Transition delay and skin friction drag reduction by considering boundary layer flow over flexible aerodynamic surface [AIAA PAPER 66-430] 13 p2106 A67-27585

Skin friction drag coefficient at supersonic-hypersonic speeds as function of transition on delta wing 13 p2051 A67-27597

Hypersonic turbulent boundary layers transformation to incompressible

form 14 p2297 A67-28137

Natural boundary layer transition on ogive nose cylinders in zero and adverse pressure gradient analyzed for fluid dynamics, using smoke visualization 14 p2306 A67-29052

Transition functions occurring in diffraction theory of plane stratified medium with increasing refractive index 14 p2349 A67-29063

Laminar boundary layer transition in hypersonic shock tunnel of cone, noting effect of high Mach numbers and tip surface roughness, using surface heat transfer gauges [AIAA PAPER 66-494] 15 p2418 A67-30191

Wake from bluff bodies interaction with initially laminar boundary layer [AIAA PAPER 66-126] 17 p2793 A67-33005

Laminar-turbulent boundary layer transition over aircraft components measured by method using negative-temperature-coefficient resistors compared to hot wire measurements 19 p3230 A67-35573

Critical Reynolds number of laminar-turbulent transition for Newtonian flow in rectangular ducts to verify minimum in curve as function of duct aspect ratio 19 p3210 A67-35616

Transition region of hypersonic boundary layer on flat plate surveyed with hot wires, giving analysis for limited wire calibration 19 p3212 A67-35765

Gas-side heat transfer at high temperature combustor sonic points, discussing Reynolds number effect, boundary layer transitions, turbulence intensity, etc [AICHE PAPER 27] 20 p3552 A67-36831

Stability technique for gas flow past body impeding laminar-turbulent boundary layer transition via crossed electric and magnetic fields 21 p3686 A67-38251

Roughness induced boundary layer transition in supersonic flow over blunt bodies 21 p3614 A67-38891

Transitional and turbulent boundary layers on cold flat plate in hypersonic flow noting bluntness, Reynolds and Mach numbers effects 21 p3615 A67-39080

Effect of initial flow turbulence on optimum suction of fluid from boundary layer of porous plate 24 p4143 A67-42282

BOUNDARY LUBRICATION

Book on molecular physics of boundary friction on metal surfaces 03 p0429 A67-13333

Literature in 1965 on lubrication and bearings covering friction and wear, boundary, metal working, gear and spline lubrication, rolling element bearings, etc [ASME PAPER 66-WA/LUB-8] 04 p0629 A67-15349

Boundary conditions of journal gas bearings lubrication, studying slots effects 20 p3453 A67-36273

Lubrication and wear with reference to boundary lubrication, fluid and solid films, discussing dry and lubricated sliding and rolling theory 20 p3455 A67-37262

Lubrication and wear problems of surfaces of solid materials noting influence of contact area, adhesion, speed, etc, on friction 21 p3633 A67-38139

Frictional processes of metal surfaces under boundary lubrication conditions emphasizing initiation of seizure 23 p4010 A67-41063

Partial differential equation in lubricant pressure based on mixing-length theory, presenting full journal bearings in turbulent and laminar regimes 23 p4010 A67-41342

BOUNDARY VALUE

Propellant and time-optimum trajectories with thrust vector rotational velocity at flight beginning and termination taken as additional boundary condition analyzed, using maximum principle 01 p0146 A67-10209

Thermal stresses in isotropic circular cylinder under temperature distribution effect, reducing problem to solution of boundary value in form of Airy stress function 01 p0159 A67-10278

Temperature, stress and displacement in elastic bodies for random surface forces and randomly distributed environmental temperature 01 p0159 A67-10403

Behavior of stationary electromagnetic field produced by reflection of given incoming stationary field for small frequencies 01 p0024 A67-10523

Solvability of degenerated parabolic boundary value problem in Euclidean space

cylinder and relation to homogeneous Dirichlet problem 01 p0105 A67-10677

Uniqueness and stability theorems for BVP involving degenerated elliptic differential operator 01 p0105 A67-10678

Orthogonal expansions in physical boundary value problems characterized by homogeneous differential equation with inhomogeneous boundary data 01 p0106 A67-10734

Boundary value problem solution for sound generated at oscillating wall, propagating into half-space, for linear Boltzmann equation with general cut-off molecular potential 01 p0114 A67-10736

Asymptotic theory of elastic plate dynamics, deriving displacement equations and boundary conditions 01 p0162 A67-10822

Variational principles for plate bending problems not subjected to boundary conditions 01 p0162 A67-10850

Parabolic equation derivative solution applying results to boundary value problems, Cauchy problem and nonlinear equation 01 p0106 A67-10901

Normal burning velocity theory, considering Cauchy problem for initial equations 01 p0167 A67-10998

Discrete element technique applied to natural vibrations of deep spherical shells satisfying geometric and force boundary conditions 01 p0164 A67-11184

Mode transformation due to slightly tilted waveguide tube treated as boundary value problem 01 p0040 A67-11233

Solution properties of linear difference equations approximating differential equations in nonoscillation interval 01 p0107 A67-11251

Intrinsic electric field of rarefied ion-electron plasma in external magnetic field and plasma stability, noting use of Galerkin method to determine plasma layer slippage 01 p0126 A67-11299

Solution of boundary value problems describing two-dimensional flow in plastic regions 01 p0165 A67-11304

Integration of second order linear differential equation with boundary conditions of third kind by graphic method of Drymael 02 p0257 A67-11478

Method giving bounds for difference quotients, up to second order, of discrete function 02 p0258 A67-11555

Nonlinear Sturm-Liouville BVP with random forcing function 02 p0258 A67-11587

Point boundary value matching method calculation of current distribution in thin linear antenna 02 p0212 A67-11610

Free boundary problem for parabolic equation proving existence and uniqueness theorems for certain initial conditions 02 p0258 A67-11626

Point matching method, solving boundary value problem in uniform cylindrical waveguide with inserted conductor within conducting tube 02 p0193 A67-11781

Kantorovich theorem, Goodman-Lance method and two-point boundary value problems, noting numerical results obtained on IBM 7094 computer 02 p0259 A67-11836

Additional conditions for boundary value problem with directional derivative in heat conduction 02 p0259 A67-11920

Solution to boundary value problem of generalized moment theory of elasticity, determining mean displacement of microinhomogeneous elastic body 02 p0337 A67-11953

Solutions for boundary value problems of potential theory and elasticity theory for single cavity hyperboloids of revolution 02 p0338 A67-11955

Optical resonator theory stressing electromagnetic boundary value problem 02 p0267 A67-12026

Least squares gradient method for boundary value and optimization problems found in flight mechanics and astrodynamics 02 p0260 A67-12372

Cauchy and boundary value problems for homogeneous differential equations with two independent variables analyzed, establishing generalized solution existing on uniqueness maximal domain 02 p0260 A67-12432

Existence theorems for nonlinear boundary value problems 02 p0260 A67-12738

Existence of Green function and invariability of sign in some boundary value problems for equation $y'' + p(x)y' + q(x)y = f(x)$ 02 p0260 A67-12739

Existence and uniqueness theorem and upper and lower Chaplygin function approximations for solutions of Cauchy problem for quasi-linear first order PDE 03 p0456 A67-12884

Book on conductive heat transfer covering lumped, integral and differential formulations, two-and three-dimensional periodic functions, unsteady problems, Laplace transforms, etc 03 p0535 A67-13075

Qualitative theory of second order dynamic systems in plane and on sphere covering trajectories, equilibrium states and boundary values 03 p0390 A67-13109

Existence conditions for Green function of boundary value problem, determining and estimating subcritical intervals 03 p0457 A67-13114

Contour integral method applied to solution of three-dimensional mixed problem for second order parabolic equation under mixed type boundary conditions containing time differentiation 03 p0457 A67-13115

Variant of averaging functional errors method in solving linear integral boundary value equations 03 p0457 A67-13116

Generalization of Weber theorem for problems of coupled thermoelasticity, considering vibrations varying with time 03 p0523 A67-13502

Mathematical physics PDE problems solved by combined method using Fourier integral transform and theory of Riemann boundary value problem 03 p0459 A67-13589

Single layer potential solution to boundary value problems for heat equation in half-plane with one or two points of discontinuity in boundary conditions 03 p0459 A67-13590

Restrictions in method of solving boundary value problems for differential equations of elliptic type by reducing to difference problem 03 p0459 A67-13591

Nonlinear boundary value problem solution as applied to effect of uniformly distributed pressure and concentrated load on spherical dome 03 p0524 A67-13623

Stability of solutions for differential-difference equations with periodic coefficients, establishing necessary and sufficient criterion for boundedness of parameter 03 p0459 A67-13642

Boundary value problems of higher order equations in infinite regions, proving existence and convergence of solution for perturbed and unperturbed cases 03 p0459 A67-13643

Multimode surface waves for plane structures in generalized impedance boundary condition, noting electromagnetic field arising from magnetic dipole source located above plane structure 03 p0469 A67-13657

Nonsteady flow problems, solving fluid motion equations by characteristic method and obtaining boundary conditions 03 p0403 A67-13769

Boundary condition effect on buckling of circular shell of given thickness 03 p0524 A67-13786

Pointwise bounds for solutions of first initial boundary value problem for second order semilinear parabolic equation 03 p0460 A67-13821

Integral transform associated with boundary conditions containing eigenvalue parameter applied to initial boundary value problem arising in diffusion theory and heat flow 03 p0460 A67-13825

Existence theorem for periodic solutions to parabolic boundary value problem involving reduction to solvable operator equation 03 p0460 A67-13835

Asymptotic rate of convergence of Gauss-Seidel type iterative processes for nonlinear difference equations 03 p0460 A67-13881

Half-plane elliptic boundary value problems involving mixed boundary conditions solved by considering generalized Tricomi equation containing damped wave equation 03 p0461 A67-13942

Accuracy of central finite difference methods for solving boundary value problems in structural analysis governed by equations with variable coefficients 03 p0526 A67-13970

Heat transfer and velocity characteristics of thermal and hydrodynamic laminar flow in ducts of arbitrary cross section, considering boundary conditions at wall [ASME PAPER 65-WA/HT-13]

03 p0537 A67-14008

Radiative modes of thin infinitely long circular plasma cylinder with dipolar azimuthal field variations 03 p0484 A67-14044

Convergence of eigenfunction series expansion of nonself-conjugate boundary value problem in complex variables 03 p0461 A67-14060

Parabolic conditions for general second order PDE, discussing bicharacteristic condition, initial boundary value problem, Monge-Ampere equations and quasi-linear equation systems 03 p0461 A67-14105

Boundary value and contact problem solution using elasticity theory for transversely isotropic layer 03 p0529 A67-14165

Stress distribution in vicinity of end of crack moving steadily along boundary joining two elastic materials 03 p0529 A67-14167

Book on systematic and unified treatment of electromagnetic radiation from elementary Hertzian dipole in presence of dissipative half-space 03 p0373 A67-14273

General method of variations for univalent functions with bounded boundary rotation permitting study of extremum problems 04 p0643 A67-14583

First boundary value problem for thermal conductivity equation involving region with two angular points on boundary 04 p0721 A67-14661

Existence and evaluation of solution for periodic boundary value problem of set of ordinary differential equations 04 p0643 A67-14668

Smoothness of thermal potential and existence of solution for second and third boundary value problems with directional derivative for parabolic equation 04 p0721 A67-14669

Nonuniform network procedure for solving Dirichlet problem for Laplace equation in finite and infinite regions with canonical points 04 p0643 A67-14670

Nozzle exhaust plumes of rockets or supersonic ramjets with diffusion flames as source of UV radiation 04 p0721 A67-14702

Eigenvalue parameter in boundary conditions for elliptic equations degenerate in section of boundary 04 p0643 A67-14724

Strong solvability of Tricomi type boundary value problem for Chaplygin differential equation 04 p0643 A67-14727

Asymptotic characteristic of eigenfunctions of two-dimensional scalar wave equation with boundary conditions at equidistant curves 04 p0570 A67-14743

Transverse wave induced surface, compression and transverse waves in plasma, deriving expressions for amplitudes, phases and energies 04 p0663 A67-14744

Elasticity and shell theory solutions for long circular cylindrical shells compared by numerical analysis 04 p0709 A67-14811

Book on main linear boundary value problems for second order linear partial differential equations and systems of such equations satisfying ellipticity 04 p0645 A67-15006

Implicit difference methods for initial boundary value problems based on Wiener-Hopf factorization methods 04 p0645 A67-15085

Exact general integral for class of compressible fluids used in boundary value problems for nonlinear equations of gas dynamics 04 p0606 A67-15194

Elastic shells of revolution axisymmetrically loaded analyzed, using multisegment method for solution of boundary value problems governed by nonlinear differential equations [ASME PAPER 66-WA/APM-16] 04 p0713 A67-15407

Boundary value problems for semilinear bars made of coupled thermoelastic material solved by new functions that are corrections to classic tabulated functions [ASME PAPER 66-WA/APM-24] 04 p0714 A67-15412

In-flight bending moment and terminal drift minimization for flexible vehicle, applying two-point boundary value problem solution for optimum rigid body control system 04 p0706 A67-15422

E layer stratification, fine structure and boundary accuracy in frequency measurements based on seasonal variations in solar activity 04 p0618 A67-15574

Green function derived for heat

conduction along straight line with boundaries in steady motion 04 p0726 A67-15595

Phenomenological theory of mass transfer in binary systems near critical point applied to particular boundary value problems 04 p0727 A67-15683

Existence and uniqueness in first and second boundary value problems for nonlinear second order differential equations 04 p0647 A67-15742

Boundary value problems for ordinary nonlinear second order systems, noting subfunction definition and existence theorem 04 p0647 A67-15744

Pool film boiling based on cellular model, postulating time-averaged cell configuration to adjust itself to maximize rate of heat transfer 04 p0734 A67-15849

Optimum processes in systems with distributed parameters described by partial differential equations 04 p0647 A67-15874

Similarity constant variation method of aircraft design 04 p0552 A67-15892

Tension of homogeneous anisotropic elastic semiinfinite plate with rigid stiffener attached on segment of straight boundary 05 p0910 A67-16150

Upper and lower bounds of transverse vibrational frequencies of variable cross section cantilever bars, considering transverse shear and rotary inertia effects 05 p0910 A67-16151

Stress in helical corrugated shell under axial tension examined as boundary value problem of ODE in cylindrical coordinate system 05 p0914 A67-16215

Concentrated tensile stresses induced by concentrated external loads applied to boundary of filament winding rectangular strip plate 05 p0914 A67-16216

Zero moment boundary value problem of thin walled helicoidal shell in asymptotic lines 05 p0915 A67-16221

Approximate method for solving elastic equilibrium problems of shallow shells with holes, using computer algorithm 05 p0916 A67-16224

General elastic problem for some boundary conditions, determining coefficients via harmonic functions 05 p0916 A67-16227

Dynamic thermoelastic problem solution for body of revolution with cuts satisfying boundary conditions 05 p0810 A67-16228

Boundary value problem of hyperbolic equation with discontinuous boundary conditions 05 p0834 A67-16371

Slip and change in displacement vector in elastoplastic boundary value problems 05 p0918 A67-16424

Uniqueness and existence theorems for mixed problem of second order degenerate hyperbolic equation with discontinuous coefficients 05 p0834 A67-16494

High magnetic field effect on interband semiconductor laser, particularly electromagnetic modes and coupling and threshold current 05 p0822 A67-16673

Nonlinear boundary value problem with small parameter multiplying highest derivative 05 p0835 A67-16737

Lie series formalism applied to solution of Bessel equation describing behavior of laminary oscillating MHD fluid 05 p0854 A67-16989

Estimates of Green function in first boundary value problem of thermoconductivity equation for cylinder 05 p0927 A67-17002

Pointwise bounds for linear and nonlinear second initial boundary value problem of parabolic type 05 p0836 A67-17046

Shape and stability of liquid-gas interface in annular tank in force field determined by numerical integration of boundary value problem and eigenvalue [AIAA PAPER 66-425] 05 p0793 A67-17218

Optimum thrust programming for sounding rocket extended by reducing state to single variable to obtain sufficient conditions for specific extremal solution 05 p0906 A67-17225

Finite element method for problems in structural mechanics extended to beam vibration including shear and rotary inertia effects 05 p0924 A67-17284

Degeneration of solutions of well-posed systems of first order partial differential equations when particular parameter approaches zero 05 p0836 A67-17315

Boundary value problem solution via direct methods of approximate analysis 05 p0925 A67-17370

Boundary value problem for heat equation, discussing Laplace transform solution and uniqueness theorem 06 p1111 A67-17645

Book on methods of determining boundary conditions for unsteady state heat transfer 06 p1111 A67-17661

Linear supersonic conical flow past lower surface of triangular wing, obtaining homogeneous boundary value problem for analytical function of complex variable 06 p0936 A67-17739

Boundary value analysis of static problems of transversely isotropic solid and hollow elastic cylinders 06 p1099 A67-17864

Newton-Raphson method generalized for solution of two-point boundary value problems of nonlinear optimal control theory for digital solution 06 p0974 A67-17923

Two supercavitating flat plate hydrofoils near free surface with ensuing boundary value problem converted to mixed boundary value problem 06 p0984 A67-18126

Mathematical analysis of jet flap with high lift coefficient, solving numerically integral equation obtained from boundary value problem [AIAA PAPER 67-2] 06 p0938 A67-18247

Numerical method solution of nonlinear two-point boundary value problem associated with optimum transfer of spacecraft [AIAA PAPER 67-58] 06 p1023 A67-18267

Yielding and brittle cracking of orthotropic strip, using Wiener-Hopf technique and asymptotic method for isotropic case 06 p1102 A67-18317

Transient linear transfer problem solution via integral equations for corresponding boundary value problems 06 p1117 A67-18390

Book on mixed boundary value problems in potential theory 06 p1024 A67-18427

Numerical analysis of free boundary problem inviscid incompressible flow field of impinging jet and two-dimensional Joukowski airfoil in sheared wind tunnel flow [AIAA PAPER 67-217] 06 p0988 A67-18460

Nonequilibrium boundary layer problem solution by direct treatment of two-point boundary value problem [AIAA PAPER 67-219] 06 p0990 A67-18515

Estimating interval of nonoscillation of finite difference equation 06 p1024 A67-18556

Plane elastic problem for bodies with almost periodic fast oscillating elastic parameters, obtaining asymptotic solution for boundary value problems 06 p1106 A67-18625

Boundary conditions for two-dimensional steady heat flow in rectangular region with temperature discontinuity at corners 06 p1119 A67-18650

Boundary value problem for determination of stationary combustion regimes in semiinfinite combustion chamber 06 p1119 A67-18818

Error estimation for approximate solutions of differential equations, using functional analysis 07 p1213 A67-19153

Approximations to Navier-Stokes equations corresponding to steady two-dimensional incompressible viscous flow about circular cylinders 07 p1167 A67-19156

Well posed problems for PDEs, discussing continuous dependence and error bounds 07 p1213 A67-19158

Galerkin procedure for multipoint boundary value problems of general nonlinear systems 07 p1213 A67-19160

Certain properties of solutions to ordinary linear differential equations with bounded coefficients 07 p1214 A67-19178

Modification of functional scheme of Chaplygin method applied to solution of first boundary value problem for class of quasi-linear second order parabolic equation 07 p1215 A67-19220

Existence and uniqueness of 2k-fold continuously differentiable solutions to Dirichlet problem for nonlinear integrodifferential equations 07 p1215 A67-19476

Eigenfunction expansion of self-adjoint operator generated by elliptic differential boundary value problem with eigenvalue in boundary condition 07 p1215 A67-19581

Algebraic theory of finite systems of linear inequalities based on Minkowski theorem and boundary solution principle 07 p1216 A67-19582

Finite difference method solution of linear and nonlinear second order boundary value problems by reduction to matrices 07 p1216 A67-19628

Mixed boundary value problem of elasticity with parabolic boundary 07 p1263 A67-19732

Digital simulation of boundary value problems of trajectory optimization, using variational and functional analysis and IBM-FORMAC language [AAS PAPER 66-116] 07 p1149 A67-19976

First boundary value problem for general case of axisymmetric stressed state of body of revolution, using biharmonic solution of Love and Grodskil 07 p1264 A67-20037

Invariant imbedding and numerical integration of boundary value problem for unstable linear systems of ordinary differential equations 07 p1218 A67-20214

Monograph on creep and creep rupture as applied to aeronautics field noting problems in boundary and initial value, stability, stressed state, etc 07 p1264 A67-20301

Scalar wave equation of annular membrane for origin symmetric motion and arbitrary initial and boundary conditions 08 p1415 A67-20476

Partial differential equations for plate motion, considering transverse shear and rotary inertia, solved for plates bounded by elliptical and hyperbolic cylinders 08 p1416 A67-20489

Boundary value problem for potentials in volume conductor based on Green theorem 08 p1288 A67-20601

Soviet book on boundary value problems for analytic functions as applied to integral equations with Cauchy and Hilbert kernels 08 p1347 A67-20760

Monograph on integral equations covering Fredholm and Volterra equations, applications to theory of differential equations, properties of Cauchy type integrals, etc 08 p1348 A67-20761

Quasi-static and dynamic linear viscoelasticity boundary value problems and elastic wave propagation theory 08 p1419 A67-20882

Schauder type boundary estimates for solution of directional-derivative problem of parabolic equation in noncylindrical region 08 p1348 A67-21153

Stress distribution in elastic plate with circular hole, noting particular cases of general solution for simple boundary tractions 08 p1422 A67-21167

Truncated elliptic systems of partial differential equations for reducing two-point boundary value problems in vector space to initial value problems by projection 08 p1348 A67-21192

Galerkin method analysis of solvability of boundary value problems for second order quasi-linear elliptic differential equations with discontinuous coefficients 08 p1349 A67-21197

Mixed boundary value problem of flexure of elastic plate 08 p1422 A67-21201

Fredholm integral equation system for magnetic currents induced on wedge under impedance boundary condition 08 p1295 A67-21273

Boundary value problem for electrostatic field external to slender axisymmetric conductor 08 p1413 A67-21301

Soviet book on numerical solution of nonlinear boundary value problems for differential equation systems, determining eigenvalues and eigenfunctions 08 p1349 A67-21337

Boundary value problem for Poisson-Vlasov equations resulting from interaction of conducting body and supersonic flow of rarefied plasma solved, using iterative method 08 p1363 A67-21368

Initial and boundary value problems in compressible fluid flow with moving boundaries governed by Navier-Stokes equation 08 p1322 A67-21384

Rosen restricted variational principle used to obtain surface integral applicable to solution of kinetic theory boundary value problems 08 p1324 A67-21408

Discrete ordinate method for unsteady linearized Boltzmann Bhatnagar-Gross-Krook equation of rarefied gas flow 08 p1324 A67-21409

Large deflection of asymmetrically layered plate, using parametric expansion techniques to extract system of differential equations

governing scaling of stresses and displacement component for boundary conditions 09 p1574 A67-21756

Minimization of MHD generator duct with fixed boundary values as criterion in determining expansion shape 09 p1443 A67-21801

Generalization of Gaussian arbitrary constant sign curvature to shallow shells by introducing corrections in Lauricella-Sherman potentials 09 p1575 A67-21927

Closed form solution for tricom boundary value problem, noting application to transonic dynamics 09 p1524 A67-21929

Bending oscillations of hinged and clamped three-layer beams 09 p1575 A67-22219

Goursat problem for partial differential equation shown not to possess classical solution even under suitable hypothesis 09 p1525 A67-22624

Boundary value solutions for current density and radiation patterns in spiral excited sheath antennas in terms of Hankel function 09 p1482 A67-22696

Reflection of spherical shock wave from concentric spherical surface, using method of characteristics starting from initial boundary value problem 10 p1623 A67-22863

MHD channel flow under transverse electromagnetic field, analyzing effect of various geometries and boundary conditions 10 p1684 A67-22875

Boundary value problems for thin elastic plates, discussing flexural stresses in neighborhood of crack, bending, etc 10 p1715 A67-22915

Complex solution of equations in two-dimensional thermal stress theory applied to solution of boundary value problems 10 p1716 A67-22942

Relation of scattering matrix, Riccati equation and boundary conditions 10 p1673 A67-22964

Modified first boundary value problem for linear elliptic nonself-adjoint partial differential equation in two-dimensional plane 10 p1674 A67-23077

Stresses and displacements in small circular stress-free crack at interface between thick elastic incompressible layer and rigid foundation 10 p1717 A67-23082

Quasi-linearization determination of optimum finite thrust and impulsive orbital transfers 10 p1706 A67-23130

Field method application to linear differential equation for numerical solution of two-point boundary value problems in structural mechanics 10 p1679 A67-23147

Oscillations of plate in plane treated by finite difference method 10 p1721 A67-23645

Navier-Stokes equation solution in region with smooth boundary, using linear elliptic equations 10 p1675 A67-23676

Generalized reciprocity law relating behavior of elastic body and static and geometric boundary conditions 10 p1721 A67-23686

Deformation of laminated shell structures under axisymmetric loading, deriving differential equation by considering boundary conditions at both ends 10 p1731 A67-23846

Wave propagation in hot plasma in cylindrical waveguide with arbitrary axial magnetic field, treating boundary value problem by perturbation expansion 11 p1826 A67-23874

Scattering matrix equations for waveguide structure of varying surface impedance boundaries 11 p1751 A67-23968

Heat flux in rarefied gas calculated via transport equations, noting validity of boundary temperature discontinuities 11 p1881 A67-24028

Dual integral equation and dual series analysis and application to mixed boundary value problems in elasticity, hydrodynamics and electrostatics 11 p1812 A67-24150

Dual integral equations in elasticity theory, noting Mehler-Fok transformation of spherical functions, Fredholm equation and application to mixed boundary value problems 11 p1812 A67-24151

Conical shell stability under hydrostatic pressure for various in-plane boundary conditions, stressing axial restraint effect 11 p1873 A67-24214

Supersonic shear flow over cavity investigated, constructing velocity and shear stress coefficient profiles satisfying

boundary conditions 11 p1778 A67-24218

Approximate mode decomposition for treating boundary value problems for uniform compressible anisotropic plasma 11 p1753 A67-24307

Axisymmetric deformation of elastic slab with external crack interpreted as steady state problem of heat conduction 11 p1813 A67-24313

Free oscillations of plates, strips, rods and cylinders subjected to arbitrary dynamic edge load 11 p1874 A67-24314

Gas jet expansion near crossed axisymmetric channel, reducing problem to solution of Laplace equation for second-kind boundary conditions 11 p1779 A67-24321

Optimal solutions to mixed initial boundary value problems for control processes described by semilinear hyperbolic partial differential equations in two independent variables 11 p1770 A67-24423

Cartesian formulation of membrane theory, discussing equations of equilibrium, strain energy, variation formulation and boundary conditions 11 p1875 A67-24431

Existence and preservation of algebraic sign in Green function for two-point boundary value problem 11 p1813 A67-24519

Moisture transfer and thermal influx equations solutions for atmospheric boundary conditions of preinversion intramass strata evolution scheme 11 p1816 A67-24522

Elastic deformation of unbounded transversely isotropic body with internal plane circular slot under slot surface load 11 p1876 A67-24681

Green matrix estimates for homogeneous parabolic boundary value problems, showing proof of integral operator 11 p1813 A67-24850

Cauchy problem and mixed boundary value problem of linear and quasi-linear degenerate hyperbolic second order equations applied to cylinder 11 p1814 A67-24851

Bound solutions for elliptical equation in n-dimensional vector space obtained, using linear transformation into Martin boundary 11 p1814 A67-24852

Integral equations of second boundary value problem of equilibrium of elastic body of revolution, treating cylinder under pressure 11 p1878 A67-24877

Two-dimensional problem of thermoelasticity solved using analytic functions 11 p1879 A67-24885

Optimum distributed parameter system described by N-dimensional wave equation with unconstrained boundary control function 11 p1770 A67-24889

Analog computer applied to solve two-point boundary value problem for fourth order optimal control problem with applied Pontryagin maximum principle 11 p1771 A67-24893

Modified collocation method for linear boundary value problem for integrodifferential equation, giving approximate solutions which converge to exact solution 11 p1814 A67-25048

Series method of solving boundary value problems for nonlinear ordinary differential equations 11 p1814 A67-25050

Stress function boundary conditions along perfectly free edges of membrane-like disks and shells loaded by optionally distributed forces 11 p1881 A67-25096

Stress field in infinite plate with three circular holes under action of concentrated forces determined by solving associated boundary value problem 12 p2016 A67-25435

Boundary value problem solution by approximation method of Kupradze with differential operators and given and unknown functions 12 p1960 A67-25440

Boundary value problem for region with arbitrary smooth boundary solved, using second order degenerate elliptical equations 12 p1961 A67-25441

Boundary value problem of smooth closed contour dividing plane in inward and outward region solved by successive approximations 12 p1961 A67-25442

Approximate solutions for boundary value problems of cylindrical shells of arbitrary geometry 12 p2021 A67-25576

Stress-strain state of cylindrical shell analyzed based on elasticity theory, noting boundary value problem 12 p2022 A67-25583

Rigidly reinforced conical shell stability under external load investigated for

boundary conditions 12 p2027 A67-25622

effect Modified quasi-linearization method for numerically solving trajectory optimization problems with undetermined terminal time 12 p2008 A67-25913

Cylindrical partially filled waveguides of rectangular cross section, formulating boundary value problem and characteristic equation 12 p1906 A67-25980

Acoustic measurement method for following motion of solid-liquid interface, obtaining solution for transient heat conduction problem 12 p1946 A67-25985

Upper and lower bounds on distance between zeros of components of solutions of second order ordinary nonlinear differential equations 12 p1961 A67-26062

Generalized Bubnov-Galerkin-Kantorovich method for approximate solution of boundary value problem 12 p1962 A67-26106

Boundary value problems solution for bodies with rapidly varying elastic properties using boundary layer type equations 12 p2032 A67-26107

Fluid vibratory behavior in rigid containers, noting surface wave behavior governed by linearized boundary value solution 12 p1931 A67-26182

Discrete ordinate method for evaluating function described by particular integral applied to boundary value problems in gas kinetics 12 p1962 A67-26192

Wind and pressure fields diagnostic relations substituted for classical equation of stream function and solved as boundary value problem 13 p2149 A67-26273

Elasticity problems for bounded connected region consisting of finite number of rectangles solved by relaxation techniques 13 p2215 A67-26372

Fundamental solution of thermoconductivity equations for thin walled shallow shells and infinite plates with various instantaneous interval heat sources 13 p2221 A67-26374

Mixed problem for linear hyperbolic partial differential equation asymptotically represented and reduced to boundary value problem and Cauchy problem 13 p2144 A67-26377

First boundary value problem for second order elliptic partial differential equations, analyzing smoothness and continuity of generalized solution 13 p2144 A67-26378

Index and solvability of general linear boundary value problem for composite type system of equations 13 p2144 A67-26380

Uniqueness of quasi-regular solution to boundary value problem for Chaplygin equation 13 p2145 A67-26444

Vibration characteristics and fundamental frequency of circular plate with arbitrary cross section reinforcing ring 13 p2216 A67-26534

Surface temperature of one-dimensional homogeneous thermally isotropic body impervious to radiation 13 p2222 A67-26610

Finite length inductive MHD generator, solving inlet and outlet effects on boundary value problem 13 p2165 A67-26613

Lower bounds for periodic solutions of steady state hydrodynamic boundary value problem 13 p2093 A67-26617

Spacecraft guidance problem, examining general and one specific solution using boundary value problem and correction function 13 p2153 A67-26620

Thin elastic plate with uniformly distributed load over area and Navier condition on edge solved for deflection 13 p2217 A67-26631

Method of characteristics used in solving nonlinear boundary value problem of thickness of delta wing with transonic leading edge 13 p2049 A67-26646

Axisymmetric problem in elasticity for simply connected body and elastic space containing axisymmetric cavity 13 p2218 A67-26687

Differential equation and boundary conditions for sandwich shells, noting bending resistance and shear deformation 13 p2219 A67-26906

Potential flow about two-dimensional hydrofoils with zero velocity boundary condition 13 p2095 A67-26910

Discrete ordinate method for boundary value problems in gas dynamics using differential equations yields solutions to Couette flow 13 p2101 A67-26962

- Numerical solution of initial and boundary value Rayleigh problems for nonlinear Krook equation at large wall velocities 13 p2102 A67-26968
- Rarefied multicomponent gas flow boundary conditions over subliming wall determined through Navier-Stokes approximation, noting distribution function of each component 13 p2105 A67-27054
- Heat conduction equation for inhomogeneous body, obtaining integrable solutions applicable to boundary value problems 13 p2224 A67-27055
- Temperature field in plates and shallow shells with internal heat sources noting solutions for various boundary conditions 13 p2224 A67-27056
- Continuation in shooting methods for two-point boundary value problems 13 p2146 A67-27146
- Elliptic regularization for symmetric positive system of linear first order partial differential equations with irregular boundaries 13 p2147 A67-27178
- Characteristic initial value problem for linear second order hyperbolic partial differential equation 13 p2147 A67-27180
- Boundary value problem for differential equations of perturbed satellite motion assuming perturbing accelerations defined by Vinti potential 13 p2200 A67-27323
- Boundary imperfections in buckling of clamped spherical caps 13 p2220 A67-27452
- Stability of solutions of Navier-Stokes equations for boundary value problem and convergence to steady state 13 p2106 A67-27455
- Numerical solution of boundary value problem for quasi-linear equation 13 p2148 A67-27498
- Digital simulation of boundary value problems of trajectory optimization, using variational and functional analysis and IBM-FORMAC language [AAS PAPER 66-116] 13 p2074 A67-27531
- Boundary value problems involving shallow cylindrical shells of given arbitrary configuration solved, using Vlasov moment theory 14 p2395 A67-27837
- Solution algorithm for boundary problem generated by necessary conditions for optimality in variational problem 14 p2341 A67-27840
- Plastic buckling of eccentrically stiffened circular cylindrical shells 14 p2399 A67-28121
- Transient vibration of viscoelastic body, showing dynamic displacement expression in terms of static boundary value problem 14 p2400 A67-28143
- Collisionless plasma flow around conducting sphere in uniform magnetic field 14 p2357 A67-28206
- Self-consistent distribution theory of charged particles and electric potential in wake of conducting body moving rapidly in rarefied plasma 14 p2357 A67-28208
- Heat equation for free boundary problem with prescribed flux at fixed and melting interface of semilinear slab 14 p2405 A67-28255
- Difference method for solution of plane problems in dynamic elasticity, noting equations of dynamic/elastic deformations under plain strain conditions 14 p2400 A67-28256
- Fourier series solutions of boundary-value and mixed problems in mathematical physics by integrating partial differential equations 14 p2348 A67-28287
- Linearization of equation of thermal explosion and stability of solutions for boundary conditions of third kind 14 p2406 A67-28310
- Two-dimensional mixed boundary value problem of heat and mass transfer with characteristic equation containing multiple roots 14 p2406 A67-28312
- Inertial criterion relation for determining effect of mass transfer, phase transformation, and Kossovich number on heat and mass transfer 14 p2406 A67-28313
- Characteristic momentary pictures of two-dimensional electromagnetic wave fields with all boundaries conformally transformed into parallel planes, taken from motion picture 14 p2268 A67-28447
- Macroscopic linear fluid model of plasma radiation and scattering restricted to bounded media, emphasizing physical interpretation of wave constituents 14 p2359 A67-28463
- Theory of nonself-adjoint ordinary second order differential operators, discussing solution algorithms 14 p2343 A67-28478
- Theory of singular integrodifferential operators on compact manifolds, discussing basic principles, concept of uniformly nonelliptic systems, etc 14 p2343 A67-28503
- Constant and variable coefficient initial and boundary value problems for second order differential equations 14 p2343 A67-28626
- Majorizing functions for Dirichlet problem in n-dimensional space 14 p2343 A67-28631
- Necessary and sufficient conditions for solvability in two-space of second order elliptic differential equations with smooth irregular continuous differentiable boundary 14 p2344 A67-28634
- Mutually adjoint boundary value problems for linear systems of first order equations of composite type with two independent variables 14 p2344 A67-28670
- Influence coefficients for stresses at circular holes in shallow cylindrical shells with both flat and curved reinforcements [AIAA PAPER 67-365] 14 p2401 A67-28733
- Steady state heat conduction approximation solution based on effective boundary conditions 14 p2408 A67-28805
- Uniqueness of solutions for Cauchy problem and some boundary value problems of general parabolic systems in class of increasing Holder functions 14 p2344 A67-28894
- Dual formulation of variational problems with differential inequality constraints, noting relation between mathematical programming and variational calculus 14 p2345 A67-28908
- Uniqueness theorems for Adler fourth and fifth boundary value problems for heat conduction differential equation 14 p2409 A67-28936
- Vaporization under laser radiation in terms of gas-dynamics, formulating boundary conditions 14 p2334 A67-29074
- Necessary and sufficient conditions for boundary of absolute stability domain of nonlinear automatic control systems 15 p2455 A67-29120
- Boundary perturbation theory in electromagnetism noting application to conducting sphere with surface perturbation 15 p2435 A67-29186
- Solving three-dimensional electrostatics problems with mixed boundary values by reduction to standard Fredholm integral equation 15 p2522 A67-29196
- Boundary conditions for Navier-Stokes equations in rarefied monatomic gas with distribution function given a priori 15 p2470 A67-29234
- Boundary value problems of continuous dislocation theory reduced to elasticity theory, deriving Green formula for internal stresses 15 p2572 A67-29235
- Monte Carlo method applied to heat conduction problems, discussing steady state and transient situations with linear and nonlinear boundary conditions [ASME PAPER 65-WA/HT-1] 15 p2578 A67-29318
- Stationary functionals construction for linear boundary value problem solution or solution derivatives at specified but arbitrary point 15 p2509 A67-29383
- Parameter and domain dependence of eigenvalues of elliptic partial differential equations 15 p2509 A67-29461
- Statistical model for size effect in electrical conduction 15 p2517 A67-29485
- Finite difference solution of third boundary value problem for heat conduction equation, obtaining conditions for coefficients from stability requirements 15 p2510 A67-29521
- Finite difference method solution of periodic parabolic problem solution subject to nonlinear boundary condition 15 p2510 A67-29522
- Barrier-layer FET frequency behavior solved, deriving inner transistor quadrupole parameters by way of boundary value problem 15 p2447 A67-29644
- Fractional powers of operators applied to boundary value problems of quasi-linear elliptic equations 15 p2510 A67-29661
- Small parameter method to study steady state flow of viscous incompressible fluid in journal bearing 15 p2493 A67-29692
- Interaction of supersonic gas stream with inclined surface, calculating parameters and boundary of fluid spreading 15 p2472 A67-29776
- Stability boundaries and critical frequencies for semilinearly elastically restrained plate determined at different boundary stiffnesses 15 p2575 A67-29858
- Transformation of class of boundary value to initial value problems in terms of one-or two-parameter group of transformations for ordinary differential equations 15 p2511 A67-29892
- Unique iterative solution to degenerate quasi-linear elliptic equations and systems 15 p2511 A67-30001
- Perturbation method for solution of linear matrix differential equations subject to initial and two-point boundary conditions applied to transmission lines 15 p2511 A67-30018
- Vibrations of helicopter rotor in Cardan suspension, dividing problem into three boundary value setups with special conditions at hub 15 p2576 A67-30175
- Exact solution of three-dimensional problem to derive algorithm for development of applied theories of improved accuracy for circular cylindrical shell 15 p2576 A67-30179
- Bulk elastic deformation of continuous medium with coaxial stress-strain deviators, analyzing deformations in body with specified boundary conditions 15 p2576 A67-30181
- Holzer method extended to analysis of free vibration of spherical shells, solving boundary value problem as set of initial value problems until all boundary conditions can be satisfied 15 p2577 A67-30193
- Arc operation under nonsteady electrical inputs noting initial conditions, energy equation solution, temperature profiles, application of Green function for moving boundary problem, etc [AIAA PAPER 66-480] 15 p2531 A67-30204
- Flat plate, simultaneous heat and mass transfer for Newtonian fluids in free convection analyzed, using group theory 15 p2582 A67-30217
- Numerical techniques for process identification in automatic control systems, discussing methods such as autocorrelation, spectral density, differential approximation, etc 15 p2460 A67-30310
- Effect of magnetic field gradients at inlet and outlet on linear two-dimensional induction MHD generator calculated by bilateral Laplace transform 16 p2605 A67-30579
- Polynomial substitution formulas for complicated equations of multipoint boundary value and optimization problems in flight mechanics and astrodynamics 16 p2695 A67-30733
- Boundary conditions for thin shells and physical meaning analyzed according to Kirchhoff-Love theory 16 p2764 A67-30862
- Fluctuating function method for approximate solution of boundary value problems for linear differential equations with reduced variational problems 16 p2696 A67-31013
- Numerical solution of nonlinear integral equations with variable upper limit, applicable to Cauchy and boundary value problems 16 p2696 A67-31142
- Index formula of boundary value problem for system of two harmonic functions 16 p2696 A67-31143
- Steady state heat flow and temperature fields in flat rectangular configurations with mixed boundary conditions 16 p2779 A67-31206
- Solution of uniform heat conduction equation with movable boundaries applied to problem of electric contacts 16 p2779 A67-31207
- Hilbert boundary problem extension for flexural problems of cracks in mixed media, noting Cauchy integrals, Plemelj formulae, etc 16 p2770 A67-31292
- Numerical methods for elliptic partial differential equations with coefficients singular on boundary portion, constructing barrier functions and establishing existence and convergence theorems 16 p2697 A67-31330
- Monotone iterations for nonlinear elliptic differential equations in boundary-value problems applied to Gauss-Seidel

methods 16 p2697 A67-31331
 Pointwise bounds for solution of Cauchy problem for nonlinear and linear elliptic system, noting application to biharmonic equation 16 p2697 A67-31422
 Boundary conditions influence on flutter critical boundary character considering nonlinearities of physical nature 16 p2776 A67-31471
 Stabilization method for solution of boundary value problems for second order nonlinear ordinary differential equation 16 p2698 A67-31482
 Incoherent scattering of plane electromagnetic waves on cylindrical plasma column with fluctuating charge-density 16 p2628 A67-31499
 Optimization of numerical solution to linear ordinary differential equation with homogeneous boundary value conditions 16 p2698 A67-31546
 Suboptimal control function sequence generation by combining approximation in control policy space with stability criteria from direct method of 16 p2648 A67-31658
 Liapunov 16 p2650 A67-31670
 Optimal trajectories for linear discrete system with respect to minimax criteria using standard programming code 16 p2652 A67-31687
 Solvability and methods of solution of boundary value problems noting uniqueness, potential theory application in solving polyharmonic equations and second-order equation 16 p2698 A67-31737
 Boundary value problems containing positive linear differential operators and monotone functions of dependent variable analyzed via nonlinear heat generation 17 p2967 A67-32040
 Iterative procedure for solving linear differential equations with given boundary conditions on analog computer 17 p2818 A67-32296
 Cesium thermionic converter extinguished-mode operation theory, deriving expressions for forward and reverse saturation output current densities and open circuit voltages 17 p2803 A67-32365
 Voltage gradient determination throughout two-dimensional electric field by electro-optic analog, noting applicability to boundary value problems satisfying Laplace equation 17 p2818 A67-32418
 Method of finite integral transforms as format for employment of incomplete eigenfunctions, discussing application of equilateral transform 17 p2876 A67-32423
 Radiation conditions for derivatives of radiating functions, omitting prescribed asymptotic behavior 17 p2877 A67-32562
 Fabry-Perot resonator excitation using integral equations corresponding to boundary value functions 17 p2868 A67-32667
 Linear boundary value problem solution using iterative method 17 p2877 A67-32678
 Periodic solution of boundary value problem involving motion equation of viscous fluid 17 p2838 A67-32681
 MHD flow, deriving equation system and boundary conditions for gas dynamic process 17 p2903 A67-32682
 All Markov transition functions in denumerable state space satisfying prescribed initial condition with given matrix 17 p2878 A67-32734
 Martin boundary for invariant Markov processes investigated on group of affine transformations of straight line 17 p2878 A67-32736
 Bounded solutions of boundary value problem with skew derivative studied by probability methods 17 p2878 A67-32737
 Boundary value problem of linear partial differential equation reduced to linear equation system with block-tridiagonal matrix by difference approximation 17 p2820 A67-32801
 Contour integral representation of eigenvalues of first boundary value problem of elasticity theory 17 p2962 A67-32832
 Soviet papers on mathematical physics covering solution of boundary value problems, structural analyses, etc. 17 p2884 A67-32867
 Iterative solution of boundary value problem for optimal trajectory, applying

smoothing procedure 17 p2830 A67-32869
 Steady state temperature field of uniform body containing heat sources, examining nonlinear boundary value problems of unsteady thermal radiation 17 p2971 A67-32870
 Critical compressive forces causing instability of rigidly-fastened rectangular plate determined by method of summary representations 17 p2962 A67-32871
 Mixed boundary value problem for x-analytic function solved through Fredholm integral equation of second kind 17 p2879 A67-32872
 Iterative solution through boundary value problem and integral equations for axisymmetric deformation of body remote from symmetry axis 17 p2962 A67-32874
 Boundary value problem solution for three-dimensional layer in axisymmetric case 17 p2885 A67-32882
 Analytical solution for sloshing of liquid in vessel of complex geometry using homogeneous boundary condition 17 p2839 A67-32886
 Exact linear elastic analysis of end effect problems for isotropic cylinders 17 p2963 A67-33019
 Limiting value calculation for temperature field criteria, analyzing heat-conduction equation solution and boundary value problems 17 p2972 A67-33068
 Numerical methods for solving thermal explosion and combustion problems on electronic computers, examining Cauchy problems solutions 17 p2973 A67-33075
 Radiation from array of parallel plate waveguide with thick walls excited by TEM modes 17 p2828 A67-33085
 Mass, momentum and energy conservation at wave fronts in coupled thermoplasticity, noting propagation velocities for isothermal/adiabatic discontinuities 17 p2964 A67-33134
 Boundary value problem for electrical potential and ion distribution function obeying Poisson-Vlasov equations when applied to rarefied plasma disturbance by supersonic body 17 p2909 A67-33205
 Solution to boundary value problem of generalized moment theory of elasticity, determining mean displacement of microinhomogeneous elastic body 17 p2965 A67-33270
 Solutions for boundary value problems of potential theory and elasticity theory for single cavity hyperboloids of revolution 17 p2966 A67-33272
 Interaction between gliding contour and ideal fluid flow 18 p3022 A67-33413
 Unsteady temperature field of thin cylindrical shell of finite length determined, using quadratic trinomial form 18 p3145 A67-33570
 Interpolation methods for solving nonlinear algebraic/transcendental equations applied to maximum principle boundary value problems 18 p3071 A67-33679
 Temperature range approximation determination in unsteady thermal boundary layer formed in plane parallel flow around body, solving equation with boundary conditions 18 p3025 A67-33680
 Vacancy source and sink effect on behavior of nonequilibrium concentration of vacancies in diffusion region during creep process 18 p3141 A67-33768
 Bending oscillations of hinged and clamped three-layer beams 18 p3141 A67-33770
 Stress analysis of loaded boundaries in two-dimensional second boundary problems, studying mechanical and thermal strain, knife-edge device, etc. 18 p3142 A67-33899
 [SESA PAPER 1194]
 Transient heat conduction in inhomogeneous solids with periodic temperature boundary conditions, using Keller perturbation method 18 p3159 A67-34007
 Differential and boundary layer equations for free convection flow along vertical hot wall, investigating existence question 18 p3027 A67-34009
 Electromagnetic wave scattering from plasma wave analyzed using Vlasov equations for anisotropic plasma, applying formulas to boundary value problems 18 p3088 A67-34090
 Neumann boundary value problem for second order elliptic equation system with

many independent variables 18 p3071 A67-34169
 Axisymmetric mixed boundary value problem for solid elastic cylinder under torsion 18 p3144 A67-34173
 Supersonic fluid flow past elliptical and circular conical bodies at large angles of attack, using straight line method 18 p2984 A67-34211
 Combination variational-difference numerical method applied to nonlinear boundary value problems, noting numerical functional minimization 18 p3071 A67-34264
 Nonlinear hyperbolic equation solution formulation based on Riemann invariants 18 p3072 A67-34288
 Vector wave functions for boundary value problems in compressible plasma for spherical geometry, noting Fourier series, acoustic wave, etc. 18 p3090 A67-34382
 Existence theorems for defining solubility of certain boundary value problems for ordinary second order linear differential equation 18 p3072 A67-34384
 Infinitely small bending deformations of convex surfaces with boundary condition of generalized slp, formulating boundary value problem for bending of surface 18 p3144 A67-34482
 Cauchy type integral applied to second boundary value problem for elastic plane with doubly periodic system of identical holes 18 p3145 A67-34601
 Existence and uniqueness of solutions of point boundary value problem for denumerable system of differential equations 18 p3073 A67-34606
 HF backscattering from absorbing infinite strip with arbitrary face impedances 18 p3005 A67-34730
 Pulse-width modulated control system optimization, with necessary conditions derived by variational calculus, and numerical solution to resulting boundary value problem 19 p3199 A67-34783
 Dirichlet problem solution for Poisson equation on rectangle with smooth boundary values, using higher order differences 19 p3249 A67-34794
 Parametric expansions in linear theory of cylindrical shells noting loading and boundary conditions, approximation formation, fiber elongation, etc. 19 p3339 A67-35054
 Self-consistent model for cathode region of high pressure arc, showing application to 200 amp arc in argon and boundary condition matching 19 p3279 A67-35138
 Boundary value wave problem in elastoviscoplastic medium solved by approximate method using Courant concept 19 p3340 A67-35444
 Intrinsic frequencies and modes of periodic free vibrations of homogeneous beam with weakly nonlinear boundary conditions of Duffing type 19 p3340 A67-35509
 Current distribution on cylindrical dipole antenna in homogeneous warm plasma 19 p3194 A67-35515
 Short-slit directional coupler functioning mode via boundary value problem indicating Chebyshev behavior of transfer coefficient and wideband subdivision 19 p3195 A67-35560
 Electromagnetic radiation reflectivity on metal surface investigated using microscopic model to derive fields and boundary conditions 19 p3282 A67-35582
 Dispersion equation for electrodynamic boundary value problem of natural oscillations of cylindrical resonator with magnetoactive plasma 19 p3299 A67-36019
 Boundary value problem of oscillatory system with time lag quasi-linear partial differential equation 19 p3251 A67-36050
 Hybrid computer for co-current laminar-flow heat exchanger Sturm-Liouville problem 19 p3190 A67-36069
 Operators spectrum properties and corresponding singular eigenfunctions encountered in plasma problems, showing application to initial and boundary value problems 20 p3494 A67-36148
 Longitudinal oscillations and Landau damping of electron plasma with fixed ion background, discussing initial and boundary value problems 20 p3494 A67-36150
 One-dimensional directed continuum assumed to represent elastic fiber strengthened string, developing boundary conditions and constitutive

- equations 20 p3535 A67-36197
- Cascade flow in mixed flow pumps and turbines, solving boundary value problems for stream function by relaxation method 20 p3536 A67-36421
- Existence and uniqueness of classical solutions of nonstationary boundary and initial value problem in MHD 20 p3497 A67-36430
- Variational problem in optimal interaction systems with control constraints solved by dynamic programming and Pontryagin principle applications 20 p3407 A67-36440
- Approximate solution for subsonic gas flow, deriving approximation for Chaplygin function for use in boundary value problems 20 p3556 A67-36442
- Two-point boundary value problem approximate solution using Monte Carlo path integral calculation 20 p3475 A67-36481
- Boundary value problem and singular integral equation applied to automatic control theory 20 p3475 A67-36652
- Analytical method yielding solutions for transient steady heat conduction in bodies with arbitrary boundary and initial conditions [ASME PAPER 67-HT-44] 20 p3547 A67-36726
- Laminar film boiling on thin wire, determining heat-transfer coefficient and vapor dome spacing and diameter [ASME PAPER 67-HT-62] 20 p3549 A67-36744
- Transient temperature distribution of cylinder subject to radiation cooling, giving dimensionless computer-derived graphs [ASME PAPER 67-HT-71] 20 p3550 A67-36751
- Numerical digital computer solution of parabolic partial differential equations with two-point boundary conditions, using method of lines 20 p3391 A67-36820
- First boundary value problem for linear elliptic differential equations involving two small parameters 20 p3477 A67-36942
- Valentine method for maximum principle problem solution, reducing to nonlinear differential equation system with special boundary conditions 20 p3477 A67-37029
- Current distribution in MHD channel with strong magnetic field solved by reduction to Riemann type boundary value problem 20 p3500 A67-37047
- Boundary conditions at dielectric-plasma interface 20 p3501 A67-37218
- Time optimal control problem solved by calculating boundary condition changes with system structure 20 p3409 A67-37222
- Admittance function for burning surface by solving differential equation and satisfying boundary conditions, discussing frequency peaks qualities 20 p3554 A67-37255
- Thermal stresses in orthotropic sandwich plate solved by boundary value and stress distribution 20 p3541 A67-37298
- Three-dimensional hologram reconstruction and image speckle, considering three-dimensional boundary value problem 20 p3451 A67-37309
- Nonlinear sequential estimation problem from noisy measurement data using nonstatistical least squares formulation, obtaining approximate solution to two-point boundary value problem 20 p3410 A67-37319
- Optimal control theory for distributed parameter systems using dynamic programming, showing use in two-point boundary control problems involving partial differential equations 20 p3410 A67-37320
- Optimal control theory for linear distributed parameter systems, presenting solution algorithms and computational results for several problems 20 p3411 A67-37321
- Iterative technique applied to solution of problems in elasticity involving minimization of double integral subjected to certain boundary conditions 20 p3541 A67-37487
- Initial boundary value problem for Chaplygin equation using Cauchy and Dirichlet data 20 p3478 A67-37574
- Galerkin method applicability to boundary value problems and eigenfunctions and eigenvalues for integrodifferential equations with deviating arguments 20 p3478 A67-37580
- Formulating Cauchy problem and mixed problem for second order self-adjoint equation, establishing initial data and boundary value dependence 20 p3479 A67-37657
- Velocity field in axisymmetric boundary layer described by nonlinear partial differential equations 20 p3425 A67-37677
- Estimates for solutions to nonlinear boundary value problems for second order differential equation 20 p3479 A67-37719
- Second boundary value problem for differential equation of elastic equilibrium of shallow cylindrical shell 20 p3543 A67-37721
- Boundary value problem solution by approximation method of Kupradze with differential operators and given and unknown functions 20 p3479 A67-37723
- Boundary value problem for region with arbitrary smooth boundary solved, using second order degenerate elliptical equations 20 p3479 A67-37724
- Index and solvability of general linear boundary value problem for composite type system of equations 20 p3479 A67-37725
- Boundary value problems solution in steady two-dimensional compressible MHD flow past thin body 21 p3660 A67-37742
- Singularities of two-fluid plasma equations, investigating compatibility and relation to boundary conditions 21 p3661 A67-37744
- Two-stream instability calculations from phase-space boundary motion, using Vlasov equation in distribution 21 p3662 A67-37763
- Papers on functional analysis covering approximation methods and Cauchy, Dirichlet and boundary value problems 21 p3651 A67-37832
- Diffraction coefficient of open laser resonators coupled in series, discussing boundary conditions 21 p3638 A67-37864
- Galerkin method shown convergent even with selected functions not satisfying exactly all boundary conditions 21 p3715 A67-37890
- Unsteady cascade flow and blade oscillation in axial condenser as aerodynamic boundary value problem 21 p3564 A67-37892
- Infinitesimal deflections of positively Gaussian curved surfaces solved by application of p, q analytic functions after affine transformation 21 p3715 A67-37903
- Quasi-linear elliptic system of first order equations used for Riemann-Hilbert boundary value problem 21 p3651 A67-37930
- Variationally derived finite difference equations for mixed boundary value problems of thermoelastic stress and strain 21 p3716 A67-37956
- Unsteady dynamic field excited by source moving along elastic half-plane boundary 21 p3716 A67-37967
- Boundary value solutions by approximate method for variable thickness and rigidity shells using equilibrium equations 21 p3718 A67-37983
- Solution for boundary value problems in elasticity theory for ellipsoid of revolution and cavity with surface loading, determining coefficients in closed form 21 p3718 A67-37984
- Generalized indirect method solving two-point boundary value problems for rapid optimal trajectory computation 21 p3702 A67-38024
- Modified adjoint method and Friedrichs operator equation solution for two-point boundary value problems 21 p3652 A67-38025
- Long radio wave propagation in earth ionosphere waveguide channel, determining eigenvalues of boundary value problem from complex transcendental equation containing Bessel function 21 p3580 A67-38116
- Response in fundamental mode of simple single span beam with tuned viscoelastic dampers attached at discrete locations, assuming harmonic loading 21 p3719 A67-38147
- Pointwise bounds for perturbed parabolic and elliptic equations using known bounds for corresponding strictly differential problems, noting Rayleigh-Ritz procedure 21 p3652 A67-38174
- Inequality for pointwise bounds of second initial boundary value problem for second order semilinear parabolic equation, noting Rayleigh-Ritz method 21 p3652 A67-38176
- Boundary value problem describing conducting fluid motion in longitudinal magnetic field, considering magnetic Reynolds numbers, electric current density distribution and heat exchange 21 p3665 A67-38243
- Navier-Stokes equation solution in region with smooth boundary, using linear elliptic equations 21 p3652 A67-38277
- Generalized reciprocity law relating behavior of elastic body and static and geometric boundary conditions 21 p3720 A67-38287
- Thermal-stress deformed condition on heated elastic bodies boundary containing inclusions of spherical thin film with homogeneous infinite heat flow 21 p3720 A67-38295
- Linear boundary value problem for system of first order partial differential equations having real and imaginary characteristics 21 p3653 A67-38398
- Noether theory for system of singular integral equations with Carleman shift and complex conjugate unknowns as applied to boundary value problem 21 p3653 A67-38399
- Stress analysis of loaded boundaries in two-dimensional second boundary problems, studying mechanical and thermal strain, knife-edge device, etc 21 p3722 A67-38435
- Forced oscillation in distributed constant system with tunnel diode described by linear wave equation with nonlinear boundary conditions 21 p3598 A67-38606
- Electromagnetic wave pulses transmission through plasma boundary, studying boundary effects for broad and narrow frequency spectra 21 p3669 A67-38682
- Electromagnetic wave scattering by rectangular geometry dielectric wedge, using precise boundary conditions 21 p3585 A67-38686
- Network method to derive differential difference equations for boundary condition of clamped and free edges and point supports of low aspect orthotropic wings network method to derive differential-difference 21 p3724 A67-38782
- Natural frequencies and shape of axisymmetric oscillations of thin spherical shell under initial stress calculated via boundary value problem, using computer method 21 p3725 A67-38791
- Flat plate bending and two-dimensional, axisymmetric and boundary value problems in elasticity theory investigated using Vlasov initial function method 21 p3725 A67-38792
- Time symmetry in oscillating cosmologies with locally irreversible processes, obtaining formalism for statistical processes and boundary conditions 21 p3706 A67-38844
- Boundary conditions at wall for low density flow problems treated by kinetic theory, synthesizing relation between distribution functions of incident and reflected particles 21 p3614 A67-38861
- Discrete method extension for bending stability problem in sectorial plates, obtaining algorithm for solutions of boundary conditions and external loads 21 p3729 A67-38907
- Boundary condition problem at interface between immiscible fluids investigated for nonequilibrium thermodynamics 21 p3733 A67-39065
- Stress distribution on boundaries of two unequal circular holes in infinite plate determined by mapping region conformally onto annulus 21 p3730 A67-39086
- Boundary value problems of wave propagation in plane, investigating coverage, source distribution and velocity perturbations 21 p3615 A67-39093
- Fuel optimal control conditions in attitude correction of satellite in circular orbit determined using maximum principle, solving resulting boundary value problem 21 p3715 A67-39153
- Eigenstate variables for representation of optimum orbital transfer problems, discussing numerical integrations 22 p3878 A67-39154
- 9-point difference formula accuracy in Laplace equation compared to 5-point formula, discussing convergence rate and Dirichlet boundary value problem 22 p3826 A67-39195
- Flow equations for electron emitter placed in ion stream and transparent to ions, showing previous results due to incorrect choice of boundary conditions 22 p3843 A67-39262
- Lower bounds to minimum error probability for block coding on noisy discrete memoryless channels 22 p3764 A67-39296
- Statistical elasticity problems involving random stress and displacement tensor fields, proving uniqueness and minimum principle for boundary value 22 p3909 A67-39396

Arbitrary function expansion into series of functions involved in plane elasticity problem with Fourier series form satisfying boundary conditions 22 p3909 A67-39397

Ferromagnetic magnetization curve approximated for analytical solutions of boundary value problems in nonlinear electrodynamics, obtaining Riemann functions 22 p3836 A67-39420

Numerical computations for resistive plasma drift instabilities in conducting cylinder, noting finite boundary conditions effect 22 p3848 A67-39693

Perturbation theory for solving initial and boundary value problem in unsteady MHD flow past thin symmetrical bodies with inwardly diffusing magnetic field 22 p3850 A67-39707

Speedy generation of space flight guidance command signals and comparative analysis of operational schemes for generating guidance signals 22 p3832 A67-40145

Thin circular elastic plate under uniform compressive thrust, with nonlinear boundary value problems involving partial differential equations for buckled states 22 p3916 A67-40525

Existence and form of orthogonality condition on natural vibrational modes of linear elastic shell under boundary conditions 23 p4073 A67-40616

Bound functionals for limit analysis of plastic solids by variational method, discussing safety factor and sandwich structures 23 p4074 A67-40629

Equations describing one-, two-, and three-layer earth model spheroidal oscillations derived and solutions obtained, considering constant density and constants differing for each layer 23 p3994 A67-40714

Deriving stability and asymptotic stability properties of temperature fields governed by quasi-linear heat equations 23 p4081 A67-40745

Boundary value problem solution convergence conditions applied to linear ordinary differential equations involving two parameters 23 p4022 A67-40746

Estimating interval of nonoscillation of finite difference equation 23 p4022 A67-40822

Soviet book on approximate methods for boundary value problem solutions of ordinary and partial differential equations and certain integral equations 23 p4022 A67-40841

Boundary value problem theory for ordinary differential equations, discussing compact and noncompact intervals of independent variables 23 p4023 A67-41018

Parameter invariance problem for linear systems solved by obtaining necessary and sufficient conditions for invariance in optimal control systems 23 p3984 A67-41159

Thin boundary problems of bimaterial plates bonded along circular arcs behaving like crack imperfections under bending, using fracture mechanics to predict failure 23 p4078 A67-41164

Nonequilibrium boundary layer problem solution by direct treatment of two-point boundary value problem [AIAA PAPER 67-219] 23 p3991 A67-41715

Mathematical model of linear guidance law to dynamical system, noting reduction of two-point boundary value class error 23 p4026 A67-41732

Mathematical model, representing two-dimensional panel fluttering in supersonic flow, to study stability criterion via Liapunov second method 23 p4081 A67-41752

Numerical solution for two-point nonlinear boundary value problem of n-order ordinary differential equation 24 p4177 A67-41914

Dynamic boundary conditions for Kirchhoff constrained shell, obtaining symbolic scalar relationship for shell mechanics 24 p4249 A67-42152

Lower bounds for eigenvalues of differential linear elliptical operator using Rayleigh-Ritz approximation extension 24 p4177 A67-42154

Approximate solution to irregular waveguides with impedance boundary conditions based on amplitude of normal wave propagation 24 p4120 A67-42159

Stabilization method for solution of boundary value problems for second order nonlinear ordinary differential equation 24 p4177 A67-42198

Existence theorems for defining solubility of certain boundary value problems for

ordinary second order linear differential equations 24 p4177 A67-42199

Finite difference method for degenerate elliptic and parabolic equations involving various boundary value problems 24 p4178 A67-42269

Finite difference solution accuracy for potential gradient along conductor boundary near reentrant corner of thin plate 24 p4131 A67-42447

Existence theorems for partial and ordinary differential equation solutions, discussing boundary value problems for nonlinear differential equation class 24 p4178 A67-42728

Integral equations for nonlinear problems in partial differential equations, including Volterra, boundary value and initial value problems 24 p4180 A67-43088

BOUSSINESQ APPROXIMATION

Estimation of lower bounds to minimum Rayleigh number inducing state of convective motion in quasi-incompressible fluid with temperature gradient in body force direction 17 p2968 A67-32410

Convective heat flow nonlinear equations for fluid sphere having heat sources expressed in Boussinesq approximation as perturbation of steady state conduction solution 21 p3731 A67-37926

Normal modes of stellar internal motions, considering turbulent convection equations and weak-coupling approximation 23 p4068 A67-41277

BOW SHOCK

Vela II measurements of earth magnetopause and bow shock positions, showing relationship to magnetic disturbance index and thus also to solar wind velocity 07 p1180 A67-19920

Turbulent electrostatic shock in plasmas, discussing determination of structure by ion wave instabilities [SR-1] 13 p2162 A67-26281

Earth bow plasma shock wave model with ion wave instabilities as principal shock structure [SR-2] 13 p2107 A67-26301

Solar wind bulk velocity studied via Vela 3A bow shock crossings, noting velocity decrease when entering magnetosheath 13 p2190 A67-26320

Earth bow shock observations with Explorer XII satellite magnetometer 14 p2383 A67-28047

IMP II satellite measurements of magnetic fields in interplanetary space by onboard monoaxial fluxgate magnetometers 14 p2310 A67-28052

Blunt nosed reentry vehicle model with skewed magnetic field investigated in magnetoaerodynamic flow for possible bow shock distortion 14 p2244 A67-29049

Argon and nitrogen flows past sphere at low supersonic velocities analyzing formation of bow shock wave 16 p2592 A67-31103

Separation shock near base of conical bodies at hypersonic speeds noting inflections in bow shock shape 17 p2793 A67-33044

Steady state magnetic field in transition region between magnetosphere and bow shock by MHD equations, noting solution by approximation method 17 p2951 A67-33186

Semilempirical methods of spillage drag prediction for two-dimensional supersonic inlets operating in transonic flight [AIAA PAPER 67-449] 18 p2982 A67-33924

Interaction of first and second shocks of blast-bow wave in double-driver shock tube, examining stagnation point pressure prediction methods 19 p3206 A67-34812

Magnetospheric features, describing magnetic field distribution, electron and proton density, plasma instabilities, bow shock and solar wind 20 p3430 A67-36903

Bow shock and combustion zone studies of spheres fired through H₂-O₂ mixtures show ignition zone separation 20 p3359 A67-37128

Quiet condition solar wind geomagnetic field interaction measurements, discussing solar plasma and bow shock wave generation 22 p3870 A67-39670

MGD reentry flow regimes analyzed, noting increased bow shock standoff distance and drag, comparing in-flight and laboratory simulation 24 p4199 A67-42920

BOW WAVE

Stream structure and bow waves in electromagnetic shock tube, establishing flow uniformity limitations through

temperature and pressure measurements 19 p3294 A67-35404

BRAGG EQUATION

Double crystal spectrometer measurement of X-ray Compton and thermal scattering accompanying Bragg reflection from Si and Ge single crystals 01 p0132 A67-10456

Reconstruction method for image with good definition via partially coherent source 13 p2119 A67-26587

X-ray laser resonator proposal involving three-dimensional puckered ring arrangement of crystals at Bragg angle, discussing polarization losses 13 p2126 A67-27012

Dynamical theory of X-ray diffraction for optical holography noting anomalous light transmission at Bragg angle 23 p4009 A67-41462

Laser pulse compression of RF signals using Bragg scattering produced in transparent solid by ultrasonic waves 24 p4188 A67-42368

RF pulse compression by chirped shear microwave sound in sapphire, inducing self-focusing of Bragg diffracted light 24 p4188 A67-42369

BRAIN

SA CEREBRAL CORTEX

SA CEREBROSPINAL FLUID

SA ELECTROENCEPHALOGRAPHY

SA HYPOTHALAMUS

SA INTRACRANIAL PRESSURE

Informal automaton simulating certain processes of information processing by human brain controlled by servosystems 03 p0365 A67-13084

Glycogen accumulation in monkey and cat brain exposed to proton irradiation, discussing astrocytes function in carbohydrate metabolism 04 p0560 A67-14489

Roentgen radiation effect on glycogen metabolism of rat brain 07 p1133 A67-19468

Interspecies communication involving human and mammalian brain as computer with programs and metaprograms [AAS PAPER 66-77] 07 p1135 A67-20000

Identification and localization of center median nucleus of Luys, noting CM projects primarily upon putamen 08 p1288 A67-21356

Brain tissue respiratory processes of rabbits subjected to hypergravity and acute hypoxia noting no significant difference between experimental and control animals 23 p3943 A67-40770

BRAIN CIRCULATION

Mechanism and pattern of human cerebrovascular regulation after rapid changes in blood carbon dioxide tension 11 p1746 A67-23989

Functional relation between oxidation, metabolism, blood flow volume rate and brain temperature in rats exposed to vibration, noting temperature decrease and blood supply and oxygen consumption stimulation 23 p3943 A67-40789

Cerebral blood flow and metabolism during combined hypoxia and hypercapnia, noting cerebral vasodilatation effect 23 p3945 A67-41080

Arterial and venous blood of brain and mixed venous blood of heart measured in dogs exposed to simulated altitude, noting body deoxygenation 24 p4111 A67-41851

BRAIN INJURY

Metabolic cerebellum changes under nonlethal hypoxia, noting system compensation during symptomatic stages and destruction of Purkinje cells at critical stages 04 p0561 A67-14629

Immediate and subsequent effects of brain damage in rats, using closed field intelligence tests 09 p1454 A67-22058

Blockage of electrically evoked pupillodilation in cat by irradiating hypothalamus with cyclotron-accelerated alpha particles 10 p1588 A67-23394

BRAKE

SA AIRCRAFT BRAKE

SA SPEED BRAKE

SA WHEEL BRAKE

Upper atmosphere density determined from satellite braking 08 p1325 A67-21002

Mechanical systems with automatic retardation /self-braking/ for application to brake mechanism and frictional transmission, analyzing Painleve paradoxes 10 p1680 A67-23607

Approach navigation accuracy and entry corridors for aerodynamic braking at Mars and Venus 13 p2212 A67-26837

Minimum of maximum overload in braking of vehicle in atmosphere, examining aerodynamic lift on basis of Pontryagin maximum principle 14 p2393 A67-27855
Spline friction effect on multiple disk brake and clutch packs, including torque and load variation and pressure distribution equations [ASME PAPER 67-LUB-26] 24 p4164 A67-42684

BRASS

X-ray diffraction analysis of polycrystalline brass deformed by tension, noting stacking fault probability, stress-strain curve, etc 18 p3064 A67-34084

BRAYTON CYCLE

Gas lubricated bearings used in Brayton cycle closed loop system turbomachinery in design of two-shaft power plant [ASME PAPER 66-GT/CLC-9] 01 p0080 A67-10871

Rankine and Brayton cycles for spacecraft power generation, discussing operation principles, advantages and performance characteristics 01 p0112 A67-11428

Closed Brayton cycle power conversion system development, discussing rotating components and single phase operating fluid [AIAA PAPER 66-889] 02 p0183 A67-12268

Nuclear power supplies for electrical propulsion including liquid metal reactor-potassium Rankine, Brayton, MHD power conversion and thermionic reactor [AIAA PAPER 66-1021] 03 p0363 A67-14153

Power output variation of solar Brayton space power plant with heat storage due to solid layer thermal resistance effects 09 p1442 A67-21698

Lubrication system design and component arrangements for several oil and gas lubricated closed looped gas turbine machines [ASME PAPER 67-GT-3] 11 p1799 A67-24791

High temperature testing and evaluation of graphite helical-screw expanders and compressors for use with inert gas Brayton cycle 15 p2492 A67-29427

Optimization of Brayton cycle consisting of heat source, MPD generator, recuperator, etc, in terms of thermal efficiency and specific power 18 p2603 A67-30567

MHD Brayton cycle power generation techniques, considering noble gases seeded with alkali metal vapors as working fluid 16 p2603 A67-30567

Jet compressors for closed Brayton cycle MPD to study momentum transfer of two high velocity gas or vapor streams of very different molecular weight 16 p2604 A67-30568

Manned space mission requirements and application of space power technology to multipurpose space stations, noting operation of Pu-238 isotope/Brayton cycle unit 17 p2953 A67-31979

Liquid-metal and plasma MHD systems for power generation in space environments, noting Rankine and Brayton cycles [JPL-TR-32-1129] 17 p2802 A67-32049

NASA test program to evaluate performance and design point characteristics of 3-kw closed recuperated Brayton cycle power conversion system 24 p4102 A67-42486

Gas bearing Brayton cycle turboalternator rotor system stability and dynamic response to electromagnet forces 24 p4102 A67-42487

Real gases examined for application as working fluid in Brayton cycle power plant, considering radiator area reduction to Rankine cycle 24 p4102 A67-42488

NASA radial flow turbine research related to Brayton cycle power generator, investigating size, Reynolds number and speed effects on efficiency and flow 24 p4102 A67-42489

SNAP-8 powered Brayton cycle system for large space stations noting components and overall design 24 p4102 A67-42490

Stirling, Brayton and Rankine dynamic cycles compatibility with isotope heat sources, emphasizing power system applications to long-duration earth orbital missions 24 p4185 A67-42542

Parametric analysis and system optimization of nuclear reactor heated Brayton cycle space power plants, discussing turbomachinery performance and shielding weight factors 24 p4186 A67-42550

Design and developmental testing of electrical components for two-shaft Brayton cycle energy conversion system, discussing

Na-Bi and Li-Te cells 24 p4108 A67-42556
Lunar electric power systems transported by Saturn V noting Brayton cycle, Rankine cycle, solar cells and thermoelectric systems [AIAA PAPER 67-902] 24 p4110 A67-43010

BRAZIL

Upper atmospheric rocket sounding experiment during solar eclipse over Brazil, noting instrumentation and participating agencies 06 p0981 A67-18382

Brazil geomagnetic anomaly and artificial radiation belt observations from Cosmos series satellites 12 p1996 A67-25773

Space research in Brazil, discussing rocket launching facility, meteorological experiments, X-ray astronomy, satellite observations, etc 19 p3320 A67-35285

BRAZING

SA SOLDERING

SA WELDING

Capacitor pressure sensor produced by furnace brazing molybdenum to itself and to zinc with pure copper and Cu-Au-Ni filler metals 04 p0630 A67-15460

Exothermically brazed tubing joints for XB-70 hydraulic system 07 p1190 A67-19212
Operational economy of dip brazing method of joining aluminum and reliability of ultrasonic printout procedures for inspection of assemblies 10 p1660 A67-23007

Wing-fuselage section panels of hypersonic aircraft built by brazing welded refractory honeycomb 10 p1660 A67-23171

Hydraulic tubing permanent joints, made by induction-brazing method, for installation on A-7A Corsair II 17 p2801 A67-32007

Ceramic-to-metal sealing method based on use of ductile nickel-titanium intermetallic compound as braze 20 p3454 A67-36518

Brazing alloys and high remelt and conventional techniques developed and evaluated for use in tantalum honeycomb structures 20 p3456 A67-37696

Low pressure diffusion welding and brazing process producing joints with mechanical properties close to titanium 6Al-4V 22 p3811 A67-39446

Beryllium braze joining for light stiff components noting structural examples and fabrication techniques, with reference to Apollo SNAP-27 radiator housing [SAE PAPER 670805] 24 p4159 A67-41991

BREAKDOWN

S ELECTRIC BREAKDOWN

S VOLTAGE BREAKDOWN

S VORTEX BREAKDOWN

BREATHING

S AIRCRAFT BREATHING APPARATUS

S HIGH ALTITUDE BREATHING

S OXYGEN BREATHING

S PRESSURE BREATHING

S RESPIRATION

BREATHING VIBRATION

Vibrations of elastic shells containing liquids 01 p0185 A67-11441

Inertia effects of internal liquid column on vibration of thin walled pressurized elastic cylindrical bellows type container [AIAA PAPER 67-38] 06 p0986 A67-18262

BREMSSTRAHLUNG

SA X-RAY

Bremsstrahlung, transient and plasma radiation as affected by surface properties of silver bombarded by electrons 02 p0291 A67-11737

Gamma, bremsstrahlung and X-ray radiation limitations in aerospace application 02 p0286 A67-12217

Plasma electron temperature measured from soft X-ray bremsstrahlung absorption by beryllium foil 02 p0274 A67-12461

X-ray emission from radio galaxies as possible bremsstrahlung radiation of hot gas, noting Crab Nebula 02 p0308 A67-12482

Solar flares, discussing continuous electromagnetic radiation, hard X-ray radiation and microwave radio bursts 02 p0310 A67-12576

Bremsstrahlung emission from electron-electron collisions in plasma, obtaining spectra of longitudinal and transverse waves 03 p0484 A67-14043

Spatial and temporal characteristics of bremsstrahlung X-ray due to energetic electron precipitation in auroral zone, noting measurement techniques 07 p1180 A67-19929

Anomalous bremsstrahlung and cyclotron emission in partially ionized plasmas 08 p1386 A67-21441

Amplification of RF wave in partially

ionized gases with large Ramsauer effect in absence of magnetic field, due to negative absorption of stimulated bremsstrahlung 08 p1366 A67-21442

Low energy cosmic ray photons in atmosphere, noting X-ray generation by bremsstrahlung effect of electron component 08 p1377 A67-21466

Production rate of secondary cosmic ray photons in upper atmosphere derived by cascade theory from stratospheric measurements of integral and differential energy spectra 09 p1561 A67-21882

Emission of bremsstrahlung X-rays caused by electrons precipitating isotropically into upper atmosphere 10 p1633 A67-23048

X-ray emission from radio galaxies as possible bremsstrahlung radiation of hot gas, noting Crab Nebula 10 p1702 A67-23350

Energy loss of high energy muons caused by nuclear interaction and fluctuation due to passage through great thickness of material corrected for standard rock 10 p1703 A67-23690

Dependence of ion energy on irradiated laser power, discussing production of ions of two discrete energies 10 p1667 A67-23793

Delta electrons formed in interstellar hydrogen-galactic ray collision 12 p1994 A67-25645

Generation of series limit continua with aid of sliding sparks for absolute measurements in vacuum UV, observing bremsstrahlung 13 p2155 A67-26271

Geomagnetic micropulsations and electron bremsstrahlung in northern auroral zone 13 p2108 A67-26321

Possible polarization of X-ray bremsstrahlung of solar flares due to sharply anisotropic electron beams 13 p2191 A67-26383

Polarization of cosmic X-ray produced by bremsstrahlung mechanism 13 p2191 A67-26713

Auroral zone electron precipitation occurring in strong transient magnetic disturbances observed by bremsstrahlung 14 p2310 A67-28056

Net polarization of celestial X-rays could lead to specification of source mechanism producing radiation 14 p2381 A67-28617

Nonthermal X-ray radiation accompanying solar flares, comparing spectral power of synchrotron radiation, Compton radiation and bremsstrahlung as possible generation mechanisms 15 p2549 A67-29141

Recording and analysis of geomagnetic pulsations of auroral zone and comparison with bremsstrahlung measurement, using two-magnetometer arrangement 15 p2474 A67-29524

Flux, energy spectrum and angular anisotropy of auroral electrons analyzed from space vehicle 16 p2670 A67-30648

Origin of X radiation from radio galaxies Cygnus A and Virgo A, hypothesizing thermal radiation and bremsstrahlung 18 p3116 A67-33855

Auroral absorption events, discussing bremsstrahlung X-rays spectrum, electron densities and temperatures measured with rockets 19 p3312 A67-35188

Customary formulas for various effects including Thomson scattering, electron-ion, bremsstrahlung, etc, in context of plasma radiation theory 19 p3284 A67-35340

Recombination and bremsstrahlung continuum radiation measurements of atomic and ionic oxygen in plasma 19 p3299 A67-36093

Book on vacuum UV spectroscopy techniques noting Lyman continuum, synchrotron radiation, Bremsstrahlung radiation, UV radiation, resolution, etc 20 p3446 A67-36664

Solar atmosphere absorption of light nuclei generated on sun indicated by satellite observation of heavy nuclei cosmic ray flux and X-ray electron bremsstrahlung 21 p3698 A67-38595

Possible polarization of X-ray bremsstrahlung of solar flares due to sharply anisotropic electron beams 21 p3698 A67-38817

Extensive cosmic ray shower bremsstrahlung in RF and optical bands noting intensity and incoherency 22 p3870 A67-39517

Electron transport theory for energy below 10 Mev, reviewing interactions, scattering, thick targets, complex geometry

and penetration in space environment [UCC/DSSD-267] 24 p4190 A67-41805

Iron radiation length unit from electromagnetic cascades produced by bremsstrahlung of horizontal cosmic ray muons 24 p4221 A67-42869

Bremsstrahlung due to collision of muon with electron at rest, discussing energy photons role 24 p4194 A67-42880

Nonthermal X-ray radiation accompanying solar flares, comparing spectral power of synchrotron radiation, Compton radiation and bremsstrahlung as possible generation mechanisms 24 p4222 A67-43064

BRIDGE

SA WHEATSTONE BRIDGE

SA WIRE BRIDGE CIRCUIT

Time domain analysis of bridge doubler circuit for varactor multiplier 02 p0218 A67-12100

Pulsed sinusoidal bridge for simultaneous measurement of volt-capacitance and volt-ampere characteristics of relaxing p-n junction barriers 08 p1303 A67-20998

Wideband miniature bridge constructed on basis of quarter wave two-conductor shielded line for UHF and SHF 11 p1757 A67-23911

Thin film superconducting bridge behavior in microwave field noting dependence of deviation from classical rectification on frequency, power, temperature and bridge width 12 p1985 A67-25848

Strain gauge bridge outputs combined during flight to measure airloads directly and inexpensively in fatigue test program 14 p2315 A67-28002

Bridge circuits with nonlinear resistances, calculating statistical characteristics by graphical method for functional transformer 20 p3451 A67-37151

Mercury fed plasma bridge neutralizers for in-flight operation of SERT II electron bombardment ion thruster [AIAA PAPER 67-670] 21 p3691 A67-38704

Wideband miniature bridge constructed on basis of quarter wave two-conductor shielded line for UHF and SHF 21 p3600 A67-38939

BRIDGMAN METHOD

Electron distribution of oxygen grown GaAs crystals after heat treatment, showing profiles due to silicon contamination 11 p1848 A67-24740

BRIGHTNESS

SA LUMINESCENCE

SA LUMINOSITY

SA SKY BRIGHTNESS

Tables of observational data on flattening, integrated brightness, brightness distribution and polarization of white corona 01 p0150 A67-10933

Radio sources and background radiation survey at 38 mc/s, presenting contour maps of brightness temperature and list of flux densities 01 p0151 A67-10966

IR brightness temperature of Uranus used to establish current lower limit at which brightness temperature of celestial object can be measured 02 p0324 A67-11773

Continuum brightness fluctuations and equivalent line widths in sunspot penumbral spectrum 02 p0330 A67-12715

Brightness curves used to determine geometrical and physical parameters of eclipsing binary systems containing component with extended spherical atmosphere 04 p0701 A67-15553

Venus brightness temperature and polarization of integral radio emission at 3.75 cm wavelength 04 p0702 A67-15566

Comet photometry using revolving table to study brightness distribution in head and determine intrinsic brightness 05 p0888 A67-16200

Photometry of comet Arend-Roland, 1956 h, calculating brightness decrease along tail streams 05 p0888 A67-16201

Intrinsic brightness of comet Alcock 1963 b obtained from visual observations in terms of stellar magnitudes 05 p0888 A67-16204

Photographic comet photometry as technique for studying comet brightness 05 p0890 A67-16332

Lunar occultation of celestial radio sources noting brightness distribution and spectral resolution 05 p0891 A67-16402

Laser brightness gain and single transverse mode operation by compensation for thermal distortion with external mirror 05 p0819 A67-16656

Mokhnach model explaining surface brightness distribution observed by miller in 1959 k comet 06 p1082 A67-17839

Statistical analysis of flare radiation intensity and brightness distribution of irregular and semiregular variables 07 p1248 A67-19486

Polarization and brightness temperature distributions across lunar disk observed with Parkes radio telescope at various wavelengths 07 p1251 A67-19854

Water vapor mass below upper limit of earth cloud cover estimated through earth brightness measurements 07 p1183 A67-20006

Transient lunar brightening, discussing attempted correlation with solar wind activity 07 p1256 A67-20160

Radio telescope-spectrophotometric scanner investigation of continuous energy distribution of four quasars 08 p1398 A67-21230

Mathematical analysis of polarization interferometry yielding polarization and brightness distribution of celestial radio sources [AFRL-67-0226] 09 p1470 A67-21608

Comet head brightness diminution during perihelion passage due to sublimation calculated, using Clapeyron-Clausius equation and insulation effect 10 p1703 A67-22719

Auroral brightness variations related to magnetic field fluctuations, especially to pearl type fluctuations 10 p1632 A67-22811

Microwave spectral brightness measurements of Venus compared with several model atmospheres 11 p1865 A67-24601

All-glass electroluminescence readout panel design with active areas integral part of connector pin 11 p1786 A67-24628

Distribution of radio brightness temperature over disk of Venus 13 p2200 A67-27333

Two-dimensional aperture synthesis in lunar CW radar astronomy, showing measurement possibility for Fourier transform components of sky brightness distribution 14 p2385 A67-28442

Number of rays and brightness of Comet Morehouse derived from photographs taken with Greenwich reflector 16 p2742 A67-30666

Brightness temperature reduction of Venus at decimeter wavelengths determined from 49.1 cm measurements 16 p2749 A67-31409

Color indices of visible meteors observed by naked eye and through color filters noting brightness dependence and meteor train distribution 16 p2751 A67-31462

Upper limit on mean mass density of luminous matter in universe from brightness of night sky 17 p2944 A67-32638

Mokhnach model explaining surface brightness distribution observed by Miller in 1959 k comet 17 p2951 A67-33214

Spectral brightness, reflectivity and polarization characteristics of clouds in IR band, measuring angular structure of underlying radiation field 18 p3073 A67-33563

Supernovae photometric properties, considering mean absolute photographic magnitude at maximum light, brightness decline rate, etc 18 p3119 A67-33857

Visible brightness features in Mariner IV photographs of Mars interpreted as clouds 18 p3123 A67-34149

Lunar surface roughness and brightness temperature anomalies from IR image study 18 p3134 A67-34537

Annular solar eclipse of May 20, 1966 visible at Bordeaux, noting active center on occultation curve 19 p3325 A67-35506

Correlating lunar eclipse brightness, solar activity and corona ellipticity data 20 p3528 A67-37462

Observational results consisting of meteor trail photographs for determining processes responsible for relative intensity of brightness and trail length 20 p3530 A67-37665

Monograph on variable stars of RR Lyrae type covering spectrophotometric investigations of periodic brightness fluctuations and oscillations stability 22 p3880 A67-39463

Auroral brightness variations related to magnetic field fluctuations, especially to pearl type fluctuations 24 p4150 A67-42148

BRIGHTNESS DISCRIMINATION

Zodiacal light brightness variation during solar activity cycle 03 p0413 A67-13454

Responses of lateral geniculate nucleus of monkey to light increment and decrement and encoding of brightness 04 p0561 A67-14592

Photometry of integrated light of Venus, inferring presence of ice in atmosphere from halo effect of brightness dispersion 05 p0892 A67-16407

Thermal coordinate analysis of lunar IR scan data for directional effects caused by surface geometry, illumination and sensor angle [AIAA PAPER 67-291] 12 p2009 A67-26008

Classification of slit spectrograms of 185 bright stars in Morgan-Keenan system 14 p2387 A67-28560

Spherically symmetrical planetary atmosphere brightness derivation using transport equation 14 p2313 A67-28766

Two-layer model of Venusian atmosphere satisfying radioastronomic and radar self-radiation measurements 17 p2941 A67-32322

Altitude variation of air scattering coefficient determined from brightness profile measurements of haze at planet limb, using spacecraft photography 20 p3432 A67-37238

Brightness thresholds and reading ability tests evaluated for male subjects under varied simulated conditions of altitude and oxygen breathing 23 p3959 A67-41694

BRILLOUIN EFFECT

Stimulated Brillouin scattering in shock-compressed acetone 01 p0116 A67-10338

Hypersonic excitations due to Brillouin scattering for case with Stokes feedback, deriving quantum equation of motion for creation of laser and Stokes modes and coupled acoustic mode 05 p0823 A67-16683

Optical heterodyne technique detecting stimulated Brillouin scattering, noting frequency shift demodulation arising from ruby laser light incidence on quartz crystal 05 p0823 A67-16688

Stimulated Brillouin scattering in liquids used for passive Q-switch applicable to visible and IR lasers 09 p1511 A67-21749

Phonon lifetime variation effect on stimulated Brillouin and Raman scattering in gases by temperature, pressure and power variation and comparison with Stokes gain theories 10 p1662 A67-22758

Hypersonic sound velocity dispersion in liquids of low viscosity analyzed using Mandelstam-Brillouin components 12 p1967 A67-26133

Multiple stimulated Brillouin scattering from liquid within Q-switched ruby laser cavity, noting changes in pulse shape, output power and spectral characteristics 20 p3457 A67-36385

Multiple stimulated Brillouin scattering used for nanosecond high intensity pulse generation combining ruby laser with liquid cell and Fabry-Perot etalon 23 p4011 A67-40786

Optical characteristics of wideband pulse compression system using Brillouin scattering for compressing time duration of frequency swept pulses of acoustic wave 23 p4012 A67-40869

Threshold power dependence on temperature and photoelasticity for stimulated Brillouin scattering in crystalline and fused quartz 24 p4204 A67-42365

Perturbation theory for exchange forces using Brillouin and Schroedinger equations 24 p4194 A67-43115

BRILLOUIN FLOW

S ELECTRON BEAM

BRILLOUIN ZONE

Landau level structure and transition matrix elements of InSb near Brillouin zone center during valence band cyclotron resonance 05 p0870 A67-17193

OPW calculation of six symmetry points in wurtzite Brillouin zone of CdS, using pseudopotential techniques 06 p1058 A67-18903

Induced absorption in far IR by impurities and defects of single crystal of potassium bromide 09 p1557 A67-22571

De Haas-van Alphen effect in bismuth telluride over range of carrier concentrations, noting existence of low mobility heavy mass band 17 p2912 A67-32268

BRISTOL-SIDDELEY OLYMPUS 593

TURBOJET ENGINE

Bench and flight tests of twin spool axial flow turbojet power plant for Concorde aircraft

[ASME PAPER 67-GT-8] 11 p1854 A67-24796
BRITTLENESS
 SA EMBRITTLEMENT
 SA HARDNESS
 Stress required for brittle fracture of alumina at room temperature based on theory of dislocation movement of cracks 01 p0092 A67-10054
 Griffith energy criterion and stress-strain environmental criterion for fractures in brittle cracked metallic plate 03 p0523 A67-13467
 Brittle fracture of Be tube under differential thermal contraction-induced plastic strain 03 p0445 A67-13470
 Book on dynamic strength, brittleness, plasticity and ductility of metals 05 p0907 A67-16031
 Brittle fracture crack theory for elastic body weakened by initially wide crack 05 p0923 A67-17179
 Tensile tests performed on alpha titanium between -321 and 75 degrees F, discussing ductile-to-brittle transition, microcrack formation and brittle fracture mechanics 06 p1014 A67-17807
 Particle microhardness and microbrittleness measured in powdered refractory compounds, noting relation to electron configuration 06 p1015 A67-17846
 Niobium addition effect on mechanical properties of steel, noting improvement of tensile strength and cold brittleness threshold decrease 06 p1018 A67-18235
 Thermostability of refractory materials and effects of high brittleness on thermal stress resistance of structural elements under single and multiple heat treatment and loads 07 p1198 A67-19128
 Hydrogen brittleness in Ti alloys, noting conditions of development 07 p1206 A67-19283
 Propagation of brittle cracks in body under compression, discussing theory of resistance of brittle bodies to compression 07 p1263 A67-20030
 Cold brittleness, impact toughness and crack resistance of titanium alloys at low temperatures 09 p1518 A67-21966
 Brittle strength of orthotropic materials investigated for proposed phenomenological fracture condition 14 p2399 A67-28103
 Cross slip and slip character related to fatigue, brittle fracture and strain hardening in crystal solids 16 p2772 A67-31299
 Fracture surface markings and topography for transgranular and intergranular paths studied with electron microscope 16 p2772 A67-31300
 Hydrostatic pressure effects on brittleness in Cr and yielding in center annealed iron specimen studying brittle-ductile transition of former 16 p2689 A67-31328
 Extension of plastic zone in direction of path of moving brittle crack, studying properties of plastic zone to crack length ratio 17 p2960 A67-32633
 Strength of single crystals, amorphous materials and other brittle materials lacking grain boundaries, noting loading rate dependence 18 p3069 A67-33491
 Brittle coatings for stress distribution analysis during static and dynamic loading, describing chemical composition and characteristics and giving formulas and diagrams 18 p3045 A67-33741
 Plasticity and brittle fracture conditions combined for stability criteria derivation 18 p3144 A67-34174
 Particle microhardness and microbrittleness measured in powdered refractory compounds, noting relation to electron configuration 20 p3471 A67-37588
 Hooke law type anisotropic fiberglass reinforced plastic, discussing elastic deformation and brittle fracture, using revised Mises ellipse equation 21 p3649 A67-37907
BROADBAND AMPLIFIER
 MOS-FET broadband frequency doubler circuit 03 p0382 A67-13671
 High power broadband traveling wave tube YH 1041 as transmitting tube for satellite radio communication, discussing mechanical layout and operational characteristics 08 p1307 A67-21446
 Electrostatically focused extended interaction S-band klystron amplifier using helical buncher resonators for interplanetary spaceborne communication systems 09 p1477 A67-22252

Small signals of wideband and high gain multicavity klystron amplifier showing similarity to traveling wave tube 09 p1478 A67-22254
 Multiple carrier measurements using TWT for application to satellite communications 15 p2438 A67-30140
 Book on analysis and synthesis of tunnel diode circuits including equivalent circuits, amplifiers, etc 16 p2636 A67-30997
 Organic dyes as broadband pulsed light amplifiers, noting input frequency relation to laser oscillation 20 p3460 A67-36855
 Compact ionospheric station for six fixed frequencies, compared with automatic station 21 p3586 A67-39047
BROMIDE
 S CESIUM BROMIDE
 S POTASSIUM BROMIDE
 S SODIUM BROMIDE
BROMINE
 Laser transition in Br 2, Br 2 and Sn in pulsed discharges of boron chloride, hydrogen bromide and stannic chloride respectively 08 p1339 A67-21379
 Gaseous chemical reaction dynamics analyzed with monochromatic laser light-induced photocatalysis 17 p2868 A67-32772
BROMINE COMPOUND
 IR chemiluminescence in hydrogen-diatomic bromine and hydrogen-hydrogen bromide IR chemiluminescence in hydrogen-diatomic bromine and hydrogen-hydrogen bromide 18 p2996 A67-33786
BRONCHIAL TUBE
 Bronchial tube diameter makes possible alveolar ventilation with minimum metabolism or entropy production in musculature 09 p1454 A67-21986
BROWNIAN MOTION
 Expression defining condition under which Brownian movement of universe affects Brownian movement of single electron 15 p2554 A67-29316
BRUDERHEIM METEORITE
 Rare earth elements distribution and component minerals in Bruderheim meteorite, using phase separation method 21 p3702 A67-38126
BUBBLE
 Nucleate boiling mechanism in superheated binary mixtures obtained from extension of theories of van Wijk, Vos and van Stralen by Scriven and Bruijn 04 p0720 A67-14637
 Incipience, growth and detachment of boiling bubbles in saturated distilled water from artificial nucleation sites of given geometry and size in heated metal surface 04 p0734 A67-15847
 Wall pressure distribution in turbulent reattachment bubble calculated by splitting bubble into large number of small control volumes 08 p1320 A67-20451
 Temperature induced surface tension variation effect on motion of bubbles and drops, noting surface active substances 08 p1321 A67-20711
 Flow visualization technique study of wake existence behind large air bubble rising through quiescent liquid 08 p1321 A67-20712
 Stability of radial motion of spherical gas bubble in incompressible inviscid fluid under external pressure 10 p1624 A67-23028
 Monograph on theory of decompression sickness and application to diving tables, including calculation of critical size of localized bubbles formed from dissolved nonrespiration-involved gases in tissues [DVL-623] 11 p1748 A67-25036
 Collapse of isolated spherical vapor-air cavitation pocket moving toward solid surface in incompressible fluid 12 p1927 A67-25320
 Surface film boiling under free convection 13 p2222 A67-26532
 Gas embolisms and gas bubble formation in tissue [DVL-615] 13 p2059 A67-26849
 Deviation from sphere shape of drop moving through viscous media and dependence on Weber number, size, etc 14 p2302 A67-28235
 Time dependent pressure distribution and threshold acceleration for bubble formation in longitudinally vibrating flexible liquid filled cylinder [ASME PAPER 67-FE-1] 14 p2304 A67-28354
 Bubble stabilization in pure viscous liquid contained in sinusoidal vibrated tank

[ASME PAPER 67-FE-3] 14 p2304 A67-28356
 Droplets and bubbles in liquids studied using general thermodynamic equilibrium criteria 17 p2971 A67-33043
 Bubble frequency, departure diameter and rise velocity relationship in nucleate boiling 20 p3553 A67-36934
 Spherical gas bubble pulsations under pressure waves analyzed in compressible and incompressible fluids 20 p3422 A67-37065
 Autopropulsion of gas bubble by rocket effect noting equivalent particle concept and applications to boiling, flow and cavitation erosion 24 p4141 A67-41904
BUBBLE CHAMBER
 SA CAPTURED AIR BUBBLE VEHICLE
 Processing and obtaining phase holograms of elementary particle tracks in gelating bubble and emulsion chambers 18 p3049 A67-34387
BUCCANEER AIRCRAFT
 S BLACKBURN B-103 AIRCRAFT
BUCKLING
 SA COMPRESSION BUCKLING
 SA CREP BUCKLING
 SA ELASTIC BUCKLING
 SA EULER BUCKLING
 SA SHELL STABILITY
 SA STRAIN
 SA THERMAL BUCKLING
 Buckling loads of reinforced cylindrical shells, discussing size and placement of stiffening members 03 p0521 A67-13019
 Boundary condition effect on buckling of circular shell of given thickness 03 p0524 A67-13786
 Modes effect on plastic buckling of compressed cylindrical shells, considering deformation theory vs incremental theory 04 p0710 A67-14852
 Shallow spherical shells with uniform and/or point loads in prebuckled or postbuckled configuration treated by approximate solution [ASME PAPER 66-WA/APM-21] 04 p0714 A67-15411
 Dynamic displacements of thin spherical shell buckling under uniform pressure 05 p0920 A67-16825
 Local buckling strength of high strength axially compressed maraging steel cylinders circumferentially prestressed with high strength epoxy-protected fiberglass filament windings 05 p0923 A67-17211
 Buckling isolator system for carrier aircraft landing and catapult shock environment allowing use of available clearance for dynamic deflection 05 p0814 A67-17459
 Generalized Stodola iteration method for computer analysis of axisymmetric buckling of ring-stiffened orthotropic shells of revolution [AIAA PAPER 67-109] 06 p1103 A67-18339
 Initial geometric and boundary condition imperfection effect on stability of shallow spherical shells under uniform pressure [AIAA PAPER 67-111] 06 p1104 A67-18453
 Buckling stability of compressed plate with transverse deflections, using energy method 06 p1109 A67-18747
 Statistical analysis discrepancy in physical experimental values of buckling pressures of spherical shells 06 p1111 A67-18876
 Inextensional buckling of thin conical shell under axial compression [AIAA PAPER 66-125] 10 p1717 A67-23129
 Buckling test data for internal integral ring-stiffened aluminum cylinders under combinations of axisymmetrical axial load and external lateral pressure 11 p1875 A67-24611
 Torsional buckling stress of orthotropic cylindrical shells with high order terms due to internal pressure rise 11 p1876 A67-24701
 Flat plate loading effects for large displacements, determining solution to plates of arbitrary shape under general loading by iterative matrix technique 13 p2217 A67-26704
 Dynamic plastic buckling of thin strips, thin and moderately thick cylindrical shells and rods under longitudinal and radial impact and compression 14 p2397 A67-28088
 Nonlinear dynamic response of thin walled shells of revolution 14 p2397 A67-28090
 Shear buckling of thin walled structural sections, noting reinforcement methods including use of swedges 17 p2957 A67-32026
 Strain amplitude and flange width-to-thickness ratio effects on dynamic buckling

in modified I-beams subjected to pure reverse bending 17 p2958 A67-32030
 High modulus high strength inorganic filament windings tested for tension and buckling-critical structures, considering weight decrease and operating temperature increase 19 p3245 A67-35553
 Differential equations and potential for simply supported anisotropic sandwich plate under compression and shear stresses above buckling limit 19 p3341 A67-35575
 Prestressed-shell buckling, using Budlanskil-Koiter tensor nonlinear equilibrium equations by numerical analysis 19 p3343 A67-35778
 Dynamic stability of spherical segments subjected to impact loading, discussing buckling in relation to rise in center and time dependence 22 p3910 A67-39456
 Curved plate postbuckling behavior, deriving curved plate effective width formula 23 p4080 A67-41475
 Curved plates tested under axial compression to prove curved plate buckling and postbuckling behavior formula, discussing stress distribution measurement 23 p4080 A67-41476

BUDGET
 SA ENERGY BUDGET
 SA HEAT BUDGET
 Planning-Programming-Budgeting System /PPBS/ implementation by Federal agencies and relation to space activities [AAS PAPER 66-150] 08 p1430 A67-20970
 Planning-Programming-Budgeting System /PPBS/ implementation by Federal agencies and relation to space activities [AAS PAPER 66-150] 13 p2232 A67-27551
 National space program planning viewpoint of Executive Branch of Federal Government [AIAA PAPER 67-628] 20 p3556 A67-37619

BUFFER
 Secretary activity of algal *Chlorella* cells effect on buffering characteristics of Tris or sodium citrate-citric acid suspending fluid 21 p3573 A67-37729
 Transmission buffer overflow prevention in telemetry data compressors using adaptive queueing control system 21 p3586 A67-38956

BUFFETING
 HF response of shell-type structures to buffeting aerodynamic environment [AIAA PAPER 66-81] 02 p0337 A67-11930
 Launch vehicle response in lateral vibration modes to nonstationary random transonic buffeting excitation 22 p3907 A67-40167
 Buffet limit for aircraft wings in transonic region based on boundary layer theory, determining transonic pressure distribution and separation points 23 p3931 A67-41311

BUILDING MATERIAL
 Clinographic polariscope for surface measurement of stress-strain in building materials, noting operation and results 14 p2395 A67-27973
 Synthetics in aircraft and rocket construction, recommending duroplastics 20 p3473 A67-36453

BUILDING STRUCTURE
 S DOOR
 S WALL

BULK MODULUS
 Fluid bulk modulus and density effect on typical hydraulic servomechanism [ASME PAPER 67-FE-19] 14 p2252 A67-28366
 Empirical equations for compressive properties of liquids, noting applicability at high pressures 17 p2841 A67-33386

BULKHEAD
 Aluminum alloy composite bulkhead fabrication under tensile stress with improved bonding uniformity 03 p0430 A67-13556

BUNDLE DRAWING
 Drawing technique for bundles of sheathed superalloy wires noting sheathing, stress relief, interfilament welding and oxide bonding 21 p3643 A67-37878

BUOY
 S FLOTATION SYSTEM

BUOYANCY
 SA RAYLEIGH NUMBER
 One-dimensional compressible flow, considering buoyancy forces as closed-form solution of Navier-Stokes equations for unknown temperature-dependent coefficient of viscosity 10 p1625 A67-23135
 Parameter values excluded by existence conditions for buoyant dissipative motions in

vertical channels 17 p2840 A67-33138
 Gravity and buoyancy effects on slip ratio, void fraction, flow model and boiling heat transfer [ASME PAPER 67-HT-63] 20 p3549 A67-36745
 Gas-solid interactions and buoyancy relation, discussing fluid density effect on Archimedes principle 24 p4119 A67-42695

BURGER EQUATION
 High resolution X-ray diffraction topography of dislocation structure of Si crystal 05 p0860 A67-16078
 Statistical initial value problem for Burger model equation of turbulence, examining velocity correlation functions, energy spectra and other statistical properties 05 p0794 A67-17419
 Wave propagation in plasma with anisotropic pressure studied using modified Burgers equations, examining effect of collisions 24 p4197 A67-42260

BURN INJURY
 Visual acuity decrement from laser lesion in fovea of stump tail macaque monkeys 05 p0756 A67-16287

BURNER
 Ignition energy, quenching distance, flame stability and gas turbine burner performance of ammonia-air mixture 18 p3109 A67-33843
 Thor SLV upper stage Burner 2 design, performance and cost 21 p3713 A67-38379

BURNING PROCESS
 SA COMBUSTION
 Combustion process monitoring in rocket engines [JPL-TR-32-1124] 13 p2188 A67-26848
 Burning velocities, temperatures and burnt gas composition of flammable methane-rich perchloric acid mixtures 14 p2406 A67-28544
 Flame properties of flammable ethylene-rich perchloric acid mixtures 14 p2406 A67-28545
 Flame properties of flammable ethane-rich perchloric acid mixtures 14 p2406 A67-28546
 Laminar flame speeds and composition flammability limits at low pressure for ternary mixtures of hydrogen and oxygen with ammonia and nitrous oxide 14 p2406 A67-28547
 Ignition response of solid propellants described with model including surface regression with verification of igniter fuel and pressure effects 15 p2581 A67-29988
 Terminating solid propellant combustion by rapid drop in pressure 15 p2582 A67-29998
 Aluminum particle combustion in solid rocket grains, noting drop formation mechanism and droplet combustion analysis [ONERA-TP-486] 17 p2926 A67-32697
 Ignition conditions of pore walls in burning of porous charge, assuming ideal pores and same charge composition throughout system 17 p2974 A67-33142
 Ignition and combustion characteristics of single aluminum and beryllium particles burning in gaseous environment, discussing oxides role 18 p3149 A67-33796
 Burning in unmixed reactants for high enthalpy inviscid flow of opposed streams studied for one-step reaction model and Lewis-Semenov number 20 p3554 A67-37132
 Admittance function for burning surface by solving differential equation and satisfying boundary conditions, discussing frequency peaks qualities 20 p3554 A67-37255
 Oxygen-hydrogen mixtures burning characteristics in shock wave tube, studying ignition processes with schlieren photographs 21 p3731 A67-38366
 Fuel burnout processes in inlet flow of secondary air stream to turbine combustion chamber determined by working mechanism in inlet section of 22 p3869 A67-40453
 Flame activation energy and combustion process order based on homogeneous reactor model for mean temperature coefficient determination 23 p4082 A67-41141
 Monograph on external burning in supersonic streams, discussing heat addition, fluid-mechanical model, use of characteristics method, Chapman-Jouget detonation, etc [TG-912] 24 p4254 A67-42386

BURNING RATE
 SA FLAME PROPAGATION
 Normal burning velocity theory, considering Cauchy problem for initial equations 01 p0187 A67-10998
 Extension of analysis of unsteady state

model for combustion of solid propellant to include nonlinearities of second order 01 p0141 A67-11158
 Hybrid propellant burning rate determination using external gamma emission source 01 p0112 A67-11420
 Steady state combustion analysis of solid propellant rocket motors extended by studying influence of grid sizes and number of steps used in numerical analysis 01 p0143 A67-11449
 Spin effects on rocket nozzle performance show higher combustion pressures and burning rates due to blockage of nozzle throat 02 p0303 A67-11947
 Mariner IV midcourse 50-lb thrust pressure-controlled monopropellant hydrazine propellant system, predicting impulse and velocity error as function of burn time [AIAA PAPER 66-948] 02 p0304 A67-12282
 Average burn rate, average pressure relationships in solid rockets 04 p0724 A67-15250
 Ignition pressure transient in solid rocket motors, examining chamber filling interval, flame propagation, heat transfer correlation, burning area, etc 05 p0873 A67-16513
 Nonlinear fluctuations in gunpowder combustion rate at various temperatures and harmonically varying pressure 05 p0927 A67-16991
 Metal fiber addition to basic propellant increases burning rate 05 p0872 A67-17215
 Liquid droplet combustion at high pressures revealing effects of vapor source distribution on predicted burning time at supercritical pressures 05 p0929 A67-17359
 Nonstationary combustion of powder under action of pressure pulse to determine temperature field variation and burning rate during transient process 06 p1112 A67-17957
 Burning rate of N powder dependence on light flux density and initial temperature range 06 p1112 A67-17958
 Solid propellant burning rate, combustion gas influx, tube geometry and propellant and tube thermophysical properties [AIAA PAPER 67-102] 06 p1074 A67-18282
 Continuous high resolution measurement of solid propellant burning rate using resonant LC circuit [AIAA PAPER 67-69] 06 p1072 A67-18450
 Combustion dynamics of solid propellants in LF range, discussing equipment and results [AIAA PAPER 67-70] 06 p1073 A67-18451
 Initial solid propellant temperature effect on constant pressure burning rate based on granular diffusion flame model /GDFM/ 08 p1375 A67-20581
 Regression rates in transient regime of composite solid rocket propellant grains upon sudden opening of exhaust port 08 p1373 A67-20803
 Rate of formation of tungsten oxide in porous sample, noting increase in rate of oxidation due to porosity effect 11 p1809 A67-24915
 Solid fueled rocket powered MHD generators with high power densities 12 p1898 A67-25382
 Propellant composition influence on finite-amplitude axial wave mode instability in solid propellant rockets [AIAA PAPER 66-600] 12 p1988 A67-25909
 Combustion of pure liquid monopropellant droplet burning in own combustion products at low Reynolds numbers 14 p2376 A67-28552
 High density moisture-proof noncrystalline family of gas generator propellants, surveying burning rates, physical properties and application 15 p2544 A67-29980
 Combustion instability, transient burning during ignition and extinction by depressurization investigated in nonsteady burning of solid propellants 15 p2580 A67-29984
 Burning rate vs pressure and other factors as function of composite solid propellant composition and oxidizer particle size distribution 15 p2580 A67-29985
 Kinetics and energetics of condensed phase thermal decomposition reactions of ammonium perchlorate composite propellants analyzed, using differential scanning calorimetry 15 p2544 A67-29989
 Parameters determining magnitude of acceleration effect on burning rate increase of aluminized and nonaluminized composite solid propellants 15 p2581 A67-29991

Combustion mechanism of ammonium perchlorate propellants, discussing gasification, decomposition, pressures, binders, burning rates, temperatures, etc 18 p3108 A67-33812

Deflagration of ammonium perchlorate studied using cleaved sections of large single crystals grown from water solution, discussing burning rate and combustion zone 18 p3108 A67-33814

HF response of local burning rate in laminar diffusion flames subjected to transverse sound waves in free stream 18 p3108 A67-33831

Metallized and nonmetallized composite solid propellant burning rates, analyzing effects of acceleration, noting agglomeration and nonnormal conditions [AIAA PAPER 67-470] 18 p3157 A67-33940

Nitrate ester monopropellants studied for heat-up, ignition and combustion in high temperature nitrogen gas under moderate/high pressures, noting burning rates [AIAA PAPER 67-480] 18 p3158 A67-33949

Effect of additives on hydrazine nitrogen trioxide droplet flame structure and burning rate [AIAA PAPER 67-482] 18 p3158 A67-33951

Combustion rate and subsurface activity of metallized burning polymers, stressing heat conduction role and applications to propellant combustion [CI PAPER 67-3] 19 p3344 A67-34998

Volt-ampere characteristics of long free-burning convection-free DC and AC arcs in nitrogen, argon and carbon dioxide 19 p3280 A67-35149

Conditions of stable burning of electric arc stabilized by gas stream in DC plasma arc torch, determining threshold current 19 p3281 A67-35150

Mariner IV midcourse 50-lb thrust pressure-controlled monopropellant hydrazine propellant system, predicting impulse and velocity error as function of burn time 21 p3712 A67-37797

Turbulent gas combustion, showing burning rate as function of combustion temperature, pressure and chemical reaction rate in flame 21 p3732 A67-38527

Liquid fuel polydisperse jet total combustion time curve determined based on droplet of fuel and medium parameters 21 p3732 A67-38528

Continuous high resolution measurement of solid propellant burning rate using resonant LC circuit [AIAA PAPER 67-69] 21 p3688 A67-38857

Microwave use in measuring burning rate of solid propellant rocket motors and in detection of porosity in nonconducting materials 22 p3795 A67-39198

Solid propellant burning rate, combustion gas influx, tube geometry and propellant and tube thermophysical properties 23 p4084 A67-41723

High density moisture-proof noncrystalline family of gas generator propellants, surveying burning rates, physical properties and application 24 p4207 A67-42921

Second order nonlinear differential equation derived for pressure-time curve required for ideal solid propellant rocket motor 24 p4208 A67-42923

BURNOUT

Extra-atmospheric coning motions of Tomahawk sounding rocket caused by dynamic instability after motor burnout 08 p1405 A67-20502

Error in application of WKB method to linearized postburnout equation of motion of sounding rocket 08 p1406 A67-20510

BURST

S METEOR BURST

S RADIO BURST

BUTADIENE

SA POLYBUTADIENE

Esterification rates of aliphatic carboxylic acids, acid terminated polybutadienes, etc, and steric environment in vicinity of acid groups 04 p0564 A67-14473

BUTYL

Resistance welds produced by butyl sealant prevent passive films formation on aluminum and magnesium alloys 12 p1948 A67-25287

BUTYLENE

S POLYISOBUTYLENE

BUTYRIC ACID

Optical resolution and configuration of

trans-2, 3-epoxybutyric acid by 07 p1137 A67-20015

BY-PASS ENGINE

Isolated nacelle design for high by-pass ratio turbofan engines, particularly pylon mounted engine [SAE PAPER 660732] 01 p0140 A67-10632

Nacelle design for high inlet pressure recovery and low external cowl drag, for high by-pass fan engine subsonic aircraft [SAE PAPER 660733] 01 p0140 A67-10633

Thrust reverser efficiency on high by-pass ratio turbofan engines [SAE PAPER 660736] 01 p0140 A67-10635

By-pass propulsion systems development for V/STOL transports including aerothermodynamic aspects [AIAA PAPER 64-606] 03 p0502 A67-12902

Optimization of power plant of short range aircraft accounting for high by-pass ratios 04 p0687 A67-14530

High by-pass vs low by-pass engine installations, discussing effects of nacelle shape, wing proximity, inlets, thrust reverses and accessory location [SAE PAPER 660735] 04 p0690 A67-15779

Short-haul airliner /Fokker F-28 Fellowship/, noting moderate size, twin by-pass engines, high speed, landing field requirements, etc 16 p2596 A67-31012

C

C-5 AIRCRAFT

C-5A aircraft design load criteria for landing gear of large aircraft that must operate from semlimproved airfields [AIAA PAPER 65-711] 03 p0360 A67-13781

Lockheed 500, derivative of USAF C-5A transport, discussing logistic capabilities, economics and representative approaches [AIAA PAPER 66-1019] 03 p0362 A67-14152

Lockheed C-5A cargo aircraft, discussing airframe construction, landing gear, weight and balance system, use of TI and honeycomb materials, etc 07 p1130 A67-20230

Lockheed C-5 cargo transport aircraft design optimization 07 p1130 A67-20231

C-5A hydraulic system design for high power and capacity application, noting landing gear and ramps 09 p1444 A67-22130

Lockheed C-5 quantitative maintainability program and application to air vehicle utilization and cost effectiveness 11 p1745 A67-24939

C-5A landing gear, discussing design and evolution of requirements such as kneeling, steering, weight and flotation 17 p2794 A67-31988

C-5A flight control system, examining subsystems, handling qualities, hydraulic power distribution and mechanical failures 17 p2794 A67-31997

C-BAND

C-band traveling wave maser for monopulse radar, analyzing saturation, recovery, duplexing and gain phase stability 08 p1293 A67-20691

Franck-Condon factors and r centroids for C-X band system of astrophysically important zirconium oxide molecule found in S type stars 08 p1354 A67-20702

Miniaturized C-band digital latching phase shifter for combined advantages of waveguide and stripline 08 p1305 A67-21227

C-band solid state YIG serrodyne theory and operation, outlining phase velocity modulation of magnetostatic modes 19 p3196 A67-35661

C LAYER

Daytime profile of electron density in C and D layers of ionosphere from measurements of surface ultralong wave fields and atmospheric pressure profile 05 p0801 A67-17131

Daytime profile of electron density in C and D layers of ionosphere from measurements of surface ultralong wave fields and atmospheric pressure profile 21 p3619 A67-38474

C-141 AIRCRAFT

Production program and MAC operational experience of C-141A jet cargo transport [AIAA PAPER 66-791] 01 p0009 A67-10534

C-141A cargo aircraft structural analysis, discussing design, load and gust criteria, flight and static test programs, vibration and noise control

[SAE PAPER 660669] 01 p0010 A67-10576

Lockheed C-141A military transport and engineering evaluation for civil certification and military acceptance, noting commercial C-5A 03 p0361 A67-14018

Category II Systems Evaluation Test of C-141A aircraft 07 p1129 A67-19616

C-141A cargo aircraft structural analysis, discussing design, load and gust criteria, flight and static test programs, vibration and noise control [SAE PAPER 660669] 07 p1131 A67-20232

C-141A engineering development test program, discussing flight, accelerated service and all-weather testing [AIAA PAPER 67-409] 15 p2422 A67-30376

Regenerative dual tandem cable servoactuator design for use in manual and automatic spoiler control system of C-141 Star Lifter 20 p3366 A67-37550

C-160 AIRCRAFT

S TRANSALL C-160 AIRCRAFT

CABIN ATMOSPHERE

SA PRESSURIZED CABIN

SA SPACE CABIN ATMOSPHERE

Spacecraft cabin atmosphere, comparing pure oxygen with two-gas atmosphere 16 p2617 A67-30776

CABLE

S COAXIAL CABLE

S SUBMARINE CABLE

S TRANSMISSION LINE

CABLE FORCE RECORDER

Equilibrium configuration and tension of flexible cable in uniform flow field, considering tangential drag force and weight effects 13 p2051 A67-27587

CADMIUM

SA NICKEL-CADMIUM BATTERY

Diffusion parameters and solubility of Cd in InAs measured with aid of radioactive isotopes compared with diffusion coefficient measurement by p-n junction method 01 p0128 A67-10082

Laser saturation of photoconductivity and determination of imperfection parameters in sensitive photoconductors such as single crystal of cadmium 02 p0251 A67-11879

Strain rate dependence of critical shear stress in cadmium single crystals used in activation energy determination 07 p1234 A67-20109

Diffusion parameters and solubility of Cd in InAs measured with aid of radioactive isotopes compared with diffusion coefficient measurement by p-n junction method 08 p1371 A67-21459

Intracrystalline field and spontaneous polarization in barium titanate studied by EPR spectrum of Cd-3 ions 09 p1554 A67-21976

Cadmium negative electrode mechanism, noting active material redistribution and anodic oxidation 09 p1445 A67-22176

Intracrystalline field and spontaneous polarization in barium titanate studied by EPR spectrum of Cd-3 ions 17 p2923 A67-33313

Time and temperature dependent diffusion of vaporized Zn and Cd in n-type InAs 19 p3299 A67-34760

Partial molal entropies of doubly ionized aqueous Zn, Cd and mercurous and mercuric ions calculated, using literature data 20 p3376 A67-36792

Quenched structures and precipitation in Al-Cu alloys with and without traces of Cd studied electromicroscopically, showing possible CD stabilizing effect 24 p4173 A67-42166

CADMIUM ALLOY

Room temperature recombination radiation induced by Lorentz field in InSb and ternary alloy of mercury, cadmium and tellurium under cross field conditions 03 p0496 A67-13675

Performance characteristics of nonstoichiometrically doped p-n junctions in Cd-Hg-Te alloy operated as IR photovoltaic detector 14 p2366 A67-28496

CADMIUM ANTIMONIDE

Tensor components of thermal emf of CdSb measured by method without producing thermoelectrical eddy currents 01 p0129 A67-10137

Hall effect and magnetoresistance effect measured on p-and n-CdSb single crystals above 77 degrees K and magnetic fields up to 7500 gauss 06 p1054 A67-18824

Galvanomagnetic effects and band structure of p-type cadmium

antimonide 06 p1064 A67-18942
Hole effective masses in p-type CdSb determined by measuring magnetoresistance effect and magnetic susceptibility 12 p1987 A67-26225
CdSb single crystals doped with Au at liquid helium temperature studied for temperature dependence and Hall effect 14 p2372 A67-28757
CdSb polycrystals of different structural patterns investigated for dependence of electrical conductivity, Hall mobility and thermal EMF 14 p2372 A67-28758
Electric and thermoelectric effects in single crystals of zinc-cadmium-antimony solid solution, measuring electrical conductivity, Hall constant and thermoelectric power 15 p2540 A67-30029
Impurities compensated p-type cadmium antimonide single crystals, determining Hall effect temperature dependence and specific resistance 21 p3876 A67-37868

CADMIUM COMPOUND

Optical and magneto-optical phenomena in CdSnAs sub 2, discussing reflection and absorption spectrum, optical activity, double refraction, dielectric constant, etc 01 p0128 A67-10094
Optical self-absorption and dielectric constant of cadmium oxide thin film in case of high electron degeneration 04 p0683 A67-15655
Photoconductivity, edge emission spectrum, longitudinal optical phonon coupling and eigenfrequencies for linear chain of Cd-Se-Cd-S-Cd... atoms 05 p0870 A67-17196
Cadmium selenide arsenide single crystals obtained free of cracks, using synthesis method 06 p1048 A67-17840
Saturation magnetization of mixed cadmium ferrites of spinel structure 06 p1050 A67-18182
Metastable exciton states of cadmium and lead iodide obtained from fundamental reflectivity spectra 06 p1060 A67-18915
Semiconductor lasers using single and double photon optical excitation 06 p1013 A67-18930
Shubnikov-de Haas effect and electron band structure of cadmium arsenide, investigating temperature and orientation dependences 06 p1064 A67-18947
Impurities effect on electrical and thermomagnetic properties of cadmium tin arsenide 13 p2184 A67-27707
EPR applied to investigation of various semiconductors containing iron, and Mn at liquid nitrogen temperature 14 p2373 A67-28968
Hall coefficient and reluctance dependence on magnetic field inductance in p-type cadmium tin arsenide samples from 250 to 411.7 degrees K 15 p2543 A67-30253
Cadmium selenide arsenide single crystals obtained free of cracks, using synthesis method 17 p2922 A67-33218
Cadmium compounds catalytic effect on ammonium perchlorate decomposition rate and ignition temperature 18 p3107 A67-33810
Temperature effect on gold diffusion in crystalline and glassy cadmium germanium arsenide samples 19 p3301 A67-34776
Thin CdAs films thermal deposited in vacuum on various substrates investigated for electric properties 19 p3305 A67-35577
Epitaxial growth of gold on cadmium iodide surface studied with transmission electron microscopy, discussing diffraction patterns and substrates preparation 21 p3687 A67-39140

CADMIUM FLUORIDE

Photoexcited electroluminescence spectra of rare earth ions in cadmium fluoride semiconductor single crystal 24 p4205 A67-42893

CADMIUM SELENIDE

Optical pumping with diode laser into Fabry-Perot resonator face of thin highly-absorbing semiconductor, noting variable mode spacing including single mode output 01 p0091 A67-10879
Cadmium selenide single crystals subjected to gas discharge saturation of current-voltage characteristic, noting section with negative differential resistance 03 p0489 A67-13146
Electron-hole pair energy in CdS and CdSe single crystals 03 p0490 A67-13155
Spectral characteristics of two-photon optical excitation and light emission from

CdSe semiconductor laser with modulated Q-factor 04 p0633 A67-15299
Time-dependent response of polycrystalline cadmium selenide thin film transistor to transient high energy radiation 04 p0589 A67-15718
Direct measurement of dispersion properties of cadmium sulfide and CdS-CdSe crystals, using Obreilmov-Fresnel diffraction method, growing crystals by synthesis 05 p0861 A67-16396
Internal modulation of IR gas laser using cadmium sulfide or selenide single crystals 05 p0824 A67-16914
HF measurements of thin film CdSe transistors, discussing equivalent circuit, stability factor and power gain 05 p0776 A67-17091
Cadmium selenide arsenide single crystals obtained free of cracks, using synthesis method 06 p1048 A67-17840
Shottky theory and electron affinity of semiconducting CdSe from DC I-V characteristics and work function of Au, Ag and Cu contacts with CdSe 07 p1231 A67-19491
Absolute value of photoconductivity in polycrystalline high resistivity CdS and CdSe SHF field and experimental determination of barrier amplification factor and intercrystalline barrier height 08 p1370 A67-20997
Laser emission from electron beam excitation of CdS crystals due to crystal uniformity and radiative transitions resulting from CD-rich growth conditions 09 p1510 A67-21569
Cadmium selenide single crystals subjected to gas discharge saturation of current-voltage characteristic, noting section with negative differential resistance 10 p1689 A67-23095
Electron-hole pair energy in CdS and CdSe single crystals 10 p1690 A67-23103
High resistivity cadmium selenide vacuum deposited films dielectric constant and electronic properties measured for different parameters 11 p1851 A67-25032
Nature of photoelectromotive force of cadmium selenide with Cu, Ag, Au, Pt vacuum-deposited on surface 14 p2367 A67-28527
Generation mechanism of laser emission in cadmium sulfide-cadmium selenide crystals in presence of two-photon excitation at various temperatures 14 p2331 A67-28534
Photoionization quantum yield in intrinsic-absorption region of cadmium selenide films 14 p2372 A67-28853
CW operation of ultrathin CdSe platelet laser excited optically by HeNe laser 15 p2500 A67-29821
Internal modulation of IR gas laser using cadmium sulfide or selenide single crystals 16 p2685 A67-30891
Refractive index dispersion of CdS_{0.9}Se and CdTe crystals in visible and infrared spectral range at room temperature 16 p2732 A67-31481
Electron radiation damage in CdSe crystals at cryogenic temperatures, noting electrical conductivity and cathodoluminescence properties before and during damage 17 p2916 A67-32838
Cadmium selenide arsenide single crystals obtained free of cracks, using synthesis method 17 p2922 A67-33218
Slow response of cadmium selenide thin film transistors related to trapping levels in insulator 18 p3015 A67-34557
Nature of photoelectromotive force of cadmium selenide with Cu, Ag, Au, Pt vacuum-deposited on surface 23 p4039 A67-40934
Generation mechanism of laser emission in cadmium sulfide-cadmium selenide crystals in presence of two-photon excitation at various temperatures 23 p4040 A67-40941

CADMIUM-SILVER BATTERY

S SILVER-CADMIUM BATTERY

CADMIUM SULFIDE

Oscillations of optical absorption in cadmium sulfide in strong electric fields, noting electron transfer between Wannier discrete level 01 p0127 A67-10070
Gamma radiation and fast neutron effects on dark resistance, photoconductivity, majority carrier mobility, recombination kinetics, etc, in CdS single crystal 01 p0128 A67-10086
Generation of current oscillations by

electroacoustic effects in semiconducting cadmium sulfide 01 p0130 A67-10199
Low energy proton bombardment damage in thin film cadmium sulfide and in single crystal silicon with silicone coating 01 p0037 A67-10476
Field effect transistors based on polycrystalline semiconducting layers of CdS deposited by silk 01 p0037 A67-10478
Spectral distribution of relative quantum yield of photoluminescence in polycrystalline cadmium sulfide films 01 p0133 A67-10510
Surface photopotential of cadmium sulphide single crystals under monochromatic illumination in alternating electric field, using voltage modulation method 01 p0134 A67-10807
Luminescence and conductivity of CdS single crystals, noting temperature effect and release mechanism of trapped electrons and holes 01 p0134 A67-10820
Two parallel carrier capture mechanisms at single recombination center in cadmium sulfide 01 p0138 A67-11298
Spectra and intensity vs excitation level and spatial distribution vs current density determined for optical radiation by electron excited cadmium sulfide 02 p0251 A67-11828
Current-voltage characteristics peculiarities of fine cadmium sulfide single crystals with nonohmic contacts 02 p0296 A67-11831
Different crystallization conditions and effect on Se surface structures on properties of p-n heterojunctions in Se-CdSe and Se-CdS rectifying cells and photocells 02 p0297 A67-11849
Impulse method for determining electron trapping parameters of cadmium sulfide-type crystals with one barrier contact exposed to continuous illumination 03 p0487 A67-12807
Laser emission in pure cadmium sulfide crystals bombarded by electron beams 03 p0433 A67-12812
Short wave length series of edge emission of cadmium sulfide single crystals at temperatures between 18 and 150 degrees K 03 p0488 A67-12813
Temperature dependence of spectral distribution of radiation, excitation and quantum output of green luminescence of cadmium sulfide films 03 p0433 A67-12889
Effect of thermal processing in various atmospheres and of additives of group I and III elements in periodic table on luminescent properties of cadmium sulfide 03 p0433 A67-12890
Electron-hole pair energy in CdS and CdSe single crystals 03 p0490 A67-13155
Time dependence of current in In-CdS-In sandwich plate system at various voltages, using X-and Z-cut monocrystal CdS 03 p0490 A67-13157
Electron-hole pair separation energy in CdS single crystal during 5 to 50 keV electron bombardment 03 p0490 A67-13160
Hall mobility, Seebeck and Nerst coefficients measured in temperature range from about 100 to 350 degrees K for scattering mechanisms of conduction electrons in n type CdS 03 p0493 A67-13351
Texture and electric conductivity of cadmium sulfide thin films 03 p0498 A67-13868
CdS thin film solar cells history, design, fabrication and performance 04 p0553 A67-14474
Cadmium sulfide film transducers for shear mode with various insertion losses, noting effect of uniformity in oblique c axes orientations 04 p0621 A67-15126
Direct measurement of dispersion properties of cadmium sulfide and CdS-CdSe crystals, using Obreilmov-Fresnel diffraction method, growing crystals by synthesis 05 p0861 A67-16396
Crystal structure defects and electroconductivity variations in CdS single crystals in oxygen ambient and effects of various surface treatments 05 p0862 A67-16605
Oscillation in CdS crystal by ruby laser induced two-photon excitation, noting proportionality of absorption coefficient to light beam intensity 05 p0821 A67-16667
Internal modulation of IR gas laser using cadmium sulfide or selenide single crystals 05 p0824 A67-16914
Charge forming in cadmium sulfide crystals under effect of applied electric

- field 05 p0868 A67-17065
- Structural changes in epitaxial CdS films grown on rock salt, mica and silver substrates analyzed by electron diffraction at various temperatures and values of electric field 06 p1047 A67-17599
- Optical energy gap of cubic CdS measured on evaporated mixed cubic-hexagonal layers 06 p1048 A67-17820
- Multilayer technique for evaporation of ohmic contacts onto CdS, noting V-I characteristics and noise spectrum of recrystallized layer 06 p1050 A67-18142
- Two-photon absorption spectrum of single crystal CdS, using polarized light and precise geometry 06 p1011 A67-18209
- OPW calculation of six symmetry points in wurtzite Brillouin zone of CdS, using pseudopotential techniques 06 p1058 A67-18903
- IR spectra of undoped and Li doped ZnSe and CdS 06 p1059 A67-18911
- Current saturation and phonon amplification induced instabilities in CdS crystals 06 p1066 A67-18958
- Threshold characteristics of photoresistors with noiseless contacts on CdS base 07 p1152 A67-19592
- Far field pattern of sheet-like laser beam from electron bombarded CdS and ZnO single crystals 07 p1196 A67-19798
- Spectral dependence of impurity photocurrent in single crystal CdS specimens in constant illumination 07 p1234 A67-20025
- Spectral distribution of photoconductance and conductance glow curves of CdS single crystals after vacuum heat treatment 07 p1237 A67-20179
- Elastic nonlinear interaction due to acoustic wave-carrier interaction in CdS, noting waveform distortion for zero acoustic dissipation 08 p1353 A67-20485
- Photovoltaic and photoresistant effects in cadmium sulfide thin films with recombination centers 08 p1368 A67-20728
- Solar cell model of CdS on copper sulfide 08 p1285 A67-20729
- Thin film CdS and CdTe solar cells compared for space applications 08 p1285 A67-20736
- Absolute value of photoconductivity in polycrystalline high resistivity CdS and CdSe SHF field and experimental determination of barrier amplification factor and intercrystalline barrier height 08 p1370 A67-20997
- Oscillations of optical absorption in cadmium sulfide in strong electric fields, noting electron transfer between Wannier discrete level 08 p1371 A67-21453
- Acoustic waves amplification in CdS crystal by electron-phonon interaction 09 p1558 A67-22591
- High field Hall effect of semiconducting CdS crystals with different mobilities, noting electron density and multiplication 10 p1689 A67-22908
- Chemisorbed oxygen effect on Hall mobility and conduction electron concentration of spray deposited CdS thin films 10 p1689 A67-22910
- Luminescence in cadmium sulfide mixed crystals of widely varying composition in presence of excitation by ruby laser emission 10 p1664 A67-23102
- Electron-hole pair energy in CdS and CdSe single crystals 10 p1690 A67-23103
- Time dependence of current in In-CdS-In sandwich plate system at various voltages, using X-and Z-cut monocrystal CdS 10 p1690 A67-23105
- Electron-hole pair separation energy in CdS single crystal during 5 to 50 kev electron bombardment 10 p1690 A67-23107
- Humidity and simulated space environment effect on various cadmium-sulfide thin film solar cells, noting degradation rates 10 p1596 A67-23163
- CdS solar cell model noting spectral response, V-I characteristic and temperature variation 10 p1596 A67-23164
- Noise in space charge limited current in CdS single crystal at low injection level 10 p1696 A67-23772
- Luminescence of CdS at low temperature excited by very high intensity laser light 10 p1667 A67-23779
- Field emission from sharply pointed CdS single crystals photon-enhanced by illumination from pulsed argon-ion laser 11 p1845 A67-24133
- Breakdown and switching in CdS single crystals, noting formation of negative resistance and thickness effect on performance 11 p1847 A67-24729
- Sublimation technique applied to high mobility PbS and CdS thin film deposition under ultrahigh vacuum equilibrium conditions 11 p1847 A67-24738
- Surface hole photoconductivity for pressed metal anode CdS ohmic cathode system, noting spectral distribution dependency on crystal heat treatment and air humidity 11 p1849 A67-24871
- Crystallographic anisotropy of electrical properties of thin film CdS photoresistors explained via potential barrier orientation theory 12 p1984 A67-25520
- Hall and electric field effects in cadmium sulfide single crystals in terms of current carrier mobility 13 p2174 A67-26369
- Stimulation of photosensitivity of cadmium sulfide single crystals by chemical etching 13 p2174 A67-26401
- Micrometeroid damage of n-p silicon and CdS solar cells 13 p2056 A67-27440
- Current-voltage characteristics of cadmium sulfide crystal diodes with indium and gold cathodes 13 p2085 A67-27731
- Cadmium sulfide crystal photoconductivity peaks near band edge, noting heat treatment, temperature and defects 14 p2364 A67-28229
- Two-step saturation of pulsed current in CdS single crystals, noting electron bunching mechanism and volt-ampere characteristics 14 p2365 A67-28238
- Second current saturation of nonohmic behavior in CdS single crystals caused by quantum mechanical interaction between drift electrons and acoustic phonons 14 p2365 A67-28239
- Temperature dependence of Hall mobility of photoelectrons and electrons produced by X radiation in cadmium sulfide single crystals 14 p2367 A67-28525
- Depth of capture levels determined from temperature dependence of kinetics of gamma-conductivity or photoconductivity of cadmium sulfide 14 p2367 A67-28526
- Generation mechanism of laser emission in cadmium sulfide-cadmium selenide crystals in presence of two-photon excitation at various temperatures 14 p2331 A67-28534
- Spectral distribution of absorption coefficient in polycrystalline films of cadmium sulfide over wide temperature range 14 p2372 A67-28852
- Charge forming in cadmium sulfide crystals under effect of applied electric field 15 p2538 A67-29796
- Ultrasonic devices for coherent optical systems, discussing CdS transducers, laser scanners and microwave signal processing 15 p2500 A67-29912
- Internal modulation of IR gas laser using cadmium sulfide or selenide single crystals 16 p2685 A67-30891
- Coherent radiation from cadmium sulfide single crystal excited by electron beam, noting transition nature in generation mode and spectral composition 17 p2915 A67-32660
- Damping effect of conduction electrons on ultrasonic surface and body waves propagating in CdS crystals, plotting damping against conductivity 17 p2921 A67-32971
- Spectral dependence of impurity photocurrent in single crystal CdS specimens in constant illumination 18 p3100 A67-33759
- Crystallographic anisotropy of electrical properties of thin film CdS photoresistors explained via potential barrier orientation theory 18 p3103 A67-34451
- Red luminescent band and photoconductivity in cadmium sulfide single crystal, discussing IR quenching of photocurrent 19 p3300 A67-34764
- Impurity photoconductivity in cadmium sulfide energy levels at red luminescence centers depth 19 p3300 A67-34765
- Copper-doping technique for obtaining p-n junctions in sintered cadmium sulfide polycrystals, suitable for use in photoelectric converters 19 p3304 A67-35427
- Electro-optical effect and Stark effect in exciton levels of cadmium sulfide 19 p3304 A67-35428
- Photomagnetic effect and kinetic photoconductivity in cadmium sulfide single crystals, determining lifetime and mobility of nonequilibrium holes 20 p3504 A67-36158
- Two-photon photoconductivity in pulsed ruby laser excited cadmium sulfide, determining carrier density and density dependence on light intensity 20 p3456 A67-36164
- Miniature resonator consisting of piezoelectric cadmium sulphide transducer evaporated onto single-crystal quartz wafer 20 p3393 A67-36176
- Cadmium sulfide edge luminescence energy shift dependence on excitation intensity and free carrier concentration 20 p3512 A67-37288
- Emission intensity dependence in CdS on laser excitation intensity for free and phonon-assisted exciton recombination at cryogenic temperature 20 p3461 A67-37295
- Threshold characteristics of photoresistors with noiseless contacts on CdS base 20 p3401 A67-37331
- Elastic bending vibrations amplitude and frequency effects on current oscillations in CdS single crystals 20 p3514 A67-37463
- Lattice relation of cuprous sulfide formed on CdS single crystal noting precisely similar orientation 21 p3677 A67-38011
- Negative differential conductivity in semiconductor in acoustic instability mode and connection with sound amplification and number of electron traps 21 p3678 A67-38097
- Hall and electric field effects in cadmium sulfide single crystals in terms of current carrier mobility 21 p3680 A67-38325
- Negative differential conductivity in viscous semiconductor with stationary sound wave propagating under sound amplification conditions 21 p3681 A67-38352
- Three- and four-phonon processes in piezoelectric cadmium sulfide observed using ultrasonic amplifier confirm nonlinear theory of multiple wave interactions 22 p3854 A67-39246
- CdS single crystal platelet growing and treating technique, relating fluorescence emissions to growth conditions 22 p3778 A67-39359
- Photoconductivity in cadmium sulfide crystals induced by light from ruby laser with Q-factor modulation, showing photocurrent dependence on laser power 22 p3814 A67-39511
- Electron beam detectors employing CdS single crystals, considering procedure for obtaining crystals characterized by high sensitivity to electron fluxes 22 p3798 A67-39568
- Design and performance of high gain amplifier consisting of cadmium sulfide single crystal and thin film transducers 23 p3977 A67-40690
- Temperature dependence of Hall mobility of photoelectrons and electrons produced by X radiation in cadmium sulfide single crystals 23 p4039 A67-40932
- Depth of capture levels determined from temperature dependence of kinetics of gamma-conductivity or cadmium sulfide 23 p4039 A67-40933
- Generation mechanism of laser emission in cadmium sulfide-cadmium selenide crystals in presence of two-photon excitation at various temperatures 23 p4040 A67-40941
- Cadmium sulfide film cell photovoltaic effect and mechanism, discussing cell structure and spectral response 23 p4046 A67-41485
- CdS solar cell model, discussing p-n junction, CdS and copper sulfide properties and microscopic junction formation and behavior 23 p4046 A67-41486
- Cleave thin film CdS solar cell fabricated with two different substrate structures noting design changes, improvements and performance characteristics 23 p3937 A67-41494
- Environmental testing of thin film solar cells, studying long term thermal cycling effect on CdS solar cell 23 p3937 A67-41496
- Si and Cd solar cell arrays compared using rigid frame Si solar cell concept 23 p3938 A67-41497
- Thin silicon, dendritic and cadmium sulfide solar cells technology and large-area lightweight arrays 23 p3939 A67-41512
- Simulated micrometeoroid bombardment effect on n/p Si and CdS solar cells performance 23 p3941 A67-41521
- CdS single crystal film trap energy spectrum studied with thermo-stimulated currents /TSC/ noting effect of SiO

layer 24 p4203 A67-42246
Solar cell/battery power systems for post-1975 satellites, discussing oriented thin film CdS solar cell array 24 p4105 A67-42515

CADMIUM TELLURIDE
Shallow hydrogenic type acceptor levels produced by Li and P doping in zinc telluride and cadmium telluride, noting heat treatment effects 02 p0280 A67-11484
Optical absorption edge in cadmium telluride, noting impurity bands and dependence on energy and temperature 02 p0281 A67-11492
Cadmium telluride optical absorption edge due to exciton creation with simultaneous absorption of longitudinal optical phonons calculated by perturbation theory 02 p0281 A67-11493
Thin layers of crystallized cadmium telluride of high electron mobility analyzed for electrical properties and photoconductivity 02 p0294 A67-11759
Interband Faraday effect in Cd-Te single crystals 04 p0676 A67-14933
Semiconductor lasers and fast IR detectors, discussing InAs, InSb and three types of mercury cadmium telluride detectors 05 p0821 A67-16668
Impurity states in CdTe analyzed by examining changes in electrical and optical properties after thermal-neutron bombardment 06 p1062 A67-18928
Copper telluride-cadmium telluride thin film heterojunction fabrication and characteristics for solar cell applications 08 p1285 A67-20730
Solar photovoltaic cell properties and preparation using thin films of copper and cadmium telluride 08 p1285 A67-20731
Photovoltaic effect in cell prepared by CdTe film deposition and copper telluride flash evaporation 08 p1285 A67-20733
Optical absorption, photoconductivity and p-n junction in cadmium telluride 08 p1368 A67-20734
Thin film CdS and CdTe solar cells compared for space applications 08 p1285 A67-20736
CdTe properties evaluated through pulse height response of surface barrier devices to monoenergetic alpha particles normally incident to surface 08 p1356 A67-21308
Anomalous IR attenuation in fast neutron irradiated GaAs and CdTe arises through scattering and absorption by highly conducting spike zones 11 p1850 A67-24910
Conduction band structure and scattering processes of cadmium mercury telluride mixed crystal determined from thermoelectric power, effective mass and electron mobility 12 p1979 A67-25178
Oriented growth of thick films of CdTe deposited on quartz plates in vacuum, discussing photovoltaic effect 12 p1982 A67-25450
Photoemission study of electronic structure of CdTe, considering two strong reflectivity peaks in optical reflectivity spectrum [AFRL-67-0405] 12 p1983 A67-25478
Volt-ampere characteristics effect on thickness of contact materials of some heterojunctions and band structures obtained by epitaxial deposition 12 p1983 A67-25515
Critical temperatures and phase composition of films obtained by vacuum deposition of sublimed cadmium telluride 15 p2537 A67-29706
Refractive index dispersion of CdSs and CdTe crystals in visible and infrared spectral range at room temperature 16 p2732 A67-31481
Mean values of characteristic temperatures and dynamic displacements of ions for lattice of solid substitution solutions of zinc telluride-cadmium telluride system 18 p3095 A67-33446
Volt-ampere characteristics effect on thickness of contact materials of some heterojunctions and band structures obtained by epitaxial deposition 18 p3103 A67-34446
Cadmium telluride electrical light absorption oscillations noting comparisons between experiment and theory, electric field, temperature range, etc 19 p3301 A67-34772
Electron mobility and trapping time in semi-insulating cadmium telluride through observing transient response to alpha

particles 19 p3308 A67-36101
Thin cadmium telluride bombardment with indium ions, finding doping efficiency dependence on ion energy and temperature 20 p3504 A67-36160
Germanium and cadmium telluride edge absorption, noting lattice imperfections causing absorption coefficient increase in indirect transition region 20 p3511 A67-37143
Physical properties of thin layers of cadmium telluride-metal systems analyzed for metal concentration and temperature of base at time of deposition 20 p3513 A67-37448
Sublimation enthalpy of CdTe thin films in high vacuum determined from 350 to 400 degrees C 20 p3514 A67-37453
Current runaway effects in n-cadmium telluride suggest current-density controlled resistivity caused by hole-electron pairs avalanche 21 p3677 A67-38006
Thin film cadmium telluride solar cells, discussing efficiencies and photoelectric properties of junction 21 p3679 A67-38224
Heat treatment effect in various gaseous media on electrical properties of CdTe films with abnormally high photovoltage, noting structural stabilization 22 p3861 A67-39924
CdTe photoemission absolute energies determined by correlating electron energy distribution structure with structure in optical data 22 p3862 A67-40001
EPR spectrum of divalent Mn ion impurity in CdTe single crystals noting concentration dependence, ion distribution and interaction nature 23 p4042 A67-41294
CdTe thin film solar cell, examining spectral response, sputtered Pt photovoltaic barrier-forming method and integrated array fabrication 23 p4046 A67-41495
Solar arrays constructed of CdTe thin film solar cells are feasible and competitive if space sunlight conversion efficiency can be maintained at level greater than 6 percent 23 p3938 A67-41498
Critical temperatures and phase composition of films obtained by vacuum deposition of sublimed cadmium telluride 24 p4199 A67-41776

CAJUN ROCKET
S NIKE-CAJUN ROCKET
CALCITE
Stimulated Raman effects in calcite oscillator crystal, measuring gain index beta relative to Stokes wave 23 p4016 A67-41191

CALCIUM
Resonance emission of H and K lines of ionized calcium during twilight spectrographically observed, suggesting meteoritic origin 06 p0998 A67-18704
Center limb variation of H-and K-lines of Ca-2 08 p1401 A67-21444
Atomic beam source for metastable Ca atoms in measuring population numbers from absorption lines 09 p1534 A67-21564
Electronic band structure calculations phase of Ca, Sr and Ba over wide range of atomic volumes under pressure electronic band structure calculations for fcc phase of Ca, Sr and Ba over wide range of 10 p1682 A67-23399
Inadequacy of formula for correction of foreshortening of Ca plages, attempting to determine directly new correction factor 10 p1712 A67-23806
Changes produced in urinary sodium, potassium, and calcium excretion in mice exposed to homogeneous magnetic field 10 p1600 A67-23819
Correlation between diurnal meteor activity and twilight emission of ionized calcium H and K lines confirmed by Quadrantides swarm observations 11 p1857 A67-24756
Profiles of cores of Ca II H and K lines in solar spectrum during maximum and minimum activity period 14 p2387 A67-28561
Resonance line profiles for Ca II and Mg II in lower solar chromosphere, noting interlocking effect 19 p3325 A67-35504
Line profiles and Stark widths of singly ionized carbon and calcium atoms measured using plasma source 19 p3299 A67-36092

CALCIUM COMPOUND
Precipitation effect of dispersed calcium titanate-rich phase on shape, organization and thickness of ferroelectric domains in barium titanate 06 p1020 A67-18047
Metastable form of C12 type calcium disilicide when under high temperature and pressure, noting X-ray diffraction powder

patterns and superconductivity 06 p1051 A67-18372
Honsel Plastic Mold /HPM/ process for high surface quality, discussing cost, materials and solidification time 21 p3637 A67-38976

CALCIUM FLUORIDE
Epitaxial deposition of Van Arkel zirconium on sodium chloride and calcium fluoride cleavages at various temperatures 02 p0286 A67-11711
Electron spin resonance with trigonal and orthorhombic symmetry in cerium oxide doped calcium fluoride 03 p0492 A67-13328
Divalent samarium ion doped calcium fluoride laser action at low temperatures obtained with giant pulse ruby laser excitation 05 p0820 A67-18661
Dysprosium doped calcium fluoride giant pulse laser with high repetition rate obtained, using DC pumping xenon lamp 05 p0822 A67-18674
Calcium fluoride-cerium fluoride with neodymium additions as active medium for lasers, discussing absorption and luminescence spectra and induced radiation 05 p0825 A67-16922
Self-lubricating properties of composites of porous nickel and nickel-chromium alloy impregnated with barium fluoride-calcium fluoride eutectic [ASLE PAPER 66AM 1C2] 08 p1335 A67-21035
Interband transitions and plasmon excitation in calcium fluoride, discussing energy loss 09 p1558 A67-22585
Optical and paramagnetic resonance of ytterbium ions in calcium fluoride, obtaining correlation between site geometry and optical absorption 12 p1984 A67-25843
Fabrication and operation of divalent dysprosium doped calcium fluoride laser, discussing magnetic field effects, Q-switching, cooling, etc 13 p2127 A67-27086
Calcium fluoride-cerium fluoride with neodymium additions as active medium for lasers, discussing absorption and luminescence spectra and induced radiation 14 p2330 A67-28262
Two-phonon absorption in ultrasonic paramagnetic resonance of uranium-doped calcium fluoride, relating wave attenuation to ultrasonic intensity and magnetic field angular variation 14 p2365 A67-28295
Quasi-continuous divalent dysprosium ion doped calcium fluoride laser with pyrotechnic excitation 16 p2686 A67-31484
Superhyperfine interactions in electron-spin-resonance spectrum of substitutional gadolinium 3 impurity in calcium fluoride single crystals under applied stress 17 p2913 A67-32367
Electron paramagnetic resonance of trivalent rare earth-monovalent alkaline earth ion pairs in calcium fluoride 21 p3676 A67-37815
Solid state CW optically pumped microwave masers using divalent Tm in calcium fluoride and strontium fluoride hosts 21 p3640 A67-38454

CALCIUM METABOLISM
Active parotin preparation to lower serum calcium levels, Ca excretion and possibly prevent decalcification, for applicability to potential system engineering 18 p2991 A67-34712

CALCIUM OXIDE
Magnetic field induced hyperfine structure in mono- and divalent iron ions in magnesium and calcium oxide, showing evidence of paramagnetic resonance 20 p3506 A67-36211

CALCIUM TUNGSTATE
Vanadium charge compensator in laser calcium tungstate, determining vanadium positions via electron spin resonance 04 p0633 A67-15306
Etching methods to visualize lattice dislocations and grain boundaries in Czochralski grown calcium tungstate crystals doped with neodymium for laser application 07 p1196 A67-19565
Stolzite and scheelite single crystal dielectric constant 20 p3505 A67-36179
Neodymium doped calcium tungstate single crystals synthesized, obtaining continuous laser action 20 p3458 A67-36494

CALCULUS
SA DIFFERENTIAL EQUATION
SA INTEGRAL EQUATION
SA OPERATIONAL CALCULUS
SA VARIATIONAL CALCULUS

SA VECTOR CALCULUS
Inaccuracies arising from measuring mean value of parameter calculated, using inertial instrument 07 p1187 A67-19739

CALIBRATION
SA STANDARDIZATION
SA WIND TUNNEL CALIBRATION
Ultrahigh vacuum measurement and total and partial pressure gauges, discussing operational and calibration problems 01 p0064 A67-10501
Calibration of pressure transducers in liquid-hydrogen to liquid-helium temperature range, using cryogenic test setup 01 p0069 A67-11018
Radiation calibration of heat flux sensors, comparing resistively heated filament and solar energy device 01 p0069 A67-11019
Black body spectral radiance calibration procedure incorporating Beckman IR-4 double-beam spectrophotometer with thermocouple, lead sulfide detector and two NBS-certified black bodies 01 p0069 A67-11023
Statistical theory using calibration data to evaluate multielement system for measuring properties of cryogenic propellants and high temperature thrusting devices 01 p0069 A67-11026
Five-million pound load cell design and compression calibration at NBS 01 p0050 A67-11097
Technique to monitor system noise and automatic digital system qualification using data obtained by shunt calibration and proper analysis 01 p0073 A67-11112
Measurement capabilities of linear digital displacement transducer with magnetically stored calibration 01 p0074 A67-11124
Thermoelectric probe in calibrating surface temperature transducers, noting results on various materials 01 p0075 A67-11134
Calibration procedures for earth albedo experimental package of Orbiting Solar Observatory 02 p0246 A67-12401
U.S. Weather Bureau calibration of solar radiation pyranometer by means of 5000 watt tungsten filament lamp 03 p0419 A67-13076
Canadian calibration of solar radiation pyranometers 03 p0419 A67-13077
Integrating hemispherical system for creating indoor artificial diffusing sky used in calibrating meteorological pyranometers 03 p0419 A67-13078
Cryogenic fluid mass flow measurement methods, noting flow meter calibration 03 p0421 A67-13768
Calibration of flow meters in liquid hydrogen at high flow rates for establishing limits of extrapolations from lower flow rate data 03 p0422 A67-13771
Gas flow calibration systems noting accuracy degree and factors contributing to errors 03 p0422 A67-13772
Laser pulse energy measurements with liquid absorption cell calorimeter 04 p0624 A67-15456
Sensors and signal conditioners, discussing operation and calibration of resistance thermometers, strain gauge pressure transducers and potentiometric transducers 04 p0626 A67-15731
Metrology requirements for Apollo project, noting control and measuring equipment and calibration procedures 05 p0814 A67-17263
Calibration of low pressure Penning gas discharge gauge and stability of discharge modes 06 p0950 A67-17748
Wavelength dependence of characteristic curve of photographic emulsion 06 p1002 A67-17977
Doetsch deflection calibration device for aircraft control surfaces 06 p0950 A67-18022
Ballistic camera calibration method and triangulation of satellite position from camera observations 07 p1188 A67-19776
Test platform isolated from random long period ground tilts used in calibration of gyroscopes, accelerometers, etc 08 p1314 A67-20580
Noise comparators and associated thermal standards to provide noise source calibration facilities at S-and X-bands 09 p1495 A67-21621
Precision power measurements of spacecraft CW signal level with microwave noise standards, noting Mariner IV application

[JPL-TR-32-1070] 09 p1495 A67-21622
Millimeter confocal wavemeter calibration and stability 09 p1470 A67-21625
Pressure calibration methods for testing response of microphones in difficult conditions of temperature, pressure and frequency 09 p1484 A67-21938
Vacuum gauge calibration error with conductance-determined pressure divider 09 p1498 A67-22109
Pressure dependence of thermoelectric power of semiconductor 09 p1499 A67-22424
Absolutely calibrated radiometer for CW laser radiation in visible and near IR bands which relies on heat flow through standard thermal impedance 09 p1502 A67-22615
Error of measurement of mean square value of fluctuation signals due to voltmeter calibration 10 p1607 A67-23451
Numerical and photoelastic solutions compared for uniform edge loading, obtaining pressure calibration by means of shear stress measurement 11 p1876 A67-24616
Intermediate band pass photometric system properties and reduction and calibration procedures 11 p1792 A67-24778
Timekeeping unit calibration, on basis of signals emitted by HBG transmitter, permitting measurement of state and performance of quartz oscillators 11 p1792 A67-24782
Dynamic Newtonian gravitational force gradient fields generator to calibrate response of dynamic gravitational gradient sensor 11 p1794 A67-24903
Automatic temperature programmed station for calibrating cryogenic sensors [ISA PAPER 12-11-2-66] 11 p1795 A67-25060
Cryostat, combination device for test and calibration of gauges for cryogenic temperature 12 p1938 A67-25187
Null-yaw and fixed direction multihole probes for aerodynamic measurements, describing calibration charts and error sources 12 p1940 A67-25352
Accelerometer mountings evaluated covering attachment, calibration, resonance frequencies, tension-compression, bending, shear interface and cantilever effect 12 p1942 A67-25680
Microwave attenuation standard derived using waveguide below critical frequency as voltage divider to determine losses in components 13 p2067 A67-26488
Calibration of vibrational transition of CO at various pressures to determine vibration-rotation wave numbers 13 p2160 A67-26600
Stability analysis of minimum variance estimations used to self-calibrate missile tracking instrumentation complex 13 p2120 A67-26815
Cryogenic fluid mass flow measurement methods, noting flow meter calibration 13 p2121 A67-27633
Laboratory calibration of piezoelectric transducer used as micrometeoroid impact gauge 15 p2486 A67-29410
Graphite cloth and felt as resistance heating elements for calibration and simulation facilities, achieving fast changes in heat flux level without sacrificing power efficiency 15 p2490 A67-30153
Evaluation and calibration of missile and space tracking systems including test-by-test analysis, lofted rockets, self-calibrating systems, etc 16 p2621 A67-30682
Sensor and calibration techniques for measurement of infrasonic and gravity waves noting error control and possible applications 16 p2677 A67-31430
Calibration system for PRESS optical aircraft program utilizing portable collimators 16 p2679 A67-31796
High hydrostatic pressure effects on load cell using foil strain gauges and calibration for small uniaxial loads 17 p2855 A67-32393
Calibration of star tracker bias errors on OAO 17 p2955 A67-32479
Probability density function of ratio of two nonzero mean Gaussian random variables derived and applied to calibrated signal using noisy calibration levels 17 p2816 A67-32624
Copper-constantan and chromel-copel microthermocouples installation in capillary tubes for measuring coolant temperature 17 p2860 A67-32831
Ultrasonic probes calibration for evaluation of propagating ultrasonic wave

during nondestructive testing of materials 18 p3046 A67-33744
Dynamometer using epoxy-bonded foil strain gauges for simultaneous two-force measurements for ultrahigh vacuum and high temperature applications, noting calibration [SESA PAPER 1209] 18 p3142 A67-33896
Computer conversion of hydrodynamic data into simulated static test of deep-throttling bipropellant rocket engine, considering inert calibration techniques [AIAA PAPER 67-427] 18 p3112 A67-33911
High pressure hydrogen atmosphere drop calorimeter for SNAP reactor fuel specific heat measurement, discussing calibration problems 18 p3052 A67-34515
Standard scintillation index method for describing ionospheric effects, discussing power calibration, scaling, deviations, etc 19 p3220 A67-35256
Surveyor spacecraft star sensor calibration and spaceborne performance 19 p3233 A67-35982
Fringe order estimation of principal stress difference in plastically deformed body shown useful for variable stress rate by calibration test in photorheological stress analysis 20 p3536 A67-36419
Radiometric technique for absolute temperature measurement of microwave noise sources under field conditions 20 p3444 A67-36521
Data analysis and reduction studies for calibration of missile tracking systems using near earth satellite 20 p3381 A67-36604
Heated thin film anemometer used to measure fluctuating velocity in airflow, noting relation of dynamic sensitivity to static calibration 20 p3447 A67-36846
JPL free piston shock tube design, calibration and performance 21 p3606 A67-37773
High pressure hypersonic gun tunnel calibration with performance estimation method compared with tests, discussing high altitude Mach 10 flight simulation 21 p3607 A67-37779
Distillation process in spherical pyranometer studied for time constants and sensitivity in calibration until reaching balanced state 21 p3627 A67-38445
Calibration for pyrgeometer with different surface heat transfer coefficients of black and gold strip 21 p3627 A67-38446
Generator installation for supersonic gust simulation to measure wing forces, discussing calibration problem 21 p3609 A67-38889
Surveyor TV system calibration, determining transfer functions for various parameters 22 p3807 A67-40376
Calibration of shock accelerometers, discussing velocity change and impact force methods with specific examples of systems in use 23 p4003 A67-41335
Test accelerometer comparison calibrations via vibration standards, discussing sensitivity, relative motion and error analysis 23 p4003 A67-41336
Comparison calibration techniques for vibration transducers using quartz accelerometer 23 p4003 A67-41337
Comparison calibration of rectilinear vibration and shock pickups 23 p4004 A67-41338
Solar and terrestrial thermal radiometer absolute calibration noting standards and methods 23 p4006 A67-41373
Thin foil heat flux sensor for radiative and convective heating rates over wide range and dynamic response, noting error mechanisms, calibration and accuracy 23 p4006 A67-41374
Radiative and convective heat flux measuring instruments calibration for aerospace industry 23 p4006 A67-41375
Pressure pulse generator-peak amplitude detector system for dynamic calibration of pressure transducers 23 p4007 A67-41388
Absolute measurement of Ar II transition probabilities using tungsten ribbon lamp as calibration standard 24 p4194 A67-41888
Ionization gauge calibration by volume expansion, flow rate and multiple orifice techniques 24 p4153 A67-42048
Differential RF voltage comparator for transfer standard and calibration of HF voltage devices at high accuracy 24 p4155 A67-42288
Calibration of optical pyrometers using

gold point black body and sectioned disks 24 p4155 A67-42292

Barium fluoride film electric hygrometer element aging and possible causes of calibration drift with time in storage 24 p4156 A67-42380

CALIBRATOR

Noise generator for calibration of radio receiver working in 1-2.6 MHz range during rocket flight 21 p3592 A67-38221

CALIFORNIUM

Type I supernova exponential decrease in light output due to spontaneous nuclear gamma ray fission of Cf 254, including detection techniques using satellite or balloon-borne telescopes 12 p1995 A67-25765

CALORIC REQUIREMENT

S DIET

S NUTRITIONAL REQUIREMENT

CALORIC STIMULUS

Caloric nystagmus in man clarified by test in weightless phase of parabolic flight 15 p2428 A67-29277

CALORIMETER

Nickel-copper cone calorimeter design and fabrication for laser energy measurements 01 p0062 A67-10193

Internal temperature distributions of present and proposed calorimeter geometries operating at high pressure and extreme heating rates compared, using one- and two-dimensional heat conduction programs 01 p0070 A67-11033

Null point or transient copper calorimeter using single temperature response measurement to determine heat flux, correlating experimental with theoretical data 01 p0070 A67-11035

Calorimeter for measuring heat flux to ablating surface, noting theory of device 01 p0071 A67-11106

Calorimeter using enameled copper wire with variable resistance for measuring laser energy and output power 03 p0437 A67-13536

Laser pulse energy measurements with liquid absorption cell calorimeter 04 p0624 A67-15456

Calorimeters used as in-line dosimeter if thin enough with respect to effective electron range to ensure that device does not degrade energy in beam 04 p0625 A67-15711

Enthalpy of reaction of sulfur and nitrogen trifluoride 06 p0955 A67-17986

Langmuir calorimetric probe to determine average energy per ion in tenuous plasma beam 06 p1076 A67-18879

Calorimetric measurement of pulsed ruby laser output energy 09 p1510 A67-21615

Ionization calorimeter performance simulation using Monte Carlo 09 p1497 A67-21900

Very low heat background calorimeter design for heat-short experiments and checking analytical predictions for propellant tank insulation 13 p2228 A67-27658

Absolute emissivity calorimeter design for low temperature measurements above 60 degrees K using liquid helium as cryogenic fluid 13 p2122 A67-27661

Ionization fluctuations due to interaction between shower particles and absorbing component of ionization calorimeter and effect on accuracy of energy measurement 17 p2855 A67-32250

Laser energy output measured using formed calibrated hollow sphere of thin insulated copper wire as calorimeter 18 p3046 A67-33747

High pressure hydrogen atmosphere drop calorimeter for SNAP reactor fuel specific heat measurement, discussing calibration problems 18 p3052 A67-34515

Nuclear active particles energy spectrum obtained on mountain tops, investigating absolute flux by using ionization calorimeter 21 p3698 A67-38293

Energies of combustion of aluminum diboride and alpha aluminum dodecaboride measured in bomb calorimeter using fluorine oxidant 22 p3758 A67-39766

Guarded cold flat plate calorimeter for measuring insulation thermoconductivity 22 p3803 A67-40296

Calorimeter for evacuated multilayer insulation materials to evaluate performance and measure heat transfer rate and thermoconductivity 22 p3803 A67-40297

Pressure, volume, temperature and internal energy data for He using constant volume calorimeter and gas thermometer,

discussing He melting 22 p3920 A67-40392

Primary proton energy spectrum determination by particle energy measurements with ionization calorimeters and particle counters onboard space stations 23 p4054 A67-41092

Fast response thin skinned calorimeters for high heat flux profiles of arc jet flows 23 p4006 A67-41381

Thick walled carbon cone calorimeter in pulsed lasers used for calibration purposes, discussing error sources 24 p4154 A67-42174

Calorimeter for measuring heat flux to ablating surface, noting theory of device 24 p4155 A67-42289

Energy fraction transfer to neutral plums during interactions with heavy nuclei measured for several energy levels, using ionization calorimeter 24 p4218 A67-42833

CALORIMETRY

SA THERMOMETRY

Calorimetric apparatus for measurement of low temperature emittance of materials as function of temperature [AIAA PAPER 65-703] 03 p0418 A67-13037

Crystallinity index measurements of poly/ethylene terephthalate/ by X-ray diffractometric and differential scanning calorimetry index methods 04 p0641 A67-14527

Effect of beryllium, boron, titanium, etc, additions on recovery and recrystallization processes in pure aluminum, using differential calorimetric techniques 04 p0637 A67-14910

Heats of solution and formation of Ti-Al alloys in region of alpha-solid solution determined, using calorimetry 07 p1204 A67-19268

Calorimetric measurements of thermionic converter/ heat pipe system, discussing electron cooling of emitter, thermal emissivity and thermal balance 09 p1448 A67-22342

Calorimetric measurement of source and broadband spectral absorptances of spacecraft thermal control coatings during exposure to UV in vacuum environment 09 p1534 A67-22452

Latent heat of fusion of titanium 10 p1670 A67-23640

Vacuum multilayer insulation for cryogenic space propulsion vehicles noting self-evacuation system and calorimetric test 10 p1734 A67-23728

Low to moderately high temperature emissometer, based on calorimetric method, to measure total hemispherical emittance of metals and coatings in vacuum [AIAA PAPER 67-299] 12 p1946 A67-26014

Total hemispherical emittance of transparent materials at low temperatures measured using calorimetry 13 p2159 A67-27356

Formation heat of boron trifluoride measured by elements direct combination in bomb calorimeter 16 p2620 A67-31762

Calorimetric investigation of role of ballistic modifier in nitrocellulose propellants combustion [CI PAPER 67-1] 19 p3309 A67-34996

CAMBERED WING

Vented profile in free surface flow of finite depth, computing lift and drag 03 p0402 A67-13449

F-111 wing sweep actuator with irreversible Acme-thread jackscrew driven by hydraulic servomotor 05 p0752 A67-16157

CAMERA

SA BAKER-NUNN CAMERA

SA BALLISTIC CAMERA

SA FRAMING CAMERA

SA HIGH SPEED CAMERA

SA SCHMIDT CAMERA

SA TELEVISION CAMERA

Transmittance measurements and consequent cloud top determination by Gemini V hand-held spectrographic camera 01 p0061 A67-11396

Panoramic facsimile camera for unmanned space operation providing 360 degrees IR and visible spectrum imagery [SMPTE PREPRINT 100-40] 03 p0423 A67-13806

Brightness angular velocity and geometry of moving object relationship to camera parameter to determine exposure and focal length and contrast for optimum recording 05 p0808 A67-17032

Satellite camera of Potsdam Geodetic Institute 07 p1187 A67-19763

Maryland-Minnesota-Mississippi Echo I satellite observation triangle, discussing principles of triangulation method, camera systems and office data reduction techniques 07 p1176 A67-19765

High resolution aerial photography, detailing photographic films, optical design, camera systems and methods of system analysis 08 p1330 A67-20645

Tilt angles for photographs of physically and geographically diverse terrains taken with different types of gyrostabilized aerial cameras 13 p2118 A67-26463

Optical system consisting of circular sweep camera for recording useful streak images on Polaroid film 14 p2320 A67-28748

Antares triaxial tracking camera noting mounting, electronic and optical systems and performance techniques 19 p3229 A67-35267

ATS-1 spin scan camera experiment for photographic recording of weather motions 20 p3446 A67-36610

Brightness angular velocity and geometry of moving object relationship to camera parameter to determine exposure and focal length and contrast for optimum recording 21 p3627 A67-38264

Camera for multispectral color aerial photography noting four-band interpretation on companion viewer and application to target acquisition problems 22 p3797 A67-39451

ATS-1 spin scan camera experiment for photographic recording of weather motions 24 p4156 A67-42405

CAMERA SHUTTER

Rotating shutter telescopic observation for optical measurement of faint meteor velocity 05 p0897 A67-16805

Near field power density incident on eyes due to reflection from CW laser reduced by optical lens and shutter rearrangement 10 p1665 A67-23415

Shutter speed and illumination data for cinematographic documentation of total solar eclipse 15 p2555 A67-29576

Surveyor variable and fixed focal length TV camera lenses, discussing zoom lens design criteria, focal plane shutter and color filter wheel 22 p3807 A67-40375

CANADA

Roughness data and statistical analysis of off-runway landing areas in Canada, using aerial photography for profile measurement 10 p1622 A67-23388

Canadian space research, detailing sounding rocket and satellite launchings 19 p3320 A67-35288

Canadian program for IQSY including aurora studies, solar observation, space research, etc 19 p3224 A67-35498

Development of major air terminal buildings at Canadian airports by maximum operational-capacity, land availability, noise contours and capital investment 22 p3779 A67-39377

SST aircraft effect on overall situation of commercial airline traffic in Canada [SAE PAPER 670901] 24 p4257 A67-42019

CANADAIR CL-84 AIRCRAFT

Mobile model test rigs and model instrumentation for CL-84 V/STOL aircraft 01 p0073 A67-11120

CANADIAN SATELLITE

S ALOUETTE I SATELLITE

S ISIS-A

S ISIS SATELLITE

CANONICAL PROBLEM

State variable equation transformation to phase variable canonical form 01 p0047 A67-11222

Nonsingular linear transformation of time-invariant linear dynamic system into canonical /phase-variable/ form 01 p0048 A67-11223

Formal integral construction of Hamiltonian system of n degrees of freedom near equilibrium point 03 p0457 A67-13163

Curvature effect on reflection coefficient of layered absorbers, examining backscattering from coated cylinder and sphere 03 p0370 A67-13852

Optimal steering and cut-off reflight in orbital transfers, using orbital parameters as state variables for greater accuracy in calculations 05 p0905 A67-16519

Perturbed motion stability in critical cases, examining canonical systems 06 p1032 A67-18034

Canonical transformation to investigate rotational motion of uniaxial orbiting rigid

body influenced by gravity gradient torque [AIAA PAPER 67-125] 06 p1084 A67-18288

Canonical transformation in two-dimensional three-body problem giving power series Hamiltonian 08 p1380 A67-20387

Transfer phenomena in polygenous solutions, noting canonic form of component flow equation 09 p1553 A67-21905

Diagonalization procedure for Hamiltonian of ferromagnetic thin film, applying canonical transformation in direction of film thickness 11 p1845 A67-23992

Method of averaging applied to solution of canonical equation system describing particle motion at high altitude in gravitational field of nonspherical planet 14 p2388 A67-28637

Canonical elements for variables of Levi-Civita regularizing binary collisions in restricted three-body problem, noting existence of periodic orbits 15 p2557 A67-29878

Difficulties arising in applying Liapunov first method to solution of canonical systems and ways to overcome them 15 p2511 A67-29885

Free rotation of solid body analyzed using homogeneous canonical transformation 15 p2519 A67-30225

Integration of regularizing canonical and corresponding Hamilton-Jacobi equation applied to two-body problem for construction of perturbation theory 19 p3249 A67-34795

Canonical form of filtering problems with solution identical to control problem 19 p3205 A67-35911

Parametric resonance in near-canonical systems with critical frequencies and instability boundary domain formulas derived from Yakubovich results 21 p3657 A67-37989

Weierstrass canonical product analog for integral functions of many complex variables, discussing existence problems and canonical function construction 22 p3827 A67-39215

Von Zeipel method to eliminate short period terms in first order general planetary theory noting system transformation into canonical equations 22 p3881 A67-39514

Independent variable changes in dynamical systems and applications to systems regularization, giving canonical and Lagrangian motion equations with tensor notation 23 p4027 A67-41006

Canonical decomposition of nonlinear error covariance difference equation derived for discrete estimation problems 24 p4177 A67-42188

CANOPY

Human body resistance limit for ejection through aircraft canopy 14 p2257 A67-28215

CANTILEVER BEAM

Linear solutions for large deflections of diamond-shaped frames under compressive loading 01 p0160 A67-10404

Upper and lower bounds of transverse vibrational frequencies of variable cross section cantilever bars, considering transverse shear and rotary inertia effects 05 p0910 A67-16151

Numerical analysis of constraint effects on trial function selection in variational calculus problem of pure torsional vibration of cantilever beam of thin walled open cross section 05 p0917 A67-16418

Bending moment change of curvature relation for large elastoplastic deflection of thin circular-arc cantilever beam, taking strain hardening materials into account 05 p0918 A67-16425

Instability modes of cantilevered bars induced by fluid flow through attached pipes, examining cases of torsional and transverse flutter and torsional buckling 05 p0921 A67-16882

Closed form solution for transverse-symmetric and asymmetric loadings on circular fixed beam 06 p1110 A67-18842

Tuned viscoelastic vibration dampers effect on responses of cantilever and clamped-clamped beams subject to Euler-Bernoulli beam equation, discussing loss factors based on transmissibility spectra 06 p1110 A67-18859

Double cantilever beam specimen for determining plain strain fracture toughness of metals 12 p1956 A67-25946

Stability of cantilevered elastic bar with end under compressive follower force, noting shear deformation, rotational inertia

and internal damping 17 p2959 A67-32420

forces 17 p2959 A67-32420

Single frequency vibrations of beams and girders solved by applying asymptotic methods 17 p2962 A67-32881

Transverse vibrations of tapered cantilever beam solved in terms of generalized hypergeometric function by Frobenius method [ASME PAPER 67-APM-25] 17 p2964 A67-33153

Upper bounds for cantilever beam natural oscillation frequency error determined when approximately calculated frequency values approach exact values of problem 18 p3143 A67-34168

Horizontal, solid, cantilever-beam profile with constant density, width and elasticity modulus determined, using Pontryagin principle 19 p3340 A67-35524

Multilayer cantilever beam subjected to varying load, studying cases where slip region propagates from edge to interior 19 p3341 A67-35579

Uniform cantilevered bar subject to eccentric compressive follower force, considering warping rigidity, bending-torsional flutter and stability 20 p3538 A67-36674

Triangular finite element under plane stress analyzed using stiffness matrix, including in-plane concentrated moments and nodal rotation 20 p3538 A67-36676

Multipoint equivalent cross section method for calculating finite deflections of beams of strain hardening material 20 p3541 A67-37285

Stress corrosion characteristics of Ti alloy evaluated using cantilever beam testing procedure 20 p3470 A67-37465

Parametric resonance in near-canonical systems with critical frequencies and instability boundary domain formulas derived from Yakubovich results 21 p3657 A67-37989

Response in fundamental mode of simple single span beam with tuned viscoelastic dampers attached at discrete locations, assuming harmonic loading 21 p3719 A67-38147

Elastic stability of cantilever column having fixed compressive and circulatory nonconservative loadings, determining critical loads 21 p3729 A67-39084

Double cantilever beam /DCB/ specimen for fracture toughness testing, discussing elastic strain energy release rate and load and crack length extension relation 23 p4018 A67-40928

CANTILEVER PLATE

Bending problem of isotropic shallow helical cantilever shell under distributed normal load 05 p0915 A67-16220

Supersonic flutter characteristics of thin cantilever plate surfaces with low aspect ratio 08 p1416 A67-20530

Supersonic flutter characteristics of thin cantilever plate surfaces with low aspect ratio 19 p3343 A67-35775

Compounded normal modes of free vibration of cantilever plates, determining component modes 20 p3541 A67-37491

Approximate solutions obtained in closed forms for low aspect wing stressed state under transverse load 21 p3724 A67-38780

Cantilever plate calculation under load and deflection by variation method, reducing problems to solutions of differential equations with constant or variable coefficients 21 p3724 A67-38781

Upper and lower bounds for frequencies of free vibration developed for uniform rectangular cantilever plates 21 p3730 A67-39094

CANTILEVER WING

Mach number effect on flutter characteristics of thin cantilever wings analyzed in transonic blowdown wind tunnel, presenting results as flutter speed ratios 05 p0747 A67-18440

Spanwise distribution of aerodynamic shear and bending-moment on cantilever tapered wings 13 p2215 A67-28485

CAPACITANCE

SA RLC CIRCUIT

Elastic behavior of load cell operating on variable capacitance principle designed to fit spaces restricted in one dimension 01 p0034 A67-10296

Capacitance pickups with nonelectrical quantity causing transverse bending of plates and change in transducer capacitance,

used in recordings of mechanical quantities 01 p0063 A67-10416

Transistor behavior in phase inverter at LF as function of type /p-n-p or n-p-n/ and value of internal capacity 01 p0038 A67-10770

Transient phenomena in capacitance of Schottky barrier diodes 01 p0137 A67-11066

Capacitive pressure transducer featuring exceptional sensitivity, hysteresis, resolution and repeatability, detailing sensing element and measuring circuit design 01 p0071 A67-11102

Maximum power transformed by nonlinear capacitance of semiconductor diode on closed p-n junction 02 p0210 A67-11510

Theory of influence of surface states on impedance of semiconductor-insulator interface, determining relaxation times which directly affect cut-off frequency of device 03 p0487 A67-12810

Parametric excitation of spectrotron with controllable p-n junction capacitance and intrinsic voltage feedback 03 p0378 A67-13241

Excitation of parametron with p-n junction capacitance produced by inverted impurity concentration gradient in base of junction 03 p0378 A67-13246

Electrical parameters of chemical current sources in determining capacitance by measuring emf, voltage and short circuit current 03 p0363 A67-13597

Emitter sidewall junction capacitance in double diffused transistors, using linearly graded junction equation and two-dimensional impurity distribution 03 p0382 A67-13679

Emitter barrier capacitance effect on frequency characteristic of current amplification factor in drift transistors with accelerating field for minority carriers 04 p0585 A67-15502

Resonant frequency change of oscillatory circuit due to nonlinear capacitance of semiconductor diode used as amplitude detector 04 p0586 A67-15677

Frequency multiplication using diffusion capacitance with derivation of efficiency expression 05 p0766 A67-17165

Bias voltage dependence of capacitance in n-type silicon p-n junctions with voltage breakdown 05 p0869 A67-17171

Transistorized circuit modelling high-Q capacitances depending on voltage and having high maximum-to-minimum ratios 06 p0972 A67-18896

Landau quantization and removal of spin degeneracy effect on capacitance of p-n junction 06 p1065 A67-18951

Illumination effect on capacitance of metal-SiO-Si system with various biases 07 p1152 A67-19591

Distribution of capacitive photo-emf over surface of semiconductor determined by measuring value created by scanning surface of sample with narrow modulated-light beam 08 p1367 A67-20415

Pulsed sinusoidal bridge for simultaneous measurement of volt-capacitance and volt-ampere characteristics of relaxing p-n junction barriers 08 p1303 A67-20998

Capacitance voltage and V-I characteristics of four-layer p-n-nu-n semiconductor diode structures 08 p1303 A67-21054

Linear transformation of normalized static capacitance matrix used to describe TEM propagation on array of parallel conductors 08 p1304 A67-21224

Cut-off frequency, breakdown voltage and capacitance calculations for diffused junctions in thin epitaxial silicon layer for microwave device design 09 p1556 A67-22206

Large area 200-v planar voltage-variable capacitance diodes 09 p1475 A67-22207

Optimum design method for variable capacitance diodes with m-th power characteristic for wide voltage range, emphasizing impurity distribution 09 p1476 A67-22213

MOS structure studied by measuring variations in capacitance and charge injection into oxide 09 p1558 A67-22586

Diffused base punchthrough avalanche transistor /PAT/ at high recurrence frequency having capacitance dependence of pulse width 10 p1609 A67-22839

Capacitance of abrupt p-n heterojunctions and effects of interface states, noting capacitance-voltage characteristics 10 p1612 A67-23372

Amplification processes in parametrically regenerated circuit with simultaneous

complex variation of capacitance and attenuation 10 p1607 A67-23446

Standing wave solution of homogeneous waveguide field distribution for H₁₀ wave after conformal mapping and effect of capacitive and inductive irises 10 p1607 A67-23571

P-n junction capacitance in transition region currents obtained by integral of holes or electron concentration 11 p1759 A67-24136

Piezoelectric accelerometer capacitance measurement and computation involved in conversion of accelerometer voltage sensitivity from one external circuit capacitance to another 12 p1947 A67-26186

Micropower electronics noting effects of input capacitance and container and wiring capacitances on HF characteristics 12 p1917 A67-26206

Parametric coupling between two waves noting losses 13 p2086 A67-26511

Current-voltage characteristics of germanium-silicon isotype heterojunctions with regard to capacitance and photoelectric measurements 13 p2183 A67-27569

Electrical parameters of chemical current sources in determining capacitance by measuring EMF, voltage and short circuit current 14 p2247 A67-27843

Maximum power transformed by nonlinear capacitance of semiconductor diode on closed p-n junction 14 p2283 A67-28073

Analog multiplier using p-n junction dynamic capacitance, noting decays in RC circuit current 14 p2290 A67-28928

Input impedance of short dipole antennas on Nike-Apache rocket 15 p2444 A67-29504

Reactive characteristics of diffused p-n junctions in p-and n-silicon at high injection levels and in strong electric fields 16 p2726 A67-30817

Oscillating circuit with nonlinear capacitance in free oscillating regime, obtaining formula for envelope of free oscillation differing from exponent 17 p2829 A67-32311

GaAs diodes measured for capacitance at 77 degrees K, noting change due to traps photoexcited in space charge layer 17 p2914 A67-32655

Depletion layer capacitance of p-n step junction with inclusion of effect of spillover charge as function of voltage 20 p3504 A67-36167

Capacitance reduction in active RC synthesis noting RLC, transfer functions, canonic sections, etc 20 p3409 A67-37109

Illumination effect on capacitance of metal-SiO₂-Si system with various biases 20 p3401 A67-37330

Two-beam capacitive converter for automatic systems reduced to synthesis of single beam converter 22 p3795 A67-39229

Capacitance between strands of braided cable composed of identical insulated conductors 22 p3747 A67-39340

Junction potential measurement in irradiated tunnel diode showing no oscillation in any bias voltage 22 p3767 A67-39369

CAPACITIVE FUEL GAUGE

Disturbance of capacitive liquid level gauges by nuclear radiation 13 p2122 A67-27684

CAPACITOR

Harmonic linearization technique to examine characteristics of oscillatory circuits with nonlinear capacitors 01 p0038 A67-10715

Physics of failure techniques applied in reliability failure analysis of intermittent operation of ceramic capacitors 01 p0041 A67-11358

Capacitance and optical thickness of fatty acid monolayers sandwiched between Al-films 02 p0290 A67-11732

Precision of thin film resistors and capacitors mounted on single base as affected by fabrication factors 03 p0491 A67-13242

Loss angle tangent of film capacitors with rectangular Al films and dielectric silicon monoxide interlayer 03 p0378 A67-13243

Integrated circuits with evaporated thin film conductors, resistors and capacitors 03 p0387 A67-13999

Capacitor pressure sensor produced by furnace brazing molybdenum to itself and to zircon with pure copper and Cu-Au-Ni filler metals 04 p0630 A67-15460

High energy electron bombardment of MIS capacitor with subsequent positive charge

introduction into insulator investigated by C-V and G-V measurements 04 p0588 A67-15712

Impurity concentration profiles in silicon epitaxial wafer determined, using MOS capacitors 05 p0866 A67-16985

Small signal MIS capacitance vs bias characteristics measured over wide range of biases and sweep speeds 06 p1002 A67-17979

Inductorless band pass filter to prove validity of hypothesis that all inductors in LC filter can be replaced by gyrator-capacitor equivalents 07 p1154 A67-19615

Evaporated thin film capacitor from silicon oxide, noting electron diffraction patterns and IR adsorption peaks 09 p1555 A67-22102

Semiconductor dielectric interface characterization from study of complex capacity of metal/oxide/semiconductor structures 09 p1557 A67-22557

Conductivity of plasma capacitors in inhomogeneous plasma found to increase with frequency due to density gradient and resonance 12 p1969 A67-25194

Thin film capacitor dielectrics of silicon oxides and various metal oxides, noting influence on vacuum deposited compounds 12 p1918 A67-26210

Grounding of capacitors in integrated circuits noting insertion of gyrators 13 p2078 A67-26783

Reliability of integrated circuit amplifier improved by using nonlinear variable capacitances at LF 13 p2081 A67-27293

Thin film resistive and capacitive circuit design 14 p2287 A67-28611

Space charge varactor compared to p-n junction varactor, noting applications 15 p2449 A67-29804

Thin-film and diffused passive component comparison, describing resistor and capacitor fabrication by using sputtered tantalum and inductors through nichrome/gold 16 p2640 A67-31528

Response of capacitors irradiated by pulses of transient nuclear radiation 17 p2828 A67-32863

Fourier analysis of amplifier commutated capacitor type integrator output signal 18 p3011 A67-34107

Destructive breakdown conduction in aluminum-silicon oxide-aluminum capacitors, discussing voltage threshold, etc 18 p3105 A67-34630

Thin film circuits for narrow band radar receivers, discussing manufacture of inductors, capacitors and LC resonant circuits 21 p3589 A67-37917

Metal-silicon nitride-silicon /MNS/ capacitor charge storage variation with temperature and time 22 p3787 A67-39257

Superconducting coils used for capacitors in pulsed operations to reduce size and weight of energy storage systems 22 p3747 A67-39900

CAPE KENNEDY

Communications systems at Kennedy Space Center /KSC/ and future prospects 02 p0230 A67-12121

Instrumentation grounding at Cape Kennedy, noting characteristics of ground system used for safety and clean space signals 20 p3398 A67-36837

CAPILLARY

Thermomolecular pressure differential in wide capillaries at low Knudsen numbers calculated, using irreversible thermodynamics 02 p0343 A67-12678

Capillary emitter of electrons and Cs ions for use in thermionic converters 04 p0664 A67-15015

Knudsen limiting law in free molecular gaseous flow in various capillaries with temperature gradient 04 p0739 A67-15948

Differential equation of motion of meniscus of MHD fluid in capillary in TM field due to surface tension 06 p1044 A67-18681

CAPILLARY CIRCULATION

Small oscillations of viscous liquid-metal droplet under capillary force and in presence of magnetic field 01 p0120 A67-10182

Microstructural study of adhesive behavior of powdered bakelite in intergrain pores of carbon-graphite compacts in terms of capillary attraction forces 11 p1810 A67-23900

Compressible fluid flow in capillary tubes, discussing reduction in variation of pressure difference/mass flow ratio 14 p2303 A67-28350

Optimization of capillary pumping of

microgrooved heat pipes, discussing transport equation 24 p4255 A67-42552

CAPILLARY WAVE

Geometric dimensional, plasma temperature and pressure effects on capillary discharge with evaporating wall /CDEW/ 17 p2897 A67-32177

CAPSULE

S ESCAPE CAPSULE

S MERCURY CAPSULE

S SPACE CAPSULE

CAPTURE

S ELECTRON CAPTURE

CAPTURE EFFECT

Temperature dependence of lifetime of electrons and holes in GaAs, noting trapping effect of recombination centers and capture levels 01 p0128 A67-10091

Two parallel carrier capture mechanisms at single recombination center in cadmium sulfide 01 p0138 A67-11298

Telemetry receivers capture ratio effect on overall system accuracy, determining effect of IF filter characteristics 02 p0197 A67-12022

Captured proton intensity measurement in inner radiation belt in Brazilian anomaly, using satellites Proton I and II 05 p0878 A67-16089

Formation mechanism of ionospheric narrow sporadic E layers by high energy electron fluxes captured by geomagnetic field 07 p1179 A67-19835

GaAs injection lamp efficiency correlated with presence of trapping levels, noting experimental technique and results 17 p2911 A67-32192

Capture probability at Venus resonant rotation rate implying fluid core similar to earth 18 p3136 A67-34587

Captured proton intensity measurement in inner radiation belt in Brazilian anomaly, using satellites Proton I and II 24 p4212 A67-42765

CAPTURED AIR BUBBLE VEHICLE

Structural, seal and sideboard design, propulsion and cavitation problems relevant to operational requirements of captured air bubble vehicle 14 p2245 A67-28729

[AIAA PAPER 67-346] 14 p2245 A67-28729

Captured air bubble /CAB/ vehicle

[AIAA PAPER 67-348] 14 p2246 A67-28730

Captured Air Bubble /CAB/ vehicle stability tests

[AIAA PAPER 67-349] 14 p2246 A67-28731

CARBIDE

SA ALUMINUM CARBIDE

SA BORON CARBIDE

SA CHROMIUM CARBIDE

SA HAFNIUM CARBIDE

SA MOLYBDENUM CARBIDE

SA NIOBIUM CARBIDE

SA SILICON CARBIDE

SA STEEL

SA TANTALUM CARBIDE

SA TITANIUM CARBIDE

SA TUNGSTEN CARBIDE

SA VANADIUM CARBIDE

SA ZIRCONIUM CARBIDE

Cutting ability of high melting binder cemented carbides with Cr and V alloys 01 p0100 A67-10724

Dispersion-strengthening by formation of carbides of Hf, Zr, Ta, Ti and Nb in wrought and recrystallized Cr, discussing structural stability 01 p0100 A67-10766

Refractory metal chlorides reacted with methane and nitrogen in hydrogen jet to form carbides and nitrides 03 p0440 A67-12925

Substructural strengthening of carbide precipitation hardened molybdenum alloy by swaging and wire drawing 11 p1805 A67-24108

Hypereutectic carbides from carbide graphite alloys exhibiting high thermal shock resistance 11 p1809 A67-25004

Structure, composition and morphology of carbide phases of nickel superalloy 13 p2131 A67-26573

Ductile failure initiation by fractured carbides in austenitic stainless steel 13 p2133 A67-27008

Polyhedral boundary precipitations of complex heat resistant nickel alloy in carbide phase caused by boron and cerium 14 p2338 A67-28674

Solid solutions of titanium, tungsten, chromium prepared by carbidization of mixtures in hydrogen medium and obtained as fine-grained carbide powders 16 p2691 A67-31587

- Methods of producing coatings based on metal-like high temperature materials 19 p3244 A67-34957
- Carbide inclusions and distribution effect on fatigue behavior of open hearth and electric-arc furnace steels 20 p3464 A67-36478
- CARBOHYDRATE**
- SA CELLULOSE
- SA GLUCOSE
- SA GLYCOGEN
- SA NUCLEOSIDE
- Oxygen, carbohydrates, proteins, etc, produced by unicellular algae through photosynthesis, finding optimum efficiency of process 02 p0186 A67-11861
- CARBOHYDRATE METABOLISM**
- Glycogen accumulation in monkey and cat brain exposed to proton irradiation, discussing astrocytes function in carbohydrate metabolism 04 p0560 A67-14489
- Roentgen radiation effect on glycogen metabolism of rat brain 07 p1133 A67-19468
- Hydrazine effect, alone and with nicotinic acid, on oxygen consumption, respiratory quotient, carbohydrate pool and heat losses in rats studied using gradient calorimeter 18 p2992 A67-34714
- Hydrazine effect on carbohydrate metabolism in vivo and in vitro, studying hyperlactatemia, hypoglycemia, oxygen consumption inhibition, etc 18 p2992 A67-34720
- Monomethylhydrazine effects on metabolism and heat balance using various calorimetric methods 23 p3954 A67-41601
- Toxic metabolic effects of MMH, discussing methemoglobinemia as indicator of exposure dosage in animal study 23 p3955 A67-41602
- CARBON**
- SA CHARCOAL
- SA DIAMOND
- SA FERRITE
- SA FUEL
- SA GRAPHITE
- Ceylon and artificial graphite behavior under very high pressure, examining problem of metallic phase of carbon 01 p0104 A67-10833
- Proton-I satellite measurement effective cross section of inelastic interaction of protons with carbon nuclei at extremely high energies 02 p0315 A67-12757
- Solubility of carbon in Mo, Re and W determined by isothermal carburization method 03 p0439 A67-12845
- Structural carbon yarn for reinforcement of composite plastics 03 p0454 A67-13424
- Fiber formation and performance properties of carbon-silica fibers and use in plastic composites 03 p0454 A67-13425
- Diffusion constant of carbon in carbide phases of tantalum determined from growth rate of carbide layers forming on tantalum surfaces 04 p0636 A67-14908
- Total carbon abundances in enstatite chondrites 05 p0886 A67-16024
- Electron density, optical thickness and temperature of ruby laser-induced carbon plasma 05 p0852 A67-16654
- Basal plane contraction and annealing of degraphitized carbon examined via X-ray diffraction techniques 05 p0833 A67-16891
- Rapid micro dry combustion determination of carbon, hydrogen and nitrogen in high explosives 05 p0759 A67-17154
- Titanium, zirconium and hafnium effect on recrystallization temperature and strength of alloys of molybdenum with carbon 05 p0832 A67-17508
- Diffusion coefficient of carbon in nonstoichiometric tantalum monocarbide at very high temperatures, noting increase with decreasing carbon content 06 p1016 A67-17901
- Carbon content effects on properties of WC-TiC-Co alloys vacuum sintered 06 p1017 A67-17968
- Mechanical properties of continuous carbon filament/graphite binder composite including tensile, compressure, flexure, fatigue and shear properties [AIAA PAPER 67-173] 06 p1021 A67-18509
- Neutron induced dimensional changes in turbostratic carbons used as coatings on nuclear fuel particles, presenting densification curves 08 p1346 A67-21542
- Carbon fibers of high strength and high breaking strain noting heat treatment, structure and mechanical properties 09 p1520 A67-21988
- Effects of additions of carbon, nitrogen or oxygen on properties of vapor deposited tungsten 09 p1519 A67-22348
- Approximation equations of thermodynamic data of air-carbon plasma with arbitrary carbon content in atomic region 10 p1732 A67-22919
- Heat sterilization of activated carbon at 135 degrees C for 24 hr or 165 degrees C for 3 hr for application to spacecraft 11 p1749 A67-24788
- Shock tube study of oscillator strength of diatomic molecular carbon Swan bands 11 p1750 A67-25066
- Model for concentrated interstitial solid solutions applied to carbon solution in gamma iron 13 p2131 A67-26574
- Positive effect of carbon on microstructure and mechanical properties of niobium alloys 16 p2687 A67-30845
- Melting point and microhardness of carbon-saturated TiC-VC solid solutions, noting temperature of eutectic of TiC-VC with graphite 16 p2691 A67-31588
- Carbon formation in oxygen premixed acetylene and benzene flames 18 p3151 A67-33808
- Effect of copper chromite, carbon and other potential catalysts on thermal decomposition and ignition of ammonium perchlorate 18 p3108 A67-33813
- High modulus carbon fiber fracture path, orientation and crystallite size effects on physical properties 19 p3248 A67-35425
- High strength high modulus carbon fiber microstructure, studying crystallite size, orientation effect, electron micrographs and X-ray diffraction 19 p3248 A67-35426
- Solar identifications for forbidden carbon I lines in solar spectrum 19 p3324 A67-35435
- Line profiles and Stark widths of singly ionized carbon and calcium atoms measured using plasma source 19 p3299 A67-36092
- Refractory properties and mechanical characteristics of graphites and carbons, discussing maximum compatibility temperature of graphite 20 p3472 A67-36110
- Endor double paramagnetic resonance in cane-sugar carbon at room temperature, noting electron-proton interaction 20 p3508 A67-36398
- Lunar crater Alphonsus emission flare noting C-2 Swan system proposal 20 p3528 A67-37470
- Titanium, zirconium and hafnium effect on recrystallization temperature and strength of alloys of molybdenum with carbon 21 p3644 A67-38036
- Carbon content effect on properties and structures of nickel and nickel-iron base superalloys 22 p3818 A67-39223
- Proton I satellite measurements of effective cross section of inelastic interaction of protons with carbon nuclei at extremely high energies 22 p3876 A67-40259
- Densified carbon and graphite production methods /carbon, metal and resin and carbon with carbon impregnation/ for glass-to-metal sealing jigs 24 p4174 A67-41913
- Carbon thermodynamic activity in molybdenum carbide alloyed with small additions of Fe, Ni and Ti 24 p4171 A67-41962
- Total carbon content and primordial rare gases in chondrites 24 p4236 A67-42641
- IR C atom multiplet in solar spectrum at 10,700 angstroms, noting C abundance dependence on convective velocities and deviations from black body function and local thermodynamic equilibrium 24 p4237 A67-42655
- Dewrinkling and diffusion mass transport mechanisms in high temperature tensile and shear plastic deformation of pyrolytic carbons [JPL-TR-32-1137] 24 p4177 A67-42711
- Cosmic particle recording facility at Tskhra-Tskaro, giving data on free path of nuclear active particles in carbon with high energies 24 p4219 A67-42845
- CARBON ARC**
- Spectral radiance of low current graphite arc anode determined, using high accuracy spectroradiometer 05 p0846 A67-16787
- Near IR atmospheric absorption over 25-km horizontal path at sea level 10 p1629 A67-22744
- High powered carbon arcs for solar simulation with increased radiant energy output 12 p1921 A67-25697
- Trapped plasma build-up in magnetic field by ionization of injected atomic beam, noting ionization cross section parameters 17 p2908 A67-33115
- CARBON COMPOUND**
- SA FLUOROCARBON
- SA HYDROCARBON
- Carbon dioxide solid matrix study of carbon trioxide production, IR spectrum and molecular structure 05 p0759 A67-16838
- Integral hemispherical and monochromatic radiative capacity of carbon compounds at high temperatures 09 p1497 A67-21877
- Melting temperatures of ZrC-HfC, TaC-ZrC and TaC-HfC compacts obtained via Pirani method 09 p1518 A67-21879
- Carbon fiber composite, noting incorporation into epoxy resin and inverse correlation of shear strength with fiber modulus 10 p1671 A67-23495
- Carbon diffusion mobility in fused carbides of vanadium and titanium, giving carbon diffusion coefficient temperature dependence equations 14 p2337 A67-28285
- Graphite cloth and felt as resistance heating elements for calibration and simulation facilities, achieving fast changes in heat flux level without sacrificing power efficiency 15 p2490 A67-30153
- Carbon silica reaction during erosion of silica-phenolic composites noting silica removal mechanisms 17 p2809 A67-33034
- High temperature fuel cells with molten carbonate mixtures as electrolyte analyzed at high temperature 20 p3366 A67-37545
- Spectral line wavelengths of solar violet bands of carbon /isotope/ nitride and hydride molecules, determining solar abundance ratios 22 p3889 A67-40207
- CARBON DIOXIDE**
- Inexpensive carbon dioxide molecular gas laser using plano-concave eyeglass lenses 01 p0090 A67-10827
- Atmospheric and surface temperature profile measurement using balloon mounted IR spectrometer 01 p0061 A67-11391
- Model of nonequilibrium properties of high temperature carbon dioxide and other gas mixtures in connection with studies for vehicles entering Martian atmosphere 01 p0008 A67-11436
- Radiative transition probabilities between laser vibrational levels of carbon dioxide, noting relaxation time and dipole moment 02 p0252 A67-11891
- Completely regenerative spacecraft life support systems, discussing loop closure techniques and possible conversion methods for metabolic wastes [AIAA PAPER 66-935] 02 p0187 A67-12278
- Overlapping of bands of nitrogen oxide, CO and carbon dioxide in 4.5 micron region determined for inversion experiments 02 p0246 A67-12368
- Thermal atmospheric sounding, discussing carbon dioxide transmission function parameters, water vapor and temperature effect 02 p0239 A67-12377
- Role of amplification due to impacts of second kind in emission of nitrogen and CO molecular bands in mixture of nitrogen-argon and CO-Ar in glow discharge 02 p0270 A67-12674
- Population inversion of upper laser level of carbon dioxide molecules, noting electron-molecule collision and effect of neon addition 03 p0437 A67-13297
- Heat transfer and friction drag for supercritical laminar flow of carbon dioxide through tube at constant thermal flux density at wall 03 p0536 A67-13612
- Carbon dioxide content in troposphere and lower stratosphere measured at various altitudes, showing seasonal variations 03 p0414 A67-14086
- Carbon dioxide abundance at 200 degrees K determined from high dispersion IR spectrograms of Mars 03 p0514 A67-14309
- Self-modulation characteristics of carbon dioxide laser and use in measuring detector response and atmospheric propagation characteristics 03 p0439 A67-14399
- Carbon dioxide condensation on Martian polar caps 04 p0694 A67-14494
- Compatibility of artificial gas mixtures dependent on carbon dioxide and oxygen partial pressures 04 p0562 A67-14573
- Population inversion of upper laser level of carbon dioxide molecules, noting electron-molecule collision and effect of neon addition 04 p0631 A67-14722
- Surface property effects on effectiveness of mass transfer cooling in laminar boundary

layers with hydrogen injected into free stream of nitrogen or carbon dioxide 04 p0733 A67-15840

Gemini carbon dioxide sensor for monitoring in closed loop breathing system useful for many gas measurements 05 p0806 A67-16549

Tube diameter influence on output power and efficiency of gas laser 05 p0816 A67-16629

Molecular gas laser Q-switching techniques, determining rotational collision sections for carbon dioxide and cross sections for vibrational relaxation 05 p0816 A67-16632

Carbon dioxide solid matrix study of carbon trioxide production, IR spectrum and molecular structure 05 p0759 A67-16838

Double probe and microwave resonance measurements of gas additives effect on radial variation of electron temperature and density with partial pressures in carbon dioxide-nitrogen-helium gas laser 05 p0826 A67-17274

Quantitative intensity of weak carbon dioxide triad in 1 micron spectral region obtained, using pressure broadening techniques 06 p1031 A67-17870

Spectral emissivity measurements of carbon dioxide band made at high temperatures identifying hot transitions through Q-branches 06 p1118 A67-18539

Laval nozzle configuration for sharply bounded carbon dioxide jet in vacuum 06 p0943 A67-18781

Ventilatory response to carbon dioxide stimulus at spontaneous and consciously regulated rebreathing rates 07 p1133 A67-19479

Scaling of binary titanium alloys in carbon dioxide at high temperatures using kinetic, metallographic and electron probe microanalysis [AAS PAPER 66-190] 08 p1341 A67-20763

Carbon dioxide abundance and surface pressure of Martian atmosphere, noting self-broadening correction 08 p1400 A67-21250

Gas desorption following Q-switched laser beam bombardment of tungsten target in vacuum 08 p1338 A67-21310

Q-switched carbon dioxide laser with internal concave rotating mirror, discussing detection with pyroelectric thermal detector 09 p1511 A67-21769

Carbon dioxide study in Mercury atmosphere yields negative results from observations made with IR spectrometer and 61 inch reflector 09 p1565 A67-22016

Total and spectral reflectance of carbon dioxide cryodeposits on test vehicles and space simulator walls as function of deposit thickness, rate of formation, angle of incidence of light, etc 09 p1533 A67-22121

Longitudinal modes of carbon dioxide laser cavity by varying optical length of cavity 10 p1663 A67-22846

Temperature dependence of total intensity in difference band systems, difference transitions between nondegenerate vibrations compared with carbon dioxide band 11 p1821 A67-23960

Optical power gain characteristics of continuous wave carbon dioxide laser studied parametrically with single-pass amplifier 11 p1800 A67-24244

Compact nonresonant five-pass carbon dioxide laser amplifier structure giving small signal gains 11 p1800 A67-24245

Martian transient phenomena correlations among mass motion of water in atmosphere, polar cap growth and white cloud appearance frequency 11 p1862 A67-24501

Eckert reference temperature yields approximations for heat transfer, skin friction and recovery temperature in high speed laminar diatomic nitrogen and carbon dioxide boundary layers 11 p1883 A67-24576

Vacuum integrating sphere for in situ spectral reflectance measurements of carbon dioxide cryodeposits from 0.5 to 10 microns [AIAA PAPER 67-298] 12 p1926 A67-26013

Powerful gas lasers using carbon dioxide noting oscillation level lifetime, inversion mechanism, temperature effect, etc 13 p2125 A67-26388

Carbon dioxide laser history, development stages, performance and applications 13 p2125 A67-26389

Beryllium corrosion in carbon dioxide under pressure at high temperatures 13 p2136 A67-27108

Carbon dioxide purge and thermal protection system for liquid hydrogen tanks of hypersonic aircraft, comparing with helium purge system 13 p2227 A67-27647

Spontaneous visible light emission due to laser action in carbon dioxide laser plasma, examining plasma current change with phase-lock technique 14 p2331 A67-28494

Gain of flowing carbon dioxide laser systems, noting extent of diameter dependence of gain, population variations, etc 15 p2497 A67-29390

Carbon dioxide laser output observation by high resolution thermographic screen 15 p2497 A67-29393

Equilibrium radiant heat transfer to bodies at hypersonic velocities in carbon dioxide atmosphere noting shock layer, shock standoff distance, shock velocity, etc 15 p2582 A67-30216

Statistical band model used to compute spectral emissivity in carbon dioxide micronband as function of pressure, optical path and temperature 15 p2521 A67-30429

Prediction and measurement of metabolic energy cost for space suit system operation, noting procedure and test results 16 p2618 A67-30781

Heat transfer in turbulent carbon dioxide pipeflow at supercritical region 16 p2780 A67-31777

Continuous IR chemical mass action in carbon dioxide, using chemi-optical resonant pumping 17 p2866 A67-32275

Carbon dioxide ions with electrons dissociative recombination measurements with microwave-afterglow differentially pumped quadrupole mass-spectrometer apparatus, noting Martian atmosphere model [SRCC-55] 17 p2888 A67-32826

Carbon dioxide laser emission, discussing extension of wavelength range with carbon isotopes 17 p2869 A67-33062

Laval nozzle configuration for sharply bounded carbon dioxide jet in vacuum 18 p2982 A67-33723

Nitrogen oxide and carbon dioxide high pressure unimolecular decomposition noting high pressure rate constants, transition probabilities, potential surface shape, etc 18 p3082 A67-33793

Michelson type carbon dioxide laser for AC discharge analysis, noting apparatus design and performance 18 p3060 A67-34014

Design, operation, characteristics and applications of carbon dioxide lasers with DC excitation and fixed mirrors 18 p3061 A67-34350

Heat transfer and friction drag for supercritical laminar flow of carbon dioxide through tube at constant thermal flux density at wall 18 p3161 A67-34477

Adsorption, surface reaction and mutual displacement of carbon monoxide, carbon dioxide and oxygen on titanium film, using mass spectrometer 19 p3244 A67-34941

Volt-ampere characteristics of long free-burning convection-free DC and AC arcs in nitrogen, argon and carbon dioxide 19 p3280 A67-35149

Calculation of vibration level populations of polyatomic molecules in electronic ground state 20 p3457 A67-36216

Mass transfer cooling of carbon dioxide-nitrogen binary system in laminar boundary layer, stressing dissociation effect [ASME PAPER 67-HT-70] 20 p3550 A67-36750

Radio carbon dioxide fixation, glutamate labeling and Krebs cycle in ribose-grown *Hydrogenomonas facilis* 20 p3370 A67-36796

Autotrophic and heterotrophic carbon dioxide fixation regulation in *Hydrogenomonas*, discussing two Calvin cycle enzymes 20 p3370 A67-36797

Passive Q-switching of carbon dioxide laser with cavity containing saturable absorber, noting peak power and pulse rate 20 p3460 A67-36854

Carbon dioxide breathing effects on forearm blood vessels, discussing vascular resistance and carbon dioxide role in blood flow regulation 20 p3373 A67-37584

Radiative heat transfer in nonisothermal nongray gas model, measuring absorption and emission in carbon dioxide and water gases [ASME PAPER 66-WA/HT-25] 20 p3555 A67-37607

Multipath cell with White mirror system using carbon dioxide and molecular nitrogen

gas mixture for gas laser amplifier and oscillator operation 21 p3625 A67-37854

Molecular and atomic, neutral and ion gas laser advances, noting high power CW carbon dioxide laser 21 p3639 A67-38062

Rapid scan spectrometer for carbon dioxide laser studies noting time dependent effects 21 p3641 A67-38460

Carbon dioxide and water vapor band emissivities determination, discussing spectral absorption, radiative heat transfer and energy distribution 22 p3918 A67-40042

Attenuation of plane sinusoidal acoustic waves due to electromagnetic radiative properties of carbon dioxide and water vapor bands 22 p3829 A67-40232

Atmospheric absorption of carbon dioxide laser radiation calculation from laboratory absorption coefficient measurements, discussing effects on power transmission and communications 22 p3816 A67-40237

Planetary atmosphere radiation spectral distribution sounded with 4.3 micron carbon dioxide band to determine temperature profile 22 p3805 A67-40355

UV light photolyzing ozone dispersed in solid carbon dioxide matrix causes formation of new substance showing IR absorption 23 p3971 A67-40970

Dog adaptation to increased carbon dioxide levels in normoxic environment, noting effects on arterial pH and bicarbonate level 23 p3950 A67-41537

Chronic hypercapnia effects on pH level, Ca and P metabolism and electrolyte metabolism in normal sedentary man 23 p3955 A67-41605

IR lasers using vibrational rotational transitions of carbon dioxide 24 p4166 A67-41799

Upper limit of carbon dioxide abundance in Mercury atmosphere 24 p4225 A67-41836

Dynamic mass transfer equation for design parameters of regenerable absorption beds for carbon dioxide removal in spacecraft life support system [SAE PAPER 670842] 24 p4115 A67-41996

Spectral reflectance of water and carbon dioxide cryodeposits in vacuum integrating sphere as function of incidence angle, substrate material and cryodeposit thickness 24 p4252 A67-42046

CARBON DIOXIDE CONCENTRATION

Growth rate limitations with interactions of light and carbon dioxide investigated for two species of *Chlorella* 20 p3369 A67-36791

Platinum wire heating in sealed carbon dioxide laser results in catalyzing effect permitting high carbon dioxide concentration 23 p4011 A67-40784

CARBON DIOXIDE REMOVAL

SA AIR PURIFICATION

Molecular sieves using regenerable carbon dioxide solid adsorbents for spacecraft life support systems 20 p3374 A67-36611

Food, water and oxygen regeneration and reclamation techniques for long duration space flights, considering carbon dioxide removal, water reclamation from urine and contamination control 22 p3755 A67-40340

Physicochemical techniques for gas separation emphasizing pulsed gas chromatography for carbon dioxide removal in spacecraft 23 p3964 A67-41555

Carbonation Cell System for removing carbon dioxide from space cabin atmosphere using electrochemical process 23 p3965 A67-41578

Regenerable sorbent /GAT-O-SORB/ in granular form for carbon dioxide removal from air, discussing design and performance tests of laboratory prototype [SAE PAPER 670844] 24 p4115 A67-41997

CARBON DIOXIDE TENSION

Mechanism and pattern of human cerebrovascular regulation after rapid changes in blood carbon dioxide tension 11 p1746 A67-23989

CARBON DISULFIDE

Carbon disulfide oxidation noting self-ignition temperature, explosion limits, reaction products, cool flame propagation, etc 04 p0566 A67-15093

Beam wavelength and laser intensity effect on attenuation in carbon disulfide induced by ruby laser indicate two-photon absorption 10 p1667 A67-23776

Carbon disulfide P-branch transitions with J equals 28 to 46 for 001-100 vibrational transition identified as laser lines in N-carbon disulfide gas

system 23 p4011 A67-40789

CARBON MONOXIDE

Nonthermal radiation of Na in CO medium, analyzing temperature, pressure and composition variation effects of ambient 01 p0166 A67-10051

Equilibrium carbon monoxide pressures measured by torsion effusion studies of reaction of graphite with hafnium and uranium dioxides at high temperatures 01 p0018 A67-10763

Diffusion and dissociation of CO molecules in solar atmosphere 01 p0151 A67-11284

Overlapping of bands of nitrogen oxide, CO and carbon dioxide in 4.5 micron region determined for inversion experiments 02 p0246 A67-12368

Rotational intensity distribution of vacuum UV absorption spectrum bands of carbon monoxide arising through mixing of D state with neighboring states 02 p0269 A67-12450

Carbon monoxide reaction with oxygen noting effects of various hydrogen-containing compounds, discrepancies in explosion limits, etc 04 p0565 A67-15092

Forbidden absorption bands of carbon monoxide in vacuum UV region, noting rotational and vibrational constants and perturbations 05 p0848 A67-16847

Closed ecological systems and endogenous formation of CO in plant and animal tissues 07 p1136 A67-19107

Solar wavelength measurements for approximately 14 bands of CO fourth positive group in solar rocket UV spectrum 08 p1399 A67-21235

Motion of structures in coma and tail of Morehouse comet compared with hydrodynamic model interaction between solar wind and cometary plasma 10 p1704 A67-22720

Calibration of vibrational transition of CO at various pressures to determine vibration-rotation wave numbers 13 p2160 A67-26600

Inelastic collisions of proton beam with carbon monoxide target molecules, determining ionization cross section and charge transfer 14 p2390 A67-28943

Laser output reduced by rare gas impurities in molecular neutral CO and nitrogen gas lasers 15 p2500 A67-29910

Carbon monoxide chemisorption on polycrystalline molybdenum studied by radiotracer, noting desorption at various temperatures as time function 15 p2434 A67-30099

Carbon monoxide and atomic oxygen recombination in expansion wave of single-pulse shock tube at high temperatures 18 p2997 A67-33790

Ignition kinetics of carbon monoxide-oxygen reaction 18 p3155 A67-33846

Adsorption, surface reaction and mutual displacement of carbon monoxide, carbon dioxide and oxygen on titanium film, using mass spectrometer 19 p3244 A67-34941

Spectral transmittance of mixture of carbon monoxide and nitrous oxide for overlapping absorption bands 19 p3266 A67-35696

Plasma flow and generation in CO comet due to electron-collisional ionization under influence of solar wind 22 p3885 A67-40081

Radiation intensity measurements in systems containing atomic oxygen and carbon monoxide by shock tube heating, deriving spectral intensity distribution for radiative combination 23 p4029 A67-40972

CARBON STEEL

S STEEL

CARBON TETRACHLORIDE

CW He-Ne laser compared with mercury arc source, obtaining Raman spectra of carbon tetrachloride by three methods of excitation 03 p0438 A67-13912

CARBON TETRACHLORIDE POISONING

Comparative pathology of animals continuously exposed to varied concentrations of carbon tetrachloride vapor in altitude chamber 21 p3573 A67-38070

CARBON TETRAFLUORIDE

Electronic and molecular radial distribution functions for liquid carbon tetrafluoride using X-ray diffraction, determining orientational effects of carbon tetrachloride and temperature dependency 01 p0117 A67-10885

Heats of combustion in fluorine of Teflon and graphite and heats of formation of carbon tetrafluoride and carbon hexafluoride 15 p2433 A67-29765

CARBON 13

Solar content of carbon isotope 13 obtained by examining solar atmosphere at center of disk 02 p0324 A67-11770

Solar spectrum reexamination determining lower limit for C12/C13 isotopic abundance ratio in photosphere [AFCR-67-0480] 09 p1566 A67-22231

CARBON 14

Evolution of radiocarbon concentration at low latitudes of Northern Hemisphere during past nine years explained by south equatorial maritime current 09 p1492 A67-22592

Geomagnetic field intensity influence on atmospheric C-14 production, using two-reservoir model 21 p3620 A67-38981

CARBONACEOUS METEORITE

Neutron exposure ages of meteorites, estimating amount of shielding which surrounds samples in space from Co-60 and Ar-39 activity data 06 p1082 A67-17871

Biotic signature distribution reflecting geologic, atmospheric and oceanographic environmental orders 06 p0954 A67-19018

Diffusive fractionation and two-component models for trapped meteoritic neon and isotopic composition of neon in carbonaceous chondrites 07 p1249 A67-19536

Sulfur compound in carbonaceous chondrites explained by oxidation of troilite by oxygen and HOOH 07 p1249 A67-19539

Optical rotation of lipids extracted from soils, sediments and Orgueil carbonaceous meteorite 08 p1289 A67-21173

Orgueil carbonaceous meteorite composition and mineral texture including petrogenesis and origin of organic content and mineralized microstructures 10 p1710 A67-23628

Mercury abundance in chondrite meteorites determined by neutron activation and separation by volatilization over temperature range 13 p2210 A67-27603

Nogoya type II carbonaceous chondrite noting cosmogenic, radiogenic and primordial noble gas components 14 p2390 A67-28890

Element abundance in various chondrite groups determined by neutron activation technique 14 p2391 A67-28950

Abundant lithophile element fractionations in chondrites with special reference to aluminum and calcium 14 p2391 A67-28951

Argon, krypton and xenon in chondrites noting constant abundance ratios and correlation of concentration to disequilibrium 16 p2750 A67-31436

Olivine composition in chondrites relative abundances and classification 16 p2751 A67-31455

Condensation history of cooling gas of cosmic composition, stressing chondrite fractionation patterns 20 p3526 A67-37172

Abundance of volatile elements in meteorites, comparing chondrite decrease for evidence of fractionations in solar nebula 20 p3526 A67-37173

Meteoritic organic chemical analyses since 1900, considering volatile materials distribution and carbonaceous chondrites 21 p3704 A67-38502

Magnetite crystals of asymmetrical shape observed in Alais, Ivuna and Orgueil carbonaceous meteorites noting particle corrosion 22 p3881 A67-39496

Origin of round body structures in Orgueil meteorite 24 p4113 A67-42455

Precious metal concentrations in carbonaceous and enstatite chondrites using neutron activation analysis 24 p4233 A67-42617

Type I carbonaceous chondrite flakes from British Columbia meteorite fall 24 p4233 A67-42618

Xenon data from Murray and Renazzo carbonaceous chondrites reinterpreted, discussing large presence of fissionogenic xenon 24 p4234 A67-42626

Aromatic compounds in benzene eluate fractions from carbonaceous chondrites by high resolution capillary gas-liquid chromatography 24 p4236 A67-42640

Olivine and pyroxene composition distribution in type II carbonaceous chondrites, discussing metamorphic effects and gas-dust fractionation 24 p4237 A67-42651

CARBONATE

SA POLYCARBONATE

Oxygen solubility in fused carbonates and corrosion behavior of Ag and Cu oxide, air and carbon dioxide cathodes in molten

carbonate fuel cells 09 p1458 A67-22182

Isomerization rate of iminocarbonates, discussing electronegative hetero-atom bonded to imino carbon 09 p1459 A67-22363

Stable isotope distribution in carbonates 14 p2310 A67-27970

CARBONIZATION

Surface hardening of titanium alloys by carbon and nitrogen, using high-frequency induction heating 19 p3242 A67-34919

CARBONYL

Chemiluminescent reactions of atomic oxygen with carbonyl sulfide and hydrogen sulfide in flow system as function of reaction time and reactant concentrations 14 p2260 A67-28781

Carbonyl compounds reaction with N-salicylideneglycinatoaquocopper (II) syntheses of beta-hydroxy alpha-amino acid from glycine 20 p3376 A67-36877

CARBOXYL GROUP

Hydrolysis of phthallimide ring with carboxylate group linked through alkyl group as anionic intramolecular catalyst 10 p1602 A67-23159

CARBOXYLIC ACID

SA DICARBOXYLIC ACID

Prebiotic synthesis of monocarboxylic acids suggested from mixture of methane and water exposed to semicorona discharge 19 p3181 A67-35882

CARCINOTRON

Harmonic mixing and heterodyne detection of laser radiation 19 p3240 A67-35623

Carcinotron hyperfrequency power oscillator with tube of same noise characteristics as control developed for space telecommunications 23 p3982 A67-41431

CARDIOGRAM

S ELECTROCARDIOGRAM

S VIBROCARDIOGRAM

CARDIOGRAPHY

SA ELECTROCARDIOGRAPHY

Long term biomedical monitoring of human heart rate through lithium chloride impregnated balsa electrodes, noting space flight application 15 p2431 A67-29918

Vibrophonocardiographic techniques for monitoring cardiac dynamics in flight environment 17 p2806 A67-31954

Vibrophonocardiograph developed for use in shirt-sleeve flight environment, previous design miniaturized without sacrificing performance characteristics 23 p3970 A67-41661

CARDIOLOGY

Cardiac changes under hypoxia, experimental morphological study 13 p2058 A67-26756

CARDIORESPIRATORY SYSTEM

SA BLOOD CIRCULATION

SA LUNG

Cardiac output during rest and work determined via carbon dioxide method at 3800 m altitude 10 p1598 A67-23392

Backward, forward and transverse acceleration effects on cardiopulmonary systems of men and dogs 10 p1599 A67-23810

Effects of breathing pure oxygen under pressure on autonomous regulatory systems /nervous, respiratory, circulatory/ of man 14 p2257 A67-28225

Maximum aerobic work correlation with anthropometric and spirometric parameters, studying ventilatory capacity coefficient 16 p2614 A67-31472

Cardiorespiratory functioning in flight monitored on carrier pilots in combat 17 p2805 A67-31956

In-flight aeromedical monitoring of cardiorespiratory response of naval pilots during aircraft carrier combat operations, discussing physiological effects determination 23 p3963 A67-41541

CARDIOTACHOMETRY

Analog circuit for presenting fixed pulse output corresponding to each cardiac cycle of given electrocardiogram and highly unresponsive to noise interference 09 p1455 A67-21715

Special preprocessing circuit for cardiac beat recognition discriminates against noise artifacts in electrocardiogram 15 p2432 A67-29920

Digital cardiometer design noting binary counter, clock, operation cycle, etc 15 p2432 A67-29921

Lithium chloride impregnated balsa wood and surgically implanted electrodes for continuous heart rate recording over long periods of time 23 p3965 A67-41571

CARDIOVASCULAR SYSTEM

SA ARTERY

SA BLOOD CIRCULATION

SA CAPILLARY

Space technology utilization in detection and prevention of cardiovascular disease, discussing instrumentation for monitoring microcirculatory system

[AIAA PAPER 66-951] 02 p0187 A67-12285
Cardiovascular changes and vasodepressor effect in reoxygenation of cats 03 p0364 A67-14290

Cardiovascular responses of anesthetized dogs to repeated rapid decompressions in near vacuum 03 p0365 A67-14296

Objective statistical approach to tilt table data analysis using computer to define characteristics of cardiovascular deconditioning resulting from bed rest, water immersion and space flight 05 p0754 A67-16276

Absolute bed rest and recumbent exercise during bed rest effects on pulse rate response to submaximal work, cardiovascular functional capacity /maximal oxygen intake/, physical work capacity and orthostatic tolerance 05 p0755 A67-16283

Cardiovascular changes due to orthostasis, evaluating influence of intravascular instrumentation on orthostatic tolerance of normal men 06 p0953 A67-18776

Cardiovascular health of air traffic controllers age-matched with noncontrollers 07 p1134 A67-19859

Cardiovascular response of 37 patients with heart disease to prolonged passive upright tilt compared with normal subjects 07 p1135 A67-19866

Radiographic analysis of thoracic cardiovascular rupture during abrupt deceleration associated with crashes [ARL-TR-67-17] 08 p1287 A67-20614

Cardiovascular deconditioning caused by microcirculatory changes which reduce proprioceptor sensory input of unanesthetized rat 09 p1452 A67-21714

Multifocal premature ventricular contractions found in ECG, evaluating cardiovascular system significance in flight stress tolerance 09 p1453 A67-21735

Cardiovascular and respiratory reactions of cosmonauts during Voskhod II orbital flight 09 p1454 A67-22384

Wave dispersion phenomena in blood vessels analyzed as measures of cardiovascular parameters 11 p1748 A67-23990

Cardiovascular and renal 24 hr synchronized and desynchronized circadian rhythm 11 p1747 A67-24785

Diurnal rhythm of cardiovascular responses to active orthostasis and Schneider test performance in function diagnostics of peripheral cycle regulation [DVL-620] 11 p1747 A67-25035

Prolonged weightlessness exposure and expected effects on man 12 p1902 A67-25725

Nervous reflex mechanisms of hemodynamic shift control during rapidly and slowly increasing acceleration 13 p2058 A67-26757

Prophylaxis for negative effect of hypokinesia on human cardiovascular system 13 p2059 A67-26764

Ballistographic, glucose and Masterov methods applied to pilot examination for coronary defects 14 p2255 A67-28223

Weightlessness simulation by bed rest and water immersion, evaluating validity of protective measures, recovery time and tilt response 15 p2424 A67-29102

Plasma volume and tilt table response of humans to water immersion deconditioning experiments, using extremity cuffs to study protective effect 15 p2428 A67-29271

Cardiovascular changes at onset of whole body, X-axis sinusoidal vibration in anesthetized mongrel dogs and unsedated humans 15 p2428 A67-29272

Weightlessness effect on human cardiovascular system noting mechanical forces, amount of work done to overcome hydrostatic pressure, etc 16 p2612 A67-30773

Effect upon cardiovascular system of weightlessness simulated by immersion in brine 17 p2805 A67-31952

Tilt table response and plasma volume changes in experimental subjects evaluated before and after short term periods of deconditioning 17 p2805 A67-31953

Aortic insufficiency in flying personnel, discussing case histories and cardiovascular

system 17 p2806 A67-31965
Extremity cuffs or leotards effect in preventing or controlling cardiovascular deconditioning of bed rest 18 p2992 A67-34715

Heat and exercise induced hypohydration effects upon physical performance of women, showing some deterioration in cardiovascular system 20 p3372 A67-37033

Hemodynamic responses of conscious dogs exposed to various centrifugation levels and back angles to determine optimum angle for positioning astronauts 22 p3750 A67-39593

Rentgenographic kymography in evaluating cardiovascular apparatus in middle aged pilots 22 p3753 A67-40543

Dog adaptation to increased carbon dioxide levels in normoxic environment, noting effects on arterial pH and bicarbonate level 23 p3950 A67-41537

Cardiovascular acceleration-stress reactions during G acceleration of dogs, noting blood pressure, blood velocity and pressure waves 23 p3951 A67-41551

Canine cardiac displacement and cardiovascular dynamic response during abrupt deceleration impact, discussing traumatic ruptures and pressure effects 23 p3951 A67-41552

Inactivity and water immersion effects on fluid balance and tilt-table performance in dehydrated subjects, assessing vasopressin and positive pressure breathing effects 23 p3951 A67-41557

Field Effect Monitor for biomonitoring cardiovascular variables and LF physiological phenomena 23 p3966 A67-41582

Experiments for relief of astronauts from cardiovascular and respiratory distress during EVA 23 p3953 A67-41586

Leg volume changes in response to lower body negative pressure due to blood redistribution 23 p3955 A67-41619

Cardiovascular integrity restoration in post myocardially infarcted aviation personnel 23 p3957 A67-41637

Vibrocadiogram used as cardiovascular monitor, applying signal averaging methods for parameter evaluation during severe subject stress 23 p3959 A67-41660

Restoration of cardiovascular integrity in post myocardially infarcted aviation personnel 23 p3971 A67-41709

CARGO AIRCRAFT
S TRANSPORT AIRCRAFT
CARNOT ENGINE

Carnot cycle diagrams using heat and work as coordinates in addition to several thermodynamic variables 01 p0166 A67-10505

Criterion for minimum weight Carnot limited space power systems 24 p4103 A67-42496

CAROTENE
Deaggregation of chlorophyll by xanthophylls 09 p1454 A67-21990

Chromatographic accumulation of primary and secondary carotenoids in Spongiochloris typica over 8-week period 14 p2254 A67-28065

CAROTID SINUS REFLEX
Blood pressure response to carotid sinus pressure in normal and vasomotor instability subjects evaluated for personnel selection for flying training 05 p0756 A67-16290

CARRIER
SA AIRCRAFT CARRIER
SA MAJORITY CARRIER
SA MINORITY CARRIER

Optical nonlinearities due to conduction band electrons in InAs, InSb, GaAs and PbTe studied, using Q-switched carbon dioxide laser radiation 02 p0254 A67-12524

Optical mixing due to conduction band electrons in semiconductor 02 p0254 A67-12525

Analog magnetic recording in ground telemetry stations 03 p0418 A67-12896

Cyclotron absorption in n type lead telluride with wide range of carrier concentrations, showing increase in transverse effective mass and decrease in anisotropic mass ratio 03 p0493 A67-13352

Equivalent noise current equations and spontaneous fluctuations of leakage current due to carrier generation in depletion layer of reverse-biased junction diode 03 p0379 A67-13479

Temperature dependence of current-carrier concentration and electrical conductivity of p-type germanium containing beryllium and phosphorus 04 p0679 A67-15144

Temperature variation of electric conductivity and carrier mobility in diffused germanium resistors doped with antimony for thermometry 05 p0773 A67-16464

Excess carrier lifetime in semiconductors by measuring photoconductive phase shift of spreading resistance under point contact 05 p0861 A67-16501

Current-controlled NDR, electron-hole generation and switching to higher current lower voltage state in GaAs 05 p0870 A67-17275

Analogy between radiation angular spectrum reflected from rough surface and frequency spectrum of carrier burst related to radio propagation 06 p0957 A67-17579

Size effects in electroconductivity of semiconductors with several groups of carriers with large intergroup relaxation time 06 p1064 A67-18944

Optical phonons role in determining form of free carrier distribution function in semiconductors and nonohmic behavior of strongly piezoelectric crystals 06 p1065 A67-18952

Semiconducting properties of ferroelectrics estimating free carrier densities in n and p regions and distributions over plate thickness 08 p1367 A67-20314

Hall effect on hot carriers in p-type Ge semiconductor in microwave field as function of field strength 08 p1369 A67-20993

Carrier drift velocity measurements in silicon at high electric fields, using time-of-flight technique 10 p1690 A67-23167

Temperature effect on microwave-gain characteristics of bulk GaAs amplifier, interpreting results in terms of changing carrier concentration 10 p1612 A67-23371

Magnetic resistance and Hall effect dependence on external electric field in semiconductors, noting difference for parabolic and nonparabolic law of carrier dispersion 10 p1695 A67-23661

Temperature dependence of current-carrier concentration and electrical conductivity of p-type germanium containing beryllium and phosphorus 12 p1979 A67-25167

Lifetime for nonequilibrium current carriers in n-type indium antimonide crystals from generation-recombination noise measurements at various temperatures 12 p1984 A67-25523

Current carrier concentration gradient in InSb, investigating effect on transverse reluctance coefficient and Hall effect dependence on magnetic field intensity 13 p2173 A67-26360

Current carrier concentration distribution in semiconductor with intrinsic anisotropy created by strong electric field 13 p2173 A67-26362

Hot carrier DC conduction in elemental semiconductors germanium and silicon 13 p2183 A67-27568

Nonlinear volt-ampere characteristic of photosensitive GaAs plus copper atoms in strong electric field 14 p2368 A67-28532

Multiple carrier measurements using TWT for application to satellite communications 15 p2438 A67-30140

Current carrier distribution in GaAs-Ge heterojunctions measured for energy band diagram 15 p2542 A67-30241

Origin of forced oscillation in space-charge density of free current carriers in semiconductors ascribed to periodic generation of carriers 15 p2542 A67-30243

Isochronous and isothermal annealing of indium antimonide irradiated by X-rays and gamma rays, studying changes in current-carrier concentration 15 p2542 A67-30247

Traveling wave amplification by interaction of drifting carriers in semiconductors with external slow wave circuit 17 p2826 A67-32656

Irradiated germanium observed for carrier concentration variations, using Hall coefficient measurements 17 p2918 A67-32853

Magnetic resistance and Hall effect dependence on external electric field in semiconductors, noting difference for parabolic and nonparabolic law of carrier dispersion 17 p2924 A67-33342

Free carrier absorption coefficients in 6H and 15R silicon carbide, showing probable ellipsoids of revolution 18 p3102 A67-34279

Lifetime for nonequilibrium current

- carriers in n-type indium antimonide crystals from generation-recombination noise measurements at various temperatures 18 p3103 A67-34454
- Excess carrier distribution in inhomogeneous semiconducting rectangular plate under two illumination conditions 19 p3308 A67-36026
- Nonequilibrium current carrier lifetime in p-type InSb samples alloyed with Cu and Ge, noting hole concentration and temperature effects 20 p3510 A67-36761
- Cadmium sulfide edge luminescence energy shift dependence on excitation intensity and free carrier concentration 20 p3512 A67-37288
- Excess carrier lifetime in semiconductors by measuring photoconductive phase shift of spreading resistance — under point contact 20 p3512 A67-37317
- Density and recombination coefficients of nonequilibrium carriers in Ge and GaAs as function of laser excitation intensity 20 p3513 A67-37437
- Transient heating and cooling of current carriers in semiconductors and highly ionized plasma analyzed, using effective temperature method 20 p3513 A67-37438
- Carrier spatial redistribution under magnetic field effect of current in semiconducting crystal with intrinsic conductivity noting I-V curve shape 21 p3678 A67-38098
- Current carrier concentration gradient in InSb, investigating effect on transverse reluctance coefficient and Hall effect dependence on magnetic field intensity 21 p3680 A67-38317
- Current carrier concentration distribution in semiconductor with intrinsic anisotropy created by strong electric field 21 p3680 A67-38319
- Nonlinear volt-ampere characteristic of photosensitive GaAs plus copper atoms in strong electric field 23 p4039 A67-40939
- Free carrier effect on higher harmonic generation in semiconductors from nonlinear Boltzmann equation 24 p4202 A67-41985
- CARRIER FREQUENCY**
- SA RADIO FREQUENCY**
- Analog carrier frequency multiplier using Hall effect in multiplier element 04 p0581 A67-14892
- Emitter barrier capacitance effect on frequency characteristic of current amplification factor in drift transistors with accelerating field for minority carriers 04 p0585 A67-15502
- Simultaneous estimate of delay time and drift of carrier frequency during nonoptimum reception against correlated noise background 05 p0766 A67-17166
- Frequency modes of Gunn effect oscillator 05 p0872 A67-17531
- Convective heat transfer in tube with gaseous heat carrier pulsating at frequency corresponding to second resonance harmonic 07 p1266 A67-19182
- Dual frequency VLF timing system for synchronization of remotely located clocks, noting WWVL radio carrier frequency, signal generator, etc 09 p1494 A67-21619
- Amplitude and phase frequency characteristics of linear system determined from transfer characteristics 11 p1772 A67-24980
- Hall and electric field effects in cadmium sulfide single crystals in terms of current carrier mobility 13 p2174 A67-26369
- Active and reactive resistance components of p-n-n diodes with minimum distribution of steady state carrier concentration in base 13 p2182 A67-27282
- HF photoconductive phase responses in single crystal n-type indium arsenide, deriving carrier lifetimes 14 p2364 A67-28104
- Galvanomagnetic properties of single crystal antimony as function of temperature, deriving carrier mobilities and densities, detailing nature of Fermi surface 14 p2364 A67-28105
- Radio pulse sequences selection according to carrier frequency by analyzing filter operation 14 p2261 A67-28278
- Pulse measuring system for observing structure of pulsed signals in rectangular phase-time coordinates 15 p2444 A67-29414
- Carrier instability influence on noise immunity of discrete communication systems, with results presented graphically for uniform and normal random frequency distributions 16 p2620 A67-30477
- Strong reflection from underlying surface effect on range-only radar measurements, deriving phase angle between side-and carrier-frequency oscillation vectors 16 p2624 A67-31030
- Hot carrier galvanomagnetic characteristics of n-type germanium of intermediate carrier concentration, noting Maxwellian distribution 16 p2731 A67-31172
- Altimeter using pulse repetition frequency /PRF/ tracking design with solid state X-band frequency source 17 p2859 A67-32522
- Ideal SSB modulation theory, discussing DSB Laplace transform formalism, noting Butterworth filters for channel contaminants reduction 19 p3181 A67-34848
- CW transmission measured for carrier and modulation phase, examining carrier phase perturbations due to mode interference CW transmission measured for carrier and modulation phase, examining carrier phase 20 p3379 A67-36292
- Hall and electric field effects in cadmium sulfide single crystals in terms of current carrier mobility 21 p3680 A67-38325
- Electrical conductivity temperature dependence, Hall coefficient, current carrier mobility, melting point and density data for single crystal of AlIBIV type electrical conductivity temperature dependence, /n-m/ junction structures transient characteristics, forward and back bias cases show inductive and capacitive element behavior respectively 22 p3858 A67-39574
- Carrier frequency measurement accuracy using panoramic radio receiver, discussing statistical estimate of errors using two different reading methods 22 p3772 A67-39871
- CARRIER INJECTION**
- Current injection effect on time delay of GaAs laser radiation 01 p0087 A67-10083
- Charged particle injection into magnetic traps through mirror, using annular electron gun 01 p0122 A67-10350
- Strong injection in nondegenerated p-n junction producing electron-hole plasma in n region near junction 02 p0296 A67-11827
- Negative resistance and current density in double-injection filaments in seminsulating Si 02 p0298 A67-11886
- Electron beam scanning technique measurement of diffusion lengths in Si and GaP n junctions and recombination rate of dislocations in n-type Si 02 p0298 A67-11887
- Initial saturation voltage effects in alloy-type transistors at high injection levels 02 p0215 A67-11977
- Electromagnetic, circuit theory, quantum and statistical mechanics laws for conduction electrons in low and high injection p-n junctions 02 p0299 A67-12105
- Injection peculiarity in heterojunctions arising from band discontinuities which favor hole injection over electron injection 03 p0490 A67-13154
- Radial distribution of excess current carriers in base of p-n junction transistor with high injection levels 03 p0378 A67-13244
- Instability of Sb and Au-doped n-type germanium during carrier injection, examining current-voltage and frequency characteristics and illumination effects 03 p0499 A67-13955
- Space charge limited unipolar nonstationary currents in solid, calculating nonsteady modes in plane parallel electrode structure due to carrier injection into gap 04 p0680 A67-15155
- Photoconductivity and negative resistance caused by carrier lifetime change in response to change in injection level in SiC p-n junctions 04 p0680 A67-15156
- Recombination waves appear in sample having ohmic contacts when drift velocity of carriers in constant electric field exceeds certain value 04 p0681 A67-15290
- Static V-I relationships in transistors at high injection level 04 p0585 A67-15621
- Neutron induced degradation of carrier lifetime in n-and p-type silicon containing oxygen and dopant impurities 04 p0684 A67-15691
- Minority carrier lifetime dependence on injection level, obtaining recombination center parameters for neutron irradiated germanium, using photoconductivity 04 p0684 A67-15692
- Transient annealing following pulsed neutron exposure in silicon transistors and solar cells as function of temperature and injection level 04 p0684 A67-15693
- Silicon electrical properties at low temperatures and various carrier concentrations, noting impurity 05 p0861 A67-16502
- Current and hole distribution calculated for p-n junction acted upon by sinusoidal voltage of arbitrary amplitude-small injection level 05 p0865 A67-16910
- Storage time of drift transistors calculated as function of minority carriers effective lifetime 05 p0776 A67-17094
- Reactive properties of p-n-n semiconductor structures at high injection levels for monomolecular electron-hole recombination 06 p1049 A67-17866
- Injected carrier flow in seminsulator containing deep impurity density gradient 06 p1051 A67-18221
- Lifetime and recombination of excess carriers in silicon over seven orders of magnitude of injected carrier density 06 p0971 A67-18226
- Current injection effect on time delay of GaAs laser radiation 08 p1340 A67-21460
- Trap-free space-charge-limited current produced by space charge injection in oxygen doped n-GaAs crystals at low temperature 09 p1552 A67-21767
- High injection theories of p-n junction, commenting on corrections made in connection with junction voltage 09 p1472 A67-21953
- Injection luminescence and photoluminescence spectra of epitaxial heterojunctions in GaP-GaAs system 09 p1554 A67-21975
- MOS structure studied by measuring variations in capacitance and charge injection into oxide 09 p1558 A67-22586
- Diffused base punchthrough avalanche transistor /PAT/ at high recurrence frequency having capacitance dependence of pulse width 10 p1609 A67-22839
- Self-consistent field in HF plasma accelerator with static magnetic field gradient 10 p1683 A67-22852
- Mobile charge carrier velocity measurements in silicon at high field strengths 10 p1690 A67-23168
- Space charge conductance and electron drift velocity measurements for avalanching p-n-n diode 10 p1611 A67-23169
- High power operation of semiconductor lasers, noting differential equation of field distribution along junction 10 p1665 A67-23519
- Distribution of injected carrier densities in strongly forward biased laser junctions 10 p1666 A67-23522
- Avalanche multiplication of current carriers at low temperatures in p-n junctions of InAs, determining carrier ionization coefficient and dependence on electrical field 10 p1695 A67-23660
- Plasma parameter range for convective and absolute Harris instabilities, noting correlation with density 11 p1827 A67-23883
- Space-charge-limited currents in p-type silicon noting I-V characteristics, theoretical values agreement, Hall coefficient measurements correlation, etc 11 p1845 A67-24135
- Cut-off frequency of drift transistor, discussing function of drift field parameter 11 p1759 A67-24143
- GaAs semiconductor diodes for thermometric measurements in low and intermediate ranges, showing temperature dependence of injected current on emitter to collector voltage 11 p1766 A67-24650
- Ion acceleration region demonstrated by coupling two HF magnetic field gradient accelerators 11 p1841 A67-24767
- Specific resistance of epitaxial layers on low resistance substrates measured, using opposing probe method 11 p1792 A67-24813
- Current distribution of magnetic field in plasma coaxial injector indicating dominant role of Hall effect in plasma acceleration 11 p1841 A67-24854
- Semiconductor junction devices analyzed for diffusion and electric field currents in bulk regions 11 p1849 A67-24904
- Charged particle injection into magnetic traps through mirror, using annular electron gun 11 p1844 A67-25023
- Avalanche injection and application to fast pulse generation and switching 13 p2079 A67-26872

Total resistance of p-i-n diode calculated assuming high injection levels in base and moderate frequencies 14 p2286 A67-28530

Critical frequency dependence of p-i-n type semiconductor triodes on emitter current or injection level 14 p2289 A67-28824

Phase shift lifetime of excess carriers in semiconductors under sinusoidal injection, showing decrease as injection frequency increases 15 p2533 A67-29264

Space charge limited unipolar nonstationary currents in solid, calculating nonsteady modes in plane parallel electrode structure due to carrier injection into gap 15 p2534 A67-29342

Photoconductivity and negative resistance caused by carrier lifetime change in response to change in injection level in SiC p-n junctions 15 p2534 A67-29343

Conductivity and Hall effect in analysis of temperature dependence of current carrier concentration and mobility in silicon, explaining ionization energy 15 p2541 A67-30240

Minority carrier lifetime in p-silicon, analyzed varying temperature and injection level and studying recombination 16 p2725 A67-30807

Reactive characteristics of diffused p-n junctions in p-and n-silicon at high injection levels and in strong electric fields 16 p2726 A67-30817

Current and hole distribution calculated for p-n junction acted upon by sinusoidal voltage of arbitrary amplitude-small injection level 16 p2727 A67-30887

Negative-resistance in evaporated silicon films at room and liquid-nitrogen temperatures believed due to double injection 16 p2728 A67-31035

Electrical field distribution during injection of charged particles into two-dimensional model of magnetosphere 17 p2841 A67-32244

Quasi-particle recombination lifetimes in superconductors measured experimentally shown to differ from calculated lifetimes 17 p2913 A67-32370

Quantum efficiency in electroluminescent GaAs diodes, considering carrier concentration effect, electron injection ratio, photon absorption and radiative recombination 17 p2914 A67-32654

Injection luminescence and photoluminescence spectra of epitaxial heterojunctions in GaP-GaAs system 17 p2923 A67-33312

Avalanche multiplication of current carriers at low temperatures in p-n junctions of InAs, determining carrier ionization coefficient and dependence on electrical field 17 p2924 A67-33341

Voltage breakdown in undoped and chromium doped semiconducting GaAs 19 p3308 A67-36040

Current distribution of magnetic field in plasma coaxial injector indicating dominant role of Hall effect in plasma acceleration 20 p3502 A67-37537

P-n-p transistor overcomes bandwidth and switching time deficiencies to enhance minority carrier transport 21 p3598 A67-38570

Space charge limited (SCL) hole current in Si noting mobility, capacitance, current density, I-V characteristics and double injection 23 p4038 A67-40878

Injection and emission of hot electron in thin film tunnel diodes 23 p4039 A67-40885

Total resistance of p-i-n diode calculated assuming high injection levels in base and moderate frequencies 23 p3980 A67-40937

P-n junction performance with depletion layer subjected to sudden extreme carrier density generation noting significant local distortion 23 p4044 A67-41453

CARRIER MODULATION

SA PULSE MODULATION

HF conductivity, dispersion and temperature modulation of carrier waves and acoustic amplification in drifted semiconductor plasmas 03 p0496 A67-13558

Power spectrum improvement of multiple wave trains by concentrating power close to carrier frequency, noting constructive and destructive interference 06 p0963 A67-18401

Exact expression for transient response for step modulated carrier signal obtained, using parallel plate waveguide 06 p0964 A67-18767

LF modulation technique used aboard Canadian ionospheric research satellite ISIS-

A for tape recording of signals with VLF components 08 p1298 A67-20662

Threshold region of FM signals having carrier modulated by Gaussian baseband signal 11 p1752 A67-24124

Traveling wave IR and sub-mm light modulator design using free carrier absorption in reverse biased p-n junction diodes 11 p1759 A67-24137

Optimum system for signal detection with single-band noise modulation during carrier suppression, noting receiving system 15 p2436 A67-29413

Modulated signal nonlinear distortions from AC system resulting from system components nonlinearities 22 p3763 A67-40478

CARRIER ROCKET S LAUNCH VEHICLE

CARRIER SYSTEM

Buckling isolator system for carrier aircraft landing and catapult shock environment allowing use of available clearance for dynamic deflection 05 p0814 A67-17459

Gold doped silicon diodes consisting of compressor and expander elements designed to eliminate impedance range control and linearity problems 24 p4130 A67-42335

CARTAN SPACE

Group classification by Cartan method of equations of one-dimensional plane wave gas flow 04 p0611 A67-15982

Group classification by Cartan method of equations of one-dimensional plane wave gas flow 14 p2305 A67-28483

CARTESIAN COORDINATE

Stress-strain and Hooke law in orthotropic elasticity presented through matrix algebra and tensor coordinates 06 p1108 A67-18656

Cartesian formulation of membrane theory, discussing equations of equilibrium, strain energy, variation formulation and boundary conditions 11 p1875 A67-24431

Plane-parallel transonic flow with direct shock wave analyzed for case where Tricomi equation replaces Chaplygin equation 14 p2297 A67-27990

Gauss theorems for tensor with valence other than unity extended to include arbitrary orthogonal coordinates 14 p2349 A67-28738

Screw dislocation and crack interaction when elastic field is independent of one of three Cartesian coordinates 16 p2764 A67-30993

Hemisphere coverage by n planar phased arrays arranged in pyramids or pyramidal frustra solved by transformations leading to analytical solution 16 p2638 A67-31337

CARTOGRAPHY

SA MAPPING

Preliminary drawings of lunar limb area 05 p0896 A67-16718

Graphical method by which small local users of meteorological satellite pictures can identify geographical position of features in image [AIAA PAPER 66-439] 07 p1184 A67-19373

Cartographic representation of diurnal magnetic variations, noting longitudinal asymmetry in amplitude 10 p1631 A67-22808

New antenna techniques for Hertzian radiometric cartography 12 p1913 A67-25305

Systematic local errors in radio leveling of aircraft for different scales and tracks, using aerial camera 13 p2118 A67-26462

Potentialities of space cartographic systems evaluated for geometric map accuracy and economic aspects [AAS PAPER 67-106] 15 p2478 A67-29960

Spacecraft surveys of earth used for city growth observations, draw land-use maps, etc 19 p3221 A67-35324

Cartographic representation of diurnal magnetic variations, noting longitudinal asymmetry in amplitude 24 p4150 A67-42145

CARTRIDGE

Starter cartridges for jet engines, discussing operational problems and mechanical design, igniter and propellant development, etc 15 p2423 A67-29982

CARTRIDGE ACTUATED DEVICE

SA THRUSTOR

High pressure hot gas solid propellant cartridge starter for aircraft turbine engine [ASME PAPER 67-GT-21] 11 p1854 A67-24803

Cartridge-pneumatic dual mode jet engine starter design and function, discussing energy conversion and handling of high

pressure gas produced by starter cartridge [ASME PAPER 67-GT-49] 11 p1855 A67-24810

CASCADE

SA ELECTRON PHOTON CASCADE

Interactions of superhigh energy muons in cosmic ray nonelectromagnetic cascade showers 02 p0317 A67-12771

Possibility of realization of multicascade tunnel diode frequency doublers without intercascade amplification 05 p0777 A67-17173

Phase linearity of microwave component and interaction of cascaded devices, giving analysis of two-port device 08 p1303 A67-21029

Network analysis of frequency stability of quartz generators, showing possible reduction through additional HF cascades introduction into feedback loop 11 p1768 A67-24982

Spurious phase modulation reduction in multistage frequency multiplier using lumped-selection filters, determining cut-off angle in multiplying cascades 18 p3000 A67-34087

Interactions of superhigh energy muons in cosmic ray nonelectromagnetic cascade showers 22 p3877 A67-40273

Nuclear cascade avalanche absorption in Fe analyzed by ionization calorimeter 24 p4219 A67-42850

CASCADE FLOW

Conformal mapping of circle onto profile cascades with arbitrary parameters useful for exact computation of potential flow through cascade 01 p0005 A67-10277

Flow of compressible fluids past straight cascades of arbitrary airfoils using Karman-Tsien method, obtaining velocity distribution around airfoil through continuity equation 02 p0177 A67-11470

Compressor cascades with different irregularities in forward flow, noting special case of low aspect ratio blades 02 p0179 A67-12439

Pseudoshocks in pipe flow in supersonic compressors represented as diffusion process, noting application in cascade and rotor configuration 03 p0352 A67-13011

Supersonic retardation cascades for lossless reduction of supersonic flow to subsonic in turbines and compressors 03 p0503 A67-13012

Boundary layer measurements of friction losses due to finite thickness of leading edges of turbine blades 03 p0353 A67-14306

Compressibility effect on characteristic curve of axial-flow compressor stage, using simplified assumptions and loss-free cascade flow 03 p0353 A67-14307

Aerodynamic problems of turbomachinery, investigating effect of geometry and aerodynamic cascade parameters on flow deflection, static pressure difference and flow losses 04 p0547 A67-14985

Noncavitating water flow tests of three loaded axial flow pump rotor blades [ASME PAPER 66-WA/FE-24] 04 p0607 A67-15354

Water tunnel investigation of unsteady partial, full and supercavitation in cascade flow, determining force coefficients [ASME PAPER 66-WA/FE-25] 04 p0607 A67-15355

Streamline curvature computing procedures for turbomachinery and fluid flow problems, considering axisymmetric and nonaxisymmetric flow fields and compressible cascade flow [ASME PAPER 66-WA/GT-3] 04 p0607 A67-15358

Low speed cascade tunnel experiments for improvement of airflow and testing techniques, noting porous sidewall section effect on axial velocity changes [ASME PAPER 66-WA/GT-7] 04 p0548 A67-15385

Prediction theory for effect of shear flows on outlet angle in axial compressor cascades, taking into account effects of secondary flow, Bernoulli surface rotation and spanwise flow displacement 04 p0548 A67-15387

Forms of function connecting deviation angle and axial velocity ratio of exit flow in three-dimensional cascade flow 05 p0791 A67-16428

Cascade flow through compressor guide vanes and flow separation at top of vane profiles 05 p0750 A67-17323

Oscillations of staggered plate cascade in plane subsonic gas flow, showing fluid compressibility effect on aerodynamic

characteristics 06 p0935 A67-17729
Inflow boundary layer effect on secondary flow at blade tips of circular cascade of reaction turbine, considering tip and gap losses 06 p0937 A67-17991
Cascade flow in axial transonic compressor, examining boundary layer separation condition 07 p1127 A67-20123
Wind tunnel study of strong-deflection supersonic cascade decelerating flow past turbine blades 07 p1128 A67-20296
Application limit of inviscid small perturbation theory to secondary flow in cascade, comparing experimental and calculated vortex strength 08 p1275 A67-20406
Aerodynamic flow field past cascade of plane thin turbine blades subjected to small random vibrations [ONERA-TP-412] 09 p1439 A67-22588
Computer calculation of induced circulations and influence coefficients for turbine blades with arbitrary profiles and oscillation shift 10 p1591 A67-23044
Inviscid flow theory in internal aerodynamics, discussing irrotational, secondary and flow past thin airfoils and slender bodies 11 p1776 A67-24049
Tandem cascade of airfoils slow speed performance flow characteristics 12 p1891 A67-25349
Rotating blades cascade performance in mixed flow turbomachines, noting flow characteristics and slip factors 12 p1892 A67-25350
Theory on secondary flows through axial compressor or turbine cascade 13 p2049 A67-26530
Self-ignition and fuel combustion at blade cascade taking place at velocities and temperatures comparable to those of gas turbines 13 p2187 A67-26746
Heat transfer calculation to turbine blading in cascade in presence of secondary flow, considering flow velocity estimation, blade boundary layer and related heat transfer properties 13 p2225 A67-27465
Effect of blade row interference on cascade flutter investigated using semiactuator disk method 15 p2415 A67-29314
Flow through blade cascade studied by averaging flow parameters behind cascade for testing internal combustion turbine guide vanes 16 p2736 A67-31005
Inviscid steady partially cavitating flow through cascade of flat plate hydrofoils 16 p2662 A67-31550
Calculation of compressible subsonic potential flow through blade cascades, giving air outlet angle, velocity distribution around blade profile and critical Mach number 17 p2791 A67-32711
Tip losses in two types of turbine straight-blade cascades at several Reynolds numbers, noting vibration effect on stage performance 18 p2983 A67-33999
Low speed cascade tunnel experiments for improvement of airflow and testing techniques, noting porous sidewall suction effect on axial velocity changes [ASME PAPER 66-WA/GT-7] 18 p2983 A67-34131
Resonance effects arising during sub- and supersonic waves expansion in aerodynamic cascade 18 p2984 A67-34216
Unsteady flow past blade cascade problem solved by splicing technique instead of conformal mapping 18 p2984 A67-34217
Aerodynamic forces pressure center on profile in plane rectilinear blade cascade 19 p3169 A67-34884
Hydrogen plasmoids produced by pulsed two-cascade injectors, using electron guns for plasma ionization and acceleration 19 p3297 A67-35597
Functional sensitivity to cavitation of hydrofoil cascade, solving Fredholm type integral equations 20 p3419 A67-36188
Cascade flow in mixed flow pumps and turbines, solving boundary value problems for stream function by relaxation method 20 p3356 A67-36421
Aerodynamic characteristics of plane compressor cascades with high subsonic flow analyzed, noting application in determining flow deflection angle and pressure loss coefficient 20 p3358 A67-37079
Geometric parameters effect on aerodynamic characteristics of plane compressor cascade with high subsonic

flow 20 p3358 A67-37080
Plane compressor and guide vane cascades design, deriving relations for angle of attack, angle of lag, etc 20 p3358 A67-37081
Singularity carrier auxiliary curves for design of straight cascades of slightly curved bladings 20 p3360 A67-37596
Direct and inverse method of calculating rotating cascades with infinite number of blades and radial flow to enhance convergence 20 p3360 A67-37597
Unsteady cascade flow and blade oscillation in axial condenser as aerodynamic boundary value problem 21 p3564 A67-37892
Distribution of gas flow departure angle from annular turbine cascades 21 p3564 A67-37914
Plane compressor cascades, comparing small and large aspect blades and studying aspect ratio effect 21 p3564 A67-38045
Soviet book on aerodynamic flow calculations of axial flow turbines with subsonic and transonic blade cascade design method 21 p3565 A67-38766
Performance prediction of low solidity cascades from potential flow calculations 21 p3566 A67-39079
Flexure-torsion cascade flutter of airfoils with two degrees of translational and torsional vibration 22 p3914 A67-40040
Crossed field cascade tubes as frequency oscillators and microwave generators, discussing improved performance and interaction efficiency of devices 22 p3775 A67-40559
Solution for flow through circular array of blades contained between two surfaces of revolution separated by small variable distance obtained by Ackeret method 23 p3927 A67-40726
Turbine blade profile calculation by hybrid method 23 p3928 A67-41244
Incompressible potential flow about thick wing profiles and cascades for blade profiles with angular and round tapered trailing edges 23 p3929 A67-41254
Lifting line theory for blade cascade in subsonic shear flow, noting compressibility effect dependence on harmonic mean upstream Mach number 24 p4091 A67-42204
Streamline curvature computing procedures for turbomachinery and fluid flow problems, considering axisymmetric and nonaxisymmetric flow fields and compressible cascade flow [ASME PAPER 66-WA/GT-3] 24 p4143 A67-42459
Noncavitating water flow tests of three loaded axial flow pump rotor blades [ASME PAPER 66-WA/FE-24] 24 p4143 A67-42465
CASE
S CONTAINER
S MISSILE CASE
S MOTOR CASE
CASE HISTORY
Medical investigation of 1964/1965 fatal aircraft accidents in Southwestern U.S., noting combined effects of drugs, fatigue, alcohol and hypoxia 01 p0017 A67-10961
CASSEGRAIN ANTENNA
Structural and mechanical concept, design and testing of fully steerable radome-enclosed parabolic Haystack antenna 03 p0396 A67-13750
X-band Cassegrainian tracking antenna for space rendezvous position and rate information for navigation and guidance computations 04 p0569 A67-14502
Ground station for space communications and radar and radio physics, noting use of Cassegrain antenna computer guided pointing control, plug-in equipment box, etc 04 p0596 A67-15047
Cassegrain feed for 85-ft-diam antenna of planetary radar system noting operative conditions, polarization capabilities and performance data 04 p0596 A67-15048
Mechanical and electrical performance requirements of satellite communications antenna using Cassegrain configuration, noting relation to design 07 p1157 A67-20092
Parabolic Cassegrain antenna with low noise temperature for space telecommunication station 12 p1913 A67-25304
Primary illumination laws for parabolic reflector for maximum quality factor determined, considering multimode sources for cold antennas 12 p1913 A67-25307
Low noise receivers in transportable

satellite communication ground terminals, discussing interrelationships between antenna, receiver and cryogenics 14 p2260 A67-27782
Cassegrain monopulse feed system using end-fire polyrod radiators 15 p2451 A67-29925
Design and electrical properties of 25-meter Cassegrainian antenna installed at Raising ground station for radio communications via satellites 16 p2622 A67-30699
Large aperture, low noise, steerable antennas for ground station commercial satellite communication networks 16 p2641 A67-31532
Cassegrain antenna gain and noise temperature with dual reflector system derived from feed pattern and system geometry 17 p2824 A67-32395
Cassegrain antenna beam-pointing accuracy, analyzing reflector beam deviation and feed displacement effects 20 p3398 A67-36819
CASSEGRAIN OPTICS
Resonance scattering measurement from solar illuminated lunar atmospheric constituents 06 p1091 A67-18999
Modular xenon solar simulator for large area solar simulation, discussing source, transfer optical system and Cassegrain module, including fill-in optics 12 p1925 A67-25735
Airborne long focal length photographic system environmental effects studied with Cassegrainian type Maksutov telescope 16 p2678 A67-31793
CASSINI DOME
Cassini second and third laws are independent of first law 18 p3128 A67-34303
CASSIOPEIA A
Radio stars as signal sources for accurate measurement of radar antennas vertical polar diagrams, describing solar noise technique disadvantages 15 p2436 A67-29645
Broadband radio star Cassiopeia A scintillations observed with swept frequency interferometer [AGARDOGRAPH 95] 15 p2563 A67-30288
Radio star Cassiopeia A scintillations and spread-F in auroral zone [AGARDOGRAPH 95] 15 p2482 A67-30289
CASSIOPEIA CONSTELLATION
Radio star fadeouts and radio propagation 15 p2563 A67-30287
CASTING
Powder metallurgy techniques for thermoelectric materials particularly lead telluride, germanium bismuth telluride and zinc antimonide 01 p0099 A67-10709
Controlled solidification in casting, ingot-making and other processes including composites and highly undercooled melts 03 p0442 A67-13305
Directional solidification and single-crystal casting for jet engine turbine blades 03 p0429 A67-13541
Small additions of refractory elements effect on structure and properties of aluminum alloy castings containing Zn and Mg 07 p1201 A67-19255
Static and fatigue properties of repair welded aluminum and magnesium premium quality castings 08 p1333 A67-20360
Plastic foam pattern technique for producing vibration and shock fixtures 12 p1949 A67-25687
Design factors for aluminum castings 14 p2323 A67-27813
Honsel Plastic Mold /HPM/ process for high surface quality, discussing cost, materials and solidification time 21 p3637 A67-38976
CAT
Cardiovascular changes and vasodepressor effect in reoxygenation of cats 03 p0364 A67-14290
Electric stimulation of crossed olivocochlear cats and effect on auditory nerve responses 08 p1287 A67-20483
CATALYST
SA ENZYME
Hydrolysis of phthalimide ring with carboxylate group linked through alkyl group as anionic intramolecular catalyst 10 p1602 A67-23159
CATALYTIC ACTIVITY
SA PHOTOCATALYSIS
Catalyzed thermal decomposition of ammonium perchlorate 05 p0759 A67-17374
Heat transfer to catalytic and noncatalytic surfaces on sharp flat plate in shock tube

gas flow for checking various laminar boundary layer theories [AIAA PAPER 67-163] 06 p0989 A67-18481
Hydroxyl catalyzed chain decomposition of ozone, proposing new reaction mechanism [JPL-TR-32-1063] 07 p1138 A67-20192
Cryogenic hydrogen-oxygen ignition with hydrogen-gas entrained Raney nickel as catalyst 09 p1579 A67-21706
Extraterrestrial life detection method based on catalysis of isotopic oxygen exchange between water and oxygen-containing anions 09 p1454 A67-22015
Vitreous silica and molten Al reaction, penetration rate of Al, reaction rate and effect of Bi and Sb on rates by lamellar compound formation 10 p1669 A67-23381
Asymptotic solution method for frozen dissociated laminar boundary layer flow over flat plate surface with arbitrarily distributed catalytic 11 p1781 A67-24573
Approximate method for calculating stagnation point laminar boundary layer equations taking into account chemical reactions in gas phase and surface of body 12 p1928 A67-25673
Thermal explosion equations for first order catalytic reaction, discussing nonstationary effects superposed on quasi-stationary combustion pattern 12 p2039 A67-26111
Catalytic decarboxylation of oxaloacetic acid into pyruvic acid by thermally prepared poly-alpha-amino acids 13 p2065 A67-26589
Catalytic effect of thermal polyanhydro-alpha-amino acids on hydrolysis of p-nitrophenylacetate, noting role of histidine residues 13 p2065 A67-26732
Extraterrestrial life detection based on catalysis of oxygen exchange between labeled oxyanions and water, noting equipment 15 p2426 A67-29113
Aerodynamic heat flux measurements in frozen boundary layer flows taken in hyperthermal wind tunnel, considering surface catalytic effects 15 p2468 A67-30154
Mechanisms of atomic recombination at surfaces analyzed, considering behavior of insulators and semiconductor oxides 18 p2997 A67-33794
Cadmium compounds catalytic effect on ammonium perchlorate decomposition rate and ignition temperature 18 p3107 A67-33810
Concentration profiles in fixed laminar boundary layer with catalyst distribution on wall, discussing Schmidt number effect and approximations 18 p3159 A67-34161
Turbulent boundary layer on plane catalytic plate in nonequilibrium dissociating gas calculated by successive approximation technique 18 p3027 A67-34204
Heat transfer to catalytic and noncatalytic surfaces on sharp flat plate in shock tube gas flow for checking various laminar boundary layer theories 19 p3211 A67-35739
Lactic dehydrogenases of H4 and M4 type, preparation and catalytic and enzymological properties 20 p3377 A67-37159
Gas chromatography and IR spectrophotometry used to examine monomethyl hydrazine air oxidation, showing evidence of surface catalyzed reaction 21 p3578 A67-38841
Radiation heat transfer by flames to wire temperature sensor corrected by technique combining radiative input and catalytic activity 21 p3733 A67-38883
Platinum wire heating in sealed carbon dioxide laser results in catalyzing effect permitting high carbon dioxide concentration 23 p4011 A67-40784
Catalyzed ignition of composite propellant fuels in presence of perchloric acid studied for acceleration of rate of acid decomposition 23 p4048 A67-41761
Optically active alpha amino acids synthesized from alpha keto acids by hydrogenolytic asymmetric transamination 24 p4119 A67-42703
CATAPULT
SA LAUNCHING
SA TAKEOFF SYSTEM
Buckling isolator system for carrier aircraft landing and catapult shock environment allowing use of available clearance for dynamic deflection 05 p0814 A67-17459
High speed linear bearing to take launch uploads in aircraft-launching steam catapult 12 p1948 A67-25328

CATECHOLAMINE

Urinary catecholamine excretion in pilots relation to physical mental expenditure of energy and flight deck work loads 23 p3952 A67-41577
CATHETERIZATION
Surgical technique for implanting and maintaining arterial and venous catheters in monkeys 10 p1601 A67-23627
CATHODE
SA ANODE
SA CATION
SA COLD CATHODE
SA HOT CATHODE
SA PHOTOCATHODE
SA THERMIONIC CATHODE
Electrical properties and electron emission of sandwich cathodes prepared in vacuum by vapor phase condensation, deriving transfer constant 02 p0294 A67-11761
Annular hollow cathode discharge emitting electron beam to heat cylindrical workpiece located along axis 04 p0628 A67-15311
Zr-coated tungsten cathode in reducing divergence of electron beam emission 06 p0968 A67-18091
Physical foundations of cathode electronics - All-Union Conference, Leningrad, October 1965 06 p1036 A67-18421
Pressure difference in cathode region of MPD accelerator as affected by plasma compression and magnetic field [AIAA PAPER 67-47] 06 p0951 A67-18466
Cesium-plasma diode effect dependence on material output of cathode in vacuum, plotting short circuit current vs vapor pressure, voltage distribution, etc 08 p1357 A67-20845
Field intensities and electron distribution function in hollow cathode, graphs show potential distribution along cathode axis 08 p1358 A67-20851
Auxiliary arc electrodes for solution to cold boundary layer and cathode emissivity problems in MHD generators 09 p1444 A67-21822
Cathode spot phenomena in pulsed vacuum arc utilized for electric microthrusters, testing cathode materials by mass and momentum transfer 12 p1989 A67-25403
Thermionic converter acceleration plate and excessive current flow effects, noting collector and cathode surface secondary electron removal, determining cut-off characteristic form 14 p2246 A67-27766
Pressure difference in cathode region of MPD accelerator as affected by plasma compression and magnetic field [AIAA PAPER 66-47] 15 p2531 A67-30205
Energy distribution functions for nearly normal glow discharge using two models and statistics 19 p3273 A67-35098
Flow of positive ions from negative glow plasma into cathode dark space determined, discussing ion current density results 19 p3273 A67-35099
Self-consistent model for cathode region of high pressure arc, considering free fall sheath connection, electron and ionization region and flaring contraction 19 p3278 A67-35137
Self-consistent model for cathode region of high pressure arc, showing application to 200 amp arc in argon and boundary condition matching 19 p3279 A67-35138
Retrograde motion of electric arc discharge at low pressure with transverse magnetic field, including cathode vaporization 19 p3281 A67-35153
Cathode study using electron images of recording storage tube cathodes 19 p3197 A67-35813
Electrical breakdown association with field emission observed through electron microscopy of whiskerlike projections on cathode surface 21 p3589 A67-37824
FR-1 satellite-borne oxide cathode used to return to ground polarization current from ambient plasma 21 p3599 A67-38649
Tangential drag measurements at electrodes of arc in plasma accelerator, ion current partitioning at cathode and electrode damage 21 p3670 A67-38693
Liquid metal cathode electron bombardment thruster operable at high temperatures, noting stability in neutralizer current range [AIAA PAPER 67-667] 21 p3690 A67-38701
Low pressure argon ion laser cold

emission cathode, considering electron production by cathode sputtering owing to self-sustained arc discharge 22 p3817 A67-40413
Hollow cathode mercury laser providing improved performance, stability and reproducibility 23 p4016 A67-41226
Cathode outer oxide surface heating for pulsed emission current measured in intervals between retarding current pulses and different repetition frequencies 24 p4129 A67-42231
CATHODE RAY TUBE
SA ELECTRON GUN
Deflection-modulation display method analyzed for presenting video signals 01 p0061 A67-10018
Digital-graphic computer terminals effect on data processing equipment design, noting CRT use 01 p0029 A67-10669
System display composition, discussing analog and digital indicators, equipment operation functions and testing 04 p0626 A67-15736
Hybrid nonlinear optical filter exhibiting different transmission properties in opposite paths applied to CRT display 05 p0804 A67-16306
Image storage tubes /cathode ray tubes with memory device to store visual information/ 07 p1189 A67-20157
Computer graphic aids with applications of graph plotters, trace analyzers, cathode ray tubes, light pens, etc 13 p2073 A67-27188
Laser light deflecting methods, detailing scanlaser, laser resonator combining features of laser and cathode ray tube 13 p2128 A67-27237
CRT display provided by integrated circuit indicator packing circuitry in single plug-in-module, noting timing, sweep, generation, etc 14 p2288 A67-28769
High resolution CRT for system designers to scan film or record photosensitive materials 15 p2447 A67-29734
CRT design factors for optimum tube design for display systems 15 p2447 A67-29735
Radar display layout for aircraft safety consisting of digital computer and CRT 15 p2468 A67-30129
High resolution direct electron beam film scanner operable at 20 MHz, construction and performance 17 p2857 A67-32469
Rastering nanosecond laser sensitizer for materials responsive to short duration signals, discussing recording, sensitizer and measuring subsystem 17 p2858 A67-32482
CRT flying-spot-scanner spatial frequency response, determining film-plane modulation response to periodic sine/square wave 17 p2860 A67-32665
High speed methods of frame scanning in character output element with character point shaping on CRT screen 17 p2822 A67-33100
Systems engineering in computer-driven CRT displays for man-machine communication, emphasizing hardware-software tradeoffs and communication-transmission factors systems engineering in computer-driven CRT 18 p3005 A67-33499
Book on fundamentals of display systems covering cathode ray tubes, color techniques, photographic and electromechanical systems, etc 20 p3435 A67-36135
Computer based CRT display technique for servo system testing, discussing Saturn V display computer and simulation studies results 20 p3415 A67-36609
High precision CRT display system using raster beam positioning and computer-generated digital video 20 p3447 A67-36807
Three-dimensional projections on cathode ray tube screens noting visual transformations linking retinal image to space scene 20 p3450 A67-36985
Automatic test system employing optical and electrical input signals based on pattern recognition with CRT display 20 p3392 A67-36991
CATION
SA ANION
SA CATHODE
Positive ion emission from tungsten surfaces laser irradiated studied, using time-of-flight spectrometer 05 p0819 A67-16651
Potentials of zero charge of gold, silver and mercury electrodes as affected by cations and respective metal ion

interaction 11 p1749 A67-23920
 Ion-molecule reactions of diatomic
 deuterium cation with diatomic deuterium
 and diatomic hydrogen 18 p3083 A67-34521
 Mobility and diffusion of neon positive
 ions in neon, deriving ion energy and
 collisional cross section 19 p3271 A67-35074

CAUCHY INTEGRAL
 Nonsteady state gas flows with small
 entropy gradients corresponding to
 supersonic flight 02 p0178 A67-11629
 conditions
 Subcritical and nonoscillation intervals for
 Chaplygin theorem evaluated, using Green
 and Cauchy functions 03 p0456 A67-13112
 Soviet book on boundary value problems
 for analytic functions as applied to integral
 equations with Cauchy and Hilbert
 kernels 08 p1347 A67-20760
 Monograph on integral equations covering
 Fredholm and Volterra equations,
 applications to theory of differential
 equations, properties of Cauchy type
 integrals, etc 08 p1348 A67-20761
 Hilbert boundary problem extension for
 flexural problems of cracks in mixed media,
 noting Cauchy integrals, Plemelj formulae,
 etc 16 p2770 A67-31292
 Differential equations extremal solutions,
 introducing infrapolynomial and Cauchy
 infrapolynomial concepts 18 p3070 A67-33548
 Cauchy type integral applied to second
 boundary value problem for elastic plane
 with doubly periodic system of identical
 holes 18 p3145 A67-34601

CAUCHY LAW
 Occurrence of singularities in cosmology,
 giving testable condition implying existence
 of singularity assuming
 causality 21 p3703 A67-38493

CAUCHY PROBLEM
 Cauchy problem of compressible
 conducting perfect fluid flowing under
 perturbation influence 01 p0121 A67-10257
 Parabolic equation derivative solution
 applying results to boundary value problems,
 Cauchy problem and nonlinear
 equation 01 p0106 A67-10901
 Cauchy and boundary value problems for
 homogeneous differential equations with two
 independent variables analyzed, establishing
 generalized solution existing on uniqueness
 maximal domain 02 p0260 A67-12432
 Limit lines of generalized Cauchy problem
 for homogeneous differential equations with
 two independent variables analyzed, using
 concept of regular variables and formal
 solution of Meyer 02 p0260 A67-12433
 Existence and uniqueness theorem and
 upper and lower Chaplygin function
 approximations for solutions of Cauchy
 problem for quasi-linear first order
 PDE 03 p0456 A67-12884
 Exact and approximate solutions to
 Cauchy problem for nonlinear wave equation
 in affine connection field 03 p0457 A67-13171
 theory
 Hydrodynamic stability Cauchy problem
 for continuous spectrum of two-dimensional
 parallel flow of nonviscous incompressible
 fluid 03 p0402 A67-13172
 Cauchy problem of odd-order equations that
 are correct according to
 Petrovskii 03 p0459 A67-13644
 Computer solution of Cauchy problem of
 ordinary differential equations in form of
 Taylor series 05 p0834 A67-16377
 Uniqueness of Cauchy problem when
 initial surface contains characteristic
 points 05 p0835 A67-16739
 Three-dimensional Cauchy-Poisson problem
 for waves in viscous fluid 06 p0984 A67-18046
 Well posed problems for PDEs, discussing
 continuous dependence and error
 bounds 07 p1213 A67-19158
 Solvability of Cauchy problem for second
 order linear parabolic equations in classes of
 exponentially increasing
 functions 07 p1216 A67-19584
 Asymptotic solution of Cauchy problem
 for integrodifferential equation with small
 parameter associated with
 derivative 08 p1348 A67-21152
 Cauchy problem for nonstationary
 linearized Navier-Stokes equations for fixed
 container partially filled with
 liquid 09 p1532 A67-21873
 Covariant decomposition of tensor and
 gravitational Cauchy problem in Riemann
 space 10 p1879 A67-22841
 Cauchy problem and mixed boundary value

problem of linear and quasi-linear
 degenerate hyperbolic second order
 equations applied to
 cylinder 11 p1814 A67-24851
 Singularities causing numerical instabilities
 used in steady gas dynamic Cauchy problem
 solution, exemplifying with supersonic blunt
 body 12 p1893 A67-25932
 Weinstein results for pointwise monotone
 growth and convexity extended in norm to
 certain Cauchy problems of second order
 differential equations 12 p1961 A67-26063
 Mixed problem for linear hyperbolic
 partial differential equation asymptotically
 represented and reduced to boundary value
 problem and Cauchy
 problem 13 p2144 A67-26377
 Regularity properties in time variable of
 solutions of n-dimensional Navier-Stokes
 system 13 p2145 A67-26509
 Pointwise bounds extended for Cauchy
 problem solution by establishing Cauchy
 problem maximum property for any second
 order linear hyperbolic
 operator 13 p2146 A67-27097
 Characteristic initial value problem for
 linear second order hyperbolic partial
 differential equation 13 p2147 A67-27180
 Uniqueness of solutions for Cauchy
 problem and some boundary value problems
 of general parabolic systems in class of
 increasing Holder
 functions 14 p2344 A67-28894
 Continuous solutions of Cauchy problem
 for linear first order PDEs with
 discontinuous coefficients, noting conditions
 imposed 14 p2344 A67-28905
 Integrodifferential equation solvability by
 investigation of adjoint Cauchy
 problem 15 p2511 A67-29890
 Uniqueness and existence of Cauchy
 problem solution considering Dirichlet limits,
 studying convergence
 requirements 16 p2695 A67-30829
 Numerical solution of nonlinear integral
 equations with variable upper limit,
 applicable to Cauchy and boundary value
 problems 16 p2696 A67-31142
 Pointwise bounds for solution of Cauchy
 problem for nonlinear and linear elliptic
 system, noting application to biharmonic
 equation 16 p2697 A67-31422
 Incorrect problems of mathematical
 physics examined and illustrated by classical
 Cauchy problem for Laplace
 equation 16 p2698 A67-31736
 Cauchy problem for homogeneous linear
 difference scheme with constant complex
 coefficients, giving stability
 lemmas 17 p2877 A67-32677
 Numerical methods for solving thermal
 explosion and combustion problems on
 electronic computers, examining Cauchy
 problems solutions 17 p2973 A67-33075
 Constructing solution of Cauchy initial
 value problem when Riemann function is
 unknown for one-dimensional linear
 viscoelasticity 18 p3139 A67-33428
 Cauchy problem solution for certain
 functional equations in complete linear
 normalized space extended to include
 nonlinear space 18 p3073 A67-34603
 Uniqueness theorem for Cauchy problem,
 elliptic equations with double characteristics
 derived by imposing smoothness
 condition 20 p3475 A67-36456
 Formulating Cauchy problem and mixed
 problem for second order self-adjoint
 equation, establishing initial data and
 boundary value
 dependence 20 p3479 A67-37657
 Papers on functional analysis covering
 approximation methods and Cauchy,
 Dirichlet and boundary value
 problems 21 p3651 A67-37832
 Integration of Cauchy problem for class of
 nonlinear higher order partial differential
 equations 21 p3651 A67-37901
 Solution methods for Cauchy problem and
 ideal unstable gas motion in cylindrical and
 spherical symmetry, discussing shock wave
 occurrence 21 p3565 A67-38562
 Thermodynamic interpretation for Cauchy
 elasticity, showing formulation of
 constitutive equations in continua
 theories 21 p3733 A67-39085
 Cauchy problem for second order
 parabolic partial differential
 equation 22 p3827 A67-39432
 Cauchy problem for heat equation noting
 error analysis for numerical procedure and

Stefan problem solution 23 p4081 A67-40860
 Cauchy problem solution for linear partial
 differential equation with coefficients which
 are functions of three-dimensional variable,
 deriving maximal class of uniqueness of
 solution 23 p4024 A67-41692
 Plane shock wave disturbance
 development analysis by solving Cauchy
 problem, discussing low viscosity
 effect 24 p4141 A67-41931
 Local existence, uniqueness and regularity
 theorems for Cauchy problem solution for
 Navier-Stokes system in
 space 24 p4177 A67-42155

CAUCHY-RIEMANN EQUATION
 Rigidity of surface with flattened point
 proved by Cauchy-Riemann equations,
 considering case where contact of surface
 with tangential plane approaches
 infinity 16 p2698 A67-31912

CAVITATION
SA GASEOUS CAVITATION
SA WAKE
 Cavitation effect on braking throttle
 actuating mechanism loaded with inertial
 mass 01 p0012 A67-10496
 Minimum cavitation number and cavity
 width in plane and axisymmetric
 channels 03 p0401 A67-12872
 Cavitation erosion in Hawker Siddeley
 Trident hydraulic system and steps to find
 solution 05 p0753 A67-16748
 Cavitation effect on braking throttle
 actuating mechanism loaded with inertial
 mass 10 p1597 A67-23618
 Cavitation induced detonation of
 stoichiometric liquid
 mixtures 11 p1884 A67-24956
 Structural, seal and sideboard design,
 propulsion and cavitation problems relevant
 to operational requirements of captured air
 bubble vehicle 14 p2245 A67-28729
 [AIAA PAPER 67-346]
 Heat transfer analysis for cavitation and
 boiling, noting vapor bubble
 formation 17 p2970 A67-32463
 Cavitation erosion noting high speed
 motion picture photographic analysis of
 kinematic structure of cavitation
 zone 20 p3420 A67-36631
 Hydraulic component material properties
 relationship to particulate material removed
 due to cavitation, showing particle size
 distribution definition 20 p3469 A67-37366
 Decompression sickness studied by
 investigating cavitation at liquid-liquid
 interface 21 p3573 A67-38076

CAVITATION FLOW
 Hydrodynamic tunnel wall effect on
 minimum cavitation number in axisymmetric
 cavitation flow around
 solids 02 p0232 A67-11631
 Shear layer and internal flow arising from
 turbulent boundary layer separation and
 heat transfer over cavity 02 p0179 A67-12344
 Foil hydrodynamic design of Conair
 subcavitating hydrofoil /HYSTAD/,
 discussing cavitation-free operation, foil
 selection and sections
 [AIAA PAPER 65-449] 03 p0402 A67-12919
 Viscous shear flow past two-dimensional
 cavity of infinite depth by use of Stokes
 approximation, emphasizing flow pattern
 near dividing streamline 03 p0402 A67-13356
 Instability of ventilated cavities extending
 behind symmetric bodies, noting resonance
 frequency and pressure distribution
 fluctuation 04 p0600 A67-14457
 Nuclear-bubble hypothesis for inception of
 hydraulic cavitation examined, using free-jet
 test 04 p0606 A67-15123
 Solvability of parallel-wall cavitation flow
 problem of perfect incompressible fluid past
 symmetric smooth arc 04 p0606 A67-15195
 Single-phase and two-phase cavitating flow
 regime performance of liquid propellant
 rocket engine turbopump inducers
 [ASME PAPER 66-WA/FE-23] 04 p0554 A67-15353
 Water tunnel investigation of unsteady
 partial, full and supercavitation in cascade
 flow, determining force coefficients
 [ASME PAPER 66-WA/FE-25] 04 p0607 A67-15355
 Reynolds number and incidence angle
 effects on inducer cavitation in water
 [ASME PAPER 66-WA/FE-31] 04 p0607 A67-15363
 Cavitation pitting and flow regime in
 cavitating venturi using water and mercury
 indicate microjet impingement is most

important damaging mechanism
[ASME PAPER 66-WA/FE-39]

- 04 p0608 A67-15447
Natural convective heat transfer in closed cavity between two disks in central force field for laminar flow in boundary layers 04 p0738 A67-15893
Two supercavitating flat plate hydrofoils near free surface with ensuing boundary value problem converted to mixed boundary value problem 06 p0984 A67-18126
Mach and cavitation number effects in fluid dynamic elements and circuits such as operating pressure limit, power consumption and output 08 p1320 A67-20455
Supersonic shear flow over cavity investigated, constructing velocity and shear stress coefficient profiles satisfying boundary conditions 11 p1778 A67-24218
Formation of cavities and microjets in liquids and role in initiation and growth of explosion 11 p1883 A67-24631
Flow and cavitation erosion tests in closed circuit hydrodynamic tunnel 14 p2295 A67-27869
Cavitation correlation with sound pressure and vibration acceleration in closed circuit hydrodynamic tunnel, showing cavitation noise spectrum 14 p2295 A67-27870
Cavitation damage in alkali metal pumps, noting damage resistance and material properties for application in space power systems 15 p2494 A67-30151
Inviscid steady partially cavitating flow through cascade of flat plate hydrofoils 16 p2662 A67-31550
Bypass flow reduction in liquid hydrogen and liquid oxygen tank mounted boost pumps on Centaur launch vehicle 17 p2800 A67-31978
Steady flow in rectangular cavity with driving motion by uniform translation of one wall 17 p2836 A67-32279
Incipient cavitation calculation in hydrodynamics as example for applying quadratic programming to mechanical system subject to one-sided constraints 17 p2838 A67-32429
Functional sensitivity to cavitation of hydrofoil cascade, solving Fredholm type integral equations 20 p3419 A67-36188
Heat transfer in region of separated flow over two-dimensional rectangular cavity facing oncoming turbulent boundary layer [ASME PAPER 67-HT-14] 20 p3545 A67-36711
Cavitation in spool control valve orifices, showing effect on flow discharge coefficient over range of conditions 20 p3666 A67-37371
Frequency pattern analysis for liquid rocket pump fluid cavitation characteristics 21 p3613 A67-38437
Relation between incipient cavitation number and Reynolds number by combining bubble dynamics Rayleigh equation with cavitation number definition 22 p3787 A67-40176
Single-phase and two-phase cavitating flow regime performance of liquid propellant rocket engine turbopump inducers [ASME PAPER 66-WA/FE-23] 24 p4143 A67-42464

CAVITY

- Two-dimensional convective motion in rectangular cavity with vertical sides maintained at different temperatures, analyzing heat transfer 04 p0719 A67-14460
Momentum transfer mechanism in separated flow region of rectangular cavity facing oncoming turbulent boundary layer [AFRL-66-851] 04 p0610 A67-15924
Integral motion equations of rigid body with cavity partly filled with viscous incompressible fluid with free surface 05 p0921 A67-17005
Local radiation equilibrium temperatures in semigray enclosures, with reference to thermal design of spacecraft [AIAA PAPER 67-211] 06 p1115 A67-18327
Rectangular and inverted wedge recompression step effect on recovery factor, heat-transfer coefficient, velocity profile and pressure distribution in open cavity flow [ASME PAPER 65-WA/HT-37] 08 p1278 A67-21320
Free and forced oscillations of body with cavity partly filled with viscous fluid 10 p1679 A67-23029
Stability of rotational motion of body with cavity containing ideal fluid, considering fluid motion as potential flow, determining

- velocity potential and inertia moments 10 p1679 A67-23031
Hydrodynamic coefficients of equations of perturbed motion for body with cavity in form of circular cylinder with flat bottom 10 p1624 A67-23032
Elastic medium dynamic response to time dependent pressure in spherical cavity with cavity wall under ablation 11 p1871 A67-23964
Dynamic two-dimensional problem of moment theory of elasticity and viscoelasticity of medium with circular cylindrical cavity 11 p1879 A67-24883
Slow oscillations of fluid in rotating cavity under magnetic field to evaluate Hide theory for nondipole drift of geomagnetic field 16 p2667 A67-31554
Wing flap aerodynamic performance as affected by wing flap surface cavities, noting usefulness in flow stabilization at high pressure gradient 17 p2792 A67-32904
Diffraction of stress pulse by spherical cavity embedded in infinite linear homogeneous isotropic elastic medium [ASME PAPER 67-APM-27] 17 p2965 A67-33154
Integral motion equations of rigid body with cavity partly filled with viscous incompressible fluid with free surface 18 p3028 A67-34267
Local radiation equilibrium temperatures in semigray enclosures, with reference to thermal design of spacecraft [AIAA PAPER 67-211] 19 p3344 A67-34820
Heat transfer dependence in cavity of closed evaporative thermosyphon on device inclination angle and coolant filled fraction of cavity 21 p3625 A67-37913

CAVITY RESONANCE

SA RESONANT CAVITY

- Dynamic stresses at boundary of fluid filled cavity during passage of plane dilatational wave train 05 p0908 A67-16136
Automatic measurement of diurnal resonance frequency variations of earth/ionosphere cavity 15 p2489 A67-30071
Oscillation mode in open-ended circular cylindrical microwave cavity resonant frequency computed by Laplace transform and Wiener-Hopf techniques 17 p2828 A67-33083
Resonances of thin shell model of earth-ionosphere cavity with dipolar magnetic field 18 p3042 A67-34427
Diurnal variation of earth-ionosphere cavity resonances and properties and propagation of ELF, ULF and MHD waves 20 p3390 A67-37727
Superconductors for high-Q microwave cavities construction, noting unloaded Q and resonant frequency measurements and surface properties 22 p3865 A67-40431
Plasma column and plasma-electron beam interaction properties by Langmuir and SHF probes noting resonance, coupling and microwave surface waves 24 p4194 A67-41911

CAVITY RESONATOR

- Intrinsic noise temperature measurement in reflection type cavity maser 06 p1010 A67-17892
Parallel equivalent circuit parameters and Q-factor of cylindrical cavity resonator in TM sub 010 mode 07 p1153 A67-19613
Electron number densities measured behind shock wave in pressure-driven shock tube by microwave resonant cavity technique and by electrostatic quasi-Langmuir probe 11 p1790 A67-24451
Transient ionization levels of hypersonic velocity projectile wakes measured by open microwave resonators phase shift 11 p1790 A67-24452
HF properties of laser cavities with anisotropic dielectric filling, calculating Q-factor and shunt resistance 13 p2075 A67-26399
Dispersion characteristics of annular resonator cavity based on waveguide of rectangular cross section 13 p2077 A67-26749
Diffraction losses in resonator cavity decreased by thermal deformation of neodymium-glass crystal due to pumping with periodic pulses 13 p2130 A67-27629
Superconducting microwave filters, discussing minimum insertion loss, loss dependence on various factors and effect of peak fields on maximum power 14 p2289 A67-28915
Characteristics of open resonators, obtaining coupling and scattering

- coefficients 15 p2501 A67-30075
Gain-bandwidth product of parametric reflection amplifiers with line-type resonators 15 p2454 A67-30145
Radiation from two optically coupled cavities of compound laser identical in time and spectral composition without tuning one cavity to other 17 p2868 A67-32661
Miniaturized cavity resonator, giving criterion for evaluation of resonant frequencies of corrugated resonators 17 p2827 A67-32786
Design and operation of three-cavity solid state ruby maser 20 p3462 A67-37329
Diffraction losses in resonator cavity decreased by thermal deformation of neodymium-glass crystal due to pumping with periodic pulses 21 p3642 A67-38825
Ruby rods in concentric spherical cavities observing spiking, mode structure and output energy distribution 22 p3817 A67-40485
Reactive optical information processing maximum efficiency from phase object in laser cavity, discussing modulation depth and power gain 23 p4002 A67-41270

CELESTIAL BODY

- Flux intensity and energy spectra of galactic X-ray sources, Tau X-1 and other celestial bodies studies, using three sensitive Geiger counters 01 p0144 A67-10562
Atmospheric agitation effect on image of extended celestial light sources, showing importance in long-range tropospheric propagation of ultrashort radio wave 02 p0325 A67-11986
Comet photometry for measuring weak fluxes of light produced by heavenly bodies, analyzing photoelectromultipliers 05 p0805 A67-16336
Mechanics of celestial bodies including problems on Newton gravitation law, motion equations, two-body problem, Kepler law, etc 06 p1030 A67-17772
Astronomical theory of main features of earth crust based on fact that celestial bodies do not rotate en bloc 06 p0997 A67-18658
Lawful concept of heavenly bodies 12 p2042 A67-26138
Upper limits to hard X-ray flux from quiet sun analyzed by balloon-borne scintillation detector measuring celestial sources 13 p2189 A67-26302
Cosmogony of celestial bodies, discussing orbital data, asteroid collisions and existence of distant comet cloud 13 p2195 A67-26466
Meteor hyperbolic motion and geocentric trajectory determination 13 p2196 A67-26497
Drag effects on meteoric bodies studied by photographic observations 13 p2196 A67-26499
Number of fragments in meteor fragmentation 13 p2197 A67-26500
Meteor particle density study based on photographic observations 13 p2197 A67-26501
Orbit, luminescence and spectrum of July 5, 1962 bolide orbit, luminescence and spectrum of July 5, 1962 bolide orbit, luminescence and spectrum of July 5, 1962 13 p2197 A67-26502
Australasian tektite origin criticized regarding magnitude of atmosphere removal 14 p2390 A67-28889
Superimposed electromotive force appearing in direction of magnetic field in presence of opposed spiral motion in turbulent field 17 p2842 A67-32341
Solar system bodies gravitational fields, discussing possibility of holding satellite in orbit 19 p3323 A67-35337
Angular momentum densities of planet-satellite systems, discussing earth-moon system and origin of celestial bodies 23 p4066 A67-41009
Stellar and planetary magnetic field formation theory based on concept of existing ionized turbulent mass flow on these celestial bodies 24 p4230 A67-42352

CELESTIAL MECHANICS

SA ASTRODYNAMICS

SA PERTURBATION THEORY

- Rational mechanics principles of inertial navigation and relation to gravitational field structure in vicinity of maneuvering vehicle [ONERA-TP-352] 01 p0110 A67-11088
Kinetic moment in celestial mechanics, noting application to satellite orbit determination in terrestrial gravitational field 03 p0510 A67-13456
Aperiodic motion of two bodies of variable

mass across canonical cross section,
constructing osculating orbit and deriving
equations for variation rate 04 p0700 A67-15202

Three-body problem of orbital motion,
examining periodic librations of planetoid
around triangular equilibrium point 06 p1079 A67-17762

Stability of rotating liquid mass /e.g.
earth/, following Jeans treatment of Jacobi
ellipsoidal equilibrium configurations 06 p1080 A67-17768

Mechanics of celestial bodies including
problems on Newton gravitation law, motion
equations, two-body problem, Kepler law,
etc 06 p1030 A67-17772

Dynamical system specified by set of
generalized coordinates, considering Jacobi
and Kepler elements and Poisson and other
methods 06 p1031 A67-17774

Regularization of three-body equations for
case of binary collisions, using Sundman
equation transformation in celestial
mechanics problems 06 p1022 A67-17776

Couple due to distant mass acting on
nonspherical object determined, considering
luni-solar precession and nutation
variability 06 p1031 A67-17778

Computational methods in stellar dynamics
noting n-body problem approach, continuum
technique and statistical method 06 p1081 A67-17780

Qualitative methods in n-body problem
concerned with masses motion in inertial
space under gravity, solving motion
equation 06 p1081 A67-17781

Kalman filter, modern version of Gaussian
least squares method linear estimation of
orbital elements of celestial body 06 p0974 A67-17926

Book on moon covering motion of moon
and dynamics of earth-moon system, internal
constitution, topography, radiation and
surface structure 06 p1087 A67-18428

Solution within planetary theory with no
secular terms in metric elements applied to
problem of first order theory of Vesta
disturbed by Jupiter 07 p1250 A67-19725

Higher order perturbations of elements in
three-body problem determined using
methods of Krylov-Bogoliubov and Poincare
[AAS PAPER 66-99] 07 p1252 A67-19962

Solar and stellar systems orbit theory -
IAU Symposium, Salonika, Greece, August
1964 08 p1379 A67-20380

Numerical analysis and third integral
applications to n-body problem in stellar
dynamics and relation to celestial
mechanics 08 p1380 A67-20381

Relationships among Delaunay theory,
Diliberto periodic surface theory and Krylov-
Bogoliubov method of averaging in celestial
mechanics 08 p1347 A67-20383

Reference orbit for integration through
boundaries of activity spheres, replacing six
osculating Keplerian reference orbits 08 p1383 A67-20590

Recent developments in space flight
mechanics - Conference, Berkeley, December
1965 08 p1384 A67-20616

Periodic solutions for restricted three-
body problem 08 p1384 A67-20619

Lunar motion analysis showing slight
acceleration to that allowed by celestial
mechanics, extrapolating observed motion to
past epochs 08 p1395 A67-21162

Difference assessment between secular
and long period perturbations generated by
similar initial conditions for celestial
mechanics problems 09 p1563 A67-21637

Geometry of lunar eclipse of earth
satellite for shadow function as quartic
polynomial in cosine of true anomaly 11 p1859 A67-24357

Stellar dynamics and galactic spiral
structure analyzed using gas and plasma
dynamics 11 p1863 A67-24534

Evolution of short-period comet orbits
/1660-2060/ taking into account perturbing
effects of outer planets 15 p2552 A67-29154

Elliptical motion of material point in
terrestrial gravitational field, noting
expression for eccentricity under effect of
small tangential force 15 p2556 A67-29659

Family of periodic orbits around triangular
libration points in restricted three-body
problem 15 p2557 A67-29876

Canonical elements for variables of Levi-
Civita regularizing binary collisions in
restricted three-body problem, noting
existence of periodic

orbits 15 p2557 A67-29878

Mathematical methods of celestial
mechanics and astronautics - Conference,
West Germany, March 1964 15 p2558 A67-30034

Quasi-isomorphic response of perturbed
systems for slow coefficient variation of
matrix system differential equation 15 p2512 A67-30050

Finite terms interpretation of Groebner
method for differential equations applied to
trajectory calculations in celestial
mechanics 15 p2561 A67-30051

Runge-Kutta-Fehlberg method for systems
of ordinary first and second order
differential equations applied to numerical
solution of many-body problem 15 p2561 A67-30052

Error assessment in numerical integration
for ordinary differential equations applied to
many-body problem 15 p2512 A67-30053

Spinor representation of energetic
identities of Kepler motion, showing identity
of Lambert theorem for position triangle
and Stumpf theorem for velocity triangle 15 p2561 A67-30054

Celestial mechanics and Dirac
hypothesis 15 p2563 A67-30123

Improvement of satellite elliptical orbits
with small eccentricities using differential
formulas 16 p2743 A67-30727

Finite collision time for artificial celestial
body moving under influence of Newtonian
force from attractive center 16 p2745 A67-30744

Motion in ternary stellar system consisting
of central body and close and distant
companions 16 p2746 A67-30956

Orbit determination between two radii
vectors with specified periastron radius
distance 16 p2746 A67-30959

Second partial derivatives of position and
velocity vectors components developed with
respect to same vectors components at
arbitrary epoch 16 p2696 A67-30960

Stellar dynamics methods - Conference,
Besancon, France, September 1966 16 p2748 A67-31136

Invariant curves dissolution and
nonapplicability of third integrals explained
examining perturbation values and initial
conditions and resonance phenomena 16 p2748 A67-31140

Celestial mechanics and adaptation of
perturbation methods and numerical
integration techniques to stellar
dynamics 16 p2748 A67-31141

Three-dimensional structure of solar
plasma flow generated by solar flares, noting
geometric factors in geomagnetic storm
intensity decrease 16 p2739 A67-31415

Lapunov subcenter manifold, showing that
real C-1 Hamiltonian system of ODEs has m
distinct two-dimensional invariant
manifolds 17 p2877 A67-32558

Book on celestial mechanics presenting
solution of artificial satellite motion in earth
gravitational field, using Lagrange
equations 17 p2950 A67-33166

Action variables to take account of
essential characteristics of Delaunay lunar
theory 18 p3118 A67-33687

Economical transfers between Keplerian
orbits in time-free case, considering
hyperbolas, exterior ellipses and launching
orbits [ONERA-TP-482] 18 p3133 A67-34465

Bounded isoenergetic displacement of
periodic orbits in restricted circular three-
body problem 18 p3135 A67-34542

Hansen planetary theory representing
position of disturbed planet as deviation in
time and space from position of fictitious
planet with Keplerian motion [AIAA PAPER 67-565] 19 p3328 A67-35961

Celestial mechanics, reviewing motion
observations, solution methods and
unresolved problems 20 p3522 A67-36623

Cometary astronomy problems from
contemporary celestial mechanics viewpoint,
considering short-period comets and orbital
perturbations caused by Jupiter 20 p3524 A67-36658

Book on celestial mechanics covering
Laplace-Newcombe method, Hill planet and
lunar methods and periodic orbits methods
using differential equations 23 p4069 A67-41429

Evolution of short period comet orbits
/1660-2060/ taking into account perturbing
effects of outer planets 24 p4239 A67-43077

CELESTIAL NAVIGATION

Near planet orbital navigation by
astronauts, celestial surfaces of position
combine to define unique three-dimensional
position of observer 09 p1526 A67-22388

CELESTIAL OBSERVATION

Observations of 24 comets, 11 minor
planets and Jupiter VIII, using
computer 01 p0148 A67-10386

Combined focusing X-ray diffractometer
and nondispersive X-ray spectrometer for
lunar and planetary analysis 01 p0067 A67-10689

Thermal radio emission from Mercury,
Venus, Mars, Saturn and Uranus at various
wavelengths, using radio telescope in
Australia, determining emission
spectrum 02 p0319 A67-11452

Mean quadratic amplitude of star image
deviation from average position dependence
on zenith distance studied from stellar
observation 02 p0261 A67-11988

Atmospheric turbulence effect on quality
of star images based on telescopic
observations of stars shows pronounced
correlation 02 p0261 A67-11989

Photoelectric recording of scintillation of
stellar images by function of nature of
scintillation while carrying out
observations 02 p0326 A67-11991

Programmed telescope control systems on
equatorial mount 02 p0241 A67-11992

Scientific program and instrumentation of
comet probe 03 p0510 A67-13496

Kilston and Barbon comets detection and
observation history 03 p0511 A67-13653

Naked-eye observations of
sunspots 03 p0514 A67-14184

Variable polarization of magnetic star HD
71866 studied by observational program
between January and April 1966 04 p0697 A67-14759

Visual and photographic comet photometry
problems, noting brightness estimates
obtained by individual observers 05 p0890 A67-16330

Comet spectra observation noting emission
band abundance, atomic lines presence and
continuous spectrum with solar Fraunhofer
lines 05 p0890 A67-16337

Transient changes on moon during last
three centuries, considering type of event,
lunar phase, correlation with solar activity,
etc 05 p0895 A67-16594

Comet Ikeya-Seki observations from Mauna
Kea, Hawaii 05 p0896 A67-16719

Comet Ikeya-Seki observations from
Tucson 05 p0896 A67-16720

Visual observations of comets Everhart
and Alcock /1964-1965/ 05 p0903 A67-17314

Hyperbolic revised orbital data of comet
Cunningham /1941 I/ hyperbolic revised
orbital data of Comet Cunningham /1941
I/ 07 p1247 A67-19168

Residuals in right ascension and
declination of Mars observations made with
astrolabe in France 07 p1250 A67-19723

Observations of sun at Stanford on May
20, 1966 at 9.1 cm after annular eclipse in
Greece and Turkey 07 p1251 A67-19914

Crab Nebula X-ray spectrum from balloon
observations, noting importance of
correction for escaped iodine K
component 07 p1251 A67-19944

Balloon observation of X-ray sources in
Cygnus region in energy range 20-130
kev 08 p1377 A67-21252

Technique for observation of 24 discrete
radio emission sources at 9.6 cm in August
and September 1961 and February through
May 1962 08 p1401 A67-21351

Ground observations of Martian relief
during 1967 optimum period 09 p1565 A67-22014

Visual observations of earth, sea and sky
made by astronauts and cosmonauts during
space flights 09 p1569 A67-22604

IGY and IQSY auroral observations at
Murmansk of frequency of occurrence of
polar auroras in years of solar activity
maxima and minima 10 p1630 A67-22787

Polar auroras during minimum of solar
activity cycle, winter 1963-64 and
1964-65 10 p1631 A67-22802

Compiled data for Mars apparition in 1967
giving general visibility conditions, phases,
seasons and positions of Mars and
earth 10 p1710 A67-23562

Saturn edgewise rings rapid fading and
brightness variation on disk 10 p1710 A67-23564

Cosmological distortion effect incorporating incident magnetic type gravitational field parameter upper limits measured from galactic cluster photographs 11 p1860 A67-24484

Meridian observation of Jupiter for planet position determination, analyzing discrepancies between ephemerides and observations, noting random error 11 p1868 A67-25087

Mean declinations correction for Talcott pairs of 191 stars from zenith telescope observations 11 p1868 A67-25088

Radiometric observations of total lunar eclipse of December 19, 1964 at wavelength of 3.3 mm indicate no significant temperature difference [JPL-TR-32-1097] 12 p2011 A67-26245

Catalog of German polar aurora observations from 1882 to 1956 13 p2109 A67-26431

Soviet papers on space physics problems 13 p2195 A67-26494

Photographic meteor observations 1957-1961 at Kiev 13 p2196 A67-26495

Meteor orbital elements according to photographic observations 13 p2196 A67-26496

Linear polarization of Crab Nebula, Cygnus A and other radio sources observed at wavelength of 21.3 cm, using radio telescope 13 p2198 A67-26714

Sunspot observation methods and techniques in white light, considering requirements, diffraction limitations on resolution, site selection and local seeing and telescope choice 13 p2202 A67-27421

Sunspot fine structure ground observations, considering umbras, penumbras, boundaries and photographs 13 p2203 A67-27422

Theoretical interpretation of fine structure observations of sunspots by stratoscope, discussing stability modes and sunspot umbras 13 p2203 A67-27423

Center-to-limb variation of Evershed effect for isolated symmetrical sunspot observations interpreted in terms of mass motions in penumbral fine structure 13 p2204 A67-27430

Observational study of lunar visible emission according to study of line depths 13 p2210 A67-27601

Astronomical almanac 1967 covering chronology, solar and planetary data, time-signal transmission, etc 14 p2385 A67-28146

Jupiter observations /1965-1966/, noting activity of NEB and long duration spots in NTB 15 p2558 A67-30025

Interaction between red spot and white oval spots on Jupiter, explaining dimensional variations of WOS during conjunction 15 p2558 A67-30026

Observational evidence disproving cosmological steady state theory in favor of expanding universe 15 p2562 A67-30082

Microwave spectrum and observation at 6 cm wavelength of Venus to determine total intensity and polarization of radiation 16 p2747 A67-30987

Probability of perceiving meteor determined on basis of observation by independent counting method by group of observers 16 p2751 A67-31460

Cosmological model for universe based on astronomical observations and validity of einstein theory and existing laws of physics 16 p2752 A67-31540

Technique for observation of 24 discrete radio emission sources at 9.6 cm in August and September 1961 and February through May 1962 17 p2940 A67-31947

Solar cosmic ray observations, discussing emission spectrum, interplanetary particle distribution, diffusion coefficient, magnetic field strength, space-time distribution, etc 17 p2934 A67-32096

Cosmic ray variation determination from single series of observations by methods of random process theory 17 p2935 A67-32108

Processing results of meteor photographs using panchromatic films and program-controlled exposure time 17 p2942 A67-32328

X-ray scanning of Cygnus region with large area proportional counters flown on attitude-controlled sounding rocket 17 p2937 A67-32648

Quasar observations using interferometer baselines, noting regular fringes and small phase scintillation in Gaussian source model 17 p2947 A67-32760

Radio emission flux from local solar

sources relation to active solar regions structure, based on radio-astronomical observations 17 p2948 A67-32969

Ashen light and magnetic field of Venus 17 p2948 A67-33096

Galactic anisotropies observation, giving procedure for detecting periodicities and data on sidereal daily variation amplitude 19 p3315 A67-35484

Classification of main data on morphology and phenomenology of aurorae observed visually and with all-sky cameras during IGY 19 p3224 A67-35495

Optical polarimetric observations of quasi-stellar objects 19 p3331 A67-36083

Minor planets observational and computational results /1964/, discussing ephemeris volume 20 p3522 A67-36615

Minor planets position observations at Crimean Astrophysical Observatory during August and September 1964 20 p3522 A67-36620

Minor planets position observations at Crimean Astrophysical Observatory from October 1964 through March 1965 20 p3522 A67-36621

Celestial mechanics, reviewing motion observations, solution methods and unresolved problems 20 p3522 A67-36623

Equinox and equator corrections to FK3 system determined from meridian observations of Mars, Jupiter and minor planets 20 p3429 A67-36838

Declinations of major and minor planets /1951-1959/ determined from meridian observations and reduced to FK3 system 20 p3524 A67-36839

Red shifts of radio galaxies observed spectroscopically with 120-inch telescope, using prime focus and image tube 20 p3527 A67-37392

Astronomical research /1965/ noting New Zealand observatory, telescopes in Chile, Hawaii and China, solar activity, planet studies, etc 21 p3700 A67-37830

Discovery position plotting of various long period comets, showing tendency to cluster near sun in morning sky, orbit distribution and estimated probabilities 21 p3705 A67-38614

Diameter and position of radio source 3C 132 determined by lunar occultation, confirming identification with red galaxy 21 p3706 A67-38616

Jupiter internal structure investigated by observing visible surface and radio emission, discussing magnetic field origin and hydrodynamics of fluid regions 21 p3710 A67-39003

Photoelectric observations of 27 long period variable stars on UVB photometric system 22 p3880 A67-39415

Comet observation by 61 inch Catalina reflector noting additions to recovery-expected-soon list 22 p3880 A67-39416

Observation of annular solar eclipse of 1966 from Madrid, noting photographs application for occulted region chord measurements 22 p3888 A67-40200

O and B stars surveyed with 154 cm Catalina reflector show discrepancies from mean interstellar polarization-wavelength dependence near Orion 23 p4062 A67-40626

Venus rotation, discussing radar and optical and UV photography observations 23 p4063 A67-40800

Cosmic ray variations over celestial sphere investigated by matrices applied to distribution model 23 p4059 A67-41134

IGY and IQSY auroral observations at Murmansk of frequency of occurrence of polar auroras in years of solar activity maxima and minima 24 p4149 A67-42123

Polar auroras during minimum of solar activity cycle, winter 1963-64 and 1964-65 24 p4150 A67-42139

Radio evidence for two supernova remnants in Southern Milky Way and observations of shell type radio sources, considering shell model fitting problem 24 p4230 A67-42332

CELESTIAL SPHERE

General inequalities for regular relativistic fluid spheres, noting gravitational potential energy limit 02 p0266 A67-11696

Data interpretation for sun grazing family of comets deriving formulas for compressive and tensile stress in spherical bodies for tidal, rotational and self-gravitating fields 03 p0512 A67-13923

Satellite orbit major axis determination by

using coincidence of time when satellite crosses plane of tracking station parallel with time of crossing topocentric celestial equator 05 p0894 A67-16560

Book on space-time relations of stellar positions on celestial sphere, detailing long focus astrometry, emphasizing mathematical principles 13 p2199 A67-26933

CELL

S BIOLOGICAL CELL
S ELECTRIC CELL
S ELECTROCHEMICAL CELL
S FUEL CELL
S GALVANIC CELL
S GAS CELL
S HEXAGONAL CELL
S KERR CELL
S KNUDSEN CELL
S PHOTOCONDUCTIVE CELL
S PHOTOELECTRIC CELL
S PHOTOVOLTAIC CELL
S SOLAR CELL

CELL DIVISION

SA MITOSIS

Space flight acceleration, vibration and ionizing radiation effects on body functions, oxidizing metabolism of central nervous system and fission processes of hemopoietic tissues 01 p0015 A67-10336

Microbial cell population statistics and dynamics 05 p0757 A67-17156

Inhibitory effect of light from cool white fluorescent lamps on growth of yeast, alga and protozoa 06 p0952 A67-17872

Space flight factors effect on mutability, survival rate and dynamics of cells of inactive cultures of chlorella on board Cosmos 110 13 p2060 A67-27336

Mutation of human tissue by cosmic radiation, discussing results of cell studies from male and female subjects 16 p2611 A67-30766

Growth rate limitations with interactions of light and carbon dioxide investigated for two species of Chlorella 20 p3369 A67-36791

CELLULOSE

SA NITROCELLULOSE

SA WOOD

Zinc penetration through regenerated cellulose membrane separators shown to be growth mechanism in silver-zinc cell 22 p3758 A67-40227

CEMS SYSTEM

S AIRCRAFT MAINTENANCE

S FIST PROJECT

CENTAUR LAUNCH VEHICLE

SA ATLAS CENTAUR LAUNCH VEHICLE

Artificial sodium cloud in twilight produced by French rocket studied, using auroral spectrophotometer and cameras 03 p0412 A67-13370

Bypass flow reduction in liquid hydrogen and liquid oxygen tank mounted boost pumps on Centaur launch vehicle 17 p2800 A67-31978

Flight strain gauge system for Centaur /AC-6/ liquid hydrogen fuel tank skin 23 p4008 A67-41390

CENTAUR PROJECT

Centaur electronic packages for space flight thermal and radiative environmental control 05 p0778 A67-17453

CENTAURUS CONSTELLATION

Alpha Centauri probe and sun-orbiting concentrator to power probe 01 p0155 A67-11403

CENTRAL NERVOUS SYSTEM

SA AUTONOMIC NERVOUS SYSTEM

Space flight acceleration, vibration and ionizing radiation effects on body functions, oxidizing metabolism of central nervous system and fission processes of hemopoietic tissues 01 p0015 A67-10336

Gemini inflight experiments on space perception via measurements of ocular counterrolling as test of otolith function 13 p2062 A67-26920

Intermittent visual stimulus influence on perceptual motor skills in aviation 14 p2258 A67-28668

Human acoustic analyzer functional state studied for hypokinesia effects 20 p3368 A67-36267

Central nervous system, adenohypophysis and adrenal glands relation in oxygen deficiency 20 p3369 A67-36669

Survival times of rats studied from positive and negative acceleration test exposure in special centrifuge 22 p3753 A67-40540

Rats exposed to repeated radial acceleration studied for central nervous system adaptation and survival rates noting better adaptability of newborns 22 p3753 A67-40541

General and cerebral hemodynamics and functions of central nervous system during positive and negative accelerations 23 p3943 A67-40766

Gamma irradiation effect on spinal cord timed differently, considering time factor in reactions of nervous system in guinea pigs 23 p3943 A67-40767

Intermittency hypothesis suggesting temporal integration of data processing of human central nervous system achieved through control of clock generating time points 23 p3944 A67-41020

Decerebrate cat experiments for semicircular canal response to rotational stimulation 23 p3956 A67-41633

CENTRAL NERVOUS SYSTEM DEPRESSANT

S SECOBARBITAL

CENTRAL NERVOUS SYSTEM STIMULANT

SA STRYCHNINE

Pharmacological alterations of vibration tolerance 23 p3955 A67-41613

CENTRIFUGAL COMPRESSOR

SA TURBOCHARGER

Roy method in computing bladed supersonic diffusers for centrifugal compressors 02 p0235 A67-12792

Secondary vorticity for compressible flow in centrifugal impeller, noting parameter effects on motion 03 p0402 A67-13337

Energy transfer by circulatory and Coriolis forces in centrifugal and axicentrifugal compressors 04 p0690 A67-15897

Potential flow theory design of subsonic flow diffusers for centrifugal compressors, assuming compressible irrotational inviscid channel flow [ASME PAPER 66-WA/GT-9] 04 p0550 A67-15938

Impact and abrasion wear of axial and centrifugal helicopter compressor stages due to dust intake, showing direct proportionality to impact velocity and particle size 11 p1853 A67-24531

Slip factors for centrifugal impellers, presenting empirical expression and correction for range and number of blade angles [ASME PAPER 66-WA/FE-18] 24 p4143 A67-42463

CENTRIFUGAL FORCE

Stresses calculated in centrifugal impeller with cover disk by two-dimensional stress analysis and digital computer program [ASME PAPER 65-WA/FE-17] 01 p0080 A67-10873

Centrifugal force field with rotation or static impingement separation for water handling in absence of gravity 01 p0017 A67-10958

Animal study showing aversiveness of simulated gravity and importance of separating rotation effects from effects of G forces 02 p0189 A67-12633

Heat transfer and centrifugal force effects on hypersonic inlet boundary layer and pressure recovery [ATAA PAPER 65-605] 03 p0350 A67-12910

Changes in reproduction and growth of mice and rats under chronic centrifugation at various g force conditions 10 p1598 A67-23416

Burst strength in high speed rotor in axial blower/gas turbine, noting effect of ductility and centrifugal force 17 p2961 A67-32688

Hydraulic resistance coefficient of rotating tubes, taking into account centrifugal mass forces effect on flow inside tube 20 p3421 A67-36793

Inertial instrument testing with precision centrifuges 22 p3781 A67-40384

Feasibility of short radius centrifuge incorporation in space station, testing radius effects on operator performance of tasks 23 p3965 A67-41567

Incompressible viscous fluid rotary turbulent flow microstructure between rotating cylinders, analyzing centrifugal force effects on turbulent heat transfer processes 24 p4142 A67-42214

CENTRIFUGAL PUMP

Centrifugal pump with vapor core principle combined with spill nozzle for application to aero engine fuel and reheat

systems 01 p0014 A67-11267

Low turbulence wind tunnel driven by airfoil centrifugal blower, noting design for best performance 09 p1485 A67-22162

Bypass flow reduction in liquid hydrogen and liquid oxygen tank mounted boost pumps on Centaur launch vehicle 17 p2800 A67-31978

Slip factors for centrifugal impellers, presenting empirical expression and correction for range and number of blade angles [ASME PAPER 66-WA/FE-18] 24 p4143 A67-42463

CENTRIFUGAL STRAIN

Large deformations of zero moment orthotropic shells of revolution under action of inertial loads caused by centrifugal acceleration of shells 12 p2028 A67-25629

Blackout experimentation results, discussing centrifugation and ophthalmodynamometry blackout production and visual system effects 22 p3752 A67-39607

Arterial oxygen tension during acceleration recorded on anesthetized greyhounds using microelectrode and physiological gas analyzer 23 p3958 A67-41653

CENTRIFUGE

SA HUMAN CENTRIFUGE

SA PILOTED CENTRIFUGE

Centrifugal machines generating creep-design data by spinning specimens at identical temperature 03 p0395 A67-13542

CENTRIPETAL FORCE

Centripetal radial blowing effect on flow and heat transfer in gap between rotating disk and wall, specifically effect of Reynolds number and dimensionless flow 20 p3357 A67-36794

CEPHEID

Photoelectric observation results of short period variable DQ Cepheid star 05 p0891 A67-16405

Stellar pulsational instability phenomena calculated numerically for infinitesimal amplitude of central core motion 14 p2392 A67-28996

CERAMIC BONDING

Bonding mechanism between metals and ceramics, noting glass penetration theory 02 p0255 A67-12060

Metal-beryllium oxide bond for semiconductors noting mechanical and electrical strength, thermal conductivity and refractivity 10 p1696 A67-23691

Wear life improvement of ceramic bonded solid film lubricant by compression and artificial filling of film voids [ASLE PREPRINT 67AM 7A-2] 14 p2326 A67-28790

Ceramic-to-metal sealing method based on use of ductile nickel-titanium intermetallic compound as braze 20 p3454 A67-36518

CERAMIC COATING

Thermostability of ceramic coatings applied to W and Mo during cooling, in terms of temperature-dependent elastic modulus and linear expansion coefficients 03 p0446 A67-13638

Zr-Mo, Ca-Mo and Ni-Cr cermet, noting preparation and structural defects 05 p0830 A67-17034

Flame-sprayed ceramic coating in space technology, examining solid atomization or Rokide process 06 p1021 A67-18764

Dielectric isolation of integrated circuit via ceramic medium, discussing technique, testing and results 12 p1916 A67-25997

Thermostability of ceramic coatings applied to W and Mo during cooling, in terms of temperature-dependent elastic modulus and linear expansion coefficients 17 p2875 A67-33172

Zr-Mo, Ca-Mo and Ni-Cr cermet, noting preparation and structural defects 18 p3066 A67-34455

Spray and brush repair of zinc oxide-potassium silicate spacecraft thermal control paint, describing tests, surface preparation and coating application 22 p3826 A67-40111

High emittance coatings radiation characteristics investigated for space applications, considering thickness effect on high temperature emittance and space environment effect at moderate temperatures [ASM PAPER C6-4.3] 23 p4020 A67-41404

CERAMIC HONEYCOMB

Optimization of base thermal protection system for advanced Saturn II boosters employing strap-on solid propellant

motors 10 p1735 A67-23729

Optimization of base thermal protection system for advanced Saturn II boosters employing strap-on solid propellant motors 24 p4256 A67-42915

CERAMICS

SA CERMET

Integrated ceramic printed and thin film circuitry in microelectronic technology 01 p0043 A67-11385

Ceramic-based microcircuit manufacturing techniques 02 p0249 A67-12182

Powdered and fired ceramic materials 03 p0449 A67-13199

Strengthening mechanisms in metals and ceramics - Conference, Raquette Lake, N.Y., August 1965 03 p0441 A67-13302

Microstructure effect on creep deformation mechanisms in polycrystalline ceramic oxides including grain size, subgrain structure, porosity, diffusional creep and dislocation movement 03 p0449 A67-13304

Ceramic material strength improvement by refractory metal fiber reinforcement, noting strontium zirconate-molybdenum systems 03 p0450 A67-13312

Refractory ceramic and graphite fibers properties and strength in high temperature reinforcements 03 p0452 A67-13406

Single crystal whisker composite methodology in plastics, metals and ceramics, emphasizing alignment and handling problems 03 p0453 A67-13410

Electromechanical hysteresis and relaxation effects in piezoelectric ceramics 03 p0498 A67-13706

Polarization and volt-ampere characteristics of ferroelectrics simultaneously under static and alternating fields 03 p0382 A67-13710

Failure mechanism of ceramic fibers in fiber-metal composites determined by high amplitude fatigue tests 03 p0525 A67-13871

High grade oxide ceramics for making dielectrically transparent insulating structures in microwave power tube 04 p0641 A67-14856

Felted fibrous ceramic structures for thermal protection, fabricated by papermaking industry techniques, used for forming lightweight porous structures 04 p0642 A67-15452

Inorganic continuous ceramic fibers production, properties and application 08 p1345 A67-20426

Tensile creep properties of chromium alloys affected by type of ceramic used as heating element core 08 p1341 A67-20766

Beryllium oxide occurrence, fabrication, properties and application 09 p1520 A67-22614

Ultrasonic flow meter for directly measuring average stream velocity using sing-around velocimeter with piezoelectric ceramics 10 p1656 A67-23079

Nuclear and engineering ceramics - Conference, Harwell, Berks., England, October 1965 12 p1964 A67-25210

Hall effect and thermoelectric power in doped, conductive titanium oxide ceramics, noting dependence on doping concentration 12 p1982 A67-25452

Book on engineering properties of ceramic materials covering high melting materials, physical, thermal and mechanical properties, thermal stress, oxidation, corrosion resistance, etc 12 p1960 A67-26201

Special plastics for low loss microwave transmission devices, describing electrical properties 15 p2508 A67-29930

Densification and wear resistance of hot pressed pure and binary systems of diboride established with TaC and other refractory additives 17 p2875 A67-33407

Combination of monoclinic zirconia, second ceramic and metal in electrodes of MHD generators 18 p3099 A67-33709

Thermodynamics of ceramic systems - Conference University of London, April 1966 19 p3248 A67-34863

Superconducting transition temperatures and low field magnetization of ceramic mixed Ba, Sr and Ca-Sr titanates, showing particle nature of specimens 19 p3302 A67-35037

Ceramic material requirements for MHD generator electrodes and duct walls, discussing tests in alkali-seeded plasma 20 p3472 A67-36114

Structure and properties of glass-ceramics noting applications to space and oceanographic exploration 20 p3473 A67-36596

Ceramic materials fracture and deformation mechanisms, discussing stress role 20 p3473 A67-36645

Biaxial prestressing in ceramic plates under nonuniform thermal stress for damage reduction study 20 p3538 A67-36778

Continuous filament ceramic fibers via viscose process involving lattice forming, spinning, weaving and firing 21 p3649 A67-37885

Ceramics operating without protective atmospheres at ultrahigh temperatures, discussing tolerance formation, mechanical properties and working processes 21 p3650 A67-38194

High temperature materials assessed for properties needed for aerospace applications including metals, alloys, refractory fasteners, aluminate coats, ablative insulation and ceramic compositions 22 p3824 A67-40333

Thermal stress fracture of brittle ceramics studied for effect of relaxation by creep at high temperature under conditions of quasi-static heat flow 22 p3915 A67-40386

CEREBRAL CORTEX

Weightlessness effect on level of vigilance of cats and rats launched in rockets, examining electrical activity of cerebral cortex 03 p0364 A67-13927

Vestibular stimulation effect on activity of neurons of optical cortex of curarized cats under vertical acceleration 13 p2058 A67-26758

Cortical electroencephalographic activity /EEG/ relation to behavioral changes in chimpanzee following rapid decompression to near vacuum 18 p2991 A67-34713

CEREBROSPINAL FLUID

Pressure changes in cerebrospinal fluid in rhesus monkey cranial cavity with applied forces at abdominal wall 10 p1600 A67-23821

Acid-base relation of blood and cerebrospinal fluid with respect to respiratory regulation studied in man at high altitude 17 p2806 A67-32333

Acetazolamide effects in aiding altitude accommodation, examining action on blood and cerebrospinal fluid 23 p3951 A67-41566

CERENKOV COUNTER

Apparatus for investigating nucleon reactions with approximate energy greater than 100,000 bev, including Cerenkov and scintillation counters and spark chambers 02 p0316 A67-12765

Davis radiochemical experiment for detection of solar neutrinos and sampling techniques for detecting high energy atmospheric neutrinos 03 p0516 A67-14338

High transmission Cerenkov spectrometer carried by proton I and II satellites to measure charges of primary cosmic ray nuclei high transmission Cerenkov spectrometer carried by Proton I and II satellites to measure 09 p1497 A67-21898

Primary cosmic radiation abundance measurements on iron and heavier nuclei, using Cerenkov counter on balloon flights 11 p1856 A67-24504

Ionizing radiation in space, discussing detection techniques, devices, etc 11 p1791 A67-24619

Atmospheric electron energy spectrum in range 70-2000 mev measured, using scintillation telescope with gas Cerenkov detector and lead glass total energy spectrometer 15 p2475 A67-29615

Gallium phosphide diode-based laser generator of nanosecond light pulse sequence, noting simulation of scintillation counter photoelectric amplifiers, Cerenkov counters, etc 19 p3228 A67-34987

Low pressure gas Cerenkov detector and spectrometer coupled into charged particle telescope for cosmic ray electron spectrum measurements, discussing efficiency and instrument calibration 20 p3452 A67-37566

Apparatus for investigating nucleon reactions with approximate energy greater than 100,000 Bev, including Cerenkov and scintillation counters and spark chambers 22 p3876 A67-40267

Primary cosmic rays with various charges measured for spectral energy with Cerenkov counter onboard space stations 23 p4054 A67-41093

Heavy and superheavy nuclei energy spectra studied from measurements by Cerenkov counter onboard space stations 23 p4054 A67-41094

Proton energy spectrum azimuthal asymmetry measured with telescopes using

scintillation and Cerenkov counters 23 p4054 A67-41096

CERENKOV EFFECT

Cerenkov and cyclotron absorption of Alfven and fast magnetoacoustic waves in plasma with gas-kinetic pressure in quasi-linear approximation 01 p0124 A67-10747

Plasma in HF electric field becoming kinetically unstable due to Cerenkov effect 06 p1045 A67-18803

Plane wave growth associated with Cerenkov and cyclotron instabilities in plasma stream 08 p1358 A67-20893

Cerenkov and cyclotron absorption of Alfven and fast magnetoacoustic waves in plasma with gas-kinetic pressure in quasi-linear approximation 13 p2166 A67-26776

Possibility of Cerenkov effect in superconductors established from electromagnetic oscillation spectrum, calculating wave resistance and resonance maxima positions 14 p2375 A67-29079

Plasma in HF electric field becoming kinetically unstable due to Cerenkov effect 18 p3090 A67-34422

CERENKOV RADIATION

SA COSMIC RADIATION

SA GAMMA RADIATION

Beam-plasma amplifier with input coupler as cavity and output coupling due to Cerenkov radiation 01 p0040 A67-11313

Cerenkov radiation of beam-plasma system into dielectric, using mathematical model and mode coupling theory 01 p0040 A67-11314

Landau damping in weakly inhomogeneous plasma related to Cerenkov radiation of accelerated electrons moving in external static field causing inhomogeneity 02 p0272 A67-11636

Ion motion effect on spectral region and energy density of Cerenkov excitation produced by charge moving in cold magnetoactive plasma 02 p0274 A67-12456

High energy proton from local radio sources, using telescopic system for Cerenkov effect detection of broad atmospheric showers 02 p0311 A67-12587

Cerenkov radiation induced by cosmic ray in end-on photomultiplier and resultant fundamental noise 02 p0247 A67-12686

Gas-filled Cerenkov radiation detector combined with solid detectors to measure charge and flux of relativistic cosmic rays 02 p0247 A67-12695

Quasi-linear approximation of Cerenkov and cyclotron damping of electromagnetic waves in magnetoactive plasma, considering collisions of wave-absorbing resonance particles with plasma 03 p0475 A67-12934

Frequency range in which Vavilov-Cerenkov surface wave exists in plasma-vacuum boundary 04 p0668 A67-15273

Angular and frequency spectra of Cerenkov and cyclotron radiation from charged particle spiraling in cold magnetoplasma determined by Fourier transform method 09 p1562 A67-22228

Lack of Cerenkov emission in isotropic plasma, presenting fast electron beam experiment for verification of theory 14 p2357 A67-28204

Cerenkov radiation due to point charge moving at uniform velocity parallel to magnetostatic field in unbounded magnetoionic medium 17 p2812 A67-32314

Frequency regions for Cerenkov radiation and power spectrum in collisionless magnetoplasma calculated using refractive index 18 p3090 A67-34428

High energy cosmic ray shower detection combining perturbed magnetic field pulse and coincident optical radiation observations 23 p4051 A67-40812

Fluctuation of Cerenkov glow in atmosphere caused by shower particles 24 p4220 A67-42868

CERIUM

Paramagnetic resonance absorption spectrum of cerium in yttrium-gallium-garnet host crystal 08 p1371 A67-21312

Polyhedral boundary precipitations of complex heat resistant nickel alloy in carbide phase caused by boron and cerium 14 p2338 A67-28674

Cerium addition effects on magnesium workability evaluated by sample elongation in tension test and plate working limit in cold rolling 15 p2505 A67-30398

Magnetostriction of trivalent Yb and Ce

ions in YIG, measuring temperature dependence, noting exchange and interaction of crystal field splitting for Yb 22 p3855 A67-39363

CERIUM COMPOUND

Calcium fluoride-cerium fluoride with neodymium additions as active medium for lasers, discussing absorption and luminescence spectra and induced radiation 05 p0825 A67-16922

Dielectric properties including permittivity, losses, polarization, impurity conduction and forbidden bandwidths of thin films of praseodymium, cerium and neodymium fluorides 08 p1370 A67-20995

Calcium fluoride-cerium fluoride with neodymium additions as active medium for lasers, discussing absorption and luminescence spectra and induced radiation 14 p2330 A67-28262

Lanthanide salts replacing lithium salts in Leclanche cell electrolyte, noting good capacity over widened temperature range 22 p3748 A67-40228

CERMET

Antifrictional properties of mica and boron nitride for use instead of graphite as solid lubricant in cermet packing materials 01 p0081 A67-11246

Apparatus for measuring temperature dependence of thermoconductivity coefficient, thermal emf and specific electroresistance of cermet cylindrical shells 01 p0076 A67-11248

Cr-SiO cermet material used in precision thin film resistors for monolithic integrated circuits 03 p0381 A67-13663

High vacuum welding of cermet seals with titanium 04 p0630 A67-15632

Zr-Mo, Ca-Mo and Ni-Cr cermets, noting preparation and structural defects 05 p0830 A67-17034

Cermets as substitutes for common carbon and alloyed steels, iron and nonferrous metals, discussing powdered metal technology and applications to structural materials 06 p1015 A67-17842

Small additions of Y, La, Hf, V, Ti and Zr on structure of cleaved surfaces and viscosity of Mo cermet materials 07 p1198 A67-19184

Structure and mechanical properties of extruded Ni-Al-oxide cermet materials, noting high compression strength 09 p1517 A67-21876

Plasma jet applications, emphasizing generation of high temperatures for refractory coatings in form of intermetallic compounds and cermets 09 p1545 A67-22172

Dispersed aluminum oxides effect on size of nickel grains in sintered or extruded nickel-aluminum oxide cermets, studying compressive strength dependence 17 p2871 A67-31924

Cleaved surfaces of Mo cermet binary alloys structures annealed and fractured under static bending loads studied for surface properties 17 p2871 A67-32133

Antifrictional properties of mica and boron nitride for use instead of graphite as solid lubricant in cermet packing materials 17 p2866 A67-33169

Apparatus for measuring temperature dependence of thermoconductivity coefficient, thermal EMF and specific electroresistance of cermet cylindrical shells 17 p2861 A67-33171

Iron-chromium-bauxite cermets preparation and properties 18 p3065 A67-34260

Zr-Mo, Ca-Mo and Ni-Cr cermets, noting preparation and structural defects 18 p3066 A67-34455

Coevaporation of cermet resistor compounds investigated for resistance and stability 18 p3014 A67-34550

Cermet sealing material dry-friction characteristics over wide sliding-speed range, discussing graphite and boron nitride lubricants 19 p3247 A67-35850

Tungsten cermet emissivity study using electron heating 20 p3466 A67-36913

Porous cermet tubular element fire barriers of stainless steel powder for increased safety in gas flame processes, determining critical Peclet values 24 p4159 A67-41957

Cementite formation during sintering in cermet compositions with titanium carbide base and steel or iron binder noting CO role 24 p4171 A67-41960

Nickel on chromium carbide base cermet

polishing by synthetic diamond wheels shown to have little effect on strength 24 p4159 A67-41963

CESIUM

Spin relaxation times of ground state of atomic cesium in aromatic gases measured using optical pumping, noting dependency on temperature 04 p0660 A67-14611

Cesium ionization and transport phenomena for developing porous-surface ion sources 04 p0689 A67-15013

Cross sections for charge transfer between alkali-metal ions and cesium atoms determined as function of primary ion beam energy, noting structure consisting of oscillations 04 p0661 A67-15766

Intercomparison of hydrogen and cesium frequency standard 09 p1494 A67-21616

Concentration of cesium in argon-cesium flow determined by total radiation absorption in resonance line of cesium 09 p1538 A67-21778

Argon-cesium plasma spectroscopy, describing equipment, ionization, conductivity, recombination, concentration, etc 09 p1538 A67-21779

Measurements of conductivity, electron density and ionization rate of cesium in argon on alkali shock tube, describing MHD generator wind tunnel experiment 09 p1540 A67-21789

Output characteristics of cesium thermionic converter as function of size of electrode gap, using device with movable air-cooled stainless steel anode 09 p1444 A67-22007

Thermionic converter life-test results and failure mechanisms noting braze failure, collector deposit, emitter warpage and separation and cesium reservoir leak 09 p1447 A67-22334

High temperature adsorption reservoir for automatic control of cesium pressure for use in thermionic converter 09 p1449 A67-22349

Control system for frequency standard using frequency switching between two points on cesium resonance curve 13 p2121 A67-27226

Isobars of adsorption of Ce on faces of W crystal measured for adsorption heat dependence on atom surface density 23 p4042 A67-41298

CESIUM BROMIDE

Symmetry of phonons and rules of corresponding selection for IR absorption and Raman diffusion for two phonons 23 p4026 A67-40689

CESIUM COMPOUND

Cesium uranyl nitrate crystal near-visible absorption spectrum at 20 degrees K cesium uranyl nitrate crystal near-visible absorption spectrum at 20 degrees K 20 p3506 A67-36229

CESIUM DIODE

Inert gas effect on performance characteristics of cesium thermionic converter, noting saturation current increase 09 p1444 A67-22008

Temperature control and thermal coupling of cesium adsorption porous tungsten, charcoal and graphite reservoirs 09 p1450 A67-22350

Low voltage arc phenomena in cesium vapor investigated in connection with cesium-diode application as thermionic converter, calculating voltage-current characteristics 19 p3176 A67-35130

Cesium plasma diode investigated using ribbon electron beam probing technique, discussing stability of electric potential distribution modes 20 p3496 A67-36329

Parameter diagnostics of low temperature plasma in cesium diode, comparing probe measurements with transport equation solutions 22 p3845 A67-39425

DC potential solutions for low pressure Cs diode with zero slope at emitter noting stability, oscillations and instability for ion/electron ratios 23 p4031 A67-40886

CESIUM ENGINE

CS contact ion engine technological status, engine life and performance characteristics 04 p0689 A67-15019

Low density electron bombardment ion engine, particularly mercury engine and Cs gas discharge ion engine, for electrostatic propulsion 04 p0689 A67-15020

Electric propulsion for satellite applications, noting cesium contact microthruster ion engine system [AIAA PAPER 67-80] 07 p1240 A67-19435

Permanent magnet low thrust engines

performance and tests, starting from cesium electron bombardment ion microthruster [AIAA PAPER 67-81] 07 p1240 A67-19436

Plasma measurements in cesium electron bombardment ion engine indicate that reversed cathode-anode configuration improves radial ion distribution [AIAA PAPER 66-246] 10 p1698 A67-23121

Cesium contact ion engine ground and flight tested for ability to operate under environments of ground handling, missile launch and space ambients 16 p2736 A67-30711

Cesium impurities analyzed for behavior in thermionic converters, investigating equilibrium state as function of pressure and temperature 16 p2609 A67-31399

Cesium thermionic converter extinguished-mode operation theory, deriving expressions for forward and reverse saturation output current densities and open circuit voltages 17 p2803 A67-32365

Permanent magnet low thrust engines performance and tests, starting from cesium electron bombardment ion microthruster 21 p3689 A67-37790

Cesium bombardment ion engine performance, giving starting circuit and automatic discharge power control system [AIAA PAPER 67-666] 21 p3690 A67-38700

CESIUM FLUORIDE

Impurity free CsF effect on work function of tungsten surface, discussing amount of impurities, type and control 09 p1450 A67-22354

CESIUM IODIDE

Energy loss spectrum in CsI at small atmospheric depths, discussing time variation of 0.5-mev gamma-ray flux 16 p2739 A67-31406

Thermionic and electrical sorption properties of tungsten in alkali iodide vapors at high pressure 17 p2887 A67-32201

CESIUM ION

Cesium ion beam generation by accelerating cesium in space charge sheath located between ionizer and plasma filled region [AIAA PAPER 66-927] 02 p0303 A67-12251

Metallurgical viewpoint of current status of porous refractory materials technology related to cesium contact ionizers 04 p0638 A67-15014

Capillary emitter of electrons and Cs ions for use in thermionic converters 04 p0664 A67-15015

Sputtering yields of aluminum, copper and titanium measured as function of cesium ion energies for use as electrodes on cesium ion engines [AIAA PAPER 66-203] 05 p0871 A67-17349

Radioactive tracer technique for measurement of yield and angular distribution of molybdenum sputtered by cesium ion beam 06 p1036 A67-18139

Three-body collisional recombination coefficients calculated for cesium and argon atomic ions, assessing Gryzinski cross sections 06 p1036 A67-18151

Mass spectrometric investigation of composition of negative ion sputtering products of solid metal surfaces under cesium ion bombardment 06 p1036 A67-18425

Dominant ionic species in cesium plasma diode determined as atomic cesium ion rather than molecular cesium ion 09 p1448 A67-22337

Low thrust divergent flow cesium-on-tungsten contact ionization electrostatic thruster for satellite attitude control and stationkeeping missions [AIAA PAPER 66-569] 13 p2188 A67-26824

Porous cesium ionizer with improved lifetime obtained by adding secondary tantalum to tungsten powder [AIAA PAPER 66-219] 14 p2376 A67-28124

Pure molecular flow coupled with surface diffusion applied to cesium transport 15 p2520 A67-29494

Cesium ion emission patterns from rear-faced porous refractory metals studied by thermal emission microscope 17 p2888 A67-33059

Duo-emitter cesium thermionic converter, discussing electron and cesium ion emission to increase transport efficiency 21 p3571 A67-38610

Measurement of cesium and mercury ion-atom resonance charge exchange cross section [AIAA PAPER 67-682] 21 p3660 A67-38713

Cesium ion beam generation by accelerating cesium in space charge sheath located between ionizer and plasma filled region [AIAA PAPER 66-927] 23 p4049 A67-41736

CESIUM PLASMA

Plasma probe for dense isothermal cesium plasma, noting electron concentration and temperatures, potential distribution, etc 02 p0184 A67-12467

Thermally ionized cesium plasma confinement investigated in magnetic mirror geometry, in terms of collisional diffusion and end plate ion recombination 02 p0276 A67-12560

Nonequilibrium conductivity of argon-cesium plasma 03 p0478 A67-13614

Electron temperature and concentration in cesium plasma in low voltage arc measured, using double probe method 04 p0666 A67-15182

Fluctuation spectra of Cs and K plasmas produced by surface ionization in Q-3 device 05 p0859 A67-17443

Minimum B magnetic field geometry for LF oscillations in Cs plasma of Topsy Q device 05 p0859 A67-17444

Cesium-plasma diode effect dependence on material output of cathode in vacuum, plotting short circuit current vs vapor pressure, voltage distribution, etc 08 p1357 A67-20845

Microwave Interferometer for measurement of effective recombination coefficient of decaying argon-cesium plasma with hot electrons at various argon pressures 09 p1542 A67-21817

Excitation of ion-acoustic waves in potassium-cesium plasma when passing current through it, finding natural frequencies of system when plasma is drifting along axis 09 p1544 A67-21853

Dominant ionic species in cesium plasma diode determined as atomic cesium ion rather than molecular cesium ion 09 p1448 A67-22337

Plasma potential and particle energies in cesium plasma measured by simultaneous observation of ion and electron energy spectra 09 p1548 A67-22338

Oxygen as steady state electronegative additive in cesium thermionic converter shown to improve performance without surface corrosion 09 p1450 A67-22355

Plasma stability research program facilities for study of helical instabilities in cesium arc plasmas in axial, Ioffe and other magnetic field configurations 11 p1829 A67-23998

LF instabilities and anomalous plasma processes in cesium discharge and thermal plasmas 11 p1829 A67-24000

Cesium plasma measurements to determine steady state parameters and LF oscillation characteristics 11 p1834 A67-24379

Cesium plasma confinement time measured in Q device by observing plasma density decay after atomic beam shut off 11 p1835 A67-24385

Alkali metal plasma generator design and performance, noting characteristics of LF wave propagation parallel to magnetic field 11 p1837 A67-24396

Quiescent cesium plasma production in thermal ionization chamber at high temperatures and low ionization level 11 p1838 A67-24412

Steady MHD electric power generation, flow velocity effect on single controlled glow discharge in cesium-seeded argon 12 p1974 A67-25402

Microwave amplification by electron beam interaction with cesium plasma 13 p2166 A67-26726

Destruction of drift motion of electrons in quiescent cesium plasma by electron-plasma oscillations 13 p2166 A67-26731

Simple model atom selection for electron density calculation in low temperature nonequilibrium Cs plasmas 13 p2171 A67-27441

Current voltage characteristics of argon cesium plasma in inductive hydrodynamic shock tube 14 p2354 A67-27761

Grid probe analysis of alkaline plasma, determining density, potential and energy distribution function 15 p2527 A67-29476

Wall radiation, temperature, pressure and electric field strength effects on electric conductivity, electron density and ionization time of nonequilibrium He-Ce

plasma 16 p2709 A67-30515
 Calculating characteristics of cesium plasma in stationary state under electric field, considering excitation and ionization by inelastic electron collisions 16 p2713 A67-30868
 Momentum transfer collision frequency for electrons in cesium plasmas from electrical conductivity and plasma properties measurement in cesium arc column 16 p2719 A67-31236
 Ionization, ion temperature and density dependence of cesium plasma on pressure of added rare gas 16 p2720 A67-31244
 Ionization outside equilibrium and relaxation of ionization in cesium seeded argon 17 p2894 A67-32152
 Hall field intensity and asymptotic electron temperature of ionized argon-cesium mixture flow in transverse magnetic field with subsonic velocity 17 p2900 A67-32338
 Frequency response of DC and AC currents flowing to RF resonance probe in quiescent cesium plasma, explaining measurements 18 p3044 A67-33713
 Cesium viscosity coefficient over range of temperatures and pressures, assessing accuracy of results and collision integral values 18 p3087 A67-34050
 Nonequilibrium conductivity of argon-cesium plasma 18 p3091 A67-34479
 Cesium plasma confinement time measurement in Q machine by plasma density decay observation 18 p3093 A67-34757
 Ionization decay in cesium vapor explained in terms of dissociative recombination and diffusion, showing strong dependence on vapor pressure 19 p3271 A67-35072
 Electron-atom collision cross-section in afterglow of pulsed cesium plasma as function of electron cyclotron absorption resonance and electron temperatures 19 p3271 A67-35076
 Thermally ionized cesium plasma produced containing negative Cl ions 19 p3272 A67-35084
 Thermal conductivity ionization coefficient of cesium plasma at high temperature and low pressure 19 p3287 A67-35359
 Experiments with thermally ionized cesium plasma in magnetic field with variable curvature 19 p3288 A67-35365
 Microwave transmission through quiescent cesium plasma studied, noting apparatus for thermal ionization studies 19 p3288 A67-35370
 Stability of cesium Q-type machines analyzed for hot plasma-beam interactions in VLF range in sheath and in plasma 19 p3292 A67-35390
 Characteristics of nonequilibrium cesium plasma subjected to continuous electric field 19 p3294 A67-35417
 Cesium plasma created in diode equipped with Langmuir probe 19 p3296 A67-35588
 Influence of Langmuir probe losses on ion-density measurements in thermal cesium plasma with homogeneous magnetic field 19 p3296 A67-35589
 Cesium plasma diode investigated using ribbon electron beam probing technique, discussing stability of electric potential distribution modes 20 p3496 A67-36329
 Major difficulties encountered in open and closed cycle MHD, particularly temperature resistance of heat exchanger 20 p3362 A67-36366
 Microwave amplification when electron beam passes through cesium plasma, noting noise figure dependence on tube pressure 21 p3668 A67-38605
 Cesium plasma ionization in low voltage arc discharge, measuring electron ionization capacity, electron temperature and cesium ionization and excitation cross sections 22 p3847 A67-39510
 Hot Langmuir probe in Cs plasma studied for method of controlling current voltage characteristics 24 p4154 A67-42210

CESIUM VAPOR

Effective electron scattering cross section in helium and argon plasma with cesium vapor admixture measured by Langmuir probe theory 01 p0119 A67-10134
 Thermionic energy conversion, discussing surface and volume phenomena, vacuum and gaseous converters 01 p0013 A67-10557
 Full temperature range electron and ion emission from polycrystalline surfaces of Nb, Mo, Ta, W, Re, Os and Ir in cesium vapor 02 p0269 A67-11878

Plasma probe in thermal emission converter with high cesium vapor, noting parameters of diffusion, electron concentration, etc 02 p0184 A67-12468
 Electron temperature measurements in low voltage arc in saturated cesium vapor 02 p0275 A67-12470
 Thermalization of cathodic electron flux by Langmuir oscillations in cesium arc plasma 04 p0673 A67-15971
 Cesium vapor flow from orifices and tubes into vacuum analyzed, noting dependence of angular distribution and center line intensity on Knudsen numbers 08 p1324 A67-21495
 Free charged particles interaction with each other and neutral atoms in highly excited states effect on thermodynamic and gas dynamic parameters of shock wave propagating in cesium vapor, taking into account energy losses due to radiation 09 p1540 A67-21791
 Plasma mode work function measurement for studying thermionic emission from Hf, Th and Tl in Cs vapor at reservoir temperature of 414 degrees K 09 p1450 A67-22353
 Thermoemission properties of ZrC powder in vacuum and in cesium vapor under thermoelectronic conversion conditions 11 p1822 A67-24033
 Cesium vapor thermionic diode operation in electron-rich surface ionization mode noting transport effects 11 p1849 A67-24902
 Semipermeable Ag membrane as electron collector in oxygen diffusion process for cesium thermionic energy converters 11 p1746 A67-24923
 Cesium thermionic diode parameters including added noble gas pressure effect for ignited mode performance prediction and optimization 12 p1896 A67-25262
 Positive ion production during illumination of cesium vapor-filled thermionic cell with laser beam 12 p1973 A67-25396
 Physical properties of binary pulsed discharge plasma in helium and argon seeded with Cs and K 16 p2711 A67-30525
 Cesium-neon mixture effect on thermionic-emission converter operation measured in experimental tube with plane electrodes, discussing volt-ampere characteristics 16 p2610 A67-31783
 Heat conductivity coefficient of cesium vapor at temperatures from 1000 to 1600 degrees K and 1 to 5 torr measured by hot tungsten filament method 17 p2895 A67-32156
 Cesium-vapor vacuum diode for thermionic conversion stressing role of electrode homogeneity, space charge and transport phenomena 17 p2823 A67-32222
 Charge recombination coefficient of decaying He and Ar plasmas with Cs vapor additions at increased pressures 19 p3271 A67-35073
 Cesium vapor treatment effect on work function of high melting Ta and Zr carbides, evaporation products and graphite 19 p3176 A67-35080
 Low voltage arc phenomena in cesium vapor investigated in connection with cesium-diode application as thermionic converter, calculating voltage-current characteristics 19 p3176 A67-35130
 Dynamics of channel formation in nonisothermal pulsed discharge and nonequilibrium ionization in inert gas-cesium mixtures 19 p3278 A67-35132
 Cesium vapor ionization on porous tungsten substrate creates gradients in surface atom concentrations diminishing ionization efficiency 20 p3487 A67-36170
 Electron-ion radiative recombination influence on time-dependent luminous intensity of various spectrum lines in cesium vapor 20 p3488 A67-36436
 Plasma Separator Thruster, advanced ion thruster design based on independent operation and optimization of plasma source and plasma extraction system [AIAA PAPER 66-598] 22 p3868 A67-40084
 Externally adjustable pressure regulation of Fabry-Perot interferometer, using device to measure cesium vapor spectral absorption in D-1 line 22 p3810 A67-40522
 Cesium vapor pumping by intensive polarized light used for studying Cs buffer gas collision influence on pumping cycle and Zeeman transitions effect on polarization 23 p4016 A67-41291
 Atomic Cs vapor experimental values for

heat-transfer coefficient used to determine Cs atoms and molecules interaction potentials 24 p4253 A67-42211

CESIUM 137
 Radioactivity, using Cs137 isotope as radioactive agent, in civilian Norwegian pilots 15 p2429 A67-29283

CESSNA 336 AIRCRAFT
 Cessna tandem twin aerodynamics noting propeller slipstream variation effects, comparing front and rear engine operation [SAE PAPER 670243] 12 p1894 A67-25498

CH-47 HELICOPTER
 Structural design and fatigue life of Chinook helicopter 01 p0010 A67-10575
 Continuous mechanical ladder for troop/cargo lowering and retrieval from CH-47 helicopter 17 p2804 A67-32518

CH-53 HELICOPTER
 CH-53A military transport helicopter, discussing design constraints, drag, weight and vibration control, power plant selection, reliability, handling qualities, etc 01 p0011 A67-11266

CH-54 HELICOPTER
 Effective engine protection system for CH-54A Flying Crane helicopter, consisting of an engine-inlet air-particle separator, noting Vietnam performance [AHS PAPER 117] 16 p2737 A67-31833
 Ch-54 A Flying Crane helicopter, discussing use in Vietnam in terms of field supply, transportation to Vietnam, etc [AHS PAPER 126] 16 p2598 A67-31841

CHAMBER
 S ANECHOIC CHAMBER
 S ARC CHAMBER
 S BUBBLE CHAMBER
 S CLOUD CHAMBER
 S COMBUSTION CHAMBER
 S ENVIRONMENTAL CHAMBER
 S FLOW CHAMBER
 S ION CHAMBER
 S IONIZATION CHAMBER
 S LOW PRESSURE CHAMBER
 S PLENUM CHAMBER
 S PRESSURE CHAMBER
 S ROCKET CHAMBER
 S SPARK CHAMBER
 S TEST CHAMBER
 S VACUUM CHAMBER

CHAMBER PRESSURE
 Maximum chamber pressure obtained with topping cycle at present, future and ultimate theoretical values 01 p0141 A67-11398
 Effect on protective coatings of launch pads of exhaust products, chamber pressure, nozzle diameter, etc, from aluminized solid propellant rocket motors [AIAA PAPER 66-972] 02 p0304 A67-12294
 Ignition pressure transient in solid rocket motors, examining chamber filling interval, flame propagation, heat transfer correlation, burning area, etc 05 p0873 A67-16513
 Axial load deformation of grains with end-face limitation used in solid propellant engines 14 p2377 A67-28651
 Effect on protective coatings of launch pads of exhaust products, chamber pressure, nozzle diameter, etc, from aluminized solid propellant rocket motors [AIAA PAPER 66-972] 17 p2928 A67-32064
 Rocket chamber pressure influence on particle size measurements of heterogeneous combustion products of solid propellants containing aluminum 18 p3109 A67-33839
 Correlation between thrust chamber design parameters and combustion stability, noting stability increment with increasing injection velocity, droplet diameter and chamber pressure [AIAA PAPER 67-474] 18 p3113 A67-33944
 Factors influencing rocket ignition pressures and conditions leading to large ignition overpressures, estimating residual propellant in rocket combustor [AIAA PAPER 67-515] 18 p3114 A67-33978
 Blaxial satellite motion simulator for large space-simulation chamber, discussing temperature and pressure simulation 18 p3021 A67-34611
 Igniter performance in solid propellant rocket motors, examining mass discharge rate effect on chamber pressure transients [AIAA PAPER 66-680] 19 p3310 A67-34811
 High chamber-pressure propulsion systems and components captive testing, describing ground support system analysis, design and mechanisms 20 p3414 A67-36534

Injector inlet conditions effects on combustion delay time in liquid bipropellant rocket engine, noting propellant atomization and droplet vaporization 22 p3868 A67-40161

Isobaric mixing chamber configuration determination method for maintaining constant static pressure along flow during turbulent jet mixing 23 p3927 A67-40730

CHANCE-VOUGHT MILITARY AIRCRAFT
S A-7 AIRCRAFT
S XC-142 AIRCRAFT

CHANDRASEKHAR EQUATION
Initial value formulation of Chandrasekhar problem for diffuse reflection of radiation from planetary atmosphere 03 p0462 A67-13903

CHANNEL
Nonlinear distortion of envelope of amplitude modulated signal in selective HF channel 01 p0020 A67-10200

PCM/TDM and influence of channel on signal determined, using mathematical model 02 p0202 A67-12130

Metering and pumping equipment for test channel for high altitude permeability tests of parachute cloth, noting permeability of MIL-C-7350 B, type I 02 p0182 A67-12789

Stability of automatic systems for tracking point targets, noting nonlinear dependence of signals on channel mismatch and its limiting values 20 p3410 A67-37234

CHANNEL CAPACITY
Ground-Air-Ground /G/A/G/ communication channels analyzed in air traffic control 02 p0263 A67-12125

Digital communications system evaluator /DICOSE/ using stored program processor coupled with communication channel arrays to provide real time on-line system 02 p0230 A67-12127

Thermodynamic equilibrium of binary channel with noise at fixed temperature 03 p0372 A67-14057

Shannon model for band-limited time-continuous channel to provide more realistic model of communication system 04 p0574 A67-15075

Parallel data decoding with high transmission rates close to channel capacity for space telemetry systems design 12 p1909 A67-25781

Lower bounds on error probability for communication in presence of white Gaussian noise with no bandwidth constraint 12 p1908 A67-26086

Information capacity dependence on number of frequency-divided channels of optical communication system, investigating information loss in channel-separating receiver 16 p2623 A67-30882

Statistical analysis of observed relationship between independent air traffic and resultant communication channel loading parameters 17 p2810 A67-32110

Asynchronous pulse modulation systems developed using step and linear segment approximations of message waveforms 17 p2812 A67-32318

Perturbing factors in avionics communications noting drawbacks and advantages of satellite utilization, possible commercial applications, etc 17 p2813 A67-32498

Feedback-signal lag and channel discreteness effect on rate of information transmission over Gaussian channel with feedback during symbolized coding 18 p2999 A67-33531

Algorithm for converting binary code into uniform binary code with maximum predetermined number of zero symbols in any code combination 18 p2999 A67-33532

Reliable efficient communication channel utilization by use of sequential decoding 20 p3384 A67-37348

Lower bounds to minimum error probability for block coding on noisy discrete memoryless channels 22 p3764 A67-39296

Proactive inhibition, recency and limited channel capacity under acoustic stress 24 p4118 A67-42701

CHANNEL FLOW
SA ANNULAR FLOW
Heat exchange and friction drag coefficients for laminar flow of equilibrium dissociable hydrogen with constant heat flow density at tube wall 01 p0165 A67-10048

One-dimensional compressible gas-channel flow under thermal and mechanical effects

analyzed within generalized energy coordinates 01 p0119 A67-10170

MGD flows in channels analyzed, using transformation of hodograph for vortical velocity distribution 01 p0119 A67-10172

Braking of conducting gas by transverse magnetic field in rectangular channel, deriving one-dimensional channel flows 01 p0119 A67-10173

Potential distribution between graphite and metallic electrodes of MHD generator in nonstationary heat conditions under induced or applied electric field 01 p0011 A67-10176

Stationary free-surface mercury flow in channels under magnetic field, analyzing hydraulic jump and influence of field on location 01 p0120 A67-10179

Motion equation solution to viscous conducting flow at inlet of diverging channel using difference method, noting magnetic field effect 01 p0120 A67-10184

Surface roughness effect on laminar MHD flow through rectangular duct, deriving relation between transition friction factor and Reynolds and Hartmann numbers 01 p0120 A67-10186

Hydrodynamic thermal explosion of stationary axisymmetric non-Newtonian fluid in infinitely long cylindrical tube 01 p0052 A67-10681

Electrode tips and inhomogeneity of applied magnetic field effect on fluid flow of MHD generator 01 p0124 A67-10753

Laminar flow of elastico-viscous fluid between parallel planes obeying Noll constitutive equation, considering heat transfer 01 p0053 A67-10802

Sound propagation in streaming air within tubes having changes of cross section and flow losses, discussing reflection coefficient dependence on flow velocity 01 p0114 A67-10819

Saturation effect dependence on electrode surface temperature and bulk gas temperature in MHD generator duct 01 p0126 A67-11186

MHD channel flow for given accelerator analyzed, based on magnetic and other interaction parameters for full range of possible exit states 01 p0014 A67-11195

Unsteady laminar flow of incompressible fluid in gap between parallel disks with gap width varying with time, obtaining solutions for Navier-Stokes and thermal energy equations 02 p0231 A67-11469

Stability of plane parallel flows in finite length tube at large Reynolds numbers, noting velocity profile 02 p0233 A67-11949

Pressure losses and improved heat transfer in incompressible fluid flow through tubes containing twisted tapes 02 p0233 A67-12200

Uniform velocity MHD channel flow of nonequilibrium plasma with tensor electroconductivity 02 p0275 A67-12552

Analogy between turbulent MHD channel flow at high Reynolds numbers and moderate Hartmann numbers and turbulent boundary layer flow with suction 02 p0277 A67-12569

Channel flow interaction of plasma from coaxial plasma gun with transverse magnetic field 02 p0277 A67-12618

Fluctuations of potential isentropic supersonic gas flow in finite channel with oscillating walls 02 p0180 A67-12669

Minimum cavitation number and cavity width in plane and axisymmetric channels 03 p0401 A67-12872

Pseudoshocks in pipe flow in supersonic compressors represented as diffusion process, noting application in cascade and rotor configuration 03 p0352 A67-13011

Distribution of electromagnetic fields, density of forces and Joule losses with higher spatial harmonics in asymmetric type of MHD induction generator allowing for conducting walls 03 p0475 A67-13178

Turbulent heat transfer in tube in conditions of axial symmetry, discussing variation of mean temperature of flow as function of axisymmetrical variation of wall temperature 03 p0535 A67-13395

Aeromagnetic flutter of walls of plane infinite channel with ionized gas flow 03 p0524 A67-13503

Stabilizing effect of wall and thermal flux temperature variations over channel length on heat transfer coefficient of liquid flow 03 p0536 A67-13610

Heat transfer and friction drag for

supercritical laminar flow of carbon dioxide through tube at constant thermal flux density at wall 03 p0536 A67-13612

Plane transonic gas flow past symmetrical convex profile at zero angle of attack along axis of channel with parallel walls 03 p0352 A67-13620

Motion of medium of variable electric conductivity in rectangular channel situated in magnetic field 03 p0478 A67-13621

Current density distribution in two-electrode MHD channel operating in amplification and generation mode 03 p0479 A67-13686

Convective heat transfer formulas for cases involving tube, liquid metals, etc 03 p0536 A67-13687

Hydrodynamic and thermal characteristics of flows bounded by channel walls 03 p0403 A67-13689

Channel flow of suddenly pressurized viscoelastic and electrically conducting fluid under influence of constant transverse magnetic field 03 p0483 A67-14035

Series coefficients of flow stream functions for plane laminar flows of viscous incompressible fluids in channels and near corners at small Reynolds numbers 03 p0405 A67-14259

Numerical solutions of equations of motion and energy for heating of non-Newtonian fluids in rectilinear axisymmetric laminar flow in circular tubes extended to case of cooling at constant tube-wall temperature 04 p0720 A67-14510

Generalized Couette-type flow with variable viscosity in plane and annular channels, liquid being injected or sucked through porous surfaces 04 p0602 A67-14639

Convective heat transfer in motion of fluid in initial section of cylindrical tube 04 p0722 A67-14716

Connective heat transfer and viscous fluid friction at air pressure with high Reynolds numbers in cooled channels, noting coolant pressure effect 04 p0603 A67-14717

Continuous spatially varied open channel liquid flow analogy for gas flow, with heat addition and extraction over finite distance 04 p0604 A67-14838

Turbulence structure in pipe flow with rough surfaces 04 p0604 A67-14845

Viscous friction and heat flux for partially ionized medium flowing in plane channel with anisotropic transport coefficients 04 p0666 A67-15189

Low density gas flow through short tubes at densities varying from continuum to free-molecule regime, noting nitrogen flow [ASME PAPER 66-WA/PID-8] 04 p0606 A67-15331

Static pressure and velocity profiles of rotating flow with recirculation core in straight pipes determined by five-hole pressure probe [ASME PAPER 66-WA/FE-36] 04 p0607 A67-15367

Theoretical analysis of translational motion and angular motion of flow induced vibration of blade suspended in flow channel [ASME PAPER 66-WA/NE-1] 04 p0712 A67-15372

Hot-wire probe measurements of time average velocity, flow directions, turbulence intensities and growth of skewed three-dimensional turbulent boundary layers in low speed flow [ASME PAPER 66-WA/FE-2] 04 p0608 A67-15386

Transfer function and input impedance of pressurized fluid piping system, using distributed parameters and block diagram feedback methods [ASME PAPER 66-WA/AUT-13] 04 p0555 A67-15416

Mass and oscillation damping of rigid sphere in cylindrical tube containing viscous liquid [ASME PAPER 66-WA/UNT-5] 04 p0608 A67-15442

Numerical solution for laminar flow heat transfer in circular tubes with axial conduction and developing thermal and velocity fields [ASME PAPER 66-WA/HT-7] 04 p0726 A67-15446

Turbulent MHD flows in prismatic and cylindrical pipes, particularly pipes with slot shaped cross section 04 p0669 A67-15513

Supersonic conducting gas flow in coaxial channel in magnetic field formed by

currents flowing over plasma 04 p0669 A67-15514

Linearly expanding MHD channel with solid electrodes, noting end effects relation to electrode dimensions 04 p0669 A67-15516

Mercury device for analyzing pressure distribution, velocity profiles and resistance coefficients of turbulent flow in channels of linear induction pumps under traveling magnetic field 04 p0670 A67-15521

One-dimensional linear approximation of effects of magnetic and electric shunting of linear inductor edges on constant velocity MHD channel flow 04 p0556 A67-15524

Relative external characteristics for calculation of maximum efficiency and minimum current supply of conduction pumps 04 p0556 A67-15527

Strain gauge measurements of resistance of sphere to MHD turbulent flow of mercury in rectangular tube 04 p0670 A67-15530

Laminar heat exchange in inlet section of rectangular channel with incompressible fluid and temperature 04 p0726 A67-15590

Errors in calculating losses in diffuser elements 04 p0548 A67-15600

Methods of calculating flow velocity losses in diffusers 04 p0548 A67-15601

Hydraulic resistance determination for plane and axisymmetric channels with attached and separated flow, noting terminology 04 p0549 A67-15602

Velocity profile and friction in plane-parallel channel with developed turbulent compressible gas flow 04 p0609 A67-15684

Variation of total pressure loss coefficient with entry Mach number for conical diffusers, junction between parallel entry pipe and cone being sharp 04 p0549 A67-15748

Variational analysis of Graetz problem of forced-convective laminar heat transfer in duct, for various cross sections and given wall temperature and temperature gradient 04 p0728 A67-15802

Turbulent heat transfer to noncircular throat bodies with and without water film cooling 04 p0728 A67-15803

Forced-convective heat transfer in asymmetrically heated rectangular ducts as function of prandtl number, Reynolds number, aspect ratio and temperature difference 04 p0728 A67-15804

Finite difference solution of parabolic equation for laminar heat transfer in inlet of rectangular duct as function of wall temperature and Nusselt number for different aspect ratios 04 p0728 A67-15805

Monte Carlo method analysis of rarefied gas heat transfer between parallel plates in terms of temperature, density and Knudsen number 04 p0728 A67-15807

Laminar tube flow and heat transfer for He gas using Navier-Stokes, energy and continuity equations in finite difference form 04 p0729 A67-15809

Heat-transfer coefficient measurements in separated flow regions in heated duct with circumferential grooves, ribs and enlargements, by visual flow techniques 04 p0729 A67-15810

Unsteady heat transfer in tubes resulting from changes in heat flow, gas mass flow rate and acoustic balance 04 p0733 A67-15844

System induced instabilities of forced convection flows with subcooled boiling restricted to case of water flow in small circular channels, high L/D ratios, moderate temperature and pressure 04 p0736 A67-15858

MHD heat transfer in finite duct for fully developed flow conditions with arbitrary oriented applied magnetic field and variable heat flux boundary conditions 04 p0673 A67-15872

Rayleigh-Ritz method for turbulent heat transfer in curvilinear channel and heat flux magnitudinal and directional effects on stability of isothermal flow in laminar boundary layer 04 p0610 A67-15900

Potential flow theory design of subsonic flow diffusers for centrifugal compressors, assuming compressible irrotational inviscid channel flow [ASME PAPER 66-WA/GT-9] 04 p0550 A67-15938

Numerical solution of motion and energy equations for non-Newtonian fluid flow in tubes of circular cross section with heat transfer to or from fluid 05 p0925 A67-16271

Nucleonic quality gauging system for two-

phase hydrogen pipeflow 05 p0842 A67-16539

MHD steady laminar flow of viscous incompressible electrically conducting liquid in rectangular pipe between conducting plates 05 p0853 A67-16723

Laminar shearing flows breakdown for second order viscoelastic fluids in channels of critical width 05 p0792 A67-16724

Solid propellant regression rate in hybrid rocket motor examined via combustion process model, assuming homogeneous flow in central channel 05 p0874 A67-16766

Transient response of Couette shear flow to step function change in blowing velocity across channel 05 p0751 A67-17420

Converse of channel coding theorem, relating average probability of error to distortion measure of source sink pair 06 p0965 A67-17946

Heat transfer by steady laminar forced convection in noncircular ducts, analyzing effects of viscous dissipation due to constant axial temperature gradient 06 p1116 A67-18384

Leak current, friction and heat-transfer coefficients of compressible laminar boundary layer on insulator wall of MHD channel with anisotropic conductivity 06 p1043 A67-18673

Quasi-one-dimensional MGD channel flow calculation methods, considering Hall effect, heat transfer, friction and potential drop near sectioned electrode 06 p1043 A67-18675

Incompressible fluid flow in symmetric flat channel, for case of constant electric conductivity and low Reynolds number 06 p1043 A67-18676

Longitudinal magnetic field effect on convective heat transfer during turbulent MHD pipeflow of liquid Ga 06 p1044 A67-18682

Size and shape of roughness projections effect on resistance coefficient during turbulent pipe flow in transverse magnetic field 06 p1044 A67-18690

Wall profile construction of working zone of flat MHD channel with ideal conductors for both sides 06 p1044 A67-18691

Fluid flow through parallel cylinders when flow incidence is lateral and Reynolds numbers are small, determining particles trajectories 06 p0991 A67-18819

Asymptotic properties of fluid temperature field and Nu numbers in nonstationary heat transfer during passage of laminar flow of viscous incompressible fluid through rectilinear channel 07 p1265 A67-19125

Temperature variation in wall of square channel due to heat transfer to turbulent flow of water and Hg 07 p1265 A67-19126

Convective heat transfer through stabilized turbulent flow of chemically homogeneous liquid in circular pipe under supercritical pressure 07 p1265 A67-19127

Convective heat transfer in tube with gaseous heat carrier pulsating at frequency corresponding to second resonance harmonic 07 p1266 A67-19182

Nonstationary heat transfer coefficient and effect of nonstationary hydrodynamic conditions on heat transfer in channels 07 p1266 A67-19183

Velocity jump characteristics of boundary layer with gradient pressure for flows at inlet channel and in wake of symmetric and asymmetric bodies 07 p1169 A67-20223

Empirical expression for resistance of small bore tubes to turbulent flow of compressible fluid in terms of mass flow and total head 08 p1320 A67-20461

Wall conductance effect on MHD flow through finite cross section rectangular and circular channels 08 p1356 A67-20572

Active component of voltage behavior in channel of helium pulse discharge measured, obtaining time dependence of channel resistance, input velocity and energy magnitude 08 p1357 A67-20848

Curvature effect on heat transfer for turbulent flow in curved pipes under constant heat flux, considering boundary layer existence along wall 08 p1426 A67-20926

Boltzmann equation for rarefied gas flows between two parallel infinite plates for Maxwellian, hard sphere and BGK models 08 p1355 A67-21117

Nuclear energy deposition effect on pressure pulse generation in fissioning gas flow through semiminfinite cylindrical tube

analyzed by method of characteristics 08 p1322 A67-21121

Compressible ideal gas flow through elliptic pipe 08 p1322 A67-21169

Navier-Stokes equation for viscous incompressible fluid flow between stationary and uniformly moving parallel plates with uniform suction along stationary plate 08 p1322 A67-21179

Film boiling of saturated nitrogen flowing upward in vertical heated tube, noting annular-flow regime change to vapor matrix [ASME PAPER 65WA/HT-26] 08 p1427 A67-21319

Pressure field, Bernoulli sum variation, momentum and energy relations in laminar zone of separation 08 p1323 A67-21389

Drag on two-dimensional cylinder between parallel walls in Stokes flow calculated by perturbation methods 08 p1323 A67-21390

Core and boundary layer flows in large scale MHD generator, noting viscous friction and heat transfer at walls 09 p1442 A67-21793

MHD of flows with hot electrons in MHD ducts at low magnetic Reynolds numbers, emphasizing boundary layer and shock wave theory 09 p1541 A67-21797

Quasi-one-dimensional plasma motion in linear and radial Hall type MHD generator ducts 09 p1541 A67-21798

Minimum volume conditions for MHD conversion duct with known upstream and downstream stagnation 09 p1443 A67-21800

Minimization of MHD generator duct with fixed boundary values as criterion in determining expansion shape 09 p1443 A67-21801

Channel flow and power generation of MHD generator, stressing influence of nonequilibrium ionization 09 p1541 A67-21802

Hydraulic approximation for calculating MHD flows in ducts 09 p1541 A67-21804

Nonequilibrium excitation influence on electron density in one-dimensional MFD channel flow 09 p1542 A67-21814

Airflow characteristics and heat transfer in right angle water-jacketed bend, measuring boundary layer profile at midbend 09 p1487 A67-21831

Unsteady flow of rarefied gas under finite pressure gradient when starting from rest, varying gradient in time until steady flow is obtained 09 p1487 A67-21847

Hysteresis effects in one-dimensional conducting gas flow through rectangular MHD converter channel with constant magnetic gap and variable electron spacing 09 p1444 A67-21859

Two-dimensional isothermal liquid flow electrically conducting in channel under electromagnetic fields, finding self-modeling solutions using Jacobi functions 09 p1544 A67-21861

Compressible nonswirling rotational flows through ducts with varying hub radii 09 p1489 A67-22161

Electrode ends effect on flow of fluid in MHD generator, using iterative solution 09 p1549 A67-22563

MHD channel flow under transverse electromagnetic field, analyzing effect of various geometries and boundary conditions 10 p1684 A67-22875

Variational problem for flow of plasma with variable electrical conductivity in channel of MHD generator solved, using Lagrange method of multipliers 10 p1684 A67-23023

Density profiles in gas-solid suspension flow in round duct 10 p1626 A67-23149

Forced convection heat transfer to liquid flowing within unsymmetrically heated rectangular ducts 10 p1733 A67-23481

Pressure drop correlation in developed, isothermal, laminar and turbulent flow in rectangular ducts 10 p1627 A67-23555

Approximate heat transfer theory based on parabolic velocity distribution for channel flows 10 p1734 A67-23575

Steady flow of viscous conducting fluid in pipe under magnetic field analyzed for relations among Hartmann number, Reynolds number, skin friction, wall conductivity, etc 10 p1687 A67-23833

Stability of flow of ideal compressible gas at low magnetic Reynolds numbers in presence of longitudinal perturbations produced by crossed electromagnetic fields 11 p1832 A67-24026

Thermal differential method of determining critical points in flow past

projection in pipe 11 p1741 A67-24032
 Fluid mechanics of internal flow - Symposium, Warren, Michigan, September 1965 11 p1775 A67-24041
 One-dimensional flow through nozzle and stability of weakly ionized plasma with induced Hall current 11 p1832 A67-24155
 Flow induced vibrations of rigid plate in narrow channels, noting flow rate dependence on channel width [ASME PAPER 67-VIBR-32] 11 p1777 A67-24190
 Instability of Maxwellian fluid flow in pipe analyzed using Galerkin method 11 p1778 A67-24216
 Volumetric loading factor expression derived for side burning solid propellant grains by imposing constraint on port channel flow Mach number 11 p1851 A67-24227
 Gas jet expansion near crossed axisymmetric channel, reducing problem to solution of Laplace equation for second-kind boundary conditions 11 p1779 A67-24321
 Laminar turbulent transition of nonisothermal incompressible forced flows in pipes measured for several working fluids and temperatures, using Reynolds number as criterion 11 p1781 A67-24574
 Magnetofluid dynamics - AIAA Selected Reprint Series, Volume II 11 p1841 A67-24946
 Hydrodynamic and overheating instability of nonisothermal plasma flux in crossed electric and magnetic fields in flat dielectric walled channel 11 p1842 A67-24950
 Channel blocking effect on motion of fluid in separation region behind bluff bodies 11 p1743 A67-24960
 Hydrodynamic thermal explosion of stationary axisymmetric non-Newtonian fluid in infinitely long cylindrical tube 11 p1783 A67-25068
 Heat transfer from laminar Newtonian flow through cooled elliptic tubes with variable cross sections 12 p2033 A67-25215
 Heat transfer and friction coefficients measured for turbulent flow of non-Newtonian fluids in rectangular and circular channels 12 p2033 A67-25315
 Convective heat transfer for water flow in curvilinear short channel, noting flow and convection types at various sections 12 p2033 A67-25316
 Two-dimensional temperature field analyzed for laminar gas flow in interspace between parallel thermally thin plates 12 p2033 A67-25319
 Thermal convection in rotating fluid annulus analyzed using Navier-Stokes equations as initial value problem 12 p1963 A67-25339
 Axisymmetric thermal convection flow in rotating fluid annulus 12 p1963 A67-25340
 Velocity profiles for turbulent ducted flow systems analyzed, showing profile decay rate for flow pattern 12 p1927 A67-25351
 Conditions controlling shock wave reflection from duct end deflector plates, determining spacing of plates from pipe 12 p1928 A67-25356
 Two-dimensional nonsteady airflow in shaped duct prediction, using numerical method 12 p1928 A67-25357
 Heat transfer between turbulent supersonic air stream and circular water-cooled tube at Mach 1 to 4, using two-dimensional flow model 12 p2035 A67-25753
 Steady flow of conducting dissociating gas in channel of constant cross section in presence of magnetic field 12 p1929 A67-25756
 Transformation for uncoupling system of duct flow of conducting fluids under arbitrary oriented applied magnetic field 12 p1976 A67-25941
 Channel profiles for producing vortex flows in weakly ionized gases in transverse magnetic fields 12 p1977 A67-26076
 Incremental pressure drop in incompressible fluid laminar flow at entrance of rectilinear duct, using conformal mapping technique 12 p1930 A67-26166
 Radial flow of two-dimensional viscous conducting fluid in wedge shaped channel under magnetic field, reducing flow equation to differential equation 12 p1977 A67-26180
 Turbulent flow through concentric annuli, measuring velocity profiles, finding maximum velocity radius different from value for laminar flow and dependent on Reynolds number 13 p2092 A67-26268

Cylindrical screened electrode for measuring temperature plasma conductivity in MGD generator 13 p2055 A67-26434
 Mass limiting two-phase flow compared in straight tube and in nozzle 13 p2093 A67-26541
 Hydraulic properties of duct of constant rectangular cross section functioning in closed circuit used to measure MHD flow velocity 13 p2185 A67-26593
 Maxwell dispersion of particles of molecular gas flow at wall of circular channel described by integral equation, determining particles experiencing mirror intercollisions 13 p2158 A67-26671
 Aeromagneto flutter of plane duct of finite length 13 p2218 A67-26805
 Self-excited vibration of cylindrical shell in coaxial rigid cylindrical duct with gas flowing past 13 p2218 A67-26806
 Entrance region tube flow combined with rounded entrance flow meters to obtain theoretical solution relating flow rate, downstream pressure, pressure drop and temperature 13 p2120 A67-26932
 Two-dimensional unsteady plasma flows in coaxial channel formed by two profile electrodes calculated in case of finite conductivity in presence of Hall effect 13 p2168 A67-27301
 MHD flow past sonic velocity in channel of constant cross section, discussing conditions for smooth acceleration 13 p2169 A67-27309
 Steady three-dimensional flow of electrically conducting gas in working section of linear MHD channel 13 p2169 A67-27310
 Forces acting in electromagnetic pump channel on gas inclusions in liquid metal, assessing increase in hydraulic resistance 13 p2169 A67-27316
 Hodograph transformation in two-dimensional problems of MHD of viscous flow 13 p2170 A67-27318
 Channel flow interaction of plasma from coaxial plasma gun with transverse magnetic field 13 p2170 A67-27374
 Low temperature engine suction line response to fluid exposed internal surface coating, determining effects of varying flow rates 13 p2229 A67-27664
 Two-dimensional steady flow analysis in channels with variable cross sections under strong magnetic field action, calculating velocity distribution by series expansion 14 p2355 A67-27902
 Pressure driven flow at high Hartmann number along annular channel between nonconducting circular cylinders 14 p2355 A67-27907
 Boundary layer equations reduced to ordinary differential equations without using self-similarity assumptions, noting friction-drag and heat-transfer coefficient along MHD channel 14 p2356 A67-27978
 Model of inviscid, incompressible and variable density airflow in long channel over mountain treated mathematically 14 p2346 A67-28004
 Origin of excessive reverse current in silicon p-n junction, discussing surface layer channel formation 14 p2283 A67-28040
 Fully developed velocity profile for prediction of hydrodynamic entrance lengths for ducts of arbitrary cross section [ASME PAPER 67-FE-4] 14 p2304 A67-28357
 MHD flows in tubes in presence of longitudinal electric current 14 p2361 A67-28743
 Compressible flow analysis in three-dimensional curved duct using small perturbation method 14 p2305 A67-28976
 Approximate solution for interaction of shock wave moving in one dimension with sudden increase in cross sectional area 14 p2306 A67-29061
 Velocity profile analysis in turbulent concentric annular flow, emphasizing correlation of results in inner wall region 15 p2468 A67-29132
 Formulation of upper and lower bounds on Knudsen flow rate of gas through channel of arbitrary geometry by reciprocal variational principles 15 p2469 A67-29195
 Normal shock relations in adiabatic constant area ducts used to connect properties on two sides of shock in steady one-dimensional flow 15 p2470 A67-29441
 Change in pressure losses in MHD

generators channel, obtained from pressure gradient relation to flow rate of conducting fluid 16 p2705 A67-30449
 Steady flow of anisotropically conducting fluid in plane or annular channel of MHD generator with nonequilibrium plasma at small Reynolds numbers 16 p2600 A67-30541
 End losses in magnetohydrodynamic channels of linearly variable cross section determined using equivalent channel geometry 16 p2606 A67-30585
 Potential distribution and volt-ampere characteristics of ionized gas flows in ducts 16 p2713 A67-30598
 Steady laminar flow of viscous, incompressible, electrically conducting fluid in insulated rectangular channel, with imposed oblique transverse magnetic field 16 p2713 A67-30860
 Heat addition in channels of variable cross section area discussed for one-dimensional, inviscid flow of ideal gases with constant specific heat ratio 16 p2591 A67-30944
 Laminar flow with forced convection heat transfer in parallel plate channel under influence of intense, longitudinal, resonant acoustic field 16 p2778 A67-30947
 Gas flow through annular duct of constant cross section analyzed in terms of conservation of energy, mass and angular momentum laws 16 p2593 A67-31153
 Limits of applicability of methods based on one-dimensional model employing Reynolds analogy for gas flow in pipes 16 p2660 A67-31203
 Turbulent channel flow of mercury in presence of uniform transverse magnetic field deducing skin friction coefficient 16 p2661 A67-31224
 Turbulent channel flow of electrically conducting fluid in presence of magnetic field obtaining skin friction coefficient and velocity profiles 16 p2661 A67-31225
 Effect of temperature dependence of plasma conductivity on magnetohydrodynamic channel flows 16 p2721 A67-31392
 Laminar flow through porous annulus with constant suction velocity at walls and swirl, using differential equations 16 p2662 A67-31551
 Transverse magnetic field effect upon convective heat transfer in turbulent flow in electrically conducting fluid in channel bounded by two parallel plates 16 p2722 A67-31572
 Turbulent flow in circular cylindrical duct at various Reynolds numbers, analyzing fluctuations and mean value of velocity 16 p2663 A67-31702
 Electromagnetic field effect on heat transfer during laminar flow of electrically conducting incompressible fluid in flat channel 16 p2723 A67-31774
 Spatial correlation coefficients and transverse temperature perturbation scales during turbulent nonisothermal flow of mercury in circular pipe 16 p2724 A67-31776
 Heat transfer in turbulent carbon dioxide pipeflow at supercritical region 16 p2780 A67-31777
 Decay and dispersion of disturbance pulse in fluid lines along pipe, considering velocity and pressure characteristics [ASME PAPER 66-WA/AUT-24] 17 p2835 A67-32017
 Approximation method for steady laminar flows of incompressible viscous fluid in curved pipes, obtaining flow rate 17 p2836 A67-32038
 Unsteady convective heat transfer and hydrodynamic behavior of gas flows in channels 17 p2967 A67-32131
 Transverse magnetic field effects on heat transfer in turbulent flow of mercury in circular iron tube 17 p2899 A67-32186
 Wall suction rate effect on turbulent flow in cylindrical circular porous duct, measuring distributions of velocity, pressure, friction coefficient and Reynolds stresses 17 p2837 A67-32380
 Transverse magnetic field effect on turbulent MHD jet flow in bounded space, noting channel wall conductivity 17 p2901 A67-32565
 Kantorovich indirect variational method applied to MHD flow inside rectangular duct 17 p2906 A67-33038
 Parameter values excluded by existence conditions for buoyant dissipative motions in vertical channels 17 p2840 A67-33138

Stability of plane parallel flows in finite length tube at large Reynolds numbers, noting velocity profile 17 p2841 A67-33266

Heat exchange and friction drag coefficients for laminar flow of equilibrium dissociable hydrogen with constant heat flow density at tube wall 17 p2974 A67-33326

Flow of viscous incompressible conducting fluid in channel with porous walls 17 p2910 A67-33352

Plane shock wave velocity measurement after interaction with obstacles in form of channelled diaphragms of various diameters, discussing stabilization 18 p3028 A67-34210

Channel flow transition to jet flow, discussing turbulence determination in flow boundary layer as Reynolds number function 18 p3028 A67-34218

Stabilizing effect of wall and thermal flux temperature variations over channel length on heat transfer coefficient of liquid flow 18 p3161 A67-34475

Heat transfer and friction drag for supercritical laminar flow of carbon dioxide through tube at constant thermal flux density at wall 18 p3161 A67-34477

Viscous fluid discharge from tubes of various cross sections under constant pressure gradient with longitudinal pulse along wall, noting short period stoppage 18 p3029 A67-34615

Probability function for turbulent velocity in duct flow determined from Doppler shift of scattered laser radiation 18 p3030 A67-34752

Critical Reynolds number of laminar-turbulent transition for Newtonian flow in rectangular ducts to verify minimum in curve as function of duct aspect ratio 19 p3210 A67-35616

Unsteady discharge of compressed viscous gas from duct analyzed by finite-difference method 19 p3172 A67-35780

Turbulent flow in circular duct, obtaining velocity distribution 20 p3419 A67-36276

Forced convection of laminar flow in tubes of various cross sections, assuming constant temperature gradient and internal heat generation 20 p3420 A67-36317

Natural convection in finite nonzero length vertical channels, using integral technique to derive results for two wall conditions [ASME PAPER 67-HT-16] 20 p3545 A67-36712

Convective secondary flow in channel flow of quasi-incompressible fluid noting temperature gradient role [ASME PAPER 67-HT-28] 20 p3546 A67-36719

Hydraulic resistance coefficient of rotating tubes, taking into account centrifugal mass forces effect on flow inside tube 20 p3421 A67-36793

Arbitrary internal heat generation terms in energy equation effect upon limiting Nusselt number for heat transfer to pipeline flow of non-Newtonian fluids [AIChE PAPER 12] 20 p3552 A67-36828

Heat transfer in fully developed laminar flow through rectangular and isosceles triangular ducts, determining Nusselt numbers 20 p3553 A67-36940

Correlation method for local and average friction coefficients of laminar and turbulent gas flow through smooth tubes 20 p3422 A67-36941

Aerodynamic forces of harmonically oscillating cylindrical duct with supersonic internal flow within framework of potential flow theory 20 p3357 A67-37003

Two-dimensional problem of penetration of subsonic compressible fluid jet into channel solved by modified Chaplygin method 20 p3357 A67-37052

Velocity and pressure fields in viscous incompressible fluid flow in inlet of flat channel 20 p3423 A67-37066

Magnetic field effect on resistance coefficient of mercury flow in circular pipe 20 p3501 A67-37304

Heat transfer in circular channel containing revolving cylinder, considering turbulent flow with microvortices 20 p3359 A67-37343

Heat-transfer coefficients for laminar and transitional liquid metal flow in tube with constant wall heat flux 20 p3555 A67-37608

Physical analysis of convective heat transfer in laminar and turbulent flow through ducts and boundary layers, deriving trailing functions by variational method 21 p3730 A67-37736

Electrodeless slip-type MHD steady state acceleration of subsonic and supersonic high density gas flows for simulating reentry speeds and altitudes 21 p3607 A67-37778

Molecular gas flow through cylindrical tube, using wall pressure distribution to measure pump speed 21 p3610 A67-37823

Turbulent gas flow viscosity, thermoconductivity and friction coefficients in tube 21 p3611 A67-37912

Unsteady conducting fluid flow in MHD ducts with small magnetic Reynolds number and constant pressure gradients 21 p3663 A67-37935

Asymptotic properties of fluid temperature field and Nu numbers in nonstationary heat transfer during passage of laminar flow of viscous incompressible fluid through rectilinear channel 21 p3731 A67-38169

Temperature variation in wall of square channel due to heat transfer to turbulent flow of water and Hg 21 p3731 A67-38170

Convective heat transfer through stabilized turbulent flow of chemically homogeneous liquid in circular pipe under supercritical pressure conditions 21 p3731 A67-38171

Finite conductivity effect on two-dimensional plasma flow in coaxial channel solved numerically, obtaining steady state flow regime by build-up method 21 p3665 A67-38240

MHD channel wall boundary layer equations for low temperature plasma, determining friction and heat transfer coefficients and leakage current 21 p3665 A67-38241

Energy indicators calculated for MHD channel flow with finite sectional electrodes and wide Hall parameter variations 21 p3665 A67-38242

Electromagnetic forces and pressure and hydraulic losses of turbulent mercury flow in annular channel under traveling magnetic field effect 21 p3668 A67-38249

Steady motion of elastoviscous liquid through annulus between two coaxial right circular porous cylinders with suction and injection 21 p3613 A67-38411

Parallel conducting flow along insulating pipe under applied magnetic field, elucidating singularities of Hartmann boundary layers 21 p3668 A67-38495

Insulator boundary layers in supersonic MGD channel noting heat transfer rate, current density, stagnation, pressure distribution and skin friction [AIAA PAPER 67-717] 21 p3673 A67-38743

Linear nonequilibrium MHD generator channel, studying discharge structure and stability and convective and Lorentz forces effects on electric characteristics [AIAA PAPER 67-718] 21 p3673 A67-38744

Linear MPD channel theory with heavy component in uniform state evaluated for investigation of electrical conductivity phenomena 22 p3747 A67-39277

Incompressible two-dimensional turbulent channel flow, calculating velocity profile and obtaining resistance formula 22 p3782 A67-39409

Gas dynamic self-regulation of supersonic nozzle consisting of cylindrical channel with central body, measuring nozzle inlet and static pressures 22 p3868 A67-39544

Book on parallel laminar flow stability covering channel and pipe flows, jets, wakes, free shear and boundary layers 22 p3783 A67-39632

Nonlinear hyperbolic equations of compressible duct flow solved using centered difference method, compared with method of characteristics 22 p3784 A67-39945

Free and near-free molecular flow via cylindrical ducts using Monte Carlo method and high speed digital computer 22 p3784 A67-39946

Heat transfer of fluid flow in annular channel with rotating shafts, deriving surface heat transfer estimation without axial flow 22 p3921 A67-40457

Hydraulic angular acceleration sensor motion equation obtained by kinetostatic method 22 p3809 A67-40477

Energy dissipation and motion equations of superfluid helium flow through pores, describing technique to detect critical velocity in wide channels 22 p3839 A67-40550

Gas-air mixing in coaxial flow engine based on one-dimensional ejector theory at

subsonic flow velocities, discussing chamber design gas-air mixing in coaxial flow engine based on one-dimensional ejector theory at subsonic flow 23 p4048 A67-40638

Peristaltic viscous fluid motion through axisymmetric pipes and symmetrical channels produced by pressure gradients and cross section changes, using Stokes approximation 23 p3990 A67-41174

Linear MHD flow characteristics variation with electric conductivity and gas flow rate changes, noting transverse magnetic flow variation with magnetic Reynolds number 23 p4033 A67-41284

Inviscid steady axisymmetric flow inside closed annulus solution derived with extremal principle [ARL-66-0173] 24 p4140 A67-41807

Longitudinal turbulence intensities, autocorrelations, energy spectra and peak energy dissipation frequencies for organic solvents flowing in smooth round tubes 24 p4141 A67-41927

Boundary layer electric current temperature, velocity and density profile calculation on nonconducting MGD channel wall assuming smaller magnetic Reynolds number than unity 24 p4196 A67-42212

Critical air-water flow in converging-diverging annular venturi noting pressure profiles 24 p4143 A67-42280

MHD generation of electric power, describing motion equations for conducting fluid in electromagnetic field and duct configurations 24 p4098 A67-42413

Energy conversion MHD channel of Faraday type using hot spacers and electrodes for control 24 p4106 A67-42526

Electrofluiddynamic (EFD) power generator channel performance dependence on charge spreading for various geometries, noting stage efficiency and electric pressure 24 p4107 A67-42529

Free convection thermal transfer in narrow horizontal channels and infinitely wide channels 24 p4255 A67-42587

Hydromagnetic flow stability in infinitely long cylindrical pipe with arbitrarily smooth cross section and applied radial magnetic field 24 p4198 A67-42693

Performance characteristics of active channel of insulated gate FET for application as high gain HF amplifier 24 p4133 A67-42824

Non-Newtonian elastoviscous channel flow between rigid boundaries solved by asymptotic expansion in lubrication approximation 24 p4145 A67-43086

CHAPLYGIN EQUATION

Existence and uniqueness theorem and upper and lower Chaplygin function approximations for solutions of Cauchy problem for quasi-linear first order PDE 03 p0456 A67-12884

Subcritical and nonoscillation intervals for Chaplygin theorem evaluated, using Green and Cauchy functions 03 p0456 A67-13112

Conditions of solvability of Chaplygin problem 03 p0458 A67-13339

Strong solvability of Tricomi type boundary value problem for Chaplygin differential equation 04 p0643 A67-14727

Modification of functional scheme of Chaplygin method applied to solution of first boundary value problem for class of quasi-linear second order parabolic equation 07 p1215 A67-19220

Existence of solution for equilibrium problem of circular symmetrically loaded membrane with stress free contour proven by Chaplygin method 11 p1876 A67-24680

Hyperbolic region solutions of equation approximating Chaplygin equation near supersonic flow vacuum line in hodograph plane 12 p1962 A67-26181

Uniqueness of quasi-regular solution to boundary value problem for Chaplygin equation 13 p2145 A67-28444

Plane-parallel transonic flow with direct shock wave analyzed for case where Tricomi equation replaces Chaplygin equation 14 p2297 A67-27990

Strong and weak magnetic field effects on qualitative characteristics of compressible media analyzed using Chaplygin-Sedov hodograph method 18 p3084 A67-33421

Two-dimensional problem of penetration of subsonic compressible fluid jet into channel solved by modified Chaplygin method 20 p3357 A67-37052

Initial boundary value problem for

Chaplygin equation using Cauchy and Dirichlet data 20 p3478 A67-37574

Maximum region of applicability of Chaplygin theorem of differential inequality to elliptic difference equation 20 p3479 A67-37722

Different motion equations equivalence for nonholonomic systems from Chaplygin method 21 p3657 A67-38303

CHAPMAN-ENSKOG METHOD

SA BOLTZMANN EQUATION

Chapman-Enskog method applied to kinetic equation describing evolution of singlet distribution function in dense gas of perfectly rough spheres 04 p0658 A67-15507

Diffusion coefficients determination from viscosity measurements based on higher Chapman-Enskog approximations 04 p0658 A67-15510

Convergence of Chapman-Enskog approximations to scalar electrical conductivity of some weakly ionized real gases 06 p1046 A67-18872

Hydrodynamic equations describing motion of electrons in weakly ionized plasma in external electric field derived from Boltzmann equation, using Chapman-Enskog method 07 p1228 A67-19503

Modified Chapman-Enskog method for obtaining transport properties of nonequilibrium partially ionized gas, giving hydrodynamic equations 11 p1775 A67-23866

Third Chapman-Enskog approximation to tensor electrical conductivity of partially ionized gas applied to two conductivity mixture rules for atmospheric cesium seeded argon 12 p1975 A67-25893

Lenard-Balescu kinetic equation solved by Chapman-Enskog method for transport coefficients of plasmas noting diminishing value 15 p2522 A67-29210

Lorentzian scalar electrical conductivity as basis of mixture rules proposed for partially ionized gases in magnetic field to calculate tensor conductivity 15 p2523 A67-29218

Chapman-Enskog method modified for formulation of multicomponent laminar boundary layer problem for numerical solution 15 p2469 A67-29220

Ion mobility in gases determined, based on kinetic equation for ion velocity distribution function with particular reference to Chapman-Enskog method 16 p2704 A67-31250

Chapman-Enskog expansion applied to Fokker-Planck equation for plasma allows transport coefficients calculation without further approximation in presence/absence of magnetic field 22 p3843 A67-39266

Chapman-Enskog transport collision integrals calculated for repulsive and attractive screened Coulomb potentials in ionized gases 22 p3850 A67-39717

Accuracy of scalar electrical conductivity calculations of partially ionized plasma using third Chapman-Enskog approximation method 23 p4035 A67-41753

CHAPMAN-JOUGET FLAME

Asymptotic law of propagation of plane detonation wave where perturbed motion behind wave transforms it to Chapman-Jouguet wave 09 p1489 A67-22218

Ionized gas flow rate behind detonation wave used with Chapman-Jouguet condition to determine speed of sound in reaction products 12 p1929 A67-25752

Asymptotic law of propagation of plane detonation wave where perturbed motion behind wave transforms it to Chapman-Jouguet wave 18 p3026 A67-33758

Friction and heat transfer effects on nonsteady flow behind Chapman-Jouguet detonation to analyze transition to steady flow 23 p3993 A67-41744

Monograph on external burning in supersonic streams, discussing heat addition, fluid-mechanical model, use of characteristics method, Chapman-Jouguet detonation, etc 24 p4254 A67-42386

CHAPMAN-JOUGET THEORY

Chapman-Jouguet theorem for MHD detonation in shock tube blocked by stationary perfectly conducting surface, noting relation to magnetoacoustic wave 12 p1976 A67-26071

Transition of supersonic flow of combustible gas mixture to Chapman-Jouguet regime 18 p3028 A67-34214

CHAPMAN SHEAR LAYER

Reynolds number effect on base pressure

behind wedge in supersonic and hypersonic flow based on Chapman wake flow recompression model 23 p3930 A67-41308

CHAR

Char generation and determination of thermal conductivity function under simulated entry heating conditions [AIAA PAPER 65-640] 03 p0534 A67-13060

Transient behavior of charring ablator under various thermal environments by finite difference method 04 p0723 A67-14847

Visible and near IR spectral reflectance and emittance at high temperature of ablation chars, carbon and graphite [AIAA PAPER 67-326] 12 p2037 A67-26040

Reflectance of pyrolytic graphite and phenolic nylon chars for radiant heat rejection from nonablating heat shield 15 p2579 A67-29434

CHARACTER RECOGNITION

Holographic applications, examining character identification, imaging technique and interferometric techniques 09 p1501 A67-22555

System using holography for character recognition according to Gabor proposals 13 p2118 A67-26258

High speed methods of frame scanning in character output element with character point shaping on CRT screen 17 p2822 A67-33100

CHARACTERISTIC EQUATION

Stability and sensitivity requirements considered simultaneously in control system design, minimizing time domain sensitivity index and incorporating transient response characteristics 01 p0047 A67-11217

Accuracy of DC amplifiers solving linear differential equations with constant coefficients, examining effect of drift and grid currents 01 p0031 A67-11264

Commuting inverses of singular square matrix A existing only if dimension of A null space equals multiplicity of zero root in characteristic equation 03 p0460 A67-13938

Stability of control systems with distributed parameters and hysteresis-curve-type nonlinearity for various critical cases of system characteristic equation 05 p0781 A67-16250

Discontinuous solutions in supersonic reacting gas flows under nonequilibrium conditions 06 p0984 A67-18112

Characteristics solution breakdown near leading frozen characteristic for piston induced flow and relaxing gas flow 06 p0984 A67-18128

Nonlinear nonsteady wave propagation in plane flow analyzed by introducing perturbations of potential into equation of gas dynamics and equation of characteristics 07 p1169 A67-19731

Missile and aircraft control systems design, discussing root locus and stability curve methods for solving characteristic equation 09 p1483 A67-22489

Dynamic vibration absorber for reducing transient vibrations of one degree of freedom system with tuning criteria formulated as function of root line of characteristic equation 10 p1715 A67-22913

Longitudinal perturbed motion of aircraft with free-floating canard, obtaining differential equation corresponding to characteristic equation 10 p1595 A67-23606

Cylindrical partially filled waveguides of rectangular cross section, formulating boundary value problem and characteristic equation 12 p1906 A67-25980

Plastic deformation mechanisms of polycrystalline beryllium to analyze temperature dependence of critical shear in prismatic plane 13 p2138 A67-27121

Two-dimensional mixed boundary value problem of heat and mass transfer with characteristic equation containing multiple roots 14 p2406 A67-28312

Supersonic gas-particle flow with chemical reactions 15 p2469 A67-29225

Extension of Vainberg method for studying nonlinear integral equations with aid of Hart theorem to cover Urysohn type equations 15 p2511 A67-29888

Supersonic internal axisymmetric conical flow obeying Taylor-Maccoll equation, discussing applications to wing surfaces and supersonic inlet leading edges 15 p2418 A67-30192

Frequency and mode configurations of natural symmetric oscillations of elastically clamped cylindrical shells solved by

characteristic equation 21 p3717 A67-37974

Stability analysis of two-dimensional nonlinear multivariable systems with nonlinearities, finding limit cycle of symmetric and antisymmetric cases from characteristic equations 23 p3984 A67-41160

Shock wave reflection with vibrational relaxation times investigated by matching characteristics equation to shock wave equation 24 p4144 A67-42564

Frequency Response and direct numerical integration of governing differential equations, considering gas-lubricated tilting-pad journal bearing stability [ASME PAPER 67-LUB-8] 24 p4182 A67-42672

CHARACTERISTIC FUNCTION

Statistical properties of estimation method for one-dimensional characteristic function of stationary ergodic random process 02 p0192 A67-11639

Characteristic function method for solving optimal control problems and sufficient conditions for existence of absolute minimum 03 p0457 A67-13183

Two-dimensional characteristic function and probability-distribution density of random process which is phase modulated by normal noise 04 p0575 A67-15161

Longitudinal conduction effect on fluid temperatures in multistream counterflow heat exchanger, based on characteristic function 04 p0728 A67-15806

Numerical analysis of constraint effects on trial function selection in variational calculus problem of pure torsional vibration of cantilever beam of thin walled open cross section 05 p0917 A67-16418

Analyzer of characteristic function of random phase of quasi-harmonic signal using statistics 06 p0972 A67-18392

Stochastic input passage through class of nonlinear systems, developing functional relations between statistical properties 08 p1308 A67-20324

System with two nonlinearities separated by high pass filter, obtaining joint describing function 11 p1760 A67-24275

Output characteristic function for two-channel analog cross correlator with each channel input consisting of deterministic signal combined with stationary Gaussian noise 12 p1916 A67-26080

Characteristic vectors theory and application to study of asymptotic behavior of solutions to differential systems 14 p2342 A67-28385

Two-dimensional characteristic function and probability-distribution density of random process which is phase modulated by normal noise 15 p2435 A67-29348

Integral equation with transfer function density restrictions defining characteristic function of Markov process functional, deriving several limit theorems 22 p3827 A67-39878

CHARACTERISTIC METHOD

Characteristics method in numerical solution of one-dimensional problems of propagation 03 p0458 A67-13348

Nonsteady flow problems, solving fluid motion equations by characteristic method and obtaining boundary conditions 03 p0403 A67-13769

Supersonic nozzle producing lift force without downward deflection analyzed by characteristics method 04 p0545 A67-14440

Numerical solution of two-dimensional quasi-linear hyperbolic systems using characteristic method, obtaining approximate equations 05 p0834 A67-16436

Characteristics method applied to one-dimensional propagation problem, considering Massau grid and using partial differential equation 06 p0990 A67-18585

Shock wave incident on unknown free boundary surface calculated in spatial method of characteristics 07 p1125 A67-19141

Compatibility relations and generalized finite difference approximation for three-dimensional steady supersonic flow 08 p1320 A67-20566

Nuclear energy deposition effect on pressure pulse generation in fissioning gas flow through semifinite cylindrical tube analyzed by method of characteristics 08 p1322 A67-21121

Reflection of spherical shock wave from concentric spherical surface, using method of characteristics starting from initial boundary value problem 10 p1623 A67-22863

Strong plane shock attenuation from impact studied with numerical method of characteristics for one-dimensional unsteady flow, showing late-stage equivalence 11 p1820 A67-24905

Nonlinear equations in gas dynamics for turbulent nonpotential flows, emphasizing geometry of characteristic surfaces and numerical calculation 12 p1931 A67-26199

Interaction of shock-induced flow in ideal gas and transverse magnetic field analyzed for steady state and transient one-dimensional effects 13 p2162 A67-26280

Unsteady ideal gas flow along moving wall treated by method of characteristics 13 p2093 A67-26635

Method of characteristics used in solving nonlinear boundary value problem of thickness of delta wing with transonic leading edge 13 p2049 A67-26646

Supersonic three-dimensional flows past smooth bodies, calculating flow parameters by characteristic method with analytical approximation of gas-dynamic functions 14 p2240 A67-27992

Introduction to method of characteristics covering propagation processes, relation to long water waves, gas flows, etc 15 p2472 A67-29677

Static and dynamic parameter estimation of nonlinear transfer elements from step responses 15 p2463 A67-30331

Characteristics identifying method required for number of multiplications to be proportional to number of inputs 15 p2464 A67-30341

Supersonic jet expelled from plane nozzle solved by characteristic method to determine family of rarefaction waves and nozzles 16 p2656 A67-30455

Linearized theory for unsteady flow about bodies of revolution in sonic stream 16 p2589 A67-30790

Types of closed characteristics in bounded region of two-dimensional autonomous differential equation systems 16 p2695 A67-30856

Multidimensional unsteady flow field of inviscid fluid calculated with application of method of characteristics and digital computer 16 p2662 A67-31535

Transonic blade cascades determined by mixed analog-numerical method starting from velocity distribution law and hodograph method 16 p2594 A67-31710

Axiallysymmetric response of semilfinite truncated cone striking smooth rigid obstacle, determining early stages of motion 17 p2960 A67-32422

Shock wave incident on unknown free boundary surface calculated in spatial method of characteristics 17 p2840 A67-33213

Free jet plume expanding into vacuum investigated experimentally, comparing with ideal gas characteristics method results 18 p3152 A67-33818

Three-dimensional hypersonic flow past blunt cones calculated by modified method of characteristics, taking into account physicochemical equilibrium conversions 18 p2984 A67-34213

Dynamic stability analysis of bodies of revolution in supersonic flow, using characteristics method [AIAA PAPER 67-607] 19 p3172 A67-35998

Incompressible cylindrical jet interaction with incompressible unbounded homogeneous stream, determining contact surface 20 p3360 A67-37661

Thermoelastic coupling effect on propagating discontinuities in stresses and particle velocities studied using characteristic method 21 p3715 A67-37893

Characteristic method for determining stress field and plastic deformation mechanism during cutting, notching and punching processes 21 p3632 A67-38060

Axial shear wave radial propagation in nonhomogeneous elastic medium under axisymmetric loading solved by Laplace transform and characteristics method 21 p3719 A67-38146

Characteristics method to determine radiative energy losses of supersonic gas flows past blunt cones 21 p3564 A67-38424

Set of states reachable in given time in control problem determined by heuristic and rigorous methods 21 p3603 A67-38441

Characteristic method computer program for calculating three-dimensional supersonic flow around blunt and pointed bodies of

revolution in reasonable time 21 p3566 A67-38887

Elastic wave problems involving one space variable solved by hyperbolic partial differential equations 23 p4072 A67-40610

CHARACTERISTICS

S AERODYNAMIC CHARACTERISTICS

S AIRFOIL CHARACTERISTICS

S FLIGHT CHARACTERISTICS

S FLOW CHARACTERISTICS

S PERFORMANCE CHARACTERISTICS

S POLARIZATION CHARACTERISTICS

S VOLT-AMPERE CHARACTERISTICS

CHARCOAL

Temperature control and thermal coupling of cesium adsorption porous tungsten, charcoal and graphite reservoirs 09 p1450 A67-22350

CHARGE

SA ELECTROSTATIC CHARGING

SA EXPLOSIVE

SA ION CHARGE

SA SHAPED CHARGE

SA SPACE CHARGE

SA TRAVELING CHARGE

Charge collection velocity in semiconductor particle energy detector expressed in terms of electron and hole motion and induced charges 01 p0065 A67-10650

Electromagnetic field of accelerating charge using Coulomb law, relativity transformation relations, charge conservation, Newton third law, etc 03 p0469 A67-13719

Charge forming in cadmium sulfide crystals under effect of applied electric field 05 p0868 A67-17065

Charge forming in cadmium sulfide crystals under effect of applied electric field 15 p2538 A67-29796

CHARGE DISTRIBUTION

Charge ratio of cosmic ray muons determined by particle collection in small and wide angular ranges about vertical 01 p0144 A67-10783

Agema Gemini electric charge monitor measures static charge difference between orbiting space vehicles 01 p0074 A67-11128

Charge composition of cosmic radiation, noting results for charges $1/3$ e and $2/3$ e, experimental setup, etc 02 p0306 A67-11500

Steady state charge distribution on surface of spaceship and in plasma beam emanating from ion engine under conditions of slight decomposition 02 p0302 A67-11549

Electronic interactions in silicon-silicon dioxide system lead to various distributions of electric charges 02 p0293 A67-11752

Thermoelectric current effect on stability of electric current and charge distribution in semiconductors 03 p0489 A67-13144

Positive-to-negative charge ratio of high energy cosmic ray muons 03 p0506 A67-13516

Surface charge distribution effect on stability of conducting fluid in presence of magnetic field 03 p0481 A67-13731

Environmental wind tunnel investigation of wind velocity and discharge current effects on average charge per Trichel pulse in corona discharges 03 p0486 A67-14119

Field and charge density distributions in semiconductor with hot electrons, showing domain movement type oscillations due to stationary wave propagation 04 p0680 A67-15286

Approximation method for molecular integrals that depends on replacement of two-center charge distributions by single-center distributions, giving results in terms of Coulomb type integrals 04 p0566 A67-15547

Orientation dependence of surface charge on anodized indium antimonide from MOS capacitance measurements 05 p0869 A67-17093

Atmospheric charge density measurement by Faraday cage and Obolensky filter 05 p0803 A67-17384

Field and charge distribution in hot electron semiconductor, discussing drift and recombination nonlinearity 06 p1066 A67-18960

Nonequilibrium ionization of gas-solid suspension expanding supersonically in nozzle as function of charge distribution 07 p1227 A67-20258

Pinching of surface carriers toward center of semiconductor produced by current induced magnetic field 08 p1371 A67-21439

Continuous charge distribution with time oriented streamlines in Minkowski space-time 09 p1534 A67-22579

Thermoelectric current effect on stability of electric current and charge distribution in semiconductors 10 p1689 A67-23094

Thermal plasma measurements in magnetosphere for electron and ion density and thermal profiles, noting Maxwell energy distribution and charge neutrality 10 p1649 A67-23295

Molecular orbital electron charge density pictures, noting representation close to Hartree-Fock calculation 10 p1682 A67-23379

Three-axis ellipsoid elastostatic problem solved through analogy with equivalent electrostatic problem of charge distribution 12 p2029 A67-25665

High density one-component plasma radial distribution determination by Born-Green-Yvon Integral 13 p2162 A67-26282

Monopole motion in magnetic dipole field, comparing electric and magnetic cases 14 p2378 A67-27920

Geomagnetic field analytical representation, giving equations for moments and distribution of equivalent set of dipoles 14 p2309 A67-27948

Electrically active centers distribution in Zn and Te implantations into GaAs 15 p2536 A67-29495

Charge curves for germanium and silicon surface obtained by field effect measurements, noting nature and mechanism of effect 15 p2542 A67-30249

Surface charge density of MOS as affected by bias and temperature treatment 16 p2724 A67-30602

Plasma-particle distribution function in infinite system of alternating positive and negative electrodes, evaluating high-velocity neutron source effectiveness 16 p2718 A67-31193

Steady state charge distribution on surface of spaceship and in plasma beam emanating from ion engine under conditions of slight decomposition 16 p2736 A67-31615

Ignition conditions of pore walls in burning of porous charge, assuming ideal pores and same charge composition throughout system 17 p2974 A67-33142

Electron bunching in sweep klystron, deriving electric field equation, motion equations and continuity criteria for arbitrary charge density distribution 18 p3010 A67-33501

Glow-broadening rate dependence on initial pressure and discharge voltage in shock tube containing hydrogen plasma, studying charge distribution variations 20 p3501 A67-37145

Circular planar satellite electrostatic probe theory based on reversible particle trajectories, showing relation between boundary curve in velocity space and current-voltage characteristics 21 p3625 A67-37899

Charge instability problems in metal-nitride-semiconductors /MNS/ solved by using thin silicon dioxide layer between silicon nitride film and substrate 21 p3678 A67-38151

Conditioned distribution functions from BBGKY hierarchy distribution functions, with analogy to hydrodynamic approximation of Boltzmann distribution 21 p3675 A67-38931

BBGKY hierarchy description of plasmas, with application to ionized particle charge distribution in external electric field 21 p3675 A67-38932

Charge model for unsaturated and saturated p-n-p-n dynamic behavior using numerical integration techniques 22 p3766 A67-39249

Cold Cu electrode interaction with H plasma, measuring electrode I-V characteristics, interelectrode charge concentration, electron temperature, etc 22 p3846 A67-39505

Capture, ionization and ionization capture in collisions of protons with argon atoms 23 p4030 A67-41687

Electron emission models for evaluation of charge distribution and total energy of metal-gas interface, noting role of quantum mechanical corrections 24 p4202 A67-42087

Upper limits of fractional charge content of cosmic radiation 24 p4210 A67-42600

CHARGE EXCHANGE

SA RESONANCE CHARGE EXCHANGE

Angular and energy characteristics of proton beam in pulsed magnetic field, determining probability of proton-neutron

charge exchange for proton in forward flight 02 p0271 A67-12753
 Instability effect in n-channel silicon MOS transistors bombarded with ionizing radiation 04 p0589 A67-15716
 Energy and angular distributions of neutral atoms and charge-exchange ions from mercury electron bombardment thruster, determining particle effluxes [AIAA PAPER 87-82] 06 p1075 A67-18498
 Ion extractor system for electrostatic thrusters designed, using salient features of digital computer and electrolytic tank analog methods 06 p1075 A67-18877
 Limiting daytime flux of ionization into protonosphere, obtaining expression for maximum upward flux supported by diffusion 07 p1180 A67-19918
 Charge exchange of protons in alkali metal vapors with formation of highly excited hydrogen atoms, noting cross section, reaction mechanism, etc 08 p1358 A67-20855
 Charge exchange cross sections measurements for ion-molecule pairs of hydrogen, argon, krypton, helium and xenon 09 p1535 A67-22381
 Charge exchange method for production of molecular beams, noting production of plasma by RF discharge and ion beam generation 14 p2316 A67-28190
 Temperature dependence of properties of acceptor center in iron doped gallium arsenide, noting delocalization of cluster electron density 16 p2726 A67-30814
 Yield variation of excited hydrogen atoms formed by charge exchange with gas target thickness described by analytical model 16 p2714 A67-30874
 Algebra of factorized Regge pole residues applied to obtain relations between meson-baryon and baryon-baryon exchange processes 16 p2705 A67-31627
 Ion-molecule reactions in propane studied using mass and energy resolved ion beams in tandem mass spectrometer 17 p2810 A67-33264
 Low energy, positive ion flux from inner radiation zone, noting losses due to charge exchange, night sky emissions and lifetimes 21 p3697 A67-37996
 Mass spectrometric method for measuring double charge exchange cross sections of low energy positive ions, investigating current distribution 22 p3797 A67-39427
 Degree of ionization effect on yield of excited atoms from gas target 22 p3852 A67-39987
 Angular and energy characteristics of proton beam in pulsed magnetic field, determining probability of proton-neutron charge exchange for proton in forward flight 22 p3842 A67-40255

CHARGE SEPARATION

Radio pulse coincidence with extensive air showers, noting consistency with Cerenkov radiation and charge separation in terrestrial magnetic field 07 p1242 A67-19619
 Charge separation mechanism of auroral electrojets, noting enhanced ionospheric conductivity by electron bombardment 07 p1245 A67-19931
 Radio emission from cosmic ray showers analyzed at Jodrell Bank, determining effects of geomagnetic field and charge separation 10 p1703 A67-23490
 Charge separation effects in Ferraro-Rosenbluth cold plasma sheath model, using relativistic treatment 11 p1825 A67-23869
 Atomic collisions with negative ions, deriving transition matrices for resonance reactions and scatterings to analyze rearrangement process of associative electron detachment 14 p2350 A67-28149
 Acoustic wave mode in weakly ionized gas analyzed, noting charge separation and electroacoustic effects 17 p2909 A67-33230
 Atmospheric electric field as possible cause of radio pulses from extensive air showers 19 p3316 A67-35803

CHARGE TRANSFER

Shifts in normal state conductivity and superconducting transition temperature due to charge carrier changes in In, Tl and Sn films 02 p0291 A67-11741
 Electron conduction in discontinuous metal films by transport of activated charge carrier creation and by tunneling for island sizes 02 p0292 A67-11746
 LCAO MO calculation of charge carrier mobility in hydrogen phthalocyanine 03 p0495 A67-13525

Cross sections for charge transfer between alkali-metal ions and cesium atoms determined as function of primary ion beam energy, noting structure consisting of oscillations 04 p0661 A67-15766
 Charge transfer energies of pyromellitic dianhydride and mellitic trianhydride with aromatic hydrocarbon donors 04 p0567 A67-15952
 Generalized charge control theory derivation of transfer function of nonparametric transistor amplifier in system with common emitter 05 p0769 A67-16168
 Molecular nitrogen ion emission in twilight, discussing intensities, rotational distribution, charge transfer zenith measurement and ion-atom interchange reaction 05 p0803 A67-17409
 Charge transport equations used to determine transient waveforms of FET as function of gate current and drain current 07 p1153 A67-19614
 Photoionization mass spectrometer for charge transfer reaction analysis 07 p1137 A67-20188
 Emission occurring when mixing molecular nitrogen with helium ion following charge transfer analyzed spectroscopically 08 p1326 A67-21358
 Positive charge drift induced by hydrogen heating in silicon dioxide film on MOS transistor 09 p1552 A67-21763
 Spatial distribution of electrons and ions in neutral plasma, considering charge density 09 p1548 A67-22352
 Propagation of bounded domain with strong electric field in semiconductor with negative differential conductivity 09 p1557 A67-22558
 Radiative recombination processes in GaAs p-n junctions, noting correlation between temperature behavior and carrier transport mechanism 10 p1693 A67-23523
 Phase shift as quantitative measure of relationship between surface convection and charge relaxation 11 p1825 A67-23862
 Charge ratios of recovery abruptness and figure of merit in switching diode with base field 11 p1765 A67-24470
 Amplitude and phase frequency characteristics of linear system determined from transfer characteristics 11 p1772 A67-24980
 Ion motion under influence of electric field and density gradient with charge transfer collision between ions and neutral gas background 13 p2162 A67-26269
 Charge motion on outer silicon oxide surface of MOS structure, estimating surface resistance and dependency on humidity and other factors 13 p2176 A67-26707
 Structure of electrostatic charge transported by pulsed plasma flow produced by coaxial source 13 p2168 A67-27306
 Charge transfer prediction by classical binary-encounter theory approximation and quantum mechanical approximation 15 p2519 A67-29331
 Field effect transistor intrinsic and extrinsic transients, switching behavior and relation to time constant by charge concept 15 p2449 A67-29806
 Asymmetric proton injection into magnetosphere using Vlasov equation, with solution in terms of electric potential 16 p2666 A67-31403
 MHD behavior of inviscid fluid in limit of infinite electrical conductivity and mobility exhibiting Hall effect 17 p2908 A67-33109
 Negative oxygen ion reaction rate constants for ion loss processes in ionospheric D region obtained by laboratory measurement 17 p2851 A67-33195
 Ionizing and charge transfer processes following heavy particle collisions in ionized gas analyzed using spectroscopic technique 19 p3264 A67-35069
 Charge transfer role in formation and maintenance of molecular and metal-ion layer in E region of ionosphere 19 p3217 A67-35204
 Luminescence from ruthenium complexes, investigating charge-transfer absorption bands 19 p3181 A67-35880
 Organic phosphate shown as inhibitory factor from B. stearothermophilus for attachment of amino acids to transfer RNA 20 p3370 A67-36798
 Cross section measurement for charge transfer reactions, using crossed ion and neutral beam configuration and product ion

mass analysis in nitrogen dioxide production 20 p3377 A67-37404
 Charge compensation defects influence on UV excitation spectrum of rare earth doped crystals fluorescence 22 p3856 A67-39384
 Reflectivity spectra of YIG and YGG crystals, observing YTG structure attributed to charge transfer enhanced crystal field transitions reflectivity spectra of YIG and YGG crystals, observing YIG structure attributed to charge 22 p3863 A67-40238
 Excitation effect on single electron charge transfer collisions of Fe ions in various gases determined with different excited states of ions 23 p4030 A67-40976
 Solid state electrochemical solar cell using various anode metals and charge transfer complexes as cathodes, noting I-V characteristics and discharge curves [JPL-TR-32-1116] 24 p4097 A67-41804
 Poly-N-vinyl carbazole-iodine charge transfer photovoltaic effect spectral and intensity dependence, noting possible radiation detection and energy conversion applications [JPL-TR-32-1138] 24 p4201 A67-41899
 Hall effect, resistivity, spin resonance and thermoelectric properties of poly(N-vinyl carbazole-iodine) complex, demonstrating charge transfer state existence in system [JPL-TR-32-1074] 24 p4205 A67-42602

CHARGED PARTICLE

SA ALPHA RADIATION
 SA BETA RADIATION
 SA COULOMB POTENTIAL
 SA CYCLOTRON RESONANCE
 SA DEUTERON
 SA ELECTRON
 SA ION
 SA MESON
 SA NUCLEAR PARTICLE
 SA PARTICLE CHARGING
 SA PARTICLE TRAJECTORY
 SA POSITRON
 SA PROTON
 SA QUARK

Charged particle motion in field of traveling electromagnet waves used in studies for microwave amplifiers, particle accelerators, etc 01 p0022 A67-10352
 Charged particle traps installed in Luna X providing evidence for moon passing through tail of earth magnetosphere, noting effect of solar wind 01 p0145 A67-10908
 Electric field radial intensity distribution and charged particle density for positive plasma column between coaxial cylinders 01 p0125 A67-10924
 Logarithmic dependence of energy losses on relativistic particle velocities in polystyrene films 01 p0125 A67-10926
 Phenomenological approach to dispersion relation for hose instability of charged particle beam passing through plasma 02 p0272 A67-11525
 Integral intensity of charged particles diffusing through drift shells in earth magnetosphere with specific example for protons 02 p0306 A67-11550
 Analog computer ionization recombination parameters and balance equation of charged particles in F-2 layer 02 p0236 A67-11659
 System of equations derived governing behavior of ideal relativistic charged fluid by means of variational principle, through introduction of generalized Clebsch transform 02 p0273 A67-12195
 Charged particle solid state detectors, considering neutron intensity and energy and spectral and/or dose measurements 02 p0244 A67-12210
 Surface barrier diffused-junction lithium-compensated silicon and lithium-compensated germanium particle detectors for aerospace application 02 p0245 A67-12212
 Distribution of charged particles of different energies escaping from magnetic trap in which spiral moving electron fluxes are created 02 p0274 A67-12459
 Diagnostic measurement techniques for statistical properties of ionized particles of equilibrium turbulent plasma, using electrostatic probe and high resolution microwave probe 02 p0275 A67-12550
 Low energy charged particle measurements, describing satellite mounted spherical electrostatic analyzer 02 p0310 A67-12571
 Flux measurement of particles with charges of one-third and two-thirds electron charge, reaching sea level with relativistic

- velocities 02 p0313 A67-12636
- Perturbation of electron density at large distances from body at high velocity in collisionless plasma under steady external magnetic field 03 p0475 A67-12939
- Charged particle motions calculated in model of earth magnetosphere including magnetic and electric field 03 p0410 A67-12953
- Survey in satellite era of energetic particle radiations, plasmas and magnetic fields in space including solar wind, solar cosmic rays, etc 03 p0506 A67-13050
- Fluctuations and broadening of energy-loss spectrum of charged particles passing through semiconductor detectors 03 p0491 A67-13224
- Motion of charged particles in constant electromagnetic fields, noting effect of drift motion 03 p0481 A67-13737
- Formula for second order correction factor derived for special case of static magnetic field with axial symmetry 03 p0484 A67-14040
- Magnetic field geometric properties effect on magnetic moment and adiabatic invariants of charged particle motion 03 p0484 A67-14041
- Existence of exact solution to motion equations for charged particles in acute angled magnetic trap 03 p0486 A67-14064
- Luna X lunar-orbiter satellite observations of charged particles in lunar ionosphere, using magnetic trap 03 p0513 A67-14066
- Charged particle motion in random magnetic field, describing time evolution of particle distribution in pitch angle and position in terms of Fokker-Planck coefficients 03 p0508 A67-14317
- Charged particle collision as UV radiation source examined, using electron-excitation analytic cross section equations 04 p0660 A67-14698
- Solar radiation effect on planetary atmosphere noting charged particle bombardment, dayglow phenomena, auroral emission, etc 04 p0696 A67-14699
- Charged particle redistribution due to rockets and satellites flying in ionosphere influence on electromagnetic propagation in region of body and interpretation of Langmuir probe 04 p0664 A67-14990
- Moving and stationary fluid type facilities to simulate aerodynamics of charged particles in ionosphere 04 p0595 A67-14991
- Electric drag of satellites noting contribution of impinging ions 04 p0705 A67-14998
- Charged colloidal heavy particle propulsion and production of heavy particles 04 p0689 A67-15016
- Charged gas expansion with particle production, noting parameters and applicability to cosmological model of Hoyle 04 p0606 A67-15185
- Plasma injected into magnetic trap with aid of conical theta pinch investigated to determine ion and electron energy, lifetime and charged particle concentration variation 04 p0668 A67-15279
- Charged particle distribution in hollow cylinder shaped positive plasma column during diffusion and helical instability in longitudinal magnetic field 04 p0668 A67-15281
- Thermal radiative property behavior of materials under elementary charged particle bombardment, determining effect of combined UV plus electron exposure and low energy proton bombardment 04 p0686 A67-15873
- Explosive driven magnetic generator applied to investigate electric, optical and elastic properties of various substances, plasma physics and charged particle accelerator 05 p0786 A67-16365
- Ionospheric charged particle density measurements during IQSY by sounding rocket 05 p0798 A67-16860
- Solar charged particles acceleration and propagation through interplanetary space, galactic cosmic ray origin, radiation belt structure, etc, analyzed from space data 05 p0883 A67-16877
- Cosmic radiation directional intensity during solar activity minimum, noting altitude dependence of charged particle photon flux 05 p0883 A67-16878
- Extrasolar X-ray observation regarded as astronomy in contrast to cosmic ray observation which is considered as local geophysical phenomena 05 p0884 A67-16881
- Quasi-neutral charged particle bunches kinematics in flat electrode plasma accelerator 05 p0855 A67-16996
- Charged particle distribution in wake of fast moving body in rarefied plasma 05 p0855 A67-17123
- Charged particle collisions effect on drift instability of low pressure plasma studied, using Landau collision integral as model collision integral 05 p0860 A67-17546
- Electron temperatures and concentrations of charged particles behind strong shock wave in air measured noting techniques, maximal values and accuracy 06 p0983 A67-17878
- Linear nonrelativistic motion of charged particle in field of traveling electromagnetic wave 06 p0975 A67-18087
- Charged particle beam interaction with plasma, determining electron-ion temperatures and HF field 06 p1040 A67-18088
- Charged particle excitation by random electromagnetic field, obtaining velocity distribution function via all-order perturbation method 06 p1040 A67-18102
- Magnetic field effect on space charge neutralization in thin beam approximation [AIAA PAPER 67-83] 06 p1041 A67-18275
- Electron-neutral particle collision and electron thermal conductivity effect on upper atmospheric electron and ion temperatures 06 p0998 A67-18702
- Forced motion of charged particle in magnetic field 06 p1045 A67-18743
- Charged particle motion in magnetic field under action of laser emission 06 p1012 A67-18787
- Charged particles motion in magnetic field with regular and random components, deriving kinetic equation for distribution function and then diffusion equation 06 p1037 A67-18800
- Charged and neutral particles collision effect on LF oscillations in weakly ionized plasma in crossed electric and magnetic fields 06 p1046 A67-18827
- Charged particles for lasing, discussing manufacture of argon laser 07 p1194 A67-19083
- Origin of fossil charged particle tracks in meteorites such as cosmic radiation, fission of U 238, meson jets, spallation recoils, etc 07 p1245 A67-19941
- Tracks of primary cosmic rays with atomic number greater than or equal to 20 in meteorites, discussing relationship between track length and particle mass 07 p1245 A67-19942
- First order correction to magnetic moment invariant in Van Allen radiation belt 07 p1246 A67-19955
- Emission of electrically charged and film producing particles from sputter ion pumps, describing experimental facility and two methods for examination 07 p1190 A67-20283
- Energy loss of charged particles during passage through weakly turbulent plasma in magnetic field with HF oscillations 08 p1357 A67-20844
- Plasma spectrography in shock tube, determining charged particle concentration 08 p1358 A67-20853
- Proton I and II satellite instrumentation noting energy-charge spectrometer, gamma-quantum fluxmeter, equipment to determine chemical composition of charged cosmic ray particles, etc 08 p1376 A67-21001
- Data correlation on nonadiabatic behavior of individual charged particles in magnetic fields 08 p1362 A67-21150
- Infinite magnetic quadrupole channel, discussing operations in complete transverse plane phase space via 4×4 matrix transformations 08 p1332 A67-21172
- Differential energy spectra and fluxes of charged splash and reentrant albedo proton measurement of cosmic radiation in various energy ranges 08 p1377 A67-21467
- Explorer XII observations of charged particles in inner radiation zone after solar activity maximum and before Star Fish explosion 08 p1378 A67-21471
- Free charged particles interaction with each other and neutral atoms in highly excited states effect on thermodynamic and gas dynamic parameters of shock wave propagating in cesium vapor, taking into account energy losses due to radiation 09 p1540 A67-21791
- Concentration waves excited by internal modulation of charged particle concentrations in cross section of plasma flow analyzed for various velocities of flow 09 p1544 A67-21851
- Average diffusion coefficient and apparent effective charges of components of alloys of Ti-S system 09 p1553 A67-21906
- Relativistic theory for interaction of electric point charge and magnetic dipole 09 p1580 A67-22549
- Magnetic moment variations of charge in combination static magnetic and HF field 10 p1683 A67-22843
- Subsonic parachute-borne blunt probes for charged particle measurement in ionosphere 10 p1645 A67-23260
- Vertical drift of charged particles effect on electron density profile as cause of seasonal variations in ionospheric absorption 10 p1646 A67-23269
- Role of corpuscular radiation in lower ionosphere formation noting charged particle flux, energy spectra, etc 10 p1647 A67-23283
- Proton spectra and spatial distribution of energy protons on magnetic shells in earth radiation belts, using satellite data 10 p1702 A67-23300
- First and second adiabatic invariants of charged particle motion in calculating trajectory in combined electric-magnetic field 10 p1651 A67-23395
- Vlasov equation for stationary distribution function of charged particles in plasma and self-consistent solution of Maxwell equations 10 p1685 A67-23463
- First integrals of motion to determine stationary distribution function of charged particles and self-consistent magnetic field of plasma 10 p1685 A67-23464
- Monochromatic longitudinal wave amplification by charged particle beam in nonlinear plasma, noting amplitude dependence on coordinate 10 p1686 A67-23587
- Focusing of charged particles with pair of concentric spherical grids 10 p1658 A67-23784
- Charged particle motion in static magnetic fields without axial symmetry derived, employing Lagrange equation in transformed coordinate system and Alfvén motion 11 p1855 A67-23929
- Classical equation of motion of extended monopole charged particle without preacceleration or runaway solutions 11 p1821 A67-23977
- Van Allen belt proton measurements by pulse height analysis, using thin low-Z scintillator to minimize large angle electron scattering 11 p1856 A67-24014
- Stormer method solution of charged particle motion in field of magnetic dipole situated in external uniform magnetic field antiparallel to dipole magnetic moment vector 11 p1856 A67-24069
- Charge particle flux in earth radiation belt as observed by Cosmos XVII 11 p1856 A67-24074
- Measurement of quark flux with $2/3$ charge of electron reaching sea level with relativistic velocities 11 p1823 A67-24598
- Ionic waves in plasma in electric field interacting with beam of charged particles at relaxation time, using dispersion equation 11 p1841 A67-24869
- Asymptotic Krylov-Bogolubov computation of moving charges interacting with space modulated magnetic fields 11 p1842 A67-24967
- Charged particle motion in field of traveling electromagnetic waves used in studies for microwave amplifiers, particle accelerators, etc 11 p1755 A67-25025
- Nonequilibrium process in one dimension in presence of constant and oscillating electric field, using distribution function 11 p1824 A67-25078
- Collective effects and centrifugal instability from charged solar wind particle injected into earth magnetosphere near neutral point 12 p1991 A67-25109
- Charged particle motion in magnetosphere under sudden magnetic pulse, compiling Fokker-Planck equation for particle distribution function 12 p1992 A67-25118
- Magnetosphere phenomena investigated via atmosphere model to explain planetary nebulas and eruptive solar prominences 12 p1992 A67-25119
- Energetic molecular hydrogen ions injected into resonant nonadiabatic magnetic mirror trap, studying particle mean lifetime,

- noting cold plasma stabilizing effect 12 p1969 A67-25248
- Energetic macroscopic particle production noting possible application in controlled thermonuclear power 12 p1966 A67-25252
- Transfer coefficients of charged particles trapped in magnetic field of earth, examining concept of sudden pulses as basic mechanism 12 p1994 A67-25541
- Charged particle motion and penetration of magnetosphere in proximity of neutral point as result of solar wind-geomagnetic field interaction 12 p1975 A67-25643
- Charged particle motion in field of magnetic dipole situated in external magnetic field /magnetospheric G region/, using Stoermer method 12 p1994 A67-25644
- Cross sections for sticking electrons to spherical charged particles, considering Debye screening distance of Coulomb force field 12 p1968 A67-25750
- Elektron II satellite charged particle flux measurements at distances up to 11.6 earth radii, using three-electrode charged particle trap 12 p1998 A67-25817
- Digitized spark chamber for gamma ray and charged particle experiments on balloons and satellites noting construction, performance characteristics and results 12 p1944 A67-25854
- Radial electric field role in electrofluid dynamic conversion of flowing gas energy into electric energy 12 p1901 A67-25933
- Alpha particle spectral analysis in various lithium compounds 13 p2159 A67-26435
- Electron transfer to multiply charged ions of various gases, noting scattering characteristics 13 p2167 A67-26989
- Energy of system of particles defined as related to active gravitational mass, or to inertial mass and passive gravitational mass respectively, in expanding universe 13 p2199 A67-27004
- Interplanetary particle diffusion model analysis in terms of energy, position in space, direction and time 13 p2193 A67-27250
- Electrostatic polarization of cylindrical plasma layer in external static magnetic field, discussing transverse charged particle drift in crossed fields 13 p2168 A67-27305
- Critical particle velocity and particles frozen in given point of magnetic field line, discussing effects of plasma compression and reflection levels 13 p2204 A67-27432
- Existence of exact solution to motion equations for charged particles in acute angled magnetic trap 13 p2172 A67-27717
- Integrals of motion-equations for charged particles in axisymmetric magnetic field derived using perturbation theory 14 p2353 A67-27752
- Line element describing gravitational field of charged particle embedded in expanding universe 14 p2336 A67-27892
- Spectrum, intensity, and charge composition of primary cosmic radiation and relevance to origin and propagation of galactic radiation 14 p2379 A67-27963
- Lack of Cerenkov emission in isotropic plasma, presenting fast electron beam experiment for verification of theory 14 p2357 A67-28204
- Self-consistent distribution theory of charged particles and electric potential in wake of conducting body moving rapidly in rarefied plasma 14 p2357 A67-28208
- Plasma-vehicle interaction, discussing charged particle motion about small vehicle in ionospheric orbit 14 p2357 A67-28209
- 198 Au isotope diffusion in n-type indium arsenide at different temperatures 14 p2368 A67-28537
- Electrode shape design for cylindrical charged-particle beam formation 14 p2320 A67-28650
- Transmission energy characteristics of spherical plate electrostatic analyzers from external sources of electrons and protons 14 p2320 A67-28746
- Origin of ultrarelativistic cosmic ray particles 14 p2382 A67-29028
- General resistive instabilities of self-pinch cylindrical symmetric beam of charged particles passing through ohmic plasma channel 15 p2522 A67-29198
- Plasmoid collisions in axisymmetric magnetic field studied spectrographically for energy density, radiative power, charged particle density, etc 15 p2525 A67-29248
- Plasmoid structure, analyzing interdependence of plasmoid parameters along length 15 p2526 A67-29256
- Quark fractional electronic charge in cosmic radiation determined through pulse height distribution 15 p2549 A67-29526
- Primary cosmic radiation and interaction in atmosphere studied during minimum solar activity by balloon flights to determine effect of latitude on secondary photons 15 p2550 A67-29533
- Spark chambers and scintillation counters used to search for fractionally charged particles in cosmic rays near sea level 15 p2550 A67-29680
- Radiation by charged particle moving in spiral line between two adjacent dielectric surfaces, deriving equations for spectral density of radiation components 15 p2520 A67-29714
- Stationary concentration of charged particles in plasma created by uniform and nonuniform SHF magnetic field in electron-cyclotron resonance state 15 p2529 A67-29716
- Emissive power of air measured by determining charged particle distribution behind spark discharge generating shock wave in plasma 15 p2530 A67-29861
- Plasma spectrum, discussing electromagnetic oscillation damping on boundary of two media with different electrical properties 15 p2531 A67-30073
- Field-aligned irregularities caused by low energy charged particles penetrating to F layer heights [AGARDOGRAPH 95] 15 p2484 A67-30304
- Motion of particles trapped in magnetic field, discussing conditions leading to spiral family of trajectory curves 15 p2551 A67-30397
- Kinetic equation for electron, ion and atom concentrations for Coulomb plasma taking into account inelastic processes 16 p2715 A67-31040
- Analog computer ionization recombination parameters and balance equation of charged particles in F-2 layer 16 p2665 A67-31074
- Collection of papers on charged particles interaction with plasma, including gas discharge and plasma acceleration 16 p2716 A67-31175
- Charged particle beam passage through plasma, detailing excitation of one-dimensional oscillation expanding perpendicularly to boundary of semilinear plasma 16 p2716 A67-31176
- Nonlinear dependence of phase velocity on wave amplitude during electromagnetic propagation in plasma waveguide, describing test apparatus 16 p2718 A67-31191
- One-dimensional charged particle flow in bounded system, particularly overlapping steady state zero-temperature flow approximation solutions, noting instabilities 16 p2704 A67-31233
- Approximate solutions of spatial distributions of charged particles as gas discharge plasma obtained by two-point Jacobi expansion method 16 p2720 A67-31241
- Integral intensity of charged particles diffusing through drift shells in earth magnetosphere with specific example for protons 16 p2740 A67-31616
- Two-dimensional motion of charged particles in electromagnetic field, noting magnitude of forbidden band as function of particle energy 16 p2740 A67-31885
- Spectroscopic measurements of cold plasma charged particle concentrations, specifically spectral broadening due to Stark effect, forbidden-line intensities affected by internal electric fields and autoionization line intensities 17 p2896 A67-32161
- Electrical field distribution during injection of charged particles into two-dimensional model of magnetosphere 17 p2841 A67-32244
- Spectrometric system aboard Proton type satellite for analyzing energy and charge spectra of primary cosmic ray particles 17 p2854 A67-32245
- Spectrometers onboard satellite, studying cosmic ray particle energy spectra and chemical composition 17 p2935 A67-32248
- Energy spectrum of cosmic ray nuclei in helium through scandium range studied with Proton I and II satellites 17 p2935 A67-32249
- Ionization fluctuations due to interaction between shower particles and absorbing component of ionization calorimeter and effect on accuracy of energy measurement 17 p2855 A67-32250
- Charged particles with Alfvén velocities distribution in magnetosphere analyzed based on cold plasma density, emphasizing data ofOGO A 17 p2899 A67-32256
- Day and night ion concentration as height function 17 p2842 A67-32258
- Charged particle beam guiding and focusing by helical magnetic multipole field for relativistic and nonrelativistic cases 17 p2908 A67-33112
- Cosmic ray electrons energy spectrum and charge composition studies inadequacy due to insufficient statistics and electron flux contamination 17 p2938 A67-33198
- Energy dissipation by relativistic charged particle and magnetic field containing it shown to exceed initial energy 17 p2952 A67-33320
- Alternative approaches to particle solutions obeying Einstein gravitation theory 18 p3077 A67-33553
- Trajectories of auroral charged particles accelerated in geomagnetic tail computed, using fields of magnetosphere reconnection model 18 p3038 A67-33614
- Charged particle motion in magnetic field under action of laser emission 18 p3059 A67-33729
- Ionospheric and magnetospheric neutral and charged particles temperature vertical distribution, noting effects producing variations 18 p3040 A67-34033
- Charged particles motion in magnetic field with regular and random components, deriving kinetic equation for distribution function and then diffusion equation 18 p3083 A67-34419
- Closed-cycle generator using gasdynamic forces to transport charged particles against opposing electric field, noting enthalpy role 19 p3175 A67-34801
- Nonrelativistic charged particle transport in geomagnetic dipole field under effect of electromagnetic pulses obtained, using Fokker-Planck equation 19 p3313 A67-35212
- Negatively ionized ozone and diatomic oxygen concentration ratio determined from physicochemical processes for 10-60 km range 19 p3219 A67-35249
- Production of charged double pion in pi plus-proton scattering, noting isobar model failure to explain enhancement at 400 Mev 19 p3266 A67-36100
- Many-body system interaction with quasi-particle with assigned orbit, discussing applications to transport coefficient, plasma stability, etc 20 p3495 A67-36155
- Charge density modulation from plasma-beam interaction 20 p3504 A67-36157
- Switched Proton Electron Channeltron Spectrometer /SPECS/ developed for measurement of charged particles in space 20 p3443 A67-36517
- Discharge length influence on reflex discharge characteristics, considering conditions for charged particles extraction from discharge 20 p3498 A67-36686
- Bargmann-Wigner and Dirac formulations for field of spin 1/2 shown equivalent provided auxiliary field vanishes in electromagnetic interaction presence 20 p3489 A67-37090
- Exact equation of state for two-dimensional plasma of equal positive and negative charged particles interacting by Coulomb potential 20 p3501 A67-37293
- Charged particles of extraterrestrial ring current during geomagnetic storms, with Ogo 3 measurements of proton and electron differential energy spectrums 20 p3432 A67-37401
- Pi micropulsation subtypes, one related to charged particles impulsive bursts from magnetospheric tail and another related to auroral electrojet 20 p3433 A67-37414
- Low pressure gas Cerenkov detector and spectrometer coupled into charged particle telescope for cosmic ray electron spectrum measurements, discussing efficiency and instrument calibration 20 p3452 A67-37566
- Statistics and kinetic equations of plasma in opacity region taking into account relativistic effects 20 p3502 A67-37662
- Plasma production by pulsed laser irradiation of aluminum in space chamber vacuum 21 p3668 A67-38259
- Charged particle distribution in wake of fast moving body in rarefied plasma 21 p3668 A67-38466
- Semiconductor detector for information on charged particles of cosmic radiation,

studying characteristics of instrument 21 p3629 A67-38664

Charged particles generation by liquid subjected to high electric field for efficient bipolar microthruster [AIAA PAPER 67-728] 21 p3694 A67-38752

BBGKY hierarchy description of plasmas, with application to ionized particle charge distribution in external electric field 21 p3675 A67-38932

Mass flow rate, viscosity and conductivity changes effects on single needle colloid thruster

[AIAA PAPER 67-530] 21 p3696 A67-38957

Alfven two-dimensional problem extended to charged-particle motion in dipole magnetic field with electric field determining forbidden band size, shape and specular reflection points 21 p3621 A67-39015

Particle distribution in infinite charged cylinder in plasma vicinity, showing plasma screening effect on potential 21 p3675 A67-39033

Charged particle motion equation derivation in guiding center approximation in lowest order through Northrop averaging process 22 p3843 A67-39264

Magnetospheric energetic charged particles interrelations, discussing electron and proton energy spectra, particle population domains, trapped radiation and solar wind kinetic energy 22 p3870 A67-39673

Ground based atmospheric and ionospheric particle temperature measurements, examining methods and thermosphere heat sources 22 p3870 A67-39676

Temporary trapping device combining resonant perturbation and saddle point injection in Stormer potential configuration methods 22 p3849 A67-39697

Intense fluxes of charged particles associated with disturbances in interplanetary medium during 1966 22 p3871 A67-39797

Charged particle /ion/ collection rates using supersonic atmospheric sounding rocket with electrode at stagnation point, noting electric field effect 22 p3791 A67-39818

Plane electromagnetic wave reflection from ionization front, determining coefficient from finite thickness plasma layer and constant charged particle density 22 p3762 A67-40122

Standing waves in hot plasma traversed by quasi-neutral charged particle flux including numerical analysis of elongated wave occurrences 22 p3853 A67-40124

Charge spectrum of very heavy cosmic ray primaries studied from balloon observations in photographic emulsion detector for Texas atmosphere 23 p4050 A67-40676

Interaction between plasma stream and inhomogeneous field of electromagnetic wave studied for relation of plasma behavior to potential forces acting on charged particles 23 p4032 A67-40910

¹⁹⁸Au isotope diffusion in n-type indium arsenide at different temperatures 23 p4040 A67-40944

Primary cosmic rays with various charges measured for spectral energy with Cerenkov counter onboard space stations 23 p4054 A67-41093

Heavy nuclei intensity during solar cosmic ray intensity increase accompanying chromospheric flares, proposing magnetic field dynamic dissipation acceleration mechanism for charged particles 23 p4056 A67-41113

Cosmic ray acceleration mechanisms for fast particle generation under outer space conditions 23 p4057 A67-41114

Electron multiplier detection efficiency for positive ions determined as function of incoming ion energy, velocity and degree of ionization 23 p4000 A67-41219

Two-stream instability in plasma analyzed using magnetic field association with charged particle motion and boundary effects 23 p4034 A67-41450

Balloon-borne electronic system for heavy primary cosmic ray particle charge identification noting compactness, low power consumption and circuit design 23 p4009 A67-41479

Computer calculation of 1 Mev electron flux and irradiation degradation of solar cell I-V curves for charged particle environment 23 p3940 A67-41514

Neutral and charged particle trapping using waves, discussing wave attenuation from particle interaction, plasma waveguide and laser beam trapping 23 p4017 A67-41681

Electrode configurations producing various intense charged particle beams, deriving algorithm applicable to three-dimensional problems 24 p4153 A67-41928

Static electrification mechanism of particles in pseudofluidized bed in terms of causes of observed polarities of column wall and various particles 24 p4254 A67-42256

Upper limits of fractional charge content of cosmic radiation 24 p4210 A67-42600

Multiple charged particle production process mean characteristics determined for several energy levels 24 p4217 A67-42830

Charged particles zenithal angular distributions determined by photorecordings for mean energies of 60 Gev 24 p4217 A67-42831

Primary cosmic ray particle chemical composition changes, explaining active particle energy spectra discrepancies between measurements and calculation 24 p4218 A67-42840

Particle streams with greater than 1 Tev energy analyzed by Lobachevskii-Einstein velocity space images 24 p4193 A67-42857

Electron-photon shower creation probability by energetic particle, deriving recursion formulas 24 p4221 A67-42874

CHART

SA GRAPH

SA MAP

Nautical chart information extracted from hyperaltitude color photographs obtained on Gemini orbital flights IV, V and VII 01 p0059 A67-10322

Control system of ACIC augmented by 100 points, constructing corresponding contour map 02 p0319 A67-11457

Northern Hemisphere synoptic auroral charts on polar projection 02 p0238 A67-12035

General circular complex charts solution, considering case where two functions of unknown variable are arbitrary functions of variable 05 p0834 A67-16435

Sputnik III data application to plotting of total magnetic field intensity chart above U.S.S.R., using spherical harmonic analysis 12 p1933 A67-25652

Book on computer programs for structural analysis covering flow charts, computer languages, matrix inversion, etc 15 p2574 A67-29646

Utility charts for evaluation of data modulation methods 20 p3380 A67-36543

Radiation balance chart of earth atmosphere system for evaluation of radiation receivers on Nimbus II satellite 20 p3431 A67-36964

CHASSIS

Flutter of flat panels at low supersonic speeds, describing mounting which makes it possible to change tension of panel during testing at constant Mach number [ONERA-TP-487] 17 p2961 A67-32699

CHEBYSHEV APPROXIMATION

Optimal filtration of noise from useful signal based on statistical information and minimax principle 04 p0591 A67-14636

Numerical quadrature methods of Romberg, Chebyshev and Monte Carlo, noting analytic function and program for machine evaluation 09 p1468 A67-22047

Chebyshev approximation for calculating coefficients of rational function 09 p1469 A67-22053

Best Chebyshev approximation and approximation in Cartesian product space 10 p1674 A67-22966

Optimum microwave filters with even number of sections, using first order Chebyshev polynomial to obtain equivalent circuit 10 p1613 A67-23444

Chebyshev approximations of differentiable functions, giving uniqueness criterion 13 p2145 A67-26611

Novel type of interpolation derived by introducing operator B and Chebyshev spaces 13 p2148 A67-27472

Harmonic analysis to improve accuracy and reduce computation of coefficients in Chebyshev expansion 14 p2342 A67-27976

Astronomical data regarding longitude differences studied, deriving evening averages, time parameters, coefficients, etc, via Chebyshev approximation 14 p2384 A67-28075

Optimal control of dynamic systems with minimax type performance index, discussing application of proposed method of solution 17 p2829 A67-32014

Microwave direct-coupled cavity filter design using single insertion loss formula for case of Chebyshev equal-ripple characteristic 17 p2828 A67-33084

Chebyshev approximation principle applied to electronics problems, giving algorithm 19 p3201 A67-34909

Short-slit directional coupler functioning mode via boundary value problem indicating Chebyshev behavior of transfer coefficient and wideband subdivision 19 p3195 A67-35560

Successive approximation and Chebyshev uniform approximation method for solving Fredholm Integral equation 21 p3651 A67-37904

Analytic representation of absolute topography of isobaric surfaces by linear combination of arbitrary surfaces represented by Chebyshev polynomials 21 p3654 A67-38087

Synthesis of nonuniformly spaced antenna arrays using lambda functions to reduce space factor and prescribed radiation pattern 21 p3602 A67-39071

Structure of error curve when function is approximated in Chebyshev sense by polynomials 23 p4022 A67-40862

Solution of linear system of equations with singularity and stable with respect to small changes in matrix elements 23 p4023 A67-41048

CHECKOUT EQUIPMENT

SA SPACE VEHICLE CHECKOUT PROGRAM

Onboard checkout system capable of meeting requirements for advanced space missions [SAE PAPER 660461] 01 p0153 A67-10568

Self-contained semiautomatic and automatic onboard checkout systems for aircraft [SAE PAPER 660701] 01 p0010 A67-10595

Semiautomatic test equipment for airborne electronics equipment for reducing checkout time [SAE PAPER 660704] 01 p0049 A67-10597

Automatic and manual testing compared within framework of integrated testing system [SAE PAPER 660694] 01 p0050 A67-10622

Computer-controlled data system with remote checkout capability for airborne electronic system 01 p0030 A67-11030

Digital computers connected by data link transmission system for prelaunch space vehicle checkout 01 p0050 A67-11031

Automatic checkout system for factory checkout, acceptance firing and postfire checkout of Saturn S-IVB stage 03 p0395 A67-13381

IEEE Automatic Support Systems Symposium for Advanced Maintainability, Clayton, Missouri, November 1966 03 p0397 A67-14201

Future onboard checkout systems including integrated onboard checkout, in-flight maintenance, onboard checkout modes and onboard/ground checkout 03 p0398 A67-14202

Automatic checkout system based on digital instrumentation with input of two bits and variable data rate resulting from use of memory storage 03 p0398 A67-14203

Maintainability efforts in support of Acceptance Checkout Equipment/Apollo-Spacecraft /ACE-S/C/ program 03 p0398 A67-14205

Evaluation of automatic test equipment for airborne weapon systems from standpoint of effect on readiness of weapon system 03 p0399 A67-14206

Factory-to-launch sequences of checkout in Saturn/Apollo program, examining present and planned levels of automation 03 p0399 A67-14207

Compatibility of checkout systems for rockets and space vehicles, with application to Saturn V launch vehicle 03 p0399 A67-14209

Aerospace vehicle simulation concept defined, examining relation to major problem areas of checkout 03 p0399 A67-14210

Analysis and projections of space vehicle automatic checkout and launch 03 p0399 A67-14211

Onboard checkout equipment design requirements, considering hardware and software for manned spacecraft flight 03 p0399 A67-14212

Onboard test and decision-making requirements for spacecraft checkout system including computer and software, data link detail and test set detail 03 p0400 A67-14215

Compiler for general purpose automatic test system /GPATS/ using program language for automatic checkout equipment 03 p0376 A67-14222

Design and construction of mobile test plant for jet engines to avoid engine removal during control and checkout procedure 04 p0594 A67-14413

Automatic checkout and monitoring of phased array radar system 04 p0595 A67-14500

Checkout system for third stage of ELDO A program 04 p0595 A67-14534

Deterministic and quasi-deterministic methods of failure prediction in electronic systems for prevention strategy in system test or checkout program 04 p0581 A67-14879

Saturn V mobile launch facility design, discussing vertical assembly of space vehicle on launch platform, transfer to launch pad, automatic checkout and remote control of launch operation 05 p0788 A67-16616

Management of development, design, contracting, construction, checkout and acquisition in ballistic missile program 05 p0929 A67-16620

Automatic checkout equipment for prelaunch use, describing packaging technique 05 p0789 A67-17461

Digital computer simulation model implementation in prelaunch prediction of Saturn V launch vehicle system performance [AIAA PAPER 67-205] 06 p1096 A67-18344

Checkout equipment development over Titan I to III span and effect on GSE [AIAA PAPER 67-267] 07 p1166 A67-20076

Cost effectiveness of fully automatic checkout systems [AIAA PAPER 67-269] 07 p1269 A67-20078

Automatic checkout system /ACS/ and digital guidance programs for Titan III and Apollo automatic checkout system /ACS/ and digital guidance programs for Titan III and Apollo 08 p1297 A67-20632

Preflight and operational status test set /PTS/ for radiation testing of electronic equipment on military aircraft 08 p1303 A67-21059

Developments in fire detection equipment noting continuous wire, armored wire and surveillance detectors 09 p1439 A67-21704

UK-3 satellite electrical design and ground checkout equipment 09 p1484 A67-21828

Program checkout facility designed to perform operational checkout of navigation systems by analyzing system under simulated conditions 09 p1484 A67-21833

Aircraft sensor systems, discussing recording and evaluation tasks and performance characteristics 09 p1501 A67-22454

Computing methods and techniques in aircraft testing, discussing measurements, application of mathematical statistics, etc 09 p1469 A67-22455

Audiofrequency ILS /phase II/ used with VHF generator to check ILS instruments 11 p1745 A67-24554

Man-rated space simulation facility, emphasizing checkout and qualification of systems 12 p1921 A67-25689

Trace /tape controlled recording automatic checkout equipment/ system design to accommodate aircraft ground support task 16 p2635 A67-30834

First stage checkout techniques of satellite launcher, noting digital computer program from pulse-code-modulated telemetry 16 p2655 A67-30835

Operational computerized system for automatic surveillance of reliability and maintainability of spacecraft hardware 18 p3021 A67-34701

Digital computer simulation model implementation in prelaunch prediction of Saturn V launch vehicle system performance [AIAA PAPER 67-205] 19 p3331 A67-34807

Checkout system for third stage of ELDO A program 20 p3413 A67-36414

Remote control pneumatic pressure test system for Saturn S-IC booster checkout with manual or automatic control, using computer 20 p3415 A67-36569

Digital computer test program for automatic checkout of Saturn launch vehicles allowing manual intervention 20 p3391 A67-36574

Man-machine graphical communication device for real time monitoring with automated checkout 20 p3446 A67-36589

Automatic electronic test and checkout techniques, automatic test equipment history and high points of 1957-1959 DOD symposia 20 p3416 A67-36970

Tactical checkout missile test installations for Terrier, Tartar and Talos missiles 20 p3416 A67-36971

Apollo program automatic checkout equipment, examining computer controlled checkout concept for Apollo spacecraft 20 p3417 A67-36974

Automation techniques for stage checkout in Saturn program noting equipment, time factor, etc 20 p3417 A67-36975

Acceptance checkout equipment spacecraft for centralized control and LEM and CSM systems testing 20 p3391 A67-36976

Apollo-Saturn program automatic checkout systems, discussing ground support equipment facility automation, computer software and checkout technique applications to nuclear electronic systems 20 p3533 A67-36977

Self-contained and vehicle integrated on-board checkout systems, considering controller-evaluator and sensors 20 p3449 A67-36979

Nuclear methods and techniques applied to maintenance and checkout of complex electronic and electromechanical systems, discussing radiation-matter interaction, etc 20 p3449 A67-36981

Onboard Checkout System /OCS/ design, considering system selection techniques, design development, equipment, etc, with orientation on OCS design by NASA/MSC 20 p3417 A67-36988

High performance automatic ground checkout system for boosters, noting rate improvement and error reduction 21 p3608 A67-38203

Automatic satellite-checkout system for use under simulated space environment and stress conditions 22 p3778 A67-39192

Hazards of rocket launching noting propellant toxicity, airborne fragmentation, inadvertent ignition and nuclear radiation 22 p3900 A67-39884

Automatic test equipment for checkout and fault finding on Saab 37 Viggen 24 p4137 A67-41898

Data analysis methods for integrated data processing system for onboard in-flight checkout for launch vehicle evaluation [AIAA PAPER 67-911] 24 p4127 A67-43018

Onboard computer-based checkout simulator system to assist astronauts in monitoring data requirements of future space programs [AIAA PAPER 67-951] 24 p4127 A67-43035

Microelectronic integrated checkout equipment interfacing subsystems under test with test subsystem [AIAA PAPER 67-952] 24 p4133 A67-43036

Onboard checkout system /OCS/ impact on space station program [AIAA PAPER 67-953] 24 p4245 A67-43037

CHELATE COMPOUND

SA CHEMICAL LASER

Four-linked rare earth chelate with sodium ion obtained with benzoylacetone and europium, analyzing molecular and ionic transitions by absorption and emission spectra 02 p0251 A67-11518

Luminescence of alcoholic solution of europium chelate at low temperatures, noting changes in intensity of optical excitation at various energy levels 03 p0433 A67-12894

Energy level structure of rare earth chelates, noting existence of isolated systems of optical electrons 09 p1512 A67-21921

Laser generation through rare earth chelate solutions, requirements for working solutions and apparatus 10 p1664 A67-23068

Laser activity from terbium trifluoroacetate in p-dioxane and acetonitrile at room temperature 11 p1803 A67-24833

Energy level structure of rare earth chelates, noting existence of isolated systems of optical electrons 14 p2330 A67-28250

Liquid lasers use of rare earth ions, chelate structures, selenium oxychloride, etc 15 p2501 A67-30086

Spectral brightness of metal chelate liquid fuel-air flames [CI PAPER 67-2] 19 p3309 A67-34997

Carbonyl compounds reaction with N-salicylideneglycinatoaquocopper /II/ syntheses of beta-hydroxy alpha-amino acid from glycine 20 p3376 A67-36877

Spectroscopic properties of mixed complexes with two different ligand groups surrounding lanthanide ion, discussing energy transfer and absorption 23 p3971 A67-40747

CHEMICAL ANALYSIS

SA ANALYTICAL CHEMISTRY

Postirradiation radiochemical and spectrochemical analysis of short-cooled samples of SNAP-8 experimental reactor primary coolant 03 p0466 A67-13798

Lunar surface chemical analysis using interaction of monoenergetic alpha particles with matter [JPL-TR-32-1065] 05 p0805 A67-16463

Chemical analysis of stony meteorites, noting analytical procedures and results 05 p0895 A67-16581

Spectrochemical analysis of solid specimen from vapor formed by laser beam and excited by spark discharge 05 p0824 A67-16786

Chemical problems concerning specifications and use of nitrogen peroxide and unsymmetrical dimethyl hydrazine as propellants 06 p1071 A67-17612

Periodical components of fluctuations in chemical processes of Piccardi D-test 06 p0994 A67-17638

Chemical analysis of lunar surface composition by instruments on board soft landing probes 07 p1186 A67-19571

Mechanics and chemistry of solid propellants - Symposium on Naval Structural Mechanics, Purdue University, April 1965 08 p1418 A67-20872

Lunar surface chemical composition analysis by Surveyor-borne instrument based on alpha interaction with matter [JPL-TR-32-1090] 08 p1411 A67-20946

Ge and Ga concentration in selected Fe meteorites used to determine quantization in terms of multiple parent body hypothesis and planetary fractionation processes 09 p1564 A67-21738

Electron microscope and microprobe measurements of luster flight samples, discussing particle size distribution and nondispersive chemical analysis 10 p1707 A67-23238

Sedimentary rock analysis for aliphatic hydrocarbons, discussing methods and results 10 p1709 A67-23488

Chemical and mineralogical composition and structure of Belly River, Bluff, Bremer Voerde and Modoc meteorites 10 p1712 A67-23808

Chondritic meteorites two-dimensional classification grid based on chemical and petrologic subdivisions 14 p2391 A67-28949

Nitrogen, oxygen and hydrogen determined by spark-source mass spectrography, noting reduction of instrument blank levels 15 p2433 A67-29403

Impurities in high-purity niobium determined chemically and spectroscopically 19 p3243 A67-34927

Analytical procedures for oxygen, nitrogen and hydrogen determination in high melting metals 20 p3467 A67-37120

Lactic dehydrogenases of H4 and M4 type, preparation and catalytic and enzymological properties 20 p3377 A67-37159

Pyrolysis gas chromatography method for life detection and chemical identification of microorganisms 20 p3378 A67-37500

Chemical analysis and normative mineral composition of Winona meteorite, showing relation to chondrites 21 p3702 A67-38067

Meteoritic organic chemical analyses since 1900, considering volatile materials distribution and carbonaceous chondrites 21 p3704 A67-38502

Anoka, Minnesota, iron meteorite noting composition, chemistry, structure and cooling rate 23 p4069 A67-41449

Histochemical investigation of effect of hypothermia and hypobiosis on activity of oxidizing tissue enzymes of carbohydrate, amino acid, nucleotide and aliphatic metabolism of rats 24 p4112 A67-41853

Chemical composition analysis of Macedon and Darwin natural glass 24 p4233 A67-42615

CHEMICAL AUXILIARY POWER SOURCE

Solid and liquid propellants, considering minimum specific propellant consumption in connection with fuel selection for auxiliary power systems [SAE PAPER 670205] 12 p1987 A67-25866

CHEMICAL BOND

SA COVALENT BOND

SA HYDROGEN BOND

Interfaces in composite materials, discussing matrix-fiber interfaces, interfacial chemical interactions, microstructure and thermodynamic instability 03 p0454 A67-13426

Chemical bonds formation during interaction between individual elements explained by total valence band energy theory 06 p1035 A67-17845

Chemical behavior of metallic elements predicted by periodic table, noting formation of liquid and solid metallic solutions, binary and complex metallides and nature of chemical bond 06 p1018 A67-18233

Average energy of bond between like atoms 06 p0956 A67-18609

Structure of X-ray K absorption edge of iron in Fe compounds, noting nature of chemical bond and structure of electron energy spectrum 12 p1957 A67-26109

Book on chemical bond in semiconductors and solids, evaluating strength and determining effect on properties of substances 13 p2182 A67-27486

Microwave spectroscopy of organic semiconductors, examining EPR of chemical bonds in energy transfer 14 p2366 A67-28505

Refractory intermetallic compounds as high mobility semiconductors, noting crystal preparation and lowest carrier concentration obtained 16 p2725 A67-30806

Soviet book on thermodynamic study of chemical bond in semiconductors 18 p3093 A67-33434

Physical properties of semiconductors relation with energy and nature of interatomic bonds, discussing effect on elastic constant, thermodynamic functions, electric and dielectric properties 18 p3094 A67-33435

Dynamic theory of hybrid ionic-covalent/homopolar/ bonds applied to physical behavior of GaAs type crystals 18 p3094 A67-33436

Elastic moduli, bond parameters and effective ion charges for wurtzite and sphalerite binary crystal lattices 18 p3094 A67-33437

Fourier series applied to X-ray investigation of potential and electron density distribution in silicon lattice to study chemical bonds 18 p3094 A67-33439

Relation between molecular structure of In and Sb semiconductor compounds and fine structure of X-ray absorption spectra 18 p3095 A67-33441

Covalent bonds found more prevalent than ionic bonds in X-ray spectral study of Al and Sb in A-III B-V type semiconductor compounds 18 p3095 A67-33443

Solubility of impurities in semiconductors and mechanism for deviation from stoichiometry 18 p3096 A67-33449

Changes in InSb, GaSb and Te crystal lattice structure and chemical bonds investigated for effects on thermoconductivity, thermal EMF and microhardness 18 p3096 A67-33451

Indium arsenide-tellurium ternary compounds chemical bond, microhardness and structure 20 p3506 A67-36226

Radioactively labeled coupling agents adsorption on E-glass surfaces, noting continuous film formation with covalent bonding occurring at interface 20 p3474 A67-37269

Chemical bonds formation during interaction between individual elements explained by total valence band energy theory 20 p3490 A67-37587

Chemical bond calculations with high temperature chemistry, discussing hydride molecular energy, dissociation energies and diatomic molecules 21 p3578 A67-38394

Soviet book on physicochemical principles of semiconductor alloying covering chemical bonds, crystal structure, binary systems, etc 21 p3684 A67-38433

Hydrogen peroxide and disulphane molecules force constant and vibrational spectra investigation indicates little change

in elastic properties 22 p3757 A67-39583

Lanthanide distribution between omphacite and Garnet, noting abundance ratios to whole rock of Japanese eclogite 24 p4151 A67-42449

CHEMICAL COMPOSITION

Lunar X-rays excited by electrons of magnetospheric tail provide information on chemical composition of moon 01 p0144 A67-10563

Extensive air shower characteristics related to energy spectrum, chemical composition and anisotropy of primary cosmic rays in superhigh energy range 02 p0318 A67-12778

Kamacite and taenite superstructures and metastable tetragonal phase in iron meteorite 03 p0510 A67-13334

Principal methods determining cosmic abundances of chemical elements, emphasizing quantitative spectral analysis of sun and fixed stars 03 p0510 A67-13538

Chemical composition of primary cosmic rays in moderate energy rigidity range with aid of satellite Proton I 05 p0877 A67-16087

Mechanical properties and chemical composition of industrial niobium VN2 and VN2A at low temperatures 05 p0832 A67-17506

Chemical signatures from astronomical bodies, noting spectral results obtained from ground stations and orbiting spacecraft 06 p1092 A67-19014

Hardness variation of alloys of system Al-Cu-Cd-Mn-Li as function of composition and aging conditions 07 p1201 A67-19252

Titanium alloy mechanical and physical characteristics, noting dependence on chemical and phase composition 07 p1206 A67-19285

Chemical composition and earth origin, with estimates of primordial abundances of elements in solar system 07 p1170 A67-19336

Rare earth compound and Ba abundances in Bununu howardite 07 p1249 A67-19537

Chemical and mineralogical composition of roederite found in Indarch meteorite, presenting electron probe analysis and X-ray diffraction pattern optical data 07 p1255 A67-20012

Bununu meteorite /pyroxene-plagioclase achondrite/ composition and structure 09 p1564 A67-21736

Isotopic composition of krypton in high and low calcium achondrites, noting measurement results 09 p1569 A67-22685

Chemical and mineralogical composition of meteorites found in Australia, Africa, Ireland and Java 10 p1712 A67-23807

Chemical composition of indochinites, determining nonuniform distribution of elements via electron microprobe 11 p1886 A67-24695

Tektites and impactites composition and origin 12 p1903 A67-25430

Meteor radiation and methods of meteor spectrography, discussing chemical composition, spectral characteristics, green oxygen line and photoelectrical color sensors 13 p2197 A67-26504

Jet fuels in U.S. and Great Britain, chemical composition, technical specifications, thermal stability and corrosion effect 13 p2185 A67-27068

Cosmic origin of tektites indicated by factors other than chronology 14 p2385 A67-28145

Surface cleaning of electrical and electronic equipment through water and oil removal by chemical compositions 14 p2327 A67-28822

Solar cosmic ray generation, discussing chromospheric eruptions, spectra, chemical and nuclear composition, particle acceleration, etc 17 p2934 A67-32095

Spectrometers onboard satellite, studying cosmic ray particle energy spectra and chemical composition 17 p2935 A67-32248

Origin and abundance distribution of heavy elements in stars, discussing theories 17 p2946 A67-32694

Elemental composition effect on electron excited fluorescence of serpentines determined by spectral examination with electron microprobe 17 p2852 A67-33239

Variation of forbidden bandwidth and linear-expansion coefficient of indium phosphide-gallium arsenide alloys as function of composition 18 p3095 A67-33447

Brittle coatings for stress distribution analysis during static and dynamic loading,

describing chemical composition and characteristics and giving formulas and diagrams 18 p3045 A67-33741

Chemical structure of premixed flames of methane and perchloric acid vapor diluted with argon obtained in terms of composition, temperature and velocity profiles 18 p3109 A67-33841

Lunar rocks composition and radioactivity through satellite gamma-ray measurements indicating basaltic and ultrabasic composition 19 p3319 A67-35258

Ternary semiconductor composition found through valence equation 20 p3512 A67-37243

Compositional changes at alloy/oxide interface during protective oxidation calculated using finite difference method 20 p3468 A67-37247

Soap and nonsoap base greases physical and chemical nature, composition, characteristics and additives 20 p3455 A67-37265

Mechanical properties and chemical composition of industrial niobium and alloys VN2 and VN2A at low temperatures 21 p3644 A67-38034

High temperature alloy applications, outlining chemical composition and influencing factors in selection and economic utilization 21 p3650 A67-38533

Oxidation mechanisms for nickel-aluminum alloys studied for effects of temperature and alloy composition 21 p3645 A67-38773

Phase and chemical compositions of structural components forming in iron-nickel-chromium alloys with aluminum and titanium content 22 p3820 A67-39788

Extensive air shower characteristics related to energy spectrum, chemical composition and anisotropy of primary cosmic rays in superhigh energy range 22 p3877 A67-40280

RNA fractions base composition and labelling kinetics in presence and absence of actinomycin for rapidly labelled RNA in rabbit bone marrow rich in erythroid cells 23 p3944 A67-40801

Crystalline variation and chemical composition of meteorite found at Marburg, West Germany 24 p4232 A67-42614

Chemical composition analysis of Macedon and Darwin natural glass 24 p4233 A67-42615

Coexisting sphalerite, troilite and daubreelite in Odessa meteorite and sphalerite inclusions in kamacite in Odessa and Canon Diablo analyzed for chemical composition 24 p4233 A67-42620

Chemical analysis of glass bombs from Ries crater area investigated for textural differences due to shock melting and cooling rates 24 p4233 A67-42621

Canon Diablo octahedrite quantitative chemical and modal mineralogical composition variations in rim and plain components 24 p4235 A67-42636

Iron meteorite chemical classification, measuring Ni, Ga, Ge and Ir concentrations for Fe groups and pallasites 24 p4237 A67-42650

Molecular weight and amino acid composition of chromatium ferredoxin 24 p4113 A67-42653

Chemical composition of primary cosmic rays in moderate energy rigidity range with aid of satellite Proton I 24 p4212 A67-42763

Primary cosmic ray particle chemical composition changes, explaining active particle energy spectra discrepancies between measurements and calculation 24 p4218 A67-42840

CHEMICAL COMPOUND

SA INORGANIC COMPOUND

SA ORGANIC COMPOUND

SA ORGANOMETALLIC COMPOUND

SA POTTING COMPOUND

Sliding contact wear under very dry high altitude or space conditions due to lack of contact film prevented by using chemical compounds like graphite or lithium carbonate 02 p0221 A67-12435

Physical and chemical behavior of elements and chemical compounds, considering electron configurations, using condensed-state atom model 06 p1035 A67-17843

Physical and chemical behavior of elements and chemical compounds, considering electron configurations, using condensed-state atom model 20 p3490 A67-37585

Book on production of boranes and related

- research for high energy fuels for air breathing engines 23 p4047 A67-41443
- CHEMICAL EFFECT**
- Water and internal acidity effect upon oligomeric polyanilines 01 p0130 A67-10197
- Time analysis of Mossbauer spectrum variation and isometric shift of source Te-125m in PbTe absorber following neutron irradiation in reactor 09 p1559 A67-22661
- Chemical polishing effects on sapphire whisker strength, obtaining correlation between fracture strength and whisker diameter 20 p3473 A67-36480
- CHEMICAL ENERGY**
- Electrical parameters of chemical current sources in determining capacitance by measuring emf, voltage and short circuit current 03 p0363 A67-13597
- Implosive collapse of liners containing gas to transfer chemical energy of explosive to kinetic and internal energy of gas [AIAA PAPER 67-178] 06 p1118 A67-18485
- Physics and efficiency of direct conversion of heat, light, nuclear, thermonuclear and chemical energy to electrical energy, avoiding mechanical 10 p1597 A67-23507
- Electrical parameters of chemical current sources in determining capacitance by measuring EMF, voltage and short circuit current 14 p2247 A67-27843
- Direct lasing of conventional ruby rods requiring 200-joule xenon pump deriving energy from chemical reaction 15 p2502 A67-30437
- Electron temperature measured in acetylene/oxygen mixture flame and found twice that of gas due to chemical energy transport to electron gas 17 p2968 A67-32151
- Long range retarded interaction energies, obtaining energy term coefficient from minimal principle using Karpus and Kolker method 22 p3757 A67-39636
- CHEMICAL ENGINEERING**
- Expandable and modular structures for support on manned space missions, reviewing inflatable, chemically rigidizable, unfurlable and elastic recovery structures 02 p0333 A67-12342
- Boron filament manufacturing process using chemical vapor plating with boron trichloride and hydrogen onto tungsten filament substrate 03 p0453 A67-13419
- High pressure technology - AICE Symposium, Detroit, December 1966, Part 1 04 p0611 A67-15945
- CHEMICAL EQUILIBRIUM**
- SA MOLECULAR DISSOCIATION**
- Effects of reentry vehicle physical characteristics and trajectory constraints on variation of velocity-atmospheric density ambient value function 04 p0706 A67-15244
- Asymptotic method for solution of boundary layer equations for generalized three-dimensional flow of dissociated air at chemical equilibrium near stagnation point 06 p0984 A67-18113
- Law of mass action derivation of chemical equilibrium ionization of multitemperature system when electron and heavy particle temperature differ 09 p1544 A67-21858
- Parameters of gas behind incident and reflected shock waves calculated, using gas dynamic and chemical equilibrium equations for one-dimensional problem 12 p1930 A67-26134
- Multicomponent reacting laminar boundary layer in chemical equilibrium solved using Stefan-Maxwell relations 16 p2658 A67-30937
- Nonlinear equations governing complex chemical and phase equilibria derived from thermodynamic principles and supplemented by solving algorithms and practical applications 16 p2620 A67-31815
- Linear algebra describing equilibrium chemical systems and complex chemical mixtures, discussing hydrogen-fluorine coupling reaction at elevated temperatures 18 p2997 A67-34124
- Nitric oxide reaction with triphenylmethylperoxy radical investigated in connection with study on reversible reaction 20 p3377 A67-37138
- Equilibrium phases in annealed NiCrTiAlW alloy using optical and electron microscopy and X-ray analysis 23 p4019 A67-41078
- CHEMICAL EXPLOSION**
- Propagation velocity and other characteristics of detonations in liquid mixtures of nitropropane 2 and nitric acid, noting relation to initial temperature and water content 04 p0726 A67-15495
- Existence and stability of solutions for equations of stationary thermal explosion in bounded container 10 p1734 A67-23679
- Formation of cavities and microjets in liquids and role in initiation and growth of explosion 11 p1883 A67-24631
- Existence and stability of solutions for equations of stationary thermal explosion in bounded container 21 p3731 A67-38280
- CHEMICAL FUEL**
- Chemical propellants in Apollo program, noting Saturn launch vehicle and spacecraft propulsion 05 p0874 A67-17016
- Chemistry and rheology of gelled fuels, noting structure, thickeners, etc 10 p1696 A67-22911
- CHEMICAL KINETICS**
- Fuel cells from point of view of thermodynamics, electrochemical reaction kinetics and transport processes and state of development of representative types 01 p0013 A67-10554
- Flame ignition from hot gas pocket, minimum size of gas bubble for flame propagation, dependence on chemical kinetic parameters and transport properties 02 p0342 A67-12030
- Nitrogen adsorption at room temperature on atomically clean polycrystalline rhodium, noting dependence of sticking coefficient upon surface coverage and temperature 02 p0257 A67-12728
- Chemical reaction kinetics and gas dynamics combined to analyze processes occurring in combustion chambers and nozzles of jet and rocket engines [DVL-602] 03 p0366 A67-12999
- Hypersonic flow of air past circular cylinder with nonequilibrium oxygen dissociation, including dissociation of free stream 03 p0351 A67-13000
- Esterification rates of aliphatic carboxylic acids, acid terminated polybutadienes, etc, and steric environment in vicinity of acid groups 04 p0564 A67-14473
- Oxidation processes by treatment of composite and elementary reactions, noting chain reactions and chain branching 04 p0565 A67-15090
- Electron spin resonance application to kinetic studies of free atoms and radicals in gases, particularly OH radical 04 p0566 A67-15173
- Turbulent boundary layer-flat surface interfacial Stefan-Nusselt flow effects on apparent kinetics of heterogeneous chemical reactions in forced convective systems 04 p0567 A67-15681
- Krypton and xenon effect on dissociation rate of fluorine in presence of argon behind shock wave 04 p0567 A67-15951
- Steady state kinetics and microstructures of simultaneous internal oxidation and external scale formation of Cb-Zr and Cb-Zr-Re alloys in pure oxygen at 1000 degrees C 05 p0828 A67-16471
- Finite rate chemistry effects in diffusion controlled hydrogen-air flames noting flame position, fuel consumption, temperature, fluid velocity outside of flame and boundary conditions 05 p0926 A67-16516
- Chemical kinetics effects in supersonic combustion noting three different zones in chamber 06 p1113 A67-18027
- Shock induced supersonic combustion of fuel-air mixtures used to obtain induction time, evaluating kinetic data and effect of small contamination levels [AIAA PAPER 67-105] 06 p1114 A67-18284
- Reaction rates controlling densities of ions and electrons in F region determined so that calculated ion and electron distribution may agree with rocket observations 06 p0996 A67-18430
- Internal ballistic considerations in hybrid rocket design, noting throttling and regimes of operation involving effects of surface-or gas-phase reaction kinetics [AIAA PAPER 66-628] 07 p1240 A67-19377
- Bibliographical research of properties of air at high temperature, noting chemical kinetics and contrasting microscopic and macroscopic approaches 07 p1268 A67-20114
- Kinetics of two-phase decomposition of solid solution of magnesium-aluminum alloy using X-ray analysis, noting grain orientation and size 08 p1342 A67-20810
- Reaction rate of oxygen jet impinging on tungsten samples at high temperature and various pressures, noting activation energy and diffusion effect 09 p1457 A67-22026
- Temperature dependence and reaction energetics of free radical addition of trifluoroacetonitrile to ethylene 09 p1459 A67-22364
- Potentials of zero charge of gold, silver and mercury electrodes as affected by cations and respective metal ion interaction 11 p1749 A67-23920
- Reaction rate kinetics of combination of H atoms with NO plus third body /M/ compared with H and O atoms plus M relative to argon 11 p1749 A67-24238
- Chemical kinetic processes in gasdynamic shock wave interactions, especially vibration in four-center transition states 11 p1773 A67-24535
- Momentum and energy transfer effects on gas kinetic equations of nonequilibrium flows, analyzing diffusion problem 11 p1780 A67-24536
- Cosmochemical considerations, from thermodynamical viewpoint, of formation processes of earth, planets and meteorites 11 p1864 A67-24600
- Decomposition rates of hydrogen halides examined behind incident shock waves between 2800 to 4600 degrees K, using IR techniques 11 p1750 A67-24995
- Martian entry condition analyzed as nonequilibrium flow field phenomenon, noting chemical kinetics and radiation behind shock wave in gas mixtures [AIAA PAPER 67-322] 12 p1930 A67-26037
- CH concentration measurement in flash photolysis of methane by means of kinetic spectroscopy 12 p1904 A67-26228
- Hafnium oxidation between 300 and 1200 C, noting occurrence of faster stages in process 13 p2132 A67-26999
- Reaction of atomic oxygen with methane studied by photolysis of ozone-methane mixtures dissolved in liquid argon [JPL-TR-32-1109] 14 p2259 A67-28297
- Lead, copper and cobalt oxides effects upon ignition kinetics of paraffinic and aromatic fuels 14 p2407 A67-28550
- Fluorine compounds as propellants in upper stage propulsion units, discussing properties, suitability and performance 14 p2377 A67-28979
- Matrix formulation and resultant approximations as approach to nonlinear chemical reaction rate equations 15 p2434 A67-30023
- Reaction kinetics of liquid titanium and hafnium with carbon using layer-growth method 16 p2690 A67-31373
- Prigogine-Glansdorf local potential calculated for usual transport effects case using variational principle 16 p2661 A67-31440
- Kinetics of difluoromethylene-nitric oxide reaction, describing experimental apparatus, reaction mechanism, molecule structure and calculating heat of molecule formation 16 p2620 A67-31760
- High temperature oxidation of titanium at reduced oxygen pressures governed by dissolution of oxygen in metal 17 p2873 A67-32812
- Experiments on oxidation kinetics of refractory metals in undissociated and partly dissociated oxygen-chlorine mixtures 17 p2971 A67-33021
- Bimolecular and termolecular kinetic rate constants for reactions involving atmospheric neutral species 17 p2809 A67-33240
- Ion-molecule reactions in propane studied using mass and energy resolved ion beams in tandem mass spectrometer 17 p2810 A67-33264
- Hydrocarbon pyrolysis and H/D substitution reaction rates, using single-pulse shock tube as chemical reactor 18 p2996 A67-33788
- Nitric oxide production reaction rate measured in shock-heated air at high temperatures, with nitric oxide concentration determined by IR emission 18 p2997 A67-33791
- Propulsion-oriented subsonic boundary layer combustion research, discussing turbulent and diffusion-limited conditions, radiant heat transfer, chemical kinetics and transient phenomena 18 p3150 A67-33800
- Role of electronically excited CH in formation of C3H3 ion and contribution to overall chemiluminescence process 18 p3150 A67-33802
- Collisional de-excitation rate or quenching

of sodium in flat premixed laminar flames 18 p3150 A67-33803

High temperature kinetics of bulk beryllium metal combustion in hydrogen-oxygen-water vapor system, studying flame environments, thermal balance, etc 18 p3151 A67-33809

Mathematical model for thermal and chemi-ionization processes in turbulent nonequilibrium afterburning rocket exhausts plume, studying neutral and charged species distribution 18 p3152 A67-33820

Post-induction kinetics in shock initiated hydrogen-oxygen reactions investigated by computer methods 18 p3153 A67-33823

Steady flow adiabatic stirred reactor to study combustion mechanism of hydrogen-oxygen mixtures, determining reaction-kinetic constants 18 p3154 A67-33834

Rate constants and activation energy in bimolecular transfer reactions for halogen atoms 18 p3154 A67-33835

Ignition kinetics of carbon monoxide-oxygen reaction 18 p3155 A67-33846

Kinetic mechanisms in combustion peninsula of three-limit explosion reactions with trace inhibitors, studying quadratic chain-breaking processes by static method 18 p3156 A67-33848

Boundary layer combustion in hybrid rockets from simplified model comprising convective transport and chemical kinetic factors, analyzing fuel regression rate [AIAA PAPER 67-471] 18 p3157 A67-33941

Hydrogen-air reaction kinetics analyzed using standing wave normal shock, noting wall effects, ignition delay and recombination [AIAA PAPER 67-479] 18 p3157 A67-33948

Chain branching during induction period of hydrogen-oxygen reaction studied by shock heating 18 p2998 A67-34519

Condensed phase thermal decomposition of ammonium perchlorate, studying pressure and additives effect on kinetics 19 p3309 A67-35003

Lean hydrogen-oxygen mixture combustion, studying induction period kinetics and spikes in OH profile 19 p3345 A67-35004

Reaction rate constants for gaseous chemical species at high temperatures [CI PAPER 67-11] 19 p3345 A67-35006

Luminescence decay kinetics of trivalent Nd ions in antiferromagnetic Rb manganese fluoride, showing mechanism of transfer process of excitation energy of Mn ions 20 p3506 A67-36218

Quadrant mechanical hypothesis /QM/ on gravitation, gravitational chemistry and zero gravity effects in various chemical processes 20 p3484 A67-36546

Burning in unmixed reactants for high enthalpy inviscid flow of opposed streams studied for one-step reaction model and Lewis-Semenov number 20 p3554 A67-37132

Shock induced supersonic combustion of fuel-air mixtures used to obtain induction time, evaluating kinetic data and effect of small contamination levels [AIAA PAPER 67-162] 21 p3732 A67-38858

Hydrocarbons transformation mechanism and kinetics at low pressures in glow discharge noting three-way decomposition 22 p3757 A67-39585

Thermographic method for investigation of kinetics of heat evolution 22 p3917 A67-39586

Kinetics of flames propagating in hydrogen-nitrous oxide mixtures diluted with inert gases 23 p4082 A67-41142

CHEMICAL LASER

Laser generation through rare earth chelate solutions, requirements for working solutions and apparatus 10 p1664 A67-23068

Solution regrowth technology of electroluminescent devices noting reduced threshold current densities, external quantum efficiency and adaptation to planar technology 10 p1665 A67-23518

P-n junction fabrication in vapor phase grown GaAs-P alloys resulting in room temperature injection laser, thereby extending operation into visible spectrum 11 p1802 A67-24741

Mechanisms operating in lasers employing optical transitions of molecules in fluids 14 p2331 A67-28471

Short term stability of beat frequency of two stable single-frequency carbon dioxide-nitrogen-helium lasers 15 p2499 A67-29732

Optical ranging system with high power chemical laser noting performance characteristics 15 p2500 A67-29913

Hydrofluoric acid for chemical vibration-rotation laser emission 20 p3462 A67-37564

CHEMICAL MILLING

Chemical milling technique for space vehicle chassis and circuitry production, noting similarity and differences with photoengraving and printed circuit techniques 16 p2683 A67-31739

Chemical milling of aluminum alloy parts by dimensional etching, discussing protective coatings 23 p4009 A67-40641

CHEMICAL PROPERTY

Physical and chemical behavior of elements and chemical compounds, considering electron configurations, using condensed-state atom model 06 p1035 A67-17843

X-ray crystal structural analysis of tetraethyl titanate and monomethyltriethyl titanate, determining reason for difference in color 06 p0955 A67-17849

Chemical stability of silver graphite, molybdenum disulfide, zinc oxide, boron nitride, muscovite and phlogopite mica solid lubricants 10 p1659 A67-22829

Nickel-base superalloy technology, stressing structural stability and hot corrosion resistance 12 p1958 A67-26128

Lanthanum germanide synthesis using arc furnace, noting chemical properties 13 p2131 A67-26470

Nature of glassy state, reviewing nucleation, crystallization, chemical, physical, and electrical properties and transformation of glasses 13 p2143 A67-26696

Book on tungsten and its compounds, physical, chemical and metallurgical data 14 p2336 A67-27890

Special grade RDX for exploding bridge wire initiators noting chemical/physical properties and performance 14 p2377 A67-28955

Molybdenum disulfide compacts pressurized by explosive forming, determining specific gravity, hardness, compressive and tensile properties, etc 16 p2695 A67-31753

Extreme pressure /EP/ films from lubricants containing borate esters, studying structure and mode of action 16 p2683 A67-31756

Structure and substructure effect on thin film properties, discussing vacuum deposition mechanism of metals, alloys, dielectrics and semiconductors 17 p2920 A67-32888

Book on coatings of high temperature materials covering properties and characteristics and coated refractory metals 19 p3244 A67-34956

Refractory metals physical, mechanical and chemical properties when coated with oxidation resistant coatings 19 p3244 A67-34958

Physicochemical and mechanical properties of refractory materials at high temperature - Conference, Paris, June-July 1965 20 p3471 A67-36109

Purification and properties of nicotine oxidase suggest metalloflavoprotein having riboflavin 5-phosphate 20 p3376 A67-37032

Synthetic lubricants noting chemical and physical properties of nonhydrocarbons, classes of synthetics, etc 20 p3455 A67-37264

Physical and chemical behavior of elements and chemical compounds, considering electron configurations, using condensed-state atom model 20 p3490 A67-37585

Microchemical and microhardness properties of parallel gap welds for microstructure interpretation of metal joint 21 p3636 A67-38633

CHEMICAL PROPULSION

Structural cryogenic vessels of chemical rocket stages 05 p0874 A67-17015

Computer experiments related to chemical propulsion such as chemical kinetics, fluid dynamics, transport process, shock and detonation phenomena, combustion, etc [AIAA PAPER 67-7] 06 p1114 A67-18250

Thermodynamic limits on specific work and specific impulse of adiabatic chemical engines and nuclear engines [AIAA PAPER 67-227] 06 p1029 A67-18445

Oxygen difluoride propellant system design and operational experience at Arnold Center

[AIAA PAPER 67-279] 07 p1164 A67-20049

Book on propulsion systems covering gas-turbine engine, ramjet engine, chemical and electrical rockets, components, etc 10 p1698 A67-23689

Hot-water rocket design by dimensionless method, noting GRILLO rockets 15 p2567 A67-29840

Combined electric constant low thrust and chemical or nuclear high thrust space propulsion systems for interplanetary missions [AIAA PAPER 67-511] 18 p3114 A67-33975

Computer experiments related to chemical propulsion such as chemical kinetics, fluid dynamics, transport process, shock and detonation phenomena, combustion, etc [AIAA PAPER 67-7] 19 p3346 A67-35734

CHEMICAL REACTION

SA CARBONIZATION

SA DECOMPOSITION

SA DEHYDRATION

SA DISSOCIATION

SA ELECTROLYSIS

SA EXOTHERMIC REACTION

SA HYDROGENATION

SA HYDROLYSIS

SA ION EXCHANGE

SA IONIC REACTION

SA NEUTRALIZATION

SA OXIDATION

SA PHOTOCHEMICAL REACTION

SA POLYMERIZATION

SA SULFATION

SA SYNTHESIS

Perfluorocyclopropane production in reaction of oxygen atoms with tetrafluoroethylene 01 p0018 A67-10762

Statistical-dynamical model for total chemical reaction cross sections using activated complex concept and integral equation 01 p0019 A67-10884

Chemiluminescent gas phase reactions involving electronically excited oxygen molecules trimethylaluminum and diborane near 3 millitorr 01 p0019 A67-11007

Interstellar molecule formation as result of chemical exchange reactions between atoms of interstellar gas and atoms chemically bound to interstellar grains 02 p0323 A67-11689

Nitrogen fluorides synthesis in nitrogen plasma jet intermixed with gaseous fluorides 02 p0190 A67-12235

Decay of dynamically passive reactant in stationary isotropic turbulent velocity field investigated, using direct interaction and modified quasi-normal closures 02 p0234 A67-12549

Refractory metal chlorides reacted with methane and nitrogen in hydrogen jet to form carbides and nitrides 03 p0440 A67-12925

Boron filament preparation on fused silica substrates by decomposition of diborane 03 p0454 A67-13420

Synthesis route to form continuous filaments of SiC, noting tensile strength, elastic modulus and density of product 03 p0454 A67-13422

Rate equation for dissociation and recombination of diatomic molecules 03 p0473 A67-13521

Potassium atom reactive scattering from oriented methyl iodine molecules, determining variation of chemical reactivity over molecular surface 03 p0367 A67-13524

Hydrogen atom-molecule exchange reaction effect on transfer coefficients of dissociating mixture, noting anisotropy and collision integrals 03 p0473 A67-13606

Flash pyrolytic technique applied to McFayden-Stevens reaction for various simple aliphatic aldehydes 04 p0565 A67-14524

Powder admixtures influence on critical diameter of detonation of solid, continuous and macroscopically homogeneous explosive, noting inorganic admixtures role 04 p0723 A67-15197

Finite difference solution to nonsimilar laminar mixing of streams undergoing nonequilibrium chemical reactions 04 p0609 A67-15816

Oxygen atoms reaction with tetrafluoroethylene in presence of molecular oxygen 04 p0567 A67-15949

Chemical reaction effect on heat transfer in thermally decomposing ozone system 05 p0925 A67-16270

Thermodynamic properties of binary Cu-Pt alloys determined, using Knudsen effusion

technique 05 p0829 A67-16473
Experimental equipment for chemical reaction analysis in fluid systems based on study of partial oxidation of methane at high pressures 05 p0759 A67-17540
Spectrum of glow during gas phase reaction of germanium tetrahydride with atomic oxygen, observing new bands of D-X system 06 p0955 A67-17655
Reacting gas flow in nozzle in one-dimensional formulation taking into account nonequilibrium course of chemical reactions 06 p0935 A67-17726
Differential equations and mathematical models for gas flows with chemical activity and radiative effects, particularly effects of reentry and propulsion 06 p0983 A67-17785
Streptoligin interaction with DNA and resulting degradation and denaturation temperature of DNA from salmon sperm and *Escherichia coli* 06 p0952 A67-17873
Reaction rate of oxygen atom with C₃F₆ and hydrocarbons 06 p0955 A67-17983
Perfect gases reacting mixture flows formulated for system of differential equations 06 p0955 A67-18114
Atomization, mixing and reaction characteristics of hydrazine and nitrogen tetroxide injected from quadlet element [AIAA PAPER 67-107] 06 p1072 A67-18308
Nonisothermal changes in properties and composition during chemical and physical reactions, noting application to Knudsen cell vaporization [AIAA PAPER 67-156] 06 p0956 A67-18321
Upper atmospheric formation of electron cloud produced by chemiluminescence reactions of chemical release agents [AIAA PAPER 67-148] 06 p0995 A67-18360
High temperature condensed phase equilibria in Ti-W-O system examined, using sealed capsule technique 06 p1018 A67-18371
Oxygen atoms association and combination with nitrogen atoms, determining rate constants of reactions 06 p0956 A67-18761
Aluminum fluoride effect on propagative ignition of fuel oxidant mixtures and on combustion between aluminum and oxygen 07 p1238 A67-19070
Isothermal kinetics and self-heating in binary mixtures of Mg and sodium nitrate as function of temperature and reactant composition 07 p1238 A67-19072
Thermal expansion of chemical reaction front in condensed phase 07 p1267 A67-19310
Numerical solution for heat transfer to reversibly reacting gas in turbulent boundary on surface of rotating cylinder 07 p1268 A67-19575
Beta hydroxyvaline synthesis, resolution and configuration 07 p1137 A67-20014
Hydroxyl catalyzed chain decomposition of ozone, proposing new reaction mechanism [JPL-TR-32-1063] 07 p1138 A67-20192
Aerogel Carbothermal Process for oxygen manufacture from lunar resources, discussing experimental results from research operations 08 p1316 A67-21092
Cryochemical synthesis and processing by reacting free radical with excited state species 08 p1290 A67-21187
Complete vibrational population inversion in molecular product of chemical reactions, finding stimulated emission 09 p1511 A67-21746
Ozone formation in photolysis of oxygen and oxygen-helium mixture as function of pressure and temperature 09 p1457 A67-22025
Nickel hydroxide structure, discussing effect of current, charge and electrolyte concentration on production rate 09 p1458 A67-22183
In situ reforming methanol air cell design, construction and expected performance 09 p1445 A67-22186
Theoretical and experimental basis of high performance Mg-air cells, discussing development and performance 09 p1445 A67-22187
Kinetics and mechanism of cathodic oxygen reduction reaction on metal electrodes 09 p1458 A67-22188
Orientation of free radicals in addition reactions with unsymmetrical monolefins 09 p1459 A67-22366
Liquified propane as fog dispersing agent 10 p1676 A67-22814
Temperature measurement methods in sulfur hexafluoride compared with reaction separation 10 p1684 A67-22892
System, incorporating Teflon membrane,

to selectively remove carrier gas from column effluent prior to entry into mass spectrometer 10 p1602 A67-22946
Surface parameter measurements of stannic oxide in powder, ceramic and gel forms by nitrogen adsorption 10 p1603 A67-23398
Hydrazine synthesis from ammonia in concentric barrier discharge reactor 10 p1603 A67-23498
Matched asymptotic expansions method for developing higher order approximations to structure of laminar detonation wave supported by irreversible unimolecular chemical reaction 11 p1749 A67-23858
Constitutive theory for fluid mixtures admitting diffusion and chemical interaction with heat conduction and plane wave propagation 11 p1783 A67-25001
Reactions between alkane and cycloalkane molecular ions analyzed, using conventional and tandem mass spectrometry 12 p1903 A67-25969
Combustion parameters of powders and explosives as function of density of light flux and transparency of burning substance 12 p2039 A67-26113
Alpha particle spectral analysis in various lithium compounds 13 p2159 A67-26435
Inactivation of thermal catalytically active polyanhydro-alpha-amino acids by heating in buffered solution, noting hydrolysis of cyclic imide bonds 13 p2065 A67-26733
Monte Carlo calculation of kinetics of chemically reacting multicomponent gas for finite number of particles followed through random collision processes 13 p2102 A67-26971
Chemical recombination parameters in F layer of day ionosphere determined from electron density profiles 13 p2115 A67-27211
Conversion process and ESR in gamma-irradiated dihydrothymine noting reaction rate 14 p2259 A67-28300
Infinitesimal pressure disturbance propagation in chemically reacting gas, deriving general equation for process, solution shows wavefront propagation at sound velocity [ASME PAPER 67-FE-2] 14 p2304 A67-28355
Steady state approach in competitive-consecutive gas reactions, establishing criterion for approach time estimation 14 p2407 A67-28548
Nickel protective coating on large parts through chemical reduction of nickel salt by sodium hypophosphite, discussing technological and economic aspects 14 p2324 A67-28609
Chemical deposition of dielectrics for thin film circuits and components 14 p2369 A67-28612
Supersonic gas-particle flow with chemical reactions 15 p2469 A67-29225
Thermomechanical theory of diffusing and chemically reacting mixture and application to elastic materials mixture subject to diffusion and heat conduction 15 p2517 A67-29463
Chemiluminescent rate constant increase in reaction of nitric oxide and oxygen in upper atmosphere explained by clustering of former 15 p2434 A67-29884
Silicon nitride deposition on metal coated substrates for studying resistivity, breakdown strength and other electrical properties of thin dielectric films 15 p2540 A67-29932
Nuclear reactor use in space environment as energy source for chemical synthesis and laser action [AAS PAPER 67-115] 15 p2558 A67-29962
Heat resistance of Ti alloys, emphasizing significance of chemical interactions, polymorphic transformations and phase diagrams for high temperature performance 15 p2504 A67-30007
Chemical treatment reducing toxicity of polyvinyl chloride tapes used for insulating electric wires in space 16 p2693 A67-30910
Combustion of hydrogen and hydrazine with nitrous and nitric oxide noting flame speeds and flammability limits of ternary mixtures at sub atmospheric pressures 16 p2779 A67-31519
Sound velocities in granular ammonium perchlorate and potassium chloride, discussing chemical reaction of shocks 16 p2734 A67-31521

Vaporization by dissociation of amine-type perchlorates revealed by infrared spectroscopy, proving role of proton transfer reaction in perchlorates thermal decomposition 16 p2619 A67-31536
Solid solutions of titanium, tungsten, chromium prepared by carbidization of mixtures in hydrogen medium and obtained as fine-grained carbide powders 16 p2691 A67-31587
Chemical reactions in Ni-Ti-Nb system, examining via X-ray diffraction formation of ternary intermetallic compounds 16 p2691 A67-31593
Kinetics of difluoromethylene-nitric oxide reaction, describing experimental apparatus, reaction mechanism, molecule structure and calculating heat of molecule formation 16 p2620 A67-31760
Formation heat of boron trifluoride measured by elements direct combination in bomb calorimeter 16 p2620 A67-31762
H, C, N, O, Cl, Ca and Al negative ion formation in plasma, noting role of continuous radiation, formation temperature and metastable and stable states 17 p2893 A67-32136
Ion-molecular reactions of hydrogen with inert gases caused by low energy electrons in low temperature plasmas, considering energy level populations, reaction cross sections, etc 17 p2808 A67-32141
Kinetic equation for chemical and electron processes in low temperature plasma flows 17 p2896 A67-32169
Gaseous chemical reaction dynamics analyzed with monochromatic laser light-induced photocatalysis 17 p2868 A67-32772
Kinetic and thermodynamic conditions for detonation during chemical reaction in infinite medium involving reaction heat, thermal expansion coefficient and reactants specific volumes 17 p2809 A67-32977
Carbon silica reaction during erosion of silica-phenolic composites noting silica removal mechanisms 17 p2809 A67-33034
Production modes, physical deactivation with related electronic energy transfer and chemical reactions of D oxygen atoms, noting significance for upper atmosphere 17 p2809 A67-33203
Depopulation of vibrational energy levels in fast chemical dissociation reactions 18 p2996 A67-33780
Very low pressure pyrolysis applied to combustion kinetics 18 p3149 A67-33787
Heterogeneous reaction in metal combustion for vapor-phase burning noting collision efficiency 18 p3149 A67-33797
Atomic nitrogen-oxygen mixtures ion concentration enhancement in hydrocarbons presence, discussing atom recombination rate, etc 18 p3107 A67-33805
Gas phase reactions of hydrazine with nitrogen dioxide, nitric oxide and oxygen, determining reaction rates, activation energy and order 18 p3109 A67-33837
Metastable atomic oxygen state observed in microwave discharge of molecular oxygen, noting g factor of 2 in strong resonance 18 p3082 A67-34029
Linear algebra describing equilibrium chemical systems and complex chemical mixtures, discussing hydrogen-fluorine coupling reaction at elevated temperatures 18 p2997 A67-34124
Hydrogen atom-molecule exchange reaction effect on transfer coefficients of dissociating mixture, noting anisotropy and collision integrals 18 p3083 A67-34471
Chain branching during induction period of hydrogen-oxygen reaction studied by shock heating 18 p2998 A67-34519
Reaction mechanism between oxygen difluoride and diborane based on visual observation, gas composition and pressure-temperature relationships [CI PAPER 67-10] 19 p3309 A67-35005
Reaction rate constants for gaseous chemical species at high temperatures [CI PAPER 67-11] 19 p3345 A67-35006
Factors involved in initiation of reaction in cobalt /III/ amine azides, discussing thermal decomposition, activation energy, etc [CI PAPER 67-15] 19 p3309 A67-35009
Dynamic equations for adiabatic changes of state for mixtures of partially ionized gases with chemical reactions 19 p3286 A67-35348
Transient nature of heterogeneous

- boundary layer chemical reaction at stagnation point studied analytically, deriving stability 19 p3211 A67-35740
- Atomization, mixing and reaction characteristics of hydrazine and nitrogen tetroxide injected from quadlet element [AIAA PAPER 67-107] 19 p3310 A67-35766
- Ethylene-oxygen reaction in shock waves, studying induction period and time dependency of mixture composition, ionization and chemiluminescence 20 p3376 A67-36232
- Quadrant mechanical hypothesis /QMh/ on gravitation, gravitational chemistry and zero gravity effects in various chemical processes 20 p3484 A67-36546
- Amino acid formation by formamide thermal decomposition, noting support for hydrogen cyanide oligomerization hypothesis 20 p3376 A67-36700
- Radio carbon dioxide fixation, glutamate labeling and Krebs cycle in ribose-grown *Hydrogenomonas facilis* 20 p3370 A67-36796
- Sterically controlled synthesis of optically active alpha-amino acids from alpha-keto acids by reductive amination 20 p3376 A67-36874
- Nitric oxide reaction with triphenylmethylperoxy radical investigated in connection with study on reversible reaction 20 p3377 A67-37138
- Boundary layer theory applied to laminar flow with chemical reaction, considering coolant blown through porous wall and wall reaction with laminar boundary layer 20 p3424 A67-37345
- Cross section measurement for charge transfer reactions, using crossed ion and neutral beam configuration and product ion mass analysis in nitrogen dioxide production 20 p3377 A67-37404
- Triplet-to-singlet conversion of difluoromethylene radical by self-annihilation, noting reactions with oxygen atoms 20 p3378 A67-37561
- Boundary layer of chemically reacting unstable gas flow along generatrix of body of revolution 21 p3564 A67-38423
- Turbulent gas combustion, showing burning rate as function of combustion temperature, pressure and chemical reaction rate in flame 21 p3732 A67-38527
- Cathodoluminescence device for rapid identification of phase assemblages in solid state reaction system magnesium oxide-magnesium silicate /enstatite/ 21 p3630 A67-38848
- Reaction rates and yield for multichannel molecular collisions, introducing observable yield operator in theory, using motion equations 22 p3757 A67-39635
- Aerothermochemistry of high temperature multicomponent reactive systems, examining thermodynamic and transport characteristics and ionized and dissociated working fluid processes 22 p3921 A67-40447
- Clean MOS structure bias and temperature /BT/ treatment at high electric fields causing electrochemical reaction affecting surface charge density 22 p3774 A67-40461
- Classification of 2-oxazolidones, examining preparation, physical chemistry, properties and polymerized derivatives 23 p3971 A67-41041
- Error in calculating rate coefficients from cross section data in limited energy range, noting m-point Laguerre integration formula 23 p4030 A67-41530
- Heat transfer between gas flows and solid /carbon/ surfaces, considering chemical reactions 24 p4252 A67-41935
- Chemical reaction effect on viscous boundary layer of hypersonic flow of reacting gas mixture past blunt body 24 p4091 A67-42270
- N-vinyl carbazole reactions with anionic initiators, discussing radical anion and polymer formation and ESR spectra [JPL-TR-32-1126] 24 p4118 A67-42601
- Synthesis of biologically pertinent peptides under possible primordial conditions 24 p4118 A67-42606
- Optically active alpha amino acids synthesized from alpha keto acids by hydrogenolytic asymmetric transamination 24 p4119 A67-42703
- Liquid rocket propellant combustion processes covering liquid phase mixing, vaporization, spray formation, atomization, gas-phase mixing and chemical reaction 24 p4256 A67-42720
- Heat and mass transfer in chemically reacting gas mixture compressible boundary layer, determining temperature in reaction zone and on porous plate surface 24 p4256 A67-42734
- Chemical interactions in formation of oxidation resistant solid lubricant composites of tungsten diselenide-gallium alloys for use in ball bearing systems [ASLE PAPER 67-LC-6] 24 p4164 A67-42745
- ### CHEMICAL REACTOR
- Instrument for generation of thermal plasmas in direct current-arc discharges and expansion to walls of coaxial corotating cylinder 17 p2835 A67-33389
- ### CHEMICAL RELAXATION
- #### SA GAS FLOW
- #### SA SHOCK WAVE
- Quantum mechanical theory of microwave nonresonant absorption and dielectric and magnetic relaxation in gases 01 p0116 A67-10145
- Tetrafluoroethylene dissociation in nitrogen behind shock waves and thermoequilibrium constants studied, using shock tube and optical absorption spectroscopy 05 p0759 A67-16840
- Relaxation processes behind shock wave in free stream partially dissociated and vibrationally excited by monitoring time history of radiative emission in shock tube [AIAA PAPER 66-519] 12 p1929 A67-25905
- Digital computer methods for calculating impulsive relaxation in unbalanced hydrogen plasma 15 p2529 A67-29713
- Vibrational and/or chemical relaxation effects behind various shock waves in hypersonic air streams determined for equilibrium and nonequilibrium conditions 19 p3169 A67-34813
- Ionizational relaxation and excitation behind shock waves, proposing solution for kinetic equation system 19 p3293 A67-35403
- ### CHEMICAL STERILIZATION
- Electronic parts sterilization program noting results on capacitors, resistors, varactor diodes, microcircuits, transistors, transformers, diodes and operating temperatures 09 p1480 A67-22296
- Ethylene oxide and methyl bromide mixture for spacecraft sterilization, discussing penetrating power, effect on components and packing and toxicity 15 p2430 A67-29101
- Multifunctional chemical compounds development for use as air revitalization materials 16 p2618 A67-30778
- Spacecraft preparation and sterilization methods including heat treatment, chemical agents, etc 20 p3375 A67-36804
- ### CHEMILUMINESCENCE
- #### SA AIRGLOW
- Chemiluminescent gas phase reactions involving electronically excited oxygen molecules trimethylaluminum and diborane near 3 millitorr 01 p0019 A67-11007
- Upper atmospheric oxygen atom concentration profiles obtained via wind tunnel simulation of NO releases [AFRL-67-0053] 04 p0615 A67-14971
- Spectrum of glow during gas phase reaction of germanium tetrahydride with atomic oxygen, observing new bands of D-X system 06 p0955 A67-17655
- Chemiluminescence from oxygen atom-hydrazine flames suggesting excited NO formed by energy transfer 06 p1072 A67-17987
- Photometric measurements on deviations from equilibrium state in burnt gases of laminar premixed shielded flames at atmospheric pressure [AIAA PAPER 67-9] 06 p1072 A67-18345
- Chemiluminescence of upper atmospheric Ni and rocket probe measurement of Ni atom concentration at night 07 p1182 A67-19951
- Chemiluminescent radiation from interaction of nitric oxide with atmospheric ozone for PCA conditions [AFOSR-67-1379] 10 p1702 A67-23345
- Chemiluminescent reactions of atomic oxygen with carbonyl sulfide and hydrogen sulfide in flow system as function of reaction time and reactant concentrations 14 p2260 A67-28781
- Chemiluminescent rate constant increase in reaction of nitric oxide and oxygen in upper atmosphere explained by clustering of former 15 p2434 A67-29884
- IR chemiluminescence in hydrogen-diatomic bromine and hydrogen-hydrogen bromide IR chemiluminescence in hydrogen-diatomic bromine and hydrogen-hydrogen bromide 18 p2996 A67-33786
- Measurements of induction period, ammonia consumption rate after induction and radiation from electronically excited OH radicals in ammonia-oxygen reaction 18 p3155 A67-33836
- Chain branching during induction period of hydrogen-oxygen reaction studied by shock heating 18 p2998 A67-34519
- Chemiluminescence and chemiluminescence in low pressure fuel-oxygen flames, measuring emission intensity of CH, carbon molecule and OH electronic bands 20 p3376 A67-37094
- Chemiluminescent radiation from far wake of hypersonic spheres launched from light gas gun measured with filtered photomultiplier 23 p3931 A67-41712
- ### CHEMISORPTION
- Electron processes at semiconductor surface in presence of chemisorption, noting conductivity and impurity distribution 03 p0492 A67-13315
- Oxygen chemisorption and oxidation on tungsten ribbon studied by flash desorption, using mass spectrometer 09 p1457 A67-22023
- Impurity free CsF effect on work function of tungsten surface, discussing amount of impurities, type and control 09 p1450 A67-22354
- Detection of vibrational structure of gases adsorbed on tungsten by low energy electron scattering 13 p2160 A67-27075
- Surface reactions and structure determinations of oxides of niobium, tantalum and vanadium with /110/ surfaces from CO and oxygen absorption 15 p2504 A67-29881
- Carbon monoxide chemisorption on polycrystalline molybdenum studied by radiotracer, noting desorption at various temperatures as time function 15 p2434 A67-30099
- Electron processes at semiconductor surface in presence of chemisorption, noting conductivity and impurity distribution 16 p2724 A67-30491
- Barium adsorption on individual crystal planes of tungsten field emitter studied for thermally equilibrated and unequilibrated adsorbate layers 17 p2922 A67-33259
- Molecular sink for simulated testing of spacecraft components noting vessel construction, vacuum pump system, molecular trap array, etc 18 p3019 A67-33547
- Water adsorption on oxide covered surface of germanium, studying chemisorption dependence on p-type doping 19 p3301 A67-34935
- Structure of surfaces - Conference, Durham, N.C., November 1966 19 p3246 A67-35782
- Low energy electron diffraction /LEED/ observations of interaction of tungsten surface with adsorbates 19 p3246 A67-35785
- Measurement of work function changes of nickel films for oxygen and hydrogen chemisorption 19 p3246 A67-35787
- Radioactively labeled coupling agents adsorption on E-glass surfaces, noting continuous film formation with covalent bonding occurring at interface 20 p3474 A67-37269
- Mass spectrometric study of oxygen adsorption, determining condensation coefficient and tungsten surface work function for various concentrations 24 p4172 A67-42073
- ### CHEMISTRY
- #### SA AEROTHERMOCHEMISTRY
- #### SA ANALYTICAL CHEMISTRY
- #### SA ATMOSPHERIC CHEMISTRY
- #### SA BIOCHEMISTRY
- #### SA ELECTROCHEMISTRY
- #### SA GEOCHEMISTRY
- #### SA ORGANIC CHEMISTRY
- #### SA PHOTOCHEMISTRY
- #### SA PHYSICAL CHEMISTRY
- #### SA PHYSIOCHEMISTRY
- #### SA PLASMA CHEMISTRY
- #### SA POLYMER CHEMISTRY
- #### SA PROPELLANT CHEMISTRY
- #### SA RADIOCHEMISTRY
- #### SA STEREOCHEMISTRY
- #### SA SURFACE CHEMISTRY
- #### SA THERMOCHEMISTRY
- Soviet book on solid state chemistry and electroconductivity of chemical

- systems 06 p1052 A67-18608
- CHINOOK HELICOPTER**
- S CH-47 HELICOPTER**
- CHIRP SIGNAL**
- Digital /chirp/ radiosonde for meteorological and earth satellite measurements employing pulse bursts from voltage controlled oscillator 10 p1655 A67-22823
- RF pulse compression by chirped shear microwave sound in sapphire, inducing self-focusing of Bragg diffracted light 24 p4188 A67-42369
- CHLORELLA**
- Mixed cultures of *Chlorella pyrenoidosa* TX 71105 and various bacteria and use in closed systems for support of man 10 p1598 A67-23626
- Space flight factors effect on mutability, survival rate and dynamics of cells of inactive cultures of *Chlorella* on board Cosmos 110 13 p2060 A67-27336
- Physiological-ecological investigations of *Chlorella* cultures as link in closed ecological system 16 p2617 A67-30775
- Continuous synchronous culture of photosynthetic microorganism *Chlorella* cultivated in illuminated and dark stirred tanks 19 p3177 A67-34913
- Cell survival rates and mutation development in *Chlorella vulgaris* plants carried by Cosmos 20 p3367 A67-36256
- Human natural immunity with respect to substitution of *Chlorella* proteins for animal proteins, studying lysozyme activity in saliva and blood serum 20 p3368 A67-36269
- Growth rate limitations with interactions of light and carbon dioxide investigated for two species of *Chlorella* 20 p3369 A67-36791
- Secretory activity of algal *Chlorella* cells effect on buffering characteristics of Tris or sodium citrate-citric acid suspending fluid 21 p3573 A67-37729
- Prolonged *Chlorella* cultivation with recovery of medium without impairing production rate 24 p4114 A67-41846
- CHLORIDE**
- SA AMMONIUM CHLORIDE
- SA BERYLLIUM CHLORIDE
- SA CARBON TETRACHLORIDE
- SA COPPER CHLORIDE
- SA GERMANIUM CHLORIDE
- SA HYDROGEN CHLORIDE
- SA LANTHANUM CHLORIDE
- SA LITHIUM CHLORIDE
- SA POLYVINYL CHLORIDE
- SA POTASSIUM CHLORIDE
- SA SILICON TETRACHLORIDE
- SA SILVER CHLORIDE
- SA SODIUM CHLORIDE
- Refractory metal chlorides reacted with methane and nitrogen in hydrogen jet to form carbides and nitrides 03 p0440 A67-12925
- Lasing on Si II and Cl II lines in pulsed gaseous discharge, noting possible mechanisms for achieving population inversion 15 p2496 A67-29178
- CHLORINE**
- Three new visible CW laser lines in discharge in singly-ionized Cl 01 p0089 A67-10373
- Chlorine abundance and distribution in iron meteorites from neutron activation analysis and metallographic examination, discussing terrestrial contamination effects 24 p4232 A67-42610
- CHLORINE COMPOUND**
- S PERCHLORIC ACID**
- CHLORINE TRIFLUORIDE**
- Ignition of hydrogen-oxygen propellant combination by chlorine trifluoride 10 p1697 A67-23132
- CHLOROBENZENE**
- Mass transfer measurements of paradichloro benzene cylinders at various turbulent intensities and angles of attack, showing free flow turbulence effect on local mass transfer coefficient 04 p0548 A67-15493
- CHLOROPHYLL**
- Deaggregation of chlorophyll by xanthophylls 09 p1454 A67-21990
- CHLOROPLAST**
- Fluorescence induction in isolated chloroplasts analysis yielding method to determine amount of light used in process 07 p1134 A67-19846
- Separation of digitonin treated chloroplasts by differential centrifugation into fractions showing distinct pigment and photochemical differences 07 p1134 A67-19847
- CHOKER**
- Thermal choking in various devices having mixing processes between two flows with different stagnation enthalpies as possible limitation of mass flow rate [ONERA-TP-411] 05 p0792 A67-16934
- Multiple-winding choke design replacing separate inductors in filtering circuit and reducing power supply size and weight 20 p3399 A67-36882
- CHOLESTEROL**
- Cholesteric liquid crystals and use in visualizing small thermal gradients for thermal nondestructive testing 02 p0250 A67-12538
- CHOLINE**
- S ACETYLCHOLINE**
- CHONDRITE**
- SA ACHONDRITE
- SA CARBONACEOUS METEORITE
- Lanthanide abundance variation and coordination number, comparing abundances in terrestrial and meteoritic materials with average chondrite 03 p0413 A67-13507
- Total carbon abundances in enstatite chondrites 05 p0886 A67-16024
- Primordial argon and metamorphism of chondrites 05 p0886 A67-16025
- Chemical analysis of stony meteorites, noting analytical procedures and results 05 p0895 A67-16581
- Diffusive fractionation and two-component models for trapped meteoritic neon and isotopic composition of neon in carbonaceous chondrites 07 p1249 A67-19536
- Petrology and mineralogy of British Museum noncarbonaceous chondrites and relative abundance of primitive and recrystallized variants by isochemical recrystallization near 900 degrees C 07 p1249 A67-19538
- Chemical and mineralogical composition of roedderite found in Indarch meteorite, presenting electron probe analysis and X-ray diffraction pattern optical data 07 p1255 A67-20012
- Iron-rich silicates significance in Mezo-Madaras chondrite [AFCL-67-0012] 07 p1256 A67-20013
- Chondrite metallic minerals, thermal history and parent planets noting nickel, taenite and kamacite crystal components 08 p1397 A67-21207
- Equilibrium temperatures of Fe and Mg ions in chondritic meteorites 08 p1400 A67-21266
- Xenon 129 and tellurium 128 formation intervals in chondritic meteorites as measure of neutron induced isotope production by solar nucleosynthesis 09 p1570 A67-22694
- Origin of chondrites implied by short period and long period nuclides created by neutron fluxes 10 p1704 A67-22849
- Meteoritic, solar and terrestrial rare earth distribution abundance in chondritic or ordinary stony meteorites 10 p1851 A67-23428
- Aliphatic hydrocarbons in meteorites, examining distribution of isoprenoid and other compounds via gas chromatography and mass spectrometry 10 p1709 A67-23489
- Short period radioactive nuclides induced by secondary neutron due to solar cosmic radiation in chondrites 11 p1858 A67-24058
- Hypersthene chondrite origin and history studied using noble gas content and shock and reheating by X-ray diffraction 11 p1865 A67-24602
- Cosmic ray spallation and special anomaly in achondrites 11 p1866 A67-24696
- Amphibole richterite found in graphite nodules of iron meteorite, using electron microprobe and X-ray powder diffraction 11 p1868 A67-24873
- Xenon-iodine dating, sharp isochronism in chondrites 12 p2002 A67-25525
- Nogoya type II carbonaceous chondrite noting cosmogenic, radiogenic and primordial noble gas components 14 p2390 A67-28890
- Chondritic meteorites two-dimensional classification grid based on chemical and petrologic subdivisions 14 p2391 A67-28949
- Element abundance in various chondrite groups determined by neutron activation technique 14 p2391 A67-28950
- Abundant lithophile element fractionations in chondrites with special reference to aluminum and calcium 14 p2391 A67-28951
- Farmington chondrite meteorite observations show two small granular cristobalite xenoliths surrounded by thin diopside clinopyroxene reaction rim 15 p2556 A67-29647
- Preferred shape orientation of olivine crystals in porphyritic chondrules suggesting drawing from larger magma bodies 16 p2619 A67-30986
- Light and heavy rare gases content in St Severin meteorite and iron-enriched fractions 16 p2750 A67-31435
- Argon, krypton and xenon in chondrites noting constant abundance ratios and correlation of concentration to disequilibrium 16 p2750 A67-31436
- Petrographic and microprobe analysis of unequilibrated ordinary chondrites, studying textural, mineralogical and chemical characteristics 16 p2750 A67-31451
- Olivine composition in chondrites relative abundances and classification 16 p2751 A67-31455
- Chemical analyses of stony meteorite and iron meteorite with silicate inclusions 16 p2751 A67-31456
- Chondrites metamorphosis and equilibrium, studying iron oxide and rare gas content, petrological factors and material formation 18 p3134 A67-34494
- Primordial rare gases abundances in unequilibrated ordinary chondrites determined by mass spectrometry 19 p3317 A67-34912
- Condensation history of cooling gas of cosmic composition, stressing chondrite fractionation patterns 20 p3526 A67-37172
- Abundance of volatile elements in meteorites, comparing chondrite decrease for evidence of fractionations in solar nebula 20 p3526 A67-37173
- Chemical analysis and normative mineral composition of Winona meteorite, showing relation to chondrites 21 p3702 A67-38067
- Chondrites solidification age measured via rubidium-strontium pairs in component minerals, using phase separation method 21 p3702 A67-38125
- Ferrous ion order-disorder in meteoritic pyroxenes, using Moosbauer iron 57 absorption, noting metamorphic history of chondrites 21 p3702 A67-38128
- Meteoritic organic chemical analyses since 1900, considering volatile materials distribution and carbonaceous chondrites 21 p3704 A67-38502
- Uranium content of chondrites measured by thermal neutron activation and delayed neutron counting 21 p3704 A67-38505
- Krypton isotope composition in three unequilibrated and two gas rich chondrites, with correction for cosmic ray spallation 22 p3881 A67-39494
- Fremont Butte, Colorado, meteorite noting external form, structure and composition 23 p4069 A67-41448
- Indium concentrations determined by neutron activation in petrological suite of L-group chondrites 23 p4069 A67-41474
- Chromite composition in chondrites using electron microprobe technique, discussing petrographic origin and vanadium abundance 24 p4232 A67-42612
- Hypersthene chondrite postformational history, discussing native copper and ilmenite content of Newmann lamellae and flowage 24 p4232 A67-42613
- Iodine, uranium and tellurium abundances in various achondrites, chondrites and mesosiderites from neutron activation analysis 24 p4233 A67-42616
- Precious metal concentrations in carbonaceous and enstatite chondrites using neutron activation analysis 24 p4233 A67-42617
- Type I carbonaceous chondrite flakes from British Columbia meteorite fall 24 p4233 A67-42618
- Shaw meteorite noting chondrite composition, lack of chondrite structure and Ca content suggesting high crystallization temperature 24 p4234 A67-42624
- Xenon data from Murray and Renazzo carbonaceous chondrites reinterpreted, discussing large presence of fissionogenic xenon 24 p4234 A67-42626
- Cl, Br and I abundances in carbonaceous chondrites analyzed by neutron activation in estimating primordial halogen abundance ratios 24 p4234 A67-42628
- Coexisting minerals and interstitial groundmass of chondrules of Mezo-Madaras chondrite 24 p4235 A67-42633

Re and Os abundances in various chondrites determined by neutron activation analysis, noting
 fractionation 24 p4235 A67-42637
 Stony meteorite Fe, Ni, Co, Ca, Cr and Mn concentration determined by X-ray fluorescence 24 p4235 A67-42638
 Total carbon content and primordial rare gases in chondrites 24 p4236 A67-42641
 Chromite and chromite chondrules in chondrites noting formation at very high temperatures and rapid cooling 24 p4236 A67-42642
 Silicon abundances in chondrules from different chondrites by neutron activation analysis 24 p4236 A67-42644
 Alkali, alkaline earth and rare earth elements distribution in chondrite component minerals 24 p4236 A67-42646
 Mezo-Madaras chondrite polymict structure differs from structure in light-dark meteorites 24 p4237 A67-42648
 Olivine and pyroxene composition distribution in type II carbonaceous chondrites, discussing metamorphic effects and gas-dust fractionation 24 p4237 A67-42651
 Cosmogenic radioactivity in freshly fallen meteorites measured and compared to calculate terrestrial and exposure ages and spatial and time dependence 24 p4238 A67-42884

CHOPPER

Very high input impedance direct current chopper amplifier using field effect transistor characterized by very low gate leakage current and capacitance 03 p0389 A67-14378
 Chopper circuit theory and design methods with DC amplifier comparison 08 p1302 A67-20991
 Modulated molecular beam apparatus with chopper used in conjunction with field emission microscope for studies of atomic interactions with surfaces 09 p1499 A67-22114

CHORUS PHENOMENON

SA WHISTLER

Relations between VLF emissions of whistler and dawn chorus types and that of ULF emissions /pearl type oscillations and rapid irregular pulsations/ 04 p0617 A67-15500
 Whistler recordings on thermal plasma motions and ionization density near magnetospheric knee, noting whistler attenuation VLF noise, ion effects, electron temperature, etc 05 p0795 A67-16011
 Hook whistler discovered in VLF radio noise data from Injun III satellite, noting time delay difference between components 05 p0799 A67-16888
 ULF radio emission of upper atmosphere and other related geophysical phenomena, analyzing hisses, choruses and contribution to earth radiation belt 08 p1324 A67-20862
 Simultaneous recordings of cosmic noise absorption and VLF chorus, noting correlation from riometer recordings 08 p1327 A67-21374
 Whistler observations near Sofia and in Czechoslovakia 14 p2307 A67-27914
 Satellite and ground observations of VLF emissions, summarizing intensity, diurnal and seasonal variation, emphasizing chorus and hiss characteristics 22 p3794 A67-40083

CHROMATE

SA POTASSIUM CHROMATE

Raman effect in solutions of potassium, sodium and ammonium dichromate and potassium dichromate single crystal 19 p3240 A67-35421
 Chromate conversion process applicable to IC interconnecting aluminization reveals defective areas under normal quality control procedures 22 p3771 A67-39835

CHROMATOGRAPHY

SA GAS CHROMATOGRAPHY

SA PAPER CHROMATOGRAPHY

Gel permeation chromatography for analytical fractionation of propellant binder prepolymers and separating and purifying labile binder ingredients 04 p0686 A67-14472
 Deaggregation of chlorophyll by xanthophylls 09 p1454 A67-21990
 Spectrometric investigation of Mars in five spectral regions applied to color analysis of Martian continents and oceans for probable coloring of Martian vegetation 11 p1867 A67-24845
 Thin film circular chromatography for determination of diphenylamine derivative products in propellant

powders 13 p2185 A67-26425
 Chromatographic accumulation of primary and secondary carotenoids in Spongiochloris typica over 8-week period 14 p2254 A67-28065
 Color contrast penetration method for crack detection in aircraft engines and motor car parts 18 p3045 A67-33739
 Bezold-Brucke hue shift measurements in color naming situation using optical system 22 p3835 A67-39238
 Adsorption equilibrium data obtained at high pressure for methane and propane on silica gel using radioactive tracer pulsing 24 p4118 A67-42584

CHROMIUM

Recovery and recrystallization of high purity warm-worked chromium sheet material 03 p0439 A67-12924
 Cr-SiO cermet material used in precision thin film resistors for monolithic integrated circuits 03 p0381 A67-13663
 Quartz crystal oscillator measurements of effect of film deposition rate on resistance of chromium thin films 04 p0675 A67-14921
 X-ray Debye temperature thermal variation measurements of pure nickel and chromium 06 p1015 A67-17850
 Energy transfer from single chromium ions to closely coupled pairs of chromium ions in ruby 07 p1234 A67-20124
 Ultramafic rock content of Na, Mn, Cr, Sc and Co determined by neutron activation technique 07 p1183 A67-20142
 Self-lubricating properties of composites of porous nickel and nickel-chromium alloy impregnated with barium fluoride-calcium fluoride eutectic [ASLE PAPER 66AM IC2] 08 p1335 A67-21035

Rare earth metals effect on Neel temperature and plasticity of recrystallized chromium at 1200 degrees C in vacuum 13 p2131 A67-26450

Relation between chromium cold-shortness temperature variations and structural changes under deformation, noting dependence on initial metallographic grain size 13 p2141 A67-27284

Far IR absorption spectra of chromium and titanium ions in aluminum oxide crystal, indicating Jahn-Teller effect reduction of trigonal field and spin-orbit coupling 14 p2370 A67-28714

Hydrostatic pressure effects on brittleness in Cr and yielding in center annealed iron specimen studying brittle-ductile transition of former 16 p2689 A67-31328

Chromizing of steel by HF induction heating in vacuum using low-carbon ferrochrome and electrolytic chromium mixture 19 p3236 A67-34920

Chromium distribution in laser rubies with neutron activation 20 p3458 A67-36427

Lifetime decrease of metastable state of chromium ion in ruby and emerald due to temperature raise, showing radiative transition 21 p3676 A67-37816

Photoconductivity measurements for chromium doped seminsulating gallium arsenide, discussing response peak and possible mechanisms 22 p3855 A67-39348

CHROMIUM ALLOY

Cutting ability of high melting binder cemented carbides with Cr and V alloys 01 p0100 A67-10724

Dispersion-strengthening by formation of carbides of Hf, Zr, Ta, Ti and Nb in wrought and recrystallized Cr, discussing structural stability 01 p0100 A67-10766

Forging and solution treating nickel-chromium alloy 718 to investigate notch ductility and uniform grain size 04 p0640 A67-15459

Structural changes during oxidation of chromium-yttrium alloys determined by measuring gain in weight per unit surface of samples heated in Silt or molybdenum oven in open alumina tubes 05 p0827 A67-16327

Nitrogen behavior in Cr-Y alloy of varying interstitial concentration and thermal history 06 p1016 A67-17898

Molybdenum effect on properties of chromium-nickel alloy, noting hardness and strength 06 p1018 A67-18229

Nickel-chromium alloys with niobium in study of precipitation hardening and hardness 06 p1018 A67-18230

Atmospheric nitrogen contamination effect on tensile creep of chromium-tantalum

alloys 06 p1018 A67-18369
 Isothermal transformations in hypo-and hypereutectoid titanium-chromium alloys 07 p1200 A67-19244
 Chemical and crystal structural analysis of solid solution of titanium chromide and zirconium chromide 07 p1204 A67-19265
 Metallides 07 p1204 A67-19265
 Tensile creep properties of chromium alloys affected by type of ceramic used as heating element core 08 p1341 A67-20766
 Fracture behavior of creep resistant alloy steel and nickel-chromium alloy subjected to cyclic loading at elevated temperatures 09 p1517 A67-21556
 Deoxidative capacity and activity of titanium in nickel-chromium alloys 09 p1518 A67-21964
 Cumulative strain behavior of nickel-chromium alloy and chromium martensitic type steel under action of cyclic loading 12 p2015 A67-25420
 Internal friction in nickel chromium alloys heated to annealing temperature, noting 530 and 800 degree peaks and origin of latter 14 p2338 A67-28675
 Metallography, roentgenography and differential thermal analysis of composition temperature ranges of chromium-germanium phases 16 p2691 A67-31592
 Iron-chromium-bauxite cermets preparation and properties 18 p3065 A67-34260
 Chromium activities in binary Cr-Ti solid solutions measured by Knudsen effusion technique, noting deviations from Raoult law and free energy calculation 20 p3469 A67-37384
 Precipitation processes in Ta-Cr solid solutions investigated for temperature dependence and change in alloy properties resulting from precipitation 23 p4018 A67-40712

CHROMIUM CARBIDE

Neutron bombardment effect on titanium and chromium carbides before and after heat treatment, giving results of X-ray and micrographical analyses, electric resistance, brittleness and microhardness measurements 03 p0447 A67-13639

Vapor composition, evaporation rate and vapor pressure above chromium carbides determined by effusion method combined with mass spectrometry 03 p0456 A67-14193

Solid solutions of titanium, tungsten, chromium prepared by carbidization of mixtures in hydrogen medium and obtained as fine-grained carbide powders 16 p2691 A67-31587

Two-stage heat treatment effect on strength of high temperature Nimonic 80 alloy noting high brittleness, grain size and boundaries and fracture propagation 23 p4019 A67-41076

Nickel on chromium carbide base cermet polishing by synthetic diamond wheels shown to have little effect on strength 24 p4159 A67-41963

CHROMIUM COMPOUND

Heat resistance of Ni alloys with oxides noting experimental procedure, and effect of various additives 16 p2690 A67-31433

X-ray absorption in chromium in chromium silicon after thermal processing at high temperatures 17 p2921 A67-32893

CHROMIUM OXIDE

Electrical and optical properties of solid solutions formed by beta manganese and chromium dioxide within wide composition range, showing magnetic semiconductor behavior 01 p0134 A67-10755

Dependence of intrinsic noise temperature of ruby reflection maser on helium bath temperature and chromium trioxide doping, using circulator 10 p1665 A67-23505

Structures in Mo-Re and W-Re systems examined by X-ray powder techniques, discussing occurrence of chromium oxide type structure 17 p2873 A67-32813

Chromium oxide addition effect on ruby recrystallization in carbonate and bicarbonate solutions under hydrothermal conditions, estimating chromic oxide solubility 21 p3685 A67-38971

Chromite and chromite chondrules in chondrites noting formation at very high temperatures and rapid cooling 24 p4236 A67-42642

CHROMIUM STEEL

Mechanical properties of Kh21G7AN5 steel at liquid hydrogen temperature 04 p0636 A67-14751

- Stability of austenite in some Fe-Cr-Ni alloys under low temperature strain 04 p0636 A67-14753
- Endurance and creep of chromium steels with extended thermal treatment 06 p1018 A67-18228
- Niobium effect on structure and properties of chromium-manganese steels as active nitride and carbide forming agent increases deformation resistance 08 p1343 A67-21206
- Cumulative strain behavior of nickel-chromium alloy and chromium martensitic type steel under action of cyclic loading 12 p2015 A67-25420
- Molybdenum and niobium effect on structure and physical properties of austenitic Cr-Mn steels with or without nickel 12 p1955 A67-25439
- Aluminum content effect on stress-rupture properties of chromium-molybdenum-vanadium steel, noting notch sensitivity and ductility 16 p2693 A67-31869
- Fatigue characteristics of chromium-molybdenum steels subjected to various heat treatments, comparing tension-compression and torsion 18 p3065 A67-34258
- Mechanical properties of Kh21G7AN5 steel at liquid hydrogen temperature 18 p3066 A67-34409
- Stability of austenite in some Fe-Cr-Ni alloys under low temperature strain 18 p3066 A67-34411
- Elongation and failure of chromium-molybdenum-vanadium steel analyzed from creep test results 20 p3464 A67-36477
- Structural stability of welded joints of chromium steel used in power plant construction examined for structural stability 23 p4019 A67-41077
- Fatigue behavior of Cr steel and Ni-Cr alloy examined for influence of direction of first loading stroke of push-pull testing 23 p4019 A67-41155
- CHROMOSOME**
- SA BIOLOGICAL CELL
- SA GENETICS
- Chromosome configuration and mitosis impairment in micropores Tridacantha paludosa due to space flight effects of Voskhod I 07 p1133 A67-19109
- Recessive lethals in X chromosome of drosophila and genetic shielding during flight of spaceship 13 p2060 A67-27337
- Space flight effect on chromosomes of dry seed embryos, noting no significant change 13 p2061 A67-27344
- CHROMOSPHERE**
- Solar prominences, proton flares and chromospheric flares in intensity of corona and solar radio emission and sunspots, noting maxima during eleven-year solar activity cycle 01 p0146 A67-11281
- Radial extension of corpuscular flux from chromospheric flares and duration of earth immersion in flux 02 p0306 A67-11653
- Synthetic line profiles generated for variety of model atmospheres containing linear and quadratic velocity fields, used to analyze solar chromosphere 02 p0323 A67-11690
- Radiative energy loss from solar chromosphere and corona estimated in order to identify mechanical energy input mechanism 02 p0323 A67-11692
- Limb intensity profiles at center of hydrogen alpha calculated for several simple models of absorption coefficient at line center, showing abrupt changes in gradient 02 p0323 A67-11693
- Line emission of hydrogen alpha limb spectra beyond continuum limb analyzed to yield data about height of formation in solar chromosphere 02 p0323 A67-11694
- [AFRL-66-834]
- Spectrophotometric study of hydrogen alpha, beta, gamma, epsilon and hydrogen and K spectral lines of chromospheric flare of August 21, 1959 02 p0308 A67-11850
- H-alpha line profiles and motions of spicules in solar chromosphere studied by spectral photographs taken with noneclipse coronagraph 02 p0328 A67-12483
- He I excitation as result of ionization and recombination at chromospheric spicule temperature 02 p0328 A67-12484
- Electron concentration in metallic emission regions in chromosphere 02 p0328 A67-12485
- Relation between Forbush decreases and chromospheric flares, obtaining longitudinal distributions before and after onset, using statistics 02 p0311 A67-12592
- Solar chromospheric structure noting network pattern of absorption in He 10830 angstrom region 03 p0514 A67-14312
- Solar corona and chromosphere activity observations at lunar observatory in gamma, X-ray and XUV regions 04 p0598 A67-15071
- Spectrophotometric results for H-alpha and K line contours of August 21, 1959 chromospheric flare 05 p0892 A67-16496
- H-alpha, H-beta, H-gamma, H-epsilon, H-8, H-11, H-12 and H-13 line emission of June 25, 1960 chromospheric flare 05 p0893 A67-16497
- Large deuterium isotope effect on fluorescence emission spectra and quantum yields observed in number of chromospheres that contain proton donor groups 05 p0758 A67-16701
- Three-dimensional oscillatory motions generation and propagation in solar atmosphere 05 p0900 A67-17074
- Acoustic wave propagation characteristics in solar chromosphere, discussing resonant frequencies 05 p0900 A67-17075
- Deformation of Fraunhofer line linked to sound waves in solar disk 05 p0900 A67-17076
- Coronal temperature and temperature distribution in transition region between chromosphere and corona, assuming photospheric wave propagation as essentially one-dimensional 05 p0900 A67-17077
- Spectrophotometric study of H, K and He spectral line characteristics of chromospheric flare of June 25, 1960 07 p1247 A67-19166
- Small two-dimensional oscillations in XY plane for isothermal magnetosphere in uniform gravitational field, postulating Boltzmann equilibrium density distribution 07 p1173 A67-19699
- LF gravitational-acoustic and internal gravity mode wave propagation in temperature-stratified photosphere-low chromosphere region and solar atmospheric resonant responses 08 p1399 A67-21236
- Ionograms of chromospheric eruptions with eruptive filament of December 1965, obtaining morphological data and determining radiation frequency range 09 p1561 A67-21842
- Extreme UV emission, discussing chromospheric coarse mottling and network characteristics of He II 304 10 p1707 A67-23224
- H-alpha line profiles and motions of spicules in solar chromosphere studied by spectral photographs taken with noneclipse coronagraph 10 p1708 A67-23351
- He I excitation as result of ionization and recombination at chromospheric spicule temperature 10 p1708 A67-23352
- Electron concentration in metallic emission regions in chromosphere 10 p1708 A67-23353
- Chromospheric background intensity difference between equatorial and polar regions of sun 10 p1711 A67-23800
- Homogeneous solar photosphere and lower chromosphere model in hydrostatic and local thermodynamic equilibrium, reproducing continuous and line spectrum 11 p1858 A67-24112
- Solar chromospheric model composed of four discrete groups of filaments 12 p2001 A67-25221
- Motions of chromospheric fine structure in weak plage analyzed, using time resolved H-alpha spectra for estimating line-of-sight velocities of objects 12 p2001 A67-25222
- Evershed effect observations suggest existence of two or more streams in both photospheric and chromospheric Evershed flows 13 p2204 A67-27429
- Sunspot groups and chromospheric features associated with magnetic fields of active region in light of supergranular structure of solar atmosphere 13 p2204 A67-27434
- Sunspot structure, discussing photospheric model, magnetic field influence, MHD structure and energy balance, and photospheric and chromospheric parts 13 p2205 A67-27438
- Heating of chromosphere above sunspot due to magnetoacoustic waves which develop into weak shock waves 15 p2551 A67-29142
- Large scale structure of chromosphere examined using birefringent filter, comparing filtergrams with spectroheliograms of perturbed and active regions of solar disk 15 p2552 A67-29143
- Chromospheric solar radiation measured during solar eclipse with UV monochromator, using electromagnetic radiation photomultipliers 15 p2565 A67-29573
- Radial extension of corpuscular flux from chromospheric flares and duration of earth immersion in flux 16 p2738 A67-31068
- Chromosphere and corona UV emission spectrum provided by sounding rocket using photographic recordings 16 p2752 A67-31625
- Solar cosmic ray generation, discussing chromospheric eruptions, spectra, chemical and nuclear composition, particle acceleration, etc 17 p2934 A67-32095
- Motion of shocks through chromosphere under guidance of magnetic fields 17 p2944 A67-32642
- Kinetic energy transport outwards in transition region between chromosphere and corona discussed qualitatively, postulating connection with spicules 17 p2952 A67-33393
- Influence of dissipation of acoustic waves on temperature rise in chromosphere 18 p3125 A67-34192
- Gravitational model for chromosphere flarelike brightenings following dispartitions brusques, examining prominence and chromospheric characteristics 19 p3324 A67-35437
- Solar flare electron density measurements using half-width method, noting variations with height, development and area 19 p3314 A67-35439
- Resonance line profiles for Ca II and Mg II in lower solar chromosphere, noting interlocking effect 19 p3325 A67-35504
- Magnetic effect on polarization of resonance radiation in solar chromosphere 21 p3709 A67-38989
- Radio observations to estimate chromospheric parameters by measuring fluctuation correlation function of solar radio emission flux 22 p3886 A67-40127
- Cosmic ray intensity increase in wake of chromospheric flares from stratospheric measurements 23 p4057 A67-41115
- Velocity fields in solar photosphere and chromosphere, discussing granulation, supergranulation, magnetic fields and oscillatory motions 23 p4068 A67-41276
- Heating of chromosphere above sunspot due to magnetoacoustic waves which develop into weak shock waves 24 p4239 A67-43065
- Large scale structure of chromosphere examined using birefringent filter, comparing filtergrams with spectroheliograms of perturbed and active regions of solar disk 24 p4239 A67-43066
- CHRONOLOGY**
- German book on space chemistry covering age and origin of earth, meteorites, tektites and impactites 12 p1903 A67-25427
- Geochronology for earth and components using radiometric and thermoluminescence methods 12 p1903 A67-25428
- Research into geological history of planetary bodies without atmosphere, discussing techniques for determining time of formation of layered ejecta units 16 p2747 A67-30988
- CHRONOTRON**
- SA PULSE RATE
- SA TIME DELAY
- Multichannel tunnel diode chronotron circuit for measuring picosecond time intervals directly with sequence of timing circuits 02 p0246 A67-12684
- Chronotron type device for measuring zenith and azimuth angles of slope of axes of extensive air showers 03 p0425 A67-14263
- Chronotron type device for measuring zenith and azimuth angles of slope of axes of extensive air showers 14 p2321 A67-28775
- CHUGGING**
- Stability boundaries of double-dead-time model describing chugging in liquid bipropellant rocket engine 24 p4207 A67-42689
- CINEMATOGRAPHY**
- Film transport methods and other factors relating to high speed frame cinematography 14 p2315 A67-27871
- Characteristic momentary pictures of two-dimensional electromagnetic wave fields with all boundaries conformally transformed into parallel planes, taken from motion picture 14 p2268 A67-28447
- Special lighting equipment for high speed

cinematography delivering high intensity light pulses in nanosecond range for use in shock wave and explosion filming 14 p2319 A67-28585
Shutter speed and illumination data for cinematographic documentation of total solar eclipse 15 p2555 A67-29576
Time-microscopy methods using laser flashlight, roentgen flashlight and rapid succession spark pulses in combination with stereo cameras 17 p2864 A67-33408

CINETHEODOLITE

Mobile Cinetheodolite Mount design and operation for missile tracking 06 p1001 A67-17794

CIRCADIAN RHYTHM

Biomedical assessments of human circadian system, noting increase in subjective fatigue and psychological and physiological performance 01 p0016 A67-10955

Phase shifts of human circadian system and performance deficit during periods of transition in north-south flight 05 p0756 A67-16289

Cardiovascular and renal 24 hr synchronized and desynchronized circadian rhythm 11 p1747 A67-24785

Diurnal rhythm of cardiovascular responses to active orthostasis and Schneider test performance in function diagnostics of peripheral cycle regulation [DVL-620] 11 p1747 A67-25035

Biological clocks and cycles in man, lower animals and plants, discussing circadian rhythms 13 p2058 A67-26607

Model equation for circadian periodicity 13 p2058 A67-26629

Circadian rhythms detection, estimating parameters by cosinor procedure for temporal morphology aspects evaluation 14 p2255 A67-28480

Free-running circadian oscillations noting nature of driving oscillation, physiology of circadian organization and relation to manned space flight 15 p2425 A67-29107

Phase shifts in human circadian system noting individual differences, performance deficit, physiological changes and dissociation from time zone displacements 15 p2425 A67-29108

Human circadian rhythms in activity, body temperature and other physiological functions, discussing oscillator multiplicity, internal desynchronization and entrainment 15 p2426 A67-29110

Circadian clocks - Conference, Feldafing, West Germany, September 1964 20 p3370 A67-36805

Biological effects of time-zone changes on circadian rhythms of urinary elimination of potassium and 17-hydroxycorticosteroids 22 p3751 A67-39606

Circadian oscillations of deep body temperature and heart rate in ambulatory primate in controlled environment 23 p3951 A67-41554

Isolation effects in constant environment on cycles of physiological functions and performance levels of man 23 p3959 A67-41697

CIRCLE**SA MOHR CIRCLE****SA RING**

Conformal mapping of circle onto profile cascades with arbitrary parameters useful for exact computation of potential flow through cascade 01 p0005 A67-10277

Limiting conditions for polynomials orthonormal on unit circle for nonnegative summable 2- π -periodic weight function 03 p0456 A67-12885

Intermediate value and simultaneous convergence obtained by sequence of polynomials for pair of functions on closed set E dense on norm z equals one 07 p1215 A67-19221

CIRCUIT**SA BISTABLE CIRCUIT****SA EXPLODING CONDUCTOR CIRCUIT****SA FLIP-FLOP****SA INDUCTOR****SA INTEGRATED CIRCUIT****SA LC CIRCUIT****SA LINEAR CIRCUIT****SA LOGIC CIRCUIT****SA LOOP****SA MAGNETIC CIRCUIT****SA MICROCIRCUIT****SA MICROWAVE CIRCUIT****SA PHASE DETECTOR****SA PNEUMATIC CIRCUIT****SA PRINTED CIRCUIT****SA RLC CIRCUIT****SA SHORT CIRCUIT****SA SWITCHING CIRCUIT****SA TRANSISTOR CIRCUIT****SA VARACTOR DIODE CIRCUIT****SA WIRE BRIDGE CIRCUIT**

Tachometer measuring angular velocity from time of definite number of rotations, noting diagram of basic circuit 01 p0062 A67-10164

Natural oscillations in dissipative oscillatory circuits containing inductance coil with magnetized ferrite core in presence of strong HF field 01 p0037 A67-10544

Methods, schedules and cost of applying computer technology to circuit design, including Apollo and LEM programs 01 p0031 A67-11335

Nonlinear solution method incorporated in computer program for analysis of abnormally operating circuits, considering catastrophic part failure modes 01 p0031 A67-11337

Behavior of resonator quantum devices, using oscillating circuit with quasi-linear negative conductance 03 p0379 A67-13293

Traveling wave parametric amplifier circuit with series connected varactor diode 03 p0380 A67-13504

Computer aided circuit design, synthesis, analysis, optimization and fabrication 03 p0376 A67-14276

Universal circuit concept for fulfilling any electronic function 04 p0591 A67-14504

Lumped electric circuit device producing dispersion for pulse compression system noting design 04 p0574 A67-15054

Amplitude effect reduced on performance of nonlinear circuits by using shunt circuit, pseudolinear laws, and negative resistances, reviewing self-adaptive systems 05 p0785 A67-17271

Circuits consisting of HF oscillator, kenotron heater, rectifier, etc, for low power HF voltage generator 05 p0780 A67-17499

Upper sideband effect in parametric amplifier on positive conductance and negative resistance of circuits, deriving noise figure expression 06 p0986 A67-17575

S-band parametric amplifier pumped at J-band using balanced idler circuit with two varactor diodes incorporated in one encapsulation 06 p0966 A67-17580

Flat cable connectors design including welding and welded connectors and Pictatiny type, noting zero insertion force, withdrawal force, etc 06 p0972 A67-18403

Forced oscillations in nonlinear resonant circuit employing p-n junction capacitance 07 p1150 A67-19235

Open air lines and cables, stressing electric wave propagation along homogeneous and inhomogeneous circuits 07 p1141 A67-19340

Circuit and system theory - Allerton Conference, University of Illinois, October 1966 08 p1307 A67-20317

Algorithms for dichotomous representation of macrocircuits, considering computer programs and establishment of flow graphs 08 p1299 A67-20326

Dry circuits effect on behavior of contacts noting prediction, control and measurement techniques 08 p1306 A67-21417

Thermomagnetic generator with resonating current in load circuit to improve thermodynamic performance 09 p1452 A67-22697

Gunn effect devices high efficiency achievement, considering circuit and material from theoretical and experimental viewpoint 10 p1616 A67-23535

Wideband coupling filters with expressions for resonant frequencies, damping factors, etc 10 p1618 A67-23639

Circuit Q of self-resonant coil of niobium stannide at RF low temperatures 11 p1767 A67-24726

High input impedance obtained with junction transistors, discussing circuit design for different frequency modulators, FET properties and applications 13 p2077 A67-26661

Mathematical model describing nonlinear behavior of vortex valve in fluid circuits, noting effect of swirl on vortex valve flow characteristics 14 p2251 A67-28341

Dielectric materials characteristics analysis to obtain flexible circuitry performance and selection factors, especially for flat cable

[ASME PAPER 67-DE-52] 14 p2341 A67-28882

On-line nonlinear circuit design, discussing computer program for evaluating performance resulting from modifications 15 p2442 A67-29169

Differential equation computer simulation, examining errors in closed circuits 16 p2633 A67-30463

Analog-to-digital conversion method for measuring weak currents, giving diagram of measuring circuit 16 p2635 A67-30672

Book on analysis and synthesis of tunnel diode circuits including equivalent circuits, amplifiers, etc 16 p2636 A67-30997

Flip-component technology discussing bonding of flip chips and face bonding of semiconductor devices 16 p2642 A67-31727

Circuit of automatic multichannel secondary particle recorder of SKL type for cosmic ray station, using azimuthal muon telescope and neutron supermonitor 17 p2854 A67-32098

Oscillating circuit with nonlinear capacitance in free oscillating regime, obtaining formula for envelope of free oscillation differing from exponent 17 p2829 A67-32311

Effect of unconditional stability of loop in phase lock demodulator on threshold performance of loop, noting transfer functions role 17 p2816 A67-32782

Algorithms for dichotomous representation of macrocircuits, considering computer programs and establishment of flow graphs 18 p3005 A67-33498

Equivalent circuit of two-port antennae with application to magic-T systems 18 p3013 A67-34527

Circuit theory - Conference, Purdue University, May 1967 19 p3200 A67-34838

Equivalent transformation of electronic circuits having nonreciprocal elements studied by methods of component connection 19 p3201 A67-34908

Stability range of feedback networks determined with respect to independent circuit parameter using root hodographs 19 p3201 A67-34910

Pulse generator for semiconductor laser excitation, noting silicon controlled rectifiers and pulse shaping line 19 p3191 A67-34983

Switching tunnel diodes, discussing amplitude discrimination and binary memory 19 p3193 A67-35065

Circuit design and performance to convert DC input voltage to pulse train with width proportional to input 19 p3197 A67-35702

Bridge circuits with nonlinear resistances, calculating statistical characteristics by graphical method for functional transformer 20 p3451 A67-37151

Gyrostabilizer feedback circuit transfer function with two-phase asynchronous motor equivalent to unit having time constant as function of transmission band of amplifier 22 p3810 A67-40483

Circuit for plotting extremal values of cycle during analog computer simulation 23 p3976 A67-41339

Oscillating circuits with nonlinear active elements amplitude and phase frequency characteristics graphically plotted, noting effects on frequency devices 24 p4136 A67-42191

Klystron amplifier stability during double interaction in output circuit determined assuming zero HF potential and electron flow not bunched 24 p4129 A67-42193

Transient processes and initial conditions of excitation of lower harmonic oscillations in resistance-capacitance nonlinear inductance circuit, noting graphical integration 24 p4189 A67-42418

CIRCUIT BOARD

Graphical techniques in determining circuit-board resistance to shock and vibration 01 p0034 A67-10159

Microscopic solder silvers as cause of malfunction in high density etched circuit boards having close conductor spacings 03 p0389 A67-14279

Modular system for packaging microelectronic flat packs and miniature discrete electronic components 05 p0779 A67-17465

Machining techniques for paper-base and glass-base laminates of various grades for printed circuit boards 08 p1334 A67-20742

Etching techniques in fabrication of printed circuit boards 08 p1334 A67-20745

Multilayer laminating process in printed

circuit wiring board design and production 08 p1335 A67-20746
Manual assembly process for small volume printed circuit board 08 p1335 A67-20747
Cost-and labor-saving advantages of automatic and semiautomatic insertion of components in circuit board 08 p1335 A67-20748
Printed circuit board manufacturing process assuring crack-free plated-through hole 08 p1304 A67-21190
Visual observation of internal circuitry and interconnections of multilayer boards through failure analysis technique 08 p1307 A67-21419
Nondestructive testing techniques for multilayer printed wiring boards stressing axial transverse laminography and mutual coupling 09 p1502 A67-21867
Pulsed laser welding process, discussing wire-to-wire welds, sheet-to-sheet welds and circuit board weldings 09 p1504 A67-22139
Planar packaging concepts for avionics equipment systems and circuit boards developed from extensive use of microcircuits and thin film circuits [SAE PAPER 670251] 11 p1758 A67-23984
Interconnecting techniques for modules contained by printed circuit boards, noting usage of pin sockets and effect on maintainability and reliability 12 p1910 A67-25266
Computer-aided layout of minitick artwork 12 p1950 A67-26130
Multilayer printed circuit board system for interconnecting microelectronic components noting application of X-ray, ultrasonic, beta-ray, etc to process control 16 p2681 A67-30476
Reliability of multilayer printed wiring boards as interconnection device 16 p2642 A67-31726
Solderless-wrap lightweight interconnection board for Lunar Module landing radar, noting manufacturing details 16 p2642 A67-31919
Fluidic breadboard version of rocket engine sequence control, describing pneumatic logic package and general limitations [AIAA PAPER 67-518] 18 p3114 A67-33981
Thin film hybrid subaudio active filter design and fabrication, discussing power consumption, circuit breadboard performance, etc 18 p3015 A67-34559
Printed circuit thermal design, discussing edge-to-center temperature gradient and circuit board models 21 p3594 A67-38330
Multilayer board compared to two-sided board circuits, discussing circuit reliability, flexibility, cost, packaging density, etc 21 p3594 A67-38332
Microelectronic circuit packages, discussing interconnection wiring and optimization 21 p3594 A67-38333
Packaging of IC core memory for aerospace use, discussing design and production of boards 21 p3595 A67-38338
Multilayer circuit board fabrication, giving data on operational and standby failures 21 p3596 A67-38345
Electrode with central heat sink used for joining flat-pack leads and copper tracks on printed circuit boards 21 p3635 A67-38624

CIRCUIT BREAKER
Wideband phase-leading quadrupoles with circuit breakers and effect on envelope of modulated signal 13 p2085 A67-27706
Solid state protection and control device characteristics noting thermal, thermal magnetic and magnetic circuit breakers for circuit protection 17 p2825 A67-32514

CIRCUIT PROTECTION
Solar array output protection against individual cell failures, considering effects of paralleling 06 p0951 A67-18420
Solid state protection and control device characteristics noting thermal, thermal magnetic and magnetic circuit breakers for circuit protection 17 p2825 A67-32514
Degradation, training and instability in superconducting coils, protection of windings and related problems of superconducting magnets for use in MHD generators 18 p3099 A67-33711
Multistage receiver protector recovery period measurement, discussing nanosecond reaction time 21 p3589 A67-37819
Forced air distribution systems for electronic equipment cooling 21 p3594 A67-38331

Aircraft circuit and installation requirements referring to short time characteristics of cables and effect on circuit protection, coordination and weight saving 21 p3572 A67-39072
Protection of equipment and systems using semiconductor devices by suppression of voltage transients 22 p3766 A67-39250
Book on reusable protective packaging of military, electronic and aerospace instruments and systems 22 p3771 A67-39832
Protective devices in electrodynamic vibration exciters, examining design, operational principles and possible cause of failures 22 p3781 A67-40403

CIRCUIT RELIABILITY

Optimum tests for check of working order of system with minimal material losses of safe or fault system functioning 01 p0043 A67-10240
Reliable electronic design by suppression of adverse interactions among system levels 01 p0083 A67-11348
NASA program for microelectronic circuit and space vehicle reliability 01 p0042 A67-11364
Integrated circuit reliability survey showing relationship of failure rate and temperature 01 p0042 A67-11365
Failure rate and failure mechanism schools test philosophies combined to know and improve integrated circuits reliability 01 p0042 A67-11366
Physical and management aspects of reliability of integrated circuits for Minuteman II 01 p0042 A67-11367
Electronic system reliability prediction without relying exclusively on failure rate information 01 p0042 A67-11372
Combining IBM ECAP and propagation-of-variance moment method computer program for improved reliability circuit analysis 01 p0043 A67-11377
Radiation stress effect on component reliability of electric circuits analyzed via mathematical statistics 02 p0210 A67-11527
Transistor failure in inductive load circuits such as TV horizontal deflection circuits and relation to secondary breakdown 02 p0223 A67-12656
Computer role in electronic systems design for higher reliability at lower cost 03 p0375 A67-13712
Switching circuit malfunctions analysis, discussing modeling for failure, simulation of failure and timing problems and sequential networks 03 p0394 A67-14219
Microscopic solder slivers as cause of malfunction in high density etched circuit boards having close conductor spacings 03 p0389 A67-14279
Multiple correlation applications in design analysis of high reliability critical circuits 05 p0777 A67-17249
General equation for reliability of parallel networks and failure density function 05 p0784 A67-17255
Partial redundancy for improved reliability of computing machine [JPL-TR-32-1088] 07 p1153 A67-19604
Feasibility of employing BIT and fault-isolation circuits made possible by microminiaturization techniques applied to advanced avionics systems [AIAA PAPER 67-268] 07 p1167 A67-20077
Determination of length of deductive circuits of recycling memories and oscillators 08 p1302 A67-20835
Microcircuitry leakage path detection using scanning electron microscopy 09 p1473 A67-22017
Parameter control during vacuum deposition of electronic film circuits for obtaining acceptable tolerances 09 p1503 A67-22099
Spacecraft electrical connector criteria to insure adequate quality for desired performance 09 p1480 A67-22295
High reliability integrated circuit selection and specification by using effective screening test and analyzing failure mechanism 09 p1480 A67-22299
Screening to improve reliability of silicon integrated circuit, noting failure mode and mechanism 09 p1480 A67-22300
Design, redundancy, reliability and tradeoffs for Launch Vehicle Digital Computer and Data Adapter /LVDC/LVDA/ for uprated Saturn I and V vehicles, noting logic circuit, memory, input/output, power supply 09 p1469 A67-22301

Cost improvement for Minuteman II integrated circuits from failure rate reduction, using failure mode model and measurement system 09 p1480 A67-22305
Logical redundancy technique based on failure-erasure circuitry for masking P-1 failures in P identical elements connected in parallel 09 p1470 A67-22668
IR techniques for reliability enhancement of microelectronics 10 p1610 A67-22977
High density circuit assembly system emphasizing micromodule method 12 p1917 A67-26205
Annual National Relay Conference, Oklahoma State University, April 1967 13 p2084 A67-27693
Electronic equipment reliability improvement methods and practices in Czechoslovakia 14 p2282 A67-28039
Nuclear radiation damage to circuit elements of missile FM/FM telemetry system, analyzing changes in electric characteristics 14 p2271 A67-28685
Circuit analysis by computer, noting programs for reliability and quality control 15 p2441 A67-30408
Book on microelectronics in U.S. covering semiconductor and thin film integrated circuits, hybrid circuits, fabrication, applications, etc 16 p2637 A67-31255
Feasibility of employing BIT and fault-isolation circuits made possible by microminiaturization techniques applied to advanced avionics systems [AIAA PAPER 67-268] 17 p2834 A67-32590
Large scale integration of circuits studied for high yield, using concept of redundancy adjustment of probability 18 p3014 A67-34553
Circuit for integral majority-voting logic elements intended for satellite design, analyzing reliability and performance 18 p3007 A67-34664
Geocentric trajectories for particles of single class 18 p3016 A67-34666
Development and maintenance of equipment containing integrated circuits, discussing processing, fault isolation and human error 18 p3016 A67-34670
Servo loop electronics reliability using continuous redundancy, integral self-test circuits, etc 19 p3191 A67-34847
Reliability evaluation of MOS large scale integration devices, using simplified circuit to test individual small elements 20 p3398 A67-36800
Series/parallel connection of redundant elements in thermopile shown to increase reliability of array over simple series of thermoelectric elements 20 p3363 A67-36958
Timing considerations in sequential fluid power circuits design in terms of stray delay concept and safety of asynchronous circuit 20 p3365 A67-37362
Amplification factor stabilization or variance of transistorized radio astronomy receivers, discussing circuit diagram, performance and reliability 20 p3403 A67-37517
Reduction of RF interference in reflection-type parametric amplifiers covering spurious responses, amplifier saturation, intermodulation and cross modulation 20 p3406 A67-37655
Design procedure for production of radiation resistant NOR gate logic circuit 21 p3603 A67-38185
Multilayer board compared to two-sided board circuits, discussing circuit reliability, flexibility, cost, packaging density, etc 21 p3594 A67-38332
Cabling material problems associated with military standard connectors for space vehicles, discussing reliability, fabrication, assembly and design 21 p3595 A67-38334
Flexible circuitry method of electronic packaging stressing use of flat cables 21 p3595 A67-38336
Multilayer circuit board fabrication, giving data on operational and standby failures 21 p3596 A67-38345
Thick film design considerations covering material and micropart selection, circuit cost, reliability, substrate size and delivery schedule 21 p3596 A67-38346
Quality control methods to ensure thin film circuitry integrity and reliability, showing need for better nondestructive testing techniques 21 p3635 A67-38623
Electronic circuit packaging in Apollo lunar module signal conditioning equipment 21 p3635 A67-38628

Pure magnetic integrated logic circuit for space research, noting improvement on speed factor 21 p3588 A67-38675

Quality assurance requirements for custom thin film circuit program covering functional reliability, environmental capabilities and latent defects detection 21 p3636 A67-38696

Second breakdown in semiconductor devices, discussing measurement methods and techniques, development, breakdown mode and safe operating conditions 22 p3766 A67-39248

LF solid state equipment improves mission reliability through use of integrated molecular circuit and modular redundancy 22 p3771 A67-39840

Surveyor TV power conditioning circuit and product design, discussing weight saving features, reliability and magnetic housing 22 p3807 A67-40374

Controlled transient signal distortion by shock monitoring instrumentation circuits using piezoelectric accelerometers 23 p4007 A67-41382

CIRCULAR CONE

Radiative heat transfer through openings of variable cross section, discussing temperature distribution and numerical results of right circular cone 04 p0738 A67-15870

Axial mode helical antenna radiation and impedance improvement by using tapered feeds and terminations 13 p2076 A67-26514

Wall streamlines and detachment on circular cone at angle of incidence in supersonic flow 13 p2049 A67-26591

Wind tunnel investigation of wake structure behind cone in supersonic flow 14 p2240 A67-27994

Flow rate and pressure coefficients approximate determination for surface of symmetrical hypersonic flow past circular cone 14 p2243 A67-28656

Rott approximate method applied to steady compressible laminar boundary layer on unyawed semiinfinite solid circular cone with attached shock wave 20 p3360 A67-37595

Hypersonic boundary layer of sharp cone, considering boundary layer interaction with outer viscous flow 22 p3741 A67-40027

CIRCULAR CYLINDER

Vortex strength in wake of circular cylinders and comparison of vortex velocity distribution with that of Hoffman and Joubert, using hot-wire anemometers at various Reynolds numbers 01 p0005 A67-10256

Thermal stresses in isotropic circular cylinder under temperature distribution effect, reducing problem to solution of boundary value in form of Airy stress function 01 p0159 A67-10278

Row of parallel circular cylinders in hypersonic flow show determinant factor in boundary layer and heat transfer characteristics 01 p0006 A67-10559

Frequency equation for purely radial vibrations of infinite isotropic composite hollow cylinder with two concentric elastic layers 01 p0162 A67-10818

Scattering of plane electromagnetic wave at infinite circular cylinder with spatially varying dielectric constant 03 p0368 A67-13281

Solutions for nonlinear Ginzburg-Landau equations in cylindrical symmetry for type I superconductor 03 p0499 A67-13876

Plane electromagnetic wave diffraction at two parallel circular cylinders for TM and TE polarization 03 p0371 A67-13959

Forced small axisymmetric oscillations of elastic right circular cylinder with end plates in form of shallow spherical shell filled with heavy ideal fluid 03 p0530 A67-14174

Numerical analysis of unsteady viscous fluid flow past circular cylinder, noting effect of Reynolds number 04 p0602 A67-14617

Slow periodic motions of viscous incompressible fluid past sphere in infinitely long circular cylinder, using Navier-Stokes motion equations 04 p0602 A67-14618

Oscillations of circle solved, using method of elastic oscillations of plane with circular cut 04 p0708 A67-14788

Energy dissipation calculation of damping factor for free oscillations of viscous liquid in circular cylindrical vessel 04 p0711 A67-15196

Optimal flexure solution for Saint Venant problem in circular cylinder, using

Papkovich-Neuber stress functions [ASME PAPER 66-WA/APM-19] 04 p0714 A67-15410

Heat transfer and skin friction rates increase in gas-liquid droplet suspension system flowing over circular cylinder formulated by laminar boundary layer theory 04 p0725 A67-15439

Mass and heat transfer data from sweptback circular cylinders in Mach 2 wind tunnel with Reynolds number 100,000 04 p0549 A67-15824

Gas flow, convective heat transfer, enthalpy rise and surface mass transfer for bodies in cross flow, with application to circular cylinder 04 p0733 A67-15841

Local details of influence of vertical sound field on heat transfer from circular cylinder determined, using schlieren system 04 p0733 A67-15845

Linear local buckling theory for finite length axially compressed circular cylinder and length effect on critical load 05 p0918 A67-16421

Rotation and vibration of conducting circular cylinder in magnetic field, noting motion retardation due to induced electric current interaction with field 05 p0851 A67-16434

Initial equilibrium state stability of multilayer orthotropic circular cylindrical shell based on anisotropic shell theory 05 p0919 A67-16585

Elastoplastic deformation of circular cylindrical shells of ideally plastic incompressible material under uniform supercritical hydrostatic pressure 05 p0922 A67-17176

Rayleigh thermal instability in horizontal circular cylinder, discussing two approximate methods for calculating upper bounds to critical Rayleigh number 05 p0929 A67-17415

Time-independent radiative transfer through circular cylindrical medium, using numerical methods 06 p1111 A67-17874

General solutions to heat conduction equations for three-dimensional unsteady heating of finite solid circular cylinder 06 p1113 A67-18124

Linear shell theory for nonlinear transverse coupled vibrations of partially filled circular cylindrical elastic tank [AIAA PAPER 67-74] 06 p1101 A67-18272

Dynamic response, sloshing frequencies and stability of free surface of liquid in circular cylindrical elastic tank with flexible bottom [AIAA PAPER 67-76] 06 p0986 A67-18274

Flow field and stability of far wake of circular cylinders at hypersonic speeds, noting Reynolds number role [AIAA PAPER 67-32] 06 p0939 A67-18348

Supersonic flutter of thin walled circular cylindrical shells under compressive loading, comparing theory and experiment [AIAA PAPER 67-77] 06 p1103 A67-18354

Resistance coefficient of circular cylinder and sphere in range of Reynolds and Stuart numbers 06 p1045 A67-18692

Linearized long wave diffraction theory of supersonic inviscid flow past slender circular cylindrical bodies and thin wings 06 p0942 A67-18729

Suction-preserved steady state vortex sheet on surface of infinite porous circular cylinder in viscous MHD liquid suddenly rotated about axis 06 p1046 A67-18891

Approximations to Navier-Stokes equations corresponding to steady two-dimensional incompressible viscous flow about circular cylinders 07 p1187 A67-19156

Oscillating variables of flow past cylinder, calculating magnitude and frequency of lift 07 p1168 A67-19258

Effect of Mach number and specific heat ratio on distance of shock wave from end face of circular cylinder in axisymmetric flow 07 p1126 A67-19347

Numerical solution to time dependent Navier-Stokes equation for transient supersonic flow around right circular cylinder, using explicit-implicit finite difference method [AIAA PAPER 67-221] 07 p1169 A67-19625

Forced torsional vibration of inhomogeneous hollow cylinder solved for radial variation of shear modulus and mass density 07 p1264 A67-20234

Correct image system and conditions for vortex model of wing body interference 08 p1277 A67-20596

Transverse oscillations of vortex free fluid in circular cylinder with horizontal generatrix, determining first natural frequency by Rayleigh method 09 p1574 A67-21891

Statistical basis for modified moment theory of elasticity that takes into account contribution of all deformation-tensor-component gradients to deformation 09 p1574 A67-21914

Plane Poiseuille flow calculations extended to Couette flow between coaxial circular cylinders, plotting flow velocity curves 09 p1490 A67-22595

Hydrodynamic coefficients of equations of perturbed motion for body with cavity in form of circular cylinder with flat bottom 10 p1624 A67-23032

Multiple wave interferometer application to determine parameters of rarefied gas flow past circular cylinder 10 p1625 A67-23043

Frequency equation for harmonic wave propagation in composite circular cylindrical shells established, based on linear three-dimensional theory of elasticity 10 p1717 A67-23127

Unified theory for bending and buckling of honeycomb type sandwich shell and linearized governing equations applied to axially compressed circular cylinder shells 10 p1728 A67-23761

Elastic response of circular cylinder under torsion 11 p1871 A67-24118

Pressure measurements on surface and in wake of circular cylinder at rest and in vortex excited oscillation at subcritical Reynolds numbers [ASME PAPER 67-VIBR-31] 11 p1777 A67-24189

Stochastic thermoelastic time varying boundary effect in circular cylindrical shell 12 p2022 A67-25587

Natural magnetoelastic oscillations of circular cylindrical conducting shell 12 p2023 A67-25596

Navier-Stokes asymptotic solutions for large Reynolds number flows, emphasizing incompressible axial flow past semiinfinite circular cylinders 12 p1930 A67-26179

Pressure driven flow at high Hartmann number along annular channel between nonconducting circular cylinders 14 p2355 A67-27907

Linear effects of oscillations of liquids in right circular cylinder, determining stability of forced oscillations 14 p2296 A67-27984

Vortices in plane flow behind circular cylinder at different Mach numbers, noting staggered pattern formation 14 p2296 A67-27988

High Mach number low Reynolds number flow over two-dimensional circular cylinder, obtaining surface pressure and heat transfer distributions 14 p2242 A67-28174

Inhomogeneous sheath effect on surface currents and scattering cross section of plasma-immersed cylinder in presence of electromagnetic and electrokinetic waves 15 p2521 A67-29192

Heat transfer and skin friction rates increase in gas-liquid droplet suspension system flowing over circular cylinder formulated by laminar boundary layer theory [ASME PAPER 66-WA/HT-33] 15 p2579 A67-29322

Heat transfer through rarefied gas between concentric circular cylinders and spheres, using Krook kinetic equation 15 p2579 A67-29570

Low Reynolds number flow past heated cylinder studied for fluid properties variation and thermal and velocity slip presence at wall 16 p2779 A67-31216

Book on aerodynamic and aerothermal experiments on circular cylinders at angle of attack in supersonic flow 17 p2790 A67-32379

Stresses due to external forces and moments acting on elastic nonradial circular cylindrical nozzle attached to spherical shell 17 p2959 A67-32409

Plane wave scattering by finite circular cylinder treated by geometrical diffraction theory, obtaining formulas for radar cross section 17 p2816 A67-32789

Interferometric comparison between two nearly identical shapes by superimposing hologram reconstruction of one onto real surface of second 17 p2864 A67-33388

Flow past circular cylinder started impulsively from rest, reexamining Navier-

Stokes equations 18 p3026 A67-34008
Transition of supersonic flow of combustible gas mixture to Chapman-Jouguet regime 18 p3028 A67-34214
Contact stresses and deformations between circular cylindrical shafts and sleeves obtained by numerical method, considering contact with and without friction 18 p3054 A67-34263
Electromagnetic scattering by thin inhomogeneous circular cylinders, presenting numerical results for induced axial current and scattering cross section 18 p3004 A67-34431
Estimation method for lower bounds of natural frequencies of circular closed cylindrical shell 19 p3338 A67-34876
Inviscid hypersonic flow in stagnation region of circular cylinder with detached shock wave, considering real-gas effects 19 p3171 A67-35713
Analysis of flow and points of stagnation of fluid circulating over cylinder 19 p3210 A67-35720
Wind tunnel tests for load and pressure distributions on flat-top cylinders with thick boundary layer 20 p3421 A67-36781
Drag measurements for turbulent flow about circular cylinders joined to plane parallel walls, noting dependence on velocity profile 20 p3359 A67-37486
Stress analysis in theory of circular cylindrical shell weakened by doubly periodic system of identical circular holes 20 p3542 A67-37664
Steady motion of elasticoviscous liquid through annulus between two coaxial right circular porous cylinders with suction and injection 21 p3613 A67-38411
Exact solutions for elastic displacements and stresses in composite circular cylinder under torsion in Fourier series form 21 p3723 A67-38560
Linear shell theory for nonlinear transverse coupled vibrations of partially filled circular cylindrical elastic tank [AIAA PAPER 67-74] 21 p3727 A67-38866
Dynamic response, sloshing frequencies and stability of free surface of liquid in circular cylindrical elastic tank with flexible bottom [AIAA PAPER 67-76] 21 p3614 A67-38868
Supersonic flutter of thin walled circular cylindrical shells under compressive loading, comparing theory and experiment [AIAA PAPER 67-77] 21 p3727 A67-38869
Stress-strain state of tubular blanks expanding under uniform distributed internal load 21 p3637 A67-38925
Electromagnetic wave scattering by circular cylinder moving in free space, noting far field patterns and Doppler shift angular dependence 22 p3760 A67-39623
Triaxial state of residual stresses in long solid or hollow axisymmetric longitudinally uniform cylinder measured by boring out cut off specimen, analyzing process 22 p3913 A67-40034
TM and TE mode uncoupling in oblique wave scattering from radially inhomogeneous cylinders 22 p3763 A67-40308
Field scattering by convex cylinders solved by asymptotes expressing reduced wave equations [NYU-EM-217] 23 p3972 A67-40751
Scattering cross section reduction of metal core loaded dielectric circular cylinder using harmonic series expansion for resonance phenomena 23 p3979 A67-40830
Currents in load impedance of transmission lines near cylindrical scatterer noting antenna field 23 p3981 A67-41209
Moebius strip self-irradiation coefficient calculated as function of relative width or area of strip 23 p4083 A67-41287
Simplified equations for thin circular cylindrical shells under loading investigated for possible elimination of inconsistencies 23 p4080 A67-41664
Natural frequencies and mode shapes determined for circular cylindrical shell closed by elastic plate 23 p4080 A67-41750

CIRCULAR ORBIT

Levi-Civita regularized equation of elliptic motion of particle influenced by massive primary and perturbed by smaller primary, Part II, Applications to circular and collision orbits 01 p0147 A67-10380
Existence of class of quasi-periodic solutions of three-body problem for near-

circular inclined planetary and lunar orbits, Part I 01 p0148 A67-10382
Minimum velocity increment for deboost from circular orbit as function of orbital altitude 01 p0153 A67-10429
Satellite rendezvous guidance laws applicable to circular, near-circular and elliptical orbits, using Lagrangian formulas for position and velocity in two-body orbit 02 p0264 A67-12315
Ground track of earth-period synchronous /24-hr/ satellites, discussing equatorial, circular and elliptical orbits 04 p0704 A67-14826
Finite thrust explicit guidance law for nearly circular orbital rendezvous 05 p0906 A67-17208
Orbital guidance and rendezvous in inverse square central force field using perturbation method, considering elliptical and circular orbits [AIAA PAPER 67-55] 06 p1028 A67-18265
Optimal guidance equations for ascent trajectories into circular orbits, developing feedback guidance loop for real onboard control system [AIAA PAPER 67-56] 06 p1029 A67-18495
Preliminary circular orbit determination from single state of range-only data [AIAA PAPER 67-92] 06 p1088 A67-18501
Numerical analysis of plane restricted three-body problem with two bodies of equal mass moving on circular orbit 08 p1380 A67-20386
Optimal transfer of thrust limited vehicle between coplanar circular orbits 09 p1571 A67-21694
Rendezvous between coplanar circular orbits, comparing Hohmann transfer with simple bielliptic method 09 p1564 A67-21695
Optimization in terms of energy expenditure of problem of interorbital one- and two-pulse satellite transfer in central gravitational field 09 p1564 A67-21888
Error accumulation in numerical integration of motion equation analyzed for circular satellite orbits 11 p1859 A67-24317
Unidentified satellite as explanation of abnormal perturbations in Saturn ring 11 p1866 A67-24770
Optimum trajectories between material points moving along same orbit in gravitational field of spherically symmetric central body, obtaining numerical solutions for circular initial orbit 14 p2382 A67-27852
Approximate analytical solution for satellite circular orbits subjected to small tangential thrust or drag 14 p2384 A67-28117
Analytic solution obtained for minimum impulse transfer between two neighboring low eccentricity orbits 15 p2554 A67-29405
Two-body system connected on circular orbit by spherical hinge examined for plane oscillations, finding all equilibrium positions with respect to orbital coordinate 17 p2954 A67-32242
Optimum control of space vehicle motion along binormal to circular reference orbit for minimum fuel consumption criterion 17 p2955 A67-32255
Regularization of restricted three-body problem extended to case where three primaries of any mass revolve in circular orbits around common center of mass and fourth body of infinitesimal mass moves in their field 18 p3136 A67-34589
Graphical method predicting latitudes where satellites in circular orbit are visible, in both Northern and Southern Hemispheres 19 p3182 A67-35268
Gravitational and magnetic torque effects on rotational motion of asymmetric Pegasus satellite in circular orbit [AIAA PAPER 67-567] 19 p3335 A67-35963
Aerocruise maneuver for optimizing orbital plane change with respect to cruise speed 20 p3532 A67-36552
Minimum velocity increment for bielliptic transfer between noncoplanar circular orbits 20 p3526 A67-37126
Economical Hohmann type orbital transfer between coplanar circular orbits with fixed duration and limited thrust 20 p3527 A67-37258
Two-body problem in classical mechanics, proving existence and quantization of circular orbits 20 p3487 A67-37581
Energy accumulator and constant power propulsion system for near-circular orbit space maneuvering, considering two-vehicle encounter 21 p3689 A67-37985

Variational method used to obtain extremal flight conditions, considering flights between circular orbits and planets close to each other 21 p3705 A67-38585
Fuel optimal control conditions in attitude correction of satellite in circular orbit determined using maximum principle, solving resulting boundary value problem 21 p3715 A67-39153
Attitude continuous instability regions in parameter space and resonance frequency of spinning unsymmetrical satellite noting periodic processes 22 p3899 A67-39311
Satellite maneuverability in orbit using hypothetical elliptical orbit to demonstrate formulas used 22 p3882 A67-39563
Iterative guidance mode, deriving alternate expressions for thrust direction control angle for time savings on Saturn launches 22 p3831 A67-39957
Minimum total impulse for optimum two impulse transfer trajectory between coplanar circular close orbits 22 p3884 A67-39958
Adaptive terminal guidance scheme for circular orbit rendezvous to provide near optimal trajectory 22 p3832 A67-39964
Minimum fuel flight plans for injecting synchronous satellite into circular equatorial orbit, developing four methods 22 p3886 A67-40116
Gravity oriented satellite coupled librational motion in circular orbit analyzed for motion stability by numerical methods 24 p4231 A67-42384

CIRCULAR PLATE

Elastic behavior of load cell operating on variable capacitance principle designed to fit spaces restricted in one dimension 01 p0034 A67-10296
Exact expressions derived for deflection, swept volume and ratio of balancing force to total thrust due to pressure for flat circular plate 01 p0164 A67-11273
Gas squeeze film stiffness and damping torques on circular disk oscillating about diameter [ASME PAPER 66-LUB-4] 03 p0432 A67-13762
Axisymmetric modes of loss of stability of circular plates lying on elastic base in inhomogeneous stress field 03 p0529 A67-14163
Energy method creep analysis of elastic bending of circular plates 04 p0707 A67-14443
Shape of meridian cross section, stressed state and deflection of circular plate of uniform strength loaded symmetrically 04 p0708 A67-14785
Bending of circular plate with two square holes under uniform load distribution around hole perimeters 05 p0916 A67-16225
Discrete model construction method for vibrating circular plates 05 p0810 A67-16231
Thin isotropic circular plate bending under eccentric moment load for clamped and simply supported cases 05 p0918 A67-16419
Thermoelastic bending of solid circular plate of variable thickness 06 p1105 A67-18581
Validity of equations for bending, natural oscillations and stability of three-layer solid circular plate with rigid filling and asymmetric structure 06 p1106 A67-18628
Elastic equilibrium of circular plate with elliptical hole and tight washer, determining stress-strain state 06 p1106 A67-18631
Exact solution of transverse shear deformation effect on axisymmetric large deflection of circular sandwich plates for different loading states and boundary conditions 10 p1728 A67-23762
Axisymmetric buckling of orthotropic circular plates with variable thickness in terms of lateral plate deflection and stress distribution 11 p1876 A67-24660
Natural frequencies of bladed disks calculated from receptances 12 p2014 A67-25417
Polar coordinate analysis of free oscillations of circular plates with loosely clamped edges under large deflections, obtaining Duffing equation 12 p2031 A67-25963
Electrical simulation of finite difference calculations of problems of bending and natural oscillations of circular, annular and sector plates 12 p2032 A67-25968
Vibration characteristics and fundamental frequency of circular plate with arbitrary cross section reinforcing

- ring 13 p2216 A67-26534
- Geometrical and equilibrium equations derived for circular plates, introducing Lagrange type coordinate as independent variable 17 p2961 A67-32807
- Numerical integration solution for finite elastoplastic deflections of circularly symmetrical plates 19 p3340 A67-35511
- Stability analysis of circular plate submitted to two compressive forces acting along diameter, using Fourier series iteration 19 p3342 A67-35718
- Thermal-stress distributions in circular disk due to instantaneous heat source on radius midpoint, assuming no temperature variation over thickness 20 p3536 A67-36418
- Asymmetric stability loss of nonuniformly heated circular plate rib, determining elastic properties and critical temperature jump value 20 p3536 A67-36447
- Triangular finite element under plane stress analyzed using stiffness matrix, including in-plane concentrated moments and nodal rotation 20 p3538 A67-36676
- Circular plate on nonlinearly elastic base with uniform load force at center, tangential force and contour moments for plate deflection 20 p3539 A67-36923
- Circular planar satellite electrostatic probe theory based on reversible particle trajectories, showing relation between boundary curve in velocity space and current-voltage characteristics 21 p3625 A67-37899
- Viscous non-Newtonian fluid radial flow between circular disks solved, using model equation reduced to power law equation 21 p3612 A67-38381
- Natural vibration frequencies of cylindrically orthotropic circular plate with linearly variable thickness, solving differential equation of motion 21 p3728 A67-38898
- Hypergeometric functions studied for solution of problems on elastic equilibrium of circular plates and shells of revolution 22 p3909 A67-39398
- Koiter theorem generalized for examining unstable temperature field cyclic effects concerning progressive failure in elastoplastic bodies 22 p3910 A67-39453
- Thin circular elastic plate under uniform compressive thrust, with nonlinear boundary value problems involving partial differential equations for buckled states 22 p3916 A67-40525
- Flexural vibration of stiffened circular plates with respect to rotatory inertia, obtaining differential equation 23 p4073 A67-40613
- Homogeneous and sandwich spherical caps and circular plate torsional frequency calculations based on sandwich and spherical shell equations 23 p4073 A67-40618

CIRCULAR POLARIZATION

- Null-free antenna radiation pattern shown to contain all axial ratios of elliptical polarization 02 p0211 A67-11598
- Tuning of lens and mirror antennas with circularly polarized radiation 05 p0766 A67-17239
- X-band circularly polarized nonreciprocal ferrite phase shifter for phased array antennas 08 p1305 A67-21226
- Polarization of cosmic OH 18-cm radiation 11 p1864 A67-24565
- Solar temperatures from observations of July 1963 eclipse with horn antenna in left and right circular polarization, noting magnetization 11 p1867 A67-24779
- Electrostatic polarization of cylindrical plasma layer in external static magnetic field, discussing transverse charged particle drift in crossed fields 13 p2168 A67-27305
- Gas laser mode interaction in Zeeman laser, investigating transition in axial magnetic field 14 p2331 A67-28715
- Pseudo-isotropic radiation source as source with isotropic gain function and polarization depending on spatial direction 16 p2761 A67-30793
- Circularly polarized radiation from Crab Nebula investigated from radio telescope observations at Arecibo 19 p3316 A67-35802
- Reflection of incident right and left hand circularly polarized plane electromagnetic waves from anisotropic helium afterglow plasma 20 p3389 A67-37707
- Circular polarization in j equals 1 to j equals zero transition in gas laser shown due to different atomic relaxation processes

- rates 21 p3640 A67-38353
- Plane circularly polarized magnetoelastic and elastic wave scattering at plane discontinuity surface between ferromagnetic insulating medium and elastic medium 22 p3856 A67-39364
- Circular polarized magnetic field penetration into plasma cylinder noting penetration depth frequency dependence and MHD stability effect 22 p3846 A67-39508
- Anomalous nonlinear preference for circular polarization in He-Ne laser noting variation with gas pressure 22 p3815 A67-39522
- Magnetically induced circular dichroism and birefringence in ICl electronic spectrum, noting frequency dependence and molecular rotation effect 22 p3758 A67-39638
- Possible circular polarization of compact quasar radio and optical radiation, discussing astrophysical implications 24 p4226 A67-41884
- Circular and linear polarization of OH line radiation from NGC 6334 nebulae region using Parkes radio telescope 24 p4230 A67-42333
- Circularly polarized nonlinear electromagnetic waves in conservative centrally symmetric dielectric, considering reflection, transmission and propagation 24 p4168 A67-42481
- CIRCULAR SHELL**
- Vibration modes and relative frequencies of shells stiffened by angularly equidistant stringers, using Vlasov theory of circular cylindrical shells 01 p0183 A67-11148
- Boundary condition effect on buckling of circular shell of given thickness 03 p0524 A67-13786
- Thermoplasticity problem for circular cylindrical shell subjected to arbitrary axisymmetric heating and loading 12 p2023 A67-25593
- Stabilizing effects of viscoelastic cores on response of long circular cylindrical shells subjected to time dependent axial loads 14 p2399 A67-28118
- Plastic buckling of eccentrically stiffened circular cylindrical shells 14 p2399 A67-28121
- Exact solution of three-dimensional problem to derive algorithm for development of applied theories of improved accuracy for circular cylindrical shell 15 p2576 A67-30179
- Shells of revolution produced by fiber-wound distributing internal and boundary stresses uniformly over fiber contours 19 p3337 A67-34871
- Free axisymmetric oscillations of reinforced, closed, cylindrical circular shells, discussing natural frequencies and bending oscillations 19 p3338 A67-34877
- Creep buckling load for thin circular rings determined by tangent modulus theory together with isochronous stress-strain diagram 21 p3719 A67-38022
- Buckling loads in orthotropic circular cylindrical shells under simultaneous longitudinal and external peripheral pressure stresses 22 p3912 A67-39752
- CIRCULAR TUBE**
- Turbulent heat transfer in circular tube with circumferentially varying wall temperature and wall heat flux [ASME PAPER 66-WA/HT-3] 04 p0738 A67-15929
- Circular tube cross-sectional ovality in plastic bending 14 p2401 A67-28655
- Timoshenko beam equations modification necessary to account for normal pressure and Poisson ratio effects for application to thin walled circular tubes 14 p2403 A67-29013
- MHD flow of liquid mercury through circular pipes at high Hartmann and Reynolds numbers, plotting friction factors 16 p2712 A67-30576
- Strain due to even pressure in oval or circular tubes, calculating deformations 17 p2958 A67-32259
- Incompressible fluid drag force on sphere rolling at constant speed in closed-end tube [ASME PAPER 67-APM-18] 17 p2840 A67-33149
- Motion equation of non-Newtonian fluids in initial section of cylindrical tube 18 p3024 A67-33539
- Turbulent flow in circular duct, obtaining velocity distribution 20 p3419 A67-36276
- Vibrational frequency and amplitude effects on heat transfer intensity from vibrating cylinder into circular channel at low Reynolds numbers 20 p3554 A67-37303

- Monograph on turbulent mixing of rotating jets in circular confined duct 21 p3615 A67-39128
- Image radiance distribution of confined plasma in circular tubes noting absence of distortion 22 p3842 A67-39234
- Membrane stress state of spiral coiled tube surface, reducing stress components to second order differential equation 22 p3913 A67-40009
- Optimization of capillary pumping of microgrooved heat pipes, discussing transport equation 24 p4255 A67-42552

CIRCULATION

S ATMOSPHERIC CIRCULATION

S BLOOD CIRCULATION

S PLANETARY CIRCULATIONS

PROJECT

S WIND CIRCULATION

CIRCULATOR

- Six-port circulator with common pair of ferrite disks serving multiple junctions, used in frequency separation networks and tunnel diode amplifiers 02 p0217 A67-12094
- Reflected voltage provided by circulator for radar echo reduction, noting principle of antenna impedance loading 03 p0370 A67-13857
- Scattering matrix coefficients and relation between transmission and reflection coefficients of three-port circulator 05 p0770 A67-16170
- Isolation bandwidth characteristics of Y circulator junction modified by external tuning elements 09 p1474 A67-22087
- Extension of stripline circulator operation calculation by Davies and Cohen to include wider range of stripline geometries 13 p2076 A67-26482
- Triple-tuned broadband UHF junction circulator using lumped element technique 13 p2076 A67-26483
- Two-stage fixed-tuned parametric amplifier for satellite communications earth stations, considering circulator development and varactor 14 p2278 A67-27781
- Low temperature parametric amplifiers, discussing varactors, circulators and demands on cooling systems 14 p2278 A67-27783
- IR technology and electromagnetic spectrum, discussing manufacture of circulators and isolators using Faraday rotation in InSb 22 p3835 A67-39213
- Nonreciprocal parametric amplifier obtained by using parametric elements in frequency inverting case without uniguide or circulator 22 p3771 A67-39838
- Operating principles of Y-shaped ferrite circulator, discussing temperature and power variations effects on sensitivity 23 p4041 A67-41213

CIRCULATORY SYSTEM

SA ARTERY

SA BLOOD CIRCULATION

SA CAPILLARY

SA VEIN

- Space technology utilization in detection and prevention of cardiovascular disease, discussing instrumentation for monitoring microcirculatory system [AIAA PAPER 66-951] 02 p0187 A67-12285
- Cumulative effects of venesection and lower body negative pressure on circulation 10 p1599 A67-23813
- Prophylaxis for negative effect of hypokinesia on human cardiovascular system 13 p2059 A67-26764
- Barotrauma, circulatory constriction and other in-flight auditory troubles of civil aeronautical navigation personnel over 40 years old 14 p2257 A67-28214
- Effects of breathing pure oxygen under pressure on autonomous regulatory systems /nervous, respiratory, circulatory/ of man 14 p2257 A67-28225
- Human circulatory response to sinusoidal gravitational stimulus via Rotational Flight Simulator /RFS/, discussing heart rate variation 23 p3951 A67-41561
- Hypoxia stimulated pulmonary arterial pressure increase in dog and baboon noting hemodynamic effects 23 p3953 A67-41588
- Renin secretion measurement for human adaptation to circulatory stress from G acceleration, discussing high plasma renin levels during acceleration 23 p3956 A67-41634
- CIRCULUNAR TRAJECTORY**
- Asymptotic solution to nonplanar earth-to-moon trajectories in restricted four-body problem 21 p3705 A67-38613

CISLUNAR SPACE

Thermoradioisotope propulsion and integrated power application to cislunar and planetary space missions 01 p0155 A67-11413
Eclipse observation from moon and cislunar space 04 p0700 A67-15070
Lunar and cislunar observation of interplanetary medium including lunar magnetic field, solar wind, existence of collisionless shock wave, gegenschein, zodiacal light and recovery of interplanetary particles 04 p0700 A67-15072
Structurally regular magnetic field in circumlunar space recorded by Luna X orbiter, noting variations in intensity and solar wind effect 05 p0887 A67-16056
Space flight problems in cislunar space, noting lunar probes, high apogee satellite specifications and orbital stability 05 p0897 A67-16732
Cislunar navigation assuming availability of power for making changes in attitude, velocity and direction, considering factors affecting space navigator 08 p1351 A67-21100
Satellite measurement of magnetic fields in cislunar space and earth proximity, noting formation of confined geomagnetic field by continuous plasma flow from sun 11 p1863 A67-24549
Radar measurement of differential group delay to moon, showing large differences in total cislunar electron content above 1000 km in solar and antisolar directions 15 p2555 A67-29611
Zodiacal dust particle flux measurements from OGO 3 and Mariner IV spacecraft in cislunar and interplanetary space 19 p3318 A67-35185
Man capability to operate in cislunar space and lunar surface through Apollo program, discussing practical applications 19 p3326 A67-35644
Structurally regular magnetic field in circumlunar space recorded by Luna X orbiter, noting variations in intensity and solar wind effect 21 p3701 A67-37843

CIVIL AVIATION
SA AIR TRANSPORTATION
Total systems concept utilizing aerospace planning and preliminary design techniques as solution to future megalopolis airport requirements [AIAA PAPER 66-944] 02 p0230 A67-12279
Service abandonment aspects of movement against subsidization of airways by CAB 05 p0929 A67-16770
Fundamentals of technology and operation of SST aircraft for commercial aviation 07 p1131 A67-20292
Air freight transport development by Alitalia, noting Fiumicino terminal 08 p1429 A67-20785
Flight testing of radio navigation aids for civil aviation noting techniques, telescope and typical test 09 p1528 A67-22629
Business jet aircraft engine design for increased service life, detailing turbine nozzles, bearings, rotors, etc [SAE PAPER 670234] 11 p1851 A67-23981
Helicopter design noting speed, maneuverability, handling, carrying capacity and disk loading 11 p1743 A67-23993
British aircraft one-eleven 500 series, detailing stretched version, flight tests to begin in August 1967 with aerodynamic prototype 11 p1743 A67-24039
International aspects of aviation and attitudes of governments toward IATA 12 p2040 A67-25488
Economic regulatory powers of Civil Aeronautics Board 12 p2040 A67-25489
Three STOL commercial transports performance and cost compared with conventional transports 12 p1894 A67-25492
Thrust reversers for business jet aircraft noting limitations, performance gains, technical aspects of analysis and testing, etc [SAE PAPER 670235] 12 p1989 A67-25493
Space activities effect on International Civil Aviation Organization including navigational problems, aircraft communication, meteorological data and technological advances 12 p2043 A67-26151
DC-8 61, 62, 63 development, design and engineering 13 p2053 A67-26907
Computer /third level/ airline industry development [SAE PAPER 670241] 13 p2054 A67-27295
Yak 40, Soviet three-engine jet airliner, for operation off short natural-surface airfields 14 p2245 A67-27893

Air traffic control system, discussing effect on business aircraft operations 14 p2347 A67-28317
Technical, economic and operation criteria for airlines when switching from conventional engines to turboprops or turbojets 14 p2409 A67-28499
Civilian aircraft electrical equipment design and construction including Caravelle and Concorde 14 p2252 A67-28568
Aviation insurance characteristics, types of policy in force and regulations applying under internal law 14 p2409 A67-28933
Planning integration of Boeing 747 jet aircraft into commercial airline [AIAA PAPER 67-394] 15 p2421 A67-30361
Boeing 747 characteristics for passenger and cargo service noting economic gain, operational performance, control cabin, engine, etc [AIAA PAPER 67-397] 15 p2421 A67-30364
Piaggio-Douglas PD-808, Italian executive jet emphasizing safety [AGARDOGRAPH 95] 15 p2422 A67-30399
Operating economics in short-haul air transports noting advantages of conversion to turbine powered equipment [SAE PAPER 670357] 17 p2975 A67-32996
Unscheduled civil aircraft power plant diagnostic removals evaluated by metal detection, performance deterioration, vibration, oil consumption and nonoperational categories [SAE PAPER 670358] 17 p2930 A67-32997
German SIAT 223 Flamingo sports, trainer and cross-country aircraft, noting design, components and tabulated technical data 18 p2985 A67-33641
Hawker Siddeley 748 short-to-medium range civil transport aircraft design features including take off/landing field length, pressurized cabin, engines, payload, etc 18 p2986 A67-34074
A-300 Airbus, economic subsonic passenger transport for short and medium ranges 18 p2986 A67-34075
Tape recorder for routine auditory screening of civil aviation personnel and criticism of whispered voice auditory test 18 p2993 A67-34725
Solutions for aviation crisis of congestion, delays and noise, including problems anticipated with jumbo and SST jets 19 p3207 A67-34968
Close coordination of aviation with other transportation facilities, considering airport/heliport planning within city planning, high speed train competition, highways congestion, etc 19 p3347 A67-34969
Airlines and governmental regulatory agencies controlling competition, new entry and rate policies relationship, examining all-cargo carrier and passenger trunk line 19 p3349 A67-34980
Short-haul aircraft operations spectrum, discussing intercity, feeder, social services, etc 19 p3349 A67-35064
Three STOL commercial transports performance and cost compared with conventional transports 20 p3362 A67-37530
Philadelphia air transportation, discussing runway construction program, passenger terminal, automated cargo handling, etc 21 p3608 A67-38804
Unscheduled civil aircraft power plant diagnostic removals evaluated by metal detection, performance deterioration, vibration, oil consumption and nonoperational categories [SAE PAPER 670358] 23 p4048 A67-40866
Civil high speed intercity VTOL aircraft using fan lift engines, discussing noise, installation, aerodynamics and thrust deflection [AIAA PAPER 67-745] 23 p4048 A67-40979
Automatic landing system introduction for civil transport aircraft noting certification program and requirements and development of operable system [AIAA PAPER 67-757] 23 p4025 A67-40990
Polyimide passenger smoke hood for protection from smoke, toxic gases and flame inhalation 23 p3968 A67-41623
Decompression tests for potential hazards of ejection or fatal head injuries in small pressurized aircraft 23 p3970 A67-41693
Supersonic civil aircraft, considering journey time, safety and operating economy 24 p4093 A67-41886
Comparative projections of helicopters, compound helicopters and tilting propotor

low-disk-loading VTOL aircraft for civil applications 24 p4097 A67-43029

CL-84 AIRCRAFT
S CANADAIR CL-84 AIRCRAFT
CL-595 HELICOPTER
S XH-51 HELICOPTER
CLADDING
Passive core fiber laser does not remove completely need for optical quality in cladding material 05 p0821 A67-16666
Operating temperature effect on vacuum emission stability of vapor-deposited tungsten clad UC-ZrC and uranium dioxide 09 p1449 A67-22347
Mechanical properties of beryllium with emphasis on influence of anisotropy in forming and grain size in powder metallurgy 13 p2140 A67-27134
Soviet book on diffusion cladding of metals covering alloy surfaces diffusion saturation, glow discharge silicizing of metals, vacuum silicizing of refractory metals, etc 19 p3235 A67-34915
Structural changes due to fatigue in cladding layer of alloy D16AT studied by X-ray diffraction 21 p3642 A67-37826
Mean stress level effect on corrosion fatigue strength of aluminum clad D16AT alloy sheet under asymmetrical loads 21 p3646 A67-39008

CLAMP
Instability of thin reinforced cylindrical shell clamped at both ends and energy method calculation of critical pressure 05 p0918 A67-16422
Multiposition grips for automatic mounting of metal or plastic specimens for low temperature mechanical tests 11 p1877 A67-24819

CLASSICAL MECHANICS
Hodographic theory of Newtonian mechanics for trajectory hodograph analysis, noting powered trajectories and multiple body problems 08 p1384 A67-20618
Classical equation of motion of extended monopole charged particle without preacceleration or runaway solutions 11 p1821 A67-23977
Energy transfer during interaction of atoms with surface of ideal crystal in terms of classical mechanics 11 p1824 A67-24855
Kinetic equation for electron gas in classical limit derived from quantum mechanical transport equation, using equilibrium analogy 11 p1844 A67-25076
Motion of point of variable mass in Newtonian central gravitational field 13 p2199 A67-26894
Ionization probability of hydrogen atom by electron impact in terms of three-body problem of classical mechanics 14 p2351 A67-29072
Free rotation of solid body analyzed using homogeneous canonical transformation 15 p2519 A67-30225
First variation theory in extremal problems, noting generalization of classical variational problems and optimal control problems for functions with single independent variable 17 p2876 A67-32043
Apparent forces of analytical mechanics for several cases of motion 19 p3261 A67-35049
Energy transfer during interaction of atoms with surface of ideal crystal in terms of classical mechanics 20 p3490 A67-37538
Two-body problem in classical mechanics, proving existence and quantization of circular orbits 20 p3487 A67-37581
Permanent states of Van der Pol equation in forced sinusoidal state using first harmonic theory which relies on amplitudes of response 23 p4028 A67-40688
Solution to Burrau three-body problem including historical and scientific background 24 p4232 A67-42605

CLAY
S SOIL
CLEAN ROOM
SA ENVIRONMENTAL CONTROL
Gantry white rooms at Cape Kennedy 07 p1187 A67-20284
Clean room techniques for Apollo/Saturn Instrument Unit, noting that environmental and guidance systems parts must be supercleaned to qualify for man-rated space vehicle 11 p1773 A67-24938
Large and intermediate ultraclean vacuum chambers converted to sputter-ion and titanium sublimation pumping 12 p1921 A67-25691

Contamination control Conference, Washington, D.C., May 1967 23 p3961 A67-40842

Need for increased sampling rates of particle counters to improve monitoring system performance for clean room sampling and leak testing of HEPA filters 23 p3961 A67-40843

Comparative microbial contamination levels in clean rooms used for assembly and test of lunar spacecraft 23 p3961 A67-40851

Supercleaning processes for Lunar Orbiter calling for personnel training, clean room garments, chemical cleaners, special packaging and inspection for particulate contamination 23 p3962 A67-40854

Clean room justification guidelines including contracts, proposals, work loads, environmental requirements, equipment and personnel selection 23 p3987 A67-40855

Human microbial shedding using sterile stainless steel shedding chamber, discussing clean room clothing reducing shed rate 23 p3962 A67-40857

Part and component cleanliness maintenance for hydraulic systems, liquid propellants and spacecraft interiors, noting protective methods [SAE PAPER 670825] 24 p4159 A67-41989

CLEANING

SA PURIFICATION
Surface cleaning of electrical and electronic equipment through water and oil removal by chemical compositions 14 p2327 A67-28822

Part and component cleanliness maintenance for hydraulic systems, liquid propellants and spacecraft interiors, noting protective methods [SAE PAPER 670825] 24 p4159 A67-41989

Filters in commercial aircraft hydraulic systems, discussing cleaning methods including ultrasonics 24 p4109 A67-42710

CLEAR AIR TURBULENCE

Incident of severe low level turbulence in clear air 01 p0108 A67-10226

Output characteristics of half-wave mode Kerr cell ruby oscillator used as optical radar for clear air turbulence /CAT/ detection 02 p0198 A67-12053

Clear air turbulence characteristics in terms of measuring systems and reduction methods [AIAA PAPER 66-966] 02 p0262 A67-12289

Gust reduction equations governing numerical procedure for transforming to inertial frame continuous records of air turbulence velocity via matrix methods [AIAA PAPER 66-967] 02 p0246 A67-12290

Clear air turbulence effect on ride quality and flight profile of SST 03 p0463 A67-13922

Radar detection of tropopause and clear air turbulence 04 p0649 A67-14682

Tropospheric probe using vertically polarized signals scattered by clear air turbulence 04 p0649 A67-14683

Doppler technique application to radar measurement of clear air target motion 04 p0569 A67-14684

Radar probe of clear atmosphere confirming detectability of birds, insects and irregularities in clear air refractivity 04 p0650 A67-15172

Clear air turbulence detection with laser radar, noting airborne equipment and results 04 p0650 A67-15304

Power spectrum of horizontal components of clear air turbulence in upper troposphere, examining influence of degenerating gravity waves on nature of turbulence spectra 05 p0837 A67-16486

Clear air turbulence relation to various ranges of Richardson number, noting set of nomograms for number estimation 05 p0838 A67-16709

Nomograms and tables for calculation of Richardson number in relation to forecasting of clear air turbulence 05 p0838 A67-16710

Physical model of turbulence used in developing forecasting scheme of clear air turbulence /CAT/ over mountains [AIAA PAPER 67-184] 06 p1026 A67-18298

Clear air turbulence connection with jet stream, wind speed, convection clouds, flight hazard, etc 07 p1220 A67-19533

Clear air turbulence problems including forecasting inadequacy, detection device requirements, categories, etc 09 p1526 A67-22390

Clear air turbulence at high altitudes, showing occurrence where sharp kink in

temperature profile exists near core of jet stream 13 p2150 A67-26331

Power spectrum of horizontal components of clear air turbulence in upper troposphere, examining influence of degenerating gravity waves on nature of turbulence spectra 13 p2150 A67-26342

Incident of severe low level turbulence in clear air [AIAA PAPER 65-642] 14 p2297 A67-28108

Clear atmosphere angels origin, clear air turbulence detection, radio propagation and atmospheric radar probing 14 p2264 A67-28395

Clear air turbulence power spectra in free atmosphere near jet stream level, discussing CAT generation 15 p2513 A67-30058

Physical model of turbulence used in developing forecasting scheme of clear air turbulence /CAT/ over mountains 17 p2880 A67-32552

Clear air turbulence characteristics in terms of measuring systems and reduction methods [AIAA PAPER 66-966] 17 p2880 A67-32581

Convection in atmosphere below cloud base considered from ground and aircraft observations 19 p3253 A67-35919

Clear air turbulence /CAT/ evaluated to alleviate effects on air traffic, noting forecasting techniques and in-flight and ground-based remote detectors 19 p3254 A67-35931

Radar and aircraft simultaneous clear air turbulence /CAT/ observations 20 p3481 A67-36996

Mountain wave and air turbulence program using high altitude research aircraft measurements and stressing CAT 24 p4181 A67-42275

CLEAVAGE

Fracture surfaces, Wallner lines and crack propagation velocity in precracked W monocrystals at 20-300 degrees K 03 p0445 A67-13471

Cleavage and separation of dye-doped ice and paraffin instantaneously heated by laser pulse, measuring mechanical pulse at energy concentrations below vaporization heat 06 p1119 A67-18807

Small additions of Y, La, Hf, V, Ti and Zr on structure of cleaved surfaces and viscosity of Mo cermet materials 07 p1198 A67-19184

Cleavage method to study pulsed pressure /energy content/ in dense gas-discharge hot plasma 16 p2714 A67-31037

Fracture surface topography related to micro- and macro-mechanics of fracture for plastic, cleavage and fatigue cases 16 p2772 A67-31301

Cleaved surfaces of Mo cermet binary alloys structures annealed and fractured under static bending loads studied for surface properties 17 p2871 A67-32133

Contact potential difference between crystal surfaces of Indium antimonide cleaved in ultrahigh vacuum measured by Kelvin method 19 p3302 A67-34939

CLIMATE

SA WEATHER
Aerospace clothing hygiene, discussing climate influence on protective garment selection and physiological responses of living organisms to obtain heat balance 12 p1902 A67-25176

CLIMATOLOGY
Periodical components of fluctuations in chemical processes of Piccardi D-test 06 p0994 A67-17638

Weather forecasting - Symposium, Vienna, September 1965 06 p1026 A67-18598

Interdiurnal pressure variability as measure of kinetic energy of air masses 06 p1027 A67-18606

Surface heat balance shown to be useful thermal boundary condition at sea-air-land interface for earth surface mean temperature and macroclimate models 15 p2513 A67-30060

Integrating pyranometer operating on silicon photovoltaic solar cell for use by climatological stations and mesoscale networks 21 p3628 A67-38580

Terrestrial environment guideline documents providing natural environment extremes, means and cycles for spacecraft development 22 p3829 A67-39927

Large scale atmospheric motions control, discussing weather control, long term effect and instability 24 p4182 A67-42756

CLINICAL MEDICINE

Altitude dysbarism treatment with high pressure oxygen, reporting three cases 05 p0756 A67-16291

Psychomotor adaptation to flight evaluated clinically, describing anxiety and other aviator symptoms in aerospace 17 p2806 A67-31964

Gastroesophageal reflux in fliers measured in evaluation of hiatal hernia and possible esophageal origin of chest pain 21 p3574 A67-38084

EEG finding in aircrew personnel to obtain information about 14 and 6 per second positive spiking phenomenon 21 p3574 A67-38085

Clinicopsychopathological method applied to analysis of hallucination, depersonalization and similar effects resulting from exposure to extremal factors from standpoint of space psychology 24 p4112 A67-41856

CLOCK

SA ATOMIC CLOCK

Nonideal clock model of georotational velocity irregularities derived from astronomical observations 02 p0236 A67-11512

Clock synchronization with artificial satellites for precise time and frequency, comparing two-and one-way transmission and reception 14 p2263 A67-28391

Dynamic model for magnetic field effect on vibrations of clock balance wheel having magnetized cross bar 21 p3625 A67-37988

CLOSED CIRCUIT TELEVISION

Laser system for diamond piercing in wire-drawing dies and closed circuit TV viewing system for monitoring operation 04 p0628 A67-15309

Programmable display synthesizing system for man-machine communications research based on electronic animation technique 05 p0786 A67-16314

Building block visual simulation facility using new generation and display techniques combined with TV model image generation 08 p1314 A67-20659

X-ray sensitive TV system with image enlargement for nondestructive testing [SAE PAPER 670362] 12 p1950 A67-25882

CLOSED CYCLE

Closed Brayton cycle power conversion system development, discussing rotating components and single phase operating fluid [AIAA PAPER 66-889] 02 p0183 A67-12268

Closed cycle MHD energy converter applications 06 p0951 A67-18668

Nonequilibrium MHD generator for closed and open cycles, noting K seed ionization by energy transfer from excited N molecules 12 p1898 A67-25388

Stirling type closed cycle cooling system for masers and other microwave electronic devices 14 p2278 A67-27784

Low temperature closed cycle refrigeration for electronics, with emphasis on relationship to system effectiveness 14 p2278 A67-27785

Efficiency and thermodynamic parameters of possible closed-cycle flow schemes for base-load MHD generators 16 p2603 A67-30563

Conductivity in Faraday generator with cesium-seeded argon calculated from energy balance of electrons 16 p2603 A67-30565

Jet compressors for closed Brayton cycle MPD to study momentum transfer of two high velocity gas or vapor streams of very different molecular weight 16 p2604 A67-30568

Closed-cycle generator using gasdynamic forces to transport charged particles against opposing electric field, noting enthalpy role 19 p3175 A67-34801

CLOSED ECOLOGICAL SYSTEM

SA LIFE SUPPORT SYSTEM
SA OXYGEN PRODUCTION
SA SPACE CABIN ATMOSPHERE
SA SPACECRAFT ENVIRONMENT

Completely regenerative spacecraft life support systems, discussing loop closure techniques and possible conversion methods for metabolic wastes [AIAA PAPER 66-935] 02 p0187 A67-12278

Bioengineering parameters influencing life support systems for manned exploration of moon including mission duration and closed regenerable systems 02 p0230 A67-12310

Mineralization of human solid and liquid wastes by methods of thermal and thermocatalytic oxidation for autotrophic and heterotrophic organism use 02 p0187 A67-12326

Environmental control and closed

ecological systems, discussing control of atmosphere, temperature, food, water and waste, instrumentation, terrestrial applications, SNAP, etc 04 p0564 A67-15667

Closed ecological systems and endogenous formation of CO in plant and animal tissues 07 p1136 A67-19107

Mixed cultures of *Chlorella pyrenoidosa* TX 71105 and various bacteria and use in closed systems for support of man 10 p1598 A67-23626

Hardware and life-support systems on submarines and space vehicles, discussing oxygen supply, temperature-humidity control, etc [AIAA PAPER 67-364] 14 p2259 A67-28732

Physiological-ecological investigations of *Chlorella* cultures as link in closed ecological system 16 p2617 A67-30775

Efficiency and stability of complex closed ecological system operating on solar energy and with internal feedbacks evaluated from thermodynamic and kinetic viewpoints 16 p2618 A67-30777

Biological life support system for regenerating closed atmosphere by photosynthesis, using gas exchange between man and microalgae 19 p3180 A67-35236

Molecular sieves using regenerable carbon dioxide solid adsorbents for spacecraft life support systems 20 p3374 A67-36611

Microbial interaction in closed system by simulating space flight conditions, noting degree of crowding effect on buildup 21 p3577 A67-38899

Potential contamination of equipment by primate passenger during 30-day earth orbit, studying skin, body particulate matter and indigenous microflora 23 p3944 A67-40856

Microbial interaction factors determined between men and environment in closed systems 23 p3962 A67-40858

Unicellular algae continuous culture as autotrophic component of closed ecological system, discussing stabilization of biomass concentration to provide oxygen requirement 24 p4114 A67-41844

Biological regeneration of enclosed atmosphere with algae photosynthesis noting effect of diet change 24 p4114 A67-41845

CLOSED LOOP SYSTEM

Comparison of variances evaluated by Kolmogorov and Volterra techniques for phase locked loop subjected to white Gaussian input 01 p0044 A67-10480

Pulsed chronotron vernier for precise time expansion, discussing circuit configuration, operation and performance characteristics 01 p0067 A67-10658

Gas lubricated bearings used in Brayton cycle closed loop system turbomachinery in design of two-shaft power plant [ASME PAPER 66-GT/CLC-9] 01 p0080 A67-10871

Closed loop control system for space vehicle guidance, formulating efficient steering algorithm 01 p0154 A67-11156

Modified Bode criterion for feedback system stability 01 p0045 A67-11198

Linear optimal control techniques used as synthesis tool in designing control system for Short Range Station Keeping /SRSK/ task of assault helicopter, noting closed loop dynamics 01 p0111 A67-11201

Closed loop gain of two-loop linear feedback system calculated, using computer 01 p0047 A67-11218

Singularity in motion equations of closed loop optimal guidance systems 01 p0111 A67-11224

Closed loop realization of optimum control law superior to open loop implementation for linear system not asymptotically stable or subject to random disturbances 01 p0048 A67-11225

Restrictions placed on transfer function of linear system with input and output coordinates in presence of given plant in control loop 03 p0390 A67-13098

Externally pressurized bearings treated as hydraulic closed loop servomechanism analyzed, using transfer functions [ASME PAPER 66-LUB-7] 03 p0431 A67-13759

Closed loop gust response control system, considering airframe loading, local accelerations, turbulence, structural mode, damping, etc [AIAA PAPER 66-997] 03 p0362 A67-14146

Closed loop system with reference to different gyro stabilization loops present in

modern space vehicle inertial measuring unit, using Prony exponential series curve fitting method as analytical tool 03 p0400 A67-14218

Synchronization errors in parallel jacks system with closed loop control by hydraulic relays, using nonlinear differential equations [ASME PAPER 66-WA/AUT-5] 04 p0555 A67-15389

Closed-loop automatic control system with unvalued substantially nonlinear element, using approximation of characteristics by Fourier series 05 p0781 A67-16254

Nonstationary response of closed loop control systems with random characteristics, noting statistical analysis of error response and conversion of random control system to constant parameter system 05 p0783 A67-16443

Ripple instability in closed loop control systems with thyristor amplifiers whose sampling action is noted in presence of alternating component voltages 05 p0777 A67-17302

Optimum guidance law simulation by analog computer using logic controlled analog, spatial analog and trajectory riding techniques 06 p1028 A67-17614

Sign codes and patterns of state variables for finding all possible responses in linear third order closed loop feedback control system 06 p0978 A67-18721

Manual control dynamics for single loop systems facilitating man-machine system design 07 p1162 A67-19907

Lunar landing simulation data, noting pilot performance and manual control modes [AIAA PAPER 67-241] 07 p1165 A67-20062

Sensitivity of index of performances to variations in plant parameter for open and closed loop optimal control with one or two degrees of freedom 08 p1309 A67-20328

Fluidic binary full-adder configurations performance for subtraction function required to generate error signal in closed loop control system 08 p1280 A67-20444

Harmonic response and jump phenomena in closed loop systems with dynamic range type nonlinearity under sudden sinusoidal excitation 08 p1312 A67-20721

Graphs for frequency plot of closed loop automatic control system from phase amplitude of open loop and frequency relations between open and closed 10 p1621 A67-23852

Lubrication system design and component arrangements for several oil and gas lubricated closed looped gas turbine machines [ASME PAPER 67-GT-3] 11 p1799 A67-24791

Acoustical and aerodynamic characteristics of full scale axial flow air compressor simulation in Freon closed loop system operation [ASME PAPER 67-GT-27] 11 p1742 A67-24806

Eigenvector scalar product solutions for closed loop time optimal control of linear systems 11 p1771 A67-24897

Signal to noise ratios of transistorized constant current and constant temperature hot-wire anemometers 12 p1947 A67-26121

Extended phase detector for phase-locked loop receivers 13 p2075 A67-26408

Hydraulic properties of duct of constant rectangular cross section functioning in closed circuit used to measure MHD flow velocity 13 p2165 A67-26593

Automatic control systems classification for ordinary systems in relation to self-adaptive systems 13 p2088 A67-26800

Automatic pulse digital analyzer design to measure simultaneously all-pulse parameters used for control of closed loop systems 13 p2078 A67-26801

Moving coil and variable air gap electromagnetic actuators, discussing characteristics and applications 14 p2247 A67-28266

Quantizer optimal design for closed-loop dynamic and open-loop static systems 15 p2456 A67-29364

Acquisition behavior of phase locked loops, determining time and pull in range of loop for input step in frequency 15 p2446 A67-29590

Tracking circuit performance, discussing squaring loop, Costas loop variants and delayed decision feedback loop 15 p2436 A67-29591

Steering laws synthesis for explicit guidance, noting generalization and solution

of closed loop equations 15 p2514 A67-29603

ARGAS closed MHD loop noting technical, constructional details, intended research program and operational results 16 p2653 A67-30553

Nonequilibrium ionization existence in sufficient magnitude to investigate closed loop MPD power generation feasibility at low temperatures, discussing explanation of saturation effect 16 p2602 A67-30555

Nonequilibrium plasma properties and generator performance due to magnetically induced ionization in closed loop facility using cesium seeded helium 16 p2602 A67-30557

Liquid metal magnetohydrodynamic power generation for space vehicle use 16 p2605 A67-30583

Closed loop simulation of movement of center of gravity and optimum guidance laws for space vehicles by analog computer techniques 16 p2700 A67-30662

Realization of invariant multiloop control in case of near-critical and critical plant parameters 16 p2643 A67-31379

Off-line training technique achieving practical closed loop, suboptimal control laws and controllers 16 p2648 A67-31653

Fluid state trigger logic element and bidirectional counter 16 p2609 A67-31663

Algebraic characterization of optimal singular control for autonomous linear plants, using explicit closed form representation of singular strip 16 p2649 A67-31669

Triple input describing functions noting application to stability analysis of forced nonlinear control systems 16 p2650 A67-31673

Temperature compensated electronically controlled ferrite attenuator design and performance 17 p2825 A67-32524

Automatic control systems, discussing open and closed loop control systems, mathematical model analysis and developments 17 p2830 A67-32788

Fluidic jet engine controls for closed loop control, noting overtemperature prevention, reliability, etc 18 p2989 A67-34097

Random characteristics of second order phase locked loop with Gaussian noise input, using digital simulation 18 p3017 A67-34104

Synthesis of closed loop system consisting of pitch control adaptive autopilot for changing flight conditions, using transient characteristics 18 p3075 A67-34282

Formulation of problem of guiding low thrust spacecraft back to nominal trajectory [AIAA PAPER 67-618] 19 p3260 A67-36007

Measurement of variation of formation time of Q-switched ruby laser as function of loop gain 20 p3458 A67-36432

Near-threshold behavior of phase-locked devices, noting phase error processes 20 p3385 A67-37350

Prediction-comparison system for data compression, noting nonlinear error feedback and advantage of closed-loop predictor 20 p3412 A67-37497

Closed loop stepping motor as mechanical memory and time optimal control and digital servomechanism applications 21 p3570 A67-37787

Plant parameter uncertainties sensitivity constraint for optimal linear control synthesis, discussing Wiener-Hopf equation condition 21 p3602 A67-38026

Europa I third stage attitude control system design, discussing various model configurations and overall simulation 22 p3897 A67-39171

Lunar landing simulation data, noting pilot performance and manual control modes [AIAA PAPER 67-241] 22 p3780 A67-40100

Vehicle systems interaction effect on guidance system stability 22 p3907 A67-40194

Multivariable Popov criterion application to stable and to state feedback law linear finite-dimensional systems, noting toleration of nonlinearities 23 p3984 A67-41158

Optimal control systems synthesis using dynamic programming and closed loop system 23 p3985 A67-41671

Generalized curves of closed loop loci of peak amplitude, phase and frequency of third order control system 24 p4134 A67-42025

CLOSURE LAW

Kinetic equation derivation for one particle species fluid using closure hypothesis 17 p2883 A67-32290

Absorptivity of medium, obtaining results for spectral quantities referred to given radiation frequency values 23 p4083 A67-41288

CLOTHING

SA FLIGHT CLOTHING

SA HELMET

SA PROTECTIVE CLOTHING

Clothing hygiene with particular reference to aerospace problems 06 p0954 A67-17998

CLOUD

SA ARTIFICIAL CLOUD

SA CUMULUS CLOUD

SA ELECTRON CLOUD

SA NOCTILUCENT CLOUD

SA PARTICLE CLOUD

SA STRATUS CLOUD

SA ZODIACAL DUST CLOUD

Automatic plotting of cloud information map on Setun digital computer from Tiros meteorological satellite data 04 p0652 A67-15471

Satellite determination of cloud distribution over sky by azimuthal measurements from single point 04 p0652 A67-15476

Anisotropic nonconservative scattering in modified Schuster-Schwarzschild approximation and Venus cloud layer 08 p1385 A67-20931

Satellite Infrared Spectrometer /SIRS/ flown by balloon for cloud top and surface temperatures 22 p3829 A67-40370

CLOUD CHAMBER

High energy cosmic ray interactions analyzed at 3340 m above sea level, using Wilson cloud chambers, gas discharge counters, ionization calorimeter, etc 02 p0248 A67-12746

Cloud-ion chamber stack to measure properties of interactions in light materials of high energy cosmic ray protons and pions 17 p2863 A67-33355

Critical supersaturations for homogeneous nucleation of ethanol, hexane, etc, investigated using thermal diffusion cloud chamber 20 p3555 A67-37562

High energy cosmic ray interactions analyzed at 3340 m above sea level, using Wilson cloud chambers, gas discharge counters, ionization calorimeter, etc 22 p3801 A67-40248

Shower particles angular distribution investigated using Wilson cloud chamber, obtaining agreement with results by kinematic methods 24 p4217 A67-42828

Secondary particles angular distribution in showers studied with cloud chamber, ionization calorimeter and counters to identify particles causing shower asymmetry and symmetry 24 p4217 A67-42829

CLOUD COVER

Tiros VII satellite IR measurement data used to determine sea surface temperature gradients, examining problem of cloud cover 01 p0109 A67-10321

Fill factor of radar beams reflected from meteorological targets of various forms derived, taking antenna radiation pattern into account 01 p0025 A67-10790

Cloud cover space photography by Voskhod I and Voskhod II to determine spatial structure of clouds of various types and fields of brightness 01 p0110 A67-11429

Clear line-of-sight through atmosphere determined, using probability estimates [AFRL-66-838] 02 p0262 A67-12080

Maritime precipitation analyzed using radar data and satellite photographs of cloud cover 02 p0262 A67-12404

Meteorological observatory on moon for observations of earth atmosphere and cloud cover and solar activity 04 p0597 A67-15066

High cloud surface effect on satellite measurements of radiation temperature of stratosphere 05 p0802 A67-17376

Satellite observations determine average cloud cover over region 05 p0839 A67-17393

Cloud melting zone, noting increased antenna temperature for radiation trapping between cloud layer and ground [AIAA PAPER 67-188] 06 p1026 A67-18491

IGY study of noctilucent clouds indicates occurrence over North America as frequently as in Europe and U.S.S.R. 07 p1218 A67-19052

Soviet papers on optical radiation and ozonometric studies of atmosphere 07 p1219 A67-19451

Angular distribution of reflected cloud

and radiation fields according to IL-18 aircraft data of 1964 07 p1220 A67-19452

Actinometric radio probe measurement of effect of clouds on long wave radiation field and to locate upper cloud cover surface from vertical profile of radiative fluxes 07 p1220 A67-19454

Computer programming to predict performance of complex orbit navigation systems using simulation of landmark visibility from orbit as model 09 p1467 A67-21832

Soviet book on practical utilization of observational data from meteorological satellites covering radiation and cloud cover, emphasizing weather forming systems analysis, aerological and synoptical data comparisons, etc 10 p1676 A67-23017

Radiant energy transfer below cloud cover in Venus atmosphere, noting greenhouse effect caused by atmosphere containing components capable of IR absorption 14 p2383 A67-27859

Correlation of diameter of cirrus cloud shield and severity of thunderstorm complex 17 p2880 A67-32554

Variability in human estimation of total cloud cover data by satellite-photograph interpretation, noting use of Nimbus I photographs 17 p2880 A67-32555

Spectral brightness, reflectivity and polarization characteristics of clouds in IR band, measuring angular structure of underlying radiation field 18 p3073 A67-33563

Satellite tracking of cloud formation on earth shadow side, calculating outgoing radiation intensity under cloudless and cloudy sky 18 p3074 A67-33564

Probability of overlapping intercept by system of random intercepts and application to detection of flying objects in cloudy skies 20 p3477 A67-37036

Wind and cloudiness effects on terrestrial scintillation based on visual estimates and measurements 22 p3828 A67-39240

Cloud melting zone, noting increased antenna temperature for radiation trapping between cloud layer and ground [AIAA PAPER 67-188] 23 p4025 A67-41747

CLOUD GLACIATION

Continuous automatic and portable instrument for ice nuclei detection and counting 10 p1654 A67-22818

Noctilucent cloud formation by agglomeration of oxygen/ozone molecules in mesosphere layers 17 p2879 A67-32323

CLOUD PHOTOGRAPH

Pattern recognition, property filtering and lunar feature data experiments coupled with Tiros cloud photographs demonstrate preprocessing for systems design [SMPT PREPRINT 100-13] 03 p0376 A67-13805

Cloud photographs obtained on board ATS-I satellite with camera equipped with reflecting telescope show feasibility of short-lived weather systems from synchronous altitude 10 p1657 A67-23367

Parametrization of photographs of cloud system by satellite TV cameras, discussing brightness problems via data 18 p3073 A67-33561

Photography from aircraft of cloud-like objects in vicinity of libration points L4 and L5 of earth-moon system 19 p3251 A67-34953

CLOUD PHOTOGRAPHY

Weather satellites, discussing photographic and radiation measuring equipment and automatic picture transmission 01 p0109 A67-10768

Weather and cloud photography during Gemini space flights and effect on interpretation of satellite weather pictures 01 p0109 A67-11393

Transmittance measurements and consequent cloud top determination by Gemini V hand-held spectrographic camera 01 p0061 A67-11396

Stereo interpretation of Nimbus II automatic picture transmission photography for cloud patterns [AFRL-66-805] 02 p0241 A67-11970

Meteorological satellites ESSA II and Nimbus II and British ground facilities for receiving cloud cover 03 p0424 A67-13913

Meteorological satellites noting necessity of radiation measurements 04 p0648 A67-14409

Nimbus II AVCS, APT, HRIR and MRIR sensory data analysis 04 p0613 A67-14801

Satellite photographs received from APT facility used in analysis of old occluded depression structure, deducing jet stream position and sea-ice presence 04 p0650 A67-14868

Meteorological studies from manned spacecraft, discussing interpretation of cloud pictures and optical inhomogeneity of troposphere and stratosphere 07 p1221 A67-20008

Nimbus I spacecraft overall characteristics, performance and major subsystems, particularly performance of meteorological sensors 16 p2759 A67-30685

Clouds over equatorial and tropical Pacific investigated by comparing photographs from Tiros satellites and jet aircraft 24 p4181 A67-42667

CLOUD PHYSICS

Kinetic equation describing microphysical random condensation of cloud droplets 01 p0109 A67-10684

Polarization effects during radio wave scattering by cloud and precipitation particles, obtaining phase state from echo signal 01 p0109 A67-11249

Physical aspects of stratocumulus including temperature, liquid water content, drop size, wind effect, shape, etc 03 p0462 A67-13499

Distribution function for temperature of interstellar H-I clouds from exact statistics of cloud collisions and quantitative treatment of cooling mechanisms 04 p0694 A67-14471

Tornado angular momentum as derived from electrostatic motor type action in parent cloud 04 p0649 A67-14678

Measurements by means of vertical beaming cloud pulsed radar operating simultaneously on two wavelengths 04 p0573 A67-15036

Soviet papers on planetary atmospheric circulation and artificial earth satellites 04 p0651 A67-15467

Vortex structures of cloud systems from meteorological satellite data 04 p0651 A67-15468

Cloud vorticity effects on ocean roughness, from Tiros autumnal observations 04 p0651 A67-15469

80-column punch card prototype for statistical generalization of cloud data from meteorological satellite 04 p0651 A67-15470

Meteorological problems connected with design and future operations of supersonic transport, noting particular hazards of mountain-like cumulonimbus clouds 04 p0652 A67-15542

Low clouds effect on ILS jet landing at Bombay airport during monsoon season, noting airfield climatology data 05 p0838 A67-16711

Oxygen-A band near 7600 angstroms used by Gemini V astronauts to measure cloud top altitude, showing method of computing correction factor 06 p1026 A67-18563

Airborne photoelectric device for registration of cloud drops 07 p1189 A67-20009

Small perturbation analysis of observed organized cloud convection for arbitrary unidirectional wind profile 08 p1350 A67-20950

Cloudstreet formation by wind induced vorticity forces equal to buoyancy forces, noting Rayleigh number variation 08 p1350 A67-20951

Cumulus convective cloud formation above isolated source of heat and water vapor 09 p1491 A67-21552

Fluctuations in measurements of hurricane clouds, determining frequency domains for dominant mode of activity via variance spectrum analysis 10 p1676 A67-22817

Variation of inner scale of turbulence in upper atmosphere with height studied from density variations of alkaline clouds ejected by rockets 10 p1638 A67-23201

Sounding rocket-released artificial strontium and barium ion cloud motion in upper atmosphere, based on equations of ambipolar diffusion 10 p1644 A67-23254

Eddy coefficients for diffusion and turbulence parameters for dispersion of vapor clouds in lower thermosphere from vapor trail evidence 10 p1646 A67-23272

Cloud formation theory based on aircraft observations of low cloud layers, considering turbulent vapor and heat redistribution in layer 10 p1677 A67-23408

Fogle theory concerning possible latitudinal shift of noctilucent clouds, using cloud occurrence frequency 10 p1677 A67-23501

Polarization effects during radio wave scattering by cloud and precipitation particles, obtaining phase state from echo signal 11 p1815 A67-24120

Monograph on problems of cloud physics covering evolution of preinversion stratiforms and vertical velocities determination in lower atmospheric layer 11 p1816 A67-24521

Convection in cellular pattern of clouds in atmosphere treated by classical methods 12 p1932 A67-25191

Poisson statistics in distributions of coalescing cloud droplets analyzed using master functions 12 p1963 A67-25343

Condensation spectrum evolution of cloud droplets 13 p2151 A67-26690

Cloud height measurement by optical method compared with vertical radar procedure 13 p2152 A67-26866

Remote sensing of surface and cloud temperatures using 899 cm spectral interval 13 p2152 A67-27355

Nondeepening synoptic scale tropical disturbance showing dependence on in situ development and decay in upper troposphere 13 p2152 A67-27605

Temperature and humidity fields vertical structure determined under conditions of stratified cloudiness 14 p2346 A67-28765

Volume backscattering functions and optical extinction coefficients for visible and IR radiation and selected cloud models 17 p2817 A67-33293

Error factors in cloud and underlying surface temperature determination from weather satellites in various spectral intervals 18 p3073 A67-33558

Aircraft measurements of clouds in spectral range from 8 to 12 microns, determining albedo for stratified clouds 18 p3073 A67-33559

Darkness of clouds of upper and middle levels in various spectral intervals and in thermal spectrum range 18 p3073 A67-33560

Martian clouds analysis and topographical relationships, discussing white and yellow occurrences 18 p3124 A67-34156

Time dependent expression for droplet-size distribution function of clouds undergoing forcible modification or natural evolution 19 p3251 A67-34862

Position, shape and motion of large scale cirrus bands relationship to meteorological properties of upper troposphere 19 p3252 A67-35527

Condensation spectrum evolution of cloud droplets 21 p3654 A67-38432

Cloud measurements from Gemini 5 from reflected solar radiation spectra of oxygen A band region 22 p3807 A67-40369

Vertical distribution of cloud condensation nuclei in free atmosphere investigated by flow type onboard photoelectric apparatus to calculate washout coefficients 24 p4181 A67-42163

Radio signals from clouds to yield information on cloud physics, using superheterodyne microwave receivers 24 p4124 A67-42883

CLOUD SEEDING

Liquidified propane as fog dispersing agent 10 p1676 A67-22814

Strontium and Ba vapor releases in upper atmosphere, testing yield of evaporated metal for different chemical reactions 17 p2851 A67-33194

Visibility in warm fog produced in cloud chamber by seeding with sodium chloride particles, with application for aircraft landing clearance 22 p3828 A67-39338

CLUSTER

SA STAR CLUSTER

Chemiluminescent rate constant increase in reaction of nitric oxide and oxygen in upper atmosphere explained by clustering of former 15 p2434 A67-29884

Relaxation processes for oxygen in solid solution in niobium demonstrating clustering of atoms into groups 17 p2871 A67-32628 [AD-642957]

Clustering in AL-GP zone alloys after low temperature neutron irradiation 17 p2872 A67-32742

COALESCENCE

Condensed phase particle growth in rocket

nozzle by particle collision and coalescence [AIAA PAPER 66-639] 15 p2548 A67-30200

COANDA EFFECT

Aerodynamic characteristics of pneumatic elements with jet propulsion and Coanda effect 05 p0791 A67-16378

Coanda device as pressure maintainer and as switch or selector 08 p1281 A67-20453

Fluid logic components utilizing Coanda wall effect for control systems 17 p2802 A67-32228

Gas turbine theory based on Coanda effect and turbine efficiency from fluid flow analysis of depressive blade-fitted turbines 20 p3515 A67-36274

Coanda effect shown to be caused by periodic system of vortices arising from nozzle edges 20 p3421 A67-36811

COATING

SA BIREFRINGENT COATING

SA CERAMIC COATING

SA CLADDING

SA DOPING

SA ELECTROPLATING

SA FILM

SA FINISH

SA FLAME SPRAYING

SA GLASS COATING

SA INORGANIC COATING

SA PLASTIC COATING

SA PLATING

SA PROTECTIVE COATING

Directional reflective coating consisting of cylindrical dielectric fibers oriented perpendicular to absorbing substrate [AIAA PAPER 65-671] 03 p0467 A67-13039

Thermal conductivity and degree of blackness of aluminum oxide coatings at high temperatures, using argon plasma jets 03 p0536 A67-13608

Extremely high reflective dielectric mirror coatings with zinc selenide for laser resonator cavities and interference filters 04 p0634 A67-15654

Gallium arsenide laser output increase due to aluminum evaporated coating on silicon dioxide used as reflective coating 07 p1196 A67-19794

Coating of titanium with aluminum and silicon by immersion of titanium samples in molten aluminum or in aluminum/silicon melts 12 p1955 A67-25360

Thickness, material type, environmental and surface emittance of radiation shield effects on thermal performance of multilayer insulation system 13 p2228 A67-27660

Aluminum, Volume 3, Fabrication and finishing 14 p2323 A67-27818

Aluminum pretreating and finishing agents noting cleaning, etching, roughening and coatings 14 p2324 A67-27821

Brittle coatings for stress distribution analysis during static and dynamic loading, describing chemical composition and characteristics and giving formulas and diagrams 18 p3045 A67-33741

Thermal conductivity and degree of blackness of aluminum oxide coatings at high temperatures, using argon plasma jets 18 p3161 A67-34473

Passive orientation of space vehicle toward sun by black and white coating, analyzing free oscillation about equilibrium 21 p3713 A67-38598

COAXIAL ACCELERATOR

SA PLASMA ACCELERATOR

Current sheet velocity in coaxial accelerator and predictions from snow-plow model 02 p0273 A67-12183

Measurement of ion velocity distribution in plasma stream of pulsed coaxial accelerator agreeing with computation from momentum transfer and mass flow measurements 02 p0276 A67-12568

Mass spectrometric study of energy distribution of ions of accelerated plasma produced by coaxial source 04 p0668 A67-15216

Coaxial plasma gun performance in longitudinal magnetic field, noting conditions of generation of single plasmoid 06 p1039 A67-18084

Plasmoid structure produced by coaxial plasma gun with interchangeable polarity electrodes, noting experimental setup, particle velocity, density, energy, etc 06 p1040 A67-18085

Hydrogen density in coaxial plasma injector prior to application of high voltage to electrodes, noting experimental setup and

results 06 p1040 A67-18086

Focused coaxial xenon gun to accelerate plasmas of high atomic weight with high power fluxes, measuring ablative and radiative flux at boundaries 08 p1356 A67-20371

Langmuir probe velocity and acceleration measurements for coaxial Hall accelerators [AIAA PAPER 66-196] 08 p1375 A67-20575

Current distribution of magnetic field in plasma coaxial injector indicating dominant role of Hall effect in plasma acceleration 11 p1841 A67-24854

MHD resonance acceleration of plasma clusters and shock waves, showing advantage for parallel or coaxial conductor systems 14 p2354 A67-27762

Current layer motion in coaxial plasma gun, measuring discharge current, electric and magnetic fields and ejected ions at gun outlet 15 p2525 A67-29250

Fast hydrogen ion generation in coaxial plasma source to determine point in gun chamber where fast particles arise 15 p2525 A67-29251

Coaxial plasma gun for plasmoids showing higher mean energy when gas admission is closer to plasma source end 15 p2525 A67-29252

Mass spectrometric study of energy distribution of ions of accelerated plasma produced by coaxial source 15 p2532 A67-30264

Marshall plasma gun with titanium electrodes saturated with deuterium for filling magnetic collector 16 p2676 A67-31400

Coaxial and magnetohydrodynamic waveguide matching obtaining reflection coefficient of former and wave amplitude of latter 16 p2722 A67-31575

Theory demonstrating stability of current sheets of different shapes in coaxial accelerators 19 p3294 A67-35406

Current distribution of magnetic field in plasma coaxial injector indicating dominant role of Hall effect in plasma acceleration 20 p3502 A67-37537

Electron temperature and density distributions for helium plasma produced in coaxial accelerator measured spectroscopically, checking thermal equilibrium assumption 21 p3661 A67-37752

Plasma component velocity distribution and multiple plasmoid production indicated in spectrograms from high speed photography of coaxial injector discharge 21 p3664 A67-37939

Reversed polarity effect on propagating current sheet in coaxial plasma accelerator [AIAA PAPER 67-658] 21 p3671 A67-38694

Plasma jet front produced by coaxial gun studied using SHF diagnostics method 22 p3799 A67-39764

COAXIAL CABLE

Electric field radial intensity distribution and charged particle density for positive plasma column between coaxial cylinders 01 p0125 A67-10924

Impedance errors of coaxial air transmission lines and mechanical and electrical characteristics of Prefix connectors 02 p0213 A67-11648

TE mode-selective coaxial directional coupler with coaxial primary line and rectangular waveguide as secondary line 02 p0214 A67-11650

Multiple internal communications system concept using single coaxial cable handling information transfer by integrated circuits 13 p2083 A67-27448

Universal internal communications system /UICS/ for interconnecting avionic system components, using single coaxial cable and modules 17 p2813 A67-32472

Higher mode cut-off frequencies in coaxial cables of elliptical cross section tabulated as function of conductor dimensions 20 p3382 A67-36861

Attenuation reduction by using hybrid wave in coaxial cables and resonators having supporting surfaces of enhanced reactance 20 p3384 A67-37214

Aircraft construction techniques for terminating cables by pressure type connections, examining design factors 21 p3572 A67-39074

Permeability and permittivity values of homogeneous samples obtained by making transmission or reflection measurements in waveguides or coaxial cables 22 p3796 A67-39276

Glider towing cable configuration taking into account aerodynamic drag forces, using digital computer for numerical calculations and integrations 22 p3745 A67-39551

Power supply system consisting of two-piece coaxial cable and pulse transformer found to possess all characteristics for gas laser operation 22 p3817 A67-40414

Cylindrical antenna admittance taking into account antenna to coaxial line junction geometry, using magnetic current mathematical model 23 p3980 A67-41205

Induced interference in open and shielded wire lines due to AC and transient currents, discussing electromagnetic coupling effects 24 p4137 A67-42713

COAXIAL FLOW

Coaxial cylindrical plasma sheet motion and geomagnetic field/solar wind interaction 01 p0143 A67-10116

Solution for parallel plates in steady state Hartmann flow extended to coaxial flow between concentric cylinders, noting role of magnetic field 05 p0856 A67-17356

Dimensional analysis of turbulent MHD flow in interspace between two coaxial cylinders in rotating circular magnetic field and similarity criteria for EM power losses 06 p1042 A67-18548

Hydrogen plasma produced by coaxial gun located in magnetic mirror 13 p2163 A67-26291

Two-dimensional unsteady plasma flows in coaxial channel formed by two profile electrodes calculated in case of finite conductivity in presence of Hall effect 13 p2168 A67-27301

Structure of electrostatic charge transported by pulsed plasma flow produced by coaxial source 13 p2168 A67-27306

Luminous front in electric shock tube having coaxial gun without current crowbarbing measured by phototransistors 14 p2355 A67-27823

Coaxial plasma gun operating in longitudinal magnetic field, noting effect on plasmoid uniformity 15 p2525 A67-29253

Linear and turbulent MHD generators of conduction type considering operating conditions, efficiency and energy conversion 16 p2608 A67-30600

Diffusion of free isothermal turbulent jet of incompressible fluid flowing from nozzle into coaxial surrounding uniform stream 19 p3209 A67-35443

Steady motion of elasticoviscous liquid through annulus between two coaxial right circular porous cylinders with suction and injection 21 p3613 A67-38411

Gas-air mixing in coaxial flow engine based on one-dimensional ejector theory at subsonic flow velocities, discussing chamber design gas-air mixing in coaxial flow engine based on one-dimensional ejector theory at subsonic flow 23 p4048 A67-40638

COAXIAL TRANSMISSION

Measuring techniques and limitations as related to small reflections in precision coaxial transmission line 09 p1495 A67-21624

Magnetic field finiteness effect on coordination between gyrotronic plasma waveguide and coaxial line 16 p2718 A67-31190

RF power meter design having coaxial thin film thermocouple in-line detector to sample incident power 21 p3589 A67-37916

Microwave characteristics of coaxial mounted tunnel diodes investigated by equivalent circuit parameters 21 p3602 A67-39070

Nonreciprocity in YIG filters employing stripline or miniature coaxial line construction 22 p3772 A67-39905

Coaxial rotors natural vibrations analysis by computer showing occurrence at rpms above first critical speed 23 p4009 A67-40685

COBALT

Molecular spectroscopy of illumination effects on cobalt activated ZnS exposed to ruby laser pulses 01 p0090 A67-10683

Hall effect, electrical resistivity and optical transmission data and Co impurities in GaP studied via crystal field theory 06 p1061 A67-18926

Ultramafic rock content of Na, Mn, Cr, Sc and Co determined by neutron activation technique 07 p1183 A67-20142

Molecular spectroscopy of illumination effects on cobalt activated ZnS exposed to ruby laser pulses 11 p1804 A67-25072

Hexagonal cobalt single crystals plastic

deformation, determining stress, free enthalpy and volume activation, temperature and strain rate 17 p2873 A67-32815

Factors involved in initiation of reaction in cobalt /III/ amine azides, discussing thermal decomposition, activation energy, etc [CI PAPER 67-15] 19 p3309 A67-35009

Co effect on precipitation hardening in high strength stainless steels 23 p4018 A67-40871

Oxidation of ultrahigh purity Co at various oxygen pressures and at high temperatures 23 p4018 A67-40872

COBALT ALLOY

Strength of cobalt alloys at elevated temperatures improved by dispersion of submicron thorla particles 01 p0093 A67-10517

Principle magnetic properties of series of anisotropic alloys of Alnico type with 38 percent cobalt and coercive forces in excess of 2000 oe 01 p0093 A67-10518

Amorphous whiskers from cobalt-gold alloy by quenching molten material through electron-beam heating and anvil-cooling device 01 p0135 A67-10895

Weldability of quenched and tempered martensitic alloy steels of low to medium carbon content, particularly carbon-nickel-cobalt alloys 01 p0081 A67-11041

Atom distribution in double matrix cell of ordered solid solution in alnico-titanium alloy 02 p0254 A67-11864

Structural changes during early stages of decomposition of oversaturated solid solution of titanium in cobalt, noting secondary diffusive reflection 02 p0255 A67-11865

Thermostability of WC-Co alloys, discussing heat treatment, crack formation, bending strength and thermal shock resistance 03 p0447 A67-13641

Prior cold reduction effect on precipitation and embrittlement of cobalt base alloy /L-605/ 04 p0639 A67-15457

Thermal conductance determinations on L-605 cobalt-base alloy panels of variable geometry made to around 2000 degrees F in high vacuum and air 04 p0735 A67-15852

High temperature cobalt iron alloy for square loop and power transformer applications 05 p0864 A67-16833

Structural, physical and mechanical properties of hard alloys formed by sintering powdered VK 15 tungsten carbide alloy with nonuniformly distributed carbide phase 07 p1208 A67-19305

Aging effect on structure of cobalt alloys annealed at 1200 degrees C suggests formation of laminar regions 08 p1342 A67-20812

Titanium and aluminum additions to cobalt-base alloys improve tensile and stress rupture properties and heat resistance 11 p1807 A67-24703

Cobalt alloys precipitation hardening behavior, oxidation, thermal shock resistance and stress rupture 11 p1808 A67-24704

Co-Ni system heterodiffusion and interdiffusion coefficients variation with temperature and composition 11 p1808 A67-24772

Niobium-cobalt alloys constitution, determining equilibrium diagram by thermal analysis, microscopic metallography and X-ray diffraction techniques 14 p2338 A67-28615

Thermostability of WC-Co alloys, discussing heat treatment, crack formation, bending strength and thermal shock resistance 17 p2875 A67-33174

Structural transformations in alnico alloy with titanium studied by X-ray 19 p3245 A67-35467

COBALT COMPOUND

Crystal structure of rare earth Co compounds prepared by levitation melting process investigated by X-ray 24 p4172 A67-41975

COBALT 60

Gamma irradiation from Co 60 effect on indium antimonide, determining defect formation on dose and limiting position of Fermi level for n-and p-type material 04 p0680 A67-15283

Neutron exposure ages of meteorites, estimating amount of shielding which surrounds samples in space from Co-60 and Ar-39 activity data 06 p1082 A67-17871

Chronic acceleration and acute Co 60 whole body irradiation effects on rats, discussing weight to mass

ratio 15 p2427 A67-29268

Cobalt 60 gamma radiation effect on set of B-doped p-type silicon samples, giving radiation-induced defects. 16 p2724 A67-30472

Cobalt 60 gamma radiation effect on MOS diodes fabricated on silicon substrates, noting surface state and oxide charge densities 20 p3510 A67-38961

Co 60-Re alloy in externally fueled thermionic system shown economically desirable for multi-kwt terrestrial or undersea applications 24 p4185 A67-42535

COCHLEA

Spontaneous discharges from single units in cochlear nucleus after destruction of cochlea, noting results of animal study 06 p0952 A67-17847

Adrenal cortical activity changes correlated with pathological emotional states 06 p0952 A67-17848

Waveforms of spike potentials form neurons in anteroventral cochlear nucleus indicate spikes are composed of three components 08 p1286 A67-20367

COCKPIT

SA AIRCRAFT CABIN

Open jet wind tunnel testing of Meteor sailplane, examining aerodynamic merging of wings, fuselage and cockpit 01 p0006 A67-10970

Pilot-aircraft compatibility in landing approach 07 p1136 A67-19888

Integrated cockpit research in man-machine relationship in aircraft 08 p1350 A67-20666

COCKPIT SIMULATOR

Instrument, force and motion servos in cockpit simulation in large aerospace flight simulators, using DC analog voltages 03 p0395 A67-13386

Pilot performance in simulator training during acute hypoxia noting effect on altitude, engine power and directional control 20 p3374 A67-36264

CODE

S BINARY CODE

S ERROR DETECTING CODE

S PULSE CODE MODULATION /PCM/

S SYNCHRONIZATION CODE

CODING

SA DECODING

SA ENCODING

SA PROGRAMMING

SA PULSE COMPRESSION

PCM digital picture transmission for monochromatic still and motion pictures and color still pictures 02 p0208 A67-12167

Digital computer calculation of trigonometric series expansions arising in solid mechanics problems 03 p0524 A67-13788

Information theory research development 14 p2269 A67-28456

Coding modulation and signal processing noting algebraic coding and binary symmetric channel neglect, discussing coherent optical radiation in noise program 14 p2269 A67-28457

Automatic positioning control and problems in normalizing programming codes used in numerical control 14 p2276 A67-28956

CODING SYSTEM

SA DECODER

SA ENCODER

Coding method for transmitting digital data over IRIG-FM/FM telemetry system applied to German-American high altitude/space flight program 04 p0569 A67-14572

Probability aspects of information transmission, deriving optimum coding and decoding algorithms 04 p0592 A67-14884

Optimal parameters of binary communication system using random coding and orthogonal radio signals with unknown phase 05 p0764 A67-16901

Converse of channel coding theorem, relating average probability of error to distortion measure of source sink pair 06 p0965 A67-17946

Mathematical tool for system design of pseudorandom coded ranging system used in space programs, noting failure probabilities 07 p1145 A67-19869

Serial comparison technique for coding systems where weight of ascending bit is equal or greater than previous bit 11 p1756 A67-24266

Lower bounds to minimum error probability using block coding on noisy discrete memoryless communication channels 11 p1752 A67-24270

Picture coding systems and selection of pre-and post-quantizing filters 11 p1791 A67-24711

Image transmission by two-dimensional contour coding using edge point coordinates studied by computer simulation 11 p1791 A67-24713

Optical computing principles, techniques and configurations for communication problems noting Fourier transform, coding, etc 12 p1907 A67-25990

Properties of favorable coding schemes, applying results to text transmission through auditory and tactile senses 12 p1907 A67-26081

Communication problems connected with deep space transmissions of interplanetary distances range 14 p2268 A67-28454

Prefix coding of histograms for minimal storage 14 p2272 A67-28703

Pulse Doppler waveform coding, presenting technique of selecting pulse-period modulation codes requiring only computer calculations 15 p2437 A67-29934

Permutation modulation systems comparison based on proved-best criterion of alphabet size and minimum distance between signal vectors 15 p2439 A67-30384

Coding for numerical data transmission over binary symmetric channel, discussing effectiveness of various error-correcting codes, taking average numerical error as fidelity criterion 15 p2439 A67-30387

Optimal parameters of binary communication system using random coding and orthogonal radio signals with unknown phase 16 p2622 A67-30877

Coding system using pulse interval modulation and providing reduced quantizing noise in received message developed from decaying-step approximation of signal waveforms 17 p2813 A67-32320

Characteristics, operation, technology and reliability of telemetering systems for ESRO I, HEOS A, TD 1 and TD 2 including control factors and coding 17 p2816 A67-32747

Generalized formulation of code separation incorporating general assumptions concerning nature of channel distortion 17 p2830 A67-32827

Selection rigidity and code step optimum parameters for communications channel symmetry 18 p3000 A67-34088

Linear networks having reciprocal and nonreciprocal elements obtained using numerical-code circuit model 19 p3201 A67-34906

Power consumption reduction problems in coded telemetry measurements for ESRO I and HEOS A satellites 21 p3584 A67-38646

PCM coder, programmer and analog switch of D-2 satellite, including systems characteristics and diagrams 21 p3599 A67-38647

Data compression and error control coding in space telemetry analyzed, using performance measures similar to distortion function 21 p3586 A67-38950

Lower bounds to minimum error probability for block coding on noisy discrete memoryless channels 22 p3764 A67-39296

Multiple speed data transmission precoding by changing data rate and overall channel characteristics simultaneously 24 p4121 A67-42342

Recording methods error probability burning code message transmission with start-stop distortion ensuring authenticity by short pulses or integral method 24 p4122 A67-42376

COEFFICIENT

S ABSORPTION COEFFICIENT

S ACCOMMODATION COEFFICIENT

S AERODYNAMIC COEFFICIENT

S ATTENUATION COEFFICIENT

S BINOMIAL COEFFICIENT

S COHERENCE COEFFICIENT

S CORRELATION COEFFICIENT

S DIFFUSION COEFFICIENT

S DISCHARGE COEFFICIENT

S DRAG COEFFICIENT

S FLOW COEFFICIENT

S FRICTION COEFFICIENT

S FRICTION-LOSS COEFFICIENT

S HEAT-TRANSFER COEFFICIENT

S INFLUENCE COEFFICIENT

S INTERNAL CONVERSION COEFFICIENT

S IONIZATION COEFFICIENT

S LIFT COEFFICIENT

S NOZZLE THRUST COEFFICIENT

S PRESSURE COEFFICIENT

S RECOMBINATION COEFFICIENT

S REFLECTION COEFFICIENT

S REGRESSION COEFFICIENT

S RESISTANCE COEFFICIENT

S SCATTERING COEFFICIENT

S SEEBECK COEFFICIENT

S THERMAL ACCOMMODATION COEFFICIENT

S THERMAL EXPANSION COEFFICIENT

S TRANSPORT COEFFICIENT

COGNITION

SA RECOGNITION

Combined control system of extremal plant with alpha system corrector and open loop part, describing noise, disturbance and efficiency factors 17 p2830 A67-33099

COHENITE

Kamacite-thenite interface relationship in iron meteorite, discussing shock wave transformation 06 p1087 A67-18377

Occurrence, decomposition kinetics and phase equilibria of cohenite, noting almost exclusive presence in meteorites containing 8 percent Ni 09 p1564 A67-21737

Cohenite grains from iron meteorites studied by X-ray diffraction for establishing pressure scale, using solid state recrystallization 13 p2200 A67-27235

Low pressure diffusion of carbon to nucleation sites and graphite growth in cubic morphology suggested as origin of cliftonite in meteorites 14 p2384 A67-28144

Structure and decomposition of Goose Lake meteorite and fragments 19 p3323 A67-35424

COHERENCE COEFFICIENT

Rotating interferometer measuring spread and coherence ratio of scattered radio wave 05 p0760 A67-15997

Second order coherence theory noting microwave experiments with radiation sources simulated by noise tubes, coherence function factorization and spectral modulation of superposed beams 09 p1510 A67-21584

Radio astronomical measurements within partial coherence theory showing coherence function relation to spectrum, brightness distribution and statistical electromagnetic fields polarization 09 p1460 A67-21585

Wave propagation through random and nonrandom medium, discussing relation of phenomena to coherence theory 09 p1460 A67-21586

Partial coherence functions to investigate contribution of solar radiation and gravitational tide in causing geomagnetic variations /ionospheric tides/ 11 p1785 A67-23938

Mutual coherence factor for plane electromagnetic wave propagating in stochastic locally homogeneous and isotropic medium of dielectric turbulence 11 p1818 A67-24415

Parameter space partition in beam-plasma regime by determining lower limits of beam density yielding coherent and incoherent domains 17 p2902 A67-32674

Coherent precipitation hardening theory treats yielding in nickel base alloy containing coherent stress-free ordered particles as dynamic process 18 p3064 A67-34080

COHERENT LIGHT

Surface effect on temperature, I-V and watt-ampere characteristics of p-n junction semiconductor injection laser diode as coherent light source 01 p0087 A67-10077

Interferences between waves diffracted by circular screens or thin wires and coherent background provided by laser, producing rings or rectilinear fringes 01 p0087 A67-10231

Unidensity coherent light processing system /UNICON/ 01 p0030 A67-11034

Spatial coherence of laser light beam after extreme wavefront distortions on diffusion explained on basis of Fraunhofer and Fresnel diffraction 01 p0115 A67-11062

Fourier transform holography for diffusion of coherent laser light beam, examining distortion term in reconstructed image 01 p0070 A67-11063

Hologram process for object reflecting or diffusing quasi-monochromatic light, including effects of partial spatial coherence 01 p0070 A67-11079

Phasing system using steered beam of

coherent light for RF array 01 p0027 A67-11320

Electromagnetic theory of wave propagation modes in dielectric cylinders applied to coherent light transmission in optical fibers 02 p0190 A67-11528

Coherence theory and linear systems analysis applied to optical image processing in incoherent and coherent illumination 02 p0287 A67-12244

Giant coherent light pulse generation by Q-factor modulated laser 03 p0433 A67-12941

Wavefront reconstruction with light of finite coherence length 03 p0424 A67-13911

Interferences between coherent light background and light diffracted by small aperture in case of strongly astigmatic beam 04 p0631 A67-14416

Quantum study of optical nonlinearities in absorbing materials, energy transfer between optical waves, laws of nonlinear reflection and coherence effects 04 p0657 A67-14881

Phase locked laser loop for amplitude and phase measuring device for coherent optical wave fronts 04 p0632 A67-15076

Multiphoton absorption processes, coherence of radiation fields and statistical properties of laser light absorption 05 p0823 A67-16681

Coherence properties of light from optical fibers noting applications to interferometry 05 p0825 A67-16978

Coherence and fluctuations of light including stellar correlation interferometry, photon bunching, etc 06 p1008 A67-17569

Optical paths and variable-contrast interference at Michelson interferometer which adds two groups of two laser coherent waves 06 p1009 A67-17636

Statistical determination of correlation functions of plasma scattered coherent light 06 p1039 A67-17824

Characteristic states of electromagnetic radiation field, using quantum mechanical theory of optical coherence 06 p1036 A67-18367

Surface effect on temperature, I-V and watt-ampere characteristics of p-n junction semiconductor injection laser diode as coherent light source 08 p1339 A67-21455

Fraunhofer hologram process when illumination is partially coherent quasi-monochromatic radiation 09 p1493 A67-21589

Laser interferometry application to detection of rotation in system by splitting light from source into two coherent beams 09 p1499 A67-22150

Two-beam Mach-Zehnder and Michelson interferometers using coherence properties of lasers, construction and applications 10 p1652 A67-22709

Detectability of coherent optical signals against incoherent Gaussian background noise radiation in heterodyne receiver with laser local oscillator 11 p1800 A67-24419

Enlarged internal laser beam projecting high contrast images generated on photochromic plate within laser cavity 11 p1801 A67-24717

Coherent and noncoherent light emission in II-VI compounds, potential for laser applications in spectral region from 3200 to 7772 angstroms 11 p1801 A67-24735

Reconstruction method for image with good definition via partially coherent source 13 p2119 A67-26587

UHF intensity-modulated light emanating from plasma observed with aid of photomultiplier 13 p2167 A67-27082

Envelope representation of fluctuating classical wave amplitude of stationary optical fields [SR-4] 15 p2518 A67-29767

High resolution spectroscopy, using incoherent light mixed with coherent laser light, for astronomical purposes 17 p2854 A67-32234

Experimental techniques in making multicolor white light reconstructed holograms, discussing signal to noise ratio, coherent light and photographic emulsion 17 p2862 A67-33299

Time resolved measurements of phase fluctuations of coherent beam at emergence from turbulent layer 17 p2817 A67-33304

Probabilities for two-photon absorption processes induced by coherent and thermal light when acting on atomic system 17 p2870 A67-33317

Interferometric comparison between two

nearly identical shapes by superimposing hologram reconstruction of one onto real surface of second 17 p2864 A67-33388

Time-microscopy methods using laser flashlight, roentgen flashlight and rapid succession spark pulses in combination with stereo cameras 17 p2864 A67-33408

Real-time electrooptical spectrum analyzers with coherent detection 19 p3197 A67-35687

Laser and nonlaser light transmission through atmosphere, noting no difference in propagation 19 p3240 A67-35695

Coherent light applications in holography and spatial filtering including Fourier transform holography and pattern recognition 20 p3457 A67-36333

Bias in coherency estimation resulting from phase changes 20 p3476 A67-36787

Giant coherent light pulses generation by Q-switched laser, studying dynamics of generation and field distribution 21 p3640 A67-38373

Book on optical interferometry from coherence theory viewpoint, considering wave front and amplitude division, interference spectroscopy, multiple and laser interference, etc 21 p3658 A67-39066

Optical communication system components, discussing cost and potential information capacity factors in picture phone and newspaper transmission facilities 22 p3759 A67-39329

Coherent optics technology, presenting effective black body temperature of six radiation sources and output and pulse duration of four laser sources 22 p3817 A67-40351

Diffraction and image formation in coherent and noncoherent light with relation to Fourier transform 23 p3972 A67-40708

Structure of image of diffused surface in coherent illumination investigated for mean intensity and noise-like obscuring component 24 p4155 A67-42336

Digital computer and coherent optical image processing techniques compared, reviewing data transfer schemes and available hardware 24 p4125 A67-42438

Character recognition via holography using Gabor principle of two coherent waves falling simultaneously on photographic plate 24 p4157 A67-42456

COHERENT RADAR

Clutter suppression by complex weighting of coherent pulse train 04 p0570 A67-14878

Threshold SNR loss of coherent radar in reception of partially coherent packages, noting graph plotting 07 p1139 A67-19230

Bulldup effectiveness of sequence of quasi-coherent radio pulses by comb filter matched with ideally coherent signal 07 p1140 A67-19231

Stability requirements placed on subsystems of coherent impulse radars 07 p1140 A67-19232

Coherent responder used in distance Doppler tracking system, obtaining radial distance by using phase compression 21 p3656 A67-38650

COHERENT RADIATION

Optical surface roughness measurement using coherent radiation produced by helium-neon laser sigma-polarized at 6328 angstroms 01 p0020 A67-10020

Minimum spectral line width, threshold current density, radiation-peak displacement and possible recombination mechanism for GaSb laser diode p-n junctions in coherent radiation 01 p0087 A67-10085

Spontaneous and induced coherent radiation from indium antimonide electron-hole plasma 01 p0087 A67-10088

Coherent emission of indium arsenide phosphide p-n junction 01 p0087 A67-10101

Coherent microwave power at K-band frequencies from indium antimonide structures, presenting theory of two-stream interaction in transverse magnetic field 01 p0131 A67-10371

Continuous coherent radiation of GaAs semiconductor laser with epitaxial p-n junction at ambient temperature of 77 degrees K 01 p0090 A67-10548

Coherent amplification of RF radiation in cosmic space 01 p0144 A67-10836

Continuous coherent radiation of GaAs semiconductor laser with epitaxial p-n junction at ambient temperature of 77 degrees K 01 p0091 A67-11056

Degree of coherence for extended source,

considering electron transitions, found to depend on electron initial and final state 01 p0091 A67-11227

External ionosphere electron concentration measurement from data on Doppler shift variations in frequency of coherent radio signals from Cosmos and Elektron satellite 02 p0192 A67-11658

Laser based on excitation of gallium phosphorus arsenide solid solution by beam of fast electrons 02 p0251 A67-11824

Scattering of partially coherent radiation by neutral molecules formulated as random process 02 p0201 A67-12096

Coherent radio emission of extensive air showers determined from known threshold energy of optical signal 02 p0318 A67-12783

Laser emission in pure cadmium sulfide crystals bombarded by electron beams 03 p0433 A67-12812

Ruby laser frequency conversion technique by laser beam scattering and mixing of combined frequencies 03 p0433 A67-13094

SHF modulation techniques for laser radiation, covering Faraday, Kerr and Pockel effects, circular dichroism, etc 03 p0436 A67-13138

Coherent homodyne detection at 10.6 micrometers with aluminum-doped silicon photoconductor, presenting noise spectra and voltage 03 p0438 A67-13989

Coherent interaction of two radio waves in plasma, generation of mutually-harmonic frequency wave and application to radio transmission in ionospheric F layer 03 p0372 A67-14091

Wave interaction dynamics of far IR electromagnetic radiation generation by coherent molecular vibrations or phonons excited by stimulated Raman scattering and resonant phase matching condition 04 p0657 A67-15113

Semiconductor lasers with radiating mirrors developed by excitation, using electron beam and neodymium laser glass radiation 05 p0821 A67-16669

Degree of coherence of two points illuminated by plane quasi-monochromatic source 06 p1000 A67-17574

Electron beam spatial scanning of coherent emission of GaAs junction laser at low temperatures, making current distribution nonuniform 06 p1011 A67-18150

Emission microwave spectroscopy of OCS, observing coherent ringing, coherent radiation modulation and pulse echoes 06 p1032 A67-18208

Coherent radiation interaction with two-level atoms system in single mode approximation, obtaining equation for time dependent number of photon emission and absorption 06 p1012 A67-18804

Spectral analysis of emission of spatially separated spots in GaAs injection lasers 07 p1197 A67-20185

Coherent radiation generation in electron-hole indium antimonide plasma, discussing emission spectrum 08 p1367 A67-20418

Second order coherence properties of fluctuating vector electromagnetic fields of arbitrary spectral width, noting dyadic field spectral density and governing differential equations 09 p1460 A67-21587

Iterative solution for spherically symmetric mutual coherence function representing radiation propagating through statistically homogeneous and isotropic random medium 09 p1460 A67-21592

Statistical properties of superposition of coherent and incoherent electromagnetic fields studied in terms of coherent state formalism 10 p1667 A67-23778

Statistical properties of coherent radiation noting correlation function, experiments on photon distribution, Bose-Einstein distribution, etc 11 p1799 A67-24106

Side-looking synthetic aperture radar systems 11 p1753 A67-24440

Heterodyne detector of submillimeter radiation using CN maser as continuous wave source of coherent radiation 12 p1951 A67-25209

Doppler frequency shift for radio waves radiating coherently from satellite in ionosphere, considering electron concentration and angles of refraction 13 p2067 A67-26568

Coherent radiation frequency conversion and nonlinear optics methods, including stimulated Raman scattering and Mandelstam-Brillouin

scattering 14 p2330 A67-26467

External ionosphere electron concentration measurement from data on Doppler shift variations in frequency of coherent radio signals from Cosmos and Elektron satellite 16 p2624 A67-31073

Dependence of focusing property of aperture on coherence length of illuminating field in Fresnel diffraction from aperture 16 p2639 A67-31358

Scattering and absorption of ultrashort coherent radiation pulses passing through electron gas applied to ionosphere 17 p2812 A67-32312

Coherent radiation from cadmium sulfide single crystal excited by electron beam noting transition nature in generation mode and spectral composition 17 p2915 A67-32660

Generation of giant pulses of coherent radiation by rotating-mirror technique and by passive Q-switch using cryptocyanine 17 p2871 A67-33390

Spatial coherence and shape of emission wave front of giant pulse from ruby laser with Pockels cell shutter 18 p3058 A67-33526

Refractive index variations, Coulomb scattering and time variation of shower front effects on coherent emission of polarized radio pulses from cosmic ray showers 18 p3116 A67-34197

Coherent radiation interaction with two-level atoms system in single mode approximation, obtaining equation for time dependent number of photon emission and absorption 18 p3061 A67-34423

Solving Schroedinger equation with initial coherent radiation state 20 p3485 A67-36866

Irradiance due to square array of circular apertures from scalar Fresnel-Kirchhoff diffraction theory, giving plots of Fresnel diffraction patterns 22 p3835 A67-39235

Quantum theory of maser oscillator model consisting of radiation field mode interacting with 3-level atoms 22 p3814 A67-39436

Book on laser systems covering quantum electronics, coherent radiation, modulation and spectral, distance, velocity and communication applications 22 p3814 A67-39445

Coherent emission observation in indium phosphide excited by injection laser at 77 degrees K 22 p3814 A67-39461

Book on theory and applications of holography, mathematical analysis of process as imaging technique, limitations and partial coherence 22 p3798 A67-39633

Gas laser simulation technique to facilitate teaching of laser physics 22 p3816 A67-39923

Coherent radio emission of extensive air showers determined from known threshold energy of optical signal 22 p3878 A67-40285

Coherent Raman amplification dynamics, considering pump depletion and coupling saturation and stimulated Raman scattering by polarization waves 22 p3816 A67-40318

Coherent high power millimeter and submillimeter wave generation by various free electron beam devices, noting periodic beam has greatest development potential 22 p3774 A67-40443

Laser radiation in calibration of spectrometer scanning function by duplicating spatial coherence characteristics of radiation 23 p4014 A67-41023

Spatial coherence of radiation field across multimode He-Ne laser beam 24 p4167 A67-42091

COHERENT SCATTERING

Object-image relationships in scattered laser light 05 p0824 A67-16792

X-ray analysis of size reduction of coherent scattering regions of metal deformed in ultrasonic field 13 p2124 A67-27627

Coherent scattering of solar radiation in uniform isotropic medium containing point source surrounded by cavity 15 p2549 A67-29144

Failure of conventional adiabatic criterion in case of excitation of helium atoms by helium ions 15 p2519 A67-29330

Coherent integral method applicable to scattering calculations for arbitrarily shaped dielectric bodies of low density [TR-67-114] 16 p2626 A67-31347

Cross section of Helium 3 reaction calculated for possible solar neutrino source 16 p2741 A67-31921

Far tropospheric propagation of radio waves due to coherent scattering, explaining signal level dependence on distance and

- wavelength and signal
fading 21 p3585 A67-38814
Siegman maximum signal theorem for coherent scattering detection, estimating attenuation through scattering medium 23 p3973 A67-40835
Interferometer phase and amplitude measurements for coherence ratio and wavefront correlation, discussing scattered flux 23 p3974 A67-41197
Escape probability of photon from homogeneous plane parallel medium, discussing coherent scattering process and integral equation 24 p4191 A67-42596
Coherent scattering of solar radiation in uniform isotropic medium containing point source surrounded by cavity 24 p4222 A67-43067
- COHERENT SOURCE**
Holographic image magnification by recording wave interference and illuminating object by coherent beam 18 p3053 A67-34622
High quality holography of back-lighted objects using achromatic-fringe interferometry 20 p3450 A67-37022
- COHERENT TRANSMISSION**
Wavelength dependence of spectrum of laser beams traversing atmosphere 05 p0763 A67-16793
Dirichlet theorem and coherent imaging, discussing form of Fourier functions in Fraunhofer diffraction at infinity 07 p1185 A67-19402
Gas lens focusing of light beams, using highly transparent gas with weakly varying refractive index to guide coherent transmission with small losses 07 p1188 A67-19789
Received signal degradation for coherent pulse transmission through rain scattering volume, calculating length and energy for various paths 11 p1752 A67-24285
Error probability for transmission of M orthogonal equally probable equal-energy signals over partially coherent channel 12 p1908 A67-26091
Modulation indexes for two-channel phase coherent communication system determining data rate yielding predetermined bit-error probability [JPL-TR-32-1118] 14 p2273 A67-28709
Coherent amplification properties of antireflective coated GaAs diodes considered for application to phased array 22 p3813 A67-39254
Josephson effect and quantum coherence measurements in superconductors and superfluids, discussing perturbation theory and tunnel junctions interference effects 22 p3866 A67-40549
- COHESION**
SA ADHESION
Agreement of crack extension criteria of Griffith and Barenblatt, considering cohesive forces 15 p2504 A67-30093
Nonlocal elasticity theory for materials with long range cohesive forces derived from lattice theory by writing strain energy in integral form 22 p3908 A67-39288
- COHOMOLOGY**
SO FUNCTION SPACE
- COIL**
SA ELECTROMAGNET
SA INDUCTOR
SA MAGNETIC COIL
SA MAGNETIC FIELD COIL
SA SOLENOID
Superconducting coils used for capacitors in pulsed operations to reduce size and weight of energy storage systems 22 p3747 A67-39900
- COIN AIRCRAFT**
SO OV-10 AIRCRAFT
COKE AIRCRAFT
S ANTONOV AN-24 AIRCRAFT
- COLD ACCLIMATIZATION**
Cellular biochemical thermoregulation and organic mass changes in cold-and heat-acclimatized monkeys 04 p0560 A67-14582
Physiological responses to cold in men during extended period of sleep loss 23 p3955 A67-41615
- COLD CATHODE**
Self-activating microwave cold cathode crossed field amplifiers for modulation circuits in complex radar systems 03 p0387 A67-14121
Role of space charge and discharge mechanism in gauge with cold cathode, noting electron sheath formation 05 p0809 A67-17494
X-ray spectrometer with cold cathode, discussing equipment design, principles, operation and performance 17 p2853 A67-32046
Intense HF oscillations from plasma-beam interaction in cold cathodes PIG reflex discharge 19 p3275 A67-35109
Cold cathode ion source /CCIS/ quadrupole mass spectrometer for ultrahigh residual gas analysis 23 p4000 A67-41217
- COLD FLOW TEST**
Subscale cold-flow rocket motor model used to determine effect of purely geometric variables on acoustic performance leading to axial mode combustion instability 06 p1075 A67-18853
Liquid fluorine closed flow loop and rocket engine test position design, construction and operation 17 p2832 A67-32012
- COLD FORMING**
Cold forming properties and handling of stainless steels and superalloys noting contained extrusion and warm heading techniques 21 p3634 A67-38177
- COLD HARDENING**
Cold hardened metal adhesive /Agomet E/, discussing polymerization, pot time, setting and temperature 07 p1193 A67-20291
Alloying elements effect on austenite hardening of high-nickel-content chromium-nickel steels during cold plastic deformation 13 p2142 A67-27285
- COLD PLASMA**
S COLLISIONLESS PLASMA
S RAREFIED PLASMA
- COLD WEATHER TESTING**
Cold starting and service test evaluation of SAE 10W30 aircraft engine oil [SAE PAPER 670249] 11 p1811 A67-23982
- COLD WORKING**
X-ray diffraction-Fourier series analysis and electron microscopy analysis of annealing effects on structural properties of cold worked dispersion-strengthened alloys 01 p0097 A67-10698
Crystal layer dislocation structure of cold rolled molybdenum foil investigated by electron microscopy 01 p0101 A67-10939
Line broadening due to cold working Ta-10 percent Re and W-20 percent Re studied by Fourier analysis, integral breadth measurements and variance analysis 02 p0256 A67-12701
Prior cold reduction effect on precipitation and embrittlement of cobalt base alloy /L-605/ 04 p0639 A67-15457
Effects of cold work by rolling and by shock waves on precipitation hardening in Al-6 percent Cu alloy 08 p1343 A67-21544
Ultrahigh vacuum cold welding in dynamic load elevated temperature environment, noting surface oxide in vacuum 10 p1670 A67-23742
Stress corrosion cracking of cold reduced austenitic stainless steels noting effects of marine atmosphere exposure, cold working, welding, etc 11 p1807 A67-24586
Electron microscope study of cold working and tempering of beryllium single crystals 13 p2138 A67-27117
Internal friction of annealed and cold-worked niobium and tantalum wires containing oxygen and nitrogen measured, noting cold-work peaks in addition to Snoek peaks 15 p2503 A67-29748
Broadening of Debye-Scherrer line profiles and structure recovery studied in cold-worked Ti, Zr and Hf specimens by X-ray analysis 19 p3247 A67-35835
Initial tension and compression effects on fatigue strength of aluminum alloy structures during plastic cold working 22 p3911 A67-39549
Crystal layer dislocation structure of cold rolled molybdenum foil investigated by electron microscopy 22 p3820 A67-39792
- COLLAPSE**
SA GRAVITATIONAL COLLAPSE
Computer program for axisymmetric nonlinear behavior of stiffened elastic shells of revolution with variable thickness, calculating collapse pressures [AIAA PAPER 66-529] 08 p1417 A67-20558
Collapse of isolated spherical vapor-air cavitation pocket moving toward solid surface in incompressible fluid medium 12 p1927 A67-25320
Constitutive equation for collapse load and limit analysis of elastoplastic structures 13 p2216 A67-26609
- Monography on plastic axisymmetric collapse of ring stiffened cylindrical shells under external hydrostatic pressure 18 p3140 A67-33432
Human experiments to study somnolent and precollapoid /collapoid/ states when falling asleep and during prolonged standing tests 20 p3368 A67-36268
- COLLECTOR**
SA CONCENTRATOR
SA DUST COLLECTOR
SA SOLAR COLLECTOR
Noise measurements on pulsed four-cavity electrostatically focused S-band klystrons 09 p1477 A67-22253
Volt-ampere characteristics of grooved collector thermionic diode indicate ions generated in cavities diffuse to cavity free region and neutralize electron space charge 09 p1448 A67-22340
Collector target complex eliminating target life time and test equipment contamination by sputtered target material, applied in testing of electrical propulsion systems [AIAA PAPER 66-500] 11 p1852 A67-24341
Upper cut-off frequency and amplitude frequency response curve shape for wideband aperiodic amplifiers, examining five common transistor circuits 13 p2077 A67-26660
Transfer of electrons from emitter or space charge region to collector in thermionic energy converter by negative ions 13 p2056 A67-27002
Thermionic converter acceleration plate and excessive current flow effects, noting collector and cathode surface secondary electron removal, determining cut-off characteristic form change 14 p2246 A67-27766
One-and two-dimensional antenna synthesis for instruments of large resolving power and effective collecting area 14 p2284 A67-28433
Diffused base transistor impurity concentration measured nondestructively to determine structure 15 p2448 A67-29801
Collector conduction resistance in saturated planar transistors determined from current distribution measurement on electrolytic model 15 p2448 A67-29802
Nonuniform base width effects on h-parameters of junction transistor 16 p2635 A67-30795
Planar transistor collector current rise time determination with base driven by current step function and application procedures 20 p3395 A67-36299
Contact continuity, intermediate resistance consistency and passing signal distortion of current collector with slip rings and brushes of various metals 21 p3572 A67-38916
Back collection of charge due to ionizing alpha or beta particles by silicon p-n junction detector with space charge width less than range 22 p3797 A67-39345
- COLLISION**
SA ATOMIC COLLISION
SA COULOMB COLLISION
SA ELASTIC COLLISION
SA ELECTRON COLLISION
SA INELASTIC COLLISION
SA IONIC COLLISION
SA METEORITE COLLISION
SA MOLECULAR COLLISION
SA PARTICLE COLLISION
Vainshtein method calculation of inelastic collision of electrons with atoms 07 p1225 A67-19207
Collisional excitation of Si ion from ground state to autoionization levels at coronal temperatures 07 p1256 A67-20168
Head-on collision between stars at high initial relative velocity, considering one-dimensional driven shock motion in inhomogeneous medium 20 p3525 A67-36943
Angular momentum and vibrational energy transfer between nearly colliding stars 21 p3700 A67-37732
Aircraft/bird collision noting dispersion, flock detection and windshield protection 23 p3934 A67-41070
- COLLISION AVOIDANCE NAVIGATION**
Short range radar with 1 m resolution for FM-CW technique for vehicle guidance in fog, describing equipment 09 p1528 A67-22630
Air derived separation assurance /ADSA/ covering visual capabilities, passive visual enhancement, visual avoidance aids and nonvisual avoidance systems 15 p2515 A67-29942

Long and short range air navigation trends, discussing digital computer application, collision prevention and landing systems 19 p3256 A67-35864
 Air collision statistics, discussing air collision avoidance system 19 p3173 A67-35865
 Air traffic control /ATC/ in 1970s, discussing airports, electronic facilities and collision avoidance 20 p3482 A67-37441

COLLISION PARAMETER

Growing space charge wave phenomenon due to collision coupling in warm compressible dissipative electron plasma in uniform motion 03 p0483 A67-13995
 Quadrupole effects on gas diffusion, viscosity and thermal diffusion factors, computing collision integrals 06 p1038 A67-19046
 Collision broadening cross sections and effect of resonant interactions on gas-laser transitions 12 p1953 A67-26196
 Local measurement of SHF electromagnetic field during plasma properties observation, using dipole antennas 15 p2485 A67-29124
 Failure of conventional adiabatic criterion in case of excitation of helium atoms by helium ions 15 p2519 A67-29330
 RF characteristics of spherical probe immersed in hot low-density plasma, using sheath model 15 p2528 A67-29564
 Thermal conductances in collisionless gas between coaxial cylinders and concentric spheres obtained for arbitrary thermal accommodation coefficients 15 p2579 A67-29566
 Collision integral for Landau plasma in strong magnetic field to obtain time evolution of one-particle distribution function 15 p2532 A67-30382
 Finite collision time for artificial celestial body moving under influence of Newtonian force from attractive center 16 p2745 A67-30744
 Nonconvective instability for hot plasmas from poles colliding through negative wave numbers 17 p2899 A67-32276
 Electron impact cross sections used to determine helium collision cross sections sets 20 p3489 A67-37417
 Stochastic optimal control algorithm for pursuit process in problem of encounter of two cosmic objects 22 p3878 A67-39183
 Wave propagation in plasma with anisotropic pressure studied using modified Burgers equations, examining effect of collisions 24 p4197 A67-42260

COLLISION RATE
 Boltzmann equations in kinetic theory of rarefied gas dynamics [ONERA-TP-379] 01 p0054 A67-11092
 Photon interaction in plasma, determining energy density and collision frequency 02 p0272 A67-11583
 Existence of divergence in density expansion of viscosity and thermal conductivity coefficient of two-dimensional gas of rigid disks 02 p0234 A67-12545
 Tandem mass spectrometers for study of ion-molecule reactions, noting ion gun, deceleration lens and collision chamber 02 p0247 A67-12690
 Book on microwave breakdown in gases covering electron collisions, Boltzmann equation for ionized gas, breakdown in atmosphere, etc 03 p0369 A67-13559
 Natural and forced oscillations of sphere-array moving with collisions, analyzing quasi-elastic properties of system 03 p0432 A67-14162
 Gas kinetic theory of negative ion collisional detachment, using elastic sphere model 05 p0844 A67-16003
 Electron collision rate and density calculations for He-Ne laser plasma 05 p0815 A67-16598
 Anomalous losses in plasma confined in magnetic field, correlating loss process with tube dimensions, electron temperature, gas pressure and magnetic field 11 p1829 A67-24002
 Free electron density and effective collision frequency of ionized argon in wake of shock wave measured, using microwave probe methods 11 p1775 A67-24017
 Plasma equilibrium from gas discharge, role of electron concentration and contributions of excited atom transitions and quenching collisions 12 p1977 A67-26132
 Surface density gradient and collision frequency effects on polarization of

microwaves reflected from plasma surface 13 p2164 A67-26300
 Kinetic model with velocity dependent collision frequency applied to forced wave propagation in half-space and other unsteady problems 13 p2100 A67-26956
 Electron density variation, collision frequency and phase shift in standing striations in positive column 14 p2353 A67-27758
 Generalization of Oepik theory of planetary bodies collision to include case where orbits of both colliding bodies are ellipses 14 p2384 A67-28055
 First collision effects in rarefied high speed flows in low density wind tunnel, noting measurement techniques and apparatus used 14 p2317 A67-28197
 Ionospheric D layer structure and formation, considering free electron height variation and collision rate 14 p2311 A67-28406
 Collision frequencies in D region and stratospheric-mesospheric relations, noting oxygen as error source and electron-density height profile 14 p2311 A67-28407
 Momentum transfer collision frequency for electrons in cesium plasmas from electrical conductivity and plasma properties measurement in cesium arc column 16 p2719 A67-31236
 Collisional de-excitation rate or quenching of sodium in flat premixed laminar flames 18 p3150 A67-33803
 Ionosphere collision frequencies and densities studied by rocket measurements of magnetic field of VLF wave radiated from ground 18 p3041 A67-34233
 Plasma finite orbits instability due to plasma particle shift, discussing collision frequency role 19 p3267 A67-34896
 Reaction rate constants for gaseous chemical species at high temperatures [CI PAPER 67-11] 19 p3345 A67-35006
 Kinetic theory of transport processes in weakly turbulent plasma with and without magnetic field 19 p3286 A67-35351
 Electron density behind shock front of discharge plasma measured using interferometer 19 p3230 A67-35395
 Electron density and collision rate of shock produced plasma measured with X-band microwave reflection probe 19 p3293 A67-35398
 Air ionization behind shock wave front, estimating free electron concentration, ionization time and collision frequency 19 p3293 A67-35401
 Electron-temperature dependence of electron collision frequency in afterglow plasma 21 p3667 A67-38414
 Ion-molecule collision cross section determined from pressure broadening of ion cyclotron resonance lines at high electric field/pressure ratio 22 p3840 A67-39365
 Kramers problem for rarefied gas flow, calculating slip coefficient for various collision frequency models, noting only slight model dependence 22 p3841 A67-39718
 Theoretical collision efficiencies for cloud droplets in steady Stokes flow suggest near unity coalescence 23 p4024 A67-40636
 Ionospheric absorption from unabsorbed cosmic radio noise intensity, discussing electron density and collision frequency profiles 23 p3994 A67-40778
 Mean F-2 layer electron collision frequency computation from cosmic noise absorption 23 p3994 A67-40779

COLLISION WARNING DEVICE
 Air collision statistics, discussing air collision avoidance system 19 p3173 A67-35865

COLLISIONLESS PLASMA
 Collisionless electron heating by ion cyclotron wave attributed to Landau damping, discussing current generation 02 p0275 A67-12556
 Attenuation and dispersion of sound in nearly collisionless gases as function of sound-to-particle path 02 p0235 A67-12565
 Perturbation of electron density at large distances from body at high velocity in collisionless plasma under steady external magnetic field 03 p0475 A67-12939
 Separation constants for finite gyrotropic axially-magnetized cold collisionless plasma graphically represented near boundary of complex region 03 p0371 A67-13867
 Small amplitude electromagnetic wave

propagation in cold homogeneous ionospheric plasma including negative ions and immersed in static magnetic field 04 p0614 A67-14957
 Perturbation theory of ion concentration at great distances from body rapidly moving in collisionless plasma in constant magnetic field 05 p0855 A67-17139
 Collisionless theory of plasma sheath near infinite planar electrodes, developing new sheath model incorporating microscopic boundary conditions 05 p0857 A67-17424
 Steady oblique nonlinear waves in warm collision-free plasma 05 p0857 A67-17425
 Transverse wave instabilities in collisionless hydrogen plasmas under magnetic field 05 p0858 A67-17429
 Surface current excitation by electromagnetic and electrokinetic waves on metal cylinder immersed in uniform collisionless isotropic plasma 06 p0962 A67-18075
 Quasi-shock structure in collision free plasma in magnetic field and comparison with bow shock on solar wind near earth 08 p1359 A67-20901
 Velocity space diffusion from weak collisionless plasma turbulence in magnetic field 08 p1360 A67-21123
 Particle loss through axisymmetric cusped magnetic field containment geometry, deriving adiabatic invariant for collisionless plasma 08 p1361 A67-21133
 Causality of steady state response of collisionless plasma model to applied external field 08 p1365 A67-21405
 Potential distribution in electron-collisionless plasma in weak magnetic field 08 p1365 A67-21412
 Collisionless damping in hot plasma due to electron reflection at wall and phase mixing associated with thermal perturbation 09 p1549 A67-22552
 Second order gyroviscous stress in collisionless plasma for LF propagation quasi-perpendicular to magnetic field calculated by utilizing higher moments of Vlasov equation 10 p1685 A67-23331
 Electrostatic wave excitation growth in collisionless plasma interaction and simultaneous modification with electron beam studied for weakly unstable situations 11 p1826 A67-23875
 Dispersion relation for large amplitude circularly polarized plane wave propagation along magnetic field in hot collision-free plasma, considering distribution function 11 p1826 A67-23881
 Collisionless instabilities in thermally ionized potassium plasma and effect of magnetic shear on oscillations and diffusion 11 p1834 A67-24378
 Highly ionized plasma with excitation and damping of density and temperature drift waves in stable regime 11 p1835 A67-24382
 Gyroviscosity of collisionless plasma in strong magnetic field, duality theorem and application to linear stability analysis 11 p1839 A67-24547
 Energetic molecular hydrogen ions injected into resonant nonadiabatic magnetic mirror trap, studying particle mean lifetime, noting cold plasma stabilizing effect 12 p1969 A67-25248
 Steady state properties of collisionless cylindrical injected plasma of zero temperature in presence of longitudinal magnetic field steady state properties of collisionless cylindrical injected plasma of zero temperature in 12 p1974 A67-25455
 Modal wave solutions of isotropic plasma-filled parallel-plate waveguide examined, using cold and warm plasma models without collision 12 p1915 A67-25943
 Excitation of collisionless shock waves in low density plasma noting lifetime, discharge process, adiabatic contraction, etc 12 p1976 A67-26074
 Third order Vlasov equation solved for nonlinear plasma oscillations in classical nonrelativistic collisionless Maxwell distribution electron gas 13 p2162 A67-26283
 Damping of plane sinusoidal wave in cold collisionless plasma, studying supercritical amplitude oscillatory process 13 p2171 A67-27615
 Dispersion relation for two-component model of collisionless nonrelativistic plasma with external magnetic field acting on system 14 p2356 A67-28201
 Local electrostatic potential for collisionless plasma flow derived, obtaining

smooth solutions for self-consistent electron density distributions 14 p2356 A67-28202

Moment method treatment of collisionless plasma equilibria in confining magnetostatic fields, using Vlasov equation to determine distribution function of particles 14 p2360 A67-28554

Plasma wind tunnel facility for producing steady flow high conductivity collisionless plasma simulating solar wind interaction with magnetosphere 14 p2294 A67-29036

Collective effects in collisionless plasmas in laboratory in case of Vlasov-Maxwell equations with Landau damping 14 p2362 A67-29037

Transverse diffusion coefficient of collisionless plasma in magnetic field measured, using variations in radial plasma column density 14 p2363 A67-29067

Frequency shift associated with nonlinear extraordinary wave in cold plasma calculated using Bogoliubov method 15 p2524 A67-29230

Kelvin instability following velocity discontinuity in current-carrying cold collisionless plasmas under magnetic field, deriving dispersion relation and instability criteria from fluid equations 16 p2714 A67-30872

Drift instabilities in nonuniform collision-free plasma stabilized by magnetic shear noting longitudinal currents, electron and ion temperature gradients, etc 16 p2718 A67-31226

Numerical analysis of structure of one-dimensional unsteady magnetic compression waves propagating into collisionless plasma, using motion equations 16 p2719 A67-31232

Temperature gradient effect on stability of inhomogeneous magnetically-confined plasma with frequent ion collisions 16 p2720 A67-31239

Plane wave disturbances in infinite rotating collisionless system for wave vector normal to axis of rotation [AD-653420] 16 p2753 A67-31700

Plasma produced transit time delay of reflected pulses for collisionless inhomogeneous plasma 17 p2810 A67-32070

Microwave methods applied to plasma diagnostics restricted to steady state plasma 17 p2901 A67-32349

Collisionless shock waves in plasmas with high beta parameter, discussing Alfvén wave turbulence, firehose instability, dissipation and structure 17 p2901 A67-32528

Zero temperature cylindrical collisionless plasma in magnetic field studied for electrostatic instability, noting effect of radial velocities of electrons and ions 17 p2902 A67-32658

Hamiltonian formalism for collisionless electron plasma nonlinear kinetics using quantum statistical perturbational treatment 17 p2902 A67-32670

Hydromagnetic wave propagation in collisionless plasma based on Vlasov equation, finding Alfvén, magnetoacoustic and nonoscillating waves 17 p2902 A67-32673

Nonlinear effects in collisionless plasma during interaction with strong HF field 17 p2905 A67-32920

Plasma resonances, deriving relations between coefficients for transmission, reflection and emission of microwaves and explaining collision-free discharge 17 p2907 A67-33105

HF electrostatic instability in low density plasma stream guided by magnetic field, discussing cause and anomalous loss of diamagnetism 17 p2907 A67-33106

Longitudinal and transverse collective effects contribution to energy loss rate in relativistic isotropic plasma subject to external fields and particles 17 p2908 A67-33111

Fluctuating electric and magnetic fields due to plasma instabilities and stabilizing effect of mode coupling in collisionless plasma 17 p2909 A67-33229

Weak turbulence theory for collisionless plasmas formulated in terms of test waves 18 p3092 A67-34744

Collisionless electrostatic shock in magnetized plasma in absence of initial magnetic field 18 p3092 A67-34749

Transverse and longitudinal waves in infinite nonrelativistic collisionless plasma, using Maxwell equation 18 p3093 A67-34750

Charge, current, and self-consistent field transport properties of collisionless plasma derived using initial value solutions to

Vlasov equation 19 p3285 A67-35343

Structure of shock waves in collision-free plasma at angle to external magnetic field studied by hydrodynamic equations 19 p3288 A67-35372

Cyclotron waves in collisionless plasma column, finding three distinct waves with resonances at/near electron cyclotron frequency 19 p3288 A67-35373

Longitudinal wave echo in collisionless electron plasma with Landau damping 19 p3295 A67-35534

Entropy and free energy functionals for collisionless plasma at equilibrium in adiabatic magnetic field 19 p3298 A67-35731

Collective fluctuations in collisionless plasma, analyzing spectra fluctuations, particle distribution and wave scattering 20 p3493 A67-36139

Transport process instability theory, discussing collisionless plasma transport phenomena and relation to Ohm law 20 p3495 A67-36156

Oblique incidence millimeter wave technique using ray theory for measuring collisionless plasma electron density profile 20 p3496 A67-36311

Collisionless plasma heating by random magnetic fields using simple betatron model 21 p3662 A67-37762

Plasma hydromagnetic jump conditions derived from two-fluid plasma model, discussing relevance to collisionless plasma shock 21 p3662 A67-37764

Wave kinetics of free Alfvén oscillations using Lagrange function of collisionless plasma, calculating energy growth rate and relaxation times 21 p3667 A67-38372

Drift instabilities of inhomogeneous plasma in HF electric field 21 p3667 A67-38374

Collisionless shock wave existence in fully ionized plasma, noting shock wave internal structure 21 p3667 A67-38410

Perturbation theory of ion concentration at great distances from body rapidly moving in collisionless plasma in constant magnetic field 21 p3668 A67-38481

Tensor conductivity effect on continuum and collisionless MPD flows past slender bodies [AIAA PAPER 67-731] 21 p3674 A67-38755

Stationary state of collisionless plasma in magnetostatic and potential fields, deriving distribution functions and concentration formulas 22 p3842 A67-39243

Alfvén, fast and slow magnetoacoustic and entropy hydromagnetic wave propagation in anisotropic collisionless magnetoplasma 22 p3843 A67-39268

Finite discontinuity jump conditions for plasma in strong magnetic field determined by approximation and Maxwell equation, noting possible application to satellite data 22 p3843 A67-39269

Collisionless damping of temperature or secondary resonance spectrum of plasma column 22 p3845 A67-39482

Ion wave velocities and damping measurements in quiescent plasma used for diagnosis of temperatures and drift velocities 22 p3846 A67-39488

Stability of collisionless plasma with ions moving relative to electrons under electric field of ion cyclotron wave 22 p3852 A67-39989

Collisionless small and large amplitude electron plasma wave damping compared, showing small amplitude waves damp exponentially and large amplitude waves exhibit amplitude oscillations collisionless small and large amplitude electron 22 p3853 A67-40242

Kinetic collisionless plasma diode model stationary regimes, discussing sheath achievement density value dependence on temperature difference and trapped particle distribution 22 p3774 A67-40322

Temporal and spatial echoes can occur in collision-free plasmas at various times for different wave number combinations and various positions for different frequency combinations 24 p4194 A67-41871

COLLOID

SA ELECTROPHORESIS

SA SOLID SUSPENSION

Temperature and magnetic field gradient effects on magnetothermomechanical interaction of viscous incompressible ferrofluid with cold wall 04 p0600 A67-14446

COLLOIDAL GENERATOR

Comparison of performance of atom-ion and colloidal thruster systems for orbital transfers, noting influence of various parameters on mission capabilities 04 p0688 A67-14560

Thermodynamic flow analysis of feasibility of coolant gas addition to nozzle flow for improved particle formation efficiency in mixed flow colloid thruster [AIAA PAPER 67-85] 06 p0941 A67-18500

Comparison of performance of atom-ion and colloidal thruster systems for orbital transfers, noting influence of various parameters on mission capabilities 20 p3515 A67-36407

Colloidal electrodynamic energy converters analyzed on basis of power plant specific mass 24 p4109 A67-42888

COLLOIDAL PROPELLANT

Colloid particle electrostatic thrusters for lunar ferry missions in specific impulse range 1000-3000 sec 03 p0503 A67-13492

Propulsion through drag interaction between magnetically-accelerated iron particle suspension and air [AIAA PAPER 66-926] 03 p0504 A67-14136

Charged colloidal heavy particle propulsion and production of heavy particles 04 p0689 A67-15016

Comparison of various electrostatic thrusters and proposed low pressure colloidal power converter for high payload lunar and planetary missions [AIAA PAPER 66-211] 05 p0874 A67-17216

Computer program and mathematical model for design of electrostatic colloid thruster [AIAA PAPER 67-84] 06 p1075 A67-18499

Emulsified fuel mixture /JP-4 and water/ tested in model Allison T63 turbine engine [SAE PAPER 670368] 12 p1987 A67-25883

Emulsified fuel effect on gas turbine combustors, noting good operation in low altitude flight but inhibited combustion at start, and at high altitudes [SAE PAPER 670366] 12 p1987 A67-25884

Emulsified jet engine fuel noting lower volatility and flammability and resistivity to corrosion and acceleration [SAE PAPER 670365] 12 p1988 A67-25885

Preformed micron and submicron-sized solid particles for colloidal propulsion, investigating particle feeding and charging [AIAA PAPER 67-727] 21 p3688 A67-38751

Mass flow rate, viscosity and conductivity changes effects on single needle colloid thruster [AIAA PAPER 67-530] 21 p3696 A67-38957

Colloid microthruster technology, discussing stationkeeping application, energy loss, diagnostic techniques, etc [AIAA PAPER 67-531] 22 p3867 A67-39200

Computer program and mathematical model for design of electrostatic colloid thruster [AIAA PAPER 67-84] 22 p3868 A67-40101

COLOR PERCEPTION

Color events on moon observed through color filters alternately, noting crater Gassendi 05 p0888 A67-16155

Color vision testing criteria in analysis of results from pseudo-isochromatic plate, anomaloscope and signal lantern testing 07 p1135 A67-19865

Pseudocolor technique, noting applicability to TV data presentation from space vehicles 11 p1789 A67-24250

Color indices of visible meteors observed by naked eye and through color filters noting brightness dependence and meteor train distribution 16 p2751 A67-31462

Mars polar cap size changes, color and visibility from observations in 1963 17 p2942 A67-32330

Moon Blink project for detecting red or blue temporary color phenomena 18 p3134 A67-34535

Color normals differences, discussing classification and correlation methods 20 p3372 A67-37026

Bezold-Brucke hue shift measurements in color naming situation using optical system 22 p3835 A67-39238

COLOR PHOTOGRAPHY

Zone plate free from chromatic aberration and application to three-color holography 03 p0420 A67-13681

Observed interstellar polarization cannot be explained in terms of graphite-crystal color since polarization must increase

monotonically from IR to UV 04 p0699 A67-14982

Aerial photograph physics in correct and faulty colors, discussing recognition of relation between landscape and photographic density 05 p0804 A67-16064

Color study of lunar surface suggesting nonexistence of cosmic dust layer 05 p0901 A67-17083

Film cooling technique for color photographs of astronomical objects to diminish effects of reciprocity failure and increase light sensitivity 06 p1002 A67-17975

Telescope optics techniques for compensation for lateral color aberration arising from atmospheric refraction, using modified Schupmann medial telescope 06 p1033 A67-18535

Color image reproduction by conventional hologram techniques 09 p1496 A67-21710

Holography /recording light in three dimensions/, noting virtual and real images and color production 10 p1657 A67-23623

Lunar optical properties simulated with commercial Portland cement and maroon and black coloring powders, noting blue-green color index discrepancy 11 p1865 A67-24609

Two-color photoelectric photometry of earthshine, determining earth albedos 15 p2477 A67-29626

Multicolor image reconstruction from holograms behaving as planar diffraction gratings, excluding cross-talk images formation 15 p2491 A67-30431

Experimental techniques in making multicolor white light reconstructed holograms, discussing signal to noise ratio, coherent light and photographic emulsion 17 p2862 A67-33299

White light reflection holography, discussing recording, reconstruction and color images 20 p3438 A67-36349

Color schlieren and high speed photography technique for transient flows in wind tunnels 20 p3445 A67-36537

Aerial color photography advantages over black and white, discussing exposure, processing and viewing 22 p3797 A67-39450

Camera for multispectral color aerial photography noting four-band interpretation on companion viewer and application to target acquisition problems 22 p3797 A67-39451

COLOR TELEVISION

Color TV laser display using Ne-He and argon-ion laser in modulation and scanning system 15 p2489 A67-29914

Color radar signal parameters display system using techniques based on mathematical application of Venn-Euler diagrams 19 p3231 A67-35624

Design and characteristics of solid state UHF transmitters and receivers applicable in color TV systems 20 p3395 A67-36249

DODGE satellite TV cameras for black and white, plus color picture transmission with photometric analysis and camera optics 20 p3452 A67-37573

COLORIMETRY

IR colorimetry of Martian bright and dark areas indicates correlations with limonite terrestrial rocks and volcanic ash 02 p0319 A67-11456

Ozone determination by electrochemical and colorimetric methods compared for effects of sensor cell aging 03 p0413 A67-13931

Red-green-IR three-beam high resolution photoelectric photometry during lunar eclipse for lunar colorimetric studies 04 p0696 A67-14735

Calorimetric, titrimetric and gravimetric methods for determination of hexogen-octogen mixtures 05 p0872 A67-17153

Spectrometric and colorimetric observations of luminescence on moon surface 08 p1390 A67-21020

Brightness of night glow measured in several spectral ranges by Cosmos 92 colorimeter 10 p1647 A67-23276

Doped alkali-halogen-crystal color center origin and transformation at liquid N temperature using ruby laser, noting temporary bleaching 12 p1951 A67-25200

Flaw detection methods using penetrating fluids, emphasizing fluorescent materials and pigments 13 p2122 A67-26255

Color normals differences, discussing classification and correlation methods 20 p3372 A67-37026

Black body visible light at 2800 degrees K changed into energy distribution at 5500 degrees K via Fabry-Perot filter for white light standards for colorimetry 23 p3999 A67-41180

COLUMBIUM

S NIOBIUM

COLUMN

SA BEAM COLUMN

SA TAPERED COLUMN

SA VERTEBRAL COLUMN

SA VORTEX COLUMN

Experimental determination of column initial deflection and load eccentricity in aluminum alloy indicate minor magnitude of load eccentricity 01 p0160 A67-10561

Parametric excitation of initially straight viscoelastic column represented by spring-dashpot model 04 p0709 A67-14814

COMBUSTIBLE FLOW

Equilibrium burning of spherical nongaseous fuel drop in slow convective hot-oxidant flow in thin flame 02 p0341 A67-11562

Air velocity and temperature, stabilizer size and blockage effects on fresh mixture entrainment in recirculation zone of bluff body stabilized flames 02 p0342 A67-12029

Thermodynamic parameters of combustible mixture and ignition system characteristics effect on energy of spark ignition of homogeneous gaseous mixture 03 p0535 A67-13396

Flame separation explained in terms of processes taking place in mixing zone of internal cone in laminar burner flame 08 p1425 A67-20306

Laminar diffusion flame in Oseen flow, identifying limiting case with stoichiometric Burke-Schumann flame and frozen flow 09 p1579 A67-21548

Flame stabilization mechanism of homogeneous combustible fluid flow using air jets through peripheral slits to join main flow producing gasdynamic screens 22 p3921 A67-40455

COMBUSTION

SA BOUNDARY LAYER COMBUSTION

SA BURNING PROCESS

SA DEFLAGRATION

SA EXTERNAL COMBUSTION ENGINE

SA FLAME

SA FUEL COMBUSTION

SA HYBRID COMBUSTION

SA HYDROCARBON COMBUSTION

SA HYPERSONIC COMBUSTION

SA INTERNAL COMBUSTION ENGINE

SA METAL COMBUSTION

SA PROPELLANT COMBUSTION

SA SUPERSONIC COMBUSTION

Soviet book on gas dynamics of combustion including detonation, deflagration, accelerating flames, combustion chambers, etc 02 p0343 A67-12679

Rapid micro dry combustion determination of carbon, hydrogen and nitrogen in high explosives 05 p0759 A67-17154

Nonstationary combustion of powder under action of pressure pulse to determine temperature field variation and burning rate during transient process 06 p1112 A67-17957

Combustion and pyrolytic behavior of thermoplastic polymer spheres burning in quiescent atmospheres of air [AIAA PAPER 67-103] 06 p1114 A67-18283

Combustion and combustion systems - Conference, Karlsruhe, West Germany, April 1965 08 p1425 A67-20302

Nonlinear system of partial differential equations describing one-dimensional combustion process of gas mixture 11 p1882 A67-24158

COMBUSTION CHAMBER

SA ROCKET CHAMBER

Combustion efficiency of supersonic ramjet, noting equations for chamber 01 p0141 A67-11149

Debugging of Emeraude propulsion system of Diamant launch vehicle, stressing problems with combustion chamber instabilities, vibrations, etc 01 p0155 A67-11389

Test stand simulating high intensity heating processes which occur in combustion chambers of rocket and jet engines 02 p0231 A67-12440

Chemical reaction kinetics and gas dynamics combined to analyze processes occurring in combustion chambers and nozzles of jet and rocket engines [DVL-602] 03 p0366 A67-12999

Flame stabilization by mechanical stabilizers in ramjet combustion chamber as function of temperature and pressure of fuel mixture 04 p0691 A67-15899

Enthalpy to work conversion in gas turbines using pulsating combustion chamber 05 p0873 A67-16743

Chemical kinetics effects in supersonic combustion noting three different zones in chamber 06 p1113 A67-18027

Hot gas tunnel for determination of material behavior under convective heat transfer conditions similar to that existing in rocket combustion chambers [AIAA PAPER 67-106] 06 p0981 A67-18473

Boundary value problem for determination of stationary combustion regimes in seminfinite combustion chamber 06 p1119 A67-18818

Turbulence effect on burning velocity and physical structure of flame surface in turbojet-afterburner-like combustion chamber 07 p1265 A67-19073

Temperature field measurement behind combustion chamber of turbojet engine 09 p1560 A67-22464

Gas flow velocity and static pressure profiles experimentally measured in combustion zone of gas turbine combustion chamber model under atmospheric conditions [SAE PAPER 670201] 09 p1561 A67-22545

HF combustion pressure oscillations in gaseous propellant rocket engines analyzed for stably burning combustor design concepts [ASME PAPER 67-VIBR-34] 11 p1851 A67-24191

Annular vaporizing combustion chamber for small-size gas turbine engines, noting fuel-air flow 11 p1853 A67-24526

Combustion chamber model for self-oscillating thermoacoustic system initiated by stimulation effect of acoustic shock 11 p1884 A67-24958

Thrust chamber nozzle performance degradation with energy release and expansion ratio 13 p2188 A67-26847

Visualization of combustion through transparent chamber walls, noting problems concerning hybrid rockets, ignition lags and hybrid combustion instabilities [ONERA-TP-474] 14 p2377 A67-27895

Model for solid rocket motor instability caused by chamber and propellant combustion characteristics, relating combustion and acoustic instabilities 14 p2404 A67-28113

Axial load deformation of grains with end-face limitation used in solid propellant engines 14 p2377 A67-28651

High pressure liquid propellant rocket engines, noting high thrust, smaller engine dimensions, and combustion chamber cooling 16 p2735 A67-30704

Gas circulation effect on temperature field of cylindrical combustion chamber with axisymmetric heat-release and gas-velocity fields 16 p2779 A67-31395

Lumped parameter model for monopropellant hydrazine reaction chamber developed, using mass and energy balance and reaction and diffusion rate coefficients 17 p2927 A67-31974

Film cooling theory applied to aircraft gas turbine chambers shows slot geometry effect as negligible 17 p2967 A67-32126

Low temperature plasma production in combustion chamber for use in MHD generators, giving equations for plasma composition 17 p2833 A67-32167

Book on design and structural strength of aircraft gas turbine engines covering inlet and exhaust systems, compressors, combustion chambers, rotors, etc 17 p2928 A67-32564

Soviet book on combustion chambers of gas turbine engines covering fuels, working processes, heating, etc 18 p3111 A67-33675

Flame shape and chamber combustion efficiency relation for flame stabilized by opposed jet flameholder [AIAA PAPER 67-472] 18 p3157 A67-33942

Physical and chemical conditions in rocket combustion chamber during starting transients and steady operation described by mathematical model intended for parametric studies [AIAA PAPER 67-517] 18 p3158 A67-33980

M-1 engine system technology items noting thrust chamber assembly, gas generator, fuel

turbopump, etc
 [AIAA PAPER 67-520] 18 p3115 A67-33983
 Pressure fluctuation onset conditions in jet engine combustion chambers with supersonic nozzles, discussing design factors effect on combustion process stability 21 p3696 A67-38909
 Physicochemical combustion of turbulent air-fuel mixture in straight flow combustion chambers, noting effects of various factors and intensification methods 22 p3921 A67-40448

COMBUSTION EFFICIENCY

Gas phase pyrolysis kinetics of tetranitromethane, noting pressure effect and rate equation of thermal decomposition 01 p0019 A67-10765
 Flame study of turbulence effects induced by sonic or ultrasonic vibration on combustion of liquid hydrocarbon jet 01 p0167 A67-10942

Combustion efficiency of supersonic ramjet, noting equations for chamber 01 p0141 A67-11149

Finite rate chemistry effects in diffusion controlled hydrogen-air flames noting flame position, fuel consumption, temperature, fluid velocity outside of flame and boundary conditions 05 p0926 A67-16516

Flame ignition from spherical hot gas pocket, finding minimum size of bubble for flame propagation and dependence on kinetic parameters 06 p1114 A67-18189

Solid propellant burning rate, combustion gas influx, tube geometry and propellant and tube thermophysical properties [AIAA PAPER 67-102] 06 p1074 A67-18282

Supersonic combustion measurements by thrust system method, optical probe and gas-sample probe technique [AIAA PAPER 67-223] 06 p1004 A67-18462

Reverse flow annular combustion system for TPE331 turboprop engine, noting fabrication and combustor efficiency [ASME PAPER 67-GT-25] 11 p1854 A67-24805

Combustion of liquid fuel droplet in sound field, noting rate dependence on sound parameters 15 p2580 A67-29778

Kinetics and energetics of condensed phase thermal decomposition reactions of ammonium perchlorate composite propellants analyzed, using differential scanning calorimetry 15 p2544 A67-29989

Combustion characteristics of crystalline oxidizers noting materials used, experiments performed and results 15 p2581 A67-29990

Supersonic combustor length and contours for optimum performance determined from one-dimensional pressure-area analysis 18 p3154 A67-33832

M-1 injector baffles, ablative chamber and start system design and development, using subscale testing [AIAA PAPER 67-461] 18 p2988 A67-33932

Flame shape and chamber combustion efficiency relation for flame stabilized by opposed jet flameholder [AIAA PAPER 67-472] 18 p3157 A67-33942

Aluminum particle combustion noting changes from preignition to burnout, flame structure, particle geometry, etc [WSCI PAPER 66-3] 22 p3919 A67-40224

Solid propellant burning rate, combustion gas influx, tube geometry and propellant and tube thermophysical properties 23 p4084 A67-41723

COMBUSTION HEAT

Convective heat transfer measurements for partially dissociated carbon monoxide and hydrogen with high Lewis number [ASME PAPER 65-WA/HT-27] 03 p0537 A67-14012

Heats of combustion in fluorine of Teflon and graphite and heats of formation of carbon tetrafluoride and carbon hexafluoride 15 p2433 A67-29765

COMBUSTION INSTABILITY

Nonlinear combustion instability in liquid propellant rocket engines, describing nonsteady combustion process with aid of Crocco time-lag hypothesis 01 p0142 A67-11412

Ignition methods for strongly and weakly hypergolic hybrid propulsion systems, examining steady state combustion problems and combustion instability causes 01 p0139 A67-11416

Unstable speed of combustion of ballistite powders studied by model, examining velocity discontinuity with continuous pressure change 03 p0535 A67-13120

LF instability of liquid propellant rocket motors, noting combustion time effect on phase relations and oscillation excitation, obtaining transfer function 04 p0723 A67-15193

Effect of several injector face baffle configurations on screech in 20,000-lb thrust hydrogen-oxygen rocket 04 p0691 A67-15987

Acoustic liners to suppress screech in hydrogen-oxygen engines 04 p0691 A67-15988

Nonlinear fluctuations in gunpowder combustion rate at various temperatures and harmonically varying pressure 05 p0927 A67-16991

Combustion dynamics of solid propellants in LF range, discussing equipment and results [AIAA PAPER 67-70] 06 p1073 A67-18451

Subscale cold-flow rocket motor model used to determine effect of purely geometric variables on acoustic performance leading to axial mode combustion instability 06 p1075 A67-18853

Surface effects for solid propellant combustion, discussing flame profile and instability, surface burning mechanism, temperature distribution, etc 08 p1373 A67-20642

HF combustion pressure oscillations in gaseous propellant rocket engines analyzed for stably burning combustor design concepts [ASME PAPER 67-VIBR-34] 11 p1851 A67-24191

Vibratory type pressure oscillations in combustor with dual orifice fuel injection analyzed in gas turbine for possible elimination [ASME PAPER 67-GT-23] 11 p1854 A67-24804

Combustion chamber model for self-oscillating thermoacoustic system initiated by stimulation effect of acoustic shock 11 p1884 A67-24958

Propellant composition influence on finite-amplitude axial wave mode instability in solid propellant rockets [AIAA PAPER 66-600] 12 p1988 A67-25909

T-burner technique for determining acoustic pressure-and velocity-coupled responses of solid propellants 12 p1988 A67-25910

Internal stability of turbulent combustion, developing analysis for one-dimensional model and deriving sufficient instability criterion 12 p2039 A67-26119

Visualization of combustion through transparent chamber walls, noting problems concerning hybrid rockets, ignition lags and hybrid combustion instabilities [ONERA-TP-474] 14 p2377 A67-27895

Model for solid rocket motor instability caused by chamber and propellant combustion characteristics, relating combustion and acoustic instabilities 14 p2404 A67-28113

Surface coupled heat release effect on oscillatory amplitude of pressure coupled response in solid propellant 15 p2544 A67-29983

Combustion instability, transient burning during ignition and extinction by depressurization investigated in nonsteady burning of solid propellants 15 p2580 A67-29984

Combustion stability in solid propellant rockets, reviewing Soviet T-sub s and Q models 15 p2581 A67-29986

Model for velocity coupled axial mode combustion instability in solid propellant rocket motors, noting computer studies 15 p2547 A67-29997

Nonsteady combustion MHD open cycle generator improving power density by modulation of conductivity and particle velocity 16 p2607 A67-30595

Cellular flame under constant volume bomb conditions, demonstrating vibratory combustion over range of gas compositions and characteristic initial pressures 17 p2974 A67-33143

Small perturbations effect on internal gas dynamic structure of flame zone for slow combustion stability criterion 17 p2974 A67-33144

Cylindrical expanding detonation waves in gas mixtures, studying detonability limits, propagation velocity and instability and vibratory phenomena 18 p3153 A67-33822

Interaction of finite amplitude pressure pulse with combustion region at surface of burning solid propellant 18 p3108 A67-33830

Fluid dynamics effect on spontaneous pressure spikes in Apollo SPS thrust chamber, noting increased combustion instability, occurrence and mechanism of pops, etc [AIAA PAPER 67-513] 18 p3114 A67-33976

Solid-propellant combustion instability models describing combustion zone dynamics applied to acoustic and nonacoustic instability in low frequency regime [CI PAPER 67-13] 19 p3311 A67-35007

Spinning detonation, deflagration instability and normal detonation characteristics 19 p3346 A67-35574

Acoustic vibrations during solid-fuel combustion, studying acoustic energy increase rate and development 20 p3551 A67-36817

COMBUSTION PHYSICS

Steady state combustion analysis of solid propellant rocket motors extended by studying influence of grid sizes and number of steps used in numerical analysis 01 p0143 A67-11449

Mechanism of hydrogen combustion near lower ignition limit studied, using electron paramagnetic resonance /EPR/ measurements 03 p0536 A67-13842

Combustion rate dependence on pressure in combustion process involving relaxation as induced by mechanical strength of fuels 04 p0726 A67-15593

Solid propellant regression rate in hybrid rocket motor examined via combustion process model, assuming homogeneous flow in central channel 05 p0874 A67-16766

Ignition of seminfinte reacting space in ideal contact with hot medium having different thermophysical properties 05 p0927 A67-16990

Temperature coefficient of combustion rate for mixtures of ammonium perchlorate with various hydrocarbons 07 p1267 A67-19311

Heterogeneous combustion in chemical propellant rocket chamber 07 p1239 A67-20116

Soviet monograph on combustion physics 08 p1428 A67-21420

Track method analysis of phase transitions in particle growth and evaporation rate during combustion 08 p1428 A67-21421

Radiative heat transfer in interior of combustion chambers of solid propellant rockets 09 p1561 A67-22567

Nonstationary gunpowder combustion at various pressures analyzed for combustion rate and surface temperature dependency on pressure and initial temperature 11 p1884 A67-24957

Detonation wave interaction with hydrogen-oxygen flow fields in clarifying rocket combustion instability and supersonic combustion 12 p1929 A67-25898

Powder and solid propellant combustion, discussing heterogeneous and homogeneous systems, characteristics of foam, flizz and flame zones, etc 12 p1988 A67-26110

Thermal explosion equations for first order catalytic reaction, discussing nonstationary effects superposed on quasi-stationary combustion 12 p2039 A67-26111

Combustion parameters of powders and explosives as function of density of light flux and transparency of burning substance 12 p2039 A67-26113

Time dependent heat conduction and diffusion equations for fuel-rich H-O flame solved by finite difference method 14 p2409 A67-29064

Slow oxidation of n-octane vapor /oxygen/ nitrogen mixtures at reduced pressures and temperatures 16 p2779 A67-31518

Combustion of hydrogen and hydrazine with nitrous and nitric oxide noting flame speeds and flammability limits of ternary mixtures at sub atmospheric pressures 16 p2779 A67-31519

Aluminum particle combustion in solid rocket grains, noting drop formation mechanism and droplet combustion analysis [ONERA-TP-486] 17 p2926 A67-32697

Preignition phase of solid propellant burning, determining concentration of volatilized species as function of surface temperature 17 p2927 A67-33028

Numerical methods for solving thermal explosion and combustion problems on electronic computers, examining Cauchy

problems solutions 17 p2973 A67-33075
 Combustion - Conference, Berkeley, August 1966 18 p3146 A67-33778
 Combustion processes studied by shock tubes, discussing experimental techniques of combustion science, high temperature measurement by spectrum line reversal method, etc 18 p3019 A67-33779
 Very low pressure pyrolysis applied to combustion kinetics 18 p3149 A67-33787
 Condensation during heterogeneous combustion, discussing kinetics, radiation and gasdynamic heat release 18 p3149 A67-33798
 Classical heterogeneous combustion and aerospace research, discussing multiple factor approach and mass transfer operations 18 p3150 A67-33801
 Mixing patterns and flow configurations in model for determining combustion performance in well-stirred reactor 18 p3154 A67-33833
 Steady flow adiabatic stirred reactor to study combustion mechanism of hydrogen-oxygen mixtures, determining reaction-kinetic constants 18 p3154 A67-33834
 Kinetic mechanisms in combustion peninsula of three-limit explosion reactions with trace inhibitors, studying quadratic chain-breaking processes by static method 18 p3156 A67-33848
 Lean hydrogen-oxygen mixture combustion, studying induction period kinetics and spikes in OH profile 19 p3345 A67-35004
 Perfectly stirred reactor /PSR/ theory application to flame analysis, obtaining temperature or concentration profiles as function of time or distance 19 p3345 A67-35011
 Flame structure of hydrazine burning in oxidizing atmosphere determined by measuring temperature and specific contractions at 90 degrees from stagnation point 19 p3310 A67-35014
 Bow shock and combustion zone studies of spheres fired through H2-O2 mixtures show ignition zone separation 20 p3359 A67-37128

COMBUSTION PRODUCT

Nonlinear equations for equilibrium composition of combustion products from methane burned with ionizing admixtures over various temperature and pressure ranges 01 p0139 A67-10046
 Hall effect in low temperature plasma consisting of combustion products with admixture of KOH under variable sign magnetic field, demonstrating potential gradient existence 01 p0120 A67-10175
 Electromagnetic measurement of motion of explosion products behind detonation wavefront, calculating isentrope from mass velocity distribution 04 p0606 A67-15184
 Combustion mechanism for boron-containing air-augmented propellant based on conductive, convective and radiant heat transfer between propellant and combustion products 04 p0687 A67-15814
 Unsaturated polyester styrene, showing via gas chromatography and IR spectroscopy effect of reticulation on pyrolytic decomposition 05 p0759 A67-16768
 Polytrope index for gas detonation products determined by velocity ratio for incident and reflected wave during collision of two detonation waves 05 p0927 A67-16999
 Combustion reactions during spacecraft reentry, noting degradation of heat shields composed of hydro- and fluorocarbon compounds 05 p0928 A67-17334
 Burning rate of N powder dependence on light flux density and initial temperature range 06 p1112 A67-17958
 Chemiluminescence from oxygen atom-hydrazine flames suggesting excited NO formed by energy transfer 06 p1072 A67-17987
 Gas phase oxidation of diborane in furnace-heated vessels and flash photolysis 06 p0955 A67-18058
 Gaseous mixture theory in calculating transport coefficients of combustion product plasma of oxygen and acetylene 06 p1119 A67-18723
 Combustion and heat transfer laws for hydrocarbon flames with predetermined visual radiation 08 p1425 A67-20303
 Compression strength and strain of solid propellants, noting internal loads developed during burning process 08 p1373 A67-20720
 Temperature characteristics, electric

conductivity, electrode drop and heat loss of acetylene combustion gas mixed with seed material and nitrogen used as MHD fluid 09 p1580 A67-22151
 Variation in electric conductivity of gas products from detonation of propane-oxygen-nitrogen mixtures 09 p1581 A67-22581
 Derivation and computer method solution of equations describing thermodynamic equilibrium of gaseous products from oxidative combustion of methane 11 p1881 A67-24023
 Spectroscopic measurement of combustion gas composition in supersonic flow [AIAA PAPER 65-580] 12 p1990 A67-25899
 Combustion of pure liquid monopropellant droplet burning in own combustion products at low Reynolds numbers 14 p2376 A67-28552
 Potential distribution and volt-ampere characteristics of ionized gas flows in ducts 16 p2713 A67-30598
 Linear and turbulent MHD generators of conduction type considering operating conditions, efficiency and energy conversion 16 p2608 A67-30600
 Ionization processes in hot products of combustion processes /flame gases/ as weak plasma media noting flame properties, mass spectroscopy, electron concentration, etc 17 p2967 A67-32140
 Low temperature plasma conductivity of combustion products, particularly of exhaust gases in duct of MHD oscillator 17 p2895 A67-32155
 Nonlinear equations for equilibrium composition of combustion products from methane burned with ionizing admixtures over various temperature and pressure ranges 17 p2927 A67-33324
 Flow stability in MHD generators after extracting significant electrical power from gas 18 p2987 A67-33705
 Experiments on equilibrium and nonequilibrium electrical conductivity of seeded combustion products and theory of nonequilibrium ionization and recombination 18 p3085 A67-33706
 Carbon formation in oxygen premixed acetylene and benzene flames 18 p3151 A67-33808
 Rate constants and activation energy in bimolecular transfer reactions for halogen atoms 18 p3154 A67-33835
 Reaction zones of ammonia-oxygen and hydrazine decomposition flames, measuring temperature and concentration profiles 18 p3155 A67-33838
 Rocket chamber pressure influence on particle size measurements of heterogeneous combustion products of solid propellants containing aluminum 18 p3109 A67-33839
 Thermodynamic characteristics of equilibrium combustion products of methane-oxygen-nitrogen mixtures over wide range of parameters and compositions, using computer 18 p3159 A67-34051
 Perfluorocyclobutane-fluorine combustion studies and measurement of detonation velocities and limits 19 p3345 A67-35013
 [CI PAPER 67-23]
 Current-voltage characteristics for double probe measured in seeded combustion products by low temperature surface emission 19 p3345 A67-35079
 Energies of combustion of aluminum diboride and alpha aluminum dodecaboride measured in bomb calorimeter using fluorine oxidant 22 p3758 A67-39766
 Asymptotic method for solving differential equations, giving equilibrium composition of gaseous combustion products 24 p4178 A67-42390
 Thermodynamic and electrical properties of MHD conversion fluid /K-seeded combustion products/ obtained by hydrocarbon fuel combustion, discussing electrical conductivity calculations 24 p4099 A67-42415

COMBUSTION STABILITY
 Pressure coupled combustion dynamics of solid propellants analyzed as function of propellant variables, oscillation frequency and combustion pressure 01 p0143 A67-11448
 Impact-induced combustion in hypersonic ramjet engines, determining hypersonic fuel-air mixing from hydrogen concentration at Laval nozzle outlet 03 p0503 A67-13014
 [DVL-601]
 T-burner tests for combustion stability evaluation of hydrazine diperchlorate [AIAA PAPER 66-599] 04 p0723 A67-15246

Aluminum powder damping of HF instability in solid propellant combustion in vortex burner 06 p1115 A67-18307
 Influence of relative thickness of elastic case on acoustic stability of radial modes in solid propellant rockets 07 p1240 A67-19370
 [AIAA PAPER 66-473]
 Oscillatory burning of solid propellant studied using integral balance equation in solid gas interface, assuming Rayleigh criterion and sound wave 08 p1373 A67-20774
 Transitional combustion phenomena in solid propellant rocket engines under unsteady conditions 08 p1373 A67-20778
 Static and dynamic combustion phenomena effects on grain structural design for solid propellant rocket engine 08 p1374 A67-20876
 Pressure deflagration limit of high energy solid propellants increased to superatmospheric pressures by composition changes 10 p1696 A67-23131
 [AIAA PAPER 66-679]
 Silicon semiconductor combustion pressure transducer for high temperature HF pressure measurements within liquid rocket motor chambers 11 p1792 A67-24820
 Electric arc combustion stability in gas flow, noting relation to weakly ionized plasma conductivity 12 p2033 A67-25314
 Correlation between thrust chamber design parameters and combustion stability, noting stability increment with increasing injection velocity, droplet diameter and chamber pressure 18 p3113 A67-33944
 [AIAA PAPER 67-474]
 Conditions of stable burning of electric arc stabilized by gas stream in DC plasma arc torch, determining threshold current 19 p3281 A67-35150
 Transient nature of heterogeneous boundary layer chemical reaction at stagnation point studied analytically, deriving stability conditions 19 p3211 A67-35740
 Low pressure solid rocket motor design and application, noting advantages in high mass ratio performance and operational disadvantages 20 p3516 A67-37131
 Combustion stability of powder in semiclosed volume, taking into account propellant surface temperature dependence on pressure and temperature gradient 21 p3732 A67-38526
 Aluminum powder damping of HF instability in solid propellant combustion in vortex burner 21 p3732 A67-38860
 [AIAA PAPER 67-104]
 Pressure fluctuation onset conditions in jet engine combustion chambers with supersonic nozzles, discussing design factors effect on combustion process stability 21 p3696 A67-38909
 Small perturbation analysis on mass conservation stability in solid propellant combustor, discussing parametric model 23 p4084 A67-41721
 Asymptotic method for solving differential equations, giving equilibrium composition of gaseous combustion products 24 p4178 A67-42390
 Stability boundaries of double-dead-time model describing chugging in liquid bipropellant rocket engine 24 p4207 A67-42689

COMBUSTION TEMPERATURE
 Ignition pressure transient in solid rocket motors, examining chamber filling interval, flame propagation, heat transfer correlation, burning area, etc 05 p0873 A67-16513
 Flame propagation on liquid fuel surface, analyzing fuel heating in front of flame until ignition temperature is reached, noting radiation and convection role 09 p1581 A67-22605
 Sensitized ignitions of methane and oxygen mixtures, with nitrogen oxides and inert gases added, and suggested reaction mechanisms 14 p2407 A67-28549
 Lead, copper and cobalt oxides effects upon ignition kinetics of paraffinic and aromatic fuels 14 p2407 A67-28550
 Classical heterogeneous combustion and aerospace research, discussing multiple factor approach and mass transfer operations 18 p3150 A67-33801
 Physical and chemical wall effects on mechanism of combustion reaction in gases studied by introducing solids and measuring ignition pressure 18 p3155 A67-33847
 Ignition temperature and ignition delay of

oxyhydrogen gas as function of pressure examined in shock wave tube, using Schlieren photography 18 p3160 A67-34261

Combustion rocket engines thermodynamic cycle and specific impulse values, considering motion equations and plasma engines 19 p3311 A67-35571

Turbulent gas combustion, showing burning rate as function of combustion temperature, pressure and chemical reaction rate in flame 21 p3732 A67-38527

Dynamic ballistics of combustion termination by fluid injection in solid propellant motors, describing termination mechanisms 21 p3733 A67-38893

Flame propagation in hydrogen-oxygen mixtures at temperatures and pressures corresponding to ignition peninsula 22 p3919 A67-40223

Finite difference integration method for predicting flow velocity and temperature distribution of gaseous diffusion flame in axisymmetrical combustion chamber 24 p4091 A67-42383

COMBUSTION VIBRATION

S INSTABILITY

COMBUSTION WAVE

Self-similar problems concerning supersonic flows of gaseous fuel mixtures with detonation waves and slow combustion fronts past wedges and cones 06 p0935 A67-17725

COMBUSTION WIND TUNNEL

Aerodynamic effects of supersonic combustion studied in wind tunnels 18 p3154 A67-33829

Hot shot tunnel F operation as combustion test facility using air, discussing oxygen depletion, particle contamination and reservoir decay 21 p3606 A67-37775

COMBUSTOR

SA ROCKET COMBUSTOR

Vibratory type pressure oscillations in combustor with dual orifice fuel injection analyzed in gas turbine for possible elimination [ASME PAPER 67-GT-23] 11 p1854 A67-24804

Reverse flow annular combustion system for TPE331 turboprop engine, noting fabrication and combustor efficiency [ASME PAPER 67-GT-25] 11 p1854 A67-24805

Tests analysis of buckling caused by thermal gradient and fatigue due to thermal cycling in restrained combustor-cooling tubes 15 p2572 A67-29164

Supersonic combustor length and contours for optimum performance determined from one-dimensional pressure-area analysis 18 p3154 A67-33832

Gas-side heat transfer at high temperature combustor sonic points, discussing Reynolds number effect, boundary layer transitions, turbulence intensity, etc [AICHE PAPER 27] 20 p3552 A67-36831

COMET

Comet orbits classification noting distributions of eccentricities, inclinations and perihelion ecliptic coordinates 01 p0146 A67-10232

Observations of 24 comets, 11 minor planets and Jupiter VIII, using computer 01 p0148 A67-10386

Cometary origin of Tungusk meteorite of 1908 supported by analysis of space trajectory and observed nightglow at time of fall 01 p0151 A67-11274

Cometary motion in outer solar system region, taking galactic nucleus as perturbing body 01 p0151 A67-11286

Geomagnetic field disturbance due to earth passage through tail of Halley comet, 1910 II 02 p0236 A67-11654

Twenty-eight blue and yellow photographs of comet Humason, tabulating exposure time 02 p0326 A67-12066

Velocity requirements for orbital transfer and selection criteria for comet missions from 1967 to 1986 03 p0510 A67-13491

Scientific program and instrumentation of comet probe 03 p0510 A67-13496

Rocket probe design for studying physical structure, chemical composition and interaction with sun of Tuttle-Giacobini-Kresak comet 03 p0518 A67-13497

Solar wind-comet interaction simulation using plasma stream and carbon dioxide gas cloud sublimated from dry ice 03 p0506 A67-13575

Kilston and Barbon comets detection and observation history 03 p0511 A67-13653

Data interpretation for sun grazing family

of comets deriving formulas for compressive and tensile stress in spherical bodies for tidal, rotational and self-gravitating fields 03 p0512 A67-13923

Dynamical effect of explosive phenomena in comet Halley and nuclear rotation based on 1909-1911 observations 04 p0694 A67-14469

Five-comet probe mission, discussing velocity requirements for launch from earth orbit, cometary brightness, weight requirements and possible carrier rockets 04 p0695 A67-14532

Computer investigation of approach of Comet 1759 III to Jupiter before perihelion passage, considering possibility of capture by Jupiter 04 p0701 A67-15450

Improvement of orbital elements of comet Grigg-Skjellerup, using all observations made during previous appearances 04 p0701 A67-15451

Comet disintegration as basic source of interplanetary dust based on zodiacal isophots 04 p0701 A67-15559

Solar wind flow past comet, obtaining minimum radius of comet source 04 p0693 A67-15563

Physical parameters, absolute values and discovery dates of comets observed from 1954 through 1960 05 p0886 A67-16030

Soviet papers on physics of comets and meteors 05 p0888 A67-16199

Comet photometry using revolving table to study brightness distribution in head and determine intrinsic brightness 05 p0888 A67-16200

Photometry of comet Arend-Roland, 1956 h, calculating brightness decrease along tail streams 05 p0888 A67-16201

Halley comet head diameter change determined by converting propane and ethylene molecules in photon and corpuscular radiation field of sun 05 p0888 A67-16202

Role of solar photon and corpuscular radiation in dissociation and ionization of water molecules in cometary atmospheres 05 p0888 A67-16203

Intrinsic brightness of comet Alcock 1963 b obtained from visual observations in terms of stellar magnitudes 05 p0888 A67-16204

Tungusk comet trajectory and orbit with radiant in constellation Cetus 05 p0889 A67-16210

Soviet papers on problems of comet photometry 05 p0890 A67-16329

Visual and photographic comet photometry problems, noting brightness estimates obtained by individual observers 05 p0890 A67-16330

Visual techniques for measuring comet total brightness based on nonfocality 05 p0890 A67-16331

Photographic comet photometry as technique for studying comet brightness 05 p0890 A67-16332

Photographic technique for photometric comet observations, noting automatic polarograph and high transmission meniscus telescope 05 p0890 A67-16333

Visual, photographic and photoelectric methods for comet polarimetry 05 p0890 A67-16334

Comet photometry for measuring weak fluxes of light produced by heavenly bodies, analyzing photoelectromultipliers 05 p0805 A67-16336

Comet spectra observation noting emission band abundance, atomic lines presence and continuous spectrum with solar Fraunhofer lines 05 p0890 A67-16337

Spectrophotometry of Arend-Roland comet, estimating radiation from comet emission bands and continuous spectrum 05 p0891 A67-16338

Brightness and spatial luminosity distribution in comet heads analyzed for steady and variable emissive processes 05 p0891 A67-16339

Linear polarization of comet Na D-lines 05 p0891 A67-16406

Space probe launching conditions for accurate cometary orbit 05 p0895 A67-16574

Communications of Lunar and Planetary Laboratory /University of Arizona/, Volume 4 /Numbers 64-69/ 05 p0896 A67-16716

Comet Ikeya-Seki observations from Mauna Kea, Hawaii 05 p0896 A67-16719

Comet Ikeya-Seki observations from Tucson 05 p0896 A67-16720

Visual observations of comets Everhart and Alcock /1964-1965/ 05 p0903 A67-17314

Mokhnach model explaining surface brightness distribution observed by miller in 1959 k comet 06 p1082 A67-17839

Physical characteristics of comets, 1961-1965 06 p1083 A67-18163

Perturbed motion of comet in medium of constant low density in solar Schwarzschild field, using quasi-Newton approximation, considering electromagnetic and gravitational fields 06 p1084 A67-18164

Comet model construction assuming rectangular coordinates system, noting particle motion initial velocity and repelling acceleration 06 p1084 A67-18205

Comets hypothesized to consist of antimatter originating from parts of galaxy consisting entirely of antimatter 07 p1247 A67-19098

Hyperbolic revised orbital data of comet Cunningham /1941 I/ hyperbolic revised orbital data of Comet Cunningham /1941 I/ 07 p1247 A67-19168

Soviet book on comets covering photometric and spectral studies, solar activity, structural elements, characteristics tables and bibliography 07 p1247 A67-19300

Interplanetary gas, solar corpuscular activity and magnetic storms and zodiacal dust cloud from satellite observations during IQSY and use of cometary tail as plasma probe 07 p1248 A67-19333

Cometary dust studied by analysis of scattered sunlight in heads and tails of comets 07 p1250 A67-19668

Measurements performed from Mariner type probe during intercept with comet complement measurements performed from ground-based astronomical observatories by direct sampling 08 p1393 A67-21098

Cometary tails relationship to interplanetary gas properties and solar wind velocities deduced from observation of type I ionic cometary tails 08 p1399 A67-21238

Transverse plasma instabilities as mechanism coupling motions of solar wind and cometary plasma, using thermal diffusion and conductivity transport coefficients to describe flow 08 p1401 A67-21367

Spectrum of comet Ikeya-Seki analyzed at solar distances noting emissions, excitation temperature, abundance ratio, photoionization effect, etc 09 p1566 A67-22234

Comet head brightness diminution during perihelion passage due to sublimation calculated, using Clapeyron-Clausius equation and insulation effect 10 p1703 A67-22719

Motion of structures in coma and tail of Morehouse comet compared with hydrodynamic model interaction between solar wind and cometary plasma 10 p1704 A67-22720

Periodic comet observation methods and orbital results 10 p1705 A67-22926

Comet 1965 f /Ikeya-Seki/ interaction with solar corona produces no significant enhancement of emission at 2.2 m wavelength 10 p1706 A67-22958

Periodicity of precipitation singularities and relation to period of comets and meteor streams 11 p1815 A67-24329

Independent cometary orbit correction permitting checkout of initial coordinate and velocity components 11 p1868 A67-25084

Comet P/Wolf I motion perturbations of six planets, searching ephemeris for perihelion in August 1967 11 p1868 A67-25085

Comet Encke tail variation and apparent correlation with solar activity 12 p2000 A67-25137

Hydrodynamic axial-symmetric model of plasma flow on sunward side of comet assuming cometary gas is ionized by solar UV radiation only 12 p1993 A67-25227

Relationship between Pons-Winnecke comet and certain types of meteor showers 13 p2196 A67-26498

Catalog tabulating 1600 comet tail orientation observations 14 p2386 A67-28481

Gas condensation near comet nucleus as source of formation of entire dust component of comet 15 p2552 A67-29153

Evolution of short-period comet orbits /1660-2060/ taking into account perturbing effects of outer planets 15 p2552 A67-29154

Cometary orbit evolution of Jupiter family, considering influence of Jupiter 15 p2553 A67-29155

Visible continuous spectrum of comets rules out hypothesis of iron particles major

role in scattering solar light 15 p2554 A67-29515

Orbit of Halleys comet integrated ahead to next apparition /1986/ and predicts time perihelion passage 15 p2557 A67-29874

Physical characteristics of comets, 1961-1965 16 p2741 A67-30507

Perturbed motion of comet in medium of constant low density in solar Schwarzschild field, using quasi-Newton approximation, considering electromagnetic and gravitational fields 16 p2741 A67-30508

Number of rays and brightness of Comet Morehouse derived from photographs taken with Greenwich reflector 16 p2742 A67-30666

Comet missions, discussing spacecraft exploration criteria for short period and long period first-apparition comets 16 p2745 A67-30749

Comet mission study using space probes boosted by Atlas Agena and Atlas Centaur launch vehicles for interception from 1967 to 1975 16 p2745 A67-30750

Expulsion of ions from comets toward sun examined for source, dissociation and ionization of parent particles, velocity, etc 16 p2746 A67-30979

Geomagnetic field disturbance due to earth passage through tail of Halley comet, 1910, II 16 p2665 A67-31069

Dynamic and physical properties of Kreutz family of sun-grazing comets suggesting collision mechanism for origin 16 p2751 A67-31464

Comet Burnham C2 coma photometry, discussing error sources in isophotes and photometric scale and tabulating oval isophote size against axes mean ratio 17 p2943 A67-32442

Frothing-sloughing ablation concept explains density variations of cometary meteors obtained from photographic and radar observations 17 p2943 A67-32541

Luminosity variations of comet 1963 III related to solar and geomagnetic disturbances caused by corpuscular solar particles 17 p2946 A67-32730

Comet 1963 III spectrometric observations showing important continuous spectrum of comet, spectrum wavelengths identification, etc 17 p2946 A67-32731

Mokhnach model explaining surface brightness distribution observed by Miller in 1959 k comet 17 p2951 A67-33214

Comet model construction assuming rectangular coordinates system, noting particle motion initial velocity and repelling acceleration 17 p2951 A67-33215

In situ study of comets by solar electric propulsion spacecraft, analyzing mission characteristics 19 p3323 A67-35333

Space probe rendezvous with Halley comet, considering use of planetary gravity field to modify trajectory [AIAA PAPER 67-614] 19 p3329 A67-36003

Orbital evolution of comet Daniel over 400 years, examining approaches to earth and discovery role 20 p3522 A67-36619

Everhart comet and various minor planets positions through photographic observations at Tartu 20 p3522 A67-36622

Cometary astronomy problems from contemporary celestial mechanics viewpoint, considering short-period comets and orbital perturbations caused by Jupiter 20 p3524 A67-36658

Motion theory of comet Wolf I during 1918-1925 revolution which included close approach to Jupiter in 1922 20 p3524 A67-36659

Comet Wolf I orbit evolution over 400 years /1660-2060/, accounting for planetary perturbations and considering secular deceleration 20 p3524 A67-36660

Possibility of common origin for comets Wolf I and Barnard 20 p3524 A67-36661

Discovery position plotting of various long period comets, showing tendency to cluster near sun in morning sky, orbit distribution and estimated probabilities 21 p3705 A67-38614

Definitive orbit of comet Pereyra derived from positional observations 21 p3707 A67-38963

Sodium D lines in Comet Ikeya-Seki /1965 f/ near perihelion passage noting possible formation by resonance scattering at comet densities and temperatures 22 p3880 A67-39414

Comet observation by 61 inch Catalina reflector noting additions to recovery-

expected-soon list 22 p3880 A67-39416

Plasma flow and generation in CO comet due to electron-collisional ionization under influence of solar wind 22 p3885 A67-40081

Dynamic processes in tail of Morehouse comet, discussing velocity measurements, structures and acceleration variations 22 p3888 A67-40205

Nongravitational effects in Halley comet motion and arbitrarily rotating comet nucleus model, noting push-effect hypothesis 23 p4082 A67-40672

Nongravitational and splitting effects in comet motion and rotating comet nucleus model, using push-effect hypothesis for post-explosion analysis nongravitational and splitting effects in comet motion and rotating comet nucleus model, using Spurlous nucleus behind solid 1910 Halley Comet nucleus hypothesized as explanation for anomalous positional residuals 23 p4065 A67-41001

Experimental facilities to test antimatter hypothesis of comets and meteoric swarms 23 p4069 A67-41689

Orbital elements and motion equations of periodic comet Harrington for five perihelion times before discovery 24 p4228 A67-41964

Gas condensation near comet nucleus as source of formation of entire dust component of comet 24 p4239 A67-43076

Evolution of short period comet orbits /1660-2060/ taking into account perturbing effects of outer planets 24 p4239 A67-43077

Cometary orbit evolution of Jupiter family, considering influence of Jupiter 24 p4240 A67-43078

COMMAND CONTROL

Lunar orbiter command and telemetry data handling system at deep space stations 02 p0194 A67-11808

Command laws for DC magnetic attitude control of spin-stabilized earth satellites by means of coil of axis parallel to spin, including effects of orbital eccentricity and magnetic dipole 07 p1257 A67-19361

Visual analysis console for automatic information handling systems providing rapid data display and operator communications with high speed digital computers 15 p2488 A67-29737

Applied synthesis technique using feedback and command controller elements for strongly interacting multivariable control systems, illustrated by flight control system design 16 p2649 A67-31661

Acceptance checkout equipment spacecraft for centralized control and LEM and CSM systems testing 20 p3391 A67-36976

Real time performance, ground control and data processing of Surveyor spacecraft during maneuvers [AIAA PAPER 67-644] 20 p3419 A67-37625

COMMAND MODULE
SA SERVICE MODULE

Model tests for determination of structural response of Apollo Command Module to water impact 07 p1257 A67-19368

Manual thrust vector control development for Apollo Command and Service Module Stabilization and Control System [AIAA PAPER 67-243] 07 p1260 A67-20043

Full mission engineering simulator /FMES/ design for integrating hardware into lunar module system as hardware is made available by subcontractors 08 p1319 A67-21546

Explosive-actuated cutting mechanism for severing electrical service lines connecting Apollo command module to service module and lunar module to spacecraft-LM adapter [ASME PAPER 67-DE-33] 14 p2394 A67-28874

LEM-CSM analysis, elastic bending and propellant sloshing 17 p2955 A67-32478

Apollo command module communication and data system design, discussing environmental and reliability requirements 21 p3584 A67-38668

Program for preventing earth environment biological contamination by lunar material 23 p3961 A67-40845

COMMAND SYSTEM

SA DIGITAL COMMAND SYSTEM

Command and control display system requirements noting dependence on human visual mechanism 03 p0365 A67-13300

Extraterritorial extent of powers of aircraft commander for maintaining safety

and order on board 07 p1269 A67-19519

NORAD installation in Cheyenne Mountain, Colorado, describing data processing equipment and performance 07 p1148 A67-19840

Complex and decision feedback systems for command channels in space communications 07 p1145 A67-19872

System design decisions through static and rotating magnetic memories reliability as applied to command and control systems 08 p1299 A67-20685

Information processing requirements for command systems, using particular form of simulation of system information 08 p1299 A67-20686

NASA STADAN and Apollo network antenna systems, analyzing tracking antenna systems, command systems and operational problems 14 p2287 A67-28681

Digital command and experimental data storage system for OAO 16 p2633 A67-30670

Synthesis of specific type of automatic microprogramming systems using complex microcommand signals conditioned by functional-blocks 19 p3190 A67-36094

Jindivik Mk 103A jet propelled target drone ground and flight control systems stressing climb, cruise, approach and descent commands 21 p3570 A67-39131

Developments in tracking, telemetry and command transmission, discussing move toward higher frequencies and rain losses 22 p3763 A67-40338

Real time systems and applications 23 p3976 A67-41056

COMMERCIAL AIRCRAFT

SA LOCKHEED L-500 AIRCRAFT

SA TRANSPORT AIRCRAFT

Commercial aircraft accident causes, emphasizing accidents occurring during approach and landing [AIAA PAPER 66-804] 01 p0008 A67-10030

Twin jet business aircraft Mystere XX /fan jet Falcon/ structural material, propulsion data and circuits 05 p0752 A67-17268

VHF and UHF communications between transoceanic commercial aircraft and ground stations by means of aeronautical communication satellites 06 p0961 A67-17701

Aerodynamic development of configuration and control system of Gulfstream II business jet, discussing wing optimization, engine characteristics, etc 12 p1894 A67-25497

Small pressurized cabin design for light commercial aircraft including safe life vs fail-safe approaches, fatigue strength testing, etc [SAE PAPER 670259] 12 p2016 A67-25508

Inertial navigation system including aircraft interfaces, system modes of operation and performance [SAE PAPER 670329] 12 p1964 A67-25871

Stress-strain problems in design load of commercial aircraft, noting role of frequency distribution curves 14 p2245 A67-28060

Civilian aircraft electrical equipment design and construction including Caravelle and Concorde 14 p2252 A67-28568

Inertial navigation system and onboard navigation course computer evaluated, noting performance data and circular error 15 p2515 A67-29742

Design requirements for commercial orbital space stations intended for weather forecasting, agricultural prediction and industrial research [AAS PAPER 67-113] 15 p2557 A67-29961

JT9D turbofan engine for Boeing 747 commercial transport aircraft, analyzing design and performance potentials [AIAA PAPER 67-374] 15 p2548 A67-30346

Pilot training for future commercial transports, noting flight simulation devices for safety and economic factors [AIAA PAPER 67-388] 15 p2432 A67-30356

Program for perceived noise levels reduction on ground of turbofan-powered commercial transport by acoustically absorptive lining of ducts [AIAA PAPER 66-389] 15 p2548 A67-30357

Boeing 747 characteristics for passenger and cargo service noting economic gain, operational performance, control cabin, engine, etc [AIAA PAPER 67-397] 15 p2421 A67-30364

System engineering approach to commercial aircraft crew requirements [AIAA PAPER 67-399] 15 p2433 A67-30366

Selection of gyroscopic reference for commercial aircraft
[AIAA PAPER 67-405] 15 p2491 A67-30372

Commercial rotor VTOL for economic intercity transportation, discussing time-frame and design requirements and analyzing improvement factors
[AIAA PAPER 67-410] 15 p2422 A67-30377

VTOL aircraft with rotor or propeller lift systems for commercial transportation, discussing helicopter role in system development
[AIAA PAPER 67-411] 15 p2422 A67-30378

Design requirements of commercial supersonic aircraft engines
[AIAA PAPER 67-376] 15 p2549 A67-30423

Fokker F-28 Fellowship conceived as jet contemporary of turboprop Fokker Friendship, noting structural and operational details
16 p2597 A67-31561

Plessey constant speed drive/starter /CSDS/ application to BAC 111 commercial transport, discussing dual role
17 p2800 A67-31975

A-300 Airbus, economic subsonic passenger transport for short and medium ranges
18 p2986 A67-34075

Commercial aircraft planning and design, considering technology, market environment and manufacturers' desires and capabilities
20 p3556 A67-37446

Cabin pressurization characteristics of USAF and commercial transport aircraft, stressing decompression sickness
21 p3577 A67-38081

Problems of handling people on future giant aircraft noting reservations, ticketing, boarding procedures and baggage-handling functions
22 p3780 A67-39382

Commercial aircraft noise system solution, considering engines, nacelles, operational procedures and airport options
[AIAA PAPER 67-761] 23 p3933 A67-40992

Commercial aircraft balance and weight measurement using on-board system, discussing wind load, runway tilt, hard landings and extreme temperature variation effects
23 p4007 A67-41386

Cockpit noise levels of various airline aircraft noting propeller effect
23 p3964 A67-41556

Injury and fatality analysis in survival study of commercial jet aircraft /Boeing 727/ landing accident with subsequent interior fire
23 p3969 A67-41650

Installation problems of head-up displays in commercial aircraft
24 p4152 A67-41896

Blower compressors for high altitude pressure and climate regulation in commercial aircraft
24 p4109 A67-42709

Filters in commercial aircraft hydraulic systems, discussing cleaning methods including ultrasonics
24 p4109 A67-42710

COMMERCIAL AVIATION

Economical hangaring of commercial aircraft as implemented by Spanish airfleet
06 p0947 A67-18028

Problems involved in ditching business aircraft on ocean and subsequent recovery
14 p2245 A67-28319

Safety in business aircraft operations based on available statistics noting need for thorough pilot training
14 p2245 A67-28320

Aviation insurance characteristics, types of policy in force and regulations applying under internal law
14 p2409 A67-28933

Commercial automatic inertial navigator for subsonic and supersonic aircraft provides global navigation and guidance within ATC limits without dependence on external aids
15 p2514 A67-29739

Propulsion and vehicle systems for commercial exploitation of space, emphasizing transportation to and from earth orbit
[AIAA PAPER 67-82] 15 p2570 A67-29949

Commercial space utilization considering space transportation cost as fundamental factor
[AAS PAPER 67-134] 15 p2571 A67-29968

Commercial airline equipment selection, schedule simulation, routing and fleet planning
[AIAA PAPER 67-392] 15 p2421 A67-30360

Initial VGH data on small turbojet operations in commercial transport service relating to accelerations, airspeed operating practices and unusual events
[AIAA PAPER 67-408] 15 p2421 A67-30375

Short-haul airliner /Fokker F-28 Fellowship/, noting moderate size, twin by-

pass engines, high speed, landing field requirements, etc
16 p2596 A67-31012

British air transportation, discussing 1946 Bermuda Pact, government control and role of private enterprise
17 p2974 A67-32124

Failure safety design of rotary wing aircraft, emphasizing airline type operation
[SAE PAPER 670349] 17 p2798 A67-32991

Aviation and transportation system, Progress, profits and public interest-Conference, Hartford, December 1966, Panel I
19 p3347 A67-34967

Legal and financial problems in obtaining airline tickets for third persons
20 p3555 A67-36300

Aircraft design by statistical methods, presenting samples for interceptor fighter, shorthaul jet and light twin-engine cargo aircraft
20 p3361 A67-37170

Optimal airline aircraft selection, discussing cost efficiency factors
22 p3922 A67-39537

Technological and economic factors affecting airline progress, discussing fares, traffic, SST and terminal areas
22 p3922 A67-40062

SST aircraft effect on overall situation of commercial airline traffic in Canada
[SAE PAPER 670901] 24 p4257 A67-42019

Maintenance schedule for small commercial aircraft fleet, periodic inspection check principles and engine reliability program
24 p4094 A67-42277

Bird strikes on high speed transport jet aircraft stabilizers
24 p4094 A67-42278

Design methods to combat fatigue effects on economics of civil aircraft, discussing structural weight role, maintenance, inspection, etc
24 p4250 A67-42441

Commercial V/STOL operating characteristics in Northeast Corridor, discussing commuter design and cost analyses
[AIAA PAPER 67-769] 24 p4095 A67-42937

Commercial VTOL airline system development through advanced helicopter application noting need for government sponsorship
[AIAA PAPER 67-772] 24 p4095 A67-42940

Commercial VTOL aircraft operating costs and cost reduction evaluation
[AIAA PAPER 67-826] 24 p4096 A67-42973

VTOL aircraft operational expense estimation using standard method, measuring maintenance costs in various planning stages and in operation
[AIAA PAPER 67-828] 24 p4096 A67-42974

Highway, ramp, terminal, runway and approach congestion problems for airports, suggesting separated general aviation airports and runways to alleviate big jet airports
[AIAA PAPER 67-871] 24 p4139 A67-42992

System-safety mathematical model for commercial jet airplanes using fault-tree modeling technique
[AIAA PAPER 67-910] 24 p4096 A67-43017

V/stol concepts for short haul commercial aircraft compared for gross weight, operating cost, gust sensitivity and noise levels
[AIAA PAPER 67-938] 24 p4096 A67-43028

Commercial V/STOL transportation system, analyzing intraurban and short haul factors for concerned parties by computer simulation
[AIAA PAPER 67-969] 24 p4260 A67-43047

Commercial VTOL transport compared with conventional aircraft and ground transportation, discussing design and operating costs
[AIAA PAPER 67-970] 24 p4097 A67-43048

COMMITTEE ON SPACE RESEARCH

S COSPAR

COMMUNICATION

SA AIRCRAFT COMMUNICATION

SA GROUND-AIR-GROUND COMMUNICATION

SA INTERPLANETARY COMMUNICATION

SA INTERSTELLAR COMMUNICATION

SA LASER COMMUNICATION

SA LUNAR COMMUNICATION

SA POINT-TO-POINT COMMUNICATION

SA RADIO COMMUNICATION

SA REENTRY COMMUNICATION

SA SATELLITE COMMUNICATION

SA SPACE COMMUNICATION

SA SPACECRAFT COMMUNICATION

SA TELECOMMUNICATION

SA TELEMETRY

SA TELEVISION

SA TRANSOCEANIC COMMUNICATION

SA VOICE COMMUNICATION

SA WIDEBAND COMMUNICATION

Interspecies communication involving human and mammalian brain as computer with programs and metaprograms
[AAS PAPER 66-77] 07 p1135 A67-20000

Microwave design techniques
13 p2072 A67-27450

Nonlinear interaction between two waves of multiple frequencies in communication line, nonlinear line capacitance being periodic function of line length
19 p3185 A67-36021

Changing role of technical writers and editors during next decade
20 p3556 A67-36587

COMMUNICATION SYSTEM

SA DEFENSE COMMUNICATIONS SYSTEM /DCS/

SA DIGITAL COMMUNICATIONS SYSTEM

SA SPACECRAFT COMMUNICATIONS SYSTEM

Satellite relay techniques providing paths for aircraft-ground communication over ocean used in ATC, noting repeater electronics
01 p0021 A67-10207

Coherent echo modulation and detection for binary data transmission, noting power savings, time and frequency diversification and communication stability
01 p0026 A67-10862

Binary detection probability for optical polarization modulation communication system using Gaussian approximation, noting signal to noise ratio
01 p0026 A67-10866

Reception antenna of ONERA weightlessness laboratory in form of surface waveguide
[ONERA-TP-374] 01 p0039 A67-11004

RCA defense electronic products applied research
02 p0251 A67-11785

Scientific lunar payload communications system
02 p0196 A67-11999

Communications systems at Kennedy Space Center /KSC/ and future prospects
02 p0230 A67-12121

Ground-Air-Ground /G/A/G/ communication channels analyzed in air traffic control
02 p0263 A67-12125

PPM-frequency time hopping for multichannel communication system to transmit digital data over tropospheric scatter path
02 p0202 A67-12131

Time combined with frequency division multiplex multichannel communication system for transmission of digital information over tropospheric scatter communication channel
02 p0203 A67-12132

Voice-bandwidth communication link analyzer /CLA/ system for making measurements on communication link, using periodic pulse stream with suitable spectral filtering
02 p0203 A67-12134

Effect of feedback capacity addition to M-ary PAM communication system perturbed by white Gaussian noise
02 p0204 A67-12170

Interplanetary communication problems and available techniques
02 p0205 A67-12540

RCA papers on ground, aerospace and data communication systems
03 p0381 A67-13634

Limitation imposed a priori on class of signals in order that every signal in class be distinguishable to within given mean square error by finite number of measurements
03 p0369 A67-13799

Book on circuitry for RF, AM and FM electronic communication systems
03 p0388 A67-14272

Shannon model for band-limited time-continuous channel to provide more realistic model of communication system
04 p0574 A67-15075

Book on phase coherent communication principles based on statistical communication theory, discussing coherent receivers and analog and digital modulation systems
04 p0576 A67-15616

RF interference detection and elimination from communication systems noting signal, frequency and amplitude analysis techniques
04 p0577 A67-15730

Programmable display synthesizing system for man-machine communications research based on electronic animation technique
05 p0788 A67-16314

Optimal parameters of binary communication system using random coding and orthogonal radio signals with unknown

- phase 05 p0764 A67-16901
Recognition of fading signals transmitted by channels with unknown parameters, considering optimum reception technique based on arbitrary law 05 p0767 A67-17399
Data processing centers integration through ground and satellite telecommunications networks for global information network [AIAA PAPER 66-331] 06 p0961 A67-17700
Future pattern of communications satellite systems, reviewing world requirements for telephony, telex, TV and radio [AIAA PAPER 66-319] 06 p0961 A67-17709
Soviet papers on theory and technique of radar 07 p1138 A67-19222
High data rate laser communication system, discussing integration of laser and wideband modulator and experimental results under field conditions 08 p1292 A67-20672
Model for synthesizing and analyzing communication systems, detailing use in converting command and control information transfer into physical and performance specifications 08 p1292 A67-20673
Input-output information transfer through correlation function of electromagnetic fields, obtaining optimization of system 09 p1461 A67-21603
Background limit to sensitivity of point to point optical communication obtained through signal to noise ratio of optical point detectors under BLIP condition 09 p1462 A67-21641
Elements of laser communication system including transmission media, terminals, generators, modulators, etc 09 p1462 A67-21675
Frequency sharing and compatibility of satellite and terrestrial radio relay systems design, discussing interference effects 09 p1464 A67-22411
Range instrumentation support systems, describing approaches to timing, firing and communications systems 10 p1605 A67-22998
Laser development, deep space communication system studies and designs 10 p1606 A67-23069
Traveling wave tube amplifiers for communications systems noting amplitude transfer function, two-tone and FM intermodulation, etc 10 p1613 A67-23440
Telemetry transmitters using solid state wideband microwave voltage-controlled oscillators 11 p1753 A67-24442
MF and HF portions of radio spectrum relationship to communication systems, presenting amplitude and phase variation in conjunction with effects of fading, time and frequency spread and atmospheric noise [IEEE PAPER 19-CP-65-482] 11 p1755 A67-25080
Advances in communication systems, Volume 2 12 p1906 A67-25987
Parameters of multiple-scattered optical radiation applied to laser communication system design 12 p1906 A67-25988
Optical computing principles, techniques and configurations for communication problems noting Fourier transform, coding, etc 12 p1907 A67-25990
Synchronous satellite communication systems including altitude and motion effects, time delay, control system, antenna, etc 12 p1907 A67-25991
Manned spaceflight RF radiation communications systems including voice, telemetry, tracking and ranging, up data and TV 12 p1907 A67-25993
Properties of favorable coding schemes, applying results to text transmission through auditory and tactile senses 12 p1907 A67-26081
Error probability for transmission of M orthogonal equally probable equal-energy signals over partially coherent channel 12 p1908 A67-26091
Thin film integrated circuit, discussing development of large value resistors and capacitors 12 p1918 A67-26219
Electrical and electronics engineering - IEEE Conference, Jackson, Mississippi, April 1967 13 p2065 A67-26404
SNR and transmission error probability in pulse modulated optical communication 13 p2067 A67-26663
Computer aided design and reliability engineering /CADRE/ applied to data processing associated with communications equipment components and subassemblies 13 p2072 A67-27446
Multiple internal communications system concept using single coaxial cable handling information transfer by integrated circuits 13 p2083 A67-27448
Communication system engineering handbook covering system design, programming, modeling, switching, multiplexing, etc 14 p2269 A67-28508
Communication satellite technology development depends on compatibility with deep-sea cables, channel demands and reflector technology 14 p2270 A67-28584
Pulse modulated data channel operation over parallel optical paths, noting advantages inherent in simple processing and control circuitry 14 p2272 A67-28699
Modulation indexes for two-channel phase coherent communication system determining data rate yielding predetermined bit-error probability [JPL-TR-32-1118] 14 p2273 A67-28709
Convolutional encoder for orthogonal tree codes in presence of white Gaussian noise [JPL-TR-32-1120] 14 p2273 A67-28710
All-pass networks design method using algorithm and computer program for communications system 14 p2274 A67-28914
Avionics, ordnance and military aircraft as totally integrated system, noting need of accurate navigation, target accuracy and improved communications 15 p2444 A67-29398
Communication technology role in commercial utilization of space, considering spectrum utilization, economic benefits and satellite programs [AAS PAPER 67-78] 15 p2437 A67-29945
Business, government and possible home applications /including mail and education/ for electronic communications via satellites, discussing legal implications [AAS PAPER 67-91] 15 p2437 A67-29952
Navigation satellites of next decade, discussing services for air and sea intercontinental transportation vehicles [AAS PAPER 67-101] 15 p2570 A67-29956
Design disclosure format /DDF/ linking program managers, review teams and contractors 16 p2781 A67-30443
Carrier instability influence on noise immunity of discrete communication systems, with results presented graphically for uniform and normal random frequency distributions 16 p2620 A67-30477
Satellite communication, noting satellite and ground terminal design performance criteria 16 p2622 A67-30689
Optimal parameters of binary communication system using random coding and orthogonal radio signals with unknown phase 16 p2622 A67-30877
Information capacity dependence on number of frequency-divided channels of optical communication system, investigating information loss in channel-separating receiver 16 p2623 A67-30882
Design and operation of orbital space station, determining orbit altitude, payload weight, tracking and communication system support requirements, recovery operations, etc 16 p2761 A67-30961
Satellite relay to provide communication paths for aircraft-ground communication over ocean, considering system design for ATC using reflex repeater 16 p2629 A67-31530
Statistical analysis of observed relationship between independent air traffic and resultant communication channel loading parameters 17 p2810 A67-32110
Statistical behavior of two-way communication system with transmission delay 17 p2811 A67-32115
Universal internal communications system /UICS/ for interconnecting avionic system components, using single coaxial cable and modules 17 p2813 A67-32472
Perturbing factors in avionics communications noting drawbacks and advantages of satellite utilization, possible commercial applications, etc 17 p2813 A67-32498
Multipath effect measurement in propagation path at UHF frequencies from synchronous satellite to aircraft 17 p2816 A67-32626
Number of feasible information networks with single channel redundancy for remote control of telemechanical system 18 p3016 A67-33572
Threshold characteristics of systems for multistate orthogonal transmission of coded analog signals in communication systems 18 p3000 A67-34023
Selection rigidity and code step optimum parameters for communications channel symmetry 18 p3000 A67-34088
RF design of satellite communications ground stations, giving hardware data on receivers, transmitters, tracking systems, power amplifiers and reliability 18 p3003 A67-34349
Conceptual design of active seismic experiment for lunar surface missions, analyzing communication approaches 19 p3323 A67-35328
Program providing man-machine communication for electronic circuit analyses using time sharing computer 19 p3186 A67-35619
Radio interior communication /RADIC/ system used in Apollo program, discussing future capabilities and advantages 20 p3380 A67-36559
Multiple internal communications system dealing with diversified information forms, discussing flexibility, reliability and other advantages for weapon systems 20 p3381 A67-36567
Rocket exhaust jet plume effects on radio signal, calculating degradation by electromagnetic diffraction propagation 20 p3381 A67-36570
Optimal signal selection on background of steady additive noise in realistic communications system 20 p3382 A67-36777
Reliable efficient communication channel utilization by use of sequential decoding 20 p3384 A67-37348
Deep space communication system using sequential decoding, binary phase-shift keying and 8-level quantized decisions 20 p3384 A67-37349
Design and performance of frequency multiplexed phase-modulated communication systems 20 p3385 A67-37353
Gravitational radio wave frequency shift from satellite measurements, noting satellite-ground radio communication system 20 p3386 A67-37524
Deep Space Network /DSN/ with ground communications network, centralized control and data processing, discussing future data return and control capabilities [AIAA PAPER 67-648] 20 p3387 A67-37628
Receiver performance related to signal and interference conditions for AM voice communication system analyzed for use in systems design 20 p3387 A67-37637
Electrical communications techniques, Part 2, HF techniques 21 p3597 A67-38532
Nonline-of-sight communication with FR-1 satellite along magnetic field line of emitter, using VLF electromagnetic waves 21 p3584 A67-38656
Apollo command module communication and data system design, discussing environmental and reliability requirements 21 p3584 A67-38668
Optical communication system components, discussing cost and potential information capacity factors in picture phone and newspaper transmission facilities 22 p3759 A67-39329
Optical communication systems modulation, discussing TV link, modulator, optical waveguides and materials availability 22 p3759 A67-39330
Channel Evaluation and Call /CHEC/ system to improve air-ground-air communications by automatic selection of optimum channels 22 p3760 A67-39664
RF generation in VLF/LF thyristor transmitter for applications in long distance communications and navigation 22 p3771 A67-39842
Light Observation Helicopter Avionics Package /LOHAP/, designed for OH-6A Cayuse helicopter, providing communications and navigational capabilities 23 p3980 A67-40927
Optical communications systems capable of microwave bandwidths evaluated experimentally and theoretically 24 p4123 A67-42805
Aperture usage for random optical communication channel through turbulent atmosphere 24 p4124 A67-42814
Medium range radio communication system using artificial ionosphere consisting of ion-

electron cloud created by Cs-Al mixture explosion
 [AIAA PAPER 67-789] 24 p4152 A67-42952
 Communication constraint in ATC system modeled with Markov chain, noting data collection and reduction and data link utilization
 [AIAA PAPER 67-868] 24 p4124 A67-42991
 R and D deep space communication system planning methodology for comparing laser, IR and mm wave possibilities, analyzing tradeoff and optimizations
 [AIAA PAPER 67-973] 24 p4260 A67-43050
COMMUNICATION THEORY
SA INFORMATION THEORY
SA STATISTICAL COMMUNICATION THEORY
 Method of coherent addition of signals to calculate noise resistance of diversity reception 01 p0024 A67-10718
 Book on antennas covering electromagnetic waves, transmission line, radiators, arrays, etc 03 p0362 A67-13713
 Differential far-end-operated half-echo suppressor design for telephone circuits with long propagation time 03 p0371 A67-13990
 Probability aspects of information transmission, deriving optimum coding and decoding algorithms 04 p0592 A67-14884
 Laser application to radar signal processing and communications equipment 04 p0576 A67-15303
 Interchannel generation transfer and multichannel generation in laser with four unsplit levels, noting radiation density, temperature effect and variations in coefficients of losses 04 p0634 A67-15760
 Chernoff bound and tilted distribution argument for obtaining error probability bounds for binary signaling on slowly fading Rician channel
 [JPL-TR-32-1051] 06 p0961 A67-17943
 Optimal signal design for binary communications systems using sequential and nonsequential detection with feedback 06 p0962 A67-17944
 Signal design problem of optimal waveforms for transmission through phase incoherent channel 06 p0962 A67-17945
 Radio waves and information transmission, discussing antennas, waveguides, diffraction and scattering modulation theory, etc 06 p0962 A67-18071
 Lightweight vertical multiwire antennas for HF range, describing construction and performance 06 p0973 A67-19050
 RCA papers on laser research and engineering 07 p1193 A67-19079
 German book on transmission of communications including transmission methods and shapes, signals, radio relays, terminal devices, etc 07 p1140 A67-19337
 Modulation devices for pulsed systems, discussing signal preparation and channel grouping for time multiplex systems 07 p1150 A67-19341
 Short wave radio links, discussing frequency converters, spectrum oscillators, transmitters, etc 07 p1150 A67-19343
 Communication parameters associated with Martian flyby probes and with lander and manned vehicles 07 p1145 A67-19870
 Series solution for average wave field in medium with random inhomogeneities by using Green function for wave equation 08 p1294 A67-20814
 Geometrical approximation of amplitude and surface-curvature parameters of wave front reflected or refracted from curvilinear boundary interface 08 p1294 A67-20815
 Minimum variance estimation and prediction theory for signal parameters in presence of noise 10 p1606 A67-23084
 Reduction of peak factor in FM system design leading to reduction of thermal noise and increase in spectrum truncation distortion 11 p1752 A67-24123
 Waveguide dispersion effect on radiation pattern and directivity of series-fed linear arrays 11 p1782 A67-24289
 Dispersion of number of positive zeros as function of time for realization of quasi-harmonic random signal 11 p1754 A67-24985
 Stochastic approximation as recursive method for solving regression problems in communication engineering 12 p1907 A67-25989
 Radar resolution performance in moving target determined by cross section of desired target compared with combined

cross section of all interfering targets 12 p1907 A67-26083
 Lower bounds on error probability for communication in presence of white Gaussian noise with no bandwidth constraint 12 p1908 A67-26086
 Approximate formulas for information transmitted by discrete communication channel obtained by averaging tight and weaker bounds respectively from transition probability matrices 12 p1908 A67-26088
 Diversity distances and loss in path antenna gain, noting association with beam width 14 p2264 A67-28399
 Atmospheric noise properties possible influence on communication, measuring intensities and short term amplitude functions 14 p2266 A67-28416
 Communication problems connected with deep space transmissions of interplanetary distances range 14 p2268 A67-28454
 Coding modulation and signal processing noting algebraic coding and binary symmetric channel neglect, discussing coherent optical radiation in noise program 14 p2269 A67-28457
 Data handling system for 8-bit phase-coherent biorthogonal coded PCM telemeter 14 p2272 A67-28696
 Cross correlation bounds and positivity of nonlinear operators, examining criteria for positive composition 15 p2457 A67-29373
 Racalator as alternative to frequency synthesis noting design principles, operation and results 15 p2445 A67-29586
 Tracking circuit performance, discussing squaring loop, Costas loop variants and delayed decision feedback 15 p2436 A67-29591
 Simultaneous primary and secondary voice message monitoring, discussing methods and experimental setup 15 p2431 A67-29895
 Invariant estimation of stochastic system parameters using autoregressive models to characterize linear plants of control systems 15 p2462 A67-30325
 Book on communication principles emphasizing digital radio communication system design, frequency and binary phase shift keying, filtering, fading, etc 16 p2624 A67-31254
 Forced-erasure decoding of fading and nonfading channels compared with correlation and digital decoding 17 p2811 A67-32114
 Timing error and noisy phase reference joint effect on system performance of coded partially phase coherent reception 17 p2811 A67-32116
 Interferometer operated with independent oscillators and without wide bandwidth communication link between elements, making operation possible at very long base lines 17 p2864 A67-33363
 Algorithm for converting binary code into uniform binary code with maximum predetermined number of zero symbols in any code combination 18 p2999 A67-33532
 Book on shift register sequence theory, discussing applications in communications, computers and switching theory 19 p3187 A67-35832
 Book on probability in communication engineering covering probability theory, information and reliability theory, random processes and noise and random phasor sums 20 p3378 A67-36137
 Soviet book on information theory and application to problems in automatic monitoring and control 20 p3413 A67-37633
 Pulse code communication system for transmission of continuous random quantities 22 p3761 A67-39831
 Transmission phenomenon of inhomogeneous electromagnetic wave in negative permittivity medium 23 p3975 A67-41480
 Channel bandwidth assignment determination using prescribed fraction of total radiated power of system contained in channel, discussing spectral distribution 24 p4123 A67-42714
 Frequency assignment for communications equipments mutual interference charts /MIC/ 24 p4123 A67-42719
COMMUNICATIONS DEVICE
SA LIGHT COMMUNICATION DEVICE
 Automatic phase sensor for waveguide combiner in S-band ground tracking and space communication 07 p1149 A67-19051

Laser development, deep space communication system studies and designs 10 p1606 A67-23069
 Optimum Bayes receiver for fading channels evaluated using Nakagami m-distribution 11 p1766 A67-24645
 Cross polarization evaluation radio echo system /CERES/ concept for polarization component separation and echo depolarization evaluation 17 p2814 A67-32520
 Man-machine graphical communication device for real time monitoring with automated checkout 20 p3446 A67-36589
 Adaptive unknown-waveform pulse signal detector algorithm construction method 20 p3384 A67-37333
COMMUNICATIONS SATELLITE
SA EARLY BIRD SATELLITE
SA ECHO SATELLITE
SA INTEL SAT SATELLITE
SA RELAY SATELLITE
SA SYNCHRONOUS COMMUNICATIONS /SYNCOM/ SATELLITE
SA TELSTAR SATELLITE
 Early Bird and Thompson-Ramo-Wooldridge systems and use in worldwide communications 01 p0022 A67-10452
 ELDO launching rockets for communications satellites 01 p0153 A67-10454
 Satellite placing in synchronous orbit using ELDO PAS booster for telecommunication purposes 01 p0156 A67-11418
 Communication relay to aircraft by satellite, discussing wave propagation characteristics, standing wave pattern, signal fading rates, etc 02 p0205 A67-12306
 Technical properties of Early Bird communications satellite noting launching, positioning, worldwide system establishment, etc 03 p0367 A67-12898
 Space research and aerospace engineering in ESRO and ELDO, examining European participation in communications satellite system promoted by U.S. 03 p0537 A67-12967
 Initial defense communication satellite and military requirements 03 p0369 A67-13826
 Early Bird circuits and development of communications systems using synchronous satellites 03 p0370 A67-13830
 Communications satellite orientation with respect to earth, using structure mounted electromagnetic actuator coils 05 p0905 A67-16831
 Broadcasting of TV by satellites, examining altitude effects, stationary satellite types, FM advantages, etc 06 p0956 A67-17560
 Communications satellite systems technology, papers from AIAA Conference, Washington, D.C., May 1966 06 p0957 A67-17662
 Characteristics and performance of synchronous satellite military communication system 06 p0979 A67-17668
 Lincoln Experimental Terminal /LET/ system, ground antenna, RF and signal processing equipment for communications via several satellites 06 p0959 A67-17669
 Adaptive utilization of communication satellite systems optimizing dynamic traffic handling of combined ground and satellite communications complex, noting network configurations 06 p0959 A67-17670
 Code-division-multiplex decentralized control system for communication satellites based on use of pseudorandom PM signals of wide bandwidth 06 p0959 A67-17672
 Multiple-access worldwide satellite communication system for aircraft terminals with limited antenna gain and transmitter power 06 p0960 A67-17674
 Communications satellite system efficiency enhanced by using automatic adaptive voice multiplexer in ground terminal equipment 06 p0960 A67-17676
 Launch vehicle parameter design for optimal support of communications satellites 06 p1093 A67-17678
 Requirements for gravity gradient stabilization of medium and synchronous altitude communication satellite systems using zero gain antennas, noting stabilization accuracy, stationkeeping effects, etc 06 p1094 A67-17680
 Wideband solid state intermediate frequency repeater for communications satellites, using waveguide-cavity diode down converter transistor amplifier and varactor upconverter 06 p0960 A67-17682
 Increased oscillation stability and

efficiency of traveling wave tubes for global satellite communications systems 06 p0967 A67-17683

Implementation of electronically despun satellite antenna system, considering limits of impracticability because of excessive weight, control power, etc 06 p0967 A67-17686 [AIAA PAPER 66-325]

Nuclear power systems for future communications satellites noting reactor, radioisotope, power system and thermoelectric power conversion equipment 06 p1029 A67-17687

Direct-to-home TV broadcasting satellite system for upper UHF, describing stabilization, thermal control, antenna, power amplifier, etc 06 p1094 A67-17689 [AIAA PAPER 66-309]

Electronic self-steering techniques applied to satellite communications system with high gain antennas, noting transdirective array and self-phasing array 06 p0967 A67-17690 [AIAA PAPER 66-326]

Interference ratios in space telecasting, considering methods of control for cochannel broadcasting 06 p0960 A67-17692

Parametric analysis, penalty-effectiveness tradeoff and system selection for communications satellites, using block digital computer synthesis with subroutines for operational requirements 06 p0960 A67-17693 [AIAA PAPER 66-330]

Multiple access modulation techniques /frequency-division, time-division, spread-spectrum and pulse-address/ for use in communications satellites 06 p0960 A67-17694

Time division multiple access /TDMA/ modulation technique for satisfying anticipated demand by many small users for communication satellite facilities 06 p0961 A67-17695

Synchronous stationary satellite system for networking television and radio material to broadcast stations, noting frequency requirements and constraints 06 p0961 A67-17697

Effects of varying orbital parameters including number of satellites, orbit altitude, positioning, tracking accuracy, cost effectiveness, etc, on establishment and maintenance of communications satellite system 06 p1094 A67-17698

Parameters of satellite communication system control and scheduling function, emphasizing distinction between scheduling model and scheduling algorithm 06 p0961 A67-17699

VHF and UHF communications between transoceanic commercial aircraft and ground stations by means of aeronautical communication satellites 06 p0961 A67-17701

Post-Echo II passive communication satellites and systems and results of Comsat systems 06 p0961 A67-17702 [AIAA PAPER 66-312]

Items affecting information transmitted from payload landed on remote planet to earth via communications satellite including orbit, transmission policy and orbit injection error effect on communication capability 06 p1094 A67-17704 [AIAA PAPER 66-314]

Lunar communication satellites, discussing satellite relay, librational, random and synchronous satellite design, lunar orbits, etc 06 p0961 A67-17705 [AIAA PAPER 66-315]

Communications requirements for manned deep space missions, using optical links, with PPM, PCM/PL and coherent reception for each link 06 p0961 A67-17706 [AIAA PAPER 66-317]

International Telecommunications Satellite /INTELSAT/ Consortium and COMSAT participation in program 06 p1120 A67-17707 [AIAA PAPER 66-332]

Long range projections of demand for intercontinental communication satellite systems and use as basis for business decisions 06 p1120 A67-17708 [AIAA PAPER 66-322]

Communications satellites, legal analysis and prognosis 06 p1120 A67-17711

Experimental and operational communication satellite, discussing attitude stabilization, automatic routing, etc 06 p1094 A67-18050

Direct-to-home TV broadcasting satellite system for upper UHF, describing stabilization, thermal control, antenna, power amplifier, etc 06 p0964 A67-18414 [AIAA PAPER 66-309]

Reliability effect on design of lunar soft landing spacecraft /Surveyor/, Syncoms I, II and III, Applications Technology Satellites, Early Bird and four Intelsat IIS 09 p1582 A67-22302

Protection of communications satellites data transmission against interplanetary interference sources and Van Allen belts 10 p1604 A67-22899

Communications satellites for high power transmission of TV and VHF signals, considering synchronous satellites, antennas, stabilizing systems and weight 11 p1870 A67-24706

Degradation factors in speech channels of multiple access communications satellites 11 p1754 A67-24719

Communications satellites within framework of space law, noting relation of commercial treaties to communication systems 12 p2042 A67-26141

Global communications satellite networks and emerging customary law for outer space 12 p2043 A67-26143

International legal principles and cooperation requirements for worldwide radio and TV broadcasting by satellite telecommunications networks 12 p2043 A67-26144

U.S. communication satellites design and transmission, including antenna types offering interference-free reception 13 p2066 A67-26334

Communication satellite techniques future development 13 p2070 A67-27151

Communication satellite program research 14 p2269 A67-28455

Satellite telecommunication networks commercial, political and military implications 14 p2270 A67-28567

Communication satellite technology development depends on compatibility with deep-sea cables, channel demands and reflector technology 14 p2270 A67-28584

VHF antenna array, electronically despun, designed for spin-stabilized synchronous-altitude communications 14 p2288 A67-28693

Block coded frequency multiplexed PM communication system design and performance, considering simplification, cost and weight 14 p2271 A67-28694

RF design of communication satellite earth stations, discussing receiving, sensitivity parameters, etc 14 p2273 A67-28798

Demand, applications and technology for future satellite communications covering transoceanic and military telecommunication, TV network, weather data, etc 14 p2274 A67-28912

Feasibility and potential uses of TV satellites for direct broadcast, considering shared use by government agencies [AAS PAPER 67-95] 15 p2570 A67-29955

Low noise amplifier specifications for communication satellite earth station 16 p2635 A67-30473

Meteorological and Communication Satellites, Congress, Athens, September 1965, Volume 4 meteorological and communication satellites - IAF Conference, Athens, September 1965, Volume 4 16 p2759 A67-30684

Early Bird satellite technology including design parameters, structure, power supply, control system and test program 16 p2759 A67-30691

Early Bird project ground stations and launch-synchronizing operations, considering time delay on transmission performance 16 p2760 A67-30692

Automatic satellite navigation and communication system for aircraft and ships using cooperating ground stations 16 p2700 A67-30695

European television satellite design emphasizing coverage area, carrier frequency selection, etc 16 p2622 A67-30697

Molniva type communication satellite, discussing optimum orbital requirements for maximum coverage, phasing, etc 16 p2742 A67-30698

Design and electrical properties of 25-meter Cassegrainian antenna installed at Raisting ground station for radio communications via satellites 16 p2622 A67-30699

Communications satellite systems discussing launching, orbits economics, etc 16 p2760 A67-30700

etc 16 p2760 A67-30700

Large aperture, low noise, steerable antennas for ground station commercial satellite communication networks 16 p2641 A67-31532

Configuration study for ELDO-PAS test satellite based on communications requirements 17 p2955 A67-32396

Future satellite regional and intercontinental telecommunication network, considering weight, classes, performance and orbital factors 17 p2813 A67-32397

Narrow beam microwave integrated circuit phased array system design for tactical communications satellite requirements 17 p2956 A67-32497

Early Bird and Intelsat commercial satellite communications system and associated ground stations noting design, power supply, control system, etc 18 p3136 A67-33545

Simplex information transmission system using communication satellites, discussing technological and economical parameters 18 p3001 A67-34176

Intelsat and communications satellites economic, political and social consequences, UN General Assembly Resolutions and use of satellite facilities for distribution of TV transmissions to broadcasting stations 18 p3162 A67-34354

Worldwide satellite telecommunication system, economic and political implications and effects on CEPT 18 p3162 A67-34357

Initial defense communications satellite program giving payload characteristics and orbit analysis of 15 military launchings 18 p3137 A67-34612

Mexican space research activities noting studies in meteorology, aeronomy, solar radiation, communications, tracking, astronomy and geomagnetism 19 p3321 A67-35298

Application satellite program, discussing meteorological and communications satellites, noting ESSA 1, Syncom, etc 19 p3333 A67-35635

Early Bird satellite design features, orbital performance, use, COMSAT applications, etc 19 p3183 A67-35636

International Telecommunications Satellite Consortium /INTELSAT/ organization 19 p3349 A67-35640

Projected series of satellite launchings by COMSAT, giving size and capacity comparisons with Early Bird technology 19 p3183 A67-35646

Reliability, orbit achievement and control and increased power bandwidth as factors making communications satellites economically feasible 19 p3350 A67-35649

Space utilization by joint venture approach, discussing communications, ocean studies, etc 19 p3350 A67-35651

Satellite TV broadcasting systems with multiple independently controllable channels visualized after 1975 19 p3183 A67-35657

Policy decisions in space broadcasting, emphasizing range of possibilities allowed and limits imposed by technical factors 20 p3378 A67-36121

Despun antenna design, functioning and performance for communications satellites, discussing pattern, scanning and phase shifters 21 p3591 A67-38205

Traveling wave tube as hyperfrequency amplifier onboard satellites for reliable space communications 21 p3592 A67-38212

Multijet electrothermal systems for attitude control and stationkeeping of synchronous communications satellite [AIAA PAPER 67-723] 21 p3694 A67-38748

Designs and performance of communications satellites, discussing long life, cooling, efficiency, larger future satellites, antennas and arrays 22 p3763 A67-40337

INTELSAT I communications satellite, discussing communications gear design and U.S. domestic satellite program 23 p4086 A67-41430

Legal problems associated with telecommunications and meteorological satellites and with launching and retrieval of manned spacecraft 24 p4257 A67-42387

Lincoln experimental satellite program, discussing communications satellites applications 24 p4242 A67-42906

Instructional broadcast satellites programming methods to reduce educational cost of students time without adding to

technological cost
[AIAA PAPER 67-787] 24 p4258 A67-42950

COMMUTATION
Commuting inverses of singular square matrix A existing only if dimension of A null space equals multiplicity of zero root in characteristic equation 03 p0460 A67-13938
Necessary and sufficient condition that generalized inverse of matrix A /denoted A plus/ commutes with A is that A plus can be expressed as polynomial in A with scalar coefficients 03 p0461 A67-13939
Commutativity of two interpolation functions, solving spaces of 04 p0644 A67-14906
Airport accessibility, discussing rail extensions to airports, bus lanes and bus-rail vehicles [SAE PAPER 670322] 12 p1925 A67-25868

COMMUTATOR
Ferroelectrics for energy switching in SHF range 03 p0378 A67-13247
High power nanosecond commutator for control of spark chambers, laser shutters, etc 09 p1473 A67-22009
Fourier analysis of amplifier commutated capacitor type integrator output signal 18 p3011 A67-34107
DC motor with switching by magnetoresistant elements 21 p3571 A67-38225

COMPARATOR
Accuracy testing of Zeiss stereocomparator 03 p0419 A67-13263
BMK ballistic camera with equatorial and azimuthal mount for stellar geodetic satellite tracking and punch card controlled mono- and stereocomparators 07 p1188 A67-19773
Fluid circuits used in drilling sequence control, detailing ring counter, binary counting stage and comparator 08 p1281 A67-20458
Pure fluid four bit binary comparator design and construction 08 p1283 A67-20474
Noise comparators and associated thermal standards to provide noise source calibration facilities at S-and X-bands 09 p1495 A67-21621
Stekometer with automatic recorder for use in analytic photogrammetry for mapping and engineering surveys 09 p1497 A67-21751
Adaptive data compression systems of predictor-comparator type 12 p1907 A67-25992
Refractory materials thermal expansion at elevated temperatures measured with apparatus consisting of optical comparator and controlled gradient vacuum furnace 16 p2677 A67-31542
Voltage comparator with high speed analog-to-digital converter and tunnel diode circuit 20 p3398 A67-36771
Maintenance time reduction for multimode airborne weapons through built-in test equipment and integrated program 21 p3601 A67-38947
Differential RF voltage comparator for transfer standard and calibration of HF voltage devices at high accuracy 24 p4155 A67-42288

COMPASS
S GYROCOMPASS
S MAGNETIC COMPASS

COMPENSATION
SA TEMPERATURE COMPENSATION
Impurity and lattice vacancy effects on compensation in doped binary semiconductors 01 p0132 A67-10455
Orbiting navigation with compensation for periodic errors, using modified Kalman filtering technique 15 p2513 A67-29595

COMPENSATOR
Elastic orifice compensator in externally pressurized gas bearings for flow control, noting increased bearing stiffness 01 p0077 A67-10123
Choosing coefficients of prefiltering, series and feedback compensators for given time response specifications despite plant parameter variations 02 p0225 A67-12143
Two-phase phase control valve with reactive compensating resistances, based on two-phase transformer with axisymmetric irreversible rotating magnetic field 07 p1150 A67-19319
Formulas for using wave plates in ellipsometry 13 p2158 A67-26879
Four-plate compensators of Jamin and Lowe type for interferometers, emphasizing linear dependence of phase difference on dispersion and rotation 14 p2315 A67-28074

Sampled data feedback control system using quadratic programming to determine optimum compensator 16 p2646 A67-31636

COMPENSATORY TRACKING
Human transfer function problem and compensatory tracking, analyzing variance and determining average rate of stick motion as underlying variable 13 p2063 A67-26923
Independent effects of error magnification and field of view on compensatory tracking performance, analyzing display and optical magnification 14 p2258 A67-28667
Compensatory tracking experiments between single and two-axis tracking systems, determining training effects on model parameters of human operator 17 p2808 A67-33178
Continuous exposure to random vertical vibrations studied for effects on compensatory tracking performance, noting decrement by peak vibration acceleration power location 18 p2993 A67-34336
Image motion compensation tracking study for earth reconnaissance from space, investigating computer and manual tracking modes, control dynamics and gain and magnification 18 p2993 A67-34337

COMPILER PROGRAM
Compiler for general purpose automatic test system /GPATS/ using program language for automatic checkout equipment 03 p0376 A67-14222

COMPLEX
S LAUNCH COMPLEX

COMPLEX VARIABLE
SA ANALYTIC FUNCTION
SA MAXIMUM PRINCIPLE
Direct and inverse Markov problem in complex region 01 p0104 A67-10286
Integral representation providing one-to-one correspondence between functions of n complex variables and complex-valued harmonic functions of n plus 1 real variables 02 p0259 A67-11918
Analytical and p-analytical functions of complex variable used to solve three-dimensional axisymmetric problems in elasticity theory 02 p0338 A67-11967
Conformal mapping for obtaining loci of complex variables without tedious calculations demonstrated, using simple T filter 02 p0227 A67-12176
Growth of integral functions of many complex variables 05 p0833 A67-16315
General circular complex charts solution, considering case where two functions of unknown variable are arbitrary functions of variable 05 p0834 A67-16435
Book on principles of ideal fluid aerodynamics covering vector algebra and calculus, Euler equations, steady and unsteady acyclic motion, complex variable, lift, etc 05 p0793 A67-17151
Linear supersonic conical flow past lower surface of triangular wing, obtaining homogeneous boundary value problem for analytical function of complex variable 06 p0936 A67-17739
Relations among various definitions of order of growth of integral functions with many complex variables 06 p1024 A67-18554
Expansion of arbitrary function in terms of Bessel functions of complex index 06 p1024 A67-18555
Necessary and sufficient set conditions for continuous function analytic within internal points of set to permit smooth approximation by means of rational fractions 07 p1212 A67-19137
Intermediate value and simultaneous convergence obtained by sequence of polynomials for pair of functions on closed set E dense on norm z equals one 07 p1215 A67-19221
Flow around variable profile in analog study of Laplacian field according to Dirichlet data 07 p1128 A67-20225
Complex solution of equations in two-dimensional thermal stress theory applied to solution of boundary value problems 10 p1716 A67-22942
Monotonic growth of multivariable function with convexity under logarithm, introducing definitions regarding order and hypersurface 10 p1875 A67-23609
Gamma function concept for varying difference interval and complex argument 11 p1812 A67-23966
Unified method of numerical quadrature for integrands of certain complex analytic

functions, obtaining asymptotic expansion of error functional 13 p2145 A67-26734
Dynamic analysis of rotor motion of rigid system in hovering state using complex variables 13 p2054 A67-27588
Constructing example of isolated stationary point 14 p2343 A67-28387
Progress in linear circuit theory, discussing scattering matrices, broadband matching and distributed and mixed lumped networks 14 p2291 A67-28460
Theory of singular integrodifferential operators on compact manifolds, discussing basic principles, concept of uniformly nonelliptic systems, etc 14 p2343 A67-28503
Envelope representation of fluctuating classical wave amplitude of stationary optical fields [SR-4] 15 p2518 A67-29767
Tension equations for oval thin walled cylinders reinforced with lateral rigid ribs noting wall strength, complex bending moment computation, etc 15 p2577 A67-30185
Analytical and p-analytical functions of complex variable used to solve three-dimensional axisymmetric problems in elasticity theory 17 p2966 A67-33284
Modulo control algorithms application in circuit for finding residues 20 p3392 A67-37153
Integral integer-valued functions of several complex variables, proving Gelfond-Straus results by using modification of Schneider method 21 p3651 A67-37921
Discrete Laplace transform for analyzing pulsed automatic systems with variable parameters, noting special type of complex variable 21 p3605 A67-39112
Weierstrass canonical product analog for integral functions of many complex variables, discussing existence problems and canonical function construction 22 p3827 A67-39215
Lemmas and theorems for support functions of plurisubharmonic functions proved, discussing complex variables and linear maps 22 p3828 A67-40555
Complex representation of elliptic differential equation solution, discussing holomorphic functions, polycylindrical regions and Vekua concept 23 p4022 A67-40723
Relations among various definitions of order of growth of integral functions with many complex variables 23 p4022 A67-40820
Expansion of arbitrary function in terms of Bessel functions of complex index 23 p4022 A67-40821
LF downcoming sky wave phase calculation method, discussing complex integral representation for resultant field 23 p3973 A67-40838
Complex Fourier transform technique in variable coefficient partial differential equations applied to Cauchy-Kowalewski and Petrowski-Leray theorems 24 p4178 A67-42202
Thin toroidal elastoplastic shells of revolution loaded axisymmetrically, calculating force, moment, stress and strain interrelation for middle surface using complex representation 24 p4250 A67-42305

COMPONENT
S SPACECRAFT COMPONENT

COMPONENT RELIABILITY
Rules for maximizing component accessibility when designing electronic equipment 01 p0078 A67-10166
Optimum nonlinear inertialess conversion of signals from several devices, taking into account unreliability in operation 01 p0043 A67-10238
Matching reliability methods to real situations in system-assessment context 01 p0078 A67-10514
Fluid power support equipment for space vehicles outside earth atmosphere, based on earth environment effect on various systems [SAE PAPER 660708] 01 p0013 A67-10600
Powder metallurgy applications in space vehicle systems, discussing parts and materials actually used in successfully orbited spacecraft 01 p0100 A67-10712
Nonlinear solution method incorporated in computer program for analysis of abnormally operating circuits, considering catastrophic part failure modes 01 p0031 A67-11337
Replacement policies for aircraft and missile parts that fail according to normal log-normal or Weibull continuous probability distribution 01 p0083 A67-11339
Component performance and flight

operations of X-15 research airplane program, considering engine, auxiliary power and propellant system 01 p0011 A67-11341

Component reliability screening techniques for Syncom, Early Bird, ATS Satellites and Surveyor spacecraft 01 p0155 A67-11343

Operational reliability components in four military systems, analyzing replacement data by digital and computer type circuitry employing semiconductors 01 p0041 A67-11344

System reliability improvements based on design and reliability experience producing increased success percentage of NASA systems from 62 to 87 percent 01 p0083 A67-11345

Full-life product warranty approach in reducing military avionics support costs by tying supplier profits to reliability attainment 01 p0171 A67-11351

In-service reliability analysis in reducing maintenance costs and spares requirements 01 p0083 A67-11352

Electronic device degradation and failure analysis in terms of changes in atomic and molecular levels 01 p0041 A67-11356

Component quality assurance program used to accelerate reliability improvement of 20-amp silicon epitaxial mesa power transistor 01 p0041 A67-11357

Physics of failure techniques applied in reliability failure analysis of intermittent operation of ceramic capacitors 01 p0041 A67-11358

Fatigue failure analysis in small metallurgically-bonded joints in very small electronic components, using statistical analysis of random forces and dynamic response of member 01 p0084 A67-11359

Accelerated stress testing and reliability estimation for electronic components 01 p0085 A67-11373

Reliability tests on aerospace and missile systems research and development component assemblies 01 p0085 A67-11376

Prediction method for system reliability in early proposal and feasibility phases of program 01 p0085 A67-11379

Markov chains used in construction of reliability mathematical models for systems with dependence between components, noting differential equations 01 p0085 A67-11383

Integrated circuit reliability and nondestructive testing, noting component failure analysis, self-maintenance, network parameter determination, etc 02 p0224 A67-11526

Radiation stress effect on component reliability of electric circuits analyzed via mathematical statistics 02 p0210 A67-11527

Reliability and MTBF of electronic devices 02 p0250 A67-12429

Book on electronics reliability, calculation and design 03 p0377 A67-13232

Automatic malfunction analysis /AMA/ technique providing space-vehicle test engineer with listing of all component failures that could cause abnormal indication at any observable monitoring point 03 p0399 A67-14213

Transistor life expectancy and failure predictions from LF noise measurements 03 p0389 A67-14277

Material failure modes in engine components and improved structural design problems 03 p0505 A67-14387

Reliability of high power level ferrite phase devices 04 p0579 A67-14455

Electronic component reliability as affected by thermal doses and ethylene oxide gas used in spacecraft sterilization 04 p0563 A67-15239

Compressor blade vibration, discussing prediction of amplitudes of vibration and interpretation of results of engine strain gauge tests in terms of component service life [ASME PAPER 66-WA/GT-14] 04 p0712 A67-15369

Component part reliability concepts, examining degradation and catastrophic failure, failure modes and lot screening 04 p0584 A67-15477

Accuracy analysis method for radioelectronic circuits, noting statistical test method 04 p0586 A67-15871

Aircraft piston engine components reliability characteristics determined from defect data survey, using statistics 04 p0691 A67-15902

Reliability of finite automata determined from analysis of elements capable of misalignment, input errors and structural design 05 p0782 A67-16261

Component reliability at low stress levels and significance of failure mechanisms, considering electrical contacts and dielectric material 05 p0774 A67-16734

Component design advances with fatigue tests on hydraulic tubes and outline of seal development 05 p0753 A67-16749

Quality control program for establishing reliability critical items, emphasizing procurement, inspection and testing 05 p0812 A67-17244

Mariner IV Space Data Automation System /SDAS/ computer reliability design, pellet component concept, testing, interconnection and welding techniques 05 p0777 A67-17254

Statistical procedures for analyzing test data to determine extent of dependence of failures in redundant components 05 p0813 A67-17256

Degradation analysis and variability measurement in reliability and quality control of component parts with application to Early Bird COMSAT satellite 05 p0813 A67-17257

Statistical probabilistic analysis of error propagation and tolerance limits in structural engineering design of assembled parts 05 p0813 A67-17258

Packaging failures in reentry/recoverable aerospace equipment due to design deficiencies in parts, materials and/or processes associated with physical hardware 05 p0779 A67-17468

Reliability and temperature stability of metals used for contacts and interconnections on semiconductor devices 06 p0971 A67-18246

Aircraft equipment retrieval after long term storage for periods of up to 23 years under jungle, desert and arctic environment, discussing sealing and hydraulic systems [ATAA PAPER 67-185] 06 p0951 A67-18487

System reliability increased by introducing redundant elements or structural changes in elements 06 p1008 A67-18546

Reliability of nonlinearly elastic polymer components of structural elements exposed to random loads 07 p1261 A67-19171

Book on electronic component reliability noting effects of environmental conditions, possible faults, various circuits, wiring, transformers, etc 07 p1158 A67-20206

Environmental and experimental testing of electronic systems component reliability 08 p1302 A67-20906

Nondestructive testing techniques in radiation vulnerability analysis of electronic systems, noting ionization effects and permanent damage in semiconductors 09 p1471 A67-21868

Electronic parts sterilization program noting results on capacitors, resistors, varactor diodes, microcircuits, transistors, transformers, diodes and operating temperatures 09 p1480 A67-22296

Parts reliability control by computer programs 09 p1583 A67-22307

Troubleshooting problems in oscillator circuit solved via Bayesian computer program simulating critical behavior 09 p1456 A67-22369

Fluid amplifiers based on Coanda effect, digital and analog pure-fluid devices, applications to spacecraft control, gyrocontrol, etc 10 p1595 A67-22975

H-film /Kapton/ flexible circuits fabrication problems including tensile strength, pattern misregistration, delamination, embrittlement, etc 10 p1611 A67-23309

Analytical methods using mass spectrometry and gas chromatography for contaminants affecting component reliability in gases enclosed within electronic components 10 p1611 A67-23310

Procedures for aircraft and spacecraft contractual arrangements to procure reliable systems, considering costs, qualification tests, etc 10 p1680 A67-23430

Aviation avionics microelectronic devices stressing reliability, maintenance, circuitry, etc [SAE PAPER 670253] 11 p1758 A67-23985

Aircraft fuel gauging systems noting float type and reliability defects [SAE PAPER 670263] 11 p1789 A67-23986

Threaded fastener reliability factors noting mechanical testing 11 p1795 A67-24040

Ground station antenna steering system for satellite communication, noting design 11 p1758 A67-24061

Storage reliability for electronic systems in missiles, noting factors affecting failure rates after dormant storage 11 p1768 A67-25010

Electronic package design for rugged military field service 12 p1911 A67-25268

SST air inlet control system, considering maintainability, impact on cockpit procedures and component reliability effect on dispatch reliability [SAE PAPER 670325] 12 p1895 A67-25869

Doppler radar and Doppler navigation system capabilities, applications, cost and reliability for supersonic and subsonic aircraft [SAE PAPER 670328] 12 p1964 A67-25870

Engine design to reduce overall cost and improve power plant component for flight schedule reliability [SAE PAPER 670330] 12 p1990 A67-25872

Systems and techniques in aircraft maintenance to meet problems of parts reliability, longevity and shop cost [SAE PAPER 670338] 12 p1895 A67-25877

Universal endurance criterion for machine structural elements sustaining complex stresses, based on machine part lifetime assessment 12 p2032 A67-25964

Reliability and cost analysis of semiconductor integrated circuit and vapor deposited thin film IC, discussing failures and defects 12 p1918 A67-26207

Plastic molded transistors for hybrid integrated circuits, production and reliability 13 p2077 A67-26651

Planar silicon transistors with improved performance and reliability due to metallic protection, noting low noise and surface potential stabilization 13 p2077 A67-26652

Aircraft engine reliability, considering local surface stresses, engine component distortion under load, vibration problems and material variability 13 p2188 A67-27000

Reliability of integrated circuit amplifier improved by using nonlinear variable capacitances at LF 13 p2081 A67-27293

Computer aided design and reliability engineering /CADRE/ applied to data processing associated with communications equipment components and subassemblies 13 p2072 A67-27446

Atlas booster materials compatibility with fluorine oxidizers 13 p2186 A67-27687

Organic contaminant effects on relay reliability, discussing materials, degassing and contamination reduction 13 p2084 A67-27694

Reliability of electromechanical relays, discussing test equipment, data analysis, etc 13 p2085 A67-27698

Electronic equipment reliability improvement methods and practices in Czechoslovakia 14 p2282 A67-28039

Fluid sphere gyroscope designed for extreme shock, vibration, temperature and overrate, examining signal processing, design parameters, etc 14 p2322 A67-29081

Error possibility in temperature measurements of 30-60 km region, noting solar irradiation effects on thermistor bead 15 p2474 A67-29202

Reliability of high power level ferrite phase devices 15 p2443 A67-29292

Environmental conditions effect on engineering systems, considering vibration, climatics, pressure, radiation, corrosion, dust penetration, etc 15 p2492 A67-29502

Spacecraft system performance vs component reliability, discussing practical aspects of software tools for management purposes 15 p2493 A67-29607

Reliability, performance requirements and environment in which system must operate 15 p2583 A67-30128

Worst distribution analysis for statistical circuit design 15 p2455 A67-30406

Standard life-testing experiment in which n similar units are cycled to failure 15 p2495 A67-30414

Reliability assessment methods for dormant weapons noting failure modes, redundancy, large parameter change, system design, derating, etc 15 p2495 A67-30418

Reliability prediction relationship to system support costs, computing factors for undersupport and oversupport of tactical missile system 16 p2782 A67-31256

Reliability of multilayer printed wiring

boards as interconnection device 16 p2642 A67-31726

Mechanical properties used to estimate low cycle fatigue behavior in creep range of components in high-temperature systems 16 p2777 A67-31813

Electroinductive defectoscope circuitry and operation described noting use for fatigue cracks observation in threaded components 16 p2681 A67-31917

Semiconductor field development, discussing component reliability and miniaturization 17 p2823 A67-32299

Iterative on-line reliability calculation of automatically repaired space computer, noting reliability and performance 17 p2820 A67-32501

Conservative series-parallel approximations to study systems models for reliability analysis and display 17 p2865 A67-32585

Plane structure silicon transistors subjected to Co gamma radiation, considering electrical properties degradation to predict component survival probability 17 p2917 A67-32842

Engine design for civil operation from military supersonic engine [SAE PAPER 670316] 17 p2929 A67-32978

Reliability methods used to insure reliability of supersonic transport engine [SAE PAPER 670317] 17 p2929 A67-32979

Development, reliability and acceptance tests for third stage of ELDO satellite launcher, discussing components, time schedules, personnel training, etc 18 p3136 A67-33639

Space pressure and temperature environment simulation facility for liquid rocket space-ignition reliability testing [AIAA PAPER 67-428] 18 p3112 A67-33912

Compressor blade vibration, discussing prediction of amplitudes of vibration and interpretation of results of engine strain gauge tests in terms of component service life [ASME PAPER 66-WA/GT-14] 18 p3115 A67-34132

Telecommunication equipment reliability and maintenance costs reduction to increase availability, noting corrective method by transistorization 18 p3002 A67-34229

Predicting effects produced by environmental interactions with various components 18 p3005 A67-34650

Relationship of management to reliability aspects during Athena program 18 p3138 A67-34651

Flight failures in complex unmanned spacecraft systematically studied for Voyager spacecraft design, discussing component failure, design deficiencies and space environment 18 p3138 A67-34656

Geocentric trajectories for particles of single class 18 p3016 A67-34666

Factors degrading reliability in use phase, developing analysis method for determining optimum corrective measures 18 p3057 A67-34667

Maximum entropy principle to derive reliability functions for creep failure modes of engineering materials at high temperatures, noting stress analysis, probability distribution, etc 18 p3145 A67-34675

Metallurgical aspects of nitrated component application in unmanned satellite drive systems to remedy sliding wear and increase reliability 18 p3058 A67-34676

Risk assessment techniques for design, fabrication and testing of complex spacecraft noting component reliability, Bayesian statistics, Monte Carlo technique, etc 18 p3138 A67-34683

Maintainability and reliability cost effectiveness program /MARCEP/ applied to logic and computer limitation problems 18 p2995 A67-34689

Reliability prediction, modeling and analysis activities in Apollo program 18 p3139 A67-34697

Reliability analysis and mathematical models to evaluate crew safety applicable to system safety analysis, discussing component failure data, failure mode effect, etc 18 p3139 A67-34704

Periodic stress and heating during creep, studying deformation adaptability of material for conditions experienced by aircraft engine components 19 p3338 A67-34885

Diagnostic methods of rotating bearing defects, describing types of bearings, oils

and equipment used in tests 19 p3235 A67-34888

System reliability and effectiveness in manned and unmanned geological/geophysical space missions 19 p3332 A67-35323

SST flight control system electronic and hydraulic systems, discussing system design, components, reliability and test programs [AIAA PAPER 67-570] 19 p3174 A67-35986

Integrated nondestructive testing for determining weld integrity of space vehicles 20 p3454 A67-36586

Lunar Orbiter power subsystem reliability tradeoff, methodology, performance prediction, etc 20 p3363 A67-36594

Quality program planning criteria for NASA contracts involving NPC 20 p3556 A67-36602

Static electricity as potential reliability problem in electronic equipment production, noting transistor failure 20 p3397 A67-36608

Product reliability dependence on scatter extent determination in fatigue life, recommending testing in S-N diagram short life region 20 p3538 A67-36699

System reliability prediction and confidence limits for several component failure probability distributions, using Monte Carlo simulation on digital computer 20 p3455 A67-37314

Contamination control of hydraulic system achieved when contamination level of fluid is within contamination tolerance level of system components 20 p3365 A67-37363

Book on turbine blade vibration damping for increasing operational reliability 21 p3715 A67-37831

Cabling material problems associated with military standard connectors for space vehicles, discussing reliability, fabrication, assembly and design 21 p3595 A67-38334

Microelectronic performance degradation resistance under thermal sterilization cycling conditions 21 p3596 A67-38344

Reliability evaluation of passive electronic components of ceramic and mica condensers and carbon resistors, including defects and stress analysis 21 p3571 A67-38671

Component selection program for equipment onboard FR-1 satellite covering production facilities, qualifications, supply, reliability, etc 21 p3572 A67-38676

Approximate method for electric propulsion missions analysis, determining system components effects on performance [AIAA PAPER 67-709] 21 p3693 A67-38736

Soviet papers on vibrations and strength of aircraft engine components 21 p3726 A67-38830

Failure mechanisms in semiconductor components under thermomechanical and electrical stresses for D2 satellite application 21 p3601 A67-39061

Perturbation scheme for linear system performance determination based on component performance information 21 p3654 A67-39063

Aircraft skin friction balance components for hostile environments noting system design 22 p3795 A67-39188

Automatic satellite-checkout system for use under simulated space environment and stress conditions 22 p3778 A67-39192

FAA certification standards for SST engines and components, emphasizing thermal environment testing and high temperature materials development 22 p3867 A67-39224

Quality control organization of suppliers to provide reliability of structural component of spacecraft electronic systems 22 p3922 A67-39282

Space research experiments reliability requirements, considering structural components, project planning and measuring methods adaptation to ambient conditions 22 p3899 A67-39283

Breakdown probability calculations to determine life span and reliability of structural components subjected to oscillations 22 p3908 A67-39284

IR for electronic circuit component diagnosis, discussing design criteria, quality control and acceptance testing 22 p3769 A67-39631

System reliability increased by introducing redundant elements or structural changes in elements 22 p3812 A67-39745

Electronic parts degradations induced by assembling and packaging environments

investigated for effects upon failure modes 22 p3771 A67-39834

Performance reliability of reinforced plastics for structural load-bearing components using nondestructive testing, defining material-energy interactions 22 p3826 A67-39860

Configuration selection of turbopump for hot-bleed cycle nuclear engine, discussing performance optimization factors 22 p3834 A67-40162

Surveyor TV power conditioning circuit and product design, discussing weight saving features, reliability and magnetic housing 22 p3807 A67-40374

Electronic or electromechanical failure-prone component pinpointing using various nondestructive testing methods 23 p4009 A67-40912

Electronic system reliability statistical estimates obtained from test results of components using series expansion 23 p3982 A67-41669

Statistical analog technique for complex logic control systems to obtain within single test series required reliability characteristics for various structural versions 23 p3985 A67-41670

Structural and mechanical design of Lunar Module Descent Engine, discussing component testing effect on development schedule 24 p4207 A67-42394

Electronic equipment components unreliability in guided weapon systems, discussing packaging, environmental conditions and customer-manufacturer relations 24 p4161 A67-42479

Design and developmental testing of electrical components for two-shaft Brayton cycle energy conversion system, discussing Na-Bi and Li-Te cells 24 p4108 A67-42556

COMPOSITE FUNCTION

Composite propulsion systems for aerospace missions, considering Mach range, specific impulse, oxygen source, design characteristics, capabilities and limitations 22 p3868 A67-39890

COMPOSITE MATERIAL

SA CERMET

Energy dissipation and heating due to oscillation of polymers whose rheological properties are described by elastic heredity theory, considering homogeneous and reinforced plastics 01 p1012 A67-10220

Tungsten composites strengthened by fibered or reacted additive 01 p0098 A67-10702

Two metal-powder sintered composites reinforced with metal fibers or fiberglass for increased tensile and impact strength at various temperatures 01 p0098 A67-10705

Whisker strength measurement methods, noting role in reinforcement of ductile metal matrices 01 p0163 A67-11152

Resistance of copper-tungsten fiber composites to repeated tension cycles 02 p0254 A67-11793

Bounds for overall elastic moduli of solid composite materials with uniform phases that may be arbitrarily anisotropic 02 p0337 A67-11795

Radioactive tracers used to determine crack initiation and propagation characteristics in reinforced plastic composite materials, relating discontinuity growth to test conditions 02 p0249 A67-12222

Metallurgical and geometrical factors affecting high temperature tensile properties of discontinuous tungsten fiber reinforced composites 03 p0441 A67-13272

Fiber of oxides by hot deformation in metal matrices of unalloyed columbium or tantalum, preparing composites by powder metallurgy 03 p0441 A67-13273

Controlled solidification in casting, ingot-making and other processes including composites and highly undercooled melts 03 p0442 A67-13305

Strength characteristics of whisker crystals, microcrystals and macrocrystals influencing selection and use of composite reinforced materials design 03 p0449 A67-13306

Filament-matrix interactions in metal matrix composites considered as liquid phase layer formation by interdiffusion 03 p0442 A67-13309

Fiber-metal composites with properties related by law-of-mixture relationship 03 p0442 A67-13310

Advanced fibrous reinforced composites -

Conference, San Diego, November 1986 03 p0450 A67-13399

Thermo-oxidative stability of polyphenylene resins in asbestos reinforced laminates 03 p0451 A67-13400

Graphite fiber reinforced epoxy resin matrix composites, determining mechanical properties 03 p0452 A67-13402

Mechanical properties of silicon carbide filament reinforced epoxy resin composites fabricated by plying monolayer tapes into unidirectional and balanced bidirectional composites 03 p0452 A67-13403

Beryllium wire reinforced epoxy-plastic composites in mechanical testing under various loadings 03 p0442 A67-13404

Carbonaceous fiber yarn reinforcements in epoxy-anhydride binder, noting moisture adsorption degradation of interlaminar shear values 03 p0452 A67-13405

Boron filaments for possible use as reinforcing phase in composite materials for aerospace structures 03 p0452 A67-13407

Technique for producing continuous metallic filaments with diameter of less than 7.5 microns and composites 03 p0443 A67-13408

Boron nitride fibers in composites for aerospace application, discussing fabrication, ablative properties, etc 03 p0452 A67-13409

Single crystal whisker composite methodology in plastics, metals and ceramics, emphasizing alignment and handling problems 03 p0453 A67-13410

Single crystal fiber reinforced composites, discussing use of silicon carbide whisker as interstitial reinforcement 03 p0453 A67-13411

Mechanical properties of continuous filament-graphite matrix composite in 0.50 inch diameter rod form, discussing limitation of binder phase and interface 03 p0453 A67-13412

Laminate optimization for filamentary composites, discussing applied spectrum of load requirement 03 p0453 A67-13413

Potential payoffs of using high modulus filament reinforced composite materials in aerospace systems applications discussed in light of development programs 03 p0443 A67-13414

Hollow-rib reinforced structure design from boron filament reinforced epoxy resin, describing fabrication equipment, techniques and test results 03 p0429 A67-13417

General and mechanical property requirements for metal matrix composite materials used for aircraft gas turbine compressor blades 03 p0443 A67-13418

Structural carbon yarn for reinforcement of composite plastics 03 p0454 A67-13424

Fiber formation and performance properties of carbon-silica fibers and use in plastic composites 03 p0454 A67-13425

Interfaces in composite materials, discussing matrix-fiber interfaces, interfacial chemical interactions, microstructure and thermodynamic instability 03 p0454 A67-13426

Surface treatment and interface stability of boron filaments reinforcing plastic composite materials 03 p0455 A67-13428

Thermodynamic compatibility of B, SiC, BN, boron carbide and tin nitride with various metal matrices in fiber-reinforced composites 03 p0443 A67-13429

Compatibility and interaction characteristics of SiC and B fibers with metal matrices in composites prepared from powder metallurgy by hot pressing 03 p0444 A67-13430

Boron fiber-reinforced aluminum composites fabrication by plasma spraying and tensile testing 03 p0444 A67-13431

Residual stress effect on stress-strain curve of uniaxial composite consisting of stainless steel wire and aluminum alloy matrix 03 p0444 A67-13432

Refractory composites consisting of high strength high modulus filaments imbedded in vapor deposited refractory metals 03 p0444 A67-13433

Unidirectional solidification of eutectics for production of composite materials, avoiding problems with whiskers, interfacial bonding, matrix distribution, etc 03 p0444 A67-13435

Boron filaments for reinforcement of aluminum alloys used in turbomachinery 03 p0444 A67-13436

Fiber reinforced composites with high strength high temperature resistance, using powder metallurgy and honeycomb

structures 03 p0429 A67-13437

Silicon carbide filament properties, fabrication and use as reinforcement of metal matrix composites, noting strength retention at high temperatures 03 p0445 A67-13439

Micromechanical behavior of composite materials under static tension, bending, shear and fatigue loading investigated analytically and experimentally 03 p0455 A67-13440

Fiber, matrix and interface contributions to composite material improvement 03 p0455 A67-13441

Statistical theory for strength of laminar composites used to optimize biaxial and multidirectional tensile strength properties of laminated materials 03 p0522 A67-13442

Engineering estimates of transverse properties of unidirectional composites compared with conventional glass-reinforced plastics 03 p0522 A67-13443

Attachment concepts and problems in fibrous composite aerospace structures 03 p0523 A67-13444

Anisotropy effect of continuous filament composites on material strength, noting dependency on test specimen configuration in evaluation of mechanical properties 03 p0523 A67-13446

Nondestructive test methods for monitoring service hardware during boron composite material development and correlation with results of destructive tests 03 p0455 A67-13447

Yield surfaces for nonhomogeneous shells of revolution 03 p0523 A67-13501

Cyclic stressing of fiber composite materials elastic-plastic region, assuming equal strains in fiber and matrix 03 p0445 A67-13529

Failure mechanism of ceramic fibers in fiber-metal composites determined by high amplitude fatigue tests 03 p0525 A67-13871

Plastic reinforced composites, weight savings, strength and thermal capability [SAE PAPER 660642] 04 p0642 A67-15786

Composite materials using whisker and short fiber reinforcements, discussing specific strength and specific moduli [SAE PAPER 660640] 04 p0642 A67-15787

Composite coatings provide temperature differences at surface of hot stamped blanks, thereby making it possible to control strain distribution over surface 04 p0630 A67-15901

Organic composites reinforced with single crystal fibers manufactured, using fiberization of whiskers 05 p0832 A67-16167

Fiber diameter, length and discontinuity effects on fatigue properties of fiber-reinforced metal 06 p1099 A67-17712

Electric resistivity and electroconductivity of copper composites reinforced with fibrous felts of tungsten 06 p1015 A67-17808

Factors affecting strength of whisker reinforced metals noting characteristics [ASME PAPER 66-MD-8] 06 p1015 A67-17835

Stress waves reflection and transmission in composite laminates and parameters affecting ability to resist fracture by hypervelocity impact [AIAA PAPER 67-140] 06 p1102 A67-18289

Two fabric-reinforced plastics performance in reentry heating as function of zirconia powder, magnesia powder and Microbestos TX paper fillers [AIAA PAPER 67-154] 06 p1020 A67-18292

Mechanical and structural properties of three-dimensionally reinforced plastic, noting composite cylinder [AIAA PAPER 67-171] 06 p1020 A67-18296

Filamentary composite of boron and epoxy applied in design optimization of helicopter blade structure, considering filament orientation and stiffness [AIAA PAPER 67-176] 06 p1102 A67-18322

Coated filaments effect in controlling composite microstructures for several metal-graphite and metal-boron systems [AIAA PAPER 67-175] 06 p1019 A67-18441

Strengthening of eutectic composite fibrous wire and rod fabricated by hydrostatic extrusion [AIAA PAPER 67-172] 06 p1008 A67-18458

Mechanical properties of continuous carbon filament/graphite binder composite including tensile, compressure, flexure, fatigue and shear properties [AIAA PAPER 67-173] 06 p1021 A67-18509

Orientation effects in mechanical behavior

of anisotropic structural materials - Astm Symposium, Seattle, October-November 1965 06 p1107 A67-18653

Material orthotropy effect on directions of principal stresses and strains in fiberglass and boron composites 06 p1108 A67-18654

Filament-metal matrix composite material research, considering reinforcement and binder 06 p1019 A67-18657

Brazed graphite-stainless steel composites for tube-to-armor joints of high temperature graphite space radiators 07 p1223 A67-19462

Fabrication, properties, deformation and fracture of silica fiber reinforced aluminum, noting effect of heat treatment and stress rupture 07 p1211 A67-20260

Metal composite technology, emphasizing degree of success attained in fabricating reproducible tensile specimens by five techniques 08 p1340 A67-20358

Filamentary reinforced resin matrix composite materials for high specific strength and specific modulus necessary for aircraft structures 08 p1333 A67-20359

Reinforced plastics - SPI Conference, Washington, D.C., January-February 1987 08 p1344 A67-20420

Tensile failure of whisker reinforced composites for loading in fiber direction 08 p1344 A67-20421

Mechanical property correlation between high performance composites and cast epoxy resin data 08 p1344 A67-20423

Boron filament epoxy resin composites test program relative to mechanical design of reentry vehicle structure 08 p1345 A67-20424

Yielding phenomena in beryllium wire plastic composites, discussing static strength and moduli, failure modes and impact resistance 08 p1341 A67-20428

Light aircraft design using fiberglass reinforced plastic primary structure for fibrous composite airframe 08 p1414 A67-20429

Void effect on strength of filament reinforced composite materials 08 p1415 A67-20434

Fabrication of complex hollow rib reinforced structures of wound boron filaments and anhydride cured epoxy resin for reentry vehicle application 08 p1345 A67-20435

Quantitative analysis of wear of metal-metal/ polymer composite friction pairs as function of time and operational conditions 08 p1334 A67-20597

Ni-graphite antifriction composites capable of high temperature operation with good lubrication properties and oxidation resistance under dry friction conditions 08 p1341 A67-20599

Fiber reinforced composite material behavior examined from shear loading tests, using finite difference analysis for representative PDEs 08 p1420 A67-20908

Fiber reinforced plastics, determining composite elastic constants in terms of elastic moduli and geometric parameters of constituents 08 p1346 A67-20910

Tape production process from noncontinuous boron fibers, noting mechanical properties and process parameters 08 p1335 A67-20911

Stress distribution in unidirectional multifiber composite under external and residual shrinkage loads expressed via displacement potentials 08 p1420 A67-20912

Strength of laminar composites, discussing application of statistical theory to determine parameters 08 p1346 A67-20915

Elastic moduli of filled systems, discussing effects of filler size, shape, concentration, agglomeration, etc 08 p1421 A67-20916

Spacecraft metal-metal composites consisting of continuous filaments in metal matrix 08 p1343 A67-21523

Composite material application to solid fuel rocket motor cases, discussing performance characteristics, manufacturing techniques, etc 09 p1578 A67-22513

Elastic moduli of composite with aligned continuous fibers derived from elastic properties of constituents 10 p1715 A67-22859

Continuous filament reinforcement data, analyzing boron and silicon carbide for metal matrix applications [ASTM PAPER WES-7-75] 10 p1668 A67-23010

Combining two or more nonmetallic substances noting applications of fiber

reinforced, particulate filled and laminated composites 10 p1671 A67-23013
Eutectics use in composite material by growing single crystal whiskers aligned inside matrix 10 p1669 A67-23637
Boron fiber reinforced epoxy matrix plastic composite for application to aircraft structures 10 p1723 A67-23697
High modulus high strength reinforcements incorporated in epoxy matrix plastic composites for aerospace structural use 10 p1671 A67-23704
Fiber aspect ratio, residual stress state and geometry of multifiber arrays studied in terms of influence on local stress concentration and matrix reinforcement 10 p1671 A67-23705
Stress distribution prediction in multilayered circular cylinder subjected to combined bending and axial loading exhibiting multilinear stress-strain relationships 10 p1724 A67-23706
Dynamic effective stiffness theory of layered and unidirectionally fiber reinforced composites, detailing field equations for laminated composite 10 p1724 A67-23708
Fracture process in composite films of stressed tetrafluoroethylene and fluorinated ethylene-propylene 10 p1672 A67-23746
Fiber spacing and array geometry effect on modulus of composites of laminate configurations used in aerospace structures 10 p1729 A67-23768
Fiber reinforced composite materials, discussing high temperature behavior, strength/weight ratio, structural composition, fabrication, etc 11 p1805 A67-24221
Book on composite materials covering theory of metal strengthening, dispersion, fiber strengthened materials, material potentials, etc 11 p1807 A67-24634
Fiber reinforcement theory, considering strengthened metal behavior at elevated temperatures and under work hardening conditions 11 p1807 A67-24635
Fiber strengthening processes, advantages and limitations of fiber for composite systems and incorporation in metal matrices 11 p1811 A67-24637
Composite materials potential in structural engineering 11 p1807 A67-24638
Filamentary materials for wound structures, particularly rocket motor cases, noting fabrication equipment, physical properties, etc 11 p1811 A67-25008
Hot pressing technique for aluminum sheet and stainless steel wire to produce composite high tensile strength plate 12 p1954 A67-25289
Glass fiber reinforced composite materials for aircraft engine, discussing construction of bearing and compressor casings [SAE PAPER 670333] 12 p1958 A67-25874
Stresses and strains in dual element and fibrous to steady state creep load calculated by considering individual properties of constituent elements 12 p2031 A67-25953
Transverse normal loading of doubly periodic unidirectional elastic fiber reinforced infinite elastic matrix 14 p2398 A67-28098
Thermal conductivities of unidirectional composite materials parallel and normal to filaments, using analogy to shear loading response 14 p2404 A67-28099
Stress distribution in matrix of composite material for case of filler between one infinite and two displaced sem infinite microfibers 14 p2398 A67-28100
Elastic moduli of composite materials with anisotropic filaments 14 p2398 A67-28101
Metal matrix composite fatigue behavior in tension-tension loading as function of volume fraction 14 p2337 A67-28422
Cylindrical bending of plate composed of strengthening and binding agents with different Youngs moduli 14 p2401 A67-28734
Filament wound sleeve seal impregnated with solid lubricants dissipates heat in rubbing contact zone and provides wear characteristics for use in air compressor [ASLE PREPRINT 67AM 7A-3] 14 p2326 A67-28791
Glass reinforced structural design fundamentals, discussing basic properties of filament materials, matrix material and composite materials [ASME PAPER 67-DE-16] 14 p2402 A67-28871
Superconducting materials for solenoids,

noting simple form conductors and current carrying capacity as field function 17 p2912 A67-32264
Maximum shear stress dependence on composite materials microstructure, noting filler and binder role 18 p3069 A67-34170
Propagation of elastic waves through composite media studied with ultrasonic pulse technique, noting Poisson ratio, bulk modulus, etc 18 p3069 A67-34488
Filament-metal matrix composites for high temperature range, discussing kinetic phenomena [ASTM PAPER 1] 18 p3066 A67-34567
Sapphire whisker reinforced aluminum composites fabrication and evaluation [ASTM PAPER 2] 18 p3070 A67-34568
Deformation behavior of matrix and fibers in aluminum-boron and copper-tungsten composites studied by X-ray lattice strain techniques 18 p3067 A67-34570
Metal matrix composites compression-microstrain behavior at room temperature, discussing stress-strain curve, Youngs modulus, yielding, etc [ASTM PAPER 6] 18 p3067 A67-34571
Aluminum-boron composites stress-strain behavior, considering synergism increasing over rule of mixtures [ASTM PAPER 7] 18 p3067 A67-34572
Mechanical behavior of boron-aluminum composites subject to stress, strain and temperature, discussing melt infiltration, powder metallurgy and diffusion bonding production [ASTM PAPER 9] 18 p3067 A67-34574
Composite material with titanium strength-weight ratio and aluminum safety for aerospace vehicle construction [ASTM PAPER 15] 18 p3067 A67-34576
Structural reinforced plastic composite materials for cryogenic temperature application evaluated noting tensile, compression, shear, flexural and bearing properties [ASTM PAPER 16] 18 p3070 A67-34577
Cermets sealing material dry-friction characteristics over wide sliding-speed range, discussing graphite and boron nitride lubricants 19 p3247 A67-35850
Resistance of ideal crystal studied for plastic yielding and brittle cracking, noting composite materials devised to resist both failures 20 p3469 A67-37248
Anisotropic composites viscoelastic analysis applied to orthotropic cylinder pressurization, glass fiber cooling and relaxation shear moduli problems 20 p3474 A67-37267
Unidirectional fiber-reinforced composite under axial load, discussing power series along with point matching techniques for solving interface, matrix and filament stresses 20 p3474 A67-37268
Stress distribution in imperfect filamentary composite material 20 p3474 A67-37270
Metals, ceramics, glasses and polymers combined as composite materials, reviewing mechanical properties and considering applications to engineering design 20 p3475 A67-37714
Vapor deposition-prepared continuous silicon carbide filaments for use as reinforcement in high strength oxidation-resistant structural plastic composite 21 p3648 A67-37881
Fiber reinforced plastic composite strength and elastic modulus dependence on fiber properties, volume content, directional orientation and matrix load transfer properties 21 p3649 A67-37882
Composite technology emphasizing fiber-reinforced metal matrix composites, discussing filaments, plastics, ceramics, fabrication methods, etc 21 p3643 A67-37953
Metal composite materials for higher temperature resistance utilizing filaments, fibers and whiskers, discussing machinability and testing 21 p3643 A67-37954
Dispersion relations for elastic wave propagation in filamentary composites obtained, establishing averaging rules for elastic constants 21 p3729 A67-39055
Dispersion relations for elastic wave propagation in lamellar composite materials obtained with averaged elastic constants 21 p3729 A67-39056
Elastic properties of filled and porous epoxy composites tested in compression and tension noting Youngs modulus relation to

filler content 22 p3824 A67-39498
Electroplating for fabricating fibrous composite materials noting advantages of low temperatures and absence of mechanical working 22 p3819 A67-39560
Composite material mechanical characteristics, discussing organic polymeric materials application in wide temperature range 22 p3825 A67-39855
Reentry vehicles heat protection design emphasizing composite material selection/development for coating within acceptable weight limitations 22 p3902 A67-39938
Mission profiles involving new materials for missile and space structures reviewed for progress in computer applications 22 p3915 A67-40330
Composite materials development and application in powder metallurgy, considering laminated, fiber and particle reinforced materials 23 p4017 A67-40711
Shear modulus measurements in fiber-reinforced composites by plate-twisting test and torsion tube in terms of classical laminated plate and shell theory 23 p4021 A67-40738
High tensile strength of composite amorphous boron filament, discussing Weibull relationship and measurements 23 p4018 A67-40787
Long term strength limit and fracture propagation of AKN22 /Nimonic 80/ alloy welds and AKN22-16/13 CrNi steel composites welds 23 p4019 A67-41079
Suitability of finite element method for stresses in composite materials, examining single broken fiber in matrix 23 p4077 A67-41156
Diagrams of specific strength of materials made of fibrous compositions 24 p4246 A67-41921
Disordered composite materials overall elastic moduli derived from local elastic moduli using correlation function 24 p4248 A67-41956
Silicon carbide and B filament reinforced Ti alloy composites analyzed metallurgically and micromechanically, noting stress-strain behavior [SAE PAPER 670862] 24 p4172 A67-42004
Stress distributions within materials sealed across planar interfaces compared with values measured in composite pairs of glass 24 p4175 A67-42374
Temperature, fiber compositions and matrix resin effects on flexural properties of unidirectionally reinforced short fiber composites 24 p4175 A67-42422
Textile fabrication methods produce multidirectional materials, describing commercial use of 3-D materials 24 p4176 A67-42424
Boron and graphite filament-resin composites tensile and interlaminar shear strengths and Al foil liner cyclic life in cryogenic pressure vessel tests 24 p4176 A67-42470
Interfiber distance and temperature effects on critical aspect ratio in fiber composites obtained from modified pull-out test 24 p4173 A67-42474
Stress-rupture properties of composites containing refractory metal fibers and nickel alloys evaluated at high temperatures 24 p4174 A67-42475
Chemical interactions in formation of oxidation resistant solid lubricant composites of tungsten diselenide-gallium alloys for use in ball bearing systems [ASLE PAPER 67-LC-6] 24 p4164 A67-42745
COMPOSITE PROPELLANT
SA BIPOPELLANT
Metal fiber addition to basic propellant increases burning rate 05 p0872 A67-17215
Regression rates in transient regime of composite solid rocket propellant grains upon sudden opening of exhaust port 08 p1373 A67-20803
Mechanical properties of unfilled and filled elastomers 08 p1420 A67-20890
Solid and liquid propellants, considering minimum specific propellant consumption in connection with fuel selection for auxiliary power systems [SAE PAPER 670205] 12 p1987 A67-25866
Solid propulsion - ICRPG/AIAA Conference, Anaheim, June 1967 15 p2546 A67-29976
Burning rate vs pressure and other factors as function of composite solid propellant composition and oxidizer particle size

- distribution 15 p2580 A67-29985
Parameters determining magnitude of acceleration effect on burning rate increase of aluminized and nonaluminized composite solid propellants 15 p2581 A67-29991
Detonation characteristics evaluation of solid-composite propellant, noting hazards study program /Project SOPHY/ and critical geometry theory 15 p2544 A67-29999
Composite ammonium perchlorate propellant temperature profile beneath burning surface, discussing main decomposition energy, heat sources, etc composite ammonium perchlorate propellant 18 p3107 A67-33811
Combustion mechanism of ammonium perchlorate propellants, discussing gasification, decomposition, pressures, binders, burning rates, temperatures, etc 18 p3108 A67-33812
Metallized and nonmetallized composite solid propellant burning rates, analyzing effects of acceleration, noting agglomeration and nonnormal conditions [AIAA PAPER 67-470] 18 p3157 A67-33940
Pressure dependent surface reaction effects on acoustic response of composite solid propellants studied for various coatings 19 p3309 A67-35010
Catalyzed ignition of composite propellant fuels in presence of perchloric acid studied for acceleration of rate of acid decomposition 23 p4048 A67-41761
Stability boundaries of double-dead-time model describing chugging in liquid bipropellant rocket engine 24 p4207 A67-42689
- COMPOSITE STRUCTURE**
Frequency equation for purely radial vibrations of infinite isotropic composite hollow cylinder with two concentric elastic layers 01 p0162 A67-10818
Sonic resonator for nondestructive testing of composite structure operating only from one accessible surface 02 p0250 A67-12630
Aluminum alloy composite bulkhead fabrication under tensile stress with improved bonding 03 p0430 A67-13556
Fracture mechanism in continuous filamentary composites 04 p0641 A67-14832
Impact resistance of spacecraft structures indicate performance criterion effect on final structural configuration and importance of hypervelocity of realistic hypervelocity test specimens 04 p0705 A67-15001
Thermal conductance determinations on L-605 cobalt-base alloy panels of variable geometry made to around 2000 degrees F in high vacuum and air 04 p0735 A67-15852
Vibrational characteristics of composite shells, noting effects of circular joint connecting two components [AIAA PAPER 67-72] 06 p1104 A67-18496
Boron fibers and reinforced plastic composites, noting mechanical and physical properties, application, etc 06 p1021 A67-18855
Effective triaxial anisotropy in exchange-coupled composite three-layered uniaxial ferromagnetic thin films 07 p1231 A67-19488
Ultrasonic techniques for nondestructive testing for Saturn honeycomb heat shields 07 p1192 A67-20166
Fiber reinforced materials for composite structures noting deformation of metals, ceramics and glasses 08 p1342 A67-20903
Frequency equation for harmonic wave propagation in composite circular cylindrical shells established, based on linear three-dimensional theory of elasticity 10 p1717 A67-23127
Hypersonic reentry heating problems for glider of composite structure with critical temperature condition, buckling, etc 11 p1869 A67-24092
Dispersed-phase alloy production noting structure types, deformation and fracture behavior at various temperatures 11 p1807 A67-24636
Composite structure of glass with crystalline aluminum oxide and zirconium oxide inclusions tested for strength and elastic properties 11 p1811 A67-24642
Vibrational characteristics of composite shells, noting effects of circular joint connecting two components [AIAA PAPER 67-72] 12 p2030 A67-25916
Microstructure of aluminum alloys analyzed for composition, fabrication and thermal treatment, using electron microscopy 14 p2334 A67-27803
Transmission electron microscopy of interfacial areas in metal-matrix composites 14 p2336 A67-28096
High strength and high elastic modulus in resin-matrix composite structures of single-crystal whiskers [ASME PAPER 67-DE-9] 14 p2340 A67-28868
Composite aircraft performance potential, with helicopter comparison with compound-type aircraft, noting range, speed, weight, productivity, etc [AHS PAPER 110] 16 p2597 A67-31826
Compound aircraft flying quality improvement methods, noting VTOL characteristic and high speed as compared to pure helicopters [AHS PAPER 111] 16 p2598 A67-31827
Normal mode analysis of multispan skin-stringer structure with isolated tuned viscoelastic dampers at arbitrary surface points 17 p2960 A67-32579
Tension and compression, dynamic and static flexural loading and vibration tests of bilaminate filament wound composite [SESA PAPER 1219] 18 p3141 A67-33889
Bond-layer compliances effect on flexural responses of sandwich beam, discussing homogeneous and composite beams, deformation equations, etc [SESA PAPER 1214] 18 p3142 A67-33895
Stresses acting in oblique cross sections of composite shells computed in reference to different orientations 19 p3342 A67-35719
Temperature field distribution and heat flux in thin narrow semilinear composite plate with moving point source 19 p3347 A67-36051
High tensile strength high elasticity modulus graphite fibers preparation from polymeric fibers for composite structures 21 p3649 A67-37884
Exact solutions for elastic displacements and stresses in composite circular cylinder under torsion in Fourier series form 21 p3723 A67-38560
Nondestructive inspection of composite structures in helicopter rotor blades, discussing structure, loading and quality control capability 22 p3812 A67-39857
Fracture behavior of laminar steel composites studied to determine effect of interfacial properties on crack propagation 22 p3822 A67-40056
Structural analysis of welded joints in composite welded panels using beam column concepts 22 p3813 A67-40181
Computer aided techniques applied to structural analysis of aircraft noting design problems in aluminum fatigue life, unclad alloys, insulation and composite structures 22 p3915 A67-40331
Fabrication under tensile stress of large double contour composite structures, obtaining improved bonding [ASM PAPER C6-21.2] 23 p4010 A67-41410
- COMPOSITION**
S ATMOSPHERIC COMPOSITION
S CHEMICAL COMPOSITION
S GAS COMPOSITION
S IONOSPHERIC COMPOSITION
S LUNAR COMPOSITION
S METEORITIC COMPOSITION
S PLASMA COMPOSITION
S WATER CONTENT
- COMPOUND**
S CHEMICAL COMPOUND
S INORGANIC COMPOUND
S PLATINUM COMPOUND
S RUBIDIUM COMPOUND
- COMPRESSED AIR**
Hearing discrimination in hyperbaric air explained by fact that increased ambient pressure causes disturbances of sound conduction 09 p1453 A67-21729
Optimum pressure drop in compressed air driven turbine as function of initial pressure in air cylinder and turbine parameters 14 p2252 A67-28652
Leak detection methods in vacuum devices including compressed air, discharge tube, halogen tracers, radioactive krypton, pressure rebuild, etc 20 p3443 A67-36474
- COMPRESSIBILITY**
Galerkin method modifications to obtain static solution of indefinitely long partial-arc self-acting gas bearing 19 p3237 A67-35866
- COMPRESSIBILITY EFFECT**
Compressibility effects on rarefied gas flow in Rayleigh problem, using BGK model of Boltzmann equation 01 p0051 A67-10457
Cavitation effect on braking throttle actuating mechanism loaded with inertial mass 01 p0012 A67-10496
Thermodynamics of shock compression of metals 04 p0637 A67-14975
Approximate theory for development of steady two-dimensional turbulent free mixing shear layers from initial velocity profile, including effects of compressibility and heat transfer [ASME PAPER 66-WA/FE-17] 04 p0606 A67-15352
Compressibility effect on dual solutions recurrence in MGD boundary layer over flat plate 06 p1041 A67-18134
Weakly ionized gas flows about electrically biased bodies under effects of compressibility and electron energy [AIAA PAPER 67-100] 06 p1042 A67-18471
Compressibility factors of gases determined by using sonic velocity measurements, providing reliable representations of equations of state 07 p1168 A67-19577
Compression process for hollow cylindrical blanks using integration method, viewing deformation as sum of sequential stages of small dislocations 07 p1191 A67-19748
Cavitation effect on braking throttle actuating mechanism loaded with inertial mass 10 p1597 A67-23618
Physicochemistry of substances under impact compression, considering thermodynamic parameters, phase transformation and compressibility curves 11 p1749 A67-24324
Antenna impedance dependence on excitation of acoustic waves by biconical dipoles encased in dielectric sphere immersed in warm plasma 11 p1769 A67-25030
Aerodynamic theory of blade vibration, discussing compressibility effect, stalling and design 12 p2014 A67-25412
Bending of thin plate of aluminum with nonlinear stress-strain relation analyzed, considering material compressibility effect 13 p2215 A67-26267
Ductility of beryllium samples subjected to compression at temperatures ranging from 300 to 600 degrees C, discussing slip effects 13 p2137 A67-27113
Steady state fluid flow in thin passage analyzed using energy model and including compressibility effects 14 p2302 A67-28264
Wear life improvement of ceramic bonded solid film lubricant by compression and artificial filling of film voids [ASLE PREPRINT 67AM 7A-2] 14 p2326 A67-28790
Effect of plastic deformation under compression on superconducting properties of Re single crystals 14 p2375 A67-29069
Discontinuities of shock adiabats and multivaluedness of compressions, noting similarity to Bancroft condition 16 p2659 A67-31043
Electric field distribution inside local superconductor carrying steady case analyzed using Ginzburg-Landau equation, noting strong compressibility effect 16 p2731 A67-31171
Viscous, compressible fluid flow through narrow gap, noting compressibility effect on pressure distribution 16 p2661 A67-31420
Helicopter rotor at high Mach numbers, noting thin blade tips and compressibility effects and tests in wind tunnel [AHS PAPER 102] 16 p2595 A67-31819
Rotor blade compressibility effects on helicopter performance, describing flight test techniques and data analyses and comparing prediction and test results [AHS PAPER 103] 16 p2595 A67-31820
Compressibility effects on airfoils during high subsonic and low speed stalls, considering Reynolds and Mach number effect 19 p3170 A67-35521
Ion cyclotron instability potential and adiabatic compression of plasma in mirror machine, measuring plasma decay rate and potential 22 p3846 A67-39487
Externally pressurized gas bearings examined for mechanism of series restrictors on pressure distribution, flow quantity and load 23 p4010 A67-41064
- COMPRESSIBLE BOUNDARY LAYER**
Corresponding compressible and incompressible jets and wakes in boundary layer equations of turbulent and laminar cases 03 p0350 A67-12988

- Static electrointegrator for numerical solution of boundary layer theory problems for incompressible fluid and compressible gas 04 p0603 A67-14642
- Transverse curvature effect on axisymmetric compressible laminar boundary layer flow, obtaining asymptotic solutions for skin friction and heat transfer 05 p0791 A67-16509
- Hypersonic flow in compressed layer between tapered blunt leading edge of wing and internal shock wave forming in front when nonuniform flow moves past, considering expansion 06 p0936 A67-17733
- Supersonic laminar two-dimensional boundary layer separation in compression corner with and without cooling [AIAA PAPER 67-191] 06 p0940 A67-18361
- Turbulent boundary layer properties for strong adverse pressure gradients, obtaining layer and displacement thickness, skin friction, heat transfer, etc [AIAA PAPER 67-196] 06 p0989 A67-18489
- Correlation number for calculation of skin friction and heat transfer for laminar compressible boundary layer flow with arbitrary pressure gradient, using von Karman momentum integral 06 p0992 A67-18862
- Similar solution of compressible laminar boundary layer equations for Laval nozzle flow contour 13 p2049 A67-26639
- Transverse curvature effect on axisymmetric compressible laminar boundary layer flow, obtaining asymptotic solutions for skin friction and heat transfer 16 p2662 A67-31600
- Intensity and specific heat ratio effects for laminar compressible boundary layers arising behind traveling shock waves 17 p2837 A67-32347
- Transport property difference effect on flow prediction of blunt body stagnation region heat transfer, noting laminar flow and compressible boundary layer equations 17 p2793 A67-33025
- Correction for experimental velocity profile in compressible laminar boundary layer flow over flat plate 17 p2840 A67-33165
- Laminar boundary layer for two-dimensional flow on bodies of revolution, noting suction velocity 19 p3210 A67-35721
- Incompressible turbulent boundary layers with arbitrary pressure gradients and divergent or convergent cross flows predicted by effective viscosity hypothesis 19 p3211 A67-35738
- Compressible boundary layer-inviscid flow interactions in entrance region of internal flows, including shock tube boundary layer and effects of mass injection or suction [ASME PAPER 67-HT-2] 20 p3421 A67-36701
- Transpiration cooled vehicles correlation with compressible turbulent boundary layer with mass transfer, emphasizing high Mach number 20 p3423 A67-37256
- Rott approximate method applied to steady compressible laminar boundary layer on yawed seminfinitesimal solid circular cone with attached shock wave 20 p3360 A67-37595
- Growth of laminar compressible boundary layer with stationary origin on uniformly moving flat plate, noting analogy to shock induced flow 21 p3811 A67-37927
- Laminar compressible boundary layer induced by plane shock wave passing over flat wall using empirical viscosity-temperature relation for Prandtl number 21 p3811 A67-37928
- Numerical solution of compressible boundary layer stability equations including perpendicular flow velocity component terms 21 p3814 A67-38854
- Compressible turbulent boundary layer equations, discussing third order correlation terms role and eddy thermal conductivity definition 21 p3814 A67-38894
- Three-dimensional compressible laminar boundary layer with heat transfer in curvilinear coordinate system linked to streamlines of external flow, assuming transverse flow 21 p3815 A67-39127
- Equations for arc length derived for two-dimensional isentropic compression surface for ideal gas 22 p3742 A67-40102
- Heat transfer, skin friction and shearing stress from similar solutions to compressible laminar boundary layer equations for flow over flat plate 23 p4082 A67-41246
- Compressible laminar boundary layer on infinite swept cylinder analyzed for effects of suction on spanwise profile 23 p3993 A67-41746
- COMPRESSIBLE FLOW**
- SA CARTAN SPACE
- Cauchy problem of compressible conducting perfect fluid flowing under perturbation influence 01 p0121 A67-10257
- Graphs for momentum flux and mass flow calculations for use in subsonic compressible flow 01 p0007 A67-11268
- Inertia and pressure effects on energy potential of homogeneous and isotropic turbulence in weakly compressible medium 02 p0235 A67-12643
- Equation for laminar gas meter applied to flow coefficient derived from Hagen-Poiseuille relationship, noting effect of heat transfer, compressibility, etc, on meter performance 03 p0404 A67-13778
- One-dimensional steady state gas compression flow undergoing thermodynamic relaxation processes 03 p0405 A67-14258
- Streamline curvature computing procedures for turbomachinery and fluid flow problems, considering axisymmetric and nonaxisymmetric flow fields and compressible cascade flow [ASME PAPER 66-WA/GT-3] 04 p0607 A67-15358
- Simple waves for nonlinear system of partial differential equations applied to multidimensional compressible inviscid flows 05 p0790 A67-16045
- Subsonic compressible flow around profile obtained by conformal transformation, reducing to Dirichlet problem 05 p0749 A67-16845
- Approximate analysis of subsonic compressible flow in annular nozzle of short duct fan engines and inner wall curvature effect on pressure distributions 06 p0944 A67-18871
- Similarity law for wall region of turbulent boundary layers in compressible flow, discussing Coles theory 08 p1320 A67-20565
- Compressible ideal gas flow through elliptic pipe 08 p1322 A67-21169
- Rayleigh problem of compressible viscous heat-conducting radiating gray gas flow near flat plate set impulsively in motion in own plane 08 p1324 A67-21392
- Compressible nonswirling rotational flows through ducts with varying hub radii 09 p1489 A67-22161
- Double concurrent waves in one-dimensional nonstationary problems with discontinuous limit 10 p1624 A67-22923
- One-dimensional compressible flow, considering buoyancy forces as closed-form solution of Navier-Stokes equations for unknown temperature-dependent coefficient of viscosity 10 p1625 A67-23135
- Inviscid two-dimensional flow using extension of Hele-Shaw analogy, noting axisymmetric, compressible and MHD cases 10 p1627 A67-23554
- Dissipative wave propagation in linearized compressible MHD flow, constructing solution for arbitrary values of dimensionless parameters and field orientation 11 p1825 A67-23867
- Theory on secondary flows through axial compressor or turbine cascade 13 p2049 A67-26530
- Stewartson-Crocco equations solved by differential method for compressible laminar boundary layers 13 p2094 A67-26649
- Compressible flow analysis in three-dimensional curved duct using small perturbation method 14 p2305 A67-28976
- Pressure loss measurements of compressible flow through gauzes with different porosity 14 p2305 A67-29009
- Compression shocks in one-dimensional steady flow of Lighthill ideal dissociating gas studied, using semiempirical relation for relaxation equation 15 p2471 A67-29578
- Calculation of compressible subsonic potential flow through blade cascades, giving air outlet angle, velocity distribution around blade profile and critical Mach number 17 p2791 A67-32711
- Hypersonic weak-interaction similarity solutions for viscous heat-conducting compressible flow past flat plate, using Navier-Stokes equations 20 p3357 A67-36849
- One-dimensional nonstationary compressible gas flow studied with variational calculus, obtaining approximate analytical periodical solutions 20 p3360 A67-37678
- Boundary value problems solution in steady two-dimensional compressible MHD flow past thin body 21 p3660 A67-37742
- Extent of lubricating film for which oil flow is plane, discussing lubricant compressibility, heat release, load capacity and pressure distribution 22 p3811 A67-39317
- Nonlinear hyperbolic equations of compressible duct flow solved using centered difference method, compared with method of characteristics 22 p3784 A67-39945
- Procedure for expanding parameter in asymptotic power series of any order to investigate viscous compressible supersonic gas flow past blunt body 22 p3740 A67-40014
- Reattachment of two-dimensional compressible air jets to planes, discussing pressure maximum and inlet Mach numbers 22 p3786 A67-40068
- Compressible laminar boundary layer in pressure gradient, analyzing suction on basis of momentum and thermal integral equations 22 p3788 A67-40421
- One-dimensional compound-compressible nozzle gas flow theory, discussing choking phenomenon and three-dimensional computer calculations 23 p3927 A67-40803
- Differential equation system for reacting laminar boundary layer heat and mass transfer solved analytically, noting compressible gas and porous foil filter 23 p4081 A67-40744
- Magnetogravitational instability of uniformly rotating compressible medium due to variable amplitude perturbations, stressing Jeans theory 23 p4033 A67-41019
- Oscillating infinitely thin wing profile in inviscid subsonic compressible flow, deriving perturbation pressure 23 p3929 A67-41250
- Model for compressible free jet with moving environment in core and developed region of exhaust plume 23 p3992 A67-41731
- Inviscid steady axisymmetric flow inside closed annulus solution derived with extremal principle 24 p4140 A67-41807
- [ARL-66-0173]
- High speed computer graphic techniques for airfoil sections characteristics in two-dimensional compressible flow [SAE PAPER 67-0845] 24 p4091 A67-41998
- Streamline curvature computing procedures for turbomachinery and fluid flow problems, considering axisymmetric and nonaxisymmetric flow fields and compressible cascade flow [ASME PAPER 66-WA/GT-3] 24 p4143 A67-42459
- COMPRESSIBLE FLUID**
- Hypervelocity impact and crater formation based on earlier work describing similarity solution for impact on compressible fluid 01 p0165 A67-11444
- Flow of compressible fluids past straight cascades of arbitrary airfoils using Karman-Tsien method, obtaining velocity distribution around airfoil through continuity equation 02 p0177 A67-11470
- Energy dissipation due to deformation of magnetic field in compressible conducting medium near zero field lines 03 p0470 A67-12940
- Secondary vorticity for compressible flow in centrifugal impeller, noting parameter effects on motion 03 p0402 A67-13337
- Stability regions for compressible fluid squeeze-film journal bearing of infinite length, considering motion along axis [ASME PAPER 66-LUB-15] 03 p0431 A67-13758
- Propagation of coupled electromagnetic, electron-acoustic and ion-acoustic waves in horizontally stratified and magnetized electron-ion plasma 03 p0372 A67-13991
- Exact general integral for class of compressible fluids used in boundary value problems for nonlinear equations of gas dynamics 04 p0606 A67-15194
- Temperatures in cylindrical receiver resulting from rapid filling with compressible fluid compared with classical bottle-filling case [ASME PAPER 66-WA/PID-2] 04 p0555 A67-15380
- Temperature-vorticity analogy validity in laminar turbulent flows extended to compressible fluids, noting temperature relation to shear stress 04 p0727 A67-15680
- Velocity profile and friction in plane-

parallel channel with developed turbulent compressible gas flow 04 p0609 A67-15684

Existence theorem for two-dimensional subsonic flow of compressible fluid, following Bers method 05 p0790 A67-16044

Scattering cross section of electromagnetic waves by finite objects in compressible plasma in absence of DC magnetic field 05 p0853 A67-16802

Steady two-dimensional MHD flow of ideal inviscid perfectly conducting compressible fluid with one nonzero component 06 p1040 A67-18115

Nonuniform two-dimensional subsonic and supersonic flow of compressible fluid past body, using small parameter method 07 p1125 A67-19322

Heat transfer in compressed gas evacuated from container, using numerical integration of state equation 07 p1267 A67-19324

Electromagnetic and electroacoustic waves and scattering in compressible plasma 07 p1141 A67-19443

Optical and acoustic waves and scattering in compressible plasma treated by ray optical method 07 p1141 A67-19444

Empirical expression for resistance of small bore tubes to turbulent flow of compressible fluid in terms of mass flow and total head 08 p1320 A67-20461

Gas dynamics of nonisentropic two-dimensional MHD flow of ideal inviscid perfectly conducting compressible fluid 08 p1357 A67-20593

Hydraulic analogy applied to axisymmetric nonideal compressible gas systems, considering water table simulation of axisymmetric rocket nozzle 08 p1324 A67-21519

Flow of ideal compressible electrically conducting fluid in traveling wave accelerator, using multiple coordinate method to approximate small perturbation solution 09 p1544 A67-21849

Excitation of electroacoustic lateral waves in compressible plasma by nonelectromagnetic source 10 p1683 A67-22865

Radial flow of compressible fluids between disks solved through simpler form instead of numerical integration of differential equations 10 p1593 A67-23475

Invariant transformation for pulse and continuity equations of one-dimensional unsteady motions of ideal compressible fluid 10 p1628 A67-23678

Stability of flow of ideal compressible gas at low magnetic Reynolds numbers in presence of longitudinal perturbations produced by crossed electromagnetic fields 11 p1832 A67-24026

Integral relation technique for approximate solution of dynamic and thermal expansion of laminar radial slot gas jets along plane wall 11 p1779 A67-24322

Unsteady transonic flow of moving compressible gas filling half-space created by sudden rupture of membrane separating gas from vacuum 11 p1743 A67-24962

Two-dimensional nonsteady airflow in shaped duct prediction, using numerical method 12 p1928 A67-25357

Oscillations of cylindrical shell containing compressible gas perturbed by heat induced shock wave 12 p2023 A67-25595

Energy equation for laminar flow of compressible Newtonian fluid, calculating temperature profiles of fluid 13 p2224 A67-27049

Functional extremals approximation method applied to compressible subsonic fluid flows 13 p2050 A67-27148

Resistance and heat transfer of plate situated in turbulent MHD boundary layer in compressible fluid 13 p2169 A67-27312

Two-dimensional unsteady Navier-Stokes equations for compressible viscous gas in closed region, examining convective flow and heat transfer 14 p2296 A67-27987

Compressible fluid flow in capillary tubes, discussing reduction in variation of pressure difference/mass flow ratio 14 p2303 A67-28350

Fundamental relations for normal shock wave behavior in compressible fluid for classical and hydromagnetic cases 15 p2473 A67-30226

Integration of laminar boundary layer equations in compressible gas by asymptotic method, calculating friction and heat flux 16 p2660 A67-31135

Annular wing motion in compressible fluid axisymmetric flow, determining forces acting on wing cross section 18 p3022 A67-33411

Strong and weak magnetic field effects on qualitative characteristics of compressible media analyzed using Chaplygin-Sedov hodograph method 18 p3084 A67-33421

Dynamic phenomena in two identical cylindrical shells placed side by side in inviscid supersonic flow of compressible fluid 18 p3024 A67-33540

Soviet book on nonlinear problems of motion of compressible fluid with small disturbances, investigating pressure fronts, neighborhoods of wave fronts, etc 18 p3025 A67-33715

Vector wave functions for boundary value problems in compressible plasma for spherical geometry, noting Fourier series, acoustic wave, etc 18 p3090 A67-34382

Flow analysis of compressible fluid in wake behind body positioned symmetrically with respect to flow direction, using momentum and energy conservation equations 19 p3170 A67-35610

Flow of steady compressible gas expressed in intrinsic relations to derive equations of rotational motions in Euclidean space 19 p3212 A67-35883

Helically symmetric MHD flow of compressible fluid in circular plasma cylinder, considering waves and stability 20 p3492 A67-36132

Compressible inviscid fluid MHD motion, stressing quasi-aligned field 20 p3496 A67-36272

Two-dimensional problem of penetration of subsonic compressible fluid jet into channel solved by modified Chaplygin method 20 p3357 A67-37052

Spherical gas bubble pulsations under pressure waves analyzed in compressible and incompressible fluids 20 p3422 A67-37065

Laminar compressible plane stationary boundary layer flow described by differential equations, including momentum and energy equations 20 p3424 A67-37280

Radiation of monofrequency antenna in compressible magnetoplasma expressing far field as sum of modal plane waves 20 p3388 A67-37701

Invariant transformation for pulse and continuity equations of one-dimensional unsteady motions of ideal compressible fluid 21 p3812 A67-38279

Oscillation and stability of two irregular thin elastic cylindrical shells in potential flow of compressible fluid 21 p3720 A67-38296

Steady state problem solution in linear formulation concerning movable load influence on thin elastic plate on ideal compressible fluid 21 p3720 A67-38300

Variable length foil fluttering in supersonic compressible gas flow, particularly case with end clamping of varying edges 22 p3910 A67-39454

Imbedded magnetic field stabilization effect on infinitely conducting inviscid compressible relativistic MGD half-jet 22 p3850 A67-39706

Flow velocity profile analysis for pressure front steady motion with steady pressure on compressible fluid 22 p3784 A67-39826

Friction and heat flow resistances for three-dimensional compressible laminar gas boundary layer over ellipsoid of revolution at angle of attack 22 p3786 A67-40028

Oscillations of polytropic and compressible cylinders investigated by small perturbation method noting separate mode of gravitational instability 22 p3896 A67-40528

Force defect coefficient method applied to calculation of compressible jet flow discharge for asymmetric two-dimensional orifice 23 p3936 A67-41330

Compressible fluid with finite electrical conductivity in constant magnetic field hitting thin cylindrical obstacle, solving flow motion equations 24 p4199 A67-43080

COMPRESSION

S AXIAL COMPRESSION

S DECOMPRESSION

S METEORITIC COMPRESSION

S PULSE COMPRESSION

COMPRESSION BUCKLING

Ultimate bending moment capability of thin walled pressure stabilized cylinder with typical axial loads demonstrated to be 50

percent greater than bending moment at which compressive wrinkling occurs 03 p0522 A67-13230

Inversion of eccentricity effect in stiffened cylindrical shells buckling under external pressure 04 p0718 A67-15746

Inelastic buckling of rib-cored orthotropic sandwich cylinders under external hydrostatic pressure, evaluating rigidity factor and Poisson ratio 04 p0719 A67-15936

Buckling phenomena involving formation of indentation in thin circular cylindrical shells under axial compression 05 p0907 A67-16021

Stressed and strained state of reinforced cylindrical shell under nonuniform heating and compression, noting three solutions to buckling problem 05 p0913 A67-16190

Linear buckling of circular cylindrical shells under asymmetric axial compressive stress distributions 05 p0922 A67-17103

Anisotropic sandwich constructions characteristics for orthotropic materials used for facings and cores, considering stiffness and buckling 06 p1108 A67-18655

Cylindrical shell stability under axial compression analyzed by generalized power series method, noting half-waves and critical load 07 p1262 A67-19345

Stability of toroidal shell under uniform external pressure solved using series expansion, considering buckling modes 08 p1417 A67-20557

Stability of linear viscoelastic columns with variable cross sections, obtaining and verifying buckling load 08 p1418 A67-20594

Stability of nonprismatic and nonhomogeneous rods under compressive tangential force, calculating critical force and corresponding frequency 10 p1717 A67-22944

Torsional stiffness of ribs effect on buckling strength of longitudinally stiffened plates compressed in direction of ribs 10 p1719 A67-23474

Structural design of stiffened cylindrical shells, discussing minimum weight, prevention of buckling modes, etc 10 p1728 A67-23719

Prebuckling deformations, ring stiffeners and load eccentricity effect on buckling of stiffened cylinders 10 p1727 A67-23759

Critical axial compression buckling loads of orthotropic cylinders having stiffening patterns analyzed, considering three instability failure modes 10 p1728 A67-23760

Unified theory for bending and buckling of honeycomb type sandwich shell and linearized governing equations applied to axially compressed circular cylinder shells 10 p1728 A67-23761

Bifurcation phenomena in spherical shells under concentrated and ring loads taking into account finite prebuckling deformation 10 p1728 A67-23764

Initial postbuckling behavior of spherical shell under external pressure determined using Koiter theory, analyzing effects of imperfections on buckling strength of structures 10 p1730 A67-23835

Axisymmetric buckling of orthotropic circular plates with variable thickness in terms of lateral plate deflection and stress distribution 11 p1876 A67-24660

Ribbed circular cylindrical shell under axial compression, reducing problem to determination of deflection and stress functions 12 p2020 A67-25571

Buckling of thin walled circular cylindrical shells under external pressure treated by Sanders theory 12 p2030 A67-25940

Dent effect on buckling strength of aluminum alloy tubular columns subjected to axial compression [ASME PAPER 67-MET-12] 12 p2030 A67-25951

Stability loss in steel cylindrical shells under axial compression for case of elastic and plastic strains 13 p2219 A67-26904

Interaction between buckling and flutter of circular cylindrical shell subjected to axial compression and placed in axial supersonic flow 14 p2398 A67-28092

Dynamic buckling of ring constrained in rigid circular surface and subjected to transiently applied inertial loading 14 p2398 A67-28093

Plastic buckling of eccentrically stiffened circular cylindrical shells 14 p2399 A67-28121

Column consisting of flexible and rigid

section measured for buckling load, using Southwell method 14 p2404 A67-29057

Buckling of longitudinally reinforced rectangular panel loaded by constant edge shear and longitudinal variable compression 16 p2763 A67-30792

Buckling of compressed thin walled structural sections, noting design concepts and flat plate theories 17 p2957 A67-32025

Filament overwrapped metallic cylindrical pressure vessels show greater efficiency ratio and buckling strength 17 p2958 A67-32054

Imperfections effect on buckling of complete electroformed spherical shells under uniform external pressure examined in rigid and soft testing systems 17 p2960 A67-32454

Stiffener eccentricity effect on critical load in cylindrical shells under axial compression 17 p2961 A67-32775

Axissymmetric plastic buckling of axially compressed cylindrical shells initiated under increasing load 17 p2961 A67-32776

Stability analysis of circular plate submitted to two compressive forces acting along diameter, using Fourier series iteration 19 p3342 A67-35718

Buckling analysis of sandwich beams with elastic orthotropic cores under axial compression 20 p3537 A67-36641

Critical plastic buckling of compressed spar flanges 20 p3537 A67-36642

Critical compression stresses in cylindrical panel with clamped lateral edges and free longitudinal edge 21 p3726 A67-38796

Testing machine effect on buckling load of electroformed cylindrical shells under axial compression 22 p3909 A67-39291

Elastically filled imperfect closed cylindrical shell stability, showing initial configuration defect effects on critical load relation to filler rigidity 22 p3912 A67-39752

Buckling loads in orthotropic circular cylindrical shells under simultaneous longitudinal and external peripheral pressure stresses 22 p3912 A67-39752

Thin circular elastic plate under uniform compressive thrust, with nonlinear boundary value problems involving partial differential equations for buckled states 22 p3916 A67-40525

Bifurcation phenomena in spherical shells under concentrated and ring loads taking into account finite prebuckling deformation 23 p4080 A67-41728

Stress functions for truncated conical shell buckling under uniform static pressure 23 p4081 A67-41760

COMPRESSION LOADING

Linear solutions for large deflections of diamond-shaped frames under compressive loading 01 p0160 A67-10404

Experimental determination of column initial deflection and load eccentricity in aluminum alloy indicate minor magnitude of load eccentricity 01 p0160 A67-10561

Calculation of cylindrical minimum weight stringer shell in axial compression loading 02 p0340 A67-12662

Hardening during plastic deformation of steel samples under compression, deriving stress-strain state in cutting process 03 p0427 A67-13193

Heat transfer through metal to metal joints, determining influence of number of real contact points and compressive load 04 p0735 A67-15854

Dynamic stability of coaxial cylindrical shells in nonuniform temperature field under uniformly distributed axial compression load 05 p0913 A67-16189

Critical stresses of three-layer wing panel compressed by load distributed along two sides, determining temperature stresses in bearing layers and equilibrium equations 05 p0913 A67-16191

Time dependent deflection behavior under compression loads of stiffened panel at high temperatures 06 p1100 A67-18011

Truncated conical shell stability under axial compression loads applied parallel to axis rather than along generatrix 06 p1105 A67-18593

Elastic behavior of bodies composed of materials with different characteristics of compression and tensile strengths, noting applicability of various variational equations 06 p1106 A67-18624

Buckling stability of compressed plate with transverse deflections, using energy

method 06 p1109 A67-18747

Propagation of brittle cracks in body under compression, discussing theory of resistance of brittle bodies to compression 07 p1263 A67-20030

Imperfection sensitivity of eccentrically axial and ring stiffened cylindrical shells under axial compression and hydrostatic pressure 08 p1417 A67-20552

Column compressive tests of aluminum alloy bars, determining load eccentricity and initial straightness deviation 10 p1715 A67-22826

Skin-stiffened compression panel design with digital computer, obtaining optimal solutions for applied stress and local and general stability equation 10 p1726 A67-23720

Integrally formed compression panel efficiencies compared with other aerospace panel concepts 10 p1729 A67-23769

General solutions for linearized three-dimensional equations of elastic stability of medium compressed along one axis 11 p1870 A67-23896

Physicochemistry of substances under impact compression, considering thermodynamic parameters, phase transformation and compressibility curves 11 p1749 A67-24324

Deflection function of glass fiber reinforced circular cylindrical shells under axial supercritical compressive loading 12 p2023 A67-25590

Axissymmetrical deformation and static instability region of circular cylindrical shell under longitudinal compressive load 12 p2026 A67-25615

Lower and upper critical loads measured in process of axial compression of cylindrical shells of glass fiber reinforced resin 12 p2031 A67-25959

Compression load stability of nonuniformly rigid plates within and beyond elasticity limits solved by combined Galerkin and finite difference methods 12 p2031 A67-25961

Stress-strain state of short cylindrical shell and square panel under axial compression hinged along edges 14 p2402 A67-28897

Elastic stability of simply supported uniformly-thin rectangular plate under unequal compressive stresses at two opposite edges due to constant body force 15 p2577 A67-30218

Stability of cantilevered elastic bar with end under compressive follower force, noting shear deformation, rotary inertia and internal damping 17 p2959 A67-32420

Critical compressive forces causing instability of rigidly-fastened rectangular plate determined by method of summary representations 17 p2962 A67-32871

Fiber shells of revolution under compression loads analyzed for use in pressurized balloons 19 p3338 A67-34872

Stability of reinforced thin structurally-orthotropic cylindrical shell problem, discussing rib eccentricity, axial compression load, torsional load, etc 19 p3338 A67-34874

Differential equations and potential for simply supported anisotropic sandwich plate under compression and shear stresses above buckling limit 19 p3341 A67-35575

Matrix method for calculating behavior of rod of constant cross section stressed by bending and stretching or compression loading 19 p3343 A67-35815

Stress-strain state in braces across elliptical hole in elastic plate, obtaining solution for eccentric load 21 p3721 A67-38305

Compression strength analysis of plane and cylindrical multilayer skin panels reinforced by corrugated fillers, determining critical load and local stability loss 21 p3725 A67-38787

Elastic stability of cantilever column having fixed compressive and circulatory nonconservative loadings, determining critical loads 21 p3729 A67-39084

COMPRESSION TESTING

Rapid gas compression technique to produce simultaneous values of pressure and temperature much higher than conventional techniques 04 p0611 A67-15946

Separation of load eccentricity and initial deviation determined through column compressive tests, using aluminum alloy bars and strain gauges 05 p0919 A67-16588

High temperature effect on strength of

solidified resins and resin based materials, determining loss of weight, density, compression strength, permittivity and electric conductivity 05 p0833 A67-17098

Shape of interaction curve for axial compression vs torsional buckling of conical shells 06 p1110 A67-18858

Wall thickening of aircraft structural components by compression of blanks to produce counter force 07 p1191 A67-19749

Aircraft hollow control rods with threaded joints noting compression and testing 07 p1192 A67-19753

Compressed air gun for impulsively loading structures, measuring response by high speed photographic technique 08 p1414 A67-20374

Compression strength and strain of solid propellants, noting internal loads developed during burning process 08 p1373 A67-20720

Structure and mechanical properties of extruded Ni-Al-oxide cermet materials, noting high compression strength 09 p1517 A67-21876

Column compressive tests of aluminum alloy bars, determining load eccentricity and initial straightness deviation 10 p1715 A67-22826

Diffusion bonding of titanium sandwich structure for Saturn tank wall application 10 p1661 A67-23702

Cylindrical wave propagation in rarefied plasma, examining effect of compression on internal plasma-magnetic field by external field 11 p1842 A67-24964

Stress-strain state of thin walled zero moment shell under uniformly distributed multiple load assuming various tensile and compression strengths 12 p2020 A67-25569

Shock wave compression effect on low carbon steels, noting hardness-explosive correlation 12 p1957 A67-26117

Microstrain c-axis compression test on two Be-4.37 wt percent Cu crystals, detecting nonbasal pyramidal slip system and compression twinning 13 p2137 A67-27114

Heat resistant stainless steel honeycomb cores for cylindrical applications, measuring energy absorption characteristics [ASME PAPER 67-DE-14] 14 p2402 A67-28870

Vacuum effect on oven-dried balsa wood strength 15 p2507 A67-29554

Dispersed aluminum oxides effect on size of nickel grains in sintered or extruded nickel-aluminum oxide cermets, studying compressive strength dependence 17 p2871 A67-31924

Empirical equations for compressive properties of liquids, noting applicability at high pressures 17 p2841 A67-33386

Compression tests with superimposed hydrostatic pressure to study rheological behavior of elastomer filled with granular potassium chloride 18 p3142 A67-33891

[SESA PAPER 1224] 18 p3142 A67-33891

Flow stress of aluminum related to strain, strain rate and temperature, discussing compression testing machine and results 18 p3064 A67-34078

Metal matrix composites compression-microstrain behavior at room temperature, discussing stress-strain curve, Youngs modulus, yielding, etc [ASTM PAPER 6] 18 p3067 A67-34571

Compression tests with superimposed hydrostatic pressure to study rheological behavior of elastomer filled with granular potassium chloride 19 p3340 A67-35465

Surface morphological changes of tantalum single crystals during plastic deformation, studying orientation dependence of yield stress in tension and compression 19 p3245 A67-35727

Mechanical characteristics of materials determined using circular bending 20 p3537 A67-36476

COMPRESSION WAVE

Identical particles gas with velocities distributed regularly in plane, analyzing compression and relaxation waves present in six- and eight-velocity models 01 p0051 A67-10228

Stimulated Brillouin scattering in shock-compressed acetone 01 p0116 A67-10338

Pressures and temperatures occurring in jet engine exhaust nozzles during speed changes on basis of compression and detonation wave theory 01 p0141 A67-11150

Transverse wave induced surface, compression and transverse waves in plasma, deriving expressions for amplitudes, phases

- and energies 04 p0663 A67-14744
- One-dimensional steady solutions for shock wave propagation in class of nonlinear viscoelastic materials deduced from stated balance laws and representation theorem for compressive and expansive motions 09 p1576 A67-22410
- Dynamic problem of shell of revolution in axial rotation under action of plane compression wave 12 p2020 A67-25568
- Formation of compression shocks in calorically ideal real gases with thermodynamic relaxation analyzed in closed form 13 p2094 A67-26636
- Separated compression shock circulation in front of wedge profiles at high Mach numbers 13 p2049 A67-26640
- Similarity solutions derived for describing propagation of strong compression shock in transversely expanding gas 13 p2094 A67-26643
- Buildup of waves to shocks and subsequent weak shock wave propagation 13 p2166 A67-26647
- Numerical analysis of structure of one-dimensional unsteady magnetic compression waves propagating into collisionless plasma, using motion equations 16 p2719 A67-31232
- Experimental determination of compression and rarefaction shock waves structure causing high pressure phase formation and decay in potassium halides 23 p3989 A67-40906
- COMPRESSOR**
- SA AXIAL COMPRESSOR
- SA AXIAL FLOW COMPRESSOR
- SA CENTRIFUGAL COMPRESSOR
- SA DATA COMPRESSOR
- SA FAN
- SA MULTISTAGE COMPRESSOR
- SA SUPERSONIC COMPRESSOR
- SA TRANSONIC COMPRESSOR
- Fatigue life index as criterion for comparison of predicted life of proposed compressor with that of another compressor with known industrial performance [ASME PAPER 66-WA/MD-10]
- Cascade flow through compressor guide vanes and flow separation at top of vane profiles 05 p0750 A67-17323
- Leakage and optimum film thickness of gas lubricated high-pressure mainshaft seals for jet engine compressors 10 p1658 A67-22705
- Erratic vibration peaks, recognized as variable acoustic resonance, during tests of jet engine compressors [ASME PAPER 67-VIBR-57]
- Jet compressors for closed Brayton cycle MPD to study momentum transfer of two high velocity gas or vapor streams of very different molecular weight 16 p2604 A67-30568
- Aerodynamic characteristics of plane compressor cascades with high subsonic flow analyzed, noting application in determining flow deflection angle and pressure loss coefficient 20 p3358 A67-37079
- Geometric parameters effect on aerodynamic characteristics of plane compressor cascade with high subsonic flow 20 p3358 A67-37080
- Motion and thermodynamic conditions of free piston ballistic compressor test gas taking into account gas leakage, viscous friction and heat losses 22 p3778 A67-39351
- COMPRESSOR BLADE**
- Axial compressor blade design for improvement of strength and vibration characteristics 01 p0006 A67-10545
- General and mechanical property requirements for metal matrix composite materials used for aircraft gas turbine compressor blades 03 p0443 A67-13418
- Strains in twisted blades with rectilinear axes, examining general relations and parameters in postulated new theory 03 p0528 A67-14080
- Torsional constraints in calculation of vibrational frequencies of compressor blade 03 p0528 A67-14081
- Noncavitating water flow tests of three loaded axial flow pump rotor blades [ASME PAPER 66-WA/FE-24]
- Vibration modes, stress distribution, natural frequency and failure points in pin-fixed compressor blades [ASME PAPER 66-WA/GT-4]
- Compressor blade vibration, discussing prediction of amplitudes of vibration and interpretation of results of engine strain gauge tests in terms of component service life [ASME PAPER 66-WA/GT-14]
- Oscillogram interpretation during ultrasonic inspection of turbine and compressor blades 06 p1007 A67-18098
- Stress distribution in dovetail compressor blade joint analyzed using frozen stresses method 08 p1424 A67-21335
- Isolated compressor blade within framework of lifting line theory, expressing drag produced by tip-gap in terms of flow rate and wing loading 09 p1437 A67-21739
- Precision rolling for fabrication of small gas turbine compressor blades for use in aircraft and stationary engines [SAE PAPER 670095]
- Impact and abrasion wear of axial and centrifugal helicopter compressor stages due to dust intake, showing direct proportionality to impact velocity and particle size 11 p1853 A67-24531
- Transonic axial flow compressor blade profile design, with incidence and deviation rules incorporating thickness and Mach number effects [ASME PAPER 67-GT-47]
- Compressor blade failure due to material fatigue, using destructive testing in stationary rig 12 p2014 A67-25413
- Semiconductor piezoresistive strain gauges and application to compressor blade vibratory stresses measurement 12 p2014 A67-25416
- Vibration characteristics of turbine and compressor blading under rotation 12 p2015 A67-25418
- Noncontacting device for compressor-blade vibration measurement supplying data on all blades of one stage 15 p2545 A67-29165
- High strength Ti alloys in development of compressor blades, considering yield strength, impact energy absorption, ductility, fracture toughness and fatigue resistance [SAE PAPER 670335]
- Compressor blade vibration, discussing prediction of amplitudes of vibration and interpretation of results of engine strain gauge tests in terms of component service life [ASME PAPER 66-WA/GT-14]
- Axial compressor blades considered as thin walled elastic shells studied for vibration forms, frequencies, stress distribution and blade geometry change effects 19 p3235 A67-34882
- Soviet papers on aerodynamic characteristics of blade compressors and jet engines 20 p3358 A67-37078
- Compressor blade flutter stability in separating flow with external perturbations analyzed, using digital computer 20 p3517 A67-37488
- Plane compressor cascades, comparing small and large aspect blades and studying aspect ratio effect 21 p3564 A67-38045
- Self-oscillations of axial compressor blades, taking into account variation in natural frequency of flexural vibrations between blades 21 p3727 A67-38835
- Aerodynamic damping of turbine buckets and compressor blades noting flutter and frequency shift 23 p3927 A67-40669
- Glass fiber reinforced gas turbine engine compressor blade thermal stability for short cycle heat stress damage 24 p4249 A67-42103
- Lifting line theory for blade cascade in subsonic shear flow, noting compressibility effect dependence on harmonic mean upstream Mach number 24 p4091 A67-42204
- Vibration modes, stress distribution, natural frequency and failure points in pin fixed compressor blades [ASME PAPER 66-WA/GT-4]
- Noncavitating water flow tests of three loaded axial flow pump rotor blades [ASME PAPER 66-WA/FE-24]
- Compressor efficiency 24 p4143 A67-42465
- Mechanical properties and corrosion resistance of titanium alloy forgings used as compressor parts 01 p0093 A67-10546
- Compressor cascades with different irregularities in forward flow, noting special case of low aspect ratio blades 02 p0179 A67-12439
- Parametric analysis of supersonic compressors, determining relative efficiencies of various leading and trailing guide vane configurations 03 p0352 A67-13010
- Working diagrams, performance characteristics and loss mechanisms of ejector and compressor for mixing two liquid or two gas streams respectively 03 p0353 A67-14305
- Computer program for analysis of off-design performance characteristics of axial flow compressor [ASME PAPER 66-WA/GT-1]
- Limitations on specific outputs and compression ratio per stage in supersonic compressors 05 p0874 A67-16746
- Perturbation technique based on hydraulic analogy for estimating optimum efficiency and performance of axial flow compressor from description of geometry and aerodynamic environment 09 p1560 A67-22491
- Effect on stage characteristics of axial compressor of design procedure used for slightly elongated vanes 10 p1897 A67-23021
- Growth and operational capabilities of turboprop and reciprocating engines [SAE PAPER 670236]
- Attenuation of circumferential inlet distortion in multistage axial compressors, predicting flow field and pressure distortion via zero axial clearance approximation [AIAA PAPER 67-415]
- Plane compressor and guide vane cascades design, deriving relations for angle of attack, angle of lag, etc 20 p3358 A67-37081
- Computer program for analysis of off-design performance characteristics of axial flow compressor [ASME PAPER 66-WA/GT-1]
- Blower compressors for high altitude pressure and climate regulation in commercial aircraft 24 p4109 A67-42709
- COMPRESSOR ROTOR**
- SA TURBINE WHEEL
- Dynamic rubber wheel model to supplement digital computer analysis for prediction of frequencies, mode shapes and stress distributions of vibrating rotor stages [ASME PAPER 66-WA/GT-8]
- Control of multishaft jet engines, discussing compressor geometry, afterburner and engine fuel flow, nozzle area effects, etc [SAE PAPER 670139]
- High temperature testing and evaluation of graphite helical-screw expanders and compressors for use with inert gas Brayton cycle 15 p2492 A67-29427
- Book on design and structural strength of aircraft gas turbine engines covering inlet and exhaust systems, compressors, combustion chambers, rotors, etc 17 p2928 A67-32564
- Three-dimensional flow across supersonic single rotor axial compressor subsonic at rotor entry and exit 24 p4092 A67-42661
- COMPTON EFFECT**
- Double crystal spectrometer measurement of X-ray Compton and thermal scattering accompanying Bragg reflection from Si and Ge single crystals 01 p0132 A67-10456
- Inverse Compton effect in causing energy loss of electrons in quasi-stellar objects 03 p0508 A67-14325
- Inverse Compton effect in models of quasi-stellar objects demonstrated to be independent of magnetic field 04 p0701 A67-15544
- Inverse Compton effect limits possible mean energy of relativistic electrons, thereby restricting quasar models 04 p0702 A67-15942
- Diffuse omnidirectional inverse Compton and synchrotron X and gamma radiation from cosmic distributions of fast electrons and thermal photons 05 p0882 A67-16404
- Inverse Compton effect in quasi-stellar source and relativistic electron distribution 05 p0898 A67-16924
- Experimental verification of predictions of conventional quantum electrodynamic vacuum effects by Compton and other scattering techniques 09 p1534 A67-22021
- Compton effect produced by thermal photons on relativistic electrons in solar atmosphere 12 p2002 A67-25528
- Plasma-radiation interaction represented

- by Compton effect, utilizing Boltzmann term developed according to powers of perturbation caused by electron motion 13 p2165 A67-26598
- Anomalies in intensity of Compton diffusion of X-rays by vanadium noting energy-diffusion angle relation 13 p2181 A67-27210
- Nonthermal X-ray radiation accompanying solar flares, comparing spectral power of synchrotron radiation, Compton radiation and bremsstrahlung as possible generation mechanisms 15 p2549 A67-29141
- Electron-photon cascade process in intergalactic space, noting role of microwave radiation in gamma ray astronomy 15 p2550 A67-29750
- Renormalization theory and Compton scattering of electron interacting with monochromatic LF polarized light beam 17 p2870 A67-33365
- Nuclear radiation damage to circuits noting Compton effect, ionization current effects, resistance drops, electron-hole pair formation, etc 24 p4132 A67-42702
- Nonthermal X-ray radiation accompanying solar flares, comparing spectral power of synchrotron radiation, Compton radiation and bremsstrahlung as possible generation mechanisms 24 p4222 A67-43064
- COMPUTATION**
- SA INTERPOLATION
- Systemic computational technique for designing specific optimal controller, considering performance index 02 p0226 A67-12155
- Computation difficulty in optimal control law for dynamical system, noting three optimal conditions 10 p1619 A67-23419
- Computational errors in generation of direction cosine matrix in strapdown system 15 p2515 A67-29741
- Computer theory and physics field relationship noting signal mechanics, geometry, logical networks, etc 19 p3202 A67-35606
- COMPUTER**
- SA ANALOG COMPUTER
- SA CONTROL SIMULATOR
- SA COUNTING RATE COMPUTER
- SA CRYOGENIC COMPUTER
- SA DATA PROCESSING
- SA DATA TRANSMISSION
- SA DIGITAL COMPUTER
- SA FINITE-STATE MACHINE
- SA HYBRID COMPUTER
- SA IBM 7040 COMPUTER
- SA IBM 7090 COMPUTER
- SA IBM 7094 COMPUTER
- SA INFORMATION RETRIEVAL
- SA PARAMETRON
- SA UNIVAC 418 COMPUTER
- SA VOCODER
- IEEE Region III Convention, Atlanta, April 1966 01 p0045 A67-10664
- Mark XII and XIV microcircuit computers for real-time navigational computation on military and civil aircraft 01 p0029 A67-10668
- Reactive display system for optimum man/computer communication with time-sharing capabilities 01 p0029 A67-10670
- Computer display and control system for launch vehicle test operation 01 p0050 A67-10672
- Rolls-Royce use of computers in engineering, manufacturing and marketing operations 01 p0031 A67-11199
- Pneumatic intermittent-action computers using linear controlled resistance 03 p0375 A67-13598
- Computer dictionary and handbook 04 p0579 A67-15947
- Advances in computers, Volume 7 07 p1148 A67-19657
- Interspecies communication involving human and mammalian brain as computer with programs and metaprograms [AAS PAPER 66-77] 07 p1135 A67-20000
- IEEE Aerospace Computer Symposium, Santa Monica, October 1966 08 p1296 A67-20624
- Nortronics NDC-1051 computer design and performance for military airborne applications 08 p1296 A67-20625
- IBM System/4 PI Model EP data processor design and performance 08 p1297 A67-20626
- Electrical and electronics engineering - IEEE Conference, Jackson, Mississippi, April 1967 13 p2085 A67-26404
- Pneumatic intermittent-action computers using linear controlled resistance 03 p0375 A67-13598
- Geophysical theory and computers - Conference, Cambridge, England, June-July 1966 20 p3432 A67-37204
- COMPUTER DESIGN**
- Digital computers for navigation and guidance solving design problem by combining general purpose /GP/ and digital differential analyzer /DDA/ approaches to produce hybrid computer 01 p0111 A67-11258
- Modularized simulation system to develop generalized digital flight simulation program for use on Titan III mission, emphasizing functional design 02 p0228 A67-11804
- Open-shop remote computing terminal system using direct coupled system of IBM 7094 and 7040 computers for core-to-core transmission, discussing experience gained from using and managing it 02 p0206 A67-11805
- Univac 418 real time executive computer design having storage speeds of 2 and 4 microseconds 02 p0206 A67-11806
- Simple gates, multilevel arrays and interconnection in integrated circuits for computers 02 p0219 A67-12110
- Shared memory computer display system provides test bed for man-machine interaction, noting hardware and software design concepts 03 p0375 A67-13633
- Mariner IV Space Data Automation System /SDAS/ computer reliability design, pellet component concept, testing, interconnection and welding techniques 05 p0777 A67-17254
- Apollo computer design mechanical packaging, implementing heat and vibration model to conduct thermal vibration and sealing tests 05 p0814 A67-17460
- Man-computer graphics for computer aided design 05 p0768 A67-17514
- Data processing and control by spaceborne computer on instrumentation satellite used for analyzing space scientific properties, noting factors influencing system design 05 p0768 A67-17516
- Analog/hybrid computer design, noting inclusion of solid state and integrated circuits for reliability cost reduction and speed 05 p0769 A67-17519
- Applications of computer generated displays, technologies and systems design in man-machine interaction 05 p0769 A67-17520
- Apollo guidance and navigation by computer holding fixed program with diverse and flexible applications 05 p0809 A67-17550
- Partial redundancy for improved reliability of computing machine [JPL-TR-32-1088] 07 p1153 A67-19604
- LSI effect on aerospace computer design, considering cost, size and power consumption of logical elements 08 p1297 A67-20635
- LSI application to computer design using functional partition of control and data path structures 08 p1298 A67-20636
- Multithreading design of reliable aerospace computer, showing inverse proportionalities between speed capacity and reliability 08 p1298 A67-20667
- Stress-strain diagrams under dynamic conditions obtained by processing strain gauge data, using analog computer 09 p1492 A67-21560
- Computer logic device development, discussing interdependence of various components and packaging methods 09 p1468 A67-21683
- Computer packaging technology, discussing form lead joining, interconnection, maintainability, handling, etc 09 p1467 A67-21684
- Integrated circuit general purpose computer for use in aerospace guidance 09 p1469 A67-22174
- Design, redundancy, reliability and tradeoffs for Launch Vehicle Digital Computer and Data Adapter /LVDC/LVDA/ for uprated Saturn I and V vehicles, noting logic circuit, memory, input/output, power supply 09 p1469 A67-22301
- Mathematical formulae for yielding storage requirement and work loadings to provide requirement to computer designer for traffic conditions in controlled area 09 p1531 A67-22654
- Multipurpose satellite computer for data processing 10 p1608 A67-22974
- Book on applied kinematics covering synthesis techniques for link-and-cam motion other than uniform rotation in high speed
- high performance automatic machines 11 p1795 A67-23921
- IBM System/360 Model 91 systems design using decomposition algorithm and three-cycle multiplication 11 p1755 A67-23948
- IBM System/360 Model 91 machine organization alleviating disparity between storage time and circuit speed 11 p1755 A67-23949
- High speed floating-point algorithm of IBM System/360 Model 91 for exploiting multiple execution units 11 p1755 A67-23950
- Floating point execution unit of IBM System/360 Model 91, emphasizing design of instruction oriented units to reveal techniques employed to match burst instruction rate of one instruction per cycle 11 p1755 A67-23951
- IBM System/360 Model 91 storage system design concepts 11 p1755 A67-23952
- Aerospace computer hardware, discussing general purpose requirement on basis of various computer designs 11 p1755 A67-24247
- Man-Computer Graphics /MCG/ allows operator control through oscilloscope via light sensitive pen 11 p1756 A67-24251
- Computer programming or software techniques in relation to hardware elements of computer graphics system [ASTME PAPER WES-7-02] 11 p1756 A67-24253
- Cryoelectric memory loop cell and hybrid organization system noting economy, high speed, mass storage, etc 12 p1915 A67-25887
- Simulation of dynamic performance of pneumatic rebound-nozzle signal converters by analog computer 13 p2056 A67-27240
- Computer aided design and reliability engineering /CADRE/ applied to data processing associated with communications equipment components and subassemblies 13 p2072 A67-27446
- Integrated circuit interconnection system design exemplified by 920 M digital computer 14 p2274 A67-28025
- General purpose digital computer for airborne and spaceborne guidance and navigation systems 14 p2275 A67-28684
- Management aspects of technological capability within large hardware systems business 14 p2409 A67-28697
- Humidity, temperature, contamination and disconnection effects on gasket and grease seals for extended space mission computer connectors 15 p2442 A67-29182
- Discretionary wiring method and polycell approach to large scale integration 15 p2444 A67-29456
- Abel integral inverter discussing design, construction and performance of analog computer for solution of Abel integral equation 16 p2634 A67-31428
- Trends in digital flight simulation for training 17 p2833 A67-32489
- F-111 MK 2 avionics system evaluation and parameter tradeoff considerations 17 p2819 A67-32499
- IBM CP-2 militarized digital computer noting design, maintainability and performance 17 p2820 A67-32500
- Iterative on-line reliability calculation of automatically repaired space computer, noting reliability and performance 17 p2820 A67-32501
- Cost effectiveness criterion for instruction repertoire selection for aerospace computer 17 p2820 A67-32502
- Organizational techniques and trade-offs for low power operation in spaceborne data processing systems 17 p2820 A67-32503
- Random pulse operation and random pulse machines structural requirements, with continuous variable dependent on certain sampling time 18 p3006 A67-34063
- Pattern recognition machine construction and design, using reading machine as example 18 p3006 A67-34383
- Digital computing complex optimum configuration for future aircraft, discussing computer role 19 p3186 A67-35311
- Collection of articles on computer advances, volume 8 19 p3186 A67-35677
- Time-shared computer system design and application, noting memory, remote terminals, program debugging, etc 19 p3186 A67-35678
- Computer Conference, American Federation of Information Processing Societies, San Francisco, November 1966 19 p3187 A67-36053
- Computer program utilizing graphic data

processing system for mask artwork design of hybrid integrated circuits 19 p3188 A67-36061

Automated logic design techniques for integrated circuitry technology, with wafer design and logic arrays described for different logic functions 19 p3189 A67-36062

Fast thin film main memory system design noting 200 nsec cycle time and 160 nsec access time 19 p3189 A67-36063

Rotationally switched rod memory system with 100 nsec cycle time, discussing cost and performance factors 19 p3189 A67-36064

High speed computer memory design using plated wire elements 19 p3189 A67-36065

Integrated circuit memory with 64 eight-bit words and compatible with high speed current-mode gates for high speed computers 19 p3189 A67-36066

Static and dynamic electronic memories used in data processing systems 20 p3390 A67-36250

Modulo control algorithms application in circuit for finding residues 20 p3392 A67-37153

Computer technology - Conference, University of Manchester, England, July 1967 20 p3392 A67-37455

Computer interconnection resistance causing propagation delay in circuits, suggesting low temperature use as possible remedy 20 p3393 A67-37457

System effectiveness analysis with particular attention to availability, concepts and sample results 21 p3734 A67-38184

Satellite automatic telemetry data processing system, noting development of high speed computer for real time 21 p3588 A67-38638

Digital computers in spacecraft control complexes analyzed for design specifics, determining processors composition 22 p3764 A67-39169

Design characteristics of IBM 9020 system to provide automated aids for processing and updating flight information 23 p3976 A67-41057

Man-computer system for aircraft design and manufacture emphasizing graphic and analytical routines [AIAA PAPER 67-898] 24 p4127 A67-43007

COMPUTER METHOD

Observations of 24 comets, 11 minor planets and Jupiter VIII, using computer 01 p0148 A67-10386

Network analysis by digital computer covering methods and programs for ladder networks, nodal, electronic circuit and state variable analysis, etc 01 p0028 A67-10462

Cost effectiveness of optimum military aircraft system, evaluating design alternatives in hardware and support concepts via Monte Carlo simulation and high speed digital computers [AIAA PAPER 66-786] 01 p0009 A67-10530

Analog computer solution of simultaneous systems of linear algebraic equations, based on modified Gauss-Zeidel method 01 p0105 A67-10542

Automatic and manual testing compared within framework of integrated testing system [SAE PAPER 660694] 01 p0050 A67-10622

Computer welding skate for automatic gas tungsten-arc welding of contoured or double-contoured parts, providing control without touching work surface with transducers 01 p0081 A67-11040

Measurement systems control in rocket engine testing via real-time surveillance, computation, error correction and graphic display 01 p0076 A67-11144

Numerical trajectory optimization method based on indirect and direct approaches for computer of limited memory 01 p0046 A67-11205

Control system analysis and design using parameter space method 01 p0047 A67-11216

Improved Monte Carlo method for calculating steady state monatomic rarefied-gas flows, using computer for calculating possibility of collision in given geometrical cell 01 p0055 A67-11292

Methods, schedules and cost of applying computer technology to circuit design, including Apollo and LEM programs 01 p0031 A67-11335

Data and mission analysis in man-rating of Gemini launch vehicle 01 p0155 A67-11347

Computing Machinery Association, National Conference, Los Angeles, August-September

1966 02 p0206 A67-11798

MECCA /mechanized catalog/ system designed to produce printed library catalogs and to generate data bank for later machine retrieval 02 p0207 A67-11812

Design Language I, prototype computer-aided design system that blends graphic techniques with console written language 02 p0207 A67-11813

Kantorovich theorem, Goodman-Lance method and two-point boundary value problems, noting numerical results obtained on IBM 7094 computer 02 p0259 A67-11836

Computational method for determination corridors of launch vehicle trajectory and impact dispersions [AIAA PAPER 66-483] 02 p0325 A67-11941

Optimal feedback control for finite state systems with suitable performance criterion, using maximum principle applied to time-sharing computer systems 02 p0227 A67-12172

Abstraction problem in pattern classification, using algorithms with convergence properties 02 p0208 A67-12173

Thermal emissivity and absorptivity of trapezoidal grooves and paneled tubular radiators, obtaining parametric relations by numerical solutions via computer 02 p0342 A67-12331

Orbital resonance caused by tesseral harmonics, examining perturbations of synchronous satellite in eccentric orbits 02 p0328 A67-12400

Discrete method strength calculation for round cylindrical shells applicable to computer solution of normal external loading problems 02 p0339 A67-12442

Computer algorithm for framework diagram in synthesizing thin walled shells strengthened by ribs 02 p0340 A67-12443

Linear equations solving methods on analog computers where system parameters are reproduced, using potentiometers and admittances 02 p0209 A67-12683

Perturbed trajectories computation in earth-moon system by replacing gravitational forces with single inverse square force 02 p0330 A67-12717

Interatomic force model calculation of shear and tensile strengths, predicting stress-strain curves for crystal structures 03 p0495 A67-13532

Computer role in electronic systems design for higher reliability at lower cost 03 p0375 A67-13712

Computer and curve tracer method to generate photo masters for printed circuit microwave antennas, transmission lines and filters 03 p0383 A67-13790

Computation of electric conductivity in sunspots and photosphere from empirically determined linear logarithmic relation 03 p0511 A67-13814

Driving point impedance of asymmetrical dipole using computer method 03 p0385 A67-13861

Computer calculations permitting investigation of time characteristics of radiation in investigation of laser with passive cell 03 p0438 A67-13962

Second order autonomous differential equation stability and boundedness obtained, using computing algorithm based on tracking function method 03 p0376 A67-13987

Computer derivation of best-fit hyperbolic and parabolic surfaces using total parameter variation method 03 p0388 A67-14122

Book on Monte Carlo method, method of statistical trials 03 p0462 A67-14256

Computer aided circuit design, synthesis, analysis, optimization and fabrication 03 p0376 A67-14276

Numerical method for estimating capacity of arbitrary surface noting relation to Dirichlet problem 03 p0462 A67-14342

Computational model for predicting unsteady aerodynamic loads of rotor blades divided into spanwise segments 04 p0545 A67-14490

Elasticity and shell theory solutions for long circular cylindrical shells compared by numerical analysis 04 p0709 A67-14811

Computer investigation of approach of Comet 1759 III to Jupiter before perihelion passage, considering possibility of capture by Jupiter 04 p0701 A67-15450

Approximate method for solving elastic equilibrium problems of shallow shells with holes, using computer 05 p0916 A67-16224

Computer method for predicting servo

positioner performance 05 p0753 A67-16235

Simulation of controlled diffusion-type Markov processes applied to two stochastic equations related to problem of misadjustment on analog computer 05 p0768 A67-16263

Numerical algorithm for supersonic gas flow past blunt bodies with shock wave separation, using Dorodnitsyn method of integral correlation 05 p0791 A67-16374

Computer solution of Cauchy problem of ordinary differential equations in form of Taylor series 05 p0834 A67-16377

Approximate computer method solution to impact problem of elastoplastic wave reflection from flexible plates in resisting medium 05 p0919 A67-16495

Thin film refractive index and thickness calculated by ellipsometry 05 p0847 A67-16796

Bang-bang control for feedback systems, applying computer to optimization of switching time from state to state of linear systems 05 p0784 A67-16854

Automatic telemetry checkout station for Saturn V systems using real time signal digitizer and general purpose computer 05 p0789 A67-17044

Real time approximation of continuous system performance on digital computer using difference equations obtained from digitized transfer function 05 p0768 A67-17518

Parametric analysis, penalty-effectiveness tradeoff and system selection for communications satellites, using block digital computer synthesis with subroutines for operational requirements [AIAA PAPER 66-330] 06 p0960 A67-17693

Computational methods in stellar dynamics noting n-body problem approach, continuum technique and statistical method 06 p1081 A67-17780

Mathematical analysis of jet flap with high lift coefficient, solving numerically integral equation obtained from boundary value problem [AIAA PAPER 67-2] 06 p0938 A67-18247

Computer experiments related to chemical propulsion such as chemical kinetics, fluid dynamics, transport process, shock and detonation phenomena, combustion, etc [AIAA PAPER 67-7] 06 p1114 A67-18250

Histogram construction via algebraic Monte Carlo method, determining simultaneous effect of several input statistical variables on output variable [AIAA PAPER 67-210] 06 p1024 A67-18326

Generalized Stodola iteration method for computer analysis of axisymmetric buckling of ring-stiffened orthotropic shells of revolution [AIAA PAPER 67-109] 06 p1103 A67-18339

Regularization of motion equations in computation of vehicle trajectory going near singularity [AIAA PAPER 67-26] 06 p1087 A67-18464

Automatic telemetry checkout station for Saturn V systems using real time signal digitizer and general purpose computer 06 p1089 A67-18861

Ion extractor system for electrostatic thrusters designed, using salient features of digital computer and electrolytic tank analog methods 06 p1075 A67-18877

Vertical velocities in atmospheric front motions, noting pressure and temperature field distributions and application of computer to solve obtained equations 07 p1219 A67-19356

Trajectory possibilities for Venus swingby mission and role in manned exploration of Mars [AIAA PAPER 66-37] 07 p1248 A67-19363

Internal ballistic considerations in hybrid rocket design, noting throttling and regimes of operation involving effects of surface-or gas-phase reaction kinetics [AIAA PAPER 66-628] 07 p1240 A67-19377

Man-machine interaction in visual displays of computer output 07 p1148 A67-19658

Nonlinear PDE for magnetostatic field with variable permeability in discontinuous medium solved with digital computer 07 p1132 A67-19795

Lunar Module evaluation and test using analog and hybrid computer simulation with LM guidance and control hardware [AIAA PAPER 67-232] 07 p1164 A67-20056

Astronaut performance evaluation in Lunar Module hover and landing, separation and docking simulation

- [AIAA PAPER 67-249] 07 p1165 A67-20067
Poles and zeros of amplifier transfer functions using digital computer, noting role in network analysis 07 p1157 A67-20091
Solar radio noise storm model, determining intensities for various frequency separations 07 p1256 A67-20169
Error analysis of direct solution of linear equations with computational errors expressed as perturbations on data 07 p1149 A67-20197
IR spectroscopy using Michelson interferometer coupled with computer and wave analyzer 07 p1190 A67-20272
Solid propellant polymeric binder chemistry and high speed computer calculations of performance characteristics 08 p1373 A67-20875
Integrated circuit in optimal design of aerospace systems, discussing potential low cost and use in computer analyses of circuits 08 p1303 A67-21060
Velocity spread on modulated electron beam of finite diameter analyzed as function of drive, drift length and pervance 08 p1362 A67-21298
Soviet book on numerical solution of nonlinear boundary value problems for differential equation systems, determining eigenvalues and eigenfunctions 08 p1349 A67-21337
Solution of ill-conditioned linear equations when matrix of coefficients is not sparse or otherwise specialized, noting error analyses of elimination methods 09 p1468 A67-22045
Givens-Householder method for computing eigenvalues and eigenvectors of real symmetric matrix 09 p1468 A67-22046
Computing methods and techniques in aircraft testing, discussing measurements, application of mathematical statistics, etc 09 p1469 A67-22455
Measurement and control methods in aircraft-instrument-pilot loop, noting human limitations in possibilities of automation computer applications 09 p1457 A67-22459
Data handling systems, describing apparatus for processing of analog time varying signals in computer 09 p1501 A67-22466
Computerized decision making for air traffic control 09 p1528 A67-22631
Fourier series and integrals in analog, digital and hybrid computation 09 p1470 A67-22667
Meteorological data classification system using computer based level logical-tree method 10 p1676 A67-22820
Automatic control with prediction, discussing optimal least time systems for trajectories satisfying maximum principle 10 p1608 A67-23322
Inertialess polarization energy of charge interaction between neighboring lattice points in Ge crystal, using M-20 computer 10 p1695 A67-23657
Skin-stiffened compression panel design with digital computer, obtaining optimal solutions for applied stress and local and general stability equation 10 p1726 A67-23720
Numerical technique for time dependent calculation of two incompressible fluids interaction to study viscous and inviscid Rayleigh-Taylor instability 11 p1774 A67-23859
Derivation and computer method solution of equations describing thermodynamic equilibrium of gaseous products from oxidative combustion of methane 11 p1881 A67-24023
Computer method study of reflection and transmission coefficients in VLF range, noting effect of ionospheric D region electron density profiles 11 p1752 A67-24219
Computer application to aerospace missions, discussing operation and equipment parameters, reliability, man-machine interaction, etc 11 p1756 A67-24248
Computer solution of barotropic vorticity equation for weather forecasting 11 p1816 A67-24330
Finite difference network model method with error tolerance for spacecraft heat transfer calculation 11 p1883 A67-24356
Restoration of digitized turbulence-degraded images by corrective processing of harmonic representation according to measured optical transfer function 11 p1789 A67-24414
Computation of optimal estimators synthesis reduced through partitioning of system state vector 11 p1764 A67-24443
One-dimensional model of stellar system evolution, using computer to calculate minimum energy configuration 11 p1862 A67-24500
Space-time correlations of turbulent field measured by grid using high speed computer 11 p1780 A67-24541
Automatic technique of root location and determination of nth order polynomial equation using simple linear computing elements 11 p1756 A67-24639
Computer analysis of curve for total emission from group of separate localized emission points on surface of high vacuum metallic cathode 11 p1820 A67-24922
Bearing mounted shaft-rotor system noting harmonic and stable whirl characteristics 12 p1949 A67-25409
Computer iteration scheme for calculating arbitrary hyperbolic transfer orbit in field of attracting center, based on Gaussian equations 12 p2002 A67-25640
Environmental operations analysis function, discussing data accumulation, storage and retrieval 12 p1921 A67-25678
Relay testing under operational voltages and currents, discussing timing circuits and sequencing and computer inputs outputs 12 p1922 A67-25698
Modified perceptron procedure for nonseparable cases, minimizing error probability and introducing reinforcement factors 12 p1961 A67-26064
Computer calculation of noise temperature of high gain antennas, noting application to design and analysis of paraboloidal and Cassegrain systems 12 p1917 A67-26195
Electron generator with oscillatory anode circuit nonlinear differential equation analyzed by linearizing, applying algorithm to obtain computer solution 13 p2144 A67-26393
Computer analysis, design and optimization of linear electronic networks 13 p2088 A67-26747
Medical testing, research and control during manned space flights, discussing diagnostic algorithms for onboard computer and frequency of data collection 13 p2062 A67-26762
Electric field distribution in p region, space charge layer and n region of p-n abrupt junction germanium diode at room temperature 13 p2078 A67-26788
EEG baselines covering wide range of states of wakefulness and sleep in astronaut candidates estimated by computation and pattern recognition techniques 13 p2062 A67-26921
Phaseplot, on-line graphical output parametric display technique, noting hardware realizations and software requirements 13 p2073 A67-27063
Computer-implemented minimization techniques used to determine realizability of N-variable switching function with single threshold-element device 13 p2073 A67-27065
Distinct state assignments for synchronous sequential machines, with modification of Dolotta-McCluskey algorithm 13 p2073 A67-27066
Computer graphic aids with applications of graph plotters, trace analyzers, cathode ray tubes, light pens, etc 13 p2073 A67-27188
Digital computer languages in relation to engineering design problems 13 p2073 A67-27189
Use of computer in aircraft design problems 13 p2074 A67-27191
Flight simulator computation methods development 13 p2090 A67-27264
Computerized weather forecasting based on informational and probability logic 13 p2152 A67-27275
Astronomical refraction in polytropic atmosphere adapted to automatic computers 13 p2152 A67-27484
Cost models for complex space programs, analyzing data acquisition systems, computer routines, etc 13 p2232 A67-27547
Computer method analysis of electron temperature and density behavior on basis of glow discharge for plasma electron balance equation solution 14 p2353 A67-27755
Numerical solution of linear differential equation and Volterra linear integral equation of second kind based on Lobatto four-point quadrature formula 14 p2342 A67-27977
Stability of motion of continuous dynamical systems analyzed via computing machines 14 p2348 A67-28080
Methods in computational physics, Volume 7, Astrophysics 14 p2392 A67-28992
Problem oriented language for mechanical problems programming applied to steady state vibrations, static problems and stress-strain relation 14 p2276 A67-29000
Particle density and material functions of gases of random composition, calculating values without regard to reaction dissociation 15 p2543 A67-29090
On-line nonlinear circuit design, discussing computer program for evaluating performance resulting from modifications 15 p2442 A67-29169
Skin effect in plasma theory for case of nonlocality of relation between current and electric field 15 p2522 A67-29211
Computer partitioning for long term reliability in space, noting requirements for various phases of operation 15 p2439 A67-29306
Finite difference method for treating head-on axisymmetric interactions of blast wave and shock layer in nose region of high speed blunt body 15 p2416 A67-29432
Approximate solution to nonlinear problem of pull-in range of phase locked loops, noting filter configurations and methods of analysis 15 p2446 A67-29589
Digital computer methods for calculating impulsive relaxation in unbalanced hydrogen plasma 15 p2529 A67-29713
Hybrid computer calculation of instantaneous and peak amplitude probability distribution of random signal 15 p2440 A67-29774
Long term study for prediction of launch vehicle costs, emphasizing estimate accuracy and application of statistical analysis 15 p2568 A67-29847
Computer model of aircraft accident investigator, discussing generation and testing of kinematic hypotheses on basis of programmed empirical data 15 p2420 A67-29896
Digital cardiometer design noting binary counter, clock, operation cycle, etc 15 p2432 A67-29921
Model for velocity coupled axial mode combustion instability in solid propellant rocket motors, noting computer studies 15 p2547 A67-29997
Range sum Doppler system for early launch tracking system to get warnings of possible impact in neighborhood of critical installations 15 p2437 A67-30111
[AAS PAPER 67-42] Dynamical and statistical approach to range safety problems, noting impact-density function of space vehicle destruction at early launch stage 15 p2572 A67-30113
[AAS PAPER 67-45] Computer applications to test scheduling problem against probabilistic demand in heuristic environment 15 p2467 A67-30114
[AAS PAPER 67-46] Method of dynamic characteristics, determining controlled plant performance during operation 15 p2462 A67-30328
Identification techniques with stochastic computers for advanced automatic control systems in form of learning machines 15 p2441 A67-30344
Reverse Monte Carlo method for circuit analysis, noting computer analysis of sense amplifier 16 p2633 A67-30475
Image analysis by Fourier transformation into incoherent illumination, applied to point source of light /star/ 16 p2671 A67-30863
Shock measurement discussing Fourier spectrum, vibrating reed gauge, analog and digital techniques, etc 16 p2671 A67-31022
Dollar consequence functions for producer and consumer risks due to product faults noting optimization 16 p2782 A67-31257
Radio ray divergence in ionosphere using computer techniques, noting ionospheric models and limitations 16 p2629 A67-31512
Computerized mathematical procedures application in advanced large-scale automated systems 16 p2634 A67-31568
Process identification by decomposition method of multilevel systems analysis, noting computer estimation of state variables of discrete time systems 16 p2647 A67-31650
Self-optimizing, type-one system design discussing steady state optimization problem 16 p2649 A67-31666
Control of output variables in discrete

multivariable system at steady state noting design, application and performance 16 p2649 A67-31668

Sensitivity analysis application to nonlinear system modeling and compensation noting minimization procedure parameter determination and performance index 16 p2650 A67-31674

Computer analysis of critical fuel solution reactors with arrays of large diameter voids 16 p2702 A67-31814

Computer method using coefficient linearity along diagonal of matrices to calculate N/h/ profiles of ionosphere 16 p2669 A67-31897

General formula for homogeneous second-order differential equation by Lie series, noting computer application 17 p2876 A67-32045

Computational limitations of onboard orbiting computers such as fixed point arithmetic, limited word length and solution techniques 17 p2881 A67-32056

Computer-aided transistor design, characterization and optimization 17 p2823 A67-32198

Iterative procedure for solving linear differential equations with given boundary conditions on analog computer 17 p2818 A67-32296

Processing results of meteor photographs using panchromatic films and program-controlled exposure time 17 p2942 A67-32328

Direct numerical control by computer of 150 heating circuits for safe kinetic heating test simulation of flying conditions for large supersonic aircraft 17 p2820 A67-32748

Waveguide discontinuity problems solution by digital computer 17 p2827 A67-32792

Inversion of symmetrical matrices by computer, noting storage space advantages 17 p2820 A67-32802

Book on computer solution of linear matrix algebraic systems and errors involved, discussing Gaussian elimination, FORTRAN, ALGOL and PL/1 programs, etc 17 p2821 A67-32825

Computerized method for on-line data analysis, elucidating SLIP language, request, processing, interpretation, time sharing, background activity, etc 17 p2821 A67-32865

Frequency response of nonlinear system, analyzing saturation characteristic of amplifier by digital computer 17 p2821 A67-32933

Regularization of motion equations in computation of vehicle trajectory near singularity [AIAA PAPER 67-26] 17 p2948 A67-33039

Inertialess polarization energy of charge interaction between neighboring lattice points in Ge crystal, using M-20 computer 17 p2924 A67-33338

Nonstationary drag coefficient for unsteady flow for large Reynolds numbers determined experimentally, using analog computer method 18 p3023 A67-33425

Post-induction kinetics in shock initiated hydrogen-oxygen reactions investigated by computer methods 18 p3153 A67-33823

Lunar thermal history computed for different radioactive elements distribution 18 p3119 A67-33862

Computer conversion of hydrodynamic data into simulated static test of deep-throttling bipropellant rocket engine, considering inert calibration techniques [AIAA PAPER 67-427] 18 p3112 A67-33911

Mathematical model for computer diagnosis of system failure, developing optimal policy for searching malfunctions with observable symptoms 18 p3006 A67-34065

Navy method for integrating all reliability data by Integrated Data Plan, discussing Interagency Data Exchange and Failure Rate Data programs 18 p3007 A67-34660

Optical system for computer counting and analyzing aerosol particles on photofilm 19 p3227 A67-34861

Electronic circuits containing vacuum tubes and transistors analyzed by computer method using Bellert's algebra of structural numbers 19 p3201 A67-34907

K-multiple automata for language recognition or generation, discussing generalization from simple to multiple automata 19 p3202 A67-35607

Program providing man-machine communication for electronic circuit analyses using time sharing

computer 19 p3186 A67-35619

Computer experiments related to chemical propulsion such as chemical kinetics, fluid dynamics, transport process, shock and detonation phenomena, combustion, etc [AIAA PAPER 67-7] 19 p3346 A67-35734

Book on shift register sequence theory, discussing applications in communications, computers and switching theory 19 p3187 A67-35832

Computer solution of optimal control problems by finite difference method 19 p3202 A67-35886

Strapdown inertial reference and navigation system initial alignment utilizing coordinate-transformation matrix computer [AIAA PAPER 67-558] 19 p3257 A67-35953

Powered flight trajectory determination for Saturn V vehicles through computer method [AIAA PAPER 67-547] 19 p3258 A67-35981

Onboard computer equations for rocket vehicle guidance to elliptical orbit, discussing iteration absence from computations and digital simulation results [AIAA PAPER 67-621] 19 p3260 A67-36010

Computer Conference, American Federation of Information Processing Societies, San Francisco, November 1966 19 p3187 A67-36053

Parameter optimization by modified sequential random perturbation technique using hybrid computer, considering initial conditions and analog computer errors effect, for dynamic systems 19 p3188 A67-36058

Graphical display technique for complex curve display, discussing system components, experimental results and relevant software 19 p3188 A67-36059

Time-sharing system with single central processing unit and several graphic display consoles for single high speed computer among human operators 19 p3188 A67-36060

Reentry trajectory optimization by repetitive computations of impulse response functions and state equations 19 p3190 A67-36072

Nonlinear circuits analyzed by Monte Carlo method for computer synthesis 20 p3407 A67-36331

Computer method for evaluating hyperfine structure recordings obtained by photoelectric Fabry-Perot interferometer 20 p3440 A67-36357

Rotor blade airload and dynamic response of large tandem rotor helicopter measured, using computer programs methods 20 p3536 A67-36462

Radio interior communication /RADIC/ system used in Apollo program, discussing future capabilities and advantages 20 p3380 A67-36559

Distribution asteroids in space studied by computer analysis from selected plots of orbital elements 20 p3524 A67-36654

Numerical digital computer solution of parabolic partial differential equations with two-point boundary conditions, using method of lines 20 p3391 A67-36820

Atmospheric energetics, discussing stratospheric-tropospheric energetics differences, atmospheric radiation balance distribution, meteorological satellite data, computer studies of atmospheric circulation, etc 20 p3429 A67-36895

Apollo program automatic checkout equipment, examining computer controlled checkout concept for Apollo spacecraft 20 p3417 A67-36974

Noise rejecting algorithms for ODE solutions with computer, using redundancy, placement of control and feedback techniques 20 p3392 A67-37224

Aircraft design automation using computer techniques by linking geometrical concepts to design parameters 20 p3455 A67-37246

Algorithm for generating normally distributed variables set with given correlation matrix in digital computer simulation of electronic circuit performance 20 p3401 A67-37315

Plane and axisymmetrical boundary layer characteristics computation, estimating transition region length 20 p3424 A67-37344

Lunar mission simulators for Saturn-Apollo project noting optimal computer approach on flexibility, accuracy, cost, etc 20 p3418 A67-37482

Compressor blade flutter stability in separating flow with external perturbations

analyzed, using digital computer 20 p3517 A67-37488

Minimizing time for deployment of infantry force by airlift analyzed by computer procedures based on loading, effectiveness and productivity 20 p3361 A67-37529

Critical supersaturations for homogeneous nucleation of ethanol, hexane, etc, investigated using thermal diffusion cloud chamber 20 p3555 A67-37562

Spacecraft computer managed laboratory /CML/ for flexible decision making in space missions of 1970s 20 p3393 A67-37624

Resistance spot welding process, using heating, cooling and stress development data to compute internal behavior 20 p3456 A67-37697

Instrument engineers guide to digital computer control 21 p3587 A67-37957

Analog computer method application for determining critical frequency and critical flutter speed of wing having torsional bending vibrations in airflow 21 p3718 A67-37992

Analog and digital computer methods for research and development of fluidic circuit components, discussing scaling effects 21 p3612 A67-38106

Computers role in fluid film lubrication, computing parameters for bearings lubricated by compressible and incompressible lubricants via iterative finite difference schemes 21 p3632 A67-38135

Computer controlled metal cutting, discussing prospects, difficulties and need for systematic mathematical study 21 p3637 A67-38920

Schuster method calculation of constant geomagnetic field spherical harmonics coefficients 21 p3623 A67-39045

Automatic test equipment /ATE/ to ensure aircraft availability noting operation, circuitry, computer methods, etc 21 p3609 A67-39132

Problems of handling people on future giant aircraft noting reservations, ticketing, boarding procedures and baggage-handling functions 22 p3780 A67-39382

Open loop adaptive optimal control, calculating plant dynamic sensitivity coefficients for unknown disturbances, using digital computer on feedback path 22 p3776 A67-39411

Computer program charts for investigation of effect of temperature dependent thermal conductivity on transient temperature distribution of heated materials 22 p3916 A67-39481

Particle and energy continuity equations derived and solved by computer method ion composition and plasma temperature measured by Explorer XXII particle and energy continuity equations derived and solved by computer method for ion composition 22 p3790 A67-39804

Nondestructive readout technique for superconductive memory cells, application and comparison with previous methods 22 p3765 A67-39899

Nonlinear differential equations describing extensional motion of dumbbell satellite solved on digital computer 22 p3886 A67-40086

Mission profiles involving new materials for missile and space structures reviewed for progress in computer applications 22 p3915 A67-40330

Computer aided techniques applied to structural analysis of aircraft noting design problems in aluminum fatigue life, unclad alloys, insulation and composite structures 22 p3915 A67-40331

RCA papers on environmental sciences 22 p3781 A67-40400

Environmental test data acquisition and processing, noting pretest requirements and relative merits of analog and digital computer methods 22 p3765 A67-40406

Wing stress analysis, reviewing computer and variational methods for calculating structural strength 22 p3746 A67-40445

Curvature for variable cross section beam bending with arbitrary transverse and longitudinal loads calculated by computer 22 p3915 A67-40449

Computerized system for calculating spares quantities and providing overall adequacy within monetary, weight or volume constraint 23 p4085 A67-40583

Cost Analysis Model - Parametric /CAMP/ computer method of estimating hardware and logistics life cycle costs for air vehicles in design stage 23 p4085 A67-40589

Computerized microfilm or magnetic tape production for manned space station maintenance documentation 23 p4071 A67-40593

Two-dimensional two-fluid nonlinear computer model applicable to low beta plasma interchange modes 23 p4033 A67-40995

Writing and use of ground checkout procedures in Apollo program using computer-assisted editing, publishing and information retrieval 23 p3976 A67-41055

Computer-operated following ellipsometer for monitoring buildup and removal of thin anodic oxide film 23 p4001 A67-41260

Computer generated binary Fraunhofer holograms for mathematically known objects, discussing diffraction theory, computational and plotting procedures 23 p4002 A67-41267

Computer calculation of 1 Mev electron flux and irradiation degradation of solar cell I-V curves for charged particle environment 23 p3940 A67-41514

Book on adaptive control and optimization techniques covering basic mathematics, computer methods, differential equations, time domain, etc 24 p4133 A67-41793

Automatic test equipment for checkout and fault finding on Saab 37 Viggen 24 p4137 A67-41898

High speed computer graphic techniques for airfoil sections characteristics in two-dimensional compressible flow [SAE PAPER 670845] 24 p4091 A67-41998

Diagnostic system for jet engine malfunctions detection using digital computer sonic vibration analysis [SAE PAPER 670871] 24 p4207 A67-42008

Distant atmospheric waveform at night analyzed using digital computer for VLF phase spectra 24 p4149 A67-42068

Phase characteristics linearity of LF regenerative amplifiers with reactive elements and Chebyshev amplitude frequency responses 24 p4129 A67-42226

Sensitivity analysis method for poorly known model parameters and preliminary computer load requirements applied to radio tracking of space vehicles [ELDO-TM-F-5] 24 p4122 A67-42385

Digital computer restoration of atmospherically degraded images, studying techniques and limitations of former and mechanisms of latter 24 p4157 A67-42436

Digital image formation and reconstruction from photographic and direct electronically detected holograms 24 p4157 A67-42437

Design parameters and performance characteristics for overdriven varactor upper sideband upconverter /USBUC/ 24 p4131 A67-42446

Image shear analysis utilizing conventional coordinate and projective transformations performed on computer 24 p4157 A67-42603

Dynamic programming, deriving successive sweep method for optimal control problems, discussing discrete algorithm for numerical problems 24 p4136 A67-42694

Moiré patterns generated on computer printout when superimposing sampling grid over two-dimensional function to be plotted 24 p4158 A67-42809

Signal processing and control computer system for materials research noting use in viscoelastic studies of crystalline polymers 24 p4126 A67-42930

Aircraft fuselages, wings, fillets, ducts and other free form surfaces defined using man-machine graphical interaction with computer [AIAA PAPER 67-895] 24 p4126 A67-43004

Costs and savings of computer graphics systems used for preparing and maintaining aerospace engineering drawings [AIAA PAPER 67-899] 24 p4127 A67-43008

Numerical procedure for structural systems analysis, discussing computer application to hydrodynamic, electric, magnetic, thermodynamic, elastostatic and elastodynamic problems [AIAA PAPER 67-955] 24 p4127 A67-43038

Computer-aided design of space systems, discussing design morphology and process [AIAA PAPER 67-956] 24 p4127 A67-43039

V/STOL airbus transportation system schedules, travel times and fares for Northeast Corridor generated by computer method [AIAA PAPER 67-972] 24 p4127 A67-43049

Power conditioning subsystem failure detection provided by computer monitoring of performance, with signal for transfer to redundant unit [AIAA PAPER 67-983] 24 p4110 A67-43055

COMPUTER PROGRAM
SA DATA PROCESSING
SA FORTRAN
SA STRESS COMPUTER PROGRAM

Digital computer program SYNAC for parametric synthesis and performance analysis of military aircraft [AIAA PAPER 66-795] 01 p0009 A67-10535

Digital computer program for power spectral density analysis of vibration data, noting bandwidth variation with frequency [SAE PAPER 660715] 01 p0028 A67-10604

Stresses calculated in centrifugal impeller with cover disk by two-dimensional stress analysis and digital computer program [ASME PAPER 65-WA/FE-17] 01 p0080 A67-10873

Digital computer compensation of strain gauge data to extend measuring bandwidth to transient or HF phenomena 01 p0030 A67-11098

Strain gauge bridge outputs combined during flight to measure airloads directly and inexpensively in fatigue test program 01 p0030 A67-11103

Electronic Circuit Analysis Program /ECAP/, integrated system of digital computer programs producing DC, AC or transient network analyses from circuit topology, excitation, etc 01 p0031 A67-11336

Nonlinear solution method incorporated in computer program for analysis of abnormally operating circuits, considering catastrophic part failure modes 01 p0031 A67-11337

Reliability estimation techniques adaptable to computer implementation for complex manned systems 01 p0031 A67-11338

Combining IBM ECAP and propagation-of-variance moment method computer program for improved reliability circuit analysis 01 p0043 A67-11377

Trajectories of electromagnetic rays across terrestrial atmosphere and computer program 01 p0028 A67-11419

Computer design test program to automate checkout process of Saturn I and V space boosters gradually while retaining manual checkout 01 p0051 A67-11427

Computer program providing ion thruster design criteria and power and weight requirements for specific satellite control mission [AIAA PAPER 66-498] 02 p0302 A67-11515

Lunar orbiter command and telemetry data handling system at deep space stations 02 p0194 A67-11808

Programmed telescope control systems on equatorial mount 02 p0241 A67-11992

Test information systems improved by coupling data sources to users through remote terminals connected directly to large time sharing computing systems 02 p0207 A67-12001

Quadratic performance criteria for discrete control systems, using Liapunov matrix equation and digital computer program 02 p0225 A67-12074

Monograph on system philosophy of automatic learning systems in application to autopilots, discussing man-aircraft system cybernetics, human behavior, environmental effects, etc 02 p0186 A67-12084

All phases of pseudorandom sequence obtained by N-stage shift register generator 02 p0203 A67-12133

Algorithm for directed random search for minimum of function of n-variables 03 p0374 A67-13182

Sequential operations in computer program for digital picture processing 03 p0375 A67-13560

AEDNET system of digital computer programs for on-line simulation of nonlinear networks and oscilloscope display 03 p0375 A67-13665

Computer program to aid analysis of tracking radar towers and foundations 03 p0396 A67-13753

Digital computer calculation of trigonometric series expansions arising in solid mechanics problems 03 p0524 A67-13788

Computer program /MAST/ analyzing F-111 wing structure involving load and stress analyses 03 p0525 A67-13967

Computer program for automated design of hyperstatic truss structures under

resonant frequency used in multisatellite Agena launcher 03 p0526 A67-13968

Monte Carlo computer program for simulation of thermal radiation among opaque surfaces in vacuum [ASME PAPER 65-WA/HT-40] 03 p0537 A67-14009

Data processing activities and ancillary equipment used in advanced techniques of computer generated graphics for weather observing and forecasting system [AIAA PAPER 66-854] 03 p0376 A67-14128

Algorithms in ZAM-2 computer program to calculate recording error parameters of linear scale measuring device 04 p0621 A67-14918

Computer program for analysis of off-design performance characteristics of axial flow compressor [ASME PAPER 66-WA/GT-1] 04 p0548 A67-15357

Relativistic photoelectric cross section for two electrons of K-shell computed, using numerical program 04 p0661 A67-15763

Program selection for motion equations, parameters and control functions maximizing composite flight vehicle probability of delivering payload to given region 04 p0552 A67-15882

Mathematical model of aircraft nucleonic fuel gauging facility system allowing performance evaluation and optimization by computer techniques 05 p0842 A67-16542

Computational methods employed with Doppler observations and derivation of geodetic results 05 p0894 A67-16571

Mechanized data system for quality and reliability control, noting performance characteristics and computer program 05 p0814 A67-17264

Digital computer programs for transient and steady state thermal analysis 05 p0929 A67-17452

Computer program used for explicit definition of wiring harness and cable assembly design procedure 05 p0779 A67-17456

Autocorrelation program for moving from study arrangement to data band readable in Fortran 06 p0965 A67-17587

Computer program for digital exact representation of spectral frequency-and intensity-distribution by superposition of Gaussian components, applying least squares method, linearizing normal equations and analyzing observational errors 06 p0965 A67-18069

Digital computer analysis of mission parameters governing spacecraft thermal characteristics including ablation effects, radioisotope generator systems, etc 06 p0986 A67-18417

Numerical analysis of free boundary problem inviscid incompressible flow field of impinging jet and two-dimensional Joukowski airfoil in sheared wind tunnel flow [AIAA PAPER 67-217] 06 p0988 A67-18460

Computer program and mathematical model for design of electrostatic colloid thruster [AIAA PAPER 67-84] 06 p1075 A67-18499

Computer program for gravity and magnetic profiles across two-dimensional bodies of arbitrary shape 06 p0998 A67-18736

Filmed data and computers - Seminar, Photo-Optical Instrumentation Engineers Society, Boston, June 1966 07 p1148 A67-19741

Integrated film reading and display system, discussing characteristics of waveform display/ analyzer subsystems and scanning/recording requirements 07 p1148 A67-19742

Automatic system for classifying and delineating terrain features in aerial photography, using general purpose computer 07 p1187 A67-19744

Image scanning systems applied to filmed data processing 07 p1148 A67-19745

Zonal harmonics determination through satellite observations processed using computer program, noting necessity for increased number of satellites [AAS PAPER 66-91] 07 p1183 A67-19956

Planned encounters with asteroids in manned missions to Mars for observational purposes, using computer program [AAS PAPER 66-124] 07 p1254 A67-19983

Algorithms for dichotomous representation of macrocircuits, considering computer programs and establishment of flow

graphs 08 p1299 A67-20326
 Computer program for analytical development of planetary disturbing function 08 p1381 A67-20393
 Satellite orbit computation program with element representation based on drag-free perturbation theory coupled with differential correction procedure 08 p1383 A67-20403
 Aerodynamic stability coefficients determined from sounding rocket flight data, using computer program for numerically integrating six degrees of freedom motion equations 08 p1407 A67-20517
 Longitudinal and lateral axes orientation of uniformly rotating or rapidly rotating vehicle utilizing outputs from solar sensors and lateral magnetometer 08 p1409 A67-20538
 Real time meteorological system providing prelaunch impact prediction for unguided high altitude rocket firings, noting computer program 08 p1314 A67-20543
 Computer program for axisymmetric nonlinear behavior of stiffened elastic shells of revolution with variable thickness, calculating collapse pressures [AIAA PAPER 66-529] 08 p1417 A67-20558
 Trajectory design and computer programs for planetary mission analysis 08 p1384 A67-20617
 Random access storage of program for airborne digital computer system 08 p1297 A67-20628
 Open and closed loop tools and techniques for guidance program validation and postvalidation operations 08 p1350 A67-20629
 Software generation for airborne digital computer systems 08 p1297 A67-20630
 Automatic checkout system /ACS/ and digital guidance programs for titan III and Apollo automatic checkout system /ACS/ and digital guidance programs for Titan III and Apollo 08 p1297 A67-20632
 Computer generation of DB Margin Summaries for telecommunications links 08 p1292 A67-20653
 Error model digital computer program applied to lunar surface hybrid navigation concepts, noting accuracy requirements from 1972 to 1985 08 p1351 A67-20675
 ATC automation, discussing first stage implementation called NAS En Route Stage A, Center Computer Complex and computer programming 08 p1315 A67-20676
 Heuristic computer programming for solution of complex logic problems 08 p1299 A67-21199
 Optimization of design of input-output matching networks for transistor microwave frequency amplifiers, using computer program 08 p1305 A67-21228
 Computer manipulative algebra programs for Fourier series 08 p1299 A67-21260
 Orbit perturbations due to tesseral harmonics contained in series expansion of gravitational potential determined using computer program 09 p1487 A67-21885
 Numerical quadrature methods of Romberg, Chebyshev and Monte Carlo, noting analytic function and program for machine evaluation 09 p1468 A67-22047
 Monte Carlo computer program for calculating molecular gas flow with axisymmetric vacuum structures, showing applications on pumping speed test domes and measuring apparatus for sticking coefficients 09 p1488 A67-22105
 Parts reliability control by computer programs 09 p1583 A67-22307
 Troubleshooting problems in oscillator circuit solved via Bayesian computer program simulating critical behavior 09 p1456 A67-22369
 Correspondence between logical relations of Boolean function implicants and numerical relations between identifiers 09 p1470 A67-22669
 Computer program for solving bending of plates of any shape and with any variation in boundary conditions for static loading and transverse vibration 10 p1731 A67-23843
 Book on design and analysis of scientific experiments covering statistical estimation theory in design and testing of hypotheses, emphasizing computational techniques 12 p1961 A67-25560
 Computer-aided layout of minitick artwork 12 p1950 A67-26130
 Computer-aided design of linear integrated circuits 12 p1919 A67-26156
 Visual aspects of transstellar space flight 12 p2009 A67-26233

Vertical cut-off rigidities for specific locations of geophysical interest computed from trajectory tracing 13 p2191 A67-26325
 Program attachment to fatigue testing machines intended for two-stage programs 13 p2217 A67-26796
 Computer program providing ion thruster design criteria and power and weight requirements for specific satellite control mission [AIAA PAPER 66-498] 13 p2188 A67-26825
 Two digital computer filing programs for determining ordinates of propagation curves of ground waves in visible region 13 p2070 A67-27202
 Computer techniques for data problems encountered by task analysts 13 p2063 A67-27260
 Propagation constants of rectangular waveguide containing parallel sheets of finite conductivity using iterative computer program 13 p2083 A67-27443
 Five classes of automated general purpose computer program for circuit design analysis 13 p2074 A67-27492
 Zeros of polynomials with real or complex coefficients determined, using steepest descent method in convergent procedure 13 p2148 A67-27496
 Satellite orbit analysis and computer program for earth zonal harmonics determination, considering orbit elements and gravitational constants [AAS PAPER 66-91] 13 p2116 A67-27516
 Computer program using Birkhoff normalization of Hamiltonian of restricted problem of three-bodies problem at L sub 4 13 p2208 A67-27521
 Planned encounters with asteroids in manned missions to Mars for observational purposes, using computer program [AAS PAPER 66-124] 13 p2209 A67-27537
 Strain gauge bridge outputs combined during flight to measure airloads directly and inexpensively in fatigue test program 14 p2315 A67-28002
 MOSTSIM 2 computer program for design of integrated circuits 14 p2281 A67-28021
 Air traffic control system, discussing effect on business aircraft operations 14 p2347 A67-28317
 End wall effects in axial compressors related to displacement thickness of boundary layer theory, using computer program [ASME PAPER 67-FE-16] 14 p2242 A67-28364
 Cylindrical specimen behavior during high strain rate tensile test, using computer program 14 p2400 A67-28523
 Design concepts for stored program data acquisition system in spacecraft applications 14 p2275 A67-28690
 Computer programs for calculating curvature tensors and motion equations [JPL-TR-32-1122] 14 p2276 A67-28847
 All-pass networks design method using algorithm and computer program for communications system 14 p2274 A67-28914
 Evolution of short-period comet orbits /1860-2060/ taking into account perturbing effects of outer planets 15 p2552 A67-29154
 Night F layer behavior, considering height and electron density, noting computer program for nonsteady state continuity equation with neutral gas movement 15 p2474 A67-29523
 Surveyor guidance program for midcourse and terminal information, noting redundancy in design, decision making telecommunications, etc 15 p2514 A67-29599
 Optimization of Atlas-Agena trajectories via steepest ascent computer program 15 p2514 A67-29602
 Space rescue mission planning and targeting by computer 15 p2555 A67-29609
 Book on computer programs for structural analysis covering flow charts, computer languages, matrix inversion, etc 15 p2574 A67-29646
 Computational errors in generation of direction cosine matrix in strapdown system 15 p2515 A67-29741
 Recognition thresholds for lunar crater sizes, noting elliptical image measurements and generation of appropriate computer program 15 p2431 A67-29894
 Computer aided network sensitivity analysis 15 p2440 A67-29937

Electronic circuit tolerance analysis by digital computer, discussing data availability, analysis methods and interpretation of answers 15 p2440 A67-29938
 Air traffic control simulation, describing functions to be fulfilled and system requirements for EUROCONTROL 15 p2441 A67-30164
 Interpolating/extrapolating computer programs noting application to analysis of industrial systems 15 p2462 A67-30327
 Cabin noise reduction in DC-9 by tuned vibration absorbers attached to engine support structure [AIAA PAPER 67-401] 15 p2421 A67-30368
 Circuit analysis by computer, noting programs for reliability and quality control 15 p2441 A67-30408
 First stage checkout techniques of satellite launcher, noting digital computer program from pulse-code-modulated telemetry 16 p2655 A67-30835
 Computer program for optimizing performance of high resolution airborne photo-optical recording system using modulation transfer function analysis 16 p2678 A67-31792
 Bending strength of spur gear teeth calculating methods to optimize design for high speed, lightweight aircraft gearing [AHS PAPER 118] 16 p2684 A67-31834
 Computer program for design and routing of external plumbing of aircraft gas turbine engines 17 p2928 A67-32006
 Book on FORTRAN with engineering applications covering case studies, graded exercises, etc 17 p2818 A67-32331
 DIALOG /computer implemented retrieval system/ capabilities, design, philosophy and performance 17 p2819 A67-32468
 Computer program for synthesizing and analyzing performance of preliminary designs of hypervelocity cruise vehicles 17 p2819 A67-32474
 Digital computer program FORTRAN coded, analyzing electric power distribution system of aerospace vehicle 17 p2804 A67-32511
 Environmental technology and extrapolation into future, noting government role 17 p2834 A67-32592
 Computer graphics for surface generation, stressing Coons surfaces and parametric representation 17 p2820 A67-32783
 Book on control systems and linear vibrational mechanical systems emphasizing use of analog and digital computers, frequency response, complex plane and root locus plots, FORTRAN method, etc 17 p2822 A67-33133
 Algorithms for dichotomous representation of macrocircuits, considering computer programs and establishment of flow graphs 18 p3005 A67-33498
 Integral equation solution of hydrodynamic problem through computer program 18 p3024 A67-33543
 Unconfined nitromethane transient initiation, determining differential conservation, state and reaction rate equations, using two-dimensional computations 18 p3153 A67-33824
 Scramjet engine nozzle contours noting expansion-deflection, bell, plug and arbitrary annular nozzles, with optimum nozzle design and computer program for performance prediction [AIAA PAPER 67-453] 18 p2983 A67-33927
 Nonlinear decision surfaces determined by pattern-recognizing adaptive threshold device via generation of polynomial discriminant functions and computer programs 18 p3006 A67-34064
 Computer application to planning and operating simultaneous access European ground station network 18 p3003 A67-34355
 High resolution flying-spot scanner as input device for computer simulation of optical character-recognition systems 18 p3006 A67-34403
 Computer program for handling of transform between spatial coordinate representation and spatial frequency representation of image 18 p3007 A67-34599
 Maintainability and reliability cost effectiveness program /MARCEP/ applied to logic and computer limitation problems 18 p2995 A67-34689
 Sensitivity coefficients through flowgraphic representation of network function, discussing algorithmic computer

- program 19 p3200 A67-34846
- Complex partial differential equations solutions by channel analog memory used with analog computer 19 p3186 A67-34966
- Systems approach combining human experience and logic with computer technology to implement navigation management function 19 p3254 A67-35313
- Slope derivation from lunar orbiter photography using photometric model and computer program 19 p3230 A67-35322
- Formula manipulation by computer, noting simplification, pattern matching, complex number handling, etc 19 p3187 A67-35679
- Ground track location on contour map for given terrain elevation profile, using digital computer 19 p3232 A67-35926
- Orbit determination for Lunar Orbiter, describing computer program and studying Doppler residuals [AIAA PAPER 67-545] 19 p3328 A67-35944
- Steepest-ascent optimization program developed for flight path of current vehicles, particularly supersonic transport vehicles 19 p3257 A67-35958
- Linear segment pitch rate program for near optimum trajectory for rocket boosters 19 p3335 A67-35976
- Random variables generation in computer, explaining procedure for beta and chi-square variates and normal distribution 19 p3188 A67-36056
- Computer program utilizing graphic data processing system for mask artwork design of hybrid integrated circuits 19 p3188 A67-36061
- Computer program for calculating optimal launch windows for orbiting satellites 19 p3190 A67-36071
- Physical electronics formulas tabulated, with solid state physics variables dimensionally coded and resultant nondimensional products cataloged, using computer routine 20 p3506 A67-36235
- Computer program for heat transfer calculation by temperature distribution along wall surface, using Fourier-Bessel series to determine distribution coefficients 20 p3544 A67-36450
- Spacecraft computers role on advanced manned missions 20 p3391 A67-36549
- Radar designation by computer and real time reentry tracking for future Apollo manned space flight 20 p3381 A67-36592
- Apollo Range Instrumentation Aircraft /ARIA/ deployment model to determine flight plans for support of translunar injection phase of Apollo mission 20 p3361 A67-36600
- Minor planets observational and computational results /1964/, discussing ephemeris volume 20 p3522 A67-36615
- Computer program for determining net thermal energy incident on satellite by computing projected surface area [ASME PAPER 67-HT-56] 20 p3549 A67-36738
- Computer program for reproducing operational conditions and simulating environment in which weapons system operates 20 p3416 A67-36765
- COSMOS, Courtauld's system for matrix operations and statistics 20 p3391 A67-36932
- Automation techniques for stage checkout in Saturn program noting equipment, time factor, etc 20 p3417 A67-36975
- Apollo-Saturn program automatic checkout systems, discussing ground support equipment facility automation, computer software and checkout technique applications to nuclear electronic systems 20 p3533 A67-36977
- Digital diagnostic program evaluation based on selective path simulation, tracing option and backtrace method 20 p3392 A67-37456
- HF skywave propagation computer model for interference prediction 20 p3387 A67-37646
- Real time meteorological system providing prelaunch impact prediction for unguided high altitude rocket firings, noting computer program 21 p3607 A67-37812
- Photographically recorded spectra for absolute intensity processed by computer program, providing digitally recorded densities on magnetic tape 21 p3624 A67-37851
- Digital switching functions and pattern recognition realization through computer-programable algorithm for designing feed-forward threshold logic
- nets 21 p3588 A67-38182
- Digital computer program SYNAC for parametric synthesis and performance analysis of military aircraft 21 p3568 A67-38534
- Digital program for stability-augmentation system-gain values yielding desired pole-zero locations for vehicle transfer functions of flight conditions 21 p3568 A67-38539
- Characteristic method computer program for calculating three-dimensional supersonic flow around blunt and pointed bodies of revolution in reasonable time 21 p3566 A67-38887
- Master matrix containing initial values of geomagnetic inclination and gyrofrequencies for storage in computer memory to calculate ionospheric vertical profiles 21 p3623 A67-39046
- Computer program based on tracking function method setup for investigating nonlinear second order autonomous system stability and boundedness 21 p3604 A67-39076
- Computer formulation of motion equations using tensor calculus to extend area of application of digital computers 22 p3827 A67-39418
- Heuristic computer programming for solution of complex problems 22 p3764 A67-39866
- Prediction of lunar surface temperature through digital computer program noting heat transfer equations 22 p3884 A67-39930
- Manned lifting reentry vehicle optimization using Optimum Compromise between Conflicting Operational Factors /OCCOF/ computer program 22 p3902 A67-39947
- Secondary payload for Saturn launch vehicle evaluation according to experiment/mission effectiveness and compatibility by computer program methodology 22 p3903 A67-39950
- Spacecraft ephemeris, orbit compatibility and scheduling in AAP mission experiments 22 p3885 A67-39959
- Computer program and mathematical model for design of electrostatic colloid thruster [AIAA PAPER 67-84] 22 p3868 A67-40101
- Gravity gradiometer digital computer program for simulated rotating gravitational mass sensor and gradient contour mapping 23 p4000 A67-41218
- Least squares deconvolution technique for reducing Fabry-Perot spectrometer data to Voigt profiles 23 p4002 A67-41262
- FORTTRAN program for B number computation applied to solid state physics 23 p3977 A67-41458
- Computer program for predicting silicon solar cell current-voltage characteristics as function of incident solar intensity and cell temperature over heliocentric distances 23 p3939 A67-41513
- Conformal representation of ring on complex doubly connected symmetrical region bounded externally by circumference and internally by star shape curve 24 p4249 A67-42106
- Digital computer compensation of strain gauge data to extend measuring bandwidth to transient or HF phenomena 24 p4155 A67-42290
- Computerized imaging techniques - Conference, Washington, D.C., June 1967 24 p4156 A67-42428
- Three-dimensional surface projection method by computer plotting program applicable to surfaces with large amount of detail 24 p4125 A67-42430
- Computer program for analysis of off-design performance characteristics of axial flow compressor [ASME PAPER 66-WA/GT-1] 24 p4092 A67-42458
- Computer applications in electronic circuits design, discussing optimal man/computer interface and data handling processes 24 p4126 A67-42477
- Systems optimization methodology to analyze radioisotope thermoelectric generators /RTG/ for spacecraft applications, discussing computer program 24 p4184 A67-42504
- Multifaceted solar array performance determination 24 p4104 A67-42509
- Atmospheric spectral analysis of planets and stars by using computer, telescope and interferometer system 24 p4232 A67-42572
- Mathematical model to aid in determination of need for technological advances in transportation [AIAA PAPER 67-799] 24 p4258 A67-42960
- AGM-69A program-managment system using CRT display for PERT/Time and Cost Control data translation [AIAA PAPER 67-920] 24 p4260 A67-43019
- Spaceborne computer-managed laboratory for experiments and instruments control in future space missions [AIAA PAPER 67-957] 24 p4140 A67-43040
- Evolution of short period comet orbits /1660-2060/ taking into account perturbing effects of outer planets 24 p4239 A67-43077
- ## COMPUTER PROGRAMMING
- ### SA LINEAR PROGRAMMING
- ### SA REDUNDANCY ENCODING
- Multiprogramming system for computer controlled telemetry data reduction system 02 p0206 A67-11807
- Automatic mathematical translation /AMTRAN/ system, remote terminal conversational-mode computer system that eliminates need for specialist programmer for large class of routine problems 02 p0206 A67-11811
- ELDO missile second stage automatic control system, noting programming control sequences, analysis of measurement results, etc 03 p0502 A67-12899
- Unsolvability of recognition of linear context-free language, searching for algorithm and generalizing to metalinear languages 03 p0375 A67-13562
- Dynamic system with unknown parameters identified through iterative and least squares methods suitable for computer programming 03 p0392 A67-13658
- General purpose computer used in automatic photointerpretation process in relation to pattern recognition 05 p0768 A67-17513
- Haystack antenna used for satellite communications and celestial observation, noting digital computer for control system and data processing 05 p0790 A67-17517
- Model estimation programming to determine optimum design criteria for rocket propulsion system using estimating function, approximation solved by Lagrange method [AIAA PAPER 67-208] 06 p1024 A67-18330
- Digital simulation program for systems design of long-duration space station of MORL type [AIAA PAPER 67-206] 06 p0981 A67-18512
- Holographic synthesis of computer generated holograms 07 p1188 A67-19796
- Convex programming procedure yielding algorithm for tuning out system from possible resonance zone 08 p1353 A67-20837
- Picture generation by computer for concept demonstration, subsequently photographed with automated microfilm camera 08 p1299 A67-21050
- Nonlinear programming and control problems in terms of variations, maximum principle and dynamic programming 10 p1619 A67-23418
- Optimal control for investment program, obtaining solution through convex programming 10 p1620 A67-23426
- Book on applied kinematics covering synthesis techniques for link-and-cam motion other than uniform rotation in high speed high performance automatic machines 11 p1795 A67-23921
- Energy techniques and matrix method for computer programming of dynamic response due to random and harmonic loading on structural systems [ASME PAPER 67-VIBR-56] 11 p1873 A67-24203
- Torsional vibration and steady state response of geared system, noting computer programming [ASME PAPER 67-VIBR-63] 11 p1797 A67-24205
- Man-computer system for aerospace problems, discussing terminology, methods of organization, problem solution, numerical analysis, etc 11 p1755 A67-24246
- On-line computation and man-computer interactive languages, discussing JOSS, MADCAP and Klerer-May systems 11 p1756 A67-24249
- Computer programming or software techniques in relation to hardware elements of computer graphics system [ASTME PAPER WES-7-02] 11 p1756 A67-24253

Random walks computer experiments on ensembles of random binary homogeneous velocity fields, using Eulerian and Lagrangian statistics 11 p1756 A67-24542

Electronic computer usage to control temperature during creep and long term strength tests of heat resistant steels 11 p1877 A67-24818

Tunguska meteorite transfer from heliocentric to geocentric orbit proved impossible by computer 11 p1868 A67-24847

Modified perceptron procedure for nonseparable cases, minimizing error probability and introducing reinforcement factors 12 p1961 A67-26064

Control systems functions and programming approaches, Volume B, covering electronic data processing, factory automation and computer center administration 13 p2153 A67-26664

Stability analysis of computer controlled linear hydraulic antenna control system 13 p2088 A67-26996

Automatic radiosonde data processing system providing azimuth and elevation angles, temperature, humidity, etc 13 p2069 A67-27019

Ordinary and time lag root locus diagram generating algorithm for adaptation to programming on digital computer 13 p2074 A67-27223

Machine independent axiomatic theory of complexity of recursive functions 13 p2148 A67-27497

Magnification problems facing aircraft designers analyzed by computerized iterative procedures 14 p2245 A67-28062

On-line computers in radio astronomy for measuring radio source flux, position and width and for increasing Dicke radiometer sensitivity 14 p2275 A67-28439

Computer controlled dynamic test facility to provide data on flight characteristics of Apollo-Saturn V launch vehicle by measuring vibration amplitudes 14 p2293 A67-28593

Automatic positioning control and problems in normalizing programming codes used in numerical control 14 p2276 A67-28956

Three-photo orientation solution to analytic aerotriangulation problem, investigating mathematical concepts and computer programming methods 15 p2486 A67-29298

Spaceborne programming language for Surveyor guidance, discussing impact on flight software development 15 p2439 A67-29600

Software tools for certifying operational flight programs 15 p2440 A67-29604

Mathematical programming on analog computers solved by saddle point and extremum methods, using differential equations 17 p2817 A67-32225

Cost effectiveness criterion for instruction repertoire selection for aerospace computer 17 p2820 A67-32502

Radar system using real-time on-line computer applied to adaptive control of beam direction and transmitter modulation 17 p2816 A67-32790

Operational computerized system for automatic surveillance of reliability and maintainability of spacecraft hardware 18 p3021 A67-34701

Collection of articles on computer advances, volume 8 19 p3186 A67-35677

Time-shared computer system design and application, noting memory, remote terminals, program debugging, etc 19 p3186 A67-35678

Programming system design for incremental data assimilation in open ended man-computer information systems 19 p3187 A67-35680

Software aspects of space navigation including computer programming, mission planning, error analysis and reliability realization 19 p3187 A67-35688

Flow pattern caused by low speed splash of liquid drop into pool computer examined, obtaining configuration plots various splash stages 19 p3212 A67-35895

Analog translational trajectory program replacing digital program for orbiting and reentry vehicles 19 p3190 A67-36070

Computer principles-equipment and programming for instrumentation systems, comparing digital computers with analog computers 20 p3390 A67-36463

Crank-Nicolson technique for first order

linear time-invariant differential equation solution, discussing truncation error 20 p3477 A67-36933

Automatic test computer programming problems, discussing system planning, documentation, personnel, system compromises, etc 20 p3391 A67-36972

Computer programming method for analysis of complex systems 20 p3392 A67-37194

Spurious response identifying equations for more realistic P and Q values on multiple conversion 20 p3404 A67-37636

Instrument engineers guide to digital computer control 21 p3587 A67-37957

Mathematical programming problem for automating design of optimum thin walled systems, noting stress-strain state factors 21 p3728 A67-38903

Algorithm for selecting optimum parameters for mathematical programming problem in thin walled systems, noting stress-strain state characteristics 21 p3728 A67-38904

Linear equation solving for gaseous mixture quantitative determination, based on combined cognitive system use of computing and programming devices 21 p3831 A67-39116

Acquisition phase of satellite with passive magnetic attitude stabilization, discussing programming difficulties and modified Rayleigh model for German 625A-1 satellite 22 p3898 A67-39173

Duration of dynamic system output for given input time calculated by computer programming 22 p3784 A67-39336

Discrete stress analysis method for shallow shells of double curvature and rectangular planform with various end conditions 23 p4075 A67-40679

Multiprocessing features of IBM 9020 system, discussing breakdown of information into subprograms with operational priorities 23 p3976 A67-41058

Operational error analysis program /OEAP/ use with multiprocessing in air traffic control application 23 p3976 A67-41059

Application of IBM 9020 multiprocessing system to air traffic control 23 p3976 A67-41060

Algorithm for processing primary motor characteristics of human motions on digital computer 24 p4114 A67-41857

Fourier transformation theory for shock and vibration data analysis, discussing programming considerations and computational efficiency [SAE PAPER 670874] 24 p4248 A67-42011

Image processing by computer generated binary filters 24 p4156 A67-42432

Computer and information sciences - Conference, Columbus, Ohio, August 1966 24 p4136 A67-42696

Automatic systems optimization, adaptation and learning 24 p4136 A67-42697

State variable approach to linear differential equations, coding for digital computation 24 p4179 A67-42933

Boeing Huntsville Simulation Center emphasizing ALPINE system and Interim Time Sharing System /ITSS/ [AIAA PAPER 67-896] 24 p4126 A67-43005

COMPUTER SIMULATION

SA ANALOG SIMULATION

SA DIGITAL SIMULATION

Computer-simulated mathematical model of thermal environmental effects on expulsion system design parameters for liquid-propellant gas-generator rocket engine [AIAA PAPER 66-686] 02 p0303 A67-11944

Scheduling and simulation of manned orbital operations using modular system of computer programs [AIAA PAPER 66-907] 02 p0230 A67-12249

Computer simulation for turbulence/upset studies on jet transports, emphasizing time dependency and nonlinear aerodynamics [AIAA PAPER 66-1002] 02 p0181 A67-12304

Diffusion of fully ionized plasma across magnetic field in computer model consisting of one thousand charged rods in two-dimensional motion 02 p0276 A67-12558

Guidance equations for multistage boosters offer target change on launch pad and in flight 02 p0265 A67-12718

Tracking interruption probability in second order astatic system, obtaining solution from Fokker-Planck equation and computer simulation 03 p0390 A67-13100

Approximation of variable time delays and

design of constant and variable delay circuits, noting simulation of delays in automatic control systems by computers 03 p0390 A67-13104

Cost and effectiveness of surveillance device for antiaircraft weapon system 03 p0538 A67-13695

Switching circuit malfunctions analysis, discussing modeling for failure, simulation of failure and timing problems and sequential networks 03 p0394 A67-14219

Satellite to satellite communications experiment simulation via digital computer, proving existence of whispering gallery propagation in lower ionosphere [RASSA PAPER 1-10-148] 03 p0373 A67-14255

Advanced feedback system simulation technique for strategic planning in business, noting manpower allocation 04 p0739 A67-14498

Mathematical model for adaptive signal processor, noting eye adaptation to changes in signal intensity and bandwidth 04 p0563 A67-14799

Flight simulation techniques covering digital computers, visual simulation and displays [ASME PAPER 66-WA/AV-1] 04 p0599 A67-15394

Computer simulation of hydraulic system using time delay elements independently of boundary conditions [ASME PAPER 66-WA/AUT-18] 04 p0555 A67-15413

In-flight bending moment and terminal drift minimization for flexible vehicle, applying two-point boundary value problem solution for optimum rigid body control system 04 p0706 A67-15422

Nonstationary problem of linear filtering in presence of additive noise solved by computer simulation 05 p0782 A67-16262

Computer simulated calculation of simple fluid properties using Monte Carlo method 05 p0927 A67-16890

Consistency technique for associating parts of patterns and results of computer simulation 06 p0965 A67-18057

Simulation of deployment dynamics of spinning spacecraft, discussing test methods emphasizing gravity compensating techniques [AIAA PAPER 67-207] 06 p0980 A67-18325

Digital simulation program for systems design of long-duration space station of MORL type [AIAA PAPER 67-206] 06 p0981 A67-18512

Comparison between Monte Carlo and PERT models, noting PERT errors and Monte Carlo simulation for Voyager spacecraft development [AIAA PAPER 67-209] 06 p1097 A67-18513

Computer simulation of perceptron predicting result of cyclic process 07 p1147 A67-19150

Random number modeling on digital computer 07 p1147 A67-19226

Temperature fluctuation of thin walled satellite passing periodically from sun to shade simulated by hybrid computer 07 p1257 A67-19375

Parameter optimization procedure in three degree of freedom trajectory simulation computer program for multistage vehicles [AAS PAPER 66-111] 07 p1253 A67-19970

Hybrid simulation for design of Apollo guidance navigation and control system [AIAA PAPER 67-233] 07 p1222 A67-20042

Apollo engineering simulation activity, particularly analog-digital real time hybrid simulation for guidance and control [AIAA PAPER 67-230] 07 p1164 A67-20055

Test procedure for direct use of digital computer, noting utilization of software simulation technique and various applications [AIAA PAPER 67-235] 07 p1149 A67-20058

Mechanized hybrid real time simulation for Gemini crew to use in rendezvous procedures [AIAA PAPER 67-250] 07 p1166 A67-20068

Apollo spacecraft hybrid real time flight simulation ensuring 40 msec sampling interval [AIAA PAPER 67-255] 07 p1166 A67-20071

Three-dimensional chaff simulator to provide video inputs to operational radar equipment for exposing operators to jamming 08 p1314 A67-20656

Computer logic cost effectiveness modeling applied to integrated circuits, discussing comparisons between existing

equipment, Conalag and redesigns 08 p1311 A67-20657
 Mathematical models for use in hybrid computer simulation for design of Integrated Helicopter Avionics System /IHAS/, analyzing operational modes of automatic flight control system 08 p1350 A67-20658
 FAA simulation systems for air traffic control noting computer simulated radar target generation, display equipment, etc 08 p1315 A67-20678
 Heat-transfer coefficients during dropwise condensation on randomly distributed nucleation sites analyzed through computer simulated model 08 p1426 A67-20925
 MORL system reliability analysis, discussing Monte Carlo simulation, major parameters, constraints, program contingencies, etc 08 p1411 A67-21073
 Full mission engineering simulator /FMES/ design for integrating hardware into lunar module system as hardware is made available by subcontractors 08 p1319 A67-21546
 Computer programming to predict performance of complex orbit navigation systems using simulation of landmark visibility from orbit as model 09 p1467 A67-21832
 Troubleshooting problems in oscillator circuit solved via Bayesian computer program simulating critical behavior 09 p1456 A67-22369
 Computer simulation of GaAs Gunn diode in resonant circuit noting frequency, efficiency and load characteristics 10 p1612 A67-23370
 Computer graphic display for dynamic response of nonuniform beam treated by lumped mass-spring representation of structure 10 p1608 A67-23739
 Computer simulation of anomalous diffusion, discussing scaling laws, quasi-steady state, plasma instabilities growth, steady diffusion, wall effects, etc 11 p1830 A67-24009
 Time varying electromagnetic field pattern of prolate spheroid antenna with rotationally symmetric current distribution motion pictures generated by 11 p1758 A67-24115
 Terrain following pulsed radar system without continuous scanning noting computer simulation, antenna and pitch control 11 p1752 A67-24259
 Dynamic control study for solar mirror aboard spacecraft using breadboard apparatus and computer simulation method 11 p1745 A67-24274
 Simulation of sampled data systems for pure servo delay by analog computer using potentiometer 12 p1919 A67-25203
 Air traffic control systems analyzed by simulation techniques 12 p1964 A67-25229
 Heat flow mechanisms and thermodynamics of supercritical cryogenic storage problems solved by digital computer simulation, using finite difference approximation 12 p1925 A67-25722
 Elastic collisions in simulating one-dimensional plasma diodes on computer 13 p2164 A67-26294
 Analog computer simulation of motions of gyroscopic pendulum, showing imbalance tolerance relationship to error 13 p2118 A67-26350
 Computer processed air traffic control, automatic weather data collection and forecasting 13 p2153 A67-26665
 Human transfer function problem and compensatory tracking, analyzing variance and determining average rate of stick motion as underlying variable 13 p2063 A67-26923
 Flight simulator computation methods development 13 p2090 A67-27264
 Comparison of computed and experimental spectral transmissions through haze 13 p2152 A67-27357
 Parameter optimization procedure in three degree of freedom trajectory simulation computer program for multistage vehicles [AAS PAPER 66-111] 13 p2214 A67-27527
 Statistical testing on digital computers for simulating current and voltage distribution in semiconductor rectifier circuits 15 p2439 A67-29416
 Simulation and error analysis of range-only location and tracking utilizing satellite system to obtain range

measurements 15 p2514 A67-29597
 Sonagrams for micropulsations, computer simulated, using equations for cyclotron instability and quasi-linear diffusion of protons in bounded plasma 15 p2476 A67-29618
 Diode and transistor transient switching characteristics determined from analog computer simulation of differential equations 15 p2449 A67-29803
 Second order optimal control system simulation by computer, describing method for generating time optimal controls 15 p2458 A67-29907
 Book on creation and use of computer simulation models and routines for study of systems 15 p2440 A67-30133
 Accuracy of satellite orbit prediction for rendezvous mission related to ground-based tracking network sensors by digital computer simulation 15 p2441 A67-30165
 Interlocking plan for entire countdown checkout process by combining subsystems simulated as partially controlled stochastic process 15 p2441 A67-30166
 Rate variation of aerodynamic parameters of pitching equation for aircraft, identifying them with linear plant model for simulation studies 15 p2420 A67-30340
 Differential equation computer simulation, examining errors in closed circuits 16 p2633 A67-30463
 Thermal gradients on surface of orbiting cylindrical stabilization boom determined, using computer simulation of earth orbital environment 16 p2764 A67-30957
 Sensitivity tests required to verify nonnormality in sample population, studied by computer simulation techniques 16 p2634 A67-31525
 Triple input describing functions noting application to stability analysis of forced nonlinear control systems 16 p2650 A67-31673
 Extravehicular activity /EVA/ simulator for zero gravity environment using servodrive and computer control 17 p2832 A67-31994
 Neighbor model for computer simulation of field ion images in fcc point lattice 17 p2887 A67-32205
 Systems analysis with computer techniques to examine future weapons system, discussing logistic simulation, interpretation, maintenance, engineering, management, documentation and reliability 17 p2833 A67-32490
 Computer simulation model for cost effectiveness of built-in test equipment /BITE/ in airborne radar systems 17 p2833 A67-32491
 Digital analog simulation program for IBM 7040 based on signal flow diagram, noting use of Runge-Kutta integration method 17 p2821 A67-32803
 Unidentified landmark navigation from orbiting vehicle by computer simulation, noting instrumentation accuracies 17 p2882 A67-33018
 Computer simulated flights of manual control for VTOL IFR operations indicate display and control subsystem deficiencies 17 p2808 A67-33183
 Hybrid simulators used for aerospace and military programs consisting of analog computers, digital computers and interface units for handling data flow 18 p3019 A67-33635
 Rocket engine turbopump assembly test capability design, facilities, cryogenic systems, control requirements, computer simulation, activation and checkout [AIAA PAPER 67-441] 18 p3112 A67-33918
 Digital computer simulations of pseudorandom noise generators, determining empirical sum distribution approximation of binomial variable 18 p3006 A67-34066
 Electron beam passing through low pressure gas generates plasma, computer simulated beam trajectory studies explain beam profile and pinch effect 19 p3275 A67-35106
 Dislocation in field-ion micrograph analyzed by computer-simulated Ranganathan hypothesis using Moore shell model 19 p3266 A67-35603
 Stability criterion for bandpass tunnel diode amplifier, determining limitations on diode series inductance as function of negative resistance 19 p3196 A67-35662
 Digital computer simulation of orbital launch window problem for departure-

trajectory analyses 19 p3329 A67-36004
 [AIAA PAPER 67-615]
 Hybrid simulation for analysis and design of nuclear reactors feedback control systems 19 p3189 A67-36068
 Computer simulation model for Saturn V launch vehicle system analysis 20 p3414 A67-36536
 Computer based CRT display technique for servo system testing, discussing Saturn V display computer and simulation studies results 20 p3415 A67-36609
 Computer program for reproducing operational conditions and simulating environment in which weapons system operates 20 p3416 A67-36765
 Fuel cell performance under operating conditions of local nonuniformity in temperature, concentration, potential or current simulated with computer program 20 p3363 A67-37014
 Magnetoresonant gyroscopes simulation by converting motion equations to rotating coordinates system 20 p3451 A67-37154
 Aperture antennas near field radiation patterns calculated by computer program based on semisimulated method 20 p3405 A67-37645
 Variational approach to error analysis in dynamic system computer simulation, applying maximum principle and Liapunov second method 21 p3588 A67-38180
 Saturn computer design and fault simulation on IBM 7090 21 p3588 A67-38181
 Digital computer for simulating and analyzing fluid turbulence by applying laws governing behavior and energy transfer of fluid elements 21 p3612 A67-38193
 Book on simulation of mechanical systems giving analytical, graphic and analog computer methods 21 p3588 A67-38252
 Operational analysis and DC design of Esaki diode pair bistable circuit used in high speed counting network performed by analog computer simulation 21 p3604 A67-38603
 Minimum variance simulation for satellite attitude determination reliability using magnetic and solar measurements 21 p3715 A67-39150
 Suboptimal radial guidance scheme based on cubic time function of optimal trajectories radius vector modulus from simultaneous data analysis 22 p3830 A67-39164
 Computer analysis and simulation of Mars soft landing descent control system combining inertial and radar sensing techniques 22 p3898 A67-39177
 Lunar rendezvous spacecraft guidance system performance for various initial conditions and instrument errors simulated by Monte Carlo computer program 22 p3832 A67-39965
 Prediction of Saturn V launch vehicle effectiveness during prelaunch phase using computer simulation [SMPT PAPER 102-27] 22 p3908 A67-40371
 Surveyor TV system signal processing and transmission, analyzing performance and computer simulation of some effects [SMPT PAPER 102-41] 22 p3808 A67-40379
 Apollo Crawler System analyzed by computer simulation for dynamic interactions of transporter and umbilical tower 22 p3782 A67-40466
 Unresolvable targets producing single radar return estimation from slow amplitude fluctuation, discussing scattering cross section effects and computer simulation verification 23 p3974 A67-41198
 Circuit for plotting extremal values of cycle during analog computer simulation 23 p3976 A67-41339
 Solar cell array model constrained at four points, with computer simulating V-I characteristics for environmental temperature and illumination intensity effects 23 p3940 A67-41515
 Errors in state vector from amplitude quantization in feedback control loop, noting finite word length in hybrid computer simulation 24 p4134 A67-42023
 Computer simulation of biological pattern generation processes 24 p4118 A67-42453
 Multifaceted solar array performance determination 24 p4104 A67-42509
 V/STOL airline economics simulated with computerized dynamic programming model [AIAA PAPER 67-841] 24 p4096 A67-42979

Boeing Huntsville Simulation Center emphasizing ALPINE system and Interim Time Sharing System /ITSS/ [AIAA PAPER 67-896] 24 p4126 A67-43005

Graphics system for space vehicle design and flight plan via light pen, trajectory computation and performance curve display on scope [AIAA PAPER 67-897] 24 p4126 A67-43006

Implementation of safety provisions in manned systems [AIAA PAPER 67-937] 24 p4096 A67-43027

Onboard computer-based checkout simulator system to assist astronauts in monitoring data requirements of future space programs [AIAA PAPER 67-951] 24 p4127 A67-43035

Commercial V/STOL transportation system, analyzing intraurban and short haul factors for concerned parties by computer simulation [AIAA PAPER 67-969] 24 p4260 A67-43047

CONCENTRATION

S ATOM CONCENTRATION

S CARBON DIOXIDE CONCENTRATION

S STRESS CONCENTRATION

CONCENTRATOR

SA COLLECTOR

Alpha Centauri probe and sun-orbiting concentrator to power 01 p0155 A67-11403

Carbonation Cell System for removing carbon dioxide from space cabin atmosphere using electrochemical process 23 p3965 A67-41578

CONCENTRIC CYLINDER

Stability of inviscid flows of perfectly conducting fluid between two concentric circular cylinders with axial volume current distribution 03 p0403 A67-13732

Motion induced by electric and magnetic fields on initially static fluid between two concentric tubes [ASME PAPER 66-WA/FE-35] 04 p0668 A67-15366

Solution for parallel plates in steady state Hartmann flow extended to coaxial flow between concentric cylinders, noting role of magnetic field 05 p0856 A67-17356

Hydromagnetic stability of dissipative flow between rotating permeable cylinders 06 p1040 A67-18129

Thermal conductances in collisionless gas between coaxial cylinders and concentric spheres obtained for arbitrary thermal accommodation 15 p2579 A67-29566

Inclusion problems involving tubular shells of isotropic incompressible materials yielding large deformations 16 p2766 A67-31099

Convective heat transfer in fluid between concentric cylinders with inner heated cylinder rotating and outer cooled cylinder stationary 20 p3543 A67-36422

Plane motion of container formed by two concentric cylinders and radial partitions partly filled with small vibrating ideal fluid 22 p3786 A67-40029

CONCORDE AIRCRAFT

Concorde SST aircraft, discussing airframe, engine, ancillary power plant, afterburner, etc 01 p0081 A67-11253

Design and construction of Franco-British Concorde SST, examining cabin, noise problem, production and tests 02 p0180 A67-12040

British-French cooperation in aeronautics, discussing Concorde SST, variable geometry aircraft, Olympus 593 turbojet, etc 03 p0362 A67-14379

Oxygen pressure vessels for prototype BAC/Sud Concorde manufactured from stainless steel 06 p0952 A67-18734

Test rig for fuel system in Concord aircraft noting construction, control system, equipment, installation and operation 10 p1623 A67-23548

Bench and flight tests of twin spool axial flow turbojet power plant for Concorde aircraft [ASME PAPER 67-GT-8] 11 p1854 A67-24796

Accident recording system for Concorde and protection from moisture, shock, fire and rough seas 12 p1939 A67-25231

Mach 2 plus Olympus 593 turbojet power plant for Anglo-French SST, analyzing fuel system, lubrication and cooling on test run 13 p2187 A67-26701

Hydraulic, pneumatic and electric circuits for twin loop engine control system of

Olympus 593 in Concorde

SST 13 p2187 A67-26702

Ground simulation of Concorde aerodynamic heating effects by blowing air through ducts built over specimen surface 15 p2465 A67-29501

Concorde automatic flight control system noting autostabilization, autopilot, electric trim, autothrottle, etc 15 p2419 A67-29508

Concorde jet engine silencer concept and characteristics [AIAA PAPER 67-391] 15 p2549 A67-30359

Concorde structural development noting effects of temperature on fatigue and creep strength of aluminum alloys [AIAA PAPER 67-402] 15 p2578 A67-30369

Concorde SST third and fourth flying prototypes described, discussing structural design, power plant, control systems, landing gear, etc 16 p2597 A67-31785

Concorde aircraft fuel, discussing fuel transfer, problem of boiling, in-flight environment simulation, payload/mass ratio, etc 16 p2734 A67-31809

SST Concorde hydraulic system noting design and hydraulic fluid selection resulting from high ambient temperatures, weight and space limitations, etc 17 p2800 A67-31971

Engine design for civil operation from military supersonic engine [SAE PAPER 670316] 17 p2929 A67-32978

Fuel requirements for Concorde SST stressing flame luminosity, radiant heat, spontaneous ignition, fuel viscosity and density 18 p3110 A67-34533

Atmospheric condition effects on SST aircraft, noting Concorde performance data analysis results 19 p3173 A67-35309

Navigation system for Concorde aircraft, considering inertial navigation 19 p3255 A67-35805

High altitude variable Mach number test cell for testing intake system of Concorde aircraft Olympus 593 20 p3414 A67-36497

Concorde fire protection system based on Firewire Triple FD equipment, discussing extinguishant toxicity, low vapor pressure, etc 20 p3364 A67-37245

Concorde SST economics noting short/medium haul characteristics, flight times, sonic boom problems, load factor, etc 22 p3744 A67-39339

Engine air intake design and development for Concorde aircraft, discussing design constraints [AIAA PAPER 67-752] 23 p4048 A67-40986

Engine test facilities on Concorde examined for effect on supersonic Olympus engine development [AIAA PAPER 67-753] 23 p4049 A67-40987

CONCRETE

Concrete pavement performance at ten civil airports, examining durability of surfaces, jointing subbase thickness and maintenance 02 p0229 A67-11841

Deformation characteristics of light concrete statistically compared to second concrete, determined through parameter similarity 19 p3341 A67-35630

CONDENSATION

SA CORONAL CONDENSATION

SA FILM CONDENSATION

SA LIQUEFACTION

SA NUCLEATION

Preparation temperature and condensation rate effect on current carrier mobility in lead selenide and telluride films 01 p0128 A67-10089

Li, Na, K, Rb and Cs vacuum tests as coolants and working fluids in high temperature compact space power plant 07 p1223 A67-19464

Mathematical model for condensation point of first order phase transitions, examining free energy singularity and metastable phase 07 p1268 A67-20089

Adiabatic flow of K vapor in supersaturated state noting supercompression, supercooling and equilibrium through condensation jump 11 p1881 A67-24029

Liquid metal MHD cycles with condensation by multistage injection of liquid 12 p1897 A67-25379

Condensation spectrum evolution of cloud droplets 13 p2151 A67-26690

Condensation of cytidylic acid in presence of polyphosphoric acid 13 p2065 A67-27183

Liquid nuclei formation at condensation centers in atmosphere analyzed for various degrees of saturation 14 p2346 A67-27908

Condensation droplet growth in supersaturated vapor and inert carrier gas, noting thermal and diffusion effects 15 p2582 A67-30198

Air condensation in hypersonic wind tunnel strongly related to flow expansion rate 16 p2657 A67-30708

Condensation during heterogeneous combustion, discussing kinetics, radiation and gasdynamic heat release 18 p3149 A67-33798

Local condensation in early stage of universe suggested from observation of spatial inhomogeneity of cosmic black-body radiation 19 p3312 A67-34893

Condensation history of cooling gas of cosmic composition, stressing chondrite fractionation patterns 20 p3526 A67-37172

Condensation spectrum evolution of cloud droplets 21 p3654 A67-38432

Upper limit for condensation of fluctuations in primordial fireball determined by considering effects of radiative diffusion 21 p3711 A67-39120

CONDENSATION PUMP

SA VACUUM PUMP

Pumping power of liquid nitrogen cooled cryosurface, showing reduced efficiency in presence of nitrogen via mass spectrometry 09 p1503 A67-22117

CONDENSER

SA CAPACITOR

SA GERDIEN CONDENSER

SA JET CONDENSER

Unsteady cascade flow and blade oscillation in axial condenser as aerodynamic boundary value problem 21 p3564 A67-37892

Transistorized time delay system based on measurement of condenser discharge time to predetermined voltage 21 p3590 A67-37952

Reliability evaluation of passive electronic components of ceramic and mica condensers and carbon resistors, including defects and stress analysis 21 p3571 A67-38671

CONDENSER RADIATOR

Condenser parameter effect on maximum heat transport in heat pipes for nonradiative and radiative cases 13 p2222 A67-26844

CONDITIONED RESPONSE

SA LEARNING

Reinforcing effect of informative stimulus that is not positive discriminative stimulus 11 p1748 A67-25065

Visual arousal interaction and specificity of nystagmic habituation 17 p2805 A67-31958

Influence on hits and false alarms of response and signal events on preceding trial 20 p3372 A67-36962

Quantification of response suppression in conditioned anxiety training with fixed duration preaversive stimulus /CS/ 20 p3373 A67-37577

Transverse accelerations remote aftereffect on conditioned alimentary reflexes of rats, discussing prolonged depression of higher nervous activity 23 p3943 A67-40771

Combined effect of acceleration and ionizing radiations on conditioned reflexes of rats noting alleviation on radiation leukopenia 23 p3943 A67-40772

Conditioned falling reflex of analyzer systems effect on change of human posture and spatial position 24 p4114 A67-41848

CONDUCTING MEDIUM

MHD rotation of conducting viscoplastic fluid between two coaxial cylinders in crossed fields 01 p0120 A67-10180

Small oscillations of viscous liquid-metal droplet under capillary force and in presence of magnetic field 01 p0120 A67-10182

Helical flow of conducting fluid between porous cylinders and disk electrodes in radial magnetic field, calculating electric power and efficiency 01 p0120 A67-10183

Approximate solution of stationary boundary layer problems involving flow of viscous incompressible conducting fluid around flat plate in presence of magnetic field 01 p0123 A67-10540

Alfven standing wave generation by current injection and/or electromagnetic induction in conducting liquid 02 p0272 A67-11520

Energy dissipation due to deformation of magnetic field in compressible conducting medium near zero field lines 03 p0470 A67-12940

MHD flow past bodies in electroconductive viscous incompressible

flow 03 p0482 A67-13743
 Secular variation of earth magnetic field 03 p0414 A67-13944
 Conducting surface boundary effect on current plasma instability in terms of potential fluctuations 04 p0667 A67-15208
 X and Z components of ponderomotive forces acting on conductive strip of finite width in EM field produced by unidirectional inductor 04 p0556 A67-15525
 Effect of finite length of conducting body on ponderomotive forces acting on traveling magnetic field 04 p0670 A67-15526
 Contactless flow meter, based on spatial MHD drifting, for flow velocity measurements on electroconductive fluid 04 p0624 A67-15531
 Coefficient of hydraulic resistance derived for plane flow of electrically conducting fluid in traveling magnetic field 04 p0670 A67-15534
 Current distribution on half-wave dipole antenna embedded in conducting half-space, noting case where dissipative medium has average earth constants 05 p0769 A67-16006
 Electric and magnetic field components produced by vertical and horizontal dipole antennas located at surface of conducting earth derived for quasi-static range 05 p0769 A67-16007
 Rotation and vibration of conducting circular cylinder in magnetic field, noting motion retardation due to induced electric current interaction with field 05 p0851 A67-16434
 MHD steady laminar flow of viscous incompressible electrically conducting liquid in rectangular pipe between conducting plates 05 p0853 A67-16723
 Electromagnetic scattering from perfectly conducting strips, wedges and notched circular cylinders 05 p0763 A67-16850
 Plane explosion in conducting gas with initial magnetic field having intensity vector directed at angle to plane 05 p0855 A67-17022
 Single parameter MHD flow of ideal incompressible infinitely electroconductive gas 05 p0855 A67-17114
 Motion of magnetic lines of force including analysis of fluids with finite high conductivity 06 p1030 A67-17561
 Optimum MHD generators using anisotropic plasma, discussing conducting-gas MHD flow, Hall effect, ion slip effect, etc 06 p0950 A67-18089
 Low magnetic Reynolds number two-dimensional and axisymmetric MHD flow of conducting ideal gas through supersonic nozzle 06 p1043 A67-18669
 Transverse oscillation stability in quasi-one-dimensional flow of conducting gas in magnetic field 07 p1227 A67-19119
 Turbulent flow of conducting fluid with free surface in presence of crossed magnetic and electric fields 07 p1227 A67-19321
 Wall conductance effect on MHD flow through finite cross section rectangular and circular channels 08 p1356 A67-20572
 MHD flow of viscous conducting fluid jets and MHD flows with nonlinear temperature dependent conductivity 09 p1541 A67-21807
 Approximation of electrical conductivity change in ideally conducting gas in turbulent MGD flow 09 p1544 A67-21860
 Steady flow of viscous conducting fluid in pipe under magnetic field analyzed for relations among Hartmann number, Reynolds number, skin friction, wall conductivity, etc 10 p1687 A67-23833
 Plane electromagnetic wave diffraction by conducting half-plane embedded in uniaxial anisotropic medium 11 p1753 A67-24315
 Green integrals extended to movement of incompressible viscous conductive fluid in which magnetic field is generated 11 p1840 A67-24620
 Partial differential equation of MHD converters, noting effects of converter width, side conductor materials and velocity distribution 12 p1896 A67-25374
 Plasma models and methods used to study wave propagation phenomena, considering particle orbit, single species moment equations, velocity distribution function, etc 12 p1975 A67-25527
 Oscillations and stability of cylindrical shell in conducting gas flow in presence of magnetic field 12 p2021 A67-25581
 Steady flow of conducting dissociating gas in channel of constant cross section in presence of magnetic field 12 p1929 A67-25756

Heat transfer in conducting and radiating gas analyzed, using governing equations reformulated as Lagrangian equations through introduction of potential 12 p2035 A67-25926
 Electromagnetic scattering from rough finitely conducting surface of uniform infinitely extended medium, considering intensity and polarization 12 p1906 A67-25945
 Nonhomogeneous turbulent motion of conducting fluid stabilized by longitudinal magnetic field 12 p1976 A67-26069
 Extension of Loitsianskii hypothesis concerning localism of turbulent transfer processes in viscous flows to MHD flows, noting results for friction coefficient 12 p1976 A67-26070
 Homogeneous solutions of Einstein-Lichnerowicz equations for electrically charged fluid with infinite conductivity universes 12 p1962 A67-26178
 Radial flow of two-dimensional viscous conducting fluid in wedge shaped channel under magnetic field, reducing flow equation to differential equation 12 p1977 A67-26180
 Velocity measurement in electrically conducting fluid flow in presence of uniform magnetic induction normal to flow direction 13 p2167 A67-27206
 Electrically conductive self-similar gas flow in medium with given back pressure, assuming medium conductivity as function of temperature and density 13 p2169 A67-27307
 Steady three-dimensional flow of electrically conducting gas in working section of linear MHD channel 13 p2169 A67-27310
 Laminar flow of incompressible conducting fluid in diffuser in presence of transverse magnetic field 13 p2169 A67-27313
 Plane conducting fluid-into-fluid jet in presence of transverse magnetic field, examining series expansion of stream function 13 p2169 A67-27317
 Technique of fabricating inhomogeneous mediums and behavior of dipole 13 p2082 A67-27407
 Plane explosion in conducting gas with initial magnetic field having intensity vector directed at angle to plane 14 p2359 A67-28484
 Nonrelativistic approximation for electromagnetic radiation in conducting medium moving with uniform velocity with respect to source 15 p2521 A67-29194
 Relativistic MHD shock wave stability in infinitely conducting plasma with magnetic field parallel to shock wave 15 p2523 A67-29216
 Current carrying incompressible viscous fluid past nonconducting sphere taking fluid inertia into account, noting eddy formation and flow separation 15 p2469 A67-29224
 Plasma acceleration in flat electrode plasma source simulated by ideally conducting bridge described electrostatically 15 p2525 A67-29249
 Eddy currents in nonmagnetic conductors calculated by finite difference successive overrelaxation technique on digital computer 15 p2541 A67-30142
 Conducting surface boundary effect on current plasma instability in terms of potential fluctuations 15 p2532 A67-30256
 Change in pressure losses in MHD generators channel, obtained from pressure gradient relation to flow rate of conducting fluid 16 p2705 A67-30449
 Material limitations in MHD induction generator, discussing effect of conducting channel walls and thermal insulation on performance 16 p2605 A67-30582
 Turbulent channel flow of electrically conducting fluid in presence of magnetic field obtaining skin friction coefficient and velocity profiles 16 p2661 A67-31225
 Conducting Bingham plastic fluids considered as lubricants in rheostatic bearing in presence of constant magnetic field [ASME PAPER 67-LUBS-4] 16 p2682 A67-31382
 Thermal radiation dependence of perfectly conducting materials on large and small surface roughnesses thermal radiation dependence of perfectly conducting materials on large and small surface 16 p2779 A67-31502
 Laminar jet flow of electrically conducting fluid over plane solid surface in transverse magnetic field solved using motion and

continuity equations 16 p2722 A67-31571
 Transverse magnetic field effect upon convective heat transfer in turbulent flow in electrically conducting fluid in channel bounded by two parallel plates 16 p2722 A67-31572
 Laminar flow of electrically-conducting fluid suddenly expanding in magnetic field calculated by approximate method 16 p2722 A67-31573
 Transverse magnetic field effect on barrier wake oscillation in electrically conducting liquid 16 p2723 A67-31714
 Self-similar motions in variable conducting fluid in strong magnetic field 16 p2724 A67-31782
 Maintenance of electromagnetic field by dynamo effect in homogeneous isotropic turbulence without mirror symmetry 17 p2883 A67-32355
 Steady flow of ideal gas with conductivity past thin wedge in magnetic field studied for asymptotic properties of flow field 17 p2902 A67-32671
 MHD behavior of inviscid fluid in limit of infinite electrical conductivity and mobility exhibiting Hall effect 17 p2908 A67-33109
 Flow of viscous incompressible conducting fluid in channel with porous walls 17 p2910 A67-33352
 Determination of magnetic field of spreading currents in continuous conducting media separated by spheroidal surface 18 p3079 A67-34035
 Longitudinal magnetic field effect on conducting fluid turbulent flow found limited to dissipation mechanism occurrence 18 p3028 A67-34215
 Electric field of AC solenoid of finite length in Hall conducting medium 18 p2990 A67-34500
 Traveling-wave bulk electroconvection induced in slightly conducting liquid with temperature gradient, giving velocity profile equations for plane flow 18 p3029 A67-34736
 Discontinuity problem solution between unloaded rectangular waveguide and same waveguide completely loaded with transversely magnetized ferrite 20 p3380 A67-36381
 Free convection of conducting fluid in coupled vertical channels for case of steady motion with lateral heating 20 p3500 A67-37051
 Electromagnetic plane wave scattering cross section from plasma coated conducting cylinder using TE and TM modes of polarization with respect to cylinder axis 20 p3389 A67-37706
 Transverse oscillation stability in quasi-one-dimensional flow of conducting gas in magnetic field 21 p3664 A67-38164
 Boundary value problem describing conducting fluid motion in longitudinal magnetic field, considering magnetic Reynolds numbers, electric current density distribution and heat exchange 21 p3665 A67-38243
 Velocity profiles of boundary layer of conducting fluid rotating over stationary dielectric disk of infinite radius in magnetic field 21 p3665 A67-38246
 Parallel conducting flow along insulating pipe under applied magnetic field, elucidating singularities of Hartmann boundary layers 21 p3668 A67-38495
 Asymptotic solution for planar electromagnetic wave diffraction on ideally conducting cylinder surrounded by inhomogeneous plasma layer 21 p3585 A67-38811
 Numerical computations for resistive plasma drift instabilities in conducting cylinder, noting finite boundary conditions effect 22 p3848 A67-39693
 Imbedded magnetic field stabilization effect on infinitely conducting inviscid compressible relativistic MGD half-jet 22 p3850 A67-39706
 Precise and approximate formulations for unsteady flows of conducting fluid in MHD channels with external electric circuit 22 p3853 A67-40023
 Polarized and depolarized scattering from perfectly conducting rough surface, theory based on Fourier transform and small perturbations polarized and depolarized scattering from perfectly conducting rough surface, using theory 22 p3762 A67-40078
 Parallel plate antenna for LF transmission and reception in conducting

medium 22 p3773 A67-40307
 HF approximation to diffraction of plane wave by conducting strip, using cylindrical wave terms for higher order patterns 23 p3979 A67-40831
 Radiative heat transfer in radiating and conducting media, calculating heat flux and temperature distribution for semisotropic model 23 p4083 A67-41718
 Scattering from half-loop on conducting plane obtained through image theory, considering electric and magnetic dipole contributions 24 p4121 A67-42265

CONDUCTION
S IONIC CONDUCTION
CONDUCTION BAND
 Electron-based superconductivity mechanism involving two overlapping conduction bands in alloys 01 p0127 A67-10062
 Optical reflection, transparency and Faraday effect for indium antimonide, calculating effective electron mass, relation between energy and wave number, etc 01 p0128 A67-10095
 State density for highly doped semiconductor in magnetic field, obtaining results at near Fermi level energies and at bottom of conduction band 01 p0128 A67-10096
 Effective mass Hamiltonian for conduction band g factor anisotropy of indium antimonide in magnetic field 01 p0134 A67-10785
 Bulk GaAs Gunn effect oscillators and amplifiers and electron transfer between high mobility and low mobility conduction bands 02 p0218 A67-12099
 Optical nonlinearities due to conduction band electrons in InAs, InSb, GaAs and PbTe studied, using Q-switched carbon dioxide laser radiation 02 p0254 A67-12524
 Optical mixing due to conduction band electrons in semiconductor 02 p0254 A67-12525
 Anisotropy of magnetoresistance and Hall effect in n-GaAs, discussing conduction band structure in vicinity of edge 03 p0487 A67-12806
 Electron conduction band structure of NaI crystals, using Hartree-Fock-Slater modified equation 03 p0495 A67-13513
 Lattice vibration spectra and energies of two-phonon summation bands and reststrahlen bands in gallium arsenide phosphide single crystals 03 p0495 A67-13514
 Anomalous high temperature Hall data for GaSb explained as effect of electrons in $1/100$ conduction band minima 03 p0501 A67-14346
 Sulfur donor level associated with conduction bands of gallium antimonide in measurements of Hall coefficient vs temperature and resistivity vs pressure 04 p0673 A67-14476
 Large signal AC field effect measurements on A and B real surfaces of InSb exposed to different ambients 05 p0862 A67-18604
 Band structure of n-type HgTe by use of model of band structure based on observation of Shubnikov-de Haas effect 05 p0864 A67-18900
 Photoconductivity, edge emission spectrum, longitudinal optical phonon coupling and eigenfrequencies for linear chain of Cd-Se-Cd-S-Cd... atoms 05 p0870 A67-17196
 Band structure and conduction phenomena in semiconductors of groups III-V, particularly in GaAs, noting signal instabilities and Gunn effect 05 p0871 A67-17325
 Experimental evidence of conduction band of semiconducting strontium titanate 06 p1059 A67-18906
 Impurity band tails in degenerate semiconductors, showing relation between decay in density of states and screening density 06 p1061 A67-18923
 Impurity centers arising from sulfur in silicon identified, using IR absorption technique and uniaxial stress effect 06 p1061 A67-18924
 Ground state energies of P, As and Sb donors in Si taking account of dielectric screening of donor potential 06 p1061 A67-18925
 Conduction band structure and anisotropy of electron scattering in n-GaAs, analyzing magnetoresistance and Hall effect 06 p1064 A67-18943

Electron motion in crossed fields with arbitrary ratio of electric and magnetic fields, considering simultaneously valence and conduction bands 06 p1069 A67-18978
 Band structure of Bi-Sb alloy system, using Shubnikov-de Haas technique with supplemental transport measurements 06 p1070 A67-18983
 Two energy gaps in superconducting compounds studied by NMR techniques 08 p1371 A67-21443
 Multiquantum electron transfers within conductivity band of semiconductors accompanied by emission or absorption of acoustic phonon, calculating absorption coefficient of electromagnetic emission 10 p1695 A67-23658
 Conduction band structure and scattering processes of cadmium mercury telluride mixed crystal determined from thermoelectric power, effective mass and electron mobility 12 p1979 A67-25178
 Approximate quantum numbers for d-band states in transition metals 13 p2179 A67-27155
 Shubnikov-De Haas oscillation analysis in n-type bismuth telluride indicates multivalley conduction band structure 14 p2369 A67-28596
 Quantum oscillation of magnetoresistivity in n-type mercury telluride crystals, obtaining electron mass 14 p2369 A67-28598
 Photoionization quantum yield in intrinsic-absorption region of cadmium selenide films 14 p2372 A67-28853
 Space-charge-wave growth and differential negative resistance conditions in two-valley semiconductors obtained from impedance 15 p2442 A67-29179
 Electron emission current density for semiconductors for all conditions between limits of thermionic and field emission 16 p2725 A67-30805
 De Haas-van Alphen effect in bismuth telluride over range of carrier concentrations, noting existence of low mobility heavy mass band 17 p2912 A67-32268
 Multiquantum electron transfers within conductivity band of semiconductors accompanied by emission or absorption of acoustic phonon, calculating absorption coefficient of electromagnetic emission 17 p2924 A67-33339
 Free carrier absorption coefficients in 6H and 15R silicon carbide, showing probable ellipsoids of revolution 18 p3102 A67-34279
 Thermistor theory and special applications 18 p3050 A67-34503
 Conduction band structure in n-type strontium titanate investigated by measuring oscillatory magnetoresistance in high magnetic fields 18 p3104 A67-34592
 Composition law of thermal resistance in contact between parallel bands 19 p3347 A67-35790
 Nonparabolic conduction energy band in semiconductors produces electron plasma excitations of sum and difference frequencies under strong DC electric field 20 p3505 A67-36210
 Electroluminescent diodes emission efficiency factor for application to lasers 21 p3591 A67-38153
 Electron energy band structure of semiconductor films determined by analysis of structural symmetry of germanium and silicon samples 22 p3861 A67-39919
 Interband and free carrier Faraday rotation in n-type InAs at room and low temperature, determining conduction band parameters 22 p3863 A67-40204
 Exact calculation of indirect exchange interaction isotropic and nonisotropic terms in rare earth metals, with free electron model for conduction band 24 p4203 A67-42110
 Semiconducting mixed titanate superconducting transition observed at 0.5 degrees K ascribed to change in valley numbers in conduction band 24 p4205 A67-43099

CONDUCTION ELECTRON
 Surface effects in quasi-classical energy quantization of conduction electron subject to arbitrary law of dispersion in metallic film 01 p0133 A67-10748
 Momentum loss rate by conduction electrons of polar semiconductors for known energy and momentum distribution 02 p0280 A67-11486
 Abnormal skin effect in thin films of noble metals near IR, taking into account

wave penetration and magnitude of conducting electrons mean free path 02 p0288 A67-11723
 Ferromagnetic semiconductors with exchange interaction due to conduction electrons 02 p0296 A67-11826
 DC and RF I-V characteristics, device fabrication and structure of epitaxial depletion mode n-type MOS-FET 02 p0218 A67-12103
 Electromagnetic, circuit theory, quantum and statistical mechanics laws for conduction electrons in low and high injection p-n junctions 02 p0299 A67-12105
 Hall mobility, Seebeck and Nernst coefficients measured in temperature range from about 100 to 350 degrees K for scattering mechanisms of conduction electrons in n type CdS 03 p0493 A67-13351
 Highly spin polarized carriers for studying neutral impurity scattering in P doped silicon 06 p1063 A67-18937
 Paramagnetic Knight shift in metals and semiconductors as affected by temperature and magnetic and electric field intensity 09 p1554 A67-21972
 Conduction phenomena in collector zone of saturated transistor 09 p1482 A67-22569
 Conduction electrons interaction with deformation potential and piezoelectric phonons to explain hot electron results in n-type InSb, taking into account screening of scattering potential 09 p1558 A67-22619
 Exponential sintering temperature dependence of conduction electrons density and attendant decrease of mobility due to ionized impurity scattering in cadmium oxide 10 p1691 A67-23503
 Surface effects in quasi-classical energy quantization of conduction electron subject to arbitrary law of dispersion in metallic film 13 p2176 A67-26777
 Optical absorption coefficient due to conduction electrons in nondegenerate semiconductors derived using Plakida method, noting light scattering 14 p2372 A67-28808
 N-type InSb electron thermoconductivity temperature dependence, lattice thermoconductivity and thermal resistance 16 p2730 A67-31163
 Damping effect of conduction electrons on ultrasonic surface and body waves propagating in CdS crystals, plotting damping against conductivity 17 p2921 A67-32971
 Paramagnetic Knight shift in metals and semiconductors as affected by temperature and magnetic and electric field intensity 17 p2923 A67-33309
 Operator for spin-phonon interaction between conduction electrons and polarization-induced longitudinal oscillations of semiconductor lattice 18 p3099 A67-33697
 Screened electron-phonon interaction effect on mobility of conduction electrons in semiconductors at low temperatures 20 p3509 A67-36433
 Conduction electron ground state and anomalous magnetic moment in antiferromagnetic semiconductor, considering magnetic polaron 22 p3857 A67-39462
 Anderson model Hamiltonian exchange character application to conduction electron Green function determination 22 p3861 A67-39994

CONDUCTIVE HEAT TRANSFER
S THERMOCONDUCTIVITY
CONDUCTIVITY
 SA AIR CONDUCTIVITY
 SA ATMOSPHERIC CONDUCTIVITY
 SA ELECTRIC CONDUCTIVITY
 SA IONOSPHERIC CONDUCTIVITY
 SA PHOTOCONDUCTIVITY
 SA PLASMA CONDUCTIVITY
 SA SUPERCONDUCTIVITY
 SA THERMOCONDUCTIVITY
 Dependence of conductivity on microhardness of p-doped n-type silicon, examining effect of gamma radiation 02 p0300 A67-12477
 Three diagonal conducting wall MHD generators, discussing time averaged behavior, instabilities and working fluid conductivity 12 p1898 A67-25381
 Current carrier concentration gradient in InSb, investigating effect on transverse reluctance coefficient and Hall effect dependence on magnetic field intensity 13 p2173 A67-26360
 Conductivity of cleaved surfaces of GaAs

- in liquid nitrogen 13 p2174 A67-26371
Current carrier concentration gradient in InSb, Investigating effect on transverse reluctance coefficient and Hall effect dependence on magnetic field intensity 21 p3680 A67-38317
Conductivity of cleaved surfaces of GaAs in liquid nitrogen 21 p3680 A67-38326
- CONDUCTIVITY METER**
Plasma jet electrical conductivity, using inductances with different diameters as measurement device 17 p2895 A67-32154
Electrodeless probe, consisting of single-layer coil enclosed in insulating tube, for plasma conductivity measurements 17 p2854 A67-32164
- CONDUCTOR**
S ELECTRIC CONDUCTOR
S EXPLODING CONDUCTOR
S PHOTOCONDUCTOR
S SEMICONDUCTOR
S SUPERCONDUCTOR
S THERMAL CONDUCTOR
S TRANSMITTER
- CONE**
SA CIRCULAR CONE
SA NOSE CONE
SA ROTATING CONE
SA SLENDER CONE
Pressure, heat transfer and Pitot pressure profiles measured on wedges and cones at high Mach and Reynolds numbers in hypersonic tunnel 04 p0600 A67-15822
Tip bluntness, surface roughness and angle of attack effects on laminar boundary layer for 10 degree cone, measuring heat transfer and detecting transition 04 p0549 A67-15823
Heat transfer tests of blunt nosed cone containing cylindrical protuberances tested in AEDC tunnel, including effects of local Mach number, Reynolds number and sweepback angle 04 p0549 A67-15832
Ballistic coefficients for power law body shapes compared with those for conical bodies having identical lengths, diameters and specific weights 05 p0750 A67-17360
Hot-wire anemometer measurements of transition in incompressible wake of cone at low Reynolds number 05 p0751 A67-17439
Schlieren techniques used in free flight range study of far wake of hypersonic cones [AIAA PAPER 67-31] 06 p0938 A67-18261
Expression for surface field components obtained for plane electromagnetic wave at nose-on incidence on seminfinte cone 14 p2261 A67-28376
Laminar boundary layer transition in hypersonic shock tunnel of cone, noting effect of high Mach numbers and tip surface roughness, using surface heat transfer gauges [AIAA PAPER 66-494] 15 p2418 A67-30191
Mach and Reynolds number, cone angle, base geometry, etc, effect on near wake flow of conical vehicle moving at high speed 15 p2418 A67-30215
Axisymmetric response of seminfinte truncated cone striking smooth rigid obstacle, determining early stages of motion 17 p2960 A67-32422
Time lag effect on dynamic stability determined, using wind tunnel tests with 10 degree cone as test body simulating ablation process by gas injection into boundary layer [AIAA PAPER 66-757] 17 p2792 A67-33004
Schlieren techniques used in free flight range study of far wake of hypersonic cones [AIAA PAPER 67-31] 17 p2793 A67-33006
Cone and disk laminar flows of power-law fluids similarity solution by Navier-Stokes equation 17 p2793 A67-33040
Supersonic fluid flow past elliptical and circular conical bodies at large angles of attack, using straight line method 18 p2984 A67-34211
50 degree semivertex angle sphere-cone Voyager configuration wind tunnel tested in dry nitrogen for aerodynamic characteristics, pressure and heat transfer distribution 20 p3356 A67-36562
Drag measurements of cones in rarefied flow regime extended to higher and lower cone semivertex angles 21 p3565 A67-38884
Base pressure measurements on elliptic cones in supersonic flow with turbulent boundary layer as function of geometry 21 p3566 A67-39083
- CONFERENCE**
Mechanics Conference, Ukrainian Academy of Sciences, Institute of Mechanics, Kiev, April 1966 01 p0157 A67-10214
Remote sensing of environment - USAF and USN Symposium, University of Michigan, Ann Arbor, April 1966 01 p0057 A67-10307
High speed nuclear electronics - Colloquium, Polytechnic Institute and Nuclear Study Center, Grenoble, France, February 1966 01 p0065 A67-10649
IEEE Region III Convention, Atlanta, April 1966 01 p0045 A67-10664
X-ray analysis applications - Conference, Denver, August 1965 01 p0095 A67-10665
Modern developments in powder metallurgy - International Conference, New York, June 1965, Volume I, Fundamentals and methods 01 p0096 A67-10691
Powder metallurgy - International Conference, New York, June 1965, Volume 2, Applications 01 p0097 A67-10696
Modern developments in powder metallurgy - International Conference, New York, June 1965, Volume 3 01 p0099 A67-10706
ISA National Aerospace Instrumentation Symposium, Philadelphia, May 1966 01 p0072 A67-11108
Reliability Symposium, San Francisco, January 1966 01 p0081 A67-11332
Basic problems of thin film physics - International Conference, Clausthal-Goettingen, West Germany, September 1965 02 p0281 A67-11701
Computing Machinery Association, National Conference, Los Angeles, August-September 1966 02 p0206 A67-11798
Telemetry - ITC Conference, Los Angeles, October 1966, Volume 2 02 p0195 A67-11996
National Electronics Conference, Chicago, October 1966 02 p0199 A67-12086
Radioisotopes for aerospace - symposium, Dayton, February 1966, Part 1, Advances and techniques 02 p0243 A67-12207
Cosmic ray physics - All-Union Conference, Apatity, U.S.S.R., August 1964 02 p0308 A67-12570
Perturbation theory and quantum mechanical applications - Seminar, University of Wisconsin, Madison, October 1965 02 p0270 A67-12721
Cosmic ray physics - All-Union Conference, Moscow, November 1965 02 p0313 A67-12744
Yearbook of European Aeronautical Congress, Munich, September 1965 03 p0354 A67-12965
Atomic interactions and space physics - Symposium, Goddard Space Flight Center, Greenbelt, Maryland, August 1965 03 p0470 A67-13216
Strengthening mechanisms in metals and ceramics - Conference, Raquette Lake, N.Y., August 1965 03 p0441 A67-13302
Aerospace instrumentation - ISA National Symposium, Los Angeles, October 1965 03 p0395 A67-13377
Advanced fibrous reinforced composites - Conference, San Diego, November 1966 03 p0450 A67-13399
Ferroelectricity - All-Union Conference, Rostov, U.S.S.R., September 1964 03 p0497 A67-13696
MHD - Seminar, Indian Institute of Science, Bangalore, May 1963 03 p0479 A67-13722
Deep space and missile tracking antennas - ASME Conference, New York, November-December 1966 03 p0383 A67-13748
Flow measurement - ASME Conference, Pittsburgh, September 1966 03 p0421 A67-13766
Atmospheric chemistry, circulation and aerosols - International Symposium, Visby, Sweden, August 1965 03 p0414 A67-14065
IEEE Automatic Support Systems Symposium for Advanced Maintainability, Clayton, Missouri, November 1966 03 p0397 A67-14201
Radio astronomical and satellite studies of atmosphere - USAF Symposium, Boston, October 1965 03 p0415 A67-14234
Nondestructive material testing - International Colloquium, Aachen, West Germany, December 1965 04 p0641 A67-14586
Solid state circuits - IEEE Conference, Philadelphia, February 1966, Part 1 04 p0580 A67-14594
Radar meteorology - AMS Conference, Oklahoma, October 1966 04 p0648 A67-14672
Vacuum microbalance techniques - Conference on Vacuum Microbalance Techniques, Princeton, September 1965, Volume 5 04 p0619 A67-14730
Fluid dynamic aspects of space flight - NATO-AGARD Specialists Meeting, Marseille, April 1964, Volume 1 04 p0605 A67-14987
Physics and technology of ion motors - AGARD Conference, Athens, July 1963 04 p0688 A67-15012
Radar techniques for detection tracking and navigation - AGARD Avionics Symposium, London, September 1964 04 p0571 A67-15028
Geological and astronomical research - Lunar International Laboratory Symposium, Athens, September 1965 04 p0596 A67-15062
Blaxial fracture strength of textured titanium alloy for design of liquid fuel tankage 04 p0711 A67-15242
Annual Electron and Laser Beam Symposium, University of Michigan, Ann Arbor, April 1966 04 p0622 A67-15300
Nuclear and space radiation effects - IEEE Conference, Stanford University, July 1966 04 p0586 A67-15687
Heat transfer - AICE International Conference, Chicago, August 1966, Volume 1, Single phase forced convection 04 p0727 A67-15800
Heat transfer - AICE International Conference, Chicago, August 1966, Volume 2, Single phase forced convection and natural convection 04 p0729 A67-15815
Heat transfer - AICE International Conference, Chicago, August 1966, Volume 3, Single phase, mass transfer and vibrations 04 p0732 A67-15837
Heat transfer - AICE International Conference, Chicago, August 1966, volume 4 04 p0734 A67-15846
Heat transfer - AICE International Conference, Chicago, August 1966, Volume 5, Flow boiling and radiation 04 p0736 A67-15859
High pressure technology - AICE Symposium, Detroit, December 1966, Part 1 04 p0611 A67-15945
Energy supply in space - Symposium, Stuttgart, West Germany, December 1965 04 p0557 A67-15953
Cosmic ray physics - All-Union Conference, Moscow, November 1965 05 p0875 A67-16081
Heat and mass transfer research - AICE Symposium, Detroit, December 1966, Part 2 05 p0925 A67-16269
Society for Information Display, Symposium, Boston, October 1966 05 p0804 A67-16305
Applied mechanics - Japan National Congress, Kyoto University, September 1964 05 p0844 A67-16415
Radioisotopes for aerospace - Symposium, Dayton, February 1966, Part 2, Systems and applications 05 p0840 A67-16528
Trajectories of artificial celestial bodies - Symposium, Paris, April 1965 05 p0893 A67-16554
Space age facilities - ASCE Conference, Cocoa Beach, Florida, November 1965 05 p0786 A67-16606
IAU General Assembly, Hamburg, August-September 1964 05 p0899 A67-17068
Bioengineering and food processing - AICE Meeting, Minneapolis, September 1965 05 p0757 A67-17155
American Society for Quality Control, Conference, New York, June 1966 05 p0812 A67-17240
Astronomical Society Conference, Gottingen, West Germany, September 1966 05 p0885 A67-17265
Electronic Packaging and Production Conference, New York, June 1966 05 p0778 A67-17450
Communications satellite systems technology, papers from AIAA Conference, Washington, D.C., May 1966 06 p0957 A67-17662
Space mathematics - Seminar, Cornell University, July-August 1963, Part 2 06 p1079 A67-17761
Space mathematics - Seminar, Cornell University, July-August 1963, Part 1 06 p1080 A67-17771
Space mathematics - Seminar, Cornell University, July-August 1963, Part 3 06 p0983 A67-17782
Noise and loading actions on helicopters, V/STOL aircraft and ground effect machines - Symposium, University of Southampton, August-September 1965 06 p0945 A67-17905

Test pilots report on aircraft and spacecraft - SETP Symposium, Beverly Hills, September 1966 06 p0947 A67-18196

Physical foundations of cathode electronics - All-Union Conference, Leningrad, October 1965 06 p1036 A67-18421

Weather forecasting - Symposium, Vienna, September 1965 06 p1026 A67-18598

Orientation effects in mechanical behavior of anisotropic structural materials - Astm Symposium, Seattle, October-November 1965 06 p1107 A67-18653

Semiconductor physics - Conference, Kyoto, September 1966 06 p1054 A67-18901

Planetology and space mission planning - Conference, New York, November 1965 06 p1090 A67-18993

Numerical solutions of nonlinear differential equations - Conference, U.S. Army Mathematics Research Center, Madison, May 1966 07 p1212 A67-19152

Self-adaptive control systems theory - IFAC Symposium, Teddington, Middx., England, September 1965 07 p1159 A67-19192

Earth science advances - Conference, MIT, Cambridge, September-October 1964 07 p1170 A67-19330

Materials for large space power systems - Symposium, American Nuclear Society, Washington, D.C., November 1965 07 p1222 A67-19459

Filmed data and computers - Seminar, Photo-Optical Instrumentation Engineers Society, Boston, June 1966 07 p1148 A67-19741

European geodetic network by satellite observation - Conference, Paris, December 1964 07 p1175 A67-19756

Physics of dislocations - Colloquium, Toulouse, March 1966 07 p1210 A67-20161

Mediterranean cooperation on solar energy use - General Spring Session, University of Marseille, May 1966 07 p1132 A67-20285

Combustion and combustion systems - Conference, Karlsruhe, West Germany, April 1965 08 p1425 A67-20302

Circuit and system theory - Allerton Conference, University of Illinois, October 1966 08 p1307 A67-20317

Solar and stellar systems orbit theory - IAU Symposium, Salonika, Greece, August 1964 08 p1379 A67-20380

Reinforced plastics - SPI Conference, Washington, D.C., January-February 1967 08 p1344 A67-20420

Empirical expression for resistance of small bore tubes to turbulent flow of compressible fluid in terms of mass flow and total head 08 p1320 A67-20461

Sounding rocket vehicle technology - AIAA Conference, Williamsburg, February-March 1967 08 p1402 A67-20491

SAE Stapp Car Crash Conference, Holloman AFB, New Mexico, November 1966 08 p1288 A67-20609

Recent developments in space flight mechanics - Conference, Berkeley, December 1965 08 p1384 A67-20616

IEEE Aerospace Computer Symposium, Santa Monica, October 1966 08 p1296 A67-20624

Aerospace and electronic systems - IEEE Convention, Washington, D.C., October 1966 08 p1290 A67-20646

Mechanics and chemistry of solid propellants - Symposium on Naval Structural Mechanics, Purdue University, April 1965 08 p1418 A67-20872

Measuring technology and automation - Conference, Dusseldorf, October 1965 08 p1313 A67-21004

Physics of moon and environment - Conference, London, June 1965 08 p1388 A67-21008

Post Apollo space exploration - AAS Meeting, Chicago, May 1965 08 p1391 A67-21064

Post Apollo space exploration - AAS Meeting, Chicago, May 1965 08 p1392 A67-21087

Polarization-optical method for investigation of stresses - All-Union Conference, Leningrad, June 1964 08 p1423 A67-21329

Precision electromagnetic measurement - IEEE Conference, Boulder, June 1966 09 p1493 A67-21612

Aerospace and electronic systems - Convention, Los Angeles, February 1967 09 p1466 A67-21674

Communications and information -

Conference, Frankfurt am Main, September 1966 09 p1463 A67-21757

MHD electrical power generation - Conference, Salzburg, July 1966, Volume I 09 p1536 A67-21773

Solid state physics - Conference, Klev, June 1965 09 p1580 A67-21903

Acoustic noise and control - Conference, London, January 1967 09 p1532 A67-21937

International Vacuum Conference, Stuttgart, June-July 1965, Volume 2, Part I 09 p1488 A67-22098

International Vacuum Congress, Stuttgart, June-July 1965, Volume 2, Part II 09 p1533 A67-22110

International Vacuum Congress, Stuttgart, June-July 1965, Volume 2, Part III 09 p1484 A67-22116

Aerospace fluid power - Conference, Detroit, October-November 1966 09 p1444 A67-22126

Laser welding and machining - Seminar, Pennsylvania State University, June-July 1965 09 p1504 A67-22137

Lubrication and wear - IME Convention, Scheveningen, Netherlands, May 1966 09 p1505 A67-22190

Fire resistance of hydraulic fluids - ASTM and SAE Symposium, New Orleans, January 1966 09 p1520 A67-22244

Microwave and optical generation and amplification - International Conference, Cambridge, England, September 1966 09 p1476 A67-22251

Reliability - Symposium, Washington, D.C., January 1967 09 p1581 A67-22286

Thermionic conversion - IEEE Specialist Conference, Houston, November 1966 09 p1448 A67-22330

Measuring and calculating methods in testing of aircraft - Conference, Prague, April 1966 09 p1500 A67-22453

Aircraft research and testing - Conference, Prague, November 1966 09 p1440 A67-22470

Microwave receivers with low noise - Colloquium, Paris, May 1966 09 p1481 A67-22477

Structural adhesives bonding - Symposium, Stevens Institute of Technology, Hoboken, September 1965 09 p1521 A67-22499

Air traffic control systems engineering and design - Conference, London, March 1967 09 p1527 A67-22626

Fundamental problems of metrology - Symposium, Warsaw, April 1967 10 p1654 A67-22755

Space research - Symposium, Vienna, May 1966, Volume 2 10 p1634 A67-23176

Space research - COSPAR International Symposium, Vienna, May 1966, Volume 1 10 p1641 A67-23246

Control theory and applications - IBM Symposium, Yorktown Heights, N.Y., October 1964 10 p1619 A67-23417

Structural fatigue in aircraft - ASTM Symposium, Seattle, October-November 1965 10 p1594 A67-23429

Gallium arsenide - International Symposium, Reading, Berks., England, September 1966 10 p1613 A67-23509

Hydraulics and fluid mechanics - Australasian Conference, University of Auckland, December 1965 hydraulics and fluid mechanics - Australasian Conference, University of Auckland, December 10 p1626 A67-23553

Structures, structural dynamics and materials - AIAA/ASME Conference, Palm Springs, March 1967 10 p1721 A67-23696

Plasma instability and anomalous transport - Conference, University of Miami, Coral Gables, May 1966 11 p1828 A67-23997

Fluid mechanics of internal flow - Symposium, Warren, Michigan, September 1965 11 p1775 A67-24041

Italian society of physics - Conference, Bologna, November 1965 11 p1818 A67-24102

Theoretical and applied mechanics - Conference, Haifa, May 1966 11 p1871 A67-24117

Aviation and astronautics - Conference, Tel-Aviv and Haifa, February 1967 11 p1777 A67-24212

Meteorology - Conference, Liblice, Czechoslovakia, October 1964 11 p1815 A67-24325

Physics of quiescent plasmas - Conference, Frascati, Italy, January 1967 11 p1832 A67-24367

Quiescent plasma physics - Conference, Frascati, Italy, January 1967, Part

2 11 p1836 A67-24369

Double Langmuir probe measurement of turbulent structure and ionization intensity of hypervelocity projectile and spectral characteristics of probe signal fluctuation 11 p1790 A67-24449

Dynamics of fluids and plasmas - Conference, University of Maryland, October 1965 11 p1779 A67-24532

Crystalline solids deformation - Conference, Ottawa, August 1966, Part 1 11 p1806 A67-24566

Rheology - Modern developments in mechanics of continua - Conference, Syracuse University, August 1965 11 p1781 A67-24569

Preparation and properties of electronic materials for radiative processes control - AIME Conference, Boston, August 1966 11 p1847 A67-24734

Interdisciplinary perspectives of time - Conference, New York, January 1966 11 p1820 A67-24935

Deformation of crystalline solids - Conference, Ottawa, August 1966, Part 2 11 p1810 A67-25089

Solar-terrestrial physics - Conference, Belgrade, August-September 1966 12 p1990 A67-25106

Nuclear and engineering ceramics - Conference, Harwell, Berks., England, October 1965 12 p1964 A67-25210

Physics of thin ferromagnetic films - Conference, Klev, June 1966 12 p1980 A67-25236

Electronic circuit packaging - Conference, University of Southern California, Los Angeles, August 1966 12 p1910 A67-25263

Low noise level microwave receivers - Conference, Paris, May 1966, Part 2 12 p1912 A67-25294

Lubrication and wear - IME Conference, Plymouth, England, May 1967 12 p1946 A67-25327

Thermodynamics and fluid mechanics - Conference, Liverpool, April 1966 12 p1927 A67-25345

MHD engineering - Conference, Stanford University, March 1967 12 p1971 A67-25373

Applied mechanics - IME Conference, Cambridge, England, April 1966 12 p2013 A67-25407

Thermionic Conversion Specialist Conference, IEEE, San Diego, October 1965 12 p1889 A67-25559

Theory of shells and plates - Conference, Baku, Azerbaidzhan SSR, September 1966 12 p2017 A67-25561

Environmental Sciences Institute - Conference, Washington, D.C., April 1967, Volume I 12 p1920 A67-25676

IES conference, Washington, D.C., April 1967, Volume 2, covering space and earth environments, shock and vibration, instrumentation and acoustics IES Conference, Washington, D.C., April 1967, Volume 2, covering space and earth environments, 12 p1922 A67-25705

Space research - Conference, Mar del Plata, Argentina, May 1965 12 p2003 A67-25759

Instrumentation in space and laboratory - Conference, Boston, October 1966 12 p1943 A67-25850

International outer space law - IAF Conference, Madrid, October 1966 12 p2041 A67-26195

Zeeman Centennial Conference, Amsterdam, September 1965 12 p1987 A67-26234

Electrical and electronics engineering - IEEE Conference, Jackson, Mississippi, April 1967 13 p2085 A67-26404

Applied mathematics and mechanics - Symposium, Darmstadt Technical University, April 1966 13 p2156 A67-26605

Advances in materials - Symposium, Manchester, England April 1964 13 p2132 A67-26691

Rarefied gas dynamics - Conference, Oxford University, July 1966, Volume I 13 p2096 A67-26934

Metallurgy of beryllium - Conference, Grenoble, France, May 1965 metallurgy of beryllium - Conference, Grenoble, France, May 1965 13 p2134 A67-27101

Magnetism and Magnetic Materials Conference, Washington, D.C., November 1966 13 p2178 A67-27137

Cosmic ray research - Conference, Huntington Beach, California, April

- 1966 13 p2192 A67-27242
Simulation and training - Conference, New York, April 1967 13 p2063 A67-27259
Sunspots - Conference, Arcetri, Italy, September 1964 13 p2206 A67-27415
Space age in fiscal year 2001 - AAS Conference, Washington, D.C., March 1966 13 p2230 A67-27501
AAS Space Flight Mechanics Specialist Conference, University of Denver, July 1966 13 p2206 A67-27515
Management of aerospace programs - AAS Conference, University of Missouri, November 1966 13 p2231 A67-27545
Advances in cryogenic engineering, Volume 12 - Conference, Boulder, June 1966 13 p2225 A67-27634
Annual National Relay Conference, Oklahoma State University, April 1967 13 p2084 A67-27693
Electronics and vacuum physics - Conference, Prague, September 1965 14 p2352 A67-27747
Low temperature refrigeration for microwave systems - Conference, Frankfurt am Main, April 1966 14 p2277 A67-27774
Symmetry principles at high energy - Conference, University of Miami, January 1966 14 p2350 A67-27798
Integrated circuits - Conference, Eastbourne, Sussex, England, May 1967 14 p2279 A67-28011
Dynamic stability of structures - Conference, Northwestern University, October 1965 14 p2396 A67-28078
Rarefied gas dynamics - conference, Oxford University, July 1966 14 p2298 A67-28160
Fluid control systems - Conference, Pennsylvania State University, July 1965 14 p2247 A67-28263
Fluidics - ASME Conference, Chicago, May 1967 14 p2248 A67-28322
Radio science, Part 1, Radio standards and measurements, troposphere, ionosphere, magnetosphere and noise of terrestrial origin - Conference, Munich, September 1966 14 p2262 A67-28388
Radio science, Part 2, Radio astronomy, radio waves and circuits and radio electronics - Conference, Munich, September 1966 14 p2266 A67-28428
Telemetry - Conference, San Francisco, May 1967 14 p2270 A67-28679
Planetary exploration - Conference, Roquencourt, Seine-et-Oise, France, December 1966 14 p2391 A67-28958
Radio spectroscopy and quantum electronics - Conference, Poznan, Poland, April 1966 14 p2332 A67-28967
Phonons and hypersound - Conference, University of Grenoble, March-April 1966 14 p2373 A67-28980
Plasma dynamics - AIAA and Northwestern University Conference, Evanston, August 1965 14 p2361 A67-29034
Life sciences and space research - Conference, Vienna, May 1966 15 p2423 A67-29096
Liquid crystal - Conference, Kent State University, August 1965, Part 1 15 p2429 A67-29297
Effects of space environment on materials - Conference, St. Louis, April 1967 15 p2505 A67-29534
Frequency generation and control for radio systems - Conference, London, May 1967 15 p2444 A67-29580
Nonhardware aspects of space navigation - Conference, Los Angeles, March 1967 15 p2513 A67-29594
Tube techniques - Conference, New York, September 1966 15 p2447 A67-29751
Semiconductor device measurements and test methods - Conference, Budapest, April 1967 15 p2448 A67-29799
Test methods and measurements of semiconductor devices - Conference, Budapest, April 1967, Part 2 15 p2449 A67-29809
Space technology - Conference, Palo Alto, May 1967 15 p2565 A67-29828
1967 SWIEECO record - IEEE Conference, Dallas, April 1967 15 p2450 A67-29901
Solid propulsion - ICRPG/AIAA Conference, Anaheim, June 1967 15 p2546 A67-29976
Mathematical methods of celestial mechanics and astronautics - Conference, West Germany, March 1964 15 p2558 A67-30034
Digital simulation in operational research - NATO Conference, Hamburg, September 1965 15 p2441 A67-30163
Network planning - Conference, London, June 1967 15 p2583 A67-30221
Spread-F and effects upon radiowave propagation and communication - NATO/AGARD Conference, Copenhagen, August 1964 15 p2479 A67-30273
Identification in automatic control systems - Conference, Prague, June 1967, Part 1 15 p2459 A67-30309
Identification in automatic control systems - Conference, Prague, June 1967, Part 2 15 p2462 A67-30329
American Society for Quality Control - Conference, Chicago, May-June 1967 15 p2494 A67-30401
Electricity from MHD - Conference, Salzburg, July 1966, Volume 2 16 p2706 A67-30512
Electricity from MHD - Conference, Salzburg, Austria, July 1966, Volume 3 16 p2607 A67-30592
Spacecraft systems, International Astronautical Congress, Athens, September 1965, Volume 1 spacecraft systems - IAF Conference, Athens, September 1965, Volume 1 16 p2755 A67-30622
Guidance and control, International Astronautical Congress, Athens, September 1965, Volume 2 guidance and control - IAF Conference, Athens, September 1965, Volume 2 16 p2699 A67-30649
Supporting equipment for space vehicles - Conference, Athens, September 1965 supporting equipment for space vehicles - IAF Conference, Athens, September 1965, Volume 3 16 p2620 A67-30667
Meteorological and Communication Satellites, Congress, Athens, September 1965, Volume 4 meteorological and communication satellites - IAF Conference, Athens, September 1965, Volume 4 16 p2759 A67-30684
Propulsion and reentry - IAF Conference, Athens, September 1965, Volume 5 16 p2735 A67-30701
Astrodynamics - IAF Conference, Athens, September 1965, Volume 6 astrodynamics - IAF Conference, Athens, September 1965, Volume 6 16 p2742 A67-30723
Life in spacecraft, International Astronautical Congress, Athens, Greece, September 1965 life in spacecraft - IAF Conference, Athens, September 1965, Volume 7 16 p2615 A67-30751
Astronautics and Education, International Astronautical Congress, Athens September 1965, Volume Eight astronautics and education - IAF Conference, Athens, September 1965, Volume 8 16 p2781 A67-30783
Heat transfer and fluid mechanics - Conference, La Jolla, Calif., June 1967 16 p2590 A67-30934
Stellar dynamics methods - Conference, Besancon, France, September 1966 16 p2748 A67-31136
Fracture - Conference, Sendai, Japan, September 1965, Volume I fracture - Conference, Sendai, Japan, September 1965, Volume I 16 p2767 A67-31275
Fracture - Conference, Sendai, Japan, September 1965, Volume 2 16 p2771 A67-31298
Fracture - Conference, Sendai, Japan, September 1965, Volume 3 16 p2773 A67-31314
Automatic control - Conference, University of Pennsylvania, Philadelphia, June 1967 16 p2644 A67-31634
Electronic components - IEEE and EIA Conference, Washington, May 1967 16 p2641 A67-31721
Physics of ferro- and antiferromagnetism - Conference, Sverdlovsk, USSR, July 1965 16 p2733 A67-31729
Airborne photo-optical instrumentation - Conference, Cocoa Beach, Florida, February 1967 16 p2678 A67-31791
Aerospace systems - SAE Conference, Los Angeles, June 1967 17 p2798 A67-31967
Effects of repeated loading of materials and structures - Conference, Mexico City, September 1966, Volume 3 17 p2957 A67-32027
Effects of repeated loading of materials and structures - Conference, Mexico City, September 1966, Volume 4 17 p2958 A67-32029
Low temperature plasma - Conference, Moscow, July 1965 17 p2890 A67-32134
Applied MHD - Conference, Jena, East Germany, April 1966 17 p2899 A67-32334
Interaction of radiation with solids - Conference, American University at Cairo, September 1966 17 p2913 A67-32371
Aerospace electronics - Conference, Dayton, May 1967 17 p2855 A67-32467
Hydroaerodynamics of carrying surfaces - Conference, Kiev, October 1965 17 p2792 A67-32901
Physical basis of yield and fracture - Conference, Oxford, England, September 1966 18 p3062 A67-33481
Aurora and airglow - NATO Conference, Keele University, England, August 1966 18 p3031 A67-33578
Liquid crystal - Conference, Kent State University, August 1965, Part II 18 p2990 A67-33632
Liquid crystal - Conference, Kent State University, August 1965, Part III 18 p2991 A67-33633
Energy conversion methods, MHD power generation - Conference, London, November 1965 18 p3085 A67-33701
Nondestructive testing - Conference, Warsaw, October 1966, Volume 1 18 p3044 A67-33733
Nondestructive testing - Conference, Warsaw, October 1966, Volume 2 18 p3045 A67-33738
Solar physics and hydrodynamics - Conference, Tatranska Lomnica, Czechoslovakia, October 1964 18 p3118 A67-33749
Numerical calculation and applied mathematics - Conference, Lille, France, 1964 18 p3071 A67-33751
Combustion - Conference, Berkeley, August 1966 18 p3146 A67-33778
Moon and planets - Conference, Vienna, May 1966 18 p3120 A67-34134
Orbital analysis - Conference, London, October 1966 18 p3125 A67-34234
Measure of moon - Conference, Manchester University, England, May-June 1966 18 p3127 A67-34301
Temperature Measurements Society Conference, Hawthorne, California, March 1967 18 p3050 A67-34501
Microelectronics for expanding economy - IEEE Conference, St. Louis, June 1967 18 p3013 A67-34547
Reliability and maintainability - Conference, Cocoa Beach, Florida, July 1967, Volume 6 18 p3055 A67-34648
Circuit theory - Conference, Purdue University, May 1967 19 p3200 A67-34838
Thermodynamics of ceramic systems - Conference University of London, April 1966 19 p3248 A67-34863
Aviation and transportation system, Progress, profits and public interest - Conference, Hartford, December 1966, Panel I 19 p3347 A67-34967
Aviation and transportation system - Progress, profits and public interest - Conference, Hartford, December 1966, Panel 2, Aviation and technological progress 19 p3347 A67-34970
Aviation and transportation system - Progress, profits and public interest - Conference, Hartford, December 1966, Panel 4, Aviation and public policy 19 p3348 A67-34975
Phenomena in ionized gases - Conference, Belgrade, August 1965, Volume 1, electronic and ionic collision phenomena, surface phenomena, electrical discharges 19 p3268 A67-35067
Phenomena in ionized gases - Conference, Belgrade, Yugoslavia, August 1965, Volume 2, Plasma physics 19 p3282 A67-35338
Phenomena in ionized gases - Conference, Belgrade, Yugoslavia, August 1965, Volume II 19 p3295 A67-35585
Automata Theory - Conference, Hanover, West Germany, October 1965 19 p3201 A67-35604
Practical space applications - Conference, San Diego, February 1966 19 p3326 A67-35634
Structure of surfaces - Conference, Durham, N.C., November 1966 19 p3246 A67-35782
Identification, optimalization and stability of automatic systems - Conference, Saclay, France, May 1965 19 p3203 A67-35901

Computer Conference, American Federation of Information Processing Societies, San Francisco, November 1966 19 p3187 A67-36053

Physicochemical and mechanical properties of refractory materials at high temperature - Conference, Paris, June-July 1965 20 p3471 A67-36109

Cellular injury and resistance in freezing organisms - Conference, Sapporo, Japan, August 1966, Volume 2 20 p3367 A67-36141

Magneto-fluid and plasma dynamics - Conference, New York, April 1965 20 p3493 A67-36142

Particle accelerator - Conference, Washington, D.C., March 1967 20 p3413 A67-36180

Electronics - Conference, Rome, June 1966, Volume 1 20 p3393 A67-36234

New methods of instrumental spectroscopy - Conference, Paris University, April 1966 20 p3436 A67-36334

Aerospace instrumentation - Conference, Cranfield, Beds., England, March 1966, Volume 4 20 p3441 A67-36457

Relation of testing and service performance - ASTM Conference, Atlantic City, June 1966 20 p3416 A67-36697

Spectral analysis of time series - Conference, University of Wisconsin, October 1966 20 p3476 A67-36782

Circadian clocks - Conference, Feldafing, West Germany, September 1964 20 p3370 A67-36805

Automation in electronic test equipment - Conference, New York, August-September 1966, Volume 3, Built-in test and continuous monitoring 20 p3416 A67-36969

Automation in electronic test equipment - Conference, New York, August-September 1966, Volume 4, Built-in test and continuous monitoring 20 p3448 A67-36978

Automation in electronic test equipment - Conference, New York University, August-September 1966, Volume 5, Built-in test and continuous monitoring 20 p3417 A67-36987

Geophysical theory and computers - Conference, Cambridge, England, June-July 1966 20 p3432 A67-37204

Fluid power research - Conference, Oklahoma State University, July 1967 20 p3365 A67-37360

Computer technology - Conference, University of Manchester, England, July 1967 20 p3392 A67-37455

Heat transfer - Conference, Chicago, August 1966, Volume 6 20 p3555 A67-37460

Nucleon-nucleon interaction - Conference, University of Florida, March 1967 20 p3490 A67-37612

Electromagnetic compatibility - IEEE Conference, Washington, DC, July 1967 20 p3404 A67-37635

Hypervelocity techniques - Conference, University of Denver, March 1967, Volume 1, Advanced experimental techniques for study of hypervelocity flight 21 p3605 A67-37787

High temperature resistance fibers - ACS conference, Phoenix, January 1966 21 p3647 A67-37870

Thin films applications in electronic engineering - Conference, London, July 1966 21 p3589 A67-37915

Fluid power - Conference, London, September 1966 21 p3570 A67-38101

Lubrication and wear - IME Conference, London, September 1967, Session 2, Fluid film lubrication 21 p3632 A67-38134

Lubrication and wear - Conference, London, September 1967, Session 4, Lubrication and materials 21 p3632 A67-38138

Lubrication and wear - IME Conference, London, September 1967, Session 5, Specific environments 21 p3633 A67-38140

Lubrication and wear - Conference, London, September 1967, Session 6, Synthesis 21 p3633 A67-38144

Industrial electronics measurement and control - Conference, Budapest, August 1967 21 p3591 A67-38157

Electronic packaging and production - Conference, Long Beach, California, January-February 1967 and New York, June 1967 21 p3593 A67-38327

High temperature technology - Conference, Pacific Grove, California, September 1967 21 p3578 A67-38390

Electronic packaging - SAE Conference, New York, February 1967 21 p3634 A67-38618

Magnetism and cosmos - Conference, University of Newcastle-upon-Tyne, England,

April 1965 21 p3707 A67-38977

Liquid metal properties - Conference, Upton, N.Y., September 1966, Part 1 21 p3685 A67-39101

Liquid metal properties - Conference, Upton, New York, September 1966, Part 2 21 p3686 A67-39103

Properties of liquid metals - Conference, Upton, New York, September 1966, Part 3 21 p3686 A67-39107

Reliability engineering - Conference, Nuremberg, April 1967 22 p3921 A67-39279

Developments in optics and applications in industry - Conference, Sussex, April 1967 22 p3836 A67-39328

Airport terminal facilities - Conference, Houston, April 1967 22 p3778 A67-39373

Symmetry principles at high energy - Conference, University of Miami, January 1967 22 p3840 A67-39582

Solar-terrestrial physics and magnetosphere - Conference, Belgrade, August-September 1966 22 p3882 A67-39687

Plastics stability - Conference, Washington, D.C., September 1967 22 p3824 A67-39850

Magnetics - Conference, Washington, D.C., April 1967 22 p3859 A67-39895

Missiles and aerospace vehicles sciences - AAS Conference, Huntsville, Alabama, December 1966, Volume 1 22 p3900 A67-39926

Missiles and aerospace vehicles sciences - Conference, Huntsville, Alabama, December 1966, Volume 2 22 p3904 A67-40134

Nonmechanical electric power sources - Conference, Brighton, England, September 1966 22 p3748 A67-40226

Cosmic ray physics - Conference, Moscow, November 1965 22 p3874 A67-40246

Thermal conductivity measurements of insulating materials at cryogenic temperatures - ASTM Conference, Philadelphia, February 1967, Committee C-16 22 p3802 A67-40289

Electromagnetic sensing of earth from satellites - Conference, University of Florida, November 1965 22 p3804 A67-40350

Liquid helium technology - Conference, Boulder, June 1966 22 p3838 A67-40388

Physics of superconducting devices - Conference, University of Virginia, April 1967 22 p3864 A67-40430

Gravitational instability and star and galaxy formation and structure - Conference, Liege, Belgium, June 1966 22 p3890 A67-40491

Logistics in 1970s - Conference, Washington, D.C., September 1967 23 p4084 A67-40579

Dynamical processes in solid state optics - Conference, Oiso, Japan, August-September 1966, Part 1 23 p4037 A67-40756

Contamination control - Conference, Washington, D.C., May 1967 23 p3961 A67-40842

Lunar probe data interpretation - AAS Conference, Huntington Beach, California, September 1966 23 p4063 A67-40946

Laser applications - Conference, Paris, July 1967 23 p4013 A67-41021

Laser applications - Conference, Paris, July 1967 23 p4014 A67-41034

Laser safety - Conference, London, November 1966 23 p4015 A67-41049

Cosmic ray physics - Conference, Alma-Ata, Kazakh SSR, October 1966 23 p4051 A67-41089

Magnetic materials and applications - Conference, London, September 1967 23 p4040 A67-41181

Aerodynamic phenomena in stellar atmospheres - Conference, Nice, France, September 1965 23 p4067 A67-41275

ISA Conference, Chicago, September 1967, Volume 22, Part I, Measurement standards instrumentation 23 p4003 A67-41334

ISA Conference, Chicago, September 1967, Volume 22, Part II, Physical and mechanical instrumentation 23 p4004 A67-41367

ISA Conference, Chicago, September 1967, Volume 22, Part III, Advances in instrumentation including data handling and computation 23 p4008 A67-41419

ISA Conference, Chicago, September 1967, Volume 22, Part IV, Applications in industry and science 23 p4008 A67-41423

Photovoltaics - IEEE Conference, Cocoa Beach, Florida, March 1967, Volume 1, Thin film cells 23 p3936 A67-41482

Photovoltaics - IEEE conference, Cocoa

Beach, Florida, March 1967, Volume 2, Spacecraft power systems, solar cell mathematical model 23 p3938 A67-41505

Photovoltaics - IEEE Conference, Cocoa beach, March 1967, Volume 3, Radiation and micrometeoroid effects on solar cells, lithium in silicon cells 23 p3940 A67-41516

Aerospace Medical Association Conference, Washington, D.C., April 1967 23 p3946 A67-41534

Fatigue crack propagation - ASTM Conference, Atlantic City, June-July 1966 24 p4247 A67-41941

Space simulation - Conference, Philadelphia, September 1967 24 p4137 A67-42028

Advanced fasteners - SAE Conference, Los Angeles, October 1967 24 p4180 A67-42076

Earth-moon system - NASA Goddard Institute for Space Studies, Conference, New York, January 1964 24 p4228 A67-42310

Reinforced plastics - Conference, Cleveland, October 1967 24 p4175 A67-42419

Computerized imaging techniques - Conference, Washington, D.C., June 1967 24 p4156 A67-42428

Advances in energy conversion engineering - ASME Conference, Miami Beach, August 1967 24 p4099 A67-42485

Computer and information sciences - Conference, Columbus, Ohio, August 1966 24 p4136 A67-42696

Cosmic ray physics - All-Union Conference, Moscow, November 1965 24 p4211 A67-42757

Cosmic ray physics - All-Union Conference, Alma-Ata, Kazakh SSR, October 1966 24 p4215 A67-42826

Nonlinear partial differential equations - Conference, University of Delaware, December 1965 24 p4179 A67-43081

CONFIDENCE LIMIT

Confidence limits for pointing error of gimbal sensor relative to off-gimbal reference, detailing sources of error and statistical properties 04 p0620 A67-14872

Failure occurrence paradox capable of resolution by small change of attitude 04 p0584 A67-15480

Error probability density distribution and selection of measurement accuracies and decision tolerances 08 p1336 A67-21057

Determining theoretical minimum signal that can be detected by optical detection system noting dependence on integration time, noise, etc 12 p1905 A67-25475

[SMPT PAPER 101-91] System reliability prediction and confidence limits for several component failure probability distributions, using Monte Carlo simulation on digital computer 20 p3455 A67-37314

CONFIGURATION

S AIRCRAFT CONFIGURATION
S LAUNCH VEHICLE CONFIGURATION
S PLANETARY CONFIGURATION
S PROPULSION CONFIGURATION
S SATELLITE CONFIGURATION
S SPACECRAFT CONFIGURATION

CONFINEMENT

SA PLASMA CONFINEMENT
SA REACTOR CONTROL
Bounded and confined turbulent jets compared to two-dimensional turbulent free jet 14 p2302 A67-28323

CONFORMAL MAPPING

Conformal mapping of circle onto profile cascades with arbitrary parameters useful for exact computation of potential flow through cascade 01 p0005 A67-10277

Stable convexity criteria of region in one-sheeted conformal mapping 01 p0104 A67-10287

Nonuniformly spaced planar arrays in which elements are located on lattice derivable from conformal mapping of uniform lattice 02 p0211 A67-11599

Conformal mapping for obtaining loci of complex variables without tedious calculations demonstrated, using simple T filter 02 p0227 A67-12176

Theoretical derivation of modification of shape of given airfoil which reduces moment values and sustains original lift 04 p0545 A67-14411

Two types of slit-coupled strip transmission lines especially useful for realization of multisection components, using printed circuit techniques 04 p0592 A67-14862

Electromagnetic wave propagation around cylinder surrounded by nonmagnetic

isotropic medium with dielectric constant function of radius, using conformal mapping 06 p0962 A67-18076

Dynamic stress concentration for plate with square hole, using approximate method of boundary shape perturbation and conformal mapping 06 p1109 A67-18665

Lemma for solution of conformal mapping problems of particular class of Fourier series with bounded partial sums and absolutely convergent on convergence circumference 07 p1215 A67-19475

Lateral efflux from flow along wall into suction slot computed by conformal mapping contraction coefficient 10 p1627 A67-23559

Standing wave solution of homogeneous waveguide field distribution for H-10 wave after conformal mapping and effect of capacitive and inductive irises 10 p1607 A67-23571

Incremental pressure drop in incompressible fluid laminar flow at entrance of rectilinear duct, using conformal mapping technique 12 p1930 A67-26166

Plane problems of elasticity theory solved numerically using conformal mapping 13 p2220 A67-27621

Transforms for regularizing two-body collisions in plane two-and three-body systems with aid of conformal mapping and function theory 15 p2559 A67-30037

Extremal problems of conformal mapping for doubly and triply connected regions, noting formulation and proof of pertinent theorems 16 p2698 A67-31913

Electrical simulation method of conformal mapping used in solving engineering problems in elasticity theory 21 p3727 A67-38839

Stress distribution on boundaries of two unequal circular holes in infinite plate determined by mapping region conformally onto annulus 21 p3730 A67-39086

Conformal mapping method for overcoming difficulties caused by limiting line in computing flow field about blunt body supporting paraboloidal shock wave 23 p3932 A67-41730

Conformal representation of ring on complex doubly connected symmetrical region bounded externally by circumference and internally by star shape curve 24 p4249 A67-42106

Electromagnetic wave propagation along arbitrary cross sectional imperfectly conducting metallic cylinder employing conformal mapping 24 p4120 A67-42230

CONFORMAL TRANSFORMATION

Thermal conductor of arbitrary shape, analogy with rectangular array of electrical resistance, detailing conformal transformation 01 p0187 A67-11015

Subsonic compressible flow around profile obtained by conformal transformation, reducing to Dirichlet problem 05 p0749 A67-16845

Einsteinian gravitation equations stated in terms of three-dimensional tensor analysis as applied in conformal space 08 p1354 A67-20843

Complex vectorial formalism in general relativity, discussing Riemann connection related to representation of Lorentz group by three-dimensional linear space 09 p1525 A67-22625

Characteristic momentary pictures of two-dimensional electromagnetic wave fields with all boundaries conformally transformed into parallel planes, taken from motion picture 14 p2268 A67-28447

More general form of metric for explicitly solving field equations of Hoyle-Narlikar conformal theory of gravitation 21 p3657 A67-37924

Conformal representation using Jacobi and Weierstrass elliptic function applied to extremal problems, noting electric modeling solutions 23 p4023 A67-40924

CONICAL FLOW

Shock-shock interactions for slender cone in theory and experiment 01 p0055 A67-11183

Pressure and density measurements of heat flux convected on sharp pointed cone placed in incidence in hypersonic flow 02 p0177 A67-11499

Asymptotic representation of solutions for boundary layers near weak shock waves in conical flows 03 p0352 A67-13631

Experiments on effect of subsonic inlet Mach number on performance of conical diffusers 05 p0748 A67-16811

Quasi-conical supersonic flow around lifting system with curved leading edge 05 p0749 A67-16843

Three-dimensional flow past blunt nosed cones 05 p0751 A67-17478

Unsteady supersonic flow about conical wing fuselage system with LF harmonic oscillatory motion 07 p1127 A67-20224

Quasi-conical motions applied to theory of wings with curved leading edges 07 p1128 A67-20235

Flow field around porous wedge or cone immersed at zero angle of attack in uniform supersonic free stream when contact surface is straight 08 p1276 A67-20571

Behavior of inviscid supersonic conical flow fields near crossflow stagnation points studied by constructing coordinate expansions of exact conical flow equations [AIAA PAPER 66-491] 10 p1591 A67-23112

Inviscid conical flow around pointed cone at angle of attack transformed into hyperbolic flow 10 p1592 A67-23136

Relative eddy flows mechanism in mixed flow turbomachines 12 p1891 A67-25348

Boundary layer transition displacement as function of nose bluntness, angle of attack and boundary layer cooling of half-angle cone [AIAA PAPER 66-495] 12 p1893 A67-25903

Transition sticking in wake of slender hypersonic cone as Reynolds number increases 12 p1893 A67-25927

Aerodynamic characteristics of sphere and blunt cone in highly rarefied gas flow, noting molecular collision effect 13 p2052 A67-27620

Rotating vortex flow and transition phenomena in conical diffuser [AIAA PAPER 66-426] 14 p2240 A67-28109

Supersonic internal axisymmetric conical flow obeying Taylor-Maccoll equation, discussing applications to wing surfaces and supersonic inlet leading edges 15 p2418 A67-30192

Numerical integration of differential equation describing gas flow in laminar boundary layer for core of conical external flow 16 p2658 A67-30454

Approximate solution for hypersonic flow past unyawed cone by small disturbance stream function equation 17 p2793 A67-33024

Quasi-conical motion past wing-body lifting system, determining pressure distribution, potential expression and axial disturbance velocity 20 p3356 A67-36278

Velocity distribution determination method for supersonic flow around zero incidence cones in equilibrium air, discussing motion equation and flow field parameters 22 p3742 A67-40098

Optimum design of ring airfoil device for maintaining pressure recovery efficiency of conical diffuser 22 p3743 A67-40168

High speed internal flow past cone with large wall injection velocities, calculating pressure of outer flow using contact surface initial slope as parameter 24 p4092 A67-42398

CONICAL INLET

Variation of total pressure loss coefficient with entry Mach number for conical diffusers, junction between parallel entry pipe and cone being sharp 04 p0549 A67-15748

Diffuser use in low density hypersonic wind tunnel and method of evaluating global performance for diffusers with conical inlet followed by cylindrical mixing section 05 p0748 A67-16763

CONICAL NOZZLE

Oblique shock detection in conical nozzle with circular arc throat, noting measurement techniques 04 p0547 A67-14833

Optimum geometry for rectilinear diffuser with rectangular, conical or annular cross section noting flow regime, performance characteristics and boundary layer effect 11 p1741 A67-24050

Test program assessing propulsion performance of cryogenic and ambient temperature gaseous parahydrogen expanded through conical thrust nozzles 16 p2734 A67-30705

Turbulent boundary layer and heat-transfer coefficients for air in conical nozzles, noting uncooled inlet length and convergence angle effects [ASME PAPER 67-HT-28] 20 p3357 A67-36721

Efficiency of conical thrust nozzles with various lengths and cone angles, determining optimization coefficient 24 p4093 A67-42922

CONICAL SHELL

Stability of thin walled conical shells under axially symmetric loading determined from nonlinear shell theory [DVL-605] 03 p0521 A67-13020

Radar scattering cross section for seminfinite perfectly conducting blunted cones 03 p0370 A67-13854

Electromagnetic excitation of metallic cone, deriving systems of linear algebraic equations for coefficients of expansion of electric and magnetic fields 04 p0575 A67-15152

Bubnov-Galerkin and energy method solutions of stability and oscillatory motion equations for conical shell under inertial loading 04 p0717 A67-15890

Thermal stress determination in thin conical shells of revolution using real function expression for forces, moments and displacements occurring during cyclic deformation 05 p0914 A67-16198

Axisymmetric modes and frequency vibration of thin conical shells subjected to rapid surface heating 06 p1100 A67-18000

Buckling of truncated conical shells due to directional thermal loadings [AIAA PAPER 67-112] 06 p1103 A67-18355

Vibration mode of conical shells measured, showing variation with conical angle and circumferential wave number 06 p1105 A67-18591

Stability of truncated conical thin shells under torsional load 06 p1105 A67-18592

Truncated conical shell stability under axial compression loads applied parallel to axis rather than along generatrix 06 p1105 A67-18593

Shape of interaction curve for axial compression vs torsional buckling of conical shells 06 p1110 A67-18858

Designing antisymmetrically loaded conical shells and elastic systems consisting of rings, plates and shells for machine elements 08 p1424 A67-21427

Vibration modes of conical frustum shells with free ends [AIAA PAPER 66-450] 08 p1424 A67-21533

Asymptotic and particular solutions of conical shells subjected to lateral normal loads, discussing membrane forces, bending effects and boundary conditions for moments and shearing force 09 p1573 A67-21754

Inextensional buckling of thin conical shell under axial compression [AIAA PAPER 66-125] 10 p1717 A67-23129

Resonant frequencies compared with associated mode shapes of truncated conical shells with both edges free 10 p1718 A67-23455

Linear motion equations including effects of transverse shear deformation and rotary inertia derived for thin elastic isotropic conical shells of revolution 10 p1729 A67-23767

Conical shell stability under hydrostatic pressure for various in-plane boundary conditions, stressing axial restraint effect 11 p1873 A67-24214

Natural oscillations of elastic truncated conical shells of revolution under composite static load 12 p2026 A67-25613

Rigidly reinforced conical shell stability under external load investigated for boundary conditions 12 p2027 A67-25622

Variational methods for calculating small axisymmetrical oscillations of conical shell of revolution partially filled with ideal incompressible fluid 12 p2028 A67-25633

Shallow conical shell stability acted upon by external hydrostatic pressure 12 p2028 A67-25635

Stressed state of conical shell with circular hole subject to tension and torsion 13 p2218 A67-26888

Electromagnetic excitation of metallic cone, deriving systems of linear algebraic equations for coefficients of expansion of electric and magnetic fields 15 p2435 A67-29339

Cross sectional shape and thickness ratio variation effect on maximum high lift/drag ratio examined, using flat-topped conical bodies 17 p2789 A67-32071

Moire topography techniques for partial slope and macroscopic curvature measurements of cylindrical and conical shells due to loading 17 p2960 A67-32455

Separation shock near base of conical

bodies at hypersonic speeds noting inflections in bow shock shape 17 p2793 A67-33044

Quasi-static equilibrium of truncated conical shell of revolution discussed in terms of zero-moment theory, when under cyclic load 19 p3341 A67-35631

Thermal buckling of conical shells under circumferential temperature gradients analyzed using Rayleigh-Ritz method 19 p3343 A67-35772

Thor SLV upper stage Burner 2 design, performance and cost 21 p3713 A67-38379

Conical shell of low aspect wing type, analyzing strength under distributed high/low pressures on surface, deriving equations and formulas for stresses 21 p3724 A67-38779

Buckling of truncated conical shells due to directional thermal loadings [AIAA PAPER 67-112] 21 p3728 A67-38873

Durability of conical rotating disks having asymmetric profiles and arbitrarily varying thickness 22 p3812 A67-39534

Stiffness matrix of unsymmetric nodal ring element for matrix displacement analysis of rib stiffened conical shells 22 p3914 A67-40191

Radiation pattern, absorption and impedance measurements of conical antenna plasma sheath about dielectric coated metal cone excited by axial radiating slot 23 p3973 A67-40840

Constant thickness elastic conical shells subject to lateral loads, deriving asymptotic solution 23 p4080 A67-41727

Stress functions for truncated conical shell buckling under uniform static pressure 23 p4081 A67-41760

Thin elastic shell nonlinear buckling theories, studying circular cylinder and truncated cone cases 24 p4252 A67-43096

CONJUGATED SYSTEM

Conjugate gradients method extended to function space for optimal control 01 p0044 A67-10483

Power gain sensitivity of transistors with conjugate matched two-port amplifier 12 p1910 A67-25260

Attainable sets and generalized geodesic spheres, noting set properties and meaning of conjugate points 13 p2088 A67-27096

Conjugate gradients providing convergent means to solve optimal-control problems for linear systems with quadratic performance index 16 p2651 A67-31678

World maps indicating geomagnetically conjugate locations and L parameters 17 p2844 A67-32547

Noether theory for system of singular integral equations with Carleman shift and complex conjugate unknowns as applied to boundary value problem 21 p3653 A67-38399

CONNECTOR

SA DISCONNECT DEVICE

SA ELECTRIC CONNECTOR

Impedance errors of coaxial air transmission lines and mechanical and electrical characteristics of Precifix connectors 02 p0213 A67-11648

Interconnection patterns for slice-level subsystems of integrated circuits 04 p0585 A67-15490

Humidity, temperature, contamination and disconnection effects on gasket and grease seals for extended space mission computer connectors 15 p2442 A67-29182

Impedance measurements in coaxial waveguide systems propagating TEM wave, using precision coaxial line standards and connectors 17 p2815 A67-32805

Flat pack interconnection technique using hot gas soldering, discussing inspection and control requirements 21 p3635 A67-38626

CONSERVATION EQUATION

Mode characteristics of solid state lasers from analytical solution of conservative equation 03 p0437 A67-13208

Ion velocity in rotating plasma treated by conservation equations of plasma constituents 03 p0485 A67-14053

Electromagnetic field in induction type plasma generator in steady state, from Maxwell equations and heat conservation equations 04 p0671 A67-15612

Optical transitions in semiconductors satisfying principle of momentum conservation through mutual interaction between free current carriers 06 p1059 A67-18912

Nonequilibrium air dissociation and

ionization in stagnation region of blunt body investigated in merged layer regime 16 p2592 A67-30955

Unconfined nitromethane transient initiation, determining differential conservation, state and reaction rate equations, using two-dimensional computations 18 p3153 A67-33824

Shock thickness for monatomic Maxwell molecule gas calculated using conservation and moment equations 18 p3030 A67-34753

Mass injection effect on compressible three-dimensional laminar boundary layers analyzed for nonreacting gas, using conservation equations for flow velocity profiles 21 p3613 A67-38852

CONSERVATION LAW

Cauchy and boundary value problems for homogeneous differential equations with two independent variables analyzed, establishing generalized solution existing on uniqueness maximal domain 02 p0280 A67-12432

Nuclear interaction similarity with Dirac monopole interaction with electromagnetic field, noting equality in number of conservation laws acting in either interaction 02 p0271 A67-12751

MHD and ionizing shock waves and conservation laws 05 p0851 A67-16416

Energy conservation analysis of step in negative resistance region of voltage-current characteristic curve of oscillating tunnel diode 11 p1759 A67-24132

Book on principles of continua with applications 12 p1986 A67-25557

Energy conservation during propagation of unsteady waves, obtaining formula for complex intensity 14 p2349 A67-28633

Nonlinear nonconservative systems stability analysis by approximate method based on principle of energy conservation 15 p2519 A67-30194

Ionization wave velocity in nonisothermal, low temperature plasma discussed, using generalized Ohm law, law of conservation of electron energy and SAHA equation 16 p2711 A67-30540

Conservative fields of force admitting spiral trajectories and dependence on constancy of energy level 16 p2748 A67-31137

Gas flow through annular duct of constant cross section analyzed in terms of conservation of energy, mass and angular momentum laws 16 p2593 A67-31153

Energy conservation law concerning electromagnetohydrodynamics of viscous electrically conducting fluid showing that total energy in fixed volume changes 16 p2721 A67-31549

Infinitesimal driven plane wave characteristics in uniform plasma with finite electron drift velocity found, using Navier-Stokes and Poisson equations, energy conservation continuity and perfect gas law 19 p3290 A67-35376

Exchange invariance in dissipationless fluid systems, deriving conservation law and stability conditions and application to gyro-stabilized magnetoplasma 20 p3419 A67-38151

Properties of kinetic energy and squared vorticity in two-dimensional inviscid turbulent flow, using Navier-Stokes equation and conservation laws 21 p3609 A67-37735

Nuclear interaction similarity with Dirac monopole interaction with electromagnetic field, noting equality in number of conservation laws acting in either interaction 22 p3841 A67-40253

Relativity theory accounting for energy conservation properties in elementary particle interactions and small size and high energy emission of quasars 22 p3892 A67-40499

CONSTANT

S COUPLING CONSTANT

S DIELECTRIC CONSTANT

S ELASTIC CONSTANT

S GRAVITATIONAL CONSTANT

S GRUNEISEN CONSTANT

S SOLAR CONSTANT

S TIME CONSTANT

CONSTELLATION

S CASSIOPEIA CONSTELLATION

S CENTAURUS CONSTELLATION

S CYGNUS CONSTELLATION

S ORION CONSTELLATION

S SAGITTARIUS CONSTELLATION

S SCORPIO CONSTELLATION

CONSTRUCTION

S AIRCRAFT CONSTRUCTION

S INSTALLATION

S MISSILE CONSTRUCTION

S SANDWICH CONSTRUCTION

S SPACECRAFT CONSTRUCTION MATERIAL

CONTACT

SA ELECTRIC CONTACT

SA ROLLING CONTACT

SA SLIDING CONTACT

Contact angle measurements for epoxy resin on boron filaments, demonstrating surface treatment effects 03 p0429 A67-13427

Legendre series solution to contact problem of torsion of elongated ellipsoid of revolution under arbitrary torsional loading 03 p0530 A67-14199

Two contact problems involving cylindrical shells reinforced with elastic frames 04 p0717 A67-15889

Temperature distribution effect on roughness of contacting surfaces of two juxtaposed solid materials 05 p0926 A67-16596

Four methods of solving elasticity theory contact problem and correlation of methods 05 p0923 A67-17180

Contact problem for elastic rectangle solved by reducing problem to solution of quasi-fully regular infinite set of linear algebraic equations with bounded free terms 11 p1876 A67-24679

CONTACT LENS

Medical complications of contact lenses and aeromedical implications 18 p2993 A67-34723

CONTACT POTENTIAL

Vibrating capacitor type device for measuring semiconductor contact potential and changes due to illumination or ambient atmosphere 06 p1005 A67-18728

Saha-Langmuir formula applied to description of temperature dependence of positive ion current in surface ionization of silicon atoms, comparing work functions by methods using contact potential, thermionic emission and Richardson graphs 09 p1554 A67-22006

Contact problem of half-plane inelasticity theory using Jacobi polynomials and taking into account thermal stresses and presence of adhesion and friction in contact area 11 p1876 A67-24677

Contact potential difference between crystal surfaces of indium antimonide cleaved in ultrahigh vacuum measured by Kelvin method 19 p3302 A67-34939

Surface potential of semiconducting gallium arsenide through temperature dependence measurements of transverse conductivity of clamped contact 21 p3676 A67-37869

Electron beam retarding potential method to measure work function changes resulting from Cs, oxygen- and hydrogen adsorption on /110/ Ta single crystal 24 p4201 A67-41892

Phenomena between evaporated metal and semiconductor surface affecting potential barrier by metal electrons extraction potential and semiconductor fast state concentration 24 p4204 A67-42410

CONTACT RESISTANCE

Contact resistance variation effect ion strength tests, noting strain gauge reading error magnitudes 02 p0340 A67-12444

Thermal conductance at interface of two materials in contact, investigating surface and lubrication effects [AIAA PAPER 65-662] 03 p0534 A67-13068

Figure contact resistance between Al and Cr sputtered conductive and resistive films 03 p0491 A67-13248

Thermal contact resistance between smooth rigid isothermal planes separated by elastically deformed smooth spheres [AIAA PAPER 66-461] 05 p0928 A67-17223

Metal-beryllium oxide bond for semiconductors noting mechanical and electrical strength, thermal conductivity and refractivity 10 p1896 A67-23691

Sliding electrical contact material for ultrahigh vacuum with 300 amp/sq inch current density, 425 in./min sliding velocity and 10 psi brush pressure 11 p1805 A67-24345

Electrical resistance of semiconducting diamond measured by pulse method 12 p1939 A67-25332

Electrically active centers distribution in Zn and Te implantations into GaAs 15 p2536 A67-29495

Metallic adhesion between Mo-Mo and Ti-Ti couples, showing contact resistance useful in determining contamination at conducting

- interface 17 p2871 A67-32465
Composition law of thermal resistance in contact between parallel bands 19 p3347 A67-35790
Similar or dissimilar materials thermal contact resistance in vacuum with negligible film effect, obtaining constriction resistance 20 p3555 A67-37609
Lubrication and wear problems of surfaces of solid materials noting influence of contact area, adhesion, speed, etc, on friction 21 p3633 A67-38139
- CONTAINER**
SA CARTRIDGE
SA CRUCIBLE
SA FUEL TANK
SA PACKAGING
SA TANK
Axial temperature and velocity measurements made in water at various aspect ratios, Grashof number and bottom-to-side heat flux ratios for turbulent free convection in closed container 04 p0731 A67-15827
Heat transfer in compressed gas evacuated from container, using numerical integration of state equation 07 p1267 A67-19324
Mass spectrometer and helium gas application in NDT for deleterious leaks in double-wall vessels for storing and shipping liquid oxygen and nitrogen 12 p1948 A67-25288
Fluid vibratory behavior in rigid containers, noting surface wave behavior governed by linearized boundary value solution 12 p1931 A67-26182
Fuel container design for space vehicles, discussing impact protection, reusability and long term cryogenic storage 13 p2212 A67-27218
Fluid motion in shallow trapezoidal container, noting dimensionless quantity relating frequencies to volume and rim dimensions, sloshing modes, eigenvalues, etc 16 p2661 A67-31421
Soviet book on numerical methods for calculating natural oscillation frequencies of liquids in bounded volumes 18 p3026 A67-33772
Low velocity detonations /LVD/ of liquid explosives indicate shape and container material and presence of witness plate affect initiation 23 p4081 A67-40635
Weldability of Al when used in low temperature container construction noting shielding with rare gases 24 p4159 A67-41839
- CONTAMINANT**
S CONFINEMENT
CONTAMINANT
Metallic couples ultrahigh vacuum adhesion experiments show contaminant dispersal as major barrier 15 p2492 A67-29493
Contaminant concentration in liquid breathing oxygen of aircraft converter determined by gas chromatography 16 p2619 A67-31475
- CONTAMINATION**
SA DECONTAMINATION
SA FUEL CONTAMINATION
SA RADIOACTIVE CONTAMINATION
SA SPACECRAFT CONTAMINATION
Micrometeoroid sampling with Luster sounding rocket during Leonid meteor shower, detailing contamination control program 04 p0699 A67-14966
Aircraft hydraulic systems contamination by particles from wear or external sources 09 p1445 A67-22131
Comparative evaluation of methods for determining microbial contamination on various types of surfaces 10 p1601 A67-23348
Contaminant control in oxygen for breathing in aviation solved by gas chromatography 12 p1902 A67-25173
Organic contaminant effects on relay reliability, discussing materials, degassing and contamination reduction 13 p2084 A67-27694
Miniature cryogenic refrigeration systems design for masers and parametric amplifiers, investigating efficiency and contamination 14 p2277 A67-27775
Experimental forging of titanium by techniques not requiring machining 14 p2324 A67-28629
Thermal control surface contamination due to rocket exhaust plumes and effects on solar absorptance and IR emittance of protective coatings 17 p2833 A67-32076
Metallic adhesion between Mo-Mo and Ti-Ti couples, showing contact resistance useful in determining contamination at conducting interface 17 p2871 A67-32465
Detection of contaminating processes in integrated circuits, describing characteristics associated with incipient failure in operational equipment 18 p3057 A67-34665
Growth of terrestrial microorganisms on Mars noting possibility of planetary contamination 19 p3178 A67-35896
Contamination control in hydraulic system of Saturn S-IVB stage, noting five-fold approach to anticontamination procedure 20 p3363 A67-36801
Contamination control of hydraulic system achieved when contamination level of fluid is within contamination tolerance level of system components 20 p3365 A67-37363
Contamination control Conference, Washington, D.C., May 1967 23 p3961 A67-40842
Contamination detection by analytical instrumentation considering sampling, IR, atomic absorption spectrophotometer, gas chromatography, colorimetry and polarography 23 p3998 A67-40844
Program for preventing earth environment biological contamination by lunar material 23 p3961 A67-40845
In-Line-Filter-Holder and Counter /ILFHC/ designed for high and low pressure systems to verify particulate cleanliness levels in modern fluid systems 23 p3935 A67-40846
Sampling bottle with valves and high pressure filter holder for fuel and oxidizer, by weighing bottle before and after sampling amount of fuel passing through filter can be calculated 23 p3998 A67-40849
Contamination control program developed for investigation and elimination of contaminant particles from 1965 Leonid Meteor Shower micrometeoroids collected by rocket payload 23 p3986 A67-40850
Supercleaning processes for Lunar Orbiter calling for personnel training, clean room garments, chemical cleaners, special packaging and inspection for particulate contamination 23 p3962 A67-40854
Vacuum chamber contaminants, discussing silicone pumping fluid from diffusion pumped systems 24 p4138 A67-42035
- CONTINUITY EQUATION**
Flow of compressible fluids past straight cascades of arbitrary airfoils using Karman-Tsien method, obtaining velocity distribution around airfoil through continuity equation 02 p0177 A67-11470
Continuity equation for electrons in F-2 layer obtained for region near geomagnetic equator at noon including photoionization, recombination, drift, etc 04 p0614 A67-14954
Radiative transfer in inhomogeneous medium derived on basis of continuity equation for radiative energy density in coordinate space and group velocity space 05 p0761 A67-16340
Dynamical model of steady state self-gravitating stellar system with finite total mass 05 p0897 A67-16804
Northern Hemispheric mean meridional circulation determined, using angular momentum and continuity equations 09 p1490 A67-21549
Invariant transformation for pulse and continuity equations of one-dimensional unstabilized motions of ideal compressible fluid 10 p1628 A67-23678
Air gauge circuit analysis extended to fluidic restrictor circuits and complex resistor circuits, using Bernoulli and continuity equations 14 p2252 A67-28353
Computer solution for current density, continuity and Poisson equation to obtain electron density and electrostatic potential in p-n junction 14 p2290 A67-28931
Night F layer behavior, considering height and electron density, noting computer program for nonsteady state continuity equation with neutral gas movement 15 p2474 A67-29523
Numerical solution of boundary layer equations by finite difference integration 15 p2473 A67-30189
Motion and continuity equations for atomic and molecular oxygen density solved numerically as time dependent problem 16 p2664 A67-30975
Continuity equation for electron density in F-2 layer, noting solution for given diffusion, loss, time dependence, etc 17 p2853 A67-33245
Relationship between stability and continuity for dynamical systems analyzed using functional analysis, discussing connection to boundedness 18 p3079 A67-34286
Turbodynamic disk stress-strain state, with final deformations under unsteady operational conditions, noting plastic flow, continuity, tension, and disk equilibrium equations 19 p3234 A67-34880
Ideal fluid energy-momentum tensor derivation of Crocco-Vazsonyi equation for ideal fluid relativistic hydrodynamics, discussing continuity equation for specific entropy 19 p3210 A67-35707
Excess carrier distribution in inhomogeneous semiconductor rectangular plate under two illumination conditions 19 p3308 A67-36026
Ram effect similarity criteria determination from partial differential equation system noting composite similarity, simulation possibilities, continuity equation, etc 20 p3419 A67-36190
Invariant transformation for pulse and continuity equations of one-dimensional unstabilized motions of ideal compressible fluid 21 p3612 A67-38279
Plasma continuity equations, deriving oscillation frequency equations for LF oscillations in partially ionized gases 22 p3844 A67-39383
Momentum equation examined by curvature of streamlines downstream from shock wave 22 p3783 A67-39727
Particle and energy continuity equations derived and solved by computer method ion composition and plasma temperature measured by Explorer XXII particle and energy continuity equations derived and solved by computer method for ion composition 22 p3790 A67-39804
Real gas jet equations of motion, energy and continuity derived, transformed and solved for mixing region, discussing approximate state equation construction 23 p3989 A67-40729
Time reversible difference procedures including Lorentz and continuity equations, relativistic orbits and gyrocenter motion 23 p4027 A67-40996
- CONTINUOUS FLOW SYSTEM**
Continuous horizontal zone refining system for purification of organic compounds, inorganic salts, metals, etc 02 p0247 A67-12691
Generalized mixing length argument in turbulent diffusion, obtaining integral equation for continuous case 04 p0603 A67-14648
Existence or nonexistence of continuous shockless transonic flow around symmetric wing profile, using Oswatitsch integral equation 06 p0942 A67-18586
Laminar and turbulent flow and heat transfer in boundary layer on continuous moving surface 10 p1732 A67-22728
Continuous flow cryostat system for open cycle cold fluid 14 p2404 A67-27786
AC MHD power generator and turbine described noting working fluid flow 16 p2605 A67-30581
- CONTINUOUS FUNCTION**
Solution of second order differential equation containing continuous function expandable in Maclaurin series, using Volterra integral equation 02 p0260 A67-12668
Optimal control problems, considering arbitrary piecewise-continuous function with finite number of discontinuities of first kind 03 p0392 A67-13626
Continuous periodic function approximation by Fourier series 03 p0462 A67-14108
Triangular iteration method of vector-matrix equation, noting role of continuous function 03 p0462 A67-14328
Approximation of functions of many variables by Bernstein polynomials, using method based on conjugate operators 04 p0646 A67-15258
Quasi-static equilibrium of thin plate heated by stationary circular source, obtaining expression for elastoplastic region at heating center, using continuous function 05 p0912 A67-16179
Necessary and sufficient set conditions for continuous function analytic within internal points of set to permit smooth approximation by means of rational fractions 07 p1212 A67-19137

Parabolic equations with continuous coefficients 07 p1212 A67-19139

Order of approximation of continuous functions through Hermite-Feier polynomial along entire axis 07 p1213 A67-19161

Stability of integrals of differential equations for periodic motions 10 p1680 A67-23666

Single parameter apparatus for approximation of set of continuous functions 11 p1813 A67-24849

Approximation problem in curve gamma, which is continuous image of interval I 12 p1960 A67-25257

First boundary value problem for second order elliptic partial differential equations, analyzing smoothness and continuity of generalized solution 13 p2144 A67-26378

De la Vallee Poussin linear homogeneous differential equation of nth order with continuous functions as coefficients 13 p2147 A67-27467

Harmonic analysis to improve accuracy and reduce computation of coefficients in Chebyshev expansion 14 p2342 A67-27976

Extension of Zygmund approximation series to two dimensions, noting periodic function role 14 p2345 A67-28938

Strong approximation of continuously differentiated function by means of differentiated expressions of finite line matrix 14 p2345 A67-28940

Method of solving for Fourier coefficients expressing dependent variable as piecewise continuous function assuming various conditions of continuity and smoothing 16 p2698 A67-31543

Proof of continuity of Haar measurable almost periodic functions 17 p2876 A67-32385

Existence theorems for linear optimal control problems with nonlinear cost functionals 20 p3408 A67-37076

Stability of integrals of differential equations for periodic motions 21 p3657 A67-38267

Helly problem of moment theory and optimum approximation of finite defect by subspace elements of continuous functions, examining uniqueness and existence 21 p3653 A67-38400

Polygonal approximation method for systems with nonlinear characteristics analyzed using continuous functions 21 p3657 A67-38551

Sample continuous second order martingale process, determining existence of limit of stochastic processes using approximation theorems 21 p3654 A67-38966

CONTINUOUS NOISE

SA IMPULSE NOISE

Derivation of moments of continuous stochastic system 15 p2459 A67-30131

Continuous /24 hr/ wide band noise effect on human body, discussing subjective/objective fatigue 20 p3369 A67-36670

CONTINUOUS WAVE

SA MODULATED CONTINUOUS WAVE

Time variation in intensity of light emitted from CW GaAs laser diodes 01 p0088 A67-10243

CW laser using 3-inch ruby crystals with 15 percent mirror transmission, pumping power of double threshold value and 1.6 watt power output 01 p0088 A67-10244

Book on statistical communications theory, digital communications, AM and FM CW communications, binary communications and noise 01 p0021 A67-10306

Three new visible CW laser lines in discharge in singly-ionized Cl 01 p0089 A67-10373

Output autocorrelation function and spectral density of CW and FM signals passed through TWT 01 p0025 A67-10858

Extensometer for measuring small changes of specimen on tensile testing vacuum furnace at high temperatures, using CW gas laser as light source 01 p0070 A67-11036

Voice-bandwidth communication link analyzer /CLA/ system for making measurements on communication link, using periodic pulse stream with suitable spectral filtering 02 p0203 A67-12134

Performance of two-photon laser operating in continuous wave mode, deriving formula for pulse frequency 03 p0437 A67-13292

Crystal absorption and lamp emission spectra for CW pumping of Nd-doped YAG by water-cooled Kr arcs 03 p0437 A67-13576

CW He-Ne laser compared with mercury

arc source, obtaining Raman spectra of carbon tetrachloride by three methods of excitation 03 p0438 A67-13912

Range safety and tracking systems, discussing C-band beacon, CW transponder and command-destruct receiver operation and testing 04 p0577 A67-15729

Line width of CW GaAs lasers measured using homodyne detection and autocorrelation 05 p0821 A67-18670

Argon discharge characteristics used in continuous action ion laser for analysis of inversion production mechanism 05 p0823 A67-18680

Laser studies at RCA Victor Research Laboratories, Montreal, discussing spectroscopic, interferometric and plasma diagnostic research 07 p1194 A67-19082

Relative intensities and cascade transition ratio in CW Ar II laser near 4103.9 angstroms 07 p1195 A67-19560

CW interference and white noise effect on second order phase lock loop, using reciprocal of loop mean square phase error as index of performance 07 p1161 A67-19878

Hellum-neon CW laser oscillation at 1.1523 microns observed in high velocity gas flow system, using rapid mixing of metastable helium atoms with initially unexcited neon 09 p1510 A67-21568

Scattering of coherent and incoherent light compared, using CW He-Ne gas laser sources 09 p1510 A67-21600

Precision power measurements of spacecraft CW signal level with microwave noise standards, noting Mariner IV application [JPL-TR-32-1070] 09 p1495 A67-21622

Traveling wave electro-optic modulator tested at 6328 angstroms with CW drive power 09 p1471 A67-21644

Continuous waves from synchronized pulsed bulk GaAs oscillators operating in microwave region 09 p1471 A67-21645

Absolutely calibrated radiometer for CW laser radiation in visible and near IR bands which relies on heat flow through standard thermal impedance 09 p1502 A67-22615

Plane shock formed by steepening of continuous wave into shock in atmosphere having exponentially decreasing density 10 p1624 A67-22969

Near field power density incident on eyes due to reflection from CW laser reduced by optical lens and shutter rearrangement 10 p1665 A67-23415

Gunn effect oscillators constructed from epitaxially grown n-type GaAs on n-plus substrate to obtain CW oscillations with frequencies from 3 to 35 gc 10 p1615 A67-23530

Epitaxial advantages over melt grown GaAs in construction of continuous wave and pulsed Gunn effect oscillators 10 p1616 A67-23531

Statistical survey of CW transferred electron oscillators /Gunn diode/ made from epitaxial gallium arsenide 10 p1616 A67-23532

Optical power gain characteristics of continuous wave carbon dioxide laser studied parametrically with single-pass amplifier 11 p1800 A67-24244

Microwave optical field distribution patterns visualized using IR thermosensitive transducer method 11 p1792 A67-24714

Central tuning dip in power output of continuous wave submillimeter molecular laser to measure radiative lifetime and collision line broadening 11 p1803 A67-24932

Heterodyne detector of submillimeter radiation using CN maser as continuous wave source of coherent radiation 12 p1951 A67-25209

Water cooled mercury arc discharge lamp for room temperature optimum optical pumping of CW lasers 12 p1952 A67-25331

Effect of multiple zinc diffusions on threshold and CW output power of semiconductor laser 13 p2125 A67-26522

Set of curves relating statistical properties of envelope detector output to SNR of CW signal in narrow band Gaussian noise at input 13 p2070 A67-27154

Bistatic CW radar observations of Venus conducted by U.S.S.R. and Great Britain during 1966 14 p2265 A67-28403

CW solid state lasers, considering principal laser crystals 14 p2330 A67-28470

Competitive and cascade coupling between transitions in CW water vapor laser 14 p2331 A67-28498

Frequency spread in ionospheric radio propagation 14 p2273 A67-28712

Single frequency, far IR and high power gas laser design and manufacturing 14 p2333 A67-28970

Magnetic field strength effects on pulse and CW operation of large diameter ionized gas lasers 15 p2496 A67-29173

CW operation of ultrathin CdSe platelet laser excited optically by HeNe laser 15 p2500 A67-29821

Modular distance measurement using geometric model for electronic continuous wave distance measuring equipment 15 p2511 A67-29893

Airborne ground profiler using CW and pulsed lasers range finders discussing performance 16 p2679 A67-31798

Laser research and development in France and applications to holography, metrology and gyros 17 p2868 A67-32745

Continuous wave signals from Lunar Orbiter I after reflection from lunar surface, noting mapping use 17 p2817 A67-33364

CW transmission measured for carrier and modulation phase, examining carrier phase perturbations due to mode interference CW transmission measured for carrier and modulation phase, examining carrier phase 20 p3379 A67-36292

Quasi-CW oscillation at 4880 angstrom of wide-bore AR II ion laser by plasma inductive excitation 20 p3458 A67-36387

Satellite orbit determination by measuring arrival angle of two transmitted waves with different frequencies 20 p3382 A67-36774

High efficiency optical pumping system for crystal laser rods with application to CW output 20 p3461 A67-37290

RF mixer and limiting IF models for RFI analysis of local oscillator control in FM-CW receivers, using digital computer simulation 20 p3405 A67-37649

Continuous wave laser ground-space-ground experiment in conjunction with Explorer XXII satellite tracking 21 p3578 A67-37858

Molecular and atomic, neutral and ion gas laser advances, noting high power CW carbon dioxide laser 21 p3639 A67-38062

Junction temperature current dependence in CW operated gallium arsenide laser diodes 21 p3639 A67-38256

Solid state CW optically pumped microwave masers using divalent Tm in calcium fluoride and strontium fluoride hosts 21 p3640 A67-38454

RF generation in VLF/LF thyristor transmitter for applications in long distance communications and navigation 22 p3771 A67-39842

Laser lines observation in Freon-He mixtures in CW gas discharge 22 p3817 A67-40489

Threshold properties of CW laser oscillation at 7525.5 angstroms in DC-excited KrII discharge 22 p3818 A67-40490

Carbon disulfide P-branch transitions with J equals 28 to 46 for 001-100 vibrational transition identified as laser lines in N-carbon disulfide gas system 23 p4011 A67-40789

Absolute frequency measurements on continuous wave hydrogen cyanide submillimeter laser lines 24 p4166 A67-41861

Silicon avalanche oscillators under continuous operation at millimeter wavelengths, discussing efficiency and power densities 24 p4133 A67-42815

CONTINUOUS WAVE /CW/ RADAR

Doppler system for missile and bullet velocity measurements noting design parameters, equipment used and range improvement obtained 04 p0653 A67-15044

Continuous wave radar application for obtaining velocity and range information on single targets at large distances 04 p0574 A67-15046

High power CW radar transmitter, discussing design parameters, development and performance characteristics 04 p0596 A67-15051

Range determination with CW tracking radar controlling rms error, noting SNR role in holding target echo 06 p0957 A67-17593

Vertical incidence CW Doppler phase path sounder spectral analysis of ionospheric motions and irregularities due to atmospheric wave propagation into ionosphere from below 07 p1182 A67-19952

Principles, methods of operation,

techniques and limitations of phase comparison position-determining CW and pulse type systems 10 p1605 A67-22996
 Meteor trains detection and study of motions in upper atmosphere using Garchy meteor radar with continuous wave 13 p2195 A67-26467
 Two-dimensional aperture synthesis in lunar CW radar astronomy, showing measurement possibility for Fourier transform components of sky brightness distribution 14 p2385 A67-28442
 Doppler effect method for measuring effective scatter area in laboratory 15 p2443 A67-29286
 Time average of autocorrelation function measured by CW radar illuminating moon calculated without lunar surface properties knowledge 21 p3703 A67-38189

CONTINUUM

Approximate analysis of electrostatic probe on reentry vehicle for electron density measurements in laminar boundary layer of continuum plasma 04 p0705 A67-15231
 Thermoelasticity theorems for harmonic vibrations of continuum, examining spherical wave propagation 07 p1264 A67-20222
 Equations for continuous media in finite case formulated in Eulerian and Lagrangian form 11 p1819 A67-24621
 Book on principles of continua with applications 12 p1966 A67-25557
 One-dimensional directed continuum assumed to represent elastic fiber strengthened string, developing boundary conditions and constitutive equations 20 p3535 A67-36197

CONTINUUM FLOW

Heat flux to SNAP reactor system models in hypersonic continuum flow measured in shock and hyperthermal wind tunnels, using thin film resistance thermometer 01 p0112 A67-11022
 Asymptotic theory for near-continuum gas flows applied to BGKW equation, deriving slip coefficient 13 p2101 A67-26964
 Free stream variables from continuum effect followed experimentally into transition flow regime to investigate impact probe in rarefied hypersonic flows of atomic gases 14 p2294 A67-27794
 Sphere drag coefficients measured using ultralightweight models launched from two-stage light-gas gun 14 p2242 A67-28172
 Ionospheric satellite trail, noting relation between length scales of medium properties and scales determined by body dimensions 14 p2302 A67-28207
 Rarefied gas axisymmetric stagnation point flow, clarifying relationship between continuum and Knudsen layer flow 22 p3784 A67-39836
 IR line intensity of planetary nebula NGC 7027, noting presence of measurable continuum flux of stellar radiation 24 p4225 A67-41830
 Algebraic equations to predict time response to step input in free molecule, transition and continuum flow regimes 24 p4155 A67-42293

CONTINUUM MECHANICS

SA DYNAMICS

SA FLUID MECHANICS

SA STATISTICAL MECHANICS

Behavior of magnet and ball in gravitational field in five-dimensional continuum 01 p0060 A67-10366
 Continuum theory of dislocations for polar elastic materials, each material point having three associated directors 01 p0162 A67-10848
 Continuum with director and constitutive equations for anisotropic fluids, obtaining solutions for simple shear, Poiseuille and Couette flows 01 p0053 A67-10849
 Proposed modification of Wetzel model of direct ionization by primary continuum in light of recent steady state precursor electron density measurements ahead of Ar shocks 01 p0118 A67-11193
 Best-possible error bounds in deformation theory 01 p0165 A67-11308
 Equations for one-dimensional model of macroscopically homogeneous linearly elastic medium of complex structure with spatial dispersion 02 p0337 A67-11952
 Dynamic reciprocal theorem for sinusoidal oscillation of elastic medium treated as extension of static reciprocal theorem of Betti and Rayleigh, using continuum mechanics

[ASME PAPER 65-WA/MD-21]

Elastic-plastic continua with unstable elements obeying normality and convexity relations 04 p0708 A67-14622
 Special relativity theory mechanical and thermodynamics laws for continuum 04 p0659 A67-15795
 Special relativity theory of electromagnetic interactions with thermoelastic solids, thermoviscous liquids and EM materials in continuum 04 p0659 A67-15796
 Motion theory of discrete defects in linear elastic continuum 05 p0908 A67-16038
 Nonlinear continuum mechanics of viscoelastic materials with application to solid propellants 08 p1419 A67-20879
 Fundamental field equations of continuum thermomechanics derived from balance of energy equation and entropy production inequality, using invariance considerations 11 p1819 A67-24533
 Rheology - Modern developments in mechanics of continua Conference, Syracuse University, August 1965 11 p1781 A67-24569
 Constitutive theory for fluid mixtures admitting diffusion and chemical interaction with heat conduction and plane wave propagation 11 p1783 A67-25001
 Continuum mechanics of Cosserat type, discussing kinematics generalization and existence of higher order displacement gradients in internal energy density equation 12 p1968 A67-26200
 Dynamic properties of elastic one- and two-dimensional continua using matrix method on digital computer and Hermitian polynomials 13 p2216 A67-28621
 Digital computer languages in relation to engineering design 13 p2073 A67-27189
 Noether theorems describing continuum mechanics material applied to Hamiltonian principle for motion of piezotropic fluid or ideal gas undergoing polytropic process 13 p2105 A67-27397
 Stability of motion of continuous dynamical systems analyzed via computing machines 14 p2348 A67-28080
 Solution of nonlinear flow problems through parametric differentiation 15 p2469 A67-29221
 Plastic behavior of material continua in terms of Riemannian and non-Riemannian differential geometry 16 p2787 A67-31276
 Physical state of material analyzed using non-Riemannian plasticity theory 16 p2768 A67-31278
 Fracture mechanics energy balance analysis using Griffith type fracture criterion 16 p2770 A67-31289
 Mechanical strength of medium formulated as microscopic behavior in continuum obtaining time-dependent macroscopic fracture strength 16 p2771 A67-31295
 Book on continuum mechanics including kinematics, principles and linear theories of continuum mechanics, elasticity and viscoelasticity 17 p2963 A67-33092
 Singularities due to concentrated couples in infinite linear elastic isotropic Cosserat continuum, noting dissimilar singular solutions 17 p2964 A67-33141
 Equations for one-dimensional model of macroscopically homogeneous linearly elastic medium of complex structure with spatial dispersion 17 p2965 A67-33269
 Viscoelasticity and rubber-like elasticity continuum mechanical description under stress relaxation conditions [AIAA PAPER 67-489] 18 p3143 A67-33955
 Relativistic mechanics of continuous media reviewed on basis of variable eigenmass dynamics, with criticism and rejection of various energy flux concept 19 p3263 A67-35833
 Orthonormalized vector reference in coupling between symmetrical tensors in continuum mechanics, deriving expansion coefficients 21 p3717 A67-37971
 Thermodynamic interpretation for Cauchy elasticity, showing formulation of constitutive equations in continua theories 21 p3733 A67-39085
 Axiomatic foundation for continuum thermodynamics theory, discussing first law and second law inequality 22 p3918 A67-39741
 D-region mobility and constituents abundance spectrometer device based on

continuum concepts 22 p3799 A67-39816
 Motor fields analysis in Cosserat continuum noting differential forms of stress and strain 22 p3837 A67-40006
 Equilibrium conditions of Cosserat continuum by complete stress function representation 22 p3837 A67-40007
 Elastic equilibrium of jointed cylinder of elastic nonlinear resilient materials obtained by relations of two-dimensional nonlinear theory of elasticity 23 p4075 A67-40682
 Plane problems with contained elastoplasticity, considering thin plates with small apertures as free boundary problem in continuum mechanics 23 p4077 A67-40754
 Mathematical reduction of three-dimensional continua to one and two dimensions expressed by equilibrium equations with identical form 23 p4078 A67-41195
 Deformation continuum mechanics near cracks, discussing fatigue load propagation applications and elastoplastic models 24 p4248 A67-41948
 Fatigue microcrack and macrocrack propagation in aluminum alloys, discussing continuum mechanics approach 24 p4248 A67-41952
 Book on mechanics of continua covering elasticity, fluid dynamics, heat conduction, thermoelasticity and viscoelastic materials equations 24 p4189 A67-42382

CONTINUUM RADIATION

Continuous coherent radiation of GaAs semiconductor laser with epitaxial p-n junction at ambient temperature of 77 degrees K 01 p0090 A67-10548
 Continuous coherent radiation of GaAs semiconductor laser with epitaxial p-n junction at ambient temperature of 77 degrees K 01 p0091 A67-11056
 Continuum brightness fluctuations and equivalent line widths in sunspot penumbral spectrum 02 p0330 A67-12715
 Radiation sources from high temperature equilibrium air noting measurements, equipment and results [AIAA PAPER 67-95] 06 p1114 A67-18279
 Radio telescope-spectrophotometric scanner investigation of continuous energy distribution of four quasars 08 p1398 A67-21230
 Spectrophotometric data correlations between color and red shifts of quasars 08 p1398 A67-21231
 Detectability of ion recombination free-free emission from H II regions 12 p2011 A67-26252
 Nightglow continuum emission 14 p2313 A67-28576
 Stimulated inverse Raman effect, noting experimental laser setup and theory based on optical phonon emission 14 p2333 A67-28985
 Monograph on quasi-stellar objects including identification, line spectra, radio emission, continuum radiation, red shift and models 23 p4069 A67-41438
 Energy distribution of photometric spectra in solar UV continuum in 1550 to 2100 angstrom range, discussing radiation temperature decrease 24 p4225 A67-41835

CONTOUR

Noncontour transpiration cooled heat shield for possible application to hypersonic atmospheric flight 04 p0725 A67-15435
 Polynomials orthogonal with respect to contours, examining analytic function representation via Fourier series expansion of such polynomials 06 p1025 A67-18695
 Boundary value problem of smooth closed contour dividing plane in inward and outward region solved by successive approximations 12 p1961 A67-25442
 Sufficiency proofs for problem of optimum transversal contour of slender conical body 13 p2051 A67-27457
 Singularity carrier auxiliary curves for design of straight cascades of slightly curved bladings 20 p3360 A67-37596
 Stretched sail behavior in sonic, supersonic and hypersonic flows, discussing profile dependence on angle of attack and free-stream Mach number 21 p3563 A67-37889

CONTRACT

Configuration management, method for current and precise documentation which attempts to assure customer and builder that final hardware is what they agreed on 04 p0739 A67-14424

Military prime contract awards distribution with respect to states 07 p1269 A67-19470
 Cost incentive contract effects on research and development 08 p1431 A67-21287
 Procedures for aircraft and spacecraft contractual arrangements to procure reliable systems, considering costs, qualification tests, etc 10 p1860 A67-23430
 Management of aerospace programs, discussing budgeting and contracting procedures 19 p3350 A67-35879
 Legal and financial problems in obtaining airline tickets for third persons 20 p3555 A67-36300
 Lessons from spacecraft industry experiences in 1960s and trends for 1970s, discussing subsystem performance experience, data acquisition, contracting, reliability, etc [AIAA PAPER 67-639] 20 p3557 A67-37622
 Trends in contracting that will influence spacecraft design and development in 1970s [AIAA PAPER 67-641] 20 p3557 A67-37623

CONTRACTION**SA BOUNDARY CONTRACTION METHOD**

Effect of fairing contraction into two-dimensional supersonic nozzle for wind tunnel, avoiding pressure gradients along walls unfavorable to boundary layer flow development 07 p1126 A67-19630
 Polytropic process of variations in state of system composed of gas and solid particles 12 p2033 A67-25317

CONTRACTOR

Management control systems, incompatibility between risk and controls, relations between government and contractors and implementation procedures [ASME PAPER 66-WA/MGT-16] 04 p0740 A67-15335

Management of development, design, contracting, construction, checkout and acquisition in ballistic missile program 05 p0929 A67-16620
 NASA quality assurance program and NASA industry quality relationships, particularly for large space systems procurement 05 p0930 A67-17242

CONTROL

S ADAPTIVE CONTROL
 S AIRCRAFT CONTROL
 S ALTITUDE CONTROL
 S APPROACH CONTROL
 S ATTITUDE CONTROL
 S AUTOMATIC CONTROL
 S AUTOMATIC DEPOSITION CONTROL
 S AUTOMATIC GAIN CONTROL /AGC/
 S BANG-BANG CONTROL
 S BOUNDARY LAYER CONTROL
 S COMMAND CONTROL
 S CONTROLLED FUSION
 S DIRECTIONAL CONTROL
 S DYNAMIC CONTROL
 S ELECTRIC CONTROL
 S ELECTROHYDRAULIC CONTROL
 S ELECTROMAGNETIC CONTROL
 S ELECTRONIC CONTROL
 S ENGINE CONTROL
 S ENVIRONMENTAL CONTROL
 S FIRE CONTROL
 S FLAP CONTROL
 S FLIGHT CONTROL
 S FREQUENCY CONTROL
 S FUEL CONTROL
 S GIMBALLED CONTROL
 S GROUND CONTROL
 S GUIDANCE AND CONTROL
 S HELICOPTER CONTROL
 S HYDRAULIC CONTROL
 S INVENTORY CONTROL
 S JET CONTROL
 S LATERAL CONTROL
 S LONGITUDINAL CONTROL
 S MAGNETIC CONTROL
 S MANUAL CONTROL
 S MISSILE CONTROL
 S NUMERICAL CONTROL
 S OPTIMAL CONTROL
 S PHASE CONTROL
 S PITCH CONTROL
 S PNEUMATIC CONTROL
 S PROPORTIONAL CONTROL
 S QUALITY CONTROL
 S RADAR APPROACH CONTROL /RAPCON/
 S RADIATION CONTROL
 S RANGE CONTROL
 S REACTION CONTROL
 S REACTOR CONTROL

S RECOVERY CONTROL CENTER**/RCC/**

S REGULATION
 S REMOTE CONTROL
 S ROLL CONTROL
 S SATELLITE CONTROL
 S SEQUENTIAL CONTROL
 S SERVOCONTROL
 S SERVOSTABILITY CONTROL
 S SHOCK WAVE CONTROL
 S SPACE VEHICLE CONTROL
 S SPACECRAFT CONTROL
 S STABILITY AND CONTROL
 S TEMPERATURE CONTROL
 S THRUST CONTROL
 S TIP CONTROL
 S TRAFFIC CONTROL
 S TRAJECTORY CONTROL
 S VECTOR CONTROL
 S VISUAL CONTROL
 S WEATHER CONTROL

CONTROL AREA

Control region construction in phase space for linear differential equation system 02 p0224 A67-11627
 Mathematical formulae for yielding storage requirement and work loadings to provide requirement to computer designer for traffic conditions in controlled area 09 p1531 A67-22654

CONTROL DEVICE**SA PITCH CONTROLLER****SA SILICON CONTROL RECTIFIER****/SCR/**

Inside-out differential transformer with control element placed outside exciting and sensing coils 01 p0075 A67-11137
 Invariant control device synthesis in multidimensional nonlinear automatic control systems 03 p0391 A67-13187
 Integrated circuit adoption for optimal mixture with remaining discrete devices, particularly gimbal loops 05 p0770 A67-16236
 Motion stability concepts of synthesis of control devices, with example for harmonic oscillator 06 p1032 A67-18243
 High power nanosecond commutator for control of spark chambers, laser shutters, etc 09 p1473 A67-22009
 Fluid amplifiers based on Coanda effect, digital and analog pure-fluid devices, applications to spacecraft control, gyrocontrol, etc 10 p1595 A67-22975
 Magnetic device design optimization for satellite attitude control, noting equations and charts 15 p2572 A67-30385
 Gas laser applications in construction, mechanics, communications, biology and medicine for control, measurement and experimental work 17 p2867 A67-32366
 Solid state protection and control device characteristics noting thermal, thermal magnetic and magnetic circuit breakers for circuit protection 17 p2825 A67-32514
 Soviet book on photoelectric sensors in monitoring, control and regulation systems noting design principles, operational requirements, etc 18 p3011 A67-33716
 Solid state microwave device technology concerning generators, low noise and control devices, discussing computerized technique for circuit analysis and design 18 p3015 A67-34595
 Compressed-air control system for lift capacity and maneuverability increment of Buccaneer type aircraft during landing and takeoff 19 p3173 A67-35876
 Modulo control algorithms application in circuit for finding residues 20 p3392 A67-37153
 Photoelectric device measuring cutting-tool temperature for automatic control of state of cutting edges 21 p3626 A67-38059
 Emission wavelength selection in multicolor-emission noble gas laser using linear polarization control device 23 p4014 A67-41025
 Fluidic actuator for direct digital control, converting computer information into mechanical motion 23 p3942 A67-41710
 ADP electro-optic crystal in laser emission control tested in beam deflection device and Michelson interferometer modulator, noting refractive index changes 24 p4167 A67-42239
 Asynchronous finite state sequential nonlinear controller synthesis with few flip-flops for dynamic space vehicle systems [AIAA PAPER 67-988] 24 p4127 A67-43060

CONTROL PANEL

Control-display association preferences for concentric controls 14 p2258 A67-28665

Control display linkages tested with human subjects for response time 18 p2993 A67-34338
 Book on inertial navigation covering laws of rational mechanics, gyroscopes, accelerometers, platform stabilization and control panels 23 p4025 A67-40633
 Internal light applied to opaque-faced edge-lighted plastic display panels [SAE PAPER 670196] 24 p4097 A67-41986

CONTROL ROCKET

Control rockets covering very low thrust operation, gas generation problems, gas expansion, etc 20 p3516 A67-36881

CONTROL SIMULATOR**SA COMPUTER****SA FLIGHT SIMULATOR**

Full mission engineering simulator /FMES/ design for integrating hardware into lunar module system as hardware is made available by subcontractors 08 p1319 A67-21546
 Adaptive processes of human operator during control tasks involving sudden change of controlled plant dynamics 21 p3576 A67-37948

CONTROL STABILITY

Direct approach to model referenced adaptive control systems using state space methods, showing simplicity in implementing adaptation equations 02 p0225 A67-12135
 Human pilot dynamic characteristics effects on manual satellite attitude control system stability, using root locus analysis of mathematical models 02 p0186 A67-12226
 Stability of control systems with distributed parameters and hysteresis-curve-type nonlinearity for various critical cases of system characteristic equation 05 p0781 A67-16250
 Popov method for random parameter control system asymptotic stability in mean with respect to bounded perturbations 05 p0784 A67-16777
 Frequency criteria of absolute stability of nonlinear control systems with periodically varying parameters 05 p0784 A67-17238
 Stability and asymptotic stability of control systems with multiple nonlinearities and inputs, using frequency criterion in connection with transfer function matrix 06 p0973 A67-17601
 Stabilization of steady motions of nonlinear control system in critical case of pair of pure imaginary roots 06 p0975 A67-18035
 Sufficient conditions for stabilization of motion of nonstationary controlled system 06 p0975 A67-18036
 Dynamics of self-adaptive systems with stabilized frequency characteristics 06 p0976 A67-18405
 Structural compliance induced cross axis coupling effect on gimbaling system stability of rocket engine two-axis attitude TVC system [AIAA PAPER 67-42] 06 p1097 A67-18448
 Bounded input of nonlinear feedback system yielding bounded output according to Popov theorem 06 p0977 A67-18528
 Stability of model reference control systems determined by direct Liapunov method 07 p1160 A67-19197
 Stability and transient response of nonlinear control systems treated by parameter plane techniques and describing function theory 08 p1310 A67-20342
 Steady state trajectory and stability of nonlinear sampled data systems with constant sampling frequencies described by finite difference equations 08 p1312 A67-20755
 Insensitivity zone used for stabilizing nonlinear automatic control systems 08 p1313 A67-21323
 Stability region for automatic nonlinear control systems unstable as whole 09 p1532 A67-21913
 Adaptation scheme applied to pitch axis control system of supersonic aircraft, using stability analysis for system design 09 p1440 A67-22387
 Missile and aircraft control systems design, discussing root locus and stability curve methods for solving characteristic equation 09 p1483 A67-22489
 Stability of automatic control systems with nonlinearity and nonunique equilibrium state 10 p1619 A67-23318
 Dissipative gyroscopic force effects on mechanical system, noting necessary and

- sufficient conditions for stability and controllability 11 p1818 A67-24146
- Reduction of order technique pertaining to plant and reference model in controller design for linear plants transfer functions with zeros and slowly varying parameters 11 p1771 A67-24895
- Adaptive feedback paths of adaptive aircraft control system in small signal stability analysis 11 p1772 A67-25081
- Simultaneous stability and quality control of pulse regulation, discussing computation of sum of squares of difference 13 p2086 A67-26474
- Book on modern control systems covering feedback control theory within framework of frequency and time domain analysis 16 p2643 A67-30621
- Behavior of high-order linear control systems analyzed using Liapunov second method, by finding low-order model with closely approximate response behavior of high order linear control systems analyzed, using Liapunov second method, 16 p2647 A67-31648
- Frequency response of longitudinal control transmission of transonic aircraft 19 p3176 A67-35570
- Nonstationary automatic control systems design by reaction quenching method 20 p3410 A67-37235
- Boundary between stable operation of multistage axial flow compressor and rotational flow separation region, using variational condition 21 p3689 A67-38046
- Stability margins for hybrid continuous discrete data control systems, developing open loop transfer function 22 p3778 A67-40157
- Sloshing stability of three-stage ELDO A launch vehicle during first stage flight 24 p4241 A67-42396
- Structural compliance induced cross axis coupling effect on gimbaling system stability of rocket engine two-axis attitude TVC system [AIAA PAPER 67-42] 24 p4242 A67-42909
- ## CONTROL SURFACE
- SA AILERON
- SA ELEVATOR
- SA ELEVON
- SA FIN
- SA RUDDER
- SA STABILIZER
- B-52 structural response to random turbulence with various stability augmentation systems, noting rigid body motions, normal vibration modes and control surface rotations [AIAA PAPER 66-998] 02 p0181 A67-12302
- F-111 aircraft wing spoilers controlled by hydraulic servactuators 05 p0753 A67-16182
- Aircraft autopilot actuators move control surfaces in response to electric signals and include facilities for performing full automatic landing 05 p0754 A67-17048
- Heating and effectiveness of control surfaces on lifting reentry vehicle or hypersonic aircraft [ONERA-TP-365] 05 p0750 A67-17403
- Doetsch deflection calibration device for aircraft control surfaces 06 p0950 A67-18022
- Control surface instabilities of lifting body configurations at very high speeds and with separated flows analyzed by wind tunnel tests for unsteady control surface load problems [AIAA PAPER 67-15] 07 p1258 A67-19430
- Rolling friction studies of intermetallic and zirconium oxide for control surface bearings for space reentry vehicle [ASLE PAPER 66AM 5D4] 08 p1335 A67-21037
- Matched asymptotic expansion for singular pressure loading behavior for oscillating wings or control surface edges 10 p1593 A67-23712
- Minimax time elapsing until meeting of pursuing and pursued controlled motion 13 p2085 A67-26382
- Airplane automatic-flare system actuating flaps and elevators as lift and moment controllers 15 p2418 A67-29313
- Acceptance criteria of space materials, discussing materials for surveyor 15 p2508 A67-29559
- Thermal control surface contamination due to rocket exhaust plumes and effects on solar absorptance and IR emittance of protective coatings 17 p2833 A67-32076
- Minimax time elapsing until meeting of pursuing and pursued controlled motion 21 p3604 A67-38818
- ## CONTROL SYSTEM
- SA ADAPTIVE CONTROL SYSTEM
- SA DATA CONTROL SYSTEM
- SA FEEDBACK CONTROL SYSTEM
- Nonlinearities such as limitation of linear characteristics, dead band, hysteresis, etc, in aircraft gas turbine control system 01 p0011 A67-10167
- Harmonic linearization of logic law control systems, deriving complex equivalent transmission coefficient for nonlinear part of circuit with variable structural elements 01 p0044 A67-10241
- Book on fluid power circuits and controls engineering 01 p0012 A67-10305
- Instrumentation and control for magnetic pulse metal forming including pulse generation, energy transfer, electrical operations, etc [SAE PAPER 660066] 01 p0078 A67-10569
- Real time digital simulation of linear and nonlinear control systems with large sampling intervals, determining optimization criterion by nonlinear multipoint boundary value problem 01 p0045 A67-10874
- Evaluation of residue integral for finite number of poles in behavior function of control circuit 01 p0045 A67-10796
- Speech commands in control systems, discussing operation of bandpass, formant, scanning, harmonic and correlation voice coders 01 p0016 A67-10823
- Air monitoring instruments used in detection and control of air pollution 01 p0050 A67-11037
- Digital electronic programmable turbine engine control system for reducing time and cost in engine-control system matching 01 p0030 A67-11094
- Measurement systems control in rocket engine testing via real-time surveillance, computation, error correction and graphic display 01 p0076 A67-11144
- Linear optimal control techniques used as synthesis tool in designing control system for Short Range Station Keeping /SRSK/ task of assault helicopter, noting closed loop dynamics 01 p0111 A67-11201
- Control system analysis and design using parameter space method 01 p0047 A67-11216
- Stability and sensitivity requirements considered simultaneously in control system design, minimizing time domain sensitivity index and incorporating transient response characteristics 01 p0047 A67-11217
- Asymptotic stability of nonlinear systems, noting application to systems with control and Liapunov function role 01 p0048 A67-11318
- Low thrust reaction control system utilizing solid propellant which sublimates into low molecular weight vapor, noting heat sources 01 p0142 A67-11407
- Control system of ACIC augmented by 100 points, constructing corresponding contour map 02 p0319 A67-11457
- Optimization of control systems with nonlinear plants, using Pontryagin maximum principle 02 p0224 A67-11511
- Weight, efficiency and control requirements of subsystems of electric propulsion applied to Mars missions, selecting power-conditioning modules for ion propulsion engines [AIAA PAPER 66-501] 02 p0302 A67-11516
- Minimax rendezvous time of two linear uniform control plants, constructing optimal pursuit 02 p0225 A67-11956
- Damping linear system with aftereffect 02 p0225 A67-11962
- Quadratic performance criteria for discrete control systems, using Liapunov matrix equation and digital computer program 02 p0225 A67-12074
- Monograph on system philosophy of automatic learning systems in application to autopilots, discussing man-aircraft system cybernetics, human behavior, environmental effects, etc 02 p0188 A67-12084
- Bayesian statistics in dual control schemes for discrete-time noisy extremum systems 02 p0226 A67-12145
- Iterative procedure for changing constraint minimization problem to mathematical programming formulation in solving discrete terminal control problem 02 p0226 A67-12152
- Observability and controllability in providing heuristic understanding of control problems, noting Kalman filter theory 02 p0227 A67-12159
- Variations in friction and inertia characteristics of rotary control determined, noting preference ratings of control characteristics 02 p0186 A67-12229
- Operator reorientation of attitude of simulated remote maneuvering unit /RMU/ using on-off acceleration command control system 02 p0186 A67-12230
- Operation and control of satellite equipment, discussing automatic, semiautomatic, human and teleoperator /man-extension system/ methods [AIAA PAPER 66-918] 02 p0204 A67-12250
- Manned Orbital Research Laboratory /MORL/ design studies stressing stabilization and control and electric power subsystems, water supply, etc [AIAA PAPER 66-932] 02 p0332 A67-12277
- Propellant combinations evaluation for minimum weight of high energy propellant reaction control systems [AIAA PAPER 66-947] 02 p0304 A67-12281
- Design of gust alleviation controls for boost phase flight of missiles incorporating random winds, time-varying missile dynamics, control problem, etc [AIAA PAPER 66-969] 02 p0332 A67-12292
- Gust Alleviation and Structural Dynamic Stability Augmentation System /GASDSAS/ design analysis [AIAA PAPER 66-999] 02 p0183 A67-12303
- Voyager spacecraft guidance and control system analysis, examining systems design requirements, problems of redundancy implementation for critical functions and gyro system 02 p0265 A67-12381
- Singular perturbation theory of differential equations applied in control engineering, noting asymptotic expansion of solution 02 p0227 A67-12681
- Describing function determination for case of piecewise linear-nonlinear characteristics with discontinuities of first kind 02 p0227 A67-12682
- ELDO missile second stage automatic control system, noting programming control sequences, analysis of measurement results, etc 03 p0502 A67-12899
- Control method excluding static and dynamic stability aspects of aircraft from guidance problem 03 p0464 A67-13003
- Partially invariant relay systems 03 p0389 A67-13085
- Synthesis of linear automatic control system with constant parameters for integral Q-factor, noting effect of small parameters on properties of optimum system 03 p0390 A67-13097
- Restrictions placed on transfer function of linear system with input and output coordinates in presence of given plant in control loop 03 p0390 A67-13098
- Solution of optimum filtering problems when input signals of automatic control system are described by different differential equations at successive time intervals 03 p0390 A67-13099
- Linearized motion equation of self-adaptive systems with stabilized frequency characteristics, considering effect of control and noise signals in basic control loop 03 p0390 A67-13101
- Coordination of integral and relay components in algorithms for adjusting control coefficients in model-reference self-adaptive control systems described by differential equations 03 p0390 A67-13102
- Transfer function of pulse amplitude modulated sampled data control systems with element generating arbitrarily shaped pulses and first order element series connected with constant parameter elements 03 p0390 A67-13103
- Approximation of variable time delays and design of constant and variable delay circuits, noting simulation of delays in automatic control systems by computers 03 p0390 A67-13104
- Soviet book on theory of automatic control systems of regular linear, special linear and nonlinear types 03 p0390 A67-13108
- Soviet papers on complex control systems 03 p0390 A67-13180
- Invariance and sensitivity theories applied to automatic control system design 03 p0391 A67-13186
- Command and control display system requirements noting dependence on human

visual mechanism 03 p0365 A67-13300
 Stabilization of steady state motion of controlled system described by nonlinear differential equations with time delays 03 p0392 A67-13588
 Graphical analysis of step-by-step extremal control system adapted to process with second order inertia before static characteristic 03 p0393 A67-13884
 Closed loop gust response control system, considering airframe loading, local accelerations, turbulence, structural mode, damping, etc [AIAA PAPER 66-997] 03 p0362 A67-14146
 Discrete gyroscopic servocontrol in presence of multidimensional random noise, ensuring optimal reproduction of input signal 03 p0465 A67-14157
 Suboptimal policies for fuel optimal control and energy optimal control problems for linear time invariant system obtained, using Liapunov functions 04 p0590 A67-14418
 Statistical linearization for minimization of mean square error between time derivatives for actual and model outputs for zero and special memory nonlinearities 04 p0591 A67-14420
 Optimum control problems for systems described by differential equation with deviating argument 04 p0591 A67-14667
 Optimal control of systems described by elliptic differential operators 04 p0593 A67-15491
 Ordnance systems and devices noting composition, function, operation and testing procedures 04 p0557 A67-15734
 Stationary points of nonlinear maximum problems in Banach space B [DVL-642] 04 p0594 A67-15880
 Time constant and control channel lag effects on size and configuration of platform stability region 04 p0552 A67-15883
 Control of water moderated nuclear reactor using neutron absorbing helium 3 gas control elements 04 p0658 A67-15989
 Dual circuit hydraulic powered brake control system for effective short landing of F-111 aircraft 05 p0753 A67-16164
 Pneumatic transmission line model for use in fluidic control systems, noting nomographs determining gain-vs-frequency curves 05 p0753 A67-16237
 Optimization of linear control systems when placing step limitations on control, using functional analysis 05 p0781 A67-16251
 Synthesis problem of optimum dynamic characteristics of multivariate linear control systems with random input signals 05 p0781 A67-16252
 Optimum control of two-dimensional oscillating system when placing limitations on control, using Butkovskii L-problem of moments 05 p0781 A67-16253
 Closed-loop automatic control system with unvalued substantially nonlinear element, using approximation of characteristics by Fourier series 05 p0781 A67-16254
 Approximation method determining follow-up failure conditions for nonlinear automatic systems in presence of control and noise signals 05 p0781 A67-16255
 Optimal control problem of variable structure system, deriving necessary and sufficient conditions for existence of trajectories 05 p0781 A67-16256
 Comparison of nonoptimum and optimum strategies in dual control of inertialess plants in presence of noise in feedback loop 05 p0781 A67-16257
 Equation for conditional overshoot density of normal stationary process in centralized and positional control, noting error estimate 05 p0782 A67-16267
 Transfer function parameters of stationary controlled plants in identification problem estimated, using Laplace transform and least squares method 05 p0782 A67-16319
 Automatic system auto-oscillations when transmission coefficient of nonlinear part of system depends on amplitude and frequency of input signal 05 p0782 A67-16323
 Synthesis and control strategy of optimal final value linear system under random environment statistically considered, using Bellman dynamic programming 05 p0783 A67-16442
 Nonstationary response of closed loop control systems with random characteristics, noting statistical analysis of error response and conversion of random control system to constant parameter

system 05 p0783 A67-16443
 Periodic and almost periodic limiting operational conditions for control systems with nonlinear units 05 p0784 A67-17020
 LF analog-linear circuitry and reduction of electromechanical control system requirements to realizable microelectronic circuits 05 p0778 A67-17038
 Automatic three-dimensional model measuring machine using data programming for aircraft contour measurement 05 p0811 A67-17047
 Metrology requirements for Apollo project, noting control and measuring equipment and calibration procedures 05 p0814 A67-17263
 Transient analysis of control system with nonlinear damping and frequency 05 p0785 A67-17301
 Haystack antenna used for satellite communications and celestial observation, noting digital computer for control system and data processing 05 p0790 A67-17517
 Autonomy in multiply connected variable structure automatic control systems 05 p0786 A67-17542
 Early Bird hydrogen peroxide control system maneuvers to place satellite into final stationary position 06 p1093 A67-17663
 Code-division-multiplex decentralized control system for communication satellites based on use of pseudorandom PM signals of wide bandwidth 06 p0959 A67-17672
 Parameters of satellite communication system control and scheduling function, emphasizing distinction between scheduling model and scheduling algorithm 06 p0961 A67-17699
 Linear frequency-domain analysis technique for examining stability and performance characteristics in optimal-control design of control systems 06 p0973 A67-17718
 Advances in control systems, Volume 3, covering reentry and aerospace vehicle guidance and control, BVP techniques, optimal control, Kalman filtering techniques and state space methods for navigation problems 06 p0973 A67-17921
 Book on advances in control systems including algorithms for sequential optimization, trajectory optimization, optimal control, etc 06 p0974 A67-17929
 Approximation techniques generating algorithm for iteratively solving sequential optimization of nonlinear control systems 06 p0974 A67-17930
 Optimum control of multidimensional and multilevel systems, discussing linear systems, load distribution, cyclic optimization and aggregated systems 06 p0974 A67-17933
 Closedness of set of trajectories or of solutions of contingent equation used in existence problems of optimal control and variational calculus 06 p0975 A67-18100
 Control law determination procedure for structural synthesis of combined automatic control systems for nonlinear plants 06 p0976 A67-18237
 Inverse method of structural analysis of automatic control systems described by nonlinear differential motion equations 06 p0976 A67-18238
 Automatic control system synthesis for fatigue testing of structural elements under random loads 06 p1101 A67-18239
 Optimal processes in sampled data control system 06 p0976 A67-18404
 Boundary curves for jump resonance criteria of nonlinear control systems and conditions in second order servo system with idealized saturation 06 p0977 A67-18528
 Control system synthesis based on approximation principle using transfer function expansion in MacLaurin series 06 p0978 A67-18559
 Flexibility and rigidity requirements imposed on vibration damping systems of optimized precision devices 06 p1106 A67-18618
 Design procedure for meeting step-input specifications in piecewise single-valued nonlinear multivariate control system design 06 p0978 A67-18720
 Attitude control for sun-pointing scientific satellites, considering control loop, sun sensor and actuator control 06 p1098 A67-18765
 Linear and nonlinear attitude control law synthesis for spinning aerospace vehicles,

including analog simulation for control designs based on frequency symmetry 07 p1257 A67-19359
 Asynchronous control of information transmission in networks consisting of independent sequential circuits 07 p1161 A67-19884
 Sufficient conditions of optimality for discrete controlled systems 07 p1162 A67-20023
 LM guidance and control systems performance verification [AIAA PAPER 67-244] 07 p1165 A67-20064
 Apollo external visual simulation display systems, discussing optical methods applied during navigation, guidance and control tests [AIAA PAPER 67-253] 07 p1189 A67-20085
 Model reference control systems design using Liapunov synthesis technique 07 p1162 A67-20203
 Multiparameter sensitivity index for control systems noting synthesis method for minimization of sensitivity 08 p1309 A67-20329
 Extremal control problem of undamped oscillatory plant analyzed using bounded phase-coordinate control theory 08 p1309 A67-20330
 Optimal control systems without complex controllers using variational calculus, for application to submarine diving control 08 p1309 A67-20331
 Quadratic control regulator problem with energy constraint analyzed, considering availability of limited control energy or as method of limiting maximum control amplitude 08 p1309 A67-20332
 Identification of unknown transfer function in nonlinear sampled data systems, using iterative method 08 p1310 A67-20336
 Pneumatic digital step optimizing device consisting of logic elements of ZPA system for process control 08 p1280 A67-20441
 Dual redundancy digital computer for improved reliability in real time processes and control situations where fault results in fatality or mission failure 08 p1298 A67-20638
 Aerospace and electronic systems - IEEE Convention, Washington, D.C., October 1966 08 p1290 A67-20646
 System design decisions through static and rotating magnetic memories reliability as applied to command and control systems 08 p1299 A67-20685
 Angular acceleration sensor for control system stabilization using MHD principles, obtaining transfer function 08 p1331 A67-20697
 Laws for aircraft control in terrain-following and formation-flight modes of operation, applying solution of Euler-Poisson equation 08 p1351 A67-20700
 Progress in control engineering, Volume 3, covering dynamic programming, adaptive control systems, sampled data systems, etc 08 p1312 A67-20751
 Dynamic programming for control system synthesis, noting invariant embedding and optimality principle use in optimum design problems 08 p1312 A67-20752
 Multivariable control systems with random inputs for nonlinear and linear cases 08 p1312 A67-20754
 Linear servomotor for high speed rectilinear response 08 p1286 A67-20992
 Management of engineering changes in manufacturing processes to prevent design or systems deficiencies resulting from poor control of changes 08 p1430 A67-21049
 Self-adjusting control systems with models, reviewing basic theoretical problems of analysis and synthesis 08 p1313 A67-21328
 Cost reduction and avoidance by value engineering to yield lowest overall cost for performance, reliability and maintainability requirement 09 p1581 A67-22157
 Survey and bibliography of works on optimum control system design and statistical signal descriptions 09 p1483 A67-22386
 Measurement and control methods in aircraft-instrument-pilot loop, noting human limitations in possibilities of automation computer applications 09 p1457 A67-22459
 Optimum transient response for bang-bang control system with finite time control activation 09 p1483 A67-22609
 Air traffic control systems engineering and design - Conference, London, March 1967 09 p1527 A67-22826
 Focal distance of lens controlled digitally

- using electro-optics 10 p1653 A67-22750
- Spacecraft instrumentation, discussing selection criteria for signal conditioning, transducer sensors, photographic equipment, etc 10 p1655 A67-23000
- Prevention system of short circuit in vacuum chambers due to glow discharges 10 p1622 A67-23316
- Control theory and applications - IBM Symposium, Yorktown Heights, N.Y., October 1964 10 p1619 A67-23417
- Liapunov stability theory applied to control system, noting stability of function and stochastic differential equations 10 p1620 A67-23427
- Stochastic control problems, considering dynamic model selection for physical system under random perturbation 10 p1620 A67-23427
- Controllability of quasi-linear systems proved by Picard classical method of successive approximation 10 p1681 A67-23682
- Synthesis of near optimum high order control systems from simple convenient control functions equivalent with respect to sign 10 p1621 A67-23850
- Nomograms for analysis and synthesis of astatic automatic control systems 10 p1621 A67-23851
- Graphs for frequency plot of closed loop automatic control system from phase amplitude of open loop and frequency relations between open and closed 10 p1621 A67-23852
- Book on modern control systems covering feedback control system, root locus and frequency response method, time-domain analysis, etc 11 p1769 A67-24062
- Minimax problem for pursuit problem of two linearly controlled objects describable by identical differential equations 11 p1812 A67-24145
- Dynamic control study for solar mirror aboard spacecraft using breadboard apparatus and computer simulation method 11 p1745 A67-24274
- Solution of optimal control problems using hybrid computers 11 p1770 A67-24426
- Packaging integrated circuit airborne tape control unit 12 p1911 A67-25273
- Aerodynamic development of configuration and control system of Gulfstream II business jet, discussing wing optimization, engine characteristics, etc 12 p1894 A67-25497
- Book on hydraulic control systems covering fluid flow theory, hydraulic pumps, motors, valves, power elements, etc 12 p1899 A67-25558
- Mechanical cascade toroidal servo flight control system tested using simulator [SAE PAPER 670269] 12 p1895 A67-25867
- SST air inlet control system, considering maintainability, impact on cockpit procedures and component reliability effect on dispatch reliability 12 p1895 A67-25869
- Positive control system for placing aircraft under precisely described flight path [SAE PAPER 670340] 12 p1895 A67-25878
- Boeing SST inlet, control and power system development, discussing test program, design objectives and cost [SAE PAPER 670318] 12 p1990 A67-25886
- Conditional stability of class of controlled systems, noting aircraft controlled by autopilot 12 p1919 A67-26104
- Root trajectory theory use in automation schemes for analysis and synthesis of optimum control systems, outlining applications 13 p2085 A67-26394
- Electrical and electronics engineering - IEEE Conference, Jackson, Mississippi, April 1967 13 p2085 A67-26404
- Soviet book on pulsed self-adjusting and extremal automatic control systems covering theory and practice 13 p2086 A67-26459
- Simultaneous stability and quality control of pulse regulation, discussing computation of sum of squares of difference 13 p2086 A67-26474
- Matrix algorithm for calculating mean square error for synthesis of optimum control systems 13 p2087 A67-26612
- Control systems functions and programming approaches, Volume B, covering electronic data processing, factory automation and computer center administration 13 p2153 A67-26664
- Analytic measure for difficulty of human control as constrained by capability, training and stress 13 p2061 A67-26709
- Time optimal control problems of linear systems with state and control vectors 13 p2087 A67-26723
- Indeterminate recognition / game type/ and prediction systems 13 p2088 A67-27022
- Automatic signal gain control system under constraints, determining time constants for signal filtering 13 p2088 A67-27041
- Control system for frequency standard using frequency switching between two points on cesium resonance curve 13 p2121 A67-27226
- Travel-time effects on quasi-steady state operation characteristics occurring from electron optical characteristics of two-grid-controlled photomultiplier 14 p2277 A67-27769
- Stability problems in control system of Saturn launch vehicles 14 p2393 A67-28085
- Automatic pressure stepping control and recycling system for use with Fabry-Perot interferometer 14 p2315 A67-28158
- Fluid control systems - Conference, Pennsylvania State University, July 1965 14 p2247 A67-28263
- Power jet and single control bubble region portion of fluid jet modulator modeled for studying static and dynamic properties 14 p2248 A67-28271
- Fluid flight control systems, discussing attitude and angular rate stabilization systems 14 p2248 A67-28273
- Control flow effect on power jet reattachment location and pressure in separation bubble enclosed by power jet for fluidic devices 14 p2250 A67-28336
- Static operating characteristics of diaphragm pneumatic logic device 14 p2275 A67-28347
- Liapunov function analysis applied to derivation of general stability criterion for control system 14 p2292 A67-28898
- Necessary and sufficient conditions for boundary of absolute stability domain of nonlinear automatic control systems 15 p2455 A67-29120
- Efficiency criterion in form of probability of task completion estimated for dynamic systems with random parameters 15 p2455 A67-29121
- Pulse-time modulation of first kind and block diagram of pulse time modulator studied for control system applications 15 p2455 A67-29122
- Step-by-step self-adaptive algorithm for selective systems with automatic control 15 p2455 A67-29123
- Sensitivity of cost functional in optimal control system with random variable parameters, noting system performance detection techniques 15 p2457 A67-29375
- Loc types presented in Chang paper for systems with particular open-loop transfer function are only types possible for third order systems with no open-loop zeros regardless of nature of open-loop poles 15 p2457 A67-29375
- Astronomical radio telescope control, noting altazimuth and equatorial modes of operation, overall accuracy, etc 15 p2492 A67-29532
- Lunar module onboard guidance equipment design, noting operational strategies, control systems, etc 15 p2514 A67-29601
- Liapunov second method and extensions used in control problems of differential systems 15 p2574 A67-29633
- Solution stability of parametric nonlinear differential equation system, noting validity of Popov criterion 15 p2518 A67-29660
- Stability of nonlinear controlled systems with infinite degrees of freedom 15 p2458 A67-29696
- Spatially distributed automatic control system used in plasma plant stabilization 15 p2530 A67-29724
- Display/control system of Mission Control Center, Houston, operation and performance 15 p2467 A67-29736
- Flight control requirements of reusable launch vehicles 15 p2570 A67-29857
- Nonlinear system analysis by subdividing total motion of system into fast and slow components, noting application to control systems 15 p2458 A67-29886
- Second order optimal control system simulation by computer, describing method for generating time optimal controls 15 p2458 A67-29907
- Linear single input optimal cooperative rendezvous problem with quadratic performance index solved using variational calculus 15 p2458 A67-29909
- Management control system for technical, production, financial and contractual management of large scale or technical industry programs [AAS PAPER 67-153] 15 p2583 A67-29969
- Optimal final value control theory, applying variational calculus and functional analysis to control function selection for dynamic systems 15 p2459 A67-30020
- Approximation of functions describing control loops output signals for various values of controller parameters 15 p2459 A67-30132
- Attitude stabilization and control system for rotationally symmetric gyroscopic body with two degrees of freedom 15 p2490 A67-30156
- Air traffic control simulation, describing functions to be fulfilled and system requirements for EUROCONTROL 15 p2441 A67-30164
- Stability of systems with controlled plant and correcting system, based on analysis of stabilizability conditions in certain natural frequency regions 15 p2518 A67-30176
- Identification in automatic control systems - Conference, Prague, June 1967, Part 1 15 p2459 A67-30309
- Identification of continuous time invariant systems from input-output data, analyzing state determination problem for distributed parameter systems 15 p2460 A67-30312
- Operator parameter identification on basis of digital treatment of experimental data, using algebraic means and static programming 15 p2460 A67-30313
- Input/output model of system with finite settling time, using error correcting technique employed in pattern recognition 15 p2460 A67-30314
- Human response model identification in manual control system applied to study of stability and performance of man-machine system 15 p2432 A67-30315
- Limitations of observability and controllability of dynamic system determined, using approximation of performance matrix and iterative procedure 15 p2461 A67-30316
- Control system identification and loop stability limit, noting dominant components of time functions and classification of substitute functions 15 p2461 A67-30317
- Accuracy of mathematical models in control system identification estimated on basis of deterministic test signals for simulation in time and frequency domains 15 p2461 A67-30318
- Control system identification for noise corrupted input/output data, using algorithmic approach and iteration procedure 15 p2461 A67-30320
- Invariant estimation of stochastic system parameters using autoregressive models to characterize linear plants of control systems 15 p2462 A67-30325
- Random noise and measurement errors limitation upon system identification in time domain 15 p2463 A67-30332
- Characteristics identifying method required for number of multiplications to be proportional to number of inputs 15 p2464 A67-30341
- Identification techniques with stochastic computers for advanced automatic control systems in form of learning machines 15 p2441 A67-30344
- Nonuniformity of mm wave detected by wideband frequency sweep control backward wave oscillator 16 p2643 A67-30896
- Effectiveness for automatic control systems estimated by comparing performance with ideally functioning systems 16 p2643 A67-30919
- Nonlinear automatic control systems with random processes studied using orthogonal polynomials with Hermitian series expansion 16 p2643 A67-30924
- Transient processes in nonlinear automatic control systems 16 p2643 A67-30926
- Parallel operation of same frequency transmitters on common antenna examining several designs 16 p2637 A67-31003
- Automatic control - Conference, University of Pennsylvania, Philadelphia, June 1967 16 p2644 A67-31634
- Quantization error effect for digital control system design 16 p2646 A67-31637

Liapunov function for modeling and bounding solutions of distributed processes defined by interacting subsystems describable by stable differential equation 16 p2646 A67-31638

Second order discontinuous attitude control system using fixed impulse, determining average number of switchings before escape from vertical switch line 16 p2762 A67-31640

Liapunov-derived fixed gain flight control system design to fulfil response requirements over wide range of parametric variations 16 p2763 A67-31644

Maintainability system operating parallel with cruise-mode spacecraft attitude-control system, noting application to Ranger III spacecraft 16 p2763 A67-31646

Synthesis and design of on-line self-organizing control of multiple goal, multiple actuator systems 16 p2648 A67-31654

Adaptation technique for on-line steady-state optimizing control using updated control algorithm 16 p2648 A67-31655

Control of output variables in discrete multivariable system at steady state noting design, application and performance 16 p2649 A67-31668

Triple input describing functions noting application to stability analysis of forced nonlinear control systems 16 p2650 A67-31673

Analysis of discrete nonlinear time-varying systems, noting computational simplicity, application to feedback system, etc 16 p2650 A67-31675

Modern control theory applied to digitally controlled tracking telescope design, emphasizing accuracy and response time 16 p2629 A67-31688

Describing functions for nonlinearity consisting of bang-bang with dead zone characteristic followed by linear integrator with constrained integration range 16 p2652 A67-31690

Continuous monitoring and control of primary mirror figure of orbiting, diffraction limited astronomical telescope for optimum performance 16 p2680 A67-31802

Fluidics applications to ramjet control systems incorporating sensing, logic and actuation functions to inlet duct, flow-air ratio and coolant control 17 p2927 A67-31981

Surface tension principles for propellant management devices, discussing static retention and dynamic control of spacecraft fuels 17 p2801 A67-31985

Static and dynamic sealing concepts and materials for propellant feed systems and pneumatic and hydraulic control systems of liquid propellant rocket engines 17 p2864 A67-31990

Hardware characteristics of control moment gyro /CMG/, determining nonlinearity effects on performance by simulation 17 p2853 A67-31995

XC-142A flight control and stability augmentation systems 17 p2794 A67-31996

C-5A flight control system, examining subsystems, handling qualities, hydraulic power distribution and mechanical failures 17 p2794 A67-31997

Fluid logic components utilizing Coanda wall effect for control systems 17 p2802 A67-32228

Interconnecting fluid elements and hardware components for construction of complex systems 17 p2802 A67-32229

Generalized linear programming applied to control theory noting use of differential equations 17 p2829 A67-32430

Rod configuration determined optimum for gyro torquer controlled spinning space station subject to impulse disturbance 17 p2955 A67-32477

Calibration of star tracker bias errors on OAO 17 p2955 A67-32479

Control theory of hyperbolic PDEs examined, noting application to distributed parameter systems 17 p2877 A67-32561

Automatic control systems, discussing open and closed loop control systems, mathematical model analysis and developments 17 p2830 A67-32788

Applicability to elastic flight vehicle control system of two variants for realization of invariance conditions 17 p2882 A67-33097

Perceptron system for correcting average line position of open loop portion of control system, discussing pole interaction and self-organization 17 p2830 A67-33098

Combined control system of extremal plant with alpha system corrector and open loop part, describing noise, disturbance and efficiency factors 17 p2830 A67-33099

Book on control systems and linear vibrational mechanical systems emphasizing use of analog and digital computers, frequency response, complex plane and root locus plots, FORTRAN method, etc 17 p2822 A67-33133

Pilot describing function measurements in multiloop control task to provide data for multiloop pilot model refinement 17 p2808 A67-33177

Inertia and muscle tone level effects on intermittence sampling frequency in hand movement control system 17 p2808 A67-33180

Minimax rendezvous time of two linear uniform control plants, constructing optimal pursuit 17 p2831 A67-33273

Damping linear system with aftereffect 17 p2831 A67-33279

Controllability methods on VTOL transporters, developing model of pilot dynamic reaction to aircraft machinery 18 p2993 A67-33457

Early Bird and Intelsat commercial satellite communications system and associated ground stations noting design, power supply, control system, etc 18 p3136 A67-33545

Transfer function parameters of stationary controlled plants in identification problem estimated, using Laplace transform and least squares method 18 p3017 A67-33870

Automatic system auto-oscillations when transmission coefficient of nonlinear part of system depends on amplitude and frequency of input signal 18 p3017 A67-33875

Fluidic fuel control system for subsonic combustion ramjet engine, describing components, breadboard model and performance characteristics [AIAA PAPER 67-497] 18 p3113 A67-33961

Lunar orbiter velocity control system design, discussing interface problems between actuator electronics and flight control system [AIAA PAPER 67-504] 18 p3137 A67-33968

Automatic control system for parameter evaluation, reducing stochastic errors by repeated measurements 18 p3017 A67-33991

Synthesis of optimal and quasi-optimal sampled data control systems applied to various order plants 18 p3017 A67-34281

Requirements of optimal controller for system with constraints imposed on control magnitude 18 p3018 A67-34283

Control integration for lunar mapping 18 p3131 A67-34321

Image motion compensation tracking study for earth reconnaissance from space, investigating computer and manual tracking modes, control dynamics and gain and magnification 18 p2993 A67-34337

Process control program including failure mode and effects analysis, critical characteristics determination, safety features and test equipment 18 p3058 A67-34673

Pulse-width modulated control system optimization, with necessary conditions derived by variational calculus, and numerical solution to resulting boundary value problem 19 p3199 A67-34783

Empirical formulas for optimal operation of extremal controllers, design data generation and cost index determination 19 p3201 A67-34992

Quantization error bounds for hybrid control systems by time varying function 19 p3202 A67-35625

Structural and systems design characteristics of British launch vehicle noting control and guidance system, flight development and test 19 p3333 A67-35841

Compressed-air control system for lift capacity and maneuverability increment of Buccaneer type aircraft during landing and takeoff 19 p3173 A67-35876

Computer solution of optimal control problems by finite difference method 19 p3202 A67-35886

Existence problem in control theory noting time independence and control set 19 p3204 A67-35905

Mathematical model for optimization problem obtaining equations generalizing Bellman equation 19 p3205 A67-35908

Damped mass expulsion for space vehicle

attitude control reducing propellant consumption and pulsing frequency [AIAA PAPER 67-535] 19 p3334 A67-35937

Jet attitude control system analysis when subjected to external disturbing torques [AIAA PAPER 67-537] 19 p3174 A67-35939

Linear optimal control technique for flexible-booster control system design, showing drift minimum model with matrix transformations for closed-loop dynamics 19 p3336 A67-35988

Bad weather landing of VTOL aircraft noting landing profiles, meteorological parameters and control system 20 p3361 A67-36455

Laser frequency control system using two optical discriminators for long and short term stability 20 p3459 A67-36519

High chamber-pressure propulsion systems and components captive testing, describing ground support system analysis, design and mechanisms 20 p3414 A67-36534

Efficiency of using self-adjustment with respect to input signal in automatic control systems, estimating gain and stability 20 p3409 A67-37198

Synthesis of control systems with minimum complexity, noting application to filter discrimination of nonstationary signals 20 p3409 A67-37223

Optimal system determined from maximum probability criteria of target hitting 20 p3410 A67-37226

Minimum control system optimization, noting adaptation with respect to minimum mean square error, statistical criterion calculation, etc 20 p3410 A67-37227

Switching surface construction using one to one correspondence between points in controllability region and points on surface of nth order system 20 p3410 A67-37230

Accuracy problems in control systems, discussing error assessment and accuracy estimates of optimal control 20 p3410 A67-37231

Suboptimal controller generating linear combination of state coordinates shown to give optimal performance when using linear controller preceding relay 20 p3410 A67-37251

Digital computer control system for aerodynamically unstable vehicles 20 p3534 A67-37257

Fluid control system design by third order linear differential equation with transient response, showing relationship to frequency response 20 p3366 A67-37370

Soviet papers on complex control systems 20 p3411 A67-37372

Complex multi-aircraft control systems with hierarchical control structure with imposed universal optimality criterion 20 p3411 A67-37373

Aircraft flight dynamics optimized in angle of attack by variational calculus, analyzing control system 20 p3361 A67-37377

Nonlinear automatic control systems characteristics analyzed for various possible error accumulations 20 p3412 A67-37382

Book on mechanics of controlled body including control system realization, motion programming, dynamic error assessment and three-dimensional problems 20 p3482 A67-37459

Control system of mounting of cross-type radio telescope east-west line, discussing parabolic trusses 20 p3402 A67-37505

Regenerative dual tandem cable servomotor design for use in manual and automatic spoiler control system of C-141 Star Lifter 20 p3366 A67-37550

Soviet book on time-frequency remote control systems theory and design 20 p3412 A67-37632

Soviet book on information theory and application to problems in automatic monitoring and control 20 p3413 A67-37633

Associative memory system of persistent current bit-cells using cryotrons in selection and control network 21 p3587 A67-37955

Direct fluidic sensors for fluid control circuitry design, discussing aerodynamic and acoustic flow and obstacle sensing 21 p3625 A67-37958

Plant parameter uncertainties sensitivity constraint for optimal linear control synthesis, discussing Wiener-Hopf equation condition 21 p3602 A67-38026

Aircraft fuel tank pressurization, discussing pressure supply sources and control system, tank venting, system integration and equipment

used 21 p3571 A67-38104
Analytical methods for control systems applied to engine governor 21 p3602 A67-38129
Onboard receiver-decoder control unit for ESRO I and II consisting essentially of four-state signal corresponding to time modulated pulses 21 p3581 A67-38201
Rocket control using analog computers, determining thrust vectors for trajectory 21 p3655 A67-38208
Electronic control system for triaxial control of geocentric satellite and second stage of CORALIE 21 p3656 A67-38231
Controllability of quasi-linear systems proved by Picard classical method of successive approximation 21 p3653 A67-38283
Thermal design of electronic packaging of Nimbus satellite control system 21 p3594 A67-38328
Advances in control systems, Theory and applications Volume 5, covering optimal control and optimization advances in control systems, Theory and applications, Volume 5, covering optimal control 21 p3603 A67-38438
Set of states reachable in given time in control problem determined by heuristic and rigorous methods 21 p3603 A67-38441
Resistojet control system for MORL analyzed for requirements and applications [AIAA PAPER 67-721] 21 p3714 A67-38747
Computer controlled metal cutting, discussing prospects, difficulties and need for systematic mathematical study 21 p3637 A67-38920
Optimal choice of prototype set by mathematical-statistics estimation theory, using active part of set for identifying control image 21 p3605 A67-39113
Pressure transducer for speech articulation to detect minute changes in articulator gesture for possible application as control element 22 p3754 A67-39163
Computer analysis and simulation of Mars soft landing descent control system combining inertial and radar sensing techniques 22 p3898 A67-39177
Man-machine design for Apollo spacecraft navigation, guidance and control systems 22 p3830 A67-39180
Test and control planning concepts for space travel projects, considering third stage of booster rocket Europa 22 p3921 A67-39281
Error control techniques covering parity check, longitudinal redundancy check and hamming and cyclic codes 22 p3776 A67-39372
Learning control systems, discussing adaptive time, searching, strategy, teaching, association, principle and behavior 22 p3776 A67-39412
Multivariable linear system noninteracting control realized by relays sliding motions 22 p3777 A67-39839
Equations for mode analysis in multichannel extremal control systems with harmonic probe signals, discussing synthesis of optimizers and phase shift automatic compensation 22 p3777 A67-39864
Book on continuous and scanning control systems optimization and random processes theory including numerical techniques, harmonic analysis and Gaussian transformation 22 p3777 A67-40070
Discrete methods for control network implementation using integrated circuitry to reduce inertial navigation systems complexity 22 p3800 A67-40184
Distribution theory in control system design, discussing sensitivity improvement by feedback for application to time invariant systems 23 p3984 A67-40755
Real time systems and applications 23 p3976 A67-41056
Multiprocessing features of IBM 9020 system, discussing breakdown of information into subprograms with operational priorities 23 p3976 A67-41058
Statistical analog technique for complex logic control systems to obtain within single test series required reliability characteristics for various structural versions 23 p3985 A67-41670
Optimal control systems synthesis using dynamic programming and closed loop system 23 p3985 A67-41671
Nonlinear sampled data automatic control system optimization by statistical method 23 p3985 A67-41673
Sun pointing attitude control acquisition

by space vehicle with jet control system 24 p4182 A67-41974
Generalized curves of closed loop loci of peak amplitude, phase and frequency of third order control system 24 p4134 A67-42025
Digital controller design for tracking telescope, discussing tracking accuracy and response time 24 p4154 A67-42176
Bounded-input bounded-output stability on nonlinear time varying discrete control system using Liapunov function 24 p4135 A67-42183
Transient behavior of autonomous nonlinear control system phase space domains, finding relative stability domains for special time dependent Liapunov function 24 p4135 A67-42186
Inductive energy storage and control system using ignitron 24 p4197 A67-42249
Spacecraft motion with limited power jet engine, applying simulation technique to determine operation modes for engine and control system 24 p4240 A67-42296
Triggering controller dynamic model with magnetoelectric drive, examining phase volume by point transformation technique 24 p4155 A67-42297
Minimizing maximum control deviation problem reduced to motion equation numerical integration 24 p4188 A67-42301
Nuclear subsystem controls and instrumentation for NERVA noting automatic startup, override, power and temperature controller testing 24 p4183 A67-42471
Automatic systems optimization, adaptation and learning 24 p4136 A67-42697
Synthesis of automatic systems optimum in mean noting difficulties arising from no restrictions on control law 24 p4137 A67-42722
Signal processing and control computer system for materials research noting use in viscoelastic studies of crystalline polymers 24 p4126 A67-42930
All-weather flight requirements of VTOL aircraft, suggesting artificial stabilization by automatic control system [AIAA PAPER 67-798] 24 p4096 A67-42959
CONTROL VALVE
Two-phase phase control valve with reactive compensating resistances, based on two-phase transformer with axisymmetric irreversible rotating magnetic field 07 p1150 A67-19319
Logic methods using conventional piston valves applied to general automation 08 p1282 A67-20470
Vortex valve performance power index 14 p2251 A67-28343
Hydraulic research data concerning control valve sizing and arrangement, noting liquid and gas control-valve formulas with limitations, Reynolds number effect, etc 15 p2423 A67-30400
Linearized differential equations for invariant servodrive with hydraulic actuator controlled by throttle slide valve 16 p2609 A67-31378
Cavitation in spool control valve orifices, showing effect on flow discharge coefficient over range of conditions 20 p3366 A67-37371
CONTROLLED FUSION
Convective type drift instability in collisional and collisionless regimes due to magnetic shear effects driven by density gradient 10 p1685 A67-23462
Plasma instability as obstacle to controlled nuclear fusion noting causes, effects, forbiddenness phenomenon, etc 11 p1831 A67-24016
Plasma instabilities and controlled thermonuclear reactions 13 p2164 A67-26387
Thermally ionized low density alkali-metal plasma for simulating controlled fusion processes, noting high particle losses and instability 14 p2362 A67-29038
CONTROLLED STABILITY
Controllability limit of human pilot for unstable second order system with positive static stability analyzed by modified transfer function and servomechanism theory 05 p0757 A67-17354
CONVAIR CV-990 AIRCRAFT
Null-field static dischargers location and maintenance on Convair 880/880M and 990 aircraft 22 p3745 A67-39733
CONVAIR MILITARY AIRCRAFT
S F-106 AIRCRAFT

S F-111 AIRCRAFT
CONVAIR 48 AIRCRAFT
S OV-10 AIRCRAFT
CONVECTION
SA ADVECTION
SA FORCED CONVECTION
SA FREE CONVECTION
SA THERMAL CONVECTION
Combined effect of gravitational and vibrational forces on formation of convection studied by method of averaging with respect to small vibrations 03 p0401 A67-12870
Small perturbation analysis of observed organized cloud convection for arbitrary unidirectional wind profile 08 p1350 A67-20950
Characteristics of atmospheric convection, obtained by vertical and horizontal heat transport processes and represented by difference equation, used to derive analytical solution 09 p1491 A67-21553
Cellular cumulus convection confined to cylindrical column in conditionally unstable atmosphere 20 p3480 A67-36505
CONVECTION CURRENT
SA ELECTRON BUNCHING
Secular variation of earth magnetic field 03 p0414 A67-13944
Convective vortex over horizontal surface caused by nonuniform heating 04 p0612 A67-14652
Internal turbulence scale for convection jets determined, using measurements of light intensity fluctuations 07 p1220 A67-20003
Airborne long focal length photographic system environmental effects studied with Cassegrainian type Maksutov telescope 16 p2678 A67-31793
Turbulence in upper atmosphere possibly due to density fluctuations accompanying internal gravity waves 17 p2843 A67-32538
Tectonic activity on Venus compared with earth, discussing convection currents and temperature gradients in crust and mantle 24 p4227 A67-42222
Poynting vectors difference obtained by using convection and polarization current models of moving plasma in Minkowski theory 24 p4124 A67-42812
CONVECTIVE FLOW
Hydrodynamic stability equations for free convection flow over vertical uniform flux plate 01 p0055 A67-11189
Retarded time integral expression rearrangement for study radiation from dipole distribution in inhomogeneous convective motion 01 p0115 A67-11305
Pressure and density measurements of heat flux convected on sharp pointed cone placed in incidence in hypersonic flow 02 p0177 A67-11499
Solar wind-magnetosphere system simulation, testing hypothesis that observed convective pattern is established by earth rotation 03 p0506 A67-12959
Convective effects role in exciting axisymmetric oscillations in plasma cylinder in magnetic field with aid of radius restricted electron beam 04 p0668 A67-15271
Laminar free convection of radiation absorbing-emitting fluid along flat plate noting interaction effects, solving problem by singular perturbation 04 p0727 A67-15682
Two-dimensional transient laminar natural convection heat transfer in partially filled liquid propellant tanks, solving vorticity and energy equations 04 p0731 A67-15826
Electromagnetic waves produced by charge traveling at constant velocity in medium with convective instability 05 p0762 A67-16353
Energy methods of subcritical convective instability theory and critical Rayleigh number dependence on Nusselt number 05 p0928 A67-16816
Subcritical convective instability, discussing effects of internal heat generation and spatial variation of gravity field on onset of thermal convection 05 p0928 A67-16817
Cumulus convective cloud formation above isolated source of heat and water vapor 09 p1491 A67-21552
Numerical finite difference solution of three-dimensional equations of motion for laminar natural convection, noting Navier-Stokes equation transformation 11 p1774 A67-23861
Diffusion measurements in potassium magnetoplasmas based on volume plasma

loss properties of variable length single-ended Q device 11 p1835 A67-24386

First azimuthally varying mode in mercury vapor plasma discharge, predicting growth of hose-like instability of electron beam 11 p1841 A67-24928

Convection in cellular pattern of clouds in atmosphere treated by classical methods 12 p1932 A67-25191

Method to describe finite amplitude convection time dependence 14 p2295 A67-27901

Two-dimensional unsteady Navier-Stokes equations for compressible viscous gas in closed region, examining convective flow and heat transfer 14 p2296 A67-27987

Model for radial and axial structure of geophysical vortices involving Boussinesq boundary-layer equations similarity solution in point heat source 16 p2778 A67-30949

Numerical calculations for two-dimensional Benard convection between rigid boundaries compared with other results 16 p2660 A67-31215

Pressure distribution and convective heat flux at slender bodies of revolution surface, considering sphericity influence of free hypersonic flow 16 p2594 A67-31468

Turbulent thermal convection properties measured in air between constant temperature horizontal plates, discussing structure 17 p2968 A67-32281

Estimation of lower bounds to minimum Rayleigh number inducing state of convective motion in quasi-incompressible fluid with temperature gradient in body force direction 17 p2968 A67-32410

Convection coefficient distribution in supersonic flow, noting wind tunnel measurement results at Mach 3.3 and at various angles of attack 17 p2791 A67-32702

Existence of affine solutions in natural convection along vertical flat heating plate, deriving expressions for thermal and dynamic boundary layers 18 p3025 A67-33685

Differential and boundary layer equations for free convection flow along vertical hot wall, investigating existence question 18 p3027 A67-34009

Lower thermal boundary layer of solar convection zone within framework of mixing length theory 18 p3133 A67-34376

Heat transfer characteristics of several aliphatic hydrocarbons in nucleate and film boiling during forced flow in heated tubes [ASME PAPER 67-HT-7] 20 p3544 A67-36705

Convective secondary flow in channel flow of quasi-incompressible fluid noting temperature gradient role [ASME PAPER 67-HT-26] 20 p3546 A67-36719

Rainfall associated with atmospheric convective activity estimated by radio ray attenuation model 21 p3582 A67-38577

Turbulent convective eddies effect on solar concentrated magnetic fields, plotting force lines 21 p3709 A67-38991

Solar hydrogen convection zone mean stratification derived from mixing length theory, discussing zone structure dependence on temperature and density dependence of opacity 23 p4068 A67-41278

Penetrative motion of individual elements in earth atmosphere and prediction of velocity field from convective overshoot 23 p4024 A67-41279

Diffusion flame shape in wake of falling droplet taken as point source of fuel, limiting analysis to Lewis and Prandtl numbers unity 23 p4083 A67-41720

Cellular convection patterns from instability of horizontal fluid layer uniformly heated and cooled from above 24 p4255 A67-42563

CONVECTIVE HEAT TRANSFER

Hot-wire probe measurement of friction temperature and convection coefficient of low pressure flows and wake of cylinder 01 p0006 A67-10757

Convective and radiative heat transfer in shock layer of hypersonic blunt body, noting asymptotic behavior of Navier-Stokes equation and energy transfer 01 p0168 A67-11421

Convective heat transfer in radiating gas, examining boundary layer equations and boundary conditions involving luminescence 03 p0532 A67-12866

Perturbation solutions in differential analysis of radiation interactions with conduction and convection 03 p0378 A67-13288

Convective heat transfer formulas for cases involving tube, liquid metals, etc 03 p0536 A67-13687

Hydrodynamic and thermal characteristics of flows bounded by channel walls 03 p0403 A67-13689

Convection heat transfer for turbulent flow in subsonic diffusers [ASME PAPER 65-HT-64] 03 p0352 A67-14010

Convective heat transfer measurements for partially dissociated carbon monoxide and hydrogen with high Lewis number [ASME PAPER 65-WA/HT-27] 03 p0537 A67-14012

Two-dimensional convective motion in rectangular cavity with vertical sides maintained at different temperatures, analyzing heat transfer 04 p0719 A67-14460

Separating composite heat transfer into radiative and convective components 04 p0722 A67-14715

Convective heat transfer in motion of fluid in initial section of cylindrical tube 04 p0722 A67-14716

Connective heat transfer and viscous fluid friction at air pressure with high Reynolds numbers in cooled channels, noting coolant pressure effect 04 p0603 A67-14717

Reynolds number assessment in analytical relations for convective heat transfer and viscous fluid friction 04 p0722 A67-14718

Convective heat transfer in accelerated heated air flows through cooled conical supersonic nozzles of three different configurations 04 p0723 A67-14837

Thermal similarity theory in accounting for convective heat transfer in arc discharge 04 p0667 A67-15192

Performance of thermal regenerators in which rapid flow cycling is accompanied by large pressure variations with time [ASME PAPER 66-WA/PID-1] 04 p0724 A67-15379

Temperature distribution and fluid flow in horizontal layer of liquid heated from below, having rigid-rigid and rigid-free upper surfaces 04 p0726 A67-15679

Variational analysis of Graetz problem of forced-convective laminar heat transfer in duct, for various cross sections and given wall temperature and temperature gradient 04 p0728 A67-15802

Forced-convective heat transfer in asymmetrically heated rectangular ducts as function of prandtl number, Reynolds number, aspect ratio and temperature difference 04 p0728 A67-15804

Simultaneous conductive-convective heat-transfer coefficient and heat flux temperature relation at solid moving liquid interface 04 p0730 A67-15817

Mach number and temperature ratio effects on convective heat-transfer coefficient to flat plate through turbulent boundary layer in air and Stanton number calculation in terms of drag coefficient 04 p0731 A67-15820

Convective heat transfer from bluff bodies analyzed, particularly small electrically heated cylinders at low Reynolds numbers, noting correlation with Nusselt and Prandtl numbers 04 p0732 A67-15831

Laminar convective heat transfer to cavities in hypersonic low density flow 04 p0732 A67-15833

Gas flow, convective heat transfer, enthalpy rise and surface mass transfer for bodies in cross flow, with application to circular cylinder 04 p0733 A67-15841

Free convective heat transfer measurements of sodium boiling on surface of horizontal tube 04 p0736 A67-15860

Boiling Na free-and forced-convective heat transfer rates, surface temperature and pool-boiling heat-transfer coefficient measurements 04 p0737 A67-15861

Natural convective heat transfer in closed cavity between two disks in central force field for laminar flow in boundary layers 04 p0738 A67-15893

Thermoelastic wave propagation in elastic layer with convective heat transfer between layer surfaces and surrounding medium, considering relations between temperature field and dynamic displacement 05 p0913 A67-16188

Convective and radiative heat transfers at stagnation point of hemisphere cylinder model immersed in high enthalpy partially ionized supersonic flow in plasma wind tunnel 05 p0747 A67-16432

Ignition pressure transient in solid rocket motors, examining chamber filling interval, flame propagation, heat transfer correlation, burning area, etc 05 p0873 A67-16513

Solar hydrogen convection zone interaction with photosphere restricted to relation of convection theory to granulation and supergranulation 05 p0899 A67-17070

Computing velocities and convective energy transport in stars of different spectral types and luminosities 05 p0899 A67-17071

Convective and radiative heat transfer to reentry vehicles at superorbital velocities [AIAA PAPER 66-106] 05 p0928 A67-17336

Atmospheric argon effect on hypersonic stagnation point convective heat transfer, using arc-heated shock tube simulating flight velocities up to 34,000 fps [AIAA PAPER 66-29] 05 p0928 A67-17337

Convective heating in shoulder regions of flat-faced cylinder with large favorable pressure gradient [AIAA PAPER 67-162] 06 p1114 A67-18293

Heat transfer by steady laminar forced convection in noncircular ducts, analyzing effects of viscous dissipation due to constant axial temperature gradient 06 p1116 A67-18384

Hot gas tunnel for determination of material behavior under convective heat transfer conditions similar to that existing in rocket combustion chambers [AIAA PAPER 67-106] 06 p0981 A67-18473

Longitudinal magnetic field effect on convective heat transfer during turbulent MHD pipeflow of liquid Ga 06 p1044 A67-18682

Equilibrium air study extended to reentry speeds up to 70,000 fps, using transport and thermodynamic properties to examine stagnation point convective heat transfer including blowing rates 06 p0943 A67-18843

Free convective heat transfer between hot and cold rotating disks in laminar steady azimuthally symmetric flow in zero-gravity field 06 p1119 A67-18864

Convective heat transfer through stabilized turbulent flow of chemically homogeneous liquid in circular pipe under supercritical pressure conditions 07 p1265 A67-19127

Convective heat transfer in tube with gaseous heat carrier pulsating at frequency corresponding to second resonance harmonic 07 p1266 A67-19182

Nonstationary heat transfer coefficient and effect of nonstationary hydrodynamic conditions on heat transfer in channels 07 p1266 A67-19183

Equations for nonstationary temperature field of n-layer plate, noting convective heat transfer on free surface of plate 07 p1267 A67-19327

Curvature effect on heat transfer for turbulent flow in curved pipes under constant heat flux, considering boundary layer existence along wall 08 p1428 A67-20926

Solid particle drag, convective heat transfer and ablation effects on structure of normal shock wave in nonreacting mixture of gas and ablating dust, using Runge-Kutta integration 08 p1427 A67-21120

Crustal features of moon and Mars analyzed for mantle convections, noting correspondence to spherical harmonics of various orders 08 p1397 A67-21208

Convective laminar heat transfer to hypersonic vehicle, deriving similarity relations between stagnation temperature profile and mass fractions of chemical species 09 p1579 A67-21699

Quasi-stationary regime during radiative-convective heating of infinite plate and cylinder, noting time dependent temperature variation 10 p1732 A67-23020

Forced convection heat transfer to liquid flowing within unsymmetrically heated rectangular ducts 10 p1733 A67-23481

Turbulent transfer in diabatic conditions, deriving formulas for wind and temperature profiles 10 p1677 A67-23574

Convective heat transfer effect on plasmatron efficiency 11 p1843 A67-24970

Convective heat transfer for water flow in curvilinear short channel, noting flow and convection types at various sections 12 p2033 A67-25316

Sound and vibration effects on convective heat transfer rates 12 p2039 A67-26167

Dissipative energy effect on laminar heat

transfer from disk rotating in uniform forced stream 13 p2221 A67-26531
Surface film boiling under free convection 13 p2222 A67-26532
Priestley constant H of free convection temperature profile approaching atmospheric value for increasing Rayleigh number 13 p2151 A67-26737
Sunspot magnetic field affecting convective energy transport so that resulting pressure gradient together with gravity force balances magnetic field 13 p2204 A67-27436
Two-dimensional unsteady Navier-Stokes equations for compressible viscous flow in closed region, examining convective flow and heat transfer 14 p2296 A67-27987
Low velocity flow measurements by inexpensive thermistor probe 14 p2318 A67-28342
Prediction of solid propellant hot-gas ignition based on preignition transient convective heat transfer model [AIAA PAPER 66-87] 15 p2582 A67-30196
Interaction of convection and radiation heat transfer in axisymmetric two-dimensional stagnation point low-speed flow of gray absorbing and emitting gas 16 p2591 A67-30942
Flow equations for convective heating associated with recirculating flow in clustered engine boosters for free viscous shear layer along exhaust jet boundary 16 p2591 A67-30942
Laminar flow with forced convection heat transfer in parallel plate channel under influence of intense, longitudinal, resonant acoustic field 16 p2778 A67-30947
Vacuum UV radiation measurement from high temperature nitrogen, detecting radiation from shock layer of ballistic model 16 p2675 A67-31267
Laminar natural convection heat transfer between vertical plate and power-law fluid with high Prandtl number 16 p2780 A67-31553
Transverse magnetic field effect upon convective heat transfer in turbulent flow in electrically conducting fluid in channel bounded by two parallel plates 16 p2722 A67-31572
Unsteady convective heat transfer and hydrodynamic behavior of gas flows in channels 17 p2967 A67-32131
Transverse magnetic field effects on heat transfer in turbulent flow of mercury in circular iron tube 17 p2899 A67-32186
Wave number and Rayleigh numbers effect on stability of two-dimensional convection in layer heated from below 18 p3159 A67-34003
Turbulent boundary layer flow in conical supersonic nozzle, discussing convective heat transfer and adverse pressure gradient effect 19 p3169 A67-34814
Simultaneous heat and mass transfer in laminar free convection boundary layer at vertical surface with moving interface 19 p3346 A67-35613
Convection in atmosphere below cloud base considered from ground and aircraft observations 19 p3253 A67-35919
Model of nonradiative energy transport in sunspots, in which Alfvén waves generated in convectively unstable layer propagate upward into overlying stable layer 19 p3330 A67-36079
Convective heat transfer in fluid between concentric cylinders with inner heated cylinder rotating and outer cooled cylinder stationary 20 p3543 A67-36422
Convection initiation Rayleigh number in closed cell and Nusselt number-Rayleigh number relation after convection initiation [ASME PAPER 67-HT-4] 20 p3544 A67-36703
Role of Rosseland approximation in convection-radiation interaction, considering flow of gray gas in laminar boundary layer [ASME PAPER 67-HT-9] 20 p3545 A67-36707
Linear heat transfer problems inside equilateral region solved by integral transform series [ASME PAPER 67-HT-67] 20 p3550 A67-36748
Nonconstant gravity field effect on free convective heat transfer to or from isothermal flat plate [AICHE PAPER 2] 20 p3552 A67-36825
Fin surface geometry optimization with respect to gross heat-transfer coefficient [AICHE PAPER 6] 20 p3552 A67-36827
Thermal boundary layer theory for steady cellular convection in viscous rotating

flow 20 p3553 A67-36937
Convective heat transfer stability in fluid contained in cubic chamber shown from temperature measurements 20 p3422 A67-37064
Physical analysis of convective heat transfer in laminar and turbulent flow through ducts and boundary layers, deriving trailing functions by variational method 21 p3730 A67-37736
Convective heat flow nonlinear equations for fluid sphere having heat sources expressed in Boussinesq approximation as perturbation of steady state conduction solution 21 p3731 A67-37926
Convective heat transfer through stabilized turbulent flow of chemically homogeneous liquid in circular pipe under supercritical pressure conditions 21 p3731 A67-38171
Viscous dissipation effect on heat transfer rates for laminar boundary layer flow of gray gas across flat plate 21 p3732 A67-38878
Convective motion of low pressure plasma confined by strong magnetic field taking into account heat and mass transfer 21 p3675 A67-39014
Forced convective film boiling heat transfer to H studied from experiments on cooling down Cu test section by liquid H 22 p3918 A67-40092
Laminar free convection of absorbing emitting gas analyzed in region of stagnation point of horizontal cylinder 22 p3920 A67-40418
Forced convective heat transfer in straight pipe rotating around parallel axis with large angular velocity 22 p3920 A67-40419
Thin plate temperature distribution from solving conduction equation, considering boundary convection losses and moving discrete heat source 22 p3920 A67-40424
Numerical solution of Poiseuille flow with variable fluid properties, solving coupled momentum and energy equations [ASME PAPER 66-WA/FE-22] 23 p3989 A67-40930
Convective heat transfer between tube and airflow in tube for pulsating flow with pressure fluctuation frequency deviating from resonant frequency 23 p4082 A67-41285
Temperature field and critical thermal loads for fuel elements with varying convective heat transfer coefficient and ambient temperature 23 p4082 A67-41286
Radiative and convective heat transfer between solid body and heat generating medium in motion, calculating thermal conductivity 23 p4083 A67-41289
Thin foil heat flux sensor for radiative and convective heating rates over wide range and dynamic response, noting error mechanisms, calibration and accuracy 23 p4006 A67-41374
Convective heating in shoulder regions of flat-faced cylinder with large favorable pressure gradient [AIAA PAPER 67-162] 23 p3932 A67-41714
Net convective and radiative heat flow to electrodes of coaxial plasma generator may exceed heat flow from moving arc spot within arc burning region 24 p4098 A67-42250
Semiempirical solution for heat transfer during turbulent natural convection near vertical impermeable flat surfaces 24 p4253 A67-42251
Free convection thermal transfer in narrow horizontal channels and infinitely wide channels 24 p4255 A67-42587
Free thermal convection in axisymmetric rotating cavities 24 p4255 A67-42588
CONVERGENCE
Convergence theorems for sequence of expected values or random variables of stochastic learning process with time-dependent probabilities 01 p0104 A67-10280
Determination of maximum number of nonzero elements in nonnegative matrix and first power for which maximum density is assumed 01 p0105 A67-10731
Convergence theorem for second-order linear three-level difference scheme for class of quasi-linear parabolic differential equation 02 p0258 A67-11556
Kantorovich theorem, Goodman-Lance method and two-point boundary value problems, noting numerical results obtained on IBM 7094 computer 02 p0259 A67-11836
Erdős and Turán theory of fine and rough convergence of interpolation and quadrature processes 02 p0259 A67-11919

Abstraction problem in pattern classification, using algorithms with convergence properties 02 p0208 A67-12173
Convergence of eigenfunction series expansion of nonself-conjugate boundary value problem in complex variables 03 p0461 A67-14060
Successive approximation solution of initial value problem, noting convergence of sequence 04 p0642 A67-14481
Menshov theorem of enhanced C-properties applied to Walsh series convergence 05 p0835 A67-17003
Approximation of functions of several variables, using one-dimensional analogy to determine rapidity of convergence 06 p1022 A67-17566
Convergence rate of method of gradients relationship to singularity of second variation operator in optimal programming problems 06 p0975 A67-17935
Retrospection of nondiverging waves, noting phase velocity dependence on atmospheric stability 06 p1027 A67-18603
Convergence of Chapman-Enskog approximations to scalar electrical conductivity of some weakly ionized real gases 06 p1046 A67-18872
Intermediate value and simultaneous convergence obtained by sequence of polynomials for pair of functions on closed set E dense on norm z equals one 07 p1215 A67-19221
Fourier convergence of Lebesgue integrable functions 07 p1215 A67-19473
Fourier convergence of analytic functions 07 p1215 A67-19474
Lemma for solution of conformal mapping problems of particular class of Fourier series with bounded partial sums and absolutely convergent on convergence circumference 07 p1215 A67-19475
Ultraconvergence of sequence of optimal approximation polynomials 07 p1216 A67-19583
Numerical solution of Fredholm integral equation of second kind with real analytic and periodic functions, noting eigenvalues 07 p1216 A67-19883
Convergence rate of approximate Ritz and Bubnov-Galerkin method in application to equations having solutions in form of linear combination of functions 08 p1349 A67-21200
Rational iteration function with high order convergence for solving equations compared with other methods 08 p1349 A67-21258
Time varying weight functions effect on convergence of polynomial expansions of isotropic distribution 08 p1323 A67-21385
Finite difference approximation of balance wind equation, discussing convergence of Liebmann relaxation process, Coriolis term and computer time 09 p1525 A67-21551
Proof that Tandoni theorem gives best estimate for convergence rates of orthogonal series 09 p1524 A67-21911
Straightforward method consistent with virtual work principle for accelerating convergence to exact solution in shell analysis by matrix displacement method 10 p1725 A67-23714
Summation of convergent series for cyclotron harmonic wave dispersion for numerical and analytic work 11 p1827 A67-23986
Modified collocation method for linear boundary value problem for integrodifferential equation, giving approximate solutions which converge to exact solution 11 p1814 A67-25048
Mechanical quadrature theory and convergence problems 13 p2148 A67-27469
Zeros of polynomials with real or complex coefficients determined, using steepest descent method in convergent procedure 13 p2148 A67-27496
Convergence of methods of tangential parabolas and hyperbolas used in nonlinear equation solution with nondifferentiable operators convergence of methods of tangential parabolas and hyperbolas used in nonlinear equation solution 13 p2149 A67-27619
Schroeder fixed point theorem for convergence rate of iteration series extended to concave operators which need not remain constant 14 p2345 A67-28937
Optimal control applications of Fletcher-Reeves conjugate gradient minimization

method and comparison with second variational technique 15 p2456 A67-29362

Iterative technique for calculating electromagnetic propagating structures with nonuniform gross perturbations obtaining convergence improvement 16 p2626 A67-31346

Interior penalty method for inequality constrained optimal control problems concerning convergence 16 p2651 A67-31677

Conjugate gradients providing convergent means to solve optimal-control problems for linear systems with quadratic performance index 16 p2651 A67-31678

General solution of linear differential equation of first order with quasi-periodic coefficients 17 p2879 A67-32880

Convergence of solutions for AC and DC electric conductivity of plasma with collisions 19 p3286 A67-35352

Steady two-dimensional laminar flow of incompressible viscous fluid, noting asymptotic convergence of velocity profile in Prandtl boundary layer 19 p3212 A67-36031

Collocation method convergence in problems other than general linear problem of ordinary integral equations and those with homogeneous kernel 19 p3250 A67-36047

Search for extremum of real function in presence of noise, using maximum principle 20 p3477 A67-37111

Direct and inverse method of calculating rotating cascades with infinite number of blades and radial flow to enhance convergence 20 p3360 A67-37597

Galerkin method shown convergent even with selected functions not satisfying exactly all boundary conditions 21 p3715 A67-37890

Convergence of perturbed Galerkin method to construct general theory of approximate methods for nonlinear equations 21 p3653 A67-38419

Rapidly converging iterative solutions to Min-H strategy applicable to trajectory optimization and payload maximization 22 p3888 A67-40148

Methods of increasing rate of convergence in convergence processes for improper integral of first kind 23 p4022 A67-40861

General convergence theorems for Newton method applied to convex operators for partially ordered topological linear spaces 23 p4023 A67-40863

CONVERGENT-DIVERGENT NOZZLE

Nonequilibrium expansion of high temperature diatomic gas through hypersonic convergent-divergent nozzle 02 p0180 A67-12547

Boundary layer development in throat region of converging-diverging nozzle, obtaining self-consistent solutions 08 p1277 A67-20589

Heat transfer effect in converging-diverging nozzle flow, considering polytropic process 08 p1278 A67-21526

Nonequilibrium quasi-one-dimensional nozzle flows in limit when relaxation time is large compared with characteristic flow time 19 p3172 A67-35800

Polytropic exponent along axis shown to approach adiabatic exponent at throat of convergent-divergent nozzle 22 p3742 A67-40112

Critical air-water flow in converging-diverging annular venturi noting pressure profiles 24 p4143 A67-42280

CONVERGENT NOZZLE

Shock wave strengthening by area convergence with viscous correction [JPL-TR-32-1067] 08 p1321 A67-20707

Extended plug nozzles in suppression of jet noise in small turbojet engines [SAE PAPER 670157] 09 p1561 A67-22544

Turbulent boundary layer and heat-transfer coefficients for air in conical nozzles, noting uncooled inlet length and convergence angle effects [ASME PAPER 67-HT-28] 20 p3357 A67-36721

Re-reflected shock wave from convergent cylindrical channel, showing secondary shock wave overtaking primary 22 p3783 A67-39720

CONVERSION

S BINARY-TO-DECIMAL CONVERSION

S DATA CONVERSION

S ENERGY CONVERSION

S FREQUENCY CONVERSION

S INTERNAL CONVERSION

COEFFICIENT

S ISOMERIZATION

S ORTHO-PARA CONVERSION

S PHOTOVOLTAIC CONVERSION

S POWER CONVERSION

S THERMIONIC CONVERSION SYSTEM

S THERMOELECTRIC CONVERSION SYSTEM

S THERMOMAGNETIC CONVERSION SYSTEM

CONVERTER

SA ANALOG-TO-DIGITAL CONVERTER

SA DATA CONVERTER

SA DIGITAL-TO-ANALOG CONVERTER

SA DOWN-CONVERTER

SA ENERGY CONVERTER

SA FREQUENCY CONVERTER

SA IMAGE CONVERTER

SA PULSE WIDTH AMPLITUDE CONVERTER

SA SOLAR CONVERTER

SA THERMIONIC CONVERTER

SA TRANSFORMER

SA TURBOCONVERTER

SA UPCONVERTER

Transistorized logarithmic amplitude converter for recording pulses of radiation detector, automatic switching of conversion scale permits amplitude measurement 01 p0062 A67-10160

HF design of DC-DC converters with low weight and high performance for spacecraft power systems 02 p0183 A67-12181

Construction of functional converter with several inputs 05 p0782 A67-16322

Functional converters of magnetic type for mathematical operations with analog computers 09 p1498 A67-22032

Negative impedance converter circuits deducible from one basic NIC, noting similarity to Steimel vacuum tube circuits 11 p1769 A67-24129

Restoration of distorted signals for linear and nonlinear process 13 p2088 A67-27021

Construction of functional converter with several inputs 18 p3017 A67-33874

Two-beam capacitive converter for automatic systems reduced to synthesis of single beam converter 22 p3795 A67-39229

CONVOLUTION THEORY

Parabolic convolution type equations in bounded cylindrical and noncylindrical regions, discussing smooth operators in half-space 02 p0259 A67-11871

Quantum theory of optical coherence in twisted convolution formalism 08 p1354 A67-20871

Synthesis of time functions with finite number of discontinuities by constructing functional scheme of system from Laplace transform of output 11 p1769 A67-24122

General heat flow problem with convolution integrals eliminated and unsteady temperature distribution expressed as sum of quasi-steady and transient fields, noting region geometry 12 p2040 A67-26185

Structures of solutions and expansion of radial heat equation with pole type data function 13 p2145 A67-26492

Quasi-invariance and ergodicity in binary sequence space with respect to discrete groups of Bernoulli schemes, noting finite entropy distance formulation of measure equivalence 14 p2343 A67-28502

Solution of incorrect magnetometric and gravimetric problems represented by integral equations of convolution type with unstable solutions 16 p2663 A67-30866

Convolution type integral equation solution via reduction to Riemann problem in class of generalized functions 16 p2698 A67-31735

Convolution technique applied to time domain to evaluate system capability 19 p3186 A67-35326

CONVULSION

S CONTRACTION

COOLANT

SA ENGINE COOLANT

Coolant injection in turbulent boundary layer for protection of surfaces from effects of high temperature and high energy gas flows 03 p0536 A67-13526

Li, Na, K, Rb and Cs vacuum tests as coolants and working fluids in high temperature compact space power plant 07 p1223 A67-19464

Copper-constantan and chromel-copel microthermocouples installation in capillary tubes for measuring coolant temperature 17 p2860 A67-32831

COOLING

SA ABLATION

SA AIR COOLING

SA CRYOGENICS

SA EVAPORATION COOLING

SA FILM COOLING

SA LIQUID COOLING

SA QUENCHING

SA RADIATION COOLING

SA REGENERATIVE COOLING

SA SUBCOOLING

SA SUPERCOOLING

SA SURFACE COOLING

SA THERMOELECTRIC COOLING

SA TRANSPIRATION COOLING

Cooling effect of emission current on square wave modulated noise diode cathode 01 p0033 A67-10024

Delayed energy produced by fission product decay when restart of nuclear rocket engine is considered, noting effects of cooldown requirements [AIAA PAPER 66-551] 05 p0844 A67-17222

Electron cooling in polar semiconductor by application of electric field 06 p1048 A67-17816

Thermal explosion laws under cooling conditions, examining linear cooling as method for studying thermal explosion of strongly self-accelerating reactions 06 p1112 A67-17962

Cooling requirements for intrinsic photoconductive IR detector, comparing theory and experiment 06 p1005 A67-18713

Cooling rate from homogenization temperature effect on structure and properties of forged alloy KhN77TiLuR 07 p1199 A67-19241

Free cooling of thin rod in constant temperature medium, finding temperature field for thermodynamics application 09 p1579 A67-21862

Thermoconductivity of heat resistant materials during cooling at room temperature, using photopyrometer to record temperature gradients 11 p1789 A67-24021

Iron and stony meteorite cooling rates determined by measuring kamacite bandwidth, bulk nickel content and composition 11 p1868 A67-24872

Heat transfer from laminar Newtonian flow through cooled elliptic tubes with variable cross sections 12 p2033 A67-25215

Iron and iron-stony meteorites cooling rates in relation to Ni content and Widmanstätten structure suggest development in different thermal environments 16 p2750 A67-31453

Experimental assembly for measuring true heat capacity of heat resistant insulating materials during natural cooling at temperatures from 1200 to 2400 degrees K 16 p2678 A67-31784

Integration of propulsion system into airframe of hypersonic cruise aircraft, discussing configurations, cooling and supersonic combustion 17 p2796 A67-32475

Lunar thermal anomalies exhibiting slower cooling rates during eclipse, discussing IR observations 18 p3135 A67-34546

Cooling and illumination effect on Gunn oscillators resulting in abrupt shift from transit-time frequency mode to higher frequency 19 p3305 A67-35628

Cooling losses in cooled gas turbines, correlating Cooling Loss Factor /CLF/ and Cooling Number /CN/ 20 p3517 A67-37484

Cooling of cylinder moving through fluid assuming fluid properties permit boundary layer approximations 22 p3918 A67-39782

Hot rolling finishing temperature and cooling rate effects on aged 250 grade 18 Ni maraging steel fracture toughness 22 p3822 A67-40057

Interstellar gas cloud collision, heating, possible gravitational instability and subsequent cooling 22 p3894 A67-40513

Interstellar gas cloud gravitational collapse for models initially in gravitational equilibrium without mass motions, analyzing cooling and density distribution effects numerically 22 p3895 A67-40514

Anoka, Minnesota, iron meteorite noting composition, chemistry, structure and cooling rate 23 p4069 A67-41449

Cooling rates for Widmanstätten pattern formation in iron meteorites used to obtain data on parent meteorite bodies 24 p4234 A67-42627

COOLING FIN

Analytical solution for determining inlet and outlet temperature for space radiator with heat rejection rate for steady state conditions and zero irradiation environment 08 p1429 A67-21511
Steady state and transient temperature profiles for straight fins of trapezoidal profile with radiative heat transfer [ASME PAPER 67-HT-73] 20 p3550 A67-36753
Optimal geometry of certain isolated heat-conducting circular fins cooled by radiation 20 p3554 A67-37067
Model for straight fin nucleate boiling onset criterion, discussing boiling section length expression, heat flux and temperature profile distribution 22 p3919 A67-40387

COOLING SYSTEM

SA GAS COOLING SYSTEM

SA REFRIGERATION

SA VENTILATION

Amorphous whiskers from cobalt-gold alloy by quenching molten material through electron-beam heating and anvil-cooling device 01 p0135 A67-10895
Materials for ablative cooling processes for rocket engines, noting structure and properties of porous and solid materials 02 p0306 A67-12791
Heat transfer and circulation data for rotating mixed convection thermosyphon geometry for application to cooling certain rotating components 04 p0731 A67-15828
Cooling induced hydraulic and thermodynamic energy losses in high pressure turbine and turbojet engines 04 p0690 A67-15896
Variable sweep wing F-111 aircraft cooling systems for temperature control of hydraulic fluid of type II system 05 p0752 A67-16161
Water cooled vest with insulated icebox and electric pump to reduce thermal strain and increase comfort for aircrew members in hot humid climates 05 p0756 A67-16284
Cooling gas turbine blades by heat pipe effect for stationary blades and thermosyphon effect for moving blades 05 p0874 A67-16747
Relation between packaging design and cooling, vibration, RF interference and reliability of microelectronic systems used in space vehicles 05 p0779 A67-17467
Thermoelectric cooling vs conventional cooling of electronic units 08 p1427 A67-21416
Testing of transpiration air cooled turbine, discussing blade fabrication [ASME PAPER 67-GT-29] 11 p1854 A67-24807
Synthetic pink-ruby crystal demagnetization characteristics when employed as coolant in cryostat, noting temperature dependence 11 p1851 A67-25033
MHD generator working fluid temperature reduction 12 p1973 A67-25395
Cooling system for maintaining uniform low temperature environment under low gravity conditions 13 p2227 A67-27645
Low temperature engine suction line response to fluid exposed internal surface coating, determining effects of varying flow rates 13 p2229 A67-27664
Cooling system for maser amplifier for ground station satellite communication 14 p2277 A67-27778
Low temperature parametric amplifiers, discussing varactors, circulators and demands on cooling systems 14 p2278 A67-27783
Stirling type closed cycle cooling system for masers and other microwave electronic devices 14 p2278 A67-27784
Continuous flow cryostat system for open cycle cold fluid refrigeration 14 p2404 A67-27786
Space simulation chamber for industry and research 14 p2292 A67-28063
Energy losses due to bleeding air from compressor for cooling systems of gas turbines 14 p2377 A67-28648
Solid film sublimation cooling effect in Couette gas flow simulating real rarefied gas flow heat transfer, for jet engine application 14 p2408 A67-28800
Large space simulation chamber for studying low temperature, absolute vacuum and solar radiation effects 15 p2466 A67-29571
Cryogenically cooled primary winding system for AC MHD generator, considering real machine data 16 p2605 A67-30580

Temperature fields in cross section of gas turbine blade with internal coolant during variation of local heat-transfer coefficient 17 p2973 A67-33076
Micro-orifice injector rocket motors covering efficiency, nominal thrust, size, performance, cooling, design factors, etc [AIAA PAPER 67-462] 18 p3113 A67-33933
Time and cryogenic liquid calculation required for cryogenic system cooling, considering low/high flow rate effects on system components [AIAA PAPER 67-475] 18 p3157 A67-33945
Book on generation of high magnetic fields, discussing solenoids, cooling systems, superconducting and pulsed coils, etc 20 p3483 A67-36452
Coolant passage axial curvature effect on heat transfer to endothermically dissociating supercritical nitrogen tetroxide [ASME PAPER 67-HT-59] 20 p3549 A67-36741
Rapid adiabatic cooling of gas systems for population inversion 21 p3638 A67-37942
Forced air distribution systems for electronic equipment 21 p3594 A67-38331
Cryogenically cooled rocket nozzle thermal fatigue analysis by thermal-cycle testing of specimens 22 p3834 A67-40183
Conductive cooling method for pressure applications in body heat loss promotion at high exercise rate 23 p3964 A67-41558
Energy expenditure in space suits studied for controlled cooling during high work rates 23 p3965 A67-41562
Liquid transport cooling system for aircrew evaluated by collecting in-flight sweat rate on fighter aircraft flying combat and training in tropics 23 p3966 A67-41581
Heat exchanger cooling system for controlling aircraft high temperature and thermal inorganic salt for protection against cold for flying personnel 23 p3967 A67-41612
Coolant selection for radiative cooling circuit of space vehicles, considering flow rate, heat transfer rate, etc 24 p4253 A67-42217

COORDINATE

S ASTRONOMICAL COORDINATE

S CARTESIAN COORDINATE

S GEOCENTRIC COORDINATE

S LAGRANGE COORDINATE

S OBLIQUE COORDINATE

S POLAR COORDINATE

COORDINATE GEOMETRY

S ANALYTIC GEOMETRY

COORDINATE SYSTEM

SA INERTIAL COORDINATE SYSTEM

SA QUATERNION

Standard earth geodetic coordinate system and Baker-Nunn camera station positions 01 p0056 A67-10038
Corrections to Smithsonian astrophysical observing station coordinates and nonzonal harmonics from combination of dynamical and geometrical method 01 p0056 A67-10039
One-dimensional compressible gas-channel flow under thermal and mechanical effects analyzed within generalized energy coordinates 01 p0119 A67-10170
Steady state two-coordinate problem of MGD solved for subsonic attached flow past simply connected profile 01 p0119 A67-10171
Carnot cycle diagrams using heat and work as coordinates in addition to several thermodynamic variables 01 p0168 A67-10505
Satellite orbit calculation using cylindrical coordinates 02 p0321 A67-11547
Polarization angle of linear feed antenna on polar mounted paraboloid relative to az-el coordinate system 02 p0212 A67-11611
Solutions of nonstationary equations of plane laminar MHD boundary layer, using transformation to specialized form of curvilinear coordinates 03 p0477 A67-13527
Motion equation and measurement of angles of aircraft closely approaching vertical plane, using new coordinate system 04 p0704 A67-14776
Steady state axisymmetric thermoelastic problems in bispherical coordinate system [ASME PAPER 66-WA/APM-12] 04 p0713 A67-15403
Stress in helical corrugated shell under axial tension examined as boundary value problem of ODE in cylindrical coordinate system 05 p0914 A67-16215
Optimum radar measurement of multiple target coordinates with unknown signal amplitudes and phases 05 p0765 A67-16960

Exact solutions in theory of orbits using Hamilton-Jacobi and Laplace equations 05 p0903 A67-17294
Eckert-Brouwer orbit correction formula in general perturbations theory, expressed in rectangular coordinates and variation of astronomical elements, applied to planetary theory 05 p0904 A67-17391
System of n first order differential equations relating coordinates and time, using matrix methods for solution 06 p1022 A67-17773
Dynamical system specified by set of generalized coordinates, considering Jacobi and Kepler elements and Poisson and other methods 06 p1031 A67-17774
Canonical transformation to investigate rotational motion of uniaxial orbiting rigid body influenced by gravity gradient torque [AIAA PAPER 67-125] 06 p1084 A67-18288
Euler angles sets, particularly right-handed coordinate systems and positive rotations, with solutions for angular velocities 06 p1032 A67-18527
Graphical method for converting geocentric satellite coordinates into topocentric, determining azimuth, elevation angle, etc 06 p0964 A67-18577
Approximation method of determining statistical characteristics of phase coordinates of linear automatic control systems 06 p0978 A67-18792
General solution of two-dimensional linear elasticity problem in polar coordinates in term of stress function satisfying biharmonic equation 06 p1111 A67-18873
Vela II measurements of earth magnetopause and bow shock positions, showing relationship to magnetic disturbance index and thus also to solar wind velocity 07 p1180 A67-19920
Hellmann-Feynman theorem in curvilinear coordinates for exact and for floating variational wave functions 07 p1138 A67-20189
Longitudinal and lateral axes orientation of uniformly rotating or rapidly rotating vehicle utilizing outputs from solar sensors and lateral magnetometer 08 p1409 A67-20538
Coordinates determining relative altitudes on lunar surface obtained through coordinate measuring instrument 08 p1398 A67-21216
Damped least squares method for kinematic synthesis of plane curves described by paired coordinates for four-bar linkage mechanism [ASME PAPER 66-MECH-13] 08 p1336 A67-21318
Tesseral harmonics of coordinates using Baker-Nunn data and geopotential and dynamical procedures, noting iterative cycle for correction determination 10 p1636 A67-23178
Photographing satellites, using optical system and image converter for determining coordinates 10 p1606 A67-23184
Image transmission by two-dimensional contour coding using edge point coordinates studied by computer 11 p1791 A67-24713
Field equations for spreading resistance of variable capacitance diode and point contact variable resistance diode derived in terms of frequency, material characteristics and physical parameters 11 p1767 A67-24731
Independent cometary orbit correction permitting checkout of initial coordinate and velocity components 11 p1868 A67-25084
Space vehicle orientation with respect to rotating system of coordinates 12 p2011 A67-25641
Equations for small oscillations of mechanical system with solid components divided into groups by system of generalized coordinates 12 p1967 A67-25661
Location of center of gravity of sensitive element of pendulum effect on stable equilibrium positions of gyrocompass in geographically oriented coordinate system 13 p2118 A67-28349
Time dependent orientation of body fixed coordinate system relative to stars for spinning rigid torque-free body 13 p2154 A67-26816
Molecule dissociation in meteoric trains, discussing coordinate system to determine cross sections for dissociation of magnesium and silicon oxides 14 p2383 A67-27945
Boltzmann equation and deduced moment equations containing moments up to fourth order in arbitrary orthogonal curvilinear

coordinates 14 p2297 A67-27998
 Lie series solution of equations resulting from separation of Helmholtz equation in special coordinate systems 15 p2509 A67-29266
 Conservative systems motion stability, generalizing precession and nutation of gyroscope with respect to noncyclic coordinate 15 p2518 A67-29685
 Equations of Hill plane lunar problem for two rectangular coordinates in rotating system reduced to one differential equation for radius vector 15 p2560 A67-30039
 Spheroidal coordinate method for obtaining gravitational potential of oblate planet 15 p2560 A67-30042
 Spherical coordinates near apogee of Cosmos 41 satellite determined with TV system and meniscus telescope 16 p2621 A67-30683
 Gravitational stabilization of satellites with respect to orbital system of coordinates 16 p2760 A67-30740
 Theodolitic device for measuring coordinates of center of gravity of photographed missile in flight 16 p2674 A67-31120
 Satellite orbit calculation using cylindrical coordinates 16 p2752 A67-31613
 Spherical analysis of geomagnetic maps to determine asymptotic directions of cosmic rays for Soviet station network 17 p2933 A67-32091
 McIlwain coordinates correlated with vertical cut-off rigidities, estimating cosmic ray rigidities 17 p2936 A67-32537
 Soviet book on moon figure and motion covering coordinate systems, surface features positions, rotational parameters, etc 17 p2948 A67-33118
 Catalog of selenocentric rectangular coordinates, selenographic longitudes and latitudes and absolute altitudes of lunar surface features 17 p2949 A67-33119
 Coordinate systems for lunar surface detail positions, accuracy and practical value and corrections for system conversion 17 p2949 A67-33120
 Moon rotational parameters determined by refractometric observations of craters position angles, tabulating selenographic and topocentric coordinates, reference system conversion corrections, etc 17 p2949 A67-33121
 Curves in polar plot representing auroral arcs over polar region organized in geomagnetic coordinate system and corrected by spherical harmonic terms 17 p2850 A67-33189
 Airfoil unsteady motion problem near screen in incompressible fluid with given horizontal/ vertical velocity 18 p2981 A67-33410
 Airglow and auroral phenomena, discussing ideal coordinate system, electric fields, morphology, solar wind-magnetosphere interactions, and particle precipitation 18 p3039 A67-33625
 Regions forbidden to motion in three-body problem determined in barycentric coordinate system for nonzero modulus of momentum vector 18 p3117 A67-33627
 Astronomical determination of position on moon 18 p3120 A67-33864
 Book on theory of orbits covering restricted problem of three bodies, two bodies in rotating coordinate system and periodic orbits 18 p3120 A67-34032
 Absolute lunar coordinate determination methods based on stereoscopic method 18 p3131 A67-34322
 Approximation method of determining statistical characteristics of phase coordinates of linear automatic control systems 18 p3018 A67-34457
 Soviet book on aircraft navigation covering theory, earth shape, map use, coordinate systems, instrumentation and aeronautical astronomy 19 p3254 A67-34894
 Conditions for optimal planar intermediate-thrust /singular/ trajectory in inverse-square-law field analyzed graphically 19 p3333 A67-35749
 Mathematical models of multichannel radio equipment in presence of noise, including guidance and coordinate measurement systems 19 p3185 A67-36095
 Azimuth and zenith distance determined from simultaneous observations of topocentric coordinates of artificial satellite transformed into astronomical and geodetic

quantities 20 p3428 A67-36483
 Gravitational theory with all curvilinear coordinate systems and space-time avoided illustrated by applying method to Dirac field case 20 p3484 A67-36836
 Highly asymmetric equation for MHD resonance of guided poloidal mode solved using dipole coordinates 20 p3502 A67-37427
 Book on mechanics of controlled body including control system realization, motion programming, dynamic error assessment and three-dimensional problems 20 p3482 A67-37459
 Inclination of quasi-geocentric coordinate system from satellite observations 20 p3434 A67-37548
 Radar station with antenna system for three target coordinates simultaneous measurements 21 p3582 A67-38498
 Satellite methods to determine absolute coordinates for geodetic points and to bridge continents 21 p3620 A67-38520
 Computer formulation of motion equations using tensor calculus to extend area of application of digital computers 22 p3827 A67-39418
 Coordinate system with straight current and magnetic field lines used for hydromagnetic resistive interchange instabilities studies in toroidal configurations provides negative criterion generalization 22 p3846 A67-39486
 Integral correlation technique used for first approximation solution in polar coordinate system to determine plane supersonic jet incidence on plane at arbitrary angle 22 p3786 A67-40020
 Absolute coordinates of 910 lunar features determined by stereoscopic method 23 p4065 A67-41005
 Spherical and cylindrical dipole fields in different coordinate systems, discussing differential distances 23 p3975 A67-41211
 Mechanical system motion with point moving on surface, imposing limitations on system mass distribution, obtaining fixed coordinate system 24 p4188 A67-42302
 Stationary motion stability of gyrostat satellite in Newtonian force field, defining body position in coordinate system 24 p4241 A67-42400
 Radar information automatic extraction by digital techniques, outlining information quantization, target detection and coordinate measurement principles 24 p4122 A67-42407
 Anharmonic method of photogrammetry rectification point by point, deriving positions from minimum control data 24 p4158 A67-42604
COORDINATE TRANSFORMATION
SA SCHWARZSCHILD METRIC
 Spherical diffraction solution obtained by reducing it to solution of diffraction problem for circular cylinder via coordinate transformation 02 p0205 A67-12529
 Uncoupled form for plasma resonance probe in magnetic field obtained, using special coordinate transformation 06 p1041 A67-18145
 Nonlinear transformations for solution of variational problems 06 p0976 A67-18407
 Derivative components of unit tangent vectors to parametric curves of curvilinear coordinate system in general Riemann space 10 p1675 A67-23792
 Reductive determination of refraction-free photographic coordinates of lunar limb profile points and disk 11 p1860 A67-24458
 Scale transfer for lunar photographs, using selenodetic controls with suitable point pattern 11 p1860 A67-24460
 Systematic errors in earthward coordinates of selenodetic points, noting results of triangulation 11 p1860 A67-24461
 Lunar rotational constants determined from measurements on scaled and oriented photographs, using least squares analysis and rigorous formalism 11 p1860 A67-24462
 Measures and reductions for 1868 points on Yerkes lunar photograph No. 1269, listing uncorrected and refraction-free photographic coordinates 11 p1860 A67-24463
 Transformation for uncoupling system of duct flow of conducting fluids under arbitrary oriented applied magnetic field 12 p1976 A67-25941
 Spherical diffraction solution obtained by reducing it to solution of diffraction problem for circular cylinder via coordinate transformation 14 p2261 A67-28006

Computational errors in generation of direction cosine matrix in strapdown system 15 p2515 A67-29741
 Selection of two regularizing functions reduced to one by evaluating relations between them in restricted three-body problem 15 p2557 A67-29875
 Nonlinear system analysis by subdividing total motion of system into fast and slow components, noting application to control systems 15 p2458 A67-29886
 Hemisphere coverage by n planar phased arrays arranged in pyramids or pyramidal frustra solved by transformations leading to analytical solution 16 p2638 A67-31337
 Matric generalization of polar coordinate transformation to second order matrix differential system 17 p2877 A67-32563
 One-dimensional three-body problem, noting shell model for two particles and coordinate transformation 17 p2888 A67-32926
 Book on variational principles of mechanics covering basic concepts, calculus of variation, equations of motion, etc 18 p3079 A67-34100
 Relativistic transformation formula for thermodynamics, with correspondence between energy change of reference system and energy change of moving body 18 p3159 A67-34119
 Strapdown inertial reference and navigation system initial alignment utilizing coordinate-transformation matrix computer [AIAA PAPER 67-556] 19 p3257 A67-35953
 Magneto resonant gyroscopes simulation by converting motion equations to rotating coordinates system 20 p3451 A67-37154
 Rotating observer relative to inertial observer in relativity 20 p3486 A67-37501
 Three-dimensional generalization of Birkhoff transformation for regularization of Keplerian motion in three-body problem noting differential equations system 22 p3881 A67-39513
 Orthogonal transformation of neighboring quantum states into classical two-component plasmas, using WKB approximation 24 p4195 A67-42107
COOT AIRCRAFT
S ILYUSHIN IL-18 AIRCRAFT
COPOLYMER
 Simultaneous copolymerization of Leuchs anhydrides of 18 amino acids common to protein, discussing nutritional significance 20 p3377 A67-37397
 Thermostable fibers from ordered heterocycle amide copolymers tested for tensile and high temperature properties 21 p3647 A67-37872
 Copolymers containing imidazopyrrolone and imide groups tested for thin film tensile properties, degradation by strong acids and bases and thermal stability 22 p3824 A67-39851
COPPER
 Resistance of copper-tungsten fiber composites to repeated tension cycles 02 p0254 A67-11793
 Thermal emf in plastic deformation of copper, considering effects of crystal lattice defects and lattice elastic distortions 02 p0301 A67-12740
 Hydromagnetic approximation in stability of axisymmetric mode in case of mercury cylinder enclosing copper rod with electric current 03 p0480 A67-13728
 Friction and adhesion coefficients of copper on copper measured in vacuum at temperatures ranging from minus 270 to 1000 degrees F and in controlled pressures of dry air [ASME PAPER 66-LUB-3] 03 p0431 A67-13754
 Recoil ranges of products from reactions of Cu-65 with 11-35-mev He-3 ions 03 p0473 A67-13926
 Effect of copper on excess and tunneling current of As-doped Ge tunnel junctions 05 p0866 A67-16986
 Electric resistivity and electroconductivity of copper composites reinforced with fibrous felts of tungsten 06 p1015 A67-17808
 Anisotropic resistivity of dislocations produced by deformation measured in high purity Au, Ag and Cu single crystals 07 p1209 A67-19638
 Momentum transfer of positively ionized nitrogen molecule incident on copper target, measuring accommodation coefficient with torsion balance 13 p2098 A67-26945
 Mono- and polycrystalline samples of Al

and Cu bombardment by argon ions in presence of oxygen and by oxygen and nitrogen ions under vacuum 14 p2351 A67-28513
 Ni XIX, Cu XX and Zn XXI spectra observation using vacuum spark chamber 14 p2389 A67-28840
 Yield and angular distribution of cesium ion-sputtered copper, noting dependence on angle of incidence, target temperature and energy 16 p2728 A67-31056
 Thermionic work functions and electron emission S curves for contaminated copper surface in oxygen and cesium vapors, separate and mixed 17 p2887 A67-32203
 Copper-doping technique for obtaining p-n junctions in sintered cadmium sulfide polycrystals, suitable for use in photoelectric converters 19 p3304 A67-35427
 Copper and its solid solutions retarding force profiles studied for explanation of Cottrell-Stokes law 20 p3464 A67-36220
 Simultaneous and independent potentiostatic control of rotating ring and disk electrode and application to CuII/CuI/Cu system 20 p3446 A67-36655
 Carbon influence on copper precipitation in dislocation free silicon single crystals with low oxygen, discussing growth mechanism and edge dislocation 21 p3686 A67-39136
 High speed read-only memory with waffle iron structure noting ease of information change and high bit density 22 p3765 A67-39904
COPPER ALLOY
SA BRASS
 Thermodynamic properties of binary Cu-Pt alloys determined, using Knudsen effusion technique 05 p0829 A67-16473
 Superlattice formation and lattice spacing changes in copper-gold alloys annealed for various periods 05 p0862 A67-16506
 Direct observation on precipitation and aging behavior in Cu-Ti alloys by transmission electron microscopy 11 p1809 A67-24948
 Recovery of deformed copper-palladium and gold-palladium alloys by isothermal and isochronal annealing, noting vacancy and interstitial migration 13 p2133 A67-27007
 Magnetization ripple in multilayer films, noting dependence on copper layer 13 p2179 A67-27143
 Activities and relative partial molar free energies of CuPt alloys, noting formation mechanism, ordering temperatures, etc 17 p2872 A67-32739
 Copper-constantan and chromel-copel microthermocouples installation in capillary tubes for measuring coolant temperature 17 p2860 A67-32831
 Fatigue crack initiation, comparing alpha brass and Al-Mg-Zn alloy, noting effect of increasing maximum pressure value in contact region [ASLE PAPER 67-LC-5] 24 p4174 A67-42744
COPPER CHLORIDE
 Luminescence spectrum of CuCl at low temperatures excited by double photon absorption from high intensity laser beam 06 p1010 A67-17822
COPPER COMPOUND
 Attenuation length of photoexcited electrons in evaporated layers of CuBr estimated by measuring photoemission yield as function of thickness 03 p0500 A67-14332
 Thermochromic materials application in display devices 05 p0860 A67-16307
 Energy spectrum of semiconductor compounds with chalcopyrite structure analyzed, using perturbation theory, noting changes resulting from crystalline and spin-orbital interactions 05 p0861 A67-16393
 Copper telluride-cadmium telluride thin film heterojunction fabrication and characteristics for solar cell applications 08 p1285 A67-20730
 Solar photovoltaic cell properties and preparation using thin films of copper and cadmium telluride 08 p1285 A67-20731
 Photovoltaic effect in cell prepared by CdT film deposition and copper telluride flash evaporation 08 p1285 A67-20733
 Copper phthalocyanine single crystal measurements for electric, thermoelectric and galvanomagnetic properties 14 p2376 A67-29086
 Effect of copper chromite, carbon and other potential catalysts on thermal

decomposition and ignition of ammonium perchlorate 18 p3108 A67-33813
 Space charge limited currents in copper phthalocyanine thin films measured as function of voltage, temperature, thickness and illumination 18 p3104 A67-34626
 Currents in copper phthalocyanine thin films measured as function of temperature and ambient noting effect on conductivity, trap density, etc 18 p3104 A67-34627
 Thin films of cuprous sulfide, selenide and telluride prepared by flash evaporation, discussing resistivity and absorption coefficient 18 p3106 A67-34637
 Carbonyl compounds reaction with N-salicylideneglycinatoaquocopper /II/ syntheses of beta-hydroxy alpha-amino acid from glycine 20 p3376 A67-36877
COPPER OXIDE
 Temperature effect on equilibrium carrier concentrations and intrinsic lattice defects in semiconductor with self-activated conductivity, considering cuprous oxide 07 p1237 A67-20177
COPPER SULFIDE
 Solar cell model of CdS on copper sulfide 08 p1285 A67-20729
 Lattice relation of cuprous sulfide formed on CdS single crystal noting precisely similar orientation 21 p3677 A67-38011
 CdS solar cell model, discussing p-n junction, CdS and copper sulfide properties and microscopic junction formation and behavior 23 p4046 A67-41486
CORE
S EARTH CORE
S HONEYCOMB CORE
S MAGNETIC CORE
S REACTOR CORE
CORE FLOW
 Capture probability at Venus resonant rotation rate implying fluid core similar to earth 18 p3136 A67-34587
 Secular changes in surface flow motion in earth core noting dynamo theories of earth main field 23 p3996 A67-40816
CORIOLIS EFFECT
 Longitudinal proper motion of sunspot groups shown to be function of size and relative extension in longitude [AFCLR-66-801] 01 p0149 A67-10804
 Solid body motion equation about stationary point fixed at earth surface 02 p0267 A67-11961
 Gravitational and magnetogravitational stability of rotating fluid layers of uniform thickness under Coriolis force and magnetic field 03 p0482 A67-13744
 Energy transfer by circulatory and Coriolis forces in centrifugal and axicentrifugal compressors 04 p0690 A67-15897
 Finite difference approximation of balance wind equation, discussing convergence of Liebmman relaxation process, Coriolis term and computer time 09 p1525 A67-21551
 Stability of points of equilibrium in restricted problem as influenced by perturbations of Coriolis force 11 p1866 A67-24773
 Superimposed electromotive force appearing in direction of magnetic field in presence of opposed spiral motion in turbulent field 17 p2842 A67-32341
 Solid body motion about stationary point fixed at earth surface 17 p2886 A67-33278
 Far IR CN laser action shown due to HCN molecule, explaining intense spectral lines around 337 microns 20 p3458 A67-36391
 Vestibular, tactual and proprioceptive information in judging Coriolis rotation and attitudes during rotation and pitching on piloted flight simulator 22 p3751 A67-39605
 Habituation transference in Coriolis stimulation for change from passive lateral chair tilts to various active head tilts during rotation 23 p3953 A67-41585
 Coriolis force effect on gross reach movements for instrument control consoles 23 p3956 A67-41630
CORNEA
 Physiological regeneration on cornea epithelium and intestines exposed to fractional irradiation with fission neutrons, studying mitotic index and chromosome aberrations content 16 p2613 A67-30909
 Medical complications of contact lenses and aeromedical implications 18 p2993 A67-34723
CORONA
SA AURORA

Solar causes of occurrence of selected geomagnetic storms and geomagnetic quiet, using data of coronal structure at central solar meridian 01 p0060 A67-10789
 Tables of observational data on flattening, integrated brightness, brightness distribution and polarization of white corona 01 p0150 A67-10933
 Anisotropic distributions of suprathermal electrons as explanation of observed line splitting for type II solar radio outburst and indirect determination of coronal magnetic fields 02 p0307 A67-11691
 Radiative energy loss from solar chromosphere and corona estimated in order to identify mechanical energy input mechanism 02 p0323 A67-11692
 Solar corona temperature measurements, noting discrepancy between results from observations of forbidden emission lines and ionization balance calculations 03 p0470 A67-13218
 Fe spectrum energy levels for various subshell configurations, calculating oscillator strengths and transition probabilities 03 p0511 A67-13649
 Photometric cross section of nonradial coronal structure in 5303 angstrom line following proton flares with cosmic, subcosmic and corpuscular emissions 03 p0507 A67-13810
 Sunspot cycle coronal Fe XIV 5303 angstrom radiation emission and type IV bursts in solar flares 03 p0507 A67-13811
 Radar experiments of sun at 38 mc/s, presenting results on echo variation with sunspot number, coronal irregularities, etc 03 p0514 A67-14311
 Alfvén wave in outward corona as natural explanation of fast drift bursts 04 p0691 A67-14485
 Interferometric radio observations of Quiet Sun at 49 cm 04 p0694 A67-14486
 Solar corona and chromosphere activity observations at lunar observatory in gamma, X-ray and XUV regions 04 p0598 A67-15071
 Solar coronal reflection and occultation of 38 mc/sec galactic radio energy, using Taurus A and galactic equatorial continuum as occulted sources 05 p0891 A67-16403
 Coronal temperature and temperature distribution in transition region between chromosphere and corona, assuming photospheric wave propagation as essentially one-dimensional 05 p0900 A67-17077
 O-to-Fe ratio determined in active solar corona from intensity ratio of O-8 to Fe-17 lines and in quiet corona from O-7 to Fe-14 ratio 06 p1083 A67-18068
 Coronal temperature-gradient regions analyzed, using data of Lyot and corona condensation spectrum 06 p1083 A67-18154
 Viscous effects in expanding solar corona under conduction heating 06 p1078 A67-18158
 Electron-neutral particle collision and electron thermal conductivity effect on upper atmospheric electron and ion temperatures 06 p0998 A67-18702
 Signal delay transmission on several frequencies from solar orbiting spacecraft to terrestrial receiver used for continuous coronal electron density profile 06 p1091 A67-18996
 Monograph on physics of solar corona including history, observational methods, data analysis, coronal gas, magnetic fields, temperature, density and radiative processes 07 p1251 A67-19838
 Shock waves in interplanetary medium caused by sudden expansion of solar corona following flare [AFOSR-66-2638] 07 p1251 A67-19848
 Origin of solar type I noise storm radiation seen in cyclotron radiation from electron streams gyrating in spot field configurations in corona 07 p1244 A67-19852
 Solar corona observations of Surveyor I, discussing extent of measurable radiance and occurrence of streamer 08 p1386 A67-20943
 Coronal observations during solar eclipse in Bolivia, discussing equipment used and results 08 p1391 A67-21044
 Solar corona and interplanetary gas corotation with sun and effects of solar wind, considering poloidal magnetic field of rotating star 08 p1399 A67-21239
 Active region corona and type I bursts supposedly generated by plasma oscillations excited by electron beam 08 p1377 A67-21445
 Ionized medium effect on synchrotron

emission spectra in solar corona proposed to account for LF cut-off in type IV radio bursts 08 p1402 A67-21464

Magnetic fields in solar corona, observing bursts with frequency splitting to determine correlation with plasma radiation theory 09 p1565 A67-21981

Rise and decay times of spike burst during type IV event of February 5, 1965, noting electron stream velocities and coronal temperature 09 p1562 A67-22233

Generation of oscillations in solar atmosphere by separate granules modeled by bottom zone of isothermal gravitating photospheric layer overlaid by hot corona 10 p1704 A67-22721

Photometry of coronal emission line 5303 angstrom on Mt. Lomnický 10 p1705 A67-22897

Comet 1965 f /Ikeya-Seki/ interaction with solar corona produces no significant enhancement of emission at 2.2 m wavelength 10 p1706 A67-22958

Solar corona and occurrence of solar wind and influence on evolution of red giant star 11 p1858 A67-24095

Relative solar abundance for O, Si and Fe determined from intensities of far UV emission lines of solar corona 12 p2001 A67-25225

Fe IR line excitation in solar corona, noting abundance of iron relative to H and linear polarization of IR lines in coronal streamer 12 p2010 A67-26242

Galactic cosmic ray intensity depression by convective region and by surrounding static barrier of expanding corona 13 p2191 A67-26323

Scattering angle of spherical radio waves on isotropic and radially elongated inhomogeneities of supercorona of sun 13 p2197 A67-26543

Solar corona broadening mechanism studied using microscopic model including kinetic equations, determining proton escape velocity from sun 13 p2194 A67-27340

Polytropic heat sources effect on ejection of stationary symmetrical plasma from sun 14 p2378 A67-27915

Solar corona temperature from intensity gradients measured during total eclipse of May 30, 1965 14 p2387 A67-28564

Maser effect hypothesized as cause of 21 cm radiation in clouds of interstellar hydrogen in galactic corona 15 p2551 A67-29139

Finite-ion Larmor radius effect on wave propagation in rarefied rotating plasma, noting solar corona application 15 p2533 A67-30396

Coronal temperature-gradient regions analyzed, using data of Lyot and corona condensation spectrum 16 p2741 A67-30498

Viscous effects in expanding solar corona under conduction heating 16 p2741 A67-30502

Forbush effect causing solar flares not originating from same active solar region, discussing long connection to sun and interlocking 16 p2739 A67-31458

Chromosphere and corona UV emission spectrum provided by sounding rocket using photographic recordings 16 p2752 A67-31625

Dielectronic recombination and autoionization included in ionization formula for solar corona 17 p2952 A67-33392

Kinetic energy transport outwards in transition region between chromosphere and corona discussed qualitatively, postulating connection with spicules 17 p2952 A67-33393

Dome formation in corona around prominence during February 1961 eclipse, describing observed features and proposing three-dimensional model 17 p2953 A67-33399

Lightning theories from Mount San Salvatore /Switzerland/ observations, noting corona currents 18 p3074 A67-33995

Corona temperature and logarithmic intensity gradients determined by pointwise three-color photoelectric photometry during solar eclipse 19 p3318 A67-35017

Corona observation within one solar radius of photosphere, identifying emission lines and explaining continuous spectrum and Fraunhofer lines reduced depth 19 p3318 A67-35055

Quiescent solar prominences general appearance described by theoretical model 19 p3324 A67-35436

Solar flare electron density measurements using half-width method, noting variations with height, development and

area 19 p3314 A67-35439

Statistical correlation of type III solar radio burst activity with coronal green line over solar cycle 19 p3316 A67-36029

Central data system for solar probe to map particle and radiation fields of solar corona 20 p3391 A67-36597

Correlating lunar eclipse brightness, solar activity and corona ellipticity data 20 p3528 A67-37462

Extreme UV solar spectrum, reviewing echelle spectrum, soft X-rays and coronal emission 20 p3528 A67-37467

Coronal heating extent placed at 1.6 solar radii by 38 MHz radar investigation studies, noting agreement with coronal density calculation 20 p3528 A67-37477

Highly ionized S, Cl, Ar and K resonance lines recorded, noting application for coronal Ca ions 20 p3528 A67-37478

Radio sources fluctuations due to inhomogeneities of solar supercorona and interplanetary plasma, studying solar wind and brightness distribution 20 p3520 A67-37513

Solar supercorona observations using three-base interferometer with correlation radiometer, discussing concentration ellipses, supercoronal inhomogeneities and interference fringe modulation 20 p3529 A67-37515

Steady state model of system consisting of solar corona and interplanetary plasma, noting plasma efflux from sun 20 p3529 A67-37520

Spicules and inhomogeneities in corona and interplanetary plasma compared assuming mutual relationship spicules and inhomogeneities in corona and interplanetary plasma compared assuming mutual 21 p3711 A67-39028

Interplanetary space properties from satellite observations, discussing solar wind, geomagnetic field, comet tail effects, coronal plasma kinetic properties, etc 22 p3883 A67-39668

Solar wind general dynamical theory, discussing interplanetary space condition determined by coronal expansion 22 p3883 A67-39669

Coronal line spectra of 1952 total solar eclipse, noting emitted energies and isothermic coronal region 22 p3889 A67-40206

Solar type IV burst centimeter and decimeter polarization and spectral variabilities examined in helical electron stream cyclotron radiation hypothesis for solar corona model 23 p4050 A67-40776

X-ray emissions from coronal condensation regions studied with pinhole camera, obtaining intensity profiles along intense X-ray regions 24 p4224 A67-41821

Wavelengths and intensities of IR coronal lines of silicon and magnesium ions from airborne total solar eclipse observations 24 p4224 A67-41822

Mean intensity photospheric H-alpha radiation profile for prominences in solar corona, noting profile dependence on height, velocity and direction 24 p4209 A67-41965

Soviet noneclipse coronagraph structure, tracking system and artificial eclipse mechanism 24 p4154 A67-42111

Horizontal telescope used for solar corona photography during total eclipse /1966/, determining radii passing through solar magnetic poles 24 p4227 A67-42153

Solar corona spectra during total eclipse /1966/ using polaroid camera 24 p4154 A67-42157

Maser effect hypothesized as cause of 21 cm radiation in clouds of interstellar hydrogen in galactic corona 24 p4239 A67-43062

CORONA DISCHARGE

Measurement and control of corona-generated noise in aircraft, noting charge rate during takeoff via potential gradient method 02 p0190 A67-11501

Operational alpha counting characteristics for point plane counter in air working in corona streamer mode 02 p0241 A67-11680

X-ray emission from old novae noting possibility that hot coronas may arise from vibration 02 p0308 A67-12032

Environmental wind tunnel investigation of wind velocity and discharge current effects on average charge per Trichel pulse in corona discharges 03 p0486 A67-14119

Jovian atmosphere simulation with energy from corona discharge, producing simple

organic molecules 07 p1246 A67-19057

Light pulse generator circuit using hydrogen corona-discharge tube and thyatron generator of nanosecond light pulses 19 p3228 A67-34968

Prebiotic synthesis of monocarboxylic acids suggested from mixture of methane and water exposed to semicorona discharge 19 p3181 A67-35882

Corona discharge propulsion system with space charge limited emission of negative ions, noting ion mobility performance and efficiency 21 p3696 A67-38856

Electrofluidynamic /EFD/ power generator unipolar charge generation using corona discharge, noting pressure and geometry effects on ion currents and attractor voltage 24 p4107 A67-42528

CORONAGRAPH

Photometric measurements of ash-moon, using large coronagraph 06 p1082 A67-18014

Design of simplified noneclipse coronagraph, describing optical system and basic performance characteristics of instrument 09 p1495 A67-21636

Spectrographic observations of late stages of limb flare by achromatic coronagraph 14 p2381 A67-28835

Lyot-coronagraph with 53 cm lens, grating spectrograph, 12.6 cm solar disk image at spectrograph slit and one angstrom per mm dispersion 23 p4001 A67-41238

Soviet noneclipse coronagraph structure, tracking system and artificial eclipse mechanism 24 p4154 A67-42111

CORONAL CONDENSATION

Condensation path of cooling gas of solar composition calculated considering barriers to homogeneous nucleation of condensed phase 16 p2751 A67-31454

Coronal condensation analysis observed photographically during total solar eclipse, finding good correspondence of loop system spatial trajectories to force line configurations 17 p2945 A67-32690

Cosmic ray yearly variation during solar activity cycle, discussing flare and acceleration mechanisms, stable coronal condensation and sunspot magnetic field 22 p3874 A67-40045

CORONARY CIRCULATION

Rentgenographic kymography in evaluating cardiovascular apparatus in middle aged pilots 22 p3753 A67-40543

CORPUSCULAR RADIATION

Luna X shielded gas-discharge counter data on soft corpuscular radiation, noting solar contribution to magnetospheric tail 01 p0145 A67-10907

Properties of solar and geophysical phenomena analyzed, concluding that magnetic field of corpuscular fluxes has forceless structure 02 p0311 A67-12590

Corpuscular stream parameters based on data from Mariner II concerning cosmic ray variations on earth surface during geomagnetic storms 05 p0881 A67-16121

Halley comet head diameter change determined by converting propane and ethylene molecules in photon and corpuscular radiation field of sun 05 p0888 A67-16202

Role of solar photon and corpuscular radiation in dissociation and ionization of water molecules in cometary atmospheres 05 p0888 A67-16203

Specific type of geomagnetic pulsations corresponding to solar corpuscular radiation, noting flux geometry and intensity variations 05 p0884 A67-17134

Corpuscular intrusions into earth magnetosphere involving entire auroral zone and occurring only on night side 07 p1174 A67-19713

Soviet lunar probe measurements of gamma spectrometry, magnetic and gravitational fields, corpuscular radiation intensity, etc 08 p1411 A67-20999

Corpuscular streams and photodetachment of electrons reaction effect on formation of D layer of ionosphere 09 p1491 A67-21894

Role of corpuscular radiation in lower ionosphere formation noting charged particle flux, energy spectra, etc 10 p1647 A67-23283

Polar orbiting satellite measurements correlating ionospheric irregularities with trapped and precipitated energetic particles in South American energetic region 12 p1996 A67-25776

Corpuscular emission role in formation of lower ionosphere 13 p2194 A67-27329

- Geomagnetic pulsations and auroral activity, using magnetosphere simplified model 15 p2474 A67-29505
- Search for solar M-regions complicated by velocity decrease near active sun, considering corpuscular streams as enhanced solar wind 16 p2749 A67-31414
- Luminosity variations of comet 1963 III related to solar and geomagnetic disturbances caused by corpuscular solar particles 17 p2946 A67-32730
- Specific type of geomagnetic pulsations corresponding to solar corpuscular radiation, noting flux geometry and intensity variations 21 p3698 A67-38477
- 27-day cosmic ray intensity variations noting possible selective effects of active spots on solar hemispheres and plasma corpuscular fluxes 23 p4056 A67-41110
- Corpuscular stream parameters based on data from Mariner II concerning cosmic ray variations on earth surface during geomagnetic storms 24 p4214 A67-42797
- ## CORRELATION
- S ANGULAR CORRELATION
- S AUTOCORRELATION
- S CROSS CORRELATION
- S DATA CORRELATION
- S IMAGE CORRELATION
- S STATISTICAL CORRELATION
- ## CORRELATION COEFFICIENT
- Analog device for measuring coefficient of space-time signal correlations and applications to statistical mechanics of turbulent fluids and random noise 01 p0054 A67-11090
- Coefficient of mutual correlation of noises for two-antenna phase type direction finder 03 p0386 A67-13957
- Atmospheric turbulence compared with associated radar echoes, noting correlation coefficient for standard deviation of derived gust velocity with maximum radar reflectivity 04 p0649 A67-14687
- Liquid and gas viscosity correlation at 1 atm with reduced density for parahydrogen 05 p0873 A67-17224
- Nozzle submergence loss in solid propellant rocket engine, correlating loss percentage of specific impulse with dimensionless groups 05 p0875 A67-17366
- Quantile system of data compression for space telemetry, discussing operation, efficiency and advantages [JPL-TR-32-772] 07 p1145 A67-19873
- Exhaust cloud diffusion from solid rocket motors correlated with measurable meteorological variables [AIAA PAPER 67-280] 07 p1221 A67-20084
- Simultaneous recordings of cosmic noise absorption and VLF chorus, noting correlation from riometer recordings 08 p1327 A67-21374
- Diffusion in solutions in nearly critical states, noting increased cross effects and linear dependence of flows near critical points 09 p1580 A67-21908
- Optical effects of thermal structure in lower atmosphere 10 p1679 A67-22745
- Impurity distribution in GaAs noting growth rate, concentration and crystallographic orientation 10 p1693 A67-23515
- Diffusion coefficient measurement based on relationship between correlation coefficient for density fluctuations and density coefficient 11 p1829 A67-24003
- Nucleation of titanium and titanium oxide thin films correlation to thickness obtained from fluorescent intensity measurement 12 p1981 A67-25276
- Two uncorrelated Gaussian dependent random variables with non-Gaussian joint distribution may have any maximal correlation coefficient 12 p1980 A67-25313
- Two-velocity spatial correlation coefficients and lengths measured for wall jets 13 p2049 A67-26590
- Frequency dependence of radio star scintillations 15 p2555 A67-29621
- Correlation measurement in two-dimensional zero pressure gradient boundary layer, noting velocity fluctuation patterns 15 p2471 A67-29652
- Partial correlation coefficients between ionospheric, solar and geomagnetic parameters and spread-F occurrence probability [AGARDOGRAPH 95] 15 p2481 A67-30283
- Spatial correlation coefficients and transverse temperature perturbation scales during turbulent nonisothermal flow of mercury in circular pipe 16 p2724 A67-31776
- Airborne Astrographic Camera System using meteor orbit theory to observe reentry trajectory discussing data reduction theory and photo-optical instrumentation 16 p2679 A67-31795
- Forced-erasure decoding of fading and nonfading channels compared with correlation and digital decoding 17 p2811 A67-32114
- Transverse and longitudinal electron effective masses for wurtzite type crystals 17 p2913 A67-32273
- Enhancement of signal to noise ratio of turbulence measurements by cross correlation and heat transfer transducer 18 p3050 A67-34499
- Electron fluctuations variance and correlation coefficients computed for sensitized GaAs, comparing noisiness of deep recombination levels 19 p3306 A67-35732
- Algorithm for generating normally distributed variables set with given correlation matrix in digital computer simulation of electronic circuit performance 20 p3401 A67-37315
- Compressible turbulent boundary layer equations, discussing third order correlation terms role and eddy thermal conductivity definition 21 p3614 A67-38894
- Correlation coefficient dependence on angular dispersion and ratio between antenna directivity and width of energy spectrum of waves scattered by troposphere 22 p3759 A67-39433
- Odd value correlation coefficient and wave amplitude fluctuation effects on mean radiation pattern and antenna amplification losses 23 p3977 A67-40599
- Correlation calculus applied in metrology, estimating correlation coefficient 23 p4008 A67-41397
- ## CORRELATION DETECTION
- Correlation measurement of stellar interferometer at Narrabri, Australia 01 p0063 A67-10284
- Qualitative biological data conversion into pseudovariables permitting use of correlation analysis and prediction, considering occupation relation to cholesterol 01 p0017 A67-10956
- Equisignal zone technique for correlation-interference direction finder using commutable delay line 05 p0774 A67-16918
- Optimum quadratic detection of sample vector from signal random process imbedded in Gaussian noise 05 p0765 A67-17041
- Space-time correlation measurements in fluctuating turbulent wakes behind projectiles [AIAA PAPER 67-19] 06 p0940 A67-18434
- Mathematical tool for system design of pseudorandom coded ranging system used in space programs, noting failure probabilities 07 p1145 A67-19869
- Solar radio noise storm model, determining intensities for various frequency separations 07 p1256 A67-20169
- Quantization, sampling frequency and statistical scattering in correlation measurements 08 p1313 A67-21006
- Optimal extremal control systems synthesized by nonlinear filtering compared to those synthesized by correlation method of control 08 p1313 A67-21326
- Normal approximation of error transition probability for correlation receiver preceded by wideband hard limiter 09 p1459 A67-21579
- Space-time correlations of turbulent field measured by grid using high speed computer 11 p1780 A67-24541
- Modulation indexes for two-channel phase coherent communication system determining data rate yielding predetermined bit-error probability [JPL-TR-32-1118] 14 p2273 A67-28709
- Equisignal zone technique for correlation-interference direction finder using commutable delay line 16 p2623 A67-30895
- Correlation reception of wideband signals from ionospheric inhomogeneities, considering effectiveness for signal distortion discrimination 16 p2632 A67-31909
- Voltage amplitude limiting for improving stability of correlation detector of electronic cross correlation systems, noting variation of SNR 18 p3012 A67-34524
- Jet flow turbulence energy balance, measuring point-pressure/velocity correlations and spatial mean gradients, giving energy equation 19 p3170 A67-35412
- Correlation detection for extracting reflected radar signal from noise 19 p3195 A67-35550
- Correlation position device for autonomous orbital navigation system 20 p3481 A67-36553
- Correlation measurement in turbulent flow with hot wire anemometer downstream from grid, considering velocity effects 22 p3783 A67-39704
- Linear correlation-detection transducer arrays for directional noise field signals, giving N-element coherent detector performance in propagating and turbulent boundary layer 22 p3801 A67-40233
- Error correcting codes for white Gaussian channel at low signal to noise ratio, discussing properties and performance criteria 23 p3984 A67-40752
- ## CORRELATION FUNCTION
- Output autocorrelation function and spectral density of CW and FM signals passed through TWT 01 p0025 A67-10858
- LF spectrum of density correlation function, obtaining diffusion coefficient of right order of magnitude using quiet plasma 01 p0124 A67-10911
- Directional correlation of first forbidden beta group and gamma ray in decay of antimony at four beta energies 02 p0269 A67-11863
- Correlation function of stellar image fluctuations and pulsations due to earth atmospheric influences for two stars separated by small angular distances 02 p0325 A67-11984
- First and second order correlation functions for field obtained by superposition of two laser modes through Youngs experiment, used to determine coherence and statistical properties 02 p0254 A67-12634
- Plasma kinetic theory calculation via direct perturbation expansion of singular distribution for single system, comparing Dupree and Dawson-Nakayama version of BBGKY hierarchy 02 p0279 A67-12800
- Incoherent scattering measurements of ionospheric power spectrum and autocorrelation function at geomagnetic equator to determine electron and ion temperatures, ion composition and ion density 03 p0408 A67-12834
- Asymptotic form of correlation functions facilitated by use of Hamiltonian 03 p0458 A67-13342
- Statistical analysis for pulsed flow measurement evaluation using correlation and regression techniques 03 p0403 A67-13777
- Ratio of Lagrange and Euler correlation scales determined from correlation of time fluctuation of transverse wind velocity and temperature variation 03 p0464 A67-14229
- Approximation method for calculating autocorrelation function of quantized noise 04 p0567 A67-14405
- Correlation scheme for mean velocity distributions in turbulent boundary layers developing in arbitrary adverse pressure gradients 04 p0601 A67-14459
- Transport properties of model fluid whose molecules interact according to square-well potential used to calculate transport coefficients of krypton, xenon and argon 04 p0720 A67-14507
- Wideband multipoint real time device automatically calculating correlation functions of acoustic signals 04 p0620 A67-14890
- Autocorrelation function in statistical analysis of geomagnetic activity 04 p0613 A67-14897
- Harmonic generation by traveling waves in nonlinear dispersive medium for quasi-monochromatic signals, obtaining correlation function and spectrum of second harmonic for Gaussian processes 04 p0657 A67-15146
- Fluctuation-dissipative ratio between correlation functions of fluctuating parameters and dissipative properties in thermodynamic-nonequilibrium systems with spatial dispersion 04 p0673 A67-15968
- Motion of cosmic radiation source effect on frequency spectrum of amplitude and phase fluctuations in turbulent atmosphere 05 p0761 A67-16344
- Correlator for determining envelope of autocorrelation function of wideband HF signal, using narrow band video amplifier 05 p0764 A67-16902

Multivariate statistical analysis of wind sounding data, applying high degree of correlation between two wind parameters and empirical density function [AIAA PAPER 66-353] 05 p0838 A67-17214

Linear system providing maximum signal to noise ratio for given parameters of correlation function of incoming quasi-harmonic signal mixed with white noise 05 p0767 A67-17396

Statistical determination of correlation functions of plasma scattered coherent light 06 p1039 A67-17824

Self-diffusion coefficients of simple liquids as predicted by Rice-Allnatt theory, noting friction coefficient and correlation function 06 p1035 A67-17989

Correlation number for calculation of skin friction and heat transfer for laminar compressible boundary layer flow with arbitrary pressure gradient, using von Karman momentum 06 p0992 A67-18862

Oscillations in stationary gas discharge, describing device for calculation of correlation function for electrical signals 07 p1227 A67-19120

Passage of pulsed coherent useful and noise signals through two-channel time discriminator 07 p1140 A67-19237

Statistical characteristics of atmospheric ozone distribution, determining autocorrelation and cross correlation functions, concentration and temperature profiles 07 p1170 A67-19357

Point source detection using signals propagating in quantum field, in terms of correlation functions of thermal field fluctuations 07 p1142 A67-19585

Effect of a priori known relation between random signal and noise voltages at output of two channels 07 p1143 A67-19593

Correlation of time variations of proton and electron intensity of outer radiation belt and dependence on geomagnetic environment 07 p1243 A67-19828

Frequency correlation of ionospheric radio waves in inhomogeneous thin layer medium and effect of irregular horizontal ionization gradients 07 p1144 A67-19836

Doppler radar measurements of wind velocity horizontal components variation in rain and snow, calculating time correlation and structural functions for neutral and unstable stratifications 07 p1221 A67-20004

Coupled Green function equations for Helsenberg ferromagnet approximated via differential equations 07 p1237 A67-20141

Correlation functions and power spectra of stochastic processes with statistical structure defined by stationary Markov chains 07 p1217 A67-20196

Frequency response functions determined from correlation functions of force and response, using Bartlett triangular weighting function 08 p1353 A67-20592

Performance of wideband interferometers using interferometer ambiguity function for radar application 08 p1300 A67-20680

High resolution radar correlometer measurement of spatial correlation radius of RF radiation scattered by disturbed ocean surface 08 p1294 A67-20819

Artificial pseudorandom binary noise generation for flight testing and aircraft control systems and correlation function and frequency spectra of noise 08 p1279 A67-21005

Generalized Gaussian distribution functional for weak plasma turbulence neglecting three-point correlation function 08 p1366 A67-21415

Integral equation for propagation of second order correlation function assuming statistical independence of wave function and refractive index fluctuations 09 p1460 A67-21594

Correlation radiometry examination of radiation emission in beam plasma discharge at harmonics of electron cyclotron frequency 09 p1536 A67-21601

Input-output information transfer through correlation function of electromagnetic fields, obtaining optimization of system 09 p1461 A67-21603

Coherent electromagnetic wave analysis using spectral density function in terms of wave vector 09 p1462 A67-21605

Approximation method to general solutions yielding coherence tensors of electromagnetic waves excited by source

distribution with known coherence properties 09 p1462 A67-21606

Three-dimensional correlation function for modulating bell shaped and rectangular radar probing pulses 09 p1463 A67-21961

Radio source scintillations caused by electron density fluctuations extended to regime with large phase fluctuations, discussing autocorrelation function for any regime 09 p1565 A67-22222

Statistical quantities needed to fix scattering regime obtained from observations of radio scintillations, showing correlation length in electron density fluctuations 09 p1565 A67-22223

Spectra and joint correlation function for PSK signal modulation 10 p1604 A67-22979

Correlation of nitrogen vibrational-translational relaxation times for various measuring methods, noting temperature distribution of rate 10 p1733 A67-23151

Statistical properties of dispersive waves in upper atmosphere analyzed, using correlation technique 10 p1639 A67-23206

Pulse sequences with good autocorrelation properties 10 p1608 A67-23330

Amplitude spectra of complex signals with known autocorrelation functions 10 p1607 A67-23458

Carbon fiber composite, noting incorporation into epoxy resin and inverse correlation of shear strength with fiber modulus 10 p1671 A67-23495

Pressure drop correlation in developed, isothermal, laminar and turbulent flow in rectangular ducts 10 p1627 A67-23555

Photospheric brightness fluctuations recorded photoelectrically across solar disk center simultaneously for two regions of continuum, deriving autocorrelation functions and spatial power spectra 10 p1711 A67-23796

Statistical properties of coherent radiation noting correlation function, experiments on photon distribution, Bose-Einstein distribution, etc 11 p1799 A67-24106

Complex correlation function application to describe correlation between signals from two antennas of radio interferometer 11 p1762 A67-24287

Frequency redistribution function of noncoherently scattered radiation, noting effect on source functions of two-level atoms 11 p1823 A67-24490

Kraichnan turbulence theory analyzed by computer calculated solutions with correlation and regression functions derived from experiment, shows good agreement with theory 11 p1780 A67-24539

Astatic gyroscope accuracy dependence on random fluctuations of dry friction moment when under oscillatory motion of bearings, giving correlation function of error dispersion 11 p1794 A67-25044

Ratio of Lagrange and Euler correlation scales determined from correlation of time fluctuation of transverse wind velocity and temperature variation 12 p1964 A67-25485

Measurements 12 p1964 A67-25485

Output characteristic function for two-channel analog cross correlator with each channel input consisting of deterministic signal combined with stationary Gaussian noise 12 p1916 A67-26080

Output correlation function for N-step symmetric amplitude quantizer with summed sine wave and Gaussian noise input, noting approximations for low SNR 12 p1908 A67-26084

Space-time cross correlation function for antennas generalized by complex antenna-height function 12 p1917 A67-26089

Use of limiters for estimating signal to noise ratio 12 p1908 A67-26090

Higher order time correlations, skewness, flatness and nonGaussian probability density distribution in turbulent field 13 p2092 A67-26278

Pair correlations function in stable homogeneous plasma 13 p2164 A67-26295

Relation between correlation functions of stationary random input and output for linear discrete systems 13 p2144 A67-26430

Tropospheric condition effect on near-ground ultrashort wave radio signal field-amplitude fluctuation, determining space-time correlation dependencies by radar observation 13 p2067 A67-26688

Correlation method for generating sensitivity coefficients of dynamic system on high speed iterative analog

computer 13 p2073 A67-27061

Irregular fields effect on aperture reception characteristics 13 p2071 A67-27402

Asymptotic form of correlation functions facilitated by use of Hamiltonian 13 p2149 A67-27713

Correlation function and pressure change of slow waves in nonisothermal plasma 14 p2360 A67-28604

Transitional impurity effects on superconducting critical temperature of normal metals, stressing localized states with no magnetic moments 14 p2371 A67-28727

Perturbation factors in angular correlation function for multidomain ferromagnetic materials determined taking into account magnetic field fluctuations 14 p2371 A67-28728

Geopotential and wind field calculations for Northern Hemisphere using statistical models 14 p2346 A67-28764

Influence of higher order contributions to correlation function of intensity fluctuation in laser near threshold determined using Fokker-Planck equation 15 p2496 A67-29091

Harmonic generation by traveling waves in nonlinear dispersive medium for quasi-monochromatic signals, obtaining correlation function and spectrum of second harmonic for Gaussian processes 15 p2517 A67-29333

Empirical correlation formulas for density and viscosity of equilibrium air, noting pressure variation at high enthalpies 15 p2579 A67-29436

Operator parameter identification on basis of digital treatment of experimental data, using algebraic means and static programming 15 p2460 A67-30313

Reducing disturbances of certain form to zero by generating modified form of test signal to be applied to cross correlator 15 p2461 A67-30322

Plasma radiation analyzed by spectral line broadening theory as relaxation of excited atom, noting frequency dependent width and shift operators 15 p2532 A67-30380

Energy spectrum and correlation characteristics of PCM signal studied by Levin method, calculating correlation moments of code group symbols 16 p2620 A67-30478

Statistical methods and application to treatment of information in space domain, noting correlation functions 16 p2633 A67-30671

Correlator for determining envelope of autocorrelation function of wideband HF signal, using narrow band video amplifier 16 p2622 A67-30878

Probability that random function with known correlation function will not fall outside regions with given boundaries within given time 16 p2696 A67-30920

Cost function to evaluate quasi-optimal amplitude meter for signal with random initial phase on white noise background with random correlation function 16 p2623 A67-31015

Receiving directional antenna effect on magnitude of frequency correlation in fluctuations of received radio emission 16 p2640 A67-31497

Laser scattering from gas particles and diffuse surfaces, noting difference in intensity of speckle patterns formed 16 p2686 A67-31882

Day and night ion concentration as height function 17 p2842 A67-32258

Correlation function for random process energy spectrum at linear system output, obtaining expression of envelope distribution for radio signals 18 p2999 A67-33506

Correlation function method in superconductivity theory, formulating electric current density in terms of distribution function in phase space 18 p3100 A67-33712

Mean-square value and autocorrelation function for fluctuations of geometrical optical paths 18 p3000 A67-34025

Signal and noise FM modulated random process characteristics determined by equation for correlation function, giving energy spectrum relationship of modulated process phase 18 p3001 A67-34177

Receiving system for detecting binary random signals in white noise, determining correlation functions and error probability 18 p3001 A67-34180

High pressure equations of state including electron gas correlation energy, giving

density vs pressure curves for various elements 18 p3104 A67-34594

Image velocity sensing technique applying moving reticle scanners, with time-dependent correlation function analyzed by frequency discriminator 19 p3231 A67-35689

Correlation position device for autonomous orbital navigation system 20 p3481 A67-36553

Surface pressure spatial correlation function for rigid infinitely long cylinder in three-dimensional diffuse sound field 20 p3537 A67-36646

Nonstationary correlation analysis using correlator in which bandwidths of two filters resolve errors 20 p3484 A67-36695

Integral equations for weight function of optimum filter and correlation function of random absolute error 20 p3408 A67-37040

Three-dimensional correlation function for modulating bell-shaped and rectangular radar probing pulses 20 p3363 A67-37191

Design of adaptive systems with forced oscillations, using correlation and filter methods 20 p3410 A67-37228

Point source detection using signals propagating in quantum field, in terms of correlation functions of thermal field fluctuations 20 p3364 A67-37322

Effect of a priori known relation between random signal and noise voltages at output of two channels 20 p3384 A67-37332

Classical nonisothermal two-component plasma correlation functions and pressure contribution from Coulomb interaction 20 p3502 A67-37603

Autocorrelation function of signal scattered incoherently from ionosphere, observing resonance at multiples of proton gyroperiod 21 p3578 A67-37758

Oscillations in stationary gas discharge, describing device for calculation of correlation function for electrical signals 21 p3664 A67-38165

Tropospheric condition effect on near-ground ultrashort wave radio signal field-amplitude fluctuation, determining space-time correlation dependencies by radar observation 21 p3582 A67-38430

Evaluation technique for correlation functions and power spectrum of randomly shaped pulse train using stationary point process 21 p3604 A67-38948

Essential additional operator, essential transformed system and cross correlation function methods for self-adjusting circuit design, considering sign of gradient component 21 p3604 A67-39110

Turbulence theory from local equilibrium breakdown macroscopic approach by imposing suitable conditions on correlation functions, discussing stochastic Navier-Stokes equations 22 p3782 A67-39500

Combined frequency and space correlation of wave fields scattered by rough surfaces where conditions of applicability of Kirchhoff approximation hold true 22 p3760 A67-39660

Two particle correlation theory for static plasma from Poisson equation theory 22 p3848 A67-39689

Integral correlation technique used for first approximation solution in polar coordinate system to determine plane supersonic jet incidence on plane at arbitrary angle 22 p3786 A67-40020

Radio observations to estimate chromospheric parameters by measuring fluctuation correlation function of solar radio emission flux 22 p3886 A67-40127

Geomagnetic field structure determination by method used to divide geomagnetic field observed along limited magnetic profile derived from mathematical apparatus of correlation analysis 23 p3994 A67-40715

Disordered composite materials overall elastic moduli derived from local elastic moduli using correlation function 24 p4248 A67-41958

Electromagnetic wave fluctuations in semiminfinite plasmas, deriving correlation functions for electromagnetic parameters, considering surface waves 24 p4195 A67-42075

Statistical entropy of nonequilibrium plasma assuming binary correlation functions, obtaining distribution function equation 24 p4196 A67-42158

System parameters of linear time-variant space communication channels from input-output viewpoint, measuring correlation functions and Doppler spread 24 p4123 A67-42476

Cross correlated photons of laser used to determine correlation functions by applying thermodynamic Green function 24 p4168 A67-42594

Correlation between entropy of envelope fluctuation of UHF radio signal and corresponding thermodynamic stability of tropospheric common volume 24 p4124 A67-42810

CORROSION

SA DEGRADATION

SA ELECTROCHEMICAL CORROSION

SA EROSION

SA ETCHING

SA FRETTEING CORROSION

SA FUEL CORROSION

SA METAL CORROSION

SA STRESS CORROSION

SA WEAR

Storable propellant pressure vessel design for Titan launch vehicles and compatibility and stress-load-corrosion analysis [SAE PAPER 660677] 01 p0160 A67-10582

Corrosive effects of chlorides in aqueous environment on pickled and anodized sheet beryllium 04 p0640 A67-15618

Stress-strain state and corrosion and erosion produced by aggressive gas flows in surface layers of gas turbine nozzle blades of Zr56-K alloy 13 p2187 A67-26451

CORROSION PREVENTION

Corrosion control requirements of P-3 Orion aircraft, including six steps to corrosion control and remedial measures 01 p0011 A67-11012

Aircraft corrosion protection, discussing eloxation and electrophoretic deposition of multilayer synthetic resin coatings 04 p0636 A67-14576

Zr-Mo, Ca-Mo and Ni-Cr cermets, noting preparation and structural defects 05 p0830 A67-17034

Aircraft exfoliation corrosion, discussing methods for prevention in fastener holes 07 p1210 A67-20087

Material corrosion control techniques, considering initial structure design, coatings application and protective coatings specifications 11 p1773 A67-24940

Surface cleaning of electrical and electronic equipment through water and oil removal by chemical compositions 14 p2327 A67-28822

Zr-Mo, Ca-Mo and Ni-Cr cermets, noting preparation and structural defects 18 p3066 A67-34455

Surface treatment of metal to ensure strength of bonded joints, discussing causes of aluminum-alloy corrosion during pickling 19 p3237 A67-35822

Microbiological organisms in jet aircraft wing fuel tanks as major corrosion sources, with fuel additives tested to inhibit microbial growth 20 p3515 A67-36485

Aluminum corrosion behavior stressing surface oxide film condition 20 p3465 A67-36635

Beryllium corrosion occurrence, causes, effects, prevention and advantages over steel and aluminum 20 p3465 A67-36636

Magnesium and magnesium alloy corrosion, discussing treatments for prevention of various kinds of corrosion 20 p3466 A67-36637

Microbial contamination of jet aircraft fuel systems [SAE PAPER 670869] 24 p4206 A67-42007

Auxiliary electrodes for sealed alkaline electrochemical cells, noting application as charge control and scavenger elements 24 p4105 A67-42519

CORROSION RESISTANCE

Mechanical properties and corrosion resistance of titanium alloy forgings used as compressor parts 01 p0093 A67-10546

Metal single crystal use in structural design of stress resisting devices 06 p1013 A67-17795

Heat treatment effect on structure, hardness, microhardness and corrosion resistance of VT1 titanium and OT4 titanium manganese-aluminum alloy sheets 06 p1018 A67-18236

Hot corrosion of aircraft gas turbine alloys operating in marine environment reproduced in laboratory test, analyzing nature of attack 11 p1804 A67-23918

Corrosion test on turbine blades with nickel and cobalt base conducted in burner rigs, using metallographic examinations [ASME PAPER 67-GT-2] 11 p1808 A67-24790

Dependence of creep, corrosion and

thermal fatigue of gas turbine vanes and blades upon inlet temperature and rate of change [ASME PAPER 67-GT-17] 11 p1808 A67-24801

Simple and stress corrosion problems in aircraft design emphasizing protection of joints 12 p1954 A67-25127

Corrosion resistance of yttrium is higher at higher pH because of slower anodic process 12 p1954 A67-25358

Corrosion of rhenium in various acids and hydroxides is electrochemical in nature and determined by kinetics of anodic and cathodic processes 12 p1955 A67-25359

Nickel-base superalloy technology, stressing structural stability and hot corrosion resistance 12 p1958 A67-26128

Book on stress corrosion of metals covering mechanisms, resistance techniques and tests 13 p2141 A67-27174

Stress corrosion resistance and control for aluminum alloys, noting types, causes and methods 14 p2335 A67-27806

Thermal, mechanical stress and moisture resistance reliability tests of plastic encapsulated transistors 15 p2444 A67-29457

Reinforced plastics composites for jet lift engines 15 p2508 A67-29671

Cladding effect on corrosion resistance and fatigue behavior of duralumin, noting role of alternating stresses in cladding layer 15 p2504 A67-29827

Hardness, toughness, stress relaxation, corrosion resistance, etc. of niobium-aluminum alloy with stable elastic modulus 15 p2504 A67-29973

GE T64 engine operation on emulsified fuel (JDI), noting corrosion effects on fuel system components due to water additive [SAE PAPER 670369] 17 p2927 A67-33002

Alloys for failure-safe structures tested, determining fracture toughness, fatigue strength and stress-corrosion cracking resistance 17 p2875 A67-33048

Maraging stainless steel for high temperature applications, discussing properties, heat treatment and solution temperature effect 17 p2875 A67-33049

MHD conversion of heat into electricity noting nozzle behavior during long-lasting experiments, corrosion resistant conducting materials and electrical insulators 18 p2989 A67-34121

Atmospheric corrosion resistance of titanium alloys [ASTM PAPER 31] 18 p3068 A67-34579

Wear, scaling and chemical resistance of carbide and boride diffusion coatings on refractory metals 19 p3243 A67-34921

Aluminum corrosion behavior stressing surface oxide film condition 20 p3465 A67-36635

Titanium susceptibility to corrosion, achieving protection by passive self-healing films forming on metal surface 20 p3466 A67-36638

Amine-tin antioxidant systems for aliphatic hydrocarbons and related alkyl substituted fluids 20 p3474 A67-37594

Heat treatment practices for precipitation hardening steels noting use in missile and aerospace applications 21 p3634 A67-38178

Heat resistant stainless steels evaluated experimentally for fatigue properties, corrosion resistance, creep limit and tensile strength 21 p3646 A67-39010

High structural efficiency of aircraft materials emphasizing fatigue characteristics, fracture toughness and corrosion resistance 22 p3823 A67-40332

CORROSION TEST

Corrosion detection of metal surface under protective coating, using beta radiation probe 02 p0245 A67-12218

Corrosion test on turbine blades with nickel and cobalt base conducted in burner rigs, using metallographic examinations [ASME PAPER 67-GT-2] 11 p1808 A67-24790

Continuous total immersion stress corrosion testing of beryllium in synthetic sea water, discussing relationship between time-to-failure and tensile stress 14 p2336 A67-28147

Test procedure and apparatus for evaluating oxidation-corrosion characteristics of aircraft gas turbine engine lubricants at high temperature 14 p2326 A67-28794

Strength corrosion cracking of high strength steels and titanium alloys in flowing sea water using cantilever loaded

- test specimen 16 p2690 A67-31385
Stress corrosion test method determined from test program on precipitation hardening semiaustenitic steels 20 p3465 A67-36486
Automatic apparatus for flooding or spraying test specimens with liquid corrosive media according to predetermined program 21 p3715 A67-37827
Mean stress level effect on corrosion fatigue strength of aluminum clad D16AT alloy sheet under asymmetrical loads 21 p3646 A67-39008
Variable loading effect on durability of D16T aluminum alloy exposed to continuous action of corrosive medium 21 p3642 A67-39009
Oxygen diffusion through lubricant to metal surface examined for influence in corrosive wear [ASLE PAPER 67-LC-4] 24 p4164 A67-42743
- CORRUGATED PLATE**
Choke slots or corrugated structure in walls of horn antenna for reducing sidelobe and backlobe level by controlling illumination of E-plane edge 02 p0211 A67-11601
Deflection and stresses in corrugated diaphragm rigidly clamped on contour with distributed pressure and concentrated central force, using finite difference approximation 21 p3717 A67-37977
- CORRUGATED SHELL**
Stress in helical corrugated shell under axial tension examined as boundary value problem of ODE in cylindrical coordinate system 05 p0914 A67-16215
Membrane solution of spirally corrugated shell under axial and torsional loading determined from thin shell bending equations 06 p1110 A67-18856
Compression strength analysis of plane and cylindrical multilayer skin panels reinforced by corrugated fillers, determining critical load and local stability loss 21 p3725 A67-38787
- CORTI ORGAN**
S COCHLEA
CORTICOSTEROID
Plasma 17 hydroxycorticosteroids in healthy subjects after water immersion of 12 hr duration shows no stressful effect 15 p2427 A67-29270
Biological effects of time-zone changes on circadian rhythms of urinary elimination of potassium and 17-hydroxycorticosteroids 22 p3751 A67-39606
- CORUNDUM**
Epitaxy of semiconductor on insulating monocrystalline base of corundum, noting electronic characteristics of silicon layers 02 p0294 A67-11755
- COSINE SERIES**
Cosine series analysis of nonuniform internal pressure effect on crack extension in infinite body 04 p0716 A67-15797
Real time Fourier transform synthesizer for spectral distribution of interferogram 20 p3437 A67-36341
- COSMIC DUST**
SA INTERPLANETARY DUST
SA ZODIACAL DUST CLOUD
IR observations of R Monocerotis preplanetary system, reporting on flux density and circumstellar dust 03 p0510 A67-13506
Comet disintegration as basic source of interplanetary dust based on zodiacal isophots 04 p0701 A67-15559
Color study of lunar surface suggesting nonexistence of cosmic dust layer 05 p0901 A67-17083
Near-earth cosmic dust cloud and data obtained from satellite, rocket and ground measurement 06 p1083 A67-18161
Solar wind effect on cathode scattering of cosmic dust particles in earth proton belt and shortening of lifetime of captured particles 06 p1078 A67-18162
High altitude balloon top collections of cosmic dust shows evidence of absence of crystal structure in 10 p1708 A67-23239
Near-earth cosmic dust cloud and data obtained from satellite, rocket and ground measurement 16 p2741 A67-30505
Solar wind effect on cathode scattering of cosmic dust particles in earth proton belt and shortening of lifetime of captured particles 16 p2737 A67-30506
Ferromagnetic dust concentration variations in upper atmosphere during meteor shower 16 p2668 A67-31707
Dust content in upper atmosphere of earth from satellite light absorption measurements 17 p2842 A67-32257
Temperature gradient and thermal effects on ceramic transducer sensors used on spacecraft for cosmic dust experiments 19 p3229 A67-35170
Effective collection time for collecting cosmic dust in altitude ranges of cosmic and terminal velocities of particles, using rockets 19 p3318 A67-35195
Optical and stereoscan microscope scanning combined with X-ray microanalysis used to investigate results on collection surfaces of space probes 19 p3339 A67-35197
Sensors used in cosmic dust experiments studied for response to microparticle hypervelocity impacts, noting relationship to velocity 19 p3229 A67-35210
Interstellar material, emphasizing chemical characterization of dust by absorption spectroscopy 19 p3323 A67-35331
Windborne dust collections on Barbados Islands investigated by mesh technique for origin of cosmic dust 20 p3432 A67-37174
Compact and dispersed cosmic matter using morphological approach to discovery, invention and research in astronomy 22 p3890 A67-40429
Microwave background in steady state universe explained by starlight absorption and microwave reemission by interstellar dust, discussing young spiral galaxies 24 p4226 A67-41875
Solar and galactic low energy cosmic ray nuclear ionizing and interaction effects on meteorite surface isotopic composition, estimating particle fluxes 24 p4210 A67-42634
- COSMIC GAS**
Astrobleme in Australia analyzed for origin of eruptive gas 10 p1706 A67-22956
Condensation history of cooling gas of cosmic composition, stressing chondrite fractionation patterns 20 p3526 A67-37172
Two-body relaxation term in N-body self-gravitating gases of one and three dimensions and validity of Vlasov equation 22 p3894 A67-40508
- COSMIC NOISE**
Radiation absorption by ionized hydrogen in plane of galaxy to explain brightness profiles for declination minus 37 degrees 02 p0307 A67-11688
Sudden cosmic noise absorption and X-ray flares noting peak, nature of decay and theoretical and experimental values [RASSA PAPER 1-10-139] 03 p0373 A67-14247
Enhancement factor and true absorption of VHF cosmic radio noise associated with solar flares 05 p0884 A67-16929
Satellite observation of radiation belt and absorption of cosmic noise in polar aurora during magnetic storms of February 1964 07 p1243 A67-19683
Simultaneous recordings of cosmic noise absorption and VLF chorus, noting correlation from riometer recordings 08 p1327 A67-21374
Noise on short waves including terrestrial, extraterrestrial, radio sources, etc 12 p1904 A67-25303
Sudden cosmic noise absorption correlated with solar microwave flux to establish daily mean value 13 p2190 A67-28311
Relation between ionospheric no-echo conditions and absorption of cosmic radio noise measured using riometer, plotting diurnal variation values 13 p2114 A67-26794
Solar cosmic ray interaction with earth ionosphere and resultant cosmic radio noise absorption 13 p2194 A67-27254
Cosmic noise intensity at 25 MHz noting nighttime variation dependence on solar activity 13 p2201 A67-27392
Short-period oscillations of auroral cosmic noise absorption 16 p2669 A67-31910
Pulsations in cosmic noise absorption of auroral zone, noting magnitude, shape and form of occurrence 17 p2841 A67-32213
Pi micropulsation subtypes, one related to charged particles impulsive bursts from magnetospheric tail and another related to auroral electrojet 20 p3433 A67-37414
Antarctic riometer observations of PCA event of February 1965 compared with satellite measurements of solar proton flux and spectrum during same event 22 p3872 A67-39803
Polarizations of Pc 1 micropulsations intermittently recorded in Alaska with analysis of data for presence of right and left hand waves 22 p3793 A67-40078
Ionospheric absorption from unabsorbed cosmic radio noise intensity, discussing electron density and collision frequency profiles 23 p3994 A67-40778
Mean F-2 layer electron collision frequency computation from cosmic noise absorption 23 p3994 A67-40779
Equivalent noise temperature of antennas located on earth surface, discussing cosmic, tropospheric and man-made noise classification 23 p3980 A67-41043
- COSMIC PLASMA**
Electron and ion acceleration by cosmic plasma waves, examining contribution of these processes to radiation belt formation 04 p0701 A67-15555
Experimental detection and evaluation of plasma instabilities, discussing research state in connection with thermonuclear and cosmic problems 14 p2360 A67-28556
Cosmic plasma flow effect on cosmic radiation polarization, deriving difference between normal waves refractive indices in two-component medium 16 p2628 A67-31494
Magnetic field in moon proximity constructed from Lunik x satellite plasma and magnetic measurements 16 p2755 A67-31889
- COSMIC RADIATION**
SA CERENKOV RADIATION
SA PRIMARY COSMIC RADIATION
Book on natural neutron background of atmosphere and earth crust including effect of primary and secondary cosmic radiation, solar neutrons, presence in rocks, etc 01 p0143 A67-10042
Spacecraft shielding combinations for astronaut protection, comparing magnetic, electrostatic and passive methods on basis of dosage and mission duration 01 p0153 A67-10425
Wide angle counter telescope measurement of cosmic ray equator position near zero meridian 01 p0149 A67-10738
Energy transfer into electron-photon avalanche by high energy nucleons compared to data of air shower and particle spectra 01 p0144 A67-10745
Charge ratio of cosmic ray muons determined by particle collection in small and wide angular ranges about vertical 01 p0144 A67-10783
Profile and fine structure of diurnal variation of cosmic ray intensity during high and low solar activity 01 p0144 A67-10810
Lunar gamma radiation intensity and spectral composition from Luna X data, deducing cosmic ray and radioactive decay origins 01 p0150 A67-10905
Recurrent cosmic-ray modulation phenomena with Forbush decrease characteristics correlated with M-region magnetic storms, concluding that each series results from shock wave solar initiated 01 p0145 A67-10919
Cosmic ray electrons with energies above 12 gev, constructing differential energy spectrum for deduction of universal black body radiation 01 p0145 A67-10921
Azimuthal asymmetry in distribution of shower particles around shower axis, using Geiger-Muller counter telescopes 01 p0145 A67-11230
Energy dissipation channels of nuclear and electron components of cosmic rays in Galaxy and Metagalaxy 01 p0145 A67-11276
Charge composition of cosmic radiation, noting results for charges 1/3 e and 2/3 e, experimental setup, etc 02 p0306 A67-11500
Neutron component diurnal variation in cosmic radiation during period of coil type magnetic disturbances in tail of geomagnetic storm 02 p0306 A67-11656
Seasonal changes in cosmic ray intensity including barometric effect in neutron component, effect of earth seasonal position, etc 02 p0307 A67-11665
Temperature effect in neutron component of cosmic rays and seasonal changes in intensity affected by interplanetary magnetic field 02 p0307 A67-11666
Cosmic ray intensity changes for various values of cut-off rigidity determined using barometric coefficient 02 p0307 A67-11667
Screen effect on cosmic ray intensity measurement by comparing data from various rocket and satellite soundings 02 p0307 A67-11668

Frequency dependence of enhanced absorption of cosmic radio emission during abrupt ionospheric disturbance 02 p0307 A67-11676

Energy spectra and abundances of elements He through Si of galactic cosmic ray above 20 mev per nucleon in nuclear charge range between 2 and 26 02 p0307 A67-11687

Location of X-ray source Sco X-1 determined by instrumented payload flown on stabilized Aerobee rocket 02 p0308 A67-11771

Neutron activation analysis applied to determination of Ar 40 and K 41 content of iron meteorites 02 p0326 A67-12045

Spallation produced Ar 40 in iron meteorites for determining cosmic ray exposure ages from radiogenic Ar 40 content 02 p0326 A67-12308

Power energy spectrum of cosmic rays as solution of general covariant kinetic equation 02 p0308 A67-12491

Cosmic ray physics - All-Union Conference, Apatity, U.S.S.R., August 1964 02 p0308 A67-12570

Stratospheric cosmic ray intensity, discussing Soviet measurements above Antarctica 02 p0310 A67-12573

Fundamental problems in cosmic radiation astrophysics 02 p0310 A67-12577

Cosmic radiation investigated by using meteorites 02 p0310 A67-12580

Cosmic ray variations studied by effects on Zaisan chondrite 02 p0310 A67-12581

Neutron-group fluxes and variations with solar activity during IYQS observed by Elektron II 02 p0310 A67-12583

Cosmic ray 27-day variations using periodograms, with measured data processed continuously from 1957 to 1964 02 p0311 A67-12591

Secular changes in stratospheric cosmic ray intensity from 1962 to 1964 02 p0311 A67-12595

Increase with latitude of Forbush effects and secular variations in cosmic ray intensity explained by worldwide data obtained with meson detectors 02 p0311 A67-12596

Energy spectrum of variations in cosmic ray intensity and changes in spectrum with decreasing solar activity calculated for additional particle flux 02 p0311 A67-12597

27-day changes in solar diurnal variation from 1957 to 1958 based on neutron component data, noting modulation of cosmic ray anisotropy 02 p0312 A67-12600

Magnetic storm accompanied by cosmic ray intensity increase analyzed, considering Forbush effect and determining all peaks 02 p0312 A67-12601

Ionizing accompaniment of near 170 bev nucleons at 2000 m altitude recorded by spark chamber/Geiger counter/ionization chamber apparatus 02 p0312 A67-12609

Secondary particle generation in satellite walls due to 0.1 to 20 bev pi-mesons and protons 02 p0312 A67-12610

Production of low energy cosmic ray electrons, investigating energy inputs to injected secondary electrons by possible low magnitude solar electric field and possible galactic Fermi acceleration 02 p0312 A67-12635

Flux measurement of particles with charges of one-third and two-thirds electron charge, reaching sea level with relativistic velocities 02 p0313 A67-12636

Cerenkov radiation induced by cosmic ray in end-on photomultiplier and resultant fundamental noise 02 p0247 A67-12688

Gas-filled Cerenkov radiation detector combined with solid detectors to measure charge and flux of relativistic cosmic rays 02 p0247 A67-12695

Cosmic ray physics - All-Union Conference, Moscow, November 1965 02 p0313 A67-12744

Hypothesis of meson resonances produced in cosmic ray interactions, explaining multiple birth characteristics of secondary particles 02 p0314 A67-12745

High energy cosmic ray interactions analyzed at 3340 m above sea level, using Wilson cloud chambers, gas discharge counters, ionization calorimeter, etc 02 p0248 A67-12746

Peripheral nonelastic interactions described, using amplitude characteristics of

elastic cosmic ray particle interaction and complex orbital moment 02 p0315 A67-12749

Statistical analysis of cosmic ray particle elastic scattering, noting isotropic nature of angular distribution 02 p0315 A67-12750

Electron-photon shower measurement using ionization calorimeter type device 02 p0271 A67-12755

Pion energy transmission during inelastic interaction of cosmic particles with Pb nuclei 02 p0315 A67-12758

Ionization calorimeter measurements of energy transmission by photons in cosmic nuclear-active pion and nucleon interactions with various nuclei 02 p0316 A67-12761

Elimination of certain contradictions in data concerning high energy cosmic rays explained by means of hypothesis of existence of passive S-state of baryon 02 p0316 A67-12766

Barometric pressure coefficient, correcting terrestrial neutron monitor intensities, dependency on magnitude variations related to changes of atmospheric water vapor content 03 p0505 A67-12958

Survey in satellite era of energetic particle radiations, plasmas and magnetic fields in space including solar wind, solar cosmic rays, etc 03 p0506 A67-13050

Quarks in cosmic rays investigated using counter telescope 03 p0506 A67-13261

Positive-to-negative charge ratio of high energy cosmic ray muons 03 p0506 A67-13516

ESRO II satellite structural design, testing and material selection noting functions, vibration testing results, etc 03 p0518 A67-13600

Solar flare mechanism, explaining absence of cosmic ray flares and occurrence of PCA events in years of sunspot minimum 03 p0506 A67-13651

Extraterrestrial radiation source spectrum determined by comparing main beam and sidelobe signal power received on suitable bandwidth 03 p0371 A67-13946

Forbush effect relation to location of large solar flares, noting association of magnetic bottles with phenomena 03 p0507 A67-14003

Recurrent variations of cosmic radiation during solar cycle 04 p0691 A67-14417

Existence of cosmic-ray-produced Mg-28 radionuclide in rain 04 p0692 A67-14495

Tritium production in atmosphere by galactic cosmic rays, by solar flare accelerated particles and accretion from sun 04 p0613 A67-14855

Spectral characteristics of long term change of cosmic ray intensity during 1963-65 compared with Forbush decrease of September 1963 04 p0692 A67-14880

Cosmic radiation measurements in stratosphere from 39 sounding balloons 04 p0692 A67-14901

Cosmic ray electron spectrum indicates universal 3 degrees K black body radiation confinement to galactic disk 04 p0692 A67-14948

Energy spectrum of cosmic ray heavy nuclei, using stack of nuclear emulsions exposed during Quiet Sun on balloon flight 04 p0692 A67-14960

Atmospheric cosmic ray fluxes measured on series of USAF jet aircraft flights [AFCRL-67-0099] 04 p0693 A67-14961

Isotropic component of cosmic X-rays at balloon altitude 04 p0693 A67-14963

Riometer data analysis results concerning cosmic ray event of April 18, 1965 04 p0693 A67-14973

Modes in spatial distribution of neutron density within cosmic ray neutron monitor, each mode having distinct lifetime, using diffusion theory 04 p0681 A67-15615

Intensity of characteristic spectral lines of Si, Al and Mg of lunar surface rock made fluorescent by solar X-rays determined from Luna X measurements 05 p0886 A67-16051

Lunar gamma radiation measured by spectrometer on Luna X orbiter noting lunar rock radiation level, effect of cosmic rays, etc 05 p0887 A67-16055

Cosmic ray physics - All-Union Conference, Moscow, November 1965 05 p0875 A67-16081

Cosmic ray variations classification and account possible interference between meteorological effects 05 p0877 A67-16082

Radioactive isotopes in iron meteorite

used to determine cosmic ray origin and to study nuclear processes in early history of solar system 05 p0877 A67-16084

Geographic position of cosmic ray equator from results of on board Proton I satellite measurements 05 p0878 A67-16090

Preliminary measurements of variations in cosmic ray intensity using device consisting of gas discharge counters, telescope and ionization chamber mounted on Kosmos XXV satellite 05 p0878 A67-16092

Helium isotope formation in cosmic rays during light nuclei fragmentation due to high energy proton interaction 05 p0878 A67-16093

Boltzmann equation for cosmic ray particle motion in random magnetic field 05 p0878 A67-16094

Energy loss of cosmic electron in interstellar space due to ionization, bremsstrahlung and Compton effect 05 p0878 A67-16095

Aurora photometry and stratospheric cosmic ray intensity, noting electron intrusion and correlation between aurora intensity and X-ray emission 05 p0879 A67-16102

Intensity of ionizing and neutron component of cosmic rays, noting correlation for sporadic cyclic variations and solar activity cycles 05 p0879 A67-16103

Magnitude of lunar neutron emission due to cosmic rays estimated from atmospheric measurements 05 p0879 A67-16105

Cosmic radiation intensity measurement using automatic interplanetary stations with on board Geiger counters 05 p0879 A67-16106

Cosmos 53 satellite radiation data using on board gas discharge counter 05 p0879 A67-16107

Change in cosmic ray cut-off rigidity caused by currents from trapped particle motion, according to Chapman-Akasofu radiation belt model 05 p0880 A67-16111

Solar cosmic ray generation during chromospheric flares, noting increased neutron intensity 05 p0880 A67-16112

Relation between cosmic ray cut-off rigidity and L parameter, solving approximately 7th degree algebraic equation 05 p0880 A67-16113

Asymptotic directions of cosmic rays for Soviet cosmic ray stations 05 p0880 A67-16114

Interplanetary space properties studied from IMP-I satellite data on cosmic ray variations 05 p0880 A67-16115

Temporal distribution of first and second harmonic of solar diurnal variation of cosmic rays after radio bursts of fourth type 05 p0881 A67-16116

Variation of seasonal diurnal distribution of sudden changes in cosmic ray neutron component intensity related to solar activity changes 05 p0881 A67-16118

Solar diurnal variation of cosmic ray neutron component in Antarctic during minimum activity period, using harmonic analysis 05 p0881 A67-16119

Anisotropy in stellar diurnal cosmic ray variations in Northern and Southern Hemispheres, noting distributions of stellar and antistellar vectors 05 p0881 A67-16120

Corpuscular stream parameters based on data from Mariner II concerning cosmic ray variations on earth surface during geomagnetic storms 05 p0881 A67-16121

Amplitude of 27-day cosmic ray modulation in relation to solar and geomagnetic activities 05 p0881 A67-16122

Barometric coefficient of cosmic ray variations determined from observation of Forbush effects and cosmic ray flare effects 05 p0881 A67-16123

Intensity of various secondary cosmic ray components in cut-off rigidity range from 0.3 to 10 Bev 05 p0881 A67-16124

Coupling coefficients of cosmic ray neutron component according to data from schooner Zaria 05 p0882 A67-16125

Coupling coefficients for vertical and oblique cosmic ray components 05 p0882 A67-16126

Geomagnetic cut-off rigidity effect on cosmic ray intensity and coupled coefficients 05 p0882 A67-16127

Motion of cosmic radiation source effect on frequency spectrum of amplitude and phase fluctuations in turbulent atmosphere 05 p0761 A67-16344

Cosmic ray origin and space plasmas 05 p0882 A67-16362

Diffuse omnidirectional inverse Compton and synchrotron X and gamma radiation from cosmic distributions of fast electrons and thermal photons 05 p0882 A67-16404

Proton flares and types of spot groups in 11-year cycle, discussing time-latitude occurrence combined with emissions of cosmic and subcosmic radiation 05 p0883 A67-16808

Cosmic X-ray research with discussion of possible mechanism of X-ray generation with reference to observed spectra 05 p0883 A67-16875

Solar charged particles acceleration and propagation through interplanetary space, galactic cosmic ray origin, radiation belt structure, etc, analyzed from space data 05 p0883 A67-16877

Cosmic radiation directional intensity during solar activity minimum, noting altitude dependence of charged particle photon flux 05 p0883 A67-16878

Altitude variation of cosmic ray intensity in atmosphere, checking accuracy of flux data from rockets and satellites 05 p0883 A67-16879

Rocket sounding of intensity distribution of proton and electron fluxes at high altitudes, noting secondary particle emission from radiation belt 05 p0883 A67-16880

Extrasolar X-ray observation regarded as astronomy in contrast to cosmic ray observation which is considered as local geophysical phenomena 05 p0884 A67-16881

Cosmic ray intensity variations using gas discharge counters onboard Soviet satellites, noting Forbush effects 05 p0884 A67-17025

Distribution of cosmic rays on sphere and reception vector of radiation 05 p0884 A67-17121

Quasi-spiral nature of change in 27-day cosmic ray variation with solar activity shown by harmonic analysis 05 p0884 A67-17137

Seasonal changes in solar diurnal and semidiurnal variations of cosmic ray neutron component due to earth rotation axis and anisotropy sources 05 p0885 A67-17138

Rotation of vector of solar diurnal variation in intensity of cosmic radiation neutron component during solar activity minimum 05 p0885 A67-17497

Geophysical and heliophysical characteristics for enhanced cosmic radiation intensity during magnetic storm in February 1959 05 p0885 A67-17498

Low energy heavy nuclei analyzed by slicing emulsion in connection with solar activity studies 06 p1076 A67-17634

Cosmic ray nuclei observed from satellites and balloons by nuclear emulsions in stacks of plastic sheets 06 p1076 A67-17641

Cosmic ray analysis with Holborn scintillator stacks to determine existence of quarks 06 p1076 A67-17650

Neutron production in cosmic radiation, neutron measurements and geophysical effects 06 p1077 A67-17875

High altitude balloon flights with gamma ray spark chamber for search of cosmic gamma ray source in Cygnus 06 p1078 A67-18212

Exponent in expression relating nuclear interaction cross section to atomic weight of absorber determined from absorption path of nuclear active particles of cosmic radiation 06 p1078 A67-18795

Cosmic X-ray source scanning for 21 cm wavelength radiation, using radiometer and parabolic reflector 07 p1247 A67-19063

Statistical analysis of distribution of cosmic ray ages of stone meteorites 07 p1249 A67-19540

Hysteresis effect on cosmic ray intensity of solar cycle variations 07 p1242 A67-19620

Bibliography on cosmic rays for use as teaching aid for college physicists 07 p1242 A67-19622

Solar system geometric effect in diurnal, annual and semiannual cosmic ray variations 07 p1243 A67-19807

Solar modulation of galactic protons and He nuclei during last solar cycle analyzed according to Parker 07 p1244 A67-19913

Depression of low energy cosmic ray cut-offs relation to permanent geomagnetic tail using model calculation, explaining PCA midday recovery 07 p1245 A67-19927

Barometric coefficient for neutron monitor noting long term and altitude

dependence 07 p1188 A67-19954

Geomagnetic, auroral, ionospheric and cosmic ray perturbations, interdependence and relationship with solar activity 07 p1183 A67-20174

Radiation belts, energetic charged particle flux and trapped radiation in geomagnetic field as result of neutron albedo decay and plasma-magnetic field interactions 07 p1246 A67-20297

Penetrating radiation measurement on moon surface obtained by Luna IX spacecraft 08 p1385 A67-20841

Low energy cosmic ray photons in atmosphere, noting X-ray generation by bremsstrahlung effect of electron component 08 p1377 A67-21466

Galactic radio sources noting disk model brightness distribution, relativistic particle energies, continuous particle acceleration and ratio between proton and electrical component of cosmic radiation 09 p1563 A67-21629

Star collapse observation by detection of high energy neutrino fluxes produced by cataclysmic star contraction 09 p1561 A67-21630

Ionization capability of cosmic rays in low ionosphere, considering relativistic energies and high energy 09 p1561 A67-21841

Low ionosphere with suitable selected track for absorption observation as indicator of galactic cosmic rays modulation by solar wind 09 p1561 A67-21843

Production rate of secondary cosmic ray photons in upper atmosphere derived by cascade theory from stratospheric measurements of integral and differential energy spectra 09 p1561 A67-21882

Magnetosonic wave effect on anisotropic relativistic plasma component, obtaining cosmic ray plasma instability when wave frequencies are less than electron cyclotron frequency 09 p1546 A67-22230

Cosmic ray protons and helium nuclei intensity measured as function of energy or magnetic rigidity, determining particle intensity gradient under equilibrium conditions for diffusion 09 p1562 A67-22241

Pioneer VI detector to measure degree of anisotropy of cosmic radiation at various energy ranges 09 p1500 A67-22427

Cosmic ray effects on solar system and on galactic scale, discussing energy spectrum, particle diffusion and motion, solar wind, etc 09 p1562 A67-22530

Isotopic composition of krypton in high and low calcium achondrites, noting measurement results 09 p1569 A67-22685

Track densities and production rates with increase of heavy cosmic nuclei inside meteorite 09 p1570 A67-22690

Cosmic ray distribution, discussing method of diurnal variations, zonal harmonics and spherical analysis 10 p1698 A67-22778

Parameters of simultaneous amplitude phase modulation of periodic cosmic ray variations obtained from satellite observations 10 p1698 A67-22779

Cosmic ray intensity variation detection with respect to sidereal time on basis of simultaneous amplitude phase modulation 10 p1698 A67-22780

Cosmic ray neutron component intensity during magnetic perturbations, considering effect of magnetospheric deformation 10 p1699 A67-22781

Rapid and slow spreading absorption of cosmic rays over polar cap 10 p1699 A67-22790

Dead time instability effect on neutron monitor performance 10 p1699 A67-22799

Atmospheric reaction with energetic particles and resultant production of atomic oxygen, atomic nitrogen and nitric oxide 10 p1637 A67-23191

Power energy spectrum of cosmic rays as solution of general covariant kinetic equation 10 p1703 A67-23359

Radio emission from cosmic ray showers analyzed at Jodrell Bank, determining effects of geomagnetic field and charge separation 10 p1703 A67-23490

Cosmic ray nucleon interaction with high energies, estimating transition probability and interaction cross section of baryon in passive state 10 p1703 A67-23588

Charged particle motion in static magnetic fields without axial symmetry derived, employing Lagrange equation in transformed coordinate system and Alfvén

motion 11 p1855 A67-23929

Solar wind region magnitude, scattering transport path of particles and spectral variation of magnetic inhomogeneities analyzed on basis of 11-year cosmic ray cycle 11 p1855 A67-23930

Differential spectrum of cosmic protons at various latitudes and years surveyed by balloons 11 p1855 A67-23932

Short period radioactive nuclides induced by secondary neutron due to solar cosmic radiation in chondrites 11 p1858 A67-24058

Cosmic radiation measurements beyond radiation belts as observed by Cosmos XVII 11 p1856 A67-24075

Cosmic ray and space research through direct measurement of particles, radiation, magnetosphere, etc 11 p1856 A67-24105

Cosmic microwave background measurements along celestial equator, using Dicke radiometer to study anisotropy of cosmic black body radiation 11 p1864 A67-24564

Polarization of cosmic OH 18-cm radiation 11 p1864 A67-24565

Measurement of quark flux with 2/3 charge of electron reaching sea level with relativistic velocities 11 p1823 A67-24598

Cosmic ray intensities under sea water and under rock 11 p1857 A67-24617

Cosmic ray spallation and special anomaly in achondrites 11 p1866 A67-24696

Discovery of or setting upper limit to strength of features of small angular size when studying isotropy of cosmic background radiation 11 p1857 A67-25000

Solar cosmic ray diffusion coefficient dependence on cosmic ray energy and distance to sun studied via solar flares 12 p1991 A67-25111

Solar wind particle propagation and scattering path in interplanetary space according to data of 11-yr cosmic ray variations 12 p1991 A67-25115

Weak cosmic ray burst relation to austral axis pole geomagnetic activity characteristics and propagation in interplanetary space of energetic solar cosmic rays 12 p1992 A67-25116

Cosmic ray secondary components yearly changes of intensity determined as function of earth heliolatitude 12 p1992 A67-25120

Long term variation in magnitude of diurnal anisotropy of solar cosmic rays analyzed quantitatively by applying statistical techniques to recorded data 12 p1993 A67-25205

He 3 nuclei in low energy primary cosmic radiation determined, using stack of nuclear emulsions 12 p1993 A67-25479

Secular variations of cosmic ray intensity governed by 11-year solar cycle 12 p1994 A67-25532

Cosmic radiation intensity fluctuation in stratosphere, noting absence of explanation for anomaly 12 p1994 A67-25542

Modified RK-1 radiosonde circuit for stratospheric cosmic ray measurements 12 p1941 A67-25555

Delta electrons formed in interstellar hydrogen-galactic ray collision 12 p1994 A67-25645

Cosmic X-ray sources attributed to thermal emission of hot condensations from supernova remnants in our galaxy or other galaxies 12 p1995 A67-25764

Geomagnetic field anomalies in Southern Hemisphere and effects on cosmic rays, geomagnetically trapped radiation and ionosphere 12 p1933 A67-25770

South Atlantic proton radiation anomaly measurements using rocket flown spectrometer, examining variation of counting rates with altitude 12 p1995 A67-25771

Vertical cut-off rigidities in South Atlantic analyzed via sixth degree simulation of geomagnetic field, obtaining results from trajectory analysis of cosmic rays [AFCRL-67-0082] 12 p1996 A67-25774

Stochastic differential equations for obtaining probability distribution of cosmic ray particles counted in given time interval sounding rocket detector 12 p1996 A67-25783

Characteristic effects of deformed geomagnetic field on trajectories and asymptotic directions of arrival of medium energy cosmic rays 12 p1998 A67-25819

Nuclear abundances of galactic and solar cosmic rays, discussing detector electronics system for measurement of particle energy

- spectrum 12 p1944 A67-25852
Device for studying high energy nuclear active particles of cosmic rays interaction and determination of energy spectrum 12 p1947 A67-26095
Cosmic X-ray sources concentration toward galactic plane and variability 12 p1999 A67-26172
Primordial element formation, primordial magnetic fields and universe isotropy, showing correctness of big-bang relativistic theory, early anisotropy of universe, etc 12 p2010 A67-26240
Magnetospheres of self-gravitating bodies with reference to radio sources and cosmic ray acceleration 12 p1999 A67-26251
Galactic cosmic ray intensity depression by convective region and by surrounding static barrier of expanding corona 13 p2191 A67-26323
Solar activity relationship to terrestrial magnetic and associated auroral, ionospheric and cosmic ray effects 13 p2109 A67-26418
Dependence of diurnal cosmic ray variations on angle which is proportional to shortest distance from earth to axis of corpuscular stream 13 p2191 A67-26546
Pulse amplitude measurement from scintillation cosmic-ray counter 13 p2119 A67-26560
Geomagnetic activity and earth heliollatitude effect on diurnal variation of cosmic radiation, based on IGY neutron component observations 13 p2191 A67-26564
Statistical and instrumental fluctuations effect on distribution of first-harmonic amplitude and phase in harmonic analysis of cosmic radiation variation 13 p2191 A67-26565
Polarization of cosmic X-ray produced by bremsstrahlung mechanism 13 p2191 A67-26713
Energy transfer into electron-photon avalanche by high energy nucleons compared to data of air shower and particle spectra 13 p2192 A67-26774
Cosmic ray research - Conference, Huntington Beach, California, April 1966 13 p2192 A67-27242
Measurement of atmospheric cosmic ray fluxes over large portions of globe as comparison evaluation for different cut-off rigidity models 13 p2192 A67-27245
Multiaircraft measurements of cosmic ray spectrum and geomagnetic cut-off rigidity 13 p2193 A67-27246
Charge and energy spectra of galactic cosmic rays during solar minimum from satellite and Skyhook balloon data 13 p2193 A67-27248
Solar and galactic particle spectra and composition measured with cosmic ray telescope mounted on satellite 13 p2193 A67-27249
Effect of decrease in intensity of cosmic ray nuclear component during magnetic storms with sudden commencement studied by superposition of epochs 13 p2194 A67-27332
High energy photons, cosmic X-rays and hard radiation production mechanisms in interstellar gas, galactic halo and intergalactic medium 14 p2380 A67-27964
Radioactive isotopes from cosmic ray action in atmosphere and nonatmospheric sources, discussing geophysical mixing and dispersion 14 p2380 A67-27967
Techniques for determining cosmic ray age and stable and radioactive nuclide production rates in meteorites 14 p2380 A67-27968
Cosmic radiation problems in space flights and in SST flights, examining biological effects, shielding methods, dosimetry and warning systems 14 p2255 A67-28217
Radiobiological aspects of radiation safety in cosmic flights 14 p2255 A67-28222
Radio galactic X-ray emission noting possible cosmic radiation mechanism, history of X-ray astronomy, etc 14 p2381 A67-28427
Stability of interstellar gas to perturbations in gas pressure, magnetic field and cosmic ray pressure from hydromagnetic viewpoint taking rotation into account 14 p2388 A67-28832
Spark chamber telescope observations on cosmic ray neutral primary sources 14 p2381 A67-28846
Radiation levels on Gemini IV flight including Van Allen belt and South Atlantic Anomaly 15 p2425 A67-29105
Quasi-biennial cycles in cosmic ray intensity 15 p2549 A67-29203
Quark fractional electronic charge in cosmic radiation determined through pulse height distribution 15 p2549 A67-29526
Solar wind modulation of low energy galactic cosmic radiation, estimating primary source spectra, proton and helium fluxes 15 p2550 A67-29614
Gravitational fields for observation of soft cosmic neutrino and neutretto background predicted by different cosmological theories 15 p2555 A67-29641
Spark chambers and scintillation counters used to search for fractionally charged particles in cosmic rays near sea level 15 p2550 A67-29680
Annual cosmic ray variations and changes in cosmic radiation intensity as function of earth heliollatitude 15 p2550 A67-30012
Primeval fireball /cosmic radio radiation/ concept based on Hubble observation of universe expansion, discussing predictions on its nature 15 p2562 A67-30085
Solar velocity with respect to distant galaxies estimated from red shift for nearby galaxies, noting cosmic microwave background 15 p2563 A67-30160
X-ray astronomy emphasizing interpretation of observational results and relationship to radio and optical astronomy and cosmic ray physics 15 p2551 A67-30224
Mutation of human tissue by cosmic radiation, discussing results of cell studies from male and female subjects 16 p2611 A67-30766
Hypothesis attributing most energetic cosmic ray proton source to powerful radio galaxies noting pair production effect on cosmic ray sources 16 p2738 A67-30822
Cosmic radiation protection during manned space flight, considering use of radiation warning devices and protective drugs 16 p2612 A67-30901
Neutron component diurnal variation in cosmic radiation during period of coil type magnetic disturbances in tail of geomagnetic storm 16 p2738 A67-31071
Seasonal changes in cosmic ray intensity including effect in neutron component, effect of earth seasonal position, etc 16 p2738 A67-31080
Temperature effect in neutron component of cosmic rays and seasonal changes in intensity affected by interplanetary magnetic field 16 p2738 A67-31081
Cosmic ray intensity changes for various values of cut-off rigidity determined using barometric coefficient 16 p2738 A67-31082
Screen effect on cosmic ray intensity measurement by comparing data from various rocket and satellite soundings 16 p2738 A67-31083
Frequency dependence of enhanced absorption of cosmic radio emission during abrupt ionospheric disturbance 16 p2738 A67-31091
Cosmic plasma flow effect on cosmic radiation polarization, deriving difference between normal waves refractive indices in two-component medium 16 p2628 A67-31494
Dynamic phenomena in diurnal variation of cosmic rays used to determine width and existence of separate flows in interplanetary medium 16 p2740 A67-31898
Barometric and temperature coefficients determined from solar-diurnal, antisideral variation, atmospheric showers 16 p2741 A67-31900
Ionization loss effect on energy spectra of cosmic ray nuclei undergoing Fermi acceleration 17 p2930 A67-32041
Effective volume of asymmetric solar wind shown to be independent of primary cosmic radiation energy, noting role of 27-day variation 17 p2932 A67-32085
Cosmic ray intensity, discussing modulation due to earth heliollatitude variation 17 p2932 A67-32086
Hysteresis phenomena in curves describing cosmic ray intensity dependence on number of sunspots 17 p2933 A67-32087
Temperature effect on diurnal variation of hard cosmic ray component based on radio probe observations 17 p2933 A67-32089
Atmospheric temperature effect on latitudinal curve of cosmic ray intensity determined from radio probe observations 17 p2933 A67-32090
Spherical analysis of geomagnetic maps to determine asymptotic directions of cosmic rays for Soviet station network 17 p2933 A67-32091
Coupling coefficient and latitude distribution in intensity of cosmic rays inclined component measured by Soviet ship 17 p2933 A67-32093
Latitude variation of effective geomagnetic cut-off rigidity of cosmic rays in presence of penumbra and constant geomagnetic field 17 p2934 A67-32094
Circuitry of transistorized azimuthal supertelescope designed for measurement of general ionization component of cosmic rays 17 p2854 A67-32097
Biochemical reactions in human organism as indicator of cosmic ray variation, showing relationship between solar activity and erythrocytes in blood 17 p2934 A67-32099
Barometric correction in cosmic ray studies using partial barometric coefficient 17 p2934 A67-32105
Simultaneous amplitude and phase modulation of periodic cosmic ray variations by using two frequencies 17 p2934 A67-32106
Cosmic ray variation analysis using theory of random processes 17 p2935 A67-32107
Spectrometers onboard satellite, studying cosmic ray particle energy spectra and chemical composition 17 p2935 A67-32248
Energy spectrum of cosmic ray nuclei in helium through scandium range studied with Proton I and II satellites 17 p2935 A67-32249
Concentration ratios of cosmic ray-produced isotopes of helium, neon and argon measured and effective irradiation hardening parameter calculated 17 p2942 A67-32358
Helium and neon content and isotopic composition in iron meteorites, noting He 3 deficiency in hexahedrites due to tritium loss 17 p2942 A67-32359
McIlwain coordinates correlated with vertical cut-off rigidities, estimating cosmic ray rigidities 17 p2936 A67-32537
Thermal and synchrotron cosmic X-ray sources 17 p2937 A67-32639
Cosmological model covering early and late stages, presenting period time when matter density equaled radiation density 17 p2947 A67-32759
Atmospheric variations effects on cosmic radiation records from plastic scintillation monitors, calculating pressure coefficients 17 p2938 A67-32795
Interplanetary structure revealed through study of cosmic ray storm effects in February 1962 17 p2845 A67-32797
Cosmic ray motion in interplanetary electromagnetic field for isotropic/anisotropic diffusion situations presented by convective diffusion models assuming spherical symmetry for solar cavity 17 p2938 A67-33188
Cosmic ray electrons energy spectrum and charge composition studies inadequacy due to insufficient statistics and electron flux contamination 17 p2938 A67-33198
Cosmic radiation anisotropy variation with time and direction described on intensity contour map, noting application for neutron monitors data reduction 17 p2938 A67-33209
Cloud-ion chamber stack to measure properties of interactions in light materials of high energy cosmic ray protons and pions 17 p2863 A67-33355
Cosmic radiation dose, estimating contributions due to mu meson and electron-photon cascade shower components 18 p2990 A67-33516
Radiation and weightlessness effect on human organism in space flights, discussing galactic cosmic, solar and Van Allen belt radiation 18 p3116 A67-33700
Possibility of determining content of natural radioactive uranium, thorium and potassium in lunar rocks and of estimating chemical composition of rocks from cosmic ray induced radioactivity 18 p3122 A67-34142
Exponent in expression relating nuclear interaction cross section to atomic weight of absorber determined from absorption path of nuclear active particles of cosmic radiation 18 p3116 A67-34414
Local condensation in early stage of universe suggested from observation of spatial inhomogeneity of cosmic black-body radiation 19 p3312 A67-34893
Time dependency, anisotropy degree and spectral composition of cosmic radiation generated during July 1966 solar flares as observed by Pioneer VI 19 p3314 A67-35270
Energy spectrum of cosmic X-rays background component, proving

experimentally rocketborne detector counting rate proportionality to field of view 19 p3314 A67-35278

Stratosphere and mesosphere wind and temperature measurements, noting additional cosmic radiation measurements during 1966 solar eclipse in Argentina 19 p3320 A67-35287

Space research in West Germany noting ionospheric physics, magnetosphere and solar and cosmic radiation 19 p3321 A67-35293

Density gradient of cosmic radiation perpendicular to plane of ecliptic as cause of variations in amplitude and phase of solar diurnal variation 19 p3315 A67-35490

Interplanetary space magnetic clouds velocity and spatial distribution obtained from cosmic ray modulation data, noting relation to solar activity 19 p3325 A67-35493

Underground cosmic ray intensity variation measurements to determine solar modulation processes 19 p3315 A67-35494

Electron component observation in studying solar modulation of galactic cosmic rays, discussing Parker model and Gloeckler-Jokipii model 19 p3315 A67-35496

National IQSY research programs /1964-1965/ 19 p3325 A67-35497

Wave propagation and geometrical optics in random media, considering applications to solar corona heating by energy transfer, stellar scintillation and cosmic ray acceleration 19 p3261 A67-35507

Cosmic ray intensity short-period variations investigated by high-counting rate detector indicating fluctuations related to geomagnetic cutoff rigidity periodic changes 19 p3315 A67-35537

Sea level and stratosphere measurement of cosmic ray intensity latitude distribution, coupling coefficients and multiplicities 19 p3316 A67-35563

Cosmic radiation origin shown inconceivable in radio galaxies 19 p3316 A67-36088

Cell survival rates and mutation development in *Chlorella vulgaris* plants carried by Cosmos satellite 20 p3367 A67-36256

Sudden commencement of November 13, 1960 caused by cosmic ray flare of November 12 20 p3517 A67-36284

Satellite observations made by two or more satellites simultaneously on interplanetary medium 20 p3521 A67-36501

Multi-input photomultiplier pulse height photographic recording system using dual beam oscilloscope for cosmic ray experiments 20 p3444 A67-36525

Aerodynamic lift, studying production of cosmic energy level supporting mechanism, explaining electromagnetic Magnus effect for gravity-free device 20 p3484 A67-36821

Quasar sources studies set limits on possible density inhomogeneity magnitudes in universe by measuring cosmic microwave background isotropy and homogeneity 20 p3525 A67-36868

Antiproton abundance upper limit in low energy galactic cosmic radiation determined by exposing nuclear stack to residual atmosphere 20 p3518 A67-36872

Cosmic-ray electron spectrum in disk-halo galactic model, studying inconsistencies in Ramaty and Lingenfelter analysis 20 p3518 A67-36946

Periodic fluctuations of cosmic ray diurnal variation statistically studied, using neutron and meson component data 20 p3518 A67-36993

He 3 ratio to He nuclei in cosmic rays, determining He nuclei path length in space, considering kinetic energy power spectrum 20 p3518 A67-37088

Phase relationship between solar activity changes and changes in solar wind parameters over 11-year cycle 20 p3519 A67-37395

Cosmic ray secondary nucleon production of multiple neutrons observed and energy spectra measured, using multiplicity monitor 20 p3452 A67-37407

Galactic cosmic ray density distribution anisotropy in solar system, discussing outward convection of cosmic rays by solar wind and inward diffusion model 20 p3520 A67-37474

Cosmic X-ray sources in 20-180 keV energy range detected in balloon flights, giving energy spectra 20 p3520 A67-37475

Intensity of characteristic spectral lines of Si, Al and Mg of lunar surface rock made

fluorescent by solar X-rays determined from Luna X measurements 21 p3701 A67-37838

Lunar gamma radiation measured by spectrometer on Luna X orbiter noting lunar rock radiation level, effect of cosmic rays, etc 21 p3701 A67-37842

Distribution of cosmic rays on sphere and reception vector of radiation detector 21 p3698 A67-38464

Quasi-spiral nature of change in 27-day cosmic ray variation with solar activity shown by harmonic analysis 21 p3698 A67-38480

X-ray spectrum and location measurements of several cosmic X-ray sources, using rocketborne proportional counters 21 p3698 A67-38564

Semiconductor detector for information on charged particles of cosmic radiation, studying characteristics of instrument 21 p3629 A67-38664

Reception vectors for first and second spherical harmonics of cosmic ray distribution calculated for neutron monitor stations 21 p3699 A67-39018

Interplanetary magnetic field normal to ecliptic plane influence on interplanetary cosmic ray flux, discussing solar origin of field 21 p3699 A67-39019

Cause of cosmic radiation intensity increase before magnetic storms associated with Forbush effects 21 p3699 A67-39029

Seasonal changes in solar diurnal and semidiurnal variations of cosmic ray neutron component due to earth rotation axis and anisotropy sources 21 p3700 A67-39048

Radiation protection from cosmic rays during space flights, considering shielding, observation and warning, dosimetry and medical provisions 22 p3754 A67-39286

Time dependency, anisotropy, propagation and spectral properties of cosmic radiation released by solar flares during sunspot activity 22 p3871 A67-39796

Observatory building for ultrahigh energy cosmic ray and cascade phenomena /air showers/ observation, describing Fresnel lens system 22 p3873 A67-39973

Double sunspot cycle or 22-yr variation in cosmic ray diurnal variation phase, discussing streaming mechanisms 22 p3874 A67-40046

Low latitude cosmic ray neutron monitor multiplicity distribution, discussing monitor geometry and latitude 22 p3874 A67-40047

Solar cosmic ray multiple neutron production increase on January 28, 1967 from Antarctica cosmic ray neutron monitor measurements 22 p3874 A67-40048

Cosmic ray physics - Conference, Moscow, November 1965 22 p3874 A67-40246

Hypothesis of meson resonances produced in cosmic ray interactions, explaining multiple birth characteristics of secondary particles 22 p3876 A67-40247

High energy cosmic ray interactions analyzed at 3340 m above sea level, using Wilson cloud chambers, gas discharge counters, ionization calorimeter, etc 22 p3801 A67-40248

Peripheral nonelastic interactions described, using amplitude characteristics of elastic cosmic ray particle interaction and complex orbital moment technique 22 p3876 A67-40251

Statistical analysis of cosmic ray particle elastic scattering, noting isotropic nature of angular distribution 22 p3841 A67-40252

Electron-photon shower measurement using ionization calorimeter type device 22 p3842 A67-40257

Pion energy transmission during inelastic interaction of cosmic particles with Pb nuclei 22 p3876 A67-40258

Ionization calorimeter measurements of energy transmission by photons in cosmic nuclear-active pion and nucleon interactions with various nuclei 22 p3876 A67-40263

Elimination of certain contradictions in data concerning high energy cosmic rays explained by means of hypothesis of existence of passive S-state of baryon 22 p3877 A67-40268

Cosmic ray intensity from balloon sounding, discussing proton to He ratio behavior as time function within Parker solar modulation model 23 p4051 A67-40809

Intensities of cosmic ray produced deuterium and tritium in atmosphere measured from high altitude balloons 23 p3995 A67-40811

Cosmic ray diurnal anisotropy component annual means variation with two solar cycles 23 p4051 A67-40817

Radiobiological risk of SST flights from heavy ions of cosmic radiation, discussing methods of radiation detection 23 p3945 A67-41074

Cosmic ray physics - Conference, Alma-Ata, Kazakh SSR, October 1966 23 p4051 A67-41089

Makeup low energy spectra and electron component of cosmic rays and solar particle production with curves for element abundance 23 p4053 A67-41090

Heavy and superheavy nuclei energy spectra studied from measurements by Cerenkov counter onboard space stations 23 p4054 A67-41094

Probes containing various scintillators for measuring electron energy spectrum at high altitude in cosmic ray flux 23 p4054 A67-41095

Low energy cosmic ray measurements during solar activity minimum suggesting changes in cosmic ray composition due to solar wind 23 p4054 A67-41097

Cosmic ray measurements during low geomagnetic activity using scintillation, gas discharge and semiconductor proton counters mounted on Cosmos satellite 23 p4055 A67-41099

Cosmic ray regional variations in intensity and ionization magnitude and duration indicating heavy nucleus and low energy particle influx accompanying solar flares 23 p4055 A67-41100

Interplanetary space cosmic ray intensity variation with time and distance from sun measured by Zond III and Venera II simultaneously 23 p4055 A67-41102

Galactic cosmic ray intensity measurements in stratosphere and at various atmospheric depths, studying secular variation energy spectra during solar cycle 23 p4055 A67-41103

Nuclear cosmic ray component intensity variation related to 27-day solar activity variation in Elektron II and IV analysis of modulating effect 23 p4055 A67-41104

Cosmic ray intensity solar cycle variations in terms of solar wind properties defined by solar activity characteristics parameters 23 p4056 A67-41106

Cosmic ray intensity variation mechanisms due to motion of solar system and quasi-radial interplanetary magnetic field 23 p4056 A67-41107

Cosmic ray intensity 27 day variations during low and high solar activity periods noting lower amplitude and softer spectrum 23 p4056 A67-41108

Cosmic ray intensity 19, 20 and 24 day quasi-periodic global variations in stratosphere related to solar activity variations, comparing amplitudes with Forbush effects 23 p4056 A67-41109

27-day cosmic ray intensity variations noting possible selective effects of active spots on solar hemispheres and plasma corpuscular fluxes structure 23 p4056 A67-41110

Cosmic ray acceleration mechanisms for fast particle generation under outer space conditions 23 p4057 A67-41114

Latitude variation in neutron component of cosmic ray intensity within cut-off rigidity at atmospheric depths from 280 to 315 mb 23 p4057 A67-41119

Earth axis inclination influence on diurnal amplitude of cosmic ray variation, discussing yearly modulation effect 23 p4058 A67-41126

Atmospheric temperature effect on cosmic ray hard component diurnal variation in high latitude regions, discussing anomalous diurnal variation 23 p4058 A67-41127

True and false sidereal diurnal cosmic ray variation, examining modulating effects leading to false variations 23 p4058 A67-41128

Sidereal diurnal cosmic ray variation caused by modulation in solar system, discussing variations in coordinate systems 23 p4059 A67-41129

Sidereal cosmic ray diurnal variations, taking into account data correction for barometric pressure and temperature effects 23 p4059 A67-41130

Solar active formations relation to annual cosmic ray variations, discussing spot group, chromospheric flares and calcium flocculi area distributions 23 p4059 A67-41132

Space time distribution of cosmic rays as

- function of plasma efflux from sun, magnetic field intensity, topology and scale irregularities 23 p4059 A67-41133
- Cosmic ray variations over celestial sphere investigated by matrices applied to distribution model 23 p4059 A67-41134
- Cosmic ray equator position at zero meridian measured, noting substantial difference in location from magnetic equator position 28 p4059 A67-41135
- Intensity of ionizing and neutron components measured in stratosphere as function of geomagnetic rigidity, obtaining coupling coefficients for cosmic ray variations 23 p4059 A67-41136
- East-west asymmetry effect in cosmic rays obtained together with ionizing and hard components, using crossed telescope 23 p4060 A67-41137
- Cosmic ray intensity measurement data from Soviet 1966 expedition in Arctic Ocean 23 p4060 A67-41138
- Cosmic X-ray sources spectra obtained by proportional counters and electronic systems on sounding rockets 23 p4001 A67-41222
- Cosmic ray distribution, discussing method of diurnal variations, zonal harmonics and spherical analysis 24 p4209 A67-42114
- Parameters of simultaneous amplitude phase modulation of periodic cosmic ray variations obtained from satellite observations 24 p4209 A67-42115
- Cosmic ray intensity variation detection with respect to sidereal time on basis of simultaneous amplitude phase modulation 24 p4209 A67-42116
- Cosmic ray neutron component intensity during magnetic perturbations, considering effect of magnetospheric deformation 24 p4209 A67-42117
- Rapid and slow spreading absorption of cosmic rays over polar cap 24 p4209 A67-42126
- Dead time instability effect on neutron monitor performance 24 p4209 A67-42135
- Neutrino behavior in beta decay, proton-neutrino and proton-proton reactions, discussing astronomical implications of neutrino radiation 24 p4227 A67-42197
- Proton space station design and onboard instruments used for high energy cosmic ray study 24 p4210 A67-42391
- Friedman cosmological models describing spatially homogeneous and isotropic universe 24 p4231 A67-42454
- Penetrating particles in cosmic radiation deep underground in Kolar gold field experiment, discussing muon-neutrino interaction 24 p4210 A67-42582
- Upper limits of fractional charge content of cosmic radiation 24 p4210 A67-42600
- Galactic cosmic ray solar cycle and secular variations in bombardment of meteorites at average meteoroid solar distance and 1 AU from radioactive isotope 24 p4210 A67-42622
- Al 26 content of stony meteorites by coincidence spectrometry noting cosmic ray exposure ages for eight meteorites 24 p4234 A67-42630
- Solar and galactic low energy cosmic ray nuclear ionizing and interaction effects on meteorite surface isotopic composition, estimating particle fluxes 24 p4210 A67-42634
- Cosmic ray physics - All-Union Conference, Moscow, November 1965 24 p4211 A67-42757
- Cosmic ray variations classification and origin taking into account possible interference between meteorological effects 24 p4212 A67-42758
- Radioactive isotopes in iron meteorite used to determine cosmic ray origin and to study nuclear processes in early history of solar system 24 p4212 A67-42760
- Geographic position of cosmic ray equator from results of onboard Proton I satellite measurements 24 p4212 A67-42766
- Preliminary measurements of variations in cosmic ray intensity using device consisting of gas discharge counters, telescope and ionization chamber mounted on Kosmos XXV satellite 24 p4213 A67-42768
- Helium isotope formation in cosmic rays during light nuclei fragmentation due to high energy proton interaction 24 p4213 A67-42769
- Boltzmann equation for cosmic ray particle motion in random magnetic field 24 p4213 A67-42770
- Energy loss of cosmic electron in interstellar space due to ionization, bremsstrahlung and Compton effect 24 p4213 A67-42771
- Aurora photometry and stratospheric cosmic ray intensity, noting electron intrusion and correlation between aurora intensity and X-ray emission 24 p4213 A67-42778
- Intensity of ionizing and neutron component of cosmic rays, noting correlation for sporadic cyclic variations and solar activity cycles 24 p4213 A67-42779
- Magnitude of lunar neutron emission due to cosmic rays estimated from atmospheric measurements 24 p4213 A67-42781
- Cosmic radiation intensity measurement using automatic interplanetary stations with onboard Geiger counters 24 p4213 A67-42782
- Cosmos 53 satellite radiation data using onboard gas discharge counter 24 p4213 A67-42783
- Change in cosmic ray cut-off rigidity caused by currents from trapped particle motion, according to Chapman-Akasofu radiation belt model 24 p4214 A67-42787
- Solar cosmic ray generation during chromospheric flares noting increased neutron intensity 24 p4214 A67-42788
- Relation between cosmic ray cut-off rigidity and L parameter, solving approximately 7th degree algebraic equation 24 p4214 A67-42789
- Asymptotic directions of cosmic rays for Soviet cosmic ray stations 24 p4214 A67-42790
- Interplanetary space properties studied from IMP-I satellite data on cosmic ray variations 24 p4214 A67-42791
- Temporal distribution of first and second harmonics of solar diurnal variation of cosmic rays after radio bursts of fourth type 24 p4214 A67-42792
- Variation of seasonal diurnal distribution of sudden changes in cosmic ray neutron component intensity related to solar activity changes 24 p4214 A67-42794
- Solar diurnal variation of cosmic ray neutron component in Antarctic during minimum activity period, using harmonic analysis 24 p4214 A67-42795
- Anisotropy in stellar diurnal cosmic ray variations in Northern and Southern Hemispheres, noting distributions of stellar and antistellar vectors 24 p4214 A67-42796
- Corpuscular stream parameters based on data from Mariner II concerning cosmic ray variations on earth surface during geomagnetic storms 24 p4214 A67-42797
- Amplitude of 27-day cosmic ray modulation in relation to solar and geomagnetic activities 24 p4214 A67-42798
- Barometric coefficient of cosmic ray variations determined from observation of Forbush effects and cosmic ray flare effects 24 p4214 A67-42799
- Intensity of various secondary cosmic ray components in cut-off rigidity range from 0.3 to 10 BeV 24 p4215 A67-42800
- Coupling coefficients of cosmic ray neutron component according to data from schooner Zaria 24 p4215 A67-42801
- Coupling coefficients for vertical and oblique cosmic ray components 24 p4215 A67-42802
- Geomagnetic cut-off rigidity effect on cosmic ray intensity and coupled coefficients 24 p4215 A67-42803
- High energy gamma quanta from high energy cosmic particle interaction with carbon and air nuclei, noting three superhigh energy electron/photon cascades recorded 24 p4218 A67-42835
- High energy nucleon interactions with X-ray films and nuclear emulsions aboard aircraft, with diagram of gamma quanta energy spectra 24 p4218 A67-42836
- Multiparticle mechanism of cosmic ray-atomic nuclei interactions assuming particle formation 24 p4218 A67-42842
- Cross section of inelastic interactions and free path between nuclear active cosmic particles and lead nuclei at high energies 24 p4219 A67-42844
- Nuclear cosmic particle interactions cross section in iron, using Bartlett S-function for particle free path determination 24 p4219 A67-42846
- High energy cosmic ray nuclear interaction cross section dependence on interacting material atomic weight determined by ionization calorimeter and Geiger counters 24 p4219 A67-42847
- Nuclear active cosmic ray particles and Fe atom nuclei inelastic interaction cross section 24 p4219 A67-42849
- Nuclear cascade avalanche absorption in Fe analyzed by ionization calorimeter 24 p4219 A67-42850
- Iron radiation length unit from electromagnetic cascades produced by bremsstrahlung of horizontal cosmic ray muons 24 p4221 A67-42869
- Penetrating component of high energy cosmic rays below ground measured for intensity 24 p4221 A67-42876
- High energy cosmic ray muon integral angular and integral spectrum below earth surface 24 p4222 A67-42877
- Hard component penetration of cosmic rays investigated by ionization calorimeter and hodoscopic counters 24 p4222 A67-42878
- Photonuclear interaction effect on large angle scattering of high energy muons 24 p4222 A67-42881
- Cosmogenic radioactivity in freshly fallen meteorites measured and compared to calculate terrestrial and exposure ages and spatial and time dependence 24 p4238 A67-42884
- COSMIC RADIO WAVE**
- Polarization measurements of distribution of ionized interstellar gas near galactic plane using two galactic region models 02 p0322 A67-11645
- Orbiting radio telescope for cosmic radio wave frequency and amplitude detection 02 p0334 A67-12360
- Thermal and nonthermal cosmic radio sources explained by short circuit breakdown of predischarged field initiated by breakdown to thermally ionized arc discharge 04 p0691 A67-14433
- Negative absorption in cosmic radio sources of synchrotron radiation 04 p0700 A67-15200
- Optimum wavelength and spectral bandwidth for measuring polarization of distributed cosmic RF radiation 05 p0786 A67-17228
- Long wave cosmic radio emission in interplanetary space 06 p1077 A67-17746
- Search for 21 cm radiation near cosmic X-ray sources 07 p1242 A67-19062
- Auroral absorption of cosmic radio radiation recorded by shipboard station drifting in North Geographic Pole region in winter 1963-64 07 p1178 A67-19824
- Depolarization of cosmic radio emission due to dispersion of Faraday rotation of planes of polarization of radio waves 08 p1376 A67-20813
- Height distributions of enhanced lower ionospheric ionization estimated from cosmic radio noise absorption 10 p1634 A67-23059
- Cosmic radio wave absorption dependence on frequency and number of electron-ion collisions during atmospheric magnetic storms 12 p1933 A67-25548
- Cosmic radio emission at 725 and 1525 kc measured for intensity by direct amplification receivers on Elektron II satellite 12 p1995 A67-25769
- Dependence of angular dimensions of discrete cosmic radio emission source on radiation flux density and frequency 15 p2549 A67-29140
- Excess cosmic microwave background temperature of 2 degrees K at 1.5 cm wavelength 15 p2551 A67-30161
- Depolarization problem and correlation method for cosmic radio emission polarization measurements in interstellar space 22 p3761 A67-39757
- Equivalent temperature of cosmic microwave background radiation at 3.2 cm wavelength, discussing Dicke type sources 23 p4063 A67-40922
- Dependence of angular dimensions of discrete cosmic radio emission source on radiation flux density and frequency 24 p4222 A67-43063
- COSMIC RAY**
- SA HEAVY COSMIC RAY PRIMARY**
- SA SOLAR COSMIC RAY**
- Energy loss of high energy muons caused by nuclear interaction and fluctuation due to passage through great thickness of material corrected for standard rock 10 p1703 A67-23690
- Origin of ultrarelativistic cosmic ray particles 14 p2382 A67-29028
- Isotope fractionation processes and

reproducibility of age of iron meteorites studied from cosmic ray exposure ages 15 p2556 A67-29664

Soviet book on cosmic rays including solar-diurnal, 11-year and 27-day variations, temperature effect, geomagnetic field effect, etc 17 p2930 A67-32077

Diurnal variation of hard component near minimum solar activity, emphasizing temperature effects 17 p2932 A67-32080

Statistical analysis of solar-diurnal and semidiurnal variations of cosmic ray neutron component with respect to geomagnetic field perturbations 17 p2932 A67-32081

Relation between frequency distribution of sudden changes in cosmic ray intensity and solar-diurnal variation 17 p2932 A67-32082

Cosmic ray intensity 11-year variation energy characteristics, discussing spectrum bending due to integral modulation in interplanetary space 17 p2932 A67-32083

Temperature effect measurement of neutron cosmic ray component, noting results of Chicago and Hobart geophysical stations 17 p2933 A67-32088

Cosmic ray variations methodology, considering solar system geometry, interstellar cosmic ray gradient, phase and amplitude modulation, etc 17 p2934 A67-32103

Integral multiplicity calculation procedure for meson component of cosmic rays based on three-dimensional elementary event model, noting meteorological effects 17 p2934 A67-32104

Cosmic ray variation determination from single series of observations by methods of random process theory 17 p2935 A67-32108

Galactic and solar ray behavior equations, with cosmic ray drift velocity and diffusion tensor determined for interstellar space in anisotropic-diffusion approximation 17 p2935 A67-32109

Cosmic ray nuclei fragmentation without particle production, noting nuclear emulsions and high energy 17 p2936 A67-32363

Temperature effect of cosmic ray neutron component 17 p2936 A67-32381

Low pressure gas Cerenkov detector and spectrometer coupled into charged particle telescope for cosmic ray electron spectrum measurements, discussing efficiency and instrument calibration 20 p3452 A67-37566

TV system with spark chamber detector for analysis and transmission of cosmic ray pictures to earth from satellites 21 p3599 A67-38655

Cosmic rays interaction with solar and terrestrial magnetic fields, noting interplanetary plasma flows and solar activity 21 p3699 A67-39006

Interplanetary magnetic field magnitude determination by considering particle motion along magnetic lines of force and trajectories divergence in earth vicinity during cosmic ray bursts 21 p3700 A67-39030

Cosmic ray trajectories in geomagnetic field, discussing asymptotic directions, rigidities, crossed telescope measurements and focusing effect 23 p4050 A67-40693

Cosmic ray intensity increase in wake of chromospheric flares from stratospheric measurements 23 p4057 A67-41115

Secular modulation of cosmic ray intensity in interplanetary space using Parker diffusion model 23 p4057 A67-41117

Forbush effects variations during solar activity cycle using hard cosmic ray component data 23 p4057 A67-41118

Solar activity cycle effect on cosmic ray anisotropy diurnal variation 23 p4057 A67-41120

Cosmic ray anisotropy in solar system, considering diurnal variation in terms of anisotropic diffusion 23 p4058 A67-41121

Diurnal variation in cosmic ray anisotropy from observations during solar activity minimum, giving amplitudes and phases distribution 23 p4058 A67-41122

Cosmic ray diurnal variation during magnetic storms from neutron monitors and meson telescope data 23 p4058 A67-41124

Cosmic ray physics - All-Union Conference, Alma-Ata, Kazakh SSR, October 1966 24 p4215 A67-42826

Multiple charged particle production process mean characteristics determined for several energy levels 24 p4217 A67-42830

Stack of alternating lead layers, nuclear emulsions, X-ray films with graphite cosmic-ray receiving shield on top used for determining distribution in time of

events 24 p4217 A67-42832

COSMIC RAY ALBEDO

Relative intensity contribution and time dependency of primary cosmic rays, splash albedo and reentrant albedo measured by polar orbiting satellite 20 p3517 A67-36306

Reentrant cosmic ray albedo intensity, considering nuclear interaction and trajectory spiraling effects 23 p4050 A67-40808

COSMIC RAY PROPAGATION

Cosmic ray electromagnetic acceleration mechanism, calculating motion of charged relativistic particles in applied fields 02 p0311 A67-12586

Planetary distribution and interpretation of abrupt increases in cosmic ray intensity observed during periods of maximum solar activity but not related to visible solar phenomena 02 p0312 A67-12602

Charged particle motion in random magnetic field, describing time evolution of particle distribution in pitch angle and position in terms of Fokker-Planck coefficients 03 p0508 A67-14317

Cosmic ray isotropy mechanism, examining plasma beam instability and cosmic ray scattering at plasma turbulent pulsations 04 p0693 A67-15554

Effect of higher harmonics of geomagnetic field on cosmic ray trajectories, noting reception cones of Soviet stations 07 p1243 A67-19685

Cosmic ray nuclei propagation in interstellar space and solar system examined from balloon, rocket and satellite soundings 08 p1378 A67-21473

Solar cosmic ray event characteristics 1962-1966, solar minimum vs solar maximum 10 p1700 A67-23187

Upper limits on cosmic gamma ray flux obtained using OSO-I and sodium iodide scintillation counters 12 p1995 A67-25763

Geomagnetic field influence on cosmic rays simulated by electron beam and terrella situated in vacuum tank 13 p2192 A67-27243

Cosmic ray particle trajectories for various cut-off rigidity values in different points on earth surface, noting integration of motion equations of charged particle 13 p2192 A67-27244

Spectrum, intensity, and charge composition of primary cosmic radiation and relevance to origin and propagation of galactic radiation 14 p2379 A67-27963

Interplanetary electromagnetic field effects on cosmic ray intensity noting geomagnetism, modulation mechanisms and solar flare particle propagation 14 p2380 A67-27965

Steady state propagation of cosmic ray nuclei, discussing energy spectrum and path lengths 19 p3317 A67-36099

Cosmic ray diffusion in interplanetary magnetic field, examining statistical homogeneity and isotropy 20 p3520 A67-37473

Intense fluxes of charged particles associated with disturbances in interplanetary medium during 1966 22 p3871 A67-39797

Cosmic ray propagation processes studied from measurement of anisotropic character of cosmic radiation 22 p3871 A67-39798

Mathematical model for solution of anisotropic diffusion equations of solar cosmic ray propagation 22 p3872 A67-39809

Energy changes between solar wind and cosmic rays, discussing particle motion description by Fokker-Planck differential equation 22 p3874 A67-40079

Drift equation supplemented by collision terms for describing interplanetary regular magnetic field and solar wind velocity fluctuation effects on cosmic ray propagation 23 p4056 A67-41105

Streaming and spatial gradient equations of cosmic ray particles in interplanetary medium model, discussing Fokker-Planck equation and heliocentric field modulation 24 p4208 A67-41832

Low energy cosmic ray proton flux as representative of interstellar medium, discussing electron density in neutral H I regions 24 p4208 A67-41833

Cosmic ray propagation through atmosphere, developing model for elementary particles 24 p4218 A67-42837

Isobar decay mechanism for high energy pion generation in cosmic rays propagating

through atmosphere 24 p4218 A67-42841

Cosmic particle recording facility at Tskhira-Tskaro, giving data on free path of nuclear active particles in carbon with high energies 24 p4219 A67-42845

Cross section of inelastic interaction between cosmic ray neutrons and carbon nuclei at energies of 100 Gev 24 p4219 A67-42848

COSMIC RAY SHOWER

Rms particle numbers calculated for electrons and photons in three-dimensional theory of electromagnetic showers 01 p0143 A67-10543

Radio pulse pattern from EAS monitored at Yorkshire, England, observed on oscilloscope against galactic noise background 01 p0144 A67-10888

High energy proton from local radio sources, using telescopic system for Cerenkov effect detection of broad atmospheric showers 02 p0311 A67-12587

Spectrum of primary cosmic radiation determined for ultrahigh energies, based on international data on electron and meson air showers 02 p0311 A67-12588

Primary cosmic rays of superhigh energy using extensive air shower data, noting Geiger-Muller counters, scintillation counters and muon detector 02 p0311 A67-12589

Extensive atmospheric showers as means of gaining insight into energy spectrum and composition of primary cosmic radiation 02 p0312 A67-12603

Atmospheric showers and high energy nuclear-active particles 02 p0312 A67-12608

Ionization calorimeter measurement of contribution of ionizing particles of star radiation to electron induced ionization of cosmic ray shower 02 p0271 A67-12754

Data on fragmentation of energy in nuclear reactions in atmospheric showers compared with calculations results for predicted energy 02 p0316 A67-12764

Energy moments of inverse problem in theory of nuclear cascade determined, using first order Volterra integral equation 02 p0317 A67-12769

High energy cosmic ray muons studied, using ionization calorimeter and hodoscope counters 02 p0317 A67-12770

Interactions of superhigh energy muons in cosmic ray nonelectromagnetic cascade showers 02 p0317 A67-12771

EAS with zenith angle between 30 and 45 degrees and fixed number of muons and electrons 02 p0318 A67-12777

Extensive air shower characteristics related to energy spectrum, chemical composition and anisotropy of primary cosmic rays in superhigh energy range 02 p0318 A67-12778

Muon groups at depth of 40 mwe not responsible for substantial energy leakage from extensive air showers 02 p0318 A67-12779

Muon flux measurement with aid of spark chamber at depth of 20 mwe used for spatial distribution near axis of extensive air showers 02 p0318 A67-12780

Ionization luminescence of air and possibilities of using it to record extensive air showers 02 p0318 A67-12781

Total energy of slow particle radio emission and real delta electron emission determined in extensive air showers 02 p0318 A67-12782

Coherent radio emission of extensive air showers determined from known threshold energy of optical signal 02 p0318 A67-12783

Monte Carlo method for calculating longitudinal and transverse development of extensive air showers, considering fluctuations 02 p0318 A67-12784

Leading particle model of formation of extensive air showers, showing determination of energy spectrum 02 p0319 A67-12785

Isobaric pions role in interaction between nucleons and pions on one hand and nuclei of air atoms on other 02 p0319 A67-12786

Extensive near-vertical air shower analysis at sea level for nucleon-air-nucleus and pion-air-nucleus interaction 03 p0506 A67-13517

Determining total number of charged particles in extensive atmospheric shower and position of axis of shower 03 p0507 A67-14059

Chronotron type device for measuring zenith and azimuth angles of slope of axes of extensive air showers 03 p0425 A67-14263

Multiplate spark chamber as linear high energy electron and photon detector 03 p0425 A67-14264

Giant airshower recorder using liquid scintillators to record collision of cosmic rays with atmospheric nuclei 03 p0508 A67-14388

Upper limits to high energy gamma flux from quasars 3C 147, 3C 196 and 3C 273 from Crab Nebula and from 53 Cam magnetic variable star 05 p0900 A67-17079

Radio pulses from air shower detection, noting correlation between shower arrival direction and antenna pattern and shower size and pulse frequency 06 p1076 A67-17554

Muon momenta, signs and densities in cosmic air showers determined, using magnet spectrograph with visual display 06 p1076 A67-17651

Radio pulse coincidence with extensive air showers, noting consistency with Cerenkov radiation and charge separation in terrestrial magnetic field 07 p1242 A67-19619

High energy solar cosmic ray spectrum during solar flare of February 23, 1956 07 p1243 A67-19805

Four-momentum transfer, inelasticity and mass of target isobars in cosmic ray jets 07 p1246 A67-20278

Transition of extensive air showers in atmosphere with determination of lateral structure, mean free path and inelasticity 08 p1377 A67-21437

Intensity gradient of galactic cosmic rays, analyzing modulation induced by solar activity 10 p1699 A67-22801

Lateral distribution of radio emission flux of extensive air showers /EAS/ of cosmic rays 12 p1940 A67-25337

Primary cosmic ray intensity and structure of air showers at high altitudes investigated by aircraft, balloons and sounding rockets 13 p2193 A67-27247

Handbook of Physics, Volume 46/2, Cosmic radiation 14 p2379 A67-27960

Electron cascade showers, examining elementary processes, general behavior, three-dimensional theories and large angle single scattering 14 p2379 A67-27961

Thermodynamical, dynamical, and possible third mechanisms responsible for features in high energy cosmic ray interactions and multiple production of shower secondaries 14 p2379 A67-27962

Electron number density profiles and polar cap absorption of radio waves time history during weak solar cosmic ray event 14 p2380 A67-28042

Chronotron type device for measuring zenith and azimuth angles of slope of axes of extensive air showers 14 p2321 A67-28775

Multiplate spark chamber as linear high energy electron and photon detector 14 p2321 A67-28776

Space-time distribution of heavy penetrating particles in extensive air showers, applying scale transformation properties of distribution to integration over primary particle spectrum 15 p2550 A67-29749

Anisotropic phase of cosmic ray flares analyzed using kinetic equation in Fokker-Planck approximation 16 p2740 A67-31891

Ionization fluctuations due to interaction between shower particles and absorbing component of ionization calorimeter and effect on accuracy of energy measurement 17 p2855 A67-32250

Amplitude and polarization of radio pulse from extensive cosmic ray air shower indicating geomagnetic deflection mechanism of emission 18 p3116 A67-34196

Refractive index variations, Coulomb scattering and time variation of shower front effects on coherent emission of polarized radio pulses from cosmic ray showers 18 p3116 A67-34197

Cosmic ray and interplanetary medium and magnetic field studies in Bolivia 19 p3320 A67-35284

Extensive air showers due to extragalactic primary photons demonstrated, considering production process 19 p3316 A67-35798

Atmospheric electric field as possible cause of radio pulses from extensive air showers 19 p3316 A67-35803

Extensive cosmic ray shower bremsstrahlung in RF and optical bands noting intensity and incoherency 22 p3870 A67-39517

Cosmic ray fluctuations without imposing limitations on particle scattering, deriving

expressions using three-dimensional cascade shower theory 22 p3873 A67-39880

Observatory building for ultrahigh energy cosmic ray and cascade phenomena /air showers/ observation, describing Fresnel lens system 22 p3873 A67-39973

Cosmic ray physics - Conference, Moscow, November 1965 22 p3874 A67-40246

Ionization calorimeter measurement of contribution of ionizing particles of star radiation to electron induced ionization of cosmic ray shower 22 p3842 A67-40256

Data on fragmentation of energy in nuclear reactions in atmospheric showers compared with calculations results for predicted energy 22 p3876 A67-40266

Energy moments of inverse problem in theory of nuclear cascade determined, using first order Volterra integral equation 22 p3842 A67-40271

High energy cosmic ray muons investigated, using ionization calorimeter and hodoscope counters 22 p3877 A67-40272

Interactions of superhigh energy muons in cosmic ray nonelectromagnetic cascade showers 22 p3877 A67-40273

EAS with zenith angle between 30 and 45 degrees and fixed number of muons and electrons 22 p3877 A67-40279

Extensive air shower characteristics related to energy spectrum, chemical composition and anisotropy of primary cosmic rays in superhigh energy range 22 p3877 A67-40280

Muon groups at depth of 40 mwe not responsible for substantial energy leakage from extensive air showers 22 p3877 A67-40281

Muon flux measurement with aid of spark chamber at depth of 20 mwe used for spatial distribution near axis of extensive air showers 22 p3877 A67-40282

Ionization luminescence of air and possibilities of using it to record extensive air showers 22 p3878 A67-40283

Total energy of slow particle radio emission and real delta electron emission determined in extensive air showers 22 p3878 A67-40284

Coherent radio emission of extensive air showers determined from known threshold energy of optical signal 22 p3878 A67-40285

Monte Carlo method for calculating longitudinal and transverse development of extensive air showers, considering fluctuations 22 p3878 A67-40286

Leading particle model of formation of extensive air showers, determining energy spectrum 22 p3878 A67-40287

Isobaric pions role in interaction between nucleons and pions on one hand and nuclei of air atoms on other 22 p3878 A67-40288

Storm time increase and anomalous type of daily variation during cosmic ray storms caused by lowered threshold rigidities and excess cosmic ray streaming respectively 23 p4050 A67-40695

High energy cosmic ray shower detection combining perturbed magnetic field pulse and coincident optical radiation observations 23 p4051 A67-40812

Primary cosmic ray energy and jet CMS velocity estimations by three methods corrected by analyzing known energy interactions 23 p4051 A67-40913

Intensity gradient of galactic cosmic rays, analyzing modulation induced by solar activity 24 p4209 A67-42138

Photoemulsion data analysis of high energy nuclear interactions in nuclear emulsions exposed to air showers during flights 24 p4192 A67-42827

Shower particles angular distribution investigated using Wilson cloud chamber, obtaining agreement with results by kinematic methods 24 p4217 A67-42828

Secondary particles angular distribution in showers studied with cloud chamber, ionization calorimeter and counters to identify particles causing shower asymmetry and symmetry 24 p4217 A67-42829

Asymmetry in angular distribution of secondary particles in cosmic ray showers 24 p4218 A67-42838

Effective lambda and sigma hyperons and K-meson production cross section dependence on target element atomic weight during cosmic rays interaction with various nuclei 24 p4220 A67-42851

Air shower nuclear active component spectra noting need for mechanism of

energy transfer from nucleons into electron-photon avalanches 24 p4220 A67-42862

Air shower muon generation altitude determination from relative positive-negative muon distribution shift 24 p4220 A67-42863

Extensive air showers accompanying high energy nuclear active particles, discussing nuclear interaction processes and energy transformation 24 p4220 A67-42864

Shower producing capability of various particle groups at 40 mwe below ground, evaluating muon energy spectra 24 p4220 A67-42865

Energy flux fluctuation of nuclear active component in extensive air shower stem for given fixed muon and electron numbers 24 p4220 A67-42867

Fluctuation of Cerenkov glow in atmosphere caused by shower particles 24 p4220 A67-42868

Electromagnetic showers in lead recorded with ionization calorimeter, discussing cascade curve 24 p4221 A67-42870

Expressions for angular distribution function of electrons at various depths in cascade showers with given primary particle energy 24 p4221 A67-42872

Electron-photon shower creation probability by energetic particle, deriving recursion formulas 24 p4221 A67-42874

Cascade particles interaction functions with substance determined by inverse problem method 24 p4221 A67-42875

Muon properties investigated for mean energy by spark calorimeter at various depths 24 p4222 A67-42879

COSMOLOGY

SA GALACTIC EVOLUTION

Radio source counts interpretation in support of evolutionary cosmologies 01 p0147 A67-10358

Space-time singularities and Einstein equations 01 p0151 A67-11291

Quasars history, properties and nature 02 p0326 A67-12046

Structure of universe and role of gravitation in determining dynamic behavior, indicating that universe will stop expanding at certain critical maximum size 03 p0516 A67-14339

Quasi-stellar radio sources analysis including red shift, spectra, variability, etc, discussing possibility of local or cosmological objects 04 p0695 A67-14514

Vector field C defined at each point of space-time when curvature is zero, leading to series of cosmological models that satisfy Hoyle relativistic equations 04 p0698 A67-14809

Charged gas expansion with particle production, noting parameters and applicability to cosmological model of Hoyle 04 p0606 A67-15185

Homogeneous anisotropic cosmological model with magnetic field for solution of Einstein gravitational and Maxwell equations in space filled with ideal matter 04 p0702 A67-15984

Cosmological solutions of linear field theory, showing possible representation in form of hypersurface of second degree in five-dimensional affine space 05 p0897 A67-16773

Cosmology in last 150 years reviewed, discussing Hubble expansion of universe, Einstein theories on gravity and present concepts 05 p0897 A67-16775

Mach principle as consequence of de Sitter universe filled with Dirac dust 05 p0847 A67-16803

Correlation between position and red shift of quasars indicating anisotropic universe or galactic origin of quasars 05 p0898 A67-16887

Symmetry of time axis and solar observations, offering counterworld alternative to Stannard 06 p1079 A67-17605

Meteoritic origin from planetary disintegration 06 p1089 A67-18659

Cosmological principles of interzonal couplings, noting cyclic and secular change, planetary evolution, terrestrial magnetism, etc 06 p0999 A67-19006

Anisotropic uniform model of universe with uniform intergalactic field 07 p1248 A67-19482

Statistical analysis of errors in angular measurement of distant objects due to gravitational scattering along light path 08 p1398 A67-21232

Linearized perturbation equations integrated for cosmological model, giving

energy density fluctuations, rotational perturbations, gravity waves and estimated anisotropy of microwave radiation 08 p1398 A67-21233

Cosmological principle and field equations used in analysis of Einstein, de Sitter, Friedmann and Hoyle-Narlikar models 09 p1563 A67-21652

Anisotropic cosmological solution with energy density determined only by neutrinos moving along one axis, noting expansion 10 p1708 A67-23334

Gravitational radiation measurements by HF gravitational wave detector 10 p1652 A67-23545

Singularities of cosmological solutions of gravitational equations for space filled with matter 10 p1710 A67-23588

Antimatter and cosmology 11 p1858 A67-23994

Age and helium content correlations from recent mass determinations of two low mass binary star systems used in stellar evolution theory. 11 p1858 A67-23996

Cold star relativistic collapse kinematics, noting equilibrium and collapse of point masses system interacting by gravitation only 11 p1858 A67-24013

Gravitational instability from reformulation of Lifshitz relativistic theory for galaxy formation in expanding universe and comparison with Bonnor approach 11 p1859 A67-24121

Gravitational instability due to small irregularities and implications for early universe and galaxy formation 11 p1860 A67-24483

One-dimensional model of stellar system evolution, using computer to calculate minimum energy configuration 11 p1862 A67-24500

Quasi-stellar objects red shift and optical magnitude measurements, noting discrepancies with zero and nonzero cosmological constant 11 p1863 A67-24508

Confirmation of reality of Gilsa geomagnetic polarity event, discussing experimental techniques and results 11 p1788 A67-24700

Magnetosphere phenomena investigated via atmosphere model to explain planetary nebulas and eruptive solar prominences 12 p1992 A67-25119

German book on space chemistry covering age and origin of earth, meteorites, tektites and impactites 12 p1903 A67-25427

Homogeneous solutions of Einstein-Lichnerowicz equations for electrically charged fluid with infinite conductivity universes 12 p1962 A67-26178

Element production in early stages of homogeneous expanding universe and within stars, noting nature of background microwave radiation 12 p2010 A67-26239

Primordial element formation, primordial magnetic fields and universe isotropy, showing correctness of big-bang relativistic theory, early anisotropy of universe, etc 12 p2010 A67-26240

Soviet papers on space physics problems 13 p2195 A67-26494

Neutrinos in stellar evolution and cosmological processes, discussing production processes 14 p2383 A67-27969

Homogeneous anisotropic cosmological model with magnetic field for solution of Einstein gravitational equations and Maxwell equations in space filled with ideal matter 14 p2386 A67-28485

Shear-free flows of gravitating gas investigated on basis of Newtonian mechanics 14 p2348 A67-28580

Association of radio sources with peculiar galaxies in symmetrically distributed pairs 14 p2388 A67-28830

UBV values and red shifts of quasars interpreted within steady state and Friedman cosmological models 14 p2392 A67-28965

Density fluctuations and thermal conditions in expanding universe and creation of stars, quasars, galactic clusters and galaxies 15 p2551 A67-29138

Gravitational fields for observation of soft cosmic neutrino and neutretto background predicted by different cosmological theories 15 p2555 A67-29641

Observational evidence disproving cosmological steady state theory in favor of expanding universe 15 p2562 A67-30082

Primeval fireball /cosmic radio radiation/ concept based on Hubble observation of universe expansion, discussing predictions on its nature 15 p2562 A67-30085

Space studies of Mars and Jupiter through cislunar and interplanetary rocket probes in near future [AAS PAPER 67-32] 15 p2562 A67-30105

Celestial mechanics and Dirac hypothesis 15 p2563 A67-30123

Solar velocity with respect to distant galaxies estimated from red shift for nearby galaxies, noting cosmic microwave background 15 p2563 A67-30160

Excess cosmic microwave background temperature of 2 degrees K at 1.5 cm wavelength 15 p2551 A67-30161

Optical astronomy opportunities in cosmology, stressing need for additional telescopes located in Southern Hemisphere 15 p2563 A67-30393

Cosmological model for universe based on astronomical observations and validity of einstein theory and existing laws of physics 16 p2752 A67-31540

Neutrino occurrence in universe noting postcreation and relic neutrinos, energy density, relic neutrino concentration, cosmic ray-neutrino interaction, etc 17 p2940 A67-32102

Solar spin-down problem, noting oblateness effect on perihellion precession of Mercury 17 p2940 A67-32208

Pulsating gravitation, noting geological evidence such as ocean transgressions, regressions, climate variations, etc 17 p2841 A67-32211

Upper limit on mean mass density of luminous matter in universe from brightness of night sky 17 p2944 A67-32638

Cosmological model covering early and late stages, presenting period time when matter density equaled radiation density 17 p2947 A67-32759

Line element not precluding peculiar motions or assuming isotropy and homogeneity of mass distribution of universe, considering kinematical consequences 18 p3117 A67-33427

Quantum cosmology, discussing continuous fluid models as representations of early dense universe 18 p3117 A67-33515

Phobos and Deimos origin in equatorial circular orbits or asteroid capture and tidal modification 18 p3125 A67-34160

Gravitational instability of homogeneous anisotropic cosmological models 18 p3133 A67-34432

Superdense cosmical object model, discussing negative mass defect necessary for expansion to diffuse state 18 p3133 A67-34433

Origin of elements, discussing element formation and abundances, nucleosynthesis and cosmological theories 19 p3263 A67-35869

Luminous and intergalactic matter, background radiation, radio sources, quasars, cosmic rays and other observational data relevant to cosmological models 19 p3327 A67-35870

Stellar evolution and Brans-Dicke cosmological theory used to construct color-magnitude diagram of star cluster 19 p3330 A67-36077

Gravitational effects and cosmic phenomena reconciliation with Einstein relativity scalar-tensor theories 20 p3524 A67-36834

Occurrence of singularities in cosmology, giving testable condition implying existence of singularity assuming causality 21 p3703 A67-38493

Gravitation wave radiation rate from binary stars, using Brans-Dicke general relativity theory 21 p3706 A67-38842

Time symmetry in oscillating cosmologies with locally irreversible processes, obtaining formalism for statistical processes and boundary conditions 21 p3706 A67-38844

Magnetism and cosmos - Conference, University of Newcastle-upon-Tyne, England, April 1965 21 p3707 A67-38977

Stellar magnetic field origin theories, discussing fossil, dynamo and battery theories 21 p3708 A67-38985

Planet Jupiter research, noting unresolved questions of cosmology, interior structure and Great Red Spot 21 p3711 A67-39092

Analytical solution to cosmological model containing radiation and matter assuming spatial homogeneity and isotropy, stress-

energy and adiabatic expansion 21 p3711 A67-39121

Tensor calculation of origin of local concentration of matter in universe model, considering effect of gravitational perturbations 22 p3880 A67-39314

Cosmology and elementary particles, noting relationship hypothesis between cosmological asymmetry and particles via vacuum 22 p3880 A67-39337

Spectral line changes caused by Rydberg constant shift detectable by observing very distant galaxies, discussing gravitational and cosmological theory 22 p3882 A67-39611

Nonzero cosmological constant effect /precise and trivial/, calculating perihellion precession from Schwarzschild exterior solution 22 p3889 A67-40382

Origin of large scale structures in universe, discussing instability and primordial-structure hypotheses 22 p3891 A67-40492

Inhomogeneity formation probability in initially homogeneous Friedman universe inhomogeneity formation probability in initially homogeneous Friedman universe 22 p3891 A67-40493

Clustering process, examining self-gravitating system separation from expanding cosmic distribution 22 p3891 A67-40494

Oscillating relativistic universe model from Einstein field equations, discussing Friedman model matter and velocity distribution, Hubble law and universe volume oscillating relativistic universe model from 22 p3892 A67-40496

Thermal instabilities in homogeneous primeval medium theory shown to play no role in galactic evolution 22 p3892 A67-40497

Microwave background radiation angular distribution anisotropy lower limit estimated from perturbations of cosmological model 22 p3892 A67-40498

Nonrandom optical red shift distribution of radio sources leading to uniform density over large volume 22 p3892 A67-40500

Spiral arm magnetic field configuration model simplifies star formation theory, discussing theoretical and observational evidence 22 p3893 A67-40505

Free-free radiation absorption from discrete radio sources calculated for various isotropic world models as red shift, electron density and temperature function 23 p4063 A67-40777

Bolometric magnitude, angular diameter and radioflux density of various world models and red shift values, calculating universe and horizon age 24 p4228 A67-42259

Time dependent gravitational constant theory, studying earth rotation secular acceleration 24 p4229 A67-42321

Cl, Br and I abundances in carbonaceous chondrites analyzed by neutron activation in estimating primordial halogen abundance ratios 24 p4234 A67-42628

Density fluctuations and thermal conditions in expanding universe and creation of stars, quasars, galactic clusters and galaxies 24 p4239 A67-43061

COSMONAUT

S ASTRONAUT

COSMOS II SATELLITE

UV solar radiation absorption in upper atmosphere determined from measurement of photoelectron currents emitted by planar metallic orthogonal photocathodes onboard Cosmos II satellite 10 p1647 A67-23282

COSMOS III SATELLITE

Radioactivity of Cosmos III satellite after U.S. thermonuclear explosion over Johnston Island 07 p1242 A67-19112

COSMOS V SATELLITE

Star Fish debris from Cosmos V observation of gamma radiation burst 03 p0506 A67-12962

Periodic frequency change in signals from Cosmos V possibly due to solar cell output fluctuations 06 p0964 A67-18766

Variations in position of mirror points of high energy electrons determined from Cosmos V satellite data 10 p1647 A67-23281

Soft electrons and ions study by traps on Cosmos V satellite 12 p1994 A67-25529

COSMOS XII SATELLITE

Low energy charged particle measurements, describing satellite mounted spherical electrostatic

analyzer 02 p0310 A67-12571
COSMOS XLI SATELLITE
 Spherical coordinates near apogee of
 Cosmos 41 satellite determined with TV
 system and meniscus
 telescope 16 p2621 A67-30683
COSMOS SATELLITE
 Location and radiation intensity variation
 in upper radiation belts determined, using
 scintillation counters aboard Cosmos
 satellites 02 p0311 A67-12598
 Radio observation of Cosmos satellites
 with flight path inclination angle of 65 and
 51 degrees, discussing signal audibility,
 atmospheric density and ionospheric
 effects 03 p0518 A67-13540
 Cosmos 53 satellite radiation data using on
 board gas discharge 05 p0879 A67-16107
 Energy spectrum of electrons recorded by
 fluorescent screen indicators onboard
 Cosmos satellites, noting ratio of electron
 intensities 07 p1170 A67-19101
 Physical pattern of high altitude fission
 cloud and motion of gamma and beta fission
 fragments captured by geomagnetic field
 and observed by Cosmos 07 p1242 A67-19102
 Cosmos LXI spectrophotometric
 measurements of atmosphere-reflected UV
 radiation spectra 07 p1178 A67-19801
 Biological satellite research, discussing
 radiation effects on living organism as
 measured by Cosmos 110 07 p1136 A67-19867
 Cosmic space exploration in U.S.S.R.,
 discussing results obtained from Cosmos and
 Elektron earth satellites 08 p1394 A67-21110
 Cosmos satellites physical
 research 09 p1570 A67-21654
 Cosmos XLIX measurements of magnetic
 field intensity compared with calculation
 from spherical harmonic
 coefficients 10 p1632 A67-22812
 Heat radiation spectra of earth as
 measured by Cosmos satellites, comparing
 experimental and calculated
 results 10 p1637 A67-23194
 Cosmos 65 spectrophotometric
 measurements of atmosphere-reflected UV
 radiation spectra 10 p1647 A67-23277
 Brazil geomagnetic anomaly and artificial
 radiation belt observations from Cosmos
 series satellites 12 p1996 A67-25773
 Relation between electron and proton
 distributions and existence of electric fields
 in magnetosphere 12 p1936 A67-25808
 Low energy proton and electron outer
 radiation belt satellite Cosmos 41 indicate
 capture and acceleration
 mechanism 12 p1997 A67-25810
 Relativistic-electron diffusion wave in
 outer radiation belt recorded by device
 mounted on Cosmos XLI satellite in high
 geomagnetic latitudes 13 p2191 A67-26545
 Space flight factors effect on mutability,
 survival rate and dynamics of cells of
 inactive cultures of chlorella on board
 Cosmos 110 13 p2060 A67-27336
 Angular, spectral and geographical
 distributions of outgoing fluxes of thermal
 radiation and earth albedo measured, using
 Cosmos satellite 14 p2306 A67-27861
 Soviet space effort and Cosmos satellites,
 deducing orbital parameters, transmission
 frequencies, launching time/place, nature of
 experiments, etc 17 p2956 A67-32724
 Air drag effect on six Cosmos satellites
 orbits having low perigee, discussing diurnal
 air density variation at 280 km
 height 18 p3042 A67-34256
 Soviet northern cosmodrome location
 determination from data obtained through
 radio/visual observation of Cosmos
 satellites 18 p3004 A67-34358
 Cell survival rates and mutation
 development in Chlorella vulgaris plants
 carried by Cosmos 20 p3367 A67-36256
 Cosmic ray regional variations in intensity
 and ionization magnitude and duration
 indicating heavy nucleus and low energy
 particle influx accompanying solar
 flares 23 p4055 A67-41100
 Cosmos XLIX measurements of magnetic
 field intensity compared with calculations
 from spherical harmonic
 coefficients 24 p4150 A67-42149
 Cosmos 53 satellite radiation data using
 onboard gas discharge
 counter 24 p4213 A67-42783

COSPAS
 COSPAR manual on establishment of
 rocket launch facility 06 p0979 A67-17553
 Space research - COSPAR International
 Symposium, Vienna, May 1966, Volume
 1 10 p1641 A67-23246
 Reassessment of COSPAR
 recommendations concerning planetary
 quarantine and spacecraft sterilization,
 particularly for Martian
 environment 10 p1601 A67-23579
 Russian and American practices and
 policies regarding planetary contamination in
 connection with COSPAR
 requirements 10 p1601 A67-23580
COST ESTIMATE
 Comparative evaluations of alternative
 weapon systems, discussing penetration cost
 effectiveness, attrition ratio, survivability,
 etc [AIAA PAPER 66-782] 01 p0169 A67-10528
 Cost effectiveness of optimum military
 aircraft system, evaluating design
 alternatives in hardware and support
 concepts via Monte Carlo simulation and
 high speed digital computers [AIAA PAPER 66-786] 01 p0009 A67-10530
 Carrier Onboard Delivery aircraft,
 discussing cost effectiveness by reduced
 delivery time of critical spare parts [AIAA PAPER 66-790] 01 p0009 A67-10533
 System concept effectiveness evaluation
 for system selection [SAE PAPER 660728] 01 p0169 A67-10628
 Overall system performance optimization
 for specified cost [SAE PAPER 660730] 01 p0170 A67-10630
 KC-70 low cost inertial navigation system
 noting use of inertial sensors and digital
 computers 01 p0076 A67-11256
 Findings, conclusions and
 recommendations of Weapon System
 Effectiveness Industry Advisory Committee
 /WSEIAC/, noting concept of cost
 effectiveness 01 p0170 A67-11334
 Mathematical model for determining
 optimal maximum operating times for
 aircraft engines, using discrete failure rate
 to determine cost 01 p0141 A67-11340
 Inaccurate estimate effect on national
 budgets when evaluating systems
 efficiency 01 p0170 A67-11349
 Reliability improvement effect on cost in
 tactical aircraft, examining obsolescence,
 risk factor determination, etc 01 p0170 A67-11350
 Unified treatment of costs yields and
 reliability in semiconductor
 manufacture 01 p0171 A67-11380
 Reliability optimization relation to
 program time and costs and schedule for
 cost reduction keeping time
 constant 01 p0085 A67-11384
 System design analysis of Edwards high
 range UHF telemetry receiving station
 network, considering reliability, availability,
 design adequacy, antennas, initial and
 operating costs, etc 02 p0229 A67-12007
 British procurement procedures for
 military aircraft noting cost estimate,
 feasibility study, development contract and
 production stages 02 p0343 A67-12242
 Reusable space vehicles role in overall
 space program, noting orbital missions in
 future and economic impact [AIAA PAPER 66-862] 02 p0343 A67-12261
 Method for propulsion system selection,
 design and optimization on total space
 program cost effectiveness basis [AIAA PAPER 66-976] 02 p0305 A67-12298
 Weight and cost comparative analysis of
 ablative and combined ablative/radiative
 heat shields for SV-5 and SV-32 lifting
 reentry vehicles [AIAA PAPER 66-990] 02 p0333 A67-12301
 Optimal tradeoff function where expense
 is increased for saving time in orbital
 transfer to rendezvous, considering impulse
 modes 02 p0328 A67-12407
 Cutting and milling processes in
 aeronautical industry, effect on costs and
 production rates 03 p0427 A67-13024
 Statistical model of cost of elements of
 system undergoing gradual breakdown,
 giving optimal distribution of mean relative
 deviations of input and output
 parameters 03 p0389 A67-13090
 Accomplishments and costs of airline
 flight recording for aircraft
 maintenance 03 p0420 A67-13380

Cost and effectiveness of surveillance
 device for antiaircraft weapon
 system 03 p0538 A67-13695
 Future short haul air transportation in
 northeast corridor of U.S., considering
 conventional, STOL and VTOL air transport
 systems 03 p0538 A67-13783
 Capabilities of passenger aircraft for
 short-range operations, noting design and
 economic suitability [AIAA PAPER 66-945] 03 p0361 A67-14022
 Component part reliability concepts,
 examining degradation and catastrophic
 failure, failure modes and lot
 screening 04 p0584 A67-15477
 Helicopter capabilities in solving
 interurban mass transport problems,
 particularly cost and time considerations
 [SAE PAPER 660336] 04 p0552 A67-15611
 System and cost effectiveness analysis
 throughout program life cycle of weapon or
 support system to aid decision making
 [SAE PAPER 660724] 04 p0740 A67-15780
 Correlation between increased
 performance demands and cost of
 lightweight airframe structures [SAE PAPER 660674] 04 p0716 A67-15783
 Cost and power requirements influence on
 aircraft hydraulic pump
 design 05 p0753 A67-16751
 Quality evaluation review technique
 /QERT/ for management facilitation of
 program planning and scheduling, noting
 time and cost estimation 05 p0930 A67-17246
 Acceptance vibration testing program
 costs, benefits and test
 control 05 p0813 A67-17248
 Degradation analysis and variability
 measurement in reliability and quality
 control of component parts with application
 to Early Bird COMSAT
 satellite 05 p0813 A67-17257
 Mission requirements and cost
 effectiveness comparison of Syncom
 satellites and associated network synthesis
 for defense communications systems 06 p0960 A67-17677
 Ground-based steerable paraboloid
 spherical reflector and multiplate type
 antennas, noting cost per unit area for unit
 wind speed of 30 mph and frequency of 1400
 mc, performance, restrictions, etc [AIAA PAPER 66-324] 06 p0967 A67-17685
 Minimum cost ground receiving station for
 synchronous satellite system [AIAA PAPER 66-311] 06 p0979 A67-17691
 Effects of varying orbital parameters
 including number of satellites, orbit altitude,
 positioning, tracking accuracy, cost
 effectiveness, etc, on establishment and
 maintenance of communications satellite
 system 06 p1094 A67-17698
 Economic aspects of educational TV
 distribution system, using comprehensive
 total cost model [AIAA PAPER 66-321] 06 p1120 A67-17710
 Aerospacecraft, reusable self-contained
 man-rated vehicle, noting economy,
 propulsion system and possible
 configurations 06 p1098 A67-19022
 Educational problems including costs,
 teacher training, management, government
 support, etc 06 p1120 A67-19042
 Cost function gradient estimation for
 optimum control of nonlinear stochastic
 systems 07 p1159 A67-19193
 Feasibility of employing BIT and fault-
 isolation circuits made possible by
 microminiaturization techniques applied to
 advanced avionics systems [AIAA PAPER 67-268] 07 p1167 A67-20077
 Cost effectiveness of fully automatic
 checkout systems [AIAA PAPER 67-269] 07 p1269 A67-20078
 VTOL technique and advanced aircraft
 design 07 p1130 A67-20220
 Reinforced plastic facings as sandwich
 materials instead of metal skins noting cost
 effectiveness, weight efficiency and layup
 times 08 p1414 A67-20430
 Rocket vehicles for synoptic meteorology,
 evaluating vehicle concepts, performance
 characteristics and costs 08 p1404 A67-20497
 Computer logic cost effectiveness
 modeling applied to integrated circuits,
 discussing comparisons between existing
 equipment, Conalag and
 redesigns 08 p1311 A67-20657
 Cost-and labor-saving advantages of
 automatic and semiautomatic insertion of
 components in circuit

board 08 p1335 A67-20748
 Cost analysis for large scale development/
 production programs 08 p1429 A67-20968
 [AAS PAPER 66-148]
 Unmanned spacecraft program costs
 estimation through empirical studies of past
 and current NASA programs 08 p1429 A67-20969
 [AAS PAPER 66-149]
 Planned interdependency incentive method
 /PIIM/ for Gemini program at lowest cost
 and best performance 08 p1430 A67-20974
 [AAS PAPER 66-157]
 Integrated circuit in optimal design of
 aerospace systems, discussing potential low
 cost and use in computer analyses of
 circuits 08 p1303 A67-21060
 Apollo extension systems, discussing
 current space technology and
 accomplishments 08 p1391 A67-21066
 High energy booster and upper stage
 combinations for space research, discussing
 mission capabilities, cost factors, reliability,
 etc 08 p1412 A67-21075
 Space systems performance, components
 and modes of operation, showing merits in
 terms of entire space program 08 p1431 A67-21108
 Cost incentive contract effects on research
 and development 08 p1431 A67-21287
 Predicting structural reliability by recent
 developments in statistics, reliability, cost
 effectiveness analysis and decision theory
 [AIAA PAPER 66-503] 08 p1424 A67-21524
 Cost reduction and avoidance by value
 engineering to yield lowest overall cost for
 performance, reliability and maintainability
 requirement 09 p1581 A67-22157
 Cost improvement for Minuteman II
 integrated circuits from failure rate
 reduction, using failure mode model and
 measurement system 09 p1480 A67-22305
 Reliability-cost trade-off analysis of
 complex system using mathematical model
 involving constant percentage increase in
 MTTE with cost 09 p1572 A67-22306
 Interface between reliability cost and
 performance resulting from application of
 microelectronics to Sergeant Artillery
 Guided Missile Ground Electronics 09 p1572 A67-22309
 Rules for comparing designs of aerospace
 transporters and selecting optimum
 configuration, based on overall cost
 criterion 10 p1713 A67-23482
 Economic impact of defense and space
 programs 10 p1735 A67-23629
 Advanced structures and materials in
 future launch vehicles evaluated by design
 synthesis technique for component weight
 reduction, equivalent payload gained and
 cost ratio 10 p1723 A67-23699
 Solid motor case technology, evaluating
 materials, fabrication, segmented case joint
 design and cost comparisons for large rocket
 motors 10 p1661 A67-23703
 Costs involved in delays occasioned by
 either ATC or airport acceptance rate for
 New York-Boston-Washington complex
 [SAE PAPER 670264] 11 p1884 A67-23987
 Low speed wind tunnel design, structure,
 performance and cost 11 p1773 A67-24640
 Improvements in management control of
 complex projects, considering network
 analysis 11 p1885 A67-24656
 Lockheed C-5 quantitative maintainability
 program and application to air vehicle
 utilization and cost 11 p1745 A67-24939
 Systems and techniques in aircraft
 maintenance to meet problems of parts
 reliability, longevity and shop cost
 [SAE PAPER 670336] 12 p1895 A67-25877
 Nonlinear programming model for launch
 vehicle design and costing 12 p2013 A67-26193
 Semiconductor integrated circuits,
 discussing hybrid, multichip and beam-lead
 methods in digital and linear circuit
 applications 12 p1917 A67-26203
 Reliability and cost analysis of
 semiconductor integrated circuit and vapor
 deposited thin film IC, discussing failures
 and defects 12 p1918 A67-26207
 Large scale monolithic integration of
 subassemblies combined with upside-down
 assembly technique for more complex low
 cost high performance
 microcircuits 13 p2077 A67-26658
 Estimating maintenance man-hours per
 flight hour for business turbojet airplanes
 [SAE PAPER 670228] 13 p2053 A67-27294

Cost models for complex space programs,
 analyzing data acquisition systems, computer
 routines, etc 13 p2232 A67-27547
 Cost analysis for large scale development/
 production programs 13 p2232 A67-27549
 [AAS PAPER 66-148]
 Unmanned spacecraft program costs
 estimation through empirical studies of past
 and current NASA programs 13 p2232 A67-27550
 [AAS PAPER 66-149]
 Planned interdependency incentive method
 /PIIM/ for Gemini program at lowest cost
 and best performance 13 p2233 A67-27558
 [AAS PAPER 66-157]
 Structures cost effectiveness in
 optimization weight-cost design in aerospace
 structures 13 p2220 A67-27590
 [AIAA PAPER 66-505]
 Stability in electronic
 equipment 14 p2285 A67-28438
 Rocket cost dependence on weight and
 airframe resistance studied for design
 problem solutions 14 p2245 A67-28638
 Management aspects of technological
 capability within large hardware systems
 business 14 p2409 A67-28697
 Loss structure models concerning age
 replacement policies, discussing
 mathematical aspects of maintenance with
 dynamic programming 14 p2345 A67-28909
 Sensitivity of cost functional in optimal
 control system with random variable
 parameters, noting system performance
 detection techniques 15 p2457 A67-29368
 Weight and cost comparative analysis of
 ablative and combined ablative/radiative
 heat shields for SV-5 and SV-32 lifting
 reentry vehicles 15 p2564 A67-29421
 [AIAA PAPER 66-990]
 Project initiation emphasizing market,
 product /design, cost and timing/ and
 resources to market 15 p2583 A67-29667
 Defense procurement procedures and task
 of project manager 15 p2583 A67-29668
 Systems approach to reliability, integrating
 cost and performance and demonstrating
 tradeoff decisions 15 p2448 A67-29800
 Near term reusable rocket launch vehicle
 concepts 15 p2566 A67-29831
 Low cost rocket launch vehicles for
 various payload capacities 15 p2566 A67-29832
 Advanced space vehicle planning analyzed
 from economic approach to decision making,
 noting cost decrease with
 time 15 p2566 A67-29833
 Ballistic vs lifting body and winged
 recovery techniques for space launch
 vehicles, noting cost and operational
 capabilities 15 p2567 A67-29834
 Earth-orbital transport systems noting
 configurations, cost, capabilities, operational
 requirements, etc 15 p2567 A67-29835
 Fixed wing reusable horizontal landing
 boosters, comparing weight, cost, technical
 difficulty and availability 15 p2567 A67-29836
 rate 15 p2567 A67-29839
 European aerospace transporter feasibility
 and worth 15 p2567 A67-29839
 Space transportation systems, considering
 recovery facilities, reusable boosters, cost,
 etc 15 p2568 A67-29846
 Long term study for prediction of launch
 vehicle costs, emphasizing estimate accuracy
 and application of statistical
 analysis 15 p2568 A67-29847
 Reusable booster concept, economic
 justification, cost characteristics and
 management planning 15 p2569 A67-29850
 Spaceport facilities, technology and
 economics 15 p2487 A67-29943
 Cost reduction of space vehicle structures
 and materials 15 p2575 A67-29948
 [AAS PAPER 67-81]
 Propulsion and vehicle systems for
 commercial exploitation of space,
 emphasizing transportation to and from
 earth orbit 15 p2570 A67-29949
 [AIAA PAPER 67-82]
 Potentialities of space cartographic
 systems evaluated for geometric map
 accuracy and economic aspects 15 p2478 A67-29960
 [AAS PAPER 67-106]
 Design requirements for commercial
 orbital space stations intended for weather
 forecasting, agricultural prediction and
 industrial research 15 p2557 A67-29961
 [AAS PAPER 67-113]
 Space tourism potential, cost estimate of
 equipment, management, etc

[AAS PAPER 67-127] 15 p2558 A67-29965
 Impact of performance improvements and
 reuse on cost of space transportation, noting
 size, configuration, mission requirements and
 commercial possibilities 15 p2570 A67-29966
 [AAS PAPER 67-130]
 Commercial space utilization considering
 space transportation cost as fundamental
 factor 15 p2571 A67-29968
 [AAS PAPER 67-134]
 Future radar developments noting range
 instrumentation deployment and
 employment, tracking, data acquisition radar
 sensors, changing cost patterns, etc 15 p2438 A67-30119
 [AIAA PAPER 67-55]
 Management and cost factors involved in
 operation of modern integrated missile
 range 15 p2468 A67-30121
 [AAS PAPER 67-59]
 Cost of titanium, steel and aluminum
 alloys in high performance aircraft
 production 15 p2505 A67-30367
 [AIAA PAPER 67-400]
 Quality cost accounting and management
 decisions in performance of various
 functions 15 p2584 A67-30420
 Sampling plan for destructive testing,
 relating quality protection to
 cost 15 p2584 A67-30421
 Communications satellite systems
 discussing launching, orbits economics,
 etc 16 p2760 A67-30700
 Economic factors controlling development
 of high capacity supersonic transport
 aircraft 16 p2782 A67-30838
 Evaluation of relative scientific
 effectiveness of various lunar exploration
 programs through analysis of results from
 hypothetical missions to selected earth-
 analog sites 16 p2747 A67-30991
 Cost function to evaluate quasi-optimal
 amplitude meter for signal with random
 initial phase on white noise background with
 random correlation 16 p2623 A67-31015
 Reliability prediction relationship to
 system support costs, computing factors for
 undersupport and oversupport of tactical
 missile system 16 p2782 A67-31256
 Dollar consequence functions for producer
 and consumer risks due to product faults
 noting optimization 16 p2782 A67-31257
 Space project management noting job
 definition and organization for
 implementation and control 16 p2783 A67-31630
 Empty-weight control in helicopters, with
 cost estimation of excess weight on
 helicopters sold to government 16 p2783 A67-31828
 [AHS PAPER 112]
 Optimum speed capability evaluation of
 aerial weapons system in relation to value
 and cost, noting aircraft performance
 characteristics 16 p2783 A67-31830
 Computer simulation model for cost
 effectiveness of built-in test equipment
 /BITE/ in airborne radar
 systems 17 p2833 A67-32491
 Cost effectiveness criterion for instruction
 repertoire selection for aerospace
 computer 17 p2820 A67-32502
 Carrier Onboard Delivery aircraft,
 discussing cost effectiveness by reduced
 deliver time of critical spare
 parts 17 p2797 A67-32572
 Capabilities of passenger aircraft for short
 range operations, noting design and
 economic suitability 17 p2797 A67-32583
 [AIAA PAPER 66-945]
 Feasibility of employing BIT and fault-
 isolation circuits made possible by
 microminiaturization techniques applied to
 advanced avionics systems 17 p2834 A67-32590
 [AIAA PAPER 67-268]
 Aerospace industry quality control
 requirements and specification, noting small
 business role 17 p2974 A67-32818
 Supersonic transport size determination
 for competitive operation in air traffic
 market using traffic volume, aircraft type
 and flight frequency forecasts 18 p2985 A67-33569
 [SAE PAPER 670371]
 Value analysis technique to compare
 competing high performance insulation
 systems on basis of differences in
 performance and cost 18 p3162 A67-33939
 [AIAA PAPER 67-469]
 Factors degrading reliability in use phase,
 developing analysis method for determining
 optimum corrective measures 18 p3057 A67-34667

Development of quantitative logistics performance parameters related to time, resources and cost in Concept Formulation Phase and Contractual Definition Phase 18 p3162 A67-34678

Maintainability and reliability cost effectiveness program /MARCEP/ applied to logic and computer limitation problems 18 p2995 A67-34689

Empirical formulas for optimal operation of extremal controllers, design data generation and cost index determination 19 p3201 A67-34992

Method for assigning numerical value to space scientific payload effectiveness toward satisfying mission goals 19 p3322 A67-35319

Reliability, orbit achievement and control and increased power bandwidth as factors making communications satellites economically feasible 19 p3350 A67-35649

Management of aerospace programs, discussing budgeting and contracting procedures 19 p3350 A67-35879

Rotationally switched rod memory system with 100 nsec cycle time, discussing cost and performance factors 19 p3189 A67-36064

Upgraded Saturn V vehicles and intermediate payload Saturn vehicles, studying costs, flexibility, performance and boost-assist components 20 p3531 A67-36539

TSIS fire control equipment family, considering maximum cost effectiveness, discussing use in Dassault Mirage M-5 and RCAF CF-5 aircraft 20 p3364 A67-37244

General utility spacecraft family, orbital bus and multiple orbit/payload launch missions for reducing unmanned space research and development costs [AIAA PAPER 67-637] 20 p3534 A67-37617

Multiple payload and multipurpose spacecraft evaluated for cost reduction in USAF space operations [AIAA PAPER 67-636] 20 p3535 A67-37621

Spacecraft and space station reliability by orbital maintenance and extravehicular activity, comparing redundancy on system and cost effectiveness [AIAA PAPER 67-652] 20 p3535 A67-37629

Operational and cost-influencing characteristics of low orbit space operations compared from manned orbital base and earth base [AIAA PAPER 67-654] 20 p3530 A67-37631

Worldwide satellite communications requirements, financial aspects and projects 21 p3581 A67-38211

Thor SLV upper stage Burner 2 design, performance and cost 21 p3713 A67-38379

Cost effectiveness of VTOL short range jet airlines, discussing significance of block time [AIAA PAPER 67-797] 21 p3568 A67-38543

Cost effectiveness of digital and voice accident recorders in small fighter and military aircraft for low level missions, reconnaissance, flight testing and training 21 p3631 A67-39129

Optical communication system components, discussing cost and potential information capacity factors in picture phone and newspaper transmission facilities 22 p3759 A67-39329

Automatic navigation trends, discussing cost effectiveness, transportation objectives and application rate 22 p3831 A67-39465

Optimal airline aircraft selection, discussing cost efficiency factors 22 p3922 A67-39537

Utility aircraft costs lower than specialized aircraft in meeting mixed mission requirements in counterinsurgency environment, considering changes, uncertainty and logistics 22 p3745 A67-39618

Hovercraft principle application noting development, sea-keeping problems, predicted capability and costs 22 p3745 A67-39663

Boeing SST competition, cost, operation, design, airport noise and sonic boom 22 p3746 A67-39882

Multiple payload mission planning for multiple and single earth orbits and apogee motor delivery, evaluating cost and performance 22 p3903 A67-39952

Technological and economic factors affecting airline progress, discussing fares, traffic, SST and terminal areas 22 p3922 A67-40062

Cost comparisons between UK aircraft industry and competing industries elsewhere 22 p3922 A67-40065

Life cycle cost concept adaptation by DOD affecting logistics engineer, discussing reliability relation, maintainability, etc 23 p4084 A67-40580

Engineering change proposals /ECP/ implementation cost emphasizing collateral cost evaluation 23 p4085 A67-40585

Life cycle cost covering accessibility, automated fault isolation, corrosion control, maintenance, etc 23 p4085 A67-40586

Cost Analysis Model - Parametric /CAMP/ computer method of estimating hardware and logistics life cycle costs for air vehicles in design stage 23 p4085 A67-40589

SST fleet size, flight time, station stop time, seat mile costs, fuel consumption, noise and sonic boom problems affecting airline economics [AIAA PAPER 67-749] 23 p3933 A67-40983

Bayes estimate of regression coefficients in cost function selection in presence of unsteady noise 24 p4134 A67-41796

Commercial V/STOL operating characteristics in Northeast Corridor, discussing commuter design and cost analyses [AIAA PAPER 67-769] 24 p4095 A67-42937

Instructional broadcast satellites programming methods to reduce educational cost of students time without adding to technological cost [AIAA PAPER 67-787] 24 p4258 A67-42950

Space structure design cost effectiveness studies for materials and configurations [AIAA PAPER 67-808] 24 p4252 A67-42965

Cost estimating techniques for military and NASA programs, comparing spacecraft resource forecasting with expenditure estimates [AIAA PAPER 67-809] 24 p4259 A67-42966

Advanced systems planning with limited funds in terms of payoff from advancing technology through R and D [AIAA PAPER 67-811] 24 p4259 A67-42967

Commercial VTOL aircraft operating costs and cost reduction evaluation [AIAA PAPER 67-826] 24 p4096 A67-42973

VTOL aircraft operational expense estimation using standard method, measuring maintenance costs in various planning stages and in operation [AIAA PAPER 67-828] 24 p4096 A67-42974

Public and private financing of vertiports /VTOL aircraft terminals/ for intercity service, investigating financial self-supporting possibilities [AIAA PAPER 67-829] 24 p4259 A67-42975

V/STOL airline economics simulated with computerized dynamic programming model [AIAA PAPER 67-841] 24 p4096 A67-42979

Commuter airline planning using systems analysis to examine technical, managerial, legal and economic aspects [AIAA PAPER 67-843] 24 p4259 A67-42981

Reusable shuttle transportation system for lunar base logistics, estimating cost and performance [AIAA PAPER 67-874] 24 p4140 A67-42995

Costs and savings of computer graphics systems used for preparing and maintaining aerospace engineering drawings [AIAA PAPER 67-899] 24 p4127 A67-43008

Booster recovery systems development, payload and operational costs evaluated using postulated space program [AIAA PAPER 67-909] 24 p4245 A67-43016

AGM-69A program-management system using CRT display for PERT/Time and Cost Control data translation [AIAA PAPER 67-920] 24 p4260 A67-43019

Commercial V/STOL transportation system, analyzing intraurban and short haul factors for concerned parties by computer simulation [AIAA PAPER 67-969] 24 p4260 A67-43047

Commercial VTOL transport compared with conventional aircraft and ground transportation, discussing design and operating costs [AIAA PAPER 67-970] 24 p4097 A67-43048

COUETTE FLOW

Continuum with director and constitutive equations for anisotropic fluids, obtaining solutions for simple shear, Poiseuille and Couette flows 01 p0053 A67-10849

Spectrum of small perturbations of plane parallel Couette flow calculated, using Galerkin method 01 p0053 A67-11000

Taylor vortices intensity and viscous losses determined for viscous flow of liquid between concentric rotating cylinders,

solving equation by numerical method 03 p0405 A67-14030

Generalized Couette-type flow with variable viscosity in plane and annular channels, liquid being injected or sucked through porous surfaces 04 p0602 A67-14639

Aerodynamic coefficients of symmetrical wing profiles and fuselages in rarefied gas calculated for free molecular flow 04 p0547 A67-14992

Linearized Couette flow problem in rarefied gas solved, using one-dimensional radiative heat transfer analogy 04 p0606 A67-15183

Successive approximations applied to optimal control equation for self-similar viscous Couette flow between one stationary and one moving wall 04 p0610 A67-15885

Parallel Couette and Poiseuille flows of multicomponent viscous plasma in presence of pressure gradient and electric field 05 p0854 A67-16894

Velocity and temperature profiles of optically thick planar Couette flow, obtaining heat transfer rates for Rosseland mean absorption coefficient variation with temperature 05 p0793 A67-17343

Transient response of Couette shear flow to step function change in blowing velocity across channel 05 p0751 A67-17420

Heat transfer in short circuit generalized MHD Couette flow for velocity field and temperature distribution, when walls are at equal and unequal temperatures in transverse magnetic field 06 p1039 A67-18070

Plastic flow effects on MHD Couette flow in annular gap between two coaxial cylinders in radial magnetic field 06 p1044 A67-18680

Instability of plane Couette-Poiseuille flow of two superposed layers of different viscosities between two horizontal plates 08 p1321 A67-20709

Nonlinear viscoelastic fluids, discussing Couette flow, steady flow, periodic motion, wave propagation, thermomechanical coupling, etc 08 p1419 A67-20881

Viscosity variation effect on heat transfer and friction coefficient at wall during Couette flow 09 p1490 A67-22547

Plane Poiseuille flow calculations extended to Couette flow between coaxial circular cylinders, plotting flow velocity curves 09 p1490 A67-22595

Rarefied gas flow analyzed through transport equation in gas kinetics using bimodal two-stream distribution functions, with application to Couette flow 10 p1624 A67-22914

Thirteen moment equation solved for problem of plane Couette flow by iteration scheme, showing functional dependence on Mach and Knudsen numbers 11 p1774 A67-23863

Stability of incompressible fluid in Couette flow between coaxial circular cylinders, using Galerkin method to obtain critical Taylor number 11 p1781 A67-24570

Heat transfer of fully developed laminar flow of Bingham material between parallel plates and linearly varying wall temperature noting equations of state, velocity and temperature distribution 11 p1883 A67-24944

Linear stability of symmetrical parabolic flows of various types 13 p2092 A67-26276

Rarefied gas flow between parallel plates based on discrete ordinate method 13 p2092 A67-26277

Cylindrical Couette flow of rarefied monatomic gas calculated by double flow method 13 p2095 A67-26898

Couette flow and heat transfer of rarefied gas between parallel plates analyzed by Monte Carlo method 13 p2223 A67-26961

Discrete ordinate method for boundary value problems in gas dynamics using differential equations yields solutions to Couette flow 13 p2101 A67-26962

Two component equivalent of two-stream distribution function solution to plane Couette flow, studying nonlinear effects 13 p2101 A67-26965

Solid film sublimation cooling effect in Couette gas flow simulating real rarefied gas flow heat transfer, for jet engine application 14 p2408 A67-28800

Laminar Couette flow analyzed for gas injection effects on heat transfer to surface, temperature profile and convection interaction with radiation 15 p2578 A67-29129

Rayleigh problem solution and accuracy

and utility of discrete ordinate method for time dependent problems as applied to Couette flow problems 15 p2473 A67-30214
 Rarefied gas cylindrical Couette flow noting Knudsen number, Bhatnagar-Gross-Krook model for Boltzmann equation, transport integrodifferential equation, etc 18 p3029 A67-34738
 Taylor instability in circular Couette flow reexamined as eigenvalue problem noting suppression of geometry effect 23 p3988 A67-40601
 Prandtl limit behavior near zero skin friction, with perturbation methods generalizing Poiseuille and Couette flows 24 p4142 A67-42170

COULOMB COLLISION

Coulomb collision damping on peculiar solutions for plasma oscillation equations 01 p0124 A67-10749
 Static and dynamic properties of servomechanical transducers for nonelectrical signals with help of electrical signals 04 p0618 A67-14412
 Instability of contrastreaming plasmas investigated by taking into account Coulomb collisions via Fokker-Planck coefficients in Boltzmann equation 04 p0662 A67-14519
 Excitonic effects in interband absorption of semiconductors noting electron-hole interaction, Coulomb interaction energy maxima and minima and scattering cross sections 04 p0676 A67-14926
 Galvanomagnetic effect of anisotropic electron energy spectrum on acoustical branch perturbation spectrum of system of electrons and ions in homogeneous magnetic field 04 p0680 A67-15289
 Energy transfer rate between electrons and ions in plasma, noting velocity dependence of Coulomb logarithm 04 p0672 A67-15775
 Hugoniot-Rankine conditions, dissociation and ionization of hydrogen and nitrogen gas behind high speed shock wave and radiation effects 05 p0790 A67-16036
 Charged particle collisions effect on drift instability of low pressure plasma studied, using Landau collision integral as model collision integral 05 p0860 A67-17546
 Coulomb interaction in two-zone superconductor model, noting variation of critical electron-temperature and effect on superconductivity 08 p1369 A67-20838
 Coulomb interaction influence upon electron distribution in radiation belts at low altitudes in magnetic anomaly region 10 p1702 A67-23299
 Oriented velocity and temperature relaxation in Coulomb type plasma with particle velocities distributed according to Maxwellian law, evaluating Coulomb collisions effect on plasma components 10 p1685 A67-23410
 Linear Fokker-Planck collision operator expanded in terms of surface spherical harmonics, showing distribution function governed by differential-integral equations and eigenvalue spectrum 12 p1962 A67-26177
 Coulomb long range interaction effect on refractive index dependence on light frequency and on absorption lines shape of dipole active excitons 13 p2173 A67-26365
 Coulomb collision damping on peculiar solutions for plasma oscillation equations 13 p2166 A67-26778
 Coulomb interaction effect on time dependent variations of electron distributions in Van Allen belt, using kinetic equation 14 p2378 A67-27918
 Coulomb collisions effect on transverse wave along external magnetic field in dense plasma, noting damping of whistler mode and use of Fokker-Planck equation 16 p2713 A67-30608
 Kinetic equation for electron, ion and atom concentrations for Coulomb plasma taking into account inelastic processes 16 p2715 A67-31040
 Convergence of solutions for AC and DC electric conductivity of plasma with collisions 19 p3286 A67-35352
 Electron distribution function in steady state plasma with Coulomb and excitation collisions obtained analytically by simplifying Fokker-Planck terms 21 p3661 A67-37746

COULOMB POTENTIAL

Impact expansions and interference patterns in atomic scattering theory for cases of forward scattering, backscatter, inversion problem and screened Coulomb

potential approximation 01 p0112 A67-10143
 Isospin impurity mixing in distorted deuteron reaction 02 p0270 A67-12526
 Screening effect on Coulomb interaction, electron-ion recombination and surface neutralization 03 p0473 A67-13512
 Nonequilibrium conductivity of argon-cesium plasma 03 p0478 A67-13614
 Electromagnetic field of accelerating charge using Coulomb law, relativity transformation relations, charge conservation, Newton third law, etc 03 p0469 A67-13719
 Approximation method for molecular integrals that depends on replacement of two-center charge distributions by single-center distributions, giving results in terms of Coulomb type integrals 04 p0566 A67-15547
 Atomic energy levels in plasma, considering energy spectrum of hydrogen-like atom in plasma based on cut-off Coulomb potential model 06 p1039 A67-17881
 Impurity energy levels in semiconductors described by equivalent Schrodinger equation containing short range as well as conventional terms for long range Coulomb potential 07 p1230 A67-19060
 Coulomb friction in gyroscopic system analyzed, solving motion equation 09 p1498 A67-22033
 Viscous and Coulomb-friction forces effect on precessional motion of gyroscope mounted on stationary base 09 p1498 A67-22034
 Spin waves in two-band ferromagnetic metal assuming electron interaction via Coulomb potential 13 p2178 A67-27138
 Energy dependence on wave vector in valence band of diamond, Si, Ge and SiC, obtaining Coulomb and resonance integrals 15 p2541 A67-30237
 Exact solutions for spatial distribution of potential within space-charge region of non-degenerate semiconductor in contact with metal 16 p2727 A67-30850
 Extension to three dimensions of Wentzel-Krammer-Brillouin approximation method for quasi-classical wave function, applicable to axisymmetrical problems 16 p2703 A67-31920
 He-He ground state and first excited state potentials obtained from differential scattering cross sections 17 p2889 A67-33257
 Nonequilibrium conductivity of argon-cesium plasma 18 p3091 A67-34479
 Friedel sum rule applied to semiconductors, discussing Born approximation role 18 p3104 A67-34591
 Screened Coulomb potential solutions of Schrodinger equation using nonlinear method 19 p3266 A67-36091
 Exact equation of state for two-dimensional plasma of equal positive and negative charged particles interacting by Coulomb potential 20 p3501 A67-37293
 Quantum transport theories and multiple scattering in doped semiconductors evaluated for screened Coulomb potentials 21 p3682 A67-38387
 Chapman-Enskog transport collision integrals calculated for repulsive and attractive screened Coulomb potentials in ionized gases 22 p3850 A67-39717

COUNTDOWN

Launch-on-time probability, showing dependence on initial countdown reliability and cumulative percentage of failures [AIAA PAPER 67-271] 07 p1260 A67-20080
 Interlocking plan for entire countdown checkout process by combining subsystems simulated as partially controlled stochastic process 15 p2441 A67-30166
 Launch-on-time probability, showing dependence on initial countdown reliability and cumulative percentage of failures [AIAA PAPER 67-271] 21 p3712 A67-37808
 Launch time prediction with mathematical appendix [AIAA PAPER 67-906] 24 p4244 A67-43013

COUNTER

SA CERENKOV COUNTER
 SA GAS DISCHARGE COUNTER
 SA GEIGER COUNTER
 SA IONIZATION COUNTER
 SA NEUTRON COUNTER
 SA PARTICLE COUNTER
 SA PROPORTIONAL COUNTER
 SA QUANTUM COUNTER
 SA RADIATION COUNTER
 SA SCINTILLATION COUNTER
 Error theory for counter frequency meter 01 p0063 A67-10415

Bidirectional counter and fluid state trigger element using high pressure recovery bistable amplifier with decoupled outputs 01 p0014 A67-11032
 Reversible dekatron counter pulse-to-voltage converter, noting maximum conversion error 03 p0425 A67-14265
 Reversible dekatron counter pulse-to-voltage converter, noting maximum conversion error 14 p2321 A67-28777
 Miniaturized no-moving-parts fluid pulse counter development for ordnance application 19 p3176 A67-34806
 Reversible counter using decimal register compared to conventional flip-flop counters 22 p3809 A67-40475

COUNTERBALANCE SYSTEM
 S COMPENSATOR
 COUNTERMEASURE
 S ELECTRONIC COUNTERMEASURE

COUNTING RATE COMPUTER
 Apparatus used to study exoelectronic emission from metallic surfaces, detailing Geiger counter, high voltage rectifier, scaling device and counting rate meter 07 p1201 A67-19256

COUPLED MODE
 Cerenkov radiation of beam-plasma system into dielectric, using mathematical model and mode coupling theory 01 p0040 A67-11314
 Mutual coupling between TEM and TE 01 parallel-plate waveguides calculated, using wedge diffraction techniques 02 p0211 A67-11596
 Variational expression for dominant mode coupling coefficients between elements of infinite array 02 p0212 A67-11604
 Modal analysis of mutual coupling effects of triangular grid array of waveguide radiators having nonzero wall thickness 02 p0212 A67-11614
 TE mode-selective coaxial directional coupler with coaxial primary line and rectangular waveguide as secondary line 02 p0214 A67-11650
 Plane stressed state in plane contact problem of coupled plates under symmetrical load conditions 02 p0340 A67-12445
 Reflection coefficient of tapered waveguide determined via coupled mode theory, noting error estimation and design of reflectionless tapers 03 p0376 A67-12802
 McIver and coupled mode theory derivations of equations for traveling wave transistor 03 p0382 A67-13667
 Propagation of coupled electromagnetic, electron-acoustic and ion-acoustic waves in horizontally stratified and magnetized electron-ion plasma 03 p0372 A67-13991
 Linear optimal control via root square locus to design simple effective structural bending control for four XB-70 coupled longitudinal bending modes [AIAA PAPER 66-970] 03 p0361 A67-14142
 Wave interaction dynamics of far IR electromagnetic radiation generation by coherent molecular vibrations or phonons excited by stimulated Raman scattering and resonant phase matching condition 04 p0657 A67-15113
 Coupling of turbomachine blade vibrations through rotor or disk in causing variations of natural frequencies and amplitudes [ASME PAPER 66-WA/GT-5] 04 p0711 A67-15360
 Energy method analysis of flutter instabilities in turbojet engine rotors caused by interaction between unsteady air loading and coupled vibration modes [ASME PAPER 66-WA/GT-6] 04 p0713 A67-15384
 High magnetic field effect on interband semiconductor laser, particularly electromagnetic modes and coupling and threshold current 05 p0822 A67-16673
 Quenching of one pulsed ruby laser oscillation by another, noting coupled rate equations for steady state and transient behavior 05 p0823 A67-16682
 Hypersonic excitations due to Brillouin scattering for case with Stokes feedback, deriving quantum equation of motion for creation of laser and Stokes modes and coupled acoustic mode 05 p0823 A67-16683
 Radiation transport in spectral lines as consecutive photon absorptions and emissions, discussing contemporary theories, approximation methods and applications spark shadow projections in air for giant

- pulse 06 p1010 A67-18090
- TEM mode coupling between transmission lines applied to wideband directional couplers 06 p0969 A67-18118
- Linear shell theory for nonlinear transverse coupled vibrations of partially filled circular cylindrical elastic tank [AIAA PAPER 67-74] 06 p1101 A67-18272
- Electron plasma oscillations excited by two-beam instability and nonlinear coupling between them 06 p1046 A67-18828
- Mutual coupling and edge effects in finite scanning arrays 07 p1154 A67-19784
- First order coupled wave equations for propagation in planar stratified compressible electron plasmas 07 p1230 A67-19851
- Higher order waveguide mode radiation incorporated antenna feed systems for performance improvement, evaluating S-and C-band dual frequency Cassegrain feed 08 p1300 A67-20681
- Elastic postbuckling involves coupled modes when critical loads corresponding to buckling modes of two degrees of freedom system are equal 08 p1422 A67-21032
- Direct-coupled confocal resonators used as band pass filters at mm wavelengths 08 p1305 A67-21229
- Energy coupling among electron acoustic, ion acoustic and transverse electromagnetic waves at two-fluid plasma density discontinuity 08 p1364 A67-21397
- Phase locking of longitudinal modes of gas laser by cavity mirror translation at constant velocity 09 p1510 A67-21575
- Dynamic properties of coupled systems derived from experimentally determined frequency response functions of component systems, noting cross correlation 09 p1573 A67-21752
- Operation of coupled mutually loaded tunnel diodes, considering short circuit mode 09 p1473 A67-21963
- Two positive kinetic power waves coupled in interaction for DC pumped quadrupole amplifier having low noise and high efficiency 09 p1478 A67-22260
- Internally modulated gas laser at 100 and 4000 MHz, describing electromagnetic field in Fabry-Perot resonator in terms of natural oscillation modes and coupling 09 p1514 A67-22269
- Coupled laser quenching and transient buildup in rate equation analysis, noting spike suppression 09 p1514 A67-22274
- Attenuation and coupling impedance of backward dipole surface wave on cylindrical plasma column with reference to oscillator design 09 p1546 A67-22281
- Dispersion of mode couplings of wave propagation in waveguide containing plasma electron beam system 09 p1550 A67-22582
- Statistical energy analysis for multimodal random vibration of complex system, discussing power flow, modal responses, kinetic energies, etc [ASME PAPER 67-VIBR-8] 11 p1872 A67-24168
- Mode coupling effect on response of rigid body to random excitation analyzed, using two degree of freedom model [ASME PAPER 67-VIBR-36] 11 p1873 A67-24193
- Rectangular to cylindrical waveguide transducer which couples dominant rectangular and cylindrical transverse electromagnetic modes 11 p1767 A67-24733
- Directional coupler classification 12 p1915 A67-25977
- Nonuniform distributed network problems solved by Lie algebras 12 p1919 A67-25979
- Coupling of laser optical modes by intracavity time varying perturbation 13 p2125 A67-26407
- Ruby maser with two synchronous symmetrical quarter-wave-coupled cavities, noting frequency gain 13 p2128 A67-27227
- Equivalent classical source for weakly coupled quantum-mechanical source, estimating approximation extent 13 p2159 A67-27732
- Power spectrum and difference frequency spectrum for energy exchange oscillations between three modes of He-Ne laser 14 p2331 A67-28603
- Propagation of coupled electromagnetic and electroacoustic waves in magnetized compressible stratified electron plasma 15 p2521 A67-29177
- Internal and coupling modulation and mode locking of continuous ruby laser 15 p2499 A67-29729
- Mutual coupling between sectoral horns side-by-side formulated in terms of rays, modes and mode caustics excited in each horn 16 p2639 A67-31355
- LEM-CSM analysis, elastic bending and propellant sloshing 17 p2955 A67-32478
- Coupled integral equations for transverse and axial currents for asymmetrically cylindrical antenna driven by EMF 17 p2826 A67-32618
- Dispersion relations for coupled electromagnetic and longitudinal waves propagating along isotropic inhomogeneous cylindrical hot plasma 17 p2908 A67-33107
- Fluctuating electric and magnetic fields due to plasma instabilities and stabilizing effect of mode coupling in collisionless plasma 17 p2909 A67-33229
- Energy method analysis of flutter instabilities in turbojet engine rotors caused by interaction between unsteady air loading and coupled vibration modes [ASME PAPER 66-WA/GT-6] 18 p3115 A67-34130
- Resonances of thin shell model of earth-ionosphere cavity with dipolar magnetic field 18 p3042 A67-34427
- Weak turbulence theory for collisionless plasmas formulated in terms of test waves 18 p3092 A67-34744
- RF plasma at electron cyclotron frequency produced with axially slotted metal cylinder 19 p3275 A67-35111
- Mode conversion in rectangular waveguides, describing results in terms of plane wave diffraction by grating 19 p3183 A67-35545
- Short-slit directional coupler functioning mode via boundary value problem indicating Chebyshev behavior of transfer coefficient and wideband subdivision 19 p3195 A67-35560
- Nonlinear resonant coupling between damped and undamped vibrations for damping roll in TRAAC and elastic dumbbell satellites [AIAA PAPER 67-568] 19 p3329 A67-35964
- Stability of three-dimensional oscillations of solid body coupled to periodically vibrating base by elastic springs 20 p3485 A67-36917
- Operation of coupled mutually loaded tunnel diodes, considering short circuit mode 20 p3400 A67-37193
- Electromagnetic plane wave scattering cross section from plasma coated conducting cylinder using TE and TM modes of polarization with respect to cylinder axis 20 p3389 A67-37706
- Ionospheric radio wave theory using coupled vacuum modes with set of coupled wave equations 20 p3389 A67-37709
- Full wave solutions for coupled modes corresponding to ionospheric propagation in vacuum, stressing numerical swamping problem 20 p3389 A67-37710
- Diffraction coefficient of open laser resonators coupled in series, discussing boundary conditions 21 p3638 A67-37864
- Linear shell theory for nonlinear transverse coupled vibrations of partially filled circular cylindrical elastic tank [AIAA PAPER 67-74] 21 p3727 A67-38866
- Unstable coupling between slow space charge mode of electron beam and lowest plasma electron band modes in finite geometry 22 p3847 A67-39643
- Mathematical model for linear memory arrays cross coupling problems, discussing signal distortion due to common mode capacitance effect 22 p3765 A67-39912
- TM and TE mode uncoupling in oblique wave scattering from radially inhomogeneous cylinders 22 p3763 A67-40308
- Helix spurious mode effects on TW amplifier performance analyzed for methods of elimination 22 p3775 A67-40462
- Coupled electromagnetic whispering gallery modes in large dielectric cylinders, discussing circumferential phase velocity, boundary region and axial wave number 23 p3974 A67-41203
- Normal modes of stellar internal motions, considering turbulent convection equations and weak-coupling approximation 23 p4088 A67-41277
- Spin characteristics of VJ 101 C VTOL airplane via numerical integration of motion equations including mass coupling effects and nonlinear aerodynamics 23 p3934 A67-41313
- Far IR spectra and space group of crystalline hydrazine and hydrazine-d4 noting coupling of translational and librational motions 23 p4048 A67-41532
- Population noise in semiconductor laser junctions calculated by quantum mechanical Langevin method 24 p4166 A67-41887
- Coupling of turbomachine blade vibrations through rotor or disk in causing variations of natural frequencies and amplitudes [ASME PAPER 66-WA/GT-5] 24 p4251 A67-42461
- Complex wave propagation and coupling in inhomogeneous media, discussing WKB type amplitude coefficients and electromagnetic and space charge waves 24 p4123 A67-42657
- COUPLED STRESS
- Plane problems of moment theory of elasticity for plane weakened by finite number of circular apertures, obtaining uniqueness of solutions 02 p0338 A67-11954
- Boundary value problems for semiinfinite bars made of coupled thermoelastic material solved by new functions that are corrections to classic tabulated functions [ASME PAPER 66-WA/APM-24] 04 p0714 A67-15412
- Constitutive equations derived based on thermodynamics of irreversible processes and coupled thermoelasticity, formulating variational and reciprocity theorems 05 p0910 A67-16165
- Linearized elasticity theory of coupled stresses effect on stress concentration around finite crack 05 p0921 A67-16884
- Coupled system of thin elastic shells, giving response to static or harmonically oscillating loads or to unloaded natural frequencies and mode shapes, using Green matrix [AIAA PAPER 67-45] 06 p1103 A67-18351
- Force distribution and stress displacement relations for two-dimensional elasticity with coupled stresses 06 p1107 A67-18651
- Viscoelasticity for micropolar solids, obtaining constitutive equations of strain and microrotation rate dependent materials 08 p1422 A67-20979
- Statistical basis for modified moment theory of elasticity that takes into account contribution of all deformation-tensor-component gradients to deformation energy 09 p1574 A67-21914
- Equations for continuous media in finite case formulated in Eulerian and Lagrangian form 11 p1819 A67-24621
- Stress distribution in matrix of composite material for case of filler between one infinite and two displaced semiinfinite microfibers 14 p2398 A67-28100
- Torsion or coupled bending torsional wave theory for thin walled open section beams 17 p2959 A67-32413
- Singularities due to concentrated couples in infinite linear elastic isotropic Cosserat continuum, noting dissimilar singular solutions 17 p2964 A67-33141
- Plane problems of moment theory of elasticity for plane weakened by finite number of circular apertures, obtaining uniqueness of solutions 17 p2966 A67-33271
- Elastic stress distribution in infinite plate having circular hole, applying coupled stresses theory 18 p3140 A67-33666
- Reciprocal theorem in linearized theory of couple stresses for perfectly elastic nonhomogeneous anisotropic materials 20 p3540 A67-37281
- Plane waves propagation in microelastic medium having only coupled stresses 20 p3542 A67-37681
- Thermoelastic coupling effect on propagating discontinuities in stresses and particle velocities studied using characteristic method 21 p3715 A67-37893
- Bending of orthotropic strip to anticlastic surface by uniform moment, determining strain along neutral axis, bending moment and couple action 22 p3913 A67-40008
- Matrix displacement method for coupled bending-bending vibrations of pretwisted blading 23 p4078 A67-41329
- Surface waves in medium with coupled stresses, using Cosserat type medium for analysis of properties 23 p4079 A67-41417
- COUPLING
- SA ANTENNA COUPLER
- SA CROSS COUPLING
- SA GYROSCOPIC COUPLING
- SA MICROWAVE COUPLING

SA OPTICAL COUPLING
 SA SPIN DECOUPLING
 SA SPIN-SPIN COUPLING
 SA THERMOCOUPLE
 SA THERMODYNAMIC COUPLING

Close-coupling calculation of resonant structure of scattering amplitude of excited-state atoms and molecules in continuum 03 p0471 A67-13221

Generalization of Weber theorem for problems of coupled thermoelasticity, considering vibrations varying with time 03 p0523 A67-13502

Numerical results of slot couplings of rectangular single mode waveguides as function of length, width, position and wavelength 05 p0775 A67-16957

Input device for quadrupole amplifiers in form of sequential oscillators with inductive coupling used to widen frequency band of output 05 p0785 A67-17472

Passband narrowing due to coupling between passive oscillating system and active substance contained in resonator cavity represented by RLC circuit 05 p0780 A67-17474

Couple due to distant mass acting on nonspherical object determined, considering luni-solar precession and nutation variability 06 p1031 A67-17778

Effect of degree of coupling between resonator system and load on generation zones and regenerative amplification of pulsed magnetron, noting characteristics 08 p1305 A67-21271

Temperature and tolerance behavior of transistor determined, based on equivalent drift sources of transistor obtained from intrinsic series coupling 09 p1482 A67-22611

Effect of varying magnetic field, vacuum and ion density at 27 MHz on properties of cylindrical argon plasma column, using capacitive and inductive coupling 10 p1686 A67-23504

RF plasma torch coupling efficiency shown insensitive to input power and gas flow rate 12 p1976 A67-25925

Transformation for uncoupling system of duct flow of conducting fluids under arbitrary oriented applied magnetic field 12 p1976 A67-25941

Resonance transition probabilities in intermediate coupling for some neutral nonmetals, noting radiative lifetime measurements by phase shift 12 p1968 A67-26246

Frequencies of turbine blade vibrations calculated by iteration method, considering coupling between bending and torsion 13 p2217 A67-26744

Induced impedance dependence on scanning angle and array parameters calculated, analyzing edge effects 14 p2279 A67-28005

Competitive and cascade coupling between transitions in CW water vapor laser 14 p2331 A67-28498

Optimum energy coupling of multimode gas laser determined experimentally 14 p2333 A67-28971

Diffraction coefficients in Keller theory extended to near-field and shadow-boundary regions of edge, introducing two correction factors 16 p2627 A67-31365

Suboptimal control of large scale dynamic system consisting of two weakly coupled subsystems using aggregation 16 p2647 A67-31645

Nature of axis coupling for Kater pendulum assuming weightless rod and mass point loads 17 p2883 A67-31929

Parametric coupling between ion and electron waves noting coefficients, growth rate amplification, etc 17 p2906 A67-33061

Laminar slow wave coupler applied to waveguide to detect very low power slow waves in indium antimonide subjected to combined effects of applied electric and magnetic fields 17 p2922 A67-33087

Transition temperature of phonon-coupling superconductor merged with that of type II superconductor critical field to obtain strong coupling corrections to critical field 17 p2925 A67-33378

Electromagnetic field coupling action through holes in metal screen, noting hole polarizability calculation and hole equivalent dipoles effect on resonators 18 p2999 A67-33530

Symmetrical traveling-wave antenna design with given sidelobe level and amplification

factor, determining coupling coefficient and maximum utilization 18 p3011 A67-34178

Coupled systems stability constraints and oscillatory behavior, discussing feedback path nonlinearities using differential equations 19 p3200 A67-34849

Critical fields in strong coupling superconductors, using Ginsburg-Landau equations 19 p3303 A67-35042

Modes and eigenvalues of symmetric cylindrical Fabry-Perot laser resonator with circular output-coupling apertures 20 p3460 A67-37024

Free convection of conducting fluid in coupled vertical channels for case of steady motion with lateral heating 20 p3500 A67-37051

Radioactively labeled coupling agents adsorption on E-glass surfaces, noting continuous film formation with covalent bonding occurring at interface 20 p3474 A67-37269

Orthonormalized vector reference in coupling between symmetrical tensors in continuum mechanics, deriving expansion coefficients 21 p3717 A67-37971

S-matrix computations for quantum transitions, considering close coupling case of homonuclear diatomic molecular rotational excitation 21 p3659 A67-38005

Different motion equations equivalence for nonholonomic systems from Chaplygin method 21 p3657 A67-38303

Synchronous motions in dynamic bearing system of nonlinear plants with one degree of freedom interacting through weak coupling 22 p3836 A67-39395

Parametric amplification of traveling wave tube through coupled wave method noting role of phase velocities of space charge waves 24 p4130 A67-42241

Frequency and intensity of laser light analyzed for reaction of coupled optical resonator 24 p4168 A67-42574

COUPLING CONSTANT

Material strength parameter /coupling modulus/ dependence on crack propagation velocity when accounting for rupture kinetics 03 p0529 A67-14166

Coupling coefficients for vertical and oblique cosmic ray components 05 p0882 A67-16126

Geomagnetic cut-off rigidity effect on cosmic ray intensity and coupled coefficients 05 p0882 A67-16127

Coupling coefficients of waves in variable cross section waveguides with impedance wall 07 p1143 A67-19602

Simple metal spin-density-wave state analyzed using electron-electron exchange interaction 12 p1985 A67-25849

Special purpose analog computer for analyzing wideband signals in two parts of network, with automatically plotting and coupling factor as function of frequency 13 p2089 A67-26410

Field solution of TE sub k zero mode wave incidence on inductive iris in rectangular waveguide 13 p2066 A67-26475

Composite resonant system behavior with and without stub tuner, tabulating internal, external, loaded Qs and coupling coefficient 13 p2076 A67-26480

Spin-projected unrestricted self-consistent field /SCF/ methods for spin density calculations used to determine hyperfine coupling constants 13 p2160 A67-26540

Characteristics of open resonators, obtaining coupling and scattering coefficients 15 p2501 A67-30075

Latitudinal effect on neutron-monitor data taken by Soviet ship in North Pacific, obtaining relation between coupling constant and cut-off rigidity 17 p2933 A67-32092

Coupling coefficient and latitude distribution in intensity of cosmic rays inclined component measured by Soviet ship 17 p2933 A67-32093

Far IR measurements used to determine superconducting energy gap widths in niobium alloys 17 p2925 A67-33373

Sea level and stratosphere measurement of cosmic ray intensity latitude distribution, coupling coefficients and multiplicities 19 p3316 A67-35563

Nonlinear coupling between fast and slow waves of cold homogeneous plasma slab partially filling parallel plate waveguide 20 p3492 A67-36126

Coupling coefficients for nonlinear

interaction between two transverse waves and electron plasma wave in magnetic field 20 p3501 A67-37181

Hyperfine structure in rotational spectrum of HDO and deuterium oxide analyzed by beam maser spectroscopy, evaluating coupling constants 20 p3461 A67-37287

Coupling coefficients of waves in variable cross section waveguides with impedance wall 20 p3401 A67-37341

Spin-spin coupling constants from perturbation-variation and first order perturbed trial function assumptions 21 p3658 A67-38003

Spin-disorder resistivity measurements in Gd-Yt alloys noting temperature and concentration effects 22 p3863 A67-40203

Hyperfine coupling constants of lithium energy levels, using Weiss 4s-configuration wave functions 24 p4190 A67-42097

Strong coupling superconductivity in intermetallic compounds, possibly due to all electrons having same kinetic energy 24 p4205 A67-42738

Coupling coefficients for vertical and oblique cosmic ray components 24 p4215 A67-42802

Geomagnetic cut-off rigidity effect on cosmic ray intensity and coupled coefficients 24 p4215 A67-42803

Structural studies of FeNi-FeNiMn type thin films with ferro-antiferromagnetic coupling by Lorentz electron microscopy 24 p4206 A67-43109

COUPLING NETWORK

Shielded coupled strip transmission line with three center conductors, noting electrical behavior, cross section dimension evaluation from characteristic immittances, etc 02 p0193 A67-11777

Synthesis of TEM directional couplers and fixed phase shifters consisting of multiple parallel coupled quarter wave sections 02 p0214 A67-11778

Effect of couplings and losses on frequency stability in self-oscillatory system with three circuits 02 p0221 A67-12418

Slot couplings of rectangular single-mode waveguides analyzed by equivalent circuit and concentrated parameter methods 03 p0385 A67-13952

Automatic phase sensor for waveguide combiner in S-band ground tracking and space communication network 07 p1149 A67-19051

Laser variable output coupler, construction, performance and applications 10 p1662 A67-22753

Diode type lossless network description with excellent transient response and less settling time than conventional branch-line coupler phase shifter 10 p1613 A67-23414

Parametric coupling analyzed in electrical RLC circuit coupled with mechanical system through nonlinear inductance [ASME PAPER 67-VIBR-30] 11 p1797 A67-24188

Parametric coupling between two waves noting losses 13 p2086 A67-26511

Two coupled resonant mechanical circuits with parameter in coupling element allowed to vary periodically 15 p2494 A67-29772

Concentric ring array application to space tapering of planar arrays, noting obtainable frequency ranges and scan angles 16 p2640 A67-31526

Coherent electromagnetic oscillation from voltage biasing of superconducting weak link producing coupled quantum oscillators 17 p2926 A67-33380

Coupling factor between microwave resonator and transmission line determined by oscillographic recording of microwave field 18 p3010 A67-33508

Generalized dynamical thermoelasticity theory formulated via heat transfer equation, considering temperature/strain rate coupling effect 24 p4252 A67-41955

Induced interference in open and shielded wire lines due to AC and transient currents, discussing electromagnetic coupling effects 24 p4137 A67-42713

COVALENT BOND

Dynamic theory of hybrid ionic-covalent /homopolar/ bonds applied to physical behavior of GaAs type crystals 18 p3094 A67-33436

Covalent bonds found more prevalent than ionic bonds in X-ray spectral study of Al and Sb in A-III B-V type semiconductor compounds 18 p3095 A67-33443

- Impurity crystal-field spectra in II-VI and III-V compound semiconductors used to predict unexplored systems spectra impurity crystal-field spectra in II-VI and III-V compound semiconductors used to predict 21 p3682 A67-38388
- COVARIANCE**
- Kalman filter estimation of covariance parameters of linear system subjected to Gaussian driving 02 p0227 A67-12157
- Log amplitude covariance for horizontal and nonhorizontal propagation path of plane wave through turbulent atmosphere, noting refractive index effect 06 p1033 A67-18537
- Covariance of log amplitude fluctuations for propagation of spherical wave in turbulent medium over horizontal path to obtain phase structure 10 p1678 A67-22712
- Covariant decomposition of tensor and gravitational Cauchy problem in Riemann space 10 p1679 A67-22841
- Law of propagation of covariance in matrix form obtained from least squares adjustment 10 p1674 A67-23004
- Filter and error-covariance equations developed for optimal fixed-point smoothing for continuous linear systems 16 p2648 A67-31652
- Local turbulent properties of shear layer derived from covariance of two crossed perpendicular beams of radiation 17 p2855 A67-32282
- Canonical decomposition of nonlinear error covariance difference equation derived for discrete estimation problems 24 p4177 A67-42188
- COVER**
- S CLOUD COVER**
- COWLING**
- Retractable airfoil and hinged cowl modifications of supersonic inlet to reduce drag below choking point for subsonic operations 17 p2791 A67-32575
- CRAB NEBULA**
- Solar and stellar X-ray astronomy, noting Crab Nebula occultation experiment 01 p0144 A67-10900
- Elliptical polarization of Crab Nebula radiation possibly explained without synchrotron hypothesis by analyzing photoelectric observations of Stokes parameters 05 p0882 A67-16593
- Upper limits to high energy gamma flux from quasars 3C 147, 3C 196 and 3C 273 from Crab Nebula and from 53 Cam magnetic variable star 05 p0900 A67-17079
- Interferometer radio observations of two lunar occultations of Crab Nebula 10 p1705 A67-22941
- X-ray source in Crab Nebula size and position, showing visible light distribution having common center within 15-inch precision of measurement and finite angular extent 13 p2189 A67-26263
- Linear polarization of Crab Nebula, Cygnus A and other radio sources observed at wavelength of 21.3 cm, using radio telescope 13 p2198 A67-26714
- Circularly polarized radiation from Crab Nebula investigated from radio telescope observations at Arecibo 19 p3318 A67-35802
- Radio emission polarization of Crab Nebula on February 1963 with Soviet radio telescope 20 p3529 A67-37516
- Synchrotron X-ray radiation by high energy electrons in magnetic field with enhancement due to outward propagating hydromagnetic waves proposed as Crab Nebula emission mechanism 23 p4051 A67-40914
- CRACK**
- SA FAILURE**
- SA FATIGUE**
- SA MICROCRACK**
- SA STRAIN**
- SA SURFACE CRACK**
- Stress distribution due to pressurized exterior crack in infinite isotropic elastic medium with coaxial cylindrical cavity 04 p0717 A67-15799
- Diffraction of plane longitudinal wave in interior of elastic solid, where wave is harmonic in time and impinging on surface of penny shaped crack 09 p1573 A67-21663
- Materials failure laws based on combined analysis of cracks and fractures 09 p1575 A67-22166
- CRACK FORMATION**
- Organic glass disintegration induced by pulsed laser beams 02 p0257 A67-12241
- Microhardness of n-type InSb single crystals and crack formation near indentation area 03 p0489 A67-13093
- Thermostability of WC-Co alloys, discussing heat treatment, crack formation, bending strength and thermal shock resistance 03 p0447 A67-13641
- Augmented strain concept and Vrestraint test for hot-cracking sensitivity and weldability of filler metals 03 p0430 A67-13694
- Fatigue cracks and fatigue cycles effect on brittle fracture behavior of annealed 4140 steel [ASME PAPER 66-WA/MET-17] 04 p0639 A67-15332
- Cracking during welding of aluminum alloy noting effect of strain, maximum temperature and cooling rate [ASME PAPER 66-WA/MET-5] 04 p0639 A67-15341
- Strains, slip lines and onset of cracks in thin chromium foils investigated by electron microscopy 04 p0640 A67-15977
- Statistical dislocation theory of crystal brittle fracture seen as stochastic process with microcrack formation and propagation under plastic deformation 05 p0919 A67-16504
- Tensile tests performed on alpha titanium between -321 and 75 degrees F, discussing ductile-to-brittle transition, microcrack formation and brittle fracture mechanics 06 p1014 A67-17807
- Penny shaped crack embedded in isotropic material treated by linear elasticity, noting stress singularities 06 p1109 A67-18732
- Micro- and macrocrack formation in organic glass by focusing of laser beam 06 p1021 A67-18808
- Hot cracking and strain-age cracking in heat affected zone of Rene 41 alloy weldments 07 p1198 A67-19215
- Gas saturation effect on titanium alloys undergoing heat treatment, discussing microhardness and surface crack formation 07 p1205 A67-19277
- Laser beam effect on hydrodynamic bearings, discussing microcracks and critical energy, explaining breakdowns 08 p1337 A67-20840
- Energy balance criteria during slow crack growth and at inception of catastrophic rupture in high strength ductile metals, noting necking phenomena in tensile test 08 p1421 A67-20953
- Lower bounds for crack tip stress intensity factors of irregularly shaped planar cracks 08 p1422 A67-20956
- Test method for aluminum and titanium alloys, estimating tendency toward brittle failure and recording kinetics of crack formation 08 p1342 A67-21176
- Second order strain accumulation in aluminum in reversed cyclic torsion at elevated temperatures 09 p1517 A67-21753
- Cold brittleness, impact toughness and crack resistance of titanium alloys at low temperatures 09 p1518 A67-21966
- High speed photography of laser radiation damage to transparent materials and analysis of destruction mechanisms involved 09 p1516 A67-22660
- Axisymmetric crack formation problem in elastoplastic material including energy dissipation and face displacement calculations, noting agreement with Griffith theory 10 p1716 A67-22939
- Plasticity correction for single edge cracked specimen in uniaxial tension, estimating axial rigidity 10 p1717 A67-23016
- Stresses and displacements in small circular stress-free crack at interface between thick elastic incompressible layer and rigid foundation 10 p1717 A67-23082
- Fracture initiation in sheet specimens, noting correlation of crack-opening displacement and fracture toughness and dependence on applied stress 10 p1718 A67-23172
- Random-loading fatigue crack growth behavior of airframe aluminum and titanium alloys under sinusoidal, narrow band and broad band random loading 10 p1669 A67-23434
- Stress corrosion cracking of cold reduced austenitic stainless steels noting effects of marine atmosphere exposure, cold working, welding, etc 11 p1807 A67-24586
- Failure mode at tip of crack predicted using cleavage strength and shear strength of perfect crystals, noting tungsten and iron 11 p1880 A67-25090
- Wiener-Hopf and Aleksandrov methods solve plane and axisymmetric problems of equilibrium longitudinal cracks in thin plates with edges free of stresses 12 p2019 A67-25565
- Aluminum oxide whiskers structure and properties 13 p2141 A67-27186
- Westergaard method of crack analysis extended for crack problems within infinite medium with cracks under applied loads at infinity 16 p2765 A67-30995
- Fracture stresses of cracked plates and flow stresses of polycrystalline aggregates as related to stresses and strains at ends of plano-discontinuities 16 p2769 A67-31285
- Hilbert boundary problem extension for flexural problems of cracks in mixed media, noting Cauchy integrals, Plemelj formulae, etc 16 p2770 A67-31292
- Crack resistance properties of high strength aluminum alloys, noting test results on fracture toughness enhancement 16 p2688 A67-31308
- Time dependent fracture of viscoelastic materials, considering defect initiation relation as approximation to crack growth history 16 p2773 A67-31312
- Fatigue in quasi-brittle materials, fatigue in creep range at elevated temperatures and cumulative fatigue damage 16 p2774 A67-31316
- Minimum alternating stress causing given length microcrack to grow and macrocrack growth rate 16 p2774 A67-31317
- Energy necessary for fracture shown independent of lattice defects by low cycle fatigue tests at constant true mean stress amplitude 16 p2774 A67-31318
- Plastic accommodation in Mg O idealized as linear array of continuously distributed edge dislocations to study crack nucleation 16 p2775 A67-31326
- Compaction pressure and sintering temperature effect on initiation and propagation of cracks during bend testing of Ni and Mo specimens 16 p2691 A67-31586
- Temperature effect on low-cycle fatigue behavior of Udmet 700 superalloy, noting internal and surface cracking 16 p2693 A67-31870
- Electroinductive defectoscope circuitry and operation described noting use for fatigue cracks observation in threaded components 16 p2681 A67-31917
- Thermostability of WC-Co alloys, discussing heat treatment, crack formation, bending strength and thermal shock resistance 17 p2875 A67-33174
- Yielding effects in stress corrosion cracking in susceptible alloys 18 p3063 A67-33487
- Silicon and phosphorus role in crack formation in manually welded high temperature resistant steel plate 18 p3063 A67-33673
- Color contrast penetration method for crack detection in aircraft engines and motor car parts 18 p3045 A67-33739
- Aluminum alloy examined for dislocation arrangements and susceptibility to intergranular stress corrosion cracking, using electron microscopy 18 p3063 A67-34000
- Crack nucleation in high strength low alloy steel, comparing fatigue processes in quenched and tempered martensite with those in pure metals 18 p3064 A67-34082
- Partial cone crack formation in brittle material loaded with sliding spherical indenter 18 p3144 A67-34275
- Statistical probability of fractures in polymethylmethacrylate by laser radiation 20 p3473 A67-36161
- Statistical dislocation theory of crystal brittle fracture seen as stochastic process with microcrack formation and propagation under plastic deformation 20 p3541 A67-37318
- Strain age cracking characteristics in welded Rene 41 nickel base alloy, discussing test procedure used with circular patch test to evaluate contributing factors 20 p3471 A67-37698
- Self-focusing of laser light pulses in ruby and leucosapphire crystals, noting different damage forms for fundamental and second harmonics 21 p3639 A67-38094
- Laser thermal and radiation effect on metals, discussing mechanical damage 21 p3646 A67-39011
- Microcracking susceptibility studies of

Inconel 718 weld heat affected zones, noting hot ductibility, weld circle patch and fillerless fusion welding 22 p3818 A67-39222

Kinetics of structural changes and failure formation and growth in high temperature alloys undergoing creep 22 p3818 A67-39320

Heat treatment effects on mechanical properties of steel-forged gas turbine rotor shafts, including microcracks formation and growth and structural strength 22 p3819 A67-39323

Hot-cracking and microstructure characteristics in weld heat resistant Ni alloys evaluated by synthetic specimen technique 22 p3819 A67-39449

Circumferential crack in pressurized cylindrical shell analyzed for extensional and bending components of stresses 22 p3911 A67-39678

Crack opening displacement and fracture toughness analyzed for uniaxial tension and edge-cracked plate 22 p3911 A67-39681

Environmentally induced delayed failure process incubation period of precracked steel from film formation 22 p3822 A67-40060

Elastic strain energy change rate as related to notch depth considered for edge notches with finite radius 23 p4074 A67-40664

Fracture in engineering design in terms of fracture mechanics 23 p4076 A67-40696

Infinitesimal dislocation theory applied to materials with cracks and cylindrical hole, straight boundary between bonded materials and cylindrical insert subject to antiplane shearing stress 23 p4078 A67-41165

Fatigue crack research effect on structural design of flight vehicle structures, discussing temperature effects, multiaxial strain effects and fatigue crack growth equations 24 p4247 A67-41942

Double linear damage rule for predicting cumulative fatigue damage, crack initiation and propagation and fatigue life, noting improved accuracy 24 p4170 A67-41951

Microstructure of SGBF graphite under tensile and compressive stresses noting crack generation in layer planes [ACS PAPER 6-N-66F] 24 p4175 A67-42372

Fatigue crack initiation, comparing alpha brass and Al-Mg-Zn alloy, noting effect of increasing maximum pressure value in contact region [ASLE PAPER 67-LC-5] 24 p4174 A67-42744

CRACK PROPAGATION

Electron microscopy study of fracture surface topography permitting identification of fine scale fracture surface features, relating them to fracture formation mechanisms [AIAA PAPER 66-814] 01 p0077 A67-10034

Tenfold increase in fatigue life of 1100 aluminum in reverse bending at vacuum level below 10-2 torr due to retardation of crack propagation phase of fatigue process 01 p0092 A67-10053

Stress required for brittle fracture of alumina at room temperature based on theory of dislocation movement of cracks 01 p0092 A67-10054

LiF single crystal destruction as function of laser beam energy, examining dislocation pattern arising from crack propagation 01 p0086 A67-10071

Continuity gauge measurement of crack growth on flat and curved surfaces at cryogenic temperatures 01 p0102 A67-11028

Fatigue crack propagation under random cyclic loading extended, obtaining zero-order solution from mean crack lengths 02 p0337 A67-11794

Radioactive tracers used to determine crack initiation and propagation characteristics in reinforced plastic composite materials, relating discontinuity growth to test conditions 02 p0249 A67-12222

Time evolution of laser induced fractures in glass, noting crack propagation accompanied by sparking 02 p0253 A67-12508

Critical load equations for plate weakened by sharp stress raisers extended to account for effect of arbitrarily oriented external forces 03 p0522 A67-13122

Griffith energy criterion and stress-strain environmental criterion for fractures in brittle cracked metallic plate 03 p0523 A67-13467

Closed form pseudostatic solutions for Kirchhoff bending stress fields associated with semiminfinite crack extending at uniform velocity in elastic plate 03 p0523 A67-13468

Plastic yielding effect on stress and deformation of edge notch subject to longitudinal shearing stress 03 p0523 A67-13469

Fracture surfaces, Wallner lines and crack propagation velocity in precracked W monocrystals at 20-300 degrees K 03 p0445 A67-13471

Ultrasonic apparatus using echo method to record automatically formation and propagation of fatigue cracks on smooth specimens 03 p0420 A67-13567

Crack propagation in heat-affected zone during HF AC current gas-tungsten arc welding of Al alloy test 03 p0430 A67-13693

Fatigue mechanisms for fcc metals and alloys, reviewing research on crack initiation and propagation 03 p0447 A67-13800

Work of fracture and measurement in metals, ceramics and other materials 03 p0525 A67-13872

Material strength parameter /coupling modulus/ dependence on crack propagation velocity when accounting for rupture kinetics 03 p0529 A67-14166

Stress distribution in vicinity of end of crack moving steadily along boundary joining two elastic materials 03 p0529 A67-14167

Thickness effect on fatigue crack propagation in notched alclad sheet under cyclic tensile loading and transition from tensile fracture mode to shear mode 03 p0532 A67-14386

Stress-corrosion cracking, evaluating role of mechanical, electrochemical and surface energy theories of causation, including hydrogen and other factors 04 p0636 A67-14804

Metastable dislocation crack transformation into polygonal walls of edge dislocations caused by diffusion over crack surface 04 p0711 A67-15282

Moisture effect on slow crack propagation in thin sheets of SAE 4340 steel under static and cyclic loading [ASME PAPER 66-WA/MET-6] 04 p0639 A67-15340

Numerical analysis of crack propagation in cyclic loaded structures, taking into account load ratio and instability at onset of fast fracture [ASME PAPER 66-WA/MET-4] 04 p0711 A67-15342

Fatigue crack propagation rates for aluminum cantilever beams in reversed bending under two-level constant amplitude and random excitation, noting stress cycle effect [ASME PAPER 66-WA/MET-3] 04 p0639 A67-15343

Diffraction of plane harmonic polarized shear waves by half-plane crack extending under antiplane strain [ASME PAPER 66-WA/APM-18] 04 p0714 A67-15409

Cosine series analysis of nonuniform internal pressure effect on crack extension in infinite body 04 p0716 A67-15797

Distributions of screw dislocations in finite slab, examining crack extension with and without plasticity 04 p0718 A67-15798

Stresses in infinitely long strip of finite width containing semiminfinite crack calculated for displaced clamped boundaries, using Wiener-Hopf technique 04 p0718 A67-15923

Effect of structure of beta titanium alloy on crack propagation resistance 04 p0641 A67-15985

Low cycle fatigue crack propagation characteristics of high strength steels, noting technique for life estimation of structure by numerical integration [ASME PAPER 66-MET-3] 05 p0827 A67-16213

Brittle fracture crack theory for elastic body weakened by initially wide crack 05 p0923 A67-17179

Fatigue crack propagation in sheet metal, noting usefulness of McClintock formula 05 p0924 A67-17332

Fatigue crack growth in metal due to plastic deformation, predicting crack growth coefficient 05 p0924 A67-17333

Plane strain fracture toughness, strain instability, slow crack growth and different modes of cracking in metal alloys 06 p1014 A67-17806

Crack growth rate and measurements of temperature effect on low pressure fatigue

of Al 06 p1019 A67-18561

Crack propagation in polymers and polymer type materials 06 p1106 A67-18626

Propagation of brittle cracks in body under compression, discussing theory of resistance of brittle bodies to compression 07 p1263 A67-20030

Electron microscope analysis of stress corrosion crack failure 07 p1211 A67-20250

Finite difference method for finding stress fields around parallel edge cracks 08 p1421 A67-20914

Craggs propagating crack model for isotropic solid extended for general elastic anisotropy, obtaining propagation theory under tensile or shear stress 08 p1421 A67-20952

Stress distribution at tip of crack expanded as power series, noting relation of various terms to crack propagation 08 p1421 A67-20954

Fracture initiation at low stress concentration, noting effect of energetic conditions and independence of plastic zone length from applied stress and defect length 08 p1421 A67-20955

LiF single crystal destruction as function of laser beam energy, examining dislocation pattern arising from crack propagation 08 p1339 A67-21454

Boundary value problems for thin elastic plates, discussing flexural stresses in neighborhood of crack, bending, etc 10 p1715 A67-22915

Thermal stress distribution around crack in elastic solid of transversely isotropic material 10 p1716 A67-22934

Nonlinearities in elastic energy release rate during load-deflection measurements of specimens with varying crack length 10 p1718 A67-23327

Electron microscopy study of fracture surface topography permitting identification of fine scale fracture surface features, relating them to fracture formation mechanisms [AIAA PAPER 66-809] 10 p1661 A67-23552

Stress corrosion cracking of titanium alloys, noting tensile test data, crack propagation in salt solution and in pure solvents and metallurgical and electrochemical factors 10 p1670 A67-23701

Fracture criterion from application of energy principle to elastic plastic crack model, showing positive nature of energy change during propagation 10 p1730 A67-23829

Isolated force solution as Green function for formulation of plane problems for cracks along interface of two bonded half-spaces 10 p1731 A67-23848

Reducing stress levels on crack propagation growth rate investigated for aircraft design problems 11 p1804 A67-24037

Crack propagation for stainless steel and Ti alloy at stresses below fatigue limit, noting of alternating stress cycles crack propagation for stainless steel and Ti alloy at stresses below fatigue limit, noting role 11 p1806 A67-24365

Stress intensity analysis for flat plates loaded close to edge crackline, giving intensity dependence on crack length and specimen shape 11 p1875 A67-24588

Singular integral equations with constant coefficients solved by Jacobi polynomials and applied to problems in fluid dynamics, crack propagation, plane elastic theory, etc 11 p1813 A67-24678

Microstructural variations of Ti-Mo-Al alloys due to stress corrosion cracking, noting increased resistance through heat treatment [ASME PAPER 67-GT-5] 11 p1808 A67-24793

Stress distribution in hole weakened shells of negative Gaussian curvature, noting linear nature of distribution and propagation direction of perturbation 11 p1879 A67-24888

Crack propagation kinetics by thermal fluctuation induction, considering endurance and breakdown of metallic and semimetallic materials 12 p2029 A67-25666

Double cantilever beam specimen for determining plain strain fracture toughness of metals 12 p1956 A67-25946

Thermal stress field effects on materials for idealized situation, discussing problem of half-space and elastic layer under nonuniform surface heating, crack, etc 12 p2032 A67-26198

Book on stress corrosion of metals

covering mechanisms, resistance techniques and tests 13 p2141 A67-27174

Hydrogen influence on fracture propagation of titanium alloy during tension tests 14 p2337 A67-28286

Fracture concept for two-phase structures analyzed on basis of crack-tip displacement, discussing macro-and microstructural cases 14 p2400 A67-28424

Effect of structure of beta titanium alloy on crack propagation resistance 14 p2338 A67-28488

Agreement of crack extension criteria of Griffith and Barenblatt, considering cohesive forces 15 p2504 A67-30093

Periodically fluctuating loading fracture propagation analysis with damage summation principle in stress and cracking time terms, deriving differential equation for fracture length 15 p2576 A67-30183

Screw dislocation and crack interaction when elastic field is independent of one of three Cartesian coordinates 16 p2764 A67-30993

Loading asymmetry effect introduced by short single edge crack specimen loaded in tension along center line 16 p2764 A67-30994

External dislocation effect on conditions for complete fracture from coplanar wedge-shaped crack in presence of applied stress 16 p2765 A67-30996

Crack problems analyzed using Tresca yield conditions to obtain continuous distributions of dislocations 16 p2768 A67-31280

Elastic interactions of cracks and dislocations of screw type in two-dimensional model 16 p2768 A67-31281

Fatigue crack analysis via Bilby, Cottrell and Swinden crack theory, noting inadequacy of energy criterion 16 p2769 A67-31283

Interaction between elastic cracks, dislocation cracks and slip bands describing various characteristics of each case 16 p2769 A67-31284

Crack extension and propagation experiments defining plane-stress regime and providing rationale for Dugdale-Muskhelishvili model, noting stress-strain relations 16 p2769 A67-31286

Plastic yielding near crack tip, noting general solution for deformation and stress distributions for various loads 16 p2769 A67-31288

Fatigue crack propagation in thin plates under fluctuating plane extension and cylindrical bending 16 p2770 A67-31290

Craggs propagating crack model extended to general elastic anisotropy deriving general theory for tensile or shear stress fracture propagation 16 p2770 A67-31291

Electron fractography and analytical fracture mechanics application to fatigue crack propagation, noting stress-intensity-factor role 16 p2771 A67-31296

Cycles required to start crack, and cycles for crack propagation to failure estimated for notched specimen 16 p2771 A67-31297

Fracture - Conference, Sendai, Japan, September 1965, Volume 2 16 p2771 A67-31298

Cross slip and slip character related to fatigue, brittle fracture and strain hardening in crystal solids 16 p2772 A67-31299

Fracture surface markings and topography for transgranular and intergranular paths studied with electron microscope 16 p2772 A67-31300

Fracture surface topography related to micro-and macro-mechanics of fracture for plastic, cleavage and fatigue cases 16 p2772 A67-31301

Fracture surface appearance and crack propagation velocity variation with stress and temperature in tungsten 16 p2688 A67-31302

Activation energies of nucleation of crack and dislocation loops in crystals, noting crack propagation theories and temperature effect 16 p2772 A67-31303

Semibrittle crack propagation dynamical criterion, noting relaxation rate increase with time 16 p2772 A67-31305

Internal fracture of solids analyzing initiation by converging tensile pulses in prolate spheroid and crack propagation in infinite solid 16 p2773 A67-31315

Fatigue in quasi-brittle materials, fatigue in creep range at elevated temperatures and cumulative fatigue

damage 16 p2774 A67-31316

Minimum alternating stress causing given length microcrack to grow and macrocrack growth rate 16 p2774 A67-31317

Fatigue crack growth rates in metals under random loading correlated to cyclic load tests 16 p2774 A67-31320

Plastic energy dissipation rate at onset of rapid crack growth for predicting biaxial fracture 16 p2775 A67-31324

Transient analysis of displacement, strain and stress fields around running crack tip in epoxy plate with central notch using Moire method 16 p2775 A67-31325

Slip step role in early stages of stress corrosion cracking in face centered iron-nickel-chromium alloy thin foils 16 p2690 A67-31384

Strength corrosion cracking of high strength steels and titanium alloys in flowing sea water using cantilever loaded test specimen 16 p2690 A67-31385

Compaction pressure and sintering temperature effect on initiation and propagation of cracks during bend testing of Ni and Mo specimens 16 p2691 A67-31586

Extension of plastic zone in direction of path of moving brittle crack, studying properties of plastic zone to crack length ratio 17 p2960 A67-32633

Monatomic step patterns on /100/ cleavage and tensile crack faces of NaCl crystals originate from dislocation processes of crack tip released by shear stress distribution 18 p3097 A67-33482

Shear stress distribution and dislocation processes at moving crack tips in ionic crystals 18 p3097 A67-33483

Thermal fatigue of 18-8 and 13 Cr steels under transient cross-sectional temperature gradients, noting crack mechanics, tensile stresses, plastic strain range, etc 18 p3140 A67-33651

Hertzian fracture of brittle solid under spherical indenter, discussing path and stability crack in nonuniformly directed stress field 18 p3144 A67-34274

Electron fractography applied to fatigue studies of fracture appearance, morphology of striations and fracture surface microdetails [ASTM PAPER 42] 18 p3068 A67-34580

Electron fractographic techniques for failure analysis, examining fracture direction, differentiation between hydrogen embrittlement and stress corrosion in steels and cyclic stress [ASTM PAPER 44] 18 p3145 A67-34581

Critical loads required for crack propagation terminating at curvilinear hole edge in plate decrease with decreasing radius of corners 19 p3343 A67-35846

Critical loading for crack propagation in structures weakened by holes 19 p3344 A67-35847

Uniformly moving crack in infinite body, in antiplane strain, driven by loads in simultaneous travel 20 p3536 A67-36415

Resistance of ideal crystal studied for plastic yielding and brittle cracking, noting composite materials devised to resist both failures 20 p3469 A67-37248

Supersonic transport structural materials design, considering fatigue behavior, crack propagation and residual static strength under temperature and cyclic load effects 22 p3819 A67-39457

Crack line loading methods for measuring fracture toughness noting advantages over remote loading test procedures 22 p3820 A67-39630

Potential energy release of stressed elastic body due to material removal and crack extension 22 p3911 A67-39679

Crack propagation in solid undergoing cyclic loading using Griffith model, stressing work hardening effect 22 p3911 A67-39680

Fracture theory for amorphous high polymers below glass transition temperature, considering viscoelastic effects on structural defect stress concentration 22 p3824 A67-39740

Safety design for high strength low toughness materials assumed to have hidden flaws, formulating stress intensity factor for fracture mechanics 22 p3913 A67-39982

Gaseous environment influence on fatigue fracture mode in quenched and tempered ultrahigh strength steel investigated by fractographic analysis 22 p3821 A67-40051

Fracture behavior of laminar steel

composites studied to determine effect of interfacial properties on crack propagation 22 p3822 A67-40056

Stress intensity factors for infinite plate subjected to cylindrical bending with radial cracks from internal hole 23 p4073 A67-40615

Crack propagation through mild steel plates investigated by method using stress values at several places near crack and at crack tip 23 p4074 A67-40665

Transient displacement and strain distributions in fracturing notched magnesium plate, using moire-fringe technique and Q-spoiled laser 23 p4076 A67-40736

Double cantilever beam /DCB/ specimen for fracture toughness testing, discussing elastic strain energy release rate and load and crack length extension relation 23 p4018 A67-40928

Cleavage, plastic, creep, fatigue and other types of fracture noting initiation, propagation, mode, behavior, microstructure and appearance 23 p4019 A67-41033

Two-stage heat treatment effect on strength of high temperature Nimonic 80 alloy noting high brittleness, grain size and boundaries and fracture propagation 23 p4019 A67-41076

Long term strength limit and fracture propagation of AKN22 /Nimonic 80/ alloy welds and AKN22-16/13 CrNi steel composites welds 23 p4019 A67-41079

Crack stability for fracture of nonworkhardening elastoplastic material in plane strain or plane stress, using energy criterion 23 p4078 A67-41162

Crack propagation related to stress wave emission number and amplitude for high strength steel, Al and Ti alloys 23 p4078 A67-41163

Thin boundary problems of bimaterial plates bonded along circular arcs behaving like crack imperfections under bending, using fracture mechanics to predict failure 23 p4078 A67-41164

Tensile mean stress effect on dormancy of fatigue edge crack in mild steel 23 p4079 A67-41344

Fatigue crack propagation - ASTM Conference, Atlantic City, June-July 1966 24 p4247 A67-41941

Crack propagation rate and residual static strength of fatigue cracked Ti and steel cylinders for SST design data 24 p4247 A67-41943

Fatigue crack propagation rate in sheet specimens under various loadings simulating rivet forces 24 p4247 A67-41944

Metal fatigue in controlled gaseous environment stressing test variables effects on crack propagation mechanism 24 p4248 A67-41945

Fatigue fracture surface macroscopic and microscopic appearance as affected by prevailing stress intensity conditions at moving crack tip 24 p4170 A67-41946

Transmission electron microscopy for microstructure observations at growing fatigue crack tips in aluminum alloys, discussing plastic dislocation morphology and density 24 p4170 A67-41947

Deformation continuum mechanics near cracks, discussing fatigue load propagation applications and elastoplastic models 24 p4248 A67-41948

High strength aluminum alloy panel resistance to fatigue crack propagation, discussing axial load fatigue machine 24 p4170 A67-41949

Tensile to shear transition behavior of fatigue crack fronts during cycling of sheet materials, noting correlation of shear with crack stress intensities 24 p4170 A67-41950

Double linear damage rule for predicting cumulative fatigue damage, crack initiation and propagation and fatigue life, noting improved accuracy 24 p4170 A67-41951

Fatigue microcrack and macrocrack propagation in aluminum alloys, discussing continuum mechanics approach 24 p4248 A67-41952

Fatigue crack propagation in ultrahigh strength steels, noting rate sensitivity to moisture and plane strain fracture toughness 24 p4171 A67-41953

Fatigue crack propagation in aluminum alloy studied for influence of maximum stress, stress range and sequence of load application 24 p4171 A67-41954

Life tests of tapered roller bearings in

mineral oils and synthetic fluids, demonstrating lubrication effect on contact fatigue crack propagation [ASME PAPER 67-LUB-20] 24 p4163 A67-42678

Ultrasonic monitoring technique for fatigue damage and crack formation and propagation in aircraft structures [AIAA PAPER 67-793] 24 p4251 A67-42954

CRANE

SA GANTRY CRANE

CRANE HELICOPTER

SA MIL MI-10 HELICOPTER

MI-10 Soviet flying crane, very high four-wheeled landing gear enables it to drive over load and clamp it by hydraulically operated grips 02 p0181 A67-12201

Hovering stability of crane helicopter with hanging load, noting effects of supporting point of wire and length, using root locus method 05 p0751 A67-16439

Ch-54 A Flying Crane helicopter, discussing use in Vietnam in terms of field supply, transportation to Vietnam, etc [AHS PAPER 126] 16 p2598 A67-31841

Continuous mechanical ladder for troop/cargo lowering and retrieval from CH-47 helicopter 17 p2804 A67-32518

CRANIUM

SA INTERCRANIAL CIRCULATION

Intracranial pressure measurements and electroplethysmographic examination of blood content in dog cranial cavity for transverse acceleration up to 40 g 13 p2057 A67-26456

CRASH INJURY

Dynamics of commercial aircraft seats with viscous dampers and elastic couplings during crash landing [ASME PAPER 66-WA/SAF-1] 04 p0551 A67-15329

Impact tests on animals at velocity changes suggestive of automobile crash conditions, confirming effect of isovolumetric containment of torso on increased survival limits 08 p1289 A67-20612

Stress-strain analysis of effects of rapid loading rate of restraint harness webbing, especially during air crash 08 p1289 A67-20613

Radiographic analysis of thoracic cardiovascular rupture during abrupt deceleration associated with crashes [ARL-TR-67-17] 08 p1287 A67-20614

Air Force biodynamic research on injury due to impact during air crash or ejection 08 p1289 A67-20615

Medicolegal problems in aircraft flight accidents and traumatic mechanisms 21 p3575 A67-38508

Human spinal column stiffness under deflection rate /axial compression/ produced by impact 23 p3954 A67-41592

Animal study of irreversible trauma in lateral impact when restrained only by aircraft lap seat belt 23 p3954 A67-41595

Injury and fatality analysis in survival study of commercial jet aircraft /Boeing 727/ landing accident with subsequent interior fire 23 p3969 A67-41650

Death and survival during water immersion in plane crashes near Cape Cod and Hamilton Bay 23 p3970 A67-41707

CRATER

SA LUNAR CRATER

SA METEORITIC CRATER

SA METEOROID CRATER

Catalog for interpretation of objects in eastern sector of far side of moon 11 p1867 A67-24844

CRATERING

SA HYPERVELOCITY CRATERING

SA PENETRATION

Martian craters, crater analysis techniques, impact velocities, etc, compared to lunar cratering and possibility of biological existence from Mariner IV photographs 04 p0696 A67-14736

Stochastic model of cratering and survival of craters on moon, discussing approximate diameter distribution of primary and secondary craters 04 p0696 A67-14739

Model for hemispherical cratering of structural metals by hypervelocity impact, determining elastic-plastic threshold stress by true tensile strength measurement 17 p2958 A67-32217

Lunar surface evolution model implying partial melting due to impacts as only cause of primitive plutonic activity 20 p3525 A67-36948

CREEP

SA DEFORMATION

SA DUCTILITY

SA PLASTIC FLOW

SA SHEAR CREEP

SA STEADY STATE CREEP

SA TENSILE CREEP

Book on creep in structural engineering and uniaxial and multiaxial states of stress for stationary and nonstationary creep 03 p0525 A67-13818

Environmental effects on mechanical behavior of metals in vacuum and gases normally found in atmosphere, considering surface oxide layer 04 p0638 A67-14996

Heat treatment and microstructural observations in wrought Ni-base superalloy Udimet 700 in static creep, determining fracture and deformation properties 06 p1015 A67-17809

Torsional creep and creep recovery behavior of amorphous 1, 3, 5-tri-alpha-naphthyl benzene close to or below glass transition temperature 06 p1019 A67-17827

Asymptotic representation of integral operator used in describing time-varying load function in quasi-static and dynamic elastic heredity problems of creep materials 06 p1107 A67-18638

Creep ductility, stress rupture and high temperature irradiation embrittlement of neutron-irradiated Hastelloy N 08 p1343 A67-21195

Long time mechanical and thermal stability of polymeric materials predicted from accelerated testing at increased temperature-time relations 10 p1672 A67-23743

Worm motion of domain walls in Permalloy films using Kerr magneto-optic apparatus under pulse drive with nanosecond rise time 22 p3860 A67-39901

CREEP ANALYSIS

Creep role in powder metallurgy sintering processes, considering plastic deformation, stresses and material transport mechanism 01 p0096 A67-10692

Dislocation model to explain creep curves, predicting linear relation between dislocation density and strain, for small strain 01 p0100 A67-10751

Resolving kernel for analysis of creep and relaxation processes in materials possessing rheological properties 02 p0338 A67-12236

Constant load creep test determination of creep ductility and dimensional instability of nickel at 500 and 525 degrees C 02 p0256 A67-12702

Analytical model developed for using creep data at constant stress to predict creep behavior under linearly increasing stress 03 p0447 A67-13797

Energy method creep analysis of elastic bending of circular plates 04 p0707 A67-14443

Test on nickel and aluminum of Bailey-Orowan equation in relation to work hardening and recovery in creep 04 p0640 A67-15623

Stress concentration in nonlinear creep of thin circular cylindrical shell loaded at one edge by symmetrical radial shear and bending moment 04 p0718 A67-15917

Creep problems during small, periodic, slow or rapid changes in temperature field, noting role of thermal stresses 05 p0912 A67-16176

Differential equation derivation for creep analysis using plastic interaction curve and associated flow rule 05 p0917 A67-16299

Equations representing combined first and second stage creep behavior 05 p0829 A67-16472

Steady state creep stress in shells under uniform internal pressure derived, using transition theory of Seth 05 p0920 A67-16722

Ramberg-Osgood relation that adequately describes stress-strain curve of strain hardening material extended to formulate constitutive laws for creep 05 p0830 A67-16812

Rate controlling mechanism in graphite creep, noting basal slip systems causing general deformation 05 p0833 A67-16892

Cyclic load and temperature effects on creep behavior of Ni-base alloy Mar-M 200 between 1800 and 1900 degrees F 06 p1014 A67-17802

High temperature steady state creep rate analysis of pure Ag and internally ionized Ag-Mg alloys 06 p1014 A67-17805

Torsional creep measurements on natural

rubber vulcanizates cross linked to various degrees complement studies on stress relaxation behavior and dynamic mechanical response 06 p1020 A67-17869

Time dependent deflection behavior under compression loads of stiffened panel at high temperatures 06 p1100 A67-18011

General nonlinear law of hereditary creep 06 p1107 A67-18636

Mechanical properties of alloys in descriptive approach, noting data on precipitation hardening, plastic strain and creep 07 p1211 A67-20176

Monograph on creep and creep rupture as applied to aeronautics field noting problems in boundary and initial value, stability, stressed state, etc 07 p1264 A67-20301

Three-dimensional creep, stress relaxation and viscoelastic measurements of nonlinear viscoelastic materials in continuum 08 p1419 A67-20884

Creep, stress relaxation and vibrational measurements, sinusoidal torsional forced oscillations and stress wave propagation in polymeric linear viscoelastic solids 08 p1419 A67-20885

Plasticity and creep problems solution using conventional elastic optically active materials 08 p1423 A67-21331

Instrument design for analyzing biaxial strain field in thin plate under creep, noting use of moire effect 08 p1332 A67-21461

Correlation among room temperature creep stresses, fatigue and proportional limit in titanium alloys 10 p1669 A67-23325

Nickel-base alloy static and dynamic creep test, examining fatigue zone fracture surface 11 p1806 A67-24364

Oscillation of oscillator with elastically hereditary and weakly nonlinear characteristics, applying operational method to analysis in terms of hereditary creep theory 11 p1876 A67-24682

Gas turbine bucket alloy improvement via heat treatment, noting performance evaluation results from creep rupture tests [ASME PAPER 67-GT-55] 11 p1808 A67-24811

Creep index determination by tests on stress relaxation with elastic members, noting importance of stress distribution at initial moment of loading 11 p1877 A67-24815

Relaxation resistance of metals determined from creep test results, comparing calculated and experimental results 11 p1877 A67-24816

Stress rupture and creep behavior in binary and ternary vanadium alloys including tensile strength and activation energy, noting titanium role 12 p1954 A67-25140

Cyclic loading of thick tube with creep, plasticity and thermal effects 12 p2016 A67-25424

Three-layer shell with lightweight filler under creep studied for initial forms of equilibrium 12 p2024 A67-25598

Approximate solution of creep and relaxation problem for plates and shells subject to bending moments and tensile forces 12 p2025 A67-25610

Stresses and strains in dual element and fibrous to steady state creep load calculated by considering individual properties of constituent elements 12 p2031 A67-25953

Polycrystalline beryllium creep at high temperature 13 p2139 A67-27122

Reciprocal theorem applied to linear and angular displacements due to creep or plastic strains in inelastic bodies 14 p2398 A67-28097

Creep behavior at different stresses approximated through density of dislocation velocity, deriving strain time relation 14 p2400 A67-28420

Behavior study of titanium alloys of interest to aeronautics industry, stressing creep resistance 14 p2338 A67-28628

Creep deformation of composite beam subjected to combined axial and bending loads 14 p2403 A67-29002

Iterative procedures for elastic, plastic and creep deformation of beams 14 p2339 A67-29003

Creep behavior of materials in nuclear reactors, gas turbines and electric power plants, noting aluminum alloy and high temperature material fatigue 15 p2502 A67-29506

Fatigue in quasi-brittle materials, fatigue in creep range at elevated temperatures and cumulative fatigue damage 16 p2774 A67-31316

- Low cycle fatigue behavior of metals at creep range temperature related to equivalent ductility and strain rate 16 p2774 A67-31321
- Creep properties of glass fiber reinforced plastics for long-term bearing structures, noting elastic strain, creep rate, etc 16 p2694 A67-31486
- Creep effects in structures obtained by elastic solution applied to pressurized shells containing discontinuities 16 p2776 A67-31558
- Mechanical properties used to estimate low cycle fatigue behavior in creep range of components in high-temperature systems 16 p2777 A67-31813
- Deformation and distribution of stresses in rotating disk with variable thickness and temperature gradient 17 p2960 A67-32687
- Vacancy source and sink effect on behavior of nonequilibrium concentration of vacancies in diffusion region during creep process 18 p3141 A67-33768
- Photoelastoplastic method using creep and stress characteristics of epoxy resins under thermal cycle, discussing stress-strain behavior [SESA PAPER 1191] 18 p3141 A67-33886
- Maximum entropy principle to derive reliability functions for creep failure modes of engineering materials at high temperatures, noting stress analysis, probability distribution, etc 18 p3145 A67-34675
- Periodic stress and heating during creep, studying deformation adaptability of material for conditions experienced by aircraft engine components 19 p3338 A67-34885
- Boron filaments mechanical properties and chemical compatibility compared with nickel and titanium matrices 19 p3245 A67-35728
- Reports on progress in physics, Volume 29, Part I, covering creep in metals and plasma spectroscopy 19 p3263 A67-35853
- Logarithmic, diffusion and high temperature creep in metals 19 p3248 A67-35854
- Thin walled structure bending in uniform temperature field, calculating stresses, deformations and creep 20 p3536 A67-36446
- Elongation and failure of chromium-molybdenum-vanadium steel analyzed from creep test results 20 p3464 A67-36477
- Crystal deformation and uniaxial failure under complex loading due to stress and temperature variations, applying physical state equation 20 p3540 A67-37057
- Lifetime of structural sections subjected to creep deformation at high temperatures, showing relation to energy dissipation forces 20 p3540 A67-37058
- Stress concentration effects on stress rupture strength, noting applicability to short term creep 21 p3717 A67-37970
- Aluminum alloy creep rates with changing temperature and stresses in hollow sphere, using time dependent viscosity coefficient 21 p3643 A67-38019
- Heat resistant stainless steels evaluated experimentally for fatigue properties, corrosion resistance, creep limit and tensile strength 21 p3646 A67-39010
- Creep properties of sheet materials in SST environment for selection of optimal airframe materials 22 p3818 A67-39225
- Kinetics of structural changes and failure formation and growth in high temperature alloys undergoing creep 22 p3818 A67-39320
- Low temperature transient creep behavior of polycrystalline aluminum investigated experimentally for recovery of surface layer stress 22 p3821 A67-40054
- Thermal stress fracture of brittle ceramics studied for effect of relaxation by creep at high temperature under conditions of quasi-static heat flow 22 p3915 A67-40386
- Metal creep behavior under step function stress application including elastic and plastic deformation 23 p4018 A67-40717
- Cleavage, plastic, creep, fatigue and other types of fracture noting initiation, propagation, mode, behavior, microstructure and appearance 23 p4019 A67-41033
- Dislocation of aluminum during creep investigated for change in block structure 23 p4020 A67-41301
- Torsion creep theory for circular and noncircular tubes using Bredt equation, measuring anisotropy in tubes, calculating torsion stresses 24 p4250 A67-42381
- CREEP BUCKLING**
- Nonuniform temperature distribution effects on creep bending characteristics of linear viscoelastic columns of polymethyl methacrylate 01 p0180 A67-10560
- Variations in tensile and creep-rupture properties of niobium caused by nitrogen additions that produce single-phase and two-phase structures studied at room and high temperatures 02 p0256 A67-12703
- Microstructure effect on creep deformation mechanisms in polycrystalline ceramic oxides including grain size, subgrain structure, porosity, diffusional creep and dislocation movement 03 p0449 A67-13304
- Pore formation, lifetime and microstructure of thin electrolytic metal films under load and high temperature at grain boundaries 12 p1955 A67-25448
- Longitudinal bending and buckling of elastoplastic rods with allowance for creep 15 p2577 A67-30184
- Short time tensile and long time creep-rupture properties of HF and HH iron-chromium-nickel alloys at high temperatures [ASTM PAPER 52] 18 p3068 A67-34582
- Creep buckling load for thin circular rings determined by tangent modulus theory together with isochronous stress-strain diagram 21 p3719 A67-38022
- Pore formation, lifetime and microstructure of thin electrolytic metal films under load and high temperature at grain boundaries 21 p3646 A67-38827
- Axisymmetric creep in cylindrical shells, noting creep buckling collapse after high temperature compression loading 21 p3727 A67-38872
- Long cylindrical two-layer shell critical asymmetric buckling time for steady creep due to external pressure and axial compression, applying variational principle 24 p4250 A67-42306
- High temperature low cycle creep range strain fatigue behavior estimation from tensile and stress rupture properties 24 p4251 A67-42483
- CREEP DIAGRAM**
- Grain boundary relaxation in high purity fcc metal using LF torsion pendulum, noting tests for internal friction and creep at constant stress 06 p1016 A67-17899
- Stress relaxation, creep and uniaxial elongation of polycrystals relationship as part of cumulative plastic deformation processes 06 p1109 A67-18809
- Wall creeping in thin magnetic Ni-Fe films analyzed as function of thickness, field pulse amplitude, etc, comparing results with existing theories 11 p1845 A67-23953
- Low temperature mechanical properties of E1827 alloy investigated under static uniaxial elongation, noting ultimate strength increases with decreasing temperature 12 p1955 A67-25370
- CREEP RESISTANCE**
- Prolonged high temperature creep and endurance testing of refractory materials in vacuum or inert media 01 p0051 A67-11247
- Creep deformation of hot-rolled Zn-Ti alloys, noting secondary flow originating from strain induced grain growth 03 p0440 A67-13251
- Refractory metal alloys mechanical properties, metallurgical behavior and applications 05 p0829 A67-16741
- Vacuum testing machine to determine tensile and creep properties of heavily drawn W wires at temperatures up to 2500 degrees F 06 p1013 A67-17799
- Carburization of niobium and tantalum-base alloys through exposure to gaseous mixture of benzene-hydrogen, noting results of creep rupture tests 08 p1341 A67-20765
- Fracture behavior of creep resistant alloy steel and nickel-chromium alloy subjected to cyclic loading at elevated temperatures 09 p1517 A67-21556
- Postquenching deformation effect on mechanical properties and creep resistance of aluminum alloys 09 p1519 A67-22156
- Test method for metal resistance to thermal fatigue under active creep conditions 09 p1519 A67-22168
- Dependence of creep, corrosion and thermal fatigue of gas turbine vanes and blades upon inlet temperature and rate of change [ASME PAPER 67-GT-17] 11 p1808 A67-24801
- Vacuum apparatus for testing flat and cylindrical specimens of high melting point materials for creep and long term strength 11 p1877 A67-24817
- Structural changes effect on creep resistance of heat resistant alloys 12 p1955 A67-25371
- Refractory metal alloys tested in ultrahigh vacuum, measuring creep extension 16 p2690 A67-31524
- Prolonged high temperature creep and endurance testing of refractory materials in vacuum or inert media 17 p2835 A67-33170
- Mechanicochemical treatment for high temperature strength increase in metals, noting effects on creep strength, stress relaxation, etc 19 p3247 A67-35852
- CREEP TESTING MACHINE**
- Centrifugal machines generating creep-design data by spinning specimens at identical temperature 03 p0395 A67-13542
- Phenomenological process in thermal fatigue research, equipment, tests and evaluation 09 p1576 A67-22475
- Creep measurement associated with adhesive bonding of aircraft structures, particularly creep of metal-metal lap joints and bonded sandwich structures creep measurement associated with adhesive bonding 09 p1522 A67-22505
- Electronic computer usage to control temperature during creep and long term strength tests of heat resistant steels 11 p1877 A67-24818
- Refractory metal alloys tested in ultrahigh vacuum, measuring creep extension 16 p2690 A67-31524
- CREW**
- S AIRCREW
- S ASTRONAUT
- S FLYING PERSONNEL
- S GROUND CREW
- S PILOT
- S SPACECREW
- CRITICAL FREQUENCY**
- Phase reversal in lunar variations of critical frequencies of F-2 layer at Waltair, India 01 p0060 A67-11232
- Diurnal variations of boundary frequencies of sporadic c-type E layer, deriving cosine law not dependent on sunspot cycle 01 p0061 A67-11289
- Critical frequencies of F-2 and E layers in ionosphere relation to total daily influx of solar wave radiation into earth atmosphere 05 p0800 A67-17128
- Diurnal and short period h sporadic E layer and critical frequency sporadic E layer variations analyzed from data obtained at Ashkhabad station 05 p0800 A67-17129
- Statistical distribution of monthly median noon critical frequency of F-2 layer from ionospheric stations at mid-latitudes, auroral regions and at polar cap 07 p1174 A67-19703
- Critical ionization frequencies in F-2 layer in near-polar region observed at Northern Hemisphere high latitude stations 07 p1179 A67-19832
- Calculation of time behavior of forenoon anomaly in diurnal variations of critical frequency of normal E layer 07 p1183 A67-20118
- Tidal force effect on variations of critical frequencies of sporadic E layer 10 p1631 A67-22806
- Ionization density as decisive factor in integral radio wave absorption increase accompanying increase in critical sporadic E layer frequency 10 p1631 A67-22807
- Freely precessible gyroscope viscous fluid nutation damping response to translational and vibration accelerations near critical frequencies 12 p1942 A67-25679
- F layer critical frequency perturbations due to low altitude nuclear explosion 13 p2107 A67-26309
- Microwave attenuation standard derived using waveguide below critical frequency as voltage divider to determine losses in components 13 p2067 A67-26488
- Sporadic E layer generated by meteoritic ionization noting critical frequency 13 p2111 A67-26601
- Revised ionization-equilibrium equation to obtain criterion for presence of winter anomaly in E layer 14 p2307 A67-27912
- Radio waves effect on ionospheric F layer, showing decrease in critical frequency and disturbance of stationary electron and ion concentration 14 p2307 A67-27923
- Ionospheric index of solar activity obtained together with quadratic equation regression coefficients by minimizing standard error of F-2 layer critical

frequency 14 p2311 A67-28375
 Quiet sun current system effects on seasonal variations of critical frequency in E region, noting dependence on local time and latitude 14 p2312 A67-28569
 Critical frequency dependence of p1-4 type semiconductor triodes on emitter current or injection level 14 p2289 A67-28824
 Occurrence frequency of midlatitude blanketing sporadic E studied for seasonal, diurnal and latitudinal variations 15 p2476 A67-29622
 Stability boundaries and critical frequencies for semiminfinite elastically restrained plate determined at different boundary stiffnesses 15 p2575 A67-29858
 Strong ionospheric effects observed on ionograms after high altitude detonation including changes in F layer critical frequency, height and spread [AGARDOGRAPH 95] 15 p2484 A67-30306
 Magnetic storm effects on F-2 layer near equatorial zone boundary causing variations in critical frequency of layer 16 p2663 A67-30970
 Diurnal variations asymmetry in critical frequency ratio of E layer for morning and evening values 16 p2668 A67-31895
 Relationship between variations of critical frequencies of sporadic E layer and solar activity cycle 16 p2669 A67-31903
 27-day cycle variation in various noncosmic ray electromagnetic complex phenomena 17 p2932 A67-32084
 Seasonal variations in afternoon and evening maxima of F-2 layer and dependence of temperature and frequency on minimum zenith angle of sun 17 p2842 A67-32384
 Plane wave propagation in kinetic theory, discussing Boltzmann equation use and asymptotic results beyond critical frequency 17 p2905 A67-32927
 Design concept for piezoelectric resonator through mathematical formulation, determining critical frequencies and electron drift rates 18 p3043 A67-33462
 Noise analysis in He-Ne laser during RF and DC excitation, noting relation between critical frequency and lifetime of metastable atom 18 p3058 A67-33648
 Iranian ionospheric observations, giving monthly median values of vertical-incidence data and critical frequency graphs 19 p3224 A67-35489
 Screening frequency dependence on reflection cut-off frequency in sporadic E layer 20 p3428 A67-36762
 Parametric resonance in near-canonical systems with critical frequencies and instability boundary domain formulas derived from Yakubovich results 21 p3657 A67-37989
 Analog computer method application for determining critical frequency and critical flutter speed of wing having torsional bending vibrations in airflow 21 p3718 A67-37992
 Critical frequencies of F-2 and E layers in ionosphere relation to total daily influx of solar wave radiation into earth atmosphere 21 p3618 A67-38471
 Diurnal and short period h sporadic E layer and critical frequency sporadic E layer variations analyzed from data obtained at Ashkhabad station 21 p3618 A67-38472
 Planetary distribution of horizontal gradients of F-2 layer critical frequency and diurnal, seasonal and solar cycle variations 21 p3622 A67-39034
 F-2 layer critical frequencies variation with solar activity, evaluating criteria for unperturbed state based on magnetically inactive days 21 p3622 A67-39035
 Latitude variation of critical frequency of F-2 layer in equatorial region during geomagnetic disturbance, discussing ionization density 21 p3622 A67-39036
 Duration of continuous occurrence of sporadic E layer dependence on incidence of sporadic E layer critical frequency maximum value 21 p3623 A67-39039
 Ionospheric F-1 layer critical frequency at sunspot minimum and maximum, discussing critical frequency diurnal variation 22 p3789 A67-39476
 Temperature dependence of carrier drift type transistor characteristic frequency, discussing temperature and diffusion coefficients 23 p3983 A67-41676
 Tidal force effect on variations of critical

frequencies of sporadic E layer 24 p4150 A67-42143
 Ionization density as decisive factor in integral radio wave absorption increase accompanying increase in critical sporadic E layer frequency 24 p4150 A67-42144
 E layer critical frequency calculation for 80 selected diurnal variations, considering forenoon anomaly effect 24 p4151 A67-42704
CRITICAL INCLINATION THEORY
 Mathematical investigation of satellite motion in vicinity of critical inclination, analyzing singularity 14 p2384 A67-28077
CRITICAL LOADING
 Stability of thin walled conical shells under axially symmetric loading determined from nonlinear shell theory [DVL-605] 03 p0521 A67-13020
 Critical load equations for plate weakened by sharp stress raisers extended to account for effect of arbitrarily oriented external forces 03 p0522 A67-13122
 Laminate optimization for filamentary composites, discussing applied spectrum of load requirement 03 p0453 A67-13413
 Load concentration effects on stability of rigidly reinforced strictly convex shell, determining upper critical load 03 p0526 A67-14063
 Conical shell stability during axial compression and internal pressure under conditions of heating, noting reduction of critical load 05 p0913 A67-16192
 Linear local buckling theory for finite length axially compressed circular cylinder and length effect on critical load 05 p0918 A67-16421
 Brittle fracture crack theory for elastic body weakened by initially wide crack 05 p0923 A67-17179
 Stability of elastic systems in small and in large, determining bending deformation of rod, noting presence of upper and lower critical loads 06 p1108 A67-18663
 Elastic postbuckling involves coupled modes when critical loads corresponding to buckling modes of two degrees of freedom system are equal 08 p1422 A67-21032
 Linearization of hyperbolic equation for data analysis of stability of elastic column and plate structures, determining critical load 11 p1874 A67-24224
 Cylindrical shell stability under external pressure, presenting critical load value and nature of undulation 11 p1880 A67-25054
 Closed cylindrical shell stability under combined bending and axial compression taking into account original arbitrary imperfection of shell form 12 p2020 A67-25567
 Cylindrical shell stability under external radial load noting stress-strain states, critical load, etc 12 p2020 A67-25572
 Cylindrical shell stability under nonuniform load, noting critical load dependence on subtending angle 12 p2020 A67-25573
 Lower critical load determination of elastic spherical shell with rigidly fastened edge 12 p2021 A67-25580
 Matrix integral equations to calculate critical stresses and natural frequencies of oscillation of thin walled isotropic shells of revolution 12 p2022 A67-25585
 Deflection function of glass fiber reinforced circular cylindrical shells under axial supercritical compressive loading 12 p2023 A67-25590
 Lower and upper critical loads measured in process of axial compression of cylindrical shells of glass fiber reinforced resin 12 p2031 A67-25959
 Lower critical load for deformation of cylindrical shell in torsion and hinged along edges 13 p2215 A67-26376
 Goldenveizer technique to determine stability loss by shells of negative Gaussian curvature 13 p2218 A67-26891
 Load concentration effects on stability of rigidly reinforced strictly convex shell, determining upper critical load 13 p2221 A67-27722
 Stress-strain state of short cylindrical shell and square panel under axial compression hinged along edges 14 p2402 A67-28897
 Direct matrix method for analysis of critical loads and associated buckling modes for struts having various end constraints 14 p2403 A67-29017
 Stability of equilibrium of nonconservative

continuous systems with slight damping 17 p2959 A67-32414
 Stiffener eccentricity effect on critical load in cylindrical shells under axial compression 17 p2961 A67-32775
 Critical compressive forces causing instability of rigidly-fastened rectangular plate determined by method of summary representations 17 p2962 A67-32871
 Large deflections of columns of variable flexural rigidity, assuming bending moment is proportional to curvature 17 p2963 A67-33020
 Partial cone crack formation in brittle material loaded with sliding spherical indenter 18 p3144 A67-34275
 Critical loads required for crack propagation terminating at curvilinear hole edge in plate decrease with decreasing radius of corners 19 p3343 A67-35846
 Critical loading for crack propagation in structures weakened by holes 19 p3344 A67-35847
 Critical plastic buckling of compressed spar flanges 20 p3537 A67-36642
 Maximum strengths of aluminum alloy and metal columns under parameter variation, using mathematical model 20 p3538 A67-36780
 Circular cylindrical shell buckling mode and upper critical load under external transverse pressure, considering dynamic edge effect on shell stability 21 p3717 A67-37975
 Creep buckling load for thin circular rings determined by tangent modulus theory together with isochronous stress-strain diagram 21 p3719 A67-38022
 Shell of revolution stability under axial compressive loading with changes in curvature due to initial imperfections effects 21 p3719 A67-38053
 Compression strength analysis of plane and cylindrical multilayer skin panels reinforced by corrugated fillers, determining critical load and local stability loss 21 p3725 A67-38787
 Elastic stability of cantilever column having fixed compressive and circulatory nonconservative loadings, determining critical loads 21 p3729 A67-39084
 Plate stability loss criterion for critical external load values without determining initial stresses applied to rectangular plate Sommerfeld problem 22 p3909 A67-39401
 Unloaded thin walled spherical shell rigidly hinged along edge noting existence of nontrivial form of equilibrium and negative lower critical load 22 p3910 A67-39402
 Elastically filled imperfect closed cylindrical shell stability, showing initial configuration defect effects on critical load relation to filler rigidity 22 p3912 A67-39685
 Squeeze film journal bearing load support capability, noting axial pressure distribution in finite case is considerably greater than infinite case [ASME PAPER 67-LUB-14] 24 p4163 A67-42675
CRITICAL MACH NUMBER
 Calculation of compressible subsonic potential flow through blade cascades, giving air outlet angle, velocity distribution around blade profile and critical Mach number 17 p2791 A67-32711
CRITICAL MASS
 Change in critical mass of large reflector moderated gaseous-fueled cavity reactor due to presence of hot hydrogen gas in cavity 12 p1965 A67-25908
CRITICAL PATH ANALYSIS
 Critical Path Analysis /CPA/ system based on network techniques, coordinating separate development programs of ELDO member states 15 p2583 A67-30223
CRITICAL POINT
 Turbulent reattachment of supersonic jet noting recompression region of flow, critical points and similarity law in evolution of wall pressures [ONERA-TP-326] 01 p0053 A67-11002
 Semiautomatic potentiometer measurement of nitrogen specific heat at small intervals, noting applicability of logarithmic law for other temperature ranges 03 p0532 A67-12929
 Superconducting critical temperatures of nonstoichiometric transition metal carbides and nitrides, correlating data with valence electron concentration 03 p0491 A67-13256
 Critical conditions of waveguide with dielectric bushing for case of

nonsymmetrical waves 03 p0378 A67-13287
 Phenomenological theory of mass transfer in binary systems near critical point applied to particular boundary value problems 04 p0727 A67-15683
 Critical phenomena in fluids with reference to liquid hydrogen 05 p0928 A67-17011
 Near wake uniqueness and criticality condition in Crocco-Lees mixing theory, obtaining critical point from boundary layer equations of motion [AIAA PAPER 67-65] 07 p1168 A67-19433
 Growth of critical temperature of small superconductor samples explained within framework of BCS superconductivity theory without using electron pairing 08 p1372 A67-21502
 Parallel critical field calculation of tunneling barrier extended to all temperatures in dirty limit 09 p1552 A67-21745
 Spatial dispersion of viscosity coefficients of liquids near critical point 09 p1487 A67-21904
 Diffusion in solutions in nearly critical states, noting increased cross effects and linear dependence of flows near critical points 09 p1580 A67-21908
 Motion equations and boundary conditions for viscous liquid, noting operator characteristics of viscosity coefficients near critical point 09 p1487 A67-21909
 Thermal differential method of determining critical points in flow past projection in pipe 11 p1741 A67-24032
 Critical point thermodynamics, refuting criticism concerning Planck-Gibbs equation 11 p1882 A67-24036
 Probable upper limit of critical field for ternary and higher order ductile transition metal superconducting alloys 11 p1850 A67-24925
 Upper critical field limits for bulk type II superconductors 11 p1850 A67-24933
 Binary van der Waals mixture near solution critical point, noting anomalous behavior of heat capacity, shear viscosity and bulk viscosity 11 p1884 A67-24990
 Thermodynamic investigation of singularity properties of critical point of vapor-liquid equilibrium 13 p2230 A67-27725
 Two-zone superconductor with nonmagnetic impurity, noting correspondence of thermodynamic values to single-zone pure state except for density 14 p2369 A67-28672
 Transitional impurity effects on superconducting critical temperature of normal metals, stressing localized states with no magnetic moments 14 p2371 A67-28727
 Critical region determination in viscous fluid flow using dye stream fuzziness or pressure drop discontinuity as measure of flow turbulence 14 p2305 A67-28801
 Critical temperatures and phase composition of films obtained by vacuum deposition of sublimed cadmium telluride 15 p2537 A67-29706
 Critical field dependence on pressure, tube radius and ion mass derived from ion-acoustic instability growth in low pressure RF discharge 15 p2531 A67-29904
 Atmospheric pressure discharges in inert gases seeded with alkali metal vapor, noting transition to low voltage high current discharge 16 p2709 A67-30513
 Scaling-law equation of state for gases in critical region 16 p2778 A67-31061
 Hysteretic superconductor, analyzing critical state and constrained reversibility relations in diamagnetic and temperature paths 17 p2912 A67-32269
 Superconductors and ferromagnetic domains proximity effects at critical temperature in resistive and tunneling effect measurements 17 p2912 A67-32271
 Critical parameters for vanadium-niobium alloys superconduction, giving curves for transition temperature and measuring critical electric fields 17 p2874 A67-32973
 Mean free path effects on critical field and density of states of small superconducting spheres 17 p2924 A67-33370
 Thin superconducting films behavior in perpendicular magnetic fields, studying sample geometry effect on reversible magnetization curve 19 p3303 A67-35041
 Critical fields in strong coupling superconductors, using Ginsburg-Landau equations 19 p3303 A67-35042

Asymmetric stability loss of nonuniformly heated circular plate rib, determining elastic properties and critical temperature jump value 20 p3536 A67-36447
 Critical surface between superconducting and normal state determined for commercial niobium stannide ribbon and Nb-Zr wire 20 p3512 A67-37346
 Superconducting critical temperature of sandwich of two semiconducting films in contact 20 p3512 A67-37434
 Superconducting critical temperature below Kondo temperature for metal solutions with magnetic impurities calculated, using Green function 21 p3680 A67-38350
 Boundary layer flow incident on smooth axisymmetric body in vicinity of critical point 21 p3613 A67-38422
 Nuclear relaxation time measurement in superconducting niobium near upper critical field 21 p3684 A67-38563
 Mixed state existence in type I superconducting thin film, discussing microwave power absorption variation with perpendicular magnetic field 22 p3856 A67-39437
 Limited instability and flux jumping variation with magnetic field for flux pinning and Lorentz forces equilibrium in mixed state of type II superconductor 22 p3856 A67-39438
 Generalized Ginsburg-Landau parameters and magnetic properties of type II superconductors near upper critical field 22 p3857 A67-39440
 Lattice type gas heat capacity discontinuity near critical point 22 p3790 A67-39509
 Temperature field and critical thermal loads for fuel elements with varying convective heat transfer coefficient and ambient temperature 23 p4082 A67-41286
 Critical temperatures and phase composition of films obtained by vacuum deposition of sublimed cadmium telluride 24 p4199 A67-41776
 Critical temperature near superconducting phase transition investigated for alloys and pure superconductors 24 p4200 A67-41867
 Porous cermet tubular element fire barriers of stainless steel powder for increased safety in gas flame processes, determining critical Peclet values 24 p4159 A67-41957
 Long cylindrical two-layer shell critical asymmetric buckling time for steady creep due to external pressure and axial compression, applying variational principle 24 p4250 A67-42306

CRITICAL PRESSURE

Instability of thin reinforced cylindrical shell clamped at both ends and energy method calculation of critical pressure 05 p0918 A67-16422
 Statistical analysis discrepancy in physical experimental values of buckling pressures of spherical shells 06 p1111 A67-18876
 Lower bound for limit pressure of cylindrical pressure vessel with unreinforced hole obtained by restricting stress directions of cylinder 08 p1421 A67-20921
 Shallow conical shell stability acted upon by external hydrostatic pressure 12 p2028 A67-25635
 Graphic representation of Mises formula for stability analysis of cylindrical shell, discussing critical pressure and time and labor saving 19 p3338 A67-34875
 Possibility of pressure destroying superconductivity in various metals, studying transition temperatures, critical pressures, etc 19 p3303 A67-35043
 Safety control requirements in thermal-vacuum testing involving protection against electric equipment operation in pressure range for glow discharge 22 p3782 A67-40404
 Rat adrenal gland responses to increased oxygen tension at ambient temperature, noting oxygen critical threshold partial pressure affecting survival time 23 p3950 A67-41538
 Turbojet engine gasdynamic parameters dependence on reduced rotational velocity for in-flight characteristics determination, assuming variable compression and critical pressure ratio 24 p4207 A67-41916
 Critical air-water flow in converging-diverging annular venturi noting pressure profiles 24 p4143 A67-42280

CRITICAL REYNOLDS NUMBER

Pressure measurements on surface and in wake of circular cylinder at rest and in vortex excited oscillation at subcritical Reynolds numbers [ASME PAPER 67-VIBR-31] 11 p1777 A67-24189
 Karman vortices in heat exchanger, noting no vortex shedding in supercritical Reynolds number range and wake turbulence 11 p1782 A67-24657
 Critical region determination in viscous fluid flow using dye stream fuzziness or pressure drop discontinuity as measure of flow turbulence 14 p2305 A67-28801
 Far wake behavior of hypersonic spheres analyzed using schlieren techniques 15 p2417 A67-30190
 Hydrodynamic stability of plane incompressible viscous wall jet subjected to small disturbances, determining critical Reynolds number, eigenvalues and eigenfunctions 16 p2660 A67-31213
 Oscillations of electric arcs with superimposed gas flow in cylindrical nozzle and rectangular channel, determining critical Reynolds number 19 p3280 A67-35147
 Critical Reynolds number of laminar-turbulent transition for Newtonian flow in rectangular ducts to verify minimum in curve as function of duct aspect ratio 19 p3210 A67-35616

CRITICAL SPEED

Monograph on higher modes of critical speed of shafts with elastic clamping moment at bearings 02 p0250 A67-12710
 Thin rod bending and twisting theory applied to critical speed of rotating shaft under axial loading and tangential torsion, using Galerkin approximation [ASME PAPER 66-WA/MD-1] 04 p0629 A67-15348
 Fluid film and rolling element bearings effect on turbomachinery rotor dynamics including critical speeds, imbalance response, instability, turbulence, etc [SAE PAPER 670059] 09 p1508 A67-22533
 Gyroscopic moment effect on critical speeds of shaft-disk system mounted in short end bearings, obtaining frequency equations [ASME PAPER 67-VIBR-9] 11 p1795 A67-24169
 Unbalanced rotor deceleration through critical speed tested, considering maximum deflection increment and bending stress in rotor shaft [ASME PAPER 67-VIBR-17] 11 p1796 A67-24176
 Angular precession and critical speed of two-bearing machines with overhung weight determined, considering shear deformation, gyroscopic moment and rotatory inertia [ASME PAPER 67-VIBR-19] 11 p1796 A67-24178
 Supercritical speed helicopter power transmission shaft for rotor synchronizing, noting viscous damper for controlling shaft vibrations [ASME PAPER 67-VIBR-20] 11 p1796 A67-24179
 General solution for motion equation of rotating shaft with changing angular velocity, noting transition through critical speed 12 p1949 A67-25408
 Turbomachine rotating shaft and rotor systems critical speeds taking into account bearing support stiffness and clearances, noting vibration mode 12 p1949 A67-25410
 Vibration problems in high speed turbines including stability, critical speeds and support structure effect on rotor response [ASME PAPER 67-DE-8] 14 p2402 A67-28867
 Critical rolling speed of aircraft tires calculated and experimentally verified 16 p2596 A67-31002
 Critical speed control by squeeze-film oil damper between two nonrotating parts in parallel with flexible bearing support, using mathematical model [SAE PAPER 670347] 17 p2865 A67-32989
 Dynamic modeling of complex rotor system to determine critical velocities, noting influence of number of mass concentrations on accuracy 21 p3689 A67-37951
 Critical fluid flow rate analysis of two-phase nitrogen at stagnation pressure of 25 psia 22 p3784 A67-39967
 Coaxial rotors natural vibrations analysis

by computer showing occurrence at rpms above first critical speed 23 p4009 A67-40685
Taylor vortices and turbulence in flow between eccentric rotating cylinders [ASME PAPER 67-LUB-12] 24 p4145 A67-42673

CRITICAL STRESS

Amplitude-dependent internal friction and defect structures in aluminum, measuring critical alternating shearing stress by bridge-circuit method 01 p0101 A67-10845
General critical stressed state of strictly convex shell under arbitrary load distributed over edge 04 p0719 A67-15983
Critical stresses of three-layer wing panel compressed by load distributed along two sides, determining temperature stresses in bearing layers and equilibrium equations 05 p0913 A67-16191
Lower bounds for crack tip stress intensity factors of irregularly shaped planar cracks 08 p1422 A67-20956
Critical stresses of compressed three-layer cylindrical shell of asymmetrical structure in presence of variable temperature 12 p2026 A67-25614
Equation for relation between critical stresses of cylindrical shell loading and minimum natural-oscillation frequency of unloaded shell 12 p2027 A67-25623
Plastic deformation mechanisms of polycrystalline beryllium to analyze temperature dependence of critical shear in prismatic plane 13 p2138 A67-27121
General critical stressed state of strictly convex shell under arbitrary load distributed over edge 14 p2400 A67-28492
Structural modifications effect on PBI fiber critical properties, discussing strain-stress characteristics, target properties and crystallization 21 p3648 A67-37875
Critical compression stresses in cylindrical panel with clamped lateral edges and free longitudinal edge 21 p3726 A67-38796
Three layer cylinders and cylindrical and plane panel optimum parameters using critical stress expressions from nonlinear elasticity theory 21 p3729 A67-38915

CROCCO-LEE THEORY

Two-dimensional shock induced separated flows in turbulent boundary layer, applying Crocco-Lee theory and calculating pressure rise coefficient 02 p0231 A67-11522
Near wake uniqueness and criticality condition in Crocco-Lees mixing theory, obtaining critical point from boundary layer equations of motion [AIAA PAPER 67-65] 07 p1168 A67-19433
Mixing function parameter behavior in boundary layer separations by Crocco-Lees method, noting linearized Glick differential equations 17 p2840 A67-33031

CROCCO METHOD

Linearized Crocco equation for zero pressure gradient and constant viscosity density product applied to boundary layer problem 12 p1929 A67-25907
Difference method of solving boundary layer equation for laminar suction boundary layer using Crocco form 17 p2790 A67-32260
Ideal fluid energy-momentum tensor derivation of Crocco-Vazsonyi equation for ideal fluid relativistic hydrodynamics, discussing continuity equation for specific entrophy 19 p3210 A67-35707

CROSS CORRELATION

Low noise receivers to achieve high sensitivity and accurate cross correlation measurement of antenna patterns, using radio star sources 02 p0213 A67-11617
Two spatial distributions transformed simultaneously with single lens heterodyning Fourier transform of spatial spectra 03 p0423 A67-13904
Frequency fluctuations of laser field determined by measuring cross correlation function at two points 05 p0815 A67-16625
Remote sensing cross-beam cross correlation methods of determining spatially resolved average thermodynamic properties [AIAA PAPER 67-149] 06 p1004 A67-18477
Dynamic properties of coupled systems derived from experimentally determined frequency response functions of component systems, noting cross correlation functions 09 p1573 A67-21752
Stabilized cross correlation radiometer for use at decametric wavelength, using two feedback loops controlling four noise diodes 11 p1762 A67-24288
Cross correlation and statistical

dependence between envelope and frequency deviation of sine wave plus random noise, noting possible application to frequency demodulation 11 p1753 A67-24646
Output characteristic function for two-channel analog cross correlator with each channel input consisting of deterministic signal combined with stationary Gaussian noise 12 p1918 A67-26080
Space-time cross correlation function for antennas generalized by complex antenna-height function 12 p1917 A67-26089
Cross correlation /by superposed epoch method/ between upper atmospheric sodium and stratospheric warmings at high latitude 13 p2110 A67-26441
Impulse response of dynamic systems using cross correlation techniques 13 p2081 A67-27220
Cross correlation bounds and positivity of nonlinear operators, examining criteria for positive composition 15 p2457 A67-29373
Stability of feedback systems with monotone and odd monotone nonlinearities 15 p2457 A67-29374
Reducing disturbances of certain form to zero by generating modified form of test signal to be applied to cross correlator 15 p2461 A67-30322
Recursive procedures for determining relationships between random parameter of linear system and resulting output random variable 16 p2652 A67-31691
Local turbulent properties of shear layer derived from covariance of two crossed perpendicular beams of radiation 17 p2855 A67-32282
Enhancement of signal to noise ratio of turbulence measurements by cross correlation and heat transfer transducer 18 p3050 A67-34499
Voltage amplitude limiting for improving stability of correlation detector of electronic cross correlation systems, noting variation of SNR 18 p3012 A67-34524
Essential additional operator, essential transformed system and cross correlation function methods for self-adjusting circuit design, considering sign of gradient component 21 p3604 A67-39110
Combined frequency and space correlation of wave fields scattered by rough surfaces where conditions of applicability of Kirchhoff approximation hold true 22 p3760 A67-39660

CROSS COUPLING

Modal analysis of mutual coupling effects of triangular grid array of waveguide radiators having nonzero wall thickness 02 p0212 A67-11614
Structural compliance induced cross axis coupling effect on gimballing system stability of rocket engine two-axis attitude TVC system [AIAA PAPER 67-42] 06 p1097 A67-18448
Quasi-optimum three-axis attitude control law for minimum time of rigid body, noting gyroscopic cross axis coupling 22 p3899 A67-39190
Mathematical model for linear memory arrays cross coupling problems, discussing signal distortion due to common mode capacitance effect 22 p3765 A67-39912
Cross coupling effects in strapdown orbital gyrocompass to determine attitude of vehicle with respect to planet-centered coordinate system 22 p3801 A67-40188
Structural compliance induced cross axis coupling effect on gimballing system stability of rocket engine two-axis attitude TVC system [AIAA PAPER 67-42] 24 p4242 A67-42909

CROSS LINKING

Torsional creep measurements on natural rubber vulcanizates cross linked to various degrees complement studies on stress relaxation behavior and dynamic mechanical response 06 p1020 A67-17869
Free energy of polymer solid consisting of entangled long chain molecules when deformed by elastic strain 22 p3826 A67-40201

CROSS RELAXATION

Temperature dependence of paramagnetic resonance spectral shifts in chromium-doped titanium oxide crystal of cross relaxation rutile maser 07 p1196 A67-19676
Nonexponential electron spin cross relaxation measurement in dilute ruby 17 p2924 A67-33369

CROSS SECTION

S ABSORPTION CROSS SECTION
S IONIZATION CROSS SECTION
S NEUTRON CROSS SECTION
S RADAR CROSS SECTION
S SCATTERING CROSS SECTION
CROSSED FIELD

MHD rotation of conducting viscoplastic fluid between two coaxial cylinders in crossed fields 01 p0120 A67-10180
Crossed electric and magnetic fields effect on quasi-liquefaction process of nonconducting particles by electrolyte 01 p0121 A67-10189
Repetitive plasma breakdown in flat electrode accelerator causing relatively low plasma velocity 02 p0275 A67-12472
Room temperature recombination radiation induced by Lorentz field in InSb and ternary alloy of mercury, cadmium and tellurium under cross field conditions 03 p0496 A67-13675
Semiconductor plasma slab subject to crossed electric and magnetic fields, examining plasma density wave instability caused by gradient in carrier density perpendicular to magnetic field 04 p0674 A67-14612
Solar wind plasma penetration into geomagnetic field under effects of drift in crossed electric-geomagnetic fields 05 p0884 A67-17120
Charged and neutral particles collision effect on LF oscillations in weakly ionized plasma in crossed electric and magnetic fields 06 p1046 A67-18827
Electron motion in crossed fields with arbitrary ratio of electric and magnetic fields, considering simultaneously valence and conduction bands 06 p1069 A67-18978
Boundary layer at electrode and center of flow of plane MHD generator calculated numerically by one-dimensional theory for subsonic and supersonic velocities 09 p1443 A67-21808
Microwave and optical generation and amplification - International Conference, Cambridge, England, September 1966 09 p1476 A67-22251
Energy characteristics of magnetically stabilized plasmatron effect on output power in crossed fields 09 p1547 A67-22316
Absorption coefficient of light in semiconductors in crossed electric and magnetic fields, examining conditions for Franz-Keldysh effect occurring in magnetic field 10 p1693 A67-23590
Cross field diffusion coefficient measurement from volume loss properties of single ended Q device plasma column 11 p1830 A67-24005
Minimum B magnetic field geometry effect on spontaneous oscillations and anomalous cross field plasma transport in TOPSY Q device with uniform axial magnetic field 11 p1835 A67-24388
Ion acceleration by drift resonance caused by crossed magnetostatic and space charge electrostatic fields 11 p1841 A67-24768
Electrostatic polarization of cylindrical plasma layer in external static magnetic field, discussing transverse charged particle drift in crossed fields 13 p2168 A67-27305
Growth and damping rates of resistive instability in gaseous plasma in crossed fields determined from empirical observations 15 p2530 A67-29823
Azimuthal motion of glow discharge plasma in space between two coaxial dielectric cylinders in crossed radial magnetic and axial electric fields 16 p2723 A67-31580
Weakly ionized inhomogeneous plasma in crossed fields, discussing magnetic field strength effect on stability against perturbations 18 p3089 A67-34296
Macroscopic cross-field instability occurring in ionized plasma studied by computer, discussing wave interactions between Fourier modes 18 p3092 A67-34746
Ionizing wave in plasma gun with crossed electric-magnetic fields, obtaining burning voltage of discharge and bias magnetic field ratios 19 p3277 A67-35123
Operation of ion source with cylindrical symmetry of crossed electric and magnetic fields 19 p3297 A67-35596
Turbulent MHD boundary layer in liquid with linear pressure gradient, discussing numerical integration, flow velocity and magnetic field

- distribution 21 p3665 A67-38244
- Stability technique for gas flow past body impeding laminar-turbulent boundary layer transition via crossed electric and magnetic fields 21 p3666 A67-38251
- Resonance and noise microwave emission thresholds for InSb electron hole plasma subject to crossed electric and magnetic fields, noting Hall effect 21 p3683 A67-38403
- Solar wind plasma penetration into geomagnetic field under effects of drift in crossed electric-geomagnetic fields 21 p3698 A67-38463
- Current distribution and electron temperature profiles in nonequilibrium crossed field devices, considering nonuniformities, thermal diffusion, boundary layers and finite reaction rates effects [AIAA PAPER 67-715] 21 p3673 A67-38741
- Stable motion of rarefied plasma ions and electrons in crossed electric and magnetic fields 22 p3853 A67-40024
- One-dimensional plasma flow variables relations analyzed in crossed electric and magnetic fields with small magnetic Reynolds numbers 24 p4196 A67-42216
- CROSSED FIELD AMPLIFIER**
- Self-activating microwave cold cathode crossed field amplifiers for modulation circuits in complex radar systems 03 p0387 A67-14121
- Small signal thin beam theory application to design of amplifiers, noting electronic gain as function of various parameters 09 p1478 A67-22261
- Effect of tunnel diode amplifier V-I characteristics on cross modulation products in electromagnetic spectrum 09 p1557 A67-22266
- Magnetron type microwave amplifier gain increase, discussing electron beam interaction region M-type device gain calculations 22 p3770 A67-39654
- Crossed field cascade tubes as frequency oscillators and microwave generators, discussing improved performance and interaction efficiency of devices 22 p3775 A67-40559
- ROTCHET**
- \$ GEOMAGNETIC CROTCHET**
- RUCIBLE**
- Optimal thickness of protective action of rucible lining in smelting of titanium 07 p1200 A67-19250
- RUCIFORM WING**
- Wind tunnel investigation of dynamic instabilities in cruciform finned missiles due to rolling motion 08 p1413 A67-21531
- Shape of minimum drag cruciform wing of symmetrical thickness in supersonic flow 20 p3355 A67-36192
- RUISE**
- Aerocruise maneuver for optimizing orbital plane change with respect to cruise speed 20 p3532 A67-36552
- RYOCYCLE**
- Large helium refrigerators for very high speed cryopumping techniques required in space simulation facilities 12 p1924 A67-25716
- CRYOGENIC COMPUTER**
- Cryogenic computers based on superconductivity phenomena, discussing building and operating feasibility in outer space 01 p0031 A67-11443
- Cryogenic computers in space based on phenomenon of superconductivity 10 p1608 A67-22770
- Magnetics - Conference, Washington, D.C., April 1967 22 p3859 A67-39895
- Large capacity cryoelectric random access memories, examining three-wire cells and hybrid system for batch fabrication, redundancy, electric parameters, tolerances and noise 22 p3764 A67-39898
- CRYOGENIC EQUIPMENT**
- SA REFRIGERATING EQUIPMENT**
- Cryogenic liquid level sensor consisting of diode heated by resistor 01 p0062 A67-10194
- Calibration of pressure transducers in liquid-hydrogen to liquid-helium temperature range, using cryogenic test setup 01 p0069 A67-11018
- Cryogenic techniques for space power generators based on superconductivity, discussing MHD converters 04 p0560 A67-15967
- Nucleonic cryogenic quality meter design and development and fluid monitoring through hydrogen vent line on Saturn S-IVB stage under orbital conditions 05 p0842 A67-16540
- Silicon surface barrier detector beta gauge for density measurements in liquid hydrogen 05 p0842 A67-16541
- Accuracy ratio and traceability of flow metrology noting uncertainty values, cryogenic standards, gas leakage detection, etc 05 p0809 A67-17377
- Remote vibration testing facility for components while using hazardous cryogens [AIAA PAPER 67-278] 07 p1167 A67-20083
- German space simulation chamber, discussing influences of cryogenic panel and solar simulation on vacuum system 09 p1485 A67-22123
- Ruby maser operating with microrefrigerator at low temperature, noting broadband and bandwidth 11 p1800 A67-24467
- Automatic temperature programmed station for calibrating cryogenic sensors [ISA PAPER 12-11-2-66] 11 p1795 A67-25060
- Space simulation using contamination-free test facilities combining several cryogenic techniques to produce all cryogenic system 12 p1924 A67-25717
- Thermal performance of insulated current carrying leads for cryogenic apparatus 13 p2229 A67-27663
- Low temperature refrigeration for microwave systems - Conference, Frankfurt am Main, April 1966 14 p2277 A67-27774
- Miniature cryogenic refrigeration systems design for masers and parametric amplifiers, investigating efficiency and contamination 14 p2277 A67-27775
- Aluminum, Volume 2, Design and application 14 p2322 A67-27811
- Kantowitz-Grey molecular beam generator performance, noting high source pressure due to high pumping speed, background gas scattering, etc 14 p2316 A67-28189
- Steel cryogenic vessel AC welding method using special emission coated electrodes nullifying arc blow effect 14 p2327 A67-28820
- Energy exchange mechanism of cryogenic sensor dynamic behavior, noting error sources 15 p2490 A67-30155
- He-Cs blow-down MPD facility, discussing generator duct feasibility, nonequilibrium ionization effects, performance and test results 16 p2653 A67-30549
- Microwave ferrite devices describing applications at metric and decimetric wavelengths, at very low temperatures and at high power levels 17 p2826 A67-32744
- Problem areas within cryogenic chemical and nuclear propulsion systems for space missions, noting available technology and limitations [AIAA PAPER 67-454] 18 p3110 A67-33928
- AC motor design for operation in He in cryogenic to room temperature range, noting performance parameters and design considerations [AIAA PAPER 67-456] 18 p2988 A67-33930
- Time and cryogenic liquid calculation required for cryogenic system cooling, considering low/high flow rate effects on system components [AIAA PAPER 67-475] 18 p3157 A67-33945
- High insulating effectiveness required of cryogenic insulations, evaluating insulation capacities of powders, fibers, foams, honeycomb, etc 20 p3553 A67-36885
- Discharge line fluid conditions in cryogenic container with self-pressurized draining, using Bernoulli, continuity and general energy equations and fluid properties 22 p3784 A67-39968
- Cryogenic insulation thermoconductivity measuring apparatus operable at high vacuum and nonsteady state conditions 22 p3803 A67-40295
- Guarded cold flat plate calorimeter for measuring insulation 22 p3803 A67-40296
- Cryogenic thermoconductivity heat flow meter apparatus for felt, powder and block materials at atmospheric pressure 22 p3803 A67-40298
- CRYOGENIC FLUID**
- Cryogenic fluid mass flow measurement methods, noting flow meter calibration 03 p0421 A67-13768
- Dynamic instability in undamped bellows face seals operating in cryogenic environment with torsional oscillation and diametrical rocking as primary motion [ASLE PAPER 66AM 2C2] 08 p1336 A67-21039
- Cryogenic fluid mass flow measurement methods, noting flow meter calibration 13 p2121 A67-27633
- True air life support system, describing concept for deriving fixed percentage binary gas from two steady state cryogenic liquids 13 p2064 A67-27638
- Dielectrophoretic methods for positioning cryogenic liquids in zero gravity environment, solving one-dimensional nonlinear problem for time history 13 p2106 A67-27642
- Semilempirical description of stratification in wall heated containers of cryogenic fluids, noting decrease due to bottom heating 13 p2227 A67-27644
- Absolute emissivity calorimeter design for low temperature measurements above 60 degrees K using liquid helium as cryogenic fluid 13 p2122 A67-27661
- Pool boiling of methane over pressure range from 1 atm to critical pressure in both nucleate and stable film boiling regimes 13 p2229 A67-27667
- Pressure drop study of near saturation Freon 11, noting flowing fluid quality condition for estimates 13 p2106 A67-27668
- Disturbance of capacitive liquid level gauges by nuclear radiation 13 p2122 A67-27684
- Electric breakdown, dielectric constant and dissipation factors of cryogenic liquid nitrogen, hydrogen and helium 14 p2341 A67-28891
- Book on cryogenic fluids covering safety principles, design data, first aid and hazard control procedures 15 p2543 A67-29233
- Time and cryogenic liquid calculation required for cryogenic system cooling, considering low/high flow rate effects on system components [AIAA PAPER 67-475] 18 p3157 A67-33945
- Low temperature effect on physical and mechanical properties of engineering materials and cryogenic fluids, discussing heat generation and removal at rubbing surfaces 21 p3633 A67-38141
- Double-guarded cold plate apparatus for measuring thermal conductivity of multilayer insulations, powders, fibers and foams 22 p3803 A67-40294
- Cryogenic liquid propellant rocket engine technology and design [AIAA PAPER 67-978] 24 p4208 A67-43053
- CRYOGENIC GYROSCOPE**
- Inertial sensors, discussing magnetic resonance and superconductor gyroscopes, ring lasers, fluid dynamical devices, electrostatic gyroscopes, etc 05 p0806 A67-16517
- Superconducting gyroscope for gimbaled platform application 13 p2122 A67-27683
- CRYOGENIC PROPELLANT**
- Statistical theory using calibration data to evaluate multielement system for measuring properties of cryogenic propellants and high temperature thrusting devices 01 p0069 A67-11026
- Dielectrophoretic propellant orientation systems design, noting electrode requirements and avoidance of electrohydrodynamic instabilities [AIAA PAPER 66-922] 02 p0301 A67-12275
- Vacuum multilayer insulation for cryogenic space propulsion vehicles noting self-evacuation system and calorimetric test 10 p1734 A67-23728
- Temperature-dependent thermoconductivity of metal film on insulation laminations in relation to bulk parent material in insulation systems of cryogenic propellants [AIAA PAPER 67-295] 12 p2035 A67-26010
- Conservation of cryogenic propellants on long duration space missions by reliquefaction of vapor 13 p2091 A67-27636
- Low gravity liquid hydrogen tank venting, considering systems with heat exchange for space missions 13 p2057 A67-27640
- Low temperature engine suction line response to fluid exposed internal surface coating, determining effects of varying flow rates 13 p2229 A67-27664
- Test program assessing propulsion performance of cryogenic and ambient temperature gaseous parahydrogen expanded through conical thrust nozzles 16 p2734 A67-30705
- Spaceflight application of cryogenic techniques including cooling magnets, noise reduction in parametric amplifiers and quantum-electronic, superconductive and IR sensing devices 16 p2702 A67-30717

- Liquid hydrogen heat exchanger for servicing Saturn V S-II stage 17 p2954 A67-32011
- Thermodynamic system for zero g venting, storage and transfer of cryogenic propellants, discussing heat exchanger 17 p2954 A67-32074
- Cryogenic rocket upper stage structural design, fabrication and testing 22 p3899 A67-39533
- Space cryogenic propellant storage utilizing vent gas recovery noting storability spectrum plot 22 p3906 A67-40164
- Analytical prediction of cryogenic propellant venting effects on orbital vehicle dynamic behavior, emphasizing vent thrusting and gas impingement 22 p3906 A67-40165
- CRYOGENIC STORAGE**
- Cryogenic associative memory system for information retrieval 02 p0208 A67-12163
- Heat flux measurements of liquid-nitrogen superinsulation systems, noting effects of material types and assembly techniques 04 p0720 A67-14531
- Structural cryogenic vessels of chemical rocket stages 05 p0874 A67-17015
- Liquid hydrogen tank insulation, content gauging and design of transfer lines and valves 05 p0789 A67-17018
- Mass spectrometer and helium gas application in NDT for deleterious leaks in double-wall vessels for storing and shipping liquid oxygen and nitrogen 12 p1948-A67-25288
- Heat flow mechanisms and thermodynamics of supercritical cryogenic storage problems solved by digital computer simulation, using finite difference approximation 12 p1925 A67-25722
- Cryogenic fluid behavior in passive storage tank as function of tank configuration, wall heating and acceleration 12 p2034 A67-25729
- Cryoelectric memory loop cell and hybrid organization system noting economy, high speed, mass storage, etc 12 p1915 A67-25887
- Cryogenic fluid storage on moon surface, considering Lambert reflection law, thermal insulation performance, incident heat flux and boil-off rates [AIAA PAPER 67-296] 12 p1926 A67-26011
- One-dimensional conduction model for predicting pressure variation of nonvented cryogenic propellant tanks in low gravity field [AIAA PAPER 67-338] 12 p2039 A67-26052
- Heat flux measurements of liquid-nitrogen superinsulation systems, noting effects of material types and assembly techniques 13 p2222 A67-26580
- Fuel container design for space vehicles, discussing impact protection, reusability and long term cryogenic storage 13 p2212 A67-27218
- Heat leak and pressure decay for single phase cryogenic storage in nonequilibrium calculated for spherical tanks, using simplifying assumptions 13 p2227 A67-27641
- Stratification similitude laws for liquid hydrogen determined and extrapolated to full size tanks from small tank data 13 p2186 A67-27643
- Cooling system for maintaining uniform low temperature environment under low gravity conditions 13 p2227 A67-27645
- Thermal performance of liquid hydrogen in horizontal hypersonic vehicle fuel tank 13 p2186 A67-27646
- Carbon dioxide purge and thermal protection system for liquid hydrogen tanks of hypersonic aircraft, comparing with helium purge system 13 p2227 A67-27647
- Minimum weight combinations of shields and spacers for lowest heat flux, noting mounting technique and leakage effect 13 p2228 A67-27653
- Propellant leakage degradation of multilayer insulation system of cryogenic storage tank 13 p2186 A67-27654
- Klegecell G-300 mechanical and thermal properties tested for thermal insulation for cryogenic stage for liquid hydrogen on space vehicle 13 p2228 A67-27659
- Dissimilar metal transition joints employing roll-bonded and friction welded components 13 p2124 A67-27685
- Two-phase cryogenic propellant storage under low gravity, discussing impact on vented and unvented vehicle design and performance 16 p2757 A67-30633
- Thermal problems peculiar to cryogenics stored in reduced gravity environment 17 p2966 A67-32010
- Cryogenic fluid storage subsystems for Gemini program, noting more advanced designs for Apollo, Lunar Module, Biosatellite, Manned Orbiting Laboratory, etc 17 p2954 A67-32013
- Multicycling metallic bladders for positive expulsion of cryogenic fluids stored in tanks [AIAA PAPER 67-444] 18 p3054 A67-33921
- Polymeric materials in expulsion bladders for cryogenic liquids, describing fabrication, flexibility, permeability, storage, transfer, control factors, etc [AIAA PAPER 67-457] 18 p3069 A67-33931
- Active thermal insulator technique for long term cryogenic storage 19 p3207 A67-34836
- Blastasis /suspended animation/ by frozen storage investigated for application to interstellar voyages, noting possible damage prevention during space trips 19 p3181 A67-35325
- Space cryogenic propellant storage utilizing vent gas recovery noting storability spectrum plot 22 p3906 A67-40164
- Cryogenically stored helium pressurization system for LEM descent stage propulsion system, discussing weight advantages and liquid helium heat transfers 22 p3749 A67-40394
- Adhesives to bond metal linings to filament-wound cryogenic pressure vessels evaluated by test series simulating fabrication and service conditions 23 p4010 A67-41347
- Long term cryogenic propellant storage in space, considering rigid open cell polyurethane foam as spacer in multilayer insulation system 24 p4254 A67-42480
- CRYOGENIC TEMPERATURE**
- Mechanical properties of Kh21G7AN5 steel at liquid hydrogen temperature 04 p0636 A67-14751
- Plastic deformation in titanium at low temperatures, noting prevalence of twinning and suitability as construction material in cryogenic technology 04 p0636 A67-14752
- Threshold energy for electron radiation damage in Ag compared for liquid He and liquid Ni temperatures 04 p0638 A67-15115
- Chromium ion concentration and temperature effects on spin-lattice relaxation times in ruby at liquid He temperatures in zero magnetic field 05 p0817 A67-16637
- Adiabatic demagnetization of ruby to obtain cryogenic temperatures 06 p1047 A67-17760
- Temperature dependence of thermoconductivity of dysprosium between 1 and 4 degrees K 06 p1048 A67-17821
- Varactor diode impedance behavior in parametric amplifiers under low temperature conditions 07 p1152 A67-19551
- Cryochemical synthesis and processing by reacting free radical with excited state species 08 p1290 A67-21187
- Cryogenic low pressure seal to seal aluminum or stainless steel flanges 08 p1336 A67-21498
- IR laser emission at cryogenic temperatures and various wavelengths obtained from diodes of lead tin selenide and lead tin telluride 09 p1551 A67-21571
- Cryogenic thermoconductivity of impure tin in superconducting and normal state, noting anisotropy and superconducting energy gap independence from impurity type 10 p1687 A67-22761
- Correlation of anisotropic energy gap with thermal conductivity in pure and impure superconducting tin 10 p1687 A67-22762
- Granular superconductor with thin insulating layer at boundary of each homogeneous superconductor grain, using isospin formulation of microscopic theory 10 p1687 A67-22763
- Millimeter microwave transmission and reflection through 50 angstrom superconducting tin and indium films near critical temperature 10 p1688 A67-22764
- Cryogenic stability, kinetics and energetics of lower boron hydrides explored with negative results, using mass spectrometry 10 p1603 A67-23385
- Dependence of intrinsic noise temperature of ruby reflection maser on helium bath temperature and chromium trioxide doping, using circulator 10 p1665 A67-23505
- Anisotropic properties of acoustic electron scattering in Si samples in 8 mm wavelength and liquid nitrogen temperature 10 p1695 A67-23664
- Adiabatic flow of K vapor in supersaturated state noting supercompression, supercooling and equilibrium through condensation jump 11 p1881 A67-24029
- Gallium arsenide electron photon transistor electrical properties at cryogenic and room temperature, determining total internal quantum yield of photons 11 p1765 A67-24475
- Thermal conductivity of low temperature silicon and germanium irradiated by fast neutrons noting differences, additive thermal resistivity and possible scattering mechanisms 11 p1849 A67-24899
- Cryostat, combination device for test and calibration of gauges for cryogenic temperature 12 p1938 A67-25187
- Low temperature mechanical properties of E1827 alloy investigated under static uniaxial elongation, noting ultimate strength increases with decreasing temperature 12 p1955 A67-25370
- Closed form solution for determining total emissivity of metals and radiation conductivity of radiation shield for nongray metallic surfaces at low temperature [AIAA PAPER 67-335] 12 p2038 A67-26049
- Cryogenic fracture toughness behavior 13 p2220 A67-27671
- Notch toughness of some aluminum alloy castings at cryogenic temperatures 13 p2221 A67-27672
- Test program of Al-Zn-Mg alloy /A25G/ to determine strength, fracture toughness, weldability and physical properties for cryogenic application 13 p2142 A67-27673
- Statistical analysis of aluminum welds tested at cryogenic temperatures 13 p2124 A67-27674
- Age hardenable low-expansion alloy for cryogenic service 13 p2142 A67-27675
- Mechanical properties of several nickel-base alloys at room and cryogenic temperatures 13 p2142 A67-27676
- Maraging steels retaining toughness at cryogenic temperatures by suitable heat treatment 13 p2142 A67-27677
- Radiation effects on shear strength of several alloys at liquid hydrogen environment 13 p2143 A67-27678
- Low temperature effects on detonation velocity and other explosive parameters for linear shaped charge systems 13 p2230 A67-27686
- Corrosion of metals by flowing liquid fluorine compounds 13 p2143 A67-27688
- Low temperature closed cycle refrigeration for electronics, with emphasis on relationship to system effectiveness 14 p2278 A67-27785
- Aluminum and aluminum alloys properties for service at cryogenic temperatures 14 p2323 A67-27816
- Book on experimental superfluidity covering He properties, low temperature production, temperature measurement, two-fluid model and macroscopic quantization, generalized hydrodynamic equations, etc 15 p2517 A67-29265
- Current-voltage characteristic determination for n-InSb Corbino disk, noting capacitance and internal resistance current source at cryogenic temperature 15 p2534 A67-29359
- Cryogenically cooled primary winding system for AC MHD generator, considering real machine data 16 p2605 A67-30580
- Negative-resistance in evaporated silicon films at room and liquid-nitrogen temperatures believed due to double injection 16 p2728 A67-31035
- Tensile and torsional fracture of low carbon steel at cryogenic temperatures, studying temperature and stress gradient effect 16 p2689 A67-31309
- Heat transfer in cryogenic range, noting heat flux measurements, use of semiconductor, etc 16 p2780 A67-31533
- Bypass flow reduction in liquid hydrogen and liquid oxygen tank mounted boost pumps on Centaur launch vehicle 17 p2800 A67-31978
- Thermal conductivities below one degree K of various very pure metals, noting normal and superconducting states 17 p2912 A67-32265
- Upper limit data about reported very low

- temperature distributed-source microwave background radiation and small-scale angular distribution 17 p2945 A67-32653
- Electrical resistance of niobium single crystal at very low temperature from beginning of superconductivity transition 17 p2916 A67-32805
- Electron radiation damage in CdSe crystals at cryogenic temperatures, noting electrical conductivity and cathodoluminescence properties before and during damage 17 p2916 A67-32838
- Low temperature thermal conductivity measurement of fast-neutron-irradiated silicon and germanium, showing difference between bombardment induced scattering in two materials 17 p2919 A67-32855
- Annealing kinetics of n-type germanium exposed to electron bombardment at cryogenic temperature 17 p2919 A67-32861
- Silicon photoconductivity measurements after electron irradiation at cryogenic temperature 17 p2920 A67-32864
- Temperature dependence of sound velocity in liquid helium at saturation vapor pressure and cryogenic temperatures 17 p2886 A67-33231
- Anisotropic properties of acoustic electron scattering in Si samples in 8 mm wavelength and liquid nitrogen temperature 17 p2924 A67-33345
- Magnetization measurements in applied magnetic fields at cryogenic temperatures of dirty type II superconducting transition metal alloys 17 p2925 A67-33375
- NERVA radiation effects tests at cryogenic temperatures [AIAA PAPER 67-477] 18 p3076 A67-33947
- Mechanical properties of Kh21G7AN5 steel at liquid hydrogen temperature 18 p3066 A67-34409
- Plastic deformation in titanium at low temperatures, noting prevalence of twinning and suitability as construction material in cryogenic technology 18 p3066 A67-34410
- Temperature sensing device development for temperature ranges from cryogenic to ambient 18 p3051 A67-34510
- Metal lined glass filament-wound pressure vessel performance at cryogenic temperatures, discussing fibers, resins and liners [ASTM PAPER 17] 18 p3067 A67-34578
- Insulating foams at liquid hydrogen temperature, describing methods for measuring thermoconductivity, specific heat and density 19 p3346 A67-35567
- Cesium uranyl nitrate crystal near-visible absorption spectrum at 20 degrees K cesium uranyl nitrate crystal near-visible absorption spectrum at 20 degrees K 20 p3506 A67-36229
- Emission intensity dependence in CdS on laser excitation intensity for free and phonon-assisted exciton recombination at cryogenic temperature 20 p3461 A67-37295
- Plasma wave propagation dispersion in sodium and potassium at cryogenic temperature using Landau-Fermi liquid theory 20 p3514 A67-37570
- Odd and even photomagnetic effect oscillations in InSb, measuring EMF at low temperatures and strong fields 21 p3677 A67-38095
- Superconducting critical temperature below Kondo temperature for metal solutions with magnetic impurities calculated, using Green function 21 p3680 A67-38350
- Conductivity and Hall coefficient measurements for electron mobilities in strontium titanate, discussing electron-phonon coupling and cryogenic experiments 22 p3863 A67-40002
- Cryogenically cooled rocket nozzle thermal fatigue analysis by thermal-cycle testing of specimens 22 p3834 A67-40183
- Thermal conductivity measurements of insulating materials at cryogenic temperatures - ASTM Conference, Philadelphia, February 1967, Committee C-16 22 p3802 A67-40289
- Guarded hot plate technique for measuring thermal conductivity of low conductivity materials at cryogenic temperatures 22 p3802 A67-40290
- Guarded hot plate apparatus for measuring thermal conductance of multilayer cryogenic insulation under vacuum 22 p3802 A67-40291
- Thermal conductivities of cryogenic insulation systems determined by two methods using calorimetry measurement of boil-off rate of liquid cryogen 22 p3802 A67-40292
- Heat flow meter apparatus for rapidly measuring thermal conductivity of flat insulation specimens under cryogenic temperatures 22 p3802 A67-40293
- Calorimeter for evacuated multilayer insulation materials to evaluate performance and measure heat transfer rate and thermoconductivity 22 p3803 A67-40297
- Pressure, volume, temperature and internal energy data for He using constant volume calorimeter and gas thermometer, discussing He melting 22 p3920 A67-40392
- Polymeric materials for extreme temperature emphasizing thermal stability 23 p4021 A67-41228
- Collection efficiency of plane acting as pump in vacuum system, discussing parameter measurements, partial pressure analyzer and kinetic theory values 23 p4004 A67-41354
- Testing procedure for determining strain gauge elongation limit, discussing gauge applications to strain measurements at LOX temperatures 23 p4007 A67-41389
- Cryogenic valve testing facility for nuclear rockets using liquid hydrogen at high pressures and flow rates 23 p3936 A67-41425
- Vacuum jacketed cryogenic globe valve design providing tight sealing, low heat leak, low cool-down mass and high flow 23 p3936 A67-41426
- Magnetization measurements for pure superconducting tin cylinders, discussing superheating effects 23 p4044 A67-41441
- Basic guidelines for fastener system selection for use in exotic environment with unusual stress condition 24 p4160 A67-42077
- Ultrahigh molecular weight poly(ethylene terephthalate)/synthesized, studying catalyst, particle size, reaction temperature and time and carrier gas flow rate 24 p4176 A67-42467
- Cryogenic flexibility of single and multiple ply thin polymeric film tested for porosity, cycle life and film thickness relation 24 p4176 A67-42468
- CRYOGENICS**
- SA COOLING
- SA NERNST HEAT THEOREM
- SA REFRIGERATION
- Two-stage parametric amplifier using GaAs cooled in closed cycle cryogenic refrigeration system applied to satellite communications 01 p0033 A67-10029
- Ionized impurity scattering mechanisms causing energy and momentum losses in n-type InSb below 77 degrees K 01 p0134 A67-10806
- Cryogenic strain gauge application to circumferential loads of Centaur hydrogen tank insulation while in launch configuration 01 p0069 A67-11016
- Si semiconductor strain sensors and miniature pressure transducers for cryogenic pressure measurements 01 p0069 A67-11017
- Continuity gauge measurement of crack growth on flat and curved surfaces at cryogenic temperatures 01 p0102 A67-11028
- Temperature and stress dependence of electron lifetime in p-type Si-B and Ge-Zn between 1.5 and 4.2 degrees K 02 p0301 A67-12523
- Cryogenic temperature resistant plastics in space program, discussing insulation, adhesives, seals, gaskets and expulsion of cryogenic propellant in zero gravity environment [SAE PAPER 660638] 04 p0642 A67-15788
- Pure and applied cryogenics, Volume 5, Liquid hydrogen 05 p0927 A67-17010
- Vacuum integrating sphere for in situ spectral reflectance measurements of carbon dioxide cryodeposits from 0.5 to 10 microns [AIAA PAPER 67-298] 12 p1926 A67-26013
- Advances in cryogenic engineering, Volume 12 - Conference, Boulder, June 1966 13 p2225 A67-27634
- Ultralow noise receiver configurations for cryogenically cooled microwave traveling wave masers and parametric amplifiers 14 p2260 A67-27776
- Two-stage parametric amplifier system cooled to 20 degrees K, as low noise amplifier in receiving equipment for satellite communication 14 p2278 A67-27780
- Vacuum simulation developments and trends, noting solar simulator hardware advances with cryogenic systems 17 p2834 A67-32597
- Safety program for nuclear rocket engine testing, discussing role of cryogenics 20 p3482 A67-36565
- Cryogenic mechanical properties of poly(ethylene terephthalate)/ film studied for effects of stretch and heat set temperature and time 24 p4176 A67-42469
- CRYOPUMPING**
- Cryogenic pumping capability of liquid helium cooled plate in supersonic flow field at simulated high altitude 04 p0606 A67-14999
- Superhigh vacuum created by cryopump, using liquid nitrogen and helium 06 p0950 A67-17940
- Monte Carlo computer program for calculating molecular gas flow with axisymmetric vacuum structures, showing applications on pumping speed test domes and measuring apparatus for sticking coefficients 09 p1488 A67-22105
- Pumping power of liquid nitrogen cooled cryosurface, showing reduced efficiency in presence of nitrogen via mass spectrometry 09 p1503 A67-22117
- Nonuniform molecular density, pumping power and gas temperature distribution in evacuated space simulator 09 p1503 A67-22118
- Low contamination space chamber design employing cryopanel array configurations with near unity sticking coefficients 09 p1485 A67-22122
- Molecular beam chamber for cryopumping studies and capture coefficient data 11 p1773 A67-24344
- Cryopumps incorporated into liquid N shrouds for small space simulation chambers 12 p1900 A67-25710
- Large helium refrigerators for very high speed cryopumping techniques required in space simulation facilities 12 p1924 A67-25716
- Space simulation using contamination-free test facilities combining several cryogenic techniques to produce all cryogenic system 12 p1924 A67-25717
- Cryogenic and cryosorption pumping of residual gases for clean test volume 13 p2106 A67-27648
- Space simulation using cryogenic adsorption pumping 17 p2884 A67-32595
- High - vacuum pump selection requirements, discussing contamination problems 17 p2884 A67-32596
- Superhigh vacuum created by cryopump, using liquid nitrogen and helium 18 p2988 A67-33776
- Internal combustion engine fuelled with cryogenic hydrogen and oxygen [AIAA PAPER 67-421] 18 p2988 A67-33906
- Cryosorption pumping of helium and hydrogen in high vacuum, describing refrigerated panels and space environment simulation application 22 p3838 A67-40396
- Book on vacuum engineering covering space vacuum simulation, pressure measurement, gas flow and load, vacuum systems and technology 23 p4028 A67-41353
- CRYOSORPTION**
- Cryogenic and cryosorption pumping of residual gases for clean test volume 13 p2106 A67-27648
- Cryosorption pumping of helium and hydrogen in high vacuum, describing refrigerated panels and space environment simulation application 22 p3838 A67-40396
- Helium sorption by nitrogen, oxygen and argon cryodeposits, discussing pumping speeds and capture coefficients 24 p4115 A67-42047
- CRYOSTAT**
- SA TEMPERATURE CONTROL
- Synthetic pink-ruby crystal demagnetization characteristics when employed as coolant in cryostat, noting temperature dependence 11 p1851 A67-25033
- Cryostat, combination device for test and calibration of gauges for cryogenic temperature 12 p1938 A67-25187
- Continuous flow cryostat system for open cycle cold fluid refrigeration 14 p2404 A67-27786
- Double-walled cryostat with copper holder for probe measurements of temperature dependence of semiconductor galvanomagnetic effects 16 p2730 A67-31158
- CRYOTRAPPING**
- Helium sorption by nitrogen, oxygen and argon cryodeposits, discussing pumping speeds and capture coefficients 24 p4115 A67-42047
- CRYOTRON**
- Performance characteristics of cryotron

memory cell for measuring pulses arriving at input from current 06 p0966 A67-18242

Superconducting switching and storage elements, examining physical properties, cryotron and continuous film memory cell 06 p0972 A67-18433

Low temperature components for data processing, low noise amplifiers and microwave technology, noting superconductor elements like cryotron 09 p1463 A67-21760

Current stretch sensing for removing limitations to usable density of cryotron storage cells of random access memories 11 p1765 A67-24625

Crossed film cryotron as single stage high gain amplifier, noting design features and performance 16 p2640 A67-31431

High density cryotron array production in associative memory application, using lock-out design feature 18 p3014 A67-34556

Associative memory system of persistent current bit-cells using cryotrons in selection and control network 21 p3587 A67-37955

Large capacity cryoelectric random access memories, examining three-wire cells and hybrid system for batch fabrication, redundancy, electric parameters, tolerances and noise 22 p3764 A67-39898

CRYSTAL

SA BODY CENTERED CUBIC /BCC/ CRYSTAL

SA CUBIC CRYSTAL

SA IONIC CRYSTAL

SA METAL CRYSTAL

SA PIEZOELECTRIC CRYSTAL

SA POLYCRYSTAL

SA SINGLE CRYSTAL

SA YTTRIUM-ALUMINUM GARNET /YAG/ CRYSTAL

SA YTTRIUM-IRON GARNET /YIG/ CRYSTAL

MHD effects in liquid crystals 05 p0846 A67-16736

Ruby and neodymium glass lasers sum frequency generation using nonlinear electro-optical KDP crystal 06 p1009 A67-17754

Attenuating electron waves in crystals corresponding to energy values in forbidden band used in calculating current across n-p junction 13 p2172 A67-26354

Attenuating electron waves in crystals corresponding to energy values in forbidden band used in calculating current across n-p junction 21 p3679 A67-38311

Spectroscopic investigations of emission under free generation and Q-switching conditions of mixed-fluoride crystal lasers 21 p3682 A67-38370

LiF crystals doped with Ti studied for electrical and optical properties, finding atomically dispersed Ti fractions in form of doubly positively charged centers 21 p3687 A67-39137

Electrical characteristics of thin triangular barium titanate crystals in strong electric fields 22 p3859 A67-39579

CRYSTAL DISLOCATION

Stress required for brittle fracture of alumina at room temperature based on theory of dislocation movement of cracks 01 p0092 A67-10054

Dislocation structure in tantalum single crystals deformed in tension to various strains at 373 degrees K studied by transmission electron microscopy 01 p0092 A67-10057

Room temperature microstrain behavior of zone-refined single crystal beryllium examined as function of prestrain 01 p0092 A67-10058

LiF single crystal destruction as function of laser beam energy, examining dislocation pattern arising from crack propagation 01 p0086 A67-10071

Dislocation-free silicon web crystal growth controlling supercooling and resistivities, noting elastic strains 01 p0131 A67-10367

Dislocation model to explain creep curves, predicting linear relation between dislocation density and strain, for small strain 01 p0100 A67-10751

Continuum theory of dislocations for polar elastic materials, each material point having three associated directors 01 p0162 A67-10848

Amplitude dependent attenuation in normal and superconducting lead for ultrasonic determination of superconducting energy gap 01 p0135 A67-10916

Crystal layer dislocation structure of cold rolled molybdenum foil investigated by electron microscopy 01 p0101 A67-10939

Crystal orientation of grains during fatigue and plastic deformation analyzed on copper using X-ray diffraction, noting crystal behavior 02 p0254 A67-11467

Electron beam scanning technique measurement of diffusion lengths in Si and GaP p-n junctions and recombination rate of dislocations in n-type Si 02 p0298 A67-11887

Ultrasonic attenuation of alkali halide crystals in 120 to 180 degrees K range, noting thermal annealing of dislocation pinning centers 02 p0298 A67-11888

Deformation theory for medium with continuous distribution of dislocations 02 p0338 A67-11966

Thermal dilation of titanium alloys during repeated cycling through alpha-beta transformation 03 p0440 A67-13252

Plastic behavior of simple solids in terms of atomistic processes, emphasizing high strength and ductility 03 p0442 A67-13303

Microstructure effect on creep deformation mechanisms in polycrystalline ceramic oxides including grain size, subgrain structure, porosity, diffusional creep and dislocation movement 03 p0449 A67-13304

Topographic X-ray analysis of deformation in tension of silicon crystal 03 p0493 A67-13452

X-ray anomalous transmission used in analysis of gallium arsenide crystal perfection with various dislocation densities, determining ratios of anomalous absorption coefficient 04 p0674 A67-14620

Loops and spirals on freshly cleaved surfaces of laboratory grown single crystals of NaCl thermally etched by placing them in muffle furnace on platinum lid 04 p0675 A67-14761

Crystal dislocation effect on electric properties of germanium 2, noting elastic carrier scattering 04 p0677 A67-14938

Displacement and stress fields in isotropic elastic solids determined by integrating displacements for point nuclei of strain 04 p0711 A67-15102

Stress-strain time relation in gallium doped p-type germanium, noting crystal dislocation and creep parameter temperature dependence 04 p0677 A67-15121

Rough surface recrystallization of heated polyethylene extended-chain crystals 04 p0566 A67-15201

Dislocation-induced relaxation in silicon single crystals by measuring internal friction and Young's modulus at temperatures from 77 to 300 degrees K 04 p0681 A67-15294

Test on nickel and aluminum of Bailey-Orowan equation in relation to work hardening and recovery in creep 04 p0640 A67-15623

Displacement effects in n-and p-type silicon when exposed to energetic radiation, using electron spin resonance and galvanomagnetic techniques 04 p0684 A67-15689

Transient radiation effects on microcircuits 04 p0588 A67-15701

Substructure of aluminum monocrystals in relation to silicon content 05 p0827 A67-16075

Dislocation structure of crystals with diamond type lattice analysis made possible by growing silicon monocrystals along growth axis 05 p0860 A67-16076

Dislocation reaction in crystals with diamond type structure analyzed on silicon grown by Czochralski method along /100/ axis 05 p0860 A67-16077

High resolution X-ray diffraction topography of dislocation structure of Si crystal 05 p0860 A67-16078

Dislocation mechanisms for prismatic and basal slip in Ti at low temperatures, measuring critical shearing stress and temperature dependence of activation volume 05 p0828 A67-16467

Polygonization in silicon single crystal by chemical etching, determining activation energy, noting dependence on annealing temperature 05 p0862 A67-16503

Statistical dislocation theory of crystal brittle fracture seen as stochastic process with microcrack formation and propagation under plastic deformation 05 p0919 A67-16504

Etching and X-ray spectrometric techniques to investigate distribution and density of dislocations in deformed and annealed GaAs and InSb

crystal 05 p0865 A67-16920

Dislocation loops by gold diffusion into silicon crystals analyzed, using X-ray diffraction topography and optical microscopy 05 p0866 A67-16974

Kinetics of formation and healing of damage caused by laser pulse in lithium fluoride single crystals 05 p0867 A67-17057

Manganese aluminate precipitation effect on primary recrystallization in metal systems, indicating softening processes in metals 06 p0105 A67-17810

Thermally activated deformation relating flow stress to square root of dislocation density 06 p0103 A67-18755

Anisotropic resistivity of dislocations produced by deformation measured in high purity Au, Ag and Cu single crystals 07 p1209 A67-19638

Dislocation density and magnetic hysteresis in superconducting state of 110-oriented Nb single crystals as function of angle of torsion 07 p1209 A67-19646

Calculation of dislocation precipitated profile for ideal complementary error-function diffusion profile of phosphorus in silicon 07 p1234 A67-19890

Structure of rolling texture of bcc metals and alloys under various external deformation conditions 07 p1210 A67-20107

Physics of dislocations - Colloquium, Toulouse, March 1966 07 p1210 A67-20161

Semiconductor dislocation noting velocities and effect on transport properties 07 p1237 A67-20162

Dislocations in Be, discussing twinning and deformation by climbing, stacking faults and condensation vacancies 07 p1210 A67-20163

Crystal deformation by electrostriction produced by laser beam 08 p1336 A67-20315

Surface oxide films and lifetime of vacancies in thin crystals analyzed for pure aluminum and dilute aluminum alloys 08 p1369 A67-20794

Elastic interaction between dislocation loops and straight dislocations in orthotropic anisotropic materials analyzed for various graphite configurations 08 p1346 A67-20797

Energy factors of infinite straight dislocations and stresses of piecewise straight dislocation configurations expressed through Green functions of elasticity 08 p1418 A67-20798

Proof of Lothe theorem showing that knowledge of stresses around infinite straight dislocations leads to solution of dislocation problems 08 p1418 A67-20799

Plastic flow peculiarities analysis based on X-ray diffraction effects obtained by deforming single crystal molybdenum of various orientations 08 p1342 A67-20809

LiF single crystal destruction as function of laser beam energy, examining dislocation pattern arising from crack propagation 08 p1339 A67-21454

Thermal etching study of rod shaped formations caused by structural dislocations during heating and cooling of Ti-Mo-Fe-Al system 09 p1518 A67-21967

Microstructural dislocation tangling and related changes in tensile properties of Hastelloy X-280 following thermomechanical treatments 10 p1668 A67-23174

Stacking fault tetrahedra in fatigued stainless steel, describing mechanism for nucleation of triangular Frank dislocation loop during cyclic load 11 p1805 A67-24109

Temperature effect, including liquid helium temperature, on yield stress of commercial purity alpha titanium 11 p1805 A67-24111

Micrographs of thin Ti layers through electron microscope showing dislocation distribution 11 p1806 A67-24428

Crystalline solids deformation - Conference, Ottawa, August 1966, Part 1 11 p1806 A67-24568

Temperature, strain rate and purity effects on alpha-titanium deformation yield and flow stresses, ascertaining thermal activation rate controlling mechanism 11 p1807 A67-24567

Discontinuous yield phenomena for slip band dislocations, when frictional stress that hinders dislocation motion undergoes static or dynamic drop 11 p1807 A67-24568

Stress and temperature dependence of motion of edge dislocations in nickel single crystals 11 p1809 A67-24920

Deformation of crystalline solids - Conference, Ottawa, August 1966, Part

2 Tantalum alloy slip line observations, stress-strain curves, yield stresses and anisotropic elastic constants in compression deformation 11 p1810 A67-25091

Beryllium single crystal dislocation and twinning induced by compression deformation 11 p1810 A67-25093

Coherent ordered precipitates formation in Ni-Cr-Al alloy, discussing spacing, shape and size of gamma prime particles as function of time 12 p1954 A67-25344

Crystal lattice defects as centers promoting dislocations during plastic deformation of ionic crystals 13 p2175 A67-26448

Temperature dependence of yield point of crystals described in terms of thermally activated motion of dislocations in external forces field 13 p2131 A67-26449

Dislocation behavior in crystalline materials, examining agreement between theory and experiment 13 p2132 A67-26695

Stress dependence of dislocation configuration in deformed niobium 13 p2133 A67-27010

Dislocation velocity measurements and thermally activated motion in molybdenum 13 p2133 A67-27011

Electron microscope observations on matrix precipitation in beryllium 13 p2136 A67-27106

Transmission electron microscopy of dislocation structure produced in beryllium by specific deformation 13 p2138 A67-27116

Electron microscope study of cold working and tempering of beryllium single crystals 13 p2138 A67-27117

Friction stress acting upon moving dislocation derived by microstrain methods is meaningful under limited conditions 13 p2141 A67-27181

Relation between chromium cold-shortness temperature variations and structural changes under deformation, noting dependence on initial metallographic grain size 13 p2141 A67-27284

Chemical influence of holes and electrons on dislocation velocity in semiconductors 13 p2184 A67-27692

Etching and X-ray spectrometric techniques to investigate distribution and density of dislocations in deformed and annealed Ga-As and InSb crystal 14 p2365 A67-28260

Creep behavior at different stresses approximated through density of dislocation velocity, deriving strain time relation 14 p2400 A67-28420

Chemical etching examination of dislocations and stacking-fault structure of epitaxial gallium arsenic phosphide, considering doping level, growth rate and composition effects 14 p2366 A67-28421

Misfit dislocations at diamond-sphalerite interface of thin epitaxial Ge layer deposited on GaAs 14 p2366 A67-28497

Precipitate and dislocation structures associated with peak effect in niobium examined using electron microscopy 14 p2375 A67-28999

Electron microscope study of dislocation structures in deformed niobium single crystals 14 p2339 A67-29031

Kinetics of formation and healing of damage caused by laser pulse in lithium fluoride single crystals 15 p2538 A67-29788

Crystal dislocation in InSb by fast neutron bombardment assuming displacement wedges with electron type conductivity 15 p2541 A67-30234

Fatigue crack analysis via Bilby, Cottrell and Swinden crack theory, noting inadequacy of energy criterion 16 p2769 A67-31283

Interaction between elastic cracks, dislocation cracks and slip bands describing various characteristics of each case 16 p2769 A67-31284

Slip step role in early stages of stress corrosion cracking in face centered iron-nickel-chromium alloy thin foils 16 p2690 A67-31384

Oxygen caused bright spots in field ion microscope patterns of tungsten, noting oxygen variation effects 16 p2693 A67-31873

Niobium-iron binary alloys structural study, noting phase instabilities for various added impurities 17 p2871 A67-32042

Neutron irradiation effects in pure Mo,

noting formation of prismatic dislocation loops 17 p2872 A67-32740

Hexagonal cobalt single crystals plastic deformation, determining stress, free enthalpy and volume activation, temperature and strain rate 17 p2873 A67-32815

Disordered regions produced by fast neutron irradiation effect on semiconductor properties of silicon 17 p2919 A67-32859

Deformation theory for medium with continuous distribution of dislocations 17 p2966 A67-33283

Frozen vacancies effect on microhardness and electrical resistance of nickel ferrite and yttrium garnet 18 p3097 A67-33480

Monatomic step patterns on /100/ cleavage and tensile crack faces of NaCl crystals originate from dislocation processes of crack tip released by shear stress distribution 18 p3097 A67-33482

Shear stress distribution and dislocation processes at moving crack tips in ionic crystals 18 p3097 A67-33483

Pressurization produced free dislocations effect on yielding and fracture in bcc metals 18 p3063 A67-33484

Temperature and composition effect on ductility transitions, yield stress and dislocation pinning strength in iron base alloys due to change in slip 18 p3063 A67-33485

Stress effects on structure of oriented crystallizing polymers, noting long periods changes due to displacement of crystallites in amorphous layers 18 p3068 A67-33489

Flow stress of fresh dislocations in titanium and vanadium doped MgO single crystals, measuring dependence on heat treatment and test temperature 18 p3097 A67-33492

Structural dislocations effect on formation of micropylasmas during avalanche breakdown of silicon p-n junction 18 p3099 A67-33698

Aluminum alloy examined for dislocation arrangements and susceptibility to intergranular stress corrosion cracking, using electron microscopy 18 p3063 A67-34000

Plastic deformation of single crystals of vanadium by bending and compressing at 298 and 77 degrees K showed etching but no evidence of mechanical twinning 18 p3101 A67-34077

X-ray diffraction analysis of polycrystalline brass deformed by tension, noting stacking fault probability, stress-strain curve, etc 18 p3064 A67-34084

Effect of dislocations in GaAs single crystals on diffused p-n junctions structure and recombination radiation parameters 19 p3300 A67-34768

Etch pitting and electron microscopy used for tungsten single crystals dislocation density measurements at different strain levels 19 p3248 A67-36028

Heat treatment of indium antimonide crystals with various dislocation densities noting change in conductivity 20 p3506 A67-36227

Statistical dislocation theory of crystal brittle fracture seen as stochastic process with microcrack formation and propagation under plastic deformation 20 p3541 A67-37318

Temperature /K-state/ effect on dislocation blocking stresses in nickel alloy studied by mechanical hysteresis method 20 p3471 A67-37558

Dilute magnesium addition effect on growth and shrinkage of dislocation loops in aluminum studied by isothermal annealing of thin foils 21 p3644 A67-38088

Steady state diffusional creep for materials with large grains and dislocations forming sinks for vacancies, obtaining strain rate 21 p3719 A67-38089

Spontaneous decomposition of helical dislocations in metal crystal into row of pinched-off loops plus straight dislocation line 21 p3677 A67-38092

Nature, distribution and causes of structural imperfections and dislocations in epitaxial Si layers with base layer orientation /111/ 21 p3681 A67-38359

Carbon influence on copper precipitation in dislocation free silicon single crystals with low oxygen, discussing growth mechanism and edge dislocation 21 p3686 A67-39136

Anomalous phosphorus diffusion in Si at high surface concentrations explained by excess vacancy generation at edge jogs on gliding dislocations 22 p3855 A67-39347

Crystal layer dislocation structure of cold rolled molybdenum foil investigated by electron microscopy 22 p3820 A67-39792

Adsorbed ions and organic molecules effect on mobility of half-loops dislocation introduced by indenter into MgO surfaces 23 p4035 A67-40655

Aluminum-magnesium alloy dislocation networks structure and formation investigated by thin foil technique after rapid solidification 23 p4017 A67-40658

Dislocation structure of tension deformed Si samples investigated by electron microscopy 23 p4042 A67-41296

Dislocation of aluminum during creep investigated for change in block structure 23 p4020 A67-41301

Radiation field asymmetry and anomalous beam angle divergence of ruby lasers linked to dislocations in ruby crystals prepared by Verneuil method 24 p4166 A67-42070

Microstructure of SGBF graphite under tensile and compressive stresses noting crack generation in layer planes [ACS PAPER 6-N-66F] 24 p4175 A67-42372

Thermal treatment at melting temperature inducing acceptors of electric conductivity in indium antimonide crystals 24 p4204 A67-42577

Steel dislocation structure under adsorption fatigue investigated by electron microscope, discussing surface active medium effect 24 p4174 A67-42724

Laser pulses producing local dislocation process in AlIBV semiconductor compounds 24 p4168 A67-42725

CRYSTAL GROWTH

SA HYDROTHERMAL CRYSTAL GROWTH

Dislocation-free silicon web crystal growth controlling supercooling and resistivities, noting elastic strains 01 p0131 A67-10367

Sintering mechanisms in powdered compacts of carbides, oxides and metals, examining grain growth, pore decrease and diffusion coefficients 01 p0096 A67-10694

Dispersion-strengthening by formation of carbides of Hf, Zr, Ta, Ti and Nb in wrought and recrystallized Cr, discussing structural stability 01 p0100 A67-10766

Temperature dependence of grain size in nonstoichiometric NbC between 1600 and 3300 degrees K in vacuum and Ar 01 p0102 A67-11245

Nucleation theories, emphasizing relation with oriented growth of thin films condensing on solid foreign substrate 02 p0285 A67-11702

Deposition conditions effect upon growth and structure of evaporated and sputtered films and significance in relation to electrical, magnetic and mechanical behavior 02 p0285 A67-11703

Vacuum deposited metal film structure analyzed over wide temperature range, using electron diffraction and electron microscopy techniques 02 p0285 A67-11705

Thermally grown silicon dioxide and resulting silicon-silicon dioxide interface, noting potential difference effect on n-type inversion layer 02 p0293 A67-11753

Growth of spherulitic structure in thin layers of tellurides, noting nucleations and multiplicity of phases 02 p0295 A67-11766

Structural orientation, purity and perfection of molybdenum single crystals grown by zonal electron-beam melting process 02 p0255 A67-11867

Solution grown epitaxial red light emitting p-n junctions in GaP preparation, electrical and optical properties, examining I-V characteristics 02 p0297 A67-11876

Recovery and recrystallization of high purity warm-worked chromium sheet material 03 p0439 A67-12924

Rate dependent melting of polytetrafluoroethylene by differential thermal analysis, noting that amount of superheating is larger with higher molecular weight 04 p0641 A67-14528

Epitaxial growth of SiC film on silicon substrate and electron diffraction analysis of crystal structure 04 p0675 A67-14762

Temperature dependence of migration of double positioning boundaries during growth of gold films inside electron microscope 04 p0675 A67-14924

Crystal and biological nucleation processes and mechanisms and roles of energy, charged particles, shocks, grain size and impurities 04 p0565 A67-15080

Metal addition effect on grain growth of matrix oxides, noting inhibitive results in most cases 04 p0642 A67-15086

Electron beam float-zone melting process applied to dielectric compound aluminum trioxide to obtain sapphire crystals 04 p0628 A67-15320

Grain oriented growth in beryllium condensates, discussing acicular structure of transverse sections of films 04 p0641 A67-15979

Soviet papers on growth and imperfections of metallic crystals 05 p0826 A67-16074

Dislocation reaction in crystals with diamond type structure analyzed on silicon grown by Czochralski method along /100/ axis 05 p0860 A67-16077

Electron beam zonal fusion growth of Mo, W and Ta single crystals without using crucible 05 p0827 A67-16079

Electron beam zonal vacuum fusion growth of Mo-Nb alloy single crystals 05 p0827 A67-16080

Direct measurement of dispersion properties of cadmium sulfide and CdS-CdSe crystals, using Obreimov-Fresnel diffraction method, growing crystals by synthesis 05 p0861 A67-16396

Ruby crystals grown by Czochralski technique using induction heated iridium crucible, noting laser oscillations in pulled crystals 05 p0866 A67-16975

Tantalum interaction with nitrogen and air show retardation of grain growth 05 p0832 A67-17507

Stress relaxation, creep and uniaxial elongation of polycrystals relationship as part of cumulative plastic deformation processes 06 p1109 A67-18809

Kinetics of growth of beta grain in titanium alloy 07 p1200 A67-19245

Spectral properties of Nd doped yttrium vanadate grown from melt, noting reduced Stark splitting leading to laser action 07 p1195 A67-19559

Etching methods to visualize lattice dislocations and grain boundaries in Czochralski grown calcium tungstate crystals doped with neodymium for laser application 07 p1196 A67-19565

Crystalline structure of ZnTe thin films as function of stoichiometric and growth conditions 07 p1233 A67-19645

Surface oxide films and lifetime of vacancies in thin crystals analyzed for pure aluminum and dilute aluminum alloys 08 p1369 A67-20794

Laser emission from electron beam excitation of CdS crystals due to crystal uniformity and radiative transitions resulting from CD-rich growth conditions 09 p1510 A67-21569

Thin films of indium antimonide for active devices grown by various methods including atomic mixing, flash evaporation, etc 09 p1474 A67-22112

Single crystal thin semiconducting films prepared by short distance evaporation diffusion under isothermal conditions 09 p1557 A67-22573

Gallium arsenide - International Symposium, Reading, Berks., England, September 1966 10 p1613 A67-23509

Gallium arsenide epitaxial technology noting deposition rate and impurity profile, Hall mobility and morphology of deposits 10 p1692 A67-23511

Gallium arsenide characteristics and preparation noting epitaxial deposition and liquid phase, mobility, impurity and Hall effect data 10 p1692 A67-23512

Pyramid formation in epitaxially deposited GaAs layers, postulating vapor-liquid-solid formation mechanism 10 p1692 A67-23513

Impurity distribution in GaAs noting growth rate, concentration and crystallographic orientation 10 p1693 A67-23515

Properties of gallium arsenide crystals produced by pulling single crystals from melt of gallium arsenide covered by molten boric oxide 10 p1693 A67-23516

Synthesis of undoped GaAs single crystals by horizontal Bridgman method, noting maximum mobility value obtained 10 p1693 A67-23517

Solution regrowth technology of electroluminescent devices noting reduced threshold current densities, external quantum efficiency and adaptation to planar technology 10 p1665 A67-23518

Eutectics use in composite material by growing single crystal whiskers aligned inside matrix 10 p1669 A67-23637

Efficiency of electroluminescent lamps, noting dependence on arsenic pressure and temperature during GaAs crystal growth 11 p1845 A67-24140

Breakdown and switching in CdS single crystals, noting formation of negative resistance and thickness effect on performance 11 p1847 A67-24729

Electron distribution of oxygen grown GaAs crystals after heat treatment, showing profiles due to silicon contamination 11 p1848 A67-24740

Direct observation on precipitation and aging behavior in Cu-Ti alloys by transmission electron microscopy 11 p1809 A67-24948

Oriented growth of thick films of CdTe deposited on quartz plates in vacuum, discussing photovoltaic effect 12 p1982 A67-25450

Trap density is lower in epitaxially grown GaAs crystals than in crystals grown by either horizontal Bridgman /HB/ or floating zone /FZ/ technique 12 p1983 A67-25457

Crystal growing technology for application to semiconductor production noting methods, impurity control, etc 12 p1950 A67-26211

Growth mechanisms and crystalline quality of diamond type compounds and crystals in III-V and II-VI groups 13 p2177 A67-27009

Low pressure diffusion of carbon to nucleation sites and graphite growth in cubic morphology suggested as origin of clintonite in meteorites 14 p2384 A67-28144

Ion temperature, cell temperature, cell voltage and current in electrolytic technique for reproducible growth of molybdenum /IV/ oxide crystals 15 p2533 A67-29295

Spin-lattice relaxation times in grown ruby in one phonon region, noting temperature dependence and undulation of lattice planes 16 p2728 A67-31054

Collection of articles on complex semiconductors investigating conductivity, thermal, electrical and other properties, and preparation methods 16 p2729 A67-31154

Growth of dendriform crystal contaminant in hydrocarbon fuel or hydraulic system during stagnant storage, discussing possible effects and corrections 17 p2801 A67-31991

Impurity diffusion and segregation effects in p-n junctions in compensated solution grown GaP 17 p2921 A67-33053

Temperature dependence of grain size in nonstoichiometric NbC between 1600 and 3300 degrees K in vacuum and Ar 17 p2875 A67-33168

Crystal growth, nucleation, supercooling, solidification, glass forming and kinetics of 1, 3, 5-tri-alpha-naphthylbenzene 17 p2809 A67-33255

Soviet book on production of homogeneous semiconductor crystals, discussing nonuniformities in structural composition 18 p3100 A67-33773

Surface hillock-like features in epitaxially grown gallium arsenide studied by X-ray diffraction topography 18 p3106 A67-34636

Particle growth during coalescence of fine phases of metallic alloys 19 p3245 A67-35469

Nickel-base single crystal superalloy tensile and creep properties, comparing single and multiple slip orientations 20 p3470 A67-37387

Tantalum interaction with nitrogen and air show retardation of grain growth 21 p3644 A67-38035

Alnico alloys containing Ti studied for columnar crystal growth, noting Ti content influence on crystal structure formation 21 p3645 A67-38376

Apparatus for refractory single crystal fusion growth at high temperature using arc melting 21 p3636 A67-38769

Chromium oxide addition effect on ruby recrystallization in carbonate and bicarbonate solutions under hydrothermal conditions, estimating chromic oxide solubility 21 p3685 A67-38971

Carbon influence on copper precipitation in dislocation free silicon single crystals with low oxygen, discussing growth mechanism and edge dislocation 21 p3686 A67-39136

Epitaxial growth of gold on cadmium iodide surface studied with transmission electron microscopy, discussing diffraction patterns and substrates 21 p3687 A67-39140

preparation 21 p3687 A67-39140

Limitations imposed on performance of large area p-n junctions by quality of silicon material, discussing defect-free processing techniques 22 p3766 A67-39247

CdS single crystal platelet growing and treating technique, relating fluorescence emissions to growth conditions 22 p3778 A67-39359

Chemical vapor deposition method to grow epitaxial YIG on YAG using high temperature hydrolysis oxidation at seed surface 22 p3860 A67-39896

Optical properties of new and stable nonlinear optical ferroelectric potassium lithium niobate single crystal 22 p3863 A67-40236

Anisotropic energy gap measurements in niobium single crystals by tunneling 22 p3865 A67-40440

Epitaxial silicon layers grown by electron microscopy with small quantities of gold, discussing possible growth mechanisms 23 p4036 A67-40656

Epitaxial growth of aluminum nitride on silicon carbide studied for influence of substrate temperature on perfection of crystal deposit 23 p4037 A67-40722

Equilibrium state of two-dimensional lattice liquid-gas system using cluster variation method for nucleation and thin film growth studies 23 p4040 A67-40967

Ice single crystal growth rate in supercooled water explained on basis of combined heat dissipation mechanism and molecular growth kinetics 23 p4024 A67-40973

Mass spectrometry used for simultaneous measurements of adsorption and crystal nucleation processes 23 p4043 A67-41355

Vapor growth of single crystal heterojunctions of GaAs on Ge or InAs on GaAs using iodine process in closed tube system 23 p4043 A67-41432

Ti additive effect on aluminum oxide particle growth in Ni matrix from 1000 to 1350 degrees C 24 p4171 A67-41959

CRYSTAL LATTICE
Si single crystal lattice parameter measurement using double-diffraction effect 01 p0135 A67-10894

Kinetics of stored energy buildup in alkali halide crystals after proton irradiation noting dependence on lattice energy of crystal 01 p0136 A67-11050

Atom distribution in double matrix cell of ordered solid solution in alnico-titanium alloy 02 p0254 A67-11864

Mg-Nd alloy structure development during plastic deformation at high temperature, noting lattice distortions and recrystallization process 02 p0255 A67-11868

Plastic deformation of indium and indium-thallium alloys, noting change of pure indium lattice to fcc with increase of thallium content 02 p0255 A67-11869

Neutron irradiation effect on twinning behavior and transition temperature of niobium-vanadium alloy 02 p0256 A67-12709

Optical phonons role in thermal conductivity of GaSb doped with Zn and Te in temperature range 80 to 600 degrees K 03 p0488 A67-12811

Harmonic approximation of infinite crystal dynamics problem, noting collisional case and action of external force on atoms 03 p0520 A67-12930

Kamacite and taenite superstructures and metastable tetragonal phase in iron meteorite 03 p0510 A67-13334

Crystal morphological features of Tucson meteorite 03 p0510 A67-13350

Atomic planes and positions in bulk thinned specimens of crystalline Ge determined, using electron microscopy 03 p0501 A67-14345

Niobium-aluminum alloys elasticity, shear cubic compressibility moduli, Poisson ratio, characteristic temperature and crystal lattice structure 04 p0635 A67-14431

Optical transitions and k conservation in crystalline solids explained in terms of localization of hole produced by excitation 04 p0674 A67-14526

Thermal conductivity of lanthanum and monochalcogenides, noting role and temperature dependence of crystal-lattice conductivity 04 p0680 A67-15287

Molecular pair distribution function in perfect crystalline solids, using method based on cell cluster theory 05 p0758 A67-16129

- Impurity atom behavior in diatomic InSb and GaSb crystal lattices analyzed, using nuclear gamma resonance, measuring absolute values of f , chemical displacements and line widths 05 p0861 A67-16392
- Superlattice formation and lattice spacing changes in copper-gold alloys annealed for various periods 05 p0862 A67-16506
- Local variations in spacing and orientation of lattice plane in silicon single crystal, measuring angular positions of diffraction peak by double crystal spectrometer 05 p0866 A67-16977
- Optical absorption due to direct intervalence band transitions in Ge, noting effect of lattice temperature 05 p0869 A67-17192
- Lattice IR reflection and transmission spectra and Raman spectrum of monocrystalline and hot pressed pellets of ZnSe 06 p1059 A67-18909
- Negative magnetoresistance in semiconductors caused by magnetic system in random lattice of impurity atoms 06 p1067 A67-18965
- X-ray line broadening in deformed magnesium by Fourier analysis of line shapes and analysis of line widths, noting lattice distortion 07 p1210 A67-20108
- Ruby laser-induced effect of pulsed pressure on KDP crystal surface and thermal bulk effect on excitation of ultrasonic oscillation in crystal 08 p1337 A67-20417
- Admissible configurations and diffusive motions of molecular chains on quadratic lattice narrow channels 08 p1356 A67-21299
- X-ray structural and spectral analysis of changes in lattice constant, linear expansion coefficient and K-absorption edge of iron and manganese in ferrite with spinel structure 08 p1372 A67-21492
- Lattice constant of thin silicon specimens determined using electron diffraction techniques 09 p1553 A67-21881
- Inertialess polarization energy of charge interaction between neighboring lattice points in Ge crystal, using M-20 computer 10 p1695 A67-23657
- Entropy function relationship to properties of pure metals, noting correlation with lattice parameters at 298 degrees K 11 p1805 A67-24360
- Energy transfer during interaction of atoms with surface of ideal crystal in terms of classical mechanics 11 p1824 A67-24855
- X-ray analysis of lattice strain and crystallite size changes in tungsten carbide compressed at high pressure, noting annealing effect 11 p1809 A67-24949
- Absorption spectra and luminescence of p-type copper diffusion doped Ga-As crystals, noting appearance of temperature dependent narrow spectral lines 12 p1984 A67-25522
- Optical and paramagnetic resonance of ytterbium ions in calcium fluoride, obtaining correlation between site geometry and optical absorption 12 p1984 A67-25843
- Formula for thermal accommodation coefficient as basis for accommodation coefficient of monatomic gas-solid system calculation 12 p2040 A67-26229
- Thermal accommodation of rare gases on clean metal surfaces, computing energy interaction with linear nearest-neighbor lattice 13 p2098 A67-26941
- Hafnium oxidation between 300 and 1200 C, noting occurrence of faster stages in process 13 p2132 A67-26999
- Dynamics of beryllium lattice noting dispersion curves of wave frequencies 13 p2137 A67-27109
- Current-voltage characteristics of germanium-silicon isotope heterojunctions with regard to capacitance and photoelectric measurements 13 p2183 A67-27569
- Nb-N system diagram for five stable nitride phases, giving two reactions governing high temperature phase fields 14 p2337 A67-28419
- Triangular flux line lattices observation by electron microscope in type II superconductors 14 p2369 A67-28599
- Lattice thermoconductivity noting local equilibrium hypothesis theory, thermal resistance mechanism, etc 14 p2374 A67-28981
- Thermal lattice conductivity at high temperatures in compound semiconductors, linking dilatation coefficient of molecular theory to ionic nature of interatomic bonds 14 p2374 A67-28984
- Ultrasonic measurement of temperature dependence of longitudinal sound absorption coefficient for main crystallographic directions in superconducting indium 14 p2375 A67-29070
- Temperature dependence of lifetime and Hall coefficient in InSb, measuring lifetime by phase shift method, concluding that recombination centers are lattice defects 15 p2535 A67-29483
- Infrared lattice vibration spectra of II-VI compounds analyzed by Drude dispersion, obtaining transverse-optical-mode frequency 16 p2724 A67-30603
- Exchange interaction between f-electrons and s-electrons in atomic shells of crystal lattice of rare earth metals, examining calculation methods for Hamiltonian of s-f exchange 16 p2733 A67-31730
- IR lattice spectra of rare earth iron garnets noting absorption in low frequency bands and molecular weights 16 p2733 A67-31880
- Neighbor model for computer simulation of field ion images in fcc point lattice 17 p2887 A67-32205
- Gamma ray radiation effects on laser glasses, noting ionization and atom displacements in lattice 17 p2887 A67-32374
- Kronig-Penney model for electron potential in crystal adapted to semiconductor, discussing cubic lattice 17 p2914 A67-32386
- Activities and relative partial molar free energies of CuPt alloys, noting formation mechanism, ordering temperatures, etc 17 p2872 A67-32739
- Inertialess polarization energy of charge interaction between neighboring lattice points in Ge crystal, using M-20 computer 17 p2924 A67-33338
- Nonexponential electron spin cross relaxation measurement in dilute ruby 17 p2924 A67-33369
- Elastic moduli, bond parameters and effective ion charges for wurtzite and sphalerite binary crystal lattices 18 p3094 A67-33437
- Relation between changes in ferrite lattice parameter at magnetic conversion temperature and changes in ferrite metal ion charges due to electron exchange 18 p3095 A67-33444
- Mean values of characteristic temperatures and dynamic displacements of ions for lattice of solid substitution solutions of zinc telluride-cadmium telluride system 18 p3095 A67-33446
- Changes in InSb, GaSb and Te crystal lattice structure and chemical bonds investigated for effects on thermoconductivity, thermal EMF and microhardness 18 p3096 A67-33451
- Liquid crystal - Conference, Kent State University, August 1965, Part II 18 p2990 A67-33632
- Gallium arsenide single crystal lattice dielectric constant measured noting broad resonance 18 p3101 A67-34010
- Absorption spectra and luminescence of p-type copper diffusion doped Ga-As crystals, noting appearance of temperature dependent narrow spectral lines 18 p3103 A67-34453
- Deformation behavior of matrix and fibers in aluminum-boron and copper-tungsten composites studied by X-ray lattice strain techniques 18 p3067 A67-34570
- Knoop hardness anisotropy in unalloyed titanium and iodide titanium sheets, discussing orientation, hardness variations, rolling, cross section planes and indentation [ASTM PAPER 53] 18 p3068 A67-34583
- Dislocation in field-ion micrograph analyzed by computer-simulated Ranganathan hypothesis using Moore shell model 19 p3266 A67-35603
- Type II superconductor suspended on elastic fiber in magnetic field investigated for oscillation dampings 20 p3505 A67-36203
- Nickel aluminide structure, examining arrangement of Ti, Cr and W in lattice via X-ray spectroscopy 20 p3467 A67-37116
- IR absorption in alkali-halide crystals containing molecular ion impurities caused by intralattice vibrations 20 p3511 A67-37140
- Spectral variations resulting from thermal processes in crystals subjected to focused ruby laser beam 20 p3460 A67-37146
- Energy transfer during interaction of atoms with surface of ideal crystal in terms of classical mechanics 20 p3490 A67-37538
- Heat conductivity in materials ascribed to phonons, noting phonon radiation effects 20 p3515 A67-37715
- Lattice relation of cuprous sulfide formed on CdS single crystal noting precisely similar orientation 21 p3677 A67-38011
- Flux line lattice and laminar magnetic structure of mixed state in type II superconductors consisting primarily of lead 21 p3681 A67-38351
- Point defect concentration in GaAs determined from lattice constant 21 p3685 A67-38970
- Nonlocal elasticity theory for materials with long range cohesive forces derived from lattice theory by writing strain energy in integral form 22 p3908 A67-39288
- Elastic constants and interatomic interaction parameters of niobium alloyed with tantalum, titanium and vanadium 22 p3820 A67-39789
- Lattice parameter of bcc Nb-Hf alloy with interstitial solid solution of oxygen 22 p3823 A67-40210
- Magnetic moments of sublattices and of yttrium garnet calculated including biquadratic temperature dependent exchange 23 p4043 A67-41302
- Crystal structure of rare earth Co compounds prepared by levitation melting process investigated by X-ray 24 p4172 A67-41975
- Atom arrangement in crystalline materials considering lattice, planes and structure, discussing effect on mechanical properties, particularly friction 24 p4164 A67-42733
- CRYSTAL OPTICS**
- Spontaneous electro-optical effect in triglycin sulfate crystals spectrally studied, noting changes in double refraction along three crystallographic axes during ferroelectric phase transition 01 p0129 A67-10138
- Optical harmonic generation and first order sum and difference frequencies in plane parallel crystal plate within framework of phenomenological theory 01 p0089 A67-10361
- Nonlinear optical materials properties discussed on basis of Soviet and foreign studies involving lasers 01 p0115 A67-11011
- Light modulation by large single crystal ZnS with negligible strain 01 p0138 A67-11330
- Birefringence and impurity states in optical absorption spectra of nonmetallic crystals in pseudopotential theory 02 p0281 A67-11489
- Voice communications system using GaAs room-temperature injection laser and TV communications system using GaAs crystals as modulators for laser beams 02 p0194 A67-11786
- Gallium arsenide crystal properties for use in optical filter 03 p0488 A67-12858
- Perturbation theory analysis of spatial dispersion effects on frequency addition in crystals 03 p0434 A67-13125
- Fracture mechanism of transparent crystals interacting with ruby laser beam 03 p0435 A67-13128
- Quantum study of optical nonlinearities in absorbing materials, energy transfer between optical waves, laws of nonlinear reflection and coherence effects 04 p0657 A67-14881
- Possible stabilization of AgCl crystals against solar radiation effects by addition of Cu, Ni, Zn, Cs, S or Hg 04 p0685 A67-15752
- Doubling of frequency of light in nonlinear medium with random nonuniformities 05 p0762 A67-16348
- General theory for parametric oscillation in optical region 05 p0817 A67-16639
- Optical harmonic generation and first order sum and difference frequencies in plane parallel crystal plate within framework of phenomenological theory 06 p1009 A67-17619
- Optical scattering dependence on heat treatment of monocrystalline silicon containing nitrogen 06 p1050 A67-18183
- Soviet book on electronic properties of semiconductor solid solutions, noting relation between probability theory and ideal crystals theory 07 p1232 A67-19580
- Optical beam deflection method based on polarization change of acoustically deflected light as compared to incident beam 09 p1510 A67-21574
- Optical quenching effect and spectral distribution of photoconductivity and optical transmission of KRS-5 single

- crystals 09 p1552 A67-21673
- Cylindrical optics in converting laser emission into second harmonic in ADP and KDP crystals, obtaining high conversion efficiency 09 p1511 A67-21916
- Nonlinear optical materials properties discussed on basis of Soviet and foreign studies involving lasers 12 p1966 A67-25361
- Cylindrical optics in converting laser emission into second harmonic in ADP and KDP crystals, obtaining high conversion efficiency 14 p2329 A67-28245
- Refractive index dispersion of CdSe and CdTe crystals in visible and infrared spectral range at room temperature 16 p2732 A67-31481
- Crystals for UV and IR optics, discussing solubility, hardness, melting, expansion coefficients and design factors 18 p3078 A67-33565
- Optical properties of magnesium fluoride in EUV from reflectivity measurements on crystal and thin films 18 p3099 A67-33692
- Appearance of extraordinary rays from double refraction in ruby laser crystals with polished rectangular prisms 20 p3507 A67-36330
- Maxwell equations solved for Gaussian beam form in anisotropic medium, discussing laser applications 24 p4167 A67-42092
- ADP electro-optic crystal in laser emission control tested in beam deflection device and Michelson interferometer modulator, noting refractive index changes 24 p4167 A67-42239
- CRYSTAL STRUCTURE**
- SA ANISOTROPY
- SA FACE CENTERED CUBIC /FCC/ CRYSTAL
- SA ISOTROPISM
- SA MORPHOTROPISM
- SA YTTRIUM-ALUMINUM GARNET /YAG/ CRYSTAL
- SA YTTRIUM-IRON GARNET /YIG/ CRYSTAL
- Electron mobility in p-type indium antimonide, noting entrainment of minority carriers by majority carriers 01 p0129 A67-10098
- Paramagnetic resonance of praseodymium and uranium ions in calcium fluoride analyzed via fitting to spin Hamiltonian 01 p0129 A67-10146
- Vapor flux of trichloromethylsilane affects morphology of pyrolytic deposits of silicon carbide 01 p0103 A67-10252
- Gunn effect noting negative bulk conductivity, creation of external negative conductance and zones with different field intensities in semiconductor crystals 01 p0130 A67-10253
- Sintered Ni-base heat resistant alloys, discussing composition-creep strength relation, grain size, prealloyed-powder production and thermal and structural shock properties 01 p0098 A67-10700
- Dysprosium crystalline structure and phase transition from helical antiferromagnetism to paramagnetism 01 p0133 A67-10744
- Complex band structure properties in diamond type crystals, discussing symmetry of various surface states with and without spin-orbit coupling 01 p0134 A67-10786
- Clathrates exhibiting metallic conductivity and superconductivity at specific temperatures, noting transition temperature of nitrate salt 01 p0135 A67-10917
- Light modulation by large single crystal ZnS with negligible strain 01 p0138 A67-11330
- Deposition conditions effect upon growth and structure of evaporated and sputtered films and significance in relation to electrical, magnetic and mechanical behavior 02 p0285 A67-11703
- Vacuum deposited metal film structure analyzed over wide temperature range, using electron diffraction and electron microscopy techniques 02 p0285 A67-11705
- Low seated interfaces effect on electron transport in thin continuous metal films in presence of magnetic or electric fields 02 p0292 A67-11743
- Properties of Si-Si interface subjected to thermal oxidation in dry and wet oxidizing gases, thermal decomposition of ethyltriethoxysilane and vacuum evaporation of SiO and quartz 02 p0293 A67-11751
- Epitaxy of semiconductor on insulating monocrystalline base of corundum, noting electronic characteristics of silicon layers 02 p0294 A67-11755
- Growth of spherulitic structure in thin layers of tellurides, noting nucleations and multiplicity of phases 02 p0295 A67-11766
- Bounds for overall elastic moduli of solid composite materials with uniform phases that may be arbitrarily anisotropic 02 p0337 A67-11795
- Surface states and additional structure in McMillan-Anderson model for Tomasch effect in superconducting films 02 p0296 A67-11822
- Structural changes during early stages of decomposition of oversaturated solid solution of titanium in cobalt, noting secondary diffusive reflection 02 p0255 A67-11865
- Mg-Nd alloy structure development during plastic deformation at high temperature, noting lattice distortions and recrystallization process 02 p0255 A67-11868
- Temperature dependence of elastic wave losses for bismuth germanium oxide, noting possible application for information storage VHF and microwave frequencies 02 p0300 A67-12507
- Crystallographic structure of hexagonal ferrites of BaO-MeO-ferric oxide system and applications in UHF and microwave regions 02 p0301 A67-12787
- Statistical effects during generation of second harmonic in optically transparent crystals, noting coefficient of correlation between harmonic and fundamental radiation power of solid state laser 03 p0467 A67-12928
- Sliding friction characteristics in vacuum of single and polycrystalline aluminum oxide in contact and with various metals 03 p0428 A67-13231
- Room temperature microhardness anisotropy, slip and twinning in molybdenum carbide single crystals noting orientation dependence, elastic modulus, electric resistivity and measurement techniques 03 p0441 A67-13254
- Ti-Mg alloy production under high pressure, noting existence of solid solution of one weight-percent Mg 03 p0441 A67-13255
- Strength characteristics of whisker crystals, microcrystals and macrocrystals influencing selection and use of composite reinforced materials 03 p0449 A67-13306
- Electron spin resonance absorption spectrum of Pt in YAG at low temperatures, noting ionic orientation 03 p0492 A67-13326
- Electron spin resonance with trigonal and orthorhombic symmetry in cerium oxide doped calcium fluoride 03 p0492 A67-13328
- Crystal structure of alpha- and beta-indium selenide semiconductor 03 p0493 A67-13361
- Interfaces in composite materials, discussing matrix-fiber interfaces, interfacial chemical interactions, microstructure and thermodynamic instability 03 p0454 A67-13426
- High temperature reaction between refractory whiskers of silicon nitride and Al and Ni, observing results by electron microscopy 03 p0445 A67-13528
- Interatomic force model calculation of shear and tensile strengths, predicting stress-strain curves for crystal structures 03 p0495 A67-13532
- Secondary scattering of low energy electrons by rows of atoms, obtaining diffraction pattern 03 p0496 A67-13648
- Domain structure of strontium ferrite investigated by Bitter powder pattern method in basal planes, showing dependence on magnetic field intensity, temperature and thickness of crystals 04 p0673 A67-14482
- Epitaxial growth of SiC film on silicon substrate and electron diffraction analysis of crystal structure 04 p0675 A67-14762
- Substructure of aluminum monocrystals in relation to silicon content 05 p0827 A67-16075
- Growth condition effect on perfection of single crystals of niobium examined, using X-ray diffraction techniques 05 p0828 A67-16470
- Heat treatment conversion of large grain n-type indium antimonide single crystals and twin crystals into p-type samples 05 p0862 A67-16507
- X-ray structural analysis of superconducting Nb based alloys, noting two-phase region in annealed samples 05 p0863 A67-16690
- Phase recrystallization effect on structure and mechanical properties of cast monophasic titanium alloys 05 p0830 A67-16760
- Ternary alloys compounded with Ti, Zr, Hf, Fe, Ni, Co, Cu, Al, Ga, noting crystalline structures 05 p0830 A67-16919
- Laser as source of optical Fourier analysis of atomic structure of crystals 05 p0824 A67-16921
- Structure and mechanical properties of molybdenum-niobium system monocrystalline melts prepared by electron beam zonal melting 05 p0830 A67-17024
- Annealing temperatures effect on Young modulus, temperature coefficient and crystallographic texture of Fe-Ni-Ti alloys after deformation 05 p0831 A67-17485
- Structural changes in epitaxial CdS films grown on rock salt, mica and silver substrates analyzed by electron diffraction at various temperatures and values of electric field 06 p1047 A67-17599
- X-ray crystal structural analysis of tetraethyl titanate and monomethyltriethyl titanate, determining reason for difference in color 06 p0955 A67-17849
- Precipitation effect of dispersed calcium titanate-rich phase on shape, organization and thickness of ferroelectric domains in barium titanate 06 p1020 A67-18047
- Metastable form of C12 type calcium disilicide when under high temperature and pressure, noting X-ray diffraction powder patterns and superconductivity 06 p1051 A67-18372
- Empirical corrections to energy band models of diamond, Si, Ge and grey Sn [AFCLR-67-0382] 06 p1058 A67-18902
- Niningerite composition and optical, physical and crystallographic properties 07 p1247 A67-19064
- Small additions of refractory elements effect on structure and properties of sheets of Al-Zn-Mg alloy in various states 07 p1201 A67-19254
- Small additions of refractory elements effect on structure and properties of aluminum alloy castings containing Zn and Mg 07 p1201 A67-19255
- Chemical and crystal structural analysis of solid solution of titanium chromide and zirconium chromide metalides 07 p1204 A67-19265
- Structural changes in titanium alloys during heat treatment 07 p1205 A67-19271
- Structure of system Ti-Mo-Cr-Fe-Al alloys when quenched from beta region, noting maximum hardness at aging temperatures 07 p1205 A67-19272
- Interaction between helicon waves and drift currents in layered lead telluride structure 07 p1232 A67-19555
- Crystalline structure of ZnTe thin films as function of stoichiometric and growth conditions 07 p1233 A67-19645
- Structure of rolling texture of bcc metals and alloys under various external deformation conditions 07 p1210 A67-20107
- Temperature variation of spin-lattice relaxation time and spin-spin relaxation time in superconducting and normal states of vanadium compounds 07 p1236 A67-20139
- Single niobium crystal deformation, discussing stress-strain curves, slippage, orientation and asymmetry of slip 07 p1211 A67-20164
- Optical spectrum of normal excitons in deformed and nondeformed n-type Ge single crystal layers for four orientations 08 p1367 A67-20409
- Nucleation during pulse remagnetization of thin films, showing domain structure of formation, growth of nuclei, etc 08 p1367 A67-20603
- Quasi-equilibrium states during pulse remagnetization of thin ferromagnetic films, discussing domain structure 08 p1367 A67-20604
- Aging effect on structure of cobalt alloys annealed at 1200 degrees C suggests formation of laminar regions 08 p1342 A67-20812
- Structural changes and changes in elastic properties of cold rolled Ti and Zr during recrystallization heating 08 p1342 A67-21003
- Paramagnetic resonance absorption spectrum of cerium in yttrium-gallium-garnet host crystal 08 p1371 A67-21312
- Crystalline structure of amorphous boron fibers noting glass-like nature of fiber as exhibited by diffraction patterns 08 p1343 A67-21313
- Single crystal film structure of fcc metals evaporated in ultrahigh vacuum onto alkali

halide surfaces cleaved in air and in situ 09 p1552 A67-21671
Intracrystalline field and spontaneous polarization in barium titanate studied by EPR spectrum of Cd-3 09 p1554 A67-21976
X-ray analysis of lattice structure of terbium crystals at 120 to 300 degrees K 09 p1555 A67-22066
Vapor-deposited tungsten formed by hydrogen reduction of tungsten hexachloride or hexafluoride, noting effect of crystal orientation and surface treatment on work function 09 p1451 A67-22357
Crystallization phase in Pbnm orthorhombic space group of yttrium manganite under pressure and high temperature 09 p1557 A67-22572
Second harmonic generation in liquid crystals, noting absence of effective center in molecular configuration 09 p1517 A67-22680
Semiconductor lasers for discrete outputs in broad spectral range determined by material characteristics, noting electronic applications 10 p1688 A67-22824
Spectrum of second order Raman lines in coupling of radiation and matter, using Green function 10 p1663 A67-22855
Phase transformations in heat treated nickel-rich Ni-Co-Cr-Al-Ti-C cast alloys noting sigma formation 10 p1668 A67-23173
Uniaxial stress and static electric field effects on energy band structure of strontium titanate and derivation of optical selection rules in region of perturbed crystals 10 p1691 A67-23403
Anisotropic vector functions of vector argument connected with crystal symmetry 11 p1812 A67-24148
Stimulated Raman effects in anisotropic crystal potassium dihydrogen phosphate with Stokes generations 11 p1800 A67-24243
Solid state material analysis inducing controlled density variations and crystal structure changes via high pressure techniques 11 p1846 A67-24618
Dispersed-phase alloy production noting structure types, deformation and fracture behavior at various temperatures 11 p1807 A67-24636
Composite structure of glass with crystalline aluminum oxide and zirconium oxide inclusions tested for strength and elastic properties 11 p1811 A67-24642
C domain wall motion in barium titanate crystals is dependent on A domains and activation fields throughout whole crystal 11 p1849 A67-24900
Doped alkali-halogen-crystal color center origin and transformation at liquid N temperature using ruby laser, noting temporary bleaching 12 p1951 A67-25200
Hyperfine structure and modified Zeeman effect in trivalent holmium in hexagonal lanthanum trichloride 12 p1987 A67-26237
Dislocation behavior in crystalline materials, examining agreement between theory and experiment 13 p2132 A67-26695
Charge motion on outer silicon oxide surface of MOS structure, estimating surface resistance and dependency on humidity and other factors 13 p2176 A67-26707
Dysprosium crystalline structure and phase transition from helical antiferromagnetism to paramagnetism 13 p2176 A67-26773
Oxidation of Be thin films in oxygen and carbon dioxide, noting decomposition of Be-carbide and effects of heating by electron beam 13 p2132 A67-26998
Recrystallization of Ge and Si thin films and structural changes due to electron bombardment and thermal annealing 13 p2177 A67-27071
Uniaxial anisotropy and rotational hysteresis in thin gadolinium films 13 p2179 A67-27144
Superconductivity of Nb3-Al-Mo3Al binary system 13 p2184 A67-27631
Aluminum alloy systems physical and structural characteristics and phase diagrams 14 p2334 A67-27802
Thermal processing of precipitation-hardenable aluminum alloys, noting changes in structural and mechanical properties 14 p2335 A67-27804
Ternary alloys compounded with Ti, Zr, Hf, Fe, Ni, Co, Cu, Al, Ga, noting crystalline structures 14 p2337 A67-28259
Laser as source of optical Fourier transforms in analysis of atomic structure of

crystals 14 p2330 A67-28261
Titanium-vanadium alloy microstructure investigated under quenching and aging through electron microscopy 14 p2338 A67-28423
Structure and mechanical properties of molybdenum-niobium system monocrystalline melts prepared by electron beam zonal melting 14 p2338 A67-28491
Enthalpy changes in ammonium perchlorate during linear heating, noting crystal structure transformation and subsequent decomposition 14 p2376 A67-28903
Effect of plastic deformation under compression on superconducting properties of Re single crystals 14 p2375 A67-29069
Structure of thin tungsten films as function of nature and temperature of substrate, noting partial crystallization of fcc structure 15 p2535 A67-29477
Vacuum effect on tensile, creep and fatigue properties of magnesium polycrystals and on tensile properties of oriented magnesium single crystals 15 p2503 A67-29561
Polymorphism in IV-VI compounds induced by high pressure and thin film epitaxial growth 15 p2539 A67-29822
X-ray structural analysis of superconducting Nb based alloys, noting two-phase region in annealed samples 15 p2539 A67-29860
Surface reactions and structure determinations of oxides of niobium, tantalum and vanadium with /110/ surfaces from CO and oxygen absorption 15 p2504 A67-29881
Temperature homogenization effect on structure of industrial aluminum, determining mechanical properties dependency on Fe/Si ratio 15 p2504 A67-29975
Combustion characteristics of crystalline oxidizers noting materials used, experiments performed and results 15 p2581 A67-29990
Carbon monoxide chemisorption on polycrystalline molybdenum studied by radiotracer, noting desorption at various temperatures as time 15 p2434 A67-30099
Gold, silver, copper and tin condensed films, investigating dependence of structure and conductivity on substrate material 15 p2540 A67-30122
Energy dependence on wave vector in valence band of diamond, Si, Ge and SiC, obtaining Coulomb and resonance integrals 15 p2541 A67-30237
Valence band structure of wurtzite type crystals 16 p2725 A67-30802
Irradiation of gallium arsenide and gallium antimonide monocrystals by electrons, fast neutrons and relativistic protons, discussing Hall coefficient variation 16 p2727 A67-30869
Activation energies of nucleation of crack and dislocation loops in crystals, noting crack propagation theories and temperature effect 16 p2772 A67-31303
Titanium alloys crystal structures determined using single crystal X-ray and powder neutron diffraction method, noting mechanical properties temperature dependence and martensitic transition 16 p2688 A67-31307
Twinning of copper, silver, iron, and gold alloys of beryllium pressurized in solid medium noting structural changes 16 p2690 A67-31371
Orthorhombic, low temperature alpha modification of niobium and vanadium carbide 16 p2691 A67-31598
Tungsten-carbon phase relations from DTA, X-ray and electron diffraction measurements noting disordered, ordered hexagonal and orthorhombic modifications 16 p2692 A67-31599
Book on intermetallic compounds discussing bonding, crystal structure, microstructure, formation, stability, kinetics, transformations and properties 16 p2692 A67-31867
Digital accelerometer converts data into pulse format without analog-digital conversion, noting bias stability determination by crystal characteristics 17 p2855 A67-32438
Electron microscopy of titanium alloys noting preparation, heat treatment of samples, crystallographic structure, etc 17 p2872 A67-32722
Structural characteristics of Ni-Mo alloys analyzed using electron microscopy and X-

ray diffusion scattering 17 p2872 A67-32723
Etch pitting analysis of slips in Fe-Si bicrystals under plastic strains, noting effect of impingement of pure edge and pure screw slip bands 17 p2872 A67-32738
Si-Fe deformation in tension/compression noting orientation dependence of yield stress, slip band formation and direction of screw dislocations 17 p2872 A67-32741
Structure of Ge-Sn thin films vacuum deposited on glass substrates analyzed by electron diffraction methods 17 p2920 A67-32891
Molybdenum/tungsten films obtained by thermal decomposition in vacuum analyzed, noting surface morphological changes with temperature changes 17 p2921 A67-32892
X-ray spectral analysis of bent aluminum single crystals with crystallographic plane parallel to reflecting surface of crystal 17 p2874 A67-32895
Twin orientation in epitaxial gallium arsenide, noting relation to stellite feature 17 p2922 A67-33065
Intracrystalline field and spontaneous polarization in barium titanate studied by EPR spectrum of Cd-3 17 p2923 A67-33313
Energy band structure of crystals of groups IV, III-V and II-VI and magnesium silicide type crystals 18 p3095 A67-33448
Stress effects on structure of oriented crystallizing polymers, noting long periods changes due to displacement of crystallites in amorphous layers 18 p3068 A67-33489
Optical methods used for study of ruby crystals uniformity, discussing Twyman interferometer design 18 p3098 A67-33576
Liquid crystal - Conference, Kent State University, August 1985, Part III 18 p2991 A67-33633
Soviet book on production of homogeneous semiconductor crystals, discussing nonuniformities in structural composition 18 p3100 A67-33773
Measuring IR Faraday rotation and Hall effect in 6H and 15R polytypes of silicon carbide 18 p3102 A67-34278
Field ion microscopy of Ni-Mo alloys 18 p3065 A67-34364
PbTe thin films vacuum-vaporized onto amorphous or oriented substrates studied for crystallographic properties as function of deposition temperature, film thickness, etc 19 p3304 A67-35422
High superconducting transition temperatures in molybdenum carbide compounds stressing crystal structures 19 p3245 A67-35729
Sliding friction characteristics in vacuum of single and polycrystalline aluminum oxide in contact and with various metals 19 p3237 A67-35838
Crystal deformation and uniaxial failure under complex loading due to stress and temperature variations, applying physical state equation 20 p3540 A67-37057
Resistance of ideal crystal studied for plastic yielding and brittle cracking, noting composite materials devised to resist both failures 20 p3469 A67-37248
Meteorite minerals characteristic constituents, describing crystalline form, frequency of occurrence, percentage, nature and terrestrial effects 21 p3700 A67-37766
Structural modifications effect on PBI fiber critical properties, discussing strain-stress characteristics, target properties and crystallization 21 p3648 A67-37875
Change patterns in melting point and forbidden bandwidth for anion and cation substituted compounds of AIIIBV group 21 p3676 A67-37932
Niobium and niobium alloy structural changes during heating after pressing and rolling deformation 21 p3644 A67-38031
Sputtered films stable fcc modification of several metals deposited at high temperatures, obtaining normal structures over 400 degrees C 21 p3677 A67-38091
Field ion images from single crystals of titanium carbide, noting development of two crystallographic regions 21 p3645 A67-38093
Structural properties of Si anodic oxide layers studied by X-ray analysis, using Laue photograph method 21 p3681 A67-38360
Alnico alloys containing Ti studied for columnar crystal growth, noting Ti content influence on crystal structure formation 21 p3645 A67-38376
Impurity crystal-field spectra in II-VI and

III-V compound semiconductors used to predict unexplored systems spectra impurity crystal-field spectra in II-VI and III-V compound semiconductors used to predict 21 p3682 A67-38388

Soviet book on physicochemical principles of semiconductor alloying covering chemical bonds, crystal structure, binary systems, etc 21 p3684 A67-38433

Superconductivity of Nb₃Al-Mo₃Al binary system superconductivity of Nb₃Al-Mo₃Al binary system 21 p3685 A67-38828

X-ray structural analysis of ferromagnetic /ferrimagnetic/ bismuth ferrite single crystal 21 p3685 A67-38967

Photoelectric polarimeter for measuring rotational, electro-optical and electrogyrational effects and optical activity in ferroelectrics 21 p3631 A67-38969

Powder X-ray structural analysis of compounds of Nb-Ni and Ta-Ni systems, establishing homogeneity region for NbNi 21 p3646 A67-38973

Qualitative and quantitative variation in alloy phase composition with temperature and age hardening length, studying structural diagram 22 p3818 A67-39321

Silicon AC strain gauges performance investigated by employing oriented p-Si crystals operating in static and dynamic modes 22 p3798 A67-39569

X-ray analysis of hydrate of diethylamine three-dimensional crystal structure, determining bond distances and angles 22 p3757 A67-39634

Phase and chemical compositions of structural components forming in iron-nickel-chromium alloys with aluminum and titanium content 22 p3820 A67-39788

Reflectivity spectra of YIG and YGG crystals, observing YTG structure attributed to charge transfer enhanced crystal field transitions reflectivity spectra of YIG and YGG crystals, observing YIG structure attributed to charge 22 p3863 A67-40238

Change in brittle fracture work during combined impact and tensile load of polymer noting variation according to maximum law 23 p4072 A67-40595

IR absorption and Raman scattering spectra of diagonal cubic crystal structures 23 p4037 A67-40758

Soviet book on present state of semiconductor technology covering theory, material properties and semiconductor devices 23 p3978 A67-40797

Cleavage, plastic, creep, fatigue and other types of fracture noting initiation, propagation, mode, behavior, microstructure and appearance 23 p4019 A67-41033

Flexible anisotropic ferrite magnets preparation, noting influence of binder in orientation of crystals 23 p4041 A67-41183

Domain structures in YIG slices after polishing strains elimination, noting spike domains 23 p4041 A67-41185

Temperature effect on structure of W films prepared by triode pulverization at low pressure and low power 23 p4041 A67-41194

Bi and Ag nucleation on evaporated substrates studied as function of substrate temperature and impinging flux using electron microscopy 23 p4044 A67-41455

Far IR spectra and space group of crystalline hydrazine and hydrazine-d₄ noting coupling of translational and librational motions 23 p4048 A67-41532

Crystal structure of rare earth Co compounds prepared by levitation melting process investigated by X-ray 24 p4172 A67-41975

Quenched structures and precipitation in Al-Cu alloys with and without traces of Cd studied electromicroscopically, showing possible CD stabilizing effect 24 p4173 A67-42166

Twin lamellae in magnesium examined by electron microscopy reconfirms double twinning sequence 24 p4173 A67-42345

Crystalline variation and chemical composition of meteorite found at Marburg, West Germany 24 p4232 A67-42614

Atom arrangement in crystalline materials considering lattice, planes and structure, discussing effect on mechanical properties, particularly friction 24 p4164 A67-42733

CRYSTAL STRUCTURE DEFECT
SA INTERSTITIAL ATOM
SA LATTICE IMPERFECTION
SA PLASTIC DEFORMATION
 Charged and neutral impurities effect on

heat conductivity of bismuth telluride crystal lattice 01 p0127 A67-10073

Photo-Hall effect and photoconductivity on compensated p-InSb at low temperatures, examining temperature dependence of carrier mobility 01 p0128 A67-10093

Impurity and lattice vacancy effects on compensation in doped binary semiconductors 01 p0132 A67-10455

Damage rate deduced from room temperature conductivity measurements on n-and p-type floating zone silicon samples subject to electron irradiation at energies from 0.3 to 2.0 mev 01 p0133 A67-10752

Amplitude-dependent internal friction and defect structures in pure aluminum from bridge-circuit measurements performed by combined kHz-mHz method 01 p0101 A67-10844

Elastic interaction energies between edge and screw dislocations and tetragonal defects in anisotropic NaCl lattice 02 p0298 A67-11885

Thermal emf in plastic deformation of copper, considering effects of crystal lattice defects and lattice elastic distortions 02 p0301 A67-12740

Mechanical characterization and structural perfection of alpha aluminum oxide wool whiskers in diameter range of 0.6 to 4.0 microns 03 p0449 A67-13307

IR transmission micrography and X-ray microanalysis of anomalous etching on surface of Si single crystals grown in Ar gas 04 p0875 A67-14769

Model of metastable defects in germanium, noting Frenkel defects 04 p0677 A67-14939

Gamma irradiation from Co 60 effect on indium antimonide, determining defect formation on dose and limiting position of Fermi level for n-and p-type material 04 p0680 A67-15283

Defect impurity relation in electron damaged p-type silicon and electron irradiation effect on float zone n-type silicon 04 p0684 A67-15690

Neutron induced degradation of carrier lifetime in n-and p-type silicon containing oxygen and dopant 04 p0684 A67-15691

Motion theory of discrete defects in linear elastic continuum 05 p0908 A67-16038

Soviet papers on growth and imperfections of metallic crystals 05 p0826 A67-16074

Relation between electrical properties and structural features of gold-and antimony-doped germanium single crystals, noting abrupt decrease in mobility 05 p0861 A67-16398

Crystal structure defects and electroconductivity variations in CdS single crystals in oxygen ambient and effects of various surface treatments 05 p0862 A67-16605

Rate controlling mechanism in graphite creep, noting basal slip systems causing general deformation 05 p0833 A67-16892

Annealing behavior and uniaxial stress response of radiation induced defects in Si causing 1.8, 3.3 and 3.9 micron IR absorption bands examined via EPR studies 05 p0870 A67-17194

Metallographic, X-ray and electron microscope studies of dislocation substructure and fatigue life extension in bending-fatigued Al and Ag crystals 06 p1013 A67-17798

Disordered regions and energy level position in germanium produced by electron irradiation 06 p1048 A67-17832

Electron microscope structure and lattice defects of martensite in commercially pure titanium 06 p1017 A67-17966

Paired defect production rate in silicon created in single electron scattering event 06 p1053 A67-18711

Hall effect, electrical resistivity and optical transmission data and Co impurities in GaP studied via crystal field theory 06 p1061 A67-18926

X-ray study of component atomic scattering and structural defects for titanium and carbide atoms in titanium carbide 07 p1208 A67-19306

X-ray diffraction study of crystallographic transistor defects causing secondary breakdown 07 p1156 A67-19896

Resistivity changes in thin metallic wires with lattice defects measured by various methods 08 p1368 A67-20717

Plastic deformation of diamonds due to differences in initial defect distribution examined by birefringence, X-ray topography and electron microscopy 08 p1346 A67-20795

Oxygen precipitation consisting of point defects as explanation of structural changes of silicon single crystals during thermal treatment 08 p1370 A67-21205

Relation in silicon between annealing rates, residual damage and defect concentrations, noting link to activation energy increase 09 p1557 A67-22420

Occurrence, size and distribution of lattice defects in type III superconductor analyzed using electron microscopy, noting defect influence on critical current density 09 p1557 A67-22437

Induced absorption in far IR by impurities and defects of single crystal of potassium bromide 09 p1557 A67-22571

Chemical etching of dislocation and stacking fault structure of epitaxial GaAs, noting possible effect on electroluminescence 10 p1692 A67-23514

Impurity distribution in GaAs noting growth rate, concentration and crystallographic orientation 10 p1693 A67-23515

Baddeleyite inclusion in Marthas Vineyard tektite identified by electron microscopy 11 p1858 A67-24065

Hydrostatic pressure effect on surface microstructure, dislocation substructure and stress-strain behavior of beryllium 11 p1805 A67-24110

Chemical impurities and native defects observed in GaAs using photoluminescence at 20 degrees K, noting role of optical activation energy 11 p1848 A67-24742

Aging kinetics and lattice defects in Al-Zn and Al-Zn-Mg alloys 11 p1809 A67-24947

Structure effect on magnetization and critical current density in transverse magnetic field of superconducting V and Nb foils with different grain boundary orientations 12 p1986 A67-26067

Radiative recombination through free carriers and localized states in silicon single crystals containing gamma-induced defects 13 p2172 A67-26357

Optical quenching of photoconductivity in silicon resulting from minority carrier capture by centers created by irradiation 13 p2173 A67-26358

High resistivity regions in silicon exposed to photon bombardment 13 p2173 A67-26364

Brittle fracture at grain boundaries in samples of electron-beam molybdenum prepared by forging in air after extrusion 13 p2130 A67-26447

Crystal lattice defects as centers promoting dislocations during plastic deformation of ionic crystals 13 p2175 A67-26448

Transmission electron microscopy of dislocation structure produced in beryllium by specific deformation 13 p2138 A67-27116

Book on high temperature oxidation of metals and alloys, fundamental aspects and reaction mechanisms 13 p2141 A67-27176

Cadmium sulfide crystal photoconductivity peaks near band edge, noting heat treatment, temperature and defects 14 p2364 A67-28229

Chemical etching examination of dislocations and stacking-fault structure of epitaxial gallium arsenic phosphide, considering doping level, growth rate and composition effects 14 p2366 A67-28421

Dislocation-free Ge structural and electrical characteristics after cooling, considering quenching defects effect 14 p2372 A67-28761

Equivalent circuit model for solid state junction devices with single energy level defect centers including transient properties 15 p2456 A67-29170

Localized defects in semiconductors, using solid state scattering theory to calculate energies of bound states 15 p2534 A67-29325

Radiation polarization in ruby laser with resonator shaped like rectangular parallelepiped 15 p2499 A67-29701

Fast neutron bombardment and temperature effects on conductivity, photoconductivity and resistivity of Si single crystals, determining energy levels of defects 15 p2541 A67-30236

Semiconductor crystal structure defects caused by irradiation with energetic particles and photons 17 p2913 A67-32372

- Recovery Stage III in neutron irradiated Al-Cu alloy, discussing vacancies and interstitials 17 p2873 A67-32743
- Electron radiation damage in CdSe crystals at cryogenic temperatures, noting electrical conductivity and cathodoluminescence properties before and during damage 17 p2916 A67-32838
- Impurity atoms and defects distributions in Si and Ge bombarded by different ions of medial energies calculated by Monte Carlo method 17 p2916 A67-32839
- Electron paramagnetic resonance /EPR/ studies of interaction of irradiation-produced defects with impurities and other defects in silicon semiconductors 17 p2918 A67-32854
- Radiation effects on carrier recombination and mobility and on lifetime of semiconductor devices 17 p2919 A67-32858
- Soviet book on study of defects of crystalline structure of metals and alloys including X-ray analysis of aluminum single crystals, radiation effects on niobium, etc 17 p2874 A67-32894
- Electron microscopy used to investigate various defects forming in phase resulting from martensitic transformation 17 p2874 A67-32896
- Defects in single crystal foils of compound bismuth telluride caused by irradiation with protons 17 p2921 A67-33050
- Electronic structure of irradiation defects in ionic solids vacancies, interstitials and dislocations, explaining electronic relaxation 19 p3306 A67-35673
- Surface bombardment damage on molybdenum and tungsten crystals by inert gas ions 19 p3246 A67-35784
- Structural defects of reciprocally oriented polycrystalline bismuth-antimony films analyzed by moire method 20 p3510 A67-36813
- Raman spectra vibrational structure theory concerning crystal impurity centers, giving intensity distribution formulas and radiation model calculations 20 p3511 A67-37031
- Deformations and residual stresses in polycrystalline microstructures, using photoelastic coating method 20 p3540 A67-37059
- Characteristics of niobium annealed at 2000 C, describing texture development and crystal perfection variation with annealing time 20 p3470 A67-37391
- Polycrystalline boron nitride fibers structure, determining density, defects, resistance, thermostability, etc 21 p3649 A67-37886
- Self-focusing of laser light pulses in ruby and leucosapphire crystals, noting different damage forms for fundamental and second harmonics 21 p3639 A67-38094
- Radiative recombination through free carriers and localized states in silicon single crystals containing gamma-induced defects 21 p3679 A67-38314
- Optical quenching of photoconductivity in silicon resulting from minority carrier capture by centers by irradiation 21 p3679 A67-38315
- High resistivity regions in silicon exposed to photon bombardment 21 p3680 A67-38321
- Nature, distribution and causes of structural imperfections and dislocations in epitaxial Si layers with base layer orientation /111/ 21 p3681 A67-38359
- Electron beams applied during pressworking of sheet materials to provide temperatures favorable to microstructure defect healing 21 p3637 A67-38927
- Crystal block structure and slip plane influence on laser radiation, discussing radiation energy distribution in space and divergence determination 21 p3642 A67-38968
- Hall effect measurements on heat treated and quenched p-type silicon crystals, noting donor centers appearance due to vacancy cluster 21 p3687 A67-39138
- Nature of defects in InSb induced by gamma and X-ray irradiation, discussing recovery process 21 p3687 A67-39143
- Limitations imposed on performance of large area p-n junctions by quality of silicon material, discussing defect-free processing techniques 22 p3766 A67-39247
- Vacancy concentration in dislocation enhanced diffusion model as explanation of phosphorus and boron anomalous diffusion in silicon 22 p3855 A67-39346
- Charge compensation defects influence on UV excitation spectrum of rare earth doped crystals fluorescence 22 p3856 A67-39384
- Divalent Eu ion ground state splitting in C3h symmetry sites and associated color centers in EPR spectrum study of Eu ion doped lanthanum trichloride 22 p3863 A67-40003
- Twinning and low temperature mechanical properties of high purity polycrystalline niobium and molybdenum, discussing grain size effects 22 p3823 A67-40208
- Interstitial oxygen solubility in niobium using X-ray diffraction, micrographic and thermal techniques, discussing lattice structure 22 p3823 A67-40209
- Superconductivity enhancement in fine grained tungsten films, discussing structural changes and theoretical models 23 p4036 A67-40702
- Laser induced damage reduction in lithium tantalate and niobate crystals, proposing mechanism to explain observed reduction 23 p4012 A67-40876
- Defects in surface layer of silicon crystals during deep diffusion of phosphorus studied by X-ray diffraction 23 p4042 A67-41295
- Structural defects in Ge and Si alloyed semiconductor junction devices caused by improper technological processing, noting microscopic photographs 23 p4043 A67-41365
- Radiation polarization in ruby laser with resonator shaped like rectangular parallelepiped 24 p4166 A67-41771
- Linear defects imaging in single crystals by interpreting anomalous behavior of propagating X-rays ascribed to structural defects 24 p4202 A67-42072
- Single crystal silicon films on insulating substrates, discussing preparation methods and chemical and structural perfection for use in field effect and bipolar devices 24 p4202 A67-42089
- Thermal vacancies in Ni-Al investigated by comparing separately determined dilatometric and lattice parameter of /100/ single crystal 24 p4173 A67-42165
- Coexisting minerals and interstitial groundmass of chondrules of Mezo-Madaras chondrite 24 p4235 A67-42633
- CRYSTAL SURFACE**
- Surface photopotential of cadmium sulphide single crystals under monochromatic illumination in alternating electric field, using voltage modulation method 01 p0134 A67-10807
- Surface structure effect of evaporation deposited film and substrate crystal on epitaxy of film studied by electron diffraction and electron microscope 02 p0286 A67-11710
- Crystal structure defects and electroconductivity variations in CdS single crystals in oxygen ambient and effects of various surface treatments 05 p0862 A67-16605
- Second harmonic generation of light by focused laser beams in nonlinear crystals at exit surface 05 p0817 A67-16640
- Alkali ion scattering coefficient from tungsten single crystals surface and dependence on incidence angle 06 p1036 A67-18424
- Oscillatory magnetoconductance in inverted surfaces of p-type silicon 06 p1063 A67-18940
- Corbino magnetoresistance experiments for n-type surface layers on p-type indium arsenide crystals as function of surface electric field 06 p1064 A67-18941
- Fermi surface of tin telluride approximated by four distorted surfaces located at L points of Brillouin zone as shown by Fourier analysis 06 p1065 A67-18950
- Ternary system Ti-Al-V alloys analyzed using thermal, microstructural, etc, methods, plotting solidus surface in crystallization region of beta-solid solution 07 p1205 A67-19273
- Crystal symmetry, optical properties and ferroelectric polarization of barium titanate single crystals 07 p1234 A67-20096
- Picosecond laser pulse widths measurement by method using special symmetry properties of second harmonic generation at GaAs crystal surface 07 p1234 A67-20097
- Oxide film surface effect on electrophysical characteristics of Ge surface, noting potential changes and recombination rate 08 p1367 A67-20412
- Interaction energy of single atom adsorption at any point on single crystal planes of bcc structure, using Lennard-Jones potential 08 p1355 A67-20719
- Energy transfer during interaction of atoms with surface of ideal crystal in terms of classical mechanics 11 p1824 A67-24855
- Surface hole photoconductivity for pressed metal anode CdS ohmic cathode system, noting spectral distribution dependency on crystal heat treatment and air humidity 11 p1849 A67-24871
- Conductivity of cleaved surfaces of GaAs in liquid nitrogen 13 p2174 A67-26371
- Vacuum thermionic work function and thermal stability measurements on crystal surfaces, discussing results on carbides, diborides and disilicides 15 p2535 A67-29486
- Numerical calculations of interactions of monatomic gas particles with ideal and contaminated crystal surfaces at epithelial energies 15 p2434 A67-30197
- Barium adsorption on individual crystal planes of tungsten field emitter studied for thermally equilibrated and unequilibrated adsorbate layers 17 p2922 A67-33259
- Surface hillock-like features in epitaxially grown gallium arsenide studied by X-ray diffraction topography 18 p3106 A67-34636
- Contact potential difference between crystal surfaces of indium antimonide cleaved in ultrahigh vacuum measured by Kelvin method 19 p3302 A67-34939
- 180 degree domain formation in ferroelectric crystals unaffected by presence of shorted electrodes due to surface layer properties differing from bulk 19 p3304 A67-35047
- Structure of surfaces Conference, Durham, N.C., November 1966 19 p3246 A67-35782
- Surface bombardment damage on molybdenum and tungsten crystals by inert gas ions 19 p3246 A67-35784
- Adsorption of oxygen on tungsten surface, discussing electron diffraction 19 p3246 A67-35786
- Energy transfer during interaction of atoms with surface of ideal crystal in terms of classical mechanics 20 p3490 A67-37538
- Conductivity of cleaved surfaces of GaAs in liquid nitrogen 21 p3680 A67-38326
- Self-decoration effect in thermally etched polycrystalline lithium ferrite, discussing geometric symmetry relation to crystallographic surface orientation 22 p3855 A67-39344
- LiF freshly cleaved crystal reflectance spectrum between UV and 28 ev, computing dielectric response function and measuring gamma exciton band 23 p4038 A67-40774
- Laser irradiation effect on semiconductor crystals surfaces using pulsed ruby laser 23 p4045 A67-41470
- Atoms interaction with solid body surface, noting pair interaction law effect on characteristic energy accommodation coefficient and motion equation solution 24 p4190 A67-41938
- CRYSTALLIZATION**
- SA RECRYSTALLIZATION**
- Polarized light crystallization microanalysis for supercooled water droplets with additives applied to spherical single crystals of ice during droplet freezing 01 p0109 A67-11010
- Different crystallization conditions and effect on Se surface structures on properties of p-n heterojunctions in Se-CdSe and Se-CdS rectifying cells and photocells 02 p0297 A67-11849
- Crystallinity index measurements of poly(ethylene terephthalate) by X-ray diffractometric and differential scanning calorimetry index methods 04 p0641 A67-14527
- Crystallization of boric anhydride obtained only through maintaining high water content in reactive agent during thermal treatment 13 p2143 A67-26812
- Magmatic origin of chondrule meteorites, considering structure, electron probe microanalysis, crystallization and equilibrium 13 p2200 A67-27234
- Germanium films crystallization when deposited by evaporation on silicon single crystals studied by optical microscopy and electron diffraction 20 p3509 A67-36473
- Tektite glasses crystallizing tendency studied by subjecting them to heat treatments above strain point and CN slow cooling from melting 20 p3527 A67-37274
- Lanthanide partition coefficient for

crystallization under calcium effect, noting inflectional pattern for inverse ionic radius variation 21 p3617 A67-38123

CRYSTALLOGRAPHY

Crystallographic structure of hexagonal ferrites of BaO-MeO-ferric oxide system and applications in UHF and microwave regions 02 p0301 A67-12787

Thermal conductivity of laminated GaSe monocrystals studied in two crystallographic directions between 90 and 600 degrees K and effect of uniaxial compression 07 p1233 A67-19649

Qualitative and quantitative methods for correlating preferred crystallographic orientation with biaxial strengths of titanium alloys 08 p1340 A67-20363

Crystallographic anisotropy of electrical properties of thin film CdS photoresistors explained via potential barrier orientation theory 12 p1984 A67-25520

Gas laser properties, noting usefulness in physics, chemistry and optics 13 p2129 A67-27364

Liquid crystal - Conference, Kent State University, August 1965, Part 1 15 p2429 A67-29297

Liquid crystal - Conference, Kent State University, August 1965, Part III 18 p2991 A67-33633

Crystallographic anisotropy of electrical properties of thin film CdS photoresistors explained via potential barrier orientation theory 18 p3103 A67-34451

Omega phase morphology by transmission electron microscopy of Ti-Nb indicating ellipsoids with major axes parallel to /111/ directions in matrix 23 p4017 A67-40653

CUBIC CRYSTAL

SA BODY CENTERED CUBIC /BCC/

CRYSTAL

SA FACE CENTERED CUBIC /FCC/

CRYSTAL

SA GRUNEISEN CONSTANT

Anomalous polarity-dependent electro-optic effect with noncubic symmetry observed in cubic single crystals of ZnS and ZnTe 03 p0496 A67-13569

Kinetic phenomena in impure ionic semiconductors of cubic symmetry, finding region for dominant scattering mechanism 04 p0675 A67-14923

Phenomenological theory of longitudinal Hall effect in cubic crystals, assuming anisotropic dispersion law and tensorial relaxation time 04 p0681 A67-15291

Optical energy gap of cubic CdS measured on evaporated mixed cubic-hexagonal layers 06 p1048 A67-17820

Anisotropy and temperature dependence of upper critical field of type II superconductor single crystals with cubic structure 07 p1236 A67-20136

Superconducting energy gap of cubic and hexagonal LA obtained by point contact tunneling to bulk samples, noting V-I characteristics and temperature dependency 11 p1846 A67-24585

Coulomb long range interaction effect on refractive index dependence on light frequency and on absorption lines shape of dipole active excitons 13 p2173 A67-26365

IR absorption and Raman scattering spectra of diagonal cubic crystal structures 23 p4037 A67-40758

Translucent material /Zyttrite/ obtained from cubic phase stabilization of Y and Zr alkoxides at low temperatures, noting high surface activity 24 p4175 A67-42373

CULTURE /BIOL/

Mixed cultures of *Chlorella pyrenoidosa* TX 71105 and various bacteria and use in closed systems for support of man 10 p1598 A67-23626

Continuous synchronous culture of photosynthetic microorganism *Chlorella* cultivated in illuminated and dark stirred tanks 19 p3177 A67-34913

Unicellular algae continuous culture as autotrophic component of closed ecological system, discussing stabilization of biomass concentration to provide oxygen requirement 24 p4114 A67-41844

CULTURE TECHNIQUE

Growth rate limitations with interactions of light and carbon dioxide investigated for two species of *Chlorella* 20 p3369 A67-36791

Survival of desert algae at extremely low temperatures and diurnal freeze thaw cycles 23 p3945 A67-41346

Continuous culture system for

Hydrogenomonas bacteria in waste management of life support system [SAE PAPER 670854] 24 p4115 A67-42002

CUMULUS CLOUD

Nonstationary models of cumuli and thermals in stratified atmosphere 02 p0262 A67-12641

Physical aspects of stratocumulus including temperature, liquid water content, drop size, wind effect, shape, etc 03 p0462 A67-13499

Wind, temperature, vertical motions and degree of turbulence measurements of cumulonimbus clouds interacting with wind field 03 p0463 A67-14224

Cumulus convective cloud formation above isolated source of heat and water vapor 09 p1491 A67-21552

Characteristics of atmospheric convection, obtained by vertical and horizontal heat transport processes and represented by difference equation, used to derive analytical solution 09 p1491 A67-21553

Wind, temperature, vertical motions and degree of turbulence measurements of cumulonimbus clouds interacting with wind field 12 p1963 A67-25480

Vertical gust components in altocumulus clouds measured by airborne instruments 13 p2152 A67-26741

Cellular cumulus convection confined to cylindrical column in conditionally unstable atmosphere 20 p3480 A67-38505

UHF serics detection system receiving and display components for remote sensing by satellite of convective cloud development 22 p3806 A67-40358

CURIE TEMPERATURE

Dielectric properties of complete solid solutions with perovskite structures in barium titanate-barium stannate and barium titanate-barium ferrotantalate systems 07 p1231 A67-19489

Spin wave theory of thin ferromagnetic films, Curie temperature decreases monotonically with decreasing film thickness spin wave theory of thin ferromagnetic films analyzed, showing Curie temperature decreases 12 p1981 A67-25239

Ferroelectric, electro-optic and dielectric properties of tetragonal potassium-niobate-strontium-niobate crystal 24 p4204 A67-42366

CURING

SA AGING

Nuclear magnetic resonance and nuclear quadrupole resonance techniques for nondestructive testing of reinforced plastics for curing and internal stresses 08 p1345 A67-20425

Automatic rigidizing of expandable fabric impregnated space structures, detailing gelatin system 08 p1345 A67-20433

Medium temperature curing general purpose structural adhesive system for use on helicopter 09 p1523 A67-22515

Vapor cured resins for aerospace applications 15 p2506 A67-29544

1, 3-diones and beta-ketoesters with cobalt for room temperature curing of unsaturated polyester resins by organic peroxide 24 p4175 A67-42420

CURRENT

S AIR CURRENT

S BEAM CURRENT

S CONVECTION CURRENT

S EARTH CURRENT

S EDDY CURRENT

S ELECTRIC CURRENT

S ION CURRENT

S IONOSPHERIC CURRENT

S LINE CURRENT

S RING CURRENT

S TELLURIC CURRENT

S THERMAL CURRENT

S THRESHOLD CURRENT

CURRENT AMPLIFIER

Amplifier design using multistage transistor current mode, feedback systems and minimized voltage swings 03 p0386 A67-13977

Current gain and collector-base saturation current and breakdown voltage in aged silicon transistors 15 p2453 A67-30064

Small signal current gain of p-n-p-n section of four-layer Si structure as function of current, noting effect of base width, minority carrier lifetime and doping level 17 p2911 A67-32193

Measuring assembly containing logarithmic-response electrometric amplifiers for sounding rockets 21 p3592 A67-38222

Power amplifiers using IC, calculating average and peak power dissipation by final transistors of push-pull circuit with resistive and reactive load 24 p4131 A67-42411

CURRENT DENSITY

Origin of polarization of radiation from GaAs diodes, noting intensity dependence on current density and effect of anisotropic electron velocity distribution 01 p0034 A67-10090

Current density resulting from integration over energy of transport equation applicable to dielectric film 02 p0295 A67-11763

Negative resistance and current density in double-injection filaments in seminsulating Si 02 p0298 A67-11886

Ripples in acceleration potential affect ion beam of electrostatic propulsion system by superimposing AC potential of 50 cps of variable amplitude on constant acceleration potential 02 p0306 A67-12790

AC measurements on hard superconductors exposed to magnetic field, obtaining critical surface current and density from voltage-time curves 03 p0487 A67-12809

Maximum current carrying capacity of type III hard superconducting wire in zero external field before superconductivity breaks down 03 p0488 A67-12814

Current carrying capacity of hard superconducting wire in zero external field determined from considerations of flux density distribution 03 p0488 A67-12815

Dependence of peak inverse voltage of n-Si and p-Ge on specific resistance and concentration and mobility of current carriers 03 p0488 A67-12817

Linear theory of self-excitation of oscillations in semiconductors in presence of large current density inhomogeneity 03 p0489 A67-13147

Mean static current density over cross section of arc moving in slot chamber under action of external magnetic field effectively measured by probing technique 03 p0476 A67-13179

Forward voltage characteristics of thyristors in fired state, depending on injection level for high current density 03 p0380 A67-13482

Current density distribution in two-electrode MHD channel operating in amplification and generation mode 03 p0479 A67-13686

Temperature dependence of current-carrier concentration and electrical conductivity of p-type germanium containing beryllium and phosphorus 04 p0679 A67-15144

Recombination radiation from Ga-Sb p-n junctions, noting spectral composition as function of current density and impurity concentration 04 p0681 A67-15297

Optical coupling using gallium arsenide laser for variation of frequency of diode emission through small change in current density 05 p0814 A67-16390

Radiation intensity dependence for various spectral bands of diffused gallium arsenide p-n junctions on current density 05 p0861 A67-16391

Dember effect, bulk photovoltaic effect and current density in illuminated inhomogeneous semiconductor 05 p0863 A67-16702

Increase in superconducting critical current density in diffusion layers of proton-irradiated niobium stannide and decrease at higher dosage 06 p1048 A67-17817

Current carrier behavior during field and diffusion injection of electron hole plasma into semiconductor 06 p1049 A67-17865

Current and frequency dependent differential resistance and diffusion capacity of junctions of p-n-n structures at high current densities 06 p1049 A67-17868

DC amplifier with capacitive feedback as correcting device in recording currents while studying magnetoplasma generator 06 p0952 A67-18693

Measuring equipment for critical current density of superconductors in strong magnetic field 06 p1005 A67-18722

Current in channel with symmetrical end electrodes, noting stepwise dependence of near-electrode potential on current density 06 p1045 A67-18812

Nonlinear second harmonic generation of current density in inhomogeneous magnetoplasma and reflected electromagnetic wave from free space

- interface 06 p1046 A67-18825
- Boltzmann transfer equation consisting of DC electric field and two AC electric fields for nonlinear second harmonic generation and combination frequencies in homogeneous plasma 06 p1046 A67-18826
- Current saturation and phonon amplification induced instabilities in CdS crystals 06 p1066 A67-18958
- Boltzmann equation for GaAs, noting coupling constant scattering between low and high mass valleys 06 p1067 A67-18963
- Spin lattice relaxation times of donor electrons in Si, noting electric field effect on relaxation rate 06 p1068 A67-18971
- Recombination radiation from GaAs p-n junctions with and without Fabry-Perot resonator, noting parameter dependence on current density 08 p1337 A67-20413
- Current density distribution in MPD arc jet exhaust measured, using Hall effect sensors [AIAA PAPER 66-116] 08 p1375 A67-20573
- Microwave third harmonic generation in homogeneous semiconductors at low temperatures, noting ionized impurity scattering effect 08 p1368 A67-20701
- Self-consistent field approximation to ion-beam-plasma boundary interaction noting effect on ion beam structure, boundary conditions and resulting current density 08 p1363 A67-21307
- Stress-dependence of Si p-n junctions with dense generation-recombination centers, showing that shifts in bias I-V characteristics are due to bandgap changes 09 p1553 A67-21947
- Pinning fluxoids by spatial inhomogeneities of Ti-Pb and Pb-In alloys, noting I-H characteristics and type II superconductor resistance 09 p1556 A67-22135
- Occurrence, size and distribution of lattice defects in type III superconductor analyzed using electron microscopy, noting defect influence on critical current density 09 p1557 A67-22437
- Boundary value solutions for current density and radiation patterns in spiral excited sheath antennas in terms of Hankel function 09 p1482 A67-22696
- Effect of liquation inhomogeneity on superconducting properties of ternary alloy, noting enhancement of critical current density in wire prepared from this alloy 10 p1689 A67-23089
- Zirconium-niobium alloy analyzed by oxide replica technique, noting superconductivity and tunnel effect, determining relation between superconductivity current critical density and sample structural characteristics 10 p1689 A67-23090
- Linear theory of self-excitation of oscillations in semiconductors in presence of large current density inhomogeneity 10 p1689 A67-23096
- Field dependent mobility effects in excess noise of junction gate FETs 10 p1612 A67-23376
- Stimulated emission in GaSb injection lasers with steep flat p-n junction, noting dependence of luminescence intensity on current density 10 p1667 A67-23665
- Electron beam experimental methods for current density distributions, electron velocities and determining parameters for microwave tube design 11 p1758 A67-24094
- Anodic behavior of GaAs single crystals at increased current densities in alkaline and acidic solutions, discussing etch tunnels 11 p1848 A67-24743
- Semiconductor junction devices analyzed for diffusion and electric field currents in bulk regions 11 p1849 A67-24904
- Microwave amplification and negative conductance for GaAs, InP and CdTe 11 p1850 A67-24916
- Temperature dependence of current-carrier concentration and electrical conductivity of p-type germanium containing beryllium and phosphorus 12 p1979 A67-25167
- Electromagnetic state theory applied to solar flares by analogy between ionized current-carrying plasma processes and solar flare conditions 12 p2001 A67-25224
- Diagnostic techniques for atmospheric pressure arc plasmas, noting that integrated current density measurements are consistent with measured total arc current 12 p1973 A67-25393
- Impurity effect on electroluminescence of gallium phosphide diodes, noting dependence of spectrum on current density through p-n junction 12 p1914 A67-25438
- Recombination radiation spectra of InAs with different current carrier concentrations in initial material and different current densities 12 p1914 A67-25516
- Constant density theory leads to analytical forms for current-voltage characteristics and electrical resistance associated with shock tube sidewall electrostatic probe problem 12 p1925 A67-25902
- Structure effect on magnetization and critical current density in transverse magnetic field of superconducting V and Nb foils with different grain boundary orientations 12 p1986 A67-26067
- Latitudinal cross section of ionospheric current density profile of equatorial electrojet from rocketborne magnetometers 13 p2107 A67-26307
- Possibility of using p-i-n /p-n-n, n-p-p/ structure with heterojunctions for rectifier designed for ultrahigh current densities 13 p2174 A67-26366
- Current density combination frequency derived for homogeneous magnetoplasma due to alternating electric fields, considering distribution function isotropic and anisotropic parts 13 p2167 A67-26994
- Transient phenomena in capacitance and reverse current for n-type GaAs Schottky barrier diodes at different carrier concentrations 14 p2364 A67-27827
- Anode emission influence on thermionic diode energy converter maximum efficiency 14 p2247 A67-28033
- Surface current change between critical paramagnetic and critical diamagnetic induced by temperature variation in type II superconductor immersed in static magnetic field 14 p2365 A67-28296
- Current density variation determination in plasma accelerated by traveling waves [ONERA-TP-472] 14 p2359 A67-28509
- Bilinear current density induction of double-frequency laser beam from superconducting metal 14 p2371 A67-28722
- Electromagnetic properties of impure anisotropic strong-coupling superconductors, using Green function to obtain response, current density and Josephson tunneling current 14 p2371 A67-28724
- Computer solution for current density, continuity and Poisson equation to obtain electron density and electrostatic potential in p-n junction 14 p2290 A67-28931
- Precipitate and dislocation structures associated with peak effect in niobium examined using electron microscopy 14 p2375 A67-28999
- Instrumentation using quantum effects in weakly coupled superconductors 14 p2375 A67-29043
- Current dependent modes in pulsed avalanche diodes 15 p2442 A67-29174
- Variation of series resistance and junction capacity in tunnel diodes used in microwave switching 15 p2449 A67-29808
- Escalation effect by interaction of conduction and induction currents in niobium alloy wires 15 p2539 A67-29826
- Transverse magnetic field effect on induced emission of GaAs diodes 15 p2543 A67-30251
- Current density distribution in MHD duct with segmented electrodes of finite size analytically described, noting experimental agreement 16 p2800 A67-30537
- Effective conductivity tensor of nonhomogeneous plasma in homogeneous external magnetic field 16 p2711 A67-30539
- Electrode-to-plasma conduction process effect on MHD generator performance, noting current saturation conditions and results 16 p2801 A67-30550
- Experiments with 100-kw MHD generator free from secondary effects by choosing MHD interaction parameter values greater than unity 16 p2802 A67-30559
- Conductivity in Faraday generator with cesium-seeded argon calculated from energy balance of electrons 16 p2803 A67-30565
- Stabilization of current intensity in superconducting coils noting two characteristic intensities, measurements of niobium compounds, effects of added copper, etc 16 p2807 A67-30593
- Electron emission current density for semiconductors for all conditions between limits of thermionic and field emission 16 p2725 A67-30805
- Irreducible tensorial components of two-electron operator and second-order density matrix for spin-projected single-determinantal wave function 16 p2705 A67-31759
- GaAs injection lamp efficiency correlated with presence of trapping levels, noting experimental technique and results 17 p2911 A67-32192
- Superconducting materials for solenoids, noting simple form conductors and current carrying capacity as field function 17 p2912 A67-32264
- Microwave attenuation change and harmonic generation by n-type GaAs in strong microwave electric fields, determining current density relation to field strength 17 p2913 A67-32310
- Cesium thermionic converter extinguished-mode operation theory, deriving expressions for forward and reverse saturation output current densities and open circuit voltages 17 p2803 A67-32365
- Relationship between microhardness of niobium and other variables characterizing superconductivity 17 p2915 A67-32720
- Electrical resistance of niobium single crystal at very low temperature from beginning of superconductivity transition 17 p2916 A67-32805
- Stimulated emission in GaSb injection lasers with steep flat p-n junction, noting dependence of luminescence intensity on current density 17 p2870 A67-33346
- Nonexistence of critical current for pinching in electron-hole plasmas 18 p3098 A67-33523
- Correlation function method in superconductivity theory, formulating electric current density in terms of distribution function in phase space 18 p3100 A67-33712
- Frequency response of DC and AC currents flowing to RF resonance probe in quiescent cesium plasma, explaining measurements 18 p3044 A67-33713
- Recombination radiation spectra of InAs with different current carrier concentrations in initial material and different current densities 18 p3012 A67-34447
- Threshold current density dependency on photon energy in diffused and epitaxial p-n junction GaAs injection lasers 19 p3238 A67-34774
- Zirconium-niobium alloys investigated for oxygen impurity effects on critical current density and superconducting properties 19 p3243 A67-34925
- Theory demonstrating stability of current sheets of different shapes in coaxial accelerators 19 p3294 A67-35408
- Saturation current measurement in diffusion transistors by method yielding current amplification factors and voltage dependence of emitter current 19 p3197 A67-35726
- Current saturation in evaporated gallium arsenide films observed noting temperature effect, X-ray measurements, etc 20 p3505 A67-36177
- E/k_z-relation for complex insulator band structure, explaining polarity effect on tunneling through asymmetric barrier 20 p3508 A67-36425
- Electromagnetic field energy absorption in cold rotating plasma, obtaining electric current density and plasma electric field relationship and cyclotron resonance 20 p3497 A67-36677
- Emission properties of vacuum spark plasma arising in production of high current electron beam 20 p3498 A67-36684
- Longitudinal vibration formation by high density electric current pulses in rod, discussing thermoelastic excitation and electrodynamic radial compression 20 p3486 A67-37060
- Electric conductivity of surface space charge layers in semiconductors, solving Boltzmann equation and determining current density and carrier mobility 20 p3511 A67-37144
- Injection lasers threshold current densities, emission spectra, emission polarization and power characteristics 21 p3639 A67-37943
- Laser-diode impulse generator construction by four-layer diodes and thyristors supplying high current intensity short impulses to low resistance load 21 p3639 A67-37945
- Current runaway effects in n-cadmium

telluride suggest current-density controlled resistivity caused by hole-electron pairs avalanche 21 p3677 A67-38006

Ionspheric conductivities, electric currents and field height variations in equatorial electrojet region calculated from model, including solar activity 21 p3617 A67-38066

Quantum size effects in electric conductivity of thin films 21 p3678 A67-38099

Tunnel and excess currents in Esaki diodes compatible with reversible introduction of active intermediate tunneling levels 21 p3590 A67-38152

Boundary value problem describing conducting fluid motion in longitudinal magnetic field, considering magnetic Reynolds numbers, electric current density distribution and heat exchange 21 p3665 A67-38243

Junction temperature current dependence in CW operated gallium arsenide laser diodes 21 p3639 A67-38256

Possibility of using p-i-n /p-n-n, n-p-p/ structure with heterojunctions for rectifier designed for ultrahigh current densities 21 p3680 A67-38322

Moving high field domain and current saturation in optically excited n-InSb 21 p3683 A67-38404

Solution grown GaAs laser diodes with Fabry-Perot cavity, measuring threshold current density variation with reciprocal laser diode length 21 p3641 A67-38457

Density, electric field and volt-ampere characteristics for spherical electrostatic Langmuir probe in collision plasma with weak ionization and recombination, using asymptotic method [AIAA PAPER 67-705] 21 p3672 A67-38732

Insulator boundary layers in supersonic MGD channel noting heat transfer rate, current density, stagnation, pressure distribution and skin friction [AIAA PAPER 67-717] 21 p3673 A67-38743

Reflex klystron for 1.5 mm wavelength noting high current density cathodes, RF section simplification and better heat dissipation 22 p3768 A67-39493

High oxygen Nb-Ti alloy solid solution critical superconducting current density and workability dependence on Th, Gd and Y solute content 23 p4036 A67-40705

Space charge limited /SCL/ hole current in Si noting mobility, capacitance, current density, I-V characteristics and double injection 23 p4038 A67-40878

Magnetic field critical current density characteristics of Nb-Zr-Ti superconducting alloys, discussing peak effect and barrier height random distribution 23 p4044 A67-41451

Destruction of superconductivity in niobium by current and external magnetic field intensity 23 p4047 A67-41691

Data analysis on electric potential gradient and air-to-earth current density 24 p4181 A67-41792

Different surface potential barrier models studied for T-F emission current density, energy distribution and Nottingham effect 24 p4201 A67-41893

Space charge effect on potential barrier in field emission, obtaining expression for work function increase using electrical image method 24 p4201 A67-41894

Plasma nonequilibrium electric conductivity in induced electric field investigated by MHD generator with Ar-K working fluid 24 p4196 A67-42209

Omega phase precipitation and superconducting critical transport currents in Ti-Nb wire samples 24 p4173 A67-42347

CURRENT DISTRIBUTION

Geometrical /current distribution/ influence on magnetoresistance effect in indium antimonide and indium arsenide at 34 gc/s 01 p0132 A67-10467

Excitation of metal sphere with large electric diameter by arbitrary electric and magnetic current distribution 02 p0191 A67-11577

Complex wave number, current distribution, admittance and radiating efficiency of cylindrical antennas made of imperfect conductors evaluated numerically 02 p0210 A67-11591

Point boundary value matching method calculation of current distribution in thin linear antenna 02 p0212 A67-11610

Current distribution in eddy configuration

of atmospheric gas discharge, noting flow surface deformation rate and measurement techniques 02 p0180 A67-12441

Width and rate of propagation of plasma current layer along accelerating electrodes of plasma gun at initial phase of discharge 02 p0278 A67-12621

Thermal instability affecting factors for current distribution in power transistor 02 p0222 A67-12651

Stationary phase technique synthesis of continuous linear antenna and integral equation for determining radiation pattern 03 p0378 A67-13284

Voltage generator consisting of quadrupole injectors where output voltage is complex function of previously chosen input voltages 03 p0392 A67-13450

Cut-off frequency of diffusion transistor calculated, using series expansion for current transport factor 03 p0382 A67-13685

Induction drag of long cylindrical satellites and Alfvén waves emitted from them, determining potential and current distribution and effect on energy loss [AIAA PAPER 66-478] 04 p0704 A67-14829

Electric potential and current density distribution in MHD channel allowing for anisotropy in conductivity 04 p0686 A67-15190

Current distribution on half-wave dipole antenna embedded in conducting half-space, noting case where dissipative medium has average earth constants 05 p0789 A67-16006

Current and hole distribution calculated for p-n junction acted upon by sinusoidal voltage of arbitrary amplitude-small injection level 05 p0865 A67-16910

Reactive properties of p-n-n semiconductor structures at high injection levels for monomolecular electron-hole recombination 06 p1049 A67-17866

Electron beam spatial scanning of coherent emission of GaAs junction laser at low temperatures, making current distribution nonuniform 06 p1011 A67-18150

Electrode geometry effect on current and potential distributions in MPD arcs 06 p1074 A67-18335

Latitudinal and vertical current components effects included in longitudinal current system supporting steady state distribution in geomagnetic anomaly 06 p0998 A67-18703

Axial current distribution in exhaust of magnetic annular arc, examining effect of entrainment on thrust measurement 06 p1075 A67-18850

Optical transitions in semiconductors satisfying principle of momentum conservation through mutual interaction between free current carriers 06 p1059 A67-18912

Directional radiation pattern for circular arc antenna, using three-step method in which current distribution is treated as truncated Fourier series 07 p1152 A67-19550

Thermally stimulated current peak distribution changes with illumination time and intensity for semi-insulating gallium arsenide 07 p1234 A67-20102

Semiconducting properties of ferroelectrics estimating free carrier densities in n and p regions and distributions over plate thickness semiconducting properties of ferroelectrics, estimating free carrier densities in n and p 08 p1367 A67-20314

Radial current density distribution in homopolar, noting deviation of magnetic field and nature of current distribution around anode 08 p1358 A67-20850

Fredholm integral equation system for magnetic currents induced on wedge under impedance boundary condition 08 p1295 A67-21273

Forward bias V-I characteristics for heterojunction in which tunneling dominates, noting temperature effect 09 p1551 A67-21666

Balanced helical wire antenna excited by delta function generator, obtaining integral equation for current distribution 09 p1481 A67-22445

Asymmetrically fed linear antenna loaded with loading impedance analyzed in terms of two coexistent current distributions 10 p1609 A67-22774

Fourier transform for exact solution of current distribution and input admittance of infinite cylindrical dielectric-coated antenna 11 p1757 A67-23972

Distribution formula for unloaded prolate

spheroidal receiving and scattering antenna 11 p1758 A67-23974

Quasi-static potential distribution in inhomogeneous volume conductor analyzed using Green theorem 11 p1746 A67-23991

Criterion of accuracy for given approximate current distribution based on difference between variationally computed stationary and nonstationary antenna impedances 11 p1759 A67-24131

Current distribution and input admittance of infinitely long cylindrical antenna driven by slice generator and immersed in anisotropic plasma 11 p1761 A67-24284

Absolute speed determination from measurement of induced EMF resulting from movement in geomagnetic field 11 p1791 A67-24455

Measured efficiency departure in power varactor converters from theoretical estimation, finding three-frequency current spectrum responsible 11 p1766 A67-24647

Current distribution of magnetic field in plasma coaxial injector indicating dominant role of Hall effect in plasma acceleration 11 p1841 A67-24854

Current distribution in incompressible fluid flow in magnetic field at low Reynolds number, estimating Lorentz force effect 11 p1842 A67-24952

DC current density distribution in plasma electron gap obtained by simulation method 11 p1843 A67-24968

Test program for induction coupled MHD generator using liquid sodium as working fluid, noting equivalent single phase circuit for electrical characteristics 12 p1897 A67-25376

Containment of transparent plasma produced by field of traveling wave in circular waveguide, noting plasma ion-current distribution 12 p1976 A67-26066

Fringe effects in MHD generator channels, determining potential and current distribution and estimating lossess 12 p1901 A67-26078

Current carrier concentration distribution in semiconductor with intrinsic anisotropy created by strong electric field 13 p2173 A67-26362

Radiation field of monopole antenna hinged on spherical conducting support calculated with Green function technique 13 p2081 A67-27200

Carrier distribution function in degenerate p-type germanium in presence of hole scattering on acoustic phonons, considering heating in arbitrary electric and magnetic fields 13 p2181 A67-27281

Width and rate of propagation of plasma current layer along accelerating electrodes of plasma gun at initial phase of discharge 13 p2170 A67-27377

Current diagram plotting by graphical integration method for diurnal solar magnetic variations in especially quiet days 14 p2309 A67-27939

Ionspheric micropulsations induced by enhanced conductivity of current due to meteors, noting end effect from finite ion trail length 14 p2383 A67-28044

Integral expression derived for current distribution on infinite antenna aligned with magnetic field immersed in plasma, using generalized eigenfunctions 14 p2284 A67-28378

Behavior of RF sources embedded in plasma, determining antenna properties by configuration, current distribution and surrounding sheath properties 14 p2359 A67-28464

Large antenna radiation from radio astronomy Explorer satellite determined on basis of antenna current distribution 14 p2286 A67-28507

Critical surface transport currents in type II superconductors interpreted by surface flux pinning model 14 p2370 A67-28718

Magnet consisting of superconductive solenoid of niobium-zirconium wire with ferromagnetic insertions 15 p2422 A67-29127

Statistical testing on digital computers for simulating current and voltage distribution in semiconductor rectifier circuits 15 p2439 A67-29416

Collector conduction resistance in saturated planar transistors determined from current distribution measurement on electrolytic model 15 p2448 A67-29802

Fat cylindrical antenna admittance measured noting behavior similar to that of

thin antenna admittances 15 p2454 A67-30137
 Conductivity and Hall effect in analysis of temperature dependence of current carrier concentration and mobility in silicon, explaining ionization 15 p2541 A67-30240
 Current carrier distribution in GaAs-Ge heterojunctions measured for energy band diagram 15 p2542 A67-30241
 Current distribution parallel connected semiconductor triodes based on approximate transfer characteristics of diodes 16 p2634 A67-30462
 Effect of capture levels on current-voltage characteristic of semiconductor p-n diode with ohmic back contact 16 p2635 A67-30471
 Internal resistance, potential fall and current distribution for staggered electrode geometry in MHD generator of Faraday type 16 p2599 A67-30528
 Current distribution in Faraday MHD generator measured with potassium resonance lines 16 p2599 A67-30529
 Current and potential distribution for thermally-stable plasma of Faraday-type segmented electrode MHD generator, taking into account nonequilibrium ionization 16 p2599 A67-30530
 Performance of linear series of MHD generators noting electrical properties, effect of electrode scattering, etc 16 p2600 A67-30531
 Ionization saturation and duct shape effects on losses near walls, including large Hall effects, regular current distribution, and plasma conductivity regularization 16 p2711 A67-30536
 Argon-potassium plasma electrical conductivity investigation showing that optimum increase in conductivity corresponds to optimum electrode length 16 p2602 A67-30560
 Current and hole distribution calculated for p-n junction acted upon by sinusoidal voltage of arbitrary amplitude-small injection level 16 p2727 A67-30887
 Resistive antenna receiving properties determined via transmitting antenna driving-point impedance and short circuit current 16 p2638 A67-31338
 Plasma sheath detuning effect on small loaded dipole in free space investigated 16 p2627 A67-31367
 Variationally computed antenna impedances and accuracy of resulting current distributions 17 p2824 A67-32301
 Digital computer program FORTRAN coded, analyzing electric power distribution system of aerospace vehicle 17 p2804 A67-32511
 Coupled integral equations for transverse and axial currents for asymmetrically cylindrical antenna driven by EMF 17 p2826 A67-32618
 Winter and summer equivalent current systems of polar solar-diurnal variations studied from observations obtained during IGY 17 p2847 A67-32949
 Nonuniform electrical conduction in MHD channels analyzed by differential equations 17 p2906 A67-33011
 Au, Zn or Ni doped silicon diodes studied for current distribution over base cross section with negative resistance 18 p3010 A67-33577
 Current flow patterns in cross connected MHD generator with four electrodes 18 p2987 A67-33704
 Thunderstorm electric circuit physics with atmospheric electric conductivity and variation with height, noting atmospheric electric fields and currents 18 p3074 A67-33996
 Determination of magnetic field of spreading currents in continuous conducting media separated by spheroidal surface 18 p3079 A67-34035
 Current distribution and element spacings for beam efficiency and gain optimization of antenna array 18 p3012 A67-34429
 Electromagnetic scattering by thin inhomogeneous circular cylinders, presenting numerical results for induced axial current and scattering cross section 18 p3004 A67-34431
 Vortical structure of current and magnetic field distribution along superconducting film with magnetic field parallel to surface, discussing possible observation by optical diffraction 19 p3301 A67-34899
 Nonuniform stationary states of current in

semiconductors having S-shaped current-voltage characteristics 19 p3301 A67-34900
 Transverse forces acting on arbitrarily curved current carrying plasma cylinder in transverse magnetic field 19 p3281 A67-35151
 Interaction of plasma stream with three-dimensional magnetic dipole field, discussing current distribution in cavity 19 p3221 A67-35368
 Current distribution on cylindrical dipole antenna in homogeneous warm plasma 19 p3194 A67-35515
 Flood beams incidence angle and current density distribution effects on half-tone reproduction of visual storage tube with cathode collimator 19 p3194 A67-35543
 Electric arc blowing in plasma of nonuniform conductivity and inclusion of effect in MHD flow 19 p3298 A67-35760
 Field determination when produced by symmetrical plasmoid with time dependent current distribution traveling along cylindrical waveguide, using Wiener-Hopf method 20 p3497 A67-36860
 Current distribution in MHD channel with strong magnetic field solved by reduction to Riemann type boundary value problem 20 p3500 A67-37047
 Differential equations governing steady state current flow in semiconductors computed, considering variations as function of distance, hole and electron densities, etc 20 p3400 A67-37216
 Current distribution coefficients determination and antenna impedances 20 p3400 A67-37219
 Operating characteristics of induction pump with asymmetrical current supply, calculating magnetic induction, currents and forces in liquid metal layer 20 p3365 A67-37307
 Current distribution of magnetic field in plasma coaxial injector indicating dominant role of Hall effect in plasma acceleration 20 p3502 A67-37537
 Transient response and current distribution of thin vertical antenna coupled to pulse generator by electric network, determining radiation field 21 p3590 A67-38117
 Current carrier concentration distribution in semiconductor with intrinsic anisotropy created by strong electric field 21 p3680 A67-38319
 Plasma rotation in MPD arc measured for electric and magnetic field distribution and current and electron density distribution [AIAA PAPER 67-655] 21 p3689 A67-38691
 Current sheet propagation transition to steady pattern in pulsed plasma accelerator, noting breakdown and current characteristics [AIAA PAPER 67-656] 21 p3689 A67-38692
 Distributions of current, potential, electron density and pressure and ion velocity vector orientation in MPD arc, verifying electromagnetic effects presence [AIAA PAPER 67-676] 21 p3671 A67-38709
 Current distribution and electron temperature profiles in nonequilibrium crossed field devices, considering nonuniformities, thermal diffusion, boundary layers and finite reaction rates effects [AIAA PAPER 67-715] 21 p3673 A67-38741
 Mass spectrometric method for measuring double charge exchange cross sections of low energy positive ions, investigating current distribution 22 p3797 A67-39427
 Soviet monograph on skin effect theory, deriving relations defining electromagnetic field distribution in bulk conductors and plates 22 p3768 A67-39566
 n-m/ junction structures transient characteristics, forward and back bias cases show inductive and capacitive element behavior respectively 22 p3858 A67-39574
 Active impedance and current distribution in infinite, planar and collinear arrays of cylindrical antennas, deriving Fourier series for antenna current 22 p3769 A67-39629
 Impedance strip directional properties when excited through slot in metallic half-plane, noting case of reflector antenna with decreasing impedance 22 p3770 A67-39763
 Nonreflecting resistive loaded dipole antenna with step function internal impedance, measuring current amplitude, input admittance and radiation field pattern 23 p3978 A67-40826
 Electrically thick monopole transmitting

antenna integral equation for current distributions and admittance 23 p3981 A67-41207
 Cylindrical tube current distribution determined by digital computer solution of Fredholm integral equations 23 p3981 A67-41208
 Field of loop antenna with arbitrary current distribution located inside cylinder with arbitrary dielectric constant studied for effects on radiation pattern 23 p3982 A67-41666
 Ekman pumping in solar core noting slow meridional-current distribution in spinning core determined by energy balance 24 p4225 A67-41834
 Distributive circuit element model for computation of optimum gridding of solar cells 24 p4098 A67-42086
 Geomagnetic dynamo laboratory model self-excitation conditions determined from solutions of electrodynamic equations, diagramming magnetic field and current distribution 24 p4231 A67-42353
CURRENT SHEET
 Current layer dynamics in flat electrode accelerator, relating plasma acceleration and polarization field potential 01 p0122 A67-10345
 Current sheet velocity in coaxial accelerator and predictions from snow-plow model 02 p0273 A67-12183
 Conical current sheet implosion forming of axial pinch in z-pinch plasma gun 07 p1230 A67-20257
 Current layer dynamics in flat electrode accelerator, relating plasma acceleration and polarization field potential 11 p1843 A67-25018
 Propagation constants of rectangular waveguide containing parallel sheets of finite conductivity using iterative computer program 13 p2083 A67-27443
 Large-dimensional inverse pinch discharge study of impulsive plasma acceleration, gas dynamics and stability of unrestrained current sheet [AIAA PAPER 66-482] 14 p2356 A67-28123
 Current strip in cold magnetoplasma, noting radiation resistance of Hertzian dipole for large frequency ranges 15 p2521 A67-29185
 Current layer motion in coaxial plasma gun, measuring discharge current, electric and magnetic fields and ejected ions at gun outlet 15 p2525 A67-29250
 Single-fluid model accounting for behavior of MHD shock producing devices with unseparated shock and driving current sheet 15 p2528 A67-29565
 Magnetic field annihilation rate prediction in current pinches attributed to magnetic energy dissipation by ways other than ohmic losses 17 p2909 A67-33248
 Interpretation of multiple structure of auroral arc 18 p3035 A67-33598
 Theory demonstrating stability of current sheets of different shapes in coaxial accelerators 19 p3294 A67-35406
 Super-Alfvénic counterpart of transient sub-Alfvénic aligned-fields flow past airfoil 19 p3170 A67-35538
 Offset impedance sheet effect on admittance of slot antenna in conducting plane 19 p3197 A67-35823
 Particle trajectories for two model configurations of electric and magnetic fields in geomagnetic tail, noting application to auroral acceleration 20 p3433 A67-37415
 Reversed polarity effect on propagating current sheet in coaxial plasma accelerator [AIAA PAPER 67-658] 21 p3671 A67-38694
 Rotating current spoke in MPD engine, existence and connection with exhaust fluctuations [AIAA PAPER 67-689] 21 p3693 A67-38720
 Signal extraction and scattering of telluric currents studied for random sheets, semiinfinite medium and interface separating medium of different resistivities 24 p4152 A67-42885
CURRENT STABILIZER
 Wide temperature and parameter range transistor amplifier stage stabilization circuit design based on linear approximation of characteristics in terms of H parameters for CE circuit 04 p0586 A67-15669
 Current sheet propagation transition to steady pattern in pulsed plasma accelerator, noting breakdown and current characteristics

CURVE

[AIAA PAPER 67-656] 21 p3689 A67-38692
Current fluctuations in Josephson
superconducting tunnel
junctions 22 p3865 A67-40433

CURVED BEAM

Closed form solution for transverse-symmetric and asymmetric loadings on circular fixed beam 06 p1110 A67-18842
Natural frequencies of elastic toroids experimentally determined compared with theoretical results 13 p2219 A67-27091
Stress concentration of plane curved beams with uniform cross section determined from photoelastic experiments 20 p3540 A67-37210

CURVED PANEL

Moire pattern method of determining fringes representing constant curvature of bent plates 05 p0921 A67-16827
Boundary conditions influence on flutter critical boundary character considering nonlinearities of physical nature 16 p2776 A67-31471
Critical compression stresses in cylindrical panel with clamped lateral edges and free longitudinal edge 21 p3726 A67-38796

CURVED SURFACE

Plasma trap configuration parameters inside solenoid wound about circular torus, noting magnetic surface distortion as function of screw axis period and curvature 01 p0121 A67-10342
Unsteady interaction between blunt bodies and shock wave, comparing reflected shock wave velocity decrease for plane spherically blunted cylinders 01 p0008 A67-11294
Curvature effect on reflection coefficient of layered absorbers, examining backscattering from coated cylinder and sphere 03 p0370 A67-13852
Pivoted slider bearing under external magnetic field analyzed, considering pad surface curvature 05 p0811 A67-16981
Quasi-conical motions applied to theory of wings with curved leading edges 07 p1128 A67-20235
Curvature effect on heat transfer for turbulent flow in curved pipes under constant heat flux, considering boundary layer existence along wall 08 p1426 A67-20926
Fibrous model of shell shaped grid noting discrete network, properties of cross section surface and stress 10 p1715 A67-22920
Boundary value problem solution governed by system of partial differential equations applied to analysis of curved thin walled shells of revolution 10 p1729 A67-23765
Derivative components of unit tangent vectors to parametric curves of curvilinear coordinate system in general Riemann space 10 p1675 A67-23792
Plasma trap configuration parameters inside solenoid wound about circular torus, noting magnetic surface distortion as function of screw axis period and curvature 11 p1843 A67-25015
Convective heat transfer for water flow in curvilinear short channel, noting flow and convection types at various sections 12 p2033 A67-25316
Mechanism of fluid jet separation from curved surface 14 p2302 A67-28324
Formulas for correcting errors in aerial-photograph and planar-model coordinates due to atmospheric refraction and earth curvature 14 p2318 A67-28371
Three-dimensional rotational stagnation point flow solution noting surface curvature influence 17 p2789 A67-32039
Electromagnetic wave diffraction by convex spherical surface considered in terms of mutual impedance between two radial electric dipoles, using integral equation 17 p2817 A67-32930
Longitudinal surface curvature effects on steady, two-dimensional incompressible laminar boundary layers, noting partial differential equations, computer solution, velocity profile, etc 19 p3209 A67-35415
Coolant passage axial curvature effect on heat transfer to endothermically dissociating supercritical nitrogen tetroxide [ASME PAPER 67-HT-59] 20 p3549 A67-36741
Infinitesimal deflections of positively Gaussian curved surfaces solved by application of p , q /analytic functions after affine transformation 21 p3715 A67-37903
Shell curvature variation parameter noting

influence on equilibrium equations and error in equations of strain compatibility 21 p3718 A67-37981
Integral equation for asymptotic expansions of plane electromagnetic and acoustic fields diffracted by convex surfaces of variable curvature 22 p3836 A67-39389
Momentum equation examined by curvature of streamlines downstream from shock wave 22 p3783 A67-39727
Curved plate postbuckling behavior, deriving curved plate effective width formula 23 p4080 A67-41475
Curved plates tested under axial compression to prove curved plate buckling and postbuckling behavior formula, discussing stress distribution measurement 23 p4080 A67-41476
Longitudinal wall curvature effect on boundary layer flow stability and generalization of Rayleigh theorems for nonviscous instability 23 p3992 A67-41733
Transverse curvature parameter in hypersonic flow regime for modifying effects on velocity profile slope, skin friction and heat transfer rate 23 p3993 A67-41755

CUT-OFF

Plasma expansion wave propagation in vacuum after current cut-off 02 p0278 A67-12628
Sharp cut-off nonlinear filter design with jump effect for rapid gain increase with small frequency increment 03 p0386 A67-13981
Maximum negative feedback depth in transistorized AC amplifier as function of cut-off frequency of logarithmic amplitude-frequency characteristic for given phase reserve 05 p0772 A67-16455
Transient cut-off processes of transistorized switch with LC load 05 p0773 A67-16460
Cut-off wavelength of lowest TE mode in rectangular waveguide having coaxial cylindrical conductor 05 p0773 A67-16511
Depression of low energy cosmic ray cut-offs relation to permanent geomagnetic tail using model calculation, explaining PCA midday recovery 07 p1245 A67-19927
Cut-off turning test on 40 mm Al bar, effect of mineral oil and kerosene on cutting depth and speed and of feed on tangential force and chip size 11 p1809 A67-24945
Vertical cut-off rigidities for specific locations of geophysical interest computed from trajectory tracing process 13 p2191 A67-26325
Characteristic cut-off frequencies of transistors determined from simple LF measurements 13 p2077 A67-26659
Upper cut-off frequency and amplitude frequency response curve shape for wideband aperiodic amplifiers, examining five common transistor circuits 13 p2077 A67-26660
Cosmic ray particle trajectories for various cut-off rigidity values in different points on earth surface, noting integration of motion equations of charged particle 13 p2192 A67-27244
Measurement of atmospheric cosmic ray fluxes over large portions of globe as comparison evaluation for different cut-off rigidity models 13 p2192 A67-27245
Multialcraft measurements of cosmic ray spectrum and geomagnetic cut-off rigidity 13 p2193 A67-27246
Plasma expansion wave propagation in vacuum after current cut-off 13 p2171 A67-27386
Latitudinal effect on neutron-monitor data taken by Soviet ship in North Pacific, obtaining relation between coupling constant and cut-off rigidity 17 p2933 A67-32092
Latitude variation of effective geomagnetic cut-off rigidity of cosmic rays in presence of penumbra and constant geomagnetic field 17 p2934 A67-32094
Pulse rebalance system in conjunction with pulse accumulator and comparator for precision velocity cut-off signals, presenting data and system characteristics 17 p2858 A67-32485
Photomultiplier gate for stimulated spontaneous light scattering discrimination, showing high cut-off efficiency, linearity and absence of spurious effect 17 p2863 A67-33353
Spurious phase modulation reduction in

SUBJECT INDEX

multistage frequency multiplier using lumped-selection filters, determining cut-off angle in multiplying cascades 18 p3000 A67-34087
Cut-off amplifiers in frequency stabilization klystron designed to cut off only HF wave applied to discriminator 20 p3396 A67-36327
Higher mode cut-off frequencies in coaxial cables of elliptical cross section tabulated as function of conductor dimensions 20 p3382 A67-36861
Magnetron cut-off characteristics modification via altering electron cloud resonant properties by injecting positive ions in interaction space 20 p3489 A67-37105
Penumbra influence on cosmic ray effective cut-off rigidity calculated, noting case of primary variations and constant magnetic field 21 p3699 A67-39017
Turbulence effect on accuracy of microwave cut-off measurements of plasma density suggests electromagnetic wave scattering 22 p3845 A67-39430

CUTANEOUS PERCEPTION

Cutaneous sensitivity communications, discussing information situations, applications and subsystems 09 p1456 A67-22375

CUTTING

Cutting ability of high melting binder cemented carbides with Cr and V alloys 01 p0100 A67-10724
Explosive-actuated cutting mechanism for severing electrical service lines connecting Apollo command module to service module and lunar module to spacecraft-LM adapter [ASME PAPER 67-DE-33] 14 p2394 A67-28874

CV-990 AIRCRAFT

S CONVAIR CV-990 AIRCRAFT

CW RADAR

S CONTINUOUS WAVE /CW/ RADAR

CYANATE

S ISOCYANATE

CYANIDE

SA HYDROGEN CYANIDE
Equivalent width of weak solar line at lambda 8668 angstroms as CN 08 p1400 A67-21247
Peak and average output power of cyanide laser in far IR measured, indicating usefulness of available oversize waveguide instrumentation at HF 11 p1801 A67-24715
Harmonic mixing and heterodyne detection of laser radiation 19 p3240 A67-35623
Far IR CN laser action shown due to HCN molecule, explaining intense spectral lines around 337 microns 20 p3458 A67-36391
Laser emission mode splitting of CN laser, discussing wavelength to resonance length and Fabry-Perot interferometer permitting line splitting observation 23 p4012 A67-40893

CYANINE DYE

Two-photon absorption in organic dyes for various wavelengths, extinction coefficients and concentrations 05 p0815 A67-16626
Biological macromolecule detection using thiacarbocyanine dye and observation of absorption spectra changes 15 p2426 A67-29115
Second order absorption spectra of symmetric cyanine dyes in methanol solution using spectrophotometer 22 p3757 A67-39444

CYANO COMPOUND

Zeeman field spatial orientation of paramagnetic spin-lattice relaxation for 2T2 states in rhombic symmetry, emphasizing application to Fe-doped potassium cobalticyanide and potassium ferricyanide 01 p0129 A67-10150

CYANOGEN

Laser action in optically pumped CN, discussing vibrational-rotational transitions 01 p0089 A67-10370
Electronic absorption spectrum observed during cyanogen azide flash photolysis 13 p2177 A67-26988

CYBERNETICS

SA HUMAN ENGINEERING
Bioastronautics role in population explosion and technological evolution problems, noting biocybernetics, and aerospace systems engineering 16 p2782 A67-30787
Cybernetics methods suited to complex systems associated with bioastronautics 16 p2618 A67-30788

CYCLE

S BRAYTON CYCLE
S CLOSED CYCLE
S CRYOCYCLE

S RANKINE CYCLE
S REGENERATIVE CYCLE
S SOLAR CYCLE
S STIRLING CYCLE
S STRESS CYCLE
S SUNSPOT CYCLE
S TOPPING CYCLE
S WORK-REST CYCLE
CYCLIC HYDROCARBON
SA ANTHRACENE
Laser beam effect on benzene and other organic compounds, noting formation of dark readily coagulating deposit 05 p0759 A67-17028
Calorimetric, titrimetric and gravimetric methods for determination of hexogen-octogen mixtures 05 p0872 A67-17153
Perfluorocyclobutane-fluorine combustion studies and measurement of detonation velocities and limits 19 p3345 A67-35013
[CI PAPER 67-23]
Classification of 2-oxazolidones, examining preparation, physical chemistry, properties and polymerized derivatives 23 p3971 A67-41041
CYCLIC LOAD
Fatigue crack propagation under random cyclic loading extended, obtaining zero-order solution from mean crack lengths 02 p0337 A67-11794
Cyclic stressing of fiber composite materials elastic-plastic region, assuming equal strains in fiber and matrix 03 p0445 A67-13529
Strength criterion for complex loading, possible development based on strength criterion for symmetrical cyclic loading 03 p0529 A67-14168
Thickness effect on fatigue crack propagation in notched alclad sheet under cyclic tensile loading and transition from tensile fracture mode to shear mode 03 p0532 A67-14386
Moisture effect on slow crack propagation in thin sheets of SAE 4340 steel under static and cyclic loading
[ASME PAPER 66-WA/MET-6]
04 p0639 A67-15340
Numerical analysis of crack propagation in cyclic loaded structures, taking into account load ratio and instability at onset of fast fracture
[ASME PAPER 66-WA/MET-4]
04 p0711 A67-15342
Shearing stress failure theory for high cycle fatigue employing rotating principal stress axes and nonsynchronous stresses
[ASME PAPER 66-WA/MET-9]
04 p0712 A67-15374
Longitudinal waves in viscoelastic rod caused by sinusoidal stress applied at one end, noting temperature dependency of mechanical properties of rod
[ASME PAPER 66-WA/APM-29]
04 p0714 A67-15423
Elastoplastic calculation of turbine disks, considering cyclic plastic deformation 05 p0810 A67-16177
Stressed and deformed state of plastic disk under cyclic loading in variable temperature field, using increments method 05 p0810 A67-16178
Thermal stress determination in thin conical shells of revolution using real function expression for forces, moments and displacements occurring during cyclic deformation 05 p0914 A67-16198
Heating and cooling rates, hold time at maximum temperature, phase temperature between temperature and strain cycling effects on thermal fatigue of stainless steel 05 p0921 A67-17085
Cyclic load and temperature effects on creep behavior of Ni-base alloy Mar-M 200 between 1800 and 1900 degrees F 06 p1014 A67-17802
Equation of cylindrical shell under cyclic loads, using asymptotic method 06 p1106 A67-18629
Cyclic torsion interaction with axial load, showing torsion angle larger than fatigue limit and applied tensile stress larger than Bauschinger yield 10 p1669 A67-23438
Discrete element method for plastic analysis of complex built-up structures subjected to cyclic loading causing membrane stress and stress reversal 10 p1725 A67-23713
Stacking fault tetrahedra in fatigued stainless steel, describing mechanism for nucleation of triangular Frank dislocation

loop during cyclic load 11 p1805 A67-24109
Adhesive properties testing and damping behavior of thin viscoelastic material under different cyclic loadings
[ASME PAPER 67-VIBR-25]
11 p1872 A67-24183
Cumulative strain behavior of nickel-chromium alloy and chromium martensitic type steel under action of cyclic loading 12 p2015 A67-25420
Elastic-plastic deformation around circular hole in plate under cyclic loading, recording strain distributions, development of plastic zone, etc 12 p2016 A67-25423
Cyclic loading of thick tube with creep, plasticity and thermal effects 12 p2016 A67-25424
Low endurance fatigue analysis for steel and Al alloy under cyclic torsion with controlled shear strain 12 p2016 A67-25425
Metal matrix composite fatigue behavior in tension-tension loading as function of volume fraction 14 p2337 A67-28422
Reinforcements 14 p2337 A67-28422
Cyclic extension of elastic fiber with elastic-plastic coating when obeying Tresca yield condition 14 p2341 A67-29060
Fatigue process theory for general broadband random loading, calculating mean damage and survival probability 15 p2576 A67-30094
Periodically fluctuating loading fracture propagation analysis with damage summation principle in stress and cracking time terms, deriving differential equation for fracture length 15 p2576 A67-30183
Stochastic model to structural fatigue, obtaining probability distribution for number of load repetitions necessary for fatigue failure 15 p2578 A67-30270
Upper and lower bounds of survivorship function of redundant structure subjected to fatigue 16 p2774 A67-31319
Fatigue crack growth rates in metals under random loading correlated to cyclic load tests 16 p2774 A67-31320
Low strain rate and temperature effects on crack initiation and growth, recovery and boundary migration for Al and Al alloy 16 p2689 A67-31368
Effects of repeated loading of materials and structures - Conference, Mexico City, September 1966, Volume 3 17 p2957 A67-32027
Cumulative fatigue at root of circular notch of coupon type aluminum alloy specimens subjected to low cycle compression-tension strains 17 p2957 A67-32028
Effects of repeated loading of materials and structures - Conference, Mexico City, September 1966, Volume 6 17 p2958 A67-32029
Electron fractographic techniques for failure analysis, examining fracture direction, differentiation between hydrogen embrittlement and stress corrosion in steels and cyclic stress 18 p3145 A67-34581
[ASTM PAPER 44]
Cumulative damage observed for biaxial fatigue stress tests on tubular steel specimens 19 p3341 A67-35552
Quasi-static equilibrium of truncated conical shell of revolution discussed in terms of zero-moment theory, when under cyclic load 19 p3341 A67-35631
Interaction between environment, oxide layer and surface slip formation in aluminum during cyclic bending 19 p3247 A67-35788
Mean stress level effect on corrosion fatigue strength of aluminum clad D16AT alloy sheet under asymmetrical loads 21 p3646 A67-39008
Supersonic transport structural materials design, considering fatigue behavior, crack propagation and residual static strength under temperature and cyclic load effects 22 p3819 A67-39457
Crack propagation in solid undergoing cyclic loading using Griffith model, stressing work hardening effect 22 p3911 A67-39680
Metal stress relaxation effects under cyclic thermal loads, with endurance vs stress relaxation diagrams 22 p3912 A67-39686
Cyclic stress-strain in annealed and cold worked fcc polycrystalline metals and alloys studied for hardening and softening by transmission electron microscopy 22 p3821 A67-40033
Yielding behavior of materials and

structures examined via one-dimensional models noting stress-strain relations 23 p4072 A67-40605
Kinetic approach to fatigue investigation in calculation of cyclic lifetime from static test data 23 p4074 A67-40663
CYCLING
S THERMAL CYCLING
CYCLOHEXANE
Second harmonic generations and mixings of Raman lines produced in cyclohexane, acetone, benzene and carbon disulfide, photographing first order Stokes radiation 02 p0252 A67-12052
Diffusion broadening in inelastic light scattering of cyclohexane-polystyrene near critical point for mixing 06 p1035 A67-17829
CYCLONE
Tornado angular momentum as derived from electrostatic motor type action in parent cloud 04 p0649 A67-14678
CYCLOPROPANE
Vapor phase IR spectrum of planar structure of trimethylenecyclopropane 04 p0566 A67-15511
CYCLOTRIMETHYLENE TRINITRAMINE /RDX/
Cool burning smokeless propellants for gas generator applications and low signature missiles evaluated against criteria 15 p2544 A67-29981
CYCLOTRON
S ION CYCLOTRON
CYCLOTRON FREQUENCY
Cold beam plasma interaction theory for finite transverse dimensions and finite magnetic fields determined by computer solution of dispersion relations 02 p0272 A67-11884
Quasi-linear theory of plasma cyclotron instability for one-dimensional oscillation spectrum, noting energy of interaction with electromagnetic field, ion velocities, etc 03 p0475 A67-12933
Microwave radiation measurements from internal plasma resonance of positive column near electron cyclotron harmonic frequencies 03 p0476 A67-13355
Higher harmonics of anomalous cyclotron emission from partially ionized plasma ascribed to negative absorption 03 p0476 A67-13358
Anomalous pulsed microwave emission at cyclotron frequency in partially ionized plasmas analysis extended to show that emission is not stationary with time 04 p0663 A67-14615
Electron cyclotron echo production from plasmas by repeated pulsing, developing theory based on electron neutral momentum transfer collisions 04 p0665 A67-15105
Operating possibility of axisymmetric electron beam so that plasma frequency will exceed electron cyclotron frequency of magnetic focusing field at some point or throughout beam 04 p0624 A67-15326
Anomalous emission at electron cyclotron frequency in partially ionized plasmas 05 p0854 A67-16895
Electrostatic ion cyclotron oscillations excitation by electrode immersed in plasma 05 p0859 A67-17435
Electron-cyclotron heating of plasma via high power oscillator, noting experimental setup and characteristics 06 p1039 A67-18082
Particle concentration and luminescence intensity correlation with electron cyclotron frequency in stationary SHF argon discharge in magnetic field 06 p1040 A67-18094
Generation of longitudinal plasma oscillation harmonics near electron cyclotron frequencies 06 p1046 A67-18831
Excitation and propagation of Bernstein modes in nonuniform plasmas near electron cyclotron harmonics 08 p1361 A67-21130
Correlation radiometry examination of radiation emission in beam plasma discharge at harmonics of electron cyclotron frequency 09 p1536 A67-21601
Magnetosonic wave effect on anisotropic relativistic plasma component, obtaining cosmic ray plasma instability when wave frequencies are less than electron cyclotron frequency 09 p1546 A67-22230
Two positive kinetic power waves coupled in interaction for DC pumped quadrupole amplifier having low noise and high efficiency 09 p1478 A67-22260
Electrical conductivity tensor effect on flow in MHD generator, considering transport of ionized gas and solution of

symmetric problem 09 p1550 A67-22575
 Summation of convergent series for cyclotron harmonic wave dispersion for numerical and analytic work 11 p1827 A67-23886
 Negative ions in night ionosphere, discussing sub-ELF emission and excitation of ion acoustic oscillations in plasma by electron drifts 11 p1784 A67-23933
 Cooperative effect among electrons in presence of radial density gradient in cyclotron echo phenomena 11 p1836 A67-24391
 Current flow through plasma sheath into magnetized plasma, noting negative resistance characteristics of sheath upon ion cyclotron frequency oscillation 11 p1837 A67-24397
 Instabilities in DC electron beam/plasma experiment noting dependence on beam current, magnetic field strength, beam velocity and plasma density 11 p1837 A67-24400
 Electron-cyclotron wave instability in plasma noting dispersion relation, growth rate frequency, destabilizing effect of electrons, etc 13 p2163 A67-26286
 Sonagrams for micropulsations, computer simulated, using equations for cyclotron instability and quasi-linear diffusion of protons in bounded plasma 15 p2476 A67-29618
 Pc 1 micropulsation signals classified as hydromagnetic whistlers and periodic hydromagnetic emissions, suggesting cyclotron instability process as generation mechanism of latter 17 p2853 A67-33253
 Cyclotron instabilities of two-component electron plasma 18 p3089 A67-34295
 RF plasma at electron cyclotron frequency produced with axially slotted metal cylinder 19 p3275 A67-35111
 Cyclotron harmonic wave propagation in warm magnetoplasmas predicted theoretically for perpendicular and oblique damping 19 p3288 A67-35371
 Cyclotron waves in collisionless plasma column, finding three distinct waves with resonances at/near electron cyclotron frequency 19 p3288 A67-35373
 High power microwave radiation from nonequilibrium plasma discharge near electron cyclotron frequency 19 p3291 A67-35386
 Ion cyclotron frequency wave generation in plasma confined in magnetic well for maximal density 19 p3295 A67-35419
 Plasma absorption of microwaves, noting 20 resonant maxima near harmonics of electron cyclotron frequency 20 p3498 A67-36692
 Counterstreaming ion electrostatic instability at cyclotron frequency to enhance trapping of injected ion beam 21 p3661 A67-37748
 Electrostatic ion cyclotron waves excitation in plasma and ion heating due to cyclotron damping 21 p3667 A67-38407
 Charged particle motion equation derivation in guiding center approximation in lowest order through Northrop averaging process 22 p3843 A67-39264
 Resonant cavity electric field excitation placed in magnetic field near electron cyclotron frequency studied for expressions of self-excitation current 22 p3816 A67-40126
 Two and three-pulse echo trains stimulated in magnetoplasma by repeated electron cyclotron frequency pulsing studied with single particle collision theory 23 p4031 A67-40889
 Plasma potential oscillations in traps, discussing flute instabilities, cyclotron instabilities and resonance electron wave excitation 23 p4034 A67-41680

CYCLOTRON RADIATION
 Cyclotron ion wave interaction with HF plasma oscillations measured, using vacuum chamber and electron gun 04 p0667 A67-15209
 Induced electron cyclotron radiation application to generation and amplification of high power electromagnetic traveling waves 05 p0824 A67-16915
 Origin of solar type I noise storm radiation seen in cyclotron radiation from electron streams gyrating in spot field configurations in corona 07 p1244 A67-19852
 Correlation between pearl pulsations and interplanetary magnetic field sector boundaries 07 p1182 A67-19946
 Anomalous bremsstrahlung and cyclotron

emission in partially ionized plasmas 08 p1366 A67-21441
 Angular and frequency spectra of Cerenkov and cyclotron radiation from charged particle spiraling in cold magnetoplasma determined by Fourier transform method 09 p1562 A67-22228
 Cyclotron instability range in earth radiation belt analyzed taking into account wave absorption in atmosphere, using measurements of perturbation effects 14 p2378 A67-27916
 Nonlinear theory of cyclotron instability of earth radiation belt covering time-dependent instability evolution, radiation belt stationary state, etc 14 p2379 A67-27930
 Synchronous and cyclotron wave behavior of electron flux in resonator with transverse electric field varying sinusoidally along wave propagation direction 14 p2288 A67-28807
 Cyclotron ion wave interaction with HF plasma oscillations measured, using vacuum chamber and electron gun 15 p2532 A67-30257
 Induced electron cyclotron radiation application to generation and amplification of high power electromagnetic traveling waves 16 p2685 A67-30892
 Faraday effect in microwave region used for electron density determination in argon and helium low pressure plasmas and comparison with cyclotron radiation data 19 p3297 A67-35592
 Solar type IV burst centimeter and decimeter polarization and spectral variabilities examined in helical electron stream cyclotron radiation hypothesis for solar corona model 23 p4050 A67-40776

CYCLOTRON RESONANCE
 HF heating of dense plasma by resonance excitation of cyclotron-type ion waves and fast magnetoacoustic waves 02 p0274 A67-12460
 Temperature and stress dependence of electron lifetime in p-type Si-B and Ge-Zn between 1.5 and 4.2 degrees K 02 p0301 A67-12523
 Spatial waveform of azimuthal electric field of Faraday shielded Stix coils for ion cyclotron resonance heating of plasma to thermonuclear temperatures 02 p0279 A67-12685
 Quasi-linear approximation of Cerenkov and cyclotron damping of electromagnetic waves in magnetoactive plasma, considering collisions of wave-absorbing resonance particles with plasma 03 p0475 A67-12934
 Cyclotron absorption in n type lead telluride with wide range of carrier concentrations, showing increase in transverse effective mass and decrease in anisotropic mass ratio 03 p0493 A67-13352
 Experimental results of microwave absorption by magnetoplasma indicate peaks result from excited electromagnetic wave propagation 03 p0476 A67-13357
 Confinement times and density of deuterium plasma produced by ion cyclotron resonance heating in C stellator 03 p0485 A67-14049
 Gas discharge in argon maintained within waveguide by microwave signal at cyclotron resonance, observing second harmonic radiation 05 p0850 A67-16046
 Properties of dense plasma with preheated electrons in ion cyclotron resonance region, using magnetic mirror 05 p0853 A67-16755
 Landau level structure and transition matrix elements of InSb near Brillouin zone center during valence band cyclotron resonance 05 p0870 A67-17193
 Electric propulsion unit using electron cyclotron resonance plasma thruster for spacecraft 06 p1074 A67-18418
 Cyclotron resonance in tellurium at submillimeter wavelengths, deducing relation time anisotropy 06 p1061 A67-18920
 Electron scattering by neutralized acceptors investigated in Ge and Si through cyclotron resonance 06 p1063 A67-18939
 Relaxation time of electrons in pure germanium and silicon measured from line width of cyclotron resonance at liquid helium temperatures taking into account quantum limit 06 p1064 A67-18945
 IR transmission measurements in single crystal thin film semiconductors, observing absorption band near plasma frequency 06 p1071 A67-18992
 Cyclotron resonance amplification of VLF

and ULF whistlers, evaluating power transfer for various whistler distributions 07 p1179 A67-19915
 Plasma ringing phenomena stimulated by Alouette I and other ionospheric probes at upper hybrid frequency and cyclotron frequency harmonics in near zero group velocity regions 07 p1179 A67-19916
 Plane wave growth associated with Cerenkov and cyclotron instabilities in plasma stream 08 p1358 A67-20893
 Resonant particle instabilities in uniform magnetic field of plasma waves propagating at arbitrary angle 08 p1359 A67-20897
 Cyclotron resonance instability of ion cyclotron and magnetosonic waves propagating at angle to magnetic field in infinite uniform plasma 08 p1359 A67-20898
 Drift cyclotron oscillations of inhomogeneous collision plasma propagating across magnetic field, taking into account particle collisions with aid of Landau collision integral 10 p1686 A67-23595
 Anisotropic properties of acoustic electron scattering in Si samples in 8 mm wavelength and liquid nitrogen temperature 10 p1695 A67-23664
 Electron cyclotron resonance heating of alkali plasmas by electromagnetic resonant absorption 11 p1838 A67-24407
 Cyclotron echo formation in rare gas and nitrogen afterglow plasma in presence of inhomogeneous magnetic field, stressing velocity-dependent collision frequency case 14 p2356 A67-28150
 Interaction between SHF field and created plasma in electron-cyclotron resonance state 15 p2529 A67-29715
 Stationary concentration of charged particles in plasma created by uniform and nonuniform SHF magnetic field in electron-cyclotron resonance state 15 p2529 A67-29716
 Scattering method for observing plasma instability near electron gyrofrequency harmonics 16 p2715 A67-31062
 Energy losses of modulated azimuthal current in magnetoplasma, discussing specifically electron cyclotron resonance 16 p2716 A67-31177
 Quasi-linear theory of plasma cyclotron instability, analyzing transverse oscillations propagating along external magnetic field 16 p2717 A67-31179
 Anisotropic properties of acoustic electron scattering in Si samples in 8 mm wavelength and liquid nitrogen temperature 17 p2924 A67-33345
 Anisotropy of electron energy distribution measurement in electron cyclotron-resonance plasma using diamagnetic loop 18 p3093 A67-34756
 Electron-atom collision cross-section in afterglow of pulsed cesium plasma as function of electron cyclotron absorption resonance and electron temperatures 19 p3271 A67-35076
 Electron cyclotron resonance absorption of microwaves in oxygen magnetoplasma used to alter electron attachment and detachment rate coefficients 19 p3271 A67-35077
 Argon plasma ionization by oscillator supplying power near electron cyclotron resonance, measuring density variation 19 p3276 A67-35116
 HF magnetic fields for plasma sheath with perpendicularly superimposed static magnetic field and resonance excitation of electron cyclotron waves 19 p3276 A67-35117
 Impedance measurements of RF discharge in single turn coil with superimposed static magnetic field, noting dependences and two resonances 19 p3276 A67-35119
 Cyclotron waves in collisionless plasma column, finding three distinct waves with resonances at/near electron cyclotron frequency 19 p3288 A67-35373
 Electromagnetic field energy absorption in cold rotating plasma, obtaining electric current density and plasma electric field relationship and cyclotron resonance 20 p3497 A67-36677
 Magnetic curvature effect on drift cyclotron instabilities, considering density gradients, Maxwell plasmas and resonance 21 p3661 A67-37749
 Ion cyclotron wave propagation in plasma, considering Larmor radius effects, quasi-static dispersion relation, phase velocity and cyclotron resonance 21 p3661 A67-37750
 Electron-cyclotron harmonic resonances interactions in RFF excited electrodeless

hollow discharges, discussing magnetic field position measurement and plasma simulation 21 p3662 A67-37757

Indium antimonide hole surfaces approximated within second order perturbation theory, discussing energy contours, Baggeley cyclotron resonance data and maximum energy value 21 p3679 A67-38255

Plasma rotation effect on cyclotron resonance, noting electromagnetic field energy absorption 21 p3669 A67-38679

Plasma acceleration by electromagnetic microwave discharge in static magnetic field gradient, discussing microwave-plasma energy transfer at electron cyclotron resonance [AIAA PAPER 67-660] 21 p3671 A67-38696

Electromagnetic wave propagation in nonuniformly magnetized plasma with wave frequency near second electron cyclotron harmonic 22 p3843 A67-39263

Ion-molecule collision cross section determined from pressure broadening of ion cyclotron resonance lines at high electric field/pressure ratio 22 p3840 A67-39365

Double probe method for determining electron temperature and density variations in HF hydrogen plasma during second harmonic cyclotron resonance 22 p3848 A67-39650

Cyclotron harmonic resonances in plasma frequency conversion output due to harmonic interactions with incident waves 22 p3851 A67-39724

Negative cyclotron resonance absorption due to electron elastic collisions with noble gas atoms, comparing results with kinetic plasma wave theory predictions 22 p3842 A67-40346

Microwave production of plasma in trap at electron cyclotron resonance, investigating absorption and density 23 p4035 A67-41684

CYGNUS CONSTELLATION

Energy spectrum of X-ray source in Cygnus constellation with 2 to 60 kev 03 p0507 A67-13917

High altitude balloon flights with gamma ray spark chamber for search of cosmic gamma ray source in Cygnus 06 p1078 A67-18212

Balloon observation of X-ray sources in Cygnus region in energy range 20-130 kev 08 p1377 A67-21252

Wavelength dependence of polarization of IR star in Cygnus measured by far IR lead sulfide photopolarimeter 11 p1863 A67-24509

Linear polarization of Crab Nebula, Cygnus A and other radio sources observed at wavelength of 21.3 cm, using radio telescope 13 p2198 A67-26714

Radio stars as signal sources for accurate measurement of radar antennas vertical polar diagrams, describing solar noise technique disadvantages 15 p2436 A67-29645

X-ray scanning of Cygnus region with large area proportional counters flown on attitude-controlled sounding rocket 17 p2937 A67-32648

Optical search of sky near X-ray positions of Cyg X-1 and Cyg X-2 for identification purposes 17 p2937 A67-32649

Origin of X radiation from radio galaxies Cygnus A and Virgo A, hypothesizing thermal radiation and bremsstrahlung 18 p3116 A67-33855

Secular behavior of optical properties of X-ray emitting object near Cygnus X-2 19 p3331 A67-36084

CYLINDER

SA AIRYS STRESS FUNCTION

SA CIRCULAR CYLINDER

SA CONCENTRIC CYLINDER

SA ELASTIC CYLINDER

SA ELLIPTICAL CYLINDER

SA HEMISPHERE CYLINDER BODY

SA MONOCOQUE CYLINDER

SA ORTHOTROPIC CYLINDER

SA OSCILLATING CYLINDER

SA PLASMA CYLINDER

SA ROTATING CYLINDER

SA VISCOELASTIC CYLINDER

Dynamic problems of elasticity theory for transversal-isotropic cylinder 02 p0338 A67-11968

Elastoplastic deformation of cylinder under torque and tensile stress based on stress stabilization in yield zones 04 p0708 A67-14796

Oscillation effect on instantaneous local heat transfer in forced convection from

cylinder measured by optical method and theoretically calculated by power series expansion method 04 p0733 A67-15843

Approximate solution of thermoconductivity equation for multilayer cylinder in constant-temperature medium 04 p0738 A67-15891

Inelastic buckling of rib-cored orthotropic sandwich cylinders under external hydrostatic pressure, evaluating rigidity factor and Poisson ratio 04 p0719 A67-15936

Axial flow dynamics of flexible slender cylindrical body immersed in fluid, emphasizing flow velocity, frictional forces, buckling and oscillatory instabilities 05 p0920 A67-16815

Scattering by infinite cylinders of arbitrary cross section treated by method of finite difference 05 p0764 A67-16952

Estimates of Green function in first boundary value problem of thermoconductivity equation for cylinder 05 p0927 A67-17002

Electromagnetic wave propagation around cylinder surrounded by nonmagnetic isotropic medium with dielectric constant function of radius, using conformal mapping 06 p0962 A67-18076

Convective heating in shoulder regions of flat-faced cylinder with large favorable pressure gradient [AIAA PAPER 67-162] 06 p1114 A67-18293

Plastic strains in thick cylindrical segment under mechanical and thermal loads [AIAA PAPER 67-113] 06 p1102 A67-18309

Fluid flow through parallel cylinders when flow incidence is lateral and Reynolds numbers are small, determining particles trajectories 06 p0991 A67-18819

Real gas effects on time required for establishing detached bow shock in front of cylinder 06 p0992 A67-18882

Aerodynamic characteristics of rough cylinders, noting effect on head drag coefficient and Reynolds number 07 p1126 A67-19323

Perturbations caused by cylindrical body in plasma, obtaining electric field and electron and ion concentration dependences on distance 07 p1250 A67-19811

Lower bound for limit pressure of cylindrical pressure vessel with unreinforced hole obtained by restricting stress directions of cylinder 08 p1421 A67-20921

Drag on two-dimensional cylinder between parallel walls in Stokes flow calculated by perturbation methods 08 p1323 A67-21390

Free molecular flow rate and mass distributions through various length cylindrical nozzles 09 p1488 A67-22106

Power spectrum of irradiance for precessing cylinder computed as function of time for given value of phase angle 10 p1652 A67-22714

Quasi-stationary regime during radiative-convective heating of infinite plate and cylinder, noting time dependent temperature variation 10 p1732 A67-23020

Plastic flow and instability behavior of thin walled tubes of nickel-chrome steel subjected to constant ratio tensile stress 10 p1719 A67-23485

Inverse problem of unsteady heat conduction equation for unbounded hollow cylinder, determining specific heat 11 p1882 A67-24031

Stress-strain state of circular cylindrical rod coupled to half-space when applying torsion to free end 11 p1879 A67-24884

Semifinite cylinder dynamic torsional problem, considering self-balanced and self-unbalanced boundary perturbation expansion 12 p2029 A67-25664

Stresses and displacements for any strain state of hollow cylinder 13 p2218 A67-26890

Radiative heat exchange between surfaces of telescoped cylinders, determining angular radiation coefficients 14 p2406 A67-28308

Cylindrical specimen behavior during high strain rate tensile test, using computer program 14 p2400 A67-28523

Heat resistant stainless steel honeycomb cores for cylindrical applications, measuring energy absorption characteristics [ASME PAPER 67-DE-14] 14 p2402 A67-28870

Time dependent problems of heat transfer in laminar flow of viscous incompressible fluid in cylinder and cylindrical annulus 14 p2408 A67-28892

High frequency asymptotic behavior of

wave field in two-dimensional diffraction problem on inhomogeneous cylinder of arbitrary cross section 16 p2628 A67-31505

Series solution for end effect in semifinite transversely isotropic cylinders, noting elastic analysis 17 p2962 A67-33014

Dynamic problems of elasticity theory for transversal-isotropic cylinder 17 p2966 A67-33285

High intensity heat flux formation during heat transfer on steel cylinder in region of incident shock wave in supersonic flow 18 p3027 A67-34206

Ionized gas flow past cylinder and sphere, determining ionization and dissociation effect on displaced shock wave form 18 p3170 A67-35449

Principal polarization radar cross sections as function of azimuth angle for rectangular cylinder 19 p3183 A67-35518

Inviscid hypersonic axisymmetric flow over cylinder and sphere near stagnation point, including dissociation and detached shock wave 19 p3171 A67-35722

Compressible laminar spanwise boundary layer on yawed infinite cylinder with disturbed suction calculated using momentum equation 19 p3342 A67-35724

Surface pressure spatial correlation function for rigid infinitely long cylinder in three-dimensional diffuse sound field 20 p3537 A67-36646

Transient temperature distribution of cylinder subject to radiation cooling, giving dimensionless computer-derived graphs [ASME PAPER 67-HT-71] 20 p3550 A67-36751

Three-dimensional boundary layer for gas flow past generatrix of cylinder of arbitrary transverse cross section 20 p3360 A67-37658

Diffraction by cylinder in locally uniaxial medium with azimuthal optic axis, using Maxwell equation solution for plasma frequency 20 p3389 A67-37705

Cooling of cylinder moving through fluid assuming fluid properties permit boundary layer approximations 22 p3918 A67-39782

Cylinder residual stress measurement, discussing stress distribution from Sachs equations 22 p3913 A67-40035

Convective heating in shoulder regions of flat-faced cylinder with large favorable pressure gradient [AIAA PAPER 67-162] 23 p3932 A67-41714

Compressible laminar boundary layer on infinite swept cylinder analyzed for effects of suction on spanwise profile 23 p3993 A67-41746

Electromagnetic wave propagation along arbitrary cross sectional imperfectly conducting metallic cylinder employing conformal mapping 24 p4120 A67-42230

CYLINDRICAL AFTERBODY

Gas ejection and boat-tailing effect on cylindrical afterbody in supersonic flow 17 p2793 A67-33041

Mean flow and motion turbulence characteristics after separation from conical afterbody for various initial boundary layer thickness and convergence angles 23 p3927 A67-40631

CYLINDRICAL SHELL

Sanders equation for circular cylindrical elastic shell reduced to fourth order PDE 01 p0159 A67-10400

Eigenfrequencies of flexural vibrations of circular cylindrical shells calculated by various methods and compared with measured values 01 p0162 A67-10839

Buckling tests on uniformly heated thin cylindrical shells, noting load and temperature effects 01 p0163 A67-11013

Vibration modes and relative frequencies of shells stiffened by angularly equidistant stringers, using Vlasov theory of circular cylindrical shells 01 p0163 A67-11148

Loading rate effect on critical behavior of cylindrical shell responses 01 p0164 A67-11187

Vibrations of elastic shells containing liquids 01 p0165 A67-11441

Propagation characteristics of cylindrical waveguide partially filled with dielectric light modulation material 02 p0193 A67-11780

Point matching method, solving boundary value problem in uniform cylindrical waveguide with inserted conductor within conducting tube 02 p0193 A67-11781

Parabolic convolution type equations in bounded cylindrical and noncylindrical regions, discussing smooth operators in half-space 02 p0259 A67-11871

Second order variation of system potential

energy of axially compressed circular cylindrical shell with ring-stiffened edges evaluated for purely inextensional deformation 02 p0339 A67-12345

Discrete method strength calculation for round cylindrical shells applicable to computer solution of normal external loading problems 02 p0339 A67-12442

Carrying capacity of cylindrical shells of arbitrary cross section calculated under transverse and longitudinal stresses 02 p0340 A67-12660

Calculation of cylindrical minimum weight stringer shell in axial compression loading 02 p0340 A67-12662

Dynamic stress field of cylindrical shell subject to internal stresses 02 p0341 A67-12664

Buckling loads of reinforced cylindrical shells, discussing size and placement of stiffening members 03 p0521 A67-13019

Variation equation for steady state creep applied to semimomentless cylindrical shell 03 p0522 A67-13206

Steady state response of viscoelastic cylindrical shells to moving loads, obtaining exact solution with correction for shear deformation and rotatory inertia effects via Fourier transforms 03 p0522 A67-13211

Uniform wall suction effect on inlet flow of porous cylindrical tube, noting laminar to turbulent transition 03 p0404 A67-13973

Strength of cylindrical shells under local radial loads and circumferential bending moments conveyed by reinforcing elements 03 p0527 A67-14069

Simulation of isotropic and structurally orthotropic shells by laminated models and constructing limiting relations between generalized stresses 03 p0530 A67-14170

Axissymmetric deformation of cylindrical shell reinforced by frames located at arbitrary distance from each other and having different geometrical and elastic characteristics 03 p0530 A67-14171

Stress state of cylindrical cantilever shell under action of concentrated normal force applied to free edge 04 p0708 A67-14784

Elasticity and shell theory solutions for long circular cylindrical shells compared by numerical analysis 04 p0709 A67-14811

Modes effect on plastic buckling of compressed cylindrical shells, considering deformation theory vs incremental theory 04 p0710 A67-14852

Plastic analysis of rib reinforced cylindrical shells using strain mapping method for Tresca yield conditions [ASME PAPER 66-WA/APM-14] 04 p0713 A67-15406

Inversion of eccentricity effect in stiffened cylindrical shells buckling under external pressure 04 p0716 A67-15746

Simultaneous free and parametric oscillations of elastic cylindrical shell of infinite length and subsonic flow of ideal gas in shell 04 p0717 A67-15888

Two contact problems involving cylindrical shells reinforced with elastic frames 04 p0717 A67-15889

Axissymmetric motions of Timoshenko type cylindrical shells composed of two elastic isotropic layers of different materials and thicknesses connected by perfect bond 04 p0717 A67-15909

Stress concentration in nonlinear creep of thin circular cylindrical shell loaded at one edge by symmetrical radial shear and bending moment 04 p0718 A67-15917

Nonlinear equations for supercritical axisymmetric elastic deformation of circular cylindrical shell under longitudinal impact from rigid body 05 p0907 A67-16015

Buckling phenomena involving formation of indentation in thin circular cylindrical shells under axial compression 05 p0907 A67-16021

Dynamic surface loads, transient displacement and stresses in elastic cylindrical shell under radial and torsional vibration and elastic spherical shell under radial symmetric vibration, using finite Hankel transformation 05 p0908 A67-16138

Elastic cylindrical shell under arbitrary impulsive pressure distribution, discussing membrane and flexural stresses 05 p0909 A67-16139

Lifting capacity of two-layer cylindrical shell made of different elastically hardening materials, considering temperature effect 05 p0912 A67-16180

Elastoplastic axisymmetric stressed state of circular cylindrical shell under unsteady temperature field, internal pressure and axial force, using differential equation 05 p0912 A67-16181

Elastoplastic deformation of cylindrical shell under cyclic axisymmetric unsteady temperature field 05 p0912 A67-16182

Free hinged cylindrical shell problem with radial load on outer edge of cross section solved via linear differential equations 05 p0915 A67-16222

Aircraft skin panel fatigue failure under hypersonic conditions, noting effect of natural vibration frequency and axisymmetric oscillations 05 p0916 A67-16229

Cylindrical shell subjected simultaneously to axial compression and internal pressure 05 p0917 A67-16246

Differential equation derivation for creep analysis using plastic interaction curve and associated flow rule 05 p0917 A67-16299

Instability of thin reinforced cylindrical shell clamped at both ends and energy method calculation of critical pressure 05 p0918 A67-16422

Initial equilibrium state stability of multilayer orthotropic circular cylindrical shell based on anisotropic shell theory 05 p0919 A67-16585

Elastoplastic deformation of circular cylindrical shells of ideally plastic incompressible material under uniform supercritical hydrostatic pressure 05 p0922 A67-17176

Bending stresses in cylindrical shell with rigid circular inclusion examined under axial tension and internal pressure [AIAA PAPER 66-525] 05 p0924 A67-17351

Inertia effects of internal liquid column on vibration of thin walled pressurized elastic cylindrical bellows type container [AIAA PAPER 67-38] 06 p0986 A67-18262

Supersonic flutter of thin walled circular cylindrical shells under compressive loading, comparing theory and experiment [AIAA PAPER 67-77] 06 p1103 A67-18354

Analytical and empirical results on shell panel flutter boundaries compared, using nonlinear Donnell theory and linear piston theory approximation [AIAA PAPER 67-78] 06 p1104 A67-18452

Characteristic method analysis of linear system of dynamic cylindrical equation for axisymmetric motion, including rotary inertia and shear correction factor [AIAA PAPER 67-79] 06 p1104 A67-18497

Stability of circular cylindrical shell in supersonic nonviscous conducting gas flow with unperturbed velocity and under magnetic field 06 p1106 A67-18622

Equation of cylindrical shell under cyclic loads, using asymptotic method 06 p1106 A67-18629

Rib elasticity effect on stressed state of circular cylindrical shell with rectangular cut in torsion 06 p1107 A67-18632

Approximate solution of temperature field of thin isotropic cylindrical shell heated by time dependent thermal fluxes from two ambient media 07 p1266 A67-19162

Cylindrical shell stability under axial compression analyzed by generalized power series method, noting half-waves and critical load 07 p1262 A67-19345

Free vibration analysis for ring and stringer stiffened cylindrical shell, using Rayleigh-Ritz technique [AIAA PAPER 67-71] 07 p1262 A67-19434

Compression process for hollow cylindrical blanks using integration method, viewing deformation as sum of sequential stages of small dislocations 07 p1191 A67-19748

Wave interaction between linear viscoelastic medium and thin cylindrical shell imbedded within it solved for uniform harmonic stress input applied to shell 08 p1415 A67-20486

Axissymmetric plane-strain vibrations of thick layered orthotropic shell under internal and external pressures analyzed, using Fourier series for eigenmodes determination 08 p1415 A67-20487

Imperfection sensitivity of eccentrically axial and ring stiffened cylindrical shells under axial compression and hydrostatic pressure 08 p1417 A67-20552

Axially loaded cylindrical structures analyzed for optimum weight construction consistent with cost constraint, emphasizing beryllium-aluminum alloys 08 p1424 A67-21521

Weight savings derived from use of contrasting ring, stringer and wall materials in J-stiffened axially compressed cylinders [AIAA PAPER 66-508] 08 p1424 A67-21522

Thermal buckling of prestressed cylindrical shells and rings where expansion coefficient of external layer is smaller [ONERA-TP-422] 09 p1574 A67-21848

Buckle pattern representation for isotropic cylinder rendering results of critical stress and role of buckle pattern upon ratio of critical stress 09 p1575 A67-22164

Quasi-static theory of cylindrical impedance probe for magnetoplasma extended to include vacuum sheath effects 09 p1549 A67-22451

Flow vortices in hollow cylinder made of type II superconductor 09 p1482 A67-22662

Fibrous model of shell shaped grid noting discrete network, properties of cross section surface and stress 10 p1715 A67-22920

Plastic analysis of cylindrical shell deflections noting support against sliding, shell with clamped edges and with longitudinal force and membrane solution 10 p1715 A67-22922

Frequency equation for harmonic wave propagation in composite circular cylindrical shells established, based on linear three-dimensional theory of elasticity 10 p1717 A67-23127

Stiffness and consistent mass matrices for finite cylindrical shell element with admissible displacement state 10 p1717 A67-23128

Load carrying capacity of plane and reinforced cylindrical shells clamped along edges and subjected to uniformly distributed internal pressure 10 p1720 A67-23600

Dynamic stability of cylindrical shell reinforced by thin walled rigid longitudinal ribs 10 p1721 A67-23604

Nonlinear behavior of elastic structural systems, approximating displacement patterns, stress-strain ratios, post buckling behavior, etc 10 p1726 A67-23717

Structural design of stiffened cylindrical shells, discussing minimum weight, prevention of buckling modes, etc 10 p1726 A67-23719

Glass-fabric reinforced plastic shells fabrication and full scale structural evaluation 10 p1727 A67-23732

Prebuckling deformations, ring stiffeners and load eccentricity effect on buckling of stiffened cylinders 10 p1727 A67-23759

Critical axial compression buckling loads of orthotropic cylinders having stiffening patterns analyzed, considering three instability failure modes 10 p1728 A67-23760

Unified theory for bending and buckling of honeycomb type sandwich shell and linearized governing equations applied to axially compressed circular cylinder shells 10 p1728 A67-23761

Asymptotic solution of typical bay in hydrostatically loaded ring-reinforced noncircular cylinder of finite length 10 p1729 A67-23766

Asymptotic expansion procedure applied to Donnell equations for cylindrical shell, obtaining solution for interaction of infinite cylinder reinforced by radially loaded ring [ASME PAPER 66-WA/APM-27] 10 p1730 A67-23839

Basic equations for shells with circular parallel sections including shells of revolution 10 p1731 A67-23844

Instability of cylindrical shells stiffened with rings and stringers of nonuniform cross sections, noting load and weight savings 11 p1874 A67-24225

Radiating slot on dielectric clad cylinder, solving wave equations and finding field expressions via harmonic series representation 11 p1761 A67-24280

Buckling test data for internal integral ring-stiffened aluminum cylinders under combinations of axisymmetrical axial load and external lateral pressure 11 p1875 A67-24611

Shear modulus magnitude effect on stress concentration at circular hole in cylindrical shell for various ratios of Youngs moduli 11 p1878 A67-24881

Cylindrical shell stability under external pressure, presenting critical load value and nature of undulation 11 p1880 A67-25054

Approximate solution of Novozhilov equilibrium equation for noncircular cylindrical shells by small parameter

method 12 p2019 A67-25562

Closed cylindrical shell stability under combined bending and axial compression taking into account original arbitrary imperfection of shell form 12 p2020 A67-25567

Ribbed circular cylindrical shell under axial compression, reducing problem to determination of deflection and stress functions 12 p2020 A67-25571

Cylindrical shell stability under external radial load noting stress-strain states, critical load, etc 12 p2020 A67-25572

Cylindrical shell stability under nonuniform load, noting critical load dependence on subtending angle 12 p2020 A67-25573

Approximate solutions for boundary value problems of cylindrical shells of arbitrary geometry 12 p2021 A67-25576

Stressed and strained state of orthotropic cylindrical shell weakened by circular hole 12 p2021 A67-25578

Oscillations and stability of cylindrical shell in conducting gas flow in presence of magnetic field 12 p2021 A67-25581

Partial differential equations applied to calculation of extended cylindrical shells under arbitrary curvilinear and rectilinear edge loading 12 p2022 A67-25582

Stress-strain state of cylindrical shell analyzed based on elasticity theory, noting boundary value problem 12 p2022 A67-25583

Approximate theory for stress-strain state of thin cylindrical shell reinforced with elastic ribs having bending rigidity 12 p2022 A67-25584

Stochastic thermoelastic time varying boundary effect in circular cylindrical shell 12 p2022 A67-25587

Elastic filler effect on thin cylindrical sandwich shell stability subjected to compression along generatrix 12 p2023 A67-25592

Thermoplasticity problem for circular cylindrical shell subjected to arbitrary axisymmetric heating and loading 12 p2023 A67-25593

Oscillations of cylindrical shell containing compressible gas perturbed by heat induced shock wave 12 p2023 A67-25595

Natural magnetoelastic oscillations of circular cylindrical conducting shell 12 p2023 A67-25596

Stress-strain state of thin cylindrical shell under effect of local forces 12 p2024 A67-25601

Approximate solution of equilibrium problem for shallow cylindrical shell of rational profile under pressure distribution from convex side 12 p2024 A67-25603

Free oscillations of closed freely supported cylindrical shell of concentrated mass, determining frequency and bending moments 12 p2025 A67-25604

Heat equation of thin closed cylindrical shell exact solution analyzed using least squares method 12 p2024 A67-25606

Displacements, stresses and moments in orthotropic and bimetallic cylindrical shells under radial concentrated forces determined via computer method 12 p2025 A67-25608

Longitudinal impact of two reinforced cylindrical shells coupled to each other at ribs against solid body 12 p2025 A67-25611

Stability of cylindrical shell of oval cross section compressed along generatrix and under external pressure analyzed, using Laplace transforms 12 p2025 A67-25612

Critical stresses of compressed three-layer cylindrical shell of asymmetrical structure in presence of variable temperature 12 p2026 A67-25614

Axisymmetrical deformation and static instability region of circular cylindrical shell under longitudinal compressive load 12 p2026 A67-25615

Rigid plastic cylindrical shell axisymmetrical deformations in terms of Tresca yield condition and gradient law when under load 12 p2026 A67-25618

Initial imperfection effects on free oscillation frequencies of cylindrical shell under static axial load 12 p2026 A67-25619

Reinforced cylindrical shell stability under external pressure, considering irregular frame disposition effect 12 p2027 A67-25620

Equation for relation between critical stresses of cylindrical shell loading and minimum natural-oscillation frequency of unloaded shell 12 p2027 A67-25623

Vlasov engineering theory of equilibrium of shells used to study stress-strain state of closed circular cylindrical shell loaded by internal pressure 12 p2028 A67-25632

Asymptotic integration of elasticity theory equations applied to two-dimensional dynamic theory for cylindrical shells 12 p2029 A67-25636

Buckling of thin walled circular cylindrical shells under external pressure treated by Sanders theory 12 p2030 A67-25940

Axisymmetrical stability loss problem in thin walled cylindrical shell with continuous elastic filler 12 p2031 A67-25958

Lower and upper critical loads measured in process of axial compression of cylindrical shells of glass fiber reinforced resin 12 p2031 A67-25959

Vibration of cylindrical shell containing flowing incompressible perfect fluid 13 p2215 A67-26528

Self-excited vibration of cylindrical shell in coaxial rigid cylindrical duct with gas flowing past 13 p2218 A67-26806

Stress and stability of stringer-reinforced circular cylindrical shell 13 p2218 A67-26892

Boundary value problems involving shallow cylindrical shells of given arbitrary configuration solved, using Vlasov moment theory 14 p2395 A67-27837

Dynamic plastic buckling of thin strips, thin and moderately thick cylindrical shells and rods under longitudinal and radial impact and compression 14 p2397 A67-28088

Stabilizing effects of viscoelastic cores on response of long circular cylindrical shells subjected to time dependent axial loads 14 p2399 A67-28118

Stability of inhomogeneous anisotropic cylindrical shells containing elastic cores under pressure, axial load and torsion 14 p2399 A67-28119

Plastic buckling of eccentrically stiffened circular cylindrical shells 14 p2399 A67-28121

Two-dimensional thermal conductivity problems for hollow cylinder heated at constant rate, estimating axial heat flux effect 14 p2406 A67-28306

Anisotropic circular cylindrical shell stability under linear axial stress and internal pressure 14 p2400 A67-28642

Vlasov variational method applied to circular cylindrical shell design for local loading 14 p2400 A67-28643

Inversely symmetrical edge effect in circular cylindrical shell with distributed stresses and moments 14 p2401 A67-28644

Cylindrical shell stability under circumferential band load effect applied to freely supported edge 14 p2401 A67-28645

Influence coefficients for stresses at circular holes in shallow cylindrical shells with both flat and curved reinforcements [AIAA PAPER 87-365] 14 p2401 A67-28733

Moment stress effect on natural oscillation frequency, deriving motion equations of circular cylindrical shell 14 p2401 A67-28735

Cylindrical shell stability under longitudinal impact, examining buckling processes with high speed motion picture camera 14 p2401 A67-28736

Cylindrical elastic shell under axial compression studied for stability loss, considering large axial strains 14 p2401 A67-28737

Stress-strain state of short cylindrical shell and square panel under axial compression hinged along edges 14 p2402 A67-28897

Tensile creep behavior of thick walled aluminum titanium alloy cylinders under internal pressure at high temperature 14 p2339 A67-29001

Thickness transition configurations for cylindrical pressure vessels with hemispherical heads, noting weight, load effects, etc 15 p2573 A67-29419

First order finite difference numerical analysis of thin elastic orthotropic and inhomogeneous cylindrical shells with small deformations from external forces 15 p2574 A67-29471

Temperature field of hollow cylinder with spatially distributed heat source, examining transient temperature distribution and thermal stresses in cylinder 15 p2574 A67-29775

Exact solution of three-dimensional problem to derive algorithm for development of applied theories of improved accuracy for circular cylindrical

shell 15 p2576 A67-30179

Transversally isotropic cylindrical shell under periodically spaced axisymmetric band loads, comparing expressions derived for stresses and displacements by elasticity and shell theories 15 p2578 A67-30271

Noncircular cylindrical shell of orthotropic material under distributed load numerically analyzed by shell theory 15 p2578 A67-30272

Thermal stresses in three-layer cylindrical sandwich shell of finite length with rigid filler having temperature as function of radius only 16 p2765 A67-31049

Inclusion problems involving tubular shells of isotropic incompressible materials yielding large deformations 16 p2766 A67-31099

Thermoelasticity of thin cylindrical shells for linear temperature distribution and temperature independent elastic constants, deriving differential equations of heat conduction 17 p2958 A67-32034

Filament overwrapped metallic cylindrical pressure vessels show greater efficiency ratio and buckling strength 17 p2958 A67-32054

Moire topography techniques for partial slope and macroscopic curvature measurements of cylindrical and conical shells due to loading 17 p2960 A67-32455

Stiffener eccentricity effect on critical load in cylindrical shells under axial compression 17 p2961 A67-32775

Axisymmetric plastic buckling of axially compressed cylindrical shells initiated under increasing load 17 p2961 A67-32776

Axially symmetric wave propagation in infinitely long two-layered cylinder, detailing displacement and stress distribution 17 p2961 A67-32778

Generalized power series method applied to compressed cylindrical shells stability analysis, giving formulas for direct shell designing 17 p2961 A67-32808

Axisymmetrical temperature fields for minimum functional of elastic deformation energy in infinite cylindrical shell 17 p2962 A67-32968

Orthotropic circular cylindrical shell of elastic material instability under combined torsion and hydrostatic pressure investigated for simply supported and clamped ends 17 p2963 A67-33016

Shell theory applied to anisotropy problem in axisymmetric cylindrical shells, illustrating shear deformation, twisting couple and circumferential displacement [ASME PAPER 87-APM-28] 17 p2965 A67-33155

Monography on plastic axisymmetric collapse of ring stiffened cylindrical shells under external hydrostatic pressure 18 p3140 A67-33432

Dynamic phenomena in two identical cylindrical shells placed side by side in inviscid supersonic flow of compressible fluid 18 p3024 A67-33540

Unsteady temperature field of thin cylindrical shell of finite length determined, using quadratic trinomial form 18 p3145 A67-33570

Stability of cylindrical shells under torsion 18 p3144 A67-34171

Stability of reinforced thin structurally-orthotropic cylindrical shell problem, discussing rib eccentricity, axial compression load, torsional load, etc 19 p3338 A67-34874

Graphic representation of Mises formula for stability analysis of cylindrical shell, discussing critical pressure and time and labor saving 19 p3338 A67-34875

Estimation method for lower bounds of natural frequencies of circular closed cylindrical shell 19 p3338 A67-34876

Free axisymmetric oscillations of reinforced, closed, cylindrical circular shells, discussing natural frequencies and bending oscillations 19 p3338 A67-34877

Forced bending oscillations for three-layer cylindrical shell under pulsed internal pressure 19 p3338 A67-34878

Parametric expansions in linear theory of cylindrical shells noting loading and boundary conditions, approximation formation, fiber elongation, etc 19 p3339 A67-35054

Axisymmetrical vibrations of cylindrical shell during HF internal pressure pulsations of gas flow containing uniformly distributed burning fuel droplets 20 p3536 A67-36445

Differential equation for axisymmetric

deformation of thin circular cylindrical shell stiffened by circumferential rings and subjected to lateral and axial pressure 20 p3537 A67-38495

Stress analysis in theory of circular cylindrical shell weakened by doubly periodic system of identical circular holes 20 p3542 A67-37664

Second boundary value problem for differential equation of elastic equilibrium of shallow cylindrical shell 20 p3543 A67-37721

Infinitesimal deflections of positively Gaussian curved surfaces solved by application of p , q / analytic functions after affine transformation 21 p3715 A67-37903

Limiting equilibrium of crosswise reinforced cylindrical shells of waffle type, allowing interaction between vertical and horizontal ribs 21 p3717 A67-37972

Hydrodynamic pressure on elastic cylindrical shell from acoustic shock wave, using higher order asymptotic approximations 21 p3717 A67-37973

Frequency and mode configurations of natural symmetric oscillations of elastically clamped cylindrical shells solved by characteristic equation 21 p3717 A67-37974

Circular cylindrical shell buckling mode and upper critical load under external transverse pressure, considering dynamic edge effect on shell stability 21 p3717 A67-37975

Random thermoelastic stress concentration near edge of circular cylindrical shell determined using axisymmetric formulation 21 p3718 A67-37979

Stress analysis of closed cylindrical shell under concentrated loading at free edge, solving differential equation by expanding functions into Fourier series 21 p3718 A67-37982

Shell of revolution stability under axial compressive loading with changes in curvature due to initial imperfections effects 21 p3719 A67-38053

Pulse magnitude and distribution due to energy release in liquid, on walls of shells submerged in liquid, used to calculate loads 21 p3611 A67-38056

Oscillation and stability of two irregular thin elastic cylindrical shells in potential flow of compressible fluid 21 p3720 A67-38296

Dynamic instability of longitudinal oscillations of cylindrical shell charged with ideal fluid established by approximate reduction of nonlinear equations 21 p3720 A67-38297

Oscillation stability of rotating cylindrical shell filled with ideal incompressible weightless fluid, determining instability region distribution 21 p3721 A67-38302

Cylindrical shell deflection by radial concentrated force, using digital computer for stability analysis 21 p3721 A67-38309

Soviet papers on strength and stability of elements of thin walled structures 21 p3723 A67-38778

Flexible ring reinforcing cylindrical shell under external load strength, considering ring cross-sectional shape change effect on bending moment 21 p3724 A67-38783

Laterally flattened cylindrical shells under internal pressure representing aircraft sections strength analyzed, deriving formulas for stress-strain distribution 21 p3724 A67-38784

Elastic stability of three-layer cylindrical shell filled with corrugated metallic sheets under combined loads, deriving linear equations 21 p3724 A67-38786

Panel flutter analysis of hinged closed circular cylindrical shell in supersonic gas flow, considering axial compression and structural damping 21 p3725 A67-38788

Stress analysis for rib-reinforced cylindrical shell subjected to rapidly varying pressure, calculating deflections and bending moments 21 p3725 A67-38790

Two-layer circular cylindrical shell stability under axial compression with transverse displacements, analyzing axisymmetric deformation of longitudinal strip 21 p3725 A67-38793

Elpatievskii method applied to axisymmetric deformation of two-layer cylindrical shell with helical glass fiber reinforcements, obtaining equations for stressed state 21 p3725 A67-38795

Critical compression stresses in cylindrical

panel with clamped lateral edges and free longitudinal edge 21 p3726 A67-38796

Triple layer cylindrical shells stability beyond elastic limit studied based on plastic deformations, loading principle and shallow shell theory 21 p3727 A67-38838

Supersonic flutter of thin walled circular cylindrical shells under compressive loading, comparing theory and experiment [AIAA PAPER 67-77] 21 p3727 A67-38869

Long cylindrical shell with externally loaded reinforcing ring, solving stress distributions and displacements 21 p3727 A67-38871

Axisymmetric creep in cylindrical shells, noting creep buckling collapse after high temperature compression loading 21 p3727 A67-38872

Thick walled cylindrical shell mobility over wide frequency range, predicting vibration response based on normal mode series convergence solution 21 p3729 A67-39059

Testing machine effect on buckling load of electroformed cylindrical shells under axial compression 22 p3909 A67-39291

Flutter of two cylindrical panels bonded by elastic filler in supersonic gas flow, showing flutter velocity increase with increasing filler elasticity 22 p3910 A67-39455

Circumferential crack in pressurized cylindrical shell analyzed for extensional and bending components of stresses 22 p3911 A67-39678

Cracked cylindrical shell stress-strain state under symmetric load, discussing shell curvature effect and integral equation solution 22 p3911 A67-39684

Elastically filled imperfect closed cylindrical shell stability, showing initial configuration defect effects on critical load relation to filler rigidity 22 p3912 A67-39685

Buckling loads in orthotropic circular cylindrical shells under simultaneous longitudinal and external peripheral pressure stresses 22 p3912 A67-39752

Mode acceleration method for axisymmetric dynamic response due to time dependent loading in spherical and cylindrical shells 22 p3914 A67-40190

Cylindrical thin walled open section structures heated nonuniformly, calculating various elastic parameters, torsion properties and shearing stress 22 p3916 A67-40450

Blade-spar thick walled cylindrical shell deformed under elastoplastic torsion, analyzing stress-strain ratio and torsional strain and displacement 22 p3916 A67-40458

Simplified equations for thin circular cylindrical shells under loading investigated for possible elimination of inconsistencies 23 p4080 A67-41664

Natural frequencies and mode shapes determined for circular cylindrical shell closed by elastic plate 23 p4080 A67-41750

Long cylindrical two-layer shell critical axisymmetric buckling time for steady creep due to external pressure and axial compression, applying variational principle 24 p4250 A67-42306

Thin elastic shell nonlinear buckling theories, studying circular cylinder and truncated cone cases 24 p4252 A67-43096

CYLINDRICAL TANK

Free surface distortion and subsequent gas ingestion in emptying cylindrical tank, emphasizing maximum height of liquid surface when gas reaches outlet 02 p0233 A67-11945

Axisymmetric sloshing oscillations of liquid in U-tube type connected cylindrical tanks, obtaining velocity, pressure and wave height 03 p0522 A67-13213

Stress distribution due to pressurized exterior crack in infinite isotropic elastic medium with coaxial cylindrical cavity 04 p0717 A67-15799

Exact solution /by Hankel and Laplace transforms/ of unsteady motion of viscous MHD fluid in cylindrical vessel in axisymmetric constant strength magnetic field 05 p0850 A67-16134

Nonlinear lateral sloshing in rigid tanks of various geometries, noting frequency-amplitude response 05 p0790 A67-16135

Diffuser use in low density hypersonic wind tunnel and method of evaluating global performance for diffusers with conical inlet followed by cylindrical mixing section 05 p0748 A67-16763

Damping of liquid oscillations in

cylindrical tanks, determining rigid and flexible baffle loss coefficients, baffle efficiency and maximum bending stress [AIAA PAPER 66-97] 05 p0793 A67-17210

Linear shell theory for nonlinear transverse coupled vibrations of partially filled circular cylindrical elastic tank [AIAA PAPER 67-74] 06 p1101 A67-18272

Dynamic response, sloshing frequencies and stability of free surface of liquid in circular cylindrical elastic tank with flexible bottom [AIAA PAPER 67-76] 06 p0986 A67-18274

Critical volume of cylindrical reactors calculated using n-group diffusion theory 10 p1675 A67-23396

Damping coefficients for rigid and flexible ring baffles for slosh suppression 15 p2470 A67-29438

Liquid sloshing at simulated low gravity in rigid cylindrical tank, noting analytical model and experimental results [ASME PAPER 67-APM-14] 17 p2840 A67-33147

Gas temperature increase effect on thin walled container during prepressurization of high pressure blowdown systems [AIAA PAPER 67-443] 18 p3137 A67-33920

Linear shell theory for nonlinear transverse coupled vibrations of partially filled circular cylindrical elastic tank [AIAA PAPER 67-74] 21 p3727 A67-38866

Dynamic response, sloshing frequencies and stability of free surface of liquid in circular cylindrical elastic tank with flexible bottom [AIAA PAPER 67-76] 21 p3614 A67-38868

Translational excitation mechanical model applied to space vehicle longitudinal excitation, examining sloshing phenomena 22 p3786 A67-40104

Liquid sloshing cylindrical tank with elastic bottom for investigating surface tension effect at liquid gas interface of partly filled container 22 p3787 A67-40179

Forced resonant nonlinear oscillation of liquid in cylindrical tank 22 p3787 A67-40192

CYLINDRICAL WAVE

Scattering of line-source radiation by circular cylinder, noting plane wave approximation 03 p0374 A67-14356

Behavioral equations derived for caustic that envelops locally-plane cylindrical wave incident on plane surface of layered plasma wedge 05 p0765 A67-16962

Dissipative effects in converging cylindrical symmetric shock wave, considering ion and electron heat conductivity, ion viscosity and energy exchange 06 p0984 A67-18029

Cylindrical wave propagation in rarefied plasma in presence of strong noncollision dissipation 07 p1227 A67-19308

D'Alembert initial value problem for cylindrical waves, obtaining linearized potential equation for plane and symmetrically spherical case 09 p1488 A67-21932

Cylindrical wave propagation in rarefied plasma, examining effect of compression on internal plasma-magnetic field by external field 11 p1842 A67-24964

Shock wave propagation in cylindrical tube, comparing theoretical and experimental results concerning light front, pressure and magnetic field 13 p2094 A67-26641

Energy accumulation of spherical and cylindrical shock waves in inhomogeneous gas 15 p2472 A67-29694

Dispersion relations for coupled electromagnetic and longitudinal waves propagating along isotropic inhomogeneous cylindrical hot plasma column 17 p2908 A67-33107

Cylindrical expanding detonation waves in gas mixtures, studying detonability limits, propagation velocity and instability and vibratory phenomena 18 p3153 A67-33822

Plane deformation problem of instantaneous elasticity theory application to expansion of stationary elastic waves in infinite medium with cylindrical cavity 21 p3720 A67-38294

Transient gas motions for various waves, analyzing motion equations and classifying integral curve fields 21 p3565 A67-38556

Oscillations of polytropic and compressible cylinders investigated by small perturbation method noting separate mode of gravitational instability 22 p3896 A67-40526

HF approximation to diffraction of plane wave by conducting strip, using cylindrical wave terms for higher order patterns 23 p3979 A67-40831

CYTIDYLIC ACID

Condensation of cytidylic acid in presence of polyphosphoric acid 13 p2065 A67-27183

CYTOGENESIS

S BIOLOGICAL CELL

CYTOLOGY

Enzymatic activity and inhibition, thermal stability and electrophoretic properties of induced and constitutive acid phosphatases of *Euglena gracilis* 10 p1598 A67-23397

Genetic transcription as affected by ionizing radiation and hydrogen peroxide 11 p1747 A67-24786

Space flight effect on chromosomes of dry seed embryos, noting no significant change 13 p2061 A67-27344

Factors involved in use of thymine by uninfected cells in metabolism of *Escherichia coli* 20 p3370 A67-36799

Indigenous biology in Venus clouds, proposing isopycnic float bladder macroorganism ingesting water and minerals blown up from surface by pinocytosis 22 p3750 A67-39556

RNA fractions base composition and labelling kinetics in presence and absence of actinomycin for rapidly labelled RNA in rabbit bone marrow rich in erythroid cells 23 p3944 A67-40801

Acute and chronic cellular level effects of low energy proton irradiation in rat skin 23 p3957 A67-41644

Prolonged *Chlorella* cultivation with recovery of medium without impairing production rate 24 p4114 A67-41846

CZECHOSLOVAKIA

Electronic equipment reliability improvement methods and practices in Czechoslovakia 14 p2282 A67-28039

Space research activities in Czechoslovakia, discussing satellite observation, aerospace medicine, solar physics, etc 19 p3320 A67-35282

D

D-1 SATELLITE

Testing facility and methods for FR-1 and D-1 satellite control 07 p1163 A67-19530

Diademe satellites design including laser beam range determination reflectors for spatial geodesy, laser telemetry, etc 10 p1712 A67-22860

High stability quartz master oscillator for D-1 satellite transmitter control 21 p3591 A67-38206

Telemetry antenna of instrument container of D-1 satellites 21 p3592 A67-38218

Sensors for acquisition and aiming of solar direction aboard D-2 satellite, discussing operating principles 21 p3629 A67-38666

D LAYER

Ionospheric D-region concentration of neutral NO estimated, based on dissimilarity of sunspot cycle variation 01 p0056 A67-10111

D region equilibrium solution using absorption measurements, considering region as nonsteady plasma under special conditions 01 p0061 A67-11288

Rocket payload with weight of 9 lb for release of sodium and lithium in aurora for study of D-region ion concentration and emission 03 p0413 A67-13375

Seasonal and solar-cyclic variations of nondeviate absorption in ionospheric D region 04 p0617 A67-15570

Sunrise effect on atmospheric radio noise intensity, directional variations and formation of D region 04 p0618 A67-15575

Radio Aurora and formation mechanism of ionospheric D and F regions, examining HF and VLF propagation via computer ray tracing, ionospheric storms and equatorial sporadic E layers 05 p0795 A67-16010

Daytime profile of electron density in C and D layers of ionosphere from measurements of surface ultralong wave fields and atmospheric pressure profile 05 p0801 A67-17131

Recombination coefficient in D region determined by comparing electron density profile with ionization rate 06 p0995 A67-18073

Winter radio absorption anomaly at middle latitudes theory in terms of temperature

and nitric oxide distributions in D region 07 p1171 A67-19415

Rocket measurement of quiet D-region electron number density profiles near sunrise 08 p1379 A67-21488

Corpuscular streams and photodetachment of electrons reaction effect on formation of D layer of ionosphere 09 p1491 A67-21894

Measurements of positive ion composition of mesosphere and ionospheric D layer from rocket experiments 10 p1645 A67-23284

Possible major effect of minor neutral constituents of mesosphere on free electron density in D layer 10 p1645 A67-23285

Ionospheric absorption effects in D and E layers, noting refraction role and effective collision frequency 10 p1646 A67-23270

Rocket observations of lowest ionosphere at sunrise and sunset 12 p1935 A67-25798

Electron production time variations in D layer during solar activity 14 p2378 A67-27909

Additional electron production in lower D layer due to solar radiation penetration 14 p2378 A67-27910

Correlation of measurements of precipitated electrons with ionospheric effects of winter anomaly in midlatitude D layer 14 p2310 A67-28043

Ionospheric D layer structure and formation, considering free electron height variation and collision rate 14 p2311 A67-28406

Collision frequencies in D region and stratospheric-mesospheric relations, noting oxygen as error source and electron-density height profile 14 p2311 A67-28407

Seasonal variations and attenuation of ionospheric absorption, using A3 method 14 p2312 A67-28570

Vertical incidence ionospheric absorption measurements from ground station criteria for recognizing winter anomaly 15 p2476 A67-29623

Equipment used in rocketborne LF propagation experiment to measure electron distribution in D region of ionosphere 15 p2489 A67-30136

Solar flares, analyzing X-ray emission, radio emission and superposition of ionospheric effect 16 p2739 A67-31459

Vertical electron density profile method for determining altitude of lower boundary of ionosphere 17 p2842 A67-32383

Negative oxygen ion reaction rate constants for ion loss processes in ionospheric D region obtained by laboratory measurement 17 p2851 A67-33195

Twilight observations for 80-100 km region, noting orthohelium measurements for solar radiation and dust and alkali-metal concentrations for D-region ionic constitution 18 p3035 A67-33601

Day-and nighttime electron density profiles in ionospheric D layer 19 p3218 A67-35227

Negatively ionized ozone and diatomic oxygen concentration ratio determined from physicochemical processes for 10-60 km range 19 p3219 A67-35249

D-region positive ion density during solar eclipse of May, 1966 observed by cylindrical Langmuir probe onboard rocket 19 p3222 A67-35454

Two-ion D region model for polar cap absorption events 20 p3426 A67-36302

Daytime profile of electron density in C and D layers of ionosphere from measurements of surface ultralong wave fields and atmospheric pressure profile 21 p3619 A67-38474

D-region mobility and constituents abundance spectrometer device based on continuum concepts 22 p3799 A67-39816

Laboratory measurements of ionospheric ion-molecule reaction rates noting unmeasured reactions in D region 23 p3993 A67-40565

Electric field heating of D-region electrons shown to be inadequate to raise temperature above gas temperature [AFCRIL-67-0121] 24 p4146 A67-41808

D-LINE

SA SODIUM D-LINE

Externally adjustable pressure regulation of Fabry-Perot interferometer, using device to measure cesium vapor spectral absorption in D-1 line 22 p3810 A67-40522

DACRON

S NYLON

DAMAGE

SA IMPACT DAMAGE

SA METEORITIC DAMAGE

SA PROTON DAMAGE

Loaded oil-lubricated steel ball bearings operating in vacuum and air investigated for electric current effect on damage [ASLE PREPRINT 67AM 1C-1] 14 p2325 A67-28783

Sonic boom effect on structural behavior 15 p2573 A67-29401

Fatigue process theory for general broadband random loading, calculating mean damage and survival probability 15 p2576 A67-30094

Cavitation damage in alkali metal pumps, noting damage resistance and material properties for application in space power systems 15 p2494 A67-30151

Silicon surface depth damage determination technique, with confirmation by Sirtl etching, oxidation and epitaxial deposition 18 p3103 A67-34565

Loaded oil-lubricated steel ball bearings operating in vacuum and air investigated for electric current effect on damage [ASLE PREPRINT 67AM 1C-1] 22 p3813 A67-40218

Individual section dampers relation to modal damping of series mass spring in lumped parameter systems 10 p1729 A67-23770

Attitude errors of inertially coupled gravity gradient satellite with solar radiation pressure as dominant disturbance, noting slot problems in stabilized package accommodating damper motion 24 p4241 A67-42904

DAMPER

SA VIBRATION DAMPER

Individual section dampers relation to modal damping of series mass spring in lumped parameter systems 10 p1729 A67-23770

Attitude errors of inertially coupled gravity gradient satellite with solar radiation pressure as dominant disturbance, noting slot problems in stabilized package accommodating damper motion 24 p4241 A67-42904

Attitude errors of inertially coupled gravity gradient satellite with solar radiation pressure as dominant disturbance, noting slot problems in stabilized package accommodating damper motion 24 p4241 A67-42904

DAMPING

SA DOPING

SA ELASTIC DAMPING

SA HYSTERESIS

SA JET DAMPING

SA LANDAU DAMPING

SA TRANSIENT OSCILLATION

SA VIBRATION DAMPING

SA VISCOELASTIC DAMPING

SA VISCOUS DAMPING

Damping linear system with aftereffect 02 p0225 A67-11962

Eddy current damping effect on motion equation of magnetization vector in thin ferromagnetic film switching by coherent rotation 05 p0860 A67-16070

Imperfect excitation effect on vibration test results such as admittance, phase curve, damping coefficient, etc 05 p0920 A67-16769

Thermal diffusion separation of damping fluids in floated gyroscopes 07 p1168 A67-19381

Collisionless damping of magnetospheric MHD waves 07 p1172 A67-19541

General mechanization in vehicular coordinates of gimballess inertial system for space navigation, obtaining equations for position errors and error damping method 08 p1351 A67-20698

Landau type damping of plasma oscillations and Bernstein mode electrostatic propagation perpendicular to weak magnetic field 08 p1360 A67-21129

Collisionless damping in hot plasma due to electron reflection at wall and phase mixing associated with thermal perturbation 09 p1549 A67-22552

Annealing effect on damping rods for magnetic field stabilized satellites 12 p2011 A67-25212

Damping coefficients for rigid and flexible ring baffles for slosh suppression 15 p2470 A67-29438

Active damping concept for gravity gradient satellite attitude control to reduce oscillation time constant, initial capture time and oscillation magnitude 17 p2954 A67-32073

Response of one degree of freedom system with power law time dependent damping and restoring forces using WKB approximation 17 p2958 A67-32128

Damping linear system with aftereffect 17 p2831 A67-33279

Satellite stabilization in geomagnetic field by applying magnet to satellite axis and using damping elements of soft magnetic materials 21 p3713 A67-38375

Tungsten strain amplitude dependent dislocation damping measured as temperature function, discussing inconsistency with Friedel thermally activated breakaway theory 22 p3819 A67-39352

Quantum damping theory formulated in coherent state representation, giving Green function solution to damped harmonic oscillator Fokker-Planck equation, noting density operator 22 p3817 A67-40486

DAMPING IN YAW

Damping in yaw on jet-flap blowing model measured by decaying oscillation technique 06 p0979 A67-17919

DAMPING TESTING MACHINE

Vertical vee gyro damping system for gravity gradient satellite, considering scaling, inertia, time and torque factors and viscosity change effects 12 p1920 A67-25122

DARK ADAPTION**SA NIGHT VISION**

Effects of irritation of vestibular apparatus on adaptability of human eye to darkness, studying rate of recovery of sharpness of vision 16 p2614 A67-30918

DARK PLASMA**S IONIC WAVE****DASSAULT MYSTERE XX AIRCRAFT**

Twin jet business aircraft Mystere XX /fan jet Falcon/ structural material, propulsion data and circuits 05 p0752 A67-17268

DATA**S ANALOG DATA****S BINARY DATA****S DIGITAL DATA****S INFORMATION****S RADAR DATA****S SAMPLED DATA****S VIDEO DATA****S WORLD DATA CENTER****DATA ACQUISITION****SA SATELLITE TRACKING AND DATA ACQUISITION NETWORK**

NASA program involving orbiting satellite studies of natural and cultural resources 01 p0168 A67-10326

Data acquisition techniques and system accuracies for static testing of solid propellant rocket engines 01 p0051 A67-11109

Digital data processing consideration in acquisition-reduction system engineering with reference to solid rocket engine testing 01 p0030 A67-11110

Packaging, manufacturing and design techniques used in total-system-in-box concept for integrated circuits 01 p0039 A67-11116

Multiple input data acquisition system /MIDAS/ centralized computer controlled data system 01 p0031 A67-11119

Auroral spectrograph data, 1959 02 p0238 A67-12036

Evolution of Tiros meteorological satellite operational system noting orbital inclination, solar illumination, data storage ground stations, etc 02 p0334 A67-12371

Worldwide meteorological data acquisition capability proposal for improving upper air observations, noting satellite system role 02 p0231 A67-12383

Integrated air-ground problem of flight data acquisition 03 p0374 A67-13379

Centrifugal machines generating creep-design data by spinning specimens at identical temperature 03 p0395 A67-13542

Stability experiments on partially grooved gas journal bearing, comparing data with previous theoretical analysis [ASME PAPER 66-LUB-6]

03 p0432 A67-13764

NASA FM telemetry system for data acquisition and processing from Ariel satellites including methods for storage, transmission, handling, etc 04 p0568 A67-14437

Data acquisition system for Blue Streak flight trials noting telemetry and radar and relation to trajectory, autopilot, structure, etc 04 p0568 A67-14438

Laser guidance system for rendezvous and docking providing data acquisition for guidance computer 04 p0655 A67-15663

Control data acquisition during takeoff and landing of VTOL type vehicles 05 p0841 A67-16535

Sample acquisition from planetary surface by unmanned probes in life detection experiments [AAS PAPER 66-70] 07 p1189 A67-19999

Automatic real time data acquisition and processing for ATS communications experiments 08 p1298 A67-20669

Pulsed ruby laser rangefinder with high maximum repetition frequency and digital range readout for data acquisition for

determining airborne target trajectories 09 p1465 A67-22622

Integral fuel tank maintenance, summarizing tank-sealant repair data 09 p1442 A67-22678

Launch vehicle preparation and firing, discussing instrumentation, missile safety and range operations 10 p1622 A67-23001

Atmospheric density scale height and variation law at different heights obtained from San Marco satellite data 10 p1712 A67-23212

High resolution density data from radar observations of low altitude polar orbiting satellites reveal longitudinal and geomagnetic variation, noting regression analysis 10 p1640 A67-23216

Compiled data for Mars apparition in 1967 giving general visibility conditions, phases, seasons and positions of Mars and earth 10 p1710 A67-23562

Constant Reynolds number applied to data evaluation for turbulent jet flow in converging-diverging axisymmetric tube using free turbulent jet 11 p1742 A67-24272

Cosmic ray measurements in interplanetary space and on moon noting intensity increase 12 p1992 A67-25123

Field testing of self-powered recorder for vibration data in environmental studies 12 p1942 A67-25682

Portable self-powered magnetic tape recorder for gathering data on vibration, temperature and shock on ground and in-flight aircraft 12 p1942 A67-25688

Instrumentation and data acquisition system used in Saturn V dynamic test program for design of flight control system 12 p1923 A67-25709

Satellite size via experiment design, demonstrating advantages and drawbacks of small and large satellites 12 p2007 A67-25784

Nanosecond fluorimeter for measuring emission kinetics of chromophores 12 p1946 A67-25981

Book on engineering properties of ceramic materials covering high melting materials, physical, thermal and mechanical properties, thermal stress, oxidation, corrosion resistance, etc 12 p1960 A67-26201

Satellite radiation data application to synoptic weather analysis including cloud pattern mapping, tropospheric relative humidity and vertical cloud structure inference 13 p2149 A67-26274

Rectangular guide receiver passband, estimating boundary effect, noting data characterizing interrelation of arrayed transmitters 13 p2069 A67-27032

Lunar scientific exploration requirements in post-Apollo period, discussing lunar and earth geophysics 13 p2199 A67-27212

Book on tungsten and its compounds, physical, chemical and metallurgical data 14 p2336 A67-27890

Design concepts for stored program data acquisition system in spacecraft applications 14 p2275 A67-28690

Test methods to determine wear coefficients and design calculations for solid film lubricants, covering wide temperature range [ASLE PREPRINT 67AM 5A-5] 14 p2325 A67-28787

Noncontacting device for compressor-blade vibration measurement supplying data on all blades of one stage 15 p2545 A67-29165

Flight recorder system designed to satisfy present and future mandatory requirements in accident recording and to provide economic solution to limited maintenance recording 15 p2487 A67-29510

Global ocean data acquisition by remote sensor operating from spacecraft for oceanographic studies 15 p2477 A67-29698

Evolution of Tiros meteorological satellite operational system noting orbital inclination, solar illumination, data storage ground stations, etc 15 p2565 A67-29761

Data acquisition, processing and display in computer based ATC system using radar with automatic position-reporting data link 15 p2515 A67-29941

Environmental prediction using orbital sensors [AAS PAPER 67-104] 15 p2478 A67-29959

Onboard data systems selection and design and relation to ground networks [AAS PAPER 67-54] 15 p2440 A67-30118

Future radar developments noting range instrumentation deployment and

employment, tracking, data acquisition radar sensors, changing cost patterns, etc [AIAA PAPER 67-55] 15 p2438 A67-30119

Physiological diagnostic information collection in prolonged space flight and data handling transmission systems 16 p2617 A67-30763

Book on microelectronics in U.S. covering semiconductor and thin film integrated circuits, hybrid circuits, fabrication, applications, etc 16 p2637 A67-31255

Radio telemetry system for aerodynamic data acquisition from free-flight models in supersonic wind tunnels 16 p2675 A67-31259

Pilot describing function measurements in multiloop control task to provide data for multiloop pilot model refinement 17 p2808 A67-33177

Sine wave tracking, studying operator manual control performance 17 p2808 A67-33179

Data and orbit analysis supporting Navy satellite Doppler system Tranet, discussing editing and archiving of Doppler data and orbital ephemerides generation 18 p3003 A67-34245

Apollo lunar landing mission noting lunar geodetic, cartographic and topographic information deficiencies and correction programs 18 p3132 A67-34329

Incident/accident information exchange system for hazard information flow to safety teams 18 p3163 A67-34692

Empirical formulas for optimal operation of extremal controllers, design data generation and cost index determination 19 p3201 A67-34992

Telecommunication system for lunar, planetary and deep space flight mission control and data acquisition 19 p3207 A67-35224

Mesosphere and lower thermosphere density variations related to solar cycle obtained, using rocket grenades 19 p3219 A67-35231

East germany space research in satellite tracking, coupling processes, upper atmosphere, high energy particles, etc 19 p3321 A67-35294

Highly eccentric orbit satellite /HEOS/ for solar wind, cosmic ray and magnetic field data collection, noting design and mission program 20 p3531 A67-36412

Performance characteristics of XB-70 flight test data acquisition system 20 p3442 A67-36467

Electromagnetic interference and tape recorder jitter control problems in data management system for manned spacecraft 20 p3442 A67-36468

Data acquisition systems for ESRO receiving, recording, display, telecommand and timing sections 20 p3443 A67-36471

Stress corrosion test method determined from test program on precipitation hardening semiaustenitic steels 20 p3465 A67-36486

S-band telemetry data during spacecraft launch phases, discussing mission support problems 20 p3380 A67-36561

Radar designation by computer and real time reentry tracking for future Apollo manned space flight 20 p3381 A67-36592

Optical data acquisition by NASA for National Geodetic Satellite Program flash photography 20 p3382 A67-36888

Electronic satellite position and motion measurement for satellite geodesy, with rapid data reduction, day-night capability and optical accuracy 20 p3383 A67-36889

Ionosphere information via rocket and satellite measurements covering ion temperatures and concentration, electron content variation, etc 20 p3430 A67-36907

PCM telemetry system for ELD program, discussing data acquisition and processing 20 p3392 A67-37162

Lessons from spacecraft industry experiences in 1960s and trends for 1970s, discussing subsystem performance experience, data acquisition, contracting, reliability, etc [AIAA PAPER 67-639] 20 p3557 A67-37622

Deep Space Network /DSN/ with ground communications network, centralized control and data processing, discussing future data return and control capabilities [AIAA PAPER 67-648] 20 p3387 A67-37628

Image tube properties in astronomical data acquisition, discussing photographic plate failure and various image intensifier

applications 22 p3799 A67-39774
 Gemini booster launch photographic
 recording with 50 cameras collecting
 engineering data and motion pictures of
 prelaunch, launch and
 postlaunch 22 p3807 A67-40372
 Environmental test data acquisition and
 processing, noting pretest requirements and
 relative merits of analog and digital
 computer methods 22 p3765 A67-40406
 Real time systems and
 applications 23 p3976 A67-41056
 Aircraft flyover noise recording system,
 considering calibration, weather tape
 recording and synchronization system
 equipment 23 p3999 A67-41145

DATA ANALYSIS
 Screen effect on cosmic ray intensity
 measurement by comparing data from
 various rocket and satellite
 soundings 02 p0307 A67-11668
 Ground-Air-Ground /G/A/G/
 communication channels analyzed in air
 traffic control 02 p0263 A67-12125
 Effects of various diets and simulated
 space conditions on human waste and water
 consumption applied to life support system
 development 02 p0188 A67-12339
 Meteorological Rocket Network /MRN/
 probing of stratosphere and lower
 mesosphere and analysis of acquired
 data 02 p0239 A67-12535
 Data on fragmentation of energy in
 nuclear reactions in atmospheric showers
 compared with calculations results for
 predicted energy 02 p0316 A67-12764
 Elimination of certain contradictions in
 data concerning high energy cosmic rays
 explained by means of hypothesis of
 existence of passive S-state of
 baryon 02 p0316 A67-12766
 Test arrangement and statistical data
 analysis for remote sensing of local flow
 instabilities and
 turbulence 03 p0422 A67-13773
 Analytical model developed for using
 creep data at constant stress to predict
 creep behavior under linearly increasing
 stress 03 p0447 A67-13797
 Data interpretation for sun grazing family
 of comets deriving formulas for compressive
 and tensile stress in spherical bodies for
 tidal, rotational and self-gravitating
 fields 03 p0512 A67-13923
 Book of physics and mathematics as
 foundation for application of satellites to
 geodesy including spherical harmonics,
 matrices, orbital geometry, statistical
 implications and data analysis 04 p0611 A67-14466
 Mass and heat transfer data from
 sweptback circular cylinders in Mach 2 wind
 tunnel with Reynolds number
 100,000 04 p0549 A67-15824
 Diurnal and short period h sporadic E
 layer and critical frequency sporadic E layer
 variations analyzed from data obtained at
 Ashkhabad station 05 p0800 A67-17129
 Data from Lunar Orbiter spacecraft used
 to test validity of corrections to lunar
 ephemeris reveals residual patterns
 [JPL-TR-32-1087] 05 p0901 A67-17201
 Reentry trim angle of attack and lift-drag
 ratios from Gemini flights compared to wind
 tunnel data for aerodynamic studies
 [AIAA PAPER 67-166] 06 p0939 A67-18295
 Aerodynamic and structural data on
 supersonic decelerators, determining
 problem areas and voids
 [AIAA PAPER 67-201] 06 p0948 A67-18301
 Superconductivity in germanium telluride,
 noting critical magnetic field
 data 06 p1069 A67-18981
 Optical and radio orbit tracking facilities,
 analyzing data accuracy levels, minitrack
 functions, etc 09 p1464 A67-22055
 Semiannual variations of magnetic
 activity 10 p1630 A67-22796
 Soviet book on practical utilization of
 observational data from meteorological
 satellites covering radiation and cloud cover,
 emphasizing weather forming systems
 analysis, aerological and synoptical data
 comparisons, etc 10 p1676 A67-23017
 Planetary mapping mission system
 requirements for photography, IR and radar
 imagery, radar reflectivity and spectroscopy
 with data analysis 11 p1859 A67-24438
 Solar flare data computerized, reducing
 reported values of importance and area to

standard scales, considering universal time
 and day 11 p1856 A67-24497
 Structural and mechanical properties of
 lunar maria surface material derived from
 satellite and earth-based
 data 11 p1864 A67-24557
 Test conditions effects on glass fiber
 strength data 11 p1811 A67-24587
 Cosmic ray intensities under sea water
 and under rock 11 p1857 A67-24617
 Superconductive magnets at Lewis
 Research Center of
 NASA 12 p1978 A67-25105
 Air traffic control systems analyzed by
 simulation techniques 12 p1964 A67-25229
 Mass transfer rates for axisymmetrically
 rotating bodies, using diffusion controlled
 electrode reaction system 12 p2033 A67-25277
 High volume data processing techniques
 applied to Ranger acoustic
 testing 12 p1924 A67-25713
 Saturn IVB flight data evaluation,
 discussing heat transfer effect on fluid
 system as function of gravity
 changes 12 p2034 A67-25721
 Preliminary results of magnetic field
 measurements in vicinity of magnetosphere
 and interplanetary space from Mariner
 IV 12 p2007 A67-25822
 Cosmogony of celestial bodies, discussing
 orbital data, asteroid collisions and existence
 of distant comet cloud 13 p2195 A67-26466
 Systems producing germanide phases
 noting phase diagrams of germanides of s-
 elements, ds-elements, fds-elements and sp-
 elements 13 p2175 A67-26469
 Sea-level pressure specification from 700-
 mb height by applying screening regression
 techniques to 17 years of synoptic
 data 13 p2114 A67-26740
 Computerized weather forecasting based
 on informational and probability
 logic 13 p2152 A67-27275
 Orbit determination of stationary satellites
 through data analysis, noting perturbation
 effect and estimation of Early Bird satellite
 orbit 13 p2208 A67-27522
 Earth-based navigation for two-spacecraft
 missions using analytical techniques for
 POLYDOP tracking data 13 p2155 A67-27526
 Solar activity cycle effect on northern
 hemisphere pressure field solar activity
 cycle effect on Northern Hemisphere
 pressure field 13 p2117 A67-27632
 Reliability of electromechanical relays,
 discussing test equipment, data analysis,
 etc 13 p2085 A67-27698
 Test method used in analysis of statistical
 distribution functions for fatigue strength
 response data of aluminum
 sheet 13 p2221 A67-27738
 Airborne radio telemetry equipment
 transmitting in-flight data to ground station
 for monitoring and analysis, using frequency-
 and time-division
 multiplexing 14 p2261 A67-28038
 Astronomical data regarding longitude
 differences studied, deriving evening
 averages, time parameters, coefficients, etc,
 via Chebyshev
 approximation 14 p2384 A67-28075
 Photographs of sunspots analyzed to
 obtain magnetic field strength
 data 14 p2384 A67-28076
 Astronomical almanac 1967 covering
 chronology, solar and planetary data, time-
 signal transmission, etc 14 p2385 A67-28146
 Captured air bubble /CAB/ vehicle
 [AIAA PAPER 67-348] 14 p2246 A67-28730
 Information on early history of solar
 system material obtained for neutron
 buildup processes of heavy element
 synthesis in stars 15 p2519 A67-29156
 Analysis of management methods
 applicable to aerospace industry, considering
 introduction of integrated information
 systems 15 p2583 A67-29669
 Jupiter observations /1965-1966/, noting
 activity of NEB and long duration spots in
 NTB 15 p2558 A67-30025
 Data analysis from oblique incidence
 soundings during spread-F conditions
 [AGARDOGRAPH 95] 15 p2481 A67-30280
 Data reduction with maintenance recording
 system onboard BAC 111 aircraft, noting use
 of automatic mode initiation logic, data
 compression, etc 15 p2420 A67-30348
 [AIAA PAPER 67-377] 15 p2420 A67-30348
 Hydraulic research data concerning control
 valve sizing and arrangement, noting liquid
 and gas control-valve formulas with

limitations, Reynolds number effect,
 etc 15 p2423 A67-30400
 Reliability assessment on incomplete and
 inaccurate field removal data, using
 reliability scoreboard 15 p2496 A67-30419
 Structure and composition of Jupiter
 atmosphere, noting laboratory and
 observational data supporting hypothesis of
 consistency with solar elements
 abundance 16 p2746 A67-30932
 Screen effect on cosmic ray intensity
 measurement by comparing data from
 various rocket and satellite
 soundings 16 p2738 A67-31083
 Sensitivity tests required to verify
 nonnormality in sample population, studied
 by computer simulation
 techniques 16 p2634 A67-31525
 Rotor blade compressibility effects on
 helicopter performance, describing flight
 test techniques and data analyses and
 comparing prediction and test results
 [AHS PAPER 103] 16 p2595 A67-31820
 Atmospheric noise data for various
 frequencies and various latitudes and
 longitudes 16 p2632 A67-31861
 Reentry trim angle of attack and lift-drag
 ratios from Gemini flights compared to wind
 tunnel data for aerodynamic studies
 [AIAA PAPER 67-166] 17 p2789 A67-32061
 Statistically designed experiments in wind
 tunnel test programs dealing with exhaust
 nozzles, discussing data analysis techniques
 [AIAA PAPER 66-742] 17 p2834 A67-32571
 Computerized method for on-line data
 analysis, elucidating SLIP language, request,
 processing, interpretation, time sharing,
 background activity, etc 17 p2821 A67-32865
 Mesospheric wind components via rocket
 measurements of Northern and Southern
 Hemispheres, noting semiannual wind
 fluctuation near equator 18 p3030 A67-33552
 Predicting effects produced by
 environmental interactions with various
 components 18 p3005 A67-34650
 Air Force programs for development of
 effectiveness and reliability data analysis
 systems 18 p3007 A67-34658
 Navy method for integrating all reliability
 data by Integrated Data Plan, discussing
 Interagency Data Exchange and Failure Rate
 Data programs 18 p3007 A67-34660
 Process control program including failure
 mode and effects analysis, critical
 characteristics determination, safety features
 and test equipment
 complexity 18 p3058 A67-34673
 Short-haul aircraft operations spectrum,
 discussing intercity, feeder, social services,
 etc 19 p3349 A67-35064
 Rocket optical studies of daylit day-time
 auroras, discussing luminosity-height data of
 emission lines 19 p3214 A67-35168
 Launch operations optimization for mission
 planning through analysis of performance
 data from past programs 20 p3532 A67-36557
 Data analysis and reduction studies for
 calibration of missile tracking systems using
 near earth satellite 20 p3381 A67-36604
 Weightlessness effect on human body
 noting brain hemodynamics, cardiovascular
 system, calcium metabolism, task
 performance, etc 20 p3369 A67-36668
 IGY data from magnetic observatories
 analyzed for luni-solar daily variations of
 geomagnetic field 20 p3525 A67-36869
 Meteorological satellites data
 interpretation and
 application 20 p3430 A67-36900
 Main geomagnetic field data, discussing
 data conversion to computer-readable
 form 20 p3430 A67-36901
 Lunar data covering mass, shape,
 dimensions, earth-moon relations, orbits,
 selenography, etc 20 p3530 A67-37549
 High strength high modulus glass fibers,
 discussing mechanical properties and
 design 21 p3648 A67-37879
 Diurnal and short period h sporadic E
 layer and critical frequency sporadic E layer
 variations analyzed from data obtained at
 Ashkhabad station 21 p3618 A67-38472
 Space vehicle tracking noting significance
 of accuracy and rapidity in determination of
 position, velocity and
 acceleration 21 p3583 A67-38642
 Semiannual wind variation in equatorial
 stratosphere analyzed for origin from rocket
 sounding data 22 p3828 A67-39466
 Solar RF radiation in mm wavelength
 evaluated for information on solar flare

activity 22 p3882 A67-39591
 Low altitude atmospheric turbulence analysis methods 22 p3828 A67-39665
 Geomagnetic perturbation data from high altitude nuclear weapon detonations, deriving theoretical model based upon MHD resonance, noting Alfvén wave behavior 22 p3792 A67-39932
 Data on fragmentation of energy in nuclear reactions in atmospheric showers compared with calculations results for predicted energy 22 p3876 A67-40266
 Elimination of certain contradictions in data concerning high energy cosmic rays explained by means of hypothesis of existence of passive S-state of baryon 22 p3877 A67-40268
 Auroral proton precipitation and hydrogen emissions 23 p3993 A67-40564
 Measured acceleration time histories analyzed for automatic handling of recorded data, discussing advantage of amplitude distribution method 23 p3986 A67-40719
 Lunar probe data interpretation - AAS Conference, Huntington Beach, California, September 1966 23 p4063 A67-40946
 Ranger, Surveyor and Orbiter probe lunar surface photographic data, discussing lunar event distribution, lunar craters and maria distribution 23 p4065 A67-40953
 Satellite and probe data analysis on ionizing component, primary cosmic rays and albedo particle flux intensity near atmospheric outer boundary 23 p4055 A67-41098
 Explorer XXII amplitude recordings, analyzing duration, strength and frequency of ionospheric electron density horizontal gradients 23 p3974 A67-41177
 Reduction and analysis of nonstationary missile flight vibration data, obtaining power spectral density 23 p4007 A67-41385
 Data analysis on electric potential gradient and air-to-earth current density 24 p4181 A67-41792
 Fourier transformation theory for shock and vibration data analysis, discussing programming considerations and computational efficiency [SAE PAPER 670874] 24 p4248 A67-42011
 Equatorial electrojet currents studied from IGY data from South American stations 24 p4148 A67-42065
 Sq currents in American equatorial zone during IGY 24 p4148 A67-42066
 Semiannual variations of magnetic activity 24 p4149 A67-42132
 Earth rotation variation in historical time using day length, eclipses and earth angular velocity 24 p4151 A67-42317
 Paleontological evidence of earth rotation rate 24 p4151 A67-42318
 Adsorption equilibrium data obtained at high pressure for methane and propane on silica gel using radioactive tracer pulsing 24 p4118 A67-42584
 Field strength data correlation with meteorological cyclonic parameters, noting possible prediction of scatter signal losses during frontal disturbances 24 p4124 A67-42823
 Penetrating component of high energy cosmic rays below ground measured for intensity 24 p4221 A67-42876
 Muon properties investigated for mean energy by spark calorimeter at various depths 24 p4222 A67-42879
 Data analysis methods for integrated data processing system for onboard in-flight checkout for launch vehicle evaluation [AIAA PAPER 67-911] 24 p4127 A67-43018

DATA COMPRESSOR
 Pathcount and coding matrices for sequence time encoding and decoding for data compression 01 p0028 A67-10022
 Monitoring events occurring during testing of space vehicle by data compression techniques and time shared computer-controlled checkout system [SAE PAPER 660696] 01 p0049 A67-10593
 Signal-space quantization and bandwidth compression examined, using theory of mappings of signal spaces with Riemann matrices 01 p0027 A67-11239
 Channel noise forces adaptive sampling system to operate at lower bit error probability than equivalent PCM system 02 p0197 A67-12016
 Adaptive technique determination of optimum operations for pure prediction of discrete time series with respect to mean

square error cost function 02 p0207 A67-12138
 Data compression with digital filtering by fan method and step reduction method 04 p0569 A67-14585
 Digital and analog TV transmission from spacecraft compared, noting data compression and development of hybrid system 06 p0964 A67-18415
 Redundancy reduction methods for data compression, noting application to photographs of Tiros, Gemini and Ranger 09 p1470 A67-22676
 Redundancy reduction for conserving bandwidth and/or power in aerospace communication and telemetry 11 p1756 A67-24708
 Adaptive data compression techniques, principles and advantages 11 p1756 A67-24709
 Floating aperture predictor, zero order interpolator and fan interpolator for redundancy removal bandwidth compression 11 p1757 A67-24710
 Picture coding systems and selection of pre- and post-quantizing filters 11 p1791 A67-24711
 Advances in communication systems, Volume 2 12 p1906 A67-25987
 Adaptive data compression systems of predictor-comparator type 12 p1907 A67-25992
 Data compression for analog signal transmission with smaller bandwidth requirement obtained from reduced signal redundancy and simulation of techniques 14 p2275 A67-28683
 Biotelemetry improvements in manned space flights, emphasizing bit rate reduction required for electrocardiogram data transmission to earth 17 p2807 A67-32900
 Logarithmic compression of digitally telemetered data for constant maximum percentage error throughout encoded range 18 p3006 A67-34115
 Prediction-comparison system for data compression, noting nonlinear error feedback and advantage of closed-loop predictor 20 p3412 A67-37497
 Data compression and error control coding in space telemetry analyzed, using performance measures similar to distortion function 21 p3586 A67-38950
 Transmission buffer overflow prevention in telemetry data compressors using adaptive queueing control 21 p3586 A67-38956
 Video digital data compression technique, time-buffered coarse-fine /TBCF/, for redundancy reduction 24 p4123 A67-42806

DATA CONTROL SYSTEM
 Multiple input data acquisition system /MIDAS/ centralized computer controlled data system 01 p0031 A67-11119
 Floating point execution unit of IBM System/360 Model 91, emphasizing design of instruction oriented units to reveal techniques employed to match burst instruction rate of one instruction per cycle 11 p1755 A67-23951
 Sampled data control system analysis, determining gain margin in unsampled loops 13 p2086 A67-26416
 Z-transform and W-transform theory applied to dynamic compensation of linear sampled data control systems for attitude control of large booster 21 p3713 A67-38027
 Stability of nonlinear sampled data control systems, investigating pulse frequency modulation using Liapunov function 22 p3777 A67-39829
 Stability margins for hybrid continuous discrete data control systems, developing open loop transfer function 22 p3778 A67-40157
 Anharmonic method of photogrammetry rectification point by point, deriving positions from minimum control data 24 p4158 A67-42604

DATA CONVERSION
 Qualitative biological data conversion into pseudovariables permitting use of correlation analysis and prediction, considering occupation relation to cholesterol 01 p0017 A67-10956
 Conversion of frequency spectrum of pulse-position-modulated signal passing through delay device and amplifier switched by input undelayed signal 07 p1139 A67-19229
 Transformation of spectrum of AM periodic sequence of video pulse by inertial detector 07 p1140 A67-19234
 Transformation of spatial coordinates of

controlled plant into electrical signal 07 p1184 A67-19318
 Digital accelerometer converts data into pulse format without analog-digital conversion, noting bias stability determination by crystal characteristics 17 p2855 A67-32438
 Comparison of lunar limb profiles referred to system of reference points and limb region maps, giving data conversion formulas and map inaccuracies 17 p2949 A67-33124
 Computer conversion of hydrodynamic data into simulated static test of deep-throttling bipropellant rocket engine, considering inert calibration techniques [AIAA PAPER 67-427] 18 p3112 A67-33911
 Effective collection time for collecting cosmic dust in altitude ranges of cosmic and terminal velocities of particles, using rockets 19 p3318 A67-35195
 Main geomagnetic field data, discussing data conversion to computer-readable form 20 p3430 A67-36901
 Fracture-toughness tests described to obtain fracture data for transformation into allowable design stresses 23 p4079 A67-41413

DATA CONVERTER
 Pure fluid binary to decimal converter using wall attachment OR/NOR elements 08 p1282 A67-20466
 Simulation of dynamic performance of pneumatic rebound-nozzle signal converters by analog computer 13 p2056 A67-27240

DATA CORRELATION
 Mechanical property correlation between high performance composites and cast epoxy resin data 08 p1344 A67-20423
 Film cooling data correlation using boundary layer model 08 p1427 A67-20930
 Data correlation on nonadiabatic behavior of individual charged particles in magnetic fields 08 p1362 A67-21150
 Spectrophotometric data correlations between color and red shifts of quasars 08 p1398 A67-21231
 Nucleate boiling heat transfer correlations graphically estimated for design purposes to compute heat flux and wall superheat 17 p2966 A67-32033
 Associative processors and application to automatic radar tracking and correlation, using digital computer 17 p2813 A67-32471
 Turbulent heat-transfer coefficients and eddy diffusivity profiles for momentum and heat in Newtonian and non-Newtonian fluids, giving equation for data correlation 19 p3344 A67-34869
 Viscoelastic theories evaluated for ability to correlate linear dynamic data with nonlinear viscosity and normal stress data 19 p3210 A67-35614
 Rohsenow nucleate pool-boiling data correlation, stressing coefficients dependence on surface preparation and liquid-surface combination [ASME PAPER 67-HT-33] 20 p3547 A67-36723
 Bubble frequency, departure diameter and rise velocity relationship in nucleate boiling 20 p3553 A67-36934
 Correlation method for local and average friction coefficients of laminar and turbulent gas flow through smooth tubes 20 p3422 A67-36941
 Correlating lunar eclipse brightness, solar activity and corona ellipticity data 20 p3528 A67-37462
 Correlation of airsickness in early flight training with subjective anxiety 21 p3575 A67-38086
 Alkali plasma Hall accelerator /ALPHA/ thruster performance, discussing acceleration mechanisms and correlating data [AIAA PAPER 67-687] 21 p3692 A67-38718

DATA HANDLING SYSTEM
 Computer-controlled data system with remote checkout capability for airborne electronic system evaluation 01 p0030 A67-11030
 Lunar orbiter command and telemetry data handling system at deep space stations 02 p0194 A67-11808
 Test information systems improved by coupling data sources to users through remote terminals connected directly to large time sharing computing systems 02 p0207 A67-12001
 Silicon integrated circuit data encoder for Isis A satellite particle counting experiment, noting design and construction 05 p0770 A67-16292
 Mariner IV Space Data Automation System

/SDAS/ computer reliability design, pellet component concept, testing, interconnection and welding techniques 05 p0777 A67-17254

Mechanized data system for quality and reliability control, noting performance characteristics and computer program 05 p0814 A67-17264

Numerical handling of data in statistical study of servomechanism, noting circuitry and random function generator 06 p0966 A67-17586

Laser displays application, performance and status of existing devices 06 p1001 A67-17887

Data handling systems, describing apparatus for processing of analog time varying signals in computer 09 p1501 A67-22466

Learning machines used for classifying measurement data of objects representable as points in n-dimensional space after training by forced learning 10 p1654 A67-22757

Meteorological data classification system using computer based level logical-tree method 10 p1676 A67-22820

Range instrumentation ships as major range subsystems, noting equipment used, accuracy and sources of errors 10 p1622 A67-22999

IBM System/360 Model 91 machine organization alleviating disparity between storage time and circuit speed 11 p1755 A67-23949

High speed floating-point algorithm of IBM System/360 Model 91 for exploiting multiple execution units 11 p1755 A67-23950

Floating point execution unit of IBM System/360 Model 91, emphasizing design of instruction oriented units to reveal techniques employed to match burst instruction rate of one instruction per cycle 11 p1755 A67-23951

Electrochemical machining data handling, discussing standards of surface integrity, process data, application steps and records [ASTME PAPER WES-7-10] 11 p1798 A67-24255

Versatile digital data handling system designed to accept and control output of space radiation scintillation spectrometer 12 p1909 A67-25864

General purpose digital computer for airborne and spaceborne guidance and navigation systems 14 p2275 A67-28684

Data handling system for 8-bit phase-coherent biorthogonal coded PCM telemetry 14 p2272 A67-28696

High data rate storage for Nimbus B satellite noting signal processing, checkout and retrieval operations 14 p2276 A67-28918

Visual analysis console for automatic information handling systems providing rapid data display and operator communications with high speed digital computers 15 p2488 A67-29737

Onboard data management systems for manned space laboratory performing experiments, development tests and quasi-operational data gathering 16 p2633 A67-30669

Computer memory systems for handling Air Force information, discussing types of memory, storage techniques and device technologies 17 p2819 A67-32473

Electronic systems in Ariel III satellite detailing power distribution, storage control, telecommand, telemetry and data handling 17 p2827 A67-32822

Operational system for handling and processing aerospace-system human-factors task data in government/contractor environment 18 p2994 A67-34343

Programming system design for incremental data assimilation in open ended man-computer information systems 19 p3187 A67-35680

Scientific data handling system using passive magnetostrictive multichannel delay line memory 20 p3390 A67-36251

Deep space communication system data rate increase using relay satellite 20 p3380 A67-36542

Data handling and reduction evolution for SNAP-10A from manual methods to completely electronic and computerized flight test telemetry 20 p3482 A67-36957

Nondestructive testing of electronic circuits with fiber optic scintillators, vidicon data sampling and pattern recognition displays, discussing TV data handling 20 p3449 A67-36982

Contour-volumetric displays for processing and handling data in nuclear experiment 20 p3450 A67-36986

KHz to GHz wide predetector bandwidth receiving system applicable to EMI evaluations of high data rate digital equipment 20 p3406 A67-37656

Ariel III satellite design, development, mechanisms, power supply and data handling systems 22 p3898 A67-39178

TV camera reseau for engineering information on planetary missions and reducing geometric distortion [SMPT E PAPER 102-39] 22 p3808 A67-40377

High level transistor/transistor logic 16-bit memory element function, characteristics and applications 23 p3975 A67-40698

Multiprocessing features of IBM 9020 system, discussing breakdown of information into subprograms with operational priorities 23 p3976 A67-41058

ISA Conference, Chicago, September 1967, Volume 22, Part III, Advances in instrumentation including data handling and computation 23 p4008 A67-41419

Johnson touch display for updating flight data combining visual display and keyboard functions 24 p4152 A67-41780

Multichannel image data handling and processing system using multispectral analysis for remote agricultural sensing and surveying from aerospace platforms 24 p4157 A67-42435

Computer applications in electronic circuits design, discussing optimal man/computer interface and data handling processes 24 p4126 A67-42477

Data handling capabilities of periodic time function for given bandwidth using Fourier series in sinusoidal spectrum analysis 24 p4124 A67-42931

AIDS data processing and analysis system for automated fault diagnosis and equipment trend prediction, describing methods applied to aircraft [AIAA PAPER 67-792] 24 p4126 A67-42953

NASA National Space Science Data Center operation [AIAA PAPER 67-946] 24 p4260 A67-43032

Onboard computer-based checkout simulator system to assist astronauts in monitoring data requirements of future space programs [AIAA PAPER 67-951] 24 p4127 A67-43035

DATA LINK

All-weather carrier landing system using precision tracking radar and microelectronic data link aboard carrier 01 p0026 A67-10969

Digital computers connected by data link transmission system for prelaunch space vehicle checkout 01 p0050 A67-11031

Onboard test and decision-making requirements for spacecraft checkout system including computer and software, data link detail and test set detail 03 p0400 A67-14215

Microwave data link system development for deep space communication 04 p0568 A67-14499

Short wave radio links, discussing frequency converters, spectrum oscillators, transmitters, etc 07 p1150 A67-19343

Computer generation of DB Margin Summaries for telecommunications links 08 p1292 A67-20653

Flight trial determination of range and reliability of LF ground-to-air data link for air traffic control 09 p1529 A67-22642

Data acquisition, processing and display in computer based ATC system using radar with automatic position-reporting data link 15 p2515 A67-29941

Telecommunication equipment reliability and maintenance costs reduction to increase availability, noting corrective method by transistorization 18 p3002 A67-34229

Control display linkages tested with human subjects for response time 18 p2993 A67-34338

Microwave amplifier using varactor diode with coaxial signal, lumped element idler and waveguide pump circuit for broadband radio link at 20 db 20 p3401 A67-37357

Direct and relay links capabilities for returning data to earth from Mars lander compared on effective radiated power basis [AIAA PAPER 67-647] 20 p3387 A67-37627

Communication constraint in ATC system modeled with Markov chain, noting data collection and reduction and data link utilization

[AIAA PAPER 67-868] 24 p4124 A67-42991

DATA PROCESSING

SA AUTOMATIC DATA PROCESSING SYSTEM

SA COMPUTER PROGRAM

SA INFORMATION

SA INFORMATION PROCESSING

SA INTERSERVICE DATA EXCHANGE PROGRAM /IDEP/

SA VOICE DATA PROCESSING SYSTEM

Coherent optical systems for processing data collected by sidelooking synthetic-aperture radars 01 p0022 A67-10430

Operational notation characterizing basic optical elements as block diagrams gives results identical to those of Fresnel-Kirchhoff diffraction formula 01 p0028 A67-10433

Fast-acting memory storage advances for data processing application, noting classification of types 01 p0029 A67-10663

ISA National Aerospace Instrumentation Symposium, Philadelphia, May 1966 01 p0072 A67-11108

Digital data processing consideration in acquisition-reduction system engineering with reference to solid rocket engine testing 01 p0030 A67-11110

Rolls-Royce use of computers in engineering, manufacturing and marketing operations 01 p0031 A67-11199

Physiological measurements of Soviet cosmonauts in Voskhod spacecraft, noting human performance characteristics and detection techniques 02 p0185 A67-11546

Integrated circuit eliminating pilot tones in digital data by simultaneously phase modulating binary data and bit-timing signals on carrier 02 p0194 A67-11797

Telemetering - ITC Conference, Los Angeles, October 1966, Volume 2 02 p0195 A67-11996

Data abbreviation application to actual range telemetry data recorded on magnetic tape, noting redundancy removal, processing time reduction, etc 02 p0197 A67-12017

Pattern recognition preprocessing by similarity functionals, examining relationship between measurement, selection and feature definition 02 p0207 A67-12137

Problem solving under sequential and batch display conditions, noting effects of data density 02 p0186 A67-12231

Data processing activities and ancillary equipment used in advanced techniques of computer generated graphics for weather observing and forecasting system [AIAA PAPER 66-854] 03 p0376 A67-14128

NASA FM telemetry system for data acquisition and processing from Ariel satellites including methods for storage, transmission, handling, etc 04 p0568 A67-14437

Weather information interpretation and utilization for air traffic control 04 p0650 A67-14688

Statistically optimum optical data processing with automatic focus estimation 04 p0578 A67-14875

Low pressure environmental chamber for estimation of gas exchange ratio during exposure of animals under controlled conditions [ASME PAPER 66-WA/HT-52] 04 p0599 A67-15438

Aircraft piston engine components reliability characteristics determined from defect data survey, using statistics 04 p0691 A67-15902

Meteor train drift observation, describing apparatus and data processing used by Kharkov Polytechnic Institute 05 p0889 A67-16208

Data display for Real Time Telemetry Data System /RTTDS/ 05 p0765 A67-17042

Automatic three-dimensional model measuring machine using data programming for aircraft contour measurement 05 p0811 A67-17047

Statistical problems in use of EM data for remote sensing of geological attributes of lithosphere-atmosphere interface 05 p0803 A67-17387

Data processing and control by spaceborne computer on instrumentation satellite used for analyzing space scientific properties, noting factors influencing system design 05 p0768 A67-17516

Haystack antenna used for satellite communications and celestial observation, noting digital computer for control system

- and data processing 05 p0790 A67-17517
Image orthicon TV system and application to auroral observations, noting data acquisition mechanism 06 p0993 A67-17563
Data processing centers integration through ground and satellite telecommunications networks for global information network [AIAA PAPER 66-331] 06 p0961 A67-17700
Pacific equilibrium longitude for stationary satellite, discussing processing of Syncom III data, drift rate calculations, etc [AIAA PAPER 67-91] 06 p1086 A67-18338
SRT Daylight Display System for ATC in which radar video signals are passed through data processor 07 p1221 A67-19543
Filmed data and computers - Seminar, Photo-Optical Instrumentation Engineers Society, Boston, June 1966 07 p1148 A67-19741
Integrated film reading and display system, discussing characteristics of waveform display/ analyzer subsystems and scanning/recording requirements 07 p1148 A67-19742
Holloman data center for reduction of ABRES test data noting film reading equipment, data analysis and data reduction report 07 p1148 A67-19743
Image scanning systems applied to filmed data processing 07 p1148 A67-19745
NORAD installation in Cheyenne Mountain, Colorado, describing data processing equipment and performance 07 p1148 A67-19840
Communication parameters associated with Marlian flyby probes and with lander and manned vehicles 07 p1145 A67-19870
Quantile system of data compression for space telemetry, discussing operation, efficiency and advantages [JPL-TR-32-772] 07 p1145 A67-19873
Queueing model of many-instrument visual sampling 07 p1136 A67-20172
IBM System/4 PI Model EP data processor design and performance 08 p1297 A67-20626
Airborne environment, compatibility and memory for airborne software 08 p1297 A67-20631
Lunar AIMP photographic data processing system which transforms photographic scans of moon into rectified lunar pictures, particularly ground processor system 08 p1330 A67-20661
Automatic real time data acquisition and processing for ATS communications experiments 08 p1298 A67-20669
Digital data processing, transfer and display equipment applied to ATC terminal operations, using surveillance radars and radar beacons 08 p1351 A67-20677
Information processing requirements for command systems, using particular form of simulation of system information environment 08 p1299 A67-20686
Internal lunar structure considered from direct measurements and extrapolation of data on constitution of solar system bodies and meteorites 08 p1395 A67-21161
Stress-strain diagrams under dynamic conditions obtained by processing strain gauge data, using analog computer 09 p1492 A67-21560
Radar applications to ATC, pictorial display and role of paper flight strip, present and future 09 p1484 A67-21678
Fluid logic elements for data processing 09 p1467 A67-21759
UK-3 satellite electrical design and ground checkout equipment 09 p1484 A67-21828
Medium flow parameter measurement via stationary sensors for simulated test stages of axial compressor 09 p1438 A67-22456
Strain gauge measurement data on rotating impeller blades of aircraft turbines, discussing errors in determination of stress amplitude 09 p1576 A67-22458
Meteorological data classification system using computer based level logical-tree method 10 p1676 A67-22820
High resolution measurement of air temperatures and temperature differences applied in conjunction with data processing equipment 10 p1654 A67-22821
Free flight hypersonic wind tunnel testing technique noting pneumatic launcher, data acquisition and processing 10 p1622 A67-23390
Computer programming or software techniques in relation to hardware elements of computer graphics system [ASTME PAPER WES-7-02] 11 p1756 A67-24253
Serial comparison technique for coding systems where weight of ascending bit is equal or greater than previous bit 11 p1756 A67-24266
Horizon sensor data processing with compensation for statistical properties of errors, noting application of optimal filtering theory 11 p1817 A67-24336
Elastic-plastic body and elastic work hardening materials under static loading, using maximum principle for computing procedures 11 p1876 A67-24622
High volume data processing techniques applied to Ranger acoustic testing 12 p1924 A67-25713
Telemetry data processing problems noting error sources, probability distribution of counts in counting processes, sensor relay during motion in varying field, etc 12 p1905 A67-25779
Use of onboard data processing for eliminating irrelevant information telemetered from satellite experiment 12 p1909 A67-25780
Parallel data decoding with high transmission rates close to channel capacity for space telemetry systems design 12 p1909 A67-25781
Multiparameter data sorting technique for one-parameter information represented by simple distribution described by appropriate transformation coefficients 12 p1909 A67-25863
Data processing and reduction on board spacecraft and on ground using generalized information system 12 p1909 A67-25865
Legal and political aspects of international meteorological data collection and distribution system, including use of satellites 12 p2044 A67-26153
Control systems functions and programming approaches, Volume B, covering electronic data processing, factory automation and computer center administration 13 p2153 A67-26664
Optimal control theory in design of aerodynamic shapes, flight paths, guidance and control logic, data processing logic, etc 13 p2072 A67-26814
Computer techniques for data problems encountered by task analysts 13 p2063 A67-27260
Computer aided design and reliability engineering /CADRE/ applied to data processing associated with communications equipment components and subassemblies 13 p2072 A67-27446
Cost models for complex space programs, analyzing data acquisition systems, computer routines, etc 13 p2232 A67-27547
Data utilization in Air Defense Command /ADC/ weapon systems management 13 p2233 A67-27560
Algorithm construction for processing of telemetry data in determination of space vehicle trajectories, applying dynamic filtering method 14 p2382 A67-27853
Data processing of signal reception from Soviet satellites indicates radio signals scintillation caused by diffraction of waves from ionospheric nonuniformities 14 p2260 A67-27857
Harmonic and impulse techniques for flight vibration testing to reduce data processing time [ONERA-TP-477] 14 p2395 A67-27899
Diaphragm element for digital logic requirements of data processing equipment, discussing functions and integrated circuit employed 14 p2274 A67-28346
Panoramic photograph processing theory 14 p2318 A67-28372
Surveyor guidance program for midcourse and terminal information, noting redundancy in design, decision making telecommunications, etc 15 p2514 A67-29599
Data acquisition, processing and display in computer based ATC system using radar with automatic position-reporting data link 15 p2515 A67-29941
Digital computer application to direct control of system dynamics and implementation of adaptive/ learning loop 15 p2441 A67-30268
Processing satellite data at Goddard Center noting Tiros IR data, cloud pictures and Imp measurements 16 p2633 A67-30668
Information capacity dependence on number of frequency-divided channels of optical communication system, investigating information loss in channel-separating receiver 16 p2623 A67-30882
Antenna resolution by data processing noting limitations due to noise 16 p2639 A67-31339
Digital onboard checkout system for SST and other commercial/military aircrafts to discover in-flight malfunctions digital onboard checkout system for SST and other commercial/military aircraft to discover in-flight 16 p2596 A67-31493
Physiological measurements of Soviet cosmonauts in Voskhod spacecraft, noting human performance characteristics and detection techniques 16 p2614 A67-31612
Task distribution, overall network, flow diagram and data processing of PERT method controlling development of ELDO-A rocket third stage 16 p2783 A67-31632
Coordination graph and electro-optical data visualization unit for digital computers noting details 16 p2634 A67-31633
DIALOG /computer implemented retrieval system/ capabilities, design, philosophy and performance 17 p2819 A67-32468
Self-optimizing dual input Wiener digital filter by live input data processing derived for zero mean input case, noting applications to hybrid navigation systems 17 p2882 A67-32527
Airborne analyzer and digital recording system to assess, diagnose and predict turbojet engine health on immediate and long term basis [SAE PAPER 670359] 17 p2861 A67-32998
Parametrization of photographs of cloud system by satellite TV cameras, discussing brightness problems via data processing 18 p3073 A67-33561
Radioscopy for testing cast-steel parts, welding seams, etc, noting radiation protection, radioscope video control and information storage 18 p3045 A67-33737
Redundancy reduction techniques and error correction coding of digital communication systems including waveform, pattern recognition, vocoding, etc 18 p3004 A67-34613
Navy method for integrating all reliability data by Integrated Data Plan, discussing Interagency Data Exchange and Failure Rate Data programs 18 p3007 A67-34660
Rapid Availability of Information and Data for Safety /RAIDS/ system as tool of system safety engineering 18 p3007 A67-34703
Nonrecurring phenomena analysis and detection describing optimum criteria recording and data processing facility 19 p3230 A67-35329
Instrument for processing and storing gas pressure data noting digital integrator, core storage unit and printer 19 p3230 A67-35565
Multistage linear dynamic systems with sequentially correlated noise, evaluating filtering, prediction and smoothing procedures 19 p3206 A67-35941
Computer program utilizing graphic data processing system for mask artwork design of hybrid integrated circuits 19 p3188 A67-36061
Static and dynamic electronic memories used in data processing systems 20 p3390 A67-36250
Equivalent circuits derived by mathematical model from experimental data on diffused planar transistor 20 p3396 A67-36378
Data reduction system noting magnetic tape data collection, data transfer, random data analyzer, system analysis with transfer function analysis, etc 20 p3442 A67-36460
Integrated data processing for turbojet and turboprop engines high altitude test facility 20 p3413 A67-36464
Data processing using digital computer, multiplexing and analog-to-digital conversion equipment for flight control and evaluation 20 p3390 A67-36465
Electromagnetic interference and tape recorder jitter control problems in data management system for manned spacecraft 20 p3442 A67-36468
Central data system for solar probe to map particle and radiation fields of solar corona 20 p3391 A67-36597
Meteorological satellites data interpretation and application 20 p3430 A67-36900
COSMOS, Courtaulds system for matrix operations and statistics 20 p3391 A67-36932
Real time performance, ground control

and data processing of Surveyor spacecraft during maneuvers
[AIAA PAPER 67-644] 20 p3419 A67-37625

Deep Space Network /DSN/ with ground communications network, centralized control and data processing, discussing future data return and control capabilities
[AIAA PAPER 67-648] 20 p3387 A67-37628

Pacific equilibrium longitude for stationary satellite, discussing processing of Syncom III data, drift rate calculations, etc
[AIAA PAPER 67-91] 22 p3886 A67-40085

Optimal filtering theory for horizon sensor data processing for orbital navigation, examining statistical characteristics
22 p3834 A67-40196

Environmental test data acquisition and processing, noting pretest requirements and relative merits of analog and digital computer methods
22 p3765 A67-40406

Lunar soil cohesive and disruptive properties from Surveyor I data, discussing micrometeorite impacts, thermal fracturing, metal vapor deposition and atomic adhesion
23 p4064 A67-40949

Operational error analysis program /OEAP/ use with multiprocessor in air traffic control application
23 p3976 A67-41059

Continuously operating transonic wind tunnel at Aerodynamic Research Institute noting design, electronic data processing equipment and tunnel calibration
23 p3987 A67-41312

Algorithm for processing primary motor characteristics of human motions on digital computer
24 p4114 A67-41857

Low gravity slosh simulation parameters and scaling law used to extrapolate data to full scale spacecraft systems
24 p4141 A67-42032

Digital imaging techniques used in sinusoidal frequency response modification with or without computer control and display on operator console
24 p4125 A67-42429

Digital computer restoration of atmospherically degraded images, studying techniques and limitations of former and mechanisms of latter
24 p4157 A67-42436

Digital computer and coherent optical image processing techniques compared, reviewing data transfer schemes and available hardware
24 p4125 A67-42438

Digital computer system for testing complex aerospace subsystems
24 p4126 A67-42932

Data analysis methods for integrated data processing system for onboard in-flight checkout for launch vehicle evaluation
[AIAA PAPER 67-911] 24 p4127 A67-43018

AGM-69A program-management system using CRT display for PERT/Time and Cost Control data translation
[AIAA PAPER 67-920] 24 p4260 A67-43019

Numerical procedure for structural systems analysis, discussing computer application to hydrodynamic, electric, magnetic, thermodynamic, elastostatic and elastodynamic problems
[AIAA PAPER 67-955] 24 p4127 A67-43038

DATA PROCESSOR

Digital communications system evaluator /DICOSE/ using stored program processor coupled with communication channel arrays to provide real time on-line system
02 p0230 A67-12127

DATA CORE, integrated launch area telemetry data system using high speed digital computers and analog or digital display
03 p0375 A67-13382

All-weather satellite navigation system using AN/SRN-9 Doppler data equipment
05 p0839 A67-17389

Dynamic range of data processor /correlator/ associated with synthetic aperture mapping radar system, considering film grain noise
08 p1293 A67-20688

Moving-window detector for binary integration on quantized data, discussing possible application to multiple-range-element radar
12 p1916 A67-26079

Star tracker using camera tube sensors and electronic scanning noting system errors reduction
13 p2154 A67-27491

Military radar intercept calculator, discussing small size, low power supply, high performance and MOS memory
15 p2439 A67-29161

Target location systems functioning in daylight, darkness and under adverse weather conditions
17 p2814 A67-32507

Equipment for processing data giving optimum performances of Doppler radar
17 p2816 A67-32750

High density cryotron array production in associative memory application, using lock-out design feature
18 p3014 A67-34556

Time-sharing system with single central processing unit and several graphic display consoles for single high speed computer among human operators
19 p3188 A67-36060

Digital simulation of clutter rejection MTI radars
20 p3388 A67-37651

DATA READOUT SYSTEM

Graphical method by which small local users of meteorological satellite pictures can identify geographical position of features in image
[AIAA PAPER 66-439] 07 p1184 A67-19373

Pulsed ruby laser rangefinder with high maximum repetition frequency and digital range readout for data acquisition for determining airborne target trajectories
09 p1465 A67-22622

Nondestructively optically read ferroelectric bismuth titanate single crystal memory device
22 p3787 A67-39261

Magnetics - Conference, Washington, D.C., April 1967
22 p3859 A67-39895

Nondestructive readout technique for superconductive memory cells, application and comparison with previous methods
22 p3765 A67-39899

DATA RECORDER

SA WEATHER DATA RECORDER

Circuit of automatic multichannel secondary particle recorder of SKL type for cosmic ray station, using azimuthal muon telescope and neutron supermonitor
17 p2854 A67-32098

Photoelectric recording of Raman spectra excited by ruby laser
19 p3240 A67-35546

DATA RECORDING

Transducers role in problems associated with accurate and precise measurements during static firing tests of solid propellant motors
01 p0073 A67-11111

Multichannel Data Logging System for recording short-term simultaneous analog data from 25 to 100 parallel input channels
01 p0076 A67-11142

Lunar craters, quadrant IV, designation, diameter, position, central peak information, etc
01 p0152 A67-11331

Magnetic recording of various types of monopulse, PPI and MTI radar signals, with application to airborne data acquisition recorder and ground reproducer
02 p0196 A67-12004

Data record and readout systems dependence on precise spot and line scan methods, using diffraction limited spots of laser generated light
04 p0623 A67-15321

80-column punch card prototype for statistical generalization of cloud data from meteorological satellite
04 p0651 A67-15470

Radiation hardened sampled data recording system design, fabrication and testing incorporating parallel write-in, variable rate sampling and tunnel diode memory
04 p0625 A67-15709

Solid state diode matrix display using gallium phosphide light sources to investigate use as data recording device
05 p0771 A67-16313

LF modulation technique used aboard Canadian ionospheric research satellite ISIS-A for tape recording of signals with VLF components
08 p1298 A67-20662

Automatic multichannel system for data recording and processing obtained in studies of ionospheric structural inhomogeneities containing magnetic-tape memory and device for digital computer input
13 p2119 A67-26561

Data reduction with maintenance recording system onboard BAC 111 aircraft, noting use of automatic mode initiation logic, data compression, etc
[AIAA PAPER 67-377] 15 p2420 A67-30348

Multiparameter recording on DC-9 jet aircraft for advancing maintenance techniques, discussing use in engine, fire warning and air conditioning systems performance
[AIAA PAPER 67-378] 15 p2420 A67-30349

Aircraft accident prevention dynamics and data recording role noting repetitive causal factors, limitations and information loss
17 p2796 A67-32218

Nonrecurring phenomena analysis and detection describing optimum criteria

recording and data processing facility
19 p3230 A67-35329

Optimal wave path parameters determined by experimentally recorded pulsed signals processing, using least squares method
21 p3580 A67-38120

High resolution interferometer data from radio source 3C 273 recorded at NASA deep space stations in Australia
21 p3712 A67-39122

Computerized microfilm or magnetic tape production for manned space station maintenance documentation
23 p4071 A67-40593

DATA REDUCTION

Bias and variability errors in analog data reduction equipment
[SAE PAPER 660716] 01 p0028 A67-10605

LEM data reduction system performing real-time telemetry conversion and data processing
01 p0030 A67-11118

Multiprogramming system for computer controlled telemetry data reduction system
02 p0206 A67-11807

Clear air turbulence characteristics in terms of measuring systems and reduction methods
[AIAA PAPER 66-966] 02 p0262 A67-12289

Simultaneous visual tracking data reduction for satellite period
05 p0763 A67-16558

Tensile analog data reduction technique for determination of principal stress differences history at points of two nonhomogeneous photoviscoelastic models
05 p0921 A67-16826

Downrange radar and optical data reduction used for evaluation of ejection velocities of ballistic missile penetration aids at deployment
[AIAA PAPER 66-405] 05 p0902 A67-17209

Spectrum signature data applied to interference analysis, noting data truncation
05 p0781 A67-17538

Error determination for transient heat transfer experiments using least squares method
06 p1024 A67-18389

Holloman data center for reduction of ABRES test data noting film reading equipment, data analysis and data reduction report
07 p1148 A67-19743

Maryland-Minnesota-Mississippi Echo I satellite observation triangle, discussing principles of triangulation method, camera systems and office data reduction techniques
07 p1176 A67-19765

Triangulation by photogrammetric use of geodetic satellites and data reduction methods
07 p1177 A67-19777

Automatic carpet plotting applicability to reduction of wind tunnel data
08 p1278 A67-21530

Measurement accuracy of deflection data for industrial specimens
08 p1333 A67-21534

Comparison of distribution functions from reduced data records for scattering of electromagnetic waves by randomly moving spheres in container
09 p1461 A67-21598

Qualitative vibration data reduction techniques for application to design problems, noting examples involving power spectra and probability-density functions
10 p1680 A67-23315

Solar X-ray emission measurement below 25 angstroms using airborne Bragg spectrometers, with data reduced by computer
11 p1867 A67-24839

Data processing and reduction on board spacecraft and on ground using generalized information system
12 p1909 A67-25865

Stability analysis of minimum variance estimations used to self-calibrate missile tracking instrumentation complex
13 p2120 A67-26815

Automatic radiosonde data processing system providing azimuth and elevation angles, temperature, humidity, etc
13 p2069 A67-27019

Postsampling exponential first order digital filter and application to data reduction for trend analysis and noisy phenomena
14 p2288 A67-28687

Data reduction with maintenance recording system onboard BAC 111 aircraft, noting use of automatic mode initiation logic, data compression, etc
[AIAA PAPER 67-377] 15 p2420 A67-30348

Airborne Astrographic Camera System using meteor orbit theory to observe reentry trajectory discussing data reduction theory and photo-optical instrumentation
16 p2679 A67-31795

Clear air turbulence characteristics in terms of measuring systems and reduction methods
 [AIAA PAPER 66-966] 17 p2880 A67-32581
 Lens arrays use in holograms 17 p2860 A67-32619
 Cosmic radiation anisotropy variation with time and direction described on intensity contour map, noting application for neutron monitors data reduction 17 p2938 A67-33209
 Rates of surface chemical reactions in well-defined flow systems theoretically investigated by data reduction techniques and quantitative predictions 18 p2997 A67-33795
 Maintainability demonstration methods and statistical techniques for test data reduction 18 p3163 A67-34700
 Internal states minimization of sequential machines by developing algorithm 19 p3200 A67-34844
 Data reduction system noting magnetic tape data collection, data transfer, random data analyzer, system analysis with transfer function analysis, etc 20 p3442 A67-36460
 Data analysis and reduction studies for calibration of missile tracking systems using near earth satellite 20 p3381 A67-36604
 IR scanning nondestructive testing program for microwelds to evaluate quality 20 p3454 A67-36666
 Geometric satellite triangulation for position of fourth satellite, with position equations solved by least squares method and applied to geodetic satellites 20 p3429 A67-36890
 Reduction of dynamic data from geodetic satellites noting satellite tracking station position, gravitational potential, gravity coefficients, synchronous satellites, etc 20 p3429 A67-36891
 Data handling and reduction evolution for SNAP-10A from manual methods to completely electronic and computerized flight test telemetry 20 p3482 A67-36957
 Surveyor project composite telemetry processing system including signal processor, ground equipment, computer data program, etc 20 p3393 A67-37458
 Reduction and analysis of nonstationary missile flight vibration data, obtaining power spectral density 23 p4007 A67-41385
 Communication constraint in ATC system modeled with Markov chain, noting data collection and reduction and data link utilization
 [AIAA PAPER 67-868] 24 p4124 A67-42991

DATA RETRIEVAL
SA INFORMATION RETRIEVAL
 MECCA /mechanized catalog/ system designed to produce printed library catalogs and to generate data bank for later machine retrieval 02 p0207 A67-11812
 Ancillary benefits of automated R and D resources allocation system used as aid to management of USAF laboratory include data retrieval and effective management planning
 [ASME PAPER 66-WA/MGT-18] 04 p0740 A67-15336
 Self-contained midcourse guidance system with space velocity meter /SVM/ used in returning probe to earth vicinity for data retrieval and orbit control 08 p1331 A67-21101
 Maximum data recovery from interplanetary reconnaissance probe by returning vehicle to earth vicinity, using space velocity meter as navigation instrument 08 p1332 A67-21102
 NASA applications technology stressing stabilization and pointing systems, data retrieval, etc
 [AAS PAPER 67-77] 15 p2557 A67-29944
 Range instrumentation ships electronic capabilities, operation, electronic systems function, accuracy and future role
 [AAS PAPER 67-52] 15 p2468 A67-30117
 Associative processors and application to automatic radar tracking and correlation, using digital computer 17 p2813 A67-32471
 Environmental technology and extrapolation into future, noting government role 17 p2834 A67-32592
 Flight measurement data retrieval on real time basis from worldwide range stations possible through Range Support Satellite system 20 p3531 A67-36470
 NASA National Space Science Data Center operation
 [AIAA PAPER 67-946] 24 p4260 A67-43032

DATA SMOOTHING

Construction method for rms-optimal digital smoothing devices, noting case of astatic systems 05 p0782 A67-16268
 Exponential smoothing for prediction of reliability growth having advantages of tracking data precisely while retaining in memory only few historical statistics 05 p0811 A67-16828
 Data smoothing, signal processing and exact minimum mean square error procedures 07 p1218 A67-20267
 Optimal smoothing filter and smoothing error covariance matrix equations for discrete linear systems, using orthogonal projection 11 p1770 A67-24422
 Ries Kessel meteoritic crater /Germany/ analyzed by Fourier data smoothing technique, noting impact center, entry direction, etc 11 p1864 A67-24559
 Smoothing experimental values of function based on choice of regularity and repeatability criteria, noting infinite number values, derivatives, spline functions, etc [ONERA-TP-463] 18 p3072 A67-34460
 Regularity of generalized solutions of general nonlinear and nonstationary Navier-Stokes equations, improving differential properties by data smoothness 19 p3209 A67-35445
 Numerical differentiation and smoothing of equally and nonequally spaced experimental data in independent variable 19 p3250 A67-35615
 Position fix and range data techniques for preliminary orbit determination for lunar satellites, using least squares method for data smoothing 22 p3879 A67-39310
 Secularly smoothed data on sunspot frequency minima and maxima 23 p4067 A67-41240

DATA STORAGE
SA MAGNETIC TAPE
SA MEMORY STORAGE UNIT
 Extremely wideband information storage and retrieval systems employing laser or electron beam on silver halide or electron beam on thermoplastic film 01 p0077 A67-11437
 Tape recorder design for spaceborne data storage using isoelectric drive principle of peripherally driving tape packs to obtain high reliability 02 p0242 A67-12018
 Comparative analysis of magnetization modes for magnetic storage of LF signals, using flux-sensitive and inductive reproducing heads in magnetic recorders 07 p1147 A67-19632
 Magnetic recording process in dynamic magnetic storage method with bias magnetization, using Preisach magnetic particle model for case of static transparency in information carrier 07 p1147 A67-19633
 Random access storage of program for airborne digital computer system 08 p1297 A67-20628
 GSFC program in telemetry data archiving, discussing necessity of data accessing capability 09 p1467 A67-21685
 IBM System/360 Model 91 machine organization alleviating disparity between storage time and circuit speed 11 p1755 A67-23949
 IBM System/360 Model 91 storage system design concepts 11 p1755 A67-23952
 Current stretch sensing for removing limitations to usable density of cryotron storage cells of random access memories 11 p1765 A67-24625
 Environmental operations analysis function, discussing data accumulation, storage and retrieval 12 p1921 A67-25678
 Jackquard loom modification for assembling read-only braid transformer memories, describing self-contained model 13 p2123 A67-26803
 Design concepts for stored program data acquisition system in spacecraft applications 14 p2275 A67-28690
 Prefix coding of histograms for minimal storage 14 p2272 A67-28703
 Computer memory systems for handling Air Force information, discussing types of memory, storage techniques and device technologies 17 p2819 A67-32473
 Inversion of symmetrical matrices by computer, noting storage space advantages 17 p2820 A67-32802
 Nonvolatile block-oriented random access memory /BORAM/ combining thin magnetic

films and scanning strain waves 18 p3012 A67-34347
 Centralized parts and materials reliability information center /PRINCE/APIC/, explaining data storage and retrieval 18 p3007 A67-34659
 Rapid Availability of Information and Data for Safety /RAIDS/ system as tool of system safety engineering 18 p3007 A67-34703
 Deflected laser beam use in TV, machining, photo etching, space navigation and data storage 19 p3239 A67-35060
 Instrument for processing and storing gas pressure data noting digital integrator, core storage unit and printer 19 p3230 A67-35565
 Specific storage volume and surface signal density in rotating magnetic data-storage devices investigated for capacity increase 19 p3186 A67-35584
 Time-shared computer system design and application, noting memory, remote terminals, program debugging, etc 19 p3186 A67-35678
 High data rate storage system for Nimbus B tested by simulation 20 p3445 A67-36547
 Analog treatment of digital telemetering signals using a priori information about transmission, noting Q-factor, storage and use of existing emissions 21 p3584 A67-38660
 High sensitivity information storage filter for spectrum analysis 21 p3601 A67-39067
 Information Service, computerized storage and retrieval system for Apollo spacecraft parts, materials and processes 22 p3765 A67-39951
 Apparatus for digital determination and storage of gas pressure variations, showing pressure curve diagram and numerical representation 22 p3804 A67-40328
 Human Error Research and Analysis Program /HERAP/ for man-machine system, investigating pilot error and performance and aircraft accident prevention
 [AIAA PAPER 67-848] 24 p4117 A67-42984

DATA TRANSMISSION
SA COMPUTER
SA PULSE TRANSMISSION SYSTEM
SA REDUNDANCY ENCODING
 Cost effective error control for coded or M-ary signal reception 01 p0023 A67-10485
 IEEE Region III Convention, Atlanta, April 1968 01 p0045 A67-10664
 Coherent echo modulation and detection for binary data transmission, noting power savings, time and frequency diversification and communication stability 01 p0026 A67-10862
 Real time data transmission systems with error detection, block retransmission capabilities and buffer storage unit treated as Markov process 02 p0194 A67-11810
 Apollo launch data telemetry system development from inception through planning and into final hardware implementation 02 p0195 A67-11997
 Optimum telemetry system characteristics for shock, vibration and acoustic measurements and data bandwidth sufficiency 02 p0196 A67-12009
 Vestigial sideband FM modem combined with three-level coding for data transmission at 4800 bauds 02 p0201 A67-12119
 Troposcatter transmission technique called frequency time shift keying, deriving optimum noncoherent receiver configuration and error performance 02 p0202 A67-12123
 Troposcatter test program for evaluating megabit digital transmission system, using wideband frequency shift keyed modem 02 p0202 A67-12126
 Simulcast /simultaneous broadcasting technique/ has higher average signal power than one transmitter alone and low data rate 02 p0202 A67-12128
 PPM-frequency time hopping for multichannel communication system to transmit digital data over tropospheric scatter path 02 p0202 A67-12131
 Error probability of binary receivers for digital transmission over radio channels characterized by specular and selective fading components 02 p0203 A67-12166
 PCM digital picture transmission for monochromatic still and motion pictures and color still pictures 02 p0208 A67-12167
 Quantum effects in noise-free communication channels with infinite and limited pass bands in channels with noise, in quantum counters and coherent amplifiers 03 p0368 A67-13140
 Noise stability for wideband analog

methods of information transmission based on analysis of probability distribution density, using normal rms error and anomalous error
 probability 03 p0369 A67-13581
 Thermodynamic equilibrium of binary channel with noise at fixed temperature 03 p0372 A67-14057
 Noise rejection of various types of modulation in data transmission with multiple noise 04 p0568 A67-14454
 Coding method for transmitting digital data over IRIG-FM/FM telemetry system applied to German-American high altitude/space flight program 04 p0569 A67-14572
 Weather satellite for automatic photo transmission, noting Tiros and Nimbus 04 p0651 A67-15454
 Functioning period of remote control systems in sporadic data transmission determined, using mathematical methods of queueing theory 05 p0782 A67-16266
 Scheme reducing decoding failures due to atmospheric noise in coherent-phase-shift-keyed data transmissions by ground wave 05 p0767 A67-17523
 Items affecting information transmitted from payload landed on remote planet to earth via communications satellite including orbit, transmission policy and orbit injection error effect on communication capability [AIAA PAPER 66-314] 06 p1094 A67-17704
 Bit synchronization during transmission of heavily biased information on PCM data systems 06 p0963 A67-18110
 German book on transmission of communications including transmission methods and shapes, signals, radio relays, terminal devices, etc 07 p1140 A67-19337
 Limitations in tilted fluxgate magnetometer data from Explorer XVIII satellite due to ambient dynamic field effects 07 p1182 A67-19943
 Data transmission capabilities of Mars probes and landing capsules [AAS PAPER 66-62] 07 p1146 A67-19998
 Transfer logic of double dialog high security data transmission system using long loop principle 07 p1146 A67-20159
 Input-output information transfer through correlation function of electromagnetic fields, obtaining optimization of system 09 p1461 A67-21603
 Communications and Information Conference, Frankfurt am Main, September 1966 09 p1463 A67-21757
 Threshold signals and optimal modulation parameters of analog methods of transmitting information under conditions of ideal reception 10 p1604 A67-22984
 Picture quality in PCM transmission of low resolution monochrome still pictures as affected by system parameter changes 11 p1791 A67-24712
 Noise rejection of remote control command information transmission in system with comparison circuit, using error detecting and correcting codes 11 p1772 A67-25041
 Approximate formulas for information transmitted by discrete communication channel obtained by averaging tight and weaker bounds respectively from transition probability matrices 12 p1908 A67-26088
 Satellite Telecommunications with Automatic Routing /STAR/ system transmission system operation and modulation techniques 13 p2068 A67-26719
 Multiple internal communications system concept using single coaxial cable handling information transfer by integrated circuits 13 p2083 A67-27448
 Information theory research development 14 p2269 A67-28456
 Design of simple circuit for high speed transmission gating of analog signals with fast switching diode and small overshoot 14 p2287 A67-28686
 Variable data rate modem for digital signal transmission on HF radio circuits 14 p2272 A67-28705
 Noise rejection of various types of modulation in data transmission with multiple noise 15 p2435 A67-29291
 Coding for numerical data transmission over binary symmetric channel, discussing effectiveness of various error-correcting codes, taking average numerical error as fidelity criterion 15 p2439 A67-30387
 Signal field energy distribution

optimization ensuring minimum error dispersion during digital information transmission through channels with noise fluctuations 16 p2623 A67-31014
 Error correction block encoding for high speed HF digital data transmission system 17 p2811 A67-32112
 Time statistics for reliable transmission of binary data in presence of atmospheric noise burst 17 p2811 A67-32113
 Spacecraft and ground equipment of Lunar Orbiter telecommunications system 17 p2811 A67-32119
 System for information transmission over optical path using microwave subcarrier, noting satisfactory SNR 17 p2812 A67-32237
 Algorithm for converting binary code into uniform binary code with maximum predetermined number of zero symbols in any code combination 18 p2999 A67-33532
 Simplex information transmission system using communication satellites, discussing technological and economical parameters 18 p3001 A67-34176
 Frequency modulated transmitter and receiver for audio high speed data transmission including discriminator for analyzing and distinguishing waveforms 20 p3379 A67-36247
 Electromagnetic interference and tape recorder jitter control problems in data management system for manned spacecraft 20 p3442 A67-36468
 Deep space communication system data rate increase using relay satellite 20 p3380 A67-36542
 Utility charts for evaluation of data modulation methods 20 p3380 A67-36543
 Multiple internal communications system dealing with diversified information forms, discussing flexibility, reliability and other advantages for weapon systems 20 p3381 A67-36567
 Real time telemetry data system for Air Force Eastern Test Range 20 p3381 A67-36614
 Noise effect on synthesis of discrete systems with and without feedback channel for transmitting continuous messages, using binary signal and criterion of minimum rms error 20 p3383 A67-37071
 Data return advantages of earth-Mars-earth flyby trajectories over more conventional Mars trajectories [AIAA PAPER 67-646] 20 p3530 A67-37626
 Direct and relay links capabilities for returning data to earth from Mars lander compared on effective radiated power basis [AIAA PAPER 67-647] 20 p3387 A67-37627
 High reliability PCM digital telemetry system for onboard data transmission of analog and digital signals 21 p3583 A67-38635
 Apollo command module communication and data system design, discussing environmental and reliability requirements 21 p3584 A67-38668
 Coded information transmission with reduced band emphasizing pulse prediction through redundancy, information quantity and delta signal 21 p3585 A67-38763
 Bandwidth reduction for holographic data transmission systems noting application to TV 22 p3796 A67-39260
 Developments in tracking, telemetry and command transmission, discussing move toward higher frequencies and rain losses 22 p3763 A67-40338
 Microwave multichannel communication system using PCM, noting low power output requirement and suitability for digital data transmission 22 p3763 A67-40460
 Modulator-demodulator device using phase shifts between signals in successive time intervals to speed handling of data in HF band 22 p3764 A67-40557
 Deep-space communication capability spectral dependence analysis indicates optical transmissions would be several orders of magnitude poorer than RF technology 22 p3764 A67-40558
 Analog and digital data processes for interplanetary photoscience with reference to Mariner Mars flyby mission, discussing telemetric transmission and SNR [IEEE PAPER 19-TP-66-1134] 23 p3998 A67-40740
 Most efficient use of voice band channel in digital data transmission by direct use of passband [IEEE PAPER 19-TP-67-1262] 23 p3972 A67-40741
 Multiple speed data transmission

precoding by changing data rate and overall channel characteristics 24 p4121 A67-42342
 NASA National Space Science Data Center operation [AIAA PAPER 67-946] 24 p4260 A67-43032
 Measuring instrument for assessing digital data transmission channels performance using bit error counting combined with peak telegraph distortion 24 p4159 A67-43116
DATING
 SA RADIOACTIVE DATING
 Terrestrial origin hypothesis for tektites, moldavites and impact glass supported by krypton-argon and fission track measurements 11 p1866 A67-24693
 Geochronology for earth and components using radiometric and thermoluminescence methods 12 p1903 A67-25428
DAZZLE PROJECT
 S RADAR TRACKING
DC
 S DIRECT CURRENT /DC/
DC-9 AIRCRAFT
 S DOUGLAS DC-9 AIRCRAFT
DCS
 S DEFENSE COMMUNICATIONS SYSTEM /DCS/
DE HAVILLAND DH-121 AIRCRAFT
 Automatic landing development in autopilot and autoflares for Trident aircraft 03 p0464 A67-13002
 Cavitation erosion in Hawker Siddeley Trident hydraulic system and steps to find solution 05 p0753 A67-16748
 Leakages in hydraulic system of Hawker Siddeley Trident jet transport due to cavitation erosion 07 p1132 A67-20149
DE LAVAL NOZZLE
 Two-dimensional nonvertical shock-wave gas flow through Laval nozzle 03 p0350 A67-12886
 Laval nozzle configuration for sharply bounded carbon dioxide jet in vacuum 06 p0943 A67-18781
 Laval nozzle configuration for sharply bounded carbon dioxide jet in vacuum 18 p2982 A67-33723
 Laval nozzles performance under off-design conditions, noting shock wave formation in region of supersonic velocity 21 p3564 A67-38420
 Base pressure behind circular projection in Laval nozzles, measuring dependence on specific heat ratio at different Mach numbers by varying gas 22 p3741 A67-40021
 Optimum blowing angle of gas into supersonic nozzle determined by supersonic wind tunnel investigation of flow interaction 22 p3743 A67-40452
 Numerical method together with stable difference scheme used to calculate sub-, trans- and supersonic flows in Laval nozzle inverse problem 24 p4091 A67-42160
DEAFNESS
 S HEARING LOSS
DEATH
 Gastrointestinal symptoms and drug use as possible contributing causes of fatal crash of race pilot 09 p1456 A67-21734
 Fourth-week syndrome in addition to normal medullary syndrome in DBA/2J mouse strain response to acute ionizing lethal irradiation 13 p2059 A67-26868
 Human factors in fatal and nonfatal general aviation accidents, discussing cause of death and relationship of experience, occupation and alcohol 23 p3971 A67-41708
DEBRIS
 SA SPACE DEBRIS
 Debris ingestion into engine arising from ground erosion effects on jet lift V/STOL aircraft 06 p0945 A67-17906
 Radiance of debris cloud ejected from manned spacecraft, effect on optical environment and astronomical observations 20 p3525 A67-37099
DEBUGGING
 Debugging of Emeraude propulsion system of Diamant launch vehicle, stressing problems with combustion chamber instabilities, vibrations, etc 01 p0155 A67-11389
DEBYE FUNCTION
 Calculation of statistical sum of bounded states of electron in atom in Debye plasma 03 p0478 A67-13615
 Pair distribution function and conductance for symmetrical electrolytes up to all powers of Bjerrum parameter, using Debye screening to eliminate long range

divergence 04 p0670 A67-15579
Atomic energy levels in plasma, considering energy spectrum of hydrogen-like atom in plasma based on cut-off Coulomb potential model 06 p1039 A67-17881
Cross sections for sticking electrons to spherical charged particles, considering Debye screening distance of Coulomb force field 12 p1968 A67-25750
Equation of state for Debye continuum governing nonlinear propagation of perturbations terminating in shock wave at distance 14 p2374 A67-28982
Calculation of statistical sum of bounded states of electron in atom in Debye plasma 18 p3091 A67-34480

DEBYE TEMPERATURE

Heat capacity and Debye temperature of NdS, LaSe and LaTe 05 p0867 A67-17056
Si and Ge heat capacities in terms of equivalent Debye temperature, obtaining coefficient of leading anharmonic contribution to free energy 05 p0870 A67-17199
X-ray Debye temperature thermal variation measurements of pure nickel and chromium 06 p1015 A67-17850
Heat capacity and Debye temperature of NdS, LaSe and LaTe 15 p2538 A67-29787
Variation of forbidden bandwidth and linear-expansion coefficient of indium phosphide-gallium arsenide alloys as function of composition 18 p3095 A67-34447
Lattice heat capacities, Debye temperatures, heat capacity, free formation energy and thermodynamic functions of groups II-IV semiconductors 23 p4047 A67-41533

DECARBONATION

Electrochemical generator concept noting compactness, adaptability, methods of adding active agents, evacuation of reaction products and decarbonation 14 p2253 A67-29020

DECAY

S ALPHA DECAY
S DEGRADATION
S NEUTRON DECAY
S ORBIT DECAY
S PARTICLE DECAY
S PLASMA DECAY
S RADIOACTIVE DECAY

DECAY RATE

Bulk minority carrier lifetime measured directly in solar cell by measuring short circuit current decay constant which is dependent on cell thickness and carrier type 04 p0554 A67-15128
Gas temperature decay characteristics for interrupted high pressure arcs at various current intensities 05 p0850 A67-16068
Energy transfer from single chromium ions to closely coupled pairs of chromium ions in ruby 05 p0862 A67-16659
Fluorescence decay time of NO, determining transition moment variation 05 p0848 A67-16837
Aerothermochemical eddy diffusion model for predicting rapid wake ionization decay behind hypersonic slender clean cone obtained in free flight ballistic range [AIAA PAPER 67-21] 06 p0938 A67-18257
MHD equations for spectral energy tensors of weak homogeneous magnetoturbulent field and derivation of asymptotic decay law by method of steepest descent 08 p1359 A67-21122
Rise and decay times of spike burst during type IV event of February 5, 1965, noting electron stream velocities and coronal temperature 09 p1562 A67-22233
Oxygen IV transition multiplet relative intensities for measuring decay rates, using triply ionized emitters 10 p1678 A67-22718
Gamma decay of Se 73 and Se 81 isomeric pairs with half-lives, energies and decay schemes 11 p1822 A67-23980
Velocity profiles for turbulent ducted flow systems analyzed, showing profile decay rate for flow pattern 12 p1927 A67-25351
Lifetime for nonequilibrium current carriers in n-type indium antimonide crystals from generation-recombination noise measurements at various temperatures 12 p1984 A67-25523
Xenon-iodine dating, sharp isochronism in chondrites 12 p2002 A67-25525
Mass spectrometers operational performance characteristics, effects on sensitivity decay rate related to time, pressure and ionizing

current 12 p1942 A67-25694
Nighttime ionosphere maintained by downward flux of electrons from protonosphere as shown by columnar electron contents measurements, noting decay rate 13 p2107 A67-26305
Volt-ampere characteristics, generation and decay of interrupted and AC arcs in nitrogen, air, argon and carbon dioxide at zero gravity 14 p2354 A67-27760
Long term measurement of trapped-electron environment in narrow region of space at lower edge of inner radiation belt 14 p2380 A67-28051
Decay of persistent currents in small ring-shaped superconductors due to detectable internal thermodynamic fluctuations 14 p2370 A67-28717
Gas condensation near comet nucleus as source of formation of entire dust coma 15 p2552 A67-29153
Pressure measuring instrumentation response requirements for computing decay rate in solid propellant termination systems 17 p2926 A67-32069
Structure and decay of artificial radiation belt produced by high altitude nuclear explosion 17 p2936 A67-32534
Lifetime for nonequilibrium current carriers in n-type indium antimonide crystals from generation-recombination noise measurements at various temperatures 18 p3103 A67-34454
Grid geometry effect on longitudinal and lateral turbulence intensities, determining decay rate dependence 18 p3030 A67-34740
Nonleptonic sigma decay modes described by four complex amplitudes with phases given by time-reversal invariance 19 p3263 A67-34892
Electric conductance exponential decay in column of wall stabilized nitrogen arc after current interruption 19 p3282 A67-35157
Vertical distribution of meteor showers obtained by measuring distribution in decay times of underdense radio echoes 20 p3521 A67-36303
Electron-ion three-body recombination rate in nonequilibrium dense nitrogen plasma measured spectroscopically [AIAA PAPER 67-703] 21 p3672 A67-38730
Ion cyclotron instability potential and adiabatic compression of plasma in mirror machine, measuring plasma decay rate and potential 22 p3846 A67-39487
Viscoelastic fluid isotropic turbulence decay approximating non-Newtonian effects by perturbation method 22 p3787 A67-40221
Spectrum line observation of decay transition of structure of gas laser 23 p4016 A67-41324
Gas condensation near comet nucleus as source of formation of entire dust coma 24 p4239 A67-43076

DECELERATION

SA ACCELERATION
SA IMPACT DECELERATION
Aerodynamic deceleration systems, discussing basic materials and fabrication techniques of BALLUTE program [AIAA PAPER 66-988] 02 p0181 A67-12299
Correlation of changes in serum enzyme behavior in rats with pathological injuries due to short transverse decelerations 06 p0953 A67-17996
Wind tunnel study of strong-deflection supersonic cascade decelerating flow past turbine blades 07 p1128 A67-20296
Impact tests on animals at velocity changes suggestive of automobile crash conditions, confirming effect of isovolumetric containment of torso on increased survival limits 08 p1289 A67-20612
Radiographic analysis of thoracic cardiovascular rupture during abrupt deceleration associated with crashes [ARL-TR-67-17] 08 p1287 A67-20614
Approximate formulas for determining speed reduction, maximum deceleration and orbit modifications for ballistic vehicle that grazes atmosphere 08 p1394 A67-21106
Electron plasma frequency instability, correlating coherent deceleration of electron beam with compression of interference pattern 11 p1827 A67-23890
Unbalanced rotor deceleration through critical speed tested, considering maximum deflection increment and bending stress in rotor shaft

[ASME PAPER 67-VIBR-17]

11 p1796 A67-24176
Muller maneuver /forced inhalation with closed glottis/ improves tolerance to negative G 12 p1901 A67-25172
Sonic booms attributed to subsonic flight 12 p1895 A67-25936
DECELERATOR
SA ACCELERATOR
SA PARACHUTE
Aerodynamic and structural data on supersonic decelerators, determining problem areas and voids [AIAA PAPER 67-201] 06 p0948 A67-18301
Ballute aerodynamic characteristics in 0.1 to 10-Mach number region for various applications [AIAA PAPER 67-228] 06 p0942 A67-18518
Hypersonic decelerator deployment investigated for interactions between decelerator, connecting cable and wake of forebody it tails 14 p2244 A67-29055
Rotary wing decelerator for sonic and supersonic operation, noting components and potential application areas 17 p2796 A67-32517
Ballute aerodynamic characteristics in 0.1 to 10-Mach number region for various applications [AIAA PAPER 67-228] 19 p3169 A67-34817
DECIMAL-TO-BINARY CONVERSION
S BINARY-TO-DECIMAL CONVERSION
DECISION ELEMENT
Development of pneumatic logical elements and systems 13 p2056 A67-27239
DECISION MAKING
System effectiveness in weapon system development and acquisition decisions [SAE PAPER 660722] 01 p0169 A67-10626
Bayesian statistics applicability to reliability estimation and decision-making 01 p0085 A67-11381
Pattern recognition systems with fixed linear structure changing to nonlinear as result of repetitive generation and selection of relations among input measurements 02 p0208 A67-12141
Adaptive machine using weighted matrix structure in generating decision space for fault detection or process control signals 02 p0243 A67-12144
Onboard test and decision-making requirements for spacecraft checkout system including computer and software, data link detail and test set detail 03 p0400 A67-14215
System and cost effectiveness analysis throughout program life cycle of weapon or support system to aid decision making [SAE PAPER 660724] 04 p0740 A67-15780
Probabilistic displays and decision making effectiveness in situation with uncertain or fallible information 05 p0757 A67-16308
Reliability in improving program quality and design decisions as in planetary exploration program 07 p1259 A67-19617
Numerical solution of sequential decision problems involving parabolic equations with moving boundaries 08 p1349 A67-21256
Reliability criteria application to improvement of program and design decision quality during preliminary design 09 p1582 A67-22291
Computerized decision making for air traffic control 09 p1528 A67-22631
Man-computer system for aerospace problems, discussing terminology, methods of organization, problem solution, numerical analysis, etc 11 p1755 A67-24246
Reliable decisions from unreliable measurements of electronic equipment via statistical method 12 p1949 A67-25524
Planning and decision-making system in technological evolution and revolution 13 p2231 A67-27506
Systems approach to reliability, integrating cost and performance and demonstrating tradeoff decisions 15 p2448 A67-29800
Quality cost accounting and management decisions in performance of various functions 15 p2584 A67-30420
Nonlinear decision surfaces determined by pattern-recognizing adaptive threshold device via generation of polynomial discriminant functions and computer programs 18 p3006 A67-34064
Maintainability technology and controls developed during F-111 design 18 p2986 A67-34663
Book on optimization covering inequality constraints, decomposition strategy, direct methods, etc 22 p3775 A67-39270

- Ejection capability vs decision to eject 22 p3754 A67-39596
- Test planning and decision making in environmental testing approached from program formulation involving resources and equipment, degree of simulation and optimum levels 22 p3781 A67-40402
- Life cycle cost covering accessibility, automated fault isolation, corrosion control, maintenance, etc 23 p4085 A67-40586
- Cost Analysis Model - Parametric /CAMP/ computer method of estimating hardware and logistics life cycle costs for air vehicles in design stage 23 p4085 A67-40589
- DECISION THEORY**
- SA STATISTICAL DECISION THEORY**
- Phase cancellation of sinusoidal signals in presence of Gaussian noise for comparison and threshold decision schemes 01 p0025 A67-10860
- Markovian division process application for solving multicomponent preventive maintenance, work sampling and search theory problems 01 p0106 A67-10930
- Model for synthesizing and analyzing communication systems, detailing use in converting command and control information-transfer into physical and performance specifications 08 p1292 A67-20673
- Planetary quarantine and biological search strategy, discussing Voyager-Mars mission configuration, sterilization, back-contamination and decisions 19 p3180 A67-35233
- Orthogonal signaling in sequential decision feedback on communication over additive white Gaussian noise channel, obtaining expression for error probability 22 p3775 A67-39295
- DECODER**
- Decoder signaling system of Eldo satellite employing PCM telemetry channel, examining counters, shift registers, flip-flop circuit, etc 02 p0192 A67-11651
- Cryoelectric memory loop cell and hybrid organization system noting economy, high speed, mass storage, etc 12 p1915 A67-25887
- DECODING**
- Pathcount and coding matrices for sequence time encoding and decoding for data compression 01 p0028 A67-10022
- Adaptive decoding technique for analyzing information-carrying signals in order to control signal to noise ratio during transmission time of single compound signal 05 p0768 A67-17401
- Scheme reducing decoding failures due to atmospheric noise in coherent-phase-shift-keyed data transmissions by ground wave 05 p0767 A67-17523
- Secondary surveillance radar system design, discussing interrogator interference, decoding and display systems 09 p1530 A67-22648
- Parallel data decoding with high transmission rates close to channel capacity for space telemetry systems design 12 p1909 A67-25781
- Information theory research development 14 p2269 A67-28456
- Convolutional encoder for orthogonal tree codes in presence of white Gaussian noise [JPL-TR-32-1120] 14 p2273 A67-28710
- Forced-erasure decoding of fading and nonfading channels compared with correlation and digital decoding 17 p2811 A67-32114
- Variational procedure for sequential decoding scheme with mean error probability dependence on code limitation approximately same as for optimal decoding 19 p3185 A67-36096
- Reliable efficient communication channel utilization by use of sequential decoding 20 p3384 A67-37348
- Deep space communication system using sequential decoding, binary phase-shift keying and 8-level quantized decisions 20 p3384 A67-37349
- Sequential decoding algorithm with memoryless channel, obtaining lower bound to distribution of computation and limiting factor [JPL-TR-32-1121] 20 p3412 A67-37494
- Errorless code transmission in specific nonbinary cyclic channels, describing effective decoding process 24 p4136 A67-42409
- DECOMPOSITION**
- SA ABLATION**
- SA CARBONIZATION**
- SA DEGENERATION**
- SA DEGRADATION**
- SA DISSOCIATION**
- SA ELECTROLYSIS**
- SA HYDROLYSIS**
- SA PHOTOLYSIS**
- SA PROPELLANT DECOMPOSITION**
- SA THERMAL DECOMPOSITION**
- Competing alternative pathways for formation of particular ion in mass spectra of substituted benzophenones 01 p0018 A67-10105
- Comparison of decomposition rate for pure ammonium perchlorate, chlorate ion doped ammonium perchlorate and X-rayed ammonium perchlorate at 236 degrees C 04 p0687 A67-14635
- Hydroxyl catalyzed chain decomposition of ozone, proposing new reaction mechanism [JPL-TR-32-1063] 07 p1138 A67-20192
- Process identification by decomposition method of multilevel systems analysis, noting computer estimation of state variables of discrete time systems 16 p2647 A67-31650
- Cadmium compounds catalytic effect on ammonium perchlorate decomposition rate and ignition temperature 18 p3107 A67-33810
- Decomposition of polytetrafluoroethylene in glow discharge studied using helium, helium plus oxygen or oxygen as carrier gas 18 p2998 A67-34369
- Spectral emittance of melting or decomposing polystyrene determined, describing apparatus and experimental technique 20 p3446 A67-36663
- Spontaneous decomposition of helical dislocations in metal crystal into row of pinched-off loops plus straight dislocation line 21 p3677 A67-38092
- DECOMPRESSION**
- Possible decompression effects in supersonic transport cabin in terms of biomedical considerations for passenger safety 14 p2258 A67-28666
- Cortical electroencephalographic activity /EEG/ relation to behavioral changes in chimpanzee following rapid decompression to near vacuum 18 p2991 A67-34713
- Rapid decompression effect on lymph pressure of dog, discussing immediate and delayed rise phases 22 p3751 A67-39600
- Decompression tests, evaluating hazards of ejections and fatal injuries following window failure in small pressurized aircraft 23 p3965 A67-41575
- Decompression tests for potential hazards of ejection or fatal head injuries in small pressurized aircraft 23 p3970 A67-41693
- High venous pressures during exposure of dogs to near-vacuum conditions 23 p3960 A67-41699
- DECOMPRESSION SICKNESS**
- Cardiovascular responses of anesthetized dogs to repeated rapid decompressions in near vacuum 03 p0365 A67-14296
- Altitude dysbarism treatment with high pressure oxygen, reporting three cases 05 p0756 A67-16291
- Decompression sickness in high altitude flying, discussing degrees of bends pain among squadron members during five year period [SAM-TR-66-305] 10 p1600 A67-23826
- Monograph on theory of decompression sickness and application to diving tables, including calculation of critical size of localized bubbles formed from dissolved nonrespiration-involved gases in tissues [DVL-623] 11 p1748 A67-25036
- Physiological effects in baboon of prolonged decompressions simulating loss of cabin pressure 13 p2060 A67-26924
- Emergency recompression procedures during space flight studied by exposure of chimpanzees to near vacuum 14 p2257 A67-28219
- Effectiveness of therapeutic modalities upon mongrel dogs subjected to dysbarism by overcompression-decompression 16 p2611 A67-30770
- Decompression sickness studied by investigating cavitation at liquid-liquid interface 21 p3573 A67-38076
- Scuba diving relation to development of aviator decompression sickness, investigating decompression time before flying 21 p3574 A67-38078
- Permeation of neon, nitrogen and sulfur hexafluoride through living tissue in rats, using subcutaneous gas pockets as decompression sickness bubbles model 21 p3574 A67-38079
- Cabin pressurization characteristics of USAF and commercial transport aircraft, stressing decompression sickness 21 p3577 A67-38081
- Pulmonary isotopic scanning technique in dog to assess embolism before and after lethal decompression 22 p3751 A67-39602
- Terminology, pathophysiology, treatment, prevention and clinical aspects of altitude decompression sickness 23 p3950 A67-41545
- Radioisotopic color coded pulmonary lung scanning, diagnostic test in experimental decompression sickness 23 p3956 A67-41626
- Seven year follow-up X-ray survey for bone changes in low pressure chamber operators to determine long term effects of altitude decompression sickness 23 p3957 A67-41641
- Treatment for relief of altitude decompression sickness for operations requiring extravehicular activity 23 p3960 A67-41702
- DECONTAMINATION**
- SA CONTAMINATION**
- Decontamination techniques and sterilization environment, discussing compatibility with components and hardware of lunar orbiting spacecraft 02 p0249 A67-12386
- High vacuum pump selection requirements, discussing contamination problems 17 p2884 A67-32596
- Antimicrobial properties for various spacecraft materials, discussing impregnation methods for bactericides and two-stage sterilization 19 p3179 A67-35229
- Vapor phase decontamination for removing residual hypergolic propellants in Apollo propulsion system 20 p3516 A67-36578
- DEEP SPACE**
- Lunar orbiter command and telemetry data handling system at deep space stations 02 p0194 A67-11808
- Deep space and missile tracking antennas - ASME Conference, New York, November-December 1966 03 p0383 A67-13748
- Primary electric propulsion systems for deep space missions with reference to SERT II program and compatibility with other spacecraft programs [AIAA PAPER 67-424] 18 p3111 A67-33908
- Control and measurement of temperatures of Mariner IV 18 p3052 A67-34514
- Deep space navigation and guidance technology, emphasizing simplification of onboard navigation procedures 19 p3255 A67-35856
- High resolution interferometer data from radio source 3C 273 recorded at NASA deep space stations in Australia 21 p3712 A67-39122
- Deep-space communication capability spectral dependence analysis indicates optical transmissions would be several orders of magnitude poorer than RF technology 22 p3764 A67-40558
- R and D deep space communication system planning methodology for comparing laser, IR and mm wave possibilities, analyzing tradeoff and optimizations [AIAA PAPER 67-973] 24 p4260 A67-43050
- DEEP SPACE INSTRUMENTATION FACILITY /DSIF/**
- Unmanned spacecraft systems design for deep space probes, examining flyby and orbiter missions, attitude stabilization, etc [AIAA PAPER 66-887] 02 p0331 A67-12266
- Design, fabrication and erection of 210-ft parabolic fully steerable tracking antenna for deep space instrumentation facility /DSIF/ 03 p0383 A67-13751
- Unmanned spacecraft systems design for deep space probes, examining flyby and orbiter missions, attitude stabilization, etc 21 p3712 A67-37781
- DEEP SPACE NETWORK /DSN/**
- Deep space communication system data rate increase using relay satellite 20 p3380 A67-36542
- Deep Space Network /DSN/ with ground communications network, centralized control and data processing, discussing future data return and control capabilities [AIAA PAPER 67-648] 20 p3387 A67-37628
- Deep-Space Network /DSN/ planning, discussing support for lunar and planetary flight support and applied research applications [AIAA PAPER 67-975] 24 p4260 A67-43051

DEFECT

S CRYSTAL STRUCTURE DEFECT
S INHOMOGENEITY
S POINT DEFECT
DEFENSE
SA AIR DEFENSE SYSTEM
SA MILITARY TECHNOLOGY
SA MISSILE DEFENSE
SA SPACE SURVEILLANCE SYSTEM
Economic impact of defense and space programs 10 p1735 A67-23629
DEFENSE COMMUNICATIONS SYSTEM
/DCS/

Initial defense communication satellite and military requirements 03 p0369 A67-13826
Characteristics and performance of synchronous satellite military communication system 06 p0979 A67-17668
Mission requirements and cost effectiveness comparison of Syncom satellites and associated network synthesis for defense communications systems 06 p0960 A67-17677
NORAD installation in Cheyenne Mountain, Colorado, describing data processing equipment and performance 07 p1148 A67-19840
Requirements for military communications for flexible response, noting limitations /survivability, error rate, delay time, cost, etc/ and Digital Distributed Communications Network /DDC/ 09 p1463 A67-21676
Initial defense communications satellite program giving payload characteristics and orbit analysis of 15 military launchings 18 p3137 A67-34612

DEFENSE INDUSTRY

System effectiveness in weapon system development and acquisition decisions [SAE PAPER 660722] 01 p0169 A67-10626
RCA defense electronic products applied research 02 p0251 A67-11785
Management control systems, incompatibility between risk and controls, relations between government and contractors and implementation procedures [ASME PAPER 66-WA/MGT-16] 04 p0740 A67-15335
Aerospace company characteristics and problems 12 p2041 A67-25742
Defense procurement procedures and task of project manager 15 p2583 A67-29668

DEFLAGRATION

Soviet book on gas dynamics of combustion including detonation, deflagration, accelerating flames, combustion chambers, etc 02 p0343 A67-12679
Pressure deflagration limit of high energy solid propellants increased to superatmospheric pressures by composition changes [AIAA PAPER 66-679] 10 p1696 A67-23131
Self-deflagration process of hydrazine diphosphate studied for three suggested pressure regimes 14 p2376 A67-28551
Materials evaluation and selection for compatibility with manned spacecraft environment 15 p2507 A67-29551
Ignition response of solid propellants described with model including surface regression with verification of igniter flux and pressure effects 15 p2581 A67-29988

DEFLECTION

SA FLOW DEFLECTION
Abruptly varying random processes with determinate deflection, discussing phase space in form of Banach space 04 p0646 A67-15260
Iterative solution for large deflection analysis of rotationally symmetric nonlinear membranes 04 p0715 A67-15658
Bending moment change of curvature relation for large elastoplastic deflection of thin circular-arc cantilever beam, taking strain hardening materials into account 05 p0918 A67-16425
Doetsch deflection calibration device for aircraft control surfaces 06 p0950 A67-18022
Invariants of triangular shell element stiffness matrices associated with polyhedral deflection distribution, discussing effect of geometry [AIAA PAPER 67-114] 06 p1103 A67-18356
Simplified equations for equilibrium problem in large deflection theory for thin annular plates 08 p1414 A67-20348
Measurement accuracy of deflection data for industrial specimens 08 p1333 A67-21534
Deflection absorption of radio waves in ionosphere 09 p1491 A67-21845

Distribution theory application to derive formula for deflections of vertical from Stokes formula 09 p1492 A67-22681
Plastic analysis of cylindrical shell deflections noting support against sliding, shell with clamped edges and with longitudinal force and membrane solution 10 p1715 A67-22922
Unbalanced rotor deceleration through critical speed tested, considering maximum deflection increment and bending stress in rotor shaft [ASME PAPER 67-VIBR-17] 11 p1796 A67-24176

Discrete rational approximation problem, procedure for solution 13 p2145 A67-26615
Thin elastic plate with uniformly distributed load over area and Navier condition on edge solved for deflection 13 p2217 A67-26631
Iteration solution for system of equations for nonlinear deflection and stability of anisotropic plates 13 p2217 A67-26632
Deflection limits on plate-twisting test 14 p2399 A67-28102
Static deflection of parallelogram plates with clamped edges subjected to uniformly distributed pressure studied by energy method 15 p2573 A67-29312
Rectangular sandwich plates large deflection equations solved by successive approximation method 19 p3342 A67-35770
Multipoint equivalent cross section method for calculating finite deflections of beams of strain hardening material 20 p3541 A67-37285
Infinitesimal deflections of positively Gaussian curved surfaces solved by application of /p, q/ analytic functions after affine transformation 21 p3715 A67-37903
Deflection and stresses in corrugated diaphragm rigidly clamped on contour with distributed pressure and concentrated central force, using finite difference approximation 21 p3717 A67-37977

DEFLECTOR

SA BLAST DEFLECTOR
SA FLAME DEFLECTOR
Conditions controlling shock wave reflection from duct end deflector plates, determining spacing of plates from pipe 12 p3715 A67-25356
Deflected laser beam use in TV, machining, photo etching, space navigation and data storage 19 p3239 A67-35060

DEFORMATION

SA AXISYMMETRIC DEFORMATION
SA CREEP
SA DISTORTION
SA ELASTIC DEFORMATION
SA PLASTIC DEFORMATION
SA STATIC DEFORMATION
SA TENSILE DEFORMATION
Deformation theory for medium with continuous distribution of dislocations 02 p0338 A67-11966
Subsonic wind tunnel analysis of wake deformations produced by secondary velocities using models with flat base but various cross sections 02 p0233 A67-12228
Second order variation of system potential energy of axially compressed circular cylindrical shell with ring-stiffened edges evaluated for purely inextensional deformation 02 p0339 A67-12345
Large deformations of circular membrane attached to ring subjected to action of uniform load 04 p0708 A67-14795
Degree of deformation effect on superconducting properties of niobium and vanadium 04 p0686 A67-15986
Inversion formula for principal integral representation of class of P-analytic functions applicable to axisymmetrical problems of elastic bodies 05 p0923 A67-17185
Microstructure and mechanical properties as functions of degree of deformation of pressed rods of TsM2A alloy at 1300 degrees C 05 p0832 A67-17509
Impurity effect /primarily O/ in reactions between liquid alloys and solid metals undergoing deformation 06 p1017 A67-17951
Deformation potential of valence band of indium antimonide, using piezoemission technique of shifting intrinsic recombination under uniaxial stress 06 p1062 A67-18932
Deformation potential effect on helicon-phonon interaction in multivalley semiconductor 06 p1071 A67-18991
Forces deforming rib cage during breathing efforts 07 p1133 A67-19480

Unalloyed titanium properties dependence on deformation and temperature 07 p1211 A67-20290
Large deflection of asymmetrically layered plate, using parametric expansion techniques to extract system of differential equations governing scaling of stresses and displacement component for boundary conditions 09 p1574 A67-21756
Titanium alloy thin foil preparation using window method and electropolishing conditions, noting phase transformation 10 p1668 A67-23175
Stress relaxation dependence on heat deformation regime in Ti alloys VT14, VT3-1 and VTS-1 12 p1955 A67-25368
Recovery of deformed copper-palladium and gold-palladium alloys by isothermal and isochronal annealing, noting vacancy and interstitial migration 13 p2133 A67-27007
Deformed laser resonator mode, studying diffraction losses, amplitude and phase distribution during pumping pulse 13 p2127 A67-27087
Enstatite characteristics in enstatite achondrite meteorites, discussing mineralogy and composition 13 p2200 A67-27236
Deviation from sphere shape of drop moving through viscous media and dependence on Weber number, size, etc 14 p2302 A67-28235
Degree of deformation effect on superconducting properties of niobium and vanadium 14 p2366 A67-28489
Motion of single-component electrically charged gas in elliptical cylindrical cavity analyzed for relative deformation when applying magnetic field 16 p2656 A67-30456
Deformation effects on thermal conductivity, microhardness, and thermal EMF of annealed bismuth telluride bars 16 p2730 A67-31160
High purity single crystal molybdenum electrical resistivity dependence on deformation 16 p2689 A67-31370
Nonlinear macroscopic rheological behavior of dilute suspensions of deformable spheres 17 p2887 A67-32280
Rectangular network analysis of displacement in disks and plates, developing differential equations and giving minimum conditions for potential energy 17 p2961 A67-32714
Deformation theory for medium with continuous distribution of dislocations 17 p2966 A67-33283
Polymer fracture mechanism hypothesized as competition between localized hardening by molecular orientation and localized softening during deformation 18 p3068 A67-33488
Free radical formation correlated with breaking time and creep rate in solid polymers subject to crushing, breakdown and deformation 18 p3068 A67-33490
Dimensional changes of metals under simultaneous effects of thermal cycling and external load due to surplus point defects directional displacement 19 p3244 A67-34929
Deformation characteristics of light concrete statistically compared to second concrete, determined through parameter similarity 19 p3341 A67-35630
Logarithmic, diffusion and high temperature creep in metals 19 p3248 A67-35854
Microstructure and mechanical properties as functions of degree of deformation of pressed rods of TsM2A alloy at 1300 degrees C 21 p3644 A67-38037
Work of deformation during expansion of tubular blanks with varying hardening characteristics under uniform loading 21 p3631 A67-38054

DEGASSING

Kinetics of degassing of tantalum-nitrogen solid solutions by annealing in high vacuum at various high temperatures 04 p0637 A67-14909
Specific degassing of high polymers placed in simulated space environment studied by residual gas analyzer 05 p0832 A67-16304
Degassing or other external causes as possible mechanism for anomalous increases in radiation from moon 08 p1398 A67-21219
Minimum N and O content in degassing determined from equilibrium pressures in Nb-O and Ta-O systems 09 p1518 A67-22125

DEGENERATION

SA DECOMPOSITION
Semiconductor integrated circuit negative

feedback amplifier design with high response characteristics for carrier terminal equipment application 01 p0040 A67-11241
High performance LF wideband discriminators with negative voltage feedback 01 p0040 A67-11316
Maximum negative feedback depth in transistorized AC amplifier as function of cut-off frequency of logarithmic amplitude-frequency characteristic for given phase reserve 05 p0772 A67-16455
Degeneration of solutions of well-posed systems of first order partial differential equations when particular parameter approaches zero 05 p0836 A67-17315
Spectral characteristics of solid state laser with large angular divergence of light, showing contribution from degenerate modes 19 p3239 A67-34903

DEGRADATION

SA CORROSION

SA DECOMPOSITION

SA THERMAL DEGRADATION

Component reliability screening techniques for Syncom, Early Bird, ATS Satellites and Surveyor spacecraft 01 p0155 A67-11343
Ionizing radiation effects on silicon planar bipolar transistors determine degradation mechanisms 04 p0588 A67-15707
Degradation analysis and variability measurement in reliability and quality control of component parts with application to Early Bird COMSAT satellite 05 p0813 A67-17257
Streptonigrin interaction with DNA and resulting degradation and denaturation temperature of DNA from salmon sperm and Escherichia coli 06 p0952 A67-17873
Image degradation comparison between photographic and image orthicon systems, discussing image orthicon receptor advantages when used for space applications 20 p3446 A67-36606

DEGREE OF FREEDOM

SA MULTIPLE-DEGREE-OF-FREEDOM SYSTEM

Periodic solutions for difference-differential autonomous nonlinear oscillatory system with one degree of freedom 01 p0113 A67-10290
Hamilton-Ostrogradskii integral variational principle for holonomic systems with linear constraints 01 p0114 A67-10991
Excitation of vibrational degrees of freedom in molecular collision from vibrational relaxation data and molecular beam elastic scattering experiments 01 p0118 A67-11302
Formal integral construction of Hamiltonian system of n degrees of freedom near equilibrium point 03 p0457 A67-13163
Existence theorems for periodic solutions of coupled nonlinear systems of two or more degrees of freedom, including normal mode vibrations 03 p0524 A67-13654
Periodic perturbations accumulation in linear system with one degree of freedom 03 p0469 A67-14178
Response curves of steady state forced vibrations, cosinelike functions and periodic functions possessing amplitude 04 p0656 A67-14444
Normal modal vibrations for some damped n degree of freedom nonlinear systems 04 p0659 A67-15935
Mechanical system with two degrees of freedom conditioned for oscillatory motion, using differential equations 05 p0908 A67-16042
Hypersonic flow past sphere by relaxing gas with internal degrees of freedom in nonequilibrium 06 p0935 A67-17731
Theorems concerning eigenvalue problems and oscillatory conditions for multiple degree of freedom mechanical systems 07 p1224 A67-20103
Geometric analysis of vibration of nonlinear systems with one degree of freedom 08 p1353 A67-20311
Sensitivity of index of performances to variations in plant parameter for open and closed loop optimal control with one or two degrees of freedom 08 p1309 A67-20328
Dynamic behavior of large flexible bodies in orbital motion around gravitating center, emphasizing response and stability of elastic degrees of freedom 08 p1383 A67-20562
Elastic postbuckling involves coupled modes when critical loads corresponding to buckling modes of two degrees of freedom system are equal 08 p1422 A67-21032

General method of averaging applied to slightly damped librations problem in perturbed one degree of freedom system 08 p1424 A67-21435
Equations describing orbital plane rotation of satellites, noting analogy between equations for oscillations of mechanical system with one degree of freedom 09 p1564 A67-21887
Stationary resonance solutions for rotating systems with one degree of freedom applied to satellite rotation 09 p1532 A67-21910
Equation of relaxation hydrodynamics for diatomic perfect gas when rotational and translational degrees of freedom are in equilibrium and dissipation has not set in 10 p1590 A67-23024
Effective degrees of freedom of vibrating structure 10 p1718 A67-23153
Fully stalled airfoil steady state pitching oscillations in one degree of freedom, deriving torsional flutter equation [ASME PAPER 67-VIBR-12] 11 p1872 A67-24172

Multidegree of freedom linear system analysis by dividing method for relations between system constants and solutions 13 p2156 A67-26527
Behavior of quasi-linear stochastic differential equations with one degree of freedom subjected to effect of random periodic excitation 16 p2696 A67-31009
Free undamped oscillations of nonlinear conservative systems with several degrees of freedom with small nonlinearities 16 p2765 A67-31048
Response of one degree of freedom system with power law time dependent damping and restoring forces using WKBJ approximation 17 p2958 A67-32128
Successive release evaluation by periodometer and memory oscillograph of viscous damping of one degree of freedom system 17 p2884 A67-32698
Soviet book on unsteady oscillations of mechanical systems with any number of degrees of freedom 18 p3078 A67-33678
Gyromotor electromechanical moment effect on drift of triaxial gyrostabilizer exposed to platform vibrations, formulating rotor motion equations 18 p3047 A67-33992
Landing characteristics of SV-5P lifting body vehicle analyzed using six degree of freedom piloted simulation, noting gust effect [AIAA PAPER 67-574] 20 p3533 A67-37133
Inertia of two-phase asynchronous motor effect on operation of interlamb correction system of three degree-of-freedom gyroscope 20 p3451 A67-37156
Dynamic compliance of two degrees of freedom nonrotating beam undergoing flexural vibrations, taking into account internal friction 21 p3726 A67-38833
Optimal shock absorbers synthesis, showing reduction to variational problem and equations for one degree of freedom mass 22 p3776 A67-39394
Number of degrees of freedom for observation of motion of steady signal from uncontrolled plant 22 p3836 A67-39775
Electrostatic energy per degree of freedom of two-temperature plasma examined for validity of resonant approximations in ion wave region 22 p3852 A67-39986
Fundamental statistical oscillation characteristics expressions for quasi-harmonic self-excited oscillators with low noise and many degrees of freedom 24 p4129 A67-42225
Book on stability of nonlinear mechanical systems covering qualitative methods, one degree of freedom systems, etc 24 p4188 A67-42375

DEHYDRATION

Water-salt metabolism changes during prolonged confinement in bed following exposure to acceleration indicating dehydration and decalcification 16 p2613 A67-30916
Heat and exercise induced hyohydration effects upon physical performance of women, showing some deterioration in cardiovascular system 20 p3372 A67-37033
Aromatic poly-1, 3, 4-oxadiazole fiber preparation noting thermostability, property retention at high temperature and resistance to hydrolytic degradation 21 p3648 A67-37877
Inactivity and water immersion effects on

fluid balance and tilt-table performance in dehydrated subjects, assessing vasopressin and positive pressure breathing effects 23 p3951 A67-41557

DEHYDROGENATION

S HYDROGENATION

DEICING SYSTEM

Electrically heated mats used to combat ice formation on aerofoil surfaces and engine intakes or to produce controlled breakdown of ice already formed 07 p1129 A67-19673
Ice removal from solid nonmetallic aircraft propeller blade by nonsteady-state heating 14 p2405 A67-28305

DEIONIZATION

SA IONIZATION

Seasonal and annual variations of electron density in ionospheric F layer interpreted as changes in production rate and ionization loss caused by atmospheric composition variations from neutral atmosphere 10 p1647 A67-23274

DELAY

S LAG

S TIME DELAY

DELAY LINE

YIG dispersive delay line in ultrawide bandwidth pulse compression radar system 01 p0132 A67-10435
Time measurement with semiconductor device, noting parameter variation effect and experimental results 01 p0066 A67-10652
Varactor diode series resistance loss responsible for bandwidth loss in parametric delay lines used for signal processing 01 p0027 A67-11323
Continuously variable optical delay line using acoustic waves to diffract and frequency shift portion of argon ion laser beam 02 p0253 A67-12517
Approximation of variable time delays and design of constant and variable delay circuits, noting simulation of delays in automatic control systems by computers 03 p0390 A67-13104
Acoustic propagation for solid state microwave delay line, discussing generation and propagation of phonon signals in passive media providing fixed delays 04 p0580 A67-14607
Moving target indication /MTI/ in theory and technique including description of delay lines, stalos, transistors, phase detectors and modulator 04 p0573 A67-15037
Internally scanned laser beam having high deflection rate produced by pulsed optical delay line 05 p0818 A67-16647
Equisignal zone technique for correlation-interference direction finder using commutable delay line 05 p0774 A67-16918
Single wave approximation of fields of cylindrical delay system with basic E-type wave propagating at variable phase velocity 05 p0767 A67-17398
Magnetic delay line vibration isolation system as heart of airborne special purpose computer in USN E-2A early warning aircraft 05 p0779 A67-17458
Conversion of frequency spectrum of pulse-position-modulated signal passing through delay device and amplifier switched by input undelayed signal 07 p1139 A67-19229
Performance and wave growth of type-M transverse-field tubes in broad delay system 08 p1302 A67-20834
Equisignal zone technique for correlation-interference direction finder using commutable delay line 16 p2623 A67-30895
Solid state microwave delay lines noting advantages, operation principles, fixed variable construction, etc 16 p2637 A67-31196
Amplification of traveling-wave tube calculated to determine effect of continuous current interception along delay system 16 p2640 A67-31506
Predetection telemetry tape combiner 17 p2813 A67-32496
Microwave delay-line techniques using YIG crystal, examining solid state dispersion characteristics 20 p3507 A67-36241
Scientific data handling system using passive magnetostrictive multichannel delay line memory 20 p3390 A67-36251
Approximate method for evaluation of processing loss in delay line MTI receiver 22 p3758 A67-39211
Backward waves effect on excitation of delay line by modulated electron beam with zero transit angle 22 p3767 A67-39422
Solid state and electron beam delay line

features compared in optimal selection for radar system target simulation 23 p3982 A67-41503
Active delay line with amplifiers converting electromagnetic oscillations into ultrasonic vibrations and back again 24 p4130 A67-42237

DELAY LOCK

SA PHASE LOCK

Extended phase detector for phase-lock loop receivers 13 p2075 A67-26408

DELTA DART

S F-106 AIRCRAFT

DELTA FUNCTION

Maxwellian and delta distribution models of reflected atoms in terms of mass, momentum and energy exchange 05 p0749 A67-17109
Interpretation of class of divergent integrals in terms of limit sums, using generalized function theory 08 p1349 A67-21193
Balanced helical wire antenna excited by delta function generator, obtaining integral equation for current distribution 09 p1481 A67-22445
Electrically thick cylindrical antenna driven by delta function generator, discussing numerical solutions to two different mathematical models 23 p3980 A67-41206

DELTA MODULATION

Time combined with frequency division multiplex multichannel communication system for transmission of digital information over tropospheric scatter communication channel 02 p0203 A67-12132
Asynchronous delta modulation system for cases with no time division multiplexing such as asynchronous multiplex communication 10 p1606 A67-23063
Troposcatter techniques reviewed proposing analog voice waveform conversion into digital form by delta modulation or PCM for upgrading present operational systems 16 p2628 A67-31492
Multidigit delta modulation system using individual optimized stages developed by successive approximation of message waveform 17 p2812 A67-32319

DELTA WING

Hypersonic flow past lower surface of slender delta wing for wide-range of angle of attack, determining velocity component, pressure and density distribution 03 p0350 A67-12874
Three-dimensional flow separation over structures with various geometric configurations, calculating limiting streamlines for subsonic laminar boundary layer conditions 05 p0747 A67-16293
Spin calculations corroborating vertical wind tunnel tests on delta wing aircraft, noting aerodynamic parameters [ONERA-TP-388] 05 p0751 A67-16477
Gap size effect on pressure and aerodynamic heating over flap of blunt delta wing in hypersonic flow [AIAA PAPER 66-408] 05 p0749 A67-17220
Three-dimensional boundary layer flow over windward side of flat delta wing in hypersonic flow at moderate angle of attack, examining viscous-inviscid interaction [AIAA PAPER 66-492] 06 p0943 A67-18848
Aerodynamic effect of volume addition to high lift to drag wing-body ratio at Mach 6 07 p1126 A67-19382
Wind tunnel investigation of effect of ground level on static aerodynamic characteristics of sideslip for rectangular and delta wing with rudder assembly 07 p1126 A67-19886
Antisymmetrical thin delta wing with flow separation at subsonic leading edge 07 p1128 A67-20236
Linearized supersonic theory for favorable thickness distributions and drag reduction for wings in supersonic flow [AIAA PAPER 65-716] 08 p1276 A67-20559
Vortex separated delta wing leading edge in supersonic flow, noting effect on pressure distribution and role of flow equation 09 p1438 A67-22496
Mach number effect on hypersonic flow past delta wing with blunt edges at zero angle of attack 10 p1590 A67-23036
Supersonic delta wing problem, discussing new approach in determining flow parameters 10 p1593 A67-23687
Aerodynamic characteristics of wedge wings determined for hypersonic viscous

flow 11 p1742 A67-24347
Method of characteristics used in solving nonlinear boundary value problem of thickness of delta wing with transonic leading edge 13 p2049 A67-26646
Vortex breakdown effects on lift, drag and pitching moment coefficients of slender sharp-edged delta wings with different aspect ratios 13 p2050 A67-27194
Skin friction drag coefficient at supersonic-hypersonic speeds as function of transition on delta wing 13 p2051 A67-27597
Four combat aircraft designs /tailless delta, swept wing, variable geometry and VTO aircraft/ using same bypass engines /Pratt Whitney-SNECMA TF-306s/ 15 p2419 A67-29670
Supersonic flow past windward side of delta wings with angles of attack from 0 to 80 degrees, verifying experimental and theoretical values 18 p2984 A67-34208
Flow around thin delta wing under supersonic conditions, considering flow separation at leading edges 19 p3170 A67-35542
Quasi-conical motion past wing-body lifting system, determining pressure distribution, potential expression and axial disturbance velocity 20 p3356 A67-36278
Supersonic delta wing problem, discussing new approach in determining flow parameters 21 p3564 A67-38288
Supersonic three-dimensional flow fields of inviscid nonconducting gas around delta wing with blunt edges 22 p3741 A67-40025
Hypersonic wave rider flow and aerodynamic problems, discussing shaping, leading edge cooling and supersonic combustion propulsion 23 p3929 A67-41251
Delta wing with leading edge vortices, calculating inviscid incompressible flow field near center of rolled up vortex sheet assuming conical velocity field 24 p4092 A67-42570

DEMODULATION

Threshold value lowering in synchronous demodulation, determining output SNR as function of input SNR 08 p1294 A67-20771
Equivalent resistance of traveling wave phototube for large modulation index 16 p2636 A67-30897
Numerical spectrum analysis procedures, discussing fast Fourier transform techniques, classical spectrum windows and complex demodulation process for time series studies 20 p3476 A67-36784
Electric vector expression of amplitude-modulated electromagnetic wave propagating in nonlinear dispersive medium 20 p3499 A67-36992

DEMODULATOR

SA FREQUENCY COMPRESSION DEMODULATOR
SA PHASE DEMODULATOR
SA PHASE LOCK DEMODULATOR
Performance characteristics of transistorized synchronous demodulator 02 p0219 A67-12113
Equivalent resistance divided by interaction impedance of CEF photodemodulators for coherent light 09 p1479 A67-22278
Thin film single-sideband demodulator using time-varying RC networks and containing extremely selective filter 17 p2825 A67-32600
Determination of limits of correct operation of comparison and decision circuits in Akima model band subdivision demodulator 18 p3002 A67-34222
Frequency locked loop FM demodulator with high noise threshold 20 p3385 A67-37352

DENMARK

Space research activities in Denmark /1966-1967/, discussing instrumentation design and development, experiments, etc 19 p3319 A67-35281

DENSITOMETER

S GRAVIMETER

S MICRODENSITOMETER

DENSITY

SA ATMOSPHERIC DENSITY
SA CURRENT DENSITY
SA ELECTRON DENSITY
SA ENERGY DENSITY
SA FLUX DENSITY
SA GAS DENSITY
SA ION DENSITY
SA MAGNETOSPHERIC ELECTRON DENSITY
SA MAGNETOSPHERIC ION DENSITY

SA METEORITE DENSITY

SA OPTICAL DENSITY

SA PACKING DENSITY

SA PHOTON DENSITY

SA PLASMA DENSITY

SA POWER DENSITY

SA PROBABILITY DENSITY

SA PROTON DENSITY

SA SPACE DENSITY

Effect of temperature, density, and amount of stabilization on elastic modulus of zirconia 16 p2695 A67-31701

DENSITY DISTRIBUTION

State density for highly doped semiconductor in magnetic field, obtaining results at near Fermi level energies and at bottom of conduction band 01 p0128 A67-10096
Electric field radial intensity distribution and charged particle density for positive plasma column between coaxial cylinders 01 p0125 A67-10924
Estimated amplitude of echo-signal for uniform, Rayleigh and a priori distribution of probability density of noise amplitudes 02 p0194 A67-11976
Density gradient effect on development of turbulent wake of reentry object determined by studying wake of heated object at low speed 02 p0179 A67-12356
Internal structure models for earth, Venus and Mars, discussing earth density distribution and seismic results 02 p0329 A67-12497
Existence of divergence in density expansion of viscosity and thermal conductivity coefficient of two-dimensional gas of rigid disks 02 p0234 A67-12545
Radial electron density distribution in induced pulsed discharge from wave refraction in planes passing through and normal to plasma cylinder axis 02 p0278 A67-12624
Kinetic equation derivation from density matrix for case of quantum generation of secondary optical harmonic in laser cavity under various optical pumping conditions 03 p0435 A67-13127
Electron oscillations of uniform plasma slab in presence of strong magnetic field, noting orthogonality condition of normal modes density gradients and profile and dispersion relation 03 p0482 A67-13747
Solitary waves in compressible atmosphere with arbitrary wind and density profiles, obtaining solution for critical speed by perturbation scheme 03 p0463 A67-14032
Resonances of impedance of RF probe in low density plasma introduced by finite electron temperature 04 p0663 A67-14614
Submerged nonisothermal turbulent jets analyzed over wide temperature range, noting expansion angle and profile configuration dependency on initial density ratio 04 p0602 A67-14638
Dispersion and damping of oscillations in Maxwellian plasmas with zero order density gradients examined, using Vlasov and Maxwell equations 04 p0665 A67-15103
Field and charge density distributions in semiconductor with hot electrons, showing domain movement type oscillations due to stationary wave propagation 04 p0680 A67-15286
Equation for conditional overshoot density of normal stationary process in centralized and positional control, noting error estimate 05 p0782 A67-16267
Stability and dynamical response of small portions of differentially rotating stellar disks, noting decaying nonaxisymmetrical instabilities, epicyclic frequency, surface density, etc 05 p0892 A67-16410
Output probability density distribution of stationary random noise containing regular signal components after mean squaring circuit 05 p0783 A67-16446
Accuracy and limit analysis of statistical distribution of EM radiation field by photoelectron counting distributions from photodetector for single mode laser near threshold 05 p0815 A67-16624
Concentration and density distributions of particle flux near body moving in rarefied plasma 05 p0855 A67-17122
Multivariate statistical analysis of wind sounding data, applying high degree of correlation between two wind parameters and empirical density function [AIAA PAPER 66-353] 05 p0838 A67-17214
Luminosity and density evolution

- hypotheses concerning distribution of flux densities of quasars, testing validity with Einstein-de Sitter model 05 p0903 A67-17328
- Plasma in Ar positive column DC discharge examined for wavelike perturbations about equilibrium, noting striation dispersion relation, density variations and electron temperature 05 p0857 A67-17427
- Probability estimation, discussing types, Bayesian method for binomial and multinomial distributions, sampling methods, etc 06 p1022 A67-17646
- Hydrogen density in coaxial plasma injector prior to application of high voltage to electrodes, noting experimental setup and results 06 p1040 A67-18086
- Plasma stabilization mechanism for electron beam caused density variation, noting use of nonlinear effects 06 p1040 A67-18097
- Closed form solution methods for blast wave propagation in solid media assuming power law density profile 06 p1102 A67-18290 [AIAA PAPER 67-141]
- Radial current density distribution in homopolar, noting deviation of magnetic field and nature of current distribution around anode 08 p1358 A67-20850
- Earth density and elasticity variation reexamined by applying data on earth oscillations and considering earth inertial moment 08 p1325 A67-20985
- Error probability density distribution and selection of measurement accuracies and decision tolerances 08 p1336 A67-21057
- Laser interferometric measurement of power spectral density of integrated particle density fluctuations in turbulent exhaust of sonic jet 08 p1337 A67-21142
- Gas ionization by fast electron beam directed along waveguide leading to longitudinal distribution of secondary electron concentration 09 p1545 A67-22002
- Incompressible potential flow about arbitrary body shapes calculated, using singularity distribution over body surface computed as solution of integral equation 10 p1589 A67-22871
- Density profiles in gas-solid suspension flow in round duct 10 p1626 A67-23149
- Internal structure models for earth, Venus and Mars, discussing earth density distribution and seismic results 10 p1709 A67-23365
- Shock wave structure theory using Navier-Stokes character of shock wings and measured thickness, noting dependence on number density 11 p1775 A67-23879
- Wall temperature and speed ratio effects on free molecule flow number density distribution about flat plate 11 p1881 A67-23880
- Density attenuation within crossed particulate beams analyzed under steady state interaction, giving more exact solution than Beer law approximation 11 p1818 A67-24318
- Ion-acoustic wave excitation by vertical density gradients, noting effect of resulting instability on ionospheric fine structure 11 p1786 A67-24398
- Conductivity of plasma capacitors in inhomogeneous plasma found to increase with frequency due to density gradient and resonance 12 p1969 A67-25194
- Two uncorrelated Gaussian dependent random variables with non-Gaussian joint distribution may have any maximal correlation coefficient 12 p1960 A67-25313
- P atoms distribution in doped surface layer of silicon photoconverter for various thermodiffusion conditions exhibiting typical concentration curves 12 p1982 A67-25322
- Oscillation frequency and frequency density distribution equations derived for thin elastic shells of revolution clamped along two parallels, using differential equations 12 p2027 A67-25627
- Pulsation properties of star models with linear density distribution, considering radial, adiabatic contraction and dynamical stability 12 p2011 A67-26253
- Magnetospheric electron density distribution determined from analytical calculations, using whistler travel-time integral 13 p2111 A67-26576
- States density in vicinity of Fermi surface obtained from values of paramagnetic susceptibility for gold-palladium alloys 13 p2133 A67-27006
- Radial electron density distribution in induced pulsed discharge from wave refraction in planes passing through and normal to plasma cylinder axis 13 p2171 A67-27380
- Refraction and reflection of shock waves from interface between media having different densities 13 p2105 A67-27414
- Static magnetic field effect on normal distribution of pressure, temperature and density in solar atmosphere, considering sunspots and velocity field effects [AFCLR-66-679] 13 p2204 A67-27435
- Shear flow, determined by velocity and density profiles, is stable for small disturbances of all wavelengths and Richardson numbers, enumerating eigenvalues 14 p2295 A67-27904
- Model of inviscid, incompressible and variable density airflow in long channel over mountain treated mathematically 14 p2346 A67-28004
- Upper atmospheric turbulence velocity probability density investigated in 90 to 110 km region 14 p2346 A67-28058
- Boundary layer in nozzle of arc-heated wind tunnel, obtaining velocity, temperature and density profiles 14 p2299 A67-28171
- Hypersonic low density flow analysis with shock tunnel and electron beam densitometer, noting density profiles at various Mach and Knudsen numbers 14 p2300 A67-28176
- Density of states of pure type II superconductors in high magnetic fields, deriving approximate expression for Green function 15 p2533 A67-29089
- Density fluctuations and thermal conditions in expanding universe and creation of stars, quasars, galactic clusters and galaxies 15 p2551 A67-29138
- Effect of payload weight, density and type on performance and design of reusable launch systems 15 p2568 A67-29841
- Effective pair potential obtained for quantum electron gas to determine thermodynamic properties over large temperature and density range 15 p2533 A67-30383
- Current density distribution in MHD duct with segmented electrodes of finite size analytically described, noting experimental agreement 16 p2600 A67-30537
- I-V curve related to state densities on both sides of n-p junction of tunneling system 16 p2725 A67-30808
- Aircraft flutter testing using free-air turbulence as exciter 16 p2764 A67-30861
- Field distribution in plasma waveguide at LF and large densities, noting dispersion properties of E and H waves 16 p2718 A67-31189
- Probability density and random distribution function derived from finite series for instantaneous voltage measurements of ideal multiplying device 16 p2653 A67-31718
- Lunar structure from lunar moments of inertia, noting thick layer denser than lead near surface 17 p2947 A67-32757
- Plasma injection into closed magnetic trap, studying effects of helical magnetic field on containment time, density and cross section distribution 17 p2903 A67-32910
- Radial hydromagnetic oscillation frequency of plasma cylinder, calculating g-factor and plasma mass 17 p2909 A67-33117
- Hydrogen and helium lateral flow in collisionless exosphere calculated on model for various sinusoidal temperature and concentration variations over exobase surface 17 p2852 A67-33235
- Tunneling into thin superconducting films in magnetic field, measuring field effect on density of states for finite mean free path 17 p2924 A67-33371
- Fourier series applied to X-ray investigation of potential and electron density distribution in silicon lattice to study chemical bonds 18 p3094 A67-33439
- Mathematical model for thermal and chemi-ionization processes in turbulent nonequilibrium afterburning rocket exhausts plume, studying neutral and charged species distribution 18 p3152 A67-33820
- Mean density of cosmological matter determined from quasi-stellar sources observations, analyzing apparent-magnitude and red shift methods 18 p3119 A67-33856
- Matter density and other physical properties of Martian surface estimated from radio and IR observations 18 p3119 A67-33860
- Lunar thermal history computed for different radioactive elements distribution 18 p3119 A67-33862
- Density redistribution of plasma electrons and ions caused by strong microwave field 18 p3087 A67-34040
- Martian surface atmospheric pressure via photometric observations of Phobos eclipses 18 p3124 A67-34155
- Concentration profiles in fixed laminar boundary layer with catalyst distribution on wall, discussing Schmidt number effect and approximations 18 p3159 A67-34161
- Plasma-density distribution produced in gas by tubular electron beam 19 p3278 A67-35128
- Temperature, electron density, and relative particle density radial distribution and mass separation effect in free burning DC arc 19 p3281 A67-35156
- Daytime ozone density distribution of mesospheric layer measured by using UV photometers in rockets 19 p3217 A67-35203
- Rotational velocity and ion density profiles of plasma vortices by measuring radial electric field 19 p3288 A67-35361
- Lower ionosphere electron density distribution estimated through impact ionization and photoionization 19 p3221 A67-35433
- Density gradient of cosmic radiation perpendicular to plane of ecliptic as cause of variations in amplitude and phase of solar diurnal variation 19 p3315 A67-35490
- Microwave refraction technique for determining electron density profiles in transient plasma column 19 p3295 A67-35517
- Flood beams incidence angle and current density distribution effects on half-tone reproduction of visual storage tube with cathode collimator 19 p3194 A67-35543
- Saccharomyces cerevisiae light particle fraction containing fatty acid synthetase analyzed by density gradient method 19 p3178 A67-35873
- Atmospheric drag influence on orbital elements of satellites having highly eccentric orbits 20 p3522 A67-36616
- Rate of diffusion and degree of density during activated sintering of tungsten-molybdenum powders, noting influence of nickel additive 20 p3466 A67-36911
- Magnetic curvature effect on drift cyclotron instabilities, considering density gradients, Maxwell plasmas and resonance 21 p3661 A67-37749
- Electron temperature and density distributions for helium plasma produced in coaxial accelerator measured spectroscopically, checking thermal equilibrium assumption 21 p3661 A67-37752
- Scintillation depth measurement relationship with probability density of amplitude distribution 21 p3617 A67-38002
- Concentration and density distributions of particle flux near body moving in rarefied plasma 21 p3668 A67-38465
- Particle distribution in infinite charged cylinder in plasma vicinity, showing plasma screening effect on potential 21 p3675 A67-39033
- Concentration distribution time for heavy gas diffusing in light gas steady flow field 22 p3917 A67-39714
- Interstellar gas cloud gravitational collapse for models initially in gravitational equilibrium without mass motions, analyzing cooling and density distribution effects numerically 22 p3895 A67-40514
- One-dimensional unstable cloud hydrodynamics analyzed numerically, noting collapse primarily in center and little density growth in outer region 22 p3895 A67-40515
- Secondary temperature resonances in magnetized plasma slab with nonsymmetric inhomogeneous density profile, noting spectrum degeneracy in symmetric nonuniform profile 23 p4034 A67-41359
- P-n junction performance with depletion layer subjected to sudden extreme carrier density generation noting significant local distortion 23 p4044 A67-41453
- Self-gravitating isothermal nonrotating gas layer stability, discussing amplitude density distributions in space 24 p4225 A67-41826
- Relation between earth-moon orbital

inclinations indicates incompatibility of dynamical figures with assumptions of hydrostatic equilibrium and homogeneous density distribution 24 p4229 A67-42320

Density variation in shock tube across nonstationary shock wave separating from nitrogen gas fluorescence excited by fast electron beam 24 p4145 A67-42663

Density fluctuations and thermal conditions in expanding universe and creation of stars, quasars, galactic clusters and galaxies 24 p4239 A67-43061

DENSITY MEASUREMENT

SA X-RAY DENSITY MEASUREMENT

LF spectrum of density correlation function, obtaining diffusion coefficient of right order of magnitude using quiet plasma 01 p0124 A67-10911

Pressure and density measurements of heat flux convected on sharp pointed cone placed in incidence in hypersonic flow 02 p0177 A67-11499

Radioisotope and radiation techniques for terrestrial and planetary gas and solid measurements 02 p0245 A67-12223

Electron density measurement in shock waves or plasma based on low power UHF wave attenuation 03 p0478 A67-13578

Density wave type flow oscillations in boiling Freon 11 examined, noting effects of partial evaporation superheat and liquid inlet temperature on stability [ASME PAPER 66-WA/HT-49] 04 p0725 A67-15433

Silicon surface barrier detector beta gauge for density measurements in liquid hydrogen 05 p0842 A67-16541

Ion density profiles and ionization rate in air behind high speed shock waves [AIAA PAPER 67-94] 06 p1037 A67-18502

Upper atmospheric density, pressure and temperature profile obtained from drag acceleration measurements on falling sphere 07 p1181 A67-19938

High resolution density data from radar observations of low altitude polar orbiting satellites reveal longitudinal and geomagnetic variation, noting regression analysis 10 p1640 A67-23216

Plasma confinement time in helium discharge determined by electron density and helium radiation intensity measurements 11 p1827 A67-23887

Atmospheric density determination from drag of eleven low altitude satellites, discussing correlation with geomagnetic activity and daily periodicity 11 p1784 A67-23937

Diffusion coefficient measurement based on relationship between correlation coefficient for density fluctuations and density coefficient 11 p1829 A67-24003

Density measurements in Q-device by resonance fluorescence scattering, Langmuir probe and microwave methods compared, examining causes of discrepancy 11 p1838 A67-24405

Langmuir probe and microwave transmission methods compared for plasma density measurement 12 p1939 A67-25256

Axisymmetric compressible turbulent wake fluctuating characteristics measured using supersonic wind tunnel, including radial velocity and temperature distribution, density, etc 12 p1893 A67-25928

Temperature and density measurements in supersonic free jets of nitrogen and shock waves 13 p2093 A67-26279

Saturn S-IB stage fuel system, studying LOX density fluctuations, heat transfer and boiling under various weather conditions 13 p2186 A67-27637

Rocketsonde and radiosonde temperature comparisons and evaluation of computed rocketsonde pressure and density 14 p2347 A67-28885

Densities of individual meteoritic, glacial and volcanic spherules, suggesting nonvolcanic origin of polar spherules 14 p2390 A67-28886

Empirical correlation formulas for density and viscosity of equilibrium air, noting pressure variation at high enthalpies 15 p2579 A67-29436

Local gas density measurements, using large angle scattering from electron beam passing through rarefied gas flow 15 p2490 A67-30152

Rarefied gas flow density measurement by determining changes in electron beam-electron concentration while crossing

flow 16 p2673 A67-31107

Density of lithium, sodium and potassium up to 1600 degrees C, using pycnometer method, showing dependence of density on temperature 16 p2692 A67-31773

Frothing-sloughing ablation concept explains density variations of cometary meteors obtained from photographic and radar observations 17 p2943 A67-32541

Cosmological model covering early and late stages, presenting period time when matter density equaled radiation 17 p2947 A67-32759

Density contour determination for magnetically confined plasma by energetic molecular ion beam probe of plasma and atomic ion measurement from collisional dissociation 17 p2910 A67-33356

Mach and Reynolds numbers effect on rarefied supersonic gas flow pattern near forward stagnation point of blunt body, noting decrease in 18 p3028 A67-34209

Graphite material strength prediction by nondestructive test techniques consisting of bulk density and eddy current measurements [ASTM PAPER 54] 18 p3070 A67-34584

Argon plasma ionization by oscillator supplying power near electron cyclotron resonance, measuring density variation 19 p3276 A67-35116

Physical changes in exploding wires before gas ionization observed by X-ray technique, studying resistivity variation with density 19 p3281 A67-35161

Exospheric density variation as related to solar activity determined from satellite orbits 19 p3217 A67-35211

Mesosphere and lower thermosphere density variations related to solar cycle obtained, using rocket grenades 19 p3219 A67-35231

Shock waves generated electromagnetically in T-tube studied with Mach-Zehnder interferometer 19 p3208 A67-35396

Solar flare electron density determination by half-width method, discussing errors due to measurement and method 19 p3314 A67-35438

Solar flare electron density measurements using half-width method, noting variations with height, development and area 19 p3314 A67-35439

Air density variation at 220 km altitude shown due to increased solar activity, from satellite orbit observation 19 p3222 A67-35458

Insulating foams at liquid hydrogen temperature, describing methods for measuring thermoconductivity, specific heat and density 19 p3346 A67-35567

Plasma electron density measurement method using beat frequencies between two dual frequency lasers 19 p3231 A67-35594

Plasma spectroscopy, discussing line profiles, local thermal equilibrium, methods of measuring number densities and temperatures 19 p3298 A67-35855

Etch pitting and electron microscopy used for tungsten single crystals dislocation density measurements at different strain levels 19 p3248 A67-36028

Upper atmosphere density measurement systematic errors in orbiting pressure gauges by neglecting adsorption and desorption 20 p3450 A67-37103

Nonthermal plasma electron density calculated from ratio of spectral line intensities of given ion 20 p3501 A67-37294

Electron density time and location dependence in Z-pinch calculated from emission measurements 20 p3502 A67-37528

Differential magnetic loop, density profile and gas laser interferometer measurements of beta, n and ion temperature in theta pinch operation 21 p3662 A67-37755

Resonance spectrum of plasma column excited by SHF field investigated for nonlinear phenomena 21 p3666 A67-38354

Microwave methods of plasma diagnostics based on attenuation, reflection or refraction measurements compared to double probe density measuring technique 21 p3670 A67-38688

Rayleigh scattered laser light technique for point measurements of time averaged neutral gas density in turbulent wake behind hypersonic velocity body 21 p3565 A67-38876

Sensitivity of film with and without image intensifier compared, using emulsion

densities as function of number of incident quanta 22 p3796 A67-39278

Dielectric susceptibility and ion density measurement for polarized hydrogen plasma moving through transverse magnetic field 22 p3845 A67-39424

Turbulence effect on accuracy of microwave cut-off measurements of plasma density suggests electromagnet wave scattering 22 p3845 A67-39430

Helium argon mixture shock wave density profile measurements, discussing shock wave production in flow field at supersonic nozzle exit 22 p3783 A67-39709

Room temperature density-dose behavior of neutron and gamma irradiated polytetrafluoroethylene (PTFE) noting crystallinity variations 23 p4021 A67-40781

Lunar surface layer soil density limits estimated in simulation study of adhesion, composition, grain size and grain shape effects 23 p4066 A67-41008

Microwave production of plasma in trap at electron cyclotron resonance, investigating absorption and density 23 p4035 A67-41684

Earth density/pressure relation and mantle and core mean atomic weight used to construct mass-mean density curve for planets 24 p4231 A67-42448

DENTISTRY

Dental aspects of manned spaceflight, discussing preventive measures 06 p0954 A67-19030

Emergency dental kit for prolonged space flight, discussing filler materials 23 p3965 A67-41564

DEOXYRIBONUCLEIC ACID (DNA)

Adenine and guanine amounts in DNA determined spectrophotometrically by dialysis of DNA 04 p0564 A67-14406

Streptonigrin interaction with DNA and resulting degradation and denaturation temperature of DNA from salmon sperm and Escherichia coli 06 p0952 A67-17873

Physical characteristics of residual DNA in bacterial cells after degradation due to ionizing radiation 06 p0953 A67-18774

DNA-agar annealing of residual DNA after degradation by ionizing radiation 11 p1746 A67-23919

Alteration in pyrimidine metabolism occurring after infection of E. coli with T-even bacteriophage 20 p3370 A67-36795

Factors involved in use of thymine by uninfected cells in metabolism of Escherichia coli 20 p3370 A67-36799

DEPENDENT VARIABLE

Extension of Pontryagin maximum principle to variable control region, using Hamilton equation 11 p1812 A67-24208

Method of solving for Fourier coefficients expressing dependent variable as piecewise continuous function assuming various conditions of continuity and smoothing 16 p2698 A67-31543

Thermodynamic basis of plasticity, noting loading and unloading stress-strain relations 20 p3541 A67-37283

DEPERSONALIZATION

Clinicopsychopathological method applied to analysis of hallucination, depersonalization and similar effects resulting from exposure to extremal factors from standpoint of space psychology 24 p4112 A67-41856

DEPOLARIZER

Depolarization of cosmic radio emission due to dispersion of Faraday rotation of planes of polarization of radio waves 08 p1376 A67-20813

Cross polarization evaluation radio echo system /CERES/ concept for polarization component separation and echo depolarization evaluation 17 p2814 A67-32520

DEPOSITION

S AUTOMATIC DEPOSITION CONTROL

S ELECTRODEPOSITION

S EPITAXIAL DEPOSITION

S SEDIMENT

S VACUUM DEPOSITION

S VAPOR DEPOSITION

DEPRIVATION

S CONFINEMENT

S SENSORY DEPRIVATION

S SLEEP DEPRIVATION

DEPTH MEASUREMENT

Anomalous skin depths and magnetic probe measurement of oscillating magnetic field penetrating into plasma cylinder 03 p0477 A67-13534

Equatorial electrojet width and intensity analyzed with ground level magnetic field

- measurements from Peru and Nigeria 14 p2312 A67-28572
- Scintillation depth measurement relationship with probability density of amplitude distribution 21 p3617 A67-38002
- DEPTH PERCEPTION**
- SA STEREOSCOPIC VISION
- Holography characteristics and possible future uses noting properties, resolution limits and depth of field of high resolution holographic microscopy 18 p3043 A67-33546
- DERIVATIVE**
- S NEWCOMB DERIVATIVE
- DERMATOLOGY**
- S SKIN /BIOL/
- DESCENT**
- Descent engine for lunar module specifications and operational requirements covering throttling, firing duration, crushable nozzle skirt, etc [AIAA PAPER 67-521] 18 p3115 A67-33984
- Cryogenically stored helium pressurization system for LEM descent stage propulsion system, discussing weight advantages and liquid helium heat transfers 22 p3749 A67-40394
- DESCENT TRAJECTORY**
- Terminal descent design for unmanned vehicle soft lunar landing in Surveyor project [AIAA PAPER 64-644] 02 p0263 A67-11923
- Ascent or descent from initially Keplerian orbit by constant low thrust analyzed by two-variable expansion procedure 04 p0704 A67-14828
- Lunar terrain uncertainties effect on trajectory optimization using Kalman filter during lunar landing powered descent [AIAA PAPER 67-543] 19 p3256 A67-35942
- Ascent and descent gravity turn trajectories of rocket in constant gravitational field, considering drag forces in motion equation [AIAA PAPER 67-596] 19 p3336 A67-35992
- Aerodynamic characteristics of helicopter main rotor during steep descent, using ring vortices method 20 p3356 A67-36443
- Flight phase constraints effect on design of Voyager orbiter-capsule mission 20 p3532 A67-36564
- Lighting and viewing conditions posing visibility problems for lunar landing mission 20 p3521 A67-36598
- Computer analysis and simulation of Mars soft landing descent control system combining inertial and radar sensing techniques 22 p3898 A67-39177
- Parachute descent training for USAF pilots using Para-Sail ascending parachute 23 p3967 A67-41609
- DESERT**
- Ecological patterns of microorganisms in desert soils 15 p2426 A67-29112
- DESERT ADAPTATION**
- Aircraft equipment retrieval after long term storage for periods of up to 23 years under jungle, desert and arctic environment, discussing sealing and hydraulic systems [AIAA PAPER 67-185] 06 p0951 A67-18487
- Soil, moisture and other requirements for microorganism survival in simulated Martian environment 19 p3177 A67-35220
- DESIGN**
- S AIRCRAFT DESIGN
- S AMPLIFIER DESIGN
- S COMPUTER DESIGN
- S ENGINE DESIGN
- S EQUIPMENT SPECIFICATIONS
- S EXPERIMENT DESIGN
- S FACTORIAL DESIGN
- S HELICOPTER DESIGN
- S LENS DESIGN
- S LOGICAL DESIGN
- S REACTOR DESIGN
- S SATELLITE DESIGN
- S SPACECRAFT DESIGN
- S STRUCTURAL DESIGN
- S SYSTEMS DESIGN
- DESPINNING**
- SA SPIN REDUCTION
- Electronically despun switched antenna using variable phase shifters to control phase of incident power to circular array of elements 06 p0967 A67-17684
- Implementation of electronically despun satellite antenna system, considering limits of impracticability because of excessive weight, control power, etc [AIAA PAPER 66-325] 06 p0967 A67-17686
- DESTRUCTION**
- Ballistic aspects, structure and destructive power of Tungusk meteorite do not support thermal explosion hypothesis 15 p2558 A67-30010
- Ballistic aspects, structure and destructive power of Tungusk meteorite do not support thermal explosion hypothesis 20 p3530 A67-37534
- DESTRUCTIVE TESTING**
- SA NONDESTRUCTIVE TESTING
- Static and fracture tests with C-160 /Transall/ transport 01 p0048 A67-10212
- Graphical method for ascertaining acceptance number and size of sample in destructive and expensive testing 09 p1506 A67-22197
- Thermal IR inspection technique for bond flaw inspection in simulated solid propellant rocket engines 09 p1508 A67-22528
- Book on fracture of structural materials covering relation between design and fracture occurrence, fracture types, fracture resistance testing, etc 12 p2013 A67-25362
- Compressor blade failure due to material fatigue, using destructive testing in stationary rig 12 p2014 A67-25413
- Treatise on adhesion and adhesives, Volume 1, Theory 14 p2340 A67-27793
- Standard life-testing experiment in which n similar units are cycled to failure 15 p2495 A67-30414
- Sampling plan for destructive testing, relating quality protection to cost 15 p2584 A67-30421
- Destructive and nondestructive testing of thickness of oxide coatings on Al and Al alloys 22 p3798 A67-39552
- Methodology used to implement high reliability objectives for Surveyor pressure vessels, tabulating burst test results [ASM PAPER C6-2.1] 23 p4071 A67-41411
- DETECTION**
- S AIRCRAFT DETECTION
- S CORRELATION DETECTION
- S ERROR DETECTING CODE
- S FLAW DETECTION
- S INSPECTION
- S SEQUENTIAL DETECTION
- S SIGNAL DETECTION
- S WAVE DETECTION
- DETECTOR**
- SA AIRPORT SURFACE DETECTION
- EQUIPMENT /ASDE/
- SA ELECTRON DETECTOR
- SA INDICATOR
- SA INFRARED DETECTOR
- SA LIFE DETECTOR
- SA NEUTRON DETECTOR
- SA PARTICLE DETECTOR
- SA PHASE DETECTOR
- SA PHOTODETECTOR
- SA PHOTOELECTROMAGNETIC DETECTOR
- SA RADAR DETECTOR
- SA RADIATION DETECTOR
- SA SIGNAL DETECTOR
- SA SILICON RADIATION DETECTOR
- SA SOUND DETECTOR
- SA SYNCHRONOUS DETECTOR
- Geometrical factor and radiation pattern for single crystalline detectors and coaxial telescope 02 p0240 A67-11542
- Diode detector with exponential voltage characteristics 04 p0579 A67-14452
- Leakage measurement, resolution and accuracy of leak detection unit and theoretical and practical minimum leak detectable 04 p0556 A67-15630
- Sensitivity increase in leak detector by using grid to eliminate residual gas from scattered ions 04 p0625 A67-15631
- Helium leak detector characteristics and reception specifications 05 p0804 A67-16302
- Transformation of spectrum of AM periodic sequence of video pulse by inertial detector 07 p1140 A67-19234
- Signal to noise ratio of optical-heterodyne detection system as affected by atmospheric distortion of optical wave front 07 p1144 A67-19786
- Eddy current test systems using magnetic reaction analyzer with Hall element for detector, noting applications to welding, thickness measurement, stress monitoring, etc 09 p1502 A67-21869
- Relay, connector and switch operation simulation, discussing design and performance of chatter and transfer detectors 12 p1943 A67-25702
- Diode detector with exponential voltage characteristics 15 p2443 A67-29289
- Geometrical factor and radiation pattern for single crystalline detectors and coaxial telescope 16 p2677 A67-31608
- Clear air turbulence /CAT/ evaluated to alleviate effects on air traffic, noting forecasting techniques and in-flight and ground-based remote detectors 19 p3254 A67-35931
- Stellar detectors components, describing optical receiving, image tracking and photometric devices 21 p3628 A67-38651
- Spacecraft power conditioning reliability using standby redundancy at functional component level and performance monitoring automatic failure detector 24 p4108 A67-42539
- Power conditioning subsystem failure detection provided by computer monitoring of performance, with signal for transfer to redundant unit [AIAA PAPER 67-983] 24 p4110 A67-43055
- DETERMINANT**
- Solution method for determinantal equation of matrix polynomial 02 p0258 A67-11799
- Sufficient conditions for obtaining finite form solution of ordinary second order differential equations with zero and nonzero determinants 07 p1214 A67-19179
- Number of completely nonsingular $n \times n$ matrices with elements 0, 1 14 p2345 A67-28934
- Recursive formula for updating determinant of covariance matrix of state estimation error after incorporation of measurement 15 p2512 A67-30213
- Stability criterion derivation involving Markov determinants using second method of Liapunov 23 p4022 A67-40648
- DETONABLE GAS MIXTURE**
- Initiation of explosive reaction in liquid mixture of tetranitromethane and benzene by methane-oxygen detonation 06 p1112 A67-17954
- Enthalpy of formation and dissociation of explosion of mixtures of hydrogen and excess nitrogen 06 p0955 A67-17985
- Variation in electric conductivity of gas products from detonation of propane-oxygen-nitrogen mixtures 09 p1581 A67-22581
- Propagation velocity of stable detonation wave in gaseous mixtures measured using Doppler effect resulting from reflection of electromagnetic wave from front of detonation wave 17 p2970 A67-32806
- Detonative ignition induced by shock merging ahead of accelerating flame in hydrogen-oxygen mixture analyzed by stroboscopic laser-schlieren photography 18 p3153 A67-33826
- Chain branching during induction period of hydrogen-oxygen reaction studied by shock heating 18 p2998 A67-34519
- Detonation properties in heterogeneous systems involving mixture of fuel with gaseous oxidant 20 p3551 A67-36815
- Incident step shock wave propagation through convergent channel containing explosive gaseous mixture, discussing detonation initiation 20 p3423 A67-37095
- DETONATION**
- SA EXPLOSION
- SA FIRING
- Soviet book on gas dynamics of combustion including detonation, deflagration, accelerating flames, combustion chambers, etc 02 p0343 A67-12679
- Lead azide and pentaerythrite tetranitrate explosion triggered by laser radiation 07 p1195 A67-19315
- Cavitation induced detonation of stoichiometric liquid mixtures 11 p1884 A67-24956
- Hydrodynamic detonation theory, noting equations of state, nonsteady detonation, further problem areas, etc 16 p2778 A67-30837
- Kinetic and thermodynamic conditions for detonation during chemical reaction in infinite medium involving reaction heat, thermal expansion coefficient and reactants specific volumes 17 p2809 A67-32977
- Electrical detonator characteristics and safety precautions in handling and use,

noting untimely functioning and misfiring as causes of accidents 17 p2927 A67-33093

Unconfined nitromethane transient initiation, determining differential conservation, state and reaction rate equations, using two-dimensional computations 18 p3153 A67-33824

Explosion theory, reviewing chain and thermal theories unification, fuel consumption effects, spatial distribution effects, etc 18 p3155 A67-33845

Perfluorocyclobutane-fluorine combustion studies and measurement of detonation velocities and limits [CI PAPER 67-23] 19 p3345 A67-35013

DETONATION WAVE

Velocity propagation of stable detonations in gas mixtures determined, using Doppler effect obtained by electromagnetic wave reflection 01 p0166 A67-10229

Pyrotechnic shock testing, discussing equipment reliability and performance improvement, shock level reduction and applications [SAE PAPER 660717] 01 p0139 A67-10606

Pressures and temperatures occurring in jet engine exhaust nozzles during speed changes on basis of compression and detonation wave theory 01 p0141 A67-11150

Mach interactions and propagation mode of spinning detonation wave front in stoichiometric oxyhydrogen 02 p0232 A67-11564

Laser light source controlled by Kerr cell coupled with Z-type schlieren optical system to produce multiple flash photographs of detonation wave development 02 p0245 A67-12227

Text describing physical phenomena and experimental apparatus for observing and measuring shock waves and detonations in gases 02 p0235 A67-12680

Supersonic flow past sphere by hot gas mixture with detonation wave in cases when wave does not split and when splitting occurs 03 p0349 A67-12864

Artificial shock wave from TNT explosion in aurora, in attempt to determine effects on auroral emission and temperature 03 p0413 A67-13374

Oscillations in burnt gas coupling to gas dynamical interactions occurring at detonation wave front 03 p0402 A67-13465

Transition to detonation in gaseous medium experimentally studied, based on self-sustained detonation front and adaptation of amplitude modulated giant pulse laser system 03 p0535 A67-13500

Flame reaction rate enhancement by electric fields 03 p0537 A67-14050

Electromagnetic measurement of motion of explosion products behind detonation wavefront, calculating isentrope from mass velocity distribution 04 p0606 A67-15184

Powder admixtures influence on critical diameter of detonation of solid, continuous and macroscopically homogeneous explosive, noting inorganic admixtures role 04 p0723 A67-15197

Polytrope index for gas detonation products determined by velocity ratio for incident and reflected wave during collision of two detonation waves 05 p0927 A67-16999

Plane, cylindrical and spherical shock propagation from point source explosion in gas with counterpressure 05 p0793 A67-17099

Self-similar problems concerning supersonic flows of gaseous fuel mixtures with detonation waves and slow combustion fronts past wedges and cones 06 p0935 A67-17725

Smear camera used to measure detonation front velocity of explosive or propellant 06 p1001 A67-17793

Mass velocity profile measured using electromagnetic device to record emf changes in metal probe embedded in nitromethane flow 06 p1112 A67-17953

Similarity in propagation of detonation waves in gaseous and liquid explosives with respect to homogeneity explained in terms of single detonation reaction 06 p1112 A67-17960

Prediction and scaling of reflected impulse from strong blast wave, with experimental correlation 06 p0984 A67-18059

Turbulence in reaction zone of detonating liquid explosives, noting pressure irregularities in and around shock wave front 06 p1113 A67-18143

Closed form solution methods for blast

wave propagation in solid media assuming power law density profile [AIAA PAPER 67-141] 06 p1102 A67-18290

Streak and open shutter photography of planar detonation wave in channel transmitting through orifice, obtaining induction distance for transition from deflagration to detonation 06 p1119 A67-18596

Plane wave generation in metal plates by detonation of contact explosives, developing elastic-plastic deformation theory for finite stress-strain components 08 p1422 A67-21290

Synchronized shadow photochronographic investigation of wire explosion shock waves in air 09 p1532 A67-22064

Asymptotic law of propagation of plane detonation wave where perturbed motion behind wave transforms it to Chapman-Jouquet wave 09 p1489 A67-22218

Shock and detonation waves in strong localized explosion in combustible gas mixture solved approximately 10 p1733 A67-23040

Elastoplastic properties of copper, aluminum alloys and brass under explosive load, noting increased temperature effect on elastoplastic wave parameters 10 p1668 A67-23092

Uniform shock driven by gaseous detonation induced by exploding wire in single-diaphragm shock tube 10 p1625 A67-23137

Trajectory of rebounding detonation wave in approximate analytic solution of nonlinear equation of motion 10 p1626 A67-23152

Converging cylindrical and spherical detonation wave behavior in polytropic perturbed medium, noting self-similar solution 10 p1628 A67-23684

Nonlinear hydrodynamic stability theory of one-dimensional detonations based on perturbation techniques, detailing cases of ideal gas unimolecular reactions 11 p1774 A67-23857

Matched asymptotic expansions method for developing higher order approximations to structure of laminar detonation wave supported by irreversible unimolecular chemical reaction 11 p1749 A67-23858

Ionized gas flow rate behind detonation wave used with Chapman-Jouquet condition to determine speed of sound in reaction products 12 p1929 A67-25752

Detonation wave interaction with hydrogen-oxygen flow fields in clarifying rocket combustion instability and supersonic combustion 12 p1929 A67-25898

Gas dynamic stability of plane detonation wave propagating in ideal gas mixture, in terms of small perturbations that may result in surface bending and changes in thickness 12 p1930 A67-25965

Chapman-Jouquet theorem for MHD detonation in shock tube blocked by stationary perfectly conducting surface, noting relation to magnetoacoustic wave 12 p1976 A67-26071

Parameters of supercompressed detonation wave in solid propellant system noting wavefront pressure, density and propagation rate dependence on displacement rate of interface 12 p1930 A67-26116

Energy release effects on unsteady gas flow in explosion [AIAA PAPER 66-517] 13 p2106 A67-27582

Low temperature effects on detonation velocity and other explosive parameters for linear shaped charge systems 13 p2230 A67-27686

Stable implosion initiation through converging detonation wave, discussing experimental techniques and results 14 p2293 A67-28141

Finite difference method for treating head-on axisymmetric interactions of blast wave and shock layer in nose region of high speed blunt body 15 p2416 A67-29432

Ionizing detonation wave model with electrical conductivity jumping from zero to infinity characterized by exothermal energy release and magnetoacoustic speed propagation 15 p2528 A67-29567

Detonation characteristics evaluation of solid-composite propellant, noting hazards study program /Project SOPHY/ and critical geometry theory 15 p2544 A67-29999

Changes in structure of gas detonation wave with changes in initial pressure 16 p2656 A67-30452

Asymptotic law of propagation of plane detonation wave where perturbed motion

behind wave transforms it to Chapman-Jouquet wave 18 p3026 A67-33758

Cylindrical expanding detonation waves in gas mixtures, studying detonability limits, propagation velocity and instability and vibratory phenomena 18 p3153 A67-33822

Speed deficits of oxyacetylene detonation waves passing through MHD channel in electromagnetic field explained by Hall effects altering boundary layer 18 p3086 A67-33825

Hydrodynamic structure of exothermic reaction zone behind one-dimensional shock fronts in gaseous detonation studied by optical method 18 p3153 A67-33827

Transverse wave structure in detonations investigated using smoked-foil technique in gas mixtures, showing dependence on tube geometry and heat capacity 18 p3153 A67-33828

Integral curves of two-dimensional shock and detonation waves in gas with varying density 18 p3028 A67-34273

Laser driven plasma detonation waves in gases observed with Schlieren system, discussing shock wave growth 18 p3092 A67-34734

Collapsing shocks and detonation waves gasdynamic problem, evaluating perturbations due to counterpressure and to heat release 19 p3209 A67-35411

Spinning detonation, deflagration instability and normal detonation characteristics 19 p3346 A67-35574

Pressure transducers for use in high temperature and pressure gaseous detonation wave phenomena, discussing performance and application 20 p3443 A67-36514

Detonation properties in heterogeneous systems involving mixture of fuel with gaseous oxidant 20 p3551 A67-36815

Incident step shock wave propagation through convergent channel containing explosive gaseous mixture, discussing detonation initiation 20 p3423 A67-37095

Converging cylindrical and spherical detonation wave behavior in polytropic perturbed medium, noting self-similar solution 21 p3612 A67-38285

Ionization gauge circuit for studies of solid explosives initiation by gaseous detonation waves and reflected wave trajectories in shock tunnels 21 p3630 A67-38770

Imploding shocks and detonations propagation investigated by similarity solution extended to early imploding processes, using Oshima quasi-similar approximation 23 p3992 A67-41722

Friction and heat transfer effects on nonsteady flow behind Chapman-Jouquet detonation to analyze transition to steady flow 23 p3993 A67-41744

Monograph on external burning in supersonic streams, discussing heat addition, fluid-mechanical model, use of characteristics method, Chapman-Jouquet detonation, etc [TG-912] 24 p4254 A67-42386

DETONATOR

Low velocity detonations /LVD/ of liquid explosives indicate shape and container material and presence of witness plate affect initiation 23 p4081 A67-40635

DEUTERIDE

Energetic and angular studies of argon deuteride and nitrogen deuteride positive ion formation using angular ion scattering apparatus 05 p0848 A67-16835

DEUTERIUM

SA HYDROGEN

Nuclear magnetic resonance and microwave spectra of some deuterio derivatives of 2, 4-dicarbaclavoheptaborane-7/ [JPL-TR-32-1038] 01 p0019 A67-11146

Galactic deuterium and energy spectrum above 20 mev per nucleon measured by IMP-III satellite near minimum solar activity 03 p0472 A67-13390

Deuterium nuclei generation in galactic cosmic radiation 05 p0878 A67-16096

Large deuterium isotope effect on fluorescence emission spectra and quantum yields observed in number of chromospheres that contain proton donor groups 05 p0758 A67-16701

Energy distributions of hydrogen and deuterium ions from dissociative ionization of hydrogen and

deuterium 17 p2889 A67-33226
Hydrocarbon pyrolysis and H/D
substitution reaction rates, using single-pulse
shock tube as chemical
reactor 18 p2996 A67-33788
Selective enhancement of molecular
spectra of HD and diatomic deuterium in
argon and krypton
discharges 18 p3083 A67-34518
Ion-molecule reactions of diatomic
deuterium cation with diatomic deuterium
and diatomic hydrogen 18 p3083 A67-34521
Optical pumping of sodium vapor with
deuterium light, discussing optical
transparency in excited state mixing cross
sections 21 p3639 A67-38018
Deuterium-tritium plasma temperature
measurement using neutron detector,
assuming Kerr cell ruby laser produced
thermonuclear reaction heating in
gas 23 p4031 A67-40892
Deuterium nuclei generation in galactic
cosmic radiation 24 p4213 A67-42772

DEUTERIUM OXIDE
SA HYDROGEN DEUTERIUM OXIDE
Frequency measurement of gas laser
transitions in heavy water and acetylene
discharges 16 p2685 A67-30824
Hyperfine structure in rotational spectrum
of HDO and deuterium oxide analyzed by
beam maser spectroscopy, evaluating
coupling constants 20 p3461 A67-37287
Far IR maser oscillators with water and
deuterium oxide, presenting construction
and operating
characteristics 21 p3639 A67-38253

DEUTERIUM PLASMA
Confinement times and density of
deuterium plasma produced by ion cyclotron
resonance heating in C
stellatorator 03 p0485 A67-14049
Radial implosion of deuterium in theta
pinch in which initial level of ionization was
controlled, relating diamagnetism of plasma
to mass of gas in motion 04 p0671 A67-15646
Deuterium plasma heating by multiply
charged hot impurity ions 19 p3287 A67-35357
Deuterium plasmod structure, impurity
distribution, passage through pulsed
magnetic barrier and capture by longitudinal
magnetic field with mirror
geometry 19 p3288 A67-35364

DEUTERON
Isospin impurity mixing in distorted
deuteron reaction 02 p0270 A67-12526
Deuteron ion fluxes studied using plasma
accelerator called Pleiade 04 p0672 A67-15647
Primary cosmic ray proton and deuteron
flux near geomagnetic equator determined
by nuclear emulsion 10 p1703 A67-23543
Absolute cross sections and isomeric yield
ratios for /d,p/ reactions up to 15 mev in
various metals 14 p2350 A67-27790

DEUTERON IRRADIATION
Peak effect in critical current of
superconductors observed during deuteron
irradiation at low
temperature 01 p0135 A67-10880
Low temperature deuteron irradiation
effect on type II superconductors noting
atomic displacement, resistivity increase and
transition temperature
decrease 12 p1985 A67-25845

DEVIATION
S ABERRATION
S ECCENTRICITY
S PHASE DEVIATION
S STANDARD DEVIATION

DEVICE
S CARTRIDGE ACTUATED DEVICE
S COMMUNICATIONS DEVICE
S CONTROL DEVICE
S DISCONNECT DEVICE
S DRAG DEVICE
S ELECTROEXPLOSIVE DEVICE
S ELECTROMECHANICAL DEVICE
S ERROR CORRECTING DEVICE
S EXPLOSIVE DEVICE
S FANLIFT DEVICE
S FEEDING DEVICE
S HEAT REJECTION DEVICE
S HOMING DEVICE
S INFLATABLE DEVICE
S INSTRUMENT
S LANDING DEVICE
S LAUNCHING DEVICE
S LIFT DEVICE
S PROPELLANT ACTUATED DEVICE
S RECOVERY DEVICE
S RESISTANCE DEVICE

S SAFETY DEVICE
S SAMPLING DEVICE
S SCANNING DEVICE
S SEMICONDUCTOR DEVICE
S SOLID STATE DEVICE
S STORAGE DEVICE
S SUN TRACKER DEVICE
S WARNING DEVICE

DEWAR SYSTEM
Liquid hydrogen use in nuclear rocket
testing, noting Kiwi reactor, Dewar system,
transfer line, etc 05 p0789 A67-17013
Light-weight liquid helium dewar for use
on Apollo spacecraft 13 p2057 A67-27682
Lightweight liquid helium dewar for LEM
program, with 670 liter capacity, 10 percent
ullage and 1.5 percent boiloff per
day 22 p3808 A67-40391

DH-121 AIRCRAFT
S DE HAVILLAND DH-121 AIRCRAFT

DIAGNOSIS
SA FUNCTION TEST
Value of routine abdominal X-ray during
aeromedical evaluation, noting number and
significance of abnormalities
detected 10 p1601 A67-23828
Medical testing, research and control
during manned space flights, discussing
diagnostic algorithms for onboard computer
and frequency of data
collection 13 p2062 A67-26762
Mathematical model for computer
diagnosis of system failure, developing
optimal policy for searching malfunctions
with observable
symptoms 18 p3006 A67-34065

DIAGRAM
S BENDING DIAGRAM
S CREEP DIAGRAM
S ENTHALPY-ENTROPY DIAGRAM
S EQUILIBRIUM DIAGRAM
S EUTECTIC DIAGRAM
S FATIGUE DIAGRAM
S FEYNMAN DIAGRAM
S GRAPH
S HERTZSPRUNG-RUSSELL DIAGRAM
S PHASE DIAGRAM
S S-N DIAGRAM
S STRESS-STRAIN DIAGRAM

DIAMAGNETISM
Behavior of diamagnetic particles in
moving magnetic field with respect to
propulsion and MHD technology in space
vehicles 04 p0687 A67-14546
Radial implosion of deuterium in theta
pinch in which initial level of ionization was
controlled, relating diamagnetism of plasma
to mass of gas in motion 04 p0671 A67-15646
Energy required to confine static shielded
magnetic dipole field, immersed in highly
conducting medium, by transient
diamagnetic surface as function of dipole
moment and disturbance
field 06 p1030 A67-17658
Inductance, flow current and external
magnetic field effects caused by
diamagnetism of superconducting solenoid
winding 06 p1051 A67-18207
Exciton and oscillatory magnetoabsorption
spectra in layer type semiconductors in high
magnetic fields 06 p1060 A67-18917
Hall coefficient and transverse
magnetoresistance behavior in n-GaSb at 4.2
degrees K, using DC high magnetic
fields 06 p1064 A67-18946
Shubnikov-de Haas effect and electron
band structure of cadmium arsenide,
investigating temperature and orientation
dependencies 06 p1064 A67-18947
Quantum oscillations in magnetoresistance
of n-type pure HgTe used to estimate
electron effective mass and g value close to
band edge 06 p1065 A67-18948
Energy surfaces of tellurium investigated
with oscillatory magnetoresistance
/Shubnikov-de Haas
effect/ 06 p1065 A67-18949
Fermi surface of tin telluride
approximated by four distorted surfaces
located at L points of Brillouin zone as
shown by Fourier analysis 06 p1065 A67-18950
De Haas-van Alphen effect in arsenic,
noting two kinds of oscillations /Fermi
surface and thin cylindrical surface/ and
doping effect 06 p1070 A67-18982
Band structure of Bi-Sb alloy system,
using Shubnikov-de Haas technique with
supplemental transport
measurements 06 p1070 A67-18983
De Haas-Shubnikov effect observation
method and application to measurements on

bismuth 07 p1155 A67-18891
Surface current change between critical
paramagnetic and critical diamagnetic
induced by temperature variation in type II
superconductor immersed in static magnetic
field 14 p2365 A67-28296
Diamagnetic properties of plasma
described by extended field equations
suggest existence of steady state inductive
power transfer between plasma and
magnetic fields 17 p2898 A67-32178
Hysteretic superconductor, analyzing
critical state and constrained reversibility
relations in diamagnetic and temperature
paths 17 p2912 A67-32269
HF electrostatic instability in low density
plasma stream guided by magnetic field,
discussing cause and anomalous loss of
diamagnetism 17 p2907 A67-33106
Inductance, flow current and external
magnetic field effects caused by
diamagnetism of superconducting solenoid
winding 17 p2922 A67-33221
Superconducting devices utilizing
transition, zero resistivity and diamagnetic
properties of materials in that
state 22 p3808 A67-40398

DIAMANT LAUNCH VEHICLE
Debugging of Emerald propulsion system
of Diamant launch vehicle, stressing
problems with combustion chamber
instabilities, vibrations,
etc 01 p0155 A67-11389
Diamant program research and
development in servomotor, first stage
engine and structural
vibration 07 p1131 A67-19520
Diamant solid propellant booster
development 07 p1240 A67-19521
Diamant third stage and nose
cone 07 p1258 A67-19522
Diamant mechanical subsystems and
programmer 07 p1258 A67-19524
DI satellite structure noting rigidity and
shock absorbing
properties 07 p1258 A67-19526
French space program /1966-1970/
techniques and installations for satellite
launching and tracking 14 p2409 A67-28605
Hypersonic reentry, inertial guidance tests
and construction of two-stage Diamant
satellite launcher 15 p2571 A67-30089
Diamant satellite series, describing design
and construction of Diapason and Diadem
orbital satellites 17 p2956 A67-32746
Solid propellant stages development from
experience acquired in France to future
large space projects 20 p3516 A67-36878
High reliability sequence programmers for
DIAMANT satellite booster switching
functions 21 p3655 A67-38207
Diamant launcher transmitter
characteristics noting anomalies during first
two firings 21 p3581 A67-38226

DIAMOND
Electric-field-induced IR absorption in
diamond type crystals with Raman-active
vibration modes 03 p0492 A67-13260
Laser system for diamond piercing in
wire-drawing dies and closed circuit TV
viewing system for monitoring
operation 04 p0628 A67-15309
Magnetic field strength effects on excited
acceptor states of semiconducting diamond
determined, using Zeeman splittings of main
excited lines 06 p1062 A67-18927
Plastic deformation of diamonds due to
differences in initial defect distribution
examined by birefringence, X-ray topography
and electron microscopy 08 p1346 A67-20795
Hexagonal diamond content of Canyon
Diablo and Goapara
meteorites 08 p1400 A67-21264
Band-to-band radiative recombination in
semiconductor groups IV, VI and III-V,
presenting data on diamond, Si, Ge, Se and
Te 09 p1558 A67-22601
Electrical resistance of semiconducting
diamond measured by pulse
method 12 p1939 A67-25332
Growth mechanisms and crystalline quality
of diamond type compounds and crystals in
III-V and II-VI groups 13 p2177 A67-27009
Diamond electronic structure studied by
absolute reflectance measurements,
obtaining dielectric response function over
broad energy range 22 p3862 A67-39999
Semiconducting diamonds photoconductive
response measured noting correlation with
activation energy 23 p4044 A67-41454

DIAPHRAGM

Waves with complex propagation constants in diaphragmed circular waveguide, solving dispersion equation for various frequencies and structural parameters of waveguide 04 p0575 A67-15214

Partial diaphragm when applying supersonic Mach box method for steady state condition and uniform downwash on wing compared with complete diaphragm 06 p0944 A67-18875

System for rupturing diaphragms in single pulse shock tube, noting time decay role 13 p2090 A67-27060

Static operating characteristics of diaphragm pneumatic logic device 14 p2275 A67-28347

Waves with complex propagation constants in diaphragmed circular waveguide, solving dispersion equation for various frequencies and structural parameters of waveguide 15 p2438 A67-30262

Plane shock wave velocity measurement after interaction with obstacles in form of channeled diaphragms of various diameters, discussing stabilization 18 p3028 A67-34210

Deflection and stresses in corrugated diaphragm rigidly clamped on contour with distributed pressure and concentrated central force, using finite difference approximation 21 p3717 A67-37977

Limiting driven conditions corresponding to optimum expansion and low density shock tube flow for overexpanded nozzle 21 p3809 A67-38886

Constrained torsion computation for multispar box with elastic diaphragms assuming applied stresses at end ribs 21 p3728 A67-38906

HF plane waves diffraction on plane circular diaphragm solved by functional theoretic methods for integral equation for Fourier transform of screen covering 22 p3912 A67-39783

DIATOMIC GAS

Oscillatory relaxation of heavy two-atom molecules during single-quantum energy transitions in light-gas 02 p0269 A67-12422

Diatomic gas flow past blunt bodies, noting effect of oscillation and dissociation relaxation on mean energy 02 p0180 A67-12465

Nonequilibrium expansion of high temperature diatomic gas through hypersonic convergent-divergent nozzle 02 p0180 A67-12547

Pressure induced monochromatic translational absorption coefficients for homopolar and nonpolar gases and gas mixtures, with application to molecular hydrogen 03 p0515 A67-14323

Plasma formation by dissociation of diatomic hydrogen ions by Lorentz force 04 p0671 A67-15645

Thermodynamic functions of diatomic gases with molecules in 3-sigma electron state 07 p1225 A67-19121

Diatomic molecular ion composition and variation of effective recombination coefficient in ionosphere in terms of altitude, time of day, solar activity, temperature, etc 10 p1630 A67-22788

Equation of relaxation hydrodynamics for diatomic perfect gas when rotational and translational degrees of freedom are in equilibrium and dissipation has not set in 10 p1590 A67-23024

Quantum mechanical kinetic theory of gas loaded spheres to obtain limit of transport coefficients and relaxation time 10 p1682 A67-23383

Interactions of homonuclear diatomic gas molecules with fcc solid surfaces calculated by digital computer 13 p2098 A67-26938

Free stream variables from continuum effect followed experimentally into transition flow regime to investigate impact probe in rarefied hypersonic flows of diatomic gases 14 p2294 A67-27794

Shock structure in diatomic gas described using Mott-Smith bimodal distribution function, including relaxation effects 15 p2469 A67-29217

Diatomic gas vibrational relaxation by master equation analysis, discussing quasi-steady state vibrational population distribution and transition probability increases 18 p3081 A67-33782

Ion-molecule reactions of diatomic deuterium cation with diatomic deuterium

and diatomic hydrogen 18 p3083 A67-34521
Mach number effect on electron temperature structure of partially ionized monatomic and diatomic gas shocks 21 p3610 A67-37760

Thermodynamic functions of diatomic gases with molecules in 3-sigma electron state 21 p3659 A67-38166

Diatomic molecular ion composition and variation of effective recombination coefficient in ionosphere in terms of altitude, time of day, solar activity, temperature, etc 24 p4149 A67-42124

DIATOMIC MOLECULE

Vibrational-rotational motion effect on electric and magnetic properties of diatomic molecules, calculating magnetic susceptibility and rotational magnetic moment 01 p0117 A67-10784

Continued fraction in theory of electron energy for ground state of one-electron diatomic molecule near united atom 01 p0118 A67-10886

Franck-Condon factors and transition probabilities of electron oscillatory transfers in diatomic molecules 03 p0471 A67-13314

Rate equation for dissociation and recombination of diatomic molecules 03 p0473 A67-13521

Atomic and molecular absorption and emission in middle UV region of electromagnetic spectrum, noting energy levels, electronic transitions and oscillator strengths 04 p0660 A67-14692

Rotational relaxation times for homonuclear diatomic molecules 06 p1037 A67-19043

Energetic metastable diatomic oxygen molecule excited by electron impact studied with high sensitivity molecular beam apparatus 10 p1682 A67-23386

Shock tube study of oscillator strength of diatomic molecular carbon Swan bands 11 p1750 A67-25066

Transport coefficient expressions for collisions between rigid diatomic molecules, using perturbation method 14 p2259 A67-28298

Franck-Condon factors and transition probabilities of electron oscillatory transfers in diatomic molecules 16 p2703 A67-30490

Attenuation cross section at Lyman alpha for Xe deviation from Beer law indicating diatomic Xe molecule formation 20 p3491 A67-37688

Electron scattering from diatomic molecules in fixed nucleus approximation using polarized single-center orbitals method applied to positively ionized hydrogen 20 p3491 A67-37689

S-matrix computations for quantum transitions, considering close coupling case of homonuclear diatomic molecular rotational excitation 21 p3659 A67-38005

Dissociation and recombination of diatomic molecules by invert third bodies described by stochastic theory 22 p3756 A67-39386

DIAZIRINE

Imines reacting with difluoramine produce diazirines and other products having potential as missile propellant components 01 p0020 A67-11147

DIBORANE

Gas phase oxidation of diborane in furnace-heated vessels and flash photolysis 06 p0955 A67-18058

Reaction mechanism between oxygen difluoride and diborane based on visual observation, gas composition and pressure-temperature relationships [CI PAPER 67-10] 19 p3309 A67-35005

DIBORIDE

SA TITANIUM DIBORIDE

X-ray microstructural and chemical analysis of sintering of zirconium diboride-molybdenum disilicide alloys 01 p0102 A67-11242

High temperature thermal expansion of Ti, Zr, Hf, Nb and Ta diborides 10 p1697 A67-23380

X-ray, microstructural and chemical analysis of sintering of zirconium diboride-molybdenum disilicide alloys 17 p2875 A67-33167

DICARBOXYLIC ACID

Esterification rates of aliphatic carboxylic acids, acid terminated polybutadienes, etc, and steric environment in vicinity of acid groups 04 p0564 A67-14473

DICKE TYPE RADIOMETER

Cosmic microwave background

measurements along celestial equator, using Dicke radiometer to study anisotropy of cosmic black body radiation 11 p1864 A67-24564

Microwave radiometric measurements of planetary disk temperature of Venus, Mars, Jupiter and Saturn 11 p1869 A67-25094

On-line computers in radio astronomy for measuring radio source flux, position and width and for increasing Dicke radiometer sensitivity 14 p2275 A67-28439

Ionization-enhanced microwave resonant radiation from model rocket exhausts studied using Dicke type radiometer 20 p3543 A67-36233

Radiometric determination of absorption by earth atmosphere and solar brightness temperature at 5.65 mm frequency 22 p3897 A67-40560

Equivalent temperature of cosmic microwave background radiation at 3.2 cm wavelength, discussing Dicke type radiometer and error sources 23 p4063 A67-40922

DICTIONARY

Computer dictionary and handbook 04 p0579 A67-15947

DIE

Hot pressing of electrolytic grade CR beryllium, noting powder manufacturing process and quality control procedure 01 p0099 A67-10707

Laser system for diamond piercing in wire-drawing dies and closed circuit TV viewing system for monitoring operation 04 p0628 A67-15309

Influence of explosive forming characteristics on springback based upon tests in forming of gore sections for Saturn V rocket 10 p1660 A67-23170

Photomask application to microelectronics chip and die fabrication, discussing systems for step-and-repeat operation elimination in image array making 19 p3236 A67-35021

DIELECTRIC CONSTANT

Optical and magneto-optical phenomena in CdSnAs sub 2, discussing reflection and absorption spectrum, optical activity, double refraction, dielectric constant, etc 01 p0128 A67-10094

Far IR absorption and dielectric constant of liquid water 01 p0115 A67-11082

Permittivity determination based on change in polarization of wave at reflection 02 p0191 A67-11578

Emission of point oscillator located in medium having permittivity varying according to traveling wave law 02 p0192 A67-11643

Dielectric behavior and point imperfections of high temperature KCl in microwave frequency range 02 p0299 A67-11896

Criteria for cold plasma density necessary to stabilize grade B drift waves in finite length energetic plasmas 02 p0275 A67-12554

Dielectric constant of homogeneous fully ionized two-temperature plasma for determining conditions under which ion waves can be found 02 p0275 A67-12555

Induced absorption coefficients in atmosphere model measured for calculation of Venus lower atmosphere properties from radio observations 03 p0394 A67-12949

Mechanical pressure effect on polarization processes in barium titanate single crystals and barium titanate-zinc oxide solid solutions 03 p0489 A67-13145

Low intensity shock wave transformation into rarefaction wave in nonconducting media in presence of external electric field 03 p0476 A67-13203

Shallow donor potential in silicon 03 p0493 A67-13363

Permittivity of barium titanate single crystals with laminar domain structure 03 p0497 A67-13699

Slow polarization processes of barium titanate in weak field 03 p0497 A67-13702

Classification of ions capable of replacing Ti in barium titanate 03 p0497 A67-13703

Permittivity of barium titanate ferroceramic materials determined by various methods 03 p0498 A67-13705

Radiative modes of thin infinitely long circular plasma cylinder with dipolar azimuthal field variations 03 p0484 A67-14044

Radio data suggests dielectric constant variations in troposphere limited to discrete scale sizes [RASSA PAPER 1-10-141] 03 p0417 A67-14249

- Comparison of decomposition rate for pure ammonium perchlorate, chlorate ion doped ammonium perchlorate and X-rayed ammonium perchlorate at 236 degrees C 04 p0687 A67-14635
- TE modes propagation in rectangular waveguides containing two dielectric slabs, computing cut-off frequencies and propagation constants 04 p0570 A67-14860
- Dielectric permittivity of barium titanate monocrystals with anisotropic stratified domain structure 04 p0678 A67-15131
- Resistivity, dielectric constant and junction depth changes in semiconductor materials by exposure to electron beam 04 p0681 A67-15314
- Optical self-absorption and dielectric constant of cadmium oxide thin film in case of high electron degeneration 04 p0683 A67-15655
- Vacuum resonant-cavity dielectrometer for in situ measurements of complex permittivity in simulated space environment 04 p0625 A67-15708
- Wave scattering by smooth and rough finite cylinder situated in layer with randomly varying dielectric constant analyzed by approximation of physical optics 05 p0762 A67-16349
- Frequency modulation of GaAs semiconductor laser by ultrasonic wave modulation of dielectric constant 05 p0821 A67-16671
- Temperature dependence of dielectric constant and existence of microwave dispersion in barium titanate above Curie point 05 p0868 A67-17060
- Thin film dielectric constant and loss tangent measured by HF capacitance meter 05 p0871 A67-17483
- Precipitation effect of dispersed calcium titanate-rich phase on shape, organization and thickness of ferroelectric domains in barium titanate 06 p1020 A67-18047
- Electromagnetic wave propagation around cylinder surrounded by nonmagnetic isotropic medium with dielectric constant function of radius, using conformal mapping 06 p0962 A67-18076
- Corrections for dielectric-constant tensor and conductivity tensor resulting from effect of electric field induced by plasmoid 07 p1229 A67-19517
- Discrete spectrum of electromagnetic waves caused by excitation of dielectric layer on ideally conducting plane in homogeneous absorbing plasma 08 p1295 A67-20832
- Lunar observation in wavelength range one to three mm, noting brightness temperature drop during total eclipse, obtaining dielectric constant 08 p1390 A67-21022
- Lunar radio brightness distribution measured at various wavelengths, determining surface temperature decrease and dielectric constant 08 p1390 A67-21023
- Complex dielectric constant and EM plane wave propagation in flame plasma 08 p1359 A67-21045
- Dielectric relaxation of gases and sharp rise in microwave absorption coefficient in Cytherean atmosphere 08 p1401 A67-21372
- Semiconductor conductivity in strong SHF electric fields, measuring dielectric constant and Fourier component 10 p1657 A67-23567
- Inertialess polarization energy of charge interaction between neighboring lattice points in Ge crystal, using M-20 computer 10 p1695 A67-23657
- Dielectric constant of very low loss materials at mm wavelengths measured by oversized rectangular waveguide technique 11 p1792 A67-24764
- Dielectric and electro-optic properties of lead magnesium niobate, noting second order ferroelectric transition 11 p1803 A67-24834
- High resistivity cadmium selenide vacuum deposited films dielectric constant and electronic properties measured for different parameters 11 p1851 A67-25032
- Dielectric permittivity of barium titanate monocrystals with anisotropic stratified domain structure 12 p1978 A67-25155
- Thin film capacitor dielectrics of silicon oxides and various metal oxides, noting influence on vacuum deposited compounds 12 p1918 A67-26210
- Dielectric properties applied determination of degree of reticulation of polymers during polymerization, noting losses due to free electrons and dipoles 14 p2340 A67-27898
- [ONERA-TP-476]
- Barium titanate polycrystal dielectric constant aging, discussing 90 degree splitting in domain structure 14 p2364 A67-28228
- Electric breakdown, dielectric constant and dissipation factors of cryogenic liquid nitrogen, hydrogen and helium 14 p2341 A67-28891
- Electric conductivity of p-Ga-Te polycrystals and single crystals in strong electric fields 14 p2375 A67-29085
- Transconductance and voltage gain of MOS/FET using hafnium dioxide 15 p2442 A67-29171
- Impedance and effective dielectric constant analysis for transmission line, with approximate theoretical solutions and experimental verification 15 p2444 A67-29455
- Absolute reflectance of RbI and KI between 300 and 77 degrees K, noting spin orbit interaction effects and values of dielectric parameters 15 p2520 A67-29768
- Temperature dependence of dielectric constant and existence of microwave dispersion in barium titanate above Curie point 15 p2538 A67-29791
- Significant-structure theory of liquids applied to rocket fuels, calculating vapor pressure, thermal expansion, dielectric constant, etc 16 p2734 A67-31537
- Dielectric constant measurement of solids at microwave frequencies, noting performance of solid dielectrics as temperature function 16 p2678 A67-31720
- Inertialess polarization energy of charge interaction between neighboring lattice points in Ge crystal, using M-20 computer 17 p2924 A67-33338
- Gallium arsenide single crystal lattice dielectric constant measured noting broad resonance 18 p3101 A67-34010
- Customary formulas for various effects including Thomson scattering, electron-ion, bremsstrahlung, etc, in context of plasma radiation theory 19 p3284 A67-35340
- Plasma wave influences on metal surface reflectivity investigated using Maxwell equation, calculating dielectric constant and conductivity 19 p3262 A67-35581
- Inhomogeneous plasma oscillations, studying drift and flute instabilities and dielectric constant 20 p3492 A67-36130
- Quantum mechanical transition time shown to be electron tunneling characteristic time 20 p3505 A67-36178
- Stolzite and scheelite single crystal dielectric constant 20 p3505 A67-36179
- Nonresonant third order dielectric susceptibility coefficients of gases measured in four-wave mixing experiment to calculate harmonic radiation in laser beam 21 p3639 A67-38008
- Ferroelectricity of barium titanate thin films noting dielectric, temperature, polarization and electric field variations 21 p3687 A67-39142
- Dielectric susceptibility and ion density measurement for polarized hydrogen plasma moving through transverse magnetic field 22 p3845 A67-39424
- Diamond electronic structure studied by absolute reflectance measurements, obtaining dielectric response function over broad energy range 22 p3862 A67-39999
- Dielectric cover effect on resonant frequency of slots in rectangular waveguide, using Stevenson free space theory and plane-wave reflection coefficient 23 p3978 A67-40824
- Laser mode synchronization by electro-optical crystal dielectric constant modulation mounted inside resonator 23 p4013 A67-40903
- Field of loop antenna with arbitrary current distribution located inside cylinder with arbitrary dielectric constant studied for effects on radiation pattern 23 p3982 A67-41666
- Dielectric function of semiconductor in external electric field, discussing effect on plasma frequency 24 p4201 A67-41979
- Ferroelectric, electro-optic and dielectric properties of tetragonal potassium-niobate-strontium-niobate crystal 24 p4204 A67-42366
- Conversion of solar-thermal to electrical energy by capacitance-change pumping of thermoelectric thin films, noting space environmental chamber tests 24 p4108 A67-42555
- Oscillation of fluid metal droplet, free or immersed in fluid dielectric, in steady and uniform magnetic field 01 p0120 A67-10181
- MHD effects during motion of dielectric shell in electrolyte in presence of external magnetic field 01 p0120 A67-10185
- Excitation of phosphor suspensions in solid dielectric by mechanical energy analyzed via impact theory 01 p0113 A67-10354
- Ellipsometer study of anomalous absorption in very thin dielectric films on evaporated metals 01 p0138 A67-11075
- Optical scattering cross sections for polydispersions of dielectric spheres, showing dependence on ratio of third to second moment of shape and size distribution function 01 p0115 A67-11077
- Impedance matching of infinite phased array by dielectric sheets, noting radiation pattern dependence on beam scan angle 01 p0040 A67-11312
- Cerenkov radiation of beam-plasma system into dielectric, using mathematical model and mode coupling theory 01 p0040 A67-11314
- Electromagnetic theory of wave propagation modes in dielectric cylinders applied to coherent light transmission in optical fibers 02 p0190 A67-11528
- Artificial nonlinearization method of solving linear second order equations with variable coefficients, with application to two-dimensional electromagnetic propagation along inhomogeneous dielectric layers 02 p0191 A67-11572
- Plane problem of surface electromagnetic wave scattering along rectangular dielectric wedge 02 p0191 A67-11579
- Substantial size reduction of conical log-spiral antenna by loading with magnetodielectric material 02 p0212 A67-11612
- Propagation constant derived for electromagnetic waves propagating along array of parallel thin wires located in plane dielectric layer 02 p0192 A67-11642
- Internal stresses of thin metallic and dielectric films, discussing methods for stress measurement, stress models and formulas 02 p0287 A67-11717
- Current density resulting from integration over energy of transport equation applicable to dielectric film 02 p0295 A67-11763
- Propagation characteristics of cylindrical waveguide partially filled with dielectric light modulation material 02 p0193 A67-11780
- Dielectrophoretic propellant orientation systems design, noting electrode requirements and avoidance of electrohydrodynamic instabilities [AIAA PAPER 66-922] 02 p0301 A67-12275
- Ferrite resonant isolators on coaxial, strip and rectangular waveguides with dielectric 02 p0223 A67-12670
- Composite metallic and dielectric insulators for high current arc electrodes 02 p0250 A67-12697
- Value and sign of phase jump taking place during light reflection from multilayer dielectric film 03 p0467 A67-12892
- Critical conditions of waveguide with dielectric bushing for case of nonsymmetrical waves 03 p0378 A67-13287
- Diffraction of plane wave at sinusoidally stratified dielectric grating, using hologram analysis 03 p0423 A67-13905
- Thin film piezoelectric transducers properties used in microwave acoustic delay lines and phonon generators for analysis of phonon-phonon interactions in dielectric materials 04 p0621 A67-15116
- Millimeter wavelength transmission line deficiencies reduced by using channeling systems in form of elastic dielectric tape on which are mounted thin metallic strips 04 p0575 A67-15167
- Electron beam float-zone melting process applied to dielectric compound aluminum trioxide to obtain sapphire crystals 04 p0628 A67-15320
- Combined free and forced convection over electrically insulating vertical plate of constant temperature with transverse magnetic field with plate moving up or down [ASME PAPER 66-WA/HT-38] 04 p0724 A67-15429
- Extremely high reflective dielectric mirror coatings with zinc selenide for laser resonator cavities and interference filters 04 p0634 A67-15654

Spontaneous dielectric breakdown in Plexiglas sheets due to pulsed electrons with breakdown plane influenced by embedded metal foils 04 p0659 A67-15699

Antenna feed eliminating compromise between antenna illumination and spillover efficiencies by placing dielectric guiding structures between primary feed and reflector 04 p0590 A67-15903

Electromagnetic field emission of infinite package of impedance half-planes produced by cophasal linear sources 05 p0762 A67-16352

Josephson current in alternating field between two superconductors separated by dielectric barrier 05 p0853 A67-16697

Electromagnetic wave emission excited by electron stream over diffraction grating lying on boundary of semiinfinite anisotropic dielectric 05 p0766 A67-17163

Approximation of space wave plus complex wave using modified saddle point technique 05 p0766 A67-17297

Optical properties of interstellar grains, noting complex index of refraction as function of wavelength 06 p1087 A67-18410

Continuous high resolution measurement of solid propellant burning rate using resonant LC circuit [AIAA PAPER 67-69] 06 p1072 A67-18450

Spectral transmission of far IR Michelson interferometer with dielectric film beam-dividers 06 p1005 A67-18716

Value and sign of phase jump taking place during light reflection from multilayer dielectric film 06 p1034 A67-18770

Dielectric properties of complete solid solutions with perovskite structures in barium titanate-barium stannate and barium titanate-barium ferrotantalate systems 07 p1231 A67-19489

Sensitivity of dielectric rod terminal impedance to surface wave coupling when no resonance regions exist within energy-carrying cross section 07 p1158 A67-20299

Steady state heat flow in dielectric cylinders in boundary scattering limit, considering liquid helium 08 p1426 A67-20716

Equations for ionized positive plasma column of gas discharge between infinite dielectric planes under oblique magnetic field with component in direction of external electric field 08 p1358 A67-20849

Dielectric properties including permittivity, losses, polarization, impurity conduction and forbidden bandwidths of thin films of praseodymium, cerium and neodymium fluorides 08 p1370 A67-20995

Bibliography on thin dielectric films, interfaces and surfaces 08 p1370 A67-21188

Envelope and phase velocities for laser pulse propagating in nonlinear dielectric with intensity dependent index of refraction 09 p1511 A67-21748

Electrostatic oscillations in dielectric, semiconductor and plasma in presence and absence of external magnetic field 09 p1555 A67-22011

Dielectric isolation techniques for elements of integrated circuit 10 p1610 A67-22971

Nondestructive testing of dielectric materials by microwave techniques 10 p1660 A67-23014

Refractive index of microwave lenses made of ferrite material changed by varying DC magnetic field 11 p1752 A67-24125

Radiating slot on dielectric clad cylinder, solving wave equations and finding field expressions via harmonic series representation 11 p1761 A67-24280

Transmission line approach for determining input admittance of slotted antenna array covered by dielectric sheet 11 p1762 A67-24293

Impedance of strip antenna embedded in dielectric layer overlain by cold plasma, considering reflection coefficient and static magnetic field effect 11 p1763 A67-24305

Laser-produced dielectric breakdown at particle sites in liquids with resulting absorption of secondary light beam 11 p1801 A67-24560

Hydrodynamic and overheating instability of nonisothermal plasma flux in crossed electric and magnetic fields in flat dielectric walled channel 11 p1842 A67-24950

Excitation of phosphor suspensions in solid dielectric by mechanical energy analyzed via impact theory 11 p1851 A67-25027

Dielectric isolation of integrated circuit via ceramic medium, discussing technique, testing and results 12 p1916 A67-25997

HF properties of laser cavities with anisotropic dielectric filling, calculating Q-factor and shunt resistance 13 p2075 A67-26399

Anodic oxides of titanium, tantalum and niobium from thin dielectric film preparations compared, determining nature and characteristics 13 p2175 A67-26654

Anisotropy in thin dielectric films of tantalum and titanium anodic oxide from various measurements explained by transistor-like model 13 p2175 A67-26655

Microwave interferometer with dielectric rods as waveguides for measuring electron density in small volume inside plasma 13 p2120 A67-26859

Vacuum deposition techniques for production of optical film materials for neutral density filters and sunglasses, discussing dielectric, metallic, reflecting and semitransparent films 13 p2158 A67-27076

Transition temperature change for thin tin and thallium superconducting films after deposition of dielectric substances 13 p2182 A67-27360

Laminar boundary flow over dielectric disk with homogeneous magnetic field perpendicular to plane of disk, obtaining liquid velocity and electric field density 14 p2358 A67-28282

Thin film passive elements for monolithic integrated circuits, using cermet and dielectrics 14 p2286 A67-28610

Chemical deposition of dielectrics for thin film circuits and components 14 p2369 A67-28612

Dielectric materials characteristics analysis to obtain flexible circuitry performance and selection factors, especially for flat cable [ASME PAPER 67-DE-52] 14 p2341 A67-28882

Organic dielectric materials for spacecraft, selection and evaluation 15 p2508 A67-29556

Josephson current in alternating field between two superconductors separated by dielectric barrier 15 p2530 A67-29868

Silicon nitride deposition on metal coated substrates for studying resistivity, breakdown strength and other electrical properties of thin dielectric films 15 p2540 A67-29932

Ultrasonic wave amplification by supersonic flux of drift electrons in sandwich structure of piezoelectric dielectric and semiconductor 15 p2542 A67-30245

Langmuir-Blodgett multimonolayers of stearic acid investigated as thin film dielectric 16 p2728 A67-31020

Coherent integral method applicable to scattering calculations for arbitrarily shaped dielectric bodies of low density [TR-67-114] 16 p2626 A67-31347

Azimuthal motion of glow discharge plasma in space between two coaxial dielectric cylinders in crossed radial magnetic and axial electric fields 16 p2723 A67-31580

Dielectric constant measurement of solids at microwave frequencies, noting performance of solid dielectrics as temperature function 16 p2678 A67-31720

Silicon oxide and nitride film thickness determined with interference technique, using spectrophotometer in UV and visible wavelength range 17 p2854 A67-32191

External noise levels effect on angular accuracy of tracking radar pencil-beam antennas, emphasizing radome noise and dielectric coating characteristics 17 p2826 A67-32685

Temperature autostabilizing nonlinear dielectric element /TANDEL/ for electric measurement circuits and measurement transducers 17 p2828 A67-32829

Optical behavior of graphite as interstellar matter, discussing appearance as metal or dielectric particle, extinction and optical conductivity 18 p3117 A67-33513

Energy transport concentration around homogeneous lossless dielectric cylinder, calculating electric field strength distribution and limiting radius of several wave modes 18 p2999 A67-33529

Focusing of electromagnetic waves by lenses, calculating field distribution near focus by diffraction theory magnitude of convergence 18 p3010 A67-33646

Thermal processes role in thin semiconducting and dielectric films,

discussing current-voltage characteristics, thermal inertia, etc 18 p3100 A67-33766

Strain and strain-rate sensor for measurements under dynamic conditions and without physical contact with deformation field being sensed 18 p3141 A67-33888

Thin films deposited onto substrates cooled to low temperatures investigated for transition temperature in structures of superconductor-dielectric-superconductor 18 p3101 A67-33989

Characteristics of dielectric rod excited with dominant propagating mode 18 p3011 A67-34020

Growth rate of oxide and other dielectric contact films on metal crystals computed for ionic diffusion and electron tunneling 18 p3103 A67-34590

Launching efficiency of PE-20 and PM-11 modes in dielectric-loaded trough waveguide excited by dielectric-loaded rectangular waveguide 19 p3194 A67-35514

Offset impedance sheet effect on admittance of slot antenna in conducting plane 19 p3197 A67-35823

Electron tunneling through thin dielectric films and damping relation to electron energy calculated, using band model and matrix methods 20 p3508 A67-36424

Wave interference and radiation tunneling phenomena influences on thermal radiation energy transfer between two separated solid dielectrics, noting spacing effect [ASME PAPER 67-HT-21] 20 p3546 A67-36716

Boundary conditions at dielectric-plasma interface 20 p3501 A67-37218

Laminar MHD boundary layer over finite dielectric disk in presence of magnetic field, determining velocity profiles 20 p3501 A67-37305

Oscillation of liquid sodium drop in dielectric medium in presence of constant magnetic field 21 p3665 A67-38245

Electromagnetic wave scattering by rectangular geometry dielectric wedge, using precise boundary conditions 21 p3585 A67-38686

Continuous high resolution measurement of solid propellant burning rate using resonant LC circuit [AIAA PAPER 67-69] 21 p3688 A67-38857

Dielectric thin film negative resistors for oscillator circuits compared to multilayer p-n-p-n structures for output frequency voltage temperature dependence 22 p3769 A67-39576

Damping constant of electromagnetic wave in plane parallel waveguide with ferrite resonant isolator, using perturbation theory, considering dielectric and magnetic losses 22 p3770 A67-39659

Radome antenna systems design utilizing dielectric structure applicable in aircraft, spacecraft and missile systems 22 p3775 A67-40468

EM radiation reflection, absorption and transmission through dielectric medium measured, studying other aspects by electric dipole oscillator model 23 p4037 A67-40757

Surface wave pole contribution to admittance of rectangular waveguide-fed slot into dielectric slab 23 p3979 A67-40825

Scattering cross section reduction of metal core loaded dielectric circular cylinder using harmonic series expansion for resonance phenomena 23 p3979 A67-40830

Coupled electromagnetic whispering gallery modes in large dielectric cylinders, discussing circumferential phase velocity, boundary region and axial wave number 23 p3974 A67-41203

Electromagnetic mode propagation in anisotropic dielectric p-n junction waveguide models noting Pockel effect of electric field on light 23 p3982 A67-41466

Strongly enhanced radiation from antenna surrounded by dielectric layer and plasma sheath, noting resonance at given operating frequency for certain plasma densities 24 p4121 A67-42266

Planar dielectric waveguide excitation at p-n junctions by externally incident electromagnetic field 24 p4121 A67-42337

Low loss mechanically or magnetically tunable 1 to 12 GHz hybrid ferrimagnetic dielectric microwave bandpass filter with improved power handling 24 p4132 A67-42808

Mutual admittance of infinite conducting slot antennas covered by dielectric layer and impedance sheet, noting losses effects on waveguide modes 24 p4133 A67-42818

DIELECTRIC PERMEABILITY

Barium titanate single crystals at infralow frequencies investigated for polarization, effective permittivity and coercive field 03 p0497 A67-13697

Reversing permittivity of barium titanate single crystals measured, using lithium chloride solution for electrodes 03 p0497 A67-13698

Electric field penetration of electrodes incorporated into theory of electron tunneling through dielectric layer 10 p1689 A67-22961

Plane electromagnetic wave reflection and refraction by semiinfinite dielectric medium moving uniformly parallel to surface analyzed for arbitrary incidence plane orientation 11 p1820 A67-24909

E and H waves in planar dielectric waveguides mounted on dielectric bases, deriving equations for wave dispersion and damping 13 p2069 A67-27028

Radiation by charged particle moving in spiral line between two adjacent dielectric surfaces, deriving equations for spectral density of radiation components 15 p2520 A67-29714

Permeability and permittivity values of homogeneous samples obtained by making transmission or reflection measurements in waveguides or coaxial cables 22 p3796 A67-39276

Capacitance between strands of braided cable composed of identical insulated conductors 22 p3747 A67-39340

DIELECTRIC POLARIZATION

Quantum mechanical theory of microwave nonresonant absorption and dielectric and magnetic relaxation in gases 01 p0116 A67-10145

Ordinary and dielectric second virial coefficients for dipolar gases calculated by off-center dipole model using series expansion 11 p1821 A67-23962

Depolarization of linearly polarized EM waves backscattered from rough metals and inhomogeneous dielectrics with known statistical properties 13 p2158 A67-26878

Temperature dependence of complex permittivity and spontaneous polarization of SbSI single-crystal whiskers in phase transformation region 15 p2537 A67-29707

Temperature dependence of complex permittivity and spontaneous polarization of SbSI single-crystal whiskers in phase transformation region 24 p4199 A67-41777

Circularly polarized nonlinear electromagnetic waves in conservative centrally symmetric dielectric, considering reflection, transmission and propagation 24 p4168 A67-42481

DIELECTRICS

SA SPARK GAP

Diffraction of plane plasma wave in rectangular dielectric wedge, considering cases of E-wave and H-wave 01 p0020 A67-10139

Transmission power of dielectric waveguide 01 p0038 A67-10716

Electron transport through thin insulating barriers in various diodes, analyzing current dependence on temperature and film thickness for perfect and imperfect dielectrics 02 p0294 A67-11760

Disintegration of alkali halide single crystals, polymers and glasses under laser radiation, noting parameters of disintegration region 03 p0439 A67-14367

Auger mechanism of recombination of electron emission from semiconductors and dielectrics 06 p1051 A67-18422

Turbulent MHD boundary layer flow of constant-electroconductivity incompressible fluid past dielectric plate in TM field, for small magnetic Reynolds numbers 06 p1043 A67-18672

Semiconductor dielectric interface characterization from study of complex capacity of metal/oxide/semiconductor structures 09 p1557 A67-22557

Radiation from dielectric antenna, noting erroneous radiation formula applications 17 p2824 A67-32308

DIESEL ENGINE

Exhaust manifold design for two-cycle diesel engine with turbosupercharger using physical simulation, discussing simulation criteria for gasdynamic processes 21 p3696 A67-38908

DIET

SA FOOD

SA NUTRITIONAL REQUIREMENT

SA SPACE FLIGHT FEEDING

Cosmonauts diets on short, intermediate and long space flights, with suggestions and concepts of onboard natural-food production 20 p3374 A67-36253

Human natural immunity with respect to substitution of Chlorella proteins for animal proteins, studying lysozyme activity in saliva and blood serum 20 p3368 A67-36269

Biological regeneration of enclosed atmosphere with algae photosynthesis noting effect of diet change 24 p4114 A67-41845

DIFFERENCE EQUATION

Motion equation solution to viscous conducting flow at inlet of diverging channel using difference method, noting magnetic field effect 01 p0120 A67-10184

Difference equations of nonlinear sampled data systems and resultant recurrence formula for system response calculation 01 p0043 A67-10201

Periodic solutions for difference-differential autonomous nonlinear oscillatory system with one degree of freedom 01 p0113 A67-10290

Difference equations of absolute motion applied to universal rendezvous guidance scheme 01 p0110 A67-10427

Asymptotic behavior of characteristic exponents and associated eigenfunctions for periodic differential difference equations 01 p0105 A67-10521

Infinitely divisible distributions of first passage times and hitting points in ordinary random walk solved by Bessel functions 01 p0106 A67-10735

Dynamic programming recursive estimation of modal trajectory for nonlinear non-Gaussian noise and comparison with Bayesian estimation and case of Gaussian white noise 01 p0047 A67-11214

Solution properties of linear difference equations approximating differential equations in nonoscillation interval 01 p0107 A67-11251

Method giving bounds for difference quotients, up to second order, of discrete function 02 p0258 A67-11555

Block successive overrelaxation method /BSOR/ compared with direct method for solving fourth order partial differential equation 02 p0258 A67-11800

Book on differential and difference equations including first order equations, linear equations, Laplace transforms, numerical and series solutions, etc 02 p0260 A67-12473

Stability of stochastic difference systems in case of continuous perturbations subject to Markov random effect 03 p0467 A67-13111

Restriction and stability in solutions of difference equations 03 p0457 A67-13113

Restrictions in method of solving boundary value problems for differential equations of elliptic type by reducing to difference problem 03 p0459 A67-13591

Stability of solutions for differential-difference equations with periodic coefficients, establishing necessary and sufficient criterion for boundedness of parameter 03 p0459 A67-13642

Self-sustained periodic solution in nonlinear difference differential equation proved under appropriate assumptions for various parameters 03 p0459 A67-13655

Asymptotic rate of convergence of Gauss-Seidel type iterative processes for nonlinear difference equations 03 p0460 A67-13881

Finite difference equation for biharmonic equation of plane 05 p0833 A67-16032

Real time approximation of continuous system performance on digital computer using difference equations obtained from digitized transfer function 05 p0768 A67-17518

Difference equations for heat transfer from liquid to solid and conductivity for solid applied to calculation of local temperatures within multilayer walls 06 p1113 A67-17990

Estimating interval of nonoscillation of finite difference equation 06 p1024 A67-18556

Inequalities for difference and pseudodifferential operators, providing sharp form of Garding inequality 06 p1025 A67-18642

Nine-point Laplace difference equation in square solved by modified alternating

direction implicit method 08 p1299 A67-21257

Consistent difference equations for displacement components in thin elastic disk of variable thickness subjected to given body forces and edge tractions for various coordinate directions 09 p1573 A67-21755

Solution properties and stability for system of nonlinear difference equations 09 p1524 A67-21926

Stability of linear systems with time delay analyzed by introducing stability indicative function, noting applications to differential-difference equations 10 p1679 A67-22916

Steady hypersonic inviscid flow, including detached shock, around blunt body, using finite difference computations 10 p1593 A67-23633

Generalized maximum likelihood estimators with proof of asymptotic efficiency, considering Markov chain and stochastic difference equations 11 p1812 A67-24098

Finite difference network model method with error tolerance for spacecraft heat transfer calculation 11 p1883 A67-24356

Periodic limiting regime for sets of difference equation 11 p1813 A67-24517

Discrete analysis in plate and shell theory based on method of constructing difference equation, using strain energy of system 12 p2023 A67-25591

Solvable convergent difference schemes for nonlinear elliptic equations using variational method applied to differential equation 13 p2145 A67-26445

Iteration process by difference scheme for numerical solution to Dirichlet problem of two-dimensional Poisson equation 13 p2148 A67-27613

Single parameter family of two-layer difference schemes with decomposing operators for general linear second order parabolic equations with mixed derivatives and variable coefficients 13 p2149 A67-27614

Difference methods for parabolic equations and alternating direction implicit methods for elliptic equations 14 p2342 A67-28155

Numerical solutions of Poisson and motion equations for electron gun design, examining truncation error via perturbation theory 14 p2287 A67-28677

Nonlinear partial differential equations of stellar evolution theory solved under assumption of spherical symmetry of star 14 p2392 A67-28995

Stellar pulsational instability phenomena calculated numerically for infinitesimal amplitude of central core motion 14 p2392 A67-28996

Optimal control of random dynamical systems analyzed, using first order vector differential or difference equations 14 p2292 A67-29062

Optimization of system described by differential and finite differential equations when including constraints 15 p2455 A67-29119

Computational error caused by finite word length of aerospace computers 15 p2439 A67-29596

Wiener-Hopf technique for class of nonhomogeneous difference-differential-integral equations 17 p2877 A67-32560

Cauchy problem for homogeneous linear difference scheme with constant complex coefficients, giving stability lemmas 17 p2877 A67-32677

Dynamic system single-and multifrequency random oscillations described by differential-difference equations and solved through probability distribution 17 p2885 A67-32876

State variable difference equation method for HF solution of ordinary differential equations in digital simulation with nonlinearity 18 p3005 A67-33662

Synthesis of time optimal control for discrete plants described by difference equations, deriving algorithm defining surface in phase space of variables 18 p3017 A67-33872

Combination variational-difference numerical method applied to nonlinear boundary value problems, noting numerical functional minimization 18 p3071 A67-34264

Properties of solutions of linear homogeneous differential-difference equations with linear coefficients and real differences 18 p3073 A67-34614

Grid functions from nodal values on rectangular surface used to solve potential

equation by finite difference method 19 p3342 A67-35717
 Higher order differences used in solution of Dirichlet problem for Poisson equation of rectangle 20 p3475 A67-36651
 Linear equation system with coefficient matrix of multiple diagonal bands solved by direct method, reducing numerical solution error 20 p3476 A67-36675
 Maximum region of applicability of Chaplygin theorem of differential inequality to elliptic difference equation 20 p3479 A67-37722
 Variationally derived finite difference equations for mixed boundary value problems of thermoelastic stress and strain 21 p3716 A67-37956
 Cordwood packaging concept for electronics thermal control in LEM, obtaining electronic package temperature field from finite difference equations 21 p3594 A67-38329
 9-point difference formula accuracy in Laplace equation compared to 5-point formula, discussing convergence rate and Dirichlet boundary value problem 22 p3826 A67-39195
 Estimating interval of nonoscillation of finite difference equation 23 p4022 A67-40822
 Sensitivity analysis of linear differential-difference equations with hereditary influences 24 p4134 A67-42026
 Noninteraction and deadbeat response in linear sampled data multivariable systems synthesis by state difference equation 24 p4134 A67-42027
 Canonical decomposition of nonlinear error covariance difference equation derived for discrete estimation problems 24 p4177 A67-42188
 Difference methods for soft solutions to partial differential equations, discussing initial value problem 24 p4180 A67-43090
 Extrapolated Crank-Nicolson difference scheme for quasi-linear parabolic equations 24 p4180 A67-43091

DIFFERENTIAL ALGEBRA

Differential and Clifford matrix algebra relationship in relativity theory, generalizing Dirac and quaternion algebras to Riemann spaces 21 p3656 A67-37923

DIFFERENTIAL AMPLIFIER**SA SEMICONDUCTOR DEVICE**

Theoretical study of common-mode rejection factor of differential amplifier, with application to valve and transistor type amplifiers at LF 04 p0586 A67-15628
 Ultrahigh input impedance for measuring electrical activity of biological cell 05 p0773 A67-16512
 Electron bombardment type ionization gauge with logarithmic differential circuit 10 p1610 A67-22950
 Equation for solid state differential amplifier-circuit configuration effect on overall system accuracy and performance 11 p1768 A67-24823
 Servo loop electronics reliability using continuous redundancy, integral self-test circuits, etc 19 p3191 A67-34847
 Small signal interaction impedance of bulk semiconductor amplifier with nonuniform doping profile, noting two-dimensional representation 21 p3588 A67-37818
 Pole shifting methods for differential amplifiers noting comparisons, singularities, alternative techniques and schematic diagrams of cascade stages 22 p3771 A67-39862
 Logarithmic nature of I-V characteristics of silicon junction diodes for design of analog multiplier with differential operational amplifier 24 p4131 A67-42478

DIFFERENTIAL ANALYZER

AC differential correlator for measuring small delays between two identical binary output waveforms 01 p0037 A67-10482
 Digital computers for navigation and guidance solving design problem by combining general purpose /GP/ and digital differential analyzer /DDA/ approaches to produce hybrid computer 01 p0111 A67-11258
 Accuracy of DC amplifiers solving linear differential equations with constant coefficients, examining effect of drift and grid currents 01 p0031 A67-11264
 Zeta transformation applied to numerical integration operator to determine stability of solution to system of linear differential equations on digital differential analyzer 13 p2072 A67-26348

DIFFERENTIAL EQUATION

SA BALANCE EQUATION
 SA BERNOULLI EQUATION
 SA BIHARMONIC EQUATION
 SA DUFFING EQUATION
 SA FALKNER-SKAN EQUATION
 SA HILL EQUATION
 SA LAPLACE EQUATION
 SA MATHIEU FUNCTION
 SA PARTIAL DIFFERENTIAL EQUATION
 SA RAYLEIGH EQUATION
 SA REYNOLDS EQUATION
 SA RICCATI EQUATION
 SA RITZ AVERAGING METHOD
 SA RUNGE-KUTTA INTEGRATION
 Special functions for solving second-order or higher linear differential equations with variable coefficients in elasticity theory problems 01 p0158 A67-10215
 Steady state oscillations and rotations, discussing time independency of parametric differential equations 01 p0113 A67-10285
 Series integration of linear differential equations with deviating argument 01 p0104 A67-10289
 Periodic solutions for difference-differential autonomous nonlinear oscillatory system with one degree of freedom 01 p0113 A67-10290
 Oscillation theorems for second order differential equations 01 p0105 A67-10522
 Undetermined coefficients method for obtaining particular solution of linear ordinary system with constant coefficients, solving final matrix 01 p0105 A67-10729
 Extension of Waltman theorems regarding oscillation and asymptotic behavior of solutions of nonlinear differential equation, proving solution existence for initial value problem 01 p0105 A67-10730
 Lateral motion of simply supported axially loaded viscoelastic column governed by system of linear ordinary differential equations with periodic coefficients 01 p0106 A67-10732
 Orthogonal expansions in physical boundary value problems characterized by homogeneous differential equation with inhomogeneous boundary data 01 p0106 A67-10734
 Nonlinear dispersive wave propagation analyzed by linearization, obtaining solution as Fourier integral through differential equation 01 p0024 A67-10737
 Limiting theorem for weak convergence of solutions of differential equations with random right hand part to Markov process 01 p0106 A67-10922
 Simultaneous effect of transverse curvature and fluid injection on boundary layer flow over parabola of revolution, obtaining iterative solution to differential equation 01 p0055 A67-11175
 Numerical solution of nonlinear differential equations governing finite axisymmetric deformation of thin shells of revolution 01 p0164 A67-11176
 Liapunov method application to adaptive loop redesign, using differential equations for model system errors coupled with squares of parameter differences 01 p0045 A67-11202
 Frequency-time domain asymptotic stability criterion for autonomous continuous systems 01 p0046 A67-11209
 Algorithm for reducing linear time-invariant differential systems to state form applied to systems described by transfer functions 01 p0047 A67-11219
 Deterministic optimal control, discussing Bellman dynamic programming method, Pontryagin maximum principle, orbital transfer, interplanetary guidance, etc 01 p0047 A67-11220
 Differential equation solution by separation of multiplicative derivative, by perturbation method, by reduction to Volterra equation and by integral series 01 p0107 A67-11250
 Solution properties of linear difference equations approximating differential equations in nonoscillation interval 01 p0107 A67-11251
 Markov chains used in construction of reliability mathematical models for systems with dependence between components, noting differential equations 01 p0085 A67-11383
 Integration of second order linear

differential equation with boundary conditions of third kind by graphic method of Drymael 02 p0257 A67-11478
 Geometrical study of Picard method of successive approximations for solving first order differential equations 02 p0257 A67-11479
 Continued fraction rational approximations to solution of second-order nonlinear equation, including Riccati equations treated by Merkes, Scott and Fair 02 p0258 A67-11558
 Control region construction in phase space for linear differential equation system 02 p0224 A67-11627
 Solution method for determinantal equation of matrix polynomial 02 p0258 A67-11799
 Numerical solution of ordinary differential equations at remote terminal, commenting on integration in on-line mode 02 p0259 A67-11802
 Kantorovich theorem, Goodman-Lance method and two-point boundary value problems, noting numerical results obtained on IBM 7094 computer 02 p0259 A67-11836
 Near circular orbit of satellite in terrestrial gravitational field analyzed, using approximate solution of perturbed Kepler motion 02 p0327 A67-12373
 Cauchy and boundary value problems for homogeneous differential equations with two independent variables analyzed, establishing generalized solution existing on uniqueness maximal domain 02 p0260 A67-12432
 Book on differential and difference equations including first order equations, linear equations, Laplace transforms, numerical and series solutions, etc 02 p0260 A67-12473
 Existence of periodic solutions for infinite system of integro-differential equation 02 p0260 A67-12537
 Solution of second order differential equation containing continuous function expandable in Maclaurin series, using Volterra integral equation 02 p0260 A67-12668
 Singular perturbation theory of differential equations applied in control engineering, noting asymptotic expansion of solution 02 p0227 A67-12681
 First order linear differential equation describing line-of-sight system of air-to-air missiles in two-dimensional case 02 p0265 A67-12731
 Influence on stability of masses which are in relative motion with respect to projectile determined, noting engine thrust effect on attitude control system performance 03 p0517 A67-13027
 Solution of optimum filtering problems when input signals of automatic control system are described by different differential equations at successive time intervals 03 p0390 A67-13099
 Coordination of integral and relay components in algorithms for adjusting control coefficients in model-reference self-adaptive control systems described by differential equations 03 p0390 A67-13102
 Qualitative theory of second order dynamic systems in plane and on sphere covering trajectories, equilibrium states and boundary values 03 p0390 A67-13109
 Thermal field of cutting area of aircraft structural material analyzed, using differential equations of thermoconductivity 03 p0427 A67-13191
 Quasi-rotational oscillatory solution to equation system with arbitrary degree of freedom with respect to parameter in given region 03 p0468 A67-13338
 Conditions of solvability of Chaplygin problem 03 p0458 A67-13339
 Differential moduli of differential spaces on ring or on differential solid with variable coefficients 03 p0458 A67-13460
 Qualitative study of first order homogeneous equation, by introducing auxiliary variables, plane curve is associated with differential equation 03 p0459 A67-13587
 Stabilization of steady state motion of controlled system described by nonlinear differential equations with time delays 03 p0392 A67-13588
 Restrictions in method of solving boundary value problems for differential equations of elliptic type by reducing to difference problem 03 p0459 A67-13591
 Stability problem of steady motions, using differential equations with time

delay 03 p0468 A67-13616
 Stability of solutions for differential-difference equations with periodic coefficients, establishing necessary and sufficient criterion for boundedness of parameter 03 p0459 A67-13642
 Boundary value problems of higher order equations in infinite regions, proving existence and convergence of solution for perturbed and unperturbed cases 03 p0459 A67-13643
 Self-sustained periodic solution in nonlinear difference differential equation proved under appropriate assumptions for various parameters 03 p0459 A67-13655
 Exact monotonic and approximate oscillatory solutions of nonlinear differential equations of high order 03 p0460 A67-13656
 Displacement potential for solutions of displacement equilibrium equations obtained by Mindlin for linear elastic medium where stresses are functions of strains and strain gradients 03 p0524 A67-13661
 Liapunov function of ninth order system represented by differential equation which, in phase variable form, can be represented by matrix equation 03 p0392 A67-13682
 Spectral properties of two possible generalizations of Jacobi matrices for use in difference methods for numerical solutions of differential equations 03 p0460 A67-13820
 Conditions of existence of unbounded solution to unforced second order differential equation, considering global asymptotic stability 03 p0460 A67-13822
 Approximate solution to nonlinear differential Riccati equation, using Bessel function 03 p0460 A67-13879
 Patching method applied to nonlinear differential equation of forced oscillation of second order relay system with damping 03 p0393 A67-13901
 Accuracy of central finite difference methods for solving boundary value problems in structural analysis governed by equations with variable coefficients 03 p0526 A67-13970
 Second order autonomous differential equation stability and boundedness obtained, using computing algorithm based on tracking function method 03 p0376 A67-13987
 Order reduction of equations for gyroscopic systems, using results of Tikhonov study on differential equations with small parameter in front of highest derivative 03 p0424 A67-14159
 Error equations for Schuler vertical, estimating discrepancy between solutions for various changes in coefficients 03 p0465 A67-14160
 Plane oscillations of elastic pendulum with shaft undergoing bending deformation, determining principal zone of instability for action by longitudinal harmonic force 03 p0469 A67-14161
 Stability of forced oscillations described by second order nonlinear differential equation determined by Pinnl asymptotic method 03 p0530 A67-14177
 Vibration shielding and shock absorbing systems design noting control function 03 p0530 A67-14180
 First order differential equations with homogeneous right sides to construct Liapunov function and stability behavior 03 p0462 A67-14257
 Quasi-periodic solutions for sets of differential equations containing small parameter 04 p0643 A67-14660
 Existence of periodic solution for set of quasi-linear differential equations 04 p0643 A67-14662
 Existence and evaluation of solution for periodic boundary value problem of set of ordinary differential equations 04 p0643 A67-14668
 Reducibility and induction of set of ordinary differential equations in vicinity of smooth integral manifold 04 p0643 A67-14726
 Ascent or descent from initially Keplerian orbit by constant low thrust analyzed by two-variable expansion 04 p0704 A67-14828
 Periodic solutions for nonautonomous differential equations, discussing existence and stability criteria 04 p0644 A67-14853
 Book on qualitative behavior of trajectories of system of differential equations characterizing rate of growth of solutions by Liapunov indices 04 p0645 A67-15011

Electrostatic polarization of plasma in applied electric field, excluding case for steady current flow 04 p0666 A67-15180
 Differential equations describing wave transformation in weakly inhomogeneous plasma 04 p0668 A67-15217
 Synchronization errors in parallel jacks system with closed loop control by hydraulic relays, using nonlinear differential equations [ASME PAPER 66-WA/AUT-5] 04 p0555 A67-15389
 Elastic shells of revolution axisymmetrically loaded analyzed, using multisegment method for solution of boundary value problems governed by nonlinear differential equations [ASME PAPER 66-WA/APM-16] 04 p0713 A67-15407
 Dynamic systems identification by digital computer modeling in state space formulation of ordinary differential equation [ASME PAPER 66-WA/AUT-10] 04 p0593 A67-15418
 Optimal control of systems described by elliptic differential operators 04 p0593 A67-15491
 Rational approximation of generalized Duffing equation, damped mass spring oscillator equation and generalized second order Riccati equation 04 p0647 A67-15660
 Asymptotic simplification of self-adjoint differential equations with parameter 04 p0647 A67-15741
 Existence and uniqueness in first and second boundary value problems for nonlinear second order differential equations 04 p0647 A67-15742
 Global stability of second order autonomous differential equations 04 p0647 A67-15743
 Boundary value problems for ordinary nonlinear second order systems, noting subfunction definition and existence theorem 04 p0647 A67-15744
 Differential equations for local interfacial and wall shear stresses for one-dimensional annular two-phase flow 04 p0735 A67-15857
 Bounded-input bounded-output stability of time-varying differential system analyzed through extension of Yoshizawa definitions and methods 04 p0594 A67-15877
 Book on optimal control theory of deterministic dynamical systems governed by ordinary differential equations in presence of control and state constraints 04 p0594 A67-15943
 Stability region of complex linear self-conjugate systems of differential equations containing skew-Hermitian matrix 04 p0647 A67-15980
 Mechanical system with two degrees of freedom conditioned for oscillatory motion, using differential equations 05 p0908 A67-16042
 Variational problem of rocket dynamics in homogeneous gravitational field in empty space reduced to differential equation system 05 p0904 A67-16049
 Elastoplastic axisymmetric stressed state of circular cylindrical shell under unsteady temperature field, internal pressure and axial force, using differential equation 05 p0912 A67-16181
 Stress in helical corrugated shell under axial tension examined as boundary value problem of ODE in cylindrical coordinate system 05 p0914 A67-16215
 Stress concentration for steep spherical shell with arbitrary elliptic hole 05 p0916 A67-16223
 Three-dimensional elastic problem of bodies of revolution, deriving Lamé and generalized Hooke equations in matrix form 05 p0916 A67-16226
 Computer method for predicting servo positioner performance 05 p0753 A67-16235
 Nonstationary problem of linear filtering in presence of additive noise solved by computer simulation 05 p0782 A67-16262
 Differential equation derivation for creep analysis using plastic interaction curve and associated flow rule 05 p0917 A67-16299
 First-kind operator equation solution by reduction to dual extremum problem, proving existence and convergence 05 p0834 A67-16375
 One-dimensional self-similar motion of relaxing gas, noting ODEs of process and gas dynamic parameters of flow field 05 p0791 A67-16376
 Computer solution of Cauchy problem of

ordinary differential equations in form of Taylor series 05 p0834 A67-16377
 Newton-Raphson quasi-linearization applied to orbit determination from angular data, range and range rate, noting linear differential equations controlling orbit 05 p0894 A67-16563
 Operational calculus for functions of one continuous and one discrete variable 05 p0834 A67-16725
 Nonlinear boundary value problem with small parameter multiplying highest derivative 05 p0835 A67-16737
 Cosmological solutions of linear field theory, showing possible representation in form of hypersurface of second degree in five-dimensional affine space 05 p0897 A67-16773
 Jordan form matrix algorithm of Wasow for reducing systems of first order ordinary differential equations with turning point 05 p0835 A67-16779
 Spence integrodifferential equation for flow around slender slightly curved profile with jet at trailing edge 05 p0749 A67-16842
 Equivalent circuit of piezoelectric quartz pressure transducer used with measuring circuit with small input resistance for solving gasdynamic problems 05 p0808 A67-17111
 One-dimensional inverse problem of scattering theory, noting differential equation reduction, determining traveling wave coefficient 05 p0765 A67-17158
 Asymptotic solution for one-dimensional MHD generator scaling numerical values to obtain correct results for zero initial current and velocity 05 p0856 A67-17365
 Reduction of systems of linear differential equations to generalized L-diagonal form 05 p0836 A67-17487
 Error bounds for asymptotic solutions of differential equations, using Volterra equations for actual and formal solution vectors 06 p1021 A67-17565
 Stability theorem for damped dynamic systems based on commutativity of class of mathematical models 06 p1099 A67-17644
 Boundary value problem for heat equation, discussing Laplace transform solution and uniqueness theorem 06 p1111 A67-17645
 Nonperiodic librational motions in restricted three-body problem for relatively elliptic motion of two finite masses 06 p1080 A67-17766
 System of n first order differential equations relating coordinates and time, using matrix methods for solution 06 p1022 A67-17773
 Regularization of three-body equations for case of binary collisions, using Sundman equation transformation in celestial mechanics problems 06 p1022 A67-17776
 Drag free motion of satellite of oblate planet determined by differential equation expressing planet gravitational potential as spherical harmonics 06 p1081 A67-17777
 Differential equations and mathematical models for gas flows with chemical activity and radiative effects, particularly effects of reentry and propulsion 06 p0983 A67-17785
 Matrix and vector computational procedures for solution of partial and ordinary differential equations 06 p1022 A67-17788
 Two variable expansion procedure for approximate asymptotic solution to nonlinear differential equation 06 p1022 A67-17789
 Time dependent geopotential variations analyzed, using straight line techniques 06 p0994 A67-17863
 Improving estimates of solutions of linear perturbed-motion equations of mechanical systems with variable coefficients 06 p1023 A67-18038
 Closedness of set of trajectories or of solutions of contingent equation used in existence problems of optimal control and variational calculus 06 p0975 A67-18100
 Perfect gases reacting mixture flows formulated for system of differential equations 06 p0955 A67-18114
 Inviscid linearized perturbations of supersonic entropy layers analyzed, using approximating partial differential equations by simultaneous ordinary differential equations [AIAA PAPER 67-6] 06 p0938 A67-18249
 Dynamic characteristics of variable mass slender elastic body, solving vector differential equations

[AIAA PAPER 67-41] 06 p1095 A67-18263
Base pressure behind supersonic vehicle, calculating existence conditions for wake solutions and location of stable and unstable singularities

[AIAA PAPER 67-60] 06 p0986 A67-18269
Attitude stability of spinning rigid symmetric satellite in elliptic orbit examined for motion about equilibrium position with spin axis normal to orbit plane

[AIAA PAPER 67-124] 06 p1095 A67-18312
Nonequilibrium boundary layer problem solution by direct treatment of two-point boundary value problem

[AIAA PAPER 67-219] 06 p0990 A67-18515
Uniqueness of extremal controls for minimum fuel problems pertaining to single input linear time-invariant systems

06 p1098 A67-18523
Filtering for nonlinear dynamical systems with white Gaussian noise

06 p1029 A67-18532
Analytical solution for axially symmetric membranes made of neo-Hookean materials solved by simultaneous differential equations

06 p1107 A67-18652
Fundamental frequency of natural oscillations of plate, using integrodifferential equations derived from elasticity theory in form of power series

06 p1108 A67-18662
Ordinary differential equation in boundary layer theory of reversed flow

06 p1025 A67-18730
Coherent radiation interaction with two-level atoms system in single mode approximation, obtaining equation for time dependent number of photon emission and absorption

06 p1012 A67-18804
Artificial heat conduction mechanism, introducing viscosity term into momentum and energy equations to account for shock discontinuities in flow problems

06 p0992 A67-18830
Structure of radiation resisted hypersonic shock in simple dissociating gas examined via quasi-equilibrium field for radiation field

06 p0993 A67-18893
Optimality conditions of systems containing components with distributed parameters

07 p1159 A67-19138
Numerical solutions of nonlinear differential equations - Conference, U.S. Army Mathematics Research Center, Madison, May 1966

07 p1212 A67-19152
Error estimation for approximate solutions of differential equations, using functional analysis

07 p1213 A67-19153
Error bounds in numerical solution of ordinary differential equations, considering monotonic majorants

07 p1213 A67-19154
Second order method for nonlinear optimal control problems resulting in Riccati differential equations

07 p1213 A67-19155
Approximations to Navier-Stokes equations corresponding to steady two-dimensional incompressible viscous flow about circular cylinders

07 p1167 A67-19156
Galerkin procedure for multipoint boundary value problems of general nonlinear systems

07 p1213 A67-19160
Variability and nonvariability of solutions to second order nonlinear differential equations

07 p1213 A67-19172
Expansion of solutions of integrodifferential equation not having holomorphic solutions vanishing with x in vicinity of x equals zero

07 p1213 A67-19173
Existence of solutions to differential and integrodifferential equations possessing asymptotic parabolas

07 p1214 A67-19174
Certain properties of solutions to ordinary linear differential equations with bounded coefficients

07 p1214 A67-19178
Sufficient conditions for obtaining finite form solution of ordinary second order differential equations with zero and nonzero determinants

07 p1214 A67-19179
Existence of bounded solutions of second order differential equations

07 p1214 A67-19180
Approximate solutions for differential and integral equations in form of second order asymptotic polynomials

07 p1214 A67-19216
Bessel function applications of two Sonin theorem formulations compared for range of applicability

07 p1215 A67-19472
Partial error analysis of Fowler z transform root-locus method for digital simulation of complex system

07 p1148 A67-19892
Minimum energy problems in Hilbert

function space for continuous and discrete linear systems, noting operator transformation into linear differential equations

07 p1216 A67-19908
Duality relation in differential equations and some associated functional equations

07 p1217 A67-20020
Theorems concerning eigenvalue problems and oscillatory conditions for multiple degree of freedom mechanical systems

07 p1224 A67-20103
Coupled Green function equations for Helsenberg ferromagnet approximated via differential equations

07 p1237 A67-20141
Solvability of class of linear differential equations with polynomial coefficients

07 p1217 A67-20152
Remedies for deficiencies in approximations near transition point in asymptotic methods used for estimates of solutions to differential equations governing axisymmetric vibrations of thin elastic shells

08 p1414 A67-20346
Existence theorem for n th order linear stochastic ordinary differential equations

08 p1347 A67-20356
Selection of constants defining reference orbit of planet and use in differential equations of motion

08 p1382 A67-20394
Reduction of differential equations of Hill lunar problem using Jacobi integral

08 p1382 A67-20396
Shear deformation and rotary inertia effects on modal data of nonuniform beam, with complex behavior defined by ordinary differential equations

08 p1416 A67-20533
Asymptotic solution of Cauchy problem for integrodifferential equation with small parameter associated with derivative

08 p1348 A67-21152
Eigenfunction expansions for fourth order differential equations

08 p1348 A67-21170
Generalization of multistep methods for ordinary differential equations, noting associated operators and local discretization error

08 p1348 A67-21191
Galerkin method analysis of solvability of boundary value problems for second order quasi-linear elliptic differential equations with discontinuous coefficients

08 p1349 A67-21197
Stability of fourth order Runge-Kutta method for solving differential equation

08 p1349 A67-21259
Numerical solution of integrodifferential equations

08 p1349 A67-21261
Reformation processes effect on stress-time-to-fracture behavior of solids, considering governing differential equation

08 p1423 A67-21302
Transient processes in linear automatic control systems dependent on parameters which appear when differential equations of analyzing system are transformed by Laplace-Karson method

08 p1313 A67-21324
Optimal control analysis of system behavior described by linear stochastic differential equations

08 p1313 A67-21325
Soviet book on numerical solution of nonlinear boundary value problems for differential equation systems, determining eigenvalues and eigenfunctions

08 p1349 A67-21337
Wave propagation through random and nonrandom medium, discussing relation of phenomena to coherence theory

09 p1460 A67-21586
Second order coherence properties of fluctuating vector electromagnetic fields of arbitrary spectral width, noting dyadic field spectral density and governing differential equations

09 p1460 A67-21587
Ordinary linear differential equations with variable coefficients solved by phase plane displacements

09 p1524 A67-21648
Large deflection of asymmetrically layered plate, using parametric expansion techniques to extract system of differential equations governing scaling of stresses and displacement component for boundary conditions

09 p1574 A67-21756
Gradient method solution for class of optimal control problems, minimizing mean square value of finite state components of object in motion

09 p1482 A67-21871
Structural equations with variable coefficients for nonstationary one-dimensional gas flows, using Cartan method

09 p1487 A67-21912
Stability of stepwise solution methods of initial value problems for second order

differential equations

09 p1524 A67-21935
Stability of Fehlberg method when applied to solution of initial value problems for second order differential equations

09 p1524 A67-21936
Variation of functional determined on trajectories of differential equation systems with discontinuities, discussing application to optimal control problems

09 p1525 A67-22076
Nonlinear system response to pulse excitation, solving problem via Poincare perturbation method

09 p1533 A67-22153
Optimization of thermionic diode, with electrical conduction and heat transport represented by differential equations

09 p1448 A67-22336
Fatigue mechanism of materials, deriving parametric differential equations from group of postulates

09 p1578 A67-22546
Dynamic simulation of linear differential equations

09 p1469 A67-22620
Stability of linear systems with time delay analyzed by introducing stability indicative function, noting applications to differential-difference equations

10 p1679 A67-22916
Double concurrent waves in one-dimensional nonstationary problems with discontinuous limit conditions

10 p1624 A67-22923
Relation of scattering matrix, Riccati equation and boundary conditions

10 p1673 A67-22964
Explicit bounds for solutions of certain second order nonlinear differential equations

10 p1674 A67-22967
Field method application to linear differential equation for numerical solution of two-point boundary value problems in structural mechanics

10 p1679 A67-23147
Polynomial solutions for differential equations describing thermoelastic equilibrium of thin anisotropic plates

10 p1718 A67-23405
Lapunov stability theory applied to control system, noting stability of function and stochastic differential equations

10 p1620 A67-23422
Radial flow of compressible fluids between disks solved through simpler form instead of numerical integration of differential equations

10 p1593 A67-23475
Numerical solution of class of nonlinear high order differential equations with two-point asymptotic boundary conditions for thermal boundary layers in laminar and turbulent flow

10 p1627 A67-23560
Longitudinal perturbed motion of aircraft with free-floating canard, obtaining differential equation corresponding to characteristic equation

10 p1595 A67-23606
Dynamic behavior of multidimensional system described by ODE

10 p1675 A67-23608
Stability of integrals of differential equations for periodic motions

10 p1680 A67-23666
Stability of linear integro-differential equations for processes with distributed parameters

10 p1681 A67-23667
Differential equations of motion for permanent rotation heavy gyro with fixed point

10 p1657 A67-23668
Optimization problem described by differential equations and related to Bellman equation

10 p1675 A67-23681
Unloading wave expanding in elastoplastic rod determined by integration of differential equation in quadratures

10 p1721 A67-23685
Deformation of laminated shell structures under axisymmetric loading, deriving differential equation by considering boundary conditions at both ends

10 p1731 A67-23846
Radial distribution function differential equation solution studied numerically and analytically for plasma parameters, using closure approximation

11 p1826 A67-23871
Scattering matrix equations for waveguide structure of varying surface impedance boundaries

11 p1751 A67-23968
Averaging method in nonlinear mechanics, discussing results of Bogolubov studies

11 p1818 A67-24089
Minimax problem for pursuit problem of two linearly controlled objects describable by identical differential equations

11 p1812 A67-24145
Expansion of arbitrary function of Mehler-Fok integral form in terms of spherical functions

11 p1812 A67-24149
Radiating slot on dielectric clad cylinder, solving wave equations and finding field

expressions via harmonic series representation 11 p1761 A67-24280

Stability of bilaterally symmetrical object towed in air along straight line, obtaining characteristic equation as test for lateral or longitudinal stability 11 p1743 A67-24309

Forced oscillations of generalized Lienard equation, examining harmonic solutions in x, y plane with confined trajectories 11 p1812 A67-24311

Reentry guidance by threshold network storage of precomputed optimum commands, using analogy of surface approximation problem in N plus one-dimensional space [AIAA PAPER 66-52] 11 p1869 A67-24338

Optimal solutions to mixed initial boundary value problems for control processes described by semilinear hyperbolic partial differential equations in two independent variables 11 p1770 A67-24423

Cartesian formulation of membrane theory, discussing equations of equilibrium, strain energy, variation formulation and boundary conditions 11 p1875 A67-24431

Motion stability during final time interval for case of two zero roots determined by analysis of nonlinear functions structure 11 p1813 A67-24518

Relativity theory for solid media model design, deriving equations of state and closed system of differential equations based on variational principle 11 p1819 A67-24675

Absence conditions for periodical trajectories in regions of possible existence 11 p1819 A67-24686

Phase locking in phase plane on modulation of driver and self-excited oscillator, using differential equation 11 p1754 A67-24725

Periodic solutions for nonautonomous differential equations, discussing existence and stability criteria 11 p1813 A67-24730

Existence and uniqueness of periodic solution to ordinary differential equations, defining position in plane of closed integral curves 11 p1813 A67-24749

Galerkin method applied to approximation of periodic solution of system of singular differential equations 11 p1819 A67-24762

Nonradial oscillations of homogeneous sphere examined on basis of general fourth order problem 11 p1819 A67-24783

Undetermined coefficient method compared with confluent hypergeometric functions for solving first order perturbation equation for refractive index of He 11 p1813 A67-24787

Two-dimensional problem of thermoelasticity solved using analytic functions 11 p1879 A67-24885

Multidimensional linear differential equations with almost periodic coefficients analyzed for error of exact solution 11 p1814 A67-24977

Modified collocation method for linear boundary value problem for integrodifferential equation, giving approximate solutions which converge to exact solution 11 p1814 A67-25048

Series method of solving boundary value problems for nonlinear ordinary differential equations 11 p1814 A67-25050

General formula for numerical solution of ODE of any order and linear and nonlinear systems 12 p1960 A67-25434

Ribbed circular cylindrical shell under axial compression, reducing problem to determination of deflection and stress functions 12 p2020 A67-25571

Algorithms for operator partitioning method in reducing shell equations solution to calculation of solid intersecting rod systems 12 p2026 A67-25617

Geometrically nonlinear theory of elastic stability of anisotropic shells and linear stability of orthotropic plates, using differential equations 12 p2028 A67-25628

Acoustic measurement method for following motion of solid-liquid interface, obtaining solution for transient heat conduction problem 12 p1946 A67-25985

Stability and asymptotic behavior of perturbed nonlinear systems of ordinary differential equations 12 p1961 A67-26060

Upper and lower bounds on distance between zeros of components of solutions of second order ordinary nonlinear differential equations 12 p1961 A67-26062

Weinstein results for pointwise monotone growth and convexity extended in norm to certain Cauchy problems of second order

differential equations 12 p1961 A67-26063

Channel profiles for producing vortex flows in weakly ionized gases in transverse magnetic fields 12 p1977 A67-26076

Solution to Bogolubov differential equation for distribution functions of particle system by functional integration technique 12 p1962 A67-26174

Closed contour for equation expressing periodic solutions of second order differential equations 12 p1962 A67-26184

Handbook of engineering sciences, Volume 1, Basic sciences 13 p2155 A67-26266

Dispersion equations obtained for numerical forecasting of meteorological fields from basic hydrothermodynamic equations, using Reynolds stresses 13 p2149 A67-26272

Zeta transformation applied to numerical integration operator to determine stability of solution to system of linear differential equations on digital differential analyzer 13 p2072 A67-26348

Static characteristics of radial gas dynamic bearing, using differential equation for pressure distribution calculation 13 p2122 A67-26351

Electron generator with oscillatory anode circuit nonlinear differential equation analyzed by linearizing, applying algorithm to obtain computer solution 13 p2144 A67-26393

Stability and asymptotic stability conditions for coefficients of system of linear first order differential equations 13 p2144 A67-26443

Solvable convergent difference schemes for nonlinear elliptic equations using variational method applied to differential equation 13 p2145 A67-26445

Vibration characteristics and fundamental frequency of circular plate with arbitrary cross section reinforcing ring 13 p2216 A67-26534

Generalization of differential equation of dynamo theory of geomagnetic variations to include unsteady dynamo effect in ionosphere 13 p2110 A67-26548

Alserman problem concerning absolute stability of zero solution to nonlinear third order system of differential equations 13 p2087 A67-26616

Solutions for piecewise linear differential equation obtained by plotting exciter amplitude against exciter frequency in treating pulling-in phenomena 13 p2145 A67-26625

Diurnal variations in structural parameters of upper atmosphere determined via differential equations of hydrodynamics 13 p2112 A67-26669

Differential equation and boundary conditions for sandwich shells, noting bending resistance and shear deformation 13 p2219 A67-26906

Discrete ordinate method for boundary value problems in gas dynamics using differential equations yields solutions to Couette flow 13 p2101 A67-26962

Dynamic errors in electronic analog computers, noting expressions for shift in characteristic roots of equations under solution 13 p2073 A67-27064

Dynamical equations for optimal nonlinear filtering and representation of conditional expectation as solution to stochastic differential equation 13 p2146 A67-27094

Proof of Kupka and Smale approximation theorem concerning differential equations defined on compact manifold 13 p2146 A67-27095

Equilibrium states of buckled elastic rings under stress 13 p2219 A67-27147

Conditions required for Reynolds operator to be idempotent over Banach algebra 13 p2146 A67-27149

Boundary value problem for differential equations of perturbed satellite motion assuming perturbing accelerations defined by Vinti potential 13 p2200 A67-27323

De la Vallée Poussin linear homogeneous differential equation of nth order with continuous functions as coefficients 13 p2147 A67-27467

Hankel transforms applied to generalized functions theory 13 p2148 A67-27470

Convergence considerations on second order method of parabolic equations approximate solution 13 p2148 A67-27473

Linear positive operator construction in approximation theory 13 p2148 A67-27474

Existence theorem for initial value problems in differential equation leading to Volterra integral equation in several variables 13 p2149 A67-27736

Nonlinear differential equation for shock wave of several circular arc airfoils integrated to give shock wave location 14 p2239 A67-27797

Solution algorithm for boundary problem generated by necessary conditions for optimality in variational problem 14 p2341 A67-27840

Numerical solution of linear differential equation and Volterra linear integral equation of second kind based on Lobatto four-point quadrature formula 14 p2342 A67-27977

Boundary layer equations reduced to ordinary differential equations without using self-similarity assumptions, noting friction-drag and heat-transfer coefficient along MHD channel 14 p2356 A67-27978

Asymptotic and numerical solutions of Goulard integrodifferential equation describing hypersonic flow near stagnation point past blunt bodies, allowing for radiative transfer effects 14 p2296 A67-27981

Elastic rod, string or torsional member under effect of accelerating axial load, solving differential equation of motion in fixed end condition 14 p2399 A67-28140

Differential equations for heat and mass transfer in laminar boundary layer of binary gas mixture flow past porous wet flat plate 14 p2242 A67-28307

Synthesis of optimal controls for nonlinear plant described by second order differential equation 14 p2291 A67-28383

Dynamical systems control problem in connection with differential equations with lagging arguments 14 p2291 A67-28384

Qualitative analysis of nonlinear systems described by ordinary or partial differential equations or by functional equations 14 p2291 A67-28452

Theory of singular integrodifferential operators on compact manifolds, discussing basic principles, concept of uniformly nonelliptic systems, etc 14 p2343 A67-28503

Constant and variable coefficient initial and boundary value problems for second order differential equations 14 p2343 A67-28626

Necessary and sufficient conditions for solvability in two-space of second order elliptic differential equations with smooth irregular continuous differentiable boundary 14 p2344 A67-28634

Cylindrical shell stability under circumferential band load effect applied to freely supported edge 14 p2401 A67-28645

Calculation of diffusive gas flame in turbulent wake, reducing problem to differential equations of motion 14 p2407 A67-28649

Theorems derived from approximate methods of analysis applied to collocation, moment and Galerkin methods for solving linear integral and differential equations 14 p2344 A67-28671

Feedback control theory for constant temperature hot-wire anemometers using differential equation applied to frequency response optimization 14 p2320 A67-28750

Linearization of oscillation differential equations containing even nonlinearities, using asymptotic polynomials 14 p2344 A67-28810

Numerical solution of Cauchy problem class of nonlinear integrodifferential equations 14 p2344 A67-28896

Real autonomous smooth ODE system in neighborhood of critical point, noting stability dependence on sign of eigenvalue 14 p2345 A67-28906

Strong approximation of continuously differentiated function by means of differentiated expressions of finite line matrix 14 p2345 A67-28940

Behavior at infinity of specific intensity in plane-parallel atmosphere 14 p2391 A67-28946

Optimization of system described by differential and finite differential equations when including constraints 15 p2455 A67-29119

General resistive instabilities of self-pinched cylindrically symmetric beam of charged particles passing through ohmic plasma channel 15 p2522 A67-29198

Chapman-Enskog method modified for formulation of multicomponent laminar

boundary layer problem for numerical solution 15 p2469 A67-29220

Solution of nonlinear flow problems through parametric differentiation 15 p2469 A67-29221

Linear integrodifferential equations describing oscillatory processes, with asymptotic solutions in terms of parameter μ through WKB method 15 p2509 A67-29232

Lie series solution of equations resulting from separation of Helmholtz equation in special coordinate systems 15 p2509 A67-29266

Monte Carlo method applied to heat conduction problems, discussing steady state and transient situations with linear and nonlinear boundary conditions [ASME PAPER 65-WA/HT-1] 15 p2578 A67-29318

Computational worst error algorithm for linear systems and quadratic error criteria, showing flowgraph and computer execution results 15 p2457 A67-29367

Extent of system parameter change insuring system performance within specified limit 15 p2457 A67-29369

Two-person zero sum games with differential equation rules, noting location of optimal trajectories, separation properties, etc 15 p2509 A67-29404

Thickness transition configurations for cylindrical pressure vessels with hemispherical heads, noting weight, load effects, etc 15 p2573 A67-29419

P-n semiconductor junction widening due to impurity diffusion and drift, noting first order differential equations describing space-charge width variation with time 15 p2535 A67-29488

Irreducible systems existence in class of linear differential equations with quasi-periodic coefficients having frequencies represented by algebraic numbers 15 p2510 A67-29629

Linear theory of elastic Cosserat plate, noting bending theory which corresponds to bending of transversely isotropic three-dimensional plate 15 p2510 A67-29630

Order and asymptotic form of error of numerical methods for solving initial value problem for differential equations 15 p2471 A67-29632

Liapunov second method and extensions used in control problems of differential systems 15 p2574 A67-29633

Barrier-layer FET frequency behavior solved, deriving inner transistor quadrupole parameters by way of boundary value problem 15 p2447 A67-29644

Turbulent energy equation converted into differential equation for boundary layer development calculation 15 p2472 A67-29657

Solution stability of parametric nonlinear differential equation system, noting validity of Popov criterion 15 p2518 A67-29660

Motion stability described by differential equations of perturbed motion 15 p2518 A67-29695

Difficulties arising in applying Liapunov first method to solution of canonical systems and ways to overcome them 15 p2511 A67-29885

Nonlinear system analysis by subdividing total motion of system into fast and slow components, noting application to control systems 15 p2458 A67-29886

Transformation of class of boundary value to initial value problems in terms of one or two-parameter group of transformations for ordinary differential equations 15 p2511 A67-29892

Nonlinear differential equations of systems describable by state model solved by incremental linearization technique 15 p2458 A67-29908

Self-similar solutions for recombination plasma decay problem, considering plane and spherical symmetry 15 p2531 A67-30011

Perturbation method for solution of linear matrix differential equations subject to initial and two-point boundary conditions applied to transmission lines 15 p2511 A67-30018

Matrix formulation and resultant approximations as approach to nonlinear chemical reaction rate equations 15 p2434 A67-30023

Equations of Hill plane lunar problem for two rectangular coordinates in rotating system reduced to one differential equation for radius vector 15 p2560 A67-30039

Perturbation theory applied to periodic motions in three-body restricted problem 15 p2560 A67-30040

Perturbation theory methods as applied to first order differential equation 15 p2560 A67-30041

Quasi-isomorphic response of perturbed systems for slow coefficient variation of matrix system differential equation 15 p2512 A67-30050

Finite terms interpretation of Groebner method for differential equations applied to trajectory calculations in celestial mechanics 15 p2561 A67-30051

Runge-Kutta-Fehlberg method for systems of ordinary first and second order differential equations applied to numerical solution of many-body problem 15 p2561 A67-30052

Error assessment in numerical integration for ordinary differential equations applied to many-body problem 15 p2512 A67-30053

Derivation of moments of continuous stochastic system 15 p2459 A67-30131

Stability of systems with controlled plant and correcting system, based on analysis of stabilizability conditions in certain natural frequency regions 15 p2518 A67-30176

Extremal principle of possible simultaneous variations of stressed and strained states which follows from origin of virtual velocities 15 p2576 A67-30182

Periodically fluctuating loading fracture propagation analysis with damage summation principle in stress and cracking time terms, deriving differential equation for fracture length 15 p2576 A67-30183

Differential equations describing wave transformation in weakly inhomogeneous plasma 15 p2532 A67-30265

Technique based on Fokker-Planck equation for estimating statistics of randomly varying parameters in dynamic systems with known differential equation 15 p2461 A67-30323

Dynamic model parameter estimation using method of generalized least squares 15 p2462 A67-30326

Parameter estimation representing differential equation coefficient of controlled system for quick-response adaptive identification 15 p2464 A67-30338

Numerical integration of differential equation describing gas flow in laminar boundary layer for core of conical external flow 16 p2656 A67-30454

Differential equation computer simulation, examining errors in closed circuits 16 p2633 A67-30463

Types of closed characteristics in bounded region of two-dimensional autonomous differential equation 16 p2695 A67-30856

Algorithm for statistical estimation of nonlinear function of signal containing noise 16 p2643 A67-30921

Numerical solutions to differential equations governing earth electric field near surface obtained by Runge-Kutta method 16 p2664 A67-30974

Behavior of quasi-linear stochastic differential equations with one degree of freedom subjected to effect of random periodic excitation 16 p2696 A67-31009

Conditions for stability of solutions of second order linear differential equation with periodic coefficients 16 p2696 A67-31010

Fluctuating function method for approximate solution of boundary value problems for linear differential equations with reduced variational problems 16 p2696 A67-31013

Refined plate bending theory taking into account edge effect 16 p2765 A67-31050

Unsteady motion stability over given time interval of mechanical systems described by nonlinear differential equations 16 p2702 A67-31052

Linearized differential equations for invariant servodrive with hydraulic actuator controlled by throttle slide valve 16 p2609 A67-31378

Iterative solution methods for minimizing convex, differentiable function in Euclidean space 16 p2697 A67-31424

Particle trajectory analysis with perturbation series, noting position and velocity error estimation for restricted three-body problems 16 p2749 A67-31425

Stabilization method for solution of boundary value problems for second order

nonlinear ordinary differential equation 16 p2698 A67-31482

Optimization of numerical solution to linear ordinary differential equation with homogeneous boundary value conditions 16 p2698 A67-31546

Laminar flow through porous annulus with constant suction velocity at walls and swirl, using differential equations 16 p2662 A67-31551

Liapunov function for modeling and bounding solutions of distributed processes defined by interacting subsystems describable by stable differential equation 16 p2646 A67-31638

Algebraic characterization of optimal singular control for autonomous linear plants, using explicit closed form representation of singular strip 16 p2649 A67-31669

Conjugate gradients providing convergent means to solve optimal-control problems for linear systems with quadratic performance index 16 p2651 A67-31678

Solvability and methods of solution of boundary value problems noting uniqueness, potential theory application in solving polyharmonic equations and second-order equation 16 p2698 A67-31737

Book on engineering mathematics covering differential equation solutions by numerical method, partial differential equations, Fourier series, integrals, vector analysis, etc 17 p2876 A67-31930

Theory and design methods of torsional-flexural buckling of thin walled elastic struts of open cross section, deriving basic differential equations 17 p2957 A67-32024

Thermoelasticity of thin cylindrical shells for linear temperature distribution and temperature independent elastic constants, deriving differential equations of heat conduction 17 p2958 A67-32034

General formula for homogeneous second-order differential equation by Lie series, noting computer application 17 p2876 A67-32045

First slip time of phase locked loop of arbitrary order shown as solution of first order linear differential equation 17 p2811 A67-32117

Response of one degree of freedom system with power law time dependent damping and restoring forces using WKB approximation 17 p2958 A67-32128

Mathematical programming on analog computers solved by saddle point and extremum methods, using differential equations 17 p2817 A67-32225

Ventilatory mechanical system response to stepwise-increasing pressure stress studied with Laplace-Carson transform, giving characteristics of linear differential equation governing system 17 p2807 A67-32238

Difference method of solving boundary layer equation for laminar suction boundary layer using Crocco form 17 p2790 A67-32260

Stationary flow in viscous fluid film on rotating body of revolution, using differential equations 17 p2836 A67-32261

Stationary laminar boundary layer equations of Ostwald-de Waele power law fluids, flow and temperature boundary layer differential equation 17 p2836 A67-32262

Iterative procedure for solving linear differential equations with given boundary conditions on analog computer 17 p2818 A67-32296

Generalized linear programming applied to control theory noting use of differential equations 17 p2829 A67-32430

Nusselt results concerning heat transfer extended to include surface tension effect on heat transfer coefficient 17 p2970 A67-32461

Liapunov subcenter manifold, showing that real C-1 Hamiltonian system of ODEs has m distinct two-dimensional invariant manifolds 17 p2877 A67-32558

Wiener-Hopf technique for class of nonhomogeneous difference-differential-integral equations 17 p2877 A67-32560

Matric generalization of polar coordinate transformation to second order matrix differential system 17 p2877 A67-32563

Algorithm for constructing state equations corresponding to linear time varying system of differential equations 17 p2829 A67-32627

Linear boundary value problem solution using iterative method 17 p2877 A67-32678

Transformation of van der Pol equation into piecewise linear differential equation, determining periodic solution from asymptotic expansion 17 p2878 A67-32712

Rectangular network analysis of displacement in disks and plates, developing differential equations and giving minimum conditions for potential energy 17 p2961 A67-32714

Martin boundary for invariant Markov processes investigated on group of affine transformations of straight line 17 p2878 A67-32736

Differential equations determining time-dependent torsional moment and stresses in thin walled rods in creep presence 17 p2821 A67-32830

Soviet papers on mathematical physics covering solution of boundary value problems, structural analyses, etc 17 p2884 A67-32867

Hypersonic gas flow past slender body, obtaining pressure coefficient and shock wave curvature by linearizing differential equations involving stream function 17 p2791 A67-32868

Dynamic system single- and multifrequency random oscillations described by differential-difference equations and solved through probability distribution 17 p2885 A67-32876

Numerical analytical method for periodic systems described by ordinary differential equations 17 p2879 A67-32877

Averaging principle applied to stochastic differential equations describing oscillatory system subject to white noise 17 p2885 A67-32878

Bogoliubov existence theorem for one-dimensional integral manifold and two-dimensional local integral manifold extended to Hilbert space 17 p2879 A67-32879

General solution of linear differential equation of first order with quasi-periodic coefficients 17 p2879 A67-32880

Properties of solutions of second order nonlinear nonautonomous ordinary differential equations from study of truncated version of 17 p2879 A67-32884

Nonuniform electrical conduction in MHD channels analyzed by differential equations 17 p2906 A67-33011

Dynamic characteristics of variable mass slender elastic body, solving vector differential equations [AIAA PAPER 67-41] 17 p2956 A67-33013

Mixing function parameter behavior in boundary layer separations by Crocco-Lees method, noting linearized Glick differential equations 17 p2840 A67-33031

Differential transport equation system in n-dimensional anisotropic space solved using matrices, discussing heat conduction equations 17 p2972 A67-33070

Separation of variables method for cylinder cooling with turbulent fluid flow parallel to axis 17 p2972 A67-33072

Formation of high energy plasma in toroidal system by neutral atom injection, discussing differential equations 17 p2908 A67-33110

Averaging method extended to physical systems described by differential equations simultaneously dependent on almost periodic fast time and periodic slow time 17 p2885 A67-33140

Sufficient conditions guaranteeing asymptotic stability of class of linear dynamic systems with bounded narrow band parametric excitation [ASME PAPER 67-APM-24] 17 p2830 A67-33152

Flow of viscous incompressible conducting fluid in channel with porous walls 17 p2910 A67-33352

Self-consistency equation for nucleation of superconductivity in presence of magnetic field 17 p2924 A67-33372

Steady state wave propagation in homogeneous anisotropic media governed by symmetric hyperbolic partial differential equations 18 p3077 A67-33429

Single circuit parametron with pulsed balance-modulated pumping voltage, showing existence of two independent subharmonic components 18 p3005 A67-33503

Differential equations extremal solutions, introducing infrapolution and Cauchy infrapolution concepts 18 p3070 A67-33548

Existence of solutions to differential equations with multiple-valued right

side 18 p3070 A67-33554

Stability and instability of tridiagonal linear system, noting application to stability analysis of differential equation system 18 p3070 A67-33644

Plane plastic strain problem analyzed assuming absence of time effects and of intermediate principal stress 18 p3140 A67-33656

State variable difference equation method for HF solution of ordinary differential equations in digital simulation with nonlinearity 18 p3005 A67-33662

A priori bound on difference between free boundary positions in two Stefan problems derived in terms of initial conditions and heat influxes 18 p3071 A67-33664

Oscillator analysis for particular class of adiabatic invariants 18 p3117 A67-33686

Transition probabilities for molecular collision excitation by differential equation matrix, approximations, perturbation theory, etc 18 p3081 A67-33785

Differential and boundary layer equations for free convection flow along vertical hot wall, investigating existence question 18 p3027 A67-34009

Finite propagation velocity in heat conduction, diffusion and viscous shear motion, studying assumptions of differential equation derivation 18 p3159 A67-34070

Predictor-corrector for solving ordinary differential equations, discussing influence of rounding-off errors on accuracy of solution 18 p3071 A67-34266

Inertial motion of solid body in space of constant curvature, obtaining solution to differential equation 18 p3079 A67-34372

Existence theorems for defining solubility of certain boundary value problems for ordinary second order linear differential equation 18 p3072 A67-34384

Reduction of differential equation to dynamic system when equation is invariant for single parameter group 18 p3072 A67-34392

Algorithm for construction of discrete approximations to linear differential expressions in terms of ordinates 18 p3072 A67-34394

Parallel numerical integration formulas for differential equations 18 p3072 A67-34395

Coherent radiation interaction with two-level atoms system in single mode approximation, obtaining equation for time dependent number of photon emission and absorption 18 p3061 A67-34423

Dirichlet problem for elliptic system of differential equation which does not satisfy Lopatinski condition where characteristic equation of system has simple roots 18 p3073 A67-34481

Critical stability cases of almost periodic motions, showing reduction to solution of differential equations of steady motion 18 p3080 A67-34602

Solid body of variable mass with cavities filled with ideal incompressible fluid, analyzing differential equations of motion 18 p3080 A67-34604

Definition of asymptotic stability conditions and instability of zero solutions of differential equations 18 p3080 A67-34605

Existence and uniqueness of solutions of point boundary value problem for denumerable system of differential equations 18 p3073 A67-34606

Properties of solutions of linear homogeneous differential-difference equations with linear coefficients and real differences 18 p3073 A67-34614

Book on optimal control covering theory and application of linear algebra, vector analysis, Euclidean space, Pontryagin principle, etc 18 p3018 A67-34758

Exact dynamical equation derived for conditional density mode representing stochastic process 19 p3199 A67-34778

Dirichlet problem solution for Poisson equation on rectangle with smooth boundary values, using higher order differences 19 p3249 A67-34794

Single-step numerical integration stability analysis applied to linear differential equations with known root locations 19 p3249 A67-34839

Lapunov function from quadratic polynomial for n-order nonlinear differential equations 19 p3250 A67-34842

Gyroscope circuit model and oscillation

behavior analyzed through nonlinear differential equation derived from Euler equation 19 p3227 A67-34843

Coupled systems stability constraints and oscillatory behavior, discussing feedback path nonlinearities using differential equations 19 p3200 A67-34849

Circular planform peripheral jet ground effect machine heaving motion analyzed using motion equations 19 p3172 A67-34867

Estimation method for lower bounds of natural frequencies of circular closed cylindrical shell 19 p3338 A67-34876

Single-mesh circuits design for driving xenon flashlamps, solving normalized nonlinear differential equation 19 p3192 A67-35015

Plasma-metal interface electric field intensity, deriving dimensionless formula from nonlinear second order differential equation 19 p3277 A67-35125

DC discharge parameters solution using pressure theory with generation terms stressing one- and two-dimensional cases 19 p3277 A67-35126

Ion-density data modifications due to temperature variations, discussing normalization and electron density relationship 19 p3224 A67-35491

Differential equations and potential for simply supported anisotropic sandwich plate under compression and shear stresses above buckling limit 19 p3341 A67-35575

Stability analysis of steady combination oscillations of single loop circuit, obtaining equations relating voltage harmonic of nonlinear capacitances 19 p3262 A67-35706

Integrodifferential equations for product surface area changes and grinding process development obtained by assuming proportionality between fracturing probability and particle size 19 p3236 A67-35725

Attitude stability of spinning rigid symmetric satellite in elliptic orbit examined for motion about equilibrium position with spin axis normal to orbit plane 19 p3333 A67-35747

Buckling of aging linearly viscoelastic beam columns with time variable mechanical properties, deriving integrodifferential equations and stability conditions 19 p3343 A67-35781

Inhomogeneous second order linear differential equation solution based on Lie formalism, presenting physical applications 19 p3250 A67-35891

Motion equation for four-body system attracting one another according to Newtonian law, obtaining series of functions converging toward solution 19 p3328 A67-35899

Macroscopic physical system with behavior described in terms of differential equation system studied for stability in presence of small delay 19 p3205 A67-35912

Book on viscoelasticity covering linear theory as part of applied mechanics, differential equations, hereditary integrals, etc 20 p3535 A67-36138

Impact characterization and length, determining contact energy with Hertz equation and integrating nonlinear differential equation for system motion 20 p3483 A67-36195

Calculation of frequency characteristics of hydraulic main line sections with parameters varying continuously along length 20 p3363 A67-36444

Two-point boundary value problem approximate solution using Monte Carlo path integral calculation 20 p3475 A67-36481

Differential equation for axisymmetric deformation of thin circular cylindrical shell stiffened by circumferential rings and subjected to lateral and axial pressure 20 p3537 A67-36495

Size and longitudinal conduction influence on wall temperature field and effectiveness of heat exchangers determined by differential equations [ASME PAPER 67-HT-80] 20 p3551 A67-36758

Mutual pulling system between two klystrons, deriving equations for pulling bandwidth and for various system responses 20 p3398 A67-36772

Differential equations for stressed thin orthotropic plates of variable thickness derived and solved in cylindrical coordinates 20 p3539 A67-36919

Crank-Nicolson technique for first order

linear time-invariant differential equation solution, discussing truncation error 20 p3477 A67-36933
 Analog simulation of differential equation system for Cardan-suspended gyro, considering dry friction, support and aircraft motion 20 p3454 A67-36954
 Vibrating annular membrane problem, including load per unit area and asymmetry of load and vibration, using finite transform derivation 20 p3539 A67-37006
 Valentine method for maximum principle problem solution, reducing to nonlinear differential equation system with special boundary conditions 20 p3477 A67-37029
 Stability of periodic solution of nonlinear systems with coefficients dependent on amplitude and frequency 20 p3408 A67-37043
 Harmonic linearization, estimating quality of oscillatory transients in nonsearching self-adjusting systems described by high order differential equations 20 p3408 A67-37045
 Group properties of differential equations describing axisymmetric thin layer jet flow of ideal fluid propagating along surface of revolution 20 p3422 A67-37063
 Asymptotic approximations for analysis of nonlinear resonant circuits through differential equations, assuming oscillation processes similar to harmonic system processes 20 p3409 A67-37113
 Transistor circuit containing magnetic cores with rectangular hysteresis loop analyzed for switching processes using differential equations 20 p3399 A67-37114
 Gyrotachcelerometer errors in measuring object angular velocity and acceleration relative to one axis, deriving differential equations of motion 20 p3451 A67-37155
 Variational equations solved by numerical integration along with nonlinear differential equations with less computing and storage and higher accuracy 20 p3478 A67-37212
 Differential equations governing steady state current flow in semiconductors computed, considering variations as function of distance, hole and electron densities, etc 20 p3400 A67-37216
 Noise rejecting algorithms for ODE solutions with computer, using redundancy, placement of control and feedback techniques 20 p3392 A67-37224
 Three-dimensional incompressible flow with colinear magnetic field, studying stability by numerical method 20 p3423 A67-37242
 Particle paths in central force field derived through second order differential equation for inverse separation, noting perturbation potential 20 p3526 A67-37254
 Admittance function for burning surface by solving differential equation and satisfying boundary conditions, discussing frequency peaks qualities 20 p3554 A67-37255
 Laminar compressible plane stationary boundary layer flow described by differential equations, including momentum and energy equations 20 p3424 A67-37280
 Differential equation for bending of homogeneous plates of variable stiffness 20 p3541 A67-37284
 Multipoint equivalent cross section method for calculating finite deflections of beams of strain hardening material 20 p3541 A67-37285
 Plane-strain problem of plasticity theory with two yield conditions applied to stress and velocity fields defined by differential equilibrium equations 20 p3541 A67-37299
 Nonlinear fluid mechanical systems design using numerical least squares method in fitting second order differential equation to straight line approximation of state variable 20 p3366 A67-37368
 Approximate solutions for nonlinear differential equations to study periodic motions for analysis of pressure relief system 20 p3366 A67-37369
 Fluid control system design by third order linear differential equation with transient response, showing relationship to frequency response 20 p3366 A67-37370
 Multiple integration method for determining coefficients and differential equation order for linear dynamic systems 20 p3412 A67-37378
 Motion equations for elastically deforming body containing cavity partly filled with ideal fluid 20 p3481 A67-37380
 Self-similar solutions for recombination plasma decay problem, considering plane and

spherical symmetry 20 p3502 A67-37536
 Kato perturbation theorems applied to ordinary differential equations in Banach space 20 p3478 A67-37575
 Soviet papers on theory of differential equations with deviating argument, Volume 4 20 p3478 A67-37578
 Laplace transformation of solution of linear differential equations with variable coefficients and time lags, analyzing motion stability 20 p3478 A67-37579
 Galerkin method applicability to boundary value problems and eigenfunctions and eigenvalues for integrodifferential equations with deviating arguments 20 p3478 A67-37580
 Optimality and invariance conditions for linear free-time problem 20 p3412 A67-37582
 Plane waves propagation in microelastic medium having only coupled stresses 20 p3542 A67-37681
 Wave propagation in nonuniform slightly gyrotropic medium with parameter less than one solved by differential equations 20 p3389 A67-37708
 Asymptotic series in theory of nonlinear systems of ordinary differential equations 20 p3479 A67-37718
 Estimates for solutions to nonlinear boundary value problems for second order differential equation 20 p3479 A67-37719
 Asymptotic behavior of solutions for nonlinear differential equations 20 p3479 A67-37720
 Second boundary value problem for differential equation of elastic equilibrium of shallow cylindrical shell 20 p3543 A67-37721
 Maximum region of applicability of Chaplygin theorem of differential inequality to elliptic difference equation 20 p3479 A67-37722
 Rotation effect on growth of discontinuity across Alfvén wavefront, solving differential equations 21 p3662 A67-37761
 Variational problem of rocket dynamics in homogeneous gravitational field in empty space reduced to differential equation system 21 p3701 A67-37836
 Stretched sail behavior in sonic, supersonic and hypersonic flows, discussing profile dependence on angle of attack and free-stream Mach number 21 p3563 A67-37889
 Perturbation method using stream function for investigating anisotropic wave propagation describable by hyperbolic differential equations 21 p3611 A67-37891
 Solution behavior of second order nonlinear differential equation with restriction on one constant 21 p3651 A67-37922
 Stress analysis of closed cylindrical shell under concentrated loading at free edge, solving differential equation by expanding functions into Fourier series 21 p3718 A67-37982
 Dynamic model for magnetic field effect on vibrations of clock balance wheel having magnetized cross bar 21 p3625 A67-37988
 Generalized indirect method solving two-point boundary value problems for rapid optimal trajectory computation 21 p3702 A67-38024
 Asymptotic representations of Whittaker functions /with terms of standard equation coefficients equal/ applicable to wave propagation in inhomogeneous media 21 p3652 A67-38109
 Pointwise bounds for perturbed parabolic and elliptic equations using known bounds for corresponding strictly differential problems, noting Rayleigh-Ritz procedure 21 p3652 A67-38174
 Positive linear second order differential equation solutions, with proof of general theorems about qualitative asymptotic behavior 21 p3652 A67-38195
 Approximate method for design of FM systems using variable capacitance varactor diodes, noting time varying differential equation 21 p3593 A67-38234
 Stability of integrals of differential equations for periodic motions 21 p3657 A67-38267
 Stability of linear integro-differential equations for processes with distributed parameters 21 p3657 A67-38268
 Differential equations of motion for permanent rotation heavy gyro with fixed point 21 p3627 A67-38269
 Optimization problem described by differential equations and related to Bellman

equation 21 p3653 A67-38282
 Unloading wave expanding in elastoplastic rod determined by integration of differential equation in quadratures 21 p3720 A67-38286
 Nonlinear differential equations for elastic spherical wedge distortion assuming isotropy, homogeneity and incompressibility 21 p3721 A67-38380
 Runge-Kutta method applied to Fredholm type integrodifferential equations 21 p3653 A67-38421
 Stability and instability properties of differential system, discussing matrix and roots 21 p3653 A67-38558
 P-n junction devices static behavior assuming Van Roosbroeck differential equations in bulk and transition regions 21 p3598 A67-38571
 Cantilever plate calculation under load and deflection by variation method, reducing problems to solutions of differential equations with constant or variable coefficients 21 p3724 A67-38781
 Network method to derive differential difference equations for boundary condition of clamped and free edges and point supports of low aspect orthotropic wings network method to derive differential difference 21 p3724 A67-38782
 Optimization analysis for axisymmetric rocket motor nozzle design based on assumptions for gas particle flow [AIAA PAPER 66-538] 21 p3565 A67-38875
 Natural vibration frequencies of cylindrically orthotropic circular plate with linearly variable thickness, solving differential equation of motion 21 p3728 A67-38898
 Position of real singular point of solution function of differential equation of Prandtl boundary layer theory 21 p3615 A67-39096
 Matrix method proposed for systems of linear differential equations governing satellite attitude control in elliptical orbits, considering integral criteria calculation 22 p3897 A67-39160
 Statistical method for determining satellite orientation and rotation based on differential motion equation model 22 p3878 A67-39168
 Optimal parameters of transfer function of low thrust power limited engines by approximate solution of differential equation 22 p3898 A67-39181
 Optimal control problem with state variables subject to inequality conditions, deriving Pontryagin principle and differential equation 22 p3826 A67-39194
 Static Green function for elastic electron scattering by hydrogen atoms, using integrodifferential equations to determine resonance energies 22 p3839 A67-39204
 Linear differential games associated with vector differential equation in arbitrary dimensional space noting square matrix and convex sets 22 p3826 A67-39214
 Quasi-periodic solutions of nonlinear systems of differential equations containing small parameter 22 p3827 A67-39304
 Optimal control of quasi-linear system perturbed motion, developing approximation method 22 p3776 A67-39305
 Steady state solutions for system of partial differential equations with two independent variables describing small perturbations of transonic gas flow near transition point 22 p3844 A67-39391
 Three-dimensional generalization of Birkhoff transformation for regularization of Keplerian motion in three-body problem noting differential equations system 22 p3881 A67-39513
 Navier-Stokes differential equations for unsteady incompressible viscous fluid motion solution method, considering quadratic inertial terms 22 p3783 A67-39682
 Approximate integrodifferential equations determining ensemble mean and covariance of particle distribution function of Vlasov plasma, discussing incompressible Navier-Stokes turbulence 22 p3850 A67-39703
 Numerical recursion method for calculation of characteristic exponent of Mathieu differential equation 22 p3827 A67-39744
 Peripheral jet GEM pitching characteristics analysis by longitudinal static stability and dynamic pitching motion 22 p3745 A67-39837
 Multivariable linear system noninteracting control realized by relays sliding

motions 22 p3777 A67-39839
 Nonstationary second order linear differential equation for near time optimal space vehicle guidance system design solved by linear transform 22 p3832 A67-39966
 Membrane stress state of spiral coiled tube surface, reducing stress components to second order differential equation 22 p3913 A67-40009
 Energy changes between solar wind and cosmic rays, discussing particle motion description by Fokker-Planck differential equation 22 p3874 A67-40079
 Nonlinear differential equations describing extensional motion of dumbbell satellite solved on digital computer 22 p3886 A67-40086
 Angle of attack determination from rotational body rates, formulating ordinary differential equations 22 p3741 A67-40093
 Mathematical classification of differential equations governing elastic-plastic waves in plane strain 22 p3914 A67-40193
 Differential equations describing stressed state of revolving shell beyond elastic limit and solutions adaptable to computer programming 23 p4075 A67-40681
 Differential equations maximum parameter values for single mass nonlinear system passage through resonance point determined with approximate methods based on small parameter method 23 p4026 A67-40686
 Complex representation of elliptic differential equation solution, discussing holomorphic functions, polycylindrical regions and Vekua 23 p4022 A67-40723
 Differential equation system for reacting laminar boundary layer heat and mass transfer solved analytically, noting compressible gas and porous foil filter 23 p4081 A67-40744
 Boundary value problem solution convergence conditions applied to linear ordinary differential equations involving two parameters 23 p4022 A67-40746
 Soviet book on approximate methods for boundary value problem solutions of ordinary and partial differential equations and certain integral equations 23 p4022 A67-40841
 Nonlinear differential equations solutions extended analytically by parameter substitution method applied to Rayleigh equation 23 p4023 A67-40926
 Boundary value problem theory for ordinary differential equations, discussing compact and noncompact intervals of independent variables 23 p4023 A67-41018
 Shock curvature and flow variable gradients at tip of pointed axisymmetric body in nonequilibrium flow, solving linear differential equations and singularity 23 p3928 A67-41176
 Spherical and cylindrical dipole fields in different coordinate systems, discussing differential distances 23 p3975 A67-41211
 Algebraic and transcendental equations solutions using analog computer model described by differential equations, noting Liapunov stability theorem and asymptotic equilibrium 23 p3976 A67-41392
 Explicit nonlinear numerical integration method for solution of large systems of ordinary differential equations 23 p4024 A67-41394
 Nonequilibrium boundary layer problem solution by direct treatment of two-point boundary value problem [AIAA PAPER 67-219] 23 p3991 A67-41715
 Mathematical model of linear guidance law to dynamical system, noting reduction of two-point boundary value class error 23 p4026 A67-41732
 Book on adaptive control and optimization techniques covering basic mathematics, computer methods, differential equations, time domain, etc 24 p4133 A67-41793
 Book on thermoelasticity associating elasticity and heat conduction theories for thermodynamics of irreversible processes and differential equation problems 24 p4246 A67-41891
 Numerical solution for two-point nonlinear boundary value problem of n-order ordinary differential equation 24 p4177 A67-41914
 Plane and turbulent fluid jets dynamic and thermal behavior expanding in magnetic field described by differential equations system 24 p4195 A67-41930

Sensitivity analysis of linear differential difference equations with hereditary influences 24 p4134 A67-42026
 Temperature variations of satellite with radiatively coupled isothermal inner shell having heat source analyzed via perturbation method for differential equations 24 p4253 A67-42051
 Distributive circuit element model for computation of optimum gridding of solar cells 24 p4098 A67-42086
 Controllability and observability concepts defined for feedback system, with finite dimensional differential equation representations 24 p4136 A67-42189
 Stabilization method for solution of boundary value problems for second order nonlinear ordinary differential equation 24 p4177 A67-42198
 Existence theorems for defining solubility of certain boundary value problems for ordinary second order linear differential equations 24 p4177 A67-42199
 Asymptotic method for solving differential equations, giving equilibrium composition of gaseous combustion products 24 p4178 A67-42390
 Second order nonlinear differential equation derived for pressure-time curve required for ideal solid propellant rocket motor 24 p4208 A67-42923
 State variable approach to linear differential equations, coding for digital computation 24 p4179 A67-42933
 Uniformization of asymptotic expansions, constructing counterterms by nesting increasing number of extensions for both secular and singular perturbation terms 24 p4190 A67-43094
 Stability boundary of periodic oscillation described by third order differential equations near Liapunov critical case 24 p4137 A67-43108
 Perturbation theory for exchange forces using Brillouin and Schroedinger equations 24 p4194 A67-43115
DIFFERENTIAL GEOMETRY
SA PROJECTIVE-DIFFERENTIAL GEOMETRY
 Galilean relativity principle in analytic mechanics of holonomous systems with infinite degrees of freedom 05 p0846 A67-16735
 Bending strain in linear shell theory, noting surface differential geometry and rotation vector and tensor [ASCE PAPER 268] 11 p1874 A67-24430
 Constructing example of isolated stationary point 14 p2343 A67-28387
 Motor fields analysis in Cosserat continuum noting differential forms of stress and strain 22 p3837 A67-40006
DIFFERENTIAL INTERFEROMETRY
 Observations with birefringent interferometer and photoelectric spectrophotometer of Martian surface materials composition, noting strong band at 3.1 micron suggesting hydrated minerals 11 p1865 A67-24603
 Holographic interferometry by superimposed holograms before or after photographic development 19 p3232 A67-35890
DIFFERENTIAL OPERATOR
 Fundamental solutions to certain singular partial differential equations with constant coefficients, using Bessel iteration operator and Fourier-Bessel transforms 01 p0105 A67-10676
 Uniqueness and stability theorems for BVP involving degenerated elliptic differential operator 01 p0105 A67-10678
 Parabolic convolution type equations in bounded cylindrical and noncylindrical regions, discussing smooth operators in half-space 02 p0259 A67-11871
 Existence theorem for periodic solutions to parabolic boundary value problem involving reduction to solvable operator equation 03 p0460 A67-13835
 Linear continuous operators in analytic space exchangeable with differential operators 04 p0646 A67-15261
 Self-conjugacy of semibounded Schroedinger operator 04 p0646 A67-15262
 Uniqueness of Cauchy problem when initial surface contains characteristic points 05 p0835 A67-16739
 Inequalities for difference and pseudodifferential operators, providing sharp form of Garding

inequality 06 p1025 A67-18642
 Trace formulas of difference between two ordinary differential operators of higher order 07 p1214 A67-19175
 Computational methods for determining lower bounds for eigenvalues of operators in Hilbert space 07 p1217 A67-20018
 Class of nonlinear operators and necessary and sufficient condition of solvability of quasi-linear elliptic equations 10 p1674 A67-23076
 Operator calculus, based on momentum operator choice, designed to take account of finite domain of wave functions in quantum mechanics 10 p1682 A67-23349
 Rodrigues type formula for generalized Laguerre polynomials based upon semigroup property for solutions of heat equation and generating function related to source solution 10 p1675 A67-23630
 Coercivity inequalities for second order elliptical operators with increasing coefficients 11 p1814 A67-24978
 Boundary value problem solution by approximation method of Kupradze with differential operators and given and unknown functions 12 p1960 A67-25440
 Conditions required for Reynolds operator to be idempotent over Banach algebra 13 p2146 A67-27149
 Mysovskikh theorem concerning convergence of Newton method for finding zeros of nonlinear operators between Banach spaces 13 p2147 A67-27172
 Elliptic regularization for symmetric positive system of linear first order partial differential equations with irregular boundaries 13 p2147 A67-27178
 Novel type of interpolation derived by introducing operator B and Chebyshev spaces 13 p2148 A67-27472
 Linear positive operator construction in approximation theory 13 p2148 A67-27474
 Single parameter family of two-layer difference schemes with decomposing operators for general linear second order parabolic equations with mixed derivatives and variable coefficients 13 p2149 A67-27614
 Convergence of methods of tangential parabolas and hyperbolas used in nonlinear equation solution with nondifferentiable operators convergence of methods of tangential parabolas and hyperbolas used in nonlinear equation solution 13 p2149 A67-27619
 Hilbert space methods in elliptic partial differential equations 14 p2341 A67-27849
 Theory of nonself-adjoint ordinary second order differential operators, discussing solution algorithms 14 p2343 A67-28478
 Integrodifferential equation solvability by investigation of adjoint Cauchy problem 15 p2511 A67-29890
 Boundary value problems containing positive linear differential operators and monotone functions of dependent variable analyzed via nonlinear heat generation 17 p2967 A67-32040
 German book on differential operators of mathematical physics covering Hilbert space h, Schroedinger spectral theory, etc 20 p3475 A67-36434
 Kato perturbation theorems applied to ordinary differential equations in Banach space 20 p3478 A67-37575
 Boundary value problem solution by approximation method of Kupradze with differential operators and given and unknown functions 20 p3479 A67-37723
 Approximate solutions of Prandtl boundary layer problem for incompressible laminar flow derived, using Nagumo-Westphal theorem on parabolic differential operators 21 p3563 A67-37888
 Characterization of eigenvalues of singular nonself-adjoint differential operator of second order 21 p3653 A67-38557
 Coupled linearized equations for laser-induced optical radiation instabilities in liquids and gases, obtaining differential operator and Green function 23 p4027 A67-41024
 Lower bounds for eigenvalues of differential linear elliptical operator using Rayleigh-Ritz approximation extension 24 p4177 A67-42154
DIFFERENTIAL THERMAL ANALYSIS
/DTA/
 Rate dependent melting of polytetrafluoroethylene by differential thermal analysis, noting that amount of

- superheating is larger with higher molecular weight 04 p0641 A67-14528
- Phase diagram of vanadium-gallium system by differential thermal analysis of thirty-five 10-g V-Ga alloy samples prepared in arc oven 05 p0827 A67-16326
- Thermal differential method of determining critical points in flow past projection in pipe 11 p1741 A67-24032
- Metallography, roentgenography and differential thermal analysis of composition temperature ranges of chromium-germanium phases 16 p2691 A67-31592
- ### DIFFERENTIAL THERMAL ANALYZER
- Tungsten-carbon phase relations from DTA, X-ray and electron diffraction measurements noting disordered, ordered hexagonal and orthorhombic modifications 16 p2692 A67-31599
- Differential RF voltage comparator for transfer standard and calibration of HF voltage devices at high accuracy 24 p4155 A67-42288
- ### DIFFRACTION
- SA ELECTRON DIFFRACTION
- SA FRESNEL DIFFRACTION
- SA LAUE DIFFRACTION
- SA LIGHT TRANSMISSION
- SA NEUTRON DIFFRACTION
- SA PULSE DIFFRACTION
- SA WAVE DIFFRACTION
- SA X-RAY DIFFRACTION
- Space-time diffraction for asymptotic solution of Klein-Gordon dispersive hyperbolic equation in bounded domain 07 p1218 A67-20270
- Periodic relaxation pulses caused by thermal resonance drift, studying diffraction loss and other effects on transverse modes in crystal lasers 17 p2867 A67-32362
- ### DIFFRACTION GRATING
- Surface color explained using backscattering angle and diffraction properties of germanium films vacuum deposited onto heated substrate 01 p0138 A67-11076
- Light generation from rectangular cross section electron beam interacting with metallic diffraction 03 p0468 A67-13593
- Tracing rays through hologram treated as generalized case of tracing rays through diffraction grating, determining local diffracting power by geometry and wavelength of beams 03 p0423 A67-13906
- Strain distribution measurement by optical grating 05 p0918 A67-16441
- Diffraction grating technique for measuring dynamic plastic strain exceeding 4 percent deformation at high strain rates in variable intensity light source 05 p0920 A67-16824
- Electromagnetic wave emission excited by electron stream over diffraction grating lying on boundary of semilinear anisotropic dielectric 05 p0766 A67-17163
- Diffraction of angular spectrum of radio waves by phase changing screen 06 p0962 A67-17969
- Moiré method of surface strain measurement 07 p1262 A67-19387
- Electromagnetic plane wave diffraction on anisotropically conducting plane and shielding and reflecting activity of dense radial grating 07 p1143 A67-19589
- Numerical computation of phenomena due to electromagnetic wave diffraction on tapered grid 07 p1143 A67-19595
- Nonhomogeneous Helmholtz equation for optical gratings with perfectly conducting boundaries solved, using distribution theory 08 p1353 A67-20349
- Optical incremental shaft resolver using plastic radial gratings 08 p1331 A67-20864
- Prisms for dispersion compensation and single plane diffraction grating as correcting element for achromatizing white light reconstruction of two-beam surface hologram 09 p1492 A67-21567
- Electromagnetic wave diffraction on perfectly black screen in Kottler theory 09 p1464 A67-22054
- Interferometer producing focusing hologram diffraction grating, noting photograph of spectrum 10 p1658 A67-23788
- Electro-optical spectrograph producing dynamic spectrograph continuous in both frequency and time 14 p2319 A67-28444
- Spectral narrowing and tunability over wide spectral range demonstrated in solid/liquid dye lasers using diffraction gratings as cavity reflectors 15 p2500 A67-29817
- Multicolor image reconstruction from holograms behaving as planar diffraction gratings, excluding crosstalk images formation 15 p2491 A67-30431
- Time resolved measurements of phase fluctuations of coherent beam at emergence from turbulent layer 17 p2817 A67-33304
- Limitations arising during reconstruction of plane-grating hologram with characteristic X radiation to operate at optical wavelengths 18 p3047 A67-33884
- Mode conversion in rectangular waveguides, describing results in terms of plane wave diffraction by grating 19 p3183 A67-35545
- Wave field behind transmission grating illuminated by plane wave examined by Fourier spectrometry based on grating resonances 20 p3437 A67-36338
- High resolution far IR lamellar grating interferometer with double beam differencing 20 p3438 A67-36347
- High quality holography of back-lighted objects using achromatic-fringe interferometry 20 p3450 A67-37022
- Electromagnetic plane wave diffraction on anisotropically conducting plane and shielding and reflecting activity of dense radial grating 20 p3384 A67-37326
- Pulsed water vapor laser single wavelength operation using three diffraction gratings to make resonator frequency-selective 23 p4011 A67-40783
- Diffraction of H-polarized plane wave on metal grating with narrow slits 23 p3975 A67-41683
- Interferometer employing diffraction grating investigated for applicability to quantitative study of gas dynamics 24 p4158 A67-42723
- ### DIFFRACTION PATH
- Laser mirror design in lens form for decoupling diffraction limited parallel beam, based on theorems concerning Gaussian beam imaging and behavior 05 p0826 A67-17327
- ### DIFFRACTION PATTERN
- Epitaxial temperature for Si films vacuum deposited on silicon as function of substrate crystallographic orientation observed by low energy electron diffraction patterns 01 p0132 A67-10372
- Nearest neighbor electron scattering in silicon, showing existence of diffuse rings association with Kikuchi pattern 01 p0135 A67-10877
- Si single crystal lattice parameter measurement using double-diffraction effect 01 p0135 A67-10894
- Born approximation theory of nonlinear scattering of microwaves from oscillating plasma column, noting diffraction patterns and frequency shifts 01 p0027 A67-11324
- Absolute intensity and angular distribution of microwaves scattered from oscillating plasma column, noting diffraction patterns and frequency shifts 01 p0027 A67-11325
- Low energy electron diffraction techniques for niobium /110/ surface, noting argon ion bombardment 02 p0257 A67-12729
- Properties of equatorial sporadic E layer irregularities studied by HF observation, including scattering spectrum and diffraction pattern formed by reflection from ground 03 p0406 A67-12823
- Nighttime F layer irregularities at equator responsible for scintillation of signals from radio sources and satellites 03 p0407 A67-12828
- Spaced receiver method for measuring ground diffraction pattern of vertically reflected radio waves 03 p0407 A67-12830
- Secondary scattering of low energy electrons by rows of atoms, obtaining diffraction pattern 03 p0496 A67-13648
- Straight edge fence design for control of radar site environment from clutter return, pattern interference, tracking errors and high power hazard to personnel 03 p0396 A67-13853
- Radio data suggests dielectric constant variations in troposphere limited to discrete scale sizes [RASSA PAPER 1-10-141] 03 p0417 A67-14249
- Stripe pattern characteristic of voltage-controlled negative resistance and LF electric oscillation observed in SbSI due to diffraction effect 04 p0674 A67-14619
- Electron diffraction patterns for GaP semiconducting thin films deposited on indium oxide substrates, determining structure as function of film thickness 04 p0686 A67-15970
- Second harmonic generation of light by focused laser beams in nonlinear crystals at exit surface 05 p0817 A67-16640
- Iron and chromium films prepared at 4 degrees K analyzed by radial distribution, showing electron diffraction patterns of amorphous state 05 p0866 A67-16976
- Hexagonal indexing of tungsten boride phase in reaction of boron with tungsten core, obtaining X-ray powder diffraction pattern 06 p1016 A67-17904
- Short wave asymptotics of diffraction field at sphere for incident plane transverse waves 06 p1100 A67-18032
- Optical properties of zinc oxide analyzed by exposing samples to mechanical and thermal treatments and UV radiation [AIAA PAPER 67-214] 06 p1052 A67-18514
- Angular power pattern for circular aperture receiving plane wave perturbed by passage through turbulent atmosphere 06 p1033 A67-18538
- Specific stacking fault energy of deformed fcc metals determined from electron microscope diffraction contrast of stacking fault dipoles 07 p1208 A67-19637
- Chemical and mineralogical composition of roederite found in Indarch meteorite, presenting electron probe analysis and X-ray diffraction pattern optical data 07 p1255 A67-20012
- Crystalline structure of amorphous boron fibers noting glass-like nature of fiber as exhibited by diffraction patterns 08 p1343 A67-21313
- Fringe counting in laser interferometers and phase quadrature signals for bidirectional counting at good efficiency without mechanical or optical complications 09 p1493 A67-21613
- Spectral differentiation and hologram filtering in reducing optical signal comparison to signal correlation 09 p1497 A67-21826
- Evaporated thin film capacitor from silicon oxide, noting electron diffraction patterns and IR adsorption peaks 09 p1555 A67-22102
- Hologram copies by recording interference pattern between undiffracted and diffracted waves 10 p1654 A67-22754
- Traveling wave V antenna, discussing parameter variation effect on radiation patterns 11 p1761 A67-24283
- Microwave thermography used to measure microwave optical field patterns, using Czerny IR thermosensitive transducer process 12 p1939 A67-25196
- Radiation pattern of irregular antennas, using digital computer and superimposition of components to determine composite pattern 12 p1915 A67-25974
- System using holography for character recognition according to Gabor proposals 13 p2118 A67-26258
- Measurement of angular spectrum of radio waves from sources outside solar system 14 p2386 A67-28445
- Li film structure on compact tungsten faces by diffraction method, using free electron beams 14 p2372 A67-28760
- Lunar occultations of two radio sources observed at various frequencies, estimating emersion time 14 p2389 A67-28841
- Modes in unstable optical resonators and lens waveguides, noting spherical wave characteristics of geometrical eigenmodes 15 p2497 A67-29391
- Lambda functions describe antenna/diffraction patterns, showing familiar patterns from linear, rectangular and circular apertures 16 p2635 A67-30474
- Focusing of electromagnetic waves by lenses, calculating field distribution near focus by diffraction theory magnitude of convergence 18 p3010 A67-33646
- Holographic moiré patterns as white light viewing technique for aerodynamic flow visualization 19 p3232 A67-35699
- Differential cross sections for inelastic large angle alpha particle scattering from unnatural parity states in Mg showing diffraction pattern 20 p3488 A67-36393
- Diffraction coefficient of open laser resonators coupled in series, discussing boundary conditions 21 p3638 A67-37864
- Stacking fault energy estimation in polycrystalline brass during tensile

- deformation by analyzing X-ray diffraction patterns 21 p3645 A67-38090
- Epitaxial growth of gold on cadmium iodide surface studied with transmission electron microscopy, discussing diffraction patterns and substrates 21 p3687 A67-39140
- Irradiance due to square array of circular apertures from scalar Fresnel-Kirchhoff diffraction theory, giving plots of Fresnel diffraction patterns 22 p3835 A67-39235
- Omega phase morphology by transmission electron microscopy of Ti-Nb indicating ellipsoids with major axes parallel to /111/ directions in matrix 23 p4017 A67-40653
- HF approximation to diffraction of plane wave by conducting strip, using cylindrical wave terms for higher order patterns 23 p3979 A67-40831
- Electromagnetic backscatter from edge scattering centers found on cylinders and flat-backed cones, discussing hemispheric scattering 23 p3973 A67-40839
- DIFFRACTION PROPAGATION**
- Electromagnetic beam propagation in unbounded gyrotropic media taking spatial dispersion into account 02 p0192 A67-11641
- Total specular reflectance of rough metal surfaces calculated, using Maxwell equations and approximation via Kirchhoff diffraction theory [AIAA PAPER 65-424] 04 p0723 A67-15232
- Diffraction limited performance achieved for flying spot recording and readout, using concentric optical system, applied to laser scanner 04 p0658 A67-15322
- Antenna height protection against microwave diffraction fading determined, using digital computer to evaluate residue series for grazing conditions 09 p1464 A67-22444
- Optical image producing method of complex ultrasonic field using light diffraction of laser beam 15 p2487 A67-29498
- Rocket exhaust jet plume effects on radio signal, calculating degradation by electromagnetic diffraction propagation 20 p3381 A67-36570
- Velocity of sound in liquids measurement using ultrasonic interferometry and laser diffraction spectra 21 p3630 A67-38772
- Diffraction and image formation in coherent and noncoherent light with relation to Fourier transform 23 p3972 A67-40708
- Light propagation in electrically and magnetically anisotropic medium and diffraction by birefringent cylinder using coupled integrodifferential equations 24 p4119 A67-41889
- DIFFRACTOMETER**
- SA PARTICLE SIZE**
- Combined focusing X-ray diffractometer and nondispersive X-ray spectrometer for lunar and planetary analysis 01 p0067 A67-10689
- Direct measurement of dispersion properties of cadmium sulfide and CdS-CdSe crystals, using Obreimov-Fresnel diffraction method, growing crystals by synthesis 05 p0861 A67-16396
- DIFFUSE RADIATION**
- Spatial coherence of laser light beam after extreme wavefront distortions on diffusion explained on basis of Fraunhofer and Fresnel diffraction 01 p0115 A67-11062
- Fourier transform holography for diffusion of coherent laser light beam, examining distortion term in reconstructed image 01 p0070 A67-11063
- Thermal emittance and reflectance of diffuse-bottomed specular-walled groove in solar radiant-flux environment [AIAA PAPER 66-459] 02 p0342 A67-11939
- Intensity distribution of earth surface as seen at various altitudes above atmosphere due to Rayleigh scattering and diffused reflection from earth surface [AIAA PAPER 65-666] 03 p0411 A67-13046
- Initial value formulation of Chandrasekhar problem for diffuse reflection of radiation from planetary atmosphere 03 p0462 A67-13903
- Diffuse reflection of radiation from nonstationary plane-parallel layer solved on basis of Ambartsumian invariance principle 04 p0695 A67-14657
- Radiation effect on satellite in presence of partly diffuse and partly specular reflecting body 05 p0905 A67-16567
- Diffuse polychromatic light reflection from infinitely deep one-dimensional medium of atoms with three energy levels, with all interlevel transitions allowed 07 p1248 A67-19484
- Line profiles and equivalent widths for diffuse reflection of sunlight from model planetary atmosphere calculations, using invariant imbedding 10 p1710 A67-23635
- Radiation diffusion in medium of finite optical thickness, computation of source function and tabulation of matrices 14 p2382 A67-27832
- Global and diffuse solar radiation measurements by Macerata observatory, noting Robitsch pyranographs, Moll thermopiles, and global radiation results 16 p2698 A67-31023
- Image reconstruction of diffusely reflecting objects using pulsed hologram technique 19 p3233 A67-36102
- DIFFUSER**
- SA MAGNETIC DIFFUSER**
- SA NOZZLE**
- SA SUPERSONIC DIFFUSER**
- Optimal subsonic flow diffusers based on Walz laminar and turbulent boundary layer theory 01 p0006 A67-10648
- Convection heat transfer for turbulent flow in subsonic diffusers [ASME PAPER 65-HT-64] 03 p0352 A67-14010
- Unstalled two-dimensional diffusers performance prediction by method based on turbulent boundary layer integral theory [ASME PAPER 66-WA/FE-15] 04 p0548 A67-15351
- Errors in calculating losses in diffuser elements 04 p0548 A67-15600
- Methods of calculating flow velocity losses in diffusers 04 p0548 A67-15601
- Prediction of turbulent boundary layer development in conical diffusers, using kinetic energy deficit equation 04 p0549 A67-15750
- Potential flow theory design of subsonic flow diffusers for centrifugal compressors, assuming compressible irrotational inviscid channel flow [ASME PAPER 66-WA/GT-9] 04 p0550 A67-15938
- Diffuser use in low density hypersonic wind tunnel and method of evaluating global performance for diffusers with conical inlet followed by cylindrical mixing section 05 p0748 A67-16763
- Experiments on effect of subsonic inlet Mach number on performance of conical diffusers 05 p0748 A67-16811
- Curvilinear annular turbine outlet diffusers, discussing effects of geometric parameters on diffuser effectiveness 06 p0942 A67-18553
- Optimum geometrical parameters for diffuser of high pressure axial fan with straight blades 07 p1126 A67-19349
- High altitude supersonic isokinetic filter paper sampler for ALARR rocket, examining subsonic 3-D stagnation flow diffuser 08 p1276 A67-20500
- Entrance conditions and flow separation effect on rectangular diffuser performance, showing importance of secondary flows 10 p1627 A67-23557
- Optimum geometry for rectilinear diffuser with rectangular, conical or annular cross section noting flow regime, performance characteristics and boundary layer effect 11 p1741 A67-24050
- Laminar flow of incompressible conducting fluid in diffuser in presence of transverse magnetic field 13 p2169 A67-27313
- Rotating vortex flow and transition phenomena in conical diffuser [AIAA PAPER 66-426] 14 p2240 A67-28109
- Two-dimensional curved diffuser design by comparison with flow regime and performance data, obtaining diffuser shape and pressure distribution criteria [ASME PAPER 67-FE-6] 14 p2242 A67-28358
- Effect of wide angle screened diffuser on turbulent velocity fluctuations [ASME PAPER 67-FE-23] 14 p2243 A67-28368
- Subsonic diffuser with vortex generator as integral design feature for supersonic transport aircraft inlet [AIAA PAPER 67-464] 18 p2983 A67-33935
- High altitude supersonic isokinetic filter paper sampler for ALARR rocket, examining subsonic 3-D stagnation flow diffuser 21 p3563 A67-37803
- Optimum design of ring airfoil device for maintaining pressure recovery efficiency of conical diffuser 22 p3743 A67-40168
- Internal flow turbulent boundary layer separation for variable angle two-dimensional diffuser, discussing analytical model and model limitations [ASME PAPER 66-WA/FE-14] 23 p3989 A67-40929
- DIFFUSION**
- SA AMBIPOLAR DIFFUSION**
- SA ATMOSPHERIC DIFFUSION**
- SA EDDY DIFFUSION**
- SA ELECTRON DIFFUSION**
- SA GASEOUS DIFFUSION**
- SA IONIC DIFFUSION**
- SA MOLECULAR DIFFUSION**
- SA PARTICLE DIFFUSION**
- SA PERFUSION**
- SA PLASMA DIFFUSION**
- SA SELF-DIFFUSION**
- SA THERMAL DIFFUSION**
- SA TURBULENT DIFFUSION**
- Vanadium-gallium wires with good superconducting properties fabricated by new stepwise diffusion process 01 p0137 A67-11064
- Electron beam scanning technique measurement of diffusion lengths in Si and GaP p-n junctions and recombination rate of dislocations in n-type Si 02 p0298 A67-11887
- Isolation-diffusion of phosphorus in silicon with low surface concentration, with applicability to preparation of integrated solid state circuits 02 p0223 A67-12736
- Phosphorus-diffusion method in silicon with thin phosphorus containing layer used to produce working area of planar strain gauges 02 p0248 A67-12737
- Diffusion of antimony and indium in germanium in range from 700 to 855 degrees C, taking into account effect of internal electric field 03 p0489 A67-13149
- Average diffusion cross section for elastic collisions of electrons with heavy particles, comparing calculated and measured values 09 p1534 A67-21864
- Diffusion of antimony and indium in germanium in range from 700 to 855 degrees C, taking into account effect of internal electric field 10 p1690 A67-23098
- Diffused GaAs varactor diodes, showing planar processes applied to production of diode based on metal-GaAs junction 10 p1615 A67-23529
- Diffusion saturation of industrial iron, molybdenum, Kh18N9T steel and Zhs6-K alloy with powdered beryllium mixture 12 p1955 A67-25369
- Temperature effect on gold diffusion in crystalline and glassy cadmium germanium arsenide samples 19 p3301 A67-34776
- Soviet book on diffusion cladding of metals covering alloy surfaces diffusion saturation, glow discharge silicizing of metals, vacuum silicizing of refractory metals, etc 19 p3235 A67-34915
- W-Ta-Re system equilibrium diagrams examined, measuring diffusion layer element concentration by X-ray spectral analysis method 20 p3468 A67-37180
- Planar diffused p-n junction profile geometry using scanning electron microscope and electron probe with computer calculations 22 p3855 A67-39360
- DIFFUSION BONDING**
- Deformation and diffusion bonding of Al, Ti and stainless steel alloys, discussing surface condition, time, temperature, cold work, heat treatment and intermediate materials 03 p0430 A67-13692
- Diffusion bonding of Be, Mo and W by interdiffusion of mating surfaces through solid or liquid-state reactions 07 p1192 A67-20248
- Metal composite technology, emphasizing degree of success attained in fabricating reproducible tensile specimens by five techniques 08 p1340 A67-20358
- Diffusion bonding of titanium sandwich structure for Saturn tank wall application 10 p1661 A67-23702
- Solid state diffusion bonding effect on structural design 10 p1662 A67-23733
- Future Air Force requirements for base metal forms and metal-working techniques including hot strength alloy forgings, fine wire, etc 12 p1948 A67-25286
- Welding processes covering high purity metals, plasma arcs, resistive slags, high energy beams and solid state 15 p2493 A67-29681
- Alloy effects in low pressure diffusion bonding of superalloys, presenting time,

pressure, bond strength and temperature curves 17 p2866 A67-33200

Fracture behavior of laminar steel composites studied to determine effect of interfacial properties on crack propagation 22 p3822 A67-40056

DIFFUSION COEFFICIENT

Diffusion coefficient of lithium in p-type silicon determined by method using electrophotographic developing agents 01 p0127 A67-10061

Diffusion and electrical transfer of zinc in indium arsenide as affected by temperature 01 p0127 A67-10068

Diffusion parameters and solubility of Cd in InAs measured with aid of radioactive isotopes compared with diffusion coefficient measurement by p-n junction method 01 p0128 A67-10082

Sintering of crystalline oxides through volume diffusion, noting sintering rates 01 p0096 A67-10693

Sintering mechanisms in powdered compacts of carbides, oxides and metals, examining grain growth, pore decrease and diffusion coefficients 01 p0096 A67-10694

Sintering of cobalt-nickel powder mixtures during formation of solid solutions, noting shrinkage and diffusion coefficients 01 p0096 A67-10695

LF spectrum of density correlation function, obtaining diffusion coefficient of right order of magnitude using quiet plasma 01 p0124 A67-10911

Radial transport of cesium plasma governed by resistive diffusion as shown by stellarator experiments in which surface recombination losses within plasma volume were negligibly small 01 p0125 A67-10914

Temperature dependence of diffusion coefficient of Li in InSb prepared in wafer form 01 p0137 A67-11067

Vaporization rate and diffusion of Cu, Mg and Cr in arc discharge plasma determined from curves of spectral-line emission energies 02 p0279 A67-12743

Stable domain propagation in gallium arsenide for nonzero constant diffusion coefficient, based on analytic approximation to velocity field characteristic 03 p0493 A67-13461

Thermoconductivity-temperature-diffusion coefficient relations for pure and mixed polyatomic gases 03 p0535 A67-13518

Diffusion coefficient for electroactive impurity in semiconductor based on current carrier concentration variations during successive removal of surface layers 03 p0498 A67-13841

Specific radioactivity of Sb-124 and effect on diffusion of antimony in Sb-doped n-type Ge single crystals and Ga-doped p-type Ge single crystals 03 p0500 A67-14067

Diffusion constant of carbon in carbide phases of tantalum determined from growth rate of carbide layers forming on tantalum surfaces 04 p0636 A67-14908

Dynamic resistance of Si p-n junction and diffusion length for minority carriers measured, using pulsed electron beam irradiation 04 p0584 A67-15317

Diffusion coefficients determination from viscosity measurements based on higher Chapman-Enskog approximations 04 p0658 A67-15510

Phenomenological theory of mass transfer in binary systems near critical point applied to particular boundary value problems 04 p0727 A67-15683

Electric field effect on donors diffusion into intrinsic semiconductor 05 p0861 A67-16397

Diffusion influence on radio determination of meteor velocity by diffraction method 05 p0897 A67-16807

Internal electric field effect on simultaneous diffusion of donors and acceptors in semiconductors, considering case of indium and antimony diffusing into germanium 05 p0867 A67-17051

Antimony diffusion into germanium using vacuum furnace, giving graphs with variation of antimony concentration and depth of diffused p-n junction 05 p0869 A67-17089

Plasma density, electron temperature and potential distribution measured across magnetic field, determining ion and electron-diffusion coefficients in plasma column 05 p0858 A67-17432

Plasma loss in single-ended Q device measured as function of magnetic field

strength, obtaining diffusion coefficient directly 05 p0859 A67-17445

Origin of Moung Nong type tektites detached by meteoritic impact, considering lunar origin based on diffusion rates in silicates 06 p1078 A67-17562

Current and frequency dependent differential resistance and diffusion capacity of junctions of p-n structures at high current densities 06 p1049 A67-17868

Diffusion coefficient of carbon in nonstoichiometric tantalum monocarbide at very high temperatures, noting increase with decreasing carbon content 06 p1018 A67-17901

Self-diffusion coefficients of simple liquids as predicted by Rice-Allnatt theory, noting friction coefficient and correlation function 06 p1035 A67-17989

Time lag in thermal coefficient of resistivity of Ge whisker explained in terms of point defect diffusion 06 p1050 A67-18144

Fuel injection parameters effects on mixing of gaseous hydrogen fuel with supersonic air stream for hypersonic ramjet, determining turbulent diffusion coefficient 06 p1117 A67-18387

Surface recombination velocities and diffusion lengths in GaAs determined by variation of cathodoluminescence intensity with voltage of exciting electron beam 06 p1063 A67-18938

Mutual diffusion characteristics of titanium-tungsten mixtures at high temperatures, noting discontinuity on concentration curve due to two-phase region presence 07 p1204 A67-19268

Ambipolar diffusion theory for describing diffusion of nonuniformities in ionosphere including F region 07 p1230 A67-19717

Photolization mass spectrometer for ion-molecule reaction studies, determining ion residence times, drift velocities, diffusion coefficients and ion temperatures 07 p1137 A67-20187

LF wave frequency-and amplitude-dependent transverse anomalous diffusion coefficient in fully ionized magnetoplasma in Q-machine 08 p1360 A67-21125

Effective electron and ion diffusion coefficients measured for positive magnetic field gradients show reduced plasma diffusion 08 p1364 A67-21400

LF electron density microscopic fluctuations in bounded plasma examined by method having virtue of being exact at zero frequency 08 p1365 A67-21404

Diffusion coefficient of lithium in p-type silicon determined by method using electrophotographic developing agents 08 p1371 A67-21447

Diffusion and electrical transfer of zinc in indium arsenide as affected by temperature 08 p1371 A67-21451

Diffusion parameters and solubility of Cd in InAs measured with aid of radioactive isotopes compared with diffusion coefficient measurement by p-n junction method 08 p1371 A67-21459

Average diffusion coefficient and apparent effective charges of components of alloys of Ti-S system 09 p1553 A67-21906

Decay kinetics of He plasma, examining pair collision, metastable atom diffusion coefficient and afterglow mechanism via spectroscopy 09 p1544 A67-21918

Sorption process for determining sticking probability of molecules on surface of sorbents, diffusion coefficient of molecules through sorbents and adsorption isotherms 09 p1533 A67-22115

Cosmic ray protons and helium nuclei intensity measured as function of energy or magnetic rigidity, determining particle intensity gradient under equilibrium conditions for diffusion 09 p1562 A67-22241

Wind velocity, direction and diffusion coefficients determined with aid of artificial luminescent cloud 10 p1675 A67-22795

Diffusion coefficient measurement based on relationship between correlation coefficient for density fluctuations and density coefficient 11 p1829 A67-24003

Cross field diffusion coefficient measurement from volume loss properties of single ended Q device plasma column 11 p1830 A67-24005

Plasma turbulence and diffusion across magnetic field investigated by plasma instabilities in case of large amplitudes of oscillation measured by Langmuir probes 11 p1834 A67-24376

Potassium plasma current instability, turbulence and diffusion across magnetic field for large amplitudes of oscillations treated as ionic sound waves 11 p1834 A67-24377

Collisionless instabilities in thermally ionized potassium plasma and effect of magnetic shear on oscillations and diffusion 11 p1834 A67-24378

Diffusion of particles across magnetic lines in dense and quiescent plasma compared with Bohm and collisional values 11 p1835 A67-24383

Transverse diffusion of particle perpendicular to magnetic field by assembly of random Alfvén waves explains increase in electric field energy 11 p1840 A67-24753

Co-Ni system heterodiffusion and interdiffusion coefficients variation with temperature and composition 11 p1808 A67-24772

Solar cosmic ray diffusion coefficient dependence on cosmic ray energy and distance to sun studied via solar flares 12 p1991 A67-25111

Velocity space diffusion coefficient of electrons in thermal radiation field, using Hamilton-Jacobi theory 12 p1969 A67-25192

Relativistic electron plasma diffusion, calculating dynamical friction and diffusion coefficient in Landau approximation 12 p1969 A67-25193

Ionization and diffusion cross sections of Ca, Fe, Si and Mg atoms of disintegrated meteors 12 p2002 A67-25551

Anomalous high diffusion coefficients determined from dispersion of chemical contaminant releases and long lasting meteor trails at various altitudes 12 p1935 A67-25792

Effective diffusion cross section for meteor atoms in atmosphere, using Thomas-Fermi-Dirac and dumbbell molecule models 13 p2111 A67-26553

Initial radius of ionized meteor track, taking into account dependence of effective diffusion cross section of meteor atoms in atmosphere on relative velocity 13 p2198 A67-26554

Numerical integrations of equation for turbulent diffusion in atmosphere 13 p2152 A67-26863

Factors affecting current methods of sizing Aitken nuclei 13 p2152 A67-26865

Self-diffusion in high-purity tellurium between 300-400 degrees C 13 p2179 A67-27156

Niobium self-diffusion in alloys with tungsten, showing dependence on specimen composition 13 p2141 A67-27283

Plasma in diffusion regime situated in nonhomogeneous RF field with rotation symmetry 14 p2354 A67-27765

Upper atmosphere densities and temperatures at 105-165 km from diffusion and spectral intensity of aluminum oxide trails 14 p2310 A67-28050

Decay kinetics of He plasma, examining pair collision, metastable atom diffusion coefficient and afterglow mechanism via spectroscopy 14 p2358 A67-28247

Carbon diffusion mobility in fused carbides of vanadium and titanium, giving carbon diffusion coefficient temperature dependence equations 14 p2337 A67-28285

198 Au isotope diffusion in n-type indium arsenide at different temperatures 14 p2368 A67-28537

Propagation of small disturbances in general three-dimensional unsteady nonequilibrium MGD, noting influence of various parameters 14 p2361 A67-28904

Diffusion due to ion-ion collisions between different ion species, stressing impurities diffusion in rotating plasmas 14 p2363 A67-29066

Transverse diffusion coefficient of collisionless plasma in magnetic field measured, using variations in radial plasma column density 14 p2363 A67-29067

Turbulent state and diffusion of plasma during drift instability, noting increase with oscillation amplitude 14 p2363 A67-29068

Internal electric field effect on simultaneous diffusion of donors and acceptors in semiconductors, considering case of indium and antimony diffusing into germanium 15 p2537 A67-29782

Diffusion, solubility and electrical behavior of lithium in gallium antimonide 16 p2726 A67-30811

Properties of uniformly propagating stable

domains in gallium arsenide calculated on basis of velocity-field and diffusion-field characteristics 16 p2727 A67-30851

Multicomponent reacting laminar boundary layer in chemical equilibrium solved using Stefan-Maxwell relations 16 p2658 A67-30937

Transport coefficients calculated from adiabatic excitation transfer in atomic gases 16 p2661 A67-31222

Dispersion equation for stability of steady turbulent state obtained from perturbation theory and applied to drift cyclotron instability of plasma 16 p2719 A67-31230

Turbulent plasma state from unstable, current driven drift waves, noting ion damping effect on amplitude of spectrum, density gradient, etc 16 p2719 A67-31231

Drift waves in fully ionized potassium magnetoplasma in single-ended Q machine, measuring effect on transverse diffusion coefficient 16 p2720 A67-31242

Diffusion coefficient dependence on solar particle energy and distance from sun noting time variation 16 p2740 A67-31892

Lumped parameter model for monopropellant hydrazine reaction chamber developed, using mass and energy balance and reaction and diffusion rate coefficients 17 p2927 A67-31974

Solar cosmic ray observations, discussing emission spectrum, interplanetary particle distribution, diffusion coefficient, magnetic field strength, space-time distribution, etc 17 p2934 A67-32096

Computer-aided transistor design, characterization and optimization 17 p2823 A67-32198

Tritium diffusion from iron meteorite shortly after fall established by artificial proton irradiation 17 p2942 A67-32357

High temperature oxidation of titanium at reduced oxygen pressures governed by dissolution of oxygen in metal 17 p2873 A67-32812

Accelerated antimony diffusion in germanium due to excess vacancies from proton irradiation, determining migration energy and diffusion length of vacancies 17 p2919 A67-32862

Two oxidation mechanisms for Ti-Al alloys based on increased diffusion rate and decreased oxidation rate 17 p2875 A67-33175

Cosmic ray motion in interplanetary electromagnetic field for isotropic/anisotropic diffusion situations presented by convective diffusion models assuming spherical symmetry for solar cavity 17 p2938 A67-33188

Strontium and Ba vapor releases in upper atmosphere, testing yield of evaporated metal for different chemical reactions 17 p2851 A67-33194

Lifetime and diffusion coefficient of lowest excited state of molecular nitrogen from intensity decay measurements of Vegard-Kaplan band 17 p2889 A67-33243

Trapping of hydrogen ions in molybdenum, titanium, tantalum and zirconium measured by mass spectrometric technique 17 p2810 A67-33384

Impurity diffusion role in silicon device technology, discussing error function distribution 18 p3096 A67-33455

Influence of fast proton and electron irradiation on diffusion of substitution impurities in silicon 18 p3100 A67-33750

Vacancy source and sink effect on behavior of nonequilibrium concentration of vacancies in diffusion region during creep process 18 p3141 A67-33768

Time and temperature dependent diffusion of vaporized Zn and Cd in n-type InAs 19 p3299 A67-34760

Diffusion saturation methods of alloy surfaces by metals and metalloids classified by physicochemical characteristics of active phase of diffusing element 19 p3242 A67-34916

Changes in experimental relationship between preexponential factor in diffusion equation and activation energy for solid solutions 19 p3243 A67-34928

Ionization decay in cesium vapor explained in terms of dissociative recombination and diffusion, showing strong dependence on vapor pressure 19 p3271 A67-35072

Positive column and striations of low pressure discharge of noble gas 19 p3273 A67-35097

Diffusion of nickel in solid solution and two-phase alloys of nickel-titanium

system 19 p3245 A67-35468

Simultaneous diffusion of gallium and arsenic in silicon from gallium arsenide source, obtaining profiles at various temperatures 19 p3308 A67-36035

Temperature dependence of diffusion coefficient of zinc in gallium arsenide 20 p3504 A67-36162

Fluctuation spectrum in most stable state of turbulent plasma 20 p3496 A67-36213

Rate of diffusion and degree of density during activated sintering of tungsten-molybdenum powders, noting influence of nickel additive 20 p3466 A67-36911

Viscosity, heat conduction and diffusion coefficients for two-temperature three-component plasma 20 p3500 A67-37049

Unsteady transverse diffusion of passive impurity and mass and heat transfer in granular layer described by cell type models 20 p3554 A67-37054

Grain boundary diffusion coefficients in tungsten at high temperatures, obtaining activation energy 20 p3470 A67-37388

Cosmic ray diffusion in interplanetary magnetic field, examining statistical homogeneity and isotropy 20 p3520 A67-37473

Temperature effect on diffusion coefficient of radioactive phosphorus in epitaxial Si layer 21 p3681 A67-38361

Chemical diffusion coefficients and heats of activation in nickel-aluminum intermetallic phases and solid solution calculated from layer growth experiments 21 p3645 A67-38775

Vacancy concentration in dislocation enhanced diffusion model as explanation of phosphorus and boron anomalous diffusion in silicon 22 p3855 A67-39346

Anomalous phosphorus diffusion in Si at high surface concentrations explained by excess vacancy generation at edge jogs on gliding dislocations 22 p3855 A67-39347

Thermal particles parallel velocity and transverse spatial diffusion coefficients found by studying test particle motion in weakly turbulent Vlasov magnetoplasma 22 p3849 A67-39702

Mathematical model for solution of anisotropic diffusion equations of solar cosmic ray propagation 22 p3872 A67-39809

Heterodiffusion of metallic impurities in body-centered phases of doped zirconium and titanium, determining diffusion coefficients via radioactive isotopes 22 p3820 A67-39823

Na and K introduced into Si by diffusion from thin layer of alkali metal and during electrolysis of molten alkali halogenides 23 p4037 A67-40721

Turbulent plasma state and diffusion across magnetic field due to ion acoustic instability noting diffusion coefficient increment with instability excitation 23 p4032 A67-40905

198 Au isotope diffusion in n-type indium arsenide at different temperatures 23 p4040 A67-40944

Temperature dependence of carrier drift type transistor characteristic frequency, discussing temperature and diffusion coefficients 23 p3983 A67-41676

Wind velocity, direction and diffusion coefficients determined with aid of artificial luminescent cloud 24 p4181 A67-42131

DIFFUSION EFFECT

SA SURFACE DIFFUSION EFFECT

Carbon diffusion in refractory metals with bcc lattice at temperatures of 1100 to 1600 degrees C, considering activation energy and frequency factor 01 p0101 A67-10937

Diffusive separation of helium-argon mixtures in underexpanded free jets and normal shock waves studied by electron beam 02 p0234 A67-12543

Diffusion effect on thermal stresses in neighborhood of macrodefects in solid solution resulting in time dependent change of stress-strain state 03 p0521 A67-13121

Influence of polarized atoms diffusion on spatial distribution of optically oriented atoms 03 p0437 A67-13388

Interferometric holography in diffused light, obtaining interferogram of phase shifting object 03 p0420 A67-13451

Various combinations of preanneal and diffusion anneal conditions used in experiments for determining environmental effects on diffusion of Ta 182 in bcc titanium 04 p0637 A67-14937

Dislocation loops by gold diffusion into silicon crystals analyzed, using X-ray diffraction topography and optical microscopy 05 p0866 A67-16974

Diffusion-viscosity coupling in stationary flow of nitrous oxide-carbon dioxide mixture in case of Maxwellian intermolecular forces 05 p0794 A67-17380

Parametric action in back biased p-n junctions carrying injected currents, discussing photoparametric frequency converters, transistor amplifiers and frequency doublers 06 p0969 A67-18106

Variable laminar boundary layer equations for air flows over flat plate with injection of foreign gases through solid surface 06 p1116 A67-18380

Turbulent wake of slender body analyzed to include dominant mode of laminar diffusion, deriving solution for linear electron chemistry 06 p0943 A67-18870

Occurrence of collisions between ionized and neutral particles based on analysis of spectrum diffused by E region 10 p1646 A67-23268

Internal flow analysis noting interaction with wall, frictional effects, boundaries and method of analysis 11 p1776 A67-24042

Momentum and energy transfer effects on gas kinetic equations of nonequilibrium flows, analyzing diffusion problem 11 p1780 A67-24536

Complementary variational principles in neutron diffusion theory 11 p1824 A67-24632

Reversed speed effect and grain boundary diffusion as explanations of discrepancy of activation energy values for strain aging under fatigue or simple stress conditions 12 p2013 A67-25284

Effect of multiple zinc diffusions on threshold and CW output power of semiconductor laser 13 p2125 A67-26522

Photochemical reaction and turbulent diffusion effect studied using mesospheric model, establishing relation between composition and dynamic state 13 p2113 A67-26681

Stability of arbitrary one-dimensional hydrodynamical flow in quasi-isothermal case 13 p2105 A67-27413

Diffusive separation due to electrical coupling of ions and hot electrons and effect on shock wave structure in plasmas 15 p2470 A67-29227

Condensation droplet growth in supersaturated vapor and inert carrier gas, noting thermal and diffusion effects 15 p2582 A67-30198

Vacuum siliconization of refractory metals in Mo-Si system noting thermodiffusion layers, vapor phase, chemical reaction, diffusion and temperature gradient 19 p3236 A67-34918

Diffusion and epitaxial equipment controlling doping level in semiconductor integrated circuits, discussing fabrication materials and techniques 19 p3236 A67-35019

Alkali-metal magnetoplasma properties related to enhanced diffusion, showing relationship to beam-plasma interaction 19 p3287 A67-35360

Balloon-borne diffusing system designed to measure absorption of minor atmospheric constituents, as sun set and passed below horizon 19 p3232 A67-35697

Saturation current measurement in diffusion transistors by method yielding current amplification factors and voltage dependence of emitter current 19 p3197 A67-35726

X-ray diffusion intensity by transverse polarization phonons in indium antimonide at various temperature ranges 19 p3307 A67-35793

Generalized Mott-Smith functions for shock wave structure in binary mixtures, relative diffusion velocity obtained and compared with Diakov solution 20 p3421 A67-36678

Steady state diffusional creep for materials with large grains and dislocations forming sinks for vacancies, obtaining strain rate 21 p3719 A67-38089

Photochemical reaction and turbulent diffusion effect studied using mesospheric model, establishing relation between composition and dynamic state 21 p3618 A67-38426

Perturbation theory for solving initial and boundary value problem in unsteady MHD flow past thin symmetrical bodies with

inwardly diffusing magnetic field 22 p3850 A67-39707

Concentration distribution time for heavy gas diffusing in light gas steady flow field 22 p3917 A67-39714

Steady laser oscillation by Maxwell equations, with allowance for diffusion effects, shows no qualitative changes in field distribution pattern 22 p3815 A67-39759

Carbon diffusion in refractory metals with bcc lattice at temperatures of 1100 to 1600 degrees C, considering activation energy and frequency factor 22 p3820 A67-39791

Defects in surface layer of silicon crystals during deep diffusion of phosphorus studied by X-ray diffraction 23 p4042 A67-41295

Spontaneous annealing models of lithium-diffused Si solar cells, discussing defect compensation and metastable defect formation 23 p3941 A67-41523

Escape probability of photon from homogeneous plane parallel medium, discussing coherent scattering process and integral equation 24 p4191 A67-42596

DIFFUSION ELECTRODE

Limit diffusion flux on rotating ring electrode surface in turbulent regime, determining mass transfer constant 24 p4146 A67-43112

DIFFUSION FLAME

Laminar diffusion flame stability analyzed, examining transient characteristics to infinitesimal disturbances of steady state solutions 02 p0342 A67-12028

Diffusion flame in transition region of gas flow 02 p0343 A67-12536

Nozzle exhaust plumes of rockets or supersonic ramjets with diffusion flames as source of UV radiation 04 p0721 A67-14702

Combustion of gaseous fuel jets in oxidizing atmosphere 04 p0728 A67-15453

Finite rate chemistry effects in diffusion controlled hydrogen-air flames noting flame position, fuel consumption, temperature, fluid velocity outside of flame and boundary conditions 05 p0926 A67-16516

Aerodynamics of diffuse combustion in laminar boundary layer of two plane-parallel accompanying flows, emphasizing flame structure 06 p1112 A67-17961

Mean velocity and mean static pressure distribution on stability and space requirements of turbulent diffusion flames 08 p1425 A67-20304

Initial solid propellant temperature effect on constant pressure burning rate based on granular diffusion flame model /GDFM/ 08 p1375 A67-20581

Laminar diffusion flame in Oseen flow, identifying limiting case with stoichiometric Burke-Schumann flame and frozen flow 09 p1579 A67-21548

Diffusion flame stability criteria for one-dimensional model at unity Lewis number 13 p2221 A67-26260

Calculation of diffusive gas flame in turbulent wake, reducing problem to differential equations of motion 14 p2407 A67-28649

Endothermic hydrocarbon fuels for supersonic aircraft, noting heat sink capacity effect in overcoming thermal thickening and usability as engine fuel 15 p2543 A67-29305

Intensity of light scattered from soot particles in diffusion flame of hydrocarbons burning in air 18 p3149 A67-33799

High temperature kinetics of bulk beryllium metal combustion in hydrogen-oxygen-water vapor system, studying flame environments, thermal balance, etc 18 p3151 A67-33809

HF response of local burning rate in laminar diffusion flames subjected to transverse sound waves in free stream 18 p3108 A67-33831

Counterflow diffusion flame in forward stagnation region of porous cylinder, detailing flame stability and velocity gradient 18 p3155 A67-33842

Hydrogen fire visualization detection techniques including application of photography, TV and image converter in IR and UV regions 20 p3445 A67-36540

Diffusion flame shape in wake of falling droplet taken as point source of fuel, limiting analysis to Lewis and Prandtl numbers unity 23 p4083 A67-41720

Finite difference integration method for predicting flow velocity and temperature distribution of gaseous diffusion flame in axisymmetrical combustion

chamber 24 p4091 A67-42383

DIFFUSION THEORY

Diffusion phenomena in rarefied gases treated, using Boltzmann equation expanded in Sonine Legendre polynomials in velocity space 02 p0234 A67-12544

Three-component diffusion theory applied to calculation of three-component metallic solid solutions, examining interstitial and substitutional systems with different boundary conditions 02 p0256 A67-12707

Pseudoshocks in pipe flow in supersonic compressors represented as diffusion process, noting application in cascade and rotor configuration 03 p0352 A67-13011

Feynman space-time path formulation of nonrelativistic quantum mechanics applied to classical diffusion 03 p0469 A67-13718

Integral transform associated with boundary conditions containing eigenvalue parameter applied to initial boundary value problem arising in diffusion theory and heat flow 03 p0460 A67-13825

Finite difference method solution of diffusion equations, including analyses of stability and truncation errors 03 p0537 A67-14013

Diffusion theory of vibration-dissociation coupling used to analyze transient effects in dissociation reactions behind shock waves 03 p0474 A67-14025

Modes in spatial distribution of neutron density within cosmic ray neutron monitor, each mode having distinct lifetime, using diffusion theory 04 p0661 A67-15615

Angular distribution of radiation at boundary of homogeneous diffusion sphere, with isotropic central point source calculated by Monte Carlo 05 p0838 A67-16491

Charged particles motion in magnetic field with regular and random components, deriving kinetic equation for distribution function and then diffusion equation 06 p1037 A67-18800

Diffusion in solutions in nearly critical states, noting increased cross effects and linear dependence of flows near critical points 09 p1580 A67-21908

Ionospheric diffusion spectra, obtaining information on neutral atmospheric winds and ionosphere dynamics 10 p1632 A67-22858

Plasma diffusion across static magnetic fields in electrodeless E type RF discharges 11 p1830 A67-24008

Drift effect on diffusion spreading of plasma inhomogeneities in magnetic field, deriving expression for Fourier component potential and magnetic field perturbations 12 p1933 A67-25546

Angular distribution of radiation at boundary of homogeneous diffusion sphere, with isotropic central point source calculated by Monte Carlo 13 p2155 A67-26346

Semiconductor diffusion by entrainment of impurity in gas phase 13 p2176 A67-26657

Comparison of effect of various diluent gases in evoking flyer bends in simulated orbital flights 13 p2062 A67-26916

Diffusion phenomena of increasing mean free path with altitude in rarefied gas analyzed, incorporating gravitational field effect in Boltzmann equations 13 p2099 A67-26952

Turbulent mixing at interface of two different density media under influence of pressure gradient, considering diffusion 13 p2105 A67-27411

Solution of one-dimensional diffusion equation of heat flow normal to surfaces, prescribing potential and flow rate along moving parametric curve 14 p2405 A67-28254

Thermally ionized low density alkali-metal plasma for simulating controlled fusion processes, noting high particle losses and instability 14 p2362 A67-29038

Temperature dependence and order of magnitude of barium titanate and strontium titanate determined from three-phonon diffusion process 17 p2915 A67-32706

Charged particles motion in magnetic field with regular and random components, deriving kinetic equation for distribution function and then diffusion equation 18 p3083 A67-34419

Thermomdiffusion term in particle flux equation, showing large electron temperature variation across low voltage arc plasma 19 p3279 A67-35140

Iterative solution for directional emissivities of two-dimensional semiinfinite slab of absorbing-scattering medium with gray isothermal dispersion [ASME PAPER 87-HT-12] 20 p3545 A67-36710

Outer Van Allen radiation zone intensity maximum position dependence on electron energy and magnetic activity, noting relation to diffusion theory 22 p3870 A67-39620

DIFFUSION WAVE

Nonself-similar energy diffusion of thermal radiation front for plane parallel geometry, giving series and parametric solutions 23 p4081 A67-40887

DIFFUSION WELDING

Diffusion processes for fabricating integrated circuits, examining open and sealed tube techniques 01 p0080 A67-10971

Diffusion welding of aluminum alloys and austenitic stainless steel tubular joints 07 p1190 A67-19214

Diffusion zones formed during soldering of AT3 OT4 Ti alloys 07 p1190 A67-19296

Diffusion bonding of titanium and stainless steel at high temperatures using pneumatic hammer 09 p1520 A67-22436

Diffusion welding of commercially pure titanium investigated for process parameters, noting temperature effect 19 p3234 A67-34792

Low pressure diffusion welding and brazing process producing joints with mechanical properties close to titanium 6Al-4V 22 p3811 A67-39446

DIGESTIVE SYSTEM

SA ESOPHAGUS

SA GASTROINTESTINAL SYSTEM

SA INTESTINE

Transverse accelerations remote aftereffect on conditioned alimentary reflexes of rats, discussing prolonged depression of higher nervous activity 23 p3943 A67-40771

DIGITAL CAPACITANCE SYSTEM

Synthesis of capacitive converters of angular displacements into digital code 06 p1003 A67-18175

Pulsed power technique and capacitive coupling between digital integrated circuits provide micropower redundant circuits with automatic error correction 07 p1155 A67-19844

DIGITAL COMMAND SYSTEM

Relays, ICs and hybrid /two-chip/ driver circuit for Motorola Digital Test Command System /DTCS/ 08 p1303 A67-21028

Design chart for parameter derivation of basic digital synthesizer, noting advantage in handling of tradeoffs 14 p2276 A67-28919

Spacecraft and ground equipment of Lunar Orbiter telecommunications system 17 p2811 A67-32119

Fluidic actuator for direct digital control, converting computer information into mechanical motion 23 p3942 A67-41710

DIGITAL COMMUNICATIONS SYSTEM

Book on statistical communications theory, digital communications, AM and FM CW communications, binary communications and noise 01 p0021 A67-10306

Integrated circuit eliminating pilot tones in digital data by simultaneously phase modulating binary data and bit-timing signals on carrier 02 p0194 A67-11797

Digital communications system evaluator /DICOSE/ using stored program processor coupled with communication channel arrays to provide real time on-line system 02 p0230 A67-12127

Error probability of binary receivers for digital transmission over radio channels characterized by specular and selective fading components 02 p0203 A67-12166

Data compression with digital filtering by fan method and step reduction method 04 p0569 A67-14585

Satellite ground terminal design considerations using adaptive digital communications techniques, noting analog to digital conversion 06 p0960 A67-17675

Tunnel diode circuits for fast digital circuits, noting shift generator and comparator generator 06 p0970 A67-18203

Mathematical tool for system design of pseudorandom coded ranging system used in space programs, noting failure probabilities 07 p1145 A67-19869

Digital communications on pseudonoise tracking link using sequence inversion modulation, noting bit error probability 09 p1459 A67-21581

Wideband video data transmission from near earth orbiting vehicle and over leased telephone lines 09 p1460 A67-21583

Continuous phase binary FSK communications system operating over linear time-variant random parameter chaff scatter channel 09 p1462 A67-21604

Requirements for military communications for flexible response, noting limitations /survivability, error rate, delay time, cost, etc/ and Digital Distributed Communications Network /DDC/ 09 p1463 A67-21676

All-digital real time display system for ground monitoring of manned space flight including computers, software, output devices, etc 09 p1483 A67-21677

Air-to-ground asynchronous digital communications system with premium error detection for air traffic control 09 p1529 A67-22639

Digital synthesis technique for automatic frequency search 10 p1604 A67-22970

Pulse sequences with good autocorrelation properties 10 p1608 A67-23330

High Noise Immunity Logic Family /HNIL/ digital switching microcircuits for long distance signal transmission operating at high voltage 14 p2282 A67-28028

Variable data rate modem for digital signal transmission on HF radio circuits 14 p2272 A67-28705

Error rate expression for canonic binary receivers, evaluating performance of incoherent detection 14 p2272 A67-28706

Power advantage of optimum system achieved with suboptimum feedback function for sequential binary detection system 14 p2292 A67-28707

Permutation modulation systems comparison based on proved-best criterion of alphabet size and minimum distance between signal vectors 15 p2439 A67-30384

Book on communication principles emphasizing digital radio communication system design, frequency and binary phase shift keying, filtering, fading, etc 16 p2624 A67-31254

Digital pulse compression radar receiver with digital-pulse compression advantages and disadvantages, noting target acquisition, range tracking and antenna scanning system 16 p2630 A67-31738

Time statistics for reliable transmission of binary data in presence of atmospheric noise burst 17 p2811 A67-32113

Systems engineering in computer-driven CRT displays for man-machine communication, emphasizing hardware-software tradeoffs and communication-transmission factors systems engineering in computer-driven CRT 18 p3005 A67-33499

Computer application to planning and operating simultaneous access European ground station network 18 p3003 A67-34355

Redundancy reduction techniques and error correction coding of digital communication systems including waveform, pattern recognition, vocoding, etc 18 p3004 A67-34613

Digital telemetry system for maximum transmission efficiency of measurements performed on space vehicle 20 p3394 A67-38245

KHz to GHz wide predetector bandwidth receiving system applicable to EMI evaluations of high data rate digital equipment 20 p3406 A67-37656

Optimum word length for signal simultaneous digital transmission in real time through single channel 21 p3581 A67-38179

Analog treatment of digital telemetering signals using a priori information about transmission, noting Q-factor, storage and use of existing emissions 21 p3584 A67-38660

Microwave multichannel communication system using PCM, noting low power output requirement and suitability for digital data transmission 22 p3763 A67-40460

Broad bandwidth digital laser communication system utilizing pulse coded polarization modulation and binary detection including optical communication link and performance data 23 p3973 A67-41039

DIGITAL COMPUTER

SA ANALOG COMPUTER

SA HYBRID COMPUTER

Automatic testing and fault-isolation capabilities in advanced avionics systems 01 p0034 A67-10272

Avionic computer testing and fault-locator

of weapons systems and system control 01 p0034 A67-10273

Network analysis by digital computer covering methods and programs for ladder networks, nodal, electronic circuit and state variable analysis, etc 01 p0028 A67-10462

Optimization of aircraft design for counter-insurgency /COIN/ operations using digital computers and wind tunnel tests, considering cost effectiveness [AIAA PAPER 66-779] 01 p0009 A67-10526

Digital computer program SYNAC for parametric synthesis and performance analysis of military aircraft [AIAA PAPER 66-795] 01 p0009 A67-10535

Monitoring events occurring during testing of space vehicle by data compression techniques and time shared computer-controlled checkout system [SAE PAPER 660696] 01 p0049 A67-10593

Digital computer program for power spectral density analysis of vibration data, noting bandwidth variation with frequency [SAE PAPER 660715] 01 p0028 A67-10604

Implementation of air data computers with solid state transducing and computing techniques 01 p0029 A67-10667

Digital-graphic computer terminals effect on data processing equipment design, noting CRT use 01 p0029 A67-10669

Digitally-driven display system for graphic man-computer communication in aerospace industry 01 p0029 A67-10671

Digital computers connected by data link transmission system for prelaunch space vehicle checkout 01 p0050 A67-11031

Digital computer compensation of strain gauge data to extend measuring bandwidth to transient or HF phenomena 01 p0030 A67-11098

Multiple input data acquisition system /MIDAS/ centralized computer controlled data system 01 p0031 A67-11119

Closed loop gain of two-loop linear feedback system calculated, using computer 01 p0047 A67-11218

KC-70 low cost inertial navigation system noting use of inertial sensors and digital computers 01 p0076 A67-11256

Digital computers for navigation and guidance solving design problem by combining general purpose /GP/ and digital differential analyzer /DDA/ approaches to produce hybrid computer 01 p0111 A67-11258

Electronic Circuit Analysis Program /ECAP/, integrated system of digital computer programs producing DC, AC or transient network analyses from circuit topology, excitation, etc 01 p0031 A67-11336

Dynamic analysis of reaction control system /RCS/ propellant feed network on lunar module using digital computers 01 p0142 A67-11435

Digital computer controlled telemetry ground station, examining six subsystems 02 p0229 A67-12002

Digital integrated circuits and methods of testing for AC, DC and ground noise margins, dynamic impedance, capacitance and inductance factors 02 p0207 A67-12112

Strap-down guidance systems using conventional inertial hardware, discussing computer function, computer selection and system errors 03 p0465 A67-13364

DATA CORE, integrated launch area telemetry data system using high speed digital computers and analog or digital display 03 p0375 A67-13382

Nonprocedural programming formal system for differentiation of mathematical formulas by digital computer 03 p0375 A67-13561

Digital computer calculation of trigonometric series expansions arising in solid mechanics problems 03 p0524 A67-13788

Ground station for space communications and radar and radio physics, noting use of Cassegrain antenna computer guided pointing control, plug-in equipment box, etc 04 p0596 A67-15047

Real time evaluation of radar signals processed by digital detector used in automatic target tracking 04 p0574 A67-15058

Digital computer-aided circuit sensitivity analysis using symbols, with example of band pass filter analysis 04 p0578 A67-15088

Dynamic systems identification by digital computer modeling in state space formulation of ordinary differential equation [ASME PAPER 66-WA/AUT-10] 04 p0593 A67-15418

Automatic plotting of cloud information

map on Setun digital computer from Tiros meteorological satellite 04 p0652 A67-15471

Book on electronic testing covering RF interference, tracking systems, receivers and transmitters, flight control equipment, digital computers, etc 04 p0577 A67-15726

Digital computer testing procedure, noting error isolation and location technique via process of elimination 04 p0579 A67-15738

Iteration method of general linear programming on digital computer using penalty functions compared to equilibrium problem of mechanical system 05 p0781 A67-16259

Test system for static tests on combinative unit for comparing two quantities given in binary code 05 p0768 A67-16265

Construction method for rms-optimal digital smoothing devices, noting case of astatic systems 05 p0782 A67-16268

Digital computer driven electroluminescent solid state vertical scale indicator design, development and fabrication emphasizing size, weight, power, reliability and display readability 05 p0805 A67-16310

Microelectronics in digital subsystems of logic, memory, input/output and power supply 05 p0784 A67-17037

Digital computer programs for transient and steady state thermal analysis 05 p0929 A67-17452

High speed digital computer packaging for minimum transmission line wire length, backplane, module connections and maximum computation speed 05 p0778 A67-17455

Parametric analysis, penalty-effectiveness tradeoff and system selection for communications satellites, using block digital computer synthesis with subroutines for operational requirements [AIAA PAPER 66-330] 06 p0960 A67-17693

Newton-Raphson method generalized for solution of two-point boundary value problems of nonlinear optimal control theory for digital solution 06 p0974 A67-17923

Digital computer analysis of mission parameters governing spacecraft thermal characteristics including ablation effects, radioisotope generator systems, etc 06 p0966 A67-18417

Book on computer matrix analysis of structures 06 p1105 A67-18520

Ion extractor system for electrostatic thrusters designed, using salient features of digital computer and electrolytic tank analog methods 06 p1075 A67-18877

Laser digital devices, discussing use as switching circuit in digital computer 07 p1194 A67-19088

Random number modeling on digital computer 07 p1147 A67-19226

Pressure variation in solid propellant rocket engine determined by digital computer in terms of propellant properties and engine design 07 p1239 A67-19351

NORAD installation in Cheyenne Mountain, Colorado, describing data processing equipment and performance 07 p1148 A67-19840

Test procedure for direct use of digital computer, noting utilization of software simulation technique and various applications [AIAA PAPER 67-235] 07 p1149 A67-20058

Poles and zeros of amplifier transfer functions using digital computer, noting role in network analysis 07 p1157 A67-20091

Computer generation of error probability distribution for linear system response to random conditions 07 p1217 A67-20117

Nonlinear DC circuits analyzed by digital computer for application to path integrals and stability problems 08 p1346 A67-20333

MARCO 4418 binary computer for strapdown guidance system in LEM/AGS 08 p1297 A67-20627

Random access storage of program for airborne digital computer system 08 p1297 A67-20628

Software generation for airborne digital computer systems 08 p1297 A67-20630

Dual redundancy digital computer for improved reliability in real time processes and control situations where fault results in fatality or mission failure 08 p1298 A67-20638

RCA Variable Instruction Computer /VIC/ for high reliability applications 08 p1298 A67-20639

Digital computer CPU control of kinetic heating processes in engine of supersonic aircraft under simulated flight conditions 08 p1315 A67-21007

Power supply design for avionics digital computer systems 08 p1286 A67-21031

Digital computer control of automatic test equipment 08 p1299 A67-21058

Mathematical methods for digital computers, Volume 2, covering programming languages, numerical linear algebra, etc 09 p1467 A67-22044

Algorithm for analyzing general electric circuits with lumped parameters in transient state by automatic digital computer 09 p1469 A67-22440

Fourier series and integrals in analog, digital and hybrid computation 09 p1470 A67-22667

Digital computer analysis of inviscid two-dimensional parallel flow stability, using finite difference method to solve resulting initial value problem 11 p1778 A67-24220

Radar scan-antenna angle transmission over DC voltage in binary form for digital computer or display 11 p1760 A67-24269

Aspect system on Pioneer VI and VII incorporates digital computer for accurate time sector division of spin stabilized vehicle 11 p1870 A67-24441

Synthetic target scenes generation technique by general purpose digital computer for early analytical evaluation of sensor concepts 11 p1791 A67-24456

Computer applications in checkout of individual Saturn stages and in prelaunch checkout of complete Saturn vehicle 13 p2089 A67-26409

Digital and hybrid pulse analyzer designs for automatic measuring pulse characteristics digital and hybrid pulse analyzer designs for automatically measuring pulse characteristics 13 p2075 A67-26411

Automatic multichannel system for data recording and processing obtained in studies of ionospheric structural inhomogeneities containing magnetic-tape memory and device for digital computer input 13 p2119 A67-26561

Automatic pulse digital analyzer design to measure simultaneously all-pulse parameters used for control of closed loop systems 13 p2078 A67-26801

Digital real time spectral analysis with fast Fourier transform algorithm, using two special purpose computer configurations to estimate power spectrum 13 p2073 A67-27062

Digital computer languages in relation to engineering design problems 13 p2073 A67-27189

Digital computer used for on-line control of jet engine 13 p2074 A67-27190

Two digital computer filing programs for determining ordinates of propagation curves of ground waves in visible region 13 p2070 A67-27202

Computer aided design and reliability engineering /CADRE/ applied to data processing associated with communications equipment components and subassemblies 13 p2072 A67-27446

Integrated circuit interconnection system design exemplified by 920 M digital computer 14 p2274 A67-28025

Linear lumped component three-terminal transformerless RC circuits analyzed using digital computers 14 p2291 A67-28459

General purpose digital computer for airborne and spaceborne guidance and navigation systems 14 p2275 A67-28684

Statistical testing on digital computers for simulating current and voltage distribution in semiconductor rectifier circuits 15 p2439 A67-29416

Computational error caused by finite word length of aerospace computers 15 p2439 A67-29596

Visual analysis console for automatic information handling systems providing rapid data display and operator communications with high speed digital computers 15 p2488 A67-29737

Electronic circuit tolerance analysis by digital computer, discussing data availability, analysis methods and interpretation of answers 15 p2440 A67-29938

Radar display layout for aircraft safety consisting of digital computer and CRT 15 p2468 A67-30129

Book on creation and use of computer simulation models and routines for study of

systems 15 p2440 A67-30133

Accuracy of satellite orbit prediction for rendezvous mission related to ground-based tracking network sensors by digital computer simulation 15 p2441 A67-30165

Interlocking plan for entire countdown checkout process by combining subsystems simulated as partially controlled stochastic process 15 p2441 A67-30166

Digital computer application to direct control of system dynamics and implementation of adaptive/ learning loop 15 p2441 A67-30266

Large deflection bending of simply supported rectangular sandwich plates with isotropic core under uniform normal pressure, solving governing differential equations by digital computer 15 p2577 A67-30269

Solar spectrum observations in oxygen regions, describing prism-grating spectrometer, photoelectric recording and scan-averaging by digital computer [AFCRL-67-0478] 16 p2749 A67-31417

Differential Doppler effect on earth satellite radio signal and application to ionospheric electron density studies 16 p2627 A67-31463

Digital onboard checkout system for SST and other commercial/military aircrafts to discover in-flight malfunctions digital onboard checkout system for SST and other commercial/military aircraft to discover in-flight 16 p2596 A67-31493

Multidimensional unsteady flow field of inviscid fluid calculated with application of method of characteristics and digital computer 16 p2662 A67-31535

Coordinatograph and electro-optical data visualization unit for digital computers noting details 16 p2634 A67-31633

Digital sequencing systems containing error-detecting and -correcting properties 16 p2647 A67-31647

F-111 MK 2 avionics system evaluation and parameter tradeoff considerations 17 p2819 A67-32499

IBM CP-2 militarized digital computer noting design, maintainability and performance 17 p2820 A67-32500

Digital computer program FORTRAN coded, analyzing electric power distribution system of aerospace vehicle 17 p2804 A67-32511

Photospheric mean alpha hydrogen radiation intensity profile computed for various heights above solar surface taking into account limb-darkening effect 17 p2946 A67-32729

Book on control systems and linear vibrational mechanical systems emphasizing use of analog and digital computers, frequency response, complex plane and root locus plots, FORTRAN method, etc 17 p2822 A67-33133

Digital and analog computers evolution, discussing microelectronics, speed, accuracy, bulk and human brain 18 p3010 A67-33551

Soviet book on digital processing of radar information covering signal processing, algorithms, discretization, etc 18 p3006 A67-33717

Lunar forced physical librations calculation improved by using digital computer programmed to generate iterative solutions 18 p3129 A67-34307

Digital computing complex optimum configuration for future aircraft, discussing computer role 19 p3186 A67-35311

Enhancement of faint photographic spectra using signal averaging digital computer 19 p3232 A67-35698

Future traffic control system for ensuring flight safety and automatic functioning by automatic radar observation and aircraft-movements control 19 p3255 A67-35806

Long and short range air navigation trends, discussing digital computer application, collision prevention and landing systems 19 p3256 A67-35864

Two-beam interferometric spectroscopy, discussing digital computers role and quality of spectral and angular measurements 19 p3232 A67-35872

Computer principles-equipment and programming for instrumentation systems, comparing digital computers with analog computers 20 p3390 A67-36463

Data processing using digital computer, multiplexing and analog-to-digital conversion equipment for flight control and

evaluation 20 p3390 A67-36465

Sofar bomb signature identification by separation of desired signal from multipath signals with digital computer 20 p3484 A67-36558

Digital computer test program for automatic checkout of Saturn launch vehicles allowing manual intervention 20 p3391 A67-36574

Digital image formation from electronically detected holograms noting advantage in imagery of weak objects 20 p3448 A67-36852

Digital computers for built-in self-test in airborne weapon system, with examples of mechanized tests from F-106/MA-1 system 20 p3392 A67-36988

Functional analysis applied to optimum control by reduction of variational problem to finite dimensional analysis and calculation of algorithms for use with digital computer 20 p3477 A67-37034

Maximum probability criterion on output coordinates of system for selection of parameters of optimal nonlinear control system 20 p3408 A67-37042

Digital computer control system for aerodynamically unstable vehicles 20 p3534 A67-37257

Soviet book on electronic and semiconductor devices of servosystems, examining theoretical principles, computational methods, design principles, analog and digital computers, etc 20 p3406 A67-37700

Instrument engineers guide to digital computer control 21 p3587 A67-37957

Analog and digital computer methods for research and development of fluidic circuit components, discussing scaling effects 21 p3612 A67-38106

Digital computer for simulating and analyzing fluid turbulence by applying laws governing behavior and energy transfer of fluid elements 21 p3612 A67-38193

Cylindrical shell deflection by radial concentrated force, using digital computer for stability analysis 21 p3721 A67-38309

Digital computer program SYNAC for parametric synthesis and performance analysis of military aircraft 21 p3568 A67-38534

Soviet book on microminiaturized aerospace digital computers noting production problems, reliability, electronics, storage units and foreign computers 21 p3588 A67-38765

Strapped-down inertial navigation computational problems solved by Euler parameter algorithms require less computer time 21 p3656 A67-38951

Digital computers in spacecraft control complexes analyzed for design specifics, determining processors composition 22 p3764 A67-39169

Finite difference method for axisymmetrical and plane elasticity problems using high speed computer 22 p3908 A67-39290

Duration of dynamic system output for given input time calculated by computer programming 22 p3764 A67-39336

Computer formulation of motion equations using tensor calculus to extend area of application of digital computers 22 p3827 A67-39418

Glider towing cable configuration taking into account aerodynamic drag forces, using digital computer for numerical calculations and integrations 22 p3745 A67-39551

Complex technical systems servicing, considering operation cost as optimization criterion 22 p3812 A67-39746

Digital temperature compensation and statistical filtering procedures for fast reaction alignment of inertial navigators 22 p3831 A67-39886

Free and near-free molecular flow via cylindrical ducts using Monte Carlo method and high speed digital computer 22 p3784 A67-39946

Orbital attitude reference system working model using strapped down principles and digital computer 22 p3907 A67-40187

Cross coupling effects in strapdown orbital gyrocompass to determine attitude of vehicle with respect to planet-centered coordinate system 22 p3801 A67-40188

Guidance and navigation sensors and systems, discussing spacecraft facilitated by microelectronics, computer technology, optimal filtering and gyroscopic sensor

- design 22 p3834 A67-40335
- Spacecraft flight control and computerized systems, discussing redundant systems, integrated circuits and simulation for man-machine interaction and lack of response 22 p3908 A67-40336
- Rapid Evaluation System To Repair Equipment /RESTORE/ approach to technical manual preparation on digital equipment 23 p4085 A67-40582
- Cylindrical tube current distribution determined by digital computer solution of Fredholm integral equations 23 p3981 A67-41208
- Bioastronautics Laboratory Research Tool /BIO-ALERT/ as automatic biomedical monitoring system composed of digital computer, analog-digital converters and input-outputs 23 p3964 A67-41548
- Digital computer compensation of strain gauge data to extend measuring bandwidth to transient or HF phenomena 24 p4155 A67-42290
- Digital computer restoration of atmospherically degraded images, studying techniques and limitations of former and mechanisms of latter 24 p4157 A67-42436
- Digital image formation and reconstruction from photographic and direct electronically detected holograms 24 p4157 A67-42437
- Digital computer and coherent optical image processing techniques compared, reviewing data transfer schemes and available hardware 24 p4125 A67-42438
- Computer simulation of biological pattern generation processes 24 p4116 A67-42453
- Digital computer system for testing complex aerospace subsystems 24 p4126 A67-42932
- State variable approach to linear differential equations, coding for digital computation 24 p4179 A67-42933
- Measuring instrument for assessing digital data transmission channels performance using bit error counting combined with peak telegraph distortion 24 p4159 A67-43116
- DIGITAL DATA**
- Digital data processing consideration in acquisition-reduction system engineering with reference to solid rocket engine testing 01 p0030 A67-11110
- Sequential operations in computer program for digital picture processing 03 p0375 A67-13560
- Book on digital transistor circuits in semiconductor devices based on Boolean algebra and logical and switching circuit principles 04 p0622 A67-15268
- Direct digital display with high precision for audio frequencies 05 p0865 A67-16944
- Digital data processing, transfer and display equipment applied to ATC terminal operations, using surveillance radars and radar beacons 08 p1351 A67-20677
- Signal field energy distribution optimization ensuring minimum error dispersion during digital information transmission through channels with noise fluctuations 16 p2623 A67-31014
- Digital error performance of transportable troposcatter facility evaluated as function of path length 17 p2811 A67-32118
- Logarithmic compression of digitally telemetered data for constant maximum percentage error throughout encoded range 18 p3006 A67-34115
- Apparatus for digital determination and storage of gas pressure variations, showing pressure curve diagram and numerical representation 22 p3804 A67-40328
- Magnetoelectric device development to measure and register weak signals in digital form in converters of automatic control systems 22 p3809 A67-40475
- Analog and digital data processes for interplanetary photoscience with reference to Mariner Mars flyby mission, discussing telemetric transmission and SNR [IEEE PAPER 19-TP-66-1134] 23 p3998 A67-40740
- Most efficient use of voice band channel in digital data transmission by direct use of passband [IEEE PAPER 19-TP-67-1262] 23 p3972 A67-40741
- Digital imaging techniques used in sinusoidal frequency response modification with or without computer control and display on operator console 24 p4125 A67-42429
- Brightness distortions quantitative determinations in digitized Tiros/ESSA satellite vidicon data to normalize scene to uniformly illuminated image 24 p4156 A67-42431
- Video digital data compression technique, time-buffered coarse-fine /TBCF/, for redundancy reduction 24 p4123 A67-42806
- Measuring instrument for assessing digital data transmission channels performance using bit error counting combined with peak telegraph distortion 24 p4159 A67-43116
- DIGITAL INTEGRATOR**
- Ballistic integrator features and overall capacities, noting integration start-stop and peak detection 01 p0076 A67-11140
- Dynamic programming and Liapunov function for optimization of systems employing digital controllers 11 p1770 A67-24210
- MOS transistor digital switch integrating methods, presenting operating conditions and design factors for IC inverter 12 p1918 A67-26218
- Formula manipulation by computer, noting simplification, pattern matching, complex number handling, etc 19 p3187 A67-35679
- DIGITAL NAVIGATION SYSTEM**
- Onboard digital computer navigation, guidance and control of reentry and aerospace vehicles 06 p1028 A67-17922
- Automatic checkout system /ACS/ and digital guidance programs for titan III and Apollo automatic checkout system /ACS/ and digital guidance programs for Titan III and Apollo 08 p1297 A67-20632
- AVNI low cost IC airborne digital inertial navigation system with analog input and display, using MOS LSI techniques 08 p1297 A67-20633
- Self-optimizing dual input Wiener digital filter by live input data processing derived for zero mean input case, noting applications to hybrid navigation systems 17 p2882 A67-32527
- DIGITAL SIMULATION**
- Computer programmed simulation for supporting resources of aircraft weapon systems from concept through production [AIAA PAPER 66-785] 01 p0169 A67-10529
- Cost effectiveness of optimum military aircraft system, evaluating design alternatives in hardware and support concepts via Monte Carlo simulation and high speed digital computers [AIAA PAPER 66-786] 01 p0009 A67-10530
- Real time digital simulation of linear and nonlinear control systems with large sampling intervals, determining optimization criterion by nonlinear multipoint boundary value problem 01 p0045 A67-10874
- Real time digital simulation of stabilization and control systems /SCS/ for manned spacecraft noting transport delays, thruster duration, etc 02 p0228 A67-11788
- Modularized simulation system to develop generalized digital flight simulation program for use on Titan III mission, emphasizing functional design 02 p0228 A67-11804
- Digital simulation results for random approximation solutions of binary signal detection problems 02 p0204 A67-12169
- AEDNET system of digital computer programs for on-line simulation of nonlinear networks and oscilloscope display 03 p0375 A67-13665
- Digital simulation of Gaussian random load forcing function and motion equations of nonlinear vibration of damped elastic beam 04 p0656 A67-14447
- Optimal temperature control design using IBM 7094 digital computer program for thermal environment simulation of stabilized multisurfaced earth-orbiting spacecraft structure [ASME PAPER 66-WA/HT-44] 04 p0724 A67-15430
- Optimum switching function of relay servosystem subjected to stationary Gaussian random input found by perturbation method 05 p0783 A67-16445
- Real time approximation of continuous system performance on digital computer using difference equations obtained from digitized transfer function 05 p0768 A67-17518
- Digital computer simulation model implementation in prelaunch prediction of Saturn V launch vehicle system performance [AIAA PAPER 67-205] 06 p1096 A67-18344
- Digital computer simulation of nonstationary Gaussian processes using Gaussian white noise, with application to simulation of structural response, ground acceleration, velocity and displacement of earthquake 06 p1109 A67-18839
- Partial error analysis of Fowler z transform root-locus method for digital simulation of complex system 07 p1148 A67-19892
- Digital simulation of boundary value problems of trajectory optimization, using variational and functional analysis and IBM-FORMAC language 07 p1149 A67-19976
- Digital computer use to provide controllable display of star field for use with spacecraft simulator for optical sightings [AIAA PAPER 67-254] 07 p1149 A67-20051
- Digital radar simulator capable of displaying 40 aircraft for air traffic control 09 p1528 A67-22632
- Relay, connector and switch operation simulation, discussing design and performance of chatter and transfer detectors 12 p1943 A67-25702
- Future potential and requirements of digital simulation noting design, construction, cost, etc 13 p2090 A67-27265
- Self-adjustable orthogonal digital filters for system identification and optimization 13 p2088 A67-27409
- Digital simulation of boundary value problems of trajectory optimization, using variational and functional analysis and IBM-FORMAC language 13 p2074 A67-27531
- Fluidic pulse switching network hazards at high operating speeds, suggesting digital computer simulation to anticipate and rectify hazards before hardware fabrication 14 p2251 A67-28348
- Comparison of operator performance when using rotary selector, thumbwheel and digital pushbutton switches 15 p2430 A67-29135
- Digital simulation in operational research - NATO Conference, Hamburg, September 1965 15 p2441 A67-30163
- Air traffic control simulation, describing functions to be fulfilled and system requirements for EUROCONTROL 15 p2441 A67-30164
- Adjoint simulation technique extended to signals consisting of continuous, sampled and multirate sampled systems with random inputs 16 p2652 A67-31684
- Forced-erasure decoding of fading and nonfading channels compared with correlation and digital decoding 17 p2811 A67-32114
- Trends in digital flight simulation for training 17 p2833 A67-32489
- Digital simulation role in advanced avionics system development such as air to air/air to ground weapon delivery, noting advantages, performance, etc 17 p2833 A67-32492
- Digital analog simulation program for IBM 7040 based on signal flow diagram, noting use of Runge-Kutta integration method 17 p2821 A67-32803
- State variable difference equation method for HF solution of ordinary differential equations in digital simulation with nonlinearity 18 p3005 A67-33662
- Random characteristics of second order phase locked loop with Gaussian noise input, using digital simulation 18 p3017 A67-34104
- Digital computer simulation model implementation in prelaunch prediction of Saturn V launch vehicle system performance [AIAA PAPER 67-205] 19 p3331 A67-34807
- Project 666a Automatic Terrain Following Program and Automatic Flight Control System /AFCS/, with digital and analog simulation and test results 19 p3174 A67-35965
- Simulation evaluation of closed form lifting reentry guidance [AIAA PAPER 67-597] 19 p3259 A67-35993
- Digital computer simulation of orbital launch window problem for departure-trajectory analyses 19 p3329 A67-36004
- Velocity and altitude at bottom of first plunge for reentry-vehicle pitch-plane maneuvers compared with digital simulation 20 p3532 A67-36577
- System reliability prediction and confidence limits for several component

failure probability distributions, using Monte Carlo simulation on digital computer 20 p3455 A67-37314

Digital diagnostic program evaluation based on selective path simulation, tracing option and backtrace method 20 p3392 A67-37456

RF mixer and limiting IF models for RFI analysis of local oscillator control in FM-CW receivers, using digital computer simulation 20 p3405 A67-37649

Digital simulation of clutter rejection MTI radars 20 p3388 A67-37651

Acquisition phase of satellite with passive magnetic attitude stabilization, discussing programming difficulties and modified Rayleigh model for German 625A-1 satellite 22 p3898 A67-39173

Propellant sloshing effect on vehicle dynamics under zero gravity conditions studied by programming motion equation into digital simulation of spacecraft, control and propellant 22 p3907 A67-40180

Gravity gradiometer digital computer program for simulated rotating gravitational mass sensor and gradient contour mapping 23 p4000 A67-41218

Digital controller design for tracking telescope, discussing tracking accuracy and response time 24 p4154 A67-42176

DIGITAL TECHNIQUE

Semiconductor device measuring pulsed nanosecond currents produced in detectors by alpha particles 01 p0065 A67-10651

Multichannel Data Logging System for recording short-term simultaneous analog data from 25 to 100 parallel input channels 01 p0076 A67-11142

Linearization of nonlinear transducer output transfer function by digital voltmeter 01 p0076 A67-11143

PCM digital picture transmission for monochromatic still and motion pictures and color still pictures 02 p0208 A67-12167

Transient radiation response and permanent radiation damage in monolithic silicon-junction-transistorized integrated circuit 04 p0589 A67-15720

Computer program for digital exact representation of spectral frequency and intensity-distribution by superposition of Gaussian components, applying least squares method, linearizing normal equations and analyzing observational errors 06 p0965 A67-18069

Level quantization effect in statistical analysis of closed loop digital automatic systems 06 p0976 A67-18406

Digital and analog TV transmission from spacecraft compared, noting data compression and development of hybrid system 06 p0964 A67-18415

Optimal allocation of n test points within redundant digital system for prelaunch and in-flight spacecraft reliability estimate 08 p1300 A67-20637

Focal distance of lens controlled digitally using electro-optics 10 p1653 A67-22750

Digital /chirp/ radiosonde for meteorological and earth satellite measurements employing pulse bursts from voltage controlled oscillator 10 p1655 A67-22823

Digital synthesis technique for automatic frequency search 10 p1604 A67-22970

Diaphragm element for digital logic requirements of data processing equipment, discussing functions and integrated circuit employed 14 p2274 A67-28346

Low cost accurate mechanical timers [ASME PAPER 67-DE-39] 14 p2321 A67-28877

Design procedures for practical elliptic function filter with high selectivity in very compact configuration, noting bandpass and band-stop applications 15 p2444 A67-29453

Optical ranging system with high power chemical laser noting performance characteristics 15 p2500 A67-29913

Large scale integration of arithmetic functions utilizing picosecond circuits, noting ease of fabrication, flexibility and module multipliers 15 p2452 A67-29936

Operator parameter identification on basis of digital treatment of experimental data, using algebraic means and static programming 15 p2460 A67-30313

First stage checkout techniques of satellite launcher, noting digital computer program from pulse-code-modulated telemetry 16 p2655 A67-30835

Digital technique for recording of step-

frequency ionospheric soundings, obtaining maximum and lowest observed frequencies 16 p2625 A67-31340

Extrapolation of time series with discrete Laguerre polynomials, deriving general recursion relation for expansion coefficients 16 p2697 A67-31418

Digital accelerometer converts data into pulse format without analog-digital conversion, noting bias stability determination by crystal characteristics 17 p2855 A67-32438

Waveguide discontinuity problems solution by digital computer 17 p2827 A67-32792

Instrument for processing and storing gas pressure data noting digital integrator, core storage unit and printer 19 p3230 A67-35565

Sonic film memory for digital information storage, discussing block-oriented random access memory /BORAM/ 19 p3189 A67-36067

High precision CRT display system using raster beam positioning and computer-generated digital video 20 p3447 A67-36807

Closed loop stepping motor as mechanical memory and time optimal control and digital servomechanism applications 21 p3570 A67-37787

Noisy signal improvement through compact instrument, giving circuit and operational aspects and applications in ionospheric research 21 p3582 A67-38396

Fluidic digital component design utilizing wave phenomena produced by two interacting low entropy pneumatic jets, discussing nozzle geometry and fluidic oscillators 23 p3936 A67-41421

Book on MOS-FET device operation and characteristics, discussing circuit parameters and digital applications 23 p3983 A67-41766

Radar information automatic extraction by digital techniques, outlining information quantization, target detection and coordinate measurement principles 24 p4122 A67-42407

DIGITAL-TO-ANALOG CONVERTER

DATA CORE, integrated launch area telemetry data system using high speed digital computers and analog or digital display 03 p0375 A67-13382

Reversible dekatron counter pulse-to-voltage converter, noting maximum conversion error 03 p0425 A67-14265

High speed analog-digital converter with fast response time of discriminator obtained by error correction system 04 p0593 A67-15636

Transformation of spatial coordinates of controlled plant into electrical signal 07 p1184 A67-19318

Reversible dekatron counter pulse-to-voltage converter, noting maximum conversion error 14 p2321 A67-28777

Digital to analog pulser system for integral and differential testing pulse height analyzers [JPL-TR-32-1049] 18 p3049 A67-34485

Bioastronautics Laboratory Research Tool /BIO-ALERT/ as automatic biomedical monitoring system composed of digital computer, analog-digital converters and input-outputs 23 p3964 A67-41548

DIGITAL TO VOICE TRANSLATOR /DIVOT/ S VOCODER

DIGITAL TRANSDUCER

ISA National Aerospace Instrumentation Symposium, Philadelphia, May 1966 01 p0072 A67-11108

Technique to monitor system noise and automatic digital system qualification using data obtained by shunt calibration and proper analysis 01 p0073 A67-11112

Measurement capabilities of linear digital displacement transducer with magnetically stored calibration 01 p0074 A67-11124

Digital force-balance pressure transducer providing parallel binary output suitable for direct input to digital computer 01 p0075 A67-11135

Electrical transducers for fluidic systems in computer peripherals 08 p1330 A67-20449

Microwave direction-finding receiver with digital output for blind aircraft landing and navigational uses 19 p3254 A67-35551

DILATATIONAL WAVE

Approximate solution for interaction of shock wave moving in one dimension with sudden increase in cross sectional area 14 p2306 A67-29061

Plane wave approximation for dilatational mode response of thin hollow spherical shell embedded in elastic medium and subjected to asymmetric pressure

wave 21 p3718 A67-38020

DILATOMETER

Dilatometer for measurement of thermal expansion coefficient of solids and variation with temperature 01 p0062 A67-10195

Field-polar forces interaction effect on viscoelastic properties of polypropylene oxide, measuring dilatometric, modulus and damping constants [JPL-TR-32-1026] 24 p4174 A67-41806

DIMENSION

Dimensions effect on efficiency of radiant energy cells 11 p1745 A67-24437

Foundation of theory of physical dimensions 13 p2157 A67-26606

Dimensions effect on efficiency of radiant energy cells 20 p3362 A67-36235

DIMENSIONAL ANALYSIS

Small-perturbation hover dynamics motion equations, characteristic modes, stability derivatives and dimensional analysis [SAE PAPER 660576] 01 p0010 A67-10570

Dimensional effect in electric conductivity of semiconductors during heating of electric field when electron energy relaxation length exceeds mean free path 04 p0679 A67-15137

Mathematical theory of dimensional analysis and similitude, application to spacecraft thermal design and experimental results 05 p0926 A67-16514

Dimensional analysis of turbulent MHD flow in interspace between two coaxial cylinders in rotating circular magnetic field and similarity criteria for EM power losses 06 p1042 A67-18548

Qualitative and quantitative descriptions of penetration of solids by high power density electron beams in welding, calculating penetration vs welding velocity and current curves 06 p1008 A67-18696

Equivalent circuit synthesis for microwave band pass filter design consisting of interdigital or comb structure EM line-coupled resonators 07 p1149 A67-19132

Measurement of dimensions and inertial properties of 50th percentile anthropometric dummy 08 p1289 A67-20611

Normalization technique for analysis of heat transfer, considering thermal entrance length, ablation and tektite problems 10 p1732 A67-22931

Dimensional effect in electric conductivity of semiconductors during heating of electric field when electron energy relaxation length exceeds mean free path 12 p1979 A67-25160

Dimensional analysis of heat transfer correlations for nucleate boiling in free convection, including critical heat flux conditions 14 p2408 A67-28932

Interaction between red spot and white oval spots on Jupiter, explaining dimensional variations of WOS during conjunction 15 p2558 A67-30026

Technique based on dimensional analysis for deriving set of dimensionless parameters in problems involving large number of variables, using matrix calculations 15 p2518 A67-30078

High altitude jet structure for two-dimensional and axisymmetric cases with very large exit/ambient pressure ratio 15 p2418 A67-30208

Book on fluid mechanics and thermodynamics of turbomachinery covering application of dimensional analysis and performance laws 15 p2418 A67-30395

Prandtl shear stress theory applied to similarity models of free turbulence 16 p2657 A67-30857

Book on similarity theory applications to heat and mass transfer in moving medium 17 p2970 A67-32464

Thermal scaling for test models in heat transfer studies of bodies enveloped in large luminous flames [ASME PAPER 67-HT-60] 20 p3549 A67-36742

Dimensional analysis method for determining similarity criteria for MHD processes in liquid metals and alloys 21 p3665 A67-38248

Pressure dependence of heat transfer by evaporation, obtaining parameters from dimensional analysis 21 p3732 A67-38499

FORTAN program for B number computation applied to solid state physics 23 p3977 A67-41458

Similarity analysis of partial differential equations, discussing free parameter analysis, variables separation method, group theory approach and dimensional analysis 24 p4180 A67-43082

DIMENSIONAL STABILITY

Neutron induced dimensional changes in turbostratic carbons used as coatings on nuclear fuel particles, presenting densification curves 08 p1346 A67-21542
Micro-yield stress determinations of cast and extruded beryllium as measure of dimensional stability 13 p2138 A67-27119
Fiberglass-reinforced thermoplastic production processes, discussing strength, rigidity, dimensional stability, etc 17 p2875 A67-31931
High temperature properties of aromatic polyimide fibers, noting thermal and dimensional stability 21 p3648 A67-37874
Self-gravitating isothermal nonrotating gas layer stability, discussing amplitude density distributions in space 24 p4225 A67-41826

DIODE

SA CESIUM DIODE
SA ESAKI DIODE
SA JUNCTION DIODE
SA P-I-N DIODE
SA PARAMETRIC DIODE
SA PHOTODIODE
SA THERMIONIC DIODE
SA TUNNEL DIODE
SA VARACTOR DIODE
SA ZENER DIODE

Fundamental theorem for diode switches proved, using scattering matrix formulation permitting generalization of theorem to nonreciprocal structures 01 p0032 A67-10010

Phase locking, mode selection and noise problems in synchronous operation of microwave silicon avalanche diode oscillators to obtain large coherent output power 01 p0033 A67-10016

Cooling effect of emission current on square wave modulated noise diode cathode 01 p0033 A67-10024

Spectrum of galactic radio emission measured using diode noise sources whose output spectra is calibrated for various frequencies 01 p0147 A67-10360

Exact solution, using Laplace transform, for problem of transient characteristic of semiconductor diode, challenging Nosov view 01 p0035 A67-10398

Reversal of diode with delay between last direct pulse and first reversed pulse 01 p0035 A67-10399

Microwave mixer point contact diode with X-band intermediate frequency for good value of conversion loss 01 p0036 A67-10438

Transistor behavior in phase inverter at LF as function of type /p-n-p or n-p-n/ and value of internal capacity 01 p0038 A67-10770

Saturated transistor logic circuit using rectifier diodes to provide nonlinear current feedback from collector to base of transistor 01 p0038 A67-10817

Transient phenomena in capacitance of Schottky barrier diodes 01 p0137 A67-11066

Microwave power generation by avalanche-transit time diodes, noting noise and excess heat problems 01 p0040 A67-11255

Modulation phase lag in causing overheating of semiconductor diodes as frequency of rectified voltage increases 02 p0209 A67-11508

Low noise figure 94 gc gallium arsenide mixer diode for minimum crystal noise ratio and minimum package parasitics 02 p0213 A67-11649

Electron transport through thin insulating barriers in various diodes, analyzing current dependence on temperature and film thickness for perfect and imperfect dielectrics 02 p0294 A67-11760

Stability of counterstreaming flow of electrons and ions in heavily biased diodes theoretically studied by space charge wave and Nyquist analysis 02 p0214 A67-11883

Avalanche transistor pulser designed to drive GaAs radar-laser diode 03 p0376 A67-12964

Gallium arsenide microwave diodes prepared by vapor phase growth method with highest combination of reverse breakdown voltages and cut-off frequencies 03 p0379 A67-13477

Threshold current density dependency on photon energy in gallium arsenide laser diodes 03 p0379 A67-13480

Spectral intensity of short-circuited noise current of space-charge-limited solid state diodes 03 p0380 A67-13486

Rectification and detection characteristics of space-charge-limited solid state diode at VHF 03 p0380 A67-13488

Closed form expression for storage time of arbitrary base diode, noting diode transient behavior 03 p0380 A67-13489

Secondary breakdown relaxation oscillations and I-V characteristics of point contact n-type Ge diode 03 p0386 A67-13964
Diode detector with exponential volt-ampere characteristics 04 p0579 A67-14452
Quadratic detector with diodes, based on linear interpolation of parabola 04 p0581 A67-14891

Current voltage characteristics of Cd-GaSe-Bi diode structure, rectification coefficient, activation energy and photocurrent spectral distribution 04 p0676 A67-14930

Thermionic energy converters in West Germany, discussing vacuum magnetic triodes, Cs diodes and rare gas triodes 04 p0554 A67-15026

Small signal theory of space charge limited unipolar diodes, calculating impedance and negative conductance 04 p0582 A67-15097

Spectral response of short circuit photocurrent of niobium pentoxide metal diodes 04 p0582 A67-15125

Localized breakdown in Ge mesa diodes due to inclusions 04 p0584 A67-15486

Equilibrium photocurrents in silicon switching diodes from nondestructively measured electrical parameters 04 p0588 A67-15698

Basic diode and triode sputtering processes, describing channeled diode system and sheet beam triode 04 p0631 A67-15996

Optical coupling using gallium arsenide laser for variation of frequency of diode emission through small change in current density 05 p0814 A67-16390

Phase locked oscillations of silicon avalanche diodes noting hysteresis 05 p0775 A67-16984

HF plasma oscillations in planar diodes, noting boundary conditions in plasma electrode interspace 05 p0866 A67-16993

Nanosecond lifetime measurement for minority carriers in long diodes 05 p0775 A67-17004

Small signal negative resistance and avalanche region of impact ionization avalanche transit time /IMPATT/ diodes, particularly Read diodes 05 p0777 A67-17319

Low 1/f noise mixer diodes, comparing Schottky barrier diode with backward diode type 05 p0780 A67-17528

Glass encapsulation for various miniature diodes 06 p0968 A67-18096

Backward diode fabrication and properties for SHF detection, noting germanium diode 06 p0969 A67-18120

Avalanche drift diode and application in microwave technology, analyzing dynamic negative resistance formation, volt-ampere characteristics and output power 06 p0970 A67-18169

Thermal noise limitation in space-charge-limited solid state diodes and triodes 06 p0971 A67-18224

Performance of vortex diode, scroll diode and fluid flow rectifier 08 p1283 A67-20473

Cesium-plasma diode effect dependence on material output of cathode in vacuum, plotting short circuit current vs vapor pressure, voltage distribution, etc 08 p1357 A67-20845

IR laser emission at cryogenic temperatures and various wavelengths obtained from diodes of lead tin selenide and lead tin telluride 09 p1551 A67-21571

Gunn diode efficiency for mixed resonant transit time and suppressed modes, using dynamic drift velocity field strength characteristic 09 p1474 A67-22039

Large area 200-v planar voltage-variable capacitance diodes 09 p1475 A67-22207

Noise generation in Gunn diodes suggests dependence on avalanching of charges in bulk material, making bulk oscillations irregular 09 p1556 A67-22263

Gunn diode self-pumped parametric oscillator, showing power derived from variation of domain capacity at second harmonic of oscillation frequency 09 p1479 A67-22267

Circuit load effects on microwave properties of Gunn diodes, discussing equivalent circuit and graphical analysis of quenched and inhibited modes of operation 09 p1479 A67-22268

Triangular low filament laser diodes, considering alteration of internal reflection to achieve phase shift phenomena 10 p1662 A67-22716

Statistical survey of CW transferred electron oscillators /Gunn diode/ made from epitaxial gallium arsenide 10 p1616 A67-23532

Potential distribution in emitter diode measured in single ended Q machine, using ribbon electron beam 11 p1764 A67-24373

Transient switching process of semiconductor planar diode with retarding electric field in base operated by short forward current pulses 11 p1764 A67-24469

Charge ratios of recovery abruptness and figure of merit in switching diode with base field 11 p1765 A67-24470

Heat resistance of GaAs laser diodes from 77 to 300 degrees K, showing relationship to thermal conductivity 11 p1802 A67-24744

Semiconductor diode light sources, discussing phenomenon of p-n junction luminescence and potential application in optical displays and data transmission 12 p1979 A67-25169

Breakdown voltage characteristics of Ge bonded diode in relation to microwave oscillation, noting avalanche breakdown 12 p1914 A67-25458

Temperature dependence of volt-ampere characteristics of silicon space charge limited diode compared with ordinary diodes 12 p1914 A67-25459

Recombination radiation spectra of InAs with different current carrier concentrations in initial material and different current densities 12 p1914 A67-25516

Elastic collisions in simulating one-dimensional plasma diodes on computer 13 p2164 A67-26294

Time-integrated and time-resolved spectra of GaAs laser diode, noting temperature effect on spectral emission 13 p2125 A67-26427

Transient characteristics of doped silicon diodes with negative resistance, determining electron lifetime vs current, noting space charge role 13 p2076 A67-26489

Si avalanche diode with p-n-n mesa structure, noting high efficiency and high power output at UHF 13 p2076 A67-26519

Active and reactive impedance components of total resistance of p-n-n structures at high injection levels 13 p2081 A67-27278

Interference effects in far field patterns of semiconductor diode lasers 13 p2128 A67-27288

Digital circuits in resistor-transistor, diode-transistor and transistor-transistor logic 13 p2082 A67-27388

Step recovery diode as frequency multiplier, discussing p-n barrier layer diode 13 p2082 A67-27389

Silicon avalanche diode behavior for short duration surge current in reverse direction 13 p2084 A67-27576

Current-voltage characteristics of cadmium sulfide crystal diodes with indium and gold cathodes 13 p2085 A67-27731

HF negative resistance in dielectric diodes with high density of shallow traps taking into account transit time 14 p2367 A67-28521

Double injection and oscillations of current-voltage dependence of alloyed diodes prepared on basis of p-type gallium phosphide 14 p2286 A67-28594

Design of simple circuit for high speed transmission gating of analog signals with fast switching diode and small overshoot 14 p2287 A67-28686

Gunn diodes using Sn-Ag and In-Au contacts studied for electrical properties and failure mechanisms 14 p2290 A67-28927

Current dependent modes in pulsed avalanche diodes 15 p2442 A67-29174

Diode detector with exponential volt-ampere characteristics 15 p2443 A67-29289

Simulation of nonlinear radiant heat transfer for constant emitting heat source by circuit, using semiconductor and pentode 15 p2579 A67-29323

Processes influencing radiative decay in compound semiconductors 15 p2536 A67-29634

Diode and transistor transient switching characteristics determined from analog computer simulation of differential equations 15 p2449 A67-29803

Transverse magnetic field effect on induced emission of GaAs diodes 15 p2543 A67-30251

Noise and HF input conductance measurement of double-injection germanium

space-charge-limited diode, noting transit-time effect 16 p2637 A67-31034

Impurity concentration and temperature dependence of reverse current in indium antimonide diodes, determining components 16 p2637 A67-31162

Large dynamic range, high-burnout microwave varistor diode construction and planar technique for Schottky barrier diode array fabrication described 16 p2642 A67-31723

Space-charge-limited dielectric diode with quadratic I-V characteristics, noting shallow trap effects on detection 17 p2823 A67-32199

Cesium-vapor vacuum diode for thermionic conversion stressing role of electrode homogeneity, space charge and transport phenomena 17 p2823 A67-32222

Quantum efficiency in electroluminescent GaAs diodes, considering carrier concentration effect, electron injection ratio, photon absorption and radiative recombination 17 p2914 A67-32654

GaAs diodes measured for capacitance at 77 degrees K, noting change due to traps photoexcited in space charge layer 17 p2914 A67-32655

Deficiencies of pulse-parameter representation used for semiconductor diodes, discussing generalized parameter describing transient processes relaxation 18 p3009 A67-33474

Au, Zn or Ni doped silicon diodes studied for current distribution over base cross section with negative resistance 18 p3010 A67-33577

Structure of wafer type point-contact diodes 18 p3011 A67-34021

Recombination radiation spectra of InAs with different current carrier concentrations in initial material and different current densities 18 p3012 A67-34447

Electrical characteristics of degenerate n-type germanium diode with gold or indium as metallic element 18 p3105 A67-34635

Diode with anode glow type discharge analyzed for relationship between discharge quenching current and structural elements of discharge gap 19 p3282 A67-35160

Cesium plasma created in diode equipped with Langmuir probe 19 p3296 A67-35588

Low temperature dependence of relative efficiency of forward biased InAs diode emitter 19 p3198 A67-36046

Semiconductor metal diodes operation principles, emphasizing lack of minority carrier storage 20 p3509 A67-36491

Power semiconductor devices, emphasizing thyristors and silicon rectifier diodes applications 20 p3397 A67-36643

Cobalt 60 gamma radiation effect on MOS diodes fabricated on silicon substrates, noting surface state and oxide charge densities 20 p3510 A67-36961

Superconducting diode behavior in resonant electromagnetic radiation field, studying current-voltage-magnetic field relationship 20 p3511 A67-37241

Avalanche drift diode and application in microwave technology, analyzing dynamic negative resistance formation, volt-ampere characteristics and output power 20 p3404 A67-37592

P-n-p diode noise measured by standard techniques and explained using theoretical model, considering internal feedback and additional amplification 21 p3589 A67-37820

Laser-diode impulse generator construction by four-layer diodes and thyristors supplying high current intensity short impulses to low resistance load 21 p3639 A67-37945

Electroluminescent diodes emission efficiency factor for application to lasers 21 p3591 A67-38153

P-n-p diode volt-ampere characteristic qualitative calculation, analyzing device negative resistance with avalanche multiplication 21 p3593 A67-38289

Diode volt-ampere characteristics, considering space charge in base barrier layer and rear contact oxide film, noting vertical section appearing on direct branch 21 p3593 A67-38291

Solution grown GaAs laser diodes with Fabry-Perot cavity, measuring threshold current density variation with reciprocal laser diode length 21 p3641 A67-38457

Second breakdown in semiconductor devices, discussing measurement methods and techniques, development, breakdown

mode and safe operating conditions 22 p3766 A67-39248

Microminialurized matrix preparation using welded and diffused Si diodes assembled in two groups of perpendicular metal strips 22 p3769 A67-39581

Pulse generation method for high power modulators in Doppler radars studied, using step recovery diode to construct compression network 22 p3772 A67-39897

Energy state of recombination level of thermally hardened silicon diode base, considering spatial lifetime of minority carriers 22 p3773 A67-39920

Kinetic collisionless plasma diode model stationary regimes, discussing sheath achievement density value dependence on temperature difference and trapped particle distribution 22 p3774 A67-40322

Nonreciprocal waveguide device consisting of ferrite loaded coaxial branch and crystal diode useful as isolator, modulator and filter 22 p3774 A67-40459

Two-terminal GaAs laser diode communication system noting laser driver component selection, system performance, construction, design and ranging and tracking applications 23 p3975 A67-41379

Internal quantum efficiency of red emitting GaP diodes noting low values due to nonradiative recombination 23 p4045 A67-41460

Edge effects in tunneling characteristics of thin film aluminum diodes in superconducting state, showing anomalies associated with quasi-particle tunneling through film edges 24 p4128 A67-41868

Gold doped silicon diodes consisting of compressor and expander elements designed to eliminate impedance range control and linearity problems 24 p4130 A67-42335

DIOPHANTINE EQUATION

Automatic optimization problem for linear Diophantine plant via analysis of discrete extremal problems 11 p1770 A67-24209

DIOXANE

Laser activity from terblum trifluoroacetylacetate in p-dioxane and acetonitrile at room temperature 11 p1803 A67-24833

DIOXIDE

S CARBON DIOXIDE

DIPHENYLACETYLENE

Reaction of lithium diphenyl phosphide with diphenylacetylene producing high yields of stereochemically pure vinyl phosphides in presence of primary or secondary amine 04 p0565 A67-14523

DIPHENYLAMINE

Thin film circular chromatography for determination of diphenylamine derivative products in propellant powders 13 p2185 A67-26425

Decomposition and stability of diphenylamine compounds in nitrocellulose powder, determining activation energies 15 p2543 A67-29889

DIPLOLE

SA DIELECTRIC POLARIZATION

SA ELECTRIC DIPOLE

SA MAGNETIC DIPOLE

SA ORBITING DIPOLE

Retarded time integral expression rearrangement for study radiation from dipole distribution in inhomogeneous convective motion 01 p0115 A67-11305

Book on systematic and unified treatment of electromagnetic radiation from elementary Hertzian dipole in presence of dissipative half-space 03 p0373 A67-14273

Impedance and admittance measurements of periodically time-varying dipole and application to microwave varactor diode 10 p1610 A67-22925

Association energy of vacancy-impurity dipole obtained from electrical conductivity of magnesium fluoride-doped lithium fluoride at ambient temperature 12 p1978 A67-25149

Dipole transition integrals for nonmetal resonance transitions 13 p2160 A67-26442

High altitude dipole equivalence of geomagnetic field properties verified by satellite-detected electron belt investigation 14 p2308 A67-27932

Current function of three eccentric dipoles representing main geomagnetic field 16 p2670 A67-31911

Improved dipole shutter, optalmic transparency for protection against high intensity flashes 23 p3965 A67-41565

DIPLOLE ANTENNA

Broadside log-periodic antenna, noting lab dimensions of models, power patterns and input impedance 01 p0036 A67-10472

Imperfectly conducting cylindrical transmitting antenna design, examining contribution by ohmic resistance to distribution of current and impedance 02 p0210 A67-11590

Electromagnetic fields of oscillating electric dipole located over half-space with anisotropic conductivity and dielectric constant 02 p0204 A67-12194

Reradiation pattern of Van Atta reflector consisting of half-wave dipoles 03 p0384 A67-13846

Fields of horizontal dipole over stratified anisotropic half-space 03 p0370 A67-13858

Driving point impedance of asymmetrical dipole using computer method 03 p0385 A67-13861

Excitation of dipole wave in circular small delay dielectric waveguide by sources with amplitudes and phases variously distributed over apertures 03 p0385 A67-13953

Current distribution on half-wave dipole antenna embedded in conducting half-space, noting case where dissipative medium has average earth constants 05 p0769 A67-16006

Electric and magnetic field components produced by vertical and horizontal dipole antennas located at surface of conducting earth derived for quasi-static range 05 p0769 A67-16007

Synphase antenna with broadband active reflector 05 p0778 A67-17394

Radiation from linear resonant antenna in lossy compressible weakly ionized plasma and dependence on ratio of source to plasma frequency 07 p1227 A67-19428

LF ionospheric measurement of admittances of three orthogonal shock dipoles, noting impedance variation with respect to frequency attitude and voltage 10 p1648 A67-23286

Impedance measurement of 39.5 meter tip-to-tip dipole antenna made during ionospheric rocket flight 10 p1611 A67-23292

Absolute gain measurements of vertically polarized HF test antennas over imperfect ground 11 p1761 A67-24278

Radar echo model from random collection of rotating dipole scatterers 11 p1764 A67-24435

Antenna impedance dependence on excitation of acoustic waves by biconical dipoles encased in dielectric sphere immersed in warm plasma 11 p1769 A67-25030

Space-time cross correlation function for antennas generalized by complex antenna-height function 12 p1917 A67-26089

Technique of fabricating inhomogeneous mediums and behavior of dipole 13 p2082 A67-27407

Induced impedance dependence on scanning angle and array parameters calculated, analyzing edge effects 14 p2279 A67-28005

Local measurement of SHF electromagnetic field during plasma properties observation, using dipole antennas 15 p2485 A67-29124

Input impedance of short dipole antennas on Nike-Apache rocket 15 p2444 A67-29504

Log periodic antenna theory and applications including HF, VHF, UHF and SHF aerials 15 p2454 A67-30139

Radio gain between simple dipole antennas for single propagation paths, noting effect of resistance from imperfect ground 16 p2625 A67-31342

Plasma sheath detuning effect on small loaded dipole in free space investigated 16 p2627 A67-31367

Spherical dipole for Italian satellite, calculating radiation impedance and pattern, input admittance, efficiency, radiated field and antenna Q factor 17 p2826 A67-32780

Resonances of thin shell model of earth-ionosphere cavity with dipolar magnetic field 18 p3042 A67-34427

Current distribution on cylindrical dipole antenna in homogeneous warm plasma 19 p3194 A67-35515

Approximate method for calculating electromagnetic field structure of vertical antenna 21 p3590 A67-38118

Nonreflecting resistive loaded dipole antenna with step function internal impedance, measuring current amplitude, input admittance and radiation field

- pattern 23 p3978 A67-40826
- Electromagnetic field components of vertical and horizontal dipole antennas in quasi-near range 23 p3979 A67-40828
- Impedance of dipole antennas in isotropic He plasma measured at X band 23 p3979 A67-40833
- Finite ground plane influence on raised electric dipole far field radiation pattern 23 p3980 A67-41202
- Magnetic and electric dipole antennas located above earth surface, deriving quasi-static electric and magnetic field components 23 p3981 A67-41210
- Harmonic analysis of half-wave dipole and director parallel to reflecting plane 24 p4132 A67-42715
- DIPOLE MOMENT**
- SA PYROELECTRICITY**
- Phenomena accompanying geomagnetic field reversal, using measurements performed on samples of core Papagayo 3G 04 p0617 A67-15543
- Equivalent dipole moment of geomagnetic field in terms of earth radius deduced from spherical harmonic analyses 10 p1652 A67-23492
- Critical binding of electron by electric dipole, noting value of dipole moment 11 p1824 A67-24996
- Geomagnetic field analytical representation, giving equations for moments and distribution of equivalent set of dipoles 14 p2309 A67-27948
- Lagrangian for interaction of electric charge with field induced by scalar magnetic charge to determine electrical dipole moment 17 p2883 A67-32100
- Magnetic and electric charge interaction, noting neutrino electric dipole moment 17 p2887 A67-32101
- Geomagnetic eccentric dipole shown equivalent to multipoles superposition, giving geometric parameters and procedure for determining true magnetic poles 18 p3042 A67-34351
- Magnetospheric free boundary representation synthesis problem, discussing relaxation solution, dipole moment and stream direction 22 p3854 A67-40347
- DIRAC EQUATION**
- Nuclear interaction similarity with Dirac monopole interaction with electromagnetism field, noting equality in number of conservation laws acting in either interaction 02 p0271 A67-12751
- Mach principle as consequence of de Sitter universe filled with Dirac dust 05 p0847 A67-16803
- Classical equation of motion of extended monopole charged particle without preacceleration or runaway solutions 11 p1821 A67-23977
- Celestial mechanics and Dirac hypothesis 15 p2563 A67-30123
- Gravitational theory with all curvilinear coordinate systems and space-time avoided illustrated by applying method to Dirac field case 20 p3484 A67-36836
- Bargmann-Wigner and Dirac formulations for field of spin 1/2 shown equivalent provided auxiliary field vanishes in electromagnetism interaction presence 20 p3489 A67-37090
- Differential and Clifford matrix algebra relationship in relativity theory, generalizing Dirac and quaternion algebras to Riemann spaces 21 p3656 A67-37923
- Nuclear interaction similarity with Dirac monopole interaction with electromagnetism field, noting equality in number of conservation laws acting in either interaction 22 p3841 A67-40253
- DIRECT CURRENT /DC/**
- SA ALTERNATING CURRENT /AC/**
- HF design of DC-DC converters with low weight and high performance for spacecraft power systems 02 p0183 A67-12181
- Instrument, force and motion servos in cockpit simulation in large aerospace flight simulators, using DC analog voltages 03 p0395 A67-13386
- Emissive capacity of argon in direct current arc at high pressure and temperature, noting experimental setup and results 03 p0478 A67-13602
- Electrical parameters of DC MHD generator with arbitrary connected electrodes 04 p0553 A67-14475
- Flux jumps in hard superconductor AC and DC magnetic fields 04 p0682 A67-15328
- Macroelectrodynamics equations for low temperature intermediate state of type I superconductors, noting magnetic field effect on structure 05 p0863 A67-16695
- Plasma in Ar positive column DC discharge examined for wavelike perturbations about equilibrium, noting striation dispersion relation, density variations and electron temperature 05 p0857 A67-17427
- Quadrupole calculation of zero-level drift in transistorized DC amplifiers 06 p0970 A67-18172
- Pulse width modulated series switch with input and output filtering for automatic impedance matching in DC circuits regardless of load or source characteristics 08 p1311 A67-20650
- DC-to-DC prime converter for anchored interplanetary monitoring platform spacecraft /AIMP/ transforming power from solar array into suitable level for instrumentation electronics 08 p1284 A67-20695
- Direct current electrical discharge investigated in gas flow in magnetic field perpendicular to flow direction 09 p1542 A67-21816
- Two positive kinetic power waves coupled in interaction for DC pumped quadrupole amplifier having low noise and high efficiency 09 p1478 A67-22260
- Photomultipliers in DC output mode for extreme UV 10 p1653 A67-22737
- Aircraft DC electronic controls and generators for voltage regulation and system protection [SAE PAPER 670250] 11 p1745 A67-23983
- Time behavior of radiation field of infinite cylindrical antenna upon DC voltage pulse at input 11 p1762 A67-24292
- Response of superconducting sheath state of lead-indium in AC and DC magnetic fields studied, noting transition changes response of superconducting sheath state of lead-indium in AC and DC magnetic fields studied, 12 p1985 A67-25847
- Substrate doping, source bias and bulk contact effect upon DC characteristics of silicon MOS transistors 12 p1916 A67-26068
- Direct current MHD generator having channel of constant cross section and using NaK as working fluid 13 p2056 A67-27315
- Hot carrier DC conduction in elemental semiconductors germanium and silicon 13 p2183 A67-27568
- Electromagnet design for experimental DC MHD generator 14 p2247 A67-27950
- DC operation of FET at liquid helium temperature noting transfer and drain characteristics similar to those at room temperature 14 p2290 A67-28926
- DC and AC parameters of germanium tunnel diodes in 3 to 5 millamp range measured by ammeter dC and AC parameters of germanium tunnel diodes in 3 to 5 millamp range measured by ammeter 15 p2449 A67-29807
- Macroelectrodynamics equations for low temperature intermediate state of type I superconductors, noting magnetic field effect on structure 15 p2539 A67-29866
- Stability conditions for gas stabilized DC electric arc in plasma-arc torch determined, using small perturbation technique schematic feed circuit 17 p2897 A67-32173
- Weak DC signals conversion into electric pulses by magnetic semiconductor pulse width modulator using AC generator 17 p2823 A67-32224
- Circuitry and operation of instrument measuring entire DC response of tunnel diodes, describing measurement method 17 p2823 A67-32298
- Voltage breakdown measurement in various gases at low pressures during simultaneous excitation by RF in superimposed DC field 17 p2902 A67-32672
- Simultaneous AC and DC in ring-shaped hard superconductors, confirming critical AC and superimposed DC existence 18 p3098 A67-33521
- Emissive capacity of argon in direct current arc at high pressure and temperature, noting experimental setup and results 18 p3090 A67-34467
- Ionization rate at higher electron densities in DC fields measured in toroidal discharge tube 19 p3272 A67-35078
- DC discharge parameters solution using pressure theory with generation terms stressing one-and two-dimensional cases 19 p3277 A67-35126
- Circuit design and performance to convert DC input voltage to pulse train with width proportional to input 19 p3197 A67-35702
- Effect of angular direct current magnetic field on radiation of slot antenna located on metal cylinder covered by plasma sheath 19 p3184 A67-35811
- Polarity reversal with DC bias in hot-carrier microwave diode 19 p3198 A67-36038
- Continuous DC EMF in semiconductor with symmetrical nonlinear conductivity analyzed in variable AC waveguide magnetic field 20 p3513 A67-37449
- Operational analysis and DC design of Esaki diode pair bistable circuit used in high speed counting network performed by analog computer simulation 21 p3604 A67-38603
- Measuring method for minority carriers recombination rate at base surfaces of /n-m/ contact without passing DC through contact 22 p3858 A67-39575
- Modulated signal nonlinear distortions from AC system resulting from system components nonlinearities 22 p3763 A67-40478
- Threshold properties of CW laser oscillation at 7525.5 angstroms in DC-excited KrII discharge 22 p3818 A67-40490
- DIRECTION FINDER**
- S RADAR DIRECTION FINDER**
- S RADIO DIRECTION FINDER**
- DIRECTIONAL ANTENNA**
- Optimization of directive gain and SNR of arbitrary antenna array with or without constraint on array Q-factor 01 p0035 A67-10431
- Automatic directional-antenna position control system for ATS synchronous orbit spin-stabilized satellite 01 p0156 A67-11426
- Polarization angle of linear feed antenna on polar mounted paraboloid relative to az-el coordinate system 02 p0212 A67-11611
- Synthesis of TEM directional couplers and fixed phase shifters consisting of multiple parallel coupled quarter wave sections 02 p0214 A67-11778
- Amplitude and phase direction-finding characteristics of monopulse automatic tracking system operating on sum-difference principle 02 p0214 A67-11904
- Spatial radiation patterns of curved high-directivity antenna array as function of amplitude distribution and directivity 02 p0214 A67-11906
- Angular section errors effect on directive gain coefficient of parabolic antenna with automatic phasing 02 p0215 A67-11975
- Coefficient of mutual correlation of noises for two-antenna phase type direction finder 03 p0386 A67-13957
- Treatment of surface of directional radar antenna with RF absorption material for sidelobe reduction 03 p0389 A67-14349
- Ionospheric sporadic E layer propagation characteristics and signal strength calculation, noting decrease in antenna gain when using highly directional antennas 04 p0576 A67-15503
- Factors governing amplitudes of reradiated signals from tall obstacles distorting VHF and UHF transmission 05 p0766 A67-17296
- Angular resolving power limitations for linear arrays of equispaced elements receiving EM or acoustic waves, in cases of mechanical rotation and electron beam scanning 06 p0966 A67-17576
- Directional radiation pattern for circular arc antenna, using three-step method in which current distribution is treated as truncated Fourier series 07 p1152 A67-19550
- Distribution function of modulus of directivity characteristic of antenna grid shown as modified Rayleigh distribution 07 p1143 A67-19596
- Bidirectional waveguide theorems derived directly from transverse and longitudinal components of Maxwell equation and generalization to include nonbidirectional waveguides 09 p1464 A67-22091
- Generalized method of calculating multielement antenna and feeder system 10 p1611 A67-22981
- Optimum antenna aperture distribution for finite line source and desired radiation pattern with given superdirective ratio upper boundary 11 p1768 A67-24943
- High directional gap antenna, considering radiation sources of equal energy located on concentric rings 12 p1914 A67-25311

Directivity factor of convex SHF pencil-beam antennas with given magnetic currents, noting planar cophasal aperture 13 p2080 A67-27025

Triode version of active LF directional coupler compared to passive coupler 13 p2081 A67-27198

Three-dimensional multielement transponder array designed to give directional replies toward source of interrogating signals 13 p2071 A67-27404

Statistical performance of wide aperture sampling linear array in HF direction finding 13 p2082 A67-27405

Maximization of directive gain for circular and elliptical arrays 13 p2082 A67-27406

Directivity factor of linear antenna array with Chebyshev radiation pattern 14 p2289 A67-28862

Helical antenna radiation characteristics under backfire operating conditions, noting improvement over endfire conditions 14 p2290 A67-29008

Nagelberg formula locating Fresnel region phase center of aperture antennas examined by calculating phase patterns of radiation field 16 p2639 A67-31357

Receiving directional antenna effect on magnitude of frequency correlation in fluctuations of received radio emission 16 p2640 A67-31497

Satellite receiving and transmission antenna orientation effects obtained by Faraday rotation measurements 16 p2628 A67-31507

Phase diagrams for axisymmetric and asymmetric antennas analyzed by Kirchhoff integral method 18 p3010 A67-33504

Short-slit directional coupler functioning mode via boundary value problem indicating Chebyshev behavior of transfer coefficient and wideband subdivision 19 p3195 A67-35560

Directional maximum gain of antennas with discrete propagation elements 20 p3398 A67-36775

Distribution function of modulus of directivity characteristic of antenna grid shown as modified Rayleigh distribution 20 p3384 A67-37335

Transient response and current distribution of thin vertical antenna coupled to pulse generator by electric network, determining radiation field 21 p3590 A67-38117

Earth finite conductivity effect on directivity patterns of vertical antennas taking into account attenuation factor 21 p3590 A67-38119

High gain directional antenna networks for space communications 21 p3600 A67-38670

Atmospheric inhomogeneities effect on large antenna directive gain, noting dependence on length and wave field 21 p3600 A67-38812

Correlation coefficient dependence on angular dispersion and ratio between antenna directivity and width of energy spectrum of waves scattered by troposphere 22 p3759 A67-39433

Linear correlation-detection transducer arrays for directional noise field signals, giving N-element coherent detector performance in propagating and turbulent boundary layer 22 p3801 A67-40233

Handbook on HF directional antennas covering performance characteristics and applications 24 p4128 A67-41794

DIRECTIONAL CONTROL

Jet direction variation via secondary fluid injection resulting in booster trajectory control, increased payload and reliability 01 p0142 A67-11409

Direct method for determining space directions and adjustment of satellite triangulation net 10 p1637 A67-23181

Continuous nonlinear feedback law for controlling thrust direction to produce minimum time spacecraft rendezvous with nonmaneuvering target 16 p2758 A67-30651

Hardware characteristics of control moment gyro /CMG/, determining nonlinearity effects on performance by simulation 17 p2853 A67-31995

Lateral-directional flying qualities for power landing approach simulated, studying roll effects and damping [AIAA PAPER 67-577] 19 p3175 A67-35972

Iterative guidance mode, deriving alternate expressions for thrust direction control angle for time savings on Saturn launches 22 p3831 A67-39957

DIRECTIONAL STABILITY

Mean and mean square directivity factor of antenna array in presence of phase and amplitude distortions 04 p0583 A67-15164

Mean and mean square directivity factor of antenna array in presence of phase and amplitude distortions 15 p2443 A67-29351

Lateral-directional stability equations for aircraft with nonzero product of inertial flying along steep flight path gradient 17 p2796 A67-32219

Equilibrium configuration for nonspherical cold gas cloud permeated by magnetic field in gravitationally collapsed state 22 p3895 A67-40518

DIRICHLET PROBLEM

Steady state elastic oscillations in case of plane deformation for infinite plane weakened by round arbitrarily arranged holes 01 p0159 A67-10224

Ljapunov second method applied to elastostatic stability, discussing applicability of Dirichlet principle and Galerkin method 01 p0161 A67-10647

Solvability of degenerated parabolic boundary value problem in Euclidean space cylinder and relation to homogeneous Dirichlet problem 01 p0105 A67-10677

Numerical method for estimating capacity of arbitrary surface noting relation to Dirichlet problem 03 p0462 A67-14342

Nonuniform network procedure for solving Dirichlet problem for Laplace equation in finite and infinite regions with canonical points 04 p0643 A67-14870

Exterior Dirichlet problem for reduced wave equation treated by numerical method 05 p0835 A67-16738

Subsonic compressible flow around profile obtained by conformal transformation, reducing to Dirichlet problem 05 p0749 A67-16845

Dirichlet problem for strongly connected elliptical systems 05 p0835 A67-16939

Dirichlet theorem and coherent imaging, discussing form of Fourier functions in Fraunhofer diffraction at infinity 07 p1185 A67-19402

Existence and uniqueness of 2k-fold continuously differentiable solutions to Dirichlet problem for nonlinear integrodifferential equations 07 p1215 A67-19476

Nine-point Laplace difference equation in square solved by modified alternating direction implicit method 08 p1299 A67-21257

Dirichlet problem of toroidal segment, noting integral transformation of spherical function 10 p1675 A67-23669

Expansion of arbitrary function of Mehler-Fok integral form in terms of spherical functions 11 p1812 A67-24149

Estimations for majorizing functions for solutions of Dirichlet problem for second order elliptic equations or inequalities 12 p1961 A67-25670

Regularity properties in time variable of solutions of n-dimensional Navier-Stokes system 13 p2145 A67-26509

Iteration process by difference scheme for numerical solution to Dirichlet problem of two-dimensional Poisson equation 13 p2148 A67-27613

Numerical methods for elliptic problems, discussing application of finite difference and solution of large algebraic systems 14 p2342 A67-28156

Majorizing functions for Dirichlet problem in n-dimensional space 14 p2343 A67-28631

Necessary and sufficient conditions for solvability in two-space of second order elliptic differential equations with smooth irregular continuous differentiable boundary 14 p2344 A67-28634

Contour integral representation of eigenvalues of first boundary value problem of elasticity theory 17 p2962 A67-32832

Dirichlet problem for elliptic system of differential equation which does not satisfy Lopatinski condition where characteristic equation of system has simple roots 18 p3073 A67-34481

Dirichlet problem solution for Poisson equation on rectangle with smooth boundary values, using higher order differences 19 p3249 A67-34794

Elastic potential used to study Green and Neumann tensors through series expansion for Dirichlet problem 19 p3341 A67-35541

Higher order differences used in solution of Dirichlet problem for Poisson equation of

rectangle 20 p3475 A67-36651

Zero moment elliptical paraboloid translational shell under uniformly distributed load, reducing solution to Dirichlet problem 20 p3539 A67-36924

Papers on functional analysis covering approximation methods and Cauchy, Dirichlet and boundary value problems 21 p3651 A67-37832

Dirichlet problem of toroidal segment, noting integral transformation of spherical function 21 p3652 A67-38270

9-point difference formula accuracy in Laplace equation compared to 5-point formula, discussing convergence rate and Dirichlet boundary value problem 22 p3826 A67-39195

DISCHARGE

S ARC DISCHARGE

S CORONA DISCHARGE

S ELECTRIC DISCHARGE

S EXHAUST

S EXPLOSION

S GAS DISCHARGE

S GLOW DISCHARGE

S PENNING DISCHARGE

S PLASMA DISCHARGE

S RADIO FREQUENCY DISCHARGE

S RING DISCHARGE

S SPARK

S SPARK DISCHARGE

S TOROIDAL DISCHARGE

S TOWNSEND DISCHARGE

DISCHARGE COEFFICIENT

Airflow instability with square edge circular orifice, discussing hysteresis effect on discharge coefficient 04 p0601 A67-14487

Outflow of perfect ponderable fluid from opening in bottom of cylindrical container measured by numerical integration method by finite differences 07 p1169 A67-20207

Steady state theory of discharge column, giving solutions to density and potential profiles for planar and cylindrical geometry 08 p1361 A67-21134

Injection coefficients of hydrogen and oxygen during buildup of discharge in homogeneous electric field 13 p2160 A67-26813

Swirling mass flow in supersonic nozzle indicates discharge coefficient falls nonlinearly with swirl 22 p3739 A67-39527

Force defect coefficient method applied to calculation of compressible jet flow discharge for asymmetric two-dimensional orifice 23 p3936 A67-41330

DISCHARGE TUBE

SA ELECTRON TUBE

SA THYRATRON

Propagation of nonaxisymmetric Alfvén waves in linear discharge tube filled with nonuniform plasma 03 p0485 A67-14045

Afterglow decay of number density and electron temperature of plasma with rare collisions between electrons and molecules 03 p0487 A67-14343

Tube diameter influence on output power and efficiency of gas laser 05 p0816 A67-16629

Response of trigger discharge gauge, noting ion current component 06 p0950 A67-17750

Structural book properties on and operational modes of electron-optic current controlling high vacuum gas-filled and solid state discharge devices 06 p0968 A67-17894

Impulse discharge tubes for laser employing industrial glass 07 p1195 A67-19506

Center frequency shifts of 6328 angstrom neon transition in Zeeman discharge cell measured in terms of discharge current and gas pressure 07 p1197 A67-20100

Vacuum UV resonance lamp design to eliminate difficulty of window seal caused by discharge 08 p1329 A67-20354

Radial particle density profile in neon negative glow plasma in cylindrical discharge tube measured by double probe method 08 p1362 A67-21288

Gain curves in multifrequency optical oscillators, measuring vanishing frequencies as function of losses in resonator, noting attenuation in laser discharge tube 09 p1514 A67-22271

Rate equation solution for density of excited atoms in He-Ne discharge for steady state 10 p1863 A67-22893

Frequency stabilization of gas laser by discriminant, using discharge tube with gain profile split by AC magnetic field 11 p1801 A67-24664

- Water cooled mercury arc discharge lamp for room temperature optimum optical pumping of CW lasers 12 p1952 A67-25331
- Rectangular pulse thyatron-type generator design and operational principles 13 p2081 A67-27276
- Current layer motion in coaxial plasma gun, measuring discharge current, electric and magnetic fields and ejected ions at gun outlet 15 p2525 A67-29250
- High power argon ion laser with wall stabilized arc discharge determining laser output 16 p2685 A67-30825
- Photographic recording of fast moving plasma clouds during pulsed discharges in rarefied gas using Topler apparatus 16 p2721 A67-31396
- Pinch radiation in quartz discharge chamber spectrographically studied for use as sources of short pulsed radiation with continuous spectrum 17 p2904 A67-32919
- Voltage drop near electrode during plasma and electric field interaction in electrical discharge tube, giving plasma current-voltage curves 17 p2907 A67-33090
- Active medium radial variation in density of neon atoms. metastable level as explanation of anomalous laser oscillation 18 p3060 A67-34013
- Plasma behavior in shock tubes with parallel conductors, discussing shape of front and velocity dependence on pressure and gas composition 18 p3089 A67-34297
- Light pulse generator circuit using hydrogen corona-discharge tube and thyatron generator of nanosecond light pulses 19 p3228 A67-34988
- Leak detection methods in vacuum devices including compressed air, discharge tube, halogen tracers, radioactive krypton, pressure rebuild, etc 20 p3443 A67-36474
- Electron density time and location dependence in Z-pinch calculated from emission measurements 20 p3502 A67-37528
- Discharge line fluid conditions in cryogenic container with self-pressurized draining, using Bernoulli, continuity and general energy equations and fluid properties 22 p3784 A67-39968
- Temperature distribution measurements behind shock wave front in discharge tube with air and Ar indicate undisturbed thermodynamic equilibrium of plasmas 24 p4141 A67-41936
- He-Ne gas mixture DC discharge electron temperature and concentration dependence on tube diameter, pressure and composition, using two-probe method 24 p4196 A67-42242
- DISCONNECT DEVICE**
- Thermal gradients effect on separable tube connectors, discussing structural elements 17 p2864 A67-32009
- DISCONTINUITY**
- SA SHOCK DISCONTINUITY**
- Necessary and sufficient conditions of invariance and autonomy of multidimensional nonlinear automatic control systems with right-hand discontinuities in describing differential equations 03 p0391 A67-13188
- Vorticity jump across discontinuity surface which is not contact surface obtained on kinematical basis, recovering Hayes formula for gas dynamic discontinuity 04 p0600 A67-14456
- Discontinuous solutions in supersonic reacting gas flows under nonequilibrium conditions 06 p0984 A67-18112
- Deformation of surface of removable wave front discontinuity in acoustically anisotropic medium with variable sound velocity 06 p1032 A67-18396
- Synthesis of time functions with finite number of discontinuities by constructing functional scheme of system from Laplace transform of output 11 p1769 A67-24122
- Waveguide discontinuity problems solved through matrix iterative analysis 11 p1760 A67-24237
- Stability of discontinuous solutions of gas dynamic equations noting doubtful case with imaginary eigenvalues 13 p2093 A67-26379
- Limitations in conventional radar compared to new multichannel radar with discontinuous pulse compression 13 p2070 A67-27203
- Plane shock wave in ideal gas characterized by infinitesimally thin discontinuity, determining width and distribution function 13 p2105 A67-27412
- Ionospheric discontinuity motion in E layer at 100 km, using long distance ultrashort-wave propagation data obtained by diversity-reception method 15 p2479 A67-30148
- Discontinuities of shock adiabats and multivaluedness of compressions, noting similarity to Bancroft condition 16 p2659 A67-31043
- Book on electromagnetic radiation discontinuities presenting solution of Helmholtz and harmonic Maxwell equations and derivation of discontinuities formulas by generalized functions 16 p2629 A67-31628
- Waveguide discontinuity problems solution by digital computer 17 p2827 A67-32792
- Discontinuity problem solution between unloaded rectangular waveguide and same waveguide completely loaded with transversely magnetized ferrite 20 p3380 A67-36381
- Rotation effect on growth of discontinuity across Alfvén wavefront, solving differential equations 21 p3662 A67-37761
- Thermoelastic coupling effect on propagating discontinuities in stresses and particle velocities studied using characteristic method 21 p3715 A67-37893
- Wave propagation rate in elastoplastic bodies under completely plastic conditions, noting discontinuity magnitude 21 p3716 A67-37968
- Discontinuous systems proved for stability and instability, using almost-reducible linear approximations 21 p3654 A67-38850
- Asymptotic formulas for propagating discontinuity diffusion in magnetoplasma, considering discontinuity shape, diffusion and lifetime 21 p3621 A67-39020
- Discontinuity problem between empty rectangular waveguide and one filled with transversely magnetized ferrite solved by introducing metal surface wave 22 p3758 A67-39272
- Plane circularly polarized magnetoelastic and elastic wave scattering at plane discontinuity surface between ferromagnetic insulating medium and elastic medium 22 p3856 A67-39364
- Discontinuous integrands in calculus of variations formulations of trajectory optimization and maximum payload problems with discontinuous state variables 22 p3827 A67-39954
- Dominant mode field reflection at air-ferrite interface junction in anisotropic rectangular waveguide, deriving singular integral equations for discontinuity problem 23 p3973 A67-40880
- DISCRETE FUNCTION**
- Discrete element technique applied to natural vibrations of deep spherical shells satisfying geometric and force boundary conditions 01 p0184 A67-11184
- Method giving bounds for difference quotients, up to second order, of discrete function 02 p0258 A67-11555
- Discrete method strength calculation for round cylindrical shells applicable to computer solution of normal external loading problems 02 p0339 A67-12442
- Optimality conditions for nonlinear discrete systems, showing that at limit these conditions become Pontryagin maximum principle for continuous systems 05 p0782 A67-16320
- Sufficient conditions of absolute stability of nonlinear discrete systems based on matrix majorant concept 06 p0978 A67-18793
- Discrete continuous feedback control systems with signal dependent sampling constraints, analyzing sampling interval criteria 09 p1483 A67-22608
- Nonlinear sampled system with parameters in functional dependence on sign of error at discrete instants of sampling 11 p1769 A67-24056
- Automatic optimization problem for linear Diophantine plant via analysis of discrete extremal problems 11 p1770 A67-24209
- Discrete ordinate method for evaluating function described by particular integral applied to boundary value problems in gas kinetics 12 p1962 A67-26192
- Rarefied gas flow between parallel plates based on discrete ordinate method 13 p2092 A67-26277
- Discrete rational approximation problem, procedure for solution 13 p2145 A67-26615
- Discrete ordinate method for boundary value problems in gas dynamics using differential equations yields solutions to Couette flow 13 p2101 A67-26962
- Rayleigh problem solution and accuracy and utility of discrete ordinate method for time dependent problems as applied to Couette flow problems 15 p2473 A67-30214
- Optimal control theory applied to extremum control in dynamic programming equation derivation for simplified extremum control problem 15 p2465 A67-30343
- Optimal control and convex programming, discussing problem of admissible investment program control for production constraints 17 p2829 A67-32431
- Optimality conditions for nonlinear discrete systems, showing that at limit these conditions become Pontryagin maximum principle for continuous systems 18 p3017 A67-33871
- Sufficient conditions of absolute stability of nonlinear discrete systems based on matrix majorant concept 18 p3018 A67-34458
- Estimation and filtering in discrete linear systems with reference to Gaussian statistical hypothesis 19 p3250 A67-35910
- Corrective force selection for bringing nonlinear discrete system to predetermined phase space point in fixed instant of time 20 p3487 A67-37659
- Discrete errors in continuous angle-modulation systems, considering conventional fidelity /SNR/ criterion and probabilistic theory 21 p3584 A67-38653
- Discrete method extension for bending stability problem in sectorial plates, obtaining algorithm for solutions of boundary conditions and external loads 21 p3729 A67-38907
- Discrete Laplace transform for analyzing pulsed automatic systems with variable parameters, noting special type of complex variable 21 p3605 A67-39112
- Final probabilities of ergodic Markov chain calculated by methods based on topological properties of stochastic graph 22 p3777 A67-39830
- Load and response design values determination by statistical method for structural systems such as launch vehicles, considering discrete forcing functions 22 p3907 A67-40178
- Interpolation of Poisson equation by method adjusting equations to insure existence of discrete solution 23 p4023 A67-40865
- Bounded-input bounded-output stability on nonlinear time varying discrete control system using Liapunov function 24 p4135 A67-42183
- Design procedure for estimating state vector of discrete-time linear stochastic system with constrained memory estimator 24 p4135 A67-42185
- DISCRIMINATION**
- S BRIGHTNESS DISCRIMINATION**
- S SENSORY DISCRIMINATION**
- S SPEECH DISCRIMINATION**
- S TACTILE DISCRIMINATION**
- S TIME DISCRIMINATION**
- S VISUAL DISCRIMINATION RECOVERY**
- DISCRIMINATOR**
- SA SIGNAL DISCRIMINATOR**
- Mode discrimination of laser cavity exploiting transmission characteristics of Fabry-Perot interferometer 10 p1663 A67-22835
- Frequency stabilization of gas laser by discriminant, using discharge tube with gain profile split by AC magnetic field 11 p1801 A67-24664
- Discriminator threshold and SNR above threshold response when demodulating FM signal undergoing selective fading 14 p2273 A67-28711
- Cut-off amplifiers in frequency stabilization klystron designed to cut off only HF wave applied to discriminator 20 p3396 A67-36327
- Laser frequency control system using two optical discriminators for long and short term stability 20 p3459 A67-36519
- DISEASE**
- SA EYE DISEASE**
- SA HEART DISEASE**
- SA VIRUS**
- Mice inoculated with tetanus exposed to high pressure oxygen /OHP/ under immediate and delayed administration 09 p1453 A67-21727
- Disease vector transport by aircraft as international health hazard 15 p2429 A67-29284
- DISINTEGRATION**
- Disintegration of alkali halide single

crystals, polymers and glasses under laser radiation, noting parameters of disintegration region magnitude 03 p0439 A67-14367

Cleavage and separation of dye-doped ice and paraffin instantaneously heated by laser pulse, measuring mechanical pulse at energy concentrations below vaporization heat 06 p1119 A67-18807

Disintegrating liquid jet penetrating high speed gas stream investigated for amplification of capillary and acceleration waves [AIAA PAPER 67-495] 18 p3026 A67-33959

DISK

SA ACTUATOR DISK

SA LUNAR DISK

SA PLANETARY DISK

SA PLATE

SA ROTATING DISK

SA ROTOR DISK

Arbitrary profile disk design, taking into account temperature gradient, based on simultaneous solution of integral equations 03 p0429 A67-13331

Classical elasticity theory determination of computational error of fibrous body treated as simply connected multiple hole disks 05 p0907 A67-16037

Stressed and deformed state of plastic disk under cyclic loading in variable temperature field, using increments method 05 p0810 A67-16178

Temperature distribution, stress distribution and displacement components for circular disk when temperature distribution at disk rim is step function of time, considering inertial terms in thermoelasticity equations 08 p1418 A67-20723

Stress function boundary conditions along perfectly free edges of membrane-like disks and shells loaded by optionally distributed forces 11 p1881 A67-25096

Hydrodynamic boundary layer velocity profile on disks in transverse airflow analyzed theoretically and by wind tunnel tests 12 p1891 A67-25318

Rigid disk impact against ideal fluid surface in cylinder, deriving formula for impulse pressure at disk surface 12 p1928 A67-25669

Molecular spectra of sunspots and solar disk 13 p2203 A67-27428

Laminar boundary flow over dielectric disk with homogeneous magnetic field perpendicular to plane of disk, obtaining liquid velocity and electric field density 14 p2358 A67-28282

Impact stage of impacting jet amplifiers studied by interposing disk between two opposing coaxial jets, obtaining pressure gain 14 p2250 A67-28332

Stresses computation at surface of contact between disk and circular ring under influence of concentrated loads 15 p2577 A67-30186

Sun effective disk temperature from measurement of solar radiation during May 1966 eclipse 18 p3125 A67-34195

Stress analysis by polar coordinate system of turbine disks produced in various wound-fiber configuration 19 p3234 A67-34873

Near IR grating spectrometer converted to multiplex instrument by adding encoding disk in spectrum plane 20 p3437 A67-36339

Astroloy /Ni base superalloy/ disks for jet engine application, discussing chemical composition, basic ingot structure, forging and heat treatment 22 p3818 A67-39226

DISLOCATION

SA CRYSTAL DISLOCATION

SA DISPLACEMENT

SA EDGE DISLOCATION

SA SCREW DISLOCATION

Indium antimonide specimens plastically bent to introduce excess of dislocations, examining dependence of lower yield stress for bending on direction of bend 03 p0498 A67-13870

Friction stress acting upon moving dislocation derived from microstrain studies 09 p1518 A67-22020

Bubble raft analog for analyzing short range repulsive forces at small strains that govern fractures 16 p2768 A67-31279

Infinitesimal dislocation theory applied to materials with cracks and cylindrical hole, straight boundary between bonded materials and cylindrical insert subject to antiplane shearing stress 23 p4078 A67-41165

DISPERSION

SA MAGNETIC DISPERSION
SA PLASMA DISPERSION

Approximation method for deriving expressions for small angle polydispersed indicatrix of gamma distribution of particles in light field 01 p0107 A67-10125

Thermogravimetric analysis and electron microscopy of agglomeration and chemical instability of submicron refractory dispersoids in tungsten 01 p0097 A67-10699

Nonlinear dispersive wave propagation analyzed by linearization, obtaining solution as Fourier Integral through differential equation 01 p0024 A67-10737

Frequency dependences of amplification index of linear amplifier at 3.39 micron wavelength for various excitation levels 02 p0191 A67-11576

Karmers-Kronig dispersion relationship for simultaneous determination of index and thickness of thin metallic film 02 p0289 A67-11726

Computational method for determination corridors of launch vehicle trajectory and impact dispersions [AIAA PAPER 66-483] 02 p0325 A67-11941

Equations for one-dimensional model of macroscopically homogeneous linearly elastic medium of complex structure with spatial dispersion 02 p0337 A67-11952

Dispersion equation for interaction of helical flux of relativistic electrons with wave field of rectangular guide 03 p0367 A67-13089

Ruby laser generation from two R lines by prismatic light dispersion in resonator 03 p0433 A67-13095

Perturbation theory analysis of spatial dispersion effects on frequency addition in crystals 03 p0434 A67-13125

Dispersion of refractive index of NO in fundamental vibration-rotation band 03 p0468 A67-13473

Relative dispersion of particle pairs in homogeneous turbulence using Lagrangian-history direct interaction closure approximation for convected scalar field, obtaining Richardson diffusion equation 03 p0405 A67-14031

Complex roots of dispersion relations involving transcendental analytic functions 03 p0486 A67-14056

Dispersion formula for waveguide irises with rounded inner edges 04 p0579 A67-14415

Lumped electric circuit device producing dispersion for pulse compression system noting design 04 p0574 A67-15054

Dispersive network of apparatus producing dispersion in pulse compression system, noting role of relatively low center frequency 04 p0574 A67-15055

Piezoelectric grating /PEG/ dispersive device using ultrasonic propagation in prismatic quartz block 04 p0574 A67-15056

Fluctuation-dissipative ratio between correlation functions of fluctuating parameters and dissipative properties in thermodynamic-nonequilibrium systems with spatial dispersion 04 p0673 A67-15968

Direct measurement of dispersion properties of cadmium sulfide and CdS-CdSe crystals, using Obreimov-Fresnel diffraction method, growing crystals by synthesis 05 p0861 A67-16396

Self-focusing due to intensity dependent anomalous dispersion effect on electromagnetic radiation, emphasizing laser radiation in saturated amplifying medium 05 p0819 A67-16649

Optical constants of Ge in XUV verified using Kronig-Kramers dispersion relation, optical oscillator strength sum rule, correlation methods and electron energy loss distribution 05 p0864 A67-16784

Hot electron emission from polar semiconductors with nonparabolic dispersion law, specifically qualitative effect of nonparabolicity and field on electron emission 06 p1052 A67-18423

Concentration effect on light absorption and dispersion by impurity centers in case of weak electron-phonon coupling 07 p1233 A67-19648

COTIR wind weighting technique to reduce impact dispersion of sounding rockets 08 p1313 A67-20541

Prisms for dispersion compensation and single plane diffraction grating as correcting element for achromatizing white light reconstruction of two-beam surface

hologram 09 p1492 A67-21567

Eddy coefficients for diffusion and turbulence parameters for dispersion of vapor clouds in lower thermosphere from vapor trail evidence 10 p1646 A67-23272

Rectangular terminal block in rectangular waveguide and dispersion equation for surface wave propagating along waveguide 10 p1613 A67-23445

Dispersion and damping characteristics due to flexural vibrations in elastic plate with viscoelastic coating, obtaining energy loss resulting from dissipation [ASME PAPER 66-WA/APM-20] 10 p1731 A67-23841

Dispersed-phase alloy production noting structure types, deformation and fracture behavior at various temperatures 11 p1807 A67-24636

Linear waves in weakly ionized multicomponent plasmas investigated using dispersion relation 13 p2172 A67-27728

Four-plate compensators of Jamin and Lowe type for interferometers, emphasizing linear dependence of phase difference on dispersion and rotation angle 14 p2315 A67-28074

Statistical dispersion methods for identification of nonlinear controlled plants 15 p2462 A67-30324

Magnetohydrodynamic wave dispersion theory at open end of semilinear plasma waveguide closed by conducting diaphragm 16 p2722 A67-31574

Dispersion of longitudinal or extensional waves in isotropic linear elastic bars with rectangular cross section [ASME PAPER 67-APM-17] 17 p2964 A67-33148

Equations for one-dimensional model of macroscopically homogeneous linearly elastic medium of complex structure with spatial dispersion 17 p2965 A67-33269

COTIR wind weighting technique to reduce impact dispersion of sounding rockets 19 p3207 A67-34837

Roll-rate reversal dispersion effects of ballistic reentry body due to mass and aerodynamic asymmetries 22 p3742 A67-40117

EM radiation reflection, absorption and transmission through dielectric medium measured, studying other aspects by electric dipole oscillator model 23 p4037 A67-40757

DISPERSION HARDENING

Strength of cobalt alloys at elevated temperatures improved by dispersion of submicron thorium particles 01 p0093 A67-10517

Nickel-thorium powder produced by pressure hydrometallurgy techniques and dispersion-strengthened by compaction and rolling, noting tensile stress-rupture properties revealed by optical and electron microscopy 01 p0097 A67-10698

X-ray diffraction-Fourier series analysis and electron microscopy analysis of annealing effects on structural properties of cold worked dispersion-strengthened alloys 01 p0097 A67-10698

Dispersion-strengthening by formation of carbides of Hf, Zr, Ta, Ti and Nb in wrought and recrystallized Cr, discussing structural stability 01 p0100 A67-10766

High temperature hardening and creation of highly heat resistant alloys of refractory metals 05 p0831 A67-17501

Electron microscopy analysis of dissolved hydrogen induced fracture in room temperature cantilever bend fatigue testing of dispersion strengthened aluminum-aluminum oxide alloy 06 p1013 A67-17796

Oxide dispersion hardening of intermetallic NiAl and FeAl compounds for improved high temperature strength 06 p1014 A67-17803

Heat resistance in air of dispersion hardened nickel alloys containing certain oxides prepared by powder metallurgy methods 14 p2336 A67-27867

High temperature superalloys for gas turbine applications noting alloys based on cobalt, iron, nickel and dispersion hardening 16 p2686 A67-30487

Niobium alloys under annealing and aging analyzed, noting formation of oxide, nitride and carbide phases followed by coagulation and brittleness 16 p2687 A67-30844

High temperature hardening and creation of highly heat resistant alloys of refractory metals 21 p3643 A67-38028

DISPLACEMENT

SA DISLOCATION

- Statistical methods for evaluating displacement in increasing number of fasteners depending on nominal sizes and tolerances of fasteners and pairs of holes 02 p0336 A67-11776
- Neutron collision cross section and calculation of energy loss of displaced Si atoms to ionization 03 p0494 A67-13481
- Stresses in infinitely long strip of finite width containing semiinfinite crack calculated for displaced clamped boundaries, using Wiener-Hopf technique 04 p0718 A67-15923
- Slip and change in displacement vector in elastoplastic boundary value problems 05 p0918 A67-16424
- Dynamic displacements of thin spherical shell buckling under uniform pressure 05 p0920 A67-16825
- Differential residual displacements of Fraunhofer lines in solar spectrum 05 p0901 A67-17116
- Displacement formulations of first order linear thin elastic shell equations in terms of stress resultant and middle surface, using modified Kirchhoff hypothesis 08 p1417 A67-20551
- Consistent difference equations for displacement components in thin elastic disk of variable thickness subjected to given body forces and edge tractions for various coordinate directions 09 p1573 A67-21755
- Reciprocal theorem applied to linear and angular displacements due to creep or plastic strains in inelastic bodies 14 p2398 A67-28097
- Axially symmetric wave propagation in infinitely long two-layered cylinder, detailing displacement and stress distribution 17 p2961 A67-32778
- Permanent displacement-induced effects in silicon semiconductor devices as function of radiation type and energy 17 p2917 A67-32847
- Elastic plates linear theories for micropolar and director displacements, deriving plate equations by asymptotic expansion method 17 p2966 A67-33349
- Mean values of characteristic temperatures and dynamic displacements of ions for lattice of solid substitution solutions of zinc telluride-cadmium telluride system 18 p3095 A67-33446
- Implications and ramifications of theory of cutouts in displacement method 19 p3343 A67-35771
- Circumferential displacement and shearing stresses in out-of-plane elasticity problem for solid torus 20 p3538 A67-36672
- Displacement effects analyzed for one beam of laser streak interferometer relative to another on image intensity distribution 22 p3795 A67-39199
- ## DISPLAY
- ### S RADAR DISPLAY
- ### S VISUAL DISPLAY
- ## DISPLAY SYSTEM
- ### SA IMAGE
- Deflection-modulation display method analyzed for presenting video signals 01 p0061 A67-10018
- Digital-graphic computer terminals effect on data processing equipment design, noting CRT use 01 p0029 A67-10669
- Reactive display system for optimum man/computer communication with time-sharing capabilities 01 p0029 A67-10670
- Digitally-driven display system for graphic man-computer communication in aerospace industry 01 p0029 A67-10671
- Computer display and control system for launch vehicle test operation 01 p0050 A67-10672
- Visual or environmental factors which affect usefulness of training simulator experimentally studied, examining problems of measuring transfer of training 02 p0186 A67-12072
- Problem solving under sequential and batch display conditions, noting effects of data density 02 p0186 A67-12231
- Display method for investigating disturbance and wave propagation in discharge plasma 02 p0247 A67-12687
- All-weather landing system for C-141 jet cargo transport using vertical navigation computer for military operations 03 p0464 A67-12907
- Optimization of display configurations for group viewing 03 p0365 A67-13299
- Command and control display system requirements noting dependence on human visual mechanism 03 p0365 A67-13300
- Shared memory computer display system provides test bed for man-machine interaction, noting hardware and software design concepts 03 p0375 A67-13633
- Human engineering aspects of design of future military high performance aircraft, noting automatic control and display system requirements 04 p0562 A67-14535
- Method for piloting aircraft along prescribed paths, particularly for manually controlled complete instrument landings 04 p0550 A67-14548
- Simulator program which uses modified head-up display unit from British Buccaneer aircraft 04 p0653 A67-14882
- Radar data handling and display systems used with pulsed radars, detailing military type for use of weapons control officer 04 p0578 A67-15057
- Terminal configuration with alphanumeric display and center-metrolplex equipment for automation implementation in radar tracking data for expanding ATC 04 p0654 A67-15061
- Flight simulation techniques covering digital computers, visual simulation and displays [ASME PAPER 66-WA/AV-1] 04 p0599 A67-15394
- Navigation functional display requirements associated with early manned lunar exploration vehicles 04 p0655 A67-15862
- System display composition, discussing analog and digital indicators, equipment operation functions and testing 04 p0626 A67-15736
- Society for Information Display, Symposium, Boston, October 1966 05 p0804 A67-16305
- Thermochromic materials application in display devices 05 p0860 A67-16307
- Digital computer driven electroluminescent solid state vertical scale indicator design, development and fabrication emphasizing size, weight, power, reliability and display readability 05 p0805 A67-16310
- Information display for weather forecasters 05 p0836 A67-16311
- Solid state diode matrix display using gallium phosphide light sources to investigate use as data recording device 05 p0771 A67-16313
- Programmable display synthesizing system for man-machine communications research based on electronic animation technique 05 p0786 A67-16314
- Direct digital display with high precision for audio frequencies 05 p0865 A67-16944
- Spacecraft extravehicular control and display system 05 p0788 A67-16968
- Data display for Real Time Telemetry Data System/RTTDS/ 05 p0765 A67-17042
- Applications of computer generated displays, technologies and systems design in man-machine interaction 05 p0769 A67-17520
- Electronic display in flight instrumentation, with reference to integrated flight system, qualitative and quantitative displays and qualitative-quantitative combinations 06 p1000 A67-17598
- Integrated film reading and display system, discussing characteristics of waveform display/ analyzer subsystems and scanning/recording requirements 07 p1148 A67-19742
- Computer logic cost effectiveness modeling applied to integrated circuits, discussing comparisons between existing equipment, Conalag and redesigns 08 p1311 A67-20657
- Digital data processing, transfer and display equipment applied to ATC terminal operations, using surveillance radars and radar beacons 08 p1351 A67-20677
- All-digital real time display system for ground monitoring of manned space flight including computers, software, output devices, etc 09 p1483 A67-21677
- Laser sources emphasizing TV display output power needs 09 p1515 A67-22362
- Landing task and pilot acceptance of displays for landing in reduced weather minimums [AIAA PAPER 65-722] 09 p1457 A67-22493
- Scan-converted bright displays for air traffic control systems 09 p1528 A67-22635
- Visual presentation of data required for ATC task, noting possible traffic display and attributes 09 p1529 A67-22646
- Secondary surveillance radar system design, discussing interrogator interference, decoding and display systems 09 p1530 A67-22648
- Two electronic displays for aircraft using basic elements necessary for flight path control in problem of easy assimilation of information by pilot 10 p1601 A67-22905
- Transducers, transmission systems and display and implementation systems of radio telemetry and effect upon measurement 10 p1605 A67-22997
- Airport traffic control tower instrument panel displaying continuously telemetered data on current weather conditions of runway complex 10 p1656 A67-23087
- Enlarged internal laser beam projecting high contrast images generated on photochromic plate within laser cavity 11 p1801 A67-24717
- X-ray sensitive TV system with image enlargement for nondestructive testing [SAE PAPER 670362] 12 p1950 A67-25882
- Oscilloscope plotting of Langmuir probe and double probe characteristics corresponding to time varying plasma properties 12 p1947 A67-26122
- Phaseplot, on-line graphical output parametric display technique, noting hardware realizations and software requirements 13 p2073 A67-27063
- Computer graphic aids with applications of graph plotters, trace analyzers, cathode ray tubes, light pens, etc 13 p2073 A67-27188
- Piloted flight simulator studies influence on design of SST instruments, discussing pitch indicator, landing and sonic boom limitation display systems 13 p2154 A67-27269
- SST ground and flight personnel training program for system operation, discussing expected role of piloted flight simulator 13 p2091 A67-27270
- Simulator design, discussing control information category and presenting representative fixed and moving base research simulators to describe display design and motion cue effects 13 p2091 A67-27271
- Human factors in air traffic control displays 13 p2064 A67-27563
- Medical factors involving ATC information displays 13 p2064 A67-27564
- PSIN /P region, Seminsulating region, N region/ diode array fabrication, performance, characteristics and applications 14 p2282 A67-28029
- Panel layout for rectilinear instruments 14 p2257 A67-28661
- Peripheral vision displays for dynamic tracking information during difficult flight control tasks improve operator performance 14 p2258 A67-28663
- Control-display association preferences for concentric controls 14 p2258 A67-28665
- Independent effects of error magnification and field of view on compensatory tracking performance, analyzing display and optical magnification 14 p2258 A67-28667
- CRT display provided by integrated circuit indicator packing circuitry in single plug-in module, noting timing, sweep, generation, etc 14 p2288 A67-28769
- On-line nonlinear circuit design, discussing computer program for evaluating performance resulting from modifications 15 p2442 A67-29169
- Large screen displays for group interaction simulation noting cost factors, techniques and performance 15 p2486 A67-29302
- CRT design factors for optimum tube design for display systems 15 p2447 A67-29735
- Display/control system of Mission Control Center, Houston, operation and performance 15 p2467 A67-29736
- Visual analysis console for automatic information handling systems providing rapid data display and operator communications with high speed digital computers 15 p2488 A67-29737
- Radar display layout for aircraft safety consisting of digital computer and CRT 15 p2468 A67-30129
- Air traffic control operations forecasting, stressing proposed STOL and VTOL port [AIAA PAPER 67-398] 15 p2515 A67-30365
- Instrument-landing displays evaluated in IFR landing approaches with helicopter, noting flight performance and pilot evaluation of display concepts [AHS PAPER 106] 16 p2680 A67-31823
- Systems recommended to meet area

navigation requirements, considering pictorial display/ course line computer /PD/CLD/ application 17 p2881 A67-32391

Raster scan parameters influencing target identification in image recognition experiments using video display 17 p2859 A67-32508

Integrated electronic display for V/STOL flight evaluated, considering vehicle dynamics, handling qualities, etc., and presenting performance data 17 p2861 A67-33182

Systems engineering in computer-driven CRT displays for man-machine communication, emphasising hardware-software tradeoffs and communication-transmission factors systems engineering in computer-driven CRT 18 p3005 A67-33499

Electron image manipulation and charge-image storage perform equivalent of incoherent optical-image transformation 18 p3047 A67-33881

Control display linkages tested with human subjects for response time 18 p2993 A67-34338

Evoked potential display procedures yielding photographic superposition of large number of average responses 19 p3179 A67-34955

Color radar signal parameters display system using techniques based on mathematical application of Venn-Euler diagrams 19 p3231 A67-35624

Design of time-shared multiformat display medium to improve guidance and control displays in manned spacecraft [AIAA PAPER 67-552] 19 p3257 A67-35949

Graphical display technique for complex curve display, discussing system components, experimental results and relevant software 19 p3188 A67-36059

Time-sharing system with single central processing unit and several graphic display consoles for single high speed computer among human operators 19 p3188 A67-36060

Book on fundamentals of display systems covering cathode ray tubes, color techniques, photographic and electromechanical systems, etc 20 p3435 A67-36135

Computer based CRT display technique for servo system testing, discussing Saturn V display computer and simulation studies results 20 p3415 A67-36609

High precision CRT display system using raster beam positioning and computer-generated digital video 20 p3447 A67-36807

Predictor display instrument for optimal manual control, noting use in manned spacecraft missions and time factor 20 p3447 A67-36840

Sensors and display systems covering fiber optics, sensing of parameters for built-in equipment and passive monitors, passive chemical vapor/gas detection, etc 20 p3449 A67-36980

Nondestructive testing of electronic circuits with fiber optic scintillators, vidicon data sampling and pattern recognition displays, discussing TV data handling 20 p3449 A67-36982

Recording and display programs illustrating relative capabilities of thermoplastic and direct electron beam on photographic film recording 20 p3449 A67-36984

Three-dimensional projections on cathode ray tube screens noting visual transformations linking retinal image to space scene 20 p3450 A67-36985

Contour-volumetric displays for processing and handling data in nuclear experiment 20 p3450 A67-36986

Devices for information exchange between man and machine, emphasizing video display equipment 21 p3577 A67-38158

Diode function generator for empirical functions representation 22 p3775 A67-40562

Application of IBM 9020 multiprocessing system to air traffic control 23 p3976 A67-41060

Scanning laser device using modified electro-optic display tube and potassium phosphate crystal mode selector 23 p4017 A67-41393

Johnson touch display for updating flight data combining visual display and keyboard functions 24 p4152 A67-41780

Installation problems of head-up displays in commercial aircraft 24 p4152 A67-41896

Internal light applied to opaque-faced

edge-lighted plastic display panels [SAE PAPER 670196] 24 p4097 A67-41986

Multidimensional data stereoscopic graphic display principles, viewing and use in engineering design 24 p4157 A67-42434

AGM-69A program-management system using CRT display for PERT/Time and Cost Control data translation [AIAA PAPER 67-920] 24 p4260 A67-43019

DISSOCIATION

SA ELECTROLYSIS

SA GAS DISSOCIATION

SA MOLECULAR DISSOCIATION

SA PHOTODISSOCIATION

SA THERMAL DISSOCIATION

Decomposition rates of hydrogen halides examined behind incident shock waves between 2800 to 4600 degrees K, using IR techniques 11 p1750 A67-24995

Riometric data on ionospheric absorption applied to determination of dissociative recombination coefficient, noting atmospheric ionization by fragment gamma-radiation 14 p2306 A67-27858

Expulsion of ions from comets toward sun examined for source, dissociation and ionization of parent particles, velocity, etc 16 p2746 A67-30979

Nocturnal recombination processes in ionospheric F region for nitrogen and oxygen based on 5200 and 6300 angstrom lines 18 p3040 A67-33693

Bacillus brevis var. G-B survival ratio dependence on space flight factors, noting no induction of dissociation products nor appearance of auxotrophic mutants 21 p3577 A67-38597

DISTANCE

S MISS-DISTANCE

S RANGE

DISTANCE MEASURING EQUIPMENT

Integrated Trajectory System, measuring spatial positions, velocities, accelerations and scalar and vector miss distances for targets 04 p0654 A67-15045

In-flight instrumentation for prompt miss distance measurement using gamma ray techniques 05 p0841 A67-16533

Error due to multiple propagation in distance measurement by comparison of modulation phases on transmitted and reflected laser beam 07 p1186 A67-19606

Calculation method for energetic photoelectric photometry system for tracing behind radiative source or for distance measurement 08 p1331 A67-21055

Laser Interferometer for precise measurement of long distances, noting function and industrial use 09 p1499 A67-22149

UHF distance measuring equipment /DME/ using new type of ground beacon and only thermionic devices in transmitter power stage 09 p1530 A67-22650

Principles, methods of operation, techniques and limitations of phase comparison position-determining CW and pulse type systems 10 p1605 A67-22996

Aircraft UHF radio system for distance measurements between airplane and two ground stations, noting onboard antenna 11 p1793 A67-24863

MSQ-1 radar system for rocket tracking used to measure distance, elevation and azimuth during May 20, 1966 solar eclipse 15 p2467 A67-29574

Modular distance measurement using geometric model for electronic continuous wave distance measuring equipment 15 p2511 A67-29893

Changes in length measured by tandem laser device investigating mirror separation modulation by piezoelectric materials 16 p2671 A67-30823

Laser measurements of long distances using laser interferometers, modulated laser beams and laser radar 17 p2867 A67-32613

Earth to lunar ground points measurement by lasers, describing experimental set-up, transmitting and receiving apparatus, etc 18 p3130 A67-34316

Interferometer standing on L-shaped base for velocity and distance measurements, noting tests on aircraft and rockets and solar reflections effect 21 p3599 A67-38643

Coherent responder used in distance Doppler tracking system, obtaining radial distance by using phase compression 21 p3656 A67-38650

Calculation method for energetic photoelectric photometry system for tracing

behind radiative source or for distance measurement 22 p3797 A67-39417

Moon-earth distance and moon-earth system astrometric parameters by laser ranging, describing artificial light reflector design 23 p4066 A67-41037

Performance limits of laser rangefinder for design of all-weather terrestrial rangefinder, discussing echo signal, backscatter noise and TPG 23 p3999 A67-41040

DISTANCE PERCEPTION

S DEPTH PERCEPTION

S PERSPECTIVE

DISTILLATION APPARATUS

Distillation process in spherical pyranometer studied for time constants and sensitivity in calibration until reaching balanced state 21 p3627 A67-38445

DISTORTION

SA DEFORMATION

SA FLOW DISTORTION

SA SIGNAL DISTORTION

SA SURFACE DISTORTION

Cosmological distortion effect incorporating incident magnetic type gravitational field parameter upper limits measured from galactic cluster photographs 11 p1860 A67-24484

Nonuniformity of mm wave detected by wideband frequency sweep control backward wave oscillator 16 p2643 A67-30896

DISTRIBUTION

S AMPLITUDE DISTRIBUTION

ANALYZER

S ANGULAR DISTRIBUTION

S BOLTZMANN DISTRIBUTION

S CHARGE DISTRIBUTION

S CURRENT DISTRIBUTION

S DENSITY DISTRIBUTION

S ELECTRON DISTRIBUTION

S ENERGY DISTRIBUTION

S FLOW DISTRIBUTION

S FORCE DISTRIBUTION

S FREQUENCY DISTRIBUTION

S GAUSSIAN DISTRIBUTION

S HOLE DISTRIBUTION

S ION DISTRIBUTION

S LIFT DISTRIBUTION

S LOAD DISTRIBUTION

S MASS DISTRIBUTION

S MAXWELL DISTRIBUTION

S MOMENT DISTRIBUTION

S NEUTRON DISTRIBUTION

S NORMAL DISTRIBUTION

S PATTERN DISTRIBUTION

S POISSON DISTRIBUTION

S PRESSURE DISTRIBUTION

S PROBABILITY DISTRIBUTION

S RADIAL DISTRIBUTION

S RADIATION DISTRIBUTION

S RANDOM DISTRIBUTION

S RAYLEIGH DISTRIBUTION

S SPATIAL DISTRIBUTION

S SPECTRAL ENERGY DISTRIBUTION

S STRESS DISTRIBUTION

S STRESS-STRAIN DISTRIBUTION

S TEMPERATURE DISTRIBUTION

S VELOCITY DISTRIBUTION

S VERTICAL DISTRIBUTION

S WALL TEMPERATURE DISTRIBUTION

S WEIBULL DISTRIBUTION

DISTRIBUTION FUNCTION

SA CHAPMAN-ENSKOG METHOD

Approximation method for deriving expressions for small angle polydispersed indicatrix of gamma distribution of particles in light field 01 p0107 A67-10125

Electronic and molecular radial distribution functions for liquid carbon tetrafluoride using X-ray diffraction, determining orientational effects of carbon tetrachloride and temperature dependency 01 p0117 A67-10885

Optical scattering cross sections for polydispersions of dielectric spheres, showing dependence on ratio of third to second moment of shape and size distribution function 01 p0115 A67-11077

Improved Monte Carlo method for calculating steady state monatomic rarefied-gas flows, using computer for calculating possibility of collision in given geometrical cell 01 p0055 A67-11292

Distribution of maintenance manhour intervals for tasks on military aircraft compared with logarithmic normal distribution, presenting histograms and cumulative distributions 01 p0171 A67-11382

Red shifts and colors correlated for quasars leading to smoothed mean energy

distribution and new values for
K-correction 02 p0322 A67-11686
Distribution function and electron mobility
in polar semiconductors for nonparabolic
dispersion law 02 p0296 A67-11825
Structure of shock wave in monatomic gas
analysis using orthogonal polynomial solution
of Boltzmann equation, noting Mott-Smith
distribution function 02 p0234 A67-12541
Shock wave structure in binary mixture,
using Mott-Smith distribution postulating
flow velocity and temperature of subsonic
mode as position 02 p0234 A67-12542
functions
Three-dimensional eigenmodes for
collisionless electronic Vlasov plasma
imbedded in magnetic field in electrostatic
approximation, noting plasma
stability 02 p0275 A67-12553
Ion mobility in gas formed by ions,
defining gas temperature, obtaining solution
of kinetic equation for ion distribution
function 02 p0270 A67-12625
Quasi-linear approximation of Cerenkov
and cyclotron damping of electromagnetic
waves in magnetoactive plasma, considering
collisions of wave-absorbing resonance
particles with plasma 03 p0475 A67-12934
Instability of nonlinear stationary
oscillations of potential in electron-ion flows
useful in distribution functions of ions and
electrons 03 p0470 A67-12935
Algorithm for directed random search for
minimum of function of
n-variables 03 p0374 A67-13182
Asymptotic behavior of distribution of
maximum for class of processes with
independent increments 03 p0458 A67-13340
Size distribution of electron avalanches in
methane gas under electric field no longer
satisfy Furry distribution due to first
Townsend ionization 03 p0473 A67-13463
Instrument methods determining function
and density of length distribution of random
radio emissions 03 p0369 A67-13586
Distribution function for temperature of
interstellar H-I clouds from exact statistics
of cloud collisions and quantitative
treatment of cooling mechanisms 04 p0694 A67-14471
Axiomatic formulation for stationary point
processes interpreted as ordered sequences
of points randomly located on real line,
noting relation to set
theory 04 p0643 A67-14521
Probability density and distribution
function of random function threshold
overshooting 04 p0657 A67-14888
Two-dimensional characteristic function
and probability-distribution density of
random process which is phase modulated
by normal noise 04 p0575 A67-15161
Partially ionized two-temperature plasma,
deriving distribution function of first
approximation associated with
viscosity 04 p0668 A67-15186
Convective excitation of ionic oscillations
in plasma by inhomogeneous electron beam
as result of spatial gradient of distribution
function 04 p0668 A67-15270
Conductance theory for electrolytes and
weakly ionized plasmas using pair
distribution function in space in presence of
short range forces 04 p0670 A67-15578
Pair distribution function and conductance
for symmetrical electrolytes up to all
powers of Bjerrum parameter, using Debye
screening to eliminate long range
divergence 04 p0670 A67-15579
Vacuum UV photolysis of solid ethane
films, measuring product distributions,
presenting evidence for quenching of
excited ethane and
ethylene 05 p0758 A67-16128
Molecular pair distribution function in
perfect crystalline solids, using method
based on cell cluster
theory 05 p0758 A67-16129
Shear relaxation in liquids, criticizing
Knollman, Miles and Hamamoto relaxation
time distribution measurement
method 05 p0758 A67-16133
Output probability density distribution of
stationary random noise containing regular
signal components after mean squaring
circuit 05 p0783 A67-16446
Quasi-linear relaxation in unsteady states
of noncollision plasma, noting electron beam
distribution function and Langmuir plasma

oscillations 05 p0852 A67-16696
Short and long range redistribution of
solute in weld fusion zones of alloy systems
through data from electron microprobe
analyses 05 p0811 A67-16830
Generalization of kinetic theory of gases,
deriving Boltzmann kinetic equation for use
in singly-partial distribution
function 05 p0849 A67-17021
Statistical properties of amplitude and
phase of output signal of electron beam
quadrupole amplifier with superposition of
regular signal plus Gaussian noise at
input 05 p0765 A67-17162
Size distribution of lunar craters from
Ranger pictures show that frequency of
crater occurrence is inversely proportional
to square of diameter 05 p0903 A67-17293
Fielder analysis on diameter frequency
and distribution of centers and number
density of lunar craters 05 p0903 A67-17295
Distribution function for probability
density of random process at output of
multiplier acted upon by envelopes
consisting of Gaussian noise and pulse
signal 05 p0767 A67-17397
Molecular fluxes in lunar atmosphere
relationship to gas source distribution,
surface temperature and gas emission
laws 05 p0904 A67-17404
Solution to chain of kinetic gas equations,
showing effect of fast reversible and slow
irreversible processes on particle
distribution function 05 p0847 A67-17541
Probability estimation, discussing types,
Bayesian method for binomial and
multinomial distributions, sampling methods,
etc 06 p1022 A67-17646
Dead time corrections to photocount
distributions using time interval probability
density of counts, noting application to laser
light 06 p1009 A67-17652
Iterative computation of a posteriori
probability for M-ary nonsupervised
adaptation 06 p0965 A67-17947
Histogram construction via algebraic
Monte Carlo method, determining
simultaneous effect of several input
statistical variables on output variable
[AIAA PAPER 67-210] 06 p1024 A67-18326
Hot electron emission from polar
semiconductors with nonparabolic dispersion
law, specifically qualitative effect of
nonparabolicity and field on electron
emission 06 p1052 A67-18423
Charged particles motion in magnetic field
with regular and random components,
deriving kinetic equation for distribution
function and then diffusion
equation 06 p1037 A67-18800
Optical phonons role in determining form
of free carrier distribution function in
semiconductors and nonohmic behavior of
strongly piezoelectric
crystals 06 p1065 A67-18952
Contact effects in degenerate
semiconductors at low temperature based on
Hall study of tunnel
junctions 06 p1069 A67-18976
WKB approximation of quantum radial
distribution function for neon intermolecular
pair potential taking into account particle
exchange effect 06 p1038 A67-19044
Velocity distribution function relaxation
and runaway of electrons in weakly ionized
plasmas 07 p1228 A67-19510
Plasma instabilities induced by charge
convection across perturbing electric field
and magnetic field 07 p1228 A67-19511
Energy distribution function in cathode
drop space of glow discharges in hydrogen
derived by numerical integration of
simplified Boltzmann
equations 07 p1229 A67-19516
Distribution function of modulus of
directivity characteristic of antenna grid
shown as modified Rayleigh
distribution 07 p1143 A67-19596
Scattering in semiconductors, calculating
collision term in Boltzmann equation for
acoustic modes and differential collision
operator for isotropic part of distribution
function 07 p1237 A67-20180
Nonhomogeneous Helmholtz equation for
optical gratings with perfectly conducting
boundaries solved, using distribution
theory 08 p1353 A67-20349
Field intensities and electron distribution
function in hollow cathode, graphs show
potential distribution along cathode
axis 08 p1358 A67-20851

Dispersion equation for whistler mode for
velocity distribution with loss cone,
discussing critical
stability 08 p1324 A67-20894
Lunar cratering statistics interpretation in
terms of meteoroid impact hypothesis,
noting equilibrium distribution function
[AAS PAPER 66-183] 08 p1387 A67-20958
Particle loss through axisymmetric cusped
magnetic field containment geometry,
deriving adiabatic invariant for collisionless
plasma 08 p1361 A67-21133
Time varying weight functions effect on
convergence of polynomial expansions of
isotropic distribution
functions 08 p1323 A67-21385
Toroidal plasma containment, noting
equilibrium theory consistency with first
order orbit theory 08 p1364 A67-21395
Generalized Gaussian distribution
functional for weak plasma turbulence
neglecting three-point correlation
function 08 p1366 A67-21415
Comparison of distribution functions from
reduced data records for scattering of
electromagnetic waves by randomly moving
spheres in container 09 p1461 A67-21598
Stochastic approximation method for
determining real number from observation
of random variables 09 p1524 A67-21933
Gardenhose instability for ultrarelativistic
plasma in magnetic field, showing that
instability criterion for particular non-
Maxwellian distribution function is not
met 09 p1546 A67-22229
Cosmic ray distribution, discussing method
of diurnal variations, zonal harmonics and
spherical analysis 10 p1698 A67-22778
Rarefied gas flow analyzed through
transport equation in gas kinetics using
bimodal two-stream distribution functions,
with application to Couette
flow 10 p1624 A67-22914
Asymptotic properties of solutions to
kinetic coefficient equation system, noting
mass velocity dependence on
time 10 p1625 A67-23042
Vlasov equation for stationary distribution
function of charged particles in plasma and
self-consistent solution of Maxwell
equations 10 p1685 A67-23463
First integrals of motion to determine
stationary distribution function of charged
particles and self-consistent magnetic field
of plasma 10 p1685 A67-23464
Impurity distribution in GaAs noting
growth rate, concentration and
crystallographic
orientation 10 p1693 A67-23515
Source function, distribution function,
damping constant, etc, determined from high
resolution Fraunhofer line profiles in solar
or stellar spectra 10 p1711 A67-23797
Radial distribution function differential
equation solution studied numerically and
analytically for plasma parameters, using
closure approximation 11 p1826 A67-23871
Toroidal machine velocity space
instabilities, rapidly saturating, with long
time scale remaining
relaxation 11 p1826 A67-23876
Shock wave structure theory using Navier-
Stokes character of shock wings and
measured thickness, noting dependence on
number density 11 p1775 A67-23879
Relaxation in space of electron velocity
distribution due to electron-ion collisions,
obtaining time independent
solution 11 p1833 A67-24372
Potential distribution in emitter diode
measured in single ended Q machine, using
ribbon electron beam 11 p1764 A67-24373
RF energy absorption by plasma column
surrounded by periodic coupling structure,
noting similarities with Landau damping and
measurements of non-Maxwellian
distributions 11 p1838 A67-24402
Electrostatic separation probe to measure
electronic velocity distribution function,
showing evolution of distribution function
relationship to plasma oscillation
growth 11 p1789 A67-24409
1/s line intensity distribution function for
molecular spectra representation using
growth curves calculated for Lorentz
lines 11 p1822 A67-24416
Transport coefficients for dense gases via
Bogolubov theory of two-particle
nonequilibrium distribution
function 11 p1823 A67-24538
Interaction of plasma oscillation with

electrons with positive distribution function, noting oscillation amplitude relation to function deformation 11 p1840 A67-24766

Time discretization method applied to determination of peak duration distribution of normal noise envelope 11 p1754 A67-24987

Calculations of plasma distributions and field configurations with particle containment and stability within particular framework 11 p1843 A67-24997

Dynamical irreversible evolution of gas with short range repulsive forces, using n-particle distribution function with many-body interactions 11 p1824 A67-25077

Nonequilibrium process in one dimension in presence of constant and oscillating electric field, using distribution function 11 p1824 A67-25078

Stress function boundary conditions along perfectly free edges of membrane-like disks and shells loaded by optionally distributed forces 11 p1881 A67-25096

Charged particle motion in magnetosphere under sudden magnetic pulse, compiling Fokker-Planck equation for particle distribution function 12 p1992 A67-25118

Moments of distribution function of perfect fluid calculated and used in studies of orthogonal polynomials on Minkowski hyperboloid 12 p1966 A67-25144

Electron and ion temperature difference necessary to develop instability connected with loss cone of plasma with hot electrons placed in magnetic mirror trap 12 p1971 A67-25334

Lateral distribution of radio emission flux of extensive air showers /EAS/ of cosmic rays 12 p1940 A67-25337

Plasma models and methods used to study wave propagation phenomena, considering particle orbit, single species moment equations, velocity distribution function, etc 12 p1975 A67-25527

Formation of Maxwell and non-Maxwell distribution in gases, noting reduction of time reversible to time irreversible equations 12 p1968 A67-26114

Linear Fokker-Planck collision operator expanded in terms of surface spherical harmonics, showing distribution function governed by differential-integral equations and eigenvalue spectrum 12 p1962 A67-26177

Discrete ordinate method for evaluating function described by particular integral applied to boundary value problems in gas kinetics 12 p1962 A67-26192

Relaxation effects in initially non-Maxwellian high temperature theta pinch using Fokker-planck equation for particle velocity distribution function relaxation effects in initially non-Maxwellian 13 p2163 A67-26288

Relaxation time for spatially homogeneous electron gas calculated by direct numerical integration of linearized Fokker-Planck equation 13 p2164 A67-26297

Anomalous photovoltages in CdSe and CdS thin layers 13 p2175 A67-26429

Probability density functions for power from Rayleigh target 13 p2067 A67-26520

Reliability analysis of active, standby and active-standby redundant system, discussing Poisson-binomial probability distribution function 13 p2123 A67-26828

Diffusion phenomena of increasing mean free path with altitude in rarefied gas analyzed, incorporating gravitational field effect in Boltzmann equations 13 p2099 A67-26952

Nonequilibrium processes, analyzing required number of additional conditions and region of applicability of most probable distribution function, noting relation to Boltzmann equation 13 p2100 A67-26954

Generalized spatially uniform distribution functions for monatomic rarefied gas describing one-dimensional heat transfer in nonuniform flow 13 p2100 A67-26958

Two component equivalent of two-stream distribution function solution to plane Couette flow, studying nonlinear effects 13 p2101 A67-26965

Velocity distribution function of re-emitted molecules effect on slip flow boundary conditions 13 p2102 A67-26970

Orthogonal polynomial method to determine distribution function for equilibrium of single species two-temperature gas mixture 13 p2102 A67-26972

Boltzmann equation and statistical properties for two-dimensional gas, analyzing

integral iteration for shock wave flow 13 p2103 A67-26975

Distribution function structure in gas kinetic flows as given by BGK model in plane weak shock in monatomic gas 13 p2104 A67-26981

Distribution function and temperatures in monatomic gas under steady expansion into vacuum determined by integrating Bhatnagar-Gross-Krook /BGK/ model equation and moment equations respectively 13 p2104 A67-26982

Current density combination frequency derived for homogeneous magnetoplasma due to alternating electric fields, considering distribution function isotropic and anisotropic parts 13 p2187 A67-26994

Rarefied multicomponent gas flow boundary conditions over subliming wall determined through Navier-Stokes approximation, noting distribution function of each component 13 p2105 A67-27054

Carrier distribution function in degenerate p-type germanium in presence of hole scattering on acoustic phonons, considering heating in arbitrary electric and magnetic fields 13 p2181 A67-27281

Ion mobility in gas formed by ions, defining gas temperature, obtaining solution of kinetic equation for ion distribution function 13 p2161 A67-27381

Plane shock wave in ideal gas characterized by infinitesimally thin discontinuity, determining width and distribution function 13 p2105 A67-27412

Test method used in analysis of statistical distribution functions for fatigue strength response data of aluminum sheet 13 p2221 A67-27738

Integrals of motion-equations for charged particles in axisymmetric magnetic field derived using perturbation theory 14 p2353 A67-27752

Anisotropic velocity distribution function measurements in jet flows using electron beam fluorescence technique 14 p2300 A67-28181

Time of flight distribution measurement of weak molecular beam, noting limitations due to signal to noise ratio 14 p2316 A67-28185

Velocity distribution function measurement in rarefied gas flow, using principle based on time of flight of metastable molecules 14 p2316 A67-28193

Velocity distribution function of gas measured with laser, noting relation to frequency variation of absorption coefficient across spectral line 14 p2317 A67-28194

Pressure and temperature in orifice set in body located in free molecular flow, checking first moment of distribution function 14 p2302 A67-28198

Linearized Fokker-Planck kinetic equation, describing approach to equilibrium of test electrons injected into electron plasma in thermal equilibrium 14 p2356 A67-28203

Self-consistent distribution theory of charged particles and electric potential in wake of conducting body moving rapidly in rarefied plasma 14 p2357 A67-28208

Nonlinear harmonic generation in magnetoplasma using Boltzmann equation, noting sharp resonance peaks 14 p2358 A67-28236

Scattering function derivation using lunar limb occultation of solar disk during partial eclipse 14 p2386 A67-28475

Generalization of kinetic theory of gases, deriving Boltzmann kinetic equation for use in singly-partial distribution function 14 p2351 A67-28482

Eigenvalue distribution in random Hermitian matrices, considering self-adjoint operators in N dimensional unitary space 14 p2343 A67-28501

Doping distribution optimum for minimizing minority carrier transit time through base to improve overall HF performance of diodes and transistors 14 p2287 A67-28676

Total number and number of distinct particles in equilibrium system of recurrent Markov processes 14 p2345 A67-28907

Two-dimensional distribution of radio sources measured for random positioning using Poisson distribution function 14 p2393 A67-29026

Shock structure in diatomic gas described using Mott-Smith bimodal distribution function, including relaxation

effects 15 p2469 A67-29217

Solution for shock wave of bimodal distribution using Bhatnagar-Gross-Krook models, noting symmetry property destruction and recovery by using modified BGK model 15 p2470 A67-29226

Boundary conditions for Navier-Stokes equations in rarefied monatomic gas with distribution function given a priori 15 p2470 A67-29234

Two-dimensional characteristic function and probability-distribution density of random process which is phase modulated by normal noise 15 p2435 A67-29348

Statistical model for size effect in electrical conduction 15 p2517 A67-29485

Space-time distribution of heavy penetrating particles in extensive air showers, applying scale transformation properties of distribution to integration over primary particle spectrum 15 p2550 A67-29749

Measurement of position of polarization plane of radiation emitted by neodymium-glass laser 15 p2499 A67-29758

Emissive power of air measured by determining charged particle distribution behind spark discharge generating shock wave in plasma 15 p2530 A67-29861

Quasi-linear relaxation in unsteady states of noncollision plasma, noting electron beam distribution function and Langmuir plasma oscillations 15 p2530 A67-29867

Book on optimization of stochastic systems noting probability distribution functions, random variables, Bayesian optimization convergence, linear and nonlinear system estimation, etc 15 p2459 A67-30024

Randomly distributed initial energy input effect on unbounded rotating barotropic atmosphere, noting energy density function as initial condition 15 p2478 A67-30056

Dynamical and statistical approach to range safety problems, noting impact-density function of space vehicle destruction at early launch stage [AAS PAPER 67-45] 15 p2572 A67-30113

Evolutionary concept for mass transportation system [AIAA PAPER 67-381] 15 p2420 A67-30351

Collision integral for Landau plasma in strong magnetic field to obtain time evolution of one-particle distribution function 15 p2532 A67-30382

Thermal slip rate of gas near solid surface determined by measuring gas-flow distribution function according to Bhatnagar, Gross and Krook 15 p2582 A67-30390

Electron drift mobility and electron and ion temperatures difference in two-component plasma obtained from momentum and energy balance equations 16 p2706 A67-30450

Solution of Boltzmann and rate equations for electron distribution function and state populations in nonequilibrium MHD plasmas 16 p2710 A67-30519

One-dimensional probability distribution density of sum of pulsed and fluctuation noises 16 p2623 A67-31016

Heating of ions in current carrying nonisothermal plasma deriving noise spectral density and electron and ion distribution functions 16 p2715 A67-31047

Quasi-linear theory of plasma cyclotron instability, analyzing transverse oscillations propagating along external magnetic field 16 p2717 A67-31179

Plasma-particle distribution function in infinite system of alternating positive and negative electrodes, evaluating high-velocity neutron source effectiveness 16 p2718 A67-31193

Velocity distribution functions in statistical theory of turbulence, deriving moment equations and comparing properties with kinetic theory 16 p2660 A67-31220

Dispersion equation for stability of steady turbulent state obtained from perturbation theory and applied to drift cyclotron instability of plasma 16 p2719 A67-31230

Electron velocity distribution function obtained for partially ionized gas in weak, steady electric field by solving Boltzmann-Fokker-Planck equation 16 p2704 A67-31235

Ion mobility in gases determined, based on kinetic equation for ion velocity distribution function with particular reference to Chapman-Enskog method 16 p2704 A67-31250

Probability density and random distribution function derived from finite

- series for instantaneous voltage measurements of ideal multiplying device 16 p2653 A67-31718
- Electron velocity distribution function in nonequilibrium plasma having spatial distribution governed by electron-electron and inelastic collisions 16 p2723 A67-31768
- Electrical field distribution during injection of charged particles into two-dimensional model of magnetosphere 17 p2841 A67-32244
- Spectral distribution of turbulent energy, noting space-time correlations, instantaneous motion of fluid, existence of nonlinear inertial forces, etc 17 p2837 A67-32289
- Model of dust distribution in interplanetary space accounting for solar effects 17 p2947 A67-32758
- Impurity atoms and defects distributions in Si and Ge bombarded by different ions of medial energies calculated by Monte Carlo method 17 p2916 A67-32839
- Solution of linearized Boltzmann collision equation for ion motion through gas in inhomogeneous electric field, describing energy distribution functions for hydrogen ions 17 p2907 A67-33102
- Boundary value problem for electrical potential and ion distribution function obeying Poisson-Vlasov equations when applied to rarefied plasma disturbance by supersonic body 17 p2909 A67-33205
- Ion radial distribution functions for primitive model of electrolyte solution using Percus-Yevick and convolution-hypernetted-chain integral equations 17 p2810 A67-33256
- Correlation function for random process energy spectrum at linear system output, obtaining expression of envelope distribution for radio signals 18 p2999 A67-33506
- Superposition approximation for dense gases and liquids equilibrium theory, using phase-space distribution functions from maximization of information entropy 18 p3078 A67-33669
- Correlation function method in superconductivity theory, formulating electric current density in terms of distribution function in phase space 18 p3100 A67-33712
- Classical hydrodynamics equations accounting for dissipative processes 18 p3027 A67-34089
- Distribution coefficients for impurities in gallium and indium arsenides as periodic function of atomic weight decreasing with increasing atomic number 18 p3102 A67-34289
- Charged particles motion in magnetic field with regular and random components, deriving kinetic equation for distribution function and then diffusion equation 18 p3083 A67-34419
- Emission statistics of nonresonant feedback laser produced by radiation scattering, showing fluctuations intensity, distribution function, etc 18 p3062 A67-34621
- Time dependent expression for droplet-size distribution function of clouds undergoing forcible modification or natural evolution 19 p3251 A67-34862
- Zero-crossing times for signals, performing transformations of time sequence to determine distribution functions 19 p3201 A67-34905
- Electron distribution function in plasma determined using electrostatic separation probe 19 p3267 A67-34947
- Velocity distribution function in positive column plasma and implications for electron energy transfer mechanism on microscopic scale 19 p3267 A67-34948
- Energy distribution functions for nearly normal glow discharge using two models and statistics 19 p3273 A67-35098
- Electrical conductivity of weakly turbulent plasma calculated by behavior of electron distribution function 19 p3287 A67-35354
- Transport phenomena in electronic plasma as initial value problem noting distribution function relaxation 19 p3287 A67-35355
- Electron distribution function of homogeneous imperfect Lorentz plasma disturbed by electric field 19 p3295 A67-35418
- Book on combinatorial methods in theory of stochastic processes covering ballot theorem, random variables, dam and storage processes, etc 19 p3250 A67-35572
- Quasi-linear plasma waves model, considering Vlasov approximation, deriving distribution functions and electric field equations solution 20 p3494 A67-36149
- Computer program for heat transfer calculation by temperature distribution along wall surface, using Fourier-Bessel series to determine distribution coefficients 20 p3544 A67-36450
- Second derivative of two-probe current measurement method for determining electron energy distribution in gas discharge, noting low sensitivity to noise 20 p3498 A67-36687
- Fabry-Perot resonator with nonuniform reflectors, analyzing resonant modes amplitude/phase distribution and diffraction/reflection losses 20 p3447 A67-36767
- Base impurity distribution design consideration for figure of merit of HF transistors, considering accelerating, decelerating and neutral electric field 20 p3398 A67-36770
- Screw dislocation distribution on intersecting planes using theoretical model to discuss errors 20 p3540 A67-37020
- Fokker-Planck equation for distribution function over laser observable values derived from quantum-mechanical laser master equation by expanding statistical operator 20 p3461 A67-37182
- Laser Fokker-Planck equation transient solution in threshold region investigated for laser distribution function, mean intensity and mean squared deviation 20 p3461 A67-37183
- Probability distribution errors effect in linear and planar impulse orbital transfers, considering angular orientation and impulsive velocity 20 p3527 A67-37259
- He-Ne laser light intensity distribution cumulants for nonlinear oscillation threshold operation 20 p3461 A67-37289
- Algorithm for generating normally distributed variables set with given correlation matrix in digital computer simulation of electronic circuit performance 20 p3401 A67-37315
- Distribution function of modulus of directivity characteristic of antenna grid shown as modified Rayleigh distribution 20 p3384 A67-37335
- Sequential decoding algorithm with memoryless channel, obtaining lower bound to distribution of computation and limiting factor [JPL-TR-32-1121] 20 p3412 A67-37494
- Radial distribution functions for liquid methanol and ethanol at room temperature, observing intermolecular hydrogen bonding 20 p3378 A67-37560
- Power series expansion of electron velocity distribution function, computing harmonic electric current densities in plasma 21 p3661 A67-37745
- Electron distribution function in steady state plasma with Coulomb and excitation collisions obtained analytically by simplifying Fokker-Planck terms 21 p3661 A67-37746
- Two-stream instability calculations from phase-space boundary motion, using Vlasov equation in distribution function 21 p3662 A67-37763
- Wind profile criterion for structural design of launch vehicles, representing wind statistically by bivariate-normal distribution function 21 p3712 A67-37813
- Giant coherent light pulses generation by Q-switched laser, studying dynamics of generation and field distribution 21 p3640 A67-38373
- Parametric excitation of electron plasma frequency derived using Boltzmann and Poisson equations 21 p3667 A67-38415
- Instability of plasma with anisotropic ion velocity distribution, deriving equations for temperature variations and magnetic field energy changes 21 p3669 A67-38680
- Electromagnetic wave propagation in plasma layer bounded by external constant magnetic field, using kinetic theory with Maxwell equations and distribution function 21 p3670 A67-38685
- Diagnostic probe for low density plasma beam ion velocity distribution measurement in steady state and pulsed plasma exhausts [AIAA PAPER 67-706] 21 p3872 A67-38733
- Boundary conditions at wall for low density flow problems treated by kinetic theory, synthesizing relation between distribution functions of incident and reflected particles 21 p3614 A67-38861
- Conditioned distribution functions from BBGKY hierarchy distribution functions, with analogy to hydrodynamic approximation of Boltzmann distribution 21 p3675 A67-38931
- Visual image description with aid of spectral power redistribution functions, discussing input arrangement in TV recognition system 21 p3605 A67-39114
- Stationary state of collisionless plasma in magnetostatic and potential fields, deriving distribution functions and concentration formulas 22 p3842 A67-39243
- Relaxation toward Maxwell distribution function of classical gas with initial nonequilibrium distribution function as velocity modulus function 22 p3782 A67-39406
- Nonlinear theory of longitudinal plasma waves, formulating distribution function and Maxwell equation for electric field 22 p3845 A67-39421
- Al impurity redistribution near Si semiconductor surface subjected to high temperature oxidation 22 p3857 A67-39502
- LF noise spectrum of p-n junction using arbitrary pulse duration distribution functions 22 p3858 A67-39573
- Approximate integrodifferential equations determining ensemble mean and covariance of particle distribution function of Vlasov plasma, discussing incompressible Navier-Stokes turbulence 22 p3850 A67-39703
- Ionized plasma electric conductivity calculation using Druyvesteyn and Maxwellian distribution for electrons and ions respectively 22 p3851 A67-39725
- Quasi-linear perturbation expansion used to study evolution of localized disturbance in plasma 22 p3851 A67-39985
- Distribution function of durability in light structural alloys based on mass fatigue tests analyzed for influence of scale factor and stress concentration 22 p3915 A67-40301
- Interstellar extinction wavelength dependence, assuming ice particle radii distribution function obeys decreasing power law and graphite particles have Gaussian distribution function 22 p3889 A67-40304
- Spiral field rotation with motion integrals as distribution function arguments, discussing potential, density and spiral arm stability 22 p3893 A67-40507
- Corrections for three results in asymptotic solution of nonideal Bose-Einstein particle system nonlinear integral equations 23 p4026 A67-40718
- Distribution theory in control system design, discussing sensitivity improvement by feedback for application to time invariant systems 23 p3984 A67-40755
- Electron beam interaction with plasma investigated for spatial distribution of intensity and oscillation spectrum in stationary mode 23 p4032 A67-40904
- Quasi-linear relaxation dynamics of unstable distribution function for potential drift waves, deriving law governing average wave number time variation 23 p4032 A67-40911
- Numerical results for source distribution estimation from external radiation field measurements, investigating transport processes in slab bounded by parallel planes 23 p4082 A67-40993
- Selection probability from multivariable normal populations in terms of noncentrality parameters 23 p4024 A67-41084
- Infinitesimal dislocation theory applied to materials with cracks and cylindrical hole, straight boundary between bonded materials and cylindrical insert subject to antiplane shearing stress 23 p4078 A67-41165
- Optical signal detector performance, deriving outlet electron distribution function 24 p4166 A67-41797
- Space distribution function of Knudsen gas in closed volume investigated using gas model noting dependence of time 24 p4190 A67-41902
- Integral turbulent transfer model using velocity distribution function to develop mixing length flow theory 24 p4141 A67-41933
- Cosmic ray distribution, discussing method of diurnal variations, zonal harmonics and spherical analysis 24 p4209 A67-42114
- Statistical entropy of nonequilibrium plasma assuming binary correlation functions, obtaining distribution function equation 24 p4196 A67-42158
- Steady random process phase overshoot length distribution determined over given level as well as relationships for mean value and distribution dispersion 24 p4136 A67-42194

- Decrement of Balmer line widths and H-alpha profiles when distributing fine components as function of radial velocity in optical prominences 24 p4232 A67-42595
- Quantitative analysis of negative excess of electrons in electromagnetic cascade showers on basis of energy distribution functions 24 p4221 A67-42871
- Expressions for angular distribution function of electrons at various depths in cascade showers with given primary particle energy 24 p4221 A67-42872
- Equilibrium angular distribution function computer calculations for cascade particle numbers in iron and lead reveal dependence on primary particle energy 24 p4221 A67-42873
- DISTURBANCE**
- S MAGNETIC FIELD DISTURBANCE**
- S SATELLITE ATTITUDE DISTURBANCE**
- S SHEAR DISTURBANCE**
- S SUDDEN IONOSPHERIC DISTURBANCE /SID/**
- S VORTEX DISTURBANCE**
- DISTURBANCE THEORY**
- Disturbance theory linearized initial value problems for free trajectories passively moving above smooth earth surface 02 p0320 A67-11465
- Power source disturbance method for linear theory of flow past bodies 05 p0749 A67-17006
- Relation between terrestrial gravitational and magnetic field variations and time-dependent changes in shape, density and magnetization of disturbing bodies 05 p0799 A67-17027
- Power source disturbance method for linear theory of flow past bodies 18 p2984 A67-34268
- Distributive systems interaction between feedback and sensitivity noting parameter variations effects on external characteristics 23 p3983 A67-40644
- Laminar boundary layer subject to local three-dimensional disturbance, studying growth, flow field and transition to turbulence 23 p3991 A67-41175
- DISTURBING FUNCTION**
- Particle motion in vicinity of triangular libration point in earth-moon system solved in form of analytical expressions with time-dependent coordinates 06 p1079 A67-17763
- Successive approximations determining radiation pressure effect on and disturbing function of motion equations of artificial satellite 06 p1081 A67-17787
- Long period effects in nearly commensurable cases of restricted three-body problem analyzed via Poincare, isolating secular and critical terms of disturbing function 08 p1381 A67-20389
- Computer program for analytical development of planetary disturbing function 08 p1381 A67-20393
- Nonlinear automatic control with random parameters, noting change of system operator as function of disturbances on system 11 p1770 A67-24211
- Molodensky integral equation solvability 13 p2114 A67-26853
- Resonance effects for satellites with nominally constant ground track 16 p2744 A67-30731
- First order generalized planetary theory from Poisson form, deriving trigonometric expansion of disturbing functions, periodic inequalities, etc 18 p3120 A67-33865
- DIURESIS**
- High gradient acceleration effect on human renal clearances of free water and creatinine following moderate water load 05 p0758 A67-16288
- Urine composition in twelve dehydrated subjects in periods of activity, water immersion and reclining in deck chair [SAM-TR-66-305] 09 p1453 A67-21730
- Urinary output patterns relationship to arterial pressure, pulse rate and parameters of hemoconcentration in study of homeostatic circulation regulation during prolonged gravitational stress 15 p2428 A67-29273
- Positive pressure breathing effects on inhibition of diuresis during water immersion 18 p2992 A67-34721
- Vasopressin-aldoosterone interrelation in diuresis and antidiuresis to explain body fluid weight loss in astronauts during space travel 21 p3574 A67-38082

- Biological effects of time-zone changes on circadian rhythms of urinary elimination of potassium and 17-hydroxycorticosteroids 22 p3751 A67-39606
- DIURNAL RHYTHM**
- S CIRCADIAN RHYTHM**
- DIURNAL VARIATION**
- Dynamo theory interpretation of magnetospheric-ionospheric electric current system associated with N-S asymmetry of magnetic daily variation at time of equinox 01 p0057 A67-10113
- Profile and fine structure of diurnal variation of cosmic ray intensity during high and low solar activity 01 p0144 A67-10810
- Phase reversal in lunar variations of critical frequencies of F-2 layer at Waltair, India 01 p0060 A67-11232
- Diurnal variations of boundary frequencies of sporadic c-type E layer, deriving cosine law not dependent on sunspot cycle 01 p0061 A67-11289
- Neutron component diurnal variation in cosmic radiation during period of coil type magnetic disturbances in tail of geomagnetic storm 02 p0306 A67-11856
- Latitudinal effect and universal time effect on diurnal variations in auroral activity 02 p0236 A67-11864
- Diurnal and seasonal variations of ionospheric turbidity 02 p0238 A67-11870
- Relation of sporadic E layer to magnetic fluxes based on observations of diurnal variations 02 p0237 A67-11875
- Magnetic field of M-element interaction with geomagnetic field as second possible cause of irregular fluctuations in velocity of earth diurnal rotation 02 p0237 A67-11878
- Cosmic ray 27-day variations using periodograms, with measured data processed continuously from 1957 to 1964 02 p0311 A67-12591
- Stellar diurnal variation determined during reduced solar activity from crossed-telescope and neutron monitor data 02 p0311 A67-12594
- 27-day changes in solar diurnal variation from 1957 to 1958 based on neutron component data, noting modulation of cosmic ray anisotropy 02 p0312 A67-12800
- Diurnal and latitudinal variation of satellite scintillation during local summer at low southern geomagnetic latitudes 03 p0406 A67-12821
- Systematic measurement of ionospheric absorption at vertical incidence made by pulse reflection method at frequencies in range 2-3 mc at Colombo, Ceylon 03 p0406 A67-12822
- Beacon satellite measurement of Faraday rotation and diurnal and seasonal variations of total electron content of ionosphere near Nairobi 03 p0406 A67-12825
- Diurnal variations in F layer at Ibadan exhibit peak before noon during sunspot maximum and after noon during sunspot minimum 03 p0407 A67-12826
- Monthly and seasonal variation of magnetic horizontal component in Eastern Africa on international quiet and disturbed days from February 1964 to January 1965 03 p0408 A67-12838
- Time-dependent photochemical model for space-time variations of oxygen allotropes in 20 to 100 km layer 03 p0414 A67-14087
- Statistical analysis of auroral radar echoes reveals changes in shape of diurnal variation curve with level of magnetic disturbance and seasonal variation with peaks at equinoxes 03 p0513 A67-14112
- Radio astronomical and satellite studies of atmosphere - USAF Symposium, Boston, October 1965 03 p0415 A67-14234
- Explorer XXII satellite measurement of total electron content from Faraday rotation recordings, noting correlation with solar activity above 80 solar flux units [RASSA PAPER 1-10-124] 03 p0416 A67-14235
- Latitudinal and diurnal variation of ionospheric electron content in auroral zone proximity [RASSA PAPER 1-10-126] 03 p0416 A67-14237
- Early Bird satellite measurement of ionospheric electron content by determining polarization twist of VHF radio signals [RASSA PAPER 1-10-130] 03 p0417 A67-14241
- Early Bird satellite measurement of ionospheric electron content obtained from Faraday rotation data [RASSA PAPER 1-10-131] 03 p0417 A67-14242
- Jovian decametric pulses compared with satellite and radio star scintillations in

- terrestrial ionosphere [RASSA PAPER 1-10-134] 03 p0373 A67-14245
- Two-dimensional dynamic model of diurnal variation of thermosphere 04 p0611 A67-14651
- 24 hr history of radar angle activity at 3.2, 10.7 and 71.5 cm wavelengths 04 p0649 A67-14681
- Diurnal variations of ionospheric ion composition over Arecibo at various altitudes for solar minimum winter and summer conditions 04 p0614 A67-14955
- Midlatitude semidiurnal tide in lower thermosphere determined from trails of chemiluminescent vapor 04 p0615 A67-14969
- Diurnal variation of sporadic E at high latitude as function of geomagnetic activity 04 p0615 A67-14972
- E-2 and F-0 intermediate ionospheric layer morphology, occurrence, electron density and signal reflection variations 04 p0616 A67-15220
- Seasonal and diurnal variations of geomagnetic field in equatorial regions 04 p0616 A67-15224
- Temporal distribution of first and second harmonic of solar diurnal variation of cosmic rays after radio bursts of fourth type 05 p0881 A67-16116
- Temperature effect on diurnal variation of meson intensity at high latitudes, finding wave maximum amplitude in spring 05 p0796 A67-16117
- Variation of seasonal diurnal distribution of sudden changes in cosmic ray neutron component intensity related to solar activity changes 05 p0881 A67-16118
- Solar diurnal variation of cosmic ray neutron component in Antarctic during minimum activity period, using harmonic analysis 05 p0881 A67-16119
- Anisotropy in stellar diurnal cosmic ray variations in Northern and Southern Hemispheres, noting distributions of stellar and antistellar vectors 05 p0881 A67-16120
- Upper atmospheric turbulence measurements based on radiolocational observation of meteor trains 05 p0796 A67-16211
- Diurnal atmospheric oscillations and wind systems producing geomagnetic variations 05 p0798 A67-16859
- Height profile of Sq current in ionosphere, showing dependence on electric field direction 05 p0799 A67-16872
- Diurnal and short period h sporadic E layer and critical frequency sporadic E layer variations analyzed from data obtained at Ashkhabad station 05 p0800 A67-17129
- Seasonal changes in solar diurnal and semidiurnal variations of cosmic ray neutron component due to earth rotation axis and anisotropy sources 05 p0885 A67-17138
- Temporal variations in values of variability characteristic of parameters of ionosphere cross sections below principal maximum 05 p0801 A67-17142
- Changeability laws in quiet solar diurnal magnetic variations in 1964 and relation to state of ionosphere resulting from dynamo effect 05 p0802 A67-17147
- Rotation of vector of solar diurnal variation in intensity of cosmic radiation neutron component during solar activity minimum 05 p0885 A67-17497
- Horizontal variability of properties of model thermosphere with seasonal changes 06 p0996 A67-18564
- Comparison of VLF emissions of two conjugate stations, noting statistical results for diurnal variation, magnetic activity, hiss, etc 06 p0997 A67-18698
- Diurnal variation of hydrogen exosphere treated by simulation technique involving critical circle and magnetopause circle 06 p0997 A67-18701
- Diurnal variation of Schumann resonances explained by geometrical factors relating position of sources and observational point, noting propagation difference between EW and NS 06 p0998 A67-18707
- Ten years ionospheric drift measurements in LF range 07 p1171 A67-19420
- VLF atmospheric noise level fluctuations, discussing daily variations as function of solar zenithal angles, sunrise and sunset and confusion of ionospheric propagation 07 p1171 A67-19422
- Tabulation and plotting of VLF radio wave diurnal phase changes as function of frequency and path 07 p1142 A67-19450

Diurnal and seasonal altitude variations of E and F layers analyzed for geomagnetic activity from rocket measurement of electron concentration 07 p1173 A67-19686

Fluctuations in diurnal variations of ionization of F-2 layer interfering with radio wave propagation determined by series expansion 07 p1173 A67-19687

Longitudinal variations of characteristics of F-1 layer compared for periods of high and low solar activity 07 p1173 A67-19688

Vertical measurement of ionospheric absorption at continuously varying frequency, showing diurnal variation of absorption 07 p1174 A67-19706

Solar system geometric effect in diurnal, annual and semiannual cosmic ray variations 07 p1243 A67-19807

Diurnal and seasonal variations of sporadic layer in auroral zone 07 p1178 A67-19823

Electron temperature and concentration at 1000 km altitude, obtaining resolution of two full diurnal cycles of ionospheric behavior 07 p1181 A67-19935

Calculation of time behavior of forenoon anomaly in diurnal variations of critical frequency of normal E layer 07 p1183 A67-20118

Mean noon profile of mesospheric electron number density at 35 degrees S latitude preceding solar eclipse 08 p1378 A67-21483

Equatorial enhancement of micropulsation p1-2 obtained from magnetograms during IGY, noting diurnal variation and latitudinal dependency similarity to other disturbances 08 p1329 A67-21540

Cosmic ray distribution, discussing method of diurnal variations, zonal harmonics and spherical analysis 10 p1698 A67-22778

Parameters of simultaneous amplitude phase modulation of periodic cosmic ray variations obtained from satellite observations 10 p1698 A67-22779

Cosmic ray intensity variation detection with respect to sidereal time on basis of simultaneous amplitude phase modulation 10 p1698 A67-22780

Diurnal variations in arch azimuths of extended polar auroral formations determined from diurnal winter observations 10 p1630 A67-22786

Cartographic representation of diurnal magnetic variations, noting longitudinal asymmetry in amplitude distribution 10 p1631 A67-22808

Strong geomagnetic disturbances distribution in space and time analyzed for correlation of magnetic activity with auroral brightness 10 p1632 A67-22809

Eigenvalue and Hough functions for diurnal and semidiurnal components and both symmetric and antisymmetric modes of atmospheric tides 10 p1634 A67-23052

S-N wind components analyzed for diurnal and semidiurnal variations, noting results on amplitude and phase of components 10 p1638 A67-23200

Rocket measurement of diurnal variation of ozone profiles above maximum concentration level 10 p1638 A67-23202

Shape and location of diurnal bulge in upper atmosphere, analyzing density and temperature distribution at high latitude from satellite drag data 10 p1639 A67-23208

Upper atmosphere dynamics, noting role of horizontal and vertical winds in shifting density phase and amplitude and UV radiation as energy source 10 p1640 A67-23218

Free sodium atom distribution in upper atmosphere related to diurnal and nocturnal variation 10 p1645 A67-23262

Winter anomaly of nondeviative ionospheric absorption of radio waves and relation to diurnal, seasonal, local and solar cycle variations 10 p1646 A67-23267

Diurnal variation of difference between dipole and measured field for quiet magnetosphere from Elektron satellite data 10 p1649 A67-23296

Diurnal variation of primary auroral electrons, average energy spectrum of 20-150 keV X-rays and time dependence of intensity and morphology 10 p1702 A67-23305

Approximate method for diurnal variation of peak electron density in F-2 layer, estimating effect of time varying drifts 10 p1650 A67-23336

Diurnal and latitudinal variations in 5577 angstrom zenith nightglow intensity compared with 6300 angstrom

calibrations 10 p1650 A67-23337

Diurnal and seasonal variation of total columnar ionospheric electron content at magnetic equator analyzed, using Faraday rotation technique 10 p1651 A67-23341

Diurnal variation of telluric currents near magnetic equator during IGY and IQSY suggests equatorial electrojet as main source for current 10 p1651 A67-23343

Atmospheric density determination from drag of eleven low altitude satellites, discussing correlation with geomagnetic activity and daily periodicity 11 p1784 A67-23937

Partial coherence functions to investigate contribution of solar radiation and gravitational tide in causing geomagnetic variations /ionospheric tides/ 11 p1785 A67-23938

Diurnally oscillating component of thermospheric east-west pressure acceleration at equator, noting balancing effect of viscous diffusion, ion distribution, etc 11 p1785 A67-23939

Long term variation in magnitude of diurnal anisotropy of solar cosmic rays analyzed quantitatively by applying statistical techniques to recorded data 12 p1993 A67-25205

Rocket and satellite measurements of electron and ion thermal structure of ionospheric F region 12 p1935 A67-25796

Rocket observations of lowest ionosphere at sunrise and sunset 12 p1935 A67-25798

Time variations of intensity in outer belt and near boundary deduced from Elektron I and II data, noting comparison with magnetic field variations 12 p1997 A67-25815

Unstable diurnal and seasonal variation of ionization of F region of ionosphere during years of minimum solar activity over Ashkhabad 12 p1938 A67-26100

Nighttime ionosphere maintained by downward flux of electrons from protonosphere as shown by columnar electron contents measurements, noting decay rate 13 p2107 A67-26305

Diurnal and annual variation of absorption of short waves in ionosphere 13 p2066 A67-26486

Diurnal, annual and seasonal variations of high altitude turbulent motions in upper atmosphere through observation of meteor trails by coherent pulse method 13 p2110 A67-26506

Dependence of diurnal cosmic ray variations on angle which is proportional to shortest distance from earth to axis of corpuscular stream 13 p2191 A67-26546

Diurnal variation in principal direction of E and H vectors of Petropavlosk-Kamchatka K index of geomagnetic field in horizon and planetary relation 13 p2111 A67-26558

Geomagnetic activity and earth heliolatitude effect on diurnal variation of cosmic radiation, based on IGY neutron component observations 13 p2191 A67-26564

Diurnal variations in sporadic E layer parameters during solar cycle based on Moscow observations 13 p2111 A67-26570

Diurnal cyclic intensity variations of atmospheric radio noise at stations widely spaced over globe 13 p2111 A67-26571

Diurnal variations in structural parameters of upper atmosphere determined via differential equations of hydrodynamics 13 p2112 A67-26669

Temperature and wind fields in stratosphere obtained with rocket probes, noting diurnal and annual temperature variation differences for heights beyond 35 km 13 p2113 A67-26879

Relation between ionospheric no-echo conditions and absorption of cosmic radio noise measured using riometer, plotting diurnal variation values 13 p2114 A67-26794

Mars atmosphere and ionosphere analyzed by measuring effect on radio occultation of planet, determining shape, atmosphere density profile, diurnal variations, etc [JPL-TR-32-1157] 13 p2199 A67-26819

Earth aerospace thermodynamic properties from 100 to 100,000 km alt predicted, considering diurnal and extreme solar activity variations for engineering applications 13 p2114 A67-26821

Ionization transport from equator along magnetic lines of force may contribute to formation of diurnal ionization anomaly of F region in intermediate zone 13 p2117 A67-27708

Crossing rates of atmospheric radio noise in high range of threshold field strength measured and compared with integrated field strength 14 p2306 A67-27881

Diurnal and seasonal variations in radio echo observations from meteoric trains during forward ultrashortwave scattering 14 p2383 A67-27924

Micropulsations of earth electromagnetic field relation to disturbed diurnal solar variation 14 p2308 A67-27925

Seasonal and diurnal variation of parameters of vertical electron density distribution 14 p2308 A67-27934

Current diagram plotting by graphical integration method for diurnal solar magnetic variations in especially quiet days 14 p2309 A67-27939

Omicron I satellite measurements of total ionospheric electron content, comparing values at Houghton, Michigan, with others for different latitudes 15 p2474 A67-29193

Diurnal and seasonal variations in occurrence probability of screening and semitransparent types of sporadic E layer 15 p2474 A67-29387

Free atomic sodium distribution in daytime upper atmosphere, noting thin layer formation and radiative transfer theory 15 p2475 A67-29616

Pc-1 micropulsations, noting harmonic curve for diurnal variations and effect of magnetic and solar activity 15 p2476 A67-29619

Occurrence frequency of midlatitude blanketing sporadic E studied for seasonal, diurnal and latitudinal variations 15 p2476 A67-29622

Diurnal and annual variations of occurrence frequency and dispersion of whistlers during IGY and IQSY 15 p2478 A67-30068

Automatic measurement of diurnal resonance frequency variations of earth/ionosphere cavity 15 p2489 A67-30071

Satellite topside sounder investigation of spread echoes at mid and high latitudes in Northern Hemisphere [AGARDOGRAPH 95] 15 p2480 A67-30276

Diurnal, annual, latitudinal and sunspot cycle-influenced variations of spread-F intensity at very high latitudes [AGARDOGRAPH 95] 15 p2481 A67-30281

Diurnal, seasonal and geographic variations of frequency of spread-F occurrence over Antarctica [AGARDOGRAPH 95] 15 p2481 A67-30282

Statistical analysis of spread-F and scintillation data in middle latitude noting diurnal and seasonal variations [AGARDOGRAPH 95] 15 p2481 A67-30284

Measurements on scintillation observed on radio signals from Discoverer satellite, noting intensity increase with latitude and data on diurnal variation [AGARDOGRAPH 95] 15 p2483 A67-30293

Diurnal temperature change effect on F-2 layer, noting maximum electron density height dependence on neutral-gas temperature variations 16 p2663 A67-30967

Daily geomagnetic variations superpositional nature studied by factorizing frequency functions describing day-to-day variability 16 p2664 A67-30971

Neutron component diurnal variation in cosmic radiation during period of coil type magnetic disturbances in tail of geomagnetic storm 16 p2738 A67-31071

Latitudinal effect and universal time effect on diurnal variations in auroral activity 16 p2665 A67-31079

Diurnal and seasonal variation of ionospheric turbidity 16 p2665 A67-31085

Relation of sporadic E layer to magnetic fluxes based on observations of diurnal variations 16 p2665 A67-31090

Magnetic field of M-element interaction with geomagnetic field as second possible cause of irregular fluctuations in velocity of earth diurnal rotation 16 p2665 A67-31093

Ion temperature measurements in upper atmosphere to determine diurnal variation 16 p2666 A67-31416

Vlf transequatorial wave propagation, noting phase cycle slipping during sunrise transition 16 p2630 A67-31848

Periodic field strength variations during sunrise on vlf signals in long path propagation noting amplitude minima and stepwise phase increase 16 p2630 A67-31849

Multimode propagation and mode

conversion at sunrise and sunset lines explaining diurnal variations on vlf paths 16 p2631 A67-31852

Airborne field strength measurements in NPM antipode region noting variation with inverse square root of distance over sections of antipodal area 16 p2631 A67-31855

Time and space distribution of anomalous ionization in ionospheric F-2 layer above Southern Hemisphere, noting maximums of ionization distribution 16 p2668 A67-31893

Diurnal variations asymmetry in critical frequency ratio of E layer for morning and evening values 16 p2668 A67-31895

Dynamic phenomena in diurnal variation of cosmic rays used to determine width and existence of separate flows in interplanetary medium 16 p2740 A67-31898

Barometric and temperature coefficients determined from solar-diurnal, antisidereal variation, atmospheric showers etc 16 p2741 A67-31900

Photochemical analysis of diurnal variations of electron concentration and temperature of upper ionosphere 16 p2669 A67-31902

Semitransparency range of sporadic E layer as solar radiation function, noting diurnal and seasonal variations 16 p2669 A67-31904

Drift data harmonic analysis correlation between solar quiet diurnal variation and ionospheric drift 16 p2669 A67-31908

Soviet book on cosmic rays including solar-diurnal, 11-year and 27-day variations, temperature effect, geomagnetic field effect, etc 17 p2930 A67-32077

Statistical correlation between phase and amplitude in first harmonic solar-diurnal variation of neutron component, noting longitude effect 17 p2931 A67-32078

Solar-diurnal variations of neutron and muon components of cosmic rays based on IGY data, analyzing temperature effect 17 p2931 A67-32079

Diurnal variation of hard component near minimum solar activity, emphasizing temperature effects 17 p2932 A67-32080

Statistical analysis of solar-diurnal and semidiurnal variations of cosmic ray neutron component with respect to geomagnetic field perturbations 17 p2932 A67-32081

Relation between frequency distribution of sudden changes in cosmic ray intensity and solar-diurnal variation 17 p2932 A67-32082

Temperature effect on diurnal variation of hard cosmic ray component based on radio probe observations 17 p2933 A67-32089

Biochemical reactions in human organism as indicator of cosmic ray variation, showing relationship between solar activity and erythrocytes in blood 17 p2934 A67-32099

Diurnal characteristics of geomagnetic micropulsations noting period, amplitude, continuity, time of occurrence, etc, proving existence of hydromagnetic waves generated at magnetosphere 17 p2841 A67-32212

Electron heating in diurnal ionosphere noting electron and ion temperatures as function of altitude 17 p2842 A67-32295

Measurement of solar extreme UV radiation atmospheric attenuation to establish daytime variations in upper atmosphere composition 17 p2843 A67-32535

Pearl type oscillations studied by recording ground currents, discussing 24-hr and seasonal variations 17 p2847 A67-32944

Winter and summer equivalent current systems of polar solar-diurnal variations studied from observations obtained during IGY 17 p2847 A67-32949

Diurnal variations in He twilight emission intensity determined using photoelectric spectrometer 17 p2849 A67-32958

Auroral belt dynamics including edge displacement rate, width, asymmetry of sides and relation to polar geomagnetic disturbances 17 p2850 A67-33184

Diurnal and seasonal variation of electron content and diurnal variation of slab thickness investigated, emphasizing relation between electron content and scintillation occurrence 17 p2850 A67-33190

Diurnal variations of ionospheric ion/electron temperatures predicted assuming solar UV radiation heating, collisional cooling and heat transport by conduction 17 p2850 A67-33192

Alpha diurnal and seasonal intensity variations in geocorona indicating hydrogen content build-up during

night 17 p2851 A67-33202

Solar diurnal wave from underground muon detectors and relationship to solar activity over 11-year cycle, noting phase changes 18 p3116 A67-33514

Atmospheric emissions and electron and proton precipitation latitude and diurnal variations measurements from satellite-borne photometric studies 18 p3039 A67-33623

Atmospheric density determination from satellite drag, noting effects of magnetic storms, diurnal and semiannual variations, solar activity, etc 18 p3041 A67-34253

Air drag effect on six Cosmos satellites orbits having low perigee, discussing diurnal air density variation at 280 km height 18 p3042 A67-34256

Lower thermosphere physical properties, studying satellite drag for density profiles, composition, data comparison, etc 19 p3215 A67-35171

Upper atmosphere diurnal and seasonal latitudinal variations satellite data, showing diurnal bulge migration with subsolar point, 2 PM bulge peak, etc 19 p3215 A67-35178

Developments in upper atmosphere research noting atmospheric density, temperature, diurnal variations, solar and geomagnetic activity effects, etc 19 p3218 A67-35225

Day-and nighttime electron density profiles in ionospheric D layer 19 p3218 A67-35227

Upper atmosphere densities and scale heights from Soviet earth satellite drag data, noting diurnal variation 19 p3219 A67-35252

Molecular and atomic ion concentration in earth upper atmosphere observed from low altitude satellite, discussing diurnal variation and solar effect 19 p3220 A67-35262

Lower thermosphere composition and mean molecular weight analyzed for diurnal and latitude effects, using mass spectrometric measurements 19 p3220 A67-35265

Hydrogen and hydroxyl emissions in nightglow 19 p3223 A67-35483

Galactic anisotropies observation, giving procedure for detecting periodicities and data on sidereal daily variation amplitude 19 p3315 A67-35484

Density gradient of cosmic radiation perpendicular to plane of ecliptic as cause of variations in amplitude and phase of solar diurnal variation 19 p3315 A67-35490

Underground cosmic ray intensity variation measurements to determine solar modulation processes 19 p3315 A67-35494

Daily and seasonal changes in numbers, dimensions and shapes of micrometeoritic particles over period of two years, discussing origin 19 p3327 A67-35878

Temperature and wind profiles in stratosphere and mesosphere during winter and summer determined by grenade soundings, noting diurnal variations 19 p3226 A67-35924

MHD instability of sub-Alfvén equations for zonal flow outside diurnally oscillating boundary layer of precessing spheroid 20 p3494 A67-36147

Auroral zone diurnal tidal effect studied by high resolution spectrum analysis, noting large diurnal conductivity variation giving rise to lunar auroral electrojet 20 p3521 A67-36298

Screening frequency dependence on reflection cut-off frequency in sporadic E layer 20 p3428 A67-36762

IGY data from magnetic observatories analyzed for luni-solar daily variations of geomagnetic field 20 p3525 A67-36869

Daily magnetic variations over England, noting difference between values obtained for summer IQD and other days of year 20 p3429 A67-36870

Upper atmospheric dynamics, considering day-night density and pressure variation, wind structure, gravity waves, etc 20 p3429 A67-36896

Structure and composition of upper atmosphere above stratopause, discussing temperature, density and wind variations 20 p3430 A67-36904

Diurnal variation investigated by rocket, discussing ionospheric electric currents and magnetosphere-ionosphere electric field 20 p3431 A67-36908

Periodic fluctuations of cosmic ray diurnal variation statistically studied, using neutron and meson component

data 20 p3518 A67-36993

Ionogram data used to identify high absorption periods, analyzing diurnal variations of critical frequency F-2 layer showing no echo occurrences 20 p3432 A67-37275

Galactic cosmic ray density distribution anisotropy in solar system, discussing outward convection of cosmic rays by solar wind and inward diffusion model 20 p3520 A67-37474

Diurnal variation of earth-ionosphere cavity resonances and properties and propagation of ELF, ULF and MHD waves 20 p3390 A67-37727

Lunar tide in E layer, diurnal/semidiurnal components and seasonal variation 21 p3616 A67-37997

Ionosphere thermal nonequilibrium during sunspot minimum noting electron density and temperature measurements and daily variations 21 p3616 A67-37999

Diurnal and short period h sporadic E layer and critical frequency sporadic E layer variations analyzed from data obtained at Ashkhabad station 21 p3618 A67-38472

Temporal variations in values of variability characteristic of parameters of ionosphere cross sections below principal maximum 21 p3619 A67-38484

Changeability laws in quiet solar diurnal magnetic variations in 1964 and relation to state of ionosphere resulting from dynamo effect 21 p3619 A67-38489

Planetary distribution of horizontal gradients of F-2 layer critical frequency and diurnal, seasonal and solar cycle variations 21 p3622 A67-39034

Seasonal changes in solar diurnal and semidiurnal variations of cosmic ray neutron component due to earth rotation axis and anisotropy sources 21 p3700 A67-39048

Lower ionospheric drift studied from signal recordings from distant medium wave broadcasting stations 22 p3788 A67-39467

Seasonal and diurnal variations of trough and ionospheric electron content and slab thickness, using S-66 satellite observation 22 p3789 A67-39471

Annual and diurnal variations of geomagnetic anomaly in Australasian Zone during sunspot minimum, stressing role in transequatorial propagation of VHF radio signals 22 p3759 A67-39473

Ionospheric F-1 layer critical frequency at sunspot minimum and maximum, discussing critical frequency diurnal variation 22 p3789 A67-39476

Short bursts of scintillation of satellite radio signals from S-66 satellite, discussing diurnal variation correlation with spread of occurrences 22 p3759 A67-39478

Lunar semidiurnal air tide distribution and small lunar gravitational excitation noting lunar diurnal tide detectable only with wind data 22 p3882 A67-39557

Ionospheric observations using Elektron I and III satellites, discussing state of ionosphere, electron concentration variation, etc 22 p3760 A67-39734

Cosmic ray propagation processes studied from measurement of anisotropic character of cosmic radiation /1965-1966/ 22 p3871 A67-39798

Electron flux and energy spectrum measurements near polar cap investigated for diurnal intensity variations 22 p3872 A67-39802

Radiative transfer in lunar surface diurnal heat flow, studying geometric model of porous medium 22 p3885 A67-39980

Double sunspot cycle or 22-yr variation in cosmic ray diurnal variation phase, discussing streaming mechanisms 22 p3874 A67-40046

Satellite and ground observations of VLF emissions, summarizing intensity, diurnal and seasonal variation, emphasizing chorus and hiss characteristics 22 p3794 A67-40083

Neutral atmospheric temperatures calculated from data provided by incoherent scatter soundings of ionosphere 22 p3794 A67-40474

Storm time increase and anomalous type of daily variation during cosmic ray storms caused by lowered threshold rigidities and excess cosmic ray streaming respectively 23 p4050 A67-40695

Diurnal, latitudinal and seasonal variations of midlatitude topside ionosphere electron density profiles and plasma scale heights

calculated from Alouette I ionograms 23 p3994 A67-40775
Cosmic ray diurnal anisotropy component annual means variation with two solar cycles 23 p4051 A67-40817
Solar activity cycle effect on cosmic ray anisotropy diurnal variation 23 p4057 A67-41120
Cosmic ray anisotropy in solar system, considering diurnal variation in terms of anisotropic diffusion 23 p4058 A67-41121
Diurnal variation in cosmic ray anisotropy from observations during solar activity minimum, giving amplitudes and phases distribution 23 p4058 A67-41122
Solar diurnal variation and sudden changes in cosmic ray intensity from yearly neutron component data 23 p4058 A67-41123
Cosmic ray diurnal variation during magnetic storms from neutron monitors and meson telescope data 23 p4058 A67-41124
Solar activity effect on distribution of source power of solar diurnal cosmic ray variation in relation to ecliptic plane 23 p4058 A67-41125
Earth axis inclination influence on diurnal amplitude of cosmic ray variation, discussing yearly modulation effect 23 p4058 A67-41126
Atmospheric temperature effect on cosmic ray hard component diurnal variation in high latitude regions, discussing anomalous diurnal variation 23 p4058 A67-41127
True and false sidereal diurnal cosmic ray variation, examining modulating effects leading to false variations 23 p4058 A67-41128
Sidereal diurnal cosmic ray variation caused by modulation in solar system, discussing variations in coordinate systems 23 p4059 A67-41129
Sidereal cosmic ray diurnal variations, taking into account data correction for barometric pressure and temperature effects 23 p4059 A67-41130
Differentiation between true variation amplitude and statistical instrument error, deriving diurnal variation amplitude and phase distribution expressions 23 p4059 A67-41131
Solar neutron observations with boron fluoride counter on OSO-1, discussing absence of diurnal variation 23 p4061 A67-41236
Ionospheric electron distribution observed and computed values discrepancy analyzed, noting diurnal variation role 24 p4146 A67-41785
Electron content of topside ionosphere studied for equatorial anomaly during diurnal variations 24 p4148 A67-42063
Diurnal variations of electron concentration in topside ionosphere studied at low and middle latitudes using satellite data, noting secondary nighttime maximum 24 p4148 A67-42064
Sq currents in American equatorial zone during IGY 24 p4148 A67-42066
Cosmic ray distribution, discussing method of diurnal variations, zonal harmonics and spherical analysis 24 p4209 A67-42114
Parameters of simultaneous amplitude phase modulation of periodic cosmic ray variations obtained from satellite observations 24 p4209 A67-42115
Cosmic ray intensity variation detection with respect to sidereal time on basis of simultaneous amplitude phase modulation 24 p4209 A67-42116
Diurnal variations in arch azimuths of extended polar auroral formations determined from diurnal winter observations 24 p4149 A67-42122
Cartographic representation of diurnal magnetic variations, noting longitudinal asymmetry in amplitude distribution 24 p4150 A67-42145
Strong geomagnetic disturbances distribution and time analyzed for correlation of magnetic activity with auroral brightness 24 p4150 A67-42146
Periodic length of day /lod/ fluctuations, interplanetary torques and variations in earth rotation 24 p4229 A67-42313
Earth rotation variation in historical time using day length, eclipses and earth angular velocity 24 p4151 A67-42317
Earth core growth rate by convection used to calculate earth inertia moment changes, hypothesizing day length variation with age 24 p4151 A67-42319
E layer critical frequency calculation for 80 selected diurnal variations, considering

forenoon anomaly effect 24 p4151 A67-42704
Temporal distribution of first and second harmonics of solar diurnal variation of cosmic rays after radio bursts of fourth type 24 p4214 A67-42792
Temperature effect on diurnal variation of meson intensity at high latitudes, finding wave maximum amplitude in spring 24 p4152 A67-42793
Variation of seasonal diurnal distribution of sudden changes in cosmic ray neutron component intensity related to solar activity changes 24 p4214 A67-42794
Solar diurnal variation of cosmic ray neutron component in Antarctic during minimum activity period, using harmonic analysis 24 p4214 A67-42795
Anisotropy in stellar diurnal cosmic ray variations in Northern and Southern Hemispheres, noting distributions of stellar and antistellar vectors 24 p4214 A67-42796
DIVERGENT NOZZLE
SA CONVERGENT-DIVERGENT NOZZLE
Five calculations of plasma accelerators using quasi-one-dimensional and two-dimensional model for different nozzle shapes 02 p0274 A67-12337
Nonequilibrium-transition patterns of quasi-one-dimensional dissociating-gas flow through diverging supersonic nozzle 19 p3211 A67-35759
Limiting driven conditions corresponding to optimum expansion and low density shock tube flow for overexpanded nozzle 21 p3609 A67-38886
DNA
S DEOXYRIBONUCLEIC ACID /DNA/
DOCKING
Gemini program evaluation, discussing information gained from experiments performed during flights [AIAA PAPER 66-1027] 04 p0704 A67-14979
Laser guidance system for rendezvous and docking providing data acquisition for guidance computer 04 p0655 A67-15663
Docking mechanisms for spacecraft systems noting hard vs soft and in-line vs off-set systems [AIAA PAPER 67-908] 24 p4244 A67-43015
DODGE SATELLITE
DODGE TV system for evaluating attitude control system in gravity gradient stabilization at synchronous altitude 20 p3452 A67-37571
DODGE satellite vidicon cameras and information processing system electronics design and performance 20 p3452 A67-37572
DODGE satellite TV cameras for black and white, plus color picture transmission with photometric analysis and camera optics 20 p3452 A67-37573
Gravity gradient stabilization experiments using DODGE satellite at synchronous orbit 21 p3714 A67-39149
DOG
Cardiovascular responses of anesthetized dogs to repeated rapid decompressions in near vacuum 03 p0365 A67-14296
GUT, GPT, MDH, LDH, SDH and aldolase serum enzyme activity in dogs subjected to moderate impact 06 p0953 A67-17997
Spermatogenesis condition of experimental dogs after 22-day space flight and reproduction function in first offspring generation 20 p3387 A67-38257
DOMAIN WALL MOTION
Intrinsic damping and eddy current-limited domain wall mobility in Ni-Fe alloy ferromagnetic thin films 02 p0298 A67-11890
Stable domain propagation in gallium arsenide for nonzero constant diffusion coefficient, based on analytic approximation to velocity field 03 p0493 A67-13461
Field and charge density distributions in semiconductor with hot electrons, showing domain movement type oscillations due to stationary wave propagation 04 p0680 A67-15286
Elastic and inelastic flux switching, explaining different types of domain wall displacement in terms of variations of energy gradient vs wall position 05 p0774 A67-16832
Precipitation effect of dispersed calcium titanate-rich phase on shape, organization and thickness of ferroelectric domains in barium titanate 06 p1020 A67-18047
C domain wall motion in barium titanate crystals is dependent on A domains and activation fields throughout whole

crystal 11 p1849 A67-24900
Barium titanate polycrystal dielectric constant aging, discussing 90 degree splitting in domain structure 14 p2364 A67-28228
One-dimensional propagation of stable negative-resistance domains for carriers interacting with single type of impurity level 16 p2727 A67-30852
Worm motion of domain walls in Permalloy films using Kerr magneto-optic apparatus under pulse drive with nanosecond rise time 22 p3860 A67-39901
Gunn effect, describing electron transfer, domain propagation and space charge instabilities in GaAs 22 p3841 A67-40073
Domain structures in YIG slices after polishing strains elimination, noting spike domains 23 p4041 A67-41185
DONNELL EQUATION
Applicability of Southwell plot to interpretation of test data from instability studies of shell bodies, based on modified Donnell equations 10 p1728 A67-23763
Asymptotic expansion procedure applied to Donnell equations for cylindrical shell, obtaining solution for interaction of infinite cylinder reinforced by radially loaded ring [ASME PAPER 66-WA/APM-27] 10 p1730 A67-23839
DONOR
Shallow donor potential in silicon 03 p0493 A67-13363
Sulfur donor level associated with conduction bands of gallium antimonide in measurements of Hall coefficient vs temperature and resistivity vs pressure 04 p0673 A67-14476
Donor electron IR absorption coefficients in semiconductors in 3-10 micron range used to study wavelength dependence 04 p0674 A67-14608
Auger effect radiative recombination of excitons bound to neutral donors of GaP and Si and generation of luminescent spectrum C line 04 p0682 A67-15463
Ground state energies of P, As and Sb donors in Si taking account of dielectric screening of donor 06 p1061 A67-18925
Electron distribution of oxygen grown GaAs crystals after heat treatment, showing profiles due to silicon contamination 11 p1848 A67-24740
Donor surface states and bulk acceptor traps in silicon on sapphire films due to activation of absorbed impurities 21 p3677 A67-38012
Ground state and four lowest optically excited states of shallow donor in Si calculated using isotropic effective mass 22 p3854 A67-39245
DOOR
Main landing gear door and aerodynamic speed brake combination in F-111 aircraft, considering weight minimization and control of landing gears 05 p0753 A67-16163
DOPING
Impurity and lattice vacancy effects on compensation in doped binary semiconductors 01 p0132 A67-10455
Specific radioactivity of Sb-124 and effect on diffusion of antimony in Sb-doped n-type Ge single crystals and Ga-doped p-type Ge single crystals 03 p0500 A67-14067
Seebeck and Hall coefficients, electrical and thermal conductivity and figure of merit measured as function of dopant concentration of n-type CuBr doped bismuth antimonide telluride 03 p0501 A67-14350
Temperature dependence of electroconductivity of pure barium titanate and Fe-and Co-doped barium titanate crystals 04 p0678 A67-15130
Neutron induced degradation of carrier lifetime in n-and p-type silicon containing oxygen and dopant impurities 04 p0684 A67-15691
Dependence of intrinsic noise temperature of ruby reflection maser on helium bath temperature and chromium trioxide doping, using circulator 10 p1665 A67-23505
Temperature dependence of electroconductivity of pure barium titanate and Fe-and Co-doped barium titanate crystals 12 p1978 A67-25154
P atoms distribution in doped surface layer of silicon photoconverter for various thermodiffusion conditions exhibiting typical concentration curves 12 p1982 A67-25322
Doping of aircraft and

rockets 13 p2124 A67-27500
 Injection electroluminescence of p-n junctions in GaP doped with tellurium, zinc, ZnO, etc 14 p2368 A67-28531
 Doping distribution optimum for minimizing minority carrier transit time through base to improve overall HF performance of diodes and transistors 14 p2287 A67-28676
 Mass analysis of ion beams from low voltage spark ion source for ion-implantation doping of semiconductors 15 p2536 A67-29496
 Temperature dependence of properties of acceptor center in iron doped gallium arsenide, noting delocalization of cluster electron density 16 p2726 A67-30814
 Au and P doped n-type Si, noting formation of p-type surface layer of increasing thickness when heat treated 19 p3299 A67-34761
 Water adsorption on oxide covered surface of germanium, studying chemisorption dependence on p-type doping 19 p3301 A67-34935
 Diffusion and epitaxial equipment controlling doping level in semiconductor integrated circuits, discussing fabrication materials and techniques 19 p2326 A67-35019
 Zn doped polycrystalline GaAs film electrical properties temperature variation 20 p3514 A67-37602
 Small signal interaction impedance of bulk semiconductor amplifier with nonuniform doping profile, noting two-dimensional representation 21 p3588 A67-37818
 LiF crystals doped with Ti studied for electrical and optical properties, finding atomically dispersed Ti fractions in form of doubly positively charged centers 21 p3687 A67-39137
 Interband and free carrier Faraday rotation in n-type InAs at room and low temperature, determining conduction band parameters 22 p3863 A67-40204
 Injection electroluminescence of p-n junctions in GaP doped with tellurium, zinc, ZnO, etc 23 p4039 A67-40938

DOPPLER EFFECT

SA STELLAR DOPPLER SHIFT

Nonlinear attenuation or gain characteristics of Doppler-broadened atomic resonance involving levels with small splittings, noting mode coupling of gas laser 01 p0087 A67-10152
 Velocity propagation of stable detonations in gas mixtures determined, using Doppler effect obtained by electromagnetic wave reflection 01 p0166 A67-10229
 Doppler tolerant pulse train design, noting signal processing by delay line with fixed taps for significant changes in pulse spacing 01 p0023 A67-10464
 Frequencies of radar echoes from Mercury and Venus measured, for testing Doppler formula 01 p0026 A67-10920
 Inhomogeneity parameter over cross section of spectral line contour for case of Doppler distribution 01 p0125 A67-11046
 External ionosphere electron concentration measurement from data on Doppler shift variations in frequency of coherent radio signals from Cosmos and Elektron satellite 02 p0192 A67-11658
 Optical frequency translation of pulses from mode locked laser, noting Doppler shifts of large magnitude 02 p0253 A67-12506
 Hydrodynamics of lower solar photosphere, examining connection between small-scale oscillatory Doppler shifts and exponentially decaying continuum granulation 03 p0511 A67-13650
 Relation between sidelobe level and radar performance in clutter for nonresolvable difference between target and clutter Doppler 03 p0369 A67-13680
 Effect of Doppler and impact line broadening of spectral characteristics of gas laser, noting standing monochromatic wave saturation 03 p0439 A67-14197
 Red shifts and blue shifts relative frequency distribution for QSO 03 p0515 A67-14321
 Doppler technique application to radar measurement of clear air target motion 04 p0569 A67-14684
 System Utilizing Signal-processing for Automatic Navigation, for moving vehicles, using time delays and frequency multiplication 04 p0653 A67-14870
 Special modulation and detection processes enable radar target to be analyzed

into dimensions of time delay and Doppler shift simultaneously 04 p0699 A67-15031
 Radar target resolution and limits as function of environment, number of targets and size of delay Doppler space 04 p0572 A67-15034
 Integrated Trajectory System, measuring spatial positions, velocities, accelerations and scalar and vector miss distances for targets 04 p0654 A67-15045
 Continuous wave radar application for obtaining velocity and range information on single targets at large distances 04 p0574 A67-15046
 Gas laser spectroscopic analysis of hyperfine structure, paramagnetic properties, radiative lifetimes and Doppler-broadened transition saturation behavior of excited states of Xe 129 04 p0661 A67-15462
 Mossbauer nuclear resonance fluorescence effect spectrometer using Doppler principle, with applications to aerospace 05 p0843 A67-16544
 Doppler and impact broadening of spectral lines and pressure effects on power output of gas laser 05 p0818 A67-16643
 Differential Doppler measurements of satellite radio emissions for obtaining ionospheric electron content 05 p0764 A67-16930
 Observational techniques and detection of solar turbulence by local Doppler shifts of Fraunhofer lines 05 p0899 A67-17069
 Doppler effect on emission spectrum and energy of moving oscillator and intensity of surface wave excited by it 05 p0765 A67-17160
 Doppler profiles of nocturnal green line /5577 angstroms/ nonthermal emission resulting from molecular oxygen ion dissociative recombination 05 p0803 A67-17411
 Installation for measuring Doppler effect of satellites, investigating limits, optimization, SNR and orbital parameter accuracy 06 p0979 A67-18018
 Photoexcited electron lifetimes measured in extrinsic germanium photoconductors using Doppler shift and rotating mirror square light pulse method 06 p1005 A67-18715
 Elastic wave and IR light interactions with moving high field domain in piezoelectric semiconductor, noting acoustic impedance 07 p1232 A67-19556
 Radar range and Doppler effect simulation by stationary target outlining passive electronic countermeasure technique 07 p1146 A67-19882
 Center frequency shifts of 8328 angstrom neon transition in Zeeman discharge cell measured in terms of discharge current and gas pressure 07 p1197 A67-20100
 Complex Doppler effect in dense cold magnetized plasma 08 p1357 A67-20818
 Satellite orbit effect on establishment of global communications network 08 p1296 A67-21505
 Molecular vibrational rotational parameters measured with IR heterodyning technique 09 p1535 A67-22136
 Total electron content calculated by measurement of Faraday and Doppler effects of satellites 10 p1604 A67-22987
 Navy navigation satellite system developed by APL, using Doppler frequency measurements for navigation fix 10 p1677 A67-23183
 Ionospheric movement measurement with LF radio waves, using triangulation coupled with cross spectrum analysis of signal fading 11 p1784 A67-23936
 Inhomogeneous formations and disturbances of electron concentrations in outer ionosphere indicated by Doppler shift differences measured by Elektron I satellite 12 p1936 A67-25800
 Neel temperature in NiO and MnO with divalent Fe measured using Mossbauer effect 12 p1985 A67-25844
 Meteor trains detection and study of motions in upper atmosphere using Garchy meteor radar with continuous wave 13 p2195 A67-26467
 Doppler frequency shift for radio waves radiating coherently from satellite in ionosphere, considering electron concentration and angles of refraction 13 p2067 A67-26568
 Propagation effects on distance, arrival angle and Doppler effect measurements with reference to tropospheric

influence 14 p2264 A67-28400
 Effect of Doppler and impact line broadening of spectral characteristics of gas laser, noting standing monochromatic wave saturation 14 p2331 A67-28542
 Total electron content calculation by measuring Faraday and Doppler effects of satellites on reception frequency 14 p2270 A67-28607
 Highly adaptive phase lock coherent receiving system fulfilling requirements of data and Doppler tracking receivers 14 p2271 A67-28691
 Gas laser mode interaction in Zeeman laser, investigating transition in axial magnetic field 14 p2331 A67-28715
 Doppler effect application to solution of tracking problems with aid of artificial earth satellites 14 p2347 A67-28991
 Doppler effect method for measuring effective scatter area in laboratory 15 p2443 A67-29286
 Mean variations of total electron density with latitude and local time during winter obtained from dispersive Doppler investigations 15 p2477 A67-29666
 Range sum Doppler system for early launch tracking system to get warnings of possible impact in neighborhood of critical installations 15 p2437 A67-30111
 [AAS PAPER 67-42] 15 p2437 A67-30111
 Ionospheric electron density profiles obtained by dispersive Doppler from beacons on research rockets, noting inhomogeneities [AGARDOGRAPH 95] 15 p2483 A67-30296
 External ionosphere electron concentration measurement from data on Doppler shift variations in frequency of coherent radio signals from Cosmos and Elektron satellite 16 p2624 A67-31073
 Navigation system by measurement of Doppler shift in radio transmissions from satellite and equipment for measurement 16 p2701 A67-31272
 Differential Doppler effect on earth satellite radio signal and application to ionospheric electron density studies 16 p2627 A67-31463
 Calculation of Doppler shift of radio waves propagating through changing ionosphere by Fermat principle 16 p2629 A67-31516
 Eldorado low altitude detection and short reaction time defense system, examining Doppler effect and Mirador pulse radar 17 p2816 A67-32751
 Measuring laminar flow development in square duct using laser Doppler flow meter [ASME PAPER 67-APM-37] 17 p2861 A67-33161
 Measurement of Doppler-broadened emission line width by Fabry-Perot interferometer to study ion temperature of pulsed plasma 17 p2862 A67-33292
 Fabry-Perot interferometer for discriminating gas laser modulation at frequencies less than Doppler bandwidth 17 p2869 A67-33294
 Exact expression for line profile of stigmatic spectrograph without vignetting, noting results with foil-excited ions as light source 18 p3082 A67-33877
 Electromagnetic radiation from electric dipole moving with uniform relativistic velocity 18 p3000 A67-34022
 Woodward ambiguity function extended to broadband signals including Doppler distortions of modulation function 18 p3001 A67-34114
 Data and orbit analysis supporting Navy satellite Doppler system Tranet, discussing editing and archiving of Doppler data and orbital ephemerides generation 18 p3003 A67-34245
 Probability function for turbulent velocity in duct flow determined from Doppler shift of scattered laser radiation 18 p3030 A67-34752
 Rocket observation of ionospheric electron density using VLF doppler shift formula, determining wave polarization 19 p3215 A67-35180
 Orbit determination for Lunar Orbiter, describing computer program and studying Doppler residuals [AIAA PAPER 67-545] 19 p3328 A67-35944
 Time variation of Doppler broadened resonance line profile determined by assuming complete frequency redistribution 19 p3329 A67-36030
 Doppler effect wave radiation experiment correction equations developed for source,

observer and medium motion 20 p3486 A67-37005

Radar moving target indicating filters performance, describing method for including target Doppler frequency statistics in gain probability 20 p3386 A67-37498

Frequency stability of molecular beam laser in space environment during prolonged continuous and repeatedly interrupted operation 21 p3582 A67-38594

Telemetry receiving station and remote control system for satellites and missiles, measuring Doppler effect, demodulation and diversity combiners 21 p3583 A67-38639

Coherent responder used in distance Doppler tracking system, obtaining radial distance by using phase compression 21 p3656 A67-38650

Doppler frequency measurement error due to short fading relative to time constant of automatic phase control loop 21 p3584 A67-38674

Doppler effect method application to satellites and space vehicles motion, giving formulas for satellite velocity, orbital shape and position 22 p3831 A67-39588

Degradation of moving clutter attenuation efficiency due to Doppler-frequency shift in MTI radar systems 23 p3972 A67-40642

Photoelectric records of DE and LZE in solar photosphere velocity fields, analyzing oscillations onset and lifetimes 23 p4066 A67-41229

Spectrum line observation of decay transition of structure of gas laser 23 p4016 A67-41324

System parameters of linear time-variant space communication channels from input-output viewpoint, measuring correlation functions and Doppler spread 24 p4123 A67-42476

DOPPLER-FIZEAU EFFECT

Doppler-Fizeau frequency effect in ionospheric satellites measuring device based on wave refraction 01 p0057 A67-10233

Nonionized atmosphere effect on radial velocity measurement of satellite via Doppler-Fizeau method 03 p0369 A67-13530

DOPPLER RADAR

SA PULSED DOPPLER SYSTEM

Lunar and planetary terminal point guidance using optical correlator 02 p0264 A67-12317

Lunar landing type of Doppler radar system evaluated by space dynamic simulation testing, using helicopter and various types of terrain 02 p0205 A67-12412

Optical and UHF Doppler /UDOP/ tracking for lift-off phase of Saturn SA-5 launch vehicle 03 p0368 A67-13383

Velocity azimuth display technique analysis of wind parameters, noting fundamental limitations 04 p0648 A67-14674

Pulse Doppler radar performance in presence of random fading to study ambiguity diagram and nature of variance with respect to Doppler frequency 04 p0653 A67-14876

Airborne Doppler navigation techniques and configurations 04 p0653 A67-15041

Doppler system for missile and bullet velocity measurements noting design parameters, equipment used and range improvement obtained 04 p0653 A67-15044

AN/SRN-9 integral Doppler equipment for use with navigation satellites to determine ship position at sea 05 p0839 A67-17388

All-weather satellite navigation system using AN/SRN-9 Doppler data equipment 05 p0839 A67-17389

Pulse Doppler radar theory using Fourier transformation integrals applied to analysis of spectrum of all signals 06 p0957 A67-17592

Blind height effect in radar measurements of aircraft cruising speed treated by repetition frequency wobbling 07 p1139 A67-19228

Fabry-Perot interferometers with electronic determination of Doppler line widths, discussing effect of hyperfine and isotopic structure 07 p1185 A67-19399

Doppler frequency measurements in satellite transmissions and use for geometric geodesy 07 p1144 A67-19771

Vertical incidence CW Doppler phase path sounder spectral analysis of ionospheric motions and irregularities due to atmospheric wave propagation into ionosphere from below 07 p1182 A67-19952

Doppler radar measurements of wind velocity horizontal components variation in

rain and snow, calculating time correlation and structural functions for neutral and unstable stratifications 07 p1221 A67-20004

Frequency scanned filter in radar signal processing system designed to extract range and Doppler resolution, using properties of ambiguity function 09 p1466 A67-22695

Errors in R-meter measurement of velocity spread of meteorological targets resulting from radar frequency instabilities 10 p1676 A67-22816

Book on range instrumentation covering optical, radar, support systems, etc 10 p1604 A67-22992

Doppler tracking systems as velocity measuring systems, including introduction methods for necessary position knowledge, one-and two-way systems analyses, etc 10 p1605 A67-22995

Doppler frequency-measuring tracking system in which tracking filter or retuned heterodyne is used for definition of signal with unknown frequency 10 p1607 A67-23452

Doppler phenomena arising in rotation of system of electromagnetic wave emitters and reflectors 11 p1750 A67-23908

Side-looking synthetic aperture radar systems 11 p1753 A67-24440

Radar measurements of Doppler spectra and power reflectivity of Mars interpreted as surface elevation differences between dark and bright areas 11 p1867 A67-24776

Doppler radar and Doppler navigation system capabilities, applications, cost and reliability for supersonic and subsonic aircraft [SAE PAPER 670328] 12 p1964 A67-25870

Landing radar system for Apollo lunar module using three-beam Doppler velocity sensor and single-beam altimeter 14 p2318 A67-28290

Pulse Doppler waveform coding, presenting technique of selecting pulse-period modulation codes requiring only computer calculations 15 p2437 A67-29934

Matched-filter systems waveform dependence investigated for signal detection in nonstationary clutter 15 p2438 A67-30135

New navigation system/ADVANCE/ consisting of two-degrees-of-freedom gyro and accelerometer noting UTM grid-zone distribution system 16 p2701 A67-30928

Radar waveforms for suppression of extended clutter, discussing confinement of matched filter response in delay and Doppler or ambiguity function 16 p2625 A67-31270

Optimum mixer-filter for aircraft navigation systems consisting of inertial platform aided by Doppler and/or Loran designed, using Kalman filtering 17 p2825 A67-32525

Equipment for processing data giving optimum performances of Doppler radar 17 p2816 A67-32750

U.S. Navy Doppler geodetic Tranet system configuration and operation, discussing tropospheric and ionospheric refraction, timing and frequency errors 18 p3003 A67-34241

Lunar landing module Doppler radar system in guidance navigation and control system, studying mathematical model performance 19 p3260 A67-38011

Doppler phenomena arising in rotation of system of electromagnetic wave emitters and reflectors 21 p3585 A67-38936

Pulse generation method for high power modulators in Doppler radars studied, using step recovery diode to construct compression network 22 p3772 A67-39897

Updated inertial navigation of continuously powered space vehicle during lunar landing mission, utilizing altimeter and Doppler radar 22 p3833 A67-40195

Solid state and electron beam delay line features compared in optimal selection for radar system target simulation 23 p3982 A67-41503

DOSAGE

S RADIATION DOSE

DOSIMETER

Calorimeters used as in-line dosimeter if thin enough with respect to effective electron range to ensure that device does not degrade energy in beam 04 p0625 A67-15711

DOUBLE BASE PROPELLANT

Double-and multiple-based nitrate propellants and gunpowders with tabulated characteristics analyzed, particularly

nitrocellulose-nitroglycerin, diglycol-dinitrate, nitroguanidine and ammonium nitrate compounds 13 p2185 A67-26337

X-band attenuation by rocket exhaust plume measured with AM/PM noise for various propellant systems 15 p2436 A67-29429

System requirements effect on ballistic and hardware design of cast double-base solid propellant rocket motors 15 p2548 A67-30000

Thermal conductivity variation of double-base solid propellants under acoustic irradiation compared with polymethyl methacrylate 15 p2545 A67-30199

DOUBLE RESONANCE

Intermolecular double resonance and Overhauser effect in organic liquids 01 p0019 A67-10825

Klystron amplifier performance, noting increased efficiency by using double interaction in output circuit 02 p0222 A67-12531

Klystron amplifier performance, noting increased efficiency by using double interaction in output circuit 14 p2279 A67-28008

Optical pumping and double resonance used to study magnetic resonance and Zeeman effect 14 p2333 A67-28969

Endor double paramagnetic resonance in cane-sugar carbon at room temperature, noting electron-proton interaction 20 p3508 A67-36398

DOUBLE-SIDEBAND RADIO COMMUNICATION

Optimum reception criteria for double beam channels with fluctuating noise, signal phase and amplitude characteristics 02 p0205 A67-12532

Mixed single and double sideband interferometer receiving system having phase processing and delay simplicity and multiple RF return cable 11 p1764 A67-24308

Optimum reception criteria for double beam channels with fluctuating noise, signal phase and amplitude characteristics 14 p2261 A67-28009

DOUGLAS DC-9 AIRCRAFT

DC-9 aerodynamic design features and control systems [AIAA PAPER 65-738] 03 p0354 A67-12905

Multiparameter recording on DC-9 jet aircraft for advancing maintenance techniques, discussing use in engine, fire warning and air conditioning systems performance [AIAA PAPER 67-378] 15 p2420 A67-30349

Cabin noise reduction in DC-9 by tuned vibration absorbers attached to engine support structure [AIAA PAPER 67-401] 15 p2421 A67-30368

DC-9 environmental control design and first year service experiences [AIAA PAPER 67-407] 15 p2423 A67-30374

DC-9 wing and high lift system aerodynamic design and development, discussing STOL field length design goals and flight test results [SAE PAPER 670846] 24 p4093 A67-41999

DOUGLAS PD-808 AIRCRAFT

S PIAGGIO-DOUGLAS PD-808 AIRCRAFT DOWN-CONVERTER

Avalanche transit time diode used as sideband translator and combination local oscillator-mixer at X-band 03 p0381 A67-13666

Down-converter in reflection cavity configuration using bulk semiconductors as detection medium, considering optimum conditions 09 p1515 A67-22277

Low noise parametric down-converter by using two incommensurable pumping generators, noting gain bandwidth product and minimum noise temperature 17 p2824 A67-32315

DOWNRANGE MEASUREMENT

Reflection-type amplifier in downrange guidance system, examining noise figure optimization, pump power requirements, bandwidth and input resistance 01 p0035 A67-10410

Calibration system for PRESS optical aircraft program utilizing portable collimators 16 p2679 A67-31796

DOWNWASH

SA GROUND EFFECT

SA LIFT AUGMENTATION

SA WAKE

Partial diaphragm when applying supersonic Mach box method for steady state condition and uniform downwash on

wing compared with complete diaphragm 06 p0944 A67-18875

Rotor downwash angle and tunnel geometry effect on maximum size rotor that can be tested in closed throat wind tunnel 13 p2091 A67-27595

DRAFTING MACHINE

Costs and savings of computer graphics systems used for preparing and maintaining aerospace engineering drawings [AIAA PAPER 67-899] 24 p4127 A67-43008

DRAG

SA BOUNDARY LAYER

SA ELECTROSTATIC DRAG

SA FRICTION DRAG

SA INTERFERENCE DRAG

SA MINIMUM DRAG

SA PRESSURE DRAG

SA SATELLITE DRAG

SA SKIN FRICTION DRAG

SA SUPERSONIC DRAG

SA VISCOUS DRAG

SA WAKE

SA WAVE DRAG

Fuselage interference effect on annular airfoils determined by measuring lift and drag of model aircraft equipped with annular wing for each semispan and empenage 03 p0352 A67-13313

BGK intermolecular collision model of sphere drag at high Knudsen numbers and low Mach numbers 08 p1322 A67-21140

Optimum hypersonic shapes for outer flow region, using Newtonian approximative model 10 p1589 A67-22734

Forward facing jets effect on blunt configurations aerodynamic characteristics from wind tunnel tests at Mach 6, emphasizing drag increase 11 p1742 A67-24354

Magnetoaerodynamic drag and flight control available to vehicle entering earth atmosphere calculated, including induced magnetic fields effects and nonscalar conductivity 14 p2394 A67-29041

Semiempirical methods of spillage drag prediction for two-dimensional supersonic inlets operating in transonic flight [AIAA PAPER 67-449] 18 p2982 A67-33924

Wing shape and size selection for hypersonic velocities formulated as extremum problem of drag, aerodynamic property, temperature and coolant consumption for given wing volume 22 p3741 A67-40015

Boundary layer control by suction at trailing edge to reduce profile drag of helicopter rotor blades 22 p3742 A67-40133

MGD reentry flow regimes analyzed, noting increased bow shock standoff distance and drag, comparing in-flight and laboratory simulation 24 p4199 A67-42920

DRAG BALANCE

S LIFT-DRAG RATIO

DRAG COEFFICIENT

SA LIFT-DRAG RATIO

Gas bearing torques acting on sphere gyroscopically precessing within rotating housing, examining effect of tilt angle 01 p0077 A67-10124

Aerodynamics of nacelle used in selection and integration of exhaust systems producing highest thrust-minus drag cruise performance [SAE PAPER 660734] 01 p0140 A67-10634

Blunt cone laminar friction drag evaluated, using Reynolds analogy 01 p0007 A67-11181

Aerodynamic coefficients of symmetrical wing profiles and fuselages in rarefied gas calculated for free molecular flow 04 p0547 A67-14992

Water tunnel investigation of unsteady partial, full and supercavitation in cascade flow, determining force coefficients [ASME PAPER 66-WA/FE-25] 04 p0607 A67-15355

Mach number and temperature ratio effects on convective heat-transfer coefficient to flat plate through turbulent boundary layer in air and Stanton number calculation in terms of drag coefficient 04 p0731 A67-15820

Difference of dynamic and photometric mass of meteors cannot be explained in terms of differences in constants of drag and light curve equations alone 05 p0897 A67-16806

Ballistic coefficients for power law body shapes compared with those for conical bodies having identical lengths, diameters and specific weights 05 p0750 A67-17360

Source model for predicting drag force on

moving arc column in cross flow velocity and balancing magnetic field [AIAA PAPER 67-97] 06 p0986 A67-18280

Magnification in profile drag of airfoil due to effect of pressure gradients on boundary layer downstream of isolated roughness element 06 p0990 A67-18748

Aerodynamic characteristics of rough cylinders, noting effect on head drag coefficient and Reynolds number 07 p1126 A67-19323

Source model for predicting aerodynamic drag on moving arc column in crossflow yields relationship between crossflow velocity and balancing magnetic field 08 p1356 A67-20579

Drag coefficients of hypersonic optimum bodies at nonoptimum Mach numbers 12 p1892 A67-25744

Drag coefficient of particles in rocket nozzle 12 p1930 A67-25924

Drag coefficient for cylinder rotating in rarefied gas, comparing numerical method and approximate analytical solution 13 p2101 A67-26963

Kinetic theory description of flow over right circular cylinder at low speed based on Lees moment method 13 p2102 A67-26969

Skin friction drag coefficient at supersonic-hypersonic speeds as function of transition on delta wing 13 p2051 A67-27597

Sphere drag coefficients measured using ultralightweight models launched from two-stage light-gas gun 14 p2242 A67-28172

Interval size effect on minimum drag coefficients and optimum shapes of bodies of revolution determined from Newtonian impact theory 15 p2416 A67-29407

Computational method for high altitude atmosphere density, orbital elements, drag coefficients and potentials from satellite displacement and velocity measurements 15 p2562 A67-30069

Turbulent boundary layer flow properties predicting velocity profiles in region of velocity maximum decay downstream 16 p2657 A67-30614

Elliptic nose shape bluntness effect on drag of bodies of revolution in axisymmetric subsonic flow 16 p2589 A67-30791

Collection of papers on aerophysical studies of supersonic flows covering shock tube experiments, gas density, interferometer and photographic measurements, etc 16 p2672 A67-31101

Drag coefficient of moving body during ballistic tests calculated from given space-time dependence 16 p2592 A67-31121

Drag coefficient of sphere at supersonic velocities dependence on specific heat ratio of argon, air, carbon dioxide and freon 16 p2593 A67-31122

Probe measurements of friction drag coefficient and velocity profile of turbulent flow of mercury in circular tube in presence of longitudinal magnetic field 16 p2721 A67-31394

Limit of circulatory lift on wings with finite span, deriving lift and drag for flat and rolled up vortex sheets 17 p2789 A67-32035

Engine nacelle location, size and shape effects on drag due to wing thickness and drag due to lift [AIAA PAPER 66-665] 17 p2791 A67-32567

Incompressible fluid drag force on sphere rolling at constant speed in closed-end tube [ASME PAPER 67-APM-18] 17 p2840 A67-33149

Soviet book on high velocity hydrodynamics including airfoil motion at distances from screen, hodograph method in MGD, drag coefficient determination, etc 18 p3021 A67-33409

Two-dimensional steady flows of viscous fluid in external infinite region on basis of fourth order nonlinear Helmholtz equation in vortex terms 18 p2981 A67-33420

Nonstationary drag coefficient for unsteady flow for large Reynolds numbers determined experimentally, using analog computer method 18 p3023 A67-33425

Nonlinear theory of lifting wing surface of arbitrary aspect ratio, deriving velocity potential, lift coefficient and induced drag 18 p2981 A67-33536

Drag measurements for turbulent flow about circular cylinders joined to plane parallel walls, noting dependence on velocity profile 20 p3359 A67-37486

Drag coefficients for random and planar

tumbling satellites 21 p3563 A67-37809

Drag forces on body with nonuniform velocity distribution, considering gradient flow effects on drag coefficients 22 p3740 A67-39941

Drag coefficients used to evaluate normal force and pitching moment characteristics of revolving body at angle of attack 22 p3740 A67-39943

Thrust history to produce maximum altitude for two-stage launch vehicle determined using simplifying assumptions and atmospheric drag 22 p3904 A67-40089

Wind tunnel data predicted vertical forces for rocket sleds compared with measurement on test track noting disagreement 22 p3780 A67-40095

Approximate solution for turbulent jet expansion in opposite gas flow, discussing hydraulic drag coefficient formula derivation 23 p3989 A67-40731

Exponential vertical flow shear effect on induced drag of elliptically loaded lifting line 23 p3932 A67-41735

Orbit-and sun-oriented solar cell concepts compared, discussing aerodynamic drag penalties 24 p4105 A67-42517

DRAG DEVICE

SA BALLUTE

Aerial delivery concepts including drag cones, lift platforms, gliding parachutes, ballute parachute, ultrafast-opening parachute, etc 17 p2796 A67-32519

DRAG EFFECT

Two-component drag force anemometer design and performance, noting method for wind bearing and velocity measurements 05 p0808 A67-17308

Orbital decay, considering drag force expression, motion equation, atmospheric structure, King-Hele theory, etc 06 p1081 A67-17786

Span loading of swept wing which produces minimum induced drag with constraints on lift and pitching moment 06 p0937 A67-18010

Subsonic drag rise for airfoil determined by limit line analysis in hodograph plane [AIAA PAPER 67-4] 06 p0938 A67-18248

Drag effects on meteoric bodies studied by photographic observations 13 p2196 A67-26499

Minimum power requirements of V/STOL aircraft 13 p2054 A67-27586

Subsonic-transonic drag of supersonic, two-dimensional and axisymmetric plug inlets 13 p2051 A67-27592

Subsonic drag rise for airfoil determined by limit line analysis in hodograph plane [AIAA PAPER 67-4] 13 p2051 A67-27599

Approximate analytical solution for satellite circular orbits subjected to small tangential thrust or drag 14 p2384 A67-28117

Free molecular flow region, calculating drag on plate, sphere and general body, considering drag effect on satellite orbit 15 p2561 A67-30045

Relation between drag and dissipation in incompressible flows 17 p2839 A67-32710

Atmospheric density determination from satellite drag, noting effects of magnetic storms, diurnal and semiannual variations, solar activity, etc 18 p3041 A67-34253

Air drag effect on six Cosmos satellites orbits having low perigee, discussing diurnal air density variation at 280 km height 18 p3042 A67-34256

Media with cold homogeneous isotropic lossless plasma dispersion characteristics exhibiting no electromagnetism drag 19 p3298 A67-35828

Ascent and descent gravity turn trajectories of rocket in constant gravitational field, considering drag forces in motion equation [AIAA PAPER 67-596] 19 p3336 A67-35992

Atmospheric drag influence on orbital elements of satellites having highly eccentric orbits 20 p3522 A67-36616

Modifying effect of base bleed investigated photographically for incompressible wake behind two-dimensional bluff body, estimating base pressure 20 p3421 A67-36844

Drag forces on body with nonuniform velocity distribution, considering gradient flow effects on drag coefficients 22 p3740 A67-39941

DRAG MEASUREMENT

Induced drag for idealized ground effect wing for optimum lift

- distribution 01 p0006 A67-10809
- Drag measurements of isolated lamellae and cylinders in rarefied gases with low velocity 03 p0404 A67-13972
- Turning-arm apparatus operating in rarefied gas chamber and low pressure wind tunnel for drag measurements 04 p0596 A67-14993
- Upper atmospheric density, pressure and temperature profile obtained from drag acceleration measurements on falling sphere 07 p1181 A67-19938
- Tangential drag measurements at electrodes of arc in plasma accelerator, ion current partitioning at cathode and electrode damage 21 p3670 A67-38693
- Drag measurements of cones in rarefied flow regime extended to higher and lower cone semivertex angles 21 p3565 A67-38884
- DRAG REDUCTION**
- Lift augmentation through drag reduction and variable wing profile in light aircraft 01 p0005 A67-10265
- Linearized supersonic theory for favorable thickness distributions and drag reduction for wings in supersonic flow [AIAA PAPER 65-716] 08 p1276 A67-20559
- Transition delay and skin friction drag reduction by considering boundary layer flow over flexible aerodynamic surface [AIAA PAPER 66-430] 13 p2106 A67-27585
- Retractable airfoil and hinged cowl modifications of supersonic inlet to reduce drag below choking point for subsonic operations 17 p2791 A67-32575
- Gas ejection and boat-tailing effect on cylindrical afterbody in supersonic flow 17 p2793 A67-33041
- Shape of minimum drag cruciform wing of symmetrical thickness in supersonic flow 20 p3355 A67-36192
- Aircraft fuselage shapes analysis for drag reduction and maximum useful space based on streamlined bodies found in nature 20 p3375 A67-36887
- Thrust and drag response to heat input directly behind and before body moving supersonically or subsonically 21 p3563 A67-37887
- Aircraft wing drag noting relation between Mach number, thickness chord ratio, aspect ratio, airfoil shape and wing configuration 23 p3930 A67-41306
- Drag problems of Belfast aircraft solved by modifications developed in wind tunnel program 24 p4092 A67-42443
- DRAWING**
- S BUNDLE DRAWING
- S MECHANICAL DRAWING
- DRIFT**
- SA GYROSCOPIC DRIFT
- SA IONOSPHERIC DRIFT
- SA YAW
- Quadrupole calculation of zero-level drift in transistorized DC amplifiers 06 p0970 A67-18172
- Drift field, field gradient and diffused impurity effects on minority carriers and quantum efficiency in silicon photocells 11 p1746 A67-24914
- Drift effect on diffusion spreading of plasma inhomogeneities in magnetic field, deriving expression for Fourier component potential, and magnetic field perturbations 12 p1933 A67-25546
- DRIFT RATE**
- Superposed electric field effect on longitudinal drift rate of geomagnetically trapped electron 01 p0056 A67-10109
- Ionospheric F-2 layer inhomogeneities attributed to plasma flute instability, using kinetic drift equations to describe plasma oscillations 02 p0236 A67-11669
- Repetitive plasma breakdown in flat electrode accelerator causing relatively low plasma velocity 02 p0275 A67-12472
- Drift velocity dependence on electric field in GaAs measured by analysis of reverse biased Schottky barrier response to step input of light 02 p0253 A67-12504
- Hydrodynamic drift-dissipation instability of plasma with nonuniform temperature 03 p0476 A67-13296
- Stable domain propagation in gallium arsenide for nonzero constant diffusion coefficient, based on analytic approximation to velocity field 03 p0493 A67-13461
- Magnetic activity effect on sporadic E region drifts, comparing plot of K index vs drift velocities 03 p0413 A67-13684
- Hydrodynamic drift-dissipation instability of plasma with nonuniform temperature 04 p0663 A67-14721
- Inelastic collisions by drifting ions studied by series of experiment in which mass analyzed ion beam is injected into drift tube containing gas 04 p0661 A67-15509
- Magnetic field effect on velocity of electron drift produced by electrical field in dense plasma 04 p0671 A67-15580
- Drift waves in finite pressure plasma, noting oscillation caused instabilities induced by Alfvén type and slow magnetoacoustic wave interaction 05 p0852 A67-18693
- Nonlinear theory on effect of drifting cone plasma instability on particle drift from adiabatic trap 05 p0860 A67-17545
- Charged particle collisions effect on drift instability of low pressure plasma studied, using Landau collision integral as model collision integral 05 p0860 A67-17546
- Pacific equilibrium longitude for stationary satellite, discussing processing of Syncom III data, drift rate calculations, etc [AIAA PAPER 67-91] 06 p1086 A67-18338
- Interaction between helicon waves and drift currents in layered lead telluride structure 07 p1232 A67-19555
- Drift velocity variation with electric field calculated in GaAs, using Boltzmann equation and incorporating additional scattering process 07 p1232 A67-19561
- Photolionization mass spectrometer for ion-molecule reaction studies, determining ion residence times, drift velocities, diffusion coefficients and ion temperatures 07 p1137 A67-20187
- Ambipolar diffusion and drift of plasma of added carriers in semiconductor in presence of magnetic field 08 p1369 A67-20900
- Ion beam excitation of drift waves in alkali plasma, discussing sinusoidal signal propagation characteristics, variations with beam velocity and with modulation frequency 08 p1361 A67-21135
- Anomalous diffusion arising from drift instability in collision-free equilibrium plasma cylinder 08 p1366 A67-21440
- Adiabatic invariant analysis of charged particle motion in model magnetosphere 08 p1378 A67-21474
- High field mobility degradation effect on characteristics of insulated gate FET, considering drift velocity proportional to field square root and constant drift velocity 09 p1471 A67-21944
- Gunn diode efficiency for mixed resonant transit time and suppressed modes, using dynamic drift velocity field strength characteristic 09 p1474 A67-22039
- Temperature and tolerance behavior of transistor determined, based on equivalent drift sources of transistor obtained from intrinsic series coupling 09 p1482 A67-22611
- Excitation and damping of drift waves in stable regime of ionized plasma radially confined by axial magnetic field 09 p1550 A67-22679
- Low temperature alkali plasmas in strong magnetic fields interpreted in terms of collisional drift modes 10 p1684 A67-23073
- Carrier drift velocity measurements in silicon at high electric fields, using time-of-flight technique 10 p1690 A67-23187
- Cut-off frequency of drift transistor, discussing function of drift field parameter 11 p1759 A67-24143
- Cesium plasma measurements to determine steady state parameters and LF oscillation characteristics 11 p1834 A67-24379
- Ion radial drift velocity in argon ion laser discharge tube 11 p1803 A67-24931
- Double shutter drift tube for measuring electron drift velocities and momentum transfer cross sections in methane, ethane, ethylene, etc 11 p1824 A67-24994
- Ponderomotive forces and geomagnetic westward drift in regard to MHD theory and earth core flows 13 p2114 A67-28855
- Temperature and carrier concentration effect on threshold electric field of current saturation and saturation drift velocity in gallium arsenide 14 p2364 A67-27826
- Second current saturation of nonohmic behavior in CdS single crystals caused by quantum mechanical interaction between drift electrons and acoustic phonons 14 p2365 A67-28239
- Negative-resistance Gunn effect in gallium arsenide and indium phosphide due to field excited electron transfer 14 p2366 A67-28474
- Fine structure profiles of solar radio bursts observed with high time resolution 14 p2381 A67-28579
- Drift waves in finite pressure plasma, noting oscillation caused instabilities induced by Alfvén type and slow magnetoacoustic wave interaction 15 p2530 A67-29864
- Reducing disturbances of certain form to zero by generating modified form of test signal to be applied to cross correlator 15 p2461 A67-30322
- Measurements at Ibadan of drift velocity of ionospheric irregularities for E and F layers during IQSY 16 p2663 A67-30969
- Ionospheric F-2 layer inhomogeneities attributed to plasma flute instability, using kinetic drift equations to describe plasma oscillations 16 p2665 A67-31084
- Drift instability of discharge plasma with oscillating electrons 16 p2717 A67-31180
- Turbulent plasma state from unstable, current driven drift waves, noting ion damping effect on amplitude of spectrum, density gradient, etc 16 p2719 A67-31231
- Galactic and solar ray behavior equations, with cosmic ray drift velocity and diffusion tensor determined for interstellar space in anisotropic-diffusion approximation 17 p2935 A67-32109
- Long term gyro drift rate evaluation involving time series detrending and autoregression, periodogram, autocorrelation, spectral density and mathematical model analysis 17 p2858 A67-32486
- Concepts of wind drift and lateral maneuver applied in flight mechanics 17 p2798 A67-32591
- Design concept for piezoelectric resonator through mathematical formulation, determining critical frequencies and electron drift rates 18 p3043 A67-33462
- Gyro-stabilized inertial navigation platform system upgraded by applying sampled model reference system, estimating gyro drift rates by stochastic approximation method 18 p3075 A67-34106
- Thermocouple drift on Chromel-P vs Constantan under vacuum, high temperatures and time factor conditions 18 p3052 A67-34516
- Nitrogen ion drift velocities in plasma jet flowing into vacuum chamber noting ion mobilities in parent and foreign gas 19 p3271 A67-35075
- Time variations of electron intensity in outer radiation belt observed by satellites, studying electron radial diffusion and drift velocity 19 p3313 A67-35257
- Drift instabilities and related phenomena in inhomogeneous plasma confined by strong magnetic fields 19 p3292 A67-35388
- Electron mobility and trapping time in semi-insulating cadmium telluride through observing transient response to alpha particles 19 p3308 A67-36101
- Inhomogeneous plasma oscillations, studying drift and flute instabilities and dielectric constant 20 p3492 A67-36130
- Rate of transequatorial plasma diffusion along geomagnetic field lines in topside ionosphere, considering electron distribution asymmetries in equatorial F-2 layer 20 p3431 A67-37098
- Electron drift velocity and mobility in InSb calculated from conductivity and Hall effect measurements, noting microwave emission occurrence 20 p3514 A67-37544
- Stabilization conditions of isothermal plasma drift in magnetic trap for comparable electron and ion temperatures 21 p3663 A67-37936
- Energy band nonparabolicity effect on GaAs drift velocity vs field curve, especially near Gunn threshold 21 p3680 A67-38348
- Drift instabilities of inhomogeneous plasma in HF electric field 21 p3667 A67-38374
- Drift and ion acoustic waves and coupled waves in highly ionized dense plasma of finite ion temperature 21 p3667 A67-38412
- Western and equatorial components of geomagnetic field drift, noting noncoincidence of rotation axis with earth rotation axis 21 p3622 A67-39028
- Ion wave dispersion relation in mercury vapor plasma, explaining cut-off frequency dependence on electron drift velocity 22 p3842 A67-39207
- Ion wave velocities and damping measurements in quiescent plasma used for diagnosis of temperatures and drift

velocities 22 p3846 A67-39488
Pacific equilibrium longitude for
stationary satellite, discussing processing of
Syncom III data, drift rate calculations, etc
[AIAA PAPER 67-91] 22 p3886 A67-40085
Electrostatic gyro characteristics, design
implications, numerical analysis of
parameters and corresponding drift
rates 22 p3800 A67-40185
Efficient inertial navigation system with
He 2 superfluid persistent current gyro
element having small drift
rate 22 p3808 A67-40395
Kinetic equation for steady state electron-
ion system with electrons drifting under
electric field, calculating HF resistivity drift
velocity dependence 23 p4033 A67-40962
Fading rate relation to ionospheric drift
speed of radio waves, estimating size of
irregularities 23 p3996 A67-41083
Flare positions relative to neutral line in
longitudinal components of photospheric
magnetic fields, stressing drift
rate 23 p4060 A67-41231

DRILL

Ion beam generation for drilling thin
metallic coatings deposited on glass-ceramic
substrates 03 p0432 A67-14269
Fluid circuits used in drilling sequence
control, detailing ring counter, binary
counting stage and
comparator 08 p1281 A67-20458
Laser as drilling and welding tool, noting
industrial guidelines, pulse control
techniques, micromachining,
etc 09 p1504 A67-22140
Laser as drilling tool 09 p1504 A67-22142
Industrial laser application, giving
background information on laser
theory 09 p1505 A67-22145
Ion beam generation for drilling thin
metallic coatings deposited on glass-ceramic
substrates 14 p2325 A67-28779

DRIVE

SA GEAR
SA PROPELLER DRIVE
SA ROTARY DRIVE
SA WIND TUNNEL DRIVE
High speed drive for rotating shafts inside
high vacuum chambers
[ASME PAPER 66-WA/PID-7] 04 p0628 A67-15330
Aircraft alternator test drives and
specification
requirements 13 p2081 A67-27238
Axial gear differential /AGD/ design and
selection for constant speed AC generator
drive for aircraft engines 17 p2800 A67-31976
Roller traction drive unit for extremely
quiet power transmission compared with
planetary-gear drive
[AIAA PAPER 67-429] 18 p3053 A67-33913

DRONE

Aerodynamic deceleration system for
target drone recovery with reduced impact
damage, discussing design
improvements 17 p2797 A67-32573

DROP

SA LIQUID DROP
Condensation droplet growth in
supersaturated vapor and inert carrier gas,
noting thermal and diffusion
effects 15 p2582 A67-30198
Spherical shape changes of droplet of
viscous substance of high surface tension
under variable external force and small
deformation 18 p3028 A67-34220
Solution drops motion in diffusing binary
gas mixture, analyzing
velocity 20 p3421 A67-36812
Relative velocity effect on vaporization
times and heat-transfer coefficients of water
drops in Leidenfrost film boiling on heated
rotating wheel
[AIChE PAPER 32] 20 p3552 A67-36833
Particle mass spectrum development in
rocket nozzle, assuming droplet growth by
collision and agglomeration as dominant
mechanism 20 p3516 A67-37130

DROP SIZE

Airborne photoelectric device for
registration of cloud
drops 07 p1189 A67-20009
Stable size and reaction of molten metal
droplets with rarefied atmosphere as
consequence of surface oxide film, treating
beryllium 10 p1733 A67-23124
Mean droplet size for cross stream water
injection into Mach 8 air flow determined by
scattered light angular variation
measurement 11 p1779 A67-24366

Evaporation kinetics of small droplets is
dependent on size, liquid and gas state and
gas-liquid interface 11 p1884 A67-24989
Condensation spectrum evolution of cloud
droplets 13 p2151 A67-26690
Deviation from sphere shape of drop
moving through viscous media and
dependence on Weber number, size,
etc 14 p2302 A67-28235
Heat transfer by dropwise condensation,
evaluating average heat
flux 17 p2969 A67-32447
Aluminum particle combustion in solid
rocket grains, noting drop formation
mechanism and droplet combustion analysis
[ONERA-TP-486] 17 p2926 A67-32697
Correlation between thrust chamber
design parameters and combustion stability,
noting stability increment with increasing
injection velocity, droplet diameter and
chamber pressure
[AIAA PAPER 67-474] 18 p3113 A67-33944
Apparatus for uniform sized liquid drop
production by ultrasonic wave action on
fluid jet, with drop formation recorded by
photography 18 p3052 A67-34610
Time dependent expression for droplet-
size distribution function of clouds
undergoing forcible modification or natural
evolution 19 p3251 A67-34862
Bubble frequency, departure diameter and
rise velocity relationship in nucleate
boiling 20 p3553 A67-36934
Condensation spectrum evolution of cloud
droplets 21 p3654 A67-38432
Q-switched laser use as light source for
photographing droplets in spray containing
fluorescent dye excited by second harmonic
of ruby light 22 p3797 A67-39492
Liquid surface tension effect on maximum
particle size in two-phase nozzle flow,
discussing drag exerted by accelerating gas
stream 22 p3787 A67-40225
Theoretical collision efficiencies for cloud
droplets in steady Stokes flow suggest near
unity coalescence 23 p4024 A67-40636

DROP TEST

IC emitter follower line driver with input
filtering for PWM signal conditioning,
solving onboard high impedance problems in
drop tests with piezoelectric
accelerometer 23 p4005 A67-41372

DROSOPHILA

Recessive lethals in X chromosome of
drosophila and genetic shielding during
flight of spaceship
Voskhod 13 p2060 A67-27337

DRUG

SA ALKALOID
SA AMMONIUM CHLORIDE
SA ANESTHETICS
SA ANTIBACTERIALS
SA CENTRAL NERVOUS SYSTEM
STIMULANT
SA MOTION SICKNESS DRUG
SA PHARMACOLOGY
Gastrointestinal symptoms and drug use as
possible contributing causes of fatal crash of
race pilot 09 p1456 A67-21734

DRY CELL BATTERY

SA STORAGE BATTERY
Nonrechargeable batteries for miniaturized
components, discussing dry, electrochemical,
alkaline and mercury
cells 07 p1131 A67-19531

DRY FRICTION

Astatic gyroscope accuracy dependence on
random fluctuations of dry friction moment
when under oscillatory motion of bearings,
giving correlation function of error
dispersion 11 p1794 A67-25044
Cermet sealing material dry-friction
characteristics over wide sliding-speed
range, discussing graphite and boron nitride
lubricants 19 p3247 A67-35850
Dry friction servo system dynamics with
relay delay in random noise
case 20 p3451 A67-37152
Triggering controller dynamic model with
magnetoelectric drive, examining phase
volume by point transformation
technique 24 p4155 A67-42297
Gyro power stabilizer in unsteady
equilibrium state becoming stable under dry
friction defined for controllability in phase
space 24 p4155 A67-42299
Synthetic molybdenum sulfide film
examined for lubricating performance under
extreme pressure conditions in air and

immersed in fluids
[ASLE PAPER 67-LC-15] 24 p4165 A67-42749

DRY HEAT

Spacecraft sterilization for microflora and
microorganisms using dry heat for
instruments, liquid straining and gas for
surfaces 15 p2430 A67-29100
Antimicrobial properties for various
spacecraft materials, discussing impregnation
methods for bactericides and two-stage
sterilization 19 p3179 A67-35229

DSIF

S DEEP SPACE INSTRUMENTATION
FACILITY /DSIF/

DTA

S DIFFERENTIAL THERMAL ANALYSIS
/DTA/

DUAL CONTROL PROBLEM

Comparison of nonoptimum and optimum
strategies in dual control of inertialess
plants in presence of noise in feedback
loop 05 p0781 A67-16257
Duality and a priori estimates in
Markovian nonlinear stochastic optimal
control problems 05 p0784 A67-16778
Dual control of plant with random
amplification factor as Bayesian
problem 06 p0976 A67-18408
Static and kinematic formulation of plastic
analysis of structures and duality in linear
programming 11 p1876 A67-24623
Book on nonlinear programming covering
various methods and use in
control 17 p2818 A67-32424
Duality method in dynamic optimization
problem 19 p3204 A67-35907

DUAL THRUST

Performance and feasibility of staged
propulsion during terminal phase of Mars
soft landing
[AIAA PAPER 67-987] 24 p4246 A67-43059

DUCT

SA ACOUSTIC DUCT
SA AIR DUCT
SA INLET
SA ORIFICE

Frictional pressure drop for isothermal
incompressible flow in isosceles triangular
duct, with correlations for laminar and
turbulent flow
[ASME PAPER 67-FE-18] 14 p2243 A67-28365
Energy transmitting characteristics and
wall local energy absorption distribution of
curved specular reflecting duct irradiated by
collimated beam 23 p4028 A67-41271

DUCTED BODY

Inviscid flow characterized by annular
elliptical region between shock wave and
ducted body calculated by integral relation
method, noting contraction coefficient
values 10 p1591 A67-23045
Transonic gas flow past ducted bodies of
revolution indicates shock wave asymptotic
attenuation at infinity 14 p2296 A67-27989
Burst strength in high speed rotor in axial
blower/gas turbine, noting effect of ductility
and centrifugal force 17 p2961 A67-32688
Ducted silo launchers transient pressures
caused by rocket engine ignition and
shutdown, treating wave propagation by one-
dimensional theory 22 p3780 A67-40091

DUCTED FAN

Flight tests of two X-22A dual tandem
rotatable ducted propeller V/STOL research
aircraft 06 p0948 A67-18201

DUCTED FAN ENGINE

Approximate analysis of subsonic
compressible flow in annular nozzle of short
duct fan engines and inner wall curvature
effect on pressure
distributions 06 p0944 A67-18871

DUCTED FLOW

MHD generators theory and operation
including superheat conductivity, strong
magnetic field generation and MGD flow
structure in ducts 17 p2803 A67-32335
Current distribution in segmented
electrode MHD duct and sufficient condition
for preventing current leakage between
adjacent segments of
generator 18 p2987 A67-33703
High pressure helium arc plasma behavior
in cylindrical duct explained by theoretical
model with different electron and heavy
particle temperatures 19 p3280 A67-35145

DUCTILITY

SA CREEP
SA PLASTICITY
Book on dynamic strength, brittleness,
plasticity and ductility of
metals 05 p0907 A67-16031

- Superplastic effect in cr-30 at pct Co alloy, noting low temperature bend ductility in quenched metastable single phased and near equilibrium conditions 05 p0829 A67-16474
- Creep ductility, stress rupture and high temperature irradiation embrittlement of neutron-irradiated Hastelloy N 08 p1343 A67-21195
- Titanium carbide dispersion-strengthened nickel by internal carburization, with fair ductility and stress rupture properties at high temperatures 11 p1806 A67-24361
- Ductile fracture with rotation under shear and normal stresses, noting relationship between fracture strain and stress state for given inclusion content [ASME PAPER 67-MET-9] 12 p1956 A67-25950
- Ductility of beryllium samples subjected to compression at temperatures ranging from 300 to 600 degrees C, discussing slip effects 13 p2137 A67-27113
- Plastic flow in beryllium under fluid pressure at room temperature 13 p2139 A67-27123
- Molybdenum ductility improvement by electrowinning with yttrium 14 p2338 A67-28616
- Low cycle fatigue behavior of metals at creep range temperature related to equivalent ductility and strain rate 16 p2774 A67-31321
- Aluminum content effect on stress-rupture properties of chromium-molybdenum-vanadium steel, noting notch sensitivity and ductility 16 p2693 A67-31869
- Effect of thermomechanical treatments on tensile properties of metastable austenitic steels 16 p2693 A67-31872
- Thermal exposure effect on recrystallization and ductility of TZM molybdenum alloy sheet and foil 19 p3234 A67-34793
- Factors affecting tensile ductility minimum behavior of silicide coated niobium alloys investigated in air for intermediate temperature range 22 p3821 A67-40052
- DUFFING EQUATION**
- SA PROBABILITY**
- Rational approximation of generalized Duffing equation, damped mass spring oscillator equation and generalized second order Riccati equation 04 p0647 A67-15660
- Forced nonlinear vibration of Duffing type experimentally simulated with models of isolating systems, obtaining response curves [ASME PAPER 67-VIBR-35] 11 p1873 A67-24192
- Polar coordinate analysis of free oscillations of circular plates with loosely clamped edges under large deflections, obtaining Duffing equation 12 p2031 A67-25963
- Macroscopic physical system with behavior described in terms of differential equation system studied for stability in presence of small delay 19 p3205 A67-35912
- Steady random natural frequency variation and subharmonic resonance, discussing periodic right hand side Duffing type equation describing system 22 p3836 A67-39405
- DUMBBELL SPACE PROBE**
- Nonlinear resonant coupling between damped and undamped vibrations for damping roll in TRAAC and elastic dumbbell satellites [AIAA PAPER 67-568] 19 p3329 A67-35964
- DUMMY**
- Measurement of dimensions and inertial properties of 50th percentile anthropometric dummy 08 p1289 A67-20611
- DUOPLASMATRON**
- High current duoplasmatron ion source with ferrite permanent magnets and extraction lens system 02 p0279 A67-12694
- Diagnostic studies of gas discharge and contact ion sources including test equipment, instrumentation, design and characteristics of propulsion concept 03 p0504 A67-13494
- Pressure dependence of mean electron energy of plasma emerging from anode aperture of duoplasmatron ion source 04 p0683 A67-14768
- Physical mechanisms and operational principles of electron bombardment ion sources with reference to Lewis geometry and duoplasmatron configuration 04 p0664 A67-15017
- Cathode sputtering thin film preparation at low pressure, describing duoplasmatron and sputron ion sources 10 p1661 A67-23693
- Pressure gradient in duoplasmatron ion source as function of parameters of discharge 14 p2359 A67-28512
- Duoplasmatron ion source study with Langmuir probe, finding that pressure dependent discharge characteristics relate to magnetic field radial components 17 p2902 A67-32659
- Modified duoplasmatron in cusp fields to produce highly ionized and high density quiescent plasma, using DC discharge, noting helium plasma generation 19 p3274 A67-35104
- Discharge model for relative abundances of different ions extracted from Ar duoplasmatron from Langmuir probe measurements 23 p4033 A67-41190
- Mass species abundance ratio of hydrogen ion beam from Oak Ridge type duoplasmatron ion source, discussing pressure dependent characteristics 23 p4034 A67-41436
- DUPLEXER**
- Step recovery varactors in constant-component and microstrip CW duplexers 18 p3011 A67-34067
- DUST**
- SA COSMIC DUST**
- SA INTERPLANETARY DUST**
- SA LUNAR DUST**
- SA METEOR DUST CLOUD**
- SA METEORITIC DUST**
- SA TERRESTRIAL DUST BELT**
- SA ZODIACAL DUST CLOUD**
- Flow induced by infinite flat oscillating plate in incompressible dusty gas 02 p0234 A67-12548
- Shock wave propagation in gas-dust medium, examining motion and velocities of gas and dust at distance approaching infinity 04 p0701 A67-15556
- Atmospheric dust content estimation, using solar radiation depletion by particulate matter and separating attenuation by gases and water vapor 10 p1700 A67-23086
- Dust content of air flow created by piston engine Mi-1 and Mi-4 helicopters in landing and takeoff 11 p1744 A67-24530
- Impact and abrasion wear of axial and centrifugal helicopter compressor stages due to dust intake, showing direct proportionality to impact velocity and particle size 11 p1853 A67-24531
- Allison T63 engine sand and dust tolerance development and field experience [SAE PAPER 670334] 12 p1990 A67-25875
- Gas turbine blade erosion from dust, discussing momentum separators and erosion-resistant coating 12 p1990 A67-25947
- Detectability of massive star from opaque dust cocoon through IR radiation 14 p2388 A67-28833
- DUST COLLECTOR**
- High altitude balloon top collections of cosmic dust shows evidence of absence of crystal structure in particles 10 p1708 A67-23239
- Windborne dust collections on Barbados Islands investigated by mesh technique for origin of cosmic dust 20 p3432 A67-37174
- DYADIC**
- SA QUATERNION**
- Book on elasticity covering engineering, Cartesian tensor and vector-dyadic notation, etc 14 p2395 A67-27891
- Multiple scattering of electromagnetic waves by arbitrary configurations extended to three-dimensional vector case 15 p2435 A67-29197
- Dyadic formalism to prove Herglotz-Noether theorem for flat manifolds [JPL-TR-32-1125] 17 p2879 A67-32929
- DYE**
- SA CYANINE DYE**
- Pumping of organic dyes in organic solvents, using pulsed ruby laser 02 p0253 A67-12515
- Fluorescein family organic dyes exhibiting laser action when excited by ruby and neodymium second harmonics 12 p1953 A67-25748
- Organic dyes as broadband pulsed light amplifiers, noting input frequency relation to laser oscillation 20 p3460 A67-36855
- DYNAMIC CONTROL**
- Matrix formulation of output controllability conditions for dynamic systems 01 p0048 A67-11293
- Dynamic analysis of reaction control system /RCS/ propellant feed network on lunar module using digital computers 01 p0142 A67-11435
- Dynamic control for two-phase liquid-gas medium under weightlessness solved by surface energy, using computer for boundary value problem involved 02 p0231 A67-11540
- Dynamic behavior of electric angle drive unit in linear automatic control system, noting nonlinearity 02 p0227 A67-12197
- Optimality of totally singular vector controls governing dynamical systems and extension of Green theory approach to higher dimensions to evaluate optimality of such controls 04 p0594 A67-15875
- Dynamic characteristics of human operator in tracking system under spaceflight conditions onboard Voskhod II spacecraft dynamic characteristics of human operator in tracking system under space flight conditions 07 p1135 A67-19106
- Dynamic control study for solar mirror aboard spacecraft using breadboard apparatus and computer simulation method 11 p1745 A67-24274
- Dynamical systems control problem in connection with differential equations with lagging arguments 14 p2291 A67-28384
- Optimal control of random dynamical systems analyzed, using first order vector differential or difference equations 14 p2292 A67-29062
- Quantizer optimal design for closed-loop dynamic and open-loop static systems 15 p2456 A67-29364
- Optimal averaging theories of controls of dynamic systems 15 p2458 A67-29687
- Determining control functions and choosing parameters governing transfer of dynamic system from initial to final state 16 p2744 A67-30732
- Dynamic control for two-phase liquid-gas medium under weightlessness solved by surface energy, using computer for boundary value problem involved 16 p2663 A67-31606
- Suboptimal control of large scale dynamic system consisting of two weakly coupled subsystems using aggregation 16 p2647 A67-31645
- Elimination of electrical transients in high performance sleeve induction motors for missile guidance control systems 16 p2609 A67-31664
- Distributed parameter concepts of propagation, reflection and characteristic termination applied to dynamic analysis and control of bending vibration 16 p2776 A67-31686
- Duality method in dynamic optimization problem 19 p3204 A67-35907
- Dynamic identification of loop system consisting of square-law operator, with behavior function of input signal and initial conditions 19 p3206 A67-35916
- Asynchronous finite state sequential nonlinear controller synthesis with few flip-flops for dynamic space vehicle systems [AIAA PAPER 67-988] 24 p4127 A67-43060
- DYNAMIC LOAD**
- Dynamic load analysis of Titan III booster structure using dynamically scaled model in vibration survey [SAE PAPER 660684] 01 p0154 A67-10588
- Formulation of dynamic three-dimensional problem of homogeneous isotropic and linearly elastic bodies in terms of stresses 03 p0523 A67-13459
- Inertial force effect on propagation of plastic deformation in specimen under dynamic load 05 p0921 A67-16936
- Stress distribution measurement by vibration method, applying hand-held extensometer place by place on surface of structure subjected to dynamic load of finite amplitude 06 p1100 A67-18001
- Dynamic stress concentration for plate with square hole, using approximate method of boundary shape perturbation and conformal mapping 06 p1109 A67-18665
- Explosive loading and structural response measurement techniques for predicting large elastic-plastic dynamic and permanent deformations of shells under dynamic loading conditions 07 p1262 A67-19411
- Dynamic stress concentration due to elastic wave analyzed by high speed photoelasticity to clarify difference between dynamic and static stress distribution 07 p1262 A67-19414
- Testing machine for evaluating high

temperature fabrics under dynamic loading and heating conditions 07 p1212 A67-20262

Axisymmetric plane-strain vibrations of thick layered orthotropic shell under internal and external pressures analyzed, using Fourier series for eigenmodes determination 08 p1415 A67-20487

Calculating method for parachute opening forces, system velocity, cloth pressure loading and filling time for horizontal and vertical deployment 11 p1743 A67-24348

Dynamics of rigid plastic thin walled shells for short term constant high intensity load 12 p2025 A67-25607

Semiinfinite cylinder dynamic torsional problem, considering self-balanced and self-unbalanced boundary perturbation expansion 12 p2029 A67-25664

Instrumentation and data acquisition system used in Saturn V dynamic test program for design of flight control system 12 p1923 A67-25709

Dynamic snap-through buckling of shallow spherical caps of elastic material 12 p2030 A67-25923

Flight Load Survey program, written in Fortran IV, for accurate and rapid sounding of wind-induced loads on aerospace launch vehicle [AIAA PAPER 66-470] 13 p2212 A67-26820

Steady and dynamic loads on tandem rotor, controls and airframe flight tested with Army helicopter, using automatic data processing 13 p2054 A67-27596

Book on safety of structures 14 p2395 A67-28030

Single mode analysis of dynamic buckling of imperfection-sensitive elastic structure prone to catastrophic failure under time dependent load 14 p2396 A67-28083

Dynamic plastic buckling of thin strips, thin and moderately thick cylindrical shells and rods under longitudinal and radial impact and compression 14 p2397 A67-28088

Secure mechanically fastened assemblies in static and dynamic stress, showing effect of tightening preload [ASME PAPER 67-DE-3] 14 p2327 A67-28865

Structural dynamic load and instability problems in launch vehicles and spacecraft in lunar exploration emphasizing reliability, crew safety and mission success 16 p2654 A67-30677

High speed plastic deformation of bar studying relation of breaking strain vs tensile velocity and comparing values of former to static case 16 p2775 A67-31329

Dynamic response of rigid-plastic material ring subjected to arbitrarily distributed impulse load 17 p2959 A67-32412

Soviet book on dynamic effects of moving loads on beams supported by linear and nonlinear bearings and elastic bases 18 p3140 A67-33661

Soviet book on stability and oscillations of elastic systems covering theory, equilibrium breakdown, dynamic loading, aeroelastic oscillations, etc 18 p3140 A67-33674

Brittle coatings for stress distribution analysis during static and dynamic loading, describing chemical composition and characteristics and giving formulas and diagrams 18 p3045 A67-33741

Tension and compression, dynamic and static flexural loading and vibration tests of bilaminate filament wound composite [SESA PAPER 1219] 18 p3141 A67-33889

Uniformly moving crack in infinite body, in antiplane strain, driven by loads in simultaneous travel 20 p3536 A67-36415

Rapid deformation in tubular blank during expansion by pulsed loading studied by high speed motion picture photography 21 p3631 A67-38055

Shallow spherical shell dynamic stability under variable moment load 22 p3911 A67-39683

Rolling element bearing fatigue life for cyclic race oscillation, analyzing variation with load, speed and oscillation amplitude via Weibull statistics [ASME PAPER 67-LUB-22] 24 p4163 A67-42680

DYNAMIC MODEL

Dynamic load analysis of Titan III booster structure using dynamically scaled model in vibration survey [SAE PAPER 660684] 01 p0154 A67-10588

Forced oscillations of two-mass dynamic system with impact

reaction 02 p0248 A67-11964

Dynamic rubber wheel model to supplement digital computer analysis for prediction of frequencies, mode shapes and stress distributions of vibrating rotor stages [ASME PAPER 66-WA/GT-8] 04 p0712 A67-15364

Electromagnetic wave scattering measurements using spheres moving randomly within slab region container, obtaining data for coherent phase, average intensity, etc 09 p1461 A67-21597

Stochastic control problems, considering dynamic model selection for physical system under random perturbation 10 p1620 A67-23427

Dynamic behavior model for gas shock wake motion and reflection in semiinfinite volume laterally bounded 11 p1782 A67-24954

Dynamic problem of shell of revolution in axial rotation under action of plane compression wave 12 p2020 A67-25568

Dynamic filtering fundamentals, considering mathematical modeling 13 p2086 A67-26414

Algorithm for minimal realization of linear finite-dimensional dynamical system displayed by Markov parameters 14 p2291 A67-28066

Ground effect of static circular peripheral jet, comparing derived relations between jet flow, base pressure and hover height with experimental model 15 p2415 A67-29262

Approximate model for simplification of linear dynamic system, neglecting effect of higher order time constants 15 p2457 A67-29370

Limitations of observability and controllability of dynamic system determined, using approximation of performance matrix and iterative procedure 15 p2461 A67-30316

Dynamic model parameter estimation using method of generalized least squares 15 p2462 A67-30326

Dynamic characteristics of normal exploitation processes determined with controlled equivalent model 15 p2464 A67-30335

Similarities between model-reference adaptive control systems and parameter identification by adjustable models 15 p2464 A67-30337

Adjustment uniqueness in defining dynamic characteristics with help of self-adjusting model 15 p2464 A67-30339

Continuous estimation of frequency response of linear system directly from random input and output data measurements 15 p2465 A67-30345

Steady-state mercury flow along open trough in transverse magnetic field, measuring electric and hydraulic characteristics and providing plasma motion model 16 p2713 A67-30578

Flow through blade cascade studied by averaging flow parameters behind cascade for testing internal combustion turbine guide vanes 16 p2736 A67-31005

Shock-wave separation dependence on bluntness degree, Mach number and gas type during supersonic motion of ellipsoids of revolution 16 p2875 A67-31130

Shape dependence of detached shock wave in supersonic gas flow of blunt-nosed models on Mach number, heat capacity and bluntness ratio 16 p2593 A67-31131

Supersonic unsteady flow of cylindrical body past diaphragm model at interface between density-differing gases, studying flow patterns 16 p2593 A67-31133

Ablation of low melting models on ballistic facility, giving ballistic trajectory optimum conditions and ablation parameters calculation method 16 p2593 A67-31134

Fracture theory statistical models, static and stochastic approach 16 p2771 A67-31294

Realization of invariant multiloop control in case of near-critical and critical plant parameters 16 p2643 A67-31379

Stress waves propagating in half-space due to point load on surface studied initially in three-dimensional dynamic photoelasticity 17 p2959 A67-32415

Dynamic system single- and multifrequency random oscillations described by differential-difference equations and solved through probability distribution 17 p2885 A67-32876

Forced oscillations of two-mass dynamic system with impact

reaction 17 p2866 A67-33281

Relationship between stability and continuity for dynamical systems analyzed using functional analysis, discussing connection to boundedness 18 p3079 A67-34286

Reduction of differential equation to dynamic system when equation is invariant for single parameter group 18 p3072 A67-34392

Static and dynamic inventory control models for logistics planning and operational readiness with cost constraints 18 p3162 A67-34680

High pressure helium arc plasma behavior in cylindrical duct explained by theoretical model with different electron and heavy particle temperatures 19 p3280 A67-35145

Thermodynamic model for laser induced gas discharges accounting for transmitted light attenuation, plasma heating, etc 19 p3239 A67-35163

Concentrated vortex model for Karman street in two-dimensional viscous incompressible laminar flow past bluff body 19 p3210 A67-35446

Hydraulic line models for fluid control system analysis, discussing frequency and transient response calculation simplification 20 p3366 A67-37365

Wavelength dependence and aspect sensitivity of radar auroral echoes show Booker field-aligned scattering model inadequate 20 p3433 A67-37411

RF mixer and limiting IF models for RFI analysis of local oscillator control in FM-CW receivers, using digital computer simulation 20 p3405 A67-37649

Toroidal plasma instabilities analyzed, justifying use of two-dimensional slab models with varying gravitational field simulating magnetic lines curvature effect 21 p3861 A67-37747

Collisionless plasma heating by random magnetic fields using simple betatron model 21 p3662 A67-37762

Dynamic modeling of complex rotor system to determine critical velocities, noting influence of number of mass concentrations on accuracy 21 p3689 A67-37951

Method for determining physical interactions in system of bodies with arbitrary perturbations, using vector form equation 21 p3657 A67-37987

Dynamic model for magnetic field effect on vibrations of clock balance wheel having magnetized cross bar 21 p3625 A67-37988

Performance prediction calculations for double junction n-p-n silicon solar cells, discussing simplified model limits and space radiation environment 21 p3571 A67-38232

Nonlinear mechanical model with mathematical pendulums for solid bodies containing nonlinearly oscillating liquid in motion 21 p3612 A67-38307

DC electric arc in superimposed gas flow behavior in arc tunnel, discussing electrode geometry [AIAA PAPER 67-675] 21 p3671 A67-38708

Sodium-potassium alloy thermodynamic properties and ordering, with pairing model for configurational entropy loss 21 p3733 A67-39106

Charge model for unsaturated and saturated p-n-p-n dynamic behavior using numerical integration techniques 22 p3766 A67-39249

Duration of dynamic system output for given input time calculated by computer programming 22 p3764 A67-39336

Plasma physics of thermionic converters, discussing simple physical models, I-V curve and converter operation region processes 22 p3747 A67-39342

Gas separation effects in Ranque-Hilsch vortex tube explained by dynamic model of axial flow 22 p3917 A67-39512

Fluid model for magnetosphere shape, calculating flow velocity, density and temperature between shock and boundary 22 p3883 A67-39671

Quasi-one-dimensional nonequilibrium argon plasma flow equation, discussing kinetic model with atom-atom and electron-atom impact ionization 22 p3850 A67-39708

Saturn V S-IVB stage propellant slosh amplification minimization at boost thrust termination analysis, simulating slosh wave motion by time varying nonlinear spring-mass model 22 p3903 A67-39970

Model for straight fin nucleate boiling onset criterion, discussing boiling section length expression, heat flux and temperature profile distribution 22 p3919 A67-40387

Pressure effects on fatigue reported for Fe, Al and Ni wires subjected to oscillating strains, discussing several fatigue models 23 p4075 A67-40666

Superconductivity enhancement in fine grained tungsten films, discussing structural changes and theoretical models 23 p4036 A67-40702

Internal flow turbulent boundary layer separation for variable angle two-dimensional diffuser, discussing analytical model and model limitations [ASME PAPER 66-WA/FE-14] 23 p3989 A67-40929

Dynamical theory of X-ray diffraction for optical holography noting anomalous light transmission at Bragg angle 23 p4009 A67-41462

Approximate investigation of standard model reference adaptive systems with random input effects based on filtering properties of automatic control systems 23 p3985 A67-41675

Mathematical model of linear guidance law to dynamical system, noting reduction of two-point boundary value class error 23 p4026 A67-41732

Infrasound wave anisotropic radiation from moving auroras analyzed using shock wave model, discussing sound propagation and ray tracing 24 p4147 A67-41882

Deformation continuum mechanics near cracks, discussing fatigue load propagation applications and elastoplastic models 24 p4248 A67-41948

Triggering controller dynamic model with magnetoelectric drive, examining phase volume by point transformation technique 24 p4155 A67-42297

Coupled earth core-mantle model for earth precessional torques, discussing precession energy dissipation and experiments on model 24 p4151 A67-42314

Plasma energy and heat transfer to surface with and without electric current, discussing various energy transfer models 24 p4197 A67-42331

High energy nucleon and pi-and K-mesons inelastic interaction cross sections from quasi-linear approximation of optical model 24 p4192 A67-42852

DYNAMIC MODULUS

Dynamic equations for adiabatic changes of state for mixtures of partially ionized gases with chemical reactions 19 p3286 A67-35348

Poincare continuation method using simple pendulum problem, deriving elliptic functions as power series [AIAA PAPER 67-564] 19 p3250 A67-35960

Low dose reactor irradiation effect on temperature dependence of dynamic modulus and internal friction of as-deposited pyrolytic graphite 23 p4021 A67-41075

DYNAMIC PRESSURE

Aerodynamic detector measuring dynamic pressure distribution in laminar He jet heated by electric arc 05 p0850 A67-18035

Dynamic pressures in helium and argon plasma jets in ambient atmosphere measured with sensitive probes 09 p1549 A67-22554

Nike rocket boosted 20-ft-diam ribbon parachute for deployment at dynamic pressures above 400 psf 13 p2054 A67-27598

Ballistic reentry vehicle recovery via low speed water impact or air snatch after vehicle has flown unperturbed trajectory down to altitude of maximum dynamic pressure 15 p2564 A67-29424

DYNAMIC PROGRAMMING

Dynamic programming recursive estimation of modal trajectory for nonlinear non-Gaussian noise and comparison with Bayesian estimation and case of Gaussian white noise 01 p0047 A67-11214

Deterministic optimal control, discussing Bellman dynamic programming method, Pontryagin maximum principle, orbital transfer, interplanetary guidance, etc 01 p0047 A67-11220

Structural design optimization by nonlinear programming noting Sequential Unconstrained Minimization Technique, use of variable metric, Powell direct search method, etc 02 p0209 A67-12711

Optimum processes in systems with

distributed parameters described by partial differential equations 04 p0647 A67-15874

Programmable display synthesizing system for man-machine communications research based on electronic animation technique 05 p0786 A67-18314

Synthesis and control strategy of optimal final value linear system under random environment statistically considered, using Bellman dynamic programming 05 p0783 A67-18442

Optimum switching function of relay servosystem subjected to stationary Gaussian random input found by perturbation method 05 p0783 A67-18445

Adaptive utilization of communication satellite systems optimizing dynamic traffic handling of combined ground and satellite communications complex, noting network configurations 06 p0959 A67-17870

Second order method for nonlinear optimal control problems resulting in Riccati differential equations 07 p1213 A67-19155

Dynamic programming for control system synthesis, noting invariant embedding and optimality principle use in optimum design problems 08 p1312 A67-20752

Existence and uniqueness theorem for functional equation of optimal control problems, noting stability of solution 09 p1524 A67-21874

Synthesis of control device for one class of nonlinear sampled data systems, obtaining processes with minimum control time 09 p1483 A67-22082

Nonlinear programming and control problems in terms of variations, maximum principle and dynamic programming 10 p1619 A67-23418

Dynamic programming relationship to calculus of variations, developing second order transversality condition 10 p1620 A67-23420

Dynamic programming and Liapunov function for optimization of systems employing digital controllers 11 p1770 A67-24210

Stochastic optimal control with noisy observations, obtaining Hamilton-Jacobi stochastic equation in function space [ASME PAPER 66-WA/FE-6] 11 p1770 A67-24276

Seismological equipment for space research applied to earthquake-resistant structural design 13 p2120 A67-27217

Optimal suspension systems synthesis, discussing dynamic programming theory 13 p2159 A67-27300

Loss structure models concerning age replacement policies, discussing mathematical aspects of maintenance with dynamic programming formulation 14 p2345 A67-28909

Two-person zero sum games with differential equation rules, noting location of optimal trajectories, separation properties, etc 15 p2509 A67-29404

Formulation and analysis of class of optimization problems based on contraction mappings in theory underlying dynamic programming 15 p2511 A67-29891

Backward and forward algorithms of dynamic programming for time dependent systems, noting advantages of forward algorithm for optimization of system 15 p2440 A67-30157

Optimal control theory applied to extremum control in dynamic programming equation derivation for simplified extremum control problem 15 p2465 A67-30343

System reliability study via detailed allocation method, selecting optimal solution in context of tradeoff analysis 15 p2512 A67-30409

Space vehicle optimal control, studying maximum principle application, developing numerical algorithms of dynamic programming type and describing variational problems 16 p2742 A67-30664

Suboptimal, adaptive solutions to sampled data problem for quadratic performance index minimization by obtaining control law and sampling scheme 16 p2649 A67-31660

Dynamic programming used for proof of distributed parameter maximum principle, exemplifying with boundary condition 16 p2652 A67-31687

Optimal control of dynamic systems with minimax type performance index, discussing application of proposed method of solution 17 p2829 A67-32014

Linear continuous time stochastic optimal control process, obtaining optimum performance achievable as function of total effort at initiation of optimization period 17 p2830 A67-33012

Optimal control methods of Bellman and Pontryagin, discussing maximum rule and dynamic programming for optimization in presence of constraints 18 p3018 A67-34284

Multistage linear dynamic systems with sequentially correlated noise, evaluating filtering, prediction and smoothing procedures 19 p3206 A67-35941

Synthesis of specific type of automatic microprogramming systems using complex microcommand signals conditioned by functional-blocks properties 19 p3190 A67-36094

Variational problem in optimal interaction systems with control constraints solved by dynamic programming and Pontryagin principle applications 20 p3407 A67-36440

Dynamic programming for optimal algorithm for extremal control in presence of noise at system input and output 20 p3408 A67-37072

Optimal control theory for distributed parameter systems using dynamic programming, showing use in two-point boundary control problems involving partial differential equations 20 p3410 A67-37320

Apollo Crawler System analyzed by computer simulation for dynamic interactions of transporter and umbilical tower 22 p3782 A67-40466

Optimal control systems synthesis using dynamic programming and closed loop system 23 p3985 A67-41671

Dynamic programming, deriving successive sweep method for optimal control problems, discussing discrete algorithm for numerical problems 24 p4136 A67-42694

Numerical solution methods for partial differential equations, discussing dynamic programming, Laplace transform and quadrature technique 24 p4180 A67-43084

DYNAMIC PROPERTY

Dynamic system with unknown parameters identified through iterative and least squares methods suitable for computer programming 03 p0392 A67-13658

Liquid-vapor interface in weightless environment noting dynamic behavior, configuration parameters and dependence on model size 04 p0605 A67-14988

Dynamic resistance of Si p-n junction and diffusion length for minority carriers measured, using pulsed electron beam irradiation 04 p0584 A67-15317

Synthesis problem of optimum dynamic characteristics of multivariate linear control systems with random input signals 05 p0781 A67-18252

Dynamic properties of coupled systems derived from experimentally determined frequency response functions of component systems, noting cross correlation functions 09 p1573 A67-21752

Dynamic plane shear of incompressible viscoelastic material with temperature dependent viscosity determined, using electric transmission line analog 09 p1533 A67-22152

Dynamic properties of linear system with damping analyzed by matrix technique 09 p1575 A67-22160

Dynamic characteristics of thermionic converter noting influence of emitter heat transfer 09 p1447 A67-22335

Statistical dynamics applications to evaluate system dynamic characteristics from operational data 09 p1469 A67-22480

Direct measurement of aeroelastic parameters of aircraft wings, using dynamically similar models fitted on auxiliary rocket devices 09 p1576 A67-22462

Amplifying elements ensuring required dynamic properties of resolving amplifier without calculating entire amplifier circuitry 10 p1811 A67-22983

Dynamic behavior of multidimensional system described by ODE 10 p1675 A67-23608

Equations for elastic system free oscillations with parallelogram shaped hysteresis loop derived from kinetic energy changes, describing system time dependent dynamic behavior 12 p1967 A67-25660

Dynamic and physical testing of metals, discussing yield point, plastic deformation and oscillation damping

characteristics 13 p2215 A67-26452
 Dynamic characteristics of pneumatic transmission lines in regulation loops noting parameters effects, calculation methods, etc 13 p2055 A67-26799
 Correlation method for generating sensitivity coefficients of dynamic system on high speed iterative analog computer 13 p2073 A67-27061
 One-dimensional small signal linear model of fluid transmission line using finite lumped parameter elements and Navier-Stokes equations 14 p2247 A67-28265
 Static and dynamic performance of pancake vortex flow field and application to pressure amplification 14 p2248 A67-28272
 Missile dynamic behavior analysis using linear aeroballistic theory in conjunction with numerical computations of motion equation 14 p2395 A67-29058
 Energy exchange mechanism of cryogenic sensor dynamic behavior, noting error sources 15 p2490 A67-30155
 Method of dynamic characteristics, determining controlled plant performance during operation 15 p2462 A67-30328
 Dynamic and physical properties of Kreutz family of sun-grazing comets suggesting collision mechanism for origin 16 p2751 A67-31464
 Soviet book on supersonic gas flows in perforated boundaries covering flow characteristics, dynamic property, supersonic nozzles, velocity regulation, etc 17 p2789 A67-32019
 Tangentially injected plane jet spreading in slipstream at various Reynolds numbers at jet inlet slot studied in wind tunnel for dynamic behavior 17 p2839 A67-32906
 Synthesis of mechanical system with variator having drive unit in steady or steadily increasing motion, deriving and solving dynamic equations 17 p2885 A67-32967
 Experimental data applicability for DC arcs in construction of AC plasmotrons 18 p3088 A67-34058
 Nonideal type II superconductors, discussing flux motion and density, pinning force, magnetization, hysteresis, relaxation and energy loss 21 p3683 A67-38402
 Automatic check system for investigation of dynamic characteristics of stabilization system for carrier and space vehicle, noting system reliability 22 p3830 A67-39172
 Dynamics of single channel extremal systems having plants in linear and nonlinear elements and control units in form of self-oscillating type optimizer 22 p3777 A67-39777
 Unsteady continuity and motion equations describing F layer dynamic characteristics under time dependent electric and magnetic fields 23 p3996 A67-41178
 Plane and turbulent fluid jets dynamic and thermal behavior expanding in magnetic field described by differential equations system 24 p4195 A67-41930
 Steady state and dynamic properties of cylindrical floating ring journal bearing with pressurized lubricant supply, considering turbulent flow and whirl instability [ASME PAPER 67-LUB-13] 24 p4162 A67-42674

DYNAMIC RESPONSE

Combined linear and vibratory accelerations effects on human body dynamics and pilot performance capabilities 02 p0189 A67-12409
 General recursion formula for dynamic response of pressure measuring systems considered as series connection of tubes and volumes 03 p0418 A67-12998
 Automatic adjustment of amplification factor of control systems in response to perturbation 03 p0389 A67-13080
 Fiber reinforced rotor blades, discussing composite material selection for research, mass balance, dynamic response tuning and material design properties 03 p0453 A67-13416
 Closed loop gust response control system, considering airframe loading, local accelerations, turbulence, structural mode, damping, etc [AIAA PAPER 66-997] 03 p0362 A67-14146
 Moire method in determining dynamic response of thin membranes 03 p0531 A67-14362
 Human dynamic force response to impact examined, using spring-mass-damper system with refined parameter

values 04 p0564 A67-15401
 Dynamic response of cylindrical sandwich shell under axially symmetric moving ring load, considering steady state behavior 04 p0713 A67-15404
 Stability and dynamical response of small portions of differentially rotating stellar disks, noting decaying nonaxisymmetrical instabilities, epicyclic frequency, surface density, etc 05 p0892 A67-16410
 Dynamic response, sloshing frequencies and stability of free surface of liquid in circular cylindrical elastic tank with flexible bottom [AIAA PAPER 67-76] 06 p0986 A67-18274
 Filtering for nonlinear dynamical systems with white Gaussian noise processes 06 p1029 A67-18532
 Model tests for determination of structural response of Apollo Command Module to water impact 07 p1257 A67-19368
 Atmospheric density, winds and turbulence relative influence on Saturn V vehicle control system and structural bending moment response during Atlantic Missile Range ascent flight [AIAA PAPER 66-341] 07 p1257 A67-19372
 Perturbation technique used to study random response of airplanes to effect of runway roughness 08 p1279 A67-20480
 Dynamic behavior of large flexible bodies in orbital motion around gravitating center, emphasizing response and stability of elastic degrees of freedom 08 p1383 A67-20562
 Fluid film and rolling element bearings effect on turbomachinery rotor dynamics including critical speeds, imbalance response, instability, turbulence, etc [SAE PAPER 670059] 09 p1508 A67-22533
 Computation difficulty in optimal control law for dynamical system, noting three optimal conditions 10 p1619 A67-23419
 Unsteady aerodynamic forces and dynamic response of flexible aircraft structure to continuous turbulence in supersonic flight 10 p1595 A67-23736
 Dynamic response of periodic liquid flow systems as function of structural support motions, noting resonance points and pressure amplitudes 10 p1628 A67-23737
 Computer graphic display for dynamic response of nonuniform beam treated by lumped mass-spring representation of structure 10 p1608 A67-23739
 Elastic medium dynamic response to time dependent pressure in spherical cavity with cavity wall under ablation process 11 p1871 A67-23964
 Energy conservation analysis of step in negative resistance region of voltage-current characteristic curve of oscillating tunnel diode 11 p1759 A67-24132
 Approximate normal mode technique, providing solution to sinusoidal and white noise randomly excited damped linear multi-degree of freedom system, for application to mathematical model [ASME PAPER 67-VIBR-2] 11 p1871 A67-24164
 Quasi-static analysis of nonsynchronous response effect of gas bearing pivoted pad design variables and application to operating machinery [ASME PAPER 67-VIBR-15] 11 p1796 A67-24175
 Mode coupling effect on response of rigid body to random excitation analyzed, using two degree of freedom model [ASME PAPER 67-VIBR-36] 11 p1873 A67-24193
 Energy techniques and matrix method for computer programming of dynamic response due to random and harmonic loading on structural systems [ASME PAPER 67-VIBR-56] 11 p1873 A67-24203
 Equation for linear dynamic systems simplification applicable to all cases irrespective of nature of eigenvalues and eigenvectors 11 p1772 A67-24898
 Dynamic measurements of heavy landings on experimental helicopter platform and of response to heavy vehicle loads on steel-and-concrete deck flyover 11 p1880 A67-25056
 Dynamic response of clamped shallow thin elastic spherical shells under time dependent loads [AIAA PAPER 66-446] 12 p2030 A67-25915
 Laboratory test program to study problems associated with flight instrument parameter measurement 12 p1947 A67-26187

Impulse response of dynamic systems using cross correlation techniques 13 p2081 A67-27220
 Nonlinear dynamic response of thin walled shells of revolution 14 p2397 A67-28090
 Moving coil and variable air gap electromagnetic actuators, discussing characteristics and applications 14 p2247 A67-28266
 Motion of holonomic mechanical system of points with variable mass under action of active forces 15 p2517 A67-29464
 Static and dynamic parameter estimation of nonlinear transfer elements from step responses 15 p2463 A67-30331
 Superlimiting phased-array receiving system in two-source environment 16 p2638 A67-31271
 Dynamics of electromechanical metering servosystems calculated by harmonic linearization method 16 p2644 A67-31380
 Gas bearing stability determination by step-jump response using observation of growth or decay of motion amplitude [ASME PAPER 67-LUBS-5] 16 p2682 A67-31383
 Dynamic response of sailplanes to longitudinal maneuvers based on steady lift coefficients on wing and tails 16 p2596 A67-31465
 Dynamic response of sailplanes to elevator control in longitudinal maneuvers, discussing load factors and tail loads as function of aerodynamic and inertial parameters 16 p2597 A67-31786
 Vibro-acoustic test system for simulation of Saturn V dynamic launch environment on major space vehicle structures, discussing design and operation characteristics 17 p2832 A67-32005
 Pressure measuring instrumentation response requirements for computing decay rate in solid propellant termination systems 17 p2926 A67-32069
 Acceleration stress effects on pilot performance and dynamic response 17 p2808 A67-33176
 Controllability methods on VTOL transporters, developing model of pilot dynamic reaction to aircraft machinery 18 p2993 A67-33457
 Uniqueness of response of nonlinear continuous servosystem subjected to any signal 18 p3017 A67-34185
 Dynamic system with state at any instant represented by point in Euclidean space of n dimensions 19 p3203 A67-35902
 Multiple scaling for analyzing flight vehicle performance and dynamic behavior [AIAA PAPER 67-560] 19 p3335 A67-35957
 Lift penetration and growth effects on space vehicle response based on slender body theory 19 p3337 A67-35999
 Rotor blade airload and dynamic response of large tandem rotor helicopter measured, using computer programs methods 20 p3536 A67-36462
 Ceramic materials fracture and deformation mechanisms, discussing stress role 20 p3473 A67-36645
 Elastic and dynamic response of viscoelastic plate with finite thickness to rigid body impact 20 p3539 A67-36920
 Dynamic response of nondegenerate electron hole plasma in semiconductor, obtaining frequency spectrum and Landau damping rate of plasma oscillation 20 p3499 A67-36945
 Adaptive processes of human operator during control tasks involving sudden change of controlled plant dynamics 21 p3576 A67-37948
 Dynamic response, sloshing frequencies and stability of free surface of liquid in circular cylindrical elastic tank with flexible bottom [AIAA PAPER 67-76] 21 p3614 A67-38868
 Multivariable linear system noninteracting control realized by relays sliding motions 22 p3777 A67-39839
 Spherical entry vehicle used to define planetary atmosphere structure and composition from dynamic response during entry, discussing aerodynamic characteristics 22 p3907 A67-40177
 Mode acceleration method for axisymmetric dynamic response due to time dependent loading in spherical and cylindrical shells 22 p3914 A67-40190
 Canine cardiac displacement and cardiovascular dynamic response during

- abrupt deceleration impact, discussing
traumatic ruptures and pressure
effects 23 p3951 A67-41552
- Algebraic equations to predict time
response to step input in free molecule,
transition and continuum flow
regimes 24 p4155 A67-42293
- Indirectly corrected gyro vertical used to
determine vertical on power plant,
considering random plant motion and
gyroscopic drift 24 p4155 A67-42298
- Dynamic response of large flexible space
systems subjected to motion inputs and
arbitrary force, analyzing joined Timoshenko
beams 24 p4240 A67-42395
- Gas bearing Brayton cycle turboalternator
rotor system stability and dynamic response
to electromagnetic forces 24 p4102 A67-42487
- Wind profiles properties application to
launch vehicle design and operation,
emphasizing wind shears and turbulence
effects on vehicle dynamic
response 24 p4242 A67-42918
- DYNAMIC STABILITY**
- Stability analysis of steady state dynamic
holonomic mechanical systems using Rouse,
Kelvin, Poincare and Chetaev
theorems 02 p0267 A67-11959
- Gust Alleviation and Structural Dynamic
Stability Augmentation System /GASDSAS/
design analysis 02 p0183 A67-12303
- [AIAA PAPER 66-999] 02 p0183 A67-12303
- Dynamic stability and critical flutter of
axial-flow-turbine blades in cascade, for
natural frequencies slightly
mismatched 03 p0520 A67-12880
- Qualitative dynamic stability analysis of
motion equations with two zeros and
trajectories near singular
line 03 p0467 A67-12887
- Qualitative theory of second order
dynamic systems in plane and on sphere
covering trajectories, equilibrium states and
boundary values 03 p0390 A67-13109
- Invariance theory for automatically
controlled underwater wings ensuring ship
motion stability in perturbed
medium 03 p0359 A67-13189
- Stability regions for compressible fluid
squeeze-film journal bearing of infinite
length, considering motion along axis
[ASME PAPER 66-LUB-15] 03 p0431 A67-13758
- Bubnov-Galerkin and energy method
solutions of stability and oscillatory motion
equations for conical shell under inertial
loading 04 p0717 A67-15890
- Thermoelastic wave propagation in elastic
layer with convective heat transfer between
layer surfaces and surrounding medium,
considering relations between temperature
field and dynamic
displacement 05 p0913 A67-16188
- Dynamic stability of coaxial cylindrical
shells in nonuniform temperature field
under uniformly distributed axial
compression load 05 p0913 A67-16189
- Numerical procedure for optimizing
stability of linear dynamic system by
applying steepest descent
method 05 p0845 A67-16437
- Lagrange variational equation application
to dynamic stability problems of plates in
gas flow 05 p0923 A67-17188
- Stability theorem for damped dynamic
systems based on commutativity of class of
mathematical models 06 p1099 A67-17644
- Liapunov theory of stochastic stability,
discussing use to obtain information about
random trajectories 06 p0974 A67-17931
- Motion stability concepts of synthesis of
control devices, with example for harmonic
oscillator 06 p1032 A67-18243
- Inviscid equilibrium gas stability
characteristics for pointed and spherically
blunt bodies in unsteady supersonic flight in
Mars atmosphere 07 p1258 A67-19380
- Fluid mechanical model of electric arc
balanced magnetically in gas flow, based on
photographs showing arc must simulate solid
body [AIAA PAPER 67-96] 07 p1240 A67-19437
- Book on rotor stability self-excited
vibration and nonlinear
resonances 07 p1263 A67-19631
- Dynamic instability in undamped bellows
face seals operating in cryogenic
environment with torsional oscillation and
diametrical rocking as primary motion
[ASLE PAPER 66AM 2C2] 08 p1336 A67-21039
- General dynamical system in metrical
space, extending Liapunov method to
analyze stability properties by using single
Liapunov functional 09 p1532 A67-21661
- Normal form and stability of coupled
nonlinear RLC networks with possible
interconnected elements of like
type 10 p1618 A67-22703
- Dynamic stability of cylindrical shell
reinforced by thin walled rigid longitudinal
ribs 10 p1721 A67-23604
- Motion stability of dynamic system whose
equation has two small positive
roots 10 p1681 A67-23680
- Singular characteristics of dynamic
systems with steady state motion, noting
effect of constantly acting small
perturbations 11 p1818 A67-24147
- Liapunov stability of motion of heavy rigid
body with fixed point moving along
spherical surface 11 p1818 A67-24163
- Loads on bodies in wakes resulting from
crossflow at submerged body or from wake
translation over submerged body, noting
dynamic instability 11 p1742 A67-24350
- Liapunov functions generated by
transformation of Companion matrix to
Routh or Schwarz canonical forms, for
asymptotically stable linear time-invariant
multivariable systems 11 p1814 A67-24942
- Gas dynamic stability of plane detonation
wave propagating in ideal gas mixture, in
terms of small perturbations that may result
in surface bending and changes in
thickness 12 p1930 A67-25965
- Pulsation properties of star models with
linear density distribution, considering
radial, adiabatic contraction and dynamical
stability 12 p2011 A67-26253
- Total asymptotic stability by nonlinear
compensation 13 p2086 A67-26415
- Dynamic equations for interacting
connected rigid bodies 13 p2212 A67-26838
- Equilateral position stability of
equilibrium in planar restricted problem of
three bodies for mass ratio
values 13 p2205 A67-27477
- Dynamic analysis of rotor motion of rigid
system in hovering state using complex
variables 13 p2054 A67-27588
- Dynamic stability of structures -
Conference, Northwestern University,
October 1965 14 p2396 A67-28078
- Dynamic stability of structures, discussing
parametric resonance, impulsive loading,
circulatory loads, aeroelastic and buckling
problems 14 p2396 A67-28079
- Stability of motion of continuous
dynamical systems analyzed via computing
machines 14 p2348 A67-28080
- Stability and asymptotic behavior of
dynamical systems defined by autonomous
functional or partial differential equation
and conditions for applying Liapunov
theorem 14 p2342 A67-28081
- Dynamic stability problems in actual
structures in vehicle
design 14 p2397 A67-28084
- Dynamic buckling under step loading
studied on basis of general nonlinear theory
of elastic stability 14 p2397 A67-28089
- Dynamic stability of pin-ended column
under different types of random axial
loading 14 p2397 A67-28091
- Dynamic buckling of ring constrained in
rigid circular surface and subjected to
transiently applied inertial
loading 14 p2398 A67-28093
- Static and dynamic characteristics of
interaction region for fluid jet and receiver-
load system, examining stability
conditions 14 p2248 A67-28270
- Natural transverse vibrations of sandwich
plates with rigid and lightweight fillers,
deriving stability equations from eigenvalue
equivalent problem 14 p2402 A67-28901
- Mathematical model used to determine
influence of nonlinear induced roll moment
and yawing moment on dynamic stability of
cruciform tailed bomb 15 p2416 A67-29428
- Liapunov direct method applied to
Hermite theorem on number of positive real
part zeros of complex polynomial and
stability theory of linear
motions 15 p2458 A67-29899
- Sensible heat transfer influence on
dynamic stability of harmonic perturbations
superimposed on zonal current, using
Lorentz two-level model 15 p2512 A67-30057
- Random instability of nonlinear oscillations
of dynamic system with time behavior
described by equation 16 p2702 A67-30447
- Book on design and development of
helicopters, Vol. 2 - Vibrations and dynamic
stability 16 p2597 A67-31812
- Dynamic stability of low disk loading
propeller-rotors as function of various
dimensionless parameters characterizing
design [AHS PAPER 132] 16 p2777 A67-31846
- Time lag effect on dynamic stability
determined, using wind tunnel tests with 10
degree cone as test body simulating ablation
process by gas injection into boundary layer
[AIAA PAPER 66-757] 17 p2792 A67-33004
- Dynamic stability of homogeneous and
inhomogeneous sandwich columns with
pinned ends under pulsating periodic loads
governed by Mathieu
equation 17 p2963 A67-33036
- Sufficient conditions guaranteeing
asymptotic stability of class of linear
dynamic systems with bounded narrow band
parametric excitation [ASME PAPER 67-APM-24] 17 p2830 A67-33152
- Stability analysis of steady state dynamic
holonomic mechanical systems using Rouse,
Kelvin, Poincare and Chetaev
theorems 17 p2886 A67-33276
- Bounded isoenergetic displacement of
periodic orbits in restricted circular three-
body problem 18 p3135 A67-34542
- Adiabatic pulsations of inhomogeneous
gaseous mass consisting of convective core
and radiative envelope 19 p3261 A67-35502
- Stability analysis of steady combination
oscillations of single loop circuit, obtaining
equations relating voltage harmonic of
nonlinear capacitances 19 p3262 A67-35706
- Dynamic stability of beam columns
undergoing weakly nonlinear vibrations
studied using Ritz-Galerkin
procedure 19 p3342 A67-35758
- Navy variable stability studies of
longitudinal handling qualities in simulated
carrier approach [AIAA PAPER 67-576] 19 p3174 A67-35971
- Dynamic stability analysis of bodies of
revolution in supersonic flow, using
characteristics method [AIAA PAPER 67-607] 19 p3172 A67-35998
- Existence and stability conditions of
several-quanta flux lines in type II
superconductors 20 p3505 A67-36206
- Dynamical consequences of thermostatic
concept of stability within general
framework of modern
thermodynamics 20 p3543 A67-36428
- Trajectory prediction for moving
stochastic systems 20 p3392 A67-37196
- Thermodynamics of nonlinear materials
with internal state variables, analyzing
evolution equation, dynamic stability,
dissipation, etc 20 p3555 A67-37563
- Dynamic flight stability characteristics of
5 inch projectile with nonlinear Magnus
moment, noting Mach number, wind tunnel
data, etc 21 p3563 A67-37805
- Motion stability of dynamic system whose
equation has two small positive
roots 21 p3657 A67-38281
- Dynamic instability of longitudinal
oscillations of cylindrical shell charged with
ideal fluid established by approximate
reduction of nonlinear
equations 21 p3720 A67-38297
- Dynamic compliance of two degrees of
freedom nonrotating beam undergoing
flexural vibrations, taking into account
internal friction 21 p3726 A67-38833
- Dynamic stability of spherical segments
subjected to impact loading, discussing
buckling in relation to rise in center and
time dependence 22 p3910 A67-39456
- Dynamic destabilization for hypersonic
flow around slender cone with severely
blunt nose analyzed by blast wave
analogy 22 p3742 A67-40109
- Stability of stellar systems with different
velocity distributions, considering nonlinear
wave in stellar sheet leading to galactic
stellar velocity distribution
evolution 22 p3894 A67-40510
- Interstellar gas cloud collision, heating,
possible gravitational instability and
subsequent cooling 22 p3894 A67-40513
- Equilibrium configuration for nonspherical
cold gas cloud permeated by magnetic field
in gravitationally collapsed
state 22 p3895 A67-40518
- Nonlinear problems of parametric

excitation of rings solved by equations, considering normally and centrally directed pressures 23 p4074 A67-40651

Beta equals one theta pinch dynamic stabilization in all modes of m equal to or greater than one 23 p4031 A67-40793

Popov method extension for absolute stability of nonlinear feedback systems containing distributed elements 23 p3984 A67-40870

Dynamic longitudinal stability of rigid glider towed by rigid aircraft with elastic cable subjected to aerodynamic loads, deriving motion differential equations 23 p3935 A67-41418

Interstellar gas dynamic instability caused by galactic cosmic rays and magnetic field, showing turbulent and fragmentation enhancement of ambipolar diffusion 24 p4223 A67-41813

Interstellar gas and magnetic field periodic system stability noting free-fall time 24 p4224 A67-41814

Extended dynamical systems in Banach space and use of invariance principle for stability theory of partial differential equations 24 p4178 A67-42652

Frequency Response and direct numerical integration of governing differential equations, considering gas-lubricated tilting-pad journal bearing stability [ASME PAPER 67-LUB-8] 24 p4162 A67-42672

Earth and planetary atmosphere entry problems for blunt nosed slender vehicles noting aerodynamics, stability, heating, ablation and interaction of effects [AIAA PAPER 67-803] 24 p4243 A67-42963

DYNAMIC SUPPRESSOR

Ride quality improvement on flexible aircraft by means of elastic structural bending mode suppression design technique [AIAA PAPER 67-571] 19 p3174 A67-35967

DYNAMICS

SA AERODYNAMICS

SA ASTRODYNAMICS

SA BIODYNAMICS

SA CONTINUUM MECHANICS

SA ELASTODYNAMICS

SA ELECTRODYNAMICS

SA GAS DYNAMICS

SA GEOMETRODYNAMICS

SA HYDRODYNAMICS

SA KINEMATICS

SA KINETICS

SA PLASMA DYNAMICS

SA SPIN DYNAMICS

SA STRUCTURAL DYNAMICS

SA THERMODYNAMICS

Lapunov method for estimating statistical averages of randomly perturbed system 04 p0647 A67-15740

Book on optimal control theory of deterministic dynamical systems governed by ordinary differential equations in presence of control and state constraints 04 p0594 A67-15943

Dynamical system specified by set of generalized coordinates, considering Jacobi and Kepler elements and Poisson and other methods 06 p1031 A67-17774

Simulation of deployment dynamics of spinning spacecraft, discussing test methods emphasizing gravity compensating techniques [AIAA PAPER 67-207] 06 p0980 A67-18325

Optimization of stochastic dynamic system with noisy output 06 p0977 A67-18525

Optimal parameter problem of controlled dynamic systems, considering antagonism between designer and nature, applying results to space flight mechanics 06 p1088 A67-18616

Lagrangian dynamical system determined under parametric form of motions applied to two- and three-body problems 07 p1216 A67-19722

Theorems on interaction of parts of mechanical system with smooth holonomic constraints 07 p1224 A67-20038

Nose selection and vehicle motion dynamics for second stage of two-stage sounding rocket system, discussing nose shapes effect on altitude performance, overall vehicle stability, bending moments, etc 08 p1406 A67-20513

Dynamics of beryllium lattice noting dispersion curves of wave frequencies 13 p2137 A67-27109

Efficiency criterion in form of probability of task completion estimated for dynamic systems with random

parameters 15 p2455 A67-29121

Variational principle of dynamics applied to linear theory of elasticity and given in form of two integrals 15 p2575 A67-30002

Celestial mechanics and adaptation of perturbation methods and numerical integration techniques to stellar dynamics 16 p2748 A67-31141

Variational principle of dynamics applied to linear theory of elasticity and given in form of two integrals 18 p3141 A67-33769

Dynamics of narrowing effect of surface and spatial dispersing agents on radiation line of ruby laser with nonresonance feedback 18 p3061 A67-34416

Book on methods for applying principles of dynamics to engineering problems covering three-dimensional approach, free-body system and derivation of motion equations 18 p3080 A67-34566

DYNAMO THEORY

Dynamo theory interpretation of magnetospheric-ionospheric electric current system associated with N-S asymmetry of magnetic daily variation at time of equinox 01 p0057 A67-10113

MHD and plasma physics and application to cosmic and geophysical phenomena 03 p0479 A67-13723

Objection to Martin ionospheric drift theory based on dynamo electric field, atmospheric tidal wind field and F-2 layer drift motion 05 p0796 A67-16063

Transient variation of ionospheric dynamo current systems obtained from sounding rocket measurements of geomagnetic field activities 05 p0797 A67-16582

Changeability laws in quiet solar diurnal magnetic variations in 1964 and relation to state of ionosphere resulting from dynamo effect 05 p0802 A67-17147

Dynamo mechanism for formation of stellar magnetic field, considering effects of EM radiation emission and celestial body rotation 06 p1089 A67-18773

Generalization of differential equation of dynamo theory of geomagnetic variations to include unsteady dynamo effect in ionosphere 13 p2110 A67-26548

Field aligned structure of ionization associated with boundaries of spread-F at middle latitudes studied by combining topside and fast-sweeping ground-based ionograms [AGARDOGRAPH 95] 15 p2480 A67-30277

Maintenance of electromagnetism field by dynamo effect in homogeneous isotropic turbulence without mirror symmetry 17 p2883 A67-32355

Ionospheric winds required to produce lunar daily geomagnetic variations deduced from atmospheric dynamo theory, estimating electric conductivity 20 p3425 A67-36281

Changeability laws in quiet solar diurnal magnetic variations in 1964 and relation to state of ionosphere resulting from dynamo effect 21 p3619 A67-38489

Stellar magnetic field origin theories, discussing fossil, dynamo and battery theories 21 p3708 A67-38985

Secular changes in surface flow motion in earth core noting dynamo theories of earth main field 23 p3996 A67-40816

Geomagnetic dynamo laboratory model self-excitation conditions determined from solutions of electrodynamic equations, diagramming magnetic field and current distribution 24 p4231 A67-42353

DYNAMOMETER

SA OPHTHALMODYNAMOMETRY

Dynamometer using epoxy-bonded foil strain gauges for simultaneous two-force measurements for ultrahigh vacuum and high temperature applications, noting calibration [SESA PAPER 1209] 18 p3142 A67-33896

Factors in recovery from performance decrement, activation, inhibition and warm-up [NAVTRADEVEN-IH-72] 24 p4114 A67-41809

DYNAVERT AIRCRAFT

S CANADAIIR CL-84 AIRCRAFT

DYNODE

S ELECTRON MULTIPLIER

DYSBARISM

Altitude dysbarism treatment with high pressure oxygen, reporting three cases 05 p0756 A67-16291

Pathogenesis of focal neurological dysbarism in pilots during altitude

decompression sickness 10 p1600 A67-23827

Effectiveness of therapeutic modalities upon mongrel dogs subjected to dysbarism by overcompression-decompression 16 p2611 A67-30770

Radiol isotopic color coded pulmonary lung scanning, diagnostic test in experimental decompression sickness 23 p3956 A67-41626

DYSPROSIUM

Anisotropy of Hall effect dependence on field and temperature in dysprosium crystal 01 p0133 A67-10743

Dysprosium crystalline structure and phase transition from heliocoid antiferromagnetism to paramagnetism 01 p0133 A67-10744

Stark and Zeeman splitting in far IR spectra of erbium, dysprosium and samarium ethyl sulphate 04 p0686 A67-15778

Dysprosium doped calcium fluoride giant pulse laser with high repetition rate obtained, using DC pumping xenon lamp 05 p0822 A67-16674

Temperature dependence of thermoconductivity of dysprosium between 1 and 4 degrees K 06 p1048 A67-17821

Anisotropy of Hall effect dependence on field and temperature in dysprosium crystal 13 p2176 A67-26772

Dysprosium crystalline structure and phase transition from heliocoid antiferromagnetism to paramagnetism 13 p2176 A67-26773

E

E-2 LAYER

E-2 and F-0 intermediate ionospheric layer morphology, occurrence, electron density and signal reflection variations 04 p0616 A67-15220

Relation between E-2 and F-0 ionospheric layer formation and geomagnetic phenomena 04 p0616 A67-15221

Seasonal variations in incidence of E-2 layer from 1960 through 1965 19 p3221 A67-35429

E LAYER

SA SPORADIC E LAYER

Long term variation in relations of solar indices to E and F region character figures interpreted without assuming changes in solar radiation 01 p0056 A67-10110

Horizontal drift measurements in E and F regions of ionosphere over magnetic equator in India 03 p0407 A67-12829

Spaced antenna technique for determining drift and anisometry of equatorial E and F region irregularities 03 p0407 A67-12833

Magnetic activity effect on sporadic E region-drifts, comparing plot of K index vs drift velocities 03 p0413 A67-13684

Electron density profiles of Nike-Apache rocket observations of nitric oxide ionization by Lyman alpha radiation in E region at sunrise 03 p0415 A67-14114

Drift of small scale E and F layer inhomogeneities in Black Sea coastal region 04 p0616 A67-15222

Correction for characteristic number of E layer based on electron transport processes and seasonal variations 04 p0618 A67-15573

E layer stratification, fine structure and boundary accuracy in frequency measurements based on seasonal variations in solar activity 04 p0618 A67-15574

Critical frequencies of F-2 and E layers in ionosphere relation to total daily influx of solar wave radiation into earth atmosphere 05 p0800 A67-17128

Geomagnetic activity effect on electron concentration at heights of 100 and 110 km 05 p0801 A67-17143

Changeability laws in quiet solar diurnal magnetic variations in 1964 and relation to state of ionosphere resulting from dynamo effect 05 p0802 A67-17147

Order of recombination coefficient in E layer determined, using ionospheric data 06 p0999 A67-18737

Diurnal and seasonal altitude variations of E and F layers analyzed for geomagnetic activity from rocket measurement of electron concentration 07 p1173 A67-19686

E layer ionization and characteristic number as affected by solar X radiation in 44-60 angstrom range 07 p1178 A67-19822

Calculation of time behavior of forenoon anomaly in diurnal variations of critical frequency of normal E layer 07 p1183 A67-20118

- Positive ion layers in E region explained by wind shear theory, obtaining steady state solutions for simple model 08 p1326 A67-21359
- Deflection absorption of radio waves in ionosphere 09 p1491 A67-21845
- Ionospheric rocket sounding, measuring ion density and electron temperature between E and F layers 10 p1633 A67-22948
- Occurrence of collisions between ionized and neutral particles based on analysis of spectrum diffused by E region 10 p1646 A67-23268
- Ionospheric absorption effects in D and E layers, noting refraction role and effective collision frequency 10 p1646 A67-23270
- Model ionosphere with homogeneous isotropic turbulence investigated for values of kinematic viscosity and dissipation rate of turbulent energy determined from rocket measurements 10 p1646 A67-23273
- Ion composition and effective recombination coefficient variation of ionosphere in study of X and UV radiation ionization of E layer 10 p1647 A67-23280
- Variations in position of mirror points of high energy electrons determined from Cosmos V satellite data 10 p1647 A67-23281
- Ionospheric probes for measuring electron density in E region through detection of plasma resonances 10 p1656 A67-23285
- Atomic ions of meteoric origin indicated as source of midlatitude E region in IQSY rocket measurement 10 p1648 A67-23289
- Hydromagnetic gradient waves theory extended to weakly ionized medium-density magnetized plasma of type expected in ionospheric E layer 11 p1783 A67-23923
- Relation between diurnal, seasonal and cyclic variations of stratifications in E layer and fine structure of sporadic E layer and E-2 layer 13 p2110 A67-26550
- Variations of ionizing radiation of E layer, eliminating aeronomic effects by considering seasonal variations of ionization index 13 p2191 A67-26767
- Ionospheric structural studies via absorption measurements 14 p2378 A67-27911
- Revised ionization-equilibrium equation to obtain criterion for presence of winter anomaly in E layer 14 p2307 A67-27912
- Spatial HF radio focusing caused by electron distribution between ionospheric layers, even in absence of horizontal density gradients 14 p2281 A67-28048
- Lower E-region positive ion concentrations measured at time of declining solar activity by rocket installed mass spectrometer 14 p2310 A67-28049
- Ionospheric E region dynamical processes, discussing energy phenomena of planetary waves, tidal oscillations and gravity waves 14 p2311 A67-28408
- Quiet sun current system effects on seasonal variations of critical frequency in E region, noting dependence on local time and latitude 14 p2312 A67-28569
- Ionospheric discontinuity motion in E layer at 100 km, using long distance ultrashort-wave propagation data obtained by diversity-reception method 15 p2479 A67-30148
- Measurements at Ibadan of drift velocity of ionospheric irregularities for E and F layers during IQSY 16 p2663 A67-30969
- Diurnal variations asymmetry in critical frequency ratio of E layer for morning and evening values 16 p2668 A67-31895
- Ionization in E region due to influx of micrometeorites 17 p2943 A67-32542
- Auroral oval between outer boundary of trapping region and ionosphere and dynamical and atomic interactions between magnetospheric plasma and neutral atmosphere 18 p3035 A67-33597
- NO role in sunrise E region compared to Barth NO distribution, determining density profiles, relative ion ratios, etc 19 p3218 A67-35191
- Electron temperature observation in E region with Langmuir probes on Nike Apache rockets, discussing solar radiation effect 19 p3218 A67-35193
- Charge transfer role in formation and maintenance of molecular and metal-ion layer in E region of ionosphere 19 p3217 A67-35204
- Ion layer formation in E region, assuming sinusoidal vertical motions and ion-electron recombination following attachment law 19 p3222 A67-35456
- Winter anomaly in ionospheric E-layer 19 p3225 A67-35617
- Ionospheric pulse absorption study of measurements taken in Bulgaria during solar eclipse of May 1966 21 p3616 A67-37995
- Lunar tide in E layer, diurnal/semidiurnal components and seasonal variation 21 p3616 A67-37997
- Critical frequencies of F-2 and E layers in ionosphere relation to total daily influx of solar wave radiation into earth atmosphere 21 p3618 A67-38471
- Geomagnetic activity effect on electron concentration at heights of 100 and 110 km 21 p3619 A67-38485
- Changeability laws in quiet solar diurnal magnetic variations in 1964 and relation to state of ionosphere resulting from dynamo effect 21 p3619 A67-38489
- Nighttime E region electron concentration profile valley structure variations for quiet and disturbed geomagnetic activity 22 p3791 A67-39814
- Effective recombination coefficient in upper-E and F-1 layers at sunset from rocketborne gyroplasma probe measurements of electron density profile 22 p3793 A67-40044
- Ionospheric electron distribution observed and computed values discrepancy analyzed, noting diurnal variation role 24 p4146 A67-41785
- Geomagnetic field aligned irregularities, explaining ionospheric E-region scattered wave propagation 24 p4120 A67-42150
- E layer critical frequency calculation for 80 selected diurnal variations, considering forenoon anomaly effect 24 p4151 A67-42704
- EAR**
- S ARTIFICIAL EAR
- S AUDITORY PERCEPTION
- S LABYRINTH
- S VESTIBULAR APPARATUS
- EARDRUM**
- External ear replica for acoustical testing noting sensing element, ear canal and eardrum impedance 21 p3577 A67-38148
- EARLY BIRD SATELLITE**
- Early Bird and Thompson-Ramo-Wooldridge systems and use in worldwide communications 01 p0022 A67-10452
- Ground signal station tasks and problems, examining Early Bird satellite and Raisting station in Germany 01 p0023 A67-10453
- Component reliability screening techniques for Syncom, Early Bird, ATS Satellites and Surveyor spacecraft 01 p0155 A67-11343
- Ionospheric studies using tracking beacon on Early Bird synchronous satellite, noting scintillations due to irregularities 03 p0407 A67-12832
- Technical properties of Early Bird communications satellite noting launching, positioning, worldwide system establishment, etc 03 p0367 A67-12898
- Early Bird circuits and development of communications systems using synchronous satellites 03 p0370 A67-13830
- Early Bird satellite measurement of ionospheric electron content by determining polarization twist of VHF radio signals [RASSA PAPER 1-10-130] 03 p0417 A67-14241
- Early Bird satellite measurement of ionospheric electron content obtained from Faraday rotation data [RASSA PAPER 1-10-131] 03 p0417 A67-14242
- Random tropospheric angle error prediction in microwave observations of Early Bird satellite 04 p0574 A67-15074
- Early Bird hydrogen peroxide control system maneuvers to place satellite into final stationary position 06 p1093 A67-17663
- Effective radiated power, receiving sensitivity, bandwidth and nonlinear performance of Early Bird satellite 06 p0959 A67-17664
- Performance of Early Bird communications satellite and associated ground stations 06 p0959 A67-17665
- User reaction test results for comparison of telephone quality via Early Bird and via cable circuits based on callback interviews, service observations and circuit rejection counts 06 p0959 A67-17666
- Subjective evaluation of telephone communications via Early Bird satellite and cable circuits 06 p0959 A67-17667
- International Telecommunications Satellite /INTELSAT/ Consortium and COMSAT participation in program [AIAA PAPER 66-332] 06 p1120 A67-17707
- Amplitude fluctuations of VHF beacon of Early Bird synchronous satellite observed from stations in Italy and Massachusetts 10 p1640 A67-23233
- Latitudinal variations of ionospheric irregularities studied via synchronous and 1000 km satellites, noting Early Bird data, scintillation index graphs, radio star signals, etc 10 p1640 A67-23234
- Orbit determination of stationary satellites through data analysis, noting perturbation effect and estimation of Early Bird satellite orbit 13 p2208 A67-27522
- Early Bird satellite technology including design parameters, structure, power supply, control system and test program 16 p2759 A67-30691
- Early Bird project ground stations and launch-synchronizing operations, considering time delay on transmission performance 16 p2760 A67-30692
- Early Bird satellite design features, orbital performance, use, COMSAT applications, etc 19 p3183 A67-35636
- Attitude determination and hydrogen peroxide control system for spacecraft orientation in Syncom, Early Bird and ATS [AIAA PAPER 67-532] 19 p3334 A67-35934
- INTELSAT I communications satellite, discussing communications gear design and U.S. domestic satellite program 23 p4086 A67-41430
- EARLY WARNING SYSTEM**
- Airborne Early Warning /AEW/ system designed to provide low altitude coverage in detection of enemy aircraft 04 p0573 A67-15040
- Magnetic delay line vibration isolation system as heart of airborne special purpose computer in USN E-2A early warning aircraft 05 p0779 A67-17458
- Range sum Doppler system for early launch tracking system to get warnings of possible impact in neighborhood of critical installations [AAS PAPER 67-42] 15 p2437 A67-30111
- EARTH**
- SA TERRESTRIAL RADIATION**
- Earth science advances - Conference, MIT, Cambridge, September-October 1964 07 p1170 A67-19330
- Chemical composition and earth origin, with estimates of primordial abundances of elements in solar system 07 p1170 A67-19336
- Water vapor mass below upper limit of earth cloud cover estimated through earth brightness measurements 07 p1183 A67-20006
- Proposal for computation of unknown parts of gravitation field of earth from successive satellite passages 10 p1636 A67-23180
- EARTH ALBEDO**
- Interdependent microwave radar-and radiometer-sensor measurements of backscatter and albedo characteristics of earth surface 01 p0021 A67-10333
- Calibration procedures for earth albedo experimental package of Orbiting Solar Observatory 02 p0246 A67-12401
- Undulatory radiation in space and simulation in space test chambers 03 p0395 A67-13495
- Meteorological satellites noting necessity of radiation measurements 04 p0648 A67-14409
- Second order scattering effect on earth albedo calculations in middle UV, noting distribution functions and parameters used 04 p0613 A67-14696
- High energy primary gamma quanta flux outside atmosphere estimated with aid of Proton I satellite 05 p0877 A67-16088
- Photometric measurements of ash-moon, using large coronagraph 06 p1082 A67-18014
- Height dependence of albedo in earth upper atmosphere, calculating total quantity of neutral hydrogen in ionosphere 07 p1170 A67-19103
- Albedo upper and lower fluctuation bounds determined by astrophysical comparison and three other methods 12 p2003 A67-25684
- Albedo and earth-radiation measurements from OSO-II compared with other results, noting limb-brightening effect [AIAA PAPER 67-330] 12 p1938 A67-26044
- Earth albedo calculation using Pegasus I thermal data, discussing Rayleigh scattering, spacecraft position, atmospheric reflection effects, etc [AIAA PAPER 67-332] 12 p1938 A67-26046

- Normal distributions of various quantities related to radiation budgets of tropospheric column, earth surface and troposphere-earth system over Northern Hemisphere 13 p2116 A67-27458
- Angular, spectral and geographical distributions of outgoing fluxes of thermal radiation and earth albedo measured, using Cosmos satellite 14 p2306 A67-27861
- Two-color photoelectric photometry of earthshine, determining earth albedos 15 p2477 A67-29626
- Errors of IR-horizon pickups due to satellite determination of vertical 18 p2677 A67-31607
- Spectral measurements of reflected solar and emitted thermal radiations from earth and clouds, using spectrometer with interference filter wedge 19 p3225 A67-35690
- Electrical circuits for earth IR radiation emission measurements, describing apparatus and incorporated miniaturized pneumatic receiver 21 p3629 A67-38661
- Luminance of lunar surface site predicted by direct solar and earth reflected illumination together with local albedo variations 22 p3887 A67-40143
- Rocketborne UV radiometers for solar spectral intensity distribution, calculating irradiance and earth reflectivity 22 p3794 A67-40363
- Earth shine illuminated lunar surface TV picture taking by modifying Surveyor equipment to provide light integration [SMPE PAPER 102-40] 22 p3808 A67-40378
- Balloon sounding data for atmospheric secondary and reentrant albedo proton intensity values, discussing empirical atmospheric secondary proton spectrum 23 p4051 A67-40610
- Satellite and probe data analysis on ionizing component, primary cosmic rays and albedo particle flux intensity near atmospheric outer boundary 23 p4055 A67-41098
- High energy primary gamma quanta flux outside atmosphere estimated with aid of Proton I satellite 24 p4212 A67-42764
- Actinometric measurements from aircraft of short wave radiation fluxes and radiation balance, determining absorption coefficient for clouds and true albedo 24 p4182 A67-42882
- EARTH ATMOSPHERE**
- SA IONOSPHERE**
- SA LOWER ATMOSPHERE**
- SA MID-LATITUDE ATMOSPHERE**
- SA TROPOSPHERE**
- Fluid power support equipment for space vehicles outside earth atmosphere, based on earth environment effect on various systems [SAE PAPER 660708] 01 p0013 A67-10600
- Soviet papers on optical instability of earth atmosphere 02 p0261 A67-11982
- Chemical aspects of evolution of terrestrial atmosphere, noting role of photolysis in oxygen production 03 p0414 A67-14089
- Meteorological observatory on moon for observations of earth atmosphere and cloud cover and solar activity effects 04 p0597 A67-15066
- Primitive earth atmosphere model suggesting that in early history of earth, reducing atmosphere could be stable against gravitational escape 04 p0701 A67-15545
- Criticism of photometric results of Ney and Pepin findings regarding link layer in terrestrial atmosphere 05 p0802 A67-17330
- Mechanism regulating total amount of earth and Mars atmosphere transparent to visible and IR radiation 06 p0995 A67-18052
- Atmospheric Sciences Laboratory proposed under Apollo applications program [AIAA PAPER 67-186] 06 p1088 A67-18488
- Structures of terrestrial and extraterrestrial atmospheres 06 p1091 A67-18997
- LF galactic emissions, noting spiral arms and spherical halo on galactic hub, signal strength variation and terrestrial atmosphere role 08 p1385 A67-20866
- Relationship between terrestrial and Jovian atmospheric circulations due to solar activity 08 p1398 A67-21215
- Tunguska meteorite transfer from heliocentric to geocentric orbit proved impossible by computer calculation 11 p1868 A67-24847
- Solar-terrestrial physics - Conference, Belgrade, August-September 12 p1990 A67-25106
- Mechanical and electrical modes of energy transfer occurring in free and forced oscillations in earth magnetosphere 12 p2000 A67-25107
- Wave propagation in earth-ionosphere waveguide, obtaining modal solutions 12 p1904 A67-25216
- Rayleigh scattering and Lambert ground reflection effect on solar energy absorbed by ozone in earth molecular atmosphere evaluated on basis of transfer equation 12 p1932 A67-25341
- Mechanism for connection between seismic earth and solar activity on atmosphere and lithosphere of earth 13 p2111 A67-26558
- Earth aerospace thermodynamic properties from 100 to 100,000 km alt predicted, considering diurnal and extreme solar activity variations for engineering applications 13 p2114 A67-26821
- Tropospheric refractive index variation measurement technique 14 p2264 A67-28394
- Tropospheric turbulence and structure derived from phenomenon of electromagnetic wave propagation 14 p2264 A67-28397
- Earth atmosphere effect on propagation of radio waves from space, image formation, phase stability, technical problems and multiaperture instruments 14 p2285 A67-28437
- Generating time series for amount of solar radiation falling on horizontal surface of unit area at top of atmosphere per unit time 15 p2477 A67-29628
- Spaceport meteorology by satellite observation of earth atmosphere and cloud systems [AAS PAPER 67-47] 15 p2513 A67-30115
- Multiple light scattering in inhomogeneous spherically symmetrical planetary atmosphere with exponentially varying attenuation coefficient 16 p2698 A67-31096
- Soviet book on meteors in earth atmosphere studied by radar discussing meteor trails, upper atmosphere winds, etc 18 p2754 A67-31866
- Zonal and meridional distributions of 5-day averaged outgoing long wave radiation and relation to Northern Hemisphere circulation 17 p2879 A67-32548
- Geophysical instrumentation for environmental studies, elucidating atmospheric and near-space mechanisms, geodesy, gravimetry, etc 17 p2860 A67-32692
- Soviet book on geomagnetic field studies 17 p2845 A67-32934
- Advances in geophysics, Volume 12, covering problems of earth crust and mantle, atmosphere interaction with sea surface, etc 18 p3040 A67-34092
- Oxygenic concentrations in primitive earth atmosphere, discussing Martian atmosphere composition 18 p3041 A67-34095
- Near earth and outer ionosphere plasma waves and oscillations in VLF and ELF bands 19 p3317 A67-34932
- Isolated solar events effects on neutral and charged earth atmosphere studied in West Germany during IQSY 1964-1965 19 p3223 A67-35479
- Molecular oxygen absorption line equivalent widths measurement at 5 mm wavelength obtained from model atmosphere to determine earth atmospheric temperature 20 p3427 A67-36370
- Braking and heating effects of atmosphere on meteors in zodiacal dust to 1-meter size, discussing interaction at air cap, entry, etc 20 p3525 A67-36949
- Radiation balance chart of earth atmosphere system for evaluation of radiation receivers on Nimbus II satellite 20 p3431 A67-36964
- Terrestrial environment guideline documents providing natural environment extremes, means and cycles for spacecraft development 22 p3829 A67-39927
- Electromagnetic sensing of earth from satellites - Conference, University of Florida, November 1965 22 p3804 A67-40350
- Microwave and mm radiometric sensor for passive satellite reconnaissance of earth atmosphere and terrain thermal noise 22 p3805 A67-40353
- Weighting function calculation for remote temperature sensing of terrestrial atmosphere using selective chopper radiometer 22 p3805 A67-40356
- Earth atmosphere humidity profiles and cloud densities interpreted from 1 cm microwave absorption measurement, water vapor resonance and radiosonde measurement 22 p3806 A67-40359
- Motion of small spherical particles entering upper atmosphere of earth with cosmic velocities studied for terminal velocities 22 p3890 A67-40472
- Dynamical interaction of interplanetary particles with upper atmosphere studied by simplification of motion equation 22 p3890 A67-40473
- Radiometric determination of absorption by earth atmosphere and solar brightness temperature at 5.65 mm frequency 22 p3897 A67-40560
- Six-stage monogram for refraction of radio wave entering earth atmosphere in terms of meteorological conditions and wave elevation angle 23 p3975 A67-41212
- Penetrative motion of individual elements in earth atmosphere and prediction of velocity field from convective overshoot 23 p4024 A67-41279
- Wakes in two-dimensional flows studied by comparing mesoscale eddies in earth atmosphere with Karman vortex street, calculating wake parameters 24 p4146 A67-41786
- EARTH AXIS**
- Effect of precession of earth axis of rotation on satellite motion 05 p0894 A67-16565
- Earth axis orbital path, using Horrebow-Talcott method for determination of polhody 13 p2110 A67-26465
- Systematic clockwise rotation of asymmetry axis of main phase decrease during geomagnetic storm lifetime 16 p2666 A67-31412
- Earth axis inclination influence on diurnal amplitude of cosmic ray variation, discussing yearly modulation effect 23 p4058 A67-41126
- EARTH CORE**
- Earth density and elasticity variation reexamined by applying data on earth oscillations and considering earth inertial moment 08 p1325 A67-20985
- Frozen field estimation of surface flow of earth core and effects of secular change resulting from flow pattern nonuniformity 08 p1329 A67-21485
- Interstellar polarization with graphite grains covered with dirty ice mantles matched with entire range of observed interstellar extinction 09 p1569 A67-22439
- Cosmochemical considerations, from thermodynamical viewpoint, of formation processes of earth, planets and meteorites 11 p1864 A67-24600
- Ponderomotive forces and geomagnetic westward drift in regard to MHD theory and earth core flows 13 p2114 A67-28855
- Magnetic shielding properties of earth mantle obtained from power spectrum, deducing transfer function of mantle 14 p2314 A67-28887
- MHD of terrestrial liquid core noting geomagnetic field variation, earth mantle movements, etc 17 p2845 A67-32773
- Incompressible hydromagnetic fluid oscillation in rotating spherical shell pervaded by strong toroidal and weak poloidal magnetic field for geomagnetic secular variation 21 p3621 A67-38983
- Hypothesis Earth core surface fluid velocity patterns and magnetic field secular change at earth surface for various epochs 23 p3996 A67-40815
- Earth core growth rate by convection used to calculate earth inertia moment changes, hypothesizing day length variation with age 24 p4151 A67-42319
- Lunar origin related to earth rotational instability due to earth core formation 24 p4230 A67-42324
- Earth density/pressure relation and mantle and core mean atomic weight used to construct mass-mean density curve for planets 24 p4231 A67-42448
- EARTH CRUST**
- Book on natural neutron background of atmosphere and earth crust including effect of primary and secondary cosmic radiation, solar neutrons, presence in rocks, etc 01 p0143 A67-10042
- Wave propagation in continents and adjacent shelf areas used for study of seismic crustal refraction and reflection measurements 01 p0060 A67-10502
- Absolute age of earth, heavy elements and

- meteorites determined by radioactive decay measurements, comparing present and initial ratios of uranium 235 and 238 02 p0329 A67-12496
- Seismic refraction measurements, computing statistics for depth to Moho, crustal thickness and upper mantle velocity for geographical and geological provinces 05 p0796 A67-16152
- Astronomical theory of main features of earth crust based on fact that celestial bodies do not rotate en bloc 06 p0997 A67-18658
- Earth crust measurement techniques and use in studying other planetary lithospheres 06 p1091 A67-19001
- Geochemical differentiation in terrestrial environments, noting vertical planetary differentiation 06 p0999 A67-19015
- Electrical conductivity of earth interior from data concerning annual geomagnetic variations for all years of solar cycle 07 p1178 A67-19826
- Geochemical cycle of chemical species movement within and into earth crust and relaxation time needed to reach equilibrium 08 p1325 A67-21212
- Geochemical studies of Wyoming Precambrian graywackes concerning composition of early and ancient North American crust 08 p1326 A67-21267
- Absolute age of earth, heavy elements and meteorites determined by radioactive decay measurements, comparing present and initial ratios of uranium 235 and 238 10 p1709 A67-23364
- Mercury abundance in various meteorite and rock types determined by neutron activation analysis, relating data to evolution of meteorites and earth 11 p1858 A67-24064
- Thermal history of earth based on thermal conductivity equation 13 p2110 A67-26453
- Mechanism for connection between seismic earth and solar activity on atmosphere and lithosphere of earth 13 p2111 A67-26556
- Geomagnetic field secular variation forecasting method suggesting inclusion of anomalies 17 p2847 A67-32947
- Advances in geophysics, Volume 12, covering problems of earth crust and mantle, atmosphere interaction with sea surface, etc 18 p3040 A67-34092
- Deformations of earth crust produced by known forces of luni-solar and surface types 18 p3040 A67-34093
- Lunar missions evaluated for scientific effectiveness via use of earth analogs assuming hypothetical terrestrial objectives parallel to lunar program 22 p3887 A67-40142
- Equations describing one-, two-, and three-layer earth model spheroidal oscillations derived and solutions obtained, considering constant density and constants differing for each layer 23 p3994 A67-40714
- Tectonic activity on Venus compared with earth, discussing convection currents and temperature gradients in crust and mantle 24 p4227 A67-42222
- Lunar origin related to earth rotational instability due to earth core formation 24 p4230 A67-42324
- EARTH CURRENT**
- SA GEOELECTRICITY
- SA TELLURIC CURRENT
- Earth electrical conductivity, determined from data concerning northern and vertical components of cyclic geomagnetic variations, suggests increases with depth 07 p1174 A67-19714
- Equatorial electrojet parameters in India 19 p3221 A67-35431
- S-current intensity variation and 10.7 cm radio noise flux show agreement with Schmidt sunspot numbers 19 p3221 A67-35432
- EARTH MANTLE**
- Spheroidal disturbances propagation on surface of heterogeneous spherical earth studied by superposition of contributions from normal free spheroidal vibration modes 02 p0237 A67-11790
- Mars constitution examined on assumption of similarity to earth, noting Emden equation and Lyttleton results 05 p0902 A67-17290
- Geochemical differentiation in terrestrial environments, noting vertical planetary differentiation 06 p0999 A67-19015
- Thermodynamic possibility of thermal convection in earth mantle 13 p2117 A67-27577
- Magnetic shielding properties of earth mantle obtained from power spectrum, deducing transfer function of mantle 14 p2314 A67-28887
- MHD of terrestrial liquid core noting geomagnetic field variation, earth mantle movements, etc 17 p2845 A67-32773
- Geomagnetic field secular variation forecasting method suggesting inclusion of anomalies 17 p2847 A67-32947
- Advances in geophysics, Volume 12, covering problems of earth crust and mantle, atmosphere interaction with sea surface, etc 18 p3040 A67-34092
- Equations describing one-, two-, and three-layer earth model spheroidal oscillations derived and solutions obtained, considering constant density and constants differing for each layer 23 p3994 A67-40714
- Coupling mechanism of earth liquid core and mantle during luni-solar precession 24 p4151 A67-42315
- Earth density/pressure relation and mantle and core mean atomic weight used to construct mass-mean density curve for planets 24 p4231 A67-42448
- EARTH-MARS RENDEZVOUS**
- Compiled data for Mars apparition in 1967 giving general visibility conditions, phases, seasons and positions of Mars and earth 10 p1710 A67-23562
- EARTH-MARS RENDEZVOUS TRAJECTORY**
- Trajectory design for spacecraft which returns in vicinity of earth after Mars encounter analyzed by patched conic model [AAS PAPER 66-126] 07 p1254 A67-19985
- Total equilibrium shock layer radiation data for Martian entry body shapes at various angles of attack extrapolated to trajectory condition [AIAA PAPER 67-324] 12 p1894 A67-26039
- EARTH-MOON SYSTEM**
- Dynamics of physical librations of moon, refining standard theory by using reduced estimate of mechanical ellipticity of lunar equator 01 p0149 A67-10803
- Time variance of earth-moon distance, discussing meteoroidal accretion mechanism effect on capture phenomena 02 p0319 A67-11453
- Collision paths of free particle in Newtonian gravitational field examined, using analogy of circular restricted three-body problem 02 p0328 A67-12403
- Exploration of role of Lagrangian points of earth-moon system within solar system exploration program, using libration point satellites 02 p0328 A67-12405
- Calculating past states of earth-moon system based on three time scales for dynamical change 04 p0698 A67-14854
- Lunar origin, tidal evolution of earth-moon system, thermal background of lunar interior, figure and composition of moon and radial density profile 04 p0702 A67-15560
- Functional relation between mass, radius and angular velocity of earth, solar mass and corresponding lunar quantities shown via reciprocity principle 04 p0702 A67-15582
- Particle motion in vicinity of triangular libration point in earth-moon system solved in form of analytical expressions with time-dependent coordinates 06 p1079 A67-17763
- Couple due to distant mass acting on nonspherical object determined, considering luni-solar precession and nutation variability 06 p1031 A67-17778
- Solar perturbation effect on motion near collinear earth-moon libration points [AIAA PAPER 67-24] 06 p1084 A67-18259
- Book on moon covering motion of moon and dynamics of earth-moon system, internal constitution, topography, radiation and surface structure 06 p1087 A67-18428
- Scientific value of manned lunar exploration 06 p1093 A67-19036
- Tidal friction theory of lunar origin and dynamic evolution [AAS PAPER 66-192] 08 p1387 A67-20965
- Dynamical capture of moon by earth 08 p1389 A67-21014
- Tidal friction and effect on evolution of earth-moon system with respect to moon capture 08 p1389 A67-21015
- Lunar crater distortion implication on past shape of moon, noting earth-moon system evolution 08 p1389 A67-21016
- Lunar motion analysis showing slight acceleration to that allowed by celestial mechanics, extrapolating observed motion to past epochs 08 p1395 A67-21162
- Lunar orbit evolution caused by tidal friction in earth and moon interiors 09 p1563 A67-21634
- Error analysis shows laser-radar method improves accuracy of astronomical parameters of earth-moon system, taking into account physical libration 13 p2200 A67-27327
- Periodic motion around triangular libration point in restricted four-body problem of earth-moon-sun system 13 p2205 A67-27478
- Computer program using Birkhoff normalization of Hamiltonian of restricted problem of three-bodies problem at L sub 4 13 p2208 A67-27521
- Magnetosphere, turbulent transition region and shock wave characteristics and dimensions examined with regard to possible active or passive interaction with moon 14 p2388 A67-28619
- Astronomical unit determination by dynamical method 15 p2555 A67-29577
- Earth to lunar ground points measurement by lasers, describing experimental set-up, transmitting and receiving apparatus, etc 18 p3130 A67-34316
- Photography from aircraft of cloud-like objects in vicinity of libration points L4 and L5 of earth-moon system 19 p3251 A67-34953
- Nonlinear analysis of earth-moon system motion stability in three dimensions near L4 libration point when perturbed by sun 19 p3328 A67-35962
- Lunar data covering mass, shape, dimensions, earth-moon relations, orbits, selenography, etc 20 p3530 A67-37549
- Lead 206/lead 204 vs lead 207/lead 204 plots for young mantle-derived volcanics support upheaval predicted by lunar capture hypothesis 22 p3881 A67-39554
- Corrected derivation of earth-moon mass and various astronomical constants from Eros orbital motion 23 p4061 A67-40620
- Numerical integration of Eros orbital motion normals, obtaining earth-moon mass and various astronomical constants 23 p4061 A67-40621
- Program for preventing earth environment biological contamination by lunar material 23 p3961 A67-40845
- Minimum distance and orbit inclination in earth-moon system, considering tidal friction effects 23 p4065 A67-41000
- Angular momentum densities of planet-satellite systems, discussing earth-moon system and origin of celestial bodies 23 p4068 A67-41009
- Angular momentum density vs mass log-log plot extended from planetary mass range to asteroids, noting support for constant period law 23 p4066 A67-41010
- Moon-earth distance and moon-earth system astrometric parameters by laser ranging, describing artificial light reflector design 23 p4066 A67-41037
- Earth-moon system - NASA Goddard Institute for Space Studies, Conference, New York, January 1964 24 p4228 A67-42310
- Coupling mechanism of earth liquid core and mantle during luni-solar precession 24 p4151 A67-42315
- Friction in solid parts of earth and moon considered as sink for tidal energy and as geophysical thermal energy source 24 p4229 A67-42316
- Relation between earth-moon orbital inclinations indicates incompatibility of dynamical figures with assumptions of hydrostatic equilibrium and homogeneous density distribution 24 p4229 A67-42320
- Lunar origin and earth-moon system, discussing dynamical requirements based on secular variation of some parameters 24 p4230 A67-42322
- Fission hypothesis of lunar origin, reviewing energy, dynamics, angular momentum, geology and physical properties 24 p4230 A67-42323
- Earth-moon system origin assuming moon was formed from terrestrial material ejected from earth during rotational instability 24 p4230 A67-42325
- EARTH-MOON TRAJECTORY**
- SA MOON-EARTH TRAJECTORY**
- Perturbed trajectories computation in earth-moon system by replacing gravitational forces with single inverse square force 02 p0330 A67-12717
- Space flight problems in cislunar space, noting lunar probes, high apogee satellite specifications and orbital

- stability 05 p0897 A67-16732
 Regularization of motion equations in computation of vehicle trajectory going near singularity
 [AIAA PAPER 67-26] 06 p1087 A67-18464
 Motion of vehicle in transition region of restricted three-body problem in which earth centered and moon centered conics were connected at mean sphere of action /MSA/ [AAS PAPER 66-97] 07 p1252 A67-19961
 Feedback control system to position satellite in vicinity of unstable collinear libration point with application to lunar communication problem [AAS PAPER 66-132] 07 p1146 A67-19991
 NRL lunar radar system applied to long term earth-moon distance measurements, using pulse compression for signal processing; noting high SNR 08 p1293 A67-20689
 Feedback control system to position satellite in vicinity of unstable collinear libration point applied to lunar communication problem [AAS PAPER 66-132] 13 p2210 A67-27543
 Earth-moon and moon-earth trajectory parameters related to lunar orbit conditions for synthesizing lunar orbit trajectory 13 p2210 A67-27616
 Iterative guidance mode with application to three-dimensional upper stage vacuum flight 17 p2881 A67-32058
 Regularization of motion equations in computation of vehicle trajectory near singularity [AIAA PAPER 67-26] 17 p2948 A67-33039
 Asymptotic solution to nonplanar earth-to-moon trajectories in restricted four-body problem 21 p3705 A67-38613
 Lunar rendezvous spacecraft guidance system performance for various initial conditions and instrument errors simulated by Monte Carlo computer program 22 p3832 A67-39965
 Minimum distance and orbit inclination in earth-moon system, considering tidal friction effects 23 p4065 A67-41000
 Reuseable shuttle transportation system for lunar base logistics, estimating cost and performance [AIAA PAPER 67-874] 24 p4140 A67-42995
- EARTH MOTION**
 Geomagnetic field disturbance due to earth passage through tail of Halley comet, 1910 II 02 p0236 A67-11654
 Amplitude variations in earth free and forced polar motion indicate periodic solar activity and moon tidal forces influence 10 p1631 A67-22798
 Earth axis orbital path, using Horrebow-Talcott method for determination of polhody 13 p2110 A67-26465
 Geomagnetic field disturbance due to earth passage through tail of Halley comet, 1910, II 16 p2685 A67-31069
 Observational consequences of geocentric dust cloud whose particles are concentrated toward plane of ecliptic and which contribute to zodiacal light 19 p3222 A67-35460
 Amplitude variations in earth free and forced polar motion indicate periodic solar activity and moon tidal forces influence 24 p4149 A67-42134
 Coupled earth core-mantle model for earth precessional torques, discussing precession energy dissipation and experiments on model 24 p4151 A67-42314
- EARTH ORBIT**
 Variant of analytical determination /in terms of osculating-orbit elements/ of moments of entry into and emergence from earth shadow of artificial satellite 02 p0321 A67-11548
 Integrated logistics system capable of supporting earth orbital operations and sufficiently flexible for demanding applications of space and lunar operations [AIAA PAPER 66-864] 02 p0331 A67-12262
 Flight experience of earth-orbiting gravity gradient stabilization systems 02 p0334 A67-12362
 Heliocentric earth orbit precursor satellite, noting position outside earth and moon gravitational fields, orbital stability for solar phenomena evaluation, etc 02 p0335 A67-12410
 Cosmic ray secondary components yearly changes of intensity determined as function of earth heliolatitude 12 p1992 A67-25120
- NASA earth orbital photographic experiments planned for 1967-1969 as supplement to Mercury and Gemini efforts 12 p1940 A67-25433
 Propulsion and vehicle systems for commercial exploitation of space, emphasizing transportation to and from earth orbit [AIAA PAPER 67-82] 15 p2570 A67-29949
 Earth orbital transportation, proposing airline type system and composite nuclear-airbreathing engines for reusability with minimum refurbishment [AAS PAPER 67-84] 15 p2546 A67-29950
 Annual cosmic ray variations and changes in cosmic radiation intensity as function of earth heliolatitude 15 p2550 A67-30012
 Variant of analytical determination /in terms of osculating-orbit elements/ of moments of entry into and emergence from earth shadow of artificial satellite 16 p2752 A67-31614
 Multiple payload mission planning for multiple and single earth orbits and apogee motor delivery, evaluating cost and performance 22 p3903 A67-39952
 Earth orbital mission utilizing propellant transfer techniques based on fluid management under low gravity environment 22 p3906 A67-40163
 Earth orbital integrated logistics system extendable to space and lunar operations, considering technical and economic feasibility 23 p4061 A67-40592
 Design integration of reactor, shielding and power conversion systems for manned earth orbital station 24 p4186 A67-42547
 Design requirements of reactor power systems for manned earth orbital space station 24 p4186 A67-42548
 Heat pipe performance in zero gravity field, discussing isothermal operation of water heat pipe in earth orbit 24 p4256 A67-42926
 Manned space flight safety through mission trajectory design, considering hardware, software and operational constraints [AIAA PAPER 67-822] 24 p4243 A67-42970
 Economic exploitation of lunar mineral resources for near earth orbit manufacturing [AIAA PAPER 67-872] 24 p4238 A67-42993
- EARTH ORBITAL RENDEZVOUS /EOR/**
 Gemini VII star sightings analyzed, using handheld space sextant in Gemini VI, discussing effect of bias, timing angle measurement and trajectory errors 13 p2154 A67-26817
 Space rescue mission planning and targeting by computer program 15 p2555 A67-29609
- EARTH RADIATION**
S TERRESTRIAL RADIATION
EARTH ROTATION
 Nonideal clock model of georotational velocity irregularities derived from astronomical observations 02 p0236 A67-11512
 Position of oval zone of polar aurora on earth nocturnal side on magnetically quiet days 02 p0236 A67-11663
 Magnetic field of M-element interaction with geomagnetic field as second possible cause of irregular fluctuations in velocity of earth diurnal rotation 02 p0237 A67-11678
 Solar wind-magnetosphere system simulation, testing hypothesis that observed convective pattern is established by earth rotation 03 p0506 A67-12959
 Solar corpuscular streams effect on magnetospheric loop and on earth rotational velocity 05 p0801 A67-17135
 Seasonal changes in solar diurnal and semidiurnal variations of cosmic ray neutron component due to earth rotation axis and anisotropy sources 05 p0885 A67-17138
 Stability of rotating liquid mass /e.g. earth/, following Jeans treatment of Jacobi ellipsoidal equilibrium configurations 06 p1080 A67-17768
 Equilibrium position of Sperry MK19 gyrocompass axis and effects of earth rotation and motion of body on which gyroscope is mounted 06 p1003 A67-18178
 Resonant oscillations of artificial earth satellite with nearly repetitive path relative to rotating primary with longitudinally varying gravitational field 08 p1401 A67-21362
 Astronomic data error effect on position of reference surface trigonometric net with regard to earth axis of rotation 11 p1787 A67-24593
- Terrestrial rotation fluctuations and volcanic activity analyzed, considering existence of viscous and liquid masses at interior of earth 11 p1788 A67-24780
 Earth rotational and orbital motions interrelated by Lofitsianskii theorem for turbulent fluid motion 12 p1932 A67-25190
 Solar activity and irregular variations in earth rotational rate 12 p1933 A67-25553
 Earth rotation synthesis using arrays of small antennas for better low declination sensitivity 14 p2284 A67-28434
 Position of oval zone of polar aurora on earth nocturnal side on magnetically quiet days 16 p2665 A67-31093
 Magnetic field of M-element interaction with geomagnetic field as second possible cause of irregular fluctuations in velocity of earth diurnal rotation 16 p2665 A67-31093
 Expression analytically representing progressive and long-term variations of earth rotation velocity 16 p2667 A67-31442
 Rotational time scale and analytical representation by single formula for earth rotation variation 16 p2750 A67-31443
 Effect of atmospheric parameter changes on terrestrial surface, discussing Coriolis forces, atmospheric circulation, etc 16 p2668 A67-31567
 Michelson interferometer and ring laser compared for measurement of relativistic rotational effects of earth 17 p2883 A67-32361
 Harmonic spectrum of variations in earth rotation, noting seasonal variation and effects of lunar tides 17 p2843 A67-32444
 Stability of motion of symmetrical rotor gyrost at about fixed point on rotating earth surface 18 p3078 A67-33555
 Radio interferometry method using precision clocks for earth rotation period measurement 18 p3043 A67-34528
 Earth rotation measurement by radio interferometry, discussing rate changes in slowdown, Love number, etc 18 p3043 A67-34529
 Solar corpuscular streams effect on magnetospheric loop and on earth rotational velocity 21 p3619 A67-38478
 Western and equatorial components of geomagnetic field drift, noting noncoincidence of rotation axis with earth rotation axis 21 p3622 A67-39026
 Seasonal changes in solar diurnal and semidiurnal variations of cosmic ray neutron component due to earth rotation axis and anisotropy sources 21 p3700 A67-39048
 Long term changes of earth RD length with respect to AD due to superposition of linear and alternating components 23 p3993 A67-40675
 Biennial component of seasonal variation in earth rotation rate using time observation data, calculating stratospheric zonal wind effect 23 p3996 A67-41085
 Irregular earth rotation velocity variation analyzed by comparing universal time with atomic time 24 p4150 A67-42312
 Periodic length of day /lod/ fluctuations, interplanetary torques and variations in earth rotation 24 p4229 A67-42313
 Coupling mechanism of earth liquid core and mantle during luni-solar precession 24 p4151 A67-42315
 Earth rotation variation in historical time using day length, eclipses and earth angular velocity 24 p4151 A67-42317
 Paleontological evidence of earth rotation rate 24 p4151 A67-42313
 Time dependent gravitational constant theory, studying earth rotation secular acceleration 24 p4229 A67-42321
 Lunar origin related to earth rotational instability due to earth core formation 24 p4230 A67-42324
- EARTH SHAPE**
 Geodetic satellites determination of positions of earth surface points, earth shape, gravitational field parameters, direct mapping and navigation 01 p0154 A67-10852
 Earth oblateness effect on torque experienced in nonuniform geogravitational field by satellite with unequal principal moments of inertia 01 p0154 A67-11194
 Satellite surveying of earth size and shape, discussing ANNA, GEOS A and PAGEOS 05 p0797 A67-16776
 Earth size, shape and mass determination using satellites 05 p0800 A67-17049
 Equilibrium shape of earth, discussing space science discoveries and hydrostatic flattening mechanism 06 p0994 A67-17767

Equatorial radius of earth and zero-order undulation of geoid obtained from data on equatorial gravity, earth flattening and product of gravity constant and mass 08 p1325 A67-20933
Book for amateurs on observing earth satellites including methods and discoveries about upper atmosphere and shape of earth 10 p1608 A67-23620
Earth figure determination from relation between gravitational potential and vertical gradient anomalies and surface and sea level potential 11 p1783 A67-23899
Molodensky integral equation solvability 13 p2114 A67-26853
Geodetic satellites determination of positions of earth surface points, earth shape, gravitational field parameters, direct mapping and navigation 14 p2394 A67-28241
Orbits of artificial satellites for suitable variables, noting oblate shape of earth and air resistance 16 p2743 A67-30725
Soviet book on aircraft navigation covering theory, earth shape, map use, coordinate systems, instrumentation and aeronautical astronomy 19 p3254 A67-34894
Minimum time-of-flight aircraft trajectory between two points, with account of earth sphericity 20 p3481 A67-37202
Soviet monograph on geometry of earth ellipsoid describing analytic geometry methods for solving geodetic problems on spheroid surface 21 p3616 A67-37965
Earth gravitational potential on geoid expressed by vertical and horizontal gradients for gravitational anomalies useful in earth figure 21 p3618 A67-38199
Satellite methods to determine absolute coordinates for geodetic points and to bridge continents 21 p3620 A67-38520
Shape of earth studied for irregularities other than flattening at poles as revealed by perturbation of artificial satellite orbits 22 p3792 A67-39894
Theory on earth shape, considering surface of geoid assumed as equipotential surface at sea level, obtaining relations between zonal and tesseral harmonics coefficients 22 p3792 A67-39933

EARTH SURFACE
SA HYDROSPHERE
Solid body motion equation about stationary point fixed at earth surface 02 p0267 A67-11961
Intensity distribution of earth surface as seen at various altitudes above atmosphere due to Rayleigh scattering and diffused reflection from earth surface [AIAA PAPER 65-666] 03 p0411 A67-13046
Liapunov stability of gyroscope motion, with Cardan suspension center moving over earth surface 03 p0424 A67-14179
Formulas for extraterrestrial potential, anomalous gravity force gradient on earth topographic surface, deflections of vertical, etc 04 p0617 A67-15565
Propagation constant of electromagnetic waves over earth surface 05 p0760 A67-18001
Electric and magnetic field components produced by vertical and horizontal dipole antennas located at surface of conducting earth derived for quasi-static range 05 p0769 A67-18007
Statistical problems in use of EM data for remote sensing of geological attributes of lithosphere-atmosphere interface 05 p0803 A67-17387
Liapunov function for motion stability of solid body on earth surface having fixed point and internal gyro 06 p1004 A67-18619
Continental-oceanic boundaries of earth and relevance to tectonic speculations about moon and planets, noting role of radiogenic heat 06 p1091 A67-19003
Power aspects of radar survey of limited earth surface regions 07 p1139 A67-19225
Atmospheric potential gradient near ground in polar region correlation with solar radio emission on 1000 mc 07 p1172 A67-19423
Tangential magnetic field on earth surface excited by LF plane electromagnetic wave 07 p1142 A67-19449
Kinematics of free gyro with gimbal suspension on rotating earth 07 p1186 A67-19627
Propagation of magnetodynamic disturbance through loss ionosphere and entry into earth surface 07 p1174 A67-19718
Earth topography in spherical harmonic

analysis of land, ocean and ice 08 p1325 A67-20937
Microscopic particles from various deposits analyzed for possible extraterrestrial origin 09 p1570 A67-22693
Electromagnetic wave propagation across land-sea boundary on flat earth near coastline 11 p1751 A67-23967
NASA earth orbital photographic experiments planned for 1967-1969 as supplement to Mercury and Gemini efforts 12 p1940 A67-25433
Magnetic field of ring current on earth surface according to observations during IGY 13 p2111 A67-26557
Cosmic ray particle trajectories for various cut-off rigidity values in different points on earth surface, noting integration of motion equations of charged particle 13 p2192 A67-27244
Normal distributions of various quantities related to radiation budgets of tropospheric column, earth surface and troposphere-earth system over Northern Hemisphere 13 p2116 A67-27458
Formulas for correcting errors in aerial-photograph and planar-model coordinates due to atmospheric refraction and earth curvature 14 p2318 A67-28371
Terrain irregularity influences on radio wave propagation and reflection 14 p2264 A67-28398
Equatorial electrojet width and intensity analyzed with ground level magnetic field measurements from Peru and Nigeria 14 p2312 A67-28572
Convective self-propulsion of continents 14 p2313 A67-28620
Geographical distribution of surface temperature of ground and/or clouds and mean relative humidity of upper troposphere 15 p2513 A67-30059
Surface heat balance shown to be useful thermal boundary condition at sea-air-land interface for earth surface mean temperature and macroclimate models 15 p2513 A67-30060
Effect of atmospheric parameter changes on terrestrial surface, discussing Coriolis forces, atmospheric circulation, etc 16 p2668 A67-31567
Solid body motion about stationary point fixed at earth surface 17 p2886 A67-33278
Luminance profiles of earth sunlit limb through visible spectrum for navigation and research 19 p3213 A67-34804
Legal aspects of use of satellites in exploiting earthbound or near-in natural resources 19 p3349 A67-35641
Earth surface influence on radiation polarimetry in vicinity of radio horizon 20 p3382 A67-36776
X-band propagation over rough earth when illuminated by radiation, studying scattering problems 20 p3388 A67-37647
Soviet monograph on geometry of earth ellipsoid describing analytic geometry methods for solving geodetic problems on spheroid surface 21 p3616 A67-37965
Attenuation function of surface wave propagating over spherical earth having surface layers with different electric impedances, studying interaction with space wave 21 p3580 A67-38122
Limb darkening of earth deduced from statistical analysis of IR radiance data from measurements by Tiroc satellites 21 p3655 A67-38579
Possibility of antimatter meteor reaching earth surface on basis of collision theory between matter and antimatter 22 p3882 A67-39589
Launcher for trapped surface waves over ice-covered sea by ferrite loaded horn device 22 p3763 A67-40306
MF surface wave launching over earth, considering field strength at ground for given radiated power 22 p3763 A67-40315
Microwave and mm radiometric sensor for passive satellite reconnaissance of earth atmosphere and terrain thermal noise 22 p3805 A67-40353
Terrestrial surface spectral IR emissivities determined in situ interferometrically, noting igneous and sedimentary rock composition and texture 22 p3805 A67-40354
Airborne measurement of microwave emission from earth surface and atmosphere for potential application of radiometry to weather satellite reconnaissance 22 p3806 A67-40361

Microwave multiband spectral reconnaissance of earth and space vehicles using imaging radar on spacecraft 22 p3806 A67-40362
Earth core surface fluid velocity patterns and magnetic field secular change at earth surface for various epochs 23 p3996 A67-40815
Secular changes in surface flow motion in earth core noting dynamo theories of earth main field 23 p3996 A67-40816
Perturbing gravitational potential of earth expanded with Taylor series along earth relief levels 23 p3996 A67-40859
Performance limits of laser rangefinder for design of all-weather terrestrial rangefinder, discussing echo signal, backscatter noise and TPG 23 p3999 A67-41040
Equivalent noise temperature of antennas located on earth surface, discussing cosmic, tropospheric and man-made noise classification 23 p3980 A67-41043
Ground and water surface temperature measurements using IR radiometers onboard aircraft 24 p4181 A67-41789
Satellites and balloons for earth surface observation surveyed by types noting operations concerning geodesy, weather, oceanography, vegetation and wildlife 24 p4150 A67-42201
Earth core growth rate by convection used to calculate earth inertia moment changes, hypothesizing day length variation with age 24 p4151 A67-42319
Forestry applications for remote sensing from earth orbiting vehicles for inventory and evaluation of resources [AIAA PAPER 67-765] 24 p4258 A67-42934

EARTHQUAKE
SA SEISMIC WAVE
Digital computer simulation of nonstationary Gaussian processes using Gaussian white noise, with application to simulation of structural response, ground acceleration, velocity and displacement of earthquake 06 p1109 A67-18839
Seismological equipment for space research applied to earthquake-resistant structural design 13 p2120 A67-27217
Solar gravitational effect on earth seismic activity, showing relation between annual variations and earth-sun radius 19 p3221 A67-35430
Short period seismic radiation patterns from underground nuclear explosions and small magnitude earthquakes, noting propagation characteristics [SR-1] 20 p3434 A67-37430

EBERT SPECTROMETER
Excitation temperature of low pressure magnetically confined argon plasma, using spectroscopic transition probability 20 p3499 A67-37028

EBULLITION
S BOILING

ECCENTRICITY
Inversion of eccentricity effect in stiffened cylindrical shells buckling under external pressure 04 p0716 A67-15746
Thin isotropic circular plate bending under eccentric moment load for clamped and simply supported cases 05 p0918 A67-16419
Isotropic mass loss effect on binary star system orbital elements and period eccentricity relationship 08 p1380 A67-20385
Simplified resonance-amplitude analysis of unbalance vibration superimposed upon steady state eccentricity in aerodynamic bearings 09 p1509 A67-22613
New integral in restricted three-body problem expressed in terms of Delaunay variables 15 p2557 A67-29877
Time of flight expressed in terms of perturbed true anomaly in case of large eccentricities 16 p2743 A67-30726
Improvement of satellite elliptical orbits with small eccentricities using differential formulas 16 p2743 A67-30727
Orbit determination between two radii vectors with specified periastron distance 16 p2746 A67-30959
Eccentricity change for satellite in librational resonance shown periodic due to gravity dependence on longitude 19 p3220 A67-35254
Intersection points for satellite orbit and earth shadow /shadow equation/ solved for small eccentricities by iteration method 20 p3523 A67-36624

ECHO

SA ANECHOIC CHAMBER
SA AURORAL ECHO
SA LUNAR ECHO
SA RADAR ECHO
SA RADIO ECHO

Cyclotron echo formation in rare gas and nitrogen afterglow plasma in presence of inhomogeneous magnetic field, stressing velocity-dependent collision frequency case 14 p2356 A67-28150

Circular disk error magnitude determination by measuring rear-wall echo with angular probe 18 p3044 A67-33736

Longitudinal wave echo in collisionless electron plasma with Landau damping 19 p3295 A67-35534

Two and three-pulse echo trains stimulated in magnetoplasma by repeated electron cyclotron frequency pulsing studied with single particle collision theory 23 p4031 A67-40889

Temporal and spatial echoes can occur in collision-free plasmas at various times for different wave number combinations and various positions for different frequency combinations 24 p4194 A67-41871

ECHO I CARRIER ROCKET

Echo I orbit determined from field-reduced Baker-Nunn observations 18 p3127 A67-34248

ECHO I SATELLITE

Maryland-Minnesota-Mississippi Echo I satellite observation triangle, discussing principles of triangulation method, camera systems and office data reduction techniques 07 p1176 A67-19765

Geodetic linking of France and North Africa by synchronous photographs of Echo I satellite 07 p1176 A67-19767

Photometric studies of eclipses of Echo I and II satellites, noting period of rotation from luminosity curves and 180 degree phase shift 12 p2008 A67-25832

ECHO II SATELLITE

Photometric studies of eclipses of Echo I and II satellites, noting period of rotation from luminosity curves and 180 degree phase shift 12 p2008 A67-25832

ECHO SATELLITE

Positions of Echo satellites during reentry stage observed at Asiago in 1964 03 p0509 A67-13105

Experimental and operational communication satellite, discussing attitude stabilization, automatic routing, etc 06 p1094 A67-18050

Cooperative European geodetic observation of luminous objects at high altitude using Echo type satellite 07 p1176 A67-19762

Astrometric processing of synchronous photographic observations of Echo I satellite 07 p1144 A67-19769

ECHO SUPPRESSION

Coherent echo modulation and detection for binary data transmission, noting power savings, time and frequency diversification and communication stability 01 p0028 A67-10862

Differential far-end-operated half-echo suppressor design for telephone circuits with long propagation time 03 p0371 A67-13990

Echo suppressor for reducing speech interference in telephone relaying by satellite 10 p1603 A67-22771

Working principle of echo suppressor used in telephone link with high propagation time based on selective attenuation by frequency and time divisions 11 p1754 A67-24651

ECLIPSE

SA LUNAR ECLIPSE
SA SOLAR ECLIPSE

Maximum and minimum eclipse time of earth satellites with circular and elliptical orbits, considering dependence on argument of orbital perigee 13 p2201 A67-27339

Photometric theory of artificial satellite elipse by earth with application to atmospheric study 16 p2745 A67-30746

Illumination impinging on geocentric satellite during eclipse by earth 16 p2761 A67-30958

ECLIPSING BINARY STAR

Brightness curves used to determine geometrical and physical parameters of eclipsing binary systems containing component with extended spherical atmosphere 04 p0701 A67-15553

Representation of rotating gaseous emission rings in eclipsing binary systems

by periodic orbits around more massive component in restricted three-body problem 17 p2944 A67-32640

Beta Lyrae intrinsic polarization amount and phase dependence in visual, blue and UV light observed, analyzing polarization curves 20 p3528 A67-37471

ECOLOGICAL SYSTEM

SA CLOSED ECOLOGICAL SYSTEM

Energy-exchange simulation in artificial three-component ecological system 02 p0188 A67-12327

Indigenous microflora as determined in men undergoing simulated space conditions, considering microbe shock postulated on long term missions 23 p3958 A67-41656

ECOLOGY

Life sciences in fiscal year 2001, advanced concepts with emphasis on neurophysiological and behavioral problems 13 p2061 A67-27505

Ecological patterns of microorganisms in desert soils 15 p2426 A67-29112

Numerical estimation of microbial contamination on surfaces of spacecraft using swab samples, environmental settling strips and air samples 23 p3962 A67-40853

ECONOMICS

Game theory of economic incentive payment reliability demonstration and prediction 01 p0171 A67-11374

Reusable space vehicles role in overall space program, noting orbital missions in future and economic impact [AIAA PAPER 66-862] 02 p0343 A67-12261

Airline strategy for domination of Northeast Corridor despite improvements in high speed ground transportation [AIAA PAPER 66-942] 03 p0361 A67-14021

Economic and technological analysis of jet transport and cargo aircraft relation to future air traffic problems [AIAA PAPER 66-820] 03 p0538 A67-14134

Light aviation, problems, prospects and performance 04 p0739 A67-14434

Nondestructive quality control testing, discussing thermoelectric, magnetic particle and fluorescent penetrant, ultrasonic and linear measurement methods 05 p0813 A67-17259

Space technology influence on general progress of technology and effects on standard of living and economy 05 p0930 A67-17539

Economical hanging of commercial aircraft as implemented by Spanish airfleet 06 p0947 A67-18028

Aircraft engine design and economic pressures effect on development 06 p0949 A67-18735

Economics of U.S. space program, effect on overall economy, research, geographical regions, manpower, etc 06 p1120 A67-19038

Air transport effect on Italian balance of payments 08 p1429 A67-20767

Economic impact of defense and space programs 10 p1735 A67-23629

Cutting tool and cutting fluid evaluation, economic considerations for aerospace manufacturing [ASTME PAPER WES-7-27] 11 p1798 A67-24256

Engine design to reduce overall cost and improve power plant component for flight schedule reliability [SAE PAPER 670330] 12 p1990 A67-25872

Book on air transport economics in supersonic era covering air cargo operational problems, mechanical loading, VTOL transport operation, etc 13 p2052 A67-26256

U.S. overall economic outlook in light of space technology and systems to year 2001 13 p2231 A67-27511

Commercial possibilities in space exploration programs, considering transportation and fuel costs 13 p2231 A67-27512

Technical, economic and operation criteria for airlines when switching from conventional engines to turboprops or turbojets 14 p2409 A67-28499

Economics of military space launching systems 15 p2566 A67-29830

Advanced space vehicle planning analyzed from economic approach to decision making, noting cost decrease with time 15 p2566 A67-29833

Partially reusable space vehicle systems examined and compared for operational costs, savings, feasibility, flexibility, simplification, etc 15 p2569 A67-29851

Impact of performance improvements and reuse on cost of space transportation, noting size, configuration, mission requirements and commercial possibilities [AAS PAPER 67-130] 15 p2570 A67-29966

Selection of gyroscopic reference for commercial aircraft [AIAA PAPER 67-405] 15 p2491 A67-30372

Commercial rotor VTOL for economic intercity transportation, discussing time-frame and design requirements and analyzing improvement factors [AIAA PAPER 67-410] 15 p2422 A67-30377

Economic factors controlling development of high capacity supersonic transport aircraft 16 p2782 A67-30838

Computerized mathematical procedures application in advanced large-scale automated systems 16 p2634 A67-31568

Airport economics application to new airports, considering social implications, cost, profit and land value [SAE PAPER 670356] 17 p2974 A67-32995

Operating economics in short-haul air transports noting advantages of conversion to turbine powered equipment [SAE PAPER 670357] 17 p2975 A67-32996

Boeing SST maintenance requirements considered in terms of aircraft characteristics, economics, facilities, operations, etc [SAE PAPER 670373] 17 p2798 A67-33003

A-300 Airbus, economic subsonic passenger transport for short and medium ranges 18 p2986 A67-34075

European heavy launching vehicle development potential and economy, discussing communication satellites, thrust augmentation, zero stages, synchronous orbit, etc 18 p3137 A67-34353

Intelsat and communications satellites economic, political and social consequences, UN General Assembly Resolutions and use of satellite facilities for distribution of TV transmissions to broadcasting stations 18 p3162 A67-34354

Aviation and transportation system - Progress, profits and public interest - Conference, Hartford, December 1966, Panel 2, Aviation and technological progress 19 p3347 A67-34970

Aviation and transportation system - Progress, profits and public interest - Conference, Hartford, December 1966, Panel 4, Aviation and public policy 19 p3348 A67-34975

Potential capital and profits growth in air transportation, discussing government, management and industry 19 p3348 A67-34978

Economic trends interrelationship with future investment climate for airline securities 19 p3349 A67-34979

International aspects of space applications and political, legal and economic problems involved 19 p3349 A67-35639

Economic considerations of space operations noting cost identification, program planning, maximum utilization, etc 19 p3350 A67-35648

Economic benefits from space systems used to survey food producing areas and weather 19 p3350 A67-35650

Economics related to practical extraction of logistics and water from moon, nearby planets and asteroids 19 p3327 A67-35652

Philadelphia International Airport facility planning based on forecasts, population and business growth, economic factors and historic trends 21 p3734 A67-38805

Book on optimization covering inequality constraints, decomposition strategy, direct methods, etc 22 p3775 A67-39270

Concorde SST economics noting short/medium haul characteristics, flight times, sonic boom problems, load factor, etc 22 p3744 A67-39339

Optimal airline aircraft selection, discussing cost efficiency factors 22 p3922 A67-39537

Logistics resource development and approaches to life cycle economics in 1970s 23 p4085 A67-40587

Supersonic civil aircraft, considering journey time, safety and operating economy 24 p4093 A67-41886

Design methods to combat fatigue effects on economics of civil aircraft, discussing structural weight role, maintenance, inspection, etc 24 p4250 A67-42441

V/STOL aircraft scheduling for passenger demand and equipment mix, optimizing

airline earnings with mathematical programming model [AIAA PAPER 67-801] 24 p4259 A67-42961
Traffic prediction for high speed aircraft and surface vehicles and VTOL aircraft city-center to city-center transportation [AIAA PAPER 67-802] 24 p4259 A67-42962
Advanced systems planning with limited funds in terms of payoff from advancing technology through R and D [AIAA PAPER 67-811] 24 p4259 A67-42967
Public and private financing of vertiports /VTOL aircraft terminals/ for intercity service, investigating financial self-supporting possibilities [AIAA PAPER 67-829] 24 p4259 A67-42975
Potential benefits of lunar resources, discussing water deposits location, mining and processing [AIAA PAPER 67-876] 24 p4238 A67-42996
Man in space programs, examining costs and benefits [AIAA PAPER 67-927] 24 p4117 A67-43023
Comparative projections of helicopters, compound helicopters and tilting propotor low-disk-loading VTOL aircraft for civil applications 24 p4097 A67-43029
Commercial VTOL transport compared with conventional aircraft and ground transportation, discussing design and operating costs [AIAA PAPER 67-970] 24 p4097 A67-43048
EDDY CURRENT
Tensor components of thermal emf of CdSb measured by method without producing thermoelectrical eddy currents 01 p0129 A67-10137
Scattering of electromagnetic waves in plasma, noting effect of eddy current fluctuations 03 p0367 A67-12938
Eddy current damping effect on motion equation of magnetization vector in thin ferromagnetic film switching by coherent rotation 05 p0860 A67-16070
Eddy current conductivity technique for monitor of heat effects in nondestructive testing of 2014 Al alloy weldments 05 p0813 A67-17260
Fusion weld evaluation in 2014-T6 material by eddy current, electric conductivity and hardness plots, noting aging effects, mechanical property degradation, etc 06 p1007 A67-17640
Eddy current test systems using magnetic reaction analyzer with Hall element for detector, noting applications to welding, thickness measurement, stress monitoring, etc 09 p1502 A67-21869
Large part inspection via ultrasonic and eddy current techniques, discussing surface and discontinuity dimension analysis 10 p1660 A67-23324
Space charge and eddy currents in ionized gas flow in MHD channel determined, showing effect of cold electrode boundary layer on electrical performance 11 p1746 A67-24874
Relative eddy flows mechanism in mixed flow turbomachines 12 p1891 A67-25348
Eddy currents in nonmagnetic conductors calculated by finite difference successive overrelaxation technique on digital computer 15 p2541 A67-30142
Graphite material strength prediction by nondestructive test techniques consisting of bulk density and eddy current measurements [ASTM PAPER 54] 18 p3070 A67-34584
Eddy configuration plasma heated by induced currents, discussing electromagnetic radiation absorption 21 p3664 A67-38047
Turbulent convective eddies effect on solar concentrated magnetic fields, plotting force lines 21 p3709 A67-38991
Large scale eddy terms for balancing mean meridional circulation in winter, discussing terms magnitudes in different latitudes 22 p3828 A67-39326
Large angle flux reversal of Permalloy magnetic films investigated from experimental results of switching characteristics 22 p3860 A67-39903
Turbulence onset from small eddies in shear flow analyzed by nonlinear approach 23 p3990 A67-41173
EDDY DIFFUSION
Relative dispersion of particle pairs in homogeneous turbulence using Lagrangian-history direct interaction closure approximation for convected scalar field, obtaining Richardson diffusion

equation 03 p0405 A67-14031
Mixing length flow theory of turbulent incompressible flow integral diffusion model extended for boundary layer, channel and Couette flows 04 p0609 A67-15811
Aerothermochemical eddy diffusion model for predicting rapid wake ionization decay behind hypersonic slender clean cone obtained in free flight ballistic range [AIAA PAPER 67-21] 06 p0938 A67-18257
Thermal and momentum eddy diffusivities computed from wind profile and turbulence of rocket released chemical clouds 08 p1328 A67-21478
Average rate of eddy mixing obtained from some eddy transport problems in thermosphere, noting molecular diffusion 10 p1646 A67-23271
Eddy coefficients for diffusion and turbulence parameters for dispersion of vapor clouds in lower thermosphere from vapor trail evidence 10 p1646 A67-23272
Circulation patterns in upper atmosphere, using sounding rockets from Indian equatorial station during monsoon and winter periods 12 p1935 A67-25791
Surface mass addition into turbulent boundary layer for attaining equilibrium velocity profiles, determining development from start of injection 12 p1930 A67-25929
Model for vertical eddy heat flux in stable atmosphere 13 p2149 A67-26275
Characteristic scales of thermal convection in unstable atmosphere, discussing time evolution of total kinetic energy and lifetime for dry air case 13 p2116 A67-27460
Three-layer atmospheric model for use in two-dimensional diffusion equation for steady state conditions incorporating eddy diffusion of momentum 13 p2153 A67-27607
Temperature distribution for asymmetric heat transfer in turbulent flow between parallel plates 15 p2469 A67-29133
Current carrying incompressible viscous fluid past nonconducting sphere taking fluid inertia into account, noting eddy formation and flow separation 15 p2469 A67-29224
Laminar flow through porous annulus with constant suction velocity at walls and swirl, using differential equations 16 p2662 A67-31551
Grid geometry effect on longitudinal and lateral turbulence intensities, determining decay rate dependence 18 p3030 A67-34740
Turbulent heat-transfer coefficients and eddy diffusivity profiles for momentum and heat in Newtonian and non-Newtonian fluids, giving equation for data correlation 19 p3344 A67-34869
Heat transfer in region of separated flow over two-dimensional rectangular cavity facing oncoming turbulent boundary layer [ASME PAPER 67-HT-14] 20 p3545 A67-36711
Compressible turbulent boundary layer equations, discussing third order correlation terms role and eddy thermal conductivity definition 21 p3614 A67-38894
EDDY VISCOSITY
Turbulence structure of equilibrium boundary layers, discussing shear stress, thickness, eddy motion and intensity spectra 23 p3990 A67-41168
EDEMA
Blood pressure changes and pulmonary edema in rat associated with hyperbaric oxygen 15 p2428 A67-29275
EDGE
SA LEADING EDGE
SA TRAILING EDGE
Induced impedance dependence on scanning angle and array parameters calculated, analyzing edge effects 14 p2279 A67-28005
EDGE DISLOCATION
Elastic interaction energies between edge and screw dislocations and tetragonal defects in anisotropic NaCl lattice 02 p0298 A67-11885
Metastable dislocation crack transformation into polygonal walls of edge dislocations caused by diffusion over crack surface 04 p0711 A67-15282
Edge dislocations effect on electrical noise in n-type silicon analyzed and results compared with Shockley-Read model 11 p1849 A67-24906
Stress and temperature dependence of motion of edge dislocations in nickel single crystals 11 p1809 A67-24920
External dislocation effect on conditions for complete fracture from coplanar wedge

shaped crack in presence of applied stress 16 p2765 A67-30996
Plastic accommodation in Mg O idealized as linear array of continuously distributed edge dislocations to study crack nucleation 16 p2775 A67-31326
Defects in single crystal foils of compound bismuth telluride caused by irradiation with protons 17 p2921 A67-33050
EDGE LOADING
Quadrature solution method for bending of arbitrarily loaded thin slab whose circular edge is supported by elastic rod 01 p0158 A67-10223
Dispersion formula for waveguide irises with rounded inner edges 04 p0579 A67-14415
Stress state of cylindrical cantilever shell under action of concentrated normal force applied to free edge 04 p0708 A67-14784
Stress concentration in nonlinear creep of thin circular cylindrical shell loaded at one edge by symmetrical radial shear and bending moment 04 p0718 A67-15917
General critical stressed state of strictly convex convex shell under arbitrary load distributed over edge 04 p0719 A67-15983
Transverse shear and edge condition effect on nonlinear vibration and dynamic buckling of homogeneous and sandwich plates 05 p0910 A67-16146
Tension of homogeneous anisotropic elastic semiinfinite plate with rigid stiffener attached on segment of straight boundary 05 p0910 A67-16150
Stress-strain state of elements of thin walled shells of revolution with hinged meridional edges under effect of force and thermal distributed load satisfying end conditions 10 p1720 A67-23601
Rectangular plate under periodic in-plane edge load investigated for transition mechanisms attendant to parametric vibrations [ASME PAPER 67-VIBR-5] 11 p1871 A67-24165
Numerical and photoelastic solutions compared for uniform edge loading, obtaining pressure calibration by means of shear stress measurement 11 p1876 A67-24616
Stress function boundary conditions along perfectly free edges of membrane-like disks and shells loaded by optionally distributed forces 11 p1881 A67-25096
Lower critical load determination of elastic spherical shell with rigidly fastened edge 12 p2021 A67-25580
Partial differential equations applied to calculation of extended cylindrical shells under arbitrary curvilinear and rectilinear edge loading 12 p2022 A67-25582
Elastoplastic equilibrium of rectangular compressible and incompressible plates under load concentrated near edge determined by elastic solutions and finite difference 12 p2031 A67-25960
Approximate method for solving bending problem of rectangular plates of nonuniform thickness under arbitrary external edge loading 12 p2031 A67-25962
Polar coordinate analysis of free oscillations of circular plates with loosely clamped edges under large deflections, obtaining Duffing equation 12 p2031 A67-25963
Boundary imperfections in buckling of clamped spherical caps 13 p2220 A67-27452
General critical stressed state of strictly convex shell under arbitrary load distributed over edge 14 p2400 A67-28492
Inversely symmetrical edge effect in circular cylindrical shell with distributed stresses and moments 14 p2401 A67-28644
Cylindrical shell stability under circumferential band load effect applied to freely supported edge 14 p2401 A67-28645
Bending of circular and elliptical slabs clamped along contours under loads described by certain algebraic polynomials 15 p2573 A67-29465
Numerical realization of partitioning method in case of rectangular plate bending with end loading, using bar scheme 15 p2576 A67-30180
Elastic stability of simply supported uniformly-thin rectangular plate under unequal compressive stresses at two opposite edges due to constant body force 15 p2577 A67-30218
Buckling of longitudinally reinforced rectangular panel loaded by constant edge shear and longitudinal variable

compression 16 p2763 A67-30792
 Loading asymmetry effect introduced by short single edge crack specimen loaded in tension along center line 16 p2764 A67-30994
 Book on thin walled structures covering frame buckling, elastic buckling of rectangular flat plates, edge loading, anisotropic plate structures, etc 17 p2956 A67-32021
 Dynamic stability of homogeneous and inhomogeneous sandwich columns with pinned ends under pulsating periodic loads governed by Mathieu equation 17 p2963 A67-33036
 Infinite edge-stiffener load diffusion into semiinfinite elastic sheet, noting interface sheet stress variation stiffener force distribution [ASME PAPER 67-APM-35] 17 p2965 A67-33160
 Stress-strain state of rod with end load and time variable load on other end, discussing forced and free oscillations 19 p3338 A67-34879
 Multilayer cantilever beam subjected to varying load, studying cases where slip region propagates from edge to interior 19 p3341 A67-35579
 Random thermoelastic stress concentration near edge of circular cylindrical shell determined using axisymmetric formulation 21 p3718 A67-37979
 Stress analysis of closed cylindrical shell under concentrated loading at free edge, solving differential equation by expanding functions into Fourier series 21 p3718 A67-37982
 Strain energy method for analyzing large deflections of trapezoidal plates with constant thickness and rigidly clamped edges under uniformly distributed load 21 p3725 A67-38794
 Anisotropic plate with two elliptical holes studied for stresses under edge load by solving linear algebraic equations infinite system 22 p3910 A67-39452
 Variable length foil fluttering in supersonic compressible gas flow, particularly case with end clamping of varying edges 22 p3910 A67-39454
 Stress-strain relationship effect on r-power steady creep of pressurized thin spherical shell with sealed opening for various edge load boundary conditions 23 p4079 A67-41343
 Tensile mean stress effect on dormancy of fatigue edge crack in mild steel 23 p4079 A67-41344
 Elastic buckling loads of shallow spherical shells supported by edge rings including nonlinear prebuckling effects 23 p4080 A67-41729

EDUCATION
 Educational problems including costs, teacher training, management, government support, etc 06 p1120 A67-19042
 Bibliography on cosmic rays for use as teaching aid for college physicists 07 p1242 A67-19622
 Project NERO /near earth rescue and operations/ design study of MIT students as part of advanced space systems engineering course 13 p2214 A67-27700
 Astronautics and Education, International Astronautical Congress, Athens September 1965, Volume Eight astronautics and education - IAF Conference, Athens, September 1965, Volume 8 16 p2781 A67-30783
 Space systems design course for fourth- and fifth-year students at MIT noting departmental, industrial and governmental cooperation 16 p2781 A67-30784
 Space systems engineering course, noting unmanned Mars exploration vehicle project and world weather system project 16 p2782 A67-30785
 Astronautics education for RAF and USAF officers 16 p2782 A67-30786
 Bioastronautics role in population explosion and technological evolution problems, noting biocybernetics, and aerospace systems engineering 16 p2782 A67-30787
 Space law education 16 p2782 A67-30789
 Technical obsolescence of engineers and scientists, considering knowledge explosion impact in terms of organizations and individuals [SAE PAPER 670833] 24 p4257 A67-41993

EDUCATIONAL TELEVISION
 Economic aspects of educational TV

distribution system, using comprehensive total cost model [AIAA PAPER 66-321] 06 p1120 A67-17710
 World-educational space-televasting technical and operational problems 16 p2622 A67-30696
 Instructional broadcast satellites programming methods to reduce educational cost of students time without adding to technological cost [AIAA PAPER 67-787] 24 p4258 A67-42950
 Stationary satellite to provide educational TV to underdeveloped lands noting design, transmission terminals and safeguards against control and propaganda [AIAA PAPER 67-963] 24 p4260 A67-43042

EEG
 S ELECTROENCEPHALOGRAPH /EEG/

EFFECT
 S ATMOSPHERIC CONDITION EFFECT
 S BACKGROUND EFFECT
 S BARKHAUSEN EFFECT
 S BIOLOGICAL EFFECT
 S BRILLOUIN EFFECT
 S CAPTURE EFFECT
 S CERENKOV EFFECT
 S CHEMICAL EFFECT
 S COANDA EFFECT
 S COMPRESSIBILITY EFFECT
 S COMPTON EFFECT
 S CORIOLIS EFFECT
 S DIFFUSION EFFECT
 S DOPPLER EFFECT
 S DOPPLER-FIZEAU EFFECT
 S DRAG EFFECT
 S ETTINGSHAUSEN EFFECT
 S ETTINGSHAUSEN-NERNST EFFECT
 S EVERSHED EFFECT
 S FARADAY EFFECT
 S FORBUSH EFFECT
 S FREE STREAM EFFECT
 S GEOMAGNETIC EFFECT
 S GRAVITATIONAL EFFECT
 S GREENHOUSE EFFECT
 S GROUND EFFECT
 S GUNN EFFECT
 S HALL EFFECT
 S HEAT EFFECT
 S JAHN-TELLER EFFECT
 S KERR EFFECT
 S LONG PERIOD EFFECT
 S LUNAR EFFECT
 S MAGNETIC EFFECT
 S MAGNUS EFFECT
 S MEISSNER EFFECT
 S MOSSBAUER EFFECT
 S NONOHMIC EFFECT
 S NUCLEAR EFFECT
 S PATHOLOGICAL EFFECT
 S PELTIER EFFECT
 S PHOTOELECTROMAGNETIC /PEM/ EFFECT
 S PINCH EFFECT
 S POCKEL EFFECT
 S PRESSURE EFFECT
 S PSYCHOLOGICAL EFFECT
 S RADIATION EFFECT
 S RAMAN EFFECT
 S REENTRY EFFECT
 S RELATIVISTIC EFFECT
 S RESONANCE EFFECT
 S REYNOLDS NUMBER EFFECT
 S SAGNAC EFFECT
 S SCALE EFFECT
 S SCHOTTKY EFFECT
 S SCREEN EFFECT
 S SOLAR ACTIVITY EFFECT
 S SOLAR EFFECT
 S STARK EFFECT
 S SURFACE ROUGHNESS EFFECT
 S TEMPERATURE EFFECT
 S THERMAL EFFECT
 S THOMSON EFFECT
 S THRUST EFFECT
 S TURBULENCE EFFECT
 S VACUUM EFFECT
 S VIBRATIONAL EFFECT
 S VIBRATION EFFECT
 S WIND EFFECT
 S ZEEMAN EFFECT

EFFICIENCY
 S COMBUSTION EFFICIENCY
 S COMPRESSOR EFFICIENCY
 S ENERGY CONVERSION EFFICIENCY
 S NOZZLE EFFICIENCY
 S POWER EFFICIENCY
 S PROPELLER EFFICIENCY
 S PROPULSIVE EFFICIENCY
 S THERMAL EFFICIENCY
 S THERMODYNAMIC EFFICIENCY
 S TRANSMISSION EFFICIENCY

EFFUSION
 Equilibrium carbon monoxide pressures measured by torsion effusion studies of reaction of graphite with hafnium and uranium dioxides at high temperatures 01 p0018 A67-10763
 Vapor composition, evaporation rate and vapor pressure above chromium carbides determined by effusion method combined with mass spectrometry 03 p0456 A67-14193

EGYPT
 Lunar research at Egyptian observatory at Kottamia 18 p3020 A67-34310

EIGENFUNCTION
 Amplitudes of two-mass single-spring system, using Rayleigh approach to determination of eigenfrequencies 01 p0159 A67-10282
 Asymptotic behavior of characteristic exponents and associated eigenfunctions for periodic differential difference equations 01 p0105 A67-10521
 Eigenvalues and eigenfunctions of free oscillations of viscous incompressible fluid in arbitrarily shaped vessel under gravitational field, asymptotically expressed 02 p0233 A67-11950
 Convergence of eigenfunction series expansion of nonself-conjugate boundary value problem in complex variables 03 p0461 A67-14060
 Eigenfunction expansion solution for axisymmetric vibrations of shallow spherical shell with concentrated mass 05 p0910 A67-16147
 Hydrodynamic stability problems solved through approximate and numerical methods involving eigenvalue spectrum and Orr-Sommerfeld equation for parallel flow 11 p1781 A67-24552
 Transform using eigenfunction as kernel generates universal solution for structural member vibration, noting application to Timoshenko beam 16 p2763 A67-30616
 Hydrodynamic stability of plane incompressible viscous wall jet subjected to small disturbances, determining critical Reynolds number, eigenvalues and eigenfunctions 16 p2660 A67-31213
 Method of finite integral transforms as format for employment of incomplete eigenfunctions, discussing application of equitriangular transform 17 p2876 A67-32423
 Variational principle for determining fluid flow stability in differentially rotating self-gravitating stars and galaxies and for studying eigenfunctions properties 17 p2947 A67-32756
 Separation of variables method for cylinder cooling with turbulent fluid flow parallel to axis 17 p2972 A67-33072
 Radiative transfer for electron scattering atmosphere, obtaining eigenfunctions of transport equations 17 p2950 A67-33164
 Eigenvalues and eigenfunctions of free oscillations of viscous incompressible fluid in arbitrarily shaped vessel under gravitational field asymptotically expressed 17 p2841 A67-33267
 Soviet book on waveguide theory covering resonators, Maxwell equations role, eigenfunctions, etc 18 p3000 A67-33677
 Accidental degeneracy of hydrogen atom levels using Schroedinger equation, deriving eigenfunctions 18 p3083 A67-34072
 Operators spectrum properties and corresponding singular eigenfunctions encountered in plasma problems, showing application to initial and boundary value problems 20 p3494 A67-36148
 Galerkin method applicability to boundary value problems and eigenfunctions and eigenvalues for integrodifferential equations with deviating arguments 20 p3478 A67-37580
 Biorthogonality relation derived between eigenfunctions of operator representing linearized anisotropic multilayer warm plasma and eigenfunctions of adjoint operator 20 p3503 A67-37711
 Stabilizing effect of ion-ion collisions on collisional types of interchange instability, giving numerical solution of relevant normal mode equations 22 p3845 A67-39484
 Vector eigenfunctions solution of three-dimensional elastic theory problems, reviewing literature on bodies of revolution in various coordinates 24 p4248 A67-42101
 Recurrence formulas extending term computations in asymptotic expansions for eigenvalues of Sturm-Liouville systems and eigenfunction expansions using Horn

- method 24 p4178 A67-42692
- EIGENVALUE**
- Direct and inverse problems of optimization of quadratic functional in linear autonomous and controlled systems 10 p1621 A67-23612
- Stability of almost stationary periodic solution of Navier-Stokes equation, examining spectrum of relevant stationary problem 10 p1675 A67-23677
- Equation for linear dynamic systems simplification applicable to all cases irrespective of nature of eigenvalues and eigenvectors 11 p1772 A67-24898
- Liapunov functions generated by transformation of Companion matrix to Routh or Schwarz canonical forms, for asymptotically stable linear time-invariant multivariable systems 11 p1814 A67-24942
- Eigenvalue density in problems involving oscillations of elastic plates and shells, establishing existence of natural frequency bunching point 12 p2022 A67-25586
- Equation for relation between critical stresses of cylindrical shell loading and minimum natural-oscillation frequency of unloaded shell 12 p2027 A67-25623
- Linear Fokker-Planck collision operator expanded in terms of surface spherical harmonics, showing distribution function governed by differential-integral equations and eigenvalue spectrum 12 p1862 A67-26177
- Stability of discontinuous solutions of gas dynamic equations noting doubtful case with imaginary eigenvalues 13 p2093 A67-26379
- Eigenvalues of Laplace equation for diurnal and semidiurnal tidal oscillations solved using Galerkin method 13 p2112 A67-26668
- Doubly symmetric orbits about collinear Lagrangian points, computing jacobians eigenvalues 13 p2205 A67-27482
- Shear flow, determined by velocity and density profiles, is stable for small disturbances of all wavelengths and Richardson numbers, enumerating eigenvalues 14 p2295 A67-27904
- Eigenvalue distribution in random Hermitian matrices, considering self-adjoint operators in N dimensional unitary space 14 p2343 A67-28501
- Natural transverse vibrations of sandwich plates with rigid and lightweight fillers, deriving stability equations from eigenvalue equivalent problem 14 p2402 A67-28901
- Real autonomous smooth ODE system in neighborhood of critical point, noting stability dependence on sign of eigenvalue 14 p2345 A67-28906
- Bounds for natural frequency eigenvalues of simply supported uniform beam with constant end load and uniformly distributed axial load 14 p2403 A67-29005
- Parameter and domain dependence of eigenvalues of elliptic partial differential equations 15 p2509 A67-29461
- Hydrodynamic stability of plane incompressible viscous wall jet subjected to small disturbances, determining critical Reynolds number, eigenvalues and eigenfunctions 16 p2860 A67-31213
- Fluid motion in shallow trapezoidal container, noting dimensionless quantity relating frequencies to volume and rim dimensions, sloshing modes, eigenvalues, etc 16 p2861 A67-31421
- Eigenvalue method prediction of two-phase fluid critical flow rates via energy model, comparing empirical and theoretical results 17 p2838 A67-32689
- Contour integral representation of eigenvalues of first boundary value problem of elasticity theory 17 p2962 A67-32832
- Propagation in rectangular waveguide solved for traveling wave maser design by Rayleigh-Ritz method reduced to matrix eigenvalue problem 17 p2828 A67-33086
- Eigenvalues and eigenfunctions of free oscillations of viscous incompressible fluid in arbitrarily shaped vessel under gravitational field asymptotically expressed 17 p2841 A67-33267
- Three-space optical resonator model, deriving properties responsible for undesired natural frequencies suppression, noting selection characteristics 18 p3058 A67-33528
- Continuous spectrum of eigenvalues related to Fokker-Planck collision integral 19 p3285 A67-35341
- Linearized system of water waves initial value problem, obtaining eigenvalue with parameter in boundary condition 19 p3210 A67-35703
- Higher mode cut-off frequencies in coaxial cables of elliptical cross section tabulated as function of conductor dimensions 20 p3382 A67-36861
- Modes and eigenvalues of symmetric cylindrical Fabry-Perot laser resonator with circular output-coupling apertures 20 p3460 A67-37024
- Galerkin method applicability to boundary value problems and eigenfunctions and eigenvalues for integrodifferential equations with deviating arguments 20 p3478 A67-37580
- Long radio wave propagation in earth ionosphere waveguide channel, determining eigenvalues of boundary value problem from complex transcendental equation containing Bessel function 21 p3580 A67-38116
- Stability of almost stationary periodic solution of Navier-Stokes equation, examining spectrum of relevant stationary problem 21 p3653 A67-38278
- Characterization of eigenvalues of singular nonself-adjoint differential operator of second order 21 p3653 A67-38557
- Matrix method to calculate energy eigenvalues and orbital wave functions for various singlet states of helium isoelectronic sequence 22 p3841 A67-40202
- Compact integral operator base problem for Hilbert-Schmidt integral operators existence, discussing Schmidt classical operator approximations and eigenvalues 22 p3828 A67-40554
- Taylor instability in circular Couette flow reexamined as eigenvalue problem noting suppression of geometry effect 23 p3988 A67-40601
- Explicit nonlinear numerical integration method for solution of large systems of ordinary differential equations 23 p4024 A67-41394
- Asymptotic solutions of eigenvalue problem with two transition points applied to Graetz problem involving heat transfer in fluid 23 p4083 A67-41668
- Lower bounds for eigenvalues of differential linear elliptical operator using Rayleigh-Ritz approximation 24 p4177 A67-42154
- Recurrence formulas extending term computations in asymptotic expansions for eigenvalues of Sturm-Liouville systems and eigenfunction expansions using Horn method 24 p4178 A67-42692
- Asymptotic functional dependences and eigenvalues of guided wave modes in uniform and nonuniform structures deduced by ray-optical techniques 24 p4124 A67-42807
- Improvement of understated eigenvalue approximations 24 p4179 A67-43079
- EIGENVECTOR**
- Sinkhorn theorem on diagonal equivalence of nonnegative matrix to stochastic matrix, using Mennon homogeneous positive nonlinear operator T and uniqueness of eigenvectors of T 04 p0645 A67-15082
- Givens-Householder method for computing eigenvalues and eigenvectors of real symmetric matrix 09 p1468 A67-22046
- Eigenvector scalar product solutions for closed loop time optimal control of linear systems 11 p1771 A67-24897
- Equation for linear dynamic systems simplification applicable to all cases irrespective of nature of eigenvalues and eigenvectors 11 p1772 A67-24898
- EINSTEIN EQUATION**
- SA RELATIVITY THEORY**
- Langvin reasoning, used to establish Einstein energy inertia formula from energy conservation principle, applied to heat transformation in special theory of relativity 01 p0166 A67-10772
- Einstein A coefficient for lambda doublet transitions of ground state of OH 01 p0114 A67-10898
- Space-time singularities and Einstein equations 01 p0151 A67-11291
- Homogeneous anisotropic cosmological model with magnetic field for solution of Einstein gravitational and Maxwell equations in space filled with ideal matter 04 p0702 A67-15984
- Exact solutions of Einstein-Maxwell equation of Petrov class N when propagation vector of gravitational field is hypersurface orthogonal 07 p1218 A67-20281
- Einsteinian gravitation equations stated in terms of three-dimensional tensor analysis as applied in conformal

space 08 p1354 A67-20843
 Static axisymmetric interior solution of Einstein field equations which matches smoothly to one of Weyl exterior solutions 09 p1531 A67-21639
 Cosmological principle and field equations used in analysis of Einstein, de Sitter, Friedmann and Hoyle-Narlikar models 09 p1563 A67-21652
 Evaluating accuracy of substitute term in Einstein equation, noting inconsistency with zero and second law of thermodynamics 10 p1680 A67-23496
 Post-Galilean transformation to which Einstein-Infeld-Hoffmann motion equation is invariant, considering transformation to center of mass system 12 p1965 A67-25125
 M-dimensional interpretation of n-dimensional Einstein equation 12 p1966 A67-25143
 Homogeneous solutions of Einstein-Lichnerowicz equations for electrically charged fluid with infinite conductivity universes 12 p1962 A67-26178
 Integration of Einstein gravitational equations implies that corpuscle be rigidly connected with particular Fermi space-time system of reference 13 p2158 A67-27298
 Homogeneous anisotropic cosmological model with magnetic field for solution of Einstein gravitational equations and Maxwell equations in space filled with ideal matter 14 p2386 A67-28485
 Adiabatic gravitational collapse of spherically symmetrical distribution of matter, investigating nonvanishing internal pressure gradient, using Einstein field equation 16 p2746 A67-30865
 Gravitation equations different from Einstein derived from Lagrangian in general form corresponding to general relativity theory 16 p2702 A67-31045
 Wave surfaces of Einstein-Schrodinger theory and nonlinear electrodynamics brought together using antisymmetric tensor 18 p3078 A67-33688
 Congruences of geodesic rays of Einstein vacuum spaces 18 p3078 A67-33690
 Integrability 18 p3078 A67-33690
 Einstein gravitation theory relation to general and special relativity, space time, unified four-dimensional continuum metric and chronogeometric theories 18 p3079 A67-34133
 Schwarzschild criterion for convective instability in general relativity extended to Einstein hydrostatics to formulate buoyancy principle with aid of initial value problem 18 p3133 A67-34375
 Approximation method for Einstein-Maxwell field equations successive solution applied to Weyl canonical problems and field equations for point particle 19 p3262 A67-35576
 Kerr metric as Einstein field equations solution, considering Sygne g method as possible Kerr metric source 20 p3486 A67-37089
 Einstein vacuum equation solution Interpretation for gravitation, space and time concepts, using vector fields oriented in time and Riemann tensorial equations 20 p3487 A67-37684
 Evolution problem investigated for invariant Einstein vacuum equation, discussing existence and uniqueness theorems 20 p3487 A67-37685
 Occurrence of singularities in cosmology, giving testable condition implying existence of singularity assuming causality 21 p3703 A67-38493
 Radial motion of spherical self-gravitating mass undergoing gravitational collapse or expansion using Einstein general relativity theory 22 p3892 A67-40495
 Oscillating relativistic universe model from Einstein field equations, discussing Friedmann model matter and velocity distribution, Hubble law and universe volume oscillating relativistic universe model from 22 p3892 A67-40496
 Rigorously geodesic inertial motion of extended object in Einstein gravitational field, using relativistic hydrodynamics 23 p4027 A67-41148
 Axisymmetric stationary gravitational field Einstein field equations in rigid uniformly rotating ideal fluid 23 p4028 A67-41149
 Einstein-Maxwell fields exact solutions constructed from Einstein vacuum fields,

discussing vacuum metric and transformations 23 p4028 A67-41150
 Einstein special relativity theory disproof based on four clocks 24 p4187 A67-41879
 Rebuttal of Dingle disproof of Einstein special relativity theory 24 p4187 A67-41880
 Einstein field equations derived for thin spherical shell of charged dust falling on spherically symmetric field of massive charged body, considering bounce 24 p4189 A67-42599
EJECTION
SA BAILOUT
SA PARACHUTING
 Downrange radar and optical data reduction used for evaluation of ejection velocities of ballistic missile penetration aids at deployment 05 p0902 A67-17209
 Mean number of random process ejections over arbitrary time period at output of receiver with time and frequency selectivity 06 p0965 A67-18897
 Gas ejection and boat-tailing effect on cylindrical afterbody in supersonic flow 17 p2793 A67-33041
 Ejection capability vs decision to eject 22 p3754 A67-39596
EJECTION INJURY
 Air Force biodynamic research on injury due to impact during air crash or ejection 08 p1289 A67-20615
 Human body resistance limit for ejection through aircraft canopy 14 p2257 A67-28215
 Fatal injuries resulting from extreme water impact studied from necropsy data on persons jumping from Golden Gate Bridge 21 p3573 A67-38069
 Radiological findings from pilots afflicted with vertebral fractures from ejection injuries 21 p3575 A67-38510
 Decompression tests for potential hazards of ejection or fatal head injuries in small pressurized aircraft 23 p3970 A67-41693
EJECTION SEAT
 Pilots and passengers protection and escape from aircraft after accident 03 p0381 A67-14096
 Military pilot escape, survival, search and rescue 05 p0752 A67-17102
 LW-3B escape system for low and medium performance V/STOL aircraft 17 p2794 A67-32000
 Evolution and future objectives of ejection-seat escape systems design, noting characteristics and deficiencies in conventional ejection seats 17 p2795 A67-32002
EJECTION TRAINING
S PILOT TRAINING
EJECTOR
SA JET PUMP
 Method for matching jet engine intake and ejector pumping characteristics to evaluate static and in-flight performance of air-augmented nozzles, considering external aerodynamics influence 03 p0350 A67-12903
 Working diagrams, performance characteristics and loss mechanisms of ejector and compressor for mixing two liquid or two gas streams 03 p0353 A67-14305
 Similarity parameters for gas generators obtained from equations governing gas-stream ejection 15 p2423 A67-30080
 Wind tunnel ejector and hot water supply for ramjet power plant attitude test stand, noting synchronization of ejector with test section 17 p2834 A67-32817
 Theory of supersonic gas ejector with cylindrical mixing chamber, discussing low and high pressure gas flow 20 p3358 A67-37085
 Optimization of staged ejector systems noting mathematical model development to represent performance characteristics 22 p3787 A67-40150
EKMAN LAYER
 Motion induced by sources and sinks distributed along vertical boundary of rotating fluid, noting role of Ekman layers 09 p1489 A67-22416
 Rotating Ekman boundary layer stability and transition for two-dimensional roll vortices superimposed upon basic boundary layer flow 11 p1781 A67-24543
 Instabilities of Ekman layer measured using hot-wire anemometers 15 p2471 A67-29655

Nonlinear steady motions produced by stable stratification in rapidly rotating fluid, discussing Ekman layers 23 p3990 A67-41170
 Ekman pumping in solar core noting slow meridional-current distribution in spinning core determined by energy balance 24 p4225 A67-41834
ELASTIC BAR
 Unstabilized rod buckling from impact load with longitudinal compression wave reflection 01 p0165 A67-11303
 Exact field equations for motion of hyperelastic rod derived from general three-dimensional theory 03 p0522 A67-13391
 Tension and bending of two-layer rods under nonuniform heating and loading 03 p0527 A67-14077
 Dynamic elastic modulus of thin rod at elevated temperatures measured in terms of rapid-heating induced longitudinal oscillation [ASME PAPER 66-WA/MET-12] 04 p0712 A67-15376
 Progressive buckling of rectangular cross section bar under cyclic variations in temperature 05 p0913 A67-16193
 Optimum design of bar profile, considering bending and torsion effect and variation of wall thickness 05 p0918 A67-16242
 Complementary energy method for flexural buckling of initially straight elastic bars 06 p1110 A67-18840
 Mathematical analysis of certain problems concerning longitudinal oscillations of compound bars consisting of elastic and elastoviscous sections 07 p1214 A67-19176
 Stress concentration factors for two circular notches of variable radius and position superposed at edges of strip 09 p1574 A67-21839
 Bending oscillations of hinged and clamped three-layer beams 09 p1575 A67-22219
 Column compressive tests of aluminum alloy bars, determining load eccentricity and initial straightness deviation 10 p1715 A67-22826
 Computer graphic display for dynamic response of nonuniform beam treated by lumped mass-spring representation of structure 10 p1608 A67-23739
 Linearization of hyperbolic equation for data analysis of stability of elastic column and plate structures, determining critical load 11 p1874 A67-24224
 Stress-strain state of circular cylindrical rod coupled to half-space when applying torsion to free end 11 p1879 A67-24884
 Fokker-Planck-Kolmogorov method analysis of nonlinear systems described by stochastic partial differential equations 15 p2517 A67-29658
 Stability of cantilevered elastic bar with end under compressive follower force, noting shear deformation, rotary inertia and internal damping forces 17 p2959 A67-32420
 Transverse oscillations of elastic inhomogeneous rod with Young's modulus varying along length, solved in Bessel functions infinite series form 17 p2962 A67-32873
 Dispersion of longitudinal or extensional waves in isotropic linear elastic bars with rectangular cross section [ASME PAPER 67-APM-17] 17 p2964 A67-33148
 Axisymmetric two-dimensional elastic wave propagation equations for finite elastic bar, considering continuous and discontinuous loadings at impact end [ASME PAPER 67-APM-22] 17 p2964 A67-33151
 Cross sectional strain and stress distributions in cylindrical elastic bars subjected to pressure-step and velocity-impact loading [ASME PAPER 67-APM-33] 17 p2965 A67-33158
 Elastic-plastic rods theory using thermodynamical restrictions, examining straight rod motions 17 p2966 A67-33348
 Plastic resonance problem for longitudinal elastoplastic waves in finite bar solved, considering bodies with rigid unloading characteristics 18 p3140 A67-33465
 Bending oscillations of hinged and clamped three-layer beams 18 p3141 A67-33770
 Linear theory of initially straight elastic rods, discussing wave propagation, thermal effects for extension and flexure and

- torsion 18 p3144 A67-34287
Flexural center location and torsional rigidity of bar calculated using elasticity theory and variational calculus 19 p3340 A67-35512
Vibrating elastic bar motion equation reduced to integral equations system for solutions to boundary value problems 20 p3476 A67-36667
Uniform cantilevered bar subject to eccentric compressive follower force, considering warping rigidity, bending-torsional flutter and stability 20 p3538 A67-36674
Minimum mass bar design for axial vibration of beam with load distribution at specified natural frequency 21 p3728 A67-38890
Normal stresses induced by temperature effects in thin walled bars, assuming nondeformability of contour and no displacements in middle surface 21 p3728 A67-38905
- PLASTIC BENDING**
Monograph on higher modes of critical speed of shafts with elastic clamping moment at bearings 02 p0250 A67-12710
Closed form pseudostatic solutions for Kirchhoff bending stress fields associated with semilinear crack extending at uniform velocity in elastic plate 03 p0523 A67-13468
Plane oscillations of elastic pendulum with shaft undergoing bending deformation, determining principal zone of instability for action by longitudinal harmonic force 03 p0469 A67-14161
Energy method creep analysis of elastic bending of circular plates 04 p0707 A67-14443
Digital simulation of Gaussian random load forcing function and motion equations of nonlinear vibration of damped elastic beam 04 p0656 A67-14447
Distributed parameter transmission matrix analysis of bending vibrations of nonuniform elastic beam [SAE PAPER 660719] 04 p0716 A67-15782
Combined elastic solutions-finite difference method for bending of compressible or incompressible rectangular metal plate beyond elastic limit 05 p0907 A67-16017
Optimum design of bar profile, considering bending and torsion effect and variation of wall thickness 05 p0916 A67-16242
Elastic plate bending mechanical analog to two-dimensional thermoelastic problem, solving thermal stresses of solid propellant grain 05 p0917 A67-16417
Thermoelastic bending of solid circular plate of variable thickness 06 p1105 A67-18581
Buckle pattern representation for isotropic cylinder rendering results of critical stress and role of buckle pattern upon ratio of critical stress 09 p1575 A67-22164
Analytical solution, based on stress functions, for deflection of plastics sandwich beam under bending loads at center, agreeing with experimental results for short duration loading 09 p1579 A67-22612
Large deflections of beam loaded and supported at two points 11 p1871 A67-24088
Bending strain in linear shell theory, noting surface differential geometry and rotation vector and tensor [ASCE PAPER 268] 11 p1874 A67-24430
Bending under transverse load of isotropic plate with elastic base, using Ambartsumian theory of anisotropic plates 11 p1878 A67-24857
Approximate solution using finite difference method of bending of rectangular plate beyond elastic limit 11 p1879 A67-24886
Stressed and strained state of infinite plate lying on elastic base weakened by finite number of arbitrarily located circular holes 11 p1879 A67-25053
Plate bending by Reissner method and asymptotic method 12 p2026 A67-25616
Bending of thin plate of aluminum with nonlinear stress-strain relation analyzed, considering material compressibility effect 13 p2215 A67-26267
Stability equation of multilayer sandwich plates with isotropic homogeneous facing layers and orthotropic homogeneous core layers 15 p2577 A67-30267
Large deflection bending of simply supported rectangular sandwich plates with isotropic core under uniform normal pressure, solving governing differential equations by digital computer 15 p2577 A67-30269
Thin walled unsymmetrical beam under bending and torsion studied for nonlinear elastic behavior 17 p2957 A67-32023
LEM-CSM analysis, elastic bending and propellant sloshing 17 p2955 A67-32478
Flexural center location and torsional rigidity of bar calculated using elasticity theory and variational calculus 19 p3340 A67-35512
Ride quality improvement on flexible aircraft by means of elastic structural bending mode suppression design technique [AIAA PAPER 67-571] 19 p3174 A67-35967
Mechanical characteristics of materials determined using circular bending 20 p3537 A67-36476
Differential equation for bending of homogeneous plates of variable stiffness 20 p3541 A67-37284
Elastic bending vibrations amplitude and frequency effects on current oscillations in CdS single crystals 20 p3514 A67-37463
Transverse deflection of rectangular plate with trapezoidal cross section subjected to uniform longitudinal curvature, comparing theory with experiment 21 p3722 A67-38436
Flat plate bending and two-dimensional, axisymmetric and boundary value problems in elasticity theory investigated using Vlasov initial function method 21 p3725 A67-38792
Long cylindrical shell with externally loaded reinforcing ring, solving stress distributions and displacements 21 p3727 A67-38871
Curvature for variable cross section beam bending with arbitrary transverse and longitudinal loads calculated by computer 22 p3915 A67-40449
Stress intensity factors for infinite plate subjected to cylindrical bending with radial cracks from internal hole 23 p4073 A67-40615
Elastic wing twisting effect on longitudinal stability and controllability of glider, considering wing rigidity 24 p4094 A67-42021
- ELASTIC BODY**
Local three-dimensional static and dynamic contact reactions between elastic isotropic bodies 01 p0158 A67-10216
Temperature, stress and displacement in elastic bodies for random surface forces and randomly distributed environmental temperature 01 p0159 A67-10403
Universal relations for static deformations in isotropic compressible elastic bodies determined by method that may be applied to isotropic incompressible elastic bodies 01 p0162 A67-10799
Wave solutions for plane waves propagating in isotropic elastic solid using isentropic approximation 01 p0162 A67-10847
Stability equation of elastic bodies subjected to body and pressure forces derived using virtual work principle, noting specialization to thin shells 01 p0165 A67-11307
Formulation of dynamic three-dimensional problem of homogeneous isotropic and linearly elastic bodies in terms of stresses 03 p0523 A67-13459
Dynamic reciprocal theorem for sinusoidal oscillation of elastic medium treated as extension of static reciprocal theorem of Betti and Rayleigh, using continuum mechanics [ASME PAPER 65-WA/MD-21] 03 p0525 A67-13832
Two contact problems involving cylindrical shells reinforced with elastic frames 04 p0717 A67-15889
Initial stress influence on frequency of three-dimensional vibrations of plates and rods 04 p0717 A67-15912
Three-dimensional stress concentration around cylindrical hole in semilinearly elastic body 05 p0909 A67-18140
Relations between mean stresses and strains of elastic body consisting of soldered isotropic layers, noting thermal effect 05 p0912 A67-18184
Brittle fracture crack theory for elastic body weakened by initially wide crack 05 p0923 A67-17179
Inversion formula for principal integral representation of class of P-analytic functions applicable to axisymmetrical problems of elastic bodies 05 p0923 A67-17185
Generalized Lagrangian for system of gravitating elastic bodies derived from Fokker Lagrangian 05 p0847 A67-17495
One-dimensional acceleration waves and higher order waves propagating in general nonlinear Maxwellian materials with fading memory 06 p1099 A67-17834
Linear shell theory for nonlinear transverse coupled vibrations of partially filled circular cylindrical elastic tank [AIAA PAPER 67-74] 06 p1101 A67-18272
Dynamic response, sloshing frequencies and stability of free surface of liquid in circular cylindrical elastic tank with flexible bottom [AIAA PAPER 67-76] 06 p0986 A67-18274
Elastic behavior of bodies composed of materials with different characteristics of compression and tensile strengths, noting applicability of various variational equations 06 p1106 A67-18624
Plane elastic problem for bodies with almost periodic fast oscillating elastic parameters, obtaining asymptotic solution for boundary value problems 06 p1106 A67-18625
Finite difference method solution of motion equations for free vibrations of initially disturbed thin elastic rings 06 p1109 A67-18838
Formulas for stress determination on surface of elastic right cylinder, sphere and circular cone taking into account geometrical nonlinearity 07 p1261 A67-19218
Diffraction of plane longitudinal wave in interior of elastic solid, where wave is harmonic in time and impinging on surface of penny shaped crack 09 p1573 A67-21663
Optimal control of elastic flight vehicles, describing axis oscillations by equations of beam with variable cross section 09 p1439 A67-22075
Stress field near surface of elastic solid during short time interval when heat flow occurs analyzed through strain theory for fracture location and probability 09 p1576 A67-22422
Thermal stress distribution around crack in elastic solid of transversely isotropic material 10 p1716 A67-22934
Gurtin variational principles extended in application to dynamic problems of elasticity with finite deformation 10 p1720 A67-23598
Generalized reciprocity law relating behavior of elastic body and static and geometric boundary conditions 10 p1721 A67-23686
Equations for continuous media in finite case formulated in Eulerian and Lagrangian form 11 p1819 A67-24621
Elastic-plastic body and elastic work hardening materials under static loading, using maximum principle for computing procedures 11 p1876 A67-24622
Nonlinear oscillation effect on motion equation of elastic object under free flight conditions 12 p2032 A67-25966
Spherical wave propagation in infinite elastic body with transverse isotropy 13 p2217 A67-26633
Random thermal-stress analysis for linearly elastic body assuming zero-stress state, uniform temperature and freely deformable surface of body 13 p2217 A67-26634
Natural frequencies of elastic toroids experimentally determined compared with theoretical results 13 p2219 A67-27091
Equilibrium states of buckled elastic rings under stress 13 p2219 A67-27147
Elastic rod, string or torsional member under effect of accelerating axial load, solving differential equation of motion in fixed end condition 14 p2399 A67-28140
Transient vibration of viscoelastic body, showing dynamic displacement expression in terms of static boundary value problem 14 p2400 A67-28143
Geometrical and statistical relations of theory of nonlinearly elastic body presented in connection with bifurcation of equilibrium of ideally elastic body 15 p2574 A67-29690
Elastic components influence on attitude stability of motion of spinning satellite 16 p2761 A67-30742
Thin elastic circular ring equilibrium stability in rigid cavity subjected to parallel loading, considering small ring separation region at buckling [ASME PAPER 67-APM-19] 17 p2958 A67-32406
Stability analysis of deformable space vehicle in torque free state noting gravitational effect, stability of spin motion,

- characteristic motion equations, etc 17 p2956 A67-32779
- Cauchy type integral applied to second boundary value problem for elastic plane with doubly periodic system of identical holes 18 p3145 A67-34601
- Magnetoelasticity/magnetothermoelasticity theories concerned with externally applied magnetic field interacting effects on elastic/thermoelastic deformations of solid body 19 p3262 A67-35799
- One-dimensional directed continuum assumed to represent elastic fiber strengthened string, developing boundary conditions and constitutive equations 20 p3535 A67-36197
- Stability condition for inhomogeneous elastic body subjected to internal stresses 20 p3535 A67-36392
- Motion equations for elastically deforming body containing cavity partly filled with ideal fluid 20 p3481 A67-37380
- Wave propagation rate in elastoplastic bodies under completely plastic conditions, noting discontinuity 21 p3716 A67-37968
- Generalized reciprocity law relating behavior of elastic body and static and geometric boundary conditions 21 p3720 A67-38287
- Thermal-stress deformed condition on heated elastic bodies boundary containing inclusions of spherical thin film with homogeneous infinite heat flow 21 p3720 A67-38295
- Linear shell theory for nonlinear transverse coupled vibrations of partially filled circular cylindrical elastic tank [AIAA PAPER 67-74] 21 p3727 A67-38866
- Dynamic response, sloshing frequencies and stability of free surface of liquid in circular cylindrical elastic tank with flexible bottom [AIAA PAPER 67-76] 21 p3614 A67-38868
- General theory advanced for analysis of statically loaded elastic structures using concept of finite members interconnected in finite loaded joints 22 p3911 A67-39559
- Potential energy release of stressed elastic body due to material removal and crack extension 22 p3911 A67-39679
- Saint Venant principle in linear and nonlinear plane elasticity in two-dimensional isotropic body 22 p3912 A67-39743
- Book on linear mechanics of elastic structures covering work and energy, Saint Venant theory of torsion, stress analysis, etc 23 p4071 A67-40566
- Steady state vertical displacements at surface of elastic half-space due to Rayleigh waves from sonic boom, obtaining shock amplification factors 23 p4074 A67-40632
- Stress-strain relation in viscoelastoplastic bodies noting static instability under conservative load 24 p4246 A67-41932
- Composite, reinforced and porous elastic body isotropic deformation, deriving macroscopic moduli, mean stress and strain values and dispersion 24 p4249 A67-42102
- Constrained torsion of thin walled rods with closed or open profiles, discussing stress-strain state of cross section sealed at one point 24 p4250 A67-42307
- ELASTIC BUCKLING**
- Skin effect association with anisotropy of medium in solid mechanics, analyzing surface instability, internal buckling and surface wave propagation 01 p0113 A67-10406
- Unstabilized rod buckling from impact load with longitudinal compression wave reflection 01 p0165 A67-11303
- Stability problems of sandwich plates, considering buckling and wrinkling 02 p0341 A67-12713
- Linear local buckling theory for finite length axially compressed circular cylinder and length effect on critical load 05 p0918 A67-16421
- Initial postbuckling behavior of double curvature shell segments under several loading conditions determined, using Koiter theory 05 p0921 A67-16885
- Finite difference method stability analysis of deformed eccentrically stiffened shells of revolution, accounting for finite prebuckling rotations [AIAA PAPER 67-110] 06 p1101 A67-18285
- Complementary energy method for flexural buckling of initially straight elastic bars 06 p1110 A67-18840
- Elastic postbuckling involves coupled modes when critical loads corresponding to buckling modes of two degrees of freedom system are equal 08 p1422 A67-21032
- Buckle pattern representation for isotropic cylinder rendering results of critical stress and role of buckle pattern upon ratio of critical stress 09 p1575 A67-22164
- Dynamic snap-through buckling of shallow spherical caps of elastic material 12 p2030 A67-25923
- Boundary imperfections in buckling of clamped spherical caps 13 p2220 A67-27452
- Dynamic stability of structures, discussing parametric resonance, impulsive loading, circulatory loads, aeroelastic and buckling problems 14 p2396 A67-28079
- Single mode analysis of dynamic buckling of imperfection-sensitive elastic structure prone to catastrophic failure under time dependent load 14 p2396 A67-28083
- Dynamic buckling under step loading studied on basis of general nonlinear theory of elastic stability 14 p2397 A67-28089
- Book on thin walled structures covering frame buckling, elastic buckling of rectangular flat plates, edge loading, anisotropic plate structures, etc 17 p2956 A67-32021
- Elastic buckling of thin walled frames, discussing restraint effect on stability, symmetry effect on critical behavior and dead loads effect 17 p2957 A67-32022
- Theory and design methods of torsional-flexural buckling of thin walled elastic struts of open cross section, deriving basic differential equations 17 p2957 A67-32024
- Finite difference method stability analysis of deformed eccentrically stiffened shells of revolution, accounting for finite prebuckling rotations [AIAA PAPER 67-110] 17 p2963 A67-33015
- Rayleigh-Ritz method used to predict elastic buckling of prolate spheroidal shells under hydrostatic pressure 17 p2963 A67-33017
- Large deflections of columns of variable flexural rigidity, assuming bending moment is proportional to curvature 17 p2963 A67-33020
- Blaxial buckling behavior of 45 degrees eccentric-stiffened waffle cylinders using prediction theory 19 p3341 A67-35525
- Buckling of aging linearly viscoelastic beam columns with time variable mechanical properties, deriving integrodifferential equations and stability conditions 19 p3343 A67-35781
- Buckling analysis of sandwich beams with elastic orthotropic cores under axial compression 20 p3537 A67-36641
- Elastic and residual strains caused by friction load in polymer surface layers studied for dependence, slip rate and friction load duration 20 p3473 A67-36842
- Elastic spherical shell stability under thermal stresses from abrupt temperature change at shell equator solved, using Fredholm integral equation 21 p3721 A67-38308
- Approximate solution of elastic buckling of radially constrained circular ring under uniformly distributed loading 22 p3908 A67-39287
- Elastic buckling loads of shallow spherical shells supported by edge rings including nonlinear prebuckling effects 23 p4080 A67-41729
- Thin elastic shell nonlinear buckling theories, studying circular cylinder and truncated cone cases 24 p4252 A67-43096
- ELASTIC COLLISION**
- Phase-space collision domains corresponding to hard-sphere N-body problem in gas transport 01 p0112 A67-10144
- Effective cooling of free electrons in plasma due to ambipolar diffusion and elastic collision with ions and neutrals 01 p0122 A67-10346
- Peripheral nonelastic interactions described, using amplitude characteristics of elastic cosmic ray particle interaction and complex orbital moment technique 02 p0315 A67-12749
- Transverse elastic impact of isotropic sphere against thin rectangular anisotropic plate 05 p0922 A67-17174
- Asymmetrical angular elastic scattering distribution of electrons on helium atoms, using Monte Carlo method 06 p1034 A67-17648
- Average diffusion cross section for elastic collisions of electrons with heavy particles, comparing calculated and measured values 09 p1534 A67-21864
- Effective cooling of free electrons in plasma due to ambipolar diffusion and elastic collision with ions and neutrals 11 p1843 A67-25019
- Longitudinal impact of two reinforced cylindrical shells coupled to each other at ribs against solid body 12 p2025 A67-25611
- Elastic collisions in simulating one-dimensional plasma diodes on computer 13 p2164 A67-26294
- Electrostatic relaxation wave dispersion in isotropic Lorentz gas, considering Landau damping and balancing of elastic electron-atom collisions 22 p3848 A67-39692
- Peripheral nonelastic interactions described, using amplitude characteristics of elastic cosmic ray particle interaction and complex orbital moment technique 22 p3876 A67-40251
- Negative cyclotron resonance absorption due to electron elastic collisions with noble gas atoms, comparing results with kinetic plasma wave theory predictions 22 p3842 A67-40346
- ELASTIC CONSTANT**
- SA YOUNGS MODULUS**
- Recording assembly for measurement of flexural and torsional moduli and internal friction at various frequencies and temperatures of small samples, using constant amplitude undamped oscillations 01 p0062 A67-10163
- Bounds for overall elastic moduli of solid composite materials with uniform phases that may be arbitrarily anisotropic 02 p0337 A67-11795
- Elastic modulus, Youngs modulus and Poisson ratio for solids containing foreign inclusions imbedded in matrix 03 p0524 A67-13785
- Longitudinal and shear wave velocities in polycrystalline sample of magnesium thorium alloy measured by pulse transmission technique as function of temperature [ASME PAPER 66-WA/MET-11] 04 p0639 A67-15375
- Variation of elastic constants of molten silica at high temperatures measured, using pulse method 04 p0683 A67-15499
- Electron-phonon interaction in semiconductors, considering three-phonon process and third order elastic constant 06 p1066 A67-18957
- Third order elastic constant for NaCl and KCl single crystals by ultrasonic pulse techniques 07 p1238 A67-20218
- Stress induced velocity variations of longitudinal and shear ultrasonic waves in steel, Al and Cu, calculating third order elastic constant 08 p1415 A67-20481
- Energy factors of infinite straight dislocations and stresses of piecewise straight dislocation configurations expressed through Green functions of elasticity 08 p1418 A67-20798
- Laminated thin shell theory applied to calculation of elastic coefficients of fiber reinforced shells [AIAA PAPER 66-526] 12 p2030 A67-25914
- Electromagnetic wave propagation in type II superconductors, noting Hall angles influence 13 p2175 A67-26428
- Hardness, toughness, stress relaxation, corrosion resistance, etc, of niobium-aluminum alloy with stable elastic modulus 15 p2504 A67-29973
- Elastic constants of directionally solidified Ni base superalloy considering consequences of anisotropy to design analysis 16 p2693 A67-31874
- Physical properties of semiconductors relation with energy and nature of interatomic bonds, discussing effect on elastic constant, thermodynamic functions, electric and dielectric properties 18 p3094 A67-33435
- Dispersion relations for elastic wave propagation in filamentary composites obtained, establishing averaging rules for elastic constants 21 p3729 A67-39055
- Dispersion relations for elastic wave propagation in lamellar composite materials obtained with averaged elastic constants 21 p3729 A67-39056
- Elastic constants and interatomic interaction parameters of niobium alloyed with tantalum, titanium and

vanadium 22 p3820 A67-39789
 Niobium stannide, V-Ga and V-Si
 paramagnetic susceptibility, elastic constants
 and electric resistivity temperature
 dependence 23 p4038 A67-40794
 Temperature dependence of elastic
 constants of 1060 and 6061-T6 aluminum
 using ultrasonic pulse echo method,
 estimating high pressure state
 equation 23 p4021 A67-41469

ELASTIC CYLINDER

Stress-strain state for elastic deformation
 of two-layer compressible nonlinearly elastic
 cylinder under internal and external
 loading 02 p0341 A67-12666
 Stresses in elliptical cross section rod
 subjected to elastoplastic torsion, using
 Legendre transforms 03 p0524 A67-13622
 Torsion of infinite hollow cylinder with
 axially symmetric load, discussing
 deformations in terms of integral
 equations 03 p0529 A67-14164
 Forced small axisymmetric oscillations of
 elastic right circular cylinder with end
 plates in form of shallow spherical shell
 filled with heavy ideal
 fluid 03 p0530 A67-14174
 Simultaneous free and parametric
 oscillations of elastic cylindrical shell of
 infinite length and subsonic flow of ideal
 gas in shell 04 p0717 A67-15888
 Magnetoelastic vibrations due to step
 function of mechanical radial force acting on
 perfectly conducting isotropic elastic
 cylinder placed in magnetic
 field 05 p0847 A67-17278
 Boundary value analysis of static problems
 of transversely isotropic solid and hollow
 elastic cylinders 06 p1099 A67-17864
 Inertia effects of internal liquid column
 on vibration of thin walled pressurized
 elastic cylindrical bellows type container
 [AIAA PAPER 67-38] 06 p0986 A67-18262
 Elastic response of circular cylinder under
 torsion 11 p1871 A67-24118
 Treating bending-torsion problem of
 straight beam using Trefftz definition of
 shear center 15 p2572 A67-29311
 Rolling friction with axial thrust analyzed
 for elastic cylinder, assuming Coulomb
 friction law and using integral
 equation 17 p2865 A67-32263
 Exact linear elastic analysis of end effect
 problems for isotropic
 cylinders 17 p2963 A67-33019
 Torsion of finite elastic cylindrical rod
 welded to elastic half-space
 [ASME PAPER 67-APM-30] 17 p2965 A67-33156

Cross sectional strain and stress
 distributions in cylindrical elastic bars
 subjected to pressure-step and velocity-
 impact loading
 [ASME PAPER 67-APM-33] 17 p2965 A67-33158

Axisymmetric mixed boundary value
 problem for solid elastic cylinder under
 torsion 18 p3144 A67-34173
 Free vibrations frequency of ideal fluid in
 elastic bottom cylinder in form of spherical
 shell 20 p3420 A67-36441
 Three layer cylinders and cylindrical and
 plane panel optimum parameters using
 critical stress expressions from nonlinear
 elasticity theory 21 p3729 A67-38915
 Asymptotic solution for class of integral
 equations of first kind with application to
 contact problem of infinite elastic
 cylinder 22 p3909 A67-39400
 Elastic equilibrium of jointed cylinder of
 elastic nonlinear resilient materials obtained
 by relations of two-dimensional nonlinear
 theory of elasticity 23 p4075 A67-40682

ELASTIC DAMPING

Oscillations induced by two forces in
 system with nonlinear elastic force and
 nonlinear damping 07 p1224 A67-20211
 Applicability to elastic flight vehicle
 control system of two variants for
 realization of invariance
 conditions 17 p2882 A67-33097
 Optimal functional parameters of
 elastically damping turbine rotor bearing to
 determine critical velocities of
 shaft 21 p3695 A67-38832

ELASTIC DEFORMATION

Elastic strain distribution in structure of
 quasi-isotropic polycrystalline
 titanium 01 p0093 A67-10100
 Steady state elastic oscillations in case of
 plane deformation for infinite plane

weakened by round arbitrarily arranged
 holes 01 p0159 A67-10224
 Elastic wave propagation in heterogeneous
 plates, discussing various plate theories,
 frequency equations, transverse shear
 deformations, etc 01 p0160 A67-10407
 Capacitance pickups with nonelectrical
 quantity causing transverse bending of
 plates and change in transducer capacitance,
 used in recordings of mechanical
 quantities 01 p0063 A67-10416
 Elasticity parameters for finite static
 deformations of rubber-like materials, noting
 natural and latex rubber 01 p0161 A67-10797
 Buckling tests on uniformly heated thin
 cylindrical shells, noting load and
 temperature effects 01 p0163 A67-11013
 Best-possible error bounds in deformation
 theory 01 p0165 A67-11308
 Maxwell-Green tensor relating forces to
 displacements in structural elastic beam,
 showing role of Maxwell influence
 coefficient 02 p0336 A67-11482
 Gradient-elastic tensor of ions in sodium
 chloride and sodium bromide crystals
 determined from effects of static elastic
 strain on nuclear magnetic
 resonance 02 p0280 A67-11485
 Homogeneous elastic stresses in
 evaporated gallium films, noting transition
 from compression to tensile
 stress 02 p0287 A67-11718
 Solution to boundary value problem of
 generalized moment theory of elasticity,
 determining mean displacement of
 microinhomogeneous elastic
 body 02 p0337 A67-11953
 Equilibrium equations, boundary conditions
 and constitutive relations for nonlinear
 theory of elastic directed curves, examining
 double stress without
 moment 02 p0267 A67-12057
 Plane large deformation of heated
 viscoelastic cylinder with internal and
 external pressure in generalized Boltzmann
 superposition principle 02 p0338 A67-12238
 Plane stressed state in plane contact
 problem of coupled plates under
 symmetrical load 02 p0340 A67-12445
 Stress-strain state for elastic deformation
 of two-layer compressible nonlinearly elastic
 cylinder under internal and external
 loading 02 p0341 A67-12666
 Thermal emf in plastic deformation of
 copper, considering effects of crystal lattice
 defects and lattice elastic
 distortions 02 p0301 A67-12740
 Deformation of rectangular slender
 webplates with boundary stiffeners flexible
 in plate plane under shear and
 compression 03 p0525 A67-13898
 Finite deformations of elastic oriented
 solid with Cosserat trihedrons taken as
 initial schema 03 p0528 A67-13971
 Elastic axisymmetric deformation of
 circular two-layer plate with closely spaced
 rod couplings compliant to radial
 shear 03 p0527 A67-14070
 Deformation of disk with nonsymmetric
 rim and hub 03 p0528 A67-14075
 Imbalance of elastically deformed rotor
 after starting only once with trial load,
 noting role of oscillation modes of
 rotor 03 p0528 A67-14078
 Deformations and rupture criteria under
 cyclic loading using stress-strain
 diagram 03 p0531 A67-14361
 Electrical pinch in elastically deformed
 germanium, examining redistribution of
 carriers across sample and current-voltage
 characteristics 04 p0675 A67-14922
 Dynamic elastic response of ring loaded
 transiently on both edges 04 p0718 A67-15921
 Nonlinear equations for supercritical
 axisymmetric elastic deformation of circular
 cylindrical shell under longitudinal impact
 from rigid body 05 p0907 A67-16015
 Finite difference equation for biharmonic
 equation of plane 05 p0833 A67-16032
 Quasi-static stresses due to moving
 temperature discontinuity on plane
 boundary 05 p0908 A67-16137
 Spherical elastic inclusion in transversely
 isotropic material under axisymmetric
 torsion field 05 p0910 A67-16149
 Thermal stress determination in thin
 conical shells of revolution using real
 function expression for forces, moments and
 displacements occurring during cyclic
 deformation 05 p0914 A67-16198

Supercritical deformation energy of thin
 elastic shell with clamped
 edge 05 p0921 A67-16940
 Motion analysis of elastic deformable body
 visualized as rigid frame and elastic
 particles 05 p0923 A67-17183
 Hole-weakened spherical body represented
 by deformation of two spherical shells with
 reinforcing rings under uniform internal
 load beyond elastic limit 05 p0923 A67-17187
 Book on aeroelastic static phenomena
 covering aerodynamic load characteristics,
 elastic deformation, drag effect on lift
 distribution, etc 05 p0924 A67-17227
 Dynamic characteristics of distributed
 elastic structures in passive analog
 simulation, noting plate
 loading [AIAA PAPER 67-40] 06 p1102 A67-18334
 Exact expression for thermodynamic
 potential in reversible-transformation
 continuums, for isothermic case of finite
 deformations of homogeneous and isotropic
 elastic bodies without inner
 constraints 06 p1119 A67-18583
 Stress-strain relations and relaxation in
 creep materials with elastic heredity and
 simple flow 06 p1107 A67-18637
 Asymptotic representation of integral
 operator used in describing time-varying
 load function in quasi-static and dynamic
 elastic heredity problems of creep
 materials 06 p1107 A67-18638
 Analytical solution for axially symmetric
 membranes made of neo-Hookean materials
 solved by simultaneous differential
 equations 06 p1107 A67-18652
 Stability of elastic systems in small and in
 large, determining bending deformation of
 rod, noting presence of upper and lower
 critical loads 06 p1108 A67-18663
 Logarithmic particular solutions of
 nonhomogeneous equation of cyclic
 deformation of shallow conical shell under
 nonuniform heating 06 p1109 A67-18664
 Finite elastic deformation theory applied
 to transverse nonlinear oscillation of cables
 in rubber-like materials 06 p1111 A67-18863
 Explosive loading and structural response
 measurement techniques for predicting large
 elastic-plastic dynamic and permanent
 deformations of shells under dynamic
 loading conditions 07 p1262 A67-19411
 Time dependent stress behavior of
 incompressible elastic fluid for various
 homogeneous deformation
 histories 07 p1169 A67-19728
 Compression process for hollow cylindrical
 blanks using integration method, viewing
 deformation as sum of sequential stages of
 small dislocations 07 p1191 A67-19748
 Changes in microhardness, elastic modulus
 and shear orientation at boundary between
 plastic and plastic deformation in steel
 under tensile stress 07 p1210 A67-20011
 Structure of rolling texture of bcc metals
 and alloys under various external
 deformation conditions 07 p1210 A67-20107
 Solid rocket engine propellant grain
 structural dynamics including elastic and
 viscoelastic deformations, stress and shear
 vibration modes, natural frequency
 calculations, etc, using Fourier inversions
 and transforms 08 p1376 A67-20883
 Terrestrial behavior under action of time
 dependent periodic potential, treating earth
 as Maxwell body for shear
 processes 08 p1325 A67-21211
 Elastic and inelastic lattice strain at oxide
 window edges determined from
 imperfections of n and p
 type 08 p1370 A67-21297
 Elastic deformation due to structural
 weight sustained by 22-meter parabolic
 reflector of RT-22 radio telescope of
 U.S.S.R. Physics Institute 08 p1424 A67-21354
 Elastic strains created in parabolic
 reflector/radio telescope antenna/ mounted
 on four supports by weight of structure in
 vertical position 08 p1424 A67-21355
 Postquenching deformation effect on
 mechanical properties and creep resistance
 of aluminum alloys
 [ONERA-TP-423] 09 p1519 A67-22156
 Effect of mass distribution and loading
 sequence on elastic rod, solving eigenvalue
 problem by Galerkin
 method 10 p1715 A67-22912
 Action of concentrated loads in plane
 problem of mechanics of deformable
 solids 10 p1715 A67-22921
 Sandwich plate problem involving

subjection to concentrated force of plate having filler flexural rigidity only, giving solution in form similar to that of thin isotropic plate 10 p1716 A67-22937

Sandwich plate problem involving plate having filler flexibility only, giving solution via reciprocity theorem based on Rayleigh-Green equality in thin plate theory 10 p1716 A67-22938

Nonlinearities in elastic energy release rate during load-deflection measurements of specimens with varying crack length 10 p1718 A67-23327

Incremental elastic-plastic analysis of two-dimensional stress system by finite element method 10 p1719 A67-23456

Gurtin variational principles extended in application to dynamic problems of elasticity with finite deformation 10 p1720 A67-23598

Nonlinear membrane equations for extremely thin shell of revolution of very deformable material, assuming large displacements, rotations and strains 10 p1730 A67-23836

Elastic response of circular cylinder under torsion 11 p1871 A67-24118

Boundary between applicability ranges of network and steepest descent methods in equation integration of Timoshenko theory in analysis of plate deformation 11 p1871 A67-24159

Material hysteresis model for transient dynamic analysis 11 p1874 A67-24358

Nb embrittlement by H at ambient temperatures under work hardening effect, noting correlation between elastic limit and deformability in H 11 p1806 A67-24427

Theoretical calculations for minimum anticlastic cross section deformations of thin elastic strips with optimally tapered edges verified by moire method 11 p1875 A67-24613

Elastic deformation of unbounded transversely isotropic body with internal plane circular slot under slot surface load 11 p1876 A67-24681

Integral equations of second boundary value problem of equilibrium of elastic body of revolution, treating cylinder under pressure 11 p1878 A67-24877

Perturbation solutions for finite inflation, under internal pressure, of elastic toroidal membrane of circular cross section 11 p1879 A67-25002

Tantalum alloy slip line observations, stress-strain curves, yield stresses and anisotropic elastic constants in compression deformation 11 p1810 A67-25091

Dent effect on buckling strength of aluminum alloy tubular columns subjected to axial compression [ASME PAPER 67-MET-12] 12 p2030 A67-25951

Lower critical load for deformation of cylindrical shell in torsion and hinged along edges 13 p2215 A67-26376

Temperature dependence of bcc metals elastic limit at low temperature, assuming sessile-dissociated screw dislocations formation during microdeformation, stressing stacking fault energy effect 13 p2130 A67-26438

Flutter and dynamic stability of closed thin walled elastic cylindrical shell filled with liquid 13 p2219 A67-26903

Elastic deformation effects on stability of rotating satellite composed of elastically connected rigid bodies 13 p2212 A67-26905

Stress dependence of dislocation configuration in deformed niobium 13 p2133 A67-27010

Difference method for solution of plane problems in dynamic elasticity, noting equations of dynamic/elastic deformations under plain strain conditions 14 p2400 A67-28256

Supercritical deformation energy of thin elastic shell with clamped edge 14 p2400 A67-28493

General method based on reciprocity theorem developed for problem solutions in elasticity theory 14 p2402 A67-28740

Iterative procedures for elastic, plastic and creep deformation of beams 14 p2339 A67-29003

Computer program for solution of large deflection nonlinear problems of elastic flat plates using grid analogy 14 p2403 A67-29015

Cyclic extension of elastic fiber with elastic-plastic coating when obeying Tresca yield condition 14 p2341 A67-29060

Matrix calculation of structures by parallel

methods of forces and displacements [ONERA-TP-412] 15 p2576 A67-30125

Bulk elastic deformation of continuous medium with coaxial stress-strain deviators, analyzing deformations in body with specified boundary conditions 15 p2576 A67-30181

Elastic deformation calculation using linear real tension-elongation law 16 p2764 A67-30855

Inclusion problems involving tubular shells of isotropic incompressible materials yielding large deformations 16 p2766 A67-31099

Deformation energy of thin elastic shell expressed as function of deformations of reference surface other than mean surface 16 p2777 A67-31708

Finite inflation of isotropic elastic toroidal membrane possessing strain-energy function by uniform internal pressure 17 p2956 A67-31932

Elastic deformation due to structural weight sustained by 22-meter parabolic reflector of RT-22 radio telescope of U.S.S.R. Physics Institute 17 p2956 A67-31950

Elastic strains created in parabolic reflector/radio telescope antenna/ mounted on four supports by weight of structure in vertical position 17 p2956 A67-31951

Metal-to-metal seal for separable joints/Bobbin seal/ utilizing elastic and plastic responses of seal structure and interface 17 p2864 A67-31993

Axisymmetrical temperature fields for minimum functional of elastic deformation energy in infinite cylindrical shell 17 p2962 A67-32968

Solution to boundary value problem of generalized moment theory of elasticity, determining mean displacement of microinhomogeneous elastic body 17 p2965 A67-33270

Local stress measurement technique in metals using temperature changes due to elastic deformation 18 p3141 A67-33887

Viscoelasticity and rubber-like elasticity continuum mechanical description under stress relaxation conditions [AIAA PAPER 67-489] 18 p3143 A67-33955

Periodic stress and heating during creep, studying deformation adaptability of material for conditions experienced by aircraft engine components 19 p3338 A67-34885

Small elastic-plastic deformation /caused by internal pressure/ of thin walled tube clamped at one end to rigid support 19 p3341 A67-35715

Magnetoelasticity/magnetothermoelasticity theories concerned with externally applied magnetic field interacting effects on elastic/thermoelastic deformations of solid body 19 p3262 A67-35799

Nonlinear approximation of thin elastic plane plates noting influence of elastic medium and strain tensor deformations 20 p3535 A67-36279

Thin walled structure bending in uniform temperature field, calculating stresses, deformations and creep 20 p3536 A67-36446

Linear equation for micropolar elastic solids deformation, including radial displacements with axial and radial symmetries 20 p3540 A67-37021

Deformations and residual stresses in polycrystalline microstructures, using photoelastic coating method 20 p3540 A67-37059

Motion equations for elastically deforming body containing cavity partly filled with ideal fluid 20 p3481 A67-37380

Parameters for motion of flight vehicle as solid body and for elastic deformations 20 p3482 A67-37381

Nonlinear elastic anisotropic wedge deformation for short time loading moment applied to apex, approximating stress function 20 p3542 A67-37660

Stress distribution in homogeneous isotropic body under finite elastic deformation rotating with constant angular velocity 20 p3542 A67-37680

Hooke law type anisotropic fiberglass reinforced plastic, discussing elastic deformation and brittle fracture, using revised Mises ellipse equation 21 p3649 A67-37907

Wheel acceleration influence on landing gear operation at touchdown, noting effect on shock absorption system and elastic deformation of supporting

legs 21 p3566 A67-37949

Strain energy in thin isotropic elastic shells subject to arbitrary temperature distribution, considering large deflections and buckling 21 p3718 A67-38021

Plane deformation problem of instantaneous elasticity theory application to expansion of stationary elastic waves in infinite medium with cylindrical cavity 21 p3720 A67-38294

Nonlinear differential equations for elastic spherical wedge distortion assuming isotropy, homogeneity and incompressibility 21 p3721 A67-38380

Birefringent properties of Voigt type viscoelastic medium and Noll hygrosteric material during stress relaxation 21 p3657 A67-38409

Book on inelastic shell theory and research covering field equations, viscous and plastic response, viscoelasticity, elastoplastic deformation, limit analysis, steady creep, etc 21 p3722 A67-38531

Displacements and temperature accompanying deformation in unbounded thermoelastic medium determined for concentrated force and heat source, using Green functions 21 p3723 A67-38559

Exact solutions for elastic displacements and stresses in composite circular cylinder under torsion in Fourier series form 21 p3723 A67-38560

Approximate solution of elastic buckling of radially constrained circular ring under uniformly distributed loading 22 p3908 A67-39287

Approximate shell theory for unrestricted elastic deformation, discussing treatment of motion equations 22 p3909 A67-39293

Extent of lubricating film for which oil flow is plane, discussing lubricant compressibility, heat release, load capacity and pressure distribution 22 p3811 A67-39317

Structural elastic deformations effect on aerodynamic steering loads of glider, examining lift changes caused by wing geometry variations 23 p3933 A67-40640

Differential equations describing stressed state of revolving shell beyond elastic limit and solutions adaptable to computer programming 23 p4075 A67-40688

Metal creep behavior under step function stress application including elastic and plastic deformation 23 p4018 A67-40717

Deformation continuum mechanics near cracks, discussing fatigue load propagation applications and elastoplastic models 24 p4248 A67-41948

Composite, reinforced and porous elastic body isotropic deformation, deriving macroscopic moduli, mean stress and strain values and dispersion 24 p4249 A67-42102

Shallow spherical shell stress and displacement distribution calculated by integral equation 24 p4249 A67-42104

Elastomer elastic deformation response in multiaxial stress field shown identical to uniaxial stress response 24 p4250 A67-42367

ELASTIC MEDIUM

Linear solutions for large deflections of diamond-shaped frames under compressive loading 01 p0160 A67-10440

Elasticity parameters for finite static deformations of rubber-like materials, noting natural and latex rubber 01 p0161 A67-10797

Equations for nonlinear wave propagation in incompressible heat-conducting elastic material, noting propagation of shocks in isotropic material 01 p0162 A67-10846

Continuum theory of dislocations for polar elastic materials, each material point having three associated directors 01 p0162 A67-10848

Mechanical constitutive theory and methods of stress analysis for physically nonlinear solid propellants [AIAA PAPER 66-124] 01 p0139 A67-11155

Finite-amplitude longitudinal plane wave propagation in elastic solids 02 p0336 A67-11792

Equations for one-dimensional model of macroscopically homogeneous linearly elastic medium of complex structure with spatial dispersion 02 p0337 A67-11952

Wave propagation in elastic materials, noting extension to materials with memory 03 p0536 A67-13659

Displacement potential for solutions of displacement equilibrium equations obtained by Mindlin for linear elastic medium where stresses are functions of strains and strain gradients 03 p0524 A67-13661

Stress distribution in vicinity of end of

- crack moving steadily along boundary joining two elastic materials 03 p0529 A67-14167
- Hole-drilling method of measuring residual stresses in elastic materials determined by empirically derived relation between magnitudes of principle stresses and strain relaxation about hole 03 p0531 A67-14360
- Courant-Hilbert ray theory and Thomas singular surfaces theory of wave propagation in anisotropic homogeneous linearly elastic medium, based on growth equation 04 p0657 A67-15083
- Displacement and stress fields in isotropic elastic solids determined by integrating displacements for point nuclei of strain 04 p0711 A67-15102
- Stress distribution due to pressurized exterior crack in infinite isotropic elastic medium with coaxial cylindrical cavity 04 p0717 A67-15799
- Motion theory of discrete defects in linear elastic continuum 05 p0908 A67-16038
- Thermoelastic wave propagation in elastic layer with convective heat transfer between layer surfaces and surrounding medium, considering relations between temperature field and dynamic displacement 05 p0913 A67-16188
- Energy dissipation effect on vibrations of elastic element with one degree of freedom excited by steady state random Gaussian disturbance 05 p0923 A67-17182
- Stresses in elastic half-plane with rectilinear notch 06 p1101 A67-18181
- Dynamic characteristics of variable mass slender elastic body, solving vector differential equations [AIAA PAPER 67-41] 06 p1095 A67-18263
- Impact problem of passage of longitudinal and transverse waves arising in elastic infinite thread over sequence of absolutely smooth nonrotating pulleys 07 p1261 A67-19163
- Rotational motion of rigid sphere about z axis in elastic medium taking into account surface adhesion 07 p1223 A67-19219
- Stress-strain state inside elastic quarter space activated by periodic or local normal loads at interfaces 07 p1264 A67-20221
- Consistent difference equations for displacement components in thin elastic disk of variable thickness subjected to given body forces and edge tractions for various coordinate directions 09 p1573 A67-21755
- Dynamic plane shear of incompressible viscoelastic material with temperature dependent viscosity determined, using electric transmission line analog 09 p1533 A67-22152
- Plane problem of rigid die penetration into elastic medium solved, using divergent series form 10 p1721 A67-23671
- General solutions for linearized three-dimensional equations of elastic stability of medium compressed along one axis 11 p1870 A67-23896
- Elastic medium dynamic response to time dependent pressure in spherical cavity with cavity wall under ablation 11 p1871 A67-23964
- Ordinary waves in viscoelastic mediums analyzed, using Green tensor relation to Kirchhoff tensor 11 p1877 A67-24750
- Three-axis ellipsoid elastostatic problem solved through analogy with equivalent electrostatic problem of charge distribution 12 p2029 A67-25665
- Boundary value problems solution for bodies with rapidly varying elastic properties using boundary layer type equations 12 p2032 A67-26107
- Thermal stress field effects on materials for idealized situation, discussing problem of half-space and elastic layer under nonuniform surface heating, crack, etc 12 p2032 A67-26198
- Theory of Rayleigh waves at surface of elastic half-space, determining ratio of horizontal to vertical component of motion 13 p2156 A67-26602
- Thermodynamics of elastic materials using corollary of Clausius-Duhem inequality 13 p2224 A67-27145
- Transverse normal loading of doubly periodic unidirectional elastic fiber reinforced infinite elastic matrix 14 p2398 A67-28098
- Boundary value problems of continuous dislocation theory reduced to elasticity theory, deriving Green formula for internal stresses 15 p2572 A67-29235
- Screw dislocation and crack interaction when elastic field is independent of one of three Cartesian coordinates 16 p2764 A67-30993
- Plane and volume stressed states of discrete medium, analyzing deformation work of continuous elastic medium 16 p2766 A67-31144
- Elastic interactions of cracks and dislocations of screw type in two-dimensional model 16 p2768 A67-31281
- Dynamic characteristics of variable mass slender elastic body, solving vector differential equations [AIAA PAPER 67-41] 17 p2956 A67-33013
- Singularities due to concentrated couples in infinite linear elastic isotropic Cosserat continuum, noting dissimilar singular solutions 17 p2964 A67-33141
- Potential equations for hydrodynamic and thermoelastodynamic linear wave motions applied to linear wave motion of isotropically thermally conducting elastic solids and viscous fluids [ASME PAPER 67-APM-32] 17 p2886 A67-33159
- Equations for one-dimensional model of macroscopically homogeneous linearly elastic medium of complex structure with spatial dispersion 17 p2965 A67-33269
- Evaluation of stored-energy function for elastomeric materials based on biaxial experiments [JPL-TR-32-1006] 18 p3145 A67-34486
- Plane elastic strip with stress-free edges concept studied, noting mechanical coherence for elasticity and bending, expressing results by meromorphic function 19 p3340 A67-35450
- Inhomogeneous elastic medium with nonlocal interaction, considering case of point defects and obtaining Green tensor 20 p3540 A67-37056
- Plane waves propagation in microelastic medium having only coupled stresses 20 p3542 A67-37681
- Plane wave approximation for dilatational mode response of thin hollow spherical shell embedded in elastic medium and subjected to asymmetric pressure wave 21 p3718 A67-38020
- Axial shear wave radial propagation in nonhomogeneous elastic medium under axisymmetric loading solved by Laplace transform and characteristics method 21 p3719 A67-38146
- Plane problem of rigid die penetration into elastic medium solved, using divergent series form 21 p3719 A67-38272
- Solution for elastic medium stressed state under axisymmetrical load, considering spherical cavity influence and moment stresses 21 p3720 A67-38301
- Stress rupture strength and durability of elastic materials 22 p3824 A67-39221
- Linear equations of motion of concentrated defect in elastic medium using variational principle 22 p3909 A67-39292
- Flutter of two cylindrical panels bonded by elastic filler in supersonic gas flow, showing flutter velocity increase with increasing filler elasticity 22 p3910 A67-39455
- Crack stability for fracture of nonworkhardening elastoplastic material in plane strain or plane stress, using energy criterion 23 p4078 A67-41162
- ### ELASTIC MODULUS
- Room temperature microhardness anisotropy, slip and twinning in molybdenum carbide single crystals noting orientation dependence, elastic modulus, electric resistivity and measurement techniques 03 p0441 A67-13254
- Boron filament manufacturing process using chemical vapor plating with boron trichloride and hydrogen onto tungsten filament substrate 03 p0453 A67-13419
- Boron carbide filament production by vapor deposition from organoboranes 03 p0454 A67-13421
- Synthesis route to form continuous filaments of SiC, noting tensile strength, elastic modulus and density of product 03 p0454 A67-13422
- Tensile test equipment and methods to determine modulus of elasticity and ultimate tensile strength of single boron filaments at room and elevated temperatures 03 p0455 A67-13445
- Niobium-aluminum alloys elasticity, shear cubic compressibility moduli, Poisson ratio, characteristic temperature and crystal lattice structure 04 p0635 A67-14431
- Dynamic elastic modulus of thin rod at elevated temperatures measured in terms of rapid-heating induced longitudinal oscillation [ASME PAPER 66-WA/MET-12] 04 p0712 A67-15376
- Piezomagnetic coefficients in magnetostriuctive equations, permeability extrema and elastic moduli of Ni-Co-Mn ferrites 05 p0863 A67-16703
- Boron fibers and reinforced plastic composites, noting mechanical and physical properties, application, etc 06 p1021 A67-18855
- Modulus of elasticity of metals and titanium alloys as function of electron structure and binding energy 07 p1206 A67-19279
- Alloying effect on elastic modulus, strength and plasticity of titanium in temperature range from -196 to 800 degrees 07 p1206 A67-19280
- Titanium alloy mechanical and physical characteristics, noting dependence on chemical and phase composition 07 p1206 A67-19285
- Solution hardening in niobium by Ta, V, Zr and W, showing linearity with composition and relationship to sum of atomic size and elastic modulus differences 07 p1209 A67-19642
- Fiber reinforced plastics, determining composite elastic constants in terms of elastic moduli and geometric parameters of constituents 08 p1346 A67-20910
- Tape production process from noncontinuous boron fibers, noting mechanical properties and process parameters 08 p1335 A67-20911
- Elastic moduli of filled systems, discussing effects of filler size, shape, concentration, agglomeration, etc 08 p1421 A67-20916
- Shear modulus determination from free flexural vibrations of sandwich beams with steel facing, using filled elastomer as core 09 p1574 A67-21838
- Adhesive bonding of solid propellants in rocket motors, emphasizing propellant liner interface and bonding at interface 09 p1578 A67-22514
- Elastic moduli of composite with aligned continuous fibers derived from elastic properties of constituents 10 p1715 A67-22859
- Tensile strength and cross sectional area measurement of aluminum oxide whiskers 10 p1669 A67-23326
- Carbon fiber composite, noting incorporation into epoxy resin and inverse correlation of shear strength with fiber modulus 10 p1671 A67-23495
- High modulus high strength reinforcements incorporated in epoxy matrix plastic composites for aerospace structural use 10 p1671 A67-23704
- Fiber spacing and array geometry effect on modulus of composites of laminate configurations used in aerospace structures 10 p1729 A67-23768
- Plastic zone about circular hole in infinite plate under uniform hydrostatic tension 11 p1879 A67-24887
- Stress-strain state of thin walled zero moment shell under uniformly distributed multiple load assuming various tensile and compression strengths 12 p2020 A67-25569
- Young's modulus and shear modulus of inorganic filaments of tungsten and boron measured by oscillation technique 13 p2144 A67-27187
- Elastic moduli of composite materials with anisotropic filaments 14 p2398 A67-28101
- High strength and high elastic modulus in resin-matrix composite structures of single-crystal whiskers [ASME PAPER 67-DE-9] 14 p2340 A67-28868
- Elastic vibrations in superconductors noting vortex effects, weaknesses of elastic moduli changes and decrease in ultrasonic attenuation 14 p2375 A67-28988
- Reinforcing fiber orientation effect on elastic moduli of materials, noting results on long and finite fibers 15 p2578 A67-30178
- Elastic properties of hardened Ti alloys discussed for behavior of elastic and shear moduli vs annealing temperature 16 p2687 A67-30848
- Bubble raft analog for analyzing short range repulsive forces at small strains that govern fractures 16 p2768 A67-31279
- Sapphire whisker strength coated with

thin metal film determined at room and elevated temperatures 16 p2694 A67-31522

Sapphire whiskers mechanical behavior obtained by static tension 16 p2694 A67-31523

Creep effects in structures obtained by elastic solution applied to pressurized shells containing discontinuities 16 p2776 A67-31558

Effect of temperature, density, and amount of stabilization on elastic modulus of zirconia 16 p2695 A67-31701

Third order moduli of GaAs by measurement of ultrasonic wave velocities as function of applied stress 17 p2922 A67-33057

Elastic moduli, bond parameters and effective ion charges for wurtzite and sphalerite binary crystal lattices 18 p3094 A67-33437

Tension and compression, dynamic and static flexural loading and vibration tests of bilaminate filament wound composite [SESA PAPER 1219] 18 p3141 A67-33889

Horizontal, solid, cantilever-beam profile with constant density, width and elasticity modulus determined, using Pontryagin principle 19 p3340 A67-35524

Correlation and analysis of ultrasonic test results in evaluating reinforced resin laminates 19 p3249 A67-35554

Loading rate effect on unidirectional fiberglass reinforced plastics under tension, examining mechanical characteristics and determining tensile strength and elastic modulus 21 p3649 A67-37908

I-beam ratio of depth to flange width for minimum weight obtained via modulus of rupture 21 p3722 A67-38546

Highly elastic materials temperature dependence of contact area and sliding friction forces affected by elastic modulus decrease with temperature under load 23 p4021 A67-40596

Disordered composite materials overall elastic moduli derived from local elastic moduli using correlation function 24 p4248 A67-41956

ELASTIC PLATE

Stress distribution in elastic anisotropic plate with row of elliptical holes reinforced by elastic rings 01 p0158 A67-10221

Asymptotic theory of elastic plate dynamics, deriving displacement equations and boundary conditions 01 p0162 A67-10822

Closed form pseudostatic solutions for Kirchhoff bending stress fields associated with semiinfinite crack extending at uniform velocity in elastic plate 03 p0523 A67-13468

Eigenfrequencies of elastic plate containing cavities filled with incompressible moving fluid, obtaining eigenfrequencies dependence on velocity of fluid motion 03 p0530 A67-14173

Boundary bending conditions for anisotropic plates with free, hinged or rigidly clamped edge 03 p0531 A67-14200

Behavior of eigenvalues in stability of elastoplastic plates used in low rigidity structures 04 p0708 A67-14786

Maximum thermoelastic stress and deflection in plate or beam as function of cross sectional shape, temperature and end conditions [ASME PAPER 66-WA/APM-1] 04 p0714 A67-15426

Semiinfinite strip reinforced by flanges under concentrated load 04 p0719 A67-15933

Tension of homogeneous anisotropic elastic semiinfinite plate with rigid stiffener attached on segment of straight boundary 05 p0910 A67-16150

Deflection of centrally loaded thin circular elastic plates on equally spaced point supports 05 p0917 A67-16366

Linear theory of homogeneous anisotropic elastic shells and plates without considering Love-Kirchhoff assumptions 05 p0921 A67-16883

Stability of elastic plates of arbitrary shape treated approximately 05 p0925 A67-17476

Quasi-steady aerodynamic and von Karman large deflection plate theory equations of nonlinear oscillations of fluttering plate for single mode subsonic and sonic or coupled mode supersonic oscillations [AIAA PAPER 67-13] 06 p1101 A67-18252

Sound diffraction by semiinfinite elastic plate in moving medium 06 p1032 A67-18398

Bending equations for thin elastic anisotropic plates, using Goldenveizer method 06 p1106 A67-18630

Analytical solution for axially symmetric membranes made of neo-Hookean materials solved by simultaneous differential equations 06 p1107 A67-18652

Fundamental frequency of natural oscillations of plate, using integrodifferential equations derived from elasticity theory in form of power series 06 p1108 A67-18662

Governing equation for bending of multilayered sandwich elastic plates composed of n membranes developed by variational method 06 p1110 A67-18857

Stress distribution in elastic plate with circular hole, noting particular cases of general solution for simple boundary tractions 08 p1422 A67-21167

Mixed boundary value problem of flexure of elastic plate 08 p1422 A67-21201

Stresses and displacements in small circular stress-free crack at interface between thick elastic incompressible layer and rigid foundation 10 p1717 A67-23082

Bassall theory to calculate bending, twisting moments and shearing forces for thin elastic plates under transverse flexure for structural design 10 p1720 A67-23569

Dispersion and damping characteristics due to flexural vibrations in elastic plate with viscoelastic coating, obtaining energy loss resulting from dissipation [ASME PAPER 66-WA/APM-20] 10 p1731 A67-23840

Free vibration and resonance of vibrating plate interacting with sound waves in surrounding air 11 p1874 A67-24228

Stressed and strained state of infinite plate lying on elastic base weakened by finite number of arbitrarily located circular holes 11 p1879 A67-25053

Eigenvalue density in problems involving oscillations of elastic plates and shells, establishing existence of natural frequency bunching point 12 p2022 A67-25586

Nonlinear oscillations of elastic plates under simultaneous effect of harmonic and random load 12 p2024 A67-25597

Flexible plate elastic stability under effect of suddenly applied and short term forces 12 p2024 A67-25599

Stress-strain state of thin sandwich plate consisting of arbitrary number of elastic isotropic layers rigidly coupled to each other 12 p2024 A67-25602

Thin elastic plate with uniformly distributed load over area and Navier condition on edge solved for deflection 13 p2217 A67-26631

Computer program for solution of large deflection nonlinear problems of elastic flat plates using grid analogy 14 p2403 A67-29015

Linear theory of elastic Cosserat plate, noting bending theory which corresponds to bending of transversely isotropic three-dimensional plate 15 p2510 A67-29630

Free vibrations of unsupported elliptical plates of lenticular section with flat or uniformly curved middle surfaces 16 p2764 A67-30841

Stress distribution in thin plates containing curvilinear holes of various shapes 16 p2766 A67-31100

Thermal stress concentration in physically nonlinear elastic plate with hole in presence of uniform heat flux 16 p2766 A67-31148

Elasto-plastic stresses and strains in cracked plates analyzed by numerical method, noting stress singularities and stress-strain fields 16 p2769 A67-31287

Pointwise bounds for solution of Cauchy problem for nonlinear and linear elliptic system, noting application to biharmonic equation 16 p2697 A67-31422

Analytic solution for finite radial expansion and consecutive unloading of circular hole in infinite elastic-plastic plate of initially varying thickness 17 p2966 A67-33347

Elastic plates linear theories for micropolar and director displacements, deriving plate equations by asymptotic expansion method 17 p2966 A67-33349

Elastic stress distribution in infinite plate having circular hole, applying coupled stresses theory 18 p3140 A67-33666

Nonlinear approximation of thin elastic plane plates noting influence of elastic medium and strain tensor 20 p3535 A67-36279

Elastic and dynamic response of viscoelastic plate with finite thickness to

rigid body impact 20 p3539 A67-36920

Circular plate on nonlinearly elastic base with uniform load force at center, tangential force and contour moments for plate deflection 20 p3539 A67-36923

Steady state problem solution in linear formulation concerning movable load influence on thin elastic plate on ideal compressible fluid surface 21 p3720 A67-38300

Stress-strain state in braces across elliptical hole in elastic plate, obtaining solution for eccentric load 21 p3721 A67-38305

Stress determination in elastic plate with remanent elasticity and cylindrical anisotropy, using integral-operational method 21 p3723 A67-38555

Quasi-steady aerodynamic and von Karman large deflection plate theory equations of nonlinear oscillations of fluttering plate for single mode subsonic and sonic or coupled mode supersonic oscillations [AIAA PAPER 67-13] 21 p3727 A67-38870

Thin circular elastic plate under uniform compressive thrust, with nonlinear boundary value problems involving partial differential equations for buckled states 22 p3916 A67-40525

Numerical data for plane thermal stresses in isotropic elastic square plate bounded by edge stiffeners and under symmetric temperature distributions 23 p4073 A67-40611

Natural frequencies and mode shapes determined for circular cylindrical shell closed by elastic plate 23 p4080 A67-41750

ELASTIC PROPERTY

Stresses in symmetrical three-layer circular disk rotating about own axis, with solutions in form of Fourier-Bessel integrals 01 p0080 A67-10777

Boundary value and contact problem solution using elasticity theory for transversely isotropic layer 03 p0529 A67-14165

Elasticity and shell theory solutions for long circular cylindrical shells compared by numerical analysis 04 p0709 A67-14811

Approximate method for solving elastic equilibrium problems of shallow shells with holes, using computer algorithm 05 p0916 A67-16224

Three-dimensional elastic problem of bodies of revolution, deriving Lamé and generalized Hooke equations in matrix form 05 p0916 A67-16226

Boundary value problem solution via direct methods of approximate analysis 05 p0925 A67-17370

Elastic nonlinearity due to acoustic wave-charger carrier interaction in CdS, noting waveform distortion for zero acoustic dissipation 08 p1353 A67-20485

Finite difference method for finding stress fields around parallel edge cracks 08 p1421 A67-20914

Variational principle for anisotropic and nonhomogeneous elasticity theory in terms of elastic polarization tensor 08 p1422 A67-20981

Structural changes and changes in elastic properties of cold rolled Ti and Zr during precrystallization heating 08 p1342 A67-21003

Boundary value problems for thin elastic plates, discussing flexural stresses in neighborhood of crack, bending, etc 10 p1715 A67-22915

H-film /Kapton/ flexible circuits fabrication problems including tensile strength, pattern misregistration, delamination, embrittlement, etc 10 p1611 A67-23309

Generalized reciprocity law relating behavior of elastic body and static and geometric boundary conditions 10 p1721 A67-23686

Elastic properties of tektites measured using resonant sphere technique 11 p1864 A67-24558

Propagation of acceleration waves in elastic and viscoelastic materials 11 p1875 A67-24572

Oscillation of oscillator with elastically hereditary and weakly nonlinear characteristics, applying operational method to analysis in terms of hereditary creep theory 11 p1876 A67-24682

Temperature dependence of elastic constants of molybdenum single crystals measured, using thin rod resonance techniques 11 p1809 A67-24908

- Boundary value problems solution for bodies with rapidly varying elastic properties using boundary layer type equations 12 p2032 A67-26107
- Elastic properties of Ti alloys of ternary system Ti-Zr-Cr, showing sensitivity to heat treatment 13 p2143 A67-27710
- Deflection limits on plate-twisting test 14 p2399 A67-28102
- Thermal and elastic properties of ternary diamond-like semiconductor compounds, determining ultrasonic wave propagation rates 18 p3096 A67-33452
- Photoelastoplastic method using creep and stress characteristics of epoxy resins under thermal cycle, discussing stress-strain behavior [SESA PAPER 1191] 18 p3141 A67-33886
- Strain-energy function of hyperelastic material in terms of extension ratios, with natural rubber as example 18 p3145 A67-34642
- Homogeneous beam consisting of two isotropic bars with different elastic properties but identical cross sections studied for perimeters stress-strain state under torsion 20 p3535 A67-36122
- Asymmetric stability loss of nonuniformly heated circular plate rib, determining elastic properties and critical temperature jump value 20 p3536 A67-36447
- Multipoint equivalent cross section method for calculating finite deflections of beams of strain hardening material 20 p3541 A67-37285
- Viscoelastic properties of capron under torsion at infrasonic frequencies and polymer resin complex shear modulus temperature dependence 21 p3647 A67-37866
- Generalized reciprocity law relating behavior of elastic body and static and geometric boundary conditions 21 p3720 A67-38287
- Elastic properties of filled and porous epoxy composites tested in compression and tension noting Youngs modulus relation to filler content 22 p3824 A67-39498
- Hydrogen peroxide and disulphane molecules force constant and vibrational spectra investigation indicates little change in elastic properties 22 p3757 A67-39583
- Free energy of polymer solid consisting of entangled long chain molecules when deformed by elastic strain 22 p3826 A67-40201
- Cylindrical thin walled open section structures heated nonuniformly, calculating various elastic parameters, torsion properties and shearing stress 22 p3916 A67-40450
- Longitudinal oscillations with multiple degree of freedom obtained over sections of adopted stress-strain diagram, characterizing elastoplastic properties 23 p4076 A67-40683
- Critical strain parameter concept for adhesive bond joints noting strength dependence on geometry and material elastic properties [SAE PAPER 670856] 24 p4160 A67-42003
- ELASTIC SCATTERING**
- SA INELASTIC SCATTERING**
- Oscillatory semiconductor photoconductivity dependence on photon energy periodic in longitudinal-optical phonon energy treated by Boltzmann equation, noting elastic scattering 02 p0280 A67-11488
- Quasi-stationary techniques for calculating energies and widths of resonances occurring in electron-atom and electron-molecule scattering 02 p0269 A67-12449
- Statistical analysis of cosmic ray particle elastic scattering, noting isotropic nature of angular distribution 02 p0315 A67-12750
- Angular dependence of elastic scattering resonance structure in atomic hydrogen 04 p0660 A67-14946
- Gas transport cross sections, angular distribution of elastic scattering of colliding gas particles and transport equation degeneration 07 p1225 A67-19129
- Potential-well characteristics from energy dependence of glory extrema in total elastic scattering cross sections 09 p1535 A67-22028
- Scattering of plane monochromatic sound wave by semiinfinite elastic pipe in moving medium, emphasizing axisymmetric oscillations 10 p1680 A67-23644
- Energy dependence of effective total cross sections of elastic scattering involving H and He atoms and H molecules 13 p2159 A67-26384
- Position and width of lowest elastic scattering resonances in three-body atomic system, showing resonance shape dependence upon observation angle and angular resolution 14 p2351 A67-28152
- Scattering of plane monochromatic sound wave by semiinfinite elastic pipe in moving medium, emphasizing axisymmetric oscillations 18 p3080 A67-34413
- Gas transport cross sections, angular distribution of elastic scattering of colliding gas particles and transport equation degeneration 21 p3659 A67-38172
- Differential cross sections for elastic scattering of alpha particles by oxygen, giving angular distributions and resonances 21 p3659 A67-38517
- Differential cross sections of elastic scattering of alpha particles by oxygen, measuring angular distributions 21 p3659 A67-38518
- Energy dependence of effective total cross sections of elastic scattering involving H and He atoms and H molecules 21 p3660 A67-38822
- Static Green function for elastic electron scattering by hydrogen atoms, using integrodifferential equations to determine resonance energies 22 p3839 A67-39204
- Statistical analysis of cosmic ray particle elastic scattering, noting isotropic nature of angular distribution 22 p3841 A67-40252
- Cross section data for molecular oxygen and electron collision processes, discussing elastic scattering, attachment, rotational transitions and Born cross section 23 p4030 A67-41481
- Solar neutrino observation, considering inverse nuclear beta decay and elastic scattering by orbital electrons 24 p4210 A67-42583
- Proton-proton and pion and kaon elastic scattering from protons at high energy, deriving approximate formula for differential cross section, noting nucleon structure 24 p4193 A67-42855
- ELASTIC SHEET**
- Infinite edge-stiffener load diffusion into semiinfinite elastic sheet, noting interface sheet stress variation stiffener force distribution [ASME PAPER 67-APM-35] 17 p2965 A67-33160
- Netting analysis of reinforced sheets for load envelopes which combine tension and shear, determining optimum fiber arrangements 21 p3729 A67-39082
- Reinforced plastics pressed sheet materials series based on chrysotile asbestos fibers and thermoplastic resin combinations or thermoplastic and thermosetting resins 24 p4176 A67-42423
- ELASTIC SHELL**
- Sanders equation for circular cylindrical elastic shell reduced to fourth order PDE 01 p0159 A67-10400
- Frequency equation for purely radial vibrations of infinite isotropic composite hollow cylinder with two concentric elastic layers 01 p0162 A67-10818
- Dynamic stresses in thick walled spherical shell of Voigt material subjected to internal pressure load 01 p0164 A67-11174
- Torsional oscillations of hollow cylinder of finite length encased in thin elastic shell 02 p0337 A67-11932
- Thin walled elastic shell response to thermal excitation [AIAA PAPER 66-84] 04 p0709 A67-14841
- Elastic shells of revolution axisymmetrically loaded analyzed, using multisegment method for solution of boundary value problems governed by nonlinear differential equations [ASME PAPER 66-WA/APM-16] 04 p0713 A67-15407
- Natural frequencies and mode shapes for axisymmetric vibration of thin elastic and ellipsoidal shells 04 p0714 A67-15424
- Nonlinear elastic thin shell theory in parallel approach based on Kirchhoff hypothesis 04 p0715 A67-15585
- Axisymmetric motions of Timoshenko type cylindrical shells composed of two elastic isotropic layers of different materials and thicknesses connected by perfect bond 04 p0717 A67-15909
- Infinite series and finite difference solutions of elastic response of thin walled spherical shell to axisymmetric transient blast loading [ASME PAPER 66-APM-EE] 04 p0718 A67-15918
- Stress calculation comparison of computer data and photoelastic data for series of pressure vessels with hemispherical and torispherical heads [ASME PAPER 66-WA/PVP-5] 04 p0719 A67-15931
- Dynamic surface loads, transient displacement and stresses in elastic cylindrical shell under radial and torsional vibration and elastic spherical shell under radial symmetric vibration, using finite Hankel transformation 05 p0908 A67-16138
- Elastic cylindrical shell under arbitrary impulsive pressure distribution, discussing membrane and flexural stresses 05 p0909 A67-16139
- Linear theory of homogeneous anisotropic elastic shells and plates without considering Love-Kirchhoff assumptions 05 p0921 A67-16883
- Stress-strain relations of linear theory of shells extended to corresponding inversion with more complex results 06 p1100 A67-18111
- Coupled system of thin elastic shells, giving response to static or harmonically oscillating loads or to unloaded natural frequencies and mode shapes, using Green matrix [AIAA PAPER 67-45] 06 p1103 A67-18351
- Rib elasticity effect on stressed state of circular cylindrical shell with rectangular cut in torsion 06 p1107 A67-18632
- Influence of relative thickness of elastic case on acoustic stability of radial modes in solid propellant rockets [AIAA PAPER 66-473] 07 p1240 A67-19370
- Free oscillation of thin elastic shell, using asymptotic method for integrating dynamic equations in classical linear theory 07 p1263 A67-20031
- Remedies for deficiencies in approximations near transition point in asymptotic methods used for estimates of solutions to differential equations governing axisymmetric vibrations of thin elastic shells 08 p1414 A67-20346
- Displacement formulations of first order linear thin elastic shell equations in terms of stress resultant and middle surface, using modified Kirchhoff hypothesis 08 p1417 A67-20551
- Computer program for axisymmetric nonlinear behavior of stiffened elastic shells of revolution with variable thickness, calculating collapse pressures [AIAA PAPER 66-529] 08 p1417 A67-20558
- Scattering of plane monochromatic sound wave by semiinfinite elastic pipe in moving medium, emphasizing axisymmetric oscillations 10 p1680 A67-23644
- Linear motion equations including effects of transverse shear deformation and rotary inertia derived for thin elastic isotropic conical shells of revolution 10 p1729 A67-23767
- Nonlinear membrane theory for thin elastic inflatable shells during pressurization phase 11 p1875 A67-24432
- Variational principle as basis for dynamics of elastic shell theory, discussing motion described by Timoshenko type equation 11 p1877 A67-24853
- Variational principles and reciprocity theorems for dynamic problems of elastic shell theory, particularly motion described by linear equations of Timoshenko type 12 p2019 A67-25563
- Lower critical load determination of elastic spherical shell with rigidly fastened edge 12 p2021 A67-25580
- Eigenvalue density in problems involving oscillations of elastic plates and shells, establishing existence of natural frequency bunching point 12 p2022 A67-25586
- Oscillation and stability of system of thin elastic shells in potential inviscid and incompressible fluid flow 12 p2023 A67-25589
- Natural oscillations of elastic truncated conical shells of revolution under composite static load 12 p2026 A67-25613
- Oscillation frequency and frequency density distribution equations derived for thin elastic shells of revolution clamped along two parallels, using differential equations 12 p2027 A67-25627
- Equilibrium equations modified in nonlinear theory of thin walled elastic shells 12 p2028 A67-25634
- Asymptotic integration of elasticity theory

equations applied to two-dimensional dynamic theory for cylindrical shells 12 p2029 A67-25636

Cylindrical elastic shell under axial compression studied for stability loss, considering large axial strains 14 p2401 A67-28737

Transversally isotropic cylindrical shell under periodically spaced axisymmetric band loads, comparing expressions derived for stresses and displacements by elasticity and shell theories 15 p2578 A67-30271

Boundary conditions for thin shells and physical meaning analyzed according to Kirchhoff-Love theory 16 p2764 A67-30862

Deformation energy of thin elastic shell expressed as function of deformations of reference surface other than mean surface 16 p2777 A67-31708

Stress calculation comparison of computer data and photoelastic data for series of pressure vessels with hemispherical and torispherical heads [ASME PAPER 66-WA/PVP-5] 18 p3143 A67-34127

Scattering of plane monochromatic sound wave by semilinear elastic pipe in moving medium, emphasizing axisymmetric oscillations 18 p3080 A67-34413

Axial compressor blades considered as thin walled elastic shells studied for vibration forms, frequencies, stress distribution and blade geometry change effects 19 p3235 A67-34882

Resolving equations of linear theory of isotropic viscoelastic shells subject to external load and steady temperature field 19 p3340 A67-35508

Small elastic-plastic deformation /caused by internal pressure/ of thin walled tube clamped at one end to rigid support 19 p3341 A67-35715

Variational principle as basis for dynamics of elastic shell theory, discussing motion described by Timoshenko type equation 20 p3542 A67-37541

Truncated elastic shell of revolution stability under tensile stress 21 p3718 A67-37978

Strain energy in thin isotropic elastic shells subject to arbitrary temperature distribution, considering large deflections and buckling 21 p3718 A67-38021

Harmonic oscillations and bending of elastic isotropic shells with variable curvature solved using Fourier transform 21 p3721 A67-38383

Ideal incompressible fluid axisymmetrical oscillations in elastic cylindrical shell, determining normal modes and natural frequencies of shell and fluid 21 p3613 A67-38789

Existence and form of orthogonality condition on natural vibrational modes of linear elastic shell under boundary conditions 23 p4073 A67-40616

Constant thickness elastic conical shells subject to lateral loads, deriving asymptotic solution 23 p4080 A67-41727

Invariant form of strain-energy function of linearized elastic potential of isotropic thin shell using three-dimensional theory 24 p4249 A67-42156

Thin elastic shell neutral equilibrium under axial compression and hydrostatic pressure, obtaining parametric terms for expressions by using quadratic functional 24 p4249 A67-42303

Revolving thin elastic shell free axisymmetric oscillation described by equation system derived by asymptotic integration technique with single reversal point 24 p4250 A67-42304

ELASTIC STABILITY

Elastic stability theory formation by combining thermodynamic and mechanical stability 01 p0159 A67-10402

Liapunov second method applied to elastostatic stability, discussing applicability of Dirichlet principle and Galerkin method 01 p0161 A67-10647

Elastic general instability of orthotropically stiffened cylinders under axial compression [AIAA PAPER 66-139] 01 p0163 A67-11154

Dynamic problems of elasticity theory for transversal-isotropic cylinder 02 p0338 A67-11968

Elastic equilibrium of isotropic plane weakened by bi-periodic series of identical circular holes with sealed-in elastic rings of

different material 02 p0340 A67-12659

Stability of transverse oscillation of thin finned elastic beam of revolution in gas flow acted upon by tracking force 03 p0520 A67-14172

Reissner variational method stability analysis of small eccentricity nonlinearly elastic thin circular ring 03 p0531 A67-14230

Adjoint field in elastic stability problems for nondissipative nonconservative systems 04 p0709 A67-14834

Sandwich plate stability analysis by linear geometric and physical equations, for rigid and light cores 06 p1099 A67-17585

Stability-instability transition of equilibrium configuration of linear elastic system under nonconservative follower forces 06 p1105 A67-18589

Elastic equilibrium of circular plate with elliptical hole and tight washer, determining stress-strain state 06 p1106 A67-18631

Small oscillations and stability of hyperelastic incompressible rectangular strip under uniformly distributed biaxial load 06 p1111 A67-18892

Book on rotor stability self-excited vibration and nonlinear resonances 07 p1263 A67-19631

Dynamic behavior of large flexible bodies in orbital motion around gravitating center, emphasizing response and stability of elastic degrees of freedom 08 p1383 A67-20562

Finite element displacement method extended to bifurcation buckling of shells of revolution under axisymmetric loading 10 p1725 A67-23715

Skin-stiffened compression panel design with digital computer, obtaining optimal solutions for applied stress and local and general stability equation 10 p1728 A67-23720

General solutions for linearized three-dimensional equations of elastic stability of medium compressed along one axis 11 p1870 A67-23896

Amplitude control of wind induced oscillation in antenna system through cross section shape [ASME PAPER 67-VIBR-39] 11 p1777 A67-24194

Axisymmetric buckling of orthotropic circular plates with variable thickness in terms of lateral plate deflection and stress distribution 11 p1876 A67-24660

Elastic stability theory according to three-dimensional linearized equations, noting necking process under tension 11 p1878 A67-24876

Flexible plate elastic stability under effect of suddenly applied and short term forces 12 p2024 A67-25599

Geometrically nonlinear theory of elastic stability of anisotropic shells and linear stability of orthotropic plates, using differential equations 12 p2028 A67-25628

Stability of elastically clamped annular plate for nonuniform stress field 13 p2218 A67-26889

Stability of nonlinearly elastic thin rectangular plates subject to compression 13 p2218 A67-26901

Direct matrix method for analysis of critical loads and associated buckling modes for struts having various end constraints 14 p2403 A67-29017

Geometrical and statistical relations of theory of nonlinearly elastic body presented in connection with bifurcation of equilibrium of ideally elastic body 15 p2574 A67-29690

Stability boundaries and critical frequencies for semilinearly elastically restrained plate determined at different boundary stiffnesses 15 p2575 A67-29858

Elastic stability of simply supported uniformly-thin rectangular plate under unequal compressive stresses at two opposite edges due to constant body force 15 p2577 A67-30218

Effect of temperature, density, and amount of stabilization on elastic modulus of zirconia 16 p2895 A67-31701

Orthotropic circular cylindrical shell of elastic material instability under combined torsion and hydrostatic pressure investigated for simply supported and clamped ends 17 p2963 A67-33016

Dynamic problems of elasticity theory for transversal-isotropic cylinder 17 p2966 A67-33285

Stability analysis of circular plate submitted to two compressive forces acting along diameter, using Fourier series

iteration 19 p3342 A67-35718

Stability condition for inhomogeneous elastic body subjected to internal stresses 20 p3535 A67-38392

Uniform cantilevered bar subject to eccentric compressive follower force, considering warping rigidity, bending-torsional flutter and stability 20 p3538 A67-38674

Structural rigidity of rotating parabolic reflector obtained by solving elastic strain problem 20 p3542 A67-37511

Second boundary value problem for differential equation of elastic equilibrium of shallow cylindrical shell 20 p3543 A67-37721

Stability criteria in stress-rupture strength theory, deriving stress and moment influence functions and damage tensor 21 p3717 A67-37969

Elastic stability of three-layer cylindrical shell filled with corrugated metallic sheets under combined loads, deriving linear equations 21 p3724 A67-38786

Three layer cylindrical shell stability in elastic and inelastic domains under separate and joint loads, considering filler layer deformation 21 p3727 A67-38840

Elastic stability of cantilever column having fixed compressive and circulatory nonconservative loadings, determining critical loads 21 p3729 A67-39084

Hypergeometric functions studied for solution of problems on elastic equilibrium of circular plates and shells of revolution 22 p3909 A67-39398

Elastically filled imperfect closed cylindrical shell stability, showing initial configuration defect effects on critical load relation to filler rigidity 22 p3912 A67-39685

Plastics stability - Conference, Washington, D.C., September 1967 22 p3824 A67-39850

Elastic equilibrium of jointed cylinder of elastic nonlinear resilient materials obtained by relations of two-dimensional nonlinear theory of elasticity 23 p4075 A67-40682

Elastohereditary /viscoelastic/ media mechanics, analyzing linear and nonlinear equilibrium equations, uniqueness and existence theorems and solution methods 23 p4077 A67-40750

Orthotropically stiffened cylinders elastic instability under torsional load 23 p4080 A67-41745

ELASTIC STRENGTH

Minimum weight structural designs for various types of behavior specifications including stiffness, elastic and plastic strength and stability 03 p0531 A67-14365

Book on strength under high transient loads and nonlinear elastic and elastoplastic wave propagation 04 p0715 A67-15617

Electronic computer usage to control temperature during creep and long term strength tests of heat resistant steels 11 p1877 A67-24818

High temperature strength of thermomechanical nickel dependent upon previous thermal and mechanical history, measuring elastic strain energy in matrix 14 p2337 A67-28418

Series solution for end effect in semilinearly transversely isotropic cylinders, noting elastic analysis 17 p2962 A67-33014

Correlations between elastic limit, tensile strength and elongation in foundry aluminum alloys used in control reliability 20 p3465 A67-36479

Bending strength dependence on porosity of sintered powdered glass beam 20 p3473 A67-36779

Maximum strengths of aluminum alloy and metal columns under parameter variation, using mathematical model 20 p3538 A67-36780

Stress concentration effects on stress rupture strength, noting applicability to short term creep 21 p3717 A67-37970

Pure plastic bending of sheet and strip at strains exceeding elastic limit analyzed by arbitrary stress-strain diagram 21 p3721 A67-38382

Stress rupture strength and durability of elastic materials 22 p3824 A67-39221

Programmer for operational strength tests during aircraft construction 22 p3912 A67-39755

High temperature polyimide laminates for radomes and other supersonic aircraft components, discussing index flexural strength, dielectric constant and dissipation

- factor 22 p3825 A67-39853
- U-shaped bellow fatigue strength under axial loading, discussing elastic and plastic fatigue tests using specially designed machine 22 p3913 A67-40037
- Primary and secondary strengthening precipitates in 18Ni/250/Al, V and Ti maraging steels 22 p3822 A67-40059
- Nickel on chromium carbide base cermet polishing by synthetic diamond wheels shown to have little effect on strength 24 p4159 A67-41963
- ELASTIC SYSTEM**
- Elastic-plastic continua with unstable elements obeying normality and convexity relations 04 p0708 A67-14622
- General elastic problem for some boundary conditions, determining coefficients via harmonic functions 05 p0916 A67-16227
- Transient stress-strain state of elastic system developing combination resonance analyzed, using approximate method 06 p1106 A67-18621
- Stability of elastic systems in small and in large, determining bending deformation of rod, noting presence of upper and lower critical loads 06 p1108 A67-18663
- Stability of equilibrium of elastic systems under nonconservative load, discussing criteria of stability, modes of instability, follower force problems, etc 08 p1422 A67-21048
- Dynamic vibration absorber for reducing transient vibrations of one degree of freedom system with tuning criteria formulated as function of root line of characteristic equation 10 p1715 A67-22913
- Dual integral equation and dual series analysis and application to mixed boundary value problems in elasticity, hydrodynamics and electrostatics 11 p1812 A67-24150
- Dual integral equations in elasticity theory, noting Mehler-Fok transformation of spherical functions, Fredholm equation and application to mixed boundary value problems 11 p1812 A67-24151
- Cylinders of rectangular section as aeroelastic nonlinear oscillators, theory of galloping oscillation and force measurements on stationary cylinder [ASME PAPER 67-VIBR-50] 11 p1777 A67-24200
- Stresses and strains in nonlinear viscous elasticity, examining tensors in abstract form 12 p2016 A67-25444
- Equations for elastic system free oscillations with parallelogram shaped hysteresis loop derived from kinetic energy changes, describing system time dependent dynamic behavior 12 p1967 A67-25660
- Dynamic stability of pin-ended column under different types of random axial loading 14 p2397 A67-28091
- Elastic deformation calculation using linear real tension-elongation law 16 p2764 A67-30855
- Soviet book on stability and oscillations of elastic systems covering theory, equilibrium breakdown, dynamic loading, aeroelastic oscillations, etc 18 p3140 A67-33674
- Stresses and strains in nonlinear viscous elasticity, examining tensors in abstract form 21 p3726 A67-38829
- Finite difference method for axisymmetrical and plane elasticity problems using high speed computer 22 p3908 A67-39290
- Fatigue in fibers and plastics, use of cumulative extension testing and time dependent effects in fatigue tests 22 p3824 A67-39562
- Aircraft flutter characteristics calculated from electromechanical analog using elastic mass vibration model and analog computer 22 p3746 A67-40451
- Stability of elastic structure in rest state based on break-point determinant, discussing bound, conjugated, affine and space and body-fixed load 23 p4078 A67-41196
- ELASTIC WAVE**
- SA MAGNETOELASTIC WAVE**
- Second-order effects in propagation of elastic waves through homogeneous isotropic media 01 p0113 A67-10405
- Diffraction of elastic waves in formulation of Young, including form of tensor potential for longitudinal waves 01 p0114 A67-10868
- Temperature dependence of elastic wave losses for bismuth germanium oxide, noting possible application for information storage
- VHF and microwave frequencies 02 p0300 A67-12507
- Longitudinal oscillations of infinitely long linear viscoelastic rods to yield wave propagation in elastic rods 04 p0707 A67-14404
- Oscillations of circle solved, using method of elastic oscillations of plane with circular cut 04 p0708 A67-14788
- Thermoelastic wave expansion in infinite medium discussed on basis of Duhamel-Neumann equation 04 p0715 A67-15577
- Exact and variational solutions to elastic wave propagation eigenvalue problem in constant Poisson ratio linear viscoelastic material 05 p0909 A67-16141
- Dynamic stress concentration due to elastic wave analyzed by high speed photoelasticity to clarify difference between dynamic and static stress distribution 07 p1262 A67-19414
- Elastic wave and IR light interactions with moving high field domain in piezoelectric semiconductor, noting acoustic impedance 07 p1232 A67-19556
- Quasi-static and dynamic linear viscoelasticity boundary value problems and elastic wave propagation 08 p1419 A67-20882
- Elastic wave diffraction around elliptical hole in thin plate, obtaining dynamic stress concentration coefficient through approximate solution 11 p1870 A67-23897
- Free oscillations of plates, strips, rods and cylinders subjected to arbitrary dynamic edge load 11 p1874 A67-24314
- Elastic surface waves excitation method in quartz at high frequencies, noting absorption temperature dependence 11 p1848 A67-24835
- Nonuniform elastic unloading wave propagation into perfectly plastically deformed region, obtaining solution of displacement field 11 p1879 A67-24941
- Light diffraction by elastic waves in YIG noting values of photoelastic tensor components 12 p1864 A67-25746
- Diffusion of protons and nuclei having elastic interactions at 27 GeV/c, using probability distribution for events outside Gaussian limit of multiple scattering 13 p2160 A67-26436
- Elastic wave propagation in Cosserat continuum with free surface 13 p2217 A67-26630
- Pulsed laser beam induced elastic waves in metals, noting experimental techniques and role of radiation pressure in wave generation 14 p2374 A67-28987
- Axisymmetric two-dimensional elastic wave propagation equations for finite elastic bar, considering continuous and discontinuous loadings at impact end [ASME PAPER 67-APM-22] 17 p2964 A67-33151
- Diffraction of stress pulse by spherical cavity embedded in infinite linear homogeneous isotropic elastic medium [ASME PAPER 67-APM-27] 17 p2965 A67-33154
- Plastic resonance problem for longitudinal elastoplastic waves in finite bar solved, considering bodies with rigid unloading characteristics 18 p3140 A67-33465
- Propagation of elastic waves through composite media studied with ultrasonic pulse technique, noting Poisson ratio, bulk modulus, etc 18 p3069 A67-34488
- Finite amplitude elastic wave motions with only constitutive nonlinearities 20 p3540 A67-37282
- Plane deformation problem of instantaneous elasticity theory application to expansion of stationary elastic waves in infinite medium with cylindrical cavity 21 p3720 A67-38294
- Dispersion relations for elastic wave propagation in filamentary composites obtained, establishing averaging rules for elastic constants 21 p3729 A67-39055
- Dispersion relations for elastic wave propagation in lamellar composite materials obtained with averaged elastic constants 21 p3729 A67-39056
- YIG magnetically induced elastic wave dispersion, acoustic Faraday rotation and group velocity dispersion measured using Bragg diffraction 22 p3855 A67-39358
- Plane circularly polarized magnetoelastic and elastic wave scattering at plane discontinuity surface between ferromagnetic insulating medium and elastic medium 22 p3856 A67-39364
- Elastic wave problems involving one space variable solved by hyperbolic partial differential equations 23 p4072 A67-40610
- ELASTICITY**
- SA AEROELASTICITY**
- SA AIRYS STRESS FUNCTION**
- SA BIHARMONIC EQUATION**
- SA FLEXIBILITY**
- SA HUGONIOT EQUATION OF STATE**
- SA HYPOELASTICITY**
- SA MAGNETOELASTICITY**
- SA PHOTOELASTICITY**
- SA PHOTOVISCOELASTICITY**
- SA PLASTICITY**
- Elastic orifice compensator in externally pressurized gas bearings for flow control, noting increased bearing stiffness 01 p0077 A67-10123
- Special functions for solving second-order or higher linear differential equations with variable coefficients in elasticity theory problems 01 p0158 A67-10215
- Concentration of stresses around curvilinear holes in thin shells solved with nonlinear law of elasticity, reducing problem by boundary shape perturbation method 01 p0158 A67-10218
- Functional analysis of plane problem of elastostatic theory for multiply-connected regions with given surface traction 01 p0160 A67-10516
- Shell theory results compared with results obtained by asymptotic integration of three-dimensional equations of elasticity theory and error correction methods 01 p0163 A67-10986
- Elastic interaction energies between edge and screw dislocations and tetragonal defects in anisotropic NaCl lattice 02 p0298 A67-11885
- Plane problems of moment theory of elasticity for plane weakened by finite number of circular apertures, obtaining uniqueness of solutions 02 p0338 A67-11954
- Solutions for boundary value problems of potential theory and elasticity theory for single cavity hyperboloids of revolution 02 p0338 A67-11955
- Analytical and p-analytical functions of complex variable used to solve three-dimensional axisymmetric problems in elasticity theory 02 p0338 A67-11967
- Harmonic approximation of infinite crystal dynamics problem, noting collisional case and action of external force on atoms 03 p0520 A67-12930
- Elasticity problem treated by method of reduction to second order partial differential equations 04 p0710 A67-14911
- Timoshenko beam theory equations and shear coefficient formula derived from three-dimensional elasticity theory [ASME PAPER 66-APM-C] 04 p0717 A67-15916
- Classical elasticity theory determination of computational error of fibrous body treated as simply connected multiple hole disks 05 p0907 A67-18037
- Classical elasticity theory determination of stress distribution on boundary plane of elastic half-space due to internal body force distribution 05 p0908 A67-18040
- Solution to external biharmonic problem for simply connected region bounded by Liapunov curve given in form of Fourier series and applied to elasticity theory 05 p0908 A67-18041
- Lifting capacity of two-layer cylindrical shell made of different elastically hardening materials, considering temperature effect 05 p0912 A67-18180
- Stressed state of viscoelastic cylinder with star shaped cavity caused by steady temperature field and distributed surface load in problem of elasticity 05 p0912 A67-18185
- Linearized elasticity theory of coupled stresses effect on stress concentration around finite crack 05 p0921 A67-18884
- Four methods of solving elasticity theory contact problem and correlation of methods 05 p0923 A67-17180
- Asymptotic solution to elasticity theory problem for hollow isotropic cylinder of finite dimensions and small thickness under axisymmetric load distributed over entire surface 06 p1100 A67-18033
- Stability of plane Poiseuille flow between elastic boundaries 06 p0984 A67-18044
- Force distribution and stress displacement

relations for two-dimensional elasticity with coupled stresses 06 p1107 A67-18651

Stress-strain and Hooke law in orthotropic elasticity presented through matrix algebra and tensor coordinates 06 p1108 A67-18656

Penny shaped crack embedded in isotropic material treated by linear elasticity, noting stress singularities 06 p1109 A67-18732

General solution of two-dimensional linear elasticity problem in polar coordinates in term of stress function satisfying biharmonic equation 06 p1111 A67-18873

Mixed boundary value problem of elasticity with parabolic boundary 07 p1263 A67-19732

Power series technique applied to single edge notches in semilinear region in plane elasticity problems, using mapping function and Muskhelishvili theory 08 p1414 A67-20347

Craggs propagating crack model for isotropic solid extended for general elastic anisotropy, obtaining propagation theory under tensile or shear stress 08 p1421 A67-20952

Statistical basis for modified moment theory of elasticity that takes into account contribution of all deformation-tensor-component gradients to deformation energy 09 p1574 A67-21914

Frequency equation for harmonic wave propagation in composite circular cylindrical shells established, based on linear three-dimensional theory of elasticity 10 p1717 A67-23127

Asymptotic integration of elasticity theory equations and analysis of stressed state of anisotropic shell 11 p1871 A67-24160

Contact problem of half-plane inelasticity theory using Jacobi polynomials and taking into account thermal stresses and presence of adhesion and friction in contact area 11 p1876 A67-24677

Singular integral equations with constant coefficients solved by Jacobi polynomials and applied to problems in fluid dynamics, crack propagation, plane elastic theory, etc 11 p1813 A67-24678

Contact problem for elastic rectangle solved by reducing problem to solution of quasi-fully regular infinite set of linear algebraic equations with bounded free terms 11 p1876 A67-24679

Approximation methods for multiply connected problems in two-dimensional theory of elasticity 11 p1878 A67-24875

Dynamic two-dimensional problem of moment theory of elasticity and viscoelasticity of medium with circular cylindrical cavity 11 p1879 A67-24883

Stress-strain state of cylindrical shell analyzed based on elasticity theory, noting boundary value problem 12 p2022 A67-25583

Asymptotic integration of elasticity theory equations applied to two-dimensional dynamic theory for cylindrical shells 12 p2029 A67-25636

Elasticity problems for bounded connected region consisting of finite number of rectangles solved by relaxation techniques 13 p2215 A67-26372

Axisymmetric problem in elasticity for simply connected body and elastic space containing axisymmetric cavity 13 p2218 A67-26887

Plane problems of elasticity theory solved numerically using conformal mapping 13 p2220 A67-27621

Book on elasticity covering engineering, Cartesian tensor and vector-dyadic notation, etc 14 p2395 A67-27891

Certain integral equations of first kind reduced to Abel equation and equation of second kind when solving elasticity and hydrodynamic problems 14 p2344 A67-28742

Asymptotic method for solving equations of theory of elasticity and mathematical physics 15 p2574 A67-29691

Variational principle of dynamics applied to linear theory of elasticity and given in form of two integrals 15 p2575 A67-30002

Contour integral representation of eigenvalues of first boundary value problem of elasticity theory 17 p2962 A67-32832

Book on continuum mechanics including kinematics, principles and linear theories of continuum mechanics, elasticity and viscoelasticity 17 p2963 A67-33092

Plane problems of moment theory of elasticity for plane weakened by finite number of circular apertures, obtaining uniqueness of solutions 17 p2966 A67-33271

Solutions for boundary value problems of potential theory and elasticity theory for single cavity hyperboloids of revolution 17 p2966 A67-33272

Analytical and p-analytical functions of complex variable used to solve three-dimensional axisymmetric problems in elasticity theory 17 p2966 A67-33284

Variational principle of dynamics applied to linear theory of elasticity and given in form of two integrals 18 p3141 A67-33769

Wing twist distortion effect on glider static longitudinal stability with stick fixed 18 p2986 A67-34373

Slip band length in plate with circular hole determined in terms of linear theory of elasticity 19 p3344 A67-35848

Circumferential displacement and shearing stresses in out-of-plane elasticity problem for solid torus 20 p3538 A67-36672

Triangular finite element under plane stress analyzed using stiffness matrix, including in-plane concentrated moments and nodal rotation 20 p3538 A67-36676

Circumferentially symmetrical stressed state of half-space determined using Polozhnyi formulas in axisymmetric elasticity theory and p-analytic functions 20 p3538 A67-36918

Relativistic elasticity, discussing solution of field equations in transient unidirectional motion 20 p3486 A67-37279

Reciprocal theorem in linearized theory of couple stresses for perfectly elastic nonhomogeneous anisotropic materials 20 p3540 A67-37281

Iterative technique applied to solution of problems in elasticity involving minimization of double integral subjected to certain boundary conditions 20 p3541 A67-37487

Solution for boundary value problems in elasticity theory for ellipsoid of revolution and cavity with surface loading, determining coefficients in closed form 21 p3718 A67-37984

Electrical simulation method of conformal mapping used in solving engineering problems in elasticity 21 p3727 A67-38839

Constrained torsion computation for multipar box with elastic diaphragms assuming applied stresses at end ribs 21 p3728 A67-38906

Nonlocal elasticity theory for materials with long range cohesive forces derived from lattice theory by writing strain energy in integral form 22 p3908 A67-39288

Statistical elasticity problems involving random stress and displacement tensor fields, proving uniqueness and minimum principle for boundary value 22 p3909 A67-39396

Arbitrary function expansion into series of functions involved in plane elasticity problem with Fourier series form satisfying boundary conditions 22 p3909 A67-39397

Saint Venant principle in linear and nonlinear plane elasticity in two-dimensional isotropic body 22 p3912 A67-39743

Stress distribution in shear-strained Cosserat prism containing deep notch 22 p3913 A67-40005

Soviet book on elasticity and plasticity covering perforated plates and shells and elastoheredity media 23 p4077 A67-40748

Elastic bending of thin shells and plates perforated with holes in various arrays, calculating stress distribution and concentration 23 p4077 A67-40749

Book on thermoelasticity associating elasticity and heat conduction theories for thermodynamics of irreversible processes and differential equation problems 24 p4246 A67-41891

Vector eigenfunctions solution of three-dimensional elastic theory problems, reviewing literature on bodies of revolution in various coordinates 24 p4248 A67-42101

ELASTODYNAMICS

Governing mechanical and thermal equations in Lagrangian coordinates, reviewing isentropic theory 06 p1099 A67-17643

Gurtin variational principles extended in application to dynamic problems of elasticity with finite deformation 10 p1720 A67-23598

Scattering of plane monochromatic sound wave by semilinear elastic pipe in moving medium, emphasizing axisymmetric oscillations 10 p1680 A67-23644

Longitudinal impact of two reinforced cylindrical shells coupled to each other at ribs against solid body 12 p2025 A67-25611

Dynamic properties of elastic one- and two-dimensional continua using matrix method on digital computer and Hermitian polynomials 13 p2216 A67-28621

Scattering of plane monochromatic sound wave by semilinear elastic pipe in moving medium, emphasizing axisymmetric oscillations 18 p3080 A67-34413

Parameters governing high resistance of reinforced resins, stressing elastomechanical equilibrium at interface [ONERA-TP-468] 18 p3069 A67-34462

Elastodynamic problems using kinetic stress functions 22 p3909 A67-39399

Validity range of Flugge bending and Donnell theories established by comparing results with elasticity theory based results 23 p4074 A67-40630

ELASTOHYDRODYNAMICS

Elastohydrodynamic lubrication in rolling bearings for avoiding oil-film breakdown in contact zone 01 p0079 A67-10728

Optical elastohydrodynamic system for evaluation of lubricants using interference pattern obtained from metal ball rolling against plate glass [ASLE PAPER 67-LC-12] 24 p4164 A67-42747

ELASTOMER

SA PLASTIC

SA SYNTHETIC RUBBER

Elastomer application in spacecraft launching, flight and reentry such as binder, sealant, base for adhesives, heat shielding, etc [ONERA-TP-407] 05 p0833 A67-18479

Mechanical properties of unfilled and filled elastomers 08 p1420 A67-20890

Filler effects on deformation and rupture of amorphous gum elastomers with various molecular structures, noting failure envelopes [JPL-TR-32-922] 08 p1420 A67-20892

Space environmental effects on filled elastomers, nylon parachute material and adhesion of metals 15 p2506 A67-29540

Elastomeric materials thermostability in simulated spacecraft environment tested to obtain ignition point 15 p2466 A67-29545

Mechanical response of highly filled elastomer in complex triaxial tensile stress field; demonstrating dewetting effect, need for more testing, etc 15 p2575 A67-29978

Evaluation of stored-energy function for elastomeric materials based on biaxial experiments [JPL-TR-32-1006] 18 p3145 A67-34486

Viscoelastic behavior of pure gum rubbers and relationship between filler characteristics and mechanical properties of inert filled composite materials 19 p3249 A67-35888

Elastomer elastic deformation response in multiaxial stress field shown identical to uniaxial stress response 24 p4250 A67-42367

ELASTOPLASTICITY

Elastoplastic deformation under plane stress conditions determined, using method of photoelastic coatings 02 p0336 A67-11628

Elastic-plastic solution for circular rigid inclusion in unidirectionally stressed flat plate of linearly strain-hardening material 02 p0336 A67-11633

Stress concentration in plate weakened by infinite sequence of uniform holes and subject to elastoplastic strain 02 p0337 A67-11844

Elastoplastic equilibrium of thin arbitrary shells of revolution with finite deflection comparable to shell thickness 02 p0340 A67-12661

Cyclic stressing of fiber composite materials elastic-plastic region, assuming equal strains in fiber and matrix 03 p0445 A67-13529

Stresses in elliptical cross section rod subjected to elastoplastic torsion, using Legendre transforms 03 p0524 A67-13622

Elastic axisymmetric deformation of circular two-layer plate with closely spaced rod couplings compliant to radial shear 03 p0527 A67-14070

Behavior of eigenvalues in stability of elastoplastic plates used in low rigidity structures 04 p0708 A67-14786

Elastoplastic deformation of cylinder under torque and tensile stress based on stress stabilization in yield

- zones 04 p0708 A67-14796
- Elastic-plastic torsion of shafts with hyperbolic notches solved for Ramberg-Osgood and bilinear stress-strain curve 04 p0627 A67-14977
- Book on strength under high transient loads and nonlinear elastic and elastoplastic wave propagation 04 p0715 A67-15617
- Large elastoplastic deflection of simply supported plate subjected to uniform load, noting steel specimens 04 p0718 A67-15920
- Combined elastic solutions-finite difference method for bending of compressible or incompressible rectangular metal plate beyond elastic limit 05 p0907 A67-16017
- Elastoplastic deformation of nonuniformly heated rotating disk determined to verify validity of theory under nonisothermal load 05 p0907 A67-16019
- Plane strain equations for elastoviscoplastic compressible bodies without strain hardening 05 p0908 A67-16039
- Elastoplastic calculation of turbine disks, considering cyclic plastic deformation 05 p0810 A67-16177
- Quasi-static equilibrium of thin plate heated by stationary circular source, obtaining expression for elastoplastic region at heating center, using continuous function 05 p0912 A67-16179
- Elastoplastic axisymmetric stressed state of circular cylindrical shell under unsteady temperature field, internal pressure and axial force, using differential equation 05 p0912 A67-16181
- Slip and change in displacement vector in elastoplastic boundary value problems 05 p0918 A67-16424
- Bending moment change of curvature relation for large elastoplastic deflection of thin circular-arc cantilever beam, taking strain hardening materials into account 05 p0918 A67-16425
- Approximate computer method solution to impact problem of elastoplastic wave reflection from flexible plates in resisting medium 05 p0919 A67-16495
- Elastoplastic deformation of circular cylindrical shells of ideally plastic incompressible material under uniform supercritical hydrostatic pressure 05 p0922 A67-17176
- Small plastic deformation theory determination of elastoplastic stressed state of thin walled isotropic incompressible shell of revolution under axisymmetric power loads and nonuniform heating 05 p0922 A67-17177
- Hole-weakened spherical body represented by deformation of two spherical shells with reinforcing rings under uniform internal load beyond elastic limit 05 p0923 A67-17187
- General solution of two-dimensional nonlinear problems of elastoplasticity using finite element method, piecewise linear load deflection relationship and computational algorithm [AIAA PAPER 67-144] 06 p1104 A67-18457
- Compression and tension of rod and plate with distribution of residual stresses such that deformation is partially plastic and elastic 06 p1107 A67-18633
- Rotation of thin walled elastoplastic tube of circular cross section after bending 06 p1107 A67-18635
- Elastic-plastic plane stress configuration analysis by matrix displacement method, using quadrilateral finite elements 06 p1111 A67-18883
- Elastic-plastic torsion of square bar twisted by terminal couples formulated as variational minimum problem 07 p1264 A67-20293
- Axisymmetric crack formation problem in elastoplastic material including energy dissipation and face displacement calculations, noting agreement with Griffith theory 10 p1716 A67-22939
- Stresses produced in elastoplastic sphere with spherical cavity by surface heating-cooling, reducing problem solution to first order ordinary differential equation and functional equation 10 p1716 A67-22940
- Elastoplastic properties of copper, aluminum alloys and brass under explosive load, noting increased temperature effect on elastoplastic wave parameters 10 p1668 A67-23092
- Fracture initiation in sheet specimens, noting correlation of crack-opening displacement and fracture toughness and dependence on applied stress 10 p1718 A67-23172
- Unloading wave expanding in elastoplastic rod determined by integration of differential equation in quadratures 10 p1721 A67-23685
- Elastic-plastic analysis showing relationship between tangent modulus and initial strain methods 10 p1726 A67-23718
- Wave dispersion phenomena in blood vessels analyzed as measures of cardiovascular parameters 11 p1748 A67-23990
- Material hysteresis model for transient dynamic analysis 11 p1874 A67-24358
- Numerical solution of elastoplastic torsion of rods by method of local variations 12 p2029 A67-25667
- Elastoplastic equilibrium of rectangular compressible and incompressible plates under load concentrated near edge determined by elastic solutions and finite difference 12 p2031 A67-25960
- Constitutive equation for collapse load and limit analysis of elastoplastic structures 13 p2216 A67-26609
- Longitudinal bending and buckling of elastoplastic rods with allowance for creep 15 p2577 A67-30184
- Elasto-plastic stresses and strains in cracked plates analyzed by numerical method, noting stress singularities and stress-strain fields 16 p2769 A67-31287
- Extension of plastic zone in direction of path of moving brittle crack, studying properties of plastic zone to crack length ratio 17 p2960 A67-32633
- Boundary value wave problem in elastoviscoplastic medium solved by approximate method using Courant concept 19 p3340 A67-35444
- Numerical integration solution for finite elastoplastic deflections of circularly symmetrical plates 19 p3340 A67-35511
- Quasi-static equilibrium of truncated conical shell of revolution discussed in terms of zero-moment theory, when under cyclic load 19 p3341 A67-35631
- Friction data, elastoplastic deformation and surface geometry of rubbing surfaces 19 p3237 A67-35851
- Formulation of problem of elastoplastic torsion of rectangular or regular polygonal bar as variational problem 20 p3536 A67-36429
- Wave propagation rate in elastoplastic bodies under completely plastic conditions, noting discontinuity magnitude 21 p3716 A67-37968
- Unloading wave expanding in elastoplastic rod determined by integration of differential equation in quadratures 21 p3720 A67-38286
- Birefringent properties of Voigt type viscoelastic medium and Noll hydrostatic material during stress relaxation 21 p3657 A67-38409
- Koiter theorem generalized for examining unstable temperature field cyclic effects concerning progressive failure in elastoplastic bodies 22 p3910 A67-39453
- Mathematical classification of differential equations governing elastic-plastic waves in plane strain 22 p3914 A67-40193
- Homogeneous isotropic elastoplastic thin flat plate under uniform unidirectional stress, studying plastic flow, fracture, distortion and slip plane inclination 22 p3915 A67-40220
- Blade-spar thick walled cylindrical shell deformed under elastoplastic torsion, analyzing stress-strain ratio and torsional strain and displacement 22 p3916 A67-40458
- Longitudinal oscillations with multiple degree of freedom obtained over sections of adopted stress-strain diagram, characterizing elastoplastic properties 23 p4076 A67-40683
- Plane problems with contained elastoplasticity, considering thin plates with small apertures as free boundary problem in continuum mechanics 23 p4077 A67-40754
- Crack stability for fracture of nonworkhardening elastoplastic material in plane strain or plane stress, using energy criterion 23 p4078 A67-41162
- Thin toroidal elastoplastic shells of revolution loaded axisymmetrically, calculating force, moment, stress and strain interrelation for middle surface using complex representation 24 p4250 A67-42305
- ELASTOSTATICS**
- Three-axis ellipsoid elastostatic problem solved through analogy with equivalent electrostatic problem of charge distribution 12 p2029 A67-25665
- Three-dimensional elastostatic problems for infinite solid with geometric discontinuities solved using potential functions 13 p2221 A67-27735
- ELBOW**
- Muscle system participation in bending and straightening of elbow joint muscle system participation in bending and straightening of elbow joint 07 p1133 A67-19346
- ELDO LAUNCH VEHICLE**
- Metallic material compatibility with medium energy hypergolic propellant components hydrazine/UDMH and nitrogen tetroxide, used in ELDO rocket 01 p0139 A67-10211
- Design, development and main assemblies of third stage of ELDO satellite launcher 01 p0078 A67-10409
- Reflection-type amplifier in downrange guidance system, examining noise figure optimization, pump power requirements, bandwidth and input resistance 01 p0035 A67-10410
- ELDO launching rockets for communications satellites 01 p0153 A67-10454
- Satellite placing in synchronous orbit using ELDO PAS booster for telecommunications purposes 01 p0156 A67-11418
- Optimal design configuration for third stage of European launching vehicle 02 p0334 A67-12376
- ELDO missile second stage automatic control system, noting programming control sequences, analysis of measurement results, etc 03 p0502 A67-12899
- Space research and aerospace engineering in ESRO and ELDO, examining European participation in communications satellite system promoted by U.S. 03 p0537 A67-12967
- Optimization of high energy turbopump unit engine for ELDO-B carrier rocket, employing system specific impulse 03 p0503 A67-13013
- Vacuum simulation facility near Munich for testing third stage of ELDO rocket 03 p0394 A67-13031
- Checkout system for third stage of ELDO A program 04 p0595 A67-14534
- Second and third stage separation for ELDO A simulated in vacuum test 04 p0595 A67-14540
- ELDO guidance station in Australia for control of third stage and orbit placement of payload, noting interferometric complex 04 p0654 A67-15625
- ELDO guidance station noting master antenna for automatic tracking of third stage 04 p0576 A67-15627
- ELDO-PAS configuration consisting of fourth-stage addition to three-stage Europa I launcher, with apogee motor integrated in satellite, for telecommunications 06 p1093 A67-17557
- PCM telemetry system for satellite test vehicle of ELDO program using transistorized printed circuit technology 06 p0957 A67-17613
- Facility for testing third stage of ELDO rocket, discussing high vacuum equipment in Ottobrunn laboratory 09 p1485 A67-22124
- Guidance station for ELDO third stage, describing equipment and function 16 p2700 A67-30657
- German firm participation in designing and constructing third stage of ELDO launch vehicle EUROPA I 16 p2763 A67-31789
- Development, reliability and acceptance tests for third stage of ELDO satellite launcher, discussing components, time schedules, personnel training, etc 18 p3136 A67-33639
- European heavy launching vehicle development potential and economy, discussing communication satellites, thrust augmentation, zero stages, synchronous orbit, etc 18 p3137 A67-34353
- Second and third stage separation for ELDO A simulated in vacuum test 20 p3413 A67-36413
- Checkout system for third stage of ELDO A program 20 p3413 A67-36414
- ELDO-A satellite launcher engine assembly and shell section production and testing 20 p3533 A67-37166
- Inertial guidance system in ELDO-A satellite launch vehicle performance assessed using onboard computer 20 p3481 A67-37167

Gyrocompassing method used for alignment of inertial platform allows gyro-torque calibration and gyro drift trimming during procedure 22 p3830 A67-39158

P4 double test stand for ground testing third stage of ELDO launch vehicle 23 p3987 A67-41325

Sloshing stability of three-stage ELDO A launch vehicle during first stage flight 24 p4241 A67-42396

ELDO SATELLITE

Decoder signaling system of Eldo satellite employing PCM telemetry channel, examining counters, shift registers, flip-flop circuit, etc 02 p0192 A67-11651

Italian sensing devices for measuring temperature, pressure, acceleration, heat shield and vibration on ELDO satellite 17 p2854 A67-32227

Configuration study for ELDO-PAS test satellite based on communications requirements 17 p2955 A67-32396

ELDO-PAS program principles, objectives, ground stages, orbital injection, etc 17 p2955 A67-32399

ELECTRET

S BARIUM TITANATE

ELECTRIC ANALOGY

Thermal conductor of arbitrary shape, analogy with rectangular array of electrical resistance, detailing conformal transformation 01 p0167 A67-11015

Slender body theory application in obtaining aerodynamic stability derivatives for reentry vehicles via electrical analogy 03 p0354 A67-12918

Analogous studies of simultaneous conductive and radiative heat transfer across transparent laminar gas space, showing position of radiation shield between bounding surfaces 03 p0535 A67-13464

Waveguide-slot antenna design, considering interaction of radiators on principal wave 03 p0385 A67-13951

Temperature and heat transfer conditions determination on rotating turbine wheel in jet power plant, using electric analogy 04 p0688 A67-14571

Phase effect during rectangular pulsations of heat transfer coefficient 07 p1267 A67-19325

Electric analog and mechanical model used to investigate single particle impact dampers 07 p1262 A67-19410

Electroanalogue analysis of convective and conductive heat transfer and transient temperature field in solid propellant rocket nozzle head 07 p1268 A67-19568

Dynamic plane shear of incompressible viscoelastic material with temperature dependent viscosity determined, using electric transmission line analog 09 p1533 A67-22152

Electron density determination from plasma resonance measurements, using electric analogy for circuit 10 p1610 A67-22951

Short method measurement of Reynolds stresses in turbulent flow, using constant current hot-wire anemometer 10 p1629 A67-23845

Exact calculation of electrical performance of rectangular waveguide T-junction having arbitrary cross section used to find equivalent circuit 11 p1767 A67-24732

Weak inhomogeneous plasma wave energy redistribution during quasi-normal oscillation expansion in resonance regions, noting electric analogy 11 p1842 A67-24953

Electrothermal analogies for heat transfer simulation by equivalent electrical circuits 11 p1884 A67-25047

Relay, connector and switch operation simulation, discussing design and performance of chatter and transfer detectors 12 p1843 A67-25702

Electrical simulation of finite difference calculations of problems of bending and natural oscillations of circular, annular and sector plates 12 p2032 A67-25968

Signal duration effect on detection in presence of masking noise by human auditory system, using electric analogy for testing purposes 12 p1903 A67-26126

Asymmetric R and RC networks as electrical analogs for solving nonlinear equation of nonstationary thermal conductivity 14 p2274 A67-28315

Electric network analogy for square matrix inversion 14 p2292 A67-28902

Static /time-discrete/ electrical model for

mathematical analogy of heat transfer processes and application to solution of nonlinear heat conduction equations 17 p2821 A67-33079

Static /time-discrete/ electrical integrators for solution of boundary layer equations 17 p2821 A67-33080

Combined electrical modeling technique for solution of two-and three-dimensional problems of unsteady heat conduction 17 p2973 A67-33081

Electrical analogy calculation of incompressible and rotational axisymmetric flow around variable-circulation streamlined propeller 18 p3025 A67-33681

Transonic jet flow study with electric analogy methods, solving Frankl and Tricomi problems for mixed type PDE 18 p2982 A67-33684

Equivalent resistance circuit of solar cell taking into account all sources of linear resistance 19 p3177 A67-36037

Analogy between electric, thermal and magnetic phenomena considered in terms of molecular transfer theory, noting pure mathematical meaning with no physical content 22 p3837 A67-40213

ELECTRIC ARC

SA SPARK

Solderability of 15 CDV 8 25 mm thick steel using argon arc and electric arc, noting mechanical properties of resulting alloy 01 p0078 A67-10270

Electron temperature measurements in low voltage arc in saturated cesium vapor 02 p0275 A67-12470

Electron temperature and concentration in cesium plasma in low voltage arc measured, using double probe method 04 p0666 A67-15182

Electric arc stabilization mechanism for nonconducting gas flow in chamber of DC plasma generator 04 p0666 A67-15191

Electromagnetic field in induction type plasma generator in steady state, from Maxwell equations and heat conservation equations 04 p0671 A67-15612

Heat transfer in plasma jet generators, considering electric arc types and thermal regime of electrodes 04 p0672 A67-15671

High temperature vacuum furnace using electric furnace parts 06 p0950 A67-17751

Source model for predicting drag force on moving arc column in cross flow velocity and balancing magnetic field [AIAA PAPER 67-97] 06 p0986 A67-18280

MHD phenomena in open electric arc, determining role in formation of plasma configurations of arc 06 p1044 A67-18688

Fluid mechanical model of electric arc balanced magnetically in gas flow, based on photographs showing arc must simulate solid body [AIAA PAPER 67-96] 07 p1240 A67-19437

Source model for predicting aerodynamic drag on moving arc column in crossflow yields relationship between crossflow velocity and balancing magnetic field 08 p1356 A67-20579

Electric arc behavior in argon gas flowing through magnetic field, measuring flow velocity, electron temperature, spatial distribution, etc 09 p1543 A67-21824

Electric arc model in longitudinal gas flow through annular gap between rod cathode and cylindrical anode 09 p1546 A67-22314

Symptomatic behavior and anode regimes of arc for electric arc with superimposed subsonic flow of argon [AIAA PAPER 66-479] 10 p1685 A67-23123

Electric arc combustion stability in gas flow, noting relation to weakly ionized plasma conductivity 12 p2033 A67-25314

Volt-ampere characteristics, generation and decay of interrupted and AC arcs in nitrogen, air, argon and carbon dioxide at zero gravity 14 p2354 A67-27760

Thermal and electrical conductivity equations for constricted water-cooled arc 15 p2523 A67-29229

Uniform flow ionization in MHD generators produced by electric arc investigated for preionized gas stream 18 p2712 A67-30547

Spectral linewidth and shift of Ti I lines produced by neutral argon atoms analyzed using high pressure arc as light source 16 p2703 A67-30665

Composition, heat conduction and radiative energy transfer characteristics of hydrogen and argon plasmas produced by arc in

cylindrical channel with cooled walls 17 p2897 A67-32172

Stability conditions for gas stabilized DC electric arc in plasma-arc torch determined using small perturbation technique schematic feed circuit 17 p2897 A67-32172

Sodium effect on dwell time and transport rates of various elements using DC arc stressing spectral consequences 17 p2888 A67-32377

Arc oscillation in argon in cross flow facility noting parameter ranges, electrode spacing effects, etc 17 p2906 A67-33037

Lithium plasma source current-voltage characteristics in vacuum, obtaining parameters valid for arcs burning under atmospheric pressure and nonzero magnetic fields 17 p2906 A67-33081

Radial mass flow effect on electric arcs obtaining higher axis temperature and enthalpy densities 17 p2910 A67-33366

Temperature field and electron concentration in electric arc moving along parallel electrodes in magnetic field, giving propagation rate, arc intensity, etc 18 p3087 A67-34044

High current arc operation characteristics in vortical-scheme plasmatron, determining current voltage characteristics 18 p3088 A67-34057

Confined electric arc developed for gas transport properties determination, noting measurement of flow pressure drop radiative heat transfer, spectral temperature distribution, etc 18 p3091 A67-34731

Energy balance of electric arcs in argon without and with superimposed gas flow investigated at various pressures [DVL-626] 19 p3280 A67-35144

Oscillations of electric arcs with superimposed gas flow in cylindrical nozzle and rectangular channel, determining critical Reynolds number [DVL-629] 19 p3280 A67-35144

Radial instreaming mass flow effect on cylindrically-symmetric arc with transpiration cooling, noting heat flux reduction 19 p3280 A67-35144

Volt-ampere characteristics of long free burning convection-free DC and AC arcs in nitrogen, argon and carbon dioxide 19 p3280 A67-35144

Conditions of stable burning of electric arc stabilized by gas stream in DC plasma arc torch, determining threshold current 19 p3281 A67-35156

Transverse forces acting on arbitrarily curved current carrying plasma cylinder in transverse magnetic field 19 p3281 A67-35156

Column effects in arc interaction with transverse magnetic fields 19 p3281 A67-35156

Retrograde motion of electric arc discharge at low pressure with transverse magnetic field, including cathode vaporization 19 p3281 A67-35156

Electric arcs in cross flow with variable magnetic field across electrode space 19 p3281 A67-35156

Measurement of column resistance during recovery of rapidly interrupted low current wall stabilized DC arc 19 p3282 A67-35156

Electric arc blowing in plasma of nonuniform conductivity and inclusion of effect in MHD flow 19 p3298 A67-35769

Tangential drag measurements at electrodes of arc in plasma accelerator, ion current partitioning at cathode and electrode damage 21 p3670 A67-38669

Convective electric arc stability and slanting in thermionic rail accelerator [AIAA PAPER 67-874] 21 p3671 A67-38700

DC electric arc in superimposed gas flow behavior in arc tunnel, discussing electrode geometry [AIAA PAPER 67-875] 21 p3671 A67-38700

Temperature determination of wire explosion plasma from expansion and resistivity measurements, showing existence of two phases of electric arcs 22 p3847 A67-39644

ELECTRIC BREAKDOWN

SA SHORT CIRCUIT

SA VOLTAGE BREAKDOWN

Impedance measurement of silver bonded Ge diode at X band and in mm wave region improving performance by usage in breakdown region 01 p0033 A67-10022

Effective hot carrier ionization rate in epitaxial gallium arsenide p-n junction determined from photomultiplier

measurements 02 p0299 A67-12186
Second breakdown in transistor with power-handling capabilities 02 p0222 A67-12648
Second breakdown and hot spot formation in simplified HF silicon power transistor with interdigitated comb emitter structure 02 p0222 A67-12649
Statistical model of cost of elements of system undergoing gradual breakdown, giving optimal distribution of mean relative deviations of input and output parameters 03 p0389 A67-13090
Nanosecond pulse microwave breakdown in air 04 p0657 A67-15120
Electric breakdown in gas discharges in nitrogen and hydrogen at high pressure 04 p0661 A67-15652
Spontaneous dielectric breakdown in Plexiglas sheets due to pulsed electrons with breakdown plane influenced by embedded metal foils 04 p0659 A67-15699
Microplasma effects arising in avalanche type breakdown in deep-seated large-area p-n junction in silicon 05 p0867 A67-17052
Formative time lag for pulsed RF breakdown in dry air as function of gas pressure and power of slot antenna 07 p1153 A67-19607
Self-healing electric breakdown in MOS structures noting magnitude duration, temperature and propagation characteristics 07 p1157 A67-19904
Delay time of avalanche discharge in silicon p-n junction as function of overvoltage 07 p1238 A67-20256
Effective field for microwave breakdown for gas in external DC magnetic field and electric field valid for any stationary random signal 09 p1462 A67-21646
Avalanche breakdown voltages of diffused silicon p-n junction calculated, using impact ionization rates 09 p1556 A67-22205
Gas pressure effect on electrical breakdown and field emission, discussing ion bombardment and whisker formation 11 p1820 A67-24921
Approximate similarity criterion for arc with self-adjusting length, burning in plasmatron with gas vortex stabilization, determined by shunting 11 p1843 A67-24969
Diffusion by microwave breakdown of weakly ionized helium plasma in metal chamber immersed in magnetic field 14 p2358 A67-28293
Electric breakdown, dielectric constant and dissipation factors of cryogenic liquid nitrogen, hydrogen and helium 14 p2341 A67-28891
Gunn diodes using Sn-Ag and In-Au contacts studied for electrical properties and failure mechanisms 14 p2290 A67-28927
Microplasma effects arising in avalanche type breakdown in deep-seated large-area p-n junction in silicon 15 p2538 A67-29783
Structural dislocations effect on formation of microplasmas during avalanche breakdown of silicon p-n junction 18 p3099 A67-33698
Destructive breakdown conduction in aluminum-silicon oxide-aluminum capacitors, discussing voltage threshold, etc 18 p3105 A67-34630
Mercury-argon low pressure discharge initiation stressing positive column establishment, examining breakdown effects by spectrographic techniques 19 p3272 A67-35088
Thermodynamic model for laser induced gas discharges accounting for transmitted light attenuation, plasma heating, etc 19 p3239 A67-35163
Trigatron spark gap using low voltage plasma jet as switch analyzed for properties, time lag and mechanisms 19 p3298 A67-35602
Laser induced gas electrical breakdown theories, predicting high threshold field strengths invalidated by single mode, phase-locked and laser measurements 20 p3459 A67-36851
Electrical breakdown association with field emission observed through electron microscopy of whiskerlike projections on cathode surface 21 p3589 A67-37824
Breakdown temperature of pulsed switching circuit using high power transistors depends on transistor property 22 p3771 A67-39827
Time dependent relation between coloring and spontaneous conductivity increase in barium titanate single crystals by strong electric field 22 p3861 A67-39918

ELECTRIC CELL

SA FISSION ELECTRIC CELL
Design and developmental testing of electrical components for two-shaft Brayton cycle energy conversion system, discussing Na-Bi and Li-Te cells 24 p4108 A67-42556
ELECTRIC CONDUCTIVITY
SA IONOSPHERIC CONDUCTIVITY
SA RESISTANCE
SA SUPERCONDUCTIVITY
Energy levels in forbidden band of gallium arsenide alloyed with silver or gold, determining impurity levels from temperature dependence of electric conductivity and Hall constant 01 p0129 A67-10104
Relation between acid-basic state and conductivity for polyaniline macromolecular semiconductors such as emeraldines 01 p0130 A67-10196
Water and internal acidity effect upon oligomeric polyanilines semiconductivity 01 p0130 A67-10197
Gunn effect noting negative bulk conductivity, creation of external negative conductance and zones with different field intensities in semiconductor crystals 01 p0130 A67-10253
Electroabsorption measurements on rutile in clarifying band structure and dichroic nature at absorption edge 01 p0131 A67-10339
Electric conductivity on clean cleaved surface of degenerate germanium 01 p0131 A67-10340
MHD power generation, presenting electrical conduction in gases, seeding and ionization, equations, conversion efficiency, electrical losses, compressible flow theory and application to various cycles 01 p0013 A67-10556
Resistivity and Hall coefficient measurement of n-and p-type gold-diffused silicon over wide temperature range 01 p0134 A67-10754
Luminescence and conductivity of CdS single crystals, noting temperature effect and release mechanism of trapped electrons and holes 01 p0134 A67-10820
Clathrates exhibiting metallic conductivity and superconductivity at specific temperatures, noting transition temperature of nitrate salt 01 p0135 A67-10917
Current transmission through semiconductors with impurities, calculating V-I characteristics at high temperatures during acceptor level creation 01 p0135 A67-10925
Electrode losses in MHD generators with nonequilibrium and equilibrium ionization compared, attributing differences to coupling between conductivity and local dissipation 01 p0014 A67-11159
Electric conductivity, electrode temperature and potential distribution across channel in potassium seeded-argon atmospheric-pressure Faraday accelerator [AIAA PAPER 66-75] 01 p0014 A67-11177
Saturation effect dependence on electrode surface temperature and bulk gas temperature in MHD generator duct 01 p0126 A67-11186
Pure selenium conductivity, thermal emf and Hall effect 01 p0138 A67-11297
Relaxation effect in electrical conductivity of semiconductors and metals, taking into account scattering by ionized impurities and Debye cloud polarization 02 p0280 A67-11480
Electron conduction in discontinuous metal films by transport of activated charge carrier creation and by tunneling for island sizes 02 p0292 A67-11746
Electric conductivity in microcrystalline metal films in theory based on Kubo type formula and Bardeen-Harrison-Stratton treatment of tunneling 02 p0292 A67-11748
Electric conductivity due to tunnel effect in aluminum-alumina-silver sandwich structures, determining potential barrier in alumina and absorption coefficient of hot electrons 02 p0295 A67-11762
Conductivity, Hall coefficient and magnetoresistance of monophase InSb films as function of film thickness 02 p0295 A67-11765
Shielded coupled strip transmission line with three center conductors, noting electrical behavior, cross section dimension evaluation from characteristic immittances, etc 02 p0193 A67-11777
Electron-hole conductivity effect on temperature variations of Hall coefficient

and Nernst-Ettingshausen effect in semiconductor 02 p0296 A67-11829
Thermal emf and electric conductivity in solid and liquid semiconducting copper-antimony-ditelluride 02 p0297 A67-11846
Emf and electric conductivity in ionized gas produced by detonation of Sakura dynamite to estimate explosion rate 02 p0288 A67-12500
Theoretical semiconductor electroconductivity dependence on intensities of strong electric and magnetic fields 03 p0490 A67-13158
Ohm law deviation in island-structure thin metallic films and current dependence on field strength 03 p0490 A67-13159
Figure contact resistance between Al and Cr sputtered conductive and resistive films 03 p0491 A67-13248
Electron processes at semiconductor surface in presence of chemisorption, noting conductivity and impurity distribution 03 p0492 A67-13315
Electrical conductivity and Hall coefficient temperature dependence in pure and alloyed Te 03 p0492 A67-13344
MHD stability of dense plasma jets flowing into transverse magnetic field, discussing effect of conductivity and Hall factor 03 p0477 A67-13462
Electrical conductivity, Hall coefficient and absolute thermoelectric power of liquid antimonides and tellurides 03 p0495 A67-13533
Plasma electric conductivity around 2000 degrees K measured, using double probe with interelectrode section of controllable length 03 p0478 A67-13603
Ionized gas electric conductivity measurement based on magnetic flux changes and deflection of lines of forces during gas-magnetic field interaction 03 p0478 A67-13604
Motion of medium of variable electric conductivity in rectangular channel situated in magnetic field 03 p0478 A67-13621
Computation of electric conductivity in sunspots and photosphere from empirically determined linear logarithmic relation 03 p0511 A67-13814
Diffusion coefficient for electroactive impurity in semiconductor based on current carrier concentration variations during successive removal of surface layers 03 p0498 A67-13841
Texture and electric conductivity of cadmium sulfide thin films 03 p0498 A67-13868
Tunnel diode circuit stability, equivalent circuit and conductivity 03 p0386 A67-13965
Channel flow of suddenly pressurized viscoelastic and electrically conducting fluid under influence of constant transverse magnetic field 03 p0483 A67-14035
Electron bombardment induced electroconductivity, with application to image tubes 03 p0387 A67-14092
Decay of K-state in Ni-Cr, Ni-Cr-Mo and Fe-Ni-Cr-Mo alloys studied in terms of electric conductivity during plastic deformation 04 p0635 A67-14429
Atmospheric electrical conductivity of air at high temperatures 04 p0684 A67-14777
V-I characteristics of stagnation point electrodes in lightly ionized atmospheric pressure plasma, calculating electric resistance from conductivity measurements 04 p0684 A67-14821
Electrical conductivity of p-GaSe single crystals in strong electric fields 04 p0676 A67-14929
Temperature dependence of electroconductivity of pure barium titanate and Fe-and Co-doped barium titanate crystals 04 p0678 A67-15130
Dimensional effect in electric conductivity of semiconductors during heating of electric field when electron energy relaxation length exceeds mean free path 04 p0679 A67-15137
Temperature dependence of current-carrier concentration and electrical conductivity of p-type germanium containing beryllium and phosphorus 04 p0679 A67-15144
Nonstationary flow of gas in transverse magnetic field, noting electric conductivity dependence on compressibility and temperature 04 p0685 A67-15178
Conductivity changes in thin layer of silicon oxide induced by electron beam of scanning electron

microscope 04 p0682 A67-15318
 Temperature perturbations produced by internal sensors embedded parallel to heated surface of low conductivity material [ASME PAPER 66-WA/HT-8] 04 p0724 A67-15427
 Conductance theory for electrolytes and weakly ionized plasmas using pair distribution function in space in presence of short range forces 04 p0670 A67-15578
 Pair distribution function and conductance for symmetrical electrolytes up to all powers of Bjerrum parameter, using Debye screening to eliminate long range divergence 04 p0670 A67-15579
 Thermal power and electrical conductivity of SnTe-InTe crystals, discussing temperature effect 04 p0683 A67-15581
 Anomalous high photoconductivity of indium antimonide thin films due to negative charge transfer to oxide surface layer during illumination 04 p0683 A67-15650
 MHD heat transfer in finite duct for fully developed flow conditions with arbitrary oriented applied magnetic field and variable heat flux boundary conditions 04 p0673 A67-15872
 MHD wave propagation emphasizing viscosity, heat and electrical conductivity, Hall current, nonequilibrium phenomena and effect of medium inhomogeneity 05 p0851 A67-16364
 Temperature variation of electric conductivity and carrier mobility in diffused germanium resistors doped with antimony for thermometry 05 p0773 A67-16464
 Electric conduction through tantalum oxide thin films, showing dependence of V-I characteristics on tunneling and Schottky effect 05 p0862 A67-16525
 Crystal structure defects and electroconductivity variations in CdS single crystals in oxygen ambient and effects of various surface treatments 05 p0862 A67-16605
 Thermoelectric powers and conductivities of vanadium dioxide whiskers measured from 273 to 335 degrees K 05 p0864 A67-16898
 Electric conductivity and luminescence increase in luminophorous zinc sulfide films as aftereffect of negative resistance 05 p0866 A67-17023
 Current carrier scattering mechanism in PbTe determined from ratio of electric conductivity and Wiedemann-Franz ratio 05 p0868 A67-17067
 High temperature effect on strength of solidified resins and resin based materials, determining loss of weight, density, compression strength, permittivity and electric conductivity 05 p0833 A67-17098
 Single parameter MHD flow of ideal incompressible infinitely electroconductive gas 05 p0855 A67-17114
 Electric conductivity of hexamethylbenzene explained by molecular interaction conductivity change at transition point 05 p0871 A67-17379
 Fusion weld evaluation in 2014-T6 material by eddy current, electric conductivity and hardness plots, noting aging effects, mechanical property degradation, etc 06 p1007 A67-17640
 Electric resistivity and electroconductivity of copper composites reinforced with fibrous felts of tungsten 06 p1015 A67-17808
 Spectroscopic measurement of temperature, electron density and conductivity in RF plasma torch 06 p1039 A67-17825
 Electric conductivity of naphthalene and beta-methylnaphthalene in liquid and solid state as affected by electric field 06 p1049 A67-17857
 Pinch effect in InSb degenerate plasma, discussing electric conductivity and recombination emission spectra 06 p1049 A67-17879
 Electric conductivity of liquid metals as function of electron oscillation frequency 06 p1032 A67-18125
 Soviet book on solid state chemistry and electroconductivity of chemical systems 06 p1052 A67-18608
 Temperature dependence of electroconductivity of As-Su-Ge system in vitreous state 06 p1052 A67-18610
 Electric conductivity of AsSeGe-AsSGe glasses 06 p1052 A67-18611
 Impurity effects on electroconductivity of

vitreous AsSe 06 p1053 A67-18612
 Temperature effect on electroconductivity of complex vitreous systems of K-Tl-Pb 06 p1053 A67-18613
 Electric conductivity of vitreous As-Se semiconductor 06 p1053 A67-18614
 Electric conductivity of vitreous As-S-Th 06 p1053 A67-18615
 Turbulent MHD boundary layer flow of constant-electroconductivity incompressible fluid past dielectric plate in TM field, for small magnetic Reynolds numbers 06 p1043 A67-18672
 Turbulent flow of electrically conducting fluid in pipe located in longitudinal magnetic field 06 p1044 A67-18689
 Convergence of Chapman-Enskog approximations to scalar electrical conductivity of some weakly ionized real gases 06 p1046 A67-18872
 Oscillatory magnetoconductance in inverted surfaces of p-type silicon 06 p1063 A67-18940
 Size effects in electroconductivity of semiconductors with several groups of carriers with large intergroup relaxation time 06 p1064 A67-18944
 Oscillations in conductivity of electron-hole plasma in semiconductors due to nonlinearity of volt-ampere characteristics 06 p1070 A67-18988
 Discharge plasma in He and argon with cesium and potassium vapor admixtures noting electric field, conductivity, electron temperature and emission spectrum 07 p1227 A67-19115
 Electron components for electrical, thermal conductivity and viscosity coefficients of gas mixtures calculated via molecular kinetic theory 07 p1225 A67-19116
 Existence of maximum conductivity of ionized gas mixture as function of thermodynamic parameters 07 p1225 A67-19117
 Quantum theory of electrical conductivity of semiconductors with nonstandard energy band 07 p1233 A67-19639
 Earth electrical conductivity, determined from data concerning northern and vertical components of cyclic geomagnetic variations, suggests increases with depth 07 p1174 A67-19714
 Electrical conductivity of earth interior from data concerning annual geomagnetic variations for all years of solar cycle 07 p1178 A67-19826
 Correction of Fatkullin expressions for LF conductivities of homogeneous plasma in presence of electron-ion collisions in ionosphere 07 p1179 A67-19834
 Nonohmic conductivity in n-type GaAs accompanied by negative photoconductivity and giant magnetoresistance, noting electron injection at cathode 07 p1234 A67-20099
 Temperature effect on equilibrium carrier concentrations and intrinsic lattice defects in semiconductor with self-activated conductivity, considering cuprous oxide 07 p1237 A67-20177
 Plasma transport properties, discussing application of ionization level as indicator for electric conductivity and viscosity 08 p1357 A67-20591
 Electric conduction models for biological tissues as anisotropic medium 08 p1288 A67-20602
 Electroconductivity variations in CdS and CdSe single crystals with SHF electric field strength, intensity of bias lighting and temperature in minus 70 to plus 70 degrees C interval 08 p1370 A67-20996
 Electric conductivity of lunar interior assuming olivine predominance and analogy to earth mantle conductivity 08 p1389 A67-21019
 RF bridge technique determining electric conductivity of plasma sheath around reentry vehicle 08 p1366 A67-21514
 Thickness dependence of Hall constant, electrical conductivity and Hall mobility in polycrystalline thin layers of InSb 09 p1551 A67-21565
 Measuring apparatus for scalar and tensor plasma conductivity in AC MHD generators and accelerators 09 p1538 A67-21775
 Boundary layer at electrode and center of flow of plane MHD generator calculated numerically by one-dimensional theory for subsonic and supersonic velocities 09 p1443 A67-21808
 Electric conductivity and kinetic energy in

seeded and unseeded airflow MHD experiments in hypersonic shock tunnels for aerospace applications 09 p1542 A67-21809
 Increased electric conductivity of gas in MHD generator obtained, using small auxiliary electrodes 09 p1443 A67-21810
 Electrical conductivity measurement of He 3 plasma induced by neutron irradiation 09 p1542 A67-21813
 Plasma characteristics of partially dissociated and ionized air due to alpha emissions from radioisotope surface material 09 p1543 A67-21819
 Conductivity of working fluid in MHD generator using thermionic emission from suspended lanthanum conductivity of working fluid in MHD generator using thermionic emission from suspended lanthanum hexaboride powder 09 p1543 A67-21820
 Two-dimensional isothermal liquid flow electrically conducting in channel under electromagnetic fields, finding self-modeling solutions using Jacobi functions 09 p1544 A67-21861
 Electric conductivity of high temperature nitrogen jet as affected by impurity particles of potassium, metals and metal oxides 09 p1547 A67-22321
 Optimization of thermionic diode, with electrical conduction and heat transport represented by differential equations 09 p1448 A67-22336
 Four-electrode device for measurement of electrical conductivity of shock ionized air 09 p1549 A67-22570
 Electrical conductivity tensor effect on flow in MHD generator, considering transport of ionized gas and solution of symmetric problem 09 p1550 A67-22575
 Variation in electric conductivity of gas products from detonation of propane-oxygen-nitrogen mixtures 09 p1581 A67-22581
 Free carrier electro-magneto-optical phenomenon in semiconductors, noting conductivity tensor, Faraday effect, Derr effect and Voigt effect 09 p1558 A67-22602
 Electrical and thermal conductivity of tin films investigated in search for surface superconductivity induced by electric field 10 p1888 A67-22765
 High field Hall effect of semiconducting CdS crystals with different mobilities, noting electron density and multiplication 10 p1889 A67-22908
 High resolution external probe for measuring electrical conductivity of argon plasma behind shock wave 10 p1884 A67-22963
 Variational problem for flow of plasma with variable electrical conductivity in channel of MHD generator solved, using Lagrange method of multipliers 10 p1884 A67-23023
 Theoretical semiconductor electroconductivity dependence on intensities of strong electric and magnetic fields 10 p1890 A67-23106
 Measuring Hall effect in high specific resistance materials by using alternating magnetic field and DC current 10 p1891 A67-23502
 Semiconductor conductivity in strong SHF electric fields, measuring dielectric constant and Fourier component 10 p1857 A67-23567
 Conductivity of almost intrinsic infinite p-n junction semiconductor, noting volume charge effect on behavior of junction 10 p1895 A67-23662
 Deformation of velocity profile in inhomogeneous magnetic field, noting anisotropic conductivity of flow 10 p1886 A67-23670
 Test set for automatically compensating for error sources in calculating FET transconductance values 11 p1760 A67-24258
 P-type Au compensated Si diode with negative resistance, determining reversed conductivity recovery time 11 p1768 A67-24861
 Semiconductor junction devices analyzed for diffusion and electric field currents in bulk regions 11 p1849 A67-24904
 Edge dislocations effect on electrical noise in n-type silicon analyzed and results compared with Shockley-Read model 11 p1849 A67-24906
 Geometrical optics approximation of plane electromagnetic wave reflection from ideally electrically conducting triaxial ellipsoid 11 p1754 A67-24986

Association energy of vacancy-impurity dipole obtained from electrical conductivity of magnesium fluoride-doped lithium fluoride at ambient temperature 12 p1978 A67-25149

Temperature dependence of electroconductivity of pure barium titanate and Fe-and Co-doped barium titanate crystals 12 p1978 A67-25154

Dimensional effect in electric conductivity of semiconductors during heating of electric field when electron energy relaxation length exceeds mean free path 12 p1979 A67-25160

Temperature dependence of current-carrier concentration and electrical conductivity of p-type germanium containing beryllium and phosphorus 12 p1979 A67-25187

AC conductivity of glass semiconductor measured over various frequency and temperature ranges, noting activation energy 12 p1980 A67-25181

Spontaneous polarization and electric conductivity in fluorite single crystals doped with lime 12 p1980 A67-25182

Electric conductivity of calcium fluoride single crystals doped with uranium dioxide 12 p1980 A67-25183

Cesium seeded argon plasma at atmospheric pressure, noting electron heating effect on conductivity curve and applicability to MHD conversion 12 p1970 A67-25253

Magnetic ordering effect on electrical properties of antiferromagnetic semiconductor MnTe indicate temperature anomaly above 440 degrees K 12 p1982 A67-25326

Plasma column deviation from static state analyzed for time constants, considering conductivity and temperature change rates 12 p1973 A67-25394

Electric current conduction between cold electrodes in shock-ionized air plasmas, noting current-voltage characteristics in flow behind shock wave 12 p1974 A67-25401

Forbidden band structure of PbTe and electrical conductivity and Hall effect measurements at high temperatures 12 p1983 A67-25513

Third Chapman-Enskog approximation to tensor electrical conductivity of partially ionized gas applied to two conductivity mixture rules for atmospheric cesium seeded argon 12 p1975 A67-25893

Electrical conductivity measurements of NaCl as function of particle size and temperature used to study subsurface diffusion 12 p1987 A67-26191

Current carrier concentration distribution in semiconductor with intrinsic anisotropy created by strong electric field 13 p2173 A67-26362

Field effect kinetics on pure germanium surface, measuring surface conductivity relaxation time by compensation-bridge techniques 13 p2174 A67-26403

Radiation-induced electroconductivity and secondary emission in alkali halide single crystals under positive ion bombardment 13 p2177 A67-27073

Effect of mutual entrainment of electrons and phonons on Wiedemann-Franz law for semiconductors, calculating thermoelectricity 13 p2181 A67-27280

Electrically conductive self-similar gas flow in medium with given back pressure, assuming medium conductivity as function of temperature and density 13 p2169 A67-27307

Hollow electrically conducting fluid jet stabilization in presence of uniform magnetic field 13 p2169 A67-27314

Hot carrier DC conduction in elemental semiconductors germanium and silicon 13 p2183 A67-27568

Evaporated silicon thin-film transistors operating by field effect conductivity modulation of n-type inversion layer at p-type film surface 13 p2083 A67-27573

Electrical conductivity and Hall coefficient temperature dependence in pure and alloyed Te 13 p2184 A67-27718

Temperature dependence of electrical conductivity and Hall effect of barium-titanate crystals reduced by hydrogen, observing electron spin resonance and optical absorptions 14 p2363 A67-27824

Semiconductor conductivity measurement from propagation irregularities of SHF electromagnetic waves in medium containing semiconductor 14 p2364 A67-27836

Self-sustaining high temperature and

electrically conducting gas layer formation observed in nonsteady interaction of compressible electrically conducting medium with magnetic field 14 p2355 A67-27839

RC network project for stabilization of tunnel diode, noting stability conditions, negative differential resistances, etc 14 p2283 A67-28041

Resistivity and magnetoresistance for metallic impurity conduction in phosphorus doped silicon at low temperature with various donor concentrations 14 p2365 A67-28232

Time varying magnetic field in shock tube, analyzing electric current diffusion layer 14 p2358 A67-28234

Electric conductivity and luminescence increase in luminophorous zinc sulfide films as aftereffect of negative resistance 14 p2366 A67-28487

Differential negative conductivity in n-type GaAs, using microwave electron heating 14 p2369 A67-28595

Large microwave field and small parallel DC field applied across GaAs sample altering conductivity related to carrier velocity-field characteristic 14 p2369 A67-28601

CdSb polycrystals of different structural patterns investigated for dependence of electrical conductivity, Hall mobility and thermal EMF 14 p2372 A67-28758

Dislocation-free Ge structural and electrical characteristics after cooling, considering quenching defects effect 14 p2372 A67-28761

Electric conductivity of p-Ga-Te polycrystals and single crystals in strong electric fields 14 p2375 A67-29085

Particle density and material functions of gases of random composition, calculating values without regard to reaction dissociation 15 p2543 A67-29090

Lorentzian scalar electrical conductivity as basis of mixture rules proposed for partially ionized gases in magnetic field to calculate tensor conductivity 15 p2523 A67-29218

Thermal and electrical conductivity equations for constricted water-cooled arc 15 p2523 A67-29229

Magnetic field influence on AC surface field effect in germanium resulting from change in sample conductance and not from change in surface barrier height 15 p2533 A67-29263

Gas-ionizing shock wave with zero electrical conductivity of gas in front of shock wave and infinite conductivity behind 15 p2470 A67-29310

Temperature dependence of electrical conductivity, Hall effect and resistance in transverse magnetic field for tin-doped InSb 15 p2534 A67-29385

Statistical model for size effect in electrical conduction 15 p2517 A67-29485

Hole mobility produced by single pulses of electrons in films of polyvinyl acetate semiconductors with sputtered gold electrodes, determining relation between film conductivity and mobility 15 p2537 A67-29703

Current carrier scattering mechanism in PbTe determined from ratio of electric conductivity and Wiedemann-Franz ratio 15 p2539 A67-29798

Electric and thermoelectric effects in single crystals of zinc-cadmium-antimony solid solution, measuring electrical conductivity, Hall constant and thermoelectric power 15 p2540 A67-30029

Gold, silver, copper and tin condensed films, investigating dependence of structure and conductivity on substrate material 15 p2540 A67-30122

Crystal dislocation in InSb by fast neutron bombardment assuming displacement wedges with electron type conductivity 15 p2541 A67-30234

Low temperature conductivity of semiconductors in electric and magnetic fields analyzed, noting electron-photon interactions and photon heating effect 15 p2542 A67-30248

Electron processes at semiconductor surface in presence of chemisorption, noting conductivity and impurity distribution 16 p2724 A67-30491

Electrical conductivity and electron energy balance in nonequilibrium plasma calculated over wide range of conditions on basis of ionization theory 16 p2709 A67-30516

Schwarz transformation methods for

electrical studies of MHD generators with tensor conductivity 16 p2600 A67-30535

Nonequilibrium plasma properties and generator performance due to magnetically induced ionization in closed loop facility using cesium seeded helium 16 p2602 A67-30559

Experiments with 100-kw MHD generator free from secondary effects by choosing MHD interaction parameter values greater than unity 16 p2602 A67-30559

Conductivity in Faraday generator with cesium-seeded argon calculated from energy balance of electrons 16 p2603 A67-30565

Electrical conductivity measurement of liquid-vapor potassium mixture flowing in circular steel tube simulating MHD oscillator conditions 16 p2712 A67-30575

Nonsteady combustion MHD open cycle generator improving power density by modulation of conductivity and particle velocity 16 p2607 A67-30595

Shock tube measurement of plasma electric conductivity, using Maxwell equation for quasi-steady state electromagnetic field 16 p2673 A67-31111

Collection of articles on complex semiconductors investigating conductivity, thermal, electrical and other properties, and preparation methods 16 p2729 A67-31154

Electric and thermal conductivity and Hall effect in solid solution of complex semiconductors noting temperature dependence 16 p2729 A67-31155

Double-walled cryostat with copper holder for probe measurements of temperature dependence of semiconductor galvanomagnetic effects 16 p2730 A67-31158

SnTe samples under uniform load studied for relation between electrical and thermal conductivity, thermal EMF and microhardness 16 p2730 A67-31165

Electron velocity distribution function obtained for partially ionized gas in weak, steady electric field by solving Boltzmann-Fokker-Planck equation 16 p2704 A67-31235

Plasma anomalous resistive instability shown independent from microinstability and caused by poor conductivity parallel to magnetic lines 16 p2720 A67-31240

Electrical conductivity and Hall effect of indium arsenide solid solutions, noting temperature dependence and hole mobility 16 p2732 A67-31480

Energy conservation in magnetohydrodynamics of plasmas, noting energy equation in plasma 16 p2721 A67-31548

Electrical and thermal conductivity and integral degree of blackness of tantalum at temperatures above 1000 degrees C 16 p2692 A67-31771

Electromagnetic field effect on heat transfer during laminar flow of electrically conducting incompressible fluid in flat channel 16 p2723 A67-31774

Admissible film thickness in probe measurements of electrical conductivity of semiconductor samples 17 p2910 A67-31928

Correlation of measurement data on electrical conductivity of nonequilibrium plasma with impurities 17 p2895 A67-32153

Plasma jet electrical conductivity, using inductances with different diameters as measurement device 17 p2895 A67-32154

Low temperature plasma conductivity of combustion products, particularly of exhaust gases in duct of MHD oscillator 17 p2895 A67-32155

Plasma conductivity measurement, applying Fishbeck nonperturbing method 17 p2896 A67-32165

Various experiments explaining fundamental properties of probes used in measurements of plasma arc columns 17 p2896 A67-32166

Electron radiation damage in CdSe crystals at cryogenic temperatures, noting electrical conductivity and cathodoluminescence properties before and during damage 17 p2916 A67-32838

Nonuniform electrical conduction in MHD channels analyzed by differential equations 17 p2906 A67-33011

MHD behavior of inviscid fluid in limit of infinite electrical conductivity and mobility exhibiting Hall effect 17 p2908 A67-33109

Magnetic field annihilation rate prediction in current pinches attributed to magnetic energy dissipation by ways other than ohmic losses 17 p2909 A67-33248

Conductivity of almost intrinsic infinite p-n junction semiconductor, noting volume charge effect on behavior of junction 17 p2924 A67-33343

Magnetic diffusion effects in sunspot region assuming Schroeter value for electric conductivity 17 p2952 A67-33395

Conduction mechanism in GaSb tunnel p-n junctions from 77 to 380 degrees K, noting temperature dependence of basic parameters, V-I characteristics, etc 18 p3098 A67-33573

Temperature and/or velocity modulation of plasmas for generating MHD power 18 p3085 A67-33702

Experiments on equilibrium and nonequilibrium electrical conductivity of seeded combustion products and theory of nonequilibrium ionization and recombination 18 p3085 A67-33706

Combination of monoclinic zirconia, second ceramic and metal in electrodes of MHD generators 18 p3099 A67-33709

Leakage current on insulating walls in MHD channel calculations, evaluating variable electrical conductivity in plasma boundary layer plasma boundary layer leakage current on insulating walls in MHD 18 p3088 A67-34061

Forbidden band structure of PbTe and electrical conductivity and Hall effect measurements at high temperatures 18 p3103 A67-34444

Plasma electric conductivity around 2000 degrees K measured, using double probe with interelectrode section of controllable length 18 p3090 A67-34468

Ionized gas electric conductivity measurement based on magnetic flux changes and deflection of lines of forces during gas-magnetic field interaction 18 p3090 A67-34469

Electric field of AC solenoid of finite length in Hall conducting medium 18 p2990 A67-34500

Traveling-wave bulk electroconvection induced in slightly conducting liquid with temperature gradient, giving velocity profile equations for plane flow 18 p3029 A67-34736

Thin semiconductor layers, studying surface conductivity variation with semiconductor thickness and surface band curvature 19 p3299 A67-34759

Transverse Nernst-Ettingshausen thermomagnetic effect in intrinsic conductivity region in InSb single crystals subjected to magnetic field 19 p3300 A67-34763

Band structure and current carrier scattering in hole-type SnTe, studying temperature dependence of electric conductivity, thermal EMF, Hall effect, etc 19 p3300 A67-34766

Temperature dependence of electric conductivity and Hall effect in epitaxial layers of undoped and Fe-doped n-type GaAs samples 19 p3300 A67-34770

Fast neutron irradiation effect on electrical conductivity and Hall effect in Zn doped n-type indium arsenide single crystals 19 p3301 A67-34771

Dark and photo-conductivity of organic semiconductors, noting measurement techniques and effect of purity, materials, pressure, etc 19 p3302 A67-34995

Electron conductivities calculated for sodium-xenon and sodium-xenon-mercury plasmas assuming local thermal equilibrium, estimating plasma temperatures and electron number densities 19 p3278 A67-35134

Electric conductance exponential decay in column of wall stabilized nitrogen arc after current interruption 19 p3282 A67-35157

High temperature plasma generation from dense plasma with moving metallic walls, evaluating electrical conductivity and energy breakdown periods 19 p3282 A67-35159

Convergence of solutions for AC and DC electric conductivity of plasma with collisions 19 p3286 A67-35352

Electrical conductivity of weakly turbulent plasma calculated by behavior of electron distribution function 19 p3287 A67-35354

Ohm law extended to electrical conduction of partially ionized plasmas and nonneutral ionized gases 19 p3287 A67-35356

Interactions produced by shock wave running into magnetic field perpendicular to wave direction 19 p3294 A67-35405

Plasma wave influences on metal surface reflectivity investigated using Maxwell

equation, calculating dielectric constant and conductivity 19 p3262 A67-35581

Conductivity profiles investigated as function of ion energy, total flux and annealing schedule, when implanting boron into silicon 19 p3307 A67-35812

Neutron irradiation effect on n-type and p-type semiconductors thermophysical parameters 19 p3307 A67-35874

Steady flow of perfectly conducting inviscid liquid past thin symmetrical airfoil of finite conductivity in aligned magnetic field 20 p3494 A67-36146

Adsorption effect of various metals on electrical conductivity and Hall effect of thin nickel films 20 p3504 A67-36166

Nonohmic electrical conduction of semiconducting thin films in strong electric fields analyzed using electron temperature approximation 20 p3506 A67-36219

Heat treatment of indium antimonide crystals with various dislocation densities noting change in conductivity 20 p3506 A67-36227

Alfven waves in ionized plasma of finite electrical conductivity, giving equations for semiphenomenological model 20 p3496 A67-36271

Temperature dependence of electrical conductivity in organic semiconductors, examining compounds during transition from solid to liquid state 20 p3508 A67-36404

Electrical conductivity variation of low and high resistance germanium due to X-ray radiation absorption 20 p3508 A67-36405

Semiconductivity of molybdenum-oxygen systems, analyzing solid phase effect on solution mechanism 20 p3510 A67-36816

Durability and electrical conductivity of metallic fiber materials noting influence of oxidation on properties 20 p3466 A67-36912

Millimeter wave reflectance for semiconductor panel, air space and metal reflector arranged planarly, discussing reflectance variation with conductivity and complete absorption 20 p3510 A67-37025

Electric conductivity variation with temperature for solid ammonium perchlorate, determining energy barrier and enthalpy of lattice defect formation and migration 20 p3377 A67-37134

Electric conductivity of surface space charge layers in semiconductors, solving Boltzmann equation and determining current density and carrier mobility 20 p3511 A67-37144

I-V characteristics of many-valley semiconductors in strong electric field deviating from Ohm law with scattering by phonons 20 p3513 A67-37439

Electron drift velocity and mobility in InSb calculated from conductivity and Hall effect measurements, noting microwave emission occurrence 20 p3514 A67-37544

Germanium conductivity dependence on surface and space charges in transverse magnetic field 21 p3876 A67-37862

Dispersion equation of radioactive compressible nonviscous plasma with finite electric conductivity under gravitational and axial magnetic fields 21 p3863 A67-37918

Carrier spatial redistribution under magnetic field effect of current in semiconducting crystal with intrinsic conductivity noting I-V curve shape 21 p3878 A67-38098

Quantum size effects in electric conductivity of thin films 21 p3878 A67-38099

Earth finite conductivity effect on directivity patterns of vertical antennas taking into account attenuation factor 21 p3590 A67-38119

Discharge plasma in He and argon with cesium and potassium vapor admixtures noting electric field, conductivity, electron temperature and emission spectrum 21 p3864 A67-38160

Electron components for electrical, thermal conductivity and viscosity coefficients of gas mixtures calculated via molecular kinetic theory 21 p3859 A67-38161

Existence of maximum conductivity of ionized gas mixture as function of thermodynamic parameters 21 p3859 A67-38162

Steady motion of electrically conducting viscous fluid due to slow rotation of thin dielectric disk inside housing immersed in magnetic field 21 p3865 A67-38247

Deformation of velocity profile in inhomogeneous magnetic field, noting

anisotropic conductivity of flow 21 p3866 A67-38271

Current carrier concentration distribution in semiconductor with intrinsic anisotropy created by strong electric field 21 p3880 A67-38319

Relation between electric conductivity and Hall coefficient in solid solutions, determining sample composition and temperature for forbidden band width concentration dependence 21 p3684 A67-38449

Indium antimonide-indium arsenide solid solution carrier mobility related to sample composition and temperature, measuring Hall coefficient and electrical conductivity 21 p3884 A67-38452

Base region thickness, minority carrier lifetime and impurity concentration effects on conduction characteristics of silicon diodes and thyristors 21 p3597 A67-38523

Velocity and pressure distributions and free shape of conducting liquid in rotating circular cylinder under magnetic and electric fields 21 p3868 A67-38561

Transistor oscillator design stressing output, efficiency and frequency stability at maximum load 21 p3598 A67-38602

Electrical conductivity of nitrogen plasma seeded with potassium, noting nonuniform temperature profile in flow [AIAA PAPER 67-716] 21 p3673 A67-38742

Tensor conductivity effect on continuum and collisionless MPD flows past slender bodies [AIAA PAPER 67-731] 21 p3674 A67-38755

Deep subterranean electric conductivity using 30-year cyclic geomagnetic field variation data 21 p3622 A67-39025

Geomagnetic aperiodic variation effect on earth electric conductivity in electromagnetic induction theory for flat earth model 21 p3622 A67-39027

Electrical conductivity and transport properties of pure liquid metals 21 p3886 A67-39108

LIF crystals doped with Ti studied for electrical and optical properties, finding atomically dispersed Ti fractions in form of doubly positively charged centers 21 p3687 A67-39137

Electrical conductivity, Hall coefficient and thermo-EMF measurements in Zn and Te doped gallium antimonide crystals for minority carrier role in impurity conduction 21 p3887 A67-39141

Electrical conductivity temperature dependence, Hall coefficient, current carrier mobility, melting point and density data for single crystal of AIBIV type electrical conductivity temperature dependence, 21 p3687 A67-39144

Linear MPD channel theory with heavy component in uniform state evaluated for investigation of electrical conductivity phenomena 22 p3747 A67-39277

Ionized plasma electric conductivity calculation using Druyvesteyn and Maxwellian distribution for electrons and ions respectively 22 p3851 A67-39725

Niobium and tantalum nitrides physical properties including microhardness, electric and thermal conductivities, Hall coefficient and thermal EMF 22 p3861 A67-39917

Irradiation damage in germanium monitored by electric conductivity measurements, noting carrier population depletion by introducing acceptor levels into forbidden gap 22 p3862 A67-39997

Curves for Hall effect logarithms, current carrier mobility and electric conductivity vs high pressure and temperature effects in InSb 22 p3864 A67-40323

Electrical conductivity or magnetic Reynolds number of shock produced plasma flow, discussing interaction between magnetic field and plasma flow 23 p4031 A67-40881

Evaporated thin Au and Ni films electric conductivity measurements, obtaining electron mean free path and bulk resistivity 23 p4040 A67-41016

Electrically thick monopole transmitting antenna integral equation for current distributions and admittance 23 p3981 A67-41207

Linear MHD flow characteristics variation with electric conductivity and gas flow rate changes, noting transverse magnetic flow variation with magnetic Reynolds number 23 p4033 A67-41284

High temperature thermal EMF and electrical conductivity in intense electric field for semiconductors with low charge carrier mobility 23 p4043 A67-41299

Accuracy of scalar electrical conductivity calculations of partially ionized plasma using third Chapman-Enskog approximation method 23 p4035 A67-41753

Two-phase mixture passing through magnetic field in MHD generator studied for effective electric conductivity 23 p3942 A67-41758

Electrical conductivity of high void fraction two-phase flow with and without magnetic field in MHD generator 23 p3942 A67-41759

Hole mobility produced by single pulses of electrons in films of polyvinyl acetate semiconductors with sputtered gold electrodes, determining relation between film conductivity and mobility 24 p4199 A67-41773

Plasma nonequilibrium electric conductivity in induced electric field investigated by MHD generator with Ar-K working fluid 24 p4196 A67-42209

Continuous shock wave profile found in MHD fluid where Whitham condition for wave profile discontinuity is satisfied 24 p4143 A67-42356

Thermodynamic and electrical properties of MHD conversion fluid /K-seeded combustion products/ obtained by hydrocarbon fuel combustion, discussing electrical conductivity 24 p4099 A67-42415

Thermal treatment at melting temperature inducing acceptors of electric conductivity in indium antimonide crystals 24 p4204 A67-42577

Electrical conductivity of ionized plasma taking into account particle impenetrability, using Boltzmann and collision at distance integrals 24 p4198 A67-42662

Compressible fluid with finite electrical conductivity in constant magnetic field penetrating thin cylindrical obstacle, solving flow motion equations 24 p4198 A67-43080

ELECTRIC CONDUCTOR

SA DIELECTRICS

High temperature electrical material reevaluation for Rankine cycle [SAE PAPER 660662] 01 p0094 A67-10571

Integrated circuits with evaporated thin film conductors, resistors and capacitors 03 p0387 A67-13999

Stability of flexible conductor in longitudinal magnetic field, using scalar potential to determine disturbed state 06 p1040 A67-18095

Flat cable connectors design including welding and welded connectors and Picatinny type, noting zero insertion force, withdrawal force, etc 06 p0972 A67-18403

Effects of gases flowing in magnetic field analogous to galvanomagnetic Hall effect in conductors analyzed using oxygen 07 p1230 A67-20144

Boundary value problem for potentials in volume conductor based on Green theorem 08 p1288 A67-20601

Quasi-static potential distribution in inhomogeneous volume conductor analyzed using Green theorem 11 p1746 A67-23991

Testing instrument for determination of lead wire mechanical properties and bond strengths within semiconductor devices 12 p1911 A67-25270

Conducting loop resonant size determination and geometrical shape effect on resonant size in anechoic chamber experiment 16 p2639 A67-31356

Higher mode cut-off frequencies in coaxial cables of elliptical cross section tabulated as function of conductor dimensions 20 p3382 A67-36861

Acceleration of plasma formed in electric explosion of foil in air 20 p3502 A67-37604

Capacitance between strands of braided cable composed of identical insulated conductors 22 p3747 A67-39340

Liquid mercury conductor flow in annular gap electromagnetically accelerated by Lorentz force, showing restricted nonexistence proof for inviscid problem 23 p3992 A67-41742

ELECTRIC CONNECTOR

Simple gates, multilevel arrays and interconnection in integrated circuits for computers 02 p0219 A67-12110

Electrical parameters of DC MHD generator with arbitrary connected electrodes 04 p0553 A67-14475

Computer program used for explicit definition of wiring harness and cable assembly design 05 p0779 A67-17456

Flat cable connectors design including welding and welded connectors and Picatinny type, noting zero insertion force, withdrawal force, etc 06 p0972 A67-18403

Semiconductor integrated circuits, discussing fabrication processes, component characteristics and electrical isolation methods 08 p1301 A67-20788

Spacecraft electrical connector criteria to insure adequate quality for desired performance 09 p1480 A67-22295

Aerospace electrical and electronic equipment reliability requirements with reference to technology of miniature electrical connection devices 15 p2454 A67-30230

Cabling material problems associated with military standard connectors for space vehicles, discussing reliability, fabrication, assembly and design 21 p3595 A67-38334

Aircraft construction techniques for terminating cables by pressure type connections, examining design factors 21 p3572 A67-39074

ELECTRIC CONTACT

Welmer triode with contact rectifier for use as component of microminiature radio circuits, noting effect of contact rectification on current-voltage characteristics and amplifying power of such triodes 01 p0035 A67-10397

Checking ohmic back contact on semiconductor wafers before fabrication of diode, using four-point probe 01 p0077 A67-11315

Contact effect between superconductor and normal conductor and between two different superconductors, noting transition temperature 02 p0291 A67-11740

Photovoltaic effect in thin telluride layers and in contacts between layers and various metal electrodes, noting dependence on angle of deposition 02 p0294 A67-11758

Make-before-break contacts effect on degree of complexity of film and hybrid microelectronic nodes 02 p0215 A67-11913

Sliding contact wear under very dry high altitude or space conditions due to lack of contact film prevented by using chemical compounds like graphite or lithium carbonate 02 p0221 A67-12435

Potential distribution, I-V characteristics and pulse shape of n-type Ge with sealed-in Sn, In-Sb, Sn-Sb and Pb-Sb contacts in strong electrical field 02 p0300 A67-12480

Magnesium wire as in-contact masking material, with surfaces precoated with thin silver layer 03 p0494 A67-13490

Plug contact configurations and characteristics 04 p0580 A67-14589

Recombination waves appear in sample having ohmic contacts when drift velocity of carriers in constant electric field exceeds certain value 04 p0681 A67-15290

Ohmic contacts prepared by chemical deposition of metal films on gallium arsenide 06 p1050 A67-17939

Reliability and temperature stability of metals used for contacts and interconnections on semiconductor devices 06 p0971 A67-18246

Alternating method of measuring Hall constant by modulation of voltage amplitude on arbitrarily shaped plates 06 p1005 A67-18727

Mechanical stresses in silicon single crystal containing p-n junction and ohmic contact measured by photoelastic method, determining birefringence 08 p1423 A67-21332

Dry circuits effect on behavior of contacts noting prediction, control and measurement techniques 08 p1306 A67-21417

Separation of effects of two factors controlling real contact area of superconducting contacts through number of individual contacts and size 10 p1688 A67-22904

Sliding electrical contact material for ultrahigh vacuum with 300 amp/sq inch current density, 425 in/min sliding velocity and 10 psi brush pressure 11 p1805 A67-24345

Metal-semiconductor electric contacts for GaAs bulk effect device noting uniformity, linearity, usefulness, adaptability,

etc 13 p2183 A67-27567

Volume electroluminescence observation during HF excitation of GaAs using neutral /indium/ contacts and unipolar voltage pulses 14 p2368 A67-28538

Forward conduction characteristics of contacts between gold n-type silicon measured at different temperatures 14 p2373 A67-28925

Solution of uniform heat conduction equation with movable boundaries applied to problem of electric contacts 16 p2779 A67-31207

Relation between current, voltage and magnetic field of weakly connected double-contact junctions in superconductors 17 p2926 A67-33406

Current-voltage characteristic of metal semiconductor point contact, taking into account rectifying effect of junction gap and majority and minority current carrier 18 p3097 A67-33476

Ohmic contacts prepared by chemical deposition of metal films on gallium arsenide 18 p3100 A67-33775

Structure of wafer type point-contact diodes 18 p3011 A67-34021

Processes and instrumentation for forming contacts on microelectronics devices 19 p3236 A67-35022

Determining resistivity and Hall coefficient using four point contacts placed on Hall plate isotropic uniformly thick two-dimensional sheet with perpendicular magnetic field 19 p3308 A67-36041

Aircraft AC electrical systems using changeover contactors and rapid fault clearance, discussing reliability and maintenance 20 p3362 A67-36316

Potential field distribution in n-GaAs devices before and after switching indicate carrier generation in narrow region near anode 20 p3510 A67-36853

Superconducting critical temperature of sandwich of two semiconducting films in contact 20 p3512 A67-37434

Contact continuity, intermediate resistance consistency and passing signal distortion of current collector with slip rings and brushes of various metals 21 p3572 A67-38916

Current-voltage characteristics of semiconductor diode with spheroidal contact 22 p3769 A67-39571

Two base diode circuit having rectangular voltage pulse applied to one of base contacts investigated for front pulse delay phenomenon 22 p3769 A67-39572

Measuring method for minority carriers recombination rate at base surfaces of /n-m/ contact without passing DC through contact 22 p3858 A67-39575

Surface states effect on frequency dependence of elements of equivalent circuit of n-type semiconductor/metal contact 22 p3859 A67-39578

Voltage-biased superconducting point contact Josephson radiation line width investigation for thermal noise contributions useful for low temperature thermometer 23 p4038 A67-40790

Evaporated metallic contacts to conducting strontium titanate single crystals measured for electric properties evaporated metallic contacts to conducting strontium titanate single crystals measured for 23 p4038 A67-40874

Volume electroluminescence observation during HF excitation of GaAs using neutral /indium/ contacts and unipolar voltage pulses 23 p4040 A67-40945

ELECTRIC CONTROL

Generalized charge control theory derivation of transfer function of nonparametric transistor amplifier in system with common emitter 05 p0769 A67-16168

Optimal discrete binary system of electrical control of beam position of phased linear antenna array 10 p1611 A67-22982

Simultaneous and independent potentiostatic control of rotating ring and disk electrode and application to CuII/CuI/Cu system 20 p3446 A67-36655

ELECTRIC CURRENT

SA ALTERNATING CURRENT /AC/

SA DIRECT CURRENT /DC/

SA EDDY CURRENT

SA JOSEPHSON CURRENT

SA LIGHTNING

SA PONDEROMOTIVE FORCE

SA POTENTIOMETRY

SA TELLURIC CURRENT

High current discharge effect on magnetically confined argon laser 01 p0086 A67-10012

Space charge formation during flow of electric current in plasma moving under thermal emission of electrons 01 p0118 A67-10043

Efficiency criterion for semiconductors, using equations for flux density of electric current and energy for isotropic semiconductor in absence of magnetic field 01 p0129 A67-10103

Azimuthal current effect on electrical efficiency of MHD vortex generator 01 p0120 A67-10174

Magnetic surfaces of straight helical magnetic field in presence of axial current 01 p0122 A67-10344

Reversal of diode with delay between last direct pulse and first reversed pulse 01 p0035 A67-10399

Peak effect in critical current of superconductors observed during deuteron irradiation at low temperature 01 p0135 A67-10880

Signal conditioning variable resistance transducer excited by constant current power supply 01 p0071 A67-11099

Driving-point impedance and current for long resonant cylindrical antennas 02 p0212 A67-11605

Electron transport through thin insulating barriers in various diodes, analyzing current dependence on temperature and film thickness for perfect and imperfect dielectrics 02 p0294 A67-11760

Tunnel-current measurements of sandwich configurations, determining metal/metal-oxide work function 02 p0295 A67-11764

Deep-level localized current oscillations in n-type silicon crystal 02 p0298 A67-11892

Electronic equipment for measuring peak and valley currents of tunnel diodes 02 p0216 A67-12037

Ion acoustic oscillations in collisionless region of fully ionized plasma excited by electric current 02 p0277 A67-12612

AC measurements on hard superconductors exposed to magnetic field, obtaining critical surface current and density from voltage-time curves 03 p0487 A67-12809

Characteristics and performance of two solid state devices, using FM principle for measurements of low currents, suitable for space vehicles 03 p0377 A67-13107

Time dependence of current in In-CdS-In sandwich plate system at various voltages, using X-and Z-cut monocrystal CdS 03 p0490 A67-13157

NGe-pGaAs heterojunctions, diffusion or emission theories of current transport do not explain electrical characteristics but validate Anderson model, considering tunneling as transport mechanism 03 p0494 A67-13478

Electrical current passage across neutral or ionized argon flow in presence of accelerating or decelerating magnetic field 03 p0478 A67-13605

Electric current oscillation mode beyond Gunn effect threshold in n-type GaAs 03 p0496 A67-13669

Bulk minority carrier lifetime measured directly in solar cell by measuring short circuit current decay constant which is dependent on cell thickness and carrier type 04 p0554 A67-15128

Stability of spatially inhomogeneous current-carrying plasma in various frequency regions 04 p0671 A67-15641

Anomalous photocurrent generation in transistors, noting carrier generation and transport processes 04 p0685 A67-15696

Equilibrium photocurrents in silicon switching diodes from nondestructively measured electrical parameters 04 p0588 A67-15698

Anomalous permanent changes in transistor gain after low exposure dosage of electron and/or gamma radiation related to recombination current-component buildup 04 p0588 A67-15705

Gas temperature decay characteristics for interrupted high pressure arcs at various current intensities 05 p0850 A67-16068

Rotation and vibration of conducting circular cylinder in magnetic field, noting motion retardation due to induced electric current interaction with field 05 p0851 A67-16434

Harmonic components of current of HF transistor under sinusoidal excitation, using piecewise parabolic approximation 05 p0772 A67-18456

Current dependence on voltage in Sn-Sn and Pb-Pb tunnel junctions attributed to electric gap anisotropy 05 p0863 A67-18754

Effects of parameters of series circuit on current pulse in active load, using computer to calculate series circuit 05 p0785 A67-17470

Component, due to recombination-generation process, of overall noise from semiconductors under electric current, measuring probability densities by statistics 06 p0966 A67-17588

Surface current excitation by electromagnetic and electrokinetic waves on metal cylinder immersed in uniform collisionless isotropic plasma 06 p0962 A67-18075

Mean value of current in flat channel of MHD generator with short circuited electrodes taking into account induced fields 06 p0952 A67-18687

Current in channel with symmetrical end electrodes, noting stepwise dependence of near-electrode potential on current density 06 p1045 A67-18812

Reverse tunneling currents in GaSb tunnel diodes as function of temperature and voltage explained through band structure 06 p0972 A67-18977

Current and voltage measuring methods for impact ionization analysis including lag and avalanche time, peak fields, etc, noting instability 06 p1070 A67-18987

Amplitudes and phase angles of harmonic components of output current of operating circuits of transistorized magnetic amplifiers 07 p1150 A67-19209

Persistent current loops in hard superconducting wire formed when wire is magnetized by static transverse external field 07 p1232 A67-19554

Interaction between helicon waves and drift currents in layered lead telluride structure 07 p1232 A67-19555

Experimental tests of critical state model of hysteresis in type II superconductors, considering critical currents in field and transport currents in zero 07 p1233 A67-19842

Current-voltage-temperature dependence of symmetric tunnel junctions, noting role of insulator thickness 07 p1237 A67-20184

Sample standard resistor combination to shunt pulsed currents used to study superconducting-to-normal transition in short wire samples 08 p1367 A67-20378

Radiation characteristics of current sources perpendicular to magnetostatic field for cylindrical column of free space surrounded by loss-free magnetotonic medium 08 p1357 A67-20715

Equivalent circuits of MHD generators with segmented electrodes electrically connected in various ways 08 p1286 A67-20738

Cesium-plasma diode effect dependence on material output of cathode in vacuum, plotting short circuit current vs vapor pressure, voltage distribution, etc 08 p1357 A67-20845

Steady state temperature distribution in disk with radial flow of electric current derived with and without heat transfer conditions 08 p1427 A67-20929

Dry circuits effect on behavior of contacts noting prediction, control and measurement techniques 08 p1308 A67-21417

Ignition systems for turbine engines, discussing low and high energy, semiconductor spark plugs, effects of electric constants on performance, etc 09 p1559 A67-21691

Direct current electrical discharge investigated in gas flow in magnetic field perpendicular to flow 09 p1542 A67-21816

Excitation of ion-acoustic waves in potassium-cesium plasma when passing current through it, finding natural frequencies of system when plasma is drifting along axis 09 p1544 A67-21853

Theory of lateral transistor current gain and frequency response 09 p1472 A67-21948

Gunn diode efficiency for mixed resonant transit time and suppressed modes, using dynamic drift velocity field strength characteristic 09 p1474 A67-22039

Electric current flow in moving decaying plasma and plasma diagnostics, deriving

nonlinear V-I characteristics 09 p1547 A67-22317

Integral short circuit current of solar converters determined from spectral distribution of solar radiation energy, using simulator and SiO photocell films 09 p1451 A67-22531

Thermomagnetic generator with resonating current in load circuit to improve thermodynamic performance 09 p1452 A67-22697

Time dependence of current in In-CdS-In sandwich plate system at various voltages, using X-and Z-cut monocrystal CdS 10 p1690 A67-23105

Ambipolar diffusion of plasma cloud imbedded in ionized gas with homogeneous magnetic field, assuming electric current is not vanishing 10 p1648 A67-23293

Current instability in inhomogeneous plasma formed by drift and ion-acoustic waves with oscillation frequencies 10 p1685 A67-23461

LF current oscillations excitation in n-type semiconductors analyzed using dispersion equation, noting role of external electric field 11 p1849 A67-24870

Low bias non-Esaki current in tunneling p-n junction diodes with large excess currents 11 p1768 A67-24926

Magnetic surfaces of straight helical magnetic field in presence of axial current 11 p1843 A67-25017

Diagnostic techniques for atmospheric pressure arc plasmas, noting that integrated current density measurements are consistent with measured total arc current 12 p1973 A67-25393

Thermodynamics of vortex flow in superconductors, using combination of electrical currents and thermal gradient 12 p1983 A67-25477

Signal to noise ratios of transistorized constant current and constant temperature hot-wire anemometers 12 p1947 A67-26121

Ion acoustic oscillations in collisionless region of fully ionized plasma excited by electric current 13 p2170 A67-27368

Silicon avalanche diode behavior for short duration surge current in reverse direction 13 p2084 A67-27576

Thermionic converter acceleration plate and excessive current flow effects, noting collector and cathode surface secondary electron removal, determining cut-off characteristic form 14 p2246 A67-27766

Origin of excessive reverse current in silicon p-n junction, discussing surface layer channel formation 14 p2283 A67-28040

Two-step saturation of pulsed current in CdS single crystals, noting electron bunching mechanism and volt-ampere characteristics 14 p2365 A67-28238

Second current saturation of nonohmic behavior in CdS single crystals caused by quantum mechanical interaction between drift electrons and acoustic phonons 14 p2365 A67-28239

Superconductor dynamic intermediate state DC voltage caused by flux motion shown by frequency spectrum measurements of noise voltage 14 p2369 A67-28600

Two cases of critical surface current magnitude change in type II superconductors after transport current direction reversal 14 p2370 A67-28719

MHD flows in tubes in presence of longitudinal electric current 14 p2361 A67-28743

Loaded oil-lubricated steel ball bearings operating in vacuum and air investigated for electric current effect on damage [ASLE PREPRINT 67AM IC-1] 14 p2325 A67-28783

Electric discharge in vacuum consisting of two successive phases, arc formation characterized by X-ray emission and weak current and arc characterized by light emission 14 p2349 A67-28899

Current instabilities in GaAs for applied electric field along piezoelectric direction attributed to electron-phonon coupling, determining additional parameters from experimental data 14 p2374 A67-28983

Inhomogeneous sheath effect on surface currents and scattering cross section of plasma-immersed cylinder in presence of electromagnetic and electrokinetic waves 15 p2521 A67-29192

Precautions required when using

- continuous gas flow in high current ion
lasers 15 p2497 A67-29394
- Anisotropic macroscopically neutral plasma
excitations by arbitrary current described by
potentials, noting electroacoustic wave
propagation 15 p2527 A67-29482
- Origin of forced oscillation in space-charge
density of free current carriers in
semiconductors ascribed to periodic
generation of carriers 15 p2542 A67-30243
- Noise suppression in p-n junction biased
in direction of current, noting effect of
space charge on current
modulation 15 p2543 A67-30252
- Stabilization of current intensity in
superconducting coils noting two
characteristic intensities, measurements of
helium compounds, effects of added
copper, etc 16 p2607 A67-30593
- Phenomenological theory for
thermomagnetic effects in type II
superconductor flux flow
state 16 p2724 A67-30609
- Current saturation and oscillation in
photosensitive GaAs explained by high
electric fields 16 p2725 A67-30611
- Analog-to-digital conversion method for
measuring weak currents, giving diagram of
measuring circuit 16 p2835 A67-30672
- Magnetic field dependence of current
oscillations in piezoelectric
semiconductors 16 p2725 A67-30804
- Impurity concentration and temperature
dependence of reverse current in indium
antimonide diodes, determining
components 16 p2637 A67-31162
- Magnetoplasma diffusion equation of F-2
layer allowing electric currents and
temperature variations, noting transverse
drift of field 16 p2686 A67-31402
- Surface leakage current and reverse
current flow in silicon p-n junction diode
affected by positive ion bombardment and
oxygen adsorption 17 p2911 A67-32202
- Static equilibrium for two-dimensional
coroidal plasma configurations with inner
fields and purely meridional electric
currents 17 p2903 A67-32709
- Space charge formation during flow of
electric current in plasma moving under
thermal emission of
electrons 17 p2910 A67-33321
- Thermal stabilization of inverse current of
p-n junction by additional gate for minority
carriers extraction 18 p3009 A67-33478
- Current distribution in segmented
electrode MHD duct and sufficient condition
for preventing current leakage between
adjacent segments of
generator 18 p2987 A67-33703
- Correlation function method in
superconductivity theory, formulating
electric current density in terms of
distribution function in phase
space 18 p3100 A67-33712
- Relation between current and voltage in
type II superconductors situated in
transverse magnetic field in flux-flow
regime 18 p3101 A67-33987
- Electrical current passage across neutral
or ionized argon flow in presence of
accelerating or decelerating magnetic
field 18 p3091 A67-34470
- Current growth rate instabilities in high
current mercury vapor discharges, giving
damage converter
photographs 19 p3265 A67-35091
- Measurement of column resistance during
recovery of rapidly interrupted low current
wall stabilized DC arc 19 p3282 A67-35158
- Diode with anode glow type discharge
analyzed for relationship between discharge
quenching current and structural elements
of discharge gap 19 p3282 A67-35160
- Solar magnetic fields studied by measuring
Fraunhofer line shifts with circular-
polarization analyzer, showing relationship to
gravity center
displacement 19 p3325 A67-35505
- Revised London theory of
superconductivity destruction by current,
using numerical methods for optimum phase-
boundary configuration 20 p3505 A67-36208
- Planar transistor collector current rise
time determination with base driven by
current step function and application
procedures 20 p3395 A67-36299
- Time-dependent current flow equations
solved for insulator with traps if injected
space charge produces negligible
perturbation on external electric
field 20 p3509 A67-36506
- Differential equations governing steady
state current flow in semiconductors
computed, considering variations as function
of distance, hole and electron densities,
etc 20 p3400 A67-37216
- Elastic bending vibrations amplitude and
frequency effects on current oscillations in
CdS single crystals 20 p3514 A67-37463
- Fields with boundaries radiated by electric
or magnetic current phased-line
distributions, interpreting field constituents
as geometric-optical and diffracted
contributions 20 p3388 A67-37702
- Electric conduction in solids, considering
impurity, temperature and light effects on
resistivity to electric
currents 20 p3515 A67-37716
- Ionospheric conductivities, electric
currents and field height variations in
equatorial electrojet region calculated from
model, including solar
activity 21 p3617 A67-38066
- MOS transistors surface properties and
leakage current affected by gold, showing
positive charge
production 21 p3678 A67-38150
- Rotating current spoke in MPD engine,
existence and connection with exhaust
fluctuations
[AIAA PAPER 67-689] 21 p3693 A67-38720
- Contact continuity, intermediate resistance
consistency and passing signal distortion of
current collector with slip rings and brushes
of various metals 21 p3572 A67-38916
- LF permeabilities of superconductor due
to surface currents calculated for magnetic
field conditions 22 p3856 A67-39439
- Maximum current and total light output of
triggered lightning strokes at close range
upon ship deck, noting photographs of
discharge 22 p3793 A67-39979
- Loaded oil-lubricated steel ball bearings
operating in vacuum and air investigated for
electric current effect on damage
[ASLE PREPRINT 67AM 1C-1] 22 p3813 A67-40218
- Current oscillations in Co-doped Si p-n
diode devices noting
characteristics SCL I-V 23 p3978 A67-40788
- Drop-across-reactance method found
satisfactory for accurate current
measurements in high voltage RF plasma
discharges 23 p4001 A67-41224
- Linear current-voltage characteristics in
type II superconductors under flux flow
conditions 23 p4044 A67-41440
- Rise rate dependence of transition current
of superconducting solenoids on presence of
electrical short circuit 23 p4045 A67-41457
- Electric stimulus effect on vestibular
apparatus responses to acceleration
increasing or decreasing reactions depending
on applied voltage 24 p4112 A67-41859
- polarity 24 p4112 A67-41859
- Boundary layer electric current
temperature, velocity and density profile
calculation on nonconducting MGD channel
wall assuming smaller magnetic Reynolds
number than unity 24 p4196 A67-42212
- Plasma energy and heat transfer to
surface with and without electric current,
discussing various energy transfer
models 24 p4197 A67-42331
- Thermionic energy converter operation
showing anomalous electron and ion currents
in plasma mode, discussing heating power
and emitter temperature 24 p4103 A67-42502
- ELECTRIC DIPOLE**
- SA MAGNETIC DIPOLE**
- SA QUADRUPOLE**
- Electromagnetic fields of oscillating
electric dipole located over half-space with
anisotropic conductivity and dielectric
constant 02 p0204 A67-12194
- Magnetic particle motion, analyzing effect
of earth electric dipole
field 02 p0311 A67-12585
- Warm plasma excitation by electric
dipole 03 p0475 A67-13173
- Quark confusion with electric-dipole
transition in far UV
solar spectrum 04 p0694 A67-14479
- Radiation resistance and modes of
oriented electric dipole in loss-free
magnetoplasma 05 p0853 A67-16848
- Retarded potentials and fields of
oscillating electric dipole undergoing
accelerated relativistic
motions 10 p1679 A67-22730
- Ordinary and dielectric second virial
coefficients for dipolar gases calculated by
off-center dipole model using series
expansion 11 p1821 A67-23962
- Critical binding of electron by electric
dipole, noting value of dipole
moment 11 p1824 A67-24996
- Combined resonance transition in indium
antimonide induced by single photon
absorption 13 p2178 A67-27083
- Radiation characteristics from electric
dipole immersed in lossy anisotropic plasma
taking into account collision
effects 16 p2713 A67-30797
- Fields generated by infinitesimal,
arbitrarily oriented, electric-dipole source
located in isotropic medium bounded by
parallel plane-stratified, anisotropic
media 16 p2632 A67-31858
- Lagrangian for interaction of electric
charge with field induced by scalar magnetic
charge to determine electrical dipole
moment 17 p2883 A67-32100
- Magnetic and electric charge interaction,
noting neutrino electric dipole
moment 17 p2887 A67-32101
- Electromagnetic radiation from electric
dipole moving with uniform relativistic
velocity 18 p3000 A67-34022
- Propagation and radiation of waves
excited by electric dipole in dispersionless
unaxial moving medium 18 p3002 A67-34199
- Highly asymmetric equation for MHD
resonance of guided poloidal mode solved
using dipole coordinates 20 p3502 A67-37427
- Transient radiation of electric dipole in
uniaxially anisotropic plasma examined for
signal frequency greater and less than
plasma frequency 20 p3388 A67-37704
- Asymptotic solution for electromagnetic
field of electric dipole above stratified half-
space 22 p3763 A67-40311
- Finite ground plane influence on raised
electric dipole far field radiation
pattern 23 p3980 A67-41202
- Spherical and cylindrical dipole fields in
different coordinate systems, discussing
differential distances 23 p3975 A67-41211
- Optical absorption, refractivity and
electron scattering used to construct model
dipole spectrum of molecular nitrogen and
calculate dipole
properties 24 p4190 A67-42096
- Scattering from half-loop on conducting
plane obtained through image theory,
considering electric and magnetic dipole
contributions 24 p4121 A67-42265
- ELECTRIC DISCHARGE**
- SA ARC DISCHARGE**
- SA CORONA DISCHARGE**
- SA GAS DISCHARGE**
- SA GLOW DISCHARGE**
- SA LIGHTNING**
- SA PENNING DISCHARGE**
- SA RADIO FREQUENCY DISCHARGE**
- SA SPARK**
- High current discharge effect on
magnetically confined argon
laser 01 p0086 A67-10012
- Point discharge from multiple points in
irregular configuration, space-charge theory
and plant discharge 01 p0107 A67-10114
- Point separation dependence of starting
voltages in two-point
discharger 01 p0107 A67-10115
- Electron temperature in electric discharge
applied to argon ion laser 01 p0090 A67-10550
- Electron temperature in electric discharge
applied to argon ion laser 01 p0091 A67-11058
- Characteristics of normal atmospheric,
discussing VLF characteristics due to return
strokes 01 p0109 A67-11228
- Nitric oxide molecular laser obtained by
dissociation of NO-Cl in pulsed electrical
discharge 02 p0253 A67-12510
- Introductory text on electrical discharges
in gases, emphasizing physical behavior of
electrons and ions in ionized
state 02 p0279 A67-12720
- Electric discharges in condensed hydrogen
beams in high vacuum 03 p0475 A67-12922
- Discharge current, discharge voltage
pressure and radius of discharge channel for
discharge in water induced by tungsten
filaments 03 p0476 A67-13210
- Current pause during circuit overloading
accompanied by filament
explosion 06 p1031 A67-17867
- Direct current electrical discharge
investigated in gas flow in magnetic field
perpendicular to flow

direction 09 p1542 A67-21816
 Energy balance of stationary discharges in quartz containers filled with gas at various pressures, determining relation of heat and light loss of discharge to gas pressure and discharge power 09 p1544 A67-21854
 Gas laser measurement of electron density in xenon pulse discharge 09 p1512 A67-21922
 Hydrazine synthesis from ammonia in concentric barrier discharge reactor 10 p1603 A67-23498
 Power output at 119 micron in water vapor laser, noting inhibition of laser action during discharge current pulse 11 p1801 A67-24728
 Electrostatic motor action in rotational momentum of tornado funnels, noting that driving power removal by electric discharge may cause dissipation 12 p1963 A67-25383
 Thermal electrode boundary layer for shock wave ionized air ohmic heating in discharge chamber, noting Joule heat consumption effect 12 p1975 A67-25894
 Lightning strikes on aircraft in flight from 1949 to 1966 12 p1896 A67-26170
 Molecular laser action on vibrational-rotational transitions between low lying vibrational levels on hydrogen and deuterium halides 13 p2127 A67-27018
 Oscillation discharge by reactive circuit elements in two-terminal line controlled by movable poles of circuit in complex plane 13 p2085 A67-27723
 Luminous front in electric shock tube having coaxial gun without current crowbaring measured by phototransistors 14 p2355 A67-27823
 Electrostatic, induction and radiation field effects of lightning discharge on intensity spectrum of atmospheric source signals 14 p2346 A67-27880
 Gas laser measurement of electron density in xenon pulse discharge 14 p2330 A67-28251
 Atmospheric characteristics at source and propagation 14 p2265 A67-28412
 Performance of low energy-density electric shock tube in helium driver 14 p2293 A67-28752
 Electric discharge in vacuum consisting of two successive phases, arc formation characterized by X-ray emission and weak current and arc characterized by light emission 14 p2349 A67-28899
 Bibliography on electrical discharges in vacuum and properties of vacuum as electrical insulator 15 p2516 A67-29200
 Stimulated emission from pulsed electrical discharge through helium with wavelength measured and transition identified with interferometer 15 p2497 A67-29395
 Quark fractional electronic charge in cosmic radiation determined through pulse height distribution 15 p2549 A67-29526
 Alkali metal vapor and inert gas mixtures with alkali seeding radiation properties, noting nonequilibrium argon-krypton plasma parameter determination in electrical discharge 16 p2710 A67-30522
 Experimental results on CN laser operated with pulsed or DC discharges 16 p2684 A67-30605
 Mechanism of electrode erosion by supersonic flame jets during pulsed discharge 16 p2724 A67-31775
 Energy distribution of shock wave created by wire explosion and electrical discharge in air, studying attenuation, dimensional effects and energy conversion 17 p2883 A67-31927
 Electrodeless annular discharges in argon and air 17 p2897 A67-32174
 Existence in alkali-metal-seeded rare gases of mode of nonequilibrium electric discharge with constricted positive column 17 p2910 A67-33385
 Lightning theories from Mount San Salvatore /Switzerland/ observations, noting corona currents 18 p3074 A67-33995
 Fabry-Perot interferometric observation of spectral line to investigate ionization rate of electrical discharge used for argon ion laser 18 p3061 A67-34044
 Noise theory for self-sustaining discharge verified for low frequencies, noting temperature dependence, silicon, etc 18 p3106 A67-34638
 Modified dioplasmatron in cusp fields to produce highly ionized and high density quiescent plasma, using DC discharge, noting helium plasma generation 19 p3274 A67-35104
 Current-voltage characteristics of low

pressure discharge in magnetron, giving integral equations and current stability 19 p3277 A67-35120
 Shock waves and spectrographic properties of emitted light during high energy linear discharge in ionized gaseous filament 19 p3176 A67-35133
 Laser emission from HF molecules rotational transition initiated by pulsed electrical discharge, listing wavelengths 19 p3241 A67-36103
 Stacking faults in tungsten specimen heated rigidly for short time by electric discharge 20 p3484 A67-36225
 Discharge length influence on reflex discharge characteristics, considering conditions for charged particles extraction from discharge 20 p3498 A67-36686
 Alpha aminonitriles formation by electric discharge through anhydrous methane and ammonia mixture, showing hydrolysis to amino acid as possible bearing on chemical evolution 20 p3369 A67-36764
 Nonthermal radio emission from electric discharges within Venus water clouds 20 p3529 A67-37480
 Laser population inversion using Fabrikant method, analyzing electron energy distribution in hollow cathode discharge 21 p3638 A67-37940
 Fast production of semiconductor and refractory metals by reducing silicon tetrachloride and molybdenum trioxide with hydrogen in electric discharge 21 p3681 A67-38358
 Gaseous mercury discharges through orifice as ion beam neutralizer for electrostatic thrusters [AIAA PAPER 67-669] 21 p3691 A67-38703
 Formation mechanism of luminous gas sphere /ionized vortex configuration/ due to atmospheric electrical discharge 21 p3655 A67-38902
 NI plasma acceleration in axisymmetric electric discharge by self-induced magnetic field, determining reaction force 22 p3844 A67-39356
 Null-field static dischargers location and maintenance on Convair 880/880M and 990 aircraft 22 p3745 A67-39733
 Maximum current and total light output of triggered lightning strokes at close range upon ship deck, noting photographs of discharge 22 p3793 A67-39979
ELECTRIC ENERGY
 Electrical efficiency of MHD generator cycles, determining external load resistance 01 p0012 A67-10178
 Helical flow of conducting fluid between porous cylinders and disk electrodes in radial magnetic field, calculating electric power and efficiency 01 p0120 A67-10183
 Thermionic energy conversion principles and conversion systems for satellite and space use 04 p0554 A67-15025
 High electric power production for short periods, anticipating magnetoaerodynamic power stage combined with conventional alternators 06 p0949 A67-17567
 Power plants for electric equipment in aircraft 06 p0950 A67-18117
 Alkaline vapor refueling of solar thermionic converters, concept, development and tests 07 p1132 A67-20287
 Power plants for electric equipment in aircraft 08 p1286 A67-20905
 MHD electrical power generation - Conference, Salzburg, July 1966, Volume I 09 p1536 A67-21773
 Orion P-3 electrical power system changes effect on weapons system, noting power distribution and generation systems 09 p1452 A67-22677
 Physics and efficiency of direct conversion of heat, light, nuclear, thermonuclear and chemical energy to electrical energy, avoiding mechanical energy 10 p1597 A67-23507
 Radiolotope applications to space science, discussing selection criteria for electric energy production and/or space propulsion 11 p1817 A67-24096
 Transverse diffusion of particle perpendicular to magnetic field by assembly of random Alfvén waves explains increase in electric field energy 11 p1840 A67-24753
 Point charges interaction energy in semiconductor thin film 18 p3101 A67-34091
 Source and load parameter effects on electrical explosion of wires noting voltage, capacity, inductance, specific resistance,

diameter, resistance, etc 20 p3483 A67-36401
 Solar photovoltaic cell design for lower temperature operation, noting application to near-sun missions 21 p3570 A67-37785
 Gamma radiation energy direct conversion into electrical energy by electrochemical recombination of radiolysis products, proposing new sealed battery 22 p3748 A67-40198
 MHD generation of electric power, describing motion equations for conducting fluid in electromagnetic field and duct configurations 24 p4098 A67-42413
 Electric power generation with closed cycle MHD conversion fluid having gases with high equilibrium conductivity discussing ionization and electrothermal instability 24 p4099 A67-42416
 Electric power generation using two-phase liquid-metal cycles in MHD converter, discussing liquid metal dynamics 24 p4099 A67-42417
 Lunar electric power systems transported by Saturn V noting Brayton cycle, Rankine cycle, solar cells and thermoelectric systems [AIAA PAPER 67-902] 24 p4110 A67-43010
ELECTRIC ENERGY STORAGE
 Storage of solar electric energy by electrolysis of water, separate storage and subsequent recombination of gases by fuel cells 07 p1132 A67-20288
 Optimization of electric energy storage for solar thermal space power systems 24 p4108 A67-42543
ELECTRIC EQUIPMENT
SA Q-FACTOR
 Component reliability at low stress levels and significance of failure mechanisms, considering electrical contacts and dielectric material 05 p0774 A67-16734
 Photomultiplier tubes for satellite instrumentation, discussing application as circuit components and star trackers 07 p1185 A67-19397
 Electrical systems except data acquisition and instrumentation for ground testing of large booster [AIAA PAPER 67-270] 07 p1167 A67-20079
 Topological properties of networks containing resistors, capacitors, self-inductors and controlled current generators 07 p1162 A67-20200
 Electric power generating equipment for aircraft noting brushless rectifier AC generator, solid rotor AC generator and brushless DC generator 09 p1451 A67-22666
 Aircraft DC electronic controls and generators for voltage regulation and system protection [SAE PAPER 67-0250] 11 p1745 A67-23983
 Soft magnetic materials metallurgy for several types of electrical equipment 13 p2178 A67-27140
 Civilian aircraft electrical equipment design and construction including Caravelle and Concorde 14 p2252 A67-28568
 Surface cleaning of electrical and electronic equipment through water and oil removal by chemical compositions 14 p2327 A67-28822
 Gradient compensated large volume degasser noting inner and outer coils magnetic field generators and construction and performance specifications 15 p2517 A67-29491
 Thin films as passive and active electrical components in microminiaturization, noting characteristics obtained by vacuum evaporation, cathode sputtering, diffusion and epitaxial growth 15 p2447 A67-29684
 Aerospace electrical and electronic equipment reliability requirements with reference to technology of miniature electrical connection devices 15 p2454 A67-30230
 Aircraft electric power systems and future use of solid state high power devices integrated microcircuits and solid rotor generator 17 p2804 A67-32511
 Solid state switching applied to aircraft electric systems noting design, performance and contactless switching concept 17 p2825 A67-32511
 Temperature autostabilizing nonlinear dielectric element /TANDEL/ for electric measurement circuits and measurement transducers 17 p2828 A67-32821
 Semiconductor strain gauge theory, application and installation 18 p3047 A67-33899
 Aircraft AC electrical systems using

- changeover contactors and rapid fault clearance, discussing reliability and maintenance 20 p3362 A67-36316
- Electrical circuits for earth IR radiation emission measurements, describing apparatus and incorporated miniaturized pneumatic receiver 21 p3629 A67-38661
- Protection of equipment and systems using semiconductor devices by suppression of voltage transients 22 p3766 A67-39250
- Fire in Apollo 204 spacecraft noting alterations in oxygen and electrical systems, escape hatch, materials and communications 22 p3900 A67-39888
- Electrically tunable low pass filter using permalloy films near resonance 22 p3772 A67-39906
- Safety control requirements in thermal-vacuum testing involving protection against electric equipment operation in pressure range for glow discharge 22 p3782 A67-40404
- ELECTRIC FIELD**
- ATMOSPHERIC ELECTRIC FIELD**
- ELECTROMAGNETISM**
- FIELD EMISSION**
- SPARK GAP**
- Surface charge after annealing of aluminum-silicon dioxide-silicon structures in inert atmospheres, analyzing effect of trapped electric field 01 p0032 A67-10004
- Superposed electric field effect on longitudinal drift rate of geomagnetically trapped electron 01 p0056 A67-10109
- Potential distribution between graphite and metallic electrodes of MHD generator in stationary heat conditions under induced or applied electric field 01 p0011 A67-10176
- Anisotropies and harmonics of inhomogeneous Lorentz plasma under electric field, using approximation 01 p0121 A67-10230
- Spectral energy density of turbulent plasma determined from spatial autocorrelation functions of electric fields of HF oscillations 01 p0121 A67-10235
- Longitudinal electric field penetration into magnetoplasma layer in constant magnetic field 01 p0122 A67-10356
- Maser oscillation intensity and frequency dependence on constant electric and magnetic fields acting on molecular beam in front of resonator 01 p0089 A67-10396
- Effect of shifting radial electrical field sign on instability state of inhomogeneous plasma produced by arc discharge in equipotential volume 01 p0123 A67-10741
- Intrinsic electric field of rarefied ion-electron plasma in external magnetic field and plasma stability, noting use of Galerkin method to determine plasma layer thickness 01 p0126 A67-11299
- Oscillatory low temperature photoconductive spectral response of p-type indium antimonide as function of electric field strength and temperature 02 p0280 A67-11487
- Purity concentration and electric field distribution determined in drift region of silicon p-i-n detectors from capacity as function of reverse voltage 02 p0296 A67-11823
- Current instability of plasma injected into germanium, noting effect of strong electric field in presence of temperature gradient 02 p0297 A67-11833
- Drift velocity dependence on electric field in GaAs measured by analysis of reverse biased Schottky barrier response to step input of light 02 p0253 A67-12504
- Random phase approximation for plasma, establishing perturbed electron distribution in oscillating electric field 02 p0276 A67-12557
- Low intensity shock wave transformation into rarefaction wave in nonconducting media in presence of external electric field 03 p0476 A67-13203
- Uniform electric field quadrupole polarizabilities and shielding factors for S-state atoms and ions, demonstrating independence of factors from existence of field gradient 03 p0472 A67-13321
- Virial theorem for electron plasma obtained by defining potential tensor and superpotential of electric field 03 p0482 A67-13746
- Space charge fields of planar magnetron calculated taking account of effect of conducting planes of cathode and anode 03 p0385 A67-13954
- Potential distribution and field dependence of electron velocity in bulk GaAs measured with point contact probe 03 p0499 A67-13985
- Flame reaction rate enhancement by electric fields 03 p0537 A67-14050
- Ionization probability of bound state of atoms in variable electric field 03 p0474 A67-14375
- TE modes propagation in rectangular waveguides containing two dielectric slabs, computing cut-off frequencies and propagation constants 04 p0570 A67-14860
- Simple asymptotic formula for motion of simultaneous electric field and conductivity domains in semiconductors in terms of electrodynamics on basis of Poisson and continuity equations 04 p0677 A67-14936
- Electromagnetic excitation of metallic cone, deriving systems of linear algebraic equations for coefficients of expansion of electric and magnetic fields 04 p0575 A67-15152
- Conditional probability density of phase derivative of narrow-band normal noise determined for case when noise envelope is greater than electric field 04 p0575 A67-15162
- Electrostatic polarization of plasma in applied electric field, excluding case for steady current flow 04 p0666 A67-15180
- Plasma flux cut-off in uniform magnetic field by transverse electric field 04 p0667 A67-15213
- Magnetic field effect on velocity of electron drift produced by electrical field in dense plasma 04 p0671 A67-15580
- Instability due to nonlinear coupling of electron plasma oscillation and ion acoustic oscillation to driving transverse field extended to longitudinal driving field 04 p0672 A67-15771
- Electric and magnetic field components produced by vertical and horizontal dipole antennas located at surface of conducting earth derived for quasi-static range 05 p0769 A67-16007
- Electric field effect on donors diffusion into intrinsic semiconductor 05 p0861 A67-16397
- Hydrogen atom excitation by Lyman alpha radiation absorption in electric field 05 p0848 A67-16795
- Parallel Couette and Poiseuille flows of multicomponent viscous plasma in presence of pressure gradient and electric field 05 p0854 A67-16894
- Temperature effect on impact ionization coefficient in SiC semiconductor p-n junctions with reversed current in strong electric field 05 p0865 A67-16916
- Tunneling through junctions with nonuniform electric field, calculating probabilities and currents by WKB method 05 p0866 A67-16973
- Internal electric field effect on simultaneous diffusion of donors and acceptors in semiconductors, considering case of indium and antimony diffusing into germanium 05 p0867 A67-17051
- Charge forming in cadmium sulfide crystals under effect of applied electric field 05 p0868 A67-17065
- Ohm law in multicomponent nonisothermal plasmas derived as function of electric and magnetic fields and temperature and pressure gradients, using transport equation 05 p0857 A67-17422
- Plasma density, electron temperature and potential distribution measured across magnetic field, determining ion and electron-diffusion coefficients in plasma column 05 p0858 A67-17432
- Space electric field measurement techniques 06 p0993 A67-17582
- Structural changes in epitaxial CdS films grown on rock salt, mica and silver substrates analyzed by electron diffraction at various temperatures and values of electric field 06 p1047 A67-17599
- Electron cooling in polar semiconductor by application of electric field 06 p1048 A67-17816
- Differential Stark effect in second excited state of alkali metal atoms described, using electric field level crossing spectroscopy 06 p1035 A67-17830
- Electric conductivity of naphthalene and beta-methylnaphthalene in liquid and solid state as affected by electric field 06 p1049 A67-17857
- Plasma instability in HF electric and constant magnetic field for sufficiently low pressure 06 p1039 A67-18081
- Spherical coupler for fastening mirrors and plane-parallel plates at Brewster angle in gas laser 06 p1011 A67-18394
- Hot electron emission from polar semiconductors with nonparabolic dispersion law, specifically qualitative effect of nonparabolicity and field on electron emission 06 p1052 A67-18423
- Reflection and transmission of birefringent plates surrounded by semiinfinite birefringent media with incident waves having polarized electric fields 06 p1033 A67-18544
- Nonlinear instability of nonisothermal plasma in external electric field, determining ion-acoustic noise spectrum and time dependent variations in kinetic energy of plasma electrons and ions 06 p1045 A67-18801
- Plasma in HF electric field becoming kinetically unstable due to Cerenkov effect 06 p1045 A67-18803
- Boltzmann transfer equation consisting of DC electric field and two AC electric fields for nonlinear second harmonic generation and combination frequencies in homogeneous plasma 06 p1046 A67-18826
- Corbino magnetoresistance experiments for n-type surface layers on p-type indium arsenide crystals as function of surface electric field 06 p1064 A67-18941
- Transport properties of electrons in GaAs in connection with traveling domains of high electric field in material 06 p1066 A67-18959
- Spin lattice relaxation times of donor electrons in Si, noting electric field effect on relaxation rate 06 p1068 A67-18971
- Electron motion in crossed fields with arbitrary ratio of electric and magnetic fields, considering simultaneously valence and conduction bands 06 p1069 A67-18978
- State density of strongly alloyed semiconductor in external constant electric field 07 p1149 A67-19188
- Turbulent flow of conducting fluid with free surface in presence of crossed magnetic and electric fields 07 p1227 A67-19321
- Electric field induced optical refractivity changes /Franz-Keldysh effect/ and nonlinear light scattering, light beam deflection and modulation in neutron-irradiated Si at 95 degrees K 07 p1231 A67-19487
- Electron capture cross section by protons in hydrogen atom obtained, using perturbed wave functions due to electric field 07 p1226 A67-19501
- Hydrodynamic equations describing motion of electrons in weakly ionized plasma in external electric field derived from Boltzmann equation, using Chapman-Enskog method 07 p1228 A67-19503
- Instability of inhomogeneous weakly ionized plasma in crossed electric and magnetic fields in 07 p1228 A67-19508
- Quasi-approximation 07 p1228 A67-19508
- Corrections for dielectric-constant tensor and conductivity tensor resulting from effect of electric field induced by plasmoid 07 p1229 A67-19517
- Effect of longitudinal plasma oscillations excited by external electric field on plasma stability, deriving dispersion relations by using Vlasov equation 07 p1229 A67-19518
- Drift velocity variation with electric field calculated in GaAs, using Boltzmann equation and incorporating additional scattering process 07 p1232 A67-19561
- Perturbations caused by cylindrical body in plasma, obtaining electric field and electron and ion concentration dependences on distance 07 p1250 A67-19811
- Spatial growth of ionization in molecular hydrogen, using thin film cathode 07 p1226 A67-19853
- Electric field domain motion in Ge samples with Au and Sb impurities, noting temperature and illumination effect on V-I characteristics 08 p1367 A67-20411
- Infinite plate consisting of monopolar semiconductor of given thickness under effect of electric field results in change in galvanomagnetic, piezoresistance and optical properties 08 p1367 A67-20416
- Plasma instability in HF electric field perpendicular to given magnetic field under low pressures 08 p1357 A67-20847
- Equations for ionized positive plasma column of gas discharge between infinite dielectric planes under oblique magnetic

field with component in direction of external electric field 08 p1358 A67-20849

Kinetic equation for unstable homogeneous plasma in uniform magnetic field when subjected to sudden uniform electric field 08 p1360 A67-21127

Energetic particle scattering by laboratory plasmas, deriving expressions for scattering coefficients in terms of electric field autocorrelation function 08 p1361 A67-21136

Langmuir probe experiments on electric and magnetic field, density and temperature profiles, I-V characteristic, etc, for rotating plasma in B-3 stellarator 08 p1361 A67-21137

Treatments of drift wave velocities in Cs and K plasmas, noting radial electric field effect made negligible by reducing cathode temperature gradient 08 p1362 A67-21147

Effective field for microwave breakdown for gas in external DC magnetic field and electric field valid for any stationary random signal 09 p1462 A67-21646

Spectrum of ionic waves in plasma located in electrical field and interacting with charged particle beam, obtaining dispersion equation 09 p1544 A67-21846

Pinning fluxoids by spatial inhomogeneities of Ti-Pb and Pb-In alloys, noting I-H characteristics and type II superconductor resistance 09 p1556 A67-22135

Electron plasma behavior and stability in presence of time dependent electric field 09 p1549 A67-22553

Electrical migration of Li and Cu in GaAs, noting ionic charge decrease due to drag by electrons 09 p1558 A67-22603

Electrical and thermal conductivity of tin films investigated in search for surface superconductivity induced by electric field 10 p1688 A67-22765

Electric field penetration of electrodes incorporated into theory of electron tunneling through dielectric layer 10 p1689 A67-22961

Electric fields due to electron-plasma and ion-acoustic waves associated with sunspot magnetic field variation as main cause of electron acceleration in solar flares 10 p1700 A67-23056

Silicon solar cell with drift fields of various widths and magnitudes, considering performance changes before and after radiation 10 p1596 A67-23161

Carrier drift velocity measurements in silicon at high electric fields, using time-of-flight technique 10 p1690 A67-23167

Semiconductor conductivity in strong SHF electric fields, measuring dielectric constant and Fourier component 10 p1657 A67-23567

Nonlinear dependence of current in electric field in thin semiconductor film in quantizing magnetic field 10 p1694 A67-23591

Perturbation theory applied to study of electron states and interband optical transfers in strong electric fields of semiconductors 10 p1695 A67-23659

Avalanche multiplication of current carriers at low temperatures in p-n junctions of InAs, determining carrier ionization coefficient and dependence on electrical field 10 p1695 A67-23660

Magnetic resistance and Hall effect dependence on external electric field in semiconductors, noting difference for parabolic and nonparabolic law of carrier dispersion 10 p1695 A67-23661

Strong electrical field effect on Faraday effect in n-type InSb 10 p1695 A67-23663

Flute instability in low beta plasma in presence of nonuniform electric field perpendicular to magnetic field 11 p1828 A67-23891

Molecular beam electric resonance /MBER/ spectrometer for hyperfine structure of rubidium fluoride 11 p1821 A67-23961

Line source antenna radiation pattern computed from complex voltage patterns measured at various range lengths in near field 11 p1763 A67-24301

Electric field effect in Q machine with uniform end plate temperature, noting deviation from thermal equilibrium and increment in ion loss rate for certain range of particle densities 11 p1833 A67-24370

Nonisothermal alkali plasma collisional drift instability in radial electric field 11 p1834 A67-24380

Magnetically confined cesium plasma analyzed under radial electric field, noting radial plasma loss rate 11 p1835 A67-24384

Undamped plasma oscillations in nonpolar semiconductors doped with impurities in external electric field, determining phase velocity 11 p1846 A67-24472

Electric field in MHD channels in presence of near-electrode potential drop 11 p1840 A67-24671

Electrostatic oscillations in electron plasma, noting effect of external electric field on electron velocity distribution 11 p1848 A67-24868

LF current oscillations excitation in n-type semiconductors analyzed using dispersion equation, noting role of external electric field 11 p1849 A67-24870

Electric field intensity distribution over length of plasmatron arc stabilized by longitudinal vortex air flow 11 p1843 A67-24972

Longitudinal electric field penetration into magnetoplasma layer in constant magnetic field 11 p1844 A67-25029

Electrical field in solar atmosphere caused by pressure gradient in case of partially ionized gas 12 p2000 A67-25133

Plasma conductivity in external electric fields calculated by LF longitudinal oscillation, using Boltzmann equation 12 p1970 A67-25249

Resonance properties of semiconductor with moving electrical domains, showing periodic variation with illumination intensity 12 p1983 A67-25517

Time dependent large scale electric potential field effect on motion of geomagnetically trapped particles 12 p1997 A67-25809

Local magnetic field, ion density flow and electric field in plasma measured downstream of theta-pinch accelerator in presence of uniform guide field [AIAA PAPER 68-155] 12 p1975 A67-25895

Radial electric field role in electrofluid dynamic conversion of flowing gas energy into electric energy 12 p1901 A67-25933

Propagation characteristics in waveguide loaded with cylindrical semiconductor rod, calculating electric field distribution 12 p1918 A67-26222

Ion motion under influence of electric field and density gradient with charge transfer collision between ions and neutral gas background 13 p2162 A67-26269

Hall and electric field effects in cadmium sulfide single crystals in terms of current carrier mobility 13 p2174 A67-26369

IR surface photoconductivity of silicon as function of surface potential and current carrier parameters 13 p2174 A67-26397

Effect of shifting radial electrical field sign on instability state of inhomogeneous plasma produced by arc discharge in equipotential volume 13 p2166 A67-26770

Injection coefficients of hydrogen and oxygen during buildup of discharge in homogeneous electric field 13 p2160 A67-26813

Current density combination frequency derived for homogeneous magnetoplasma due to alternating electric fields, considering distribution function isotropic and anisotropic parts 13 p2167 A67-26994

Frequency shift in emission spectrum of complex atom in uniform electric field, noting numerical results for Al I 13 p2168 A67-27208

Plasma acceleration under combined axial magnetic and electric fields, noting experimental setup and results 14 p2353 A67-27750

Temperature and carrier concentration effect on threshold electric field of current saturation and saturation drift velocity in gallium arsenide 14 p2364 A67-27826

Magnetosphere rotation problem in presence of solar wind analyzed for auroral particle acceleration, noting perturbing field of induced electric current 14 p2307 A67-27917

Domain originated functional integrated circuits with possible solid-state bulk effect extension from microwave systems to whole of electronics 14 p2281 A67-28022

Argon plasma thermal conductivity at atmospheric pressure and various temperatures determined in central zone of arc column 14 p2404 A67-28031

Hydrodynamic equations for electric field in steady collision-dominated three-component plasma 14 p2358 A67-28240

Laminar boundary flow over dielectric disk with homogeneous magnetic field perpendicular to plane of disk, obtaining liquid velocity and electric field density 14 p2358 A67-28282

Motion and dispersion of inhomogeneity in unbounded plasma in magnetic and electric fields 14 p2359 A67-28504

Nonlinear volt-ampere characteristic of photosensitive GaAs plus copper atoms in strong electric field 14 p2368 A67-28532

P-type silicon IR photoconductivity burst in nonequilibrium field effect 14 p2368 A67-28536

Superconductor dynamic intermediate state DC voltage caused by flux motion shown by frequency spectrum measurements of noise voltage 14 p2369 A67-28600

Large microwave field and small parallel DC field applied across GaAs sample altering conductivity related to carrier velocity-field characteristic 14 p2369 A67-28601

Magnetactive plasma quasi-linear oscillations equations, determining damping decrements of plasma electric field components 14 p2361 A67-28753

Synchronous and cyclotron wave behavior of electron flux in resonator with transverse electric field varying sinusoidally along wave propagation direction 14 p2288 A67-28807

Forward conduction characteristics of contacts between gold n-type silicon measured at different temperatures 14 p2373 A67-28925

Current instabilities in GaAs for applied electric field along piezoelectric direction attributed to electron-phonon coupling, determining additional parameters from experimental data 14 p2374 A67-28983

Argon plasma accelerator producing diamagnetic discharge measured along axis for plasma properties 14 p2362 A67-29046

Electron mobility and temperature due to electric field in polar semiconductor investigated assuming displaced Maxwellian velocity distribution 14 p2375 A67-29065

Electric field effect in terms of drifted Maxwellian distribution, considering nonparabolic electron scattering where dominant energy-loss mechanism is optical polar mode scattering 14 p2376 A67-29088

Particle velocity distribution calculation in current-carrying electron-proton plasma by Lenard-Balescu-Guernsey form of Fokker-Planck equation 15 p2522 A67-29204

Steady state velocity distribution in fully ionized plasma in DC electric field obtained through Bhatnagar-Gross-Krook equation 15 p2522 A67-29206

Screw instability in linear Hall accelerator 15 p2522 A67-29207

Skin effect in plasma theory for case of nonlocality of relation between current and electric field 15 p2522 A67-29211

Electrically conducting compressible viscous free jet in presence of transverse magnetic and electric fields solved analytically by perturbation technique 15 p2523 A67-29215

Current layer motion in coaxial plasma gun, measuring discharge current, electric and magnetic fields and ejected ions at gun outlet 15 p2525 A67-29250

Electric field device to generate short plasmoids free from plasma contamination through contact with metal 15 p2526 A67-29255

Electromagnetic excitation of metallic cone, deriving systems of linear algebraic equations for coefficients of expansion of electric and magnetic fields 15 p2435 A67-29331

Conditional probability density of phase derivative of narrow-band normal noise determined for case when noise envelope is greater than electric field 15 p2435 A67-29341

Pure molecular flow coupled with surface diffusion applied to cesium transport 15 p2520 A67-29494

Plasma flow layer, acceleration and other parameters investigated under several operation conditions in coaxial plasma gun 15 p2529 A67-29718

Internal electric field effect on simultaneous diffusion of donors and acceptors in semiconductors, considering case of indium and antimony diffusing into germanium 15 p2537 A67-29781

Charge forming in cadmium sulfide crystals under effect of applied electric field 15 p2538 A67-29794

Microwave emission from magnetic-field

- free electron hole plasma in p-type InSb at 15 p2539 A67-29820
- Recombination-regeneration formula for hole-electron pairs in randomly doped semiconductor materials 15 p2539 A67-29915
- Low temperature conductivity of semiconductors in electric and magnetic fields analyzed, noting electron-photon interactions and photon heating effect 15 p2542 A67-30248
- Plasma flux cut-off in uniform magnetic field by transverse electric 15 p2532 A67-30261
- Polyatomic gaseous impurity effect on electric conductivity of alkaline plasma from axial field and electron temperature measurements 16 p2710 A67-30520
- Nonequilibrium plasma production via plasma electron heating with electric field induced in MHD 16 p2601 A67-30552
- Experiments with 100-kw MHD generator free from secondary effects by choosing MHD interaction parameter values greater than unity 16 p2602 A67-30559
- Argon-potassium plasma electrical conductivity investigation showing that optimum increase in conductivity corresponds to optimum electrode length 16 p2602 A67-30560
- Surface charge density of MOS as affected by bias and temperature 16 p2724 A67-30602
- Current saturation and oscillation in photosensitive GaAs explained by high electric fields 16 p2725 A67-30611
- Reactive characteristics of diffused p-n junctions in p- and n-silicon at high injection levels and in strong electric fields 16 p2726 A67-30817
- Calculating characteristics of cesium plasma in stationary state under electric field, considering excitation and ionization by inelastic electron collisions 16 p2713 A67-30868
- Stabilization of ion cyclotron plasma in mirror machines by energy spreading and application of high frequency electric field 16 p2714 A67-30873
- Temperature effect on impact ionization coefficient in SiC semiconductor p-n junctions with reversed current in strong electric field 16 p2727 A67-30893
- Sign-discriminating field mill design using one rotor and one stator 16 p2671 A67-30972
- Electrostatic wave propagating into region of decreasing electron density calculated using one-dimensional plasma with uniform electron density 16 p2715 A67-31063
- Electric field distribution inside local superconductor carrying steady case analyzed using Ginzburg-Landau equation, noting strong compressibility effect 16 p2731 A67-31171
- Mutual coupling between sectoral horns side-by-side formulated in terms of rays, modes and mode caustics excited in each horn 16 p2639 A67-31355
- Plasma sheath detuning effect on small loaded dipole in free space investigated 16 p2627 A67-31367
- Pulsed resistivity and Hall effect measurements of n-type GaAs in high electric fields at room temperature below microwave oscillation threshold 16 p2731 A67-31449
- Hyperfrequency amplification using electric field effect for conduction modulation of single crystal germanium sheet 16 p2732 A67-31705
- Atmospheric noise data for various frequencies and various latitudes and longitudes 16 p2632 A67-31861
- Two-dimensional motion of charged particles in electromagnetic field, noting magnitude of forbidden band as function of particle energy 16 p2740 A67-31885
- Magnetic and electric charge interaction, noting neutrino electric dipole moment 17 p2887 A67-32101
- Electric field effect on magnetoresistance of p-type indium arsenide surface in high magnetic fields at low temperatures 17 p2911 A67-32206
- Electrical field distribution during injection of charged particles into two-dimensional model of magnetosphere 17 p2841 A67-32244
- Microwave attenuation change and harmonic generation by n-type GaAs in strong microwave electric fields, determining current density relation to field strength 17 p2913 A67-32310
- Book on effects of hot electrons associated with carrier concentration in semiconductors at very low temperatures 17 p2914 A67-32378
- Voltage gradient determination throughout two-dimensional electric field by electro-optic analog, noting applicability to boundary value problems satisfying Laplace equation 17 p2818 A67-32418
- Microwave emission intensity from InSb, examining dependence on angle between DC electric and magnetic fields 17 p2914 A67-32615
- Effects of electric fields and configurations on thermal annealing and radiation hardening of MOSFETs 17 p2916 A67-32835
- Electric vortex-field integrator using aluminum foil sheet and external field to simulate circular flow about wing profile at various angles of attack 17 p2834 A67-32905
- Plasmoid motion in longitudinal, transverse and two-dimensional multipole magnetic fields, investigating electric fields and plasmoid parameters 17 p2904 A67-32916
- Nonadiabatic theory for plasma behavior in strong electric field, discussing plasma instability conditions 17 p2905 A67-32924
- Solution of linearized Boltzmann collision equation for ion motion through gas in inhomogeneous electric field, describing energy distribution functions for hydrogen ions 17 p2907 A67-33102
- Whistler method detection of magnetospheric electric field associated with polar substorm 17 p2851 A67-33197
- Fluctuating electric and magnetic fields due to plasma instabilities and stabilizing effect of mode coupling in collisionless plasma 17 p2909 A67-33229
- Perturbation theory applied to study of electron states and interband optical transfers in strong electric fields of semiconductors 17 p2924 A67-33340
- Avalanche multiplication of current carriers at low temperatures in p-n junctions of InAs, determining carrier ionization coefficient and dependence on electrical field 17 p2924 A67-33341
- Magnetic resistance and Hall effect dependence on external electric field in semiconductors, noting difference for parabolic and nonparabolic law of carrier dispersion 17 p2924 A67-33342
- Strong electrical field effect on Faraday effect in n-type InSb 17 p2924 A67-33344
- Energy loss factors for slow electrons in hot gases determined by measuring electron temperature variation with HF electric field power 17 p2890 A67-33367
- Electron bunching in sweep klystron, deriving electric field equation, motion equations and continuity criteria for arbitrary charge density distribution 18 p3010 A67-33501
- Static electric fields produced in magnetosphere and effects such as motion of visual and radio aurora and currents in ionosphere 18 p3035 A67-33600
- Spectral data and energy level diagrams from magnetic and electric field passage through barium cloud 18 p3036 A67-33606
- Airglow and auroral phenomena, discussing ideal coordinate system, electric fields, morphology, solar wind-magnetosphere interactions, and particle precipitation 18 p3039 A67-33625
- Nonlinear instability of nonisothermal plasma in external electric field, determining ion-acoustic noise spectrum and time dependent variations in kinetic energy of plasma electrons and ions 18 p3090 A67-34420
- Plasma in HF electric field becoming kinetically unstable due to Cerenkov effect 18 p3090 A67-34422
- Resonance properties of semiconductor with moving electrical domains, showing periodic variation with illumination intensity 18 p3103 A67-34448
- Cadmium telluride electrical light absorption oscillations noting comparisons between experiment and theory, electric field, temperature range, etc 19 p3301 A67-34772
- Closed-cycle generator using gasdynamic forces to transport charged particles against opposing electric field, noting enthalpy role 19 p3175 A67-34801
- Ionization rate at higher electron densities in DC fields measured in toroidal discharge tube 19 p3272 A67-35078
- Average dwell times and velocities of Ba, Sr, Li, Tl, Sn, Bi, Be, Zn, and Hg in arc plasma 19 p3281 A67-35155
- Charge, current, and self-consistent field transport properties of collisionless plasma derived using initial value solutions to Vlasov equation 19 p3285 A67-35343
- Unsteady state of infinite plane layer of isotropic homogeneous plasma situated in steady electric field normal to layer 19 p3286 A67-35349
- Cylindrical plasma column subjected to axial magnetic field measured for electric field oscillations by movable probe within ionized gas 19 p3288 A67-35374
- Electric field due to double grid excitation in circular waveguide partially filled with warm homogeneous plasma in infinite magnetostatic fields 19 p3290 A67-35379
- Electric and magnetic field measurements in collisionless shock wave propagating through highly ionized magnetized plasma 19 p3294 A67-35408
- Characteristics of nonequilibrium cesium plasma subjected to continuous electric field 19 p3294 A67-35417
- Electron distribution function of homogeneous imperfect Lorentz plasma disturbed by electric field 19 p3295 A67-35418
- Solar wind velocity and interplanetary magnetic field components obtained by IMP II related to geomagnetic field variation 19 p3222 A67-35473
- Quasi-linear plasma waves model, considering Vlasov approximation, deriving distribution functions and electric field equations solution 20 p3494 A67-36149
- Nonparabolic conduction energy band in semiconductors produces electron plasma excitations of sum and difference frequencies under strong DC electric field 20 p3505 A67-36210
- Stationary moving domains in hot electron semiconductors, obtaining criteria for soft and hard regimes of domain excitation 20 p3506 A67-36222
- Theory of small signal current transients applied to study of electron trapping in amorphous selenium 20 p3509 A67-36507
- Electric field produced by polarization in plasmoid injected across field in closed system 20 p3497 A67-36681
- Base impurity distribution design consideration for figure of merit of HF transistors, considering accelerating, decelerating and neutral electric field 20 p3398 A67-36770
- Tracer experiments using tritiated ethanol on surface of MOS capacitor to indicate field-induced proton transport 20 p3510 A67-36857
- Electromagnetic wave propagation in waveguides calculated together with electric and magnetic fields by perturbation method 20 p3382 A67-36862
- Vortical stabilization of plasma column within radial electric field 20 p3500 A67-37062
- Thermal EMF in semiconductors with electric fields caused by hot carriers, showing energy relaxation of high energy electrons 20 p3513 A67-37451
- Plasma conductivity tensor in steady magnetic field in terms of electric field correlation using Kubo transport theory 20 p3503 A67-37692
- Theta pinch plasma sheath and fields time development for relaxing radial electric field 21 p3662 A67-37754
- Maser output pulsations by varying active particles entering resonator through electric or magnetic field 21 p3638 A67-37941
- Simplified formulas and curves for electromagnetic wave diffraction on small ideally conducting sphere, examining electric field components 21 p3580 A67-38121
- Interaction between plane electromagnetic wave and separating boundary, considering electric field with component normal to boundary 21 p3581 A67-38292
- Hall and electric field effects in cadmium sulfide single crystals in terms of current carrier mobility 21 p3680 A67-38325
- Drift instabilities of inhomogeneous plasma in HF electric field 21 p3667 A67-38374

Electromagnetic wave focusing in nonlinear medium with small nonlinear polarizability 21 p3670 A67-38684

Density, electric field and volt-ampere characteristics for spherical electrostatic Langmuir probe in collision plasma with weak ionization and recombination, using asymptotic method [AIAA PAPER 87-705] 21 p3672 A67-38732

Conditioned distribution functions from BBGKY hierarchy distribution functions, with analogy to hydrodynamic approximation of Boltzmann distribution 21 p3675 A67-38931

BBGKY hierarchy description of plasmas, with application to ionized particle charge distribution in external electric field 21 p3675 A67-38932

Alfven two-dimensional problem extended to charged-particle motion in dipole magnetic field with electric field determining forbidden band size, shape and specular reflection points position 21 p3621 A67-39015

Ferroelectricity of barium titanate thin films noting dielectric, temperature, polarization and electric field variations 21 p3687 A67-39142

Sidelobe reduction by stepping E-plane field distribution on rectangular horn antenna aperture, finding values of geometrical parameters 22 p3767 A67-39273

Steady state plasma in strong microwave electric field acting on electron component 22 p3845 A67-39431

Electric domains in high resistance GaAs single crystals, measuring electric field intensity with Pockels electro-optic effect noting surface state role 22 p3857 A67-39459

Dispersion relation for wave propagation in electro-magneto-ionic medium under electric and magnetic fields obtained using Maxwell-Boltzmann-Vlasov equations, discussing cut-off frequency 22 p3788 A67-39469

Stability of collisionless plasma with ions moving relative to electrons under electric field of ion cyclotron wave 22 p3852 A67-39989

Precise and approximate formulations for unsteady flows of conducting fluid in MHD channels with external electric circuit 22 p3853 A67-40023

Resonant cavity electric field excitation placed in magnetic field near electron cyclotron frequency studied for expressions of self-excitation current 22 p3816 A67-40126

Relative equilibrium of liquid cylinder investigated for uniform rotation in uniform axial electric field 22 p3787 A67-40135

Branch cut contribution to longitudinal electric field in relativistic Maxwell plasma using non-Laplace transformation procedure 22 p3854 A67-40319

N-type InSb microwave noise emission at low temperatures in low electric field regime, measuring magnetic field threshold and background continuum 22 p3864 A67-40345

Clean MOS structure bias and temperature /BT/ treatment at high electric fields causing electrochemical reaction affecting surface charge density 22 p3774 A67-40461

Measurements on YIG crystals showing magnetic crystal symmetry lowering by strong electric field 23 p4035 A67-40654

DC potential solutions for low pressure Cs diode with zero slope at emitter noting stability, oscillations and instability for ion/electron ratios 23 p4031 A67-40886

Index of refraction measurements near damage spots in KTN due to laser beam and electric field simultaneous presence 23 p4013 A67-40895

Nonlinear volt-ampere characteristic of photosensitive GaAs plus copper atoms in strong electric field 23 p4039 A67-40939

P-type silicon IR photoconductivity burst in nonequilibrium field 23 p4040 A67-40943

He ions beam passing through electric field and inducing light intensity fluctuations when emitted from fine structure levels observed via Stark interference 23 p4029 A67-40956

Kinetic equation for steady state electron-ion system with electrons drifting under electric field, calculating HF resistivity drift velocity dependence 23 p4033 A67-40962

Unsteady continuity and motion equations describing F layer dynamic characteristics under time dependent electric and magnetic

fields 23 p3996 A67-41178

Magnetic and electric dipole antennas located above earth surface, deriving quasi-static electric and magnetic field components 23 p3981 A67-41210

High temperature thermal EMF and electrical conductivity in intense electric field for semiconductors with low charge carrier mobility 23 p4043 A67-41299

Electric field heating of D-region electrons shown to be inadequate to raise temperature above gas temperature [AFCRL-87-0121] 24 p4146 A67-41808

Axial component of electric field intensity in vortex stabilized arc measured by sectional channel and electrode spacing 24 p4195 A67-41940

Dielectric function of semiconductor in external electric field, discussing effect on plasma frequency 24 p4201 A67-41979

Strong electric field effects on parabolic energy band semiconductor magnetoresistance and Hall coefficients, discussing scattering mechanisms 24 p4202 A67-41982

Electric and magnetic field measurement by energy density antenna applicable to reducing signal fading encountered on mobile radio transmission path 24 p4131 A67-42340

Second harmonic power generation associated with simultaneous application of DC fields and gas laser beams to narrow band gap semiconductors 24 p4168 A67-42364

Gravitational effect on free falling electrons in vacuum, showing gravitational induction of electric field outside metal surface 24 p4189 A67-42740

Read type and avalanche type oscillations in silicon varactor diodes, noting parasitic series resistance and electric field peak effects 24 p4133 A67-42820

ELECTRIC FIELD STRENGTH

Autocorrelation function of radiation electric field measurement from clipped correlation function and spacing estimation for optimally efficient SNR determination 01 p0114 A67-10808

Electric field radial intensity distribution and charged particle density for positive plasma column between coaxial cylinders 01 p0125 A67-10924

Magnetic particle motion, analyzing effect of earth electric dipole field 02 p0311 A67-12585

Field intensity probe measurements of potential distribution and I-V characteristics in AC arc plasma 03 p0475 A67-13087

Theoretical semiconductor electroconductivity dependence on intensities of strong electric and magnetic fields 03 p0490 A67-13158

Ohm law deviation in island-structure thin metallic films and current dependence on field strength 03 p0490 A67-13159

Cylindrical electronic microwave tubes, deriving expressions for zero and first approximations of physical parameters 05 p0774 A67-16906

Hall effect on hot carriers in p-type Ge semiconductor in microwave field as function of field strength 08 p1369 A67-20993

Electroconductivity variations in CdS and CdSe single crystals with SHF electric field strength, intensity of bias lighting and temperature in minus 70 to plus 70 degrees C interval 08 p1370 A67-20996

Theoretical semiconductor electroconductivity dependence on intensities of strong electric and magnetic fields 10 p1690 A67-23106

Analytical expression for steady state rate of electric domain movement in semiconductors in terms of electric field distribution at domain center 11 p1846 A67-24482

Electric field distribution in p region, space charge layer and n region of p-n abrupt junction germanium diode at room temperature 13 p2078 A67-26788

Electric field meter /E-meter/ measurement of field strength at given point on spacecraft surface [AIAA PAPER 86-74] 13 p2120 A67-26835

Autoelectric emission in superconductors near transition point noting variation with total field energy and normal component 14 p2370 A67-28673

Electric conductivity of p-Ga-Te polycrystals and single crystals in strong electric fields 14 p2375 A67-29085

Influence of strong HF electrical fields on plasma instability originated in buildup of potential field oscillations 15 p2530 A67-29728

Electron concentration and temperature, gas temperature, electrical field intensity and conductivity of Hg-Cs nonequilibrium plasma 16 p2709 A67-30517

Cylindrical electronic microwave tubes, deriving expressions for zero and first approximations of physical parameters 16 p2636 A67-30883

Electrical conductivity of plasma /produced in toroidal discharge chamber by injection method/ relation to electric field 16 p2721 A67-31483

Electric field enhanced Raman scattering and linear frequency shift of strontium titanate soft mode in random domain orientation and reorientation 18 p3098 A67-33520

Energy transport concentration around homogeneous lossless dielectric cylinder, calculating electric field strength distribution and limiting radius of several wave modes 18 p2999 A67-33529

Plasma-metal interface electric field intensity, deriving dimensionless formula from nonlinear second order differential equation 19 p3277 A67-35125

Rotational velocity and ion density profiles of plasma vortices by measuring radial electric field 19 p3288 A67-35361

Electron deflection instrument for measuring surface electric field strength 20 p3444 A67-36524

Electric field effects on condensation heat transfer, discussing heat-transfer coefficient dependence on electric field and instability appearance at liquid film interface [ASME PAPER 87-HT-39] 20 p3547 A67-36724

Moving high field domain and current saturation in optically excited n-InSb 21 p3683 A67-38404

Charged particles generation by liquid subjected to high electric field for efficient bipolar microthruster [AIAA PAPER 87-728] 21 p3694 A67-38752

Charged particle /ion/ collection rates using supersonic atmospheric sounding rocket with electrode at stagnation point, noting electric field effect 22 p3791 A67-39818

Shielding factors for electrostatic aeriels 24 p4129 A67-41973

ELECTRIC GROUNDING

Instrumentation grounding at Cape Kennedy, noting characteristics of ground system used for safety and clean space signals 20 p3398 A67-36837

ELECTRIC IMPEDANCE

Currents in elements of linear uniformly spaced antenna array when mutual impedance-between neighboring elements is taken into account 01 p0041 A67-11326

Driving-point impedance and current for long resonant cylindrical antennas 02 p0212 A67-11605

Impedance errors of coaxial air transmission lines and mechanical and electrical characteristics of Precifix connectors 02 p0213 A67-11648

Characteristic impedance of TEM mode transmission lines, extracting upper and lower bounds on finite difference solution of Laplace equation 02 p0194 A67-11784

Aperture admittance, material loading and higher order modes effect on rectangular cavity slot antenna design 02 p0218 A67-12098

Input impedances calculated for parametric up-converters, examining overall signal behavior 02 p0220 A67-12205

Network analysis shortcut by topological representation of impedance in node and loop equations 03 p0389 A67-12963

Multimode surface waves for plane structures in generalized impedance boundary condition, noting electromagnetic field arising from magnetic dipole source located above plane structure 03 p0469 A67-13657

Grating-lobe series for impedance variation with phasing in infinite planar array of elements with periodic spacing 03 p0384 A67-13848

Impedance of finite insulated cylindrical antenna in cold plasma with longitudinal magnetic field 03 p0385 A67-13850

Impedance of finite insulated antenna in cold plasma with perpendicular magnetic field 03 p0385 A67-13851

Reflected voltage provided by circulator

For radar echo reduction, noting principle of antenna impedance 03 p0370 A67-13857

Loading 03 p0370 A67-13857

Driving point impedance of asymmetrical dipole using computer 03 p0385 A67-13861

Method 03 p0385 A67-13861

Synthesis of networks incorporating semiuniform loss by transformation into networks with near ideal reactances 03 p0393 A67-13974

Radio propagation in microwave terrestrial model waveguide of variable surface impedance, using reciprocity theorem 04 p0570 A67-14865

Plasma sheath simulation used to analyze effects of sheath discontinuities and inhomogeneities on slot antenna radiation pattern and input impedance 05 p0769 A67-16000

Impedance cardiac output values simultaneously compared with dye dilution techniques under rest and exercise conditions 05 p0755 A67-16278

Tunnel diode amplifier distortion by finite impedance at zero frequency and second harmonic frequency 05 p0775 A67-16945

Surface impedance of nonhomogeneous plasma with sharply varying parameters, noting skin effect and permittivity gradient 05 p0766 A67-17231

Small signal admittance parameters of field effect transistors treated as analog RC transmission lines 05 p0777 A67-17298

RC active circuit under effect of amplifier finite input impedance, nonzero output impedance and nonzero source impedance 05 p0785 A67-17299

Input resistance of short filamental antenna in warm plasma according to kinetic theory and hydrodynamic equations 07 p1151 A67-19445

Varactor diode impedance behavior in parametric amplifiers under low temperature conditions 07 p1152 A67-19551

Coupling coefficients of waves in variable cross section waveguides with impedance wall 07 p1143 A67-19602

Sensitivity of dielectric rod terminal impedance to surface wave coupling when no resonance regions exist within energy-carrying cross section 07 p1158 A67-20299

Current, input impedance and far field pattern of cylindrical antenna with tapered resistive loading 09 p1481 A67-22446

Semiconductor dielectric interface characterization from study of complex capacity of metal/oxide/semiconductor structures 09 p1557 A67-22557

Generalized method of calculating multielement antenna and feeder system 10 p1611 A67-22981

Computer simulation of GaAs Gunn diode resonant circuit noting frequency, efficiency and load characteristics 10 p1612 A67-23370

Simulator measurements of active impedance of phased array antenna element at two different scan angles by single element in waveguide 11 p1763 A67-24299

Ionospheric plasma resonances studied by four-electrode probe, calculating mutual impedance as function of orientation and excitation frequency 12 p1931 A67-25152

Axial mode helical antenna radiation and impedance improvement by using tapered feeds and terminations 13 p2076 A67-26514

Analytical representations of admittance matrix of transistors, describing methods of obtaining quality coefficients, equivalent circuit synthesis, etc 13 p2081 A67-27199

Active and reactive impedance components of total resistance of p-n-n structures at high injection levels 13 p2081 A67-27278

Microwave design techniques for calculating even and odd mode characteristic impedances of miniature microstrip transmission lines 13 p2071 A67-27445

Antenna in interplanetary plasma, noting fluctuation noise in exosphere and radiation impedance when exposed to solar wind 14 p2279 A67-27856

HF negative resistance in dielectric diodes with high density of shallow traps taking into account transit time 14 p2367 A67-28521

Effects of strong coupling and spin-flip scattering by magnetic impurities on superconductors, calculating conductivity and surface impedance at finite temperatures 14 p2371 A67-28725

Space-charge-wave growth and differential negative resistance conditions in two-valley

semiconductors obtained from impedance 15 p2442 A67-29179

Impedance and effective dielectric constant analysis for transmission line, with approximate theoretical solutions and experimental verification 15 p2444 A67-29455

Experiments of internal impedance of MHD generator show wide range of working conditions as slowly varying function of applied current 17 p2802 A67-32182

Variationally computed antenna impedances and accuracy of resulting current distributions 17 p2824 A67-32301

Active filter design employing impedance converters, amplifiers and gyrators, providing equations for component values 17 p2824 A67-32394

Inductive characteristics of junction transistors, showing Q-factor increase achieved by using negative impedance produced by avalanche multiplication 18 p3009 A67-33479

Linear microcircuits evaluation and application covering offset voltage and current, noise properties, input impedance, etc 18 p3013 A67-34548

HF backscattering from absorbing infinite strip with arbitrary face impedances 18 p3005 A67-34730

Variational formula for antenna impedance in warm magnetoplasma, considering force and fluid-flux distribution 19 p3194 A67-35513

Mutual admittance of slot antennas measured for free space and ionized environment by different techniques 19 p3194 A67-35516

Offset impedance sheet effect on admittance of slot antenna in conducting plane 19 p3197 A67-35823

Current distribution coefficients determination and antenna impedances 20 p3400 A67-37219

Coupling coefficients of waves in variable cross section waveguides with impedance wall 20 p3401 A67-37341

Small signal interaction impedance of bulk semiconductor amplifier with nonuniform doping profile, noting two-dimensional representation 21 p3588 A67-37818

Attenuation function of surface wave propagating over spherical earth having surface layers with different electric impedances, studying interaction with space wave 21 p3580 A67-38122

Reflex klystron electron admittance dependence on potential distribution in repeller space, showing electrode structure and space charge effects 21 p3598 A67-38604

Characteristic impedance of waveguides from equivalent voltage and current definitions 22 p3765 A67-39212

Metal bolometer impedance and noise generation, discussing Johnson and temperature fluctuation noises 22 p3797 A67-39343

Radiation pattern of linear antenna erected over tapered ground screen, noting system surface impedance variation 22 p3760 A67-39628

Characteristic admittances of comb-type and undulating waveguide filters, considering diaphragm thickness and TE propagation mode 22 p3770 A67-39662

Design formulas for predicting dependence of resistance and reactance of diffused microwave p-i-n diodes on reverse bias voltage 22 p3770 A67-39730

Impedance strip directional properties when excited through slot in metallic half-plane, noting case of reflector antenna with decreasing impedance 22 p3770 A67-39763

Superconducting parametric amplifier for measurements of small DC voltages in low impedance circuits 22 p3886 A67-40441

Nonreflecting resistive loaded dipole antenna with step function internal impedance, measuring current amplitude, input admittance and radiation field pattern 23 p3978 A67-40826

Surface wave pole contribution to admittance of rectangular waveguide-fed slot into dielectric slab 23 p3979 A67-40829

Impedance of dipole antennas in isotropic He plasma measured at X band 23 p3979 A67-40833

Electromagnetic scattering from free-space impedance homogeneous spheres, discussing null production in backscattering cross section 23 p3973 A67-40882

Cylindrical antenna admittance taking into account antenna to coaxial line junction

geometry, using magnetic current mathematical model 23 p3980 A67-41205

Currents in load impedance of transmission lines near cylindrical scatterer noting antenna field equations 23 p3981 A67-41209

Shielding factors for electrostatic aerials 24 p4129 A67-41973

Approximate solution to irregular waveguides with impedance boundary conditions based on amplitude of normal wave propagation 24 p4120 A67-42159

Gold doped silicon diodes consisting of compressor and expander elements designed to eliminate impedance range control and linearity problems 24 p4130 A67-42335

Linear and planar phased array antennas investigated for radiation impedance as function of scan variable 24 p4130 A67-42339

Mutual admittance of infinite conducting slot antennas covered by dielectric layer and impedance sheet, noting losses effects on waveguide modes 24 p4133 A67-42818

ELECTRIC IMPULSE

Iterative method determination of output signal, impulse response and transfer function of variable parameter linear sampled data system 05 p0784 A67-16705

ELECTRIC INSULATION

SA ASBESTOS

SA DIELECTRICS

High grade oxide ceramics for making dielectrically transparent insulating structures in microwave power tube 04 p0641 A67-14856

Dielectric isolation techniques for elements of integrated circuit 10 p1610 A67-22971

Preferential epitaxial growth method for electrical element isolations in IC, noting no lattice defect effect on electrical characteristics of element 12 p1918 A67-26217

Heat removal from high density packaged electronics by bonded metallic heat sink [ASME PAPER 67-DE-47] 14 p2408 A67-28880

Bibliography on electrical discharges in vacuum and properties of vacuum as electrical insulator 15 p2516 A67-29200

Chemical treatment reducing toxicity of polyvinyl chloride tapes used for insulating electric wires in space cabins 16 p2693 A67-30910

Electrode and insulator behavior in experimental MHD generator electrically producing temperature modulation of gas stream 18 p2988 A67-33708

Cesium propellant systems utilizing surface tension to position and transfer liquid propellant in zero-g environment studied with high voltage electrical isolation methods [AIAA PAPER 67-681] 21 p3692 A67-38712

Solar electric propulsion for space missions, evaluating modularized ion propulsion systems to determine effect of electric isolation on system reliability, weight, etc [AIAA PAPER 67-699] 21 p3697 A67-38959

ELECTRIC LEAD

Axial lead package and stack design of batch fabricated matrices to speed integrated circuit assembly 11 p1760 A67-24260

Thermal performance of insulated current carrying leads for cryogenic apparatus 13 p2229 A67-27663

Wideband phase-leading quadrupoles with circuit breakers and effect on envelope of modulated signal 13 p2085 A67-27706

Rocketsonde thermistor mount noting thin film configuration and long lead mount for heat dissipation 23 p4025 A67-41446

ELECTRIC MEASUREMENT

SA MAGNETIC MEASUREMENT

Resonance methods for measuring input admittance of low power electronic tubes of type used in telemetry, radar and TV over frequency range from 50 to 1000 MHz 02 p0279 A67-11462

Permittivity determination based on change in polarization of wave at reflection 02 p0191 A67-11578

Statistical topological analysis of electric measurement precision and accuracy 04 p0657 A67-14887

Atmospheric charge density measurement by Faraday cage and Obolensky filter 05 p0803 A67-17384

Wideband multichannel transient monitoring system for detection and analysis of electrical transient 05 p0809 A67-17537

Small signal MIS capacitance vs bias characteristics measured over wide range of biases and sweep speeds 06 p1002 A67-17979

Well logging methods for study of composition of planetary near surface layers, noting electric, nuclear and acoustic measurement methods 06 p1092 A67-19016

Resonant cavity technique for measurement of k/β diagrams /dispersion relations/ of leaky wave structures 07 p1153 A67-19612

Electric field measuring methods, showing Stark effect in rotational spectra of gases as most promising 08 p1311 A67-20652

Measuring technology and automation - Conference, Dusseldorf, October 1965 08 p1313 A67-21004

Current-voltage characteristics of moving argon plasma, noting variation of plasma conductance with flush and filament electrodes 09 p1540 A67-21786

Plasma diffusion across static magnetic fields in electrodeless E type RF discharges 11 p1830 A67-24008

Electric field meter /E-meter/ measurement of field strength at given point on spacecraft surface [AIAA PAPER 66-74] 13 p2120 A67-26835

Measurement of resistance of thin metal films and kinetics of charge drain from surface 15 p2485 A67-29126

Transistor failure analyses by measuring electric parameters, repeating production phases on opened transistors, destructive testing and defect production by extreme artificial stress 15 p2449 A67-29811

Electrical conductivity measurement of liquid-vapor potassium mixture flowing in circular steel tube simulating MHD oscillator conditions 16 p2712 A67-30575

Admissible film thickness in probe measurements of electrical conductivity of semiconductor samples 17 p2910 A67-31928

Temperature autostabilizing nonlinear dielectric element /TANDEL/ for electric measurement circuits and measurement transducers 17 p2828 A67-32829

First order prediction of equilibrium photocurrent in silicon switching diodes and radiation storage time in silicon low power planar and mesa transistors from electrical measurements 17 p2918 A67-32851

Resonance method for measuring microwave resonators Q-factor and its small variations 19 p3191 A67-34982

Electric field measurements with isolated electrodes ejected near apex, finding continuous changes near 100 and 80 km 19 p3217 A67-35199

Saturation current measurement in diffusion transistors by method yielding current amplification factors and voltage dependence of emitter current 19 p3197 A67-35726

Electron deflection instrument for measuring surface electric field strength 20 p3444 A67-36524

Electrometer and varactor devices for onboard low current measurements in space probes 21 p3599 A67-38634

Analytic model for output voltage of fluxgate magnetometer, demonstrating excitation function and core squareness effects 22 p3800 A67-39911

Soviet papers on thermoelectric measurements and monitoring 22 p3801 A67-40212

Direct measurement of transfer curve slope of active quadrupole circuit to determine drain current and gate voltage of field effect transistors 22 p3773 A67-40305

Superconducting parametric amplifier for measurements of small DC voltages in low impedance circuits 22 p3866 A67-40441

Test procedure for Si microcircuit production consisting of bulk and junctions electric measurement, oxide thickness and junction position 23 p3977 A67-40660

Threshold voltage for onset of image-spot blurring of field-ion microscope screen and function of tip temperature 23 p3998 A67-40896

Device for metering variety of metals for high vacuum evaporation designed for thin film metal-insulator-metal diodes fabrication 23 p4001 A67-41223

Pyroelectric effect using single barium titanate crystals with liquid electrodes extending ferroelectric switching time measurements to low

fields 24 p4203 A67-42090

ELECTRIC MOMENT

S NUCLEAR-ELECTRIC MOMENT

ELECTRIC MOTOR

Electric motor energized by microwaves in waveguides at S-band, investigating speed, torque and frequency characteristics 02 p0183 A67-12116

DC motor with switching by magnetoresistant elements 21 p3571 A67-38225

ELECTRIC NETWORK

SA RC NETWORK

SA TRANSMISSION LINE

High speed cameras with image converter tubes noting electrical circuits 01 p0067 A67-10774

Real function interpolation method for synthesis of electric networks in time domain by sinusoidal exponential series 03 p0458 A67-13505

Delay equalization in UHF range by allpass networks with symmetric three-conductor transmission lines 11 p1760 A67-24231

Electrothermal analogies for heat transfer simulation by equivalent electrical circuits 11 p1884 A67-25047

Electronic and ultrasonic principles defining pulse-echo high resolution and application to electronic and electroacoustic circuitry for testing aerospace structures 12 p1948 A67-25218

Low cost time delay and multiple programmer for space research 12 p1909 A67-25230

Electronic circuit tolerance analysis by digital computer, discussing data availability, analysis methods and interpretation of answers 15 p2440 A67-29938

Coordinate photodiode matrix with photocells positioned at current-conducting busbar intersections, describing preparation technique 18 p3009 A67-33471

Installation for measuring wear rate, friction force, etc. of plane surfaces in alternating motion 20 p3453 A67-36198

Equivalent electrical circuit model, corresponding to laser energy-level model, used to describe laser action in terms of circuit theory 20 p3459 A67-36768

Receiver mixer design characteristics effect on prediction of spurious response levels 20 p3405 A67-37648

Frequency characteristics of planar and spherical plasma resonance probes and RF impedance probe in magnetic field, considering equivalent electric circuit 20 p3503 A67-37670

Large capacity cryoelectric random access memories, examining three-wire cells and hybrid system for batch fabrication, redundancy, electric parameters, tolerances and noise 22 p3764 A67-39898

Series and parallel pulse forming feed networks for generating microwave signals, comparing output parameters and limitations 22 p3774 A67-40444

Electronic network analysis using topological techniques of signal flow graphs, flow graphs and k-trees 22 p3778 A67-40556

ELECTRIC POTENTIAL

SA BIOELECTRIC POTENTIAL

SA VOLTAGE

Configurations of HF discharge plasma and dependence on gas pressure and annular electrode potential 01 p0122 A67-10348

Surface photopotential of cadmium sulphide single crystals under monochromatic illumination in alternating electric field, using voltage modulation method 01 p0134 A67-10807

Radiosonde for measurement of electric potential gradient in atmosphere at high altitudes 01 p0068 A67-10870

Thermally grown silicon dioxide and resulting silicon-silicon dioxide interface, noting potential difference effect on n-type inversion layer 02 p0293 A67-11753

Electric conductivity due to tunnel effect in aluminum-alumina-silver sandwich structures, determining potential barrier in alumina and absorption coefficient of hot electrons 02 p0295 A67-11762

Potential distribution, I-V characteristics and pulse shape of n-type Ge with sealed-in Sn, In-Sb, Sn-Sb and Pb-Sb contacts in strong electrical field 02 p0300 A67-12480

Electric potential and current density distribution in MHD channel allowing for anisotropy in conductivity 04 p0666 A67-15190

Variation of floating potential formed

between electrodes by injection of electronegative gas is logarithmic function of electron attachment coefficient on neutral particles 04 p0669 A67-15496

Dember effect, bulk photovoltaic effect and current density in illuminated inhomogeneous semiconductor 05 p0863 A67-16702

Current in channel with symmetrical end electrodes, noting stepwise dependence of near-electrode potential on current density 06 p1045 A67-18812

Waveforms of spike potentials from neurons in anteroventral cochlear nucleus indicate spikes are composed of three components 08 p1286 A67-20303

Potentials of zero charge of gold, silver and mercury electrodes as affected by cations and respective metal ion interaction 11 p1749 A67-23920

Potential buildup on electron emitting ionospheric satellite, noting limitation on current emission by geomagnetic field 11 p1869 A67-23941

Potential distribution in emitter diode measured in single ended Q machine, using ribbon electron beam 11 p1764 A67-24373

Configurations of HF discharge plasma and dependence on gas pressure and annular electrode potential 11 p1844 A67-25021

Fringe effects in MHD generator channels determining potential and current distribution and estimating losses 12 p1901 A67-26078

Electric potential distribution in flame for electronegative gas layer present between two electrodes 13 p2165 A67-26597

Self-consistent distribution theory of charged particles and electric potential in wake of conducting body moving rapidly in rarefied plasma 14 p2357 A67-28206

Computer solution for current density continuity and Poisson equation to obtain electron density and electrostatic potential in p-n junction 14 p2290 A67-28931

Asymmetric proton injection into magnetosphere using Vlasov equation, with solution in terms of electric potential 16 p2666 A67-31403

Probability density and random distribution function derived from finite series for instantaneous voltage measurements of ideal multiplying device 16 p2653 A67-31718

Surface potential contrast induced by electron beam of scanning microscope on unbiased planar transistors, investigating beam voltage effect on contrast formation 17 p2823 A67-32197

Fourier series applied to X-ray investigation of potential and electron density distribution in silicon lattice to study chemical bonds 18 p3094 A67-33433

Evoked potential display procedures yielding photographic superposition of large number of average responses 19 p3179 A67-34955

Active impurities concentration in p-type semiconductors by measuring temperature at zero thermoelectric potential 19 p3308 A67-35875

Cesium plasma diode investigated using ribbon electron beam probing technique discussing stability of electric potential distribution modes 20 p3496 A67-36323

Simultaneous and independent potentiostatic control of rotating ring and disk electrode and application to CuI/CuI/Cu system 20 p3446 A67-36655

Connections between superconductivity and electromagnetic potentials, presenting model for flow of superconducting electrons and quantization of fluxoid 22 p3863 A67-40196

Electrostatic and magnetostatic potentials for slender bodies of revolution in axially symmetric external fields 23 p4026 A67-40755

Data analysis on electric potential gradient and air-to-earth current density 24 p4181 A67-41799

Electrification of single crystals of semiconductor compounds of AIIIBVI and AIIIBV type after exposure to ruby laser pulses 24 p4167 A67-42168

Pump frequency reduction in Adler tubes examining spatial harmonics of quadrupole structure field and suggesting use of cophase connection 24 p4130 A67-42244

Differential RF voltage comparator for transfer standard and calibration of HV voltage devices at high

- accuracy 24 p4155 A67-42288
Charge time determined as circuit constants function in designing linear detectors 24 p4158 A67-42716
- ELECTRIC POWER CONVERSION**
SA MAGNETOHYDRODYNAMIC GENERATOR
Power amplifier used in electrodynamic shakers for transforming electrical into mechanical vibrations, examining range, deformations, humming and impedance 03 p0363 A67-13398
Space satellite power converter-regulator design for minimum magnetic disturbance 05 p0754 A67-17462
Steady MHD electric power generation, flow velocity effect on single controlled glow discharge in cesium-seeded argon 12 p1974 A67-25402
Radial electric field role in electrofluid dynamic conversion of flowing gas energy into electric energy 12 p1901 A67-25933
Mobile hydrogen generators for alkaline electrolyte cells and medium temperature fuel cells for autonomous hydrocarbon electricity units 14 p2253 A67-29021
Direct energy conversion techniques in generating electric power in space for future astronautic systems 14 p2253 A67-29044
Digital computer program FORTRAN coded, analyzing electric power distribution system of aerospace vehicle 17 p2804 A67-32511
Flow stability in MHD generators after extracting significant electrical power from gas 18 p2987 A67-33705
MHD equation simplifications and MHD converter model for problem solving, discussing electrical and thermodynamic characteristics 18 p2989 A67-34125
Electric power plant survey for space application, noting Rankine and Brayton cycles 20 p3364 A67-37017
Direct solar to electric energy conversion using superconducting flux barrier, discussing superconductive phase change and magnetic properties 22 p3748 A67-40151
NASA test program to evaluate performance and design point characteristics of 3-kw closed recuperated Brayton cycle power conversion system 24 p4102 A67-42486
Steady electric power from Cs seeded Ar plasma in nonequilibrium ionization flowing at high speed through magnetic field 24 p4109 A67-42895
- ELECTRIC PROPERTY**
SA CAPACITANCE
SA CONDUCTIVITY
SA HYSTERESIS
SA IMPEDANCE
SA INDUCTION
SA MAGNETIC PROPERTY
SA RESISTANCE
Electrical and optical properties of solid solutions formed by beta manganese and chromium dioxide within wide composition range, showing magnetic semiconductor behavior 01 p0134 A67-10755
X-ray irradiation effect on electrophysical properties of n-and p-type germanium, determining absorption coefficient 01 p0136 A67-11044
Vacuum evaporation of HgTe thin film, examining thermal treatment, electric properties as function of thickness, etc 02 p0280 A67-11463
Thin layers of crystallized cadmium telluride of high electron mobility analyzed for electrical properties and photoconductivity 02 p0294 A67-11759
Electrical properties and electron emission of sandwich cathodes prepared in vacuum by vapor phase condensation, deriving transfer constant 02 p0294 A67-11761
Electric characteristics of nGe-pGaAs heterojunctions in multistep recombination-tunneling model 02 p0299 A67-12189
Semiconducting properties of platinum arsenide with pyrite-type crystal structure 03 p0488 A67-12926
Optical and electrical properties of barrier layers in Cu doped GaP, discussing intensity region of superlinearity dependence on temperature and IR light 03 p0491 A67-13202
Temperature dependence of electrical properties of alpha-indium selenide n-type semiconductor single crystals 03 p0493 A67-13362
Boron nitride fibers in composites for aerospace application, discussing fabrication, ablative properties, etc 03 p0452 A67-13409
Anisotropic medium capacitance calculation, using method based on point-charge field behavior analysis in isotropic medium, for biconical antenna 03 p0371 A67-13866
Seebeck and Hall coefficients, electrical and thermal conductivity and figure of merit measured as function of dopant concentration of n-type CuBr doped bismuth antimonide telluride 03 p0501 A67-14350
Electrical parameters of Polish-developed silicon varactors 04 p0581 A67-14920
Crystal dislocation effect on electric properties of germanium 2, noting elastic carrier scattering 04 p0677 A67-14938
Synthesis and growth of dendritic InSb films by electron beam microzone melting of vacuum deposited composite indium and antimony films, noting electrical properties 04 p0682 A67-15319
Electrical properties of thin and thick resistive films vacuum-deposited and nonvacuum-deposited by chemical and firing process 04 p0682 A67-15485
Scattering matrix properties of symmetrical octupoles 04 p0586 A67-15673
Relation between electrical properties and structural features of gold-and antimony-doped germanium single crystals, noting abrupt decrease in mobility 05 p0861 A67-16398
Electrical properties of indium antimonide single crystals with noncompensated impurity concentration, determining position of deep-seated levels in forbidden band 05 p0861 A67-16399
Impurity microsegregation substructure in n-and p-type bismuth telluride crystals grown according to Bridgman method, measuring electrical properties, thermal emf, Hall constant, etc 05 p0861 A67-16498
Silicon electrical properties at low temperatures and various carrier concentrations, noting impurity 05 p0861 A67-16502
Temperature dependence of electrical and galvanomagnetic properties of single crystal InSb dendrites 05 p0869 A67-17092
Upper sideband effect in parametric amplifier on positive conductance and negative resistance of circuits, deriving noise figure expression 06 p0966 A67-17575
Electron irradiation effect on electric properties of gallium arsenide 06 p1049 A67-17858
Mercury telluride thin film properties and fabrication methods 06 p1050 A67-18185
Hall effect and resistivity in n-GaAs with Si as shallow donor, obtaining ionization energy and impurity band conduction values 06 p1052 A67-18570
Electric properties of gas dynamic mirror formed in wake of shock wave front 07 p1227 A67-19118
Corrections for dielectric-constant tensor and conductivity tensor resulting from effect of electric field induced by plasmoid 07 p1229 A67-19517
Soviet book on electronic properties of semiconductor solid solutions, noting relation between probability theory and ideal crystals theory 07 p1232 A67-19580
Mechanical and electrical performance requirements of satellite communications antenna using Cassegrain configuration, noting relation to design 07 p1157 A67-20092
Electrical characteristics of linear segmented electrode Hall and Faraday MHD generators, noting power output reduction due to electrode voltage losses 08 p1283 A67-20578
Built-in voltage decrease in bulk germanium and Ge tunnel diodes under irradiation, noting Fermi level 09 p1471 A67-21764
Electrical parameters of DC MHD generator determined from equivalent circuits 09 p1471 A67-21796
Electrical characteristics of thin film nickel-chromium resistors dependency on variation in processing parameters including source and film composition, deposition rate, etc 09 p1555 A67-22103
Resistivity, Hall effect and thermoelectric power of mercury selenide from 77 to 500 degrees K 09 p1557 A67-22556
Temperature dependence of electrical properties of compensated GaAs 10 p1694 A67-23655
Electric, thermal and physical properties of pyrolytic carbides and nitrides of group IV metals 11 p1804 A67-23903
Gallium arsenide electron photon transistor electrical properties at cryogenic and room temperature, determining total internal quantum yield of photons 11 p1765 A67-24475
Crystallographic anisotropy of electrical properties of thin film CdS photoresistors explained via potential barrier orientation theory 12 p1984 A67-25520
Electric conductivity, Hall effect and photoconductivity of epitaxial single crystal GaAs films obtained by gas transport method 12 p1984 A67-25521
Low temperature deuteron irradiation effect on type II superconductors noting atomic displacement, resistivity increase and transition temperature decrease 12 p1985 A67-25845
Thermal and electrical properties and width of forbidden bands of PbTe and PbSe from 90 to 800 degrees K 12 p1986 A67-26094
Electronic structure and electrophysical properties of d-transition metal sulphides 12 p1986 A67-26096
Current voltage characteristics of alloyed p-n junctions in n-type InAs, discussing contribution of tunnel current 12 p1986 A67-26099
Electric and photoelectric properties of p-n junction obtained by thermal diffusion of copper into n-ZnS-Cl single crystals 13 p2172 A67-26355
Nature of glassy state, reviewing nucleation, crystallization, chemical, physical, and electrical properties and transformation of glasses 13 p2143 A67-26696
Structure dependent electric properties of anodized and unanodized tantalum-tantalum oxide thin film resistors, discussing aging, heat treatment, etc 13 p2082 A67-27366
Technique of fabricating inhomogeneous mediums and behavior of dipole 13 p2082 A67-27407
Impurities effect on electrical and thermomagnetic properties of cadmium tin arsenide 13 p2184 A67-27707
Dielectric properties applied determination of degree of reticulation of polymers during polymerization, noting losses due to free electrons and dipoles 14 p2340 A67-27898
Nuclear radiation damage to circuit elements of missile FM/FM telemetry system, analyzing changes in electric characteristics 14 p2271 A67-28685
Gunn diodes using Sn-Ag and In-Au contacts studied for electrical properties and failure mechanisms 14 p2290 A67-28927
Electrical property change of pressure sensitive electronic components upon embedment in casting resins, noting results of inductance changes in ferrite core transformer 14 p2341 A67-28954
Copper phthalocyanine single crystal measurements for electric, thermoelectric and galvanomagnetic properties 14 p2376 A67-29086
Coaxial plasma gun for plasmoids showing higher mean energy when gas admission is closer to plasma source 15 p2525 A67-29252
Epitaxial deposition of p-GaAs on n-GaAs noting dislocations, packing defect concentrations and V-I characteristics 15 p2533 A67-29317
Current-voltage characteristic determination for n-InSb Corbino disk, noting capacitance and internal resistance current source at cryogenic temperature 15 p2534 A67-29359
Lanthanum chromite activation energy determination from electrical resistivity and Hall coefficient variation as function of temperature and IR absorption spectrum 15 p2535 A67-29478
Electrical properties of degenerate intrinsic semiconductor noting spherical energy surfaces, parabolic density of states, acoustic phonon scattering, etc 15 p2535 A67-29487
Microwave transmission measurements of electrical properties of shock ionized air noting dielectric constant, electron density, conductivity, attenuation, etc 15 p2470 A67-29490
Production of crossed field and beam microwave tubes, noting demagnetization and coercive and inductance forces of various magnetic

materials 15 p2447 A67-29753
 DC and aC parameters of germanium tunnel diodes in 3 to 5 milliamp range measured by ammeter dC and AC parameters of germanium tunnel diodes in 3 to 5 milliamp range measured by ammeter 15 p2449 A67-29807
 Variation of series resistance and junction capacity in tunnel diodes used in microwave switching 15 p2449 A67-29808
 Special plastics for low loss microwave transmission devices, describing electrical properties 15 p2508 A67-29930
 Fast neutron bombardment and temperature effects on conductivity, photoconductivity and resistivity of Si single crystals, determining energy levels of defects 15 p2541 A67-30236
 Conductivity and Hall effect in analysis of temperature dependence of current carrier concentration and mobility in silicon, explaining ionization energy 15 p2541 A67-30240
 Electrical characteristics of low current arc discharge in magnetic field determining effect of nonequilibrium plasma on conductivity 16 p2710 A67-30524
 MHD generator terminal values and other electric parameters deviations for various finite length electrodes connected in series 16 p2600 A67-30532
 Arbitrary electrode MHD generator electrical characteristics, considering end effects and determining internal conduction matrix 16 p2600 A67-30534
 Nonequilibrium linear MHD generator electrical characteristics, discussing power output and Hall potential reduction causes 16 p2602 A67-30558
 Large combustion-driven, self-excited Faraday-type MHD generator having multi-or single-circuit net power output, discussing design 16 p2608 A67-30596
 Carrousel magnetoaerodynamic generator, defining equations governing development of electric and thermodynamic properties of plasma 16 p2608 A67-30599
 Analog-to-digital conversion method for measuring weak currents, giving diagram of measuring circuit 16 p2635 A67-30672
 Refractory intermetallic compounds as high mobility semiconductors, noting crystal preparation and lowest carrier concentration obtained 16 p2725 A67-30806
 Diffusion, solubility and electrical behavior of lithium in gallium 16 p2726 A67-30811
 Hardness, electrical resistance and phase composition on Ni-Mo alloy during annealing, discussing phase transformations 16 p2687 A67-30847
 Density, crystallinity and electric properties of thin metal films deposited on rotating cylindrical substrate 16 p2727 A67-30899
 Langmuir-Blodgett multilayers of stearic acid investigated as thin film dielectric 16 p2728 A67-31020
 Attachment and detachment processes effect on plasma quenching by electronegative gases, showing usefulness of steady state nitrogen afterglow flow system 16 p2720 A67-31238
 Variables in screen printing and firing processes for thick film resistors affecting reproducibility 16 p2641 A67-31620
 Magnetic, electric and SHF properties of oxides and solid solutions of bivalent europium from 1.6 to 300 degrees K 16 p2733 A67-31732
 Book on intermetallic compounds discussing bonding, crystal structure, microstructure, formation, stability, kinetics, transformations and properties 16 p2692 A67-31867
 Space-charge-limited dielectric diode with quadratic I-V characteristics, noting shallow trap effects on detection properties 17 p2823 A67-32199
 Stress effect on electric properties of p-n junction of semiconductor diodes and means of control 17 p2912 A67-32252
 Semiconductor crystal structure defects caused by irradiation with energetic particles and photons 17 p2913 A67-32372
 Plane structure silicon transistors subjected to Co gamma radiation, considering electrical properties degradation to predict component survival probability 17 p2917 A67-32842
 Temperature dependence of electrical

properties of compensated GaAs 17 p2923 A67-33336
 Physical properties of semiconductors relation with energy and nature of interatomic bonds, discussing effect on elastic constant, thermodynamic functions, electric and dielectric properties 18 p3094 A67-33435
 Pauling empirical equation relating thermal effect of reaction to negative ionization potential of solid substances 18 p3094 A67-33438
 Paramagnetic and electrical properties of organic polyvinyl-acetate-based semiconductor films irradiated with electrons before and after heating 18 p3099 A67-33694
 Crystallographic anisotropy of electrical properties of thin film CdS photoresistors explained via potential barrier orientation theory 18 p3103 A67-34451
 Electric conductivity, Hall effect and photoconductivity of epitaxial single crystal GaAs films obtained by gas transport method 18 p3103 A67-34452
 Currents in copper phthalocyanine thin films measured as function of temperature and ambient noting effect on conductivity, trap density, etc 18 p3104 A67-34627
 Electrical characteristics of degenerate n-type germanium diode with gold or indium as metallic element 18 p3105 A67-34635
 Electrical characteristics of GaAs p-n diffusion junctions used as solar cells 19 p3300 A67-34769
 Thin CdS films thermal deposited in vacuum on various substrates investigated for electric properties 19 p3305 A67-35577
 Flowgraph models describing relationships between thermal and electrical parameters of devices and associated circuits 19 p3206 A67-36034
 Conductance and capacitance measurements on grain boundaries in p-type indium antimonide 20 p3504 A67-36173
 MOS devices electrical characteristics controlled by physical parameters studied for approximate relations between loads, potentials and surface fields 20 p3507 A67-36319
 Radiation effects on MOS devices, analyzing electrical characteristics degradation mode and conduction threshold voltage variation 20 p3396 A67-36321
 Si optical and electrical properties and energy levels with Mg as donor impurity 20 p3510 A67-36916
 Book on transistor electrical characteristics, discussing transistor model correspondence with real transistors, temperature variation effects, etc 20 p3399 A67-37010
 Zn doped polycrystalline GaAs film electrical properties temperature variation 20 p3514 A67-37602
 InBi single crystal electrophysical properties, giving temperature dependences 20 p3514 A67-37605
 Electric conduction in solids, considering impurity, temperature and light effects on resistivity to electric currents 20 p3515 A67-37716
 Electric properties of gas dynamic mirror formed in wake of shock wave front 21 p3664 A67-38163
 Electric and photoelectric properties of p-n junction obtained by thermal diffusion of copper into n-ZnS-Cl single crystals 21 p3679 A67-38312
 Phosphorus concentration influence on epitaxial silicon layers growth and electrical characteristics 21 p3681 A67-38362
 Book on electrical properties of semiconductor surfaces covering space charge layer theory, solid state theory, etc 21 p3682 A67-38365
 AlN single crystal thermally stable semiconductor optical/electrical properties, measuring space-charge-limited current and photocurrent 21 p3684 A67-38522
 Atmospheric inhomogeneities effect on large antenna directive gain, noting dependence on length and wave field 21 p3600 A67-38812
 Coherent amplification properties of antireflective coated GaAs diodes considered for application to phased array 22 p3813 A67-39254
 N-type Hall effect in high temperature Li doped ceramic sample of MnO, measuring electric transport

properties 22 p3858 A67-39521
 Electrical characteristics of thin triangular barium titanate crystals in strong electric fields 22 p3859 A67-39579
 High performance engineering thermoplastic/Polymer 360/mechanical and electrical properties and environmental factors effects 22 p3825 A67-39858
 Heat treatment effect in various gaseous media on electrical properties of CdTe films with abnormally high photovoltage, noting structural stabilization 22 p3861 A67-39924
 Low temperature electron irradiation effects on undoped GaSb resulting in impurity conduction 22 p3862 A67-40000
 Posistors barium titanate, lead titanate and potassium compound semiconductor and ferroelectric properties analyses indicating closely interrelated properties 22 p3801 A67-40215
 TI thin film microcircuit fabrication and electrical properties 23 p3977 A67-40661
 Soviet book on present state of semiconductor technology covering theory, material properties and semiconductor devices 23 p3978 A67-40797
 Evaporated metallic contacts to conducting strontium titanate single crystals measured for electric properties evaporated metallic contacts to conducting strontium titanate single crystals measured for 23 p4038 A67-40874
 Property changes of semiconductor materials during processing, discussing photoelectric methods, resistivity derivative, recombination parameters and mechanical stresses 23 p4043 A67-41364
 High voltage solar cell made by integrated circuit processes noting fabrication and electrical characteristics 23 p3937 A67-41492
 Equilateral triangular stepped helical aerial observed characteristics including impedance variation, radiation patterns, axial ratio and velocity factor 24 p4128 A67-41970
ELECTRIC PROPULSION
SA ELECTROSTATIC PROPULSION
SA IONIC PROPULSION
SA NUCLEAR-ELECTRIC PROPULSION
 Electrothermal, electromagnetics and electrostatic propulsion system design principles, operation applications and performance characteristics 01 p0142 A67-11410
 Solid propellant electrical thrusters for spacecraft attitude and trajectory control 01 p0142 A67-11433
 Weight, efficiency and control requirements of subsystems of electric propulsion applied to Mars missions, selecting power-conditioning modules for ion propulsion engines 02 p0302 A67-11516
 [AIAA PAPER 66-501] 02 p0302 A67-11516
 Cesium ion beam generation by accelerating cesium in space charge sheath located between ionizer and plasma filled region 02 p0303 A67-12251
 [AIAA PAPER 66-927] 02 p0303 A67-12251
 Solar and nuclear-electric propulsion thrusters including ion engines, plasma engines, arc jets, resistojets, etc 02 p0303 A67-12253
 [AIAA PAPER 66-830] 02 p0303 A67-12253
 Solar cell power systems for electric propulsion, considering methods of generating, controlling and conditioning onboard electric power 02 p0183 A67-12269
 [AIAA PAPER 66-891] 02 p0183 A67-12269
 Solar electropulsion developments for solar system exploration 03 p0513 A67-14097
 Nuclear power supplies for electrical propulsion including liquid metal reactor-potassium Rankine, Brayton, MHD power conversion and thermionic reactor 03 p0363 A67-14153
 [AIAA PAPER 66-1021] 03 p0363 A67-14153
 Electric propulsion status of thruster performance, promises and potentialities 03 p0504 A67-14155
 [AIAA PAPER 66-1024] 03 p0504 A67-14155
 Electric propulsion role in auxiliary and primary spacecraft propulsion 03 p0504 A67-14156
 [AIAA PAPER 66-1025] 03 p0504 A67-14156
 Rankine cycle power plant characteristics for electric propulsion manned Mars mission 03 p0504 A67-14274
 [AIAA PAPER 66-894] 03 p0504 A67-14274
 Low specific impulse electric propulsion with plasma separator thruster that prevents surface recombination, drawback of Kaufman thruster 04 p0687 A67-14428
 High altitude high voltage breakdown in electric propulsion flight test system 04 p0704 A67-14997
 CS contact ion engine technological status, engine life and performance

- characteristics 04 p0689 A67-15019
Ionization recombination mechanisms and density-time profiles for electric propulsion unit efflux 04 p0690 A67-15024
Electric thrusters and electric propulsion, examining overall efficiency as function of specific impulse 05 p0874 A67-16933
Solar electric spacecraft performance in specific Mars orbiter-lander mission evaluated, using characteristic length concept 06 p1074 A67-18276
Electric propulsion unit using electron cyclotron resonance plasma thruster for spacecraft 06 p1074 A67-18418
Photographic mapping of Martian surface with electrically propelled solar-powered photographic spacecraft placed into near polar orbit
[AIAA PAPER 67-88] 06 p1096 A67-18438
Megawatt ion-propulsion power conditioning system design for manned interplanetary missions, noting payload-mass ratio problems, advantages, etc
[AIAA PAPER 67-52] 06 p1075 A67-18449
Electric propulsion research in foreign countries
[AIAA PAPER 67-53] 06 p1075 A67-18494
Nuclear thermionic propulsion system with low specific weight as interplanetary propulsion system
[AIAA PAPER 67-229] 06 p1029 A67-18519
Electric propulsion for satellite applications, noting cesium contact microthruster ion engine system
[AIAA PAPER 67-80] 07 p1240 A67-19435
Replacement of chemical launching rockets by advanced propulsion system, with particular reference to nuclear rocket 07 p1242 A67-20264
Expressions showing possibilities to exchange independently all orbital elements of spacecraft by means of small continuous thrusts achieved through electric propulsion 08 p1413 A67-21365
Evaluation of requirements for ground testing of electric propulsion devices in vacuum, noting effects of sputtering phenomena 09 p1559 A67-22120
Book on propulsion systems covering gas-turbine engine, ramjet engine, chemical and electrical rockets, components, etc 10 p1698 A67-23689
Radioisotope applications to space science, discussing selection criteria for electric energy production and/or space propulsion 11 p1817 A67-24096
Collector target complex eliminating target life time and test equipment contamination by sputtered target material, applied in testing of electrical propulsion systems
[AIAA PAPER 66-500] 11 p1852 A67-24341
Electric propulsion for manned interplanetary mission evaluated in light of new optimum planetary transfer trajectories of power-limited flight 11 p1859 A67-24342
Suitability of Saturn IB/Centaur and Atlas/Centaur launched solar-electric propulsion vehicles for performing 0.1-AU solar probe mission
[AIAA PAPER 66-496] 11 p1852 A67-24343
Magnetically accelerating continuously operating plasma engine for spacecraft propulsion compared with electrothermal engine 11 p1855 A67-25100
Cathode spot phenomena in pulsed vacuum are utilized for electric microthrusters, testing cathode materials by mass and momentum transfer
Measurements 12 p1989 A67-25403
Maximum payload for air-scooping low thrust space propulsion system 13 p2212 A67-26893
Propulsion systems in which propulsive fluid is accelerated to high speeds by electrical or electromagnetic processes 14 p2377 A67-28962
Electric and photon propulsion systems in German-American research 16 p2736 A67-30710
Thermionic conversion system using mixed vapors for electric propulsion power 16 p2608 A67-30715
Electric drive operating parameters and design, using exploding wire type device and electromagnetic apparatus for plasma production and acceleration 16 p2736 A67-30716
Primary electric propulsion systems for deep space missions with reference to SERT II program and compatibility with other spacecraft programs
[AIAA PAPER 67-424] 18 p3111 A67-33908
Primary electric propulsion application to satellite and other space missions, considering auxiliary systems and experimental thruster systems
[AIAA PAPER 67-426] 18 p3112 A67-33910
Combined electric constant low thrust and chemical or nuclear high thrust space propulsion systems for interplanetary missions
[AIAA PAPER 67-511] 18 p3114 A67-33975
In situ study of comets by solar electric propulsion spacecraft, analyzing mission characteristics 19 p3323 A67-35333
Solar-electric powered vehicle trajectory optimization using variational calculus, assuming general forms for efficiency and solar power variation
[AIAA PAPER 67-583] 19 p3329 A67-35978
Solid propellant electric thruster /SPET/ using pulse plasma for spacecraft attitude control and stationkeeping
[AIAA PAPER 67-661] 21 p3690 A67-38697
Space electric rocket test /SERT/ II thruster system, discussing flight worthiness and mercury bombardment discharges
[AIAA PAPER 67-700] 21 p3693 A67-38728
Low thrust Jupiter flyby mission analysis for interplanetary vehicles with solar electric propulsion
[AIAA PAPER 67-708] 21 p3706 A67-38735
Approximate method for electric propulsion missions analysis, determining system components effects on performance
[AIAA PAPER 67-709] 21 p3693 A67-38736
Trajectory optimization, performance and other factors in analysis of low thrust solar electric propulsion Jupiter flyby mission
[AIAA PAPER 67-710] 21 p3706 A67-38737
High payload electric propulsion spacecraft powered by solar array for multiple interplanetary missions
[AIAA PAPER 67-711] 21 p3714 A67-38738
Spacecraft design, solar powering, electric propulsion and side-looking radar for planetary surface observation mission on Mars or Venus
[AIAA PAPER 67-712] 21 p3714 A67-38739
Satellite orbit adjustment, stationkeeping and attitude control of typical earth-and sun-synchronous satellites by electric propulsion systems
[AIAA PAPER 67-719] 21 p3694 A67-38745
Pulsed vacuum arc microthruster noting various performance data and advantages
[AIAA PAPER 67-737] 21 p3695 A67-38759
French research on electric propulsion dealing with plasma dynamics, discussing traveling wave accelerators, pulsed plasma guns, ion thrusters, etc
[AIAA PAPER 67-740] 21 p3695 A67-38762
Solar electric propulsion for space missions, evaluating modularized ion propulsion systems to determine effect of electric isolation on system reliability, weight, etc
[AIAA PAPER 67-699] 21 p3697 A67-38959
Graphic optimization technique for mass reduction in solar powered ion propulsion system with acceptable reliability constraint
[AIAA PAPER 67-701] 21 p3697 A67-38960
Electric propulsion applied to satellite stationkeeping and attitude control, noting ion engine resistor combination providing complete redundancy
[AIAA PAPER 67-722] 21 p3697 A67-38961
Electric propulsion ion engine systems using solar power source for Mars and Jupiter exploratory unmanned spacecraft is adaptable to existing launch vehicles
[AIAA PAPER 67-713] 22 p3868 A67-39844
Rankine cycle power plant for electric propulsion manned Mars mission analysis of system characteristics and mission duration effect 22 p3869 A67-40173
Synchronous orbit communication satellite electric thruster, considering space charge neutralized ion accelerator 23 p4049 A67-41428
Cesium ion beam generation by accelerating cesium in space charge sheath located between ionizer and plasma filled region
[AIAA PAPER 66-927] 23 p4049 A67-41736
Lithium-boiling potassium test facility to investigate transient and steady state characteristics of Rankine cycle system for application to spacecraft nuclear-electric propulsion 24 p4183 A67-42492
Electrical design of large lightweight solar array for electric propulsion type Mars-bound spacecraft, discussing magnetic effects and power losses 24 p4104 A67-42512
Primary electric propulsion application to satellite and other space missions, considering auxiliary systems and experimental thruster systems
[AIAA PAPER 67-426] 24 p4208 A67-42901
Electric propulsion research in foreign countries
[AIAA PAPER 67-53] 24 p4208 A67-42902
ELECTRIC PULSE
Potential distribution, I-V characteristics and pulse shape of n-type Ge with sealed-in Sn, In-Sb, Sn-Sb and Pb-Sb contacts in strong electrical field 02 p0300 A67-12480
Environmental wind tunnel investigation of wind velocity and discharge current effects on average charge per Trichel pulse in corona discharges 03 p0486 A67-14119
Short triple electric and light pulse generation noting equipment design and performance 03 p0388 A67-14270
Logic and memory circuits and operational dynamics of system of pulsed elements operating on tunnel diodes 05 p0772 A67-16451
Pulse response of MOSFET and depletion layer FET 05 p0778 A67-17324
Effects of parameters of series circuit on current pulse in active load, using computer to calculate series circuit 05 p0785 A67-17470
Interpreting short voltage pulse measurements of electron drift velocity in n-GaAs 06 p1048 A67-17815
Electrodynamics of combined operation of transistors and tunnel diodes in pulsed circuit 06 p0970 A67-18170
Performance characteristics of cryotron memory cell for measuring pulses arriving at input from current magnitude 06 p0966 A67-18242
Short pulse start/stop control of tunnel diode oscillator 07 p1153 A67-19608
Pulsed sinusoidal bridge for simultaneous measurement of volt-capacitance and volt-ampere characteristics of relaxing p-n junction barriers 08 p1303 A67-20998
Apparatus producing voltage pulses in X-band magnetrons operating on pulse lengths of tens of nanoseconds 09 p1479 A67-22262
Transient switching process of semiconductor planar diode with retarding electric field in base operated by short forward current pulses 11 p1764 A67-24469
Avalanche injection and application to fast pulse generation and switching 13 p2079 A67-26872
General equation for suppressor controlled transconductance of pentode useful for circuit analysis 16 p2635 A67-30794
Weak DC signals conversion into electric pulses by magnetic semiconductor pulse width modulator using AC generator 17 p2823 A67-32224
Delay time between current pulse and light emission of GaAs laser diodes, noting nonlinearity between current and delay time 17 p2824 A67-32316
Periodic changes, using square-wave current modulation, between diffuse and highly constricted positive column in medium-pressure rare-gas discharges 19 p3274 A67-35101
Pulsar circuit for studying large signal transient response in plasma lasers 20 p3445 A67-36530
Longitudinal vibration formation by high density electric current pulses in rod, discussing thermoelastic excitation and electrodynamic radial compression 20 p3486 A67-37060
Electrical and spectral investigation of pulsed high pressure arc produced by capacitor bank discharge in helium and hydrogen 22 p3845 A67-39426
Two base diode circuit having rectangular voltage pulse applied to one of base contacts investigated for front pulse delay phenomenon 22 p3769 A67-39572
Series and parallel pulse forming feed networks for generating microwave signals, comparing output parameters and limitations 22 p3774 A67-40444
High gain wideband amplifier with rapid pulse trains, discussing silicon transistor response time, impedance, Q-factor and correction circuit 23 p3977 A67-40691
Recovery time of carbon dioxide laser excited by electric pulse discharge noting heat conduction toward

- walls 23 p4011 A67-40692
Cathode outer oxide surface heating for pulsed emission current measured in intervals between retarding current pulses and different repetition frequencies 24 p4129 A67-42231
- ELECTRIC RESISTANCE**
SA PIEZORESISTIVE DEVICE
SA RLC CIRCUIT
SA SHORT CIRCUIT
Change in resistance of titanium films deposited in high vacuum from argon ion bombardment, noting dependence on energy value 01 p0129 A67-10099
Static accuracy of temperature stabilization in thermostat increase by using temperature dependences of heat regulators and active resistance of output transformer 01 p0064 A67-10424
Equivalent series resistance of semiconductor region of varactor diodes at UHF determined, using series resonance method 01 p0038 A67-10815
Input admittance and susceptance of microwave tetrode 01 p0038 A67-10829
Thermal conductor of arbitrary shape, analogy with rectangular array of electrical resistance, detailing conformal transformation 01 p0167 A67-11015
Voltage induced by electron beam in n-and p-type germanium bars having inhomogeneous resistivity distribution, obtaining equations from one-dimensional model 01 p0137 A67-11059
Apparatus for measuring temperature dependence of thermoconductivity coefficient, thermal emf and specific electroresistance of cermet cylindrical shells 01 p0076 A67-11248
Checking ohmic back contact on semiconductor wafers before fabrication of diode, using four-point probe 01 p0077 A67-11315
Electric resistance of titanium evaporated films in thickness range of path length effects 02 p0292 A67-11744
Effects of order-disorder state and film thickness on structure and electric conductivity of evaporated nickel, titanium and silver films 02 p0292 A67-11745
Electric resistance of discontinuous thin gold films as function of time and temperature 02 p0292 A67-11747
Inverse optimization for calculating refractive index and electrical resistivity of plasma in reentry and surface tension coefficient in ephydrodynamics 02 p0333 A67-12347
Resistivity, temperature coefficient of resistivity and Hall coefficient as function of bismuth film thickness, showing that size quantization of films leads to semiconductor metals 02 p0300 A67-12509
Aging of Ni containing maraging steel and related alloys analyzed by electrical resistivity, X-ray diffraction and hardness measurements, noting nature of Co-Mo interaction 03 p0440 A67-13250
Room temperature microhardness anisotropy, slip and twinning in molybdenum carbide single crystals noting orientation dependence, elastic modulus, electric resistivity and measurement techniques 03 p0441 A67-13254
Neutron bombardment effect on titanium and chromium carbides before and after heat treatment, giving results of X-ray and micrographical analyses, electric resistance, brittleness and microhardness measurements 03 p0447 A67-13639
V-I characteristics of stagnation point electrodes in lightly ionized atmospheric pressure plasma, calculating electric resistance from conductivity measurements 04 p0664 A67-14821
Quartz crystal oscillator measurements of effect of film deposition rate on resistance of chromium thin films 04 p0675 A67-14921
Base spreading resistance and junction temperature of uniform base junction transistors 04 p0582 A67-15098
Resistivity, dielectric constant and junction depth changes in semiconductor materials by exposure to electron beam 04 p0681 A67-15314
Resistance of DC arc gap recovering freely after interruption instantaneously measured, using voltage and current probing techniques 05 p0850 A67-18069
Excess carrier lifetime in semiconductors by measuring photoconductive phase shift of spreading resistance under point contact 05 p0861 A67-16501
Macroelectrodynamics equations for low temperature intermediate state of type I superconductors, noting magnetic field effect on structure 05 p0863 A67-16695
Two base-resistance measuring methods based on reverse-voltage-transfer-ratio measurement 05 p0807 A67-16949
Electric conductivity and luminescence increase in luminophorous zinc sulfide films as aftereffect of negative resistance 05 p0866 A67-17023
Metal resistivity change due to multiple point imperfections and lattice distortions, noting aggregate effect estimation from scattering power of isolated defects 05 p0830 A67-17190
Temperature dependence of emittance and electric resistance of tantalum, vanadium and niobium up to 2500 degrees C 05 p0831 A67-17312
Microwave surface resistance of type II superconductors, from simultaneous measurements of real part of surface impedance and magnetization 05 p0871 A67-17375
Electric resistivity and electroconductivity of copper composites reinforced with fibrous felts of tungsten 06 p0105 A67-17808
Current and frequency dependent differential resistance and diffusion capacity of junctions of p-n structures at high current densities 06 p0149 A67-17868
Resistive effects in type II superconductors near upper critical field examined, using Ginzburg-Landau equations 06 p0149 A67-17882
Multilayer technique for evaporation of ohmic contacts onto CdS, noting V-I characteristics and noise spectrum of recrystallized layer 06 p0150 A67-18142
Time lag in thermal coefficient of resistivity of Ge whisker explained in terms of point defect diffusion 06 p0150 A67-18144
Annealing of fast neutron damage in impurity conducting n-type Ge, noting small activation energy in resistivity below 10 degrees K 06 p0150 A67-18146
Excess noise and oscillations in gold-doped germanium photodiodes attributed to generation-recombination fluctuations of large bulk resistance 06 p0971 A67-18220
Hall effect, electrical resistivity and optical transmission data and Co impurities in GaP studied via crystal field theory 06 p1061 A67-18926
Impurity states in CdTe analyzed by examining changes in electrical and optical properties after thermal-neutron bombardment 06 p1062 A67-18928
Hall effect in hopping region of Si and Ge attributed to residual thermal and impact ionization 06 p1067 A67-18966
Resistivity, magnetoresistance, Hall effect and thermal conductivity in n-type In-Sb at liquid He temperatures 06 p1068 A67-18968
Annealing of neutron irradiation induced changes in impurity conduction in Sb-doped Ge 06 p1068 A67-18969
Titanium alloy mechanical and physical characteristics, noting dependence on chemical and phase composition 07 p1206 A67-19285
Anisotropic resistivity of dislocations produced by deformation measured in high purity Au, Ag and Cu single crystals 07 p1209 A67-19638
DC resistivity due to electron scattering from vacancy, octahedral and tetrahedral interstitials in beryllium computed by diffraction model concept of pseudopotentials in metal theory 07 p1209 A67-19643
Temperature dependence of residual resistivity of diffusing ions for electromigration of silver in copper and gold and self-diffusion of copper in aluminum 07 p1209 A67-19647
Niobium and tantalum purification from interstitial impurities by high vacuum annealing, noting effect on electric resistivity 07 p1210 A67-20112
Electrical resistance of manganin coil to 7 kbar and 200 degrees C, use as pressure indicator at elevated temperatures provided correction due to shift of resistance at different temperatures is made 08 p1353 A67-20373
Resistivity changes in thin metallic wires with lattice defects measured by various methods 08 p1368 A67-20717
Electrical resistance and weight increase measurements in aluminum and Al-Mg alloys, noting relation between oxidation rate and Mg content during annealing 08 p1341 A67-20796
Electrical resistance changes in quaternary alloy during simultaneous occurrence of phase solution coalescence and silicon spheroidization, noting effects of aging and various metal additions 08 p1342 A67-20807
Low temperature characteristics of Ga-As varactor diode junction properties, calculating spreading resistance 09 p1471 A67-21827
Thermal noise in space-charge-limited solid state diodes, showing equivalence of noise resistance with DC resistance 09 p1472 A67-21951
Direct coupling resistance component of transistorized voltage stabilizer 09 p1473 A67-21958
Resistivity variation in n-type germanium pellet measured with focused electron beam, showing position dependence of diffusion length as cause of error 09 p1473 A67-22018
Stability of palladium oxide resistive glaze films, describing process variables affecting resistivity and TCR 09 p1473 A67-22019
Pinning fluxoids by spatial inhomogeneities of Ti-Pb and Pb-In alloys, noting I-H characteristics and type II superconductor resistance 09 p1556 A67-22135
Equivalent resistance divided by interaction impedance of CEF photodemodulators for coherent light 09 p1479 A67-22278
Graphite fibers as internal electrical resistance heat source for curing structural adhesives demonstrated in lap shears, larger area and sandwich construction 09 p1507 A67-22516
Temperature dependence of magnetization and resistivity in SHF magnesium-aluminum ferrite 10 p1688 A67-22830
Fast neutron irradiated p-type silicon single crystals electric and photoelectric properties 10 p1691 A67-23404
Hall effect and electrical resistance of ZrC-NbC and TaC-HfC alloys at room temperature 11 p1804 A67-23904
Plasma conductivity measurement based on Hall current and Hall voltage relation to electrical resistance 11 p1839 A67-24424
Type II superconductor voltage proportionality to time varying magnetic field under constant transport current and linear field sweep conditions 11 p1846 A67-24583
Microwave surface absorption in static magnetic field affects surface resistance of superconducting alloys 11 p1846 A67-24584
Field equations for spreading resistance of variable capacitance diode and point contact variable resistance diode derived in terms of frequency, material characteristics and physical parameters 11 p1767 A67-24731
Rapid vapor phase growth of high resistivity GaP for electro-optic modulators, noting high electron mobility 11 p1848 A67-24747
Specific resistance of semiconductor plates measured by change in effective loss component of toroidal coil 11 p1792 A67-24812
Specific resistance of epitaxial layers on low resistance substrates measured, using opposing probe method 11 p1792 A67-24813
High resistivity cadmium selenide vacuum deposited films dielectric constant and electronic properties measured for different parameters 11 p1851 A67-25032
High resistance region effect in neighborhood of linear junction on series resistance analyzed for microwave varactor design 12 p1912 A67-25280
Resistance welds produced by butyl sealant prevent passive films formation on aluminum and magnesium alloys 12 p1948 A67-25287
Electrical resistance of semiconductor diamond measured by pulse method 12 p1939 A67-25332
Constant density theory leads to analytical forms for current-voltage characteristics and electrical resistance associated with shock tube sidewall electrostatic probe problem 12 p1925 A67-25902
Microwave methods for electric resistivity measurements of semiconductor materials, noting application to

- GaAs 12 p1916 A67-25999
P- and n-type silicon spectral emissivity measured at several temperatures and wavelengths for carrier concentrations and direct current resistivities
AIAA PAPER 67-302] 12 p1958 A67-26017
Plastic deformation effect on resistivity and Hall effect of copper-palladium and gold-palladium alloys 13 p2133 A67-27005
High pressure, uniaxial stress and temperature effects on GaAs electrical resistivity 13 p2180 A67-27159
Resistance and heat transfer of plate situated in turbulent MHD boundary layer in compressible fluid 13 p2169 A67-27312
Silicon photocells at high luminous flux concentrations, noting increase in multiplicity of power with series resistance 13 p2056 A67-27622
Electric conductivity and luminescence increase in luminophorous zinc sulfide films after effect of negative resistance 14 p2366 A67-28487
Hall coefficient, electrical resistivity, and Seebeck coefficient of p-type lead telluride measured, using two-valence band model 14 p2367 A67-28520
Total resistance of p-i-n diode calculated assuming high injection levels in base and moderate frequencies 14 p2286 A67-28530
Theoretical determination of polished metal emission factors, using model where emission depends on surface layer temperature and electric resistivity 14 p2407 A67-28558
Measurement of resistance of thin metal films and kinetics of charge drain from surface 15 p2485 A67-29126
Substrate resistivity effect on threshold of surface inversion in MOS system, deriving expression for threshold voltage vs impurity concentration 15 p2446 A67-29638
Collector conduction resistance in saturated planar transistors determined from current distribution measurement on electrolytic model 15 p2448 A67-29802
Macroelectrodynamical equations for low temperature intermediate state of type I superconductors, noting magnetic field effect on structure 15 p2539 A67-29866
Emitter-base voltage vs collector-current characteristic used to study stability of parallel pairs of HF high power transistors 15 p2453 A67-30017
Thermoelectric power increase in low temperature metals not explained by residual resistivity in simple model calculation 15 p2540 A67-30096
Internal resistance, potential fall and current distribution for staggered electrode geometry in MHD generator of Faraday type 16 p2599 A67-30528
High purity single crystal molybdenum electrical resistivity dependence on deformation 16 p2689 A67-31370
Pulsed resistivity and Hall effect measurements of n-type GaAs in high electric fields at room temperature below microwave oscillation threshold 16 p2731 A67-31449
Electrical resistance of niobium single crystal at very low temperature from beginning of superconductivity transition 17 p2916 A67-32805
Apparatus for measuring temperature dependence of thermoconductivity coefficient, thermal EMF and specific electroresistance of cermet cylindrical shells 17 p2861 A67-33171
Frozen vacancies effect on microhardness and electrical resistance of nickel ferrite and yttrium garnet 18 p3097 A67-33480
Hard superconductors electrical resistivity when subjected to increasing magnetic field, considering flux pinning and viscous motion of flux lines 18 p3098 A67-33518
Fatigue-damage evaluation system for transport aircraft, noting use of cumulative strain gauge that stores strain history 18 p3142 A67-33897
Co-evaporation of cermet resistor compounds investigated for resistance and stability 18 p3014 A67-34550
Thin films of cuprous sulfide, selenide and telluride prepared by flash evaporation, discussing resistivity and absorption coefficient 18 p3106 A67-34637
Physical changes in exploding wires before gas ionization observed by X-ray technique, studying resistivity variation with density 19 p3261 A67-35161
Optimum aging temperatures obtained from electric resistance of beryllium alloys containing chromium and zirconium 19 p3245 A67-35472
Indium-antimony alloy thin film preparation by vacuum evaporation, noting effect of heating and annealing on electrical resistivity 19 p3305 A67-35609
Resistance and Hall effect measurements on PbTe thin films prepared by vacuum evaporation on amorphous or oriented substrates 19 p3307 A67-35795
Equivalent resistance circuit of solar cell taking into account all sources of linear resistance 19 p3177 A67-36037
Determining resistivity and Hall coefficient using four point contacts placed on Hall plate isotropic uniformly thick two-dimensional sheet with perpendicular magnetic field 19 p3308 A67-36041
Superconductor resistive behavior as hole motion in flux lattice under peak effect influence 20 p3505 A67-36209
Source and load parameter effects on electrical explosion of wires noting voltage, capacity, inductance, specific resistance, diameter, resistance, etc 20 p3483 A67-36401
Layer removal techniques with Hall effect and sheet resistivity measurements indicate carrier concentrations exceeding thermal equilibrium solubility for antimony implants into silicon 20 p3510 A67-36856
Hardening during deformation in stoichiometric nickel manganite alloy noting temperature effect, surface characteristics and electric resistance 20 p3467 A67-37118
Volt-ampere characteristics of tunnel diode analyzed to derive dependence of differential resistance on voltage 20 p3400 A67-37150
Direct coupling resistance component of transistorized voltage stabilizer 20 p3400 A67-37188
Excess carrier lifetime in semiconductors by measuring photoconductive phase shift of spreading resistance under point contact 20 p3512 A67-37317
Distributed RC parameters influence on Hall voltage magnitude in high resistivity semiconductors, explaining voltage decrease 20 p3513 A67-37452
Computer interconnection resistance causing propagation delay in circuits, suggesting low temperature use as possible remedy 20 p3393 A67-37457
Dependence of electric resistance of thin Permalloy films on substrate temperature during evaporation and vacuum heat treatment 20 p3514 A67-37555
Changes in electric resistance of ellipsoidal plasma probe in homogeneous magnetic field, deriving equations of potential and resistance 21 p3666 A67-38250
Electron beam method for measuring resistivity variation in germanium semiconductors, calculating diffusion lengths 21 p3679 A67-38254
Pseudopotential-structure factor relation for small wave vector applied to liquid alkali metal electric resistivities and temperatures 21 p3686 A67-39102
Liquid mercury equation of state and electrical resistivity at high temperatures and pressures 21 p3686 A67-39104
Coordinate system with straight current and magnetic field lines used for hydromagnetic resistive interchange instabilities studies in toroidal configurations provides negative criterion generalization 22 p3846 A67-39486
Magnetic element impurity effects on semiconductor resistivity, calculating spin dependent scattering of free carriers 22 p3859 A67-39625
Spin-disorder resistivity measurements in Gd-Yt alloys noting temperature and concentration effects 22 p3863 A67-40203
Noise factor variations with source resistance for MOST in common-gate and common-source connections, showing advantage of low noise operation 22 p3773 A67-40309
Superconducting devices utilizing transition, zero resistivity and diamagnetic properties of materials in that state 22 p3808 A67-40398
New semiconductor compounds derived by cross substitution of group IV semiconductors, giving thermal properties and phase diagrams 23 p4036 A67-40720
Niobium stannide, V-Ga and V-Si paramagnetic susceptibility, elastic constants and electric resistivity temperature dependence 23 p4038 A67-40794
Resistance properties of thin continuous Au, Ag, Cu and Al films influenced by superimposed thin films, discussing resistance change and surface scattering 23 p4039 A67-40879
Total resistance of p-i-n diode calculated assuming high injection levels in base and moderate frequencies 23 p3980 A67-40937
Oscillating magnetic field influence on Hall effect and resistance of superconducting niobium 24 p4201 A67-41870
Equivalent circuit to study AC posistor temperature characteristics and determine active and reactive components of net resistance 24 p4130 A67-42253
Hall effect, resistivity, spin resonance and thermoelectric properties of poly(N-vinyl carbazole)/iodine complex, demonstrating charge transfer state existence in system [JPL-TR-32-1074] 24 p4205 A67-42602
Signal extraction and scattering of telluric currents studied for random sheets, semilfinite medium and interface separating medium of different resistivities 24 p4152 A67-42885
ELECTRIC STIMULUS
Electric stimulation of crossed olivocochlear cats and effect on auditory nerve responses 08 p1287 A67-20483
Reinforcing effect of informative stimulus that is not positive discriminative stimulus 11 p1748 A67-25065
Temporary irritation by anti-g and change in vestibular motor reflex action under laboratory conditions 14 p2257 A67-28224
High intensity electric field used to freeze out large quantity of droplets from supercooled artificial fog 16 p2699 A67-31717
Effects of electric stimulation of human vestibular apparatus recorded by monosynaptic H-reflex technique 20 p3369 A67-36270
Electric stimulus effect on vestibular apparatus responses to acceleration increasing or decreasing reactions depending on applied voltage polarity 24 p4112 A67-41859
ELECTRIC TERMINAL
Properties of selective filter containing inhomogeneous semiconductor RC circuit with distributed parameters 14 p2291 A67-28275
ELECTRIC WELDING
SA PLASMA ARC WELDING
Crack propagation in heat-affected zone during HF AC current gas-tungsten arc welding of Al alloy test plate 03 p0430 A67-13693
ELECTRIC WIRING
Computer program used for explicit definition of wiring harness and cable assembly design procedure 05 p0779 A67-17456
Color temperature measurement in first stage of electrical explosion of copper, silver and constantan wires as function of magnitude of energy input for various heating times 16 p2703 A67-31779
ELECTRICITY
SA ANTIFERROELECTRICITY
SA ATMOSPHERIC ELECTRICITY
SA BIOELECTRICITY
SA GEOELECTRICITY
SA PHOTOELECTRICITY
SA PIEZOELECTRICITY
SA PYROELECTRICITY
SA STATIC ELECTRICITY
SA THERMOELECTRICITY
Electricity from MHD - Conference, Salzburg, July 1966, Volume 2 16 p2706 A67-30512
Electricity from MHD - Conference, Salzburg, Austria, July 1966, Volume 3 16 p2607 A67-30592
ELECTRO-OPTICS
Optical modulator using electro-optic effect in lithium tantalate for PCM transmission systems operating at 224 megacycle bit rate 01 p0033 A67-10013
Oscillations of optical absorption in cadmium sulfide in strong electric fields, noting electron transfer between Wannier discrete level 01 p0127 A67-10070
Variable effect of external electrical field on IR photoconductivity of thin n- and p-type silicon samples with low bulk impurity contents 01 p0128 A67-10076
Spontaneous electro-optical effect in

triglycin sulfate crystals spectrally studied, noting changes in double refraction along three crystallographic axes during ferroelectric phase transition 01 p0129 A67-10138

Voice communications system using GaAs room-temperature injection laser and TV communications system using GaAs crystals as modulators for laser beams 02 p0194 A67-11786

Electro-optical properties of paraelectric perovskites indicating origin in polarization 02 p0296 A67-11821

Anomalous polarity-dependent electro-optic effect with noncubic symmetry observed in cubic single crystals of ZnS and ZnTe 03 p0496 A67-13569

Statistically optimum optical data processing with automatic focus estimation 04 p0578 A67-14875

Electro-optical imaging systems used in military aerial TV display, emphasizing variables involved in viewing related to visual interpretation 05 p0757 A67-16309

Amplifier using electro-optic junction modulator combined with photodetector, showing gain at microwave frequencies 05 p0774 A67-16822

Ruby and neodymium glass lasers sum frequency generation using nonlinear electro-optical KDP crystal 06 p1009 A67-17754

Electro-optic intra-cavity color switching in krypton ion Fabry-Perot laser 06 p1010 A67-17888

Heterodyne and photon counting receivers compared for optical communications 07 p1185 A67-19398

Book on reticles in electro-optical devices 08 p1353 A67-20757

Oscillations of optical absorption in cadmium sulfide in strong electric fields, noting electron transfer between Wannier discrete level 08 p1371 A67-21453

Modulation linearity improvement using separate analyzer assembly with each electro-optic crystal 09 p1511 A67-21643

Traveling wave electro-optic modulator tested at 6328 angstroms with CW drive power 09 p1471 A67-21644

Mosaic of photosensors for solid state imaging, discussing electro-optical conversion, structure and characteristics 09 p1476 A67-22209

Free carrier electro-magneto-optical phenomenon in semiconductors, noting conductivity tensor, Faraday effect, Derr effect and Voigt effect 09 p1558 A67-22602

Focal distance of lens controlled digitally using electro-optics 10 p1653 A67-22750

Room temperature electroreflectance spectra of several materials with Ge, zinc blende and wurtzite structures by electrolyte technique 10 p1691 A67-23401

Tunneling assisted photon absorption process /Franz-Keldysh effect/ in semiconductor junctions studied, using differential photocurrent response 10 p1691 A67-23402

Absorption coefficient of light in semiconductors in crossed electric and magnetic fields, examining conditions for Franz-Keldysh effect occurring in magnetic field 10 p1693 A67-23590

Transmission of large number of instrumentation channels over parallel pulse-modulated light beams, using electro-optical mosaic sources and detectors 11 p1764 A67-24444

Optical resolution, light intensity and true perspective effect on imaging characteristics and parallax and image brightness influence on display realism of visual simulation 11 p1749 A67-24629

Rapid vapor phase growth of high resistivity GaP for electro-optic modulators, noting high electron mobility 11 p1848 A67-24747

Dielectric and electro-optic properties of lead magnesium niobate, noting second order ferroelectric transition 11 p1803 A67-24834

Electro-optical spectrograph producing dynamic spectrograph continuous in both frequency and time 14 p2319 A67-28444

Coding modulation and signal processing noting algebraic coding and binary symmetric channel neglect, discussing coherent optical radiation in noise program 14 p2269 A67-28457

Electro-optical rectifier, types of materials generated, operational capability and lunar

and aerial photographic application 14 p2321 A67-28828

Tunable microwave-frequency light modulator consisting of rectangular cross section coaxial cavity with two electro-optical crystals 15 p2501 A67-30141

Parallel electro-optical technique for implementing linear threshold adaptive networks 17 p2860 A67-32616

System performance in electro-optical telemetry noting receiver, transmitter, silicon photodiode, shot, thermal and background noise, etc 17 p2817 A67-32931

Laser beam slitting hologram production technique using polarization controller and birefringent prism 17 p2864 A67-33359

Optical parametric oscillator with ruby laser pumping, noting values of electro-optic and rotational tuning 18 p3059 A67-34011

Electro-optical effect and Stark effect in exciton levels of cadmium sulfide 19 p3304 A67-35428

Real-time electrooptical spectrum analyzers with coherent detection 19 p3197 A67-35687

Optical subcarrier communications, noting use space-oriented missions and RF techniques optical subcarrier communications, noting use in space-oriented missions and RF techniques 20 p3378 A67-36183

Two-dimensional displays conversion to three-dimensional, using uniaxial crystals to vary optical path length and digital control with electro-optic polarization switches 20 p3447 A67-36806

Electro-optic phase modulation of visible and IR light by p-n, p-i-n and metal semiconductor junctions and heterojunctions, noting propagation modes 21 p3684 A67-38453

Photoelectric polarimeter for measuring rotational, electro-optical and electrogyrational effects and optical activity in ferroelectrics 21 p3631 A67-38969

Optical communication systems modulation, discussing TV link, modulator, optical waveguides and materials availability 22 p3759 A67-39330

Electric domains in high resistance GaAs single crystals, measuring electric field intensity with Pockels electro-optic effect noting surface state role 22 p3857 A67-39459

Temperature dependence and electro-optic coefficients in lithium niobate single crystal measured, noting relationship in paraelectric perovskites 22 p3863 A67-40235

Optical properties of new and stable nonlinear optical ferroelectric potassium lithium niobate single crystal 22 p3863 A67-40236

Fabry-Perot etalon resonator studied for incidence angles for use as filter, test instrument and control device for laser output 22 p3809 A67-40469

Laser mode synchronization by electro-optical crystal dielectric constant modulation mounted inside resonator 23 p4013 A67-40903

Emission wavelength selection in multicolor-emission noble gas laser using linear polarization control device 23 p4014 A67-41025

Scanning laser device using modified electro-optic display tube and potassium phosphate crystal mode selector 23 p4017 A67-41393

Electromagnetic mode propagation in anisotropic dielectric p-n junction waveguide models noting Pockel effect of electric field on light 23 p3982 A67-41466

ADP electro-optic crystal in laser emission control tested in beam deflection device and Michelson interferometer modulator, noting refractive index changes 24 p4167 A67-42239

Ferroelectric, electro-optic and dielectric properties of tetragonal potassium-niobate-strontium-niobate crystal 24 p4204 A67-42366

ELECTROACOUSTIC WAVE

Generation of current oscillations by electroacoustic effects in semiconducting cadmium sulfide 01 p0130 A67-10199

Energy relation for acoustic propagation modes in hot electron plasma considered in application of Helmholtz theorem 01 p0123 A67-10441

Excitation of electroacoustic lateral waves in compressible plasma by nonelectromagnetic source 10 p1683 A67-22865

LF current oscillations excitation in n-type semiconductors analyzed using dispersion equation, noting role of external electric

field 11 p1849 A67-24870

Propagation of coupled electromagnetic and electroacoustic waves in magnetized compressible stratified electron plasma 15 p2521 A67-29177

Acoustic wave mode in weakly ionized gas analyzed, noting charge separation and electroacoustic effects 17 p2909 A67-33230

Rapid randomization phenomena in unstable plasma sac for Mach numbers close to unity attributed to electron interaction with trapped electroacoustic waves 22 p3844 A67-39357

ELECTROCARDIOGRAM

Analog circuit for presenting fixed pulse output corresponding to each cardiac cycle of given electrocardiogram and highly unresponsive to noise 09 p1455 A67-21715

Interference Multifocal premature ventricular contractions found in ECG, evaluating cardiovascular system significance in flight stress tolerance 09 p1453 A67-21735

Biopotential detection, recording and design noting electrocardiogram and electroencephalogram use to monitor weightlessness in manned space programs 17 p2807 A67-32666

Glucose loading effects on electrocardiogram of pilot applicants evaluated for injection before and after diabetes test 21 p3573 A67-38068

ELECTROCARDIOGRAPHY

Carotidogram recording of left ventricular ejection, noting application as diagnostic tool in heart physiology and in pathology 04 p0561 A67-14626

Medical research in glider plane noting airborne electrocardiograph 04 p0563 A67-14630

Boundary value problem for potentials in volume conductor based on Green theorem 08 p1288 A67-20601

ECG measurement results on ascent in depressurized chamber, observing dislocation of electrical axis of heart due to diaphragm lift 08 p1287 A67-20643

Statistical analysis of heart rates of Navy carrier pilots during bombing attacks compared with those for launch and landing 09 p1455 A67-21718

Miniaturized multichannel multiplexed FM biotelemetry system designed to record physiological condition of pilot and test operational efficiency 14 p2256 A67-28210

Electrocardiogram amplifier-transmitter designed for long term heart rate monitoring on unrestrained subjects in orbiting laboratories 15 p2431 A67-29919

Biotelemetry improvements in manned space flights, emphasizing bit rate reduction required for electrocardiogram data transmission to earth 17 p2807 A67-32900

Continuous EKG recording during free fall parachuting, discussing tachycardia as normal response 23 p3964 A67-41560

Human cardiac output estimated using impedance plethysmography, discussing simultaneous indicator dilution curves /Dye/ and impedance records /Imp/ 23 p3951 A67-41563

ELECTROCHEMICAL CELL

SA NICKEL-CADMIUM BATTERY

Fuel cells from point of view of thermodynamics, electrochemical reaction kinetics and transport processes and state of development of representative types 01 p0013 A67-10554

Electrochemical power components meeting extreme requirements of space applications, used in commercial market [AIAA PAPER 66-1012] 02 p0184 A67-12305

Electrochemical deposition of Schottky contacts of copper and gold on gallium arsenide 03 p0494 A67-13484

Nonrechargeable batteries for miniaturized components, discussing dry, electrochemical, alkaline and mercury cells 07 p1131 A67-19531

Sealed Ni-Cd battery developments including oxygen recombination, temperature effect, separator reliability, electrochemical failure modes, etc 09 p1445 A67-22177

Oxygen solubility in fused carbonates and corrosion behavior of Ag and Cu oxide, air and carbon dioxide cathodes in molten carbonate fuel cells 09 p1458 A67-22182

High energy density Zn/O battery system, noting good low oxygen pressure and low temperature performance characteristics 13 p2055 A67-26836

Electrochemical generator concept noting compactness, adaptability, methods of adding active agents, evacuation of reaction products and decarbonation 14 p2253 A67-29020

Batteries and fuel cells for space power systems, discussing Ni-Cd, Ag-Cd, Ag-Zn, Bacon cell, etc 17 p2801 A67-32047

Optically pumped alkali metal vapors orientation checking by light pulse method, noting relaxation curve 17 p2869 A67-32811

System selection for hydrogen-oxygen low temperature fuel cell with aqueous KOH electrolyte 20 p3363 A67-37012

Gamma radiation energy direct conversion into electrical energy by electrochemical recombination of radiolysis products, proposing new sealed battery 22 p3748 A67-40199

Sealed silver-cadmium batteries meeting space requirements, discussing high energy plates, cell design and packaging 22 p3749 A67-40230

Alkaline concentrator appears superior to acid and solid units for possible onboard generation of oxygen 23 p3963 A67-41543

Carbonation Cell System for removing carbon dioxide from space cabin atmosphere using electrochemical process 23 p3965 A67-41578

Zero gravity perturbation mechanisms affecting electrochemical systems noting transport processes and Curie theorem 23 p3972 A67-41607

Solid state electrochemical solar cell using various anode metals and charge transfer complexes as cathodes, noting I-V characteristics and discharge curves [JPL-TR-32-1116] 24 p4097 A67-41804

Auxiliary electrodes for sealed alkaline electrochemical cells, noting application as charge control and scavenger elements 24 p4105 A67-42519

Aerospace automatically activated electrochemical battery and DC-DC high voltage converter-regulator noting storage stability 24 p4108 A67-42541

ELECTROCHEMICAL CORROSION

Stress-corrosion cracking, evaluating role of mechanical, electrochemical and surface energy theories of causation, including hydrogen and other factors 04 p0636 A67-14804

Stress corrosion cracking of titanium alloys, noting tensile test data, crack propagation in salt solution and in pure solvents and metallurgical and electrochemical factors 10 p1670 A67-23701

Corrosion resistance of yttrium is higher at higher pH because of slower anodic process 12 p1954 A67-25358

Corrosion of rhenium in various acids and hydroxides is electrochemical in nature and determined by kinetics of anodic and cathodic processes 12 p1955 A67-25359

Loaded oil-lubricated steel ball bearings operating in vacuum and air investigated for electric current effect on damage [ASLE PREPRINT 67AM 1C-1] 14 p2325 A67-28783

Hydrogen coverage at metal surface during dissolution in corrosion process 18 p3066 A67-34368

Loaded oil-lubricated steel ball bearings operating in vacuum and air investigated for electric current effect on damage [ASLE PREPRINT 67AM 1C-1] 22 p3813 A67-40218

ELECTROCHEMICAL MACHINING

Electrochemical machining, discussing relationship between total current, applied potential, electrolyte flow rate, electrolyte conductivity and electrode gap [ASME PAPER 66-PROD-5] 03 p0432 A67-13833

Mathematical analysis of electrochemical machining phenomena, discussing behavior predicting equations [ASTME PAPER WES-7-09] 11 p1798 A67-24254

Electrochemical machining data handling, discussing standards of surface integrity, process data, application steps and records [ASTME PAPER WES-7-10] 11 p1798 A67-24255

Book on nontraditional machining processes covering process parameters, shape and materials applications, tooling, chemical removal, etc 14 p2328 A67-28893

Electrostream process for drilling very

small diameter holes in superalloys for gas turbine and nozzle vane fabrication [ASTME PAPER MR67-141] 18 p3054 A67-34175

Surface geometrical variations in electrochemical shaping process for hydrodynamic removal of dissolved processed metal, deriving partial differential equations 21 p3636 A67-38897

Electrochemical shaping precision analysis, discussing efficiency, current losses, energy consumption, surface geometry and electrolyte properties 22 p3812 A67-39543

ELECTROCHEMICAL OXIDATION

Fuel cell construction principles, oxidation potentials of prospective fuels and Gemini GT-5 space capsule fuel cell 01 p0014 A67-10639

Isotope analysis of iron migration in Ni-Cd cells with pocket electrodes 09 p1458 A67-22178

Catalytic performance of silver alloys as oxygen electrodes of low temperature fuel cells 09 p1458 A67-22181

Nickel hydroxide structure, discussing effect of current, charge and electrolyte concentration on production rate 09 p1458 A67-22183

Anodic oxidation usable for efficient phase analysis technique for V-Ga alloys, identifying interference colors in absence of oxygen impurities 23 p4036 A67-40713

ELECTROCHEMISTRY

Ozone determination by electrochemical and colorimetric methods compared for effects of sensor cell aging 03 p0413 A67-13931

Fuel cells and fuel batteries, investigating hydrogen, compromise fuels and hydrocarbons, studying reliability, working life and costs 04 p0556 A67-15549

Electrochemical properties of solid refractory oxides for high temperature fuel cells 08 p1284 A67-20703

Solid electrolytes used as MHD hot electrode materials between electron conductors 08 p1284 A67-20704

Equality conditions for gold and silver electrode zero charge and transient peak potentials by pH and anion effects, using scraped electrodes 10 p1602 A67-23158

Fuel cell research noting gas porous electrodes, effect of geometry on performance and electrocatalysis 14 p2252 A67-29019

Electrophoretic coating of metals compared with icathodic and anodic synthetic depositions 18 p3054 A67-34098

Book on high energy batteries covering electrochemistry of discharge plate materials, weight factors, polarization electrolytes, parasitic effects, etc 18 p2989 A67-34265

Holographic interferometry in electrochemical studies, examining advantages in less critical alignment and preparation and observation of changes 20 p3450 A67-37137

Soviet book on semiconductor electrochemistry covering space charge layer structure, semiconductor corrosion, etc 22 p3856 A67-39413

ELECTRODE

SA ANODE

SA CATHODE

SA DIFFUSION ELECTRODE

SA PLASMA ELECTRODE

Effect of electrode tips of MHD generator and induced magnetic field on fluid flow in generator analyzed, using approximation method 01 p0121 A67-10227

Electrode tips and inhomogeneity of applied magnetic field effect on fluid flow of MHD generator 01 p0124 A67-10753

Effects of aluminum electrode and hydrogen atom on MOS structure during annealing 01 p0137 A67-11069

Saturation effect dependence on electrode surface temperature and bulk gas temperature in MHD generator duct 01 p0126 A67-11186

Photovoltaic effect in thin telluride layers and in contacts between layers and various metal electrodes, noting dependence on angle of deposition 02 p0294 A67-11758

Interaction of plasma jets ejected from electrode spots with accelerating magnetic field as possible cause of electrode polarity effect on flat-electrode-type plasma acceleration 02 p0275 A67-12471

Composite metallic and dielectric

insulators for high current arc electrodes 02 p0250 A67-12697

Variation of floating potential formed between electrodes by injection of electronegative gas is logarithmic function of electron attachment coefficient on neutral particles 04 p0669 A67-15496

Linearly expanding MHD channel with solid electrodes, noting end effects relation to electrode dimensions 04 p0669 A67-15516

Heat transfer in plasma jet generators, considering electric arc types and thermal regime of electrodes 04 p0672 A67-15871

Vacuum cup electrode in spectrographic analysis of solutions of refractory metal alloys 05 p0758 A67-16369

Sputtering yields of aluminum, copper and titanium measured as function of cesium ion energies for use as electrodes on cesium ion engines 05 p0871 A67-17349

[AIAA PAPER 66-203]

Quasi-one-dimensional MGD channel flow calculation methods, considering Hall effect, heat transfer, friction and potential drop near sectioned electrode 06 p1043 A67-18675

Current in channel with symmetrical end electrodes, noting stepwise dependence of near-electrode potential on current density 06 p1045 A67-18812

Electrical characteristics of linear segmented electrode Hall and Faraday MHD generators, noting power output reduction due to electrode voltage losses 08 p1283 A67-20578

Solid electrolytes used as MHD hot electrode materials between electron conductors 08 p1284 A67-20704

Equivalent circuits of MHD generators with segmented electrodes electrically connected in various ways 08 p1286 A67-20738

Electrode conduction processes and segmented electrode-insulator ratio effects in MHD power generation experiments 09 p1539 A67-21785

Current-voltage characteristics of moving argon plasma, noting variation of plasma conductance with flush and filament electrodes 09 p1540 A67-21786

Auxiliary arc electrodes for solution to cold boundary layer and cathode emissivity problems in MHD generators 09 p1444 A67-21822

Unusual electrode configuration for Hall effect measurements on thin films and field effect devices 09 p1472 A67-21955

Output characteristics of cesium thermionic converter as function of size of electrode gap, using device with movable air-cooled stainless steel anode 09 p1444 A67-22007

Cadmium negative electrode mechanism, noting active material redistribution and anodic oxidation 09 p1445 A67-22176

Fuel cell hydrogen electrodes prepared from preactivated Raney-Nickel catalyst powders 09 p1445 A67-22185

Kinetics and mechanism of cathodic oxygen reduction reaction on metal electrodes 09 p1458 A67-22188

Efficiency increase in vapor-filled thermionic converter anticipated by introducing intermediate electrodes between emitter and collector of vapor-filled diode 09 p1447 A67-22333

Electrode ends effect on flow of fluid in MHD generator, using iterative solution 09 p1549 A67-22563

Equality conditions for gold and silver electrode zero charge and transient peak potentials by pH and anion effects, using scraped electrodes 10 p1602 A67-23158

Plasma flows from normal and coaxial electrode contact points of arc and effect of external forces by schlieren photography 10 p1687 A67-23849

Gas pressure effect on electrical breakdown and field emission, discussing ion bombardment and whisker formation 11 p1820 A67-24921

Hot electrodes for open cycle MHD generators, noting refractory oxides 12 p1899 A67-25405

Electrode feed system for segmented electrode MHD wind tunnel 12 p1920 A67-25406

Pulsed inert gas metal-arc welding technique for titanium 721, investigating arc characteristics in argon, argon/helium and helium 12 p1950 A67-25738

Electrode shape design for cylindrical

- charged-particle beam formation 14 p2320 A67-28650
- Fuel cell research noting gas porous electrodes, effect of geometry on performance and electrocatalysis 14 p2252 A67-29019
- Annex circuits for regulating electrolyte grade, cell temperature, reactant supply, fluid circulation and generated electricity of unit cells grouped in batteries 14 p2253 A67-29024
- MHD generator terminal values and other electric parameters deviations for various finite length electrodes connected in series 16 p2600 A67-30532
- Cesium-vapor vacuum diode for thermionic conversion stressing role of electrode homogeneity, space charge and transport phenomena 17 p2823 A67-32222
- Combination of monoclinic zirconia, second ceramic and metal in electrodes of MHD generators 18 p3099 A67-33709
- Book on electrodeposition of metals in ultrasonic field, discussing effects on electrode potentials, concentration polarization, deposition rate, etc 19 p3235 A67-34914
- Electric field measurements with isolated electrodes ejected near apex, finding continuous changes near 100 and 80 km 19 p3217 A67-35199
- Electrode feed system for segmented-electrode MHD accelerator to avoid power supplies/switch gear proliferation 19 p3177 A67-35774
- Simultaneous and independent potentiostatic control of rotating ring and disk electrode and application to CuI/CuI/Cu system 20 p3446 A67-36655
- Electrode with central heat sink used for joining flat-pack leads and copper tracks on printed circuit boards 21 p3635 A67-38624
- DC electric arc in superimposed gas flow behavior in arc tunnel, discussing electrode geometry [AIAA PAPER 67-675] 21 p3671 A67-38708
- 150-180 watts at 1000 MHz tetrode, examining mechanical durability and temperature stability of metallic electrodes and ceramic insulators 22 p3772 A67-39873
- Lithium chloride impregnated balsa wood and surgically implanted electrodes for continuous heart rate recording over long periods of time 23 p3965 A67-41571
- Static electrification mechanism of particles in pseudofluidized bed in terms of causes of observed polarities of column wall and various particles 24 p4254 A67-42256
- Auxiliary electrodes for sealed alkaline electrochemical cells, noting application as charge control and scavenger elements 24 p4105 A67-42519
- Methanol-air fuel cell development, discussing electrode performance, temperature effects and catalytic agents 24 p4106 A67-42520
- ELECTRODE FILM BARRIER**
- Hall constant of semiconductors noting dependence on specimen size, film and current electrode parameters 20 p3508 A67-36406
- ELECTRODEPOSITION**
- Electrophoretic coating of metals compared with cathodic and anodic synthetic depositions 18 p3054 A67-34098
- Lubrication mechanisms defined via electrodeposited solid film systems, noting porous structure formation 19 p3233 A67-34789
- Book on electrodeposition of metals in ultrasonic field, discussing effects on electrode potentials, concentration polarization, deposition rate, etc 19 p3235 A67-34914
- Batch fabrication method for storage elements using electrophoretic deposition of ferrite on platinum wire 22 p3812 A67-39915
- ELECTRODERMAL RESPONSE**
- Cutaneous sensitivity communications, discussing information situations, applications and subsystems 09 p1456 A67-22375
- ELECTRODISSOLUTION**
- Hydrogen coverage at metal surface during dissolution in corrosion process 18 p3066 A67-34368
- ELECTRODYNAMICS**
- SA QUANTUM ELECTRODYNAMICS**
- Current layer dynamics in flat electrode accelerator, relating plasma acceleration and polarization field
- potential 01 p0122 A67-10345
- Text on high power electronics including cathodic losses in magnetrons, electrodynamic theory of grids, high frequency measurement, secondary electron emission and electromagnetic oscillations 03 p0379 A67-13301
- Simple asymptotic formula for motion of simultaneous electric field and conductivity domains in semiconductors in terms of electrodynamic on basis of Poisson and continuity equations 04 p0677 A67-14936
- Conical MHD flow of ideal conducting gas with Hall effect in magnetic field, deriving electrodynamic and energy characteristics 04 p0669 A67-15515
- Approximations of electrodynamic effects of moving media 04 p0670 A67-15529
- Umov-Poynting theorem, Lorentz lemma, complex conjugate lemmas and quadratic relations for EM field intensity in electrodynamic of moving media 05 p0844 A67-18354
- Electrohydrodynamic equilibrium showing continuum feedback control of Rayleigh-Taylor type instability 05 p0856 A67-17414
- Electrodynamic properties of homogeneous magnetoactive plasmas including wave propagation, excitation, scattering, etc 08 p1358 A67-20863
- London superconductors in local approximation, obtaining solution to equation in form of gradient expansions 09 p1556 A67-22221
- Relativistic electrodynamic of moving medium, discussing Maxwell-Minkowski equations, Born equations, field vector transformations, etc 09 p1533 A67-22449
- Plasmatron jet with vortical air stabilization of arc, correlating jet structure with nozzle geometry and electrode polarity 11 p1832 A67-24027
- Current layer dynamics in flat electrode accelerator, relating plasma acceleration and polarization field 11 p1843 A67-25018
- Electrodynamic equations for pure and doped two-band superconductors, studying upper critical magnetic field 13 p2184 A67-27630
- Electrodynamic forces and torques on charged bodies moving through rarefied and partially ionized earth magnetosphere and upper atmosphere 14 p2362 A67-29039
- Matrix inversion formula applied to moving media electrodynamic and scaling operator in Lorentz transformation 15 p2509 A67-29175
- Solving three-dimensional electrodynamic problems with mixed boundary values by reduction to standard Fredholm integral equation 15 p2522 A67-29196
- Plasma acceleration in flat electrode plasma source simulated by ideally conducting bridge described electrodynamic 15 p2525 A67-29249
- Electrodynamics applied to two-dimensional problem of determining resolution of images reproduced from ideally plane infinitely thin holograms 15 p2489 A67-30006
- Electrodynamically coupled system consisting of RCL circuit, transformer and mechanical system analyzed by mathematical analogy and analog computer 15 p2440 A67-30081
- Liquid metal energy converters using magnetohydrodynamic induction noting electrodynamic aspects 16 p2606 A67-30586
- Electrodynamic transducer for liquid-borne ultrasonic pulse intensity measurements, considering limits, inductance and measuring system dimensions 18 p3043 A67-33463
- Wave surfaces of Einstein-Schrodinger theory and nonlinear electrodynamic brought together using antisymmetric tensor 18 p3078 A67-33688
- London superconductors in local approximation, obtaining solution to equation in form of gradient expansions 18 p3100 A67-33765
- Electrodynamics applied to two-dimensional problem of determining resolution of images reproduced from ideally plane infinitely thin holograms 18 p3046 A67-33767
- Book on electrodynamic of plasmas covering analysis of collective properties of plasma based on classical and quantum-statistical mechanics 19 p3267 A67-34866
- Book on electromagnetodynamics of fluids
- covering MHD, astrophysics, plasma physics, etc 20 p3499 A67-36806
- Book on electrodynamic of moving media deriving force distribution using Hamiltonian and virtual power principles in relativistic formulations 20 p3500 A67-37087
- Electrodynamic equations for pure and doped two-band superconductors, studying upper critical magnetic field 21 p3685 A67-38826
- Ferromagnetic magnetization curve approximated for analytical solutions of boundary value problems in nonlinear electrodynamic, obtaining Riemann functions 22 p3836 A67-39421
- Electrodynamic exciter of mechanical vibration noting design, operation and characteristics 22 p3780 A67-39553
- Geomagnetic dynamo laboratory model, self-excitation conditions determined from solutions of electrodynamic equations, diagramming magnetic field and current distribution 24 p4231 A67-42353
- ELECTROENCEPHALOGRAPH (EEG)**
- EEG of pilot during orbital flight on Gemini VII used to study sleep cycles 01 p0015 A67-10954
- Alertness during visual surveillance at night, noting correlation between cortical activity and performance 04 p0561 A67-14627
- Immobilization effects on electrical activity of brain and intellectual and perceptual motor processes 11 p1748 A67-25064
- EEG data from Astronaut Borman on Gemini flight GT-7 13 p2062 A67-26919
- Emergency recompression procedures during space flight studied by exposure of chimpanzees to near vacuum 14 p2257 A67-28219
- Biopotential detection, recording and design noting electrocardiogram and electroencephalogram use to monitor weightlessness in manned space programs 17 p2807 A67-32666
- EEG and rhythmical tremor in outstretched upper extremities in man analyzed by autocorrelation and cross correlation 20 p3373 A67-37525
- ELECTROENCEPHALOGRAPHY**
- Radiotelemetric recordings of EEGs aviation pilots during long flight 01 p0017 A67-10962
- Evoked brain response to clicks as measure of vigilance tested in work-rest schedule and pressure suit-sleep experiments on man 09 p1452 A67-21721
- EEG baselines covering wide range of states of wakefulness and sleep in astronaut candidates estimated by computation and pattern recognition techniques 13 p2062 A67-26921
- Analysis of brain wave records from Gemini flight GT-VII by computations to be used in 30-day primate flight 15 p2425 A67-29104
- Cortical electroencephalographic activity /EEG/ relation to behavioral changes in chimpanzee following rapid decompression to near vacuum 18 p2991 A67-34713
- Human brain hemodynamics during prolonged hypokinesia including orthostatic and bed-rest tests, using rheoencephalographic technique 20 p3368 A67-36266
- EEG finding in aircrew personnel to obtain information about 14 and 6 per second positive spiking phenomenon 21 p3574 A67-38085
- ELECTROEROSION**
- S SPARK EROSION MACHINING**
- ELECTROEXPLOSIVE DEVICE**
- Time domain reflectometry in reliability testing, detailing applications in checkout of electroexplosive devices with spark gap and cable validation equipment connection 01 p0084 A67-11361
- Electroexplosive devices, considering safety improvement for exploding and thermal bridgewire initiators 08 p1372 A67-20526
- Control of RF hazard to electroexplosive devices 08 p1290 A67-20548
- Electrical detonator characteristics and safety precautions in handling and use, noting untimely functioning and misfiring as causes of accidents 17 p2927 A67-33093
- ELECTROFORMING**
- Coatings of nickel, chromium and Cu on SiC and aluminum oxide whiskers by electroforming and metallizing, using

electron microscope techniques 03 p0444 A67-13434

Testing techniques for shells noting tensile properties 13 p2219 A67-27184

Imperfections effect on buckling of complete electroformed spherical shells under uniform external pressure examined in rigid and soft testing 17 p2960 A67-32454

Electroplating for fabricating fibrous composite materials noting advantages of low temperatures and absence of mechanical working 22 p3819 A67-39560

ELECTROHYDRAULIC CONTROL

Fluid management techniques for control in space of functions such as liquid expulsion, vapor venting, gauging and center-of-gravity control 04 p0553 A67-14427

Component design advances with fatigue tests on hydraulic tubes and outline of seal development 05 p0753 A67-16749

Multiplex electrohydraulic actuators development, noting fault detection and feedback signals to prevent output drift 05 p0754 A67-16752

Force /or torque/ electrohydraulic servocontrols, considering transfer function, compatibility conditions and hydraulic perturbation 07 p1132 A67-20113

Pressure feedback in electrohydraulic servomechanisms for high inertia loads to increase stability, using dynamic analysis and differential equations 09 p1442 A67-21687

Equation derived for accurate approximation of viscous friction coefficient in spool and nozzle-flapper preamplifier stages of electrohydraulic servovalve 16 p2610 A67-31915

Transfer functions in electrohydraulic servo systems through feedback instability properties, discussing root locus theory and typical servomechanism properties 17 p2830 A67-32932

Dynamics of electrohydraulic servomechanism /transducer-amplifier/ for transforming signals into forces for displacing spacecraft control mechanism, examining motion equations 23 p3935 A67-40637

ELECTROHYDRODYNAMICS

EFM, interplay of electric fields with insulating fluids which cannot remain nonconductive at high temperatures, considering astronautics application 01 p0014 A67-11408

Dielectrophoretic propellant orientation systems design, noting electrode requirements and avoidance of electrohydrodynamic instabilities [AIAA PAPER 66-922] 02 p0301 A67-12275

Laminar electrohydrodynamic flow in plane diffusor, taking into account molecular diffusion of space charge 04 p0668 A67-15277

Parallel Couette and Poiseuille flows of multicomponent viscous plasma in presence of pressure gradient and electric field 05 p0854 A67-16894

Radial electric field role in electrofluid dynamic conversion of flowing gas energy into electric energy 12 p1901 A67-25933

Dielectrophoretic methods for positioning cryogenic liquids in zero gravity environment, solving one-dimensional nonlinear problem for time history 13 p2106 A67-27642

Electrohydrodynamic flow laminarization with tritium ionizer, obtaining Poiseuille flow stability 17 p2839 A67-32907

Electro-fluid dynamic power generation, discussing Mach number, charged particle mobility, pressure level and radial space charge field effects on load characteristic and conversion ratio 24 p4107 A67-42527

Electrofluiddynamic /EFD/ power generator unipolar charge generation using corona discharge, noting pressure and geometry effects on ion currents and attractor voltage 24 p4107 A67-42528

Electrofluiddynamic /EFD/ power generator channel performance dependence on charge spreading for various geometries, noting stage efficiency and electric pressure 24 p4107 A67-42529

Colloidal electrogasdynamic energy converters analyzed on basis of power plant specific mass 24 p4109 A67-42888

ELECTROJET

SA AURORAL ELECTROJET

SA EQUATORIAL ELECTROJET

Ionospheric electric current measurement,

determining vertical current density distribution and electron number density for geomagnetic field study 13 p2107 A67-26308

Electric current associated with polar magnetic substorms 14 p2313 A67-28573

Early appearance of active aurora during geomagnetic storm caused by westward traveling surges along expanded oval 14 p2313 A67-28575

Sq currents in American equatorial zone during IGY 24 p4148 A67-42066

ELECTROKINETICS

Surface current excitation by electromagnetic and electrokinetic waves on metal cylinder immersed in uniform collisionless isotropic plasma 06 p0962 A67-18075

Depth of capture levels determined from temperature dependence of kinetics of gamma-conductivity or photoconductivity of cadmium sulfide 14 p2367 A67-28526

Measurement of resistance of thin metal films and kinetics of charge drain from surface 15 p2485 A67-29126

Inhomogeneous sheath effect on surface currents and scattering cross section of plasma-immersed cylinder in presence of electromagnetic and electrokinetic waves 15 p2521 A67-29192

Depth of capture levels determined from temperature dependence of kinetics of gamma-conductivity or cadmium sulfide 23 p4039 A67-40933

ELECTROLUMINESCENCE

SA SELF-LUMINOUS BODY

Efficient electroluminescence at 300 dopant K from GaAs diode amphoteric dopant Si as dominant impurity on both sides of p-n junction 01 p0131 A67-10368

Solution grown epitaxial red light emitting p-n junctions in GaP preparation, electrical and optical properties, examining I-V characteristics 02 p0297 A67-11876

GaP electroluminescent junctions, considering feasibility of electroluminescence applications where human eye is detector 04 p0581 A67-15077

Electroluminescence, photoconductivity and I-V characteristics of niobium-niobium oxide-gold diode and possible existence of p-i-n junction in oxide 04 p0582 A67-15104

Forward current, electroluminescent intensity and short circuit current during bombardment as function of 2-mev electron irradiation 04 p0685 A67-15704

Electric conductivity and luminescence increase in luminophorous zinc sulfide films as aftereffect of negative resistance 05 p0866 A67-17023

Electroluminescence, discussing semiconductor lasers with various excitation sources, luminescent efficiency, etc 06 p1010 A67-17889

Short aging test results on GaAs diodes, noting surface changes and dependence of nonradiative excess current component on device perimeter 09 p1472 A67-21952

Chemical etching of dislocation and stacking fault structure of epitaxial GaAs, noting possible effect on electroluminescence 10 p1692 A67-23514

Quantum efficiency of optimized GaAs diodes with Zn diffused in skin layer, noting dependence on junction depth 10 p1614 A67-23524

Factors of degradation of GaAs electroluminescent diodes, discussing surface leakage and change in spectral characteristics as major causes 10 p1615 A67-23526

All-glass electroluminescence readout panel design with active areas integral part of connector pin 11 p1766 A67-24628

Semiconductor diode light sources, discussing phenomenon of p-n junction luminescence and potential application in optical displays and data transmission 12 p1979 A67-25169

Impurity effect on electroluminescence of gallium phosphide diodes, noting dependence of spectrum on current density through p-n junction 12 p1914 A67-25438

Electric conductivity and luminescence increase in luminophorous zinc sulfide films as aftereffect of negative resistance 14 p2366 A67-28487

Characteristics of electroluminescent p-n junctions prepared on base of beryllium-doped silicon carbide 14 p2387 A67-28524

Injection electroluminescence of p-n junctions in GaP doped with tellurium, zinc,

ZnO, etc 14 p2368 A67-28531

Volume electroluminescence observation during HF excitation of GaAs using neutral /indium/ contacts and unipolar voltage pulses 14 p2368 A67-28538

Cathodoluminescence detector for electron microprobe, noting components and use 16 p2677 A67-31432

Quantum efficiency in electroluminescent GaAs diodes, considering carrier concentration effect, electron injection ratio, photon absorption and radiative recombination 17 p2914 A67-32654

Design of time-shared multifunction display medium to improve guidance and control displays in manned spacecraft [AIAA PAPER 67-552] 19 p3257 A67-35949

Electroluminescent diodes emission efficiency factor for application to lasers 21 p3591 A67-38153

Cathodoluminescence device for rapid identification of phase assemblages in solid state reaction system magnesium oxide-magnesium silicate 21 p3630 A67-38848

Characteristics of electroluminescent p-n junctions prepared on base of beryllium-doped silicon carbide 23 p4039 A67-40931

Injection electroluminescence of p-n junctions in GaP doped with tellurium, zinc, ZnO, etc 23 p4039 A67-40938

Volume electroluminescence observation during HF excitation of GaAs using neutral /indium/ contacts and unipolar voltage pulses 23 p4040 A67-40945

Photoexcited electroluminescence spectra of rare earth ions in cadmium fluoride semiconductor single crystal 24 p4205 A67-42893

ELECTROLUMINESCENT LAMP

U.S. Weather Bureau calibration of solar radiation pyranometer by means of 5000 watt tungsten filament lamp 03 p0419 A67-13076

Integrating hemispherical system for creating indoor artificial diffusing sky used in calibrating meteorological pyranometers 03 p0419 A67-13078

Digital computer driven electroluminescent solid state vertical scale indicator design, development and fabrication emphasizing size, weight, power, reliability and display readability 05 p0805 A67-16310

Efficiency of electroluminescent lamps, noting dependence on arsenic pressure and temperature during GaAs crystal growth 11 p1845 A67-24140

ELECTROLYSIS

Electrochemical machining, discussing relationship between total current, applied potential, electrolyte flow rate, electrolyte conductivity and electrode gap [ASME PAPER 66-PROD-5] 03 p0432 A67-13833

High purity beryllium mechanical properties obtained by double electrolysis 13 p2139 A67-27126

Ion temperature, cell temperature, cell voltage and current in electrolytic technique for reproducible growth of molybdenum /IV/ oxide crystals 15 p2533 A67-29295

Aluminum renewal from titanium electrolytes by reacting electrolyte melt at high temperature 16 p2687 A67-30843

Aminasine injection and electrolysis effects on formatio reticularis of animals after exposure to hypoxia 20 p3367 A67-36255

Na and K introduced into Si by diffusion from thin layer of alkali metal and during electrolysis of molten alkali halogenides 23 p4037 A67-40721

Mass spectrometric analysis of electrolyte degradation during electrolysis in sulfuric acid silica gel cell for oxygen recovery 23 p3970 A67-41705

ELECTROLYTE

SA ANION

SA BATTERY

SA CATION

SA MOLTEN-SALT ELECTROLYTE

MHD effects during motion of dielectric shell in electrolyte in presence of external magnetic field 01 p0120 A67-10185

Crossed electric and magnetic fields effect on quasi-liquefaction process of nonconducting particles by electrolyte 01 p0121 A67-10189

Electrolytic tank analog for magnetic field configurations in design of plasma containment device 02 p0279 A67-12693

LF temperature pulsations in turbulent

MHD flow of electrolyte 09 p1549 A67-22385
 Room temperature electroreflectance spectra of several materials with Ge, zinc blende and wurtzite structures by electrolyte technique 10 p1691 A67-23401
 Heat transfer of electrolyte solutions, noting effect of magnetic field on turbulent flow and empirical relation to calculate Nusselt number 11 p1831 A67-24024
 Collector conduction resistance in saturated planar transistors determined from current distribution measurement on electrolytic model 15 p2448 A67-29802
 Ion radial distribution functions for primitive model of electrolyte solution using Percus-Yevick and convolution-hypernetted-chain integral equations 17 p2810 A67-33256
 Book on high energy batteries covering electrochemistry of discharge plate materials, weight factors, polarization electrolytes, parasitic effects, etc 18 p2989 A67-34265
 High temperature fuel cells with molten carbonate mixtures as electrolyte analyzed at high temperature 20 p3366 A67-37545
 Lanthanide salts replacing lithium salts in Lelanche cell electrolyte, noting good capacity over widened temperature range 22 p3748 A67-40228

ELECTROLYTIC MACHINING
SA SPARK EROSION MACHINING
 Book on nontraditional machining processes covering process parameters, shape and materials applications, tooling, chemical removal, etc 14 p2328 A67-28893

ELECTROLYTIC POLISHING
 Intermediate principal stress effect on fatigue of thick wall steel tubes under triaxial stresses 15 p2573 A67-29402
 Electrolytic polishing technique for bright field etch of Be specimens 24 p4173 A67-42349

ELECTROMAGNET
SA COIL
SA KERR EFFECT
 Low power MPD arc thruster design and performance with radiation cooled electromagnets and permanent magnets [AIAA PAPER 67-50] 06 p1074 A67-18436
 Electromagnet design for experimental DC MHD generator 14 p2247 A67-27950
 Electro-and permanent magnet configurations using different materials analyzed, determining lowest mass magnet system for MPD arcs [AIAA PAPER 67-686] 21 p3692 A67-38717

ELECTROMAGNETIC ABSORPTION
 Electromagnetic radiation absorption coefficient of atmospheric water vapor in long-wave portion of submillimeter range 02 p0190 A67-11568
 Resonance absorption of electromagnetic power by weakly ionized gas produced in cylindrical discharge tube 02 p0273 A67-12184
 Absorption of electromagnetic energy in gases in centimeter range waves measured, using optical-acoustic method of signal changes 03 p0418 A67-12895
 Order-disorder parameter determined from HF absorption in pure superconducting films 03 p0501 A67-14373
 Engineering methods for construction of electromagnetic wave absorbing walls for microwave darkroom applications at various frequency bands 04 p0576 A67-15504
 Absorption of electromagnetic energy in gases in centimeter range waves measured, using optical-acoustic method of signal changes 06 p1006 A67-18772
 Polarization and atom state distribution of excited atomic gas taking into account resonance excitation, using Boltzmann equation to determine line shape of electromagnetic wave absorption 06 p0991 A67-18799
 Electron cyclotron resonance heating of alkali plasmas by electromagnetic resonant absorption 11 p1838 A67-24407
 Acoustic wave attenuation coefficients for small gap superconductors, noting electromagnetic absorption and collisional drag as cause 16 p2729 A67-31059
 Magnetic field induced changes in Bardeen-Cooper-Schrieffer spectrum of electronic excitations in pure type I superconductor and effect on electromagnetic radiation absorption 17 p2925 A67-33374
 Polarization and atom state distribution of excited atomic gas taking into account resonance excitation, using Boltzmann

equation to determine line shape of electromagnetic wave absorption 18 p3029 A67-34418
 Computational scheme for calculation of Mie cross sections of absorbing particles 19 p3184 A67-35688
 Plasma absorption of microwaves, noting 20 resonant maxima near harmonics of electron cyclotron frequency 20 p3498 A67-36692
 Negative cyclotron resonance absorption due to electron elastic collisions with noble gas atoms, comparing results with kinetic plasma wave theory 22 p3842 A67-40346
 Microwave absorption phenomena observed in Tb, Dy, Ho and Er single crystals 23 p4036 A67-40710
 EM radiation reflection, absorption and transmission through dielectric medium measured, studying other aspects by electric dipole oscillator model 23 p4037 A67-40757
 IR absorption and Raman scattering spectra of diagonal cubic crystal structures 23 p4037 A67-40758

ELECTROMAGNETIC COMPATIBILITY
SA ELECTRONIC EQUIPMENT TESTING
 Interference Prediction Model /IPM/ for RF interference study at satellite tracking stations 01 p0023 A67-10498
 HF conducted and radiated RF interference suppression by dielectric and magnetic absorption, pseudoresonant or interfacial loss and artificial skin effect 01 p0024 A67-10500
 Graphing spurious intermodulation responses in tunable superheterodyne receiver to determine susceptibility to RF environment 03 p0383 A67-13789
 Straight edge fence design for control of radar site environment from clutter return, pattern interference, tracking errors and high power hazard to personnel 03 p0396 A67-13853
 Frequency sharing and compatibility of satellite and terrestrial radio relay systems design, discussing interference effects 09 p1464 A67-22411
 Combination tones generation by interaction of orthogonal gas laser oscillations, showing dependence on polarization states and primary oscillations 13 p2126 A67-27015
 Ionospheric dispersion of AM-FM artificial satellite signals noting distortion effects, synchronization and interference difficulties 13 p2070 A67-27197
 Electromagnetic interference and tape recorder jitter control problems in data management system for manned spacecraft 20 p3442 A67-36468
 Small and large orbiting observatory satellites compared for operational needs, interference problems, scheduling and multisampling of space phenomena [AIAA PAPER 67-634] 20 p3534 A67-37616
 Electromagnetic compatibility - IEEE Conference, Washington, DC, July 1967 20 p3404 A67-37635
 Electromagnetic compatibility operational problems aboard Apollo spacecraft tracking ship 20 p3387 A67-37641
 Titanium alloy resistivity and aircraft structure role as current return and electromagnetic shield, discussing greater use of wire for susceptible circuits to achieve EMC 20 p3405 A67-37643
 Audioconducted and RF radiated susceptibility thresholds of active low pass filter circuits, determining limitations and meeting specification requirements 20 p3406 A67-37652
 Low noise transistor switch design capable of switching 1A and meeting military current probe EMI specifications 20 p3406 A67-37653
 Flat-top pulse waveform with high transmission efficiency, confined spectra and good electromagnetic compatibility 20 p3388 A67-37654
 KHz to GHz wide predetector bandwidth receiving system applicable to EMI evaluations of high data rate digital equipment 20 p3406 A67-37656
 Electronic packaging techniques for electromagnetic compatibility covering electric and magnetic fields suppression and common impedance interference avoidance 21 p3599 A67-38627
 Electromagnetic compatibility prediction using statistical descriptions of case

emission and susceptibility 24 p4132 A67-42712
 Induced interference in open and shielded wire lines due to AC and transient currents, discussing electromagnetic coupling effects 24 p4137 A67-42713
 Aerospace system power conditioning design optimization, treating efficiency, regulation, EMI, BITE, primary power, size, weight, radiation hardening and cost [AIAA PAPER 67-985] 24 p4110 A67-43057

ELECTROMAGNETIC CONTROL
 Communications satellite orientation with respect to earth, using structure mounted electromagnetic actuator coils 05 p0905 A67-16833
 Jaeger electromagnetic powder coupler characteristics and space application 07 p1131 A67-19525

ELECTROMAGNETIC FIELD
 Linear formulation of electromagnetic field effect on supersonic gas flow 01 p0125 A67-10980
 Intensity observation of ELF electromagnetic field integral and SEA phenomena caused by solar flare-induced SID 01 p0060 A67-11240
 Rectilinear and smooth multiwave transition 02 p0215 A67-11914
 Electromagnetic fields of oscillating electric dipole located over half-space with anisotropic conductivity and dielectric constant 02 p0204 A67-12194
 Cosmic ray electromagnetic acceleration mechanism, calculating motion of charged relativistic particles in applied fields 02 p0311 A67-12586
 Nuclear interaction similarity with Dirac monopole interaction with electromagnetic field, noting equality in number of conservation laws acting in either interaction 02 p0271 A67-12751
 Criterion equations describing motion of fluid particle in conducting medium in presence of electromagnetic field and crossed electrical and magnetic fields 03 p0475 A67-13177
 Multimode surface waves for plane structures in generalized impedance boundary condition, noting electromagnetic field arising from magnetic dipole source located above plane structure 03 p0469 A67-13657
 Electromagnetic field of accelerating charge using Coulomb law, relativity transformation relations, charge conservation, Newton third law, etc 03 p0469 A67-13719
 Electric drag of satellites noting contribution of impinging ions 04 p0705 A67-14998
 Boundary layer structure between rarefied plasma and magnetic field, detailing mathematical formulation in relativistic invariant form 04 p0665 A67-15179
 Electromagnetic field in induction type plasma generator in steady state, from Maxwell equations and heat conservation equations 04 p0671 A67-15612
 Gas film MGD lubrication in transverse and tangential electromagnetic fields 05 p0810 A67-16273
 Electromagnetic field emission of infinite package of impedance half-planes produced by cophasal linear sources 05 p0762 A67-16352
 Umov-Poynting theorem, Lorentz lemma, complex conjugate lemmas and quadratic relations for EM field intensity in electrodynamics of moving media 05 p0844 A67-16354
 Approximation of space wave plus complex wave using modified saddle point technique 05 p0766 A67-17297
 Resistive effects in type II superconductors near upper critical field examined, using Ginzburg-Landau equations 06 p1049 A67-17882
 Optical phonon production, showing existence of electric field strength range at low temperature scattering in which phonon emission results in electron stoppage 06 p1010 A67-17884
 MNT-VZ-V device for simulating electromagnetic field in radio waveguides by induced current method 06 p1001 A67-17937
 LF electromagnetic field behavior in cold magnetoactive plasma near resonance layer, noting condition for energy absorption increase 06 p1039 A67-18078
 Oscillations of inhomogeneous weakly

ionized plasma situated in external electric and magnetic field, noting causes and conditions of plasma instability 06 p1039 A67-18080

Charged particle excitation by random electromagnetic field, obtaining velocity distribution function via all-order perturbation method 06 p1040 A67-18102

Electromagnetic diffraction at aperture, comparing three theories for case of partial polarized incident field 06 p1033 A67-18541

Interband electron absorption and dispersion during one- and two-photon processes in semiconductors subjected to electromagnetic field, noting laser applications 06 p1054 A67-18798

Charged and neutral particles collision effect on LF oscillations in weakly ionized plasma in crossed electric and magnetic fields 06 p1046 A67-18827

Electromagnetic induction in conducting sphere rotating in transverse field, extending results for steady state to unsteady rotation, determining magnetic moment 07 p1174 A67-19715

Exact solutions of Einstein-Maxwell equation of Petrov class N when propagation vector of gravitational field is hypersurface orthogonal 07 p1218 A67-20281

Radio astronomical measurements within partial coherence theory showing coherence function relation to spectrum, brightness distribution and statistical electromagnetic fields polarization 09 p1460 A67-21585

Input-output information transfer through correlation function of electromagnetic fields, obtaining optimization of system 09 p1461 A67-21603

Two-dimensional isothermal liquid flow electrically conducting in channel under electromagnetic fields, finding self-modeling solutions using Jacobi functions 09 p1544 A67-21861

Book on general electromagnetic fields represented by superposition of plane waves traveling in diverse directions 09 p1463 A67-21984

Dispersion and interaction impedance of slow wave structures from cold tests measured, using resonance methods 09 p1476 A67-22212

Retarded potentials and fields of oscillating electric dipole undergoing accelerated relativistic motions 10 p1679 A67-22730

MHD channel flow under transverse electromagnetic field, analyzing effect of various geometries and boundary conditions 10 p1684 A67-22875

First and second adiabatic invariants of charged particle motion in calculating trajectory in combined electric-magnetic field 10 p1651 A67-23395

Plasma stabilization by HF electromagnetic fields, noting mode spectrum spacing along sample axis and dependence on field strength 10 p1686 A67-23585

Statistical properties of superposition of coherent and incoherent electromagnetic fields studied in terms of coherent state formalism 10 p1667 A67-23778

Plasma thermoconductivity in general force fields, showing validity of Meador-Staton results in case of ambipolar diffusion and nonuniform total pressure 11 p1827 A67-23884

Ray solution for point source in medium with varying propagation constant determined, using Green function for scalar wave equation 11 p1751 A67-23969

Stability of flow of ideal compressible gas at low magnetic Reynolds numbers in presence of longitudinal perturbations produced by crossed electromagnetic fields 11 p1832 A67-24026

Time varying electromagnetic field pattern of prolate spheroid antenna with rotationally symmetric current distribution motion pictures generated by computer 11 p1758 A67-24115

Dynamic correspondence between electromagnetic field density matrix and associated classical random problem, obtaining means of quantum operators through Fokker-Planck equation 11 p1799 A67-24240

Plasma confinement by HF multipole electromagnetic field, noting role of potential accompanying rotating magnetic field 11 p1839 A67-24425

Inhomogeneous gas of weakly coupled

relativistic electrons, deriving kinetic equation for particle electromagnetic field system 11 p1782 A67-24781

Radiation MGD, considering flow problems with thermal radiation and electromagnetic field effect 12 p1975 A67-25889

RF electromagnetic fields to control state of flowing thermal plasma 12 p1975 A67-25921

Approximate technique using perturbation theory in analyzing microwave interaction with gyrotropic media 12 p1908 A67-26183

Electromagnetic field tensor created by point charge provided with universal velocity and acceleration is equal to outer product of universal vectors 13 p2156 A67-26594

Stabilizing or destabilizing effect of electromagnetic force on liquid film flow 13 p2167 A67-26930

Carrier distribution function in degenerate p-type germanium in presence of hole scattering on acoustic phonons, considering heating in arbitrary electric and magnetic fields 13 p2181 A67-27281

Characteristic momentary pictures of two-dimensional electromagnetic wave fields with all boundaries conformally transformed into parallel planes, taken from motion picture 14 p2268 A67-28447

Electromagnetic properties of impure anisotropic strong-coupling superconductors, using Green function to obtain response, current density and Josephson tunneling current 14 p2371 A67-28724

Local measurement of SHF electromagnetic field during plasma properties observation, using dipole antennas 15 p2485 A67-29124

Boundary perturbation theory in electromagnetism noting application to conducting sphere with surface perturbation 15 p2435 A67-29186

Expression defining condition under which Brownian movement of universe affects Brownian movement of single electron 15 p2554 A67-29316

Mathematical model of MHD induction generator, deriving electrical diagram 15 p2527 A67-29472

Ionizing detonation wave model with electrical conductivity jumping from zero to infinity characterized by exothermal energy release and magnetoacoustic speed propagation 15 p2528 A67-29567

Envelope representation of fluctuating classical wave amplitude of stationary optical fields [SR-4] 15 p2518 A67-29767

Invariant solutions to nonlinear electromagnetic phenomena in dense plasma with nonequilibrium electric conductivity in variable magnetic field 16 p2712 A67-30543

Shock tube measurement of plasma electric conductivity, using Maxwell equation for quasi-steady state electromagnetic field 16 p2073 A67-31111

Origin of afternoon VHF radar echo from backscattering layer near auroral electrojet explained by plasma instability and perpendicular electric and magnetic fields 16 p2627 A67-31407

Earth electromagnetic field stable micropulsations/pearls/ properties stressing apparent pearl polarization and polarization behavior 16 p2667 A67-31485

Electromagnetic field effect on heat transfer during laminar flow of electrically conducting incompressible fluid in flat channel 16 p2723 A67-31774

Light field distribution in optical resonator of Fabry-Perot type interferometer with nonparallel mirrors, using Airy function for localizing field concentration planes 17 p2853 A67-31925

Maintenance of electromagnetic field by dynamo effect in homogeneous isotropic turbulence without mirror symmetry 17 p2883 A67-32355

Exact solutions for pure total radiation state, constructing singular electromagnetic fields 17 p2884 A67-32703

Electromagnetic properties associated with presence of overlapping bands in pure superconductors, discussing temperature dependence 17 p2915 A67-32718

Rapid earth electromagnetic field variations used for plasma concentration and magnetosphere radius determination 17 p2846 A67-32937

Electromagnetic fluctuation structure associated with resonance properties of

earth-ionosphere bounded cavity 17 p2847 A67-32942

Laminar slow wave coupler applied to waveguide to detect very low power slow waves in indium antimonide subjected to combined effects of applied electric and magnetic fields 17 p2922 A67-33087

Cosmic ray motion in interplanetary electromagnetic field for isotropic/anisotropic diffusion situations presented by convective diffusion models assuming spherical symmetry for solar cavity 17 p2938 A67-33188

Coherent electromagnetic oscillation from voltage biasing of superconducting weak link producing coupled quantum oscillators 17 p2926 A67-33380

LF gravitational waves radiated by electromagnetic field of moving bodies, discussing measurement problems 18 p3117 A67-33527

Electromagnetic field coupling action through holes in metal screen, noting hole polarizability calculation and hole equivalent dipoles effect on resonators 18 p2999 A67-33530

Initial loss in TWT with lossless slow wave circuit connection to drift tube, expressing field components by sums of normal modes 18 p3010 A67-33645

MNT-VZ-V device for simulating electromagnetic field in radio waveguides by induced current method 18 p3046 A67-33774

Speed deficits of oxyacetylene detonation waves passing through MHD channel in electromagnetic field explained by Hall effects altering boundary layer 18 p3086 A67-33825

Density redistribution of plasma electrons and ions caused by strong microwave field 18 p3087 A67-34040

High pressure vortical discharge in air and argon, solving differential equations for heat conduction and electromagnetic field by digital computer 18 p3088 A67-34062

Book on plasma physics covering plasma clouds in electromagnetic force field, kinetic equations, Boltzmann equation, etc 18 p3089 A67-34370

Interband electron absorption and dispersion during one- and two-photon processes in semiconductors subjected to electromagnetic field, noting laser applications 18 p3102 A67-34417

Ionizing wave in plasma gun with crossed electric-magnetic fields, obtaining burning voltage of discharge and bias magnetic field ratios 19 p3277 A67-35123

Multiple-photon ionization of atoms and molecules in strong varying electromagnetic field, measuring ionization probability dependence on field intensity 19 p3265 A67-35164

Inhomogeneous plasma stability, considering wave drift oscillations expanding across external magnetic field and flute instability in noncompensating plasma 19 p3292 A67-35393

Interactions produced by shock wave running into magnetic field perpendicular to wave direction 19 p3294 A67-35405

Semiconductor surface electromagnetic oscillations excitation in presence of strong electric and magnetic fields, obtaining damping and dispersion law 20 p3504 A67-36163

Electromagnetic and pressure fields produced by current distributions in compressible magnetoplasmas determined using perturbation theory 20 p3496 A67-36312

Pressure gauge for plasmas subjected to large dynamic electric and magnetic fields in accelerator channel of MHD wind tunnel 20 p3444 A67-36529

Electromagnetic field energy absorption in cold rotating plasma, obtaining electric current density and plasma electric field relationship and cyclotron resonance 20 p3497 A67-36677

Field determination when produced by symmetrical plasmoid with time dependent current distribution traveling along cylindrical waveguide, using Wiener-Hopf method 20 p3497 A67-36680

Correlation of north-south component of telluric currents and brightness fluctuations in quiet form auroras 20 p3431 A67-36994

Soviet book on electromagnetic and gravitational fields theory based on relativity theories 20 p3486 A67-37207

Superconducting diode behavior in

resonant electromagnetic radiation field, studying current-voltage-magnetic field relationship 20 p3511 A67-37241

Quantum corrections to Maxwell plasma free energy in compensating electromagnetic field by method of displacements and collective variables for high temperatures 21 p3663 A67-37861

Electromagnetic and acoustic waves diffraction at smooth convex body of arbitrary shape, solving field equations 21 p3579 A67-38108

Electromagnetic forces and pressure and hydraulic losses of turbulent mercury flow in annular channel under traveling magnetic field effect 21 p3666 A67-38249

Stability technique for gas flow past body impeding laminar-turbulent boundary layer transition via crossed electric and magnetic fields 21 p3666 A67-38251

Pinch effect in degenerate indium antimonide plasma in longitudinal and transverse electromagnetic fields 21 p3666 A67-38369

Giant coherent light pulses generation by Q-switched laser, studying dynamics of generation and field distribution 21 p3640 A67-38373

Plasma rotation effect on cyclotron resonance, noting electromagnetic field energy absorption 21 p3669 A67-38679

Distributions of current, potential, electron density and pressure and ion velocity vector orientation in MPD arc, verifying electromagnetic effects presence [AIAA PAPER 67-676] 21 p3671 A67-38709

Geomagnetic aperiodic variation effect on earth electric conductivity in electromagnetic induction theory for flat earth model 21 p3622 A67-39027

Two-mode laser beam electromagnetic field statistical properties tend to Bose-Einstein form 21 p3642 A67-39117

Soviet monograph on skin effect theory, deriving relations defining electromagnetic field distribution in bulk conductors and plates 22 p3768 A67-39566

Electron affinity of helium measured by analyzing energy of electrons photodetached from negative helium ions beam passing through laser electromagnetic field 22 p3815 A67-39614

Long period hydromagnetic propagation in theta model geomagnetic tail, deriving TM and TE modes equations 22 p3791 A67-39815

Stable motion of rarefied plasma ions and electrons in crossed electric and magnetic fields 22 p3853 A67-40024

Nuclear interaction similarity with Dirac monopole interaction with electromagnetic field, noting equality in number of conservation laws acting in either interaction 22 p3841 A67-40253

Asymptotic solution for electromagnetic field of electric dipole above stratified half-space 22 p3763 A67-40311

Emissivity expressions and absorption coefficients developed for plasma particles interacting with electromagnetic field and at equilibrium 22 p3854 A67-40527

Electromagnetic field components of vertical and horizontal dipole antennas in quasi-near range 23 p3979 A67-40828

LF downcoming sky wave phase calculation method, discussing complex integral representation for resultant field 23 p3973 A67-40838

Cosmic ray intensity solar cycle variations in terms of solar wind properties defined by solar activity characteristics parameters 23 p4056 A67-41106

Einstein-Maxwell fields exact solutions constructed from Einstein vacuum fields, discussing vacuum metric and transformations 23 p4028 A67-41150

Quasi-neutral ion beam focusing by axisymmetric electromagnetic field with closed electron drift, noting ion velocity distribution effects for longitudinal and azimuthal components 23 p4035 A67-41682

One-dimensional plasma flow variables relations analyzed in crossed electric and magnetic fields with small magnetic Reynolds numbers 24 p4196 A67-42216

Planar dielectric waveguide excitation at p-n junctions by externally incident electromagnetic field 24 p4121 A67-42337

MHD generation of electric power, describing motion equations for conducting fluid in electromagnetic field and duct configurations 24 p4098 A67-42413

Gas bearing Brayton cycle turboalternator rotor system stability and dynamic response to electromagnetic forces 24 p4102 A67-42487

Nonlinear electrical problems requiring partial differential equations including magnetic saturation, parametric amplifier, electron tube, traveling wave amplifier and semiconductor diodes 24 p4133 A67-43089

ELECTROMAGNETIC INSTRUMENT

Soviet papers on electromagnetic and semiconductor devices in conversion technology 07 p1150 A67-19316

High speed electromagnetically driven shutter 10 p1658 A67-23786

Conducting gas flow in jet in front of electromagnetic accelerator nozzle exit region analyzed, giving jet shape and parameter distribution 11 p1842 A67-24951

Electromagnetic component /Vectorsyn/ for improving mass element restraint and support for three-axes acceleration measurement system 12 p1947 A67-26123

Moving coil and variable air gap electromagnetic actuators, discussing characteristics and applications 14 p2247 A67-28266

Nuclear methods and techniques applied to maintenance and checkout of complex electronic and electromechanical systems, discussing radiation-matter interaction, etc 20 p3449 A67-36981

Instrumentation systems for measuring thrust and electric power input of electromagnetic induction plasma thruster [AIAA PAPER 67-739] 21 p3695 A67-38761

Liquid helium application in electromagnetic DC, LF and HF AC devices 22 p3838 A67-40397

ELECTROMAGNETIC INTERACTION

SA PLASMA-ELECTROMAGNETIC INTERACTION

Resonance amplification of associated slightly attenuating electromagnetic and acoustic helicon waves by electron drift in semiconductors and semimetals 01 p0128 A67-10081

Thin film piezoelectric transducers properties used in microwave acoustic delay lines and phonon generators for analysis of phonon-phonon interactions in dielectric materials 04 p0621 A67-15116

Special relativity theory of electromagnetic interactions with thermoelastic solids, thermoviscous liquids and EM materials in continuum 04 p0659 A67-15796

Nonlinear interaction of two electromagnetic waves in infinite cold magnetoactive plasma 05 p0766 A67-17230

Coherent radiation interaction with two-level atoms system in single mode approximation, obtaining equation for time dependent number of photon emission and absorption 06 p1012 A67-18804

Deformation potential effect on helicon-phonon interaction in multivalley semiconductor 06 p1071 A67-18991

Resonance amplification of associated slightly attenuating electromagnetic and acoustic helicon waves by electron drift in semiconductors and semimetals 08 p1371 A67-21458

Nonreciprocal characteristics of long distance HF ionospheric propagation path interpreted as interaction of waves with transmitting and receiving antennas 11 p1754 A67-24718

Channel profiles for producing vortex flows in weakly ionized gases in transverse magnetic fields 12 p1977 A67-26076

Oscillator strengths for extreme UV resonance lines of ions in neon isoelectronic sequence calculated, based on single configurations in intermediate coupling 12 p1968 A67-26247

Matching factor for energy exchange in electromagnetic interaction between ionic and electronic gases in amplitude-amplitude ionospheric intermodulation 13 p2070 A67-27196

Resonant interactions between energetic trapped particles and transverse electromagnetic wave, suggesting geophysical applications and examining resonances suppression conditions 17 p2939 A67-33210

Coherent radiation interaction with two-level atoms system in single mode approximation, obtaining equation for time dependent number of photon emission and absorption 18 p3061 A67-34423

Laser pulse duration effect on

photonuclear processes, as affected by matter-radiation interactions, observing ionization in gases and surface photoeffects 19 p3238 A67-34897

Bargmann-Wigner and Dirac formulations for field of spin 1/2 shown equivalent provided auxiliary field vanishes in electromagnetic interaction presence 20 p3489 A67-37090

Weak electromagnetic decays of hyperons in broken SU(3) model 20 p3489 A67-37093

Effect of electromagnetic field interaction with gravitational field calculated from satellite data, determining difference between frequencies 20 p3386 A67-37523

Electromagnetic interference reduction between antennas on space vehicles 20 p3405 A67-37642

Excited nuclei electromagnetic de-excitation rate by inelastic scattering in stellar particles calculated as function of temperature, density, transition energy and multipole functions 21 p3660 A67-38846

Electromagnetic interactions in hyperfine structure of vibrational and rotational states in rubidium and potassium /isotopes/ fluorides, using electric resonance method 22 p3839 A67-39203

Long range interaction of two H atoms calculated with electrostatic Hellmann-Feynman theorem, determining part of second order molecular wave function 22 p3840 A67-39387

Connections between superconductivity and electromagnetic potentials, presenting model for flow of superconducting electrons and quantization of fluxoid 22 p3863 A67-40198

Electron-electron interaction effect on Li soft X-ray emission spectrum, liquid metal optical absorption and alkali metal dielectric response 23 p4037 A67-40760

Laser light production and properties based on quantum mechanical equations, describing nonlinear interaction between radiation and matter 23 p4011 A67-40761

Intermediate range intermolecular forces with overlapping wave functions and exchange effects calculated for ionized H molecule using perturbation theory 23 p4029 A67-40971

Light beam self-focusing, discussing electromagnetic interaction in nonlinear medium, refractive index dependence on wave intensity and geometrical optics 24 p4187 A67-41770

Hall potential difference for thin film in magnetic leakage field of domain interface between ferro- and ferrimagnetic 24 p4204 A67-42457

ELECTROMAGNETIC MEASUREMENT

Electromagnetic measurement of motion of explosion products behind detonation wavefront, calculating isentrope from mass velocity distribution 04 p0606 A67-15184

Radio measurement methods and standards, reviewing progress in atomic and quartz frequency standards, precision coaxial connectors, etc 05 p0804 A67-16008

Electromagnetic noise effect on aircraft examined, using fuselage mounted monitoring antennas 05 p0768 A67-17533

Hydraulics of electromagnetic liquid-metal metering device with constant inlet pressure, noting dose value dependence on parameters and operating conditions 06 p0951 A67-18684

Precision electromagnetic measurement - IEEE Conference, Boulder, June 1965 09 p1493 A67-21612

Fast variations of electromagnetic field measured by satellites electron I and II used as indication of state of radiation belts and magnetosphere of earth fast variations of electromagnetic field measured 12 p1994 A67-25537

Plasma spectrum, discussing electromagnetic oscillation damping on boundary of two media with different electrical properties 15 p2531 A67-30073

Flux penetration and dissipation measured on superconducting niobium slab samples with tangential applied field studied for effect of thickness 22 p3857 A67-39491

High energy cosmic ray shower detection combining perturbed magnetic field pulse and coincident optical radiation observations 23 p4051 A67-40812

Interferometer phase and amplitude measurements for coherence ratio and wavefront correlation, discussing scattered

- flux 23 p3974 A67-41197
Field Effect Monitor for biomonitoring cardiovascular variables and LF physiological electromagnetic phenomena 23 p3966 A67-41582
- ELECTROMAGNETIC METHOD**
Electromagnetic analysis of rotating fluid systems containing rigid and inhomogeneous parts within fluid by introducing additional relativistic transformation of gravitational constant 01 p0113 A67-10470
Alfvén standing wave generation by current injection and/or electromagnetic induction in conducting liquid 02 p0272 A67-11520
Electromagnetic excitation of metallic cone, deriving systems of linear algebraic equations for coefficients of expansion of electric and magnetic fields 04 p0575 A67-15152
Statistical problems in use of EM data for remote sensing of geological attributes of lithosphere-atmosphere interface 05 p0803 A67-17387
Electromagnetic excitation of metallic cone, deriving systems of linear algebraic equations for coefficients of expansion of electric and magnetic fields 15 p2435 A67-29339
Electromagnetic probing by laser, determining number densities of water, carbon dioxide and oxygen constituents of atmosphere 15 p2500 A67-29911
Mapping of fluctuation field of space and earth environment by electromagnetic techniques 22 p3884 A67-39949
Electromagnetic sensing of earth from satellites - Conference, University of Florida, November 1965 22 p3804 A67-40350
- ELECTROMAGNETIC PROPAGATION**
SA IONOSPHERIC PROPAGATION
Electromagnetic wave propagation in two waveguides with different cross section connected by long continuous slot 01 p0038 A67-10717
Waveform coefficient variation F-matrix analysis of electromagnetic wave propagation in light waveguide with gas lens, considering field distribution and impedance analogy 01 p0026 A67-11237
Self-focusing of transverse electromagnetic plane waves in magnetoplasma 02 p0191 A67-11571
Artificial nonlinearization method of solving linear second order equations with variable coefficients, with application to two-dimensional electromagnetic propagation along inhomogeneous dielectric layers 02 p0191 A67-11572
Electromagnetic beam propagation in unbounded gyrotropic media taking spatial dispersion into account 02 p0192 A67-11641
Propagation constant derived for electromagnetic waves propagating along array of parallel thin wires located in plane dielectric layer 02 p0192 A67-11642
Abnormal skin effect in thin films of noble metals near IR, taking into account wave penetration and magnitude of conducting electrons mean free path 02 p0288 A67-11723
Fast and slow electromagnetic wave propagation along annular plasma 02 p0204 A67-12187
Instabilities and dispersion during electromagnetic wave excitation and propagation in weakly turbulent plasma 02 p0278 A67-12627
Experimental results of microwave absorption by magnetoplasma indicate peaks result from excited electromagnetic wave propagation 03 p0476 A67-13357
Bar line theory for electromagnetic wave propagation in system of triperiodic parallel multiwire lines 03 p0387 A67-14094
Small amplitude electromagnetic wave propagation in cold homogeneous ionospheric plasma including negative ions and immersed in static magnetic field 04 p0614 A67-14957
Charged particle redistribution due to rockets and satellites flying in ionosphere influence on electromagnetic propagation in region of body and interpretation of Langmuir probe 04 p0664 A67-14990
Electromagnetic wave propagation along confocal lens line for variable refractive index of ambient medium 04 p0575 A67-15150
Kinetic theory of electromagnetic propagation in confined magnetoactive plasma 04 p0668 A67-15272
Transverse electromagnetic wave transformation into ion-acoustic plasma oscillations with formation of intermediate Langmuir electron wave 04 p0668 A67-15275
Transmission coefficient for passage of electromagnetic wave through circular aperture in plane diaphragm 04 p0577 A67-15657
Coupled spin, electromagnetic and plasma waves in ferrites 04 p0686 A67-15973
Propagation constant of electromagnetic waves over earth surface 05 p0760 A67-16001
Electromagnetic wave propagation in gyrotropic medium, writing linear equations for alternating field 05 p0761 A67-16207
Kinetic theory of electromagnetic wave propagation in layered plasma waveguide in strong magnetic field 05 p0761 A67-16341
Approximation method of geometric optics in theory of electromagnetic waves in gyrotropic medium 05 p0762 A67-16347
Small amplitude electromagnetic wave propagation in collisionless plasma with negative ions, noting bands and waves for various frequencies and polarizations 05 p0853 A67-16846
Longitudinal propagation of SLF electromagnetic waves through plane-laminar magnetoactive ionospheric plasma 05 p0765 A67-16955
Lunar line waveguide parameters calculated for inner conductor displacement and ratio of radii 05 p0775 A67-16958
Recognition and subsequent amplification of difference frequency in plasma-beam system with two electromagnetic waves propagating in opposite direction 05 p0766 A67-17170
Soviet book on electromagnetic shock waves associated with not-very-high powers, using Maxwell-Lorentz equations 06 p1031 A67-17949
Electromagnetic wave propagation around cylinder surrounded by nonmagnetic isotropic medium with dielectric constant function of radius, using conformal mapping 06 p0962 A67-18076
Angular power pattern for circular aperture receiving plane wave perturbed by passage through turbulent atmosphere 06 p1033 A67-18538
Reflection and transmission of birefringent plates surrounded by semiinfinite birefringent media with incident waves having polarized electric fields 06 p1033 A67-18544
Weak superconductivity electrodynamics and EM wave propagation in Josephson tunnel junction in presence of vortices 06 p1054 A67-18806
Electromagnetic wave dispersion in semiconductor plasma waveguides for case of plane wave propagation normal to magnetic field vector 07 p1231 A67-19133
Galerkin-Ritz method application to Maxwell waveguide equations for calculation of propagation constant of rectangular guide with transverse ferrimagnetic core 07 p1152 A67-19590
Amplitude and phase velocity of electromagnetic waves in 1-30 kc range near earth surface for plane and spherical earth-ionosphere waveguide 07 p1144 A67-19695
First order coupled wave equations for propagation in planar stratified compressible electron plasmas 07 p1230 A67-19851
Self-focusing of longitudinal electromagnetic waves in nonlinear plasma in strong magnetic field 08 p1357 A67-20822
Complex dielectric constant and EM plane wave propagation in flame plasma 08 p1359 A67-21045
Laser interferometric measurement of power spectral density of integrated particle density fluctuations in turbulent exhaust of sonic jet 08 p1337 A67-21142
Linear transformation of normalized static capacitance matrix used to describe TEM propagation on array of parallel conductors 08 p1304 A67-21224
EH solutions of Maxwell equations describing guided electromagnetic waves in homogeneous isotropic medium at velocity of light 09 p1465 A67-22550
Electromagnetic propagation in semiconductor with account of nonlinear effects such as skin effects arising from electron heating by field 10 p1694 A67-23592
Electromagnetic wave propagation across land-sea boundary on flat earth near coastline 11 p1751 A67-23967
Electromagnetic wave propagation in partially ionized paramagnetic gas in static magnetic field 11 p1751 A67-23970
Mutual coherence factor for plane electromagnetic wave propagating in stochastic locally homogeneous and isotropic medium of dielectric turbulence 11 p1818 A67-24415
Electrodeless electromagnetic shock tube with large discharge chamber for high velocity shock waves, applying theta pinch effect 11 p1773 A67-24592
Radio refractive index irregularities in lower troposphere examined, using helicopter mounted spaced cavity refractometer 11 p1787 A67-24644
Plasma models and methods used to study wave propagation phenomena, considering particle orbit, single species moment equations, velocity distribution function, etc 12 p1975 A67-25527
Polarized harmonic electromagnetic wave propagation in plane stratified isotropic plasma of cold lossless electron gas, resolving inconsistency near resonance region 12 p1976 A67-25944
Propagation characteristics in waveguide loaded with cylindrical semiconductor rod, calculating electric field distribution 12 p1918 A67-26222
Electron-cyclotron wave instability in plasma noting dispersion relation, growth rate frequency, destabilizing effect of electrons, etc 13 p2163 A67-26286
Instabilities and dispersion during electromagnetic wave excitation and propagation in weakly turbulent plasma 13 p2171 A67-27384
Electromagnetic wave propagation, excitation and dispersion in metals in magnetic field 14 p2366 A67-28426
Electromagnetic wave propagation characteristics in solid plasmas without magnetic induction, showing dynamic Hall effect 14 p2366 A67-28473
Electromagnetic wave propagation along confocal lens line for variable refractive index of ambient medium 15 p2435 A67-29337
Electromagnetic surface wave propagation in plasma, studying oscillation spectra dependence on surface wave field amplitude 15 p2529 A67-29712
Nonlinear dependence of phase velocity on wave amplitude during electromagnetic propagation in plasma waveguide, describing test apparatus 16 p2718 A67-31191
Axial nonuniform perturbations of electromagnetic propagating structures analyzed, using nonlinear phase progression from perturbation theory of quantum mechanics 16 p2626 A67-31345
Iterative technique for calculating electromagnetic propagating structures with nonuniform gross perturbations obtaining convergence improvement 16 p2626 A67-31346
Fields generated by infinitesimal, arbitrarily oriented, electric-dipole source located in isotropic medium bounded by parallel plane-stratified, anisotropic media 16 p2632 A67-31858
Refractive-index equation derived for electromagnetic wave propagation along static magnetic field in plasma motion direction, using relativistic transformations 17 p2812 A67-32304
Propagation loss dependence in laser ranging systems on meteorological visibility and target-receiver range, noting inverse-square law confirmation 17 p2812 A67-32305
Dispersion relations for coupled electromagnetic and longitudinal waves propagating along isotropic inhomogeneous cylindrical hot plasma column 17 p2908 A67-33107
Structure of curved space-time in which electromagnetic wave propagation takes place without tail formation 18 p3079 A67-33761
Mean-square value and autocorrelation function for fluctuations of geometrical optical paths 18 p3000 A67-34025
Three-dimensional equation for wave propagation through inhomogeneous warm compressible plasma in inhomogeneous static magnetic field 18 p3088 A67-34071
Propagation and radiation problems in linear homogeneous dispersive anisotropic media in uniform motion solved using constitutive equation 18 p3001 A67-34198
Equivalent transmission circuits for electromagnetic propagation in birefringent media 18 p3002 A67-34226

Weak superconductivity electrodynamics and EM wave propagation in Josephson tunnel junction in presence of vortices 18 p3102 A67-34425

Pump induced optical distortion in isotropic laser materials analyzed using Fermat principle, predicting ray refraction, beam divergence, etc 18 p3062 A67-34624

Analysis of flame effects on measured electromagnetic propagation data for plume shape, plume electron density distribution and signal attenuation 19 p3344 A67-34819

Progressing wave method for linear partial differential equation systems, including Maxwell equations, applied to electromagnetic waves from moving sources 19 p3184 A67-35665

Electromagnetic wave propagation in absorbing gyrotropic medium in terms of geometrical optics, considering applicability to radiowave propagation in upper atmosphere 19 p3185 A67-36015

Phase velocity and attenuation of audiofrequency electromagnetic waves to derive electron density profiles 20 p3426 A67-36288

Rocket exhaust jet plume effects on radio signal, calculating degradation by electromagnetic diffraction propagation 20 p3381 A67-36570

Antenna array simulator using acoustic waves in water to simulate electromagnetic propagation 20 p3397 A67-36580

Electromagnetic wave propagation in waveguides calculated together with electric and magnetic fields by perturbation method 20 p3382 A67-36862

Galerkin-Ritz method application to Maxwell waveguide equations for calculation of propagation constant of rectangular guide with transverse ferrimagnetic core 20 p3401 A67-37327

Wave equation for electromagnetic wave propagation in randomly varying refractive index medium, noting focusing for radio waves in interplanetary plasma 20 p3386 A67-37521

Kinetic theory of electromagnetic wave propagation in laminar plasma medium situated in steady HF or LF magnetic field normal to plasma layer 21 p3663 A67-37860

Standard equation method for normal incidence of plane monochromatic electromagnetic wave propagation in inhomogeneous anisotropic medium 21 p3579 A67-38111

Geometrical-optics approximation method for electromagnetic wave propagation in parametric medium 21 p3580 A67-38113

Electromagnetic wave propagation in plasma layer bounded by external constant magnetic field, using kinetic theory with Maxwell equations and distribution function 21 p3670 A67-38685

Electromagnetic waves passage through thin radio-transparent layer solved by asymptotic series 21 p3585 A67-38810

Far tropospheric propagation of radio waves due to coherent scattering, explaining signal level dependence on distance and wavelength and signal fading 21 p3585 A67-38814

Electromagnetic wave propagation in nonuniformly magnetized plasma with wave frequency near second electron cyclotron harmonic 22 p3843 A67-39263

Electromagnetic wave propagation in moving media filled waveguides noting nondispersive dielectric and cold plasma cases 22 p3759 A67-39361

Kinetic theory of electromagnetic propagation through magnetoactive plasma, determining reflection, transmission and absorption coefficients and plasma field configuration 22 p3761 A67-39758

Electromagnetic propagation in plasma layer in magnetic field, determining absorption coefficient 22 p3762 A67-40123

Elliptically polarized electromagnetic wave propagation in homogeneous infinite plasma, solving Vlasov equations of nonlinear theory by successive approximation 23 p4030 A67-40597

Charged particle gas interaction with EM field noting electron gas collective oscillations, EM wave propagation in anisotropic plasma and applications 23 p4037 A67-40759

Solar type IV burst centimeter and decimeter polarization and spectral

variabilities examined in helical electron stream cyclotron radiation hypothesis for solar corona model 23 p4050 A67-40776

Coupled electromagnetic whispering gallery modes in large dielectric cylinders, discussing circumferential phase velocity, boundary region and axial wave number 23 p3974 A67-41203

Electromagnetic mode propagation in anisotropic dielectric p-n junction waveguide models noting Pockel effect of electric field on light 23 p3982 A67-41466

Light propagation in electrically and magnetically anisotropic medium and diffraction by birefringent cylinder using coupled integrodifferential equations 24 p4119 A67-41889

Approximate solution to irregular waveguides with impedance boundary conditions based on amplitude of normal wave propagation 24 p4120 A67-42159

Electromagnetic wave propagation through two-layer shielded dielectric waveguide using dispersion equation 24 p4129 A67-42192

Electromagnetic wave propagation along arbitrary cross sectional imperfectly conducting metallic cylinder employing conformal mapping 24 p4120 A67-42230

Medium range radio communication system using artificial ionosphere consisting of ion-electron cloud created by Cs-Al mixture explosion [AIAA PAPER 67-789] 24 p4152 A67-42952

ELECTROMAGNETIC PROPULSION

Resistojet and axisymmetric electromagnetic space propulsion thrusters 02 p0305 A67-12340

Propulsion systems in which propulsive fluid is accelerated to high speeds by electrical or electromagnetic processes 14 p2377 A67-28962

Microwave rocket propulsion through direct electromagnetic heating of gas and powered by wireless ground-transmitted microwaves 16 p2736 A67-30712

ELECTROMAGNETIC PUMP

Magnetic field of cylindrical permanent magnet used as rotor of electromagnetic induction pump, determining induction components and permeances to fluxes 06 p0951 A67-18685

Forces acting in electromagnetic pump channel on gas inclusions in liquid metal, assessing increase in hydraulic resistance 13 p2169 A67-27316

Electric drive operating parameters and design, using exploding wire type device and electromagnetic apparatus for plasma production and acceleration 16 p2736 A67-30716

Pressure attenuation of transverse fringe effect in flat linear induction pumps 16 p2723 A67-31582

Performance characteristics of helical electromagnetic induction pumps calculated taking into account effect of duct wall and liquid metal layer 16 p2609 A67-31584

Time-growing instability existences in distributed parametric media using dispersion relation 19 p3195 A67-35620

Operating characteristics of induction pump with asymmetrical current supply, calculating magnetic induction, currents and forces in liquid metal layer 20 p3365 A67-37307

ELECTROMAGNETIC RADIATION

SA ALPHA RADIATION

SA BETA RADIATION

SA MICROWAVE RADIATION

Green function method applied to calculating resonance absorption of electromagnetic radiation for interlevel transitions in thin film 01 p0127 A67-10072

Rms particle numbers calculated for electrons and photons in three-dimensional theory of electromagnetic showers 01 p0143 A67-10543

Characteristics of normal atmospheric, discussing VLF characteristics due to return strokes 01 p0109 A67-11228

Trajectories of electromagnetic rays across terrestrial atmosphere and computer program 01 p0028 A67-11419

Electromagnetic theory of wave propagation modes in dielectric cylinders applied to coherent light transmission in optical fibers 02 p0190 A67-11528

Electromagnetic irradiation of pyroelectric hot spots and regional variation of response 02 p0299 A67-11893

Meteorological experiments possible in

manned earth orbital spacecraft with aid of remote sensing of electromagnetic radiation 02 p0239 A67-12379

Solar flares, discussing continuous electromagnetic radiation, hard X-ray radiation and microwave radio bursts 02 p0310 A67-12576

Plasma kinetic theory calculation via direct perturbation expansion of singular distribution for single system, comparing Dupree and Dawson-Nakayama version of BBGKY hierarchy 02 p0279 A67-12800

Book on systematic and unified treatment of electromagnetic radiation from elementary Hertzian dipole in presence of dissipative half-space 03 p0373 A67-14273

Self-focusing due to intensity dependent anomalous dispersion effect on electromagnetic radiation, emphasizing laser radiation in saturated amplifying medium 05 p0819 A67-16649

Book on electromagnetic wave emission, absorption and scattering processes in gaseous plasma 05 p0855 A67-17152

Angular distribution of intensity and phase of electromagnetic wave scattered by cylindrical plasma column 06 p1041 A67-18138

Correlation of meteoroid environments in solar system, analyzing meteor mass measurement results, hypervelocity impact and solar electromagnetic radiation effects [AIAA PAPER 67-151] 06 p1085 A67-18319

Characteristic states of electromagnetic radiation field, using quantum mechanical theory of optical coherence 06 p1036 A67-18367

Dynamo mechanism for formation of stellar magnetic field, considering effects of EM radiation emission and celestial body rotation 06 p1089 A67-18773

Electromagnetic radiation at satellite-borne sensor, discussing spectral, spatial and temporal distributions of radiation energy intensity 06 p1006 A67-19010

Sensors of electromagnetic radiation in UV, visible and IR ranges, noting improvement through automatic data processing 06 p1006 A67-19013

Biotic signatures, discussing detection and epistemology 06 p0954 A67-19017

High altitude balloon-borne polarization measurements relevance in research program of radiation emerging from earth atmosphere 07 p1170 A67-19393

Radiation enhancement and resonance scattering due to plasma sheath between spherical antenna and surrounding plasma layer 07 p1153 A67-19611

Electromagnetic-wave radiation peculiarities in homogeneous anisotropic dispersive magnetic plasma 08 p1294 A67-20821

Time dependent Green function for electromagnetic radiation in moving simple media 08 p1296 A67-21430

Second order coherence properties of fluctuating vector electromagnetic fields of arbitrary spectral width, noting dyadic field spectral density and governing differential equations 09 p1460 A67-21587

Effect of tunnel diode amplifier V-I characteristics on cross modulation products in electromagnetic spectrum 09 p1557 A67-22266

Natural ELF electromagnetic noise properties during solar flare of July 7, 1966, considering radiation compression effects on earth-ionosphere cavity 10 p1700 A67-23057

Multiquantum electron transfers within conductivity band of semiconductors accompanied by emission or absorption of acoustic phonon, calculating absorption coefficient of electromagnetic emission 10 p1695 A67-23658

Optimum illumination for maximum power transfer between two opposed rotationally symmetric antennas 11 p1762 A67-24291

Time behavior of radiation field of infinite cylindrical antenna upon DC voltage pulse at input 11 p1762 A67-24292

Approximate mode decomposition for treating boundary value problems for uniform compressible anisotropic plasma 11 p1753 A67-24307

Airglow and enhanced penetrating electromagnetic radiation in southern radiation anomaly observed with scintillation crystal during aircraft flight 12 p1996 A67-25775

High energy particle and electromagnetic space radiation effects on thermal control

coating, noting spectral absorptance for various conditions
 [AIAA PAPER 67-339] 12 p1959 A67-26053
 ULF electromagnetic radiations related to magnetic bays and ionospheric phenomena at high latitudes 13 p2110 A67-26455
 Electromagnetic radiation equilibrium in gas lasers, studying effect of cavity length variations on linewidth 14 p2329 A67-27952
 Radiants associated with sonic, magnetosonic and Alfvén waves and definition in terms of distribution of delta operator of infinitesimal discontinuity 14 p2359 A67-28511
 Mechanical friction occurring during oscillating motion of gas which absorbs or reflects electromagnetic radiation 14 p2349 A67-29075
 Possibility of Cerenkov effect in superconductors established from electromagnetic oscillation spectrum, calculating wave resistance and resonance maxima positions 14 p2375 A67-29079
 Nonrelativistic approximation for electromagnetic radiation in conducting medium moving with uniform velocity with respect to source 15 p2521 A67-29194
 Chromospheric solar radiation measured during solar eclipse with UV monochromator, using electromagnetic radiation photomultipliers 15 p2565 A67-29573
 Communication with and by space vehicles at GHz frequencies, using atmospheric windows [AAS PAPER 67-94] 15 p2478 A67-29954
 Overall profile of ophthalmic injury associated with ionizing and nonionizing electromagnetic radiation fields, based on human response to radiation exposure 16 p2811 A67-30769
 Pseudo-isotropic radiation source as source with isotropic gain function and polarization depending on spatial direction 16 p2761 A67-30793
 Output noise power spectrum properties of X-band ruby maser oscillator, noting frequency dependence on electromagnetic energy and cavity losses 16 p2885 A67-31055
 Amplifying electromagnetic radiation in nonequilibrium decaying plasma of various degrees of ionization, taking into account kinetics 16 p2723 A67-31577
 Book on electromagnetic radiation discontinuities presenting solution of Helmholtz and harmonic Maxwell equations and derivation of discontinuities formulas by generalized functions 16 p2629 A67-31628
 Book on solar radio exploration covering electromagnetic radiation discovery, solar physics principles, solar radio activity and research instruments 16 p2755 A67-31923
 Sky brightness temperature measurements at various millimeter wavelengths for possible isotropic electromagnetic emission in universe 17 p2935 A67-32230
 Nonlinear incoherent light scattering from two frequency-differing coherent beams of electromagnetic radiation propagating in homogeneous plasma without magnetic field 17 p2901 A67-32354
 Radiation properties of low-gain ring antenna on ground plane, showing by patterns effect of geometrical parameters and frequency 17 p2827 A67-32781
 Shock wave generation of electromagnetic radiation at magnetospheric boundary, discussing plasma oscillation excitation, plasma wave scattering, etc 17 p2846 A67-32935
 Multiquantum electron transfers within conductivity band of semiconductors accompanied by emission or absorption of acoustic phonon, calculating absorption coefficient of electromagnetic emission 17 p2924 A67-33339
 Quantum formulas for optimal filtration of useful electromagnetic signal in noise background based on maximum misinformation principle 18 p2999 A67-33533
 Electromagnetic radiation from electric dipole moving with uniform relativistic velocity 18 p3000 A67-34022
 Amplitude and polarization of radio pulse from extensive cosmic ray air shower indicating geomagnetic deflection mechanism of emission 18 p3116 A67-34196
 Propagation and radiation problems in linear homogeneous dispersive anisotropic media in uniform motion solved using constitutive equation 18 p3001 A67-34198

Propagation and radiation of waves excited by electric dipole in dispersionless uniaxial moving medium 18 p3002 A67-34199
 Soviet book on lasers and nonlinear optics covering theory, physical processes and phenomena caused by strong electromagnetic laser radiation 19 p3238 A67-34800
 Ground based solar electromagnetic radiation environment studies in visible and radio windows 19 p3323 A67-35332
 Electromagnetic radiation reflectivity on metal surface investigated using microscopic model to derive fields and boundary conditions 19 p3262 A67-35582
 Electromagnetic radiation, elementary particles and micrometeorites effects on earth satellites 19 p3327 A67-35672
 Radiation of monofrequency antenna in compressible magnetoplasma expressing far field as sum of modal plane waves 20 p3388 A67-37701
 Bilateral metal grating effect on E and H polarized radiation from plane parallel layer noting intensity, energy density and reflection at interface with medium 21 p3638 A67-37865
 Eddy configuration plasma heated by induced currents, discussing electromagnetic radiation absorption 21 p3664 A67-38047
 Book on laser systems covering quantum electronics, coherent radiation, modulation and spectral, distance, velocity and communication applications 22 p3814 A67-39445
 Attenuation of plane sinusoidal acoustic waves due to electromagnetic radiative properties of carbon dioxide and water vapor bands 22 p3829 A67-40232
 Analog simulation of electromagnetic radiation from antenna of revolution in vacuum and plasma via networks, discussing rocket nose cone shapes 23 p3977 A67-40578
 Antenna immersed in plasma problem solved using electromagnetic radiation in ionized medium principles 23 p3978 A67-40707
 Neutron component intensity variation and particle generation on sun during chromospheric flares and electromagnetic radiation during solar activity cycle 23 p4057 A67-41116
 50 Hz ruby pulse laser emission, discussing power output, electromagnetic spectrum and transverse mode interaction 23 p4016 A67-41153
 Correlation of meteoroid environments in solar system, analyzing meteor mass measurement results, hypervelocity impact and solar electromagnetic radiation effects [AIAA PAPER 67-151] 23 p4070 A67-41719
 Maxwell equations solved for Gaussian beam form in anisotropic medium, discussing laser applications 24 p4167 A67-42092
 Book on Hamilton principle and physical systems covering planetary motion, rotating bodies, electromagnetic radiation, quantum theory, etc 24 p4189 A67-42406
 Channel bandwidth assignment determination using prescribed fraction of total radiated power of system contained in channel, discussing spectral distribution 24 p4123 A67-42714
 Effects of low density, temperature, proton radiation and electromagnetic radiation on thermal control materials, using synergistic testing 24 p4177 A67-42916

ELECTROMAGNETIC SCATTERING

Combination scattering suffered by component, polarized parallel to electromagnetic wave incident on plasma cylinder, from Tonks-Dattner resonances excited by perpendicular component 01 p0020 A67-10148
 Radar scatterometer remote sensing measurement of variation of radar scattering coefficient with angle, wavelength and polarization 01 p0021 A67-10317
 Behavior of stationary electromagnetic field produced by reflection of given incoming stationary field for small frequencies 01 p0024 A67-10523
 Plane problem of surface electromagnetic wave scattering along rectangular dielectric wedge 02 p0191 A67-11579
 Diffracted field structure of plane wave incident obliquely from air onto sinusoidally modulated half-space at Rayleigh and Bragg wavelengths 02 p0204 A67-12196
 Scattering of electromagnetic waves in plasma, noting effect of eddy current fluctuations 03 p0367 A67-12938
 Scattering of plane electromagnetic wave

at infinite circular cylinder with spatially varying dielectric constant 03 p0368 A67-13281
 Point matching solution developed for scattering by conducting bodies of arbitrary shape including circular and square wire loops, plates, spheres and hemispheres 03 p0370 A67-13855
 Wave scattering by smooth and rough finite cylinder situated in layer with randomly varying dielectric constant analyzed by approximation of physical optics 05 p0762 A67-16349
 Scattering cross section of electromagnetic waves by finite objects in compressible plasma in absence of DC magnetic field 05 p0853 A67-16802
 Electromagnetic scattering from perfectly conducting strips, wedges and notched circular cylinders 05 p0763 A67-16850
 Wave scattering in plasma in presence of transformation 06 p1045 A67-18785
 Radio wave emission due to shock wave propagation in magnetospheric boundary and electromagnetic scattering in plasma wave field 07 p1243 A67-19808
 Electromagnetic wave scattering by rough surface computed by approximate method 07 p1147 A67-20237
 Relativistic mechanism of electromagnetic wave scattering at velocity fluctuations and emission from plasma in external field 08 p1295 A67-20831
 Electromagnetic wave scattering measurements using spheres moving randomly within slab region container, obtaining data for coherent phase, average intensity, etc 09 p1461 A67-21597
 Comparison of distribution functions from reduced data records for scattering of electromagnetic waves by randomly moving spheres in container 09 p1461 A67-21598
 Experimental verification of predictions of conventional quantum electrodynamics vacuum effects by Compton and other scattering techniques 09 p1534 A67-22021
 Electromagnetic wave diffraction on perfectly black screen in Kottler theory 09 p1464 A67-22054
 Radiation absorption and scattering by small spherical solid carbon particles in wavelength range 0.2 to 40 μ calculated by classical Mie theory 10 p1682 A67-23146
 [AIAA PAPER 66-134] 10 p1682 A67-23146
 Scattering of circularly polarized electromagnetic wave in Coulomb field, noting coalescence of two-wave quanta into one quantum of double frequency 10 p1666 A67-23594
 Diffraction of plane electromagnetic wave from ideally conducting ellipsoid of revolution 11 p1751 A67-23915
 Electromagnetic wave scattering from plasmas calculated in context of physical optics, noting that radar cross section for plasmas with finite conductivity is polarization dependent 11 p1820 A67-24913
 Combination scatter of electromagnetic waves by ion-acoustic oscillations in flat confined plasma layer with zero plasma density outside 12 p1974 A67-25447
 Electromagnetic scattering from rough finitely conducting surface of uniform infinitely extended medium, considering intensity and polarization 12 p1906 A67-25945
 Surface roughness effect on spectral and total emittance of platinum, noting spatial distribution of polarized components [AIAA PAPER 67-320] 12 p1957 A67-26035
 Radio propagation in inhomogeneous media with permittivity varying bilinearly with distance, noting model experiment 12 p1908 A67-26220
 Resonance scattering of electromagnetic waves on arbitrary rarefied plasma region with near zero intrinsic wave number relative to small perturbation 13 p2067 A67-26547
 Diffraction field parts of slit aperture formed by two nonplanar screens satisfy variational principle 14 p2281 A67-28106
 Radiation from plasma films and columns nonlinearly excited by incident electromagnetic waves, showing predominance of radiation on scattering 14 p2356 A67-28153
 Clear atmosphere angels origin, clear air turbulence detection, radio propagation and atmospheric radar probing 14 p2264 A67-28395
 Effects of strong coupling and spin-flip

- scattering by magnetic impurities on superconductors, calculating conductivity and surface impedance at finite temperatures 14 p2371 A67-28725
- Electromagnetic wave field probability distribution when scattering by medium with randomly varying refractive index 16 p2623 A67-30968
- Incoherent scattering of plane electromagnetic waves on cylindrical plasma column with fluctuating charge-density 16 p2628 A67-31499
- Radio ray divergence in ionosphere using computer techniques, noting ionospheric models and limitations 16 p2629 A67-31512
- Wave scattering in plasma in presence of transformation 18 p3086 A67-33727
- Electromagnetic scattering by thin inhomogeneous circular cylinders, presenting numerical results for induced axial current and scattering cross section 18 p3004 A67-34431
- Computational scheme for calculation of Mie cross sections of absorbing particles 19 p3184 A67-35688
- Electromagnetic plane wave scattering cross section from plasma coated conducting cylinder using TE and TM modes of polarization with respect to cylinder axis 20 p3389 A67-37706
- Electromagnetic scattering from adsorbing spheres near resonances calculated from extinction efficiency factor and angular scattering function dependence on refractive index 21 p3656 A67-37856
- Combination scatter of electromagnetic waves by ion-acoustic oscillations in flat confined plasma layer with zero plasma density outside combination scatter of electromagnetic waves by ion-acoustic oscillations in flat confined plasma 21 p3674 A67-38821
- Diffraction of plane electromagnetic wave from ideally conducting ellipsoid of revolution 21 p3586 A67-38943
- Integral equation for asymptotic expansions of plane electromagnetic and acoustic fields diffracted by convex surfaces of variable curvature 22 p3836 A67-39389
- Helical electromagnetic wave scattering and transformation during propagation in magnetoplasma, considering fluctuations 22 p3846 A67-39501
- Electromagnetic wave scattering by circular cylinder moving in free space, noting far field patterns and Doppler shift angular dependence 22 p3760 A67-39623
- Polarized and depolarized scattering from perfectly conducting rough surface, theory based on Fourier transform and small perturbations polarized and depolarized scattering from perfectly conducting rough surface, using theory 22 p3762 A67-40076
- Electromagnetic backscatter from edge scattering centers found on cylinders and flat-backed cones, discussing hemispheric scattering 23 p3973 A67-40839
- Electromagnetic scattering from free-space impedance homogeneous spheres, discussing null production in backscattering cross section 23 p3973 A67-40882
- ### ELECTROMAGNETIC SHIELDING
- Parabolic reflector with shields protecting feed from extraneous radio waves 08 p1318 A67-21343
- Shielding methods for electronic equipment packaging, considering magnetic, electromagnetic and RFI shielding in gamma and X-ray range 12 p1911 A67-25267
- Plane wave shielding effectiveness of thin films, using TEM mode 13 p2175 A67-26524
- Parabolic reflector with shields protecting feed from extraneous radio waves 17 p2822 A67-31939
- Electromagnetic shielding effectiveness of enclosure determined by measurement of perpendicular magnetic field along conducting wall surface, emphasizing continuity of seams 20 p3404 A67-37640
- Titanium alloy resistivity and aircraft structure role as current return and electromagnetic shield, discussing greater use of wire for susceptible circuits to achieve EMC 20 p3405 A67-37643
- ### ELECTROMAGNETIC SHOCK TUBE
- Precursor wave velocity, electron density and current content in electromagnetically driven shock tube, using hydrogen and argon 08 p1363 A67-21380
- Normal ionizing shocks propagating through hydrogen in sub-Alfvénic and trans-Alfvénic regimes in coaxial electromagnetic shock tube 08 p1363 A67-21381
- Plasma flux shaping in setup consisting of air filled discharge chamber, electromagnetic shock tube and vacuum chamber 09 p1485 A67-22324
- High velocity shock waves obtained by magnetic pressure and relaxation processes, using electromagnetic shock tubes 11 p1832 A67-24034
- Hydrocarbon pyrolysis and H/D substitution reaction rates, using single-pulse shock tube as chemical reactor 18 p2996 A67-33788
- Carbon monoxide and atomic oxygen recombination in expansion wave of single-pulse shock tube at high temperatures 18 p2997 A67-33790
- Shock wave argon ionization in constant magnetic field, showing attenuation decrease of microwave signal in plasma and modulus change curves 18 p3087 A67-34045
- Detection and measurement of precursor ionization in electromagnetic shock tube 18 p3091 A67-34727
- Shock waves generated electromagnetically in T-tube studied with Mach-Zehnder interferometer 19 p3208 A67-35396
- Plasma temperature and density measured behind luminous and preceding shock fronts in electromagnetic shock tube 19 p3293 A67-35399
- Stream structure and bow waves in electromagnetic shock tube, establishing flow uniformity limitations through temperature and pressure measurements 19 p3294 A67-35404
- Transverse magnetic field retardation of flowing plasma in electromagnetic shock tube noting conductivity 20 p3496 A67-36214
- Precursor waves in electromagnetically driven shock tube explained by considering tube as electromagnetic transmission line [AIAA PAPER 67-694] 21 p3613 A67-38723
- Plasmoid propagation at high pressures, emphasizing Bostick buttons performance compared to electromagnetic shock tube, describing button gun and photographic equipment 21 p3674 A67-38771
- Wave-like behavior of precursor electron density front in electromagnetic shock tubes explained via transmission line model 22 p3850 A67-39711
- Electron density between shock front and discharge plasma in electromagnetic shock tube determined by interferometric technique, using guided waves 22 p3810 A67-40523
- Design of gasdynamic shock tube described with measuring apparatus developed for studying ionized gas flows in magnetic field 24 p4139 A67-42357
- ### ELECTROMAGNETIC WAVE
- #### SA RADIO WAVE
- Electromagnetic oscillation excitation in plasma beam, analyzing cases of weak and strong external magnetic fields 01 p0122 A67-10349
- Charged particle motion in field of traveling electromagnetic waves used in studies for microwave amplifiers, particle accelerators, etc 01 p0022 A67-10352
- Reflection of vertically polarized exponentially varying electromagnetic waves by horizontally stratified magnetoplasma half-space 01 p0023 A67-10471
- Simultaneous excitation of electron plasma and ion-acoustic oscillations, using single electromagnetic wave for plasma oscillation generation 01 p0125 A67-10913
- Mutual coupling between TEM and TE 01 parallel-plate waveguides calculated, using wedge diffraction techniques 02 p0211 A67-11596
- Optical resonator theory stressing electromagnetic boundary value problem 02 p0287 A67-12026
- Electromagnetic wave propagation along plasma column subjected to longitudinal magnetic field, calculating dispersion curves for two dipolar modes as function of wavelength and frequency 02 p0273 A67-12062
- Quasi-linear approximation of Cerenkov and cyclotron damping of electromagnetic waves in magnetoactive plasma, considering collisions of wave-absorbing resonance particles with plasma 03 p0475 A67-12934
- Waveguide interactometer measurement of plasma parameters 03 p0477 A67-13458
- Plane electromagnetic wave diffraction at two parallel circular cylinders for TM and TE polarization 03 p0371 A67-13959
- Power spectrum of electromagnetic wave incoherently diffused by ionospheric electrons 04 p0571 A67-14896
- Depolarization of fully polarized electromagnetic waves, obtaining degree of polarization 04 p0575 A67-15151
- Millimeter wavelength transmission line deficiencies reduced by using channeling systems in form of elastic dielectric tape on which are mounted thin metallic strips 04 p0575 A67-15167
- Dispersion equation for electromagnetic waves propagating in uniform plasma layer along boundary parallel to external magnetic field 04 p0667 A67-15207
- Engineering methods for construction of electromagnetic wave absorbing walls for microwave darkroom applications at various frequency bands 04 p0576 A67-15504
- Elliptically polarized wave reception by antenna, itself elliptically polarized, for use in interferometry problems, noting relation to complex vector 04 p0658 A67-15626
- Electromagnetic waves produced by charge traveling at constant velocity in medium with convective instability 05 p0762 A67-16353
- Klystron with broad electron flux and excited traveling and standing electromagnetic waves, analyzing electron grouping 05 p0771 A67-16356
- Radiation pressure of electromagnetic and acoustic waves calculated from momentum of incident and scattered wave trains 05 p0846 A67-16583
- Induced electron cyclotron radiation application to generation and amplification of high power electromagnetic traveling waves 05 p0824 A67-16915
- Electromagnetic wave emission excited by electron stream over diffraction grating lying on boundary of semilinear anisotropic dielectric 05 p0766 A67-17163
- Wave excitation in compressible partially ionized plasma by electromagnetic and acoustic /or mechanical/ sources, describing set of linearized hydrodynamic and Maxwell equations 05 p0859 A67-17436
- ELF and VLF wave propagation in earth-ionosphere waveguide at wide frequency range, giving amplitude spectra and mean phase velocity for day and night 06 p0994 A67-17970
- Radio electronics, discussing quantum electronics, lasers, microwave devices and technology, plasma physics, etc 06 p0968 A67-18072
- Surface current excitation by electromagnetic and electrokinetic waves on metal cylinder immersed in uniform collisionless isotropic plasma 06 p0962 A67-18075
- Plasma half-space impedance for diffusive electron reflection from plasma vacuum boundary, noting damping decrement of surface electromagnetic wave, electric field Fourier components and absorption capacity 06 p1039 A67-18079
- Stationary self-consistent plasma density distribution in field of strong electromagnetic wave 06 p1045 A67-18779
- Nonlinear second harmonic generation of current density in inhomogeneous magnetoplasma and reflected electromagnetic wave from free space interface 06 p1046 A67-18825
- Helicon effect in semiconductors measured by resonant cavity method 06 p1071 A67-18990
- Open air lines and cables, stressing electric wave propagation along homogeneous and inhomogeneous circuits 07 p1141 A67-19340
- Tangential magnetic field on earth surface excited by LF plane electromagnetic wave 07 p1142 A67-19449
- Interaction between helicon waves and drift currents in layered lead telluride structure 07 p1232 A67-19555
- Electromagnetic plane wave diffraction on anisotropically conducting plane and shielding and reflecting activity of dense radial grating 07 p1143 A67-19589
- Numerical computation of phenomena due to electromagnetic wave diffraction on tapered grid 07 p1143 A67-19595
- Electromagnetic emission from growing plasma oscillations 07 p1230 A67-20146
- Electromagnetic wave diffraction problems

- solved by two-dimensional Laplace transforms 07 p1147 A67-20298
- Formation and expansion of electromagnetic shock waves in communication lines, using ferroelectric crystals 08 p1295 A67-20824
- Book on electromagnetic wave propagation and turbulent media covering invariant imbedding method, turbulence generation, statistical methods of analysis, etc 08 p1295 A67-20984
- Invariant properties of partially polarized electromagnetic waves analyzed in Poincare and Cayley-Klein models of hyperbolic space, using geometric constructions 09 p1460 A67-21588
- Electromagnetic wavefront perturbations from plane wave propagation resolved into random tilt and residual phase perturbation 09 p1461 A67-21596
- Spatial coherence measurement in 3.2 mm horizontal transmission, considering amplitude and phase fluctuations received in two spaced antennas 09 p1461 A67-21599
- Coherent electromagnetic wave analysis using spectral density function in terms of wave vector 09 p1462 A67-21605
- Hologram fixation by Gabor single beam method, using gas laser as light source 09 p1511 A67-21919
- Electron beam excitation of longitudinal transverse waves in ionic semiconductors, obtaining amplitude increments and frequencies 09 p1554 A67-21978
- Fresnel formulas for transformation of transverse electromagnetic wave into longitudinal plasma wave at dielectric-plasma interface, using Laplace transforms 09 p1464 A67-21993
- Magnetosonic wave effect on anisotropic relativistic plasma component, obtaining cosmic ray plasma instability when wave frequencies are less than electron cyclotron frequency 09 p1546 A67-22230
- Bispectral analysis of electromagnetic wave diffraction by ionosphere, obtaining information on altitude and scale of irregularities 10 p1604 A67-22888
- Plasma instabilities due to RF motion obtained by expanding fluid and electromagnetic wave equations in asymptotic series 11 p1825 A67-23870
- Doppler phenomena arising in rotation of system of electromagnetic wave emitters and reflectors 11 p1750 A67-23908
- Plane electromagnetic wave diffraction by conducting half-plane embedded in uniaxial anisotropic medium 11 p1753 A67-24315
- Harmonic power at TWT taking into account effect of space charge on electron beam bunching 11 p1765 A67-24478
- Microwave surface absorption in static magnetic field affects surface resistance of superconducting alloys 11 p1846 A67-24584
- Plane electromagnetic wave reflection and refraction by semiinfinite dielectric medium moving uniformly parallel to surface analyzed for arbitrary incidence plane orientation 11 p1820 A67-24909
- Reflection and transmission of electromagnetic waves at interface between stationary isotropic medium and moving anisotropic medium 11 p1820 A67-24919
- Geometrical optics approximation of plane electromagnetic wave reflection from ideally electrically conducting triaxial ellipsoid 11 p1754 A67-24986
- Electromagnetic oscillation excitation in plasma beam, analyzing cases of weak and strong external magnetic fields 11 p1844 A67-25022
- Charged particle motion in field of traveling electromagnetic waves used in studies for microwave amplifiers, particle accelerators, etc 11 p1755 A67-25025
- Electromagnetic wave diffraction on plasma cylinders calculated using wave equation and geometrical optics approximation 12 p1969 A67-25246
- Oblique incidence of electromagnetic wave on plasma half-space 13 p2065 A67-26290
- Electromagnetic wave propagation in type II superconductors, noting Hall angles influence 13 p2175 A67-26428
- Field solution of TE sub k zero mode wave incidence on inductive iris in rectangular waveguide 13 p2066 A67-26475
- Reflection coefficients for electromagnetic waves obliquely incident on sinusoidally stratified half-space 13 p2066 A67-26481
- Depolarization of linearly polarized EM waves backscattered from rough metals and inhomogeneous dielectrics with known statistical properties 13 p2158 A67-26878
- Formulas for using wave plates in ellipsometry 13 p2158 A67-26879
- Steady state wave propagation in homogeneous anisotropic media studied from near field behavior of Green matrix 13 p2158 A67-27179
- Energy propagation and Poynting vector for electromagnetic wave propagation in tube of square cross section 13 p2070 A67-27207
- Semiconductor conductivity measurement from propagation irregularities of SHF electromagnetic waves in medium containing semiconductor 14 p2364 A67-27836
- Dispersion of proton whistlers in plasma in motion with respect to observer 14 p2379 A67-27933
- HF conductivity of weakly ionized plasma, establishing expression for Lorentz plasma conductivity 14 p2355 A67-27954
- Hologram fixation by Gabor single beam method, using gas laser as light source 14 p2329 A67-28248
- Expression for surface field components obtained for plane electromagnetic wave at nose-on incidence on semiinfinite cone 14 p2261 A67-28376
- Tropospheric turbulence and structure derived from phenomenon of electromagnetic wave propagation 14 p2264 A67-28397
- General formulation and solution methods of electromagnetic wave diffraction and scattering problems 14 p2268 A67-28448
- Magnetactive plasma quasi-linear oscillations equations, determining damping decrements of plasma electric field components 14 p2361 A67-28753
- Equations describing forces of electromagnetic wave interaction with spherical plasmoid in free space 14 p2361 A67-28806
- Function of symmetrical gas-laser resonator analyzed to determine angle of divergence of laser beams generated by various transverse electromagnetic wave modes 14 p2332 A67-28854
- Asymptotic solution of oblique waves in inhomogeneous vertically magnetized plasma 14 p2361 A67-28922
- Electron-electron scattering in field of monochromatic laser beam, noting resonances in effective Moller scattering cross section 14 p2334 A67-29078
- Reflection coefficient for electromagnetic waves incident at various angles on plane laminar medium of unit 15 p2552 A67-29150
- Propagation of coupled electromagnetic and electroacoustic waves in magnetized compressible stratified electron plasma 15 p2521 A67-29177
- Electromagnetic wave diffraction by infinite set of parallel metallic plates, obtaining exact solution by Wiener-Hopf technique 15 p2435 A67-29191
- Inhomogeneous sheath effect on surface currents and scattering cross section of plasma-immersed cylinder in presence of electromagnetic and electrokinetic waves 15 p2521 A67-29192
- Multiple scattering of electromagnetic waves by arbitrary configurations extended to three-dimensional vector case 15 p2435 A67-29197
- Depolarization of fully polarized electromagnetic waves, obtaining degree of polarization 15 p2435 A67-29338
- Behavior of electromagnetically accelerated shock waves investigated by Mach-Zehnder interferometer 15 p2488 A67-29663
- Excitation of potential LF electromagnetic waves in electron-hole plasma of solid body for negative volt-ampere characteristics of carrier current 15 p2537 A67-29702
- Reflection coefficient for electromagnetic wave in circular cylindrical shock tube incident on moving plasma calculated numerically 15 p2531 A67-29905
- Dispersion equation for electromagnetic waves propagating in uniform plasma layer along boundary parallel to external magnetic field 15 p2532 A67-30255
- Induced electron cyclotron radiation application to generation and amplification of high power electromagnetic traveling waves 16 p2685 A67-30892
- Coherent integral method applicable to scattering calculations for arbitrarily shaped dielectric bodies of low density [TR-67-114] 16 p2626 A67-31347
- Transient plane wave magnetic field attenuation through semiinfinite plate using simplified Laplace transfer function, noting infinite product form for LPTF 16 p2626 A67-31349
- Excitation of high and low frequency electromagnetic waves in unbounded plasma by external currents, deriving wave excitation intensity expression 16 p2721 A67-31477
- Incoherent scattering of plane electromagnetic waves on cylindrical plasma column with fluctuating charge-density 16 p2628 A67-31499
- Frequency tripling of electromagnetic waves passing through hot electron gas in semiconductors, deriving third harmonic amplitude for helical wave 16 p2628 A67-31500
- Diffraction of plane electromagnetic waves on compressible plasma cylinder analyzed, obtaining scattering cross sections 16 p2628 A67-31503
- Numerical calculation of self-focusing of axisymmetric electromagnetic-wave packets in nonabsorbing cubic isotropic media based on parabolic equation 16 p2628 A67-31504
- Impedance and reflection coefficient measurement in uniconductor waveguide noting experimental techniques, coefficient standards, etc 17 p2815 A67-32606
- Nonlinear interaction between weakly ionized helium magnetoplasma produced by HF discharge and microwave field 17 p2903 A67-32676
- Propagation velocity of stable detonation wave in gaseous mixtures measured using Doppler effect resulting from reflection of electromagnetic wave from front of detonation wave 17 p2970 A67-32806
- Electromagnetic wave diffraction by convex spherical surface considered in terms of mutual impedance between two radial electric dipoles, using integral equation 17 p2817 A67-32930
- Propagation of strong ionizing front at arbitrary oblique angle relative to magnetic field, determining limits to value of electric field ahead of shock 17 p2908 A67-33114
- Resonant interactions between energetic trapped particles and transverse electromagnetic wave, suggesting geophysical applications and examining resonances suppression conditions 17 p2939 A67-33210
- Electron beam excitation of longitudinal transverse waves in ionic semiconductors, obtaining amplitude increments and frequencies 17 p2923 A67-33315
- Focusing of electromagnetic waves by lenses, calculating field distribution near focus by diffraction theory magnitude of convergence 18 p3010 A67-33646
- Stationary self-consistent plasma density distribution in field of strong electromagnetic wave 18 p3086 A67-33720
- Coupling between slow waves and convective instabilities in solids, showing interaction inhibition for electron drift velocities greater than phase velocity 18 p3101 A67-34017
- Numerical solution of electromagnetic wave equations for semiconductor junction laser using McWhorter model 18 p3060 A67-34019
- Electromagnetic wave scattering from plasma wave analyzed using Vlasov equations for anisotropic plasma, applying formulas to boundary value problems 18 p3088 A67-34090
- Electromagnetic waves in isotropic laminar plasma waveguide 18 p3090 A67-34440
- Electromagnetic wave reflection and transmission by moving plasma medium as function of velocity 18 p3091 A67-34633
- HF backscattering from absorbing infinite strip with arbitrary face impedances 18 p3005 A67-34730
- Soviet book on wave propagation in turbulent atmosphere covering geometric optics of electromagnetic and acoustic wave scattering and propagation, etc 19 p3182 A67-35206
- Nonrelativistic charged particle transport in geomagnetic dipole field under effect of electromagnetic pulses obtained, using Fokker-Planck equation 19 p3313 A67-35212
- Electromagnetic wave reflection by stratified magnetoplasma, obtaining formulas providing perturbation effect on reflection

coefficients 19 p3183 A67-35457
 Guidance of audio-frequency electromagnetic waves along earth magnetic field investigated in absence of field-aligned irregularities of ionization 19 p3225 A67-35608
 Media with cold homogeneous isotropic lossless plasma dispersion characteristics exhibiting no electromagnetic drag 19 p3298 A67-35828
 Function of symmetrical gas-laser resonator analyzed to determine angle of divergence of laser beams generated by various transverse electromagnetic wave modes 19 p3242 A67-36106
 Linear electromagnetic oscillations in homogeneous plasma described by motion and Maxwell equations 20 p3492 A67-36129
 Semiconductor surface electromagnetic oscillations excitation in presence of strong electric and magnetic fields, obtaining damping and dispersion law 20 p3504 A67-36163
 Electromagnetic properties of metal considered for strong quantization of electron states in magnetic field 20 p3464 A67-36224
 Propagation characteristics of ELF electromagnetic waves investigated below anisotropic ionosphere, considering magnetic field 20 p3379 A67-36282
 Light beam propagation in atomic vapor, with atoms undergoing magnetic resonance, describing electromagnetic wave polarization 20 p3458 A67-36435
 Electromagnetic wave generation and amplification extended from LF microwaves up to optical band 20 p3380 A67-36488
 Plasma absorption of microwaves, noting 20 resonant maxima near harmonics of electron cyclotron frequency 20 p3498 A67-36692
 Algebraic equation for refractive index of arbitrarily directed oblique electromagnetic waves in compressible general magnetoplasma 20 p3499 A67-36944
 Electric vector expression of amplitude-modulated electromagnetic wave propagating in nonlinear dispersive medium 20 p3499 A67-36992
 Attenuation reduction by using hybrid wave in coaxial cables and resonators having supporting surfaces of enhanced reactance 20 p3384 A67-37214
 Electromagnetic plane wave diffraction on anisotropically conducting plane and shielding and reflecting activity of dense radial grating 20 p3384 A67-37326
 Time delay of remote-resonance trace of polarized electromagnetic pulse propagating through topside ionosphere 20 p3527 A67-37403
 Propagation rate of electromagnetic and gravity wave front in synchronous reference system in Riemann space 20 p3486 A67-37554
 Resonance phenomena in bounded magnetoplasma shown on basis of dispersion relation as due to formation of standing waves of electromagnetic waves 20 p3503 A67-37671
 Electromagnetic point source in presence of planar interface between two anisotropic media, obtaining far fields through Fourier integral and ray optical calculation 20 p3388 A67-37703
 Reflection of incident right and left hand circularly polarized plane electromagnetic waves from anisotropic helium afterglow plasma 20 p3389 A67-37707
 Soviet papers on wave propagation and diffraction problems 21 p3579 A67-38107
 Electromagnetic and acoustic waves diffraction at smooth convex body of arbitrary shape, solving field equations 21 p3579 A67-38108
 Plane electromagnetic wave reflection from rough surface, calculating energy and polarization characteristics 21 p3580 A67-38115
 Simplified formulas and curves for electromagnetic wave diffraction on small ideally conducting sphere, examining electric field components 21 p3580 A67-38121
 Interaction between plane electromagnetic wave and separating boundary, considering electric field with component normal to boundary 21 p3581 A67-38292
 Nonline-of-sight communication with FR-1 satellite along magnetic field line of emitter, using VLF electromagnetic waves 21 p3584 A67-38656

Electromagnetic wave pulses transmission through plasma boundary, studying boundary effects for broad and narrow frequency spectra 21 p3669 A67-38682
 Electromagnetic wave focusing in nonlinear medium with small nonlinear polarizability 21 p3670 A67-38684
 Electromagnetic wave scattering by rectangular geometry dielectric wedge, using precise boundary conditions 21 p3585 A67-38686
 Plasma acceleration by electromagnetic microwave discharge in static magnetic field gradient, discussing microwave-plasma energy transfer at electron cyclotron resonance [AIAA PAPER 67-660] 21 p3671 A67-38696
 Asymptotic solution for planar electromagnetic wave diffraction on ideally conducting cylinder surrounded by inhomogeneous plasma layer 21 p3585 A67-38811
 Doppler phenomena arising in rotation of system of electromagnetic wave emitters and reflectors 21 p3585 A67-38936
 ULF radiation in polar auroral zone explained via plasma beam instability, assessing perturbation of particle fluxes in magnetosphere 21 p3621 A67-39016
 Motion rate of pendulum with two antennas moving in electromagnetic field with standing wave measured by correlation meter 21 p3631 A67-39115
 Scattering of plane electromagnetic wave obliquely incident on surface of two coaxial disks investigated via separation of variables 22 p3758 A67-39306
 Dispersion relation for wave propagation in electro-magneto-ionic medium under electric and magnetic fields obtained using Maxwell-Boltzmann-Vlasov equations, discussing cut-off frequency 22 p3788 A67-39469
 Atmospheric ground layer water vapor absorption of 183.31 GHz electromagnetic wave 22 p3759 A67-39506
 Electromagnetic wave scattering by circular cylinder moving in free space, noting far field patterns and Doppler shift angular dependence 22 p3760 A67-39623
 Damping constant of electromagnetic wave in plane parallel waveguide with ferrite resonant isolator, using perturbation theory, considering dielectric and magnetic losses 22 p3770 A67-39659
 Tenuous high temperature plasma electromagnetic wave scattering, with relativistic corrections for scattered radiation spatial and spectral distribution 22 p3849 A67-39699
 Spherical electromagnetic wave refraction on heterogeneous parabolic plasma layer using beam optics methods 22 p3760 A67-39737
 Plane electromagnetic wave reflection from ionization front, determining coefficient from finite thickness plasma layer and constant charged particle density 22 p3762 A67-40122
 TM and TE mode uncoupling in oblique wave scattering from radially inhomogeneous cylinders 22 p3763 A67-40308
 Transverse electric field generated by interaction of various longitudinal plasma waves in ion electron plasmas 23 p4033 A67-41151
 Reflection coefficient determined for plane monochromatic electromagnetic wave incident on idealized laminar plane stratified jet stream, deriving Riccati type differential equation 23 p3974 A67-41201
 Transmission phenomenon of inhomogeneous electromagnetic wave in negative permittivity medium 23 p3975 A67-41480
 Diffraction of H-polarized plane wave on metal grating with narrow slits 23 p3975 A67-41683
 Excitation of potential LF electromagnetic waves in electron-hole plasma of solid body for negative volt-ampere characteristics of carrier current 24 p4199 A67-41772
 Electromagnetic wave absorption and transformation in resonant layer of nonuniform plasma at oblique incidence 24 p4119 A67-42071
 Electromagnetic wave fluctuations in semilfinite plasmas, deriving correlation functions for electromagnetic parameters, considering surface waves 24 p4195 A67-42075
 Active delay line with amplifiers

converting electromagnetic oscillations into ultrasonic vibrations and back again 24 p4130 A67-42237
 Circularly polarized nonlinear electromagnetic waves in conservative centrally symmetric dielectric, considering reflection, transmission and propagation 24 p4168 A67-42481
 Complex wave propagation and coupling in inhomogeneous media, discussing WKB type amplitude coefficients and electromagnetic and space charge waves 24 p4123 A67-42657
 Reflection coefficient for electromagnetic waves incident at various angles on planar laminar medium of lune 24 p4239 A67-43073
ELECTROMAGNETISM
 Electromagnetic state theory applied to solar flares by analogy between ionized current-carrying plasma processes and solar flare conditions 12 p2001 A67-25224
ELECTROMECHANICAL DEVICE
 LF analog-linear circuitry and reduction of electromechanical control system requirements to realizable microelectronic circuits 05 p0776 A67-17038
 Transient self-excitation in autonomous electromechanical system consisting of pump and MHD generator 06 p0952 A67-18686
 Structural and technological problems connected with miniature electromechanical filters 10 p1609 A67-22876
 X-radiographic nondestructive testing and inspection for quality control of electronic and electromechanical devices including printed circuits, encapsulated modules, thin films, etc 10 p1611 A67-23311
 Electrodynamical vibration absorber attached to single degree of freedom vibrating system as passive or active device with or without feedback [ASME PAPER 67-VIBR-18] 11 p1796 A67-24177
 Electromechanical system for study of plant or organism growth and development in compensated gravitational fields 11 p1793 A67-24822
 Direct 'microthrust' measurement on swinging gate test stand with equalization network 11 p1774 A67-25014
 Relay, connector and switch operation simulation, discussing design and performance of chatter and transfer detectors 12 p1943 A67-25702
 Reliability of electromechanical relays, discussing test equipment, data analysis, etc 13 p2085 A67-27698
 Piezoelectric transducer electromechanical properties compared to electromagnetic actuator, noting fluid control applications 14 p2248 A67-28267
 Dynamics of electromechanical metering servosystems, calculated by harmonic linearization method 16 p2644 A67-31380
 Strain and strain-rate sensor for measurements under dynamic conditions and without physical contact with deformation field being sensed 18 p3141 A67-33888
 Gyromotor electromechanical moment effect on drift of triaxial gyrostabilizer exposed to platform vibrations, formulating rotor motion equations 18 p3047 A67-33992
 Random vibration testing by multiple electrodynamic exciter technique, analyzing electromechanics and structural feedback 19 p3339 A67-34961
 Nuclear methods and techniques applied to maintenance and checkout of complex electronic and electromechanical systems, discussing radiation-matter interaction, etc 20 p3449 A67-36981
 Electromechanical servosystem in conjunction with inductive pickup circuit for thrust measurements in jet engine bed tests 22 p3797 A67-39536
 Electromechanical simulator of wing flutter with aileron under flight conditions 22 p3912 A67-39775
 Book on electromechanical, direct and nuclear energy conversion covering transducer design, nuclear structure, photoelectric conversion, reactor theory thermionic conversion, etc 22 p3749 A67-40325
 Performance of electromechanical pressure transducers tested environmentally for static and dynamic temperature, steady acceleration and vibrational acceleration 22 p3809 A67-40464
 Dynamics of electrohydraulic servomechanism /transducer-amplifier/ for transforming signals into forces for

displacing spacecraft control mechanism, examining motion 23 p3935 A67-40637

Integral SI stress sensor with transverse and shear piezoresistance sensitivity, noting design and fabrication 23 p4005 A67-41371

ELECTROMECHANICS

Electromechanical and photomechanical effects on microhardness in semiconductors 23 p4045 A67-41472

ELECTROMETER

Wide range vibrating-reed Mariner II electrometer, describing components, performance characteristics and results 02 p0241 A67-11681

Instability zone of electrometer, noting relation to parametric resonance of needle and Hill equation form of needle motion 11 p1877 A67-24758

Measuring assembly containing logarithmic-response electrometric amplifiers for sounding rockets 21 p3592 A67-38222

ELECTROMIGRATION

Temperature dependence of residual resistivity of diffusing ions for electromigration of silver in copper and gold and self-diffusion of copper in aluminum 07 p1209 A67-19647

ELECTROMOTIVE FORCE

SA PONDEROMOTIVE FORCE

Tensor components of thermal emf of CdSb measured by method without producing thermoelectrical eddy currents 01 p0129 A67-10137

Apparatus for measuring temperature dependence of thermoconductivity coefficient, thermal emf and specific electroresistance of cermet cylindrical shells 01 p0076 A67-11248

Thermal emf and electric conductivity in solid and liquid semiconducting copper-antimony-ditelluride 02 p0297 A67-11846

Thermoconductivity and thermal emf of Zn-and Te-doped GaSb 02 p0297 A67-11847

Emf and electric conductivity in ionized gas produced by detonation of Sakura dynamite to estimate explosion rate 02 p0268 A67-12500

Thermal emf in plastic deformation of copper, considering effects of crystal lattice defects and lattice elastic distortions 02 p0301 A67-12740

Isobaric-isothermal potential and entropy and enthalpy formation of GaAs from emf measurements at 643-741 degrees K 03 p0498 A67-13840

Quantum oscillation of transverse and longitudinal magnetothermal emf in n-type indium antimonide compared with oscillations of transverse and longitudinal magnetoresistance and Hall coefficient 04 p0680 A67-15288

Surface photoelectromotive force in GaAs type semiconductors with short duration minority carriers 04 p0686 A67-15969

Emf as cause of vertical downward and upward ionization drift in F region of ionosphere during magnetic storm 05 p0801 A67-17141

Mass velocity profile measured using electromagnetic device to record emf changes in metal probe embedded in nitromethane flow 06 p1112 A67-17953

Distribution of capacitive photo-emf over surface of semiconductor determined by measuring value created by scanning surface of sample with narrow modulated-light beam 08 p1367 A67-20415

Photovoltaic emf of silicon solar cell illuminated by ruby laser 08 p1285 A67-20732

Absolute speed determination from measurement of induced EMF resulting from movement in geomagnetic field 11 p1791 A67-24455

Galvano-and thermomagnetic phenomena in semiconductors analyzed using transient method, noting extraneous EMF influence on Hall effect 11 p1792 A67-24814

Magnetic ordering effect on electrical properties of antiferromagnetic semiconductor MnTe indicate temperature anomaly above 440 degrees K 12 p1982 A67-25326

EMF induced in ionized gas across magnetic field measured for flow velocity determination 12 p1973 A67-25392

Scattering mechanisms and role of interelectron collisions in n-Pb-Te and certain other semimetals analyzed by concentration dependence of mobility and thermal EMF 12 p1983 A67-25514

Hall EMF measurement in base of negative resistance silicon diode 12 p1917 A67-26097

Electromagnetic effect in n-type InSb samples, measuring magnetic resistance, Hall effect and magnetic EMF 13 p2174 A67-26368

Conductivity, temperature dependence, thermal EMF Hall constant, thermal conductivity and resistivity of aluminides of transition metals 13 p2131 A67-26471

Apparatus for determining impurity distribution in semiconductor structure 14 p2317 A67-28281

Nature of photoelectromotive force of cadmium selenide with Cu, Ag, Au, Pt vacuum-deposited on surface 14 p2367 A67-28527

Measurement of variable Hall electromotive force component created by illumination of thin low resistance germanium samples by modulated 14 p2368 A67-28529

CdSb polycrystals of different structural patterns investigated for dependence of electrical conductivity, Hall mobility and thermal EMF 14 p2372 A67-28758

MHD effect in shock tube, studying EMF induced in motion of transverse magnetoplasma 16 p2715 A67-31112

Deformation effects on thermal conductivity, microhardness, and thermal EMF of annealed bismuth telluride bars 16 p2730 A67-31160

GeTe solid solutions reviewed considering thermal EMF, temperature dependence and current carrier mobility 16 p2730 A67-31164

SnTe samples under uniform load studied for relation between electrical and thermal conductivity, thermal EMF and microhardness 16 p2730 A67-31165

Superimposed electromotive force appearing in direction of magnetic field in presence of opposed spiral motion in turbulent fluid 17 p2842 A67-32341

Electric quadrupole-quadrupole and dipole-octupole forces contribution to dispersion energy for axially symmetric molecules, noting resonance frequencies 17 p2887 A67-32353

Coupled integral equations for transverse and axial currents for asymmetrically cylindrical antenna driven by EMF 17 p2826 A67-32618

Apparatus for measuring temperature dependence of thermoconductivity coefficient, thermal EMF and specific electroresistance of cermet cylindrical shells 17 p2861 A67-33171

Free energy, heat and entropy of formation of several semiconductors by measuring EMF 18 p3095 A67-33445

InSb-InAs solid solution thin films absorption spectra, noting band structure, temperature change and Hall EMF reduction 18 p3096 A67-33450

Changes in InSb, GaSb and Te crystal lattice structure and chemical bonds investigated for effects on thermoconductivity, thermal EMF and microhardness 18 p3096 A67-33451

Scattering mechanisms and role of interelectron collisions in n-Pb-Te and certain other semimetals analyzed by concentration dependence of mobility and thermal EMF 18 p3103 A67-34445

Thermocouple drift on Chromel-P vs Constantan under vacuum, high temperatures and time factor 18 p3052 A67-34516

Friction contact between semiconductor and rotating metal disk studied for sign shifts causing sharp temperature gradient producing thermal EMF 20 p3503 A67-36123

Anisotropy of piezothermal EMF in Si and Ge under uniaxial stress 20 p3511 A67-37147

Plasma diagnostic measurement simulation, considering electromotive effect from satellite motion through geomagnetic field 20 p3418 A67-37428

Continuous DC EMF in semiconductor with symmetrical nonlinear conductivity analyzed in variable AC waveguide magnetic field 20 p3513 A67-37449

Thermal EMF in semiconductors with electric fields caused by hot carriers, showing energy relaxation of high energy electrons 20 p3513 A67-37451

Odd and even photomagnetic effect oscillations in InSb, measuring EMF at low temperatures and strong fields 21 p3677 A67-38095

Electromagnetic effect in n-type InSb samples, measuring magnetic resistance, Hall effect and magnetic EMF 21 p3680 A67-38324

EMF as cause of vertical downward and upward ionization drift in F region of ionosphere during magnetic storm 21 p3619 A67-38483

Niobium and tantalum nitrides physical properties including microhardness, electric and thermal conductivities, Hall coefficient and thermal EMF 22 p3861 A67-39917

Copper oxide and selenium semiconductor rectifiers as heat flux sensors, describing operation and thermal EMF 22 p3801 A67-40217

Nature of photoelectromotive force of cadmium selenide with Cu, Ag, Au, Pt vacuum-deposited on surface 23 p4039 A67-40934

Measurement of variable Hall electromotive force component created by illumination of thin low resistance germanium samples by modulated light 23 p4039 A67-40936

High temperature thermal EMF and electrical conductivity in intense electric field for semiconductors with low charge carrier mobility 23 p4043 A67-41299

ELECTRON

SA CONDUCTION ELECTRON

SA FAST ELECTRON

SA FREE ELECTRON

SA HIGH ENERGY ELECTRON

SA HOT ELECTRON

SA PHOTOELECTRON

SA PHOTON-ELECTRON INTERACTION

SA POSITRON

SA TWO-ELECTRON SYSTEM

Relativistic mass-velocity relationship in empirical verification involving data on electron-proton parameters 09 p1531 A67-21650

Chemical influence of holes and electrons on dislocation velocity in semiconductors 13 p2184 A67-27692

Rocket measurements in auroral zone, considering proton and electron intensities, energy spectra and angular distribution 24 p4209 A67-42262

ELECTRON ACCELERATOR

Relativistic electron stream requirements to obtain self-magnetic confinement, noting 4 million volt pulsed electron field emission accelerator 04 p0624 A67-15325

Electron beam accelerator generating 5000 amp beam transmitted through thin window for external use, noting pulse length, energy density, etc 04 p0599 A67-15327

Single wave approximation of fields of cylindrical delay system with basic E-type wave propagating at variable phase velocity 05 p0767 A67-17398

Electron-cyclotron heating of plasma via high power oscillator, noting experimental setup and characteristics 06 p1039 A67-18082

Electric fields due to electron-plasma and ion-acoustic waves associated with sunspot magnetic field variation as main cause of electron acceleration in solar flares 10 p1700 A67-23056

Advances in microwaves, Volume 1, covering stanford accelerator design, directional couplers, waveguide singular integral equations, Lie algebras, microwave network application, etc advances in microwaves, Volume 1, covering 12 p1906 A67-25975

High intensity runaway electron fluxes accelerated by external field in toroidal plasma discharge, noting pressure effect 13 p2162 A67-26270

Microwave and type IV solar bursts, examining gyrosynchrotron emission and various electron acceleration mechanisms 17 p2939 A67-33391

Reversible betatron acceleration mechanism during geomagnetic storm 20 p3434 A67-37425

Ion source using electron bombardment without magnetic source field, studying focusing and optimal operating conditions of electron accelerating system 22 p3847 A67-39641

ELECTRON ATTACHMENT

Vibrational excitation and dissociative attachment in bombardment of hydrogen molecules by electrons of energies up to about 12 ev 01 p0117 A67-10782

Electron affinity data for various pentacyclic aromatic hydrocarbons, predicting ionization

- potentials 01 p0019 A67-10882
- Altitude dependent electron attachment rates and molecular oxygen concentrations indicating three-body attachment process in lower ionosphere 03 p0410 A67-12960
- Variation of floating potential formed between electrodes by injection of electronegative gas is logarithmic function of electron attachment coefficient on neutral particles 04 p0669 A67-15496
- Shockley theory and electron affinity of semiconducting CdSe from DC I-V characteristics and work function of Au, Ag and Cu contacts with CdSe 07 p1231 A67-19491
- Electron barrier heights of Al-Al₂O₃-SnTe and Al-Al₂O₃-GeTe tunnel junctions, noting values of Fermi level and energy gap 07 p1155 A67-19893
- Gas pressure dependence of attachment and recombination coefficients for thermalized electrons in air and oxygen 17 p2893 A67-32139
- Atomic collision processes in ionized gases, studying ambipolar diffusion, electron attachment, electron-ion recombination and Penning ionization by afterglow technique 19 p3264 A67-35070
- Electron cyclotron resonance absorption of microwaves in oxygen magnetoplasma used to alter electron attachment and detachment rate coefficients 19 p3271 A67-35077
- Kinetic behavior of electrons in air plasmas containing electrophilic gasses studied with microwaves behind reflected shock waves 24 p4196 A67-42196
- ### ELECTRON AVALANCHE
- Avalanche transistor pulser designed to drive GaAs radar-laser diode 03 p0376 A67-12964
- Size distribution of electron avalanches in methane gas under electric field no longer satisfy Furry distribution due to first Townsend ionization coefficient 03 p0473 A67-13463
- Small signal negative resistance and avalanche region of impact ionization avalanche transit time /IMPATT/ diodes, particularly Read diodes 05 p0777 A67-17319
- Avalanche characteristics and failure mechanisms in junction diodes, showing negative resistance regions due to space charge effect of carriers 07 p1156 A67-19899
- Second breakdown in transistors analyzed in terms of lumped parameters noting V-I characteristics, temperature effect, avalanche multiplication, etc 07 p1157 A67-19903
- Space charge conductance and electron drift velocity measurements for avalanche p-n-n diode 10 p1611 A67-23169
- Si avalanche diode with p-n-n mesa structure, noting high efficiency and high power output at UHF 13 p2076 A67-26519
- Injection coefficients of hydrogen and oxygen during buildup of discharge in homogeneous electric field 13 p2160 A67-26813
- Silicon avalanche diode behavior for short duration surge current in reverse direction 13 p2084 A67-27576
- Avalanche photodiode model with guarding for active area geometry 15 p2452 A67-30014
- Criteria for optimized avalanche photodiode design and for best semiconductor material choice based on carrier multiplication process 15 p2453 A67-30015
- Parametric negative resistance range and impedance matrix element values of microwave Read avalanche diode 15 p2453 A67-30016
- IMPATT diode operation based on combination of avalanche-current multiplication and transit-time delay to produce negative resistance 17 p2824 A67-32332
- Inductive characteristics of junction transistors, showing Q-factor increase achieved by using negative impedance produced by avalanche multiplication 18 p3009 A67-33479
- Structural dislocations effect on formation of microplasmas during avalanche breakdown of silicon p-n junction 18 p3099 A67-33698
- Statistics of electron avalanche generating secondary effect at cathode through photon emission, obtaining excited molecule distribution 19 p3285 A67-35087
- Current runaway effects in n-cadmium telluride suggest current-density controlled resistivity caused by hole-electron pairs avalanche 21 p3677 A67-38006
- Short circuit photocurrent of avalanche photodiode, determining frequency response and multiplication effect on bandwidth 22 p3767 A67-39362
- Noise in polarized Si semiconductor avalanche junctions at RF and microwave frequencies noting determination of impact ionization parameters 23 p3980 A67-41189
- Air shower nuclear active component spectra noting need for mechanism of energy transfer from nucleons into electron-photon avalanches 24 p4220 A67-42862
- ### ELECTRON BEAM
- #### SA BEAM-PLASMA AMPLIFIER
- Charged particle injection into magnetic traps through mirror, using annular electron gun 01 p0122 A67-10350
- Amorphous whiskers from cobalt-gold alloy by quenching molten material through electron-beam heating and anvil-cooling device 01 p0135 A67-10895
- Structural sensitivity of plastic properties of molybdenum alloys produced by electron beam fusion, investigating microstructure, failure in bending tests and grain fragmentation 01 p0101 A67-10936
- Voltage induced by electron beam in n-and p-type germanium bars having inhomogeneous resistivity distribution, obtaining equations from one-dimensional model 01 p0137 A67-11059
- Rotational temperatures measured in static low density air with electron beam probe 01 p0071 A67-11105
- Plasma electron and ion oscillations excitation by low voltage electron beams provide examples of turbulence 01 p0126 A67-11311
- Beam-plasma amplifier with input coupler as cavity and output coupling due to Cerenkov radiation 01 p0040 A67-11313
- Extremely wideband information storage and retrieval systems employing laser or electron beam on silver halide or electron beam on thermoplastic film 01 p0077 A67-11437
- Laser based on excitation of gallium phosphorus arsenide solid solution by beam of fast electrons 02 p0251 A67-11824
- Cold beam plasma interaction theory for finite transverse dimensions and finite magnetic fields determined by computer solution of dispersion relations 02 p0272 A67-11884
- Electron beam scanning technique measurement of diffusion lengths in Si and GaP p-n junctions and recombination rate of dislocations in n-type Si 02 p0298 A67-11887
- Laser, electron and plasma energy beam types and application to manufacturing technology 02 p0249 A67-12179
- Injection of helical electron beams into magnetic mirror trap, examining plasma lifetime, density and electron and ion energies produced 02 p0274 A67-12457
- Diffusive separation of helium-argon mixtures in underexpanded free jets and normal shock waves studied by electron beam 02 p0234 A67-12543
- Electron gun producing helical electron beams with prescribed high transverse-to-longitudinal electron energy ratio 03 p0475 A67-13088
- Power gain of submillimeter wave in traveling wave amplifier with periodic delay-line structure 03 p0380 A67-13557
- Light generation from rectangular cross section electron beam interacting with metallic diffraction grating 03 p0468 A67-13593
- Stimulated emission by electron beam bombardment of laser materials 03 p0439 A67-14394
- Linearized model of readout process in image tubes incorporating progressive erasure of stored image, noting increased effects of erasure with increasing beam modulation 03 p0428 A67-14396
- Vibration temperature of relaxing hypersonic gas flow measured by electron beam technique 04 p0545 A67-14542
- Plasma ion gun with Pierce electrode 04 p0663 A67-14771
- Periodicity of plasma oscillation intensity spatial distribution upon electron beam excitation 04 p0666 A67-15181
- Photographic measurement of plasma jet velocity using time shift in brightness fluctuation 04 p0666 A67-15188
- Convective excitation of ionic oscillations in plasma by inhomogeneous electron beam as result of spatial gradient of distribution function 04 p0668 A67-15270
- Annual Electron and Laser Beam Symposium, University of Michigan, Ann Arbor, April 1966 04 p0622 A67-15300
- Annular hollow cathode discharge emitting electron beam to heat cylindrical workpiece located along axis 04 p0628 A67-15311
- Resistivity, dielectric constant and junction depth changes in semiconductor materials by exposure to electron beam 04 p0681 A67-15314
- Electron beam evaporation of silicon dioxide producing storage layers for automatic picture transmission vidicon, analyzing causes of signal loss after short operating time in flight tubes 04 p0623 A67-15315
- Single pulsed electron beam used in machining and imaging modes for creating machine scan device 04 p0623 A67-15316
- Dynamic resistance of Si p-n junction and diffusion length for minority carriers measured, using pulsed electron beam irradiation 04 p0584 A67-15317
- Conductivity changes in thin layer of silicon oxide induced by electron beam of scanning electron microscope 04 p0682 A67-15318
- Synthesis and growth of dendritic InSb films by electron beam microzone melting of vacuum deposited composite indium and antimony films, noting electrical properties 04 p0682 A67-15319
- Electron beam float-zone melting process applied to dielectric compound aluminum trioxide to obtain sapphire crystals 04 p0628 A67-15320
- Generation of dense electron beams of energy half-width including tightly collimated beams of very low energy, space charge effects in deflectors, etc 04 p0623 A67-15323
- Energy relaxation in electron beams with high charge density, anomalous shiftings and broadenings and symmetrizations of energy distribution 04 p0623 A67-15324
- Relativistic electron stream requirements to obtain self-magnetic confinement, noting 4 million volt pulsed electron field emission accelerator 04 p0624 A67-15325
- Operating possibility of axisymmetric electron beam so that plasma frequency will exceed electron cyclotron frequency of magnetic focusing field at some point or throughout beam 04 p0624 A67-15326
- Electron beam accelerator generating 5000 amp beam transmitted through thin window for external use, noting pulse length, energy density, etc 04 p0599 A67-15327
- Automatic electron beam balancing plant used for plane thin film resistor combinations provides automated electron beam machining by work conditional supplementary equipment 04 p0600 A67-15479
- Calorimeters used as in-line dosimeter if thin enough with respect to effective electron range to ensure that device does not degrade energy in beam 04 p0625 A67-15711
- Semiconductor lasers with radiating mirrors developed by excitation, using electron beam and neodymium laser glass radiation 05 p0821 A67-16669
- Quasi-linear relaxation in unsteady states of noncollision plasma, noting electron beam distribution function and Langmuir plasma oscillations 05 p0852 A67-16696
- Electron beam excitation as possible explanation of relation between enhanced diffusion and HF oscillation in plasma 05 p0854 A67-16896
- Graphical data concerning drifting beams as possibility for calculation of reduction coefficient of space charge field of electron beams moving in periodic electrostatic fields 05 p0764 A67-16908
- Induced electron cyclotron radiation application to generation and amplification of high power electromagnetic traveling waves 05 p0824 A67-16915
- Structure and mechanical properties of molybdenum-niobium system monocrystalline melts prepared by electron beam zonal melting 05 p0830 A67-17024
- Electron beam rotation experiments on linear spiratron with M-type electron gun 05 p0776 A67-17169

- Focusing of electron beam from low noise gun with different magnet systems 05 p0777 A67-17279
- Instabilities and scattering in space charge focused low voltage electron beams in absence of magnetic field 05 p0849 A67-17449
- Yield point and strain aging in tantalum, identifying interstitial atom in electron-beam melted tantalum after incremental plastic deformation 06 p1015 A67-17896
- Plasma stabilization mechanism for electron beam caused density variation, noting use of nonlinear effects 06 p1040 A67-18097
- Electron beam spatial scanning of coherent emission of GaAs junction laser at low temperatures, making current distribution nonuniform 06 p1011 A67-18150
- Surface recombination velocities and diffusion lengths in GaAs determined by variation of cathodoluminescence intensity with voltage of exciting electron beam 06 p1063 A67-18936
- Plasma instabilities induced by charge convection across perturbing electric field and magnetic field 07 p1228 A67-19511
- Velocity spread on modulated electron beam of finite diameter analyzed as function of drive, drift length and convergence 08 p1362 A67-21298
- Active region corona and type I bursts supposedly generated by plasma oscillations excited by electron beam 08 p1377 A67-21445
- Laser emission from electron beam excitation of CdS crystals due to crystal uniformity and radiative transitions resulting from CD-rich growth conditions 09 p1510 A67-21569
- Electron velocity-field characteristics of insulating GaAs measured using electron beam injected electrons 09 p1551 A67-21573
- Electron beam excitation of longitudinal transverse waves in ionic semiconductors, obtaining amplitude increments and frequencies 09 p1554 A67-21978
- Gas ionization by fast electron beam directed along waveguide leading to longitudinal distribution of secondary electron concentration 09 p1545 A67-22002
- Nonsymmetric oscillations in plasma in magnetic field arising from electron beam passage through plasma, deriving dispersion equation 09 p1545 A67-22003
- Resistivity variation in n-type germanium pellet measured with focused electron beam, showing position dependence of diffusion length as cause of error 09 p1473 A67-22018
- Cross sections for excitation of upper and lower ion states by electron impact with ground state neutral argon atoms found by measuring coherent and incoherent light of laser beam 09 p1514 A67-22272
- Beam-plasma interaction with transverse modulation, obtaining growth rates 09 p1546 A67-22280
- Beam-generated plasma oscillation frequency expansion due to temperature, field and density characteristics 09 p1546 A67-22282
- Gap excitation of waveguide loaded with plasma represented as charge-free medium with tensor dielectric constant 09 p1480 A67-22283
- Numerical integration of dispersion relation for electron beam in plasma 09 p1546 A67-22313
- Dispersion of mode couplings of wave propagation in waveguide containing plasma electron beam system 09 p1550 A67-22582
- Photon absorption coefficients measured in active and passive regions of electron-beam-pumped semiconductor laser 10 p1664 A67-22909
- Steady state field distribution of semiconductor laser with nonuniform excitation pumped by electron 10 p1666 A67-23648
- Electrostatic wave excitation growth in collisionless plasma interaction and simultaneous modification with electron beam studied for weakly unstable situations 11 p1826 A67-23875
- Electron plasma frequency instability, correlating coherent deceleration of electron beam with compression of interference pattern 11 p1827 A67-23890
- Electrostatic oscillations excited in cylindrical plasma shell by electron beam, noting resultant instability 11 p1828 A67-23892
- Electron beam experimental methods for current density distributions, electron velocities and determining parameters for microwave tube design 11 p1758 A67-24094
- Potential distribution in emitter diode measured in single ended Q machine, using ribbon electron beam 11 p1764 A67-24373
- Instabilities in DC electron beam/plasma experiment noting dependence on beam current, magnetic field strength, beam velocity and plasma density 11 p1837 A67-24400
- Quantitative fast response visualization technique for low density flow fields based on electron beam fluorescence probe 11 p1790 A67-24450
- Magnetically confined helical electron beams formed by two-anode electron guns, considering effect of space charge 11 p1764 A67-24466
- Harmonic power at TWT taking into account effect of space charge on electron beam bunching 11 p1765 A67-24478
- Electron beam plasma amplification measurements in interaction region by nonperturbing technique, measuring RF growth, phase velocity, etc 11 p1841 A67-24907
- First azimuthally varying mode in mercury vapor plasma discharge, predicting growth of hose-like instability of electron beam 11 p1841 A67-24928
- Charged particle injection into magnetic traps through mirror, using annular electron gun 11 p1844 A67-25023
- Spectrum of longitudinal plasma oscillations noting instability under resonance condition 12 p1970 A67-25255
- Possible polarization of X-ray bremsstrahlung of solar flares due to sharply anisotropic electron beams 13 p2191 A67-26383
- Microwave amplification by electron beam interaction with cesium plasma 13 p2166 A67-26726
- Oxidation of Be thin films in oxygen and carbon dioxide, noting decomposition of Be-carbide and effects of heating by electron beam 13 p2132 A67-26998
- Laser light deflecting methods, detailing scanlaser, laser resonator combining features of laser and cathode ray tube 13 p2128 A67-27237
- Fabrication of small geometry planar bipolar transistors by using electron beam 13 p2084 A67-27574
- Electron density and HF spectrum of beam generated plasma as function of gas pressure and injection parameter 14 p2352 A67-27749
- Energy absorption profile and ionization rates for electron beam dependence on beam energy, altitude and atmospheric layer thickness and mass 14 p2379 A67-27921
- Shock wave structure in air at supersonic and hypersonic velocities studied by electron-beam density method 14 p2297 A67-27997
- Electron beam density survey in low density hypersonic flow field over sharp flat plate, noting results in outer and inner part of shock layer 14 p2241 A67-28167
- Hypersonic low density flow analysis with shock tunnel and electron beam densitometer, noting density profiles at various Mach and Knudsen numbers 14 p2300 A67-28176
- Anisotropic velocity distribution function measurements in jet flows using electron beam fluorescence technique 14 p2300 A67-28181
- Electron beam analysis of skimmer influence on nozzle beam formation 14 p2301 A67-28187
- Lack of Cerenkov emission in isotropic plasma, presenting fast electron beam experiment for verification of theory 14 p2357 A67-28204
- Structure and mechanical properties of molybdenum-niobium system monocrystalline melts prepared by electron beam zonal melting 14 p2338 A67-28491
- Li film structure on compact tungsten faces by diffraction method, using free electron beams 14 p2372 A67-28760
- Steady state one-dimensional carrier distribution in depth for electron beam excitation of semiconductors computed, including diffusion and surface recombination 15 p2442 A67-29180
- Production of crossed field and beam microwave tubes, noting demagnetization and coercive and inductance forces of various magnetic materials 15 p2447 A67-29753
- Prevention of burnout in high power linear beam traveling wave tubes by placing small negative electrode at end of collector opposite beam entrance 15 p2447 A67-29754
- Electron beam probing of semiconductor materials and devices 15 p2450 A67-29813
- Quasi-linear relaxation in unsteady states of noncollision plasma, noting electron beam distribution function and Langmuir plasma oscillations 15 p2530 A67-29867
- Secondary electron detector for electronic microcircuits bombarded by electron beam used to observe potential distribution in junction breakdown 15 p2453 A67-30065
- Effect of decomposition of Langmuir waves on interaction of electron beam with nonisothermal plasma 16 p2705 A67-30448
- Small signal power conservation in space charge waves of multivelocity electron beam with rectangular velocity distribution 16 p2703 A67-30796
- Graphical data concerning drifting beams as possibility for calculation of reduction coefficient of space charge field of electron beams moving in periodic electrostatic fields 16 p2636 A67-30885
- Induced electron cyclotron radiation application to generation and amplification of high power electromagnetic traveling waves 16 p2685 A67-30892
- Rarefied gas flow density measurement by determining changes in electron beam-electron concentration while crossing flow 16 p2673 A67-31107
- Charged particle beam passage through plasma, detailing excitation of one-dimensional oscillation expanding perpendicularly to boundary of semifinite plasma 16 p2716 A67-31176
- Parametric instability of infinitely wide periodically modulated electron beam with uniform cross section in terms of nonlinear theory of parametric excitation 16 p2716 A67-31178
- Electron beam interaction with plasma analyzed using nonquasi-static plasma model 17 p2895 A67-32159
- Surface potential contrast induced by electron beam of scanning microscope on unbiased planar transistors, investigating beam voltage effect on contrast formation 17 p2823 A67-32197
- High resolution direct electron beam film scanner operable at 20 MHz, construction and performance 17 p2857 A67-32469
- Electron beam and laser beam line scan recorders requirements, limits, applications and techniques 17 p2857 A67-32470
- Coherent radiation from cadmium sulfide single crystal excited by electron beam, noting transition nature in generation mode and spectral composition 17 p2915 A67-32660
- Parameter space partition in beam-plasma regime by determining lower limits of beam density yielding coherent and incoherent domains 17 p2902 A67-32674
- Irradiated germanium observed for carrier concentration variations, using Hall coefficient measurements 17 p2918 A67-32853
- Electron beam excitation of longitudinal transverse waves in ionic semiconductors, obtaining amplitude increments and frequencies 17 p2923 A67-33315
- Steady state field distribution of semiconductor laser with nonuniform excitation pumped by electron 17 p2870 A67-33329
- Oxygen concentration and strain rate effect on yield point phenomenon in electron beam refined niobium, showing relation to dislocation multiplication 18 p3063 A67-33486
- Ionizer with three-electrode electron gun, noting potential distribution between electrodes and ionization efficiency 18 p3080 A67-33722
- Beat frequency generation and multiplication and subsequent harmonic amplification in plasma-beam system, particular case of plane waves 18 p3087 A67-34037
- Use of controlled flow of electrons for analyzing and processing integrated circuits and focused electron beam as heat source for microwelding 19 p3192 A67-35023
- Electron beam passing through low pressure gas generates plasma, computer simulated beam trajectory studies explain

beam profile and pinch effect 19 p3275 A67-35106

Wave propagation and electron beam-plasma interaction in plasma column inside magnetic field, measuring plasma characteristics and spatial distribution 19 p3275 A67-35107

Plasma-density distribution produced in gas by tubular electron beam 19 p3278 A67-35128

Space-charge and potential distributions calculated for region between two plane electrodes of single collision model 19 p3265 A67-35129

Comparison of experimental and theoretical results on electron beam produced mercury-vapor discharge 19 p3290 A67-35380

UHF wave interaction between plasma and electron stream in magnetic field noting convective instability 19 p3291 A67-35382

Beam-plasma interaction in magnetic field, studying microwave field distribution and emission 19 p3291 A67-35383

Stability of cesium Q-type machines analyzed for hot plasma-beam interactions in VLF range in sheath and in plasma 19 p3292 A67-35390

Flood beams incidence angle and current density distribution effects on half-tone reproduction of visual storage tube with cathode collimator 19 p3194 A67-35543

Hollow anode glow discharge noting motion of ions and electrons in beam configuration 19 p3195 A67-35598

Space charge analyses applied to electron beam extractions from plasma cathodes, computing stability data for potential distributions and extracted current 20 p3495 A67-36168

Electron space-charge and nonzero beam-coupling impedance effects on TWT, considering weakly saturated state 20 p3395 A67-36313

Cesium plasma diode investigated using ribbon electron beam probing technique, discussing stability of electric potential distribution modes 20 p3496 A67-36329

Technological methods for depositing thin films in vacuum, considering evaporation, scattering, etc 20 p3453 A67-36472

Ionized gas properties for use in various microwave components to obtain amplification through electron beam plasma interaction 20 p3497 A67-36489

Electron beam probe for determination of local gas parameters in reentry simulation 20 p3445 A67-36588

Emission properties of vacuum spark plasma arising in production of high current electron beam 20 p3498 A67-36684

Recording and display programs illustrating relative capabilities of thermographic and direct electron beam on photographic film recording 20 p3449 A67-36984

Electron beam deflection by standing light wave of laser shows momentum transfer resulting in Bragg relationship for reflection angle 20 p3461 A67-37185

Electron beam method for measuring resistivity variation in germanium semiconductors, calculating diffusion lengths 21 p3679 A67-38254

Zinc telluride laser generation by electron-beam excitation noting high threshold values 21 p3641 A67-38458

Reflex klystron electron admittance dependence on potential distribution in repeller space, showing electrode structure and space charge effects 21 p3598 A67-38604

Microwave amplification when electron beam passes through cesium plasma, noting noise figure dependence on tube pressure 21 p3668 A67-38605

Possible polarization of X-ray bremsstrahlung of solar flares due to sharply anisotropic electron beams 21 p3698 A67-38817

Electron beams applied during pressworking of sheet materials to provide temperatures favorable to microstructure defect healing 21 p3637 A67-38927

Two-beam capacitive converter for automatic systems reduced to synthesis of single beam converter 22 p3795 A67-39229

Backward waves effect on excitation of delay line by modulated electron beam with zero transit angle 22 p3767 A67-39422

Electron beam detectors employing CdS single crystals, considering procedure for

obtaining crystals characterized by high sensitivity to electron fluxes 22 p3798 A67-39568

Ion source using electron bombardment without magnetic source field, studying focusing and optimal operating conditions of electron accelerating system 22 p3847 A67-39641

Unstable coupling between slow space charge mode of electron beam and lowest plasma electron band modes in finite geometry 22 p3847 A67-39643

Magnetron type microwave amplifier gain increase, discussing electron beam interaction region M-type device gain calculations 22 p3770 A67-39654

Structural sensitivity of plastic properties of molybdenum alloys produced by electron beam fusion, investigating microstructure, failure in bending tests and grain fragmentation 22 p3820 A67-39790

Coherent high power millimeter and submillimeter wave generation by various free electron beam devices, noting periodic beam has greatest development potential 22 p3774 A67-40443

Electron beam interaction with plasma investigated for spatial distribution of intensity and oscillation spectrum in stationary mode 23 p4032 A67-40904

Scanning laser device using modified electro-optic display tube and potassium phosphate crystal mode selector 23 p4017 A67-41393

Solid state and electron beam delay line features compared in optimal selection for radar system target simulation 23 p3982 A67-41503

Electron beam retarding potential method to measure work function changes resulting from Cs, oxygen and hydrogen adsorption on /110/ Ta single crystal 24 p4201 A67-41892

Plasma column and plasma-electron beam interaction properties by Langmuir and SHF probes noting resonance, coupling and microwave surface waves 24 p4194 A67-41911

ELECTRON BEAM WELDING

Transverse oscillated electron beam welding procedures of D6AC steel and mechanical properties evaluation show comparable results to corresponding gas tungsten arc welds 01 p0080 A67-10946

Plasma arc welding for joining thick titanium, examining data for three common titanium alloys, three welding positions and process variables such as plasma gas composition and travel rates 01 p0081 A67-11039

Narrow welded joint, discussing advantages and limitations of narrow gap, electron beam and plasma arc techniques 04 p0627 A67-14805

Nonvacuum electron beam welder noting welding head 04 p0628 A67-15312

Electron beam welding noting effects of pressure and vacuum 04 p0628 A67-15313

Electron beam welding parameters correlation for understanding welding process [ASME PAPER 66-WA/MET-18] 04 p0629 A67-15333

Electron beam zonal fusion growth of Mo, W and Ta single crystals without using crucible 05 p0827 A67-16079

Electron beam zonal vacuum fusion growth of Mo-Nb alloy single crystals 05 p0827 A67-16080

Qualitative and quantitative descriptions of penetration of solids by high power density electron beams in welding, calculating penetration vs welding velocity and current curves 06 p1008 A67-18696

Electron beam welding in vacuum and in atmosphere, describing rapid positioning, workplace guidance, beam control and observation 09 p1503 A67-22119

Laser and electron beam welding techniques, noting weld joint characteristics and tungsten inert gas arc welding 10 p1660 A67-23008

Electron beam process for vapor plating aluminum on beryllium for welding 11 p1798 A67-24264

Quality control in electron beam welding, discussing design, metallurgical aspects, etc 13 p2124 A67-27168

Use of controlled flow of electrons for analyzing and processing integrated circuits and focused electron beam as heat source for microwelding 19 p3192 A67-35023

In-space hand-held electron beam welding

gun design, testing and performance 20 p3454 A67-36575

Electron beam welded D6AC steel plates evaluated after heat treated condition /stress relief/ for mechanical properties 20 p3456 A67-37695

Electron beam welding of high temperature metals in vacuum 22 p3812 A67-39541

ELECTRON BOMBARDMENT

SA SECONDARY EMISSION

Bremsstrahlung, transient and plasma radiation as affected by surface properties of silver bombarded by electrons 02 p0291 A67-11737

Laser emission in pure cadmium sulfide crystals bombarded by electron beams 03 p0433 A67-12812

Electron-hole pair separation energy in CdS single crystal during 5 to 50 kev electron bombardment 03 p0490 A67-13160

Electron bombardment induced electroconductivity, with application to image tubes 03 p0387 A67-14092

Physical mechanisms and operational principles of electron bombardment ion sources with reference to Lewis geometry and duoplasmatron configuration 04 p0664 A67-15017

Kaufman type electron bombardment ion source with 2.5 cm diameter for satellite low thrust attitude control system 04 p0554 A67-15018

Low density electron bombardment ion engine, particularly mercury engine and Cs gas discharge ion engine, for electrostatic propulsion 04 p0689 A67-15020

Threshold energy for electron radiation damage in Ag compared for liquid He and liquid Ni temperatures 04 p0638 A67-15115

Temperature dependence of current carrier mobility in GaAs crystals irradiated with fast electrons 04 p0679 A67-15140

Nonohmic contacts, metal semiconductor point contact and soldered contact instead of p-n junctions used to measure diffusion length for minority carriers 04 p0584 A67-15481

Defect impurity relation in electron damaged p-type silicon and electron irradiation effect on float zone n-type silicon 04 p0684 A67-15690

Transient radiation effects induced in silicon irradiated by electron pulses measured, using resistivity transient response and Hall effect voltages 04 p0685 A67-15695

Spontaneous dielectric breakdown in Plexiglas sheets due to pulsed electrons with breakdown plane influenced by embedded metal foils 04 p0659 A67-15699

Forward current, electroluminescent intensity and short circuit current during bombardment as function of 2-mev electron irradiation 04 p0685 A67-15704

High energy electron bombardment of MIS capacitor with subsequent positive charge introduction into insulator investigated by C-V and G-V measurements 04 p0588 A67-15712

Insulated gate field effect transistors with silicon dioxide and silicon nitride insulation under electron irradiation, noting gate turn-on voltage reduction and source-drain leakage elimination 04 p0588 A67-15713

K-shell ionization cross sections of silver, tin and gold from electron bombardment 04 p0661 A67-15762

Dember effect, bulk photovoltaic effect and current density in illuminated inhomogeneous semiconductor 05 p0863 A67-16702

Number transmission coefficients for isotropically incident electrons determined for spacecraft shield design [AIAA PAPER 66-511] 05 p0906 A67-17219

Defects in silicon p-n solar cells with Li diffused N region produced by electron irradiation and spontaneously annealed at room temperature interpreted as Li ions 05 p0870 A67-17273

Disordered regions and energy level position in germanium produced by electron irradiation 06 p1048 A67-17832

Electron irradiation effect on electric properties of gallium arsenide 06 p1049 A67-17858

X and electron irradiation effect on current-voltage characteristics of p-n junctions in gallium arsenide 06 p1049 A67-17859

Energy and angular distributions of

neutral atoms and charge-exchange ions from mercury electron bombardment thruster, determining particle effluxes [AIAA PAPER 67-82] 06 p1075 A67-18498

Emission spectra of nitrogen excited by electron beam of 0.1 to 20 kev and oxygen and air bombarded by 13-kev electrons 07 p1225 A67-19099

Permanent magnet low thrust engines performance and tests, starting from cesium electron bombardment ion microthruster [AIAA PAPER 67-81] 07 p1240 A67-19436

Far field pattern of sheet-like laser beam from electron bombarded CdS and ZnO single crystals 07 p1196 A67-19798

Charge separation mechanism of auroral electrojets, noting enhanced ionospheric conductivity by electron bombardment 07 p1245 A67-19931

Electron and proton radiation effects on GaAs, CdS and CdTe thin film solar cells noting proton damage, estimates on cell life, etc 08 p1285 A67-20735

Built-in voltage decrease in bulk germanium and Ge tunnel diodes under irradiation, noting Fermi level 09 p1471 A67-21764

Stability of various surfaces with respect to electron bombardment heating, noting influence of roughness on electron trapping 09 p1500 A67-22428

Electron bombardment type ionization gauge with logarithmic differential circuit 10 p1610 A67-22950

Electron-hole pair separation energy in CdS single crystal during 5 to 50 kev electron bombardment 10 p1690 A67-23107

Ion thruster, including mercury feed system and shielded neutralizer, designed and tested for spacecraft station keeping and attitude control [AIAA PAPER 66-247] 10 p1698 A67-23120

Plasma measurements in cesium electron bombardment ion engine indicate that reversed cathode-anode configuration improves radial ion distribution [AIAA PAPER 66-246] 10 p1698 A67-23121

Structure, conductivity and Hall effect of electron bombardment evaporated silicon films on sapphire substrates, noting deposition temperature source doping effectiveness 11 p1845 A67-24141

Temperature dependence of current carrier mobility in GaAs crystals irradiated with fast electrons 12 p1979 A67-25163

Electron bombardment ion thrusters with two accelerator-grid systems for producing ion beams in directions 180 or 90 degrees apart [AIAA PAPER 66-284] 12 p1990 A67-25891

GaAs gas bombarded by fast electrons investigated for recombination radiation spectra, noting shift of edge emission maximum toward longer wavelengths 13 p2173 A67-26359

Electron bombardment thrusters using liquid mercury cathodes noting lifetime, propellant and power efficiency, feed system, temperature limits, etc 13 p2188 A67-26822

Recrystallization of Ge and Si thin films and structural changes due to electron bombardment and thermal annealing 13 p2177 A67-27071

Plasma-vehicle interaction, discussing charged particle motion about small vehicle in ionospheric orbit 14 p2357 A67-28209

Threshold energy of formation and stable defect spatial distribution of silicon irradiated with electrons 15 p2542 A67-30250

Irradiation of gallium arsenide and gallium antimonide monocrystals by electrons, fast neutrons and relativistic protons, discussing Hall coefficient variation 16 p2727 A67-30869

Probability of atomic excitation by electron bombardment 17 p2893 A67-32138

Degradation in silicon transistors due to particle bombardment analyzed, showing surface/ bulk recombination increase 17 p2917 A67-32845

N-and p-type silicon solar cells orientation and energy dependence of damage at room temperature under electron bombardment 17 p2918 A67-32848

Electron bombardment effect on insulated-gate and junction-gate FETs and MOS IC indicates FET resistance to ionizing radiation 17 p2918 A67-32850

N-type germanium photoconductivity spectrum studied after bombardment with electrons at very low

temperatures 17 p2919 A67-32860

Annealing kinetics of n-type germanium exposed to electron bombardment at cryogenic temperature 17 p2919 A67-32861

Silicon photoconductivity measurements after electron irradiation at cryogenic temperature 17 p2920 A67-32864

Elemental composition effect on electron excited fluorescence of serpentines determined by spectral examination with electron microprobe 17 p2852 A67-33239

Technological methods for depositing thin films in vacuum, considering evaporation, scattering, etc 20 p3453 A67-36472

Permanent magnet low thrust engines performance and tests, starting from cesium electron bombardment ion microthruster 21 p3689 A67-37790

GaAs gas bombarded by fast electrons investigated for recombination radiation spectra, noting shift of edge emission maximum toward longer wavelengths 21 p3680 A67-38316

Silicon solar cells bombarded by energetic electrons for radiation resistance 21 p3571 A67-38648

Cesium bombardment ion engine performance, giving starting circuit and automatic discharge power control system [AIAA PAPER 67-666] 21 p3690 A67-38700

Liquid metal cathode electron bombardment thruster operable at high temperatures, noting stability in neutralizer current range [AIAA PAPER 67-667] 21 p3690 A67-38701

Gaseous mercury discharges through orifice as ion beam neutralizer for electrostatic thrusters [AIAA PAPER 67-669] 21 p3691 A67-38703

Mercury electron bombardment thruster system performance as function of mass utilization and specific impulse, noting magnetic field shape and ion optical system design effects [AIAA PAPER 67-697] 21 p3693 A67-38726

Clustered mercury electron bombardment ion engine system experiments showing feasibility, discussing components [AIAA PAPER 67-698] 21 p3693 A67-38727

Ion source using electron bombardment without magnetic source field, studying focusing and optimal operating conditions of electron accelerating system 22 p3847 A67-39641

Excitation effect on single electron charge transfer collisions of Fe ions in various gases determined with different excited states of ions 23 p4030 A67-40976

Titanium-magnesium and titanium-beryllium oxides physical properties under electron bombardment in vacuum indicate usability for SHF oscillation energy absorbers 24 p4202 A67-42069

Characteristics of high energy electron radiation and temperature and effect on N/P silicon solar cells 24 p4105 A67-42513

ELECTRON BUNCHING

Klystron with broad electron flux and excited traveling and standing electromagnetic waves, analyzing electron grouping 05 p0771 A67-16356

Two-step saturation of pulsed current in CdS single crystals, noting electron bunching mechanism and volt-ampere characteristics 14 p2385 A67-28238

Electron bunching in sweep klystron, deriving electric field equation, motion equations and continuity criteria for arbitrary charge density distribution 18 p3010 A67-33501

ELECTRON CAPTURE

Cross sections for double electron capture by two 50-kev protons in single collisions with hydrogen and inert gas target 01 p0115 A67-10140

Impulse method for determining electron trapping parameters of cadmium sulfide-type crystals with one barrier contact exposed to continuous illumination 03 p0487 A67-12807

Space charge limited unipolar nonstationary currents in solid, calculating nonsteady modes in plane parallel electrode structure due to carrier injection into gap 04 p0680 A67-15155

Radial distribution of plasma formed in simple mirror machines by quantum effect field ionization of fast neutral atoms 04 p0671 A67-15644

High energy electron intensity measurement beyond atmosphere with aid of proton I and II satellites, showing capture

by geomagnetic field 05 p0878 A67-16091

Electron capture cross section by protons in hydrogen atom obtained, using perturbed wave functions due to electric field 07 p1226 A67-19501

Electron capture coefficient of A-centers in silicon at helium temperatures 10 p1694 A67-23649

Critical binding of electron by electric dipole, noting value of dipole moment 11 p1824 A67-24996

Nonlinear effects in steady state volt-ampere characteristics of zinc compensated n-type silicon single crystals 13 p2172 A67-26356

Depth of capture levels determined from temperature dependence of kinetics of gamma-conductivity or photoconductivity of cadmium sulfide 14 p2367 A67-28526

Charge transfer prediction by classical binary-encounter theory approximation and quantum mechanical approximation 15 p2519 A67-29331

Space charge limited unipolar nonstationary currents in solid, calculating nonsteady modes in plane parallel electrode structure due to carrier injection into gap 15 p2534 A67-29342

Magnetic trap electron capture lifetime dependence on magnetic field determined by scattering by residual gas, noting adiabaticity parameter critical value 15 p2526 A67-29361

Effect of capture levels on current-voltage characteristic of semiconductor p-n diode with ohmic back contact 16 p2635 A67-30471

Electron recombination and capture processes at deep centers in n-type GaAs 16 p2724 A67-30604

Space-charge-limited dielectric diode with quadratic I-V characteristics, noting shallow trap effects on detection properties 17 p2823 A67-32199

Cross sections for electron capture by protons measured for various energies in nitrogen, argon and helium 17 p2889 A67-33227

Electron capture coefficient of A-centers in silicon at helium temperatures 17 p2923 A67-33330

Mobility measurement of electron capture in hydrocarbon flames using Hall effect, noting variation when injecting chlorine 18 p3146 A67-33691

Impurity photoconductivity in cadmium sulfide energy levels at red luminescence centers depth 19 p3300 A67-34765

Nonlinear effects in steady state volt-ampere characteristics of zinc compensated n-type silicon single crystals 21 p3679 A67-38313

SbS recombination center concentration, hole capture cross sections and trap energy levels 22 p3846 A67-39503

Depth of capture levels determined from temperature dependence of kinetics of gamma-conductivity or cadmium sulfide 23 p4039 A67-40933

Capture, ionization and ionization capture in collisions of protons with argon atoms 23 p4030 A67-41687

High energy electron intensity measurement beyond atmosphere with aid of proton I and II satellites, showing capture by geomagnetic field 24 p4213 A67-42767

ELECTRON CLOUD

Two-flow equations for stationary relativistic electron cloud in self-consistent crossed fields 05 p0774 A67-16907

Upper atmospheric formation of electron cloud produced by chemiionization reactions of chemical release agents [AIAA PAPER 67-148] 06 p0995 A67-18360

Electron cloud equilibrium in toroidal magnetic and electric fields due to space and image charges 08 p1364 A67-21396

Two-flow equations for stationary relativistic electron cloud in self-consistent crossed fields 16 p2636 A67-30884

Diocotron effect in cylindrical charge layers analyzed, noting instability when layer thickness is less than critical, experimenting with plasma discharges 19 p3292 A67-35392

Magnetron cut-off characteristics modification via altering electron cloud resonant properties by injecting positive ions in interaction space 20 p3489 A67-37105

ELECTRON COLLISION

Inelastic collisions of electrons with diatomic molecules, noting effect on speed of energy exchange in nonhomogeneous

plasma 01 p0118 A67-10044
 Effective cooling of free electrons in plasma due to ambipolar diffusion and elastic collision with ions and neutrals 01 p0122 A67-10346
 Electron collisions in nitrogen studied by mass spectrometer, measuring dissociative ionization cross section of nitrogen 01 p0117 A67-10779
 Absolute excitation cross sections of helium levels colliding with low energy electrons 02 p0270 A67-12487
 Electron-ion recombination process due to electron collision in plasma with capture electrons transferred to ground level 03 p0474 A67-12853
 Electron collision cross section resonance mechanism analyzed via matrix methods, noting threshold effect application to electron scattering 03 p0470 A67-13219
 Kinetic model for three-component plasmas with ionization resulting from electron-neutral collisions 03 p0484 A67-14037
 Bremsstrahlung emission from electron-electron collisions in plasma, obtaining spectra of longitudinal and transverse waves 03 p0484 A67-14043
 Electron cyclotron echo production from plasmas by repeated pulsing, developing theory based on electron neutral momentum transfer collisions 04 p0665 A67-15105
 Cross sections for electron collisions with hydrogen atoms and hydrogen-like ions for excitation of ground and other levels 04 p0671 A67-15642
 Electron motion in gases in pressure range where electron mean free path is comparable to or less than chamber length, showing effect on ion currents 04 p0662 A67-15769
 Electron collision rate and density calculations for He-Ne laser plasma 05 p0815 A67-16598
 Ochkur and Rudge approximation for exchange in electron-atom collisions adapted for atom-atom collisions 06 p1034 A67-17649
 Velocity distribution function relaxation and runaway of electrons in weakly ionized plasmas 07 p1228 A67-19510
 Field harmonics of HF plasma discharge taking nonlinear interaction into account 08 p1357 A67-20827
 Excitation cross section of states of Ne 2, Ar 2 and Kr 2 by electron collision 08 p1339 A67-21376
 Electrostatic probe theory in moderately ionized gas taking into account effect of electron-ion collisions 08 p1324 A67-21393
 Kinetic equations for homogeneous electron gas derived to all orders in plasma parameter λ_{De} /reciprocal number of electrons per Debye sphere/ 08 p1363 A67-21394
 Potential distribution in electron-collisionless plasma in weak magnetic field 08 p1365 A67-21412
 Average diffusion cross section for elastic collisions of electrons with heavy particles, comparing calculated and measured values 09 p1534 A67-21864
 Rise and decay times of spike burst during type IV event of February 5, 1965, noting electron stream velocities and coronal temperature 09 p1562 A67-22233
 Hydrogen-molecule ion dissociation by electron collision, noting various transition states 09 p1535 A67-22378
 Electron collision with atmospheric nitrogen molecules, obtaining effective cross sections 10 p1633 A67-23047
 Ionospheric absorption effects in D and E layers, noting refraction role and effective collision frequency 10 p1646 A67-23270
 Absolute excitation cross sections of helium levels colliding with low energy electrons 10 p1682 A67-23355
 Excitation cross section of upper laser levels in ionized argon by electron collision with ground state neutral atoms measured, using incoherent light technique 10 p1665 A67-23382
 Effective cross sections of excitation of lower energy levels during electron collisions in alkaline metals, noting dependence of various levels on quantum number and atomic number 11 p1822 A67-24018
 Level populations and energy loss rate of electrons during nonelastic collisions with impurity molecules in weakly ionized two-temperature plasma 11 p1831 A67-24019

Relaxation in space of electron velocity distribution due to electron-ion collisions, obtaining time independent solution 11 p1833 A67-24372
 Magnetic effect and collision in damping of electron Langmuir oscillations 11 p1842 A67-24965
 Effective cooling of free electrons in plasma due to ambipolar diffusion and elastic collision with ions and neutrals 11 p1843 A67-25019
 Electron transport coefficients and electron energy equation closed formulation for two-temperature plasma, considering elastic and nonelastic collisions 12 p1973 A67-25397
 Scattering mechanisms and role of interelectron collisions in n-Pb-Te and certain other semimetals analyzed by concentration dependence of mobility and thermal EMF 12 p1983 A67-25514
 Cosmic radio wave absorption dependence on frequency and number of electron-ion collisions during atmospheric magnetic storms 12 p1933 A67-25548
 Electric potential distribution in flame for electronegative gas layer present between two electrodes 13 p2185 A67-26597
 Ionospheric D layer structure and formation, considering free electron height variation and collision 14 p2311 A67-28406
 Charge transfer prediction by classical binary-encounter theory approximation and quantum mechanical approximation 15 p2519 A67-29331
 Particle energy distribution in low temperature nonequilibrium plasma in diffusion approximation 16 p2720 A67-31386
 Collision cross sections and energy scattering of atoms with slow electrons 17 p2893 A67-32137
 Linear theory of collision-induced instability of partially ionized gases for waves propagating along external magnetic field 17 p2902 A67-32669
 Inelastic collisions of electrons with diatomic molecules, noting effect on speed of energy exchange in nonhomogeneous plasma 17 p2890 A67-33322
 Electron precipitation data examined to determine whether electron behavior can be understood on basis of binary collisions with atmospheric constituents and guidance by geomagnetic field 18 p3035 A67-33599
 Scattering mechanisms and role of interelectron collisions in n-Pb-Te and certain other semimetals analyzed by concentration dependence of mobility and thermal EMF 18 p3103 A67-34445
 Low-energy electron collisions and interactions with atoms and molecules, discussing vibrational excitation, ion formation, ionization cross section, etc 19 p3264 A67-35068
 Electron-atom collision cross-section in afterglow of pulsed cesium plasma as function of electron cyclotron absorption resonance and electron temperatures 19 p3271 A67-35076
 Space-charge and potential distributions calculated for region between two plane electrodes of single collision model 19 p3265 A67-35129
 Continuous spectrum of eigenvalues related to Fokker-Planck collision integral 19 p3285 A67-35341
 Initial ionization processes in shock heated argon consisting of atom-atom collisions followed by electron-atom processes 19 p3293 A67-35397
 Phase shift method for obtaining radiative lifetimes by electron collisions 20 p3488 A67-36665
 Electron-temperature dependence of electron collision frequency in afterglow plasma 21 p3667 A67-38414
 Negative cyclotron resonance absorption due to electron elastic collisions with noble gas atoms, comparing results with kinetic plasma wave theory predictions 22 p3842 A67-40346
 Mean F-2 layer electron collision frequency computation from cosmic noise absorption 23 p3994 A67-40779
 Anomalous electron heating rate in plasma region traversed by magnetic shock wave obtained by electron velocity distribution observation 24 p4198 A67-42736

ELECTRON DECAY TIME

Transient characteristics of doped silicon diodes with negative resistance, determining electron lifetime vs current, noting space charge role 13 p2076 A67-26489
 Anomalous decay of discharge plasma with oscillating electrons in strong magnetic field, using diagrams 16 p2717 A67-31181

ELECTRON DENSITY
 SA IONOSPHERIC ELECTRON DENSITY
 SA IONOSPHERIC ELECTRON DENSITY
 SA MAGNETOSPHERIC ELECTRON DENSITY
 Superconductivity of nondegenerate semiconductor thin films, dependence on current carrier concentration, impurity levels and film thickness 01 p0128 A67-10084
 Optical reflection, transparency and Faraday effect for indium antimonide, calculating effective electron mass, relation between energy and wave number, etc 01 p0128 A67-10095
 Peculiarities of Hall curves of n-type alpha silicon carbide, noting concentration of conduction electrons related to temperature 01 p0129 A67-10102
 Multibeam microwave interferometer measurement of radial distribution of electron density in plasma cylinder 01 p0119 A67-10169
 Plasma probe measurement of distribution of electron concentration, temperature and space potential throughout entire interelectrode gap of thermoelectronic converters 01 p0012 A67-10353
 Electron density fluctuations in turbulent wake, using stochastic analysis and statistical averaging [AIAA PAPER 65-818] 01 p0007 A67-11168
 Proposed modification of Wetzel model of direct ionization by primary continuum in light of recent steady state precursor electron density measurements ahead of Ar shocks 01 p0118 A67-11193
 Radio wave guiding along electron density discontinuity in magnetotonic exosphere, noting low dispersion modes 01 p0027 A67-11259
 Plasma effects in nozzle flow of hypersonic shock tunnel using air, obtaining electron density profile 01 p0126 A67-11442
 Electron density enhancement in thermal plasma by metastable atoms, computing ionization by method of Lagrange multipliers 02 p0272 A67-11519
 Linear electron density in meteoric trails determined not by vaporization rate but by number of meteoric atoms moving together with body at given moment 02 p0322 A67-11677
 Electron density effect on transition temperature of superconductivity, considering tantalum 02 p0291 A67-11742
 Three-mirror laser interferometer measuring electron densities in repetitively pulsed plasmas 02 p0241 A67-11875
 Plasma electron density and formation determined, using Fabry-Perot resonator 02 p0275 A67-12469
 Current carrier concentration and dynamic coefficients for nondegenerated and highly degenerated Fermi gases subject to nonparabolic isotropic laws of dispersion 02 p0300 A67-12475
 Electron concentration in metallic emission regions in chromosphere 02 p0328 A67-12485
 Criteria for cold plasma density necessary to stabilize grade B drift waves in finite length energetic plasmas 02 p0275 A67-12554
 Radial electron density distribution in induced pulsed discharge from wave refraction in planes passing through and normal to plasma cylinder axis 02 p0278 A67-12624
 EAS with zenith angle between 30 and 45 degrees and fixed number of muons and electrons 02 p0318 A67-12777
 Scattering of electromagnetic waves in plasma, noting effect of eddy current fluctuations 03 p0367 A67-12938
 Perturbation of electron density at large distances from body at high velocity in collisionless plasma under steady external magnetic field 03 p0475 A67-12939
 Superconducting critical temperatures of nonstoichiometric transition metal carbides and nitrides, correlating data with valence electron concentration 03 p0491 A67-13256
 Energy relaxation as explanation of

changes in electron density and temperature of helium plasma in upper hybrid resonant heating 03 p0477 A67-13360

Electron density effect on transition point of superconductors 03 p0494 A67-13508

Electron density measurement in shock waves or plasma based on low power UHF wave attenuation 03 p0478 A67-13578

Phenomena preceding shock waves in argon, evaluating electron density profile and UV brightness of 03 p0483 A67-13885

Air ionization rate behind high speed shock waves, determining electron density from IR emission 03 p0405 A67-14028

Spin temperature of intergalactic atomic hydrogen calculated as function of electron density and kinetic 03 p0515 A67-14319

Afterglow decay of number density and electron temperature of plasma with rare collisions between electrons and molecules 03 p0487 A67-14343

Transverse magnetoresistance and Hall effect measurements on n-type GaSb at various magnetic fields and temperatures, obtaining electron concentration and mobility 03 p0501 A67-14347

Plasma electron density as function of radius compared with ion cyclotron heating theory and stability criteria [AIAA PAPER 66-158] 04 p0664 A67-14823

Comparison of experimentally obtained electron effective masses for high electron concentration in InSb and InAs 04 p0677 A67-14935

Approximate analysis of electrostatic probe on reentry vehicle for electron density measurements in laminar boundary layer of continuum 04 p0705 A67-15231

Luminous density distribution of decaying hydrogen plasma recorded by photoelectronic method 04 p0672 A67-15653

Linear electron density measurement in meteor trains using radio echo observations of Geminids 1963 stream 05 p0889 A67-16206

Time resolved spectroscopic measurements of intensity and Stark width during decay of hydrogen plasma produced by ruby laser, determining electron density and temperature decay 05 p0852 A67-16653

Electron density, optical thickness and temperature of ruby laser-induced carbon plasma 05 p0852 A67-16654

Electron densities in helium plasma measured by laser amplifier with maximum gain and minimum bandwidth at point nearest threshold 05 p0820 A67-16663

Plasma electron density range measurable by microwave extended by phase angle being expanded by impedance transformation 05 p0854 A67-16982

Spatially resolved He-Ne laser heterodyne measurements of electron number densities in weakly ionized Ar pulsed discharges 05 p0856 A67-17272

Double probe and microwave resonance measurements of gas additives effect on radial variation of electron temperature and density with partial pressures in carbon dioxide-nitrogen-helium gas laser 05 p0826 A67-17274

Microwave cavity techniques to measure electron precursors in shock tube [AIAA PAPER 66-175] 05 p0856 A67-17342

Spectroscopic measurement of temperature, electron density and conductivity in RF plasma 06 p1039 A67-17825

Shock wave front structure in plasma, noting use of SHF diagnostics, electron concentration growth, etc 06 p0984 A67-18077

Plasma parameter determined from measurements of wave reflection coefficient in waveguide 06 p1041 A67-18187

Electron number density determined using interference pattern recorded by satellite ionograms at high latitudes 06 p0996 A67-18568

Generation of longitudinal plasma oscillation harmonics near electron cyclotron frequencies 06 p1046 A67-18831

Turbulent wake of slender body analyzed to include dominant mode of laminar diffusion, deriving solution for linear electron chemistry 06 p0943 A67-18870

Electric properties of gas dynamic mirror formed in wake of shock wave front 07 p1227 A67-19118

State density of strongly alloyed

semiconductor in external constant electric field 07 p1149 A67-19188

Time dependence of electron density in afterglow of electrodeless discharge in hydrogen plasma measured, using microwave interferometer 07 p1229 A67-19682

Perturbations caused by cylindrical body in plasma, obtaining electric field and electron and ion concentration dependences on distance 07 p1250 A67-19811

Equilibrium particle ionization effect on electron density of gas particle plasma 08 p1360 A67-21124

Electron space-charge neutralization in design of thermionic /heat-to-electricity/ converters 08 p1286 A67-21177

Laser effect on electron gas and excited state populations in xenon discharges 08 p1338 A67-21306

Electron temperature and density in F region analyzed for nighttime heating, using Langmuir probe measurements 08 p1327 A67-21364

LF electron density microscopic fluctuations in bounded plasma examined by method having virtue of being exact at zero frequency 08 p1365 A67-21404

Laser interferometry and photon scattering in high temperature plasma diagnostics 09 p1536 A67-21602

Ionization and temperature measurement in MHD experiment, noting microwave interferometer response as electron density function and line reversal 09 p1538 A67-21777

Measurements of conductivity, electron density and ionization rate of cesium in argon on alkali shock tube, describing MHD generator wind tunnel experiment 09 p1540 A67-21789

Nonequilibrium excitation influence on electron density in one-dimensional MFD channel flow 09 p1542 A67-21814

Electric arc behavior in argon gas flowing through magnetic field, measuring flow velocity, electron temperature, spatial distribution, etc 09 p1543 A67-21824

Gas laser measurement of electron density in xenon pulse discharge 09 p1512 A67-21922

Steady state beam induced plasma parameters and behavior when affected by HF noise oscillations and effect on electron concentration in plasma 09 p1545 A67-21997

Statistical quantities needed to fix scattering regime obtained from observations of radio scintillations, showing correlation length in electron density fluctuations 09 p1565 A67-22223

Plasma electron density determined from mutual impedance measurements obtained as function of frequency 09 p1501 A67-22561

Electron and ion densities and temperatures measured by rockets in active auroras and correlated with directly measured ionizing flux 10 p1650 A67-23307

Electron concentration in metallic emission regions in 10 p1708 A67-23353

Plasma confinement time in helium discharge determined by electron density and helium radiation intensity measurements 11 p1827 A67-23887

Radiation characteristics for slotted cylinder covered with magnetized inhomogeneous plasma sheath assuming parabolic electron density distribution 11 p1753 A67-24306

Cooperative effect among electrons in presence of radial density gradient in cyclotron echo phenomena 11 p1836 A67-24391

Plasma conductivity measurement based on Hall current and Hall voltage relation to electrical resistance 11 p1839 A67-24424

Electron number densities measured behind shock wave in pressure-driven shock tube by microwave resonant cavity technique and by electrostatic quasi-Langmuir probe 11 p1790 A67-24451

Cesium vapor thermionic diode operation in electron-rich surface ionization mode noting transport effects 11 p1849 A67-24902

Supersonic rarefied argon plasma jet, determining pressure distribution, electron concentration and temperature 11 p1842 A67-24963

Plasma probe measurement of distribution of electron concentration, temperature and space potential throughout entire interelectrode gap of thermoelectronic converters 11 p1746 A67-25026

Microwave reflection analysis of plasma surface phenomena, noting dependence on electron density and collision frequency 11 p1844 A67-25097

Mathematical theories applicable to excitation and ionization of atoms in plasmas at thermal equilibrium, determining electron density and temperature 12 p1968 A67-25432

Ionization dependence of Na, K, Ca, Mg, Al, Fe and Si on arc temperature, noting correlations between temperature and electron concentration independent of plasma composition 12 p1977 A67-26108

Plasma equilibrium from gas discharge, role of electron concentration and contributions of excited atom transitions and quenching collisions 12 p1977 A67-26132

Meteor distribution estimation attempted through radar observation, measuring kinetic energy level, velocity and electron distribution in meteor trails 13 p2197 A67-26507

Microwave interferometer with dielectric rods as waveguides for measuring electron density in small volume inside plasma 13 p2120 A67-26859

Electron mobility in semiconducting strontium titanate 13 p2180 A67-27160

Radial electron density distribution in induced pulsed discharge from wave refraction in planes passing through and normal to plasma cylinder axis 13 p2171 A67-27380

Simple model atom selection for electron density calculation in low temperature nonequilibrium Cs plasmas 13 p2171 A67-27441

Book on chemical bond in semiconductors and solids, evaluating strength and determining effect on properties of substances 13 p2182 A67-27486

Electron microscopy of biological-like structures in Orgueil carbonaceous meteorite 13 p2210 A67-27583

Electron density and HF spectrum of beam generated plasma as function of gas pressure and injection parameter 14 p2352 A67-27749

Phase shift between electron temperature, luminous intensity and electron density in stratified positive column of glow discharge 14 p2353 A67-27757

Electron density variation, collision frequency and phase shift in standing striations in positive column 14 p2353 A67-27758

Long term solar cycle and seasonal variation of whistler dispersion 14 p2307 A67-27887

Seasonal and diurnal variation of parameters of vertical electron density distribution 14 p2308 A67-27934

Magnetic field, pressure and discharge current effects on saturation electron current of electrostatic probe used to measure magnetoplasma electron density 14 p2358 A67-28237

Gas laser measurement of electron density in xenon pulse discharge 14 p2330 A67-28251

Anisotropy in tunneling density of states in pure type II superconductors, examining ideal case of perfectly specular boundary scattering at tunneling junction 14 p2365 A67-28294

Slotted-sphere antenna immersed in plasma measured for RF admittance 14 p2283 A67-28377

Spectroscopic methods applied to plasma electron temperature and density measurements 14 p2322 A67-29045

Hotshot wind tunnel for ionized wakes of models in nitrogen hypersonic flow, determining electron temperature and density [ONERA-TP-455] 15 p2416 A67-29380

RF characteristics of spherical probe immersed in hot low-density plasma, using sheath model 15 p2528 A67-29564

Electron density and temperature in plasma measured, using self-focused laser beams 15 p2488 A67-29902

Time varying high density laser induced plasmas formed in high pressure gases studied using Mach-Zehnder interferometer 15 p2488 A67-29903

Recombination-regeneration formula for hole-electron pairs in randomly doped semiconductor materials 15 p2539 A67-29915

Electron concentration and temperature, gas temperature, electrical field intensity and conductivity of Hg-Cs nonequilibrium

- plasma 16 p2709 A67-30517
 Electron number density and number density of electronic states calculated from rate equations for noble gas seeded with alkali metal 16 p2710 A67-30518
 Temperature dependence of properties of acceptor center in iron doped gallium arsenide, noting delocalization of cluster electron density 16 p2726 A67-30814
 Electrostatic wave propagating into region of decreasing electron density calculated using one-dimensional plasma with uniform electron density 16 p2715 A67-31063
 Linear electron density in meteoric trails determined not by vaporization rate but by number of meteoric atoms moving together with body at given moment 16 p2747 A67-31092
 Rarefied gas flow density measurement by determining changes in electron beam-electron concentration while crossing flow 16 p2673 A67-31107
 Concentration profile of normal and excited mercury atoms in shock wave front and wake, noting gas density and electron concentration profiles 16 p2673 A67-31108
 Plasma probe diagnostic technique in shock tube, noting electron concentration, gas temperature and plasma potential from V-T characteristics 16 p2673 A67-31110
 Radio wave trapping and guiding along magnetic field lines by irregularities in electron density 16 p2667 A67-31513
 Faraday rotation satellite observations at closely spaced frequencies, allowing electron content figure determination 16 p2629 A67-31514
 Equilibrium deviation occurring in plasma with variable kinetic temperature due to radiation transport within plasma volume and outflow beyond limits of volume 16 p2723 A67-31767
 Ionization processes in hot products of combustion processes /flame gases/ as weak plasma media noting flame properties, mass spectroscopy, electron concentration, etc 17 p2967 A67-32140
 Radiation spectra of plasma jets from IR to UV, determining electron density and argon excitation temperature, noting bremsstrahlung 17 p2893 A67-32144
 Vertical electron temperature and concentration distribution up to 480 km at middle latitudes from rockets 17 p2842 A67-32253
 De Haas-van Alphen effect in bismuth telluride over range of carrier concentrations, noting existence of low mobility heavy mass band 17 p2912 A67-32268
 Determination of electron density and temperature, gas temperature, atomic composition and flow velocity of high temperature gas stream 17 p2900 A67-32339
 Motion of artificial high density ionization cloud released in ionosphere 17 p2844 A67-32545
 Mechanism of positive low pressure column in plasma of low electron density, studying steady state conditions of nonstratified inert gas discharges 17 p2907 A67-33103
 Coupling between neutral air motion and plasma transport in model F-2 layer, noting nonlinear diffusion equation, velocity profiles, etc 17 p2852 A67-33241
 Fourier series applied to X-ray investigation of potential and electron density distribution in silicon lattice to study chemical bonds 18 p3094 A67-33439
 Auroral rocket measurements of electron flux, electron and ion density, electron temperature and auroral brightness 18 p3034 A67-33593
 Auroral backscatter theory and relationship to instability concepts 18 p3038 A67-33618
 Radiation power of He-Ne laser at 0.63, 1.15 and 3.39 microns, effect on electron concentration 18 p3060 A67-34038
 Temperature field and electron concentration in electric arc moving along parallel electrodes in magnetic field, giving propagation rate, arc intensity, etc 18 p3087 A67-34046
 Electron concentration in turbulent boundary layer of weakly ionized plasma when injecting electrons through pores in wall 18 p3087 A67-34053
 Electron density radial distribution, neutral gas temperature and ionization-caused column contraction calculated for cylindrical discharge plasma in argon 18 p3089 A67-34298
 Nonlinear and second order thermal diffusion of electrons in ionized gas, using kinetic theory 18 p3083 A67-34401
 Electron flow in low density argon gas diode analyzed by Monte Carlo method 18 p3091 A67-34641
 Detection and measurement of precursor ionization in electromagnetic shock tube 18 p3091 A67-34727
 Analysis of flame effects on measured electromagnetic propagation data for plume shape, plume electron density distribution and signal attenuation 19 p3344 A67-34819
 Electron density decay curves in helium afterglows at high electron densities and gas pressure found controlled by recombination loss process 19 p3270 A67-35071
 Ionization rate at higher electron densities in DC fields measured in toroidal discharge tube 19 p3272 A67-35078
 Positive column contraction in inert gas discharge, studying electron density and radiation intensity radial distribution and wall current 19 p3272 A67-35092
 Electron temperature, concentration and potential distribution, measurement in moving striations by Langmuir probe method 19 p3273 A67-35095
 Plasma resonance in RF discharge excited with frequency higher than collision frequency, determining electron density 19 p3276 A67-35114
 Temperature, electron density, and relative particle density radial distribution and mass separation effect in free burning DC arc 19 p3281 A67-35156
 Ionized gas produced by exploded lithium wires, presenting physical measurements, finding self-consistent solution of temperature and electron concentration 19 p3261 A67-35162
 Electron density behind shock front of discharge plasma measured using interferometer 19 p3230 A67-35395
 Electron density and collision rate of shock produced plasma measured with X-band microwave reflection probe 19 p3293 A67-35398
 Plasma-magnetic shock wave propagation in high pressure, partially ionized argon plasma 19 p3293 A67-35400
 Air ionization behind shock wave front, estimating free electron concentration, ionization time and collision frequency 19 p3293 A67-35401
 Solar flare electron density determination by half-width method, discussing errors due to measurement and method 19 p3314 A67-35438
 Solar flare electron density measurements using half-width method, noting variations with height, development and area 19 p3314 A67-35439
 Electron density and temperature measurements using RF capacitance probe and double Langmuir probe in auroral zone 19 p3222 A67-35455
 Absolute intensities of Lyman hydrogen alpha and beta lines used for interpretation of electron temperatures and density of emitting layers 19 p3325 A67-35464
 Ion-density data modifications due to temperature variations, discussing normalization and electron density relationship 19 p3224 A67-35491
 Electron temperature of H II region related to high temperature main sequence stars determined as function of electron density and radiation dilution factor 19 p3325 A67-35503
 Langmuir probe collection of ions in low density plasma flows, with electron density agreeing with microwave data 19 p3297 A67-35591
 Faraday effect in microwave region used for electron density determination in argon and helium low pressure plasmas and comparison with cyclotron radiation data 19 p3297 A67-35592
 Plasma electron density measurement method using beat frequencies between two dual frequency lasers 19 p3231 A67-35594
 Wave propagation in anisotropic plasma in presence of electron density irregularities, noting Faraday effect 19 p3184 A67-35825
 Space charge analyses applied to electron beam extractions from plasma cathodes, computing stability data for potential distributions and extracted current 20 p3495 A67-36168
 Complex reflection coefficient for finite-width boundary used for plasma diagnostics in high electron-density range, discussing modeling errors 20 p3499 A67-36959
 Differential equations governing steady state current flow in semiconductors computed, considering variations as function of distance, hole and electron densities, etc 20 p3400 A67-37216
 Nonthermal plasma electron density calculated from ratio of spectral line intensities of given ion 20 p3501 A67-37294
 Electron density time and location dependence in Z-pinch calculated from emission measurements 20 p3502 A67-37528
 Laser interferometric measurements of electron density in plasma arc discharge at atmospheric pressure 21 p3664 A67-38017
 Electric properties of gas dynamic mirror formed in wake of shock wave front 21 p3664 A67-38163
 Hydrogen plasma discharge with hot electrons, investigating plasma decay and electron and plasma density 21 p3666 A67-38368
 P-n junction devices static behavior assuming Van Roosbroeck differential equations in bulk and transition regions 21 p3598 A67-38571
 Plasma diagnostics using self-focused laser beams, determining electron density and temperature 21 p3673 A67-38734
 RF induction heating and production of low pressure plasmas, discussing plasma electron density function [AIAA PAPER 67-732] 21 p3674 A67-38756
 Electron density relation to output power in He-Ne laser and magnetic field effect, using microwave resonator technique 22 p3814 A67-39428
 Steady state plasma in strong microwave electric field acting on electron component 22 p3845 A67-39431
 Carrier concentration dependence of thermoelectric power and Hall mobility of undoped and doped lead telluride explained by two-valence model 22 p3857 A67-39490
 Double probe method for determining electron temperature and density variations in HF hydrogen plasma during second harmonic cyclotron resonance 22 p3848 A67-39650
 Wavelike behavior of precursor electron density front in electromagnetic shock tubes explained via transmission line model 22 p3850 A67-39711
 EAS with zenith angle between 30 and 45 degrees and fixed number of muons and electrons 22 p3877 A67-40279
 Electron density between shock front and discharge plasma in electromagnetic shock tube determined by interferometric technique, using guided waves 22 p3810 A67-40523
 Hypersonic reentry plasma electron density measurement in free stream wake and shock layer using hotshot wind tunnel simulation 23 p3986 A67-40574
 Spectroscopic analysis of iron meteoroid radiation by emission growth curve method covering temperature factors and atom and electron concentrations 23 p4062 A67-40674
 Faraday rotation data from Explorer XXII, determining atmospheric electron content for magnetic field aligned ionization layer location and occurrence 23 p3996 A67-40818
 Rapid scan spectrometer used to measure Stark broadened H lines in plasma column, determining electron density 23 p4032 A67-40957
 Low energy cosmic ray proton flux as representative of interstellar medium, discussing electron density in neutral H I regions 24 p4208 A67-41833
 He-Ne gas mixture DC discharge electron temperature and concentration dependence on tube diameter, pressure and composition, using two-probe method 24 p4196 A67-42242
 Ar produced in capillary arc discharge, studying charged particle density and electron temperature dependence on magnetic field intensity 24 p4196 A67-42244
 Interferometer crossed with spectrograph used for electron concentration investigation in ionized argon behind shock waves propagating at high Mach numbers 24 p4197 A67-42358
ELECTRON DENSITY PROFILE
 Stratospheric measurements of electrons and gamma radiation in cosmic rays, using

plastic scintillator and lead sheet
supplemented Geiger
counters 02 p0310 A67-12584

F region effects following two severe
magnetic storms, noting changes in electron
density profile 06 p0995 A67-17972

Signal delay transmission on several
frequencies from solar orbiting spacecraft to
terrestrial receiver used for continuous
coronal electron density
profile 06 p1091 A67-18996

Ionospheric effect of sudden magnetic
storm eruption, noting propagation of
disturbance above terrestrial
surface 07 p1174 A67-19705

Steady state theory of discharge column,
giving solutions to density and potential
profiles for planar and cylindrical
geometry 08 p1361 A67-21134

Adiabatic invariant analysis of charged
particle motion in model
magnetosphere 08 p1378 A67-21474

Mean noon profile of mesospheric electron
number density at 35 degrees S latitude
preceding solar eclipse 08 p1378 A67-21483

Spectral analysis of laser discharge in
pure and impure He, obtaining spectra of
spark at various pressures, determining
electron concentration 09 p1512 A67-22010

Hydrogen line profiles in model
atmospheres using quasi-static approximation
for electrons and ions 10 p1704 A67-22883

High field Hall effect of semiconducting
CdS crystals with different mobilities, noting
electron density and
multiplication 10 p1689 A67-22908

Electron density determination from
plasma resonance measurements, using
electric analogy for 10 p1610 A67-22951

Vertical drift of charged particles effect
on electron density profile as cause of
seasonal variations in ionospheric
absorption 10 p1646 A67-23269

Molecular orbital electron charge density
pictures, noting representation close to
Hartree-Fock calculation
method 10 p1682 A67-23379

Neutral wind structure effects on
ionospheric sporadic E layer variations,
noting daytime evolution, nighttime
characteristics and electron density
profiles 11 p1783 A67-23924

Behavior of nighttime equatorial F-2 layer
under ambipolar diffusion and
electrodynamical drift 11 p1784 A67-23935

Low altitude electron trapping boundary
collapse during magnetic storm due to field
line extension into geomagnetic
tail 11 p1785 A67-23943

Free electron density and effective
collision frequency of ionized argon in wake
of shock wave measured, using microwave
probe methods 11 p1775 A67-24017

Expression for electron contribution to
Stark broadening, using impact
approximation with Lewis or Debye
cut-offs 11 p1823 A67-24491

Elektron I and II satellite observational
data on terrestrial radiation
belt 12 p1998 A67-25816

Optical interferometry in plasma
diagnostics, discussing degree of ionization,
time dependent electron density
distribution, etc 12 p1976 A67-26073

Plasma EM instability in magnetic mirror
configuration, solving linearized Vlasov
equation for dispersion relation of
transverse EM waves 13 p2164 A67-26293

Ionospheric electric current measurement,
determining vertical current density
distribution and electron number density for
geomagnetic field study 13 p2107 A67-26308

Temperature of F region deduced from
electron number density
profiles 13 p2108 A67-26322

Magnetospheric electron density
distribution determined from analytical
calculations, using whistler travel-time
integral 13 p2111 A67-26576

Solar flare electron propagation in
interplanetary space 13 p2194 A67-27251

Plasma in diffusion regime situated in
nonhomogeneous RF field with rotation
symmetry 14 p2354 A67-27765

Ionization structure of elements H, He, C,
N, O, Ne in planetary nebulae computed for
theoretically determined electron
temperature and electron density
variation 14 p2382 A67-27847

Electron number density profiles and

polar cap absorption of radio waves time
history during weak solar cosmic ray
event 14 p2380 A67-28042

Spatial HF radio focusing caused by
electron distribution between ionospheric
layers, even in absence of horizontal density
gradients 14 p2261 A67-28048

Local electrostatic potential for
collisionless plasma flow derived, obtaining
smooth solutions for self-consistent electron
density distributions 14 p2356 A67-28202

Decrease in degree of ionization of shock-
heated argon resulting from radiative
emission 15 p2527 A67-29563

Radar measurement of differential group
delay to moon, showing large differences in
total cislunar electron content above 1000
km in solar and antisolar
directions 15 p2555 A67-29611

Range of undistorted propagation of
traveling disturbances, noting shape of
altitude-frequency characteristics of
ionosphere with parabolic electron density
distribution 15 p2479 A67-30074

French Rubis rocket flight noting high
altitude barium release experiment, high
energy proton and electron measurements,
etc 16 p2738 A67-31017

Numerical analysis of ionospheric radio
wave propagation, examining, attenuation
polarization and power flow as function of
electron density profiles 16 p2631 A67-31857

Changes of phase and signal amplitude of
VLF radio waves during solar flares noting
waveguide mode
characteristics 16 p2632 A67-31859

Nighttime profiles calculated with
allowance for ionization beyond lower bound
of frequency range of ionospheric
station 16 p2669 A67-31896

Altitude of lower boundary of ionosphere
determined by electron density profile,
considering absorption coefficient and
magnetotonic signal
components 16 p2669 A67-31906

Electron heating in diurnal ionosphere
noting electron and ion temperatures as
function of altitude 17 p2842 A67-32295

Vertical electron density profile method
for determining altitude of lower boundary
of ionosphere 17 p2842 A67-32383

Structure and decay of artificial radiation
belt produced by high altitude nuclear
explosion 17 p2936 A67-32534

Auroral rocket measurements of electron
densities, ionization rates, particle energy
fluxes, energy spectra, pitch angle
distribution, etc 18 p3034 A67-33592

Thomson scattering of Q-switched ruby
laser beam in shock wave plasma,
determining electron densities, spectral
distribution of scattered light,
etc 18 p3084 A67-33649

Electron conductivities calculated for
sodium-xenon and sodium-xenon-mercury
plasmas assuming local thermal equilibrium,
estimating plasma temperatures and electron
number densities 19 p3278 A67-35134

Rocket observations of upper atmospheric
winds, electron density, electron
temperature, and neutral temperature in
auroral region with Langmuir
probes 19 p3214 A67-35169

Lower thermosphere physical properties,
studying satellite drag for density profiles,
composition, data comparison,
etc 19 p3215 A67-35171

Auroral absorption events, discussing
bremsstrahlung X-rays spectrum, electron
densities and temperatures measured with
rockets 19 p3312 A67-35188

NO role in sunrise E region compared to
Barth NO distribution, determining density
profiles, relative ion ratios,
etc 19 p3216 A67-35191

Flux, energy distribution and density of
ions and electrons in magnetosphere plasma
during solar activity period determined by
OGO-C electrostatic
probes 19 p3217 A67-35200

Electron density measurement in
ionosphere-magnetosphere transition region
using rocketborne gyroplasma swept
frequency probe, discussing electron density
profile and plasma
medium 19 p3229 A67-35201

Ionospheric electron density profile
microstructure studied by rocketborne
gyroplasma probe discovering electron
density irregularities 19 p3217 A67-35202

Day-and nighttime electron and ion

density profiles in lower ionosphere deduced
from blunt probe theory and
measurements 19 p3218 A67-35213

Day-and nighttime electron density
profiles in ionospheric D
layer 19 p3218 A67-35227

Storm-time change and average electron
density profile of polar topside ionosphere
at sunspot minimum 19 p3218 A67-35230

Electron temperature and density profiles
in lower ionosphere at sunset, describing
temperature measurement
technique 19 p3229 A67-35246

Rocket observations of visible and UV
dayglow including emission rates and
electron density and
temperature 19 p3221 A67-35277

Microwave refraction technique for
determining electron density profiles in
transient plasma column 19 p3295 A67-35517

Attachment coefficient and transport
velocity in nighttime F region from
backscatter N-h profiles, determining loss
term integration 20 p3426 A67-36287

Phase velocity and attenuation of
audiofrequency electromagnetic waves to
derive electron density
profiles 20 p3426 A67-36288

Oblique incidence millimeter wave
technique using ray theory for measuring
collisionless plasma electron density
profile 20 p3496 A67-36311

Energetic electrons in Van Allen radiation
belt through satellite measurements, giving
intensity maps, energy spectra and pitch
angle distributions 20 p3517 A67-36371

Ionosphere information via rocket and
satellite measurements covering ion
temperatures and concentration, electron
content variation, etc 20 p3430 A67-36907

Radial profiles of carrier density and
energy in diffusion controlled
plasma 20 p3501 A67-37239

Gemini spacecraft antennas performance
during reentry into ionized medium,
discussing electron concentration profiles,
nonearth atmosphere extrapolation and
antenna breakdown effect 21 p3591 A67-38210

Plasma spatial electron density
distribution from refraction of microwave
beams with several frequency
components 21 p3670 A67-38689

Plasma rotation in MPD arc measured for
electric and magnetic field distribution and
current and electron density distribution
[AIAA PAPER 67-655] 21 p3689 A67-38691

Axial electron density profile in weakly
ionized seeded argon plasma expanding
through supersonic nozzle determined
experimentally using microwave
interferometer
[AIAA PAPER 67-704] 21 p3672 A67-38731

Smith gyrofrequency model for
determination of vertical electron
concentration distribution in magnetosphere,
using whistling atmospheric
data 21 p3621 A67-39022

Nighttime E region electron concentration
profile valley structure variations for quiet
and disturbed geomagnetic
activity 22 p3791 A67-39814

Effective recombination coefficient in
upper-E and F-1 layers at sunset from
rocketborne gyroplasma probe measurements
of electron density
profile 22 p3793 A67-40044

Star Fish high altitude nuclear explosion
effect on electron loss rate in F-2
region 22 p3793 A67-40082

Radial electron density profile and critical
longitudinal magnetic field for helical
current convective instability in hollow
plasma column via Langmuir probe
measurements 22 p3853 A67-40234

Diurnal, latitudinal and seasonal variations
of midlatitude topside ionosphere electron
density profiles and plasma scale heights
calculated from Alouette I
ionograms 23 p3994 A67-40775

Ionospheric absorption from unabsorbed
cosmic radio noise intensity, discussing
electron density and collision frequency
profiles 23 p3994 A67-40778

Ionospheric refractive irregularities and
traveling disturbances from Alouette I
satellite data, calculating electron density
profiles using lamination
method 23 p3994 A67-40780

Wave propagation in random plasma
medium with inhomogeneous parabolic
electron density profile background for

ionospheric propagation applications 23 p3974 A67-41199
 Secondary temperature resonances in magnetized plasma slab with nonsymmetric inhomogeneous density profile, noting spectrum degeneracy in symmetric nonuniform profile 23 p4034 A67-41359
 Absolute measurement of Ar II transition probabilities using tungsten ribbon lamp as calibration standard 24 p4194 A67-41888

ELECTRON DETECTOR

Secondary electron detector for electronic microcircuits bombarded by electron beam used to observe potential distribution in junction breakdown 15 p2453 A67-30065
 Electron beam detectors employing CdS single crystals, considering procedure for obtaining crystals characterized by high sensitivity to electron fluxes 22 p3798 A67-39568
 Electron multiplier detection efficiency for positive ions determined as function of incoming ion energy, velocity and degree of ionization 23 p4000 A67-41219

ELECTRON DIFFRACTION

Low energy electron diffraction study of interaction of thin deposit of amorphous boron with tungsten single crystal surfaces 01 p0093 A67-10205

Epitaxial temperature for Si films vacuum deposited on silicon as function of substrate crystallographic orientation observed by low energy electron diffraction patterns 01 p0132 A67-10372

Electron diffraction structural studies of lead bismuth selenide 01 p0136 A67-11009

Radial distribution analysis of films of bismuth and gallium prepared by low temperature condensation for electron diffraction tests 01 p0137 A67-11060

Radial distribution analysis of films of Pb-12 percent Bi and beryllium in metastable phases prepared by low temperature condensation for electron diffraction tests 01 p0137 A67-11061

Basic problems of thin film physics - International Conference, Clausthal-Goettingen, West Germany, September 1965 02 p0281 A67-11701

Vacuum deposited metal film structure analyzed over wide temperature range, using electron diffraction and electron microscopy techniques 02 p0285 A67-11705

Low energy electron diffraction techniques for niobium /110/ surface, noting argon ion bombardment 02 p0257 A67-12729

Epitaxial growth of SiC film on silicon substrate and electron diffraction analysis of crystal structure 04 p0675 A67-14762

Trivalent neodymium doped glass laser with internal imperfections due to optical pumping examined via optical metallography, transmission electron microscopy and electron diffraction techniques 04 p0632 A67-14927

Electron diffraction scanner structural analysis of Ta and Mo very thin film growth 04 p0677 A67-15101

Electron diffraction patterns for GaP semiconducting thin films deposited on indium oxide substrates, determining structure as function of film thickness 04 p0686 A67-15970

Iron and chromium films prepared at 4 degrees K analyzed by radial distribution, showing electron diffraction patterns of amorphous state 05 p0866 A67-16976

Structural changes in epitaxial CdS films grown on rock salt, mica and silver substrates analyzed by electron diffraction at various temperatures and values of electric field 06 p1047 A67-17599

Lattice constant of thin silicon specimens determined using electron diffraction techniques 09 p1553 A67-21881

Surface and volume diffusion in thin films of system Ag-Se investigated by electron diffraction and microscopic studies 12 p1979 A67-25179

InAs epitaxial layers grown on GaAs substrate investigated via sandwich method and electron diffraction 12 p1980 A67-25201

YIG epitaxial growth condition on YAG and GdIG on YAG identified by X-ray, electron diffraction, microprobe and magneto-optic studies 15 p2539 A67-29824

Vacuum deposited amorphous and semicrystalline gallium phosphide film properties analyzed by electron diffraction 16 p2729 A67-31065

Tungsten-carbon phase relations from DTA, X-ray and electron diffraction measurements noting disordered, ordered hexagonal and orthorhombic modifications 18 p2692 A67-31599

Structure of Ge-Sn thin films vacuum deposited on glass substrates analyzed by electron diffraction methods 17 p2920 A67-32891

Fractional order peaks in low energy electron diffraction /LEED/ patterns from single crystal metal surfaces 19 p3246 A67-35783

Surface bombardment damage on molybdenum and tungsten crystals by inert gas ions 19 p3246 A67-35784

Low energy electron diffraction /LEED/ observations of interaction of tungsten surface with adsorbates 19 p3246 A67-35785

Adsorption of oxygen on tungsten surface, discussing electron diffraction 19 p3246 A67-35786

Structures of glow discharge and evaporated silicon oxide films determined by measuring intensity of electron wave scattering at large angles, describing measurement method 21 p3687 A67-39139

Selected-area small angle electron diffraction using double-condenser electron microscope, noting high resolution power 22 p3798 A67-39561

ELECTRON DIFFUSION

Diffusion and lifetime of plasma charged particles in magnetic field covering instability, contraction, decay, recombination, etc 01 p0123 A67-10389

Abnormal diffusion of base dopant impurities in shallow double-diffused structures in silicon, noting cooperative diffusion in enhanced or retarded penetration of base region 02 p0298 A67-11877

Stationary waves and nonstationary multibeam flows in plasma with arbitrary electron velocity distribution 03 p0486 A67-14198

Power spectrum of electromagnetic wave incoherently diffused by ionospheric electrons 04 p0571 A67-14896

Effective diffusive scattering cross section of electrons in He and Ar plasma with K vapor additions and in pure K, based on DC plasma conductivity and microwave generator Q-factor 04 p0673 A67-15972

Effective electron and ion diffusion coefficients measured for positive magnetic field gradients show reduced plasma diffusion 08 p1384 A67-21400

Anomalous diffusion arising from drift instability in collision-free equilibrium plasma cylinder 08 p1386 A67-21440

Diffusion effect on hole mobility in base of semiconductor device with p-n-p-n structure 11 p1765 A67-24480

Semiconductor junction devices analyzed for diffusion and electric field currents in bulk regions 11 p1849 A67-24904

Short circuit current measuring technique and results of electron diffusion lengths in diffused p type and holes in uniformly doped n type GaAs 11 p1850 A67-24912

Electron and ionic temperatures from incoherent diffusion spectra, noting dependence on height and permanent thermodynamic equilibrium below 130 km 12 p1931 A67-25108

Velocity space diffusion coefficient of electrons in thermal radiation field, using Hamilton-Jacobi theory 12 p1969 A67-25192

Stability of self-gravitating two-fluid infinite plasma cylinder model in axial magnetic field 13 p2163 A67-28285

Relativistic-electron diffusion wave in outer radiation belt recorded by device mounted on Cosmos XLI satellite in high geomagnetic latitudes 13 p2191 A67-28545

Total resistance of p-n diode calculated assuming high injection levels in base and moderate frequencies 14 p2286 A67-28530

Stationary waves and nonstationary multibeam flows in plasma with arbitrary electron velocity distribution 14 p2360 A67-28543

Electron thermal diffusivity in room temperature neon afterglow plasma measured using Tonks-Dattner resonance, noting independence of electron density 15 p2532 A67-30381

Thermal conductivity of group of molten and solid chalcogenides at various temperatures, estimating heat transfer

mechanism role 16 p2731 A67-31388

Nonlinear and second order thermal diffusion of electrons in ionized gas, using kinetic theory 18 p3083 A67-34401

Time variations of electron intensity in outer radiation belt observed by satellites, studying electron radial diffusion and drift velocity 19 p3313 A67-35257

Electron beam method for measuring resistivity variation in germanium semiconductors, calculating diffusion lengths 21 p3679 A67-38254

Total resistance of p-n diode calculated assuming high injection levels in base and moderate frequencies 23 p3980 A67-40937

ELECTRON DISTRIBUTION

Thermodynamics of electronic carrier populations in pure or doped dissociable binary semiconductor 01 p0130 A67-10198

Earth radiation belt, particle motion and magnetic cavity 01 p0143 A67-10254

Intensities of L, M and N X-ray spectra for wavelengths in region from 2 to 85 angstroms 01 p0116 A67-10690

Electronic and molecular radial distribution functions for liquid carbon tetrafluoride using X-ray diffraction, determining orientational effects of carbon tetrachloride and temperature dependency 01 p0117 A67-10885

Azimuthal asymmetry in distribution of shower particles around shower axis, using Geiger-Muller counter telescopes 01 p0145 A67-11230

Plasma probe in thermal emission converter with high cesium vapor, noting parameters of diffusion, electron concentration, etc 02 p0184 A67-12468

Random phase approximation for plasma, establishing perturbed electron distribution in oscillating electric field 02 p0276 A67-12557

Unstable transverse waves in anisotropic multicomponent plasma, establishing stability criteria, noting role of electron distribution 02 p0276 A67-12562

Mean electron concentration in SHF helium discharge determined as function of discharge power and pressure 02 p0277 A67-12616

Satellite measurement of behavior of high latitude energetic electron trapping boundary, noting geomagnetic storm effects 03 p0410 A67-12951

Electron velocity distribution equation extended to small wave numbers for electron-ion plasma 03 p0483 A67-13914

Electron cloud-like distribution in ionosphere shown from phase measurements of 162 and 324 mc emissions of Transit and Anna- satellites

[RASSA PAPER 1-10-135] Spatial distribution of energetic electrons in geomagnetic tail by analyzing counting rates from solid state detector on IMP I satellite 04 p0692 A67-14953

Electron temperature and concentration in cesium plasma in low voltage arc measured, using double probe method 04 p0666 A67-15182

Collisionless shock wave excitation in plasma, determining shock front thickness 04 p0666 A67-15187

Quantum oscillations of Hall effect and longitudinal and transverse reluctance in n-indium antimonide, noting spin splitting and temperature and electron concentration effect on oscillation maximum 05 p0861 A67-16394

Current-controlled NDR, electron-hole generation and switching to higher current lower voltage state in GaAs 05 p0870 A67-17275

Dead time corrections to photocount distributions using time interval probability density of counts, noting application to laser light 06 p1009 A67-17652

Physical and chemical behavior of elements and chemical compounds, considering electron configurations, using condensed-state atom model 06 p1035 A67-17843

Physical properties of transition elements, alloys and compounds in terms of stable electron configurations, using Samsonov theory 06 p1035 A67-17844

Particle microhardness and microbrittleness measured in powdered refractory compounds, noting relation to electron configuration 06 p1015 A67-17846

Reaction rates controlling densities of ions

and electrons in F region determined so that calculated ion and electron distribution may agree with rocket observations 06 p0996 A67-18430

Retardation energy distribution of ions and electrons in hydrogen 06 p1037 A67-18762

Boltzmann equation for GaAs, noting coupling constant scattering between low and high mass valleys 06 p1067 A67-18963

Electron concentration inhomogeneities during traveling gravity wave propagation through F layer 07 p1178 A67-19809

Evening micropulsation events with rising midfrequency characteristics, discussing possible source mechanisms 07 p1182 A67-19947

Ionospheric stabilization of interchange mode calculation applied to electron debris of Star Fish event, noting role of ionospheric current 07 p1182 A67-19948

Infinite plate consisting of monopolar semiconductor of given thickness under effect of electric field results in change in galvanomagnetic, piezoresistance and optical properties 08 p1367 A67-20416

Field intensities and electron distribution function in hollow cathode, graphs show potential distribution along cathode axis 08 p1358 A67-20851

Magnetized plasma oscillations for arbitrary initial distributions of electrons and ions, obtaining dispersion equation in fifth degree 09 p1550 A67-22617

Coulomb interaction influence upon electron distribution in radiation belts at low altitudes in magnetic anomaly region 10 p1702 A67-23299

Knudsen low voltage discharge with hot cathode, determining electron distribution, velocity profiles, V-I characteristics, etc 11 p1831 A67-24020

RF energy absorption by plasma column surrounded by periodic coupling structure, noting similarities with Landau damping and measurements of non-Maxwellian distributions 11 p1838 A67-24402

Electrostatic separation probe to measure electronic velocity distribution function, showing evolution of distribution function relationship to plasma oscillation 11 p1789 A67-24409

Electron distribution of oxygen grown GaAs crystals after heat treatment, showing profiles due to silicon contamination 11 p1848 A67-24740

Interaction of plasma oscillation with electrons with positive distribution function, noting oscillation amplitude relation to function deformation 11 p1840 A67-24766

Electrostatic oscillations in electron plasma, noting effect of external electric field on electron velocity distribution 11 p1848 A67-24868

Fokker-Planck equation for geomagnetically trapped electron distribution as function of longitude, time, energy and mirror-point field intensity 12 p1995 A67-25772

Mean electron concentration in SHF helium discharge determined as function of discharge power and pressure 13 p2170 A67-27372

Coulomb interaction effect on time dependent variations of electron distributions in Van Allen belt, using kinetic equation 14 p2378 A67-27918

Autoelectric emission in superconductors near transition point noting variation with total field energy and normal component 14 p2370 A67-28673

Rocket soundings of electron angular distributions during auroral substorms, noting effects of anisotropy, intensity variations, etc 15 p2473 A67-29187

Solution of Boltzmann and rate equations for electron distribution function and state populations in nonequilibrium MHD plasmas 16 p2710 A67-30519

Heating of ions in current carrying nonisothermal plasma deriving noise spectral density and electron and ion distribution functions 16 p2715 A67-31047

Millimeter wave resonant interferometer capable of measuring spatial distribution of electrons in low density transient plasma column subject to perturbation 16 p2875 A67-31263

Electron velocity distribution function in nonequilibrium plasma having spatial distribution governed by electron-electron

and inelastic collisions 16 p2723 A67-31768

Semitransparency range of sporadic E layer as solar radiation function, noting diurnal and seasonal variations 16 p2669 A67-31904

Two peaks in emission from low pressure helium or neon discharge simulating plasma slab with second peak corresponding to plasma cut-off frequency 17 p2901 A67-32369

Synchrotron radiation spectrum of self-absorbed radio sources for various electron distributions 17 p2947 A67-32755

Analysis of flame effects on measured electromagnetic propagation data for plume shape, plume electron density distribution and signal attenuation 19 p3344 A67-34819

Electron distribution function in plasma determined using electrostatic separation probe 19 p3267 A67-34947

Statistics of electron avalanche generating secondary effect at cathode through photon emission, obtaining excited molecule distribution 19 p3265 A67-35087

Electrical conductivity of weakly turbulent plasma calculated by behavior of electron distribution function 19 p3287 A67-35354

Electron distribution function of homogeneous imperfect Lorentz plasma disturbed by electric field 19 p3295 A67-35418

Approximate electron radial functions for uniformly charged nucleus /UCN/ used in analyzing boron 12 and nitrogen 12 beta decay spectra 20 p3488 A67-36915

Physical and chemical behavior of elements and chemical compounds, considering electron configurations, using condensed-state atom model 20 p3490 A67-37585

Physical properties of transition elements, alloys and compounds in terms of stable electron configurations, using Samsonov theory 20 p3490 A67-37586

Particle microhardness and microbrittleness measured in powdered refractory compounds, noting relation to electron configuration 20 p3471 A67-37588

Electron distribution function in steady state plasma with Coulomb and excitation collisions obtained analytically by simplifying Fokker-Planck terms 21 p3661 A67-37746

Fokker-Planck equation describing distribution of geomagnetically trapped electrons as function of longitude, time, energy and mirror-point field intensity 22 p3791 A67-39808

Optical signal detector performance, deriving outlet electron distribution function 24 p4166 A67-41797

ELECTRON EMISSION

SA EXO-ELECTRON EMISSION

SA PHOTOELECTRIC EMISSION

SA RADIO FREQUENCY DISCHARGE

Cooling effect of emission current on square wave modulated noise diode cathode 01 p0033 A67-10024

Space charge formation during flow of electric current in plasma moving under thermal emission of electrons 01 p0118 A67-10043

Field electron emission measurements for determination of work function of single crystal /110/ planes of tungsten 01 p0135 A67-10878

Secondary electron emission investigated by transmission and backscatter experiments with thin films, noting maximum exit depth dependence on energy 02 p0290 A67-11733

Angular distribution of secondary electrons emitted at reverse side of aluminum films 02 p0290 A67-11734

Electrical properties and electron emission of sandwich cathodes prepared in vacuum by vapor phase condensation, deriving transfer constant 02 p0294 A67-11761

External electron emission measurement from polished n-germanium and n-silicon surfaces 02 p0296 A67-11830

Full temperature range electron and ion emission from polycrystalline surfaces of Nb, Mo, Ta, W, Re, Os and Ir in cesium vapor 02 p0269 A67-11878

Implantation of Cs and Na ions into p-type silicon, effect on hot electron emission from p-n junction 02 p0299 A67-11897

Total energy of slow particle radio emission and real delta electron emission determined in extensive air showers 02 p0318 A67-12782

Continuous helium-neon laser used to obtain short intense light pulses and to

study kinetics of autophotocathodic emission of high resistivity silicon 03 p0436 A67-13142

Energy exchange localization to cathode emitting area during field electron emission, noting dependence on temperature, work function and applied field 03 p0472 A67-13329

Temperature effect on electron emission and stability of p-n junction using silicon and silicon carbide 03 p0494 A67-13487

Electron and ion emission from iridium in lithium vapor, noting surface ionization, work functions and experimental setup 04 p0660 A67-15108

Electromagnetic wave emission excited by electron stream over diffraction grating lying on boundary of semiminfinite anisotropic dielectric 05 p0766 A67-17163

Photoemission of electrons from conduction and valence bands of n-type degenerate Si into thermally grown silicon dioxide layers 05 p0870 A67-17195

Zr-coated tungsten cathode in reducing divergence of electron beam emission 06 p0968 A67-18091

Auger mechanism of recombination of electron emission from semiconductors and dielectrics 06 p1051 A67-18422

Hot electron emission from polar semiconductors with nonparabolic dispersion law, specifically qualitative effect of nonparabolicity and field on electron emission 06 p1052 A67-18423

Origin of solar type I noise storm radiation seen in cyclotron radiation from electron streams gyrating in spot field configurations in corona 07 p1244 A67-19852

Plasma mode work function measurement for studying thermionic emission from Hf, Th and Ti in Cs vapor at reservoir temperature of 414 degrees K 09 p1450 A67-22353

Work functions of monocrystalline and polycrystalline rhenium with electron emission current measured by copper collector 09 p1451 A67-22358

Perturbed zone stability of body immersed in equilibrium plasma during surface electron emission 10 p1683 A67-22782

Electron and ion emissions from hydrogen and helium UV glows in nighttime ionosphere 10 p1633 A67-23049

Solar cosmic ray event characteristics 1962-1966, solar minimum vs solar maximum 10 p1700 A67-23187

Heat flow through Langmuir sheath in presence of electron emission and application to limitation of energy loss rate by thermal conduction 11 p1828 A67-23894

Potential buildup on electron emitting ionospheric satellite, noting limitation on current emission by geomagnetic field 11 p1869 A67-23941

Electron synchrotron as source of extreme UV radiation noting design 11 p1788 A67-23965

Electron generator with oscillatory anode circuit nonlinear differential equation analyzed by linearizing, applying algorithm to obtain computer solution 13 p2144 A67-26393

Energy distribution of electrons emitted from alkali halide films on Mo substrates during positive helium and argon ion bombardment 13 p2177 A67-27074

Frequency multiplication of microwaves by field electron emission in superconducting cavity 14 p2278 A67-27787

Additional electron production in lower D layer due to solar radiation penetration 14 p2378 A67-27910

Delta coefficient of secondary emission of monocrystal of GaAs with various doping 14 p2367 A67-28516

Autoelectric emission in superconductors near transition point noting variation with total field energy and normal component 14 p2370 A67-28673

Point-contact germanium diode static characteristics with self-heating and image forces 14 p2289 A67-28825

Thermionic and electrical sorption properties of tungsten in alkali iodide vapors at high pressure 17 p2887 A67-32201

Thermionic work functions and electron emission S curves for contaminated copper surface in oxygen and cesium vapors, separate and mixed 17 p2887 A67-32203

Space charge formation during flow of electric current in plasma moving under thermal emission of

electrons 17 p2910 A67-33321
 Vacuum UV and X-ray lasers from electron ejection from inner shells of atoms through photoionization 18 p3060 A67-34015
 Structure of ion and electron currents axial emission from cathode measured as function of magnetic field 19 p3277 A67-35121
 Intensity 19 p3277 A67-35121
 Electron emission and adsorption of potassium on tungsten single crystal faces, noting work function values 20 p3504 A67-36165
 Factors influencing secondary electron emission produced by high energy molecular beam impact on metal surface 20 p3488 A67-36438
 Electron deflection instrument for measuring surface electric field strength 20 p3444 A67-36524
 Emission properties of vacuum spark plasma arising in production of high current electron beam 20 p3498 A67-36684
 Duo-emitter cesium thermionic converter, discussing electron and cesium ion emission to increase transport efficiency 21 p3571 A67-38610
 Flow equations for electron emitter placed in ion stream and transparent to ions, showing previous results due to incorrect choice of boundary conditions 22 p3843 A67-39262
 Total energy of slow particle radio emission and real delta electron emission determined in extensive air showers 22 p3878 A67-40284
 Injection and emission of hot electron in thin film tunnel diodes 23 p4039 A67-40885
 Field induced photoelectron emission /FPE/ from Si surface barrier diodes, discussing FPE measurement using xenon arc lamp and grating monochromator 23 p3980 A67-40890
 Energy distribution deviation of electrons emitted from plasma or solid via Maxwell distribution, deriving kinetic reflection coefficient in thermionic emission current expression 23 p4047 A67-41688
 Perturbed zone stability of body immersed in equilibrium plasma during surface electron emission 24 p4195 A67-42118
 Excitation time of electronic states on nitrogen molecule at high temperatures 24 p4194 A67-42890

ELECTRON ENERGY

Damage rate deduced from room temperature conductivity measurements on n-and p-type floating zone silicon samples subject to electron irradiation at energies from 0.3 to 2.0 mev 01 p0133 A67-10752
 Continued fraction in theory of electron energy for ground state of one-electron diatomic molecule near united atom 01 p0118 A67-10886
 Cosmic ray electrons with energies above 12 gev, constructing differential energy spectrum for deduction of universal black body radiation 01 p0145 A67-10921
 Trapped particle acceleration by magnetic fluctuation produced by ionospheric currents derived from observations of sharp energy groups of high energy electrons 03 p0409 A67-12942
 Electron-hole pair energy in CdS and CdSe single crystals 03 p0490 A67-13155
 Electron-hole pair separation energy in CdS single crystal during 5 to 50 kev electron bombardment 03 p0490 A67-13160
 Adiabatic harmonic unitary transformations and relation between electron trapping energy and normal lattice modes associated with F center ground state 03 p0495 A67-13515
 Lower bound electronic energy calculations for positive H, using methods of truncated Hamiltonians and of Temple and Kato 03 p0469 A67-13943
 Inverse Compton effect in causing energy loss of electrons in quasi-stellar objects 03 p0508 A67-14325
 Rocket measurement of secondary electron energy distribution in aurora, employing 180 degree electrostatic deflection analyzer 03 p0418 A67-14357
 Pressure dependence of mean electron energy of plasma emerging from anode aperture of duoplasmatron ion source 04 p0663 A67-14768
 Criterion for deciding when effect of perturbation of electron-energy distribution in plasma by probe can be neglected 04 p0665 A67-15112

Plasma injected into magnetic trap with aid of conical theta pinch investigated to determine ion and electron energy, lifetime and charged particle concentration variation 04 p0668 A67-15279
 Galvanomagnetic effect of anisotropic electron energy spectrum on acoustical branch perturbation spectrum of system of electrons and ions in homogeneous magnetic field 04 p0680 A67-15289
 Absorption spectra of Te, Sn, Pb, PbTe and SnTe at various energy ranges, noting role of wave functions involved in absorption by d-electrons 04 p0681 A67-15295
 Electron energy spectrum for alloyed semiconductors, determining state densities via Thomas-Fermi statistical method 04 p0681 A67-15296
 Generation of dense electron beams of energy half-width including tightly collimated beams of very low energy, space charge effects in deflectors, etc 04 p0623 A67-15323
 Thermalization of cathodic electron flux by Langmuir oscillations in cesium arc plasma 04 p0673 A67-15971
 Energy loss of cosmic electron in interstellar space due to ionization, bremsstrahlung and Compton effect 05 p0878 A67-16095
 Spectral indices of radio galaxies and quasi-stellar sources explained by relativistic electron injection into magnetic field by recurring blasts 05 p0891 A67-16400
 Electron energy quantization phenomenon in thin film studied by using dielectric barrier sandwiched between semiconductor films of same conductivity type 05 p0865 A67-16966
 Substituent effects on unimolecular ion decomposition reactions, noting role of Hammett equation and electron energies 06 p0954 A67-17568
 Problems in using Langmuir probes in ionized medium for measuring electron and ion energy density, temperature and distribution 06 p1000 A67-17590
 Optical phonon production, showing existence of electric field strength range at low temperature scattering in which phonon emission results in electron stoppage 06 p1010 A67-17884
 Weakly ionized gas flows about electrically biased bodies under effects of compressibility and electron energy [AIAA PAPER 67-100] 06 p1042 A67-18471
 Error due to electron thermal energy fluctuations in mean electron temperature measurement by line intensity ratio 06 p1042 A67-18540
 Contact effects in degenerate semiconductors at low temperature based on Hall study of tunnel junctions 06 p1069 A67-18976
 Electron energy spectra analyzed in earth magnetosphere using OGO 3, noting relation to radial distance 07 p1244 A67-19926
 High energy primary electrons and universal body radiation 07 p1246 A67-20227
 Growth rate along whistler path for waves propagating at angle to geomagnetic field 08 p1328 A67-21463
 Shock tube studies of magnetically induced nonequilibrium ionization in potassium-seeded argon plasma, noting electrical conductivity, current density, wall potential, Soule dissipation and radiation loss 09 p1540 A67-21788
 Impact ionization in ionic semiconductors for arbitrary temperatures and electric field intensities 09 p1554 A67-21971
 Interband transitions and plasmon excitation in calcium fluoride, discussing energy loss 09 p1558 A67-22585
 Electron-hole pair energy in CdS and CdSe single crystals 10 p1690 A67-23103
 Electron-hole pair separation energy in CdS single crystal during 5 to 50 kev electron bombardment 10 p1690 A67-23107
 Energetic solar particle effect on ionosphere, discussing signal phase, amplitude propagation and attenuation 10 p1637 A67-23192
 Electromagnetic propagation in semiconductor with account of nonlinear effects such as skin effects arising from electron heating by field 10 p1694 A67-23592
 Double shutter drift tube for measuring electron drift velocities and momentum transfer cross sections in methane, ethane, ethylene, etc 11 p1824 A67-24994

Optically excited electrons of X minima in gallium arsenide 11 p1803 A67-24998
 Electronic Raman scattering from phosphorus donors and boron acceptor impurities in Si, noting importance of interband transitions 11 p1851 A67-24999
 Electron temperature vs plasma cell power input measured, determining electron energy loss factor for hot diatomic gases in electric field 12 p1973 A67-25398
 Energy distribution of electron tunneling through metal-insulator-metal diode noting dependence on temperature, film thickness and voltage 12 p1982 A67-25449
 Increase in mean electron energy shown to be factor leading to plasma stratification 14 p2353 A67-27756
 Thermionic converter acceleration plate and excessive current flow effects, noting collector and cathode surface secondary electron removal, determining cut-off characteristic form 14 p2246 A67-27766
 Nonstationary disturbance effect on electron producing bound s-state during slow collision of atoms 14 p2352 A67-29073
 Atmospheric electron energy spectrum in range 70-2000 mev measured, using scintillation telescope with gas Cerenkov detector and lead glass total energy spectrometer 15 p2475 A67-29615
 Spectroscopic techniques for plasma parameter measurements in high temperature range, discussing methods employed and experimental setups 15 p2533 A67-30424
 Electrical conductivity and electron energy balance in nonequilibrium plasma calculated over wide range of conditions on basis of ionization theory 16 p2709 A67-30516
 Upper atmosphere photoelectric processes contributing to low energy electron content of magnetosphere 16 p2664 A67-30973
 Transport coefficients calculated from adiabatic excitation transfer in atomic gases 16 p2661 A67-31222
 Internal conversion electron spectrum for samarium 155 to europium 155 transmutation, noting multipolarities and new lines 16 p2733 A67-31706
 Ion-molecular reactions of hydrogen with inert gases caused by low energy electrons in low temperature plasmas, considering energy level populations, reaction cross sections, etc 17 p2806 A67-32141
 Energy level shifts due to atom confinement by conducting walls 17 p2888 A67-32390
 Local electronic energy balance formulation, including radiative transport effect in nonuniform seeded plasma, described by two-temperature model 17 p2906 A67-33010
 Cross sections for electron capture by protons measured for various energies in nitrogen, argon and helium 17 p2889 A67-33227
 Impact ionization in ionic semiconductors for arbitrary temperatures and electric field intensities 17 p2923 A67-33308
 Energy loss factors for slow electrons in hot gases determined by measuring electron temperature variation with HF electric field power 17 p2890 A67-33367
 High kinetic energy electrons associated with solar flares, noting prompt and delayed types 17 p2940 A67-33401
 Negative glow diffusion model evaluated via generation function determined by discharge voltage and dependence of reduced length of cathode fall 18 p3085 A67-33668
 Anisotropy of electron energy distribution measurement in electron cyclotron-resonance plasma using diamagnetic loop 18 p3093 A67-34756
 Velocity distribution function in positive column plasma and implications for electron energy transfer mechanism on microscopic scale 19 p3267 A67-34948
 Low-energy electron collisions and interactions with atoms and molecules, discussing vibrational excitation, ion formation, ionization cross section, etc 19 p3264 A67-35068
 Electron energy distribution and thermalization measurement in Langmuir mode discharge in plasmas, using electron energy spectrometer 19 p3274 A67-35105
 Plasma bunches-microwave interaction showing electron energy and plasma ions

velocity increase 19 p3291 A67-35384
Cathode study using electron images of recording storage tube 19 p3197 A67-35813
Energetic electrons in Van Allen radiation belt through satellite measurements, giving intensity maps, energy spectra and pitch angle distributions 20 p3517 A67-36371
Second derivative of two-probe current measurement method for determining electron energy distribution in gas discharge, noting low sensitivity to noise 20 p3498 A67-36687
Dayglow photoelectron excitation rate from electron energy loss calculations, with energy transfer functions calculated from photoelectrons produced by UV solar radiation 20 p3434 A67-37421
Laser population inversion using Fabrikant method, analyzing electron energy distribution in hollow cathode discharge 21 p3638 A67-37940
Superconducting bismuth investigated using tunnel effect method to measure electron energy spectrum gap and phonon spectrum distribution 21 p3685 A67-38801
Electron energy loss calculations for nonnormal incidence in thin dielectric foil, with excitation probabilities and dispersion relations for bulk and surface plasmons 21 p3686 A67-39135
Doubly differential cross section for ejected secondary electrons energy and angular distribution calculated from He by fast protons bombardment 22 p3839 A67-39201
Electron affinity of helium measured by analyzing energy of electrons photodetached from negative helium ions beam passing through laser electromagnetic field 22 p3815 A67-39614
Outer Van Allen radiation zone intensity maximum position dependence on electron energy and magnetic activity, noting relation to diffusion theory 22 p3870 A67-39620
Electron energy band structure of semiconductor films determined by analysis of structural symmetry of germanium and silicon samples 22 p3861 A67-39919
CdTe photoemission absolute energies determined by correlating electron energy distribution structure with structure in optical data 22 p3862 A67-40001
Primary cosmic radiation electron component studies through differential energy spectrum observations, considering confinement regions and black body radiation at 3 degrees K 22 p3874 A67-40239
Temperature of metal surface irradiated by giant pulse laser beam by measuring energy of emitted thermal ions 23 p4015 A67-41035
Electron multiplier detection efficiency for positive ions determined as function of incoming ion energy, velocity and degree of ionization 23 p4000 A67-41219
Electron emission models for evaluation of charge distribution and total energy of metal-gas interface, noting role of quantum mechanical corrections 24 p4202 A67-42087
Electron photon cascades in lead scintillator devices investigated using Nagel Monte Carlo calculations for energies between 100 and 440 Mev 24 p4191 A67-42439
Energy loss of cosmic electron in interstellar space due to ionization, bremsstrahlung and Compton effect 24 p4213 A67-42771
Quantitative analysis of negative excess of electrons in electromagnetic cascade showers on basis of energy distribution functions 24 p4221 A67-42871

ELECTRON FLUX

L-3 rocket observation of proton and electron fluxes at high altitudes, using solid state detectors 01 p0144 A67-10564
Luna X shielded gas-discharge counter data on soft corpuscular radiation, noting solar contribution to magnetospheric tail 01 p0145 A67-10907
Electron current and positive ion current in flames measured by improved single-probe technique using grid and ring electrode 01 p0070 A67-11068
Stability of counterstreaming flow of electrons and ions in heavily biased diodes theoretically studied by space charge wave and Nyquist analysis 02 p0214 A67-11883
Radar observations of equatorial electrojet irregularities indicate reversal during

nighttime of daylight westward traveling electrons stream 03 p0408 A67-12837
Instability of nonlinear stationary oscillations of potential in electron-ion flows useful in distribution functions of ions and electrons 03 p0470 A67-12935
400-kev electrons precipitation in auroral zone measured with solid state detector mounted on polar satellite 03 p0410 A67-12952
Dispersion equation for interaction of helical flux of relativistic electrons with wave field of rectangular guide 03 p0367 A67-13089
Space and time characteristics of electron fluxes penetrating into terrestrial atmosphere in auroral zone, based on riometer measurements 05 p0879 A67-16101
Klystron with broad electron flux and excited traveling and standing electromagnetic waves, analyzing electron grouping 05 p0771 A67-16356
Vertical flux and energy spectra of secondary gamma rays and electrons in upper atmosphere 07 p1242 A67-19621
Formation mechanism of ionospheric narrow sporadic E layers by high energy electron fluxes captured by geomagnetic field 07 p1179 A67-19835
Satellite observations of energetic trapped electrons, August 1964 08 p1379 A67-21484
Electron flux measurement during visible aurora, using high resolution rocketborne spectrometer 09 p1491 A67-22022
Auroral zone irregularity correlated with perturbations in outer radiation belt, noting simultaneous displacement of boundary zone of perturbations 10 p1699 A67-22784
Rocket measurements of electron fluxes in upper atmosphere of middle latitude at altitudes of 200-500 km 10 p1701 A67-23219
Energy spectrum of primary electron flux and brightness of auroral light measured by rockets in active auroras used to derive electron production rate 10 p1650 A67-23306
Electron component of primary cosmic radiation 11 p1856 A67-24104
Electron spectra, pitch angle distributions and total ionization measured throughout radiation belts by satellite magnetic spectrometer and integrating ionization chamber 12 p1997 A67-25807
High intensity runaway electron fluxes accelerated by external field in toroidal plasma discharge, noting pressure effect 13 p2162 A67-26270
Satellite measurements of electron flux and electron energy spectra in inner radiation belt 13 p2191 A67-26324
Increment of constant HF electron flux in resonance probe determined for case of large constant potential, noting role of plasma 13 p2119 A67-26559
Solar flare electron propagation in interplanetary space 13 p2194 A67-27251
Corpuscular emission role in formation of lower ionosphere 13 p2194 A67-27329
Long term measurement of trapped-electron environment in narrow region of space at lower edge of inner radiation belt 14 p2380 A67-28051
Synchronous and cyclotron wave behavior of electron flux in resonator with transverse electric field varying sinusoidally along wave propagation direction 14 p2288 A67-28807
Primary cosmic ray electron flux and energy spectrum near solar minimum compared with nonthermal radio emission from high galactic latitudes 14 p2381 A67-28831
Fourier-Hermite solutions of Vlasov equations for electron motion against positive neutralizing background examined in linearized limit, noting Landau damping recovery 15 p2509 A67-29205
Oscillations of confined cylindrical plasma with hot electron current, obtaining dispersion relation for large Debye radius 15 p2531 A67-30072
Ultrasonic wave amplification by supersonic flux of drift electrons in sandwich structure of piezoelectric dielectric and semiconductor 15 p2542 A67-30245
Magnetospheric tail bursts of energetic electrons identified with auroral zone radiowave absorption 16 p2666 A67-31410
Photographic high atmosphere observations of hydroxyl and helium emission bands, determining solar UV radiation and electron flux 17 p2849 A67-32960

Two-stream instability in semiconductor InSb plasmas, noting collision conditions, surface space charge, wave growth, etc 17 p2921 A67-33052
Cosmic ray electrons energy spectrum and charge composition studies inadequacy due to insufficient statistics and electron flux contamination 17 p2938 A67-33198
Rocket observations of energy spectra of auroral electrons 18 p3034 A67-33591
Auroral rocket measurements of electron flux, electron and ion density, electron temperature and auroral brightness 18 p3034 A67-33593
Electron measurements near weak aurora during rocket flight 18 p3034 A67-33595
Electron precipitation data examined to determine whether electron behavior can be understood on basis of binary collisions with atmospheric constituents and guidance by geomagnetic field 18 p3035 A67-33599
Polar ionosphere by satellite-borne electron traps, measuring electron density, temperature, quasi-energetic electron flux, etc 19 p3215 A67-35174
Inner zone trapped electron flux measurements by satellite indicating natural environment emergence from Starfish remnants 19 p3216 A67-35186
Existence and stability conditions of several-quanta flux lines in type II superconductors 20 p3505 A67-36206
Superconductor resistive behavior as hole motion in flux lattice under peak effect influence 20 p3505 A67-36209
VLF radio noise during auroral display studied by ground and rocketborne receivers, suggesting emissions triggered by high energy electron fluxes 20 p3428 A67-36374
Electron flux and energy spectrum measurements near polar cap investigated for diurnal intensity variations 22 p3872 A67-39802
Auroral zone balloon measurement of 5 and 25 msec duration energetic electron burst fluxes 22 p3873 A67-39821
Connections between superconductivity and electromagnetic potentials, presenting model for flow of superconducting electrons and quantization of fluxoid 22 p3863 A67-40198
Computer calculation of 1 Mev electron flux and irradiation degradation of solar cell I-V curves for charged particle environment 23 p3940 A67-41514
Auroral zone irregularity correlated with perturbations in outer radiation belt, noting simultaneous displacement of boundary zone of perturbations 24 p4209 A67-42120
Klystron amplifier stability during double interaction in output circuit determined assuming zero HF potential and electron flow not bunched 24 p4129 A67-42193
Space and time characteristics of electron fluxes penetrating into terrestrial atmosphere in auroral zone based on riometer measurements 24 p4213 A67-42777

ELECTRON GAS

Dimensional effect in electric conductivity of semiconductors during heating of electric field when electron energy relaxation length exceeds mean free path 04 p0679 A67-15137
Magnetic field effect on velocity of electron drift produced by electrical field in dense plasma 04 p0671 A67-15580
Kinetic theory of quantum electron gas coupled to radiation field under uniform external magnetic field 04 p0672 A67-15770
Kinetic equations for homogeneous electron gas derived to all orders in plasma parameter lambda /reciprocal number of electrons per Debye sphere/ 08 p1363 A67-21394
Ion wave amplification in two-component plasma due to isothermal electron gas 08 p1365 A67-21414
Ionosphere as binary two-temperature gas and transfer coefficients for elastic collisions based on Boltzmann equation 10 p1640 A67-23220
Inhomogeneous gas of weakly coupled relativistic electrons, deriving kinetic equation for particle electromagnetic field system 11 p1782 A67-24781
Kinetic equation for electron gas in classical limit derived from quantum mechanical transport equation, using equilibrium analogy 11 p1844 A67-25076
Dimensional effect in electric conductivity of semiconductors during heating of electric

field when electron energy relaxation length exceeds mean free path 12 p1979 A67-25160

Polarized harmonic electromagnetic wave propagation in plane stratified isotropic plasma of cold lossless electron gas, resolving inconsistency near resonance region 12 p1978 A67-25944

Third order Vlasov equation solved for nonlinear plasma oscillations in classical nonrelativistic collisionless Maxwell distribution electron gas 13 p2162 A67-26283

Nonuniform absorption of gyro-resonant microwave energy by electron gas used to produce helical configuration in magnetoplasmas 13 p2163 A67-26289

Relaxation time for spatially homogeneous electron gas calculated by direct numerical integration of linearized Fokker-Planck equation 13 p2164 A67-26297

Matching factor for energy exchange in electromagnetic interaction between ionic and electronic gases in amplitude-amplitude ionospheric intermodulation 13 p2070 A67-27196

Motion equation for nonideal relativistic electron gas, reviewing hydrodynamics obtained from Landau equation 15 p2527 A67-29517

Electron correlations influence on plasma-broadened Lyman alpha line 15 p2520 A67-29679

Effective pair potential obtained for quantum electron gas to determine thermodynamic properties over large temperature and density range 15 p2533 A67-30383

Energy exchange between electron gas and molecular gas shown to depend on composition of latter, for application of nonequilibrium plasma 16 p2710 A67-30521

Second order conductivity tensor of isotropic electron gas theory, using thermodynamic Green functions 16 p2713 A67-30803

Heating of upper atmosphere electron gas by indirect Joule dissipation of reverse current in ambient electrons demonstrated for high fluxes 16 p2739 A67-31405

Auroral intensity ratio of green line of atomic oxygen and first negative band of nitrogen, showing rise in electron temperature above neutral particle temperature 16 p2666 A67-31413

Frequency tripling of electromagnetic waves passing through hot electron gas in semiconductors, deriving third harmonic amplitude for helical wave 16 p2628 A67-31500

Electron temperature measured in acetylene/oxygen mixture flame and found twice that of gas due to chemical energy transport to electron gas 17 p2968 A67-32151

Scattering and absorption of ultrashort coherent radiation pulses passing through electron gas applied to ionosphere 17 p2812 A67-32312

Nonlocal heating of electrons of daytime ionosphere taking account of displacement along geomagnetic field lines, comparing Dalgarno and Thomson probes 17 p2844 A67-32708

High pressure equations of state including electron gas correlation energy, giving density vs pressure curves for various elements 18 p3104 A67-34594

Continuous spectrum of eigenvalues related to Fokker-Planck collision integral 19 p3285 A67-35341

Rapid randomization phenomena in unstable plasma sac for Mach numbers close to unity attributed to electron interaction with trapped electroacoustic waves 22 p3844 A67-39357

Charged particle gas interaction with EM field noting electron gas collective oscillations, EM wave propagation in anisotropic plasma and applications 23 p4037 A67-40759

Vertical profile of concentration of atmospheric electron-ion gas flux under action of gravitational field 24 p4150 A67-42141

ELECTRON GUN

SA CATHODE RAY TUBE

Charged particle injection into magnetic traps through mirror, using annular electron gun 01 p0122 A67-10350

Electron gun producing helical electron beams with prescribed high transverse-to-longitudinal electron energy ratio 03 p0475 A67-13088

Cyclotron ion wave interaction with HF plasma oscillations measured, using vacuum chamber and electron gun 04 p0667 A67-15209

Electron beam rotation experiments on linear spiratron with M-type electron gun 05 p0776 A67-17169

Focusing of electron beam from low noise gun with different magnet systems 05 p0777 A67-17279

Design method for electron gun with specified anode shape 07 p1154 A67-19655

Magnetic field shaping for convergent confined flow electron guns to create design data to reduce trial and error work 09 p1478 A67-22256

Magnetically confined helical electron beams formed by two-anode electron guns, considering effect of space charge 11 p1784 A67-24466

Charged particle injection into magnetic traps through mirror, using annular electron gun 11 p1844 A67-25023

Control efficiency and perfect cut-off of beam current of controlled electron guns, noting focusing properties and variation in focusing with voltage 14 p2276 A67-27767

Electron lens with hyperbolic field configuration designed to focus or modulate electron lenses, noting hyperbolic application to electron guns 14 p2276 A67-27768

Numerical solutions of Poisson and motion equations for electron gun design, examining truncation error via perturbation theory 14 p2287 A67-28677

Cyclotron ion wave interaction with HF plasma oscillations measured, using vacuum chamber and electron gun 15 p2532 A67-30257

Ionizer with three-electrode electron gun, noting potential distribution between electrodes and ionization efficiency 18 p3080 A67-33722

Hydrogen plasmoids produced by pulsed two-cascade injectors, using electron guns for plasma ionization and acceleration 19 p3297 A67-35597

Electromagnetic wave generation and amplification extended from LF microwaves up to optical band 20 p3380 A67-36488

ELECTRON IMPACT

Electron impact induced transitions between principal quantum number levels in atomic hydrogen estimated via impact parameter method 01 p0124 A67-10780

Line profile in one-electron approximation compared with impact approximation 02 p0270 A67-12521

Charged particle collision as UV radiation source examined, using electron-excitation analytic cross section 04 p0660 A67-14698

Hydrogen molecule excitation by electron impact extended to D excited state, noting values for oscillator strength 04 p0662 A67-15767

Temperature effect on impact ionization coefficient in SIC semiconductor p-n junctions with reversed current in strong electric field 05 p0865 A67-16916

Small signal negative resistance and avalanche region of impact ionization avalanche transit time /IMPATT/ diodes, particularly Read diodes 05 p0777 A67-17319

Absolute cross section for dissociation of hydrogen ion by electron impact measured, using cross beam technique 09 p1535 A67-22377

Contribution of quasi-static electrons to broadening of hydrogen 2 line profile 10 p1704 A67-22884

Energetic metastable diatomic oxygen molecule excited by electron impact studied with high sensitivity molecular beam apparatus 10 p1682 A67-23386

Expression for electron contribution to Stark broadening, using impact approximation with Lewis or Debye cut-offs 11 p1823 A67-24491

Ionization probability of hydrogen atom by electron impact in terms of three-body problem of classical mechanics 14 p2351 A67-29072

Ion beam generation and applications, discussing duoplasmatron, RF source, contact ionization source and Penning discharge 15 p2488 A67-29756

Dissociation cross section of hydrogen molecule exchange excited by electron impact from ground to triplet state, using one-center wave functions 15 p2521 A67-30379

Temperature effect on impact ionization coefficient in SIC semiconductor p-n

junctions with reversed current in strong electric field 16 p2727 A67-30893

Secondary ion generation in flames by electron impact noting application of mass-spectrometry and hydrocarbon fuels analysis 16 p2780 A67-31520

Chemical reactions fluorescent and resonant scattering, electron impact and photodissociation from sunlight upon atmosphere 18 p3036 A67-33602

Angular distribution of products in electron impact dissociation of hydrogen molecule calculated following Born approximation for scattering amplitude 20 p3487 A67-36231

Transitions in neutral spectra observed in near IR wavelength region in noble gases 20 p3460 A67-36859

Absolute electron impact excitation cross section of 3914 angstrom band of positively ionized nitrogen molecule 20 p3450 A67-37104

Semiempirical electron impact cross sections for He from oscillator strengths, using Born approximation 20 p3489 A67-37416

Electron impact cross sections used to determine helium collision cross sections sets 20 p3489 A67-37417

Electron impact excitation and ionization cross sections data of molecular nitrogen synthesized using modified Born approximation 20 p3489 A67-37418

Inelastic electron impact cross sections for ionization and vibrational excitation of atmospheric molecular oxygen 20 p3489 A67-37419

Auroral transition radiation calculated from electron impact 20 p3433 A67-37420

Electron impact ionization cross sections and rate coefficients for atoms and ions of Hg, rare gas and alkali metal groups 21 p3660 A67-39098

Empirical formula for representation of cross sections for single ionization of atoms and ions from ground state by electron impact 24 p4194 A67-41890

ELECTRON INTENSITY

High energy electron intensity measurement beyond atmosphere with aid of proton I and II satellites, showing capture by geomagnetic field 05 p0878 A67-16091

Electron intensity measurement in primary cosmic radiation by high altitude balloons carrying telescope made of two plastic scintillation counters 05 p0878 A67-16097

Equilibrium concentrations for air water plasma at various temperatures tabulated for three densities, noting effect on electron concentration 05 p0850 A67-16131

Energy spectrum of electrons recorded by fluorescent screen indicators onboard Cosmos satellites, noting ratio of electron intensities 07 p1170 A67-19101

Correlation of time variations of proton and electron intensity of outer radiation belt and dependence on geomagnetic environment 07 p1243 A67-19828

Electron production time variations in D layer during solar activity 14 p2378 A67-27909

Pulsations in electron intensities in postbreakup aurora, noting possibility of distant processes affecting electrons 17 p2844 A67-32765

Inner zone electron intensity distribution model for solar activity minimum 19 p3219 A67-35238

Time variations of electron intensity in outer radiation belt observed by satellites, studying electron radial diffusion and drift velocity 19 p3313 A67-35257

High energy electron intensity measurement beyond atmosphere with aid of proton I and II satellites, showing capture by geomagnetic field 24 p4213 A67-42767

Electron intensity measurement in primary cosmic radiation by high altitude balloons carrying telescope made of two plastic scintillation counters 24 p4213 A67-42773

ELECTRON INTERACTION

SA PHOTON-ELECTRON INTERACTION

Resonance amplification of associated slightly attenuating electromagnetic and acoustic helicon waves by electron drift in semiconductors and semimetals 01 p0128 A67-10081

Time dependent perturbation theory applied to calculating probability field ionization as function of atom-metal separation 01 p0116 A67-10206

Vibrational force constants of nitrogen fluoride, using lone pair of electrons model 01 p0117 A67-10764

Shallow impurity states in semiconductor described by Green function method, considering effective-mass equation corrections 02 p0281 A67-11491

Plasma oscillation properties, excitation and attenuation in films of various thickness, noting electron excitation 02 p0290 A67-11736

Electronic interactions in silicon-silicon dioxide system lead to various distributions of electric charges 02 p0293 A67-11752

Ferromagnetic semiconductors with exchange interaction due to conduction electrons 02 p0296 A67-11826

Solar neutrino-electron interaction and use of boron-cycle solar neutrino fluxes to determine existence of neutrino and antineutrino scattering effects 02 p0317 A67-12776

Ionospheric properties and wave-electron interaction 03 p0405 A67-12801

Low energy electron-helium atom scattering, using formal optical potential in variational expression for scattering phase shifts 03 p0471 A67-13318

Excitonic effects in interband absorption of semiconductors noting electron-hole interaction, Coulomb interaction energy maxima and minima and scattering cross sections 04 p0676 A67-14926

Excited states in negative atomic oxygen ion, giving estimates of electron-atom interaction 04 p0661 A67-15764

Auroral hydrogen emission measurements and indications of proton or electron excitations 05 p0797 A67-16851

Superconductivity in degenerate semiconductors, applying Bardeen-Cooper-Schrieffer theory, calculating electron-electron interaction 06 p1069 A67-18979

Band structure effects and interacting electrons and phonons in superconductor, treating Dyson equations and various simplified models 07 p1235 A67-20133

Resonance amplification of associated slightly attenuating electromagnetic and acoustic helicon waves by electron drift in semiconductors and semimetals 08 p1371 A67-21458

Energy level structure of rare earth chelates, noting existence of isolated systems of optical electrons 09 p1512 A67-21921

Granular superconductor with thin insulating layer at boundary of each homogeneous superconductor grain, using isospin formulation of microscopic theory 10 p1687 A67-22763

Multiple-photon radiative transitions in strongly doped semiconductor, noting state density 10 p1694 A67-23652

Chandrasekhar dynamical friction theory for star in cluster adapted to Fokker-Plank electron in two-component plasma theory and including multiple encounters 10 p1711 A67-23790

Dependence of ion energy on irradiated laser power, discussing production of ions of two discrete energies 10 p1667 A67-23793

Cross sections for sticking electrons to spherical charged particles, considering Debye screening distance of Coulomb force field 12 p1968 A67-25750

Simple metal spin-density-wave state analyzed using electron-electron exchange interaction 12 p1985 A67-25849

Fast ions produced in interaction between escaping electrons and plasma 13 p2164 A67-26402

Microwave amplification by electron beam interaction with cesium plasma 13 p2166 A67-26726

Spin waves in two-band ferromagnetic metal assuming electron interaction via Coulomb potential 13 p2178 A67-27138

Angular correlation in helium atom with electron-electron interaction 13 p2161 A67-27182

Autoionization effects accompanying impairment of forbidden intercombination transfer in plasma due to atom collision with plasma electron 13 p2171 A67-27626

Energy level structure of rare earth chelates, noting existence of isolated systems of optical electrons 14 p2330 A67-28250

Second order phase transitions in ionic crystals caused by vibronic interaction analogous to Jahn-Teller effect in ideal crystals 16 p2726 A67-30813

Exchange interaction between f-electrons

and s-electrons in atomic shells of crystal lattice of rare earth metals, examining calculation methods for Hamiltonian of s-f exchange 16 p2733 A67-31730

Kinetic equation for chemical and electron processes in low temperature plasma flows 17 p2896 A67-32169

Multiple-photon radiative transitions in strongly doped semiconductor, noting state density 17 p2923 A67-33333

Renormalization theory and Compton scattering of electron interacting with monochromatic LF polarized light beam 17 p2870 A67-33365

Electron-interference experiment using laser light, discussing electron wave function phase change and electron interference pattern displacement 20 p3460 A67-36999

Small signal interaction impedance of bulk semiconductor amplifier with nonuniform doping profile, noting two-dimensional representation 21 p3588 A67-37818

Advances in electronics and electron physics, Volume 23 22 p3799 A67-39769

Solar neutrino-electron interaction and use of boron-cycle solar neutrino fluxes to determine existence of neutrino and antineutrino scattering effects 22 p3877 A67-40278

Fermi pressure shifts of highly excited states of atoms in gaseous medium due to electron particle interactions, discussing scattering contributions 23 p4029 A67-40958

Electron transport theory for energy below 10 Mev, reviewing interactions, scattering, thick targets, complex geometry and penetration in space environment [UCC/DSSD-267] 24 p4190 A67-41805

Cascade particles interaction functions with substance determined by inverse problem method 24 p4221 A67-42875

ELECTRON-ION RECOMBINATION

Electron-ion recombination process due to electron collision in plasma with capture electrons transferred to ground level 03 p0474 A67-12853

Screening effect on Coulomb interaction, electron-ion recombination and surface neutralization 03 p0473 A67-13512

Dissociative recombination coefficient of nitrosyl ion with electrons 04 p0567 A67-15765

Helium mono and divalent ion electron recombination coefficient determined as function of electron density and temperature 04 p0672 A67-15774

Electron-ion recombination behind shock waves in argon containing dilute lean mixtures of hydrocarbons and oxygen 09 p1457 A67-22024

Spatial distribution of electrons and ions in neutral plasma, considering charge density 09 p1548 A67-22352

Recombination processes determined from data of time dependence of spectral line intensities and number density in decay plasmas produced in neon and helium-neon mixtures 09 p1548 A67-22360

Recombination processes in decaying helium plasmas as indicated by time dependence of spectral line intensities and ion number density 09 p1548 A67-22361

Changes in electron concentration in lower ionosphere with temperature dependent effective recombination coefficient during transmission of pulse radio signals 10 p1630 A67-22791

Electron-ion recombination coefficients for atmospheric ions determined in laboratory and compared with ionospheric analysis 10 p1682 A67-23261

Nocturnal decline of ionospheric airglow 6300 angstrom line intensity due to diatomic oxygen ion-electron recombination 10 p1649 A67-23294

Coefficient for electron ion recombination during triple particle collision, using Boltzmann kinetic equations 14 p2363 A67-29077

Particle theory analysis of electromagnetic and electrostatic instabilities due to anisotropic velocity distributions 16 p2722 A67-31560

Gas pressure dependence of attachment and recombination coefficients for thermalized electrons in air and oxygen 17 p2893 A67-32139

Ionization outside equilibrium and relaxation of ionization in cesium seeded argon 17 p2894 A67-32152

Carbon dioxide ions with electrons

dissociative recombination measurements with microwave-afterglow differentially pumped quadrupole mass-spectrometer apparatus, noting Martian atmosphere model [SRCC-55] 17 p2888 A67-32826

Parametric coupling between ion and electron waves noting coefficients, growth rate amplification, etc 17 p2906 A67-33061

Excited state and steady state populations in high pressure plasma with heavy particle collisional ionization and electron-ion recombination 17 p2909 A67-33228

Interaction between ion and electron waves in plasma 18 p3089 A67-34186

Surface recombination velocities relationship in depletion, inversion and accumulation surface layers of p-type silicon, using ambipolar carrier transport formulation 18 p3104 A67-34593

Atomic collision processes in ionized gases, studying ambipolar diffusion, electron attachment, electron-ion recombination and Penning ionization by afterglow technique 19 p3264 A67-35070

Electron density decay curves in helium afterglows at high electron densities and gas pressure found controlled by recombination loss process 19 p3270 A67-35071

Ion layer formation in E region, assuming sinusoidal vertical motions and ion-electron recombination following attachment law 19 p3222 A67-35456

Electron-ion radiative recombination influence on time-dependent luminous intensity of various spectrum lines in cesium vapor 20 p3488 A67-36436

Parametric excitation in plasma located in oscillating electric field due to density gradient, showing predominance on electron-ion coupling 20 p3503 A67-37672

Ionization and recombination effects on MHD wave propagation through three-component magnetoplasma, deriving nonlinear motion equations 21 p3660 A67-37743

Current carrier recombination processes in pure, preheated and Cu-doped GaAs, studying temperature and concentration dependence of intrinsic and impurity photoconductivity 21 p3676 A67-37863

Electron-ion three-body recombination rate in nonequilibrium dense nitrogen plasma measured spectroscopically [AIAA PAPER 67-703] 21 p3672 A67-38730

Recombination centers in silicon transistor emitter-base junctions causing anomalous base current component studied via temperature dependence of forward characteristics 22 p3770 A67-39732

Changes in electron concentration in lower ionosphere with temperature dependent effective recombination coefficient during transmission of pulse radio signals 24 p4149 A67-42127

ELECTRON IONIZATION

Ionization cross sections of neutral atoms caused by electron impact with Maxwellian velocity distribution 02 p0269 A67-12486

Transport and ionization properties of molecular gases in transverse magnetic field, using ionization chamber 03 p0474 A67-14358

Spatial distributions of free electrons in near wakes of spheres in hypersonic flight [AIAA PAPER 66-55] 04 p0547 A67-14820

Electron induced ionization and displacement damage in n-p-n and p-n-p transistors at medium and low powers 04 p0588 A67-15706

Ionization cross sections of neutral atoms caused by electron impact with Maxwellian velocity distribution 10 p1682 A67-23354

Electron spectra, pitch angle distributions and total ionization measured throughout radiation belts by satellite magnetic spectrometer and integrating ionization chamber 12 p1997 A67-25807

Ionization threshold energy of electrons and holes in silicon 14 p2368 A67-28535

Gas stream discharge studied by using electromagnetic plasma gun to direct plasmoids toward beam 15 p2472 A67-29726

Experiments on equilibrium and nonequilibrium electrical conductivity of seeded combustion products and theory of nonequilibrium ionization and recombination 18 p3085 A67-33706

Quasi-one-dimensional nonequilibrium argon plasma flow equation, discussing kinetic model with atom-atom and electron-atom impact ionization 22 p3850 A67-39708

Plasma flow and generation in CO comet

due to electron-collisional ionization under influence of solar wind 22 p3885 A67-40081
 Ionization threshold energy of electrons and holes in silicon 23 p4040 A67-40942

ELECTRON MASS
 Optical reflection, transparency and Faraday effect for indium antimonide, calculating effective electron mass, relation between energy and wave number, etc 01 p0128 A67-10095
 Optical or inertial electron mass dependence on N-concentration in IR spectrum of n-type GaAs monocrystal with S, Se and Te impurities 03 p0490 A67-13161
 Extreme variations of electronic effective mass with temperature cannot lead to satisfactory explanation of specific heat anomaly in superconducting lead 04 p0676 A67-14934
 Comparison of experimentally obtained electron effective masses for high electron concentration in InSb and InAs 04 p0677 A67-14935
 Absorption measurements of 139-Gc microwaves for very high purity mercury telluride, deducing electron effective mass 06 p1047 A67-17653
 Electron effective mass in gallium arsenide as function of doping obtained from Faraday rotation measurements 06 p1061 A67-18921
 Quantum oscillations in magnetoresistance of n-type pure HgTe used to estimate electron effective mass and g value close to band edge 06 p1065 A67-18948
 Optical or inertial electron mass dependence on N-concentration in IR spectrum of n-type GaAs monocrystal with S, Se and Te impurities 10 p1690 A67-23108
 Quantum oscillation of magnetoresistivity in n-type mercury telluride crystals, obtaining electron mass 14 p2369 A67-28598
 Transverse and longitudinal electron effective masses for wurtzite type crystals 17 p2913 A67-32273

ELECTRON MICROSCOPE
 Coatings of nickel, chromium and Cu on SiC and aluminum oxide whiskers by electroforming and metallizing, using electron microscope 03 p0444 A67-13434
 Conductivity changes in thin layer of silicon oxide induced by electron beam of scanning electron microscope 04 p0682 A67-15318
 Scanning electron microscope used as conductive probe to measure depletion layer widening in silicon diode as function of applied voltage 04 p0584 A67-15483
 Scanning electron microscope used in emissive mode to quantitatively measure depletion layer widening in silicon mesa diode 04 p0584 A67-15484
 Localized breakdown in Ge mesa diodes due to inclusions 04 p0584 A67-15486
 Electron microscope study of plastic deformation mechanism of titanium alloy AT4 and fatigue strain mechanism in coarse grained specimens of alloy T-40 07 p1205 A67-19278
 Specific stacking fault energy of deformed fcc metals determined from electron microscope diffraction contrast of stacking fault dipoles 07 p1208 A67-19637
 Aluminum alloy with various metal additions analyzed for aging, using electron microscope 08 p1342 A67-20806
 Micrographs of thin Ti layers through electron microscope showing dislocation distribution 11 p1806 A67-24428
 Scanning microscope for studying Si p-n junctions by electron or ion bombardment 13 p2120 A67-27069
 Stroboscopic electron mirror microscope observations of Si p-n junctions in pulsed regime 13 p2120 A67-27070
 Scanning electron microscope observations of p-n junctions using small periodic bias voltages 13 p2177 A67-27072
 Electron microscope observations on matrix precipitation in beryllium 13 p2136 A67-27106
 Fabrication of small geometry planar bipolar transistors by using electron beam 13 p2084 A67-27574
 Microstructure of aluminum alloys analyzed for composition, fabrication and thermal treatment, using electron microscopy 14 p2334 A67-27803
 Electron beam probing of semiconductor materials and devices 15 p2450 A67-29813

High magnification microscopes for semiconductor research noting advantages of illumination system and light sources 21 p3630 A67-38895
 Planar diffused p-n junction profile geometry using scanning electron microscope and electron probe with computer calculations 22 p3855 A67-39360
 Selected-area small angle electron diffraction using double-condenser electron microscope, noting high resolution power 22 p3798 A67-39561
 Scanning electron microscope signal processing and application to electronic devices failures, processes variations, integrated circuits and thin film circuit continuity 22 p3774 A67-40411
 Twin lamellae in magnesium examined by electron microscopy reconfirms double twinning sequence 24 p4173 A67-42345
 Steel dislocation structure under adsorption fatigue investigated by electron microscope, discussing surface active medium effect 24 p4174 A67-42724

ELECTRON MICROSCOPY
 Electron microscopy study of fracture surface topography permitting identification of fine scale fracture surface features, relating them to fracture formation mechanisms [AIAA PAPER 66-814] 01 p0077 A67-10034
 Stacking faults in steam-oxidized silicon wafers annealed in vacuum at 800, 1000 and 1200 degrees C observed by chemical etching and transmission electron microscopy 01 p0126 A67-10052
 X-ray diffraction-Fourier series analysis and electron microscopy analysis of annealing effects on structural properties of cold worked dispersion-strengthened alloys 01 p0097 A67-10698
 Thermogravimetric analysis and electron microscopy of agglomeration and chemical instability of submicron refractory dispersoids in tungsten 01 p0097 A67-10699
 Crystal layer dislocation structure of cold rolled molybdenum foil investigated by electron microscopy 01 p0101 A67-10939
 Vacuum deposited metal film structure analyzed over wide temperature range, using electron diffraction and electron microscopy techniques 02 p0285 A67-17055
 Electron microscopy analysis of microinhomogeneities in commercial Si used in preparation of p-n junction devices 02 p0257 A67-12434
 Second breakdown in junction transistors examined, using scanning electron microscope 02 p0222 A67-12653
 Room temperature microhardness anisotropy, slip and twinning in molybdenum carbide single crystals noting orientation dependence, elastic modulus, electric resistivity and measurement techniques 03 p0441 A67-13254
 High temperature reaction between refractory whiskers of silicon nitride and Al and Ni, observing results by electron microscopy 03 p0445 A67-13528
 Atomic planes and positions in bulk thinned specimens of crystalline Ge determined, using electron microscopy 03 p0501 A67-14345
 Temperature dependence of migration of double positioning boundaries during growth of gold films inside electron microscope 04 p0675 A67-14924
 Trivalent neodymium doped glass laser with internal imperfections due to optical pumping examined via optical metallography, transmission electron microscopy and electron diffraction techniques 04 p0632 A67-14927
 Short and long range redistribution of solute in weld fusion zones of alloy systems through data from electron microprobe analyses 05 p0811 A67-16830
 Recrystallization and polygonization of pure and impure metals, noting role of vacancy supersaturation 05 p0830 A67-17311
 Electron microscopy analysis of dissolved hydrogen induced fracture in room temperature cantilever bend fatigue testing of dispersion strengthened aluminum-aluminum oxide alloy 06 p1013 A67-17796
 Transmission electron microscopy analysis of microstructural phase properties of Ti-8Al-1V-1Mo alloy after duplex and mill annealing treatments 06 p1013 A67-17797
 Transmission electron microscopy study of phase transformations of Ti-8Al-1Mo-1V

alloy 06 p1014 A67-17804
 Electron microscopic structure and lattice defects of martensite in commercially pure titanium 06 p1017 A67-17966
 Transformation twins in titanium, discussing relationship between twins and martensite crystal, using electron microscopy 06 p1017 A67-17967
 Low pressure physical adsorption and electron microscope study of surface of annealed pyrolytic graphite, using flash filament technique 06 p1020 A67-17988
 Ninnigerite composition and optical, physical and crystallographic properties 07 p1247 A67-19064
 Small additions of Y, La, Hf, V, Ti and Zr on structure of cleaved surfaces and viscosity of Mo cermet materials 07 p1198 A67-19184
 Electron microscope analysis of stress corrosion crack failure 07 p1211 A67-20250
 Scaling of binary titanium alloys in carbon dioxide at high temperatures using kinetic, metallographic and electron probe microanalysis [AAS PAPER 66-190] 08 p1341 A67-20763
 Oxidation of tantalum coated with aluminum and aluminum-chromium alloys at high temperatures and various oxygen pressures, using X-ray diffraction, electron microscopy, etc 08 p1341 A67-20764
 Plastic deformation of diamonds due to differences in initial defect distribution examined by birefringence, X-ray topography and electron microscopy 08 p1346 A67-20795
 Microcircuitry leakage path detection using scanning electron microscopy 09 p1473 A67-22017
 Occurrence, size and distribution of lattice defects in type III superconductor analyzed using electron microscopy, noting defect influence on critical current density 09 p1557 A67-22437
 Electron microscope and microprobe measurements of luster flight samples, discussing particle size distribution and nondispersible chemical analysis 10 p1707 A67-23238
 Electron microscopy study of fracture surface topography permitting identification of fine scale fracture surface features relating them to fracture formation mechanisms [AIAA PAPER 66-809] 10 p1661 A67-23552
 Hepatic effects of breathing pure oxygen for eight months upon rats, dogs and monkeys 10 p1600 A67-23818
 Baddeleyite inclusion in Marthas Vineyard tektite identified by electron microscopy 11 p1858 A67-24065
 Electron microprobe analysis for examining oxidation reduction mechanism in iron meteorites 11 p1865 A67-24606
 Metallurgical investigations by electron microscopy of rolling contact fatigue, elucidating mechanisms of failure due to shearing stress 12 p1954 A67-25329
 Transmission electron microscopy of dislocation structure produced in beryllium by specific deformation 13 p2138 A67-27116
 Electron microscopy of biological-like structures in Orgueil carbonaceous meteorite 13 p2210 A67-27583
 Transmission electron microscopy of interfacial areas in metal-matrix composites 14 p2336 A67-28096
 Titanium-vanadium alloy microstructure investigated under quenching and aging through electron microscopy 14 p2338 A67-28423
 Rutile in meteorites, noting presence of titanium oxide as result of electron microprobe studies 14 p2386 A67-28476
 Triangular flux line lattices observation by electron microscope in type II superconductors 14 p2369 A67-28599
 Precipitate and dislocation structures associated with peak effect in niobium examined using electron microscopy 14 p2375 A67-28999
 Electron microscope study of dislocation structures in deformed niobium single crystals 14 p2339 A67-29031
 Fracture surface topography related to micro- and macro-mechanics of fracture for plastic, cleavage and fatigue cases 16 p2772 A67-31301
 Cathodoluminescence detector for electron microprobe, noting components and use 16 p2877 A67-31432
 Surface potential contrast induced by

electron beam of scanning microscope on unbiased planar transistors, investigating beam voltage effect on contrast formation 17 p2823 A67-32197

Neighbor model for computer simulation of field ion images in fcc point lattice 17 p2887 A67-32205

Electron-mirror microscopy for intermediate-state pattern of superconducting samples noting bulk, thin sheet and lead films 17 p2912 A67-32266

Zr-Nb alloy structure effect on critical superconductivity parameters determined, using electron microscopy of thin films 17 p2916 A67-32721

Electron microscopy of titanium alloys noting preparation, heat treatment of samples, crystallographic structure, etc 17 p2872 A67-32722

Neutron irradiation effects in pure Mo, noting formation of prismatic dislocation loops 17 p2872 A67-32740

Electron microscopy used to investigate various defects forming in phase resulting from martensitic transformation 17 p2874 A67-32896

Damage regions in Si, GaAs and InSb irradiated with monoenergetic neutrons determined, using electron microscopy 17 p2922 A67-33060

Structures from two-step aging of aluminum-magnesium-silicon alloy, discussing effect on needle precipitation 18 p3065 A67-34362

Micrometeoroid collection experiments flown on Gemini IX and Gemini XII analyzed, using optical and electron microscopy and mass spectrometry 19 p3339 A67-35196

Pedoscope use in soil microbiological studies including ecology, infection susceptibility, etc 19 p3179 A67-35205

High strength high modulus carbon fiber microstructure, studying crystallite size, orientation effect, electron micrographs and X-ray diffraction 19 p3248 A67-35426

Ti-Al alloys ordering transformation studied by electron microscopy and electron and X-ray diffraction, showing existence of three phase fields 20 p3470 A67-37386

Electrical breakdown association with field emission observed through electron microscopy of whiskerlike projections on cathode surface 21 p3589 A67-37824

Crystal layer dislocation structure of cold rolled molybdenum foil investigated by electron microscopy 22 p3820 A67-39792

Cyclic stress-strain in annealed and cold worked fcc polycrystalline metals and alloys studied for hardening and softening by transmission electron microscopy 22 p3821 A67-40033

Phase transformations in commercial titanium alloys compared for mechanical properties, emphasizing decomposition of metastable beta phases on quenching, aging or deformation 22 p3822 A67-40055

Aluminum particle combustion noting changes from preignition to burnout, flame structure, particle geometry, etc [WSCI PAPER 66-3] 22 p3919 A67-40224

Omega phase morphology by transmission electron microscopy of Ti-Nb indicating ellipsoids with major axes parallel to //111/ directions in matrix 23 p4017 A67-40653

Epitaxial silicon layers grown by electron microscopy with small quantities of gold, discussing possible growth mechanisms 23 p4036 A67-40656

Equilibrium phases in annealed NiCrTiAlW alloy using optical and electron microscopy and X-ray analysis 23 p4019 A67-41078

Dislocation structure of tension deformed Si samples investigated by electron microscopy 23 p4042 A67-41296

Bi and Ag nucleation on evaporated substrates studied as function of substrate temperature and impinging flux using electron microscopy 23 p4044 A67-41455

Ti thin films use as getter in electron microscopy of Mo particles at high temperature with minimum oxidation 24 p4172 A67-41978

Origin of round body structures in Orgueil meteorite 24 p4113 A67-42455

Chromite composition in chondrites using electron microprobe technique, discussing petrographic origin and vanadium abundance 24 p4232 A67-42612

Preatmospheric hypervelocity impact black glass in Cachari eucrite studied by optical

microscopy, electron microprobe and X-ray diffraction 24 p4233 A67-42623

Black magnetic spherules in Pleistocene and recent beach sands, investigating origin by electron microscopy 24 p4235 A67-42635

Structural studies of FeNi-FeNiMn type thin films with ferro-antiferromagnetic coupling by Lorentz electron microscopy 24 p4206 A67-43109

ELECTRON MOBILITY

Origin of polarization of radiation from GaAs diodes, noting intensity dependence on current density and effect of anisotropic electron velocity 01 p0034 A67-10090

Electron mobility in p-type indium antimonide, noting entrainment of minority carriers by majority carriers 01 p0129 A67-10098

Variation of effective conductivity of thin metallic film with surface charge calculated by Boltzmann transport equation used with Fuchs-Sondheimer boundary conditions 01 p0130 A67-10204

Charge collection velocity in semiconductor particle energy detector expressed in terms of electron and hole motion and induced charges 01 p0065 A67-10650

Signal excitation in negatively charged antenna rod in effect of unfocused laser beam 01 p0091 A67-10835

Thin layers of crystallized cadmium telluride of high electron mobility analyzed for electrical properties and photoconductivity 02 p0294 A67-11759

Electro-optical properties of paraelectric perovskites indicating origin in polarization 02 p0296 A67-11821

Distribution function and electron mobility in polar semiconductors for nonparabolic dispersion law 02 p0296 A67-11825

Proton irradiation effect on Hall coefficient, resistivity and magnetoresistance of p-type bismuth telluride single crystals 02 p0298 A67-11882

Drift velocity dependence on electric field in GaAs measured by analysis of reverse biased Schottky barrier response to step input of light 02 p0253 A67-12504

Optical nonlinearities due to conduction band electrons in InAs, InSb, GaAs and PbTe studied, using Q-switched carbon dioxide laser radiation 02 p0254 A67-12524

Optical mixing due to conduction band electrons in semiconductor 02 p0254 A67-12525

Differential method measurement of Hall effect in presence of large constant magnetic field 03 p0487 A67-12808

Dependence of peak inverse voltage of n-Si and p-Ge on specific resistance and concentration and mobility of current carriers 03 p0488 A67-12817

Hall mobility and Nernst-Ettingshausen effect in Zn and Cd-doped p-type GaAs at temperatures from 90 to 800 degrees K 03 p0491 A67-13174

Surface state density effect on electron mobility in Si inversion layer of MOS-FET 03 p0496 A67-13577

V-I characteristics and bias field/carrier concentration-sample length diagram of Gunn effect phenomena 03 p0500 A67-13993

Anomalous high temperature Hall data for GaSb explained as effect of electrons in /100/ conduction band minima 03 p0501 A67-14346

Temperature dependence of current carrier mobility in GaAs crystals irradiated with fast electrons 04 p0679 A67-15140

Temperature and impurity ion concentration effect on minority carrier mobility in degenerate gallium arsenide 04 p0679 A67-15143

Plasma resonance measurement from radio wave scattering in cylindrical tubes which simulate meteor trail models 04 p0700 A67-15226

Tunable Raman laser obtained by electron mobility subjected to magnetic field, noting threshold pump power 05 p0823 A67-16684

Inelastic scattering of carbon dioxide laser radiation by mobile Landau-level electrons in n-InSb 06 p1009 A67-17723

Interpreting short voltage pulse measurements of electron drift velocity in n-GaAs 06 p1048 A67-17815

Transport properties of electrons in GaAs in connection with traveling domains of high electric field in material 06 p1066 A67-18959

Field and charge distribution in hot electron semiconductor, discussing drift and recombination nonlinearity 06 p1066 A67-18960

Gunn effect in GaAs caused by field induced transfer of electrons from high to low conduction band valleys 06 p1067 A67-18961

Electron mobility in AlSb, GaP and GaSb calculated by combining effects of optical polar and deformation potential scattering 06 p1067 A67-18964

Electron motion in crossed fields with arbitrary ratio of electric and magnetic fields, considering simultaneously valence and conduction bands 06 p1069 A67-18978

Resistivity, Hall coefficient and magnetoresistance of bismuth thin films at various temperatures, showing size dependence of effective mobilities of electrons and holes 06 p1070 A67-18985

Hydrodynamic equations describing motion of electrons in weakly ionized plasma in external electric field derived from Boltzmann equation, using Chapman-Enskog method 07 p1228 A67-19503

Hall mobility and thermal emf in indium antimonide with mixed electron scattering mechanism 07 p1237 A67-20182

Electron scattering mechanism in SiC polytypes, noting mobility limiting mechanism from 300 to 800 degrees K 08 p1370 A67-21293

Electron mobility measurements in n-type SiC polytypes noting temperature dependence 08 p1370 A67-21294

Pinching of surface carriers toward center of semiconductor produced by current induced magnetic field 08 p1371 A67-21439

Soviet book on electron properties of metals and alloys 08 p1371 A67-21490

Electron velocity-field characteristics of insulating GaAs measured using electron beam injected electrons 09 p1551 A67-21573

Negative slope mobility in n-GaAs from measurements of current-voltage characteristic 09 p1552 A67-21744

High field mobility degradation effect on characteristics of insulated gate FET, considering drift velocity proportional to field square root and constant drift velocity 09 p1471 A67-21944

Hole electron product of p-n junctions, plotting numerical results for electrostatic potential, quasi-Fermi levels and carrier concentration of n-p junction 09 p1553 A67-21946

Electrical migration of Li and Cu in GaAs, noting ionic charge decrease due to drag by electrons 09 p1558 A67-22603

Chemisorbed oxygen effect on Hall mobility and conduction electron concentration of spray deposited CdS thin films 10 p1689 A67-22910

Electron mobility and lifetime variations effects on drift field in silicon junction devices 10 p1612 A67-23374

Field dependent mobility effects in excess noise of junction gate FETs 10 p1612 A67-23376

Exponential sintering temperature dependence of conduction electrons density and attendant decrease of mobility due to ionized impurity scattering in cadmium oxide 10 p1691 A67-23503

Gallium arsenide epitaxial technology noting deposition rate and impurity profile, Hall mobility and morphology of deposits 10 p1692 A67-23511

Gallium arsenide characteristics and preparation noting epitaxial deposition and liquid phase, mobility, impurity and Hall effect data 10 p1692 A67-23512

Synthesis of undoped GaAs single crystals by horizontal Bridgman method, noting maximum mobility value obtained 10 p1693 A67-23517

Local potential variational method to study runaway stability of electrons in two-component plasma 11 p1826 A67-23872

Relativistic electron motion in mirror magnetic field interacting with axial electromagnetic wave calculated, comparing results with Seidl experiment 11 p1828 A67-23895

Thermal dissipation of energy in ionized cesium plasma, obtaining plasma oscillation excitation which destroys electron drift motion 11 p1837 A67-24394

Temperature effects in wave propagation on drifting carriers in

semiconductors 11 p1847 A67-24720
 Epitaxial vapor growth of GaAs noting reduction of electron concentration and increase in electron mobility 11 p1848 A67-24746
 Rapid vapor phase growth of high resistivity GaP for electro-optic modulators, noting high electron mobility 11 p1848 A67-24747
 Temperature dependence of current carrier mobility in GaAs crystals irradiated with fast electrons 12 p1979 A67-25163
 Temperature and impurity ion concentration effect on minority carrier mobility in degenerate gallium arsenide 12 p1979 A67-25166
 Conduction band structure and scattering processes of cadmium mercury telluride mixed crystal determined from thermoelectric power, effective mass and electron mobility 12 p1979 A67-25178
 Crystallographic anisotropy of electrical properties of thin film CdS photoresistors explained via potential barrier orientation theory 12 p1984 A67-25520
 Plasma-radiation interaction represented by Compton effect, utilizing Boltzmann term developed according to powers of perturbation caused by electron motion 13 p2165 A67-26598
 Destruction of drift motion of electrons in quiescent cesium plasma by electron-plasma oscillations 13 p2166 A67-26731
 Electron mobility in semiconducting strontium titanate 13 p2180 A67-27160
 Space-time description of dynamical phenomena in unbounded homogeneous linear medium, noting dispersion properties and wave structures in plasma 14 p2358 A67-28461
 Temperature dependence of Hall mobility of photoelectrons and electrons produced by X radiation in cadmium sulfide single crystals 14 p2367 A67-28525
 Schubnikow-De Haas oscillation analysis in n-type bismuth telluride indicates multivalley conduction band structure 14 p2369 A67-28596
 MOS transistor channel conductance measured as function of gate voltage, noting variation with temperature 14 p2289 A67-28924
 Electron mobility and temperature due to electric field in polar semiconductor investigated assuming displaced Maxwellian velocity distribution 14 p2375 A67-29065
 Temperature dependence of current carrier mobility in nickel and iron oxide, noting scattering due to magnetic field 15 p2533 A67-29315
 Analytic properties of finite-band models in solids as generalization of Kohn procedure 15 p2534 A67-29324
 Solitary waves, discussing electron and ion acceleration and transfer mechanism of solar wind ion kinetic energy to electrons 15 p2475 A67-29613
 Electron drift mobility and electron and ion temperatures difference in two-component plasma obtained from momentum and energy balance 16 p2706 A67-30450
 Refractory intermetallic compounds as high mobility semiconductors, noting crystal preparation and lowest carrier concentration obtained 16 p2725 A67-30806
 Properties of uniformly propagating stable domains in gallium arsenide calculated on basis of velocity-field and diffusion-field characteristics 16 p2727 A67-30851
 Conductivity, Hall effect and Seebeck coefficient measurements on single domain crystals of barium titanate 16 p2729 A67-31060
 GeTe solid solutions reviewed considering thermal EMF, temperature dependence and current carrier mobility 16 p2730 A67-31164
 Electron velocity distribution function obtained for partially ionized gas in weak, steady electric field by solving Boltzmann-Fokker-Planck equation 16 p2704 A67-31235
 Particle theory analysis of electromagnetic and electrostatic instabilities due to anisotropic velocity distributions 16 p2722 A67-31560
 Preparation of doped and undoped epitaxial InAs with open tube vapor-phase transport system noting properties, temperature effects, electron mobilities, etc 17 p2911 A67-32194
 Clustering in AL-GP zone alloys after low

temperature neutron irradiation 17 p2872 A67-32742
 Radiation effects on carrier recombination and mobility and on lifetime of semiconductor devices 17 p2919 A67-32858
 Disordered regions produced by fast neutron irradiation effect on semiconductor properties of silicon 17 p2919 A67-32859
 Mobility measurement of electron capture in hydrocarbon flames using Hall effect, noting variation when injecting chlorine 18 p3146 A67-33691
 Excitement of slow and fast recombination waves in semiconductors with mutually independent current-carrier concentrations and lifetime 18 p3099 A67-33696
 Coupling between slow waves and convective instabilities in solids, showing interaction inhibition for electron drift velocities greater than phase velocity 18 p3101 A67-34017
 Hamiltonian equations and Fourier transformations applied to free electron and gap motions in doped semiconductor 18 p3002 A67-34231
 Crystallographic anisotropy of electrical properties of thin film CdS photoresistors explained via potential barrier orientation theory 18 p3103 A67-34451
 Infinitesimal driven plane wave characteristics in uniform plasma with finite electron drift velocity found, using Navier-Stokes and Poisson equations, energy conservation continuity and perfect gas law 19 p3290 A67-35376
 Intense runaway electron stream from wave-plasma interaction in magnetic field noting microwave radiation and disruption time 19 p3291 A67-35381
 Electron mobility and trapping time in semi-insulating cadmium telluride through observing transient response to alpha particles 19 p3308 A67-36101
 Screened electron-phonon interaction effect on mobility of conduction electrons in semiconductors at low temperatures 20 p3509 A67-36433
 Theory of small signal current transients applied to study of electron trapping in amorphous selenium 20 p3509 A67-36507
 Electron drift velocity and mobility in InSb calculated from conductivity and Hall effect measurements, noting microwave emission occurrence 20 p3514 A67-37544
 Power series expansion of electron velocity distribution function, computing harmonic electric current densities in plasma 21 p3661 A67-37745
 Negative differential conductivity in semiconductor in acoustic instability mode and connection with sound amplification and number of electron traps 21 p3678 A67-38097
 Energy band nonparabolicity effect on GaAs drift velocity vs field curve, especially near Gunn threshold 21 p3680 A67-38348
 N-type InSb hot electron and nonohmic effects, noting low temperature and magnetic and electric field dependence of Hall coefficient and resistivity 21 p3683 A67-38405
 Indium antimonide-indium arsenide solid solution carrier mobility related to sample composition and temperature, measuring Hall coefficient and electrical conductivity 21 p3684 A67-38452
 Electron mobility in He, using irreversible quantum statistics theory to obtain momentum dependent relaxation time 22 p3840 A67-39210
 Current carrier mobility, Hall effect and magnetoresistance in semiconductors with nonuniform ion distribution 22 p3858 A67-39507
 Hot electron Hall mobility in n-type GaAs in negative differential mobility region 22 p3858 A67-39518
 Conductivity and Hall coefficient measurements for electron mobilities in strontium titanate, discussing electron-phonon coupling and cryogenic experiments 22 p3863 A67-40002
 Magnetic breakdown in metals covering one-electron theory, electronic motion, Bragg diffraction, de Hass-van Alfvén effect, coupled orbits and HF oscillations 22 p3866 A67-40552
 Temperature dependence of Hall mobility of photoelectrons and electrons produced by X radiation in cadmium sulfide single crystals 23 p4039 A67-40932

ELECTRON MULTIPLIER
SA PHOTOMULTIPLIER

Perseld meteor brightness studied from data of photoelectric observations by use of electronic multiplier 11 p1887 A67-24846
 Channel multiplier instrument measuring low energy electron and proton auroral fluxes from polar orbiting satellites 12 p1944 A67-25855
 Optical detectors for images and selected radiation signals using Bendix Channeltron multiplier, describing types, properties and applications 17 p2858 A67-32480
 Low power pulsed reflex klystron used to produce hyperfrequency-wave trains for short time periods 19 p3193 A67-35411
 Magnetic electron multiplier performance as photomultiplier in EUV spectral region 19 p3231 A67-35683
 Electron multiplier detection efficiency for positive ions determined as function of incoming ion energy, velocity and degree of ionization 23 p4000 A67-41219

ELECTRON OPTICS

Soviet and other papers on nuclear emission detectors, using electron-optical light amplifiers 01 p0069 A67-11006
 Structural book properties on and operational modes of electron-optic current controlling high vacuum gas-filled and solid state discharge devices 06 p0968 A67-17894
 Electron optical method for visualizing barrier layer concentrations in ceramic responsible for anomalous increase in resistivity observed in doped barium titanate 07 p1233 A67-19651
 Electron lens with hyperbolic field configuration designed to focus or modulate electron lenses, noting hyperbolic application to electron guns 14 p2276 A67-27768
 Travel-time effects on quasi-steady state operation characteristics occurring from electron optical characteristics of two-grid-controlled photomultiplier 14 p2277 A67-27769
 Soviet and other papers on nuclear emission detector, using electron-optical light amplifiers 16 p2670 A67-30494
 Electron image manipulation and charge-image storage perform equivalent of incoherent optical-image transformation 18 p3047 A67-33861

ELECTRON ORBIT

Different-orbitals-for-different-spins wave function for singlet S ground state of He expressed in Shull and Loewdin basis orbitals 03 p0473 A67-13522
 Matrix method to calculate energy eigenvalues and orbital wave functions for various singlet states of helium isoelectronic sequence 22 p3841 A67-40202
 Magnetic breakdown in metals covering one-electron theory, electronic motion, Bragg diffraction, de Hass-van Alfvén effect, coupled orbits and HF oscillations 22 p3866 A67-40552
 Solar neutrino observation, considering inverse nuclear beta decay and elastic scattering by orbital electrons 24 p4210 A67-42583

ELECTRON OSCILLATION

Dispersion relation of electron impurities in gapless superconductors and effect on period and damping of Tomasch oscillations 01 p0130 A67-10154
 Transformation of transverse oscillations of electron flux by short magnetic lenses studied by eigenvector concept 02 p0214 A67-11900
 Onset of electron oscillations in plasma with large velocity or temperature gradients 02 p0277 A67-12611
 Diffusion decay of discharge plasma with oscillating electrons in magnetic field 02 p0278 A67-12620
 Quasi-linear equations for inhomogeneous plasma in magnetic field applied to pumping of energy of Langmuir oscillations 03 p0475 A67-12936
 Electron oscillations of uniform plasma slab in presence of strong magnetic field, noting orthogonality condition of normal modes density gradients and profile and dispersion relation 03 p0482 A67-13747
 Convective excitation of ionic oscillations in plasma by inhomogeneous electron beam as result of spatial gradient of distribution function 04 p0668 A67-15270
 Convective effects role in exciting axisymmetric oscillations in plasma cylinder in magnetic field with aid of radius restricted electron beam 04 p0668 A67-15271

- Electric conductivity of liquid metals as function of electron oscillation frequency 06 p1032 A67-18125
- Performance of transferred electron oscillators produced by alloying Sn contacts on to epitaxial GaAs layers 06 p0971 A67-18225
- Paramagnetic Knight shift in metals and semiconductors as affected by temperature and magnetic and electric field intensity 09 p1554 A67-21972
- Collective oscillations of electron shells of atom, discussing energy, excitation and damping 09 p1534 A67-22004
- Statistical survey of CW transferred electron oscillators /Gunn diode/ made from epitaxial gallium arsenide 10 p1616 A67-23532
- Impurity photoconductivity spectra of p-type germanium at low temperatures, noting parameters of relative depth of equidistant minima oscillations 10 p1693 A67-23583
- Attenuating electron waves in crystals corresponding to energy values in forbidden band used in calculating current across n-p junction 13 p2172 A67-26354
- Onset of electron oscillations in plasma with large velocity or temperature gradients 13 p2170 A67-27367
- Diffusion decay of discharge plasma with oscillating electrons in magnetic field 13 p2170 A67-27376
- Negative-resistance Gunn effect in gallium arsenide and indium phosphide due to field excited electron transfer 14 p2366 A67-28474
- Plasma drift instability in discharge with oscillating electrons, measuring plasma vibration spectrum 15 p2528 A67-29711
- Drift instability of discharge plasma with oscillating electrons 16 p2717 A67-31180
- Anomalous decay of discharge plasma with oscillating electrons in strong magnetic field, using diagrams 16 p2717 A67-31181
- Associated nonuniform electron-nucleus oscillations in ferromagnetic substances studied to determine feasibility of maser, using magnetic-reversal nuclear magnetic resonance 16 p2686 A67-31731
- Axial electrostatic field forming in resonance zone of mixed structure noting ion entrainment, shock wave generation and motion of electrons 17 p2899 A67-32291
- Paramagnetic Knight shift in metals and semiconductors as affected by temperature and magnetic and electric field intensity 17 p2923 A67-33309
- Electron fluctuations variance and correlation coefficients computed for sensitized GaAs, comparing noisiness of deep recombination levels 19 p3306 A67-35732
- Plasmoid instability from inhomogeneous flow along magnetic field 20 p3498 A67-36693
- Attenuating electron waves in crystals corresponding to energy values in forbidden band used in calculating current across n-p junction 21 p3679 A67-38311
- Magnetic breakdown in metals covering one-electron theory, electronic motion, Bragg diffraction, de Hass-van Alphen effect, coupled orbits and HF oscillations 22 p3866 A67-40552
- ELECTRON PARAMAGNETIC RESONANCE**
- Polymethylmethacrylate and polystyrene exposure to ruby and neodymium-glass laser radiation, noting appearance of EPR 01 p0086 A67-10075
- Mechanism of hydrogen combustion near lower ignition limit studied, using electron paramagnetic resonance /EPR/ measurements 03 p0536 A67-13842
- Active time of two-level quantum paramagnetic amplifier increased by using only portion of spin packets, noting effect of EPR line 04 p0633 A67-15159
- EPR spectral shape and width as affected by phosphor concentration, degree of boron compensation and temperature in strongly doped n-silicon 05 p0867 A67-17055
- Annealing behavior and uniaxial stress response of radiation induced defects in Si causing 1.8, 3.3 and 3.9 micron IR absorption bands examined via EPR 05 p0870 A67-17194
- Electron paramagnetic resonance of photosensitive donors in zinc oxide with oxygen vacancies 06 p1054 A67-18832
- Paramagnetic current formation due to volume resonator microwave field interaction with dense plasma subject to RF pressure and EPR in static magnetic field 07 p1228 A67-19512
- Intracrystalline field and spontaneous polarization in barium titanate studied by EPR spectrum of Cd-3 ions 09 p1554 A67-21976
- Superfine structure of EPR spectrum of nitrogen in silicon carbide as function of nitrogen concentration and sample temperature 10 p1694 A67-23650
- Autodyne design and operational principles for EPR in weak fields, using coaxial resonator 11 p1793 A67-24865
- Optical and paramagnetic resonance of ytterbium ions in calcium fluoride, obtaining correlation between site geometry and optical absorption 12 p1984 A67-25843
- Defects in irradiated silicon, analyzing electron paramagnetic resonance and electron-nuclear double resonance of aluminum vacancy pair 13 p2180 A67-27161
- Microwave spectroscopy of organic semiconductors, examining EPR of chemical bonds in energy transfer 14 p2366 A67-28505
- EPR applied to investigation of various semiconductors containing iron, and Mn at liquid nitrogen temperature 14 p2373 A67-28968
- Active time of two-level quantum paramagnetic amplifier increased by using only portion of spin packets, noting effect of EPR line 15 p2496 A67-29346
- Gaussian and Lorentzian components separation in analyzing EPR spectrum in ruby, using variance techniques 15 p2536 A67-29499
- EPR spectral shape and width as affected by phosphor concentration, degree of boron compensation and temperature in strongly doped n-silicon 15 p2538 A67-29786
- Electron paramagnetic resonance /EPR/ studies of interaction of irradiation-produced defects with impurities and other defects in silicon semiconductors 17 p2918 A67-32854
- Hydroxyl radical formed by radiolysis of ice at 77 degrees K identified as center producing EPR lines 17 p2890 A67-33258
- EPR spectra of radicals formed during gamma irradiation of polytetrafluoroethylene 17 p2810 A67-33260
- Intracrystalline field and spontaneous polarization in barium titanate studied by EPR spectrum of Cd-3 ions 17 p2923 A67-33313
- Superfine structure of EPR spectrum of nitrogen in silicon carbide as function of nitrogen concentration and sample temperature 17 p2923 A67-33331
- Amplification characteristics of multicavity masers, determining Q-factor using chain matrix A formalism 19 p3241 A67-36027
- Endor double paramagnetic resonance in cane-sugar carbon at room temperature, noting electron-proton interaction 20 p3508 A67-36398
- Electron paramagnetic resonance of trivalent rare earth-monovalent alkaline earth ion pairs in calcium fluoride 21 p3676 A67-37815
- Divalent Eu ion ground state splitting in C3h symmetry sites and associated color centers in EPR spectrum study of Eu ion doped lanthanum trichloride 22 p3863 A67-40003
- Stimulated emission and spectroscopic investigations of double lanthanum-sodium molybdate single crystals with neodymium impurities, considering applicability in lasers 23 p4039 A67-40901
- EPR spectrum of divalent Mn ion impurity in CdTe single crystals noting concentration dependence, ion distribution and interaction nature 23 p4042 A67-41294
- ELECTRON PATH**
- Passage of hot electrons through metal film in semiconductor-metal-semiconductor system 15 p2541 A67-30239
- He 3 ratio to He nuclei in cosmic rays, determining He nuclei path length in space, considering kinetic energy power spectrum 20 p3518 A67-37088
- P-i-n structures obtained from p-type Si by Li drift studied for carriers collection efficiency and potential path distributions 23 p4044 A67-41456
- ELECTRON-PHONON INTERACTION**
- Electron collision cross section resonance mechanism analyzed via matrix methods, noting threshold effect application to electron scattering 03 p0470 A67-13219
- Superconductivity in strontium titanates and similar polar substances with transition temperature accounted for by electron-phonon interactions 03 p0491 A67-13259
- Adiabatic harmonic unitary transformations and relation between electron trapping energy and normal lattice modes associated with F center ground state 03 p0495 A67-13515
- Semiconductor photoconductivity dependence on external radiation frequency, examining electron-phonon interaction 03 p0502 A67-14374
- Dimensional effect in electric conductivity of semiconductors during heating of electric field when electron energy relaxation length exceeds mean free path 04 p0679 A67-15137
- Thermal conductivity of lanthanum and monochalcogenides, noting role and temperature dependence of crystal-lattice conductivity 04 p0680 A67-15287
- Limitation of Froehlich-Terreaux quasi-superconducting state, discussing experimental and observational difficulties 06 p1047 A67-17654
- Superconducting transition temperature of thin film, showing growth of temperature and decrease in film thickness due to phonon electron interaction 06 p1049 A67-17886
- Two-phonon IR absorption and Raman scattering spectra to provide information about phonon spectra of crystals and phonon-electron interaction in filled valence bands 06 p1059 A67-18907
- Time dependence of V-I curves in n-type In-Sb at low temperatures, determining electron-hole pair generation rate 06 p1066 A67-18955
- Electron-phonon interaction in semiconductors, considering three-phonon process and third order elastic constant 06 p1066 A67-18957
- Resistivity, magnetoresistance, Hall effect and thermal conductivity in n-type In-Sb at liquid He temperatures 06 p1068 A67-18968
- Concentration effect on light absorption and dispersion by impurity centers in case of weak electron-phonon coupling 07 p1233 A67-19648
- Scattering in semiconductors, calculating collision term in Boltzmann equation for acoustic modes and differential collision operator for isotropic part of distribution function 07 p1237 A67-20180
- Superconducting properties of vanadium silicide noting high transition temperature, electron-phonon interaction, sound absorption, etc 08 p1369 A67-20990
- Soviet book on electron properties of metals and alloys 08 p1371 A67-21490
- Theory of superconductivity on basis of phonon model for finite temperatures, comparing four-fermion/electron interaction with Bardeen hamiltonian model theory of superconductivity on basis of phonon 08 p1372 A67-21491
- Acoustic waves amplification in CdS crystal by electron-phonon interaction 09 p1558 A67-22591
- Conduction electrons interaction with deformation potential and piezoelectric phonons to explain hot electron results in n-type InSb, taking into account screening of scattering potential 09 p1558 A67-22619
- Thermal conductivity of low temperature silicon and germanium irradiated by fast neutrons noting differences, additive thermal resistivity and possible scattering mechanisms 11 p1849 A67-24899
- Dimensional effect in electric conductivity of semiconductors during heating of electric field when electron energy relaxation length exceeds mean free path 12 p1979 A67-25160
- Electron-phonon interaction and phonon spectrum observed for electron tunneling measurements in fcc alloys of Pb alloys, noting electron concentration changes 13 p2175 A67-26426
- Temperature dependence of energy levels of shallow donor impurities in silicon, noting electron-phonon interaction 13 p2176 A67-26987
- Effect of mutual entrainment of electrons and phonons on Wiedemann-Franz law for semiconductors, calculating thermoconductivity 13 p2181 A67-27280
- Second current saturation of nonohmic behavior in CdS single crystals caused by quantum mechanical interaction between drift electrons and acoustic phonons 14 p2365 A67-28239
- Numerical evaluation of voltage and polarity variation induced by electron conductivity changes created by longitudinal

phonon pressure caused by shock wave 14 p2367 A67-28514
 HF localized and LF resonant impurity modes valence effect on energy gap and transition temperature in isotropic superconductors 14 p2370 A67-28720
 Current instabilities in GaAs for applied electric field along piezoelectric direction attributed to electron-phonon coupling, determining additional parameters from experimental data 14 p2374 A67-28983
 Two-photon recombination in semiconductors with degenerate electron-hole gas taking into account damping during interaction with phonons 15 p2542 A67-30244
 Electron-phonon interaction calculation for solid state transition metals justifying matrix element presented and using augmented plane wave 16 p2731 A67-31447
 Self-consistency equation for nucleation of superconductivity in presence of magnetic field 17 p2924 A67-33372
 Operator for spin-phonon interaction between conduction electrons and polarization-induced longitudinal oscillations of semiconductor lattice 18 p3099 A67-33697
 Critical fields in strong coupling superconductors, using Ginsburg-Landau equations 19 p3303 A67-35042
 IR emission in n-type gallium arsenide samples exhibiting current oscillations due to electron-phonon coupling 20 p3508 A67-36423
 Screened electron-phonon interaction effect on mobility of conduction electrons in semiconductors at low temperatures 20 p3509 A67-36433
 I-V characteristics of many-valley semiconductors in strong electric field deviating from Ohm law with scattering by phonons 20 p3513 A67-37439
 Three- and four-phonon processes in piezoelectric cadmium sulfide observed using ultrasonic amplifier confirm nonlinear theory of multiple wave interactions 22 p3854 A67-39246
 Conductivity and Hall coefficient measurements for electron mobilities in strontium titanate, discussing electron-phonon coupling and cryogenic experiments 22 p3863 A67-40002
 Phonon assisted magnetoabsorption in direct band semiconductors 24 p4203 A67-42267

ELECTRON PHOTON CASCADE
 Rms particle numbers calculated for electrons and photons in three-dimensional theory of electromagnetic showers 01 p0143 A67-10543
 Electron-photon shower measurement using ionization calorimeter type device 02 p0271 A67-12755
 Ionization calorimeter measurements of energy transmission by photons in cosmic nuclear-active pion and nucleon interactions with various nuclei 02 p0316 A67-12761
 Ionization calorimeter measurement of absorption of energy flux of primary cosmic radiation nuclear active component in iron 02 p0316 A67-12762
 Nucleon interaction generating high energy gamma rays, discussing photon and energy spectra of electron photon cascade, pion generation and gamma quantum detection in atmospheric nuclear interactions 02 p0316 A67-12763
 Superhigh energy particle accelerators and energy spectra of cosmic ray muons in electron photon cascades 02 p0317 A67-12772
 Spatial and angular particle distributions in muon-generated electron photon cascade, using spark chamber muon detectors 02 p0317 A67-12774
 Microstructural analysis multiple electron-photon cascade resonance amplifier response to sine-square radio signal 03 p0376 A67-13091
 Production rate of secondary cosmic ray photons in upper atmosphere derived by cascade theory from stratospheric measurements of integral and differential energy spectra 09 p1561 A67-21882
 Electron cascade showers, examining elementary processes, general behavior, three-dimensional theories and large angle single scattering 14 p2379 A67-27961
 Electron-photon cascade process in intergalactic space, noting role of microwave radiation in gamma ray astronomy 15 p2550 A67-29750
 Cosmic radiation dose, estimating

contributions due to mu meson and electron-photon cascade shower 18 p2990 A67-33516
 components 18 p2990 A67-33516
 Electron-photon shower measurement using ionization calorimeter type device 22 p3842 A67-40257
 Ionization calorimeter measurements of energy transmission by photons in cosmic nuclear-active pion and nucleon interactions with various nuclei 22 p3876 A67-40263
 Ionization calorimeter measurement of absorption of energy flux of primary cosmic radiation nuclear active component in iron 22 p3842 A67-40264
 Nucleon interaction generating high energy gamma rays, discussing photon and energy spectra of electron photon cascade, pion generation and gamma quantum detection in atmospheric nuclear interactions 22 p3876 A67-40265
 Superhigh energy particle accelerators and energy spectra of cosmic ray muons in electron photon cascades 22 p3877 A67-40274
 Spatial and angular particle distributions in muon-generated electron photon cascade, using spark chamber muon detectors 22 p3877 A67-40276
 Electron photon cascades in lead scintillator devices investigated using Nagel Monte Carlo calculations for energies between 100 and 440 Mev 24 p4191 A67-42439
 Photoemulsion data analysis of high energy nuclear interactions in nuclear emulsions exposed to air showers during flights 24 p4192 A67-42827
 High energy gamma quanta from high energy cosmic particle interaction with carbon and air nuclei, noting three superhigh energy electron/photon cascades recorded 24 p4218 A67-42835
 Extensive air showers accompanying high energy nuclear active particles, discussing nuclear interaction processes and energy transformation 24 p4220 A67-42864
 Iron radiation length unit from electromagnetic cascades produced by bremsstrahlung of horizontal cosmic ray muons 24 p4221 A67-42869
 Quantitative analysis of negative excess of electrons in electromagnetic cascade showers on basis of energy distribution 24 p4221 A67-42871
 Expressions for angular distribution function of electrons at various depths in cascade showers with given primary particle energy 24 p4221 A67-42872
 Equilibrium angular distribution function computer calculations for cascade particle numbers in iron and lead reveal dependence on primary particle energy 24 p4221 A67-42873
 Electron-photon shower creation probability by energetic particle, deriving recursion formulas 24 p4221 A67-42874

ELECTRON PLASMA
 Free energy of electron gas in compensating field at high temperatures determined from displacements in collective variables, using equation of statistical sum of steady state plasma 01 p0119 A67-10133
 Energy relation for acoustic propagation modes in hot electron plasma considered in application of Helmholtz theorem 01 p0123 A67-10441
 Temperature dependence of spectral line intensity emitted by thermal plasma 01 p0124 A67-10867
 Simultaneous excitation of electron plasma and ion-acoustic oscillations, using single electromagnetic wave for plasma oscillation generation 01 p0125 A67-10913
 Landau damping in weakly inhomogeneous plasma related to Cerenkov radiation of accelerated electrons moving in external static field causing inhomogeneity 02 p0272 A67-11636
 Strong injection in nondegenerated p-n junction producing electron-hole plasma in n region near junction 02 p0296 A67-11827
 Effective capture of electrons in magnetic mirror trap with stationary field by pulse-type injection of helical electron beam 02 p0274 A67-12458
 Distribution of charged particles of different energies escaping from magnetic trap in which spiral moving electron fluxes are created 02 p0274 A67-12459
 Characteristics of one-dimensional cold electron plasma produced by uniform background of ions 02 p0278 A67-12626
 Landau damping in anisotropic electron

plasma treated by kinetic dispersion equation 03 p0474 A67-12920
 Calculation of statistical sum of bounded states of electron in atom in Debye plasma 03 p0478 A67-13615
 Virial theorem for electron plasma obtained by defining potential tensor and superpotential of electric field 03 p0482 A67-13746
 Propagation of coupled electromagnetic, electron-acoustic and ion-acoustic waves in horizontally stratified and magnetized electron-ion plasma 03 p0372 A67-13991
 Growing space charge wave phenomenon due to collision coupling in warm compressible dissipative electron plasma in uniform motion 03 p0483 A67-13995
 Laboratory-controlled nonlinear, nonresonant excitation of electron plasma oscillations with one transverse electromagnetic wave 03 p0485 A67-14052
 Instability in hot electron plasma in mirror field occurring suddenly in quietly decaying plasma generated by high power microwave 04 p0663 A67-14621
 Transverse electromagnetic wave transformation into ion-acoustic plasma oscillations with formation of intermediate Langmuir electron wave 04 p0668 A67-15275
 Nighttime magnetospheric auroral VLF hiss generation by suprathermal particle associated with coherent electron plasma radio emission 04 p0618 A67-15686
 Instability due to nonlinear coupling of electron plasma oscillation and ion acoustic oscillation to driving transverse field extended to longitudinal driving field 04 p0672 A67-15771
 Scattering cross section of electromagnetic waves by finite objects in compressible plasma in absence of DC magnetic field 05 p0853 A67-16802
 Hot electron plasma instability in magnetic mirror, discussing stabilization by cold plasma component and magnetic field line typing in conducting end plates 05 p0858 A67-17431
 Current carrier behavior during field and diffusion injection of electron hole plasma into semiconductor 06 p1049 A67-17865
 Oscillations of inhomogeneous weakly ionized plasma situated in external electric and magnetic field, noting causes and conditions of plasma instability 06 p1039 A67-18080
 Electric propulsion unit using electron cyclotron resonance plasma thruster for spacecraft 06 p1074 A67-18418
 Nonlinear instability of nonisothermal plasma in external electric field, determining ion-acoustic noise spectrum and time dependent variations in kinetic energy of plasma electrons and ions 06 p1045 A67-18801
 Electron plasma oscillations excited by two-beam instability and nonlinear coupling between them 06 p1046 A67-18828
 Oscillations in conductivity of electron-hole plasma in semiconductors due to nonlinearity of volt-ampere characteristics 06 p1070 A67-18988
 Magnetic field effect on static shielding of point charge calculated, using Green function of inverse dielectric function of electron gas plasma 06 p1071 A67-18989
 Hydrodynamic equations describing motion of electrons in weakly ionized plasma in external electric field derived from Boltzmann equation, using Chapman-Enskog method 07 p1228 A67-19503
 Wave coupling in varying density regions in hot anisotropic electron plasma, noting effect of angle width between propagation vector and static magnetic field 07 p1228 A67-19509
 Simple method for determining mean free path of primary electrons in plasma 07 p1229 A67-19515
 First order coupled wave equations for propagation in planar stratified compressible electron plasmas 07 p1230 A67-19851
 Plane wave growth associated with Cerenkov and cyclotron instabilities in plasma stream 08 p1358 A67-20893
 Electron streaming instability of plasmas with zero order density gradients from variational analysis of Vlasov-and Maxwellian-plasma perturbation wave propagation 08 p1360 A67-21128
 Landau damping and growth applied to electron plasma waves for Maxwellian

- velocity distribution in slab and cylindrical geometries 08 p1365 A67-21403
 - Kinetic equation for inhomogeneous electron plasma derived from Liouville equation by Prigogine-Balescu diagram technique 08 p1366 A67-21431
 - Microwave interferometer for measurement of effective recombination coefficient of decaying argon-cesium plasma with hot electrons at various argon pressures 09 p1542 A67-21817
 - Conductivity of high density plasma of JMH generator, noting quantum phenomena associated with overlapping electron wave functions 09 p1543 A67-21818
 - Microwave noise intensity emitted by electron plasma within framework of fluctuation theory 09 p1547 A67-22318
 - Collisionless damping in hot plasma due to electron reflection at wall and phase mixing associated with thermal perturbation 09 p1549 A67-22552
 - Electron plasma behavior and stability in presence of time dependent electric field 09 p1549 A67-22553
 - Electron-hole plasma pinch instability in InSb on application of longitudinal magnetic fields shows change to helical rotating plasma 10 p1683 A67-22760
 - Nonlinear excitation of electron plasmas in solids explained by mechanism of nonparabolic energy bands 10 p1689 A67-23075
 - Relaxation in space of electron velocity distribution due to electron-ion collisions, obtaining time independent solution 11 p1833 A67-24372
 - Cooperative effect among electrons in presence of radial density gradient in cyclotron echo phenomena 11 p1836 A67-24391
 - Electron plasma wave propagation along cylindrical plasma column in magnetic field, calculating damping and dispersion curves 11 p1837 A67-24401
 - Enhanced plasma fluctuations produced by suprathermal electron effect on emission and scattering of electromagnetic waves, noting analogy with corona plasma 11 p1839 A67-24546
 - Interaction of plasma oscillation with electrons with positive distribution function, noting oscillation amplitude relation to function deformation 11 p1840 A67-24766
 - Electrostatic oscillations in electron plasma, noting effect of external electric field on electron velocity distribution 11 p1848 A67-24868
 - Kinetic equation for electron gas in classical limit derived from quantum mechanical transport equation, using equilibrium analogy 11 p1844 A67-25076
 - Relativistic electron plasma diffusion, calculating dynamical friction and diffusion coefficient in Landau approximation 12 p1969 A67-25193
 - Plasmoid generated by Q-switched neodymium-glass laser radiation focused on solid target, estimating plasma electron temperature 12 p1986 A67-26065
 - Relaxation of velocity distribution to equilibrium in electron plasma, showing linearized collision operator covers continuous spectrum of eigenvalues 12 p1977 A67-26176
 - Electron velocities distribution in plasma, studying boltzmann equation inelastic and superelastic collision operator, considering eigenfunctions and eigenvalues for electronic excitations and deexcitations 13 p2165 A67-26437
 - Destruction of drift motion of electrons in quiescent cesium plasma by electron-plasma oscillations 13 p2166 A67-26731
 - Characteristics of one-dimensional cold electron plasma produced by uniform background of ions 13 p2171 A67-27382
 - Damping of plane sinusoidal wave in cold collisionless plasma, studying supercritical amplitude oscillatory process 13 p2171 A67-27615
 - Autoionization effects accompanying impairment of forbidden intercombination transfer in plasma due to atom collision with plasma electron 13 p2171 A67-27626
 - Linearized Fokker-Planck kinetic equation, describing approach to equilibrium of test electrons injected into electron plasma in thermal equilibrium 14 p2356 A67-28203
 - Spectroscopic methods applied to plasma electron temperature and density measurements 14 p2322 A67-29045
 - Propagation of coupled electromagnetic and electroacoustic waves in magnetized compressible stratified electron plasma 15 p2521 A67-29177
 - Particle velocity distribution calculation in current-carrying electron-proton plasma by Lenard-Balescu-Guernsey form of Fokker-Planck equation 15 p2522 A67-29204
 - Skin effect in plasma theory for case of nonlocality of relation between current and electric field 15 p2522 A67-29211
 - Magnetic moment of electron in HF plasma accelerator for case of negligible axial acceleration in resonance region 15 p2527 A67-29514
 - Excitation of potential LF electromagnetic waves in electron-hole plasma of solid body for negative volt-ampere characteristics of carrier current 15 p2537 A67-29702
 - Nonlinear instability, demonstrated for electron plasma waves driven toward instability by small ion beam but linearly stabilized by electron Landau damping 16 p2719 A67-31228
 - Electron wave resonances in bounded plasmas, examining application to average plasma density measurement 17 p2896 A67-32163
 - Hamiltonian formalism for collisionless electron plasma nonlinear kinetics using quantum statistical perturbational treatment 17 p2902 A67-32670
 - Vlasov equation for anisotropic electron plasma in external magnetic field solved by Laplace transform of density perturbation in initial value problem 17 p2907 A67-33104
 - Propagation modes and instabilities of transverse disturbances in solid state plasmas 17 p2925 A67-33377
 - Density redistribution of plasma electrons and ions caused by strong microwave field 18 p3087 A67-34040
 - Cyclotron instabilities of two-component electron plasma 18 p3089 A67-34295
 - Nonlinear instability of nonisothermal plasma in external electric field, determining ion-acoustic noise spectrum and time dependent variations in kinetic energy of plasma electrons and ions 18 p3090 A67-34420
 - Calculation of statistical sum of bounded states of electron in atom in Debye plasma 18 p3091 A67-34480
 - Collisionless electron plasma dynamics in one dimension, investigating nonlinear Vlasov equation for Landau damping and instability 18 p3092 A67-34747
 - One-dimensional electron plasma model, transport coefficient determination, Lorentz plasma conductivity measurement, decay rate, etc 18 p3092 A67-34748
 - Anisotropy of electron energy distribution measurement in electron cyclotron-resonance plasma using diamagnetic loop 18 p3093 A67-34756
 - Energy and intensity density of radiation emitted by semilfinite nonequilibrium electron plasma with non-Maxwellian particle distribution calculated, based on general fluctuation theory 19 p3267 A67-34902
 - Periodic spatial variations of parameters of positive column plasma in magnetic field along obstacle shadow due to electron wakes 19 p3273 A67-35093
 - Transport phenomena in electronic plasma as initial value problem noting distribution function relaxation 19 p3287 A67-35355
 - Intense runaway electron stream from wave-plasma interaction in magnetic field noting microwave radiation and disruption time 19 p3291 A67-35381
 - Longitudinal wave echo in collisionless electron plasma with Landau damping 19 p3295 A67-35534
 - Longitudinal oscillations and Landau damping of electron plasma with fixed ion background, discussing initial and boundary value problems 20 p3494 A67-36150
 - Nonparabolic conduction energy band in semiconductors produces electron plasma excitations of sum and difference frequencies under strong DC electric field 20 p3505 A67-36210
 - Electron-plasma oscillation damping in hot collisional plasma with external uniform magnetic field investigated using Fokker-Planck equation 20 p3503 A67-37693
 - Quantum corrections to Maxwell plasma free energy in compensating electromagnetic field by method of displacements and collective variables for high temperatures 21 p3663 A67-37861
 - HF resonance probes, giving theoretical results of nonzero electron plasma temperature effect and experimental results with plasma between plates of plane capacitor 21 p3626 A67-38220
 - Z-pinch in electron hole plasma observed by microwave probe method, noting no minimum current exists for semiconductors 21 p3666 A67-38356
 - Pinch effect in degenerate indium antimonide plasma in longitudinal and transverse electromagnetic fields 21 p3666 A67-38369
 - Hard X-ray emission by hot electron plasma trapped in discharge tube due to magnetic field rise 21 p3667 A67-38413
 - Parametric excitation of electron plasma frequency derived using Boltzmann and Poisson equations 21 p3667 A67-38415
 - Isolated longitudinal wave pulse amplitude and phase velocity dependence on trapped particle density in ion-electron and electron-positron plasmas 21 p3669 A67-38683
 - Malmberg-Wharton configuration electron plasma wave dispersion and damping 22 p3844 A67-39367
 - Solitary pulse longitudinal waves existence in electron plasma related to trapped ions presence, studying ion pulse shape and oscillation stability 22 p3845 A67-39423
 - Steady state nonlinear Landau damping of electron plasma wave obtained from random phase approximation by balancing nonlinear and collision effects 22 p3848 A67-39691
 - Hot electron plasma confinement in magnetic mirror fields with compensating curvature, discussing experimental observations and hybrid configuration formation 22 p3849 A67-39698
 - Collisionless small and large amplitude electron plasma wave damping compared, showing small amplitude waves damp exponentially and large amplitude waves exhibit amplitude oscillations collisionless small and large amplitude electron 22 p3853 A67-40242
 - Hot electron plasma production, discussing microwave power feeding across magnetic flux lines producing closed plasma shell structure 22 p3854 A67-40243
 - Elliptically polarized electromagnetic wave propagation in homogeneous infinite plasma, solving Vlasov equations of nonlinear theory by successive approximation 23 p4030 A67-40597
 - Kinetic equation for steady state electron-ion system with electrons drifting under electric field, calculating HF resistivity drift velocity dependence 23 p4033 A67-40962
 - Transverse electric field generated by interaction of various longitudinal plasma waves in ion electron plasmas 23 p4033 A67-41151
 - Maxwell-Euler equations reformulated into equivalent matrix integral equation, obtaining dispersion relation from integral equation kernel for compressible electron plasma 23 p3974 A67-41204
 - Excitation of potential LF electromagnetic waves in electron-hole plasma of solid body for negative volt-ampere characteristics of carrier current 24 p4199 A67-41772
 - Proton gyrofrequency effect on antenna resonance at electron plasma frequency using Alouette II satellite 24 p4125 A67-43111
- ELECTRON PRECIPITATION**
- Characteristics of relativistic electron precipitation events in and near auroral zone during day and night 03 p0410 A67-12957
 - Energetic electron precipitation and 5 to 40 second geomagnetic micropulsations relation to auroral substorms 04 p0615 A67-14968
 - Electron precipitation from outer radiation belt as cause of ionospheric disturbances, noting relation to time 07 p1245 A67-19928
 - Spatial and temporal characteristics of bremsstrahlung X-ray due to energetic electron precipitation in auroral zone, noting measurement techniques 07 p1180 A67-19929
 - X-ray microburst correlation with impulsive microburst 07 p1246 A67-19949
 - Emission of bremsstrahlung X-rays caused by electrons precipitating isotropically into upper atmosphere 10 p1633 A67-23048
 - Balloon observations of large scale coherent pulsating electron precipitation events in auroral zone accompanied by geomagnetic continuous pulsations

- [AFOSR-67-1314] 12 p1931 A67-25112
High energy particle precipitation into upper atmosphere at medium latitude after magnetic storms, dependence on season and latitude and correlation with geomagnetic pulsation enhancement 12 p1991 A67-25113
Polar orbiting satellite measurements correlating ionospheric irregularities with trapped and precipitated energetic particles in South American anomaly region 12 p1996 A67-25776
Ionospheric measurements at Antarctic station in south radiation anomaly region showing precipitated electron flux associated with ionospheric disturbances 12 p1934 A67-25778
Electron precipitation in conjugate regions of auroral zone latitudes examined via X-ray measurements with balloon-borne instrumentation 13 p2115 A67-27255
Auroral zone electron precipitation occurring in strong transient magnetic disturbances observed by bremsstrahlung 14 p2310 A67-28056
Relative, world-wide magnetospheric electron precipitation into lower, denser atmosphere determined, using conjugate point magnetospheric-ionospheric circuit model 16 p2667 A67-31510
Microburst precipitation of energetic electrons into auroral zone 18 p3035 A67-33596
Electron precipitation data examined to determine whether electron behavior can be understood on basis of binary collisions with atmospheric constituents and guidance by geomagnetic field 18 p3035 A67-33599
Magnetic variations relationship to magnetospheric perturbations, emphasizing particle participation near auroral zones 20 p3428 A67-36376
Auroral substorms, examining energy spectrum and flux of precipitating particles and morphology 20 p3431 A67-37100
Temporal periodicity of 10 cps observed in flux of auroral electrons by rocketborne radiation detectors 22 p3790 A67-39795
- ELECTRON PRESSURE**
Equilibrium of magnetic field confined by impact pressure of beam of ions for general direction of incidence of beam 14 p2310 A67-28046
Partition function of partially ionized hydrogen two-component plasma 19 p3285 A67-35346
Equivalent widths of line spectrum analyzed by modification of Milne-Eddington growth procedure curve 22 p3896 A67-40528
Equations governing umbra structure of single spot integrated on spot axis, consistent model can be obtained only for narrow electron pressure range at surface 23 p4067 A67-41230
- ELECTRON PROBE**
Microprobe study of impurities in hot-pressed polycrystalline MgO compact and existence of significant grain boundary volume [JPL-TR-32-1015] 01 p0131 A67-10262
Rotational temperatures measured in static low density air with electron beam probe 01 p0071 A67-11105
Bonding mechanism between metals and ceramics, noting glass penetration theory 02 p0255 A67-12060
Sample orientation and electron beam incidence angle variation effects on X-ray spectrometer performance 04 p0621 A67-15114
Chemical and mineralogical composition of roedderite found in Indarch meteorite, presenting electron probe analysis and X-ray diffraction pattern optical data 07 p1255 A67-20012
Probe measurements of intermediate and high pressure plasmas in cases where mean free path of particles is greater than probe dimension 09 p1539 A67-21783
Monograph on electron microprobe X-ray analyzer and application in mineralogy 10 p1603 A67-23632
Chemical composition of indochinites, determining nonuniform distribution of elements via electron microprobe counts 11 p1866 A67-24695
Electron microprobe analysis of quartz and alumina darkening upon solar wind ion bombardment, noting existence of iron, tungsten and carbon in samples 16 p2753 A67-31745
Electron beam probe for determination of

- local gas parameters in reentry simulation 20 p3445 A67-36588
Planar diffused p-n junction profile geometry using scanning electron microscope and electron probe with computer calculations 22 p3855 A67-39360
Germanium distribution in metallic phases of various iron meteorites by electron probe microanalysis 22 p3885 A67-39976
Probes containing various scintillators for measuring electron energy spectrum at high altitude in cosmic ray flux 23 p4054 A67-41095
Concentration and distribution of phosphorus in kamacite and taenite in Mount Edith medium octahedrite determined by electron probe microanalysis 24 p4236 A67-42643
- ELECTRON RADIATION**
Solar flares, discussing continuous electromagnetic radiation, hard X-ray radiation and microwave radio bursts 02 p0310 A67-12576
Effect of electron irradiation on silicon solar cells constituting power generator aboard Diapason IA satellite 03 p0362 A67-12897
Temporal variations of intensities of electrons of various energy ranges trapped in outer radiation zone measured by research satellite Injun III 04 p0693 A67-14962
Brittle fracture threshold of silicon, germanium and indium antimonide under pulsed electron irradiation 04 p0685 A67-15694
Gamma radiation effect on SCR correlated with electron radiation encountered by spacecraft 04 p0590 A67-15725
Photovoltage measurement across lifetime junction produced by electron irradiation and by changing surface recombination velocity 11 p1850 A67-24917
Silicon crystals composition effect on solar cells reaction to irradiation by 4 mev electrons 12 p1896 A67-25150
Book on electron radiation damage in semiconductors and metals covering lattice defects, alloys, atom displacement, EPR testing, etc 12 p1986 A67-25890
Specific resistance, EMF, Hall effect, and minority-carrier lifetime measurement of germanium whiskers bombarded by high energy electrons from linear accelerator 16 p2732 A67-31479
Subthreshold electron irradiation effects on surface recombination properties of n- and p-type germanium and silicon crystals 17 p2916 A67-32834
Electron radiation damage in CdSe crystals at cryogenic temperatures, noting electrical conductivity and cathodoluminescence properties before and during damage 17 p2916 A67-32838
Permanent displacement-induced effects in silicon semiconductor devices as function of radiation type and energy 17 p2917 A67-32847
Ionizing radiation effect on field effect MOST transistors, noting irradiation degradations 17 p2919 A67-32856
Influence of fast proton and electron irradiation on diffusion of substitution impurities in silicon 18 p3100 A67-33750
Isochronal annealing of short-circuit current of electron irradiated silicon solar cells 19 p3305 A67-35668
Electron emission utilized in evaluating metal surface properties, particularly sintered material porosity 19 p3247 A67-35849
Silicon solar cells bombarded by energetic electrons for radiation resistance 21 p3571 A67-38648
High energy electron radiation effects on silicon photocells deposited epitaxially on artificial satellite surface, discussing liberated carrier accumulation possibility 21 p3572 A67-38672
Junction potential measurement in irradiated tunnel diode showing no oscillation in any bias voltage 22 p3767 A67-39369
Irradiation damage in germanium monitored by electric conductivity measurements, noting carrier population depletion by introducing acceptor levels into forbidden gap 22 p3862 A67-39997
Low temperature electron irradiation effects on undoped GaSb resulting in impurity conduction 22 p3862 A67-40000
Si semiconductor strain gauge thermal coefficient of resistance /TCR/ reduction by

- high energy electron irradiation 23 p4008 A67-41391
Characteristics of high energy electron radiation and temperature and effect on N/P silicon solar cells 24 p4105 A67-42513
- ELECTRON RECOMBINATION**
Electron recombination in rapid cooling of magnetized plasma jet expanding into vacuum 03 p0486 A67-14195
Continuity equation for electrons in F-2 layer obtained for region near geomagnetic equator at noon including photoionization, recombination, drift, etc 04 p0614 A67-14954
Electron recombination in laser produced hydrogen discharge, noting temperature decay due to radiation, expansion cooling and electron loss 04 p0665 A67-15109
Electron recombination kinetics in diatomic and polyatomic gases expanding into emptiness 05 p0927 A67-16992
Effect of local states in forbidden band on electron processes in n-GaP crystals, diagramming absorption and photoluminescence excitation spectra 05 p0868 A67-17063
Reactive properties of p-n-n semiconductor structures at high injection levels for monomolecular electron-hole recombination 06 p1049 A67-17866
Interaction between two high resistivity layers in Mn doped GaAs separated by region of bulk material 06 p1051 A67-18222
Auger mechanism of recombination of electron emission from semiconductors and dielectrics 06 p1051 A67-18422
Stress-dependence of Si p-n junctions with dense generation-recombination centers, showing that shifts in bias I-V characteristics are due to bandgap changes 09 p1553 A67-21947
Electron recombination in argon plasma at atmospheric pressure in vicinity of 10,000 degrees K 09 p1550 A67-22584
Dielectronic recombination effect in hot dilute plasmas extended to energetically overlapping metastable levels involving matrix inversion in formal description 10 p1681 A67-22722
Electron capture coefficient of A-centers in silicon at helium temperatures 10 p1694 A67-23649
Time resolution spectroscopy applied to electron recombination in H plasma due to azimuthal pinch 11 p1841 A67-24769
Solid solution properties of niobium carbide-molybdenum carbide alloy, noting changes in electron structure 14 p2337 A67-28284
Electron recombination in rapid cooling of magnetized plasma jet expanding into vacuum 14 p2360 A67-28540
Effect of local states in forbidden band on electron processes in n-GaP crystals, diagramming absorption and photoluminescence excitation spectra 15 p2538 A67-29794
Electron recombination and capture processes at deep centers in n-type GaAs 16 p2724 A67-30604
Minority carrier lifetime in p-silicon, analyzed varying temperature and injection level and studying recombination 16 p2725 A67-30807
Solar UV spectrum interpretation taking into account dielectronic recombination processes in ionization equilibrium computation, obtaining spectral lines intensities, abundances and atmospheric structure indications 17 p2941 A67-32235
Population of atomic levels by cascade, dielectric and three-body electronic recombination, discussing spontaneous transition, electron impact and RF spectra 17 p2947 A67-32762
Radiation effects on carrier recombination and mobility and on lifetime of semiconductor devices 17 p2919 A67-32858
Electron capture coefficient of A-centers in silicon at helium temperatures 17 p2923 A67-33330
Dielectronic recombination and autoionization included in ionization formula for solar corona 17 p2952 A67-33392
Excitement of slow and fast recombination waves in semiconductors with mutually independent current-carrier concentrations and lifetime 18 p3099 A67-33696
Electron fluctuations variance and correlation coefficients computed for sensitized GaAs, comparing noisiness of deep recombination levels 19 p3306 A67-35732

- SbS recombination center concentration, whole capture cross sections and trap energy levels 22 p3846 A67-39503
- Size effects in platelets of multivalley bipolar semiconductors with long scattering and electron-hole recombination times, studying electric pinch effect 23 p4042 A67-41292
- ### ELECTRON SCATTERING
- Effective electron scattering cross section in helium and argon plasma with cesium vapor admixture measured by Langmuir probe theory 01 p0119 A67-10134
- Nearest neighbor electron scattering in silicon, showing existence of diffuse rings association with Kikuchi pattern 01 p0135 A67-10877
- Electron angular distribution in copper and gold thin films attributed to individual close interaction scattering phenomena 02 p0297 A67-11834
- Quasi-stationary techniques for calculating energies and widths of resonances occurring in electron-atom and electron-molecule scattering 02 p0269 A67-12449
- Temperature and stress dependence of electron lifetime in p-type Si-B and Ge-Zn between 1.5 and 4.2 degrees 02 p0301 A67-12523
- Energy spectra of avalanche electrons in copper, iron, aluminum and graphite determined by method of moments, considering polarization of medium and multiple scattering 02 p0316 A67-12768
- Electron collision cross section resonance mechanism analyzed via matrix methods, noting threshold effect application to electron scattering 03 p0470 A67-13219
- Low energy total and momentum-transfer scattering cross sections for electrons on He and Ar compared, using modified effective range formulas 03 p0471 A67-13319
- Secondary scattering of low energy electrons by rows of atoms, obtaining diffraction pattern 03 p0496 A67-13648
- Plasma streaming across magnetic field by beam polarization studied by Vlasov equation 03 p0484 A67-14042
- Thermal conductivity of lanthanum and monochalcogenides, noting role and temperature dependence of crystal-lattice conductivity 04 p0680 A67-15287
- Instabilities and scattering in space charge focused low voltage electron beams in absence of magnetic field 05 p0849 A67-17449
- Asymmetrical angular elastic scattering distribution of electrons on helium atoms, using Monte Carlo method 06 p1034 A67-17648
- Plasma half-space impedance for diffusive electron reflection from plasma vacuum boundary, noting damping decrement of surface electromagnetic wave, electric field Fourier components and absorption capacity 06 p1039 A67-18079
- Paired defect production rate in silicon created in single electron scattering event 06 p1053 A67-18711
- Interband electron absorption and dispersion during one-and two-photon processes in semiconductors subjected to electromagnetic field, noting laser applications 06 p1054 A67-18798
- Highly spin polarized carriers for studying neutral impurity scattering in P doped silicon 06 p1063 A67-18937
- Electron scattering by neutralized acceptors investigated in Ge and Si through cyclotron resonance 06 p1063 A67-18939
- Conduction band structure and anisotropy of electron scattering in n-GaAs, analyzing magnetoresistance and Hall effect 06 p1064 A67-18943
- Single-and double-quantum photodetachment of negative ions, giving cross sections for electron elastic scattering 07 p1225 A67-19494
- Cross sections for photodetachment of electron from negative atomic oxygen ion 07 p1225 A67-19497
- Variational bound method applied to calculation of lower bounds on S-wave phase shifts for scattering of electrons by hydrogen atoms 07 p1226 A67-19499
- DC resistivity due to electron scattering from vacancy, octahedral and tetrahedral interstitials in beryllium computed by diffraction model concept of pseudopotentials in metal theory 07 p1209 A67-19643
- Effect of spin exchange scattering by magnetic impurities on electronic properties of superconductor 07 p1235 A67-20129
- Hall mobility and thermal emf in indium antimonide with mixed electron scattering mechanism 07 p1237 A67-20182
- Electron scattering mechanism in SiC polytypes, noting mobility limiting mechanism from 300 to 800 degrees K 08 p1370 A67-21293
- Nernst-Ettingshausen coefficient calculated for scattering at short duration potential, at impurity ions and at acoustic oscillations 09 p1554 A67-21970
- Experimental verification of predictions of conventional quantum electrodynamic vacuum effects by Compton and other scattering techniques 09 p1534 A67-22021
- Electron impact spectrum of ethylene at low energy and right angle scattering, noting unresolved and forbidden transitions 09 p1458 A67-22027
- Domain formation process during passage of current through multivalley semiconductor when electron intervalley scattering drift length exceeds diffusion length 09 p1555 A67-22074
- Landau-Ginzburg theory extended to anisotropic superconducting energy gap, considering diffuse and specular boundary scattering 10 p1687 A67-22759
- Critical fields of thin superconducting films determined by specular reflection of electrons from surfaces 10 p1694 A67-23596
- Anisotropic properties of acoustic electron scattering in Si samples in 8 mm wavelength and liquid nitrogen temperature 10 p1695 A67-23664
- Van Allen belt proton measurements by pulse height analysis, using thin low-Z scintillator to minimize large angle electron scattering 11 p1856 A67-24014
- Local density and temperature measurement in wind tunnels determined by 50-keV electron scattering, using air as test gas 11 p1790 A67-24446
- Detection of vibrational structure of gases adsorbed on tungsten by low energy electron scattering 13 p2160 A67-27075
- Physics of plasmas, Volume 2, Weakly ionized gas, covering inelastic collision, free electron scattering, intermediary plasmas, etc 13 p2168 A67-27221
- Atmosphere model for pure helium star including only helium I and II transitions and electron scattering in calculating opacity 14 p2387 A67-28578
- Electron-electron scattering in field of monochromatic laser beam, noting resonances in effective Moller scattering cross section 14 p2334 A67-29078
- Electric field effect in terms of drifted Maxwellian distribution, considering nonparabolic electron scattering where dominant energy-loss mechanism is optical polar mode scattering 14 p2376 A67-29088
- Magnetic trap electron capture lifetime dependence on magnetic field determined by scattering by residual gas, noting adiabaticity parameter critical value 15 p2526 A67-29361
- Potentials occurring in excitation of highly ionized ions by electron impacts 15 p2520 A67-29527
- Local gas density measurements, using large angle scattering from electron beam passing through rarefied gas flow 15 p2490 A67-30152
- Phonon drag part of thermoelectric power in metals formula, by assuming electron scattering description by relaxation time 16 p2731 A67-31445
- Radiative transfer for electron scattering atmosphere, obtaining eigenfunctions of transport equations 17 p2950 A67-33164
- Nernst-Ettingshausen coefficient calculated for scattering at short duration potential, at impurity ions and at acoustic oscillations 17 p2923 A67-33307
- Anisotropic properties of acoustic electron scattering in Si samples in 8 mm wavelength and liquid nitrogen temperature 17 p2924 A67-33345
- Interband electron absorption and dispersion during one-and two-photon processes in semiconductors subjected to electromagnetic field, noting laser applications 18 p3102 A67-34417
- Band structure and current carrier scattering in hole-type SnTe, studying temperature dependence of electric conductivity, thermal EMF, Hall effect, etc 19 p3300 A67-34766
- Low energy electron scattering from hydrogen molecules in ground electronic and vibrational states, calculating rotational excitation cross section 20 p3491 A67-37687
- Electron scattering from diatomic molecules in fixed nucleus approximation using polarized single-center orbitals method applied to positively ionized hydrogen 20 p3491 A67-37689
- Quantum transport theories for calculating multiple scattering in doped semiconductors 21 p3682 A67-38386
- Static Green function for elastic electron scattering by hydrogen atoms, using integrodifferential equations to determine resonance energies 22 p3839 A67-39204
- Energy spectra of avalanche electrons in copper, iron, aluminum and graphite determined by method of moments, considering polarization of medium and multiple scattering 22 p3877 A67-40270
- Bond formation effect on electron scattering cross sections for molecular H, N and O 23 p4029 A67-40966
- Optical absorption, refractivity and electron scattering used to construct model dipole spectrum of molecular nitrogen and calculate dipole properties 24 p4190 A67-42096
- Frequency limitation of Gunn effect associated with relaxation time for intervalley electron scattering in small signal approximation 24 p4205 A67-42811
- ### ELECTRON SOURCE
- Electron sources from arc discharge plasma in metal vapor, using copper and tin cathodes 09 p1548 A67-22327
- Electrons energy spectrum stability dependence on spatial distribution of source, discussing cosmic ray generation 20 p3517 A67-36532
- ### ELECTRON SPECTRUM
- Power and DC spectra for electron motion due to plasma heating and diffusion in static magnetic and transverse random electric field 03 p0485 A67-14046
- Cosmic ray electron spectrum indicates universal 3 degrees K black body radiation confinement to galactic disk 04 p0692 A67-14948
- Electron energy spectrum measured near equator by satellite mounted scintillator 04 p0614 A67-14950
- Diffuse omnidirectional inverse Compton and synchrotron X and gamma radiation from cosmic distributions of fast electrons and thermal photons 05 p0882 A67-16404
- Electron spectra, pitch angle distributions and total ionization measured throughout radiation belts by satellite magnetic spectrometer and integrating ionization chamber 12 p1997 A67-25807
- Structure of X-ray K absorption edge of iron in Fe compounds, noting nature of chemical bond and structure of electron energy spectrum 12 p1957 A67-26109
- Gaussian and Lorentzian components separation in analyzing EPR spectrum in ruby, using variance techniques 15 p2536 A67-29499
- Zeeman effect of germanium I and II, discussing configuration-interaction, deriving intermediate-coupling wave functions 16 p2733 A67-31876
- Magnetic field induced changes in Bardeen-Cooper-Schrieffer spectrum of electronic excitations in pure type I superconductor and effect on electromagnetic radiation absorption 17 p2925 A67-33374
- Microburst precipitation of energetic electrons into auroral zone 18 p3035 A67-33596
- Chemical effects in X-ray spectra and inner shell photoelectron spectra of sulfur- and chlorine-oxygen anions and molecular orbital method 18 p2998 A67-34520
- Inner Van Allen belt proton dose rate and spectral charged particle environment profiles correlated, noting agreement with theoretical values 19 p3313 A67-35189
- Electron component observation in studying solar modulation of galactic cosmic rays, discussing Parker model and Gloeckler-Jokipii model 19 p3315 A67-35496
- Electron energy spectrum, showing intensity maxima from surface plasma oscillations, noting thin films effect on surface losses 19 p3307 A67-35789
- Photoelectric contribution to

magnetospheric electron density on basis of pitch redistribution of collision component 20 p3425 A67-36283

Magnesium oxide single crystal electronic spectrum obtained from reflectance spectra, observing large plasma peak in energy loss function 20 p3509 A67-36508

Switched Proton Electron Channeltron Spectrometer /SPECS/ developed for measurement of charged particles in space 20 p3443 A67-36517

Superconducting magnet spectrometer using lithium drifted silicon detectors for measurement of electron spectra 20 p3444 A67-36523

Cosmic-ray electron spectrum in disk-halo galactic model, studying inconsistencies in Ramaty and Lingenfelter analysis 20 p3518 A67-36946

Low pressure gas Cerenkov detector and spectrometer coupled into charged particle telescope for cosmic ray electron spectrum measurements, discussing efficiency and instrument calibration 20 p3452 A67-37566

Magnetically induced circular dichroism and birefringence in ICI electronic spectrum, noting frequency dependence and molecular rotation effect 22 p3758 A67-39638

Energetic outer radiation belt electron spectra spatial and time variations 22 p3873 A67-39822

LiF freshly cleaved crystal reflectance spectrum between UV and 28 eV, computing dielectric response function and measuring gamma exciton band 23 p4038 A67-40774

Probes containing various scintillators for measuring electron energy spectrum at high altitude in cosmic ray flux 23 p4054 A67-41095

Strong coupling superconductivity in intermetallic compounds, possibly due to all electrons having same kinetic energy 24 p4205 A67-42738

ELECTRON SPIN

Electron excitation cross section of transitions between spin multiplets of ground state of neutral oxygen atom calculated, using continuous state Hartree-Fock formulation 03 p0472 A67-13322

Spin localization enhancement or hindrance by superconductivity 05 p0863 A67-16757

Resistivity, magnetoresistance, Hall effect and thermal conductivity in n-type In-Sb at liquid He temperatures 06 p1068 A67-18968

Photoionization by spin-dependent electric dipole and spin-dependent magnetic quadrupole transitions with polarized electron spin 09 p1535 A67-22379

Steady state plasma belt in dipole magnetic field, measuring spatial variation of density and temperature, electron spin, gyration, etc 11 p1828 A67-23940

Irreducible tensorial components of two-electron operator and second-order density matrix for spin-projected single-determinantal wave function 16 p2705 A67-31759

Nonexponential electron spin cross relaxation measurement in dilute ruby 17 p2924 A67-33369

Operator for spin-phonon interaction between conduction electrons and polarization-induced longitudinal oscillations of semiconductor lattice 18 p3099 A67-33697

Specific heat of superconductors containing paramagnetic impurities calculated, noting effect of ordering impurity spins 19 p3303 A67-35045

Spin restricted, unrestricted, projected unrestricted and extended SCF wave functions energies compared, discussing calculation method for spin extended SCF functions 20 p3483 A67-36230

Hyperfine splitting of spin interaction energy of two hydrogen atoms, determining eigenfunctions for effective Hamiltonian 21 p3658 A67-37814

Spin-disorder resistivity measurements in Gd-Yt alloys noting temperature and concentration effects 22 p3863 A67-40203

ELECTRON SPIN RESONANCE

Electron resonance and magnetic properties of solid solution in bismuth ferrite and barium titanate system, obtaining phase diagram 01 p0127 A67-10063

Electron resonances of hydrogen ion calculated and illustrated by waves, using variational principle incorporating outgoing-wave boundary conditions 01 p0117 A67-10781

Three-body and wall recombination

coefficients of atomic nitrogen, using electron spin resonance spectrometer for concentration measurements 01 p0117 A67-10883

Electron spin resonance absorption spectrum of Pt in YAG at low temperatures, noting ionic orientation 03 p0492 A67-13326

Electron spin resonance with trigonal and orthorhombic symmetry in cerium oxide doped calcium fluoride 03 p0492 A67-13328

Electron spin resonance application to kinetic studies of free atoms and radicals in gases, particularly OH radical 04 p0566 A67-15173

Vanadium charge compensator in laser calcium tungstate, determining vanadium positions via electron spin resonance 04 p0633 A67-15306

Displacement effects in n-and p-type silicon when exposed to energetic radiation, using electron spin resonance and galvanomagnetic techniques 04 p0684 A67-15689

Electron spin resonance in phosphorus-doped silicon at various temperature ranges 05 p0861 A67-16499

Electron spin resonance of impurities in semiconductors, with attention to shallow centers 06 p1061 A67-18922

Electron double resonance for ionized impurity pairs in n-and p-type Si, noting splitting of resonance peaks and relaxation time of homopolar pair 06 p1068 A67-18970

Electron spin resonance of P doped Si at liquid He temperatures, obtaining paramagnetic susceptibility in metallic conduction region 06 p1068 A67-18972

Electron spin resonance in P-doped Si at liquid He temperature, noting effects of P concentration, impurity scattering, etc 06 p1068 A67-18973

Characteristic optical density and equilibrium of alkyl-sodium and aromatic hydrocarbons as function of temperature and wavelengths, correlating electron affinity with enthalpy values 09 p1458 A67-22214

Temperature dependence of electrical conductivity and Hall effect of barium-titanate crystals reduced by hydrogen, observing electron spin resonance and optical absorptions 14 p2363 A67-27824

Conversion process and ESR in gamma-irradiated dihydrothymine noting reaction rate 14 p2259 A67-28300

Electron spin resonance measurement of ground state population in ruby rod during optical pumping 15 p2497 A67-29389

Superhyperfine interactions in electron-spin-resonance spectrum of substitutional gadolinium 3 impurity in calcium fluoride single crystals under applied stress 17 p2913 A67-32367

Free radical formation correlated with breaking time and creep rate in solid polymers subject to crushing, breakdown and deformation 18 p3068 A67-33490

Nitric oxide reaction with triphenylmethylperoxy radical investigated in connection with study on reversible reaction 20 p3377 A67-37138

Hyperfine interaction between unpaired trapped electron and adjacent titanium 47 and 49 nuclei in F center ESR line in barium titanate 21 p3684 A67-38417

Electron-resonance spikes on Alouette I ionograms observed for proton gyro-effects in topside ionosphere 24 p4148 A67-42062

Na-acenaphthene reaction temperature dependence, studying optical density, precipitation, ion pair formation, coupling constants and hyperfine structure [JPL-TR-32-1144] 24 p4118 A67-42326

N-vinyl carbazole reactions with anionic initiators, discussing radical anion and polymer formation and ESR spectra [JPL-TR-32-1126] 24 p4118 A67-42601

Hall effect, resistivity, spin resonance and thermoelectric properties of poly(N-vinyl carbazole-iodine complex, demonstrating charge transfer state existence in system [JPL-TR-32-1074] 24 p4205 A67-42602

ELECTRON STATE

Localized electron states of semiconductor surface due to lattice defects, determining excited state, ground state and bonding energies 01 p0128 A67-10078

Degree of coherence for extended source, considering electron transitions, found to depend on electron initial and final state 01 p0091 A67-11227

Variational perturbation equations and

time-independent Schroedinger equation for two-, three- and four-electron atoms 02 p0271 A67-12724

Electron energy spectrum for alloyed semiconductors, determining state densities via Thomas-Fermi statistical method 04 p0681 A67-15296

S-D interaction in electronic band structure of transition metals represented by model Hamiltonian, treating copper band structure 07 p1238 A67-20217

Plasma oscillations of electron shell of atom, discussing natural frequency, damping, probability and participation of plasmon in atomic reactions 08 p1355 A67-20860

Localized electron states of semiconductor surface due to lattice defects, determining excited state, ground state and bonding energies 08 p1371 A67-21456

Growth of critical temperature of small superconductor samples explained within framework of BCS superconductivity theory without using electron pairing 08 p1372 A67-21502

Atomic beam source for metastable Ca atoms in measuring population numbers from absorption lines 09 p1534 A67-21564

Unrestricted projected Hartree-Fock solutions for two-electron systems, with application to special configuration superposition 09 p1535 A67-22380

Monte Carlo calculations of impurity band states in degenerate semiconductor 09 p1558 A67-22618

Perturbation theory applied to study of electron states and interband optical transfers in strong electric fields of semiconductors 10 p1695 A67-23659

Nonequilibrium states in metal-to-semiconductor junction resulting from emission of high energy holes and hot free electrons in same direction 13 p2176 A67-26861

Band structure of spinel-type semiconductors calculation, applying model potential to nearly free electron model 13 p2181 A67-27166

Silicon surface purified by argon ion bombardment and annealing, studying field effect kinetics 14 p2372 A67-28755

Perturbation theory applied to study of electron states and interband optical transfers in strong electric fields of semiconductors 17 p2924 A67-33340

Field ion microscopy of Ni-Mo alloys 18 p3065 A67-34364

Electromagnetic properties of metal considered for strong quantization of electron states in magnetic field 20 p3464 A67-36224

Scaling law derived from small angle scattering theory, interpreting data in spectroscopic manner to deduce potentials and interactions between electronic states 22 p3839 A67-39205

Ar II population inversion of 4s and 4p states in stationary arc discharge, measuring ionic and atomic spectral line shift, widths and intensities and emission power 24 p4196 A67-42245

ELECTRON TEMPERATURE

Microwave frequency measurements of radiation temperature of nitrogen afterglow plasma with Maxwellian electron velocity distributions 01 p0119 A67-10147

Electron temperature in electric discharge applied to argon ion laser 01 p0090 A67-10550

Thermalization rate of highly ionized plasma with initially hot ions and cold electrons, using laser scattering to observe time variation of electron temperature 01 p0125 A67-10912

Electron temperature in electric discharge applied to argon ion laser 01 p0091 A67-11058

Electrode losses in MHD generators with nonequilibrium and equilibrium ionization compared, attributing differences to coupling between conductivity and local dissipation 01 p0014 A67-11159

Homogeneous transfer equation in line formation, noting correlation between thermalization length and line source function of two-level atom 02 p0266 A67-1169F

Plasma electron temperature measured from soft X-ray bremsstrahlung absorption by beryllium foil 02 p0274 A67-12461

Measurement of sticking coefficient for thermal electrons in oxygen and air, using microwave circuits 02 p0274 A67-12466

Plasma probe for dense isothermal cesium

plasma, noting electron concentration and temperatures, potential distribution, etc 02 p0184 A67-12467

Electron temperature measurements in low voltage arc in saturated cesium vapor 02 p0275 A67-12470

Conductivity of plasma accelerated by progressive waves, noting wall thermal absorption effect on electron temperature [ONERA-TP-424] 02 p0279 A67-12794

Electron temperature and concentration in DC plasma arc determined from Thomson scattering of laser radiation 03 p0437 A67-13209

Electron scattering cross section of argon and atomic oxygen measured, using microwave interferometer for analysis of plasma produced in shock tube 03 p0472 A67-13320

Energy relaxation as explanation of changes in electron density and temperature of helium plasma in upper hybrid resonant heating 03 p0477 A67-13360

Electron thermal conductivity of fully ionized Lorentz gas, determining energy transfer from Landau damping of plasma waves and collision parameters 03 p0484 A67-14039

Afterglow decay of number density and electron temperature of plasma with rare collisions between electrons and molecules 03 p0487 A67-14343

Resonances of impedance of RF probe in low density plasma introduced by finite electron temperature 04 p0663 A67-14614

Shock wave structure in viscous heat conducting gas, deriving preservation law for irreversible energy flux, equation for velocity profile and expression for integral curve 04 p0604 A67-14747

Electron temperature and concentration in cesium plasma in low voltage arc measured, using double probe method 04 p0666 A67-15182

Effects of atmospheric composition and electric field on electron temperature 05 p0798 A67-16862

Current carrier scattering mechanism in PbTe determined from ratio of electric conductivity and Wiedemann-Franz ratio 05 p0868 A67-17067

Double probe and microwave resonance measurements of gas additives effect on radial variation of electron temperature and density with partial pressures in carbon dioxide-nitrogen-helium gas laser 05 p0828 A67-17274

Water-cooled electrostatic probe capability of measuring local electron temperature, electron density, floating potential and saturation current ratio in dense plasmas [AIAA PAPER 66-73] 05 p0856 A67-17344

Plasma in Ar positive column DC discharge examined for wavelike perturbations about equilibrium, noting striation dispersion relation, density variations and electron temperature 05 p0857 A67-17427

Plasma density, electron temperature and potential distribution measured across magnetic field, determining ion and electron-diffusion coefficients in plasma column 05 p0858 A67-17432

Arc diffusion measurements of electron temperature and density profile across magnetic field 05 p0858 A67-17433

Electron cooling in polar semiconductor by application of electric field 06 p1048 A67-17816

Electron temperatures and concentrations of charged particles behind strong shock wave in air measured noting techniques, maximal values and accuracy 06 p0983 A67-17878

Charged particle beam interaction with plasma, determining electron-ion temperatures and HF field 06 p1040 A67-18088

Production and diagnostic measurement of deuterium, helium and neon plasmas, stressing electron and ion heating and cooling and attendant equilibration 06 p1041 A67-18147

Error due to electron thermal energy fluctuations in mean electron temperature measurement by line intensity ratio 06 p1042 A67-18540

Electron-neutral particle collision and electron thermal conductivity effect on upper atmospheric electron and ion temperatures 06 p0998 A67-18702

Perpendicular magnetic field induced change in electron temperature of current carrying semiconducting plates 06 p1054 A67-18805

Discharge plasma in He and argon with cesium and potassium vapor admixtures noting electric field, conductivity, electron temperature and emission spectrum 07 p1227 A67-19115

Helium plasma density effect on results of spectroscopic electron temperature determination 07 p1228 A67-19514

Electron temperature and concentration at 1000 km altitude, obtaining resolution of two full diurnal cycles of ionospheric behavior 07 p1181 A67-19935

Plasma electron temperature determined from measured spectral line intensities 07 p1230 A67-20106

Coulomb interaction in two-zone superconductor model, noting variation of critical electron-temperature and effect on superconductivity 08 p1369 A67-20838

Electron temperature and density in F region analyzed for nighttime heating, using Langmuir probe measurements 08 p1327 A67-21364

Electron and ion temperature changes in sporadic E layer based on wind shear theory, using energy equation 08 p1327 A67-21366

Ion temperature profiles obtained from satellite measurements of dawn-dusk auroral zone orbits 08 p1329 A67-21482

Electron temperature variation in polar indium antimonide with dominant optical scattering 09 p1552 A67-21672

Numerical solutions for range of operating conditions in segmented linear MPD generators, using He-Cs working fluids 09 p1443 A67-21811

Law of mass action derivation of chemical equilibrium ionization of multitemperature system when electron and heavy particle temperature differ 09 p1544 A67-21858

Plasmoid density, electron temperature and radius variation during propagation through magnetic field, using electric and magnetic probes 09 p1545 A67-21996

Electron temperature higher than gas temperature in dense argon plasma in presence of electric field 09 p1547 A67-22325

Plasma potential and particle energies in cesium plasma measured by simultaneous observation of ion and electron energy spectra 09 p1548 A67-22338

Changes in electron concentration in lower ionosphere with temperature dependent effective recombination coefficient during transmission of pulse radio signals 10 p1630 A67-22791

Ionospheric diffusion spectra, obtaining information on neutral atmospheric winds and ionosphere dynamics 10 p1632 A67-22858

Ionospheric rocket sounding, measuring ion density and electron temperature between E and F layers 10 p1633 A67-22948

Electron and ion densities and temperatures measured by rockets in active auroras and correlated with directly measured ionizing flux 10 p1650 A67-23307

Langmuir probe and spectrometric electron temperature measurements in negative glow plasma compared, finding probe temperatures significantly higher 11 p1788 A67-23963

Anomalous losses in plasma confined in magnetic field, correlating loss process with tube dimensions, electron temperature, gas pressure and magnetic field 11 p1829 A67-24002

Quiescent plasma physics - Conference, Frascati, Italy, January 1967, Part 2 11 p1836 A67-24389

Electron temperature variation induced effects and Landau damping of ion acoustic waves studied in quiescent discharge tube plasma 11 p1837 A67-24395

Current flow through plasma sheath into magnetized plasma, noting negative resistance characteristics of sheath upon ion cyclotron frequency 11 p1837 A67-24397

Electron cyclotron resonance heating of alkali plasmas by electromagnet resonant absorption 11 p1838 A67-24407

Gross behavior and properties of laboratory plasma generation with combined transverse and longitudinal ionizing currents parallel to magnetic field 11 p1845 A67-25098

Electron and ionic temperatures from

incoherent diffusion spectra, noting dependence on height and permanent thermodynamic equilibrium below 130 km 12 p1931 A67-25108

Electron temperature vs plasma cell power input measured, determining electron energy loss factor for hot diatomic gases in electric field 12 p1973 A67-25398

Rocket and satellite measurements of electron and ion thermal structure of ionospheric F region 12 p1935 A67-25796

Plasmoid generated by Q-switched neodymium-glass laser radiation focused on solid target, estimating plasma electron temperature 12 p1986 A67-26065

Simple model atom selection for electron density calculation in low temperature nonequilibrium Cs plasmas 13 p2171 A67-27441

Computer method analysis of electron temperature and density behavior on basis of glow discharge for plasma electron balance equation solution 14 p2353 A67-27755

Phase shift between electron temperature, luminous intensity and electron density in stratified positive column of glow discharge 14 p2353 A67-27757

Ionization structure of elements H, He, C, N, O, Ne in planetary nebulae computed for theoretically determined electron temperature and electron density variation 14 p2382 A67-27847

Spectroscopic methods applied to plasma electron temperature and density measurements 14 p2322 A67-29045

Electron mobility and temperature due to electric field in polar semiconductor investigated assuming displaced Maxwellian velocity distribution 14 p2375 A67-29065

Diffusive separation due to electrical coupling of ions and hot electrons and effect on shock wave structure in plasmas 15 p2470 A67-29227

Plasmoid structure, analyzing interdependence of plasmoid parameters along length 15 p2526 A67-29256

Hotshot wind tunnel for ionized wakes of models in nitrogen hypersonic flow, determining electron temperature and density [ONERA-TP-455] 15 p2416 A67-29380

Current carrier scattering mechanism in PbTe determined from ratio of electric conductivity and Wiedemann-Franz ratio 15 p2539 A67-29798

Electron density and temperature in plasma measured, using self-focused laser beams 15 p2488 A67-29902

Automatic recording and computer analysis of double probe measurements in plasma research, calculating electron temperature and plasma density 15 p2489 A67-30092

Electron temperature reduction possibility in individual valleys of multivalley semiconductors, based on energy-balance equation in electron-temperature approximation 15 p2542 A67-30246

Field-aligned irregularities as effect of increased electron temperature in F-2 layer, analyzing heat production and loss mechanism 15 p2484 A67-30305

Electron drift mobility and electron and ion temperatures difference in two-component plasma obtained from momentum and energy balance equations 16 p2706 A67-30450

Mean absorption coefficient for optically thin plasma derived taking into account radiative losses, noting electron and ion temperature ratios 16 p2706 A67-30459

Polyatomic gaseous impurity effect on electric conductivity of alkaline plasma from axial field and electron temperature measurements 16 p2710 A67-30520

Boundary layer equations for two-temperature plasma, showing distinction between electron and ion thermal boundary layer thickness 16 p2712 A67-30544

Electron heating by direct discharge during plasmoid interaction involving polarization 16 p2717 A67-31182

Helium plasma electron temperature and density dependence, with/without magnetic field, on pinch discharge 16 p2718 A67-31187

Thermal plasma column instability concept applied to determine Kaufmann Criterion, calculating production coefficient, V-I characteristics, etc 16 p2719 A67-31229

Interferometrically-measured ion

- temperatures compared to electron temperatures in pure barium and barium-cesium plasmas produced by contact ionization 16 p2720 A67-31243
- Heating of upper atmosphere electron gas by indirect Joule dissipation of reverse current in ambient electrons demonstrated for high fluxes 16 p2739 A67-31405
- Auroral intensity ratio of green line of atomic oxygen and first negative band of nitrogen, showing rise in electron temperature above neutral particle temperature 16 p2666 A67-31413
- Coupling between free electron and molecular vibrational temperatures in plasma environments, noting energy distribution, application to MHD generation, etc 17 p2894 A67-32150
- Electron temperature measured in acetylene/oxygen mixture flame and found twice that of gas due to chemical energy transport to electron gas 17 p2968 A67-32151
- Correlation of measurement data on electrical conductivity of nonequilibrium plasma with impurities 17 p2895 A67-32153
- Vertical electron temperature and concentration distribution up to 480 km at middle latitudes from rockets 17 p2842 A67-32253
- Excitation temperatures of electron levels of CH molecule in photosphere 17 p2941 A67-32326
- Hall field intensity and asymptotic electron temperature of ionized argon-cesium mixture flow in transverse magnetic field with subsonic velocity 17 p2900 A67-32338
- Determination of electron density and temperature, gas temperature, atomic composition and flow velocity of high temperature gas stream 17 p2900 A67-32339
- F region and magnetosphere data obtained by incoherent-backscatter radar technique, studying ion and electron temperatures relationship to height, electron density profiles, etc 17 p2843 A67-32389
- Electron temperature/ion temperature ratio and oxygen atom ratio to sum of oxygen molecule and nitric oxide in F-1 layer obtained by radar 17 p2843 A67-32529
- Nonlinear interaction between weakly ionized helium magnetoplasma produced by HF discharge and microwave field 17 p2903 A67-32676
- Nonlocal heating of electrons of daytime ionosphere taking account of displacement along geomagnetic field lines, comparing Dalgarno and Thomson probes 17 p2844 A67-32708
- Diurnal variations of ionospheric ion/electron temperatures predicted assuming solar UV radiation heating, collisional cooling and heat transport by conduction 17 p2850 A67-33192
- Energy loss factors for slow electrons in hot gases determined by measuring electron temperature variation with HF electric field power 17 p2890 A67-33367
- Dielectronic recombination and autoionization included in ionization formula for solar corona 17 p2952 A67-33392
- Auroral rocket measurements of electron flux, electron and ion density, electron temperature and auroral brightness 18 p3034 A67-33593
- Ionospheric electron temperature incoherent backscatter measurements confirming predawn enhancement of 6300 angstroms airglow 18 p3039 A67-33624
- Argon plasma injection effect into low pressure coaxial magnetic field noting pressure, flow speed, electron temperature, etc 18 p3084 A67-33647
- Mobility measurement of electron capture in hydrocarbon flames using Hall effect, noting variation when injecting chlorine 18 p3146 A67-33691
- Carbon monoxide and hydrogen flames ionization and electron temperatures with methane premixing 18 p3151 A67-33807
- Perpendicular magnetic field inducer change in electron temperature of current carrying semiconducting plates 18 p3102 A67-34424
- Electron-atom collision cross-section in afterglow of pulsed cesium plasma as function of electron cyclotron absorption resonance and electron temperatures 19 p3271 A67-35076
- Electron temperature, concentration and potential distribution, measurement in moving striations by Langmuir probe method 19 p3273 A67-35095
- Dynamics of channel formation in nonisothermal pulsed discharge and nonequilibrium ionization in inert gas-cesium mixtures 19 p3278 A67-35132
- Thermodiffusion term in particle flux equation, showing large electron temperature variation across low voltage arc plasma 19 p3279 A67-35140
- High pressure helium arc plasma behavior in cylindrical duct explained by theoretical model with different electron and heavy particle temperatures 19 p3280 A67-35145
- Polar ionosphere by satellite-borne electron traps, measuring electron density, temperature, quasi-energetic electron flux, etc 19 p3215 A67-35174
- Auroral absorption events, discussing bremsstrahlung X-rays spectrum, electron densities and temperatures measured with rockets 19 p3312 A67-35188
- Electron temperature observation in E region with Langmuir probes on Nike Apache rockets, discussing solar radiation effect 19 p3216 A67-35193
- Electron density and temperature, solar UV radiation and upper atmosphere neutral components measured using rockets 19 p3218 A67-35215
- Ionospheric ion and electron densities and temperatures from rocket probes near geomagnetic equator 19 p3219 A67-35232
- Electron temperature and density profiles in lower ionosphere at sunset, describing temperature measurement technique 19 p3229 A67-35246
- Rocket observations of visible and UV dayglow including emission rates and electron density and temperature 19 p3221 A67-35277
- Plasmoid structure created by plasma injector and freely propagating in space, noting plasma composition, energy spectrum, electron temperature, density, etc 19 p3288 A67-35362
- Electron density and temperature measurements using RF capacitance probe and double Langmuir probe in auroral zone 19 p3222 A67-35455
- Absolute intensities of Lyman hydrogen alpha and beta lines used for interpretation of electron temperatures and density of emitting layers 19 p3325 A67-35464
- Electron temperature of H II region related to high temperature main sequence stars determined as function of electron density and radiation dilution factor 19 p3325 A67-35503
- Hot plasma corpuscular diagnostics methods, noting particle beam determination of hot plasma density, electron temperature and plasma electric fields 19 p3296 A67-35586
- Theory of Langmuir probes in plasmas with negative ions, considering different ion concentrations and electron temperatures 19 p3296 A67-35587
- Plasma production by ruby laser beam irradiation of lithium hydride particle, measuring electron temperatures 20 p3496 A67-36212
- Nonohmic electrical conduction of semiconducting thin films in strong electric fields analyzed using electron temperature approximation 20 p3506 A67-36219
- E and F region electron density and temperature measurements, using electrostatic probe and MOS electrometer 20 p3441 A67-36383
- Langmuir probe for electron density and temperature measurements in lower ionosphere 20 p3444 A67-36526
- Electron temperature and density distributions for helium plasma produced in coaxial accelerator measured spectroscopically, checking thermal equilibrium assumption 21 p3661 A67-37752
- Mach number effect on electron temperature structure of partially ionized monatomic and diatomic gas shocks 21 p3610 A67-37760
- Stabilization conditions of isothermal plasma drift in magnetic trap for comparable electron and ion temperatures 21 p3663 A67-37936
- Ionosphere thermal nonequilibrium during sunspot minimum noting electron density and temperature measurements and daily variations 21 p3616 A67-37999
- Ionospheric electron and ion temperatures during 10.7 cm-solar radio flux activity, giving scatter diagrams 21 p3616 A67-38000
- Discharge plasma in He and argon with cesium and potassium vapor admixtures noting electric field, conductivity, electron temperature and emission spectrum 21 p3664 A67-38160
- Electron-temperature dependence of electron collision frequency in afterglow plasma 21 p3667 A67-38414
- Spatial electron temperature distribution in electrodeless discharge, noting thermal conduction effect [AIAA PAPER 67-692] 21 p3672 A67-38721
- Plasma diagnostics using self-focused laser beams, determining electron density and temperature 21 p3673 A67-38734
- Current distribution and electron temperature profiles in nonequilibrium crossed field devices, considering nonuniformities, thermal diffusion, boundary layers and finite reaction rates effects [AIAA PAPER 67-715] 21 p3673 A67-38741
- Magnetic field effect on flow field and drag of blunt body in partially ionized argon plasma, obtaining electron density and temperature [AIAA PAPER 67-729] 21 p3673 A67-38753
- Electron temperature spatial variation in late He afterglow due to standing wave microwave heating 22 p3844 A67-39353
- F-2 layer contribution to vertical radio wave absorption, using information about structure, electron and ion temperatures 22 p3789 A67-39472
- Cold Cu electrode interaction with H plasma, measuring electrode I-V characteristics, interelectrode charge concentration, electron temperature, etc 22 p3846 A67-39505
- Cesium plasma ionization in low voltage arc discharge, measuring electron ionization capacity, electron temperature and cesium ionization and excitation cross sections 22 p3847 A67-39510
- Plasma electron and positive ion temperatures measurement using orbit magnetic analyzer probes 22 p3798 A67-39626
- Double probe method for determining electron temperature and density variations in HF hydrogen plasma during second harmonic cyclotron resonance 22 p3848 A67-39650
- Ionospheric and magnetospheric temperature measurements using rockets and satellites including neutral particle, ion and electrons 22 p3871 A67-39677
- Theta pinch energy loss determined and electron temperatures measured, discussing Poynting flux and plasma diamagnetism decay 22 p3849 A67-39696
- Cyclotron instability examined for plasma in magnetic mirror machines with anisotropic nonmonotonic ion distribution in velocity space 22 p3852 A67-39988
- Electron temperature measurements of powerful pulsed plasma discharge using spectral line intensity 22 p3852 A67-39991
- Ionospheric electron temperature and electron and ion density profiles from Japanese sounding rocket 23 p3997 A67-41478
- Electric field heating of D-region electrons shown to be inadequate to raise temperature above gas temperature [AFRL-67-0121] 24 p4146 A67-41808
- Differential departure from thermodynamic equilibrium and electron temperature in gaseous nebulae determined by observing RF emission lines 24 p4225 A67-41825
- Electron neutral heat transfer in plasmas, obtaining data on electron thermal diffusivity from pulsed heat flow experiments in helium afterglow 24 p4194 A67-41872
- Changes in electron concentration in lower ionosphere with temperature dependent effective recombination coefficient during transmission of pulse radio signals 24 p4149 A67-42127
- Ionospheric observation using Japanese sounding rocket, discussing electron density profile, ion density and electron temperature measurements 24 p4150 A67-42151
- Hot Langmuir probe in Cs plasma studied for method of controlling current voltage characteristics 24 p4154 A67-42210
- He-Ne gas mixture DC discharge electron temperature and concentration dependence on tube diameter, pressure and composition, using two-probe method 24 p4196 A67-42242

Ar produced in capillary arc discharge, studying charged particle density and electron temperature dependence on magnetic field intensity 24 p4196 A67-42244

ELECTRON TRAJECTORY

Fermi surface curvature of indium single crystals measured from RF size effect at reference point 01 p0133 A67-10742

Simplified 180 degrees focusing beta-ray spectrometer, noting electron trajectory radius, shape of vacuum chamber walls, etc 05 p0806 A67-16500

Focusing of electron beam from low noise gun with different magnet systems 05 p0777 A67-17279

Oscillation in finite plasma with two types of boundaries, showing dynamics of particles 05 p0859 A67-17448

Fermi surface curvature of indium single crystals measured from RF size effect at reference point 13 p2176 A67-26771

RF size effects in plane parallel metal plate, discussing skin effect in magnetic fields, electron trajectories and spherical Fermi surface 22 p3866 A67-40551

ELECTRON TRANSFER

Diffusion and electrical transfer of zinc in indium arsenide as affected by temperature 01 p0127 A67-10068

Thermoelectric generator performance, materials, technology, electron transport theory and phenomenological basis of thermoelectric effects 01 p0013 A67-10555

Low seated interfaces effect on electron transport in thin continuous metal films in presence of magnetic or electric fields 02 p0292 A67-11743

Electron conduction in discontinuous metal films by transport of activated charge carrier creation and by tunneling for island sizes 02 p0292 A67-11746

Semiconducting properties of lead telluride thin films, analyzing electron transport phenomena 02 p0294 A67-11756

Electron transport through thin insulating barriers in various diodes, analyzing current dependence on temperature and film thickness for perfect and imperfect dielectrics 02 p0294 A67-11760

Bulk GaAs Gunn effect oscillators and amplifiers and electron transfer between high mobility and low mobility conduction bands 02 p0218 A67-12099

Frank-Condon factors and transition probabilities of electron oscillatory transfers in diatomic molecules 03 p0471 A67-13314

Electron transfer in thin film tantalum-tantalum oxide diodes, noting tunnel and Schottky emission 04 p0582 A67-15106

Correction for characteristic number of E layer based on electron transport processes and seasonal variations 04 p0618 A67-15573

Similarity theory applied to electron processes in p-n junctions 06 p1048 A67-17854

Diffusion and electrical transfer of zinc in indium arsenide as affected by temperature 08 p1371 A67-21451

Electron transport phenomena in thermionic converter plasmas, emphasizing electron-ion collisions to electron momentum transfer collision frequency 09 p1450 A67-22351

Statistical survey of CW transferred electron oscillators/Gunn diode/ made from epitaxial gallium arsenide 10 p1616 A67-23532

Multiquantum electron transfers within conductivity band of semiconductors accompanied by emission or absorption of acoustic phonon, calculating absorption coefficient of electromagnetic emission 10 p1695 A67-23658

Electron transport coefficients and electron energy equation closed formulation for two-temperature plasma, considering elastic and nonelastic collisions 12 p1973 A67-25397

Electron transfer to multiply charged ions of various gases, noting scattering characteristics 13 p2187 A67-26989

Transfer of electrons from emitter or space charge region to collector in thermionic energy converter by negative ions 13 p2056 A67-27002

Autolization effects accompanying impairment of forbidden intercombination transfer in plasma due to atom collision with plasma electron 13 p2171 A67-27626

Domain originated functional integrated circuits with possible solid-state bulk effect extension from microwave systems to whole of electronics 14 p2281 A67-28022

Negative-resistance Gunn effect in gallium arsenide and indium phosphide due to field excited electron transfer 14 p2366 A67-28474

Two opposing tunnel currents determination through transition zone of metal-oxide-metal structure 14 p2367 A67-28515

Differential negative conductivity in n-type GaAs, using microwave electron heating 14 p2369 A67-28595

Equation describing electron transfer between semiconductor surface bands and space bands, applying Fermi concept 14 p2371 A67-28754

Photolization quantum yield in intrinsic-absorption region of cadmium selenide films 14 p2372 A67-28853

Frank-Condon factors and transition probabilities of electron oscillatory transfers in diatomic molecules 16 p2703 A67-30490

Recharge cross section in collisions of slow atoms or ions involving interparticle transfer of one electron 16 p2705 A67-31781

Multiquantum electron transfers within conductivity band of semiconductors accompanied by emission or absorption of acoustic phonon, calculating absorption coefficient of electromagnetic emission 17 p2924 A67-33339

Heterogeneous reaction in metal combustion for vapor-phase burning noting collision efficiency 18 p3149 A67-33797

Electron tunneling through thin dielectric films and damping relation to electron energy calculated, using band model and matrix methods 20 p3508 A67-36424

Electrical conductivity and transport properties of pure liquid metals 21 p3686 A67-39108

Gunn effect, describing electron transfer, domain propagation and space charge instabilities in GaAs 22 p3841 A67-40073

Electronic transport in graded band gap semiconductor heterojunctions without space charges, using method based on intraband transitions between complete Hamiltonian eigenstates 22 p3864 A67-40381

Electron transport theory for energy below 10 Mev, reviewing interactions, scattering, thick targets, complex geometry and penetration in space environment [UCC/DSSD-267] 24 p4190 A67-41805

ELECTRON TRANSITION

Green function method applied to calculating resonance absorption of electromagnetic radiation for interlevel transitions in thin film 01 p0127 A67-10072

Three new visible CW laser lines in discharge in singly-ionized Cl 01 p0089 A67-10373

Magnetic susceptibility studies show semiconductor to metal transition in titanium pentoxide and titanium trioxide, clarifying electronic nature of phase transition 01 p0132 A67-10376

Radiation from high energy level transitions excited in He-Ne laser during optical pumping with He lamp 01 p0090 A67-10513

Energy transfer mechanisms involving trivalent terbium and europium, noting that at 295 degrees K thermal effects cause overlap permitting dipole-dipole transfer to occur 01 p0134 A67-10874

Einstein A coefficient for lambda doublet transitions of ground state of OH 01 p0114 A67-10898

Degree of coherence for extended source, considering electron transitions, found to depend on electron initial and final state 01 p0091 A67-11227

Optical absorption edge in cadmium telluride, noting impurity bands and dependence on energy and temperature 02 p0281 A67-11492

Radiative transition probabilities between laser vibrational levels of carbon dioxide, noting relaxation time and dipole moment 02 p0252 A67-11891

Oscillatory relaxation of heavy two-atom molecules during single-quantum energy transitions in light-gas medium 02 p0269 A67-12422

Line profile in one-electron approximation compared with impact approximation 02 p0270 A67-12521

Short wave length series of edge emission of cadmium sulfide single crystals at temperatures between 18 and 150 degrees K 03 p0488 A67-12813

Nonemissive multiphonon transitions and

quantum yield for ruby R line 03 p0433 A67-12852

Absorption spectrum of activated nitrogen produced by microwave discharge in 600-1100 angstrom region [AFCLR-67-0109] 03 p0473 A67-13520

Electronic Raman scattering by neutral Zn and Mg acceptors in GaP, energy level transitions and accompanying phonon wing 04 p0673 A67-14477

Virtual transitions to low-lying continuum states in oxygen 04 p0659 A67-14478

K spectrum to obtain structure and regularities of occupation of external energy bands in transition from Sc to Cr 04 p0640 A67-15975

Radiative lifetimes of UV multiplets in Si, P, S, O, Ne 2 and Ar 2 measured via phase shift method, correcting for transition cascading 05 p0892 A67-16411

Isotope substitution effect on natural frequencies of vibrational-rotational transitions in diatomic and triatomic molecules and generation of new IR maser frequencies 05 p0816 A67-16634

Two-electron transitions in luminescence of excitons bound to neutral donors in gallium phosphide 06 p1051 A67-18210

Oscillatory magnetoabsorption of direct transition in layer compound gallium selenide near absolute 06 p1060 A67-18918

Optical absorption and oscillatory magnetoabsorption in tellurium, noting interband transition and lack of inversion symmetry 06 p1060 A67-18919

Spectral dependence of impurity photocurrent in single crystal CdS specimens in constant illumination 07 p1234 A67-20025

Electron impact spectrum of ethylene at low energy and right angle scattering, noting unresolved and forbidden transitions 09 p1458 A67-22027

Atomic collisions, excitation transfer processes and energy level transition probabilities in plasma of gas lasers 09 p1513 A67-22067

Gas laser frequency and emitted power dependence on resonator tuning 09 p1513 A67-22070

Effective excitation cross sections of helium simple levels under proton impacts 10 p1699 A67-22845

Electron collision with atmospheric nitrogen molecules, obtaining effective cross sections 10 p1633 A67-23047

Continuous spectra of atomic gases and low temperature plasma, analyzing photoionization cross section and electron transitions in neutral atom field 10 p1682 A67-23067

Exchange model of zero bias tunneling anomalies, discussing Hamiltonian, interference magnetic scattering and metal junctions 10 p1691 A67-23400

Laser emission at band-band transitions in impurity semiconductor without conservation of quasi-momentum 10 p1666 A67-23653

Combined resonance transition in indium antimonide induced by single photon absorption 13 p2178 A67-27083

Far IR electronic transitions in pure and doped solids 13 p2178 A67-27085

Stark broadening of hydrogen lines of large principal quantum number for RF transitions by electron and ion impact approximation 14 p2389 A67-28839

UV spectra of Mg III and Mg IV investigated by sliding spark in vacuum, noting various ionization charges in vacuum 14 p2351 A67-28944

Laser output reduced by rare gas impurities in molecular neutral CO and nitrogen gas lasers 15 p2500 A67-29910

Continuous spectrum emission from free-bound and free-free electron transitions into field of monatomic gas ion using shock tube 16 p2673 A67-31109

Laser emission at band-band transitions in impurity semiconductor without conservation of quasi-momentum 17 p2870 A67-33334

Spectral dependence of impurity photocurrent in single crystal CdS specimens in constant illumination 18 p3100 A67-33759

Molybdenum interband transitions noting low energy optical property anomalies and origin of two absorption bands 20 p3466 A67-36865

Solar radio emission mechanism for spin transitions of neutron beta decay electrons in external magnetic field 20 p3520 A67-37522

Ammonia inversion transition hyperfine

structure for nitrogen 14 and 15 nuclear masses measured with two-cavity maser spectrometer 20 p3462 A67-37565

Lifetime decrease of metastable state of chromium ion in ruby and emerald due to temperature raise, showing radiative transition 21 p3676 A67-37816

Circular polarization in j equals 1 to j equals zero transition in gas laser shown due to different atomic relaxation processes rates 21 p3640 A67-38353

Resonance electronic Raman effect and parametric induced anti-Stokes radiation in potassium vapor atoms 21 p3641 A67-38456

Electronic transitions optical saturations in polyatomic organic molecules with high intensity laser radiation, discussing relation to bleaching of dyes 22 p3817 A67-40487

Two-photon absorption theory extension to include vibronic mixing between different electronic states using two-photon laser excitation of polycyclic atomic molecules 23 p4013 A67-40964

ELECTRON TUBE

SA CATHODE RAY TUBE

SA DIODE

SA DISCHARGE TUBE

SA DUPLEXER

SA FIBER OPTICS

SA GAS TUBE

SA IGNITRON

SA KLYSTRON

SA MAGNETRON

SA MODULATOR

SA PHOTOTUBE

SA RESONATOR

SA SEMICONDUCTOR DEVICE

SA THYRATRON

SA TRAVELING WAVE TUBE

SA TRIODE

SA VACUUM TUBE

Resonance methods for measuring input admittance of low power electronic tubes of type used in telemetry, radar and TV over frequency range from 50 to 1000 MHz 02 p0279 A67-11462

Reflex klystron operation modes such as phase locked amplifier, regenerative amplifier, detector and mixer 03 p0387 A67-14101

Book on microwave engineering including transmission lines, resonators, waveguides, antennas, tubes, etc 04 p0583 A67-15269

Selenium stabilatron tubes for voltages of 1 v or less 07 p1149 A67-19165

Performance and wave growth of type-M transverse-field tubes in broad delay system 08 p1302 A67-20834

Comparison of electron tubes, transistors and FET noise figures as function of source impedance of generator 10 p1610 A67-22924

Field ion microscope design and operation, noting construction and experimental results 14 p2314 A67-27770

Optimum efficiency of high power klystrons for operation in fourth and fifth TV band, noting space charge effect 14 p2277 A67-27773

Performance of electron tube and solid state devices in microwave region, comparing low noise amplifier devices 14 p2289 A67-28913

Tube techniques - Conference, New York, September 1966 15 p2447 A67-29751

Electron tube requirements for space applications noting size, weight, environmental parameters, etc 15 p2447 A67-29752

Multipactor suppression properties of Ti, Cr, V and Ta determined using special electromagnetic cavities 15 p2448 A67-29757

Mutual pulling system between two klystrons, deriving equations for pulling bandwidth and for various system responses 20 p3398 A67-36772

Attenuation reduction by using hybrid wave in coaxial cables and resonators having supporting surfaces of enhanced reactance 20 p3384 A67-37214

Soviet monograph on multiphase relaxation oscillators including circuit analysis for use in automation, telematics and radio engineering 22 p3768 A67-39464

150-180 watts at 1000 MHz tetrode, examining mechanical durability and temperature stability of metallic electrodes and ceramic insulators 22 p3772 A67-39873

Nonlinear electrical problems requiring partial differential equations including magnetic saturation, parametric amplifier, electron tube, traveling wave amplifier and

semiconductor diodes 24 p4133 A67-43089

ELECTRONIC AMPLIFIER

Reflex klystron operation modes such as phase locked amplifier, regenerative amplifier, detector and mixer 03 p0387 A67-14101

Logarithmic tunnel diode amplifier design techniques and characteristics 04 p0580 A67-14597

Tunnel diode amplifier distortion by finite impedance at zero frequency and second harmonic frequency 05 p0775 A67-16945

Inductive correction effect on single stage tunnel diode RC amplifier, noting increase of upper frequency limit and shortening of wave front buildup time 06 p0970 A67-18213

Electronic analog detection and separation of oscillations slightly differing in amplitude 06 p1109 A67-18667

Small signal thin beam theory application to design of amplifiers, noting electronic gain as function of various parameters 09 p1478 A67-22261

Amplifier and self-excited oscillator employing reflex klystron with phase locking 11 p1757 A67-23907

Reduction of peak factor in FM system design leading to reduction of thermal noise and increase in spectrum truncation distortion 11 p1752 A67-24123

Conditions for minimum nonlinear distortion in power amplification of single band signal 11 p1772 A67-24983

Logarithmic amplifier designs based on follower type circuits 12 p1915 A67-25858

Power amplifier with discrimination of even harmonics in anode circuit and rectangular excitation 13 p2077 A67-26748

Noise figure expression using normal mode amplitudes for crossed field amplifiers 13 p2079 A67-26874

Aircraft alternator test drives and specification requirements 13 p2081 A67-27238

Transmittance of thin film field effect transistor with equivalent circuit with lumped constants and generalized transfer function of nonparametric 14 p2286 A67-28586

Performance of electron tube and solid state devices in microwave region, comparing low noise amplifier devices 14 p2289 A67-28913

Inductive correction effect on single stage tunnel diode RC amplifier, noting increase of upper frequency limit and shortening of wave front buildup time 16 p2635 A67-30479

Crossed film cryotron as single stage high gain amplifier, noting design features and performance 16 p2640 A67-31431

Instability in resonant amplifier and video pulse effect on amplifier resonant load during radio pulse formation 18 p3010 A67-33509

500 to 1000 MHz ultrahigh RF hybrid amplifier fabricated with microelectronic multilayer thin film technique, noting performance of components 21 p3596 A67-38342

Amplifier and self-excited oscillator employing reflex klystron with phase locking 21 p3600 A67-38935

Klystron amplifier stability during double interaction in output circuit determined assuming zero HF potential and electron flow not bunched 24 p4129 A67-42193

Active delay line with amplifiers converting electromagnetic oscillations into ultrasonic vibrations and back again 24 p4130 A67-42237

ELECTRONIC CONTROL

Aircraft DC electronic controls and generators for voltage regulation and system protection [SAE PAPER 670250] 11 p1745 A67-23983

Sensors and sensor control devices for use in high speed low altitude reconnaissance aircraft 15 p2485 A67-29162

Gain control of common emitter cascade by varying transistor regime, taking into account effect of operating frequency and temperature 16 p2637 A67-31027

Linear autodyne circuit allowing sensitivity control irrespective of oscillation level useful in NMR lines 19 p3202 A67-35791

Electronic control system for triaxial control of geocentric satellite and second stage of CORALIE 21 p3656 A67-38231

ELECTRONIC COUNTERMEASURE

Radar range and Doppler effect simulation by stationary target outlining passive electronic countermeasure technique 07 p1146 A67-19882

Passive electronics countermeasure device /chaff/ consisting of metal strips to produce radar echoes 18 p3001 A67-34118

ELECTRONIC EQUIPMENT

SA MICROMINIATURIZED ELECTRONIC EQUIPMENT

SA MINIATURE ELECTRONIC EQUIPMENT

SA SPACECRAFT ELECTRONIC EQUIPMENT

Integrated circuit application engineering and resultant advantages 01 p0034 A67-10271

Semiautomatic test equipment for airborne electronics equipment for reducing checkout time [SAE PAPER 660704] 01 p0049 A67-10597

High resolution optical shaft angle encoder with gallium arsenide diodes as light sources and compatible with integrated circuit techniques 01 p0073 A67-11113

Electronic device degradation and failure analysis in terms of changes in atomic and molecular levels 01 p0041 A67-11356

Fatigue failure analysis in small metallurgically-bonded joints in very small electronic components, using statistical analysis of random forces and dynamic response of member 01 p0084 A67-11359

RCA defense electronic products applied research 02 p0251 A67-11785

Plotting oriented graph of two-stage electronic circuit with cathode coupling 02 p0224 A67-11915

Electronic equipment for measuring peak and valley currents of tunnel diodes 02 p0216 A67-12037

National Electronics Conference, Chicago, October 1966 02 p0199 A67-12086

Reliability and MTBF of electronic devices 02 p0250 A67-12429

Book on electronics reliability, calculation and design 03 p0377 A67-13232

Universal circuit concept for fulfilling any electronic function 04 p0591 A67-14504

Book on nuclear radiation effects on electronic systems including radiation shielding, nuclear instrumentation systems and electronic design techniques 04 p0583 A67-15267

Submillimeter wavelength electronic devices, examining development of lasers and reflected wave tubes with overlapping effective wave range 05 p0825 A67-17168

Solar radiation integrator, discussing design, composition and performance characteristics 05 p0808 A67-17310

Electronic self-steering techniques applied to satellite communications system with high gain antennas, noting transdirective array and self-phasing array [AIAA PAPER 66-326] 06 p0967 A67-17690

Space radiation effect on satellite design, noting guidelines for electronic equipment shielding 06 p1078 A67-18419

Passive thermocontrol techniques for electronic equipment near descent engine skirts and plumes [AIAA PAPER 67-158] 06 p1117 A67-18479

Physical phenomena and electrical effects of various bodies in creating new automation elements 07 p1159 A67-19185

Electronic clocks, with frequency and phase variation negligible, as means of making air and space navigation exact 07 p1222 A67-19681

Book on electronic component reliability, noting effects of environmental conditions possible faults, various circuits, wiring, transformers, etc 07 p1158 A67-20206

Electronics methods used in laser technology and vice versa, emphasizing microwave photoelectronic devices, self-consistent gas discharges at optical frequencies, etc 08 p1338 A67-21269

Operation modes of electron beam generators with resonant oscillating systems and bipolar regenerative amplifiers developed from them 08 p1305 A67-21272

Thermoelectric cooling vs conventional cooling of electronic units 08 p1427 A67-21410

Environmentally induced stresses in encapsulated electronic modules measured using hydrostatically pressure-sensitive transducer, noting internal stress changes 08 p1306 A67-21410

- Failure reporting, analysis and correction on satellite programs, discussing system reliability 09 p1480 A67-22289
- Two electronic displays for aircraft using basic elements necessary for flight path control in problem of easy assimilation of information by pilot 10 p1601 A67-22905
- H-film /Kapton/ flexible circuits fabrication problems including tensile strength, pattern misregistration, delamination, embrittlement, etc 10 p1611 A67-23309
- Electronic efficiency of three types of TWT and dependences on dimensionless and dimension parameters 11 p1764 A67-24465
- Small size cylindrical gear reduction system design for servomotors of synchro systems in electronic equipment 11 p1745 A67-24553
- Electronics package for category II qualified jet business aircraft and function of system components [SAE PAPER 670254] 12 p1941 A67-25504
- Reliable decisions from unreliable measurements of electronic equipment via statistical method 12 p1949 A67-25524
- Heat sterilization in microelectronic assemblies 12 p1914 A67-25683
- High intensity acoustic test facility for electronic packages and structures 12 p1924 A67-25718
- Computer analysis, design and optimization of linear electronic networks 13 p2088 A67-26747
- Step-recovery action in transistor switch-off with current gain and reduction of load on driving source 13 p2078 A67-26784
- Avionics system development for V-STOL tactical aircraft, emphasizing onboard electrical system 13 p2053 A67-27222
- Rectangular pulse thyatron-type generator design and operational principles 13 p2081 A67-27276
- Organic contaminant effects on relay reliability, discussing materials, degassing and contamination 13 p2084 A67-27694
- Radiographic screening of relays for detection of solder balls, broken leads, cracks, etc 13 p2084 A67-27695
- Field ion microscope design and operation, noting construction and experimental results 14 p2314 A67-27770
- Low temperature closed cycle refrigeration for electronics, with emphasis on relationship to system effectiveness 14 p2278 A67-27785
- Electronic equipment reliability improvement methods and practices in Czechoslovakia 14 p2282 A67-28039
- Stability in electronic equipment 14 p2285 A67-28438
- Advances in microelectronics, emphasizing role of MOS transistors 14 p2285 A67-28458
- Surface cleaning of electrical and electronic equipment through water and oil removal by chemical compositions 14 p2327 A67-28822
- Handbook of materials and techniques for vacuum devices covering high temperature properties, materials selection, joining processes, etc 14 p2339 A67-28829
- Electronic equipment used for IR radiation measurement during space experiment, describing thermal effect detectors [ONERA-TP-465] 15 p2486 A67-29382
- Simulated space effects on microelectronic device materials 15 p2466 A67-29549
- Racalator as alternative to frequency synthesis noting design principles, operation and results 15 p2445 A67-29586
- Modular distance measurement using geometric model for electronic continuous wave distance measuring equipment 15 p2511 A67-29893
- Electronic device modelling criteria expressing physical structure, representing significant properties and leading to useful equivalent circuits for circuit analysis 15 p2452 A67-30013
- Handbook of electronic instruments and measurement techniques covering tools and instruments, components and equipment testing 15 p2490 A67-30232
- Estimation of mean overheating of casing and heated space inside air cooled electronic device 16 p2778 A67-30470
- Multilayer printed circuit board system for interconnecting microelectronic components noting application of X-ray, ultrasonic, beta ray, etc to process control 16 p2681 A67-30476
- Electronic equipment for generating delay times corresponding to missile velocity during optical recording by numerous sensors distributed along ballistic firing range 16 p2674 A67-31118
- High speed spark photography with electronic equipment, describing generating and control units and optical techniques for shock wave observation 16 p2674 A67-31127
- Cathodoluminescence detector for electron microprobe, noting components and use 16 p2677 A67-31432
- Thin-film and diffused passive component comparison, describing resistor and capacitor fabrication by using sputtered tantalum and inductors through nichrome/gold 16 p2640 A67-31528
- Thyristor assemblies /dimmers/, for control of power supply, noting operation principles and examples cited 16 p2641 A67-31566
- Off-line training technique achieving practical closed loop, suboptimal control laws and controllers 16 p2648 A67-31653
- Electronic components - IEEE and EIA Conference, Washington, May 1967 16 p2641 A67-31721
- Fluoric and electronic integrated circuits compared, presenting state of art in packaging 16 p2610 A67-31722
- All-electronic, ultra-fast scanning spectrometer utilizing image dissector for power spectral density function measurements of rapidly time varying optical emission 16 p2680 A67-31803
- Avionics equipment development for Cayuse helicopter, discussing design with respect to weight, size, maintainability and other logistical considerations [AHS PAPER 105] 16 p2680 A67-31822
- Electronic systems for V-STOL fighter aircraft, considering operational capabilities, reliability, maintenance and protection 17 p2795 A67-32032
- Computer-aided transistor design, characterization and optimization 17 p2823 A67-32198
- Operation and design principles of 200 MHz counter/shift register, noting integrated circuit fabrication techniques 17 p2824 A67-32306
- Low noise parametric down-converter by using two incommensurable pumping generators, noting gain bandwidth product and minimum noise temperature 17 p2824 A67-32315
- High power frequency multiplication using beam lead varactors in arrays noting construction, technique and conversion loss 17 p2826 A67-32623
- Acoustic hologram formation retaining holographic properties of Leith-Upatnelks holograms 17 p2860 A67-32625
- Electronic systems in Ariel III satellite detailing power distribution, storage control, telecommand, telemetry and data handling 17 p2827 A67-32822
- Materials engineering for electronic hardware, discussing design, development and construction, including tables on metallic finishes, coatings for printed wiring, etc 17 p2865 A67-33047
- Step recovery varactors in constant-component and microstrip CW duplexers 18 p3011 A67-34067
- Design and development of IR signature analysis technique for nondestructive testing of electronic and electromechanical assemblies 18 p3052 A67-34512
- Development and maintenance of equipment containing integrated circuits, discussing processing, fault isolation and human error 18 p3016 A67-34670
- Reliability prediction prospects for electronic products, considering factory-to-target progress and reliability factors 18 p3057 A67-34672
- Error effect in continuous Kalman filters used in orbit determination problems, deriving error bounds formula 19 p3199 A67-34779
- Equivalent transformation of electronic circuits having nonreciprocal elements studied by methods of component connection 19 p3201 A67-34908
- Chebyshev approximation principle applied to electronics problems, giving algorithm 19 p3201 A67-34909
- Antares triaxial tracking camera noting mounting, electronic and optical systems and performance techniques 19 p3229 A67-35267
- Space research activities in Denmark /1966-1967/, discussing instrumentation design and development, experiments, etc 19 p3319 A67-35281
- Book on electronic sensing devices covering physical-chemical-electronic effects in solids, liquids, gases, etc 19 p3230 A67-35533
- Program providing man-machine communication for electronic circuit analyses using time sharing computer 19 p3186 A67-35619
- Materials technology expansion in electronics industry, discussing complete equipment components processed on semiconductor slices and large scale integrated electronics 19 p3198 A67-36054
- Tunnel diode technology stressing electrical results 20 p3396 A67-36490
- High density packaging technique for aerospace electronic equipment of reliable and long-life qualities 20 p3397 A67-36603
- Static electricity as potential reliability problem in electronic equipment production, noting transistor failure 20 p3397 A67-36608
- Digital image formation from electronically detected holograms noting advantage in imagery of weak objects 20 p3448 A67-36852
- Space electronics in France, role in boosters, control, communication, onboard systems, etc 20 p3399 A67-36879
- Hardening technique for circuits using electrical shielding to withstand radiation effects of nuclear war 20 p3399 A67-36883
- Automation in electronic test equipment - Conference, New York, August-September 1966, Volume 3, Built-in test and continuous monitoring 20 p3416 A67-36969
- Three-dimensional projections on cathode ray tube screens noting visual transformations linking retinal image to space scene 20 p3450 A67-36985
- Contour-volumetric displays for processing and handling data in nuclear experiment 20 p3450 A67-36986
- Air traffic control /ATC/ in 1970s, discussing airports, electronic facilities and collision avoidance 20 p3482 A67-37441
- Computer interconnection resistance causing propagation delay in circuits, suggesting low temperature use as possible remedy 20 p3393 A67-37457
- Electronic system for measuring operator information retrieval in bisensory configuration, using video-record radar set and playback 20 p3419 A67-37639
- Electromagnetic compatibility operational problems aboard Apollo spacecraft tracking ship 20 p3387 A67-37641
- Soviet book on electronic and semiconductor devices of servosystems, examining theoretical principles, computational methods, design principles, analog and digital computers, etc 20 p3406 A67-37700
- Multistage receiver protector recovery period measurement, discussing nanosecond reaction time 21 p3589 A67-37819
- Thin films applications in electronic engineering - Conference, London, July 1966 21 p3589 A67-37915
- Industrial electronics measurement and control - Conference, Budapest, August 1967 21 p3591 A67-38157
- Electronic equipment in space booster, considering test methods, environment simulation and electronic packaging 21 p3592 A67-38229
- Satellite influence on microwave antenna design, discussing mount designs, multifunctional antenna feed systems, structural analysis and geometries for microwave antennas 21 p3593 A67-38233
- Forced air distribution systems for electronic equipment cooling 21 p3594 A67-38331
- Design, equipment and techniques of electronic packaging in Titan III program, stressing environmental levels and safety factors 21 p3595 A67-38335
- Noisy signal improvement through compact instrument, giving circuit and operational aspects and applications in ionospheric research 21 p3582 A67-38396
- Electrical communications techniques, Part 2, HF techniques 21 p3597 A67-38532
- Coupler type bend for double layer pillbox antennas, discussing measurements for performance characteristics 21 p3597 A67-38565

High efficiency tunable ferrite frequency doubler consisting of yttrium-iron-garnet disk at waveguide junction 21 p3598 A67-38572

Stellar detectors components, describing optical receiving, image tracking and photometric devices 21 p3628 A67-38651

Reliability evaluation of passive electronic components of ceramic and mica condensers and carbon resistors, including defects and stress analysis 21 p3571 A67-38671

Reflex klystron for 1.5 mm wavelength noting high current density cathodes, RF section simplification and better heat dissipation 22 p3768 A67-39493

Soviet monograph on skin effect theory, deriving relations defining electromagnetic field distribution in bulk conductors and plates 22 p3768 A67-39566

Inexpensive high vacuum high voltage feedthrough used in conical shock driver system for plasma research 22 p3774 A67-40348

Rapid Evaluation System To Repair Equipment /RESTORE/ approach to technical manual preparation on digital equipment 23 p4085 A67-40582

Electronic assembly loose parts detection system using nondestructive vibration testing 23 p4005 A67-41369

Balloon-borne electronic system for heavy primary cosmic ray particle charge identification noting compactness, low power consumption and circuit design 23 p4009 A67-41479

Electronic system reliability statistical estimates obtained from test results of components using series expansion 23 p3982 A67-41869

Electronic ellipsometer for measurement of very small changes in elliptically polarized light, discussing refractive index, Kerr effect and calibration 24 p4152 A67-41901

Computer applications in electronic circuits design, discussing optimal man/computer interface and data handling processes 24 p4126 A67-42477

Electronic equipment components unreliability in guided weapon systems, discussing packaging, environmental conditions and customer-manufacturer relations 24 p4161 A67-42479

Spacecraft long life and reliability, examining mechanical and electronic equipment margin testing problem [AIAA PAPER 87-880] 24 p4244 A67-43000

ELECTRONIC EQUIPMENT TESTING

Optimum tests for check of working order of system with minimal material losses of safe or fault system functioning 01 p0043 A67-10240

Computer-controlled data system with remote checkout capability for airborne electronic system evaluation 01 p0030 A67-11030

Maintainability diagnosis techniques and fields of application to electronic equipment, examining entropic methods, decreasing probability methods and linear analysis techniques 01 p0041 A67-11342

Reliability overstress testing of Gemini inertial measuring unit system electronics package, discussing vibration and temperature/altitude environment results 01 p0111 A67-11363

Electronic system reliability prediction without relying exclusively on failure rate information 01 p0042 A67-11372

Accelerated stress testing and reliability estimation for electronic components 01 p0085 A67-11373

Digital integrated circuits and methods of testing for AC, DC and ground noise margins, dynamic impedance, capacitance and inductance factors 02 p0207 A67-12112

Deterministic and quasi-deterministic methods of failure prediction in electronic systems for prevention strategy in system test or checkout program 04 p0581 A67-14879

Microwave and thermal vacuum testing to demonstrate design maturity of LEM rendezvous radar during simulated mission 04 p0576 A67-15397

Book on electronic testing covering RF interference, tracking systems, receivers and transmitters, flight control equipment, digital computers, etc 04 p0577 A67-15726

Electronic testing of transmitters and receivers noting AM and FM systems sensitivity, noise figures and image

rejection 04 p0590 A67-15727

Telemetry systems, discussing PAM/FM/FM system, airborne equipment parts, ground support system and electronic testing procedures 04 p0577 A67-15728

Range safety and tracking systems, discussing C-band beacon, CW transponder and command-destruct receiver operation and testing 04 p0577 A67-15729

RF interference detection and elimination from communication systems noting signal, frequency and amplitude analysis techniques 04 p0577 A67-15730

Sensors and signal conditioners, discussing operation and calibration of resistance thermometers, strain gauge pressure transducers and potentiometric transducers 04 p0626 A67-15731

Ordnance systems and devices noting composition, function, operation and testing procedures 04 p0557 A67-15734

Automatic flight control systems for missiles and aircraft, noting error sensing and correcting functions, calibration and testing methods 04 p0655 A67-15735

System display composition, discussing analog and digital indicators, equipment operation functions and testing 04 p0626 A67-15736

Analog computer design noting operation principles, application to guidance problems and testing and troubleshooting methods 04 p0579 A67-15737

Digital computer testing procedure, noting error isolation and location technique via process of elimination 04 p0579 A67-15738

Postmortem flaw detection methods and equipment for IC failure analysis 06 p0968 A67-18054

Printed circuit assembly testing, discussing preassembly component testing, test programming techniques, test facility requirements and economics 08 p1301 A67-20750

Environmental and experimental testing of electronic systems component reliability 08 p1302 A67-20906

Nondestructive testing techniques in radiation vulnerability analysis of electronic systems, noting ionization effects and permanent damage in semiconductors 09 p1471 A67-21868

Parameter control during vacuum deposition of electronic film circuits for obtaining acceptable tolerances 09 p1503 A67-22099

X-radiographic nondestructive testing and inspection for quality control of electronic and electromechanical devices including printed circuits, encapsulated modules, thin films, etc 10 p1611 A67-23311

Relay testing under operational voltages and currents, discussing timing circuits and sequencing and computer inputs outputs 12 p1922 A67-25698

Relay testing for Saturn program including vibration scan, radiographic inspection, etc 13 p2084 A67-27696

Optimum efficiency of high power klystrons for operation in fourth and fifth TV band, noting space charge effect 14 p2277 A67-27773

Microelectronic amplifiers, emphasizing reliability improvement and decreased sensitivity to parameter changes 15 p2443 A67-29239

Electronic checkout, environmental qualification and integration of OGO by spacecraft simulator and performance analysis system 16 p2654 A67-30639

Trace/tape controlled recording automatic checkout equipment/ system design to accommodate aircraft ground support task 16 p2635 A67-30834

Coevaporation of cermet resistor compounds investigated for resistance and stability 18 p3014 A67-34550

Reliability and maintainability case histories 18 p3005 A67-34696

Automatic high speed IC test equipment and procedure 19 p3192 A67-35027

Microelectronic failure mechanism, examining manufacture and processing methods and production of uniform and versatile material 19 p3193 A67-35029

MOS transistors handling, mounting and utilization compared to FETs 20 p3396 A67-36322

Automatic electronic test and checkout techniques, automatic test equipment history and high points of 1957-1959 DOD

symposia 20 p3416 A67-36970

Built-in test features in Minuteman II intercontinental ballistic missile weapons system electronics, discussing ground equipment including self-test features and status display techniques 20 p3417 A67-36973

Automation in electronic test equipment - Conference, New York University, August-September 1966, Volume 5, Built-in test and continuous monitoring 20 p3417 A67-36987

Digital computers for built-in self-test in airborne weapon system, with examples of mechanized tests from F-106/MA-1 system 20 p3392 A67-36989

Electronic instruments testing to ascertain environmental conditions for perfect operation, storage and transportation 21 p3589 A67-37920

IR for electronic circuit component diagnosis, discussing design criteria, quality control and acceptance testing 22 p3769 A67-39631

ELECTRONIC FILTER

SA MICROWAVE FILTER

Response of linear FM matched filter to gated noise 01 p0037 A67-10484

Counting control methods for multistable elements containing nonlinear quadrupole with comb type amplitude characteristic, using short-term action on LF filter 01 p0044 A67-10497

Notch steepness of open circuit transfer function of loaded exponentially tapered RC notch filter 01 p0041 A67-11317

Wideband elliptic-function band-stop transmission line filter design, computing characteristic impedances of filter element 02 p0214 A67-11779

Q-active filter for narrow-band noise measurement in LF range 02 p0216 A67-12038

Materials for energy transducers used in detection, generation or measurement of ultrasonic waves and materials for electrical filters 03 p0495 A67-13547

Synthesis procedure for distributed filters based on elliptic function or Cauer parameter lumped element prototype 04 p0580 A67-14859

Operational characteristics of transistorized smoothing filter working with parallel transistor 05 p0772 A67-16453

Smoothing filter with output controlled parallel transistors, discussing empirical and experimental formulas and approximate circuit calculation 06 p0971 A67-18215

Amplitude bounded noise and random measurement error smoothing, noting increased efficiency and possibility of narrow band application 06 p0975 A67-18217

Buildup effectiveness of sequence of quasi-coherent radio pulses by comb filter mated with ideally coherent signal 07 p1140 A67-19231

Filtering properties of frequency-stability transport circuits of molecular beam generator, noting design considerations for high efficiency 08 p1305 A67-21274

Probability of signal acquisition by phase locked oscillator system operating in frequency search mode, determining maximum admissible search rate without noise 08 p1295 A67-21275

Multiple sampled data systems with cyclically varying sampling rates, determining smoothing filters and periodic presampling filters 10 p1618 A67-22731

Optimum filtration of signals in presence of arbitrary interference, using orthogonal function series 10 p1607 A67-23443

Counting control methods for multistable elements containing nonlinear quadrupole with comb type amplitude characteristic, using short term action on LF filter 10 p1621 A67-23619

Wideband coupling filters with expressions for resonant frequencies, damping factors, etc 10 p1618 A67-23639

Active filter design combining flat amplitude response with flat time delay 12 p1915 A67-25973

Grounding of capacitors in integrated circuits noting insertion of gyrators 13 p2078 A67-26783

Microelectronic technique application to active filter design, noting monolithic realization of operational amplifier 14 p2280 A67-28017

Properties of selective filter containing inhomogeneous semiconductor RC circuit with distributed parameters 14 p2291 A67-28275

- Radar receiver as optimal filter and correlator, obtaining correlation and resulting ambiguity 15 p2434 A67-29181
- Design procedures for practical elliptic filter with high selectivity in very compact configuration, noting bandpass and band-stop applications 15 p2444 A67-29453
- Approximate solution to nonlinear problem of pull-in range of phase locked loops, noting filter configurations and methods of analysis 15 p2446 A67-29589
- Laser radiation control techniques using saturation filter or negative feedback circuit with resonator Q-factor depending on radiation field power 15 p2499 A67-29722
- Smoothing filter with output controlled parallel transistors, discussing empirical and experimental formulas and approximate circuit calculation 16 p2635 A67-30481
- Amplitude bounded noise and random measurement error smoothing, noting increased efficiency and possibility of narrow band application 16 p2642 A67-30483
- Thin film hybrid subaudio active filter design and fabrication, discussing power consumption, circuit breadboard performance, etc 18 p3015 A67-34559
- Optimal discrete filter corresponding to given analog filter for minimum mean square error 19 p3199 A67-34782
- Multiple-winding choke design replacing separate inductors in filtering circuit and reducing power supply size and weight 20 p3399 A67-36882
- Synthesis of control systems with minimum complexity, noting application to filter discrimination of nonstationary signals 20 p3409 A67-37223
- Design of adaptive systems with forced oscillations, using correlation and filter methods 20 p3410 A67-37228
- Output noise variance minimization, calculating smoothing coefficients for discrete time invariant filters used in sampled data systems 21 p3601 A67-38949
- High sensitivity information storage filter for spectrum analysis 21 p3601 A67-39067
- Transistorized LF LC filter with positive and negative feedback, analyzing circuit to increase Q-factor and narrow passband 22 p3772 A67-39869
- ELECTRONIC LEVEL**
- SA FORBIDDEN BAND**
- Shallow hydrogenic type acceptor levels produced by Li and P doping in zinc telluride and cadmium telluride, noting heat treatment effects 02 p0280 A67-11484
- Rotational intensity distribution of vacuum UV absorption spectrum bands of carbon monoxide arising through mixing of D state with neighboring states 02 p0269 A67-12450
- Chemiluminescence and chemionization in low pressure fuel-oxygen flames, measuring emission intensity of CH, carbon molecule and OH electronic bands 20 p3376 A67-37094
- ELECTRONIC MODULE**
- Weight, efficiency and control requirements of subsystems of electric propulsion applied to Mars missions, selecting power-conditioning modules for ion propulsion engines 02 p0302 A67-11516 [AIAA PAPER 66-501]
- Amplifier design using multistage transistor current mode, feedback systems and minimized voltage swings 03 p0386 A67-13977
- Reliable test method based on special strain gauge load transducer for embedment axial stress measurement in electronic modules 05 p0779 A67-17457
- Queueing theory applied to phased array radar maintenance problems, specifically replacement and repair of transmitter and/or receiver modules 08 p1292 A67-20668
- Interconnecting techniques for modules contained by printed circuit boards, noting usage of pin sockets and effect on maintainability and reliability 12 p1910 A67-25266
- Wire-connected electronic packaging module system providing change capability, design flexibility, arrangement freedom and volumetric efficiency 12 p1912 A67-25275
- Microwave modules using integrated circuits 15 p2451 A67-29926
- Thick film hybrid modules discussed for speed, circuit, power density and versatility 16 p2641 A67-31618
- Power supply family synthesized from series of modules evaluated for packaging design, treating module interconnection methods and optimum thermal characteristics 20 p3399 A67-36926
- ELECTRONIC PACKAGING**
- Rules for maximizing component accessibility when designing electronic equipment 01 p0078 A67-10166
- Packaging, manufacturing and design techniques used in total-system-in-box concept for integrated circuits 01 p0039 A67-11116
- Reliability overstress testing of Gemini inertial measuring unit system electronics package, discussing vibration and temperature/altitude environment 01 p0111 A67-11363
- Energetic particle monitoring satellites, discussing design and development of four IMP generations 01 p0156 A67-11415
- Miniaturized high shock package utilizing FM-modulated 19.8 megacycle transmitter and piezoresistive accelerometer for measuring deceleration 02 p0242 A67-12011
- Thermal model for transient heat transfer analysis of missile guidance systems for prediction of operating temperature 02 p0263 A67-12104
- Thermal control of Nimbus spacecraft by utilizing semipassive and passive thermal control elements to maintain temperature of overall spacecraft, subsystems and components 02 p0335 A67-12391
- Electronic Packaging and Production Conference, New York, June 1966 05 p0778 A67-17450
- Centaur electronic packages for space flight thermal and radiative environmental control 05 p0778 A67-17453
- Thermoelectric /Peltier/ refrigeration technique for cooling complex electronic equipment in avionic weapon systems line replaceable units 05 p0754 A67-17454
- High speed digital computer packaging for minimum transmission line wire length, backplane, module connections and maximum computation speed 05 p0778 A67-17455
- Automatic checkout equipment for prelaunch use, describing packaging technique 05 p0789 A67-17461
- Design technique for inertial navigation instruments makes it possible to package within instrument electronics necessary to control and operate each of its facilities 05 p0779 A67-17464
- Modular system for packaging microelectronic flat packs and miniature discrete electronic components 05 p0779 A67-17465
- Mechanical design and packaging of transceiver mounted in spacesuit helmet for intercommunication among astronauts and space vehicles 05 p0779 A67-17466
- Relation between packaging design and cooling, vibration, RF interference and reliability of microelectronic systems used in space vehicles 05 p0779 A67-17467
- Packaging failures in reentry/recoverable aerospace equipment due to design deficiencies in parts, materials and/or processes associated with physical hardware 05 p0779 A67-17468
- Failure rates and modes for nonoperating electronic packages, presenting solutions for reliability problem 05 p0780 A67-17469
- Glass encapsulation for various miniature diodes 06 p0968 A67-18096
- Thermal design of attitude translational control assembly /ACTA/ of lunar excursion module /LEM/ 08 p1303 A67-21062
- High density microelectronic circuitry, discussing interconnection through use of advanced materials and techniques 08 p1303 A67-21189
- Computer logic device development, discussing interdependence of various components and packaging methods 09 p1466 A67-21683
- Computer packaging technology, discussing form lead joining, interconnection, maintainability, handling, etc 09 p1467 A67-21684
- Electronic parts sterilization program noting results on capacitors, resistors, varactor diodes, microcircuits, transistors, transformers, diodes and operating temperatures 09 p1480 A67-22296
- Analytical methods using mass spectrometry and gas chromatography for contaminants affecting component reliability in gases enclosed within electronic components 10 p1611 A67-23310
- Planar packaging concepts for avionics equipment systems and circuit boards developed from extensive use of microcircuits and thin film circuits [SAE PAPER 670251] 11 p1758 A67-23984
- Axial lead package and stack design of batch fabricated matrices to speed integrated circuit assembly 11 p1760 A67-24260
- Storage reliability for electronic systems in missiles, noting factors affecting failure rates after dormant storage 11 p1768 A67-25010
- Electronic circuit packaging - Conference, University of Southern California, Los Angeles, August 1966 12 p1910 A67-25263
- Electronic packaging technique in thin film technology using flip-chip bonding and MTFI techniques 12 p1910 A67-25264
- Packaging method for integrated microwave transistor amplifier constructed on ceramic substrates 12 p1910 A67-25265
- Interconnecting techniques for modules contained by printed circuit boards, noting usage of pin sockets and effect on maintainability and reliability 12 p1910 A67-25266
- Shielding methods for electronic equipment packaging, considering magnetic, electromagnetic and RFI shielding in gamma and X-ray range 12 p1911 A67-25267
- Electronic package design for rugged military field service 12 p1911 A67-25268
- Percussive arc mode welding applicability to delicate components and butt type joints 12 p1948 A67-25269
- RF communication converter miniaturization and packaging techniques 12 p1911 A67-25271
- Silk screen techniques used for film circuitry implementation on integral sensor telemetry transmitter with standard components 12 p1911 A67-25272
- Packaging integrated circuit airborne tape control unit 12 p1911 A67-25273
- High density power converter using integrated circuits and thyristors, noting packaging 12 p1911 A67-25274
- Wire-connected electronic packaging module system providing change capability, design flexibility, arrangement freedom and volumetric efficiency 12 p1912 A67-25275
- Liquid cooling of integrated circuit systems to remove increased heat dissipation, noting heat transfer rates 12 p1915 A67-25888
- Dielectric isolation of integrated circuit via ceramic medium, discussing technique, testing and results 12 p1916 A67-25997
- Computer-aided layout of minilstick artwork 12 p1950 A67-26130
- High density circuit assembly system emphasizing micromodule method 12 p1917 A67-26205
- Bonding and packaging techniques in production of semiconductor integrated circuits, discussing chip, lead and thermopressure bonding methods 12 p1951 A67-26214
- Military electronics equipment packaging, discussing integrated circuits, module board design, interconnectors, nuclear radiation effect, heat dissipation, power supply design and cooling 13 p2083 A67-27447
- Integrated memory arrays, discussing packaging methods and comparing monolithic and hybrid large scale integration 14 p2280 A67-28014
- Thin film technique interconnecting integrated circuits by ultrasonic welding and multilayer thin film conductor networks 14 p2280 A67-28016
- Gate capacitance storage property of p-channel enhancement MOSTs used in achieving low power consumption values 14 p2281 A67-28020
- Heat removal from high density packaged electronics by bonded metallic heat sink [ASME PAPER 67-DE-47] 14 p2408 A67-28880
- Dielectric materials characteristics analysis to obtain flexible circuitry performance and selection factors, especially for flat cable [ASME PAPER 67-DE-52] 14 p2341 A67-28882
- Electrical property change of pressure sensitive electronic components upon embedment in casting resins, noting results of inductance changes in ferrite core transformer 14 p2341 A67-28954
- Printed circuit technology development

survey showing refining processes and techniques 16 p2641 A67-31622

Testing for leak-proof encapsulation of semiconductor devices by use of krypton 85 as radioactive tracer gas 17 p2823 A67-32297

Flip-chip bonding and dimensional transformation, low cost microcircuit production technique 18 p3014 A67-34549

Highly purified silicone junction coating resins and silicone molding compound for microelectronic packaging 18 p3069 A67-34564

Processes and instrumentation for forming contacts on microelectronics devices 19 p3236 A67-35022

Techniques for achieving contaminant-free sealed package of solid state active devices 19 p3236 A67-35024

High density packaging technique for aerospace electronic equipment of reliable and long-life qualities 20 p3397 A67-36603

Power supply family synthesized from series of modules evaluated for packaging design, treating module interconnection methods and optimum thermal characteristics 20 p3399 A67-36926

Electronic instruments testing to ascertain environmental conditions for perfect operation, storage and transportation 21 p3589 A67-37920

Electronic equipment in space booster, considering test methods, environment simulation and electronic packaging 21 p3592 A67-38229

Electronic packaging and production - Conference, Long Beach, California, January-February 1967 and New York, June 1967 21 p3593 A67-38327

Thermal design of electronic packaging of Nimbus satellite control system 21 p3594 A67-38328

Cordwood packaging concept for electronics thermal control in LEM, obtaining electronic package temperature field from finite difference equations 21 p3594 A67-38329

Microelectronic circuit packages, discussing interconnection wiring and optimization 21 p3594 A67-38333

Design, equipment and techniques of electronic packaging in Titan III program, stressing environmental levels and safety factors 21 p3595 A67-38335

Flexible circuitry method of electronic packaging stressing use of flat cables 21 p3595 A67-38336

Design and construction of power supply without hookup cables for manned lunar vehicle 21 p3571 A67-38337

Packaging of IC core memory for aerospace use, discussing design and production of boards 21 p3595 A67-38338

Packaging of satellite plated wire memory components including memory plane stack, electronic circuit modules and interconnections 21 p3595 A67-38339

Production process of hermetically sealed electronic package for aerospace use 21 p3595 A67-38340

Packaging design of modular power supplies for airborne computers 21 p3596 A67-38341

Thick film design considerations covering material and micropart selection, circuit cost, reliability, substrate size and delivery schedule 21 p3596 A67-38346

Electronic packaging - SAE Conference, New York, February 1967 21 p3634 A67-38618

Modular packaging technique using dual in-line integrated circuits, discussing advantages, interconnection matrix and conversion from logic diagram to graphic format 21 p3634 A67-38619

Electronic flat-pack processes covering sealing methods, material combinations, leakage determination, etc 21 p3634 A67-38621

Flat pack interconnection technique using hot gas soldering, discussing inspection and control requirements 21 p3635 A67-38626

Electronic packaging techniques for electromagnetic compatibility covering electric and magnetic fields suppression and common impedance interference avoidance 21 p3599 A67-38627

Electronic circuit packaging in Apollo lunar module signal conditioning equipment 21 p3635 A67-38628

Cross-wire resistance welded metal joints for aerospace electronic packing assemblies, investigating embedment, mechanical strength and materials

evaluation 21 p3635 A67-38629

Thermal stress analysis of epoxy encapsulants using mathematical model for predicting performance in thermal shock 21 p3723 A67-38630

Impurity sources in hermetic electronic packaging investigated using mass spectrography and gas chromatography, comparing packaging techniques 21 p3636 A67-38632

Plasma sprayed alumina and beryllia dielectric coatings for heat sinks in electronic packaging, emphasizing heat dissipation from heat/generating components 21 p3650 A67-38849

Book on reusable protective packaging of military, electronic and aerospace instruments and systems 22 p3771 A67-39832

Electronic parts degradations induced by assembling and packaging environments investigated for effects upon failure modes 22 p3771 A67-39834

Electronic equipment components unreliability in guided weapon systems, discussing packaging, environmental conditions and customer-manufacturer relations 24 p4161 A67-42479

ELECTRONIC PHOTOGRAPHY

SA ASTRONOMICAL PHOTOGRAPHY

Picture generation by computer for concept demonstration, subsequently photographed with automated microfilm camera 08 p1299 A67-21050

Electronic zoom by varying vidicon raster size 14 p2321 A67-28920

Performance of fiber-optics coupled cascade image intensifier systems from standpoint of overall system noise, resolution, gain, contrast degradation and information rate 17 p2859 A67-32504

ELECTRONIC RECORDING INSTRUMENT

Automatic recording equipment measuring polarization angle of Syncom III 137 mc/s radio signal and determination of ionospheric total electron content 03 p0415 A67-14110

Recording telethermometer for use at airports, noting performance characteristics including unattended reliability, rapid response time, etc 10 p1656 A67-23088

High resolution spectroscopy, using incoherent light mixed with coherent laser light, for astronomical purposes 17 p2854 A67-32234

Flow velocity measurement in shock tube using electronic Bascule Bootstrap type installation 17 p2855 A67-32287

Cosmic X-ray sources spectra obtained by proportional counters and electronic systems on sounding rockets 23 p4001 A67-41222

ELECTRONIC SIGNAL MEASUREMENT

Subnanosecond time interval measurements with recirculating transmission line memory 02 p0243 A67-12092

Rastering nanosecond laser sensitometer for materials responsive to short duration signals, discussing recording, sensitometric and measuring subsystem 17 p2858 A67-32482

ELECTRONIC STRUCTURE

Complex band structure properties in diamond type crystals, discussing symmetry of various surface states with and without spin-orbit coupling 01 p0134 A67-10786

Optical properties of thin metallic films relative to electronic structure in microcrystals 02 p0288 A67-11722

Photoelectric emission of metal films with electronic structure evolving with film thickness 02 p0290 A67-11731

Electron conduction band structure of NaI crystals, using Hartree-Fock-Slater modified equation 03 p0495 A67-13513

K spectrum to obtain structure and regularities of occupation of external energy bands in transition from Sc to Cr 04 p0640 A67-15975

Structures of divalent and trivalent metals in terms of pseudopotentials and second order perturbation theory 05 p0869 A67-17189

Increase in low temperature specific heat and change in electronic density of states of boronated graphite 05 p0833 A67-17197

Isotope effects on superconducting transition temperature of molybdenum boride and tungsten boride 06 p1047 A67-17642

Modulus of elasticity of metals and titanium alloys as function of electron structure and binding energy 07 p1206 A67-19279

Eigenvalues of five lowest lying states for three electron atomic systems obtained using conventional Rayleigh-Ritz variational method 07 p1226 A67-19500

Correlation of physical properties of transition elements with atomic electron structure, noting energetic stability of configurations 09 p1517 A67-21878

Electronic band structure calculations phase of Ca, Sr and Ba over wide range of atomic volumes under pressure electronic band structure calculations for fcc phase of Ca, Sr and Ba over wide range of 10 p1682 A67-23395

Photoemission study of electronic structure of CdTe, considering two strong reflectivity peaks in optical reflectivity spectrum [AFRL-67-0405] 12 p1983 A67-25478

Electronic structure and electrophysical properties of d-transition metal sulphides 12 p1986 A67-26096

Band structure of spinel-type semiconductors calculation, applying model potential to nearly free electron model 13 p2181 A67-27166

UV optical properties and electronic band structure of magnesium oxide 13 p2181 A67-27167

Electronic states and transitions of zirconium oxide, noting Franck-Condon factors and r centroids, calculated from Morse model 16 p2704 A67-31173

Silver-gold and silver-germanium alloys tested for Fermi surface changes with alloying, using thermoelectric power measurements 16 p2731 A67-31448

Electronic structure of irradiation defects in ionic solids vacancies, interstitials and dislocations, explaining electronic relaxation 19 p3306 A67-35673

Existence of ozone difluoride established by low temperature experiments and correlation with mass spectrometric EPR, IR and NMR 20 p3377 A67-37136

Quantum mechanical accounting for materials optical properties, considering electronic structure 20 p3515 A67-37717

Diamond electronic structure studied by absolute reflectance measurements, obtaining dielectric response function over broad energy range 22 p3862 A67-39995

ELECTRONIC SWITCH

X sub L band waveguide switches using p-i-n diodes for switching elements in SPST, SP2T, SP4T and SP8T microwave switches 04 p0580 A67-14863

Solid state pulse modulated 10 MHz/channel passband frequency switch design and reduction to microelectronic form 05 p0789 A67-17043

Electronically despun switched antenna using variable phase shifters to control phase of incident power to circular array of elements 06 p0967 A67-17684

Three-port 35-GHz ferrite circulator latching switch, discussing geometric configurations, effects on performance characteristics, ferromagnetic materials selection, etc 08 p1304 A67-21225

Integrated MOS-FET analog gate for pointing and logic of space telemetry switch 21 p3592 A67-38227

ELECTRONIC TRANSDUCER

SA ULTRASONIC WAVE TRANSDUCER

Linearization of nonlinear transducer output transfer function by digital voltmeter 01 p0076 A67-11143

Electric field forced ferroelectric-antiferroelectric state transitions in transducers 03 p0426 A67-14301

Measurement of laser frequency control characteristics of piezoelectric transducers noting effect of mechanical structure supporting transducer on frequency control characteristics 15 p2502 A67-30426

Balanced SHF transducer for microwave receiver input with separate signal and heterodyne lines coupled by directional bond openings, noting decoupled inputs 22 p3772 A67-39875

Basic displacement transducers, electromagnetic transducer theory and design 23 p4008 A67-41423

ELECTRONICS

SA AVIONICS

SA MEDICAL ELECTRONICS

SA MICROELECTRONICS

SA MOLECULAR ELECTRONICS

SA RADIO ELECTRONICS

High speed nuclear electronics

Colloquium, Polytechnic Institute and Nuclear Study Center, Grenoble, France, February 1966 01 p0065 A67-10649

Radioisotopes for aerospace - symposium, Dayton, February 1966, Part 1, Advances and techniques 02 p0243 A67-12207

Integrated circuit development noting role of NASA and industry

[AIAA PAPER 66-835] 02 p0220 A67-12254

Soviet papers on quantum electronics 03 p0434 A67-13124

Text on high power electronics including cathodic losses in magnetrons, electrodynamic theory of grids, high frequency measurement, secondary electron emission and electromagnetic oscillations 03 p0379 A67-13301

Physical foundations of cathode electronics - All-Union Conference, Leningrad, October 1965 06 p1036 A67-18421

Aerospace and electronic systems - IEEE Convention, Washington, D.C., October 1966 08 p1290 A67-20646

Aerospace and electronic systems - IEEE Convention, Los Angeles, February 1967 09 p1466 A67-21674

Preparation and properties of electronic materials for radiative processes control - AIME Conference, Boston, August 1966 11 p1847 A67-24734

Electronics and vacuum physics - Conference, Prague, September 1965 14 p2352 A67-27747

Radio spectroscopy and quantum electronics - Conference, Poznan, Poland, April 1966 14 p2332 A67-28967

Epoxy casting resins as structural material in electronic industry, with tables of various hardener characteristics, viscosities, epoxy equivalents, etc 15 p2508 A67-29683

1967 SWIEECO record - IEEE Conference, Dallas, April 1967 15 p2450 A67-29901

Book on large signal transistor circuits covering device physics and equivalent circuits 15 p2454 A67-30233

Aerospace electronics - Conference, Dayton, May 1967 17 p2855 A67-32467

SST flight control system electronic and hydraulic systems, discussing system design, components, reliability and test programs [AIAA PAPER 67-570] 19 p3174 A67-35966

Electronics - Conference, Rome, June 1966, Volume 1 20 p3393 A67-36234

Physical electronics formulas tabulated, with solid state physics variables dimensionally coded and resultant nondimensional products cataloged, using computer routine 20 p3506 A67-36235

Advances in electronics and electron physics, Volume 23 22 p3799 A67-39769

ELECTROPHORESIS

SA COLLOID

EFM, interplay of electric fields with insulating fluids which cannot remain nonconductive at high temperatures, considering astronautics application 01 p0014 A67-11408

Dielectrophoretic propellant orientation systems design, noting electrode requirements and avoidance of electrohydrodynamic instabilities [AIAA PAPER 66-922] 02 p0301 A67-12275

Aircraft corrosion protection, discussing relaxation and electrophoretic deposition of multilayer synthetic resin 04 p0636 A67-14576

Enzymatic activity and inhibition, thermal stability and electrophoretic properties of induced and constitutive acid phosphatases of *Euglena gracilis* 10 p1598 A67-23397

Wear life improvement of ceramic bonded solid film lubricant by compression and artificial filling of film voids [ASLE PREPRINT 67AM 7A-2] 14 p2326 A67-28790

Electrophoretic coating of metals compared with cathodic and anodic synthetic depositions 18 p3054 A67-34098

Batch fabrication method for storage elements using electrophoretic deposition of ferrite on platinum wire 22 p3812 A67-39915

Particle electrophoresis technique for rapid clinical microorganism identification in blood elements, noting applications in serum protein analysis and antigen antibody reaction quantitation 23 p3956 A67-41628

ELECTROPHOTOMETRY

S PHOTOELECTRIC PHOTOMETRY

ELECTROPHYSIOLOGY

High magnetic fields effect on cardiac

activity in spontaneously excited isolated turtle heart by simultaneous and separate electrical and mechanical measurement 05 p0755 A67-16282

Waveforms of spike potentials form neurons in anteroventral cochlear nucleus indicate spikes are composed of three components 08 p1286 A67-20367

Blockage of electrically evoked pupilodilation in cat by irradiating hypothalamus with cyclotron-accelerated alpha particles 10 p1598 A67-23394

Absolute threshold of cat optic nerves determined by inspection of poststimulus time histograms, computed from responses of identical flashes of white light 10 p1598 A67-23581

Electrophysiological tests performed onboard Voskhod I noting apparatus recording electroencephalograph, electrooculogram, dynamogram and motion coordination in writing of astronauts 16 p2616 A67-30760

Peripheral auditory system model relating all-or-none activity of nerve fibers to acoustic stimulation 17 p2806 A67-32044

Cortical electroencephalographic activity /EEG/ relation to behavioral changes in chimpanzee following rapid decompression to near vacuum 18 p2991 A67-34713

ELECTROPLATING

Metallizing and plating techniques for printed circuit fabrication 08 p1334 A67-20744

Printed circuit board manufacturing process assuring crack-free plated-through hole 08 p1304 A67-21190

High speed computer memory design using plated wire elements 19 p3189 A67-36065

Automatic plating system insuring quality finishes by selectively phosphating or chromating parts after zinc plating 23 p4010 A67-41351

ELECTROPLETHYSMOGRAPHY

Intracranial pressure measurements and electroplethysmographic examination of blood content in dog cranial cavity for transverse acceleration up to 40 g 13 p2057 A67-26456

ELECTRORETINOGRAM

Photochemical cells and site involved in visual adaptation, reporting electroretinogram data 06 p0953 A67-18643

ELECTROSTATIC CHARGING

Measurement and control of corona-generated noise in aircraft, noting charge rate during takeoff via potential gradient method 02 p0190 A67-11501

Structure of electrostatic charge transported by pulsed plasma flow produced by coaxial source 13 p2168 A67-27306

Electrostatic discharging systems for helicopters, discussing earth field effect and fail-safe concept [AHS PAPER 107] 16 p2610 A67-31824

ELECTROSTATIC DRAG

Electric drag of satellites noting contribution of impinging ions 04 p0705 A67-14998

ELECTROSTATIC ENGINE

Tornado angular momentum as derived from electrostatic motor type action in parent cloud 04 p0649 A67-14678

Interactions in low density plasma beams of electrostatic thrust engine exhaust, discussing neutralization, instabilities, plasma wind tunnel, etc 04 p0690 A67-15022

Computer program and mathematical model for design of electrostatic colloid thruster [AIAA PAPER 67-84] 06 p1075 A67-18499

Electrostatic ion engine timetable, noting contact ion and electron bombardment engines and application to NASA Applications Technology Satellite series 17 p2928 A67-32435

Computer program and mathematical model for design of electrostatic colloid thruster [AIAA PAPER 67-84] 22 p3868 A67-40101

ELECTROSTATIC FIELD

Rotating vane electric field meter system flown on Nike-Cajon sounding rocket to determine electrostatic potential on vehicle throughout flight 01 p0074 A67-11126

Vibrating-piston electrostatic field sensor for Gemini program, examining design improvements including unity-feedback preamplifier, noise reduction devices, etc 01 p0074 A67-11127

Particle deflection techniques for determining electrostatic field strengths,

detailing application to surface field strengths for isolated spacecraft 01 p0074 A67-11129

Graphical data concerning drifting beams as possibility for calculation of reduction coefficient of space charge field of electron beams moving in periodic electrostatic fields 05 p0764 A67-16908

Dynamics of ionized stellar winds noting anisotropic effect of stress tensors and densities, velocities and electrostatic potentials distributions [AIAA PAPER 67-146] 06 p1088 A67-18476

Uniaxial stress and static electric field effects on energy band structure of strontium titanate and derivation of optical selection rules in region of perturbed crystals 10 p1691 A67-23403

Scattering of circularly polarized electromagnetic wave in Coulomb field, noting coalescence of two-wave quanta into one quantum of double frequency 10 p1666 A67-23594

Height distribution of Sq current intensity in midlatitude ionosphere as function of electrostatic field direction 11 p1786 A67-24333

Ion acceleration region demonstrated by coupling two HF magnetic field gradient accelerators 11 p1841 A67-24767

Ion acceleration by drift resonance caused by crossed magnetostatic and space charge electrostatic fields 11 p1841 A67-24768

Drift field, field gradient and diffused impurity effects on minority carriers and quantum efficiency in silicon photocells 11 p1746 A67-24914

Graphical data concerning drifting beams as possibility for calculation of reduction coefficient of space charge field of electron beams moving in periodic electrostatic fields 16 p2636 A67-30885

Unsteady Vlasov equation for class of beam-like initial distributions associated with ion engines 17 p2928 A67-32158

Axial electrostatic field forming in resonance zone of mixed structure noting ion entrainment, shock wave generation and motion of electrons 17 p2899 A67-32291

Energy difference between metastable levels of hydrogen-like atom determined by measuring lifetime in electrostatic field, yielding average Lamb shift in Li ion 22 p3839 A67-39202

Electrostatic and magnetostatic potentials for slender bodies of revolution in axially symmetric external fields 23 p4026 A67-40753

ELECTROSTATIC GENERATOR

Electrostatic generators for space power, describing single capacitor, constant oblique field and brushless types [AIAA PAPER 64-450] 04 p0554 A67-15251

ELECTROSTATIC GYROSCOPE

Mathematical analysis of problems posed by electrostatic gyroscope with regard to suspension, starting, braking and effect of magnetic induction field on rotor 02 p0242 A67-12039

Inertial sensors, discussing magnetic resonance and superconductor gyroscopes, ring lasers, fluid dynamical devices, electrostatic gyroscopes, etc 05 p0806 A67-16517

Electrostatic gyro characteristics, design implications, numerical analysis of parameters and corresponding drift rates 22 p3800 A67-40185

ELECTROSTATIC INSTRUMENT

Low energy charged particle measurements, describing satellite mounted spherical electrostatic analyzer 02 p0310 A67-12571

Nanosecond pulse ion source for electrostatic accelerator 03 p0425 A67-14262

Rocket measurement of secondary electron energy distribution in aurora, employing 180 degree electrostatic deflection analyzer 03 p0418 A67-14357

Approximate analysis of electrostatic probe on reentry vehicle for electron density measurements in laminar boundary layer of continuum 04 p0705 A67-15231

Resistance of DC arc gap recovering freely after interruption instantaneously measured, using voltage and current probing techniques 05 p0850 A67-16069

Electron beam rotation experiments on linear spiratron with M-type electron gun 05 p0776 A67-17169

Water-cooled electrostatic probe capability

of measuring local electron temperature, electron density, floating potential and saturation current ratio in dense plasmas [AIAA PAPER 66-73] 05 p0856 A67-17344

Ion density profiles in boundary layers associated with supersonic flow of shock heated air over flat plate measured by cylindrical and flush-mounted electrostatic probes [AIAA PAPER 66-159] 05 p0856 A67-17345

Electrostatic probes for collision dominated weakly ionized plasma noting mathematical formulation, density and V-A characteristics 09 p1539 A67-21782

Theory of electrostatic probes in high pressure plasma, discussing ionization and recombination phenomena, diffusion boundary layer, spherical probe, etc 09 p1539 A67-21784

Electrostatically focused extended interaction S-band klystron amplifier using helical buncher resonators for interplanetary spaceborne communication systems 09 p1477 A67-22252

Noise measurements on pulsed four-cavity electrostatically focused S-band klystrons 09 p1477 A67-22253

Plasma diagnostics using electrostatic probes under short mean free path conditions compared with microwave measurements 11 p1827 A67-23882

Electrostatic probe techniques for low density thermally ionized plasmas 11 p1838 A67-24408

Electron number densities measured behind shock wave in pressure-driven shock tube by microwave resonant cavity technique and by electrostatic quasi-Langmuir probe 11 p1790 A67-24451

Electrostatic motor action in rotational momentum of tornado funnels, noting that driving power removal by electric discharge may cause dissipation 12 p1963 A67-25383

Constant density theory leads to analytical forms for current-voltage characteristics and electrical resistance associated with shock tube sidewall electrostatic probe problem 12 p1925 A67-25902

Uniformly valid asymptotic theory of collisionless electrostatic probes 13 p2118 A67-26298

Magnetic field, pressure and discharge current effects on saturation electron current of electrostatic probe used to measure magnetoplasma electron density 14 p2358 A67-28237

Transmission energy characteristics of spherical plate electrostatic analyzers from external sources of electrons and protons 14 p2320 A67-28746

Nanosecond pulse ion source for electrostatic accelerator 14 p2321 A67-28774

Automatic electrostatic image orthicon camera with small weight, volume and input power, having full low-light level sensitivity capability 17 p2858 A67-32481

Miniature electrostatic accelerometer featuring suspension and force rebalance systems, discussing performance, applications and accuracy acceleration measurement 17 p2858 A67-32484

Wake plasma turbulence of projectiles studied using electrostatic probe array 17 p2861 A67-33023

Ionization in ethylene flames at atmospheric pressure, using nitric oxide as oxidizer and electrostatic probe 18 p3107 A67-33804

Grid electrostatic probe for ionospheric measurement of electron density and temperature, examining measurement errors due to environmental disturbances 18 p3048 A67-34225

Diagnostic equations for electrostatic double probes for arbitrary ion Schmidt numbers 19 p3267 A67-34830

E and F region electron density and temperature measurements, using electrostatic probe and MOS electrometer 20 p3441 A67-36383

Electrostatic getter-ion pump, giving quantitative theory for maximizing ionizing efficiency and design features to attain low pressures and high pumping speed 21 p3624 A67-37821

Electrostatic getter-ion pump performance, giving pumping speeds, pressure and starting characteristics, residual gas composition and operating life 21 p3624 A67-37822

Slide wire strain gauge to measure static

strains and stresses at high temperatures 22 p3809 A67-40476

ELECTROSTATIC PLASMA

Electrostatic polarization of plasma in applied electric field, excluding case for steady current flow 04 p0666 A67-15180

Spherical electrostatic probe in stationary plasma analyzed based on kinetic theory using Krook type model for collision integral formulation 05 p0857 A67-17423

Generalized formulation of electrostatic oscillations and streaming instabilities in bounded and unbounded inhomogeneous Vlasov plasmas with transverse density gradients in strong axial magnetic field 08 p1363 A67-21305

Electrostatic probe theory in moderately ionized gas taking into account effect of electron-ion collisions 08 p1324 A67-21393

Electrical parameters of DC MHD generator determined from equivalent circuits 09 p1471 A67-21796

Electrostatic oscillations in dielectric, semiconductor and plasma in presence and absence of external magnetic field 09 p1555 A67-22011

Thin electrostatic sheath adjacent to body immersed in flowing weakly ionized continuum plasma analyzed for arbitrary Debye length mean free path ratios 11 p1825 A67-23868

Electrostatic oscillations excited in cylindrical plasma shell by electron beam, noting resultant instability 11 p1828 A67-23892

Synthesized plasma ion beams by electron injection from hot filament noting electrostatic instabilities and growth rates corresponding to nonlinear regime 11 p1838 A67-24403

Electrostatic turbulence in low beta plasma and influence on diffusion across magnetic field, noting heating system for plates of Q device 11 p1789 A67-24413

Electrostatic polarization of cylindrical plasma layer in external static magnetic field, discussing transverse charged particle drift in crossed fields 13 p2168 A67-27305

Superthermal electron production by quasi-cyclotron acceleration when interacting with monochromatic large amplitude electrostatic plasma wave 15 p2528 A67-29569

Electrostatic stability of finite-length plasmas immersed in magnetic field studied on mathematical model, discussing experiments with plasma-generating machines 16 p2714 A67-30871

Nonexistence of critical current for pinching in electron-hole plasmas 18 p3098 A67-33523

Generalized formulas and stability criteria applied to higher order electrostatic oscillation modes in Vlasov plasmas, considering double-stream amplifier designs 20 p3495 A67-36169

Counterstreaming ion electrostatic instability at cyclotron frequency to enhance trapping of injected ion beam 21 p3661 A67-37748

Malmberg-Wharton configuration electron plasma wave dispersion and damping 22 p3844 A67-39367

Electrostatic energy per degree of freedom of two-temperature plasma examined for validity of resonant approximations in ion wave region 22 p3852 A67-39986

ELECTROSTATIC PROPULSION

Low density electron bombardment ion engine, particularly mercury engine and Cs gas discharge ion engine, for electrostatic propulsion 04 p0689 A67-15020

Electrostatic propulsion using positive and negative ions, considering neutralization effects, thrust/surface and thrust/power ratios, etc 04 p0690 A67-15023

Gaseous mercury discharges through orifice as ion beam neutralizer for electrostatic thrusters [AIAA PAPER 67-669] 21 p3691 A67-38703

Conventional and composite grid designs tested with low voltage Kaufman thruster [AIAA PAPER 67-680] 21 p3692 A67-38711

Electrostatic ion propulsion and KEMAN MPD thruster research in Germany [AIAA PAPER 67-724] 21 p3694 A67-38749

ELECTROSTATIC SHIELDING

Helical instability of positive plasma column in longitudinal magnetic field, using magnetic pickup coil 11 p1829 A67-23999

Shielding factors for electrostatic

aerials 24 p4129 A67-41977

ELECTROSTATIC WAVE

Landau type damping of plasma oscillations and Bernstein mode electrostatic propagation perpendicular to weak magnetic field 08 p1360 A67-21122

Electrostatic wave excitation growth in collisionless plasma interaction and simultaneous modification with electron beam studied for weakly unstable situations 11 p1826 A67-23874

Highly ionized plasma with excitation and damping of density and temperature drift waves in stable regime 11 p1835 A67-24388

Plasma production by ruby laser pulse irradiation of LiD investigated, results suggest collisionless electrostatic shock propagation at expanding plasma balance edge 11 p1840 A67-24561

Electrostatic waves in LF noise bands as cause of diffuse traces observed by Louette satellite ionospheric probe electrostatic waves in LF noise bands as cause of diffuse traces observed by Alouette satellite 14 p2312 A67-28518

Electrostatic wave propagating into region of decreasing electron density calculated using one-dimensional plasma with uniform electron density 16 p2715 A67-31061

Electrostatic wave effect on anisotropic relativistic proton plasma in magnetic field noting instability 16 p2739 A67-31234

Interaction between electrostatic and guided electromagnetic wave, considering plasma wave amplification by pumping at microwave frequency 18 p3091 A67-34643

Collisionless electrostatic shock in magnetized plasma in absence of initial magnetic field 18 p3092 A67-34745

Magnetic moment under short wave electrostatic perturbations 18 p3093 A67-34755

Electrostatic ion cyclotron waves excitation in plasma and ion heating due to cyclotron damping 21 p3667 A67-38407

Electrostatic relaxation wave dispersion in isotropic Lorentz gas, considering Landau damping and balancing of elastic electron-atom collisions 22 p3848 A67-39692

ELECTROSTATICS

SA STATIC ELECTRICITY

Elimination of rocket motor ignition by electrostatic initiation through development of electrically insensitive igniter and nonelectric stimulus transfer system 08 p1372 A67-20525

Boundary value problem for electrostatic field external to slender axisymmetric conductor 08 p1413 A67-21301

Push-pull electrostatic loudspeaker for aircraft cockpit, helmet and ear-insert communication 11 p1767 A67-24702

Three-axis ellipsoid elastostatic problem solved through analogy with equivalent electrostatic problem of charge distribution 12 p2029 A67-25665

Mean internal potential for InSb lattice calculated, comparing empirical results with those obtained from Hartree and Thomas-Fermi-Dirac methods 18 p3095 A67-33442

Long range interaction of two H atoms calculated with electrostatic Hellmann-Feynman theorem, determining part of second order molecular wave function 22 p3840 A67-39387

ELECTROSTRICTION

SA MAGNETOSTRICTION

Crystal deformation by electrostriction produced by laser beam 08 p1336 A67-20315

ELECTROTHERMAL ENGINE

Acceleration of propellant in arcjet devices by thermal and self-magnetic forces, using various nozzle configurations 08 p1375 A67-20574

Magnetically accelerating continuously operating plasma engine for spacecraft propulsion compared with electrothermal engine 11 p1855 A67-25100

Design and performance characteristics of electrothermal microthruster systems for spacecraft functions [AIAA PAPER 67-423] 18 p2988 A67-33907

Multijet electrothermal systems for attitude control and stationkeeping of synchronous communications satellite [AIAA PAPER 67-723] 21 p3694 A67-38745

ELEKTRON I SATELLITE

Altitude-time distribution of electron concentration of outer ionosphere measured by coherent signals from Elektron I satellite 12 p1936 A67-25795

- Elektron I and III earth satellite electron and proton energy distribution correlation with geomagnetic phenomena 12 p1996 A67-25804
- ELEKTRON II SATELLITE**
- Solar X-ray emission measurements with Geiger photon counters carried by Elektron II and IV satellites 02 p0240 A67-11544
- Neutron-group fluxes and variations with solar activity during IYQS observed by Elektron II 02 p0310 A67-12583
- Temporal variations of nuclear flux of primary cosmic radiation of Elektron II and IV satellites, discussing Forbush effect in nuclear and neutron components 05 p0877 A67-16085
- Metrological characteristics of three-component magnetometers with ferromagnetic probes installed in Elektron II space station 11 p1789 A67-24079
- Elektron II satellite charged particle flux measurements at distances up to 11.6 earth radii, using three-electrode charged particle trap 12 p1998 A67-25817
- Micrometeoritic particle condensation in vicinity of earth measured by Elektron II satellite 12 p2008 A67-25825
- Ionospheric ion temperature determination from variations in collector current of ion trap mounted on rotating satellite 13 p2115 A67-27330
- Solar X-ray emission measurements with Geiger photon counters carried by Elektron II and IV satellites 16 p2677 A67-31610
- Temporal variations of nuclear flux of primary cosmic radiation of Elektron II and IV satellites, discussing Forbush effect in nuclear and neutron components 24 p4212 A67-42761
- ELEKTRON IV SATELLITE**
- Solar X-ray emission measurements with Geiger photon counters carried by Elektron II and IV satellites 02 p0240 A67-11544
- Temporal variations of nuclear flux of primary cosmic radiation of Elektron II and IV satellites, discussing Forbush effect in nuclear and neutron components 05 p0877 A67-16085
- Primary cosmic radiation investigated by Elektron II and IV satellites 12 p1998 A67-25827
- Solar X-ray emission measurements with Geiger photon counters carried by Elektron II and IV satellites 16 p2677 A67-31610
- Temporal variations of nuclear flux of primary cosmic radiation of Elektron II and IV satellites, discussing Forbush effect in nuclear and neutron components 24 p4212 A67-42761
- ELEKTRON SATELLITE**
- Radiation resistance of silicon photoconverters onboard Elektron III satellite, noting protective coating 02 p0240 A67-11543
- Low energy proton distribution in geomagnetic coordinates obtained from Elektron satellite measurements 05 p0880 A67-16108
- Elektron satellite observations on primary cosmic radiation, noting correlation between intensity variation and neutron component intensity 05 p0880 A67-16109
- Elektron I and II satellite measurements on outer radiation belt, noting geomagnetic field distortion and boundary dependence on magnetic perturbations 05 p0880 A67-16110
- Cosmic space exploration in U.S.S.R., discussing results obtained from Cosmos and Elektron earth satellites 08 p1394 A67-21110
- Diurnal variation of difference between dipole and measured field for quiet magnetosphere from Elektron satellite data 10 p1649 A67-23296
- Time variations of intensity in outer belt and near boundary deduced from Elektron I and II data, noting comparison with magnetic field variations 12 p1997 A67-25815
- Elektron I and II satellite observational data on terrestrial radiation 12 p1998 A67-25816
- Primary cosmic radiation investigated by Elektron II and IV satellites 12 p1998 A67-25827
- Measurement of total number of electrons in ionosphere, horizontal gradients, equivalent height and vertical profile from recorded Elektron satellite signals 14 p2307 A67-27922
- Radiation resistance of silicon photoconverters onboard Elektron III satellite, noting protective
- coating 16 p2677 A67-31609
- Low energy proton distribution in geomagnetic coordinates obtained from Elektron satellite measurements 24 p4214 A67-42784
- Elektron satellite observations on primary cosmic radiation, noting correlation between intensity variation and neutron component intensity 24 p4214 A67-42785
- Elektron I and II satellite measurements on outer radiation belt, noting geomagnetic field distortion and boundary dependence on magnetic perturbations 24 p4214 A67-42786
- ELEMENT**
- S DECISION ELEMENT**
- S FUEL ELEMENT**
- S HEAVY ELEMENT**
- S NEUTRAL ELEMENT**
- S ORBITAL ELEMENT**
- S RADIOACTIVE ELEMENT**
- S SWITCHING ELEMENT**
- S TRACE ELEMENT**
- S TRANSITION ELEMENT**
- ELEMENT ABUNDANCE**
- Energy spectra and abundances of elements He through Si of galactic cosmic ray above 20 mev per nucleon in nuclear charge range between 2 and 26 02 p0307 A67-11687
- Composition and surface pressure of Martian atmosphere determined from photographic spectrum of Mars obtained at March 1965 opposition 02 p0323 A67-11695
- Age determination of iron meteorites by comparing isotopic abundance of primordial potassium in inclusions with terrestrial standards 02 p0326 A67-12044
- Lanthanide abundance variation and coordination number, comparing abundances in terrestrial and meteoritic materials with average chondrite 03 p0413 A67-13507
- Principal methods determining cosmic abundances of chemical elements, emphasizing quantitative spectral analysis of sun and fixed stars 03 p0510 A67-13538
- Australites, Henbury impact glass and subgreywacke, comparison of abundances of 51 elements 03 p0512 A67-13900
- Rare earth trace element variations in anorthosite and quartz mangerite determined, using stable isotope dilution technique of analysis 03 p0513 A67-14006
- Primordial He 3 and 4 and deuterium abundances in early stages of universal expansion show dependence on time scale 03 p0515 A67-14322
- Total carbon abundances in enstatite chondrites 05 p0886 A67-16024
- Primordial argon and metamorphism of chondrites 05 p0886 A67-16025
- Radioactive isotopes in iron meteorite used to determine cosmic ray origin and to study nuclear processes in early history of solar system 05 p0877 A67-16084
- Lunar and planetary surface elemental analysis technique by analysis of gamma rays resulting from inelastic scattering of neutrons 05 p0843 A67-16545
- Neutron activation analysis of Si, Fe, Al, Mg and O content of lunar and planetary surfaces 05 p0843 A67-16546
- O-to-Fe ratio determined in active solar corona from intensity ratio of O-8 to Fe-17 lines and in quiet corona from O-7 to Fe-14 ratio 06 p1083 A67-18068
- Chemical composition and earth origin, with estimates of primordial abundances of elements in solar system 07 p1170 A67-19336
- Rare earth compound and Ba abundances in Bununu howardite 07 p1249 A67-19537
- Aerobee rockets measurement of sodium dayglow suggest equilibrium between sodium atoms and distribution of dust particles 07 p1180 A67-19917
- Oscillator strength of atomic and ionic lines, normalization of NBS gf values and solar abundances of alkali metals 07 p1256 A67-20167
- Metal deficiencies, UV excesses and other color anomalies in solar type disk population stars 08 p1400 A67-21249
- Fractional volume abundance of atmospheric nitrous oxide, considering photodissociation, microbiological reactions and mixing 08 p1327 A67-21369
- Thermodynamic equilibrium composition of all combinations of C, H, O and N at average pressure and temperature calculated for atmospheres of earth, Venus, Mars and Jupiter 09 p1566 A67-22236
- Solar X-ray spectrum of Tousey analyzed using criteria of abundance of elements of Pottasch 10 p1707 A67-23227
- Neutron activation analysis for terrestrial and meteoritic rock major element abundance, noting possible application to extraterrestrial surface analysis 11 p1749 A67-23976
- Relative solar abundance for O, Si and Fe determined from intensities of far UV emission lines of solar corona 12 p2001 A67-25225
- Element production in early stages of homogeneous expanding universe and within stars, noting nature of background microwave radiation 12 p2010 A67-26239
- Primordial element formation, primordial magnetic fields and universe isotropy, showing correctness of big-bang relativistic theory, early anisotropy of universe, etc 12 p2010 A67-26240
- Mercury abundance in chondrite meteorites determined by neutron activation and separation by volatilization over temperature range 13 p2210 A67-27603
- Element abundance in various chondrite groups determined by neutron activation technique 14 p2391 A67-28950
- Structure and composition of Jupiter atmosphere, noting laboratory and observational data supporting hypothesis of consistency with solar elements abundance 16 p2746 A67-30932
- Argon, krypton and xenon in chondrites noting constant abundance ratios and correlation of concentration to disequilibrium 16 p2750 A67-31436
- Isotopic composition and abundance of xenon and krypton in graphite of iron meteorite from Canyon Diablo examined for anomaly pattern 16 p2750 A67-31438
- Nonrotating, hydrostatic models of geochemically likely planets calculated using solar elemental abundances and equations of state for cold materials 16 p2754 A67-31748
- Slow motion gamma spectrometry for measurement of sodium 24 abundance in Saint Severin meteorite, evaluating modes of formation 16 p2754 A67-31790
- Helium origin in universe and heavy element creation 17 p2942 A67-32405
- Origin and abundance distribution of heavy elements in stars, discussing theories 17 p2946 A67-32694
- He abundance in sun suggests He stellar nucleosynthesis was responsible for increase in He abundance in interstellar gas between formation of sun and present time 17 p2947 A67-32763
- Surface helium abundance in blue horizontal branch and halo B stars, considering depletion mechanism 17 p2947 A67-32764
- Triatomic molecules formation and abundance in solar photosphere estimated for thermodynamic equilibrium 18 p3119 A67-33858
- Primordial rare gases abundances in unequilibrated ordinary chondrites determined by mass spectrometry 19 p3317 A67-34912
- Origin of elements, discussing element formation and abundances, nucleosynthesis and cosmological theories 19 p3263 A67-35869
- Lead abundance in sun computed from measurement of Pb lines equivalent widths 19 p3331 A67-36087
- Abundance of volatile elements in meteorites, comparing chondrite decrease for evidence of fractionations in solar nebula 20 p3526 A67-37173
- Atmospheric pressure at cloud top and hydrogen abundance in Jupiter atmosphere determined by analyzing methane spectral line widths 20 p3529 A67-37479
- Abundance of stable isotopes of neon, argon, krypton and xenon in Costilla Peak iron meteorite, observing spallation components 21 p3702 A67-38124
- Uranium content of chondrites measured by thermal neutron activation and delayed neutron counting 21 p3704 A67-38505
- Krypton isotope composition in three unequilibrated and two gas rich chondrites, with correction for cosmic ray spallation 22 p3881 A67-39494
- Spectral line wavelengths of solar violet bands of carbon /isotope/ nitride and hydride molecules, determining solar abundance ratios 22 p3889 A67-40207
- Rare gas isotopic analysis using ruby pulsed laser and mass

spectrometer 22 p3816 A67-40241
 Equivalent widths of line spectrum analyzed by modification of Milne-Eddington growth procedure curve 22 p3896 A67-40528
 Makeup low energy spectra and electron component of cosmic rays and solar particle production with curves for element abundance 23 p4053 A67-41090
 Wavelengths and intensities of IR coronal lines of silicon and magnesium ions from airborne total solar eclipse observations 24 p4224 A67-41822
 Upper limit of carbon dioxide abundance in Mercury atmosphere 24 p4225 A67-41836
 Energetic nuclear bombardment effects on stellar surface element abundance calculated with statistical theory in A magnetic variable star abundance anomaly 24 p4228 A67-42263
 Abundance anomalies in stellar surface layers by proton and alpha particle bombardment caused nucleus breakdown and buildup to lower and higher mass numbers respectively 24 p4228 A67-42264
 Lanthanide distribution between omphacite and Garnet, noting abundance ratios to whole rock of Japanese eclogite 24 p4151 A67-42449
 Chlorine abundance and distribution in iron meteorites from neutron activation analysis and metallographic examination, discussing terrestrial contamination 24 p4232 A67-42610
 Chromite composition in chondrites using electron microprobe technique, discussing petrographic origin and vanadium abundance 24 p4232 A67-42612
 Iodine, uranium and tellurium abundances in various achondrites, chondrites and mesosiderites from neutron activation analysis 24 p4233 A67-42616
 Precious metal concentrations in carbonaceous and enstatite chondrites using neutron activation analysis 24 p4233 A67-42617
 Cl, Br and I abundances in carbonaceous chondrites analyzed by neutron activation in estimating primordial halogen abundance ratios 24 p4234 A67-42628
 Li isotopic composition and abundance in chondrites and iron meteorites measured, noting implications for earth and meteoritic parent body formation 24 p4235 A67-42632
 Re and Os abundances in various chondrites determined by neutron activation analysis, noting fractionation 24 p4235 A67-42637
 Silicon abundances in chondrules from different chondrites by neutron activation analysis 24 p4236 A67-42644
 Rare earth and barium abundances in Ivory Coast tektites and rocks determined by isotope dilution 24 p4236 A67-42645
 Antimony abundance in meteorites, tektites and terrestrial rock by neutron activation analysis 24 p4236 A67-42647
 Solar abundance determination, discussing composition parameters and Planck gradient method 24 p4237 A67-42654
 IR C atom multiplet in solar spectrum at 10,700 angstroms, noting C abundance dependence on convective velocities and deviations from black body function and local thermodynamic equilibrium 24 p4237 A67-42655
 Radioactive isotopes in iron meteorite used to determine cosmic ray origin and to study nuclear processes in early history of solar system 24 p4212 A67-42760
 Primary cosmic ray particle chemical composition changes, explaining active particle energy spectra discrepancies between measurements and calculation 24 p4218 A67-42840

ELEMENTARY PARTICLE
 SA ANTINEUTRINO
 SA CHARGED PARTICLE
 SA DEUTERON
 SA ELECTRON
 SA FAST NEUTRON
 SA KAON
 SA LEPTON
 SA MESON
 SA NEUTRINO
 SA NEUTRON
 SA NUCLEAR PARTICLE
 SA NUCLEON
 SA PHOTON
 SA POSITRON
 SA PROTON
 SA QUARK

Cosmic ray nucleon interaction with high energies, estimating transition probability and interaction cross section of baryon in passive state 10 p1703 A67-23586
 Existence of nucleon bound state in PIN channel investigated through nonperturbative S-matrix in absence of forces arising from inelastic states 11 p1822 A67-23978
 Quark fractional electronic charge in cosmic radiation determined through pulse height distribution 15 p2549 A67-29526
 Spark chambers and scintillation counters used to search for fractionally charged particles in cosmic rays near sea level 15 p2550 A67-29680
 Processing and obtaining phase holograms of elementary particle tracks in gelatin bubble and emulsion 18 p3049 A67-34387
 General quantum relativity theory in real universe with large radius and elementary particle structure 18 p3080 A67-34728
 Electromagnetic radiation, elementary particles and micrometeorites effects on earth satellites 19 p3327 A67-35672
 Bargmann-Wigner and Dirac formulations for field of spin 1/2 shown equivalent provided auxiliary field vanishes in electromagnetic interaction presence 20 p3489 A67-37090
 Gravitation theory, general theory of relativity, field theory and gravitational interactions with elementary particles 22 p3879 A67-39294
 Cosmology and elementary particles, noting relationship hypothesis between cosmological asymmetry and particles via vacuum 22 p3880 A67-39337
 Symmetry principles at high energy - Conference, University of Miami, January 1967 22 p3840 A67-39582
 Relativity theory accounting for energy conservation properties in elementary particle interactions and small size and high energy emission of quasars 22 p3892 A67-40499
 Cosmic ray propagation through atmosphere, developing model for elementary particles behavior 24 p4218 A67-42837

ELEVATION ANGLE
 Prediction of apparent elevation angle expected for object situated in troposphere at specified values of geometrical elevation angle height 02 p0199 A67-12083
 Elevation angle of arrival of ionospherically propagated HF radio signals determined with circular antenna arrays 02 p0217 A67-12088
 Radar measurements of Doppler spectra and power reflectivity of Mars interpreted as surface elevation differences between dark and bright areas 11 p1867 A67-24776
 Antennas featuring steerable notch in omnidirectional pattern as alternative to narrow beam antenna for certain applications 16 p2638 A67-31335
 Ground track location on contour map for given terrain elevation profile, using digital computer 19 p3232 A67-35926
 Bistatic radar cross section of coherent-dot radar angel in convective thermal model 20 p3480 A67-36286
 Six-stage monogram for refraction of radio wave entering earth atmosphere in terms of meteorological conditions and wave elevation angle 23 p3975 A67-41212

ELEVATOR
 SA AILERON
 Airplane automatic-flare system actuating flaps and elevators as lift and moment controllers 15 p2418 A67-29313

ELEVON
 SA AILERON
 Wind tunnel tests of lifting reentry body at Mach numbers up to 16.5 and at angles of attack up to 50 degrees 04 p0546 A67-14567

ELIMINATION
 Ventilation-perfusion inequality effects studied in inert gas elimination from lungs 21 p3575 A67-38516

ELLIPSE
 Compressible ideal gas flow through elliptic pipe 08 p1322 A67-21169

ELLIPSOID
 SA OGIVE
 Legendre series solution to contact problem of torsion of elongated ellipsoid of revolution under arbitrary torsional loading 03 p0530 A67-14199

Stability of rotating liquid mass /e.g. earth/, following Jeans treatment of Jacob ellipsoidal equilibrium configurations 06 p1080 A67-17761
 Relation of magnetization of any homogeneous isotropic ellipsoid to local field and external applied magnetic field deduced from Maxwell equations and potential theory 07 p1234 A67-20127
 Geometrical optics approximation of plane electromagnetic wave reflection from ideally electrically conducting triaxial ellipsoid 11 p1754 A67-24986
 Light scattering by flattened ellipsoids at 90 and zero degree of incidence 12 p1965 A67-25130
 Thermal stresses in thin shell in contact with smooth rigid container 14 p2403 A67-29011
 Flattening of ellipsoid of revolution considered as mathematical surface for solution of geodetic problems 15 p2477 A67-29744
 Conrad-type probe used to determine, in boundary layer of flattened ellipsoid, mean velocity of flow 16 p2663 A67-31711
 Solution for boundary value problems in elasticity theory for ellipsoid of revolution and cavity with surface loading, determining coefficients in closed form 21 p3718 A67-37984
 Changes in electric resistance of ellipsoidal plasma probe in homogeneous magnetic field, deriving equations of potential and resistance 21 p3866 A67-38255
 Friction and heat flow resistances for three-dimensional compressible laminar gas boundary layer over ellipsoid of revolution at angle of attack 22 p3786 A67-40028

ELLIPTIC EQUATION
 Uniqueness and stability theorems for BVP involving degenerated elliptic differential operator 01 p0105 A67-10678
 Block successive overrelaxation method /BSOR/ compared with direct method for solving fourth order partial differential equation 02 p0258 A67-11800
 Integral representation providing one-to-one correspondence between functions of complex variables and complex-valued harmonic functions of n plus 1 real variables 02 p0259 A67-11911
 Restrictions in method of solving boundary value problems for differential equations of elliptic type by reducing to difference problem 03 p0459 A67-13591
 Boundary value problems of higher order equations in infinite regions, proving existence and convergence of solution for perturbed and unperturbed cases 03 p0459 A67-13644
 Eigenvalue parameter in boundary conditions for elliptic equations degenerated in section of boundary 04 p0643 A67-14721
 Regular approximation of solutions for complex elliptic equations of any order 04 p0643 A67-14721
 Book on main linear boundary value problems for second order linear partial differential equations and systems of such equations satisfying ellipticity 04 p0645 A67-15001
 Optimal control of systems described by elliptic differential operators 04 p0593 A67-15491
 Dirichlet problem for strongly connected elliptical systems 05 p0835 A67-16931
 Structure of solutions to elliptic and parabolic equations with one separable variable concerning combined action of convective and conductive transport 07 p1214 A67-19171
 Eigenfunction expansion of self-adjoint operator generated by elliptic differential boundary value problem with eigenvalue in boundary condition 07 p1215 A67-19581
 Elliptic restricted problem of periodic Trojan orbit and nonperiodic libration frequency and angular motion of Jupiter 08 p1381 A67-20381
 Truncated elliptic systems of partial differential equations for reducing two-point boundary value problems in vector space to initial value problems by projection 08 p1348 A67-21191
 Galerkin method analysis of solvability of boundary value problems for second order quasi-linear elliptic differential equation with discontinuous coefficients 08 p1349 A67-21191
 Class of nonlinear operators and necessary

and sufficient condition of solvability of
quasi-linear elliptic
equations 10 p1674 A67-23076

Modified first boundary value problem for
linear elliptic nonself-adjoint partial
differential equation in two-dimensional
plane 10 p1674 A67-23077

Navier-Stokes equation solution in region
with smooth boundary, using linear elliptic
equations 10 p1675 A67-23676

Bound solutions for elliptical equation in
n-dimensional vector space obtained, using
linear transformation into Martin
boundary 11 p1814 A67-24852

Coercivity inequalities for second order
elliptical operators with increasing
coefficients 11 p1814 A67-24978

Boundary value problem for region with
arbitrary smooth boundary solved, using
second order degenerate elliptical
equations 12 p1961 A67-25441

Estimations for majorizing functions for
solutions of Dirichlet problem for second
order elliptic equations or
inequalities 12 p1961 A67-25670

First boundary value problem for second
order elliptic partial differential equations,
analyzing smoothness and continuity of
generalized solution 13 p2144 A67-26378

Solvable convergent difference schemes
for nonlinear elliptic equations using
variational method applied to differential
equation 13 p2145 A67-26445

Formulas for using wave plates in
ellipsometry 13 p2158 A67-26879

Numerical solution of boundary value
problem for quasi-linear
equation 13 p2148 A67-27498

Hilbert space methods in elliptic partial
differential equations 14 p2341 A67-27849

Difference methods for parabolic
equations and alternating direction implicit
methods for elliptic
equations 14 p2342 A67-28155

Numerical methods for elliptic problems,
discussing application of finite difference
and solution of large algebraic
systems 14 p2342 A67-28156

Long wave type solutions for quasi-linear
elliptic equations, noting parameter lambda
for small nontrivial solutions 14 p2343 A67-28386

Majorizing functions for Dirichlet problem
in n-dimensional space 14 p2343 A67-28631

Necessary and sufficient conditions for
solvability in two-space of second order
elliptic differential equations with smooth
irregular continuous differentiable
boundary 14 p2344 A67-28634

Parameter and domain dependence of
eigenvalues of elliptic partial differential
equations 15 p2509 A67-29461

Fractional powers of operators applied to
boundary value problems of quasi-linear
elliptic equations 15 p2510 A67-29661

Unique iterative solution to degenerate
quasi-linear elliptic equations and
systems 15 p2511 A67-30001

Finite difference method of solving
degenerate elliptic and parabolic
equations 15 p2511 A67-30008

Numerical methods for elliptic partial
differential equations with coefficients
singular on boundary portion, constructing
barrier functions and establishing existence
and convergence theorems 16 p2697 A67-31330

Pointwise bounds for solution of Cauchy
problem for nonlinear and linear elliptic
system, noting application to biharmonic
equation 16 p2697 A67-31422

Soviet book on new methods for solving
elliptic equations including equations in
many-dimensional space, index problem in
functional equation theory, 17 p2878 A67-32686

Bounded solutions of boundary value
problem with skew derivative studied by
probability methods 17 p2878 A67-32737

Uniformly valid approximation of two-
dimensional subsonic flow along thin airfoil
with blunt elliptical shape 18 p2982 A67-33663

Neumann boundary value problem for
second order elliptic equation system with
many independent variables 18 p3071 A67-34169

Dirichlet problem for elliptic system of
differential equation which does not satisfy
Lopatinski condition where characteristic
equation of system has simple

roots 18 p3073 A67-34481

Alternating direction implicit /ADI/
method variant for elliptic and parabolic
partial differential equations 19 p3250 A67-34868

Uniqueness theorem for Cauchy problem,
elliptic equations with double characteristics
derived by imposing smoothness
condition 20 p3475 A67-36456

First boundary value problem for linear
elliptic differential equations involving two
small parameters 20 p3477 A67-36942

Maximum region of applicability of
Chaplygin theorem of differential inequality
to elliptic difference equation 20 p3479 A67-37722

Boundary value problem for region with
arbitrary smooth boundary solved, using
second order degenerate elliptical
equations 20 p3479 A67-37724

Pointwise bounds for perturbed parabolic
and elliptic equations using known bounds
for corresponding strictly differential
problems, noting Rayleigh-Ritz
procedure 21 p3652 A67-38174

Navier-Stokes equation solution in region
with smooth boundary, using linear elliptic
equations 21 p3652 A67-38277

9-point difference formula accuracy in
Laplace equation compared to 5-point
formula, discussing convergence rate and
Dirichlet boundary value problem 22 p3826 A67-39195

Complex representation of elliptic
differential equation solution, discussing
holomorphic functions, polycylindrical
regions and Vekua concept 23 p4022 A67-40723

Finite difference method for degenerate
elliptic and parabolic equations involving
various boundary value problems 24 p4178 A67-42269

ELLIPTIC FUNCTION

Wideband elliptic-function band-stop
transmission line filter design, computing
characteristic impedances of filter
element 02 p0214 A67-11779

Synthesis procedure for distributed filters
based on elliptic function or Cauer
parameter lumped element prototype 04 p0580 A67-14859

Poincare continuation method using simple
pendulum problem, deriving elliptic
functions as power series [AIAA PAPER 67-564] 19 p3250 A67-35960

Quasi-linear elliptic system of first order
equations used for Riemann-Hilbert
boundary value problem 21 p3651 A67-37930

Cauchy problem for second order
parabolic partial differential equation 22 p3827 A67-39432

Conformal representation using Jacobi and
Weierstrass elliptic function applied to
extremal problems, noting electric modeling
solutions 23 p4023 A67-40924

ELLIPTIC INTEGRAL

Three-body problem with all perturbations
of first order represented by elliptic
integrals 08 p1381 A67-20390

Rational approximations to incomplete
elliptic integral of first and second kinds
derived by main diagonal Padé
approximations 18 p3072 A67-34397

Integrals of motion in plane elliptic
restricted three-body problems for orbits
with small eccentricity near
primaries 18 p3136 A67-34588

Notch stress theory, discussing mapping
function and elliptic integral solutions 22 p3913 A67-40004

Elliptic integrals and numerical
representation of power series to yield
closed form approximation, presenting error
as function of modulus 24 p4178 A67-42205

ELLIPTICAL CYLINDER

Optimal design of elliptical pumping
chambers from numerical calculations
containing all geometric sizes of pumping
lamps and laser rods and reflectivity of
walls 07 p1195 A67-19490

Multiple pass effects in laser pumping
cavities, noting mercury lamp
performance 10 p1662 A67-22743

Heat transfer from laminar Newtonian
flow through cooled elliptic tubes with
variable cross sections 12 p2033 A67-25215

Tension equations for oval thin walled
cylinders reinforced with lateral rigid ribs
noting wall strength, complex bending
moment computation, etc 15 p2577 A67-30185

Motion of single-component electrically

charged gas in elliptical cylindrical cavity
analyzed for relative deformation when
applying magnetic field 16 p2656 A67-30456

Separation and stall of impulsively started
elliptic cylinder including interactions
between boundary layer and outer flow
[ASME PAPER 67-APM-31] 17 p2840 A67-33157

ELLIPTICAL ORBIT

SA EULER-LAMBERT EQUATION

Rendezvous maneuver between vehicle and
target in free orbital flight in central
gravitational field, deriving low acceleration
program for elliptical target
orbit 01 p0152 A67-10208

Levi-Civita regularized equations of
elliptic motion of particle influenced by
massive primary and perturbed by smaller
primary, Part I, Trigonometric series
solution 01 p0147 A67-10379

Levi-Civita regularized equation of elliptic
motion of particle influenced by massive
primary and perturbed by smaller primary,
Part II, Applications to circular and collision
orbits 01 p0147 A67-10380

Existence of class of quasi-periodic
solutions of three-body problem for near-
circular inclined planetary and lunar orbits,
Part I 01 p0148 A67-10382

Satellite rendezvous guidance laws
applicable to circular, near-circular and
elliptical orbits, using Lagrangian formulas
for position and velocity in two-body
orbit 02 p0264 A67-12315

Ground track of earth-period synchronous
/24-hr/ satellites, discussing equatorial,
circular and elliptical orbits 04 p0704 A67-14826

Relative motion of body about satellite in
orbit, determining impulses which cause
body to remain in satellite
vicinity 04 p0706 A67-15249

Optimal interorbital transfer between
elliptical orbits in central Newtonian force
field analyzed in terms of minimum
characteristic velocity 05 p0886 A67-16047

Orbital guidance and rendezvous in
inverse square central force field using
perturbation method, considering elliptical
and circular orbits [AIAA PAPER 67-55] 06 p1028 A67-18265

Attitude stability of spinning rigid
symmetric satellite in elliptic orbit
examined for motion about equilibrium
position with spin axis normal to orbit plane
[AIAA PAPER 67-124] 06 p1095 A67-18312

Satellite under perturbing acceleration
having constant modulus and directed along
normal to osculating plane of orbit,
calculating rotation of orbital
plane 06 p1088 A67-18620

Plane optimum transfer of point of
variable mass between two elliptical orbits
in centrally directed Newtonian force
field 07 p1247 A67-19095

Rigorous error bounds on position and
velocity of satellite derived from
Hamiltonian theory and von Zelpel method
[AAS PAPER 66-94] 07 p1252 A67-19958

Orbital change problems using Busemann
configuration space combined with
geometrical properties inherent to Keplerian
orbits [AAS PAPER 66-122] 07 p1254 A67-19981

Optimum deorbit positioning on
planetocentric elliptic orbit for single
impulse reentry treated by two coupled
quartic polynomials [AAS PAPER 66-123] 07 p1254 A67-19982

Transfer from elliptical orbit to coplanar
hyperbolic asymptote treated in terms of
limited classes of one-and two-impulse
maneuvers [AAS PAPER 66-127] 07 p1255 A67-19986

Rocket maneuvers for rendezvous with
propulsionless target satellite in elliptic
orbit 08 p1410 A67-20640

Elliptic type orbit determination in
generalized problem of two stationary
centers by integration in quadratures of
motion equations of satellite 09 p1565 A67-21902

Propellant cost optimization using
minimum characteristic velocity solutions for
extra-atmospheric part of rocket ascent
trajectory, emphasizing final elliptical orbit
of arbitrary orientation 10 p1704 A67-22877

Satellite attitude control in elliptic
orbit 11 p1869 A67-24337

Rate of satellite turn in elliptical orbit
calculated by introducing nondimensional

angle, deriving master curves, noting applicability to attitude control systems 12 p2000 A67-25124

Single-impulse transition in Newtonian central force field from hyperbolic to elliptical orbit in case of radial impulse 12 p2002 A67-25638

Earth gravitational field eccentricity effect on deviation of satellites from Kepler ellipse orbits 13 p2200 A67-27322

Sun illumination time of artificial earth satellite moving in elliptical orbit 13 p2200 A67-27338

Rigorous error bounds on position and velocity of satellite derived from Hamiltonian theory and von Zeipel method [AAS PAPER 66-94] 13 p2207 A67-27518

Optimum deorbit positioning on planetocentric elliptic orbit for single impulse reentry treated by two coupled quartic polynomials 13 p2209 A67-27536

Rendezvous between spacecraft and target flying in elliptic orbit of arbitrary eccentricity solved, using new approach [AIAA PAPER 66-537] 14 p2394 A67-28115

Elliptical motion of material point in terrestrial gravitational field, noting expression for eccentricity under effect of small tangential force 15 p2556 A67-29659

Motion analysis near triangular libration point within framework of elliptic restricted three-body problem 15 p2559 A67-30036

Librational and flexural resonances induced in satellite whose center of mass is moving in planar elliptic orbit 15 p2572 A67-30195

Molniva type communication satellite, discussing optimum orbital requirements for maximum coverage, phasing, etc 16 p2742 A67-30698

Improvement of satellite elliptical orbits with small eccentricities using differential formulas 16 p2743 A67-30727

Minimum-fuel transfers of moving body between infinitely close elliptical Keplerian orbits in central Newtonian field, considering propulsion system models 16 p2744 A67-30738

Optimal transfers between coplanar and coaxial orbits /any 16 p2745 A67-30739

Ascent of satellite of variable mass from elliptic orbit along spiral trajectories by low thrust 17 p2948 A67-33022

Attitude stability of spinning rigid symmetric satellite in elliptic orbit examined for motion about equilibrium position with spin axis normal to orbit plane 19 p3333 A67-35747

Elliptic geocentric satellite orbit for measurements of magnetosphere-nearby space region, analyzing orbital lifetimes and perturbations [AIAA PAPER 67-616] 19 p3226 A67-36005

Onboard computer equations for rocket vehicle guidance to elliptical orbit, discussing iteration absence from computations and digital simulation results [AIAA PAPER 67-621] 19 p3260 A67-36010

Shortest distance between two quasi-coplanar elliptical asteroid orbits, solving transcendental equations by consecutive approximation method 20 p3523 A67-36628

Suboptimal Hohmann orbital transfer extension to nonaligned two-impulse elliptical transfer 20 p3526 A67-37253

Optimal interorbital transfer between elliptical orbits in central Newtonian force field analyzed in terms of minimum characteristic velocity 21 p3701 A67-37834

Matrix method proposed for systems of linear differential equations governing satellite attitude control in elliptical orbits, considering integral criteria calculation 22 p3897 A67-39160

Optical determination accuracy of satellite orbits, investigating orbit elements by Gaussian averaging calculation assuming elliptical orbit 22 p3830 A67-39161

Satellite maneuverability in orbit using hypothetical elliptical orbit to demonstrate formulas used 22 p3882 A67-39563

Jacobi high energy ellipsoid orbits in barred spirals valid at galactic time scales 23 p4063 A67-40898

Pursuit trajectory plotting in central field of gravity for pursuer and fugitive assuming motion can be predicted successively at small time intervals 24 p4228 A67-42273

ELLIPTICITY

Ellipticities of moon for radial shift and rotation of unperturbed orbit of close satellite in plane of instantaneous motion 08 p1396 A67-21178

Moon mechanical ellipticity determined by modification of Habbullin method adapted to Schrutka-Rechtenstamm artifact 18 p3128 A67-34304

Photometric determination of moon limb shape during annular solar eclipse, using rotating prisms 18 p3129 A67-34313

Moon shape determined from topocentric terminator deviation, using photometry 18 p3132 A67-34334

Faraday rotation and ellipticity measurements in germanium and gallium arsenide at room temperature in weak magnetic fields 24 p4202 A67-41984

EMBOLISM

Gas embolisms and gas bubble formation in tissue 13 p2059 A67-26849

[DVL-615]

Air embolism pathogenesis and therapy in terms of problem of treatment in overpressure 13 p2059 A67-26850

[DVL-628]

EMBRITTELEMENT

SA BRITTLENESS

Prior cold reduction effect on precipitation and embrittlement of cobalt base alloy /L-605/ 04 p0639 A67-15457

Molybdenum grain boundary relaxation and embrittling effect of interstitial impurity additions 05 p0829 A67-16505

Creep ductility, stress rupture and high temperature irradiation embrittlement of neutron-irradiated Hastelloy N 08 p1343 A67-21195

Nb embrittlement by H at ambient temperatures under work hardening effect, noting correlation between elastic limit and deformability in H 11 p1806 A67-24427

Beta-Ti alloy mechanical properties variation with hydrogen content for various temperatures and hydrogen embrittlement mechanism 20 p3468 A67-37176

EMERGENCY BREATHING TECHNIQUE

S PRESSURE BREATHING

EMERGENCY LIFE SUSTAINING SYSTEM

Space rescue capability and proposed concepts to achieve it [AIAA PAPER 66-905] 02 p0332 A67-12271

Qualitative safety and survival factors in emergency escape and relation to complete ejection event via functional diagramming 23 p3964 A67-41546

Mathematical technique to determine probabilities associated with critical system performance capability measured under varying human and environmental conditions 23 p3964 A67-41547

Death and survival during water immersion in plane crashes near Cape Cod and Hamilton Bay 23 p3970 A67-41707

Space flight emergency contingency planning for survival, evaluating physiological effects and remedial system effectiveness [AIAA PAPER 67-825] 24 p4116 A67-42972

EMISSION

SA AIRGLOW

SA ATMOSPHERIC EMISSION

SA AURORAL EMISSION

SA ELECTRON EMISSION

SA EXO-ELECTRON EMISSION

SA FIELD EMISSION

SA FLUORESCENT EMISSION

SA ION EMISSION

SA LIGHT EMISSION

SA NEUTRON EMISSION

SA OPTICAL EMISSION

SA PARTICLE EMISSION

SA PHOTOELECTRIC EMISSION

SA RADIANT ENERGY

SA RADIATION EMISSION

SA RADIO EMISSION

SA SECONDARY EMISSION

SA SELF-SUSTAINED EMISSION

SA SIMULATED EMISSION

SA SPECTRAL EMISSION

SA SPONTANEOUS EMISSION

SA STEFAN-BOLTZMANN LAW

SA STIMULATED EMISSION

SA THERMAL EMISSION

SA THERMIONIC EMISSION

SA VERY LOW FREQUENCY EMISSION

RECORDER

Deformation potential of valence band of indium antimonide, using piezoemission technique of shifting intrinsic recombination

under uniaxial stress 06 p1062 A67-18932

EMISSION SPECTRUM

Hall effect and fine structure of X-ray fluorescence and absorption K spectrum of vanadium in silicides 01 p0101 A67-10935

Total emissivity and upper limit of water vapor determined from IR spectra emissivity 01 p0187 A67-10973

Numerical method to obtain emissor coefficients from emitted spectral intensities for asymmetrical plasma sources such as atomic spectral argon line 01 p0115 A67-11073

Thermal radio emission from Mercury, Venus, Mars, Saturn and Uranus at various wavelengths, using radio telescope in Australia, determining emission spectrum 02 p0319 A67-11455

Four-linked rare earth chelate with sodium ion obtained with benzoylacetone and europium, analyzing molecular and ionic transitions by absorption and emission spectra 02 p0251 A67-11518

Spontaneous emission spectra and ratio of number of photons in various oscillation modes of laser with nonlinear filter type lock 02 p0251 A67-11573

Line emission of hydrogen alpha limb spectra beyond continuum limb analyzed to yield data about height of formation in solar chromosphere 02 p0323 A67-11694

[AFCL-66-834]

Eppley-JPL solar constant measurement experiment, noting 12-channel radiometer, filter wavelength limits and high altitude measurements 02 p0328 A67-12396

Tunable dispersion resonator and broadening of laser emission spectral range to obtain operating frequency other than fundamental 03 p0435 A67-13131

Steady state laser radiation during relaxation, discussing time-dependent spectral composition, oscillation modes and polarization characteristics 03 p0435 A67-13134

Crystal absorption and lamp emission spectra for CW pumping of Nd-doped YAG by water-cooled Kr arcs 03 p0437 A67-13576

Emissive capacity of argon in direct current arc at high pressure and temperature, noting experimental setup and results 03 p0478 A67-13602

Intergalactic atomic neutral hydrogen detection in emission in clusters of galaxy and in noncluster field 03 p0514 A67-14318

SHF oscillator construction using multiphonon processes that occur in gases during dipole interactions 04 p0580 A67-14749

Light emission spectrum changes due to forced transitions during passage through finite volume with negative absorption factor 04 p0709 A67-14812

Emission spectra and I-V characteristics of diffusion p-n junctions in InP and spontaneous radiative recombination in presence of small current 04 p0679 A67-15138

Comet spectra observation noting emission band abundance, atomic lines presence and continuous spectrum with solar Fraunhofer lines 05 p0890 A67-16337

Relaxation problem of two-level molecule in dense resonance medium 05 p0762 A67-16351

CW argon ion laser scattering in argon plasma, noting resonance and correlation between data and plasma properties 05 p0820 A67-16665

Large deuterium isotope effect on fluorescence emission spectra and quantum yields observed in number of chromospheres that contain proton donor groups 05 p0758 A67-16701

Stimulated emission in triplet system of nitrogen molecule produced by pulsed laser discharge, identifying lines and interpreting intensity distribution in rotational band spectrum 05 p0824 A67-16785

Spectrochemical analysis of solid specimen from vapor formed by laser beam and excited by spark 05 p0824 A67-16786

Anomalous emission at electron cyclotron frequency in partially ionized plasmas 05 p0854 A67-16895

Doppler effect on emission spectrum and energy of moving oscillator and intensity of surface wave excited by it 05 p0765 A67-17160

Photoconductivity, edge emission spectrum, longitudinal optical phonon coupling and eigenfrequencies for linear chain of Cd-Se-Cd-S-Cd...

- 05 p0870 A67-17196
X-ray emission and absorption spectra,
electron structure and properties of metallic
compounds of titanium 05 p0831 A67-17484
Luminescence spectrum of CuCl at low
temperatures excited by double photon
absorption from high intensity laser
beam 06 p1010 A67-17822
Radiative lifetimes of UV molecular
transitions, analyzing emission spectrum in
vacuum monochromator 06 p1035 A67-17828
Emission microwave spectroscopy of OCS,
observing coherent ringing, coherent
radiation modulation and pulse
echoes 06 p1032 A67-18208
Spectral emissivity measurements of
carbon dioxide band made at high
temperatures identifying hot transitions
through Q-branches 06 p1118 A67-18539
Resonance emission of H and K lines of
ionized calcium during twilight
photographically observed, suggesting
meteoritic origin 06 p0998 A67-18704
Sharp line emission spectra due to alkali
metal doping in ZnO crystals at low
temperatures 06 p1060 A67-18914
Magnetic field strength effects on excited
acceptor states of semiconducting diamond
determined, using Zeeman splittings of main
excited lines 06 p1062 A67-18927
Optical transitions at isoelectronic traps in
GaP and ZnTe, presenting fluorescent
spectra 06 p1062 A67-18929
Emission spectrum of GaP diodes analyzed
as function of current and
temperature 06 p1062 A67-18931
X-ray astronomy of discrete sources in or
near galactic plane, noting likely X-ray
production mechanism 06 p1092 A67-19009
Emission spectra of nitrogen excited by
electron beam of 0.1 to 20 kev and oxygen
and air bombarded by 13-kev
electrons 07 p1225 A67-19099
Discharge plasma in He and argon with
cesium and potassium vapor admixtures
noting electric field, conductivity, electron
temperature and emission
spectrum 07 p1227 A67-19115
Particle number fluctuation in single cell
of Kastler photon set, discussing statistical
properties of laser emission in multimode
excitation regime 07 p1196 A67-19599
Spectral analysis of emission of spatially
separated spots in GaAs injection
lasers 07 p1197 A67-20185
Photolysis of hydrazine vapor in vacuum
UV, examining emission as function of
pressure and photolysis
time 07 p1138 A67-20190
Frequency doubling of light in ruby laser
due to laser light interaction with corundum
lattice, anti-Stokes-Raman scattering of laser
light, etc 08 p1336 A67-20316
Coherent radiation generation in electron-
hole indium antimonide plasma, discussing
emission spectrum 08 p1367 A67-20418
K beta 5 emission band and fundamental
K-edge absorption of vanadium analyzed and
results compared with vanadium spectra
from other series 08 p1342 A67-20808
Spectrum of meteorite luminescence
emission after irradiation with protons and
UV radiation, using
spectrophotometer 08 p1390 A67-21021
Spectrophotometric data correlations
between color and red shifts of
quasars 08 p1398 A67-21231
Mercury emission intensity ratios in
negative glow of Hg-hydrogen DC abnormal
glow discharge 08 p1356 A67-21296
Alloying effect on aluminum K and iron L
K-ray emission spectra in Al-Fe binary
system 08 p1343 A67-21304
Emission occurring when mixing molecular
nitrogen with helium ion following charge
transfer analyzed
spectroscopically 08 p1326 A67-21358
Center limb variation of H-and K-lines of
Ca-2 08 p1401 A67-21444
Spectrum of comet Ikeya-Seki analyzed at
polar distances noting emissions, excitation
temperature, abundance ratio,
photoionization effect, etc 09 p1566 A67-22234
Red shift and absorption line of PKS 0237-
33 09 p1567 A67-22242
Faraday rotation effects in spectral
records of Jupiter decametric
radiation 09 p1568 A67-22401
Output and emission spectra of p-n
junction diodes analyzed in connection with
laser effect in GaSb 09 p1516 A67-22600
Temperature measurement methods in
sulfur hexafluoride compared with reaction
separation 10 p1684 A67-22892
Photometry of coronal emission line 5303
angstrom on Mt. Lomnický
Stit 10 p1705 A67-22897
Emission and absorption bands in K
spectral region of titanium, using single
setup 10 p1688 A67-23093
Space correlation of main emission lines
for night sky emission spectra and altitude
distribution of sodium
luminescence 10 p1647 A67-23279
Diurnal and latitudinal variations in 5577
angstrom zenith nightglow intensity
compared with 6300 angstrom
calibrations 10 p1650 A67-23337
Luminescence of CdS at low temperature
excited by very high intensity laser
light 10 p1667 A67-23779
Spectroscopic twilight airglow
measurements for upper atmosphere
interpreted using rocket flight
data 11 p1786 A67-24263
One-dimensional weak plasma turbulence,
noting structure of spectra for various
oscillation frequencies 11 p1837 A67-24393
Solar K-line intensity and emission area at
various phases of sunspot
cycle 11 p1861 A67-24493
Detection and measurement of mm wave
difference frequency between two near laser
lines, using optical
heterodyne 11 p1803 A67-24832
Solar X-ray emission measurement below
25 angstroms using airborne Bragg
spectrometers, with data reduced by
computer 11 p1867 A67-24839
Auroral green lambda 5577 of oxygen atom
analyzed from glow discharge emission,
proposing excitation mechanism on basis of
intensity variations 11 p1824 A67-24934
Electronic Raman scattering from
phosphorus donors and boron acceptor
impurities in Si, noting importance of
interband transitions 11 p1851 A67-24999
Fluor molecule emission spectrum
between 4500 and 8500 angstroms, discussing
results of rotational vibration analysis
[DVL-624] 11 p1750 A67-25003
Emission spectra and I-V characteristics of
diffusion p-n junctions in InP and
spontaneous radiative recombination in
presence of small current 12 p1979 A67-25161
Variability of integrated K-line emission
studied during one solar
rotation 12 p2001 A67-25223
Relative solar abundance for O, Si and Fe
determined from intensities of far UV
emission lines of solar
corona 12 p2001 A67-25225
Emission spectrum of single and
multicomponent ruby laser, observing
decrease in number of modes during
transition from solid to multielement
instrument 12 p1952 A67-25436
Impurity effect on electroluminescence of
gallium phosphide diodes, noting dependence
of spectrum on current density through p-n
junction 12 p1914 A67-25438
Emission properties of sintered oxides
treated by method of empirical
generalization and by method involving
comparison of emittance in air and in
vacuum 12 p1958 A67-26016
[AIAA PAPER 67-301]
Surface roughness effect on spectral and
total emittance of platinum, noting spatial
distribution of polarized components
[AIAA PAPER 67-320] 12 p1957 A67-26035
Time-integrated and time-resolved spectra
of GaAs laser diode, noting temperature
effect on spectral
emission 13 p2125 A67-26427
Thermal radiation characteristics of
metallic surfaces, comparing metal
dispersion relationships with experimental
emissivity 13 p2130 A67-26439
Prediction of total emissivity of nitrogen-
broadened and self-broadened hot water
vapor 13 p2155 A67-26493
Optical fluorescence, thermally tunable
over significant portion of visible and near
IR spectrum, from phase-matched parametric
system 13 p2127 A67-27081
Frequency shift in emission spectrum of
complex atom in uniform electric field,
noting numerical results for Al
I 13 p2168 A67-27208
Electron density and HF spectrum of
beam generated plasma as function of gas
pressure and injection
parameter 14 p2352 A67-27749
P-type GaAs laser excited by Q-switched
ruby laser at liquid nitrogen temperature,
noting spectral shift due to Burstein
effect 14 p2329 A67-27831
Velocity distribution function of gas
measured with laser, noting relation to
frequency variation of absorption coefficient
across spectral line 14 p2317 A67-28194
Characteristics of electroluminescent p-n
junctions prepared on base of beryllium-
doped silicon carbide 14 p2367 A67-28524
Nightglow continuum
emission 14 p2313 A67-28576
OH emission in H II region W3, using
improved equipment 14 p2389 A67-28845
Threshold temperature variation, output
power and emission spectrum of short ruby
crystals operated in quasi-continuous
mode 15 p2498 A67-29665
Book on laser microemission spectrum
analysis covering laser properties, Q-
switching technique, controlled negative
feedback lasers, applications,
etc 15 p2501 A67-30147
Absorption, fluorescence and laser
emission spectra of triply ionized
neodymium yttrium in compound below
room temperature 16 p2726 A67-30810
Multiphonon relaxation in neodymium
doped lanthanum chloride, determining
transition rates between stark levels with
lifetime and quantum efficiency
measurements 16 p2728 A67-31057
Continuous spectrum emission from free-
bound and free-free electron transitions into
field of monatomic gas ion using shock
tube 16 p2673 A67-31109
Mid-IR spectral emittance measuring
apparatus, discussing range of performance,
systems response, etc 16 p2677 A67-31429
Radiative recombination mechanisms in
photoluminescence of n-type InP, discussing
emission bands 16 p2732 A67-31450
Chromosphere and corona UV emission
spectrum provided by sounding rocket using
photographic recordings 16 p2752 A67-31625
Internal conversion electron spectrum for
samarium 155 to europium 155
transmutation, noting multipolarities and
new lines 16 p2733 A67-31706
Two peaks in emission from low pressure
helium or neon discharge simulating plasma
slab with second peak corresponding to
plasma cut-off frequency 17 p2901 A67-32369
Photoelectric spectrophotometric study of
emission line spectrum of quasi-stellar
source 17 p2944 A67-32636
Interpretation of UVB measurements of
quasi-stellar sources 17 p2944 A67-32637
Solar X-ray spectrum observed by rocket
carried Bragg crystal spectrometers and
pinhole cameras array 17 p2937 A67-32650
Coherent radiation from cadmium sulfide
single crystal excited by electron beam,
noting transition nature in generation mode
and spectral composition 17 p2915 A67-32660
Population of atomic levels by cascade,
dielectric and three-body electronic
recombination, discussing spontaneous
transition, electron impact and RF
spectra 17 p2947 A67-32762
Space-time properties of hydroxyl
emission observed by
spectrophotometry, giving diagrams of
periodic variations and measurement
errors 17 p2848 A67-32954
Hydroxyl emission at high latitudes during
winter months of 1960 through 1963
measured with
spectroscope 17 p2848 A67-32955
Periodic variations in rotational
temperatures of OH emission bands
determined by spectroscopic
measurements 17 p2849 A67-32956
IQSY electrophotometric and
spectrometric measurements of annual and
nighttime variations in rotational
temperatures and integral intensity of
hydroxyl emission bands 17 p2849 A67-32957
Diurnal variations in He twilight emission
intensity determined using photoelectric
spectrometer 17 p2849 A67-32958
Helium afterglow observation at high
latitudes, determining He line intensity on
IR spectrograph and giving time-dependent
seasonal variations 17 p2849 A67-32959
Hydrogen distribution in upper
atmosphere and geocorona, relating H-alpha
emission increase to solar activity

decrease 17 p2849 A67-32961
 Elliptical patterns on emission lines of argon plasma jets attributed to antihalation backing during hypersensitization of film 17 p2863 A67-33305
 Eruption of solar flare of importance 2, describing evolution, associated optical and radio phenomena, structure of longitudinal magnetic field, etc 17 p2939 A67-33397
 X-ray K spectra of phosphorus absorption and emission in indium, gallium and boron phosphide semiconductors and red phosphorus 18 p3095 A67-33440
 Upper atmosphere observation at twilight, considering broad spectral regions and emission lines 18 p3033 A67-33585
 Dayglow emissions observation by ground-based instruments indicate atmospheric response to concurrent input of solar energy 18 p3033 A67-33586
 Cinematographic observations of fast auroral variations 18 p3033 A67-33587
 Mars emission spectrum computed for two atmospheric models, presenting weighting functions for different wave numbers 18 p3125 A67-34159
 Long-duration monochromatic emission with worldwide character in frequency spectrum of magnetic storm 18 p3041 A67-34193
 Temperature and frequency response of argon arc continuum emission coefficient, explaining unexpected deviations 18 p3089 A67-34299
 Emissive capacity of argon in direct current arc at high pressure and temperature, noting experimental setup and results 18 p3090 A67-34467
 Laser frequency variation and emission kinetics during generation process, investigating spectra at scanning rate and pumping energy ranges 18 p3061 A67-34619
 Emission recombination in n-type Si single crystals irradiated with fast neutrons or gamma quanta 19 p3301 A67-34775
 Height profile of atomic oxygen 6300 angstrom emission in night airglow determined by rocket photography 19 p3215 A67-35177
 Microwave noise radiation and scattering from cylindrical plasma column, studying dissipative processes on emission spectrum 19 p3291 A67-35387
 Magnetic electron multiplier performance as photomultiplier in EUV spectral region 19 p3231 A67-35683
 Fluorescence spectrum of activating europium ion in lutetium oxide matrix and appearance in crystalline-field model 19 p3307 A67-35794
 Spherical interferometers used in measuring time-resolved spectra of ruby laser relaxation oscillations 19 p3241 A67-35804
 Spectral-line narrowing in ruby laser during standing wave field displacement with respect to active center of ruby crystal 19 p3241 A67-36023
 Generation threshold of substance with electronic-vibrational energy level studied for laser use 19 p3309 A67-36105
 Nitrogen and oxygen dayglow emissions observed during total solar eclipse of May 1965, studying emission/continuum intensity ratio 20 p3427 A67-36368
 Chemiluminescence and chemionization in low pressure fuel-oxygen flames, measuring emission intensity of CH, carbon molecule and OH electronic bands 20 p3376 A67-37094
 Cadmium sulfide edge luminescence energy shift dependence on excitation intensity and free carrier concentration 20 p3512 A67-37288
 Particle number fluctuation in single cell of Kastler photon set, discussing statistical properties of laser emission in multimode excitation regime 20 p3462 A67-37338
 Solar X-ray emission line spectrum from 1.3 to 20 angstroms in solar flares identified as Fe XXVI through Fe XX transitions 20 p3519 A67-37396
 Lunar crater Alphonsus emission flare noting C-2 Swan system 20 p3528 A67-37470
 Laboratory investigation of laser emission line absorption by atmospheric gases in vacuum multiple-pass cell, obtaining data free of aerosol scattering 20 p3386 A67-37606
 Radiative heat transfer in nonisothermal nongray gas model, measuring absorption and emission in carbon dioxide and water

gases [ASME PAPER 66-WA/HT-25] 20 p3555 A67-37607
 Injection lasers threshold current densities, emission spectra, emission polarization and power 21 p3639 A67-37943
 Discharge plasma in He and argon with cesium and potassium vapor admixtures noting electric field, conductivity, electron temperature and emission spectrum 21 p3664 A67-38160
 Hydroxyl radical emission, hypotheses attempting to explain OH emission origin, including possible maser mechanism and interstellar communications 21 p3704 A67-38567
 21.2 cm spectra of Jupiter, Venus, Mars and Saturn noting mean effective brightness temperatures 21 p3709 A67-38993
 Boron oxide identified as radiating species causing molecular fluorescence spectrum in upper atmosphere at twilight 21 p3623 A67-39123
 Profile of night sky hydrogen Lyman alpha emission line determined using data from rocketborne hydrogen-filled filter tube 22 p3790 A67-39805
 Carbon dioxide and water vapor band emissivities determination, discussing spectral absorption, radiative heat transfer and energy distribution 22 p3918 A67-40042
 Airborne multiple scan interferometry for low temperature IR emission spectral distribution of minerals 22 p3807 A67-40368
 Fabry-Perot interferometer for emission spectra time variations observed by employing electromechanical system to vary mirror motion speed 22 p3809 A67-40416
 Spectroscopic analysis of iron meteoroid radiation by emission growth curve method covering temperature factors and atom and electron concentrations 23 p4062 A67-40674
 Charge spectrum of very heavy cosmic ray primaries studied from balloon observations in photographic emulsion detector for Texas atmosphere 23 p4050 A67-40676
 Electron-electron interaction effect on Li soft X-ray emission spectrum, liquid metal optical absorption and alkali metal dielectric response 23 p4037 A67-40760
 Pulsed water vapor laser single wavelength operation using three diffraction gratings to make resonator frequency-selective 23 p4011 A67-40783
 Characteristics of electroluminescent p-n junctions prepared on base of beryllium-doped silicon carbide 23 p4039 A67-40931
 50 Hz ruby pulse laser emission, discussing power output, electromagnetic spectrum and transverse mode 23 p4016 A67-41153
 Emission of GaSb injection lasers in pulse regime, demonstrating existence of two staggered laser lines originating in diode regions 23 p4016 A67-41193
EMITTER
 Interference Prediction Model /IPM/ for RF interference study at satellite tracking stations 01 p0023 A67-10498
 Emitter sidewall junction capacitance in double diffused transistors, using linearly graded junction equation and two-dimensional impurity distribution 03 p0382 A67-13679
 Capillary emitter of electrons and Cs ions for use in thermionic converters 04 p0664 A67-15015
 Emitter barrier capacitance effect on frequency characteristic of current amplification factor in drift transistors with accelerating field for minority carriers 04 p0585 A67-15502
 Dependence of first harmonic averaged parameters of transistor on oscillation amplitude in common-emitter circuit in absence of bias current in base circuit 07 p1149 A67-19187
 Control of polarization of radiation field of waveguide-slot antenna 07 p1153 A67-19598
 Thermal variation of emitter base voltage of bipolar transistor 07 p1155 A67-19792
 Incremental stress effects in transistors at emitter-base junction due to piezoresistive and piezoelectric effects 09 p1472 A67-21950
 Niobium and nickel as thermionic converter collector materials, comparing characteristics 09 p1447 A67-22331
 Dynamic characteristics of thermionic converter noting influence of emitter heat

transfer 09 p1447 A67-22331
 Calorimetric measurements of thermionic converter/ heat pipe system, discussing electron cooling of emitter, thermal emissivity and thermal balance 09 p1448 A67-22341
 Doppler phenomena arising in rotation of system of electromagnetic wave emitters and reflectors 11 p1750 A67-23908
 Potential distribution in emitter diode measured in single ended Q machine, using ribbon electron beam 11 p1764 A67-24371
 Porous W-Ta emitters as ion source for production of quiescent alkali plasmas of improved symmetry, reproducibility and uniformity 11 p1838 A67-24411
 Upper cut-off frequency and amplitude frequency response curve shape for wideband aperiodic amplifiers, examining five common transistor circuits 13 p2077 A67-26660
 Transfer of electrons from emitter or space charge region to collector in thermionic energy converter by negative ions 13 p2056 A67-27002
 Frequency scanning array of emitters on convex curve 13 p2069 A67-27031
 Signal spectral characteristics when reflected from rough surface exposed to monochromatic and frequency modulated oscillations from moving airborne emitter 13 p2154 A67-27038
 Nonuniform base width effects on h-parameters of junction transistor 16 p2635 A67-30795
 External mutual coupling of rectangular waveguide-slot emitters, deriving coefficient of reflection 17 p2826 A67-32683
 Low temperature dependence of relative efficiency of forward biased InAs diode emitter 19 p3198 A67-36046
 Linear operation of diffused planar transistor in common emitter connection studied by mathematical models 20 p3396 A67-36377
 Indirect measurement of differential switching parameters examined for admittance matrix of common emitter coupling for field effect and junction transistors 20 p3396 A67-36379
 Control of polarization of radiation field of waveguide-slot antenna emitter 20 p3401 A67-37337
 P-n-p transistor overcomes bandwidth and switching time deficiencies to enhance minority carrier transport 21 p3598 A67-38570
 Doppler phenomena arising in rotation of system of electromagnetic wave emitters and reflectors 21 p3585 A67-38936
 Breakdown temperature of pulsed switching circuit using high power transistors depends on transistor property 22 p3771 A67-39827
EMOTIONAL FACTOR
 Quantification of response suppression in conditioned anxiety training with fixed duration preaversive stimulus /CS/ 20 p3373 A67-37577
EMULSION
SA COLLOID
SA NUCLEAR EMULSION
SA PHOTOGRAPHIC EMULSION
 Emulsified fuel effect on gas turbine combustors, noting good operation in low altitude flight but inhibited combustion at start and at high altitudes [SAE PAPER 670366] 12 p1987 A67-25884
 Emulsified jet engine fuel noting lower volatility and flammability and resistivity to corrosion and acceleration [SAE PAPER 670365] 12 p1988 A67-25885
 Magnetohydrodynamic generator functioning by emulsion consisting of gas or vapor in liquid metal 16 p2606 A67-30588
 Nonlinear macroscopic rheological behavior of dilute suspensions of deformable spheres 17 p2887 A67-32280
 GE T64 engine operation on emulsified fuel /JD1/, noting corrosion effects on fuel system components due to water additive [SAE PAPER 670369] 17 p2927 A67-33002
 Gelled, emulsified and otherwise thickened fuels for aircraft fire safety, discussing requirements and engine operation [AIAA PAPER 67-503] 18 p3110 A67-33967
 Processing and obtaining phase holograms of elementary particle tracks in gelatin bubble and emulsion chambers 18 p3049 A67-3387
 Formulas describing hologram properties, considering emulsion thickness effect on

Recording and reconstruction 20 p3435 A67-36202
Centrifugal disk photosedimentometer used for size analysis of latex emulsions 23 p3972 A67-41066
CAPSULATION
Coating and embedding techniques for environmental protection of printed circuit assemblies 08 p1335 A67-20749
Testing for leak-proof encapsulation of semiconductor devices by use of krypton 85 as radioactive tracer gas 17 p2823 A67-32297
Techniques for achieving contaminant-free sealed package of solid state active devices 19 p3236 A67-35024
Encapsulation material and process implementation for thick film substrates noting fabrication and quality problems 21 p3596 A67-38343
Puncture sealing of meteoroid penetration in spacecraft, giving mechanical and chemical methods and self-sealing tile inner shell process 22 p3913 A67-39885
ENCKE METHOD
Encke special perturbation method of integrating motion equations of near-earth satellites modified to eliminate first-order effects of earth oblateness 01 p0148 A67-10383
Nominal trajectory in modified Encke special perturbation method, using two-body functions 01 p0148 A67-10384
Modification of Encke perturbation method for computing satellite orbits, obtaining integration of motion equations [AAS PAPER 66-93] 07 p1252 A67-19957
Modification of Encke perturbation method for computing satellite orbits, obtaining integration of motion equations [AAS PAPER 66-93] 13 p2207 A67-27517
ENCODER
Ninety-eight-channel microelectronic PCM multiplexer-encoder design and development qualified to Apollo spacecraft environments 01 p0026 A67-10864
High resolution optical shaft angle encoder with gallium arsenide diodes as light sources and compatible with integrated circuit techniques 01 p0073 A67-11113
Silicon integrated circuit data encoder for Isis A satellite particle counting experiment, noting design and construction 05 p0770 A67-16292
Fluidic digital rectilinear displacement indicator emphasizing transducer, logic circuitry and readout 08 p1281 A67-20456
Encoding and decoding techniques using integrated circuits and applicable to binary digitizing of electrical analog information 13 p2072 A67-26412
Convolutional encoder for orthogonal tree codes in presence of white Gaussian noise [JPL-TR-32-1120] 14 p2273 A67-28710
Open loop and feedback analog-to-digital conversion techniques, discussing conversion time, aperture and complexity 14 p2276 A67-28771
ENCODING
SA CODING
SA DECODING
SA REDUNDANCY ENCODING
SA SIGNAL ENCODING
Pathcount and coding matrices for sequence time encoding and decoding for data compression 01 p0028 A67-10022
Compact encoding of stationary Markov sources 12 p1919 A67-26085
END PLATE
Heat transfer to end wall of shock tube behind reflected shock wave in oxygen dissociated to varying degrees and at high temperatures 04 p0729 A67-15813
Electric field effect in Q machine with uniform end plate temperature, noting deviation from thermal equilibrium and increment in ion loss rate for certain range of particle densities 11 p1833 A67-24370
Conditions controlling shock wave reflection from duct end deflector plates, determining spacing of plates from pipe 12 p1928 A67-25356
ENDOCRINE SYSTEM
SA ADRENAL GLAND
SA HORMONE
SA PITUITARY GLAND
SA THYROID
Stress-related and other physiological variables on jet aircraft pilots participating in storm penetration and perimeter flights 17 p2805 A67-31955
Glands in two sea snakes located in oral

area compared, identified and proved not to be salt glands 21 p3573 A67-37898
ENDOCRINOLOGY
Biochemical response pattern to combat flying stress of monitored carrier aircraft pilots 17 p2805 A67-31957
ENDOSCOPE
New endoscope for internal viewing [SAE PAPER 670361] 12 p1945 A67-25881
ENDOTHERMIC FUEL
Endothermic hydrocarbon fuels for supersonic aircraft, noting heat sink capacity effect in overcoming thermal thicket and usability as engine fuel 15 p2543 A67-29305
ENERGETIC PARTICLE EXPLORER S EXPLORER SATELLITE
ENERGETIC PARTICLE EXPLORER-A S EXPLORER XII SATELLITE
ENERGETIC PARTICLE EXPLORER-B S EXPLORER XIV SATELLITE
ENERGY
SA ACTIVATION ENERGY
SA BINDING ENERGY
SA CHEMICAL ENERGY
SA ELECTRIC ENERGY
SA ELECTRON ENERGY
SA FORMATION ENERGY
SA FREE ENERGY
SA INTERFACIAL ENERGY
SA INTERNAL ENERGY
SA KINETIC ENERGY
SA MOLECULAR ENERGY
SA MOMENTUM ENERGY
SA NUCLEAR ENERGY
SA POTENTIAL ENERGY
SA PROTON ENERGY
SA RADIANT ENERGY
SA SEISMIC ENERGY
SA SOLAR ENERGY
SA STACKING FAULT ENERGY
SA STRAIN ENERGY
SA SURFACE ENERGY
SA THERMAL ENERGY
SA THERMONUCLEAR ENERGY
Laser pulse energy measurements with liquid absorption cell calorimeter 04 p0624 A67-15456
Quadratic control regulator problem with energy constraint analyzed, considering availability of limited control energy or as method of limiting maximum control amplitude 08 p1309 A67-20332
Topology of three-dimensional integral surface projection of section of energy integral by third integral 08 p1380 A67-20382
Fracture criterion from application of energy principle to elastic plastic crack model, showing positive nature of energy change during propagation 10 p1730 A67-23829
Momentum and energy of gravitational waves in terms of relativity theory 15 p2518 A67-30005
Momentum and energy of gravitational waves in terms of relativity theory momentum and energy of gravitational waves in terms of relativity theory 18 p3079 A67-33763
ENERGY ABSORPTION
Self-focusing of laser beam in plasma, solving wave equation for slab and cylindrical beam configurations 02 p0252 A67-12089
Ionization calorimeter measurement of absorption of energy flux of primary cosmic radiation nuclear active component in iron 02 p0316 A67-12762
Absorption curve and energy spectrum of high energy muons 02 p0317 A67-12775
Work of fracture and measurement in metals, ceramics and other materials 03 p0525 A67-13872
Acoustic wave energy absorption by superconductors in intermediate state 03 p0502 A67-14377
Properties of crushable impact attenuation materials used to absorb and dissipate kinetic energy of impacting body 04 p0711 A67-15238
Neutron energy deposition in silicon in ionization and elastic interactions calculated, noting effects of atomic recoils 04 p0684 A67-15688
Quasi-steady state temperature distribution in thick walled spherical satellite under solar radiation 05 p0906 A67-17368
LF electromagnetic field behavior in cold magnetoactive plasma near resonance layer, noting condition for energy absorption increase 06 p1039 A67-18078

Energy absorption characteristics of honeycomb structures under static and impact loading 10 p1727 A67-23745
RF energy absorption by plasma column surrounded by periodic coupling structure, noting similarities with Landau damping and measurements of non-Maxwellian distributions 11 p1838 A67-24402
Nonuniform absorption of gyro-resonant microwave energy by electron gas used to produce helical configuration in magnetoplasmas 13 p2163 A67-26289
Energy absorption profile and ionization rates for electron beam dependence on beam energy, altitude and atmospheric layer thickness and mass 14 p2379 A67-27921
Heat resistant stainless steel honeycomb cores for cylindrical applications, measuring energy absorption characteristics [ASME PAPER 67-DE-14] 14 p2402 A67-28870
Output energy for ruby laser with parallel mirrors for varying excitation energies, pulse lengths, mirror reflectivities and losses due to absorption, scattering and reflection 15 p2502 A67-30427
Mode-locked laser described in traveling light pulse terms, with saturable absorber, noting pulse width under steady state 16 p2686 A67-31808
Helicopter cargo restraint system program meeting prescribed operational and safety requirements [AHS PAPER 124] 16 p2598 A67-31839
GaAs single crystals excited to stable longitudinal vibrations by supersonic absorption, determining resonance curve 17 p2914 A67-32401
High strength Ti alloys in development of compressor blades, considering yield strength, impact energy absorption, ductility, fracture toughness and fatigue resistance [SAE PAPER 670335] 17 p2874 A67-32985
Radiative heating of H and He containing suspension of solid particle absorbers, noting proportionality between gas particle dispersion decrease and energy absorption [AIAA PAPER 67-501] 18 p3158 A67-33965
Emissivity and absorptivity of infinite length isothermal trapezoidal grooves with radiating gray walls 18 p3159 A67-34055
Electromagnetic field energy absorption in cold rotating plasma, obtaining electric current density and plasma electric field relationship and cyclotron resonance 20 p3497 A67-36677
Efficiency of plasma heating by HF field with excited magnetosonic wave due to energy absorption 21 p3669 A67-38678
Plasma rotation effect on cyclotron resonance, noting electromagnetic field energy absorption 21 p3669 A67-38679
Electromagnetic propagation in plasma layer in magnetic field, determining absorption coefficient 22 p3762 A67-40123
Ionization calorimeter measurement of absorption of energy flux of primary cosmic radiation nuclear active component in iron 22 p3842 A67-40264
Absorption curve and energy spectrum of high energy muons 22 p3877 A67-40277
Energy transmitting characteristics and wall local energy absorption distribution of curved specular reflecting duct irradiated by collimated beam 23 p4028 A67-41271
Titanium-magnesium and titanium-beryllium oxides physical properties under electron bombardment in vacuum indicate usability for SHF oscillation energy absorbers 24 p4202 A67-42069
ENERGY BAND
SA EXCITON
Calculation of energy band structure of gallium arsenide, using experimental Fourier coefficients for germanium in pseudopotential method 01 p0136 A67-11054
Current density resulting from integration over energy of transport equation applicable to dielectric film 02 p0295 A67-11763
Oscillatory magnetostriction in GaSb, noting stress effect on energy bands 02 p0296 A67-11819
Room temperature reflectance spectra of GaAs, GaP and typical alloys in energy range 2.5 to 20 ev and 2.5 and 6 ev at liquid nitrogen temperature 03 p0501 A67-14355
Energy gap anisotropy effects in pure single crystal superconductors investigated by factorable BCS-like model for effective electron-electron matrix element 04 p0673 A67-14518
Excitonic effects in interband absorption

of semiconductors noting electron-hole interaction, Coulomb interaction energy maxima and minima and scattering cross sections 04 p0676 A67-14926

K spectrum to obtain structure and regularities of occupation of external energy bands in transition from Sc to Cr 04 p0640 A67-15975

Change in basic barrier relation for heterojunction compared to homojunction of wide gap emitter injection laser 05 p0825 A67-17097

Chemical bonds formation during interaction between individual elements explained by total valence band energy theory 06 p1035 A67-17845

Silicon-gallium phosphide heterojunction fabricated by epitaxial deposition, presenting V-I characteristics and energy band diagrams 06 p1051 A67-18223

Tunneling measurements of energy gap anisotropy in thick and thin superconducting films of Al, Pb, In and Sn 06 p1052 A67-18571

Empirical corrections to energy band models of diamond, Si, Ge and grey Sn [AFCL-67-0382] 06 p1058 A67-18902

OPW calculation of six symmetry points in wurtzite Brillouin zone of CdS, using pseudopotential techniques 06 p1058 A67-18903

Band structure of GaAs, GaP, InP and AlSb obtained by k.p method 06 p1058 A67-18904

Band structures of gallium selenide and gallium sulfide derived by tight band approach 06 p1058 A67-18905

Deformation potential of valence band of indium antimonide, using piezoemission technique of shifting intrinsic recombination under uniaxial stress 06 p1062 A67-18932

Oscillatory magnetoconductance in inverted surfaces of p-type silicon 06 p1063 A67-18940

Galvanomagnetic effects and band structure of p-type cadmium antimonide 06 p1064 A67-18942

Band structures of group V semimetals and IV-VI semiconductors analyzed using tunneling, noting data on band edge energies 06 p1069 A67-18975

Quantum theory of electrical conductivity of semiconductors with nonstandard energy band 07 p1233 A67-19639

Band structure effects and interacting electrons and phonons in superconductor, treating Dyson equations and various simplified models 07 p1235 A67-20133

Anisotropy of energy gap in superconducting Pb analyzed using superconductive tunneling 07 p1236 A67-20137

K beta 5 emission band and fundamental K-edge absorption of vanadium analyzed and results compared with vanadium spectra from other series 08 p1342 A67-20808

Landau-Ginzburg theory extended to anisotropic superconducting energy gap, considering diffuse and specular boundary scattering 10 p1687 A67-22759

Cryogenic thermoconductivity of impure tin in superconducting and normal state, noting anisotropy and superconducting energy gap independence from impurity type 10 p1687 A67-22761

Correlation of anisotropic energy gap with thermal conductivity in pure and impure superconducting tin 10 p1687 A67-22762

Nonlinear excitation of electron plasmas in solids explained by mechanism of nonparabolic energy bands 10 p1689 A67-23075

Uniaxial stress and static electric field effects on energy band structure of strontium titanate and derivation of optical selection rules in region of perturbed crystals 10 p1691 A67-23403

Temperature dependence of total intensity in difference band systems, difference transitions between nondegenerate vibrations compared with carbon dioxide band 11 p1821 A67-23960

Waveguide dispersion effect on radiation pattern and directivity of series-fed linear arrays 11 p1762 A67-24289

Photoemission study of electronic structure of CdTe, considering two strong reflectivity peaks in optical reflectivity spectrum [AFCL-67-0405] 12 p1983 A67-25478

HF localized and LF resonant impurity modes valence effect on energy gap and

transition temperature in isotropic superconductors 14 p2370 A67-28720

Analytic properties of finite-band models in solids as generalization of Kohn procedure 15 p2534 A67-29324

Localized defects in semiconductors, using solid state scattering theory to calculate energies of bound states 15 p2534 A67-29325

Parameters for model of two valence bands of SnTe according to Hall effect measurements at high temperatures 15 p2537 A67-29709

Energy dependence on wave vector in valence band of diamond, Si, Ge and SiC, obtaining Coulomb and resonance integrals 15 p2541 A67-30237

Semiconductor nonlinear polarizability at difference frequency calculated, considering exciton states alone and combined with band energy states 15 p2541 A67-30238

Current carrier distribution in GaAs-Ge heterojunctions measured for energy band diagram 15 p2542 A67-30241

Valence band structure of wurtzite type crystals 16 p2725 A67-30802

Second order phase transitions in ionic crystals caused by vibronic interaction analogous to Jahn-Teller effect in ideal crystals 16 p2726 A67-30813

Optical reflection spectra of GaS, GaSe, and GaTe single crystal semiconductors in electron volt band energy range 16 p2730 A67-31159

Energy band structure of crystals of groups IV, III-V and II-VI and magnesium silicide type crystals 18 p3095 A67-33448

Band structure and current carrier scattering in hole-type SnTe, studying temperature dependence of electric conductivity, thermal EMF, Hall effect, etc 19 p3300 A67-34766

Light absorption of single-band semiconductor calculated from wave function of electron-hole pairs located near charged impurities, obtaining pair lifetime 19 p3300 A67-34767

Electron tunneling through thin dielectric films and damping relation to electron energy calculated, using band model and matrix methods 20 p3508 A67-36424

Molybdenum interband transitions noting low energy optical property anomalies and origin of two absorption bands 20 p3466 A67-36865

Energy band pinch effect in laser-heated GaAs, studying temperature effect on radiative recombination rate 20 p3460 A67-37106

Superconductors with overlapping bands, discussing copper pairing, heat capacity, critical field and ultrasonic attenuation 20 p3512 A67-37435

Chemical bonds formation during interaction between individual elements explained by total valence band energy theory 20 p3490 A67-37587

Energy band nonparabolicity effect on GaAs drift velocity vs field curve, especially near Gunn threshold 21 p3680 A67-38348

Parameters for model of two valence bands of SnTe according to Hall effect measurements at high temperatures 24 p4200 A67-41779

Strong electric field effects on parabolic energy band semiconductor magnetoresistance and Hall coefficients, discussing scattering mechanisms 24 p4202 A67-41982

Thermodynamic property of superconductors with nonmagnetic impurity analyzed using overlapping energy bands near Fermi energy 24 p4203 A67-42162

Phonon assisted magnetoabsorption in direct band semiconductors 24 p4203 A67-42267

ENERGY BUDGET

Energy balance equations for solar atmosphere, considering hydromagnetic and thermodynamic processes, noting turbulent eddy effects 06 p1089 A67-18738

Energy balance criteria during slow crack growth and at inception of catastrophic rupture in high strength ductile metals, noting necking phenomena in tensile test 08 p1421 A67-20953

Energy balance of stationary discharges in quartz containers filled with gas at various pressures, determining relation of heat and light loss of discharge to gas pressure and discharge power 09 p1544 A67-21854

Thermal equilibrium method for

calculating parameters of plasma arc in atmosphere of hydrogen, air and air containing 0.1 percent sodium vapor 09 p1546 A67-22318

Energy characteristics of magnetically stabilized plasmatron effect on output power in crossed fields 09 p1547 A67-22316

Comet head brightness diminution during perihelion passage due to sublimation calculated, using Clapeyron-Clausius equation and insulation effect 10 p1703 A67-22719

Satellite Telecommunications with Automatic Routing /STAR/ system modulation techniques, channel capacity and Start-Stop /SS/ operation 13 p2067 A67-26718

Vertical distribution of heating rate by radiative processes over Northern Hemisphere presented in zonal cross sections 13 p2116 A67-27459

Surface heat balance shown to be useful thermal boundary condition at sea-air-land interface for earth surface mean temperature and macroclimate models 15 p2513 A67-30060

Electron temperature reduction possibility in individual valleys of multivalley semiconductors, based on energy-balance equation in electron-temperature approximation 15 p2542 A67-30246

Conductivity in Faraday generator with cesium-seeded argon calculated from energy balance of electrons 16 p2603 A67-30565

Fracture mechanics energy balance analysis using Griffith type fracture criterion 16 p2770 A67-31289

Upper atmosphere ion temperature profile transitional behavior analyzed by fractional separation in terms of energy budget, including multiple ion effects 17 p2843 A67-32531

Enhanced radiation energy for visible and near IR during electron emission calculated by energy balance 19 p3176 A67-35081

Energy balance of high current argon arc, showing main energy supply supported by cathodic plasma beam, measuring temperature decay and field 19 p3279 A67-35143

Energy balance of electric arcs in argon without and with superimposed gas flow investigated at various pressures [DVL-626] 19 p3280 A67-35146

Jet flow turbulence energy balance, measuring point-pressure/velocity correlations and spatial mean gradients, giving energy equation 19 p3170 A67-35412

Virtual work principle shown equivalent to linear coupled thermoelasticity theory 19 p3342 A67-35763

Computer program for determining net thermal energy incident on satellite by computing projected surface area [ASME PAPER 67-HT-56] 20 p3549 A67-36738

Atmospheric energetics, discussing stratospheric-tropospheric energetics differences, atmospheric radiation balance distribution, meteorological satellite data, computer studies of atmospheric circulation, etc 20 p3429 A67-36895

Energy changes between solar wind and cosmic rays, discussing particle motion description by Fokker-Planck differential equation 22 p3874 A67-40079

ENERGY CONVERSION

SA HEAT GENERATION

Book on direct energy conversion 01 p0012 A67-10552

Photovoltaic effect application to conversion of solar radiation to electrical energy, presenting pictorial explanation of solar cell 01 p0013 A67-10553

Fuel cells from point of view of thermodynamics, electrochemical reaction kinetics and transport processes and state of development of representative types 01 p0013 A67-10554

Regenerative thermomagnetic power devices, considering state equations for ferromagnetic material, power cycle and entropy change due to magnetization [ASME PAPER 66-WA/ENER-1] 04 p0555 A67-15414

Multiplex electrohydraulic actuators development, noting fault detection and feedback signals to prevent output drift 05 p0754 A67-16752

Unsteady state analysis of heat transfer and energy transformation processes in closed cycle regenerative heat energy converters, using differential equations [AIAA PAPER 67-218] 06 p0951 A67-18329

- Implosive collapse of liners containing gas to transfer chemical energy of explosive to kinetic and internal energy of gas
[AIAA PAPER 67-178] 06 p1118 A67-18485
- Electric propulsion research in foreign countries
[AIAA PAPER 67-53] 06 p1075 A67-18494
- Closed cycle MHD energy converter applications 06 p0951 A67-18668
- MHD application for power conversion and generation, discussing methods and efficiency 06 p1076 A67-19023
- Soviet papers on electromagnetic and semiconductor devices in conversion technology 07 p1150 A67-19316
- Excited atoms effect on nonequilibrium ionization of partially ionized plasma in direct energy conversion systems, using Klein effect 09 p1543 A67-21821
- Cartridge-pneumatic dual mode jet engine starter design and function, discussing energy conversion and handling of high pressure gas produced by starter cartridge [ASME PAPER 67-GT-49] 11 p1855 A67-24810
- Energy conversion by MHD 12 p1896 A67-25184
- MHD induction generator with variable fluid and magnetic field velocity noting high power of cascading generator 12 p1897 A67-25377
- Explosively driven MHD generator, obtaining conversion efficiency dependence on magnetic Reynolds number, load-to-channel inductance ratio and magnetic/kinetic energies 12 p1901 A67-25896
- Onsager formalism of irreversible thermodynamics applied to steady state laminar hydromagnetic energy conversion, analyzing nature of coupling 13 p2055 A67-27001
- Pumping efficiency of optically pumped laser, considering electric energy conversion, absorption, etc 13 p2129 A67-27349
- Characteristics of sound formation in turbulent flow and mechanism of flow energy conversion into sound 14 p2305 A67-28519
- Direct energy conversion techniques in generating electric power in space for future astronautic systems 14 p2253 A67-29044
- Electrodeless MGD power generation during entry, using torque on magnet taken as rotating member of generator 15 p2422 A67-29443
- Solar energy conversion into electric power by GaAs and Si cells analyzed, using photovoltaic cell theory 15 p2536 A67-29503
- Noise cancelling devices for converting noise into equivalent electric energy, noting pressure, differential and throat microphones 15 p2489 A67-30088
- Rapid acquisition of sun in solar energy conversion systems based on momentum exchange from rotating flywheels to platform 15 p2423 A67-30130
- MHD conversion of thermal energy contained in cesium-seeded noble gas examined for conditions governing disk-type ducts use 16 p2603 A67-30566
- Energy conversion with liquid metal working fluids in MHD converter, proposing stepwise injection and expansion to reduce impact losses 16 p2604 A67-30572
- Liquid metal magnetohydrodynamic power generation for space vehicle use 16 p2605 A67-30583
- Fluid metal magnetohydrodynamic power conversion program results 16 p2606 A67-30584
- Liquid metal energy converters using magnetohydrodynamic induction noting electrodynamic aspects 16 p2606 A67-30586
- Liquid metal injection techniques used in magnetohydrodynamic converters 16 p2606 A67-30587
- Magnetohydrodynamic liquid metal power conversion systems investigated using thermodynamic properties 16 p2606 A67-30590
- Thermodynamics of injector of magnetohydrodynamic power unit using two-phase vapor-liquid metallic working fluid 16 p2607 A67-30591
- Linear and turbulent MHD generators of conduction type considering operating conditions, efficiency and energy conversion 16 p2608 A67-30600
- Spaceflight application of cryogenic techniques including cooling magnets, noise reduction in parametric amplifiers and quantum-electronic, superconductive and IR sensing devices 16 p2702 A67-30717
- Magnetohydrodynamic energy converters based on nonequilibrium plasmas for laser construction 16 p2686 A67-31576
- Energy distribution of shock wave created by wire explosion and electrical discharge in air, studying attenuation, dimensional effects and energy conversion efficiency 17 p2883 A67-31927
- Optimum energy conversion for MHD flows related to magnetic field value 17 p2888 A67-32180
- Thermionic work functions and electron emission S curves for contaminated copper surface in oxygen and cesium vapors, separate and mixed 17 p2887 A67-32203
- Energy conversion methods, MHD power generation - Conference, London, November 1965 18 p3085 A67-33701
- Open circuit voltage, short circuit current and maximum power for silicon solar cells at low temperatures 18 p2989 A67-34101
- MHD conversion of heat into electricity noting nozzle behavior during long-lasting experiments, corrosion resistant conducting materials and electrical insulators 18 p2989 A67-34121
- Stagnation pressure lower than atmospheric pressure in supersonic subatmospheric flow in magnetoaerodynamic generation nozzle, discussing Hall effects for energy conversion process 18 p3020 A67-34122
- Regenerative thermomagnetic power devices, considering state equations for ferromagnetic material, power cycle and entropy change due to magnetization [ASME PAPER 66-WA/ENER-1] 18 p2989 A67-34128
- Book on energy conversion covering heat engines, power sources, solar energy, SNAP generators, etc 19 p3177 A67-35892
- Major difficulties encountered in open and closed cycle MHD, particularly temperature resistance of heat exchanger 20 p3362 A67-36366
- Book on theory of energy transfers and conversions including thermodynamics and Legendre transform 20 p3484 A67-36650
- Wave propagation and flow past obstacle in fluid magnetodynamics 20 p3503 A67-37676
- Unsteady state analysis of heat transfer and energy transformation processes in closed cycle regenerative heat energy converters, using differential equations 21 p3689 A67-37791
- MHD transformation of heat energy into electricity, discussing plasmatron applications and plasma velocity and temperature measurements in MHD generators 21 p3664 A67-38236
- Gamma radiation energy direct conversion into electrical energy by electrochemical recombination of radiolysis products, proposing new sealed battery 22 p3748 A67-40199
- Book on electromechanical, direct and nuclear energy conversion covering transducer design, nuclear structure, photoelectric conversion, reactor theory, thermionic conversion, etc 22 p3749 A67-40329
- Mixing effect in dual flow turbojet engines analyzed to obtain better conversion of combustion into kinetic energy 23 p3931 A67-41317
- Advances in energy conversion engineering - ASME Conference, Miami Beach, August 1967 24 p4099 A67-42485
- Thermionic energy converter operation showing anomalous electron and ion currents in plasma mode, discussing heating power and emitter temperature 24 p4103 A67-42502
- Energy conversion MHD channel of Faraday type using hot spacers and electrodes for control 24 p4106 A67-42526
- Electro-fluid dynamic power generation, discussing Mach number, charged particle mobility, pressure level and radial space charge field effects on load characteristic and conversion ratio 24 p4107 A67-42527
- Electrofluidynamic /EFD/ power generator unipolar charge generation using corona discharge, noting pressure and geometry effects on ion currents and attractor voltage 24 p4107 A67-42528
- Electrofluidynamic /EFD/ power generator channel performance dependence on charge spreading for various geometries, noting stage efficiency and electric pressure 24 p4107 A67-42529
- Reentry vehicle solid propellant and liquid fuel compact turboalternator electric power system operating characteristics and performance 24 p4108 A67-42534
- Conversion of solar-thermal to electrical energy by capacitance-change pumping of thermoelectric thin films, noting space environmental chamber tests 24 p4108 A67-42555
- Design and developmental testing of electrical components for two-shaft Brayton cycle energy conversion system, discussing Na-Bi and Li-Te cells 24 p4108 A67-42556
- Electric propulsion research in foreign countries 24 p4208 A67-42902
- ### ENERGY CONVERSION EFFICIENCY
- Hot source temperature effect upon thermoelectric energy conversion, noting efficiency of various compounds 07 p1132 A67-20286
- Output characteristics of electroetched rhenium surface, bare and cesiated work function and performance 09 p1447 A67-22332
- Efficiency increase in vapor-filled thermionic converter anticipated by introducing intermediate electrodes between emitter and collector of vapor-filled diode 09 p1447 A67-22333
- Thermionic converter life-test results and failure mechanisms noting braze failure, collector deposit, emitter warpage and separation and cesium reservoir leak 09 p1447 A67-22334
- Flame heated thermionic converter noting electrical, material and combustion problems of design of 100 watt device 09 p1448 A67-22341
- Performance of thermionic converters, discussing voltage output, interelectrode spacing, rhenium-rhenium and rhenium-molybdenum electrode systems 09 p1449 A67-22343
- Thermionic planar electrode converter and generator tests, noting test equipment and performance tables 09 p1449 A67-22344
- Emitter material, emitter treatment, collector lateral area and interelectrode and lateral spacing effects on solar converter performance 09 p1449 A67-22345
- Oxygen as steady state electronegative additive in cesium thermionic converter shown to improve performance without surface corrosion 09 p1450 A67-22355
- Effect of concentrator orientation with respect to sun on solar energy converter performance 09 p1451 A67-22532
- Characteristics of single circuit space power installation with thermoelectric converter noting capacity, temperature and heat transfer 10 p1596 A67-23019
- Electronic conversion efficiency in gridless two-cavity klystrons for cylindrical and sheet beams 10 p1611 A67-23062
- Physics and efficiency of direct conversion of heat, light, nuclear, thermonuclear and chemical energy to electrical energy, avoiding mechanical energy 10 p1597 A67-23507
- Dimensions effect on efficiency of radiant energy cells 11 p1745 A67-24437
- Measured efficiency departure in power varactor converters from theoretical estimation, finding three-frequency current spectrum responsible 11 p1766 A67-24647
- End losses in magnetohydrodynamic channels of linearly variable cross section determined using equivalent channel geometry 16 p2606 A67-30585
- Germanium photovoltaic cells as solar conversion devices 18 p2990 A67-34464
- [ONERA-TP-478] 18 p2990 A67-34464
- Input and output voltage and efficiency of thermal-to-electric energy conversion effect on fuel cells and insulation of thermoelectric generator 19 p3177 A67-35897
- Dimensions effect on efficiency of radiant energy cells 20 p3362 A67-36239
- Photovoltaic cell characteristics, emphasizing energy conversion processes and quantum efficiency determination 20 p3362 A67-36240
- Corona discharge propulsion system with space charge limited emission of negative ions, noting ion mobility performance and efficiency 21 p3696 A67-38856
- MPD energy conversion duct using heated inert gas working fluid, discussing Hall parameter operation and efficiency factors 24 p4109 A67-42898

ENERGY CONVERTER

SA FUEL CELL
SA PHOTOELECTRIC CELL
SA TRANSDUCER

Thermionic energy conversion, discussing surface and volume phenomena, vacuum and gaseous converters 01 p0013 A67-10557

Materials for energy transducers used in detection, generation or measurement of ultrasonic waves and materials for electrical filters 03 p0495 A67-13547

Thin film photoconverters using silicon, cadmium sulfide and cadmium telluride 04 p0553 A67-14664

Space-power subsystems, evaluation of power sources 04 p0558 A67-15954

Thermomechanical energy converter for generating 500 watts, noting installation bearings testing device 04 p0559 A67-15962

Design and performance characteristics of two-bridge controlled autonomous compensation inverter for DC to AC conversion 07 p1150 A67-19317

Hysteresis effects in one-dimensional conducting gas flow through rectangular MHD converter channel with constant magnetic gap and variable electron spacing 09 p1444 A67-21859

Measured efficiency departure in power varactor converters from theoretical estimation, finding three-frequency current spectrum responsible 11 p1766 A67-24647

Energy supply and energy converters in satellites and space vehicles 14 p2247 A67-27876

Anode emission influence on thermionic diode energy converter maximum efficiency 14 p2247 A67-28033

Power supply and transformation equipment in satellites, discussing batteries, fuel cells, nuclear reactors and solar energy 14 p2252 A67-28566

Soviet book on semiconductor technology and microelectronics covering photoelectric functional converters, junction characteristics, etc 18 p3008 A67-33467

Photoelectric functional converters application to semiconductor microelectronics and optoelectronic circuits 18 p3008 A67-33468

Transverse-conduction photopotentiometer operating as functional energy converter, calculating resistive layer required for device operation 18 p3009 A67-33469

Design and performance of explosive driven magnetic generators, giving line drawings and current oscillograms 18 p2987 A67-33628

MHD jet converter research, reviewing basic equations, AC/DC generators and thermodynamic/ electric problems 19 p3268 A67-35062

Thermophile radiation receiver utilizing detector comprised of fuel cells in series studied for application to actinometry 21 p3628 A67-38530

Liquid metal MHD converters with multistage injection condensation, calculating cyclic process efficiency through thermodynamics 24 p4098 A67-42085

Sealed heat sterilizable high impact resistant battery for space missions, grafting acrylic acid and polyethylene by irradiation for separator 24 p4106 A67-42521

Apollo spacecraft H-O chemical to electric energy converting fuel cell performance degradation resulting from O electrode contamination due to inert diluent impurities in O supply 24 p4106 A67-42525

Aerospace automatically activated electrochemical battery and DC-DC high voltage converter-regulator noting storage stability 24 p4108 A67-42541

Colloidal electrogasdynamic energy converters analyzed on basis of power plant specific mass 24 p4109 A67-42888

ENERGY DENSITY

Sign and value of plane gravitational wave energy as function of reference point and wave structure 02 p0268 A67-12417

Herman and Gibbons conclusions on radiation energy concentration in ionized gas shown to be erroneous 03 p0411 A67-12961

Boundary layer phenomenon in nonlinear membrane theory, investigating problem of closing hole in membrane having John strain energy density 03 p0525 A67-13823

Electron beam accelerator generating 5000 amp beam transmitted through thin window for external use, noting pulse length, energy density, etc 04 p0599 A67-15327

Radiative transfer in inhomogeneous medium derived on basis of continuity equation for radiative energy density in coordinate space and group velocity space 05 p0761 A67-16340

Problems in using Langmuir probes in ionized medium for measuring electron and ion energy density, temperature and distribution 06 p1000 A67-17590

Constants of superconducting alloys for arbitrary temperatures and impurity concentrations, calculating free energy density by using Gorkov equation 07 p1236 A67-20140

Book on strength of materials covering energy density, plastic flow deformations, friction heating and fracture mechanisms 08 p1414 A67-20307

Nonlinear constant profile plane waves in cold Vlasov hydrogen plasma under influence of external magnetic field 08 p1359 A67-20896

Linearized perturbation equations integrated for cosmological model, giving energy density fluctuations, rotational perturbations, gravity waves and estimated anisotropy of microwave radiation 08 p1398 A67-21233

Plasma energy density, conductivity and temperature measurements at various pressures 08 p1362 A67-21303

Anisotropic cosmological solution with energy density determined only by neutrinos moving along one axis, noting expansion 10 p1708 A67-23334

Gravitational radiation measurements by HF gravitational wave detector 10 p1652 A67-23545

Continuum mechanics of Cosserat type, discussing kinematics generalization and existence of higher order displacement gradients in internal energy density equation 12 p1968 A67-26200

Interstellar gas dynamics suggests that energy density of galactic cosmic rays places firm upper limit on undetermined constant of solar modulation 13 p2189 A67-26265

Solar wind plasma properties, noting relation between positive ion component and interplanetary magnetic field as measured by Mariner II 13 p2190 A67-26304

High energy density Zn/O battery system, noting good low oxygen pressure and low temperature performance 13 p2055 A67-26836

Energy propagation and Poynting vector for electromagnetic wave propagation in tube of square cross section 13 p2070 A67-27207

Performance of low energy-density electric shock tube in helium 14 p2293 A67-28752

Plasmoid collisions in axisymmetric magnetic field studied spectrographically for energy density, radiative power, charged particle density, etc 15 p2525 A67-29248

Blast wave driven by solar flare ejecting plasma cloud proposed as origin of energy density increase causing sudden commencement of magnetic storm 15 p2478 A67-29625

Initially isotropic turbulence, characterized by three dimensionless numbers, suppressed by applying uniform magnetic field 15 p2471 A67-29856

Randomly distributed initial energy input effect on unbounded rotating barotropic atmosphere, noting energy density function as initial condition 15 p2478 A67-30056

Closed-loop MHD cycle efficiency through thermal efficiency as function of net MHD output density 16 p2803 A67-30561

Cleavage method to study pulsed pressure /energy content/ in dense gas-discharge hot plasma 16 p2714 A67-31037

Neutrino occurrence in universe noting postcreation and relic neutrinos, energy density, relic neutrino concentration, cosmic ray-neutrino interaction, etc 17 p2940 A67-32102

Critical heat-flux density dependence on dominant parameters in bilateral heating in annular channels 17 p2969 A67-32459

Ruby laser radiation transmission by Crofon plastic fiber optics 17 p2870 A67-33302

Energy transport concentration around homogeneous lossless dielectric cylinder, calculating electric field strength distribution and limiting radius of several

wave modes 18 p2999 A67-33529

Graphical integration method for calculating optical characteristics of materials used in solar radiation spectral measurements 18 p2990 A67-34492

Energy and intensity density of radiation emitted by semifinite nonequilibrium electron plasma with non-Maxwellian particle distribution calculated, based on general fluctuation theory 19 p3267 A67-34902

Energy-momentum density and superpotentials in privileged frame of reference, giving results due to Einstein and Freud pseudotensors 19 p3261 A67-35048

High photon energy densities generation and concept of exponential amplifier for use as laser probes 19 p3240 A67-35692

Relativistic mechanics of continuous media reviewed on basis of variable eigenmass dynamics, with criticism and rejection of various energy flux concept methods 19 p3263 A67-35833

Inhomogeneous elastic medium with nonlocal interaction, considering case of point defects and obtaining Green tensor 20 p3540 A67-37056

Bilateral metal grating effect on E and H polarized radiation from plane parallel layer noting intensity, energy density and reflection at interface with medium 21 p3638 A67-37865

Energy densities of polar and antipolar arrays in barium titanate including nonlinear oxygen polarizability 21 p3683 A67-38406

Vertical distribution of mechanical wave energy density in lower atmosphere and energy fraction escaping to high altitudes derived by integral transform methods 21 p3655 A67-39088

Resonant particle diffusion of nonuniform plasma across magnetic field, calculating transport coefficients 22 p3848 A67-39687

Maximum permissible energy density incident on retina determined for eye safety in viewing laser beam 23 p3962 A67-41052

Initial value problem with vanishing energy density at infinity investigated for interstellar gas oscillations 24 p4224 A67-41815

Electric and magnetic field measurement by energy density antenna applicable to reducing signal fading encountered on mobile radio transmission path 24 p4131 A67-42340

Energy flux fluctuation of nuclear active component in extensive air shower stem for given fixed muon and electron numbers 24 p4220 A67-42867

ENERGY DISSIPATION

Turbulent energy dissipation rates, eddy fluxes of sensible heat, momentum and kinetic energy measured above nonhomogeneous surface 02 p0238 A67-12076

Data on fragmentation of energy in nuclear reactions in atmospheric showers compared with calculations results for predicted energy 02 p0316 A67-12764

Auxiliary system considered simultaneously with given dissipative system in variational formulations, noting motion equations 03 p0530 A67-14175

Stimulated emission by electron beam bombardment of laser materials 03 p0439 A67-14394

Certain dissipative mechanisms of homogeneous turbulence in presence of uniform magnetic field with small magnetic Reynolds number 04 p0662 A67-14414

Adjoint field in elastic stability problems for nondissipative nonconservative systems 04 p0709 A67-14834

Energy dissipation calculation of damping factor for free oscillations of viscous liquid in circular cylindrical vessel 04 p0711 A67-15196

Energy dissipation effect on vibrations of elastic element with one degree of freedom excited by steady state random Gaussian disturbance 05 p0923 A67-17182

Thermal regeneration in power dissipating elements and effects on transistor circuit failures 06 p0971 A67-18245

Heat transfer by steady laminar forced convection in noncircular ducts, analyzing effects of viscous dissipation due to constant axial temperature gradient 06 p1116 A67-18384

Weakly dissipative fluid with schematized zone of strong gradients in perfect fluid formed by shock wave characterized by inversion of Reynolds

- number 06 p0990 A67-18726
Plasma flow in plane MHD channel in
absence of longitudinal thermal flux,
considering temperature dependence of heat
transfer and viscous energy dissipation
coefficients 06 p1045 A67-18811
Ionospheric heating by Joule dissipation of
main-phase ring current associated with
asymmetry 07 p1181 A67-19934
Energy dissipation and other problems for
alien planetary atmospheric entry at high
speeds of interplanetary
flight 08 p1394 A67-21155
Solutions for field aligned flow past
magnetic source using Green function,
estimating energy dissipation
rate 09 p1549 A67-22399
Axisymmetric crack formation problem in
elastoplastic material including energy
dissipation and face displacement
calculations, noting agreement with Griffith
theory 10 p1716 A67-22939
Nonlinearities in elastic energy release
rate during load-deflection measurements of
specimens with varying crack
length 10 p1718 A67-23327
Dispersion and damping characteristics
due to flexural vibrations in elastic plate
with viscoelastic coating, obtaining energy
loss resulting from dissipation
[ASME PAPER 66-WA/APM-20] 10 p1731 A67-23840
Numerical calculations of nonlinear
behavior of MHD shock waves in dissipative
medium 11 p1825 A67-23854
Thermal dissipation of energy in ionized
cesium plasma, obtaining plasma oscillation
excitation which destroys electron drift
motion 11 p1837 A67-24394
Response of superconducting sheath state
of lead-indium in AC and DC magnetic fields
studied, noting transition changes response
of superconducting sheath state of lead-
indium in AC and DC magnetic fields
studied, 12 p1985 A67-25847
Dissociation energy of nitrous oxide
reconciled with electron physics
data 12 p1904 A67-26230
Dissipative energy effect on laminar heat
transfer from disk rotating in uniform
forced stream 13 p2221 A67-26531
Law for turbulent boundary layer
dissipation integral 13 p2094 A67-26637
Rotational energy diffusion in shock wave
structure, examining magnitude of error in
effective number of intermolecular collisions
required for equilibrium 13 p2104 A67-26980
Friction stress acting upon moving
dislocation derived by microstrain methods
is meaningful under limited
conditions 13 p2141 A67-27181
Collective effects in collisionless plasmas
in laboratory in case of Vlasov-Maxwell
equations with Landau
damping 14 p2362 A67-29037
Fatigue crack analysis via Bilby, Cottrell
and Swinden crack theory, noting
inadequacy of energy
criterion 16 p2769 A67-31283
Griffith initiation criterion extended to
fracture initiation and growth in viscoelastic
materials using energy
formulation 16 p2773 A67-31311
Plastic energy dissipation rate at onset of
rapid crack growth for predicting biaxial
fracture 16 p2775 A67-31324
Energy dissipation and transport
coefficients temperature dependence effect
on short wave perturbation development in
magnetohydrodynamics 16 p2723 A67-31578
Electric quadrupole-quadrupole and dipole-
octupole forces contribution to dispersion
energy for axially symmetric molecules,
noting resonance
frequencies 17 p2887 A67-32353
Normal mode analysis of multispan skin-
stringer structure with isolated tuned
viscoelastic dampers at arbitrary surface
points 17 p2960 A67-32579
Magnetic field annihilation rate prediction
in current pinches attributed to magnetic
energy dissipation by ways other than ohmic
losses 17 p2909 A67-33248
Energy dissipation by relativistic charged
particle and magnetic field containing it
shown to exceed initial
energy 17 p2952 A67-33320
Influence of dissipation of acoustic waves
on temperature rise in
chromosphere 18 p3125 A67-34192
Energy dissipation in turbulent steady
isotropic homogeneous gas flow with
suspended solid particles 18 p3028 A67-34385
Stability of equilibrium of holonomic
system in critical cases by means of search
for Liapunov functions, using power
series 19 p3281 A67-35050
Power spectra and dissipation rate for
vertical velocity fluctuations measured with
sonic anemometers 19 p3251 A67-35056
Microwave noise radiation and scattering
from cylindrical plasma column, studying
dissipative processes on emission
spectrum 19 p3291 A67-35387
Energy dissipation of strong magnetosonic
waves in rarefied plasma, discussing
electrons ionizing collisions at wave
front 19 p3293 A67-35402
Hydromagnetic shock waves in dissipative
plasma, considering nonevolutionary normal
shock break-up and switch-on shock
stability 20 p3493 A67-36143
Slightly resistive plasma stability analyzed
by asymptotic methods, studying small
perturbation growth rate 20 p3493 A67-36145
Lifetime of structural sections subjected
to creep deformation at high temperatures,
showing relation to energy dissipation
forces 20 p3540 A67-37058
Low energy proton flux increases in outer
radiation belt during quiet magnetic activity
and correlation with magnetic bay
appearances 20 p3519 A67-37408
Short period seismic radiation patterns
from underground nuclear explosions and
small magnitude earthquakes, noting
propagation characteristics
[SR-1] 20 p3434 A67-37430
Energy exchanges between plasma and
excitation source sinusoidal in time and
arbitrary in space 22 p3847 A67-39642
Energy dissipation due to spatial
dispersion proven identical to dissipation
due to Landau damping for large
waves 22 p3847 A67-39649
Data on fragmentation of energy in
nuclear reactions in atmospheric showers
compared with calculations results for
predicted energy 22 p3876 A67-40266
Energy dissipation and motion equations
of superfluid helium flow through pores,
describing technique to detect critical
velocity in wide channels 22 p3839 A67-40550
Energy dissipation criteria for object
falling on viscoelastic foundation or vehicle
impacting without mass separation from
support structure 23 p4072 A67-40609
Energy expenditure in space suits studied
for controlled cooling during high work
rates 23 p3965 A67-41562
Longitudinal turbulence intensities,
autocorrelations, energy spectra and peak
energy dissipation frequencies for organic
solvents flowing in smooth round
tubes 24 p4141 A67-41927
Triggering controller dynamic model with
magnetoelectric drive, examining phase
volume by point transformation
technique 24 p4155 A67-42297
Coupled earth core-mantle model for earth
precessional torques, discussing precession
energy dissipation and experiments on
model 24 p4151 A67-42314
Power amplifiers using IC, calculating
average and peak power dissipation by final
transistors of push-pull circuit with resistive
and reactive load 24 p4131 A67-42411
- ENERGY DISTRIBUTION**
Time varying energy distribution of high
energy electrons producing solar microwave
impulsive bursts and X-ray bursts by
emission of gyrosynchrotron
radiation 01 p0145 A67-11145
Momentum loss rate by conduction
electrons of polar semiconductors for known
energy and momentum
distribution 02 p0280 A67-11486
Intensity and energy distribution of solar
plasma determined by mass spectrometers
which can separate hydrogen and helium
components of plasma
stream 02 p0247 A67-12692
Quantum mechanical perturbation theory
calculation of upper and lower bounds of
energy eigenvalues using partitioning
methods 02 p0269 A67-12727
Rocket measurement of secondary electron
energy distribution in aurora, employing 180
degree electrostatic deflection
analyzer 03 p0418 A67-14357
Criterion for deciding when effect of
perturbation of electron-energy distribution
in plasma by probe can be
neglected 04 p0665 A67-15112
Meteoritic body distribution by energies
noting consistency with mass
distribution 04 p0701 A67-15228
Energy relaxation in electron beams with
high charge density, anomalous shiftings and
broadenings and symmetrizations of energy
distribution 04 p0623 A67-15324
Energy distribution of surface states at
steam-grown silicon-silicon dioxide interfaces
determined by LF differential capacitance
measurements of MOS
structures 04 p0683 A67-15622
Spectral indices of radio galaxies and
quasi-stellar sources explained by relativistic
electron injection into magnetic field by
recurring blasts 05 p0891 A67-16400
Magnetic and kinetic energy calculated for
geomagnetic storm as function of velocity
distributions 05 p0801 A67-17133
Problems in using Langmuir probes in
ionized medium for measuring electron and
ion energy density, temperature and
distribution 06 p1000 A67-17590
Diagnostic measurements in alkali plasma
Hall accelerator /alpha/ including azimuth
and axial velocity components, energy flux,
total beam power, etc
[AIAA PAPER 67-46] 06 p1042 A67-18493
Energy and angular distributions of
neutral atoms and charge-exchange ions
from mercury electron bombardment
thruster, determining particle effluxes
[AIAA PAPER 67-82] 06 p1075 A67-18498
Retardation energy distribution of ions
and electrons in hydrogen
discharge 06 p1037 A67-18762
Energy distribution function in cathode
drop space of glow discharges in hydrogen
derived by numerical integration of
simplified Boltzmann
equations 07 p1229 A67-19516
Energy gap derived from I-V
characteristics for pressure contacts
between type II superconductors and normal
metals 07 p1233 A67-19843
Area of Safe Operation for transistors in
switching mode defined, using thermal
feedback model 07 p1157 A67-19902
Minimum energy problems in Hilbert
function space for continuous and discrete
linear systems, noting operator
transformation into linear differential
equations 07 p1216 A67-19908
Metaequilibrium state of one-dimensional
star gas computed for interesting initial
conditions corresponds to minimum energy
configuration 07 p1256 A67-20017
Superconducting energy-gap parameter
anisotropy effect on critical field in
presence of nonmagnetic
impurities 07 p1235 A67-20132
Anisotropic energy gap in superconducting
white tin obtained by expansion in
tetragonal harmonics 07 p1235 A67-20134
Time dependence of low energy proton
belts noting spatial and differential energy
distribution 08 p1378 A67-21470
Multiple pass effects in laser pumping
cavities, noting mercury lamp
performance 10 p1662 A67-22743
Prism and grating spectra obtained during
Gemini XI mission providing UV energy
distribution data and Balmer
discontinuity 10 p1706 A67-23060
Dependence of ion energy on irradiated
laser power, discussing production of ions of
two discrete energies 10 p1667 A67-23793
One-dimensional model of stellar system
evolution, using computer to calculate
minimum energy
configuration 11 p1862 A67-24500
Weak inhomogeneous plasma wave energy
redistribution during quasi-normal oscillation
expansion in resonance regions, noting
electric analogy 11 p1842 A67-24953
Longitudinal target defocusing effect on
solar reflector power parameters, noting
energy redistribution
phenomenon 12 p1896 A67-25323
Energy distribution of electron tunneling
through metal-insulator-metal diode noting
dependence on temperature, film thickness
and voltage 12 p1982 A67-25449
Satellite measurement of low energy
electrons and protons in auroral regions,
discussing use of instruments with variable
energy electrostatic thresholds and
postacceleration
techniques 12 p1944 A67-25851

Rough metal surface bidirectional reflectance, using Davies and Beckmann models [AIAA PAPER 67-319] 12 p2037 A67-26034

Inversion of spectroscopic integral equation which relates emission coefficient to integrated intensity distribution for optically thin and asymmetrical light source 12 p1968 A67-26175

OGO 3 observation of low energy protons and electrons in earth magnetosphere, noting narrow peak of relatively high low-energy particle intensities 13 p2190 A67-26312

Microwave field distribution in waveguide partially filled with solid state plasma for application to isolator 13 p2076 A67-26521

Energy distribution of electrons emitted from alkali halide films on Mo substrates during positive helium and argon ion bombardment 13 p2177 A67-27074

Kinetic energy distribution of ions produced by dissociative attachment dependence on ion thermal energy and oxygen affinity of 14 p2350 A67-28151

Spectral energy distribution of source 3C 446 between August 17 and December 12, 1966 14 p2389 A67-28850

Photolization quantum yield in intrinsic-absorption region of cadmium selenide films 14 p2372 A67-28853

Nonstationary disturbance effect on electron producing bound s-state during slow collision of atoms 14 p2352 A67-29073

Grid probe analysis of alkaline plasma, determining density, potential and energy distribution function 15 p2527 A67-29476

Stabilization of ion cyclotron plasma in mirror machines by energy spreading and application of high frequency electric field 16 p2714 A67-30873

Signal field energy distribution optimization ensuring minimum error dispersion during digital information transmission through channels with noise fluctuations 16 p2623 A67-31014

Graphical technique for phase-modulated deep-space communications links resulting in optimum power division between carrier and sine and square-wave 16 p2625 A67-31258

Particle energy distribution in low temperature nonequilibrium plasma in diffusion approximation 16 p2720 A67-31386

Energy distribution of shock wave created by wire explosion and electrical discharge in air, studying attenuation, dimensional effects and energy conversion efficiency 17 p2883 A67-31927

Coupling between free electron and molecular vibrational temperatures in plasma environments, noting energy distribution, application to MHD generation, etc 17 p2894 A67-32150

Physical parameter determination for monatomic gas flow based on energy balance, taking into account heating and ionization in thermal nonequilibrium 17 p2837 A67-32337

Electrodeless device for currentless plasmoid generation noting flowing plasma conductivity, boundary layer phenomena and potential distribution 17 p2900 A67-32344

Temperature dependence of Josephson critical current in superconductor model having anisotropic energy gap 17 p2915 A67-32719

Accelerated antimony diffusion in germanium due to excess vacancies from proton irradiation, determining migration energy and diffusion length of vacancies 17 p2919 A67-32862

Titanium plasma source design features, performance, ion mean free path, energy spectrum and energy distribution 17 p2904 A67-32912

Solution of linearized Boltzmann collision equation for ion motion through gas in inhomogeneous electric field, describing energy distribution functions for hydrogen ions 17 p2907 A67-33102

Energy distributions of hydrogen and deuterium ions from dissociative ionization of hydrogen and deuterium 17 p2889 A67-33226

Piezoelectric microphone for measuring pulsed ultrasonic radiation intensity and energy distribution, discussing principles, operating conditions and construction of instrument 18 p3046 A67-33745

Anisotropy of electron energy distribution measurement in electron cyclotron-resonance plasma using diamagnetic loop 18 p3093 A67-34756

Energy distribution functions for nearly normal glow discharge using two models and statistics 19 p3273 A67-35098

Flow of positive ions from negative glow plasma into cathode dark space determined, discussing ion current density results 19 p3273 A67-35099

Electron energy distribution and thermalization measurement in Langmuir mode discharge in plasmas, using electron energy spectrometer 19 p3274 A67-35105

Flux, energy distribution and density of ions and electrons in magnetosphere plasma during solar activity period determined by OGO-C electrostatic probes 19 p3217 A67-35200

Second derivative of two-probe current measurement method for determining electron energy distribution in gas discharge, noting low sensitivity to noise 20 p3498 A67-36687

Nonstationary random process power spectral analysis, noting evolutionary power spectra estimation methods, local energy distribution, etc 20 p3485 A67-37004

Effect of energy redistribution between ion and electron components of plasma flow in nonuniform magnetic field, deriving relativistic and polarization corrections to classical theory 20 p3500 A67-37050

Laser population inversion using Fabrikant method, analyzing electron energy distribution in hollow cathode discharge 21 p3638 A67-37940

Magnetic and kinetic energy calculated for geomagnetic storm as function of velocity distributions 21 p3619 A67-38476

Crystal block structure and slp plane influence on laser radiation, discussing radiation energy distribution in space and divergence determination 21 p3642 A67-38968

Sign of energy gain and direction of energy flow shown invariant under Lorentz transformation for two relatively moving systems possessing equal proper temperature 21 p3733 A67-39124

U-B and B-V color indices, total absorption, color excesses and reddening lines for hot black bodies, with energy curve corrections for absorption line effects 22 p3883 A67-39768

CdTe photoemission absolute energies determined by correlating electron energy distribution structure with structure in optical data 22 p3882 A67-40001

Shore hammer motion behavior, especially rebounding process frictional energy loss distribution 22 p3913 A67-40038

Carbon dioxide and water vapor band emissivities determination, discussing spectral absorption, radiative heat transfer and energy distribution 22 p3918 A67-40042

Anisotropic energy gap measurements in niobium single crystals by tunneling 22 p3865 A67-40440

Ruby rods in concentric spherical cavities observing spiking, mode structure and output energy 22 p3817 A67-40485

Superconducting niobium energy gap determination by tunneling experiments 23 p4036 A67-40703

Black body visible light at 2800 degrees K changed into energy distribution at 5500 degrees K via Fabry-Perot filter for white light standards for colorimetry 23 p3999 A67-41180

Energy distribution deviation of electrons emitted from plasma or solid via Maxwell distribution, deriving kinetic reflection coefficient in thermionic emission current expression 23 p4047 A67-41688

Energy distribution of photometric spectra in solar UV continuum in 1550 to 2100 angstrom range, discussing radiation temperature decrease 24 p4225 A67-41835

V-I characteristics correlated with energy release from arc column, noting turbulent nature of heat transfer in arc with transverse blowing 24 p4255 A67-42589

High energy cosmic ray muon integral angular and integral spectrum below earth surface 24 p4222 A67-42877

Muon properties investigated for mean energy by spark calorimeter at various depths 24 p4222 A67-42879

ENERGY EQUATION

Elastic stability theory formation by combining thermodynamic and mechanical stability 01 p0159 A67-10402

Langevin reasoning, used to establish Einstein energy inertia formula from energy conservation principle, applied to heat transformation in special theory of relativity 01 p0166 A67-10772

Heat transfer in viscous fluid flow in gap between permeable isothermal surface and rotating disk, solving energy equation 03 p0536 A67-13611

Charged particle collision as UV radiation source examined, using electron-excitation analytic cross section equations 04 p0660 A67-14698

Uniform property turbulent boundary layer heat transfer calculation, using solution of integral momentum and kinetic energy equations 04 p0731 A67-15821

Aerodynamic heating from turbulent boundary layer to swept surface symmetrical to surface line dividing flow obtained from momentum and energy integral equations 04 p0549 A67-15825

Two-dimensional transient laminar natural convection heat transfer in partially filled liquid propellant tanks, solving vorticity and energy equations 04 p0731 A67-15826

Energy methods of subcritical convective instability theory and critical Rayleigh number dependence on Nusselt number 05 p0926 A67-16816

Turbulent heat transfer at semipermeable surface during foreign gas injection, solving energy equation 05 p0927 A67-17000

Plane flow of radiating gas over semilfinite flat plate, considering upstream effect when energy equation becomes elliptical 05 p0928 A67-17358

Energy balance equations for solar atmosphere, considering hydromagnetic and thermodynamic processes, noting turbulent eddy effects 06 p1089 A67-18738

Artificial heat conduction mechanism, introducing viscosity term into momentum and energy equations to account for shock discontinuities in flow problems 06 p0992 A67-18833

Turbulent flow of conducting fluid with free surface in presence of crossed magnetic and electric fields 07 p1227 A67-19321

Electron and ion temperature changes in sporadic E layer based on wind shear theory, using energy equation 08 p1327 A67-21366

Fundamental field equations of continuum thermomechanics derived from balance of energy equation and entropy production inequality, using invariance considerations 11 p1819 A67-24533

Properties of anisotropic continuous media with energy and stresses depending on deformation tensor gradients and other tensor magnitudes 11 p1876 A67-24678

Integral energy equation for three-dimensional laminar boundary layer element on porous surface in presence of suction 11 p1783 A67-25052

Electron transport coefficients and electron energy equation closed formulation for two-temperature plasma, considering elastic and nonelastic collisions 12 p1973 A67-25397

Book on principles of continua with applications 12 p1968 A67-25557

One-dimensional heat flow to confined ideal gas solved on digital computer, discussing energy equations, thermal gradient induced fluid motion, etc [AIAA PAPER 67-337] 12 p2039 A67-26051

Thermal history of earth based on thermal conductivity equation solution 13 p2110 A67-26453

Law for turbulent boundary layer dissipation integral 13 p2094 A67-26637

Energy equation for laminar flow of compressible Newtonian fluid, calculating temperature profiles of fluid 13 p2224 A67-27049

Flow and heat transfer in viscous fluid layer expanding over rotating disk, calculating energy and motion equations 13 p2224 A67-27050

Reverse magnetization spike domains analyzed for nucleation and growth 13 p2179 A67-27141

Energy conservation during propagation of unsteady waves, obtaining formula for complex intensity 14 p2349 A67-28633

- Turbulent energy equation converted into differential equation for boundary layer development calculation 15 p2472 A67-29657
- Formula for thrust derived from thermodynamic steady flow energy equations 15 p2472 A67-29673
- Numerical solution of boundary layer equations by finite difference integration 15 p2473 A67-30189
- Arc operation under nonsteady electrical inputs noting initial conditions, energy equation solution, temperature profiles, application of Green function for moving boundary problem, etc [AIAA PAPER 66-480] 15 p2531 A67-30204
- Electron drift mobility and electron and ion temperatures difference in two-component plasma obtained from momentum and energy balance 16 p2706 A67-30450
- Energy conservation in magnetohydrodynamics of plasmas, noting energy equation in 16 p2721 A67-31548
- Unsteady plane parallel flow stability of viscous electrically conducting incompressible fluid in oscillating magnetic field 17 p2910 A67-33350
- Buildup time for nonequilibrium argon ionization at inlet of MHD generator channel 18 p2989 A67-34048
- Heat transfer in viscous fluid flow in gap between permeable isothermal surface and rotating disk, solving energy equation 18 p3161 A67-34476
- Heat transfer in steady flow of non-Newtonian fluid between two walls with periodic deformation considered, using perturbation method 18 p3161 A67-34616
- Exact dynamical equation derived for conditional density mode representing stochastic process 19 p3199 A67-34778
- Flow analysis of compressible fluid in wake behind body positioned symmetrically with respect to flow direction, using momentum and energy conservation equations 19 p3170 A67-35610
- Energy equation for laminar convective heat transfer in combined hydrodynamic and thermal entrance region bound by parallel flat plates [ASME PAPER 67-HT-48] 20 p3548 A67-36730
- Arbitrary internal heat generation terms in energy equation effect upon limiting Nusselt number for heat transfer to pipeline flow of non-Newtonian fluids [AICHE PAPER 12] 20 p3552 A67-36828
- Laminar compressible plane stationary boundary layer flow described by differential equations, including momentum and energy equations 20 p3424 A67-37280
- Temperature distributions and heat generation in viscoelastic isotropic solid resulting from mechanical deformations determined by energy equation 21 p3715 A67-37894
- Electromagnetically driven confined viscous vortex flow with high positive radial Reynolds numbers, solving energy equation for temperature distribution [AIAA PAPER 67-730] 21 p3874 A67-38754
- Discharge line fluid conditions in cryogenic container with self-pressurized draining, using Bernoulli, continuity and general energy equations and fluid properties 22 p3784 A67-39968
- Electrostatic energy per degree of freedom of two-temperature plasma examined for validity of resonant approximations in ion wave region 22 p3852 A67-39986
- Numerical solution of Poiseuille flow with variable fluid properties, solving coupled momentum and energy equations [ASME PAPER 66-WA/FE-22] 23 p3989 A67-40930
- Energy equation solution procedure for heat transfer across two-dimensional oscillating laminar boundary layer 23 p4082 A67-41243
- Turbulent boundary layer energy and motion equations, heat transfer through layers, energy exchange and phenomenological relations 23 p3991 A67-41249
- Energy-mass equivalence and relativistic transformation formulas application to extended bodies 24 p4188 A67-41905
- ENERGY EXCHANGE**
- Inelastic collisions of electrons with diatomic molecules, noting effect on speed of energy exchange in nonhomogeneous plasma 01 p0118 A67-10044
- Turbulent energy dissipation rates, eddy fluxes of sensible heat, momentum and kinetic energy measured above nonhomogeneous surface 02 p0238 A67-12076
- Energy-exchange simulation in artificial three-component ecological system 02 p0188 A67-12327
- Energy exchange localization to cathode emitting area during field electron emission, noting dependence on temperature, work function and applied field 03 p0472 A67-13329
- Gas-surface interactions, energy exchange and scattering between particles and surface 13 p2097 A67-26935
- Matching factor for energy exchange in electromagnetic interaction between ionic and electronic gases in amplitude-amplitude ionospheric intermodulation 13 p2070 A67-27196
- Power spectrum and difference frequency spectrum for energy exchange oscillations between three modes of He-Ne laser 14 p2331 A67-28603
- Energy exchange mechanism of cryogenic sensor dynamic behavior, noting error sources 15 p2490 A67-30155
- Numerical calculations of interactions of monatomic gas particles with ideal and contaminated crystal surfaces at epithermal energies 15 p2434 A67-30197
- Dissociation cross section of hydrogen molecule exchange excited by electron impact from ground to triplet state, using one-center wave functions 15 p2521 A67-30379
- Energy exchange between electron gas and molecular gas shown to depend on composition of latter, for application of nonequilibrium plasma 16 p2710 A67-30521
- Diapason satellite thermal control noting external energy exchange calculation, coating, in-space simulation tests, temperature measurements, etc 16 p2762 A67-31018
- Sokolov method of averaging functional corrections for treatment of radiant interchange between surfaces 17 p2967 A67-32068
- Inelastic collisions of electrons with diatomic molecules, noting effect on speed of energy exchange in nonhomogeneous plasma 17 p2890 A67-33322
- Rate of vibration-vibration energy exchange in gas mixtures 18 p3081 A67-33783
- Band and total emissivities estimation procedures for polyatomic molecules, discussing empirical emissivity charts and radiative exchange at local thermodynamic equilibrium 18 p3152 A67-33817
- Relativistic transformation formula for thermodynamics, with correspondence between energy change of reference system and energy change of moving body 18 p3159 A67-34119
- Entropy and free energy functionals for collisionless plasma at equilibrium in adiabatic magnetic field 19 p3298 A67-35731
- Exchange invariance in dissipationless fluid systems, deriving conservation law and stability conditions and application to gyro-stabilized magnetoplasma 20 p3419 A67-36151
- Angular momentum and vibrational energy transfer between nearly colliding stars 21 p3700 A67-37732
- Surface states effect on current-voltage characteristics of metal-semiconductor contact from kinetic coefficients of electron exchange 22 p3858 A67-39570
- Integrated and integral Hellmann-Feynman formulas for isoelectronic molecular process energy difference 22 p3757 A67-39637
- Energy exchanges between plasma and excitation source sinusoidal in time and arbitrary in space 22 p3847 A67-39642
- Anderson model Hamiltonian exchange character application to conduction electron Green function determination 22 p3861 A67-39994
- Radiating hydrogen two-dimensional equilibrium flow with variable absorption coefficient in axisymmetric nozzle analyzed in presence of gray radiation, examining transfer equation in diffusive approximation 22 p3785 A67-40013
- Turbulent boundary layer energy and motion equations, heat transfer through layers, energy exchange and phenomenological relations 23 p3991 A67-41249
- Different surface potential barrier models studied for T-F emission current density, energy distribution and Nottingham effect 24 p4201 A67-41893
- Exact calculation of indirect exchange interaction isotropic and nonisotropic terms in rare earth metals, with free electron model for conduction band 24 p4203 A67-42110
- Soviet book on molecular flow in vessels covering mass balance, energy exchange, rarefied gas, etc 24 p4191 A67-42359
- Perturbation theory for exchange forces using Brillouin and Schrodinger equations 24 p4194 A67-43115
- ENERGY LEVEL**
- SA EXCITATION**
- Localized electron states of semiconductor surface due to lattice defects, determining excited state, ground state and bonding energies 01 p0128 A67-10078
- Energy levels in forbidden band of gallium arsenide alloyed with silver or gold, determining impurity levels from temperature dependence of electric conductivity and Hall constant 01 p0129 A67-10104
- Electron impact induced transitions between principal quantum number levels in atomic hydrogen estimated via impact parameter method 01 p0124 A67-10780
- High temperature operation of diamond counters for nuclear particles 01 p0068 A67-10927
- Frequency dependences of amplification index of linear amplifier at 3.39 micron wavelength for various excitation levels 02 p0191 A67-11576
- Laser characteristics of narrow band type I solar radio burst and magnetic dipole transitions in split Zeeman sublevels of hydrogen atoms of solar corona in ground level 02 p0322 A67-11652
- Ionization calorimeter measurement of absorption of energy flux of primary cosmic radiation nuclear active component in iron 02 p0316 A67-12762
- Luminescence of alcoholic solution of europium chelate at low temperatures, noting changes in intensity of optical excitation at various energy levels 03 p0433 A67-12894
- Low energy electron-helium atom scattering, using formal optical potential in variational expression for scattering phase shifts 03 p0471 A67-13318
- Nonrelativistic energies and mass polarization shifts of excited S states of lithium cation 03 p0472 A67-13323
- Electron spectra in UV region noting excitation techniques, energy level mean lives and population distribution 03 p0472 A67-13324
- Energy gap of vanadium silicide measured by tunneling technique based on proximity effect 03 p0492 A67-13327
- Internal conversion coefficients for M4 transition in Te, noting gamma energy magnitude, nuclear size effects and eigenvalue results 03 p0472 A67-13335
- Fe spectrum energy levels for various subshell configurations, calculating oscillator strengths and transition probabilities 03 p0511 A67-13649
- Recoil ranges of products from reactions of Cu-65 with 11-35-mev He-3 ions 03 p0473 A67-13926
- Lower bound electronic energy calculations for positive H, using methods of truncated Hamiltonians and of Temple and Kato 03 p0469 A67-13943
- Electronic Raman scattering by neutral Zn and Mg acceptors in GaP, energy level transitions and accompanying phonon wing 04 p0673 A67-14477
- Atomic and molecular absorption and emission in middle UV region of electromagnetic spectrum, noting energy levels, electronic transitions and oscillator strengths 04 p0660 A67-14692
- Molecular nitrogen and oxygen properties, calculating Hartree-Fock value for energy in ground state 04 p0660 A67-14693
- Shock wave structure in viscous heat conducting gas, deriving preservation law for irreversible energy flux, equation for velocity profile and expression for integral curve 04 p0604 A67-14747
- Periodicity of plasma oscillation intensity spatial distribution upon electron beam excitation 04 p0666 A67-15181
- Cross sections for electron collisions with

hydrogen atoms and hydrogen-like ions for excitation of ground and other levels 04 p0671 A67-15642

Electrical properties of indium antimonide single crystals with noncompensated impurity concentration, determining position of deep-seated levels in forbidden band 05 p0861 A67-16399

Pulsed gas discharge lasers noting required energy level for maximum efficiency, experimental techniques and results 05 p0819 A67-16650

Loss measurement for ruby laser resonant cavity, comparing thresholds for R sub 1 and R sub 2 line operation 05 p0819 A67-16655

Optically pumped ruby noting absorption and emission spectrum, transition stages and phonon terminated amplification 05 p0820 A67-16658

Oscillation in CdS crystal by ruby laser induced two-photon excitation, noting proportionality of absorption coefficient to light beam intensity 05 p0821 A67-16667

Semiconductor lasers noting strong field behavior and absorption coefficient for saturation 05 p0821 A67-16672

Impurity states theory for semiconductors with In-Sb type band structure, calculating ionization potential and numerical values for energy levels 05 p0863 A67-16694

Differential cross sections corresponding to excitation of seven states of residual nucleus in Al-Mg reaction at 20.9 Mev 05 p0849 A67-17381

Hartree, Hartree and Swirls calculations for oxygen repeated with superposition of configurations in determining wave functions and energy 06 p1034 A67-17647

Optical energy gap of cubic CdS measured on evaporated mixed cubic-hexagonal layers 06 p1048 A67-17820

Differential Stark effect in second excited state of alkali metal atoms described, using electric field level crossing spectroscopy 06 p1035 A67-17830

Atomic energy levels in plasma, considering energy spectrum of hydrogen-like atom in plasma based on cut-off Coulomb potential model 06 p1039 A67-17881

Resistive effects in type II superconductors near upper critical field examined, using Ginzburg-Landau equations 06 p1049 A67-17882

Stimulated two quantum radiation in optical range for transitions occurring between discrete levels of impurity crystals or free atoms 06 p1010 A67-17885

Electroluminescence, discussing semiconductor lasers with various excitation sources, luminescent efficiency, etc 06 p1010 A67-17889

Two-electron transitions in luminescence of excitons bound to neutral donors in gallium phosphide 06 p1051 A67-18210

Impurity band tails in degenerate semiconductors, showing relation between decay in density of states and screening density 06 p1061 A67-18923

Electron double resonance for ionized impurity pairs in n-and p-type Si, noting splitting of resonance peaks and relaxation time of homopolar pair 06 p1068 A67-18970

Spin lattice relaxation times of donor electrons in Si, noting electric field effect on relaxation rate 06 p1068 A67-18971

Electron spin resonance in P-doped Si at liquid He temperature, noting effects of P concentration, impurity scattering, etc 06 p1068 A67-18973

Impurity energy levels in semiconductors described by equivalent Schroedinger equation containing short range as well as conventional terms for long range Coulomb potential 07 p1230 A67-19060

Thermodynamic functions of diatomic gases with molecules in 3-sigma electron state 07 p1225 A67-19121

Diffuse polychromatic light reflection from infinitely deep one-dimensional medium of atoms with three energy levels, with all interval transitions allowed 07 p1248 A67-19484

Mathematical model for condensation point of first order phase transitions, examining free energy singularity and metastable phase 07 p1268 A67-20089

Oscillator strength of atomic and ionic lines, normalization of NBS gf values and solar abundances of alkali metals 07 p1256 A67-20167

Localized electron states of semiconductor

surface due to lattice defects, determining excited state, ground state and bonding energies 08 p1371 A67-21456

Bohn ionization equation applied to helium plasma to include effect of He 2 energy levels 09 p1544 A67-21883

Energy level structure of rare earth chelates, noting existence of isolated systems of optical electrons 09 p1512 A67-21921

Fluctuation levels and induced photoconductivity in vitreous semiconductor thallium selenide and arsenic telluride mixture 09 p1553 A67-21969

Pioneer VI detector to measure degree of anisotropy of cosmic radiation at various energy ranges 09 p1500 A67-22427

Effective excitation cross sections of helium simplet levels under proton impacts 10 p1699 A67-22845

Rydberg series energy levels of oxygen molecule, comparing theoretical calculations with experimental results 10 p1681 A67-22887

Photon modulated tunneling in Te-Al oxide-Al structures, noting increased spectral response and detection range 10 p1689 A67-22907

Effective cross sections of excitation of lower energy levels during electron collisions in alkaline metals, noting dependence of various levels on quantum number and atomic number 11 p1822 A67-24018

Vacuum UV wavelength standards and energy levels in first silicon spectrum from low pressure source 11 p1822 A67-24417

Superconducting energy gap of cubic and hexagonal LA obtained by point contact tunneling to bulk samples, noting V-I characteristics and temperature dependency 11 p1846 A67-24585

Laser emission temperature dependence resulting from variation in radiationless transfer of excitation in trivalent erbium and thulium 11 p1803 A67-24836

Electronic Raman scattering from phosphorus donors and boron acceptor impurities in Si, noting importance of interband transitions 11 p1851 A67-24999

Lunar figure and orbit parameters measured by optical location method 12 p2002 A67-25647

Intrinsically safe and nonincendive electrical installations for hazardous environments 12 p1900 A67-25677

Density of energy levels in amorphous semiconductors induced by local fluctuations in atomic arrangement 13 p2172 A67-26353

Meteor distribution estimation attempted through radar observation, measuring kinetic energy level, velocity and electron distribution in meteor trails 13 p2197 A67-26507

Temperature dependence of small signal AC field effect kinetics in silicon within 170-300 K, considering majority carriers and one energy level theory 13 p2176 A67-26708

Temperature dependence of energy levels of shallow donor impurities in silicon, noting electron-phonon interaction 13 p2176 A67-26987

Approximate quantum numbers for d-band states in transition metals 13 p2179 A67-27155

Orbach spin lattice relaxation of shallow donors in silicon 13 p2180 A67-27162

Frequency shift in emission spectrum of complex atom in uniform electric field, noting numerical results for Al I 13 p2168 A67-27208

Energy level structure of rare earth chelates, noting existence of isolated systems of optical electrons 14 p2330 A67-28250

Density of states of pure type II superconductors in high magnetic fields, deriving approximate expression for Green function 15 p2533 A67-29089

Multiple ionization of rare gases analyzed in mass spectrometer with trapped ion source, noting energies of metastable levels 15 p2519 A67-29189

Gain of flowing carbon dioxide laser systems, noting extent of diameter dependence of gain, population variations, etc 15 p2497 A67-29390

Impurity states theory for semiconductors with In-Sb type band structure, calculating ionization potential and numerical values for energy levels 15 p2539 A67-29865

Spectroscopic study of gas discharge parameters in argon ion lasers to determine

level inversion mechanism in continuous or pulsed regime of generation 15 p2501 A67-30003

Liquid lasers use of rare earth ions, chelate structures, selenium oxychloride, etc 15 p2501 A67-30086

Temperature dependent noise spectra of InSb single crystals, noting deep energy level and impurity energy level 15 p2541 A67-30235

Semiconductor nonlinear polarizability at difference frequency calculated, considering exciton states alone and combined with band energy states 15 p2541 A67-30238

Laser characteristics of narrow band type I solar radio burst and magnetic dipole transitions in split Zeeman sublevels of hydrogen atoms of solar corona in ground level 16 p2747 A67-31067

Conservative fields of force admitting spiral trajectories and dependence on constancy of energy level 16 p2748 A67-31137

Amplifying electromagnetic radiation in nonequilibrium decaying plasma of various degrees of ionization, taking into account kinetics 16 p2723 A67-31577

Excitation temperatures of electron levels of CH molecule in photosphere 17 p2941 A67-32326

Energy level shifts due to atom confinement by conducting walls 17 p2888 A67-32390

Laser energy and power measurement, discussing radiation attenuation devices, measurement standards, etc 17 p2867 A67-32612

Population of atomic levels by cascade, dielectric and three-body electronic recombination, discussing spontaneous transition, electron impact and RF spectra 17 p2947 A67-32762

Isotope effect in hydrogen molecule dissociative attachment at low energy, noting short negative-ion formation lifetime and long separation time 17 p2889 A67-33223

Fluctuation levels and induced photoconductivity in vitreous semiconductor thallium selenide and arsenic telluride mixture 17 p2923 A67-33306

Plastic resonance problem for longitudinal elastoplastic waves in finite bar solved, considering bodies with rigid unloading characteristics 18 p3140 A67-33465

Auroras and airglows in relation to ionospheric phenomena 18 p3033 A67-33584

Spectral data and energy level diagrams from magnetic and electric field passage through barium cloud 18 p3036 A67-33606

Probability of tunneling across impurity level of p-n junction 18 p3099 A67-33695

Spectroscopic study of gas discharge parameters in argon ion lasers to determine level inversion mechanism in continuous or pulsed regime of generation 18 p3059 A67-33760

Depopulation of vibrational energy levels in fast chemical dissociation reactions 18 p2996 A67-33780

Emission equations describing radiation field amplitude and energy level populations of solid state laser with broad oscillation spectrum 18 p3061 A67-34388

Hall effect measurements on Te-doped GaAs crystals diffused with Cu64, studying vacancy-donor interactions, hole concentrations and energy levels 18 p3105 A67-34634

Data representing monopole antenna voltage breakdown in simulated Mars and Venus atmospheres 19 p3197 A67-35829

Initial conditions effect on transient states of linear systems 19 p3205 A67-35909

Generation threshold of substance with electronic-vibrational energy level studied for laser use 19 p3309 A67-36105

Equivalent electrical circuit model, corresponding to laser energy-level model, used to describe laser action in terms of circuit theory 20 p3459 A67-36768

Si optical and electrical properties and energy levels with Mg as donor impurity 20 p3510 A67-36916

Grazing incidence spectrometer and low inductance spark source used for energy level identification in various elements 20 p3378 A67-37468

Energy level behavior of metastable alkali atoms against autoionization and radiative decay 20 p3492 A67-37691

Vibrational energy levels leading to laser oscillation in UV, noting process using

- yman discharge 21 p3638 A67-37855
 Thermodynamic functions of diatomic
 ases with molecules in 3-sigma electron
 ate 21 p3659 A67-38166
 Density of energy levels in amorphous
 emiconductors induced by local fluctuations
 a atomic arrangement 21 p3679 A67-38310
 Evidence for relationship between solar
 ares and magnetic fields explained by
 neutral point type model, considering
 smaller flares 21 p3699 A67-38988
 Energy difference between metastable
 levels of hydrogen-like atom determined by
 measuring lifetime in electrostatic field,
 holding average Lamb shift in Li
 on 22 p3839 A67-39202
 Electromagnetic interactions in hyperfine
 structure of vibrational and rotational states
 a rubidium and potassium /isotopes/
 uorides, using electric resonance
 ethod 22 p3839 A67-39203
 Foil excitation technique used to measure
 n and 3p levels mean lifetime in He 2
 cascading and agreement with theoretical
 alue 22 p3840 A67-39206
 Resonance lines originating from
 autoionization energy levels far above
 ionization potential observed for highly
 ized atoms of Na I isoelectronic
 equence 22 p3840 A67-39237
 Ion bombardment excitation used to
 extend excited state range for level crossing
 spectroscopy studies, giving Zeeman energy
 level diagram 22 p3835 A67-39239
 Lande factors of neon atoms subjected to
 magnetic field and multimode laser
 radiation measured by observing resonant
 saturations in fluorescent light
 mitted 22 p3815 A67-39651
 Energy state of recombination level of
 thermally hardened silicon diode base,
 considering spatial lifetime of minority
 carriers 22 p3773 A67-39920
 Electron temperature measurements of
 powerful pulsed plasma discharge using
 spectral line intensity 22 p3852 A67-39991
 Ionization calorimeter measurement of
 absorption of energy flux of primary cosmic
 radiation nuclear active component in
 iron 22 p3842 A67-40264
 Primary cosmic particles energy spectrum
 measurements onboard space station with
 ionization calorimeters and energy level
 discriminators 23 p4054 A67-41091
 Hyperfine coupling constants of lithium
 energy levels, using Weiss 45-configuration
 ave functions 24 p4190 A67-42097
 Multiple charged particle production
 process mean characteristics determined for
 several energy levels 24 p4217 A67-42830
 Charged particles zenithal angular
 distributions determined by photorecordings
 or mean energies of 60
 kev 24 p4217 A67-42831
 Energy fraction transfer to neutral pions
 uring interactions with heavy nuclei
 measured for several energy levels, using
 ionization calorimeter 24 p4218 A67-42833
ENERGY LOSS
 Energy dissipation and heating due to
 oscillation of polymers whose rheological
 properties are described by elastic heredity
 theory, considering homogeneous and
 reinforced plastics 01 p0102 A67-10220
 Physical and environmental effects on
 energy dissipation characteristics of balsa
 wood
 [SAE PAPER 660657] 01 p0103 A67-10616
 Ionized impurity scattering mechanisms
 causing energy and momentum losses in n-
 type InSb below 77 degrees
 01 p0134 A67-10806
 Electron-tunneling measurements of
 energy gap in lanthanum explaining
 differences between various
 measurements 01 p0135 A67-10918
 Logarithmic dependence of energy losses
 on relativistic particle velocities in
 polystyrene films 01 p0125 A67-10926
 Energy dissipation channels of nuclear and
 electron components of cosmic rays in
 Galaxy and Metagalaxy 01 p0145 A67-11276
 Dynamic dissipation of magnetic field,
 examining mechanism by which magnetic
 energy is converted directly into fast
 particle energy 01 p0146 A67-11277
 Plasma propulsion devices and phenomena
 responsible for energy losses, considering
 plasma gun and MPD arc
 et 01 p0141 A67-11388
 Radiative energy loss from solar
 chromosphere and corona estimated in order
 to identify mechanical energy input
 mechanism 02 p0323 A67-11692
 Energy dissipation due to deformation of
 magnetic field in compressible conducting
 medium near zero field
 lines 03 p0470 A67-12940
 Emission losses in solid state laser
 resonator calculated for Nd glass
 laser 03 p0435 A67-13133
 Fluctuations and broadening of energy-loss
 spectrum of charged particles passing
 through semiconductor
 detectors 03 p0491 A67-13224
 Loss angle tangent of film capacitors with
 rectangular Al films and dielectric silicon
 monoxide interlayer 03 p0378 A67-13243
 Neutron collision cross section and
 calculation of energy loss of displaced Si
 atoms to ionization 03 p0494 A67-13481
 Mean energy and energy dissipation of
 hydrogen ions ejected from HF
 source 03 p0424 A67-14261
 V-I tunneling characteristics and energy
 gap anisotropy of Pb-Bi superconducting
 alloy, discussing mean free
 path 03 p0501 A67-14341
 Radiation losses effects on temperature
 measurements with transparent sheathed
 thermometers 03 p0426 A67-14344
 Induction drag of long cylindrical satellites
 and Alfvén waves emitted from them,
 determining potential and current
 distribution and effect on energy loss
 [AIAA PAPER 66-478] 04 p0704 A67-14829
 Cooling induced hydraulic and
 thermodynamic energy losses in high
 pressure turbine and turbojet
 engines 04 p0690 A67-15896
 Energy loss of cosmic electron in
 interstellar space due to ionization,
 bremsstrahlung and Compton
 effect 05 p0878 A67-16095
 Current dependence on voltage in Sn-Sn
 and Pb-Pb tunnel junctions attributed to
 electric gap anisotropy 05 p0863 A67-16754
 Total energy loss in weakly irregular
 multiwave waveguide accounted for by
 energy losses in weakly damped
 waves 05 p0775 A67-16965
 Vibratory energy dissipation of plates with
 riveted beams as induced by gas-pumping
 in structural joints 05 p0924 A67-17285
 Energy losses in explosions in sphere to
 determine specific heat, heats of dissociation
 and formation, chemical bond energies and
 other thermochemical
 values 06 p1113 A67-17963
 Cylindrical wave propagation in rarefied
 plasma in presence of strong noncollision
 dissipation 07 p1227 A67-19308
 Electron barrier heights of Al-Al₂O₃-SnTe
 and Al-Al₂O₃-GeTe tunnel junctions, noting
 values of Fermi level and energy
 gap 07 p1155 A67-19893
 Formation and expansion of
 electromagnetic shock waves in
 communication lines, using ferroelectric
 crystals 08 p1295 A67-20824
 Energy loss of charged particles during
 passage through weakly turbulent plasma in
 magnetic field with HF
 oscillations 08 p1357 A67-20844
 Microwave loss in reflex plasma discharge
 determined from microwave energy decay
 measurements 08 p1363 A67-21311
 Interband transitions and plasmon
 excitation in calcium fluoride, discussing
 energy loss 09 p1558 A67-22585
 Force-deflection relationship under
 arbitrary loading for structure exhibiting
 hysteretic behavior 10 p1727 A67-23751
 Nonequilibrium ionization and radiation
 effect on shock wave attenuation calculated
 using linearized theory 11 p1774 A67-23856
 Heat flow through Langmuir sheath in
 presence of electron emission and
 application to limitation of energy loss rate
 by thermal conduction 11 p1828 A67-23894
 Level populations and energy loss rate of
 electrons during nonelastic collisions with
 impurity molecules in weakly ionized two-
 temperature plasma 11 p1831 A67-24019
 Ruby laser output energy losses when
 passing from normal to passive Q-switched
 operation 11 p1800 A67-24241
 Measurement of quark flux with 2/3
 charge of electron reaching sea level with
 relativistic velocities 11 p1823 A67-24598
 Radial gas turbine losses, obtaining rotor
 loss coefficients, discussing flow pattern for
 performance prediction 12 p1891 A67-25347
 Electron temperature vs plasma cell power
 input measured, determining electron energy
 loss factor for hot diatomic gases in electric
 field 12 p1973 A67-25398
 Fringe effects in MHD generator channels,
 determining potential and current
 distribution and estimating
 losses 12 p1901 A67-26078
 Vortex breakdown theory, considering
 small energy losses and small flow force
 reduction /wave resistance
 effects/ 13 p2095 A67-26908
 General model for semiconductor-to-metal
 transition 13 p2180 A67-27163
 Flexwell waveguide as low loss flexible
 microwave transmission
 line 13 p2084 A67-27581
 Argon plasma thermal conductivity at
 atmospheric pressure and various
 temperatures determined in central zone of
 arc column 14 p2404 A67-28031
 Anode emission influence on thermionic
 diode energy converter maximum
 efficiency 14 p2247 A67-28033
 Energy losses due to bleeding air from
 compressor for cooling systems of gas
 turbines 14 p2377 A67-28648
 Mean energy and energy dissipation of
 hydrogen ions ejected from HF
 source 14 p2321 A67-28773
 Electric field effect in terms of drifted
 Maxwellian distribution, considering
 nonparabolic electron scattering where
 dominant energy-loss mechanism is optical
 polar mode scattering 14 p2376 A67-29088
 Mathematical models for loss
 measurements in thin Permalloy films with
 ramp drives 15 p2536 A67-29649
 Amplitude dependence of energy
 dissipation due to internal friction in metals
 and alloys of various lattice types under
 near-resonance loading
 vibrations 15 p2504 A67-29970
 Rotating spacecraft attitude changes due
 to energy dissipation from angular
 deformation treated by modal
 method 15 p2572 A67-30201
 Nonequilibrium linear MHD generator
 electrical characteristics, discussing power
 output and Hall potential reduction
 causes 16 p2602 A67-30558
 Closed-loop MHD cycle efficiency through
 thermal efficiency as function of net MHD
 output density 16 p2603 A67-30561
 Laminar and turbulent MHD flows of
 liquid sodium in rectangular duct with
 conducting walls, determining wall and
 magnetohydraulic losses 16 p2712 A67-30573
 Energy losses of modulated azimuthal
 current in magnetoplasma, discussing
 specifically electron cyclotron
 resonance 16 p2716 A67-31177
 Heat loss from wires in nitrogen, helium
 and mixtures measured at low Reynolds
 numbers, finding agreement with theory of
 Kassoy 16 p2779 A67-31217
 Energy loss spectrum in CsI at small
 atmospheric depths, discussing time
 variation of 0.5-mev gamma-ray
 flux 16 p2739 A67-31406
 Energy loss function of thin film
 deposited metals, using optical measurement
 method 17 p2913 A67-32294
 Local electronic energy balance
 formulation, including radiative transport
 effect in nonuniform seeded plasma,
 described by two-temperature
 model 17 p2906 A67-33010
 Longitudinal and transverse collective
 effects contribution to energy loss rate in
 relativistic isotropic plasma subject to
 external fields and
 particles 17 p2908 A67-33111
 Energy loss factors for slow electrons in
 hot gases determined by measuring electron
 temperature variation with HF electric field
 power 17 p2890 A67-33367
 Far IR measurements used to determine
 superconducting energy gap widths in
 niobium alloys 17 p2925 A67-33373
 Electron energy spectrum, showing
 intensity maxima from surface plasma
 oscillations, noting thin films effect on
 surface losses 19 p3307 A67-35789
 Temperature dependence and anisotropy
 of high temperature ferrimagnetic
 microwave resonance linewidth of Si-doped
 YIG, showing valence exchange effect on
 losses 20 p3508 A67-36390
 Magnesium oxide single crystal electronic

spectrum obtained from reflectance spectra, observing large plasma peak in energy loss function 20 p3509 A67-36508

Bounded plasma flux in magnetic field, considering plasma polarization on magnetic field boundary, noting flux deceleration 20 p3497 A67-36682

Semilempirical electron impact cross sections for He from oscillator strengths, using Born approximation 20 p3489 A67-37416

Daylong photoelectron excitation rate from electron energy loss calculations, with energy transfer functions calculated from photoelectrons produced by UV solar radiation 20 p3434 A67-37421

Low energy electron scattering from hydrogen molecules in ground electronic and vibrational states, calculating rotational excitation cross section 20 p3491 A67-37687

Electromagnetic forces and pressure and hydraulic losses of turbulent mercury flow in annular channel under traveling magnetic field effect 21 p3666 A67-38249

Nonideal type II superconductors, discussing flux motion and density, pinning force, magnetization, hysteresis, relaxation and energy loss 21 p3683 A67-38402

Characteristics method to determine radiative energy losses of supersonic gas flows past blunt cones 21 p3564 A67-38424

Electron energy loss calculations for nonnormal incidence in thin dielectric foil, with excitation probabilities and dispersion relations for bulk and surface plasmons 21 p3686 A67-39135

Colloid microthruster technology, discussing stationkeeping application, energy loss, diagnostic techniques, etc [AIAA PAPER 67-531] 22 p3867 A67-39200

Electrochemical shaping precision analysis, discussing efficiency, current losses, energy consumption, surface geometry and electrolyte properties 22 p3812 A67-39543

Potential energy release of stressed elastic body due to material removal and crack extension 22 p3911 A67-39679

Theta pinch energy loss determined and electron temperatures measured, discussing Poynting flux and plasma diamagnetism decay 22 p3849 A67-39696

Two-dimensional diffusion model for gas propagation in lunar atmosphere, discussing contamination by lunar module exhaust gases and solar wind loss mechanism 22 p3883 A67-39817

Dynamic energy losses in thin Ni-Fe films during magnetization reversal studied by observation of M-H loop 22 p3860 A67-39902

Shore hammer motion behavior, especially rebounding process frictional energy loss distribution 22 p3913 A67-40038

LiF freshly cleaved crystal reflectance spectrum between UV and 28 ev, computing dielectric response function and measuring gamma exciton band 23 p4038 A67-40774

Injection and emission of hot electron in thin film tunnel diodes 23 p4039 A67-40885

Implantation process for thin silicon solar cell fabrication, discussing leakage losses and efficiency 23 p4046 A67-41488

Spectral response of p-n semiconductor heterojunction, considering absorption effects and photocurrent loss 24 p4202 A67-41981

Electrical design of large lightweight solar array for electric propulsion type Mars-bound spacecraft, discussing magnetic effects and power losses 24 p4104 A67-42512

Energy loss of cosmic electron in interstellar space due to ionization, bremsstrahlung and Compton effect 24 p4213 A67-42771

ENERGY METHOD STRESS CALCULATION

Energy method creep analysis of elastic bending of circular plates 04 p0707 A67-14443

Energy method analysis of flutter instabilities in turbojet engine rotors caused by interaction between unsteady air loading and coupled vibration modes [ASME PAPER 66-WA/GT-6] 04 p0713 A67-15384

Bubnov-Galerkin and energy method solutions of stability and oscillatory motion equations for conical shell under inertial loading 04 p0717 A67-15890

Orthogonal function energy method calculation of stress concentration in ring under impact loads distributed along inner and outer edges 05 p0918 A67-16420

Instability of thin reinforced cylindrical shell clamped at both ends and energy

method calculation of critical pressure 05 p0918 A67-16422

Buckling stability of compressed plate with transverse deflections, using energy method 06 p1109 A67-18747

Complementary energy method for flexural buckling of initially straight elastic bars 06 p1110 A67-18840

Energy techniques and matrix method for computer programming of dynamic response due to random and harmonic loading on structural systems [ASME PAPER 67-VIBR-56] 11 p1873 A67-24203

Energy method extended to stability analysis of linear system under action of nonconservative forces 14 p2398 A67-28094

Column shape for maximum Euler buckling load determined using energy method calculations 17 p2960 A67-32421

Energy method analysis of flutter instabilities in turbojet engine rotors caused by interaction between unsteady air loading and coupled vibration modes [ASME PAPER 66-WA/GT-6] 18 p3115 A67-34130

ENERGY REQUIREMENT

SA METABOLISM

Secondary breakdown characterization technique in Ge p-n-p alloyed junction transistors with open base condition 02 p0223 A67-12655

Energy input requirements of electric shock tube determined from empirical I-V relations at electrodes 05 p0788 A67-16248

Energy required to confine static shielded magnetic dipole field, immersed in highly conducting medium, by transient diamagnetic surface as function of dipole moment and disturbance field 06 p1030 A67-17658

Plasma with axially varying equilibrium quantities, examining stability in theta pinch configuration via energy principle 08 p1361 A67-21132

Alternate mission modes for manned Mars exploration 22 p3886 A67-40136

Determination of energy, water and protein requirements of man under simulated aerospace conditions 23 p3952 A67-41573

Physiological measurements in obtaining energy expenditure and workloads during simulated lunar surface mission 23 p3959 A67-41657

ENERGY SOURCE

Optimization of working characteristics of MHD generator as power device 01 p0011 A67-10049

Human body as source of power for implanted electronic devices [AIAA PAPER 66-930] 03 p0366 A67-14137

Thermionic energy conversion principles and conversion systems for satellite and space use 04 p0554 A67-15025

Energy supply in space - Symposium, Stuttgart, West Germany, December 1965 04 p0557 A67-15953

Delayed energy produced by fission product decay when restart of nuclear rocket engine is considered, noting effects of cooldown requirements [AIAA PAPER 66-551] 05 p0844 A67-17222

Thermoelectric generators, discussing design capabilities of SNAP series and thermoelectric materials 07 p1131 A67-19191

Energy production sources in inner magnetospheric plasma near equatorial plane 10 p1634 A67-23058

Pneumatic starting systems for gas turbine engines including energy sources, system components and arrangements [ASME PAPER 67-GT-15] 11 p1854 A67-24800

Nancay radiotelescope energy collection, illumination choice and development 12 p1914 A67-25310

Step-recovery action in transistor switch-off with current gain and reduction of load on driving source 13 p2078 A67-28784

Energy supply and energy converters in satellites and space vehicles 14 p2247 A67-27876

Parametric amplifiers as reliable low noise broadband microwave amplifiers 14 p2286 A67-28465

Red shifts from absorption line spectra of quasi-stellar objects, discussing energy generation mechanism 14 p2390 A67-28851

Necessary and sufficient conditions to ensure existence of unique solutions of equations for active

networks 15 p2456 A67-29238

Nuclear reactor use in space environment as energy source for chemical synthesis and laser action [AAS PAPER 67-115] 15 p2558 A67-29962

Direct lasing of conventional ruby rods requiring 200-joule xenon pump deriving energy from chemical reaction 15 p2502 A67-30437

Optimization of working characteristics of MHD generator as power device 17 p2804 A67-33327

Bipolar Ni-Cd cells for ruby lasers and power sources to yield high energy pulses for firing pyrotechnic devices 19 p3175 A67-34803

Jupiter internal structure and energy emission 20 p3525 A67-36867

Oxidative phosphorylation effects on energy metabolism of *Thiobacillus thioparus* in cell-free system 20 p3371 A67-36927

Planetary and interplanetary environments based on experimental data and quantitative information, noting influence of sun in solar system mass 21 p3707 A67-38946

Friction in solid parts of earth and moon considered as sink for tidal energy and as geophysical thermal energy source 24 p4229 A67-42316

Lunar geothermal deposits, discussing recovery applications and energy tapping [AIAA PAPER 67-901] 24 p4239 A67-43009

ENERGY SPECTRUM

Flux intensity and energy spectra of galactic X-ray sources, Tau X-1 and other celestial bodies studies, using three sensitive Geiger counters 01 p0144 A67-10562

Cosmic ray electrons with energies above 12 gev, constructing differential energy spectrum for deduction of universal black body radiation 01 p0145 A67-10921

Energy spectra and abundances of elements He through Si of galactic cosmic ray above 20 mev per nucleon in nuclear charge range between 2 and 26 02 p0307 A67-11687

Spectra of outgoing protons for various targets using scintillation counter, interpreting data by means of impulse-approximation calculation 02 p0269 A67-11862

Radioisotope sources used for simulating space radiations, obtaining energy spectra by blending beta emitters 02 p0265 A67-12213

Diatomic gas flow past blunt bodies, noting effect of oscillation and dissociation relaxation on mean energy 02 p0180 A67-12465

Power energy spectrum of cosmic rays as solution of general covariant kinetic equation 02 p0308 A67-12491

Solar cosmic ray generation, discussing proton energy spectrum analysis and wave propagation in interplanetary space 02 p0310 A67-12572

Spectrum of primary cosmic radiation determined for ultrahigh energies, based on international data on electron and meson air showers 02 p0311 A67-12588

Primary cosmic rays of superhigh energy using extensive air shower data, noting Geiger-Muller counters, scintillation counters and muon detector 02 p0311 A67-12589

Energy spectrum of variations in cosmic ray intensity and changes in spectrum with decreasing solar activity calculated for additional particle flux 02 p0311 A67-12597

Approximate solution of Gelfand-Levitan equation leading to localized bound-state wave function examined in S-matrix approach to first order energy shift 02 p0270 A67-12637

High energy cosmic ray interactions analyzed at 3340 m above sea level, using Wilson cloud chambers, gas discharge counters, ionization calorimeter, etc 02 p0248 A67-12746

Nuclear cascade process in iron absorber of ionization calorimeter, comparing empirical and experimental values 02 p0248 A67-12747

Angular and energy characteristics of proton beam in pulsed magnetic field, determining probability of proton-neutron charge exchange for proton in forward flight 02 p0271 A67-12753

Energy spectra of avalanche electrons in copper, iron, aluminum and graphite determined by method of moments, considering polarization of medium and multiple scattering 02 p0316 A67-12768

Energy moments of inverse problem in

- theory of nuclear cascade determined, using first order Volterra integral equation 02 p0317 A67-12769
- Superhigh energy particle accelerators and energy spectra of cosmic ray muons in electron photon cascades 02 p0317 A67-12772
- Integral energy spectra and angular distribution of muons, comparing computational and experimental data 02 p0317 A67-12773
- Absorption curve and energy spectrum of high energy muons 02 p0317 A67-12775
- Extensive air shower characteristics related to energy spectrum, chemical composition and anisotropy of primary cosmic rays in superhigh energy range 02 p0318 A67-12778
- Leading particle model of formation of extensive air showers, showing determination of energy spectrum 02 p0319 A67-12785
- Quasi-linear theory of plasma cyclotron instability for one-dimensional oscillation spectrum, noting energy of interaction with electromagnetic field, ion velocities, etc 03 p0475 A67-12933
- Galactic deuterium and energy spectrum above 20 mev per nucleon measured by IMP-II satellite near minimum solar activity 03 p0472 A67-13390
- Extensive near-vertical air shower analysis at sea level for nucleon-air-nucleus and pion-air-nucleus interaction 03 p0506 A67-13517
- Energy spectrum of X-ray source in Cygnus constellation with 2 to 60 kev 03 p0507 A67-13917
- Stochastic analysis of energy spectrum of output signal of phase shift modulator in PCM systems 04 p0571 A67-14895
- Cosmic ray electron spectrum indicates universal 3 degrees K black body radiation confinement to galactic disk 04 p0692 A67-14948
- Electron energy spectrum measured near equator by satellite mounted scintillator 04 p0614 A67-14950
- Energy spectrum of cosmic ray heavy nuclei, using stack of nuclear emulsions exposed during Quiet Sun on balloon flight 04 p0692 A67-14960
- Radiometer data analysis results concerning cosmic ray event of April 18, 1965 04 p0693 A67-14973
- Mass spectrometric study of energy distribution of ions of accelerated plasma produced by coaxial source 04 p0668 A67-15216
- Galvanomagnetic effect of anisotropic electron energy spectrum on acoustical branch perturbation spectrum of system of electrons and ions in homogeneous magnetic field 04 p0680 A67-15289
- Electron energy spectrum for alloyed semiconductors, determining state densities via Thomas-Fermi statistical method 04 p0681 A67-15296
- Direct energy spectrum measurements of primary cosmic radiation in wide energy range 05 p0877 A67-16086
- Electron intensity measurement in primary cosmic radiation by high altitude balloons carrying telescope made of two plastic scintillation counters 05 p0878 A67-16097
- Change in intensity and forms of energy spectrum effects on accuracy of measuring values of meteorite preentry dimensions, weight and degree of ablation 05 p0887 A67-16099
- Aurora photometry and stratospheric cosmic ray intensity, noting electron intrusion and correlation between aurora intensity and X-ray emission 05 p0879 A67-16102
- Energy spectrum of secular variations of cosmic ray intensity in interplanetary space, using data from stratospheric measurements 05 p0879 A67-16104
- Asymptotic directions of cosmic rays for Soviet cosmic ray stations 05 p0880 A67-16114
- Interplanetary space properties studied from IMP-I satellite data on cosmic ray variations 05 p0880 A67-16115
- Motion of cosmic radiation source effect on frequency spectrum of amplitude and phase fluctuations in turbulent atmosphere 05 p0761 A67-16344
- Energy spectrum of semiconductor compounds with chalcopyrite structure analyzed, using perturbation theory, noting changes resulting from crystalline and spin-orbital interactions 05 p0861 A67-16393
- Relativistic interaction energies between atoms in degenerate states determined, using Breit-Pauli approximation 05 p0848 A67-16839
- Energy spectra of galactic X-rays observed with three types of counters borne on sounding rockets 05 p0883 A67-16876
- Barometric effect of cosmic rays with allowance for changes in D/R/ primary spectrum and cut-off 05 p0884 A67-17136
- Optical absorption due to direct intervalence band transitions in Ge, noting effect of lattice temperature 05 p0869 A67-17192
- Landau level structure and transition matrix elements of InSb near Brillouin zone center during valence band cyclotron resonance 05 p0870 A67-17193
- Photoemission of electrons from conduction and valence bands of n-type degenerate Si into thermally grown silicon dioxide layers 05 p0870 A67-17195
- Increase in low temperature specific heat and change in electronic density of states of boronated graphite 05 p0833 A67-17197
- Statistical initial value problem for Burger model equation of turbulence, examining velocity correlation functions, energy spectra and other statistical properties 05 p0794 A67-17419
- Fluctuation spectra of Cs and K plasmas produced by surface ionization in Q-3 device 05 p0859 A67-17443
- X-ray emission and absorption spectra, electron structure and properties of metallic compounds of titanium 05 p0831 A67-17484
- Energy spectrum of levels appearing in silicon single crystals irradiated by integral fluxes of fast electrons, neutrons and gamma quanta 05 p0872 A67-17547
- Low energy heavy nuclei analyzed by slicing emulsion in connection with solar activity studies 06 p1076 A67-17634
- Atomic energy levels in plasma, considering energy spectrum of hydrogen-like atom in plasma based on cut-off Coulomb potential model 06 p1039 A67-17881
- Plasmoid structure produced by coaxial plasma gun with interchangeable polarity electrodes, noting experimental setup, particle velocity, density, energy, etc 06 p1040 A67-18085
- Synchrotron nature of Sagittarius A central component radio spectrum and injection of relativistic cosmic particles 06 p1078 A67-18166
- Gunn effect in GaAs caused by field induced transfer of electrons from high to low conduction band 06 p1067 A67-18961
- Energy spectrum of electrons recorded by fluorescent screen indicators onboard Cosmos satellites, noting ratio of electron intensities 07 p1170 A67-19101
- Statistical properties of radar signals with internal coherence reflected from rough surfaces 07 p1139 A67-19223
- Energy spectrum of inelastically scattered alpha particles from alpha particle helium 3 reaction 07 p1226 A67-19563
- Vertical flux and energy spectra of secondary gamma rays and electrons in upper atmosphere 07 p1242 A67-19621
- Stratospheric recordings of solar cosmic rays from chromospheric flares, calculating and comparing diffusion coefficient of cosmic rays and energy spectrum of solar protons 07 p1243 A67-19698
- Proton energy spectrum obtained from nuclear emulsion measurements on Gemini IV and V missions 07 p1244 A67-19655
- Photoionization mass spectrometer for charge transfer reaction analysis 07 p1137 A67-20188
- Radiation noise effect on laser optical properties, noting density vs resonator characteristics, energy spectrum, etc 08 p1337 A67-20839
- Proton I and II satellite instrumentation noting energy-charge spectrometer, gamma-quantum fluxmeter, equipment to determine chemical composition of charged cosmic ray particles, etc 08 p1376 A67-21001
- Balloon observation of X-ray sources in Cygnus region in energy range 20-130 kev 08 p1377 A67-21252
- Lasering effect on electron gas and excited state populations in xenon discharges 08 p1338 A67-21306
- Growth rate along whistler path for waves propagating at angle to geomagnetic field 08 p1328 A67-21463
- Differential energy spectra and fluxes of charged splash and reentrant albedo proton measurement of cosmic radiation in various energy ranges 08 p1377 A67-21467
- Satellite observations of energetic trapped electrons, August 1964 08 p1379 A67-21484
- Galactic radio sources noting disk model brightness distribution, relativistic particle energies, continuous particle acceleration and ratio between proton and electrical component of cosmic radiation 09 p1563 A67-21629
- Plasma potential and particle energies in cesium plasma measured by simultaneous observation of ion and electron energy spectra 09 p1548 A67-22338
- Energy spectrum of primary cosmic ray alpha particles measured by nuclear photographic emulsion, estimating geomagnetic cut-off energies 09 p1562 A67-22418
- Cosmic ray effects on solar system and on galactic scale, discussing energy spectrum, particle diffusion and motion, solar wind, etc 09 p1562 A67-22530
- Background noise curve of geomagnetic variations, attributing minimum spectral energy on ground to existence of permanent static solar wind component 10 p1632 A67-22856
- Quasars, energy emission, high red shifts and relation to radio sources and visible stars 10 p1705 A67-22953
- Energy spectra of galactic X-rays from four rocket measurements, observing Cygnus and Tau X-1 10 p1700 A67-23054
- Solar cosmic ray event characteristics 1962-1966, solar minimum vs solar maximum 10 p1700 A67-23187
- Properties of solar cosmic rays causing polar cap absorption measured with satellites 10 p1700 A67-23188
- Polar cap absorption with solar cosmic ray properties from balloons and relation to processes in terrestrial atmosphere 10 p1637 A67-23189
- Polar glow aurora, discussing optical emissions generated by solar cosmic ray protons and alpha particles, energy spectrum, atmospheric and ionospheric absorption effect, etc 10 p1637 A67-23190
- Energy spectra of Tau X-1 and isotropic component of galactic X-rays, using rocketborne scintillation and GM counters 10 p1701 A67-23229
- Flux and energy spectra of primary cosmic X and gamma rays between 20 kev and 1 mev from balloon-rocket measurements 10 p1701 A67-23231
- Role of corpuscular radiation in lower ionosphere formation noting charged particle flux, energy spectra, etc 10 p1647 A67-23283
- Diurnal variation of primary auroral electrons, average energy spectrum of 20-150 kev X-rays and time dependence of intensity and morphology 10 p1702 A67-23305
- Energy spectrum of primary electron flux and brightness of auroral light measured by rockets in active auroras used to derive electron production rate 10 p1650 A67-23306
- Power energy spectrum of cosmic rays as solution of general covariant kinetic equation 10 p1703 A67-23359
- Cosmic ray nucleon interaction with high energies, estimating transition probability and interaction cross section of baryon in passive state 10 p1703 A67-23586
- Spectral characteristics of turbulence in presence of mean velocity and temperature gradients 11 p1815 A67-23955
- Knudsen low voltage discharge with hot cathode, determining electron distribution, velocity profiles, V-I characteristics, etc 11 p1831 A67-24020
- Turbulence research applicability to solution of internal flow problems 11 p1776 A67-24046
- Extraterrestrial solar radiation simulation and total flux and spectral component measurement 11 p1772 A67-24053
- Evolution of radio spectral index of supernova remnants modeled to include synchrotron radiation energy distribution 11 p1859 A67-24114
- Primary cosmic radiation abundance measurements on iron and heavier nuclei, using Cerenkov counter on balloon flights 11 p1856 A67-24504
- Nuclear abundances of galactic and solar

cosmic rays, discussing detector electronics system for measurement of particle energy spectrum 12 p1944 A67-25852

Device for studying high energy nuclear active particles of cosmic rays interaction and determination of energy spectrum 12 p1947 A67-26095

Structure of X-ray K absorption edge of iron in Fe compounds, noting nature of chemical bond and structure of electron energy spectrum 12 p1957 A67-26109

OGO 3 observation of low energy protons and electrons in earth magnetosphere, noting narrow peak of relatively high low-energy particle intensities 13 p2190 A67-26312

Satellite measurements of electron flux and electron energy spectra in inner radiation belt 13 p2191 A67-26324

Three-dimensional hard spheres theory of gas atom scattering from solid surface noting velocity distribution, energy and momentum accommodation coefficients, etc 13 p2097 A67-26936

Anomalies in intensity of Compton diffusion of X-rays by vanadium noting energy-diffusion angle relation 13 p2181 A67-27210

Charge and energy spectra of galactic cosmic rays during solar minimum from satellite and Skyhook balloon data 13 p2193 A67-27248

Solar and galactic particle spectra and composition measured with cosmic ray telescope mounted on satellite 13 p2193 A67-27249

Energy spectra of solar wind ion fluxes outside magnetosphere measured using Venus 3 space vehicle 13 p2194 A67-27331

Absorption probability for photons traversing photon gases with different spectra 13 p2161 A67-27733

Opacity of universe to high energy photons, estimating spectra and absorption probability 13 p2161 A67-27734

Primary cosmic radiation composition effect on secondary emission, examining flux, spectra, nucleon interactions, proton component and neutrons 14 p2380 A67-27966

N-type germanium doped with antimony and arsenic investigated for radiation recombination, noting energy spectrum and forbidden band changes 14 p2368 A67-28533

Primary cosmic ray electron flux and energy spectrum near solar minimum compared with nonthermal radio emission from high galactic latitudes 14 p2381 A67-28831

Spectral energy distribution of source 3C 446 between August 17 and December 12, 1966 14 p2389 A67-28850

Electron-electron scattering in field of monochromatic laser beam, noting resonances in effective Moller scattering cross section 14 p2334 A67-29078

Weak random initial magnetic field evolution in highly conducting isotropically turbulent fluid, noting exact initial growth expression of magnetic energy spectrum 15 p2469 A67-29223

Coaxial plasma gun for plasmoids showing higher mean energy when gas admission is closer to plasma source 15 p2525 A67-29252

Plasmoid structure, analyzing interdependence of plasmoid parameters along length 15 p2526 A67-29256

Modified Thomson mass spectroscopy for visual observation of energy spectra of ion component of plasmoid 15 p2486 A67-29260

Spatial distribution of electrons and protons trapped by geomagnetic field and charged particle fluxes in interplanetary space 15 p2550 A67-29536

Atmospheric electron energy spectrum in range 70-2000 mev measured, using scintillation telescope with gas Cerenkov detector and lead glass total energy spectrometer 15 p2475 A67-29615

Effect of single-axis compression on radiative impurity recombination in arsenic- and gadolinium-doped germanium 15 p2537 A67-29705

Two-photon recombination in semiconductors with degenerate electron-hole gas taking into account damping during interaction with phonons 15 p2542 A67-30244

Mass spectrometric study of energy distribution of ions of accelerated plasma produced by coaxial source 15 p2532 A67-30264

Energy spectrum and correlation

characteristics of PCM signal studied by Levin method, calculating correlation moments of code group symbols 16 p2620 A67-30478

Synchrotron nature of Sagittarius A central component radio spectrum and injection of relativistic cosmic particles 16 p2737 A67-30510

Primary cosmic ray investigation by Proton I scientific space station concerning energy spectrum, chemical composition, galactic gamma ray and solar radiation hazard 16 p2737 A67-30647

Hypothesis attributing most energetic cosmic ray proton source to powerful radio galaxies noting pair production effect on cosmic ray sources 16 p2738 A67-30822

Upper atmosphere photoelectric processes contributing to low energy electron content of magnetosphere 16 p2864 A67-30973

Energy loss spectrum in CsI at small atmospheric depths, discussing time variation of 0.5-mev gamma-ray flux 16 p2739 A67-31406

Intrinsic optical excitation spectrum of crystalline solids for hole or electron localization, considering many-body relaxation effects influencing photoemission 16 p2732 A67-31698

Two-dimensional motion of charged particles in electromagnetic field, noting magnitude of forbidden band as function of particle energy 16 p2740 A67-31885

Ionization loss effect on energy spectra of cosmic ray nuclei undergoing Fermi acceleration 17 p2930 A67-32041

Cosmic ray intensity 11-year variation energy characteristics, discussing spectrum bending due to integral modulation in interplanetary space 17 p2932 A67-32083

Spectrometric system aboard Proton type satellite for analyzing energy and charge spectra of primary cosmic ray particles 17 p2854 A67-32245

Energy spectrum and composition of primary cosmic rays in high and superhigh energy range of Proton I and II satellites 17 p2935 A67-32246

Spectrometers onboard satellite, studying cosmic ray particle energy spectra and chemical composition 17 p2935 A67-32248

Energy spectrum of cosmic ray nuclei in helium through scandium range studied with Proton I and II satellites 17 p2935 A67-32249

Spectral distribution of turbulent energy, noting space-time correlations, instantaneous motion of fluid, existence of nonlinear inertial forces, etc 17 p2837 A67-32289

Primary cosmic ray spectrum changes from differential response functions and specific yield functions of neutron monitors 17 p2936 A67-32533

Titanium plasma source design features, performance, ion mean free path, energy spectrum and energy distribution 17 p2904 A67-32912

Energy spectrum and pitch-angle distribution of protons in auroras based on H-beta line profiles 17 p2938 A67-32962

Cosmic ray electrons energy spectrum and charge composition studies inadequacy due to insufficient statistics and electron flux contamination 17 p2938 A67-33198

Low energy H and He isotope detection in cosmic radiation at solar minima via balloon mounted scintillation counter 17 p2939 A67-33246

Correlation function for random process energy spectrum at linear system output, obtaining expression of envelope distribution for radio signals 18 p2999 A67-33506

Auroral particle fluxes and effects from coordinated satellite, aircraft-and ground-based measurements 18 p3034 A67-33590

Rocket observations of energy spectra of auroral electrons 18 p3034 A67-33591

Auroral rocket measurements of electron densities, ionization rates, particle energy fluxes, energy spectra, pitch angle distribution, etc 18 p3034 A67-33592

Electron measurements near weak aurora during rocket flight 18 p3034 A67-33595

Balloon measurements of auroral X-rays, discussing flux and energy spectrum variations and bursts relation to magnetic storms 18 p3038 A67-33613

Possibility of determining content of natural radioactive uranium, thorium and potassium in lunar rocks and of estimating chemical composition of rocks from cosmic ray induced radioactivity 18 p3122 A67-34142

Signal and noise FM modulated random process characteristics determined by equation for correlation function, giving energy spectrum relationship of modulated process phase 18 p3001 A67-34177

Grid geometry effect on longitudinal and lateral turbulence intensities, determining decay rate dependence 18 p3030 A67-34740

Energy spectrum of cosmic X-rays background component, proving experimentally rocketborne detector counting rate proportionality to field of view 19 p3314 A67-35278

Plasmoid structure created by plasma injector and freely propagating in space noting plasma composition, energy spectrum electron temperature, density, etc 19 p3288 A67-35362

Electron energy spectrum, showing intensity maxima from surface plasma oscillations, noting thin films effect on surface losses 19 p3307 A67-35789

Energy spectrum and production rates for secondary antiprotons from inelastic collisions of high energy galactic cosmic radiation with interstellar gas nuclei 19 p3316 A67-36098

Steady state propagation of cosmic ray nuclei, discussing energy spectrum and path lengths 19 p3317 A67-36099

Electrons energy spectrum stability dependence on spatial distribution of source, discussing cosmic ray generation 20 p3517 A67-36532

Auroral substorms, examining energy spectrum and flux of precipitating particles and morphology 20 p3431 A67-37100

Dynamic microstrain of niobium, considering purity and temperature effects, obtaining activation energy band spectrum 20 p3469 A67-37385

Charged particles of extraterrestrial ring current during geomagnetic storms, with Ogo 3 measurements of proton and electron differential energy spectrums 20 p3432 A67-37401

Cosmic ray secondary nucleon production of multiple neutrons observed and energy spectra measured, using multiplicity monitor 20 p3452 A67-37407

Cosmic X-ray sources in 20-180 kev energy range detected in balloon flights, giving energy spectra 20 p3520 A67-37475

Nuclear active particles energy spectrum obtained on mountain tops, investigating absolute flux by using ionization calorimeter 21 p3698 A67-38293

Peak energy dependence on atomic number in inelastic alpha particle scattering at 24.8 Mev by Ni 58, Cu, Ag, Ta and Au 21 p3659 A67-38401

Barometric effect of cosmic rays with allowance for changes in D/R/ primary spectrum and cut-off rigidity 21 p3698 A67-38479

ESRO V satellite-borne solar-proton spectrometry experiment to study proton and alpha particle energy spectra emitted during solar activity 21 p3629 A67-38663

Superconducting bismuth investigated using tunnel effect method to measure electron energy spectrum gap and phonon spectrum distribution 21 p3685 A67-38801

Magnetospheric energetic charged particles interrelations, discussing electron and proton energy spectra, particle population domains, trapped radiation and solar wind kinetic energy 22 p3870 A67-39673

Temporal periodicity of 10 cps observed in flux of auroral electrons by rocketborne radiation detectors 22 p3790 A67-39795

Electron flux and energy spectrum measurements near polar cap investigated for diurnal intensity variations 22 p3872 A67-39802

Solar proton event /February 1965/, time history of low energy protons was more complex than that of higher energy particles 22 p3872 A67-39812

Solar cycle prediction based upon random number technique, Fourier curve fits and power spectra analysis 22 p3873 A67-39931

Coronal line spectra of 1952 total solar eclipse, noting emitted energies and isothermic coronal region 22 p3889 A67-40206

Wake turbulence regimes for flows behind typical hypersonic bodies 22 p3743 A67-40222

Primary cosmic radiation electron component studies through differential

energy spectrum observations, considering confinement regions and black body radiation at 3 degrees K 22 p3874 A67-40239

High energy cosmic ray interactions analyzed at 3340 m above sea level, using Wilson cloud chambers, gas discharge counters, ionization calorimeter, 22 p3801 A67-40248

Nuclear cascade process in iron absorber of ionization calorimeter, comparing empirical and experimental values 22 p3801 A67-40249

Angular and energy characteristics of proton beam in pulsed magnetic field, determining probability of proton-neutron charge exchange for proton in forward light 22 p3842 A67-40255

Energy spectra of avalanche electrons in copper, iron, aluminum and graphite determined by method of moments, considering polarization of medium and multiple scattering 22 p3877 A67-40270

Energy moments of inverse problem in theory of nuclear cascade determined, using first order Volterra integral equation 22 p3842 A67-40271

Superhigh energy particle accelerators and energy spectra of cosmic ray muons in electron photon cascades 22 p3877 A67-40274

Integral energy spectra and angular distribution of muons, comparing computational and experimental data 22 p3877 A67-40275

Absorption curve and energy spectrum of high energy muons 22 p3877 A67-40277

Extensive air shower characteristics related to energy spectrum, chemical composition and anisotropy of primary cosmic rays in superhigh energy range 22 p3877 A67-40280

Leading particle model of formation of extensive air showers, determining energy spectrum 22 p3878 A67-40287

Solar system environment, discussing solar magnetic field, flare flux and energy spectrum, interplanetary plasma and radiation, asteroids, meteoroids and comets 22 p3889 A67-40407

Secondary neutron spectral data measured by proton recoil spectrometer from targets bombarded by 160 Mev protons 23 p4028 A67-40739

N-type germanium doped with antimony and arsenic investigated for radiation recombination, noting energy spectrum and forbidden band changes 23 p4040 A67-40940

Makeup low energy spectra and electron component of cosmic rays and solar particle production with curves for element abundance 23 p4053 A67-41090

Primary cosmic particles energy spectrum measurements onboard space station with ionization calorimeters and energy level discriminators 23 p4054 A67-41091

Primary proton energy spectrum determination by particle energy measurements with ionization calorimeters and particle counters onboard space stations 23 p4054 A67-41092

Heavy and superheavy nuclei energy spectra studied from measurements by Cerenkov counter onboard space stations 23 p4054 A67-41094

Probes containing various scintillators for measuring electron energy spectrum at high altitude in cosmic ray 23 p4054 A67-41095

Proton energy spectrum azimuthal asymmetry measured with telescopes using scintillation and Cerenkov counters 23 p4054 A67-41096

Low energy cosmic ray measurements during solar activity minimum suggesting changes in cosmic ray composition due to solar wind 23 p4054 A67-41097

Galactic cosmic ray intensity measurements in stratosphere and at various atmospheric depths, studying secular variation energy spectra during solar cycle 23 p4055 A67-41103

Effect of single-axis compression on radiative impurity recombination in arsenic- and gadolinium-doped germanium 24 p4199 A67-41775

Longitudinal turbulence intensities, autocorrelations, energy spectra and peak energy dissipation frequencies for organic solvents flowing in smooth round tubes 24 p4141 A67-41927

CdS single crystal film trap energy spectrum studied with thermo-stimulated

currents /TSC/ noting effect of SiO layer 24 p4203 A67-42246

Rocket measurements in auroral zone, considering proton and electron intensities, energy spectra and angular distribution 24 p4209 A67-42262

Pulsed ion flow energy and mass spectra analyzer suitable for 1 to 3 msec duration and time variation over 10 msec 24 p4158 A67-42741

Direct energy spectrum measurements of primary cosmic radiation in wide energy range 24 p4212 A67-42762

Electron intensity measurement in primary cosmic radiation by high altitude balloons carrying telescope made of two plastic scintillation counters 24 p4213 A67-42773

Change in intensity and forms of energy spectrum effects on accuracy of measuring values of meteorite preentry dimensions, weight and degree of ablation 24 p4238 A67-42775

Aurora photometry and stratospheric cosmic ray intensity, noting electron intrusion and correlation between aurora intensity and X-ray emission 24 p4213 A67-42778

Energy spectrum of secular variations of cosmic ray intensity in interplanetary space, using data from stratospheric measurements 24 p4213 A67-42780

Asymptotic directions of cosmic rays for Soviet cosmic ray stations 24 p4214 A67-42790

Interplanetary space properties studied from IMP-I satellite data on cosmic ray variations 24 p4214 A67-42791

Relativistic particles producing ionization bursts studied for energy spectrum recorded during operation of stack of ionization chambers alternating with lead and graphite layers 24 p4218 A67-42834

High energy nucleon interactions with X-ray films and nuclear emulsions aboard aircraft, with diagram of gamma quanta energy spectra 24 p4218 A67-42836

Primary cosmic ray particle chemical composition changes, explaining active particle energy spectra discrepancies between measurements and calculation 24 p4218 A67-42840

Air shower nuclear active component spectra noting need for mechanism of energy transfer from nucleons into electron-photon avalanches 24 p4220 A67-42862

Shower producing capability of various particle groups at 40 mwe below ground, evaluating muon energy spectra 24 p4220 A67-42865

Electron tunneling into superconductors to investigate pressure induced energy shifts in Pb phonon spectrum 24 p4206 A67-43100

Laser-created alumina plasma ion-energy spectrum, measuring plasma characteristics with pentagrid energy analyzer 24 p4199 A67-43102

ENERGY STORAGE

SA ELECTRIC ENERGY STORAGE

SA THERMAL ENERGY STORAGE

Kinetics of stored energy buildup in alkali halide crystals after proton irradiation, noting dependence on lattice energy of crystal 01 p0136 A67-11050

Heat of formation of KCl-KBr solid solutions and energy storage after proton irradiation 01 p0136 A67-11051

Cryogenic techniques for space power generators based on superconductivity, discussing MHD 04 p0560 A67-15967

Network analysis with state variables describing system stored energy 05 p0781 A67-16022

Power supply and transformation equipment in satellites, discussing batteries, fuel cells, nuclear reactors and solar energy 14 p2252 A67-28566

Nonlinear nonconservative systems stability analysis by approximate method based on principle of energy conservation 15 p2519 A67-30194

Small signal power conservation in space charge waves of multivelocity electron beam with rectangular velocity distribution 16 p2703 A67-30796

Gas flow through annular duct of constant cross section analyzed in terms of conservation of energy, mass and angular momentum laws 16 p2593 A67-31153

Energy conservation law concerning electromagnetohydrodynamics of viscous electrically conducting fluid showing that

total energy in fixed volume changes 16 p2721 A67-31549

Mass, momentum and energy conservation at wave fronts in coupled thermostaticity, noting propagation velocities for isothermal/adiabatic discontinuities 17 p2964 A67-33134

Evaluation of stored-energy function for elastomeric materials based on biaxial experiments 18 p3145 A67-34486

[JPL-TR-32-1006]

Vibrating neutron stars, discussing damping, heating, energy storage and X-ray emission possibilities at 1000 years range 22 p3882 A67-39619

Superconducting coils used for capacitors in pulsed operations to reduce size and weight of energy storage systems 22 p3747 A67-39900

Flight optimization problems, considering spacecraft with energy storage and limited power engines 24 p4240 A67-42295

Elastomer elastic deformation response in multiaxial stress field shown identical to uniaxial stress response 24 p4250 A67-42367

ENERGY STORAGE DEVICE

Orbiting Energy Depot, discussing fuel regeneration and resupply to enable use of fuel cells combined with nuclear power as main onboard power 22 p3902 A67-39948

Inductive energy storage and control system using ignitron switching 24 p4197 A67-42249

ENERGY TRANSFER

SA ANTENNA COUPLER

SA HEAT TRANSFER

SA MASS TRANSFER

SA WAVE SUPERHEATER

Instrumentation and control for magnetic pulse metal forming including pulse generation, energy transfer, electrical operations, etc 01 p0078 A67-10569

Energy transfer into electron-photon avalanche by high energy nucleons compared to data of air shower and particle spectra 01 p0144 A67-10745

Energy transfer mechanisms involving trivalent terbium and europium, noting that at 295 degrees K thermal effects cause overlap permitting dipole-dipole transfer to occur 01 p0134 A67-10874

Pion energy transmission during inelastic interaction of cosmic particles with Pb nuclei 02 p0315 A67-12756

Ionization calorimeter measurements of energy transmission by photons in cosmic nuclear-active pion and nucleon interactions with various nuclei 02 p0316 A67-12761

Thermodynamic parameters of combustible mixture and ignition system characteristics effect on energy of spark ignition of homogeneous gaseous mixture 03 p0535 A67-13396

Thermal conductivity and degree of blackness of aluminum oxide coatings at high temperatures, using argon plasma jets 03 p0536 A67-13608

Electron thermal conductivity of fully ionized Lorentz gas, determining energy transfer from Landau damping of plasma waves and collision parameters 03 p0484 A67-14039

Radiative modes of thin infinitely long circular plasma cylinder with dipolar azimuthal field variations 03 p0484 A67-14044

Massive star behavior during final catastrophic evolution stages, stressing effect of electron type neutrino interactions, using numerical hydrodynamics coupled with energy transfer methods 03 p0518 A67-14340

Radiant energy transfer in absorbing medium with constant absorption coefficient 04 p0722 A67-14714

Quantum study of optical nonlinearities in absorbing materials, energy transfer between optical waves, laws of nonlinear reflection and coherence effects 04 p0657 A67-14881

Helicon wave propagation along multilayered structure, calculating Bloch waves, fields and dispersion 04 p0665 A67-15119

Energy transfer rate between electrons and ions in plasma, noting velocity dependence of Coulomb logarithm 04 p0672 A67-15775

Energy transfer by circulatory and Coriolis forces in centrifugal and axicentrifugal compressors 04 p0690 A67-15897

Energy transfer from single chromium ions to closely coupled pairs of chromium

ions in ruby 05 p0862 A67-16659
 Laser emission at 1.06 microns from ytterbium-neodymium glass, noting linearity of energy transfer with Yb 05 p0820 A67-16664
 Computing velocities and convective energy transport in stars of different spectral types and luminosities 05 p0899 A67-17071
 Matrix equations approximating integral equations of radiative energy transfer 06 p1118 A67-18551
 Optimum energy transfer from hyperbolic orbit in Newtonian central force field in absence of transfer time limitations 07 p1247 A67-19094
 Energy transfer from single chromium ions to closely coupled pairs of chromium ions in ruby 07 p1234 A67-20124
 Energy balance equations including effects of heating by electron gas, cooling and energy coupling obtained for various ion species, assuming each ion gas has Maxwellian velocity 08 p1326 A67-21363
 Atomic collisions, excitation transfer processes and energy level transition probabilities in plasma of gas lasers 09 p1513 A67-22067
 Energy transfer spectra and Joule effect dissipation in decline of homogeneous turbulence in presence of uniform magnetic field with small Reynolds number 09 p1549 A67-22565
 Transport of free molar energy in system in interdiffusion 09 p1581 A67-22597
 Matched pulses for two-layer laminates, discussing complete energy transfer to base and uniform momentum transfer 10 p1724 A67-23707
 Solar corona and occurrence of solar wind and influence on evolution of red giant star 11 p1858 A67-24095
 Momentum and energy transfer effects on gas kinetic equations of nonequilibrium flows, analyzing diffusion problem 11 p1780 A67-24536
 Ionized fluid flow analyzed by multifluid theory to evaluate energy transfer mechanisms, noting temperature and compositional nonequilibrium effects 11 p1780 A67-24537
 Energy transfer during interaction of atoms with surface of ideal crystal in terms of classical mechanics 11 p1824 A67-24855
 Hydromagnetic wave propagation and energy transfer in stratified isothermal plasma embedded in parallel uniform gravity and magnetic fields 11 p1868 A67-25083
 Mechanical and electrical modes of energy transfer occurring in free and forced oscillations in earth magnetosphere 12 p2000 A67-25107
 Nonequilibrium MHD generator for closed and open cycles, noting K seed ionization by energy transfer from excited N molecules 12 p1898 A67-25388
 Energy transfer into electron-photon avalanche by high energy nucleons compared to data of air shower and particle spectra 13 p2192 A67-28774
 Magnetospheric regions of amplification of VLF emissions and micropulsations 13 p2115 A67-26858
 Gas-solid energy exchange model, studying harmonic oscillator and free particle 13 p2098 A67-26939
 Unified theory of gas-solid energy transfer in perturbation approximation, examining physical principles 13 p2223 A67-26940
 Radiant energy transfer below cloud cover in Venus atmosphere, noting greenhouse effect caused by atmosphere containing components capable of IR absorption 14 p2383 A67-27859
 Microwave spectroscopy of organic semiconductors, examining EPR of chemical bonds in energy transfer 14 p2366 A67-28505
 Numerical evaluation of voltage and polarity variation induced by electron conductivity changes created by longitudinal phonon pressure caused by shock wave 14 p2367 A67-28514
 Transmission energy characteristics of spherical plate electrostatic analyzers from external sources of electrons and protons 14 p2320 A67-28746
 Equation of state for Debye continuum governing nonlinear propagation of perturbations terminating in shock wave at distance 14 p2374 A67-28982

Radiative energy transfer through nongray medium bounded by two flat surfaces, obtaining temperature distribution and heat flux values 15 p2578 A67-29130
 Mass dependence of behavior of stellar core undergoing gravitational collapse examined, using improved equation of state and mean free path for energy transfer 15 p2553 A67-29183
 Electron temperature reduction possibility in individual valleys of multivalley semiconductors, based on energy-balance equation in electron-temperature approximation 15 p2542 A67-30246
 Energy and momentum exchange model for interaction of gas particle with solid body surface 16 p2619 A67-30458
 Rectangular light guides transfer energy from injection type semiconductor laser to laser with logic element 16 p2684 A67-30461
 Hot electron nonequilibrium plasma use in MHD generators, considering energy transfer, plasma stability, magnetogasdynamics, etc 16 p2601 A67-30545
 Probe for measuring energy transfer between satellite surface and upper atmosphere 16 p2670 A67-30646
 Electron temperature measured in acetylene/oxygen mixture flame and found twice that of gas due to chemical energy transport to electron gas 17 p2968 A67-32151
 Rotating field pinch dynamics in terms of temperature, pressure, plasma radius and magnetic field strength, noting energy transfer efficiency 17 p2908 A67-33108
 Production modes, physical deactivation with related electronic energy transfer and chemical reactions of D oxygen atoms, noting significance for upper atmosphere 17 p2809 A67-33203
 Interaction of planetary magnetic field with solar plasma studied using hypersonic analog, estimating energy transfer rate 17 p2951 A67-33208
 Ion-molecule reactions in propane studied using mass and energy resolved ion beams in tandem mass spectrometer 17 p2810 A67-33264
 Kinetic energy transport outwards in transition region between chromosphere and corona discussed qualitatively, postulating connection with spicules 17 p2952 A67-33393
 Energy transport, cosmic ray particle storage and triggering mechanism in solar flares, considering relation with stellar flares 17 p2939 A67-33398
 Energy transport concentration around homogeneous lossless dielectric cylinder, calculating electric field strength distribution and limiting radius of several wave modes 18 p2999 A67-33529
 Combustion - Conference, Berkeley, August 1966 18 p3146 A67-33778
 Michelson type carbon dioxide laser for AC discharge analysis, noting apparatus design and performance 18 p3060 A67-34014
 Laser excited vibrational fluorescence measurements in carbon dioxide noting energy transfer rates, system kinetics, radiative coupling, etc 18 p3060 A67-34027
 Thermal conductivity and degree of blackness of aluminum oxide coatings at high temperatures, using argon plasma jets 18 p3161 A67-34473
 Energy flux in steady inhomogeneous turbulent gas flow with arbitrary mean velocity field, deriving velocity spectra and pressure-velocity correlation tensors 18 p3030 A67-34741
 Velocity distribution function in positive column plasma and implications for electron energy transfer mechanism on microscopic scale 19 p3267 A67-34948
 Water cooled copper anode operation compared to porous graphite transpiration cooled annular anode to study energy transfer in wall stabilized cascaded arc 19 p3279 A67-35141
 Wave propagation and geometrical optics in random media, considering applications to solar corona heating by energy transfer, stellar scintillation and cosmic ray acceleration 19 p3261 A67-35507
 Potential energy flux across isobaric surfaces in atmosphere indicates flux direction dependent on correlation sign between temperature and vertical velocity at surfaces 19 p3224 A67-35526
 Model of nonradiative energy transport in sunspots, in which Alfvén waves generated

in convectively unstable layer propagated upward into overlying stable layer 19 p3330 A67-36074
 Recombination and bremsstrahlung continuum radiation measurements of atomic and ionic oxygen in plasma 19 p3299 A67-36093
 Luminescence decay kinetics of trivalent Nd ions in antiferromagnetic Rb manganese fluoride, showing mechanism of transfer process of excitation energy of Mn ions 20 p3506 A67-36218
 Electronic energy transfer between metastable argon and nitrogen molecules noting rotational enhancement 20 p3487 A67-36221
 Vertical energy transfer from stationary disturbances induced by topography and diabatic heat sources and sinks, using primitive motion equations 20 p3480 A67-36504
 Book on theory of energy transfers and conversions including thermodynamics and Legendre transform 20 p3484 A67-36650
 Wave interference and radiation tunneling phenomena influences on thermal radiation energy transfer between two separated solid dielectrics, noting spacing effect [ASME PAPER 67-HT-21] 20 p3546 A67-36716
 Argon arc plasma generator with film cooled anode for producing stable high temperature gas jet [ASME PAPER 67-HT-72] 20 p3498 A67-36752
 Stratosphere and mesosphere, discussing energetics, energy transfer, ionospheric currents, magnetic fields, atmospheric trace components, solar UV radiation measurements, etc 20 p3430 A67-36897
 Heat transfer of gas between parallel plates including radiation and rarefaction effects treated, using kinetic theory 20 p3553 A67-36935
 Cadmium sulfide edge luminescence energy shift dependence on excitation intensity and free carrier concentration 20 p3512 A67-37288
 Dayglow photoelectron excitation rate from electron energy loss calculations, with energy transfer functions calculated from photoelectrons produced by UV solar radiation 20 p3434 A67-37421
 Energy transfer during interaction of atoms with surface of ideal crystal in terms of classical mechanics 20 p3490 A67-37538
 Pulse magnitude and distribution due to energy release in liquid, on walls of shells submerged in liquid, used to calculate loads 21 p3611 A67-38056
 Digital computer for simulating and analyzing fluid turbulence by applying laws governing behavior and energy transfer of fluid elements 21 p3612 A67-38193
 Plasma acceleration by electromagnetic microwave discharge in static magnetic field gradient, discussing microwave-plasma energy transfer at electron cyclotron resonance [AIAA PAPER 67-660] 21 p3671 A67-38696
 Sputtering yields and energy-transfer efficiency measurements by ion beam sputtering of liquid metals indicate no justification for incorporation into low thrustor [AIAA PAPER 67-683] 21 p3692 A67-38714
 Energy transfer and electron conduction in nonequilibrium argon arc column at one atmosphere [AIAA PAPER 67-693] 21 p3672 A67-38722
 Boundary condition problem at interface between immiscible fluids investigated for nonequilibrium thermodynamics 21 p3733 A67-39065
 Plasma model kinetic equation, discussing collision operator approximating momentum and energy transfer rates 22 p3843 A67-39265
 Quasi-linear perturbation expansion used to study evolution of localized disturbance in plasma 22 p3851 A67-39985
 High velocity tropospheric winds at 40 to 60 km altitude, discussing supergradient and subgradient winds and energy transport to mesosphere possibilities 22 p3793 A67-40032
 Atomic and molecular chemophysical processes in shock waves derived from high temperature thermal energy transfer including instrumentation, relaxation, ionization and spectroscopy 22 p3786 A67-40074
 Higher lunar radio temperatures than IR measurements using temperature dependence of radiant energy transfer,

considering thermal conductivity of lunar materials 22 p3886 A67-40119
 Analogy between electric, thermal and magnetic phenomena considered in terms of molecular transfer theory, noting pure mathematical meaning with no physical content 22 p3837 A67-40213
 Pion energy transmission during inelastic interaction of cosmic particles with Pb nuclei 22 p3876 A67-40258
 Ionization calorimeter measurements of energy transmission by photons in cosmic nuclear-active pion and nucleon interactions with various nuclei 22 p3876 A67-40263
 Integrated intensities for thermal radiation heat transfer in nongray nonscattering gas approximated, deriving effective absorption coefficient 22 p3920 A67-40442
 Spectroscopic properties of mixed complexes with two different ligand groups surrounding lanthanide ion, discussing energy transfer and absorption 23 p3971 A67-40747
 Nonself-similar energy diffusion of thermal radiation front for plane parallel geometry, solving series and parametric solutions 23 p4081 A67-40887
 Resonance transfer of energy as mechanism for quenching interaction between rare earth ions affecting fluorescent lifetime 23 p3971 A67-40974
 Turbulence onset from small eddies in shear flow analyzed by nonlinear approach 23 p3990 A67-41173
 Energy transmitting characteristics and wall local energy absorption distribution of curved specular reflecting duct irradiated by collimated beam 23 p4028 A67-41271
 Energy transfer effects on pathophysiological responses of guinea pigs and bradycardia response in monkeys under minus G impact 23 p3955 A67-41610
 Radiative heat transfer in radiating and conducting media, calculating heat flux and temperature distribution for semisotropic model 23 p4083 A67-41718
 Effective temperature for late type stars with or without water vapor opacity calculated for several masses, determining convective energy transport efficiency 24 p4224 A67-41818
 Energy transfer in sunspot model with vertical magnetic field, noting magnetic pressure distribution and magnetohydrostatic equations 24 p4226 A67-41966
 Plasma energy and heat transfer to surface with and without electric current, discussing various energy transfer models 24 p4197 A67-42331
 Energy fraction transfer to neutral pions during interactions with heavy nuclei measured for several energy levels, using ionization calorimeter 24 p4218 A67-42833
 Air shower nuclear active component spectra noting need for mechanism of energy transfer from nucleons into electron-photon avalanches 24 p4220 A67-42862

ENGINE
 S AIR BREATHING ENGINE
 S AIRCRAFT ENGINE
 S BY-PASS ENGINE
 S CARNOT ENGINE
 S CESIUM ENGINE
 S DIESEL ENGINE
 S DUCTED FAN ENGINE
 S ELECTROSTATIC ENGINE
 S ELECTROTHERMAL ENGINE
 S EXTERNAL COMBUSTION ENGINE
 S GAS GENERATOR ENGINE
 S HEAT ENGINE
 S HELICOPTER ENGINE
 S HYDRAZINE ENGINE /NIMPHE/
 S HYDROX ENGINE
 S INTERNAL COMBUSTION ENGINE
 S ION ENGINE
 S JET ENGINE
 S LOX-HYDROGEN ENGINE
 S NUCLEAR ENGINE FOR ROCKET VEHICLE /NERVA/
 S PISTON ENGINE
 S PLASMA ENGINE
 S PROPULSION
 S RAMJET ENGINE
 S RECIPROCATING ENGINE
 S RESISTOJET ENGINE
 S ROCKET ENGINE
 S SCRAMJET ENGINE
 S TURBINE ENGINE
 S TURBOFAN ENGINE
 S TURBOJET ENGINE

S TURBOPROP ENGINE
 S TURBORAMJET ENGINE
 S TWIN ENGINE
 S VERNIER ENGINE
 S WANKEL ENGINE

ENGINE CONTROL
 SA ROCKET ENGINE CONTROL
 SA TURBOJET ENGINE CONTROL
 Digital electronic programmable turbine engine control system for reducing time and cost in engine-control system matching 01 p0030 A67-11094
 Hydraulic gimbal system with closed loop design for orienting Saturn S-IVB engine 03 p0363 A67-13535
 Fluid amplifiers and sensors for jet-engine control systems 06 p0949 A67-17611
 Digital computer CPU control of kinetic heating processes in engine of supersonic aircraft under simulated flight conditions 08 p1315 A67-21007
 JR 100 H lift jet engine height control studies by NAL 11 p1852 A67-24267
 Automatic height control test equipment for V/STOL aircraft, discussing experimental setup and performance 11 p1772 A67-24268
 Control methods for parameters of helicopter gas turbine engines 11 p1853 A67-24527
 Hydraulic, pneumatic and electric circuits for twin loop engine control system of Olympus 593 in Concorde SST 13 p2187 A67-26702
 Digital computer used for on-line control of jet engine 13 p2074 A67-27190
 Rocket control with limited-power engine when approaching target 14 p2394 A67-28640
 Fuel control system of GE4 engine for supersonic transport noting main and augmentation fuel and control subsystems [SAE PAPER 670326] 17 p2929 A67-32982
 Rocket engine turbopump assembly test capability design, facilities, cryogenic systems, control requirements, computer simulation, activation and checkout [AIAA PAPER 67-441] 18 p3112 A67-33918
 Fluidic jet engine controls for closed loop control, noting overtemperature prevention, reliability, etc 18 p2989 A67-34097
 Analytical methods for control systems applied to engine governor systems 21 p3602 A67-38129

ENGINE COOLANT
 Postirradiation radiochemical and spectrochemical analysis of short-cooled samples of SNAP-8 experimental reactor primary coolant 03 p0466 A67-13798

ENGINE DESIGN
 SA ROCKET ENGINE DESIGN
 High by-pass fan engine installation in subsonic transport in terms of configuration, environmental severity, structures and systems [SAE PAPER 660737] 01 p0140 A67-10636
 Computer program providing ion thruster design criteria and power and weight requirements for specific satellite control mission [AIAA PAPER 66-498] 02 p0302 A67-11515
 Resistojet design and fabrication, using hydrogen propellant and having 3-kw power input [AIAA PAPER 66-224] 02 p0302 A67-11937
 VTOL power plant design noting jet deflection, lift fans, RB-162 engine, etc 04 p0687 A67-14435
 Ramjet external-combustion engine noting design of trailing edge, nomograms of pressure, temperature, thrust component, etc 04 p0688 A67-14578
 Supersonic combustion air breathing engines as propulsion systems for hypersonic vehicles [AIAA PAPER 66-826] 04 p0688 A67-14624
 Ion thrust motors used to overcome solar-lunar attraction, earth triaxiality, solar pressure and other forces tending to perturb satellite orbit or modify orientation 04 p0705 A67-15027
 High by-pass vs low by-pass engine installations, discussing effects of nacelle shape, wing proximity, inlets, thrust reverses and accessory location [SAE PAPER 660735] 04 p0690 A67-15779
 Thermodynamic limits on specific work and specific impulse of adiabatic chemical engines and nuclear engines [AIAA PAPER 67-227] 06 p1029 A67-18445
 Aircraft engine design and economic pressures effect on

development 06 p0949 A67-18735
 Mechanical difficulties in designing shaft, bearing and seal systems for three high speed turbine engines [SAE PAPER 670064] 09 p1560 A67-22537
 Aircraft gas turbine and fuel control design to meet engine requirement in broad environmental challenges [SAE PAPER 670140] 09 p1560 A67-22541
 Solid motor case technology, evaluating materials, fabrication, segmented case joint design and cost comparisons for large rocket motors 10 p1661 A67-23703
 Business jet aircraft engine design for increased service life, detailing turbine nozzles, bearings, rotors, etc [SAE PAPER 670234] 11 p1851 A67-23981
 Aircraft engine development and economic efficiency, discussing need for new fuels for rocket engines 11 p1853 A67-24630
 Scramjet performance analysis stressing construction problems and importance of fuel choice 11 p1853 A67-24748
 Design aspects of power plants for V/STOL aircraft, examining lift jets, thrust vectoring and lift fans [ASME PAPER 67-GT-7] 11 p1744 A67-24795
 Plane constant pressure contours determined by hodograph mapping used to design lift engine intakes 12 p1891 A67-25213
 Two-stroke cycle light aircraft engine with respect to competitive power plants 12 p1989 A67-25496
 Engine design to reduce overall cost and improve power plant component for flight schedule reliability [SAE PAPER 670330] 12 p1990 A67-25872
 Computer program providing ion thruster design criteria and power and weight requirements for specific satellite control mission [AIAA PAPER 66-498] 13 p2188 A67-26825
 Subsonic-transonic drag of supersonic, two-dimensional and axisymmetric plug inlets 13 p2051 A67-27592
 Soviet book on pilotless aircraft and missiles covering jet engine design, automatic control, radio engineering and aircraft aerodynamics 15 p2564 A67-29242
 System requirements effect on ballistic and hardware design of cast double-base solid propellant rocket motors 15 p2548 A67-30000
 System-effectiveness concept for turbine and piston engine development 15 p2584 A67-30402
 Effective engine protection system for CH-54A Flying Crane helicopter, consisting of an engine-inlet air-particle separator, noting Vietnam performance [AHS PAPER 117] 16 p2737 A67-31833
 Engine development and manufacture in Sweden 17 p2928 A67-32123
 Book on design and structural strength of aircraft gas turbine engines covering inlet and exhaust systems, compressors, combustion chambers, rotors, etc 17 p2928 A67-32564
 Engine nacelle location, size and shape effects on drag due to wing thickness and drag due to lift [AIAA PAPER 66-665] 17 p2791 A67-32567
 Engine design for civil operation from military supersonic engine [SAE PAPER 670316] 17 p2929 A67-32978
 JT9D engine design from viewpoint of incorporated noise reduction features [SAE PAPER 670331] 17 p2929 A67-32984
 Engine materials investigated for optimum low cycle fatigue resistance by pull-pull and rotating-beam fatigue testing techniques [SAE PAPER 670336] 17 p2874 A67-32986
 Supercavitating engines noting design principles, performances of existing models and connection between parameters 18 p3023 A67-33417
 Supercavitating engines, defining optimum curvature and thickness distribution, performance optimization, etc 18 p3023 A67-33418
 Soviet collection of articles on aircraft engine strength and dynamics 19 p3234 A67-34870
 Superalloys for SST engine, discussing materials properties, structures, turbine disk production, welding, alloy design, coating-base metal interactions, etc 20 p3469 A67-37358
 Single nozzle thermal storage resistojet thruster for low thrust satellite attitude and orbit control applications, noting design and

performance
[AIAA PAPER 67-662] 21 p3690 A67-38698
Design, fabrication and performance of 10-millipound resistojet operating on hydrogen or ammonia, describing heat exchanger and nozzle geometry
[AIAA PAPER 67-664] 21 p3690 A67-38699
Multitrotor trochoidal engines external balancing problems, discussing cam distribution and shaft shape
21 p3696 A67-38910
Handley Page Jetstream power plant, propeller design, turboprop engine operation and control
22 p3868 A67-40131
Configuration selection of turbopump for hot-bleed cycle nuclear engine, discussing performance optimization factors
22 p3834 A67-40162
Gas-air mixing in coaxial flow engine based on one-dimensional ejector theory at subsonic flow velocities, discussing chamber design gas-air mixing in coaxial flow engine based on one-dimensional ejector theory at subsonic flow
23 p4048 A67-40638
Engine air intake design and development for Concorde aircraft, discussing design constraints
[AIAA PAPER 67-752] 23 p4048 A67-40986
Design criteria for VTOL tactical aircraft power plant using turbojets for attack aircraft in support of land troops
23 p4049 A67-41044
Performance and design parameters for VTOL fighter aircraft engine and wings, stressing takeoff weight factor
23 p3935 A67-41316
Turboramjet engine design for aerodynamic flight vehicles up to Mach number 6
23 p4049 A67-41318
SST engines design, combustion and thrust augmentation systems, engine controls and complications facing users
[SAE PAPER 67-0865] 24 p4207 A67-42005
Thermoelectric converter designed for operation with SNAPOODLE /hybrid radioisotope thruster/ electric generator/, discussing test results
24 p4184 A67-42507

ENGINE FAILURE
Material failure modes in engine components and improved structural design problems
03 p0505 A67-14387
Aircraft piston engine components reliability characteristics determined from defect data survey, using statistics
04 p0691 A67-15902
Engine-oil-operated water/methanol system provides boosted takeoff power and maintains takeoff power at elevated temperatures
05 p0873 A67-16233
Quality control and internal combustion aircraft engine reliability from mechanical engineering viewpoint
05 p0812 A67-17243
Debris ingestion into engine arising from ground erosion effects on jet lift V/STOL aircraft
06 p0945 A67-17906
Structural predictions of mean times between failures through maintenance activity for aircraft power systems
09 p1560 A67-22287
Aircraft engine service life and reliability during series production, analyzing failure of parts
09 p1560 A67-22476
Vibration in cylindrical shafts, noting high stresses due to low mechanical damping, existence of two natural frequencies, etc
12 p1949 A67-25411
Dynamic vibration in aircraft power plant components, noting responsiveness of parts and fatigue life evaluation
[SAE PAPER 67-0237] 12 p1989 A67-25495
Aircraft engine reliability, considering local surface stresses, engine component distortion under load, vibration problems and material variability
13 p2188 A67-27000
Gas turbine auxiliary power unit design to provide boost to helicopter engine in powered and autorotational flight modes
[AHS PAPER 116] 16 p2598 A67-31832
Engine design for civil operation from military supersonic engine
[SAE PAPER 67-0316] 17 p2929 A67-32978
Diagnostic devices for sensing performance deterioration and mechanical malfunctions in supersonic aircraft engines
[SAE PAPER 67-0363] 17 p2930 A67-33000
Statistical method for demonstrating reliability of clustered liquid propellant rocket engines
18 p3116 A67-34662
Reliability in aircraft engines from start of assembly to completion and delivery
22 p3867 A67-39285

Mission flight profile, considering thrust failure prior to attaining orbital speed, analyzing instantaneous impact point /IIP/
22 p3831 A67-39610

ENGINE FAILURE INDICATOR
Diagnostic system for jet engine malfunctions detection using digital computer sonic vibration analysis
[SAE PAPER 67-0871] 24 p4207 A67-42008
Internal combustion engine vibration signals application to automatic fault diagnosis, discussing engine instrumentation and signal analysis
[SAE PAPER 67-0872] 24 p4207 A67-42009

ENGINE MONITORING SYSTEM
Aircraft engine parameter control by onboard recording instruments
14 p2315 A67-28059

ENGINE PART
SA COMBUSTION CHAMBER
SA FLYWHEEL
SA PISTON
SA VALVE
Passive thermocontrol techniques for electronic equipment near descent engine skirts and plumes
[AIAA PAPER 67-158] 06 p1117 A67-18479
Test program to evaluate characteristics of existing Atlas engine boots in flight environment and provide parameters for design change
[AIAA PAPER 67-277] 07 p1241 A67-20054
High strength nickel base alloy with improved oxidation resistance up to 2200 degrees F for applicability to gas turbine engine components
[ASME PAPER 67-GT-1] 11 p1808 A67-24789
Steady thermal strains measurement in aero and industrial turbine and engine components, discussing fine wire behavior, bonding agent, performance, requirements, etc
18 p3143 A67-33900
Configuration selection of turbopump for hot-bleed cycle nuclear engine, discussing performance optimization factors
22 p3834 A67-40162

ENGINE STARTER
Vapor replacement in propellant feed duct with subcooled liquid to meet engine starting requirement of space vehicle parked in orbit
[AIAA PAPER 66-975] 02 p0305 A67-12297
Delayed energy produced by fission product decay when restart of nuclear rocket engine is considered, noting effects of cooldown requirements
[AIAA PAPER 66-551] 05 p0844 A67-17222
Hypergolic propellant ignition experience during Project Sure Fire of Gemini program
[AIAA PAPER 67-259] 07 p1241 A67-20046
Starting phenomenon on reversed nozzle and multishock types of supersonic intakes
10 p1590 A67-22918
Pneumatic starting systems for gas turbine engines including energy sources, system components and arrangements
[ASME PAPER 67-GT-15] 11 p1854 A67-24800
High pressure hot gas solid propellant cartridge starter for aircraft turbine engine
[ASME PAPER 67-GT-21] 11 p1854 A67-24803
Cartridge-pneumatic dual mode jet engine starter design and function, discussing energy conversion and handling of high pressure gas produced by starter cartridge
[ASME PAPER 67-GT-49] 11 p1855 A67-24810
Light weight small gas turbine starter system permitting self-starting of high power turbo engines noting cost, flexibility, military application, etc
12 p1988 A67-25186
Plessey constant speed drive/starter /CSDS/ application to BAC 111 commercial transport, discussing dual role
17 p2800 A67-31975
Start characteristics of LM Ascent Engine determined by test series, noting effects of altitude variation, propellant lead time, temperature and valve slow-down
[AIAA PAPER 67-522] 18 p3115 A67-33985
Cesium bombardment ion engine performance, giving starting circuit and automatic discharge power control system
[AIAA PAPER 67-666] 21 p3690 A67-38700

ENGINE TESTING
SA ALTITUDE TEST
SA ENVIRONMENTAL TESTING
SA FLIGHT TEST
SA FUEL TESTING
SA GROUND TEST
SA PRELAUNCH TESTING
SA PROPELLANT TESTING
SA PROPULSIVE EFFICIENCY

SA SPACE ELECTRIC ROCKET TEST /SERT/

Space vacuum simulation chambers for testing of ionic, plasma and other rocket engines
01 p0048 A67-10302
Transducers role in problems associated with accurate and precise measurements during static firing tests of solid propellant motors
01 p0073 A67-11111
Transport jet engine inspection with radioactive isotopes, noting techniques and results
02 p0303 A67-12219
Instrumentation and control /I and C/ system for ground test of Nerva propulsion system
03 p0395 A67-13384
Engine test facility for measuring thrust and propellant flow in pulsating rockets
03 p0396 A67-13774
Nuclear rocket propulsion development, noting nuclear rocket engine test program
[AIAA PAPER 66-829] 03 p0466 A67-14124
Testing of NRX/EST and NRX-A5 with emphasis on startup capability, engine control and high temperature operation
[AIAA PAPER 66-1004] 03 p0466 A67-14149
Impulse measurements of small electric engines by vacuum microbalance technique, also suitable for average thrust measurements in millipound and micropound ranges
04 p0620 A67-14734
Compressor blade vibration, discussing prediction of amplitudes of vibration and interpretation of results of engine strain gauge tests in terms of component service life
[ASME PAPER 66-WA/GT-14] 04 p0712 A67-15369
Statistical procedures for analyzing test data to determine extent of dependence of failures in redundant components
05 p0813 A67-17256
Scramjet testing with wave superheater hypersonic tunnel
[AIAA PAPER 67-182] 06 p0980 A67-18343
Permanent magnet low thrust engines performance and tests, starting from cesium electron bombardment ion microthruster
[AIAA PAPER 67-81] 07 p1240 A67-19436
Diamant solid propellant booster development
07 p1240 A67-19521
Diamant third stage and nose cone
07 p1258 A67-19522
Space simulator application to development of space rocket propulsion systems, examining test problems of low pressure space engines
[AIAA PAPER 67-257] 07 p1164 A67-20052
Nonconventional rocket propulsion systems performance and base environment characteristics evaluated, using separate cold flow and combustion models
[AIAA PAPER 67-256] 07 p1241 A67-20072
Testing of three individual propulsion systems of lunar module space vehicle in preparation for man-rated flight service
[AIAA PAPER 67-258] 07 p1166 A67-20073
Electrical systems except data acquisition and instrumentation for ground testing of large booster
[AIAA PAPER 67-270] 07 p1167 A67-20079
JR 100 H lift jet engine height control studies by NAL
11 p1852 A67-24267
Automatic height control test equipment for V/STOL aircraft, discussing experimental setup and performance
11 p1772 A67-24268
Collector target complex eliminating target life time and test equipment contamination by sputtered target material, applied in testing of electrical propulsion systems
[AIAA PAPER 66-500] 11 p1852 A67-24341
Bench and flight tests of twin spool axial flow turbojet power plant for Concorde aircraft
[ASME PAPER 67-GT-8] 11 p1854 A67-24796
Metallurgical and fluid dynamic results of 2000-hr endurance test at high temperatures on two-stage 200 hp turbine in wet potassium vapor
[ASME PAPER 67-GT-9] 11 p1745 A67-24797
Allison T63 engine sand and dust tolerance development and field experience
[SAE PAPER 67-0334] 12 p1990 A67-25875
Emulsified fuel mixture /JP-4 and water/ tested in model Allison T63 turbine engine
[SAE PAPER 67-0368] 12 p1987 A67-25883
Small liquid propulsion systems testing in space environment simulator with high vacuum and low pumping capacity
13 p2089 A67-26840
Aircraft radiography for turbojet engine

integrity and serviceability determination
[AIAA PAPER 67-380] 15 p2494 A67-30350

Cesium contact ion engine ground and
flight tested for ability to operate under
environments of ground handling, missile
launch and space
16 p2736 A67-30711

Airborne analyzer and digital recording
system to assess, diagnose and predict
turbojet engine health on immediate and
long term basis
[SAE PAPER 670359] 17 p2861 A67-32998

Gas turbine environmental testing,
measuring emulsified fuel flow, direct
burning effects of JP-4 fuel on extended
engine operation, etc
[SAE PAPER 670367] 18 p3111 A67-33567

Development, reliability and acceptance
tests for third stage of ELDO satellite
launcher, discussing components, time
schedules, personnel training,
etc
18 p3136 A67-33639

Solid propellant rocket motors reliability,
discussing corrective action, retest, success
probability, requirements, capability,
simulation model, etc
[AIAA PAPER 67-435] 18 p3112 A67-33914

Phoebus 1B test /high-power-density
reactors for space propulsion/ noting reactor
design for fuel-element testing
[AIAA PAPER 67-486] 18 p3076 A67-33952

MIRA 150A variable thrust rocket engine
applied to manned lunar exploration flying
systems
[AIAA PAPER 67-505] 18 p3113 A67-33969

Vacuum-ignition phenomena in Apollo
rocket engine when oriented in upward-
firing attitude
[AIAA PAPER 67-514] 18 p3114 A67-33977

Compressor blade vibration, discussing
prediction of amplitudes of vibration and
interpretation of results of engine strain
gauge tests in terms of component service
life
[ASME PAPER 66-WA/GT-14] 18 p3115 A67-34132

Scramjet testing with wave superheater
hypersonic tunnel
[AIAA PAPER 67-182] 19 p3208 A67-35767

Permanent magnet low thrust engines
performance and tests, starting from cesium
electron bombardment ion
microthruster
21 p3689 A67-37790

Narrow and wide passband measurements
of LRBA liquid propellant motors using test
bench automatic measurement
equipment
21 p3607 A67-38202

Clustered mercury electron bombardment
ion engine system experiments showing
feasibility, discussing components
[AIAA PAPER 67-698] 21 p3693 A67-38727

FAA certification standards for SST
engines and components, emphasizing
thermal environment testing and high
temperature materials
development
22 p3867 A67-39224

NERVA components including nozzle and
associated hot gas bleed port, turbopump,
control valve, pressure vessel and
thermocouples
22 p3834 A67-40172

Structural and mechanical design of Lunar
Module Descent Engine, discussing
component testing effect on development
schedule
24 p4207 A67-42394

Nuclear subsystem controls and
instrumentation for NERVA noting
automatic startup, override, power and
temperature controller
testing
24 p4183 A67-42471

Thermoelectric converter designed for
operation with SNAPOODLE /hybrid
radioisotope thruster/ electric generator/
discussing test results
24 p4184 A67-42507

ENGINE TESTING LABORATORY

Extended plug nozzles in suppression of
jet noise in small turbojet engines
[SAE PAPER 670157] 09 p1561 A67-22544

Integrated data processing for turbojet
and turboprop engines high altitude test
facility
20 p3413 A67-36464

Mississippi Test Facility /MTF/ of NASA
noting rocket testing facilities, scientific
laboratories and industrial
complex
23 p3986 A67-40588

Sub-, super- and hypersonic air breathing
engines, examining developments on ground
test and simulation facilities
[AIAA PAPER 67-779] 24 p4208 A67-42946

ENGINEERING

SA AERONAUTICAL ENGINEERING

SA BIOENGINEERING

SA CHEMICAL ENGINEERING

SA HUMAN ENGINEERING

SA MECHANICAL ENGINEERING

SA PRODUCTION ENGINEERING

SA STRUCTURAL ENGINEERING

SA SYSTEMS ENGINEERING

SA UNDERWATER ENGINEERING

Book on microwave engineering including
transmission lines, resonators, waveguides,
antennas, tubes, etc
04 p0583 A67-15269

Book on theoretical equipment of
engineering fluid
mechanics
06 p0982 A67-17660

MHD engineering - Conference, Stanford
University, March 1967
12 p1971 A67-25373

Handbook of engineering sciences, Volume
1, Basic sciences
13 p2155 A67-26266

Mechanization effect on man-machine
relationships in flight test engineering
analysis
13 p2052 A67-26423

Advances in cryogenic engineering,
Volume 12 - Conference, Boulder, June
1966
13 p2225 A67-27634

Book on heat transfer covering basic
treatment of heat conduction, convection
and radiation
14 p2404 A67-27792

Book on radioisotope measurement
applications in engineering covering nuclear
radiation, gas detectors, scintillation,
etc
15 p2516 A67-29900

Book on engineering mathematics covering
differential equation solutions by numerical
method, partial differential equations,
Fourier series, integrals, vector analysis,
etc
17 p2876 A67-31930

Book on statistical models in engineering
covering probability theory, random
variables, frequency distributions,
etc
17 p2876 A67-32236

Book on FORTRAN with engineering
applications covering case studies, graded
exercises, etc
17 p2818 A67-32331

Thin films applications in electronic
engineering - Conference, London, July
1966
21 p3589 A67-37915

Advances in energy conversion
engineering - ASME Conference, Miami
Beach, August 1967
24 p4099 A67-42485

ENGINEERING DEVELOPMENT

Book on geometric programming detailing
theory of mathematical method for
optimizing engineering
design
09 p1469 A67-22435

Digital computer languages in relation to
engineering design
13 p2073 A67-27189

C-141A engineering development test
program, discussing flight, accelerated
service and all-weather testing
[AIAA PAPER 67-409] 15 p2422 A67-30376

Book on functional mechanisms for
engineering design, presenting kinematic
characteristics of output motion, planar
linkage and spatial cycloidal crank and
flexural mechanisms
20 p3454 A67-36766

Spacecraft atmosphere selection covering
physiological, engineering and fire criteria,
evaluating oxygen diluent and
recovery
22 p3755 A67-39889

Engineering change proposals /ECP/
implementation cost emphasizing collateral
cost evaluation
23 p4085 A67-40585

Technical obsolescence of engineers and
scientists, considering knowledge explosion
impact in terms of organizations and
individuals
[SAE PAPER 670833] 24 p4257 A67-41993

Mathematical model to aid in
determination of need for technological
advances in transportation
[AIAA PAPER 67-799] 24 p4258 A67-42960

ENGRAVING

SA ETCHING

SA PHOTOENGRAVING

Thin film and semiconductor integrated
circuits, discussing functional flexibility,
fabrication by microengraving, isolation and
computer fabrication
08 p1301 A67-20791

ENTHALPY

Exact solutions to equations for
compressible boundary layer in case of
power-law dependence of initial profile of
stagnation enthalpy on stream
function
03 p0400 A67-12867

Plasma arc tunnel tests show
thermochemical heat of ablation of magnesita
strongly dependent on stagnation enthalpy
[AIAA PAPER 65-641] 03 p0449 A67-13061

Enthalpy measurement for self-binding
silicon carbide at high
temperatures
03 p0446 A67-13609

Mean value definition in one-dimensional
gas dynamics applied to nonuniform
flow
04 p0609 A67-15747

Gas flow, convective heat transfer,
enthalpy rise and surface mass transfer for
bodies in cross flow, with application to
circular cylinder
04 p0733 A67-15841

Enthalpy to work conversion in gas
turbines using pulsating combustion
chamber
05 p0873 A67-16743

Transport of vorticity and enthalpy in
flow field in nose region of blunt body in
viscous hypersonic flow
05 p0749 A67-16820

Thermal choking in various devices having
mixing processes between two flows with
different stagnation enthalpies as possible
limitation of mass flow rate
[ONERA-TP-411] 05 p0792 A67-16934

Enthalpy of formation and dissociation of
explosion of mixtures of hydrogen and
excess nitrogen
06 p0955 A67-17985

Enthalpy of reaction of sulfur and
nitrogen trifluoride
06 p0955 A67-17986

Wall temperature effect on behavior of
hypersonic stagnation region shock layer in
incipient merged layer flow, obtaining
enthalpy function profile
08 p1278 A67-20928

Characteristic optical density and
equilibrium of alkyl-sodium and aromatic
hydrocarbons as function of temperature and
wavelengths, correlating electron affinity
with enthalpy values
09 p1458 A67-22214

Steady flow of conducting dissociating gas
in channel of constant cross section in
presence of magnetic
field
12 p1929 A67-25756

Enthalpy and position in heated tube
where liquid boiling begins, finding heat
content in turbulent liquid
flow
14 p2406 A67-28311

Enthalpy changes in ammonium
perchlorate during linear heating, noting
crystal structure transformation and
subsequent decomposition
14 p2376 A67-28903

Relative enthalpy and thermodynamic
properties of beryllium aluminate from room
temperature to melting
point
15 p2508 A67-29764

Enthalpy measurement of anhydrous
crystalline aluminum trifluoride with ice
calorimeter and drop method obtaining
thermodynamic properties
16 p2620 A67-31761

Hexagonal cobalt single crystals plastic
deformation, determining stress, free
enthalpy and volume activation, temperature
and strain rate
17 p2873 A67-32815

Probe for total enthalpy measurements in
arc jet exhausts
17 p2971 A67-33030

Radial mass flow effect on electric arcs,
obtaining higher axis temperature and
enthalpy densities
17 p2910 A67-33366

Enthalpy measurement for self-binding
silicon carbide at high
temperatures
18 p3066 A67-34474

Radial instreaming mass flow effect on
cylindrically-symmetric arc with
transpiration cooling, noting heat flux
reduction
19 p3280 A67-35148

Surrounded atom model for
thermodynamic enthalpy and entropy
characteristics of mixing in liquid binary
alloys
21 p3733 A67-39105

Chromel-alumel thermocouple for high
enthalpy gas flow temperature measurement,
discussing design and measurement
accuracy
23 p4081 A67-40569

Enthalpies of formation and bond
energies of various fluorinated amines in gas
state
23 p3971 A67-40975

Niobium carbide enthalpy, heat content
and heat capacity variation in homogeneity
domain from 1300 to 2500 degrees
K
24 p4171 A67-41958

MX solids refractory character correlation
with volatility at triple point, calculating
bond energy according to formation enthalpy
equation
24 p4173 A67-42084

ENTHALPY-ENTROPY DIAGRAM

Cooling losses in cooled gas turbines,
correlating Cooling Loss Factor /CLF/ and
Cooling Number /CN/
20 p3517 A67-37484

ENTROPY

SA ENTHALPY-ENTROPY DIAGRAM

SA NERNST HEAT THEOREM

Steady state flows without external forces
becoming parallel in thermodynamic
equilibrium at distance from body, noting
relations between drag, shear, heat transfer,
entropy, etc
01 p0005 A67-10281

Clausius-Duhem inequality in general

formulation of second law of thermodynamics 01 p0167 A67-10798

Maintainability diagnosis techniques and fields of application to electronic equipment, examining entropic methods, decreasing probability methods and linear analysis techniques 01 p0041 A67-11342

Nonsteady state gas flows with small entropy gradients corresponding to supersonic flight conditions 02 p0178 A67-11629

Shannon expression of information entropy measure and average uncertainty measure 02 p0203 A67-12168

Entropy defect and source function in gray atmosphere thermodynamics 03 p0537 A67-14314

Minimum average conditional entropy for minimum probability of error in statistical decision theory 04 p0644 A67-14885

Entropy and available energy in operation of gas turbine, considering thermodynamic efficiency, heat balance and available energy balance 05 p0873 A67-16742

Optimal one-dimensional truncated signal distribution ensuring optimal capacity or differential entropy 06 p0976 A67-18219

Inviscid linearized perturbations of supersonic entropy layers analyzed, using approximating partial differential equations by simultaneous ordinary differential equations [AIAA PAPER 67-6] 06 p0938 A67-18249

Tests at Mach 8 on cone, analyzing effect of roughness elements and variable entropy on transition and heat transfer distribution [AIAA PAPER 67-132] 06 p0940 A67-18357

Perfect thermodynamic vapor concepts and application to power conversion cycles 07 p1268 A67-19367

Classical macroscopic thermodynamics including entropy, equilibrium, accessibility, internal energy, absolute temperature, etc 07 p1268 A67-20277

Newcomb entropy method extended to stability analysis of plasma in zero magnetic field 08 p1362 A67-21144

Bronchial tube diameter makes possible alveolar ventilation with minimum metabolism or entropy production in musculature 09 p1454 A67-21986

Principle of maximum entropy and application in reliability estimation of aircraft structures 10 p1726 A67-23730

Entropy function relationship to properties of pure metals, noting correlation with lattice parameters at 298 degrees K 11 p1805 A67-24360

Entropy functional characterization of equilibrium and stability properties of plasma configuration 12 p1977 A67-26227

Nonequilibrium processes, analyzing required number of additional conditions and region of applicability of most probable distribution function, noting relation to Boltzmann equation 13 p2100 A67-26954

Quasi-invariance and ergodicity in binary sequence space with respect to discrete groups of Bernoulli schemes, noting finite entropy distance formulation of measure equivalence 14 p2343 A67-28502

Entropy of sequence Y obtained from coded sequence of random variables X 14 p2292 A67-28935

Entropy applied to theory of fuel cells, noting effect of operating temperature 14 p2252 A67-29018

Optimal one-dimensional truncated signal distribution ensuring optimal capacity or differential entropy 16 p2643 A67-30485

Nonequilibrium flow relation to flow in thermal balance, describing irreversible processes in terms of entropy source field and relaxation resistance 16 p2662 A67-31467

Relativistic generalization of Bernoulli equation from three-dimensional vector analysis of acoustic and entropy waves 18 p3084 A67-33422

Superposition approximation for dense gases and liquids equilibrium theory, using phase-space distribution functions from maximization of information entropy 18 p3078 A67-33669

Symmetry removal from linear relations between forces and fluxes, concluding that fading memory in viscoelastic materials results from irreversible entropy 18 p3159 A67-34005

Theory of available potential energy and rate of change and variational approach to atmospheric energetics 18 p3074 A67-34096

Existence of entropy as consequence of asymptotic stability 18 p3160 A67-34285

Entropy and free energy functionals for collisionless plasma at equilibrium in adiabatic magnetic field 19 p3298 A67-35731

Partial molal entropies of doubly ionized aqueous Zn, Cd and mercurous and mercuric ions calculated, using literature data 20 p3376 A67-36792

Weakly interacting system statistical mechanics relation to macroscopic thermodynamic description, deriving entropy and absolute temperature 20 p3484 A67-36835

Entropy and specific heat of superconductor in mixed state calculated using cellular model of vortex 21 p3680 A67-38349

Thermodynamic interpretation for Cauchy elasticity, showing formulation of constitutive equations in continua theories 21 p3733 A67-39085

Surrounded atom model for thermodynamic enthalpy and entropy characteristics of mixing in liquid binary alloys 21 p3733 A67-39105

Relation between entropy flux and heat flux using entropy inequality and natural invariance principle for materials with fading memory 22 p3918 A67-39742

Extraterrestrial life detection studied from knowledge of major and trace components of atmospheres 23 p3944 A67-40999

Statistical entropy of nonequilibrium plasma assuming binary correlation functions, obtaining distribution function equation 24 p4196 A67-42158

Correlation between entropy of envelope fluctuation of UHF radio signal and corresponding thermodynamic stability of tropospheric common volume 24 p4124 A67-42810

ENVIRONMENT

S EXTRATERRESTRIAL ENVIRONMENT

S FRICTIONLESS ENVIRONMENT

S HIGH ALTITUDE ENVIRONMENT

S HIGH GRAVITY ENVIRONMENT

S HIGH TEMPERATURE ENVIRONMENT

S LOW TEMPERATURE ENVIRONMENT

S LUNAR ENVIRONMENT

S PLANETARY ENVIRONMENT

S ROTATING ENVIRONMENT

S SPACE ENVIRONMENT

S SPACECRAFT ENVIRONMENT

S THERMAL ENVIRONMENT

ENVIRONMENT MODEL

Atmosphere of Mars studied using three models generated to show high, mean and low density compositions to account for gravitational and magnetic fields 22 p3887 A67-40140

Trapped radiation levels via AP1-5 and AE1-3 model environments noting long term effects 23 p4061 A67-41517

ENVIRONMENT SIMULATION

SA SPACE SIMULATION

Crew performance evaluation via behavioral and psychophysiological tests in Lunex II simulated lunar mobile laboratory 01 p0017 A67-11392

Hybrid computer simulation of reentry guidance for lifting vehicle, noting compatibility of temperature rate flight control system with other vehicle controls 01 p0051 A67-11438

Energy-exchange simulation in artificial three-component ecological system 02 p0188 A67-12327

Reentry simulation, discussing aerodynamic and thermodynamic parameters, heat transfer and simulation accuracy 02 p0335 A67-12415

Test stand simulating high intensity heating processes which occur in combustion chambers of rocket and jet engines 02 p0231 A67-12440

Wind tunnel testing of hypersonic vehicles with complete simulation of entire hypersonic environment is not yet possible 03 p0396 A67-13794

Second and third stage separation for ELDO A simulated in vacuum test 04 p0595 A67-14540

Cryogenic pumping capability of liquid helium cooled plate in supersonic flow field at simulated high altitude 04 p0606 A67-14999

McDonnell Martlan Environmental Simulation Facility, analyzing sand and dust storm behavior at low pressures 07 p1248 A67-19386

Space environment simulation noting

various testing facilities for space equipment 07 p1163 A67-19534

Effect on human performance of variations from true values in simulation of extraterrestrial visual environment [AIAA PAPER 67-251] 07 p1166 A67-20069

Graphite thermochemical response tested in simulated environment for use as thermal shield for hypersonic reentry vehicles [AIAA PAPER 65-643] 08 p1426 A67-20561

Information processing requirements for command systems, using particular form of simulation of system information environment 08 p1299 A67-20686

Hot corrosion of aircraft gas turbine alloys operating in marine environment reproduced in laboratory test, analyzing nature of attack 11 p1804 A67-23918

Design, tests, operation and limitations of Apollo man-rated environmental control system simulation 11 p1748 A67-24340

First order factors affecting driver ability to safely control typical lunar vehicle through simulated mission profile over representative terrain [SMPTE PAPER 101-54] 12 p1920 A67-25469

Laboratory techniques for utilization of shock synthesizer/analyzer 12 p1942 A67-25693

In-space visual environment simulation, discussing photometric and geometric requirements, solar illumination characteristics and effects on human performance 12 p1922 A67-25700

Space environment simulation facility for thermal control coatings to study synergistic and healing effects 12 p1924 A67-25711

JPL solar simulator design, fabrication and performance 12 p1925 A67-25733

Photometric investigations of simulated lunar surfaces confirm high porosity and low albedo without postulating necessity for fine dust layer 12 p2003 A67-25740

In situ measurements of diffuse hemispherical spectral reflectance of thermal control coatings irradiated in vacuo with various combinations [AIAA PAPER 67-342] 12 p1959 A67-26056

Computer processed air traffic control automatic weather data collection and forecasting 13 p2153 A67-26665

Flight simulators for present and future aircraft 13 p2090 A67-27263

Simulation of magnetospheric effects for possible application to ionospheric probes 14 p2294 A67-29035

NASA and USAF experiment on mans contribution to trace contaminants in space cabin simulator at 760 mm of Hg 15 p2430 A67-29278

Environmental conditions effect on engineering systems, considering vibration, climatic, pressure, radiation, corrosion, dust penetration, etc 15 p2492 A67-29502

Oxidation resistant-coated refractory alloy systems for use on reentry vehicles 15 p2466 A67-29537

Elastomeric materials thermostability in simulated spacecraft environment tested to obtain ignition point values 15 p2466 A67-29545

Refractory material as component of silicate binder having stable optical and physical properties under simulated space conditions 15 p2506 A67-29547

Thermal control materials for spacecraft, considering UV spectral distribution, radiation energy and flux, oxygen bleaching, etc 15 p2579 A67-29552

Possible degradation effects produced in uncovered and covered N/P silicon solar cells by simulated micrometeoroid exposure 15 p2423 A67-30219

In-flight simulation of fog for pilot training noting heads-up optical viewing system, daylight backscatter, photographic method, etc [AIAA PAPER 67-386] 15 p2468 A67-30354

System engineering approach to commercial aircraft crew requirements [AIAA PAPER 67-399] 15 p2433 A67-30366

Space environment simulator of CNES in France describing reproduction of low pressure atmosphere, heat sink, solar and planetary radiation, etc 16 p2654 A67-30675

Evaluation of relative scientific effectiveness of various lunar exploration programs through analysis of results from hypothetical missions to selected earth-analog sites 16 p2747 A67-30991

Manrating of space environment
 simulators, emphasizing integration of
 physical facility requirements and operation
 procedure to provide
 safety 17 p2807 A67-31960
 Lunar environment simulation test bed,
 noting lunar gravity effect on astronaut
 performance 17 p2832 A67-32003
 Space pressure and temperature
 environment simulation facility for liquid
 rocket space-ignition reliability testing
 [AIAA PAPER 87-428] 18 p3112 A67-33912
 Environmental stress use in conjunction
 with simulation testing 18 p3020 A67-34112
 Human performance relation research
 relationship with aerospace mission oriented
 simulation studies, discussing methodological
 resolution and limitation 18 p2994 A67-34341
 Interactionist models of human
 performance in complex system or formal
 work organization, discussing
 multidimensional models 18 p2994 A67-34654
 Automatic life-support system tried on
 leeches for space
 applications 19 p3180 A67-35248
 Interplanetary space environment effect
 on surface thermal radiative properties,
 noting results of exposure to simulated solar
 plasma, solar UV, solar wind,
 etc 19 p3249 A67-35748
 Data representing monopole antenna
 voltage breakdown in simulated Mars and
 Venus atmospheres 19 p3197 A67-35829
 Second and third stage separation for
 ELDO A simulated in vacuum
 test 20 p3413 A67-36413
 Analytical and simulation procedure for
 determining environment induced errors in
 missile guidance 20 p3481 A67-36605
 Coil and dipole systems for magnetic
 testing of large
 spacecraft 20 p3415 A67-36612
 Computer program for reproducing
 operational conditions and simulating
 environment in which weapons system
 operates 20 p3416 A67-36765
 Plasma diagnostic measurement simulation,
 considering electromotive effect from
 satellite motion through geomagnetic
 field 20 p3418 A67-37428
 Black and white surface coating materials
 exposed to simulated solar radiation in
 vacuum, noting deterioration of white
 coatings 21 p3650 A67-37960
 Electronic equipment in space booster,
 considering test methods, environment
 simulation and electronic
 packaging 21 p3592 A67-38229
 Automatic satellite-checkout system for
 use under simulated space environment and
 stress conditions 22 p3778 A67-39192
 Environmental simulation for aerospace
 vehicle, discussing vibration, shock and high
 temperature testing and space and nuclear
 radiation simulation 22 p3781 A67-40343
 High emittance coatings radiation
 characteristics investigated for space
 applications, considering thickness effect on
 high temperature emittance and space
 environment effect at moderate
 temperatures
 [ASM PAPER C6-4.3] 23 p4020 A67-41404
 Contaminant concentration due to human
 habitation of space cabin simulator at 258
 mm Hg and oxygen atmosphere
 environment 23 p3964 A67-41559
 Anesthetized dogs subjected to near
 vacuum condition before and after clinical
 death, comparing data of venous and arterial
 pressure 23 p3952 A67-41572
 Determination of energy, water and
 protein requirements of man under
 simulated aerospace
 conditions 23 p3952 A67-41573
 Reactions of animals exposed to pure
 oxygen space cabin atmosphere for 235 days,
 noting no systematic
 toxicity 23 p3952 A67-41574
 Oxygen consumption rate during
 ambulatory lunar surface exploration,
 describing lunar
 simulator 23 p3966 A67-41597
 Optimum cooling in ventilated
 impermeable clothing using ambient air over
 range of simulated physiological
 activity 23 p3967 A67-41604
 Biomedical safety monitoring
 instrumentation for Lunar Module oxygen
 filled internal environment
 simulator 23 p3969 A67-41640
 Vehicle volume and design criteria for

manned lunar roving vehicles investigated
 by evaluating subjects performance under
 prolonged simulated lunar
 environment 23 p3970 A67-41658
 Trace contaminant experiment for
 studying effect of hyperoxic environment at
 high total pressure on human blood
 constituents 23 p3960 A67-41703
 Low gravity slosh simulation parameters
 and scaling law used to extrapolate data to
 full scale spacecraft
 systems 24 p4141 A67-42032
 Martian sand and dust storms simulation
 and abrasive effects on spacecraft surface
 coatings, noting similarity with Earth
 deserts 24 p4227 A67-42038
 Optimum solar simulator and design of
 thermal vacuum chamber around
 it 24 p4138 A67-42042
 Manned testing of EVA equipment in
 simulated space environment, emphasizing
 crewman ingress and egress and mission
 objectives 24 p4115 A67-42049
 Cosmonaut physiological reactions during
 simulated space environment exposure
 outside Voskhod II
 spacecraft 24 p4113 A67-42054
 Lunar gravity, reduced pressure and suit
 encumbrance effects examined in lunar
 surface environment simulation test bed,
 assessing astronaut performance
 [AIAA PAPER 87-866] 24 p4117 A67-42989
 Scaling laws and hydrodynamic model
 design techniques for high fidelity
 underwater simulation of zero and partial-g
 environments for manned space activities
 [AIAA PAPER 87-925] 24 p4140 A67-43021
ENVIRONMENTAL CHAMBER
 Structural design of large space chambers,
 examining outgassing rate and thermal
 stress in material
 selection 02 p0228 A67-11839
 Physical simulation design of Martian
 surface environment in form of physically
 enclosed environmental
 chamber 02 p0230 A67-12350
 Vacuum chambers operating at larger
 dynamic gas loads at lower pressure by
 means of ions, titanium sublimation and
 liquid nitrogen cryogenic
 pumping 04 p0598 A67-15174
 Low pressure environmental chamber for
 estimation of gas exchange ratio during
 exposure of animals under controlled
 conditions
 [ASME PAPER 66-WA/HT-52] 04 p0599 A67-15438
 Large space environmental simulation
 chamber design problems arising due to
 man-rated feature
 Gantry white rooms at Cape
 Kennedy 07 p1167 A67-20284
 Man-rated space simulation facility,
 emphasizing checkout and qualification of
 systems 12 p1921 A67-25689
 Cryopumps incorporated into liquid N
 shrouds for small space simulation
 chambers 12 p1900 A67-25710
 Two 15-day experiments of three subjects
 performing work-rest cycles in isolation
 chamber studying psychological functions,
 cardiovascular system, etc 16 p2613 A67-30912
 Prolonged confinement in small chambers
 effect on biodynamic processes of walking
 and other movements in special
 positions 16 p2613 A67-30914
 Human reaction to intermittent photic
 stimulation in environmental chamber under
 IFR conditions 17 p2807 A67-31966
 Rescue teams for manned testing in
 environmental chamber for Gemini
 spacecraft noting personnel, chamber and
 personal equipment, test operations and
 rescue function and drill 17 p2807 A67-32598
 Automated system for growth and analysis
 of bacterial colonies using environmental
 chamber and computer controlled flying-spot
 scanner 20 p3453 A67-37598
 Comparative pathology of animals
 continuously exposed to varied
 concentrations of carbon tetrachloride vapor
 in altitude chamber 21 p3573 A67-38070
 Space cabin environmental changes studied
 for susceptibility of mice to viral
 infection 21 p3574 A67-38080
 Multiphase metabolimeter closed circuit
 system with servo-driven volume meter for
 animal oxygen consumption in gaseous
 artificial environments 23 p3999 A67-41088
 Conversion of solar-thermal to electrical
 energy by capacitance-change pumping of

thermoelectric thin films, noting space
 environmental chamber
 tests 24 p4108 A67-42555
ENVIRONMENTAL CONTROL
SA CLEAN ROOM
 Straight edge fence design for control of
 radar site environment from clutter return,
 pattern interference, tracking errors and
 high power hazard to
 personnel 03 p0396 A67-13853
 Waste management and physiological
 response to substandard hygiene under
 controlled environmental
 conditions 03 p0386 A67-14289
 Environmental control and closed
 ecological systems, discussing control of
 atmosphere, temperature, food, water and
 waste, instrumentation, terrestrial
 applications, SNAP, etc 04 p0564 A67-15667
 Vacuum deposition of thin films, noting
 importance of low pressure environment,
 with attention to diffusion and ion
 pumps 04 p0631 A67-15994
 Gemini carbon dioxide sensor for
 monitoring in closed loop breathing system
 useful for many gas
 measurements 05 p0806 A67-16549
 Coating and embedding techniques for
 environmental protection of printed circuit
 assemblies 08 p1335 A67-20749
 Aerojet Carbothermal Process for oxygen
 manufacture from lunar resources,
 discussing experimental results from
 research operations 08 p1316 A67-21092
 Impurity free CsF effect on work function
 of tungsten surface, discussing amount of
 impurities, type and
 control 09 p1450 A67-22354
 Sterilization environment effects on
 structural systems design for interplanetary
 spacecraft 10 p1714 A67-23758
 Clean room techniques for Apollo/Saturn
 Instrument Unit, noting that environmental
 and guidance systems parts must be
 supercleaned to qualify for man-rated space
 vehicle 11 p1773 A67-24938
 TV subsystem of Surveyor I, discussing
 operation-design constraints, camera
 configuration, video sequence, etc
 [SMPT PAPER 101-43] 12 p1904 A67-25461
 Large and intermediate ultraclean vacuum
 chambers converted to sputter-ion and
 titanium sublimation
 pumping 12 p1921 A67-25691
 Thermal radiation characteristics of
 spacecraft temperature control louvers in
 solar space environment, discussing specular
 reflection
 [AIAA PAPER 87-307] 12 p2036 A67-26022
 Laboratory test program to study
 problems associated with flight instrument
 parameter measurement 12 p1947 A67-26187
 DC-9 environmental control design and
 first year service experiences
 [AIAA PAPER 87-407] 15 p2423 A67-30374
 Environmental adjustment factors for
 operating and nonoperating failure
 rates 15 p2495 A67-30417
 Environmental control for high
 performance military aircraft covering air
 conditioning, temperature and pressure
 control and oxygen supply
 systems 21 p3572 A67-39130
 Automatic control of Block II Apollo ECS
 space radiator system, deriving linearized
 control equations for
 subsystem 22 p3916 A67-39174
 Environmentally induced delayed failure
 process incubation period of precracked
 steel from film formation 22 p3822 A67-40060
 Metabolic depression in animals exposed
 to air after living in helium-oxygen
 environment, suggesting denitrogenation
 period effect 23 p3944 A67-40823
 Comparative microbial contamination
 levels in clean rooms used for assembly and
 test of lunar spacecraft 23 p3961 A67-40851
 Clean room justification guidelines
 including contracts, proposals, work loads,
 environmental requirements, equipment and
 personnel selection 23 p3987 A67-40855
 Potential contamination of equipment by
 primate passenger during 30-day earth orbit,
 studying skin, body particulate matter and
 indigenous microflora 23 p3944 A67-40856
 Human microbial shedding using sterile
 stainless steel shedding chamber, discussing
 clean room clothing reducing shed
 rate 23 p3962 A67-40857
 Contamination control for Titan IIIB
 program, discussing MAPS, membrane filter

- technique, environment cleanliness control and particulate spectra 23 p3938 A67-41499
- Circadian oscillations of deep body temperature and heart rate in ambulatory primate in controlled environment 23 p3951 A67-41554
- Energy expenditure in space suits studied for controlled cooling during high work rates 23 p3965 A67-41562
- Indigenous biological flora of human male subjects in closed environment and effects of diet on fecal flora 23 p3957 A67-41642
- Vibrophonocardiograph developed for use in shirt-sleeve flight environment, previous design miniaturized without sacrificing performance characteristics 23 p3970 A67-41661
- Isolation effects in constant environment on cycles of physiological functions and performance levels of man 23 p3959 A67-41697
- Environmental control and life support system design for NASA Biosatellite program, discussing experimental results [SAE PAPER 670839] 24 p4114 A67-41995
- Boeing 20-ft solar simulator alignment, calibration, cleanliness, optical system, xenon light sources and vacuum system 24 p4139 A67-42045
- Manned chamber testing of lunar module environmental control subsystem, describing equipment and support systems 24 p4139 A67-42050
- ### ENVIRONMENTAL INDEX
- Manned and unmanned spacecraft structures, discussing environmental and functional requirements, influence of vibration and pressurized gas containment [SAE PAPER 660672] 01 p0153 A67-10579
- Design, equipment and techniques of electronic packaging in Titan III program, stressing environmental levels and safety factors 21 p3595 A67-38335
- ### ENVIRONMENTAL LABORATORY
- Environmental stress use in conjunction with simulation testing 18 p3020 A67-34112
- Operational requirements for modern space environment test laboratory covering thermal vacuum, shock, vibration and combined testing 22 p3781 A67-40401
- ### ENVIRONMENTAL SCIENCE
- Remote sensing of environment - USAF and USN Symposium, University of Michigan, Ann Arbor, April 1966 01 p0057 A67-10307
- Requirements for radiation detection and measuring systems in aerospace environment, considering safety, design, circuit techniques, etc 02 p0220 A67-12208
- Naval solid propellant rocket engine structural design, configurations, handling, storage and adaptation to environmental conditions 08 p1375 A67-20873
- Book on environmental biology covering effects of temperature, radiant energy, acceleration and gravity, etc 11 p1747 A67-24233
- Environmental Sciences Institute - Conference, Washington, D.C., April 1967, Volume I 12 p1920 A67-25676
- Environmental operations analysis function, discussing data accumulation, storage and retrieval 12 p1921 A67-25678
- IES conference, Washington, D.C., April 1967, Volume 2, covering space and earth environments, shock and vibration, instrumentation and acoustics IES Conference, Washington, D.C., April 1967, Volume 2, covering space and earth environments, 12 p1922 A67-25705
- Environmental conditions effect on engineering systems, considering vibration, climatics, pressure, radiation, corrosion, dust penetration, etc 15 p2492 A67-29502
- Environmental prediction using orbital sensors [AAS PAPER 67-104] 15 p2478 A67-29959
- Environmental technology and extrapolation into future, noting government role 17 p2834 A67-32592
- Geophysical instrumentation for environmental studies, elucidating atmospheric and near-space mechanisms, geodesy, gravimetry, etc 17 p2860 A67-32692
- Predicting effects produced by environmental interactions with various components 18 p3005 A67-34650
- Inner zone trapped electron flux measurements by satellite indicating natural environment emergence from Starfish remnants 19 p3216 A67-35186
- Space program applications for environmental sciences and operations including oceanography, seismology, wind direction, etc 19 p3253 A67-35647
- Terrestrial environment guideline documents providing natural environment extremes, means and cycles for spacecraft development 22 p3829 A67-39927
- RCA papers on environmental sciences 22 p3781 A67-40400
- Solar system environment, discussing solar magnetic field, flare flux and energy spectrum, interplanetary plasma and radiation, asteroids, meteoroids and comets 22 p3889 A67-40407
- Basic guidelines for fastener system selection for use in exotic environment with unusual stress condition 24 p4160 A67-42077
- Materials and structural concepts for design of entry systems, discussing environmental factors, reuse potential and high reliability [AIAA PAPER 67-805] 24 p4251 A67-42964
- ### ENVIRONMENTAL SURVEY SATELLITE /ESSA/
- ### S ESSA SATELLITE
- ### ENVIRONMENTAL TEMPERATURE
- Relation between skin temperature and environmental air supply temperatures in fixed air-ventilated clothing assembly 02 p0188 A67-12346
- Correlation between increased performance demands and cost of lightweight airframe structures [SAE PAPER 660674] 04 p0716 A67-15783
- Packaging failures in reentry/recoverable aerospace equipment due to design deficiencies in parts, materials and/or processes associated with physical hardware 05 p0779 A67-17468
- ### ENVIRONMENTAL TESTING
- ### SA MATERIAL TESTING
- Effect of plasma outside cylindrical plasma column on dipole resonance, noting increased oscillation frequency and coupling of resonances 01 p0123 A67-10459
- Changing environmental condition effects on spacecraft structure from launch through orbit to entry and recovery [SAE PAPER 660680] 01 p0154 A67-10584
- Environmental simulation techniques to supplement facility capabilities for environmental test program of Lunar Excursion Module /LEM/ [SAE PAPER 660682] 01 p0049 A67-10587
- Environmental structural testing capabilities for orbital and space vehicles [SAE PAPER 660685] 01 p0154 A67-10589
- Flight environment effect on lubrication requirements of Pratt-Whitney SST engine [SAE PAPER 660711] 01 p0013 A67-10601
- Long wave spacecraft antenna design, deployment and stabilization, noting environmental effects such as thermal expansion, solar pressure, etc [AIAA PAPER 66-848] 02 p0221 A67-12258
- Prolonged autonomous existence of humans in space suits, discussing maintenance of heat balance by physiological perspiration 02 p0187 A67-12324
- Directory of RCA environmental test facilities 03 p0396 A67-13635
- Heat, noise, vibration and acceleration simulation to determine beneficial effects of boost and reentry stresses on humans 03 p0366 A67-14389
- Environmental test program for third stage of European launch vehicle 04 p0595 A67-14570
- Space environment simulation testing as essential part of contemporary space flight development programs [AIAA PAPER 65-474] 04 p0598 A67-15229
- Environment-simulation testing effectiveness for unmanned space systems 04 p0598 A67-15230
- Thermal similarity study of models in space environmental chambers for deducing characteristics of typical space vehicle element [AIAA PAPER 66-460] 04 p0724 A67-15247
- Microwave and thermal vacuum testing to demonstrate design maturity of LEM rendezvous radar during simulated mission 04 p0576 A67-15397
- Long term effects of oxygen environment on rat colony at 210 mm Hg absolute showed no significant physiological changes and no difficulty in readaptation 05 p0755 A67-16285
- Arnold Center advanced ground test facilities for rocket and space vehicle

- environmental testing 05 p0788 A67-16617
- Arnold Engineering Development Center, discussing aircraft and space vehicle environmental simulation and testing 05 p0788 A67-16619
- Apollo computer design mechanical packaging, implementing heat and vibration model to conduct thermal vibration and sealing tests 05 p0814 A67-17460
- VTOL test bed for ground effects test, noting environmental characteristics, configuration dependence of lift and hot gas ingestion [AIAA PAPER 67-181] 06 p0980 A67-18297
- Shock and vibration test specifications contrasting approaches requiring exact duplication of environment with those simulating damaging characteristics 06 p0981 A67-18366
- Aircraft equipment retrieval after long term storage for periods of up to 23 years under jungle, desert and arctic environment, discussing sealing and hydraulic systems [AIAA PAPER 67-185] 06 p0951 A67-18487
- Test program to evaluate characteristics of existing Atlas engine boots in flight environment and provide parameters for design change [AIAA PAPER 67-277] 07 p1241 A67-20054
- Environmental and experimental testing of electronic systems component reliability 08 p1302 A67-20906
- Cold starting and service test evaluation of SAE 10W30 aircraft engine oil [SAE PAPER 670249] 11 p1811 A67-23982
- Shock spectrum synthesis and analysis as environmental test technique compared with time function shock testing 12 p2030 A67-25681
- Field testing of self-powered recorder for vibration data in environmental studies 12 p1942 A67-25682
- Plastic foam pattern technique for producing vibration and shock fixtures 12 p1949 A67-25687
- Portable self-powered magnetic tape recorder for gathering data on vibration, temperature and shock on ground and in-flight aircraft 12 p1942 A67-25688
- Allison T63 engine sand and dust tolerance development and field experience [SAE PAPER 670334] 12 p1990 A67-25875
- Pegasus thermal control lower system characteristics determined by environmental chamber testing, noting testing configuration [AIAA PAPER 67-308] 12 p2036 A67-26023
- Temperature and environmental effects on mechanical behavior of metals 13 p2132 A67-26697
- Man rating requirements of space environment simulation laboratory consisting of two large chambers with floors which can be cooled by liquid nitrogen down to 92 degrees K 13 p2090 A67-26841
- Lubricant selection for lunar missions and manned spacecraft based on compatibility with oxygen-rich environment, propellant, anodic coatings and sliding friction behavior in vacuum [ASLE PAPER 66AM-7A2] 13 p2123 A67-27100
- Thickness, material type, environmental and surface emittance of radiation shield effects on thermal performance of multilayer insulation system 13 p2228 A67-27660
- Humidity, temperature, contamination and disconnection effects on gasket and grease seals for extended space mission computer connectors 15 p2442 A67-29182
- Electronic checkout, environmental qualification and integration of OGO by spacecraft simulator and performance analysis system 16 p2654 A67-30639
- Airborne long focal length photographic system environmental effects studied with Cassegrainian type Maksutov telescope 16 p2678 A67-31793
- Gas turbine environmental testing, measuring emulsified fuel flow, direct burning effects of JP-4 fuel on extended engine operation, etc [SAE PAPER 670367] 18 p3111 A67-33567
- NERVA radiation effects tests at cryogenic temperatures [AIAA PAPER 67-477] 18 p3076 A67-33947
- Design, fabrication and testing to enable optical systems to resist space environmental degradation 20 p3445 A67-36568
- Helium-oxygen environment relation to

biological-thermal requirements of
spacecrew 20 p3374 A67-36582
Low temperature and irradiation
environment effects on mechanical
properties of engineering
materials 20 p3418 A67-37532
Electronic instruments testing to ascertain
environmental conditions for perfect
operation, storage and
transportation 21 p3589 A67-37920
Isolation of *Acinetobacter anitratus* from
subject and room area during spacecraft
environmental tests 21 p3573 A67-38072
Lithium and ammonia MPD arc thrusters
tests in low environmental pressure
[AIAA PAPER 67-685] 21 p3692 A67-38716
Aircraft skin friction balance components
for hostile environments noting system
design 22 p3795 A67-39188
High performance engineering
thermoplastic /Polymer 360/ mechanical and
electrical properties and environmental
factors effects 22 p3825 A67-39858
Environmental factors effect on stability
of high performance
polycarbonate 22 p3825 A67-39859
Gaseous environment influence on fatigue
fracture mode in quenched and tempered
ultrahigh strength steel investigated by
fractographic analysis 22 p3821 A67-40051
Superoorbital reentry environments,
discussing materials, test environments and
heat factors 22 p3919 A67-40383
Test planning and decision making in
environmental testing approached from
program formulation involving resources and
equipment, degree of simulation and
optimum levels 22 p3781 A67-40402
Air damping effect on structural fatigue
failure evaluated mathematically as power
function relating stress to number of
cycles 22 p3915 A67-40405
Environmental test data acquisition and
processing, noting pretest requirements and
relative merits of analog and digital
computer methods 22 p3765 A67-40406
Performance of electromechanical pressure
transducers tested environmentally for static
and dynamic temperature, steady
acceleration and vibrational
acceleration 22 p3809 A67-40464
Cockpit environment thermal stress effect
on psychological test performance and
biomedical parameters 22 p3753 A67-40539
Ti stress corrosion in nitrogen tetroxide,
detailing investigative techniques
[ASM PAPER C-6.22] 23 p4020 A67-41409
Clevite thin film CdS solar cell fabricated
with two different substrate structures
noting design changes, improvements and
performance characteristics 23 p3937 A67-41494
Environmental testing of thin film solar
cells, studying long term thermal cycling
effect on CdS solar cell 23 p3937 A67-41496
Flexible integrated deployable solar cell
array design, environmental testing and
performance prediction 23 p3939 A67-41511
Space cabin simulator tests in helium-
oxygen mixtures at various total pressures
and ratios of oxygen to
diluent 23 p3969 A67-41646
Metal fatigue in controlled gaseous
environment stressing test variables effects
on crack propagation
mechanism 24 p4248 A67-41945
Electronic equipment components
unreliability in guided weapon systems,
discussing packaging, environmental
conditions and customer-manufacturer
relations 24 p4161 A67-42479
Small scale Rankine cycle power
conversion system using potassium working
fluid under environmental, RF interference
and ground performance
tests 24 p4102 A67-42491
Military flight clothing tested in actual
survival conditions for ability of subject to
withstand moderate sea water environment
[AIAA PAPER 67-968] 24 p4118 A67-43046
ENZYME
SA CAROTENE
SA OXIDASE
Pituitary enzymes hydrolyzing aminoacyl
arylamides and relation to
peptidases 01 p0015 A67-10488
Enzyme-isoenzyme changes in rhesus
monkeys under gamma
irradiation 07 p1134 A67-19860
Luciferase denaturation prevention using
vacuum and molecular sieve during

sterilization temperature
exposure 10 p1597 A67-22928
ENZYME ACTIVITY
Metabolic reaction of deer mice to
temperature and altitude, analyzing various
enzyme systems 04 p0561 A67-14593
Correlation of changes in serum enzyme
behavior in rats with pathological injuries
due to short transverse
decelerations 06 p0953 A67-17996
GUT, GPT, MDH, LDH, SDH and aldolase
serum enzyme activity in dogs subjected to
moderate impact 06 p0953 A67-17997
Enzymatic activity and inhibition, thermal
stability and electrophoretic properties of
induced and constitutive acid phosphatases
of *Euglena gracilis* 10 p1598 A67-23397
Molecular sizes of diphosphopyridine
nucleotide linked dehydrogenases of
representative animal, plant and microbial
species 11 p1750 A67-24784
Enzyme activity in erythrocytes when
MICORENE is used to prevent death from
high altitude hypoxia 14 p2254 A67-28212
Rapid assay for thymidylate synthetase as
specific and sensitive measure of enzyme
activity 14 p2260 A67-28479
Exobiology and effect of physical factors
on microorganisms 15 p2427 A67-29117
Thiobarbituric acid reacted substance
reaction with ribonuclease may be possible
source of age pigment 15 p2433 A67-29296
Microbial numbers relation to phosphatase
activity in soil, discussing seasonal variation,
sterilization by irradiation and moisture
content 18 p2991 A67-33660
Pure oxygen effect on activity of
lysosomal aryl sulfatase in brain, liver and
liver tissue homogenates from
rats 18 p2992 A67-34719
Human natural immunity with respect to
substitution of *Chlorella* proteins for animal
proteins, studying lysozyme activity in saliva
and blood serum 20 p3368 A67-36269
Radio carbon dioxide fixation, glutamate
labeling and Krebs cycle in ribose-grown
Hydrogenomonas facilis 20 p3370 A67-36796
Autotrophic and heterotrophic carbon
dioxide fixation regulation in
Hydrogenomonas, discussing two Calvin cycle
enzymes 20 p3370 A67-36797
Organic phosphate shown as inhibitory
factor from *B. stearothermophilus* for
attachment of amino acids to transfer
RNA 20 p3370 A67-36798
Factors involved in use of thymine by
uninfected cells in metabolism of
Escherichia coli 20 p3370 A67-36799
Purification and properties of nicotine
oxidase suggest metalloflavoprotein having
riboflavin 5-phosphate 20 p3376 A67-37032
Lactic dehydrogenases of H4 and M4 type,
preparation and catalytic and enzymological
properties 20 p3377 A67-37159
Enzyme activity of light and heavy crude
ribosomal fractions in *Saccharomyces*
cerevisiae indicating subcellular sites of
lipid synthesis 21 p3573 A67-37919
Traumatic sickness in dogs due to high
gravity impact noting enzymatic activity
changes and immunizing
reaction 21 p3575 A67-38509
Protective effect of substrates against
ionizing radiation on enolase and lactic
dehydrogenase 24 p4111 A67-41841
[SAM-TR-66-264]
Histochemical investigation of effect of
hypothermia and hypobiosis on activity of
oxidizing tissue enzymes of carbohydrate,
amino acid, nucleotide and aliphatic
metabolism of rats 24 p4112 A67-41853
Spectrofluorimetric studies on active site
of alpha-chymotrypsin using anthraniloyl as
chromophore 24 p4119 A67-42865
EOR
S EARTH ORBITAL RENDEZVOUS
/EOR/
EPE-A
S EXPLORER XII SATELLITE
EPE-B
S EXPLORER XIV SATELLITE
EPHEMERIS
Improvement of orbital elements of comet
Grigg-Skjellerup, using all observations made
during previous
appearances 04 p0701 A67-15451
Data from Lunar Orbiter spacecraft used
to test validity of corrections to lunar
ephemeris reveals residual patterns
[JPL-TR-32-1087] 05 p0901 A67-17201
Surveillance of solar activity based on

optical observations of
satellites 10 p1606 A67-23222
Comet P/Wolf I motion perturbations of
six planets, searching ephemeris for
perihelion in August 1967 11 p1868 A67-25085
Astronomical almanac 1967 covering
chronology, solar and planetary data, time-
signal transmission, etc 14 p2385 A67-28146
Planetary masses, radii and orbital
element and astronomic unit determinations
from radar time delay and Doppler shift
measurements 15 p2556 A67-29871
Corrections to equinox and equator of
FK3 from meridian observations of Ceres,
Pallas, Juno and Vesta 15 p2557 A67-29873
Difference between ephemeris and
universal time based on observations of
lunar occultations 17 p2950 A67-33129
Data and orbit analysis supporting Navy
satellite Doppler system Tranet, discussing
editing and archiving of Doppler data and
orbital ephemerides
generation 18 p3003 A67-34245
Minor planets observational and
computational results /1964/, discussing
ephemeris volume 20 p3522 A67-36615
Orbital element periodic variations for
satellite motion about oblate planet with low
and moderate eccentricity 22 p3880 A67-39313
Spacecraft ephemeris, orbit compatibility
and scheduling in AAP mission
experiments 22 p3885 A67-39959
EPHEMERIS TIME
SA UNIVERSAL TIME
Meridian observation of Jupiter for planet
position determination, analyzing
discrepancies between ephemerides and
observations, noting random
error 11 p1868 A67-25087
Celestial mechanics and Dirac
hypothesis 15 p2563 A67-30123
U.S.S.R. astronomical almanac for
1970 21 p3703 A67-38200
Ephemeris time corrections /1900-1966/
with respect to UT after revision of Brown
lunar theory 22 p3881 A67-39516
Soviet ephemeris of minor planets for
1968 covering orbital elements, opposition
dates, time, etc 22 p3884 A67-39925
EPITAXIAL DEPOSITION
Epitaxial diffused integrated circuit
structure containing p-n-p and n-p-n
transistors 01 p0033 A67-10021
Epitaxial temperature for Si films vacuum
deposited on silicon as function of substrate
crystallographic orientation observed by low
energy electron diffraction
patterns 01 p0132 A67-10372
Induction heating contributions to solid
state technology including zone refining and
zone leveling, growth of metallic and
nonmetallic single crystals, thin film
production and epitaxial
growth 01 p0080 A67-10972
Simultaneous derivation of optical gain
factor and loss per unit length of series of
solution grown diffused GaAs injection
laser 01 p0138 A67-11072
Deposition conditions effect upon growth
and structure of evaporated and sputtered
films and significance in relation to
electrical, magnetic and mechanical
behavior 02 p0285 A67-11703
Interaction of crystalline film of one
substance growing on surface of second
substance, examining influence on film
structure 02 p0286 A67-11708
Kinetics of formation of thin continuous
films from isolated three-dimensional
nuclei 02 p0286 A67-11709
Surface structure effect of evaporation
deposited film and substrate crystal on
epitaxy of film studied by electron
diffraction and electron
microscope 02 p0286 A67-11710
Epitaxial deposition of Van Arkel
zirconium on sodium chloride and calcium
fluoride cleavages at various
temperatures 02 p0286 A67-11711
Epitaxy of semiconductor on insulating
monocrystalline base of corundum, noting
electronic characteristics of silicon
layers 02 p0294 A67-11755
Thermodynamics of epitaxial growth of
GaAs-Ge heterojunctions in closed tube
process 02 p0296 A67-11767
Solution grown epitaxial red light emitting
p-n junctions in GaP preparation, electrical
and optical properties, examining I-V
characteristics 02 p0297 A67-11876
Nucleation of epitaxial SiC on Si

surfaces 02 p0299 A67-11894
 DC and RF I-V characteristics, device fabrication and structure of epitaxial depletion mode n-type 02 p0218 A67-12103
 MOS-FET 02 p0218 A67-12103
 Single crystal transistor with metallic base, noting frequency, V-I and power characteristics, radiation resistance, etc 02 p0221 A67-12530
 Epitaxial transistor array on common heat sink with and without emitter series resistance, examining second breakdown mechanism 02 p0222 A67-12652
 Epitaxial growth and control of low-resistivity n-type silicon layers on p-type boron-doped substrates 03 p0494 A67-13485
 Carrier mobility and concentration in epitaxial silicon layers obtained by vacuum sublimation 03 p0498 A67-13869
 Epitaxial growth of SiC film on silicon substrate and electron diffraction analysis of crystal structure 04 p0675 A67-14762
 Temperature dependence of migration of double positioning boundaries during growth of gold films inside electron microscope 04 p0675 A67-14924
 Structural and magnetic properties of /111/ films of permalloy produced epitaxially on epitaxial /111/ Ag on mica 04 p0676 A67-14931
 Epitaxial gallium arsenide films prepared by vacuum evaporation of elements 04 p0678 A67-15124
 Thin film deposition techniques, presenting vacuum evaporation and sputtering 04 p0631 A67-15992
 Sputtered film deposition processes, investigating low pressure sputtered germanium films 04 p0631 A67-15995
 Impurity distribution in epitaxial films at film/ substrate interface after oxidation under different oxidation conditions for silicon planar devices 05 p0869 A67-17095
 Indium arsenide diode laser fabrication using liquid phase epitaxy, noting quantum efficiency 05 p0825 A67-17096
 Change in temperature conditions during growth of epitaxial germanium films from molecular beam in vacuum 06 p1046 A67-17551
 Effect of donor Zn and Cd additions and acceptor Se and Te additions on rate of growth and morphology of epitaxial GaAs films grown from gas phase by chemical reaction 06 p1047 A67-17552
 Structural changes in epitaxial CdS films grown on rock salt, mica and silver substrates analyzed by electron diffraction at various temperatures and values of electric field 06 p1047 A67-17599
 Performance of transferred electron oscillators produced by alloying Sn contacts on to epitaxial GaAs layers 06 p0971 A67-18225
 Semiconductor heterojunctions noting preparation, properties, measurement and results 06 p1053 A67-18756
 Vapor phase epitaxial deposition of n-type GaAs contact layers for Gunn effect X-band oscillators 07 p1153 A67-19609
 Gallium arsenide planar technology using starting material obtained by vapor growth, noting doped silicon dioxide technique 07 p1155 A67-19889
 Current mode second breakdown in epitaxial planar transistors, describing V-I behavior 07 p1156 A67-19897
 Gallium arsenide epitaxial film on germanium obtained by vapor phase transport techniques 08 p1368 A67-20726
 Optical and electrical properties of epitaxial and diffused GaAs injection lasers noting spectral characteristics, optical gain, current distribution, etc 08 p1338 A67-21289
 Elastic and inelastic lattice strain at oxide window edges determined from imperfections of n and p type 08 p1370 A67-21297
 Cut-off frequency, breakdown voltage and capacitance calculations for diffused junctions in thin epitaxial silicon layer for microwave diode design 09 p1556 A67-22206
 Crystal orientation effect on epitaxial growth gallium arsenide crystals for smooth laser junction 09 p1515 A67-22275
 Epitaxial gallium arsenide properties and preparation using arsenic trichloride 10 p1692 A67-23510
 Gallium arsenide epitaxial technology noting deposition rate and impurity profile, Hall mobility and morphology of

deposits 10 p1692 A67-23511
 Gallium arsenide characteristics and preparation noting epitaxial deposition and liquid phase, mobility, impurity and Hall effect data 10 p1692 A67-23512
 Pyramid formation in epitaxially deposited GaAs layers, postulating vapor-liquid-solid formation mechanism 10 p1692 A67-23513
 Chemical etching of dislocation and stacking fault structure of epitaxial GaAs, noting possible effect on electroluminescence 10 p1692 A67-23514
 Gunn effect oscillators constructed from epitaxially grown n-type GaAs on n-plus substrate to obtain CW oscillations with frequencies from 3 to 35 gc 10 p1615 A67-23530
 Epitaxial advantages over melt grown GaAs in construction of continuous wave and pulsed Gunn effect oscillators 10 p1616 A67-23531
 Statistical survey of CW transferred electron oscillators /Gunn diode/ made from epitaxial gallium arsenide 10 p1616 A67-23532
 Epitaxial GaAs Gunn effect oscillators, showing importance in high efficiency of preparation and method of contacting material and resonant cavity design 10 p1616 A67-23533
 Assessment of epitaxial gallium arsenide for use in Gunn effect devices from check slices on semiinsulating substrates 10 p1616 A67-23534
 Abrasion technique to improve Gunn oscillator performance using epitaxial GaAs, considering diode shape and contact structure 10 p1616 A67-23536
 Fabrication technique for planar gallium arsenide junction FET and properties 10 p1617 A67-23539
 Monolithic gallium arsenide tunnel diode construction with epitaxial layer grown on semi-insulating substrate 10 p1617 A67-23542
 Relationship between domain transit frequency and cavity controlled frequency of thin Gunn devices 11 p1759 A67-24130
 Preparation and properties of III-V compounds for radiative processes, discussing epitaxial deposition of GaAs into semi-insulating substrate for array of devices 11 p1847 A67-24736
 Epitaxial vapor growth of GaAs noting reduction of electron concentration and increase in electron mobility 11 p1848 A67-24746
 Rapid vapor phase growth of high resistivity GaP for electro-optic modulators, noting high electron mobility 11 p1848 A67-24747
 Specific resistance of semiconductor plates measured by change in effective loss component of toroidal coil 11 p1792 A67-24812
 Specific resistance of epitaxial layers on low resistance substrates measured, using opposing probe method 11 p1792 A67-24813
 InAs epitaxial layers grown on GaAs substrate investigated via sandwich method and electron diffraction 12 p1980 A67-25201
 UHF oscillations in GaAs thin epitaxial layers deposited on isolating substrates of same material 12 p1981 A67-25279
 Trap density is lower in epitaxially grown GaAs crystals than in crystals grown by either horizontal Bridgman /HB/ or floating zone /FZ/ technique 12 p1983 A67-25457
 Volt-ampere characteristics effect on thickness of contact materials of some heterojunctions and band structures obtained by epitaxial deposition 12 p1983 A67-25515
 Volt-ampere characteristics of diffused p-n junctions in epitaxial GaAsP film obtained by gas transport technique 12 p1984 A67-25519
 Electric conductivity, Hall effect and photoconductivity of epitaxial single crystal GaAs films obtained by gas transport method 12 p1984 A67-25521
 Crystal growing technology for application to semiconductor production noting methods, impurity control, etc 12 p1950 A67-26211
 Preferential epitaxial growth method for electrical element isolations in IC, noting no lattice defect effect on electrical characteristics of element 12 p1918 A67-26217
 Semiconductor device fabrication and operation, analyzing silicon, germanium, silicon carbide, InSb and GaAs 13 p2176 A67-26693
 Vacuum deposition techniques for

production of optical film materials for neutral density filters and sunglasses, discussing dielectric, metallic, reflecting and semitransparent films 13 p2158 A67-27076
 Single crystal transistor with metallic base, noting frequency, V-I and power characteristics, radiation resistance, etc 14 p2279 A67-28007
 Chemical etching examination of dislocations and stacking-fault structure of epitaxial gallium arsenic phosphide, considering doping level, growth rate and composition effects 14 p2366 A67-28421
 Misfit dislocations at diamond-sphalerite interface of thin epitaxial Ge layer deposited on GaAs 14 p2366 A67-28497
 Forward conduction characteristics of contacts between gold n-type silicon measured at different temperatures 14 p2373 A67-28925
 Epitaxial deposition of p-GaAs on n-GaAs noting dislocations, packing defect concentrations and V-I characteristics 15 p2533 A67-29317
 Polymorphism in IV-VI compounds induced by high pressure and thin film epitaxial growth 15 p2539 A67-29822
 YIG epitaxial growth condition on YAG and GdIG on YAG identified by X-ray, electron diffraction, microprobe and magneto-optic studies 15 p2539 A67-29824
 GaAs epitaxial layer in transistors with silicon nitride insulator surpasses silicon MOS device in power gain, frequency response and temperature range 15 p2455 A67-30391
 Preparation of doped and undoped epitaxial InAs with open tube vapor-phase transport system noting properties, temperature effects, electron mobilities, etc 17 p2911 A67-32194
 Fabrication and properties of p-n junction diodes, noting cut-off frequencies, junction characteristics, etc 17 p2826 A67-32620
 Twin orientation in epitaxial gallium arsenide, noting relation to stellite feature 17 p2922 A67-33065
 Epitaxial deposition of silicon on silicon substrates, discussing vapor and vacuum deposition, impurity distributions, layer thickness, etc 18 p3097 A67-33456
 Volt-ampere characteristics effect on thickness of contact materials of some heterojunctions and band structures obtained by epitaxial deposition 18 p3103 A67-34446
 Volt-ampere characteristics of diffused p-n junctions in epitaxial GaAsP film obtained by gas transport technique 18 p3103 A67-34450
 Electric conductivity, Hall effect and photoconductivity of epitaxial single crystal GaAs films obtained by gas transport method 18 p3103 A67-34452
 Silicon surface depth damage determination technique, with confirmation by Sirtl etching, oxidation and epitaxial deposition 18 p3103 A67-34565
 Surface hillock-like features in epitaxially grown gallium arsenide studied by X-ray diffraction topography 18 p3106 A67-34636
 Temperature dependence of electric conductivity and Hall effect in epitaxial layers of undoped and Fe-doped n-type GaAs samples 19 p3300 A67-34770
 Epitaxial growth of iron on tungsten field-emission points studied by field-emission microscopy 19 p3302 A67-34938
 Diffusion and epitaxial equipment controlling doping level in semiconductor integrated circuits, discussing fabrication materials and techniques 19 p3236 A67-35019
 Epitaxial gallium arsenide FET electrical characteristics, noting structural details and feasibility for use at microwave frequencies 19 p3196 A67-35629
 Soviet papers on physical properties of ultrapure metals and semiconductors, stressing epitaxial silicon layers 21 p3681 A67-38357
 Nature, distribution and causes of structural imperfections and dislocations in epitaxial Si layers with base layer orientation /111/ 21 p3681 A67-38359
 Temperature effect on diffusion coefficient of radioactive phosphorus in epitaxial Si layer 21 p3681 A67-38361
 Phosphorus concentration influence on epitaxial silicon layers growth and electrical characteristics 21 p3681 A67-38362

Gallium arsenide substrate treatment methods effects on autoeptaxial layer perfection 21 p3685 A67-38972

Epitaxial growth of gold on cadmium iodide surface studied with transmission electron microscopy, discussing diffraction patterns and substrates preparation 21 p3687 A67-39140

GaAs pulsed injection laser diode noting characteristics for room temperature operation 22 p3813 A67-39253

Hall coefficient and mobility measured for annealed polycrystalline and epitaxially grown gold, silver and copper films, discussing size effect 22 p3855 A67-39355

Chemical vapor deposition method to grow epitaxial YIG on YAG using high temperature hydrolysis oxidation at seed surface 22 p3860 A67-39896

Epitaxial silicon layers grown by electron microscopy with small quantities of gold, discussing possible growth mechanisms 23 p4036 A67-40656

Epitaxial growth of aluminum nitride on silicon carbide studied for influence of substrate temperature on perfection of crystal deposit 23 p4037 A67-40722

Heteroepitaxial Si films grown on sapphire studied for current voltage relations, finding space charge limited current 23 p4038 A67-40785

POXYDE

Boron fiber reinforced epoxy matrix plastic composite for application to aircraft structures 10 p1723 A67-23697

High modulus high strength reinforcements incorporated in epoxy matrix plastic composites for aerospace structural use 10 p1671 A67-23704

POXY RESIN

Strain gauges applied to epoxy laminates in liquid hydrogen insulation systems 01 p0072 A67-11107

Multidirectional reinforced epoxy plastics in testing mechanical response to stress 03 p0451 A67-13401

Mechanical properties of silicon carbide filament reinforced epoxy resin composites fabricated by plying monolayer tapes into unidirectional and balanced bidirectional composites 03 p0452 A67-13403

Beryllium wire reinforced epoxy-plastic composites in mechanical testing under various loadings 03 p0442 A67-13404

Carbonaceous fiber yarn reinforcements in epoxy-anhydride binder, noting moisture adsorption degradation of interlaminar shear values 03 p0452 A67-13405

Hollow-rib reinforced structure design from boron filament reinforced epoxy resin, describing fabrication equipment, techniques and test results 03 p0429 A67-13417

Refrigeration process of freezing stresses at ambient temperature improves elastic and photoelastic properties and renders them comparable to those of nonplasticized epoxy resins [ONERA-TP-367] 05 p0919 A67-16480

Molded aircraft wheels of epoxy resin reinforced with noncontinuous glass filaments 06 p1007 A67-18026

Optical resolution and configuration of trans-2, 3-epoxybutyric acid by brucine 07 p1137 A67-20015

Mechanical property correlation between high performance composites and cast epoxy resin data 08 p1344 A67-20423

Boron filament epoxy resin composites test program relative to mechanical design of reentry vehicle structure 08 p1345 A67-20424

Epoxy adhesive properties dependence on application variables according to test methods of MIL-A-8623 adhesive specification 09 p1523 A67-22525

Carbon fiber composite, noting incorporation into epoxy resin and inverse correlation of shear strength with fiber modulus 10 p1671 A67-23495

Epoxy casting resins as structural material in electronic industry, with tables of various hardener characteristics, viscosities, epoxy equivalents, etc 15 p2508 A67-29683

Photoelastoplastic method using creep and stress characteristics of epoxy resins under thermal cycle, discussing stress-strain behavior [SESA PAPER 1191] 18 p3141 A67-33886

Epoxy resins thermal degradation, discussing degradation in oxidizing atmospheres and vacuum differential

thermal analysis and hot-wire pyrolysis 19 p3248 A67-34994

Thermal stress analysis of epoxy encapsulants using mathematical model for predicting performance in thermal shock 21 p3723 A67-38630

Adhesive and water resistance properties of epoxy resin for bonding tensometers and underwater sealing 21 p3650 A67-38919

Elastic properties of filled and porous epoxy composites tested in compression and tension noting Youngs modulus relation to filler content 22 p3824 A67-39498

Ablators for severe reentry environments evaluated from modifications of reference model constructed of epoxy resin with silica fiber and phenolic filler 22 p3826 A67-39887

Reinforced plastics, evaluating epoxy resin with glass fiber reinforcements for laminates, measuring tensile, compressive and flexural strengths [ASM PAPER C6-21.1] 23 p4022 A67-41403

EQUATION

S ADIABATIC EQUATION

S BALANCE EQUATION

S BERNOLLI EQUATION

S BIHARMONIC EQUATION

S BLASIU EQUATION

S BOLTZMANN EQUATION

S BOLTZMANN-VLASOV EQUATION

S BRAGG EQUATION

S BURGER EQUATION

S CAUCHY-RIEMANN EQUATION

S CHANDRASEKHAR EQUATION

S CHAPLYGIN EQUATION

S CHARACTERISTIC EQUATION

S CONSERVATION EQUATION

S CONTINUITY EQUATION

S DIFFERENCE EQUATION

S DIFFERENTIAL EQUATION

S DIOPHANTINE EQUATION

S DIRAC EQUATION

S DONNELL EQUATION

S DUFFING EQUATION

S EINSTEN EQUATION

S ELLIPTIC EQUATION

S ENERGY EQUATION

S EULER-CAUCHY EQUATION

S EULER EQUATION

S EULER-LAGRANGE EQUATION

S EULER-LAMBERT EQUATION

S FALKNER-SKAN EQUATION

S FIRST ORDER EQUATION

S FLOW EQUATION

S FOKKER-PLANCK EQUATION

S GIBBS EQUATION

S GRAD EQUATION

S HAMILTON-JACOBI EQUATION

S HEAT EQUATION

S HELMHOLTZ EQUATION

S HILL EQUATION

S HYDRODYNAMIC EQUATION

S HYPERBOLIC EQUATION

S INTEGRAL EQUATION

S KINEMATIC EQUATION

S KINETIC EQUATION

S KLEIN-GORDON EQUATION

S KROOK EQUATION

S LAGRANGE EQUATION

S LAME WAVE EQUATION

S LAPLACE EQUATION

S LINEAR EQUATION

S LIOUVILLE EQUATION

S MACROSCOPIC EQUATION

S MAXWELL EQUATION

S MILNE EQUATION

S MOMENT EQUATION

S MOTION EQUATION

S NAVIER-STOKES EQUATION

S NONLINEAR EQUATION

S ORBIT EQUATION

S PARABOLIC EQUATION

S PERIOD EQUATION

S PLANCK EQUATION

S POISSON EQUATION

S QUADRATIC EQUATION

S RAYLEIGH EQUATION

S REISSNER EQUATION

S REYNOLDS EQUATION

S SAHA EQUATION

S SCHROEDINGER EQUATION

S SHALLOW SHELL EQUATION

S STATE EQUATION

S TRANSPORT EQUATION

S VLASOV EQUATION

S VOLTERRA EQUATION

S VON KARMAN EQUATION

S VORTICITY EQUATION

S WAVE EQUATION

S WIENER-HOPF EQUATION

EQUATOR

SA GEOMAGNETIC EQUATOR

SA MAGNETIC EQUATOR

SA TRANSEQUATORIAL PROPAGATION

Wide angle counter telescope measurement of cosmic ray equator position near zero meridian 01 p0149 A67-10738

Rapid geomagnetic variations in vicinity of equator 03 p0409 A67-12844

Geographic position of cosmic ray equator from results of on board Proton I satellite measurements 05 p0878 A67-16090

Mean monthly winds at low level calculated for equatorial station in East Africa, noting monsoon patterns and jet streams 06 p1025 A67-18024

Circulation patterns in upper atmosphere, using sounding rockets from Indian equatorial station during monsoon and winter periods 12 p1935 A67-25791

Biennial variations of zonal atmospheric circulation at equatorial latitudes analyzed using hydrothermodynamics 13 p2150 A67-26680

Corrections to equinox and equator of FK3 from meridian observations of Ceres, Pallas, Juno and Vesta 15 p2557 A67-29873

Semiannual wind variation in equatorial stratosphere analyzed for origin from rocket sounding data 22 p3828 A67-39466

Cosmic ray equator position at zero meridian measured, noting substantial difference in location from magnetic equator position 23 p4059 A67-41135

Clouds over equatorial and tropical Pacific investigated by comparing photographs from Tiros satellites and jet aircraft 24 p4181 A67-42667

Geographic position of cosmic ray equator from results of onboard Proton I satellite measurements 24 p4212 A67-42766

EQUATORIAL ELECTROJET

Horizontal drift measurements in E and F regions of ionosphere over magnetic equator in India 03 p0407 A67-12829

Radar observations of equatorial electrojet irregularities indicate reversal during nighttime of daylight westward traveling electrons stream 03 p0408 A67-12837

Monthly and seasonal variation of magnetic horizontal component in Eastern Africa on international quiet and disturbed days from February 1964 to January 1965 03 p0408 A67-12838

Origin of fluctuations in equatorial electrojet, discussing new type of geomagnetic variation of polar origin 03 p0408 A67-12840

Equatorial geomagnetic field fluctuations in frequency range of 4.0 to 0.003 c/s 03 p0408 A67-12842

Equatorial electrojet relationship with worldwide Sq currents 07 p1171 A67-19417

Spectrum of echoes from irregularities in equatorial electrojet at oblique incidence 08 p1328 A67-21465

Nike-Cajun rocket investigation of equatorial D and E region parameters and effect on electrojet 10 p1648 A67-23288

Diurnal variation of telluric currents near magnetic equator during IGY and IQSY suggests equatorial electrojet as main source for current 10 p1651 A67-23343

Height distribution of Sq current intensity in midlatitude ionosphere as function of electrostatic field direction 11 p1786 A67-24333

Rocketborne magnetometer measurements of midlatitude Sq ionospheric currents 12 p1935 A67-25794

Latitudinal cross section of ionospheric current density profile of equatorial electrojet from rocketborne magnetometers 13 p2107 A67-26307

Rocket measurements of equatorial electrojet current 13 p2114 A67-26793

Equatorial electrojet width and intensity analyzed with ground level magnetic field measurements from Peru and Nigeria 14 p2312 A67-28572

Seasonal variations in position and intensity of equatorial electrojet and correlation of latter with sunspot number 15 p2478 A67-30061

Magnetic variation measurements at Addis Ababa indicate intermittent existence of inverse direction equatorial electrojet 15 p2478 A67-30070

Time and space study of onset and early development of single occurrence of spread-F in equatorial region

[AGARDOGRAPH 95] 15 p2480 A67-30275
 Equatorial electrojet parameters in
 India 19 p3221 A67-35431
 Rocket and balloon studies of solar
 radiation, wind characteristics, equatorial
 electrojet and lower ionosphere electron
 density 19 p3223 A67-35474
 Ionospheric conductivities, electric
 currents and field height variations in
 equatorial electrojet region calculated from
 model, including solar 21 p3617 A67-38066
 activity
 Equatorial electrojet currents studied
 from IGY data from South American
 stations 24 p4148 A67-42065

EQUATORIAL ORBIT

Ground track of earth-period synchronous
 /24-hr/ satellites, discussing equatorial,
 circular and elliptical 04 p0704 A67-14826
 orbits
 Satellite orbit major axis determination by
 using coincidence of time when satellite
 crosses plane of tracking station parallel
 with time of crossing topocentric celestial
 equator 05 p0894 A67-16560
 Resonance rotation of Venus, discussing
 spin period determinations and retrograde
 nature of rotation from radar
 observations 19 p3317 A67-34952
 Mass optimal trajectory problems with
 variable endpoints solved using initial and
 terminal coasting arcs 22 p3884 A67-39955
 Minimum fuel flight plans for injecting
 synchronous satellite into circular equatorial
 orbit, developing four
 methods 22 p3886 A67-40116

EQUATORIAL SATELLITE

Equilibrium positions of synchronous
 equatorial satellite situated in directions of
 extremum positions of radius of equatorial
 section of synchronous
 geoid 02 p0327 A67-12370

EQUILIBRIUM

SA BODY SWAY TEST
 SA CHEMICAL EQUILIBRIUM
 SA LIQUID-VAPOR EQUILIBRIUM
 SA NONEQUILIBRIUM
 SA STABILIZATION
 SA STEADY STATE
 SA THERMODYNAMIC EQUILIBRIUM
 Existence of two points near any planet
 where third body, given appropriate initial
 conditions, would remain in libelle
 gravitational equilibrium 02 p0324 A67-11814
 Equilibrium equations, boundary conditions
 and constitutive relations for nonlinear
 theory of elastic directed curves, examining
 double stress without
 moment 02 p0267 A67-12057
 Existence and stability of equilibrium
 orientations of rigid body with gyrost at in
 nonuniform gravitational
 field 02 p0268 A67-12385
 Formal integral construction of
 Hamiltonian system of n degrees of freedom
 near equilibrium point 03 p0457 A67-13163
 Surface tension and equilibrium surfaces
 in weightless liquids, with application to
 spacecraft systems design 03 p0404 A67-13890
 Necessary conditions for equilibrium of
 Maxwell-Boltzmann distribution using
 analyticity of S -matrix 05 p0849 A67-17115
 Equilibrium position of Sperry MK19
 gyrocompass axis and effects of earth
 rotation and motion of body on which
 gyroscope is mounted 06 p1003 A67-18178
 Limited mutual solubility of gases above
 critical point of least volatile
 component 06 p1116 A67-18381
 Equilibrium equations of Vlasov
 engineering moment theory of shells of
 variable curvature 12 p2021 A67-25577
 Magmatic origin of chondrule meteorites,
 considering structure, electron probe
 microanalysis, crystallization and
 equilibrium 13 p2200 A67-27234
 Graphical demonstration of human reaction
 to shock or vibration input in horizontal
 plane to study physiological functions of
 equilibration 13 p2064 A67-27274
 Equilibrium configuration and tension of
 flexible cable in uniform flow field,
 considering tangential drag force and weight
 effects 13 p2051 A67-27587
 Electromagnetic radiation equilibrium in
 gas lasers, studying effect of cavity length
 variations on linewidth 14 p2329 A67-27952
 Experimental detection and evaluation of
 plasma instabilities, discussing research state
 in connection with thermonuclear and
 cosmic problems 14 p2360 A67-28556

Thin elastic circular ring equilibrium
 stability in rigid cavity subjected to parallel
 loading, considering small ring separation
 region at buckling
 [ASME PAPER 67-APM-19] 17 p2958 A67-32406

Equilibrium state for interstellar gas-
 magnetic field system as described by
 model 20 p3528 A67-37472
 Equilibrium stability conditions for
 mechanical system of solid bodies derived
 using Liapunov function 21 p3626 A67-37991
 Spacecraft-space plasma electric
 equilibrium, discussing active spacecraft
 configurations for control
 [AIAA PAPER 67-702] 21 p3714 A67-38729

EQUILIBRIUM DIAGRAM

Equilibrium diagram of niobium-nickel
 system determined by thermal analysis,
 microscopical metallography and X-ray
 techniques 05 p0828 A67-16387
 Quenching examination of phase
 equilibrium in system lead oxide-titanium
 oxide-zirconium oxide, determining
 isotherms lines, melting points,
 etc 12 p1986 A67-26188
 Niobium-cobalt alloys constitution,
 determining equilibrium diagram by thermal
 analysis, microscopical metallography and X-
 ray diffraction techniques 14 p2338 A67-28615
 Two-body system connected on circular
 orbit by spherical hinge examined for plane
 oscillations, finding all equilibrium positions
 with respect to orbital
 coordinate 17 p2954 A67-32242
 TINI-TiFe system equilibrium diagram,
 studying melting points and heat treatment
 effects on microstructure 20 p3468 A67-37179
 W-Ta-Re system equilibrium diagrams
 examined, measuring diffusion layer element
 concentration by X-ray spectral analysis
 method 20 p3468 A67-37180

EQUILIBRIUM FLOW

SA NONEQUILIBRIUM FLOW
 Electrode losses in MHD generators with
 nonequilibrium and equilibrium ionization
 compared, attributing differences to
 coupling between conductivity and local
 dissipation 01 p0014 A67-11159
 Fluid equilibrium shape under gravity
 force and surface tension analyzed via
 variational method 03 p0401 A67-12881
 Numerical determination of axisymmetric
 equilibrium shapes of interface between two
 nonmixing liquids uniformly rotating in
 vessel under weak centrifugal and capillary
 forces and zero gravity
 conditions 03 p0402 A67-12882
 Hydrodynamic stability Cauchy problem
 for continuous spectrum of two-dimensional
 parallel flow of nonviscous incompressible
 fluid 03 p0402 A67-13172
 Experimental data compared to theory for
 expansion of high temperature air in
 equilibrium and nonequilibrium flow through
 Mach number 10 contoured nozzle
 [AIAA PAPER 66-2] 05 p0750 A67-17340
 Electrohydrodynamic equilibrium showing
 continuum feedback control of Rayleigh-
 Taylor type instability 05 p0856 A67-17414
 Asymptotic method for solution of
 boundary layer equations for generalized
 three-dimensional flow of dissociated air at
 chemical equilibrium near stagnation
 point 06 p0984 A67-18113
 Equilibrium air total radiation mechanism,
 vacuum UV radiation and relation to
 hypervelocity entry studied, using shock
 tube blunt model test flow
 [AIAA PAPER 66-103] 08 p1426 A67-20569
 Equilibrium particle ionization effect on
 electron density of gas particle
 plasma 08 p1360 A67-21124
 Peak density in single ended Q machine
 described in agreement with equilibrium
 theory 11 p1833 A67-24368
 Approximate solution of equilibrium
 problem for shallow cylindrical shell of
 rational profile under pressure distribution
 from convex side 12 p2024 A67-25603
 Distribution function structure in gas
 kinetic flows as given by BGK model in
 plane weak shock in monatomic
 gas 13 p2104 A67-26981
 Instabilities of Ekman layer measured
 using hot-wire
 anemometers 15 p2471 A67-29655
 Nonequilibrium flow relation to flow in
 thermal balance, describing irreversible
 processes in terms of entropy source field
 and relaxation resistance 16 p2662 A67-31467

Solution to moment equations for near-
 equilibrium spherically-symmetric expanding
 flows by using Bernstein-Greene-Kraskal
 theory for Boltzmann
 equation 19 p3212 A67-35764
 Critical parameters of plane problem of
 transition of fluid into suspension, ignoring
 deformation of body up to point of limiting
 equilibrium 22 p3916 A67-39392
 Relative equilibrium of liquid cylinder
 investigated for uniform rotation in uniform
 axial electric field 22 p3787 A67-40135

EQUIPMENT

S AIRBORNE EQUIPMENT
 S AIRPORT SURFACE DETECTION
 EQUIPMENT /ASDE/
 S AUDIO EQUIPMENT
 S CHECKOUT EQUIPMENT
 S CRYOGENIC EQUIPMENT
 S DISTANCE MEASURING EQUIPMENT
 S ELECTRIC EQUIPMENT
 S ELECTRONIC EQUIPMENT
 S ELECTRONIC EQUIPMENT TESTING
 S GROUND SUPPORT EQUIPMENT
 S HANDLING EQUIPMENT
 S HEATING EQUIPMENT
 S HYDRAULIC EQUIPMENT
 S JACKING EQUIPMENT
 S LIGHTING EQUIPMENT
 S MEDICAL EQUIPMENT
 S OPTICAL EQUIPMENT
 S PNEUMATIC EQUIPMENT
 S POSITIONING EQUIPMENT
 S RADAR EQUIPMENT
 S RADIO EQUIPMENT
 S REFRIGERATING EQUIPMENT
 S TELEVISION EQUIPMENT
 S TEST EQUIPMENT
 S THERMONUCLEAR EQUIPMENT
 S TRAINING EQUIPMENT
 S VACUUM EQUIPMENT
 S VIDEO EQUIPMENT
 S X-RAY EQUIPMENT

EQUIPMENT SPECIFICATIONS

Design strength calculation for materials
 as function of reliability level and number
 of components 04 p0627 A67-14705
 Systematic approach using weight factor
 for apportioning mean corrective times of
 equipment based upon maintainability, usage
 and reliability data 08 p1315 A67-20670
 Percentile specifications of orthogonal
 components and of additive errors of
 guidance systems 08 p1350 A67-20674
 Book on applied kinematics covering
 synthesis techniques for link-and-cam motion
 other than uniform rotation in high speed
 high performance automatic
 machines 11 p1795 A67-23921
 Ground effect machine development, with
 table of models and specifications and
 photographs and drawings of
 configurations 11 p1744 A67-24705
 Gradient compensated large volume
 degauser noting inner and outer coils,
 magnetic field generators and construction
 and performance
 specifications 15 p2517 A67-29491
 Space vehicle lubrication methods, noting
 design and construction of test
 apparatus 15 p2492 A67-29558
 Liquid spring design characteristics noting
 fluid characteristics, precharge fluid
 pressure, friction, efficiency, gland
 configuration and application
 requirements 15 p2494 A67-30097
 Environmental adjustment factors for
 operating and nonoperating failure
 rates 15 p2495 A67-30417
 Design for light-gas gun with light piston
 by successive parameter computation of
 various parts 16 p2655 A67-31125
 Reference issue on
 fastening and
 joining 16 p2682 A67-31563
 Tactical aircraft survivability in North and
 South Vietnam, discussing missile and
 interceptor ineffectiveness and limited-war
 considerations for aircraft 17 p2796 A67-32434
 Solid propellant rocket motors reliability,
 discussing corrective action, retest, success
 probability, requirements, capability,
 simulation model, etc
 [AIAA PAPER 67-435] 18 p3112 A67-33914
 Soviet book on protective equipment for
 aviators and cosmonauts 21 p3576 A67-37934
 Design, performance and development of
 aircraft wiring cables noting need for high
 temperature operation 21 p3572 A67-39073
 FAA certification standards for SST
 engines and components, emphasizing
 thermal environment testing and high

- temperature materials
development 22 p3867 A67-39224
- ERBIUM**
Stark and Zeeman splitting in far IR spectra of erbium, dysprosium and samarium ethyl sulphate 04 p0688 A67-15778
Two photon stepwise absorption of low power He-Ne laser light in erbium doped yttrium oxide and lanthanum fluoride crystals 13 p2177 A67-27013
- ERGODIC PROCESS**
Statistical properties of estimation method for one-dimensional characteristic function of stationary ergodic random process 02 p0192 A67-11639
Ergodic theory of measurable partitions in Lebesgue space, extending Rokhlin-Sinai theory of increasing to flows generated by automorphism 04 p0644 A67-14756
Connection between flow spectrum and velocity, obtaining continuous spectrum upon velocity change to equivalent invariant measure 06 p0983 A67-17860
Stationary property of random process approximating anomalous magnetic field, noting optimum filtering 14 p2309 A67-27946
Quasi-invariance and ergodicity in binary sequence space with respect to discrete groups of Bernoulli schemes, noting finite entropy distance formulation of measure equivalence 14 p2343 A67-28502
Ergodic properties of additive functionals of recurrent Markov processes 18 p3071 A67-34182
Significance of far field portion of plasma microfield 19 p3285 A67-35344
Invariant measure existence condition derived for Markov processes, with several ergodic theorems for homogeneous Markov processes proved, noting transfer functions 22 p3827 A67-39877
Fixed point probability row vector of regular or ergodic transition matrices simplified using generalized matrix inversion theory 23 p4023 A67-41032
- ERGONOMICS**
BIOTECHNOLOGY
EROS ASTEROID
Corrected derivation of earth-moon mass and various astronomical constants from Eros orbital motion 23 p4061 A67-40620
Numerical integration of Eros orbital motion normals, obtaining earth-moon mass and various astronomical constants 23 p4061 A67-40621
- EROSION**
SA ETCHING
SA MATERIALS EROSION
SA SPARK EROSION MACHINING
SA SURFACE EROSION
SA WEAR
Flow and cavitation erosion tests in closed circuit hydrodynamic tunnel 14 p2295 A67-27869
Cavitation correlation with sound pressure and vibration acceleration in closed circuit hydrodynamic tunnel, showing cavitation noise spectrum 14 p2295 A67-27870
Cavitation erosion noting high speed motion picture photographic analysis of kinematic structure of cavitation zone 20 p3420 A67-36631
- ERROR**
SA INSTRUMENT ERROR
SA PHASE ERROR
SA PILOT ERROR
SA POINT ERROR
SA POSITION ERROR
SA RANDOM ERROR
SA RANGE ERROR
SA ROOT-MEAN-SQUARE ERROR
SA SCALE ERROR
SA TRUNCATION ERROR
SA VELOCITY ERROR
Best-possible error bounds in deformation theory 01 p0165 A67-11308
Impedance errors of coaxial air transmission lines and mechanical and electrical characteristics of Precifix connectors 02 p0213 A67-11648
Projection principle for minimization of variance of squared error 02 p0259 A67-12154
Variant of averaging functional errors method in solving linear integral boundary value equations 03 p0457 A67-13116
Strap-down guidance systems using conventional inertial hardware, discussing computer function, computer selection and system errors 03 p0465 A67-13364
Equivalent gain and error response of hysteretic system to Gaussian inputs 04 p0593 A67-15637
Probabilistic displays and decision making effectiveness in situation with uncertain or fallible information 05 p0757 A67-16308
Error estimate for approximate solution of linear parabolic equation using Kantorovich theorem on functional analysis in normalized space 05 p0836 A67-17108
Statistical probabilistic analysis of error propagation and tolerance limits in structural engineering design of assembled parts 05 p0813 A67-17258
Satellite three-dimensional triangulation accuracy, discussing orientation of camera axes and plate coordinates of satellite images as error sources 06 p0994 A67-17717
Computer program for digital exact representation of spectral frequency-and intensity-distribution by superposition of Gaussian components, applying least squares method, linearizing normal equations and analyzing observational errors 06 p0965 A67-18069
Matrix error analysis compared to algorithm optimization problems of numerical analysis 06 p1024 A67-18475
[AIAA PAPER 67-142] Error due to electron thermal energy fluctuations in mean electron temperature measurement by line intensity 06 p1042 A67-18540
Complex and decision feedback systems for command channels in space communications 07 p1145 A67-19872
Partial error analysis of Fowler z transform root-locus method for digital simulation of complex system 07 p1148 A67-19892
Rigorous error bounds on position and velocity of satellite derived from Hamiltonian theory and von Zeipel method [AAS PAPER 66-94] 07 p1252 A67-19958
Complete error budget of ballistic flight orbit prediction including force model error effects 07 p1253 A67-19966
Effects of unmodeled errors on minimum variance estimators, with application to tracking complex self-calibration estimation scheme [AAS PAPER 66-107] 07 p1216 A67-19967
Free parameters in third and fourth order pseudo-Runge-Kutta methods involving two points 07 p1218 A67-20215
Human error causes, accidents and effects of fatigue, microsleep and flicker fusion frequency 07 p1137 A67-20229
Data smoothing, signal processing and exact minimum mean square error procedures 07 p1218 A67-20267
Error in application of WKB method to linearized postburnout equation of motion of sounding rocket 08 p1406 A67-20510
Maximal error estimation arising from delay in output functions of servomechanisms provided bandwidth, maximum oscillation and slope are known 08 p1286 A67-20780
Error probability density distribution and selection of measurement accuracies and decision tolerances 08 p1336 A67-21057
Maximum errors of polynomial approximations defined by interpolation and least squares method 08 p1349 A67-21262
Recurrence relation for determining asymptotic error constant of rational function iterative methods for solving equations 08 p1349 A67-21263
Direction finding errors of method of instantaneous amplitude comparison in elliptically polarized antenna arrays 09 p1473 A67-21960
Range instrumentation ships as major range subsystems, noting equipment used, accuracy and sources of errors 10 p1622 A67-22999
Interpolation errors visualization by spectrum of sampled data 10 p1605 A67-23005
Inequality to derive error estimation of performance of automatic pulse servosystem inside interval of discreteness 11 p1772 A67-25039
Analog computer simulation of motions of gyroscopic pendulum, showing imbalance tolerance relationship to error 13 p2118 A67-26350
Rigorous error bounds on position and velocity of satellite derived from Hamiltonian theory and von Zeipel method [AAS PAPER 66-94] 13 p2207 A67-27518
Complete error budget of ballistic flight orbit prediction including force model error effects [AAS PAPER 66-106] 13 p2208 A67-27524
Effect of unmodeled errors on minimum variance estimators, with application to tracking complex self-calibration estimation scheme [AAS PAPER 66-107] 13 p2154 A67-27525
Errors arising when dividing geomagnetic field into primary and anomalous fields by simple averaging techniques 14 p2309 A67-27947
High accuracy radio guidance and tracking station, discussing relation between basic station parameters, error sources and associated error components 14 p2260 A67-27972
Independent effects of error magnification and field of view on compensatory tracking performance, analyzing display and optical magnification 14 p2258 A67-28667
Error rate expression for canonic binary receivers, evaluating performance of incoherent detection 14 p2272 A67-28706
Modulation indexes for two-channel phase coherent communication system determining data rate yielding predetermined bit-error probability [JPL-TR-32-1118] 14 p2273 A67-28709
Orbiting navigation with compensation for periodic errors, using modified Kalman filtering technique 15 p2513 A67-29595
Computational error caused by finite word length of aerospace computers 15 p2439 A67-29596
Error assessment in numerical integration for ordinary differential equations applied to many-body problem 15 p2512 A67-30053
Statistical probability distribution for determining systematic errors of potentiometer multiplier by Monte Carlo method /static testing/ 16 p2633 A67-30464
Errors of real accelerometer and instability of rotation effect on accuracy of angular velocity measurements of aircraft motion 16 p2670 A67-30466
Quantization error effect for digital control system design 16 p2646 A67-31637
Nonuniform error quantization effects on stability of feedback control systems, investigating limit cycles existence and giving optimum quantizer design procedure 17 p2829 A67-32016
Digital error performance of transportable troposcatter facility evaluated as function of path length 17 p2811 A67-32118
Comet Burnham C2 coma photometry, discussing error sources in isophotes and photometric scale and tabulating oval isophote size against axes mean ratio 17 p2943 A67-32442
Systematic errors limiting velocity measurement accuracy of longitudinal ultrasonic waves when using pulse-delay methods, for application to ultrasonic equipment 18 p3044 A67-33734
Circular disk error magnitude determination by measuring rear-wall echo with angular probe 18 p3044 A67-33736
Star occultation measurements accuracy for determining satellite orbit parameters, noting error sources 18 p3075 A67-34108
Upper bounds for cantilever beam natural oscillation frequency error determined when approximately calculated frequency values approach exact values of problem 18 p3143 A67-34168
Solar flare electron density determination by half-width method, discussing errors due to measurement and method 19 p3314 A67-35438
Quantization error bounds for hybrid control systems by time varying function 19 p3202 A67-35625
Software aspects of space navigation including computer programming, mission planning, error analysis and reliability realization 19 p3187 A67-35858
Fundamental intensity error in Fourier spectroscopy noting requirement that interferograms be inverted by Fourier transformation 20 p3437 A67-36337
Eastern Test Range time synchronization system, analyzing errors and limitations 20 p3414 A67-36535
Analytical and simulation procedure for determining environment induced errors in missile guidance 20 p3481 A67-36605
Artificial earth satellite orbital element accuracy, describing least squares method of

choosing time intervals for reducing errors 20 p3523 A67-36625

Complex reflection coefficient for finite-width boundary used for plasma diagnostics in high electron-density range, discussing modeling errors 20 p3499 A67-36959

Mean error and optimal structures for multidimensional extremal systems with random noise obtained from steady process 20 p3409 A67-37112

Direction finding errors of method of instantaneous amplitude comparison in elliptically polarized antenna arrays 20 p3400 A67-37190

Probability distribution errors effect in linear and planar impulse orbital transfers, considering angular orientation and impulsive velocity 20 p3527 A67-37259

Shell curvature variation parameter noting influence on equilibrium equations and error in equations of strain compatibility 21 p3718 A67-37981

Spacecraft trajectory parameter estimation, discussing various time-varying error components 21 p3705 A67-38587

Discrete errors in continuous angle-modulation systems, considering conventional fidelity /SNR/ criterion and probabilistic theory 21 p3584 A67-38653

Tracking interruption probability determination in radars reduced to Kolmogoroff equation in dimensionless form taking dynamic error into account 21 p3585 A67-38815

Thin foil heat flux sensor for radiative and convective heating rates over wide range and dynamic response, noting error mechanisms, calibration and accuracy 23 p4006 A67-41374

Thick walled carbon cone calorimeter in pulsed lasers used for calibration purposes, discussing error sources 24 p4154 A67-42174

Correction to parametric representations of nonsteady one-dimensional flows 24 p4145 A67-42691

ERROR CORRECTING DEVICE

Combined automatic control systems with automatic adjustment of amplification coefficient of disturbance controller for error reduction 01 p0044 A67-10242

Cosmic ray intensity changes for various values of cut-off rigidity determined using barometric coefficient 02 p0307 A67-11667

Real time data transmission systems with error detection, block retransmission capabilities and buffer storage unit treated as Markov process 02 p0194 A67-11810

Troposcatter transmission technique called frequency time shift keying, deriving optimum noncoherent receiver configuration and error performance 02 p0202 A67-12123

Flow pulsation effect on error of flow measurement by means of steady flow formula, noting manometer design requirements 03 p0403 A67-13767

Optimum continuous electrical correction of dynamic characteristics of inertial pickups 03 p0426 A67-14286

Error correcting method for star pattern and constellation identification process 04 p0619 A67-14552

Synchronization errors in parallel jacks system with closed loop control by hydraulic relays, using nonlinear differential equations [ASME PAPER 66-WA/AUT-5] 04 p0555 A67-15389

Fourier transform used in correction of instrument contour error when observing solar spectral line profile 04 p0624 A67-15564

High speed analog-digital converter with fast response time of discriminator obtained by error correction 04 p0593 A67-15636

Automatic flight control systems for missiles and aircraft, noting error sensing and correcting functions, calibration and testing methods 04 p0655 A67-15735

Data from Lunar Orbiter spacecraft used to test validity of corrections to lunar ephemeris reveals residual patterns [JPL-TR-32-1087] 05 p0901 A67-17201

Sequential trajectory estimation improved by implementing simple running estimates of observation error variances [AIAA PAPER 67-89] 06 p1086 A67-18337

DC amplifier with capacitive feedback as correcting device in recording currents while studying magnetoplasma generator 06 p0952 A67-18693

Pulsed power technique and capacitive coupling between digital integrated circuits

provide micropower redundant circuits with automatic error correction 07 p1155 A67-19844

Test set for automatically compensating for error sources in calculating FET transconductance values 11 p1760 A67-24258

Soviet book on theory of inertial navigation, autonomous systems 11 p1817 A67-24513

Heat receiver with correcting device for instantaneous temperature measurements in unsteady gas flow, discussing matching of time constants and heat-transfer coefficients 13 p2118 A67-26352

Error correcting method for star pattern and constellation identification process 13 p2153 A67-26579

Error reduction in signal reconstruction represented by segment of band-limited function 13 p2069 A67-27040

Formulas for correcting errors in aerial-photograph and planar-model coordinates due to atmospheric refraction and earth curvature 14 p2318 A67-28371

Computational errors in generation of direction cosine matrix in strapdown system 15 p2515 A67-29741

Input/output model of system with finite settling time, using error correcting technique employed in pattern recognition 15 p2460 A67-30314

Coding for numerical data transmission over binary symmetric channel, discussing effectiveness of various error-correcting codes, taking average numerical error as fidelity criterion 15 p2439 A67-30387

Cosmic ray intensity changes for various values of cut-off rigidity determined using barometric coefficient 16 p2738 A67-31082

Error damping procedures for gimballing inertial navigational systems 16 p2701 A67-31268

Digital sequencing systems containing error-detecting and -correcting properties 16 p2647 A67-31647

Error correction block encoding for high speed HF digital data transmission system 17 p2811 A67-32112

Predetection telemetry tape combiner 17 p2813 A67-32496

Predictor-corrector for solving ordinary differential equations, discussing influence of rounding-off errors on accuracy of solution 18 p3071 A67-34286

Variational procedure for sequential decoding scheme with mean error probability dependence on code limitation approximately same as for optimal decoding 19 p3185 A67-36096

Optimal correcting strategy for vehicle moving close to nominal trajectory 20 p3407 A67-36809

Optimal flexible strategies for pulsed correction of close-to-nominal space vehicle trajectory, using fuel reserve limitation criterion 22 p3878 A67-39186

Air temperature measurements at subsonic and supersonic flight speeds, discussing error sources and thermometer efficiency 22 p3797 A67-39542

Simplified fire control system for helicopters, noting helmet sight, error source corrections and sighting and tracking convenience 22 p3755 A67-39849

Error correcting codes for white Gaussian channel at low signal to noise ratio, discussing properties and performance criteria 23 p3984 A67-40752

Operational error analysis program /OEAP/ use with multiprocessing in air traffic control application 23 p3976 A67-41059

Sequential trajectory estimation improved by implementing simple running estimates of observation error variances [AIAA PAPER 67-89] 23 p4070 A67-41717

Error probability for binary signaling through multipath channel with receiver waveform comprising white Gaussian noise and time delayed frequency-shifted signal 24 p4121 A67-42341

Hydraulic failure detection system in Titan booster servo injector module featuring anticipation and correction of servomodular failure 24 p4099 A67-42426

Measuring instrument for assessing digital data transmission channels performance using bit error counting combined with peak telegraph distortion 24 p4159 A67-43116

ERROR DETECTING CODE

Cost effective error control for coded or M-ary signal reception 01 p0023 A67-10485

Differentially coherent phase-shift keying system analyzed under wide range of signal and noise conditions 01 p0025 A67-10861

Coherent echo modulation and detection for binary data transmission, noting power savings, time and frequency diversification and communication stability 01 p0026 A67-10862

Error probabilities for partially coherent diversity reception, noting linearized receiver performance during random noise output 01 p0028 A67-10863

Data and mission analysis in man-rating of Gemini launch vehicle 01 p0155 A67-11347

Channel noise forces adaptive sampling system to operate at lower bit error probability than equivalent PCM system 02 p0197 A67-12016

Digital computer testing procedure, noting error isolation and location technique via process of elimination 04 p0579 A67-15738

Errors by mutual interference in frequency-time coding in satellite communications systems, deriving expressions relating commissive and omissive error rates, simultaneous users per unit bandwidth, etc 06 p0961 A67-17696

Iterative computation of a posteriori probability for M-ary nonsupervised adaptation 06 p0965 A67-17947

Information criteria for threshold setting in simple binary hypothesis tests 06 p0962 A67-17948

Sign codes and patterns of state variables for finding all possible responses in linear third order closed loop feedback control system 06 p0978 A67-18721

Failure-correction decoding in improving error-correction block codes, using reliability estimates of received digit decisions 09 p1459 A67-21578

Instrumental accuracy of missile range instrumentation systems, discussing error sources, detection and correction 10 p1605 A67-23002

Lower bounds to minimum error probability using block coding on noisy discrete memoryless communication channels 11 p1752 A67-24270

Noise rejection of remote control command information transmission in system with comparison circuit, using error detecting and correcting codes 11 p1772 A67-25041

Lower bounds on error probability for communication in presence of white Gaussian noise with no bandwidth constraint 12 p1908 A67-26086

Error probability for transmission of M orthogonal equally probable equal-energy signals over partially coherent channel 12 p1908 A67-26091

Computational worst error algorithm for linear systems and quadratic error criteria, showing flowgraph and computer execution results 15 p2457 A67-29367

Accuracy of mathematical models in control system identification estimated on basis of deterministic test signals for simulation in time and frequency domains 15 p2461 A67-30318

Time statistics for reliable transmission of binary data in presence of atmospheric noise burst 17 p2811 A67-32113

Redundancy reduction techniques and error correction coding of digital communication systems including waveform, pattern recognition, vocoding, etc 18 p3004 A67-34613

Accuracy problems in control systems, discussing error assessment and accuracy estimates of optimal control 20 p3410 A67-37231

Data compression and error control coding in space telemetry analyzed, using performance measures similar to distortion function 21 p3586 A67-38950

Lower bounds to minimum error probability for block coding on noisy discrete memoryless channels 22 p3764 A67-39296

Error control techniques covering parity check, longitudinal redundancy check and hamming and cyclic codes 22 p3776 A67-39372

Error correcting codes for white Gaussian channel at low signal to noise ratio, discussing properties and performance criteria 23 p3984 A67-40752

Multiprocessing features of IBM 9020 system, discussing breakdown of information into subprograms with operational

- priorities 23 p3976 A67-41058
 Errorless code transmission in specific
 monbinary cyclic channels, describing
 effective decoding 24 p4136 A67-42409
 process
ERROR FUNCTION
 Error equation for accuracy of monopulse
 radar in search mode applied to monopulse
 radar systems, using logarithmic
 normalization 01 p0022 A67-10446
 Model distribution for phase error in
 second-order phase locked loop used to
 complement analytical model in signal to
 noise region
 [JPL-TR-32-1017] 01 p0026 A67-10865
 Parameter optimization in systems subject
 to worst bounded disturbance that
 maximizes chosen performance
 index 01 p0046 A67-11204
 Adaptive technique determination of
 optimum operations for pure prediction of
 discrete time series with respect to mean
 square error cost 02 p0207 A67-12138
 Autonomous satellite navigation based on
 repeatedly measuring angular position of
 ejected test probe relative to
 stars 02 p0264 A67-12311
 Mayer technique in calculus of variation
 for constrained error coefficient criterion
 function for missile trajectory optimization
 in aerospace guidance and
 control 02 p0265 A67-12389
 Unreliability of mean-time-between-failures
 concept as standard quality measure for
 mechanical systems 02 p0249 A67-12426
 Reflection coefficient of tapered
 waveguide determined via coupled mode
 theory, noting error estimation and design
 of reflectionless tapers 03 p0376 A67-12802
 Errors in thermodynamic functions of
 ideal gases determined from molecular
 data 03 p0536 A67-13607
 Error equations for Schuler vertical,
 estimating discrepancy between solutions for
 various changes in
 coefficients 03 p0465 A67-14160
 Minimum average conditional entropy for
 minimum probability of error in statistical
 decision theory 04 p0644 A67-14885
 Boundary value problems for semilinear
 stars made of coupled thermoelastic material
 solved by new functions that are corrections
 to classic tabulated functions
 [ASME PAPER 66-WA/APM-24] 04 p0714 A67-15412
 Error estimation in linear matrix equation
 systems by rounding-off
 inaccuracies 05 p0834 A67-16721
 Error bounds for asymptotic solutions of
 differential equations, using Volterra
 equations for actual and formal solution
 vectors 06 p1021 A67-17565
 Optimal Wiener values of filter
 parameters in phase-lock loop, noting
 possibility of improved performance despite
 deviations 06 p0973 A67-17615
 Chernoff bound and tilted distribution
 argument for obtaining error probability
 bounds for binary signaling on slowly fading
 Rician channel
 [JPL-TR-32-1051] 06 p0961 A67-17943
 Converse of channel coding theorem,
 relating average probability of error to
 distortion measure of source sink
 pair 06 p0965 A67-17946
 Error determination for transient heat
 transfer experiments using least squares
 method 06 p1024 A67-18389
 Relationship between optimum gain and
 time constant settings for multiple time
 constant self-adjusting
 models 06 p0977 A67-18530
 Error estimation for approximate solutions
 of differential equations, using functional
 analysis 07 p1213 A67-19153
 Error bounds in numerical solution of
 ordinary differential equations, considering
 monotonic majorants 07 p1213 A67-19154
 Calculation of dislocation precipitated
 profile for ideal complimentary error-
 function diffusion profile of phosphorus in
 silicon 07 p1234 A67-19890
 Computer generation of error probability
 distribution for linear system response to
 random conditions 07 p1217 A67-20117
 Error analysis of direct solution of linear
 equations with computational errors
 expressed as perturbations on
 data 07 p1149 A67-20197
 Normal approximation of error transition
 probability for correlation receiver preceded
 by wideband hard limiter 09 p1459 A67-21579
 Solution of ill-conditioned linear equations
 when matrix of coefficients is not sparse or
 otherwise specialized, noting error analyses
 of elimination methods 09 p1468 A67-22045
 Nonlinear sampled system with parameters
 in functional dependence on sign of error at
 discrete instants of
 sampling 11 p1769 A67-24056
 Stability analysis of symmetrically loaded
 thin walled spherical shell, noting
 construction of asymptotic expansion, error
 estimation and application of elasticity
 theory 11 p1871 A67-24152
 Error accumulation in numerical
 integration of motion equation analyzed for
 circular satellite orbits 11 p1859 A67-24317
 Optimal smoothing filter and smoothing
 error covariance matrix equations for
 discrete linear systems, using orthogonal
 projection 11 p1770 A67-24422
 Multidimensional linear differential
 equations with almost periodic coefficients
 analyzed for error of exact
 solution 11 p1814 A67-24977
 Astatic gyroscope accuracy dependence on
 random fluctuations of dry friction moment
 when under oscillatory motion of bearings,
 giving correlation function of error
 dispersion 11 p1794 A67-25044
 Unified method of numerical quadrature
 for integrands of certain complex analytic
 functions, obtaining asymptotic expansion of
 error functional 13 p2145 A67-26734
 Angular errors in antennas with
 aerodynamic radome heating due to
 temperature variability 13 p2080 A67-27034
 Dynamic errors in electronic analog
 computers, noting expressions for shift in
 characteristic roots of equations under
 solution 13 p2073 A67-27064
 Interval arithmetic methods used for error
 bounding in matrix calculations of linear
 equations 13 p2147 A67-27170
 Stable evaluation algorithm for
 polynomials, discussing minimal Newton
 forms, error estimation,
 etc 14 p2342 A67-28003
 Order and asymptotic form of error of
 numerical methods for solving initial value
 problem for differential
 equations 15 p2471 A67-29632
 Operational accuracy of inertial navigation
 system as function of accelerometer and
 integrator error 16 p2699 A67-30468
 Particle trajectory analysis with
 perturbation series, noting position and
 velocity error estimation for restricted
 three-body problems 16 p2749 A67-31425
 Filter and error-covariance equations
 developed for optimal fixed-point smoothing
 for continuous linear
 systems 16 p2648 A67-31652
 Error probabilities of matched filter
 receiver operating in additive combination
 of impulsive and Gaussian
 noise 17 p2812 A67-32120
 Book on computer solution of linear
 matrix algebraic systems and errors
 involved, discussing Gaussian elimination,
 FORTRAN, ALGOL and PL/1 programs,
 etc 17 p2821 A67-32825
 Impurity diffusion role in silicon device
 technology, discussing error function
 distribution 18 p3096 A67-33455
 Limiting values for remainder forms in
 Taylor series and error estimation
 procedures for power series approximations,
 including truncation error 18 p3072 A67-34398
 Errors in thermodynamic functions of
 ideal gases determined from molecular
 data 18 p3161 A67-34472
 Error effect in continuous Kalman filters
 used in orbit determination problems,
 deriving error bounds
 formula 19 p3199 A67-34779
 Statistical techniques for missile injection
 error analysis, discussing direct and adjoint
 methods 19 p3254 A67-34780
 Numerical differentiation and smoothing
 of equally and nonequally spaced
 experimental data in independent
 variable 19 p3250 A67-35615
 Absorbance and emittance of metal
 surfaces determined via cyclic incident
 radiation, noting error computation and
 method accuracy 19 p3346 A67-35742
 Gradient method of parametric
 identification of processes through
 mathematical model 19 p3206 A67-35915
 Relative and absolute error sign and
 magnitude shown to be functions of strain
 field, strain gauge mounting and angular
 error of mounting on test
 object 21 p3626 A67-38049
 Variational approach to error analysis in
 dynamic system computer simulation,
 applying maximum principle and Liapunov
 second method 21 p3588 A67-38180
 Space triangulation equalization method
 based on modified closing plane method,
 discussing error equations 21 p3618 A67-38196
 Predictions from barotropic vorticity
 equation in spectral form analyzed for
 errors 21 p3654 A67-38575
 Radio wave refraction and refraction-
 induced errors calculated in determination
 of artificial satellite
 trajectories 21 p3582 A67-38593
 Reinforcement intervals /RI/ effect in
 paired-associate learning using within-
 subjects, noting error dependence on
 RI 21 p3576 A67-39100
 Error divergence elimination in recursive
 minimum variance estimation of space
 vehicle trajectories 21 p3587 A67-39148
 Orthogonal signaling in sequential decision
 feedback on communication over additive
 white Gaussian noise channel, obtaining
 expression for error
 probability 22 p3775 A67-39295
 Evaluation and analysis of critical human
 performance for rating man-machine
 interface 22 p3755 A67-40154
 Structure of error curve when function is
 approximated in Chebyshev sense by
 polynomials 23 p4022 A67-40862
 Discretization error analyzed for
 accumulation during numerical solution of
 equations of orbital
 motion 23 p4023 A67-40864
 Test accelerometer comparison calibrations
 via vibration standards, discussing
 sensitivity, relative motion and error
 analysis 23 p4003 A67-41336
 Error in calculating rate coefficients from
 cross section data in limited energy range,
 noting m-point Laguerre integration
 formula 23 p4030 A67-41530
 Canonical decomposition of nonlinear error
 covariance difference equation derived for
 discrete estimation
 problems 24 p4177 A67-42188
 Elliptic integrals and numerical
 representation of power series to yield
 closed form approximation, presenting error
 as function of modulus 24 p4178 A67-42205
 Errors in measuring scattering patterns of
 arbitrary body in Fresnel region due to
 body/antenna finite distances and
 directivities 24 p4120 A67-42229
ERROR SIGNAL
 Digital feedback control system
 compensation of pulse input to improve time
 response of controlled
 variable 01 p0045 A67-10673
 Signal and clutter model of monopulse
 radar tracking errors 02 p0201 A67-12114
 Complex indicated angle extension of
 monopulse normalized error signal used to
 locate unresolved targets 02 p0201 A67-12115
 Frequency shift keyed /FSK/ digital signal
 detection using FM discriminators,
 predicting error rates for several
 sequences 02 p0201 A67-12118
 Bit and message error rate dependence on
 variation of atmospheric noise statistical
 properties 02 p0203 A67-12165
 Time limited receiver signals design for
 minimizing error probability under energy
 and frequency constraints 02 p0204 A67-12171
 Contact resistance variation effect on
 strength tests, noting strain gauge reading
 error magnitudes 02 p0340 A67-12444
 Limitation imposed a priori on class of
 signals in order that every signal in class be
 distinguishable to within given mean square
 error by finite number of
 measurements 03 p0369 A67-13799
 Trimode four channel monopulse bridge
 with reduced microwave
 components 03 p0383 A67-13828
 Balloon-borne sun seeker improvements
 through transistorized circuits and solid
 state switches 07 p1184 A67-19396
 Transfer logic of double dialog high
 security data transmission system using long
 loop principle 07 p1146 A67-20159
 Fluidic binary full-adder configurations
 performance for subtraction function

required to generate error signal in closed loop control system 08 p1280 A67-20444

Error signal generation method to control laser frequency of laser oscillator 08 p1339 A67-21378

State space methods approach to model referenced adaptive control systems design using differential equations 11 p1771 A67-24894

Telemetry data processing problems noting error sources, probability distribution of counts in counting processes, sensor relay during motion in varying field, etc 12 p1905 A67-25779

Timing error and noisy phase reference joint effect on system performance of coded partially phase coherent reception 17 p2811 A67-32116

Modes of boresight shift in conical-scan and sequential-lobing types of amplitude sensitive angle-tracking antennas 17 p2814 A67-32523

Antenna field strength measurement above 1 GHz, discussing formulas for high accuracy gain determination, multipath interference and antenna separation 17 p2815 A67-32609

Generalized formulation of code separation incorporating general assumptions concerning nature of channel distortion 17 p2830 A67-32827

Discriminator for fine automatic frequency control of reflex-klystron by error signal 19 p3228 A67-34991

Strapdown star tracker for space vehicle attitude control, using scanning and error-signal determination method [AIAA PAPER 67-551] 19 p3233 A67-35948

Control moment gyro /CMG/ and use in space-vehicle attitude-control system, emphasizing control laws [AIAA PAPER 67-589] 19 p3336 A67-35985

Frequency shift keyed /FSK/ digital signal detection using FM discriminators, predicting error rates for several sequences 20 p3385 A67-37351

Sun pointing attitude control acquisition by space vehicle with jet control system 24 p4182 A67-41974

Errors in state vector from amplitude quantization in feedback control loop, noting finite word length in hybrid computer simulation 24 p4134 A67-42023

Star tracker error signal processor for onboard current satellite attitude control over wide range of gimbal angles 24 p4154 A67-42175

Recording methods error probability burning code message transmission with start-stop distortion ensuring authenticity by short pulses or integral method 24 p4122 A67-42376

ERYTHROCYTE

Enzyme activity in erythrocytes when MICORENE is used to prevent death from high altitude hypoxia 14 p2254 A67-28212

Biochemical reactions in human organism as indicator of cosmic ray variation, showing relationship between solar activity and erythrocytes in blood 17 p2934 A67-32099

Hematologic effects of increased oxygen tension, discussing mechanisms of erythrocyte-oxygen interactions 18 p2991 A67-34710

Plasma volume, red blood cell mass and erythrocyte survival determination before and after space flight 20 p3372 A67-37429

ESAKI DIODE

Current-voltage characteristics of Esaki diode composite circuit 10 p1609 A67-22837

Design and fabrication of germanium Esaki diodes emphasizing development of planar process, using conventional oxide masking techniques 13 p2083 A67-27572

Esaki diodes noting hump in V-I characteristics, temperature variation effects, etc 17 p2826 A67-32621

Memory-cell circuit employing Esaki diodes negative resistance characteristic, developing small memory pulse amplitude useful in minimizing cycle time 20 p3397 A67-36769

Tunnel and excess currents in Esaki diodes compatible with reversible introduction of active intermediate tunneling levels 21 p3590 A67-38152

Operational analysis and DC design of Esaki diode pair bistable circuit used in high speed counting network performed by analog computer 21 p3604 A67-38603

Distributed Esaki diode pulse

characteristics in solid state transmission circuit 21 p3599 A67-38609

ESCAPE

Escape of rocket vehicle from vicinity of planet, using tangential thrust [AAS PAPER 66-120] 07 p1254 A67-19979

Nutation divergence during atmosphere exit of spin stabilized probe shown to be analogous to pendulous gyro with time dependent spring 08 p1406 A67-20511

Escape of rocket vehicle from vicinity of planet, using tangential thrust [AAS PAPER 66-120] 13 p2209 A67-27534

Escape equipment, emphasizing Robertshaw helmet design to provide facial protection and retention of high Q conditions 14 p2256 A67-27744

Optimal methods of escape from helicopter, examining rotor avoidance during ejection 14 p2256 A67-27745

LW-3B escape system for low and medium performance V/STOL aircraft 17 p2794 A67-32000

Low light level TV as aid to nighttime air rescue, describing ionoscope and image orthicon of camera 17 p2859 A67-32506

Fire in Apollo 204 spacecraft noting alterations in oxygen and electrical systems, escape hatch, materials and communications 22 p3900 A67-39888

Qualitative safety and survival factors in emergency escape and relation to complete ejection event via functional diagramming 23 p3964 A67-41546

Mathematical technique to determine probabilities associated with critical system performance capability measured under varying human and environmental conditions 23 p3964 A67-41547

ESCAPE CAPSULE

Emergency Global Rescue, Escape and Survival System /EGRESS/ to protect space crew in emergencies encountered in earth-orbital operations 05 p0906 A67-17204

F-111 crew escape module design and performance 14 p2244 A67-27739

Requirements and disadvantages of proposed escape systems for fixed and rotary wing Army aircraft 17 p2794 A67-31998

In-flight escape of helicopter personnel using Navy fuselage capsule, describing devices for recovery, protection and survival 17 p2794 A67-31999

Paracone emergency escape system for rescuing space crews from orbits at hypersonic velocities 17 p2794 A67-32001

ESCAPE VELOCITY

Abort velocity requirements for three-burn transfer maneuver out of lunar polar orbit [AAS PAPER 66-133] 07 p1255 A67-19992

Velocity requirements for scientific probe vehicles in direct flight and planetary swingby modes of operation throughout solar system 14 p2387 A67-28618

Australasian tektite origin criticized regarding magnitude of atmosphere removal 14 p2390 A67-28889

Future planning of interplanetary voyages based on capabilities and economic advantages of classical propulsion, noting high escape velocity 14 p2392 A67-28961

Finite value of escape velocity from stationary stellar system influence on residual velocities 16 p2746 A67-30836

Evolution and future objectives of ejection-seat escape systems design, noting characteristics and deficiencies in conventional ejection seats 17 p2795 A67-32002

Geometrical form for solar system escape criterion 17 p2940 A67-32075

Moon-earth trajectories, with formulas for given angular ranges of flight, obtaining optimum velocity to depart from lunar gravitational field 21 p3704 A67-38584

ESCHERICHIA

Streptolignin interaction with DNA and resulting degradation and denaturation temperature of DNA from salmon sperm and Escherichia coli 06 p0952 A67-17873

Alteration in pyrimidine metabolism occurring after infection of E. coli with T-even bacteriophage 20 p3370 A67-38795

Factors involved in use of thymine by uninfected cells in metabolism of Escherichia coli 20 p3370 A67-38799

ESOPHAGUS

Gastroesophageal reflux in fillers measured in evaluation of hiatal hernia and possible esophageal origin of chest pain 21 p3574 A67-38084

ESRO I SATELLITE

DFL mobile telemetry ground station participation in solar eclipse expedition of ESRO in Greece 06 p0980 A67-18020

Temperature control in design of ESRO I European research satellite design 13 p2222 A67-26582

ESRO I research satellite structural design test results for study of polar ionosphere, particularly auroras 13 p2211 A67-26583

German participation in solar eclipse campaign of ESRO, describing rockets and radar used 15 p2466 A67-29572

Data acquisition systems for ESRO receiving, recording, display, telecommand and timing sections 20 p3443 A67-36471

Onboard receiver-decoder control unit for ESRO I and II consisting essentially of four-state signal corresponding to time modulated pulses 21 p3581 A67-38201

Mathematical model describing magnetic damping in attitude control system of ESRO I satellite 21 p3678 A67-38216

ESRO I satellite electronic equipment design applied to aurora studies 21 p3713 A67-38217

Power consumption reduction problems in coded telemetry measurements for ESRO I and HEOS A satellites 21 p3584 A67-38846

ESRO II SATELLITE

ESRO II satellite structural design, testing and material selection noting functions, vibration testing results, etc 03 p0518 A67-13600

ESRO II satellite project, describing systems and program management 05 p0905 A67-16728

ESRO II satellite project objectives, design, testing program and mission requirements 24 p4241 A67-42402

ESSA SATELLITE

ESSA meteorological satellite system noting mission requirements, design and performance [SMPT PAPER 101-56] 12 p2011 A67-25472

ESTER

SA NITRATE ESTER

SA POLYESTER

Esterification rates of aliphatic carboxylic acids, acid terminated polybutadienes, etc, and steric environment in vicinity of acid groups 04 p0564 A67-14473

Esterification of secondary alcohols, using amino acids 06 p0956 A67-18576

Extreme pressure /EP/ films from lubricants containing borate esters, studying structure and mode of action 16 p2683 A67-31756

ETCHING

Loops and spirals on freshly cleaved surfaces of laboratory grown single crystals of NaCl thermally etched by placing them in muffle furnace on platinum lid 04 p0675 A67-14761

IR transmission micrography and X-ray microanalysis of anomalous etching on surface of Si single crystals grown in Ar gas 04 p0675 A67-14769

HF acid vapor technique for room temperature etching of photolithographic stage of planar silicon dioxide device 04 p0682 A67-15488

Polygonization in silicon single crystal by chemical etching, determining activation energy, noting dependence on annealing temperature 05 p0862 A67-16503

Etching and X-ray spectrometric techniques to investigate distribution and density of dislocations in deformed and annealed GaAs and InSb crystal 05 p0865 A67-16920

Fluidic system design and fabrication method 06 p0950 A67-18063

Etching methods to visualize lattice dislocations and grain boundaries in Czochralski grown calcium tungstate crystals doped with neodymium for laser application 07 p1196 A67-19565

Etching techniques in fabrication of printed circuit boards 08 p1334 A67-20745

Thermal etching study of rod shaped formations caused by structural dislocations during heating and cooling of Ti-Mo-Fe-Al system 09 p1518 A67-21967

Anodic behavior of GaAs single crystals at increased current densities in alkaline and

acidic solutions, discussing etch
tunnels 11 p1848 A67-24743

Stimulation of photosensitivity of cadmium
sulfide single crystals by chemical
etching 13 p2174 A67-26401

Aluminum pretreating and finishing agents
noting cleaning, etching, roughening and
coatings 14 p2324 A67-27821

Etching and X-ray spectrometric
techniques to investigate distribution and
density of dislocations in deformed and
annealed Ga-As and InSb 14 p2365 A67-28260

Chemical etching examination of
dislocations and stacking-fault structure of
epitaxial gallium arsenic phosphide,
considering doping level, growth rate and
composition effects 14 p2366 A67-28421

Surface etching effects on positively
biased current-voltage characteristics of p-n
junctions in fused indium
antimonide 16 p2730 A67-31161

Plastic deformation of single crystals of
vanadium by bending and compressing at 298
and 77 degrees K showed etching but no
evidence of mechanical
twinning 18 p3101 A67-34077

Dissolution of single crystal silicon by
aqueous solutions of hydrofluoric acid and
chromium oxide studied as function of
etchant composition 19 p3301 A67-34934

Self-decoration effect in thermally etched
polycrystalline lithium ferrite, discussing
geometric symmetry relation to
crystallographic surface
orientation 22 p3855 A67-39344

Chemical milling of aluminum alloy parts
by dimensional etching, discussing protective
coatings 23 p4009 A67-40641

Electrolytic polishing technique for bright
field etch of Be
specimens 24 p4173 A67-42349

VACUUM
Vacuum UV photolysis of solid ethane
films, measuring product distributions,
presenting evidence for quenching of
excited ethane and
ethylene 05 p0758 A67-16128

IR observations for presence of ethane in
atmospheres of Jupiter and Saturn
reanalyzed and found consistent with
previous results 08 p1398 A67-21218

Flame properties of flammable ethane-rich
perchloric acid mixtures 14 p2406 A67-28546

ETHANOL
S ETHYL ALCOHOL
ETHER
S POLYPHENYL ETHER
THYL
Stark and Zeeman splitting in far IR
spectra of erbium, dysprosium and samarium
ethyl sulphate 04 p0686 A67-15778

ETHYL ALCOHOL
Radial distribution functions for liquid
methanol and ethanol at room temperature,
observing intermolecular hydrogen
bonding 20 p3378 A67-37560

ETHYLENE
SA POLYETHYLENE
Oxygen atoms reaction with
tetrafluoroethylene in presence of molecular
oxygen 04 p0567 A67-15949

Mercury photosensitized oxidation of
tetrafluoroethylene, noting reaction process
and parameters 04 p0567 A67-15950

Electron impact spectrum of ethylene at
low energy and right angle scattering, noting
unresolved and forbidden
transitions 09 p1458 A67-22027

Temperature dependence and reaction
energetics of free radical addition of
trifluoroacetonitrile to
ethylene 09 p1459 A67-22364

Flame properties of flammable ethylene-
rich perchloric acid
mixtures 14 p2406 A67-28545

Ionization in ethylene flames at
atmospheric pressure, using nitric oxide as
oxidizer and electrostatic
probe 18 p3107 A67-33804

ETHYLENE COMPOUND
Perfluorocyclopropane production in
reaction of oxygen atoms with
tetrafluoroethylene 01 p0018 A67-10762

Tetrafluoroethylene dissociation in
nitrogen behind shock waves and
thermochemical constants studied, using
shock tube and optical absorption
spectroscopy 05 p0759 A67-16840

Ultrahigh molecular weight poly(ethylene
terephthalate) synthesized, studying catalyst,

particle size, reaction temperature and time
and carrier gas flow rate 24 p4178 A67-42467

ETHYLENE OXIDE
Electronic part sterilization program using
ethylene tetroxide gas 07 p1136 A67-19618

Ethylene oxide and methyl bromide
mixture for spacecraft sterilization,
discussing penetrating power, effect on
components and packing and
toxicity 15 p2430 A67-29101

Desiccated microbial populations of
lyophilized Staphylococcus epidermidis cells
and Bacillus subtilis spores studied for
synergism in ethylene oxide-methyl bromide
sterilization 19 p3180 A67-35279

ETTINGSHAUSEN EFFECT
Peltier and Ettingshausen effects in flux-
flow state of superconducting niobium,
considering contribution to entropy
flow 19 p3304 A67-35535

ETTINGSHAUSEN-NERNST EFFECT
Electron-hole conductivity effect on
temperature variations of Hall coefficient
and Nernst-Ettingshausen effect in
semiconductor 02 p0296 A67-11829

Nernst-Ettingshausen coefficient calculated
for scattering at short duration potential, at
impurity ions and at acoustic
oscillations 09 p1554 A67-21970

Electromagnetic effect in n-type InSb
samples, measuring magnetic resistance, Hall
effect and magnetic EMF 13 p2174 A67-26368

Galvano and thermomagnetic effects in
semiconductors determined by using Hall
effect, resistance variations in magnetic
field and Nernst-Ettingshausen transverse
effect 14 p2365 A67-28314

Quantum oscillations of Nernst-
Ettingshausen effect in indium
arsenide 14 p2376 A67-29087

Temperature dependence of transverse
and longitudinal Nernst-Ettingshausen effect
and composition effects on Hall electron
concentration in InSb-InTe solid
solution 16 p2730 A67-31157

Nernst-Ettingshausen coefficient calculated
for scattering at short duration potential, at
impurity ions and at acoustic
oscillations 17 p2923 A67-33307

Transverse Nernst-Ettingshausen
thermomagnetic effect in intrinsic
conductivity region in InSb single crystals
subjected to magnetic
field 19 p3300 A67-34763

Band structure and current carrier
scattering in hole-type SnTe, studying
temperature dependence of electric
conductivity, thermal EMF, Hall effect,
etc 19 p3300 A67-34766

Electromagnetic effect in n-type InSb
samples, measuring magnetic resistance, Hall
effect and magnetic EMF 21 p3680 A67-38324

EUCLIDEAN SPACE
Solvability of degenerated parabolic
boundary value problem in Euclidean space
cylinder and relation to homogeneous
Dirichlet problem 01 p0105 A67-10677

Partitions of n-space by hyperplanes,
examining applications in switching
theory 01 p0106 A67-10733

Differential moduli of differential spaces
on ring or on differential solid with variable
coefficients 03 p0458 A67-13460

Extreme points of copositive quadratic
forms constituting closed convex cone in
Euclidean space 05 p0836 A67-17045

Tame subsets of spheres in Euclidean-3
space, showing tameness of closed subset F
of 2-sphere S 07 p1215 A67-19507

Asymptotic behavior of curvature tensor
in certain asymptotically Euclidean
Riemannian space-time
manifold 11 p1819 A67-24763

Almost periodicity of bounded solutions to
nonlinear systems in n-dimensional Euclidean
space 13 p2144 A67-26381

Iterative methods for solving nonlinear
least squares problems by choosing linear
nonsingular transformations of finite-
dimensional Euclidean
space 13 p2147 A67-27171

Unique iterative solution to degenerate
quasi-linear elliptic equations and
systems 15 p2511 A67-30001

Iterative solution methods for minimizing
convex, differentiable function in Euclidean
space 16 p2697 A67-31424

Book on optimal control covering theory
and application of linear algebra, vector
analysis, Euclidean space, Pontryagin
principle, etc 18 p3018 A67-34758

Motion equations of classical point
particles determined by known Euclidean
symmetry of space 19 p2362 A67-35709

Flow of steady compressible gas expressed
in intrinsic relations to derive equations of
rotational motions in Euclidean
space 19 p3212 A67-35883

Dynamic system with state at any instant
represented by point in Euclidean space of
n dimensions 19 p3203 A67-35902

Almost periodicity of bounded solutions to
nonlinear systems in n-dimensional Euclidean
space 20 p3479 A67-37726

EULER BUCKLING
Stability of linear viscoelastic columns
with variable cross sections, obtaining and
verifying buckling load 08 p1418 A67-20594

Dent effect on buckling strength of
aluminum alloy tubular columns subjected to
axial compression
[ASME PAPER 67-MET-12] 12 p2030 A67-25951

Column shape for maximum Euler
buckling load determined using energy
method calculations 17 p2960 A67-32421

Buckling analysis of sandwich beams with
elastic orthotropic cores under axial
compression 20 p3537 A67-36641

EULER-CAUCHY EQUATION
Cauchy problem for Euler-Poisson-Darboux
equation solved for all values of time and
specified values of
parameter 02 p0260 A67-12431

EULER EQUATION
Book on principles of ideal fluid
aerodynamics covering vector algebra and
calculus, Euler equations, steady and
unsteady acyclic motion, complex variable,
lift, etc 05 p0793 A67-17151

Self-similar solution generalization for
Euler-Poisson wave equations, noting
application to transonic gas
dynamics 06 p1023 A67-17862

Euler angles sets, particularly right-handed
coordinate systems and positive rotations,
with solutions for angular
velocities 06 p1032 A67-18527

Tuned viscoelastic vibration dampers
effect on responses of cantilever and
clamped-clamped beams subject to Euler-
Bernoulli beam equation, discussing loss
factors based on transmissibility
spectra 06 p1110 A67-18859

Transient response of beams using lumped
parameter models calculated by Euler
method to eliminate influence coefficient
normally required 06 p1111 A67-18889

Nutation divergence during atmosphere
exit of spin stabilized probe shown to be
analogous to pendulous gyro with time
dependent spring
constant 08 p1406 A67-20511

Lagrange and Euler representations of
particle shapes and vortex theorems in
hydrodynamic flow 13 p2094 A67-26644

Intermediate-thrust arcs in central force
field satisfying optimality conditions, noting
that motions are degenerate solutions of
Euler equations 14 p2382 A67-27850

Optimum shape variations of minimum-
drag body with given lifting force and
volume solved through Euler
equations 14 p2239 A67-27983

Existence and uniqueness theorem for
axisymmetric problem with initial data for
Euler equation in case of incompressible
fluid 18 p3027 A67-34201

Perturbation scheme deriving geomagnetic
Euler potentials applied to magnetospheric
model with solar wind
effect 20 p3434 A67-37423

Strapped-down inertial navigation
computational problems solved by Euler
parameter algorithms require less computer
time 21 p3656 A67-38951

Euler motion generalization of solid body,
discussing inertial and kinetic
moments 22 p3836 A67-39403

Maxwell-Euler equations reformulated into
equivalent matrix integral equation,
obtaining dispersion relation from integral
equation kernel for compressible electron
plasma 23 p3974 A67-41204

EULER-LAGRANGE EQUATION
Project Prairie Grass diffusion
experiments analyzed to determine Hay-
Pasquill scale factor relating Lagrangian and
Eulerian turbulence
scales 02 p0262 A67-12082

Estimation of parameters of transverse
diffusion in lowest atmospheric layer using

Lagrange and Euler turbulence characteristics 16 p2698 A67-31095

EULER-LAMBERT EQUATION

SA ELLIPTICAL ORBIT

SA RENDEZVOUS

Euler-Lambert equation for orbital transfer in Newtonian field solved by approximate method 14 p2383 A67-27865

EUROPE

SA DENMARK

SA FRANCE

SA GERMANY

SA GREAT BRITAIN

SA ITALY

SA RUMANIA

SA SPAIN

SA SWEDEN

SA SWITZERLAND

SA U.S.S.R.

Future prospects of aeronautical construction in Europe 01 p0168 A67-10264

European airline depreciation practice and suggested modification 01 p0168 A67-10269

Future prospects of aeronautical construction in Europe 03 p0537 A67-12966

International factors in air transport under treaty establishing European Economic Community [SAE PAPER 670231] 12 p2040 A67-25491

EUROPEAN I SPACECRAFT

Cold rolled extra-thin stainless steel application in construction of front and rear interstage sections of second stage of Europa I rocket 01 p0160 A67-10408

Chemical problems concerning specifications and use of nitrogen peroxide and unsymmetrical dimethyl hydrazine as propellants 06 p1071 A67-17612

German firm participation in designing and constructing third stage of ELDO launch vehicle EUROPA I 16 p2763 A67-31789

Europa I third stage attitude control system design, discussing various model configurations and overall simulation 22 p3897 A67-39171

EUROPEAN SPACE PROGRAM

Space research and astronautics, importance to science and European economy 01 p0168 A67-10268

Satellites for TV distribution and broadcasting system for Western Europe, considering increased antenna gain of ground station for minimum satellite energy consumption 01 p0027 A67-11417

Satellite placing in synchronous orbit using ELDO PAS booster for telecommunications purposes 01 p0156 A67-11418

Optimal design configuration for third stage of European launching vehicle 02 p0334 A67-12376

Space research and aerospace engineering in ESRO and ELDO, examining European participation in communications satellite system promoted by U.S. 03 p0537 A67-12967

High altitude test stands of DVL rocket test range at Lampoldshausen, planning considerations and preliminary results from altitude simulation [DVL-604] 03 p0394 A67-13029

Rocket launching site in Sweden operated by ESRO for studies of polar auroras and polar cap absorption 03 p0395 A67-13498

Environmental test program for third stage of European launch vehicle 04 p0595 A67-14570

UK space projects detailing Skylark, Blue Streak, Black Knight and Black Arrow rockets 05 p0905 A67-16727

European Conference on Telecommunications by Satellites /CETS/, recommendations and patterns of cooperation 06 p1119 A67-17558

European geodetic network by satellite observation - Conference, Paris, December 1964 07 p1175 A67-19756

European satellite triangulation network, discussing scientific, technical and organizational aspects 07 p1176 A67-19761

Diademe satellites design including laser beam range determination reflectors for spatial geodesy, laser telemetry, etc 10 p1712 A67-22860

French space program /1966-1970/ techniques and installations for satellite launching and tracking 14 p2409 A67-28605

French installations for space research, describing laboratory work and industrial investments for satellite launching 14 p2320 A67-28606

Launcher for research and development on

aerodynamic reentry 15 p2564 A67-29094

European recoverable and reusable aerospace transporter 15 p2566 A67-29829

feasibility

European aerospace transporter, fundamental concepts and development 15 p2556 A67-29838

European aerospace transporter feasibility and worth 15 p2567 A67-29839

Air breathing reusable rocket launchers for European development, comparing ramrocket and turboramjet propulsion 15 p2568 A67-29844

Saphir test vehicle, two-stage guided and controlled rocket 15 p2571 A67-30090

Critical Path Analysis /CPA/ system based on network techniques, coordinating separate development programs of ELDO member states 15 p2583 A67-30223

San Marco project, joint effort of NASA and Italian Space Commission to launch satellite for atmospheric and ionospheric measurements 16 p2757 A67-30642

Space environment simulator of CNES in France describing reproduction of low pressure atmosphere, heat sink, solar and planetary radiation, etc 16 p2654 A67-30675

European television satellite design emphasizing coverage area, carrier frequency selection, etc 16 p2622 A67-30697

Diapason satellite thermal control noting external energy exchange calculation, coating, in-space simulation tests, temperature measurements, etc 16 p2762 A67-31018

Task distribution, overall network, flow diagram and data processing of PERT method controlling development of ELDO-A rocket third stage 16 p2783 A67-31632

German firm participation in designing and constructing third stage of ELDO launch vehicle EUROPA I 16 p2763 A67-31789

French Diademe satellites power supply systems and planned laser experiments 17 p2941 A67-32232

Configuration study for ELDO-PAS test satellite based on communications requirements 17 p2955 A67-32396

European Satellite Telecommunication Conference /CETS/, discussing government participation, INTELSTAT projects, European technical program and juridical and administrative operations 17 p2974 A67-32398

ELDO-PAS program principles, objectives, ground stages, orbital injection, etc 17 p2955 A67-32399

Satellite telecommunication techniques including demodulation, detection, microwave amplification, antennas, etc 17 p2813 A67-32400

Diamant satellite series, describing design and construction of Diapason and Diadem orbital satellites 17 p2956 A67-32746

Characteristics, operation, technology and reliability of telemetering systems for ESRO I, HEOS A, TD 1 and TD 2 including control factors and coding 17 p2816 A67-32747

Hybrid simulators used for aerospace and military programs consisting of analog computers, digital computers and interface units for handling data flow 18 p3019 A67-33635

German Azur research satellite program design, instrumentation, payload, etc, and NASA role 18 p3162 A67-33640

Space center under construction in French Guiana for launching rocket probes and satellites with aid of Diamant booster, discussing optical sites, storage tanks, LOX factory, etc 18 p3019 A67-33652

Development of liquid hydrogen-oxygen propulsion stage in France, discussing structure, thermal isolation, storage, etc 18 p3111 A67-33653

European heavy launching vehicle development potential and economy, discussing communication satellites, thrust augmentation, zero stages, synchronous orbit, etc 18 p3137 A67-34353

Computer application to planning and operating simultaneous access European ground station network 18 p3003 A67-34355

Worldwide satellite telecommunication system, economic and political implications and effects on CEPT 18 p3162 A67-34357

Rocket launchings of French ballistic program, discussing trajectory study techniques 18 p3020 A67-34379

Central station construction for German ground-station system for research

satellites 18 p3021 A67-34601

French laser telemetry network, noting Q-switched ruby laser, Doppler effect, measurement and local spatial geodesy, program 19 p3182 A67-35233

Tracking station network organization, equipment and operations of National Center for Space Studies /CNES/ in France 19 p3207 A67-35244

Tropospheric circulation observation through FR-2 satellite project, discussing instrumentation, ground stations, trajectory analysis, etc 19 p3332 A67-35244

Space research activities in Denmark /1966-1967/, discussing instrumentation design and development, experiments, etc 19 p3319 A67-35283

Space research activities in Czechoslovakia, discussing satellite observation, aerospace medicine, solar physics, etc 19 p3320 A67-35283

Bulgarian research in spectroscopy, solar system, ionosphere, gravitation equations, astrophysics, etc 19 p3320 A67-35283

Space research activities in Finland /1966/ detailing satellite station 19 p3320 A67-35283

French space program research on ionospheric plasma, wave emissions, wind velocity, etc 19 p3320 A67-35294

Cosmic space research activities in Hungary, discussing data recording, satellite tracking, etc 19 p3320 A67-35294

East Germany space research in satellite tracking, coupling processes, upper atmosphere, high energy particles, etc 19 p3321 A67-35294

Italian space-research activities /1966-1967/, discussing San Marco 2 satellite project 19 p3321 A67-35294

Space research organizational structure in Netherlands noting programs and experiments 19 p3321 A67-35294

Swiss space research programs noting experiments, technology, etc 19 p3321 A67-35301

Rumanian space research in meteorology, fluid mechanics, space medicine, etc 19 p3321 A67-35305

ISY geophysical work in Greece examining geomagnetism, aurora, ionosphere, airglow, solar activity, etc 19 p3223 A67-35478

Specific features of French Diademe satellites noting payload stabilization, thermal control observation carried, instrumentation, etc 19 p3333 A67-35500

Ground station for satellite communications in Italy covering TV transmission 19 p3207 A67-35568

Satellite programs for Black Arrow launch vehicle, discussing functions, tasks, tests, etc 19 p3333 A67-35842

Data acquisition systems for ESRO receiving, recording, display, telecommand and timing sections 20 p3443 A67-36471

Space electronics in France, role in boosters, control, communication, onboard systems, etc 20 p3399 A67-36875

European approaches to physiological and psychotechnical selection and training of cosmonauts 20 p3375 A67-36925

PCM telemetry system for ELDO program discussing data acquisition and processing 20 p3392 A67-37162

Activity of Satellite Servo System and Electronic Division of San Giorgio in aerospace field 20 p3400 A67-37163

Space activity and research in industry noting European participation, international cooperation /ELDO program/ and research organizations 20 p3556 A67-37164

ELDO-A satellite launcher engine assembly and shell section production and testing 20 p3533 A67-37166

Inertial guidance system in ELDO-A satellite launch vehicle performance assessed using onboard computer 20 p3481 A67-37167

Onboard receiver-decoder control unit for ESRO I and II consisting essentially of four-state signal corresponding to time modulated pulses 21 p3581 A67-38201

ESRO I satellite electronic equipment design applied to aurora studies 21 p3713 A67-38217

Diamant launcher transmitter characteristics noting anomalies during first two firings 21 p3581 A67-38222

Electronic control system for triaxial control of geocentric satellite and second stage of CORALIE 21 p3656 A67-38231

booster

Nonline-of-sight communication with FR-I

- satellite along magnetic field line of emitter, using VLF electromagnetic waves 21 p3584 A67-38656
- ESRO V satellite-borne solar-proton spectrometry experiment to study proton and alpha particle energy spectra emitted during solar activity 21 p3629 A67-38663
- French research on electric propulsion dealing with plasma dynamics, discussing traveling wave accelerators, pulsed plasma guns, ion thrusters, etc [AIAA PAPER 67-740] 21 p3695 A67-38762
- European rockets characteristics and launch firing ranges, discussing rocket probes for near-earth and space environments 21 p3714 A67-39049
- Acquisition phase of satellite with passive magnetic attitude stabilization, discussing programming difficulties and modified Rayleigh model for German 625A-1 satellite 22 p3898 A67-39173
- Test and control planning concepts for space travel projects, considering third stage of booster rocket Europa 22 p3921 A67-39281
- German capability of competing in space travel with other nations 22 p3922 A67-39532
- P4 double test stand for ground testing third stage of ELDO launch vehicle 23 p3987 A67-41325
- AZUR project /first German satellite/ cooperation with NASA, testing, signal recording, etc 23 p4071 A67-41326
- EUROPEAN SPACE RESEARCH ORGANIZATION SATELLITE S ESRO I SATELLITE S ESRO II SATELLITE
- EUROPIUM Solvent and temperature effects on fluorescent emission of europium beta diketonates 01 p0131 A67-10297
- Energy transfer mechanisms involving trivalent terbium and europium, noting that at 295 degrees K thermal effects cause overlap permitting dipole-dipole transfer to occur 01 p0134 A67-10874
- Luminescence of alcoholic solution of europium chelate at low temperatures, noting changes in intensity of optical excitation at various energy levels 03 p0433 A67-12894
- Internal conversion electron spectrum for samarium 155 to europium 155 transmutation, noting multipolarities and new lines 16 p2733 A67-31706
- Fluorescence spectrum of activating europium ion in lutetium oxide matrix and appearance in crystalline-field model 19 p3307 A67-35794
- Divalent Eu ion ground state splitting in C3h symmetry sites and associated color centers in EPR spectrum study of Eu ion doped lanthanum trichloride 22 p3863 A67-40003
- EUROPIUM COMPOUND High intensity triboluminescence in europium tetrakis /dibenzoylmethide/-triethylammonium crystals under mechanical impact 01 p0019 A67-10897
- Magnetic, electric and SHF properties of oxides and solid solutions of bivalent europium from 1.6 to 300 degrees K 16 p2733 A67-31732
- EUTECTIC ALLOY Unidirectional solidification of eutectics for production of composite materials, avoiding problems with whiskers, interfacial bonding, matrix distribution, etc 03 p0444 A67-13435
- Fine structure and microstructural effects on control of magnetic, electrical, optical, thermal and mechanical properties of eutectic alloys 06 p1018 A67-18409
- Eutectic alloys of heavy metal phases with InP compound analyzed, noting phase orientation parallel to solidification direction 09 p1552 A67-21880
- Eutectics use in composite material by growing single crystal whiskers aligned inside matrix 10 p1669 A67-23637
- Hypereutectic carbides from carbide graphite alloys exhibiting high thermal shock resistance 11 p1809 A67-25004
- Hydrogen solubility in eutectic sodium-potassium mixture, noting usefulness as nuclear reactor coolants, and dependence on pressure and temperature 16 p2619 A67-30620
- Microstructure stability of aluminum reinforced with Al-Ni whiskers, noting tensile strength and mechanical property dependence on temperature 16 p2690 A67-31372
- Melting point and microhardness of carbon-saturated TiC-VC solid solutions, noting temperature of eutectic of TiC-VC with graphite 16 p2691 A67-31588
- Unidirectionally solidified eutectic alloys noting materials preparations for thermoelectric, magnetic, optical and electronic applications 20 p3469 A67-37359
- Fe rods in Fe-Sb matrix eutectic system, measuring rod diameter and Fe volume fraction effects on magnetic properties 23 p4039 A67-40884
- EUTECTIC DIAGRAM Isothermal transformations in hypo-and hypereutectoid titanium-chromium alloys 07 p1200 A67-19244
- Phase equilibrium and physicochemical properties of titanium aluminide-titanium stannide-zirconium quasi-ternary alloy 07 p1204 A67-19264
- Titanium-chromium-vanadium system isohardness and isothermal diagrams and characteristic micrographs 11 p1806 A67-24362
- Niobium-cobalt alloys constitution, determining equilibrium diagram by thermal analysis, microscopic metallography and X-ray diffraction techniques 14 p2338 A67-28615
- EVACUATION SA GAS EVACUATION Indications and contraindications for transportation of wounded by helicopter and ambulance 12 p1902 A67-25174
- SA BOILING SA TRANSPIRATION SA VAPORIZATION Ellipsometer study of anomalous absorption in very thin dielectric films on evaporated metals 01 p0138 A67-11075
- Substrate temperature effect on structure of evaporated alloy thin films 02 p0287 A67-11716
- Evaporation process and pore development in alloy samples under tensile stresses 03 p0424 A67-14058
- Vapor composition, evaporation rate and vapor pressure above chromium carbides determined by effusion method combined with mass spectrometry 03 p0456 A67-14193
- Heating and scattering of plasma produced by giant laser pulse focused on solid target 03 p0486 A67-14194
- Thin film deposition techniques, presenting vacuum evaporation and sputtering 04 p0631 A67-15992
- Gas dynamic equations for determination of heating, vaporization and expansion of substance due to Q-switched laser radiated collimates onto surface of solids 05 p0819 A67-16652
- Evaporated thin film capacitor from silicon oxide, noting electron diffraction patterns and IR adsorption peaks 09 p1555 A67-22102
- Heating and scattering of plasma produced by giant laser pulse focused on solid target 14 p2360 A67-28539
- Constant total pressure evaporation with heat reuse by built-in engine 14 p2407 A67-28623
- Thin films of cuprous sulfide, selenide and telluride prepared by flash evaporation, discussing resistivity and absorption coefficient 18 p3106 A67-34637
- Water injection for alleviating reentry plasma sheath-induced communication blackout, analyzing spherical drop evaporation in free molecular flow 19 p3211 A67-35762
- Resistance and Hall effect measurements on PbTe thin films prepared by vacuum evaporation on amorphous or oriented substrates 19 p3307 A67-35795
- Pressure dependence of heat transfer by evaporation, obtaining parameters from dimensional analysis 21 p3732 A67-38499
- Evaporation of Saturn ice rings by UV and solar wind sputtering or by photosputtering in IR and proton bombardment 21 p3705 A67-38599
- EVAPORATION COOLING Optimum cooling in ventilated impermeable clothing using ambient air over range of simulated physiological activity 23 p3967 A67-41604
- EVAPORATION RATE Lubricant testing for supersonic aircraft, examining temperature requirements, viscosity, evaporation characteristics, etc [DVL-606] 03 p0426 A67-13016
- Quartz crystal oscillator measurements of effect of film deposition rate on resistance of chromium thin films 04 p0675 A67-14921
- Track method analysis of phase transitions in particle growth and evaporation rate during combustion process 08 p1428 A67-21421
- Evaporation process of particles in high temperature gas stream under nonadiabatic conditions 08 p1428 A67-21424
- Approximation method for calculating self-ignition delay for monodisperse air-fuel mixtures 08 p1428 A67-21425
- Evaporation kinetics of small droplets is dependent on size, liquid and gas state and gas-liquid interface properties 11 p1884 A67-24989
- High temperature corrosion and evaporation of Haynes 25 and Hastelloy X-280 in atmospheres of oxygen, carbon monoxide, carbon dioxide, water vapor and methane 14 p2336 A67-28148
- High temperature oxidation of titanium at reduced oxygen pressures governed by dissolution of oxygen in metal 17 p2873 A67-32812
- Sublimation enthalpy of CdTe thin films in high vacuum determined from 350 to 400 degrees C 20 p3514 A67-37453
- Space environmental effect on lubricants and rolling element bearings, comparing evaporative losses of solid and liquid lubricants 21 p3633 A67-38143
- Arsenic evaporation from gallium arsenide experiment used to study volatile solid evaporation suppression 21 p3686 A67-39134
- EVASIVE SATELLITE Interception satellite thrust and steering optimization for pursuing maneuverable satellite, analyzing both evader and pursuer sides with differential game concept 24 p4182 A67-42908
- EVERSHED EFFECT Sunspot phenomenon covering formation, penumbra, spot umbra, magnetic field, interpretation, radiative deficit in umbra and penumbra, energy flux through Evershed stream, etc 13 p2202 A67-27416
- Evershed effect observations suggest existence of two or more streams in both photospheric and chromospheric Evershed flows 13 p2204 A67-27429
- Center-to-limb variation of Evershed effect for isolated symmetrical sunspot observations interpreted in terms of mass motions in penumbral fine structure 13 p2204 A67-27430
- Line contours for Fe-I-6302.5 angstrom across sunspot in west solar limb measured simultaneously with magnetic field strengths and direction and Evershed velocity 15 p2554 A67-29460
- EVOLUTION SA BIOGENY SA GALACTIC EVOLUTION SA GAS EVOLUTION SA LUNAR EVOLUTION SA ORIGIN SA PLANETARY EVOLUTION SA STELLAR EVOLUTION
- Origin of life on earth, formation of nucleic acid molecules and metabolic mechanism 24 p4112 A67-42052
- EXCHANGE S CHARGE EXCHANGE S ENERGY EXCHANGE S GAS EXCHANGE S ION EXCHANGE
- EXCHANGER S HEAT EXCHANGER
- EXCITATION SA ACOUSTIC EXCITATION SA ATOMIC EXCITATION SA ENERGY LEVEL SA HARMONIC EXCITATION SA IONIZATION SA SELF-EXCITATION SA TRIPLET EXCITATION
- Excitation and relaxation mechanisms for closed molecular gas laser 05 p0816 A67-16631
- Excitation of probe near semiconductor 07 p1154 A67-19790
- Fractional excitation and ionization for argon beam extracted from arc-heated supersonic free jet, noting molecular ions and neutralization 18 p3082 A67-34028
- Absolute electron impact excitation cross section of 3914 angstrom band of positively ionized nitrogen molecule 20 p3450 A67-37104

EXCITED STATE

- Differential cross section for excitation of helium electronic states by helium ions 01 p0116 A67-10337
- Exciton and impurity states in Kr and Xe crystals and in rare-gas solids containing Xe impurity calculated by pseudopotential theory 02 p0281 A67-11490
- Normal and abnormal optical absorption in thin zinc sulfide films with excited states in forbidden band surfaces 02 p0288 A67-11724
- Spectra and intensity vs excitation level and spatial distribution vs current density determined for optical radiation by electron excited cadmium sulfide 02 p0251 A67-11828
- Quasi-stationary techniques for calculating energies and widths of resonances occurring in electron-atom and electron-molecule scattering 02 p0269 A67-12449
- He I excitation as result of ionization and recombination at chromospheric spicule temperature 02 p0328 A67-12484
- Absolute excitation cross sections of helium levels colliding with low energy electrons 02 p0270 A67-12487
- Light absorption by uranium glass in excited state, showing relaxation time relation to luminescence 03 p0436 A67-13141
- Nonrelativistic energies and mass polarization shifts of excited S states of lithium cation 03 p0472 A67-13323
- Electron spectra in UV region noting excitation techniques, energy level mean lives and population distribution 03 p0472 A67-13324
- Steady state regime and stability of two-photon laser, noting field dependence of intensity and duration of frequency pulse and resonance excitation curves 04 p0631 A67-14745
- Antenna with limited excitation region, discussing emitter design with prescribed radiation pattern and near field behavior 04 p0583 A67-15148
- Gas laser spectroscopic analysis of hyperfine structure, paramagnetic properties, radiative lifetimes and Doppler-broadened transition saturation behavior of excited states of Xe 129 04 p0661 A67-15462
- Excited states in negative atomic oxygen ion, giving estimates of electron-atom interaction 04 p0661 A67-15764
- Hydrogen molecule excitation by electron impact extended to D excited state, noting values for oscillator strength 04 p0662 A67-15767
- Nature of excited state resulting from two-quantum absorption associated with fluorescence in anthracene produced by ruby laser 05 p0814 A67-16130
- Relaxation problem of two-level molecule in dense resonance medium 05 p0762 A67-16351
- Gas laser pumped microwave emission for producing controlled excited state population for RF spectroscopy of neon 05 p0817 A67-16638
- Double resonance effects extended to case of stimulated emission in excited states of neon, using gas laser in transverse DC magnetic field 05 p0818 A67-16645
- L- and K-band absorption due to optical transitions starting from ground state of F center in alkali halide 05 p0864 A67-16801
- Fluorescence decay time of NO, determining transition moment variation 05 p0848 A67-16837
- Differential cross sections corresponding to excitation of seven states of residual nucleus in Al-Mg reaction at 20.9 Mev 05 p0849 A67-17381
- Cryochemical synthesis and processing by reacting free radical with excited state species 08 p1290 A67-21187
- Lasering effect on electron gas and excited state populations in xenon discharges 08 p1338 A67-21306
- Excitation-recombination statistics in semiconductors with donor and center interacting with both bands for given thermal disequilibrium, treating silicon 09 p1551 A67-21669
- Free charged particles interaction with each other and neutral atoms in highly excited states effect on thermodynamic and gas dynamic parameters of shock wave propagating in cesium vapor, taking into account energy losses due to radiation 09 p1540 A67-21791
- Atomic collisions, excitation transfer processes and energy level transition probabilities in plasma of gas lasers 09 p1513 A67-22067
- Molecular metastables produced in positive column of helium discharge by electron excitation 09 p1548 A67-22368
- Effective excitation cross sections of helium singlet levels under proton impacts 10 p1699 A67-22845
- Excitation and photon emission rates of auroral nitrogen first and second positive group 10 p1650 A67-23338
- He I excitation as result of ionization and recombination at chromospheric spicule temperature 10 p1708 A67-23352
- Absolute excitation cross sections of helium levels colliding with low energy electrons 10 p1682 A67-23355
- Excitation cross section of upper laser levels in ionized argon by electron collision with ground state neutral atoms measured, using incoherent light technique 10 p1665 A67-23382
- Effective cross sections of excitation of lower energy levels during electron collisions in alkaline metals, noting dependence of various levels on quantum number and atomic number 11 p1822 A67-24018
- Level populations and energy loss rate of electrons during nonelastic collisions with impurity molecules in weakly ionized two-temperature plasma 11 p1831 A67-24019
- Differential reaction cross section and internal excitation function from K and Br molecule crossed beam velocity analysis 11 p1750 A67-24991
- Rate equations for nonequilibrium excitation of neutral helium in plasmas of moderate density solved and compared with population densities 11 p1844 A67-25075
- Nonequilibrium MHD generator for closed and open cycles, noting K seed ionization by energy transfer from excited N molecules 12 p1898 A67-25388
- Spatial modulation in populations of optically pumped ruby investigated for possible application to analysis of space and time distribution of laser beam 13 p2126 A67-26860
- Anisotropy in tunneling density of states in pure type II superconductors, examining ideal case of perfectly specular boundary scattering at tunneling junction 14 p2365 A67-28294
- Density of states of pure type II superconductors in high magnetic fields, deriving approximate expression for Green function 15 p2533 A67-29089
- Antenna with limited excitation region, discussing emitter design with prescribed radiation pattern and near field behavior 15 p2443 A67-29335
- Dissociation cross section of hydrogen molecule exchange excited by electron impact from ground to triplet state, using one-center wave functions 15 p2521 A67-30379
- Long-lived impact excitation states of particles measured from cross section of nonelastic collision with second particle 17 p2809 A67-32142
- Superconducting and superheated metastable state transition to normal state by beta irradiation 17 p2912 A67-32270
- Cerenkov radiation due to point charge moving at uniform velocity parallel to magnetostatic field in unbounded magnetotonic medium 17 p2812 A67-32314
- Excitation temperatures of electron levels of CH molecule in photosphere 17 p2941 A67-32326
- GaAs diodes measured for capacitance at 77 degrees K, noting change due to traps photoexcited in space charge layer 17 p2914 A67-32655
- Inelastic differential scattering cross sections and angular distribution of Ni first-excited-state protons determined by distorted wave calculation 17 p2888 A67-32733
- Spin-exchange frequency pulling of ground state hyperfine transition in atomic hydrogen analyzed for self-excited oscillation in hydrogen maser 17 p2889 A67-33225
- Excited state and steady state populations in high pressure plasma with heavy particle collisional ionization and electron-ion recombination 17 p2909 A67-33228
- He-He ground state and first excited state potentials obtained from differential scattering cross sections 17 p2889 A67-33257
- Dielectronic recombination and autoionization included in ionization formula for solar corona 17 p2952 A67-33392
- Multiphonon orbit-lattice relaxation of lower lying excited states of Dy doped lanthanum chloride investigated, using IR fluorescence and quantum counter techniques 19 p3302 A67-35035
- Statistics of electron avalanche generating secondary effect at cathode through photon emission, obtaining excited molecule distribution 19 p3265 A67-35087
- Secondary ionization processes in mercury vapor, calculating relative populations of excited and metastable atoms per ion pair 19 p3265 A67-35090
- Stationary moving domains in hot electron semiconductors, obtaining criteria for soft and hard regimes of domain excitation 20 p3506 A67-36222
- Auroral excitation of atomic oxygen forbidden lines, giving photon emission rate vs zenith angle 20 p3426 A67-36301
- Direct excitation in argon gas from metastable state to upper laser state compared with two-step excitation 20 p3460 A67-36860
- Intermolecular hydrogen bonds energies estimated for organic semiconductors in ground and first excited states 20 p3512 A67-37301
- Inelastic electron impact cross sections for ionization and vibrational excitation of atmospheric molecular oxygen 20 p3489 A67-37419
- Dayglow photoelectron excitation rate from electron energy loss calculations, with energy transfer functions calculated from photoelectrons produced by UV solar radiation 20 p3434 A67-37421
- Low energy electron scattering from hydrogen molecules in ground electronic and vibrational states, calculating rotational excitation cross section 20 p3491 A67-37687
- Electron distribution function in steady state plasma with Coulomb and excitation collisions obtained analytically by simplifying Fokker-Planck terms 21 p3661 A67-37746
- Radio source W49 and anomalous OH emission at radio wavelengths explained as OH formation in electronically excited state by two-body process 21 p3701 A67-37896
- Optical pumping of sodium vapor with deuterium light, discussing optical transparency in excited state mixing cross sections 21 p3639 A67-38018
- Parametric excitation of electron plasma frequency derived using Boltzmann and Poisson equations 21 p3667 A67-38415
- Ion bombardment excitation used to extend excited state range for level crossing spectroscopy studies, giving Zeeman energy level diagram 22 p3835 A67-39239
- Ground state and four lowest optically excited states of shallow donor in Si calculated using isotropic effective mass 22 p3854 A67-39245
- Energy exchanges between plasma and excitation source sinusoidal in time and arbitrary in space 22 p3847 A67-39642
- Micropulsation pattern changes during magnetospheric transition from quiet to excited state, discussing influence of earth and long period and pearl-type pulsations 22 p3883 A67-39674
- Matrix method to calculate energy eigenvalues and orbital wave functions for various singlet states of helium isoelectronic sequence 22 p3841 A67-40202
- Excited levels mean life in multiply ionized oxygen and neon measured by beam-foil technique 23 p4029 A67-40955
- Fermi pressure shifts of highly excited states of atoms in gaseous medium due to electron particle interactions, discussing scattering contributions 23 p4029 A67-40958
- Excitation effect on single electron charge transfer collisions of Fe ions in various gases determined with different excited states of ions 23 p4030 A67-40976
- Semiconducting diamonds photoconductive response measured noting correlation with activation energy 23 p4044 A67-41454
- Planar dielectric waveguide excitation at p-n junctions by externally incident electromagnetic field 24 p4121 A67-42337
- Phonon annihilation during decay of two metastable fluorescent states of ionized Ba compound 24 p4205 A67-42737
- Microwave absorption by magnetic field induced surface states in superconductors, showing anomalies consistent with quasi-particle decay 24 p4205 A67-42739

Excitation time of electronic states on nitrogen molecule at high temperatures 24 p4194 A67-42890

XCITON

SA ENERGY BAND

Exciton and impurity states in optical absorption spectra of nonmetallic crystals in pseudopotential theory 02 p0281 A67-11489

Cadmium telluride optical absorption edge due to exciton creation with simultaneous absorption of longitudinal optical phonons calculated by perturbation theory 02 p0281 A67-11493

Luminescent intensity and spectral energy distribution determined for exciton luminescence of anthracene crystals for spontaneous and stimulated emission 03 p0436 A67-13136

Free current carrier formation in amorphous crystal, examining dependence of photoconductivity on magnetic field intensity 03 p0501 A67-14369

Allowed and forbidden direct interband optical transitions in anisotropic semiconductors, using effective mass theory for exciton, solving Schrodinger equation 04 p0674 A67-14610

Excitonic effects in interband absorption of semiconductors noting electron-hole interaction, Coulomb interaction energy maxima and minima and scattering cross sections 04 p0676 A67-14926

Vannier-Mott excitons effect on ultrasound absorption in piezoelectric semiconductors 04 p0678 A67-15134

Auger effect radiative recombination of excitons bound to neutral donors of GaP and Si and generation of luminescent spectrum C line 04 p0682 A67-15463

Metastable exciton states of cadmium and lead iodide obtained from fundamental reflectivity spectra 06 p1060 A67-18915

Exciton and oscillatory magnetoabsorption spectra in layer type semiconductors in high magnetic fields 06 p1060 A67-18917

Optical spectrum of normal excitons in deformed and nondeformed n-type Ge single crystal layers for four orientations 08 p1367 A67-20409

Quantum mechanical theory for IR absorption by excitons due to photoionization and intraband lattice scattering 09 p1552 A67-21670

Recombination through exciton states in semiconductors compared to interband radiative recombination 09 p1554 A67-21974

Vannier-Mott excitons effect on ultrasound absorption in piezoelectric semiconductors 12 p1978 A67-25158

Exciton molecule formation in semiconductors in case of large radius exciton, determining dissociation energy and temperature 13 p2173 A67-26363

Coulomb long range interaction effect on refractive index dependence on light frequency and on absorption lines shape of dipole active excitons 13 p2173 A67-26365

Recombination through exciton states in semiconductors compared to interband radiative recombination 17 p2923 A67-33311

Optical exciton-magnon absorption in manganese fluoride, experimental results and theory of interactions 17 p2926 A67-33382

Electro-optical effect and Stark effect in exciton levels of cadmium sulfide 19 p3304 A67-35428

Exciton molecule formation in semiconductors in case of large radius exciton, determining dissociation energy and temperature 21 p3680 A67-38320

EXECUTIVE AIRCRAFT

SA MITSUBISHI MU-2 AIRCRAFT

Design and market research aspects of Hamburger HFB 320 jet executive aircraft 03 p0357 A67-12970

Executive jet aircraft Hamburger Flugzeugbau HFB 320 Hansa development, testing and production 07 p1129 A67-19670

Aviation avionics microelectronic devices stressing reliability, maintenance, circuitry, etc [SAE PAPER 670253] 11 p1758 A67-23985

Aircraft fuel gauging systems noting float type and reliability defects [SAE PAPER 670263] 11 p1789 A67-23986

Thrust reversers for business jet aircraft noting limitations, performance gains, technical aspects of analysis and testing, etc [SAE PAPER 670235] 12 p1989 A67-25493

Aerodynamic factors effect on airframe design and power plant selection for

medium Mach twin turboprop business aircraft [SAE PAPER 670244] 12 p1894 A67-25499

Supersonic business jet designs, unswept trapezoidal wing model and delta wing model [SAE PAPER 670246] 12 p1895 A67-25501

Electronics package for category II qualified jet business aircraft and function of system components [SAE PAPER 670254] 12 p1941 A67-25504

Executive aircraft structure safe-life fatigue analysis and tests [SAE PAPER 670257] 12 p2016 A67-25507

Estimating maintenance man-hours per flight hour for business turbojet airplanes [SAE PAPER 670228] 13 p2053 A67-27294

Gulfstream II maintainability program, examining support department responsibility, insurance and material support [AIAA PAPER 67-383] 15 p2421 A67-30352

Handley Page Jetstream turboprop aircraft basic design requirements, emphasizing aerodynamic design philosophy 22 p3746 A67-40129

Decompression tests, evaluating hazards of ejections and fatal injuries following window failure in small pressurized aircraft 23 p3965 A67-41575

EXHAUST

SA AIRCRAFT EXHAUST

SA ROCKET EXHAUST

Interactions in low density plasma beams of electrostatic thrust engine exhaust, discussing neutralization, instabilities, plasma wind tunnel, etc 04 p0690 A67-15022

Ionization recombination mechanisms and density-time profiles for electric propulsion unit efflux 04 p0690 A67-15024

EXHAUST GAS

SA JET STREAM

Nozzle exhaust plumes of rockets or supersonic ramjets with diffusion flames as source of UV radiation 04 p0721 A67-14702

Spectral radiance of model rocket exhaust gases measured by rapid scanning spectrometer at simulated altitude [AIAA PAPER 67-10] 06 p1116 A67-18346

Exhaust cloud diffusion from solid rocket motors correlated with measurable meteorological variables [AIAA PAPER 67-280] 07 p1221 A67-20084

Jet engine thrust augmentation by controlled mixing of exhaust gases with ambient air 07 p1242 A67-20119

Helicopter exhaust-gas expansion and contamination of intake air under unfavorable wind conditions 11 p1853 A67-24529

Expression derived for vibrational relaxation in recombining expanding nozzle exhaust gas, assessing effect of chemical reactions on this mechanism 12 p1929 A67-25755

Short duration technique providing simulation of thermodynamic properties and composition of exhaust products of liquid and solid propellant rocket engines [AIAA PAPER 66-760] 13 p2090 A67-26843

Exhaust gases effect on satellites optical equipment calculated by determining propane attitude-control jet gas flow parameters 18 p3137 A67-34359

Spectral radiance of model rocket exhaust gases measured by rapid scanning spectrometer at simulated altitude [AIAA PAPER 67-10] 19 p3346 A67-35761

Two-dimensional diffusion model for gas propagation in lunar atmosphere, discussing contamination by lunar module exhaust gases and solar wind loss mechanism 22 p3883 A67-39817

One-dimensional compound-compressible nozzle gas flow theory, discussing choking phenomenon and three-dimensional computer calculations 23 p3927 A67-40603

EXHAUST JET

Model for gas particle exhaust flow from under expanded nozzles 10 p1592 A67-23154

Semiempirical method for predicting aerodynamic interference of circular jet exhausting at right angles from wing, showing effect on lift loss 11 p1742 A67-24659

Approximating method for predicting multiengine exhaust geometry and thermodynamic properties with single reference engine 22 p3902 A67-39940

Model for compressible free jet with moving environment in core and developed region of exhaust plume 23 p3992 A67-41731

Length of supersonic core of axisymmetric jet exhausting into quiescent atmosphere 23 p3992 A67-41739

Momentum and heat transfer in axisymmetric turbulent free jets exhausting into quiescent air, using finite difference technique 24 p4092 A67-42608

EXHAUST NOZZLE

SA ROCKET NOZZLE

Pressures and temperatures occurring in jet engine exhaust nozzles during speed changes on basis of compression and detonation wave theory 01 p0141 A67-11150

Effect on protective coatings of launch pads of exhaust products, chamber pressure, nozzle diameter, etc, from aluminized solid propellant rocket motors [AIAA PAPER 66-972] 02 p0304 A67-12294

Suppressor applications of nozzles in reduction of sound power level generated in exhaust jet wake and ground surface deterioration from VTOL lift jets 03 p0350 A67-12916

Nuclear rockets employing multiple exhaust nozzles, noting performance gain occurring because of high temperature capability of refractory nozzles [AIAA PAPER 66-925] 03 p0466 A67-14135

Nozzle requirements for hypersonic vehicle at transonic conditions, noting results of tests in high velocity wind tunnel 04 p0545 A67-14536

Aerodynamic problems due to air intake and exhaust nozzles effect on propulsion of hypersonic aircraft [ONERA-TP-416] 05 p0748 A67-16481

Supersonic combustion measurements by thrust system method, optical probe and gas-sample probe technique [AIAA PAPER 67-223] 06 p1004 A67-18462

SST nozzle geometry for high efficiency operation over large exhaust pressure variation 06 p0942 A67-18745

Effect on protective coatings of launch pads of exhaust products, chamber pressure, nozzle diameter, etc, from aluminized solid propellant rocket motors [AIAA PAPER 66-972] 17 p2928 A67-32064

Statistically designed experiments in wind tunnel test programs dealing with exhaust nozzles, discussing data analysis techniques [AIAA PAPER 66-742] 17 p2834 A67-32571

Multiple exhaust nozzles for advanced nuclear rocket engines noting design and performance prediction procedures 22 p3834 A67-40160

Steady state matching of inlets, engines and exhaust nozzle for SST [AIAA PAPER 67-754] 23 p3928 A67-40988

EXHAUST SIMULATOR

Wind tunnel test program for simulation of gas-particle rocket exhaust plume, separated flow around nozzle and base recirculation [AIAA PAPER 66-767] 11 p1773 A67-24351

EXHAUST SYSTEM

Aerodynamics of nacelle used in selection and integration of exhaust systems producing highest thrust-minus drag cruise performance [SAE PAPER 660734] 01 p0140 A67-10634

Exhaust processes of gases at high initial pressure from tubes, when flow is initiated by acceleration of solid body 02 p0235 A67-12788

Tailpipe length effect on flame stability in high velocity propane-air stream with bluff body or reverse jet flame holders [ASME PAPER 67-GT-4] 11 p1853 A67-24792

High bypass ratio turbofan engine installation noting induction system, exhaust system, thrust reverser configuration requirements, accessories, etc [AIAA PAPER 67-390] 15 p2548 A67-30358

Nonlinearity of unsteady gasdynamic processes in internal combustion engine exhaust systems, using unsteady sources and sinks 21 p3689 A67-38044

Exhaust manifold design for two-cycle diesel engine with turbosupercharger using physical simulation, discussing simulation criteria for gasdynamic processes 21 p3696 A67-38908

EXHAUST VELOCITY

Arc jet exhaust velocity compared with propagation velocity of random light fluctuations 13 p2188 A67-26839

Submerged nozzle for solid rockets, noting exhaust flow velocity and direction determination 15 p2547 A67-29994

Optimum consumption of inert mass

working fluid in limited discharge velocity engine in terms of final speed gain 21 p3689 A67-37986

Diagnostic probe for low density plasma beam ion velocity distribution measurement in steady state and pulsed plasma exhausts [AIAA PAPER 87-706] 21 p3672 A67-38733

EXISTENCE THEOREM

Series integration of linear differential equations with deviating argument 01 p0104 A67-10289

Analytic continuation method proof of existence of class of periodic orbits of three-dimensional three-body problem, Part II 01 p0148 A67-10381

Existence of class of quasi-periodic solutions of three-body problem for near-circular inclined planetary and lunar orbits, Part I 01 p0148 A67-10382

Solvability of degenerated parabolic boundary value problem in Euclidean space cylinder and relation to homogeneous Dirichlet problem 01 p0105 A67-10677

Existence, uniqueness and reversion theorems, necessary optimality criteria and nonfixed time case for optimal control problem of n-dimensional linear parabolic equations 01 p0105 A67-10679

Existence and uniqueness theorem of Riccati equation arising in solution of optimal linear regulator problems in Hilbert space 01 p0047 A67-11213

Free boundary problem for parabolic equation proving existence and uniqueness theorems for certain initial conditions 02 p0258 A67-11626

Existence of two points near any planet where third body, given appropriate initial conditions, would remain in libelle gravitational equilibrium 02 p0324 A67-11814

Existence of periodic solutions for infinite system of integro-differential equation 02 p0260 A67-12537

Existence theorems for nonlinear boundary value problems 02 p0260 A67-12738

Existence of Green function and invariability of sign in some boundary value problems for equation y super n equals $g/t/y$ 02 p0260 A67-12739

Existence and uniqueness theorem and upper and lower Chaplygin function approximations for solutions of Cauchy problem for quasi-linear first order PDE 03 p0456 A67-12884

Formulated conditions for proving existence of invariant surfaces of system not circumscribed by ordinary perturbation theory 03 p0456 A67-13110

Existence conditions for Green function of boundary value problem, determining and estimating subcritical intervals 03 p0457 A67-13114

Forced periodic vibrations of homogeneous isotropic uniformly thick plate with free edges reduced to Fredholm integral equation 03 p0524 A67-13624

Boundary value problems of higher order equations in infinite regions, proving existence and convergence of solution for perturbed and unperturbed cases 03 p0459 A67-13643

Existence theorems for periodic solutions of coupled nonlinear systems of two or more degrees of freedom, including normal mode vibrations 03 p0524 A67-13654

Conditions of existence of unbounded solution to unforced second order differential equation, considering global asymptotic stability 03 p0460 A67-13822

Existence theorem for smooth solution of short term weather forecasting problem 03 p0462 A67-13834

Existence theorem for periodic solutions to parabolic boundary value problem involving reduction to solvable operator equation 03 p0460 A67-13835

Existence of exact solution to motion equations for charged particles in acute angled magnetic trap 03 p0486 A67-14064

Parabolic conditions for general second order PDE, discussing bicharacteristic condition, initial boundary value problem, Monge-Ampere equations and quasi-linear equation systems 03 p0461 A67-14105

Existence of periodic solution for set of quasi-linear differential equations 04 p0643 A67-14662

Periodic solutions for nonautonomous differential equations, discussing existence and stability criteria 04 p0644 A67-14853

Solvability of parallel-wall cavitation flow

problem of perfect incompressible fluid past symmetric smooth arc 04 p0606 A67-15195

Pointwise bounds for solutions of semilinear parabolic equation, presenting existence theorems 04 p0647 A67-15739

Existence and uniqueness in first and second boundary value problems for nonlinear second order differential equations 04 p0647 A67-15742

Boundary value problems for ordinary nonlinear second order systems, noting subfunction definition and existence theorem 04 p0647 A67-15744

Existence theorem for two-dimensional subsonic flow of compressible fluid, following Bers method 05 p0790 A67-16044

Boundary value problem of hyperbolic equation with discontinuous boundary conditions 05 p0834 A67-16371

First-kind operator equation solution by reduction to dual extremum problem, proving existence and convergence 05 p0834 A67-16375

Uniqueness and existence theorems for mixed problem of second order degenerate hyperbolic equation with discontinuous coefficients 05 p0834 A67-16494

Error bounds for asymptotic solutions of differential equations, using Volterra equations for actual and formal solution vectors 06 p1021 A67-17565

Existence theorems in optimal control theory of linear and nonlinear systems 06 p0974 A67-17924

Existence of solutions to differential and integrodifferential equations possessing asymptotic parabolas 07 p1214 A67-18174

Existence of bounded solutions of second order differential equations 07 p1214 A67-19180

Existence and uniqueness of 2k-fold continuously differentiable solutions to Dirichlet problem for nonlinear integrodifferential equations 07 p1215 A67-19476

Periodic solutions of hyperbolic equations containing small parameter by extending Cesar method for differential equations 07 p1218 A67-20213

Existence theorem for nth order linear stochastic ordinary differential equations 08 p1347 A67-20356

Monograph on existence theorems for nonlinear equations, using functional analysis in Banach space 08 p1348 A67-21175

Existence theorems of algebraic integral equations /AIR/ with nonlinear functionals 09 p1524 A67-21649

Existence and uniqueness theorem for functional equation of optimal control problems, noting stability of solution 09 p1524 A67-21874

One-dimensional steady solutions for shock wave propagation in class of nonlinear viscoelastic materials deduced from stated balance laws and representation theorem for compressive and expansive motions 09 p1576 A67-22410

Existence, uniqueness and stability investigation of periodical solutions for nonlinear hyperbolic partial differential equations 10 p1874 A67-23387

Existence and stability of solutions for equations of stationary thermal explosion in bounded container 10 p1734 A67-23679

Existence and preservation of algebraic sign in Green function for two-point boundary value problem 11 p1813 A67-24519

Gyroviscosity of collisionless plasma in strong magnetic field, duality theorem and application to linear stability analysis 11 p1839 A67-24547

Absence conditions for periodical trajectories in regions of possible existence 11 p1819 A67-24686

Periodic solutions for nonautonomous differential equations, discussing existence and stability criteria 11 p1813 A67-24730

Existence and uniqueness of periodic solution to ordinary differential equations, defining position in plane of closed integral curves 11 p1813 A67-24749

Existence, uniqueness and reversion theorems, necessary optimality criteria and nonfixed time case for optimal control problem of n-dimensional linear parabolic equations 11 p1814 A67-25067

Existence, uniqueness, stability and approximation of solutions of Prandtl system for nonstationary boundary layer 13 p2093 A67-26603

Existence of exact solution to motion equations for charged particles in acute angled magnetic trap 13 p2172 A67-27717

Existence theorem for initial value problems in differential equation leading to Volterra integral equation in several variables 13 p2149 A67-27736

Heat equation for free boundary problem with prescribed flux at fixed and melting interface of semiinfinite slab 14 p2405 A67-28255

Concept of extremal state in topological space, discussing existence conditions and criteria concerning extremal and stationary points 14 p2343 A67-28632

Necessary and sufficient conditions to ensure existence of unique solutions of equations for active networks 15 p2456 A67-29238

Irreducible systems existence in class of linear differential equations with quasi-periodic coefficients having frequencies represented by algebraic numbers 15 p2510 A67-29629

Fractional powers of operators applied to boundary value problems of quasi-linear elliptic equations 15 p2510 A67-29661

Stochastic Liapunov function existence demonstrated for continuous strong Markov process with certain stochastic stability properties 15 p2458 A67-29898

Time independent two-dimensional Navier-Stokes equations solutions from singular perturbation theory, determining properties 16 p2657 A67-30828

Uniqueness and existence of Cauchy problem solution considering Dirichlet limits, studying convergence requirements 16 p2695 A67-30829

Existence theorems for systems of nonlinear integral equations of Hammerstein type with positive definite kernels 16 p2687 A67-30859

Numerical methods for elliptic partial differential equations with coefficients singular on boundary portion, constructing barrier functions and establishing existence and convergence theorems 16 p2697 A67-31330

Wiener-Hopf technique for class of nonhomogeneous difference-differential integral equations 17 p2877 A67-32560

Affine solutions for temperature/flux distribution on heated horizontal plate 17 p2838 A67-32701

Bogolubov existence theorem for one-dimensional integral manifold and two-dimensional local integral manifold extended to Hilbert space 17 p2879 A67-32879

Parameter values excluded by existence conditions for buoyant dissipative motions in vertical channels 17 p2840 A67-33138

Constructing solution of Cauchy initial value problem when Riemann function is unknown for one-dimensional linear viscoelasticity 18 p3139 A67-33428

Numerical solutions of multidimensional singular integral equations in problems of hydrodynamics 18 p3024 A67-33537

Existence of solutions to differential equations with multiple-valued right side 18 p3070 A67-33554

Existence of affine solutions in natural convection along vertical flat heating plate, deriving expressions for thermal and dynamic boundary layers 18 p3025 A67-33685

Differential and boundary layer equations for free convection flow along vertical hot wall, investigating existence question 18 p3027 A67-34009

Existence and uniqueness theorem for axisymmetric problem with initial data for Euler equation in case of incompressible fluid 18 p3027 A67-34201

Existence theorems for defining solubility of certain boundary value problems for ordinary second order linear differential equation 18 p3072 A67-34384

Existence and uniqueness of solutions of point boundary value problem for denumerable system of differential equations 18 p3073 A67-34606

Existence problem in control theory noting time independence and control set 19 p3204 A67-35905

Automatic control systems general theory with distributed parameters and delay, proving existence and uniqueness of solutions of partial differential equations solutions 19 p3251 A67-36048

Existence and uniqueness of classical

solutions of nonstationary boundary and initial value problem in
MHD 20 p3497 A67-36430
Existence theorems for linear optimal control problems with nonlinear cost functionals 20 p3408 A67-37076
Evolution problem investigated for invariant Einstein vacuum equation, discussing existence and uniqueness theorems 20 p3487 A67-37685
Existence and stability of solutions for equations of stationary thermal explosion in bounded container 21 p3731 A67-38280
Helly problem of moment theory and optimum approximation of finite defect by subspace elements of continuous functions, examining uniqueness and existence 21 p3653 A67-38400
Sample continuous second order martingale process, determining existence of limit of stochastic processes using approximation theorems 21 p3654 A67-38966
Compact integral operator base problem for Hilbert-Schmidt integral operators existence, discussing Schmidt classical operator approximations and eigenvalues 22 p3828 A67-40554
Thin plate strong bending generalized and smooth solutions existence 23 p4076 A67-40716
Elastohereditary /viscoelastic/ media mechanics, analyzing linear and nonlinear equilibrium equations, uniqueness and existence theorems and solution methods 23 p4077 A67-40750
Local existence, uniqueness and regularity theorems for Cauchy problem solution for Navier-Stokes system in space 24 p4177 A67-42155
Existence theorems for defining solubility of certain boundary value problems for ordinary second order linear differential equations 24 p4177 A67-42199
Duhamel principle for internal radiation field in inhomogeneous finite atmosphere based on existence and uniqueness theorem for Milne integral equation 24 p4189 A67-42598
Nonlinear equation solution existence in real Hilbert space with linear and nonlinear operator 24 p4178 A67-42721
Hyperbolic noninvariance in partial differential equations, discussing existence theorems for nonhyperbolic initial value problem systems 24 p4178 A67-42727
Existence theorems for partial and ordinary differential equation solutions, discussing boundary value problems for nonlinear differential equation class 24 p4178 A67-42728
XO-ELECTRON EMISSION
External electron emission measurement from polished n-germanium and n-silicon surfaces 02 p0296 A67-11830
Apparatus used to study exoelectronic emission from metallic surfaces, detailing Geiger counter, high voltage rectifier, scaling device and counting rate meter 07 p1201 A67-19256
Phase and structural transformations in metals and alloys studied with aid of exoelectronic emission 07 p1201 A67-19257
XOBIOLOGY
S BIOASTRONAUTICS
S EXTRATERRESTRIAL LIFE
XOSPHERE
Radio wave guiding along electron density discontinuity in magnetotonic exosphere, noting low dispersion modes 01 p0027 A67-11259
Radio propagation and ion effects in ionosphere and exosphere observed by spacecraft 05 p0783 A67-16866
Diurnal variation of hydrogen exosphere treated by simulation technique involving critical circle and magnetopause circle 06 p0997 A67-18701
Plasma concentration diagnostics in exosphere from delay time of forward frequency as function of parameter of whistler trajectory 13 p2111 A67-26563
Antenna in interplanetary plasma, noting fluctuation noise in exosphere and radiation impedance when exposed to solar wind 14 p2279 A67-27856
ULF radio emission associated with magnetic field disturbances, geomagnetic pulsations, auroras and exospheric particle acceleration 17 p2846 A67-32939
H-alpha diurnal and seasonal intensity variations in geocorona indicating hydrogen

content build-up during night 17 p2851 A67-33202
Hydrogen and helium lateral flow in collisionless exosphere calculated on model for various sinusoidal temperature and concentration variations over exobase surface 17 p2852 A67-33235
Semiannual exospheric density variation confirmed by satellite orbit analysis 17 p2852 A67-33238
Magnetosonic resonances location in exosphere, showing diagram of Alfvén velocity profile 18 p3042 A67-34389
Alfvén and magnetosonic wave generation and propagation in magnetosphere, detailing azimuth number approaching infinity 18 p3042 A67-34391
Exospheric density variation as related to solar activity determined from satellite orbits 19 p3217 A67-35211
EXOTHERMIC REACTION
Boundary value problem for determination of stationary combustion regimes in semilinear combustion chamber 06 p1119 A67-18818
Gaseous ammonia composite solid propellant ignition upon contact with oxidizing vapors such as perchloric acid vapor 06 p1073 A67-18869
Exothermal reaction zone in one-dimensional shock wave in argon diluted oxygen-hydrogen and methane-oxygen mixtures 07 p1267 A67-19309
Angular distribution of fast hydrogen atoms from exothermic reaction measured for various proton energies and scattering angles 07 p1225 A67-19495
Surface coupled heat release effect on oscillatory amplitude of pressure coupled response in solid propellant 15 p2544 A67-29983
Ammonium perchlorate solid propellant ignition characteristics recording preignition surface exotherms 17 p2927 A67-33027
High temperature kinetics of bulk beryllium metal combustion in hydrogen-oxygen-water vapor system, studying flame environments, thermal balance, etc 18 p3151 A67-33809
Hydrodynamic structure of exothermic reaction zone behind one-dimensional shock fronts in gaseous detonation studied by optical method 18 p3153 A67-33827
Criticality criteria and temperature profiles in thermal explosions, studying exothermic decomposition of gaseous methyl nitrate 18 p3156 A67-33851
Rayleigh number effect on importance of convective heat transfer in self-heating gaseous reactions checked against thermal ignition theory 18 p3156 A67-33852
Combustion characteristics of hydrazine type propellants and resultant reactions in low thrust engines prior to ignition 21 p3887 A67-37798
EXPANDABLE STRUCTURE
Expandable and modular structures for support on manned space missions, reviewing inflatable, chemically rigidizable, unfurlable and elastic recovery structures 02 p0333 A67-12342
Forming closed contour shells by straining with expandable punch 07 p1191 A67-19750
Expandable gas bag for stowable omnidirectional multiple impact landing system 10 p1714 A67-23755
U-shaped bellow fatigue strength under axial loading, discussing elastic and plastic fatigue tests using specially designed machine 22 p3913 A67-40037
Expandable gas bag for stowable omnidirectional multiple impact landing system 22 p3904 A67-40097
EXPANDING UNIVERSE THEORY
S COSMOLOGY
EXPANSION
SA GAS EXPANSION
SA NOZZLE EXPANSION
SA PRANDTL-MEYER EXPANSION
SA SERIES EXPANSION
SA THERMAL EXPANSION
Asymptotic expansion of radiating antenna field in penumbra region 23 p3973 A67-40836
EXPANSION WAVE
Competition of two types of oscillations in traveling wave laser 01 p0089 A67-10362
Plasma expansion wave propagation in vacuum after current cut-off 02 p0278 A67-12628
Expansion velocity of luminous front of plasma plume generated by giant pulse

laser 03 p0478 A67-13573
Competition of two types of oscillations in traveling wave laser 06 p1009 A67-17620
Hypersonic flow in compressed layer between tapered blunt leading edge of wing and internal shock wave forming in front when nonuniform flow moves past, considering expansion plane 06 p0936 A67-17733
Hydrogen or nitrogen gas injection at various Mach numbers from nozzle in flat plate into Mach 2.72 free air stream [AIAA PAPER 67-225] 06 p0940 A67-18444
Plasma expansion wave propagation in vacuum after current cut-off 13 p2171 A67-27386
Heat conducting supersonic gas flow around corner considered calculating viscous corrections in expansion region 16 p2660 A67-31218
Carbon monoxide and atomic oxygen recombination in expansion wave of single-pulse shock tube at high temperatures 18 p2997 A67-33790
Cylindrical expanding detonation waves in gas mixtures, studying detonability limits, propagation velocity and instability and vibratory phenomena 18 p3153 A67-33822
Resonance effects arising during sub- and supersonic waves expansion in aerodynamic cascade 18 p2984 A67-34216
Inhomogeneous plasma stability, considering wave drift oscillations expanding across external magnetic field and flute instability in noncompensating plasma 19 p3292 A67-35393
Hydrogen or nitrogen gas injection at various Mach numbers from nozzle in flat plate into Mach 2.72 free air stream 21 p3610 A67-37800
Incomplete expansion wave diffraction by corner, noting pressure discontinuity across boundary 21 p3564 A67-37929
Plane deformation problem of instantaneous elasticity theory application to expansion of stationary elastic waves in infinite medium with cylindrical cavity 21 p3720 A67-38294
Upstream influence ahead of weak uniformly moving shock or expansion wave incident on plane wall boundary layer 21 p3615 A67-39089
EXPERIMENT DESIGN
Classification of experimental methods used in analysis of thermal phenomena during metal cutting 03 p0427 A67-13194
Enthalpy measurement for self-binding silicon carbide at high temperatures 03 p0446 A67-13609
Nagoya University, Institute of Plasma Physics, Annual Review, April 1965-March 1966 04 p0662 A67-14590
Book on design and analysis of scientific experiments covering statistical estimation theory in design and testing of hypotheses, emphasizing computational techniques 12 p1961 A67-25560
Satellite size via experiment design, demonstrating advantages and drawbacks of small and large satellites 12 p2007 A67-25784
Enthalpy measurement for self-binding silicon carbide at high temperatures 18 p3066 A67-34474
Conceptual design of active seismic experiment for lunar surface missions, analyzing communication approaches 19 p3323 A67-35328
Experimental method for studying Taylor columns over hills and holes in Jupiter atmosphere 21 p3614 A67-39000
Payload integration process for space experimentation 22 p3922 A67-39962
EXPIRED AIR
S ALVEOLAR AIR
EXPLODING CONDUCTOR
MHD instability as mechanism responsible for destruction of conductor during electrical explosion 01 p0126 A67-11296
Jarrell-Ash model 75 spectrograph adapted for time resolved spectroscopy of transient plasma produced by exploding wire and shock waves 03 p0426 A67-14401
Exploding wire phenomena in air at atmospheric and reduced pressures 05 p0847 A67-17317
Current pause during circuit overloading accompanied by filament explosion 06 p1031 A67-17867
Magnetothermoelastic mechanism of exploding wire effect under high intensity current surge in pulsed generator for

- hydrodynamic and magnetoelastic pumping 08 p1354 A67-21046
- Synchronized shadow photochronographic investigation of wire explosion shock waves in air 09 p1532 A67-22064
- Uniform shock driven by gaseous detonation induced by exploding wire in single-diaphragm shock tube 10 p1625 A67-23137
- Color temperature measurement in first stage of electrical explosion of copper, silver and constantan wires as function of magnitude of energy input for various heating times 16 p2703 A67-31779
- Energy distribution of shock wave created by wire explosion and electrical discharge in air, studying attenuation, dimensional effects and energy conversion efficiency 17 p2883 A67-31927
- Physical changes in exploding wires before gas ionization observed by X-ray technique, studying resistivity variation with density 19 p3261 A67-35161
- Ionized gas produced by exploded lithium wires, presenting physical measurements, finding self-consistent solution of temperature and electron concentration 19 p3261 A67-35162
- Source and load parameter effects on electrical explosion of wires noting voltage, capacity, inductance, specific resistance, diameter, resistance, etc 20 p3483 A67-36401
- Acceleration of plasma formed in electric explosion of foil in air atmosphere 20 p3502 A67-37604
- Temperature determination of wire explosion plasma from expansion and resistivity measurements, showing existence of two phases of electric arcs 22 p3847 A67-39644
- Explosion of ovoid copper wire conductors observed with pulsed X-rays noting effect of magnetic pressure 23 p4028 A67-41461
- EXPLODING CONDUCTOR CIRCUIT**
- Special grade RDX for exploding bridge wire initiators noting chemical/physical properties and performance 14 p2377 A67-28955
- Electric drive operating parameters and design, using exploding wire type device and electromagnetic apparatus for plasma production and acceleration 16 p2736 A67-30716
- EXPLORATION**
- S LUNAR EXPLORATION
- S PLANETARY EXPLORATION
- S SPACE EXPLORATION
- EXPLORER IX SATELLITE**
- Geomagnetic activity effect derived from Explorer IX drag data, with atmospheric temperature as geomagnetic storm intensity function and atmospheric density increase 18 p3042 A67-34255
- EXPLORER VII SATELLITE**
- Composition and energy spectra of primary cosmic radiation in low energy regions from observations of Mariner II and Explorer VII 02 p0310 A67-12582
- EXPLORER XII SATELLITE**
- Magnetopause structure and attitude from Explorer XII observations 07 p1180 A67-19925
- Explorer XII observations of charged particles in inner radiation zone after solar activity maximum and before Star Fish explosion 08 p1378 A67-21471
- EXPLORER XIV SATELLITE**
- Inflation of magnetosphere near 8 earth radii in Southern Hemisphere using Explorer XIV satellite 12 p1936 A67-25805
- Long period hydromagnetic waves in magnetosphere and coupling to solar wind studied by Explorer XIV 12 p1937 A67-25812
- EXPLORER XVII SATELLITE**
- Atmospheric composition data from Explorer XVII satellite, obtaining expression for thermal diffusion factor of He 07 p1181 A67-19937
- EXPLORER XVIII SATELLITE**
- Interplanetary space properties studied from IMP-I satellite data on cosmic ray variations 05 p0880 A67-16115
- Criticism of Ivanov assumption regarding IMP-I observation of lunar wake in solar wind by magnetic field and plasma measurements 07 p1243 A67-19829
- Limitations in tilted fluxgate magnetometer data from Explorer XVIII satellite due to ambient dynamic field effects 07 p1182 A67-19943
- IMP-I earth satellite magnetic field measurement experimental results including solar wind flow effects 12 p1936 A67-25802
- Interplanetary space properties studied from IMP-I satellite data on cosmic ray variations 24 p4214 A67-42791
- EXPLORER XX SATELLITE**
- Solar radiation field interaction with flexible antenna as possible explanation of anomalous rapid spin decay of satellites [AIAA PAPER 67-39] 06 p1096 A67-18350
- EXPLORER XXII SATELLITE**
- Explorer XXII satellite measurement of total electron content from Faraday rotation recordings, noting correlation with solar activity above 80 solar flux units [RASSA PAPER 1-10-124] 03 p0416 A67-14235
- Explorer XXII satellite measurement of total electron content from observations of Faraday effect [RASSA PAPER 1-10-128] 03 p0372 A67-14239
- Ionospheric absorption determination by measuring amplitudes of wave components of satellite transmission 11 p1786 A67-24059
- Explorer XXII coherent frequency phase difference data for polar ionospheric integral electron density, discussing diurnal and seasonal variation 22 p3794 A67-40121
- Explorer XXII amplitude recordings, analyzing duration, strength and frequency of ionospheric electron density horizontal gradients 23 p3974 A67-41177
- EXPLORER XXIII SATELLITE**
- Lunar AIMP photographic data processing system which transforms photographic scans of moon into rectified lunar pictures, particularly ground processor system 08 p1330 A67-20661
- EXPLORER XXX SATELLITE**
- S INTERNATIONAL QUIET SUN YEAR /IQSY/
- EXPLORER XXXIII SATELLITE**
- Explorer XXXIII satellite magnetometric measurements of geomagnetic tail at distances beyond lunar orbit 08 p1402 A67-21468
- EXPLORER SATELLITE**
- SA RADIO ASTRONOMY EXPLORER /RAE/ SATELLITE
- Energetic particle monitoring satellites, discussing design and development of four IMP generations 01 p0156 A67-11415
- Problems of temperature data from Explorer and Ariel II satellites including magnetometer failure, poor conduction, paint degradation, etc 03 p0518 A67-13074
- Ionic composition measurements of topside ionosphere from mass spectrometer flown on Explorer XXXI satellite 06 p0996 A67-18646
- Radiation belts, energetic charged particle flux and trapped radiation in geomagnetic field as result of neutron albedo decay and plasma-magnetic field interactions 07 p1246 A67-20297
- Explorer type compared to Orbiting Observatory type satellites regarding weight, volume, reliability, data transmission, power, etc 12 p2012 A67-25785
- Nondipole region of geomagnetic field at magnetosphere boundary and effect on boundary position on daylight side 14 p2308 A67-27931
- Explorer 33 plasma measurements, discussing plasma flow parameter calculation methods, including plasma models and magnetospheric shape and size 19 p3319 A67-35245
- Small and large orbiting observatory satellites compared for operational needs, interference problems, scheduling and multisampling of space phenomena [AIAA PAPER 67-634] 20 p3534 A67-37616
- EXPLOSION**
- SA BLAST
- SA CHEMICAL EXPLOSION
- SA DETONATION
- SA GAS EXPLOSION
- SA IMPLSION
- SA LAMINAR FLAME
- SA METAL COMBUSTION
- SA NUCLEAR EXPLOSION
- SA THERMONUCLEAR EXPLOSION
- Hydrodynamic thermal explosion of stationary axisymmetric non-Newtonian fluid in infinitely long cylindrical tube 01 p0052 A67-10681
- Effect of diffusion-pump fluid contamination and degradation on explosion hazard of operating diffusion pumped system 06 p0979 A67-17632
- Explosion analogy in flows past slender blunt bodies, noting accuracy improvement by placing explosion center ahead of origin 06 p0936 A67-17732
- Initiation of explosive reaction in liquid mixture of tetranitromethane and benzene by methane-oxygen detonation 06 p1112 A67-17954
- Initiation of explosion by impact of plate against charge surface 06 p1112 A67-17955
- Ignition of explosive powder by hot gas stream, with particular attention to heat transfer between substance and surrounding medium 06 p1112 A67-17956
- Thermal explosion laws under cooling conditions, examining linear cooling as method for studying thermal explosion of strongly self-accelerating reactions 06 p1112 A67-17962
- Energy losses in explosions in sphere to determine specific heat, heats of dissociation and formation, chemical bond energies and other thermochemical values 06 p1113 A67-17963
- Elastoplastic properties of copper, aluminum alloys and brass under explosive load, noting increased temperature effect on elastoplastic wave parameters 10 p1668 A67-23092
- Hydrodynamic thermal explosion of stationary axisymmetric non-Newtonian fluid in infinitely long cylindrical tube 11 p1783 A67-25068
- Intrinsically safe and nonincendive electrical installations for hazardous environments 12 p1900 A67-25677
- Thermal explosion equations for first order catalytic reaction, discussing nonstationary effects superposed on quasi-stationary combustion pattern 12 p2039 A67-26111
- Linearization of equation of thermal explosion and stability of solutions for boundary conditions of third kind 14 p2406 A67-28310
- Ballistic aspects, structure and destructive power of Tungusk meteorite do not support thermal explosion hypothesis 15 p2558 A67-30010
- Aircraft fuel explosion problem, analyzing mechanism of lightning-induced explosions and discussing protection methods 16 p2597 A67-31810
- Numerical methods for solving thermal explosion and combustion problems on electronic computers, examining Cauchy problems solutions 17 p2973 A67-33075
- Explosion theory, reviewing chain and thermal theories unification, fuel consumption effects, spatial distribution effects, etc 18 p3155 A67-33845
- Ignition kinetics of carbon monoxide-oxygen reaction 18 p3155 A67-33846
- Kinetic mechanisms in combustion peninsula of three-limit explosion reactions with trace inhibitors, studying quadratic chain-breaking processes by static method 18 p3156 A67-33848
- Critical reaction rate for ignition, temperature rise and induction period for various geometries calculated for conductive theory, including reactant consumption 18 p3156 A67-33850
- Criticality criteria and temperature profiles in thermal explosions, studying exothermic decomposition of gaseous methyl nitrate 18 p3156 A67-33851
- Analysis of explosion hazards of large solid motors, suggesting mathematical approach in predicting blast damage [CI PAPER 67-14] 19 p3309 A67-35008
- Friction heat effect on explosion threshold noting pressure drop role in reacting system explosion 20 p3554 A67-37055
- Ballistic aspects, structure and destructive power of Tungusk meteorite do not support thermal explosion hypothesis 20 p3530 A67-37534
- EXPLOSIVE**
- SA CHARGE
- SA HIGH EXPLOSIVE
- SA NITROCELLULOSE
- SA NITROGLYCERIN
- SA PROPELLANT
- Nonlinear fluctuations in gunpowder combustion rate at various temperatures and harmonically varying pressure 05 p0927 A67-16991
- Similarity in propagation of detonation waves in gaseous and liquid explosives with respect to homogeneity explained in terms of single detonation reaction 06 p1112 A67-17960
- Condensed explosive ignition by

conductive heat inflow from low
thermoconductivity media 07 p1267 A67-19314

Nonstationary gunpowder combustion at
various pressures analyzed for combustion
rate and surface temperature dependency on
pressure and initial
temperature 11 p1884 A67-24957

Factors involved in initiation of reaction
in cobalt /III/ amine azides, discussing
thermal decomposition, activation energy,
etc
[CI PAPER 67-15] 19 p3309 A67-35009

Chemistry and technology of explosives,
Volume 3, covering rocket propellants,
mining explosives and smokeless powder
manufacture 21 p3688 A67-37900

Sensitivity of explosives to shock waves
tested by device using water as intermediate
layer 22 p3866 A67-39489

EXPLOSIVE DEVICE

SA DETONATOR

SA ELECTROEXPLOSIVE DEVICE

SA PRIMER

Ordinance systems and devices noting
composition, function, operation and testing
procedures 04 p0557 A67-15734

Explosive driven magnetic generator
applied to investigate electric, optical and
elastic properties of various substances,
plasma physics and charged particle
accelerator 05 p0786 A67-16365

Physical and hydrodynamic processes
induced in vaporizable solids by pulsed light
radiation from sources using
explosives 11 p1782 A67-24955

Cavitation induced detonation of
stoichiometric liquid
mixtures 11 p1884 A67-24956

Special grade RDX for exploding bridge
wire initiators noting chemical/physical
properties and
performance 14 p2377 A67-28955

Pyrotechnic actuation, discussing
parameters, equipment and performance of
explosive devices 15 p2543 A67-29304

Laser-energized explosive device /LEED/
for pyrotechnic device actuation noting
power source, ruby laser, metallic fiber-optic
conductor, missile design,
etc 17 p2803 A67-32437

Design and performance of explosive
driven magnetic generators, giving line
drawings and current
oscillograms 18 p2987 A67-33628

Low velocity detonations /LVD/ of liquid
explosives indicate shape and container
material and presence of witness plate
affect initiation 23 p4081 A67-40635

EXPLOSIVE FORMING

Forming of refractory materials for
rockets by explosive, magnetic and Dynapak
forming and beam welding
methods 01 p0079 A67-10638

Aluminum and tungsten carbides formed
from metal powders mixed with acetylene
black and exposed to explosive
shock 03 p0440 A67-12927

Stress corrosion resistance of explosively
deformed high strength steels and aluminum
alloy
[ASTME PAPER WES-7-63] 10 p1667 A67-23009

Influence of explosive forming
characteristics on springback based upon
tests in forming of gore sections for Saturn
V rocket 10 p1660 A67-23170

Stable implosion initiation through
converging detonation wave, discussing
experimental techniques and
results 14 p2293 A67-28141

Sound velocities in granular ammonium
perchlorate and potassium chloride,
discussing chemical reaction of
shocks 16 p2734 A67-31521

Molybdenum disulfide compacts
pressurized by explosive forming,
determining specific gravity, hardness,
compressive and tensile properties,
etc 16 p2695 A67-31753

Fatigue properties of explosively formed
parts tested by repeated axial loading and
results compared with statically formed
specimens 17 p2871 A67-32433

General equation for explosion limits from
unified thermal and chain theory, noting
application to hydrogen and oxygen
systems 18 p3156 A67-33849

Rapid deformation in tubular blank during
expansion by pulsed loading studied by high
speed motion picture
photography 21 p3631 A67-38055

High speed information generation by
projectile impact machine, explosive forming
and capacitor-discharge energy with very
high strain rates, presenting failure modes
related to forming
velocity 23 p4076 A67-40737

EXPLOSIVE GAS

SA GAS EXPLOSION

Transition to detonation in gaseous
medium experimentally studied, based on
self-sustained detonation front and
adaptation of amplitude modulated giant
pulse laser system 03 p0535 A67-13500

Asymptotic expansion applied to strong
explosion in heat-conducting
gas 06 p0984 A67-18030

Parameters and shock wave characteristics
of Tunguska explosion, postulating reaction
mechanism 10 p1710 A67-23611

Microexplosion by optical breakdown of
air in focus of laser beam, analyzing volume
of concentrated plasma by measuring
external magnetic field
perturbation 12 p1952 A67-25336

Parameters and shock wave characteristics
of Tunguska explosion, postulating reaction
mechanism 20 p3530 A67-37535

Enthalpies of formation and bond
energies of various fluorinated amines in gas
state 23 p3971 A67-40975

EXPONENTIAL FUNCTION

Functional integration analysis of
exponential behavior of nonlinear feedback
control systems 01 p0047 A67-11211

Noise rejection properties of time
discrimination method of pulsed signals
improved by using exponential rather than
selecting function 02 p0194 A67-11909

Integral representation providing one-to-
one correspondence between functions of n
complex variables and complex-valued
harmonic functions of n plus 1 real
variables 02 p0259 A67-11918

Real function interpolation method for
synthesis of electric networks in time
domain by sinusoidal exponential
series 03 p0458 A67-13505

Hydrodynamics of lower solar photosphere,
examining connection between small-scale
oscillatory Doppler shifts and exponentially
decaying continuum 03 p0511 A67-13650

Low pass filters approximating phase and
modulus of exponential function near
frequency origin 03 p0386 A67-13976

Exponential smoothing for prediction of
reliability growth having advantages of
tracking data precisely while retaining in
memory only few historical
statistics 05 p0811 A67-16828

Asymptotic exponential laws of
contraction of plane and axisymmetric jets
of weightless fluids, obtaining expressions
for stream function and velocity
component 10 p1824 A67-23039

Piezotransistor static characteristics
approximated by exponential function of two
variables 12 p1939 A67-25281

Newtonian analogues of trigonometric and
exponential functions studied by
series 13 p2146 A67-26851

Characteristic vectors theory and
application to study of asymptotic behavior
of solutions to differential
systems 14 p2342 A67-28385

Solution of MHD boundary layers with
magnetic field as exponential function of x
coordinate, extended to transverse magnetic
fields 16 p2722 A67-31570

Smoothing experimental values of function
based on choice of regularity and
repeatability criteria, noting infinite number
values, derivatives, spline functions, etc
[ONERA-TP-463] 18 p3072 A67-34460

Duration of continuous occurrence of
sporadic E layer dependence on incidence of
sporadic E layer critical frequency maximum
value 21 p3623 A67-39039

Numerical recursion method for
calculation of characteristic exponent of
Mathieu differential
equation 22 p3827 A67-39744

EXPOSURE

SA RADIATION EXPOSURE

Antilexposure assemblies evaluation in low
temperature water, recording body heat loss
and tolerance time for application to
helicopter crews 17 p2807 A67-31959

Holographic exposure times controlled by
direct viewing of reconstructed image
during exposure 18 p3048 A67-34012

EXPULSION

Computer-simulated mathematical model of
thermal environmental effects on expulsion
system design parameters for liquid-
propellant gas-generator rocket engine
[AIAA PAPER 66-686] 02 p0303 A67-11944

Heat leak and pressure decay for single
phase cryogenic storage in nonequilibrium
calculated for spherical tanks, using
simplifying assumptions 13 p2227 A67-27641

Multicycling metallic bladders for positive
expulsion of cryogenic fluids stored in tanks
[AIAA PAPER 67-444] 18 p3054 A67-33921

Damped mass expulsion for space vehicle
attitude control reducing propellant
consumption and pulsing frequency
[AIAA PAPER 67-535] 19 p3334 A67-35937

EXTENSOMETER

Extensometer for measuring small changes
of specimen on tensile testing vacuum
furnace at high temperatures, using CW gas
laser as light source 01 p0070 A67-11036

Design principles and reliability of
extensometric sensor with photodiode for
static and dynamic study of deformation
processes 04 p0621 A67-14919

Stress distribution measurement by
vibration method, applying hand-held
extensometer place by place on surface of
structure subjected to dynamic load of finite
amplitude 06 p1100 A67-18001

Laser extensometer measuring small
dimensional changes of specimen in tensile
testing furnace at high
temperatures 06 p1012 A67-18778

Hysteresis loop measurement using
Sonntag fatigue machine which produces
sinusoidal force at 30 Hz fixed
frequency 23 p4078 A67-41227

EXTERNAL COMBUSTION ENGINE

Air breathing rocket using external
combustor formed by two short
annuli 08 p1376 A67-21284

Monograph on external burning in
supersonic streams, discussing heat addition,
fluid-mechanical model, use of
characteristics method, Chapman-Jouget
detonation, etc 24 p4254 A67-42386

EXTERNAL STORE

S NACELLE

EXTINGUISHER

S FIRE EXTINGUISHER

EXTRACTION

SA HYDROLYSIS

SA ION EXTRACTION

SA SEPARATION

Ion source using Penning discharge used
to inject hydrogen ions into magnetic
field 19 p3195 A67-35599

EXTRAGALACTIC LIGHT

Absolute radio luminosity empirical
relationship with surface brightness for
extragalactic radio
sources 03 p0515 A67-14320

Galactic depolarization of 21 cm
wavelength radiation of extragalactic sources
explained as function of distance traveled
by radiation through halo 05 p0895 A67-16601

Supernovae photometric properties,
considering mean absolute photographic
magnitude at maximum light, brightness
decline rate, etc 18 p3119 A67-33857

EXTRAGALACTIC RADIATION

Identification of strong extragalactic radio
sources in declination zone zero to minus 20
degrees 04 p0697 A67-14773

Degree of polarization and position angle
measurements of linearly polarized
components of galactic and extragalactic
radio sources at short
wavelength 11 p1861 A67-24486

Extragalactic radio sources classified into
five groups via radio magnitude and spectral
index at 400 MHz 11 p1868 A67-25086

Intergalactic radiation absorption and
extragalactic sources contribution to LF
background radiation 12 p1995 A67-25766

Polarization of extragalactic radiation
sources and evidence of irregularities of
magnetic field in our
Galaxy 13 p2198 A67-26791

Extensive air showers due to extragalactic
primary photons demonstrated, considering
production process 19 p3316 A67-35796

Extragalactic radio sources interpreted as
consistent evolutionary sequence, suggesting
particle injection, relativistic gas expansion
and intergalactic gas pressure
equilibrium 23 p4069 A67-41361

EXTRATERRESTRIAL ENVIRONMENT

SA LUNAR ENVIRONMENT
SA PLANETARY ENVIRONMENT
SA SPACE ENVIRONMENT
Structures of terrestrial and extraterrestrial atmospheres 06 p1091 A67-18997
Human performance on earth and in space noting depth perception, visual acuity, walking ability, reaction time, etc 06 p1289 A67-21068
Manned orbital laboratory for biological research, discussing experimental possibilities and requirements on spacecraft 08 p1287 A67-21070
Solar energy role in lunar water production, evaluating efficiency of collector-absorber systems 08 p1317 A67-21094
Orientation and navigation in space-time 11 p1820 A67-24936
Pressure and thermal protection of man during earth-moon flight and life on moon surface 12 p1901 A67-25175
Heat sterilization in microelectronic assemblies 12 p1914 A67-25683
Conservation of cryogenic propellants on long duration space missions by reliquefaction of vapor 13 p2091 A67-27636
Extraterrestrial vestibular research in orientation of humans in space, noting possible disorders due to radiation and lack of protection 15 p2425 A67-29106
Structure and composition of Jupiter atmosphere, noting laboratory and observational data supporting hypothesis of consistency with solar elements abundance 16 p2746 A67-30932
Space environment utilization for biological and medical research, physiological studies and therapeutic purposes, discussing orbital hospital and ambulance launch vehicle 19 p3181 A67-35653

EXTRATERRESTRIAL LIFE

SA LIFE DETECTOR
Voyager project for planetary biological exploration 02 p0185 A67-11816
Construction of lunar microcosm, considering recycling based on photosynthesis 02 p0185 A67-12313
Gulliver radiol isotopic biochemical probe to detect extraterrestrial life 05 p0806 A67-16548
Terrestrial and planetary biospheres, tabulating probability values for matching 06 p0953 A67-19007
Biotic signatures, discussing detection and epistemology 06 p0954 A67-19017
Biotic signature distribution reflecting geologic, atmospheric and oceanographic environmental orders 06 p0954 A67-19018
Fusion propulsion for interstellar missions, examining requirements for detection of extra solar life 06 p1076 A67-19027
Plausibility of extra solar intelligence, suggesting electromagnetic or optical means of communication 06 p0954 A67-19039
U.S. and U.S.S.R. search for extraterrestrial civilizations [AAS PAPER 66-78] 07 p1255 A67-20001
Extraterrestrial life detection method based on catalysis of isotopic oxygen exchange between water and oxygen-containing anions 09 p1454 A67-22015
Detecting planetary life from earth 11 p1747 A67-24063
Pressure and thermal protection of man during earth-moon flight and life on moon surface 12 p1901 A67-25175
Voyager project goals, orbital operations, capsule descent, navigational systems, etc 12 p2002 A67-25232
Low barometric pressure, high carbon dioxide concentration and water availability on simulated Mars environment related to survival and growth of bacillus cereus 15 p2426 A67-29111
Extraterrestrial life detection based on catalysis of oxygen exchange between labeled oxyanions and water, noting equipment 15 p2426 A67-29113
Pasteur Probe, assay of asymmetry of D, L amino acids in detection of Martian life 15 p2433 A67-29116
Exobiology and effect of physical factors on microorganisms 15 p2427 A67-29117
Preservation of viable microbes in anabiosis in potassium salts determined improbable by failure to grow bacteria 15 p2427 A67-29118
Detection of microbial life on near planets

by measuring physical parameters 16 p2611 A67-30768
Electrolysis-Hydrogenomonas bacterial bioregenerative life support system for manned space flight of long duration 16 p2617 A67-30774
Statistical correlation of latitude with time of maximum darkening of Mars dark areas, noting consistency of 2 models 16 p2749 A67-31401
Voyager project goals, orbital operations, capsule descent, navigational systems, etc 16 p2751 A67-31487
Automated biological laboratory /ABL/, comprehensive integrated system for detection of life on Mars 16 p2762 A67-31488
Pedoscope use in soil microbiological studies including ecology, infection susceptibility, etc 19 p3179 A67-35205
Soil, moisture and other requirements for microorganism survival in simulated Martian environment 19 p3177 A67-35220
Planetary quarantine and biological search strategy, discussing Voyager-Mars mission configuration, sterilization, back-contamination and decisions 19 p3180 A67-35233
Extraterrestrial life detection methods compared, discussing sampling and method requirements 19 p3180 A67-35250
Jupiter atmosphere, interior and surface properties, speculating on possibility of life in spite of presence of noxious gases 21 p3703 A67-38191
Microelectronic performance degradation resistance under thermal sterilization cycling conditions 21 p3596 A67-38344
Indigenous biology in Venus clouds, proposing isopycnic float bladder for macroorganism ingesting water and minerals blown up from surface by pinocytosis 22 p3750 A67-39556
Extraterrestrial life detection studied from knowledge of major and trace components of atmospheres 23 p3944 A67-40999

EXTRATERRESTRIAL MATTER

Sedimentologic process which comminutes, transports and deposits material by impact on planetary surfaces 02 p0235 A67-11451
Propellant preparation from extraterrestrial materials on moon and planets rather than transportation from earth as economical source of fuel for interplanetary manned traffic 04 p0695 A67-14555
Microscopic particles from various deposits analyzed for possible extraterrestrial origin 09 p1570 A67-22693
Meteorite age and related problems of cosmic chemistry 12 p1903 A67-25429
Cosmic origin of tektites indicated by factors other than chronology 14 p2385 A67-28145
Mean density of cosmological matter determined from quasi-stellar sources observations, analyzing apparent-magnitude and red shift methods 18 p3119 A67-33856
Solid interplanetary matter in moon vicinity through piezoelectric sensors, giving impact rate, trajectory projections and increased matter density 19 p3319 A67-35275
Economics related to practical extraction of logistics and water from moon, nearby planets and asteroids 19 p3327 A67-35652
Micrometeorite flux rate for Leonid shower measured with Luster sounding rocket collecting surface 20 p3528 A67-37424
Meteorite minerals characteristic constituents, describing crystalline form, frequency of occurrence, percentage, nature and terrestrial effects 21 p3700 A67-37766
Compact and dispersed cosmic matter using morphological approach to discovery, invention and research in astronomy 22 p3890 A67-40429
Alkali, alkaline earth and rare earth elements distribution in chondrite component minerals 24 p4236 A67-42646

EXTRATERRESTRIAL RADIATION

S PLANETARY RADIATION
S SPACE RADIATION
EXTRAVEHICULAR OPERATION
SA ASTRONAUT LOCOMOTION
Requirements and alternate systems approaches for extravehicular operations in space [AFAPL-CONF-67-6] 01 p0018 A67-11400
Manned extravehicular activities and

equipment used in Gemini space flight program 01 p0018 A67-11414
Water-immersion weightlessness simulation to determine astronaut EVA capabilities and man-machine interfaces [AIAA PAPER 66-903] 02 p0187 A67-12270
Passive heat transfer system for metabolic heat removal in extravehicular activity suit 03 p0364 A67-14295
Gemini program evaluation, discussing information gained from experiments performed during flights [AIAA PAPER 66-1027] 04 p0704 A67-14979
Integrated space suit, suit loop and backpack system for intravehicular operation on interplanetary missions 04 p0563 A67-15235
Spacecraft extravehicular control and display system 05 p0788 A67-16968
Telefactor system in control of space operations, describing master-slave manipulator servomechanism with TV network and electronic communication link 13 p2063 A67-27213
Water-immersion weightlessness simulation to determine astronaut EVA capabilities and man-machine interfaces [AIAA PAPER 66-903] 15 p2431 A67-29439
Local transportation in commercial space operations, extravehicular activity evolution and space environment characteristics utilization [AAS PAPER 67-116] 15 p2432 A67-29963
Extravehicular space maneuvering units, manned and unmanned, in satellite laboratory systems, describing space flight requirements and systems configuration 16 p2615 A67-30631
Extravehicular activity /EVA/ simulator for zero gravity environment using servodrives and computer control 17 p2832 A67-31994
Spacecraft and space station reliability by orbital maintenance and extravehicular activity, comparing redundancy on system and cost effectiveness [AIAA PAPER 67-652] 20 p3535 A67-37629
Mathematical models for retrieval systems for future extravehicular operations, discussing rotational and translational motion and constraint equations 22 p3753 A67-39157
Ground based simulation program for EVA evaluation including center of mass and inertia products of model astronaut 22 p3780 A67-40153
Biomedical results for various human medical systems during weightlessness experiments of Gemini program, noting vestibular function and EVA 22 p3752 A67-40534
Solar cell array for LEM electric power system during lunar surface operation noting requirements and tradeoffs 23 p3939 A67-41510
Experiments for relief of astronauts from cardiovascular and respiratory distress during EVA 23 p3953 A67-41586
Treatment for relief of altitude decompression sickness for operations requiring extravehicular activity 23 p3960 A67-41702
Manned testing of EVA equipment in simulated space environment, emphasizing crewman ingress and egress and mission objectives 24 p4115 A67-42049
Scaling laws and hydrodynamic model design techniques for high fidelity underwater simulation of zero and partial-g environments for manned space activities [AIAA PAPER 67-925] 24 p4140 A67-43021

EXTREMELY LOW FREQUENCY /ELF/
Intensity observation of ELF electromagnetic field integral and SEA phenomena caused by solar flare-induced SID 01 p0060 A67-11240
Natural ELF electromagnetic noise properties during solar flare of July 7, 1966, considering radiation compression effects on earth-ionosphere cavity 10 p1700 A67-23057
Horizontal loop antenna for observation of whistle-like ELF radio waves between 3 and 60 c/s 14 p2306 A67-27885
ELF and micropulsations phenomena divided into earth-ionosphere cavity resonances and regular and irregular pulsations 14 p2266 A67-28415
Resonances of thin shell model of earth-ionosphere cavity with dipolar magnetic field 18 p3042 A67-34427
Magnetic variations relationship to magnetospheric perturbations, emphasizing

particle participation near auroral zones 20 p3428 A67-36376
 Diurnal variation of earth-ionosphere cavity resonances and properties and propagation of ELF, ULF and MHD waves 20 p3390 A67-37727
 ELF waveforms spectral estimation at discrete frequencies of each polarity used for statistical comparison of mean spectra show normal distribution 22 p3789 A67-39474
EXTREMUM VALUE
 General problem in pure stress analysis, obtaining direct characterization and specific properties of extremal fields 02 p0336 A67-11791
 Bayesian statistics in dual control schemes for discrete-time noisy extremum systems 02 p0226 A67-12145
 Minimization method for examining from unique functional-analytic point of view additional aspect of extremum problems and methods of solving them 03 p0456 A67-12859
 Algorithm for directed random search for minimum of function of n -variables 03 p0374 A67-13182
 Characteristic function method for solving optimal control problems and sufficient conditions for existence of absolute minimum 03 p0457 A67-13183
 Extreme value problem of constant type and extremal approximating operators with positive kernels 03 p0461 A67-14106
 General method of variations for univalent functions with bounded boundary rotation permitting study of extremum problems 04 p0643 A67-14583
 General theory of variational problems of optimum control incorporating calculus of variations and Pontryagin maximum principle 04 p0647 A67-15981
 First-kind operator equation solution by reduction to dual extremum problem, proving existence and convergence 05 p0834 A67-16375
 Cartwright-Longuet-Higgins-Rice theory on instantaneous maxima of stationary random variable for deriving instantaneous maximum gust ratio to mean wind speed 05 p0837 A67-16426
 Point and interval estimation, from one order statistic, of location parameter of extreme value distribution with known scale parameter and of scale parameter of Weibull distribution with known shape parameter 05 p0835 A67-16853
 Extreme points of copositive quadratic forms constituting closed convex cone in Euclidean space 05 p0836 A67-17045
 Optimum thrust programming for sounding rocket extended by reducing state to single variable to obtain sufficient conditions for specific extremal solution 05 p0906 A67-17225
 Oscillatory ground wind response of Atlas/Agna examined, using statistical theory of extreme values 06 p1104 A67-18492
 Bessel function applications of two Sonin theorem formulations compared for range of applicability 07 p1215 A67-19472
 Algebraic theory of finite systems of linear inequalities based on Minkowski theorem and boundary solution principle 07 p1216 A67-19582
 Absolute extrema of certain integrals from method for finding corresponding functions with prescribed endpoints 11 p1812 A67-24087
 Absolute extremum existence in Boltz-Mayer type variational problem established by optimality principle 11 p1870 A67-24685
 Concept of extremal state in topological space, discussing existence conditions and criteria concerning extremal and stationary points 14 p2343 A67-28632
 Optimal control theory applied to extremum control in dynamic programming equation derivation for simplified extremum control problem 15 p2465 A67-30343
 Extremal problems of conformal mapping for doubly and triply connected regions, noting formulation and proof of pertinent theorems 16 p2698 A67-31913
 First variation theory in extremal problems, noting generalization of classical variational problems and optimal control problems for functions with single independent variable 17 p2876 A67-32043
 Mathematical programming on analog computers solved by saddle point and extremum methods, using differential equations 17 p2817 A67-32225
 Differential equations extremal solutions, introducing infasolution and Cauchy

infasolution concepts 18 p3070 A67-33548
 Singular optimal control and attitude problem in rocket guidance [AIAA PAPER 67-582] 19 p3258 A67-35977
 Dynamic programming for optimal algorithm for extremal control in presence of noise at system input and output 20 p3408 A67-37072
 Search for extremum of real function in presence of noise, using maximum principle 20 p3477 A67-37111
 Mean error and optimal structures for multidimensional extremal systems with random noise obtained from steady process 20 p3409 A67-37112
 Maximum information principle applied to search for minimum of function 20 p3477 A67-37195
 Free vibrations and motion stability during extremum drift for one- and multidimensional pulsed optimal systems 20 p3411 A67-37374
 Variational method used to obtain extremal flight conditions, considering flights between circular orbits and planets close to each other 21 p3705 A67-38585
 Optimal control problem with state variables subject to inequality conditions, deriving Pontryagin principle and differential equation 22 p3826 A67-39194
 Dynamics of single channel extremal systems having plants in linear and nonlinear elements and control units in form of self-oscillating type optimizer 22 p3777 A67-39777
 Wing shape and size selection for hypersonic velocities formulated as extremum problem of drag, aerodynamic property, temperature and coolant consumption for given wing volume 22 p3741 A67-40015
 Rapidly converging iterative solutions to Min-H strategy applicable to trajectory optimization and payload maximization 22 p3888 A67-40148
 Booster autopilot in bounded phase coordinates subject to disturbances, determining extremal control as function of time 22 p3833 A67-40149
 Differential equations maximum parameter values for single mass nonlinear system passage through resonance point determined with approximate methods based on small parameter method 23 p4026 A67-40686
 Conformal representation using Jacobi and Weierstrass elliptic function applied to extremal problems, noting electric modeling solutions 23 p4023 A67-40924

EXTRUSION

SA COLD WORKING

Mean tensile strength of aluminum alloys using torsion tests determined at high strain levels and compared with extrusion tests values 04 p0636 A67-14907
 Strengthening of eutectic composite fibrous wire and rod fabricated by hydrostatic extrusion [AIAA PAPER 67-172] 06 p1008 A67-18458
 Manufacturing methods for continuous filament refractory fibers including extrusion and chemical vapor deposition 08 p1345 A67-20427
 Structure and mechanical properties of extruded Ni-Al-oxide cermet materials, noting high compression strength 09 p1517 A67-21876
 Micro-yield stress determinations of cast and extruded beryllium as measure of dimensional stability 13 p2138 A67-27119
 Aluminum impact extrusion process design 14 p2323 A67-27814
 Aluminum magnesium alloys prepared by powder metallurgy and hot extrusion evaluated for tension, compression, impact, fatigue and creep 22 p3821 A67-40053

EYE

SA CORNEA
 SA LENS
 SA OCULAR CIRCULATION
 SA PUPIL
 SA RETINA
 SA VISION
 Model of retinal receptor incorporating various feedback control processes consistent with physiological and psychological evidence 01 p0044 A67-10465
 Tonometric and tonographic investigations of intraocular tension in hypoxia 06 p0953 A67-17995
 Photochemical cells and site involved in visual adaptation, reporting

electroretinogram data 06 p0953 A67-18643
 Independent effect of receptor adaptation level and pupil size on production of flashblindness by high intensity short-duration flashes 13 p2060 A67-26925
 Retinal photocoagulation using solid state laser 14 p2333 A67-28973
 Gas laser IR radiation hazards to eyes tested on rabbits indicates irreversible changes in cornea leading to impaired vision 20 p3375 A67-37276
 Absorption times for gases injected into mammalian eye anterior chamber 23 p3950 A67-41536

EYE DISEASE

Bilateral conjunctival hyperemia attributed to cardio-hemo-respiratory decompensation 04 p0561 A67-14628
 Retinal angiomas and aircrew fitness noting correction by photocoagulation 23 p3945 A67-41071

EYE EXAMINATION

Physiological limits of adaptation of eye with respect to body noting increase of pressure in ophthalmic artery under different conditions of hypoxia 16 p2611 A67-30757

EYE MOVEMENT

Existence of fovea in human retina explained by blood supply interference with steady and acute vision 02 p0184 A67-11473

EYE PROTECTION

Safety program for laser hazards, discussing eye and body protection 07 p1194 A67-19089
 Near field power density incident on eyes due to reflection from CW laser reduced by optical lens and shutter rearrangement 10 p1665 A67-23415
 Advanced vision research for extended space flight 15 p2430 A67-29274
 Overall profile of ophthalmic injury associated with ionizing and nonionizing electromagnetic radiation fields, based on human response to radiation exposure 16 p2611 A67-30769
 Laser safety - Conference, London, November 1966 23 p4015 A67-41049
 Safety of personnel from laser hazards covering installation containment, operator screening and eye protection 23 p4015 A67-41053
 Improved dipole shutter, ophthalmic transparency for protection against high intensity flashes 23 p3965 A67-41565

F

F-1 LAYER

Horizontal drift and anisotropy in F-1 region during geomagnetically active and quiet conditions 01 p0057 A67-10117
 Ionospheric stratification and electron density distribution in F-1 layer by Serafimov method 04 p0618 A67-15572
 Longitudinal variations of characteristics of F-1 layer compared for periods of high and low solar activity 07 p1173 A67-19688
 Dependence of electron concentration in F-1 layer on zenith angle of sun 07 p1178 A67-19820
 Electron temperature/ion temperature ratio and oxygen atom ratio to sum of oxygen molecule and nitric oxide in F-1 layer obtained by radar 17 p2843 A67-32529
 Ionospheric F-1 layer critical frequency at sunspot minimum and maximum, discussing critical frequency diurnal variation 22 p3789 A67-39476
 Effective recombination coefficient in upper-E and F-1 layers at sunset from rocketborne gyroplasma probe measurements of electron density profile 22 p3793 A67-40044

F-2 AIRCRAFT

S HUNTER F-2 AIRCRAFT

F-2 LAYER

F-2 layer ion-atom interchange coefficients, ion-neutral diffusion coefficient and flux of solar ionizing radiation, comparing ionospheric data 01 p0056 A67-10108
 Phase reversal in lunar variations of critical frequencies of F-2 layer at Waltair, India 01 p0060 A67-11232
 Analog computer ionization recombination parameters and balance equation of charged particles in F-2 layer 02 p0236 A67-11659
 Ionospheric F-2 layer inhomogeneities

attributed to plasma flute instability, using kinetic drift equations to describe plasma oscillations 02 p0236 A67-11669

Spectral analysis of pulsed signal reflected from ionospheric F-2 layer 02 p0193 A67-11672

Equatorial ionospheric storms, analyzing sub-peak and total columnar electron content 03 p0408 A67-12841

Noon electron density variation of F-2 layer at low latitudes and associated transport processes, using modified least squares method 03 p0415 A67-14111

Continuity equation for electrons in F-2 layer obtained for region near geomagnetic equator at noon including photoionization, recombination, drift, etc 04 p0614 A67-14954

Objection to Martin ionospheric drift theory based on dynamo electric field, atmospheric tidal wind field and F-2 layer drift motion 05 p0796 A67-16063

External sources of geomagnetic field at F-2 layer altitude and effects on recurring-orbit satellites 05 p0800 A67-17119

IGY and IQSY data on maximum electron density variation in F-2 layer 05 p0800 A67-17126

Critical frequencies of F-2 and E layers in ionosphere relation to total daily influx of solar wave radiation into earth atmosphere 05 p0800 A67-17128

Number of reverse signals reflected from F-2 layer during oblique reflection sounding 05 p0802 A67-17145

Fluctuations in diurnal variations of ionization of F-2 layer interfering with radio wave propagation determined by series expansion 07 p1173 A67-19687

Relation between magnetic activity and ionospheric disturbances in F-2 layer studied on basis of 30-year data 07 p1173 A67-19702

Statistical distribution of monthly median noon critical frequency of F-2 layer from ionospheric stations at mid-latitudes, auroral regions and at polar cap 07 p1174 A67-19703

Cyclic variations in maximum electron concentration of F-2 layer with solar activity explained by upper atmosphere temperature variations 07 p1178 A67-19818

Fast phase fluctuations of signal reflected from F-2 layer 07 p1144 A67-19819

Critical ionization frequencies in F-2 layer in near-polar region observed at Northern Hemisphere high latitude stations 07 p1179 A67-19832

Cyclic curves of F-2 layer critical frequencies based on seasonal phase variations in solar cycle 07 p1179 A67-19833

Ionospheric disturbances from high altitude nuclear detonations observed as changes in F-2 layer critical frequency 07 p1181 A67-19939

Approximate method for diurnal variation of peak electron density in F-2 layer, estimating effect of time varying drifts 10 p1650 A67-23336

Behavior of nighttime equatorial F-2 layer under ambipolar diffusion and electrodynamic drift 11 p1784 A67-23935

Nature of middle latitude ionospheric perturbations 12 p1932 A67-25543

Ionospheric waveguide channels for long distance radio links below maximum of F-2 layer 13 p2071 A67-27328

Low latitude nose whistlers, estimating path latitude and electron density distribution in intermediate region of magnetosphere 14 p2306 A67-27882

Ionospheric index of solar activity obtained together with quadratic equation regression coefficients by minimizing standard error of F-2 layer critical frequency 14 p2311 A67-28375

Nuclear explosion effects on atmospheric pressure, electron density, and F-2 layer height, noting dependence on time, season, etc 15 p2478 A67-30067

Field-aligned irregularities as effect of increased electron temperature in F-2 layer, analyzing heat production and loss mechanism [AGARDOGRAPH 95] 15 p2484 A67-30305

Analog computer ionization recombination parameters and balance equation of charged particles in F-2 layer 16 p2665 A67-31074

Ionospheric F-2 layer inhomogeneities attributed to plasma flute instability, using kinetic drift equations to describe plasma oscillations 16 p2665 A67-31084

Spectral analysis of pulsed signal reflected from ionospheric F-2

layer 16 p2624 A67-31087

Magnetoplasma diffusion equation of F-2 layer allowing electric currents and temperature variations, noting transverse drift of field 16 p2666 A67-31402

Time and space distribution of anomalous ionization in ionospheric F-2 layer above Southern Hemisphere, noting maximums of ionization distribution 16 p2668 A67-31893

Drift data harmonic analysis correlation between solar quiet diurnal variation and ionospheric drift 16 p2669 A67-31908

Seasonal variations in afternoon and evening maxima of F-2 layer and dependence of temperature and frequency on minimum zenith angle of sun 17 p2842 A67-32384

Continuity equation for electron density in F-2 layer, noting solution for given diffusion, loss, time dependence, etc 17 p2853 A67-33245

Traveling ionospheric disturbances effect on and measurement of direction of movement of downcoming F-2 region perturbation 18 p3043 A67-34526

Ionospheric F-2 region equatorial anomaly dependence on geomagnetic field 20 p3426 A67-36289

Rate of transequatorial plasma diffusion along geomagnetic field lines in topside ionosphere, considering electron distribution asymmetries in equatorial F-2 layer 20 p3431 A67-37098

Scattered radio signals received during solar eclipse examined for indication of electron clouds masked by daytime high electron density 20 p3432 A67-37208

Ionogram data used to identify high absorption periods, analyzing diurnal variations of critical frequency F-2 layer showing no echo 20 p3432 A67-37275

External sources of geomagnetic field at F-2 layer altitude and effects on recurring-orbit satellites 21 p3618 A67-38462

IGY and IQSY data on maximum electron density variation in F-2 layer 21 p3618 A67-38469

Critical frequencies of F-2 and E layers in ionosphere relation to total daily influx of solar wave radiation into earth atmosphere 21 p3618 A67-38471

Number of reverse signals reflected from F-2 layer during oblique reflection sounding 21 p3619 A67-38487

Planetary distribution of horizontal gradients of F-2 layer critical frequency and diurnal, seasonal and solar cycle variations 21 p3622 A67-39034

F-2 layer critical frequencies variation with solar activity, evaluating criteria for unperturbed state based on magnetically inactive days 21 p3622 A67-39035

Latitude variation of critical frequency of F-2 layer in equatorial region during geomagnetic disturbance, discussing ionization density 21 p3622 A67-39036

Ion formation rate in F-2 layer under nocturnal ionospheric conditions, determining electron densities 21 p3623 A67-39037

F-2 layer contribution to vertical radio wave absorption, using information about structure, electron and ion temperatures 22 p3789 A67-39472

Star Fish high altitude nuclear explosion effect on electron loss rate in F-2 region 22 p3793 A67-40082

Mean F-2 layer electron collision frequency computation from cosmic noise absorption 23 p3994 A67-40779

Equatorial anomaly in F-2 layer of ionosphere, examining solar activity, seasonal variation relation to magnetic activity, lunar phase and heights 23 p3996 A67-41082

F-4 AIRCRAFT

Beryllium rudder and structures for F-4C aircraft, discussing weight factor, analysis, design, fabrication, ground tests and fail-safe flight test programs [SAE PAPER 660666] 01 p0094 A67-10574

Urinalysis assessment of physiological response of eight pilots to 18-hr flight in F-4C aircraft 03 p0364 A67-14287

Flight load maneuver data for fatigue evaluation of F-4 series aircraft 10 p1594 A67-23435

F-5 AIRCRAFT

TSIS fire control equipment family, considering maximum cost effectiveness,

discussing use in Dassault Mirage M-5 and RCAF CF-5 aircraft 20 p3364 A67-37244

F-27 AIRCRAFT

Fokker F-28 Fellowship conceived as jet contemporary of turboprop Fokker Friendship, noting structural and operational details 16 p2597 A67-31561

F-28 AIRCRAFT

S FOKKER F-28 AIRCRAFT

F CENTER

Adiabatic harmonic unitary transformations and relation between electron trapping energy and normal lattice modes associated with F center ground state 03 p0495 A67-13515

L-and K-band absorption due to optical transitions starting from ground state of F center in alkali halide 05 p0864 A67-16801

Hyperfine interaction between unpaired trapped electron and adjacent titanium 47 and 49 nuclei in F center ESR line in barium titanate 21 p3684 A67-38417

Time dependent relation between coloring and spontaneous conductivity increase in barium titanate single crystals by strong electric field 22 p3861 A67-39918

F LAYER

Direct backscatter recordings from polar cap F-layer reflections used to predict communications 01 p0020 A67-10007

Long term variation in relations of solar indices to E and F region character figures interpreted without assuming changes in solar radiation 01 p0056 A67-10110

Auroral region disturbances generating atmospheric waves in F layer that produce atmospheric mixing 01 p0056 A67-10112

Drift velocities change in F layer as function of time explained by movement of reflection point over ionospheric surface 01 p0061 A67-11262

Diurnal variations in F layer at Ibadan exhibit peak before noon during sunspot maximum and after noon during sunspot minimum 03 p0407 A67-12826

F region ionization equatorial anomaly during two periods of minimum sunspot activity in 1965 03 p0407 A67-12827

Nighttime F layer irregularities at equator responsible for scintillation of signals from radio sources and satellites 03 p0407 A67-12828

Horizontal drift measurements in E and F regions of ionosphere over magnetic equator in India 03 p0407 A67-12829

Spaced antenna technique for determining drift and anisotropy of equatorial E and F region irregularities 03 p0407 A67-12833

Rapid geomagnetic micropulsation activity in low latitude conjugate stations show definitive results on current system 03 p0408 A67-12843

Oblique echo presence during winter nights on auroral and subauroral latitudes ionograms, analyzing electron number density of nighttime F region in midlatitude trough vicinity 03 p0409 A67-12947

Coherent interaction of two radio waves in plasma, generation of mutually-harmonic frequency wave and application to radio transmission in ionospheric F layer 03 p0372 A67-14091

Spread-F occurrence dependency on F layer height variations with time, season and longitude and plasma wave generation near geomagnetic equator 03 p0415 A67-14115

Sunset peak in occurrence of F layer field-aligned echoes explained by Martyn amplification mechanism, estimating ionization vertical velocities from electron number density 04 p0615 A67-14959

E-2 and F-0 intermediate ionospheric layer morphology, occurrence, electron density and signal reflection variations 04 p0616 A67-15220

Relation between E-2 and F-0 ionospheric layer formation and geomagnetic phenomena 04 p0616 A67-15221

Drift of small scale E and F layer inhomogeneities in Black Sea coastal region 04 p0616 A67-15222

Radio Aurora and formation mechanism of ionospheric D and F regions, examining HF and VLF propagation via computer ray tracing, ionospheric storms and equatorial sporadic E layers 05 p0795 A67-16010

Emf as cause of vertical downward and upward ionization drift in F region of ionosphere during magnetic storm 05 p0801 A67-17141

Ionospheric F layer rise during

magnetically quiet night as caused by charge carrier drift induced by electric field 06 p0993 A67-17581
Loss coefficient and vertical transport velocity for nighttime F region during solar activity 06 p0995 A67-17971
F region effects following two severe magnetic storms, noting changes in electron density profile 06 p0995 A67-17972
Virtual reflection-height oscillations and ultrasonic waves in ionospheric F layer 06 p0995 A67-17974
Reaction rates controlling densities of ions and electrons in F region determined so that calculated ion and electron distribution may agree with rocket observations 06 p0996 A67-18430
Seasonal variation in temperature in nighttime F region through analysis of emission intensity of oxygen red line and upper atmosphere 06 p0996 A67-18431
Latitudinal and vertical current components effects included in longitudinal current system supporting steady state distribution in geomagnetic anomaly 06 p0998 A67-18703
Recombination rate increase in F region following magnetic activity due to passage of atmospheric wave 07 p1171 A67-19418
Diurnal and seasonal altitude variations of E and F layers analyzed for geomagnetic activity from rocket measurement of electron concentration 07 p1173 A67-19686
Electron density variation, solar activity and geomagnetic storm effects on ionospheric F-region 07 p1177 A67-19785
Electron concentration inhomogeneities during traveling gravity wave propagation through F layer 07 p1178 A67-19809
Electron-concentration distribution in ionospheric F-2 layer with vertical distribution of electron-ion 07 p1178 A67-19821
Relation between solar radiation and electron concentration up to F layer analyzed in winter and summer 07 p1179 A67-19831
Electron temperature and density in F region analyzed for nighttime heating, using Langmuir probe measurements 08 p1327 A67-21364
Normality of SD variation at dip-equatorial stations suggests origin beyond F layer 08 p1327 A67-21373
High latitude increase in ionization of F layer correlating in space and time with auroral precipitation as shown by ionospheric electron number density data 08 p1328 A67-21481
Vertical ionospheric perturbations observed from January 1963 through May 1965 10 p1630 A67-22789
Ionospheric rocket sounding, measuring ion density and electron temperature between E and F layers 10 p1633 A67-22948
Seasonal and annual variations of electron density in ionospheric F layer interpreted as changes in production rate and ionization loss caused by atmospheric composition variations from neutral atmosphere 10 p1647 A67-23274
Nocturnal decline of ionospheric airglow 3300 angstrom line intensity due to diatomic oxygen ion-electron recombination 10 p1649 A67-23294
F layer changes during solar eclipse observed at equatorial station, obtaining values for effective electron loss coefficients 10 p1651 A67-23340
Electron density variation from photochemical rates in equatorial F layer during October 1959 solar eclipse 10 p1651 A67-23342
Rocket and satellite measurements of electron and ion thermal structure of ionospheric F region 12 p1935 A67-25796
Unstable diurnal and seasonal variation of ionization of F region of ionosphere during years of minimum solar activity over Ashkhabad 12 p1938 A67-26100
F layer critical frequency perturbations due to low altitude nuclear explosion 13 p2107 A67-26309
Temperature of F region deduced from electron number density profiles 13 p2108 A67-26322
Dependence of seasonal occurrence probability of F-zero layer on level of geomagnetic activity and ionospheric activity

observed above Ashkhabad 13 p2110 A67-26549
Chemical recombination parameters in F layer of day ionosphere determined from electron density profiles 13 p2115 A67-27211
Ionization transport from equator along magnetic lines of force may contribute to formation of diurnal ionization anomaly of F region in intermediate zone 13 p2117 A67-27708
Radio waves effect on ionospheric F layer, showing decrease in critical frequency and disturbance of stationary electron and ion concentration 14 p2307 A67-27923
Spatial HF radio focusing caused by electron distribution between ionospheric layers, even in absence of horizontal density gradients 14 p2261 A67-28048
F region phenomena, discussing charged particles dynamics, equatorial and seasonal anomalies and nighttime F layer maintenance, using Alouette I data 14 p2312 A67-28409
Magnetosphere-ionosphere coupling mechanisms at middle and low latitudes 14 p2312 A67-28411
Characteristic enhancement of forbidden doublet in nitrogen excitation observed in night airglow during traveling ionospheric F region perturbation 15 p2474 A67-29479
Night F layer behavior, considering height and electron density, noting computer program for nonsteady state continuity equation with neutral gas movement 15 p2474 A67-29523
Traveling ionospheric disturbance heat conduction waves excited in neutral gas of thermosphere by hydromagnetic waves from magnetopause 15 p2475 A67-29617
Angular spread of backscattered spread-F echoes compared with that associated with normal F region returns [AGARDOGRAPH 95] 15 p2480 A67-30278
Influence of spread-F upon apparent reflection coefficients of F region for HF radio waves [AGARDOGRAPH 95] 15 p2481 A67-30279
F region irregularities studied by scintillation of radio signals from earth satellites [AGARDOGRAPH 95] 15 p2481 A67-30285
Nature of nighttime F-layer irregularities responsible for scintillation of VHF signals received from radio stars and earth satellites [AGARDOGRAPH 95] 15 p2482 A67-30290
Measurements on scintillation observed on radio signals from Discoverer satellite, noting intensity increase with latitude and data on diurnal variation [AGARDOGRAPH 95] 15 p2483 A67-30293
Large-scale structure of F layer studied by observing Faraday rotation of satellite signals, noting irregularities in total electron content 15 p2483 A67-30295
Intense fluctuations observed above Arecibo during geomagnetically disturbed conditions, using ionospheric backscatter technique 15 p2483 A67-30299
Ionospheric irregularities in F region during night hours /1958-1960/ [AGARDOGRAPH 95] 15 p2483 A67-30300
Ionospheric irregularity observation near F layer maximum, determining traveling velocities [AGARDOGRAPH 95] 15 p2484 A67-30302
Properties of irregularities responsible for spread-F, discussing hydromagnetic waves [AGARDOGRAPH 95] 15 p2484 A67-30303
Strong ionospheric effects observed on ionograms after high altitude detonation including changes in F layer critical frequency, height and spread [AGARDOGRAPH 95] 15 p2484 A67-30306
Diurnal temperature change effect on F-2 layer, noting maximum electron density height dependence on neutral-gas temperature variations 16 p2663 A67-30967
Measurements at Ibadan of drift velocity of ionospheric irregularities for E and F layers during IQSY 16 p2663 A67-30969
Magnetic storm effects on F-2 layer near equatorial zone boundary causing variations in critical frequency of layer 16 p2663 A67-30970
Morning effect on F region, noting seasonal variation of corresponding solar zenith angle and worldwide distribution of predawn minimum 16 p2664 A67-30976
F-region electron-density perturbations transmitted to magnetically conjugate

region, noting electrostatic coupling mechanism 16 p2667 A67-31509
Propagation rate distribution as function of geomagnetic latitude provides evidence for geomagnetic effects on vertical ionization drifts in F region of ionization 16 p2668 A67-31894
F region and magnetosphere data obtained by incoherent-backscatter radar technique, studying ion and electron temperatures relationship to height, electron density profiles, etc 17 p2843 A67-32389
Bates theory of atomic oxygen excitation in upper atmosphere as cause of F layer nightglow emissions 18 p3038 A67-33616
Nocturnal recombination processes in ionospheric F region for nitrogen and oxygen based on 5200 and 6300 angstrom lines 18 p3040 A67-33693
Protonosphere heating by photoelectrons escaping from F region, estimating protonosphere opacity and daytime escape flux 19 p3221 A67-35280
Traveling-ionospheric disturbances observed at midlatitudes by backscattering technique, noting auroral zone and gravity waves role 20 p3425 A67-36280
Attachment coefficient and transport velocity in nighttime F region from backscatter N-h profiles, determining loss term integration 20 p3426 A67-36287
Latitude, altitude and local time variation of forces controlling 100 to 700 km atmospheric winds, noting effects on ionospheric phenomena 21 p3654 A67-37994
EMF as cause of vertical downward and upward ionization drift in F region of ionosphere during magnetic storm 21 p3619 A67-38483
Ion and neutral particle interaction effects on F region winds, considering plasma forces 22 p3789 A67-39479
Radar-derived results for midlatitude F-region densities and temperatures at sunspot minimum noting seasonal anomalies 22 p3793 A67-40080
Unsteady continuity and motion equations describing F layer dynamic characteristics under time dependent electric and magnetic fields 23 p3996 A67-41178
Ionospheric electron content and OI nightglow in Hawaii, discussing ionization density increases throughout bottomsides F layer 24 p4147 A67-41878
Vertical ionospheric perturbations observed from January 1963 through May 1965 24 p4149 A67-42125
F-106 AIRCRAFT
Next generation interceptor aircraft to follow F-106A, including YF-12A and evolving F-111B, would serve largely as missile launching platforms 04 p0550 A67-14422
Digital computers for built-in self-test in airborne weapon system, with examples of mechanized tests from F-106/MA-1 system 20 p3392 A67-36989
F-110 AIRCRAFT
S F-4 AIRCRAFT
F-111 AIRCRAFT
Computer program /MAST/ analyzing F-111 wing structure involving load and stress analyses 03 p0525 A67-13967
Next generation interceptor aircraft to follow F-106A, including YF-12A and evolving F-111B, would serve largely as missile launching platforms 04 p0550 A67-14422
F-111 wing sweep actuator with irreversible Acme-thread jackscrew driven by hydraulic servomotor 05 p0752 A67-16157
Hydraulic power distribution system for flight control of F-111 aircraft 05 p0752 A67-16158
Horizontal tail two-stage hydraulic servoactuator for F-111 horizontal stabilizer control 05 p0752 A67-16160
Variable sweep wing F-111 aircraft cooling systems for temperature control of hydraulic fluid of type II system 05 p0752 A67-16161
F-111 aircraft wing spoilers controlled by hydraulic servoactuators 05 p0753 A67-16162
Main landing gear door and aerodynamic speed brake combination in F-111 aircraft, considering weight minimization and control of landing gears 05 p0753 A67-16163
Dual circuit hydraulic powered brake control system for effective short landing of F-111 aircraft 05 p0753 A67-16164
F-111 fixed price contract management, discussing weapon system management,

acquisition, controls and techniques to circumvent inherent problems
[AAS PAPER 66-153] 08 p1430 A67-20971

F-111 fixed price contract management, discussing weapon system management, acquisition, controls and techniques to circumvent inherent problems f-111 fixed price contract management, discussing weapon system management, acquisition, controls
[AAS PAPER 66-153] 13 p2233 A67-27554

F-111 crew escape module design and performance 14 p2244 A67-27739

Wing pivoting design for supersonic aircraft adaptability to different flight conditions, noting experiments with F-111 16 p2590 A67-30839

Flight test program for F-111A variable sweep tactical weapon system, discussing afterburning turbofan engine, crew module, escape and survival 17 p2795 A67-32214

F-111 MK 2 avionics system evaluation and parameter tradeoff 17 p2819 A67-32499

Strong forward flow of engine exhaust gas in blast deflection flow field of twin jet F-111B 17 p2797 A67-32568

Maintainability technology and controls developed during F-111 design 18 p2986 A67-34663

FABRIC

S PARACHUTE FABRIC

FABRY-PEROT INTERFEROMETER

Intensity dependent frequency shift in spectral output of monochromatic giant pulse lasers measured, using Fabry-Perot interferometer 01 p0088 A67-10251

Optical systems crossing in Fabry-Perot interferometer to determine instrumental function of spectrographic device 02 p0246 A67-12479

Fabry-Perot interferometers with electronic determination of Doppler line widths, discussing effect of hyperfine and isotopic structure 07 p1185 A67-19399

Astrospectrometer, instrument for recording high definition star spectra 07 p1186 A67-19425

Interference filter of Fabry-Perot interferometer type for studying millimeter and submillimeter plasma radiation 09 p1545 A67-22000

Modulation pyrometer measuring plasma temperature from spectral line intensity 09 p1499 A67-22328

Pressure scanned Fabry-Perot etalon for measuring ruby line widths at room temperature 10 p1662 A67-22741

Absolute gravitational acceleration determined by timing symmetrical free motion of body moving under attraction of gravity 12 p1965 A67-25126

Maximeter in monitoring thin films differing in optical thickness 13 p2181 A67-27232

Fabry-Perot interferometer construction 14 p2315 A67-27830

Automatic pressure stepping control and recycling system for use with Fabry-Perot interferometer 14 p2315 A67-28158

Ruby laser with Fabry-Perot interferometer selector studied for wavelength and thermal stability control 14 p2332 A67-28759

Mechanical friction occurring during oscillating motion of gas which absorbs or reflects electromagnetic radiation 14 p2349 A67-29075

Development of plasmoid density due to laser ionization measured using Fabry-Perot interferometer 15 p2527 A67-29474

Double sapphire plate resonator to control multiple modes of commercial laser /Korad K-1Q/ without use of saturable dye 15 p2498 A67-29497

Shape of extremely short pulses generated by helium-neon laser with mutual synchronization of intermodal beats achieved by Fabry-perot interferometer 15 p2500 A67-29760

Light field distribution in optical resonator of Fabry-Perot type interferometer with nonparallel mirrors, using Airy function for localizing field concentration planes 17 p2853 A67-31925

Laser measurements of long distances using laser interferometers, modulated laser beams and laser radar 17 p2867 A67-32613

Optical observations of daytime aurorae by means of atomic-oxygen-emission interferometry 17 p2852 A67-33212

Measurement of Doppler-broadened emission line width by Fabry-Perot interferometer to study ion temperature of pulsed plasma 17 p2862 A67-33292

Fabry-Perot interferometer for discriminating gas laser modulation at frequencies less than Doppler bandwidth 17 p2869 A67-33294

Kinetic temperature measurements of 5577 angstrom line night airglow with Fabry-Perot interferometer, discussing nightly mean temperatures 18 p3037 A67-33609

Fabry-Perot interferometric observation of spectral line to investigate ionization rate of electrical discharge used for argon ion laser 18 p3061 A67-34044

Far IR Fabry-Perot interference filters consisting of parallel close-spaced metal meshes 19 p3262 A67-35686

Computer method for evaluating hyperfine structure recordings obtained by photoelectric Fabry-Perot interferometer 20 p3440 A67-36357

Mapping of Fabry-Perot interferometer plates defects by measuring apparatus function peak displacement, describing measurement setup 20 p3440 A67-36358

Fabry-Perot interferometer improvements for high resolution rocket photography of solar Fraunhofer spectrum 20 p3440 A67-36359

Fabry-Perot interferometer with magnetostrictive scanning and SNR improves system for solar physics and airglow observations 20 p3440 A67-36360

Pressure scanned Fabry-Perot interferometer for twilight sky and zodiacal light observations 20 p3440 A67-36361

Spectrometer with two servocontrolled Fabry-Perot interferometers 20 p3441 A67-36364

Accelerometer using interference fringes of Fabry-Perot system for measurement of small vibratory disturbances 20 p3444 A67-36520

Ruby laser radiation frequency temperature dependence, observing narrow spectral width with Fabry-Perot interferometer 21 p3640 A67-38451

Fabry-Perot interferometer for emission spectra time variations observed by employing electromechanical system to vary mirror motion speed 22 p3809 A67-40416

Near IR laser transitions in pure helium studied with scanning Fabry-Perot interferometer, determining fine structure components in upper laser levels 22 p3817 A67-40488

Externally adjustable pressure regulation of Fabry-Perot interferometer, using device to measure cesium vapor spectral absorption in D-1 line 22 p3810 A67-40522

Multiple stimulated Brillouin scattering used for nanosecond high intensity pulse generation combining ruby laser with liquid cell and Fabry-Perot etalon 23 p4011 A67-40786

Laser emission mode splitting of CN laser, discussing wavelength to resonance length and Fabry-Perot interferometer permitting line splitting observation 23 p4012 A67-40893

Giant pulse ruby laser having tunable two-frequency output noting spectral measurements made with Fabry-Perot interferometer 23 p4015 A67-41038

FABRY-PEROT LASER

Optical pumping with diode laser into Fabry-Perot resonator face of thin highly-absorbing semiconductor, noting variable mode spacing including single mode output 01 p0091 A67-10879

Single mode approximation of parametric excitation and self-excitation of oscillations in Fabry-Perot resonator filled with nonlinear dispersive medium 02 p0251 A67-11575

I-V characteristic of GaAs diode with Fabry-Perot resonator, noting variations during amplification to generation transition 04 p0678 A67-15132

Semiconductor lasers with radiating mirrors developed by excitation, using electron beam and neodymium laser glass radiation 05 p0821 A67-16669

Fizeau fringes produced in laser illuminated Fabry-Perot interferometer to obtain concentration profiles in turbulent and laminar jets 05 p0794 A67-17371

Electro-optic intra-cavity color switching in krypton ion Fabry-Perot laser 06 p1010 A67-17888

Recombination radiation of p-n junctions in GaAs with and without Fabry-Perot cavity, discussing nonequilibrium current carrier kinetics and I-V characteristics 06 p1063 A67-18934

Recombination radiation from GaAs p-n junctions with and without Fabry-Perot resonator, noting parameter dependence on current density 08 p1337 A67-20413

Gain saturation effect on oscillating modes of optical masers 08 p1339 A67-21377

Internally modulated gas laser at 100 and 4000 MHz, describing electromagnetic field in Fabry-Perot resonator in terms of natural oscillation modes and coupling 09 p1514 A67-22261

Ruby laser cavity losses measurement by Fabry-Perot resonance 10 p1662 A67-22740

Mode discrimination of laser cavity exploiting transmission characteristics of Fabry-Perot interferometer 10 p1663 A67-22835

I-V characteristic of GaAs diode with Fabry-Perot resonator, noting variations during amplification to generation transition 12 p1951 A67-25156

Gaseous laser oscillations in Fabry-Perot resonator with corner-cube prism noting alignment characteristics 12 p1953 A67-25454

Laser measurements of long distances using laser interferometers, modulated laser beams and laser radar 17 p2867 A67-32613

Fabry-Perot resonator excitation using integral equations corresponding to boundary value functions 17 p2868 A67-32667

Fabry-Perot resonator free oscillations defined by complex frequency, obtaining diffraction loss and resonant frequency 17 p2868 A67-32668

Many-element lasers spiking emission for Fabry-Perot and confocal geometry, including time resolved spectroscopy and far and near field patterns 17 p2870 A67-33298

Cylindrical Fabry-Perot resonator, determining resonant modes by applying boundary conditions, noting eigenvalue and eigenfunction roles 18 p3060 A67-34024

Appearance of extraordinary rays from double refraction in ruby laser crystals with polished rectangular prisms 20 p3507 A67-36330

Modes and eigenvalues of symmetric cylindrical Fabry-Perot laser resonator with circular output-coupling apertures 20 p3460 A67-37024

Solution grown GaAs laser diodes with Fabry-Perot cavity, measuring threshold current density variation with reciprocal laser diode length 21 p3641 A67-38457

Fabry-Perot etalon resonator studied for incidence angles for use as filter, test instrument and control device for laser output 22 p3809 A67-40469

Intrinsic modes of spherical mirror resonators, noting parameters identifying beams generated by such resonators 23 p3998 A67-40709

Black body visible light at 2800 degrees K changed into energy distribution at 5500 degrees K via Fabry-Perot filter for white light standards for colorimetry 23 p3999 A67-41180

Optically concentrated laser radiation beam properties using plane and spherical faced ruby resonators 23 p4016 A67-41322

FABRY-PEROT SPECTROMETER

Plasma electron density and formation determined, using Fabry-Perot resonator 02 p0275 A67-12469

Extremely fast varying and low intensity plasma emissions analyzed with reflection multichannel Fabry-Perot interferometer 20 p3439 A67-36352

Design, construction and operation of multichannel photoelectric spectrometer, using Fabry-Perot etalon and axicon 20 p3439 A67-36353

Low intensity photoelectric signal detection by Fabry-Perot spectrometer using SNR enhancing method 20 p3439 A67-36356

Fabry-Perot spectrometer applied to upper atmospheric emission measurements of airglow and aurora 20 p3440 A67-36362

Digital recording double Fabry-Perot spectrometer, discussing pressure difference control system 20 p3440 A67-36363

Spectrometer with two servocontrolled Fabry-Perot interferometers 20 p3441 A67-36364

Aperture system using moire fringe method to execute spectral scan for Fabry-

- Perot spectrometer 23 p4001 A67-41258
Least squares deconvolution technique for reducing Fabry-Perot spectrometer data to Voigt profiles 23 p4002 A67-41262
- FACE CENTERED CUBIC / FCC/ CRYSTAL**
Thermogravimetric analysis and electron microscopy of agglomeration and chemical instability of submicron refractory dispersoids in tungsten 01 p0097 A67-10699
Kinetics of formation of thin continuous films from isolated three-dimensional nuclei 02 p0286 A67-11709
Plastic deformation of indium and indium-thallium alloys, noting change of pure indium lattice to fcc with increase of thallium content 02 p0255 A67-11869
Fatigue mechanisms for fcc metals and alloys, reviewing research on crack initiation and propagation 03 p0447 A67-13800
Grain boundary relaxation in high purity fcc metal using LF torsion pendulum, noting tests for internal friction and creep at constant stress 06 p1016 A67-17899
Tungsten films with fcc structure obtained by ion beam sputtering in vacuum onto substrates of glass, rock salt and mica at various temperatures 07 p1232 A67-19557
Specific stacking fault energy of deformed fcc metals determined from electron microscope diffraction contrast of stacking fault dipoles 07 p1208 A67-19637
Single niobium crystal deformation, discussing stress-strain curves, slippage, orientation and asymmetry of slip 07 p1211 A67-20164
Electronic band structure calculations phase of Ca, Sr and Ba over wide range of atomic volumes under pressure electronic band structure calculations for fcc phase of Ca, Sr and Ba over wide range of 10 p1682 A67-23399
Diagonalization procedure for Hamiltonian of ferromagnetic thin film, applying canonical transformation in direction of film thickness 11 p1845 A67-23992
Electron-phonon interaction and phonon spectrum observed for electron tunneling measurements in fcc alloys of Pb alloys, noting electron concentration changes 13 p2175 A67-26426
Interactions of homonuclear diatomic gas molecules with fcc solid surfaces calculated by digital computer 13 p2098 A67-26938
Structure of thin tungsten films as function of nature and temperature of substrate, noting partial crystallization of fcc structure 15 p2535 A67-29477
Slip step role in early stages of stress corrosion cracking in face centered iron-nickel-chromium alloy thin foils 16 p2690 A67-31384
Neighbor model for computer simulation of field ion images in fcc point lattice 17 p2887 A67-32205
Structural characteristics of Ni-Mo alloys analyzed using electron microscopy and X-ray diffraction scattering 17 p2872 A67-32723
Sputtered films stable fcc modification of several metals deposited at high temperatures, obtaining normal structures over 400 degrees C 21 p3677 A67-38091
Cyclic stress-strain in annealed and cold worked fcc polycrystalline metals and alloys studied for hardening and softening by transmission electron microscopy 22 p3821 A67-40033
Solubility of niobium carbide in gamma iron determined from experiments using Fe-Nb alloy in equilibrium with hydrogen-methane mixtures 24 p4173 A67-42348
- FACILITY**
S DEEP SPACE INSTRUMENTATION FACILITY /DSIF/
S GROUND HANDLING FACILITY
S HIGH FIELD MAGNET FACILITY
S LAUNCHING FACILITY
S RESEARCH FACILITY
S TEST FACILITY
- FACSIMILE TRANSMISSION**
Panoramic facsimile camera for unmanned space operation providing 360 degrees IR and visible spectrum imagery [SMPTE PREPRINT 100-40] 03 p0423 A67-13806
- FACTOR**
S AGE FACTOR
S AMPLIFICATION FACTOR
S EMOTIONAL FACTOR
S FRANK-CONDON FACTOR
S GEOMETRIC FACTOR
S HUMAN FACTOR
- S LOAD FACTOR
S MASS FLOW FACTOR
S PH FACTOR
S PHYSICAL FACTOR
S PSYCHOLOGICAL FACTOR
S Q-FACTOR
S SAFETY FACTOR
S SOCIAL FACTOR
S TIME FACTOR
S VIEW FACTOR
S WEIGHT FACTOR
- FACTOR ANALYSIS**
Second order personality factor analysis applied to air traffic control specialists 13 p2063 A67-26929
- FACTORIAL DESIGN**
Design factors for aluminum castings 14 p2323 A67-27813
Aluminum impact extrusion process design 14 p2323 A67-27814
Aluminum alloy forgings design 14 p2323 A67-27815
- FADING**
SA PHASE FADING
SA RAYLEIGH FADING
SA RICIAN FADING
SA SELECTIVE FADING
SA SIGNAL FADING
Fading and multipath propagation mechanism for communication links involving satellites and aircraft with antenna beams, assuming fading models and estimating margins required for FSK teletype transmission 06 p0960 A67-17673
Error rate expression for canonic binary receivers, evaluating performance of incoherent detection 14 p2272 A67-28706
Discriminator threshold and SNR above threshold response when demodulating FM signal undergoing selective fading 14 p2273 A67-28711
- FAI**
S FIELD-ALIGNED IRREGULARITY /FAI/
FAIL-SAFE SYSTEM
Model ten-member redundant structure under constant-amplitude loads analyzed, determining statistical distribution of consecutive failures for fail safe design applications 10 p1718 A67-23432
Electrostatic discharging systems for helicopters, discussing earth field effect and fail-safe concept 16 p2610 A67-31824
Random load fatigue life and reliability via fail-safe structural model, obtaining statistical distribution of 2024-T4 aluminum alloy bending strength 23 p4076 A67-40735
Fail-safe design, nondestructive testing and inspection facilities at design stage for aircraft structures 24 p4250 A67-42442
- FAILURE**
SA CRACK
SA ENGINE FAILURE
SA FATIGUE
SA FRACTURE
SA SHORT CIRCUIT
SA STRAIN
SA STRUCTURAL FAILURE
SA SYSTEM FAILURE
Failure rate and failure mechanism schools test philosophies combined to know and improve integrated circuits reliability 01 p0042 A67-11366
Shock and vibration test specifications, contrasting approaches requiring exact duplication of environment with those simulating damaging characteristics 06 p0981 A67-18366
Reliability in optimal control problems in terms of probability of faultless operation 07 p1162 A67-20027
Failure mechanism of solid propellant grain and stress criteria for solid motor design and evaluation 08 p1374 A67-20891
Accelerated fatigue testing using stepwise stress increase method 14 p2402 A67-28815
Fabrication, structure, possible failure and testing of coated refractory metals in applications for space technology 19 p3245 A67-34959
- FAILURE MODE**
Structural sensitivity of plastic properties of molybdenum alloys produced by electron beam fusion, investigating microstructure, failure in bending tests and grain fragmentation 01 p0101 A67-10936
Transient junction temperature rise, transient thermal resistance and failure energy in transistors by forward-potential sampling method 01 p0040 A67-11235
Nonlinear solution method incorporated in computer program for analysis of abnormally operating circuits, considering catastrophic part failure modes 01 p0031 A67-11337
Mathematical model for determining optimal maximum operating times for aircraft engines, using discrete failure rate to determine cost 01 p0141 A67-11340
Component performance and flight operations of X-15 research airplane program, considering engine, auxiliary power and propellant system 01 p0011 A67-11341
Component quality assurance program used to accelerate reliability improvement of 20-amp silicon epitaxial mesa power transistor 01 p0041 A67-11357
Physics of failure techniques applied in reliability failure analysis of intermittent operation of ceramic capacitors 01 p0041 A67-11358
Integrated circuit reliability survey showing relationship of failure rate and temperature 01 p0042 A67-11365
Game theory of economic incentive payment reliability demonstration and prediction 01 p0171 A67-11374
Reliability tests on aerospace and missile systems research and development component assemblies 01 p0085 A67-11376
Transistor failure in inductive load circuits such as TV horizontal deflection circuits and relation to secondary breakdown data 02 p0223 A67-12656
Lagrange multiplier matrix in minimum weight and fully stressed optimum structural design techniques 03 p0525 A67-13966
Hughes-USAF VATE /Versatile Automatic Test Equipment/ system for fault detection and isolation and acceptance testing of inertial guidance equipment 03 p0399 A67-14208
Automatic malfunction analysis /AMA/ technique providing space-vehicle test engineer with listing of all component failures that could cause abnormal indication at any observable monitoring point 03 p0399 A67-14213
Automated learning methods used to design fault diagnosis procedures 03 p0400 A67-14217
Modeling of magnetic drum memory system using Markov chain based on historical data 03 p0400 A67-14220
Microscopic solder slivers as cause of malfunction in high density etched circuit boards having close conductor spacings 03 p0389 A67-14279
Material failure modes in engine components and improved structural design problems 03 p0505 A67-14387
Deterministic and quasi-deterministic methods of failure prediction in electronic systems for prevention strategy in system test or checkout program 04 p0581 A67-14879
Component part reliability concepts, examining degradation and catastrophic failure, failure modes and lot screening 04 p0584 A67-15477
Failure mechanisms in silicon transistors deduced from step stress tests 04 p0584 A67-15482
Lunar surface composition, strength and failure modes, determining ability to support LEM 05 p0895 A67-16612
Causal analysis of failure modes and failure rate, time and stress dependence, kinetic sensitivity and distribution 05 p0811 A67-16852
Integrated plan for reliability demonstration through safety margin testing 05 p0813 A67-17253
Mariner IV Space Data Automation System /SDAS/ computer reliability design, pellet component concept, testing, interconnection and welding techniques 05 p0777 A67-17254
Degradation analysis and variability measurement in reliability and quality control of component parts with application to Early Bird COMSAT satellite 05 p0813 A67-17257
Failure rates and modes for nonoperating electronic packages, presenting solutions for reliability problem 05 p0780 A67-17469
Plane strain fracture toughness, strain instability, slow crack growth and different modes of cracking in metal alloys 06 p1014 A67-17806
Fracture mechanism for formation of dimpled fracture surface

morphology 06 p1105 A67-18562

Second breakdown in transistors examined by thermal concept, noting transient junction temperature rise 07 p1156 A67-19900

Book on electronic component reliability noting effects of environmental conditions, possible faults, various circuits, wiring, transformers, etc 07 p1158 A67-20206

Spacecraft failures noting iron concentration, poor machining, nitriding and anisotropy as causes 07 p1193 A67-20253

Yielding phenomena in beryllium wire plastic composites, discussing static strength and moduli, failure modes and impact resistance 08 p1341 A67-20428

Structural design of solid propellant rocket engine and failure, deformation and fracture of reinforced propellant grains 08 p1420 A67-20888

Filler effects on deformation and rupture of amorphous gum elastomers with various molecular structures, noting failure envelopes [JPL-TR-32-922] 08 p1420 A67-20892

Environmental and experimental testing of electronic systems component reliability 08 p1302 A67-20906

Visual observation of internal circuitry and interconnections of multilayer boards through failure analysis technique 08 p1307 A67-21419

Failure-correction decoding in improving error-correction block codes, using reliability estimates of received digit decisions 09 p1459 A67-21578

Lab techniques for studying unusual bearing failures, noting damage from water contaminated lubricant, pitting, etc 09 p1506 A67-22195

Thermionic converter life-test results and failure mechanisms noting braze failure, collector deposit, emitter warpage and separation and cesium reservoir leak 09 p1447 A67-22334

Structural design of stiffened cylindrical shells, discussing minimum weight, prevention of buckling modes, etc 10 p1726 A67-23719

Critical axial compression buckling loads of orthotropic cylinders having stiffening patterns analyzed, considering three instability failure modes 10 p1728 A67-23760

Dependence of creep, corrosion and thermal fatigue of gas turbine vanes and blades upon inlet temperature and rate of change [ASME PAPER 67-GT-17] 11 p1808 A67-24801

Optimal structural design with failure probability constraints 14 p2399 A67-28122

Rolling contact failure modes classification including wear, plastic flow, fatigue and bulk failure [ASLE PREPRINT 67AM 1C-3] 14 p2325 A67-28784

Loss structure models concerning age replacement policies, discussing mathematical aspects of maintenance with dynamic programming formulation 14 p2345 A67-28909

Apportioning system reliability requirements to various system components, using generalized failure mode and effects analysis for each equipment within system 15 p2492 A67-29605

Spacecraft reliability requirements, discussing design parameters and performance standards 15 p2493 A67-29606

Prevention of burnout in high power linear beam traveling wave tubes by placing small negative electrode at end of collector opposite beam entrance 15 p2447 A67-29754

Systems approach for product and test equipment failure information reporting, including cause and corrective and preventive measures 15 p2584 A67-30410

Reliability assessment methods for dormant weapons noting failure modes, redundancy, large parameter change, system design, derating, etc 15 p2495 A67-30418

Quality cost accounting and management decisions in performance of various functions 15 p2584 A67-30420

Stabilization gyros used for monitoring and detecting performance of avionics inertial navigation system, considering failure modes and effects 17 p2881 A67-32488

Reliability methods used to insure reliability of supersonic transport engine [SAE PAPER 670317] 17 p2929 A67-32979

Stress distribution in reinforced-material models consisting of isolated fiber

embedded in brittle matrix analyzed by photoelastic technique 17 p2966 A67-33387

Solid propellant rocket motors reliability, discussing corrective action, retest, success probability, requirements, capability, simulation model, etc [AIAA PAPER 67-435] 18 p3112 A67-33914

Process control program including failure mode and effects analysis, critical characteristics determination, safety features and test equipment 18 p3058 A67-34673

Maximum entropy principle to derive reliability functions for creep failure modes of engineering materials at high temperatures, noting stress analysis, probability distribution, etc 18 p3145 A67-34675

Reliability prediction, modeling and analysis activities in Apollo program 18 p3139 A67-34697

Reliability analysis and mathematical models to evaluate crew safety applicable to system safety analysis, discussing component failure data, failure mode effect, etc 18 p3139 A67-34704

Collection of papers on integrated circuit technology covering instrumentation and techniques for measurement, process and failure analysis 19 p3192 A67-35018

Microelectronic failure mechanism, examining manufacture and processing methods and production of uniform and versatile material 19 p3193 A67-35029

Reliability contribution of pilot using manual backup control for first stage of Saturn V tested using simulation [AIAA PAPER 67-554] 19 p3335 A67-35951

Apollo gyro reliability covering Guidance, Navigation and Control systems, stressing failure mode prediction 19 p3259 A67-35984

Reliability evaluation of MOS large scale integration devices, using simplified circuit to test individual small elements 20 p3398 A67-36800

Resistance of ideal crystal studied for plastic yielding and brittle cracking, noting composite materials devised to resist both failures 20 p3469 A67-37248

Multilayer circuit board fabrication, giving data on operational and standby failures 21 p3596 A67-38345

Second breakdown in semiconductor devices, discussing measurement methods and techniques, development, breakdown mode and safe operating conditions 22 p3766 A67-39248

Structural sensitivity of plastic properties of molybdenum alloys produced by electron beam fusion, investigating microstructure, failure in bending tests and grain fragmentation 22 p3820 A67-39790

Electronic parts degradations induced by assembling and packaging environments investigated for effects upon failure modes 22 p3771 A67-39834

Environmentally induced delayed failure process incubation period of precracked steel from film formation 22 p3822 A67-40060

Fracture in engineering design in terms of fracture mechanics 23 p4076 A67-40696

High speed information generation by projectile impact machine, explosive forming and capacitor-discharge energy with very high strain rates, presenting failure modes related to forming velocity 23 p4076 A67-40737

Electronic or electromechanical failure-prone component pinpointing using various nondestructive testing methods 23 p4009 A67-40912

Thin boundary problems of bimaterial plates bonded along circular arcs behaving like crack imperfections under bending, using fracture mechanics to predict failure 23 p4078 A67-41164

Probable failure mode and minimum service life prediction for spacecraft pressure vessels using fracture mechanics analysis and fracture specimen test results [ASM PAPER C6-2.3] 23 p4079 A67-41408

Thermionic converter arrays output characteristics determined as function of interconnection resistance, failure modes and patterns, etc 24 p4103 A67-42500

Spacecraft power conditioning reliability using standby redundancy at functional component level and performance monitoring automatic failure detector 24 p4108 A67-42539

Life tests of tapered roller bearings in

mineral oils and synthetic fluids, demonstrating lubrication effect on contact fatigue crack propagation [ASME PAPER 67-LUB-20] 24 p4163 A67-42678

Power conditioning subsystem failure detection provided by computer monitoring of performance, with signal for transfer to redundant unit [AIAA PAPER 67-983] 24 p4110 A67-43055

FAIRING

SA LANDING GEAR

Rigid body ejection dynamics of split-fairing system for four-stage Javelin sounding rocket under various parameter changes 08 p1408 A67-20536

Iterative method for design of bullet-like fairing, giving subsonic subcritical flow with desired velocities at junction of two wings 17 p2791 A67-32586

FALKNER-SKAN EQUATION

Exponentially decaying solution of Hartree as limiting solution for Falkner-Skan equation 04 p0604 A67-14830

Solutions to Falkner-Skan equation, making similarity solutions for pressure gradient parameter physically acceptable 12 p1893 A67-25935

Computer integration of Falkner-Skan equation in presence of normal and tangential flow velocity components on surface of body 18 p3024 A67-33538

FALLOUT

S RADIOACTIVE FALLOUT

FAN

SA COMPRESSOR

SA DUCTED FAN

SA LIFT FAN

SA VENTILATOR

Fan system of 14 by 9 ft open circuit wind tunnel structural principles and operation, discussing blade fabrication, hub design, spinner and motor fairing 03 p0397 A67-14104

Characteristics of cross flow fan determined as function of blade angle, diameter ratio of impeller and vortex position 18 p3025 A67-33650

FAN-IN-WING AIRCRAFT

Aerodynamic coefficients of finite wing with built-in lifting fans, noting additional lift and drag due to supercirculation at trailing end 01 p0006 A67-10769

VTOL and STOL aircraft comparison, discussing advantages and disadvantages of hinged and folding rotors, hinged wings, jet thrust and fan-in-wing principle 17 p2798 A67-32833

Fan-in-wing aerodynamics evaluated for datum inlet with circular arc lips with and without vanes [AIAA PAPER-67-746] 23 p3928 A67-40980

FANLIFT DEVICE

Aerodynamic coefficients of finite wing with built-in lifting fans, noting additional lift and drag due to supercirculation at trailing end 01 p0006 A67-10769

FAR FIELD

Far field pattern of sheet-like laser beam from electron bombarded CdS and ZnO single crystals 07 p1196 A67-19798

Current, input impedance and far field pattern of cylindrical antenna with tapered resistive loading 09 p1481 A67-22446

Far field radiation patterns of Advanced Antenna System presented by Surveyor I on lunar surface [JPL-TR-32-1079] 11 p1763 A67-24298

Interference effects in far field patterns of semiconductor diode lasers 13 p2128 A67-27288

Significance of far field portion of plasma microfield 19 p3285 A67-35344

Radiation of monofrequency antenna in compressible magnetoplasma expressing far field as sum of modal plane waves 20 p3388 A67-37701

Electromagnetic wave scattering by circular cylinder moving in free space, noting far field patterns and Doppler shift angular dependence 22 p3760 A67-39623

Finite ground plane influence on raised electric dipole far field radiation pattern 23 p3980 A67-41202

FAR INFRARED

Far IR absorption and dielectric constant of liquid water 01 p0115 A67-11082

Paint film thickness of spacecraft coatings, effect on spectral directional reflectance and binormal transmittance in far IR [AIAA PAPER 65-653] 03 p0447 A67-13033

Far IR reflection spectra of silicate mineral at room and liquid nitrogen temperatures
[AIAA PAPER 65-668] 03 p0508 A67-13048
Polarized radiation measurements of far IR absorption coefficient and refractive indices in lithium niobium
oxide 03 p0496 A67-13571
Parametric amplification of far IR in Te crystal pumped by carbon dioxide laser 03 p0437 A67-13572
Wave interaction dynamics of far IR electromagnetic radiation generation by coherent molecular vibrations or phonons excited by stimulated Raman scattering and resonant phase matching
condition 04 p0657 A67-15113
Possible existence of circumstellar dust clouds emitting far IR radiation 04 p0702 A67-15588
Spectral transmission of far IR Michelson interferometer with dielectric film beam-dividers 06 p1005 A67-18716
Far IR lattice bands in n-type indium antimonide single crystal 06 p1059 A67-18908
Far IR resonant absorption in n-type silicon analyzed, considering donor-pair conduction dominant mechanism 06 p1068 A67-18974
Time behavior of pulsed water vapor laser, noting spiking from far IR emission lines 07 p1197 A67-20095
Middle and far IR spectra of silicate minerals for remote sensing of lunar or planetary surface composition 08 p1385 A67-20934
Collision induced far IR absorption in rare gas mixtures with emission spectrum calculation 09 p1535 A67-22382
Induced absorption in far IR by impurities and defects of single crystal of potassium bromide 09 p1557 A67-22571
Far IR reflectivity of potassium tantalate analyzed as function of temperature, noting soft mode as temperature lowers towards Curie temperature far IR reflectivity of potassium tantalate 10 p1688 A67-22766
Peak and average output power of cyanide laser in far IR measured, indicating usefulness of available oversize waveguide instrumentation at HF 11 p1801 A67-24715
Absolute frequency measurement and spectroscopy of gas laser transitions in far IR, analyzing Zeeman effect 11 p1802 A67-24830
Far IR electronic transitions in pure and doped solids 13 p2178 A67-27085
Transmittance and reflectance measurements on wirecloth and metallic meshes using vacuum grating spectrometer for design of transmission band pass filter in far IR 13 p2121 A67-27354
Far IR absorption spectra of chromium and titanium ions in aluminum oxide crystal, indicating Jahn-Teller effect reduction of trigonal field and spin-orbit coupling 14 p2370 A67-28714
Single frequency, far IR and high power gas laser design and manufacturing 14 p2333 A67-28970
Optical constants of ionic crystals at low temperatures determined from reflection spectra, noting correlation between absorption coefficient, magnitude and phonon difference processes 14 p2374 A67-28986
Relaxation oscillations in n-type indium antimonide crystal under magnetic field effect and responsivity measurements in far IR 15 p2540 A67-29931
Three-level maser detector for far IR using double-quantum pumping 16 p2684 A67-30606
Far IR surveys of sky for thermal radiation from interstellar grains and other sources of far IR radiation, using balloon sounding 17 p2952 A67-33362
Far IR measurements used to determine superconducting energy gap widths in niobium alloys 17 p2925 A67-33373
Far IR Fabry-Perot interference filters consisting of parallel close-spaced metal meshes 19 p3262 A67-35686
Asymmetric interferogram for spectral transmittance measurements in magnitude and phase obtained by far IR Michelson interferometer 20 p3437 A67-36335
High resolution far IR lamellar grating interferometer with double beam differencing 20 p3438 A67-36347
Far IR CN laser action shown due to HCN

molecule, explaining intense spectral lines around 337 microns 20 p3458 A67-36391
Temperature dependence of far IR collision-induced absorption as probe of rare gas mixtures interatomic potentials 20 p3490 A67-37567
Josephson junctions as high speed far IR detectors, describing point contact junctions used in experiment 22 p3838 A67-40434
FAR ULTRAVIOLET
Far UV extinction curve and wavelength dependence of interstellar polarization by graphite grains 01 p0150 A67-10890
Quark confusion with electric-dipole transition in far UV solar spectrum 04 p0694 A67-14479
Optical constants of Ge in XUV verified using Kronig-Kramers dispersion relation, optical oscillator strength sum rule, correlation methods and electron energy loss distribution 05 p0864 A67-16784
Far UV radiation flux measurement by satellite-borne telescopic stellar spectrophotometer 08 p1399 A67-21234
Aerobee rocket sounding of far UV spectra of six stars in Orion, extrapolating mass ejection from resonance absorption lines 11 p1861 A67-24488
Measurement of radiation reflectively scattered from optical surfaces in far UV, noting role of overcoating with metal films 11 p1819 A67-24666
Javelin rocket soundings with far UV scanning spectrometer, noting atomic hydrogen and oxygen radiation 12 p1934 A67-25787
Solar studies in extreme UV using stabilized Skylark rockets, including data on chromospheric and coronal spectra and XUV spectroheliograms 12 p2008 A67-25826
Far UV transmitting windows, particularly lithium fluoride, and response measurements below 2000 angstroms, noting fabrication on solar blind materials 12 p1947 A67-26161
High luminosity spectrograph using inverse Wadsworth mounting constructed for recording auroral spectra in far UV 14 p2315 A67-28157
Intensity and polarization of hydrogen Lyman alpha lines in day airglow as function of altitude for principal far UV emission 14 p2314 A67-28849
Magnetic electron multiplier performance as photomultiplier in EUV spectral region 19 p3231 A67-35683
Far UV interstellar absorption lines evaluated for main-sequence B stars 19 p3330 A67-36075
Far UV spectra of brighter stars in vicinity of epsilon Orionis photographed with objective spectrograph carried by rocket 22 p3882 A67-39555
Vacuum type lensless spectrograph in intermediate and far UV for evaluating shock compressed metals resulting from hypervelocity impact 22 p3799 A67-39749
FARADAY DARK SPACE
Formulas relating detector current to average UHF power obtained for positive plasma column and dark Faraday region of glow discharge 05 p0856 A67-17235
Negative glow diffusion model evaluated via generation function determined by discharge voltage and dependence of reduced length of cathode fall 18 p3085 A67-33668
FARADAY-DOPPLER TECHNIQUE
Seasonal variations of total electron content of ionosphere during sunspot minimum 12 p1935 A67-25795
FARADAY EFFECT
Optical reflection, transparency and Faraday effect for indium antimonide, calculating effective electron mass, relation between energy and wave number, etc 01 p0128 A67-10095
Electric conductivity, electrode temperature and potential distribution across channel in potassium seeded-argon atmospheric-pressure Faraday accelerator [AIAA PAPER 66-75] 01 p0014 A67-11177
SHF modulation techniques for laser radiation, covering Faraday, Kerr and Pockel effects, circular dichroism, etc 03 p0436 A67-13138
Explorer XXII satellite measurement of total electron content from observations of Faraday effect [RASSA PAPER 1-10-128] 03 p0372 A67-14239
Intracavity time-varying perturbation of losses in gas laser using diamagnetic

Faraday effect in glasses analyzed in connection with output intensity 05 p0818 A67-16646
Equations for longitudinal Faraday and Kerr effects in gyroelectric thin films bounded by nonmagnetic medium, considering multiple inner reflections 05 p0865 A67-16971
Longitudinal Kerr and Faraday effects in Ni and permalloy films using photoelectric polarization spectrometer, choosing various refractive indices and gyroelectric constants 05 p0865 A67-16972
Singularities of Faraday effect in n-type InSb in millimeter band at 77.8 degrees K as function of sample thickness and magnetic field intensity 06 p1047 A67-17755
Depolarization of cosmic radio emission due to dispersion of Faraday rotation of planes of polarization of radio waves 08 p1376 A67-20813
Faraday effect optical isolator for IR region using lead glass rod in magnetic field as nonreciprocal element 09 p1500 A67-22425
Free carrier electro-magneto-optical phenomenon in semiconductors, noting conductivity tensor, Faraday effect, Derr effect and Voigt effect 09 p1558 A67-22602
Total electron content calculated by measurement of Faraday and Doppler effects of satellites 10 p1604 A67-22987
Strong electrical field effect on Faraday effect in n-type InSb 10 p1695 A67-23663
Faraday effect in semiconductors in cylindrical waveguides analyzed using numerical calculation 14 p2270 A67-28522
Total electron content calculation by measuring Faraday and Doppler effects of satellites on reception frequency 14 p2270 A67-28607
High time-resolution polarimeter observations of Jupiter decimeter radio bursts 14 p2388 A67-28836
Performance characteristics of Faraday and Hall MHD generators using strong magnetic fields and considering ion slip and finite electrode segmentation effects 16 p2599 A67-30527
Current distribution in Faraday MHD generator measured with potassium resonance lines 16 p2599 A67-30529
MHD power generation experiments with potassium seeded argon plasmas to study performance at Faraday and Hall parameters 16 p2601 A67-30554
Maximum power density, maximum efficiency of diagonal wall generator, Faraday generators and Hall current generators compared 16 p2608 A67-30597
Ionospheric electron content as function of longitude and latitude calculated from Faraday fading of radio waves 16 p2627 A67-31362
Strong electrical field effect on Faraday effect in n-type InSb 17 p2924 A67-33344
Faraday effect in microwave region used for electron density determination in argon and helium low pressure plasmas and comparison with cyclotron radiation data 19 p3297 A67-35592
Wave propagation in anisotropic plasma in presence of electron density irregularities, noting Faraday effect 19 p3184 A67-35825
Energy conversion MHD channel of Faraday type using hot spacers and electrodes for control 24 p4106 A67-42526
FARADAY ROTATION
Beacon satellite measurement of Faraday rotation and diurnal and seasonal variations of total electron content of ionosphere near Nairobi 03 p0406 A67-12825
Automatic recording equipment measuring polarization angle of Syncom III 137 mc/s radio signal and determination of ionospheric total electron content 03 p0415 A67-14110
Explorer XXII satellite measurement of total electron content from Faraday rotation recordings, noting correlation with solar activity above 80 solar flux units [RASSA PAPER 1-10-124] 03 p0416 A67-14235
Total electron content distribution over Europe in terms of geomagnetic activity, noting occurrence of scintillations [RASSA PAPER 1-10-125] 03 p0416 A67-14236
Faraday fading rate of satellite signal as calculated from Appleton-Hartree formula for refraction index /without collision/ near transverse propagation [RASSA PAPER 1-10-127] 03 p0372 A67-14238
Syncom III satellite measurement of time

variation of total ionospheric electron content
 [RASSA PAPER 1-10-129] 03 p0417 A67-14240
 Early Bird satellite measurement of ionospheric electron content obtained from Faraday rotation data
 [RASSA PAPER 1-10-131] 03 p0417 A67-14242
 Interband Faraday effect in Cd-Te single crystals 04 p0676 A67-14933
 Faraday rotation measurement of trapped magnetic fields in theta pinch plasma, using gas laser beam 05 p0859 A67-17447
 Electron effective mass in gallium arsenide as function of doping obtained from Faraday rotation measurements 06 p1061 A67-18921
 Time variation of positional angle of polarization plane of radio sources due to Faraday rotation 08 p1388 A67-20987
 Mean noon profile of mesospheric electron number density at 35 degrees S latitude preceding solar eclipse 08 p1378 A67-21483
 Controlled nonreciprocal microwave device using Faraday rotation in solid state plasma 09 p1474 A67-22090
 Faraday rotation effects in spectral records of Jupiter decametric radiation 09 p1568 A67-22401
 Plasma magnetization under action of circularly polarized wave, noting inverse Faraday effect 10 p1683 A67-22853
 Ionospheric electron content calculated from beacon satellite data on Faraday rotation 10 p1641 A67-23235
 Satellite measurement of ionospheric electron density, determining Faraday null times 10 p1641 A67-23236
 Diurnal and seasonal variation of total columnar ionospheric electron content at magnetic equator analyzed, using Faraday rotation technique 10 p1651 A67-23341
 Seasonal variations in ionospheric total electron content measured by observing Faraday rotation of linearly polarized wave from geostationary satellite Syncom III 10 p1651 A67-23346
 Magnetic field effect on electromagnetic wave propagation through free carrier plasmas in semiconductors, considering Faraday configuration 11 p1840 A67-24663
 Polarization of extragalactic radiation sources and evidence of irregularities of magnetic field in our Galaxy 13 p2198 A67-26791
 Ionospheric electron content obtained as function of longitude and latitude, using satellite measurements of Faraday rotation 15 p2478 A67-29923
 Large-scale structure of F layer studied by observing Faraday rotation of satellite signals, noting irregularities in total electron content 15 p2483 A67-30295
 Satellite receiving and transmission antenna orientation effects obtained by Faraday rotation measurements 16 p2628 A67-31507
 Faraday rotation satellite observations at closely spaced frequencies, allowing electron content figure determination 16 p2629 A67-31514
 Measuring IR Faraday rotation and Hall effect in 6H and 15R polytypes of silicon carbide 18 p3102 A67-34278
 Electron content measured using satellite motion and position effects on Faraday rotation 20 p3431 A67-37102
 IR technology and electromagnetic spectrum, discussing manufacture of circulators and isolators using Faraday rotation in InSb 22 p3835 A67-39213
 Interband and free carrier Faraday rotation in n-type InAs at room and low temperature, determining conduction band parameters 22 p3863 A67-40204
 Faraday rotation data from Explorer XXII, determining atmospheric electron content for magnetic field aligned ionization layer location and occurrence 23 p3996 A67-40818
 Faraday rotation in YIG studied from measurements at He-Ne laser wavelengths for applications to materials design 23 p4041 A67-41184
 Intervening galaxy effect on radiation from distant objects, studying Faraday rotation, 21-cm absorption, optical scattering and absorption lines 24 p4223 A67-41810
 Faraday rotation and ellipticity measurements in germanium and gallium arsenide at room temperature in weak magnetic fields 24 p4202 A67-41984

FAST ELECTRON

Laser based on excitation of gallium phosphorus arsenide solid solution by beam of fast electrons 02 p0251 A67-11824
 Spectra and intensity vs excitation level and spatial distribution vs current density determined for optical radiation by electron excited cadmium sulfide 02 p0251 A67-11828
 Alfvén wave in outward corona as natural explanation of fast drift bursts 04 p0691 A67-14485
 GaAs gas bombarded by fast electrons investigated for recombination radiation spectra, noting shift of edge emission maximum toward longer wavelengths 13 p2173 A67-26359
 Fast ions produced in interaction between escaping electrons and plasma 13 p2164 A67-26402
 GaAs gas bombarded by fast electrons investigated for recombination radiation spectra, noting shift of edge emission maximum toward longer wavelengths 21 p3680 A67-38316
 Fast electrons formation mechanism during flares ascribed to fast proton deceleration in flare region rather than high energy particle ionization 21 p3699 A67-39013
 He-Ne gas mixture DC discharge electron temperature and concentration dependence on tube diameter, pressure and composition, using two-probe method 24 p4196 A67-42242
 Density variation in shock tube across nonstationary shock wave separating from nitrogen gas fluorescence excited by fast electron beam 24 p4145 A67-42863

FAST NEUTRON

SA THERMAL NEUTRON
 Gamma radiation and fast neutron effects on dark resistance, photoconductivity, majority carrier mobility, recombination kinetics, etc, in CdS single crystal 01 p0128 A67-10086
 Fast and slow neutrons detected by proportional and scintillation counters 02 p0312 A67-12606
 Fast neutron latitude variations in atmosphere during solar minimum measured by high-altitude balloons, noting neutron leakage into space 03 p0505 A67-12950
 Anomalous IR attenuation in fast neutron irradiated GaAs and CdTe arises through scattering and absorption by highly conducting spike zones 11 p1850 A67-24910
 Recoil proton detectors used for rocket measurements of fast neutron intensity above Fort Churchill, Canada, during 1964 and 1965 12 p1998 A67-25828
 Circuit for discriminating neutrons, gammas and charged particles from each other in phoswich scintillator 12 p1945 A67-25857
 Radiation effects on silicon transistor parameter behavior characteristics 17 p2917 A67-32843
 Low temperature thermal conductivity measurement of fast-neutron-irradiated silicon and germanium, showing difference between bombardment induced scattering in two materials 17 p2919 A67-32855
 Disordered regions produced by fast neutron irradiation effect on semiconductor properties of silicon 17 p2919 A67-32859
 Fast neutron irradiation effect on electrical conductivity and Hall effect in Zn doped n-type indium arsenide single crystals 19 p3301 A67-34771
 Emission recombination in n-type Si single crystals irradiated with fast neutrons or gamma quanta 19 p3301 A67-34775
 Effect of irradiation of silicon by fast neutrons on switching time of alloy diode synthesized on silicon base 20 p3508 A67-36402
 Fast neutron radiation damage in narrow base p-n-p-n devices compared to one-dimensional theory, showing superiority to bipolar transistors 24 p4130 A67-42248
 Radiation resistant silicon diode fast neutron monitors, discussing fission spectra and leakage currents in damaged diodes 24 p4183 A67-42473

FAST REACTOR

Nuclear reactors for space propulsion and onboard power supply, including conversion systems 18 p3075 A67-33654

FASTENER

SA BOLT
 SA CLAMP
 SA FITTING
 SA JOINT

SA RIVET

SA SOLDER

Statistical methods for evaluating displacement in increasing number of fasteners depending on nominal sizes and tolerances of fasteners and pairs of holes 02 p0336 A67-11776
 Insert size, shape and core undercut diameter and depth effect on insert tensile strength of honeycomb sandwich fasteners 02 p0248 A67-11943
 Stress distribution in fir-tree fastenings of turbine blades in alternate bending caused by blade oscillations under static tension 03 p0528 A67-14076
 Threaded fastener developments for critical joint design requirements, considering strength, temperature, weight and cost 05 p0810 A67-16166
 Rivet type aircraft fasteners 05 p0810 A67-16232
 Aircraft exfoliation corrosion, discussing methods for prevention in fastener holes 07 p2120 A67-20087
 Threaded fastener reliability factors noting mechanical testing 11 p1795 A67-24040
 Secure mechanically fastened assemblies in static and dynamic stress, showing effect of tightening preload [ASME PAPER 67-DE-3] 14 p2327 A67-28865
 Fastener performance in commercial and aerospace application, considering component thermal expansion [ASME PAPER*67-DE-18] 14 p2327 A67-28872
 Threaded fastener design and manufacture 15 p2493 A67-29650
 Reference issue on fastening and joining 16 p2682 A67-31563
 Advanced fasteners - SAE Conference, Los Angeles, October 1967 24 p4160 A67-42076
 Basic guidelines for fastener system selection for use in exotic environment with unusual stress condition 24 p4160 A67-42077
 Strength and oxidation tests evaluated for coated fasteners in extreme temperature use 24 p4160 A67-42078
 Fastener applications for gas turbine engines noting materials selection and design 24 p4160 A67-42079
 Threaded fasteners for application to aerospace structures noting preload, torque and lubrication 24 p4160 A67-42080
 Fastener and fastened joint technology noting influence of hole preparation, surface coating, thread lubricants and fit on fatigue life 24 p4161 A67-42081
 Aircraft fasteners, airline operation and maintenance requirements and improvement of standardization 24 p4161 A67-42082

FAT

S ADIPOSE TISSUE

S LIPID

FATIGUE

SA ACOUSTIC FATIGUE
 SA BENDING FATIGUE
 SA CRACK
 SA FAILURE
 SA FLIGHT FATIGUE
 SA FRACTURE
 SA METAL FATIGUE
 SA SHEAR FATIGUE
 SA STRAIN
 SA STRAIN FATIGUE
 SA STRUCTURAL FATIGUE
 SA THERMAL FATIGUE

Cyclic torsion interaction with axial load showing torsion angle larger than fatigue limit and applied tensile stress larger than Bauschinger yield 10 p1669 A67-23436
 Stacking fault tetrahedra in fatigued stainless steel, describing mechanism for nucleation of triangular Frank dislocation loop during cyclic load 11 p1805 A67-24109
 Fracture stresses of cracked plates and flow stresses of polycrystalline aggregates as related to stresses and strains at ends of plane-discontinuities 16 p2769 A67-31285

FATIGUE /BIOL/

SA MUSCULAR FATIGUE

Fatigue failure induced by aging and disease of self-healing biological structure in mathematical model [ASME PAPER 66-WA/BHF-3]

04 p0564 A67-15399
 Phase shifts in human circadian system noting individual differences, performance deficit, physiological changes and dissociation from time zone displacements 15 p2425 A67-29100
 Continuous /24 hr/ wide band noise effect on human body, discussing

- subjective/objective
fatigue 20 p3369 A67-36670
Sudden strong stimulus effects on pilot
simple visual reaction time and fatigued
muscle strength 22 p3756 A67-40537
Subjective effects of fatigue on aircrew
expressed in work cycle terms from data of
continuing daily activity
log 23 p3959 A67-41663
- FATIGUE DIAGRAM**
Design strength of plane notched elements
under single mode vibration, obtaining
equation for fatigue stress concentration
factor 05 p0919 A67-18592
Monte Carlo simulation studies for fatigue
data analysis of rolling-contact bearings,
using Weibull equation
[ASLE PAPER 66AM 1B2]
08 p1336 A67-21038
Reversed speed effect and grain boundary
diffusion as explanations of discrepancy of
activation energy values for strain aging
under fatigue or simple stress
conditions 12 p2013 A67-25284
Aluminum and aluminum alloys properties
for service at cryogenic
temperatures 14 p2323 A67-27816
Boron filament behavior in rotating-beam
fatigue test 20 p3470 A67-37390
Diagrams of specific strength of materials
made of fibrous
compositions 24 p4246 A67-41921
- FATIGUE LIFE**
Tenfold increase in fatigue life of 1100
aluminum in reverse bending at vacuum
level below 10-2 torr due to retardation of
crack propagation phase of fatigue
process 01 p0092 A67-10053
Structural design and fatigue life of
Chinook helicopter
[SAE PAPER 660667] 01 p0010 A67-10575
Extended theory of cumulative damage in
fatigue when stress amplitude varies from
cycle to cycle throughout life of structure
[SAE PAPER 660720] 01 p0161 A67-10607
Fatigue failure analysis in small
metallurgically-bonded joints in very small
electronic components, using statistical
analysis of random forces and dynamic
response of member 01 p0084 A67-11359
Accelerated stress testing and reliability
estimation for electronic
components 01 p0085 A67-11373
Fatigue crack propagation under random
cyclic loading extended, obtaining zero-order
solution from mean crack
lengths 02 p0337 A67-11794
Fatigue mechanisms for fcc metals and
alloys, reviewing research on crack initiation
and propagation 03 p0447 A67-13800
Deformations and rupture criteria under
cyclic loading using stress-strain
diagram 03 p0531 A67-14361
Manson-Coffin relation for low cycle
fatigue life derived from considerations of
dynamical dislocation processes without
specification of crack
shape 04 p0707 A67-14512
Environmental effects on mechanical
behavior of metals in vacuum and gases
normally found in atmosphere, considering
surface oxide layer 04 p0638 A67-14996
Fatigue life index as criterion for
comparison of predicted life of proposed
compressor with that of another compressor
with known industrial performance
[ASME PAPER 66-WA/MD-10] 04 p0554 A67-15337
Performance characteristics and bearing
load-deflection equations of shaft supported
by n roller bearings
[ASME PAPER 66-WA/LUB-4] 04 p0629 A67-15339
Shearing stress failure theory for high
cycle fatigue employing rotating principal
stress axes and nonsynchronous stresses
[ASME PAPER 66-WA/MET-9] 04 p0712 A67-15374
Fatigue life of thin walled shells with
inside pressure and outside support during
axial motion
[ASME PAPER 66-WA/MET-13] 04 p0712 A67-15377
Maraging steel properties, discussing
composition, strengthening mechanism,
tensile and impact toughness, mechanical
and fatigue properties,
etc 04 p0640 A67-15458
Low cycle fatigue crack propagation
characteristics of high strength steels,
noting technique for life estimation of
structure by numerical integration
[ASME PAPER 66-MET-3] 05 p0827 A67-16213
Mean strain cumulative damage and effect
in low cycle fatigue of 2024-T351 aluminum
alloy, covering strain cycling, fatigue life,
residual ductility, etc
[ASME PAPER 65-WA/MET-5] 05 p0827 A67-16214
Aircraft skin panel fatigue failure under
hypersonic conditions, noting effect of
natural vibration frequency and
axisymmetric oscillations 05 p0916 A67-16229
Low endurance fatigue of aluminum alloy
and stainless steel in plane bending at
ambient and elevated
temperatures 05 p0920 A67-16810
Book on roller bearings noting
construction, operation and performance
characteristics 06 p1008 A67-18837
Spacecraft failures noting iron
concentration, poor machining, nitriding and
anisotropy as causes 07 p1193 A67-20253
Corrosive media effects on fatigue
strength and endurance limits of three Al
alloys used in aircraft
components 08 p1341 A67-20598
Material combination and hardness effect
in rolling contact fatigue life of high speed
tool steel, stainless steel and wear resistant
materials 09 p1505 A67-22191
Aircraft reliability as function of fatigue
life of welded joints noting static strength
variation, S-N curve and multiple safety
factor 09 p1506 A67-22471
Fatigue life on 727 aircraft structure
improved through room temperature curing
of adhesive film 09 p1577 A67-22510
Correlation among room temperature
creep stresses, fatigue and proportional limit
in titanium alloys 10 p1669 A67-23325
Helicopter rotor blade service life
substantiation through tests with rotor
excitation panels inducing blade bending
moments 10 p1622 A67-23431
Scatter factor for fatigue life of aluminum
aircraft structures subjected to identical
loading histories 10 p1594 A67-23436
Short life fatigue failures in multiaxial
stress-strain system 10 p1719 A67-23486
Vibratory motions of turbine blades,
considering frequency determination,
tangential mode, stress, damping and
excitation source
[ASME PAPER 67-VIBR-66] 11 p1798 A67-24207
Crack propagation for stainless steel and
Ti alloy at stresses below fatigue limit,
noting of alternating stress cycles crack
propagation for stainless steel and Ti alloy
at stresses below fatigue limit, noting
role 11 p1806 A67-24365
Metallurgical and fluid dynamic results of
2000-hr endurance test at high temperatures
on two-stage 200 hp turbine in wet
potassium vapor 11 p1745 A67-24797
Aircraft flight and ground strain
measurements for static strength clearance
and fatigue life assessment, noting structural
integrity evaluation 11 p1880 A67-25058
Accelerometer use for operational load
measurements in aircraft, emphasizing
automatic counting 11 p1880 A67-25059
Compressor blade failure due to material
fatigue, using destructive testing in
stationary rig 12 p2014 A67-25413
Low endurance fatigue analysis for steel
and Al alloy under cyclic torsion with
controlled shear strain
amplitude 12 p2016 A67-25425
Executive aircraft structure safe-life
fatigue analysis and tests
[SAE PAPER 670257] 12 p2016 A67-25507
ASTM 1964 references on
fatigue 12 p2032 A67-26093
Creep rupture, fatigue strength and
brittle-ductile transition of aluminum as
affected by nuclear
radiation 13 p2133 A67-27090
Five-ball fatigue tester to investigate
reduced pressure environment effect on
rolling element fatigue life with polyphenyl
ether
[ASLE PREPRINT 67AM 8A-3] 14 p2326 A67-28795
Reinforced plastics composites for jet lift
engines 15 p2508 A67-29671
Fatigue process theory for general
broadband random loading, calculating mean
damage and survival probability 15 p2576 A67-30094
Plastic behavior of material continua in
terms of Riemannian and non-Riemannian
differential geometry 16 p2767 A67-31276
Stress space theory and application to
fatigue fracture theory, noting geometrical
formulations for deformation and stress of
body 16 p2768 A67-31277
Fatigue crack analysis via Bilby, Cottrell
and Swinden crack theory, noting
inadequacy of energy
criterion 16 p2769 A67-31283
Fatigue crack propagation in thin plates
under fluctuating plane extension and
cylindrical bending 16 p2770 A67-31290
Fatigue in quasi-brittle materials, fatigue
in creep range at elevated temperatures and
cumulative fatigue 16 p2774 A67-31316
Minimum alternating stress causing given
length microcrack to grow and macrocrack
growth rate 16 p2774 A67-31317
Upper and lower bounds of survivorship
function of redundant structure subjected to
fatigue 16 p2774 A67-31319
Low cycle fatigue behavior of metals at
creep range temperature related to
equivalent ductility and strain
rate 16 p2774 A67-31321
Metal fatigue studied with X-ray
diffraction technique 16 p2774 A67-31322
Ultrahigh vacuum and air fatigue testing
of aluminum alloy observing corrosion
process influence on mechanism by
latter 16 p2689 A67-31369
Helicopter structural elements safe life
through variable-amplitude fatigue tests
[AHS PAPER 122] 16 p2777 A67-31837
Structural reliability of fatigue loaded
rotorcraft estimated through S-N and
spectrum testing
[AHS PAPER 123] 16 p2777 A67-31838
Fatigue strength calculated using fracture
criterion for multiaxial alternating stress
and combined alternating bending and
torsional stresses 17 p2960 A67-32632
Strength increase of parts or system to
prevent fatigue failure, noting bulk and
material considerations and elimination of
fretting, scoring, corrosion, sharp corners,
etc 17 p2862 A67-32824
Design criteria and configuration for long-
life aircraft gas turbines
[SAE PAPER 670344] 17 p2929 A67-32988
Product reliability dependence on scatter
extent determination in fatigue life,
recommending testing in S-N diagram short
life region 20 p3538 A67-36699
Loading frequency influence on endurance
characteristics of V95 aluminum alloy
notched for stress
concentration 21 p3644 A67-38051
Fatigue indicating meter attachment to
integrate fatigue damage over any load/time
spectra 21 p3719 A67-38130
Computer aided techniques applied to
structural analysis of aircraft noting design
problems in aluminum fatigue life, unclad
alloys, insulation and composite
structures 22 p3915 A67-40331
High structural efficiency of aircraft
materials emphasizing fatigue characteristics,
fracture toughness and corrosion
resistance 22 p3823 A67-40332
Air damping effect on structural fatigue
failure evaluated mathematically as power
function relating stress to number of
cycles 22 p3915 A67-40405
Stress interaction in cumulative fatigue
damage studied to predict remaining life of
machine structures 23 p4074 A67-40650
Kinetic approach to fatigue investigation
in calculation of cyclic lifetime from static
test data 23 p4074 A67-40663
Pressure effects on fatigue reported for
Fe, Al and Ni wires subjected to oscillating
strains, discussing several fatigue
models 23 p4075 A67-40666
Fatigue crack propagation rate in sheet
specimens under various loadings simulating
rivet forces 24 p4247 A67-41944
Double linear damage rule for predicting
cumulative fatigue damage, crack initiation
and propagation and fatigue life, noting
improved accuracy 24 p4170 A67-41951
Fatigue crack propagation in aluminum
alloy studied for influence of maximum
stress, stress range and sequence of load
application 24 p4171 A67-41954

Basic guidelines for fastener system selection for use in exotic environment with unusual stress condition 24 p4160 A67-42077

Threaded fasteners for application to aerospace structures noting preload, torque and lubrication 24 p4160 A67-42080

Fastener and fastened joint technology noting influence of hole preparation, surface coating, thread lubricants and fit on fatigue life 24 p4161 A67-42081

High temperature low cycle creep range strain fatigue behavior estimation from tensile and stress rupture properties 24 p4251 A67-42483

Life tests of tapered roller bearings in mineral oils and synthetic fluids, demonstrating lubrication effect on contact fatigue crack propagation [ASME PAPER 67-LUB-20] 24 p4163 A67-42678

Rolling element bearing fatigue life for cyclic race oscillation, analyzing variation with load, speed and oscillation amplitude via Weibull statistics [ASME PAPER 67-LUB-22] 24 p4163 A67-42680

Fatigue crack initiation, comparing alpha brass and Al-Mg-Zn alloy, noting effect of increasing maximum pressure value in contact region [ASME PAPER 67-LC-5] 24 p4174 A67-42744

Low altitude flight load spectra for light aircraft 24 p4094 A67-42755

Ultrasonic monitoring technique for fatigue damage and crack formation and propagation in aircraft structures [AIAA PAPER 67-793] 24 p4251 A67-42954

Metal-fatigue failure indicator-predictor gauge by correlating resistance changes with fatigue damage [AIAA PAPER 67-794] 24 p4251 A67-42955

FATIGUE TEST

SA FULL SCALE FATIGUE TESTING

Electron microscopy study of fracture surface topography permitting identification of fine scale fracture surface features, relating them to fracture formation mechanisms [AIAA PAPER 66-814] 01 p0077 A67-10034

Environmental structural testing capabilities for orbital and space vehicles [SAE PAPER 660685] 01 p0154 A67-10589

Strain gauge bridge outputs combined during flight to measure airloads directly and inexpensively in fatigue test program 01 p0030 A67-11103

Resistance of copper-tungsten fiber composites to repeated tension cycles 02 p0254 A67-11793

Fatigue testing facility for tubings in aviation hydraulic systems 02 p0231 A67-12447

Effect of internal fluid pressure and installation inaccuracies on fatigue resistance of line connections for aircraft hydraulic and gas systems 02 p0184 A67-12448

Acoustic fatigue tests of aircraft components, determining sound field and stresses using actual jet engine or simulation 03 p0521 A67-13021

Micromechanical behavior of composite materials under static tension, bending, shear and fatigue loading investigated analytically and experimentally 03 p0455 A67-13440

Cyclic stressing of fiber composite materials elastic-plastic region, assuming equal strains in fiber and matrix 03 p0445 A67-13529

Ultrasonic fatigue testing using magnetostrictive vibrators 03 p0524 A67-13550

Failure mechanism of ceramic fibers in fiber-metal composites determined by high amplitude fatigue tests 03 p0525 A67-13871

Strength criterion for complex loading, possible development based on strength criterion for symmetrical cyclic loading 03 p0529 A67-14168

Thickness effect on fatigue crack propagation in notched alclad sheet under cyclic tensile loading and transition from tensile fracture mode to shear mode 03 p0532 A67-14386

Behavior and fatigue strength of graphite during testing, plotting curves in semilogarithmic coordinates 04 p0641 A67-14599

Fatigue crack propagation rates for aluminum cantilever beams in reversed bending under two-level constant amplitude and random excitation, noting stress cycle effect [ASME PAPER 66-WA/MET-3] 04 p0639 A67-15343

Component design advances with fatigue tests on hydraulic tubes and outline of seal development 05 p0753 A67-16749

Heating and cooling rates, hold time at maximum temperature, phase temperature between temperature and strain cycling effects on thermal fatigue of stainless steel 05 p0921 A67-17085

Electron microscopy analysis of dissolved hydrogen induced fracture in room temperature cantilever bend fatigue testing of dispersion strengthened aluminum-aluminum oxide alloy 06 p1013 A67-17796

Metallographic, X-ray and electron microscope studies of dislocation substructure and fatigue life extension in bending-fatigued Al and Ag crystals 06 p1013 A67-17798

Rotating beam S-N fatigue curves for 18 percent Ni maraging steel bars subjected to heat treatments 06 p1014 A67-17800

Automatic control system synthesis for fatigue testing of structural elements under random loads 06 p1101 A67-18239

Shock and vibration test specifications, contrasting approaches requiring exact duplication of environment with those simulating damaging characteristics 06 p0981 A67-18366

Strain rate effects on low endurance fatigue noting constant frequency induced variations 07 p1261 A67-19059

Heat resistance and fatigue strength of Ti alloys examined, using bending techniques 07 p1207 A67-19288

Electron microscope analysis of stress corrosion crack failure 07 p1211 A67-20250

Static and fatigue properties of repair welded aluminum and magnesium premium quality castings 08 p1333 A67-20360

Literature review on effect of static fatigue on filament wound fiberglass internal pressure vessels, noting program to test and expand data 08 p1415 A67-20432

Tensile residual stress measurement in area of failure origin in helicopter rotor blade, using laboratory tests and X-ray analysis [SAE PAPER 670154] 09 p1502 A67-21772

Damage accumulation during thermal fatigue noting need for statistical analysis of law governing process 09 p1575 A67-22167

Test method for metal resistance to thermal fatigue under active creep conditions 09 p1519 A67-22168

Fatigue mechanism of materials, deriving parametric differential equations from group of postulates 09 p1578 A67-22546

Fatigue of powder metal compositions, discussing data from rotating beam and reverse bending fatigue tests 10 p1667 A67-22702

Bending fatigue tests of unmachined, mechanically machined and chemically machined panels of aluminum and titanium alloys 10 p1669 A67-23437

Roll fatigue tests of forged ZK60A-T5 magnesium and 2014-T6 aluminum wheels 10 p1661 A67-23439

Electron microscopy study of fracture surface topography permitting identification of fine scale fracture surface features, relating them to fracture formation mechanisms [AIAA PAPER 66-809] 10 p1661 A67-23552

Principle of maximum entropy and application in reliability estimation of aircraft structures 10 p1726 A67-23730

Nickel-base alloy static and dynamic creep test, examining fatigue zone fracture surface 11 p1806 A67-24364

Measurement of torsional fatigue loads on aircraft undercarriage under service conditions 11 p1880 A67-25057

Low endurance fatigue tests for reversed torsional strain cycling of two steels 12 p2015 A67-25421

Nickel and cobalt superalloys low cycle thermal fatigue test method under cyclical extension and temperature conditions, giving stress-strain-time relations [ASME PAPER 67-MET-19] 12 p1956 A67-25955

Beryllium joints and structures tested for static and repeated loading fatigue at room and high temperatures 13 p2123 A67-27132

Test method used in analysis of statistical distribution functions for fatigue strength response data of aluminum sheet 13 p2221 A67-27738

Strain gauge bridge outputs combined during flight to measure airloads directly and inexpensively in fatigue test program 14 p2315 A67-28002

Accelerated fatigue testing using stepwise stress increase method 14 p2402 A67-28815

Intermediate principal stress effect on fatigue of thick wall steel tubes under triaxial stresses 15 p2573 A67-29402

Cladding effect on corrosion resistance and fatigue behavior of duralumin, noting role of alternating stresses in cladding layer 15 p2504 A67-29821

Fatigue failure prevention noting load redistributing, stress concentration reduction, critical section size increases, mean stress reduction, etc 15 p2494 A67-30098

C-141A engineering development test program, discussing flight, accelerated service and all-weather testing [AIAA PAPER 67-409] 15 p2422 A67-30376

Inclusion type, forging ratio and heat treatment effect on properties of longitudinal and transverse steel specimens 16 p2689 A67-31310

Energy necessary for fracture shown independent of lattice defects by low cycle fatigue tests at constant true mean stress amplitude 16 p2774 A67-31318

Thermal fatigue cycling of nimonic 80A solid cylinder specimen restrained by clamps 16 p2775 A67-31323

Low strain rate and temperature effects on crack initiation and growth, recovery and boundary migration for Al and Al alloy 16 p2689 A67-31368

Bending strength of spur gear teeth calculating methods to optimize design for high speed, lightweight aircraft gearing [AHS PAPER 118] 16 p2684 A67-31834

Structural design, analysis and tests pertaining to hot cycle rotor system used on XV-9A aircraft [AHS PAPER 121] 16 p2598 A67-31836

Cumulative fatigue at root of circular notch of coupon type aluminum alloy specimens subjected to low cycle compression-tension strains 17 p2957 A67-32028

Fatigue properties of explosively formed parts tested by repeated axial loading and results compared with statically formed specimens 17 p2871 A67-32433

Engine materials investigated for optimum low cycle fatigue resistance by pull-pull and rotating-beam fatigue testing techniques [SAE PAPER 670336] 17 p2874 A67-32986

High-elongation foil strain gauges evaluation for measuring cyclic plastic strains, determining Poisson ratio 18 p3142 A67-33890

Crack nucleation in high strength low alloy steel, comparing fatigue processes in quenched and tempered martensite with those in pure metals 18 p3064 A67-34082

Fatigue characteristics of chromium-molybdenum steels subjected to various heat treatments, comparing tension-compression and torsion 18 p3065 A67-34258

Cumulative damage observed for biaxial fatigue stress tests on tubular steel specimens 19 p3341 A67-35552

Crystal deformation and uniaxial failure under complex loading due to stress and temperature variations, applying physical state equation 20 p3540 A67-37057

Low cycle thermal fatigue under uniaxial constraint, describing clamping device, time-temperature controller and programmer used 20 p3543 A67-37699

Structural changes due to fatigue in cladding layer of alloy D16AT studied by X-ray diffraction 21 p3642 A67-37826

Automatic apparatus for flooding or spraying test specimens with liquid corrosive media according to predetermined program 21 p3715 A67-37827

Rotating bending fatigue limit and true stress/true strain parameters correlation for steels extended to axial load fatigue tests 21 p3719 A67-38132

Mean stress level effect on corrosion fatigue strength of aluminum clad D16AT alloy sheet under asymmetrical loads 21 p3646 A67-39008

Variable loading effect on durability of D16T aluminum alloy exposed to continuous action of corrosive

medium 21 p3642 A67-39009
Heat resistant stainless steels evaluated experimentally for fatigue properties, corrosion resistance, creep limit and tensile strength 21 p3646 A67-39010
Endurance fatigue characteristics of weldable martensitic stainless steel, giving data for butt and spot 22 p3811 A67-39447
Supersonic transport structural materials design, considering fatigue behavior, crack propagation and residual static strength under temperature and cyclic load effects 22 p3819 A67-39457
Fatigue in fibers and plastics, use of cumulative extension testing and time dependent effects in fatigue tests 22 p3824 A67-39562
Crack propagation in solid undergoing cyclic loading using Griffith model, stressing work hardening effect 22 p3911 A67-39680
HF fatigue tests in high vacuum environment on recrystallized molybdenum base alloy TZC for elevated temperature fatigue 22 p3822 A67-40058
Distribution function of durability in light structural alloys based on mass fatigue tests analyzed for influence of scale factor and stress concentration 22 p3915 A67-40301
Random load fatigue life and reliability via fail-safe structural model, obtaining statistical distribution of 2024-T4 aluminum alloy bending strength 23 p4076 A67-40735
Fatigue behavior of Cr steel and Ni-Cr alloy examined for influence of direction of first loading stroke of push-pull testing 23 p4019 A67-41155
High vacuum environment and vacuum outgassing time effects on magnesium alloys fatigue properties under constant load and reversed bending 24 p4172 A67-42037
FATIGUE TESTING MACHINE
Ultrasonic machines used to determine fatigue strength of components subjected to repeated alternating stresses 02 p0338 A67-12043
Heating unit of device for testing small samples of sintered materials for thermal fatigue 03 p0420 A67-13545
PEM-62 electromagnetic program-controlled fatigue testing machine 03 p0420 A67-13565
Ultrasonic apparatus using echo method to record automatically formation and propagation of fatigue cracks on smooth specimens 03 p0420 A67-13567
Soviet book on high temperature strength of materials noting test stands, stresses, loads, applications to jet and rocket technologies, etc 07 p1208 A67-19299
Aircraft reliability as function of fatigue life of welded joints noting static strength variation, S-N curve and multiple safety factor 09 p1506 A67-22471
Constant-amplitude reverse bend stress fatigue testing device for extreme high vacuum, testing aluminum 10 p1658 A67-23781
Metallurgical and fluid dynamic results of 2000-hr endurance test at high temperatures on two-stage 200 hp turbine in wet potassium vapor 11 p1745 A67-24797
[ASME PAPER 67-GT-9] 11 p1745 A67-24797
Program attachment to fatigue testing machines intended for two-stage programs 13 p2217 A67-26796
Apparatus for programming thermal cycles in fatigue tests of materials 13 p2218 A67-26797
Five-ball fatigue tester to investigate reduced pressure environment effect on rolling element fatigue life with polyphenyl ether 14 p2326 A67-28795
[ASLE PREPRINT 67AM 8A-3] 14 p2326 A67-28795
Materials rolling contact fatigue strength measured by tester intended to serve as screening device 16 p2676 A67-31381
[ASME PAPER 67-LUBS-3] 16 p2676 A67-31381
Electroinductive defectoscope circuitry and operation described noting use for fatigue cracks observation in threaded components 16 p2681 A67-31917
Stress-strain curves under variable stress sequences in high stress range 22 p3913 A67-40036
U-shaped bellow fatigue strength under axial loading, discussing elastic and plastic fatigue tests using specially designed machine 22 p3913 A67-40037
Hysteresis loop measurement using

Sonntag fatigue machine which produces sinusoidal force at 30 Hz fixed frequency 23 p4078 A67-41227
Fracture-toughness tests described to obtain fracture data for transformation into allowable design stresses 23 p4079 A67-41413
High strength aluminum alloy panel resistance to fatigue crack propagation, discussing axial load fatigue machine 24 p4170 A67-41949
FATTY ACID
Capacitance and optical thickness of fatty acid monolayers sandwiched between Al films 02 p0290 A67-11732
Saccharomyces cerevisiae light particle fraction containing fatty acid synthetase analyzed by density gradient method 19 p3178 A67-35873
Prebiotic synthesis of monocarboxylic acids suggested from mixture of methane and water exposed to semicorona discharge 19 p3181 A67-35882
Enzyme activity of light and heavy crude ribosomal fractions in Saccharomyces cerevisiae indicating subcellular sites of lipid synthesis 21 p3573 A67-37919
FAULT ISOLATION BY SEMIAUTOMATIC TECHNIQUES
S FIST PROJECT
FAULT MECHANICS
SA STACKING FAULT
Modeling of magnetic drum memory system using Markov chain based on historical data 03 p0400 A67-14220
Microminiaturized systems for fault analysis and indication design and application to built-in test equipment 20 p3449 A67-36983
FBFM
S FEEDBACK FREQUENCY MODULATION /FBFM/
FCC
S FACE CENTERED CUBIC /FCC/ CRYSTAL
FEED SYSTEM
Multielement scanning feed system for parabolic cylindrical antenna by controlling phase and amplitude of signal radiating from each element 02 p0211 A67-11600
Polarization angle of linear feed antenna on polar mounted paraboloid relative to az-el coordinate system 02 p0212 A67-11611
Radiation pattern and standing wave ratio for antenna system consisting of paraboloidal cylindrical reflector and feed 02 p0213 A67-11644
Cassegrain feed for 85-ft-diam antenna of planetary radar system noting operative conditions, polarization capabilities and performance data 04 p0596 A67-15048
Broadening of frequency bandwidth of slot array antenna by adopting center feed method 04 p0585 A67-15505
Antenna feed eliminating compromise between antenna illumination and spillover efficiencies by placing dielectric guiding structures between primary feed and reflector 04 p0590 A67-15903
High efficiency S-band monopulse focal point tracking feed, discussing aperture geometry design theory 08 p1300 A67-20654
Higher order waveguide mode radiation incorporated antenna feed systems for performance improvement, evaluating S-and C-band dual frequency Cassegrain feed 08 p1300 A67-20681
Wideband feed for cross shaped antennas of parabolic cylinder type 08 p1306 A67-21340
Wideband feed with electrical scanning of radiation pattern for cross shaped radio telescope 08 p1306 A67-21341
Parabolic reflector with shields protecting feed from extraneous radio waves 08 p1318 A67-21343
Asymmetrically fed linear antenna loaded with loading impedance analyzed in terms of two coexistent current distributions 10 p1609 A67-22774
Generalized method of calculating multielement antenna and feeder system 10 p1611 A67-22981
Ion thruster, including mercury feed system and shielded neutralizer, designed and tested for spacecraft station keeping and attitude control 10 p1698 A67-23120
[AIAA PAPER 66-247] 10 p1698 A67-23120
Basic design differences illustrating paraboloidal reflector variations, noting factors contributing to or detracting from antenna efficiency 10 p1613 A67-23413

Feed system design for spherical reflector illumination specifying required field distribution and primary gain 11 p1761 A67-24281
Solid propellant highly restartable electric trigger microthruster, noting triggering electrode and feed system 11 p1746 A67-25013
Electrode feed system for segmented electrode MHD wind tunnel 12 p1920 A67-25406
Determinants of electronically steerable antenna arrays 12 p1917 A67-26158
Broadband monopulse three-element tracking feeds for spherical Luneberg lens scanning antenna, discussing radiator design, radiation pattern and cross coupling between error channels 15 p2451 A67-29924
Cassegrain monopulse feed system using end-fire polyrod radiators 15 p2451 A67-29925
Rapidly varying high pressure measurement requirements, treating pressure transducer as seismic system and analyzing feed channel distortion 16 p2671 A67-31004
Correcting feed for Arecibo Ionospheric Observatory reflector noting antenna gain 16 p2639 A67-31359
Wideband feed for cross shaped antennas of parabolic cylinder type 17 p2822 A67-31936
Wideband feed with electrical scanning of radiation pattern for cross shaped radio telescope 17 p2822 A67-31937
Parabolic reflector with shields protecting feed from extraneous radio waves 17 p2822 A67-31939
Static and dynamic sealing concepts and materials for propellant feed systems and pneumatic and hydraulic control systems of liquid propellant rocket engines 17 p2864 A67-31990
Cassegrain antenna gain and noise temperature with dual reflector system derived from feed pattern and system geometry 17 p2824 A67-32395
Liquid hydrogen pumping for Phoebus reactor, discussing feed systems, nozzles, configurations, design, testing, etc [AIAA PAPER 67-478] 18 p3077 A67-34402
LF oscillations built up in bipropellant rocket engine equipped with pressurized feeding system 19 p3311 A67-35052
Electrode feed system for segmented-electrode MHD accelerator to avoid power supplies/switch gear proliferation 19 p3177 A67-35774
Cassegrain antenna beam-pointing accuracy, analyzing reflector beam deviation and feed displacement effects 20 p3398 A67-36819
Valveless metal vapor feed system for use in pulsed plasma accelerators employing mercury as propellant 21 p3695 A67-38760
[AIAA PAPER 67-738] 21 p3695 A67-38760
Target-tracking antenna design with primary feed system suitable for slewing of mobile radar equipment 22 p3760 A67-39592
Multimode monopulse feed system optimum aperture distribution determination, obtaining maximum rate of signal change on axis 22 p3763 A67-40313
Series and parallel pulse forming feed networks for generating microwave signals, comparing output parameters and limitations 22 p3774 A67-40444
FEEDBACK
SA DEGENERATION
SA NONLINEAR FEEDBACK
SA REGENERATION
SA SENSORY FEEDBACK
Ruby laser with scattering induced feedback and absence of resonance type oscillations 01 p0090 A67-10740
Sufficient condition for absolute bounded-input-bounded-output stability for certain class of nonlinear sampled data feedback systems 02 p0224 A67-11586
Effect of feedback capacity addition to M-ary PAM communication system perturbed by white Gaussian noise 02 p0204 A67-12170
Stability analysis of spectrotron with external feedback based on time delay, inertia of nonlinear quadrupole and circuit phase shifts 03 p3377 A67-13092
Frequency oscillations in oscillator with double-loop delayed feedback 03 p0378 A67-13291
Feedback effect on current voltage characteristic of device with negative feedback and reactivity of device in negative resistance region 03 p0380 A67-13583

Ruby laser with nonresonant feedback due to radiation scattering, showing use as optical frequency 05 p0818 A87-16642

Ruby laser with scattering induced feedback and absence of resonance type oscillations 13 p2126 A87-26769

Rhombic traveling wave antenna with feedback loop to utilize larger proportion of total power 17 p2824 A87-32313

Free gyroscopes with feedbacks on each gimbal, determining feedbacks and improving operating indices 18 p3047 A87-33993

Cross-spectral method application problems in feedback system analysis, identification and linear time invariant system 20 p3407 A87-36785

Double signal modulation used to increase authenticity of information transmission in binary systems having resolving feedback 24 p4122 A87-42378

FEEDBACK AMPLIFIER

Maximum power gain and admittance matrix for neutralized amplifier stages with three-terminal amplifier devices /electron tubes and transistors/ 01 p0035 A87-10432

Circuit design measuring travel time required by low energy particle of varying mass 01 p0066 A87-10654

Semiconductor integrated circuit negative feedback amplifier design with high response characteristics for carrier terminal equipment application 01 p0040 A87-11241

Wide range vibrating-reed Mariner II electrometer, describing components, performance characteristics and results 02 p0241 A87-11681

Amplifier design using multistage transistor current mode, feedback systems and minimized voltage swings 03 p0386 A87-13977

Analogous tube and transistor tuned feedback amplifier analysis and use of nonunidirectional active network as amplifying element 04 p0586 A87-15670

Tunnel diode superregenerative amplification and detection in linear regime and volt-ampere characteristics of diode 05 p0772 A87-16450

Electron densities in helium plasma measured by laser amplifier with maximum gain and minimum bandwidth at point nearest threshold 05 p0820 A87-16663

Microwave feedback radiometers using electromechanical and all-electronic systems 07 p1155 A87-19875

Isolation bandwidth characteristics of Y circulator junction modified by external tuning elements 09 p1474 A87-22087

Theoretical realizability, design and stability of ideal gyrator with two operational amplifiers and resistance network 11 p1760 A87-24232

Twelve-channel parallel action noise spectrum analyzer for LF noise measurement, using transistorized negative feedback amplifier 11 p1769 A87-25038

Resistive transistor stage with feedback, deriving input-output impedances, amplification factors, conductance and resistance 14 p2283 A87-28276

Analysis of discrete nonlinear time-varying systems, noting computational simplicity, application to feedback system, etc 16 p2650 A87-31675

Noise effect on ideal relay element with lagging feedback analyzed using Kolmogoroff equations, comparing performance with ideal forcing element connected to linear amplifier 18 p3017 A87-33873

Fourier analysis of amplifier commutated capacitor type integrator output signal 18 p3011 A87-34107

Functional analysis of transistor amplifier with multiloop feedback, deriving equation for transfer constant increment 22 p3769 A87-39577

Gyrostabilizer feedback circuit transfer function with two-phase asynchronous motor equivalent to unit having time constant as function of transmission band of amplifier 22 p3810 A87-40483

Phase characteristics linearity of LF regenerative amplifiers with reactive elements and Chebyshev amplitude frequency responses 24 p4129 A87-42226

FEEDBACK CONTROL SYSTEM

SA SERVOMECHANISM

Model of retinal receptor incorporating various feedback control processes

consistent with physiological and psychological evidence 01 p0044 A87-10485

Digital feedback control system compensation of pulse input to improve time response of controlled variable 01 p0045 A87-10673

Variable-stability feedback control low range air speed system for X-22A aircraft 01 p0073 A87-11211

Modified Bode criterion for feedback system stability 01 p0045 A87-11198

Optimal nonlinear feedback control derived from quartic and higher order performance criteria 01 p0046 A87-11206

Stability of feedback single-loop systems with one differentiable nonlinear element, noting Popov criterion 01 p0046 A87-11210

Functional integration analysis of exponential behavior of nonlinear feedback control systems 01 p0047 A87-11211

Oscillation formation by violation of sufficient conditions of asymptotic stability in linear system 01 p0047 A87-11215

Closed loop gain of two-loop linear feedback system calculated, using computer 01 p0047 A87-11218

Stability theory application to control, circuit theory and aerospace systems 01 p0047 A87-11221

Stability of sampled data feedback systems with time-varying gain by restriction with memoryless element and nonanticipative linear time-invariant subsystem 01 p0048 A87-11226

Nonlinear servo devices examined, using simplified form of harmonic-equivalent method obtained from multilinear characteristics 02 p0224 A87-11529

Steady state output ripple performance and sampling frequency choice for single and multirate direct digital control system with stochastic input 02 p0225 A87-12073

Transient response of frequency synchronization circuit determined with or without application of radar stability circuit 02 p0203 A87-12146

Optimal feedback control for finite state systems with suitable performance criterion, using maximum principle applied to time-sharing computer systems 02 p0227 A87-12172

Pulse amplitude range estimated for which PWM system is asymptotically stable, using method of Murphy and Wu 03 p0393 A87-13983

Stability criterion for PWM feedback systems containing one integrating element 03 p0393 A87-13984

Fluid interface instability suppression via feedback, noting stability criteria and parameters 03 p0483 A87-14036

Advanced feedback system simulation technique for strategic planning in business, noting manpower allocation 04 p0739 A87-14498

Signal stabilization of memory type nonlinearity, using dual input describing function to determine effect of external sinusoidal signal on system limit cycles [ASME PAPER 66-WA/AUT-1] 04 p0593 A87-15421

Automatic flight control systems for missiles and aircraft, noting error sensing and correcting functions, calibration and testing methods 04 p0655 A87-15735

Exhaustive equivalence classes of optimal systems with separable controls 04 p0594 A87-15876

Comparison of nonoptimum and optimum strategies in dual control of inertialess plants in presence of noise in feedback loop 05 p0781 A87-16257

Synthesis of stochastic optimal control for case of discrete input of feedback vector, noting dependency on coordinates characterizing probability density of plant vector 05 p0782 A87-16316

Q-switched ruby laser configuration with feedback control, noting frequency and instability correlation with theoretical results obtained from mathematical model 05 p0822 A87-16676

Single mode 6328 angstrom units He-Ne laser having single frequency power output of 50 mwatt stabilized by feedback system whose output is neither amplitude nor frequency modulated 05 p0823 A87-16685

Bang-bang control for feedback systems, applying computer to optimization of switching time from state to state of linear systems 05 p0784 A87-16854

Electrohydrodynamic equilibrium showing

continuum feedback control of Rayleigh-Taylor type instability 05 p0858 A87-17414

Optimal signal design for binary communications systems using sequential and nonsequential detection with feedback 06 p0962 A87-17944

FM feedback system for lunar orbiter signal demodulation, discussing system composition and performance 06 p0975 A87-18108

Optimal threshold level resulting in minimum residual probability of distortion in transmission of pulse coded signals in systems with information feedback 06 p0975 A87-18211

Hypothetical control system with 30 db/decade attenuation characteristic and constant phase margin of 45 degrees, presenting phase angle stabilization technique that improves actual systems 06 p0977 A87-18416

Optimal guidance equations for ascent trajectories into circular orbits, developing feedback guidance loop for real onboard control system [AIAA PAPER 67-56] 06 p1029 A87-18495

Minimum time and fuel problems for PFM systems, deriving optimal control by heuristic argument 06 p0977 A87-18524

Optimization of stochastic dynamic system with noisy output 06 p0977 A87-18525

Bounded input of nonlinear feedback system yielding bounded output according to Popov theorem 06 p0977 A87-18528

Zero steady state error operation of feedback systems with time-varying nonlinear element 06 p0977 A87-18529

DC amplifier with capacitive feedback as correcting device in recording currents while studying magnetoplasma generator 06 p0952 A87-18693

Periodic oscillation mode of time invariant feedback system containing relay determined, using state space approach 06 p0978 A87-18719

Sign codes and patterns of state variables for finding all possible responses in linear third order closed loop feedback control system 06 p0978 A87-18721

Impact excitation of oscillation with oscillating circuit in anode and cathode 07 p1150 A87-19236

Complex and decision feedback systems for command channels in space communications 07 p1145 A87-19872

Area of Safe Operation for transistors in switching mode defined, using thermal feedback model 07 p1157 A87-19902

Feedback control system to position satellite in vicinity of unstable collinear libration point with application to lunar communication problem [AAS PAPER 66-132] 07 p1146 A87-19991

Motion reproduction, analyzing control systems, dynamic fidelity, voltage command, etc [AIAA PAPER 67-252] 07 p1166 A87-20070

Circle criterion for stability of time varying feedback systems 08 p1310 A87-20338

Instability and periodic solutions in nonlinear feedback systems obtained using perturbation theory of Hale and Cesari 08 p1310 A87-20339

Monostable fluidic amplifier with adjustable positive feedback /AF relay/ characteristics and application as oscillator, proximity switch, delay unit and in alarm annunciator systems 08 p1282 A87-20462

Self-optimizing and adaptive control systems achieved by feedback action or performance index optimization 08 p1312 A87-20753

Pressure feedback in electrohydraulic servomechanisms for high inertia loads to increase stability, using dynamic analysis and differential equations 09 p1442 A87-21687

Control of laser action, noting feedback theory conception and geometrical optics of laser modulation 09 p1513 A87-22146

Optimal type of strategy of remote control and force sensitive and stable feedback presentation in master-slave manipulators with transmission delay 09 p1456 A87-22374

Discrete continuous feedback control systems with signal dependent sampling constraints, analyzing sampling interval criteria 09 p1483 A87-22608

Self-excited oscillations of nonlinear servosystems examined, applying expression for generalized transmittance of nth order system 10 p1618 A87-22851

- Book on modern control systems covering feedback control system, root locus and frequency response method, time-domain analysis, etc 11 p1769 A67-24062
- Definition, realizability and design of active gyrator, using two controlled current sources to obtain ideal impedance inverting characteristics 11 p1789 A67-24127
- Complex correlation function application to describe correlation between signals from two antennas of radio interferometer 11 p1762 A67-24287
- Stabilized cross correlation radiometer for use at decametric wavelength, using two feedback loops controlling four noise diodes 11 p1762 A67-24288
- Optimum distributed parameter system described by N-dimensional wave equation with unconstrained boundary control function 11 p1770 A67-24889
- Optimum control integral criterion function for class of distributed parameter systems subject to control signal saturation 11 p1770 A67-24890
- Network analysis of frequency stability of quartz generators, showing possible reduction through additional HF cascades introduction into feedback loop 11 p1768 A67-24982
- Adaptive feedback paths of adaptive aircraft control system in small signal stability analysis 11 p1772 A67-25081
- Automatic control systems classification for ordinary systems in relation to self-adaptive systems 13 p2088 A67-26800
- Telefactor system in control of space operations, describing master-slave manipulator servomechanism with TV network and electronic communication link 13 p2063 A67-27213
- Design and optimal performance considerations on application of derived rate increment feedback to satellite attitude control systems in limit cycle and acquisition systems 13 p2212 A67-27297
- Feedback control system to position satellite in vicinity of unstable collinear libration point applied to lunar communication problem [AAS PAPER 66-132] 13 p2210 A67-27543
- Fluidic temperature sensor using frequency beating technique for generating analog pressure signal proportional to frequency differences 14 p2318 A67-28345
- Power advantage of optimum system achieved with suboptimum feedback function for sequential binary detection system 14 p2292 A67-28707
- Feedback control theory for constant temperature hot-wire anemometers using differential equation applied to frequency response optimization 14 p2320 A67-28750
- Frequency domain instability criteria generated from stability criteria for time varying and nonlinear feedback problems 15 p2455 A67-29167
- Parametric input/output relation of approximate controller with optimized performance index, obtaining specific optimal control designed in regard to worst initial state 15 p2456 A67-29365
- Stability of feedback systems with monotone and odd monotone nonlinearities 15 p2457 A67-29374
- Pull-in range in feedback synchronization, discussing multistage filter and results obtained with graphical, computer and theoretical methods 15 p2446 A67-29588
- Tracking circuit performance, discussing squaring loop, Costas loop variants and delayed decision feedback 15 p2436 A67-29591
- Laser radiation control techniques using saturation filter or negative feedback circuit with resonator Q-factor depending on radiation field power 15 p2499 A67-29722
- Feedback control system for hologram interference fringe stabilization, noting phase disturbances due to different effects 15 p2491 A67-30432
- Optimal threshold level resulting in minimum residual probability of distortion in transmission of pulse coded signals in systems with information feedback 16 p2642 A67-30484
- Book on modern control systems covering feedback control theory within framework of frequency and time domain analysis 16 p2643 A67-30621
- Realization of invariant multiloop control in case of near-critical and critical plant parameters 16 p2643 A67-31379
- Sampled data feedback control system using quadratic programming to determine optimum compensator 16 p2646 A67-31636
- Asymptotic stability criterion for autonomous feedback system with single odd monotonic nonlinearity, using functional analysis 16 p2646 A67-31639
- Optimal feedback control system design to account for differences between physical system and mathematical model in terms of parameters 16 p2647 A67-31641
- Feedback from observations introduced into midcourse guidance correction program, showing optimal random feedback solution obtained for deterministic optimal feedback control problems 16 p2701 A67-31657
- Applied synthesis technique using feedback and command controller elements for strongly interacting multivariable control systems, illustrated by flight control system design 16 p2649 A67-31661
- Linear pulse frequency modulated control systems, noting upper and lower bounds of optimal performance 16 p2650 A67-31671
- Indices 16 p2650 A67-31671
- Optimal control of measurement subsystems within feedback control systems 16 p2650 A67-31676
- Optimal feedback control calculation for launch vehicle synthesizing optimal controller with sensitivity constraints to reduce trajectory dispersion 16 p2763 A67-31679
- Continuous control process with random variable stopping time of known probability distribution, presenting optimal feedback control, trajectory and minimum cost 16 p2651 A67-31681
- Optimum filtering and control of randomly-sampled linear and nonlinear systems with Gaussian or non-Gaussian statistics, synthesizing generalized Kalman filter 16 p2651 A67-31683
- Nonlinear discrete system equivalence of integral pulse frequency modulation /ipfm/ feedback systems, discussing Lagrange stability criterion 16 p2652 A67-31685
- Recursive procedures for determining relationships between random parameter of linear system and resulting output random variable 16 p2652 A67-31691
- Necessary and sufficient conditions for decoupling time-invariant linear multivariable system by state variable feedback, discussing transfer matrix consequences 16 p2652 A67-31692
- Monte Carlo evaluation of linear- and eigenvector-method for estimation of pulse transfer function of linear, time-invariant dynamic feedback system 16 p2653 A67-31695
- Nonuniform error quantization effects on stability of feedback control systems, investigating limit cycles existence and giving optimum quantizer design procedure 17 p2829 A67-32016
- Transfer functions in electrohydraulic servo systems through feedback instability properties, discussing root locus theory and typical servomechanism properties 17 p2830 A67-32932
- Feedback-signal lag and channel discreteness effect on rate of information transmission over Gaussian channel with feedback during symbolized coding 18 p2999 A67-33531
- Synthesis of stochastic optimal control for case of discrete input of feedback vector, noting dependency on coordinates characterizing probability density of plant vector 18 p3016 A67-33867
- Planar highly conducting liquid jet kink mode stability in electric field and feedback stability control of spatially growing wave 18 p3029 A67-34735
- X-transform for open/closed loop sampled data system with zero-order hold device 19 p3263 A67-35927
- Feedback control system using pneumatic computing components and vibration isolators for automatic platform tilt stabilization, performance characteristics, etc [AIAA PAPER 67-548] 19 p3208 A67-35946
- Hybrid simulation for analysis and design of nuclear reactors feedback control systems 19 p3189 A67-36068
- Noise effect on synthesis of discrete systems with and without feedback channel for transmitting continuous messages, using binary signal and criterion of minimum rms error 20 p3383 A67-37071
- Time optimal feedback control using extension of Hermes approximation theorem 20 p3408 A67-37074
- Maximum principle application to optimal control procedure, minimizing transient response and decreasing effect of random changes in system parameters 20 p3410 A67-37232
- Synthesis procedure for linear automatic feedback control systems, examining time-domain response 20 p3413 A67-37679
- Motion reproduction, analyzing control systems, dynamic fidelity, voltage command, etc 21 p3608 A67-38540
- IR monitoring technique to improve accuracy of welding inspection using voltage feedback to regulate output 21 p3634 A67-38620
- Orthogonal signaling in sequential decision feedback on communication over additive white Gaussian noise channel, obtaining expression for error probability 22 p3775 A67-39295
- Open loop adaptive optimal control, calculating plant dynamic sensitivity coefficients for unknown disturbances, using digital computer on feedback path 22 p3776 A67-39411
- Stability and response time of quantified pulse-position modulation feedback control circuit consisting of nonlinear sampler and first order continuous part 22 p3776 A67-39647
- Lateral stability augmentation of supersonic aircraft using linear multichannel state-vector optimal feedback control 22 p3746 A67-40155
- Distributive systems interaction between feedback and sensitivity noting parameter variations effects on external characteristics 23 p3983 A67-40644
- Nonlinear system suboptimal feedback control technique based on method for determining approximate solutions for Hamilton-Jacobi-Bellman equation 23 p3983 A67-40645
- Popov method extension for absolute stability of nonlinear feedback systems containing distributed elements 23 p3984 A67-40870
- Parameter invariance problem for linear systems solved by obtaining necessary and sufficient conditions for invariance in optimal control systems 23 p3984 A67-41159
- Matrix version of Kalman-Yacubovich lemma for deriving stability conditions for continuous time dynamical systems with m-feedback nonlinearities 23 p3985 A67-41726
- Errors in state vector from amplitude quantization in feedback control loop, noting finite word length in hybrid computer simulation 24 p4134 A67-42023
- Sampling interval criteria with nonlinear integrands in discrete-continuous feedback control systems, obtaining performance surfaces in object function-parameter space 24 p4134 A67-42024
- Design of approximately optimal feedback controllers for systems with bounded states 24 p4134 A67-42178
- Piecewise linear switching functions design for suboptimal regulation of linear plants with relay controller in regard to transient response performance criterion 24 p4135 A67-42179
- Integral pulse FM effect on feedback control, obtaining stability of equivalent nonlinear discrete system 24 p4135 A67-42182
- Stability of feedback systems containing single odd monotonic nonlinearity 24 p4136 A67-42187
- Controllability and observability concepts defined for feedback system, with finite dimensional differential equation representations 24 p4136 A67-42189
- Controller design method for linear feedback control systems with transport lag by parameter plane and dominant root methods 24 p4136 A67-42291
- High gain phased array for satellite transmission using feedback to correct phase and amplitude parameters variations 24 p4124 A67-42816
- Linear optimal control in systems with uncertain parameters, noting application to design of compensating network for flexible booster for uncertain value of first bending mode 24 p4137 A67-42903
- FEEDBACK FREQUENCY MODULATION**
- /FBFM/
- Threshold performance of limiter

discriminator phase locked demodulator and FM feedback demodulator 06 p0969 A67-18107
 FM feedback system for lunar orbiter signal demodulation, discussing system composition and performance 06 p0975 A67-18108
 FM signals demodulation and negative feedback modulation, deriving signal to noise ratio and noise spectrum formulas 19 p3183 A67-35562
 Transmission behavior of double tuned band filters with frequency dependent feedback and stagger tuning 24 p4129 A67-42206

FEEDING DEVICE

Feeding and phase scanning in various antenna arrays 07 p1152 A67-19545
 Preformed micron and submicron-sized solid particles for colloidal propulsion, investigating particle feeding and charging [AIAA PAPER 67-727] 21 p3688 A67-38751
 Inexpensive high vacuum high voltage feedthrough used in conical shock driver system for plasma research 22 p3774 A67-40348
 Array antenna directive pattern scanning utilizing difference in phase lead between heterodyne and converted signals at feeder 24 p4130 A67-42234

FELLOWSHIP AIRCRAFT

S FOKKER F-28 AIRCRAFT

FERMAT PRINCIPLE

Calculation of Doppler shift of radio waves propagating through changing ionosphere by Fermat principle 16 p2629 A67-31516
 Pump induced optical distortion in isotropic laser materials analyzed using Fermat principle, predicting ray refraction, beam divergence, etc 18 p3062 A67-34624

FERMI-DIRAC STATISTICS

Intranuclear cascades of nucleon-nucleus interaction calculated on basis of Fermi gas model, using Monte Carlo method and three-dimensional relativistic kinematics 02 p0314 A67-12748
 Fermi-Dirac statistics, transverse magnetoresistance and galvanomagnetic properties of hexagonal-close-packed Mg and Zn 03 p0495 A67-13511
 Intranuclear cascades of nucleon-nucleus interaction calculated on basis of Fermi gas model, using Monte Carlo method and three-dimensional relativistic kinematics 22 p3876 A67-40250

FERMI STATISTICS

Production of low energy cosmic ray electrons, investigating energy inputs to injected secondary electrons by possible low magnitude solar electric field and possible galactic Fermi acceleration 02 p0312 A67-12635
 Gamma irradiation from Co 60 effect on indium antimonide, determining defect formation on dose and limiting position of Fermi level for n-and p-type material 04 p0680 A67-15283
 Shallow donor introduction in p-type Ga-As laser results in increased efficiency of radiative recombination 05 p0826 A67-17280
 Oscillatory magnetoresistance and Hall effect in single crystals of Sn-doped Bi to decrease Fermi energy 06 p1070 A67-18984
 Quasi-particle ensemble theory applied to Fermi fluid, noting relation of thermodynamic properties to grand canonical ensemble 07 p1224 A67-19504
 High injection theories of p-n junction, commenting on corrections made in connection with junction voltage 09 p1472 A67-21953
 Spatial variation of quasi-Fermi potentials in symmetrical step and linearly graded p-n junctions 09 p1556 A67-22201
 Single conduction band approximation of nature of increase with temperature of thermal conductivity of ZrC and NbC in terms of scattering and Fermi energy 11 p1804 A67-23902
 Niobium stannide, V-Ga and V-Si paramagnetic susceptibility, elastic constants and electric resistivity temperature dependence 23 p4038 A67-40794
 Fermi pressure shifts of highly excited states of atoms in gaseous medium due to electron particle interactions, discussing scattering contributions 23 p4029 A67-40958

FERMI SURFACE

State density for highly doped semiconductor in magnetic field, obtaining results at near Fermi level energies and at bottom of conduction

band 01 p0128 A67-10096
 Mechanism leading to superconductivity even for particles with purely repulsive forces between them, examining general theory for weak short-ranged pair forces between particles 01 p0129 A67-10151
 Fermi surface curvature of indium single crystals measured from RF size effect at reference point 01 p0133 A67-10742
 Inverse Hall effect of noble metals alloyed with B-group metals as affected by residual resistivity and phonon scattering 04 p0682 A67-15465
 Increase in low temperature specific heat and change in electronic density of states of boronated graphite 05 p0833 A67-17197
 Fermi surface of tin telluride approximated by four distorted surfaces located at L points of Brillouin zone as shown by Fourier analysis 06 p1065 A67-18950
 De Haas-van Alphen effect in arsenic, noting two kinds of oscillations /Fermi surface and thin cylindrical surface/ and doping effect 06 p1070 A67-18982
 Anisotropic energy gap in superconducting white tin obtained by expansion in tetragonal harmonics 07 p1235 A67-20134
 Anisotropy and temperature dependence of upper critical field of type II superconductor single crystals with cubic structure 07 p1236 A67-20136
 Fermi surface curvature of indium single crystals measured from RF size effect at reference point 13 p2176 A67-28771
 States density in vicinity of Fermi surface obtained from values of paramagnetic susceptibility for gold-palladium alloys 13 p2133 A67-27006
 Integration of Einstein gravitational equations implies that corpuscle be rigidly connected with particular Fermi space-time system of reference 13 p2158 A67-27298
 Galvanomagnetic properties of single crystal antimony as function of temperature, deriving carrier mobilities and densities, detailing nature of Fermi surface 14 p2364 A67-28105
 Equation describing electron transfer between semiconductor surface bands and space bands, applying Fermi concept 14 p2371 A67-28754
 Superconducting mixed state of concentrated Mo-Nb alloy, evaluating free area of Fermi surface in k space 16 p2726 A67-30812
 Silver-gold and silver-germanium alloys tested for Fermi surface changes with alloying, using thermoelectric power measurements 16 p2731 A67-31448
 Plasma wave propagation dispersion in sodium and potassium at cryogenic temperature using Landau-Fermi liquid theory 20 p3514 A67-37570
 Spin-density waves effect on electronic properties and Fermi surface of antiferromagnetic metals 21 p3676 A67-37817
 Magnetoacoustic attenuation in metals with Fermi surface, open orbits and magnetic breakdown calculated by solving Boltzmann equation via path-integral method generalization 22 p3861 A67-39995
 RF size effects in plane parallel metal plate, discussing skin effect in magnetic fields, electron trajectories and spherical Fermi surface 22 p3866 A67-40551
 Alloying effect on diffusion thermopower in relation to Fermi surface variations in dilute silver-gold alloys [JPL-TR-32-1095] 24 p4200 A67-41840
 Exact calculation of indirect exchange interaction isotropic and nonisotropic terms in rare earth metals, with free electron model for conduction band 24 p4203 A67-42110
 Thermodynamic property of superconductors with nonmagnetic impurity analyzed using overlapping energy bands near Fermi energy 24 p4203 A67-42162
 Microwave absorption by magnetic field induced surface states in superconductors, showing anomalies consistent with quasi-particle decay 24 p4205 A67-42739

FERRIMAGNET
 Galerkin-Ritz method application to Maxwell waveguide equations for calculation of propagation constant of rectangular guide with transverse ferrimagnetic core 07 p1152 A67-19590
 Galerkin-Ritz method application to Maxwell waveguide equations for calculation of propagation constant of rectangular guide

with transverse ferrimagnetic core 20 p3401 A67-37327
 Flexible anisotropic ferrite magnets preparation, noting influence of binder in orientation of crystals 23 p4041 A67-41183

FERRIMAGNETISM
 Resistance losses of ferrite core in strong HF field determined using oscillogram analysis, noting possibilities in wide frequency range and complex magnetization 01 p0035 A67-10414
 Vacuum deposition and mechanical properties of magnetic thin films of ferrite-borate mixtures 04 p0677 A67-15118
 Three-port 35-GHz ferrite circulator latching switch, discussing geometric configurations, effects on performance characteristics, ferromagnetic materials selection, etc 08 p1304 A67-21225
 Refractive index of microwave lenses made of ferrite material changed by varying DC magnetic field 11 p1752 A67-24125
 Temperature dependence and anisotropy of high temperature ferrimagnetic microwave resonance linewidth of Si-doped YIG, showing valence exchange effect on losses 20 p3508 A67-36390
 Wave propagation in ferrite-filled rectangular waveguide with transverse magnetization 20 p3382 A67-38864
 X-ray structural analysis of ferromagnetic /ferrimagnetic/ bismuth ferrite single crystal 21 p3685 A67-38967
 Discontinuity problem between empty rectangular waveguide and one filled with transversely magnetized ferrite solved by introducing metal surface wave 22 p3758 A67-39272
 Hall potential difference for thin film in magnetic leakage field of domain interface between ferro-and ferrimagnetic 24 p4204 A67-42457
 Low loss mechanically or magnetically tunable 1 to 12 GHz hybrid ferrimagnetic dielectric microwave bandpass filter with improved power handling 24 p4132 A67-42808

FERRITE
SA STEEL
 Temperature dependence of complex initial magnetic permeability of cobalt-zinc ferrites over 0.1-2000 mc frequency range 01 p0128 A67-10079
 Resistance losses of ferrite core in strong HF field determined using oscillogram analysis, noting possibilities in wide frequency range and complex magnetization 01 p0035 A67-10414
 Magnetic properties of YGa and YGaGd ferrites noting effect of increasing Gd content 01 p0136 A67-11052
 Inductance coefficient dependence on geometric air gap of ferrite cup cores, showing use for design of stable resonance circuits 02 p0280 A67-11464
 Ferrite-based microelements as quasi-resonant RC circuits 02 p0214 A67-11907
 Monolithic ferrite space memory system of minimum weight, power consumption and high reliability 02 p0208 A67-12162
 Gyroscope rotor configuration using barium ferrite magnets and axial rotor magnetization 02 p0184 A67-12411
 Ferrite resonant isolators on coaxial, strip and rectangular waveguides with dielectric 02 p0223 A67-12670
 Temperature dependence of phase shift in magnesium-copper ferrite-chromite phase shifter as affected by microwave permeability 02 p0301 A67-12672
 Phase shift dependence on ferrite permeability tensor of reversible ferrite phase shifter 02 p0301 A67-12673
 High current duoplasmatron ion source with ferrite permanent magnets and extraction lens system 02 p0279 A67-12694
 Crystallographic structure of hexagonal ferrites of BaO-MeO-ferric oxide system and applications in UHF and microwave regions 02 p0301 A67-12787
 Ferrite materials for resonators of magnetostrictive transducers and filters used in transmission and reception of ultrasonic waves 03 p0420 A67-13548
 Temperature and magnetic field gradient effects on magnetothermomechanical interaction of viscous incompressible ferrofluid with cold wall 04 p0600 A67-14446
 Reliability of high power level ferrite phase devices 04 p0579 A67-14455
 Domain structure of strontium ferrite investigated by Bitter powder pattern

- method in basal planes, showing dependence on magnetic field intensity, temperature and thickness of crystals 04 p0673 A67-14482
- Mossbauer investigations of stoichiometric manganese-ferrite and two magnesium-manganese ferrites made at room and liquid nitrogen temperatures 04 p0676 A67-14925
- Vacuum deposition and mechanical properties of magnetic thin films of ferrite-borate mixtures 04 p0677 A67-15118
- Coupled spin, electromagnetic and plasma waves in ferrites 04 p0686 A67-15973
- Piezomagnetic coefficients in magnetostatic equations, permeability extrema and elastic moduli of Ni-Co-Mn ferrites 05 p0863 A67-16703
- Small signal suppression and third order intermodulation products of ferrite frequency-selective limiters 05 p0780 A67-17532
- Saturation magnetization of mixed cadmium ferrites of spinel structure 06 p1050 A67-18182
- Temperature dependence of magnetization and resistivity in SHF magnesium-aluminum ferrite 10 p1688 A67-22830
- Nonreciprocal ferrite devices at microwave frequencies, detailing circulator and isolator components 11 p1758 A67-24060
- Reliability of high power level ferrite phase devices 15 p2443 A67-29292
- Microwave ferrite devices describing applications at metric and decimetric wavelengths, at very low temperatures and at high power levels 17 p2826 A67-32744
- Relation between changes in ferrite lattice parameter at magnetic conversion temperature and changes in ferrite metal ion charges due to electron exchange 18 p3095 A67-33444
- Frozen vacancies effect on microhardness and electrical resistance of nickel ferrite and yttrium garnet 18 p3097 A67-33480
- Transient effects of changes in applied radio frequency power to which latching ferrite phase shifters could be subjected in array applications 19 p3196 A67-35663
- Self-decoration effect in thermally etched polycrystalline lithium ferrite, discussing geometric symmetry relation to crystallographic surface orientation 22 p3855 A67-39344
- Magnetically tunable multisection bandpass filter in ferrite-loaded evanescent waveguide 22 p3772 A67-39907
- Temperature stable ferrite materials for laminated memory arrays compatible with integrated semiconductor drive circuit 22 p3861 A67-39914
- Batch fabrication method for storage elements using electrophoretic deposition of ferrite on platinum wire 22 p3812 A67-39915
- Launcher for trapped surface waves over ice-covered sea by ferrite loaded horn device 22 p3763 A67-40306
- Nonreciprocal waveguide device consisting of ferrite loaded coaxial branch and crystal diode useful as isolator, modulator and filter 22 p3774 A67-40459
- Dominant mode field reflection at air-ferrite interface junction in anisotropic rectangular waveguide, deriving singular integral equations for discontinuity problem 23 p3973 A67-40880
- Magnetically tunable microwave filters using MHD modes in ferrites 23 p3980 A67-41186
- Operating principles of Y-shaped ferrite circulator, discussing temperature and power variations effects on sensitivity 23 p4041 A67-41213
- Nonlinear ferrite diaphragms in waveguides, discussing magnetic field effect on cavity tuning 24 p4119 A67-41972
- FERROELECTRICS**
- SA ANTIFERROELECTRICITY**
- Spontaneous electro-optical effect in triglycin sulfate crystals spectrally studied, noting changes in double refraction along three crystallographic axes during ferroelectric phase transition 01 p0129 A67-10138
- Ferroelectric field effect device having drain current gate voltage characteristic reproducing hysteresis character of ferroelectric gate 01 p0036 A67-10463
- Ferroelectrics for energy switching in SHF range 03 p0378 A67-13247
- Superconductivity in strontium titanates and similar polar substances with transition temperature accounted for by electron-phonon interactions 03 p0491 A67-13259
- Ferroelectricity - All-Union Conference, Rostov, U.S.S.R., September 1964 03 p0497 A67-13696
- UHF dispersion in barium titanate ferroelectric crystals explained as microwave scattering 03 p0497 A67-13701
- Ferroelectric properties and morphotropic phase boundary in phase diagram of ternary system of compounds of lead, titanium and nickel 03 p0498 A67-13704
- Electric properties of thin ferroelectric films of barium titanate compound 03 p0498 A67-13708
- Polarization and volt-ampere characteristics of ferroelectrics simultaneously under static and alternating fields 03 p0382 A67-13710
- Electric field forced ferroelectric-antiferroelectric state transitions in transducers 03 p0426 A67-14301
- Optical method observations of phase transition of ferroelectric monocrystal SbSI 06 p1047 A67-17758
- Precipitation effect of dispersed calcium titanate-rich phase on shape, organization and thickness of ferroelectric domains in barium titanate 06 p1020 A67-18047
- Crystal symmetry, optical properties and ferroelectric polarization of barium titanate single crystals 07 p1234 A67-20096
- Semiconducting properties of ferroelectrics estimating free carrier densities in n and p regions and distributions over plate thickness semiconducting properties of ferroelectrics, estimating free carrier densities in n and p 08 p1367 A67-20314
- Crystal deformation by electrostriction produced by laser beam 08 p1336 A67-20315
- Far IR reflectivity of potassium tantalate analyzed as function of temperature, noting soft mode as temperature lowers towards Curie temperature far IR reflectivity of potassium tantalate 10 p1688 A67-22766
- Dielectric and electro-optic properties of lead magnesium niobate, noting second order ferroelectric transition 11 p1803 A67-24834
- Second order phase transitions in ionic crystals caused by vibronic interaction analogous to Jahn-Teller effect in ideal crystals 16 p2726 A67-30813
- Temperature autostabilizing nonlinear dielectric element /TANDEL/ for electric measurement circuits and measurement transducers 17 p2828 A67-32829
- 180 degree domain formation in ferroelectric crystals unaffected by presence of shorted electrodes due to surface layer properties differing from bulk 19 p3304 A67-35047
- MOS element utilization as impedance transformer at output of ceramic ferroelectric subminiaturized pressure pickup 20 p3435 A67-36323
- Ferroelectric phase shifter temperature compensation, showing reduction in sensitivity by connecting in series two different ferroelectric materials 21 p3679 A67-38219
- Energy densities of polar and antipolar arrays in barium titanate including nonlinear oxygen polarizability 21 p3683 A67-38406
- Photoelectric polarimeter for measuring rotational, electro-optical and electrogyrational effects and optical activity in ferroelectrics 21 p3631 A67-38969
- Ferroelectricity of barium titanate thin films noting dielectric, temperature, polarization and electric field variations 21 p3687 A67-39142
- Nondestructively optically read ferroelectric bismuth titanate single crystal memory device 22 p3767 A67-39261
- Posistors barium titanate, lead titanate and potassium compound semiconductor and ferroelectric properties analyses indicating closely interrelated properties 22 p3801 A67-40215
- Optical properties of new and stable nonlinear optical ferroelectric potassium lithium niobate single crystal 22 p3863 A67-40236
- Pyroelectric effect using single barium titanate crystals with liquid electrodes extending ferroelectric switching time measurements to low fields 24 p4203 A67-42090
- Ferroelectric, electro-optic and dielectric properties of tetragonal potassium-niobate-strontium-niobate crystal 24 p4204 A67-42366
- FERROMAGNETIC FILM**
- Intrinsic damping and eddy current-limited domain wall mobility in Ni-Fe alloy ferromagnetic thin films 02 p0298 A67-11890
- Eddy current damping effect on motion equation of magnetization vector in thin ferromagnetic film switching by coherent rotation 05 p0860 A67-16070
- Temperature and thickness dependence of critical field of superconducting Sn films measured and compared with nonlocal theoretical models 05 p0864 A67-16899
- Equations for longitudinal Faraday and Kerr effects in gyroelectric thin films bounded by nonmagnetic medium, considering multiple inner reflections 05 p0865 A67-16971
- Longitudinal Kerr and Faraday effects in Ni and permalloy films using photoelectric polarization spectrometer, choosing various refractive indices and gyroelectric constants 05 p0865 A67-16972
- Effective triaxial anisotropy in exchange-coupled composite three-layered uniaxial ferromagnetic thin films 07 p1231 A67-19488
- Nucleation during pulse remagnetization of thin films, showing domain structure of formation, growth of nuclei, etc 08 p1367 A67-20603
- Quasi-equilibrium states during pulse remagnetization of thin ferromagnetic films, discussing domain structure 08 p1367 A67-20604
- SHF susceptibility of ferromagnetic thin films for constant magnetic fields far from electromagnet resonance 08 p1367 A67-20605
- Ferromagnetic multilayer systems effect on SHF power transmission and variation of resonator parameter 08 p1368 A67-20606
- Reverse magnetization and energy of anisotropy of single crystal ferromagnetic films 08 p1368 A67-20607
- Interaction between layers of ferromagnetic films of different composition and coercivity separated by insulating quartz layer, obtaining films by vacuum deposition 08 p1369 A67-20811
- Diagonalization procedure for Hamiltonian of ferromagnetic thin film, applying canonical transformation in direction of film thickness 11 p1845 A67-23992
- Physics of thin ferromagnetic films - Conference, Kiev, June 1966 12 p1980 A67-25236
- Resistance of magnetic structure of Ni-Fe thin films deposited on metal substrate with anisotropic surface roughness to effect of orthogonal pulsed fields 12 p1980 A67-25238
- Spin wave theory of thin ferromagnetic films, Curie temperature decreases monotonically with decreasing film thickness spin wave theory of thin ferromagnetic films analyzed, showing Curie temperature decreases 12 p1981 A67-25239
- Magnetic characteristics of ferromagnetic thin films obtained by ferromagnetic and spin wave resonance techniques 12 p1981 A67-25241
- Thermal expansion coefficient of ferromagnetic thin films compared with bulky samples by electronographic technique 12 p1939 A67-25242
- Ferromagnetic film coercive force variation near supercritical state due to film thickness 12 p1981 A67-25243
- Magnetism and Magnetic Materials Conference, Washington, D.C., November 1966 13 p2178 A67-27137
- Associated nonuniform electron-nucleus oscillations in ferromagnetic substances studied to determine feasibility of maser, using magnetic-reversal nuclear magnetic resonance 16 p2686 A67-31731
- Superconductors and ferromagnetic domains proximity effects at critical temperature in resistive and tunneling effect measurements 17 p2912 A67-32271
- Nonvolatile block-oriented random access memory /BORAM/ combining thin magnetic films and scanning strain waves 18 p3012 A67-34347
- Ferromagnetic powder deposition on superconductor surface in vacuum used to obtain magnetic flux distribution in superconductors 23 p4035 A67-40652
- Hall potential difference for thin film in magnetic leakage field of domain interface between ferro- and ferrimagnetic 24 p4204 A67-42457

FERROMAGNETIC RESONANCE

Magnetic characteristics of ferromagnetic thin films obtained by ferromagnetic and spin wave resonance techniques 12 p1981 A67-25241

Width of ferromagnetic resonance curve in nickel and permalloy thin films as function of preparation and thermal treatment techniques 12 p1981 A67-25244

Magnetism and Magnetic Materials Conference, Washington, D.C., November 1966 13 p2178 A67-27137

Ferromagnetic resonance relaxation process in thin films 13 p2179 A67-27142

Temperature dependence of ferromagnetic parallel resonance line width in Ni-Fe alloy films, stressing surface oxidation role 22 p3855 A67-39350

In-plane and out-of-plane ferromagnetic resonance line widths in Ni single crystal platelets noting cubic crystalline anisotropy at 25.92 GHz 22 p3884 A67-40245

FERROMAGNETISM

SA ANTIFERROMAGNETISM

SA BARKHAUSEN EFFECT

Ferromagnetic semiconductors with exchange interaction due to conduction electrons 02 p0296 A67-11826

Galvanomagnetic effect in ferromagnetic metals, developing theory of planar Hall effect in terms of spin-orbit interaction of electrons 03 p0501 A67-14368

Temperature and magnetic field gradient effects on magnetothermomechanical interaction of viscous incompressible ferrofluid with cold wall 04 p0600 A67-14446

Ferromagnetic magnetostatic amplifier using various types of oscillations for pumping and signal amplification 04 p0583 A67-15168

Regenerative thermomagnetic power devices, considering state equations for ferromagnetic material, power cycle and entropy change due to magnetization [ASME PAPER 66-WA/ENER-1] 04 p0555 A67-15414

Nonreciprocal ferrite devices at microwave frequencies, detailing circulator and isolator components 11 p1758 A67-24060

Metrological characteristics of three-component magnetometers with ferromagnetic probes installed in Elektron II space station 11 p1789 A67-24079

Annealing effect on damping rods for magnetic field stabilized satellites 12 p2011 A67-25212

Wideband tank circuit using ferromagnetic core with negative frequency characteristic in induction coil 13 p2071 A67-27277

Perturbation factors in angular correlation function for multidomain ferromagnetic materials determined taking into account magnetic field fluctuations 14 p2371 A67-28728

Magnet consisting of superconductive solenoid of niobium-zirconium wire with ferromagnetic insertions 15 p2422 A67-29127

Ferromagnetic magnetostatic amplifier using various types of oscillations for pumping and signal amplification 15 p2443 A67-29354

Magnetic devices for microwave integrated circuits, discussing ferrite substrate use as medium for microstrip transmission lines 15 p2452 A67-29928

Transient growth of magnetostatic modes in yttrium garnet subject to pulsed longitudinal pumping 16 p2732 A67-31704

Physics of ferro-and antiferromagnetism - Conference, Sverdlovsk, USSR, July 1965 16 p2733 A67-31729

Regenerative thermomagnetic power devices, considering state equations for ferromagnetic material, power cycle and entropy change due to magnetization [ASME PAPER 66-WA/ENER-1] 18 p2989 A67-34128

Magnetic field induced hyperfine structure in mono- and divalent iron ions in magnesium and calcium oxide, showing evidence of paramagnetic resonance 20 p3506 A67-36211

Data and theories on stationary spin waves in ferromagnetic thin layers, considering modes, dispersion law and spectra interpretation 20 p3507 A67-36318

Separation of magnetic noise caused by ferromagnetic bodies in geomagnetic field 22 p3795 A67-39227

Plane circularly polarized magnetoelastic and elastic wave scattering at plane discontinuity surface between ferromagnetic

insulating medium and elastic medium 22 p3856 A67-39364

Ferromagnetic magnetization curve approximated for analytical solutions of boundary value problems in nonlinear electrodynamics, obtaining Riemann functions 22 p3836 A67-39420

Fe rods in Fe-Sb matrix eutectic system, measuring rod diameter and Fe volume fraction effects on magnetic properties 23 p4039 A67-40884

FERRY SPACECRAFT

Titan III system capability for space support and logistics, discussing parameters of assessment 08 p1412 A67-21076

Set of linearized motion equation for ferry vehicle to obtain optimal-thrust during rendezvous attempt with orbital satellite 15 p2571 A67-30049

FET

S FIELD EFFECT TRANSISTOR /FET/

FEYNMAN DIAGRAM

Feynman space-time path formulation of nonrelativistic quantum mechanics applied to classical diffusion problem 03 p0469 A67-13718

Experimental verification of predictions of conventional quantum electrodynamic vacuum effects by Compton and other scattering techniques 09 p1534 A67-22021

Renormalization theory and Compton scattering of electron interacting with monochromatic LF polarized light beam 17 p2870 A67-33365

Integrated and integral Hellmann-Feynman formulas for isoelectronic molecular process energy difference 22 p3757 A67-39637

Nuclear interactions mechanisms analyzed by method allowing comparison with Feynman diagram, determining necessary information for analysis 24 p4193 A67-42859

FIAT G-91 AIRCRAFT

Fiat G91Y and G222 aircraft at Second International Aeronautical Exhibition, Turin, noting performance, physical characteristics and component parts 09 p1439 A67-22092

FIAT G-222 AIRCRAFT

Fiat G91Y and G222 aircraft at Second International Aeronautical Exhibition, Turin, noting performance, physical characteristics and component parts 09 p1439 A67-22092

FIBER

SA BUNDLE DRAWING

SA GLASS FIBER

SA REINFORCING FIBER

SA SYNTHETIC FIBER

Boron nitride fibers in composites for aerospace application, discussing fabrication, ablativity properties, etc 03 p0452 A67-13409

Classical elasticity theory determination of computational error of fibrous body treated as simply connected multiple hole disks 05 p0907 A67-16037

Manufacturing methods for continuous filament refractory fibers including extrusion and chemical vapor deposition 08 p1345 A67-20427

Crystalline structure of amorphous boron fibers noting glass-like nature of fiber as exhibited by diffraction patterns 08 p1343 A67-21313

Elastic moduli of composite with aligned continuous fibers derived from elastic properties of constituents 10 p1715 A67-22859

Fibrous model of shell shaped grid noting discrete network, properties of cross section surface and stress 10 p1715 A67-22920

Fiber aspect ratio, residual stress state and geometry of multifiber arrays studied in terms of influence on local stress concentration and matrix reinforcement 10 p1871 A67-23705

Fiber spacing and array geometry effect on modulus of composites of laminate configurations used in aerospace structures 10 p1729 A67-23768

Heat transfer, thermal conductivity and thermal diffusivity of loose fibrous materials under vacuum 16 p2780 A67-31772

Durability and electrical conductivity of metallic fiber materials noting influence of oxidation on properties 20 p3466 A67-36912

FIBER OPTICS

SA VIDICON

Electromagnetic theory of wave propagation modes in dielectric cylinders applied to coherent light transmission in optical fibers 02 p0190 A67-11528

Fabrication of improved Focons and field flatteners and evaluation of optical performance in terms of modulation transfer

function /MTF/, vignetting and T-number measurements [SMPTE PREPRINT 100-3] 03 p0469 A67-13802

Indirect techniques such as IR and temperature sensing to overcome limitations of hard-wired test points but still monitor complete ensemble of components in built-in test equipment 03 p0388 A67-14216

Passive core fiber laser does not remove completely need for optical quality in cladding material 05 p0821 A67-16666

Coherence properties of light from optical fibers noting applications to interferometry 05 p0825 A67-16979

Measuring atomic radiation and collision cross section coefficients of plasmas 11 p1839 A67-24551

Wideband solar-burst spectrum analyzer noting antenna design and operation 14 p2382 A67-28966

Optical system for earth observation satellite with line-scan television for weather forecasting discussing photometry and fiber optics 16 p2879 A67-31797

Laser-energized explosive device /LEED/ for pyrotechnic device actuation noting power source, ruby laser, metallic fiber-optic conductor, missile design, etc 17 p2803 A67-32437

Performance of fiber-optics coupled cascade image intensifier systems from standpoint of overall system noise, resolution, gain, contrast degradation and information rate 17 p2859 A67-32504

Ruby laser radiation transmission by Crofon plastic fiber optics 17 p2870 A67-33302

Fiber optic window fitted to stainless steel field ion microscope permitting use of direct contact photography for image recording 17 p2863 A67-33354

Spaceborne fiber optics TV system emphasizing image enhanced flexible front end optical assembly 20 p3445 A67-36554

Sensors and display systems covering fiber optics, sensing of parameters for built-in equipment and passive monitors, passive chemical vapor/gas detection, etc 20 p3449 A67-36960

Nondestructive testing of electronic circuits with fiber optic scintillators, vidicon data sampling and pattern recognition displays, discussing TV data handling 20 p3449 A67-36962

FIBER STRENGTH

Fiber strengthening theory, taking into account stress transfer between matrix and fiber in both elastic and plastic regions 03 p0449 A67-13257

Fiberling of oxides by hot deformation in metal matrices of unalloyed columbium or tantalum, preparing composites by powder metallurgy 03 p0441 A67-13273

Fiber-metal composites with properties related by law-of-mixture relationship 03 p0442 A67-13310

Tensile strength affecting factors in metals reinforced with strong fibers 03 p0442 A67-13311

Ceramic material strength improvement by refractory metal fiber reinforcement, noting strontium zirconate-molybdenum systems 03 p0450 A67-13312

Single crystal fiber reinforced composites, discussing use of silicon carbide whisker as interstitial reinforcement 03 p0453 A67-13411

Boron fiber-reinforced aluminum composites fabrication by plasma spraying and tensile testing 03 p0444 A67-13431

Refractory composites consisting of high strength high modulus filaments imbedded in vapor deposited refractory metals 03 p0444 A67-13433

Boron filaments for reinforcement of aluminum alloys used in turbomachinery 03 p0444 A67-13436

Fiber, matrix and interface contributions to composite material improvement 03 p0455 A67-13441

Attachment concepts and problems in fibrous composite aerospace structures 03 p0523 A67-13444

Failure mechanism of ceramic fibers in fiber-metal composites determined by high amplitude fatigue tests 03 p0525 A67-13871

Fiber reinforced metals 03 p0456 A67-13893

Felted fibrous ceramic structures for thermal protection, fabricated by papermaking industry techniques, used for

- forming lightweight porous
structures 04 p0642 A67-15452
- Organic composites reinforced with single
crystal fibers manufactured, using
fiberization of whiskers 05 p0832 A67-16167
- Anisotropy effect on strength of unwoven
glass fiber reinforced plastic, ascertaining
nature of stressed state arising at high
temperature 05 p0912 A67-16183
- High temperature effect on strength of
solidified resins and resin based materials,
determining loss of weight, density,
compression strength, permittivity and
electric conductivity 05 p0833 A67-17098
- Properties of pyrolytically produced boron
fibers, noting strength decrease with
temperature increase 06 p1016 A67-17903
- Hexagonal indexing of tungsten boride
phase in reaction of boron with tungsten
oxide, obtaining X-ray powder diffraction
pattern 06 p1016 A67-17904
- Metallic fibers development, noting
research for continuous filaments, whiskers,
tape fibers, materials, strength,
etc 06 p1019 A67-18558
- Refractory glass fibers composition, fiber
forming characteristics, construction and
operation 07 p1212 A67-20261
- Literature review on effect of static
fatigue on filament wound fiberglass internal
pressure vessels, noting program to test and
expand data 08 p1415 A67-20432
- Void effect on strength of filament
reinforced composite materials 08 p1415 A67-20434
- Fiber reinforced materials for composite
structures noting deformation of metals,
ceramics and glasses 08 p1342 A67-20903
- Mechanical behavior of fiber reinforced
materials, discussing elastic properties,
failure theories, stress analysis, fracture
toughness, structural design, etc 08 p1342 A67-20904
- Fiber reinforced composite material
behavior examined from shear loading tests,
noting finite difference analysis for
representative PDEs 08 p1420 A67-20908
- Fiber reinforced plastics, determining
composite elastic constants in terms of
elastic moduli and geometric parameters of
constituents 08 p1346 A67-20910
- Carbon fibers of high strength and high
breaking strain noting heat treatment,
structure and mechanical properties 09 p1520 A67-21988
- Carbon fiber composite, noting
incorporation into epoxy resin and inverse
correlation of shear strength with fiber
modulus 10 p1671 A67-23495
- High modulus high strength
reinforcements incorporated in epoxy matrix
plastic composites for aerospace structural
use 10 p1671 A67-23704
- Test conditions effects on glass fiber
strength data 11 p1811 A67-24587
- High temperature polyimide
unidirectionally reinforced with silica fiber,
noting precuring process to avoid porosity
and strength degradation 11 p1811 A67-24641
- Fiber reinforced metal coating by passing
silica through molten aluminum, discussing
freezing by radial conduction of heat into
fiber 12 p1954 A67-25292
- Fiber orientation and morphology effect
on anisotropic tensile behavior of Al-Ni
whisker reinforced aluminum, studying
solidification rate, etc 18 p3067 A67-34569
- [ASTM PAPER 3] Fiber shells of revolution under
compression loads analyzed for use in
pressurized balloons 19 p3338 A67-34872
- Parametric expansions in linear theory of
cylindrical shells noting loading and
boundary conditions, approximation
formation, fiber elongation, etc 19 p3339 A67-35054
- High modulus carbon fiber fracture path,
orientation and crystallite size effects on
physical properties 19 p3248 A67-35425
- High strength high modulus carbon fiber
microstructure, studying crystallite size,
orientation effect, electron micrographs and
X-ray diffraction 19 p3248 A67-35426
- Boron filaments mechanical properties and
chemical compatibility compared with nickel
and titanium matrices 19 p3245 A67-35728
- One-dimensional directed continuum
assumed to represent elastic fiber
strengthened string, developing boundary
conditions and constitutive equations 20 p3535 A67-36197
- Testing apparatus for rapid determination
of tensile strength of fine
filaments 20 p3537 A67-36522
- High temperature resistance fibers - ACS
conference, Phoenix, January
1966 21 p3647 A67-37870
- Temperature resistant aromatic ordered
copolyamide fibers, obtaining tensile
properties and radiation
resistance 21 p3647 A67-37871
- Thermostable fibers from ordered
heterocycle amide copolymers tested for
tensile and high temperature
properties 21 p3647 A67-37872
- Fibers of ordered aromatic copolyamides,
performance characteristics and resistance
to degradation at high
temperature 21 p3647 A67-37873
- Structural modifications effect on PBI
fiber critical properties, discussing strain-
stress characteristics, target properties and
crystallization 21 p3648 A67-37875
- Poly/phenylene/hydrazide fibers
mechanical properties, thermal stability and
potential application 21 p3648 A67-37876
- High strength high modulus glass fibers,
discussing mechanical properties and
design 21 p3648 A67-37879
- Laboratory equipment for R and D on
fibrous refractory materials 21 p3649 A67-37883
- High tensile strength high elasticity
modulus graphite fibers preparation from
polymeric fibers for composite
structures 21 p3649 A67-37884
- Continuous filament ceramic fibers via
viscose process involving lattice forming,
spinning, weaving and
firing 21 p3649 A67-37885
- Polycrystalline boron nitride fibers
structure, determining density, defects,
resistance, thermostability, etc 21 p3649 A67-37886
- Composite technology emphasizing fiber-
reinforced metal matrix composites,
discussing filaments, plastics, ceramics,
fabrication methods, etc 21 p3643 A67-37953
- Metal composite materials for higher
temperature resistance utilizing filaments,
fibers and whiskers, discussing machinability
and testing 21 p3643 A67-37954
- Netting analysis of reinforced sheets for
load envelopes which combine tension and
shear, determining optimum fiber
arrangements 21 p3729 A67-39082
- Fatigue in fibers and plastics, use of
cumulative extension testing and time
dependent effects in fatigue tests 22 p3824 A67-39562
- Book on fiber reinforced materials
covering theories, principles and
experimental data noting stress distribution,
fiber orientation effects, etc 22 p3820 A67-39590
- Temperature, fiber compositions and
matrix resin effects on flexural properties
of unidirectionally reinforced short fiber
composites 24 p4175 A67-42422
- FIBERGLASS**
S GLASS FIBER
FIBRIN
In-vivo inactivation of factor VII by
hydrazine in ether anesthetized
rats 07 p1134 A67-19856
- FIELD**
S ANTENNA FIELD
S BOSON FIELD
S CROSSED FIELD
S ELECTRIC FIELD
S ELECTROMAGNETIC FIELD
S ELECTROSTATIC FIELD
S FAR FIELD
S FLOW FIELD
S FORCE FIELD
S GEOMAGNETIC FIELD
S GRAVITATIONAL FIELD
S INTERSTELLAR MAGNETIC FIELD
S MAGNETIC FIELD
S MAGNETOSTATIC FIELD
S MULTIPOLAR FIELD
S POTENTIAL FIELD
S PRESSURE FIELD
S RADIATION FIELD
S SELF-CONSISTENT FIELD /SCF/
S SOUND FIELD
S STAR FIELD
S STELLAR FIELD
S STRAIN FIELD
S TEMPERATURE FIELD
S TENSOR FIELD
S VISUAL FIELD
- FIELD-ALIGNED IRREGULARITY /FAI/**
Radio wave scattering propagation caused
by geomagnetic field aligned
irregularities 01 p0021 A67-10334
- Field aligned currents in magnetosphere
as explanation of geomagnetic fluctuation
localization to region smaller than applicable
hydromagnetic wavelength 08 p1402 A67-21476
- Field aligned structure of ionization
associated with boundaries of spread-F at
middle latitudes studied by combining
topside and fast-sweeping ground-based
ionograms [AGARDOGRAPH 95] 15 p2480 A67-30277
- Diffraction of HF radio waves by
ionospheric layer containing field-aligned
inhomogeneities [AGARDOGRAPH 95] 15 p2482 A67-30291
- Field-aligned irregularities caused by low
energy charged particles penetrating to F
layer heights [AGARDOGRAPH 95] 15 p2484 A67-30304
- Field-aligned irregularities as effect of
increased electron temperature in F-2 layer,
analyzing heat production and loss
mechanism [AGARDOGRAPH 95] 15 p2484 A67-30305
- Super-Alfvénic counterpart of transient
sub-Alfvénic aligned-fields flow past
airfoil 19 p3170 A67-35538
- Guidance of audio-frequency
electromagnetic waves along earth magnetic
field investigated in absence of field-aligned
irregularities of ionization density 19 p3225 A67-35608
- Compressible inviscid fluid MHD motion,
stressing quasi-aligned field
flows 20 p3496 A67-36272
- Ionospheric irregularities field alignment
responsible for radio signal fading analyzed,
showing no evidence for relation to
geomagnetic field 22 p3788 A67-39468
- Field-aligned irregularity instabilities in
ionization vertical gradient, showing unstable
E region for irregularities of scale size 20
m-6 km 22 p3789 A67-39475
- Faraday rotation data from Explorer XXII,
determining atmospheric electron content
for magnetic field aligned ionization layer
location and occurrence 23 p3996 A67-40818
- FIELD EFFECT TRANSISTOR /FET/**
SA METAL OXIDE SEMICONDUCTOR
/MOS/
Insulated gate FET tetrode with high
drain breakdown potential 01 p0033 A67-10025
- Linearity of MOS transistor as variable
resistor improved by keeping substrate
floating and connecting substrate to
drain 01 p0036 A67-10439
- Ferroelectric field effect device having
drain current gate voltage characteristic
reproducing hysteresis character of
ferroelectric gate insulator 01 p0036 A67-10463
- High pinch-off voltage field effect
transistor /FET/ for use as electronically
variable resistor 01 p0036 A67-10474
- Field effect transistors based on
polycrystalline semiconducting layers of CdS
deposited by silk screening 01 p0037 A67-10478
- Indium arsenide thin films for field effect
transistors prepared by coevaporation,
obtaining high Hall mobilities and good
saturation 01 p0039 A67-10876
- Thermal, excess and shot noise in
transducers, examining CW signal generator
method for measuring average noise
factor 01 p0039 A67-11196
- Integratable gyrator using metal oxide
semiconductor and bipolar transistors whose
circuit enables high Q factor inductances to
be derived from low loss
capacitors 01 p0041 A67-11329
- Surface origin of LF noise power
spectrum demonstrated via silicon MOS field
effect structures 02 p0296 A67-11820
- Junction type field effect transistors and
metal oxide semiconductor devices for
switching functions in digital
circuitry 02 p0215 A67-11971
- All-solid state airborne low level PAM
multicoder that employs N-channel FETs for
all analog switching functions of
system 02 p0216 A67-12013
- Equations for small signal sinusoidal
operation of intrinsic field effect transistor,
considering physical principles of operation
of device 02 p0216 A67-12071

DC and RF I-V characteristics, device fabrication and structure of epitaxial depletion mode n-type MOS-FET 02 p0218 A67-12103

Microelectronic applications of silicon-on-sapphire /SOS/ and MOS-FET large scale arrays /LSA/ 02 p0219 A67-12108

Surface state density effect on electron mobility in Si inversion layer of MOS-FET 03 p0496 A67-13577

MOS-FET amplifier RC network design 03 p0382 A67-13670

MOS-FET broadband frequency doubler circuit 03 p0382 A67-13671

Field effect transistor characteristics and operation 03 p0387 A67-14001

Designing with MOS field effect transistors 03 p0388 A67-14182

Very high input impedance direct current chopper amplifier using field effect transistor characterized by very low gate leakage current and capacitance 03 p0389 A67-14378

Transistor and integrated circuits applications including high input impedance amplifier using MOSFET transistor, pulse forming circuit, stable sawtooth generator, etc 04 p0579 A67-14402

Traveling wave field effect transistors, discussing method of increasing transconductance and cut-off frequency 04 p0582 A67-15096

Insulated gate field effect transistors with silicon dioxide and silicon nitride insulation under electron irradiation, noting gate turn-on voltage reduction and source-drain leakage elimination 04 p0588 A67-15713

Space radiation effect on MOSFET and metal-silicon nitride-silicon devices, noting protective methods 04 p0589 A67-15715

Transient gamma ray effect on thin film insulated gate FETs compared with FETs fabricated on silicon 04 p0589 A67-15717

HF measurements of thin film CdSe transistors, discussing equivalent circuit, stability factor and power gain 05 p0776 A67-17091

Small signal admittance parameters of field effect transistors treated as analog RC transmission lines 05 p0777 A67-17298

Pulse response of MOSFET and depletion layer FET 05 p0778 A67-17324

Equivalent circuit for field effect transistor, considering amplifying characteristics of component, noting use of thermal and shot noise 06 p0966 A67-17589

Charge transport equations used to determine transient waveforms of FET as function of gate current and drain current 07 p1153 A67-19614

Read-only memory composed of MOS-FETs on single silicon chip 07 p1155 A67-19845

Transconductance limitation in FET devices obtained through changes in Shockley theory, noting behavior and design of solid state devices 08 p1300 A67-20335

High field mobility degradation effect on characteristics of insulated gate FET, considering drift velocity proportional to field square root and constant drift velocity 09 p1471 A67-21944

Unusual electrode configuration for Hall effect measurements on thin films and field effect devices 09 p1472 A67-21955

Arbitrarily doped four-terminal field effect transistors /large and small signal models/ 09 p1475 A67-22199

Insulated gate to obtain depletion in channel of MOS-FET transistor, noting inversion layer and frequency response 09 p1475 A67-22202

Comparison of electron tubes, transistors and FET noise figures as function of source impedance of generator 10 p1610 A67-22924

Analysis of current flow for different input conditions on double-gate thin film transistor 10 p1612 A67-23373

Electron mobility and lifetime variations effects on drift field in silicon junction devices 10 p1612 A67-23374

Field dependent mobility effects in excess noise of junction gate FETs 10 p1612 A67-23376

Fabrication technique for planar gallium arsenide junction FET and properties 10 p1617 A67-23539

Gallium arsenide insulated gate field effect transistor fabrication techniques and properties 10 p1617 A67-23540

Mesa- and planar-structure gallium arsenide

junction type FETs with diffused n-type channel 10 p1617 A67-23541

Field effect transistor transition from pentode-to triode-like characteristics with increasing drain bias 11 p1759 A67-24138

Test set for automatically compensating for error sources in calculating FET transconductance values 11 p1760 A67-24258

Semiconductor devices for microcircuits, discussing MOS FET, metal base transistor, etc 12 p1918 A67-26208

Field effect kinetics on pure germanium surface, measuring surface conductivity relaxation time by compensation-bridge techniques 13 p2174 A67-26403

Static and dynamic behavior of large pulsed signal behavior of n-type MOSFET below and in constriction /pinch/ region 13 p2076 A67-26487

Anomalous shift in gate threshold voltage of high transconductance p-channel MOSFETs during exposure to space-like radiation 13 p2076 A67-26516

High input impedance obtained with junction transistors, discussing circuit design for different frequency modulators, FET properties and applications 13 p2077 A67-26661

Temperature dependence of small signal AC field effect kinetics in silicon within 170-300 K, considering majority carriers and one energy level theory 13 p2176 A67-26708

Full-wave rectifier using field effect transistor switches 13 p2078 A67-26780

Resonant gate transistor permitting high-Q frequency selection to be incorporated into silicon integrated circuits 13 p2079 A67-26870

Model for shifts in gate turn-on voltage of insulated-gate field effect devices induced by ionizing radiation 13 p2079 A67-26871

Surface fields effect on breakdown voltage of planar silicon p-n junctions 13 p2079 A67-26873

Book on MOSFET covering device theory, characteristics and usage in discrete and integrated circuit form and application to practical circuit design 13 p2079 A67-26997

Evaporated silicon thin-film transistors operating by field effect conductivity modulation of n-type inversion layer at p-type film surface 13 p2083 A67-27573

Transmittance of thin film field effect transistor with equivalent circuit with lumped constants and generalized transfer function of nonparametric amplifier 14 p2286 A67-28586

DC operation of FET at liquid helium temperature noting transfer and drain characteristics similar to those at room temperature 14 p2290 A67-28926

Transconductance and voltage gain of MOS/FET using hafnium dioxide 15 p2442 A67-29171

Magnetic field influence on AC surface field effect in germanium resulting from change in sample conductance and not from change in surface barrier height 15 p2533 A67-29263

Multichannel field effect transistor theory and experiment 15 p2446 A67-29635

Characteristics and mathematical model of junction field effect devices with small length-to-width ratios 15 p2446 A67-29636

Current saturation phenomena in junction-gate field effect transistor 15 p2446 A67-29637

Barrier-layer FET frequency behavior solved, deriving inner transistor quadrupole parameters by way of boundary value problem 15 p2447 A67-29644

MOS transistor HF behavior noting phase shift, frequency dependence, etc 15 p2449 A67-29805

Field effect transistor intrinsic and extrinsic transients, switching behavior and relation to time constant by charge concept 15 p2449 A67-29806

Two-port network design applied to FET in common source and common gate amplifier configuration 15 p2451 A67-29917

Metal oxide semiconductor field effect transistor /MOSFET/ inverter transient response determination, noting mobility dependency on gate voltage 15 p2452 A67-29940

Charge curves for germanium and silicon surface obtained by field effect measurements, noting nature and mechanism of effect 15 p2542 A67-30249

GaAs epitaxial layer in transistors with silicon nitride insulator surpasses silicon

MOS device in power gain, frequency response and temperature range 15 p2455 A67-30399

Field effect behavior of thin InSb film noting semiconductor surface properties mobility decrease with temperature and increase of impurity concentrations 16 p2732 A67-31522

Effects of electric fields and configurations on thermal annealing and radiation hardening of MOSFETs 17 p2916 A67-32833

Electron bombardment effect on insulated gate and junction-gate FETs and MOS 17 p2916 A67-32834

Indicates FET resistance to ionizing radiation 17 p2918 A67-32835

Ionizing radiation effect on field effect MOST transistors, noting irradiation degradations 17 p2919 A67-32855

Design of large scale integrated MOS-FET devices for general logic circuit applications 18 p3014 A67-34555

MOSFET approach to small scale integration of large scale circuits 18 p3014 A67-34555

Bipolar and field effect transistor combinations for high gain amplifiers discussing various circuitries 19 p3191 A67-34943

Epitaxial gallium arsenide FET electrical characteristics, noting structural details and feasibility for use at microwave frequencies 19 p3196 A67-35622

Space environment effects on integrated circuits, discussing FET-MOS type 19 p3196 A67-35677

LF noise in MOS-FET, discussing relationship to drain current and power dissipation 19 p3198 A67-36044

MOS transistors handling, mounting and utilization compared to FETs 20 p3396 A67-36323

Indirect measurement of differential switching parameters examined for admittance matrix of common emitter coupling for field effect and junction transistors 20 p3396 A67-36373

Field effect devices noting insulated gate transistor, thin single crystal silicon film deposition on sapphire single crystal etc 21 p3590 A67-38066

Integrated MOS-FET analog gate for pointing and logic of space telemetry switch 21 p3592 A67-38222

HF noise spectrum of drain and gate currents of junction FET computed from current series expansion 21 p3597 A67-38563

MOSFET gate breakdown nondestructively determined by measurement of leakage component 21 p3598 A67-38577

Junction field effect transistors for onboard satellite equipment, noting resistance to ionizing radiation 21 p3600 A67-38665

MOS-FET signal distortion avoided by taking into account turn-on voltage dependence on source bias 21 p3600 A67-38884

Switching behavior equations derived for FET with solutions applied to MOS and junction gate FET circuits 21 p3602 A67-39066

Frequency limitations of field effect transistor as amplifier in connection with impurity profile, discussing figure of merit 22 p3767 A67-39277

Semiconductor device noise theory emphasizing junction diodes, bipolar transistors and field effect transistors 22 p3770 A67-39777

Radiation effects on bipolar transistor: field effect devices and integrated circuit noting damage in degraded current gain increased saturation voltages and leakage 22 p3772 A67-39866

Direct measurement of transfer curve slope of active quadrupole circuit to determine drain current and gate voltage of field effect transistors 22 p3773 A67-40303

MOSFET integrated circuits for use in analog computers noting simplicity and switching qualities for control of hybrid devices 22 p3775 A67-40466

Book on MOS-FET device operation and characteristics, discussing circuit parameter and digital applications 23 p3983 A67-41766

Performance characteristics of active channel of insulated gate FET for application as high gain HF amplifier 24 p4133 A67-42822

FIELD EMISSION

Zr-coated tungsten cathode in reducing divergence of electron beam 06 p0968 A67-18091
 Second order coherence properties of fluctuating vector electromagnetic fields of arbitrary spectral width, noting dyadic field spectral density and governing differential equations 09 p1460 A67-21587
 Modulated molecular beam apparatus with copper used in conjunction with field emission microscope for studies of atomic interactions with surfaces 09 p1499 A67-22114
 Anisotropy of electronic metal work functions for zero and high electric fields perpendicular to surface measured by field emission and thermionic techniques 09 p1450 A67-22356
 Field emission from sharply pointed CdS single crystals photon-enhanced by excitation from pulsed argon-ion laser 11 p1845 A67-24133
 Gas pressure effect on electrical breakdown and field emission, discussing ion bombardment and whisker formation 11 p1820 A67-24921
 Computer analysis of curve for total emission from group of separate localized emission points on surface of high vacuum metallic cathode 11 p1820 A67-24922
 Frequency multiplication of microwaves by field electron emission in superconducting cavity 14 p2278 A67-27787
 Electron emission current density for superconductors for all conditions between limits of thermionic and field emission 16 p2725 A67-30805
 Barium adsorption on individual crystal planes of tungsten field emitter studied for thermally equilibrated and unequilibrium adsorbate layers 17 p2922 A67-33259
 Epitaxial growth of iron on tungsten field-emission points studied by field-emission microscopy 19 p3302 A67-34938
 Dislocation in field-ion micrograph analyzed by computer-simulated Ranganathan hypothesis using Moore shell model 19 p3266 A67-35603
 Electrical breakdown association with field emission observed through electron microscopy of whiskerlike projections on cathode surface 21 p3589 A67-37824
 Field ion images from single crystals of titanium carbide, noting development of two crystallographic regions 21 p3645 A67-38093
 Field induced photoelectron emission (FPE) from Si surface barrier diodes, discussing FPE measurement using xenon arc lamp and grating monochromator 23 p3980 A67-40890
 Different surface potential barrier models studied for T-F emission current density, energy distribution and Nottingham effect 24 p4201 A67-41893
 Space charge effect on potential barrier in field emission, obtaining expression for work function increase using electrical image method 24 p4201 A67-41894
 Electromagnetic compatibility prediction using statistical descriptions of case emission and susceptibility 24 p4132 A67-42712

FIELD INTENSITY METER

 Field intensities and electron distribution function in hollow cathode, graphs show potential distribution along cathode axis 08 p1358 A67-20851

FIELD MODE THEORY

 Mathematical reliability of model for vibrating field lines used to explain micropulsation observations 07 p1182 A67-19950
 Multimode monopulse feed system optimum aperture distribution determination, obtaining maximum rate of signal change on axis 22 p3763 A67-40313
 Dominant mode field reflection at air-ferrite interface junction in anisotropic rectangular waveguide, deriving singular integral equations for discontinuity problem 23 p3973 A67-40880

FIELD STRENGTH

SA ELECTRIC FIELD STRENGTH

SA MAGNETIC FIELD INTENSITY

 Field distribution at bends in circular zero-normal H and cylindrical surface waveguides 04 p0586 A67-15635
 Field strength measurements in multipath field using linear and circular probing 07 p1142 A67-19448
 Standing wave solution of homogeneous waveguide field distribution for H-10 wave after conformal mapping and effect of capacitive and inductive irises 10 p1607 A67-23571
 Satellite-emitted short radio wave field intensity and ionospheric parameters 11 p1751 A67-24071
 Igneous rock suitability for determination of ancient geomagnetic field intensity, discussing theory, application and results 11 p1788 A67-24697
 Periodic field strength variations during sunrise on vlf signals in long path propagation noting amplitude minima and stepwise phase increase 16 p2630 A67-31849
 Modal interference of VLF radio waves investigation from field strength data, noting isotropic case 16 p2631 A67-31850
 Airborne field strength measurements in NPM antipode region noting variation with inverse square root of distance over sections of antipodal area 16 p2631 A67-31855
 Oxygen caused bright spots in field ion microscope patterns of tungsten, noting oxygen variation effects 16 p2693 A67-31873
 Antenna field strength measurement above 1 GHz, discussing formulas for high accuracy gain determination, multipath interference and antenna separation 17 p2815 A67-32609
 Multiple-photon ionization of atoms and molecules in strong varying electromagnetic field, measuring ionization probability dependence on field intensity 19 p3265 A67-35164
 Winter anomaly of ionospheric adsorption studied by field strength recordings 21 p3617 A67-38001
 Electrical characteristics of thin triangular barium titanate crystals in strong electric fields 22 p3859 A67-39579
 Three-photon combination process used to increase laser emission frequency, determining laser field strength 22 p3815 A67-39760
 MF surface wave launching over earth, considering field strength at ground for given radiated power 22 p3763 A67-40315
 Radio wave field strengths received at Ahmedabad from Tashkent and solar X-ray emission effect, noting field strength increase with solar activity 23 p4051 A67-40915
 Field strength data correlation with meteorological cyclonic parameters, noting possible prediction of scatter signal losses during frontal disturbances 24 p4124 A67-42823

FIELD THEORY

SA FUNCTION SPACE

SA QUANTUM ELECTRODYNAMICS

SA QUANTUM THEORY

SA RELATIVITY THEORY

SA UNIFIED FIELD THEORY

 Exact and approximate solutions to Cauchy problem for nonlinear wave equation in affine connection field theory 03 p0457 A67-13171
 Phenomena accompanying geomagnetic field reversal, using measurements performed on samples of core Papagayo 3G 04 p0617 A67-15543
 Cosmological solutions of linear field theory, showing possible representation in form of hypersurface of second degree in five-dimensional affine space 05 p0897 A67-16773
 Variational derivations of field equations for relativistic mechanical, EM and gravitational fields in space-time continuum 06 p1033 A67-18582
 Dynamo mechanism for formation of stellar magnetic field, considering effects of EM radiation emission and celestial body rotation 06 p1089 A67-18773
 Point source detection using signals propagating in quantum field, in terms of correlation functions of thermal field fluctuations 07 p1142 A67-19585
 Cosmological principle and field equations used in analysis of Einstein, de Sitter, Friedmann and Hoyle-Narlikar models 09 p1563 A67-21652
 Relativistic electrodynamics of moving medium, discussing Maxwell-Minkowski equations, Born equations, field vector transformations, etc 09 p1533 A67-22449
 Magnetic moment variations of charge in combination static magnetic and HF field 10 p1683 A67-22843
 Dynamic effective stiffness theory of layered and unidirectionally fiber reinforced

composites, detailing field equations for laminated composite 10 p1724 A67-23708
 Fundamental field equations of continuum thermomechanics derived from balance of energy equation and entropy production inequality, using invariance considerations 11 p1819 A67-24533
 Soviet papers on quantum field theory and hydrodynamics 13 p2105 A67-27410
 Eigenstates of particle mixing matrices and relation to physical antiparticles 16 p2705 A67-31565
 Wave surfaces of Einstein-Schrodinger theory and nonlinear electrodynamics brought together using antisymmetric tensor 18 p3078 A67-33688
 Kerr metric as Einstein field equations solution, considering Synge g method as possible Kerr metric source 20 p3486 A67-37089
 Faster-than-light particles with spacelike four-momentum within special relativity theory, discussing quantum field theory rejection of objections 20 p3486 A67-37091
 Soviet book on electromagnetic and gravitational fields theory based on relativity theories 20 p3486 A67-37207
 Relativistic elasticity, discussing solution of field equations in transient unidirectional motion 20 p3486 A67-37279
 Point source detection using signals propagating in quantum field, in terms of correlation functions of thermal field fluctuations 20 p3384 A67-37322
 Gravitation theory, general theory of relativity, field theory and gravitational interactions with elementary particles 22 p3879 A67-39294
 Cosmology and elementary particles, noting relationship hypothesis between cosmological asymmetry and particles via vacuum 22 p3880 A67-39337
 Oscillating relativistic universe model from Einstein field equations, discussing Friedmann model matter and velocity distribution, Hubble law and universe volume oscillating relativistic universe model from 22 p3892 A67-40496
 Vector field theory of time dependent backscatter from distant slightly rough sphere for pulsed and sinusoidally steady state sources 23 p3974 A67-41200

FIGHTER AIRCRAFT

SA VTO FIGHTER AIRCRAFT

SA YF-12 AIRCRAFT

 Next generation interceptor aircraft to follow F-106A, including YF-12A and evolving F-111B, would serve largely as missile launching platforms 04 p0550 A67-14422
 Aircraft sizing methodology and hover control comparative analysis on V/STOL fighter-bomber using lift plus lift cruise propulsion [AIAA PAPER 67-133] 06 p0948 A67-18358
 Spin characteristic of fighter type aircraft investigated by using Kerr criteria, noting yawing velocity and recovery 09 p1439 A67-21836
 Supersonic combat biplane airframe, power plant, fuel, control and escape system, instrumentation and weapons system 13 p2052 A67-26420
 Electronic systems for V/STOL fighter aircraft, considering operational capabilities, reliability, maintenance and protection 17 p2795 A67-32032
 German VJ101C VTOL fighter aircraft design and testing, with description of engines and telemetric testing 19 p3173 A67-35522
 Frequency response of longitudinal control transmission of transonic aircraft 19 p3176 A67-35570
 Cost effectiveness of digital and voice accident recorders in small fighter and military aircraft for low level missions, reconnaissance, flight testing and training 21 p3631 A67-39129
 Performance and design parameters for VTOL fighter aircraft engine and wings, stressing takeoff weight factor 23 p3935 A67-41316
 Variable sweep pivoted wing fighter aircraft structural and aerodynamic design considerations, noting journal bearing endurance and aircraft fatigue life [SAE PAPER 670881] 24 p4094 A67-42015

FIGURE OF MERIT

 Figure of merit as evaluation criterion for HF transistors, using unidirectional available

power gain 04 p0585 A67-15501
Improved expressions for efficiency of infinite stage thermoelectric heat pump and generator 15 p2422 A67-29639
Frequency limitations of field effect transistor as amplifier in connection with impurity profile, discussing figure of merit 22 p3767 A67-39275

FILAMENT
SA HEATING EQUIPMENT
Coupling mechanism in passive Q-switching operation between filaments at different regions of ruby laser rod 01 p0090 A67-10813
Negative resistance and current density in double-injection filaments in seminsulating Si 02 p0298 A67-11886
Filament-matrix interactions in metal matrix composites considered as liquid phase layer formation by interdiffusion 03 p0442 A67-13309
Technique for producing continuous metallic filaments with diameter of less than 7.5 microns and composites 03 p0443 A67-13408
Mechanical properties of continuous filament-graphite matrix composite in 0.50 inch diameter rod form, discussing limitation of binder phase and interface 03 p0453 A67-13412
Laminate optimization for filamentary composites, discussing applied spectrum of load requirement 03 p0453 A67-13413
Potential payoffs of using high modulus filament reinforced composite materials in aerospace systems applications discussed in light of development programs 03 p0443 A67-13414
Boron-modified SiC continuous filament fabrication by vapor deposition on hot W wire substrate and tensile testing 03 p0454 A67-13423
Contact angle measurements for epoxy resin on boron filaments, demonstrating surface treatment effects 03 p0429 A67-13427
Surface treatment and interface stability of boron filaments reinforcing plastic composite materials 03 p0455 A67-13428
Tensile test equipment and methods to determine modulus of elasticity and ultimate tensile strength of single boron filaments at room and elevated temperatures 03 p0455 A67-13445
Temperature fluctuation in AC heated filaments and magnitude and phase of harmonic components of temperature 04 p0723 A67-15117
Current pause during circuit overloading accompanied by filament explosion 06 p1031 A67-17867
Coated filaments effect in controlling composite microstructures for several metal-graphite and metal-boron systems [AIAA PAPER 67-175] 06 p1019 A67-18441
Filament-metal matrix composite material research, considering reinforcement and binder 06 p1019 A67-18657
Filamentary reinforced resin matrix composite materials for high specific strength and specific modulus necessary for aircraft structures 08 p1333 A67-20359
Triangular low filament laser diodes, considering alteration of internal reflection to achieve phase shift phenomena 10 p1662 A67-22716
Youngs modulus and shear modulus of inorganic filaments of tungsten and boron measured by oscillation technique 13 p2144 A67-27187
Thermal conductivities of unidirectional composite materials parallel and normal to filaments, using analogy to shear loading response 14 p2404 A67-28099
Elastic moduli of composite materials with anisotropic filaments 14 p2398 A67-28101
Induced argon discharge shown to have shape of plasma filament, noting detachment from chamber walls 17 p2897 A67-32176
Filament-metal matrix composites for high temperature range, discussing kinetic phenomena [ASTM PAPER 1] 18 p3066 A67-34567
Flexible filament under transverse impact from sphere, considering friction forces 19 p3341 A67-35704
Testing apparatus for rapid determination of tensile strength of fine filaments 20 p3537 A67-36522
Stress distribution in imperfect filamentary composite material 20 p3474 A67-37270
Boron filament behavior in rotating-beam

fatigue test 20 p3470 A67-37390
Dispersion relations for elastic wave propagation in filamentary composites obtained, establishing averaging rules for elastic constants 21 p3729 A67-39055

FILAMENT WINDING
Boron filaments for possible use as reinforcing phase in composite materials for aerospace structures 03 p0452 A67-13407
Fracture mechanism in continuous filamentary composites 04 p0641 A67-14832
Concentrated tensile stresses induced by concentrated external loads applied to boundary of filament winding rectangular strip plate 05 p0914 A67-16216
Local buckling strength of high strength axially compressed maraging steel cylinders circumferentially prestressed with high strength epoxy-protected fiberglass filament windings 05 p0923 A67-17211
Filament winding techniques and design for thin wall cylindrical pressure vessels 06 p1006 A67-17622
Performance-weight relations and shape parameters for Maxwell structures design, considering filament wound isotensoid container and tension shell decelerator 06 p1111 A67-18884
Boron filament epoxy resin composites test program relative to mechanical design of reentry vehicle 08 p1345 A67-20424
Manufacturing methods for continuous filament refractory fibers including extrusion and chemical vapor deposition 08 p1345 A67-20427
Literature review on effect of static fatigue on filament wound fiberglass internal pressure vessels, noting program to test and expand data 08 p1415 A67-20432
Fabrication of complex hollow rib reinforced structures of wound boron filaments and anhydride cured epoxy resin for reentry vehicle application 08 p1345 A67-20435
Glass filament wound interlaminar shear specimen design and instrumentation 11 p1875 A67-24614
Filamentary materials for wound structures, particularly rocket motor cases, noting fabrication equipment, physical properties, etc 11 p1811 A67-25008
Filament wound sleeve seal impregnated with solid lubricants dissipates heat in rubbing contact zone and provides wear characteristics for use in air compressor [ASLE PREPRINT 67AM 7A-3] 14 p2326 A67-28791
Design considerations in material selection for rocket motor cases, considering fracture toughness, ductile-failure resistance and buckling under flight loading [AIAA PAPER 66-630] 15 p2573 A67-29418
Tension string structure of high strength filaments for ultralightweight planetary entry vehicle 15 p2573 A67-29420
Filament overwrapped metallic cylindrical pressure vessels show greater efficiency ratio and buckling strength 17 p2958 A67-32054
Tension and compression, dynamic and static flexural loading and vibration tests of bilaminate filament wound composite [SESA PAPER 1219] 18 p3141 A67-33889
Metal lined glass filament-wound pressure vessel performance at cryogenic temperatures, discussing fibers, resins and liners [ASTM PAPER 17] 18 p3067 A67-34578
Shells of revolution produced by fiber-wound distributing internal and boundary stresses uniformly over fiber contours 19 p3337 A67-34871
Stress analysis by polar coordinate system of turbine disks produced in various wound-fiber configuration 19 p3234 A67-34873
High modulus high strength inorganic filament windings tested for tension and buckling-critical structures, considering weight decrease and operating temperature increase 19 p3245 A67-35553
Continuous filament ceramic fibers via viscose process involving lattice forming, spinning, weaving and firing 21 p3649 A67-37885
Adhesives to bond metal linings to filament-wound cryogenic pressure vessels evaluated by test series simulating fabrication and service conditions 23 p4010 A67-41347
Textile fabrication methods produce

multidirectional materials, describing commercial use of 3-D materials 24 p4176 A67-42424
Boron and graphite filament-resin composites tensile and interlaminar shear strengths and Al foil liner cyclic life in cryogenic pressure vessel tests 24 p4176 A67-42470

FILLER
SA PRIMER
SA RESIN
Axisymmetric bending of circular sandwich plates with lightweight compressible filler subject to special transverse or local loads 05 p0922 A67-17175
Filler effects on deformation and rupture of amorphous gum elastomers with various molecular structures, noting failure envelopes [JPL-TR-32-922] 08 p1420 A67-20892
Elastic filler effect on thin cylindrical sandwich shell stability subjected to compression along generatrix 12 p2023 A67-25592
Axisymmetrical stability loss problem in thin walled cylindrical shell with continuous elastic filler 12 p2031 A67-25958
Alpha-beta Ti alloys weldability, considering underwater applications 14 p2327 A67-28821
Viscoelastic behavior of pure gum rubbers and relationship between filler characteristics and mechanical properties of inert filled *composite materials 19 p3249 A67-35888
Three layer cylindrical shell stability in elastic and inelastic domains under separate and joint loads, considering filler layer deformation 21 p3727 A67-38840
Emergency dental kit for prolonged space flight, discussing filler materials 23 p3965 A67-41564

FILM
SA COATING
SA FERROMAGNETIC FILM
SA HELIUM FILM
SA MAGNETIC FILM
SA METAL FILM
SA OXIDE FILM
SA PHOTOGRAPHIC EMULSION
SA PHOTOGRAPHIC FILM
SA PLASTIC FILM
SA SILICON FILM
SA SOLAR ENERGY ABSORPTION FILM
SA THERMOPLASTIC FILM
SA THICK FILM
SA THIN FILM
Gas mixture component concentration in fluid film flowing down wall, determining quantity of gas component transported by fluid per unit time 13 p2094 A67-26836
Plasma spray gun as possible method of applying resin, ceramic and metallic bonded solid film lubricants [ASLE PREPRINT 67AM 7A-4] 14 p2326 A67-28792
Holographic exposure times controlled by direct viewing of reconstructed image during exposure 18 p3048 A67-34012
Sensitivity of film with and without image intensifier compared, using emulsion densities as function of number of incident quanta 22 p3796 A67-39278

FILM BOILING
Automatic control of evaporation and deposition of thin films under vacuum 01 p0078 A67-10295
Pool film boiling based on cellular model postulating time-averaged cell configuration to adjust itself to maximize rate of heat transfer 04 p0734 A67-15841
Theoretical dimensionless correlation for vaporization times of drops in film boiling on flat plate in Leidenfrost state 04 p0734 A67-15856
Radiation effects on heat transfer and friction characteristics in natural and forced convection film boiling in boundary layer flows [ASME PAPER 66-WA/HT-6] 04 p0739 A67-15933
Film boiling of saturated nitrogen flowing upward in vertical heated tube, noting annular-flow regime change to vapor matrix [ASME PAPER 65WA/HT-26] 08 p1427 A67-21311
Electric analog simulation of periodic nonuniform heat transfer mechanism in film boiling from coated plate 08 p1427 A67-21322
Heat transfer data obtained from film

boiling for four liquid compositions, using flat plate geometry 10 p1732 A67-22729

Method Surface film boiling under free convection 13 p2222 A67-26532

Pool boiling of methane over pressure range from 1 atm to critical pressure in both nucleate and stable film boiling regimes 13 p2229 A67-27667

Heat transfer process for film boiling taking into account growth of prominences up to bubble departure and Taylor instability 18 p3160 A67-34162

Heat transfer characteristics of several aliphatic hydrocarbons in nucleate and film boiling during forced flow in heated tubes [ASME PAPER 67-HT-7] 20 p3544 A67-36705

Laminar film boiling on thin wire, determining heat-transfer coefficient and vapor dome spacing and diameter [ASME PAPER 67-HT-62] 20 p3549 A67-36744

Film boiling of potassium on horizontal plate, discussing heat fluxes relationship to Berenson equation and heat transfer [AICHE PAPER 28] 20 p3552 A67-36832

Relative velocity effect on vaporization times and heat-transfer coefficients of water droplets in Leidenfrost film boiling on heated rotating wheel [AICHE PAPER 32] 20 p3552 A67-36833

Forced convective film boiling heat transfer to H studied from experiments on cooling down Cu test section by liquid 22 p3918 A67-40092

Boiling heat transfer to liquid helium, discussing heat flux as temperature difference function and surface finish effect 22 p3920 A67-40390

FILM CONDENSATION

Field effect transistors based on polycrystalline semiconducting layers of CdS deposited by silk 01 p0037 A67-10478

Radial distribution analysis of films of bismuth and gallium prepared by low temperature condensation for electron diffraction tests 01 p0137 A67-11060

Radial distribution analysis of films of Pb-12 percent Bi and beryllium in metastable phases prepared by low temperature condensation for electron diffraction tests 01 p0137 A67-11061

Transient forced convection laminar film condensation on horizontal plate, noting film thickness changes and heat-transfer coefficient variations 01 p0168 A67-11229

Nucleation theories, emphasizing relation with oriented growth of thin films condensing on solid foreign substrate 02 p0285 A67-11702

Condensation mechanism and effect on physical properties of thin films 02 p0285 A67-11704

Surface structure effect of evaporation deposited film and substrate crystal on epitaxy of film studied by electron diffraction and electron microscope 02 p0286 A67-11710

Quantitative in situ X-ray diffractometer investigations of evaporated metal films and after annealing treatments ranging up to 370 degrees C 02 p0287 A67-11713

Optical properties of evaporated barium films investigated at various wavelengths, using ultrahigh vacuum reflectometer 03 p0499 A67-13909

Condensation heat transfer in presence of noncondensables, interfacial resistance, superheating, variable properties and diffusion 04 p0720 A67-14644

Grain oriented growth in beryllium condensates, discussing acicular structure of transverse sections of films 04 p0641 A67-15979

Effect of donor Zn and Cd additions and acceptor Se and Te additions on rate of growth and morphology of epitaxial GaAs films grown from gas phase by chemical reaction 06 p1047 A67-17552

Photovoltaic effect in cell prepared by CdTe film deposition and copper telluride flash evaporation 08 p1285 A67-20733

Heat-transfer coefficients during dropwise condensation on randomly distributed nucleation sites analyzed through computer simulated model 08 p1426 A67-20925

Formation of hydride zinc film on titanium activated for deposition of galvanic coating 14 p2336 A67-27868

Critical temperatures and phase composition of films obtained by vacuum

deposition of sublimed cadmium telluride 15 p2537 A67-29706

Gold, silver, copper and tin condensed films, investigating dependence of structure and conductivity on substrate material 15 p2540 A67-30122

Density, crystallinity and electric properties of thin metal films deposited on rotating cylindrical substrate 16 p2727 A67-30899

Heat transfer by dropwise condensation, evaluating average heat flux 17 p2969 A67-32447

Nusselt results concerning heat transfer extended to include surface tension effect on heat transfer coefficient 17 p2970 A67-32461

UV spectrophotometer for continuous measurement in vacuum systems of polyphenyl diffusion pump fluid film thickness 23 p4004 A67-41358

Critical temperatures and phase composition of films obtained by vacuum deposition of sublimed cadmium telluride 24 p4199 A67-41776

FILM COOLING

Turbulent heat transfer to noncircular throat bodies with and without water film cooling 04 p0728 A67-15803

Film cooling technique for color photographs of astronomical objects to diminish effects of reciprocity failure and increase light sensitivity 06 p1002 A67-17975

Film cooling by helium secondary flow injection into incompressible low speed airflow in turbulent boundary layer above flat plate 06 p1116 A67-18385

Film cooling data correlation using boundary layer model 08 p1427 A67-20930

Film cooled rocket engine efficiency and effects of distribution of fuel mixing ratio and characteristic velocity on performance 09 p1559 A67-22094

Cooling and heating effectiveness of plane surface in turbulent air flow by injection of air film, noting temperature effect 11 p1881 A67-23898

Wind tunnel studies of heat shield over plane surface with film cooling during injection through two tangential slots 11 p1884 A67-25055

Relationship between effectiveness of film cooling, free stream Reynolds number, slot Reynolds number and angle of injection 14 p2408 A67-28816

Film cooling theory applied to aircraft gas turbine chambers shows slot geometry effect as negligible 17 p2967 A67-32126

Argon arc plasma generator with film cooled anode for producing stable high temperature gas jet [ASME PAPER 67-HT-72] 20 p3498 A67-36752

FILM THICKNESS

Superconductivity of nondegenerate semiconductor thin films, dependence on current carrier concentration, impurity level positions and film thickness 01 p0128 A67-10084

Vacuum evaporation of HgTe thin film, examining thermal treatment, electric properties as function of thickness, etc 02 p0280 A67-11463

Peculiarities of substructure of thin metal films produced by condensation in vacuum studied by multibeam interferometric technique 02 p0285 A67-11706

Electron microscopy study using replica technique of cross section of films of Al and Si vacuum deposited on glass substrates reveal columnar growth of polycrystalline film 02 p0287 A67-11712

Correlation of X-ray diffraction lines of thin films with theoretical forms of films made from large crystals in thin slabs of uniform thickness 02 p0287 A67-11714

Film thickness determination by balance/oscillating crystal and multiple beam interferometry methods and steam-jet thickness methods 02 p0288 A67-11720

Interferometric technique for measuring thickness and optical constant of thin antimony trisulfide films 02 p0288 A67-11721

Karmers-Kronig dispersion relationship for simultaneous determination of index and thickness of thin metallic film 02 p0289 A67-11726

Index and thickness of absorbant thin film determined from reflection and transmission coefficients 02 p0289 A67-11727

Film thickness dependence of photoelectric effect of surface and volume

in single electron excitation by photon absorption 02 p0289 A67-11729

Photoelectric emission of metal films with electronic structure evolving with film thickness 02 p0290 A67-11731

Plasma oscillation properties, excitation and attenuation in films of various thickness, noting electron excitation 02 p0290 A67-11736

Hall coefficient dependency on thickness of semiconducting thin metal films 02 p0294 A67-11757

Conductivity, Hall coefficient and magnetoresistance of monophase InSb films as function of film thickness 02 p0295 A67-11765

Intrinsic damping and eddy current-limited domain wall mobility in Ni-Fe alloy ferromagnetic thin films 02 p0298 A67-11890

Gear lubrication fundamentals and principles of oil film formation on mating gear tooth surfaces 02 p0250 A67-12499

Resistivity, temperature coefficient of resistivity and Hall coefficient as function of bismuth film thickness, showing that size quantization of films leads to semiconductor metals 02 p0300 A67-12509

Paint film thickness of spacecraft coatings, effect on spectral directional reflectance and binormal transmittance in far IR [AIAA PAPER 65-653] 03 p0447 A67-13033

Turbulent annular airflows in turbulent film lubrication of high speed bearings [ASME PAPER 66-LUB-14] 03 p0403 A67-13755

Turbulent lubrication analysis in fluid film theory and turbulent shear flow, with application to bearings [ASME PAPER 66-LUB-12] 03 p0431 A67-13761

Helium 2 film free convection heat transfer, discussing mathematical analysis for vertical flat plate and horizontal circular cylinder [ASME PAPER 65-WA/HT-10] 03 p0536 A67-14007

Attenuation length of photoexcited electrons in evaporated layers of CuBr estimated by measuring photoemission yield as function of thickness 03 p0500 A67-14332

Epitaxial growth of SiC film on silicon substrate and electron diffraction analysis of crystal structure 04 p0675 A67-14762

Quartz crystal oscillator measurements of effect of film deposition rate on resistance of chromium thin films 04 p0675 A67-14921

Schottky emission as rate limiting factor in thermal oxidation of metals 04 p0677 A67-14947

Electron diffraction scanner structural analysis of Ta and Mo very thin film growth 04 p0677 A67-15101

Electrical properties of thin and thick resistive films vacuum-deposited and nonvacuum-deposited by chemical and firing process 04 p0682 A67-15485

Electron diffraction patterns for GaP semiconducting thin films deposited on indium oxide substrates, determining structure as function of film thickness 04 p0686 A67-15970

Thin film refractive index and thickness calculated by ellipsometry 05 p0847 A67-16796

Temperature and thickness dependence of critical field of superconducting Sn films measured and compared with nonlocal theoretical models 05 p0864 A67-16899

Change in temperature conditions during growth of epitaxial germanium films from molecular beam in vacuum 06 p1046 A67-17551

Device for controlling thickness of thin films prepared by sputtering in vacuum 06 p1003 A67-18195

Tunneling measurements of energy gap anisotropy in thick and thin superconducting films of Al, Pb, In and Sn 06 p1052 A67-18571

Spectral transmission of far IR Michelson interferometer with dielectric film beam-dividers 06 p1005 A67-18716

Pressure distribution between lubricated rolling bearings, comparing static and dynamic stresses in cylindrical disks, noting film thickness 08 p1333 A67-20361

Ferromagnetic multilayer systems effect on SHF power transmission and variation of resonator parameter 08 p1368 A67-20606

Thick film hybrid microcircuit technology, fabrication and performance characteristics 08 p1301 A67-20790

Load and friction torque of Rayleigh step film scheme applied to journal bearing, using Reynolds equation [ASME PAPER 65-WA/LUB-2]

08 p1335 A67-20917
Silicon oxide film thickness determined from intensity of reflected light 09 p1553 A67-21954

Electronic carrier transport in semiconductor films, stressing active thin film devices and typical behavior 09 p1555 A67-22111

Film thickness effect on pressure generation of parallel surface thrust bearing investigated, using dynamic instrumentation mounted in moving surface 09 p1505 A67-22192

Film thicknesses in elastohydrodynamic lubrication by silicone fluids obtained from oscillatory shear related to continuous shear 09 p1506 A67-22193

Selective surface obtained experimentally by deposition of stack of thin layers 09 p1558 A67-22599

Leakage and optimum film thickness of gas lubricated high-pressure mainshaft seals for jet engine compressors 10 p1658 A67-22705

Magnetically coupled superconducting films, showing fluxon size as function of film thickness 10 p1696 A67-23774

Wall creeping in thin magnetic Ni-Fe films analyzed as function of thickness, field pulse amplitude, etc, comparing results with existing theories 11 p1845 A67-23953

Thermoelectric power of thin layers of bismuth in thermocouple with solid copper 12 p1978 A67-25151

Spin wave theory of thin ferromagnetic films, Curie temperature decreases monotonically with decreasing film thickness spin wave theory of thin ferromagnetic films analyzed, showing Curie temperature decreases 12 p1981 A67-25239

Ferromagnetic film coercive force variation near supercritical state due to film thickness 12 p1981 A67-25243

Nucleation of titanium and titanium oxide thin films correlation to thickness obtained from fluorescent intensity measurement 12 p1981 A67-25276

Oriented growth of thick films of CdTe deposited on quartz plates in vacuum, discussing photovoltaic effect 12 p1982 A67-25450

Volt-ampere characteristics effect on thickness of contact materials of some heterojunctions and band structures obtained by epitaxial deposition 12 p1983 A67-25515

Thermal radiation properties of oxide films of variable thickness on metal substrates, using radio-recording spectrophotometer at various wavelengths [AIAA PAPER 67-286] 12 p1958 A67-26003

Recrystallization of Ge and Si thin films and structural changes due to electron bombardment and thermal annealing 13 p2177 A67-27071

Hydrodynamic lubrication in face seals, discussing mechanism of fluid film, surface roughness, wear, leakage, thickness, temperature, pressure, etc [BHRA PAPER E5] 14 p2324 A67-27889

Superconducting indium-bismuth alloy films immersed in strong magnetic fields parallel and perpendicular to surface, studying film thickness effect by tunneling technique 14 p2371 A67-28723

MOS oxide-film thickness estimation by extrapolating MOS capacitance-voltage curve into accumulation region at high negative bias 15 p2539 A67-29815

Thick film hybrid modules discussed for speed, circuit, power density and versatility 16 p2641 A67-31618

Variation of friction and wear of solid lubricant film with thickness theory based on junction and wear particle size 16 p2683 A67-31751

Reflectance and optical constants of evaporated iridium films measured in vacuum ultraviolet 16 p2733 A67-31878

Admissible film thickness in probe measurements of electrical conductivity of semiconductor samples 17 p2910 A67-31928

Characteristics of photovoltaic solar converters, discussing drift field, wrap around and epitaxial webbed silicon cells, minimum film thickness and radiation damage 17 p2801 A67-32048

Silicon oxide and nitride film thickness determined with interference technique, using spectrophotometer in UV and visible wavelength range 17 p2854 A67-32191

Current-voltage characteristics of clamped metal/p-silicon diodes 18 p3009 A67-33475

Volt-ampere characteristics effect on thickness of contact materials of some heterojunctions and band structures obtained by epitaxial deposition 18 p3103 A67-34446

Thin semiconductor layers, studying surface conductivity variation with semiconductor thickness and surface band curvature 19 p3299 A67-34759

PbTe thin films vacuum-vaporized onto amorphous or oriented substrates studied for crystallographic properties as function of deposition temperature, film thickness, etc 19 p3304 A67-35422

Sliding friction between spherical steel rider and gold-plated steel flat measured for varied loading, steel combinations and gold film thicknesses 19 p3237 A67-35837

Sensitivity of single-mirror schlieren system, deriving expression relating film density change with angular light deflection 20 p3441 A67-36400

Operation of Hall generator with variable thickness active layer 20 p3401 A67-37220

Sputtered films stable fcc modification of several metals deposited at high temperatures, obtaining normal structures over 400 degrees C 21 p3677 A67-38091

Thick film design considerations covering material and micropart selection, circuit cost, reliability, substrate size and delivery schedule 21 p3596 A67-38346

Natural vibration frequencies of cylindrically orthotropic circular plate with linearly variable thickness, solving differential equation of motion 21 p3728 A67-38898

Extent of lubricating film for which oil flow is plane, discussing lubricant compressibility, heat release, load capacity and pressure distribution 22 p3811 A67-39317

Destructive and nondestructive testing of thickness of oxide coatings on Al and Al alloys 22 p3798 A67-39552

Test procedure for Si microcircuit production consisting of bulk and junctions electric measurement, oxide thickness and junction position measurements 23 p3977 A67-40660

Temperature effect on structure of W films prepared by triode pulverization at low pressure and low power 23 p4041 A67-41194

UV spectrophotometer for continuous measurement in vacuum systems of polyphenyl diffusion pump fluid film thickness 23 p4004 A67-41358

Deposited Al layer thickness on Si determined using X-ray spectrometric technique 24 p4200 A67-41803

Spectral reflectance of water and carbon dioxide cryodeposits in vacuum integrating sphere as function of incidence angle, substrate material and cryodeposit thickness 24 p4253 A67-42046

Parasitic torques of squeeze-film cylindrical journal bearings in output axis of high performance gyroscopes, discussing tolerance errors [ASME PAPER 67-LUB-5]

24 p4162 A67-42669
Bounded variation method for optimum load capacity hydrodynamic one-dimensional gas slider bearing, discussing film thickness [ASME PAPER 67-LUB-6]

24 p4162 A67-42670
Analysis divided into step and ridge regions used to obtain linearized PH solution to Reynolds equation, neglecting side leakage [ASME PAPER 67-LUB-17]

24 p4163 A67-42676
Film thickness, pressure distribution and load carrying capacity of loaded line contact in presence of viscoelastic lubricant noting high pressure spike [ASME PAPER 67-LUB-23]

24 p4163 A67-42681

FILTER
SA ADAPTIVE FILTER

SA AIR FILTER

SA BAND PASS FILTER

SA ELECTRONIC FILTER

SA FLUIDIZED BED

SA HIGH PASS FILTER

SA IMAGE FILTER

SA INFRARED FILTER

SA KALMAN-SCHMIDT FILTER

SA LINEAR FILTER

SA LOW PASS FILTER

SA MICROWAVE FILTER

SA NONLINEAR FILTER

SA OPTICAL FILTER

SA PARTICULATE FILTER

SA RADAR FILTER

SA RADIO FILTER

SA SEPARATOR

SA TRACKING FILTER

SA ULTRAVIOLET FILTER

SA WAVEGUIDE FILTER

SA WIENER FILTER

Gyrator-RC filter synthesis procedure noting open circuit voltage of network configuration 01 p0032 A67-10008

Pulse shape formed during discharge of chain-type artificial line 01 p0038 A67-10719

Telemetry receivers capture ratio effect on overall system accuracy, determining effect of IF filter characteristics 02 p0197 A67-12022

Ruby laser with liquid filter, considering relation between filter efficiency and absorption curve parameters when acting as Q-factor modulator 02 p0252 A67-12423

Ferrite materials for resonators of magnetostrictive transducers and filters used in transmission and reception of ultrasonic waves 03 p0420 A67-13548

Bridge type piezoelectric filter with Zolotarev type attenuation characteristic 04 p0579 A67-14449

Data compression with digital filtering by fan method and step reduction method 04 p0569 A67-14585

Heavy current fluidic devices using self-cleaning filter with no moving parts 08 p1280 A67-20445

Efficiency of fibrous filters for radioactive particles and small ions increased, using greater flow rate 09 p1562 A67-22683

Stationary property of random process approximating anomalous magnetic field, noting optimum filtering 14 p2309 A67-27946

Postsampling exponential first order digital filter and application to data reduction for trend analysis and noisy phenomena 14 p2288 A67-28687

Gyrator type circuit which requires only three amplifiers and which, when terminated with capacitor, can replace ungrounded inductor 15 p2456 A67-29240

Equipment for processing data giving optimum performances of Doppler radar 17 p2816 A67-32750

Canonical form of filtering problems with solution identical to control problem 19 p3205 A67-35911

Nonstationary correlation analysis using correlator in which bandwidths of two filters resolve errors 20 p3484 A67-36695

Integral equations for weight function of optimum filter and correlation function of random absolute error 20 p3408 A67-37040

Characteristic admittances of comb-type and undulating waveguide filters, considering diaphragm thickness and TE propagation mode 22 p3770 A67-39662

Nonreciprocity in YIG filters employing stripline or miniature coaxial line construction 22 p3772 A67-39905

Filters in commercial aircraft hydraulic systems, discussing cleaning methods including ultrasonics 24 p4109 A67-42710

FILTRATION

Statistical description of signal filtration 01 p0043 A67-10237

Solution of optimum filtering problems when input signals of automatic control system are described by different differential equations at successive time intervals 03 p0390 A67-13099

Spatially distributed system for optimal filtration of useful signal in random noise fields 03 p0391 A67-13181

Optimal filtration of noise from useful signal based on statistical information and minimax principle 04 p0591 A67-14636

Linear filtering equations and Kalman filtering techniques for linear, quasi-linear, nonlinear and optimum mixer filter problems, orbit determination, space vehicle ballistic coefficient estimation, etc 06 p1028 A67-17720

Molecular sizes of diphosphopyridine nucleotide linked dehydrogenases of representative animal, plant and microbial species 11 p1750 A67-24784

Inaccurate determination effect of input-
signal characteristics on filtration quality,
solving equations for estimating upper limit
relative increase of rms filtration
error 17 p2829 A67-32223
Quantum formulas for optimal filtration of
useful electromagnetic signal in noise
background based on maximum
information principle 18 p2999 A67-33533
Improved filtration techniques for aircraft
hydraulic systems, noting high pressure
meter unit using paper-based element for
ground service 20 p3418 A67-37169
Mathematical models of flow and filtration
performance of wire cloth filter media in
series and parallel 20 p3365 A67-37364
Configuration 20 p3365 A67-37364
Distributed receiving system for optimal
operation of random field of space-
distributed source 20 p3385 A67-37376
Purification systems, filters and porous
materials applications to liquids and gas
systems associated with spacecraft, boosters
and ground support 21 p3570 A67-38103
Equipment 21 p3570 A67-38103
Depth sampler for testing dirt content of
jet fuels, discussing settling
effects 24 p4206 A67-42279
Reusable and disposable hydrosol filters
tested with heavy bacterial suspension for
ability to produce sterile
filtrates 24 p4116 A67-42705
COOLING FIN
Fin efficiencies in n-core stack heat
exchanger
[ASME PAPER 66-WA/HT-47] 04 p0724 A67-15432
Tallfin design effect on induced rolling
moment characteristics of sounding
rocket 08 p1405 A67-20503
Parameter management applied to roll
rate control in ballistic missile target system
[MSTS/ with fin 08 p1407 A67-20516
Black Brant sounding rocket fin design,
discussing flight characteristics, engine
selection criteria and stability
parameters 08 p1416 A67-20532
Wind tunnel investigation of dynamic
instabilities in cruciform finned missiles due
to rolling motion 08 p1413 A67-21531
Fin surface geometry optimization with
respect to gross heat-transfer coefficient
[AICHE PAPER 6] 20 p3552 A67-36827
Parameter management applied to roll
rate control in ballistic missile target system
[MSTS/ with fin 21 p3712 A67-37801
Black Brant sounding rocket fin design,
discussing flight characteristics, engine
selection criteria and stability
parameters 21 p3712 A67-37807
Model for straight fin nucleate boiling
asset criterion, discussing boiling section
length expression, heat flux and
temperature profile 22 p3919 A67-40387
FINE STRUCTURE
Profile and fine structure of diurnal
variation of cosmic ray intensity during high
and low solar activity 01 p0144 A67-10810
Irregularities in fine structure of solar
atmosphere with respect to radio emissions,
electron density, temperature and flux
density 01 p0150 A67-10891
Hall effect and fine structure of X-ray
fluorescence and absorption K spectrum of
uranium in silicides 01 p0101 A67-10935
E layer stratification, fine structure and
boundary accuracy in frequency
measurements based on seasonal variations
of solar activity 04 p0618 A67-15574
Slit size effect on magnetograph
observations of solar magnetic field in near
solar regions 06 p1082 A67-18015
Fine structure and microstructural effects
in control of magnetic, electrical, optical,
thermal and mechanical properties of
eutectic alloys 06 p1018 A67-18409
Fine structure of two-phase alloys of
titanium VT14 and structures effect on
mechanical properties 07 p1205 A67-19274
High temperature thermomechanical
treatment effects on VT10 titanium alloy
fine structure
characteristics 10 p1670 A67-23641
Motions of chromospheric fine structure in
weak plage analyzed, using time resolved H-
alpha spectra for estimating line-of-sight
velocities of objects 12 p2001 A67-25222

Prediction of total emissivity of nitrogen-
broadened and self-broadened hot water
vapor 13 p2155 A67-26493
Sunspot fine structure ground
observations, considering umbras,
penumbras, boundaries and
photographs 13 p2203 A67-27422
Theoretical interpretation of fine
structure observations of sunspots by
stratoscope, discussing stability modes and
sunspot umbras 13 p2203 A67-27423
Center-to-limb variation of Evershed effect
for isolated symmetrical sunspot
observations interpreted in terms of mass
motions in penumbral fine
structure 13 p2204 A67-27430
Atmospheric fine structure deduced from
radio observation and from turbulence
theory 14 p2311 A67-28396
Fine structure profiles of solar radio
bursts observed with high time
resolution 14 p2381 A67-28579
High time-resolution polarimeter
observations of Jupiter decimeter radio
bursts 14 p2388 A67-28836
Homogeneity of solar prominences studied
photographically in monochromatic
light 14 p2382 A67-28941
Book on thin walled structures covering
frame buckling, elastic buckling of
rectangular flat plates, edge loading,
anisotropic plate structures,
etc 17 p2956 A67-32021
Elastic buckling of thin walled frames,
discussing restraint effect on stability,
symmetry effect on critical behavior and
dead loads effect 17 p2957 A67-32022
Superhyperfine interactions in electron-
spin-resonance spectrum of substitutional
gadolinium 3 impurity in calcium fluoride
single crystals under applied
stress 17 p2913 A67-32367
Absorption lines in quasi-stellar source
analysis to obtain estimates of either
particle density in absorbing region or
distance between continuum source and
absorber 19 p3330 A67-36082
Fine structure of nitrogen 14 resonance in
hydrazine analyzed for Zeeman
effect 21 p3688 A67-38418
Solar magnetic field existence evidenced
by transverse fields in sunspots, field vector
spatial distribution around sunspots and
granular pattern inside
sunspots 21 p3708 A67-38986
Schottky tunneling measurements in GaAs
with Au noting fine
structure 22 p3861 A67-39996
Near IR laser transitions in pure helium
studied with scanning Fabry-Perot
interferometer, determining fine structure
components in upper laser
levels 22 p3817 A67-40488
He ions beam passing through electric
field and inducing light intensity
fluctuations when emitted from fine
structure levels observed via Stark
interference 23 p4029 A67-40956
Noctilucent cloud fine structure wave
form due to visibility through ice condensed
on dust particles in wave-like
pattern 24 p4146 A67-41791
Planetary nebulae IR emission intensities,
discussing radiative recombination, ionization
equilibrium and fine structure level
population 24 p4223 A67-41811
X-ray emissions from coronal condensation
regions studied with pinhole camera,
obtaining intensity profiles along intense X-
ray regions 24 p4224 A67-41821
Decrement of Balmer line widths and H-
alpha profiles when distributing fine
components as function of radial velocity in
optical prominences 24 p4232 A67-42595
FINISH
SA COATING
SA MACHINING
SA PAINT
SA PLATING
SA PRIMER
SA SURFACE FINISH
Aluminum, Volume 3, Fabrication and
finishing 14 p2323 A67-27818
Aluminum pretreating and finishing agents
noting cleaning, etching, roughening and
coatings 14 p2324 A67-27821
FINITE DIFFERENCE METHOD
Convergence theorem for second-order
linear three-level difference scheme for
class of quasi-linear parabolic differential
equation 02 p0258 A67-11556

Characteristic impedance of TEM mode
transmission lines, extracting upper and
lower bounds on finite difference solution of
Laplace equation 02 p0194 A67-11784
Laminar Prandtl boundary layer arising
during steady flow past blunt cone at angle
of attack studied by finite difference
method 03 p0349 A67-12868
Accuracy of central finite difference
methods for solving boundary value
problems in structural analysis governed by
equations with variable
coefficients 03 p0526 A67-13970
Finite difference method solution of
diffusion equations, including analyses of
stability and truncation
errors 03 p0537 A67-14013
Transient behavior of charring ablator
under various thermal environments by
finite difference method 04 p0723 A67-14847
Implicit difference methods for initial
boundary value problems based on Wiener-
Hopf factorization 04 p0645 A67-15085
Methods 04 p0645 A67-15085
Finite difference solution of parabolic
equation for laminar heat transfer in inlet
of rectangular duct as function of wall
temperature and Nusselt number for
different aspect ratios 04 p0728 A67-15805
Laminar tube flow and heat transfer for
He gas using Navier-Stokes, energy and
continuity equations in finite difference
form 04 p0729 A67-15809
Transient method for simultaneously
determining thermal conductivity and
specific heat, utilizing finite difference and
statistical procedure called nonlinear
estimation 04 p0734 A67-15851
Infinite series and finite difference
solutions of elastic response of thin walled
spherical shell to axisymmetric transient
blast loading
[ASME PAPER 66-APM-EE] 04 p0718 A67-15918
Combined elastic solutions-finite
difference method for bending of
compressible or incompressible rectangular
metal plate beyond elastic
limit 05 p0907 A67-16017
Boundary value problem of hyperbolic
equation with discontinuous boundary
conditions 05 p0834 A67-16371
Difference approximation with second
order accuracy of numerical solution for
parabolic type equations 05 p0834 A67-16372
Numerical method for calculation of finite
amplitude orographic disturbances by using
finite difference
algorithm 05 p0837 A67-16484
Scattering by infinite cylinders of
arbitrary cross section treated by method of
finite difference 05 p0764 A67-16952
Difference scheme for calculating one-
dimensional steady and unsteady Navier-
Stokes equations for compressible gas
flows 06 p0982 A67-17727
Finite difference method stability analysis
of deformed eccentrically stiffened shells of
revolution, accounting for finite prebuckling
rotations
[AIAA PAPER 67-110] 06 p1101 A67-18285
Three-dimensional laminar boundary layer
equations solved by finite difference
methods for application to boundary layer
flow on blunted cone, noting effect on
crossflow
[AIAA PAPER 67-159] 06 p0989 A67-18480
Nonequilibrium boundary layer problem
solution by direct treatment of two-point
boundary value problem
[AIAA PAPER 67-219] 06 p0990 A67-18515
Finite difference method solution of
motion equations for free vibrations of
initially disturbed thin elastic
rings 06 p1109 A67-18838
Unsteady temperature field calculated by
difference method, for application to
structures with various geometric
configurations 07 p1266 A67-19147
Numerical solution of hydrodynamic
equations adaptable to finite difference
methods 07 p1167 A67-19157
Numerical solution to time dependent
Navier-Stokes equation for transient
supersonic flow around right circular
cylinder, using explicit-implicit finite
difference method
[AIAA PAPER 67-221] 07 p1169 A67-19625
Finite difference method solution of linear
and nonlinear second order boundary value
problems by reduction to

- matrices 07 p1216 A67-19628
Nonlinear PDE for magnetostatic field with variable permeability in discontinuous medium solved with digital computer 07 p1132 A67-19795
Outflow of perfect ponderable fluid from opening in bottom of cylindrical container measured by numerical integration method by finite differences 07 p1169 A67-20207
Compatibility relations and generalized finite difference approximation for three-dimensional steady supersonic flow 08 p1320 A67-20566
Spectral stability criteria for numerical integration procedure using Z transforms, specifically finite difference operators 08 p1296 A67-20600
Finite difference method for finding stress fields around parallel edge cracks 08 p1421 A67-20914
Finite difference approximation of balance wheel equation, discussing convergence of Liebmman relaxation process, Coriolis term and computer time economy 09 p1525 A67-21551
Incremental elastic-plastic analysis of two-dimensional stress system by finite element method 10 p1719 A67-23456
Oscillations of plate in plane treated by finite difference method 10 p1721 A67-23645
Finite difference scheme for solving set of Prandtl equations for nonstationary flow of viscous incompressible fluid 10 p1628 A67-23672
Numerical finite difference solution of three-dimensional equations of motion for laminar natural convection, noting Navier-Stokes equation transformation 11 p1774 A67-23861
Natural and forced lateral vibration analysis of free-free beam by integration and finite difference methods, considering influence coefficients [ASME PAPER 67-VIBR-54] 11 p1873 A67-24202
Digital computer analysis of inviscid two-dimensional parallel flow stability, using finite difference method to solve resulting initial value problem 11 p1778 A67-24220
Finite difference network model method with error tolerance for spacecraft heat transfer calculation 11 p1883 A67-24356
Approximate solution using finite difference method of bending of rectangular plate beyond elastic limit 11 p1879 A67-24886
Penalty function method used for bounded phase coordinate optimal control problem for linear discrete systems with quadratic cost functionals 11 p1771 A67-24891
Viscous flow around spheres, considering mass efflux effect, using Navier-Stokes equations and finite difference methods 12 p1927 A67-25282
Navier-Stokes equations solved by finite difference methods at low Reynolds numbers for viscous flow around sphere, noting no flow separation 12 p1927 A67-25283
Vibration characteristics of cantilever type pretwisted turbine blading, considering effects of taper, calculating frequencies and mode shapes 12 p2014 A67-25414
Heat flow mechanisms and thermodynamics of supercritical cryogenic storage problems solved by digital computer simulation, using finite difference approximation 12 p1925 A67-25722
Elastoplastic equilibrium of rectangular compressible and incompressible plates under load concentrated near edge determined by elastic solutions and finite difference 12 p2031 A67-25960
Compression load stability of nonuniformly rigid plates within and beyond elasticity limits solved by combined Galerkin and finite difference methods 12 p2031 A67-25961
Electrical simulation of finite difference calculations of problems of bending and natural oscillations of circular, annular and sector plates 12 p2032 A67-25968
Numerical method for calculation of finite amplitude orographic disturbances by using finite difference algorithm 13 p2150 A67-26340
Numerical methods for elliptic problems, discussing application of finite difference and solution of large algebraic systems 14 p2342 A67-28156
Difference method for solution of plane problems in dynamic elasticity, noting equations of dynamic/elastic deformations under plain strain
- conditions 14 p2400 A67-28256
Hydrodynamics of gravitating stellar system numerically calculated for nonrotating spherically symmetric case 14 p2393 A67-28997
Time dependent heat conduction and diffusion equations for fuel-rich H-O flame solved by finite difference method 14 p2409 A67-29064
Finite difference method for treating head-on axisymmetric interactions of blast wave and shock layer in nose region of high speed blunt body 15 p2416 A67-29432
First order finite difference numerical analysis of thin elastic orthotropic and inhomogeneous cylindrical shells with small deformations from external forces 15 p2574 A67-29471
Finite difference solution of third boundary value problem for heat conduction equation, obtaining conditions for coefficients from stability requirements 15 p2510 A67-29521
Finite difference method solution of periodic parabolic problem solution subject to nonlinear boundary condition 15 p2510 A67-29522
Finite difference method of solving degenerate elliptic and parabolic equations 15 p2511 A67-30008
Eddy currents in nonmagnetic conductors calculated by finite difference successive overrelaxation technique on digital computer 15 p2541 A67-30142
Laminar viscous wake interaction with supersonic external inviscid flow downstream treated by implicit finite difference method [AIAA PAPER 66-454] 15 p2417 A67-30188
Numerical solution of boundary layer equations by finite difference integration 15 p2473 A67-30189
Dynamic model parameter estimation using method of generalized least squares 15 p2462 A67-30326
Successive overrelaxation iterative method for solving elliptic partial differential equations 16 p2695 A67-30830
Numerical approximation of evolution equation solution for linear and nonlinear operators by finite difference method 16 p2696 A67-31198
Scattering problem for partial difference equations with finite perturbation and inverse problem determining perturbation 17 p2817 A67-32885
Finite difference method stability analysis of deformed eccentrically stiffened shells of revolution, accounting for finite prebuckling rotations [AIAA PAPER 67-110] 17 p2963 A67-33015
Static /time-discrete/ electrical model for mathematical analogy of heat transfer processes and application to solution of nonlinear heat conduction equations 17 p2821 A67-33079
Dirichlet problem solution for Poisson equation on rectangle with smooth boundary values, using higher order differences 19 p3249 A67-34794
Long term global integrations of primitive meteorological equations for free surface model, using spherical polar coordinates 19 p3252 A67-35058
Grid functions from nodal values on rectangular surface used to solve potential equation by finite difference method 19 p3342 A67-35717
Finite difference heat conduction method for surface subliming processes in space vehicles 19 p3346 A67-35755
Underexpanded jet boundary streamline calculations by exact and approximate methods 19 p3171 A67-35768
Unsteady discharge of compressed viscous gas from duct analyzed by finite-difference method 19 p3172 A67-35780
Computer solution of optimal control problems by finite difference method 19 p3202 A67-35886
Energy equation for laminar convective heat transfer in combined hydrodynamic and thermal entrance region bound by parallel flat plates [ASME PAPER 67-HT-48] 20 p3548 A67-36730
Fourth order parabolic partial differential equation solution by explicit and implicit finite difference methods 20 p3478 A67-37211
Finite difference scheme based on Douglas-Rachford implicit alternating direction method for nonstationary Navier-
- Stokes equation initial value problems 20 p3423 A67-37212
Compositional changes at alloy/oxide interface during protective oxidation calculated using finite difference method 20 p3468 A67-37213
Variationally derived finite difference equations for mixed boundary value problems of thermoelastic stress and strain 21 p3716 A67-37929
Deflection and stresses in corrugated diaphragm rigidly clamped on contour with distributed pressure and concentrated central force, using finite difference approximation 21 p3717 A67-37930
Computers role in fluid film lubrication computing parameters for bearings lubricated by compressible and incompressible lubricants via iterative finite difference schemes 21 p3632 A67-38111
Finite difference scheme for solving set of Prandtl equations for nonstationary flow viscous incompressible fluid 21 p3612 A67-38212
Network method to derive differential difference equations for boundary conditions of clamped and free edges and supports of low aspect orthotropic wing network method to derive differential difference 21 p3724 A67-38717
Finite difference method for axisymmetrical and plane elasticity problems using high speed computer 22 p3908 A67-39212
Radiative cooling and self-absorption effects on reflected shock flow field around end wall heat transfer studied using finite difference method 22 p3917 A67-39717
Friction and heat flow resistances for three-dimensional compressible laminar gas boundary layer over ellipsoid of revolution at angle of attack 22 p3786 A67-40011
Optimum sensitivities of control functions with respect to vehicle parameter changes and state variables without using finite differences 22 p3833 A67-40111
Nonequilibrium boundary layer problem solution by direct treatment of two-point boundary value problem [AIAA PAPER 67-219] 23 p3991 A67-41717
Finite difference method for degenerate elliptic and parabolic equations involving various boundary value problems 24 p4178 A67-42211
Finite difference integration method for predicting flow velocity and temperature distribution of gaseous diffusion flame axisymmetrical combustion chamber 24 p4091 A67-42311
Finite difference solution accuracy for potential gradient along conductor boundary near reentrant corner of thin plate 24 p4131 A67-42411
Momentum and heat transfer in axisymmetric turbulent free jets exhausting into quiescent air, using finite difference technique 24 p4092 A67-42611
High order accurate difference methods for hydrodynamics 24 p4146 A67-43011
- FINITE-STATE MACHINE**
Optimal feedback control for finite state systems with suitable performance criteria using maximum principle applied to time sharing computer systems 02 p0227 A67-12111
Reliability of finite automata determined from analysis of elements capable of misalignment, input errors and structural design 05 p0782 A67-16211
Optimization of stochastic dynamic systems with noisy output 06 p0977 A67-18511
Compact encoding of stationary Markov sources 12 p1919 A67-26011
Asynchronous finite state sequential nonlinear controller synthesis with few flip flops for dynamic space vehicle system [AIAA PAPER 67-988] 24 p4127 A67-43011
- FINLAND**
Space research activities in Finland /1966 detailing satellite station 19 p3320 A67-35211
- FINNED BODY**
Wing lift and pitching moment variations due to fin on supersonic aircraft 09 p1437 A67-22111
- FIRE CONTROL**
Aircraft cabin fire tests to determine filling cabin with high expansion foam cover keep temperature within survival limits while controlling combustion products 02 p0181 A67-12211
Radioisotopes for army aviation applications, stressing need for ballistics

- protection of crew members and critical components 05 p0841 A67-16534
- Fire resistance of hydraulic fluids - ASTM SAE Symposium, New Orleans, January 09 p1520 A67-22244
- Ignition of flammable fluids by hot surfaces tested on static hot plate rig and wind tunnel rig, noting data on kerosene, lubricating oil and hydraulic fluid 09 p1580 A67-22248
- Resistance of aviation hydraulic fluids, mineral, snuffer, phosphate ester, siloxane and chlorosilicone to wheel brake fires, evaluating lab test techniques and simulation testing 09 p1521 A67-22250
- Kinematic analysis of deviation from aircraft-missile line for designing electronic missile firing simulator, with manual control comprising controlled precession microscope for last 09 p1486 A67-22419
- Eldorado low altitude detection and short reaction time defense system, examining Doppler effect and Mirador pulse radar 17 p2816 A67-32751
- Reliability demonstration during category I and III testing of missile and airborne radar fire control system, emphasizing coordination between factory and field 18 p3138 A67-34652
- ISIS fire control equipment family, considering maximum cost effectiveness, discussing use in Dassault Mirage M-5 and PAF CF-5 aircraft 20 p3364 A67-37244
- AH-56A Cheyenne compound aircraft weapon system and major subsystems, discussing fire control, navigation system and performance 21 p3568 A67-38133
- Simplified fire control system for helicopters, noting helmet sight, error source corrections and sighting and tracking convenience 22 p3755 A67-39849
- Polyimide passenger smoke hood for protection from smoke, toxic gases and flame inhalation 23 p3968 A67-41623
- Injury and fatality analysis in survival study of commercial jet aircraft /Boeing 727/ landing accident with subsequent anterior fire 23 p3969 A67-41650
- Porous cermet tubular element fire barriers of stainless steel powder for increased safety in gas flame processes, determining critical Peclet number 24 p4159 A67-41957
- FIRE EXTINGUISHER**
- Concorde fire protection system based on Firewire Triple FD equipment, discussing extinguishant toxicity, low vapor pressure, etc 20 p3364 A67-37245
- FIRE PREVENTION**
- Fuel system design criteria, discussing ways of reducing postcrash fires in aircraft 08 p1279 A67-20610
- Developments in fire detection equipment noting continuous wire, armored wire and surveillance detectors 09 p1439 A67-21704
- Closed compartment fire-resistance test for hydraulic fluids leaking near heated aircraft skin with or without electric heating 09 p1521 A67-22245
- Fire hazard testing of hydraulic fluids, coolants and lubricants in aircraft with reference to SST hot wing compartment conditions 09 p1521 A67-22246
- Fire resistance of aircraft fluids, analyzing likelihood of spontaneous ignition by flashpoint and isothermal enclosure methods 09 p1521 A67-22247
- Intrinsically safe and nonincendive electrical installations for hazardous environments 12 p1900 A67-25677
- Electrostatic discharging systems for helicopters, discussing earth field effect and all-safe concept 16 p2610 A67-31824
- SAE PAPER 107]
- Fuel emulsions for helicopters to minimize hazards associated with liquid fuel, discussing composition, stability, corrosion and flow properties 17 p2927 A67-33001
- SAE PAPER 670364]
- Gelled, emulsified and otherwise thickened fuels for aircraft fire safety, discussing requirements and engine operation 18 p3110 A67-33967
- SAE PAPER 67-503]
- Design, construction and procedure changes in Apollo following fire of January 1967 19 p3334 A67-35928
- Hydrogen fire visualization detection techniques including application of photography, TV and image converter in IR and UV regions 20 p3445 A67-36540
- Fire in Apollo 204 spacecraft noting alterations in oxygen and electrical systems, escape hatch, materials and communications 22 p3900 A67-39888
- Spacecraft atmosphere selection covering physiological, engineering and fire criteria, evaluating oxygen diluent and recovery 22 p3755 A67-39889
- Flame mechanism experiments for solid material surface, measuring flame velocity, stressing space capsule fire hazard minimization 22 p3904 A67-40110
- FIRING**
- SA DETONATION
- SA ROCKET FIRING
- SA STATIC FIRING
- SA TEST FIRING
- Range instrumentation support systems, describing approaches to timing, firing and communications systems 10 p1605 A67-22998
- FIRING TIME**
- Descent engine for lunar module specifications and operational requirements covering throttling, firing duration, crushable nozzle skirt, etc [AIAA PAPER 67-521] 18 p3115 A67-33984
- FIRST AID**
- Indications and contraindications for transportation of wounded by helicopter and ambulance 12 p1902 A67-25174
- FIRST ORDER EQUATION**
- SA REYNOLDS EQUATION
- Levi-Civita regularized equations of elliptic motion of particle influenced by massive primary and perturbed by smaller primary, Part I, Trigonometric series solution 01 p0147 A67-10379
- First order solution of economical impulse transfer between near-circular, coplanar or noncoplanar, close orbits by linearization of circular nominal orbit 01 p0152 A67-11404
- Geometrical study of Picard method of successive approximations for solving first order differential equations 02 p0257 A67-11479
- First order linear differential equation describing line-of-sight system of air-to-air missiles in two-dimensional case 02 p0265 A67-12731
- Energy moments of inverse problem in theory of nuclear cascade determined, using first order Volterra integral equation 02 p0317 A67-12769
- Existence and uniqueness theorem and upper and lower Chaplygin function approximations for solutions of Cauchy problem for quasi-linear first order PDE 03 p0456 A67-12884
- Qualitative study of first order homogeneous equation, by introducing auxiliary variables, plane curve is associated with differential equation 03 p0459 A67-13587
- First order differential equations with homogeneous right sides to construct Liapunov function and stability behavior 03 p0462 A67-14257
- Jordan form matrix algorithm of Wasow for reducing systems of first order ordinary differential equations with turning point 05 p0835 A67-18779
- Displacement formulations of first order linear thin elastic shell equations in terms of stress resultant and middle surface, using modified Kirchhoff hypothesis 08 p1417 A67-20551
- Undetermined coefficient method compared with confluent hypergeometric functions for solving first order perturbation equation for refractive index of He 11 p1813 A67-24787
- Elliptic regularization for symmetric positive system of linear first order partial differential equations with irregular boundaries 13 p2147 A67-27178
- Mutually adjoint boundary value problems for linear systems of first order equations of composite type with two independent variables 14 p2344 A67-28670
- Perturbation theory methods as applied to first order differential equation 15 p2560 A67-30041
- First slip time of phase locked loop of arbitrary order shown as solution of first order linear differential equation 17 p2811 A67-32117
- General solution of linear differential equation of first order with quasi-periodic coefficients 17 p2879 A67-32880
- Boundary value wave problem in elastoviscoplastic medium solved by approximate method using Courant concept 19 p3340 A67-35444
- Quasi-linear elliptic system of first order equations used for Riemann-Hilbert boundary value problem 21 p3651 A67-37930
- Linear boundary value problem for system of first order partial differential equations having real and imaginary characteristics 21 p3653 A67-38398
- Radio wave propagation in three-dimensional inhomogeneous magnetoactive ionosphere studied by geometrical optics method 21 p3582 A67-38592
- Radio wave refraction and refraction-induced errors calculated in determination of artificial satellite trajectories 21 p3582 A67-38593
- Energy moments of inverse problem in theory of nuclear cascade determined, using first order Volterra integral equation 22 p3842 A67-40271
- Analytic form of solutions of first order variational equations of restricted three-body problem 23 p4061 A67-40622
- FIRST PROJECT**
- Project initiation emphasizing market, product /design, cost and timing/ and resources to market product 15 p2583 A67-29667
- FISH**
- Mammalian porcine thyrocalcitonin extract effect on concentrations of serum calcium and phosphate in catfish 20 p3372 A67-37277
- FISSION**
- Spark counter for recording fission fragments in presence of high intensity alpha radiation 06 p1001 A67-17936
- Origin of fissionogenic Xe isotopes in Pasamonte achondrite 08 p1386 A67-20938
- Nuclear energy deposition effect on pressure pulse generation in fissioning gas flow through seminfinitesimal cylindrical tube analyzed by method of characteristics 08 p1322 A67-21121
- Fission-particle damage formation in semiconducting layer structures, using model based on thermal spike 17 p2918 A67-32849
- Fission hypothesis of lunar origin, reviewing energy, dynamics, angular momentum, geology and physical properties 24 p4230 A67-42323
- FISSION ELECTRIC CELL**
- Thermionic reactor with uranium diodes core array, describing in-pile reactor uses, arcjet, heat pipe and conceptual design components [AIAA PAPER 67-498] 18 p3076 A67-33962
- FISSION PRODUCT**
- Delayed energy produced by fission product decay when restart of nuclear rocket engine is considered, noting effects of cooldown requirements [AIAA PAPER 66-551] 05 p0844 A67-17222
- Surface air radioactivity and ozone measurements in Antarctica reveal fission product yearly oscillation 20 p3429 A67-36871
- Iodine isotope mass-yield distributions from spontaneous plutonium 242 fission, discussing heavy xenon isotopes from extinct plutonium 244 in meteorites 24 p4191 A67-42450
- Radiation resistant silicon diode fast neutron monitors, discussing fission spectra and leakage currents in damaged diodes 24 p4183 A67-42473
- Fast He nuclei from photoemulsion nuclear splitting induced by proton and antiproton bombardment 24 p4193 A67-42860
- Isotope ratios of fission and spallation xenon in meteorites from abundance data analysis by least squares method 24 p4238 A67-42886
- FIST PROJECT**
- Automatic checkout system based on digital instrumentation with input of two bits and variable data rate resulting from use of memory storage 03 p0398 A67-14203
- Man-machine interface and automatic test operations in Saturn S-IVB system 03 p0398 A67-14204
- Evaluation of automatic test equipment for airborne weapon systems from standpoint of effect on readiness of weapon system 03 p0399 A67-14206
- Factory-to-launch sequences of checkout in Saturn/Apollo program, examining present and planned levels of automation 03 p0399 A67-14207
- Hughes-USAFA VATE /Versatile Automatic Test Equipment/ system for fault detection and isolation and acceptance testing of

inertial guidance equipment 03 p0399 A67-14208
Analysis and projections of space vehicle automatic checkout and launch 03 p0399 A67-14211
Automatic malfunction analysis /AMA/ technique providing space-vehicle test engineer with listing of all component failures that could cause abnormal indication at any observable monitoring point 03 p0399 A67-14213
Automated learning methods used to design fault diagnosis procedures 03 p0400 A67-14217
Maintenance time reduction for multimode airborne weapons through built-in test equipment and integrated program 21 p3601 A67-38947

FITNESS

S FLIGHT FITNESS
S PHYSICAL FITNESS

FITTING

SA FASTENER
Extension fittings for A-7A bomber having hydraulic system with no flexible hose 09 p1442 A67-21659
Weldable tube fittings, welding equipment and inspection methods for connecting tubing in aircraft and aerospace hydraulic systems 17 p2864 A67-32008

FIXED FREQUENCY TOPSIDE SOUNDER

S TOPSIDE PROGRAM

FIXED POINT

Harmonic analysis of perturbed satellite motion from exact solution for point motion about two fixed centers [ONERA-TP-420] 02 p0320 A67-11494
Combination into unified setting of various results for approximate solution of fixed point equation, using iterative process 07 p1218 A67-20212
Vertical atmospheric flow mean velocity determination within fixed area from wind probe observations at fixed points 11 p1816 A67-24523
Inverse problem of relativistic motion of point of variable mass 13 p2159 A67-27362
Schroeder fixed point theorem for convergence rate of iteration series extended to concave operators which need not remain constant 14 p2345 A67-28937
Comparison of lunar limb profiles referred to system of reference points and limb region maps, giving data conversion formulas and map inaccuracies 17 p2949 A67-33124
Book on calculus of variations and optimal control theory covering function maximum and minimum theory, fixed end-point problem, etc 21 p3653 A67-38799

FIXED-WING AIRCRAFT

Flight test method for evaluating ground effect on fixed-wing aircraft in which pilot flies at constant angle of attack and power setting during landing approach [AIAA PAPER 66-468] 02 p0180 A67-11513
Flight test method for evaluating ground effect on fixed-wing aircraft in which pilot flies at constant angle of attack and power setting during landing approach [AIAA PAPER 66-468] 09 p1441 A67-22486
Requirements and disadvantages of proposed escape systems for fixed and rotary wing Army aircraft 17 p2794 A67-31998
Rotary wing role in short haul intercity transportation, comparing V/STOL and STOL advantages over fixed wing aircraft, noting need for compound helicopter 21 p3734 A67-38013

FLAME

SA CHAPMAN-JOUGET FLAME
SA COMBUSTION
SA DIFFUSION FLAME
SA FLARE
SA JET FLAME
SA LAMINAR FLAME
SA PREMIXED FLAME
Equilibrium burning of spherical nongaseous fuel drop in slow convective hot-oxidant flow in thin flame theory 02 p0341 A67-11562
Combustion and heat transfer laws for hydrocarbon flames with predetermined visual radiation 08 p1425 A67-20303
Torque effect on characteristics of burner flame based on principles of fluid mechanics 08 p1425 A67-20305
Atomic-absorption flame photometric instrumentation and techniques 13 p2120 A67-26811
Plasma behavior in laminar and turbulent hydrocarbon-air flames, discussing flame

ionization, electron concentration and recombination, detonation wave ionization data, ignition, etc 17 p2968 A67-32168
Thermal scaling for test models in heat transfer studies of bodies enveloped in large luminous flames [ASME PAPER 67-HT-60] 20 p3549 A67-36742
FLAME DEFLECTOR
Rocket launching pad exhaust deflector investigated for uncooled efflux deflectors design data, calculating heat transfer coefficient and stagnation temperature 19 p3207 A67-35520

FLAME FRONT

Aerodynamics of diffuse combustion in laminar boundary layer of two plane-parallel accompanying flows, emphasizing flame structure 06 p1112 A67-17961
Viscosity effect on stability of plane flame front, showing destabilization from linearized equations of velocity and pressure disturbances 08 p1428 A67-21423
Transfer process effect on stability of plane flame front, deriving revised approximate solution for large finite Reynolds numbers 11 p1883 A67-24672
Ionizing detonation wave model with electrical conductivity jumping from zero to infinity characterized by exothermal energy release and magnetoacoustic speed propagation 15 p2528 A67-29567
Cellular flame under constant volume bomb conditions, demonstrating vibratory combustion over range of gas compositions and characteristic initial pressures 17 p2974 A67-33143
Small perturbations effect on internal gas dynamic structure of flame zone for slow combustion stability criterion 17 p2974 A67-33144
Plane ionization wave propagation in uniform magnetic field compared with flame front expansion during slow burning 19 p3286 A67-35347
Hydrodynamic stability of flame front propagation in tube 20 p3543 A67-36396

FLAME HOLDER

Flame shape and chamber combustion efficiency relation for flame stabilized by opposed jet flameholder [AIAA PAPER 67-472] 18 p3157 A67-33942
Flame stabilization with flame holders in supersonic flow, discussing improved combustion in ramjets at supersonic velocities 18 p3116 A67-34609

FLAME INTERACTION

Flame shape and chamber combustion efficiency relation for flame stabilized by opposed jet flameholder [AIAA PAPER 67-472] 18 p3157 A67-33942

FLAME IONIZATION

Electron current and positive ion current in flames measured by improved single-probe technique using grid and ring electrode 01 p0070 A67-11068
Hydrocarbon flame ionization, discussing second process occurring in flames with acetylene and related unsaturated compounds 04 p0719 A67-14488
Radiation from flames and chemical perturbations of atmosphere, examining flame structure, irreversible processes, photoemissive events, etc 04 p0721 A67-14701
Variation of floating potential formed between electrodes by injection of electronegative gas is logarithmic function of electron attachment coefficient on neutral particles 04 p0669 A67-15496
Role of negative ions in flames and of negative droplets in mercury vapor, noting use of isotopic tracer techniques and flame behavior as gaseous semiconductors 05 p0853 A67-16886
Electric potential distribution in flame for electronegative gas layer present between two electrodes 13 p2165 A67-26597
Ionization processes in hot products of combustion processes /flame gases/ as weak plasma media noting flame properties, mass spectroscopy, electron concentration, etc 17 p2967 A67-32140
Hot flame gases ionization by electron reactions at atmospheric pressure 17 p2968 A67-32149
Role of electronically excited CH in formation of C₃H₃ ion and contribution to overall chemiluminescence 18 p3150 A67-33802
Ionization in ethylene flames at atmospheric pressure, using nitric oxide as oxidizer and electrostatic

probe 18 p3107 A67-33804
Ionization and recombination processes of alkali metal ions in hydrogen-oxygen-nitrogen flames with hydrocarbon additives 18 p3107 A67-33806
Carbon monoxide and hydrogen flames ionization and electron temperatures with methane premixing 18 p3151 A67-33807
Mathematical model for thermal and chemiluminescence processes in turbulent nonequilibrium afterburning rocket exhausts plume, studying neutral and charged species distribution 18 p3152 A67-33820
Ionization-enhanced microwave resonant radiation from model rocket exhausts studied using Dicke type radiometer 20 p3543 A67-36233
Chemiluminescence and chemiluminescence in low pressure fuel-oxygen flames, measuring emission intensity of CH, carbon molecule and OH electronic bands 20 p3376 A67-37094
FLAME PLATING
SA ACETYLENE
SA ALUMINUM OXIDE
SA TUNGSTEN CARBIDE
SA WELDING
Metal surface property improvement by thermal-spray coating noting flame plating 18 p3055 A67-34483
FLAME PROBE
Amplitude spectrum of turbulent flow rate fluctuations at flame temperatures measured via photoelectric method 05 p0927 A67-16942
Polycyclic aromatic hydrocarbons in soot of premixed acetylene-oxygen flames, discussing graphs of flame height vs mixture composition 10 p1602 A67-22960
Powder and solid propellant combustion, discussing heterogeneous and homogeneous systems, characteristics of foam, fizz and flame zones, etc 12 p1988 A67-26110
Amplitude spectrum of turbulent flow rate fluctuations at flame temperatures measured via photoelectric method 14 p2406 A67-28490
Time dependent heat conduction and diffusion equations for fuel-rich H-O flame solved by finite difference method 14 p2409 A67-29064
Secondary ion generation in flames by electron impact noting application of mass spectrometry and hydrocarbon fuels analysis 16 p2780 A67-31520
Analysis of flame effects on measured electromagnetic propagation data for plume shape, plume electron density distribution and signal attenuation 19 p3344 A67-34819
Flame structure of hydrazine burning in oxidizing atmosphere determined by measuring temperature and specific contractions at 90 degrees from stagnation point 19 p3310 A67-35014
FLAME PROPAGATION
SA BURNING RATE
Flame study of turbulence effects induced by sonic or ultrasonic vibration on combustion of liquid hydrocarbon jet 01 p0167 A67-10942
Flame ignition from hot gas pocket, minimum size of gas bubble for flame propagation, dependence on chemical kinetic parameters and transport properties 02 p0342 A67-12030
Flame reaction rate enhancement by electric fields 03 p0537 A67-14050
Ignition pressure transient in solid rocket motors, examining chamber filling interval, flame propagation, heat transfer correlation, burning area, etc 05 p0873 A67-16513
Flame ignition from spherical hot gas pocket, finding minimum size of bubble for flame propagation and dependence on kinetic parameters 06 p1114 A67-18189
Flame spreading velocity over surface of igniting solid rocket propellants as function of atmospheric pressure and chemistry and specimen surface condition 06 p1073 A67-18852
Aluminum fluoride effect on propagative ignition of fuel oxidant mixtures and on combustion between aluminum and oxygen 07 p1238 A67-19070
Turbulence effect on burning velocity and physical structure of flame surface in turbojet-afterburner-like combustion chamber 07 p1265 A67-19073
Cylindrical flame propagation in analytical solution derived from artificial reaction rate 07 p1265 A67-19076
Flammability limits of hydrogen-oxygen-nitrogen mixtures at low pressures 07 p1239 A67-19077

- Thermal expansion of chemical reaction front in condensed phase 07 p1267 A67-19310
- Normal flame propagation rates for methane-air mixtures at high pressures 07 p1239 A67-19313
- Surface effects for solid propellant combustion, discussing flame profile and instability, surface burning mechanism, temperature distribution, etc 08 p1373 A67-20642
- Flame propagation effects and combustion chemistry of nitrate ester or double base solid propellants 08 p1374 A67-20877
- Fire resistance of aircraft fluids, analyzing likelihood of spontaneous ignition by flashpoint and isothermal enclosure methods 09 p1521 A67-22247
- Flame propagation on liquid fuel surface, analyzing fuel heating in front of flame until ignition temperature is reached, noting radiation and convection 09 p1581 A67-22605
- Combustion of hydrogen and hydrazine with nitrous and nitric oxide noting flame speeds and flammability limits of ternary mixtures at sub atmospheric pressures 16 p2779 A67-31519
- Flame propagation along interface between gas and reacting medium, studying fuel heating ahead of flame, noting radiation and convection role 18 p3151 A67-33816
- Ammonia-air combustion, flame speed needed to obtain optimum performance 18 p3110 A67-33844
- Flame spreading over igniting solid propellant surface in high pressure oxygen-inert environment 19 p3344 A67-34999
- Hydrodynamic stability of flame front propagation in tube 20 p3543 A67-36396
- Fire in Apollo 204 spacecraft noting alterations in oxygen and electrical systems, escape hatch, materials and communications 22 p3900 A67-39888
- Flame mechanism experiments for solid material surface, measuring flame velocity, stressing space capsule fire hazard minimization 22 p3904 A67-40110
- Flame propagation in hydrogen-oxygen mixtures at temperatures and pressures corresponding to ignition 22 p3919 A67-40223
- Kinetics of flames propagating in hydrogen-nitrous oxide mixtures diluted with inert gases 23 p4082 A67-41142
- FLAME QUENCHING**
- Quenching diameter of premixed fuel-oxidizer flames by volatile inhibitors, noting nature of oxidizers, particularly oxygen 02 p0342 A67-12031
- Collisional de-excitation rate or quenching of sodium in flat premixed laminar flames 18 p3150 A67-33803
- Aluminum particle combustion noting changes from preignition to burnout, flame structure, particle geometry, etc [WSCI PAPER 66-3] 22 p3919 A67-40224
- FLAME SPRAYING**
- SA PLASMA SPRAYING
- SA PLATING
- Flame-sprayed ceramic coating in space technology, examining solid atomization or Rokide process 06 p1021 A67-18764
- Metal surface property improvement by thermal-spray coating noting flame plating 18 p3055 A67-34483
- FLAME STABILITY**
- Laminar diffusion flame stability analyzed, examining transient characteristics to infinitesimal disturbances of steady state solutions 02 p0342 A67-12028
- Air velocity and temperature, stabilizer size and blockage effects on fresh mixture entrainment in recirculation zone of bluff body stabilized flames 02 p0342 A67-12029
- Flame stabilization by mechanical stabilizers in ramjet combustion chamber as function of temperature and pressure of fuel mixture 04 p0691 A67-15899
- Mean velocity and mean static pressure distribution on stability and space requirements of turbulent diffusion flames 08 p1425 A67-20304
- Flame separation explained in terms of processes taking place in mixing zone of internal cone in laminar burner flame 08 p1425 A67-20306
- Tallpipe length effect on flame stability in high velocity propane-air stream with bluff body or reverse jet flame holders [ASME PAPER 67-GT-4] 11 p1853 A67-24792
- Jet flame stabilization and audible noise reduction using ultrasonic acoustic energy 11 p1883 A67-24842
- Diffusion flame stability criteria for one-dimensional model at unity Lewis number 13 p2221 A67-26260
- Mobility measurement of electron capture in hydrocarbon flames using Hall effect, noting variation when injecting chlorine 18 p3146 A67-33691
- Spectrophotometric study of multiple reaction zones of premixed trimethylaluminum-oxygen flames, emphasizing microstructure 18 p3109 A67-33840
- Counterflow diffusion flame in forward stagnation region of porous cylinder, detailing flame stability and velocity gradient 18 p3155 A67-33842
- Ignition energy, quenching distance, flame stability and gas turbine burner performance of ammonia-air mixture 18 p3109 A67-33843
- Flame stabilization with flame holders in supersonic flow, discussing improved combustion in ramjets at supersonic velocities 18 p3116 A67-34609
- Flame stabilization mechanism of homogeneous combustible fluid flow using air jets through peripheral slits to join main flow producing gasdynamic screens 22 p3921 A67-40455
- FLAME TEMPERATURE**
- Extension of analysis of unsteady state model for combustion of solid propellant to include nonlinearities of second order 01 p0141 A67-11158
- Finite rate chemistry effects in diffusion controlled hydrogen-air flames noting flame position, fuel consumption, temperature, fluid velocity outside of flame and boundary conditions 05 p0926 A67-16516
- Photometric measurements on deviations from equilibrium state in burnt gases of laminar premixed shielded flames at atmospheric pressure [AIAA PAPER 67-9] 06 p1072 A67-18345
- Time dependent temperature profile for stationary nitroglycerin powder combustion process 07 p1267 A67-19312
- Velocity and temperature measurements in turbulent swirling butane-propane air flames in high exit velocity range 11 p1882 A67-24217
- Burning velocities, temperatures and burnt gas composition of flammable methane-rich perchloric acid mixtures 14 p2406 A67-28544
- Flame properties of flammable ethylene-rich perchloric acid mixtures 14 p2406 A67-28545
- Flame properties of flammable ethane-rich perchloric acid mixtures 14 p2406 A67-28546
- Laminar flame speeds and composition flammability limits at low pressure for ternary mixtures of hydrogen and oxygen with ammonia and nitrous oxide 14 p2406 A67-28547
- Self-deflagration process of hydrazine diperchlorate studied for three suggested pressure regimes 14 p2376 A67-28551
- Electronic, vibrational and rotational temperatures in laser-produced flames measured spectroscopically 15 p2433 A67-29879
- Combustion instability, transient burning during ignition and extinction by depressurization investigated in nonsteady burning of solid propellants 15 p2580 A67-29984
- Temperature distribution field of flame studied by applying holographic techniques in obtaining interferogram of inhomogeneity created by flame 16 p2672 A67-31066
- Gas circulation effect on temperature field of cylindrical combustion chamber with axisymmetric heat-release and gas-velocity fields 16 p2779 A67-31395
- Electron temperature measured in acetylene/oxygen mixture flame and found twice that of gas due to chemical energy transport to electron gas 17 p2988 A67-32151
- Excitation and radiation of OH molecules and alkali metals in low pressure flames and rocket exhausts 18 p3152 A67-33819
- Steady flow adiabatic stirred reactor to study combustion mechanism of hydrogen-oxygen mixtures, determining reaction-kinetic constants 18 p3154 A67-33834
- Reaction zones of ammonia-oxygen and hydrazine decomposition flames, measuring temperature and concentration profiles 18 p3155 A67-33838
- Effect of additives on hydrazine nitrogen trioxide droplet flame structure and burning rate [AIAA PAPER 67-482] 18 p3158 A67-33951
- Perfectly stirred reactor /PSR/ theory application to flame analysis, obtaining temperature or concentration profiles as function of time or distance 19 p3345 A67-35011
- Radiative heat flux for free burning methanol and acetone flames of arbitrary size and geometry predicted, using transport equation [ASME PAPER 67-HT-47] 20 p3547 A67-36729
- Turbulent gas combustion, showing burning rate as function of combustion temperature, pressure and chemical reaction rate in flame 21 p3732 A67-38527
- Flame activation energy and combustion process order based on homogeneous reactor model for mean temperature coefficient determination 23 p4082 A67-41141
- FLANGE**
- SA METAL PLATE
- Semifinite strip reinforced by flanges under concentrated load 04 p0719 A67-15933
- Cryogenic low pressure seal to seal aluminum or stainless steel flanges 08 p1336 A67-21498
- Heating of flange joint solved with approximate method taking stresses at joint into account 16 p2766 A67-31205
- Critical plastic buckling of compressed spar flanges 20 p3537 A67-36842
- I-beam ratio of depth to flange width for minimum weight obtained via modulus of rupture 21 p3722 A67-38546
- FLAP**
- S JET FLAP
- S STABILIZATION
- S WING FLAP
- FLAP CONTROL**
- Airplane automatic-flare system actuating flaps and elevators as lift and moment controllers 15 p2418 A67-29313
- FLAPPING HINGE**
- Dynamic stability of low disk loading propeller-rotors as function of various dimensionless parameters characterizing design [AHS PAPER 132] 16 p2777 A67-31846
- FLARE**
- SA ILLUMINATION
- SA PYROTECHNICS
- SA SOLAR FLARE
- Statistical analysis of flare radiation intensity and brightness distribution of irregular and semiregular variables 07 p1248 A67-19486
- Optical instrument for measurement and control of tube flares in connections in liquid propulsion systems 18 p3054 A67-34366
- Flare and landing performance of glide vehicles with low lift-drag ratio, noting aerodynamic characteristics effect [AIAA PAPER 67-575] 19 p3335 A67-35970
- Sudden commencement of November 13, 1960 caused by cosmic ray flare of November 12 20 p3517 A67-36284
- Lunar crater Alphonsus emission flare noting C-2 Swan system proposal 20 p3528 A67-37470
- FLARED BODY**
- Laminar, transitional and turbulent boundary layer flows with adverse pressure gradient on axisymmetric blunted conical flared body at Mach 10 [AIAA PAPER 66-493] 06 p0943 A67-18844
- Aerodynamic characteristics of flared bodies noting geometry, Reynolds number and boundary layer state effects on stability 08 p1275 A67-20499
- Flared afterbody aerodynamic characteristic predictions for aircraft stability at high Mach numbers, discussing turbulent separation 24 p4093 A67-42924
- FLASH**
- Time resolution amplification of flash spectroscopy apparatus equipped with switched laser 13 p2126 A67-26599
- FLASH BLINDNESS**
- SA VISION
- Independent effect of receptor adaptation level and pupil size on production of flashblindness by high intensity short-duration flashes 13 p2060 A67-26925
- Light effects and aircraft safety studied for lightning strikes, noting temporary blindness and slowing of psychomotor reactions 23 p3945 A67-41069
- Improved dipole shutter, ophthalmic transparency for protection against high

intensity flashes 23 p3965 A67-41565
 Flash blindness effects on pilot performance simulating inadvertent exposure to nuclear bursts of light by xenon gas discharge tube 23 p3965 A67-41569
 Flash blindness, recovery time and aircraft control loss studied in flight simulator 23 p3966 A67-41580

FLASH TUBE
 Approximate absolute values of pumping power, threshold power and critical excess population for ruby laser determined from relative flash tube intensity measurements 01 p0088 A67-10245
 Flashlight /incoherent/ pumping of visible and IR, InSb and CdS-CdSe lasers 01 p0089 A67-10447
 Laser equipment for fusion welding of aerospace structural materials, examining ruby laser properties, flash tube and overall system 09 p1504 A67-22141
 Pumping efficiency of optically pumped laser, considering electric energy conversion, absorption, etc 13 p2129 A67-27349
 Single-mesh circuits design for driving xenon flashlamps, solving normalized nonlinear differential equation 19 p3192 A67-35015

FLAT LAYER
 Linear theory solution of eigenvalue problem for natural convection in horizontal layers giving characteristic Rayleigh numbers for first ten modes 08 p1427 A67-21139
 Thin shock layer stagnation region analysis in hypersonic flow, emphasizing lateral asymmetry for planar and perturbed axisymmetrical cases 10 p1624 A67-22936

FLAT PLATE
 Approximate solution of stationary boundary layer problems involving flow of viscous incompressible conducting fluid around flat plate in presence of magnetic field 01 p0123 A67-10540
 Impingement of supersonic jet on flat plate studied for variety of jet Mach numbers, plate incidence angles and plate locations downstream of nozzle outlet 01 p0006 A67-10792
 Laminar boundary layer on flat plate at high Prandtl number, obtaining temperature profile, recovery factor and heat transfer 01 p0052 A67-10795
 Variational principles for plate bending problems not subjected to boundary conditions 01 p0162 A67-10850
 Theory for incompressible two-dimensional flow of inviscid liquid past array of similar hydrofoils, behind each of which extends cavity of finite length 01 p0053 A67-10851
 Interaction between boundary layer and external inviscid flow, noting unsteady motion of gas around infinite plate and steady flow around semiminfinite plate 01 p0053 A67-10983
 Hypersonic flow over blunt flat plate with surface mass transfer 01 p0007 A67-11180
 Hydrodynamic stability equations for free convection flow over vertical uniform flux plate 01 p0055 A67-11189
 Transient forced convection laminar film condensation on horizontal plate, noting film thickness changes and heat-transfer coefficient variations 01 p0168 A67-11229
 Exact expressions derived for deflection, swept volume and ratio of balancing force to total thrust due to pressure for flat circular plate 01 p0164 A67-11273
 Elastic-plastic solution for circular rigid inclusion in unidirectionally stressed flat plate of linearly strain-hardening material 02 p0336 A67-11633
 Center of pressure stabilization for thin wing profile with downward deflected trailing edge, when placed in steady state flow of ideal incompressible fluid 02 p0179 A67-12438
 Viscous incompressible flow past finite flat plate obtained under Oseen approximation for large and moderate Reynolds numbers, using Wiener-Hopf technique 02 p0234 A67-12546
 Flow induced by infinite flat oscillating plate in incompressible dusty gas 02 p0234 A67-12548
 Hypersonic flow separation over simple geometries and aerodynamic controls, noting pressure gradients and heating-rate distributions [AIAA PAPER 65-753] 03 p0350 A67-12911
 Critical load equations for plate weakened

by sharp stress raisers extended to account for effect of arbitrarily oriented external forces 03 p0522 A67-13122
 Vented profile in free surface flow of finite depth, computing lift and drag 03 p0402 A67-13449
 Heat and mass transfer from vertical plates boundary layer in convection at low Reynolds number by interferometry [ASME PAPER 65-WA/HT-39] 03 p0404 A67-14011
 Pressure variational law effect along boundary layer of flat plate on formation of turbulent spots measured via hot-wire technique 04 p0602 A67-14598
 Laminar flow on adiabatic surface measured, using Stanton tube and supersonic wind tunnel 04 p0547 A67-14849
 Force measurements and visual observations made in water tunnel on fully wetted and ventilated flows past family of conical ring wing hydrofoils having flat plate section geometry [ASME PAPER 66-WA/UNT-4] 04 p0608 A67-15383
 Nongray radiation effects on laminar boundary layer of absorbing gas over flat plate at low Eckert numbers [ASME PAPER 66-WA/HT-35] 04 p0724 A67-15428
 Combined free and forced convection over electrically insulating vertical plate of constant temperature with transverse magnetic field with plate moving up or down [ASME PAPER 66-WA/HT-38] 04 p0724 A67-15429
 Free stream turbulence and pressure gradient effects on flat plate boundary layer velocity profiles and heat transfer [ASME PAPER 66-WA/HT-4] 04 p0608 A67-15448
 Interferometer measurements of laminar forced convection in entrance region between parallel flat plates [ASME PAPER 66-WA/HT-16] 04 p0608 A67-15449
 Laminar free convection of radiation absorbing-emitting fluid along flat plate noting interaction effects, solving problem by singular perturbation 04 p0727 A67-15682
 Wall shearing stress and heat transfer measurements through turbulent boundary layer on heated flat plate in accelerating and decelerating airflow 04 p0731 A67-15819
 Mach number and temperature ratio effects on convective heat-transfer coefficient to flat plate through turbulent boundary layer in air and Stanton number calculation in terms of drag coefficient 04 p0731 A67-15820
 Local heat-transfer coefficients between isothermal flat plate and two-dimensional wall jet 04 p0732 A67-15835
 Frozen layer that forms when warm liquid flows over flat plate cooled below freezing temperature of liquid by coolant flowing along other side of plate 04 p0735 A67-15856
 Uniform flow of very high temperature radiating gas over semiminfinite flat plate 04 p0737 A67-15863
 Nonsimilar free convection boundary layer from vertical flat plate with step discontinuities in surface temperature [ASME PAPER 66-WA/HT-17] 04 p0739 A67-15930
 Radiation effects on heat transfer and friction characteristics in natural and forced convection film boiling in boundary layer flows [ASME PAPER 66-WA/HT-6] 04 p0739 A67-15939
 Radiation transfer effect on equilibrium temperature for laminar boundary layer flow of absorbing-emitting gas over flat plate [ASME PAPER 66-WA/HT-48] 04 p0739 A67-15940
 Three-dimensional flow separation over structures with various geometric configurations, calculating limiting streamlines for subsonic laminar boundary layer conditions 05 p0747 A67-16293
 Two-phase flow of gas over harmonically oscillating flat plate expressed in laminar boundary layer terms, presenting liquid film thickness, heat transfer rate, skin friction, etc 05 p0793 A67-17338
 Ion density profiles in boundary layers associated with supersonic flow of shock heated air over flat plate measured by cylindrical and flush-mounted electrostatic

probes [AIAA PAPER 66-159] 05 p0856 A67-17345
 Minimum potential energy principle and Rayleigh-Ritz method derivation of flutter equations for flat rectangular orthotropic panels 05 p0924 A67-17350
 Plane flow of radiating gas over semiminfinite flat plate, considering upstream effect when energy equation becomes elliptical 05 p0928 A67-17358
 Hydromagnetic compressible boundary layer flow past flat plate analyzed via von Karman integral method 05 p0794 A67-17361
 Laminar heat transfer in thermal viscous MHD flow past semiminfinite flat plate 05 p0857 A67-17411
 Compressibility effect on dual solutions recurrence in MGD boundary layer over flat plate 06 p1041 A67-18134
 Turbulent boundary layer characteristics of compliant surfaces, using hot-wire anemometer to measure velocity profiles, Reynolds stresses and skin friction [AIAA PAPER 67-128] 06 p0987 A67-18336
 Skin friction under mass injection on porous flat plate in supersonic turbulent flow [AIAA PAPER 67-194] 06 p0987 A67-18341
 Static temperature-velocity distribution for zero pressure flat plate compressible turbulent boundary layer with heat transfer [AIAA PAPER 67-195] 06 p1116 A67-18362
 Variable laminar boundary layer equations for air flows over flat plate with injection of foreign gases through solid surface 06 p1116 A67-18380
 Heat transfer to catalytic and noncatalytic surfaces on sharp flat plate in shock tube gas flow for checking various laminar boundary layer theories [AIAA PAPER 67-163] 06 p0989 A67-18481
 Electrically conducting boundary layer flow past flat plate in TM field 06 p1043 A67-18677
 Local skin friction coefficient for turbulent boundary layers on smooth flat plates measured, using Preston tube 06 p0990 A67-18751
 Erosive burning of ammonium perchlorate solid propellants for combustion in turbulent boundary layer determined, using flat plate heat transfer correlation 07 p1238 A67-19069
 Oseen flow past semiminfinite plate and vertical force formulated by integral equations solved for drag and lifting singularities distribution, using Wiener-Hopf technique 08 p1319 A67-20350
 Velocity distribution of turbulent incompressible boundary layer along flat plate with assumed polynomials of shearing stress and mixing length 08 p1319 A67-20405
 Supersonic flutter characteristics of thin cantilever plate surfaces with low aspect ratio 08 p1416 A67-20530
 Manufacturing process and life testing of bismuth telluride alloy based flat plate thermoelectric solar cells for near earth orbits 08 p1283 A67-20648
 Approximate solution of some nonstationary boundary layer problems with allowance for magnetic field, discussing nonsteady flow of viscous incompressible electrically conducting fluid past flat plate 08 p1362 A67-21202
 Rayleigh problem of compressible viscous heat-conducting radiating gray gas flow near flat plate set impulsively in motion in own plane 08 p1324 A67-21392
 Heat transfer data obtained from film boiling for four liquid compositions, using flat plate geometry method 10 p1732 A67-22729
 Supersonic delta wing problem, discussing new approach in determining flow parameters 10 p1593 A67-23687
 Wall temperature and speed ratio effects on free molecule flow number density distribution about flat plate 11 p1881 A67-23880
 Laminar heat transfer rate to two-dimensional blunt base in supersonic flow evaluated for varying Reynolds, flow and shock Mach numbers 11 p1882 A67-24222
 Asymptotic solution method for frozen dissociated laminar boundary layer flow over flat plate surface with arbitrarily distributed catalytic 11 p1781 A67-24573
 Stress intensity analysis for flat plates loaded close to edge crackline, giving intensity dependence on crack length and specimen shape 11 p1875 A67-24588

- Viscous flow around flat plate at various angles of incidences at high Mach number to evaluate shock wave intensity variation and wall pressure distribution 11 p1742 A67-24761
- Thermal and ablative lag induced by periodic heat input to oscillating flat plate in high velocity flow, showing crossover from dynamically stabilizing to destabilizing condition as oscillation frequency increases [AIAA PAPER 67-336] 12 p2039 A67-26050
- Wire screen roughnesses effect on turbulent boundary layer along flat plate without pressure gradient 13 p2093 A67-26529
- Unsteady perturbation effect of external velocity on laminar boundary layer 13 p2094 A67-26645
- Flat plate loading effects for large displacements, determining solution to plates of arbitrary shape under general loading by iterative matrix technique 13 p2217 A67-26704
- Displacement and momentum loss thickness in boundary layer of rough flat plate at low velocities as function of wall roughness, pressure gradient, etc 13 p2095 A67-26809
- Thermal boundary layer equation reduced to ordinary differential equation for flat plate with given heat conductivity 13 p2224 A67-27048
- Viscous fluid flow stability in boundary layer on plate, applying perturbation method, calculating critical values of modified Reynolds numbers 13 p2105 A67-27051
- Temperature field in plates and shallow shells with internal heat sources noting solutions for various boundary conditions 13 p2224 A67-27056
- Transition delay and skin friction drag reduction by considering boundary layer flow over flexible aerodynamic surface [AIAA PAPER 66-430] 13 p2106 A67-27585
- Thermionic converter acceleration plate and excessive current flow effects, noting collector and cathode surface secondary electron removal, determining cut-off characteristic form 14 p2246 A67-27766
- Change Transitional rarefied flow regime noting drag on simple bodies, flows at sharp edges, lifting bodies, etc 14 p2299 A67-28161
- Viscous hypersonic flow past leading edge of sharp flat plate analyzed, using Navier-Stokes equation and velocity slip and temperature jump wall boundary conditions 14 p2299 A67-28162
- Continuum flow analysis for leading edge region of flat plate, using model based on hypersonic thin layer type of approximation 14 p2240 A67-28163
- Pressure on sharp-edged insulated flat plate in low density hypersonic flow, noting results and possible sources of error 14 p2241 A67-28164
- Flow field measurement near sharp leading edge of cooled flat plate parallel to low density hypersonic stream 14 p2241 A67-28165
- Low density hypersonic wind tunnel, noting surface pressure and flow field measurements 14 p2293 A67-28166
- Electron beam density survey in low density hypersonic flow field over sharp flat plate, noting results in outer and inner part of shock layer 14 p2241 A67-28167
- Cylindrical bending of plate composed of strengthening and binding agents with different Youngs moduli 14 p2401 A67-28734
- Flow of conducting incompressible viscous fluid near accelerated plate under parallel plate and magnetic field, noting velocity profiles and stress role 14 p2361 A67-28814
- Computer program for solution of large deflection nonlinear problems of elastic flat plates using grid analogy 14 p2403 A67-29015
- Free stream turbulence and pressure gradient effects on flat plate boundary layer velocity profiles and heat transfer [ASME PAPER 66-WA/HT-4] 15 p2470 A67-29321
- Aerodynamic heating through turbulent boundary layer of flat plate determined using Ferrari formula 15 p2415 A67-29328
- MHD boundary layer flow past semiminfinite plate, applying fluctuating magnetic field to plate 15 p2510 A67-29631
- Boundary layer problem concerned with effects of radiation absorption and emission for flow of high speed gas over flat plate [AIAA PAPER 66-521] 15 p2473 A67-30207
- Flat plate, simultaneous heat and mass transfer for Newtonian fluids in free convection analyzed, using group theory 15 p2582 A67-30217
- Hypersonic weak and strong interaction theory for case of uniform flow past flat plate, discussing boundary layer characteristics 15 p2473 A67-30220
- Shock tunnel experiments with hypersonic turbulent boundary layer flow over flat plates with blunt and sharp leading edges and wall of expansion nozzle 16 p2659 A67-30954
- Boundary layer in low speed flow over dispersively coupled system of acoustic resonators, noting excitation by flexible wall of oscillations 16 p2660 A67-31214
- Hydrodynamic stability problems solutions by numerical methods of Orr-Sommerfeld equations 16 p2661 A67-31419
- Inviscid steady partially cavitating flow through cascade of flat plate hydrofoils 16 p2662 A67-31550
- Book on thin walled structures covering frame buckling, elastic buckling of rectangular flat plates, edge loading, anisotropic plate structures, etc 17 p2956 A67-32021
- Buckling of compressed thin walled structural sections, noting design concepts and flat plate theories 17 p2957 A67-32025
- Correction for experimental velocity profile in compressible laminar boundary layer flow over flat plate 17 p2840 A67-33165
- Incompressible fluid flow past semiminfinite flat plate during ejection of another fluid from plane surface into main flow solved using motion equations 18 p3025 A67-33571
- Numerical solutions of hypersonic sharp leading edge flows, with full time-dependent Navier-Stokes equations solved 18 p2984 A67-34739
- Thermal stress concentration factors for rectangular flat plates penetrated by holes 19 p3337 A67-34823
- Temperature distribution within two-dimensional thermal boundary layer due to flow of second order fluid past flat plate 19 p3210 A67-35447
- Hot-wire anemometer response in turbulent flow studied requires correction leading to constant results when applied to flat plate bluff body wakes normal to stream 19 p3230 A67-35523
- Flow of incompressible viscous fluid past plane body, when flow boundary layer detaches from body producing aerodynamic wake 19 p3171 A67-35632
- Hypersonic rarefied flow past sharp leading edge of flat plate noting incomplete compression phenomenon 19 p3171 A67-35735
- Heat transfer to catalytic and noncatalytic surfaces on sharp flat plate in shock tube gas flow for checking various laminar boundary layer theories 19 p3211 A67-35739
- Laminar incompressible boundary layer on isothermal flat plate with strong blowing, comparing different solutions 19 p3211 A67-35754
- Transition region of hypersonic boundary layer on flat plate surveyed with hot wires, giving analysis for limited wire calibration 19 p3212 A67-35765
- Supersonic flutter characteristics of thin cantilever plate surfaces with low aspect ratio 19 p3343 A67-35775
- Mean heat transfer coefficient at flat plate with turbulent boundary layer at zero incidence Mach numbers mean heat-transfer coefficient at flat plate with turbulent boundary layer at zero incidence Mach 20 p3543 A67-36275
- Momentum integral method applied to two-dimensional flow problem between flat plates 20 p3420 A67-36420
- Laminar boundary layer flow of water over flat plates, noting heat transfer effects on velocity profile stability [ASME PAPER 67-HT-41] 20 p3547 A67-36725
- Transient mean wall temperature of flat plate with time dependent heat source and cooled by incompressible turbulent flow, discussing heat-transfer coefficient [ASME PAPER 67-HT-45] 20 p3547 A67-36727
- Approximate solution to heat transfer coefficient on flat plate in linear shearing flow [ASME PAPER 67-HT-46] 20 p3547 A67-36728
- Energy equation for laminar convective heat transfer in combined hydrodynamic and thermal entrance region bound by parallel flat plates [ASME PAPER 67-HT-48] 20 p3548 A67-36730
- Mass transfer cooling of carbon dioxide-nitrogen binary system in laminar boundary layer, stressing dissociation effect [ASME PAPER 67-HT-70] 20 p3550 A67-36750
- Nonconstant gravity field effect on free convective heat transfer to or from isothermal flat plate [AICHE PAPER 2] 20 p3552 A67-36825
- Hypersonic weak-interaction similarity solutions for viscous heat-conducting compressible flow past flat plate, using Navier-Stokes equations 20 p3357 A67-36849
- Volumetric absorption coefficient effect on Rosseland equilibrium radiative heat transfer and temperature profiles in optically thick fluid flowing past flat plate 20 p3553 A67-36936
- Simply-supported elliptic plate free vibration problem applying Rayleigh-Ritz technique to obtain fundamental frequencies 20 p3539 A67-37007
- Response of plate to fluid loading, determining fluid pressure induced by plate motion 20 p3539 A67-37009
- Turbulent boundary layer theory for streamline flow over impermeable plate, noting viscous interface effect 20 p3424 A67-37461
- Viscoelastic flow, examining boundary layer approximation for flat plate with zero angle of incidence 20 p3424 A67-37503
- Growth of laminar compressible boundary layer with stationary origin on uniformly moving flat plate, noting analogy to shock induced flow 21 p3611 A67-37927
- Supersonic delta wing problem, discussing new approach in determining flow parameters 21 p3564 A67-38288
- Flat plate bending and two-dimensional, axisymmetric and boundary value problems in elasticity theory investigated using Vlasov initial function method 21 p3725 A67-38792
- Second order weak interaction expansion for hypersonic flow past adiabatic flat plate, obtaining expressions for static pressure, displacement thickness and skin friction 21 p3566 A67-38892
- Transitional and turbulent boundary layers on cold flat plate in hypersonic flow noting bluntness, Reynolds and Mach numbers effects 21 p3615 A67-39080
- MGD boundary layer flow for thermally conducting flat plate, deriving equations for any heat transfer condition 21 p3675 A67-39090
- Rectangular plate with clamped edges studied for nonlinear cylindrical bending under uniform pressure 22 p3910 A67-39480
- Local coefficient of heat exchange by natural convection on isothermal vertical flat plate in turbulent regime 22 p3917 A67-39648
- Incompressible laminar boundary layer flow on semiminfinite flat plate with impulsive motion solved using Meksyn steady pressure gradient boundary layer method 22 p3786 A67-40039
- Heat transfer experiments with flat plate heated under constant heat flux, discussing wall temperature distribution, Prandtl number and Spalding function 22 p3918 A67-40041
- Homogeneous isotropic elastoplastic thin flat plate under uniform unidirectional stress, studying plastic flow, fracture, distortion and slip plane inclination 22 p3915 A67-40220
- Guarded hot plate technique for measuring thermal conductivity of low conductivity materials at cryogenic temperatures 22 p3802 A67-40290
- Guarded cold flat plate calorimeter for measuring insulation thermoconductivity 22 p3803 A67-40296
- Heat transfer, skin friction and shearing stress from similar solutions to compressible laminar boundary layer equations for flow over flat plate 23 p4082 A67-41246
- Influence of sweptback wing leading edge geometry on boundary layer instability using supersonic flat plates 23 p3928 A67-41247
- Skin friction under mass injection on porous flat plate in supersonic turbulent flow [AIAA PAPER 67-194] 23 p3991 A67-41713
- Temperature distribution of fluid in laminar boundary layer of flat plate and heat flow from fluid to plate wall 24 p4143 A67-42281
- Contact region of glass ball rolling on

viscoelastic plate at various velocities analyzed by interference microscope photography [ASME PAPER 67-LUB-25]

24 p4176 A67-42683

FLAT SURFACE

Turbulent boundary layer-flat surface interfacial Stefan-Nusselt flow effects on apparent kinetics of heterogeneous chemical reactions in forced convective systems

04 p0567 A67-15681

Flow field around porous wedge or cone immersed at zero angle of attack in uniform supersonic free stream when contact surface is straight

08 p1276 A67-20571

Electromagnetic wave propagation across land-sea boundary on flat earth near coastline

11 p1751 A67-23967

Heat transfer of pulsating liquid jet impinging on perpendicular flat surface and spreading laminarily

11 p1882 A67-24229

Convective heat transfer for water flow in curvilinear short channel, noting flow and convection types at various sections

12 p2033 A67-25316

Spacecraft thermal joint conduction study covering surface conditions, external pressure, use of various fillers and parent materials and vacuum environment. [AIAA PAPER 67-316]

12 p2037 A67-26031

Lift and drag of trapezoidal wing models in blown flow near free surface studied for sweepback angle effect on aerodynamic characteristics

13 p2093 A67-26595

Swell generation by means of flat paddle board in translational motion

22 p3783 A67-39646

Lloyd mirror experiment applied to testing flatness of large surfaces, using moiré technique for visualizing and measuring fringe deviation

23 p4002 A67-41263

Semilempirical solution for heat transfer during turbulent natural convection near vertical impermeable flat surfaces

24 p4253 A67-42251

FLATTENING

Tables of observational data on flattening, integrated brightness, brightness distribution and polarization of white corona

01 p0150 A67-10933

FLAW DETECTION

SA NONDESTRUCTIVE TESTING

SA X-RAY INSPECTION

Nondestructive ultrasonic detection of surface or internal flaws

03 p0430 A67-13549

Laser microprobe used to study small inclusions in metals

04 p0634 A67-15461

Postmortem flaw detection methods and equipment for IC failure analysis

06 p0968 A67-18054

Ultrasonic immersion inspection apparatus for structural defects detection in turbine blades

06 p1007 A67-18103

Quality criteria in production flaw detection work, quantitatively estimating transition probability matrix and using error theory

06 p1007 A67-18104

Microcircuitry leakage path detection using scanning electron microscopy

09 p1473 A67-22017

UVFD-1 ultrasonic velocimetric flaw detector for inspection of nonmetallic laminated structures and products

09 p1502 A67-22096

Thermal IR inspection technique for bond flaw inspection in simulated solid propellant rocket engines

09 p1508 A67-22528

Nondestructive testing of dielectric materials by microwave techniques

10 p1660 A67-23014

Nondestructive testing in aircraft industry evaluated, considering role in aircraft structural design, crack detection, etc

11 p1799 A67-24654

Nondestructive testing methods noting applicability to flaw detection and quality control

12 p1948 A67-25138

Gamma flaw detectors for radiographic inspection

13 p2122 A67-26254

Flaw detection methods using penetrating fluids, emphasizing fluorescent materials and pigments

13 p2122 A67-26255

Ultrasonic flaw detection of hidden cracks in turbine blades

14 p2395 A67-27872

Color contrast penetration method for crack detection in aircraft engines and motor car parts

18 p3045 A67-33739

Welds qualification system based on radiographically determined macrostructure defectiveness, classifying defects according

to size and distribution

18 p3053 A67-33742

Aluminum welded joints investigated by radiographic and metallographic methods for bubbles and cracks

18 p3053 A67-33743

Detection of contaminating processes in integrated circuits, describing characteristics associated with incipient failure in operational equipment

18 p3057 A67-34665

Collection of papers on integrated circuit technology covering instrumentation and techniques for measurement, process and failure analysis

19 p3192 A67-35018

Electronic parts degradations induced by assembling and packaging environments investigated for effects upon failure modes

22 p3771 A67-39834

Electronic or electromechanical failure-prone component pinpointing using various nondestructive testing methods

23 p4009 A67-40912

AIDS data processing and analysis system for automated fault diagnosis and equipment trend prediction, describing methods applied to aircraft

[AIAA PAPER 67-792]

24 p4126 A67-42953

FLEET BALLISTIC MISSILE /FBM/

WEAPON SYSTEM

S POLARIS MISSILE

FLEXIBILITY

SA ELASTICITY

SA PLASTICITY

Flexibility and rigidity requirements imposed on vibration damping systems of optimized precision devices

06 p1106 A67-18618

Book on matrices for structural analysis, including elementary algebra and detailed arithmetic of matrix methods applied to structure theory

10 p1719 A67-23476

Flexibility and mass distribution effect on vibration response of general continuous structures

[ASME PAPER 67-VIBR-44]

11 p1873 A67-24196

Implications and ramifications of theory of cutouts in displacement method

19 p3343 A67-35771

Cryogenic flexibility of single and multiple ply thin polymeric film tested for porosity, cycle life and film thickness relation

24 p4176 A67-42468

FLEXIBLE BODY

In-flight bending moment and terminal drift minimization for flexible vehicle, applying two-point boundary value problem solution for optimum rigid body control system

04 p0706 A67-15422

Externally pressurized gas bearing, noting construction applications and performance characteristics of hydrodynamic foil

05 p0812 A67-17106

Dynamic response, sloshing frequencies and stability of free surface of liquid in circular cylindrical elastic tank with flexible bottom

[AIAA PAPER 67-76]

06 p0986 A67-18274

Solar radiation field interaction with flexible antenna as possible explanation of anomalous rapid spin decay of satellites

[AIAA PAPER 67-39]

06 p1096 A67-18350

Dynamic behavior of large flexible bodies in orbital motion around gravitating center, emphasizing response and stability of elastic degrees of freedom

08 p1383 A67-20562

Aerodynamic forces on flexible plate embedded in right half-space undergoing arbitrary temporal and spatial motion

08 p1424 A67-21433

Bending of flexible tubes using variational calculus of Rayleigh-Ritz type

09 p1579 A67-22606

Optimal control of maneuver induced vibration in flexible aerospace vehicles

10 p1714 A67-23754

Systems constraints imposed on spacecraft utilizing long flexible rods with attached tip masses, specifically deployment and retraction problems

10 p1714 A67-23757

Time dependent pressure distribution and threshold acceleration for bubble formation in longitudinally vibrating flexible liquid filled cylinder

[ASME PAPER 67-FE-1]

14 p2304 A67-28354

Librational and flexural resonances induced in satellite whose center of mass is moving in planar elliptic orbit

15 p2572 A67-30195

Ride quality improvement on flexible aircraft by means of elastic structural bending mode suppression design technique

[AIAA PAPER 67-571]

19 p3174 A67-35967

Linear optimal control technique for flexible-booster control system design showing drift minimum model with matrix transformations for closed-loop dynamics

19 p3336 A67-35967

Dynamic response, sloshing frequencies and stability of free surface of liquid in circular cylindrical elastic tank with flexible bottom

[AIAA PAPER 67-76]

21 p3614 A67-38866

Empirical method predicting flexible hose flow losses, with Fanning friction factor as Reynolds number and internal hose geometry function

22 p3785 A67-39977

Liquid sloshing cylindrical tank with elastic bottom for investigating surface tension effect at liquid gas interface of partly filled container

22 p3787 A67-40171

Optimal control of maneuver induced vibration in flexible aerospace vehicles

23 p4071 A67-41722

Dynamic response of large flexible space systems subjected to motion inputs and arbitrary force, analyzing joined Timoshenko beams

24 p4240 A67-42391

Flexible membrane hydrostatic air bearing determining membrane shape, pressure distribution and air gap by Navier-Stokes and membrane analogy equations

[ASME PAPER 67-LUB-1]

24 p4162 A67-42666

FLEXIBLE WING

Flexible wing analysis based on slender body theory, calculating wing profiles, pressure distribution as function of stress and lift force values

03 p0351 A67-12992

Aerodynamic qualities of flexible wings, noting performance, lift drag ratio, application to powered aircraft and cargo gliders

03 p0359 A67-12993

Flexible wings for hypersonic vehicles allowing for safe controllable landings stressing leading edge parawing concept flow visualization, lift-drag ratio, etc

[AIAA PAPER 67-200]

07 p1258 A67-19444

Flexible sailplane designs allowing for towing cable analyzed with analog computer for gust loading

10 p1593 A67-23013

Longitudinal static stability margin of glider for small lift coefficients showing effect of torsional deformation

16 p2596 A67-31001

FLEXURE

Large deflections of beam loaded and supported at two points

11 p1871 A67-24088

Flexural vibrations of plates studied by moiré method for nodes, antinodes, local amplitude and phase distributions

12 p1966 A67-25293

Hilbert boundary problem extension for flexural problems of cracks in mixed media noting Cauchy integrals, Plemelj formulae, etc

16 p2770 A67-31292

Nonlinear flexural vibrations of rings studied without assuming zero midplane strain

17 p2963 A67-33033

Bond-layer compliances effect on flexural responses of sandwich beam, discussing homogeneous and composite beams, deformation equations, etc

[SESA PAPER 1214]

18 p3142 A67-33891

Linear theory of initially straight elastic rods, discussing wave propagation, thermal effects for extension and flexure and torsion

18 p3144 A67-34281

Flexure-torsion cascade flutter of airfoils with two degrees of translational and torsional vibration

22 p3914 A67-40044

Flexural vibration of stiffened circular plates with respect to rotatory inertia obtaining differential equation

23 p4073 A67-40611

FLIGHT

S BALLOON FLIGHT

S BUFFETING

S FREE FLIGHT

S HYPERSONIC FLIGHT

S INTERPLANETARY FLIGHT

S JET FLIGHT

S LUNAR FLIGHT

S METEOROLOGICAL FLIGHT

S OVER-WATER FLIGHT

S PARABOLIC FLIGHT

S PREFLIGHT ANALYSIS

S PREFLIGHT OPERATION

S RECORD-SETTING FLIGHT

S ROCKET FLIGHT

S SPACE FLIGHT

S SUPERSONIC FLIGHT

S TRANSONIC FLIGHT

S VERTICAL FLIGHT

FLIGHT ALTITUDE

Physiological effects of high altitude flights on human organism 12 p1903 A87-26164
Long duration random vibration effects on human response in simulated low altitude high speed flights 14 p2257 A87-28660
Night and day carrier landing pilot performance, noting altitude position estimation inaccuracy as contribution to higher accident rate 23 p3968 A87-41618

FLIGHT CHARACTERISTICS

SA AIR SPEED

Dragon rocket probe, launch history and flight modifications 03 p0517 A87-13028
Doppler system for missile and bullet velocity measurements noting design parameters, equipment used and range improvement obtained 04 p0653 A87-15044
Flights tests of XH-51A compound helicopter, discussing rigid rotor concept and results of compound flight research program

[AIAA PAPER 87-262] 07 p1130 A87-20075

Dynamic flight characteristics of spin-stabilized sounding rockets during passage through atmosphere, emphasizing roll resonance and motions leading to roll lock-in and angle of attack 08 p1407 A87-20514
Black Brant sounding rocket fin design, discussing flight characteristics, engine selection criteria and stability parameters 08 p1416 A87-20532

Nike-Tomahawk rocket aeroelastic behavior, noting occurrence of large extra-atmospheric coning angles 08 p1416 A87-20534
Computer controlled dynamic test facility to provide data on flight characteristics of Apollo-Saturn V launch vehicle by measuring vibration amplitudes 14 p2293 A87-28593

Missile dynamic behavior analysis using linear aeroballistic theory in conjunction with numerical computations of motion equation 14 p2395 A87-29058
Flight data of X-15 research aircraft noting development, operation and economic aspects of performance 15 p2420 A87-29848

Boeing 747 characteristics for passenger and cargo service noting economic gain, operational performance, control cabin, engine, etc

[AIAA PAPER 87-397] 15 p2421 A87-30364

Bell Model 286 composite VTOL aircraft, discussing tilting rotor principle for conversion from helicopter to aircraft 16 p2595 A87-30495
Optimal thrust-weight ratio for lifting engines of VTOL aircraft 18 p3110 A87-33544

Black Brant sounding rocket fin design, discussing flight characteristics, engine selection criteria and stability parameters 21 p3712 A87-37807

Turbojet engine gasdynamic parameters dependence on reduced rotational velocity for in-flight characteristics determination, assuming variable compression and critical pressure ratio 24 p4207 A87-41916

Nike-Tomahawk rocket aeroelastic behavior, noting occurrence of large extra-atmospheric coning angles 24 p4242 A87-42912

Dynamic flight characteristics of spin-stabilized sounding rockets during passage through atmosphere, emphasizing roll resonance and motions leading to roll lock-in and angle of attack 24 p4242 A87-42917

V/STOL airline economics simulated with computerized dynamic programming model [AIAA PAPER 87-841] 24 p4096 A87-42979

FLIGHT CLOTHING

SA PRESSURIZED SUIT

SA PROTECTIVE CLOTHING

Clothing hygiene with particular reference to aerospace problems 06 p0954 A87-17998
Hygiene of aerospace protective clothing, studying garments characteristics, disinfection and related skin diseases 16 p2619 A87-31476

Physiological protection by aviator flight suit coverall when on raft in open sea after downing, noting circulating water effect 23 p3967 A87-41608

Ventilated wet suit /VWS/ for varying flight cockpit environment and emergency condition thermal protection, assessing physiological responses 23 p3967 A87-41614

Military flight clothing tested in actual survival conditions for ability of subject to withstand moderate sea water environment [AIAA PAPER 87-968] 24 p4118 A87-43046

FLIGHT CONDITION

Design procedure for slender multistage fast-burning rockets, noting modified flexural behavior and aerodynamic load 08 p1416 A87-20529

Flight control requirements of reusable launch vehicles 15 p2570 A87-29857
Wing pivoting design for supersonic aircraft adaptability to different flight conditions, noting experiments with F 111 16 p2590 A87-30839

Vibrophonocardiographic techniques for monitoring cardiac dynamics in flight environment 17 p2806 A87-31954

Synthesis of closed loop system consisting of pitch control adaptive autopilot for changing flight conditions, using transient characteristics 18 p3075 A87-34282

Digital program for stability-augmentation system-gain values yielding desired pole-zero locations for vehicle transfer functions of flight conditions 21 p3568 A87-38539

FLIGHT CONTROL

SA ATTITUDE CONTROL

SA IN-FLIGHT MONITORING

SA MANEUVER

Flight control problems and techniques in space age 01 p0153 A87-10267

Hybrid computer simulation of reentry guidance for lifting vehicle, noting compatibility of temperature rate flight control system with other vehicle controls 01 p0051 A87-11438

Linearly-approximated characteristics of maneuvers correcting near-planet positions of spacecraft with pulsed flight velocity characteristics 02 p0321 A87-11536

Interactions and relationships between man and machine in flight guidance 02 p0185 A87-11551

Triplex flight control system for VTOL aircraft noting new servomotor, simple mechanical construction and increased reliability 02 p0284 A87-12206

TVC flight dynamics and trajectory optimization analysis of pulse, singular and sliding regimes 03 p0509 A87-13184

Performance requirements of dynamic flight simulators and visual display systems in man-machine flight control problems 03 p0395 A87-13385

Low weather minima flight control system consisting of autopilot, flight system and gyromagnetic compass 03 p0466 A87-14385

Adaptive flight control using parameter tracking mechanism functioning with any type of disturbance as input, for adjustment of control system parameters [ASME PAPER 86-WA/AUT-22] 04 p0552 A87-15393

Book on electronic testing covering RF interference, tracking systems, receivers and transmitters, flight control equipment, digital computers, etc 04 p0577 A87-15726

Automatic flight control systems for missiles and aircraft, noting error sensing and correcting functions, calibration and testing methods 04 p0655 A87-15735

Hydraulic power distribution system for flight control of F-111 aircraft 05 p0752 A87-16158

Powered flying control systems developments, considering reliability and autostabilization 05 p0753 A87-16750

Controllability limit of human pilot for unstable second order system with positive static stability analyzed by modified transfer function and servomechanism theory 05 p0757 A87-17354

Transfer from elliptical orbit to coplanar hyperbolic asymptote treated in terms of limited classes of one- and two-impulse maneuvers [AAS PAPER 86-127] 07 p1255 A87-19986

Flight attitude control problems of manned lunar landing vehicles emphasizing pitch control [AIAA PAPER 87-239] 07 p1129 A87-20045

Ground and flight tests to evaluate lunar landing research vehicle fly-by-wire control system [AIAA PAPER 87-273] 07 p1129 A87-20048

Lunar landing simulation data, noting pilot performance and manual control modes [AIAA PAPER 87-241] 07 p1165 A87-20062

Aerodynamics of sounding rockets, discussing stabilization by fins, conical flares, etc 08 p1275 A87-20498

Mathematical models for use in hybrid computer simulation for design of Integrated

Helicopter Avionics System /IHAS/, analyzing operational modes of automatic flight control system 08 p1350 A87-20658

Laws for aircraft control in terrain-following and formation-flight modes of operation, applying solution of Euler-Poisson equation 08 p1351 A87-20700

XV-4B vertical lift aircraft with lift engines noting stability, control, structural design, flight control system, etc 09 p1439 A87-22284

Two electronic displays for aircraft using basic elements necessary for flight path control in problem of easy assimilation of information by pilot 10 p1601 A87-22905

Flight control magnetic source interaction with ionized gas induced by bow shock ahead of blunt body in hypersonic flow 10 p1592 A87-23143

Terrain following pulsed radar system without continuous scanning noting computer simulation, antenna and pitch control 11 p1752 A87-24259

Divergent vertical helicopter oscillations resulting from physical presence of pilot in collective control loop 11 p1744 A87-24591

Automatic flight control development for general aviation, discussing fluidics, electropneumatic servoactuator and microelectronics [SAE PAPER 87-0255] 12 p1895 A87-25505

Mechanical cascade toroidal servo flight control system tested using simulator [SAE PAPER 87-0269] 12 p1895 A87-25867

Space vehicle flight control with minimum total characteristic velocity, determining optimum points for applying correcting acceleration 13 p2213 A87-27320

Man-machine compatibility in very low altitude flight determined by two-phase controlled field experiments on obstruction avoidance task 14 p2256 A87-27742

Fluid flight control systems, discussing attitude and angular rate stabilization systems 14 p2248 A87-28273

Automatic fluoric gain changer circuit for flight control systems counteracting Mach number and altitude pressure effects 14 p2251 A87-28352

Magnetohydrodynamic drag and flight control available to vehicle entering earth atmosphere calculated, including induced magnetic fields effects and nonscalar conductivity 14 p2394 A87-29041

Hover augmentation system reducing VTOL pilot task in maintaining position by providing damping signals for automatic flight modes with accurate path control 14 p2246 A87-29082

Concorde automatic flight control system noting autostabilization, autopilot, electric trim, autothrottle, etc 15 p2419 A87-29508

Software tools for certifying operational flight programs 15 p2440 A87-29604

Flight control requirements of reusable launch vehicles 15 p2570 A87-29857

Discrete interval binary-noise perturbation signal application for identification and compensation of three-variable self-adaptive flight control system 15 p2572 A87-30319

Extravehicular space maneuvering units, manned and unmanned, in satellite laboratory systems, describing space flight requirements and systems configuration 16 p2615 A87-30631

Linearly-approximated characteristics of maneuvers correcting near-planet positions of spacecraft with pulsed flight velocity characteristics 16 p2752 A87-31602

Lapunov-derived fixed gain flight control system design to fulfil response requirements over wide range of parametric variations 16 p2763 A87-31644

Applied synthesis technique using feedback and command controller elements for strongly interacting multivariable control systems, illustrated by flight control system design 16 p2849 A87-31661

Time optimal adaptive control system synthesis using off-line memorization with simple on-line calculations to determine control signal 16 p2650 A87-31672

Dynamic response of sailplanes to elevator control in longitudinal maneuvers, discussing load factors and tail loads as function of aerodynamic and inertial parameters 16 p2597 A87-31786

Turboprop lift fan concept for VTOL propulsion system, noting control capability, future potential, etc

[AHS PAPER 115] 16 p2737 A67-31831
Handbook of telemetry and remote control
considering position measuring, missile
guidance, flight control, data processing,
feedback information, communications
etc 16 p2633 A67-31916
Flight control hydraulic systems for
Boeing 2707 SST noting absence of radical
changes in operating procedures 17 p2793 A67-31968
Flight control power distribution systems
for hypersonic aircraft, considering cooled
and pulsating flow hydraulic, liquid metal,
pneumatic and mechanical systems 17 p2800 A67-31970
XC-142A flight control and stability
augmentation systems 17 p2794 A67-31996
C-5A flight control system, examining
subsystems, handling qualities, hydraulic
power distribution and mechanical failures 17 p2794 A67-31997
Controls Development /CODE/ program
for proving design validity of B2707 SST
flight control and hydraulic systems prior to
flight 17 p2795 A67-32004
Acceleration stress effects on pilot
performance and dynamic response 17 p2808 A67-33176
Computer simulated flights of manual
control for VTOL IFR operations indicate
display and control subsystem
deficiencies 17 p2808 A67-33183
Lunar orbiter velocity control system
design, discussing interface problems
between actuator electronics and flight
control system [AIAA PAPER 67-504] 18 p3137 A67-33968
Reliability prediction with inadequate data
in flight control systems, using nonelectric
approach combining failure data with
judgment 18 p3058 A67-34699
Northrop program for V/STOL aircraft
including systems studies, propulsion,
aerodynamics, flight control technology,
performance characteristics and operation
and testing northrop program for V/STOL
aircraft including 18 p2987 A67-34708
Telecommunication system for lunar,
planetary and deep space flight mission
control and data acquisition 19 p3207 A67-35224
Fokker F-28 aircraft systems fuel system,
auxiliary power unit, hydraulics, flight
controls, pressurization and electrical
systems and avionics 19 p3176 A67-35559
Project 666a Automatic Terrain Following
Program and Automatic Flight Control
System /AFCS/, with digital and analog
simulation and test results 19 p3174 A67-35965
SST flight control system electronic and
hydraulic systems, discussing system design,
components, reliability and test programs
[AIAA PAPER 67-570] 19 p3174 A67-35966
Boeing 727 automatic flight control and
landing system [AIAA PAPER 67-573] 19 p3258 A67-35969
Data processing using digital computer,
multiplexing and analog-to-digital conversion
equipment for flight control and
evaluation 20 p3390 A67-36465
Aircraft flight dynamics optimized in angle
of attack by variational calculus, analyzing
control system 20 p3361 A67-37377
Flight control system for future large
aircraft, obtaining structural fatigue
reduction, better handling and smoother
ride 21 p3570 A67-39133
Luna IX automatic station flight control
complex, detailing communication,
orientation and stabilization systems
operation after separation from acceleration
module 22 p3897 A67-39167
Fast and slow oscillatory spinning of
aircraft, examining equations of motion by
approximate methods based on Brodetsky
analysis 22 p3744 A67-39197
Low altitude atmospheric turbulence
analysis methods 22 p3828 A67-39665
Lunar landing simulation data, noting pilot
performance and manual control modes
[AIAA PAPER 67-241] 22 p3780 A67-40100
Handley Page Jetstream aircraft major
systems, auxiliary equipment and
instrumentation 22 p3748 A67-40132
Vehicle systems interaction effect on
guidance system stability 22 p3907 A67-40194
Spacecraft flight control and computerized
systems, discussing redundant systems,
integrated circuits and simulation for man-
machine interaction and lack of

response 22 p3908 A67-40336
US SST airframe prototype, surveying
hardware developments, flight control,
pivoting system, landing performance and
pilot cabin [AIAA PAPER 67-750] 23 p3933 A67-40984
Automatic landing system introduction for
civil transport aircraft noting certification
program and requirements and development
of operable system [AIAA PAPER 67-757] 23 p4025 A67-40990
Application of IBM 9020 multiprocessing
system to air traffic control 23 p3976 A67-41060
Anabatic winds caused by solar heating of
slope, investigating flow patterns useful for
soaring purposes 24 p4181 A67-42022
All-weather flight requirements of VTOL
aircraft, suggesting artificial stabilization by
automatic control system [AIAA PAPER 67-798] 24 p4096 A67-42959
Automatic flight management of future
high performance aircraft [AIAA PAPER 67-847] 24 p4183 A67-42983
FLIGHT DUTY
Relation of time between flights to
accident potential of pilots 23 p3970 A67-41696
FLIGHT FATIGUE
Reaction of human organism to time shifts
experienced during flights of modern
aircraft [DVL-611] 02 p0185 A67-12428
FLIGHT FITNESS
Ballistographic, glucose and Masterov
methods applied to pilot examination for
coronary defects 14 p2255 A67-28223
Prolonged space flight effects on crew
members health concerning crew selection
test methods 16 p2613 A67-30911
Pilot capability in low level high speed
flying analyzed for influence of roughness
fatigue, control improvements, vibration and
visual problems 23 p3963 A67-41068
Vehicle flight readiness review, technique
for assuring maximum probability of mission
success [AIAA PAPER 67-888] 24 p4140 A67-43001
FLIGHT HAZARD
Bird impact hazard to aircraft simulated
with hens propelled against windshields and
metal targets 01 p0049 A67-10539
Data and mission analysis in man-rating of
Gemini launch vehicle 01 p0155 A67-11347
Biological effects of supersonic flight,
discussing radiation at high altitudes and
preventive measures 07 p1134 A67-19532
Clear air turbulence connection with jet
stream, wind speed, convection clouds, flight
hazard, etc 07 p1220 A67-19533
Bird strike hazard and ways to combat
it 07 p1129 A67-19909
Gastrointestinal symptoms and drug use as
possible contributing causes of fatal crash of
race pilot 09 p1456 A67-21734
FLIGHT INSTRUMENT
SA HORIZON SCANNER
SA POSITION INDICATOR
Digital computer driven electroluminescent
solid state vertical scale indicator design,
development and fabrication emphasizing
size, weight, power, reliability and display
readability 05 p0805 A67-16310
Electronic display in flight
instrumentation, with reference to
integrated flight system, qualitative and
quantitative displays and qualitative-
quantitative combinations 06 p1000 A67-17598
Laboratory test program to study
problems associated with flight instrument
parameter measurement 12 p1947 A67-26187
Roll-angle indicators used for avoiding
spatial disorientation during instrument
flight 13 p2063 A67-26927
Piloted flight simulator studies influence
on design of SST instruments, discussing
pitch indicator, landing and sonic boom
limitation display systems 13 p2154 A67-27269
Flight simulator experiments test pilots
ability to disregard senses and trust only
flight control instruments 14 p2255 A67-28220
Inertial systems application to airline
operation, discussing data insertion, power
supply integrity, alignment display, dynamic
testing, etc [AIAA PAPER 67-396] 15 p2515 A67-30363
Flight instrumentation aiming at improving
safety of approach and landing of
commercial aircraft [SAE PAPER 670327] 17 p2860 A67-32983
Jindivik Mk 103A jet propelled target

drone ground and flight control system
stressing climb, cruise, approach and descent
commands 21 p3570 A67-39133
Missile and space support systems
reliability, flight equipment and
redundancy 22 p3781 A67-40340
Flight strain gauge system for Centaur
/AC-6/ liquid hydrogen fuel tank
skin 23 p4008 A67-41380
Johnson touch display for updating flight
data combining visual display and keyboard
functions 24 p4152 A67-41780
FLIGHT LOAD RECORDER
Flight Load Survey program, written in
Fortran IV, for accurate and rapid sounding
of wind-induced loads on aerospace launch
vehicle [AIAA PAPER 66-470] 13 p2212 A67-26822
FLIGHT MECHANICS
Aerodynamic penetration and radius in
drag and lift during atmospheric entry
process 06 p1094 A67-18000
Mathematical calculation and role in flight
mechanics 06 p0947 A67-18010
General lateral stability and control
equations for steep gradient aircraft in
terms of equivalent aircraft in level flight
without inertial cross coupling 06 p0949 A67-18559
Optimal parameter problem of controlled
dynamic systems, considering antagonism
between designer and nature, applying
results to space flight mechanics 06 p1088 A67-18616
Book on flight characteristics, static
stability, equations of motion, excitation and
response 06 p0949 A67-18722
Designing propeller blades with maximum
aerodynamic efficiency by vortex theory,
considering engine power, propeller
diameter, forward velocity, etc 15 p2417 A67-30076
Polynomial substitution formulas for
complicated equations of multipoint
boundary value and optimization problems in
flight mechanics and astrodynamics 16 p2695 A67-30733
Concepts of wind drift and lateral
maneuver applied in flight
mechanics 17 p2798 A67-32591
Matched asymptotic expansion method
applied to hypervelocity flight trajectories,
obtaining solutions to flight dynamic
equations 19 p3336 A67-35994
Flight mechanics of gust absorber for high
speed aircraft, discussing transient effects
and short response time 21 p3568 A67-38378
Book on inertial navigation covering laws
of rational mechanics, gyroscopes,
accelerometers, platform stabilization and
control panels 23 p4025 A67-40633
FLIGHT OPTIMIZATION
SA OPTIMUM THRUST PROGRAMMING
Flight performance and low speed
behavior of V/STOL aircraft, noting
correlation between thrust angle and aircraft
attitude 02 p0180 A67-11524
Flight path control in software system for
Lunar Orbiter, discussing optimization
program for midcourse aim point and lunar
injection point 02 p0265 A67-12382
Navigation measurement optimization
using Pontryagin maximum principle as
necessary and sufficient condition to obtain
smallest possible uncertainty 02 p0265 A67-12384
Lifting reentry vehicles for achieving
orbital plane changes by synergetic
maneuvers [AIAA PAPER 66-960] 03 p0520 A67-14141
Book on variational problems in flight
dynamics of winged aircraft and space
vehicles 04 p0705 A67-15007
Time-optimum transition of VTOL aircraft
takeoff to forward flight [DVL-627] 06 p0944 A67-17627
Lifting reentry vehicles for achieving
orbital plane changes by synergetic
maneuvers [AIAA PAPER 66-960] 13 p2212 A67-26846
Supersonic transport vehicle throttle
schedule, comparing point performance,
indirect and gradient optimization
techniques 15 p2418 A67-29406
Correctional maneuver changing space
vehicle position on planet approach,
assuming flight velocity pulsation during
correction 16 p2758 A67-30661
Determining control functions and
choosing parameters governing transfer of
dynamic system from initial to final

- state 16 p2744 A67-30732
Optimum thrust direction for horizontal
jet flight of maximum duration determined,
using variational calculus 18 p3136 A67-33557
Supersonic transport size determination
for competitive operation in air traffic
market using traffic volume, aircraft type
and flight frequency forecasts
[SAE PAPER 670371] 18 p2985 A67-33569
Optimal algorithm for single parameter
linear and nonlinear correction of
interplanetary flight, noting application to
spacecraft vehicle approach to designated
planet 22 p3230 A67-39193
Long range supersonic cruising aircraft
research and design techniques, methods
and approaches for optimizing efficiency,
drag and ATC
[AIAA PAPER 67-748] 23 p3987 A67-40982
Flight optimization problems, considering
spacecraft with energy storage and limited
power engines 24 p4240 A67-42295
Spacecraft motion with limited power jet
engine, applying simulation technique to
determine operation modes for engine and
control system 24 p4240 A67-42296
- FLIGHT PATH**
Slide rule for calculating liftoff free-
flight trajectories in resisting media by
iteration technique 02 p0240 A67-11553
Control method excluding static and
dynamic stability aspects of aircraft from
guidance problem 03 p0464 A67-13003
Radio observation of Cosmos satellites
with flight path inclination angle of 65 and
51 degrees, discussing signal audibility,
atmospheric density and ionospheric
effects 03 p0518 A67-13540
Phugoid trajectories of ballistic reentry of
hypothetical glider into variable density
atmosphere 05 p0847 A67-17009
Natural trajectory optimization for lateral
turn at constant height 06 p1098 A67-18865
Numerical solution methods for variational
problems of flight
dynamics 08 p1348 A67-21114
Two electronic displays for aircraft using
basic elements necessary for flight path
control in problem of easy assimilation of
information by pilot 10 p1601 A67-22905
Meteoritic matter investigation with Venus
II and Zond III probes, discussing impact
rate and distribution along flight
path 10 p1708 A67-23241
Positive control system for placing aircraft
under precisely described flight path
[SAE PAPER 670340] 12 p1895 A67-25878
Optimal control theory in design of
aerodynamic shapes, flight paths, guidance
and control logic, data processing logic,
etc 13 p2072 A67-26814
Velocity requirements for scientific probe
vehicles in direct flight and planetary
swingsby modes of operation throughout solar
system 14 p2387 A67-28618
Hover augmentation system reducing
VTOL pilot task in maintaining position by
providing damping signals for automatic
flight modes with accurate path
control 14 p2246 A67-29082
Range of hypersonic gliders for various
flight and reentry conditions, assuming small
flight path angle and constant bank
angle 16 p2595 A67-30963
Parallelism between edges of aerial
photographs and line of flight achieved by
automatic rotation 16 p2671 A67-31031
Lateral-directional stability equations for
aircraft with nonzero product of inertial
flying along steep flight path
gradient 17 p2796 A67-32219
Flight trajectories having apogees
unaffected by geomagnetic field, giving
numerical solution, discussing radial
propagation laws 17 p2941 A67-32239
Phugoid trajectories of ballistic reentry of
hypothetical glider into variable density
atmosphere 18 p3079 A67-34272
Future traffic control system for ensuring
flight safety and automatic functioning by
automatic radar observation and aircraft-
movements control 19 p3255 A67-35806
Multiple scaling for analyzing flight
vehicle performance and dynamic behavior
[AIAA PAPER 67-560] 19 p3335 A67-35957
Steepest-ascent optimization program
developed for flight path of current
vehicles, particularly supersonic transport
vehicles 19 p3257 A67-35958
Powered flight trajectory determination
for Saturn V vehicles through computer
method
[AIAA PAPER 67-547] 19 p3258 A67-35981
Matched asymptotic expansion method
applied to hypervelocity flight trajectories,
obtaining solutions to flight dynamic
equations 19 p3336 A67-35994
Minimum time-of-flight aircraft trajectory
between two points, with account of earth
sphericity 20 p3481 A67-37202
Statistical properties of perturbations in
rocket path determined to minimize
statistical quantities 22 p3878 A67-39182
Moving map display as cockpit navigation
device useful when flying erratic routes at
low altitude 23 p4003 A67-41283
Glider takeoff using tow winch,
emphasizing flight path and aerodynamic
loads and forces 24 p4093 A67-41917
- FLIGHT PLAN**
Automation role in air traffic control,
discussing flight route
planning 09 p1530 A67-22651
Flexible flight plan processing system
with high continuity of service, using
differing degrees of redundancy and having
comprehensive system monitoring and
control facilities 09 p1531 A67-22656
23 world helicopter records established by
YOH-6A helicopter during 10 flights, noting
details
[AHS PAPER 125] 16 p2598 A67-31840
Apollo Range Instrumentation Aircraft
/ARIA/ deployment model to determine
flight plans for support of translunar
injection phase of Apollo
mission 20 p3361 A67-36600
Minimum fuel flight plans for injecting
synchronous satellite into circular equatorial
orbit, developing four
methods 22 p3886 A67-40116
Graphics system for space vehicle design
and flight plan via light pen, trajectory
computation and performance curve display
on scope
[AIAA PAPER 67-897] 24 p4126 A67-43006
- FLIGHT RECORDER**
Flight recorder may aid aircraft accident
investigation by furnishing data from which
energy analyses, flight tracks and profiles
can be made
[AIAA PAPER 66-810] 01 p0008 A67-10033
Magnetic tape recorder for collection of
flight loads data, examining development,
test and specification 01 p0075 A67-11131
Accomplishments and costs of airline
flight recording for aircraft
maintenance 03 p0420 A67-13380
Radar applications to ATC, pictorial
display and role of paper flight strip,
present and future 09 p1484 A67-21678
Aircraft sensor systems, discussing
recording and evaluation tasks and
performance
characteristics 09 p1501 A67-22454
Flight recorder system designed to satisfy
present and future mandatory requirements
in accident recording and to provide
economic solution to limited maintenance
recording 15 p2487 A67-29510
Flight recorder may aid aircraft accident
investigation by furnishing data from which
energy analyses, flight tracks and profiles
can be made
[AIAA PAPER 66-810] 17 p2796 A67-32216
Cost effectiveness of digital and voice
accident recorders in small fighter and
military aircraft for low level missions,
reconnaissance, flight testing and
training 21 p3631 A67-39129
Design characteristics of IBM 9020 system
to provide automated aids for processing
and updating flight
information 23 p3976 A67-41057
Event recorder for in-flight measurements
of missile heat-shield
ablation 23 p4006 A67-41377
- FLIGHT SAFETY**
Pilot training, regulation, instrumentation
and airspace environment changes for
increased safety
[AIAA PAPER 66-812] 01 p0008 A67-10032
Flight safety improvement in design and
maintenance procedure brought about by jet
transport accident investigation data
[AIAA PAPER 66-809] 01 p0008 A67-10035
Airline safety rules formulation,
considering future aircraft capacities
[AIAA PAPER 66-844] 03 p0360 A67-14015
Hazards in sounding rocket assembly and
launch operations and safety techniques at
- NASA Wallops station noting storage,
explosive control, ground safety,
etc 08 p1314 A67-20547
Semipermanent repellant for aircraft
windshields to overcome effect of visual
errors caused by rain on
windshields 08 p1279 A67-21042
Hydraulic system of Boeing 737 jet
transport, noting flight safety and system
reliability throughout
design 09 p1444 A67-22129
Liquified propane as fog dispersing
agent 10 p1676 A67-22814
Flight safety improvement in design and
maintenance procedure brought about by jet
transport accident investigation data
[AIAA PAPER 66-809] 10 p1595 A67-23550
Optimal methods of escape from
helicopter, examining rotor avoidance during
ejection 14 p2256 A67-27745
Functional or reactive hypoglycemia as
potential cause of flight accidents, showing
alimentary behavior of pilot brings about
apparition of hypoglycemic
phases 14 p2254 A67-28216
Radiobiological aspects of radiation safety
in cosmic flights 14 p2255 A67-28222
Required safety standards for selection of
commuter airlines and contracted
flying 14 p2245 A67-28318
Problems involved in ditching business
aircraft on ocean and subsequent
recovery 14 p2245 A67-28319
Safety in business aircraft operations
based on available statistics noting need for
thorough pilot training 14 p2245 A67-28320
Air derived separation assurance /ADSA/
covering visual capabilities, passive visual
enhancement, visual avoidance aids and
nonvisual avoidance
systems 15 p2515 A67-29942
Soviet book on flight vehicle navigation
accuracy and reliability 17 p2881 A67-31933
Mission risk appraisal technique for
identification and quantification of high risk
areas for unmanned interplanetary
missions 18 p3163 A67-34682
Pilot medical examination frequency and
effect on safety 18 p2992 A67-34722
General aviation accident investigation
from medical and operational standpoint,
concluding pilots poor judgement was cause
of accident 18 p2996 A67-34724
Future traffic control system for ensuring
flight safety and automatic functioning by
automatic radar observation and aircraft-
movements control 19 p3255 A67-35806
Orpheus program for space flight safety
using lifeboat rescue of astronauts on Apollo
and other manned
missions 20 p3532 A67-36572
Factors for SST safety and airworthiness
requirements, discussing environment,
engineering level, learning and flying quality
[AIAA PAPER 67-751] 23 p3933 A67-40985
Gastroesophageal reflux measurements in
evaluation of hiatus hernia and chest pain in
fliers 23 p3954 A67-41599
Manned space flight safety through
mission trajectory design, considering
hardware, software and operational
constraints
[AIAA PAPER 67-822] 24 p4243 A67-42970
Manned space flight safety, discussing
system design, operations planning, staffing,
training and simulation
[AIAA PAPER 67-824] 24 p4243 A67-42971
Space flight emergency contingency
planning for survival, evaluating
physiological effects and remedial system
effectiveness
[AIAA PAPER 67-825] 24 p4116 A67-42972
Aircrew safety emphasizing prior to abort
aspects in detection of catastrophic failure
and initiation of abort sequence
[AIAA PAPER 67-934] 24 p4245 A67-43024
Reentry vehicle design characteristics and
requirements for safe reentry of radioactive
power sources, discussing heat protection
systems
[AIAA PAPER 67-966] 24 p4246 A67-43044
- FLIGHT SIMULATION**
Effect of hypoxia on psychomotor
behavior at simulated cabin altitudes of 5000
and 8000 ft 01 p0017 A67-10953
Modularized simulation system to develop
generalized digital flight simulation program
for use on Titan III mission, emphasizing
functional design 02 p0228 A67-11804
Low altitude hypersonic flow simulation
by means of supersonic compressor,

considering capability of providing true temperature sea-level flight duplication at Mach 9 02 p0229 A67-11933

Integrated logistics system capable of supporting earth orbital operations and sufficiently flexible for demanding applications of space and lunar operations [AIAA PAPER 66-864] 02 p0331 A67-12262

Propellant flow in tanks at high and low accelerations simulated, using similarity parameters obtained from dimensional analysis and motion 04 p0598 A67-15243

Flight simulation techniques covering digital computers, visual simulation and displays [ASME PAPER 66-WA/AV-1] 04 p0599 A67-15394

Piloted space flight simulation at Langley Research Center [ASME PAPER 66-WA/AV-2] 04 p0599 A67-15395

Navy simulation techniques for pilot training [ASME PAPER 66-WA/AV-3] 04 p0599 A67-15396

Three and six degrees of freedom missile subsystem design analysis using flight simulation by hybrid computer 05 p0789 A67-17515

Simulated high altitude hypersonic cold wall testing of lifting bodies, measuring lift, drag and static pitching moment 06 p0943 A67-18847

Simulation testing of modular maneuvering unit for stabilized and untethered maneuvers in free space 07 p1163 A67-19379

Apollo engineering simulation activity, particularly analog-digital real time hybrid simulation for guidance and control [AIAA PAPER 67-230] 07 p1164 A67-20055

Motion reproduction, analyzing control systems, dynamic fidelity, voltage command, etc. [AIAA PAPER 67-252] 07 p1166 A67-20070

Apollo spacecraft hybrid real time flight simulation ensuring 40 msec sampling interval [AIAA PAPER 67-255] 07 p1166 A67-20071

FAA simulation systems for air traffic control noting computer simulated radar target generation, display equipment, etc. 08 p1315 A67-20678

Digital computer CPU control of kinetic heating processes in engine of supersonic aircraft under simulated flight conditions 08 p1315 A67-21007

Preflight and operational status test set /PTS/ for radiation testing of electronic equipment on military aircraft 08 p1303 A67-21059

Sensory input overload effects on performance of civil aviation pilots during simulated instrument flights in Link AN 2550-1 trainer 09 p1455 A67-21726

Carrier landing improvements in Fresnel lens optical landing system, emphasizing compensated-meatball stabilization [AIAA PAPER 65-791] 09 p1441 A67-22494

Multiple arc performance in 8000 kw plasma facility consisting of hyperthermal blowdown tunnel for ballistic flight simulation 12 p1974 A67-25404

Articulated optical pickup system for scale model simulation providing pitch, roll and yaw motions and fixed perspective point 12 p1941 A67-25470

Mechanical cascade toroidal servo flight control system tested using simulator [SAE PAPER 670269] 12 p1895 A67-25867

SST and military aircraft simulation exercises under various terrain and traffic conditions 13 p2053 A67-26711

Roll-angle indicators used for avoiding spatial disorientation during instrument flight 13 p2063 A67-26927

Visual flight simulation, detailing all-weather operation requirements 13 p2091 A67-27287

Flight simulator use for aircrew training to circumvent costs, impractical exercises and adverse flight conditions affecting pilot programs 14 p2292 A67-28037

Remote maneuvering unit control during satellite inspection in simulated conditions 14 p2258 A67-28669

Ground simulation of Concorde aerodynamic heating effects by blowing air through ducts built over specimen surface 15 p2465 A67-29501

Rate variation of aerodynamic parameters

of pitching equation for aircraft, identifying them with linear plant model for simulation studies 15 p2420 A67-30340

Pilot training for future commercial transports, noting flight simulation devices for safety and economic factors [AIAA PAPER 67-388] 15 p2432 A67-30356

Role of ground and flight simulation test facility on past, current and future developments in aerospace propulsion 16 p2854 A67-30709

Trends in digital flight simulation for training 17 p2833 A67-32489

Direct numerical control by computer of 150 heating circuits for safe kinetic heating test simulation of flying conditions for large supersonic aircraft 17 p2820 A67-32748

Radar target designation tracking performance in simulated high speed low altitude aircraft, using closed loop analyses 17 p2830 A67-33181

Computer simulated flights of manual control for VTOL IFR operations indicate display and control subsystem deficiencies 17 p2808 A67-33183

Controllability methods on VTOL transporters, developing model of pilot dynamic reaction to aircraft machinery 18 p2993 A67-33457

Construction and operational possibilities of gimbal mounted servo-controlled aircraft model for optical simulation of flight mechanical motions 18 p3019 A67-33458

MARCEP mathematical and mission simulation models to evaluate parameters affecting maintainability of long duration manned space flights 18 p3138 A67-34688

Supersonic combustion simulation for hypersonic flight in relation to scramjet operation, discussing auto-ignition limits [CI PAPER 67-6] 19 p3344 A67-35001

Interplanetary transfer trajectory simulation, discussing planet ephemeris, coordinate systems, low and high powered and coasting segments 19 p3322 A67-35321

Wind penetration effects on flight simulations evaluated in frequency domain by solution of theoretical transfer function, showing relationship to angle of attack [AIAA PAPER 67-609] 19 p3208 A67-36000

Manual control stationkeeping simulation, studying tether visual rendezvous techniques and fuel economy [AIAA PAPER 67-617] 19 p3337 A67-36006

High altitude variable Mach number test cell for testing intake system of Concorde aircraft Olympus 593 20 p3414 A67-36497

Oblique interaction between supersonic vehicle in free flight and plane shock wave simulated, noting large unbalanced force 21 p3607 A67-37776

High pressure hypersonic gun tunnel calibration with performance estimation method compared with tests, discussing high altitude Mach 10 flight simulation 21 p3607 A67-37779

Motion reproduction, analyzing control systems, dynamic fidelity, voltage command, etc. 21 p3608 A67-38540

Microbial interaction in closed system by simulating space flight conditions, noting effect on buildup 21 p3577 A67-38899

Computer analysis and simulation of Mars soft landing descent control system combining inertial and radar sensing techniques 22 p3898 A67-39177

Saturn V S-IVB stage propellant slosh amplification minimization at boost thrust termination analysis, simulating slosh wave motion by time varying nonlinear spring-mass model 22 p3903 A67-39970

Thomson motion equation derivation for variable mass system extended for flight simulation equations for variable mass inertially guided system 22 p3832 A67-40099

Spacecraft flight control and computerized systems, discussing redundant systems, integrated circuits and simulation for man-machine interaction and lack of response 22 p3908 A67-40336

Articulated optical pickup system for scale model simulation providing pitch, roll and yaw motions and fixed perspective point 23 p3988 A67-41502

Brightness thresholds and reading ability tests evaluated for male subjects under varied simulated conditions of altitude and oxygen breathing 23 p3959 A67-41694

Treatment for relief of altitude decompression sickness for operations

requiring extravehicular activity 23 p3960 A67-41702

Water immersion simulation, studying astronaut performance characteristics in Gemini and proposed Apollo missions [AIAA PAPER 67-773] 24 p4116 A67-42941

Sub-, super- and hypersonic air breathing engines, examining developments on ground test and simulation facilities [AIAA PAPER 67-779] 24 p4208 A67-42946

Onboard computer-based checkout simulator system to assist astronauts in monitoring data requirements of future space programs [AIAA PAPER 67-951] 24 p4127 A67-43036

FLIGHT SIMULATOR

T-38 pilot trainer with mandatory stability control characteristics to meet current supersonic aircraft requirements [AIAA PAPER 66-798] 01 p0009 A67-10536

Hoverbug VTOL twin-jet flying simulator operational experience and management and construction techniques [AIAA PAPER 66-799] 01 p0009 A67-10537

Visual or environmental factors which affect usefulness of training simulator experimentally studied, examining problems of measuring transfer of training 02 p0186 A67-12072

Experimental fixed and moving-base flight simulator investigation of generalized aircraft longitudinal pilot induced oscillations [AIAA PAPER 65-793] 03 p0365 A67-12913

Airborne V/STOL simulators used for handling qualities research at National Aeronautical Establishment, Ottawa [AIAA PAPER 65-705] 03 p0394 A67-12915

Performance requirements of dynamic flight simulators and visual display systems in man-machine flight control problems 03 p0395 A67-13385

Instrument, force and motion servos in cockpit simulation in large aerospace flight simulators, using DC analog voltages 03 p0395 A67-13386

Simulator program which uses modified head-up display unit from British Buccaneer aircraft 04 p0653 A67-14882

Simulation system and hovering vehicle prototype design for use in development of VTOL aircraft 04 p0600 A67-15540

Platform with six degrees of freedom for flight simulation in pilot training 09 p1483 A67-21555

Spatial-turn simulator using rocking device rotating under effect of internal forces 10 p1655 A67-22840

DC-9 training program using classroom responder system and programmed-type learning aids 13 p2064 A67-27261

Flight simulators for present and future aircraft 13 p2090 A67-27263

Flight simulator computation methods development 13 p2090 A67-27264

Future potential and requirements of digital simulation noting design, construction, cost, etc. 13 p2090 A67-27265

Flight simulator motion enhancement and potential for flight crew training, examining human vestibular system 13 p2064 A67-27268

Piloted flight simulator studies influence on design of SST instruments, discussing pitch indicator, landing and sonic boom limitation display systems 13 p2154 A67-27265

Flight simulator acceptance and role in pilot training and checking in UK 13 p2064 A67-27272

Aircraft handling qualities research with variable static stability aircraft used as in-flight simulator [SAE PAPER 670261] 13 p2054 A67-27296

V/STOL transport testing and operational requirement, discussing hover rig, pedestal and simulator 14 p2245 A67-27746

Flight simulator experiments test pilots ability to disregard senses and trust only flight control instruments 14 p2255 A67-28220

Training programs to improve airline pilot performance, suggesting greater use of flight simulators and pedagogy methods [AIAA PAPER 67-387] 15 p2432 A67-30355

System engineering approach to commercial aircraft crew requirements [AIAA PAPER 67-399] 15 p2433 A67-30366

Manned flight simulators suitable to space research, discussing types, phases of development, operational and performance features, etc. 16 p2654 A67-30761

Vestibular, tactual and proprioceptive information in judging Coriolis rotation and

- attitudes during rotation and pitching on
piloted flight simulator 22 p3751 A67-39605
- Electromechanical simulator of wing
flutter with aileron under flight
conditions 22 p3912 A67-39779
- Human circulatory response to sinusoidal
gravitational stimulus via Rotational Flight
Simulator /RFS/, discussing heart rate
variation 23 p3951 A67-41561
- Flash blindness, recovery time and aircraft
control loss studied in flight
simulator 23 p3966 A67-41580
- Hand-held sextant capability in in-flight
spacecraft navigation measurements
[AIAA PAPER 67-775] 24 p4183 A67-42943
- FLIGHT STABILITY TEST**
- Longitudinal stability of rigid glider in
towed flight, calculating lift coefficients for
various rope-plane
configurations 09 p1441 A67-22607
- Kinematic coupling effect in stabilization
axes of flight vehicle as result of errors in
gyrocompass gimbals and coordinate
system 11 p1870 A67-25101
- Aircraft performance, stability and control
characteristics in nonsteady flight with high
accuracy instrumentation
system 20 p3442 A67-36466
- Dynamic flight stability characteristics of
6 inch projectile with nonlinear Magnus
moment, noting Mach number, wind tunnel
data, etc 21 p3563 A67-37805
- FLIGHT STRESS**
- SA SPACE FLIGHT STRESS**
- Urinalysis assessment of physiological
response of eight pilots to 18-hr flight in F-
4C aircraft 03 p0364 A67-14287
- Dose levels and hangover effect of
secobarbital on simulated pilotage
performance 03 p0366 A67-14291
- Phase shifts of human circadian system
and performance deficit during periods of
transition in north-south
flight 05 p0756 A67-16289
- Sensory input overload effects on
performance of civil aviation pilots during
simulated instrument flights in Link AN
2550-1 trainer 09 p1455 A67-21726
- Multifocal premature ventricular
contractions found in ECG, evaluating
cardiovascular system significance in flight
stress tolerance 09 p1453 A67-21735
- Human tolerance to changes in aircraft
cabin pressurization 10 p1602 A67-23825
- Maximal intensity inflight stress effects on
human tolerance investigated, noting
deceleration experiments 14 p2257 A67-28218
- Rotor system with blade angle reverse
control noting blade-angle adjustment
changes for achievement of higher flight
speeds 18 p2985 A67-33460
- Vestibular inaptitude in atmospheric and
space flight environment
[AD-640908] 19 p3178 A67-35884
- Urinary catecholamine excretion in pilots
relation to physical mental expenditure of
energy and flight deck work
loads 23 p3952 A67-41577
- FLIGHT SURGEON**
- Aeromedical examiner relationship to
accident prevention, discussing
standardization of psychological
approach 23 p3963 A67-41539
- Aeromedical incidents among Canadian Air
Force pilots, using mailed
questionnaire 23 p3963 A67-41540
- FLIGHT TEST**
- C-141A cargo aircraft structural analysis,
discussing design, load and gust criteria,
flight and static test programs, vibration and
noise control
[SAE PAPER 680669] 01 p0010 A67-10576
- Strain gauge bridge outputs combined
during flight to measure airloads directly
and inexpensively in fatigue test
program 01 p0030 A67-11103
- Flight test method for evaluating ground
effect on fixed-wing aircraft in which pilot
flies at constant angle of attack and power
setting during landing approach
[AIAA PAPER 66-468] 02 p0180 A67-11513
- Angle of attack measurements of
hypersonic reentry vehicle derived from
flight test pressure data 02 p0178 A67-11942
- Second generation Saturn vehicles,
discussing anomalies discovered during flight
tests, development, etc
[AIAA PAPER 66-839] 02 p0331 A67-12255
- Aircraft structural design criteria and
analysis methods, noting procedures which
result in discrepancies between design
loadings and actual flight test results
[AIAA PAPER 66-881] 02 p0339 A67-12263
- Flight flutter tests, related problems,
objectives and recommendations
[AIAA PAPER 66-883] 02 p0181 A67-12264
- Manned lifting body flight test program,
noting NASA M2-F2 and HL-10 and USAF
SV-5P
[AIAA PAPER 66-838] 03 p0519 A67-14127
- Data acquisition system for Blue Streak
flight trials noting telemetry and radar and
relation to trajectory, autopilot, structure,
etc 04 p0568 A67-14438
- SA 330 turbine-powered assault helicopter,
noting flight tests, speed, altitude, transport
capabilities, etc 04 p0550 A67-14468
- High altitude high voltage breakdown in
electric propulsion flight test
system 04 p0704 A67-14997
- Flight test of nucleonic fuel gauge,
discussing photon-matter interaction
principles, ground test calibration data,
aircraft environment and gauge
performance 05 p0841 A67-16537
- Test pilots report on aircraft and
spacecraft - SETP Symposium, Beverly Hills,
September 1966 06 p0947 A67-18196
- Joint NASA-USAF lifting body flight test
program and M2/F2, HL-10 and SV-5P
research vehicles 06 p0947 A67-18197
- Flight test program of North American
OV-10A COIN /counter-insurgency/
aircraft 06 p0947 A67-18199
- Flight tests of two X-22A dual tandem
rotatable ducted propeller V/STOL research
aircraft 06 p0948 A67-18201
- GHOST balloon experiments, determining
life, stability and clustering characteristics
at several altitudes 07 p1219 A67-19065
- Category II Systems Evaluation Test of C-
141A aircraft 07 p1129 A67-19616
- Small helicopter flight test report,
discussing testing procedures on 14 models
of one-man rotorcraft
[AIAA PAPER 67-264] 07 p1129 A67-20041
- Flight and operational suitability testing
of XC-142 V/STOL assault transport
[AIAA PAPER 67-261] 07 p1130 A67-20074
- Flights tests of XH-51A compound
helicopter, discussing rigid rotor concept
and results of compound flight research
program 07 p1130 A67-20075
- Gemini rendezvous experience, describing
flight test cycles, type of maneuvers needed,
ground and onboard support systems, etc
[AIAA PAPER 67-272] 07 p1260 A67-20081
- Flight testing Lear Jet Models XXIII,
XXIV and XXV noting flutter, redundancy,
hydroplaning, etc
[AIAA PAPER 67-263] 07 p1130 A67-20086
- C-141A cargo aircraft structural analysis,
discussing design, load and gust criteria,
flight and static test programs, vibration and
noise control
[SAE PAPER 680669] 07 p1131 A67-20232
- Frangible sounding rocket vehicle and
explosive fragmentation system,
determination of impact kinetic energy of
fragments and flight tests
08 p1407 A67-20521
- Terrier two-stage sounding rocket design,
fabrication, flight testing and performance
characteristics 08 p1408 A67-20527
- Optimal allocation of n test points within
redundant digital system for prelaunch and
in-flight spacecraft reliability
estimate 08 p1300 A67-20637
- Artificial pseudorandom binary noise
generation for flight testing and aircraft
control systems and correlation function and
frequency spectra of noise
generators 08 p1279 A67-21005
- Direct measurement of aeroelastic
parameters of aircraft wings, using
dynamically similar models fitted on
auxiliary rocket devices 09 p1576 A67-22462
- Temperature distribution in tail pipe of M
701 engine, based on differences between
readings obtained from onboard
thermocouples 09 p1560 A67-22463
- Longitudinal stability of L-29 aircraft,
comparing measurement results from
independent experiments 09 p1440 A67-22469
- Least squares methods for calculating
stability derivatives of aircraft from
unsteady flight data 09 p1438 A67-22474
- Flight test method for evaluating ground
effect on fixed-wing aircraft in which pilot
flies at constant angle of attack and power
setting during landing approach
- [AIAA PAPER 66-468] 09 p1441 A67-22486
- V/STOL theory for equilibrium level
flight, evaluating optimum performance over
complete velocity
spectrum 09 p1441 A67-22487
- Flight testing of radio navigation aids for
civil aviation noting techniques, telescopes
and typical test 09 p1528 A67-22629
- Saturn IB flight test loads, comparing
measured and calculated bending moment,
noting launch time wind
profile 10 p1713 A67-23734
- Aircraft control system of subsonic
airplanes operated over wide speed ranges,
noting flight test results 11 p1744 A67-24578
- Bench and flight tests of twin spool axial
flow turbojet power plant for Concorde
aircraft
[ASME PAPER 67-GT-8] 11 p1854 A67-24796
- Saturn IVB flight data evaluation,
discussing heat transfer effect on fluid
system as function of gravity
changes 12 p2034 A67-25721
- XH-51A compound research flight test
program, discussing adaptation of rigid rotor
concept 13 p2052 A67-26421
- Mechanization effect on man-machine
relationships in flight test engineering
analysis 13 p2052 A67-26423
- Airline flight testing problems, discussing
aircraft availability, equipment competency,
crew proficiency, safety, economy,
etc 13 p2052 A67-26424
- Steady and dynamic loads on tandem
rotor, controls and airframe flight tested
with Army helicopter, using automatic data
processing 13 p2054 A67-27596
- Harmonic and impulse techniques for
flight vibration testing to reduce data
processing time 14 p2395 A67-27899
- [ONERA-TP-477] 14 p2395 A67-27899
- Strain gauge bridge outputs combined
during flight to measure airloads directly
and inexpensively in fatigue test
program 14 p2315 A67-28002
- Management role in making technical and
administrative decisions regarding type of
telemetry system 14 p2272 A67-28698
- Flight test skin temperatures of
supersonic aircraft compared with
theoretical results, explaining measurement
discrepancies 14 p2243 A67-28977
- Launcher for research and development on
aerodynamic reentry 15 p2564 A67-29094
- Electronic equipment used for IR
radiation measurement during space
experiment, describing thermal effect
detectors
[ONERA-TP-465] 15 p2486 A67-29382
- Frangible sounding rocket vehicle and
explosive fragmentation system,
determination of impact kinetic energy of
fragments and flight tests
results 15 p2565 A67-29449
- Fixed wing reusable horizontal landing
boosters, comparing weight, cost, technical
difficulty and availability
rate 15 p2567 A67-29836
- Rocket nozzle design to reduce gas
misalignment noting turning moment, nozzle
geometry, cold gas tests, static and flight
trials of motors, etc 15 p2547 A67-29995
- Hypersonic reentry, inertial guidance tests
and construction of two-stage Diamant
satellite launcher 15 p2571 A67-30089
- C-141A engineering development test
program, discussing flight, accelerated
service and all-weather testing
[AIAA PAPER 67-409] 15 p2422 A67-30376
- Flow turbulence on leading edge of
attachment line of swept wing studied in
wind tunnel 18 p2589 A67-30618
- Aerothermodynamics for Apollo spacecraft
design and results of flight
tests 18 p2761 A67-30935
- Rotor blade stall, comparing power,
flapping motion blade bending and vibratory
hub shears for illustration
[AHS PAPER 101] 16 p2595 A67-31818
- Rotor blade compressibility effects on
helicopter performance, describing flight
test techniques and data analyses and
comparing prediction and test results
[AHS PAPER 103] 16 p2595 A67-31820
- Instrument-landing displays evaluated in
IFR landing approaches with helicopter,
noting flight performance and pilot
evaluation of display concepts
[AHS PAPER 106] 16 p2680 A67-31823
- Coordinated laboratory and flight test

program, determining stability of solar concentrator reflective surfaces in orbital environment 17 p2832 A67-32060

Flight test program for F-111A variable sweep tactical weapon system, discussing afterburning turbofan engine, crew module, escape and survival 17 p2795 A67-32214

Northrop program for V/STOL aircraft including systems studies, propulsion, aerodynamics, flight control technology, performance characteristics and operation and testing northrop program for V/STOL aircraft including 18 p2987 A67-34708

Performance characteristics of XB-70 flight test data acquisition system 20 p3442 A67-36467

Blue Streak launch vehicle control system, discussing destabilizing resonance effects, hydraulic system, propellant movement in tanks and testing 21 p3570 A67-38102

Aircraft structural design criteria and analysis methods, noting procedures which result in discrepancies between design loadings and actual flight test results 21 p3568 A67-38537

Motion coordination under conditions of intermittent acceleration and weightlessness during parabolic aircraft flight 24 p4112 A67-41858

DC-9 wing and high lift system aerodynamic design and development, discussing STOL field length design goals and flight test results [SAE PAPER 670846] 24 p4093 A67-41999

Astronaut role in balanced in-flight testing for manned spacecraft [AIAA PAPER 67-949] 24 p4245 A67-43033

FLIGHT TEST INSTRUMENT

SNAP-10A flight test instrumentation performance, discussing exceptions 08 p1330 A67-20655

Devices for flight speed measurement 18 p3019 A67-33461

Self-contained and vehicle integrated on-board checkout systems, considering controller-evaluator and sensors 20 p3449 A67-36979

FLIGHT TIME

Radar observations of Venus at 23 cm noting flight time and Doppler shift measurements of reflected signals 05 p0889 A67-16297

Plasma flow velocity measurement in MHD channel using time-of-flight technique, noting experimental error 05 p0854 A67-16983

Evaluation of minimum-time courses for aircraft and inherent error 07 p1222 A67-19680

Flight time estimation methods for iterative solutions of optimum trajectories by numerical integration 11 p1859 A67-24436

Directional neutron spectrometer for events in which neutron is scattered by first scintillator into second 12 p1945 A67-25859

Time of flight distribution measurement of weak molecular beam, noting limitations due to signal to noise ratio 14 p2316 A67-28185

Velocity distribution function measurement in rarefied gas flow, using principle based on time of flight of metastable molecules 14 p2316 A67-28193

Numbers, flow velocities and temperatures of positive ions emitted by He and Ar plasmas pulsed into evacuated region by plasma gun determined by time-of-flight analysis 15 p2523 A67-29214

Time of flight expressed in terms of perturbed true anomaly in case of large eccentricities 16 p2743 A67-30726

Orbit determination between two radii vectors with specified periastris radius distance 16 p2746 A67-30959

Earth-Mars round-trip flight maximum payload delivery variational problem, determining optimum trajectories and minimum flight time dependence on engine parameters 17 p2941 A67-32240

Lambert theorem used to find required trajectory to effect rendezvous in space 19 p3332 A67-34828

Steering equation derived from dynamic equation of velocity gain, as function of booster state for rocket vehicle ballistic trajectory [AIAA PAPER 67-595] 19 p3259 A67-35991

Minimum time-of-flight aircraft trajectory between two points, with account of earth sphericity 20 p3481 A67-37202

Concorde SST economics noting short/medium haul characteristics, flight

times, sonic boom problems, load factor, etc 22 p3744 A67-39339

Iterative guidance mode, deriving alternate expressions for thrust direction control angle for time savings on Saturn launches 22 p3831 A67-39957

Supersonic civil aircraft, considering journey time, safety and operating economy 24 p4093 A67-41886

Steering equation derived from dynamic equation of velocity gain as function of booster state for rocket vehicle ballistic trajectory [AIAA PAPER 67-595] 24 p4182 A67-42910

FLIGHT TRAINING

SA PILOT TRAINING

Flight simulator motion enhancement and potential for flight crew training, examining human vestibular system 13 p2064 A67-27268

SST ground and flight personnel training program for system operation, discussing expected role of piloted flight simulator 13 p2091 A67-27270

Astronaut training techniques applicability to conventional aircraft pilots training, discussing instruction and high fidelity simulation devices 13 p2064 A67-27273

Flight simulator use for aircrew training to circumvent costs, impractical exercises and adverse flight conditions affecting pilot programs 14 p2292 A67-28037

In-flight simulation of fog for pilot training noting heads-up optical viewing system, daylight backscatter, photographic method, etc [AIAA PAPER 67-386] 15 p2468 A67-30354

Correlation of airsickness in early flight training with subjective anxiety 21 p3575 A67-38086

Psychosomatic symptoms in student naval aviators 23 p3955 A67-41624

FLIGHT VEHICLE

Book on methods of determining temperature fields in thin walled elements characteristic of structure of flight vehicles and engines 04 p0723 A67-15010

Soviet book on methods of calculating temperature fields and thermal insulation of flight vehicles 07 p1266 A67-19144

Thermal insulation for flight vehicles under various conditions of gas-kinetic heating 07 p1266 A67-19146

Balancing operations for rocket vehicles and payloads, defining terms, establishing relation between static and dynamic imbalance and flight vehicle motions, etc 08 p1408 A67-20535

Optimal control of elastic flight vehicles, describing axis oscillations by equations of beam with variable cross section 09 p1439 A67-22075

Angular stabilization of flight vehicle by introduction of cubic terms of variable parameters into control law 10 p1678 A67-23319

Kinematic coupling effect in stabilization axes of flight vehicle as result of errors in gyrocompass gimbals and coordinate system 11 p1870 A67-25101

Soviet book on flight vehicle navigation accuracy and reliability 17 p2881 A67-31933

Applicability to elastic flight vehicle control system of two variants for realization of invariance conditions 17 p2882 A67-33097

Construction and uniqueness of time optimal control of multidimensional linear system with constraints on control signal amplitudes and rates 18 p3017 A67-34280

Soviet book on temperature fields and stresses in structural elements of flight vehicles, giving theoretical analysis and numerical calculation methods 18 p3145 A67-34705

Parameters for motion of flight vehicle as solid body and for elastic deformations 20 p3482 A67-37381

Soviet book on aerodynamics, flight dynamics, flight vehicle structural design and mechanical and control considerations for various aircraft 21 p3568 A67-37833

Reduction and analysis of nonstationary missile flight vibration data, obtaining power spectral density 23 p4007 A67-41385

FLIP-FLOP

Dinistor trigger circuits with counting input, discussing flip-flop circuits 03 p0377 A67-13239

Functional device based on interaction of two unijunction transistors to perform flip-flop circuit function, noting V-I

characteristics and binary counter operation 04 p0593 A67-15488

Flip-flop and OR-NOR gate design and fabrication to specification 08 p1282 A67-20467

Flip-flop type current mode switching circuits, discussing features incorporated and performance 14 p2280 A67-28012

Digital sequencing systems containing error-detecting and -correcting properties 16 p2647 A67-31647

Flip-component technology discussing bonding of flip chips and face bonding of semiconductor devices 16 p2642 A67-31727

Integrated circuit memory with 64 eight bit words and compatible with high speed current-mode gates for high speed computers 19 p3189 A67-36066

Reversible counter using decimal register compared to conventional flip-flop counters 22 p3809 A67-40476

FLOTATION SYSTEM

R/D on water launched space probes, discussing operation, applications and results 12 p2012 A67-25839

Mark 27 gyrocompass, discussing suspension by flotation 14 p2322 A67-29083

Aircraft flotation requirements, emphasizing surface strength reduction 17 p2832 A67-31986

FLOW

S AIRFLOW

S ANNULAR FLOW

S AXIAL FLOW

S AXISYMMETRIC FLOW

S BAROTROPIC FLOW

S BASE FLOW

S BELTRAMI FLOW

S BLOOD FLOW

S BOUNDARY LAYER FLOW

S CARTAN SPACE

S CASCADE FLOW

S CAVITATION FLOW

S CHANNEL FLOW

S COAXIAL FLOW

S COMBUSTIBLE FLOW

S COMPRESSIBLE FLOW

S CONICAL FLOW

S CONTINUUM FLOW

S CONVECTIVE FLOW

S CORE FLOW

S COUETTE FLOW

S DUCTED FLOW

S EQUILIBRIUM FLOW

S FREE FLOW

S FROZEN FLOW

S FUEL FLOW

S GAS FLOW

S HARTMANN FLOW

S HEAT FLOW

S HELICAL FLOW

S HYPERSONIC FLOW

S HYPERVELOCITY FLOW

S INCOMPRESSIBLE FLOW

S INDUCED FLUID FLOW

S INLET FLOW

S INVISCID FLOW

S IRRATIONAL FLOW

S ISOTHERMAL FLOW

S JET FLOW

S KNUDSEN FLOW

S LAMINAR FLOW

S LIQUID FLOW

S MAGNETOHYDRODYNAMIC FLOW

S MASS FLOW

S MERIDIONAL FLOW

S MIXED FLOW

S MOLECULAR FLOW

S MULTIPHASE FLOW

S NON-NEWTONIAN FLOW

S NONEQUILIBRIUM FLOW

S NONVISCOUS FLOW

S NOZZLE FLOW

S ONE-DIMENSIONAL FLOW

S OSCILLATING FLOW

S PIPEFLOW

S PLASMA FLOW

S PLASTIC FLOW

S POISEUILLE FLOW

S POTENTIAL FLOW

S PULSATING FLOW

S RADIAL FLOW

S RAYLEIGH NUMBER

S REATTACHED FLOW

S REVERSED FLOW

S ROTATIONAL FLOW

S SECONDARY FLOW

S SEPARATED FLOW

S SHEAR FLOW

S SINGLE-PHASE FLOW

S SLIP FLOW

- SMALL PERTURBATION FLOW
SONIC FLOW
STAGNATION FLOW
STEADY FLOW
STEADY STATE FLOW
STRATIFIED FLOW
STREAMLINE FLOW
SUBSONIC FLOW
SUPERCAVITATING FLOW
SUPERFLUID FLOW
SUPERSONIC FLOW
THREE-DIMENSIONAL FLOW
TRANSONIC FLOW
TURBULENT FLOW
TWO-DIMENSIONAL FLOW
TWO-PHASE FLOW
UNIFORM FLOW
UNSTEADY FLOW
VISCOELASTIC FLOW
VISCOUS FLOW
VORTEX FLOW
WALL FLOW
WATER FLOW
WEDGE FLOW
WING FLOW METHOD TEST
- CHAMBER
Convective heat transfer stability in fluid contained in cubic chamber shown from temperature measurements 20 p3422 A67-37064
- FLOW CHARACTERISTICS
Optimization of working characteristics of MHD generator as power device 01 p0011 A67-10049
Supersonic jet from finite length nozzle in supersonic stream at angle of attack, analyzing flow characteristics by using linearized theory 02 p0177 A67-11523
Compressor cascades with different irregularities in forward flow, noting special case of low aspect ratio blades 02 p0179 A67-12439
Propellant flow in tanks at high and low accelerations simulated, using similarity parameters obtained from dimensional analysis and motion 04 p0598 A67-15243
Flow properties in laminar and turbulent near wake of cones and wedges using hypersonic shock tunnels, obtaining wake centerline and stagnation temperature profile [AIAA PAPER 67-30] 07 p1126 A67-19432
Averaging of parameters of inhomogeneous flowing medium using as criterion degree at which flow parameters (energy, losses, momentum, flow rate) are maintained 09 p1495 A67-21689
Binary turbulent reattachment type fluid amplifier to control submerged jet of fluid 10 p1597 A67-23389
Optimum geometry for rectilinear diffuser with rectangular, conical or annular cross section noting flow regime, performance characteristics and boundary layer effect 11 p1741 A67-24050
Unsteady transonic flow of moving compressible gas filling half-space created by sudden rupture of membrane separating gas from vacuum 11 p1743 A67-24962
Thermal convection in rotating fluid annulus analyzed using Navier-Stokes equations as initial value problem 12 p1963 A67-25339
Tandem cascade of airfoils slow speed performance flow characteristics 12 p1891 A67-25349
Rotating blades cascade performance in mixed flow turbomachines, noting flow characteristics and slip factors 12 p1892 A67-25350
Recovery factor associated with moving fluid temperature measurement is dependent on thermodynamic and transport properties of fluid, noting probe errors 12 p1928 A67-25353
Zero gravity effects on boiling from flat horizontal surface for various subcoolings, fluid properties and heat transfer rates 12 p2034 A67-25720
Plane one-dimensional MHD flow in transverse magnetic field with magnetic Reynolds number equal to or greater than unity 13 p2169 A67-27311
Supersonic three-dimensional flows past smooth bodies, calculating flow parameters by characteristic method with analytical approximation of gas-dynamic functions 14 p2240 A67-27992
Defined region geometry flow characteristics for high-gain proportional amplifiers 14 p2249 A67-28326
Two-dimensional supersonic fluid amplifier flow characteristics analyzed numerically by digital computer 14 p2250 A67-28333
Mathematical model describing nonlinear behavior of vortex valve in fluid circuits, noting effect of swirl on vortex valve flow characteristics 14 p2251 A67-28341
Mach and Reynolds number, cone angle, base geometry, etc, effect on near wake flow of conical vehicle moving at high speed 15 p2418 A67-30215
Flow through blade cascade studied by averaging flow parameters behind cascade for testing internal combustion turbine guide vanes 16 p2736 A67-31005
Optimization of working characteristics of MHD generator as power device 17 p2804 A67-33327
Radial mass flow effect on electric arcs, obtaining higher axis temperature and enthalpy densities 17 p2910 A67-33366
Characteristics of cross flow fan determined as function of blade angle, diameter ratio of impeller and vortex position 18 p3025 A67-33650
Supersonic combustion characteristics of hypersonic ramjet predicted by analytical method using constant-mass tube technique, discussing flow field properties [AIAA PAPER 67-494] 18 p2983 A67-33958
Economical feasibility of open and closed cycle vortex-stabilized gaseous nuclear rocket engines, investigating vortex flow characteristics [AIAA PAPER 67-500] 18 p3076 A67-33964
Low molecular weight polymer flow behavior variation with shear rate, shear stress and temperature 20 p3473 A67-36914
Pressure drop increase in choke eliminates axial compressor stage discontinuity caused by disrupted flow formation 20 p3358 A67-37083
Short tube orifices, confined turbulent jets, jet-wall and jet-receiver interactions and characteristics of diffusion process for design of fluid amplifiers 20 p3365 A67-37361
Base flow characteristics and thermal environment of launch vehicles with strap-on solid rocket motors 22 p3902 A67-39939
Mean flow and motion turbulence characteristics after separation from conical afterbody for various initial boundary layer thickness and convergence angles 23 p3927 A67-40631
Oscillating mass flow characteristics in modified Moore variometer configuration for step, triangular and infrasonic functions 23 p4000 A67-41221
Linear MHD flow characteristics variation with electric conductivity and gas flow rate changes, noting transverse magnetic flow variation with magnetic Reynolds number 23 p4033 A67-41284
- FLOW COEFFICIENT
Tabulated data on specific losses in flow systems 02 p0233 A67-11995
Flow rate and pressure coefficients approximate determination for surface of symmetrical hypersonic flow past circular cone 14 p2243 A67-28656
Change in pressure losses in MHD generators channel, obtained from pressure gradient relation to flow rate of conducting fluid 16 p2705 A67-30449
Cavitation in spool control valve orifices, showing effect on flow discharge coefficient over range of conditions 20 p3366 A67-37371
Fan-in-wing aerodynamics evaluated for datum inlet with circular arc lips with and without vanes [AIAA PAPER 67-746] 23 p3928 A67-40980
Flow coefficient of various nozzles discharging into unbounded atmosphere for wall pressure distribution of potential rotational flow, using rheoelectric tank 23 p3989 A67-41140
- FLOW DEFLECTION
Aerodynamic problems of turbomachinery, investigating effect of geometry and aerodynamic cascade parameters on flow deflection, static pressure difference and flow losses 04 p0547 A67-14985
Curved flow effect on lift characteristics of blade using Scholz method, noting role of correction coefficient of lift curve slope and zero lift angle 05 p0791 A67-16427
Forms of function connecting deviation angle and axial velocity ratio of exit flow in three-dimensional cascade flow 05 p0791 A67-16428
- Impact of supersonic jet against surface 05 p0795 A67-17479
Three-way valve design for flow deflection, separation and mixing 08 p1286 A67-21535
Airflow characteristics and heat transfer in right angle water-jacketed bend, measuring boundary layer profile at midbend 09 p1487 A67-21831
Complex velocity and circulation around thin wing 09 p1439 A67-22564
Effects of fast expansion and consequent lip shock at shoulder of supersonic base or downstream-facing step, suggesting alleviation by shoulder modification 10 p1592 A67-23156
Strong small perturbation solutions for steady supersonic flows of inert or reacting gas mixtures around plane corner 11 p1778 A67-24230
Unsteady transonic flow of moving compressible gas filling half-space created by sudden rupture of membrane separating gas from vacuum 11 p1743 A67-24962
Viscous flow around spheres, considering mass efflux effect, using Navier-Stokes equations and finite difference methods 12 p1927 A67-25282
Internal structure of highly underexpanded transverse jets in supersonic cross stream 12 p1892 A67-25900
Low thrust divergent flow cesium-ontungsten contact ionization electrostatic thruster for satellite attitude control and stationkeeping missions [AIAA PAPER 66-569] 13 p2188 A67-26824
Plane shock wave propagation in inviscid perfect gas colliding with right angle obstacle, determining flow in perturbed region 14 p2296 A67-27979
Model of inviscid, incompressible and variable density airflow in long channel over mountain treated mathematically 14 p2346 A67-28004
Proportional momentum beam deflection fluid amplifier design 14 p2249 A67-28327
Two-dimensional flow through bends with turning vanes, using Green theorem to obtain surface pressure distributions [ASME PAPER 67-FE-13] 14 p2304 A67-28362
Flow turning angle during two-dimensional turbulent supersonic reattachment to plane wall [ASME PAPER 67-FE-20] 14 p2305 A67-28367
Flow pattern of thin jet-flapped wing with small deflection angle in proximity to ground 15 p2415 A67-29308
Formula for pressure vs flow deflection at hypersonic speeds, useful in studies involving pressure on inclined surfaces 15 p2472 A67-29675
Behavior of high speed, coherent, turbulent liquid jet in planar, standing, transverse acoustic field 16 p2658 A67-30945
Heat conducting supersonic gas flow around corner considered calculating viscous corrections in expansion region 16 p2660 A67-31218
Vibrational excitation effects on shock wave behavior calculated analytically by linearizing problem 19 p3212 A67-35773
Two-dimensional potential flow through bend profile, obtaining streamlines and velocity distributions 20 p3356 A67-36533
Aerodynamic characteristics of plane compressor cascades with high subsonic flow analyzed, noting application in determining flow deflection angle and pressure loss coefficient 20 p3358 A67-37079
Distribution of gas flow departure angle from annular turbine cascades 21 p3564 A67-37914
- FLOW DIRECTION INDICATOR
Turbulence measured by flow direction indicators used as pressure probes 01 p0076 A67-11192
Test of probes designed to determine direction of supersonic flows in wind tunnels, using schlieren photography 09 p1496 A67-21693
Nozzle form optimization from Mach distribution in supersonic region, defining perturbation functions 23 p3929 A67-41248
- FLOW DISTORTION
Instability and transition to turbulence in separated shear layer produced by laminar boundary layer separation from rearward-facing step, noting periodic spanwise structure 02 p0232 A67-11563
Steady flow of jet from orifice at nose of body and opposing supersonic free

stream 02 p0178 A67-11565
 Current distribution in eddy configuration of atmospheric gas discharge, noting flow surface deformation rate and measurement techniques 02 p0180 A67-12441
 Flat turbulent jet ejected from thin slit into cross wind in experimental and theoretical comparison 03 p0401 A67-12878
 Prediction theory for effect of shear flows on outlet angle in axial compressor cascades, taking into account effects of secondary flow, Bernoulli surface rotation and spanwise flow displacement 04 p0548 A67-15387
 Flow recirculation as affected by position and geometry of inducing obstacle 06 p0937 A67-17918
 Circumferential inlet velocity distortion effect on normal force response and stall characteristics of rotating blade in axial flow turbomachine 06 p0938 A67-18255
 Disturbance diffusion in incompressible zero pressure gradient flow 10 p1626 A67-23144
 Effect of wide angle screened diffuser on turbulent velocity fluctuations [ASME PAPER 87-FE-23] 14 p2243 A67-28368
 Attenuation of circumferential inlet distortion in multistage axial compressors, predicting flow field and pressure distortion via zero axial clearance approximation [AIAA PAPER 87-415] 18 p2982 A67-33902
 Collapsing shocks and detonation waves gasdynamic problem, evaluating perturbations due to counterpressure and to heat release 19 p3209 A67-35411
 Circumferential inlet velocity distortion effect on normal force response and stall characteristics of rotating blade in axial flow turbomachine 21 p3565 A67-38536

FLOW DISTRIBUTION
SA CHAPMAN-ENSKOG METHOD
 Numerical calculations of nonlinear behavior of MHD shock waves in dissipative medium 11 p1825 A67-23854
 Flow induced vibrations of rigid plate in narrow channels, noting flow rate dependence on channel width [ASME PAPER 87-VIBR-32] 11 p1777 A67-24190
 Existence of continuous transonic flow and model representing velocity distribution by Oswatitsch integral equation 13 p2050 A67-26808
 Plated-tube heat exchanger design for minimizing axial heat conduction losses and controlling heat transfer surfaces and core weight 13 p2229 A67-27665
 Two-dimensional curved diffuser design by comparison with flow regime and performance data, obtaining diffuser shape and pressure distribution criteria [ASME PAPER 87-FE-6] 14 p2242 A67-28358
 Relationship between geomagnetic storms with sudden commencements and perturbations of southern and northern components of meson distribution in Northern Hemisphere 17 p2938 A67-32796
 Measuring laminar flow development in square duct using laser Doppler flow meter [ASME PAPER 87-APM-37] 17 p2881 A67-33161
 Incompressible turbulent boundary layers with arbitrary pressure gradients and divergent or convergent cross flows predicted by effective viscosity hypothesis 19 p3211 A67-35738
 Molten carbonate fuel cell module featuring flexibility of construction, electrical simplicity and effective gas distribution characteristics 20 p3364 A67-37015
 Gas flow interaction with blunt body in transition flow regime between continuum and free molecule flow calculated using first collision model 22 p3743 A67-40175

FLOW EQUATION
 Parametric representation derived for one-dimensional nonsteady flows, considering two distinct solutions of Martin Monge-Ampere equation 01 p0052 A67-10520
 Laminar flow of elastico-viscous fluid between parallel planes obeying Noll constitutive equation, considering heat transfer 01 p0053 A67-10802
 Stability of solutions to general equations of steady state one-dimensional relaxed flow of perfect gas mixtures [ONERA-TP-360] 01 p0054 A67-11089
 Boundary layer equations for nonstationary plane flow of viscous incompressible fluid 02 p0232 A67-11921

Solution to boundary layer equations for unsteady flow of viscous incompressible fluid under injection or suction 02 p0233 A67-11948
 Transonic plane gas flow equations with algebraic self-similar solutions used for analysis of flow in various nozzles 02 p0178 A67-11951
 Secondary vorticity for compressible flow in centrifugal impeller, noting parameter effects on motion 03 p0402 A67-13337
 Solutions of nonstationary equations of plane laminar MHD boundary layer, using transformation to specialized form of curvilinear coordinates 03 p0477 A67-13527
 MHD flow past bodies in electroconductive viscous incompressible flow 03 p0482 A67-13743
 Nonsteady flow problems, solving fluid motion equations by characteristic method and obtaining boundary conditions 03 p0403 A67-13769
 Equation for laminar gas meter applied to flow coefficient derived from Hagen-Poiseuille relationship, noting effect of heat transfer, compressibility, etc. on meter performance 03 p0404 A67-13778
 Formulation of problem of large-scale fluid mechanics, based on definition of characteristic flow parameters, applied to molecular flows 03 p0404 A67-13882
 Taylor vortices intensity and viscous losses determined for viscous flow of liquid between concentric rotating cylinders, solving equation by numerical method 03 p0405 A67-14030
 Composite heat transfer in moving gray medium, obtaining solution based on boundary layer equations 04 p0722 A67-14712
 Solid-solid impact at hypervelocities using flow equations, noting variations of impact velocity, projectile shape and density and state equation 04 p0710 A67-15004
 Longitudinal conduction effect on fluid temperatures in multistream counterflow heat exchanger, based on characteristic function 04 p0728 A67-15806
 Successive approximations applied to optimal control equation for self-similar viscous Couette flow between one stationary and one moving wall 04 p0610 A67-15885
 Radial momentum equation of flow outward from axisymmetric turbulent wall air jet impinging on solid surface 05 p0792 A67-16819
 Spence integrodifferential equation for flow around slender slightly curved profile with jet at trailing edge 05 p0749 A67-16842
 Two-dimensional self-similar hot conducting gas outflow into vacuum, for power law variation of gas-vacuum interface temperature 05 p0793 A67-17007
 Asymptotic method for solution of boundary layer equations for generalized three-dimensional flow of dissociated air at chemical equilibrium near stagnation point 06 p0984 A67-18113
 Ordinary differential equation in boundary layer theory of reversed flow 06 p1025 A67-18730
 Three-dimensional boundary layer flow of incompressible second order viscous fluid near spinning cone 06 p0992 A67-18868
 Radiation effect on hydrodynamic shock wave parameter distribution for bodies entering dense atmospheric layers at supersonic velocities 07 p1125 A67-19110
 Nonlinear nonsteady wave propagation in plane flow analyzed by introducing perturbations of potential into equation of gas dynamics and equation of characteristics 07 p1189 A67-19731
 Hypercritical flows in MGD solved explicitly for exact solutions 07 p1230 A67-20120
 Oseen equations inadequacy in ensuring uniqueness for flow past infinite body 08 p1319 A67-20351
 Transfer phenomena in polygenous solutions, noting canonic form of component flow equation 09 p1553 A67-21905
 Structural equations with variable coefficients for nonstationary one-dimensional gas flows, using Cartan method 09 p1487 A67-21912
 Closed form solution for tricom boundary value problem, noting application to transonic dynamics 09 p1524 A67-21929
 Flow of ideal gas behind shock wave of finite amplitude analyzed, based on equation

for one-dimensional adiabatic motion 10 p1624 A67-23033
 Numerical solution of class of nonlinear high order differential equations with two-point asymptotic boundary conditions for thermal boundary layers in laminar and turbulent flow 10 p1627 A67-23560
 Finite difference scheme for solving set of Prandtl equations for nonstationary flow of viscous incompressible fluid 10 p1628 A67-23672
 Invariant transformation for pulse and continuity equations of one-dimensional unstabilized motions of ideal compressible fluid 10 p1628 A67-23678
 Plasma instabilities due to RF motion obtained by expanding fluid and electromagnetic wave equations in asymptotic series 11 p1825 A67-23870
 Radial flow of two-dimensional viscous conducting fluid in wedge shaped channel under magnetic field, reducing flow equation to differential equation 12 p1977 A67-26180
 Invariant transformation of MGD equations where plane flow is situated in transverse magnetic field 13 p2166 A67-26895
 Asymptotic short wave flow equations simplified for various viscous heat conducting gas flows 14 p2295 A67-27838
 Navier-Stokes equations governing flow linearized by using weak solution technique 14 p2295 A67-27894
 Solution of one-dimensional diffusion equation of heat flow normal to surfaces, prescribing potential and flow rate along moving parametric curve 14 p2405 A67-28254
 Axisymmetric blunt bodies shock standoff distances in hypersonic flow determined by numerical and analytic methods 14 p2244 A67-29056
 Numerical solution of boundary layer equations by finite difference integration 15 p2473 A67-30189
 Flow equations for convective heating associated with recirculating flow in clustered engine boosters for free viscous shear layer along exhaust jet boundary 16 p2591 A67-30942
 Hydrogen and helium lateral flow in collisionless exosphere calculated on model for various sinusoidal temperature and concentration variations over exobase surface 17 p2852 A67-33235
 Solution to boundary layer equations for unsteady flow of viscous incompressible fluid under injection or suction 17 p2840 A67-33265
 Transonic plane gas flow equations with algebraic self-similar solutions used for analysis of flow in various nozzles 17 p2841 A67-33268
 Two-dimensional self-similar hot conducting gas outflow into vacuum, for power law variation of gas-vacuum interface temperature 18 p3028 A67-34269
 Two-dimensional flow structure around thin body in dispersive medium, discussing flow equations and similarity law 19 p3208 A67-34901
 Binary laminar boundary layer equations with second order transverse curvature for hypersonic flow with mass injection of foreign gases into air 19 p3211 A67-35737
 Flow of steady compressible gas expressed in intrinsic relations to derive equations of rotational motions in Euclidean space 19 p3212 A67-35883
 Axisymmetric flow equations for performance prediction of axial-flow turbomachines and stage design 20 p3355 A67-36186
 Steady flow equations with symmetry of revolution, obtaining first integrals for perfect fluid 20 p3420 A67-36395
 Time-dependent current flow equations solved for insulator with traps if injected space charge produces negligible perturbation on external electric field 20 p3509 A67-36506
 Stagnation ablation of blunt body hypersonic reentry with nonreacting gas, deriving laminar flow equations 20 p3356 A67-36509
 Equations of one-dimensional aerothermodynamic flow of dissociating gas 20 p3420 A67-36599
 Mathematical models of flow and filtration performance of wire cloth filter media in series and parallel configuration 20 p3365 A67-37364
 Finite difference scheme for solving set of

Prandtl equations for nonstationary flow of viscous incompressible fluid 21 p3612 A67-38273

Invariant transformation for pulse and continuity equations of one-dimensional unsteady motions of ideal compressible fluid 21 p3612 A67-38279

Boundary layer flow incident on smooth axisymmetric body in vicinity of critical point 21 p3613 A67-38422

Flow equations for electron emitter placed in ion stream and transparent to ions, showing previous results due to incorrect choice of boundary conditions 22 p3843 A67-39262

Quasi-one-dimensional nonequilibrium argon plasma flow equation, discussing kinetic model with atom-atom and electron-atom impact ionization 22 p3850 A67-39708

Equations numerical integration for MHD fluid flows near critical point in presence of azimuthal magnetic field for several Alfvén and diffusion numbers 22 p3853 A67-40011

Precise and approximate formulations for unsteady flows of conducting fluid in MHD channels with external electric current 22 p3853 A67-40023

Velocity distribution determination method for supersonic flow around zero incidence cones in equilibrium air, discussing motion equation and flow field parameters 22 p3742 A67-40098

Numerical solution of Poiseuille flow with variable fluid properties, solving coupled momentum and energy equations [ASME PAPER 66-WA/FE-22] 23 p3989 A67-40930

Haskell viscous flow equations describing very slow linearly viscous liquid with initially crater shaped surfaces solved and applied to lunar craters 23 p4065 A67-40998

Book on fluid mechanics foundations for introductory and/or secondary fluid mechanics course, with appendices containing vector analysis, inviscid fluid flow equations, etc 23 p3991 A67-41529

Two-phase flow equations for turbulent boundary layer flows, considering solid particle effects 23 p3993 A67-41748

High speed internal flow past cone with large wall injection velocities, calculating pressure of outer flow using contact surface initial slope as parameter 24 p4092 A67-42398

FLOW FIELD

Turbulent mixing of axisymmetric jet of partially dissociated nitrogen with ambient air, establishing mixing and decay characteristics [AIAA PAPER 65-823] 01 p0055 A67-11171

Flow field about subsonic jet exhausting into quiescent and low velocity air stream [AIAA PAPER 65-704] 01 p0055 A67-11254

Predicting wake-induced nonuniform flow field in plane of rotor disk [AIAA PAPER 66-17] 03 p0354 A67-12909

Spatial distributions of free electrons in near wakes of spheres in hypersonic flight [AIAA PAPER 66-55] 04 p0547 A67-14820

Wind tunnel experiments extending range of data published in 1964 on flow field associated with sonic injection of gas 04 p0604 A67-14831

Cryogenic pumping capability of liquid helium cooled plate in supersonic flow field at simulated high altitude 04 p0606 A67-14999

Streamline curvature computing procedures for turbomachinery and fluid flow problems, considering axisymmetric and nonaxisymmetric flow fields and compressible cascade flow [ASME PAPER 66-WA/GT-3] 04 p0607 A67-15358

Energy transfer by circulatory and Coriolis forces in centrifugal and axicentrifugal compressors 04 p0690 A67-15897

Transverse curvature effect on axisymmetric compressible laminar boundary layer flow, obtaining asymptotic solutions for skin friction and heat transfer 05 p0791 A67-16509

Flow field of finite bladed propeller in forward flight regime, analyzing harmonic content, noting fluctuating part of velocity component 06 p0937 A67-18004

Discontinuous solutions in supersonic reacting gas flows under nonequilibrium conditions 06 p0984 A67-18112

Flow field associated with tangential slot gas injection in supersonic flow, presenting turbulent mixing zone and stability and spark shadowgraphs

[AIAA PAPER 67-198] 06 p0987 A67-18300

Flow field and stability of far wake of circular cylinders at hypersonic speeds, noting Reynolds number role [AIAA PAPER 67-32] 06 p0939 A67-18348

Time dependent computational method for three-dimensional blunt body flow fields traveling at supersonic speed including shock points, sphere cones and ellipsoid [AIAA PAPER 67-222] 06 p0941 A67-18461

Near-field solution for nonequilibrium transonic flow around corner near transonic-frozen flow field 06 p0942 A67-18587

Flow around variable profile in analog study of Laplacian field according to Dirichlet data 07 p1128 A67-20225

Flow field around porous wedge or cone immersed at zero angle of attack in uniform supersonic free stream when contact surface is straight 08 p1276 A67-20571

Flow field in turbulent far wake at high Mach and Reynolds numbers, obtaining solution of boundary layer equations 08 p1277 A67-20577

Book on theory of flow machines covering pumps, turbines, windmills, fluid dynamics, viscous flow fields, cascade flow, etc 08 p1321 A67-20758

Solutions for field aligned flow past magnetic source using Green function, estimating energy dissipation rate 08 p1549 A67-22399

Medium flow parameter measurement via stationary sensors for simulated test stages of axial compressor 09 p1438 A67-22456

Aerodynamic problem of steady potential flow and added mass in unsteady motion of idealized hemispherical parachute 09 p1438 A67-22485

Aerodynamic flow field past cascade of plane thin turbine blades subjected to small random vibrations [ONERA-TP-412] 09 p1439 A67-22588

Exact theory of enclosed molecular radiometer using flow field solution from Wu-revised thermal transpiration theory in two cases 10 p1681 A67-22864

Behavior of inviscid supersonic conical flow fields near crossflow stagnation points studied by constructing coordinate expansions of exact conical flow equations [AIAA PAPER 66-491] 10 p1591 A67-23112

Radiometer system with photomultiplier tube for measuring absolute radiation from hypervelocity projectile flow fields 11 p1790 A67-24447

Null-yaw and fixed direction multihole probes for aerodynamic measurements, describing calibration charts and error sources 12 p1940 A67-25352

Radiation MGD, considering flow problems with thermal radiation and electromagnetic field effect 12 p1975 A67-25889

Detonation wave interaction with hydrogen-oxygen flow fields in clarifying rocket combustion instability and supersonic combustion 12 p1929 A67-25898

MHD of thin body in oblique fields 12 p1976 A67-25939

Martian entry condition analyzed as nonequilibrium flow field phenomenon, noting chemical kinetics and radiation behind shock wave in gas mixtures [AIAA PAPER 67-322] 12 p1930 A67-26037

Flow fields of inlets for real or perfect gases determined through four methods for application to supersonic and hypersonic flight regimes [AIAA PAPER 66-805] 13 p2050 A67-26831

Nonequilibrium effects in spherical free jet expansions of polyatomic gases and gas mixtures, obtaining moment equations for flow field development 13 p2104 A67-26983

Equilibrium configuration and tension of flexible cable in uniform flow field, considering tangential drag force and weight effects 13 p2051 A67-27587

Partial differential equations for three-dimensional inviscid flow solved for flow field over blunt body shapes at various angles of attack, for application to Apollo spacecraft [AIAA PAPER 66-413] 14 p2240 A67-28110

Hydraulic analog for qualitative analysis of flow field of expansion-deflection nozzle 14 p2297 A67-28136

Flow field measurement near sharp leading edge of cooled flat plate parallel to low density hypersonic stream 14 p2241 A67-28165

Low density hypersonic wind tunnel,

noting surface pressure and flow field measurements 14 p2293 A67-28166

Local flow field measurements of static temperature, density and local impact pressure of hypersonic rarefied flow over 10 degree cone 14 p2241 A67-28169

Ionospheric aerodynamics, discussing flow field properties, satellite motion, flight characteristics, etc 14 p2242 A67-28200

Static and dynamic performance of pancake vortex flow field and application to pressure amplification 14 p2248 A67-28272

Planar incompressible free turbulent mixing with arbitrary velocity ratio and axial pressure gradient [ASME PAPER 67-FE-9] 14 p2304 A67-28359

Parameter determination for flow field in space between shock wave of nonviscous supersonic gas flow and thin spherically blunt cone 14 p2243 A67-28659

Flow field and heat transfer in radiating stagnation-point shock layer of atmospheric-entry vehicles 16 p2591 A67-30940

Circular vortex ring motion and decay in incompressible flow field considered for Navier-Stokes equations solution by boundary layer technique 16 p2660 A67-31212

Low Reynolds number flow past heated cylinder studied for fluid properties variation and thermal and velocity slip presence at wall 16 p2779 A67-31216

Multidimensional unsteady flow field of inviscid fluid calculated with application of method of characteristics and digital computer 16 p2662 A67-31535

Transverse curvature effect on axisymmetric compressible laminar boundary layer flow, obtaining asymptotic solutions for skin friction and heat transfer 16 p2662 A67-31600

Wall-turbulence interaction for infinite flat plate inserted into homogeneous isotropic turbulence, measuring growth of inhomogeneity layer 17 p2837 A67-32286

Strong forward flow of engine exhaust gas in blast deflection flow field of twin jet F-111B 17 p2797 A67-32568

Steady flow of ideal gas with conductivity past thin wedge in magnetic field studied for asymptotic properties of flow field 17 p2902 A67-32671

Local mass flux and local impact pressure measurement in arc jet exhaust flow fields 17 p2861 A67-33029

Steady state magnetic field in transition region between magnetosphere and bow shock by MHD equations, noting solution by approximation method 17 p2951 A67-33186

Attenuation of circumferential inlet distortion in multistage axial compressors, predicting flow field and pressure distortion via zero axial clearance approximation [AIAA PAPER 67-415] 18 p2982 A67-33902

Supersonic combustion characteristics of hypersonic ramjet predicted by analytical method using constant-mass tube technique, discussing flow field properties [AIAA PAPER 67-494] 18 p2983 A67-33958

Interactions produced by shock wave running into magnetic field perpendicular to wave direction 19 p3294 A67-35405

Shock wave interaction with plasma arc discharge, investigating wave refraction, arc response to pressure and temperature pulses and aftershock flow field 19 p3294 A67-35407

Model thruster designed and operated with argon and hydrogen for investigation of hybrid flow fields of plasma acceleration by thermal and magnetic forces [DVL-630] 19 p3297 A67-35601

Time dependent computational method for three-dimensional blunt body flow fields traveling at supersonic speed including shock points, sphere cones and ellipsoid [AIAA PAPER 67-222] 19 p3171 A67-35736

Compressible inviscid fluid MHD motion, stressing quasi-aligned field flows 20 p3496 A67-36272

Momentum integral method applied to two-dimensional flow problem between flat plates 20 p3420 A67-36420

Viscoelastic flow, examining boundary layer approximation for flat plate with zero angle of incidence 20 p3424 A67-37503

Differential geometry and vector analysis used to design axisymmetric lens of arbitrary shape for observing phenomena in arbitrary flow field of revolution 21 p3610 A67-37810

Approximate method for calculating interaction between flow and soft spherical

shell 21 p3717 A67-37976
 Magnetic field effect on flow field and drag of blunt body in partially ionized argon plasma, obtaining electron density and temperature 21 p3673 A67-38753
 [AIAA PAPER 67-729]
 Steady flow field from turbulent boundary layer separation in front of forward facing step, discussing pressure field 21 p3613 A67-38853
 Inviscid hypersonic flow field between barrel shock and free boundary for source flow representing high altitude jet exhaust 22 p3739 A67-39410
 Turbulent cylindrical wall jet flow field, velocity profile and surface friction coefficient noting transverse curvature effects 22 p3783 A67-39531
 Helium argon mixture shock wave density profile measurements, discussing shock wave production in flow field at supersonic nozzle exit 22 p3783 A67-39709
 Radiative cooling and self-absorption effects on reflected shock flow field and end wall heat transfer studied using finite difference method 22 p3917 A67-39710
 Concentration distribution time for heavy gas diffusing in light gas steady flow field 22 p3917 A67-39714
 Integral relations method for nonequilibrium hypersonic planetary entry, emphasizing flow fields and thermal environment determinations for blunt body vehicle configuration 22 p3740 A67-39936
 Supersonic three-dimensional flow fields of inviscid nonconducting gas around delta wing with blunted edges 22 p3741 A67-40025
 Velocity distribution determination method for supersonic flow around zero incidence cones in equilibrium air, discussing motion equation and flow field 22 p3742 A67-40098
 Laminar flow field between rotating turbine disks solved for low Reynolds number and partial admission 23 p3988 A67-40614
 Laminar boundary layer subject to local three-dimensional disturbance, studying growth, flow field and transition to turbulence 23 p3991 A67-41175
 Conformal mapping method for overcoming difficulties caused by limiting line in computing flow field about blunt body supporting paraboloidal shock wave 23 p3932 A67-41730
 Streamline curvature computing procedures for turbomachinery and fluid flow problems, considering axisymmetric and nonaxisymmetric flow fields and compressible cascade flow [ASME PAPER 66-WA/GT-3] 24 p4143 A67-42459
 Delta wing with leading edge vortices, calculating inviscid incompressible flow field near center of rolled up vortex sheet assuming conical velocity field 24 p4092 A67-42570

FLOW GEOMETRY

MHD channel flow under transverse electromagnetic field, analyzing effect of various geometries and boundary conditions 10 p1684 A67-22875
 General heat flow problem with convection integrals eliminated and unsteady temperature distribution expressed as sum of quasi-steady and transient fields, noting region geometry 12 p2040 A67-26185
 Rotor downwash angle and tunnel geometry effect on maximum size rotor that can be tested in closed throat wind tunnel 13 p2091 A67-27595
 Defined region geometry flow characteristics for high-gain proportional amplifiers 14 p2249 A67-28326
 End losses in magnetohydrodynamic channels of linearly variable cross section determined using equivalent channel geometry 16 p2606 A67-30585
 Interference of open and closed wind tunnels with ground board calculated and results applied to airfoils 16 p2590 A67-30854
 Hermetically sealed ballistic facility design and operating principles, for testing at various Mach and Reynolds numbers to calculate aerodynamic coefficients and flow geometry 16 p2655 A67-31115
 Geometry of streamlines and field lines of MHD flow, using partial differential equations 17 p2910 A67-33351
 Potential flow stability of weightless incompressible fluid for specific flow

geometries 18 p3028 A67-34219
 Analysis of flow and points of stagnation of fluid circulating over cylinder 19 p3210 A67-35720
 Base pressure measurements on elliptic cones in supersonic flow with turbulent boundary layer as function of geometry 21 p3566 A67-39083

FLOW GRAPH

SA SIGNAL FLOW GRAPH

Flowgraph teaching techniques, discussing problem formulation, construction procedures and symbolic and numerical evaluation in network analysis 01 p0030 A67-11042
 Graphs for momentum flux and mass flow calculations for use in subsonic compressible flow 01 p0007 A67-11268
 Algorithms for dichotomous representation of macrocircuits, considering computer programs and establishment of flow graphs 08 p1299 A67-20326
 Task distribution, overall network, flow diagram and data processing of PERT method controlling development of ELDO-A rocket third stage 16 p2783 A67-31632
 Algorithms for dichotomous representation of macrocircuits, considering computer programs and establishment of flow graphs 18 p3005 A67-33498
 Flowgraph models of thermal and electrical parameters interaction in solid state devices, examining performance characteristics, system stability, etc 19 p3191 A67-34845
 Sensitivity coefficients through flowgraphic representation of network function, discussing algorithmic computer program 19 p3200 A67-34846
 Flowgraph models describing relationships between thermal and electrical parameters of devices and associated circuits 19 p3206 A67-36034
 Supersonic viscous gas flow around body of revolution involving perturbation damping, analyzing Navier-Stokes and heat transfer equations for flow chart 20 p3357 A67-36810
 Coates flow graph gain formula modification by introducing loop-set and two-loop-set for linear systems analysis 23 p3984 A67-40649
 Externally pressurized gas bearings examined for mechanism of series restrictors on pressure distribution, flow quantity and load 23 p4010 A67-41064
 Gas bearings with wide pockets investigated theoretically and experimentally for pressure distribution, flow quantity and load capacity 23 p4010 A67-41065

FLOW MEASUREMENT

Heat flux measurement in very short flows in short arc wind tunnels and shock tubes 01 p0168 A67-11091
 Probe holder used in wind tunnels for shifting of flow measuring probes 02 p0228 A67-11554
 Flow measurement - ASME Conference, Pittsburgh, September 1966 03 p0421 A67-13766
 Flow pulsation effect on error of flow measurement by means of steady flow formula, noting manometer design requirements 03 p0403 A67-13767
 Cryogenic fluid mass flow measurement methods, noting flow meter calibration 03 p0421 A67-13768
 Transient air flow rates into gas turbine metered, using two critical flow circular arc venturi 03 p0421 A67-13770
 Engine test facility for measuring thrust and propellant flow in pulsating rockets 03 p0396 A67-13774
 Statistical analysis for pulsed flow measurement evaluation using correlation and regression techniques 03 p0403 A67-13777
 Laminar flow on adiabatic surface measured, using Stanton tube and supersonic wind tunnel 04 p0547 A67-14849
 Aerodynamic characteristics of wings of complex planform at subsonic velocities, calculating flows past wings at moderate angles of attack 06 p0935 A67-17730
 Fluidic test equipment for measuring rapidly varying fluid parameters and flow visualization 07 p1186 A67-19634
 Book on airflow measurement techniques and flow meters 08 p1321 A67-20759
 Cesium vapor flow from orifices and tubes into vacuum analyzed, noting dependence of

angular distribution and center line intensity on Knudsen numbers 08 p1324 A67-2149
 Averaging of parameters of inhomogeneous flowing medium using a criterion degree at which flow parameter/energy, losses, momentum, flow rate/air maintained 09 p1495 A67-2168
 Flow of ideal compressible electrical conducting fluid in traveling wave accelerator, using multiple coordinate method to approximate small perturbation solution 09 p1544 A67-2184
 Cryogenic fluid mass flow measurement methods, noting flow meter calibration 13 p2121 A67-2763
 Low velocity flow measurements inexpensive thermistor probe 14 p2318 A67-2834
 Rocket nozzle effect on acoustic losses from model motor chambers oscillating in first longitudinal mode 15 p2546 A67-2999
 Flow through blade cascade studied by averaging flow parameters behind cascade for testing internal combustion turbine guide vanes 16 p2736 A67-3100
 Argon and nitrogen shock wave damping along tube in absence of effects of oscillation excitation, gas dissociation ionization and emission 16 p2659 A67-3110
 Fuel consumption precision measurements for low thrust auxiliary rockets using impeller wheel and photometric devices [AIAA PAPER 67-507] 18 p2989 A67-3397
 Aerospace technology and hardware transference to commercial and architectural testing, noting application to flow measurements, hydraulic acoustics and helium leak detection 20 p3416 A67-3669
 Indium activity measurements to determine epithermal neutron flux in atmospheric upper layers, giving results in terms of dependence on atmospheric depth 21 p3622 A67-3903
 Ring laser use for measuring gas flow on ground and fuel and oxidizer flow in rockets 22 p3800 A67-3989

FLOW METER

Cryogenic fluid mass flow measurement methods, noting flow meter calibration 03 p0421 A67-13768
 Calibration of flow meters in liquid hydrogen at high flow rates for establishing limits of extrapolations from lower flow rate data 03 p0422 A67-13771
 Differential pressure flow meter for unsteady or transient fluid flow 03 p0422 A67-13777
 Flow meter for extremely low flow rates during steady state and pulse mode thrust operation 03 p0422 A67-13777
 Elbow flow meters, comparing average coefficients with theoretical values 03 p0422 A67-13777
 Slip table fixture design for cryogenic and vibration testing of liquid oxygen pre valves and flow meter 04 p0598 A67-15176
 Contactless flow meter, based on spatial MHD drifting, for flow velocity measurements on electroconductive fluid 04 p0624 A67-15531
 Heat flow meter with short response time measuring influence of acoustic field on forced convection 05 p0790 A67-16033
 Liquid hydrogen pressure, temperature flow and liquid level measuring techniques 05 p0807 A67-17011
 Accuracy ratio and traceability of flow metrology noting uncertainty values, cryogenic standards, gas leakage detection etc 05 p0809 A67-17377
 Low rate gas flow meter noting sealing and controlling of piston, differential pressure meter and DC servoamplifier 06 p1000 A67-17753
 Hydraulics of electromagnetic liquid-metal metering device with constant inlet pressure, noting dose value dependence on parameters and operating conditions 06 p0951 A67-16868
 Book on airflow measurement techniques and flow meters 08 p1321 A67-20759
 Ultrasonic flow meter for directly measuring average stream velocity using sing-around velocimeter with piezoelectric ceramics 10 p1656 A67-2307
 Entrance region tube flow combined with rounded entrance flow meters to obtain theoretical solution relating flow rate downstream pressure, pressure drop and temperature 13 p2120 A67-26933
 Cryogenic fluid mass flow measurement

methods, noting flow meter calibration 13 p2121 A67-27633
Incompressible two-phase mixed flow through sharp edge orifice including shear force between phases 14 p2305 A67-29012
Aircraft flow meters for simultaneous rate and volume measurements, examining equations of motion 16 p2671 A67-31006
Polarographic and mass gas flowmeter sensors incorporated into bench model for on-line continuous determination of oxygen consumption in human subjects 18 p2995 A67-34711
Heat flow meter apparatus for rapidly measuring thermal conductivity of flat insulation specimens under cryogenic temperatures 22 p3802 A67-40293
Cryogenic thermoconductivity heat flow meter apparatus for felt, powder and block materials at atmospheric pressure 22 p3803 A67-40298

FLOW PATTERN

Temperature distribution and fluid flow in horizontal layer of liquid heated from below, having rigid-rigid and rigid-free upper surfaces 04 p0728 A67-15679
Potential double waves at interface between two-dimensional nonsteady barotropic gas flow and region of undisturbed gas 07 p1169 A67-20034
Wakes behind axisymmetric blunt based bodies, noting similarity among wakes through measurements of velocity, turbulence and static pressure 08 p1277 A67-20706
Flow vortices in hollow cylinder made of type II superconductor 09 p1482 A67-22662
Airflow past wing profile with leading edge slot blowing foreign gases, noting schlieren photographs of flow patterns and concentration distribution measurement 10 p1589 A67-22724
Flow pattern in front of cylinder mounted on plate at Mach 3 in wind tunnel, noting supersonic region between cylinder surface and shock wave 10 p1590 A67-23025
Stokes flow for sphere in arbitrary external flow pattern solved using Green function, showing uniqueness solution 10 p1629 A67-23831
Axisymmetric thermal convection flow in rotating fluid annulus 12 p1963 A67-25340
Radial gas turbine losses, obtaining rotor loss coefficients, discussing flow pattern for performance prediction 12 p1891 A67-25347
Relative eddy flows mechanism in mixed flow turbomachines 12 p1891 A67-25348
Velocity profiles for turbulent ducted flow systems analyzed, showing profile decay rate for flow pattern 12 p1927 A67-25351
Analysis of steady flows of viscoelastic materials by introduction of two dimensionless groups 13 p2096 A67-26931
Two-dimensional self-similar problem for uniform penetration of plate into half-plane of perfect gas flow, determining flow pattern 14 p2239 A67-27982
Vortices in plane flow behind circular cylinder at different Mach numbers, noting staggered pattern formation 14 p2296 A67-27988
Three-dimensional gas flow in region of incidence of shock wave on cylinder situated in high supersonic flow 14 p2297 A67-27995
Apparent mass of supersonic jet stream under off-design flow conditions 14 p2242 A67-28302
Two-phase gas-liquid flow photography equipment and techniques, with applications to droplet mass transfer, flow pattern determination, etc 16 p2671 A67-30840
Supersonic unsteady flow of cylindrical body past diaphragm model at interface between density-differing gases, studying flow patterns 16 p2593 A67-31133
Two-dimensional inviscid flow pattern of gas behind shock front in neighborhood of stagnation point of cylindrical body acting as magnetic field source 16 p2723 A67-31581
Steady flow in rectangular cavity with driving motion by uniform translation of one wall 17 p2836 A67-32279
Current flow patterns in cross connected MHD generator with four electrodes 18 p2987 A67-33704
Mixing patterns and flow configurations in model for determining combustion performance in well-stirred reactor 18 p3154 A67-33833
Exhaust gas recirculation for VTOL aircraft

[AIAA PAPER 67-439] 18 p2985 A67-33916
Recirculation zone in fluid mechanics experiments on cylindrical cavity simulating gas-core nuclear rocket as heavy gas reservoir, discussing flow patterns [AIAA PAPER 67-502] 18 p3076 A67-33966
Atmospheric properties at high temperature, discussing atmosphere radiation influence on flow around reentry device and radiative heat transfer 18 p3159 A67-34126
Three-dimensional detached flow patterns forming near secondary jet injected into supersonic flow 18 p3027 A67-34207
Mach and Reynolds numbers effect on rarefied supersonic gas flow pattern near forward stagnation point of blunt body, noting decrease in density 18 p3028 A67-34209
Flow pattern caused by low speed splash of liquid drop into pool computer examined, obtaining configuration plots various splash stages 19 p3212 A67-35895
Gas turbine theory based on Coanda effect and turbine efficiency from fluid flow analysis of depressive blade-fitted turbines 20 p3515 A67-36274
Flow patterns of two-phase mixtures in cylindrical tubes, using high speed photography 20 p3423 A67-37161
Flow pattern at low Reynolds numbers about airfoil cascade illustrated by hydrogen bubble flow-visualization technique 20 p3359 A67-37483
Taylor columns occurrence criterion in Jupiter atmosphere investigated experimentally, giving flow patterns 21 p3614 A67-38999
Secular changes in surface flow motion in earth core noting dynamo theories of earth main field 23 p3996 A67-40816
Flow past disk at angle to stream with marked periodic motions caused by vortex ring shedding increasing with angle of incidence 23 p3990 A67-41171
Human respiratory system impedance simulator for dynamic testing of aircraft breathing equipment to detect possible instabilities 24 p4114 A67-41782
Structure of quasi-steady-state MHD shock wave in plasma supersonic flow, analyzing width dependence magnetic field 24 p4195 A67-41937
Anabatic winds caused by solar heating of slope, investigating flow patterns useful for soaring purposes 24 p4181 A67-42022
Incompressible viscous fluid rotary turbulent flow microstructure between rotating cylinders, analyzing centrifugal force effects on turbulent heat transfer processes 24 p4142 A67-42214
Cellular convection patterns from instability of horizontal fluid layer uniformly heated and cooled from above 24 p4255 A67-42563
Nonlinear analysis of cellular convection induced by surface tension in finite amplitude heated liquid layer, discussing prediction of hexagonal flow pattern 24 p4255 A67-42569
One-dimensional steady MGD flow of polytropic gas with finite constant electric conductivity, noting flow patterns and oblique shock wave structure 24 p4198 A67-42707

FLOW REGULATOR

Elastic orifice compensator in externally pressurized gas bearings for flow control, noting increased bearing stiffness 01 p0077 A67-10123
Supersonic retardation cascades for lossless reduction of supersonic flow to subsonic in turbines and compressors 03 p0503 A67-13012
Flow restricting devices, describing basic and special throttles and nozzles 09 p1442 A67-21647
Remote control of monochromator prism rotation using balanced-bridge system to regulate flow 20 p3451 A67-37308

FLOW RESISTANCE

Strain gauge measurements of resistance of sphere to MHD turbulent flow of mercury in rectangular tube 04 p0670 A67-15530
Hydraulic resistance determination for plane and axisymmetric channels with attached and separated flow, noting terminology 04 p0549 A67-15602
Reynolds stress maintenance by components of turbulent shear flow, noting jet mixing layer 06 p0985 A67-18133
Human perception of airflow resistance

and perception thresholds under various conditions 07 p1133 A67-19478
Empirical expression for resistance of small bore tubes to turbulent flow of compressible fluid in terms of mass flow and total head 08 p1320 A67-20461
Drag on two-dimensional cylinder between parallel walls in Stokes flow calculated by perturbation methods 08 p1323 A67-21390
Friction and heat transfer across boundary layer in external flow with transverse inhomogeneity calculated by mean-mass values method 10 p1625 A67-23041
Mercury flow in rotating torus with induction pump and magnetic field effect on flow studied for flow resistance 17 p2900 A67-32342
Slightly resistive plasma stability analyzed by asymptotic methods, studying small perturbation growth rate 20 p3493 A67-36145
Vacuum jacketed cryogenic globe valve design providing tight sealing, low heat leak, low cool-down mass and high flow 23 p3936 A67-41426

FLOW SEPARATION

Diffusion flame in transition region of gas flow 02 p0343 A67-12536
Hypersonic flow separation over simple geometries and aerodynamic controls, noting pressure gradients and heating-rate distributions [AIAA PAPER 65-753] 03 p0350 A67-12911
Shock tube flow nonuniformity analyzed where shock and contact surface have maximum separation, applying results to turbulent and laminar boundary layer for heat transfer studies 03 p0397 A67-14027
Separation points occurring in Newtonian theory of hypersonic flow locally treated by modifying shock layer equations, thus verifying free layer theory 04 p0545 A67-14463
Thrust and mass flow rate of supersonic nozzle with and without internal separation 04 p0602 A67-14568
Quantity of separated liquid deposited on wall of rectangular channel from turbulent air-water dispersed annular flow, calculating liquid flow rate 04 p0602 A67-14641
Momentum transfer mechanism in separated flow region of rectangular cavity facing oncoming turbulent boundary layer [AFCLR-66-851] 04 p0610 A67-15924
Terminal shock-boundary layer interaction on slender cone-cylinder payloads at supersonic speeds and resulting flow separation [AIAA PAPER 66-471] 05 p0924 A67-17213
Cascade flow through compressor guide vanes and flow separation at top of vane profiles 05 p0750 A67-17323
Heat transfer for wall adjacent to region of turbulent separated flow 06 p0985 A67-18131
Lip shock from separation edge of half-angle wedge and resultant static-pressure recovery distribution along wake [AIAA PAPER 67-29] 06 p0986 A67-18260
Effect of Mach number and specific heat ratio on distance of shock wave from end face of circular cylinder in axisymmetric flow 07 p1128 A67-19347
Ranque effect, based on model of two-dimensional vortex flow of viscous thermoconductive gas, explains radial temperature distribution 07 p1268 A67-19352
Antisymmetrical thin delta wing with flow separation at subsonic leading edge 07 p1128 A67-20236
Attachment time of thin turbulent jet to adjacent parallel flat plate calculated using quasi-steady analysis and correlated empirically 08 p1280 A67-20440
Pressure field, Bernoulli sum variation, momentum and energy relations in laminar zone of separation 08 p1323 A67-21389
Three-way valve design for flow deflection, separation and mixing 08 p1286 A67-21535
Effect of straightening section of airfoil contour on local supersonic flow, noting deformation of sonic line or characteristics 09 p1438 A67-22217
Vortex separated delta wing leading edge in supersonic flow, noting effect on pressure distribution and role of flow equation 09 p1438 A67-22496
Three-dimensional flow in supersonic stream in symmetry plane of region of shock boundary layer interaction in front of obstacle mounted on plate, noting

penetration in separation region 10 p1590 A67-23026

Approximate closed form solutions for supersonic separated and reattaching laminar flow problem with boundary layer/shock wave interaction 10 p1591 A67-23115

Integral relations for separating flow 10 p1626 A67-23142

Three-dimensional turbulent boundary layers over swept wing calculated using entrainment equation 10 p1626 A67-23473

Entrance conditions and flow separation effect on rectangular diffuser performance, showing importance of secondary flows 10 p1627 A67-23557

Separation and nonseparation of skewed boundary layer, considering two-dimensional wing of finite aspect ratio at large angle of incidence 11 p1777 A67-24051

Channel blocking effect on motion of fluid in separation region behind bluff bodies 11 p1743 A67-24960

Navier-Stokes equations solved by finite difference methods at low Reynolds numbers for viscous flow around sphere, noting no flow separation 12 p1927 A67-25283

High lift techniques for STOL aircraft compared based on maximum lift coefficient, noting airfoil stall characteristics and flow separation delay devices [SAE PAPER 670245] 12 p1894 A67-25500

Vortical interaction between free jet boundary layer and outer flow in separation area of hypersonic gas flow past body 12 p1892 A67-25671

Wall streamlines and detachment on circular cone at angle of incidence in supersonic flow 13 p2049 A67-26591

Three-dimensional axisymmetrical boundary layer on spinning body of revolution in two-component fluid flow, discussing velocity distribution, drag and separation 14 p2295 A67-27835

Supersonic flow separation from corner of base compared to Stokes-type flow separation 14 p2240 A67-28111

Mechanism of fluid jet separation from curved surface 14 p2302 A67-28324

Current carrying incompressible viscous fluid past nonconducting sphere taking fluid inertia into account, noting eddy formation and flow separation 15 p2469 A67-29224

Flow behavior recognition techniques using changes in boundary layer velocity diagram to predict flow separation 17 p2792 A67-32908

Separation and stall of impulsively started elliptic cylinder including interactions between boundary layer and outer flow [ASME PAPER 67-APM-31] 17 p2840 A67-33157

Effect of straightening section of airfoil contour on local supersonic flow, noting deformation of sonic line or characteristics 18 p2982 A67-33756

Unsteady flow past blade cascade problem solved by splicing technique instead of conformal mapping technique 18 p2984 A67-34217

Flow around thin delta wing under supersonic conditions, considering flow separation at leading edges 19 p3170 A67-35542

Flow of incompressible viscous fluid past plane body, when flow boundary layer detaches from body producing aerodynamic wake 19 p3171 A67-35632

Flow pattern at low Reynolds numbers about airfoil cascade illustrated by hydrogen bubble flow-visualization technique 20 p3359 A67-37483

Boundary between stable operation of multistage axial flow compressor and rotational flow separation region, using variational condition 21 p3689 A67-38046

Gas separation effects in Ranque-Hilsch vortex tube explained by dynamic model of axial flow 22 p3917 A67-39512

Internal flow turbulent boundary layer separation for variable angle two-dimensional diffuser, discussing analytical model and model limitations [ASME PAPER 66-WA/FE-14] 23 p3989 A67-40929

FLOW STABILITY

Benard and related stability problems of thin horizontal fluid layer heated from beneath 01 p0053 A67-10801

Cyclic formation of turbulence in wake of profiled obstacle with laminar boundary layer 01 p0053 A67-10943

Spectrum of small perturbations of plane parallel Couette flow calculated, using Galerkin method 01 p0053 A67-11000

Hydrodynamic stability equations for free convection flow over vertical uniform flux plate 01 p0055 A67-11189

Instability and transition of wake behind axisymmetric slender body with sound-induced velocity fluctuation amplification 02 p0177 A67-11560

Stability of plane parallel flows in finite length tube at large Reynolds numbers, noting velocity profile 02 p0233 A67-11949

Perturbation estimation theorems and stability of plane steady curvilinear flows of ideal fluid 03 p0402 A67-12883

Steady flow possessing extremal kinetic energy compared to equivortex flow for stability analysis 03 p0402 A67-13618

Stability analysis of adiabatic flow of incompressible fluid without equation linearization and by constructing functional from hydrodynamic fields 03 p0402 A67-13619

Test arrangement and statistical data analysis for remote sensing of local flow instabilities and turbulence 03 p0422 A67-13773

Shock tube flow nonuniformity analyzed where shock and contact surface have maximum separation, applying results to turbulent and laminar boundary layer for heat transfer studies 03 p0397 A67-14027

Taylor vortices intensity and viscous losses determined for viscous flow of liquid between concentric rotating cylinders, solving equation by numerical method 03 p0405 A67-14030

Airflow instability with square edge circular orifice, discussing hysteresis effect on discharge coefficient 04 p0601 A67-14487

Unstable modes of barotropic horizontally sheared zonal current in stratified atmosphere 04 p0611 A67-14650

Stability and steadiness of gas flow of argon plasma jet analyzed, using dual grating spectrograph 04 p0664 A67-14848

Protecting turbomachinery from unstable and oscillatory flow, noting resonance effect [ASME PAPER 66-WA/GT-13] 04 p0690 A67-15370

System induced instabilities of forced convection flows with subcooled boiling restricted to case of water flow in small circular channels, high L/D ratios, moderate temperature and pressure 04 p0736 A67-15858

Rayleigh-Ritz method for turbulent heat transfer in curvilinear channel and heat flux magnitudinal and directional effects on stability of isothermal flow in laminar boundary layer 04 p0610 A67-15900

Laminar shearing flows breakdown for second order viscoelastic fluids in channels of critical width 05 p0792 A67-16724

Intermittent phenomena related to entrainment process in free turbulent flows, noting indentation of surface growth and decay cycle 05 p0792 A67-16814

Energy methods of subcritical convective instability theory and critical Rayleigh number dependence on Nusselt number 05 p0926 A67-16816

Subcritical convective instability, discussing effects of internal heat generation and spatial variation of gravity field on onset of thermal convection 05 p0926 A67-16817

Stability of plane Poiseuille flow between elastic boundaries 06 p0984 A67-18044

Flow field and stability of far wake of circular cylinders at hypersonic speeds, noting Reynolds number role [AIAA PAPER 67-32] 06 p0939 A67-18348

Artificial heat conduction mechanism, introducing viscosity term into momentum and energy equations to account for shock discontinuities in flow problems 06 p0992 A67-18830

Convective heat transfer through stabilized turbulent flow of chemically homogeneous liquid in circular pipe under supercritical pressure conditions 07 p1265 A67-19127

Pressure recovery increase in bistable fluid elements by stationary latching vortices 08 p1283 A67-20475

Instability of plane Couette-Poiseuille flow of two superposed layers of different viscosities between two horizontal plates 08 p1321 A67-20709

Helmholtz velocity profile instability in atmosphere with unstable density gradient

/negative Richardson number/ 08 p1323 A67-21388

Diffusion in solutions in nearly critical states, noting increased cross effects and linear dependence of flows near critical points 09 p1580 A67-21908

Aerodynamic problem of steady potential flow and added mass in unsteady motion of idealized hemispherical parachute 09 p1438 A67-22485

Symmetrical equilibrium flow past blunt body at superorbital reentry conditions calculated by integrating motion equations across shock layer 10 p1591 A67-23109

Lapunov-Schmidt method combined with topological method show secondary flows formed after stability loss 10 p1734 A67-23673

Transverse fluid flow stability between permeable boundaries for case with exact solution of perturbation spectrum 10 p1628 A67-23675

Similarity laws for jet noise and shear flow instability as suggested by experiments 10 p1628 A67-23830

Liquid film flowing instability down inclined plane with respect to Tollmien-Schlichting wave compared with surface wave formation 11 p1774 A67-23860

Stability of flow of ideal compressible gas at low magnetic Reynolds numbers in presence of longitudinal perturbations produced by crossed electromagnetic fields 11 p1832 A67-24026

Turbulent boundary layer phenomena, discussing parameters of production processes, relation with instability, etc 11 p1776 A67-24043

Instability of Maxwellian fluid flow in pipe analyzed using Galerkin method 11 p1778 A67-24216

Digital computer analysis of inviscid two-dimensional parallel flow stability, using finite difference method to solve resulting initial value problem 11 p1778 A67-24220

Rotating Ekman boundary layer stability and transition for two-dimensional roll vortices superimposed upon basic boundary layer flow 11 p1781 A67-24543

Stability of incompressible fluid in Couette flow between coaxial circular cylinders, using Galerkin method to obtain critical Taylor number 11 p1781 A67-24570

Dynamics of baroclinic geostrophic circumpolar vortex beta-plane flow in zonal magnetic field, noting applications to solar rotation, hydromagnetic dynamo theory, etc 12 p1963 A67-25338

Nonhomogeneous turbulent motion of conducting fluid stabilized by longitudinal magnetic field 12 p1976 A67-26069

Linear stability of symmetrical parabolic flows of various types 13 p2092 A67-26276

Existence, uniqueness, stability and approximation of solutions of Prandtl system for nonstationary boundary layer 13 p2093 A67-26603

Parametric self-excited vibrations of plates of finite length in plane supersonic flow, applying linearized potential flow theory, deriving frequency equations 13 p2218 A67-26804

Stabilizing or destabilizing effect of electromagnetic force on liquid film flow 13 p2167 A67-26930

Finite ion Larmor radius effect on superposed fluid stability investigated for general perturbation direction, noting magnetically stabilized configurations become overstable 13 p2167 A67-26993

Viscous fluid flow stability in boundary layer on plate, applying perturbation method, calculating critical values of modified Reynolds numbers 13 p2105 A67-27051

Stability of arbitrary one-dimensional hydrodynamical flow in quasi-isothermal case 13 p2105 A67-27413

Stability of multiple rows of vortices created behind tripping cylinders at low Reynolds number 14 p2294 A67-27795

Hydrodynamic stabilization of plane Poiseuille flow by modulating pressure gradient 15 p2470 A67-29332

ONERA hot-shot wind tunnel flow stability and homogeneity and measurement of plasma electromagnetic field, skin friction, etc [ONERA-TP-447] 15 p2465 A67-29377

Striated layer flow of working fluid in duct of synchronous induction MGD generator studying stability by

approximation 16 p2607 A67-30594
 Mach number effect on location of heard shock wave and flow stability at slightly supersonic velocities for various body shapes 16 p2593 A67-31129
 One-dimensional charged particle flow in bounded system, particularly overlapping steady state zero-temperature flow approximation solutions, noting instabilities 18 p2704 A67-31233
 Wall jet compared to plane free jet examining equilibrium conditions of velocity profile of fluctuation and mean flow determining stress 16 p2662 A67-31470
 Aeroelastic stability of two-dimensional flat panels in subsonic and transonic flow, noting flutter and divergence 16 p2776 A67-31545
 Stability of one-dimensional polyphase flow in porous medium studied using theory of servomechanisms 16 p2609 A67-31713
 Variational principle for determining fluid flow stability in differentially rotating self-gravitating stars and galaxies and for studying eigenfunctions properties 17 p2947 A67-32756
 Wing flap aerodynamic performance as affected by wing flap surface cavities, noting usefulness in flow stabilization at high pressure gradient 17 p2792 A67-32904
 Electrohydrodynamic flow laminarization with tritium ionizer, obtaining Poiseuille flow stability 17 p2839 A67-32907
 Stability of plane parallel flows in finite length tube at large Reynolds numbers, noting velocity profile 17 p2841 A67-33266
 Unsteady plane parallel flow stability of viscous electrically conducting incompressible fluid in oscillating magnetic field 17 p2910 A67-33350
 Flow stability in MHD generators after extracting significant electrical power from gas 18 p2987 A67-33705
 Economical feasibility of open and closed cycle vortex-stabilized gaseous nuclear rocket engines, investigating vortex flow characteristics [AIAA PAPER 67-500] 18 p3076 A67-33964
 Wave number and Rayleigh numbers effect on stability of two-dimensional convection in layer heated from below 18 p3159 A67-34003
 Conditions of time-symmetry for four classes of flows, discussing instabilities 18 p3079 A67-34004
 Plane shock wave velocity measurement after interaction with obstacles in form of channelled diaphragms of various diameters, discussing stabilization 18 p3028 A67-34210
 Potential flow stability of weightless incompressible fluid for specific flow geometries 18 p3028 A67-34219
 Schwarzschild criterion validity, reducing initial value problem for hydrodynamic perturbation equation to time independent problem 18 p3029 A67-34737
 Linear theory for steady motions in rotating stratified fluid 19 p3209 A67-35410
 Cyclogenesis due to baroclinic instability in zonal and meridional basic current showing relationship by superimposing perturbation 19 p3252 A67-35528
 Stratified shear flow instability examined through two classical models 19 p3210 A67-35611
 Instability of gas-cooled nuclear reactor passages in steady laminar flow studied by time-dependent analysis 19 p3260 A67-35743
 Stability of continuous baroclinic flow in zonal magnetic field examined for zonal-flow profile of hyperbolic tangent form 19 p3253 A67-35918
 Exchange invariance in dissipationless fluid systems, deriving conservation law and stability conditions and application to gyro-stabilized magnetoplasma 20 p3419 A67-36151
 Heating rate and type effects on stationary fluids stability, noting dependence on critical Rayleigh number 20 p3553 A67-36848
 Pressure drop increase in choke eliminates axial compressor stage discontinuity caused by disrupted flow 20 p3358 A67-37083
 Three-dimensional incompressible flow with colinear magnetic field, studying stability by numerical method 20 p3423 A67-37242
 Compressor blade flutter stability in separating flow with external perturbations

analyzed, using digital computer 20 p3517 A67-37488
 Convective heat transfer through stabilized turbulent flow of chemically homogeneous liquid in circular pipe under supercritical pressure conditions 21 p3731 A67-38171
 Stability technique for gas flow past body impeding laminar-turbulent boundary layer transition via crossed electric and magnetic fields 21 p3666 A67-38251
 Liapunov-Schmidt method combined with topological method show secondary flows formed after stability loss 21 p3731 A67-38274
 Transverse fluid flow stability between permeable boundaries for case with exact solution of perturbation spectrum 21 p3812 A67-38276
 Collisionless shock wave existence in fully ionized plasma, noting shock wave internal structure 21 p3667 A67-38410
 Steady state solutions for system of partial differential equations with two independent variables describing small perturbations of transonic gas flow near transition point 22 p3844 A67-39391
 Book on parallel laminar flow stability covering channel and pipe flows, jets, wakes, free shear and boundary layers 22 p3783 A67-39632
 Inviscid compressible relativistic half-jet plasma flow stability, discussing disturbance equations and eigenvalues 22 p3850 A67-39705
 Haskell viscous flow equations describing very slow linearly viscous liquid with initially crater shaped surfaces solved and applied to lunar craters 23 p4065 A67-40998
 Vorticity component change rate expressions for arbitrary configuration inviscid flow, discussing local instabilities 23 p3990 A67-41166
 Inviscid instability of cylindrical two-dimensional free boundary layer vortex flow, using approximation by axisymmetrical vortex model 23 p3990 A67-41169
 Spiral flow in cylindrical annular chamber behind guide vanes /stators/ noting flow instability in outer region due to vortex generation 23 p3929 A67-41253
 Longitudinal wall curvature effect on boundary layer flow stability and generalization of Rayleigh theorems for nonviscous instability 23 p3992 A67-41733
 Protecting turbomachinery from unstable and oscillatory flow, noting resonance effect [ASME PAPER 66-WA/GT-13] 24 p4207 A67-42462
 Hydromagnetic flow stability in infinitely long cylindrical pipe with arbitrarily smooth cross section and applied radial magnetic field 24 p4198 A67-42693
 Viscous flow stability between concentric rotating cylinders with Taylor vortices, deriving velocity and pressure perturbation nonlinear partial differential equations 24 p4145 A67-43083
FLOW THEORY
SA FLUID MECHANICS
SA HYDRODYNAMICS
SA MIXING LENGTH FLOW THEORY
 Nonlinear MHD waves, examining hyperbolic systems of quasi-linear PDEs, simple wave and flow theory 01 p0126 A67-11252
 Thermodynamic approach to flow phenomena based on temperature dependence of specific heat 03 p0537 A67-14304
 Mixing at constant section of two flows of different enthalpies, demonstrating phenomenon with arc type reheater 04 p0802 A67-14569
 Ergodic theory of measurable partitions in Lebesgue space, extending Rokhlin-Sinai theory of increasing to flows generated by automorphism 04 p0644 A67-14756
 Power source disturbance method for linear theory of flow past bodies 05 p0749 A67-17006
 Book on theoretical equipment of engineering fluid mechanics 06 p0982 A67-17660
 Free energy of spatially homogeneous phase in approximation of self-consistent field for application to fluids and gases 07 p1168 A67-18186
 Book on inviscid hypersonic flow theory including nonequilibrium effects, flows on blunt bodies, shock layer, conical flows, etc 07 p1127 A67-20204
 Shock wave formation due to heat

addition to one-dimensional flow of ideal inviscid conducting monatomic compressible fluid under transverse magnetic field 08 p1359 A67-20980
 Ionized fluid flow analyzed by multilayer theory to evaluate energy transfer mechanisms, noting temperature and compositional nonequilibrium effects 11 p1780 A67-24537
 Hyperbolic region solutions of equation approximating Chaplygin equation near supersonic flow vacuum line in hodograph plane 12 p1962 A67-26181
 Theory on secondary flows through axial compressor or turbine cascade 13 p2049 A67-26530
 Three-dimensional supersonic flow for ideal fluids using Euler motion equation 13 p2050 A67-26648
 Two component equivalent of two-stream distribution function solution to plane Couette flow, studying nonlinear effects 13 p2101 A67-26965
 Hypersonic weak and strong interaction theory for case of uniform flow past flat plate, discussing boundary layer characteristics 15 p2473 A67-30220
 Approximate solution for hypersonic flow past unyawed cone by small disturbance stream function equation 17 p2793 A67-33024
 Finite length plate in plane supersonic flow analyzed for forced vibration by applying linearized potential flow theory 18 p3140 A67-33466
 Successive approximation method analysis of flow around single barrier extending downstream and in direction of velocity at infinity upstream 18 p3025 A67-33682
 Power source disturbance method for linear theory of flow past bodies 18 p2984 A67-34268
 Hardening function form in flow theory, showing dependence on cosine of stress velocity vector angle with normal to yield surface 20 p3539 A67-36921
 Aerodynamic forces of harmonically oscillating cylindrical duct with supersonic internal flow within framework of potential flow theory 20 p3357 A67-37003
 Empirical method predicting flexible hose flow losses, with Fanning friction factor as Reynolds number and internal hose geometry function 22 p3785 A67-39971
 Quasi-cylindrical approximation theory on swirling nozzle flow in relation to spin effect on rocket nozzle performance 22 p3742 A67-40118
 Hydrodynamic separation using compatibility conditions for Prandtl steady boundary layer equations at zero skin friction point 24 p4142 A67-42172

FLOW VELOCITY

SA MASS FLOW RATE

Sound propagation in streaming air within tubes having changes of cross section and flow losses, discussing reflection coefficient dependence on flow velocity 01 p0114 A67-10819
 Approximate method for calculating parallel flow past slender bodies of noncircular cross section 02 p0177 A67-11517
 Thermal creep in rarefied gas investigated using Boltzmann-Krook equation 03 p0402 A67-13359
 Transient air flow rates into gas turbine metered, using two critical flow circular arc venturi 03 p0421 A67-13770
 Calibration of flow meters in liquid hydrogen at high flow rates for establishing limits of extrapolations from lower flow rate data 03 p0422 A67-13771
 Eigenfrequencies of elastic plate containing cavities filled with incompressible moving fluid, obtaining eigenfrequencies dependence on velocity of fluid motion 03 p0580 A67-14173
 Vorticity jump across discontinuity surface which is not contact surface obtained on kinematical basis, recovering Hayes formula for gas dynamic discontinuity 04 p0600 A67-14456
 Low density gas flow through short tubes at densities varying from continuum to free-molecule regime, noting nitrogen flow [ASME PAPER 66-WA/PID-8] 04 p0606 A67-15331
 Optimum control of flow rate through nuclear rocket with constraint on thermal stress in fuel elements [ASME PAPER 66-WA/AUT-6] 04 p0656 A67-15419

Errors in calculating losses in diffuser elements 04 p0548 A67-15600
 Methods of calculating flow velocity losses in diffusers 04 p0548 A67-15601
 Wall shearing stress and heat transfer measurements through turbulent boundary layer on heated flat plate in accelerating and decelerating airflow 04 p0731 A67-15819
 Successive approximations applied to optimal control equation for self-similar viscous Couette flow between one stationary and one moving wall 04 p0610 A67-15885
 Forced and periodic breakdown of confined vortex rotating in opposite direction, measuring flow rates and wall pressures [ASME PAPER 66-WA/FE-7] 04 p0611 A67-15928
 Turbulent subsonic gas jets, importance of Reynolds number and geometrical configuration of nozzle in determination of flow parameter 05 p0790 A67-16033
 Forms of function connecting deviation angle and axial velocity ratio of exit flow in three-dimensional cascade flow 05 p0791 A67-16428
 Rotating Langmuir probes for flow velocity distribution measurements in highly ionized supersonic low density MPD arc 05 p0851 A67-16466
 Axial flow dynamics of flexible slender cylindrical body immersed in fluid, emphasizing flow velocity, frictional forces, buckling and oscillatory instabilities 05 p0920 A67-16815
 Plasma flow velocity measurement in MHD channel using time-of-flight technique, noting experimental error 05 p0854 A67-16983
 Friction stress and flow rate for rarefied constant density gas flow past seminfinit plate treated by approximate diffusion model 05 p0792 A67-16995
 Hybrid fuel regression rate, discussing oxydizer flow rate and burner pressure interdependence [AIAA PAPER 66-113] 05 p0873 A67-17347
 Motion of magnetic lines of force including analysis of fluids with finite high conductivity 06 p1030 A67-17561
 Connection between flow spectrum and velocity, obtaining continuous spectrum upon velocity change to equivalent invariant measure 06 p0983 A67-17860
 Source model for predicting drag force on moving arc column in cross flow velocity and balancing magnetic field [AIAA PAPER 67-97] 06 p0986 A67-18280
 Boundary layer thickness in air measured in presence of sound field, determining flow velocity distribution in layer 06 p0988 A67-18400
 Stability of circular cylindrical shell in supersonic nonviscous conducting gas flow with unperturbed velocity and under magnetic field 06 p1106 A67-18622
 Steady flow of anisotropic conducting medium in half-space under influence of magnetic field 07 p1230 A67-20033
 Velocity jump characteristics of boundary layer with gradient pressure for flows at inlet channel and in wake of symmetric and asymmetric bodies 07 p1189 A67-20223
 Source model for predicting aerodynamic drag on moving arc column in crossflow yields relationship between crossflow velocity and balancing magnetic field 08 p1356 A67-20579
 Shocked gas flow duration in small diameter shock tubes at low initial pressures 08 p1321 A67-21119
 Isolated compressor blade within framework of lifting line theory, expressing drag produced by tip-gap in terms of flow rate and wing loading 09 p1437 A67-21739
 Concentration waves excited by internal modulation of charged particle concentrations in cross section of plasma flow analyzed for various velocities of flow 09 p1544 A67-21851
 Gas flow velocity and static pressure profiles experimentally measured in combustion zone of gas turbine combustion chamber model under atmospheric conditions [SAE PAPER 670201] 09 p1561 A67-22545
 Wall friction coefficient measurement, using scale incorporated into wall 09 p1501 A67-22577
 Plane Poiseuille flow calculations extended to Couette flow between coaxial circular cylinders, plotting flow velocity

curves 09 p1490 A67-22595
 Efficiency of fibrous filters for radioactive particles and small ions increased, using greater flow rate 09 p1562 A67-22683
 Reflection of spherical shock wave from concentric spherical surface, using method of characteristics starting from initial boundary value problem 10 p1623 A67-22863
 Main parameters of two-stage hydraulic amplifier-actuator system determined with aid of pressure and flow-rate amplification factors 10 p1597 A67-23321
 Interplanetary magnetic field effect on hydrodynamic supersonic expansion of solar corona noting solar wind velocity, nonradial flow, wave motion, etc 10 p1709 A67-23546
 Inviscid two-dimensional flow using extension of Hele-Shaw analogy, noting axisymmetric, compressible and MHD cases 10 p1627 A67-23554
 Deformation of velocity profile in inhomogeneous magnetic field, noting anisotropic conductivity of flow 10 p1686 A67-23670
 Short method measurement of Reynolds stresses in turbulent flow, using constant current hot-wire anemometer 10 p1629 A67-23845
 Wall temperature and speed ratio effects on free molecule flow number density distribution about flat plate 11 p1881 A67-23880
 Adiabatic flow of K vapor in supersaturated state noting supercompression, supercooling and equilibrium through condensation jump 11 p1881 A67-24029
 Velocity and temperature measurements in turbulent swirling butane-propane air flames in high exit velocity range 11 p1882 A67-24217
 Gas jet expansion near crossed axisymmetric channel, reducing problem to solution of Laplace equation for second-kind boundary conditions 11 p1779 A67-24321
 Calculation of weight flow and velocity for real gas, obtaining correction factor 11 p1779 A67-24355
 Ionized fluid flow analyzed by multifluid theory to evaluate energy transfer mechanisms, noting temperature and compositional nonequilibrium effects 11 p1780 A67-24537
 Green integrals extended to movement of incompressible viscous conductive fluid in which magnetic field is generated 11 p1840 A67-24620
 Hydrodynamic boundary layer velocity profile on disks in transverse airflow analyzed theoretically and by wind tunnel tests 12 p1891 A67-25318
 EMF induced in ionized gas across magnetic field measured for flow velocity determination 12 p1973 A67-25392
 Steady MHD electric power generation, flow velocity effect on single controlled glow discharge in cesium-seeded argon 12 p1974 A67-25402
 MHD generator two-dimensional incompressible flow, obtaining expressions for power output, velocity, electrical efficiency, etc 13 p2055 A67-26417
 Aeromagneto flutter of plane duct of finite length 13 p2218 A67-26805
 Velocity measurement in electrically conducting fluid flow in presence of uniform magnetic induction normal to flow direction 13 p2167 A67-27206
 Heat transfer calculation to turbine blading in cascade in presence of secondary flow, considering flow velocity estimation, blade boundary layer and related heat transfer properties 13 p2225 A67-27465
 Three-dimensional axisymmetrical boundary layer on spinning body of revolution in two-component fluid flow, discussing velocity distribution, drag and separation 14 p2295 A67-27835
 Flow and cavitation erosion tests in closed circuit hydrodynamic tunnel 14 p2295 A67-27869
 Three-dimensional flow of ideal fluid past body enveloped by air cavern, deriving normal velocity components 14 p2239 A67-27985
 First collision effects in rarefied high speed flows in low density wind tunnel, noting measurement techniques and apparatus used 14 p2317 A67-28197
 Low velocity flow measurements by inexpensive thermistor

probe 14 p2318 A67-28342
 Velocity profile analysis in turbulent concentric annular flow, emphasizing correlation of results in inner wall region 15 p2468 A67-29132
 Flow velocity determination by cylindrical magnifying probe, measuring stagnation and wake pressures difference, noting magnifying factor variation under Reynolds number and stem and blockage effects 15 p2471 A67-29529
 Fluid flow measurement through optical radiation detection, determining local velocities and image-space motion 15 p2488 A67-29766
 MHD generator with uniform rectangular duct, considering ion slip and Hall effect in case of two-dimensional flow 15 p2422 A67-29906
 Submerged nozzle for solid rockets, noting exhaust flow velocity and direction determination 15 p2547 A67-29994
 Rayleigh problem solution and accuracy and utility of discrete ordinate method for time dependent problems as applied to Couette flow problems 15 p2473 A67-30214
 Effect of magnetic field gradients at inlet and outlet on linear two-dimensional induction MHD generator calculated by bilateral Laplace transform 16 p2605 A67-30579
 Boundary layer equations similar solutions obtained for incompressible flow with external velocity and suction 16 p2657 A67-30613
 Steady laminar flow of viscous, incompressible, electrically conducting fluid in insulated rectangular channel, with imposed oblique transverse magnetic field 16 p2713 A67-30860
 Liquid discharge from cylindrical container exposed to longitudinal vibration, noting flow retardation 16 p2658 A67-30946
 Turbulent boundary layer with large acceleration parameter studied for flow and heat transfer coefficient [JPL-TR-32-1119] 16 p2659 A67-30953
 Firing range for investigating Reynolds number effect on flow around bodies having complex design at transonic and supersonic velocities 16 p2655 A67-31116
 Curved mixing layer measured for probability density of turbulent velocities at several positions in curved mixing layer 16 p2860 A67-31219
 Turbulent channel flow of electrically conducting fluid in presence of magnetic field obtaining skin friction coefficient and velocity profiles 16 p2661 A67-31225
 Attachment and detachment processes effect on plasma quenching by electronegative gases, showing usefulness of steady state nitrogen afterglow flow system 16 p2720 A67-31238
 Velocity profile of vortex region formed downstream of step-shaped wall calculated, assuming flow is turbulent, using similarity hypothesis 16 p2662 A67-31469
 Turbulent flow in circular cylindrical duct at various Reynolds numbers, analyzing fluctuations and mean value of velocity 16 p2663 A67-31702
 Approximation method for steady laminar flows of incompressible viscous fluid in curved pipes, obtaining flow rate 17 p2836 A67-32038
 Flow velocity measurement in shock tube using electronic Bascul Bootstrap type installation 17 p2855 A67-32287
 Determination of electron density and temperature, gas temperature, atomic composition and flow velocity of high temperature gas stream 17 p2900 A67-32339
 Mean velocities, turbulence intensities, Reynold stresses and wall friction measurement in turbulent radial wall jet [ASME PAPER 67-APM-10] 17 p2838 A67-32419
 Flow behavior recognition techniques using changes in boundary layer velocity diagram to predict flow separation 17 p2792 A67-32908
 Field spectrum developed from monochromatic temperature oscillations in bodies due to time variation of heat transfer coefficients caused by unsteady flow velocity 17 p2972 A67-33073
 Measuring laminar flow development in square duct using laser Doppler flow meter [ASME PAPER 67-APM-37] 17 p2861 A67-33161

- Computer integration of Faulkner-Skan equation in presence of normal and tangential flow velocity components on surface of body 18 p3024 A67-33538
- Argon plasma injection effect into low pressure coaxial magnetic field noting pressure, flow speed, electron temperature, etc 18 p3084 A67-33647
- Successive approximation method analysis of flow around single barrier extending downstream and in direction of velocity at infinity upstream 18 p3025 A67-33682
- Time and cryogenic liquid calculation required for cryogenic system cooling, considering low/high flow rate effects on system components [AIAA PAPER 67-475] 18 p3157 A67-33945
- Velocity measurement in turbulent flow near smooth wall by hot-wire anemometer 18 p3027 A67-34184
- Heat flux measurements in fluid systems using joule heating accomplished with single calibration and without flow rate measurements 18 p3052 A67-34513
- Jet flow turbulence energy balance, measuring point-pressure/velocity correlations and spatial mean gradients, solving energy equation 19 p3170 A67-35412
- Flow analysis of compressible fluid in wake behind body positioned symmetrically with respect to flow direction, using momentum and energy conservation equations 19 p3170 A67-35610
- Profile velocity distribution and shape determinations for flow around thin profile with jet flap 19 p3172 A67-35819
- Stage operation compensation in multistage axial compressor during operating regimes variations along flow length 20 p3516 A67-37084
- Airflow velocity measurement device in cylindrical or rectangular tubes at low gas pressures 20 p3451 A67-37300
- Flow velocity calculation by analog computer, discussing Laplace equation 20 p3424 A67-37302
- Potential linear theory applied to oscillatory profiles moving at uniform velocity inside ideal fluid 20 p3424 A67-37593
- Poiseuille flow of rarefied gases through cylindrical tube, solving integral equation, noting variational calculation of hydrodynamic velocity 21 p3609 A67-37738
- Flows superimposition on toroidal hydromagnetic equilibrium, stressing stationary motion of plasma layers between neighboring magnetic surfaces 21 p3661 A67-37751
- Deformation of velocity profile in inhomogeneous magnetic field, noting anisotropic conductivity of flow 21 p3666 A67-38271
- Inviscid incompressible flow of normal and slightly oblique static round jet impinging on ground, noting velocity distribution 21 p3565 A67-38544
- Rigid cylinder two-dimensional motion in rotating incompressible fluid compared to motion in isotropic incompressible conducting medium under magnetic field 21 p3668 A67-38552
- Mass injection effect on compressible three-dimensional laminar boundary layers analyzed for nonreacting gas, using conservation equations for flow velocity profiles 21 p3613 A67-38852
- Numerical solution of compressible boundary layer stability equations including perpendicular flow velocity component terms 21 p3614 A67-38854
- Flow velocity and magnetic field effects on characteristics of single controlled glow discharge in cesium seeded argon 21 p3674 A67-38888
- Fluid model for magnetosphere shape, calculating flow velocity, density and temperature between shock and boundary 22 p3883 A67-39671
- Drag forces on body with nonuniform velocity distribution, considering gradient flow effects on drag coefficients 22 p3740 A67-39941
- Critical fluid flow rate analysis of two-phase nitrogen at stagnation pressure of 25 psia 22 p3784 A67-39967
- Energy dissipation and motion equations of superfluid helium flow through pores, describing technique to detect critical velocity in wide channels 22 p3839 A67-40550
- Helicopter maximum speed increase using rotor with controlled blade oscillation motion, studying flow velocity, distribution and asymmetry elimination 23 p3933 A67-40639
- Liquid drop impact on liquid, calculating velocity potential, initial pressure and time dependence of cavity depth and wall velocity 23 p3991 A67-41459
- Spray coating particle flow rate dependence on plasma jet flow velocity, specific weight and particle size measured by high speed filming 24 p4159 A67-41961
- Coolant selection for radiative cooling circuit of space vehicles, considering flow rate, heat transfer rate, etc 24 p4253 A67-42217
- Finite difference integration method for predicting flow velocity and temperature distribution of gaseous diffusion flame in axisymmetrical combustion chamber 24 p4091 A67-42383
- FLOW VISUALIZATION**
- Airflow in small wind tunnel with roughened heat transfer surface, using flow visualization techniques 04 p0727 A67-15801
- Heat-transfer coefficient measurements in separated flow regions in heated duct with circumferential grooves, ribs and enlargements, by visual flow techniques 04 p0729 A67-15810
- Tests for measuring heat-transfer coefficients in horizontal annulus filled with gas and visualization of flow 04 p0732 A67-15829
- Fluidic test equipment for measuring rapidly varying fluid parameters and flow visualization 07 p1186 A67-19634
- Submerged water-operated proportional amplifier characteristics in interaction region studied by flow visualization 08 p1280 A67-20446
- Behavior of momentum effect jet interaction proportional amplifier using flow visualization on water table and large scale pneumatic model 08 p1282 A67-20460
- Flow visualization technique study of wake existence behind large air bubble rising through quiescent liquid 08 p1321 A67-20712
- End-wall pressure distributions in confined vortex [JPL-TR-32-1099] 10 p1626 A67-23150
- Thermal differential method of determining critical points in flow past projection in pipe 11 p1741 A67-24032
- Quantitative fast response visualization technique for low density flow fields based on electron beam fluorescence probe 11 p1790 A67-24450
- Holography applications including vibration analysis, flow visualization, etc 11 p1793 A67-24837
- Fluid flow processes for secondary sonic jet injection into Mach 6 free stream, noting upstream flow into separated flow regions 12 p1893 A67-25934
- Vortex breakdown effects on lift, drag and pitching moment coefficients of slender sharp-edged delta wings with different aspect ratios 13 p2050 A67-27194
- Visualization of combustion through transparent chamber walls, noting problems concerning hybrid rockets, ignition lags and hybrid combustion instabilities [ONERA-TP-474] 14 p2377 A67-27895
- Hartmann oscillator problem studied using hydraulic analogy between supersonic compressible gas dynamics and incompressible flows with free surface 14 p2295 A67-27903
- Flow visualization, discussing schlieren process in light of Toepler, fine focusing, microscopic, phase contrast and field absorption processes 14 p2315 A67-27974
- High Mach number low Reynolds number flow over two-dimensional circular cylinder, obtaining surface pressure and heat transfer distributions 14 p2242 A67-28174
- Smoke generator control and performance for flow visualization applications [JPL-TR-32-1117] 14 p2293 A67-28751
- Natural boundary layer transition on ogive nose cylinders in zero and adverse pressure gradient analyzed for fluid dynamics, using smoke visualization 14 p2306 A67-29052
- Supersonic unsteady flow of cylindrical body past diaphragm model at interface between density-differing gases, studying flow patterns 16 p2593 A67-31133
- Magnetically driven shock tube as tool for aerodynamic studies of high velocity high enthalpy flows 16 p2594 A67-31265
- Holographic moiré patterns as white light viewing technique for aerodynamic flow visualization 19 p3232 A67-35699
- Flow pattern at low Reynolds numbers about airfoil cascade illustrated by hydrogen bubble flow-visualization technique 20 p3359 A67-37483
- Wind tunnel hypersonic flow visualizations under low flow density conditions, comparing schlieren and phase-contrast methods 23 p3985 A67-40568
- Reynolds number effect on slender high speed cones wake-neck geometry, obtaining measurements of location, diameter and closure angle 23 p3932 A67-41754
- Cellular convection patterns from instability of horizontal fluid layer uniformly heated and cooled from above 24 p4255 A67-42563
- Velocity profiles of non-Newtonian fluid /polyisobutylene solution/ in helical flow by flow visualization technique, discussing Poiseuille and viscometric flows 24 p4145 A67-42708
- FLUCTUATION THEORY /STAT MECH/**
- Fluctuation-dissipative ratio between correlation functions of fluctuating parameters and dissipative properties in thermodynamic-nonequilibrium systems with spatial dispersion 04 p0673 A67-15968
- Amplitude spectrum of turbulent flow rate fluctuations at flame temperatures measured via photoelectric method 05 p0927 A67-16942
- Statistical mechanics predictions of turbulent fluctuations in hypersonic wake from ballistic range experiments and theoretical stochastic model of gas particle motion [AIAA PAPER 67-22] 07 p1168 A67-19431
- Point source detection using signals propagating in quantum field, in terms of correlation functions of thermal field fluctuations 07 p1142 A67-19585
- Laser interferometric measurement of power spectral density of integrated particle density fluctuations in turbulent exhaust of sonic jet 08 p1337 A67-21142
- Microwave noise intensity emitted by electron plasma within framework of fluctuation theory 09 p1547 A67-22318
- Quantum mechanical theory of fluctuation and relaxation in semiconductor lasers, using Langevin method to calculate noise in quasi-Fermi electron distribution 10 p1663 A67-22891
- LF noise fluctuation anomalies in narrow doped germanium p-n junctions at low temperatures 11 p1765 A67-24476
- Performance characteristics of photosensors and limitation by statistical fluctuation in absorption rate of light quanta in primary photoprocess 11 p1766 A67-24627
- LF thermodynamic energy and pressure fluctuation-dissipation theorem for open systems with dynamic turbulence 11 p1821 A67-24974
- Cosmic radiation intensity fluctuation in stratosphere, noting absence of explanation for anomaly 12 p1994 A67-25542
- Amplitude spectrum of turbulent flow rate fluctuations at flame temperatures measured via photoelectric method 14 p2406 A67-28490
- Expression defining condition under which Brownian movement of universe affects Brownian movement of single electron 15 p2554 A67-29316
- Master equation for statistical operator of laser mode leads to photon number distribution for arbitrary pumping 15 p2501 A67-30124
- Prigogine-Glansdorf local potential calculated for usual transport effects case using variational principle 16 p2661 A67-31440
- Frequency spectra of excess noise in semiconductor devices due to characteristics fluctuations after applying signal 17 p2828 A67-33383
- Emission statistics of nonresonant feedback laser produced by radiation scattering, showing fluctuations intensity, distribution function, etc 18 p3062 A67-34621
- Energy and intensity density of radiation emitted by semimfinite nonequilibrium electron plasma with non-Maxwellian particle distribution calculated, based on general fluctuation theory 19 p3267 A67-34902
- Electron fluctuations variance and correlation coefficients computed for sensitized GaAs, comparing noisiness of deep recombination levels 19 p3306 A67-35732
- Small correlated amplitude and frequency fluctuations of stochastically-modulated radio

waves 19 p3241 A67-36025
 Fluctuation spectrum in most stable state of turbulent plasma 20 p3496 A67-36213
 Point source detection using signals propagating in quantum field, in terms of correlation functions of thermal field fluctuations 20 p3384 A67-37322
 Mapping of fluctuation field of space and earth environment by electromagnetic techniques 22 p3884 A67-39949
 Pencil-beam antenna with field distribution fluctuation determined for resolving power by mean square measuring of radiation pattern, detailing parabolic reflectors with rough surfaces 22 p3763 A67-40125
 Laser and maser noise quantum theory emphasizing equations of motion and fluctuation problem, deriving density matrix equation 23 p4011 A67-40762
 Variational methods for nonequilibrium thermodynamic processes based on fluctuation theory, noting application to viscous heat conducting flows 24 p4255 A67-42554

FLUID
 SA ANISOTROPIC FLUID
 SA BINARY FLUID
 SA BODY FLUID
 SA CEREBROSPINAL FLUID
 SA COMPRESSIBLE FLUID
 SA CRYOGENIC FLUID
 SA HIGH TEMPERATURE FLUID
 SA HYDRAULIC FLUID
 SA IDEAL FLUID
 SA INCOMPRESSIBLE FLUID
 SA LAVA
 SA LIQUID
 SA MAXWELL FLUID
 SA NEWTONIAN FLUID
 SA NON-NEWTONIAN FLUID
 SA ROTATING FLUID
 SA SUPERFLUIDITY
 SA THREE-FLUID MODEL
 SA TWO-FLUID MODEL
 SA VISCOUS FLUID
 SA WEIGHTLESS FLUID
 SA WORKING FLUID
 Computer simulated calculation of simple fluid properties using Monte Carlo method 05 p0927 A67-16890

FLUID AMPLIFICATION
 Static operating characteristics of vented single-stage momentum exchange proportional amplifiers, noting applicability for compressible and incompressible flow regimes 14 p2250 A67-28329
 Fluid amplification and fluid logic trends stressing industrial applications, comparing electronic and fluid systems performance 21 p3571 A67-38105

FLUID AMPLIFIER
 Graphical method of analyzing nonlinear problems of fluidic circuits 02 p0182 A67-11775
 Vortex amplifier performance characteristics in liquid and gas flow control and chemical processing 03 p0363 A67-13170
 Fluidic oscillators, negative and positive-gain operational amplifiers and cascade circuits 03 p0363 A67-13233
 Fluid interface instability suppression via feedback, noting stability criteria and parameters 03 p0483 A67-14036
 Turbulence as producer of noise in proportional fluid amplifiers, considering signal and noise at receiver entrance in terms of stagnation pressure 04 p0557 A67-15919
 Pneumatic transmission line model for use in fluidic control systems, noting nomographs determining gain-vs-frequency curves 05 p0753 A67-18237
 Fluidic circuit design, testing and performance noting transfer functions and differentiating and integrating circuits 05 p0754 A67-17200
 Fluid amplifiers and sensors for jet-engine control systems 06 p0949 A67-17611
 Fluidic system design and fabrication method 06 p0950 A67-18063
 Turbulence amplifiers design, characteristics and production 08 p1280 A67-20437
 Vortex devices characteristics and applications studied with vortex sink model 08 p1280 A67-20442
 Submerged water-operated proportional amplifier characteristics in interaction region studied by flow visualization 08 p1280 A67-20446

Switching time of turbulent reattachment fluid amplifier in large scale model and in theory 08 p1281 A67-20447
 Fluid circuits used in drilling sequence control, detailing ring counter, binary counting stage and comparator 08 p1281 A67-20458
 Optimal design of pneumatic control jet of fluid amplifier to obtain maximum logic gain 08 p1282 A67-20459
 Monostable fluidic amplifier with adjustable positive feedback /AF relay/ characteristics and application as oscillator, proximity switch, delay unit and in alarm annunciator systems 08 p1282 A67-20462
 Momentum interaction principle used in experiments to produce proportional fluid amplifier, discussing geometry and characteristics 08 p1282 A67-20464
 Digital fluoric amplifier of gyroscopic signals for proportional thrust control 08 p1282 A67-20465
 Fluid mechanical binary counter with bistable fluid elements 08 p1283 A67-20472
 Pressure recovery increase in bistable fluid elements by stationary latching vortices 08 p1283 A67-20475
 Main parameters of two-stage hydraulic amplifier-actuator system determined with aid of pressure and flow-rate amplification factors 10 p1597 A67-23321
 Binary turbulent reattachment type fluid amplifier to control submerged jet of fluid 10 p1597 A67-23389
 Static and dynamic performance of pancake vortex flow field and application to pressure amplification 14 p2248 A67-28272
 Proportional momentum beam deflection fluid amplifier design 14 p2249 A67-28327
 Aspect ratio effect on noise in proportional fluid amplifiers 14 p2250 A67-28330
 Two-dimensional supersonic fluid amplifier flow characteristics analyzed numerically by digital computer 14 p2250 A67-28333
 Laminar NOR unit feasibility, operating characteristics and performance 14 p2250 A67-28335
 Principle of operation and static performance data of fluoric AND gate, using wall attachment principle 14 p2251 A67-28337
 Jet driven fluoric oscillator 14 p2251 A67-28344
 Automatic fluoric gain changer circuit for flight control systems counteracting Mach number and altitude pressure effects 14 p2251 A67-28352
 Fluid state trigger logic element and bidirectional counter 16 p2609 A67-31663
 Fluoric and electronic integrated circuits compared, presenting state of art in packaging 16 p2610 A67-31722
 Fluoric solar attitude control device functioning as sensor and actuator, noting design principles and operation 17 p2954 A67-31982
 Miniaturized no-moving-parts fluid pulse counter development for ordnance application 19 p3176 A67-34806
 Short tube orifices, confined turbulent jets, jet-wall and jet-receiver interactions and characteristics of diffusion process for design of fluid amplifiers 20 p3365 A67-37361
 Proportional characteristics and signal limiting capabilities of fluoric operational amplifier, discussing analog gain block performance 24 p4098 A67-41988

FLUID BOUNDARY
 Benard and related stability problems of thin horizontal fluid layer heated from beneath 01 p0053 A67-10801
 Infinite horizontal fluid layer heated from below /classical Rayleigh thermal stability problem/ extended to fluid in rigid sphere heated nonuniformly 22 p3918 A67-39715
 Cooling of cylinder moving through fluid assuming fluid properties permit boundary layer approximations 22 p3918 A67-39782
 Flow velocity profile analysis for pressure front steady motion with steady pressure on compressible fluid surface 22 p3784 A67-39826
 Free convection thermal transfer in narrow horizontal channels and infinitely wide channels 24 p4255 A67-42587

FLUID FLOW
 S GAS FLOW
 S INDUCED FLUID FLOW
 S LIQUID FLOW
 S RECIRCULATIVE FLUID FLOW

FLUID INJECTION

SA GAS INJECTION

SA LIQUID INJECTION

Injection from half-plane located in steady viscous flow in Oseen approximation, noting skin friction 01 p0052 A67-10793
 Simultaneous effect of transverse curvature and fluid injection on boundary layer flow over parabola of revolution, obtaining iterative solution to differential equation 01 p0055 A67-11175
 Mass effect on blast wave equations of shock generation by secondary injection of fluid into hypersonic flow 01 p0141 A67-11179
 Jet direction variation via secondary fluid injection resulting in booster trajectory control, increased payload and reliability 01 p0142 A67-11409
 Coolant injection in turbulent boundary layer for protection of surfaces from effects of high temperature and high energy gas flows 03 p0536 A67-13526
 Mixing at constant section of two flows of different enthalpies, demonstrating phenomenon with arc type reheater 04 p0602 A67-14569
 Heat-transfer coefficients and shearing stress in turbulent boundary layer along porous flat plate with uniform fluid injection 04 p0733 A67-15842
 Thrust magnitude and restart control of solid propellant motor by injection of fluorine and chlorine trifluoride 08 p1376 A67-21518
 Skin friction drag of constant property turbulent boundary layer with uniform injection, corrections of experimental law-of-wall and velocity-defect law concepts 10 p1825 A67-23111
 Mean droplet size for cross stream water injection into Mach 8 air flow determined by scattered light angular variation measurement 11 p1779 A67-24366
 Relationship between effectiveness of film cooling, free stream Reynolds number, slot Reynolds number and angle of injection 14 p2408 A67-28816
 Two-dimensional wall jet effectiveness measurements and calculation procedures for injection conditions 15 p2468 A67-29128
 Separation streamline for massive flow in free stream for model injected into arc tunnel flow 17 p2839 A67-33007
 [AIAA PAPER 66-457]
 Plane incompressible wall jet ejected from slot into boundary layer in case of stationary and nonstationary external flow with and without pressure increase 20 p3420 A67-36277
 Dynamic ballistics of combustion termination by fluid injection in solid propellant motors, describing termination mechanisms 21 p3733 A67-38893
 Shock refraction effects due to velocity and temperature gradients in rocket nozzles investigated by studying leading shock in two-dimensional secondary fluid injection 23 p3992 A67-41740

FLUID JET
 SA AIR JET
 SA GAS JET
 SA VAPOR JET
 SA WATER JET
 AND EXCLUSIVE-OR passive elements based on interaction of two or more unbounded jets 08 p1280 A67-20443
 Increasing effective sensitivity of bistable device using pulsed power supply 08 p1282 A67-20463
 Collision of opposed supersonic jets in pulse discharges, noting formation of shock-constricted plasma regions between electrodes 09 p1544 A67-21855
 Asymptotic exponential laws of contraction of plane and axisymmetric jets of weightless fluids, obtaining expressions for stream function and velocity component 10 p1624 A67-23039
 Formation of cavities and microjets in liquids and role in initiation and growth of explosion 11 p1883 A67-24631
 Stability of motion of plane boundary interface between two different density coupled fluid jets analyzed to determine role of viscosity in drop formation 11 p1782 A67-24959
 Hollow electrically conducting fluid jet stabilization in presence of uniform magnetic field 13 p2169 A67-27314
 Plane conducting fluid-into-fluid jet in presence of transverse magnetic field,

examining series expansion of stream function 13 p2169 A67-27317

Fluid control systems - Conference, Pennsylvania State University, July 1965 14 p2247 A67-28263

Flow processes and static and dynamic performance characteristics of axisymmetric fluid jet modulator and single receiver-diffuser studied experimentally 14 p2248 A67-28269

Static and dynamic characteristics of interaction region for fluid jet and receiver-load system, examining stability conditions 14 p2248 A67-28270

Mechanism of fluid jet separation from curved surface 14 p2302 A67-28324

Simple impact position model for predicting subsonic mass flow for opposing axisymmetric jet 14 p2303 A67-28331

High speed liquid jet in standing acoustic field with velocity vector transverse to jet axis, testing injector orifice diameter, viscosity, etc [AIAA PAPER 67-473] 18 p3026 A67-33943

Apparatus for uniform sized liquid drop production by ultrasonic wave action on fluid jet, with drop formation recorded by photography 18 p3052 A67-34610

Planar highly conducting liquid jet kink mode stability in electric field and feedback stability control of spatially growing wave 18 p3029 A67-34735

Two-dimensional problem of penetration of subsonic compressible fluid jet into channel solved by modified Chaplygin method 20 p3357 A67-37052

Motion equations of incompressible nonisothermal fluid jet studied by closed similarity solutions, obtaining temperature distributions 20 p3423 A67-37209

Plane and turbulent fluid jets dynamic and thermal behavior expanding in magnetic field described by differential equations system 24 p4195 A67-41930

FLUID JET AMPLIFIER

Fluid jet amplifier switching mechanism, discussing effect of aspect ratio and logic element with downstream control ports 14 p2248 A67-28268

Power jet and single control bubble region portion of fluid jet modulator modeled for studying static and dynamic properties 14 p2248 A67-28271

Defined region geometry flow characteristics for high-gain proportional amplifiers 14 p2249 A67-28326

Momentum amplifier based on primary, secondary and control jet momentum fluid interaction 20 p3362 A67-38120

Coanda effect shown to be caused by periodic system of vortices arising from nozzle edges 20 p3421 A67-36811

Jet interaction low power-consumption fluid amplifier, NOR logic element switched from laminar to accelerated expansion flow mode by control signal 23 p3936 A67-41420

FLUID LOGIC

Fluid logic elements based on binary arithmetic, and/or algebra and DeMorgan inversion, using gate circuitry 03 p0374 A67-13169

Performance and flow field characteristics of vortex-flow fluid logic devices, discussing efficiency, velocity profiles and momentum profiles for amplifier, rate sensor, test apparatus, etc 06 p0982 A67-17719

Fluidic devices operating on digital signals, showing logic circuits 06 p0952 A67-18833

AND and EXCLUSIVE-OR passive elements based on interaction of two or more unbounded jets 08 p1280 A67-20443

Mach and cavitation number effects in fluid dynamic elements and circuits such as operating pressure limit, power consumption and output 08 p1320 A67-20455

Fluid switching device using free moving foil constrained in chamber 08 p1281 A67-20457

Pure fluid binary to decimal converter using wall attachment OR/NOR elements 08 p1282 A67-20466

Flip-flop and OR-NOR gate design and fabrication to specification 08 p1282 A67-20467

Logic methods using conventional piston valves applied to general automation 08 p1282 A67-20470

Reynolds number and ratio with Mach number as similarity parameters in fluidic devices with significant compressibility and

viscosity 08 p1283 A67-20471

Pure fluid four bit binary comparator design and construction 08 p1283 A67-20474

Fluid logic elements for data processing 09 p1467 A67-21759

Fluid jet amplifier switching mechanism, discussing effect of aspect ratio and logic element with downstream control ports 14 p2248 A67-28268

High speed fluidic logic circuitry for pneumatic stepping motor 14 p2251 A67-28351

Fluid amplification and fluid logic trends stressing industrial applications, comparing electronic and fluid systems performance 21 p3571 A67-38105

FLUID MECHANICS

SA AERODYNAMICS

SA CONTINUUM MECHANICS

SA GAS DYNAMICS

SA HYDRAULICS

SA HYDRODYNAMICS

SA HYDROSTATICS

SA MAGNETOHYDROSTATICS

SA THERMODYNAMICS

EFM, interplay of electric fields with insulating fluids which cannot remain nonconductive at high temperatures, considering astronautics application 01 p0014 A67-11408

Fluid mechanics of mixtures whose components are at large deviation from equilibrium with one another, considering propulsion system application 01 p0055 A67-11439

Rotating fluid dynamics with results derived from classical rules of vorticity, noting various types of waves 02 p0232 A67-11566

General inequalities for regular relativistic fluid spheres, noting gravitational potential energy limit 02 p0266 A67-11696

Tabulated data on specific losses in flow systems 02 p0233 A67-11995

Fluid motion in weightlessness, examining effects of weak forces normally suppressed by terrestrial gravitational field 02 p0233 A67-12322

Fluid equilibrium shape under gravity force and surface tension analyzed via variational method 03 p0401 A67-12881

Vented profile in free surface flow of finite depth, computing lift and drag 03 p0402 A67-13449

Equation for laminar gas meter applied to flow coefficient derived from Hagen-Poiseuille relationship, noting effect of heat transfer, compressibility, etc, on meter performance 03 p0404 A67-13778

Elbow flow meters, comparing average coefficients with theoretical values 03 p0422 A67-13779

Formulation of problem of large-scale fluid mechanics, based on definition of characteristic flow parameters, applied to molecular flows 03 p0404 A67-13882

Upper and lower bounds for solutions to transport equation obtained, using convolution method and maximum principle [DVL-479] 04 p0602 A67-14509

Fluid dynamic sources of radiation during atmospheric entry, considering equilibrium and nonequilibrium radiation, thermal radiation and relaxation processes in hypersonic flow 04 p0703 A67-14703

Kinetic relaxation equation with initial values for uniformly expanding or contracting gas and Maxwellian molecule problem 04 p0604 A67-14792

Fluid dynamic aspects of space flight - NATO-AGARD Specialists Meeting, Marseille, April 1964, Volume 1 04 p0605 A67-14987

Interferometer design for use with laser light in fluid mechanics 04 p0624 A67-15455

Fluid mechanics development in Rumania noting studies on movement of incompressible fluids, barotropic fluids, supersonic aerodynamics, filtration, etc 05 p0792 A67-16798

Instability modes of cantilevered bars induced by fluid flow through attached pipes, examining cases of torsional and transverse flutter and torsional buckling 05 p0921 A67-16882

Power source disturbance method for linear theory of flow past bodies 05 p0749 A67-17006

Book on theoretical equipment of engineering fluid mechanics 06 p0982 A67-17660

Applied mathematics of space program fluid mechanics and

aerodynamics 06 p0983 A67-17783

Fluid mechanical model of electric arc balanced magnetically in gas flow, based on photographs showing arc must simulate solid body [AIAA PAPER 67-96] 07 p1240 A67-19437

Thermal turbomachines, Volume 1, Thermodynamics and fluid mechanics calculations, covering one-dimensional turbine stage theory, blade cascades, etc 07 p1127 A67-20040

Torque effect on characteristics of burner flame based on principles of fluid mechanics 08 p1425 A67-20305

Laboratory hypersonic wake fluid mechanics transition data over range of Reynolds number structured into three laws of far and near wake and interpolation regime [AIAA PAPER 67-33] 08 p1275 A67-20379

Book on theory of flow machines covering pumps, turbines, windmills, fluid dynamics, viscous flow fields, cascade flow, etc 08 p1321 A67-20758

Dynamical effects of heat absorption or rejection on flow of electrically charged fluid considered within special relativity framework 08 p1426 A67-20923

Viscoelasticity for micropolar solids, obtaining constitutive equations of strain and microrotation rate dependent materials 08 p1422 A67-20979

Book on quantitative relationships for non-Newtonian systems, considering classification and fluid behavior of materials with anomalous flow properties 08 p1322 A67-21268

Analytical expressions developed for prediction of partially wetted rotating disk pressure, gradient development and frictional drag for different flow regimes 10 p1659 A67-22708

Asymptotic exponential laws of contraction of plane and axisymmetric jets of weightless fluids, obtaining expressions for stream function and velocity component 10 p1624 A67-23039

Hydraulics and fluid mechanics - Australasian Conference, University of Auckland, December 1965 hydraulics and fluid mechanics - Australasian Conference, University of Auckland, December 10 p1626 A67-23553

Irregular refraction of plane shock wave by hot gas wedge, analyzing relation to Mach number values 11 p1775 A67-23878

Fluid mechanics of internal flow - Symposium, Warren, Michigan, September 1965 11 p1775 A67-24041

Internal flow analysis noting interaction with wall, frictional effects, boundaries and method of analysis 11 p1776 A67-24042

Inviscid flow theory in internal aerodynamics, discussing irrotational, secondary and flow past thin airfoils and slender bodies 11 p1776 A67-24049

Fluid dynamic fields from hypersonic flow around slender bodies, using extension of Vallander tangent cone method for zero angle of attack 11 p1741 A67-24091

Rotor supported in fluid film journal bearings, eliminating self-excited vibrations through motion equation [ASME PAPER 67-VIBR-28] 11 p1797 A67-24186

Trapped fluid effect on high speed rotor vibration, discussing asynchronous and synchronous whirl for fully and partially wetted cavities [ASME PAPER 67-VIBR-29] 11 p1797 A67-24187

Dynamics of fluids and plasmas - Conference, University of Maryland, October 1965 11 p1779 A67-24532

Fundamental field equations of continuum thermomechanics derived from balance of energy equation and entropy production inequality, using invariance considerations 11 p1819 A67-24533

Kraichnan turbulence theory analyzed by computer calculated solutions with correlation and regression functions derived from experiment, shows good agreement with theory 11 p1780 A67-24539

Formal expansion schemes in predicting statistical properties of turbulent flows at high Reynolds numbers 11 p1780 A67-24540

Nonlinear mechanics of plasma-like distributed system studied with Q machine, noting mode locking 11 p1839 A67-24550

Singular integral equations with constant

coefficients solved by Jacobi polynomials and applied to problems in fluid dynamics, crack propagation, plane elastic theory, etc 11 p1813 A67-24678

Metallurgical and fluid dynamic results of 2000-hr endurance test at high temperatures on two-stage 200 hp turbine in wet potassium vapor [ASME PAPER 67-GT-9] 11 p1745 A67-24797

Dynamics of baroclinic geostrophic circumpolar vortex beta-plane flow in zonal magnetic field, noting applications to solar rotation, hydromagnetic dynamo theory, etc 12 p1963 A67-25338

Thermodynamics and fluid mechanics - Conference, Liverpool, April 1966 12 p1927 A67-25345

Recovery factor associated with moving fluid temperature measurement is dependent on thermodynamic and transport properties of fluid, noting probe errors 12 p1928 A67-25353

Large disk MHD generator studied for plasma properties and fluid mechanics, noting seed ionization effect on performance 12 p1972 A67-25386

Book on hydraulic control systems covering fluid flow theory, hydraulic pumps, motors, valves, power elements, etc 12 p1899 A67-25558

Two-velocity spatial correlation coefficients and lengths measured for wall jets 13 p2049 A67-26590

Study of transfers in mechanics of single-phase fluids, Volume 2, Boundary layer, experimental results 13 p2222 A67-26736

Potential flow about two-dimensional hydrofoils with zero velocity boundary condition 13 p2095 A67-26910

Axially symmetric potential flow about slender body, noting source strength distribution and solution via integral equations 13 p2095 A67-26911

Existence of three-dimensional solution of boundary layer equations of viscous incompressible flow in neighborhood of stagnation point 13 p2050 A67-26912

Turbulent wake under homogeneous strain noting mechanism of transport and mixing 13 p2096 A67-26915

Hydrodynamic lubrication in face seals, discussing mechanism of fluid film, surface roughness, wear, leakage, thickness, temperature, pressure, etc [BHRA PAPER E5] 14 p2324 A67-27889

Discharge characteristics of sharp and round edged orifices in transition regime noting variation of pressure ratio, magnitude of Knudsen and Reynolds numbers, etc 14 p2300 A67-28180

Nonequilibrium aspects of fluid mechanics of freely expanding jet analyzed, using aerodynamic molecular beam system 14 p2301 A67-28184

Flow processes and static and dynamic performance characteristics of axisymmetric fluid jet modulator and single receiver-diffuser studied experimentally 14 p2248 A67-28269

Incompressible fluid flow in convergent nozzle with finite aspect ratio, predicting offset on nozzle flow and jet reattachment 14 p2303 A67-28334

Natural boundary layer transition on ogive nose cylinders in zero and adverse pressure gradient analyzed for fluid dynamics, using smoke visualization 14 p2306 A67-29052

Weak random initial magnetic field evolution in highly conducting isotropically turbulent fluid, noting exact initial growth expression of magnetic energy spectrum 15 p2469 A67-29223

Thermomechanical theory of diffusing and chemically reacting mixture and application to elastic materials mixture subject to diffusion and heat conduction 15 p2517 A67-29463

Formula for thrust derived from thermodynamic steady flow energy equations 15 p2472 A67-29873

Fluid flow measurement through optical radiation detection, determining local velocities and image-space motion 15 p2488 A67-29766

Generalized streamline hypothesis for turbulent boundary layer flow with spatial variation of viscosity 15 p2473 A67-30210

Book on basic fluid mechanics, applying continuity momentum and energy relations to various practical problems through dimensional and control-volume analyses

techniques 15 p2473 A67-30231

Book on fluid mechanics and thermodynamics of turbomachinery covering application of dimensional analysis and performance laws 15 p2418 A67-30395

Heat transfer and fluid mechanics - Conference, La Jolla, Calif., June 1967 18 p2590 A67-30934

Conducting Bingham plastic fluids considered as lubricants in rheostatic bearing in presence of constant magnetic field [ASME PAPER 67-LUBS-4] 18 p2682 A67-31382

Surface tension principles for propellant management devices, discussing static retention and dynamic control of spacecraft fuels 17 p2801 A67-31985

Decay and dispersion of disturbance pulse in fluid lines along pipe, considering velocity and pressure characteristics [ASME PAPER 66-WA/AUT-24] 17 p2835 A67-32017

Kinetic equation derivation for one particle species fluid using closure hypothesis 17 p2883 A67-32290

Eigenvalue method prediction of two-phase fluid critical flow rates via energy model, comparing empirical and theoretical results 17 p2838 A67-32869

Mixing function parameter behavior in boundary layer separations by Crocco-Lees method, noting linearized Glick differential equations 17 p2840 A67-33031

Empirical equations for compressive properties of liquids, noting applicability at high pressures 17 p2841 A67-33386

Two-dimensional steady flows of viscous fluid in external infinite region on basis of fourth order nonlinear Helmholtz equation in vortex terms 18 p2981 A67-33420

Dynamic phenomena in two identical cylindrical shells placed side by side in inviscid supersonic flow of compressible fluid 18 p3024 A67-33540

Gas core reactor, discussing application of fissionable gas to heat hydrogen propellant in nuclear rocket reactor [AIAA PAPER 67-499] 18 p3076 A67-33963

Recirculation zone in fluid mechanics experiments on cylindrical cavity simulating gas-core nuclear rocket as heavy gas reservoir, discussing flow patterns [AIAA PAPER 67-502] 18 p3076 A67-33966

Fluid dynamics effect on spontaneous pressure spikes in Apollo SPS thrust chamber, noting increased combustion instability, occurrence and mechanism of pops, etc [AIAA PAPER 67-513] 18 p3114 A67-33976

Concentration profiles in fixed laminar boundary layer with catalyst distribution on wall, discussing Schmidt number effect and approximations 18 p3159 A67-34161

Power source disturbance method for linear theory of flow past bodies 18 p2984 A67-34268

Schwarzschild criterion validity, reducing initial value problem for hydrodynamic perturbation equation to time independent problem 18 p3029 A67-34737

Wind tunnel measurement of turbulent transport terms for unstable curved mixing layer of incompressible flow 18 p3030 A67-34751

Ideal fluid energy-momentum tensor derivation of Crocco-Vazsonyi equation for ideal fluid relativistic hydrodynamics, discussing continuity equation for specific entropy 19 p3210 A67-35707

Perfect fluid theory analyzed from resistance viewpoint and compared with flow past material body when viscous, discussing potential flow 20 p3419 A67-36189

Ram effect similarity criteria determination from partial differential equation system noting composite similarity, simulation possibilities, continuity equation, etc 20 p3419 A67-36190

Dynamical consequences of thermostatic concept of stability within general framework of modern thermodynamics 20 p3543 A67-36428

Book on electromagnetodynamics of fluids covering MHD, astrophysics, plasma physics, etc 20 p3498 A67-36808

Response of plate to fluid loading, determining fluid pressure induced by plate motion 20 p3539 A67-37009

Heat transfer - Conference, Chicago, August 1966, Volume 6 20 p3555 A67-37460

Wave propagation and flow past obstacle in fluid magnetodynamics 20 p3503 A67-37676

Book on fluid dynamics of multiphase systems covering momentum, heat and mass transfers and chemical reactions 20 p3425 A67-37728

Growth and attenuation of acceleration waves and higher order waves derived from nonlinear fluid theory with internal state variables 21 p3610 A67-37739

Steady flow field from turbulent boundary layer separation in front of forward facing step, discussing pressure field 21 p3613 A67-38853

Taylor columns occurrence criterion in Jupiter atmosphere investigated experimentally, giving flow patterns 21 p3614 A67-38999

Experimental method for studying Taylor columns over hills and holes in Jupiter atmosphere 21 p3614 A67-39000

Navier-Stokes differential equations for unsteady incompressible viscous fluid motion solution method, considering quadratic inertial terms 22 p3783 A67-39682

Graduate text in general fluid mechanics covering magnetofluid dynamics and vector analysis 22 p3788 A67-40324

Book on fluid mechanics foundations for introductory and/or secondary fluid mechanics course, with appendices containing vector analysis, inviscid fluid flow equations, etc 23 p3991 A67-41529

Papers on fluid mechanics and singular perturbations including Navier-Stokes equations, boundary layer theory, etc 24 p4141 A67-42167

Singular perturbation methods for two-dimensional lifting low Reynolds number flow 24 p4091 A67-42169

Hydrodynamic separation using compatibility conditions for Prandtl steady boundary layer equations at zero skin friction point 24 p4142 A67-42172

Book on mechanics of continua covering elasticity, fluid dynamics, heat conduction, thermoelasticity and viscoelastic materials equations 24 p4189 A67-42382

Gaseous nuclear rocket engine propulsion, reviewing fluid mechanics, radiant heat transfer, transparent walls, nuclear criticality, coaxial flow reactor, etc [AIAA PAPER 67-783] 24 p4187 A67-42948

High order accurate difference methods in hydrodynamics 24 p4146 A67-43095

FLUID POWER

Book on fluid power circuits and controls engineering 01 p0012 A67-10305

Fluid power support equipment for space vehicles outside earth atmosphere, based on earth environment effect on various systems [SAE PAPER 660708] 01 p0013 A67-10600

Single point charger design for A-7A aircraft fluid power accumulators 02 p0182 A67-11843

Aerospace fluid power - Conference, Detroit, October-November 1966 09 p1444 A67-22126

Management of aircraft hydraulic vacuum, deicing system and pneumatic components 09 p1581 A67-22127

BAC 111 hydraulic system, discussing service experience, reliability, maintenance, performance characteristics, etc 09 p1444 A67-22128

Piezoelectric transducer electromechanical properties compared to electromagnetic actuator, noting fluid control applications 14 p2248 A67-28267

Power jet and single control bubble region portion of fluid jet modulator modeled for studying static and dynamic properties 14 p2248 A67-28271

Fluid flight control systems, discussing attitude and angular rate stabilization systems 14 p2248 A67-28273

Control flow effect on power jet reattachment location and pressure in separation bubble enclosed by power jet for fluidic devices 14 p2250 A67-28336

Hydraulic systems reliability and maintenance, designing corrective measures to eliminate fluid leakage [AIAA PAPER 67-403] 15 p2423 A67-30370

Hydraulic power units for supersonic aircraft noting trends in component power, speed, flow, pressure, design, etc 17 p2800 A67-31969

Fluid power research - Conference, Oklahoma State University, July 1967 20 p3365 A67-37360

Timing considerations in sequential fluid power circuits design in terms of stray delay concept and safety of asynchronous circuit 20 p3365 A67-37362

Contamination control of hydraulic system achieved when contamination level of fluid is within contamination tolerance level of system components 20 p3365 A67-37363

Fluid power - Conference, London, September 1966 21 p3570 A67-38101

Advanced high Mach number aircraft secondary power system requirements, discussing high pressure hydraulic systems and complex pneumatic positioning control systems 22 p3749 A67-40341

FLUID ROTOR GYROSCOPE

Inertial sensors, discussing magnetic resonance and superconductor gyroscopes, ring lasers, fluid dynamical devices, electrostatic gyroscopes, etc 05 p0806 A67-16517

Thermal diffusion separation of damping fluids in floated gyroscopes 07 p1168 A67-19381

Maneuvering stability analysis of single rotor correctable gyrocompass with fluid torsional suspension of sensitive element 15 p2490 A67-30170

Motion of gyroscope with conical cavity filled with ideal incompressible fluid describing rotating motion 15 p2518 A67-30171

FLUID SWITCHING ELEMENT

Bidirectional counter and fluid state trigger element using high pressure recovery bistable amplifier with decoupled outputs 01 p0014 A67-11032

Switching of supersonic gas jets in convergent-divergent duct by atmospheric venting, using phenomena of boundary layer separation 08 p1279 A67-20436

Steady state and switching characteristics of OR/NOR and bistable wall attachment elements 08 p1280 A67-20438

Switching time of turbulent reattachment fluid amplifier in large scale model and in theory 08 p1281 A67-20447

Fluid switching device using free moving foil constrained in chamber 08 p1281 A67-20457

Spring controlled pneumatic switching units for switching machine operations and interlocking of machine controls 08 p1282 A67-20468

Fluid jet amplifier switching mechanism, discussing effect of aspect ratio and logic element with downstream control ports 14 p2248 A67-28268

Fluidic pulse switching network hazards at high operating speeds, suggesting digital computer simulation to anticipate and rectify hazards before hardware fabrication 14 p2251 A67-28348

Fluid state trigger logic element and bidirectional counter 16 p2609 A67-31663

Pulse-length modulated pressure waves having zero quiescent pulse width, actuating floating flapper disk switching valves of pneumatic servomechanism 16 p2609 A67-31665

Interconnecting fluid elements and hardware components for construction of complex systems 17 p2802 A67-32229

Fluidics defined, giving uses in amplification, sensing, logic, switching and computation, noting reliability under extreme environmental and radiation conditions 20 p3364 A67-37171

FLUID TRANSMISSION LINE

Nucleonic cryogenic quality meter design and development and fluid monitoring through hydrogen vent line on Saturn S-IVB stage under orbital conditions 05 p0842 A67-16540

Spacecraft plumbing systems, discussing tubing materials and types of joints 07 p1192 A67-20247

Fluid control systems - Conference, Pennsylvania State University, July 1965 14 p2247 A67-28263

One-dimensional small signal linear model of fluid transmission line using finite lumped parameter elements and Navier-Stokes equations 14 p2247 A67-28265

Experimental evaluation of fluidic transmission line theory, studying frequency response and sending impedance 14 p2251 A67-28349

Linear symmetric modes of propagation for viscous compressible liquid in rigid and elastic conduits analyzed using Navier-Stokes

equations [ASME PAPER 67-FE-12] 14 p2304 A67-28361

Hydraulic line models for fluid control system analysis, discussing frequency and transient response calculation simplification 20 p3366 A67-37365

FLUID TRANSPIRATION

Thermal diffusion and diffusion thermoconduction coupling effects on transpiration cooling of porous bronze disk at axisymmetric stagnation point 04 p0733 A67-15839

FLUIDICS

SA FLUID AMPLIFICATION

SA FLUID LOGIC

Pneumatic grating for complete measuring system, considering fluidic techniques 08 p1330 A67-20439

Fluidic binary full-adder configurations performance for subtraction function required to generate error signal in closed loop control system 08 p1280 A67-20444

Heavy current fluidic devices using self-cleaning filter with no moving parts 08 p1280 A67-20445

Electrical transducers for fluidic systems in computer peripherals 08 p1330 A67-20449

Design procedure and manufacturing techniques for multielement fluidic plate using wall attachment devices, discussing integrated arrays 08 p1281 A67-20452

Moving part vs nonmoving part elements, with reference to Reynolds 08 p1281 A67-20454

Fluidic digital rectilinear displacement indicator emphasizing transducer, logic circuitry and readout 08 p1281 A67-20456

Fluid circuits used in drilling sequence control, detailing ring counter, binary counting stage and comparator 08 p1281 A67-20458

Monostable fluidic amplifier with adjustable positive feedback /AF relay/ characteristics and application as oscillator, proximity switch, delay unit and in alarm annunciator systems 08 p1282 A67-20462

Flip-flop and OR-NOR gate design and fabrication to specification 08 p1282 A67-20467

Components and design improvement for FM and AM fluidic circuits 08 p1282 A67-20469

Performance of vortex diode, scroll diode and fluid flow rectifier 08 p1283 A67-20473

Fluidic system design including coded tape valves, vibrating reed frequency sensor, flow control, pneumatic switches, etc 08 p1286 A67-21053

Fast response fluidic sensor for absolute pressure ratio operable in adverse temperature and vibration environment 08 p1332 A67-21286

Fluid amplifiers based on Coanda effect, digital and analog pure-fluid devices, applications to spacecraft control, gyrocontrol, etc 10 p1595 A67-22975

NR fluidic elements for automatic control 12 p1896 A67-25104

Automatic flight control development for general aviation, discussing fluidics, electropneumatic servoactuator and microelectronics [SAE PAPER 670255] 12 p1895 A67-25505

Fluidics - ASME Conference, Chicago, May 1967 14 p2248 A67-28322

Control flow effect on power jet reattachment location and pressure in separation bubble enclosed by power jet for fluidic devices 14 p2250 A67-28336

Principle of operation and static performance data of fluoric AND gate, using wall attachment principle 14 p2251 A67-28337

Air gauge circuit analysis extended to fluidic restrictor circuits and complex resistor circuits, using Bernoulli and continuity equations 14 p2252 A67-28353

Fluoric pressure, temperature and angular rate sensors for military and commercial applications [ASME PAPER 67-DE-12] 14 p2252 A67-28869

Fluoric and electronic integrated circuits compared, presenting state of art in packaging 16 p2610 A67-31722

Fluidics applications to ramjet control systems incorporating sensing, logic and actuation functions to inlet duct, flow-air ratio and coolant control 17 p2927 A67-31981

Fluid logic components utilizing Coanda wall effect for control systems 17 p2802 A67-32228

Interconnecting fluid elements and

hardware components for construction of complex systems 17 p2802 A67-32229

Fluidic fuel control system for subsonic combustion ramjet engine, describing components, breadboard model and performance characteristics [AIAA PAPER 67-497] 18 p3113 A67-33961

Fluidic breadboard version of rocket engine sequence control, describing pneumatic logic package and general limitations [AIAA PAPER 67-518] 18 p3114 A67-33981

Fluidic jet engine controls for closed loop control, noting overtemperature prevention, reliability, etc 18 p2989 A67-34097

Momentum amplifier based on primary, secondary and control jet momentum flux interaction 20 p3362 A67-36120

Fluidics defined, giving uses in amplification, sensing, logic, switching and computation, noting reliability under extreme environmental and radiation conditions 20 p3364 A67-37171

Direct fluidic sensors for fluid control circuitry design, discussing aerosonic and acoustic flow and obstacle sensing 21 p3625 A67-37958

Analog and digital computer methods for research and development of fluidic circuit components, discussing scaling effects 21 p3612 A67-38106

Fluidic digital component design utilizing wave phenomena produced by two interacting low entropy pneumatic jets, discussing nozzle geometry and fluidic oscillators 23 p3936 A67-41421

FLUIDIZED BED

Interphase exchange coefficient for gas phase moving through fluidized bed analyzed by tracer gas technique 18 p3160 A67-34290

Critical parameters of plane problem of transition of fluid into suspension, ignoring deformation of body up to point of limiting equilibrium 22 p3916 A67-39392

Static electrification mechanism of particles in pseudofluidized bed in terms of causes of observed polarities of column wall and various particles 24 p4254 A67-42256

FLUORESCENCE

SA PHOSPHOR

SA PHOTOLUMINESCENCE

SA SELF-LUMINOUS BODY

SA X-RAY FLUORESCENCE

Solvent and temperature effects on fluorescent emission of europium beta diketones 01 p0131 A67-10297

Temperature dependence of threshold for stimulated emission of Nd trivalent ion in several host lattices estimated from intensity variation of laser active fluorescence component 01 p0091 A67-11085

Fluorescent emission of neodymium laser triggered by Pockels effect as function of population inversion 03 p0436 A67-13201

Population inversion variation during laser emission as shown by measurements of fluorescence intensity 04 p0634 A67-15497

Nature of excited state resulting from two-quantum absorption associated with fluorescence in anthracene produced by ruby laser 05 p0814 A67-16130

Energy transfer from single chromium ions to closely coupled pairs of chromium ions in ruby 05 p0862 A67-16659

Terminal level lifetime and fluorescence line of neodymium doped glass influence on dynamics and efficiency of Q-spooled laser 05 p0822 A67-16675

Saturable optical absorption of light flux from high intensity Q-switched ruby laser 05 p0822 A67-16677

Large deuterium isotope effect on fluorescence emission spectra and quantum yields observed in number of chromospheres that contain proton donor groups 05 p0758 A67-16701

Twilight effects of solar ionizing radiation absorption, discussing ion production rates and fluorescence 05 p0885 A67-17410

Fluorescence induction in isolated chloroplasts analysis yielding method to determine amount of light used in process 07 p1134 A67-19846

Energy transfer from single chromium ions to closely coupled pairs of chromium ions in ruby 07 p1234 A67-20124

Nucleation of titanium and titanium oxide thin films correlation to thickness obtained from fluorescent intensity measurement 12 p1981 A67-25276

Automatic photographic recording of laser

output energy vs excitation energy obtained from fluorescence of ruby used to integrate laser light 12 p1952 A67-25333

Flaw detection methods using penetrating fluids, emphasizing fluorescent materials and pigments 13 p2122 A67-28255

Absorption, fluorescence and laser emission spectra of triply ionized neodymium yttrium in compound below room temperature 16 p2726 A67-30810

Elemental composition effect on electron excited fluorescence of serpentines determined by spectral examination with electron microprobe 17 p2852 A67-33239

Resonance transfer of energy as mechanism for quenching interaction between rare earth ions affecting fluorescent lifetime 23 p3971 A67-40974

FLUORESCENT EMISSION

Two-photon absorption in organic dyes for various wavelengths, extinction coefficients and concentrations 05 p0815 A67-16626

Fluorescence decay time of NO, determining transition moment variation 05 p0848 A67-16837

Inhibitory effect of light from cool white fluorescent lamps on growth of yeast, alga and protozoa 06 p0952 A67-17872

Fluorescein family organic dyes exhibiting laser action when excited by ruby and neodymium second harmonics 12 p1953 A67-25748

Optical fluorescence, thermally tunable over significant portion of visible and near IR spectrum, from phase-matched parametric system 13 p2127 A67-27081

Hypersonic low density flow analysis with shock tunnel and electron beam densitometer, noting density profiles at various Mach and Knudsen numbers 14 p2300 A67-28176

Emission intensity and spatial distribution of fluorescence measured for transitions in He, noting resonance radiation absorption effect on 5016 angstrom light spread 14 p2317 A67-28196

Gain of flowing carbon dioxide laser systems, noting extent of diameter dependence of gain, population variations, etc 15 p2497 A67-29390

Effective cross section of stimulated emission, noting fluorescence band profile during laser emission 17 p2868 A67-32293

Boron oxide identified as radiating species causing molecular fluorescence spectrum in upper atmosphere at twilight 21 p3623 A67-39123

CdS single crystal platelet growing and treating technique, relating fluorescence emissions to growth conditions 22 p3778 A67-39359

Charge compensation defects influence on UV excitation spectrum of rare earth doped crystals fluorescence 22 p3856 A67-39384

Q-switched laser use as light source for photographing droplets in spray containing fluorescent dye excited by second harmonic of ruby light 22 p3797 A67-39492

Lande factors of neon atoms subjected to magnetic field and multimode laser irradiation measured by observing resonant saturations in fluorescent light emitted 22 p3815 A67-39651

Density variation in shock tube across nonstationary shock wave separating from nitrogen gas fluorescence excited by fast electron beam 24 p4145 A67-42683

Spectrofluorimetric studies on active site of alpha-chymotrypsin using anthraniloyl as chromophore 24 p4119 A67-42685

FLUORIDE

SA ALUMINUM FLUORIDE

SA BARIUM FLUORIDE

SA BORON FLUORIDE

SA CADMIUM FLUORIDE

SA CALCIUM FLUORIDE

SA CARBON TETRAFLUORIDE

SA CESIUM FLUORIDE

SA HYDROGEN FLUORIDE

SA LANTHANUM FLUORIDE

SA LITHIUM FLUORIDE

SA MAGNESIUM FLUORIDE

SA NITROGEN FLUORIDE

SA OXYGEN BIFLUORIDE

SA OXYGEN FLUORIDE

SA OZONE FLUORIDE

SA STRONTIUM FLUORIDE

SA TETRAFLUORIDE

Sublimation and gaseous equilibria involving neodymium fluorides and barium fluorides 03 p0387 A67-13519

Niobium and tantalum oxides from decomposition of zircon-pyrochlor concentrate by silicon 04 p0637 A67-14941

Dielectric properties including permittivity, losses, polarization, impurity conduction and forbidden bandwidths of thin films of praseodymium, cerium and neodymium fluorides 08 p1370 A67-20995

Mixed crystals with fluoride base, investigating spectrum and time behavior of laser emission for operation below room temperature 16 p2725 A67-30809

Estimation of statistical sums of states of groups of oxides and fluorides at high temperatures 16 p2704 A67-31390

Mass spectrometry of titanium subfluorides at high temperatures, determining sublimation pressures and heat and dissociation energy 20 p3377 A67-37135

Fluoride crystals for laser applications, discussing crystal absorption spectrum 24 p4166 A67-41983

FLUORINE

Krypton and xenon effect on dissociation rate of fluorine in presence of argon behind shock wave 04 p0567 A67-15951

High thrust fluorine engines and propellants 06 p1071 A67-17608

Fluor molecule emission spectrum between 4500 and 8500 angstroms, discussing results of rotational vibration analysis [DVL-624] 11 p1750 A67-25003

Potential hazards of Teflon gaskets in liquid fluorine systems 13 p2187 A67-27689

Production, handling and shipping of elemental fluorine, noting materials, health and safety precautions, aerospace applications and toxicity 16 p2734 A67-31811

Liquid fluorine closed flow loop and rocket engine test position design, construction and operation 17 p2832 A67-32012

FLUORINE COMPOUND

SA ORGANIC FLUORINE COMPOUND

Atlas booster materials compatibility with fluorine oxidizers 13 p2186 A67-27687

Corrosion of metals by flowing liquid fluorine compounds 13 p2143 A67-27688

Fluorine compounds as propellants in upper stage propulsion units, discussing properties, suitability and performance 14 p2377 A67-28979

FLUORITE

Spontaneous polarization and electric conductivity in fluorite single crystals doped with lime 12 p1980 A67-25182

Electric conductivity of calcium fluorite single crystals doped with uranium dioxide 12 p1980 A67-25183

FLUORO COMPOUND

SA PERFLUOROALKANE

SA POLYTETRAFLUOROETHYLENE

Perfluorocyclopropane production in reaction of oxygen atoms with tetrafluoroethylene 01 p0018 A67-10762

Tetrafluoroditertiary arsine preparation and coordinating properties, noting effect from introduction of fluorine atoms 01 p0135 A67-10896

9-alpha-fluorohydrocortisone and venous occlusive cuffs effects on plasma volume and orthostatic tolerance following 28 to 78 days of bed rest 01 p0016 A67-10960

Mercury photosensitized oxidation of tetrafluoroethylene, noting reaction process and parameters 04 p0567 A67-15950

Tetrafluoroethylene dissociation in nitrogen behind shock waves and thermoequilibrium constants studied, using shock tube and optical absorption spectroscopy 05 p0759 A67-16840

Gas chromatography parameters of fluoro derivatives of amino acids compared for use in packed columns or sensitivity evaluation 21 p3578 A67-38764

FLUOROAMINE

Imines reacting with difluoramine produce diazirines and other products having potential as missile propellant components 01 p0020 A67-11147

Enthalpies of formation and bond energies of various fluorinated amines in gas state 23 p3971 A67-40975

FLUOROCARBON

Trace fluorocarbon effect on vibrational relaxation in nitrogen shock waves studied by UV spectrophotometric technique 06 p0955 A67-18251

Fracture process in composite films of

stressed tetrafluoroethylene and fluorinated ethylene-propylene 10 p1872 A67-23744

Kinetics of difluoromethylene-nitric oxide reaction, describing experimental apparatus, reaction mechanism, molecule structure and calculating heat of molecule formation 16 p2820 A67-31760

Trace fluorocarbon effect on vibration, relaxation in nitrogen shock waves studied by UV spectrophotometric technique [AIAA PAPER 67-11] 17 p2809 A67-33035

Perfluorocyclobutane-fluorine combustion studies and measurement of detonation velocities and limits 19 p3345 A67-35011

[CI PAPER 67-23]

FLUOROSCOPY

Fluorimetric technique for phosphatase activity in soil based on beta-naphthol release from sodium-beta-naphthylphosphate 14 p2254 A67-28087

FLUORSPAR

S CALCIUM FLUORIDE

FLUTTER

SA AEROMAGNETO FLUTTER

SA BOUNDARY LAYER CONTROL

SA PANEL FLUTTER

SA SUBSONIC FLUTTER

SA SUPERSONIC FLUTTER

SA TRANSONIC FLUTTER

SA VIBRATION

Reconstructing serial pulse train from parallel data recorded on magnetic tape, examining flutter performance 02 p0242 A67-12021

Flexure-torsion cascade flutter of airfoils with two degrees of translational and torsional vibration 22 p3914 A67-40040

Aircraft flutter characteristics calculated from electromechanical analog using elastic mass vibration model and analog computer 22 p3746 A67-40451

FLUTTER ANALYSIS

Improved numerical procedure for harmonically deforming lifting surfaces from supersonic kernel function method [AIAA PAPER 66-78] 01 p0007 A67-11162

Flight flutter tests, related problems, objectives and recommendations [AIAA PAPER 66-883] 02 p0181 A67-12264

Dynamic stability and critical flutter of axial-flow-turbine blades in cascade, for natural frequencies slightly mismatched 03 p0520 A67-12880

Aeromagnetic flutter of walls of plane infinite channel with ionized gas flow 03 p0524 A67-13503

Bending and torsion induced symmetric flutter of aircraft in supersonic flow 04 p0708 A67-14789

Variational approximation of normal velocity on-oscillating wings including linear approximation, numerical integration and comparison to least squares method 04 p0547 A67-14842

Energy method analysis of flutter instabilities in turbojet engine rotors caused by interaction between unsteady air loading and coupled vibration modes [ASME PAPER 66-WA/GT-6] 04 p0713 A67-15384

Propeller-rotor whirl flutter and effect of hinged blades and flexible twisted blades 06 p1099 A67-17920

Quasi-steady aerodynamic and von Karman large deflection plate theory equations of nonlinear oscillations of fluttering plate for single mode subsonic and sonic or coupled mode supersonic oscillations [AIAA PAPER 67-13] 06 p1101 A67-18252

Analytical and empirical results on shell panel flutter boundaries compared, using nonlinear Donnell theory and linear piston theory approximation [AIAA PAPER 67-78] 06 p1104 A67-18452

Bending torsional flutter of uniform swept wing with velocity component aerodynamic strip theory [AIAA PAPER 66-475] 06 p1110 A67-18860

Graphical analysis of rotor flutter in hover using modified Theodorsen function 09 p1573 A67-21743

Nonlinear flutter of simply supported rectangular plate under thermal compression in supersonic gas flow 09 p1574 A67-21915

Flutter of panels mounted on wedges in hypersonic flow of perfect gas, neglecting acoustic waves 10 p1593 A67-23735

Fully stalled airfoil steady state pitching oscillations in one degree of freedom, deriving torsional flutter equation

[ASME PAPER 67-VIBR-12]

Aerodynamic theory of blade vibration, discussing compressibility effect, stalling and design 12 p2014 A67-25412
Flutter characteristics of slab tail or stabilator installation, discussing prevention and design 12 p1872 A67-24172

[SAE PAPER 670260]

Identical flutter boundaries of multibay and one-bay panels with clamped edges in high and low supersonic 12 p1895 A67-25509

Regions 12 p2030 A67-25930

Flutter and dynamic stability of closed thin walled elastic cylindrical shell filled with liquid 13 p2219 A67-26903

Energy method extended to stability analysis of linear system under action of nonconservative forces 14 p2398 A67-28094

Flutter amplitude of stressed panels analyzed in terms of amplification ratios 14 p2399 A67-28139

Effect of blade row interference on cascade flutter investigated using cascade actuator disk method 15 p2415 A67-29314

Aircraft flutter testing using free-air turbulence as exciter 16 p2764 A67-30861

Stall flutter instability of helicopter rotor blades analysis based on unsteady aerodynamic data 16 p2777 A67-31844

[AHS PAPER 130]

Stability of equilibrium of nonconservative continuous systems with slight damping 17 p2959 A67-32414

Energy method analysis of flutter instabilities in turbojet engine rotors caused by interaction between unsteady air loading and coupled vibration modes 17 p2959 A67-32414

[ASME PAPER 66-WA/GT-6]

Flutter of simply supported thin isotropic parallelogrammic flat panels in supersonic flow 19 p3342 A67-35751

Uniform cantilevered bar subject to eccentric compressive follower force, considering warping rigidity, bending-torsional flutter and stability 20 p3538 A67-36674

Response of plate to fluid loading, determining fluid pressure induced by plate motion 20 p3539 A67-37009

Compressor blade flutter stability in separating flow with external perturbations analyzed, using digital computer 20 p3517 A67-37488

Quasi-steady aerodynamic and von Karman large deflection plate theory equations of nonlinear oscillations of fluttering plate for single mode subsonic and sonic or coupled mode supersonic oscillations 21 p3727 A67-38870

[AIAA PAPER 67-13]

Variable length foil fluttering in supersonic compressible gas flow, particularly case with end clamping of varying edges 22 p3910 A67-39454

Flutter of two cylindrical panels bonded by elastic filler in supersonic gas flow, showing flutter velocity increase with increasing filler elasticity 22 p3910 A67-39455

Electromechanical simulator of wing flutter with alleron under flight conditions 22 p3912 A67-39779

Aerodynamic damping of turbine buckets and compressor blades noting flutter and frequency shift 23 p3927 A67-40669

FLUX

S ELECTRON FLUX

S HEAT FLUX

S NEUTRON FLUX

S PARTICLE FLUX

S SCALAR MAGNETIC FLUX

S SOLAR FLUX

FLUX DENSITY

Efficiency criterion for semiconductors, using equations for flux density of electric current and energy for isotropic semiconductor in absence of magnetic field 01 p0129 A67-10103

Radiant flux modulation using two lattices, for case of rectangular aperture with uniform flux distribution 01 p0022 A67-10423

Red shifts and power outputs in quasars and radio galaxies 01 p0149 A67-10889

Radio sources and background radiation survey at 38 mc/s, presenting contour maps of brightness temperature and list of flux densities 01 p0151 A67-10966

IR observations of R Monocerotis preplanetary system, reporting on flux density and circumstellar dust 03 p0510 A67-13506

Radio emission from blue stellar objects and radio galaxies, comparing upper flux densities with quasi-stellar radio source emission densities 03 p0512 A67-14002

Annual variation of quiet sun radio emission during solar cycle, noting daily mean values of flux at different frequencies 03 p0513 A67-14005

Flux densities of 67 nonthermal radio sources at 6 cm wavelength obtained, using CSIRO radio telescope 04 p0697 A67-14775

Weak radio sources observed with Cambridge one-mile telescope 04 p0698 A67-14808

Ionization recombination mechanisms and density-time profiles for electric propulsion unit efflux 04 p0690 A67-15024

Plasma flux cut-off in uniform magnetic field by transverse electric field 04 p0667 A67-15213

Variations in RF spectra of 3C 84, 3C 273, 3C 279 and other radio sources 05 p0891 A67-16401

Rocket measurement of altitude dependence of flux intensity of solar vacuum UV radiation, using ionization chambers 05 p0799 A67-16874

Number/flux density relation of radio sources in fourth Cambridge catalog 05 p0902 A67-17286

Luminosity and density evolution hypotheses concerning distribution of flux densities of quasars, testing validity with Einstein-de Sitter model 05 p0903 A67-17328

Cosmic X-ray source scanning for 21 cm wavelength radiation, using radiometer and parabolic reflector 07 p1247 A67-19063

Radio observation of quasar CT102 at various frequencies from Arecibo for possible explanation of sinusoidal variation of flux density 08 p1397 A67-21186

Supersonic flow velocity and density probe for direct measures of mass and momentum influx, noting solution of H-T diagram of argon and probe criteria 09 p1497 A67-21776

Time variations in flux density of some quasi-stellar sources, discussing relationships with component age and thickness 10 p1705 A67-22955

Extraterrestrial solar radiation simulation and total flux and spectral component measurement 11 p1772 A67-24053

X-ray spectral distributions and fluxes in low keV range of five cosmic sources at low galactic latitude and longitude, noting effective temperature 11 p1856 A67-24505

Extragalactic radio sources classified into five groups via radio magnitude and spectral index at 400 MHz 11 p1868 A67-25086

Upper limits to hard X-ray flux from quiet sun analyzed by balloon-borne scintillation detector measuring celestial sources 13 p2189 A67-26302

Measurement of atmospheric cosmic ray fluxes over large portions of globe as comparison evaluation for different cut-off rigidity models 13 p2192 A67-27245

Solar flux density absolute microwave spectra 14 p2385 A67-28441

Flux density of variable radio sources with peculiar radio spectra 14 p2386 A67-28446

Asymptotic curve for single arbitrary reflection of atom from plane with weak surface roughness, calculating total momentum and energy fluxes 14 p2351 A67-28636

Mean flux density and polarization degree of radio emission from Jupiter in centimeter spectral range 14 p2389 A67-28837

Radio sources in declination ranges of minus 07 to 20 degrees and 40 to 80 degrees using Cambridge interferometer at 178 mc 15 p2551 A67-29095

Dependence of angular dimensions of discrete cosmic radio emission source on radiation flux density and frequency 15 p2549 A67-29140

Plasma flux cut-off in uniform magnetic field by transverse electric field 15 p2532 A67-30261

Flux observations in type II superconductors when changing magnetic field suddenly, with results used to deduce flux flow resistivity 16 p2730 A67-31169

Type II superconductor flux flow resistivity theories, introducing Nozières-Vinen extension 16 p2731 A67-31170

Faint radio sources investigated for isotropy applying Scheuer statistical method rendering quasars local origin theory improbable 16 p2752 A67-31623

Radio telescopic measurements of brighter planetary nebulae indicating majority are thermal radio sources 16 p2752 A67-31624

Critical heat-flux density dependence on dominant parameters in bilateral heating in annular channels 17 p2969 A67-32459

Magnetization in superconducting Mo measured in He 3 cryostat, noting transition temperatures and critical field 17 p2925 A67-33379

Skin effect in type II superconductor, observing flux penetration into single crystal cylinder immersed in LF alternating magnetic field 17 p2926 A67-33381

Upper limit in flux density of intergalactic gas UV radiation measured from interplanetary satellite, showing temperature effect 18 p3116 A67-33524

Short wave spectrometer for measuring total and scattered sky radiation, spectral brightness and fluxes of direct and reflected solar radiation 19 p3227 A67-34860

Solar X-ray flare of July 1966 observed from satellite, giving curves describing energy flux, radiation intensity, etc 19 p3312 A67-35187

Near-earth meteor flux estimate through luminous efficiency and ionizing probability application to data on radio and photographic meteor fluxes 19 p3319 A67-35217

Variational formula for antenna impedance in warm magnetoplasma, considering force and fluid-flux distribution 19 p3194 A67-35513

Magnetic cut-off system for plasma jet, with plasma flux reduction 20 p3497 A67-36679

Red shift magnitude relation for quasi-stellar objects 21 p3701 A67-37895

Flux line lattice and laminar magnetic structure of mixed state in type II superconductors consisting primarily of lead 21 p3681 A67-38351

Nonideal type II superconductors, discussing flux motion and density, pinning force, magnetization, hysteresis, relaxation and energy loss 21 p3683 A67-38402

Limited instability and flux jumping variation with magnetic field for flux pinning and Lorentz forces equilibrium in mixed state of type II superconductor 22 p3856 A67-39438

Flux penetration and dissipation measured on superconducting niobium slab samples with tangential applied field studied for effect of thickness 22 p3857 A67-39491

Pinning force in nonideal type II superconductors 22 p3858 A67-39519

Spectral index dependence on flux density and cosmological red shift, considering model universes populated with radio sources 23 p4062 A67-40634

Power conversion derivation in nonlinear resistive element in series with linear resistors 23 p3981 A67-41395

Relative radio source flux density at 8 GHz for various radio sources 24 p4224 A67-41824

Strong radio sources at 1415 MHz, discussing flux density measurements and spectra of OQ208 source 24 p4225 A67-41831

Energy flux fluctuation of nuclear active component in extensive air shower stem for given fixed muon and electron numbers 24 p4220 A67-42867

Dependence of angular dimensions of discrete cosmic radio emission source on radiation flux density and frequency 24 p4222 A67-43063

FLUX MAPPING

SA FLOW MEASUREMENT

Elastic and inelastic flux switching, explaining different types of domain wall displacement in terms of variations of energy gradient vs wall position 05 p0774 A67-16832

Hysteresis losses in nonideal superconductors calculated, using phenomenological equations of flux motion 06 p1048 A67-17819

High field type II superconductors, analyzing flux jumps 14 p2373 A67-28916

Lunar internal heat flow measured by infrared mapping of polar regions from orbiting satellites 16 p2754 A67-31750

Time variation of magnetic flux distribution in type II superconductor under sinusoidal magnetic field, obtaining flux penetration rate, pinning forces and hysteresis loop 21 p3685 A67-39075

Ferromagnetic powder deposition on superconductor surface in vacuum used to obtain magnetic flux distribution in superconductors 23 p4035 A67-40652

FLUXMETER

Particle effects of interplanetary shock wave, noting discontinuous drop in solar proton intensities 08 p1378 A67-21469
Earth magnetic field micropulsation polarization properties at middle latitudes from three-component fluxmeter recordings 17 p2847 A67-32941

FLYBY MISSION

Reconnaissance missions to outer solar system using energy derived from midcourse planetary encounter 05 p0893 A67-16520
Mars/Venus flyby missions with manned Mars landers, showing trajectory profile for mission 05 p0902 A67-17221
Science subsystems for Jupiter flyby missions, discussing equipment selection, mission planning, spacecraft design and trajectory and constraints on vehicle configuration [AIAA PAPER 67-120] 06 p1084 A67-18287

Mars stopover mission with Venus swingby technique, discussing velocity requirements, trip times and initial mass in earth orbit [AIAA PAPER 67-27] 06 p1085 A67-18332
Manned interplanetary flights before Mars landing, using Saturn-Apollo technology 06 p1092 A67-19031
Unmanned Jupiter space flights, discussing requirements for flyby, Orbiter and low thrust missions 07 p1249 A67-19570

Communication parameters associated with Martian flyby probes and with lander and manned vehicles 07 p1145 A67-19870
Nuclear rocket engine design for near-optimum vehicle performance for mission capability 08 p1412 A67-21107
Flight trajectories to moon, Venus and Mars 08 p1394 A67-21115

Future manned planetary missions including flybys and landings, describing vehicle configurations and technological requirements [AAS PAPER 67-28] 15 p2562 A67-30103
Matched asymptotic expansions and patched conics used to simplify flyby interplanetary trajectories [AIAA PAPER 65-689] 16 p2743 A67-30728
Mars stopover mission with Venus swingby technique, discussing velocity requirements, trip times and initial mass in earth orbit [AIAA PAPER 67-27] 17 p2940 A67-32059

Asteroid belt study with spin-stabilized flyby probes 19 p3322 A67-35317
Launch vehicle, payload size, velocity requirements, etc, for probes exploring solar system and near interstellar space 19 p3323 A67-35330

Navigation and guidance analysis of Mars probe launched from manned flyby spacecraft for 1975-1976 [AIAA PAPER 67-546] 19 p3257 A67-35945

Multiplanet mission for Jupiter, Saturn, Uranus and Neptune, using swingby technique for probe launched in late 1970s [AIAA PAPER 67-613] 19 p3329 A67-36002

Spacecraft in lunar exploration by type and properties, emphasizing soft landing and orbiting mooncraft 20 p3526 A67-37249

Data return advantages of earth-Mars-earth flyby trajectories over more conventional Mars trajectories [AIAA PAPER 67-646] 20 p3530 A67-37626

Low thrust Jupiter flyby mission analysis for interplanetary vehicles with solar electric propulsion [AIAA PAPER 67-708] 21 p3706 A67-38735

Trajectory optimization, performance and other factors in analysis of low thrust solar electric propulsion Jupiter flyby mission [AIAA PAPER 67-710] 21 p3706 A67-38737

Electric propulsion ion engine systems using solar power source for Mars and Jupiter exploratory unmanned spacecraft is adaptable to existing launch vehicles [AIAA PAPER 67-713] 22 p3868 A67-39844

Alternate mission modes for manned Mars exploration 22 p3886 A67-40136

Analog and digital data processes for interplanetary photoscience with reference to Mariner Mars flyby mission, discussing telemetric transmission and SNR [IEEE PAPER 19-TP-66-1134] 23 p3998 A67-40740

FLYING
S HIGH ALTITUDE FLYING
S HIGH SPEED FLYING

FLYING PERSONNEL

SA AIRCREW
SA ASTRONAUT
SA PILOT

SST ground and flight personnel training program for system operation, discussing expected role of piloted flight simulator 13 p2091 A67-27270

Flight simulator use for aircrew training to circumvent costs, impractical exercises and adverse flight conditions affecting pilot programs 14 p2292 A67-28037

Barotrauma, circulatory constriction and other in-flight auditory troubles of civil aeronautical navigation personnel over 40 years old 14 p2257 A67-28214

Ballistographic, glucose and Masterov methods applied to pilot examination for coronary defects 14 p2255 A67-28223

Radioactivity, using Cs137 isotope as radioactive agent, in civilian Norwegian pilots 15 p2429 A67-29283

Antilexposure assemblies evaluation in low temperature water, recording body heat loss and tolerance time for application to helicopter crews 17 p2807 A67-31959

Psychomotor adaptation to flight evaluated clinically, describing anxiety and other aviator symptoms in aerospace 17 p2806 A67-31964

Aortic insufficiency in flying personnel, discussing case histories and cardiovascular system 17 p2806 A67-31965

Airline pilot recruitment, role, capability and training 18 p2993 A67-34073

Manpower planning concept assuring personnel availability for space missions 18 p3162 A67-34679

European approaches to physiological and psychotechnical selection and training of cosmonauts 20 p3375 A67-36925

Data on crew workload in C-141 aircraft used for extended mission living and working schedules, showing major disruptions in regular patterns 21 p3576 A67-38073

Gastroesophageal reflux in fliers measured in evaluation of hiatal hernia and possible esophageal origin of chest pain 21 p3574 A67-38084

Middle aged pilot medical fitness for flying, noting age-accident statistics, changes in skill, performance, senses and responses 22 p3756 A67-40535

Age limitations of flying personnel taking into account physical condition and professional capabilities 22 p3756 A67-40542

Rentgenographic kymography in evaluating cardiovascular apparatus in middle aged pilots 22 p3753 A67-40543

Laboratory psychophysiological efficiency in flying personnel of various ages covering pursuit reaction tests, serial motor activity and optico-acoustic signal analysis 22 p3753 A67-40544

Retinal angiomatosis and aircrew fitness noting correction by photocoagulation 23 p3945 A67-41071

Naval jet replacement pilot training failures examined for significant data 23 p3966 A67-41579

Liquid transport cooling system for aircrew evaluated by collecting in-flight sweat rate on fighter aircraft flying combat and training in tropics 23 p3966 A67-41581

Gastroesophageal reflux measurements in evaluation of hiatal hernia and chest pain in fliers 23 p3954 A67-41599

Medical support for SR-71 aircraft crew members, describing crew selection, flight preparation and medical examinations 23 p3966 A67-41600

Treatment of psychiatric diseases in ground staff and aircrew, discussing psychopharmacology in aeronautical medicine 23 p3967 A67-41603

Physiological protection by aviator flight suit overall when on raft in open sea after downing, noting circulating water effect 23 p3967 A67-41606

Heat exchanger cooling system for controlling aircraft high temperature and thermal inorganic salt for protection against cold for flying personnel 23 p3967 A67-41612

Ventilated wet suit /VWS/ for varying flight cockpit environment and emergency condition thermal protection, assessing physiological responses 23 p3967 A67-41614
Physiological Support Division facility for training crew members of SR-71 aircraft 23 p3968 A67-41616

Cardiovascular integrity restoration in post myocardially infarcted aviation personnel 23 p3957 A67-41637

Restoration of cardiovascular integrity in post myocardially infarcted aviation personnel 23 p3971 A67-41709

Thermo-protective systems for ejected aircraft personnel noting cream product producing heat when dissolved in water [AIAA PAPER 67-967] 24 p4117 A67-43045

Military flight clothing tested in actual survival conditions for ability of subject to withstand moderate sea water environment [AIAA PAPER 67-968] 24 p4118 A67-43046

FLYING PLATFORM

SA GROUND EFFECT MACHINE

DC-to-DC prime converter for anchored interplanetary monitoring platform spacecraft /AIMP/ transforming power from solar array into suitable level for instrumentation electronics 08 p1284 A67-20695

FLYING PLATFORM STABILITY

Research and operational results obtained with nonaerodynamic variable stability flying platform for examining problem associated with lunar landing 06 p0948 A67-18202

Optimum stabilization system for manned space station with asymptotic damping of initial angular momentum 24 p4240 A67-42088

FLYING QUALITY

Handling quality evaluation of seven general aviation aircraft of type operated under instrument flight conditions 06 p0947 A67-18200

Aircraft handling qualities research with variable static stability aircraft used as in-flight simulator [SAE PAPER 670261] 13 p2054 A67-27296

UF-XS Japanese STOL seaplane used to investigate slow speed flying quality and hydrodynamic characteristics of PX-S aircraft 14 p2245 A67-27743

Lateral-directional flying qualities for power landing approach simulated, studying roll effects and damping [AIAA PAPER 67-577] 19 p3175 A67-35972

Factors for SST safety and airworthiness requirements, discussing environment, engineering level, learning and flying quality [AIAA PAPER 67-751] 23 p3933 A67-40985

FLYWHEEL

Flywheel-augmented gravity gradient stabilization /FLAGGS/ 02 p0333 A67-12312

Finite rotation of body due to revolutions of internal flywheels determined assuming total kinetic moment of system is zero 12 p1966 A67-25658

Motion of solid body with rotating flywheels rotating at constant velocities relative to inertial space and body 15 p2493 A67-29686

Finite displacements of solid body under effect of internal rotating flywheels and translational motion of masses 15 p2518 A67-30169

FOAM

SA COLLOID

SA POLYURETHANE FOAM

Insulating foams at liquid hydrogen temperature, describing methods for measuring thermoconductivity, specific heat and density 19 p3346 A67-35567

FOAMED MATERIAL

Aircraft cabin fire tests to determine if filling cabin with high expansion foam could keep temperature within survival limits while controlling combustion products 02 p0181 A67-12232

Ground tests of 2.3-m-diam models of foldable foam-reinforced plastic paraboloidal mirrors for satellite energy supply system and optimization of optical characteristics 04 p0558 A67-15957

FOCUS

SA IMAGE CONTRAST

Statistically optimum optical data processing with automatic focus estimation 04 p0578 A67-14875

Oscillating plateholder for determining instantaneous focal length of large telescopes 11 p1791 A67-24459

Airborne long focal length photographic system environmental effects studied with Cassegrainian type Maksutov telescope 16 p2678 A67-31793

FOCUSING

Self-focusing of transverse electromagnetic plane waves in magnetoplasma 02 p0191 A67-11571

Self-focusing of ruby laser beam in NaCl

- crystals 02 p0252 A67-12481
- Relativistic electron stream requirements to obtain self-magnetic confinement, noting 4 million volt pulsed electron field emission accelerator 04 p0624 A67-15325
- Simplified 180 degrees focusing beta-ray spectrometer, noting electron trajectory radius, shape of vacuum chamber walls, etc 05 p0806 A67-16500
- Focusing of electron beam from low noise gun with different magnet 05 p0777 A67-17279
- Holographic technique for restoration of third-dimension information in recording of conventionally focused photographs 07 p1188 A67-19788
- Self-focusing of longitudinal electromagnetic waves in nonlinear plasma in strong magnetic field 08 p1357 A67-20822
- Self-focusing of elliptically polarized light resulting in formation of channels with linear polarization 08 p1340 A67-21503
- Periodic permanent magnet assemblies for traveling wave tube design, employing magnet stack design curves and demagnetization curves 09 p1476 A67-22210
- Empiric design of taper for increasing efficiency of coupled cavity traveling wave tube 09 p1476 A67-22211
- Self-focusing laser beam in inhomogeneous plasma 09 p1515 A67-22276
- Focal distance of lens controlled digitally using electro-optics 10 p1653 A67-22750
- Focusing of charged particles with pair of concentric spherical grids 10 p1658 A67-23784
- Interferometer producing focusing hologram diffraction grating, noting photograph of spectrum 10 p1658 A67-23788
- Procedure and auxiliary equipment used to focus optical elements of gas laser 12 p1952 A67-25364
- Control efficiency and perfect cut-off of beam current of controlled electron guns, noting focusing properties and variation in focusing with voltage 14 p2276 A67-27767
- Experimental determination of hydrogen atom beam density after focusing by hexapolar magnet 15 p2520 A67-29720
- Dependence of focusing property of aperture on coherence length of illuminating field in Fresnel diffraction from aperture 16 p2639 A67-31358
- Focusing of electromagnetic waves by lenses, calculating field distribution near focus by diffraction theory magnitude of convergence 18 p3010 A67-33646
- Noise and dark current reduction in photomultiplier tubes by magnetic defocusing [SRCC-43] 19 p3193 A67-35314
- Electromagnetic wave focusing in nonlinear medium with small nonlinear polarizability 21 p3670 A67-38684
- Debye-Sears effect in one-dimensional Fresnel zone plate moving at acoustic velocity causes scanning of focal spots 22 p3835 A67-39242
- Ion source using electron bombardment without magnetic source field, studying focusing and optimal operating conditions of electron accelerating system 22 p3847 A67-39641
- Quasi-neutral ion beam focusing by axisymmetric electromagnetic field with closed electron drift, noting ion velocity distribution effects for longitudinal and azimuthal components 23 p4035 A67-41682
- Light beam self-focusing, discussing electromagnetic interaction in nonlinear medium, refractive index dependence on wave intensity and geometrical optics 24 p4187 A67-41770
- Electrode configurations producing various intense charged particle beams, deriving algorithm applicable to three-dimensional problems 24 p4153 A67-41928
- FOG**
- Submillimeter wave scattering by fog, comparing experiments in clear atmosphere and dense fog 02 p0199 A67-12078
- Propagation of vertical turbulent hot gas stream in fog from point source of heat 03 p0463 A67-14225
- Fog penetrating imaging device using germanium panel, horn and waveguide 05 p0809 A67-17512
- Liquidified propane as fog dispersing agent 10 p1676 A67-22814
- Propagation of vertical turbulent hot gas stream in fog from point source of heat 12 p1963 A67-25481
- In-flight simulation of fog for pilot training noting heads-up optical viewing system, daylight backscatter, photographic method, etc [AIAA PAPER 67-386] 15 p2468 A67-30354
- High intensity electric field used to freeze out large quantity of droplets from supercooled artificial fog 16 p2699 A67-31717
- Hypersensitization procedure for spectroscopic plates, minimizing nonuniformities of plate fog by use of stop bath 18 p3047 A67-33883
- Defogging procedure for all-weather aircraft landing, with operational results 18 p3021 A67-34608
- Hologram reconstruction of objects in fog-like medium 20 p3450 A67-37027
- Visibility in warm fog produced in cloud chamber by seeding with sodium chloride particles, with application for aircraft landing clearance 22 p3828 A67-39338
- Attenuation of continuous and pulsed laser emission studied for various thicknesses of artificial water fog 22 p3816 A67-39921
- FOIL**
- SA METAL FOIL**
- Acceleration of plasma formed in electric explosion of foil in air atmosphere 20 p3502 A67-37604
- FOKKER BOND TESTER**
- Quality control system for adhesive bonding using Fokker bond tester ultrasonic resonance instrument 09 p1508 A67-22527
- FOKKER F-28 AIRCRAFT**
- Short-haul airliner /Fokker F-28 Fellowship/, noting moderate size, twin bypass engines, high speed, landing field requirements, etc 16 p2596 A67-31012
- Fokker F-28 Fellowship conceived as jet contemporary of turboprop Fokker Friendship, noting structural and operational details 16 p2597 A67-31561
- Fokker F-28 aircraft features for minimum turnaround time, noting self-sufficiency provided by auxiliary power unit 19 p3173 A67-35558
- Fokker F-28 aircraft systems fuel system, auxiliary power unit, hydraulics, flight controls, pressurization and electrical systems and avionics 19 p3176 A67-35559
- FOKKER FRIENDSHIP AIRCRAFT**
- S F-27 AIRCRAFT**
- FOKKER-PLANCK EQUATION**
- Tracking interruption probability in second order astatic system, obtaining solution from Fokker-Planck equation and computer simulation 03 p0390 A67-13100
- Charged particle motion in random magnetic field, describing time evolution of particle distribution in pitch angle and position in terms of Fokker-Planck coefficients 03 p0508 A67-14317
- Instability of contraststreaming plasmas investigated by taking into account Coulomb collisions via Fokker-Planck coefficients in Boltzmann equation 04 p0662 A67-14519
- Threshold reduction in phase locked loop by retarding phase of return signal from voltage controlled oscillator to phase detector 06 p0969 A67-18109
- High energy solar proton propagation in interplanetary magnetic field by Fokker-Planck equation 07 p1243 A67-19806
- Fokker-Planck equation extended to small amplitude waves in uniform plasma 08 p1360 A67-21126
- Chandrasekhar dynamical friction theory for star in cluster adapted to Fokker-Planck electron in two-component plasma theory and including multiple encounters 10 p1711 A67-23790
- Quantum noise theory for lasers, obtaining rate equations and noise sources with moments appropriate to shot noise and amplitude spectrum 11 p1799 A67-24239
- Dynamic correspondence between electromagnetic field density matrix and associated classical random problem, obtaining means of quantum operators through Fokker-Planck equation 11 p1799 A67-24240
- Charged particle motion in magnetosphere under sudden magnetic pulse, compiling Fokker-Planck equation for particle distribution function 12 p1992 A67-25118
- Fokker-Planck equation for geomagnetically trapped electron distribution as function of longitude, time, energy and mirror-point field intensity 12 p1995 A67-25772
- Fokker-Planck-Kolmogoroff equations extended to cover conditional probability density functions of arbitrary random processes 12 p1961 A67-26082
- Relaxation of velocity distribution to equilibrium in electron plasma, showing linearized collision operator covers continuous spectrum of eigenvalues 12 p1977 A67-26176
- Linear Fokker-Planck collision operator expanded in terms of surface spherical harmonics, showing distribution function governed by differential-integral equations and eigenvalue spectrum 12 p1962 A67-26177
- Relaxation effects in initially non-Maxwellian high temperature theta pinch using Fokker-planck equation for particle velocity distribution function relaxation effects in initially non-Maxwellian 13 p2163 A67-26288
- Relaxation time for spatially homogeneous electron gas calculated by direct numerical integration of linearized Fokker-Planck equation 13 p2164 A67-26297
- Linearized Fokker-Planck kinetic equation, describing approach to equilibrium of test electrons injected into electron plasma in thermal equilibrium 14 p2356 A67-28203
- Influence of higher order contributions to correlation function of intensity fluctuation in laser near threshold determined using Fokker-Planck equation 15 p2496 A67-29091
- Particle velocity distribution calculation in current-carrying electron-proton plasma by Lenard-Balescu-Guernsey form of Fokker-Planck equation 15 p2522 A67-29204
- Fokker-Planck-Kolmogorov method analysis of nonlinear systems described by stochastic partial differential equations 15 p2517 A67-29658
- Technique based on Fokker-Planck equation for estimating statistics of randomly varying parameters in dynamic systems with known differential equation 15 p2461 A67-30323
- Coulomb collisions effect on transverse wave along external magnetic field in dense plasma, noting damping of whistler mode and use of Fokker-Planck equation 16 p2713 A67-30608
- Anisotropic phase of cosmic ray flares analyzed using kinetic equation in Fokker-Planck approximation 16 p2740 A67-31891
- Fokker-Planck damping introduced into Fourier-Hermite representation of Vlasov equation produces Landau and Van Kampen treatments 18 p3030 A67-34754
- Nonrelativistic charged particle transport in geomagnetic dipole field under effect of electromagnetic pulses obtained, using Fokker-Planck equation 19 p3313 A67-35212
- Continuous spectrum of eigenvalues related to Fokker-Planck collision integral 19 p3285 A67-35341
- Transport coefficients of fully ionized hydrogen plasma in magnetic field calculated from Fokker-Planck equation 19 p3286 A67-35350
- Convergence of solutions for AC and DC electric conductivity of plasma with collisions 19 p3286 A67-35352
- Damping of high frequency waves in homogeneous fully ionized plasma with relative electron-ion drift calculated, using fokker-planck kinetic equation 19 p3292 A67-35391
- Validity range for weak turbulence theory in case of wave resonant interaction mechanism, treating Fokker-Planck and nonlinear optics approximations 19 p3298 A67-35792
- Fokker-Planck equation for distribution function over laser observable values derived from quantum-mechanical laser master equation by expanding statistical operator 20 p3461 A67-37182
- Laser Fokker-Planck equation transient solution in threshold region investigated for laser distribution function, mean intensity and mean squared deviation 20 p3461 A67-37183
- Electron-plasma oscillation damping in hot collisional plasma with external uniform magnetic field investigated using Fokker-Planck equation 20 p3503 A67-37693
- Electron distribution function in steady state plasma with Coulomb and excitation collisions obtained analytically by simplifying Fokker-Planck terms 21 p3681 A67-37746
- Plasma model kinetic equation, discussing collision operator approximating momentum and energy transfer rates 22 p3843 A67-39265

Chapman-Enskog expansion applied to Fokker-Planck equation for plasma allows transport coefficients calculation without further approximation in presence/absence of magnetic field 22 p3843 A67-39266

Quantum theory of maser oscillator model consisting of radiation field mode interacting with 3-level atoms 22 p3814 A67-39436

Fokker-Planck equation describing distribution of geomagnetically trapped electrons as function of longitude, time, energy and mirror-point field

Intensity 22 p3791 A67-39808

Energy changes between solar wind and cosmic rays, discussing particle motion description by Fokker-Planck differential equation 22 p3874 A67-40079

Quantum damping theory formulated in coherent state representation, giving Green function solution to damped harmonic oscillator Fokker-Planck equation, noting density operator 22 p3817 A67-40486

Linear Boltzmann equation approximation by Fokker-Planck equation leading to logical inconsistency 23 p4029 A67-40963

Streaming and spatial gradient equations of cosmic ray particles in interplanetary medium model, discussing Fokker-Planck equation and heliocentric field modulation 24 p4208 A67-41832

Relaxation of anisotropic plasmas based on Fokker-planck equation assuming elliptic distribution during process 24 p4198 A67-42440

FOLDING STRUCTURE

SA BALLOON

SA PARACHUTE

SA PARAGLIDER

Flexural instability of foldable tube with elastic recovery for use as structural elements, pipes, antennas and masts 01 p0165 A67-11387

VTOL and STOL aircraft comparison, discussing advantages and disadvantages of hinged and folding rotors, hinged wings, jet thrust and fan-in-wing principle 17 p2798 A67-32833

High speed helicopters and large transport capacity aircraft, discussing combination of rotors with wings and propeller drive, retractable blades and folding rotors 22 p3745 A67-39753

FOOD

SA DIET

SA NUTRITION

SA SPACE FLIGHT FEEDING

SA SPACE FOOD

Bioengineering and food processing - AICE Meeting, Minneapolis, September 1965 05 p0757 A67-17155

Economic benefits from space systems used to survey food producing areas and weather 19 p3350 A67-35650

FORBIDDEN BAND

Energy levels in forbidden band of gallium arsenide alloyed with silver or gold, determining impurity levels from temperature dependence of electric conductivity and Hall constant 01 p0129 A67-10104

Directional correlation of first forbidden beta group and gamma ray in decay of antimony at four beta energies 02 p0269 A67-11863

Gapless superconductivity by tunnel effect experiments on dirty superconducting alloys in high magnetic field 02 p0300 A67-12247

Optical absorption spectra of hexagonal red HgS single crystals at self-absorption edge at temperatures from 20.4 to 310 degrees K 02 p0300 A67-12476

Electrical properties of GaSe-layer-semiconductor single crystals used to determine scattering mechanisms of charge carriers, depth of impurity centers, effective mass and forbidden gap 03 p0488 A67-12816

Solar corona temperature measurements, noting discrepancy between results from observations of forbidden emission lines and ionization balance 03 p0470 A67-13218

Allowed and forbidden direct interband optical transitions in anisotropic semiconductors, using effective mass theory for exciton, solving Schrodinger equation 04 p0674 A67-14610

Temperature and doping level effect on conduction band edge of n-type semiconductors, noting doublet shifts resulting in narrower forbidden energy gaps 04 p0681 A67-15292

Electrical properties of indium antimonide single crystals with noncompensated impurity concentration, determining position of deep-seated levels in forbidden band 05 p0861 A67-16399

Forbidden absorption bands of carbon monoxide in vacuum UV region, noting rotational and vibrational constants and perturbations 05 p0848 A67-16847

Effect of local states in forbidden band on electron processes in n-GaP crystals, diagramming absorption and photoluminescence excitation spectra 05 p0868 A67-17063

Dielectric properties including permittivity, losses, polarization, impurity conduction and forbidden bandwidths of thin films of praseodymium, cerium and neodymium fluorides 08 p1370 A67-20995

Forbidden band structure of PbTe and electrical conductivity and Hall effect measurements at high temperatures 12 p1983 A67-25513

Thermal and electrical properties and width of forbidden bands of PbTe and PbSe from 90 to 800 degrees K 12 p1986 A67-28094

N-type germanium doped with antimony and arsenic investigated for radiation recombination, noting energy spectrum and forbidden band changes 14 p2368 A67-28533

Characteristic enhancement of forbidden doublet in nitrogen excitation observed in night airglow during traveling ionospheric F region perturbation 15 p2474 A67-29479

Effect of local states in forbidden band on electron processes in n-GaP crystals, diagramming absorption and photoluminescence excitation spectra 15 p2538 A67-29794

Two-dimensional motion of charged particles in electromagnetic field, noting magnitude of forbidden band as function of particle energy 16 p2740 A67-31895

Spectroscopic measurements of cold plasma charged particle concentrations, specifically spectral broadening due to Stark effect, forbidden-line intensities affected by internal electric fields and autoionization line intensities 17 p2896 A67-32161

Stoichiometric composition effect on semiconducting properties of gamma iron telluride at high temperature 17 p2911 A67-32220

Forbidden nitrogen I lines in IR solar spectrum, computing oscillation frequencies, nitrogen abundance and equivalent widths, comparing predictions to observational results 17 p2948 A67-32819

Variation of forbidden bandwidth and linear-expansion coefficient of indium phosphide-gallium arsenide alloys as function of composition 18 p3095 A67-33447

InSb-InAs solid solution thin films absorption spectra, noting band structure, temperature change and Hall EMF reduction 18 p3096 A67-33450

Forbidden band structure of PbTe and electrical conductivity and Hall effect measurements at high temperatures 18 p3103 A67-34444

Solar identifications for forbidden carbon I lines in solar spectrum 19 p3324 A67-35435

Conditions for optimal planar intermediate-thrust /singular/ trajectory in inverse-square-law field analyzed graphically 19 p3333 A67-35749

Minimum radius of line emitting regions in quasars estimation method, discussing origin problem 19 p3327 A67-35893

Auroral excitation of atomic oxygen forbidden lines, giving photon emission rate vs zenith angle 20 p3426 A67-36301

Change patterns in melting point and forbidden bandwidth for anion and cation substituted compounds of AIIIBV group 21 p3676 A67-37932

Relation between electric conductivity and Hall coefficient in solid solutions, determining sample composition and temperature for forbidden band width concentration dependence 21 p3684 A67-38449

Alfvén two-dimensional problem extended to charged-particle motion in dipole magnetic field with electric field determining forbidden band size, shape and specular reflection points 21 p3621 A67-39015

Auroras /ordinary and type with forbidden emission of atomic oxygen/, examining wind-aurora relation 22 p3790 A67-39675

Irradiation damage in germanium

monitored by electric conductivity measurements, noting carrier population depletion by introducing acceptor levels into forbidden gap 22 p3862 A67-39997

Electronic transport in graded band gap semiconductor heterojunctions without space charges, using method based on intraband transitions between complete Hamiltonian eigenstates 22 p3864 A67-40381

N-type germanium doped with antimony and arsenic investigated for radiation recombination, noting energy spectrum and forbidden band changes 23 p4040 A67-40940

Lifetimes of n-type Cd-Hg-Te alloy, showing Hall-Shockley-Read type recombination at low temperatures 24 p4205 A67-42664

FORBIDDEN TRANSITION

Photolization by spin-dependent electric dipole and spin-dependent magnetic quadrupole transitions with polarized electron spin 09 p1535 A67-22379

Laser oscillation on hyperfine transitions in ionized iodine, noting Fabry-Perot fringes 10 p1662 A67-22699

Identification of forbidden nitrogen IR multiplet in Fraunhofer spectrum 14 p2382 A67-27848

Extension to three dimensions of Wentzel-Kramer-Brillouin approximation method for quasi-classical wave function, applicable to axisymmetrical problems 16 p2703 A67-31920

IR chemiluminescence in hydrogen-diatomic bromine and hydrogen-hydrogen bromide IR chemiluminescence in hydrogen-diatomic bromine and hydrogen-hydrogen bromide 18 p2996 A67-33786

FORBUSH DECREASE

Recurrent cosmic-ray modulation phenomena with Forbush decrease characteristics correlated with M-region magnetic storms, concluding that each series results from shock wave solar initiated 01 p0145 A67-10919

Spectral characteristics of long term change of cosmic ray intensity during 1963-65 compared with Forbush decrease of September 1963 04 p0692 A67-14880

Forbush decreases associated with type IV burst flares, particularly in relation to PCA events, noting delay time and magnetic western boundary 12 p1992 A67-25129

Effect of decrease in intensity of cosmic ray nuclear component during magnetic storms with sudden commencement studied by superposition of epochs 13 p2194 A67-27332

Relationship between geomagnetic storms with sudden commencements and perturbations of southern and northern components of meson distribution in Northern Hemisphere 17 p2938 A67-32796

Underground cosmic ray intensity variation measurements to determine solar modulation processes 19 p3315 A67-35494

Forbush effects variations during solar activity cycle using hard cosmic ray component data 23 p4057 A67-41118

FORBUSH EFFECT

Relation between Forbush decreases and chromospheric flares, obtaining longitudinal distributions before and after onset, using statistics 02 p0311 A67-12592

Changes in solar cosmic ray and geomagnetic field intensities during magnetic storms accompanied by decrease in galactic cosmic ray intensity, using moving averages method 02 p0311 A67-12593

Increase with latitude of Forbush effects and secular variations in cosmic ray intensity explained by worldwide data obtained with meson detectors 02 p0311 A67-12596

Magnetic storm accompanied by cosmic ray intensity increase analyzed, considering Forbush effect and determining all peaks 02 p0312 A67-12601

Forbush effect relation to location of large solar flares, noting association of magnetic bottles with phenomena 03 p0507 A67-14003

Temporal variations of nuclear flux of primary cosmic radiation of Elektron II and IV satellites, discussing Forbush effect in nuclear and neutron components 05 p0877 A67-16085

Corpuscular stream parameters based on data from Mariner II concerning cosmic ray variations on earth surface during geomagnetic storms 05 p0881 A67-16121

Barometric coefficient of cosmic ray

variations determined from observation of
 Forbush effects and cosmic ray flare
 effects 05 p0881 A67-16123
 Cosmic ray intensity variations using gas
 discharge counters onboard Soviet satellites,
 noting Forbush effects 05 p0884 A67-17025
 Measurement of cosmic ray intensity by
 Gond III automatic space
 probe 10 p1701 A67-23230
 Solar flares causing Forbush effect,
 determining relevant parameters, variations
 with solar cycle and mutual
 relations 16 p2739 A67-31457
 Forbush effect causing solar flares not
 originating from same active solar region,
 discussing long connection to sun and
 interlocking 16 p2739 A67-31458
 Cause of cosmic radiation intensity
 increase before magnetic storms associated
 with Forbush effects 21 p3699 A67-39029
 Cosmic ray intensity 19, 20 and 24 day
 quasi-periodic global variations in
 atmosphere related to solar activity
 variations, comparing amplitudes with
 Forbush effects 23 p4056 A67-41109
 Forbush effects variations during solar
 activity cycle using hard cosmic ray
 component data 23 p4057 A67-41118
 Temporal variations of nuclear flux of
 primary cosmic radiation of Elektron II and
 IV satellites, discussing Forbush effect in
 nuclear and neutron
 components 24 p4212 A67-42761
 Corpuscular stream parameters based on
 data from Mariner II concerning cosmic ray
 variations on earth surface during
 geomagnetic storms 24 p4214 A67-42797
 Barometric coefficient of cosmic ray
 variations determined from observation of
 Forbush effects and cosmic ray flare
 effects 24 p4214 A67-42799
FORCE
 SA AERODYNAMIC FORCE
 SA CENTRIFUGAL FORCE
 SA CENTRIPETAL FORCE
 SA ELECTROMOTIVE FORCE
 SA G FORCE
 SA INERTIAL FORCE
 SA LIFT FORCE
 SA LORENTZ FORCE
 SA MEMBRANE FORCE
 SA PONDEROMOTIVE FORCE
 SA PRESSURE
 SA STRAIN
 SA TORQUE
 SA TORSION
 SA VAN DER WAALS FORCE
 Vibroplate pickups for measuring mean
 values of nonsteady state forces, noting
 maximum permissible limits of frequency
 change of pickups 01 p0064 A67-10422
 Nondissipative plasma flow past
 magnetized cylinder in absence of
 electromagnetic field, noting current force
 relation to distance between conductor and
 cylinder surface 13 p2168 A67-27303
 Symmetry removal from linear relations
 between forces and fluxes, concluding that
 fading memory in viscoelastic materials
 results from irreversible
 entropy 18 p3159 A67-34005
 Corrective force selection for bringing
 nonlinear discrete system to predetermined
 phase space point in fixed instant of
 time 20 p3487 A67-37659
FORCE DISPLACEMENT INDICATOR
 Gyro as force sensor in instrumentation
 systems, discussing types, testing and
 calibration procedures 04 p0626 A67-15732
FORCE DISTRIBUTION
 SA NORMAL FORCE DISTRIBUTION
 Classical elasticity theory determination of
 stress distribution on boundary plane of
 elastic half-space due to internal body force
 distribution 05 p0908 A67-16040
 Matrix displacement approach to discrete
 element structural analysis for thin shell
 instability, emphasizing determination of
 membrane force
 distribution 05 p0925 A67-17352
 Force distribution and stress displacement
 relations for two-dimensional elasticity with
 coupled stresses 06 p1107 A67-18651
 Large scale structure of homogeneous
 turbulence generated at initial instant by
 distribution of random impulsive forces,
 noting statistical
 properties 09 p1490 A67-22417
 Locally loaded orthotropic shells of
 revolution under radial concentrated
 forces 12 p2021 A67-25575

Displacements, stresses and moments in
 orthotropic and bimetallic cylindrical shells
 under radial concentrated forces determined
 via computer method 12 p2025 A67-25608
 Stress distribution in matrix of composite
 material for case of filler between one
 infinite and two displaced semiminfinite
 microfibers 14 p2398 A67-28100
 Force on plane wire screen at right angle
 to turbulent incompressible two-dimensional
 jet axis determined, developing approximate
 theories in terms of screen K
 factor 17 p2836 A67-32127
 Infinite edge-stiffener load diffusion into
 semiminfinite elastic sheet, noting interface
 sheet stress variation stiffener force
 distribution
 [ASME PAPER 67-APM-35] 17 p2965 A67-33160
 Variational formula for antenna impedance
 in warm magnetoplasma, considering force
 and fluid-flux distribution 19 p3194 A67-35513
 Book on electrodynamics of moving media,
 deriving force distribution using Hamiltonian
 and virtual power principles in relativistic
 formulations 20 p3500 A67-37087
 Pinning force in nonideal type II
 superconductors 22 p3858 A67-39519
 Forces on spheres inside diffusers noting
 instability onset 23 p3932 A67-41734
 Glider takeoff using tow winch,
 emphasizing flight path and aerodynamic
 loads and forces 24 p4093 A67-41917
FORCE FIELD
 Energy functionals and universal integrals
 of motion for force field symmetric about
 axis of rotation 01 p0113 A67-10680
 Vibrational force constants of nitrogen
 fluoride, using lone pair of electrons
 model 01 p0117 A67-10764
 Certain solutions to problem of motion of
 solid body with clamped point in
 homogeneous gravitational force
 field 01 p0114 A67-10990
 Three-dimensional problem of optimizing
 motion of two-stage rocket in homogeneous
 parallel force field with limited thrusts in
 engine of both stages 01 p0154 A67-10993
 Calculation method for trajectories in
 central force field with arbitrary
 potential 02 p0327 A67-12375
 Numerical determination of axisymmetric
 equilibrium shapes of interface between two
 nonmixing liquids uniformly rotating in
 vessel under weak centrifugal and capillary
 forces and zero gravity 03 p0402 A67-12882
 Natural convective heat transfer in closed
 cavity between two disks in central force
 field for laminar flow in boundary
 layers 04 p0738 A67-15893
 Optimal interorbital transfer between
 elliptical orbits in central Newtonian force
 field analyzed in terms of minimum
 characteristic velocity 05 p0886 A67-16047
 Plane problem of optimum interorbital
 transfer in central Newtonian force field,
 classifying initial orbits and transfer
 trajectories 05 p0886 A67-16048
 Shape and stability of liquid-gas interface
 in annular tank in force field determined by
 numerical integration of boundary value
 problem and eigenvalue
 [AIAA PAPER 66-425] 05 p0793 A67-17218
 Orbital guidance and rendezvous in
 inverse square central force field using
 perturbation method, considering elliptical
 and circular orbits
 [AIAA PAPER 67-55] 06 p1028 A67-18265
 Plane optimum transfer of point of
 variable mass between two elliptical orbits
 in centrally directed Newtonian force
 field 07 p1247 A67-19095
 Motion of arbitrary gyrostabilizer in
 central Newtonian force field, applying
 Liapunov stability conditions for regular
 precession 11 p1791 A67-24683
 Rarefied gas motion instability,
 constructing general solution for effect of
 various force fields 11 p1782 A67-24688
 Energy functionals and universal integrals
 of motion for force field symmetric about
 axis of rotation 11 p1821 A67-25069
 Single-impulse transition in Newtonian
 central force field from hyperbolic to
 elliptical orbit in case of radial
 impulse 12 p2002 A67-25638
 Temperature dependence of yield point of
 crystals described in terms of thermally
 activated motion of dislocations in external
 forces field 13 p2131 A67-26449

Intermediate-thrust arcs in central force
 field satisfying optimality conditions, noting
 that motions are degenerate solutions of
 Euler equations 14 p2382 A67-27850
 Optimum trajectory of pulsed coplanar
 orbital transfer in central Newtonian force
 field with restrictions placed on distance to
 attracting center 14 p2382 A67-27851
 Associated force field applied to phase
 trajectories of nonlinear systems, analyzing
 conditions of conservatism and
 normalization 14 p2349 A67-28744
 Finite collision time for artificial celestial
 body moving under influence of Newtonian
 force from attractive
 center 16 p2745 A67-30744
 Conservative fields of force admitting
 spiral trajectories and dependence on
 constancy of energy level 16 p2748 A67-31137
 Orbits and trajectories for plane motion of
 material point in conservative field of
 force 16 p2748 A67-31138
 Particle paths in central force field
 derived through second order differential
 equation for inverse separation, noting
 perturbation potential
 determination 20 p3526 A67-37254
 Optimal interorbital transfer between
 elliptical orbits in central Newtonian force
 field analyzed in terms of minimum
 characteristic velocity 21 p3701 A67-37834
 Plane problem of optimum interorbital
 transfer in central Newtonian force field,
 classifying initial orbits and transfer
 trajectories 21 p3701 A67-37835
 Field-polar forces interaction effect on
 viscoelastic properties of polypropylene
 oxide, measuring dilatometric, modulus and
 damping constants
 [JPL-TR-32-1026] 24 p4174 A67-41806
 Nonlinear growth of interstellar gas clouds
 and forces in three
 dimensions 24 p4223 A67-41812
 Stationary motion stability of gyrostabilizer
 satellite in Newtonian force field, defining
 body position in coordinate
 system 24 p4241 A67-42400
 Isothermal equilibrium of constant volume
 gas mixture under external mass forces field
 deriving from time independent
 potential 24 p4257 A67-43113
FORCE LINE
 Solar activity effect on brightness and
 polarization of zodiacal
 light 13 p2109 A67-26332
 Coronal condensation analysis observed
 photographically during total solar eclipse,
 finding good correspondence of loop system
 spatial trajectories to force line
 configurations 17 p2945 A67-32690
 Plasma stability in combined magnetic
 fields investigated for oscillation
 frequencies 20 p3500 A67-37048
 Geomagnetic tail at 1000 earth radii,
 noting possibility of magnetic force lines
 connected to earth and tail
 geometry 20 p3433 A67-37402
 Nonline-of-sight communication with FR-1
 satellite along magnetic field line of emitter,
 using VLF electromagnetic
 waves 21 p3584 A67-38656
 Direction of sunspot magnetic force lines
 at any point of solar surface by fringe
 analysis of light polarization
 ellipse 21 p3709 A67-38987
 Turbulent convective eddies effect on
 solar concentrated magnetic fields, plotting
 force lines 21 p3709 A67-38991
FORCED CONVECTION
 Transient response of vapor volumetric
 concentration to perturbation propagation
 and wave form in boiling forced convection
 system under oscillatory
 conditions 01 p0167 A67-10974
 Internal forced convection in viscoplastic
 fluids between two parallel plates with
 applied normal magnetic
 field 01 p0126 A67-11188
 Transient forced convection laminar film
 condensation on horizontal plate, noting film
 thickness changes and heat-transfer
 coefficient variations 01 p0168 A67-11229
 Forced convection effects on VHF CW and
 X-band antenna voltage breakdowns in wind
 tunnel experiments, using cold
 nonconducting gas 02 p0213 A67-11647
 Combined free and forced convection over
 electrically insulating vertical plate of
 constant temperature with transverse
 magnetic field with plate moving up or
 down

[ASME PAPER 66-WA/HT-38]

04 p0724 A67-15429

Density wave type flow oscillations in boiling Freon 11 examined, noting effects of partial evaporation superheat and liquid inlet temperature on stability

[ASME PAPER 66-WA/HT-49]

04 p0725 A67-15433

Interferometer measurements of laminar forced convection in entrance region between parallel flat plates

[ASME PAPER 66-WA/HT-16]

04 p0608 A67-15449

Turbulent boundary layer-flat surface interfacial Stefan-Nusselt flow effects on apparent kinetics of heterogeneous chemical reactions in forced convective systems

04 p0567 A67-15681

Heat transfer - AICE International Conference, Chicago, August 1966, Volume 1, Single phase forced convection

04 p0727 A67-15800

Variational analysis of Graetz problem of forced-convective laminar heat transfer in duct, for various cross sections and given wall temperature and temperature gradient

04 p0728 A67-15802

Forced-convective heat transfer in asymmetrically heated rectangular ducts as function of prandtl number, Reynolds number, aspect ratio and temperature difference

04 p0728 A67-15804

Unsteady incompressible laminar forced convection around stagnation point due to arbitrary time-wise-variant free stream velocity, considering skin friction and heat transfer

04 p0610 A67-15830

Oscillation effect on instantaneous local heat transfer in forced convection from cylinder measured by optical method and theoretically calculated by power series expansion method

04 p0733 A67-15843

System induced instabilities of forced convection flows with subcooled boiling restricted to case of water flow in small circular channels, high L/D ratios, moderate temperature and pressure

04 p0736 A67-15858

Boiling Na free-and forced-convective heat transfer rates, surface temperature and pool-boiling heat-transfer coefficient measurements

04 p0737 A67-15861

Radiation effects on heat transfer and friction characteristics in natural and forced convection film boiling in boundary layer flows

[ASME PAPER 66-WA/HT-6]

04 p0739 A67-15939

Heat flow meter with short response time, measuring influence of acoustic field on forced convection

05 p0790 A67-16034

Pressure oscillations induced by forced convection heating of dense hydrogen

13 p2107 A67-27670

Heat transfer and skin friction increase for gas stream with liquid-droplet suspension flowing over blunt-nosed body near stagnation point

14 p2405 A67-28126

Vapor volumetric fraction during forced convection, calculating true local vapor weight, volumetric fraction, location of bubble departure, etc

18 p3160 A67-34163

Forced convection of laminar flow in tubes of various cross sections, assuming constant temperature gradient and internal heat generation

20 p3420 A67-36317

Heat transfer characteristics of several aliphatic hydrocarbons in nucleate and film boiling during forced flow in heated tubes

[ASME PAPER 67-HT-7]

20 p3544 A67-36705

Gravity and buoyancy effects on slip ratio, void fraction, flow model and boiling heat transfer

[ASME PAPER 67-HT-63]

20 p3549 A67-36745

Forced convective film boiling heat transfer to H studied from experiments on cooling down Cu test section by liquid H

22 p3918 A67-40092

Forced convective heat transfer in straight pipe rotating around parallel axis with large angular velocity

22 p3920 A67-40419

FORCED OSCILLATION

Discontinuous impact vibration absorber with small auxiliary mass sliding in slit of rigid body excited by sinusoidal oscillation

01 p0161 A67-10645

Forced oscillations of two-mass dynamic system with impact reaction

02 p0248 A67-11964

Analog computer solution to autonomous systems with one degree of freedom capable of self-excited oscillation or excited by

external periodic force 02 p0209 A67-12712

Patching method applied to nonlinear differential equation of forced oscillation of second order relay system with damping

03 p0393 A67-13901

Natural and forced oscillations of sphere-array moving with collisions, analyzing quasi-elastic properties of

03 p0432 A67-14162

Forced small axisymmetric oscillations of elastic right circular cylinder with end plates in form of shallow spherical shell filled with heavy ideal fluid

03 p0530 A67-14174

Stability of forced oscillations described by second order nonlinear differential equation determined by Pinnl asymptotic method

03 p0530 A67-14177

Traveling waves interaction in gas laser, explaining forcing-of-oscillations and traveling wave suppression effect

03 p0439 A67-14371

Ritz averaging method to determine free and forced vibratory response of beams and plates undergoing large amplitude steady state harmonic oscillations

04 p0715 A67-15659

Directed graphs application to calculation of forced pressure oscillations in hydraulic systems of flight vehicles and engines

04 p0557 A67-15886

Probability density of oscillating system with piecewise-linear characteristic under action of exponentially correlated random force

05 p0844 A67-16014

Forced parametric oscillations in linear system, obtaining solutions for case where excitation frequency is twice natural frequency

05 p0916 A67-16243

Small oscillations of viscous incompressible fluid in container with free surface under action of potential force field

05 p0791 A67-16373

Forced oscillation method measurement of aerodynamic coefficient of hypersonic blowdown wind tunnel

05 p0788 A67-16764

Forced oscillations in nonlinear resonant circuit employing p-n junction capacitance

07 p1150 A67-19235

Growth of solutions of forced oscillations of nonlinear oscillator driven by white noise

07 p1218 A67-20268

Parameter plane analysis of forced oscillations and jump resonance phenomena in nonlinear systems with periodic forced signals

08 p1311 A67-20343

Causality of steady state response of collisionless plasma model to applied external field

08 p1365 A67-21405

Free and forced oscillations of body with cavity partially filled with viscous fluid

10 p1679 A67-23029

Forced and free oscillation characteristics of ideal incompressible fluid contained in cavity shaped as rectangular parallelepiped with free surface under deformations

10 p1679 A67-23030

Hydrodynamic drawing together problem for aerosol particles oscillating in sonic field at small Reynolds numbers, showing optimal field frequency-approach velocity correspondence

10 p1627 A67-23643

Dynamic theory of vibration damping by controlled impact in forced oscillations in two-mass nonlinear system

10 p1721 A67-23683

Forced oscillations of generalized Lienard equation, examining harmonic solutions in x, y plane with confined trajectories

11 p1812 A67-24311

Mechanical and electrical modes of energy transfer occurring in free and forced oscillations in earth magnetosphere

12 p2000 A67-25107

Asymptotic solutions for free and forced oscillations of solid having cavity filled with viscous fluid, considering several degrees of freedom and arbitrary cavity shapes

12 p2029 A67-25657

Inertial navigation system with damping of oscillations for enhancement of stability of stationary platform

13 p2118 A67-26375

Linear effects of oscillations of liquids in right circular cylinder, determining stability of forced oscillations

14 p2296 A67-27984

Free-running circadian oscillations noting nature of driving oscillation, physiology of circadian organization and relation to manned space flight

15 p2425 A67-29107

Existence conditions of periodic solution of equations describing nonlinear oscillations

of thin plates with allowance for damping and application of Galerkin method

15 p2575 A67-29887

Origin of forced oscillation in space-charged density of free current carriers in semiconductors ascribed to periodic generation of carriers

15 p2542 A67-30243

Forced oscillations of two-mass dynamic system with impact reaction

17 p2866 A67-33281

Hydrodynamic drawing together problem for aerosol particles oscillating in sonic field at small Reynolds numbers, showing optimal field frequency-approach velocity correspondence

18 p3029 A67-34411

Forced bending oscillations for three-layer cylindrical shell under pulsed internal pressure

19 p3338 A67-34878

Stress-strain state of rod with end load and time variable load on other end, discussing forced and free oscillations

19 p3338 A67-34879

Design of adaptive systems with forced oscillations, using correlation and filter methods

20 p3410 A67-37228

Dynamic theory of vibration damping by controlled impact in forced oscillations in two-mass nonlinear system

21 p3720 A67-38284

Linear oscillator forced motion subjected to harmonic AM perturbations studied for servomechanisms

21 p3658 A67-38554

Satellite stabilization with respect to geomagnetic field obtained by applying moments of magnetic forces

21 p3713 A67-38589

Forced oscillation in distributed constant system with tunnel diode described by linear wave equation with nonlinear boundary conditions

21 p3598 A67-38606

Forced resonant nonlinear oscillation of liquid in cylindrical tank

22 p3787 A67-40192

Integral equations with integral operators and excitation frequencies for forced oscillation, solving friction via orthogonal iteration approximation method

22 p3916 A67-40454

Measuring device for aerodynamic coefficients during wind tunnel tests by forced oscillation method

23 p3986 A67-40571

Helicopter maximum speed increase using rotor with controlled blade oscillation motion, studying flow velocity, distribution and asymmetry elimination

23 p3933 A67-40639

FORCED VIBRATION

Forced periodic vibrations of homogeneous isotropic uniformly thick plate with free edges reduced to Fredholm integral equation

03 p0524 A67-13624

Response curves of steady state forced vibrations, cosinelike functions and periodic functions possessing amplitude

04 p0656 A67-14444

Digital simulation of Gaussian random load forcing function and motion equations of nonlinear vibration of damped elastic beam

04 p0656 A67-14447

Dynamic rubber wheel model to supplement digital computer analysis for prediction of frequencies, mode shapes and stress distributions of vibrating rotor stages

[ASME PAPER 66-WA/GT-8]

Rational approximation of generalized Duffing equation, damped mass spring oscillator equation and generalized second order Riccati equation

04 p0647 A67-15660

Forced torsional vibration of inhomogeneous hollow cylinder solved for radial variation of shear modulus and mass density

07 p1264 A67-20234

Creep, stress relaxation and vibrational measurements, sinusoidal torsional forced oscillations and stress wave propagation in polymeric linear viscoelastic solids

08 p1419 A67-20885

Free and forced liquid sloshing motions in tank of arbitrary shape at low gravity environments analyzed, using Satterlee-Reynolds method

10 p1629 A67-23832

Rectangular plate under periodic in-plane edge load investigated for transition mechanisms attendant to parametric vibrations

[ASME PAPER 67-VIBR-5]

Forced nonlinear vibration of Duffing type experimentally simulated with models of isolating systems, obtaining response curves

11 p1871 A67-24165

Forced nonlinear vibration of Duffing type experimentally simulated with models of isolating systems, obtaining response curves

[ASME PAPER 67-VIBR-35]

11 p1873 A67-24192
Natural and forced lateral vibration analysis of free-free beam by integration and finite difference methods, considering influence coefficients
[ASME PAPER 67-VIBR-54]

11 p1873 A67-24202
Multidegree of freedom linear system analysis by dividing method for relations between system constants and solutions
13 p2156 A67-26527
Steady state forced sound propagation in semiminfinite gas induced by oscillating plane piston reflecting particles with Maxwellian distribution
13 p2100 A67-26957
Long period vibrometer with small spring constant and minimized solid friction by HF vibration of support
14 p2348 A67-28257
Time dependent pressure distribution and threshold acceleration for bubble formation in longitudinally vibrating flexible liquid filled cylinder
[ASME PAPER 67-FE-1] 14 p2304 A67-28354
Forced transverse vibrations of sandwich plates of symmetrical structure
16 p2776 A67-31547
Finite length plate in plane supersonic flow analyzed for forced vibration by applying linearized potential flow theory
18 p3140 A67-33466
Input signal level for stability loss or self-oscillations automatic control in system, using analysis for nonlinear systems with forced vibrations
20 p3408 A67-37041
Amplitude of forced flexural vibrations of free rotating shaft under arbitrary load with dampers, taking into account viscous friction
21 p3726 A67-38834
Dynamic response of large flexible space systems subjected to motion inputs and arbitrary force, analyzing joined Timoshenko beams
24 p4240 A67-42395

FORECASTING
S PREDICTION THEORY
S STATISTICAL FORECASTING PROJECT
S WEATHER FORECASTING

FORGING
SA SPIN FORGING
Forging and solution treating nickel-chromium alloy 718 to investigate notch ductility and uniform grain size
04 p0640 A67-15459
Newer titanium alloys compared with present production alloys from closed die forgings in typical airframe and engine configuration
06 p1017 A67-17999
Future Air Force requirements for base metal forms and metal-working techniques including hot strength alloy forgings, fine wire, etc
12 p1948 A67-25286
Aluminum alloy forgings design
14 p2323 A67-27815
Experimental forging of titanium by techniques not requiring machining
14 p2324 A67-28629
Methods for transformation of titanium alloys by forging or die stamping to meet particular requirements
14 p2324 A67-28630
Giant forging press for aircraft and aerospace components
21 p3634 A67-38198
Stream functions correctness for press-forged metals plastic flow by analyzing streamlines of various materials
21 p3637 A67-38928
Heavy section forgings of Ti and high tensile strength Ti alloys with thicknesses up to 10 inches
22 p3822 A67-40197

FORM PERCEPTION
S PERSPECTIVE

FORMALDEHYDE
Paraformaldehyde hypothesis of IR spectrum of Saturn ring
03 p0509 A67-13187
Photosynthesis of nitrosoformaldehyde and identification of spectrum consisting of diffuse band
18 p2998 A67-34277

FORMAMIDE
SA AMIDE
Amino acid formation by formamide thermal decomposition, noting support for hydrogen cyanide oligomerization hypothesis
20 p3376 A67-36700

FORMATION
SA CRACK FORMATION
SA ICE FORMATION
Table of names of formations on moon far side identified by Zond III lunar orbiter photographs
02 p0329 A67-12498
Table of names of formations on moon far side identified by Zond III Lunar Orbiter photographs
10 p1709 A67-23366

FORMATION ENERGY
Threshold energy of formation and stable defect spatial distribution of silicon irradiated with electrons
15 p2542 A67-30250
Fusion crust of meteorites noting similar properties and relations in zonal arrangement of mineral associations in their formation
16 p2750 A67-31437
Electric conductivity variation with temperature for solid ammonium perchlorate, determining energy barrier and enthalpy of lattice defect formation and migration
20 p3377 A67-37134
Enthalpies of formation and bond energies of various fluorinated amines in gas state
23 p3971 A67-40975
Lattice heat capacities, Debye temperatures, heat capacity, free formation energy and thermodynamic functions of groups II-IV semiconductors
23 p4047 A67-41533
MX solids refractory character correlation with volatility at triple point, calculating bond energy according to formation enthalpy equation
24 p4173 A67-42084

FORMATION HEAT
Heat of formation of KCl-KBr solid solutions and energy storage after proton irradiation
01 p0136 A67-11051
Enthalpy of formation and dissociation of explosion of mixtures of hydrogen and excess nitrogen trifluoride
06 p0955 A67-17985
Heats of combustion in fluorine of Teflon and graphite and heats of formation of carbon tetrafluoride and carbon hexafluoride
15 p2433 A67-29765
Kinetics of difluoromethylene-nitric oxide reaction, describing experimental apparatus, reaction mechanism, molecule structure and calculating heat of molecule formation
16 p2620 A67-31760
Formation heat of boron trifluoride measured by elements direct combination in bomb calorimeter
16 p2620 A67-31762
Free energy, heat and entropy of formation of several semiconductors by measuring EMF
18 p3095 A67-33445
Energies of combustion of aluminum diboride and alpha aluminum dodecaboride measured in bomb calorimeter using fluorine oxidant
22 p3758 A67-39766

FORMING
S COLD FORMING
S ELECTROFORMING
S EXPLOSIVE FORMING
S MAGNETIC FORMING
S METAL FORMING
S MOLECULAR FORMING
S ROLL FORMING

FORMULA
S RECURSION FORMULA

FORSTERITE
S OLIVINE
S SILICATE

FORTRAN
Autocorrelation program for moving from study arrangement to data band readable in Fortran
06 p0965 A67-17587
Digital simulation of boundary value problems of trajectory optimization, using variational and functional analysis and IBM-FORMAC language
07 p1149 A67-19976
Flight Load Survey program, written in Fortran IV, for accurate and rapid sounding of wind-induced loads on aerospace launch vehicle
13 p2212 A67-26820
[AIAA PAPER 68-470] Digital simulation of boundary value problems of trajectory optimization, using variational and functional analysis and IBM-FORMAC language
13 p2074 A67-27531
[ASAE PAPER 68-116] Three-photo orientation solution to analytic aerotriangulation problem, investigating mathematical concepts and computer programming
15 p2486 A67-29298
Book on FORTRAN with engineering applications covering case studies, graded exercises, etc
17 p2818 A67-32331
Digital computer program FORTRAN coded, analyzing electric power distribution system of aerospace vehicle
17 p2804 A67-32511
FORTRAN program for B number computation applied to solid state physics
23 p3977 A67-41458

FORWARD SCATTER
Radar detection of tropopause and clear

air turbulence
04 p0649 A67-14682
Sporadic E layer in middle latitude by method of forward ultrashort wave scattering
10 p1630 A67-22792
Laser-produced dielectric breakdown at particle sites in liquids with resulting absorption of secondary light beam
11 p1801 A67-24560
Sporadic E layer formation and possible creation of more favorable conditions by high meteor activity
13 p2201 A67-27391
Diurnal and seasonal variations in radio echo observations from meteoric trains during forward ultrashortwave scattering
14 p2383 A67-27924
Sporadic E layer in middle latitude by method of forward ultrashort wave scattering
24 p4149 A67-42128

FOUNDATION
S STRUCTURAL FOUNDATION

FOUR-BODY METHOD
Periodic solutions of elliptical and restricted four-body problems about libration points of restricted three-body problem
[AAS PAPER 66-101] 07 p1252 A67-19963
Periodic motion around triangular libration point in restricted four-body problem of earth-moon-sun system
13 p2205 A67-27478
Integration scheme for variational r sub j wave functions containing unlinked four-electron correlated terms for atoms up to neon
18 p3082 A67-34026
Regularization of restricted three-body problem extended to case where three primaries of any mass revolve in circular orbits around common center of mass and fourth body of infinitesimal mass moves in their field
18 p3136 A67-34589
Asymptotic solution to nonplanar earth-to-moon trajectories in restricted four-body problem
21 p3705 A67-38613

FOURIER ANALYSIS
Calculation of energy band structure of gallium arsenide, using experimental Fourier coefficients for germanium in pseudopotential method
01 p0136 A67-11054
Precision spectrum analyzer modification using RC network for analyzing filter applied to transient pulses for both Fourier and shock spectra
01 p0074 A67-11130
Line broadening due to cold working Ta-10 percent Re and W-20 percent Re studied by Fourier analysis, integral breadth measurements and variance analysis
02 p0258 A67-12701
Flute type instability of ideally conducting plasma in toroidal discharges with strong longitudinal magnetic field
03 p0476 A67-13343
Power spectrum improvement of multiple wave trains by concentrating power close to carrier frequency, noting constructive and destructive interference
06 p0963 A67-18401
Fermi surface of tin telluride approximated by four distorted surfaces located at L points of Brillouin zone as shown by Fourier analysis
06 p1065 A67-18950
Interpretation of class of divergent integrals in terms of limit sums, using generalized function theory
08 p1349 A67-21193
Semiconductor conductivity in strong SHF electric fields, measuring dielectric constant and Fourier component
10 p1657 A67-23567
Ries Kessel meteoritic crater /Germany/ analyzed by Fourier data smoothing technique, noting impact center, entry direction, etc
11 p1864 A67-24559
Flute type instability of ideally conducting plasma in toroidal discharges with strong longitudinal magnetic field
13 p2172 A67-27715
Fourier analysis of line profiles of X-ray-studied deformation faulting in titanium, zirconium and hafnium
14 p2340 A67-29033
Spherical wave Fourier holography modifications using different scheme for incidence of reference beam and illumination of object
15 p2486 A67-29237
Possible directional pattern forms obtainable for single-ring circular arrays, using Fourier harmonic analysis technique
15 p2454 A67-30138
Shock measurement discussing Fourier spectrum, vibrating reed gauge, analog and digital techniques, etc
16 p2871 A67-31022
Fourier integral in terms of maximum harmonic amplitudes
20 p3406 A67-37650
Convex plasma thermal radiation at UHF, determining spectral composition using

Fourier integrals 21 p3663 A67-37937
 Solar cycle prediction based upon random number technique, Fourier curve fits and power spectra analysis 22 p3873 A67-39931
 Microwave mixing with weakly coupled Josephson superconducting diodes, discussing Fourier components 22 p3865 A67-40439

FOURIER-BESSEL SERIES

Fundamental solutions to certain singular partial differential equations with constant coefficients, using Bessel iteration operator and Fourier-Bessel transforms 01 p0105 A67-10676
 Stresses in symmetrical three-layer circular disk rotating about own axis, with solutions in form of Fourier-Bessel integrals 01 p0080 A67-10777
 Solving three-dimensional electrodynamics problems with mixed boundary values by reduction to standard Fredholm integral equation 15 p2522 A67-29196

FOURIER LAW

Steady one-dimensional heat conduction in rarefied gas at rest analyzed from viewpoint of kinetic theory to determine existence or possible departure from Fourier law 05 p0925 A67-16272
 Pulse tube refrigeration heat pumping rates 13 p2229 A67-27680
 Relativistic thermodynamics in case of equilibrium with stationary co-moving metric and constant pocket temperature, deriving relativistic Fourier law of heat conduction 14 p2404 A67-27951
 Thermal propagation in gases studied through heat transfer equation resulting from Fourier law 17 p2968 A67-32221

FOURIER SERIES

Fourier integral calculation using Hurwitz and Zweifel numerical integration method and Euler transformation 02 p0258 A67-11557
 Extreme value problem of constant type and extremal approximating operators with positive kernels 03 p0461 A67-14106
 Integrable function representation by double singular integral at generalized Lebesgue point 03 p0461 A67-14107
 Continuous periodic function approximation by Fourier series 03 p0462 A67-14108
 Solution to external biharmonic problem for simply connected region bounded by Liapunov curve given in form of Fourier series and applied to elasticity 05 p0908 A67-16041
 Closed-loop automatic control system with unvalued substantially nonlinear element, using approximation of characteristics by Fourier series 05 p0781 A67-16254
 Fourier series approximation of functions with structural properties differing with segments of domain of definition 05 p0836 A67-17107
 Three-body problem of orbital motion, examining periodic librations of planetoid around triangular equilibrium point 06 p1079 A67-17762
 Long period of nonperiodic librational motion about equilateral points of restricted three-body problem 06 p1080 A67-17765
 Uniform almost periodic functions with Fourier indices having one, and only one, limit point 06 p1023 A67-17836
 Polynomials orthogonal with respect to contours, examining analytic function representation via Fourier series expansion of such polynomials 06 p1025 A67-18695
 Fourier convergence of Lebesgue integrable functions 07 p1215 A67-19473
 Fourier convergence of analytic functions 07 p1215 A67-19474
 Lemma for solution of conformal mapping problems of particular class of Fourier series with bounded partial sums and absolutely convergent on convergence circumference 07 p1215 A67-19475
 Directional radiation pattern for circular arc antenna, using three-step method in which current distribution is treated as truncated Fourier series 07 p1152 A67-19550
 Output signal of switched amplifier with arbitrary input signal analyzed, using Fourier series 07 p1154 A67-19656
 Axisymmetric plane-strain vibrations of thick layered orthotropic shell under internal and external pressures analyzed, using Fourier series for eigenmodes determination 08 p1415 A67-20487
 Computer manipulative algebra programs for Fourier series 08 p1299 A67-21260

Fourier series and integrals in analog, digital and hybrid computation 09 p1470 A67-22667
 Stability of almost stationary periodic solution of Navier-Stokes equation, examining spectrum of relevant stationary problem 10 p1675 A67-23677
 Method of images series solution converging rapidly for simply supported Euler-Bernoulli beam with high velocity moving concentrated load 10 p1730 A67-23837
 Natural frequency and mode shape for nonuniform simply supported beam, using Fourier series to approximate deflection, mass and inertia moment 11 p1874 A67-24429
 Fourier series solutions of boundary-value and mixed problems in mathematical physics by integrating partial differential equations 14 p2348 A67-28287
 Compressible flow analysis in three-dimensional curved duct using small perturbation method 14 p2305 A67-28976
 Spinor algebra application to Fourier series transformation of spherical harmonics expansion representing earth gravitational potential at space location 15 p2561 A67-30055
 Nontrivial real or complex solutions of nonlinear integral equations of Hammerstein type bifurcating from identically vanishing solution 16 p2695 A67-30858
 Double curvature influence on rigidity of shell of revolution analyzed for surface loading and cross sectional linear loading, using Fourier series 16 p2766 A67-31149
 Method of solving for Fourier coefficients expressing dependent variable as piecewise continuous function assuming various conditions of continuity and smoothing 16 p2698 A67-31543
 Wind profile analysis from balloon sounding data, using Fourier series to filter out unwanted part of spectrum 16 p2668 A67-31742
 Book on engineering mathematics covering differential equation solutions by numerical method, partial differential equations, Fourier series, integrals, vector analysis, etc 17 p2876 A67-31930
 Control theory of hyperbolic PDEs examined, noting application to distributed parameter systems 17 p2877 A67-32561
 Fourier series applied to X-ray investigation of potential and electron density distribution in silicon lattice to study chemical bonds 18 p3094 A67-33439
 Least squares method for heat problems and approximate similarity law covering orthogonal expansions and compatibility between contradictory requirements 18 p3071 A67-33752
 Optical system devised to alter relative harmonic coefficients and eliminating ringing effects for photographs represented in two-dimensional Fourier series applied to lunar photography 18 p3047 A67-33998
 Fourier analysis of amplifier commutated capacitor type integrator output signal 18 p3011 A67-34107
 Moon physical libration in longitude 18 p3129 A67-34306
 Vector wave functions for boundary value problems in compressible plasma for spherical geometry, noting Fourier series, acoustic wave, etc 18 p3090 A67-34382
 Stability analysis of circular plate submitted to two compressive forces acting along diameter, using Fourier series iteration 19 p3342 A67-35718
 Fundamental intensity error in Fourier spectroscopy noting requirement that interferograms be inverted by Fourier transformation 20 p3437 A67-36337
 Computer program for heat transfer calculation by temperature distribution along wall surface, using Fourier-Bessel series to determine distribution coefficients 20 p3544 A67-36450
 Stress analysis of closed cylindrical shell under concentrated loading at free edge, solving differential equation by expanding functions into Fourier series 21 p3718 A67-37982
 Stability of almost stationary periodic solution of Navier-Stokes equation, examining spectrum of relevant stationary problem 21 p3953 A67-38278
 Exact solutions for elastic displacements and stresses in composite circular cylinder under torsion in Fourier series form 21 p3723 A67-38560

Arbitrary function expansion into series of functions involved in plane elasticity problem with Fourier series form satisfying boundary conditions 22 p3909 A67-39397
 Active impedance and current distribution in infinite, planar and collinear arrays of cylindrical antennas, deriving Fourier series for antenna current 22 p3769 A67-39629
 Spatial filtering for altering relative harmonic coefficients in two-dimensional Fourier integral representation of astronomical photographs eliminates ringing effects 23 p3997 A67-40625
 Power conversion derivation in nonlinear resistive element in series with linear resistors 23 p3961 A67-41395
 Steady random process phase overshoot length distribution determined over given level as well as relationships for mean value and distribution 24 p4136 A67-42194
 Temperature distribution in solid rotating cylinder exposed to solar radiation using Fourier series expansion 24 p4255 A67-42482
 Data handling capabilities of periodic time function for given bandwidth using Fourier series in sinusoidal spectrum analysis 24 p4124 A67-42931

FOURIER TRANSFORM

Partial coherence theory to describe Fourier /autocorrelation/ spectroscopy, showing resolving power dependence upon parameter of measuring instrument and radiation 01 p0018 A67-10504
 Fundamental solutions to certain singular partial differential equations with constant coefficients, using Bessel iteration operator and Fourier-Bessel transforms 01 p0105 A67-10676
 Dynamic response of simple beam and rectangular plate under traveling shock wave at supersonic speed, using Fourier transforms 01 p0161 A67-10775
 Stroke and Restrick method used in Fourier transform application to spectroscopy and astronomy and in obtaining holograms 01 p0069 A67-11008
 Fourier transform holography for diffusion of coherent laser light beam, examining distortion term in reconstructed image 01 p0070 A67-11063
 Time-normalized Fourier transform of sampling function of stationary random process as bounded nonstationary random function of frequency 02 p0224 A67-11901
 Model for ionospheric drift measurements made by spaced receiver method when scattered wave has frequency above plasma frequency of scattering region 03 p0407 A67-12831
 Steady state response of viscoelastic cylindrical shells to moving loads, obtaining exact solution with correction for shear deformation and rotatory inertia effects via Fourier transforms 03 p0522 A67-13211
 Mathematical physics PDE problems solved by combined method using Fourier integral transform and theory of Riemann boundary value problem 03 p0459 A67-13589
 Two spatial distributions transformed simultaneously with single lens heterodyning Fourier transform of spatial spectra 03 p0423 A67-13904
 Fourier transformation related to real half of straight line set of positive harmonic measure 04 p0646 A67-15492
 Fourier transform used in correction of instrument contour error when observing solar spectral line profile 04 p0624 A67-15564
 Fourier transform synthesis of aperture distributions producing sector beam patterns 04 p0590 A67-15907
 Laser as source of optical Fourier analysis of atomic structure of crystals 05 p0824 A67-16921
 Pulse Doppler radar theory using Fourier transformation integrals applied to analysis of spectrum of all signals 06 p0957 A67-17592
 Electric signal transmission noting shape, properties, types, time dependency and use of Fourier transforms in calculations 07 p1141 A67-19338
 Dirichlet theorem and coherent imaging, discussing form of Fourier functions in Fraunhofer diffraction at infinity 07 p1185 A67-19402
 General purpose quadrature method for numerical evaluation of specific definite integrals 09 p1524 A67-21834
 Filter theory method applied in solving analytical construction problems for optimal

controllers, noting existence of Fourier transform and Pally-Wiener condition 09 p1482 A67-22078

Fourier transform for exact solution of current distribution and input admittance of infinite cylindrical dielectric-coated antenna 11 p1757 A67-23972

Pulsed ruby laser to obtain Fourier holograms in light reflected from diffusely scattering objects, discussing relaxation of resolving power of photographic emulsions 12 p1939 A67-25335

Optical computing principles, techniques and configurations for communication problems noting Fourier transform, coding, etc 12 p1907 A67-25990

Digital real time spectral analysis with fast Fourier transform algorithm, using two special purpose computer configurations to estimate power spectrum 13 p2073 A67-27062

Optical interference method of two-dimensional Fourier transform with spatially incoherent illumination to derive relations for transforms of images 13 p2121 A67-27290

Laser as source of optical Fourier transforms in analysis of atomic structure of crystals 14 p2330 A67-28261

Two-dimensional aperture synthesis in lunar CW radar astronomy, showing measurement possibility for Fourier transform components of sky brightness distribution 14 p2385 A67-28442

Time-dependent Green function for moving isotropic nondispersive medium 15 p2509 A67-29199

Fourier-Hermite solutions of Vlasov equations for electron motion against positive neutralizing background examined in linearized limit, noting Landau damping recovery 15 p2509 A67-29205

Image analysis by Fourier transformation into incoherent illumination, applied to point source of light/star/ 16 p2671 A67-30863

Fourier coefficients determination by calculating trapezoidal-rule approximations 16 p2697 A67-31333

Source size effect on resolution in Fourier transform holography comparing theoretical and experimental results 16 p2681 A67-31883

Numerical Fourier transform calculations for pulse testing procedures for controlled time function input systems 17 p2883 A67-32018

Electron image manipulation and charge-image storage perform equivalent of incoherent optical-image transformation 18 p3047 A67-33881

Hamiltonian equations and Fourier transformations applied to free electron and gap motions in doped semiconductor 18 p3002 A67-34231

Computer program for handling of transform between spatial coordinate representation and spatial frequency representation of image 18 p3007 A67-34599

Oscillation conditions of microwave tunnel diode theoretically and experimentally evaluated for mounting at feed point of semicircular loop antenna 19 p3196 A67-35660

Corrective image deconvolution of smearing caused by extended instrument functions in optical imaging possible by holographic Fourier transform division 20 p3435 A67-36204

Coherent light applications in holography and spatial filtering including Fourier transform holography and pattern recognition 20 p3457 A67-36333

Fourier spectroscopy problems including source noise effects on interferogram modulation and maximum SNR attainable in spectrum estimated from given interferogram 20 p3437 A67-36336

Fundamental intensity error in Fourier spectroscopy noting requirement that interferograms be inverted by Fourier transformation 20 p3437 A67-36337

Fourier spectroscopy in far IR for routine investigation through Michelson and lamellar grating interferometers 20 p3437 A67-36340

Real time Fourier transform synthesizer for spectral distribution of interferogram 20 p3437 A67-36341

Scintillation and dynamic range problems mitigated for Fourier spectrometry by rapid scanning 20 p3438 A67-36342

Planetary spectra improvement by Fourier spectroscopy, discussing modulation method reduction of atmospheric turbulence effects and fast transmission system 20 p3438 A67-36345

Very high resolution Fourier transform spectrometer, discussing path difference variation 20 p3438 A67-36346

Numerical spectrum analysis procedures, discussing fast Fourier transform techniques, classical spectrum windows and complex demodulation process for time series studies 20 p3476 A67-36784

Vibrating anular membrane problem, including load per unit area and asymmetry of load and vibration, using finite transform derivation 20 p3539 A67-37006

Electromagnetic point source in presence of planar interface between two anisotropic media, obtaining far fields through Fourier integral and ray optical calculation 20 p3388 A67-37703

Book on optimal control theory covering Fourier and Laplace transforms, automatic control, mathematical theories, etc 21 p3602 A67-37829

Harmonic oscillations and bending of elastic isotropic shells with variable curvature solved using Fourier transform 21 p3721 A67-38383

Fourier transform application to automatic pattern recognition, using photographic plate to record plane intensity distribution 22 p3764 A67-39331

HF plane waves diffraction on plane circular diaphragm solved by functional theoretic methods for integral equation for Fourier transform of screen covering 22 p3912 A67-39783

Polarized and depolarized scattering from perfectly conducting rough surface, theory based on Fourier transform and small perturbations polarized and depolarized scattering from perfectly conducting rough surface, using theory 22 p3782 A67-40076

Modulation transfer theory for frequency response of optical system in temporal or spatial domains, discussing Fourier series and transform [SMPTA PAPER 102-47] 22 p3808 A67-40380

Diffraction and image formation in coherent and noncoherent light with relation to Fourier transform 23 p3972 A67-40708

Exact equation for potential oscillations of inhomogeneous plasma cylinder via Fourier transformations, discussing drift, cyclotron oscillations and flute instability 23 p4034 A67-41679

Radiation resistance and reactance of thin film inductor in microwave integrated circuit determined using Fourier transform 24 p4128 A67-41924

Fourier transformation theory for shock and vibration data analysis, discussing programming considerations and computational efficiency [SAE PAPER 670874] 24 p4248 A67-42011

Complex Fourier transform technique in variable coefficient partial differential equations applied to Cauchy-Kowalewski and Petrowski-Leray theorems 24 p178 A67-42202

Two-dimensional optical image analysis program for image prediction and enhancement, discussing transfer function 24 p4157 A67-42433

Spatial filters for code translation and image sharpening produced by holograph in reasonably good approximation 24 p4159 A67-43097

FR-1 SATELLITE

Time multiplex telemetry equipment for FR-1 satellite that encodes data in PAM/FM wave train for transmission to ground 01 p0020 A67-10107

FR-1 satellite design difficulties such as material selection, insulation of structure, making structure perfectly conducting, etc 03 p0518 A67-13601

FR-1 satellite structure and fabrication 07 p1191 A67-19529

Testing facility and methods for FR-1 and D-1 satellite control 07 p1163 A67-19530

FR-1 satellite data on VLF propagation in lower magnetosphere 10 p1849 A67-23301

French satellite FR-1 to be launched in late 1965 by NASA for ionospheric studies, noting instrumentation, data transmission, etc 16 p2757 A67-30641

FR-1 satellite-borne oxide cathode used to return to ground polarization current from ambient plasma 21 p3599 A67-38649

Component selection program for equipment onboard FR-1 satellite covering production facilities, qualifications, supply, reliability, etc 21 p3572 A67-38676

FRACTION

S VOID FRACTION

FRACTIONATION

Gel permeation chromatography for analytical fractionation of propellant binder prepolymers and separating and purifying labile binder ingredients 04 p0686 A67-14472

Chemical composition and earth origin, with estimates of primordial abundances of elements in solar system 07 p1170 A67-19336

Separation of digitonin treated chloroplasts by differential centrifugation into fractions showing distinct pigment and photochemical differences 07 p1134 A67-19847

Stable isotope distribution in carbonates 14 p2310 A67-27970

Abundant lithophile element fractionations in chondrites with special reference to aluminum and calcium 14 p2391 A67-28951

High temperature vapor fractionation of silicate glass related to variations of oxygen isotopes in tektites 15 p2564 A67-30394

Condensation history of cooling gas of cosmic composition, stressing chondrite fractionation patterns 20 p3526 A67-37172

Chemical history of Fe traced in nebular material assuming preplanetary particles were similar to those presently discarded by sun 23 p4068 A67-41360

Re and Os abundances in various chondrites determined by neutron activation analysis, noting fractionation 24 p4235 A67-42637

Tektite composition considered from results of high temperature vapor fractionation of silicates 24 p4237 A67-42649

FRACTOGRAPHY

Electron fractography applied to fatigue studies of fracture appearance, morphology of striations and fracture surface microdetails [ASTM PAPER 42] 18 p3068 A67-34580

Electron fractographic techniques for failure analysis, examining fracture direction, differentiation between hydrogen embrittlement and stress corrosion in steels and cyclic stress [ASTM PAPER 44] 18 p3145 A67-34581

Gaseous environment influence on fatigue fracture mode in quenched and tempered ultrahigh strength steel investigated by fractographic analysis 22 p3821 A67-40051

FRACTURE

Electron microscope study of plastic deformation mechanism of titanium alloy AT4 and fatigue strain mechanism in coarse grained specimens of alloy T-40 07 p1205 A67-19278

Plastic deformation and fracture of rotating turbine rotor model 09 p1502 A67-21554

Fracture behavior of creep resistant alloy steel and nickel-chromium alloy subjected to cyclic loading at elevated temperatures 09 p1517 A67-21556

External dislocation effect on conditions for complete fracture from coplanar wedge shaped crack in presence of applied stress 16 p2765 A67-30996

Fracture in viscoelastic bodies, considering stress-strain-time properties and analyzing temperature and failure envelopes 16 p2694 A67-31313

Pressurization produced free dislocations effect on yielding and fracture in bcc metals 18 p3063 A67-33484

Radiological findings from pilots afflicted with vertebral fractures from ejection injuries 21 p3575 A67-38510

FRACTURE MECHANICS

SA GRIFFITH FRACTURE THEORY

Electron microscopy study of fracture surface topography permitting identification of fine scale fracture surface features, relating them to fracture formation mechanisms [AIAA PAPER 66-814] 01 p0077 A67-10034

Time evolution of laser induced fractures in glass, noting crack propagation accompanied by sparking 02 p0253 A67-12508

Fracture mechanism of transparent crystals interacting with ruby laser beam 03 p0435 A67-13128

Micromechanical behavior of composite materials under static tension, bending, shear and fatigue loading investigated analytically and experimentally 03 p0455 A67-13440

Brittle fracture of Be tube under differential thermal contraction-induced plastic strain 03 p0445 A67-13470

Fracture surfaces, Wallner lines and crack propagation velocity in precracked W monocrystals at 20-300 degrees K 03 p0445 A67-13471

Work of fracture and measurement in metals, ceramics and other materials 03 p0525 A67-13872

Fracture mechanism in continuous filamentary composites 04 p0641 A67-14832

Stresses in infinitely long strip of finite width containing semiinfinite crack calculated for displaced clamped boundaries, using Wiener-Hopf technique 04 p0718 A67-15923

Brittle fracture crack theory for elastic body weakened by initially wide crack 05 p0923 A67-17179

Electron microscopy analysis of dissolved hydrogen induced fracture in room temperature cantilever bend fatigue testing of dispersion strengthened aluminum-aluminum oxide alloy 06 p1013 A67-17796

Tensile tests performed on alpha titanium between -321 and 75 degrees F, discussing ductile-to-brittle transition, microcrack formation and brittle fracture mechanics 06 p1014 A67-17807

Heat treatment and microstructural observations in wrought Ni-base superalloy Udmet 700 in static creep, determining fracture and deformation properties 06 p1015 A67-17809

Ultrahigh vacuum effects on flow and fracture behavior of molybdenum 06 p1016 A67-17897

Yielding and brittle cracking of orthotropic strip, using Wiener-Hopf technique and asymptotic method for isotropic case 06 p1102 A67-18317

Fracture mechanism for formation of dimpled fracture surface morphology 06 p1105 A67-18562

Delayed fracture and brittle properties of titanium alloys 07 p1207 A67-19293

Surface defects effect on mechanical properties of sheet metal under tension and bending, tracking brittle fracture to stress concentrators 07 p1263 A67-19751

Book on strength of materials covering energy density, plastic flow deformations, friction heating and fracture mechanisms 08 p1414 A67-20307

Structural design of solid propellant rocket engine and failure, deformation and fracture of reinforced propellant grains 08 p1420 A67-20888

Fracture of viscoelastic bodies, predicting statistical variability of rupture data for uniform and nonuniform excitation histories 08 p1421 A67-20913

Energy balance criteria during slow crack growth and at inception of catastrophic rupture in high strength ductile metals, noting necking phenomena in tensile test 08 p1421 A67-20953

Fracture initiation at low stress concentration, noting effect of energetic conditions and independence of plastic zone length from applied stress and defect length 08 p1421 A67-20955

Materials failure laws based on combined analysis of cracks and fractures 09 p1575 A67-22166

Stress field near surface of elastic solid during short time interval when heat flow occurs analyzed through strain theory for fracture location and probability 09 p1576 A67-22422

Axisymmetric crack formation problem in elastoplastic material including energy dissipation and face displacement calculations, noting agreement with Griffith theory 10 p1716 A67-22939

Fracture initiation in sheet specimens, noting correlation of crack-opening displacement and fracture toughness and dependence on applied stress 10 p1718 A67-23172

Electron microscopy study of fracture surface topography permitting identification of fine scale fracture surface features, relating them to fracture formation mechanisms [AIAA PAPER 66-809] 10 p1661 A67-23552

Fracture process in composite films of stressed tetrafluoroethylene and fluorinated ethylene-propylene 10 p1672 A67-23746

Fracture criterion from application of energy principle to elastic plastic crack model, showing positive nature of energy change during

propagation 10 p1730 A67-23829

Fracture line formation in glass specimen as result of laser beam focusing, noting refractive index variation 12 p1951 A67-25148

Book on fracture of structural materials covering relation between design and fracture occurrence, fracture types, fracture resistance testing, etc 12 p2013 A67-25362

Ductile fracture with rotation under shear and normal stresses, noting relationship between fracture strain and stress state for given inclusion content [ASME PAPER 67-MET-9] 12 p1956 A67-25950

Brittle fracture at grain boundaries in samples of electron-beam molybdenum prepared by forging in air after extrusion 13 p2130 A67-26447

Ductile failure initiation by fractured carbides in austenitic stainless steel 13 p2133 A67-27008

Cryogenic fracture toughness behavior 13 p2220 A67-27671

Treatise on adhesion and adhesives, Volume 1, Theory 14 p2340 A67-27793

Brittle strength of orthotropic materials investigated for proposed phenomenological fracture condition 14 p2399 A67-28103

Hydrogen influence on fracture propagation of titanium alloy during tension tests 14 p2337 A67-28286

Metal matrix composite fatigue behavior in tension-tension loading as function of volume fraction reinforcements 14 p2337 A67-28422

Fracture concept for two-phase structures analyzed on basis of crack-tip displacement, discussing macro-and microstructural cases 14 p2400 A67-28424

Agreement of crack extension criteria of Griffith and Barenblatt, considering cohesive forces 15 p2504 A67-30093

Periodically fluctuating loading fracture propagation analysis with damage summation principle in stress and cracking time terms, deriving differential equation for fracture length 15 p2576 A67-30183

Westergaard method of crack analysis extended for crack problems within infinite medium with cracks under applied loads at infinity 16 p2765 A67-30995

Fracture - Conference, Sendai, Japan, September 1965, Volume 1 fracture - Conference, Sendai, Japan, September 1965, Volume 1 16 p2767 A67-31275

Plastic behavior of material continua in terms of Riemannian and non-Riemannian differential geometry 16 p2767 A67-31276

Physical state of material analyzed using non-Riemannian plasticity theory 16 p2768 A67-31278

Bubble raft analog for analyzing short range repulsive forces at small strains that govern fractures 16 p2768 A67-31279

Crack problems analyzed using Tresca yield conditions to obtain continuous distributions of dislocations 16 p2768 A67-31280

Effect of defects distribution on behavior of steel structures analyzed for plastically relaxed model of slit 16 p2768 A67-31282

Fatigue crack analysis via Bilby, Cottrell and Swinden crack theory, noting inadequacy of energy criterion 16 p2769 A67-31283

Interaction between elastic cracks, dislocation cracks and slip bands describing various characteristics of each case 16 p2769 A67-31284

Fracture stresses of cracked plates and flow stresses of polycrystalline aggregates as related to stresses and strains at ends of plano-discontinuities 16 p2769 A67-31285

Crack extension and propagation experiments defining plane-stress regime and providing rationale for Dugdale-Muskhishvili model, noting stress-strain relations 16 p2769 A67-31286

Elasto-plastic stresses and strains in cracked plates analyzed by numerical method, noting stress singularities and stress-strain fields 16 p2769 A67-31287

Plastic yielding near crack tip, noting general solution for deformation and stress distributions for various loads 16 p2769 A67-31288

Fracture mechanics energy balance analysis using Griffith type fracture criterion 16 p2770 A67-31289

Fatigue crack propagation in thin plates under fluctuating plane extension and

cylindrical bending 16 p2770 A67-31290

Craggs propagating crack model extended to general elastic anisotropy deriving general theory for tensile or shear stress fracture propagation 16 p2770 A67-31291

Hilbert boundary problem extension for flexural problems of cracks in mixed media, noting Cauchy integrals, Plemelj formulae, etc 16 p2770 A67-31292

Ductile fracture depending on stress/strain history and material element rotation relative to stress/strain axes proposed for asymmetrically notched specimens 16 p2770 A67-31293

Fracture theory statistical models, static and stochastic approach 16 p2771 A67-31294

Electron fractography and analytical fracture mechanics application to fatigue crack propagation, noting stress-intensity-factor role 16 p2771 A67-31296

Cycles required to start crack, and cycles for crack propagation to failure estimated for notched specimen 16 p2771 A67-31297

Fracture - Conference, Sendai, Japan, September 1965, Volume 2 16 p2771 A67-31298

Fracture surface markings and topography for transgranular and intergranular paths studied with electron microscope 16 p2772 A67-31300

Fracture surface topography related to micro-and macro-mechanics of fracture for plastic, cleavage and fatigue cases 16 p2772 A67-31301

Fracture surface appearance and crack propagation velocity variation with stress and temperature in tungsten 16 p2688 A67-31302

Tensile and torsional fracture of low carbon steel at cryogenic temperatures, studying temperature and stress gradient effect 16 p2689 A67-31309

Griffith initiation criterion extended to fracture initiation and growth in viscoelastic materials using energy formulation 16 p2773 A67-31311

Time dependent fracture of viscoelastic materials, considering defect initiation relation as approximation to crack growth history 16 p2773 A67-31312

Fracture - Conference, Sendai, Japan, September 1965, Volume 3 16 p2773 A67-31314

Internal fracture of solids analyzing initiation by converging tensile pulses in prolate spheroid and crack propagation in infinite solid 16 p2773 A67-31315

Fatigue in quasi-brittle materials, fatigue in creep range at elevated temperatures and cumulative fatigue 16 p2774 A67-31316

Fatigue crack growth rates in metals under random loading correlated to cyclic load tests 16 p2774 A67-31320

Metal fatigue studied with X-ray diffraction technique 16 p2774 A67-31322

Plastic energy dissipation rate at onset of rapid crack growth for predicting biaxial fracture 16 p2775 A67-31324

Transient analysis of displacement, strain and stress fields around running crack tip in epoxy plate with central notch using Moire method 16 p2775 A67-31325

Low strain rate and temperature effects on crack initiation and growth, recovery and boundary migration for Al and Al alloy 16 p2689 A67-31368

Physical basis of yield and fracture - Conference, Oxford, England, September 1966 16 p3062 A67-33481

Polymer fracture mechanism hypothesized as competition between localized hardening by molecular orientation and localized softening during deformation 18 p3068 A67-33488

Free radical formation correlated with breaking time and creep rate in solid polymers subject to crushing, breakdown and deformation 18 p3068 A67-33490

Plasticity and brittle fracture conditions combined for stability criteria derivation 18 p3144 A67-34174

Electron fractography applied to fatigue studies of fracture appearance, morphology of striations and fracture surface microdetails [ASTM PAPER 42] 18 p3068 A67-34580

Integrodifferential equations for product surface area changes and grinding process development obtained by assuming proportionality between fracturing

probability and particle size 19 p3236 A67-35725

Critical loading for crack propagation in structures weakened by holes 19 p3344 A67-35847

Tensile properties of fiber-reinforced metals, discussing failure at notch root 20 p3464 A67-36417

Circumferential crack in pressurized cylindrical shell analyzed for extensional and bending components of stresses 22 p3911 A67-39678

Fracture theory for amorphous high polymers below glass transition temperature, considering viscoelastic effects on structural defect stress concentration 22 p3824 A67-39740

Safety design for high strength low toughness materials assumed to have hidden flaws, formulating stress intensity factor for fracture mechanics 22 p3913 A67-39982

Fracture behavior of laminar steel composites studied to determine effect of interfacial properties on crack propagation 22 p3822 A67-40056

Homogeneous isotropic elastoplastic thin flat plate under uniform unidirectional stress, studying plastic flow, fracture, distortion and slip plane inclination 22 p3915 A67-40220

Parallel contours of fracture surface at optical magnifications obtained by method based on microhardness indentations 22 p3823 A67-40300

Change in brittle fracture work during combined impact and tensile load of polymer noting variation according to maximum law 23 p4072 A67-40595

Kinetic approach to fatigue investigation in calculation of cyclic lifetime from static test data 23 p4074 A67-40663

Fracture in engineering design in terms of fracture mechanics 23 p4076 A67-40696

Cleavage, plastic, creep, fatigue and other types of fracture noting initiation, propagation, mode, behavior, microstructure and appearance 23 p4019 A67-41033

Crack stability for fracture of nonworkhardening elastoplastic material in plane strain or plane stress, using energy criterion 23 p4078 A67-41162

Thin boundary problems of bimaterial plates bonded along circular arcs behaving like crack imperfections under bending, using fracture mechanics to predict failure 23 p4078 A67-41164

Infinitesimal dislocation theory applied to materials with cracks and cylindrical hole, straight boundary between bonded materials and cylindrical insert subject to antiplane shearing stress 23 p4078 A67-41165

Probable failure mode and minimum service life prediction for spacecraft pressure vessels using fracture mechanics analysis and fracture specimen test results [ASM PAPER C6-2.3] 23 p4079 A67-41408

Fatigue fracture surface macroscopic and microscopic appearance as affected by prevailing stress intensity conditions at moving crack tip 24 p4170 A67-41946

Fatigue crack propagation in ultrahigh strength steels, noting rate sensitivity to moisture and plane strain fracture toughness 24 p4171 A67-41953

FRACTURE RESISTANCE

Stress required for brittle fracture of alumina at room temperature based on theory of dislocation movement of cracks 01 p0092 A67-10054

Stress concentration in annular rotor with notch /or crack/ on inner surface, using integral equation 01 p0159 A67-10276

Fatigue cracks and fatigue cycles effect on brittle fracture behavior of annealed 4140 steel [ASME PAPER 66-WA/MET-17] 04 p0639 A67-15332

Short-time tensile and long-time creep rupture properties of HK-40 alloy and type 310 wrought stainless steel from room temperature to 2000 degrees F [ASME PAPER 66-WA/MET-2] 04 p0639 A67-15344

Brittle fracture threshold of silicon, germanium and indium antimonide under pulsed electron irradiation 04 p0685 A67-15694

Effect of structure of beta titanium alloy on crack propagation resistance 04 p0641 A67-15985

Stress waves reflection and transmission

in composite laminates and parameters affecting ability to resist fracture by hypervelocity impact [AIAA PAPER 67-140] 06 p1102 A67-18289

Atmospheric nitrogen contamination effect on tensile creep of chromium-tantalum alloys 06 p1018 A67-18369

Printed circuit board manufacturing process assuring crack-free plated-through hole 08 p1304 A67-21190

Long time mechanical and thermal stability of polymeric materials predicted from accelerated testing at increased relations 10 p1672 A67-23743

Conical shell stability under hydrostatic pressure for various in-plane boundary conditions, stressing axial restraint effect 11 p1873 A67-24214

Nickel-base alloy static and dynamic creep test, examining fatigue zone fracture surface 11 p1806 A67-24364

Book on fracture of structural materials covering relation between design and fracture occurrence, fracture types, fracture resistance testing, etc 12 p2013 A67-25362

Push-pull low endurance fatigue of En 25 and En 32B steels at 20 and 450 degrees C 12 p2015 A67-25422

Strengthening of sapphire single crystals by precipitates containing titanium 12 p1987 A67-26190

Texture strengthening and fracture toughness of titanium alloy sheets biaxial stress fields at room and cryogenic temperatures 13 p2142 A67-27442

Effect of structure of beta titanium alloy on crack propagation resistance 14 p2338 A67-28488

Cross slip and slip character related to fatigue, brittle fracture and strain hardening in crystal solids 16 p2772 A67-31299

Energy necessary for fracture shown independent of lattice defects by low cycle fatigue tests at constant true mean stress amplitude 16 p2774 A67-31318

High pressure hydrogen environment effects on mechanical properties of steels at high temperatures 16 p2689 A67-31327

Sapphire whiskers mechanical behavior obtained by static tension testing 16 p2694 A67-31523

Parameters governing high resistance of reinforced resins, stressing elastomechanical equilibrium at interface [ONERA-TP-468] 18 p3069 A67-34462

Structural section bending determined for fracturing tolerance 18 p3144 A67-34484

Chemical polishing effects on sapphire whisker strength, obtaining correlation between fracture strength and whisker diameter 20 p3473 A67-36480

Cross-wire resistance welded metal joints for aerospace electronic packing assemblies, investigating embedment, mechanical strength and materials evaluation 21 p3635 A67-38629

Thermal stress fracture of brittle ceramics studied for effect of relaxation by creep at high temperature under conditions of quasi-static heat flow 22 p3915 A67-40386

High strength aluminum alloy panel resistance to fatigue crack propagation, discussing axial load fatigue machine 24 p4170 A67-41949

FRACTURE TOUGHNESS

Titanium alloy forging tests covering notched tension, compression, shear, bearing, fracture toughness and smooth and axial fatigue 03 p0446 A67-13552

Fracture toughness and critical defect sizes with welds of 18 percent nickel maraging steels 03 p0446 A67-13554

Biaxial fracture strength of textured titanium alloy for design of liquid fuel tankage 04 p0711 A67-15242

Moisture effect on slow crack propagation in thin sheets of SAE 4340 steel under static and cyclic loading [ASME PAPER 66-WA/MET-6] 04 p0639 A67-15340

Numerical analysis of crack propagation in cyclic loaded structures, taking into account load ratio and instability at onset of fast fracture [ASME PAPER 66-WA/MET-4] 04 p0711 A67-15342

Statistical dislocation theory of crystal brittle fracture seen as stochastic process with microcrack formation and propagation under plastic deformation 05 p0919 A67-18504

Side grooving effect on measurements of plane strain fracture toughness 05 p0922 A67-17086

Plane strain fracture toughness, strain instability, slow crack growth and different modes of cracking in metal alloys 06 p1014 A67-17806

Fracture behavior of Ti alloys in aqueous environment, noting process to increase fracture toughness 08 p1340 A67-20364

Mechanical behavior of fiber reinforced materials, discussing elastic properties, failure theories, stress analysis, fracture toughness, structural design, etc 08 p1342 A67-20904

Reformation processes effect on stress-time-to-fracture behavior of solids, considering governing differential equation 08 p1423 A67-21302

Fracture initiation in sheet specimens, noting correlation of crack-opening displacement and fracture toughness and dependence on applied stress 10 p1718 A67-23172

Thermal mechanical treatments influence on strength, toughness and environmental failure resistance of low alloy high strength martensitic steel 11 p1806 A67-24363

Double cantilever beam specimen for determining plain strain fracture toughness of metals 12 p1956 A67-25946

Fracture toughness of 7075-T6 and -T651 sheet, plate and multilayered adhesive bonded panels, showing independence of thickness and number of layers [ASME PAPER 67-MET-4] 12 p1956 A67-25948

Pressure vessel design with ultrahigh strength steels, material strength variations, fracture toughness, minimum defect size and materials melting and fabrication practice [ASME PAPER 67-MET-18] 12 p2031 A67-25954

Cryogenic fracture toughness behavior 13 p2220 A67-27671

Evaluating mechanical and corrosion suitability of materials [ASME PAPER 67-DE-7] 14 p2339 A67-28866

Design considerations in material selection for rocket motor cases, considering fracture toughness, ductile-failure resistance and buckling under flight loading [AIAA PAPER 66-630] 15 p2573 A67-29418

Mechanical strength of medium formulated as microscopic behavior in continuum obtaining time-dependent macroscopic fracture strength 16 p2771 A67-31295

Crack resistance properties of high strength aluminum alloys, noting test results on fracture toughness enhancement 16 p2688 A67-31308

Microstructural features of Ni maraging steel weldments related to fracture toughness properties 16 p2692 A67-31868

Alloys for failure-safe structures tested, determining fracture toughness, fatigue strength and stress-corrosion cracking resistance 17 p2875 A67-33048

Statistical dislocation theory of crystal brittle fracture seen as stochastic process with microcrack formation and propagation under plastic deformation 20 p3541 A67-37318

Electron beam welded D6AC steel plates evaluated after heat treated condition /stress relief/ for mechanical properties 20 p3456 A67-37695

Stress rupture strength and durability of elastic materials 22 p3824 A67-39221

Crack line loading methods for measuring fracture toughness noting advantages over remote loading test procedures 22 p3820 A67-39630

Crack opening displacement and fracture toughness analyzed for uniaxial tension and edge-cracked plate 22 p3911 A67-39681

Hot rolling finishing temperature and cooling rate effects on aged 250 grade 18 Ni maraging steel fracture toughness 22 p3822 A67-40057

High structural efficiency of aircraft materials emphasizing fatigue characteristics, fracture toughness and corrosion resistance 22 p3823 A67-40332

Double cantilever beam /DCB/ specimen for fracture toughness testing, discussing elastic strain energy release rate and load and crack length extension relation 23 p4018 A67-40928

Probable failure mode and minimum service life prediction for spacecraft pressure vessels using fracture mechanics

analysis and fracture specimen test results [ASM PAPER C6-2.3] 23 p4079 A67-41408
 Shear spun 300-grade maraging steel evaluated for pressure vessel applications, discussing fracture toughness [ASM PAPER C6-2.4] 23 p4020 A67-41412
 Fracture-toughness tests described to obtain fracture data for transformation into allowable design stresses 23 p4079 A67-41413
 Fracture toughness and stress corrosion cracking of titanium alloy weldments indicating resistance differences between base metal and weldment 24 p4161 A67-42329
 Aluminum alloy sheet welds with high silicon and magnesium content analyzed for tensile properties and fracture toughness 24 p4161 A67-42330

FRAGMENTATION

Structural sensitivity of plastic properties of molybdenum alloys produced by electron beam fusion, investigating microstructure, failure in bending tests and grain fragmentation 01 p0101 A67-10936
 Instability of gravitating slipstreams or mixed streams and cloud fragmentation of interstellar gas 03 p0511 A67-13877
 Divergence of fragments of force-free gas-filled vessel exploded in vacuum 04 p0708 A67-14793
 Helium isotope formation in cosmic rays during light nuclei fragmentation due to high energy proton interaction 05 p0878 A67-16093
 Observed meteor luminosity and deceleration compared with theoretical values 05 p0889 A67-16209
 Frangible sounding rocket vehicle and explosive fragmentation system, determination of impact kinetic energy of fragments and flight tests 08 p1407 A67-20521
 Number of fragments in meteor fragmentation 13 p2197 A67-28500
 Frangible sounding rocket vehicle and explosive fragmentation system, determination of impact kinetic energy of fragments and flight tests 15 p2565 A67-29449
 Fragmentation parameters of multicharge component of heavy cosmic ray nuclei on emulsion hydrogen 17 p2936 A67-32251
 Structural sensitivity of plastic properties of molybdenum alloys produced by electron beam fusion, investigating microstructure, failure in bending tests and grain fragmentation 22 p3820 A67-39790
 Hazards of rocket launching noting propellant toxicity, airborne fragmentation, inadvertent ignition and nuclear radiation 22 p3900 A67-39884
 Rotation and pressure gradient effects on gravitational instability of collapsing gas clouds, discussing subsequent fragmentation 22 p3893 A67-40501
 Collapsing gas cloud noting instability for density fluctuations, rise of turbulence and fragmentation phenomena 22 p3895 A67-40516
 Fragmentation and excess angular momentum problems in star formation theories, examining relevance to simplifying assumptions and physical situation 22 p3895 A67-40517
 Helium isotope formation in cosmic rays during light nuclei fragmentation due to high energy proton interaction 24 p4213 A67-42769

FRAME
SA AIRFRAME
SA GRID

Axisymmetric deformation of cylindrical shell reinforced by frames located at arbitrary distance from each other and having different geometrical and elastic characteristics 03 p0530 A67-14171
 Straining equipment for testing aircraft structures 04 p0708 A67-14584
 Two contact problems involving cylindrical shells reinforced with elastic frames 04 p0717 A67-15889
 PCM frame synchronization with self-varying threshold detector 11 p1764 A67-24434

FRAME PHOTOGRAPHY

Optimum frame frequency and virtual exposure coefficient determination for high-and superhigh-speed cameras 01 p0067 A67-10831
 Optimization of size of film negative for aerial cameras on grounds of economic efficiency 02 p0240 A67-11532
 Frame camera for high speed aerial

photography, discussing interlacing with advances in other areas 05 p0806 A67-16700
 Analytical reduction of panoramic and strip photography to equivalent frame photography 15 p2486 A67-29299

FRAMING CAMERA

High speed cameras with image converter tubes noting electrical circuits 01 p0067 A67-10774
 Framing cameras of rotating mirror type, discussing optical principles used in American, British and Russian high speed cameras developed since original NACA camera 03 p0419 A67-13229
 Framing cameras of rotating mirror type, discussing optical principles used in American, British and Russian high speed cameras developed since original NACA camera 05 p0806 A67-16699

FRANCE

Geodetic linking of France and North Africa by synchronous photographs of Echo I satellite 07 p1176 A67-19767
 Future French Air Force combat aircraft limited to Mirage F-III or Franco-British Jaguar project variable geometry types 10 p1595 A67-23621
 French optical satellite observation network 14 p2270 A67-28589
 Geos satellite observational technique in France 19 p3182 A67-35237
 French space program research on ionospheric plasma, wave emissions, wind velocity, etc 19 p3320 A67-35290
 Space electronics in France, role in boosters, control, communication, onboard systems, etc 20 p3399 A67-36879

FRANCK-CONDON FACTOR

Franck-Condon factors and transition probabilities of electron oscillatory transfers in diatomic molecules 03 p0471 A67-13314
 Franck-Condon factors and r centroids for C-X band system of astrophysically important zirconium oxide molecule found in S type stars 08 p1354 A67-20702
 Condon loci geometry of molecular spectrum determined by plotting intensities on Deslandres diagram 10 p1681 A67-22959
 Franck-Condon factors and transition probabilities of electron oscillatory transfers in diatomic molecules 16 p2703 A67-30490
 Electronic states and transitions of zirconium oxide, noting Franck-Condon factors and r centroids, calculated from Morse model 16 p2704 A67-31173
 Partial Franck-Condon factors and r centroids for zirconium oxide molecule, noting transition probabilities 16 p2704 A67-31174
 Photoelectron energy measurement and Franck-Condon factors for vibrational transitions of molecular ions when ejected by He resonance line 17 p2888 A67-32356

FRAUNHOFER LINE
SA PHOTOSPHERE

Space bandwidth theorem for Fresnel and Fraunhofer holograms, taking into account effects of photographic film 01 p0071 A67-11083
 Comet spectra observation noting emission band abundance, atomic lines presence and continuous spectrum with solar Fraunhofer lines 05 p0890 A67-18337
 Observational techniques and detection of solar turbulence by local Doppler shifts of Fraunhofer lines 05 p0899 A67-17069
 Interpretation of profiles of middle strength Fraunhofer lines, especially strontium resonance line of microturbulence above hydrogen convection zone 05 p0899 A67-17072
 Deformation of Fraunhofer line linked to sound waves in solar disk 05 p0900 A67-17076
 Differential residual displacements of Fraunhofer lines in solar spectrum 05 p0901 A67-17116
 Fraunhofer hologram process when illumination is partially coherent quasi-monochromatic radiation 09 p1493 A67-21589
 Source function, distribution function, damping constant, etc, determined from high resolution Fraunhofer line profiles in solar or stellar spectra 10 p1711 A67-23797
 Generalized integro-exponential weighting functions allow accurate computations of Fraunhofer lines in solar intensity/stellar flux spectra 11 p1859 A67-24113
 Center-to-limb variations for continuum, faint iron lines and core of strong Fraunhofer lines measured along polar and equatorial diameters of solar

disk 11 p1861 A67-24492
 Solar continuous spectrum observations indicating limb darkening around 2500 angstroms, using optical system mounted on Veronique rocket 12 p2007 A67-25820
 Photoelectric observation of Fraunhofer line profiles by high dispersion solar spectrograph 13 p2198 A67-26706
 Identification of forbidden nitrogen IR multiplet in Fraunhofer spectrum 14 p2382 A67-27848
 Nitrogen presence in solar material, using measurements of high resolution spectrophotometric record of Fraunhofer spectrum [AFCRL-67-0479] 15 p2554 A67-29511
 Distinction between macro-and microturbulence in solar photosphere studied from line profiles 17 p2944 A67-32641
 Corona observation within one solar radius of photosphere, identifying emission lines and explaining continuous spectrum and Fraunhofer lines reduced depth 19 p3318 A67-35055
 Solar magnetic fields studied by measuring Fraunhofer line shifts with circular-polarization analyzer, showing relationship to gravity center 19 p3325 A67-35505
 Fabry-Perot interferometer improvements for high resolution rocket photography of solar Fraunhofer spectrum 20 p3440 A67-36359

FREDHOLM INTEGRAL EQUATION
 Velocity distributions at blade profiles in two-dimensional model of axial stage treated by numerical solution of Fredholm integral equations 01 p0006 A67-10525
 Analytical and p-analytical functions of complex variable used to solve three-dimensional axisymmetric problems in elasticity theory 02 p0338 A67-11967
 Forced periodic vibrations of homogeneous isotropic uniformly thick plate with free edges reduced to Fredholm integral equation 03 p0524 A67-13624
 Torsion of infinite hollow cylinder with axially symmetric load, discussing deformations in terms of integral equations 03 p0529 A67-14164
 Book on main linear boundary value problems for second order linear partial differential equations and systems of such equations satisfying 04 p0645 A67-15006
 Antenna synthesis for wide band radiation reception using Fredholm integral equation 05 p0774 A67-16912
 Numerical solution of Fredholm integral equation of second kind with real analytic and periodic functions, noting eigenvalues 07 p1216 A67-19883
 Stress-strain state inside elastic quarter space activated by periodic or local normal loads at interfaces 07 p1264 A67-20221
 Monograph on integral equations covering Fredholm and Volterra equations, applications to theory of differential equations, properties of Cauchy type integrals, etc 08 p1348 A67-20761
 Fredholm integral equation system for magnetic currents induced on wedge under impedance boundary condition 08 p1295 A67-21273
 Two-dimensional problem for layer with mixed boundary conditions, obtaining solutions for Fredholm integral equations and relations for temperature distribution 09 p1580 A67-21994
 Dual integral equation and dual series analysis and application to mixed boundary value problems in elasticity, hydrodynamics and electrostatics 11 p1812 A67-24150
 Dual integral equations in elasticity theory, noting Mehler-Fok transformation of spherical functions, Fredholm equation and application to mixed boundary value problems 11 p1812 A67-24151
 Optimum control integral criterion function for class of distributed parameter systems subject to control signal saturation 11 p1770 A67-24890
 Solving three-dimensional electrodynamics problems with mixed boundary values by reduction to standard Fredholm integral equation 15 p2522 A67-29196
 Antenna synthesis for wide band radiation reception using Fredholm integral equation 16 p2636 A67-30889
 Book on variational calculus and integral equations, examining extremum conditions,

Fredholm and Volterra integral equations, Pontryagin maximum principle, etc 16 p2696 A67-31200

Coaxial and magnetohydrodynamic waveguide matching obtaining reflection coefficient of former and wave amplitude of latter 16 p2722 A67-31575

Sokolov method of averaging functional corrections for treatment of radiant interchange between surfaces 17 p2967 A67-32068

Mixed boundary value problem for x-analytic function solved through Fredholm integral equation of second kind 17 p2879 A67-32872

Boundary value problem solution for three-dimensional layer in axisymmetric case 17 p2885 A67-32882

Torsion of finite elastic cylindrical rod welded to elastic half-space [ASME PAPER 67-APM-30] 17 p2965 A67-33156

Analytical and p-analytical functions of complex variable used to solve three-dimensional axisymmetric problems in elasticity theory 17 p2966 A67-33284

Algorithm for Fredholm type integral equation solution incorporating successive approximations, kernel replacement by degenerate kernel, averaging functional corrections and band methods 18 p3071 A67-34167

Functional sensitivity to cavitation of hydrofoil cascade, solving Fredholm type integral equations 20 p3419 A67-36188

Successive approximation and Chebyshev uniform approximation method for solving Fredholm integral equation 21 p3651 A67-37904

Runge-Kutta method applied to Fredholm type integrodifferential equations 21 p3653 A67-38421

Surface temperatures of two rubbing bodies and heat partition between them determined numerically, using Fredholm integral equation solution 21 p3638 A67-39091

Fredholm equation solution and minlmax theory for p-dimensional vector signal detection against p-dimensional Gaussian noise background 22 p3762 A67-39876

Cylindrical tube current distribution determined by digital computer solution of Fredholm integral equations 23 p3981 A67-41208

FREE ATMOSPHERE

Aircraft bumpiness conditions in free atmosphere relation to turbulence and other aerological data 02 p0263 A67-12647

Measurement techniques used in wind tunnel and free atmosphere parachute tests 06 p0979 A67-18017

Assessment of available methods for direct measurement of radiative heat influx in free atmosphere 07 p1172 A67-19458

Stratospheric free air turbulence detection from slant-range FPS-16 radar tracked Jimsphere balloons 10 p1676 A67-22815

Clear air turbulence power spectra in free atmosphere near jet stream level, discussing CAT generation 15 p2513 A67-30058

Vertical distribution of cloud condensation nuclei in free atmosphere investigated by flow type onboard photoelectric apparatus to calculate washout coefficients 24 p4181 A67-42163

FREE BOUNDARY

Free boundary problem for parabolic equation proving existence and uniqueness theorems for certain initial conditions 02 p0258 A67-11626

Boundary bending conditions for anisotropic plates with free, hinged or rigidly clamped edge 03 p0531 A67-14200

Numerical analysis of free boundary problem inviscid incompressible flow field of impinging jet and two-dimensional Joukowski airfoil in sheared wind tunnel flow [AIAA PAPER 67-217] 06 p0988 A67-18460

Free boundary flows of viscous liquid, analyzing Stokes flow at zero Reynolds number 06 p0990 A67-18641

Shock wave incident on unknown free boundary surface calculated in spatial method of characteristics 07 p1125 A67-19141

Shock wave incident on unknown free boundary surface calculated in spatial method of characteristics 17 p2840 A67-33213

A priori bound on difference between free boundary positions in two Stefan problems derived in terms of initial conditions and heat influxes 18 p3071 A67-33664

Magnetospheric free boundary representation synthesis problem, discussing relaxation solution, dipole moment and stream direction 22 p3854 A67-40347

Plane problems with contained elastoplasticity, considering thin plates with small apertures as free boundary problem in continuum mechanics 23 p4077 A67-40754

FREE CONVECTION

Hydrodynamic stability equations for free convection flow over vertical uniform flux plate 01 p0055 A67-11189

Free convective boundary layer flows of electrically conducting fluid in transverse magnetic field 03 p0481 A67-13734

Combined free and forced convection over electrically insulating vertical plate of constant temperature with transverse magnetic field with plate moving up or down [ASME PAPER 66-WA/HT-38] 04 p0724 A67-15429

Laminar free convection of radiation absorbing-emitting fluid along flat plate noting interaction effects, solving problem by singular perturbation 04 p0727 A67-15682

Two-dimensional transient laminar natural convection heat transfer in partially filled liquid propellant tanks, solving vorticity and energy equations 04 p0731 A67-15826

Axial temperature and velocity measurements made in water at various aspect ratios, Grashof number and bottom-to-side heat flux ratios for turbulent free convection in closed container 04 p0731 A67-15827

Free convective heat transfer measurements of sodium boiling on surface of horizontal tube 04 p0736 A67-15860

Boiling Na free and forced-convective heat transfer rates, surface temperature and pool-boiling heat-transfer coefficient measurements 04 p0737 A67-15861

Nonsimilar free convection boundary layer from vertical flat plate with step discontinuities in surface temperature [ASME PAPER 66-WA/HT-17] 04 p0739 A67-15930

Steady free convection in porous medium heated from below and accounting for end effects and mass discharge 06 p1113 A67-18127

Free convective heat transfer between hot and cold rotating disks in laminar steady azimuthally symmetric flow in zero-gravity field 06 p1119 A67-18864

Linear theory solution of eigenvalue problem for natural convection in horizontal layers giving characteristic Rayleigh numbers for first ten modes 08 p1427 A67-21139

Normalization technique for analysis of heat transfer, considering thermal entrance length, ablation and tektite problems 10 p1732 A67-22931

Liapunov-Schmidt method combined with topological method show secondary flows formed after stability loss 10 p1734 A67-23673

Surface film boiling under free convection 13 p2222 A67-26532

Dimensional analysis of heat transfer correlations for nucleate boiling in free convection, including critical heat flux conditions 14 p2408 A67-28932

Flat plate, simultaneous heat and mass transfer for Newtonian fluids in free convection analyzed, using group theory 15 p2582 A67-30217

Free convection oscillatory flow from horizontal plate having periodic temperature variations analyzed for LF and HF ranges 17 p2969 A67-32445

Numerical methods for calculating pseudoadiabatic characteristics of saturated air parcels 17 p2879 A67-32549

Temperature convection and vertical velocity fluctuations measured and compared with similarity theory of free convection and laboratory heated plates 19 p3252 A67-35059

Simultaneous heat and mass transfer in laminar free convection boundary layer at vertical surface with moving interface 19 p3346 A67-35613

Natural convection in finite nonzero length vertical channels, using integral technique to derive results for two wall conditions [ASME PAPER 67-HT-16] 20 p3545 A67-36712

Local heat transfer coefficients, mean temperature and velocity distributions in

turbulent natural convection boundary layer on vertical plane surface [ASME PAPER 67-HT-17] 20 p3545 A67-36713

Free convection effect on forced laminar flow of water in horizontal tube with uniform heat flux and velocity profile fully developed [ASME PAPER 67-HT-52] 20 p3548 A67-36734

Nonconstant gravity field effect on free convective heat transfer to or from isothermal flat plate [AICHE PAPER 2] 20 p3552 A67-36825

Free convection of conducting fluid in coupled vertical channels for case of steady motion with lateral heating 20 p3500 A67-37051

Liapunov-Schmidt method combined with topological method show secondary flows formed after stability loss 21 p3731 A67-38274

Laminar free convection of absorbing emitting gas analyzed in region of stagnation point of horizontal cylinder 22 p3920 A67-40418

Free thermal convection in axisymmetric rotating cavities 24 p4255 A67-42588

FREE ELECTRON

Fermi surface curvature of indium single crystals measured from RF size effect at reference point 01 p0133 A67-10742

Possible major effect of minor neutral constituents of mesosphere on free electron density in D layer 10 p1645 A67-23265

Fermi surface curvature of indium single crystals measured from RF size effect at reference point 13 p2176 A67-26771

Nonequilibrium states in metal-to-semiconductor junction resulting from emission of high energy holes and hot free electrons in same direction 13 p2176 A67-26861

Band structure of spinel-type semiconductors calculation, applying model potential to nearly free electron model 13 p2181 A67-27166

Ionospheric D layer structure and formation, considering free electron height variation and collision rate 14 p2311 A67-28406

Sporadic E layer scintillation effects on amplitude of 137 MHz radio waves from Early Bird 14 p2270 A67-28577

One-dimensional propagation of stable negative-resistance domains for carriers interacting with single type of impurity level 16 p2727 A67-30852

Point charges interaction energy in semiconductor thin film 18 p3101 A67-34091

Hamiltonian equations and Fourier transformations applied to free electron and gap motions in doped semiconductor 18 p3002 A67-34231

Comparison of classical approximations to free carrier absorption in semiconductors, using reflectivity minimum associated with plasma resonance as criteria 21 p3678 A67-38155

Exact calculation of indirect exchange interaction isotropic and nonisotropic terms in rare earth metals, with free electron model for conduction band 24 p4203 A67-42110

FREE ENERGY

Free energy of electron gas in compensating field at high temperatures determined from displacements in collective variables, using equation of statistical sum of steady state plasma 01 p0119 A67-10133

Thermodynamic properties of binary Cu-Pt alloys determined, using Knudsen effusion technique 05 p0829 A67-16473

Si and Ge heat capacities in terms of equivalent Debye temperature, obtaining coefficient of leading anharmonic contribution to free energy 05 p0870 A67-17199

Free energy of spatially homogeneous phase in approximation of self-consistent field for application to fluids and gases 07 p1168 A67-19186

Mathematical model for condensation point of first order phase transitions, examining free energy singularity and metastable phase 07 p1268 A67-20089

Transport of free molar energy in system in interdiffusion 09 p1581 A67-22597

Landau-Ginzburg theory extended to anisotropic superconducting energy gap, considering diffuse and specular boundary scattering 10 p1687 A67-22759

Magnetic properties of superconducting vanadium calculated from cellular

- model 16 p2726 A67-30816
- Free energy, heat and entropy of formation of several semiconductors by measuring EMF 18 p3095 A67-33445
- Free energy of N-particle system with far-reaching intramolecular interaction, using collective variables 18 p3085 A67-33670
- High pressure equations of state including electron gas correlation energy, giving density vs pressure curves for various elements 18 p3104 A67-34594
- Entropy and free energy functionals for collisionless plasma at equilibrium in adiabatic magnetic field 19 p3298 A67-35731
- Chromium activities in binary Cr-Ti solid solutions measured by Knudsen effusion technique, noting deviations from Raoult law and free energy calculation 20 p3469 A67-37384
- Quantum corrections to Maxwell plasma free energy in compensating electromagnetic field by method of displacements and collective variables for high temperatures 21 p3663 A67-37861
- Thermodynamic interpretation for Cauchy elasticity, showing formulation of constitutive equations in continua theories 21 p3733 A67-39085
- Second virial coefficient contribution to high temperature plasma free energy calculated by means of derived pseudopotential 22 p3851 A67-39785
- Free energy of polymer solid consisting of entangled long chain molecules when deformed by elastic strain 22 p3826 A67-40201
- FREE FALL**
- SA WEIGHTLESSNESS**
- Matrix solution to free motion of point in randomly perturbed resisting medium in rotating aspherical geogravitational field 05 p0901 A67-17110
- Fixed vertical plane surface effect on velocity of solid sphere in free fall in laminar region of incident viscous flow for various Reynolds numbers 06 p0983 A67-17928
- Time and distance measurement of freely falling body to determine acceleration due to gravity 10 p1657 A67-23317
- Absolute gravitational acceleration determined by timing symmetrical free motion of body moving under attraction of gravity 12 p1965 A67-25126
- Gravitational acceleration determination noting reversible pendulum, free fall and symmetrical free motion methods 15 p2517 A67-29507
- Weightlessness state in atmosphere and vacuum applied to satellites and space probes, noting effects on passengers and equipment 20 p3418 A67-37260
- Terminal velocity theory of freely falling body with ballistic coefficient of 200 psf and altitude region between zero and 60,000 ft 21 p3656 A67-37811
- Continuous EKG recording during free fall parachuting, discussing tachycardia as normal response 23 p3984 A67-41560
- Gravitational effect on free falling electrons in vacuum, showing gravitational induction of electric field outside metal surface 24 p4189 A67-42740
- Zero gravity orbital manufacturing noting free fall casting and blowing and zero gravity surface tension casting and foaming, discussing Serpentiator System engineering [AIAA PAPER 67-842] 24 p4165 A67-42980
- FREE FLIGHT**
- Rendezvous maneuver between vehicle and target in free orbital flight in central gravitational field, deriving low acceleration program for elliptical target orbit 01 p0152 A67-10208
- Slide rule for calculating liftoff free-flight trajectories in resisting media by iteration technique 02 p0240 A67-11553
- Radar observation of insects in free flight, noting backscatter and velocity measurement results [AFCLR-67-0127] 03 p0371 A67-13916
- Linear and nonlinear three-dimensional longitudinal stability coefficients from free flight measurements aboard missiles 04 p0703 A67-14553
- Finite thrust explicit guidance law for nearly circular orbital rendezvous 05 p0906 A67-17208
- Mach-Zehnder interferometer used with axisymmetric free flight models at hypersonic speeds, noting isopycnals and light gas gun 05 p0789 A67-17355
- Aerothermochemical eddy diffusion model for predicting rapid wake ionization decay behind hypersonic slender clean cone obtained in free flight ballistic range [AIAA PAPER 67-21] 06 p0938 A67-18257
- Schlieren techniques used in free flight range study of far wake of hypersonic cones [AIAA PAPER 67-31] 06 p0938 A67-18261
- Lift-drag ratio, lift and drag coefficients and angle of attack effects on Gemini and Apollo reentry vehicles measured in shock tunnel under free flight conditions [AIAA PAPER 67-165] 06 p0941 A67-18507
- Nanosecond pulse light sources used in free flight hypersonics for ballistic range measurements, noting less photographic blurring of motion 06 p0981 A67-18881
- Ground and flight tests to evaluate lunar landing research vehicle fly-by-wire control system [AIAA PAPER 67-273] 07 p1129 A67-20048
- Free flight response of two panels subjected to turbulent pressure fluctuations at supersonic Mach numbers 10 p1719 A67-23558
- Nonlinear oscillation effect on motion equation of elastic object under free flight conditions 12 p2032 A67-25966
- Para-Foil models tested in wind tunnel and free flight for flight capability, L/D ratios, deployment, control and maneuverability, etc 14 p2246 A67-29054
- Thrust augmentation ratio for hovercraft, lift ratio obtained by annular jets of same mass flow and total energy in ground effect and free flight conditions 15 p2419 A67-29674
- Pressure measurement at stagnation point of cylindrical missile with spherical nose cone during free flight in ballistic testing 16 p2593 A67-31123
- Radio telemetry system for aerodynamic data acquisition from free-flight models in supersonic wind tunnels 16 p2875 A67-31259
- Schlieren techniques used in free flight range study of far wake of hypersonic cones [AIAA PAPER 67-31] 17 p2793 A67-33006
- Time-resolved spectra for hypervelocity spheres and cones in free-flight ballistic range obtained by large aperture spectrograph and image converter camera 17 p2862 A67-33290
- Lift-drag ratio, lift and drag coefficients and angle of attack effects on Gemini and Apollo reentry vehicles measured in shock tunnel under free flight conditions [AIAA PAPER 67-165] 19 p3169 A67-34818
- Microsphere ablation in free-flight range observed by laser photography, giving shadowgraphs with density contour map 19 p3346 A67-35757
- Inference of vehicle and atmosphere parameters from free flight motion measurements using iterative calculations of parameter values 19 p3337 A67-35996
- Oblique interaction between supersonic vehicle in free flight and plane shock wave simulated, noting large unbalanced force 21 p3607 A67-37776
- Nose bluntness and cone angle effects on base pressure and heating in laminar hypersonic flow regime, using free flight telemetry technique 21 p3565 A67-38882
- FREE FLIGHT TEST APPARATUS**
- Steady and unsteady aerodynamic coefficients determined by free flight analysis of trajectory and attitude variations in supersonic wind tunnel 05 p0748 A67-16765
- Laser photography, discussing equipment used and shadowgraphs obtained in free flight range 08 p1330 A67-20595
- Free falling probe test during terminal descent for determining unknown planetary atmosphere profile from onboard measurements alone 10 p1629 A67-22768
- Free flight hypersonic wind tunnel testing technique noting pneumatic launcher, data acquisition and processing 10 p1622 A67-23390
- Total aerodynamic forces and moments of free flying body in wind tunnel determined from accelerations measured and telemetered by onboard instruments [AIAA PAPER 66-775] 11 p1773 A67-24349
- FREE FLOW**
- Stationary free-surface mercury flow in channels under magnetic field, analyzing hydraulic jump and influence of field on location 01 p0120 A67-10179
- Free surface distortion and subsequent gas ingestion in emptying cylindrical tank, emphasizing maximum height of liquid surface when gas reaches outlet 02 p0233 A67-11945
- Approximate theory for development of steady two-dimensional turbulent free mixing shear layers from initial velocity profile, including effects of compressibility and heat transfer [ASME PAPER 66-WA/FE-17] 04 p0606 A67-15352
- Mass transfer measurements of paradichloro benzene cylinders at various turbulent intensities and angles of attack, showing free flow turbulence effect on local mass transfer coefficient 04 p0548 A67-15493
- Intermittent phenomena related to entrainment process in free turbulent flows, noting indentation of surface growth and decay cycle 05 p0792 A67-16814
- Free turbulent shear flows and bound turbulent shear layer flows 12 p1928 A67-25355
- Free molecular flow region, calculating drag on plate, sphere and general body, considering drag effect on satellite orbit 15 p2561 A67-30045
- Incipient boiling prediction extended from forced flow water to other fluids and natural flow conditions [ASME PAPER 67-HT-61] 20 p3549 A67-36743
- Hydrodynamic stability of rotating flow with cylindrical free surface requiring Rayleigh criterion satisfaction 24 p4144 A67-42568
- Free convection thermal transfer in narrow horizontal channels and infinitely wide channels 24 p4255 A67-42587
- FREE JET**
- Turbulent mixing of axisymmetric jet of partially dissociated nitrogen with ambient air, establishing mixing and decay characteristics [AIAA PAPER 65-823] 01 p0055 A67-11171
- Induction velocimetry measurement of average velocity of free jet of ionized gas influenced by transverse uniform magnetic field 02 p0272 A67-11881
- Ventilated airfoil sections characteristics in free jet 05 p0793 A67-17321
- Source flow expansion of partially ionized gas into vacuum for predicting flow properties of low density free jet plasma expansions [AIAA PAPER 67-99] 06 p1041 A67-18281
- Iterative method for two-dimensional problem of incompressible viscous MHD free jet flow from thin slot in plane wall 08 p1361 A67-21143
- Constant Reynolds number applied to data evaluation for turbulent jet flow in converging-diverging axisymmetric tube using free turbulent jet 11 p1742 A67-24272
- Free plane jet compared with wall jet, noting more rapid lateral expansion of free jet 12 p1891 A67-25142
- Vortical interaction between free jet boundary layer and outer flow in separation area of hypersonic gas flow past body 12 p1892 A67-25671
- Temperature and density measurements in supersonic free jets of nitrogen and shock waves 13 p2093 A67-26279
- Model tests on free jet scramjet facility configurations at high Mach numbers, obtaining data on bypass flow pressure recovery and diffusion process 13 p2089 A67-26830
- Nonequilibrium effects in spherical free jet expansions of polyatomic gases and gas mixtures, obtaining moment equations for flow field development 13 p2104 A67-26963
- Molecular speed ratio in low density flows determined via stagnation point heat transfer and flat plate heat transfer measurements 14 p2301 A67-28182
- Axial and radial velocity distributions in axisymmetric free jets of pure gases and binary gas mixtures, noting molecular beam production 14 p2301 A67-28183
- Nonequilibrium aspects of fluid mechanics of freely expanding jet analyzed, using aerodynamic molecular beam system 14 p2301 A67-28184
- Kantrowitz-Grey molecular beam generator performance, noting high source pressure due to high pumping speed, background gas scattering, etc 14 p2316 A67-28189
- Bounded and confined turbulent jets compared to two-dimensional turbulent free jet 14 p2302 A67-28323
- Electrically conducting compressible viscous free jet in presence of transverse magnetic and electric fields solved

- analytically by perturbation
technique 15 p2523 A67-29215
- Wall jet compared to plane free jet
examining equilibrium conditions of velocity
profile of fluctuation and mean flow
determining stress 16 p2662 A67-31470
- Molecular nitrogen rotational relaxation
time by probing of supersonic free
jet 16 p2705 A67-31757
- Axisymmetric free turbulent jet flow with
swirling vortex motion over wide range of
swirl degree 17 p2838 A67-32417
- Velocity and temperature measurements in
turbulent swirling burning free jets of
butane-propane-air 18 p3151 A67-33815
- Mixture
Free jet plume expanding into vacuum
investigated experimentally, comparing with
ideal gas characteristics method
results 18 p3152 A67-33818
- Fractional excitation and ionization for
argon beam extracted from arc-heated
supersonic free jet, noting molecular ions
and neutralization 18 p3082 A67-34028
- Supersonic free plasma jet with axial
current, solving MGD equations for structure
modifications due to self-magnetic
forces 19 p3288 A67-35363
- Diffusion of free isothermal turbulent jet
of incompressible fluid flowing from nozzle
into coaxial surrounding uniform
stream 19 p3209 A67-35443
- Diffusing plane turbulent free jet
compared with correspondent wall jet
velocity distribution and variation and
length scales 20 p3360 A67-37492
- Model for compressible free jet with
moving environment in core and developed
region of exhaust plume 23 p3992 A67-41731
- Plane and turbulent fluid jets dynamic
and thermal behavior expanding in magnetic
field described by differential equations
system 24 p4195 A67-41930
- Momentum and heat transfer in
axisymmetric turbulent free jets exhausting
into quiescent air, using finite difference
technique 24 p4092 A67-42608
- FREE MOLECULAR FLOW**
- Aerodynamic coefficients of symmetrical
wing profiles and fuselages in rarefied gas
calculated for free molecular
flow 04 p0547 A67-14992
- Low density wind tunnel, with results of
tests on free expanding cold
jets 04 p0596 A67-14994
- Low density gas flow through short tubes
at densities varying from continuum to free-
molecule regime, noting nitrogen flow
[ASME PAPER 66-WA/PID-8] 04 p0606 A67-15331
- Knudsen limiting law in free molecular
gaseous flow in various capillaries with
temperature gradient 04 p0739 A67-15948
- Free molecular expansion into vacuum of
pulsed and steady gas flow from circular
orifice 06 p0985 A67-18190
- Shock tunnel heat transfer measurement
and hypersonic viscous flow over pointed
cones, particularly viscous-layer regime at
low Reynolds numbers 06 p0943 A67-18845
- Solid particle drag, convective heat
transfer and ablation effects on structure of
normal shock wave in nonreacting mixture
of gas and ablating dust, using Runge-Kutta
integration 08 p1427 A67-21120
- Transmission probability describing free
molecular flow through vacuum systems
obtained via Monte Carlo
program 09 p1488 A67-22104
- Free molecular flow rate and mass
distributions through various length
cylindrical nozzles 09 p1488 A67-22106
- Wall temperature and speed ratio effects
on free molecule flow number density
distribution about flat
plate 11 p1881 A67-23880
- Variational method for linearized problems
of rarefied gas dynamics applied to
cylindrical Poiseuille flow and heat transfer
from sphere, using BGK 13 p2101 A67-26966
- Monte Carlo approach to transition and
free molecular flow problems having mass as
well as thermal motion of
molecules 13 p2101 A67-26967
- Surface interaction of free molecular flows
or molecular beams, considering state
variables in highly rarefied gas in
Maxwellian equilibrium, stagnation
temperature, etc 13 p2159 A67-27299
- Wakes behind circular cylinders in free
molecule flow, noting inaccuracy in off-axis
impact pressure
measurements 14 p2300 A67-28175
- Heat loss and recovery temperature of
fine wires in transonic transitional flow
regime, noting experimental and
computational results 14 p2405 A67-28177
- Wind tunnel heat transfer measurements
from circular cylinders to transverse air
flow, noting recovery factor as function of
Knudsen number 14 p2405 A67-28178
- Free molecular flow through circular
orifice at high pressure ratios, discussing
mass flux measurement
methods 14 p2300 A67-28179
- Pressure and temperature in orifice set in
body located in free molecular flow,
checking first moment of distribution
function 14 p2302 A67-28198
- Rarefied gas flow interaction with sphere
analyzed using multiple wave interferometer,
noting transition region from continuous
medium to free molecular
flow 16 p2656 A67-30453
- Water injection for alleviating reentry
plasma sheath-induced communication
blackout, analyzing spherical drop
evaporation in free molecular
flow 19 p3211 A67-35762
- Free and near-free molecular flow via
cylindrical ducts using Monte Carlo method
and high speed digital
computer 22 p3784 A67-39946
- Multiple reflection of molecules effect on
nonconvex wing aerodynamic characteristics
for finite Mach number lateral free
molecular flow 22 p3741 A67-40022
- Aerodynamic coefficients for bodies in
free molecule flow determination method by
generalized force coefficient
equation 22 p3743 A67-40174
- Gas flow interaction with blunt body in
transition flow regime between continuum
and free molecule flow calculated using first
collision model 22 p3743 A67-40175
- Algebraic equations to predict time
response to step input in free molecule,
transition and continuum flow
regimes 24 p4155 A67-42293
- FREE OSCILLATION**
- Stability and free oscillations of three-
layer plates of symmetrical structure with
isotropic outer layers and light transversal
isotropic filler and weakened by central
rectangular cut-outs 01 p0158 A67-10219
- Dynamic stability tests of aircraft mockups
in transonic and supersonic flows, using
free-oscillation method
[ONERA-TP-390] 01 p0011 A67-11093
- Eigenvalues and eigenfunctions of free
oscillations of viscous incompressible fluid
in arbitrarily shaped vessel under
gravitational field, asymptotically
expressed 02 p0233 A67-11950
- Variational analysis of BVP of natural
oscillations of orthotropic
plates 02 p0341 A67-12663
- Free oscillations of rotating star with
equal angular velocity 04 p0698 A67-14915
- Energy dissipation calculation of damping
factor for free oscillations of viscous liquid
in circular cylindrical
vessel 04 p0711 A67-15196
- Recombination waves appear in sample
having ohmic contacts when drift velocity of
carriers in constant electric field exceeds
certain value 04 p0681 A67-15290
- Ritz averaging method to determine free
and forced vibratory response of beams and
plates undergoing large amplitude steady
state harmonic
oscillations 04 p0715 A67-15659
- Simultaneous free and parametric
oscillations of elastic cylindrical shell of
infinite length and subsonic flow of ideal
gas in shell 04 p0717 A67-15888
- Dynamic response, sloshing frequencies
and stability of free surface of liquid in
circular cylindrical elastic tank with flexible
bottom
[AIAA PAPER 67-76] 06 p0986 A67-18274
- Validity of equations for bending, natural
oscillations and stability of three-layer solid
circular plate with rigid filling and
asymmetric structure 06 p1106 A67-18628
- Free oscillation of thin elastic shell, using
asymptotic method for integrating dynamic
equations in classical linear
theory 07 p1263 A67-20031
- Advances in applied mechanics, Volume 9,
covering hydrodynamic stability, free
oscillations, nonlinear vibrations and
viscoplasticity 08 p1352 A67-20308
- Numerical calculation of free oscillations
of liquid in static
container 08 p1319 A67-20310
- Possible gravimetric study of lunar
gravity, tide and free
oscillation modes
[AAS PAPER 66-191] 08 p1387 A67-20964
- Free and forced oscillations of body with
cavity partially filled with viscous
fluid 10 p1679 A67-23029
- Forced and free oscillation characteristics
of ideal incompressible fluid contained in
cavity shaped as rectangular parallelepiped
with free surface under
deformations 10 p1679 A67-23030
- Free oscillations of plates, strips, rods and
cylinders subjected to arbitrary dynamic
edge load 11 p1874 A67-24314
- Existence and uniqueness of periodic
solution to ordinary differential equations,
defining position in plane of closed integral
curves 11 p1813 A67-24749
- Mechanical and electrical modes of energy
transfer occurring in free and forced
oscillations in earth
magnetosphere 12 p2000 A67-25107
- Approximate method for determining free
oscillation frequencies of hinged rectangular
plate with variable
thickness 12 p2021 A67-25574
- Free oscillations of closed freely
supported cylindrical shell of concentrated
mass, determining frequency and bending
moments 12 p2025 A67-25604
- Initial imperfection effects on free
oscillation frequencies of cylindrical shell
under static axial load 12 p2028 A67-25619
- Asymptotic method of integrating
differential equations applied to analysis of
axisymmetrical oscillations of thin elastic LF
shells of revolution 12 p2027 A67-25624
- Asymptotic solutions for free and forced
oscillations of solid having cavity filled with
viscous fluid, considering several degrees of
freedom and arbitrary cavity
shapes 12 p2029 A67-25657
- Equations for elastic system free
oscillations with parallelogram shaped
hysteresis loop derived from kinetic energy
changes, describing system time dependent
dynamic behavior 12 p1967 A67-25660
- Natural frequencies of free longitudinal
oscillations of circular rod with random
parameters determined by modified Krylov-
Bogolubov asymptotic
method 12 p2031 A67-25957
- Polar coordinate analysis of free
oscillations of circular plates with loosely
clamped edges under large deflections,
obtaining Duffing
equation 12 p2031 A67-25963
- Free undamped oscillations of nonlinear
conservative systems with several degrees of
freedom with small
nonlinearities 16 p2765 A67-31048
- Free vibrations of freely supported
toroidal shell, noting elastic motion
equations in terms of toroidal coordinates
and boundary conditions applicable to polar
motion 16 p2775 A67-31423
- Slow oscillations of fluid in rotating cavity
under magnetic field to evaluate Hide
theory for nondipole drift of geomagnetic
field 16 p2687 A67-31554
- Oscillating circuit with nonlinear
capacitance in free oscillating regime,
obtaining formula for envelope of free
oscillation differing from
exponent 17 p2829 A67-32311
- Fabry-Perot resonator free oscillations
defined by complex frequency, obtaining
diffraction loss and resonant
frequency 17 p2868 A67-32668
- Eigenvalues and eigenfunctions of free
oscillations of viscous incompressible fluid
in arbitrarily shaped vessel under
gravitational field asymptotically
expressed 17 p2841 A67-33267
- Free axisymmetrical oscillations of
reinforced, closed, cylindrical circular shells,
discussing natural frequencies and bending
oscillations 19 p3338 A67-34877
- Stress-strain state of rod with end load
and time variable load on other end,
discussing forced and free
oscillations 19 p3338 A67-34879
- Nonlinear mechanical model with
mathematical pendulums for solid bodies
containing nonlinearly oscillating liquid in
motion 21 p3612 A67-38307

Wave kinetics of free Alfvén oscillations using Lagrange function of collisionless plasma, calculating energy growth rate and relaxation times 21 p3667 A67-38372

Passive orientation of space vehicle toward sun by black and white coating, analyzing free oscillation about equilibrium 21 p3713 A67-38598

Dynamic response, sloshing frequencies and stability of free surface of liquid in circular cylindrical elastic tank with flexible bottom [AIAA PAPER 67-76] 21 p3614 A67-38868

Hollow torus axisymmetric circumferential natural vibration eigenfrequencies and eigenmodes dependence on thickness and torus radius ratio 22 p3908 A67-39289

Revolving thin elastic shell free axisymmetric oscillation described by equation system derived by asymptotic integration technique with single reversal point 24 p4250 A67-42304

FREE RADICAL

Free radicals in gas phase oxidation and spontaneous ignition reactions 02 p0341 A67-11502

Electron spin resonance application to kinetic studies of free atoms and radicals in gases, particularly OH radical 04 p0566 A67-15173

Cryochemical synthesis and processing by reacting free radical with excited state species 08 p1290 A67-21187

Temperature dependence and reaction energetics of free radical addition of trifluoroacetonitrile to ethylene 09 p1459 A67-22364

Free radical addition of perfluoroacetonitrile to vinyl fluoride, noting formation of one isomeric compound 09 p1459 A67-22365

Orientation of free radicals in addition reactions with unsymmetrical monoolefins 09 p1459 A67-22366

Free radical formation in amino acids exposed to thermal hydrogen atoms 13 p2065 A67-26869

Thiobarbituric acid reacted substance reaction with ribonuclease may be possible source of age pigment 15 p2433 A67-29296

Radio signals reflection by free radicals in ionosphere, observing predicted intensity and particle detection 17 p2817 A67-33233

Hydroxyl radical formed by radiolysis of ice at 77 degrees K identified as center producing EPR lines 17 p2890 A67-33258

Free radical formation correlated with breaking time and creep rate in solid polymers subject to crushing, breakdown and deformation 18 p3068 A67-33490

Increased oxygen tension causing increased free radical flux in rat kidney tissue akin to ionizing radiation exposure 23 p3958 A67-41654

FREE SPACE

Information model for manual control of astronaut motion and space orientation in free space 02 p0188 A67-12330

Elastic wave propagation in Cosserat continuum with free surface 13 p2217 A67-26630

Mutual admittance of slot antennas measured for free space and ionized environment by different techniques 19 p3194 A67-35516

Dielectric cover effect on resonant frequency of slots in rectangular waveguide, using Stevenson free space theory and plane-wave reflection coefficient 23 p3978 A67-40824

Electromagnetic scattering from free-space impedance homogeneous spheres, discussing null production in backscattering cross section 23 p3973 A67-40882

FREE STREAM

Free streamline theory of two-dimensional separated potential flow past bluff body and formation of periodic vortex turbulent wake 02 p0178 A67-12233

Free stream conditions approaching oscillating body in low speed wind tunnel, employing unsteady Bernoulli equation 03 p0352 A67-13899

Free stream turbulence effects on boundary layer transition, discussing acoustical disturbance as source of velocity fluctuations 05 p0794 A67-17364

Hydrogen or nitrogen gas injection at various Mach numbers from nozzle in flat plate into Mach 2.72 free air stream [AIAA PAPER 67-225] 06 p0940 A67-18444

Flow field around porous wedge or cone immersed at zero angle of attack in uniform supersonic free stream when contact surface is straight 08 p1276 A67-20571

Fluid flow processes for secondary sonic jet injection into Mach 6 free stream, noting upstream flow into separated flow regions 12 p1893 A67-25934

Mach and Reynolds number, cone angle, base geometry, etc, effect on near wake flow of conical vehicle moving at high speed 15 p2418 A67-30215

Turbulent jet spread issuing into parallel moving airstreams 16 p2857 A67-30615

Base pressure and geometry of separated region in boundary of supersonic accelerated flow analyzed and compared with Chapman-Korst model 16 p2592 A67-30951

Vibrational and/or chemical relaxation effects behind various shock waves in hypersonic air streams determined for equilibrium and nonequilibrium conditions 19 p3169 A67-34813

Two-dimensional incompressible fluid jet penetration analyzed kinematically via free streamline theory and notched hodograph 20 p3422 A67-36845

Hydrogen or nitrogen gas injection at various Mach numbers from nozzle in flat plate into Mach 2.72 free air stream 21 p3810 A67-37800

Integral equation for discontinuous flows and free streamline solutions for axisymmetric bodies at zero and small angles of attack 22 p3743 A67-40166

Dynamic impossibility of free stream velocity distributions admitting similarity solutions, calculating laminar boundary layers 23 p3992 A67-41741

FREE STREAM EFFECT

Transitional immersed cylinder heat transfer measurements used in conjunction with theory of boundary layer transition to determine free-stream turbulence intensity 04 p0601 A67-14508

Free stream turbulence and pressure gradient effects on flat plate boundary layer velocity profiles and heat transfer [ASME PAPER 66-WA/HT-4] 04 p0608 A67-15448

Unsteady incompressible laminar forced convection around stagnation point due to arbitrary time-wise-variant free stream velocity, considering skin friction and heat transfer 04 p0610 A67-15830

Relaxation processes behind shock wave in free stream partially dissociated and vibrationally excited by monitoring time history of radiative emission in shock tube [AIAA PAPER 66-519] 12 p1929 A67-25905

Free stream variables from continuum effect followed experimentally into transition flow regime to investigate impact probe in rarefied hypersonic flows of diatomic gases 14 p2294 A67-27794

Relationship between effectiveness of film cooling, free stream Reynolds number, slot Reynolds number and angle of injection 14 p2408 A67-28816

Free stream turbulence and pressure gradient effects on flat plate boundary layer velocity profiles and heat transfer [ASME PAPER 66-WA/HT-4] 15 p2470 A67-29321

Separation streamline for massive blowing in free stream for model injected into arc tunnel flow [AIAA PAPER 66-457] 17 p2839 A67-33007

Spark discharge generated blast wave application to shock on shock simulation, free-stream sound speed determination and hypervelocity flow measurements [AIAA PAPER 66-763] 19 p3208 A67-35753

Viscous degradation of hypersonic lift-drag ratio in manned spacecraft, noting free stream Mach and Reynolds numbers 22 p3742 A67-40113

Free VIBRATION

Spheroidal disturbances propagation on surface of heterogeneous spherical earth studied by superposition of contributions from normal free spheroidal vibration modes 02 p0237 A67-11790

Matrix-Holzer method for predicting free vibration modes of clustered launch vehicles in bending applied to first eight modes of Saturn I model 02 p0337 A67-11931

Modification of Potter method of Gaussian elimination for solving eigenvalue problems of buckling and free vibrations of shells of revolution 04 p0656 A67-14839

Free vibration of sandwich beams viscoelastic cores, examining equations of motion, natural boundary conditions and derivation of expressions for modal distribution of damping [ASME PAPER 66-WA/UNT-3] 04 p0713 A67-15382

Correspondence principle in linearized classical theory of viscoelasticity for free vibrations, emphasizing case of irrotational or solenoidal motion 05 p0909 A67-16145

Shape determination for uniform-strength clamped bar with constant dynamic stress distributions subjected to first order free vibrations 05 p0917 A67-16247

Finite difference method solution of motion equations for free vibrations of initially disturbed thin elastic rings 06 p1109 A67-18838

Motion equations for free vibrations of shaft mounted on ball bearings 07 p1191 A67-19355

Unsymmetric free vibrations of orthotropic sandwich shells of revolution treated by Rayleigh-Ritz technique 08 p1417 A67-20555

Vibration modes of conical frustum shells with free ends [AIAA PAPER 66-450] 08 p1424 A67-21533

Heated rectangular plate nonlinear free flexural vibration problem involving initial deflection, temperature change, etc 10 p1715 A67-22825

Stochastic Markov model for transient amplitude variation in systems with damped free vibration compared with deterministic solution 10 p1724 A67-23709

Free and forced liquid sloshing motions in tank of arbitrary shape at low gravity environments analyzed, using Satterlee-Reynolds method 10 p1629 A67-23832

Determination of proper frequencies of vibration of thick-bladed turbine disk with interaction between disk, blades and shrouding [ASME PAPER 67-VIBR-52] 11 p1797 A67-24201

Free vibration and resonance of vibrating plate interacting with sound waves in surrounding air 11 p1874 A67-24222

Temperature dependence of Young's modulus of tantalum alloy determined together with free-free vibrations and resonance frequency 12 p1954 A67-25141

Vibrational stress of clamped free rectangular rods of constant cross section under effect of instantaneous impulse 13 p2220 A67-27275

Transient vibration of viscoelastic body showing dynamic displacement expression in terms of static boundary value problem 14 p2400 A67-28145

Long period vibrometer with small spring constant and minimized solid friction by HK vibration of support 14 p2348 A67-28257

Holzer method extended to analysis of free vibration of spherical shells, solving boundary value problem as set of initial value problems until all boundary conditions can be satisfied 15 p2577 A67-30193

Free vibrations of unsupported elliptical plates of lenticular section with flat or uniformly curved middle surfaces 16 p2764 A67-30844

Intrinsic frequencies and modes of periodic free vibrations of homogeneous beam with weakly nonlinear boundary conditions of Duffing type 19 p3340 A67-35501

Free vibrations frequency of ideal fluid in elastic bottom cylinder in form of spherical shell 20 p3420 A67-36444

Simply-supported elliptic plate free vibration problem applying Rayleigh-Ritz technique to obtain fundamental frequencies 20 p3539 A67-37007

Free vibrations and motion stability during extremum drift for one-and multidimensional pulsed optimal systems 20 p3411 A67-37377

Parameters for motion of flight vehicle at solid body and for elastic deformations 20 p3482 A67-37388

Compounded normal modes of free vibration of cantilever plates, determining component modes 20 p3541 A67-37449

Upper and lower bounds for frequencies of free vibration developed for uniform rectangular cantilever plates 21 p3730 A67-39099

Ring finite element analysis for shells of

evolution improved by extending
polynomials representing
placements 22 p3911 A67-39499
Coaxial rotors natural vibrations analysis
computer showing occurrence at rpms
above first critical speed 23 p4009 A67-40685
Natural frequencies and mode shapes
determined for circular cylindrical shell
closed by elastic plate 23 p4080 A67-41750
FREEDOM FIGHTER AIRCRAFT
F-5 AIRCRAFT
FREEZING
One-dimensional freezing of semiinfinite
isotropic homogeneous liquid-solid system
with temperature-varying thermal
properties 01 p0166 A67-10758
Refrigeration process of freezing stresses
at ambient temperature improves elastic and
photoelastic properties and renders them
comparable to those of nonplasticized epoxy
resins
[ONERA-TP-367] 05 p0919 A67-16480
Frost phenomena on Mars examined on
basis of Martian wave of darkening, noting
necessity of deliquescent salts to attract and
retain water on surface 06 p1089 A67-18645
Fiber reinforced metal coating by passing
Al₂O₃ through molten aluminum, discussing
freezing by radial conduction of heat into
fiber 12 p1954 A67-25292
High intensity electric field used to freeze
out large quantity of droplets from
supercooled artificial fog 16 p2699 A67-31717
Cellular injury and resistance in freezing
organisms - Conference, Sapporo, Japan,
August 1966, Volume 2 20 p3387 A67-38141
FRENCH SATELLITE
FR-1 SATELLITE
FREEON
Density wave type flow oscillations in
boiling Freon 11 examined, noting effects of
partial evaporation superheat and liquid
inlet temperature on stability
[ASME PAPER 66-WA/HT-49] 04 p0725 A67-15433
Pressure drop study of near saturation
Freon 11, noting flowing fluid quality
condition for estimates 13 p2106 A67-27668
FREQUENCY
AUDIOFREQUENCY
CARRIER FREQUENCY
CRITICAL FREQUENCY
CYCLOTRON FREQUENCY
EXTREMELY LOW FREQUENCY
[ELF/
HIGH FREQUENCY
INFRASONIC FREQUENCY
IONIZATION FREQUENCY
LOW FREQUENCY
MAXIMUM USABLE FREQUENCY
MICROWAVE FREQUENCY
NATURAL FREQUENCY
OSCILLATION FREQUENCY
PLASMA FREQUENCY
RADIO FREQUENCY
RESONANT FREQUENCY
SWEEP FREQUENCY
ULTRAHIGH FREQUENCY
ULTRALOW FREQUENCY
VERY HIGH FREQUENCY
VERY LOW FREQUENCY
VIBRATIONAL FREQUENCY
FREQUENCY AMPLIFIER
INTERMEDIATE FREQUENCY
AMPLIFIER
Recognition and subsequent amplification
of difference frequency in plasma-beam
system with two electromagnetic waves
propagating in opposite
direction 05 p0766 A67-17170
Autodyne design and operational
principles for EPR in weak fields, using
coaxial resonator 11 p1793 A67-24865
Conditions for minimum nonlinear
distortion in power amplification of single
band signal 11 p1772 A67-24983
Frequency response of nonlinear system,
analyzing saturation characteristic of
amplifier by digital
computer 17 p2821 A67-32933
Traveling wave tube as hyperfrequency
amplifier onboard satellites for reliable
space communications 21 p3592 A67-38212
High efficiency tunable ferrite frequency
doubler consisting of yttrium-iron-garnet
disk at waveguide
junction 21 p3598 A67-38572
Performance characteristics of active
channel of insulated gate FET for
application as high gain HF
amplifier 24 p4133 A67-42824

FREQUENCY ANALYSIS

SA OSCILLOSCOPE
Composite surface and composite
correlation approaches to frequency
dependence and surface roughness problems
of lunar surface signal
scattering 01 p0020 A67-10019
Frequency equation for purely radial
vibrations of infinite isotropic composite
hollow cylinder with two concentric elastic
layers 01 p0162 A67-10818
Perturbation theory analysis of spatial
dispersion effects on frequency addition in
crystals 03 p0434 A67-13125
Stability of single-frequency solutions to
quasi-linear autonomous systems with two
degrees of freedom 03 p0468 A67-13625
Nonlinear instability of optical frequencies
in partially ionized plasma, noting nonlinear
frequency buildup for strong plasma
waves 05 p0852 A67-16691
Linear frequency-domain analysis
technique for examining stability and
performance characteristics in optimal-
control design of control
systems 06 p0973 A67-17718
Polonnikov generalization of Bode
amplitude approximation technique to phase
approximate evaluation 07 p1161 A67-19879
Artificial pseudorandom binary noise
generation for flight testing and aircraft
control systems and correlation function and
frequency spectra of noise
generators 08 p1279 A67-21005
Frequency stability of He-Ne lasers
analyzed by heterodyning two laser
resonators 09 p1509 A67-21558
Two-frequency correlation method for
determining time dependent mean statistical
voltage and current values for DC
arc 09 p1547 A67-22323
Continuous spectrum of nonperiodic
curves, discussing measurement of frequency
spectra of periodic voltage
curves 09 p1501 A67-22468
Graphs for frequency plot of closed loop
automatic control system from phase
amplitude of open loop and frequency
relations between open and
closed 10 p1621 A67-23852
Differential frequency discriminators
under combined action of signal and
noise 11 p1750 A67-23913
Gyroscopic moment effect on critical
speeds of shaft-disk system mounted in
short end bearings, obtaining frequency
equations
[ASME PAPER 67-VIBR-9] 11 p1795 A67-24169
Determination of proper frequencies of
vibration of thick-bladed turbine disk with
interaction between disk, blades and
shrouding
[ASME PAPER 67-VIBR-52] 11 p1797 A67-24201
Frequency analysis of continuous and
irregular geomagnetic pulsations measured
by induction magnetometer 11 p1786 A67-24332
Measured efficiency departure in power
varactor converters from theoretical
estimation, finding three-frequency current
spectrum responsible 11 p1766 A67-24647
Aerodynamic damping and frequency drift
of turbomachine blades, discussing wind
tunnel testing results for various geometric
configurations 13 p2051 A67-27205
Limiting frequencies median values
suggested as suitable characteristics of
relation between solar activity and sporadic
E layer behavior 14 p2307 A67-27913
Velocity distribution function of gas
measured with laser, noting relation to
frequency variation of absorption coefficient
across spectral line 14 p2317 A67-28194
Nonlinear instability of optical frequencies
in partially ionized plasma, noting nonlinear
frequency buildup for strong plasma
waves 15 p2530 A67-29862
Sunrise variations of phase and amplitude
of vlf signals over single long path
interpreted as interference between
waveguide modes 16 p2631 A67-31851
Response of logarithmic frequency
characteristics of dynamic linear systems to
small parameter
variations 18 p3018 A67-34441
Frequency pattern analysis for liquid
rocket pump fluid
cavitation characteristics 21 p3613 A67-38437
Noise measurement and instrumentation

used 21 p3630 A67-38900
Differential frequency discriminators
under combined action of signal and
noise 21 p3585 A67-38941
Selective circuit with FM system and
constant gain designed to determine radio
whistler arrival direction as function of
frequency 21 p3587 A67-39125
Oscillating circuits with nonlinear active
elements amplitude and phase frequency
characteristics graphically plotted, noting
effects on frequency
devices 24 p4136 A67-42191
FREQUENCY ASSIGNMENT
Synchronous stationary satellite system for
networking television and radio material to
broadcast stations, noting frequency
requirements and
constraints 06 p0961 A67-17697
Diurnal, seasonal and geographic variations
of frequency of spread-F occurrence over
Antarctica
[AGARDOGRAPH 95] 15 p2481 A67-30282
Block diagram and basic circuit for
measuring ionospheric radio wave
absorption 21 p3586 A67-39044
Compact ionospheric station for six fixed
frequencies, compared with automatic
station 21 p3586 A67-39047
Frequency assignment for communications
equipments mutual interference charts
/MIC/ 24 p4123 A67-42719
FREQUENCY BAND
SA C-BAND
SA K-BAND
SA L-BAND
SA RADIO SPECTRUM
SA S-BAND
SA X-BAND
YIG dispersive delay line in ultrawide
bandwidth pulse compression radar
system 01 p0132 A67-10435
Octantal error of frequency band over
which Adcock direction finder operates,
noting observed and true bearing relation of
arriving signal 01 p0027 A67-11327
Radiation patterns and impedance plots of
sleeve antenna over band with frequency
ratio of 4 to 1 02 p0212 A67-11607
Time slope relation to frequency
bandwidth extended to less particular
input 04 p0591 A67-14516
Frequency spectra of VLF hiss near
auroral zone analyzed by Injun III
satellite 04 p0614 A67-14958
Engineering methods for construction of
electromagnetic wave absorbing walls for
microwave darkroom applications at various
frequency bands 04 p0576 A67-15504
Broadening of frequency bandwidth of slot
array antenna by adopting center fed
method 04 p0585 A67-15505
Pulsed high energy ionizing radiation
effects on behavior and output frequency of
electronic quartz oscillator
crystals 04 p0685 A67-15700
Propagation constant of electromagnetic
waves over earth surface 05 p0760 A67-16001
Transmission loss for ionospheric
propagation over 4000 km path measured at
several frequencies in HF
band 05 p0760 A67-16005
Correlator for determining envelope of
autocorrelation function of wideband HF
signal, using narrow band video
amplifier 05 p0764 A67-16902
Phase separation and synchronization
during separation of AM signals with
overlapping frequency
spectra 05 p0764 A67-16903
Passband narrowing due to coupling
between passive oscillating system and
active substance contained in resonator
cavity represented by RLC
circuit 05 p0780 A67-17474
Analogy between radiation angular
spectrum reflected from rough surface and
frequency spectrum of carrier burst related
to radio propagation 06 p0957 A67-17579
Tabulation and plotting of VLF radio wave
diurnal phase changes as function of
frequency and path
distance 07 p1142 A67-19450
Frequency doubling of light in ruby laser
due to laser light interaction with corundum
lattice, anti-Stokes-Raman scattering of laser
light, etc 08 p1336 A67-20316
Antennas for HF radio communications
integrated with shipboard
structures 08 p1301 A67-20772
LF galactic emissions, noting spiral arms

and spherical halo on galactic hub, signal strength variation and terrestrial atmosphere role 08 p1385 A67-20866

Radio observation of quasar CTA 102 at various frequencies from Arecibo for possible explanation of sinusoidal variation of flux density 08 p1397 A67-21186

Wideband and optimum antennas, using Lepidopter antenna as example 10 p1613 A67-23506

Ionospheric absorption relationship with frequency, extending lower limiting frequency to 2 MHz 11 p1753 A67-24302

Telemetry transmitters using solid state wideband microwave voltage-controlled oscillators 11 p1753 A67-24442

High power pulsed microwave generation in gallium arsenide diode when operated at X-band frequencies 11 p1767 A67-24721

Design of broadband steerable Wullenweber antenna arrays allowing HF element rings to be within LF rings 13 p2074 A67-26257

Transistorized resonant cascade amplifier with added active resistance for amplifier stability improvement 14 p2283 A67-28277

Semiconductor nonlinear polarizability at difference frequency calculated, considering exciton states alone and combined with band energy states 15 p2541 A67-30238

Correlator for determining envelope of autocorrelation function of wideband HF signal, using narrow band video amplifier 16 p2622 A67-30878

Phase separation and synchronization during separation of AM signals with overlapping frequency spectra 16 p2622 A67-30879

Faraday rotation satellite observations at closely spaced frequencies, allowing electron content figure determination 16 p2629 A67-31514

Soviet book on SHF radio receivers covering theoretical and engineering aspects of component design, control, signal detection, etc 17 p2822 A67-32020

Electronically swept coherent frequency synthesizer for various bands 17 p2827 A67-32799

Signal generator tuning to center frequency of narrow band receivers, noting test setup and procedure 17 p2827 A67-32800

Near earth and outer ionosphere plasma waves and oscillations in VLF and ELF bands 19 p3317 A67-34932

Simultaneous absorption of two photons by transparent material at radiation frequency corresponding to only one photon 20 p3457 A67-36325

Radio parameter continuity between radio galaxies and quasars, plotting spectral indices against absolute spectral power 20 p3525 A67-36947

Modulation systems in satellite communications evaluated by criteria of baseband signal noise ratio, signal power, frequency band requirements, etc 20 p3383 A67-36956

Wideband troposcatter radio channel simulator exhibiting frequency flat or frequency selective fading over band greater than 10 MHz and centered at 70 MHz 20 p3385 A67-37354

Principles, design and operation of synthetic plasma source for studying space vehicle antennas over wide frequency band 21 p3664 A67-38214

Frequency bands and modulation methods for space communication system 21 p3581 A67-38235

FM/PM and FM/FM radio telemetry in proportional and constant band covering regulation, SNR, noise threshold, etc 21 p3587 A67-39050

FREQUENCY COMPRESSION DEMODULATOR

Statistical dependence between frequency and amplitude deviations of FM wave perturbed by white noise, describing amplitude-phase correlation FM demodulator 22 p3758 A67-39271

FREQUENCY CONTROL

SA AUTOMATIC FREQUENCY CONTROL

Frequency correlation of clutter by considering signal received by radar at time t after it has transmitted pulse 01 p0023 A67-10468

Effect of couplings and losses on frequency stability in self-oscillatory system with three circuits 02 p0221 A67-12418

Transmission line antenna tunable over

greater than octave bandwidth 03 p0384 A67-13847

Interference ratios in space telecasting, considering methods of control for cochannel broadcasting 06 p0960 A67-17692

Expansion of free turbulent air jet controlled by given frequency from disk pulsator 06 p0982 A67-17744

Error signal generation method to control laser frequency of laser oscillator 08 p1339 A67-21378

Loss in temperature compensation with varying frequency for quartz generators 11 p1757 A67-23909

Parametric double pumping mixer of down converter type for multiple-beam low noise receiving antenna 12 p1913 A67-25302

Frequency selective parametric limiting by parallel pumping of subharmonic magnetoelastic waves in YIG 13 p2077 A67-26523

Solutions for piecewise linear differential equation obtained by plotting exciter amplitude against exciter frequency in treating pulling-in phenomena 13 p2145 A67-26625

Frequency generation and control for radio systems - Conference, London, May 1967 15 p2444 A67-29580

Worldwide network of Doppler observation stations, discussing frequency and time monitoring for enhanced measurement accuracy 15 p2436 A67-29592

Environmental adjustment factors for operating and nonoperating failure rates 15 p2495 A67-30417

Measurement of laser frequency control characteristics of piezoelectric transducers, noting effect of mechanical structure supporting transducer on frequency control characteristics 15 p2502 A67-30426

Gain control of common emitter cascade by varying transistor regime, taking into account effect of operating frequency and temperature 16 p2637 A67-31027

Transistor overload in active region operated by large pulse trains, discussing thermal response and resistance and operational frequency intervals 17 p2827 A67-32784

Monolithic operational amplifiers with simplified frequency-compensated network using minimum stages and integrated circuit components 17 p2828 A67-32899

Laser frequency control system using two optical discriminators for long and short term stability 20 p3459 A67-36519

Higher mode cut-off frequencies in coaxial cables of elliptical cross section tabulated as function of conductor dimensions 20 p3382 A67-36861

Soviet papers on wideband cross-shaped radio telescope and radio astronomy studies 20 p3402 A67-37504

Spaced antenna array radiation pattern frequency control analyzed for relationship between arrival angle and heterodyne frequency 20 p3402 A67-37506

Loss in temperature compensation with varying frequency for quartz generators 21 p3600 A67-38937

Carcinotron hyperfrequency power oscillator with tube of same noise characteristics as control developed for space telecommunications 23 p3982 A67-41431

Pump frequency reduction in Adler tubes, examining spatial harmonics of quadrupole structure field and suggesting use of cophasic connection 24 p4130 A67-42240

FREQUENCY CONVERSION

Microwave mixing in paramagnetic crystal using traveling wave maser with ruby as mixer element, noting frequency conversion 01 p0086 A67-10003

Microwave mixer point contact diode with X-band intermediate frequency for good value of conversion loss 01 p0036 A67-10438

Ruby laser frequency conversion technique by laser beam scattering and mixing of combined frequencies 03 p0433 A67-13094

System Utilizing Signal-processing for Automatic Navigation, for moving vehicles, using time delays and frequency multiplication 04 p0653 A67-14870

Frequency conversion at optical wavelengths of doubly modulated light, using LF photodetectors as receivers 04 p0575 A67-15170

Sum and difference frequency mixing of visible and IR gas laser light in GaP at near reststrahl frequencies and relationship to

spontaneous Raman scattering 04 p0682 A67-15464

Matrix analysis of small signal microwave frequency conversion based on linear operation of semiconductor diode 05 p0772 A67-16449

Convex programming procedure yielding algorithm for tuning out system from possible resonance zone 08 p1353 A67-20837

Coherent radiation frequency conversion and nonlinear optics methods, including stimulated Raman scattering and Mandelstam-Brillouin scattering 14 p2330 A67-28467

Frequency conversion at optical wavelengths of doubly modulated light using LF photodetectors as receivers 15 p2443 A67-29356

UHF amplification and frequency conversion using single transistor as amplifier and base-collector junction capacitance as varactor 20 p3398 A67-38773

Cyclotron harmonic resonances in plasma frequency conversion output due to harmonic interactions with incident waves 22 p3851 A67-39724

FREQUENCY CONVERTER

SA PARAMETRIC FREQUENCY CONVERTER

Noise factor of linear receiving systems in quantum and classical regions, noting role of dual push-pull amplifier and frequency converter 01 p0022 A67-10393

Linearization of nonlinear transducer output transfer function by digital voltmeter 01 p0076 A67-11143

Performance and design characteristics of solid state microwave converters for converting VLF telemetry receivers to L-and S-bands 02 p0196 A67-12006

Nondissipatively regulated variable frequency DC to DC converter with variable on time and variable off time 02 p0183 A67-12117

Performance characteristics of tunnel diode autodyne frequency converters 05 p0774 A67-16917

Parametric action in back biased p-n junctions carrying injected currents, discussing photoparametric frequency converters, transistor amplifiers and frequency doublers 06 p0969 A67-18106

Design and performance characteristics of two-bridge controlled autonomous compensation inverter for DC to AC conversion 07 p1150 A67-19317

Short wave radio links, discussing frequency converters, spectrum oscillators, transmitters, etc 07 p1150 A67-19343

Performance and stability of germanium tunnel-diode autodyne frequency converter 09 p1472 A67-21957

Down-converter in reflection cavity configuration using bulk semiconductors as detection medium, considering optimum conditions 09 p1515 A67-22277

Metal GaAs diodes as frequency changers, discussing fabrication, performance characteristics and parameters 10 p1615 A67-23528

RF communication converter miniaturization and packaging techniques 12 p1911 A67-25271

High density power converter using integrated circuits and thyristors, noting packaging 12 p1911 A67-25274

Performance characteristics of tunnel diode autodyne frequency converters 16 p2636 A67-30894

Large-signal analysis for varactor frequency upconverter under overdriven conditions, obtaining equations for varactor charge, current and voltage 20 p3396 A67-36510

Performance and stability of germanium tunnel-diode autodyne frequency converter 20 p3400 A67-37187

Systems with low noise factor and high selectivity tuned by varying pumping frequency 22 p3767 A67-39370

Solid state laser with mode selection within active medium ensures beam collimation in one plane, noting use in second-harmonic generation and parametric frequency conversion systems 22 p3814 A67-39458

Monolithic magnetic double-balanced modulator, comparing patterns from working sample with theoretical conversion gain 22 p3773 A67-39916

FREQUENCY DISTRIBUTION
 SA POISSON DISTRIBUTION
 SA WEIGHTING /MATH/
 Frequency-time domain asymptotic
 stability criterion for autonomous continuous
 systems 01 p0046 A67-11209
 Red shifts and blue shifts relative
 frequency distribution for
 QSO 03 p0515 A67-14321
 Structure function of interstellar
 absorption, noting spatial and frequency
 distribution of dust concentrated in
 clouds 05 p0897 A67-16774
 Si and Ge heat capacities in terms of
 equivalent Debye temperature, obtaining
 coefficient of leading anharmonic
 contribution to free
 energy 05 p0870 A67-17199
 Computer program for digital exact
 representation of spectral frequency-and
 intensity-distribution by superposition of
 Gaussian components, applying least squares
 method, linearizing normal equations and
 analyzing observational
 errors 06 p0965 A67-18069
 Quantization, sampling frequency and
 statistical scattering in correlation
 measurements 08 p1313 A67-21006
 Gas laser dynamic behavior, discussing
 internal modulation, mode locking, noise and
 perturbation modes 09 p1515 A67-22431
 Frequency redistribution function of
 noncoherently scattered radiation, noting
 effect on source functions of two-level
 atoms 11 p1823 A67-24490
 Weak inhomogeneous plasma wave energy
 redistribution during quasi-normal oscillation
 expansion in resonance regions, noting
 electric analogy 11 p1842 A67-24953
 Frequency spectrum of PI_2
 micropulsation activity and relation to
 planetary magnetic
 activity 13 p2109 A67-26327
 Special purpose analog computer for
 analyzing wideband signals in two parts of
 network, with automatically plotting and
 coupling factor as function of
 frequency 13 p2089 A67-26410
 Phase distribution in laser aperture based
 on analysis of radiation in Fresnel
 zone 13 p2127 A67-27029
 Radiation diffusion in medium of finite
 optical thickness, computation of source
 function and tabulation of
 matrixes 14 p2382 A67-27832
 Stress-strain problems in design load of
 commercial aircraft, noting role of frequency
 distribution curves 14 p2245 A67-28060
 LF and HF single stage RC filters with
 steep frequency characteristic slope in
 transition region 14 p2289 A67-28863
 Model stellar atmosphere computations
 predict emergent radiation
 spectrum 14 p2392 A67-28993
 Broadening of lines emitted by tunnel
 superconductor, noting unfeasibility of
 simultaneous amplitude-frequency
 prescription of Josephson
 current 16 p2728 A67-31044
 Fluid motion in shallow trapezoidal
 container, noting dimensionless quantity
 relating frequencies to volume and rim
 dimensions, sloshing modes, eigenvalues,
 etc 16 p2661 A67-31421
 Relation between frequency distribution of
 sudden changes in cosmic ray intensity and
 solar-diurnal variation 17 p2932 A67-32082
 Frequency spectrum of annihilation
 operator for system of harmonic oscillators
 using motion equation obtained through
 Hamiltonian 17 p2870 A67-33316
 Frequency spectra of excess noise in
 semiconductor devices due to characteristics
 fluctuations after applying
 signal 17 p2828 A67-33383
 Polar cap auroras frequency patterns
 relationship to worldwide
 storms 18 p3037 A67-33611
 Ionization frequency distribution in HF
 discharge produced by long single turn
 coil 19 p3276 A67-35118
 Time variation of Doppler broadened
 resonance line profile determined by
 assuming complete frequency
 redistribution 19 p3329 A67-36030
 Combined frequency and space correlation
 of wave fields scattered by rough surfaces
 where conditions of applicability of
 Kirchhoff approximation hold
 true 22 p3760 A67-39660
 Impact crater size vs incidence analyzed

statistically in study of validity of time
 dependence on saturation for moon and
 Mars 23 p4066 A67-41007
 Multifrequency radar system performance,
 obtaining expression for detection
 probability as frequency number, false alarm
 probability and integrated pulse number
 function 24 p4122 A67-42408
FREQUENCY DIVIDER
 Data quality assurance program for
 telemetry ground station operations, noting
 frequency division and time division
 formats 02 p0198 A67-12023
 Neon tube staircase generator performing
 functions of frequency and voltage
 division 05 p0769 A67-18023
 Communications satellite system efficiency
 enhanced by using automatic adaptive voice
 multiplexer in ground terminal
 equipment 06 p0960 A67-17676
 Multiple access modulation techniques
 /frequency-division, time-division, spread-
 spectrum and pulse-address/ for use in
 communications satellites 06 p0960 A67-17694
 Bandwidth, phase and amplitude
 characteristics calculated for reflex klystron
 divider in case of multiple frequency
 division 07 p1158 A67-20243
 Working principle of echo suppressor used
 in telephone link with high propagation time
 based on selective attenuation by frequency
 and time divisions 11 p1754 A67-24651
 Variable-ratio frequency divider using
 integrated circuits of resistor-transistor-
 micrologic type 17 p2827 A67-32798
 Frequency doubler and divider using
 transistorized synchronized switching phase
 detectors with closed feedback
 circuit 22 p3762 A67-39872
FREQUENCY-DIVISION MULTIPLEXING
 Block coded frequency multiplexed PM
 communication system design and
 performance, considering simplification, cost
 and weight 14 p2271 A67-28694
 Information capacity dependence on
 number of frequency-divided channels of
 optical communication system, investigating
 information loss in channel-separating
 receiver 16 p2623 A67-30882
 Design and performance of frequency
 multiplexed phase-modulated communication
 systems 20 p3385 A67-37353
FREQUENCY MEASUREMENT
 Doppler-Flizeau frequency effect in
 ionospheric satellites measuring device
 based on wave refraction 01 p0057 A67-10233
 Sum signal of output of system consisting
 of two detuned resonators and two
 amplitude detectors used for automatic
 measurement of signal
 frequencies 01 p0022 A67-10413
 Error theory for counter frequency
 meter 01 p0063 A67-10415
 Cut-off frequency of diffusion transistor
 calculated, using series expansion for
 current transport factor 03 p0382 A67-13685
 Phase determination of signal components
 generated by parametric oscillator by
 synchronizing oscillator with respect to
 difference between frequencies of
 components 04 p0583 A67-15171
 E layer stratification, fine structure and
 boundary accuracy in frequency
 measurements based on seasonal variations
 in solar activity 04 p0618 A67-15574
 RF interference detection and elimination
 from communication systems noting signal,
 frequency and amplitude analysis
 techniques 04 p0577 A67-15730
 Erosion destruction mechanism in
 polycrystalline graphite, noting effect of gas
 flow over surfaces, flow pulsation frequency
 and generated aerodynamic
 loads 04 p0642 A67-15761
 Direct digital display with high precision
 for audio frequencies 05 p0865 A67-16944
 HF measurements of thin film CdSe
 transistors, discussing equivalent circuit,
 stability factor and power
 gain 05 p0776 A67-17091
 Maximum slope method for obtaining
 natural frequency and damping ratio of
 highly damped second order systems from
 time history data 06 p1100 A67-18012
 Installation for measuring Doppler effect
 of satellites, investigating limits,
 optimization, SNR and orbital parameter
 accuracy 06 p0979 A67-18018
 Measuring harmonic AM frequency of bell-
 shaped video-pulses train for modulation-to-
 repetition-frequency ratio greater than

unity 07 p1139 A67-19227
 Field strength measurements in multipath
 field using linear and circular
 probing 07 p1142 A67-19448
 Doppler frequency measurements in
 satellite transmissions and use for geometric
 geodesy 07 p1144 A67-19771
 Millimeter confocal wavemeter calibration
 and stability 09 p1470 A67-21625
 Zeeman effect in Ne-He gas laser
 operating in longitudinal magnetic field,
 noting dependence of frequency difference
 on field strength 09 p1512 A67-21920
 Type III solar radioburst characteristics
 determined using sweep frequency
 interferometer 10 p1699 A67-22886
 Navy navigation satellite system developed
 by APL, using Doppler frequency
 measurements for navigation
 fix 10 p1677 A67-23183
 Frequency temperature dependence of
 longitudinal and transverse hypersonic wave
 absorption coefficients in quartz and
 artificial ruby crystal 10 p1693 A67-23582
 Flute instability in mirror confined
 plasmas assuming particle drift under
 external forces 11 p1830 A67-24004
 Vibratory motions of turbine blades,
 considering frequency determination,
 tangential mode, stress, damping and
 excitation source
 [ASME PAPER 67-VIBR-66] 11 p1798 A67-24207
 Absolute frequency measurement and
 spectroscopy of gas laser transitions in far
 IR, analyzing Zeeman
 effect 11 p1802 A67-24830
 Detection and measurement of mm wave
 difference frequency between two near laser
 lines, using optical
 heterodyne 11 p1803 A67-24832
 Amplitude and phase frequency
 characteristics of linear system determined
 from transfer
 characteristics 11 p1772 A67-24980
 Characteristic cut-off frequencies of
 transistors determined from simple LF
 measurements 13 p2077 A67-26659
 Upper cut-off frequency and amplitude
 frequency response curve shape for
 wideband aperiodic amplifiers, examining
 five common transistor
 circuits 13 p2077 A67-26660
 Zeeman effect in Ne-He gas laser
 operating in longitudinal magnetic field,
 noting dependence of frequency difference
 on field strength 14 p2330 A67-28249
 Fluidic temperature sensor using
 frequency beating technique for generating
 analog pressure signal proportional to
 frequency differences 14 p2318 A67-28345
 Superconductor dynamic intermediate
 state DC voltage caused by flux motion
 shown by frequency spectrum measurements
 of noise voltage 14 p2369 A67-28600
 Phase determination of signal components
 generated by parametric oscillator by
 synchronizing oscillator with respect to
 difference between frequencies of
 components 15 p2443 A67-29357
 Occurrence frequency of midlatitude
 blanketing sporadic E studied for seasonal,
 diurnal and latitudinal
 variations 15 p2476 A67-29622
 Measurements of short term frequency or
 phase fluctuations of gas lasers, noting
 random Gaussian
 perturbation 15 p2499 A67-29730
 Frequency measurement of gas laser
 transitions in heavy water and acetylene
 discharges 16 p2685 A67-30824
 Daily geomagnetic variations
 superpositional nature studied by factorizing
 frequency functions describing day-to-day
 variability 16 p2684 A67-30971
 Digital technique for recording of step-
 frequency ionospheric soundings, obtaining
 maximum and lowest observed
 frequencies 16 p2625 A67-31340
 Differential Doppler effect on earth
 satellite radio signal and application to
 ionospheric electron density
 studies 16 p2627 A67-31463
 Nonlinear laser theory to calculate
 amplitudes, frequencies and beat frequencies
 of circularly polarized modes in laser with
 axial magnetic field 16 p2686 A67-31562
 VLF worldwide comparison of atomic
 standards, noting statistical analysis of data
 and possible sources of
 error 16 p2632 A67-31860

Differential phase-shift measurements at UHF and microwave frequencies, discussing standards, techniques and uncertainties in characteristics 17 p2815 A67-32608

Swept measurement techniques, discussing reflection coefficient and slotted line accuracy using signal flow graph 17 p2815 A67-32610

Micrometeoritic cloud existence near earth refuted by satellite incidence-frequency measurements, describing satellite measuring devices 17 p2850 A67-32975

Luna IX and Luna X near moon, studying injection phase, orbit and landing phase from transmitted frequency observations 18 p3003 A67-34242

Radar cross section measurement using standing wave method 19 p3184 A67-35826

Statistical properties of strong light intensity fluctuations propagating in ground layer of atmosphere investigated to measure frequency spectra 19 p3254 A67-36017

Scheme for obtaining zero beats using broad range of phase frequency modulations for direct determination of laser frequencies 19 p3241 A67-36024

Simply-supported elliptic plate free vibration problem applying Rayleigh-Ritz technique to obtain fundamental frequencies 20 p3539 A67-37007

Effect of electromagnetic field interaction with gravitational field calculated from satellite data, determining difference between frequencies 20 p3386 A67-37523

Doppler frequency measurement error due to short fading relative to time constant of automatic phase control loop 21 p3584 A67-38674

Measuring device for frequency and resistance change measurements in quartz crystals due to temperature variations 21 p3601 A67-38975

Base bleed effects on flow behind two-dimensional model with blunt trailing edge, measuring base pressure, shedding frequency and vortex formation 21 p3566 A67-39078

Carrier frequency measurement accuracy using panoramic radio receiver, discussing statistical estimate of errors using two different reading methods 22 p3772 A67-39871

Absolute frequency measurements on continuous wave hydrogen cyanide submillimeter laser lines 24 p4166 A67-41861

FREQUENCY MODULATION

SA FEEDBACK FREQUENCY MODULATION /FBFM/

SA PULSE AMPLITUDE MODULATION /PAM/

SA PULSE FREQUENCY MODULATION /PFM/

SA PULSE MODULATION

Phase locking, mode selection and noise problems in synchronous operation of microwave silicon avalanche diode oscillators to obtain large coherent output power 01 p0033 A67-10016

Pulse frequency multistable devices whose states differ, along with output voltage, by generated pulse rate 01 p0043 A67-10239

Book on statistical communications theory, digital communications, AM and FM CW communications, binary communications and noise 01 p0021 A67-10306

Response of linear FM matched filter to gated noise 01 p0037 A67-10484

Output autocorrelation function and spectral density of CW and FM signals passed through TWT 01 p0025 A67-10858

Paired echo sidelobe produced by ripples of Fresnel spectrum in active linear compressed-pulse frequency modulation 01 p0027 A67-11328

Reflection measurements with broadband FM using long transmission lines 02 p0193 A67-11783

Compatible double sideband/single sideband/constant bandwidth FM telemetry system for wideband data 02 p0197 A67-12010

Data quality assurance program for telemetry ground station operations, noting frequency division and time division formats 02 p0198 A67-12023

Frequency shift keyed /FSK/ digital signal detection using FM discriminators, predicting error rates for several sequences 02 p0201 A67-12118

Vestigial sideband FM mode combined with three-level coding for data transmission at 4800 bauds 02 p0201 A67-12119

Swept frequency modulation program,

emphasizing lack of design information for optimizing performance and networks design with large time bandwidth products 02 p0202 A67-12124

Analog magnetic recording in ground telemetry stations 03 p0418 A67-12896

DC parametric device in which capacitance variation of silicon p-n junctions due to input signal causes FM 03 p0377 A67-13106

Characteristics and performance of two solid state devices, using FM principle for measurements of low currents, suitable for space vehicles 03 p0377 A67-13107

Book on principles of construction and theory of main elements and assemblies of analog radio telemetry systems with frequency and time channel separation 03 p0367 A67-13123

SHF modulation techniques for laser radiation, covering Faraday, Kerr and Pockel effects, circular dichroism, etc 03 p0436 A67-13138

Internal modulation and heterodyning in construction of highly linear large-deviation VHF solid state FM oscillator /FMO/ 03 p0381 A67-13636

Noise reduction in FM receivers with negative frequency feedback by reducing IF bandwidth 03 p0381 A67-13662

Book on circuitry for RF, AM and FM electronic communication systems 03 p0388 A67-14272

Coding method for transmitting digital data over IIRIG-FM/FM telemetry system applied to German-American high altitude/space flight program 04 p0569 A67-14572

Signal design and principle of vernier FM radar system to measure surface characteristics of small target at long distance and range 04 p0570 A67-14877

Asymptotic method of synthesizing FM pulse signals from given autocorrelation function 04 p0575 A67-15160

Spectrum broadening of long-duration HF pulses by FM 04 p0577 A67-15675

Electronic testing of transmitters and receivers noting AM and FM systems sensitivity, noise figures and image rejection 04 p0590 A67-15727

Frequency modulation of GaAs semiconductor laser by ultrasonic wave modulation of dielectric constant 05 p0821 A67-16871

Stationarity conditions for FM oscillations with noise modulated frequency 05 p0766 A67-17167

FM in quartz oscillators, deriving nonlinear distortion and frequency deviation factors and analyzing effect of destabilizing factors 05 p0767 A67-17400

Threshold performance of limiter discriminator phase locked demodulator and FM feedback demodulator 06 p0969 A67-18107

Radio relay systems with frequency, single sideband and pulse phase modulation 07 p1141 A67-19342

Kerr cell properties noting four-electrode cell giving frequency shift of 60 mc for laser beam 07 p1142 A67-19552

Cancellation of unwanted spectral components in FM multivibrator system by generating cancelling component in square law device 07 p1145 A67-19871

LF modulation technique used aboard Canadian ionospheric research satellite ISIS-A for tape recording of signals with VLF components 08 p1298 A67-20662

PDM/FM high efficiency voltage regulator design, switching theory and regulation theory 08 p1286 A67-21030

FM of RC generator by connecting parametric voltage transducer output to phase shift network and applying generated voltage to transducer input through matching network 09 p1496 A67-21692

FM noise source in cavity controlled Gunn effect oscillator 09 p1474 A67-22040

Beam-plasma interaction with transverse modulation, obtaining growth rates 09 p1546 A67-22280

Gas laser dynamic behavior, discussing internal modulation, mode locking, noise and perturbation modes 09 p1515 A67-22431

Single frequency light from argon FM laser with external lithium niobate modulator, discussing overall conversion efficiency and distortion 10 p1664 A67-22906

Reduction of peak factor in FM system

design leading to reduction of thermal noise and increase in spectrum truncation distortion 11 p1752 A67-24123

Threshold region of FM signals having carrier modulated by Gaussian baseband signal 11 p1752 A67-24124

Cross correlation and statistical dependence between envelope and frequency deviation of sine wave plus random noise, noting possible application to frequency demodulation 11 p1753 A67-24646

Pulse compression parallel channel technique for evaluating channel filter characteristics effect on compressed pulse form 11 p1754 A67-24648

Parametric resonance excitation of Alfvén waves by small LF modulation of DC magnetic field imposed on ideal MHD plasma 11 p1844 A67-25062

Amplitude and frequency fluctuations in flicker noise region of transistorized quartz oscillator 13 p2075 A67-26395

High input impedance obtained with junction transistors, discussing circuit design for different frequency modulators, FET properties and applications 13 p2077 A67-26661

Alternative modulation techniques for Satellite Telecommunications with Automatic Routing, considering start-stop operation with PCM-FDM system 13 p2068 A67-26720

Effect of distortion on spectrum of pulse signal with linear frequency modulation 13 p2070 A67-27046

Ionospheric dispersion of AM-FM artificial satellite signals noting distortion effects, synchronization and interference difficulties 13 p2070 A67-27197

Modulation and demodulation methods for multiplex telemetry, discussing PCM, PSK and SSB 14 p2271 A67-28682

Discriminator threshold and SNR above threshold response when demodulating FM signal undergoing selective fading 14 p2273 A67-28711

Book on theory and practice of transistor circuits covering oscillator theory, transistor noise, frequency modulation, band filter linkage, etc 14 p2290 A67-29007

Asymptotic method of synthesizing FM pulse signals from given autocorrelation function 15 p2435 A67-29347

Internal and coupling modulation and mode locking of continuous ruby laser 15 p2499 A67-29729

Direct experimental verification of frequency modulating semiconductor injection laser using ultrasonic waves 15 p2499 A67-29731

Short term stability of beat frequency of two stable single-frequency carbon dioxide-nitrogen-helium lasers 15 p2499 A67-29732

Intermodulation distortion due to nonlinear elements in transistors analyzed using Volterra series representation 15 p2455 A67-30386

TV signal transmission over gas laser light beam with ADP crystal at 7GHz modulating frequency 16 p2684 A67-30610

Method to extend operation range of FM altimeters, with block diagram of proposed system 16 p2676 A67-31274

Ballistic range blast-traversal testing technique using scale models containing fast response FM telemetry system modulated by capacitance type pressure transducer [AIAA PAPER 66-777] 17 p2832 A67-32063

Digital error performance of transportable troposcatter facility evaluated as function of path length 17 p2811 A67-32118

Plasma jet electrical conductivity, using inductances with different diameters as measurement device 17 p2895 A67-32154

Radar system using real-time on-line computer applied to adaptive control of beam direction and transmitter modulation 17 p2816 A67-32790

Fabry-Perot interferometer for discriminating gas laser modulation at frequencies less than Doppler bandwidth 17 p2869 A67-33294

Potassium dihydrogen phosphate inside laser cavity to achieve HF modulation 17 p2869 A67-33297

Signal and noise FM modulated random process characteristics determined by equation for correlation function, giving energy spectrum relationship of modulated process phase 18 p3001 A67-34177

Noise in injection-synchronized oscillators, deriving inequality 18 p3011 A67-34221

Structure of quasi-linear and wideband
satellite transponders, discussing possible
improvements 18 p3003 A67-34356

FM laser frequency stabilization employing
stabilization discriminant derived from
residual phase variation and laser beat
note 19 p3240 A67-35622

Input-to-output amplitude and phase
modulation characteristics derived for
multicavity klystron 19 p3197 A67-35809

Estimation of fluctuation sensitivity of
measuring radio receiver modulated by
intermediate frequency amplifier 19 p3198 A67-36016

Scheme for obtaining zero beats using
broad range of phase frequency modulations
for direct determination of laser
frequencies 19 p3241 A67-36024

Small correlated amplitude and frequency
fluctuations of stochastically-modulated radio
waves 19 p3241 A67-36025

Frequency modulated transmitter and
receiver for audio high speed data
transmission including discriminator for
analyzing and distinguishing
waveforms 20 p3379 A67-36247

Near IR grating spectrometer converted to
multiplex instrument by adding encoding
disk in spectrum plane 20 p3437 A67-36339

Intermodulation interference effect on
PCM/FM error rates studied using power
series as mathematical
model 20 p3380 A67-36583

Small alternating magnetic field
modulation effects on sampled output of
rubidium magnetometer with frequency
counter 20 p3448 A67-36876

Triode system of reflex klystron, stressing
operation of modulated SHF oscillations
device 20 p3451 A67-37148

Frequency shift keyed /FSK/ digital signal
detection using FM discriminators,
predicting error rates for several
sequences 20 p3385 A67-37351

Frequency locked loop FM demodulator
with high noise threshold 20 p3385 A67-37352

RF mixer and limiting IF models for RFI
analysis of local oscillator control in FM-CW
receivers, using digital computer
simulation 20 p3405 A67-37649

Approximate method for design of FM
compression using variable capacitance varactor
diodes, noting time varying differential
equation 21 p3593 A67-38234

Short range FM transmitter-receiver
system for shock measurements required to
optimize shock absorber
design 21 p3581 A67-38395

Frequency limitations of PCM
communication, determining PCM/PM and
PCM/FM power spectra for hybrid
modulation spectra
calculations 21 p3584 A67-38652

Discrete errors in continuous angle-
modulation systems, considering conventional
fidelity /SNR/ criterion and probabilistic
theory 21 p3584 A67-38653

Traveling wave maser saturation and
signal distortion, determining magnetic
moment 21 p3642 A67-38813

FM/PM and FM/FM radio telemetry in
proportional and constant band covering
regulation, SNR, noise threshold,
etc 21 p3587 A67-39050

Waveguide dispersive line use in FM pulse
compression system outlined for high
resolution in S-band radar 21 p3601 A67-39068

Selective circuit with FM system and
constant gain designed to determine radio
whistler arrival direction as function of
frequency 21 p3587 A67-39125

High speed wideband L-band tunnel diode
frequency deviator tunable over octave
bandwidth by 160 mv change in input
voltage
[IEEE PAPER 19-TP-67-1175] 23 p3978 A67-40743

Laser mode synchronization by electro-
optical crystal dielectric constant modulation
mounted inside resonator 23 p4013 A67-40903

Wideband FM demodulation system
providing good reception with smaller radio
SNR through delayed
signal 23 p3975 A67-41677

Double signal modulation used to increase
authenticity of information transmission in
binary systems having resolving
feedback 24 p4122 A67-42378

FM oscillations spectrum component
amplitude formula for multiple frequency

modulation using Bessel
function 24 p4122 A67-42379

Book on radar signals covering FM pulse
compression signals, waveform, Doppler
shift, time factor etc 24 p4122 A67-42425

Millisecond bursts in radio emission from
Jupiter not imposed by interplanetary
scintillation but by amplitude or frequency
variation in source 24 p4231 A67-42452

FREQUENCY MULTIPLIER

Varactor diodes and frequency multiplier
surveyed for application in harmonic
generation at microwave
frequencies 01 p0034 A67-10165

Output power of frequency multiplier
using varactor diode for given output
voltage and terminal resistances at various
harmonics 01 p0039 A67-10857

Analytic performance calculation for
varactor frequency doubler with various
degrees of nonlinearity 01 p0040 A67-11234

Maximum power transformed by nonlinear
capacitance of semiconductor diode on
closed p-n junction 02 p0210 A67-11510

Time domain analysis of bridge doubler
circuit for varactor
multiplier 02 p0218 A67-12100

MOS-FET broadband frequency doubler
circuit 03 p0382 A67-13671

SHF oscillator construction using
multiphonon processes that occur in gases
during dipole interactions 04 p0580 A67-14749

Microwave varactor tuned transistor
oscillator design, considering collector base
multiplication, oscillation and load matching
conditions and theoretical tuning
curve 04 p0581 A67-14864

Analog carrier frequency multiplier using
Hall effect in multiplier
element 04 p0581 A67-14892

Frequency multiplication using diffusion
capacitance with derivation of efficiency
expression 05 p0766 A67-17165

Possibility of realization of multicascade
tunnel diode frequency doublers without
intercascade amplification 05 p0777 A67-17173

Optimal regime conditions in engineering
calculation of generating device with self-
parametric frequency multiplication, using
nonlinear inductance in ultrasonic frequency
range 06 p0970 A67-18171

UV radiation generation from output of
Nd glass laser by frequency doubling in
ammonium dihydrogen phosphate
crystals 06 p1011 A67-18712

Avalanche multiplication in Ge and GaAs
p-n junctions, comparing experimental and
theoretical ionization rates, predicting
voltage breakdown 06 p1065 A67-18954

VHF tunnel diode frequency multiplier
noting power gains and
circuit 07 p1155 A67-19793

Varactor junction diode frequency
multipliers emphasizing maximum conversion
power and efficiency 10 p1809 A67-22836

Two-cascade frequency multiplier with
traveling wave tube at various input
frequency ranges and high conversion
coefficient 10 p1613 A67-23406

AC background in phase of output
oscillation of multistage frequency
multipliers attributed to presence of HF
harmonics in automatic bias
circuit 10 p1613 A67-23448

Step-recovery action in transistor switch-
off with current gain and reduction of load
on driving source 13 p2078 A67-26784

Step recovery diode as frequency
multiplier, discussing p-n barrier layer
diode 13 p2082 A67-27389

Varactor multiplier circuit design and
equations for harmonic
currents 13 p2089 A67-27724

Frequency multiplication of microwaves by
field electron emission in superconducting
cavity 14 p2278 A67-27787

Maximum power transformed by nonlinear
capacitance of semiconductor diode on
closed p-n junction 14 p2283 A67-28073

All solid state wideband telemetry
transmitters realization by compact high-
powered frequency
multipliers 14 p2288 A67-28692

Frequency doubler using two-diode
varactor array to obtain double output
power 15 p2442 A67-29176

Frequency tripling of electromagnetic
waves passing through hot electron gas in
semiconductors, deriving third harmonic
amplitude for helical
wave 16 p2628 A67-31500

High power frequency multiplication using
beam lead varactors in arrays noting
construction, technique and conversion
loss 17 p2826 A67-32623

Beat frequency generation and
multiplication and subsequent harmonic
amplification in plasma-beam system,
particular case of plane
waves 18 p3087 A67-34037

Spurious phase modulation reduction in
multistage frequency multiplier using
lumped-selection filters, determining cut-off
angle in multiplying
cascades 18 p3000 A67-34087

Nonlinear impedances used for frequency
multiplication 19 p3182 A67-35033

P-n junction diode frequency doubler
operating in charge-storage/step-recovery
mode efficiency and power
output 20 p3395 A67-36315

Frequency multiplier operating from 10-30
GHz with easily tunable construction,
obtaining lossy element influence
approximation 20 p3398 A67-36863

Design of adaptive systems with forced
oscillations, using correlation and filter
methods 20 p3410 A67-37228

Short circuit photocurrent of avalanche
photodiode, determining frequency response
and multiplication effect on
bandwidth 22 p3767 A67-39362

Three-photon combination process used to
increase laser emission frequency,
determining laser field
strength 22 p3815 A67-39760

Frequency doubler and divider using
transistorized synchronized switching phase
detectors with closed feedback
circuit 22 p3762 A67-39872

FREQUENCY RANGE

Temperature dependence of complex
initial magnetic permeability of cobalt-zinc
ferrites over 0.1-2000 mc frequency
range 01 p0128 A67-10079

Vibroplate pickups for measuring mean
values of nonsteady state forces, noting
maximum permissible limits of frequency
change of pickups 01 p0084 A67-10422

Log periodic antennas operating in SHF
bands having nonserrated radiation
patterns 01 p0036 A67-10444

Stability theory application to control,
circuit theory and aerospace
systems 01 p0047 A67-11221

Q-active filter for narrow-band noise
measurement in LF range 02 p0216 A67-12038

TE modes propagation in rectangular
waveguides containing two dielectric slabs,
computing cut-off frequencies and
propagation constants 04 p0570 A67-14860

Dispersive network of apparatus producing
dispersion in pulse compression system,
noting role of relatively low center
frequency 04 p0574 A67-15055

Single mode 6328 angstrom units He-Ne
laser having single frequency power output
of 50 mwatt stabilized by feedback system
whose output is neither amplitude nor
frequency modulated 05 p0823 A67-16685

ELF and VLF wave propagation in earth-
ionosphere waveguide at wide frequency
range, giving amplitude spectra and mean
phase velocity for day and
night 06 p0994 A67-17970

Transistorized wideband and pulse type
amplifiers for nanosecond frequency
range 06 p0970 A67-18191

Satellite communications system noting
instrumentation, design criteria, frequency
range, propagation aspects and suitable
trajectories 07 p1141 A67-19344

Iron doped rutile traveling wave maser
operating in 34-36 GHz frequency
range 07 p1196 A67-19605

Ionospheric disturbances from high
altitude nuclear detonations observed as
changes in F-2 layer critical
frequency 07 p1181 A67-19939

Equalization and cancellation model of
binaural unmasking applied to data on
interaural just-noticeable
differences 08 p1290 A67-20482

Frequency broadening of natural
oscillations of optical resonator upon
interaction with two-level atom in
electromagnetic field 08 p1337 A67-20868

Frequency spectrum during UHF plasma
oscillation excitation by monoenergetic
primary electrons introduced into low
pressure Hg discharge 08 p1358 A67-20869

Probability of signal acquisition by phase

locked oscillator system operating in frequency search mode, determining maximum admissible search rate without noise 08 p1295 A67-21275

Upper frequency limit prediction method for Gunn oscillations 09 p1556 A67-22264

Frequency sharing and compatibility of satellite and terrestrial radio relay systems design, discussing interference effects 09 p1464 A67-22411

Radio burst produced by solar flare on August 28, 1966, analyzing flux increases as function of time and frequency 10 p1703 A67-23803

Wideband miniature bridge constructed on basis of quarter wave two-conductor shielded line for UHF and SHF 11 p1757 A67-23911

Sheath helix antenna with conducting core, noting variation of operation characteristics with core size and pitch angle 11 p1760 A67-24277

Anomalous Hall effect in microcrystalline germanium at SHF 11 p1846 A67-24471

Statistical analysis of solar dm radio bursts in frequency range 536-2000 mc/s 12 p1993 A67-25132

Contribution of propagation factors in terrestrial atmosphere to noise received by antenna at hyperfrequencies 12 p1904 A67-25308

Si avalanche diode with p-n-n mesa structure, noting high efficiency and high power output at UHF 13 p2076 A67-26519

Recording of frequencies from 0 to 1000 Hz on low priced media 13 p2119 A67-26662

Microminaturizable transistorized circuit for generating wide frequency range high Q inductances from semiconductor devices for integrated selective circuits 13 p2081 A67-27201

Two digital computer filing programs for determining ordinates of propagation curves of ground waves in visible region 13 p2070 A67-27202

Design chart for parameter derivation of basic digital synthesizer, noting advantage in handling of tradeoffs 14 p2276 A67-28919

Current strip in cold magnetoplasma, noting radiation resistance of Hertzian dipole for large frequency ranges 15 p2521 A67-29185

Stability of feedback systems with monotone and odd monotone nonlinearities 15 p2457 A67-29374

Frequency dependence of radio star scintillations 15 p2555 A67-29621

Human response model identification in manual control system applied to study of stability and performance of man-machine system 15 p2432 A67-30315

Path diversity in millimeter waves propagation through rain for various frequency 16 p2625 A67-31343

Concentric ring array application to space tapering of planar arrays, noting obtainable frequency ranges and scan angles 16 p2640 A67-31526

Atmospheric modulation noise in optical heterodyne receiver, deriving signal power variance and mean-square frequency spread from propagation statistics for wave structure function 16 p2630 A67-31807

Atmospheric noise data for various frequencies and various latitudes and longitudes 16 p2632 A67-31861

Nature of Pcl oscillations in solar cycle, discussing frequency spectra of data obtained 17 p2847 A67-32945

Frequency regions for Cerenkov radiation and power spectrum in collisionless magnetoplasma calculated using refractive index 18 p3090 A67-34428

Estimation method for lower bounds of natural frequencies of circular closed cylindrical shell 19 p3338 A67-34876

Optical auroral pulsations in various frequency ranges analyzed using automatic zenith photometer 19 p3222 A67-35459

Linear operation of diffused planar transistor in common emitter connection studied by mathematical models 20 p3396 A67-36377

Equivalent circuits derived by mathematical model from experimental data on diffused planar transistor 20 p3396 A67-36378

Degree of isolation between radar tracking data and motion of ship determined, using frequency domain 20 p3415 A67-36555

Dynamic spectrum of long-period

geomagnetic pulsations noting Pc range characteristics 20 p3433 A67-37413

Equivalent quadrupoles for analyzing ultrasonic systems using piezotransducer disks operating at any frequency 20 p3401 A67-37454

Multiply-tuned antenna array operating over certain frequency range through electric beam shifting 20 p3403 A67-37507

Scattering amplitude of frequency spectrum components of isolated exponential acoustic pulse incident on hard sphere 21 p3657 A67-38057

Meander-line antenna operated under backfire conditions studied for electrical performance and radiation properties 21 p3597 A67-38397

Solar radio spectrograph using broadband logarithmic antenna, considering receiver operation and frequency range 21 p3627 A67-38497

Electromagnetic wave pulses transmission through plasma boundary, studying boundary effects for broad and narrow frequency spectra 21 p3669 A67-38682

Wideband miniature bridge constructed on basis of quarter wave two-conductor shielded line for UHF and SHF 21 p3600 A67-38939

Thick walled cylindrical shell mobility over wide frequency range, predicting vibration response based on normal mode series convergence 21 p3729 A67-39059

Upper and lower bounds for frequencies of free vibration developed for uniform rectangular cantilever plates 21 p3730 A67-39094

Channel Evaluation and Call /CHEC/ system to improve air-ground-air communications by automatic selection of optimum channels 22 p3760 A67-39664

Deep-space communication capability spectral dependence analysis indicates optical transmissions would be several orders of magnitude poorer than RF technology 22 p3764 A67-40558

Ion wave propagation in weakly ionized gases 23 p4032 A67-40960

Dependence of decametric radio emission from Jupiter on positions of Galilean satellites with respect to sun, earth and Jovian magnetic plane 23 p4069 A67-41362

Frequency limitation of Gunn effect associated with relaxation time for intervalley electron scattering in small signal approximation 24 p4205 A67-42811

Signal processing and control computer system for materials research noting use in viscoelastic studies of crystalline polymers 24 p4126 A67-42930

FREQUENCY REGULATOR

Tunable dispersion resonator and broadening of laser emission spectral range to obtain operating frequency other than fundamental 03 p0435 A67-13131

Small signal suppression and third order intermodulation products of ferrite frequency-selective limiters 05 p0780 A67-17532

FREQUENCY RESPONSE

Amplitude and frequency characteristics of hydrogen-atom beam maser 02 p0251 A67-11574

Frequency dependences of amplification index of linear amplifier at 3.39 micron wavelength for various excitation levels 02 p0191 A67-11576

Wind tunnel technique for measuring frequency response of flexible airplane to vertical sinusoidal gusts [AIAA PAPER 65-787] 03 p0354 A67-12908

Linearized motion equation of self-adaptive systems with stabilized frequency characteristics, considering effect of control and noise signals in basic control loop 03 p0390 A67-13101

Sharp cut-off nonlinear filter design with jump effect for rapid gain increase with small frequency increment 03 p0386 A67-13981

Accelerometer frequency response and quadratic lag function amplitude response curves and relation to resonant frequency 04 p0627 A67-15792

Current and frequency dependent differential resistance and diffusion capacity of junctions of p-n-n structures at high current densities 06 p1049 A67-17868

Resistive effects in type II superconductors near upper critical field

examined, using Ginzburg-Landau equations 06 p1049 A67-17882

Inductive correction effect on single stage tunnel diode RC amplifier, noting increase of upper frequency limit and shortening of wave front buildup time 06 p0970 A67-18213

Optimal signal transmission in detection system characterized by optimal linear filtration of reflected signal 06 p0963 A67-18216

Holographic evaluation of spatial frequency response of photographic emulsions 07 p1186 A67-19493

Parameter plane analysis of forced oscillations and jump resonance phenomena in nonlinear systems with periodic forced signals 08 p1311 A67-20343

Frequency response functions determined from correlation functions of force and response, using Bartlett triangular weighting function 08 p1353 A67-20592

Dynamic properties of coupled systems derived from experimentally determined frequency response functions of component systems, noting cross correlation functions 09 p1573 A67-21752

Pressure calibration methods for testing response of microphones in difficult conditions of temperature, pressure and frequency 09 p1484 A67-21938

Theory of lateral transistor current gain and frequency response 09 p1472 A67-21948

Nonlinear automatic system with logical device analyzed in presence of external action, obtaining harmonic linearization coefficients 09 p1482 A67-22080

Simple diode parametric amplifier, discussing bandwidth and noise measurements and compensating circuits for gain-frequency response improvement 09 p1474 A67-22085

Signal and noise response of Ge avalanche photodiodes noting design, fabrication, LF photomultiplication and static V-I characteristics 09 p1475 A67-22200

Insulated gate to obtain depletion in channel of MOS-FET transistor, noting inversion layer and frequency response 09 p1475 A67-22202

Least squares methods for calculating stability derivatives of aircraft from unsteady flight data 09 p1438 A67-22474

Azimuthal modes of Kadomtsev plasma instability, describing subthreshold response spectra 11 p1829 A67-24001

Approximate normal mode technique, providing solution to sinusoidal and white noise randomly excited damped linear multi-degree of freedom system, for application to mathematical model [ASME PAPER 67-VIBR-2] 11 p1871 A67-24164

Frequency response, equation of motion, elastic restraint and structural flexibility of gyroscopic vibration absorber, noting antiresonant frequency functions [ASME PAPER 67-VIBR-13] 11 p1795 A67-24173

Torsional vibration and steady state response of geared system, noting computer programming [ASME PAPER 67-VIBR-63] 11 p1797 A67-24205

Inclined log spiral antenna, noting back radiation reduction and frequency independence 11 p1783 A67-24294

Conductivity of plasma capacitors in inhomogeneous plasma found to increase with frequency due to density gradient and resonance 12 p1969 A67-25194

Response of superconducting sheath state of lead-indium in Ac and Dc magnetic fields studied, noting transition changes response of superconducting sheath state of lead-indium in AC and DC magnetic fields studied, 12 p1985 A67-25847

Thin film superconducting bridge behavior in microwave field noting dependence of deviation from classical rectification on frequency, power, temperature and bridge width 12 p1985 A67-25848

Piezoelectric accelerometer capacitance measurement and computation involved in conversion of accelerometer voltage sensitivity from one external circuit capacitance to another 12 p1947 A67-26186

Intermodulation noise calculated for case of distortion variable in any way with frequency 13 p2070 A67-27195

Characteristics of waveguide resonant-iris filters for microwave

generators 13 p2083 A67-27444
Higher harmonic components of twecks as evidence of adequacy of waveguide mode theory of VLF propagation between earth and ionosphere 14 p2307 A67-27888
Constant temperature hot-wire anemometer circuit using solid state amplifiers, obtaining frequency response expression 14 p2315 A67-28159
Experimental evaluation of fluidic transmission line theory, studying frequency response and sending impedance 14 p2251 A67-28349
Feedback control theory for constant temperature hot-wire anemometers using differential equation applied to frequency response optimization 14 p2320 A67-28750
Analog multiplier using p-n junction dynamic capacitance, noting decays in RC circuit current 14 p2290 A67-28928
Parameter stability regions with frequency response, noting interpretation for several parameters 15 p2457 A67-29366
Time and frequency accuracies obtainable with geostationary satellites, noting measurement error sources 15 p2565 A67-29593
MOS transistor HF behavior noting phase shift, frequency dependence, etc 15 p2449 A67-29805
Oscillator with lumped parameter superconducting L-C tank circuit, noting frequency variations as function of temperature 15 p2451 A67-29916
Random noise and measurement errors limitation upon system identification in time domain 15 p2463 A67-30332
Continuous estimation of frequency response of linear system directly from random input and output data measurements 15 p2465 A67-30345
Inductive correction effect on single stage tunnel diode RC amplifier, noting increase of upper frequency limit and shortening of wave front buildup time 16 p2635 A67-30479
Optimal signal transmission in detection system characterized by optimal linear filtration of reflected signal 16 p2620 A67-30482
Book on modern control systems covering feedback control theory within framework of frequency and time domain analysis 16 p2643 A67-30621
CRT flying-spot-scanner spatial frequency response, determining film-plane modulation response to periodic sine/square wave 17 p2860 A67-32665
Frequency response of nonlinear system, analyzing saturation characteristic of amplifier by digital computer 17 p2821 A67-32933
Frequency response of DC and AC currents flowing to RF resonance probe in quiescent cesium plasma, explaining measurements 18 p3044 A67-33713
HF response of local burning rate in laminar diffusion flames subjected to transverse sound waves in free stream 18 p3108 A67-33831
Temperature and frequency response of argon arc continuum emission coefficient, explaining unexpected deviations 18 p3089 A67-34299
Pressure dependent surface reaction effects on acoustic response of composite solid propellants studied for various coatings 19 p3309 A67-35010
Temperature and frequency effects on amplitude-independent longitudinal ultrasonic attenuation in superconducting lead 19 p3304 A67-35538
Frequency response of longitudinal control transmission of transonic aircraft 19 p3176 A67-35570
Calculation of frequency characteristics of hydraulic main line sections with parameters varying continuously along length 20 p3363 A67-36444
Admittance function for burning surface by solving differential equation and satisfying boundary conditions, discussing frequency peaks qualities 20 p3554 A67-37255
Hydraulic line models for fluid control system analysis, discussing frequency and transient response calculation simplification 20 p3366 A67-37365
Fluid control system design by third order linear differential equation with transient response, showing relationship to frequency response 20 p3366 A67-37370
Spurious response identifying equations

for more realistic P and Q values on multiple conversion 20 p3404 A67-37636
Receiver mixer design characteristics effect on prediction of spurious response levels 20 p3405 A67-37648
Minimum detectable signal and frequency response of mercury-doped germanium detector, measuring response time and SNR through optical heterodyne techniques 21 p3590 A67-38009
Short circuit photocurrent of avalanche photodiode, determining frequency response and multiplication effect on bandwidth 22 p3787 A67-39362
Boiler inlet impedance frequency response in single tube heat exchanger when pumped with oscillating flow 22 p3916 A67-39390
Optically pumped vapor rotatory power as optical pumping experiment monitoring technique, discussing specific rotatory power and refractive index dependance on light frequency 22 p3816 A67-40320
Modulation transfer theory for frequency response of optical system in temporal or spatial domains, discussing Fourier series and transform [SMPT PAPER 102-47] 22 p3808 A67-40380
Phase characteristics linearity of LF regenerative amplifiers with reactive elements and Chebyshev amplitude frequency responses 24 p4129 A67-42226
Digital imaging techniques used in sinusoidal frequency response modification with or without computer control and display on operator console 24 p4125 A67-42429
Moderate bandwidth tunnel diode amplifier using directional filter as bandpass structure 24 p4131 A67-42445
Frequency and intensity of laser light analyzed for reaction of coupled optical resonator 24 p4168 A67-42574
Frequency Response and direct numerical integration of governing differential equations, considering gas-lubricated tilting-pad journal bearing stability [ASME PAPER 87-LUB-8] 24 p4162 A67-42672

FREQUENCY SCANNING

Beam scanning and beam forming techniques for phased-array radar, noting frequency and phase scan methods 04 p0596 A67-15049
Frequency and phase scanning for pencil-shaped beam antenna 07 p1152 A67-19546
Digital, matrix and intermediate frequency scanning 07 p1152 A67-19547
Frequency scanned filter in radar signal processing system designed to extract range and Doppler resolution, using properties of ambiguity function 09 p1466 A67-22695
Reception of signals reflected from ionosphere in vertical radar probing, examining frequency-difference combinations 13 p2087 A67-26569
Frequency scanning array of emitters on convex curve 13 p2069 A67-27031
Circuit for multifrequency ionospheric probing, with basic frequency scanning unit containing sawtooth pulse oscillator 14 p2315 A67-27949
Laser frequency variation and emission kinetics during generation process, investigating spectra at scanning rate and pumping energy ranges 18 p3061 A67-34619
Equations of motion of continuous single loop adaptive control system with scan modulated parameters, noting stability analysis method 20 p3408 A67-37044

FREQUENCY SHIFT

Intensity dependent frequency shift in spectral output of monochromatic giant pulse lasers measured, using Fabry-Perot interferometer 01 p0088 A67-10251
Born approximation theory of nonlinear scattering of microwaves from oscillating plasma column, noting diffraction patterns and frequency shifts 01 p0027 A67-11324
Absolute intensity and angular distribution of microwaves scattered from oscillating plasma column, noting diffraction patterns and frequency shifts 01 p0027 A67-11325
High order frequency shift measurement and general relativity 03 p0466 A67-12848
Theoretical curves for day and night time conditions for variation of peak frequency of radio atmospheric with distance computed from source spectrum and dominant propagation mode 03 p0415 A67-14117

SHF oscillator construction using multiphonon processes that occur in gases during dipole interactions 04 p0580 A67-14749
Electronic scanning of antenna beams, reducing feed complexity of large phased array by grouping of elements, tapering and array thinning 04 p0581 A67-15050
Isotope substitution effect on natural frequencies of vibrational-rotational transitions in diatomic and triatomic molecules and generation of new IR maser frequencies 05 p0816 A67-16634
Traveling wave ruby laser as radar transmitter noting power gain, coherence, frequency shift and single mode of operation 05 p0819 A67-16657
Optical heterodyne technique detecting stimulated Brillouin scattering, noting frequency shift demodulation arising from ruby laser light incidence on quartz crystal 05 p0823 A67-16688
Rising blue shift induced by acceleration in relativistically expanding objects and significance for intensity variations in quasars 05 p0898 A67-16926
Center frequency shifts of 6328 angstrom neon transition in Zeeman discharge cell measured in terms of discharge current and gas pressure 07 p1197 A67-20100
Phase locking systems and problems of frequency shifts and Doppler effect 10 p1620 A67-23508
Time dependence of coherent emission wavelength shift of GaAs-P laser diodes during flat-topped current pulsation 13 p2125 A67-26513
Doppler frequency changes of ionospheric propagating radio waves and relationship to geomagnetic variation 13 p2068 A67-26992
Frequency shift in emission spectrum of complex atom in uniform electric field, noting numerical results for Al I 13 p2168 A67-27208
Coherent radiation frequency conversion and nonlinear optics methods, including stimulated Raman scattering and Mandelstam-Brillouin scattering 14 p2330 A67-28467
Frequency shift associated with nonlinear extraordinary wave in cold plasma calculated using Bogoliubov method 15 p2524 A67-29230
Frequency shifting technique using auxiliary coil to produce magnetic field for masers in high power radar applications 15 p2439 A67-30392
Small scale trapping of laser beam and frequency shift in Raman radiations observed under various polarization conditions 16 p2884 A67-30807
Satellite tracking and data acquisition network of receiving stations /TRANET/ that acquires and processes Doppler frequency shift data 16 p2630 A67-31740
Frequency shifts on whistler mode signals from stabilized VLF transmitter from ionosphere and magnetosphere effects, noting electron density 16 p2631 A67-31856
Electric field enhanced Raman scattering and linear frequency shift of strontium titanate soft mode in random domain orientation and reorientation 18 p3098 A67-33520
IR spectra of gaseous, solid and matrix-isolated HNCS and DNCS, studying frequency shift, bending modes, fundamental vibrations, gas phase, etc 19 p3181 A67-35016
Cooling and illumination effect on Gunn oscillators resulting in abrupt shift from transit-time frequency mode to higher frequency 19 p3305 A67-35628
Frequency amplitude spectra of atmospheric from multiple stroke lightning, showing shift to VLF 20 p3480 A67-36290
Resonance frequency shift analysis of autostabilized light modulator at microwave frequencies noting heat transfer, transition temperature, etc 20 p3459 A67-36503
Gravitational radio wave frequency shift from satellite measurements, noting satellite-ground radio communication system 20 p3386 A67-37524
Steady random natural frequency variation and subharmonic resonance, discussing periodic right hand side Duffing type equation describing system 22 p3836 A67-39405
Degradation of moving clutter attenuation efficiency due to Doppler-frequency shift in MTI radar systems 23 p3972 A67-40642
Aerodynamic damping of turbine buckets and compressor blades noting flutter and

frequency shift 23 p3927 A67-40669

FREQUENCY-SHIFT KEYING

Frequency shift keyed /FSK/ digital signal detection using FM discriminators, predicting error rates for several sequences 02 p0201 A67-12118

Troposcatter transmission technique called frequency time shift keying, deriving optimum noncoherent receiver configuration and error performance 02 p0202 A67-12123

Troposcatter test program for evaluating megabit digital transmission system, using wideband frequency shift keyed modem 02 p0202 A67-12126

Time combined with frequency division multiplex multichannel communication system for transmission of digital information over tropospheric scatter communication channel 02 p0203 A67-12132

Microelectronic frequency discrimination techniques based on analyzing whole functional block and searching for circuit configurations 14 p2282 A67-28024

Frequency shift keyed /FSK/ digital signal detection using FM discriminators, predicting error rates for several sequences 20 p3385 A67-37351

FREQUENCY STABILITY

SA OUTPUT

Frequency stability of double beam ammonia laser with thermostatic quartz resonators on 3-2 line 01 p0088 A67-10247

Improved frequency stability and specific transistor characteristics of transistor oscillators with AGC 02 p0216 A67-11981

Frequency stabilization of Zeeman laser, using intensity crossover region with cavity tuning between oscillations on two orthogonally circularly polarized axial modes 09 p1513 A67-22134

LF instabilities and anomalous plasma processes in cesium discharge and thermal plasmas 11 p1829 A67-24000

Frequency stabilization of gas laser by discriminant, using discharge tube with gain profile split by AC magnetic field 11 p1801 A67-24664

Frequency stabilization of power klystron used in spectrometer for relaxation time measurement 11 p1767 A67-24752

Network analysis of frequency stability of quartz generators, showing possible reduction through additional HF cascades introduction into feedback loop 11 p1768 A67-24982

Laser measurements and standards of energy, power, attenuation and frequency stability, using pulsed ruby and gas lasers as radiation source 14 p2319 A67-28392

Integral equations in automatic control theory, deriving theorem which leads to Popov frequency domain stability criterion 14 p2292 A67-28635

Cross correlation bounds and positivity of nonlinear operators, examining criteria for positive composition 15 p2457 A67-29373

Fast warmup crystal oscillator, noting advantages and applications in equipment requiring low power consumption and frequency stability 15 p2445 A67-29584

Frequency and wavelength stabilization of gas lasers, noting wavelength shifts due to gas pressure and gain variations 17 p2815 A67-32611

FM laser frequency stabilization employing stabilization discriminant derived from residual phase variation and laser beat note 19 p3240 A67-35622

Cut-off amplifiers in frequency stabilization klystron designed to cut off only HF wave applied to discriminator 20 p3396 A67-36327

Crystal frequency stabilization in relaxation-oscillator circuit, showing similar use in astable multivibrator instead of LC circuit 20 p3384 A67-37215

High stability quartz master oscillator for D-1 satellite transmitter 21 p3591 A67-38206

Frequency stabilization of laser oscillator against reference laser amplifier, noting residual AM effects 21 p3641 A67-38461

Frequency stability of molecular beam laser in space environment during prolonged continuous and repeatedly interrupted operation 21 p3582 A67-38594

Transistor oscillator design stressing output, efficiency and frequency stability at maximum load conductance 21 p3598 A67-38602

Monograph on frequency stabilization of

LF oscillator by servo method, showing improved SNR of 21 p3587 A67-39126

Nonlinear radiation transport problem solution by reduction to linear, considering light resonant scattering in approximation of complete frequency mixing 23 p4051 A67-40909

FREQUENCY STANDARD

Radio measurement methods and standards, reviewing progress in atomic and quartz frequency standards, precision coaxial connectors, etc 05 p0804 A67-16008

Ruby laser with nonresonant feedback due to radiation scattering, showing use as optical frequency standard 05 p0818 A67-16642

Intercomparison of hydrogen and cesium frequency standard 09 p1494 A67-21616

Meteor burst radio propagation channel clock synchronization experiment to determine frequency offset between two remotely located frequency standards 09 p1494 A67-21618

Control system for frequency standard using frequency switching between two points on cesium resonance curve 13 p2121 A67-27226

Atomic and molecular frequency standards, reviewing ammonia and hydrogen masers and Cs, Tl and Rb gas frequency standards 14 p2333 A67-28975

Atomic frequency standards based on rubidium gas cell approach, noting atomic clock types and applications 15 p2487 A67-29582

Atomic frequency standards, noting cesium and thallium atomic beam devices, H maser, rubidium gas cells, optical pumping, etc 17 p2860 A67-32601

Relative merits of atomic frequency standards, discussing limitations, future outlook and applications 17 p2860 A67-32602

RF attenuation measurement methods and standards 17 p2815 A67-32607

FREQUENCY SYNCHRONIZATION

Transient response of frequency synchronization circuit determined with or without application of radar stability circuit 02 p0203 A67-12146

Electron concentration in ionosphere by coherent frequency method, examining Cosmos XI and Elektron I satellite measurement errors 09 p1491 A67-21893

Wave synchronization in gas laser with ring resonator cavity 09 p1513 A67-22063

Synchronized shadow photochronographic investigation of wire explosion shock waves in air 09 p1532 A67-22064

Crystal frequency stabilization in relaxation-oscillator circuit, showing similar use in astable multivibrator instead of LC circuit 20 p3384 A67-37215

HF oscillators phase bridge based on phase synchronization of identical and adjacent frequencies 21 p3590 A67-37947

Giant pulse ruby laser having tunable two-frequency output noting spectral measurements made with Fabry-Perot interferometer 23 p4015 A67-41038

FREQUENCY SYNTHESIS

Frequency doubling by varactor diode, expressing principal parameters as function of normalized amplitude of input voltage 01 p0039 A67-10856

Frequency fluctuations of laser field determined by measuring cross correlation function at two points 05 p0815 A67-16625

Errors by mutual interference in frequency-time coding in satellite communications systems, deriving expressions relating commissive and omissive error rates, simultaneous users per unit bandwidth, etc 06 p0961 A67-17696

Ruby and neodymium glass lasers sum frequency generation using nonlinear electro-optical KDP crystal 06 p1009 A67-17754

Power spectrum improvement of multiple wave trains by concentrating power close to carrier frequency, noting constructive and destructive interference 06 p0963 A67-18401

Method of radiation pattern synthesis for equally and unequally spaced arrays 14 p2285 A67-28451

Racalator as alternative to frequency synthesis noting design principles, operation and results 15 p2445 A67-29586

Variable-ratio frequency divider using integrated circuits of resistor-transistor-micrologic type 17 p2827 A67-32798

Electronically swept coherent frequency synthesizer for various bands 17 p2827 A67-32799

Sum generation of tunable two-frequency pulse output of gain-switched ruby laser 20 p3458 A67-36389

Digital frequency synthesizers analysis and synthesis, considering clocked-pulse and sine-wave systems to obtain guidelines for DFS system designs 21 p3601 A67-38974

FREQUENCY TRANSLATION SYSTEM

Standard frequency transfer to local oscillator, removing modulation and producing continuous stable carrier 02 p0210 A67-11530

Optical frequency translation of pulses from mode locked laser, noting Doppler shifts of large magnitude 02 p0253 A67-12506

Broadband microwave frequency translator using latching ferrite phase shifter 13 p2075 A67-26477

Tabulation of accidental coincidences between fundamental frequency of one laser and harmonic or subharmonic frequencies of another, as necessary condition for frequency translation between lasers 19 p3240 A67-35700

Active VHF translation repeater onboard ATS-1 for aircraft communication systems 20 p3381 A67-36591

FRESNEL DIFFRACTION

Operational notation characterizing basic optical elements as block diagrams gives results identical to those of Fresnel-Kirchhoff diffraction formula 01 p0028 A67-10433

Spatial coherence of laser light beam after extreme wavefront distortions on diffusion explained on basis of Fraunhofer and Fresnel diffraction 01 p0115 A67-11062

Space bandwidth theorem for Fresnel and Fraunhofer holograms, taking into account effects of photographic film 01 p0071 A67-11083

Diffusion influence on radio determination of meteor velocity by diffraction method 05 p0897 A67-16807

Fresnel-Kirchhoff diffraction theory interpretation of plane and three-dimensional hologram 06 p1003 A67-18105

Fresnel microzone plates for X-ray images of sun 10 p1707 A67-23232

Modes in unstable optical resonators and lens waveguides, noting spherical wave characteristics of geometrical eigenmodes 15 p2497 A67-29391

Dependence of focusing property of aperture on coherence length of illuminating field in Fresnel diffraction from aperture 16 p2639 A67-31358

High resolution holograms using Fresnel biprism to reduce noise 18 p3053 A67-34620

Irradiance due to square array of circular apertures from scalar Fresnel-Kirchhoff diffraction theory, giving plots of Fresnel diffraction patterns 22 p3835 A67-39235

Laser beam expansion in turbulent medium using Huygens-Kirchhoff principle and Fresnel diffraction approximation 22 p3761 A67-39739

FRESNEL INTEGRAL

Fresnel formulas for transformation of transverse electromagnetic wave into longitudinal plasma wave at dielectric-plasma interface, using Laplace transforms 09 p1464 A67-21993

Fresnel integrals for quadratures of motion for undamped vibrator, deriving equation for envelope of maximum amplitude 20 p3541 A67-37485

FRESNEL REFLECTOR

Approximation method for computation of radiation patterns from circular apertures and reflectors by single integration at wide angles and large Fresnel numbers 03 p0384 A67-13844

Optical properties of evaporated barium films investigated at various wavelengths, using ultrahigh vacuum reflectometer 03 p0499 A67-13909

Radiative transfer in heterogeneous scattering medium with Fresnel reflection at slab boundary interface, computing transmittance, reflectance and absorptance [ASME PAPER 67-HT-19] 20 p3545 A67-36714

FRESNEL REGION

Engineering method of calculating Fresnel coefficients based on use of nomograms 02 p0266 A67-11910

Approximation method for computation of radiation patterns from circular apertures

and reflectors by single integration at wide angles and large Fresnel numbers 03 p0384 A67-13844

Method for recording Fresnel transformations of two- and three-dimensional scenes illuminated by spatially incoherent light 03 p0423 A67-13907

Optical systems and holography in reconstruction of SHF antenna radiation patterns from field measurements in Fresnel zone 07 p1183 A67-19143

Phase distribution in laser aperture based on analysis of radiation in Fresnel zone 13 p2127 A67-27029

Nagelberg formula locating Fresnel region by phase center of aperture antennas examined by calculating phase patterns of radiation field 16 p2639 A67-31357

Optical systems and holography in reconstruction of SHF antenna radiation patterns from field measurements in Fresnel zone 17 p2861 A67-33222

Debye-Sears effect in one-dimensional Fresnel zone plate moving at acoustic velocity causes scanning of focal spots 22 p3835 A67-39242

Errors in measuring scattering patterns of arbitrary body in Fresnel region due to body/antenna finite distances and directivities 24 p4120 A67-42229

PRETTING

Hertz and Mindlin problems for fourth order paraboloids in contact generalized, minimizing microslips and annulus of slip [ASME PAPER 67-APM-12] 15 p2505 A67-30149

Hertz and Mindlin problems for fourth order paraboloids in contact generalized, minimizing microslips and annulus of slip [ASME PAPER 67-APM-12] 17 p2871 A67-32411

PRETTING CORROSION

SA WEAR

Lubrication and wear with reference to boundary lubrication, fluid and solid films, discussing dry and lubricated sliding and rolling theory 20 p3455 A67-37262

SA ABRASION

SA DRY FRICTION

SA INTERNAL FRICTION

SA KINETIC FRICTION

SA SKIN FRICTION

SA SLIDING FRICTION

SA STATIC FRICTION

SA WEAR

Rayleigh dissipation function and Lagrange equations of nonlinear friction forces 04 p0658 A67-15584

Asymptotic flow theory laws of friction and heat transfer in turbulent boundary layer 04 p0610 A67-15838

Friction, lubrication and wear, survey of work done during last decade 05 p0809 A67-16065

Quasi-one-dimensional MGD channel flow calculation methods, considering Hall effect, heat transfer, friction and potential drop near sectioned electrode 06 p1043 A67-18675

Book on strength of materials covering energy density, plastic flow deformations, friction heating and fracture mechanisms 08 p1414 A67-20307

Friction welding fundamentals noting bonding, heat effect, pressure, speed, etc 08 p1333 A67-20357

Quantitative analysis of wear of metal-metal/ polymer composite friction pairs as function of time and operational conditions 08 p1334 A67-20597

Motion of variable-mass mechanical system with friction described by 3N equations 13 p2159 A67-27709

Flexible filament under transverse impact from sphere, considering friction forces 19 p3341 A67-35704

Soviet papers on friction and wear in machinery covering elastorheology and equilibrium stability of rigid rotor 22 p3811 A67-39315

Minimum distance and orbit inclination in earth-moon system, considering tidal friction effects 23 p4065 A67-41000

FRICTION COEFFICIENT

Heat exchange and friction drag coefficients for laminar flow of equilibrium dissociable hydrogen with constant heat flow density at tube wall 01 p0165 A67-10048

Surface roughness effect on laminar MHD flow through rectangular duct, deriving relation between transition friction factor

and Reynolds and Hartmann numbers 01 p0120 A67-10186

Sintered-metal friction materials from metallic and nonmetallic powders, noting composition 01 p0099 A67-10710

Sliding friction characteristics in vacuum of single and polycrystalline aluminum oxide in contact and with various metals 03 p0428 A67-13231

Physical properties of metals influence on friction, adhesion, wear and welding tendency in vacuum 03 p0428 A67-13271

Friction and adhesion coefficients of copper on copper measured in vacuum at temperatures ranging from minus 270 to 1000 degrees F and in controlled pressures of dry air [ASME PAPER 66-LUB-3] 03 p0431 A67-13754

Static and dynamic properties of servomechanical transducers for nonelectrical signals with help of electrical signals 04 p0618 A67-14412

Composite heat transfer and viscous friction of moving gray medium with large optical density, using laminar boundary layer equation, noting hydrodynamic state role 04 p0722 A67-14713

Connective heat transfer and viscous fluid friction at air pressure with high Reynolds numbers in cooled channels, noting coolant pressure effect 04 p0603 A67-14717

Reynolds number assessment in analytical relations for convective heat transfer and viscous fluid friction 04 p0722 A67-14718

Fatigue life of thin walled shells with inside pressure and outside support during axial motion [ASME PAPER 66-WA/MET-13] 04 p0712 A67-15377

Velocity profile and friction in plane-parallel channel with developed turbulent compressible gas flow 04 p0609 A67-15884

Self-diffusion coefficients of simple liquids as predicted by Rice-Albatt theory, noting friction coefficient and correlation function 06 p1035 A67-17989

Correlation of local heat transfer and friction coefficients for subsonic turbulent flow of air through high temperature annulus 06 p1117 A67-18386

Leak current, friction and heat-transfer coefficients of compressible laminar boundary layer on insulator wall of MHD channel with anisotropic conductivity 06 p1043 A67-18673

Friction coefficient of compressive gas flow growth when negative pressure gradients in channel reach very high levels 06 p0991 A67-18816

Book on roller bearings noting construction, operation and performance characteristics 06 p1008 A67-18837

Wind profiles obtained from meteorological tower plotting wind velocity, normalized by value of friction velocity, as function of measurement heights 07 p1220 A67-20002

Load and friction torque of Rayleigh step film scheme applied to journal bearing, using Reynolds equation [ASME PAPER 65-WA/LUB-2] 08 p1335 A67-20917

Viscosity variation effect on heat transfer and friction coefficient at wall during Couette flow 09 p1490 A67-22547

Wall friction coefficient measurement, using scale incorporated into wall 09 p1501 A67-22577

Heat transfer and friction coefficients measured for turbulent flow of non-Newtonian fluids in rectangular and circular channels 12 p2033 A67-25315

Friction factors and velocity profiles in turbulent flow of viscoelastic non-Newtonian fluid, noting correlation between frictional characteristics and Reynolds number 12 p1929 A67-25904

Extension of Loitsianski hypothesis concerning localism of turbulent transfer processes in viscous flows to MHD flows, noting results for friction coefficient 12 p1976 A67-26070

Friction stress acting upon moving dislocation derived by microstrain methods is meaningful under limited conditions 13 p2141 A67-27181

Physical properties of metals influence on friction, adhesion, wear and welding tendency in vacuum 14 p2324 A67-28000

Solid lubricants frictional behavior in

press-fit tests, measuring sliding speed, load and surface roughness as function of time [ASLE PREPRINT 67AM 5A-2] 14 p2325 A67-28786

Test methods to determine wear coefficients and design calculations for solid film lubricants, covering wide temperature range [ASLE PREPRINT 67AM 5A-5] 14 p2325 A67-28787

MHD flow of liquid mercury through circular pipes at high Hartmann and Reynolds numbers, plotting friction factors 16 p2712 A67-30576

Influence of surface roughness and humidity on endurance of rubbed films of various lamellar solids on steel 16 p2881 A67-30853

Friction and wear properties of resins and polymers with carbon fiber examined and compared for various amounts of fiber 16 p2694 A67-31021

Variation of friction and wear of solid lubricant film with thickness theory based on junction and wear particle size 16 p2683 A67-31751

Strength and durability in friction tests of soft, vacuum deposited, thin-metal gold film lubricants, noting dependence on film-substrate interface 16 p2684 A67-31816

Equation derived for accurate approximation of viscous friction coefficient in spool and nozzle-flapper preamplifier stages of electrohydraulic servovalve 16 p2610 A67-31915

Stationary laminar boundary layer equations of Ostwald-de Waele power law fluids, flow and temperature boundary layer differential equation 17 p2836 A67-32262

Rolling friction with axial thrust analyzed for elastic cylinder, assuming Coulomb friction law and using integral equation 17 p2865 A67-32263

Wall suction rate effect on turbulent flow in cylindrical circular porous duct, measuring distributions of velocity, pressure, friction coefficient and Reynolds stresses 17 p2837 A67-32380

Contribution to friction coefficient from time correlations between hard and soft molecular interactions evaluated, using linear trajectory approximation 17 p2890 A67-33263

Heat exchange and friction drag coefficients for laminar flow of equilibrium dissociable hydrogen with constant heat flow density at tube wall 17 p2974 A67-33326

Partial cone crack formation in brittle material loaded with sliding spherical indenter 18 p3144 A67-34275

Compressible laminar spanwise boundary layer on yawed infinite cylinder with disturbed suction calculated using momentum equation 19 p3342 A67-35724

Sliding friction between spherical steel rider and gold-plated steel flat measured for varied loading, steel combinations and gold film thicknesses 19 p3237 A67-35837

Sliding friction characteristics in vacuum of single and polycrystalline aluminum oxide in contact and with various metals 19 p3237 A67-35838

Cold welding tendencies and frictional studies of clean metal combinations under ultra high vacuum 19 p3237 A67-35839

Friction and heat transfer characteristics of turbulent swirl flow under large transverse temperature gradients [ASME PAPER 67-HT-24] 20 p3546 A67-36718

Elastic and residual strains caused by friction load in polymer surface layers studied for dependence, slip rate and friction load duration 20 p3473 A67-36842

Correlation method for local and average friction coefficients of laminar and turbulent gas flow through smooth tubes 20 p3422 A67-36941

Heat transfer in circular channel containing revolving cylinder, considering turbulent flow with microvortices 20 p3359 A67-37343

Turbulent gas flow viscosity, thermoconductivity and friction coefficients in tube 21 p3611 A67-37912

MHD channel wall boundary layer equations for low temperature plasma, determining friction and heat transfer coefficients and leakage current 21 p3665 A67-38241

Optimal functional parameters of

elastically damping turbine rotor bearing to determine critical velocities of shaft 21 p3695 A67-38832

Turbulent cylindrical wall jet flow field, velocity profile and surface friction coefficient noting transverse curvature effects 22 p3783 A67-39531

Highly elastic materials temperature dependence of contact area and sliding friction forces affected by elastic modulus decrease with temperature under load 23 p4021 A67-40596

Energy dissipation criteria for object falling on viscoelastic foundation or vehicle impacting without mass separation from support structure 23 p4072 A67-40609

Frictional processes of metal surfaces under boundary lubrication conditions emphasizing initiation of seizure 23 p4010 A67-41063

Friction in solid parts of earth and moon considered as sink for tidal energy and as geophysical thermal energy source 24 p4229 A67-42316

Approximate single parameter solution for compressible turbulent boundary layer in supersonic diffuser 24 p4144 A67-42586

Spline friction effect on multiple disk brake and clutch packs, including torque and load variation and pressure distribution equations [ASME PAPER 67-LUB-26] 24 p4164 A67-42684

Atom arrangement in crystalline materials considering lattice, planes and structure, discussing effect on mechanical properties, particularly friction 24 p4164 A67-42733

Lubricating action of electroplated gold on stainless steel examined under load by single rub block loaded against rotating disk [ASLE PAPER 67-LC-16] 24 p4165 A67-42750

FRICTION DRAG

SA SKIN FRICTION DRAG

Heat exchange and friction drag coefficients for laminar flow of equilibrium dissociable hydrogen with constant heat flow density at tube wall 01 p0165 A67-10048

Blunt cone laminar friction drag evaluated, using Reynolds analogy 01 p0007 A67-11181

Self-preserving flow in turbulent boundary layer passing over surfaces with different roughness 02 p0232 A67-11561

Heat transfer and friction drag for supercritical laminar flow of carbon dioxide through tube at constant thermal flux density at wall 03 p0536 A67-13612

Friction stress and flow rate for rarefied constant density gas flow past semiinfinite plate treated by approximate diffusion model 05 p0792 A67-16995

Analytical expressions developed for prediction of partially wetted rotating disk pressure, gradient development and frictional drag for different flow regimes 10 p1659 A67-22708

Boundary layer equations reduced to ordinary differential equations without using self-similarity assumptions, noting friction-drag and heat-transfer coefficient along MHD channel 14 p2356 A67-27978

Probe measurements of friction drag coefficient and velocity profile of turbulent flow of mercury in circular tube in presence of longitudinal magnetic field 16 p2721 A67-31394

Heat exchange and friction drag coefficients for laminar flow of equilibrium dissociable hydrogen with constant heat flow density at tube wall 17 p2974 A67-33326

Heat transfer and friction drag for supercritical laminar flow of carbon dioxide through tube at constant thermal flux density at wall 18 p3161 A67-34477

Motion and thermodynamic conditions of free piston ballistic compressor test gas taking into account gas leakage, viscous friction and heat losses 22 p3778 A67-39351

Empirical method predicting flexible hose flow losses, with Fanning friction factor as Reynolds number and internal hose geometry function 22 p3785 A67-39971

Friction and heat transfer effects on nonsteady flow behind Chapman-Jouget detonation to analyze transition to steady flow 23 p3993 A67-41744

Friction-drag and heat-transfer coefficients of plate in turbulent gas flow, estimating effect of turbulent Prandtl number 24 p4143 A67-42283

FRICTION-LOSS COEFFICIENT

Boundary layer measurements of friction

losses due to finite thickness of leading edges of turbine blades 03 p0353 A67-14306

Local loss coefficients for multiplate hydraulic actuators with various working fluid temperatures 16 p2608 A67-31007

Shore hammer motion behavior, especially rebounding process frictional energy loss distribution 22 p3913 A67-40038

FRICTION MEASUREMENT

Hot-wire probe measurement of friction temperature and convection coefficient of low pressure flows and wake of cylinder 01 p0006 A67-10757

Variations in friction and inertia characteristics of rotary control determined, noting preference ratings of control characteristics 02 p0186 A67-12229

Book on molecular physics of boundary friction on metal surfaces 03 p0429 A67-13333

Dynamic components thermal characteristics determination by IR optic techniques, studying metal fatigue, wear and friction phenomena 14 p2328 A67-28873

Integration of laminar boundary layer equations in compressible gas by asymptotic method, calculating friction and heat flux 16 p2660 A67-31135

Mean velocities, turbulence intensities, Reynold stresses and wall friction measurement in turbulent radial wall jet [ASME PAPER 67-APM-10] 17 p2838 A67-32419

Two-phase liquid metal MHD generators, appraising friction losses and conductivity limitations 19 p3175 A67-34802

Surface-temperature conditions in disks and gears stressing heat transfer coefficient and lubricated contact 19 p3237 A67-35840

Friction data, elastoplastic deformation and surface geometry of rubbing surfaces 19 p3237 A67-35851

Installation for measuring wear rate, friction force, etc. of plane surfaces in alternating motion 20 p3453 A67-36198

Amplitude of forced flexural vibrations of free rotating shaft under arbitrary load with dampers, taking into account viscous friction 21 p3726 A67-38834

Wear characteristics of polytetrafluoroethylene studied under various loading and sliding speeds in air and vacuum 23 p4009 A67-41062

FRICTION PRESSURE DROP

Discontinuous yield phenomena for slip band dislocations, when frictional stress that hinders dislocation motion undergoes static or dynamic drop 11 p1807 A67-24568

Friction heat effect on explosion threshold noting pressure drop role in reacting system explosion 20 p3554 A67-37055

FRICTION REDUCTION

Different rotation bearings as method of reducing bearing friction and directional gyro errors from random disturbances 03 p0425 A67-14285

SNAP-8 reactor oscillating bearings to provide low friction self-lubrication at 1150 degrees F [ASLE PAPER 66AM 7A1] 08 p1335 A67-21034

Machinery wear, galling and scuffing reduction by using graphite and molybdenum disulfide as dry film lubricants 14 p2324 A67-27999

Long period vibrometer with small spring constant and minimized solid friction by HF vibration of support 14 p2348 A67-28257

FRICTIONLESS ENVIRONMENT

Nonlinear singularities method for calculating velocity distribution over thick wing of finite aspect ratio situated at zero angle of attack in incompressible frictionless potential flow 07 p1127 A67-19887

FRINGE

Moire pattern method of determining fringes representing constant curvature of bent plates 05 p0921 A67-16827

Moire patterns of modified intensity distribution analyzed, ascertaining fringe sharpening and multiplication 11 p1875 A67-24612

Quasar observations using interferometer baselines, noting regular fringes and small phase scintillation in Gaussian source model 17 p2947 A67-32760

Aperture system using moire fringe method to execute spectral scan for Fabry-Perot spectrometer 23 p4001 A67-41258

FRONT

S FLAME FRONT
S SHOCK FRONT
S WAVE FRONT
S WEATHER FRONT

FROUDE NUMBER

Continuous spatially varied open channel liquid flow analogy for gas flow, with heat addition and extraction over finite distance 04 p0604 A67-14838

Elliptic planform vertical submerged hydrofoils, determining circulation distribution over foil span at arbitrary Froude numbers 18 p3022 A67-33414

Nonlinear features of geostrophic adjustment in one-dimensional barotropic atmosphere number 19 p3253 A67-35917

FROZEN FLOW

Frozen layer that forms when warm liquid flows over flat plate cooled below freezing temperature of liquid by coolant flowing along other side of plate 04 p0735 A67-15856

Laminar diffusion flame in Oseen flow, identifying limiting case with stoichiometric Burke-Schumann flame and frozen flow 09 p1579 A67-21548

Asymptotic solution method for frozen dissociated laminar boundary layer flow over flat plate surface with arbitrarily distributed catalytic 11 p1781 A67-24573

Critical particle velocity and particles frozen in given point of magnetic field line, discussing effects of plasma compression and reflection levels 13 p2204 A67-27432

Nonequilibrium quasi-one-dimensional nozzle flows in limit when relaxation time is large compared with characteristic flow time 19 p3172 A67-35800

FUEL

SA AIRCRAFT FUEL
SA CARBON
SA CHARCOAL
SA CHEMICAL FUEL
SA ENDOTHERMIC FUEL
SA FLAME
SA HIGH ENERGY FUEL /HEF/
SA HYDROCARBON FUEL
SA HYDROGEN FUEL
SA JET FUEL
SA KEROSENE
SA METAL FUEL
SA NUCLEAR FUEL
SA OIL
SA PETROLEUM
SA PROPELLANT
SA REACTOR FUEL
Chemistry and rheology of gelled fuels, noting structure, thickeners, etc 10 p1696 A67-22911

FUEL-AIR RATIO

Air velocity and temperature, stabilizer size and blockage effects on fresh mixture entrainment in recirculation zone of bluff body stabilized flames 02 p0342 A67-12029

Impact-induced combustion in hypersonic ramjet engines, determining hypersonic fuel-air mixing from hydrogen concentration at Laval nozzle outlet [DVL-601] 03 p0503 A67-13014

Normal flame propagation rates for methane-air mixtures at high pressures 07 p1239 A67-19313

Annular vaporizing combustion chamber for small-size gas turbine engines, noting fuel-air flow 11 p1853 A67-24526

Mixture ratio distribution effect on rocket thrust chamber performance 15 p2545 A67-29431

Fluidics applications to ramjet control systems incorporating sensing, logic and actuation functions to inlet duct, flow-air ratio and coolant control 17 p2927 A67-31981

Density induction times for shock wave induced exothermic reaction in lean mixtures of deuterium, hydrogen, ethylene and ethane with oxygen 18 p3081 A67-33792

Spectral brightness of metal chelate liquid fuel-air flames [CI PAPER 67-2] 19 p3309 A67-34997

Ignition and extinction characteristics of liquid fuel droplets burning in oxidizing atmosphere calculated, using finite rate kinetics 19 p3214 A67-35000

Physicochemical combustion of turbulent air-fuel mixture in straight flow combustion chambers, noting effects of various factors and intensification 22 p3921 A67-40448

FUEL CELL

Fuel cells from point of view of thermodynamics, electrochemical reaction

kinetics and transport processes and state of development of representative types
 Fuel cell construction principles, oxidation potentials of prospective fuels and Gemini GT-5 space capsule fuel
 Fuel cell as low voltage power source
 Electrochemical power components meeting extreme requirements of space applications, used in commercial market [AIAA PAPER 66-1012]
 Fuel cells and fuel batteries, investigating hydrogen, compromise fuels and hydrocarbons, studying reliability, working life and costs
 Storage of solar electric energy by electrolysis of water, separate storage and subsequent recombination of gases by fuel cells
 Electrochemical properties of solid refractory oxides for high temperature fuel cells
 Catalytic performance of silver alloys as oxygen electrodes of low temperature fuel cells
 Oxygen solubility in fused carbonates and corrosion behavior of Ag and Cu oxide, air and carbon dioxide cathodes in molten carbonate fuel cells
 Nickel hydroxide structure, discussing effect of current, charge and electrolyte concentration on production
 Hydrogen fuel battery, discussing construction, operation and performance characteristics
 Fuel cell hydrogen electrodes prepared from preactivated Raney-Nickel catalyst powders
 In situ reforming methanol air cell design, construction and expected performance
 Theoretical and experimental basis of high performance Mg-air cells, discussing development and performance
 Anodic oxidation and molecular structure influence on performance of normal saturated hydrocarbons in fuel cells
 Thermal design of molten carbonate fuel cells using transpiration heating for reducing heat loss and control of temperature
 Entropy applied to theory of fuel cells, noting effect of operating temperature
 Fuel cell research* noting gas porous electrodes, effect of geometry on performance and electrocatalysis
 Electrochemical generator concept noting compactness, adaptability, methods of adding active agents, evacuation of reaction products and decarbonation
 Mobile hydrogen generators for alkaline electrolyte cells and medium temperature fuel cells for autonomous hydrocarbon electricity units
 Direct and indirect methods of using methanol in fuel cells
 Operation, structure, performance and application of solid, molten and aqueous electrolyte fuel cells
 Annex circuits for regulating electrolyte grade, cell temperature, reactant supply, fluid circulation and generated electricity of unit cells grouped in batteries
 Fuel cells such as KOH, high temperature and ion exchanger diaphragm noting applications and performance characteristics
 Batteries and fuel cells for space power systems, discussing Ni-Cd, Ag-Cd, Ag-Zn, Bacon cell, etc
 Input and output voltage and efficiency of thermal-to-electric energy conversion effect on fuel cells and insulation of thermoelectric generator
 Hydrogen-oxygen fuel cell for spacecraft power system
 System selection for hydrogen-oxygen low temperature fuel cell with aqueous KOH electrolyte
 Fuel cell systems operating at low temperatures, noting control loops, hydrogen/oxygen, nickel electrode, asbestos

systems, etc
 Fuel cell performance under operating conditions of local nonuniformity in temperature, concentration, potential or current simulated with computer program
 Molten carbonate fuel cell module featuring flexibility of construction, electrical simplicity and effective gas distribution characteristics
 Heat transfer in fuel cell battery held in isothermal bath, giving charts for maximum temperatures at different Peclet numbers
 High temperature fuel cells with molten carbonate mixtures as electrolyte analyzed at high temperature
 Thermophile radiation receiver utilizing detector comprised of fuel cells in series studied for application to actinometry
 Orbiting Energy Depot, discussing fuel regeneration and resupply to enable use of fuel cells combined with nuclear power as main onboard power
 Nonmechanical electric power sources - Conference, Brighton, England, September 1986
 30 cell 1 kw hydrogen fuel battery for room temperature operation, noting construction and performance
 Methanol-air fuel cell development, discussing electrode performance, temperature effects and catalytic agents
 Apollo fuel cell power system transient temperature and voltage response characteristics predicted by analytic model
 Compact portable high purity H generator using liquid ammonia for indirect method H-O fuel cell
 Apollo spacecraft H-O chemical to electric energy converting fuel cell performance degradation resulting from O electrode contamination due to inert diluent impurities in O supply
 Reliability assessment test program for determining capabilities and limitations of 2 kw hydrogen-oxygen fuel cell stacks

FUEL COMBUSTION

SA METAL COMBUSTION
 Quenching diameter of premixed fuel-oxidizer flames by volatile inhibitors, noting nature of oxidizers, particularly oxygen
 Combustion of gaseous fuel jets in oxidizing atmosphere
 Acoustic liners to suppress screech in hydrogen-oxygen engines
 Liquid droplet combustion at high pressures revealing effects of vapor source distribution on predicted burning time at supercritical pressures
 Shock induced supersonic combustion of fuel-air mixtures used to obtain induction time, evaluating kinetic data and effect of small contamination levels
 Aluminum fluoride effect on propagative ignition of fuel oxidant mixtures and on combustion between aluminum and oxygen
 Flame propagation on liquid fuel surface, analyzing fuel heating in front of flame until ignition temperature is reached, noting radiation and convection role
 Scramjet performance analysis stressing construction problems and importance of fuel choice
 Radical concentrations and decays in lean hydrogen-nitrogen-oxygen flames
 Self-ignition and fuel combustion at blade cascade taking place at velocities and temperatures comparable to those of gas turbines
 Supersonic flow pressure and density perturbations caused by discrete or continuous mass and heat sources
 Supersonic combustion simulation facility and duplicable static parameters for hydrogen fuel
 Book on motor fuels, performance and testing, including fuel source and nature,

gasoline combustion, diesel, turbine fuels, etc
 Soviet book on combustion chambers of gas turbine engines covering fuels, working processes, heating, etc
 Flame propagation along interface between gas and reacting medium, studying fuel heating ahead of flame, noting radiation and convection role
 Post-induction kinetics in shock initiated hydrogen-oxygen reactions investigated by computer methods
 Ignition energy, quenching distance, flame stability and gas turbine burner performance of ammonia-air mixture
 Ammonia-air combustion, flame speed needed to obtain optimum performance
 Internal combustion engine fuelled with cryogenic hydrogen and oxygen
 Nitrate ester monopropellants studied for heat-up, ignition and combustion in high temperature nitrogen gas under moderate/high pressures, noting burning rates
 Mixing, ignition and combustion in secondary combustor for air-augmented solid rockets with solid particles in primary stream
 Fuel requirements for Concorde SST stressing flame luminosity, radiant heat, spontaneous ignition, fuel viscosity and density
 Spectral brightness of metal chelate liquid fuel-air flames
 Ignition and extinction characteristics of liquid fuel droplets burning in oxidizing atmosphere calculated, using finite rate kinetics
 Axisymmetrical vibrations of cylindrical shell during HF internal pressure pulsations of gas flow containing uniformly distributed burning fuel droplets
 Hybrid rocket design combining flexibility of liquid fuel with simplicity and reliability of solid propellant rockets
 Acoustic vibrations during solid-fuel combustion, studying acoustic energy increase rate and development
 Chemiluminescence and chemionization in low pressure fuel-oxygen flames, measuring emission intensity of CH, carbon molecule and OH electronic bands
 Shock induced supersonic combustion of fuel-air mixtures used to obtain induction time, evaluating kinetic data and effect of small contamination levels
 Fuel burnout processes in inlet flow of secondary air stream to turbine combustion chamber determined by working mechanism in inlet section of chamber

FUEL CONSUMPTION

Propellant and time-optimum trajectories with thrust vector rotational velocity at flight beginning and termination taken as additional boundary condition analyzed, using maximum principle
 Analytic solution in terms of modified Bessel functions of synergetic turn in exponential atmosphere, using spacecraft engines only for drag cancellation and orbit trimming
 Comparison of piston engine with turbojet engine noting power-weight ratio, specific fuel consumption, performance characteristics, etc
 Lifting reentry vehicles for achieving orbital plane changes by synergetic maneuvers
 Finite rate chemistry effects in diffusion controlled hydrogen-air flames noting flame position, fuel consumption, temperature, fluid velocity outside of flame and boundary conditions
 Mesoscale temperature variability below 60,000 ft measured for calculation of supersonic aircraft fuel requirement
 Optimization problem associated with fuel consumption for control of satellite orientation by means of active

system 09 p1571 A67-21696
Heat regeneration and high gas temperatures for fuel economy in helicopter gas turbine engines 11 p1852 A67-24525
Peculiarities of helicopter turbine engine with direct rotor drive 11 p1853 A67-24528
Optimum stabilization problem for axisymmetric satellite, considering fuel consumption 12 p2011 A67-25639
Solid and liquid propellants, considering minimum specific propellant consumption in connection with fuel selection for auxiliary power systems [SAE PAPER 670205] 12 p1987 A67-25866
Lifting reentry vehicles for achieving orbital plane changes by synergetic maneuvers [AIAA PAPER 66-960] 13 p2212 A67-26846
Microrocket technology, deriving propellant consumption equations and explaining numerical coefficient variation 15 p2545 A67-29452
Optimal maneuvers for space rendezvous between earth satellite and propelled vehicle on circular orbits, studying fuel consumption and rendezvous time 16 p2758 A67-30652
Minimum-fuel transfers of moving body between infinitely close elliptical Keplerian orbits in central Newtonian field, considering propulsion system models 16 p2744 A67-30738
Parametric comparative study of helicopters powered with current-technology engines and advanced non-regenerative and regenerative twin-engine installations [AHS PAPER 119] 16 p2598 A67-31835
Engineering formulas to determine fuel reserve margins for fueling techniques and fuel consumption events due to incidental rocket design parameter scatter 17 p2954 A67-32241
Optimum control of space vehicle motion along binormal to circular reference orbit for minimum fuel consumption criterion 17 p2955 A67-32255
Explosion theory, reviewing chain and thermal theories unification, fuel consumption effects, spatial distribution effects, etc 18 p3155 A67-33845
Variable turbine geometry in gas turbine engines, discussing part power fuel consumption, acceleration characteristics, etc [AIAA PAPER 67-417] 18 p3111 A67-33904
Fuel consumption precision measurements for low thrust auxiliary rockets using impeller wheel and photometric devices [AIAA PAPER 67-507] 18 p2989 A67-33971
Minimax fuel requirement of aircraft angular stabilization for undetermined inertial moment probability distribution 19 p3202 A67-35887
Damped mass expulsion for space vehicle attitude control reducing propellant consumption and pulsing frequency [AIAA PAPER 67-535] 19 p3334 A67-35937
Payload and trajectories determination for consumption optimization for missiles moving in constant gravitational field, using Pontryagin maximum principle 20 p3531 A67-36409
Fan jet engine performance and operation as affected by humidity 20 p3515 A67-36448
Extremal space trajectories problems of one-impulse flights and two-impulse orbital transfers in central gravitational field 20 p3522 A67-36617
Optimal correcting strategy for vehicle moving close to nominal trajectory 20 p3407 A67-36809
Optimum consumption of inert mass working fluid in limited discharge velocity engine in terms of final speed gain 21 p3689 A67-37986
Fuel optimal control conditions in attitude correction of satellite in circular orbit determined using maximum principle, solving resulting boundary value problem 21 p3715 A67-39153
Suboptimal feedback solution to guidance and control in minimum time and fuel for low thrust orbital transfer 22 p3832 A67-40146
Two-finite burns minimum fuel rendezvous problem using dual phase plane description, determining control law 22 p3888 A67-40147
SST fleet size, flight time, station stop time, seat mile costs, fuel consumption, noise and sonic boom problems affecting airline economics [AIAA PAPER 67-749] 23 p3933 A67-40983

FUEL CONTAMINATION

Shock induced supersonic combustion of fuel-air mixtures used to obtain induction time, evaluating kinetic data and effect of small contamination levels [AIAA PAPER 67-105] 06 p1114 A67-18284
Effect of metals and alloys on thermal stability of Avtur 50 aviation kerosene from ASTM-CRC and high temperature coker tests 13 p2185 A67-26703
Growth of dendriform crystal contaminant in hydrocarbon fuel or hydraulic system during stagnant storage, discussing possible effects and corrections 17 p2801 A67-31991
Quantitative method for determining sodium in gas turbine fuels by direct spectral analysis of unashed fuel samples 21 p3688 A67-38016
Shock induced supersonic combustion of fuel-air mixtures used to obtain induction time, evaluating kinetic data and effect of small contamination levels [AIAA PAPER 67-182] 21 p3732 A67-38858
Microbial contamination of jet aircraft fuel systems [SAE PAPER 670869] 24 p4206 A67-42007
Depth sampler for testing dirt content of jet fuels, discussing settling effects 24 p4206 A67-42279
FUEL CONTROL
Fuel requirements for high altitude high-Mach number aircraft noting thermal stability, autooxidation, self-ignition, specific heat, etc [DVL-599] 03 p0502 A67-13015
Suboptimal policies for fuel optimal control and energy optimal control problems for linear time invariant system obtained, using Liapunov functions 04 p0590 A67-14418
Aviation fuel static electricity elimination by Shell additive ASA-3 05 p0872 A67-16234
Elastomer application in spacecraft launching, flight and reentry such as binder, sealant, base for adhesives, heat shielding, etc [ONERA-TP-407] 05 p0833 A67-16479
Fixed time fuel-optimal controls computed by iterative procedure developed by Pontryagin principle 06 p1097 A67-18522
Aircraft gas turbine and fuel control design to meet engine requirement in broad environmental challenges [SAE PAPER 670140] 09 p1560 A67-22541
Computer analysis of critical fuel solution reactors with arrays of large diameter voids 16 p2702 A67-31814
Fuel control system of GE4 engine for supersonic transport noting main and augmentation fuel and control subsystems [SAE PAPER 670326] 17 p2929 A67-32982
Fuel ground thermal conditioning for performance gains [AIAA PAPER 67-442] 18 p3019 A67-33919
Fluidic fuel control system for subsonic combustion ramjet engine, describing components, breadboard model and performance characteristics [AIAA PAPER 67-497] 18 p3113 A67-33961
FUEL CORROSION
Corrosion test on turbine blades with nickel and cobalt base conducted in burner rigs, using metallographic examinations [ASME PAPER 67-GT-2] 11 p1808 A67-24790
Emulsified fuel effect on gas turbine combustors, noting good operation in low altitude flight but inhibited combustion at start and at high altitudes [SAE PAPER 670366] 12 p1987 A67-25884
Emulsified jet engine fuel noting lower volatility and flammability and resistivity to corrosion and acceleration [SAE PAPER 670365] 12 p1988 A67-25885
Qualitative and quantitative prediction of corrosive environments effects on transducer performance [ASME PAPER 67-MET-14] 12 p1945 A67-25952
Jet fuels in U.S. and Great Britain, chemical composition, technical specifications, thermal stability and corrosion effect 13 p2185 A67-27068
Fuel injection system used on aircraft engines noting system layout, advantages and disadvantages, fuel corrosion, etc 14 p2377 A67-28500
FUEL ECONOMY
Iterative procedure for computing fixed-time fuel-optimal controls for problem of hitting hypersphere centered at origin at state space 02 p0303 A67-12149
Propellant preparation from

extraterrestrial materials on moon and planets rather than transportation from earth as economical source of fuel for interplanetary manned traffic 04 p0695 A67-14555
Analytical solution to determine rocket design for maximum payload energy 04 p0706 A67-15240
Uniqueness of extremal controls for minimum fuel problems pertaining to single input linear time-invariant systems 06 p1098 A67-18523
Minimum time and fuel problems for PFM systems, deriving optimal control by heuristic argument 06 p0977 A67-18524
Explicit guidance law for minimum fuel horizontal translation with bounded control 06 p1090 A67-18867
Asymptotic matching in optimization of minimum fuel power-limited interplanetary trajectory [AAS PAPER 66-114] 07 p1253 A67-19973
Minimum fuel vehicle transfers between coaxial orbits of coplanar and noncoplanar types, using impulses [AAS PAPER 66-119] 07 p1253 A67-19978
Minimum fuel impulses for space trajectories under influence of gravitational and propulsive forces 10 p1678 A67-23424
Asymptotic matching in optimization of minimum fuel power-limited interplanetary trajectory [AAS PAPER 66-114] 13 p2208 A67-27530
Minimum fuel vehicle transfers between coaxial orbits of coplanar and noncoplanar types, using impulses [AAS PAPER 66-119] 13 p2209 A67-27533
Analytic solution obtained for minimum impulse transfer between two neighboring low eccentricity orbits 15 p2554 A67-29405
Supersonic transport vehicle throttle schedule, comparing point performance, indirect and gradient optimization techniques 15 p2418 A67-29406
Manual control stationkeeping simulation, studying tether visual rendezvous techniques and fuel economy [AIAA PAPER 67-617] 19 p3337 A67-36006
Minimum fuel flight plans for injecting synchronous satellite into circular equatorial orbit, developing four methods 22 p3886 A67-40116
FUEL ELEMENT
Partially ionized gases application to industry, stressing power units incorporating plasma converters, plasma electrolytic fuel elements and MHD generators 17 p2899 A67-32187
Temperature field and critical thermal loads for fuel elements with varying convective heat transfer coefficient and ambient temperature 23 p4082 A67-41286
Thermoelectric nuclear energy conversion device operating inside reactor fuel element, discussing conversion efficiency 24 p4186 A67-42551
FUEL FLOW
Air velocity and temperature, stabilizer size and blockage effects on fresh mixture entrainment in recirculation zone of bluff body stabilized flames 02 p0342 A67-12029
Engine test facility for measuring thrust and propellant flow in pulsating rockets 03 p0396 A67-13774
Self-similar problems concerning supersonic flows of gaseous fuel mixtures with detonation waves and slow combustion fronts past wedges and cones 06 p0935 A67-17725
Control of multishaft jet engines, discussing compressor geometry, afterburner and engine fuel flow, nozzle area effects, etc [SAE PAPER 670139] 09 p1559 A67-21770
Cryogenic fluid behavior in passive storage tank as function of tank configuration, wall heating and acceleration 12 p2034 A67-25729
Low temperature engine suction line response to fluid exposed internal surface coating, determining effects of varying flow rates 13 p2229 A67-27664
Molten carbonate fuel cell module featuring flexibility of construction, electrical simplicity and effective gas distribution characteristics 20 p3364 A67-37015
Ring laser use for measuring gas flow on ground and fuel and oxidizer flow in rockets 22 p3800 A67-39892
FUEL GAUGE
SA CAPACITIVE FUEL GAUGE
Operational spacecraft fuel gauging system

based on application of radioisotope techniques 05 p0841 A67-16536
Flight test of nucleonic fuel gauge, discussing photon-matter interaction principles, ground test calibration data, aircraft environment and gauge performance 05 p0841 A67-16537
Continuous nucleonic oil quantity gauging system requiring no tank penetrations 05 p0842 A67-16538
Nucleonic quality gauging system for two-phase hydrogen pipeline 05 p0842 A67-16539
Mathematical model of aircraft nucleonic fuel gauging facility system allowing performance evaluation and optimization by computer techniques 05 p0842 A67-16542
Radiotracer propellant gauge for zero gravity space environmental conditions using radioactive krypton 85 10 p1656 A67-23078

FUEL INJECTION

SA GAS INJECTION

SA LIQUID INJECTION

Mixing gaseous propellant injector, injection velocity and momentum flux ratio, combustion pressure and propellant combination effects on HF combustion pressure oscillations in rocket motor 02 p0302 A67-11940
Working equations for dimensions and orientation of impinging propellant sheets in liquid rocket engine injectors 02 p0182 A67-11946
Atomization, mixing and reaction characteristics of hydrazine and nitrogen tetroxide injected from quadlet element [AIAA PAPER 67-107] 06 p1072 A67-18308
Propellant injection through electrodes effect on potential distribution in MPD arc [AIAA PAPER 67-49] 06 p1074 A67-18435
Fuel injection system used on aircraft engines noting system layout, advantages and disadvantages, fuel corrosion, etc 14 p2377 A67-28500
Micro-orifice injector rocket motors covering efficiency, nominal thrust, size, performance, cooling, design factors, etc [AIAA PAPER 67-462] 18 p3113 A67-33933
Propellant injection through porous media, advantages, fluid flow nature, heat transfer, characteristics and uses [AIAA PAPER 67-463] 18 p3026 A67-33934
Correlation between thrust chamber design parameters and combustion stability, noting stability increment with increasing injection velocity, droplet diameter and chamber pressure [AIAA PAPER 67-474] 18 p3113 A67-33944
Atomization, mixing and reaction characteristics of hydrazine and nitrogen tetroxide injected from quadlet element [AIAA PAPER 67-107] 19 p3310 A67-35766
Gasoline-injection system for aircraft engines noting construction details, economics, advantages, etc 19 p3312 A67-36052
Injector inlet conditions effects on combustion delay time in liquid bipropellant rocket engine, noting propellant atomization and droplet vaporization 22 p3868 A67-40161

FUEL PUMP

Centrifugal pump with vapor core principle combined with spill nozzle for application to aero engine fuel and reheat systems 01 p0014 A67-11267

FUEL SYSTEM

SA AIRCRAFT FUEL SYSTEM

Problems in fuel systems associated with chemical impurities such as sulfur and chlorine compounds, examining effects of particulate matter and free water [SAE PAPER 660714] 01 p0140 A67-10603
Liquid-vapor interface in weightless environment noting dynamic behavior, configuration parameters and dependence on model size 04 p0605 A67-14988
Fuel system design criteria, discussing ways of reducing postcrash fires in aircraft 08 p1279 A67-20610
Instrumentation and fuel systems for turbocharged and/or pressurized aircraft, discussing vapor lock problem, hydrocarbon fuels and vapor pressure equipment [SAE PAPER 670262] 12 p1899 A67-25510
Low temperature engine suction line response to fluid exposed internal surface coating, determining effects of varying flow rates 13 p2229 A67-27664
Thermodynamic evaluation of nuclear fuels, suggesting operation with deuterium-tritium and deuterium-helium

mixture 16 p2702 A67-30718
Growth of dendriform crystal contaminant in hydrocarbon fuel or hydraulic system during stagnant storage, discussing possible effects and corrections 17 p2801 A67-31991
AH-56A /AAFS/ safety engineering, failure effects method, Army role, etc 18 p2987 A67-34690
Fokker F-28 aircraft systems fuel system, auxiliary power unit, hydraulics, flight controls, pressurization and electrical systems and avionics 19 p3176 A67-35559
Hypervelocity vehicle volume decreasing method by applying dual-fuel concept [AIAA PAPER 67-559] 19 p3174 A67-35956
Gasoline-injection system for aircraft engines noting construction details, economics, advantages, etc 19 p3312 A67-36052
Handley Page Jetstream aircraft major systems, auxiliary equipment and instrumentation 22 p3748 A67-40132
Co 60-Re alloy in externally fueled thermionic system shown economically desirable for multi-kwt terrestrial or undersea applications 24 p4185 A67-42535

FUEL TANK

SA CONTAINER

SA PROPELLANT TANK

SA ROCKET FUEL TANK

SA STORAGE TANK

Structural design of hypersonic vehicle flight tank for liquid hydrogen fuel, discussing loading, material, support system, stress analysis, testing and analytical problems [SAE PAPER 660679] 01 p0161 A67-10583
Load carrying capability of thin walled pressurized tanks under compression and bending with postwrinkling included, improved by addition of jettisonable shell [SAE PAPER 660683] 01 p0161 A67-10586
Dynamics of booster rockets and spacecraft with cavities partially filled with liquid 08 p1412 A67-21113
Integral fuel tank maintenance, summarizing tank-sealant repair data 09 p1442 A67-22678
Space evacuation of NRC-2 insulation for liquid hydrogen tankage, noting vacuum test apparatus and cold plate test 10 p1734 A67-23727
Liquid hydrogen fuel tankage thermal protection in manned hypersonic vehicles, discussing results of tests in steady state conditions [AIAA PAPER 67-297] 12 p2035 A67-26012
Future supersonic and hypersonic aircraft horizontal liquid hydrogen fuel tank requirements, discussing insulation optimization using variable thickness 13 p2054 A67-27657
Bubble stabilization in pure viscous liquid contained in sinusoidal vibrated tank [ASME PAPER 67-FE-3] 14 p2304 A67-28356
Engineering formulas to determine fuel reserve margins for fueling techniques and fuel consumption events due to incidental rocket design parameter scatter 17 p2954 A67-32241
Microbiological organisms in jet aircraft wing fuel tanks as major corrosion sources, with fuel additives tested to inhibit microbial growth 20 p3515 A67-36485
Flight strain gauge system for Centaur /AC-6/ liquid hydrogen fuel tank skin 23 p4008 A67-41390
Microbial contamination of jet aircraft fuel systems [SAE PAPER 670869] 24 p4206 A67-42007
Depth sampler for testing dirt content of jet fuels, discussing settling effects 24 p4206 A67-42279

FUEL TANK PRESSURIZATION SYSTEM

Heat and mass transfer processes in rotationally symmetrical tank partially filled with liquid and subjected to external heating and acceleration in direction of longitudinal axis 04 p0720 A67-14577
Aircraft fuel tank pressurization and venting systems, evaluating refueling, defueling, inerting systems, recuperators and system integration 04 p0554 A67-14883
Test rig for fuel system in Concord aircraft noting construction, control system, equipment, installation and operation 10 p1623 A67-23548
One-dimensional conduction model for predicting pressure variation of nonvented cryogenic propellant tanks in low gravity field

[AIAA PAPER 67-338] 12 p2039 A67-26052
Development of liquid hydrogen-oxygen propulsion stage in France, discussing structure, thermal isolation, storage, etc 18 p3111 A67-33653
Aircraft fuel tank pressurization, discussing pressure supply sources and control system, tank venting, system integration and equipment used 21 p3571 A67-38104

FUEL TESTING

Propellant composition variation for improving cooling characteristics of Surveyor vernier propulsion system [AIAA PAPER 66-627] 08 p1374 A67-21517
Emulsified fuel mixture /JP-4 and water/ tested in model Allison T63 turbine engine [SAE PAPER 670368] 12 p1987 A67-25883
Lead, copper and cobalt oxides effects upon ignition kinetics of paraffinic and aromatic fuels 14 p2407 A67-28550

FUEL VALVE

Valveless metal vapor feed system for use in pulsed plasma accelerators employing mercury as propellant [AIAA PAPER 67-738] 21 p3695 A67-38760
Cryogenic valve testing facility for nuclear rockets using liquid hydrogen at high pressures and flow rates 23 p3936 A67-41425
FULL SCALE FATIGUE TESTING
High temperature lubricants for ball bearing applications, discussing bearing endurance and rolling-contact fatigue tests on synthetic paraffinic oil [ASME PAPER 67-LUB-21] 24 p4163 A67-42679

FUNCTION

S ANALYTIC FUNCTION
S APERIODIC FUNCTION
S ASYMPTOTIC FUNCTION
S BESSEL FUNCTION
S CHARACTERISTIC FUNCTION
S COMPOSITE FUNCTION
S CONTINUOUS FUNCTION
S CORRELATION FUNCTION
S DEBYE FUNCTION
S DELTA FUNCTION
S DISCRETE FUNCTION
S DISTRIBUTION FUNCTION
S DISTURBING FUNCTION
S ELLIPTIC FUNCTION
S ERROR FUNCTION
S EXPONENTIAL FUNCTION
S GAMMA FUNCTION
S GAUSS FUNCTION
S GREEN FUNCTION
S HANKEL FUNCTION
S HARMONIC FUNCTION
S HEART FUNCTION
S HYPERGEOMETRIC FUNCTION
S INTEGRAL FUNCTION
S KERNEL FUNCTION
S LAGUERRE FUNCTION
S LEGENDRE FUNCTION SERIES
S LIAPUNOV FUNCTION
S MATHIEU FUNCTION
S MUSCULAR FUNCTION
S ORTHOGONAL FUNCTION
S PERIODIC FUNCTION
S PROLATE SPHEROID FUNCTION
S PULMONARY FUNCTION
S RADIATION FUNCTION
S RATIONAL FUNCTION
S RENAL FUNCTION
S SCATTERING FUNCTION
S SPACE-TIME FUNCTION
S SPLINE FUNCTION
S STEP FUNCTION
S STREAM FUNCTION
S STRESS FUNCTION
S SWITCHING FUNCTION
S TIME FUNCTION
S TRANSCENDENTAL FUNCTION
S TRANSFER FUNCTION
S TRIGONOMETRIC FUNCTION
S WAVE FUNCTION
S WHITTAKER FUNCTION
S WORK FUNCTION

FUNCTION GENERATOR

Format method for generating Liapunov and scalar functions for autonomous and nonautonomous systems 04 p0593 A67-15415
Numerical handling of data in statistical study of servomechanism, noting circuitry and random function generator 06 p0966 A67-17586
Zener diode function generator eliminates need for external reference voltage source 08 p1307 A67-21538
Liapunov functions generating methods applicable to nonlinear and linear

autonomous systems 15 p2511 A67-30048
 Transform using eigenfunction as kernel
 generates universal solution for structural
 member vibration, noting application to
 Timoshenko beam 16 p2763 A67-30616
 Negative glow diffusion model evaluated
 via generation function determined by
 discharge voltage and dependence of
 reduced length of cathode fall 18 p3085 A67-33668
 Diode function generator for empirical
 functions representation 22 p3775 A67-40562
 Time optimal adaptive control system
 synthesized via adaptive switching
 hypersurface and function generator /off-
 line memorization and on-line
 interpolation/ 24 p4134 A67-42177

FUNCTION SPACE
SA EUCLIDEAN SPACE
SA HILBERT SPACE
 Conjugate gradients method extended to
 function space for optimal
 control 01 p0044 A67-10483
 Nonlinear transformations of probability
 measures in functional spaces, noting
 application of random-process
 theory 02 p0259 A67-11922
 Algorithm for directed random search for
 minimum of function of
 n-variables 03 p0374 A67-13182
 Limitation imposed a priori on class of
 signals in order that every signal in class be
 distinguishable to within given mean square
 error by finite number of
 measurements 03 p0369 A67-13799
 Commutativity of two interpolation
 function, solving spaces of
 functions 04 p0644 A67-14906
 Conjugate gradient minimization method in
 function space 08 p1310 A67-20337
 Microcausality principle formulation in
 axiomatic manner using generalized
 functional space 13 p2155 A67-26385
 Definition of solutions of problem that
 constitutes generalization of infrapolynomial
 problem and best approximation problem in
 normed space 13 p2148 A67-27471
 Sampling interval criteria with nonlinear
 integrands in discrete-continuous feedback
 control systems, obtaining performance
 surfaces in object function-parameter
 space 24 p4134 A67-42024
 Local existence, uniqueness and regularity
 theorems for Cauchy problem solution for
 Navier-Stokes system in
 space 24 p4177 A67-42155

FUNCTION TEST
SA DIAGNOSIS
 Test functions for testing location, scale
 and shape parameter hypotheses of Weibull
 distribution 01 p0107 A67-10931
 Diurnal rhythm of cardiovascular
 responses to active orthostasis and
 Schneider test performance in function
 diagnostics of peripheral cycle regulation
 [DVL-620] 11 p1747 A67-25035
 Pilot describing function measurements in
 multiloop control task to provide data for
 multiloop pilot model refinement 17 p2808 A67-33177
 Diagnostic system for jet engine
 malfunctions detection using digital
 computer sonic vibration analysis
 [SAE PAPER 670871] 24 p4207 A67-42008
 Internal combustion engine vibration
 signals application to automatic fault
 diagnosis, discussing engine instrumentation
 and signal analysis
 [SAE PAPER 670872] 24 p4207 A67-42009

FUNCTIONAL ANALYSIS
SA BANACH SPACE
SA SERIES EXPANSION
 Calculation of scale functions of alignment
 nomogram as applied to sets of
 functions 01 p0104 A67-10279
 Direct and inverse problems of
 optimization of quadratic functional in linear
 autonomous and controlled
 systems 01 p0044 A67-10490
 Functional analysis of plane problem of
 elastostatic theory for multiply-connected
 regions with given surface
 traction 01 p0180 A67-10516
 Energy functionals and universal integrals
 of motion for force field symmetric about
 axis of rotation 01 p0113 A67-10680
 Constructive representation of zero classes
 of differentiated functions of many variables
 based on theory of
 approximations 01 p0106 A67-10902
 Stability theory based on functional

methods, examining feedback system with
 linear time invariant and nonlinear
 elements 01 p0046 A67-11208
 Existence and uniqueness theorem of
 Riccati equation arising in solution of
 optimal linear regulator problems in Hilbert
 space 01 p0047 A67-11213
 Functional analysis method application to
 reliability testing of Polaris
 missile 01 p0155 A67-11346
 Synthesis of optimum discrete control for
 eventual state of linear stochastic system,
 reducing problem to solution of Bellman
 functional equation 02 p0225 A67-11957
 Minimization method for examining from
 unique functional-analytic point of view
 additional aspect of extremum problems and
 methods of solving them 03 p0458 A67-12859
 Asymptotic control problem of n-
 dimensional systems solved by functional
 analytic techniques 03 p0391 A67-13265
 Conditions of solvability of Chaplygin
 problem 03 p0458 A67-13339
 Duality principle for automorphic forms on
 semisimple Lie groups extended to include
 arbitrary topological unimodular
 groups 03 p0458 A67-13387
 Approximate solution to nonlinear
 differential Riccati equation, using Bessel
 function 03 p0460 A67-13879
 Extreme value problem of constant type
 and extremal approximating operators with
 positive kernels 03 p0461 A67-14106
 Integrable function representation by
 double singular integral at generalized
 Lebesgue point 03 p0461 A67-14107
 Diffuse reflection of radiation from
 nonstationary plane-parallel layer solved on
 basis of Ambartsumian invariance
 principle 04 p0695 A67-14657
 Maximum problem solution with quadratic
 nonconcave objective functions and linear
 inequalities as constraints 04 p0644 A67-14772
 Periodic solutions for nonautonomous
 differential equations, discussing existence
 and stability criteria 04 p0644 A67-14853
 Soviet papers on theory of functions,
 functional analysis and
 applications 04 p0645 A67-15256
 Optimization of linear control systems
 when placing step limitations on control,
 using functional analysis 05 p0781 A67-18251
 Function approximation from finite
 number of arbitrary points, using iteration
 methods 05 p0833 A67-18260
 General circular complex charts solution,
 considering case where two functions of
 unknown variable are arbitrary functions of
 variable 05 p0834 A67-18435
 Error estimate for approximate solution of
 linear parabolic equation using Kantorovich
 theorem on functional analysis in normed
 space 05 p0836 A67-17108
 Approximation of functions of several
 variables, using one-dimensional analogy to
 determine rapidity of
 convergence 06 p1022 A67-17566
 Minimum normed operator application to
 optimal terminal control system
 problems 06 p0974 A67-17925
 Lagrange theorem for series expansion
 with remainder for weak function whose
 argument satisfies implicit
 relation 06 p1025 A67-18731
 Error estimation for approximate solutions
 of differential equations, using functional
 analysis 07 p1213 A67-19153
 Solution approximation for nonlinear
 parabolic PDEs, using linear combination of
 finite set of selected
 functions 07 p1213 A67-19159
 Intermediate value and simultaneous
 convergence obtained by sequence of
 polynomials for pair of functions on closed
 set E dense on norm z equals
 one 07 p1215 A67-19221
 Convergence of solution of nonlinear
 functional equations, noting iteration
 processes applications 07 p1215 A67-19329
 Fourier convergence of Lebesgue
 integrable functions 07 p1215 A67-19473
 Ultraconvergence of sequence of optimal
 approximation
 polynomials 07 p1216 A67-19583
 Solvability of Cauchy problem for second
 order linear parabolic equations in classes of
 exponentially increasing
 functions 07 p1216 A67-19584
 Minimum energy problems in Hilbert
 function space for continuous and discrete
 linear systems, noting operator

transformation into linear differential
 equations 07 p1216 A67-19908
 Digital simulation of boundary value
 problems of trajectory optimization, using
 variational and functional analysis and IBM-
 FORMAC language
 [AAS PAPER 66-116] 07 p1149 A67-19976
 Duality relation in differential equations
 and some associated functional
 equations 07 p1217 A67-20020
 Stochastic input passage through class of
 nonlinear systems, developing functional
 relations between statistical
 properties 08 p1308 A67-20324
 Simultaneous approximation of function
 and derivatives, ensuring uniqueness by
 imposing linear conditions on coefficients of
 polynomials 08 p1347 A67-20368
 Monograph on existence theorems for
 nonlinear equations, using functional analysis
 in Banach space 08 p1348 A67-21175
 Interpretation of class of divergent
 integrals in terms of limit sums, using
 generalized function
 theory 08 p1349 A67-21193
 Galerkin method analysis of solvability of
 boundary value problems for second order
 quasi-linear elliptic differential equations
 with discontinuous
 coefficients 08 p1349 A67-21197
 Optimum transformation of linear system
 with minimal rms error from given point to
 fixed delta-environment of another given
 point 08 p1313 A67-21322
 Cauchy problem for nonstationary
 linearized Navier-Stokes equations for fixed
 container partially filled with
 liquid 09 p1532 A67-18783
 Synthesis of optimal Lapunov-Bellman
 function, noting sequential solution method
 for independent variables and method using
 first order partial differential
 equation 09 p1525 A67-22077
 Class of nonlinear operators and necessary
 and sufficient condition of solvability of
 quasi-linear elliptic
 equations 10 p1674 A67-23076
 Critical volume of cylindrical reactors
 calculated using n-group diffusion
 theory 10 p1675 A67-23396
 Monotonic growth of multivariable
 function with convexity under logarithm,
 introducing definitions regarding order and
 hypersurface 10 p1675 A67-23609
 Direct and inverse problems of
 optimization of quadratic functional in linear
 autonomous and controlled
 systems 10 p1621 A67-23612
 Expansion of arbitrary function of Mehler-
 Fok integral form in terms of spherical
 functions 11 p1812 A67-24149
 Forced oscillations of generalized Liénard
 equation, examining harmonic solutions in x,
 y plane with confined
 trajectories 11 p1812 A67-24311
 Periodic limiting regime for sets of
 difference equation 11 p1813 A67-24517
 Motion stability during final time interval
 for case of two zero roots determined by
 analysis of nonlinear functions
 structure 11 p1813 A67-24518
 Periodic solutions for nonautonomous
 differential equations, discussing existence
 and stability criteria 11 p1813 A67-24730
 Bound solutions for elliptical equation in
 n-dimensional vector space obtained, using
 linear transformation into Martin
 boundary 11 p1814 A67-24852
 Energy functionals and universal integrals
 of motion for force field symmetric about
 axis of rotation 11 p1821 A67-25069
 Radar resolution performance in moving
 target determined by cross section of
 desired target compared with combined
 cross section of all interfering
 targets 12 p1907 A67-26083
 Functional extremals approximation
 method applied to compressible subsonic
 fluid flows 13 p2050 A67-27148
 Asymptotic behavior of parameter-
 dependent nonlinear functional equations
 arising in signal reconstruction
 study 13 p2147 A67-27451
 Nonlinear programming in Banach space,
 considering saddle value
 problem 13 p2147 A67-27453
 Hankel transforms applied to generalized
 functions theory 13 p2148 A67-27470
 Linear positive operator construction in
 approximation theory 13 p2148 A67-27474
 Machine independent axiomatic theory of

- complexity of recursive functions 13 p2148 A67-27497
- Digital simulation of boundary value problems of trajectory optimization, using variational and functional analysis and IBM-FORMAC language 13 p2074 A67-27531
- AAS PAPER 66-116] 13 p2074 A67-27531
- Qualitative analysis of nonlinear systems described by ordinary or partial differential equations or by functional 14 p2291 A67-28452
- Functional-analytic techniques providing understanding of some nonlinear circuits action on input to output signal production 14 p2291 A67-28453
- Theory of nonself-adjoint ordinary second order differential operators, discussing solution algorithms 14 p2343 A67-28478
- Majorizing functions for Dirichlet problem in n-dimensional space 14 p2343 A67-28631
- Concept of extremal state in topological space, discussing existence conditions and criteria concerning extremal and stationary points 14 p2343 A67-28632
- Extent of system parameter change ensuring system performance within specified limit 15 p2457 A67-29369
- Stationary functionals construction for linear boundary value problem solution or solution derivatives at specified but arbitrary point 15 p2509 A67-29383
- Numerical analysis of PDEs with singular coefficients, noting equivalence of stability and convergence 15 p2510 A67-29519
- Optimal final value control theory, applying variational calculus and functional analysis to control function selection for dynamic systems 15 p2459 A67-30020
- Transforms for regularizing two-body collisions in plane two-and three-body systems with aid of conformal mapping and function theory 15 p2559 A67-30037
- Approximation of functions describing control loops output signals for various values of controller parameters 15 p2459 A67-30132
- Three-step nonlinear analysis procedure for nonlinear stability for position-control servomechanical system applications 15 p2459 A67-30143
- Subadditive functional expectations and inequality of variables 15 p2512 A67-30228
- Identification of continuous time invariant systems from input-output data, analyzing state determination problem for distributed parameter systems 15 p2460 A67-30312
- Control system identification and loop stability limit, noting dominant components of time functions and classification of substitute functions 15 p2461 A67-30317
- Lambda functions describe antenna/diffraction patterns, showing familiar patterns from linear, rectangular and circular apertures 16 p2635 A67-30474
- Analog computer method for approximation of real functions, discussing applications and limitations 16 p2634 A67-30831
- Monotone iterations for nonlinear elliptic differential equations in boundary-value problems applied to Gauss-Seidel methods 16 p2697 A67-31331
- Stationary Newton method for nonlinear functional equations in Banach spaces, formulating convergence conditions 16 p2697 A67-31332
- Asymptotic stability criterion for autonomous feedback system with single odd monotonic nonlinearity, using functional analysis 16 p2646 A67-31639
- Identification of continuous, nonlinear, time-dependent, single-input single-output systems represented by Volterra functional series model and stochastic approximation 16 p2653 A67-31694
- Convolution type integral equation solution via reduction to Riemann problem in class of generalized functions 16 p2698 A67-31735
- Optimal control of dynamic systems with minimax type performance index, discussing application of proposed method of solution 17 p2829 A67-32014
- Sokolov method of averaging functional corrections for treatment of radiant interchange between surfaces 17 p2967 A67-32068
- Time optimal control for parabolic equations, proving bang-bang principle, smoothness, existence of minimum, etc 17 p2877 A67-32559
- Control theory of hyperbolic PDEs examined, noting application to distributed parameter systems 17 p2877 A67-32561
- Cauchy problem for homogeneous linear difference scheme with constant complex coefficients, giving stability lemmas 17 p2877 A67-32677
- Simplification of linear equation of first kind with Tikhonov smoothing functionals 17 p2878 A67-32680
- Homogeneous continuous Markov process without discontinuities of second kind and form of infinitesimal operator 17 p2878 A67-32735
- Approximation method for plotting function of three independent variables 17 p2821 A67-32866
- Boundary value problem solution for three-dimensional layer in axisymmetric case 17 p2885 A67-32882
- Rotational motions of second order autonomous systems, proposing determining algorithm 17 p2885 A67-32883
- Axisymmetrical temperature fields for minimum functional of elastic deformation energy in infinite cylindrical shell 17 p2962 A67-32968
- Synthesis of optimum discrete control for eventual state of linear stochastic system, reducing problem to solution of Bellman functional equation 17 p2831 A67-33274
- Ergodic properties of additive functionals of recurrent Markov processes 18 p3071 A67-34182
- Combination variational-difference numerical method applied to nonlinear boundary value problems, noting numerical functional minimization 18 p3071 A67-34264
- Relationship between stability and continuity for dynamical systems analyzed using functional analysis, discussing connection to boundedness 18 p3079 A67-34286
- Electronic circuit theoretical analysis noting nonlinear and qualitative processes 19 p3200 A67-34904
- Linear networks having reciprocal and nonreciprocal elements obtained using numerical-code circuit model 19 p3201 A67-34906
- Method for influence range determination of stationary points of nonlinear recurrence of order greater than one corresponding to rational functions 19 p3205 A67-35913
- Functional sensitivity to cavitation of hydrofoil cascade, solving Fredholm type integral equations 20 p3419 A67-36188
- Functional analysis applied to optimum control by reduction of variational problem to finite dimensional analysis and calculation of algorithms for use with digital computer 20 p3477 A67-37034
- Existence theorems for linear optimal control problems with nonlinear cost functionals 20 p3408 A67-37076
- Maximum information principle applied to search for minimum of function 20 p3477 A67-37195
- Necessary condition for optimal control in nonlinear automatic control system determined, using method of successive approximations 20 p3410 A67-37229
- Accuracy problems in control systems, discussing error assessment and accuracy estimates of optimal control 20 p3410 A67-37231
- Papers on functional analysis covering approximation methods and Cauchy, Dirichlet and boundary value problems 21 p3651 A67-37832
- Discrete Laplace transform for analyzing pulsed automatic systems with variable parameters, noting special type of complex variable 21 p3605 A67-39112
- Functional analysis of transistor amplifier with multiloop feedback, deriving equation for transfer constant increment 22 p3769 A67-39577
- Integral equation with transfer function density restrictions defining characteristic function of Markov process functional, deriving several limit theorems 22 p3827 A67-39878
- Three-dimensional heat conduction, heat and mass transfer and thermoelasticity problems solved by approximate method using functional parameters 23 p4083 A67-41290
- Functional equations in internal radiation field in finite inhomogeneous isotropically scattering atmosphere, using invariant embedding and Duhamel principle 24 p4189 A67-42597
- ### FUNCTIONAL INTEGRATION
- Functional integration analysis of exponential behavior of nonlinear feedback control systems 01 p0047 A67-11211
- Expansion of arbitrary function in terms of Bessel functions of complex index 06 p1024 A67-18555
- Mathematical model for condensation point of first order phase transitions, examining free energy singularity and metastable phase 07 p1268 A67-20089
- Generalized Gaussian distribution functional for weak plasma turbulence neglecting three-point correlation function 08 p1366 A67-21415
- Existence theorems of algebraic integral equations /AIR/ with nonlinear functionals 09 p1524 A67-21649
- Solution to Bogolubov differential equation for distribution functions of particle system by functional integration technique 12 p1962 A67-26174
- Current diagram plotting by graphical integration method for diurnal solar magnetic variations in especially quiet days 14 p2309 A67-27939
- Soviet book on new methods for solving elliptic equations including equations in many-dimensional space, index problem in functional equation theory, etc 17 p2878 A67-32686
- Iterative methods for integration of linear partial differential equations, determining relaxation factor 18 p3071 A67-33753
- Cauchy problem solution for certain functional equations in complete linear normalized space extended to include nonlinear space 18 p3073 A67-34603
- Expansion of arbitrary function in terms of Bessel functions of complex index 23 p4022 A67-40821
- ### FUNGUS
- SA SPORE
- SA YEAST
- Response of fungi to diurnal temperature extremes, describing soil, simulated Martian temperature regime and fungi growth 09 p1454 A67-21991
- ### FURNACE
- SA IMAGE FURNACE
- SA VACUUM FURNACE
- Rotating plasma furnace and application to spheroidization of refractory powders, noting arc source 02 p0228 A67-11503
- Instrument for generation of thermal plasmas in direct current-arc discharges and expansion to walls of coaxial corotating cylinder 17 p2835 A67-33389
- ### FUSED METAL
- Surface etching effects on positively sloped current-voltage characteristics of p-n junctions in fused indium antimonide 16 p2730 A67-31161
- ### FUSELAGE
- SA AIRFRAME
- SA WING-FUSELAGE COMBINATION
- Fuselage optimization for short haul transport aircraft 02 p0181 A67-12199
- Effect of rotor control feedback loads of two-bladed rotor system on helicopter fuselage vibrations 16 p2777 A67-31847
- [AHS PAPER 133] In-flight escape of helicopter personnel using Navy fuselage capsule, describing devices for recovery, protection and survival 17 p2794 A67-31999
- Aircraft fuselage shapes analysis for drag reduction and maximum useful space based on streamlined bodies found in nature 20 p3375 A67-36887
- ### FUSELAGE MOUNTING
- Computer algorithm for framework diagram in synthesizing thin walled shells strengthened by ribs 02 p0340 A67-12443
- Aircraft fuselage design noting planning philosophy, parameters, future problems and considerations [SAE PAPER 670370] 18 p2985 A67-33568
- ### FUSION
- SA CONTROLLED FUSION
- SA NUCLEAR FUSION
- Latent heat of fusion of titanium 10 p1670 A67-23640
- ### FUSION WELDING
- Electron beam zonal fusion growth of Mo, W and Ta single crystals without using crucible 05 p0827 A67-18079
- Electron beam zonal vacuum fusion growth of Mo-Nb alloy single

crystals 05 p0827 A67-16080
 Short and long range redistribution of solute in weld fusion zones of alloy systems through data from electron microprobe analyses 05 p0811 A67-16830
 Nondestructive test development to meet inspection requirements of advanced aircraft design, discussing titanium fusion and resistance spot welds and adhesive bonding honeycomb components 05 p0808 A67-17087
 Fusion weld evaluation in 2014-T6 material by eddy current, electric conductivity and hardness plots, noting aging effects, mechanical property degradation, etc 06 p1007 A67-17640
 Fusion welding of nickel maraging steel to lower strength steels to produce leaf spring subjected to tensile impact loading 07 p1198 A67-19213
 Laser equipment for fusion welding of aerospace structural materials, examining ruby laser properties, flash tube and overall system 09 p1504 A67-22141
 Resistance welds produced by butyl sealant prevent passive films formation on aluminum and magnesium alloys 12 p1948 A67-25287
 Welding processes covering high purity metals, plasma arcs, resistive slags, high energy beams and solid state 15 p2493 A67-29681
 Integrated nondestructive testing for determining weld integrity of space vehicles 20 p3454 A67-36586
 Microcracking susceptibility studies of Inconel 718 weld heat affected zones, noting hot ductibility, weld circle patch and fillerless fusion welding tests 22 p3818 A67-39222
 Microsegregation and grain boundary liquation in heat affected zone of 18-Ni maraging steel welds 22 p3812 A67-39448
F4H AIRCRAFT
 S F-4 AIRCRAFT

G

G-91 AIRCRAFT
 S FIAT G-91 AIRCRAFT
G FORCE
 SA ACCELERATION STRESS
 Animal study showing aversiveness of simulated gravity and importance of separating rotation effects from effects of G forces 02 p0189 A67-12633
 Experiments showing occurrence of aero-atelectasis in pilots exposed to high G forces, breathing oxygen and using anti-G suit 09 p1453 A67-21733
 Time and distance measurement of freely falling body to determine acceleration due to gravity 10 p1657 A67-23317
 Changes in reproduction and growth of mice and rats under chronic centrifugation at various g force conditions 10 p1598 A67-23416
 Absolute gravitational acceleration determined by timing symmetrical free motion of body moving under attraction of gravity 12 p1965 A67-25126
 Muller maneuver /forced inhalation with closed glottis/ improves tolerance to negative G 12 p1901 A67-25172
 Periodic prolonged low-intensity acceleration stress provided by short radius centrifuge in baboons 13 p2059 A67-26917
 Hemodynamic responses of conscious dogs exposed to various centrifugation levels and back angles to determine optimum angle for positioning astronauts 22 p3750 A67-39593
 Trauma in lateral impact at high entrance velocity compared with rearward and forward facing body orientations of baboons when restrained by lap belt only 22 p3750 A67-39594
 Color photographic study of blackout during radial acceleration on human centrifuge, presenting evidence confirming central retinal arterial collapse 23 p3957 A67-41638
G-222 AIRCRAFT
 S FIAT G-222 AIRCRAFT
GADOLINIUM
 Magnetic properties of YGa and YGaGd ferrites noting effect of increasing Gd content 01 p0136 A67-11052
 Specific heat and magnetic susceptibility of yttrium solid solutions with magnetic impurities of Gd 08 p1369 A67-20870
 Uniaxial anisotropy and rotational

hysteresis in thin gadolinium films 13 p2179 A67-27144
 Thorium-gadolinium alloy magnetization curves confirming full Meissner effect, showing bulk properties of superconductors obey Abrikosov-Gorkov theory 14 p2373 A67-28859
 Superhyperfine interactions in electron-spin-resonance spectrum of substitutional gadolinium 3 impurity in calcium fluoride single crystals under applied stress 17 p2913 A67-32367
GAIN
 SA HEAT GAIN
 SA POWER GAIN
 Simultaneous derivation of optical gain factor and loss per unit length of series of solution grown diffused GaAs injection laser 01 p0138 A67-11072
 VHF antenna proposed as working gain standard, determining antenna gain by two-identical antenna method 03 p0385 A67-13859
 Equivalent gain and error response of hysteretic system to Gaussian inputs 04 p0593 A67-15637
 Relationship between optimum gain and time constant settings for multiple time constant self-adjusting models 06 p0977 A67-18530
 Effects of gain saturation by strong traveling fields in dilute laser media, noting atomic motion and line broadening 07 p1197 A67-20126
 Worst case gain sensitivity with zero phase sensitivity in active RC network 08 p1308 A67-20321
 Fluctuating effective gain of rocket telemetry links determined from signal strength data of Black Brant sounding rockets 09 p1463 A67-21829
 Automatic fluoric gain changer circuit for flight control systems counteracting Mach number and altitude pressure effects 14 p2251 A67-28352
 Gain maximization for arbitrary antenna arrays with excitation amplitude and phase and element positions are subjected to random errors 16 p2638 A67-31336
 Wideband varactor upconverters for satellites use, emphasizing transmission characteristics and stability over wide temperature range 16 p2640 A67-31531
 Random error effect on directional gain of sectional parabolic antenna with automatic phasing, setting sections effectively by three control points method 22 p3770 A67-39657
 Coates flow graph gain formula modification by introducing loop-set and two-loop-set for linear systems analysis 23 p3984 A67-40649
GALACTIC EVOLUTION
 SA STELLAR EVOLUTION
 Galactic and solar nucleosynthesis, determining formation of meteorites on basis of decay of nucleides Pu 244 and I 129 02 p0320 A67-11472
 Statistical data on space density of bright elliptical galaxies, radio galaxies, quasars, noting relation between space density and age 02 p0322 A67-11685
 Discrepancies between various mass models of galactic systems, commenting on rotation curves 02 p0324 A67-11768
 Milky Way galaxy mechanism and evolution, examining correlation between period of pulsation of intrinsic variable and galactic velocity 03 p0516 A67-14334
 Astronomical UV radiation noting galactic composition and extragalactic systems, stellar emission and molecular and atomic H 04 p0696 A67-14700
 Partial fragmentation of pregalaxy in early phase of contraction with large internal velocity difference 04 p0697 A67-14806
 Metagalactic existence of type of hypothetical particles representing stable closed Einstein microcosms 04 p0702 A67-15757
 Cosmology in last 150 years reviewed, discussing Hubble expansion of universe, Einstein theories on gravity and present concepts 05 p0897 A67-16775
 Anisotropic cosmological solution with energy density determined only by neutrinos moving along one axis, noting expansion 10 p1708 A67-23334
 Gravitational instability from reformulation of Lifshitz relativistic theory for galaxy formation in expanding universe and comparison with Bonnor approach 11 p1859 A67-24121

Gravitational instability due to small irregularities and implications for early universe and galaxy formation 11 p1860 A67-24483
 Possible initial perturbations development into galaxies with dissipative effects associated with transport processes treated via Boltzmann equation 11 p1867 A67-24838
 Evolutionary scheme of radio galaxies based on radio luminosity vs volume emissivity diagram, noting similarity and parallelism between radio and X-ray intensities 12 p2007 A67-25767
 Density fluctuations and thermal conditions in expanding universe and creation of stars, quasars, galactic clusters and galaxies 15 p2551 A67-29138
 Helium origin in universe and heavy element creation 17 p2942 A67-32405
 Quasar regarded as early stage in formation of system like galaxy nucleus, using model 19 p3317 A67-34950
 Origin of elements, discussing element formation and abundances, nucleosynthesis and cosmological theories 19 p3263 A67-35869
 Quasars and radio galaxies characteristics contrasted, drawing conclusions about evolution using radio emission synchrotron hypothesis and consistent model 20 p3526 A67-37250
 Stellar magnetic field origin theories, discussing fossil, dynamo and battery theories 21 p3708 A67-38985
 Upper limit for condensation of fluctuations in primordial fireball determined by considering effects of radiative diffusion 21 p3711 A67-39120
 Gravitational instability and star and galaxy formation and structure - Conference, Liege, Belgium, June 1986 22 p3890 A67-40491
 Origin of large scale structures in universe, discussing instability and primordial-structure hypotheses 22 p3891 A67-40492
 Clustering process, examining self-gravitating system separation from expanding cosmic distribution 22 p3891 A67-40494
 Oscillating relativistic universe model from Einstein field equations, discussing Friedmann model matter and velocity distribution, Hubble law and universe volume oscillating relativistic universe model from 22 p3892 A67-40496
 Thermal instabilities in homogeneous primeval medium theory shown to play no role in galactic evolution 22 p3892 A67-40497
 Nonlinear hydrodynamic equation term effects on rotational fluid motion in galactic plane, discussing velocity perturbations and discontinuities 22 p3893 A67-40502
 Spiral field rotation with motion integrals as distribution function arguments, discussing potential, density and spiral arm stability 22 p3893 A67-40507
 Stability of stellar systems with different velocity distributions, considering nonlinear wave in stellar sheet leading to galactic stellar velocity distribution evolution 22 p3894 A67-40510
 Protogalactic survival during metagalactic formation due to favorable orientation of equatorial planes to orbital planes 22 p3894 A67-40511
 Jacobi high energy ellipsoid orbits in barred spirals valid at galactic time scales 23 p4063 A67-40898
 Density fluctuations and thermal conditions in expanding universe and creation of stars, quasars, galactic clusters and galaxies 24 p4239 A67-43061
GALACTIC MAGNETIC FIELD
 Irregularity of galactic magnetic field structure in vicinity of sun indicated by starlight polarization, interstellar cloud motion and Milky Way photography 01 p0151 A67-11275
 Interstellar magnetic fields and influence on motion of gaseous matter in galaxies studied by Zeeman splitting and Faraday rotation techniques 03 p0516 A67-14336
 Galactic explosions, radio galaxies and quasi-stellar radio sources theories, discussing role of large scale magnetic field 05 p0902 A67-17287
 Galactic magnetic field structure in local spiral arm in accounting for radiation and polarization 05 p0902 A67-17288
 Electron component of primary cosmic radiation 11 p1856 A67-24104
 Origin of ultrarelativistic cosmic ray

- particles 14 p2382 A67-29028
- Galactic plasma dynamics related to galactic magnetic field generation and topology, discussing agreement with Hoyle-Ireland model and Morris-Berg observations 22 p3854 A67-40503
- Unified theory for galaxy spiral formation and radio galaxy and quasar evolutionary dynamics, discussing galactic dipole magnetic field generation 22 p3893 A67-40504
- Spiral arm magnetic field configuration model simplifies star formation theory, discussing theoretical and observational evidence 22 p3893 A67-40505
- Galactic rotation effects on gaseous spiral arm stability for magnetic critical wavelength less than Jeans critical wavelength case 22 p3893 A67-40506
- Cosmic ray intensity variation mechanisms due to motion of solar system and quasi-radial interplanetary magnetic field 23 p4056 A67-41107
- Interstellar gas dynamic instability caused by galactic cosmic rays and magnetic field, showing turbulent and fragmentation enhancement of ambipolar diffusion 24 p4223 A67-41813
- GALACTIC RADIATION**
- SA EXTRAGALACTIC RADIATION**
- Spectrum of galactic radio emission measured using diode noise sources whose output spectra is calibrated for various frequencies 01 p0147 A67-10360
- Flux intensity and energy spectra of galactic X-ray sources, Tau X-1 and other celestial bodies studies, using three sensitive Geiger counters 01 p0144 A67-10562
- Large multipole steerable-beam antenna built by using independent reflectors that redirect energy from desired direction to focus 02 p0210 A67-11592
- Energy spectra and abundances of elements He through Si of galactic cosmic ray above 20 mev per nucleon in nuclear charge range between 2 and 26 02 p0307 A67-11687
- Radiation absorption by ionized hydrogen in plane of galaxy to explain brightness profiles for declination minus 37 degrees 02 p0307 A67-11688
- Hazards to man on moon from flare-produced solar particle beams and galactic radiation, noting estimate for life shortening 02 p0189 A67-12394
- X-ray emission from radio galaxies as possible bremsstrahlung radiation of hot gas, noting Crab Nebula 02 p0308 A67-12482
- Galactic deuterium and energy spectrum above 20 mev per nucleon measured by IMP-III satellite near minimum solar activity 03 p0472 A67-13390
- Protective shielding for astronauts from ionizing radiation from solar and galactic cosmic rays and radiation 03 p0365 A67-13539
- Intense radio emission from galaxies may be due to large scale explosions in galactic nuclei, examining characteristics of synchrotron emission 03 p0516 A67-14335
- Cosmic ray electron spectrum indicates universal 3 degrees K black body radiation confinement to galactic disk 04 p0692 A67-14948
- Secular modulation of galactic cosmic rays in interplanetary space as function of solar activity 05 p0877 A67-16083
- Deuterium nuclei generation in galactic cosmic radiation 05 p0878 A67-16096
- Luminosity of galactic disk in 12.8 micron radiation, obtaining from volume integral stellar photon flux density and thermal radio emission rate 05 p0892 A67-16412
- Galactic depolarization of 21 cm wavelength radiation of extragalactic sources explained as function of distance traveled by radiation through halo 05 p0895 A67-16601
- Galactic emissions and LF and MF radio noises in ionosphere 05 p0898 A67-16867
- Energy spectra of galactic X-rays observed with three types of counters borne on sounding rockets 05 p0883 A67-16876
- Extrasolar X-ray observation regarded as astronomy in contrast to cosmic ray observation which is considered as local geophysical phenomena 05 p0884 A67-16881
- Correlation between position and red shift of quasars indicating anisotropic universe or galactic origin of quasars 05 p0898 A67-16887
- Galactic magnetic field structure in local spiral arm in accounting for radiation and polarization 05 p0902 A67-17288
- Long wave cosmic radio emission in interplanetary space 06 p1077 A67-17746
- Synchrotron nature of Sagittarius A central component radio spectrum and injection of relativistic cosmic particles 06 p1078 A67-18166
- Solar modulation of galactic protons and He nuclei during last solar cycle analyzed according to Parker 07 p1244 A67-19913
- LF galactic emissions, noting spiral arms and spherical halo on galactic hub, signal strength variation and terrestrial atmosphere role 08 p1385 A67-20866
- Quark radio wave line detection from quasars in galaxies with history of high intensity cosmic rays 08 p1400 A67-21246
- Radio spectrometer for polarization measurements of galactic emission in meter wave range 08 p1306 A67-21350
- Galactic radio sources noting disk model brightness distribution, relativistic particle energies, continuous particle acceleration and ratio between proton and electrical component of cosmic radiation 09 p1563 A67-21629
- Low ionosphere with suitable selected track for absorption observation as indicator of galactic cosmic rays modulation by solar wind 09 p1561 A67-21843
- Intensity gradient of galactic cosmic rays, analyzing modulation induced by solar activity 10 p1699 A67-22801
- Energy spectra of galactic X-rays from four rocket measurements, observing Cygnus and Tau X-1 10 p1700 A67-23054
- Energy spectra of Tau X-1 and isotropic component of galactic X-rays, using rocketborne scintillation and GM counters 10 p1701 A67-23229
- X-ray emission from radio galaxies as possible bremsstrahlung radiation of hot gas, noting Crab Nebula 10 p1702 A67-23350
- Galactic radio noise intensity decrease correlated with decline in solar activity, calculating D and F region absorption 11 p1784 A67-23934
- Spiral and irregular galaxies total mass to neutral hydrogen mass ratio derived from mass-luminosity relations 11 p1858 A67-23995
- Degree of polarization and position angle measurements of linearly polarized components of galactic and extragalactic radio sources at short wavelength 11 p1861 A67-24486
- Tabulated localized cosmic X-ray sources and survey of rocket probe identifications 11 p1857 A67-24633
- Delta electrons formed in interstellar hydrogen-galactic ray collision 12 p1994 A67-25645
- Cosmic x-ray sources identified using Geiger counters aboard rockets, noting clustering toward galactic disk 12 p1994 A67-25760
- Precise position and spectra of Scorpio X-ray source and location of two weaker sources in galactic plane, describing instrumentation used 12 p1995 A67-25761
- Nuclear abundances of galactic and solar cosmic rays, discussing detector electronics system for measurement of particle energy spectrum 12 p1944 A67-25852
- Cosmic X-ray sources concentration toward galactic plane and variability 12 p1999 A67-26172
- Interstellar gas dynamics suggests that energy density of galactic cosmic rays places firm upper limit on undetermined constant of solar modulation 13 p2189 A67-26265
- Galactic cosmic ray intensity depression by convective region and by surrounding static barrier of expanding corona 13 p2191 A67-26323
- Radio astronomical investigations of 18 cm ground state lambda doublet transition of OH suggest maser amplification of radiation takes place in interstellar medium 13 p2198 A67-26715
- Charge and energy spectra of galactic cosmic rays during solar minimum from satellite and Skyhook balloon data 13 p2193 A67-27248
- Solar and galactic particle spectra and composition measured with cosmic ray telescope mounted on satellite 13 p2193 A67-27249
- Spectrum, intensity, and charge composition of primary cosmic radiation and relevance to origin and propagation of galactic radiation 14 p2379 A67-27963
- Maser effect hypothesized as cause of 21 cm radiation in clouds of interstellar hydrogen in galactic corona 15 p2551 A67-29139
- Solar wind modulation of low energy galactic cosmic radiation, estimating primary source spectra, proton and helium fluxes 15 p2550 A67-29614
- Synchrotron nature of Sagittarius A central component radio spectrum and injection of relativistic cosmic particles 16 p2737 A67-30510
- Radio spectrometer for polarization measurements of galactic emission in meter wave range 17 p2822 A67-31946
- Cosmic ray intensity 11-year variation energy characteristics, discussing spectrum bending due to integral modulation in interplanetary space 17 p2932 A67-32083
- Galactic and solar ray behavior equations, with cosmic ray drift velocity and diffusion tensor determined for interstellar space in anisotropic-diffusion approximation 17 p2935 A67-32109
- Hydrogen emission lines photoelectric measures in Ton 1542 indicates radiative recombination in upper levels and sharp intensity increase in red ascribed to nonthermal sources 18 p3120 A67-33997
- Galactic anisotropies observation, giving procedure for detecting periodicities and data on sidereal daily variation amplitude 19 p3315 A67-35484
- Balloon and satellite measurements of 11-year solar modulation of low energy protons and helium nuclei in galactic cosmic rays 19 p3315 A67-35487
- Hyperfine structure of ground state of helium 3 microwave transition radiation from galactic H II regions 19 p3330 A67-36074
- Energy spectrum and production rates for secondary antiprotons from inelastic collisions of high energy galactic cosmic radiation with interstellar gas nuclei 19 p3316 A67-36098
- Antiproton abundance upper limit in low energy galactic cosmic radiation determined by exposing nuclear stack to residual atmosphere 20 p3518 A67-36872
- Optical metagalactic radiation measured by spacecraft photographic and photometric methods, reviewing Olbers paradox and night sky brightness measurements 20 p3528 A67-37127
- Galactic cosmic ray density distribution anisotropy in solar system, discussing outward convection of cosmic rays by solar wind and inward diffusion model 20 p3520 A67-37474
- Probes containing various scintillators for measuring electron energy spectrum at high altitude in cosmic ray flux 23 p4054 A67-41095
- Galactic cosmic ray intensity measurements in stratosphere and at various atmospheric depths, studying secular variation energy spectra during solar cycle 23 p4055 A67-41103
- Galactic radiation hazard for long term space missions, discussing life shortening effect 23 p3953 A67-41583
- Interstellar gas dynamic instability caused by galactic cosmic rays and magnetic field, showing turbulent and fragmentation enhancement of ambipolar diffusion 24 p4223 A67-41813
- Intensity gradient of galactic cosmic rays, analyzing modulation induced by solar activity 24 p4209 A67-42138
- Galactic cosmic ray solar cycle and secular variations in bombardment of meteorites at average meteoroid solar distance and 1 AU from radioactive isotope ratios 24 p4210 A67-42622
- Solar and galactic low energy cosmic ray nuclear ionizing and interaction effects on meteorite surface isotopic composition, estimating particle fluxes 24 p4210 A67-42634
- Secular modulation of galactic cosmic rays in interplanetary space as function of solar activity 24 p4212 A67-42759
- Deuterium nuclei generation in galactic cosmic radiation 24 p4213 A67-42772
- Maser effect hypothesized as cause of 21 cm radiation in clouds of interstellar hydrogen in galactic corona 24 p4239 A67-43062
- GALACTIC RADIO WAVE**
- Polarization measurements of distribution of ionized interstellar gas near galactic plane using two galactic region

- models 02 p0322 A67-11645
Galaxy M82, analyzing continuous optical magnetobremstrahlung and relativistic electrons 02 p0310 A67-12578
Radio emission from 18 galaxies observed, noting accompaniment of optical spectrum emission and enhancement due to production of relativistic electrons in active nuclei 04 p0697 A67-14774
Solar coronal reflection and occultation of 38 mc/sec galactic radio energy, using Taurus A and galactic equatorial continuum as occulted sources 05 p0891 A67-16403
Angular sizes of radio sources at 6, 11, and 21 cm wavelengths, using Mark II radio telescope of Jodrell Bank 09 p1565 A67-21980
Two-dimensional distribution of radio sources measured for random positioning using Poisson distribution 14 p2393 A67-29026
Galactic radio source W49 at 3.4 mm, showing no additional components in spectrum with turnover points at various frequency ranges 20 p3527 A67-37393
- GALAXY**
SA MILKY WAY
SA RADIO GALAXY
SA SPIRAL GALAXY
SA STAR
SA SUPERNOVA
Energy dissipation channels of nuclear and electron components of cosmic rays in Galaxy and Metagalaxy 01 p0145 A67-11276
Cometary motion in outer solar system region, taking galactic nucleus as perturbing body 01 p0151 A67-11286
Numerical integration of solar orbit in model of galactic system 02 p0330 A67-12714
Dynamical model of steady state self-gravitating stellar system with finite total mass 05 p0897 A67-16804
Artificial satellite UV photometry and polarimetry of galactic star clusters 06 p1077 A67-18065
Inertial frame of reference for measuring accelerations, considering external galaxies, stellar system in our galaxy and planetary system 07 p1250 A67-19678
Relative gravitational potentials through certain regions in Galaxy obtained through rotation curve in plane of Galaxy 08 p1380 A67-20384
Cosmic X-ray sources attributed to thermal emission of hot condensations from supernova remnants in our galaxy or other galaxies 12 p1995 A67-25764
Localization of radio source 3C 17 from moon occultations and identification with near galaxy 12 p2011 A67-26249
Stabilization of clusters of galaxies by ionized gas studied for recombination radiation 12 p2011 A67-26250
Solar velocity with respect to distant galaxies estimated from red shift for nearby galaxies, noting cosmic microwave background 15 p2563 A67-30160
Secular increase of stellar noncircular velocities in disk portions of galactic systems, noting gravitational disturbances [AROD-2160-19] 16 p2753 A67-31699
Upper limit on mean mass density of luminous matter in universe from brightness of night sky 17 p2944 A67-32638
Variational principle for determining fluid flow stability in differentially rotating self-gravitating stars and galaxies and for studying eigenfunctions 17 p2947 A67-32756
Rotational velocity of neutral hydrogen subsystem in outer regions of Galaxy outside galactic plane 17 p2950 A67-33163
Cosmic-ray electron spectrum in disk-halo galactic model, studying inconsistencies in Ramaty and Lingenfelter analysis 20 p3518 A67-36946
Absorption spectra of quasi-stellar objects /QSO/, suggesting origin in galaxies through which light passes on way to earth 23 p4069 A67-41442
Intervening galaxy effect on radiation from distant objects, studying Faraday rotation, 21-cm absorption, optical scattering and absorption lines 24 p4223 A67-41810
- GALERKIN METHOD**
Lapunov second method applied to elastostatic stability, discussing applicability of Dirichlet principle and Galerkin method 01 p0161 A67-10647
Spectrum of small perturbations of plane parallel Couette flow calculated, using Galerkin method 01 p0053 A67-11000
Intrinsic electric field of rarefied ion-electron plasma in external magnetic field and plasma stability, noting use of Galerkin method to determine plasma layer slippage 01 p0126 A67-11299
Book on numerical realization of variational methods, discussing Hilbert space elements, Ritz and Bubnov-Galerkin stability processes, spectral and nonlinear problems, etc 04 p0645 A67-15009
Electromagnetic excitation of metallic cone, deriving systems of linear algebraic equations for coefficients of expansion of electric and magnetic fields 04 p0575 A67-15152
Thin rod bending and twisting theory applied to critical speed of rotating shaft under axial loading and tangential torsion, using Galerkin approximation [ASME PAPER 66-WA/MD-1] 04 p0629 A67-15348
Bubnov-Galerkin and energy method solutions of stability and oscillatory motion equations for conical shell under inertial loading 04 p0717 A67-15890
Galerkin procedure for multipoint boundary value problems of general nonlinear systems 07 p1213 A67-19160
Galerkin-Ritz method application to Maxwell waveguide equations for calculation of propagation constant of rectangular guide with transverse ferrimagnetic core 07 p1152 A67-19590
Galerkin method analysis of solvability of boundary value problems for second order quasi-linear elliptic differential equations with discontinuous coefficients 08 p1349 A67-21197
Convergence rate of approximate Ritz and Bubnov-Galerkin method in application to equations having solutions in form of linear combination of functions 08 p1349 A67-21200
Effect of mass distribution and loading sequence on elastic rod, solving eigenvalue problem by Galerkin method 10 p1715 A67-22912
Dynamic analysis of sandwich plate with clamped edges executing plane strain motions, using variational motion equation and Galerkin method 10 p1717 A67-23138
Instability of Maxwellian fluid flow in pipe analyzed using Galerkin method 11 p1778 A67-24216
Stability of incompressible fluid in Couette flow between coaxial circular cylinders, using Galerkin method to obtain critical Taylor number 11 p1781 A67-24570
Galerkin method applied to approximation of periodic solution of system of singular differential equations 11 p1819 A67-24762
Bending theory for sandwich plates solved by Galerkin method assuming load distribution over upper and lower faces of plate 11 p1880 A67-25095
Compression load stability of nonuniformly rigid plates within and beyond elasticity limits solved by combined Galerkin and finite difference methods 12 p2031 A67-25961
Generalized Bubnov-Galerkin-Kantorovich method for approximate solution of boundary value problem 12 p1962 A67-26106
Eigenvalues of Laplace equation for diurnal and semidiurnal tidal oscillations solved using Galerkin method 13 p2112 A67-26668
Theorems derived from approximate methods of analysis applied to collocation, moment and Galerkin methods for solving linear integral and differential equations 14 p2344 A67-28671
Electromagnetic excitation of metallic cone, deriving systems of linear algebraic equations for coefficients of expansion of electric and magnetic fields 15 p2435 A67-29339
Existence conditions of periodic solution of equations describing nonlinear oscillations of thin plates with allowance for damping and application of Galerkin method 15 p2575 A67-29887
Buckling of longitudinally reinforced rectangular panel loaded by constant edge shear and longitudinal variable compression 16 p2763 A67-30792
Galerkin method analysis of vibrations of clamped rectangular plates, using polynomial approximation 17 p2962 A67-32823
Variational technique for temperature field determination in plane system with given heat distribution sources, based on Galerkin-Ritz method 17 p2972 A67-33069
Dynamic stability of beam columns undergoing weakly nonlinear vibrations studied using Ritz-Galerkin procedure 19 p3342 A67-35758
Galerkin method modifications to obtain static solution of indefinitely long partial-arc self-acting gas bearing 19 p3237 A67-35866
Galerkin-Ritz method application to Maxwell waveguide equations for calculation of propagation constant of rectangular guide with transverse ferrimagnetic core 20 p3401 A67-37327
Galerkin method applicability to boundary value problems and eigenfunctions and eigenvalues for integrodifferential equations with deviating arguments 20 p3478 A67-37580
Galerkin method shown convergent even with selected functions not satisfying exactly all boundary conditions 21 p3715 A67-37890
Convergence of perturbed Galerkin method to construct general theory of approximate methods for nonlinear equations 21 p3653 A67-38419
- GALLIUM**
Superconducting transition temperature and critical field curve for pure Ga single crystals 01 p0130 A67-10153
Radial distribution analysis of films of bismuth and gallium prepared by low temperature condensation for electron diffraction tests 01 p0137 A67-11060
Vanadium-gallium wires with good superconducting properties fabricated by new stepwise diffusion process 01 p0137 A67-11064
Homogeneous elastic stresses in evaporated gallium films, noting transition from compression to tensile stress 02 p0287 A67-11718
Local diffusion of Ga into Sb-doped Ge samples from Ga-doped silicon dioxide films prepared in specially designed vacuum ampoule 03 p0491 A67-13175
Longitudinal magnetic field effect on convective heat transfer during turbulent MHD pipeflow of liquid Ga 06 p1044 A67-18682
Concentration of Ni, Ga and Ge in series of Odessa and Canyon Diablo meteorite specimens 08 p1385 A67-20936
Ge and Ga concentration in selected Fe meteorites used to determine quantization in terms of multiple parent body hypothesis and planetary fractionation processes 09 p1564 A67-21738
Perpendicular critical magnetic fields of superconducting aluminum, tin and gallium small grained films examined for superconducting transition temperature enhancement 14 p2373 A67-28860
Simultaneous diffusion of gallium and arsenic in silicon from gallium arsenide source, obtaining profiles at various temperatures 19 p3308 A67-36035
Ultrasonic wave absorption in high purity gallium single crystals in magnetic field, observing large magnitude geometric oscillations at cryogenic temperature 22 p3859 A67-39653
Anodic oxidation usable for efficient phase analysis technique for V-Ga alloys, identifying interference colors in absence of oxygen impurities 23 p4036 A67-40713
- GALLIUM ALLOY**
Phase diagram of vanadium-gallium system by differential thermal analysis of thirty-five 10-g V-Ga alloy samples prepared in arc oven 05 p0827 A67-16326
P-n junction fabrication in vapor phase grown GaAs-P alloys resulting in room temperature injection laser, thereby extending operation into visible spectrum 11 p1802 A67-24741
Semiconducting alloys of gallium investigated by photometric method using gallium and xylene orange 22 p3804 A67-40299
- GALLIUM ANTIMONIDE**
Minimum spectral line width, threshold current density, radiation-peak displacement and possible recombination mechanism for GaSb laser diode p-n junctions in coherent radiation 01 p0087 A67-10085
Nonsinusoidal pumping of tunnel diode mixers, calculating noise figure for zero bias as function of pump voltage 01 p0037 A67-10477
Oscillatory magnetostriction in GaSb, noting stress effect on energy bands 02 p0296 A67-11819
Thermoconductivity and thermal emf of

- Zn- and Te-doped GaSb 02 p0297 A67-11847
Optical phonons role in thermal conductivity of GaSb doped with Zn and Te in temperature range 80 to 600 degrees K 03 p0488 A67-12811
Anomalous high temperature Hall data for GaSb explained as effect of electrons in /100/ conduction band minima 03 p0501 A67-14346
Transverse magnetoresistance and Hall effect measurements on n-type GaSb at various magnetic fields and temperatures, obtaining electron concentration and mobility 03 p0501 A67-14347
Sulfur donor level associated with conduction bands of gallium antimonide in measurements of Hall coefficient vs temperature and resistivity vs pressure 04 p0673 A67-14476
Recombination radiation from Ga-Sb p-n junctions, noting spectral composition as function of current density and impurity concentration 04 p0681 A67-15297
Impurity atom behavior in diatomic InSb and GaSb crystal lattices analyzed, using nuclear gamma resonance, measuring absolute values of f, chemical displacements and line widths 05 p0861 A67-16392
I-V characteristics of p-gallium antimonide based tunnel junction at various temperatures analyzed, finding secondary peaks exhibited by inverted diodes 05 p0861 A67-16395
Ultrasonic wave absorption in GaAs and GaSb compounds at temperatures from 95 to 300 degrees K 06 p1051 A67-18399
Hall coefficient and transverse magnetoresistance behavior in n-GaSb at 4.2 degrees K, using DC high magnetic fields 06 p1064 A67-18946
Reverse tunneling currents in GaSb tunnel diodes as function of temperature and voltage explained through band structure 06 p0972 A67-18977
Output and emission spectra of p-n junction diodes analyzed in connection with laser effect in GaSb 09 p1516 A67-22600
Temperature dependence of Hall constant and photoconductivity kinetics of gallium antimonide with different tellurium content 10 p1694 A67-23651
Stimulated emission in GaSb injection lasers with steep flat p-n junction, noting dependence of luminescence intensity on current density 10 p1687 A67-23665
Temperature dependence of thermal conductivity and phonon and electron components in solid and liquid n- and p-type semiconductors 11 p1851 A67-24975
Low temperature transport effects in n-type gallium antimonide at high magnetic fields, observing oscillatory behavior of Hall coefficient and transverse magnetoresistance 15 p2534 A67-29327
GaSb properties and perspective applications, noting junction formation, production processes, etc 15 p2538 A67-29700
Diffusion, solubility and electrical behavior of lithium in gallium antimonide 16 p2726 A67-30811
Irradiation of gallium arsenide and gallium antimonide monocrystals by electrons, fast neutrons and relativistic protons, discussing Hall coefficient variation 16 p2727 A67-30869
Electric and thermal conductivity and Hall effect in solid solution of complex semiconductors noting temperature dependence 16 p2729 A67-31155
Temperature dependence of Hall constant and photoconductivity kinetics of gallium antimonide with different tellurium content 17 p2923 A67-33332
Stimulated emission in GaSb injection lasers with steep flat p-n junction, noting dependence of luminescence intensity on current density 17 p2870 A67-33346
Conduction mechanism in GaSb tunnel p-n junctions from 77 to 380 degrees K, noting temperature dependence of basic parameters, V-I characteristics, etc 18 p3098 A67-33573
Electrical conductivity, Hall coefficient and thermo-EMF measurements in Zn and Te doped gallium antimonide crystals for minority carrier role in impurity conduction 21 p3687 A67-39141
Low temperature electron irradiation effects on undoped GaSb resulting in impurity conduction 22 p3862 A67-40000
Emission of GaSb injection lasers in pulse regime, demonstrating existence of two staggered laser lines originating in diode regions 23 p4016 A67-41193
Pressure sintered GaSb-GaAs alloys investigated for densification and thermoelectric properties 24 p4204 A67-42346
- ### GALLIUM ARSENIDE
- Epitaxial gallium arsenide Gunn effect oscillators in generating continuous wave oscillation 01 p0033 A67-10026
Trapezoidal I-V characteristics in gallium arsenide at liquid nitrogen and room temperature 01 p0033 A67-10027
Two-stage parametric amplifier using GaAs cooled in closed cycle cryogenic refrigeration system applied to satellite communications 01 p0033 A67-10029
Threshold and power characteristics of gallium arsenide diode laser operating in pulsed regime 01 p0086 A67-10066
Band structure of spectra of gallium phosphide, gallium arsenide and solid solutions determined by optical reflection techniques 01 p0086 A67-10067
Volt-ampere characteristics and other properties of GaAs lasers with tellurium and Zn-doped epitaxial p-n junction 01 p0087 A67-10080
Current injection effect on time delay of GaAs laser radiation 01 p0087 A67-10083
Origin of polarization of radiation from GaAs diodes, noting intensity dependence on current density and effect of anisotropic electron velocity distribution 01 p0034 A67-10090
Temperature dependence of lifetime of electrons and holes in GaAs, noting trapping effect of recombination centers and capture levels 01 p0128 A67-10091
Energy levels in forbidden band of gallium arsenide alloyed with silver or gold, determining impurity levels from temperature dependence of electric conductivity and Hall constant 01 p0129 A67-10104
Time variation in intensity of light emitted from CW GaAs laser diodes 01 p0088 A67-10243
Efficient electroluminescence at 300 degrees K from GaAs diode amphoteric dopant Si as dominant impurity on both sides of p-n junction 01 p0131 A67-10368
Oscillations associated with S type current controlled negative resistance in seminsulator gallium arsenide samples, examining LF instability 01 p0133 A67-10473
Microwave negative conductance due to traveling space charge waves in n-type GaAs 01 p0133 A67-10487
Continuous coherent radiation of GaAs semiconductor laser with epitaxial p-n junction at ambient temperature of 77 degrees K 01 p0090 A67-10548
Calculation of energy band structure of gallium arsenide, using experimental Fourier coefficients for germanium in pseudopotential method 01 p0136 A67-11054
Continuous coherent radiation of GaAs semiconductor laser with epitaxial p-n junction at ambient temperature of 77 degrees K 01 p0091 A67-11056
Transient phenomena in capacitance of Schottky barrier diodes 01 p0137 A67-11066
Oscillation frequency and breakdown voltage in GaAs p-n junction reverse-biased into avalanche region due to negative resistance arising from transit time effect 01 p0137 A67-11070
Simultaneous derivation of optical gain factor and loss per unit length of series of solution grown diffused GaAs injection laser 01 p0138 A67-11072
High resolution optical shaft angle encoder with gallium arsenide diodes as light sources and compatible with integrated circuit techniques 01 p0073 A67-11113
Low noise figure 94 gc gallium arsenide mixer diode for minimum crystal noise ratio and minimum package 02 p0213 A67-11649
Thermodynamics of epitaxial growth of GaAs-Ge heterojunctions in closed tube process 02 p0296 A67-11787
Voice communications system using GaAs room-temperature injection laser and TV communications system using GaAs crystals as modulators for laser beams 02 p0194 A67-11786
Semiconductor heterojunction properties of epitaxial single crystal layer of GaAs grown on Ge substrate 02 p0299 A67-11895
Bulk GaAs Gunn effect oscillators and amplifiers and electron transfer between high mobility and low mobility conduction bands 02 p0218 A67-12099
Effective hot carrier ionization rate in epitaxial gallium arsenide p-n junction determined from photomultiplier measurements 02 p0299 A67-12186
Electric characteristics of nGe-pGaAs heterojunctions in multistep recombination-tunneling model 02 p0299 A67-12189
Drift velocity dependence on electric field in GaAs measured by analysis of reverse biased Schottky barrier response to step input of light 02 p0253 A67-12504
Gallium arsenide negative conductance amplifiers used in calculation of negative mobility 02 p0221 A67-12512
Temperature induced and optical quenching of emission recombination in gallium arsenide Be-doped electroluminescent diode 02 p0254 A67-12741
Anisotropy of magnetoresistance and Hall effect in n-GaAs, discussing conduction band structure in vicinity of edge 03 p0487 A67-12806
Gallium arsenide crystal properties for use in optical filter 03 p0488 A67-12858
Avalanche transistor pulser designed to drive GaAs radar-laser diode 03 p0376 A67-12964
Steady state photoconductivity and photomagnetic effect in single crystals of n-type GaAs with various carrier concentrations 03 p0490 A67-13151
Optical or inertial electron mass dependence on N-concentration in IR spectrum of n-type GaAs monocrystal with S, Se and Te impurities 03 p0490 A67-13161
Hall mobility and Nernst-Ettingshausen effect in Zn and Cd-doped p-type GaAs at temperatures from 90 to 800 degrees K 03 p0491 A67-13174
Stable domain propagation in gallium arsenide for nonzero constant diffusion coefficient, based on analytic approximation to velocity field characteristic 03 p0493 A67-13461
Gallium arsenide microwave diodes prepared by vapor phase growth method with highest combination of reverse breakdown voltages and cut-off frequencies 03 p0379 A67-13477
Threshold current density dependency on photon energy in gallium arsenide laser diodes 03 p0379 A67-13480
Electrochemical deposition of Schottky contacts of copper and gold on gallium arsenide 03 p0494 A67-13484
Lattice vibration spectra and energies of two-phonon summation bands and reststrahlen bands in gallium arsenide phosphide single crystals 03 p0495 A67-13514
Tunnel diode combined with backward diode improves rate of response and pulse waveform in tunnel diode circuits 03 p0381 A67-13585
Electric current oscillation mode beyond Gunn effect threshold in n-type GaAs 03 p0496 A67-13669
Isobaric-isothermal potential and entropy and enthalpy formation of GaAs from emf measurements at 643-741 degrees K 03 p0498 A67-13840
Potential distribution and field dependence of electron velocity in bulk GaAs measured with point contact probe 03 p0499 A67-13985
V-I characteristics and bias field/carrier concentration-sample length diagram of Gunn effect phenomena 03 p0500 A67-13993
Temperature stability of several types of modulated radiation sources employing GaAs diodes, examining current change with temperature change 03 p0388 A67-14271
GaAs epitaxial layer ultrasonic wave transducers fabricated from seminsulator material, for generation of longitudinal waves 03 p0428 A67-14302
Room temperature reflectance spectra of GaAs, GaP and typical alloys in energy range 2.5 to 20 ev and 2.5 and 6 ev at liquid nitrogen temperature 03 p0501 A67-14355
X-ray anomalous transmission used in analysis of gallium arsenide crystal perfection with various dislocation densities, determining ratios of anomalous absorption coefficient 04 p0874 A67-14620
Compressive stress effect on band gap widening and diffusion current in GaAs junctions 04 p0877 A67-15107
Epitaxial gallium arsenide films prepared

by vacuum evaporation of elements 04 p0678 A67-15124

I-V characteristic of GaAs diode with Fabry-Perot resonator, noting variations during amplification to generation transition 04 p0678 A67-15132

Temperature dependence of current carrier mobility in GaAs crystals irradiated with fast electrons 04 p0679 A67-15140

Nonsinusoidal periodic oscillations observed in high resistivity n-type silicon compensated by zinc and phosphorus 04 p0679 A67-15142

Temperature and impurity ion concentration effect on minority carrier mobility in degenerate gallium arsenide 04 p0679 A67-15143

Temperature and doping level effect on conduction band edge of n-type semiconductors, noting doublet shifts resulting in narrower forbidden energy gaps 04 p0681 A67-15292

Surface aspects of thermal degradation of GaAs p-n junction lasers and tunnel diodes 04 p0585 A67-15620

Forward current, electroluminescent intensity and short circuit current during bombardment as function of 2-mev electron irradiation 04 p0685 A67-15704

Performance of GaAs semiconductor laser with resonator, noting dependence of forbidden zone width and absorption coefficient on free carrier concentration and incident photon energy 04 p0634 A67-15759

GaAs p-s-i-n diode exhibiting negative resistance, allowing assembly into X-Y matrix and electrical pulsing into emitting or nonemitting state 05 p0771 A67-16312

Optical coupling using gallium arsenide laser for variation of frequency of diode emission through small change in current density 05 p0814 A67-16390

Radiation intensity dependence for various spectral bands of diffused gallium arsenide p-n junctions on current density 05 p0861 A67-16391

Line width of CW Ga-As lasers measured using homodyne detection and autocorrelation 05 p0821 A67-16670

Etching and X-ray spectroscopic techniques to investigate distribution and density of dislocations in deformed and annealed GaAs and InSb crystal 05 p0865 A67-16920

Emission from p-n junctions in crystals of InP-GaAs solid solution 05 p0865 A67-16941

LF photocurrent oscillation in high resistivity n-type GaAs, noting relation between amplitude temperature and light intensity 05 p0866 A67-16987

Volt-ampere characteristics of epitaxial GaP-GaAs heterojunctions 05 p0867 A67-17054

Temperature dependence of three-phonon processes in solids noting application to Si, Ge, GaAs and InSb 05 p0870 A67-17198

Current-controlled NDR, electron-hole generation and switching to higher current lower voltage state in GaAs 05 p0870 A67-17275

Shallow donor introduction in p-type Ga-As laser results in increased efficiency of radiative recombination 05 p0826 A67-17280

Band structure and conduction phenomena in semiconductors of groups III-V, particularly in GaAs, noting signal instabilities and Gunn effect 05 p0871 A67-17325

Frequency modes of Gunn effect oscillator 05 p0872 A67-17531

Effect of donor Zn and Cd additions on rate of growth and morphology of epitaxial GaAs films grown from gas phase by chemical reaction 06 p1047 A67-17552

Interpreting short voltage pulse measurements of electron drift velocity in n-GaAs 06 p1048 A67-17815

Electron irradiation effect on electric properties of gallium arsenide 06 p1049 A67-17858

X and electron irradiation effect on current-voltage characteristics of p-n junctions in gallium arsenide 06 p1049 A67-17859

Ohmic contacts prepared by chemical deposition of metal films on gallium arsenide 06 p1050 A67-17939

Electron beam spatial scanning of coherent emission of GaAs junction laser at low temperatures, making current distribution nonuniform 06 p1011 A67-18150

Interaction between two high resistivity layers in Mn doped GaAs separated by region of bulk material 06 p1051 A67-18222

Ultrasonic wave absorption in GaAs and GaSb compounds at temperatures from 95 to 300 degrees K 06 p1051 A67-18399

Hall effect and resistivity in n-GaAs with Si as shallow donor, obtaining ionization energy and impurity band conduction values 06 p1052 A67-18570

Semiconductor heterojunctions noting preparation, properties, measurement and results 06 p1053 A67-18756

Band structure of GaAs, GaP, InP and AlSb obtained by k.p method 06 p1058 A67-18904

Electron effective mass in gallium arsenide as function of doping obtained from Faraday rotation measurements 06 p1061 A67-18921

Semiconductor lasers using single and double photon optical excitation 06 p1013 A67-18930

Absorption spectra and photoluminescence in n-and p-type GaAs before and after neutron and electron irradiation 06 p1062 A67-18933

Recombination radiation of p-n junctions in GaAs with and without Fabry-Perot cavity, discussing nonequilibrium current carrier kinetics and I-V characteristics 06 p1063 A67-18934

Surface recombination velocities and diffusion lengths in GaAs determined by variation of cathodoluminescence intensity with voltage of exciting electron beam 06 p1063 A67-18936

Conduction band structure and anisotropy of electron scattering in n-GaAs, analyzing magnetoresistance and Hall effect 06 p1064 A67-18943

Avalanche multiplication in Ge and GaAs p-n junctions, comparing experimental and theoretical ionization rates, predicting voltage breakdown 06 p1065 A67-18954

Transport properties of electrons in GaAs in connection with traveling domains of high electric field in material 06 p1066 A67-18959

Gunn effect in GaAs caused by field induced transfer of electrons from high to low conduction band 06 p1067 A67-18961

Boltzmann equation for GaAs, noting coupling constant scattering between low and high mass valleys 06 p1067 A67-18963

Light source devices for electronic functions, discussing p-n junction 07 p1231 A67-19081

GaAs room temperature laser diode application to communication and radar systems 07 p1194 A67-19086

Electric field induced IR absorption in GaAs p-n junction diodes 07 p1231 A67-19553

Drift velocity variation with electric field calculated in GaAs, using Boltzmann equation and incorporating additional scattering process 07 p1232 A67-19561

Conductivity changes in flash evaporated p-GaAs films caused by field effect and optical and thermal excitation at temperatures about 100 degrees K 07 p1232 A67-19564

Vapor phase epitaxial deposition of n-type GaAs contact layers for Gunn effect X-band oscillators 07 p1153 A67-19609

Temperature dependence for n-n-n epitaxial GaAs sandwich structures mounted on infinite half-plane of copper 07 p1155 A67-19797

Gallium arsenide planar technology using starting material obtained by vapor growth, noting doped silicon dioxide technique 07 p1155 A67-19889

Picosecond laser pulse widths measurement by method using special symmetry properties of second harmonic generation at GaAs crystal surface 07 p1234 A67-20097

Nonohmic conductivity in n-type GaAs accompanied by negative photoconductivity and giant magnetoresistance, noting electron injection at cathode 07 p1234 A67-20099

Thermally stimulated current peak distribution changes with illumination time and intensity for semi-insulating gallium arsenide 07 p1234 A67-20102

Recombination radiation from GaAs p-n junctions with and without Fabry-Perot resonator, noting parameter dependence on current density 08 p1337 A67-20413

Semiconducting compounds for thin film

photovoltaic devices using GaAs crystals, considering absorption coefficient 08 p1284 A67-20725

Gallium arsenide epitaxial film on germanium obtained by vapor phase transport techniques 08 p1368 A67-20726

Optical and electrical properties of epitaxial and diffused GaAs injection lasers noting spectral characteristics, optical gain, current distribution, etc 08 p1338 A67-21289

GaAs p-n-i-n diode as light activated switch, noting electrical and optical properties 08 p1306 A67-21295

Threshold and power characteristics of gallium arsenide diode laser operating in pulsed regime 08 p1339 A67-21449

Band structure of spectra of gallium phosphide, gallium arsenide and solid solutions determined by optical reflection techniques 08 p1339 A67-21450

Volt-ampere characteristics and other properties of GaAs lasers with tellurium and Zn-doped epitaxial p-n junction 08 p1340 A67-21457

Current injection effect on time delay of GaAs laser radiation 08 p1340 A67-21460

Electron velocity-field characteristics of insulating GaAs measured using electron beam injected electrons 09 p1551 A67-21573

Range capability of gallium arsenide injection LIDAR against extended targets and corner reflectors under both negligible and high background radiation conditions 09 p1462 A67-21640

Continuous waves from synchronized pulsed bulk GaAs oscillators operating in microwave region 09 p1471 A67-21645

Negative slope mobility in n-GaAs from measurements of current-voltage characteristic 09 p1552 A67-21744

Transient phenomena in reverse current and capacitance in gallium arsenide Schottky barrier diode in monochromatic light 09 p1471 A67-21762

Trap-free space-charge-limited current produced by space charge injection in oxygen doped n-GaAs crystals at low temperature 09 p1552 A67-21767

Low temperature characteristics of Ga-As varactor diode junction properties, calculating spreading resistance 09 p1471 A67-21827

Short aging test results on GaAs diodes, noting surface changes and dependence of nonradiative excess current component on device perimeter 09 p1472 A67-21952

Gallium arsenide laser pumped by Stokes component of induced Raman scattering in liquid nitrogen of Q-modulated ruby laser light 09 p1512 A67-21973

Injection luminescence and photoluminescence spectra of epitaxial heterojunctions in GaP-GaAs system 09 p1554 A67-21975

Hydrostatic pressure and temperature effect on current-voltage characteristics of tunnel p-n junctions in gallium arsenide 09 p1554 A67-21977

Far field radiation patterns with Hermite-Gaussian symmetry in junction plane of Ga-As lasers 09 p1513 A67-22133

Crystal orientation effect on epitaxial growth gallium arsenide crystals for smooth laser junction 09 p1515 A67-22275

Electrical migration of Li and Cu in GaAs, noting ionic charge decrease due to drag by electrons 09 p1558 A67-22603

Pulsed oscillations of microwave Gunn effect oscillator in n-type single crystal GaAs 10 p1609 A67-22838

Steady state photoconductivity and photomagnetic effect in single crystals of n-type GaAs with various carrier concentrations 10 p1690 A67-23100

Optical or inertial electron mass dependence on N-concentration in IR spectrum of n-type GaAs monocrystal with S, Se and Te impurities 10 p1690 A67-23108

Vapor deposited GaAs thin film solar cells for application to solar power systems 10 p1596 A67-23165

Gallium arsenide - International Symposium, Reading, Berks., England, September 1986 10 p1613 A67-23509

Epitaxial gallium arsenide properties and preparation using arsenic trichloride 10 p1692 A67-23510

Gallium arsenide epitaxial technology noting deposition rate and impurity profile, Hall mobility and morphology of deposits 10 p1692 A67-23511

Gallium arsenide characteristics and preparation noting epitaxial deposition and liquid phase, mobility, impurity and Hall effect data 10 p1692 A67-23512

Pyramid formation in epitaxially deposited GaAs layers, postulating vapor-liquid-solid formation mechanism 10 p1692 A67-23513

Chemical etching of dislocation and stacking fault structure of epitaxial GaAs, noting possible effect on electroluminescence 10 p1692 A67-23514

Impurity distribution in GaAs noting growth rate, concentration and crystallographic orientation 10 p1693 A67-23515

Properties of gallium arsenide crystals produced by pulling single crystals from melt of gallium arsenide covered by molten boric oxide 10 p1693 A67-23516

Synthesis of undoped GaAs single crystals by horizontal Bridgman method, noting maximum mobility value obtained 10 p1693 A67-23517

Solution regrowth technology of electroluminescent devices noting reduced threshold current densities, external quantum efficiency and adaptation to planar technology 10 p1665 A67-23518

High power operation of semiconductor lasers, noting differential equation of field distribution along junction 10 p1665 A67-23519

Reversible and irreversible limitation of maximum power output from GaAs by thermal heating and surface damage 10 p1665 A67-23520

GaAs laser diodes in pulse operation at liquid nitrogen temperature, comparing reflection and diffraction losses with absorption losses 10 p1666 A67-23521

Distribution of injected carrier densities in strongly forward biased laser junctions 10 p1666 A67-23522

Radiative recombination processes in GaAs p-n junctions, noting correlation between temperature behavior and carrier transport mechanism 10 p1693 A67-23523

Quantum efficiency of optimized GaAs diodes with Zn diffused in skin layer, noting dependence on junction depth 10 p1614 A67-23524

Systematic degradation of GaAs light emitter quantum efficiency, noting relation to current density 10 p1615 A67-23525

Factors of degradation of GaAs electroluminescent diodes, discussing surface leakage and change in spectral characteristics as major causes 10 p1615 A67-23526

GaAs Schottky diodes for integrated circuits, discussing fabrication, parameters and performance 10 p1615 A67-23527

Metal GaAs diodes as frequency changers, discussing fabrication, performance characteristics and parameters 10 p1615 A67-23528

Diffused GaAs varactor diodes, showing planar processes applied to production of diode based on metal-GaAs junction 10 p1615 A67-23529

Gunn effect oscillators constructed from epitaxially grown n-type GaAs on n-plus substrate to obtain CW oscillations with frequencies from 3 to 35 gc 10 p1615 A67-23530

Epitaxial advantages over melt grown GaAs in construction of continuous wave and pulsed Gunn effect oscillators 10 p1618 A67-23531

Epitaxial GaAs Gunn effect oscillators, showing importance in high efficiency of preparation and method of contacting material and resonant cavity design 10 p1618 A67-23533

Assessment of epitaxial gallium arsenide for use in Gunn effect devices from check slices on seminsulating substrates 10 p1618 A67-23534

Airbrasion technique to improve Gunn oscillator performance using epitaxial GaAs, considering diode shape and contact structure 10 p1618 A67-23536

Double diffused n-p-n gallium arsenide transistor, discussing ways oxygen modifies p-n junctions to increase voltage breakdown 10 p1617 A67-23537

Iron doped gallium arsenide transistor with better frequency performance and higher operating temperatures 10 p1617 A67-23538

Fabrication technique for planar gallium

arsenide junction FET and properties 10 p1617 A67-23539

Gallium arsenide insulated gate field effect transistor fabrication techniques and properties 10 p1617 A67-23540

Mesa- and planar-structure gallium arsenide junction type FETs with diffused n-type channel 10 p1617 A67-23541

Monolithic gallium arsenide tunnel diode construction with epitaxial layer grown on semi-insulating substrate 10 p1617 A67-23542

GaAs semiconductor quantum generator heating during injection pulse, analyzing temperature effect on external quantum output and generator efficiency 10 p1666 A67-23568

Steady state field distribution of semiconductor laser with nonuniform excitation pumped by electron 10 p1666 A67-23648

Temperature dependence of electrical properties of compensated GaAs 10 p1694 A67-23655

Temperature dependence of Hall coefficient of tellurium doped GaAs ternary compound, noting activation energy parameter 10 p1694 A67-23656

Efficiency of electroluminescent lamps, noting dependence on arsenic pressure and temperature during GaAs crystal growth 11 p1845 A67-24140

Gallium arsenide electron photon transistor electrical properties at cryogenic and room temperature, determining total internal quantum yield of photons 11 p1765 A67-24475

GaAs semiconductor diodes for thermometric measurements in low and intermediate ranges, showing temperature dependence of injected current on emitter to collector voltage 11 p1766 A67-24650

High power pulsed microwave generation in gallium arsenide diode when operated at X-band frequencies 11 p1767 A67-24721

High efficiency pulsed gallium arsenide avalanche diode 11 p1767 A67-24722

Preparation and properties of III-V compounds for radiative processes, discussing epitaxial deposition of GaAs into semi-insulating substrate for array of devices 11 p1847 A67-24736

Electron distribution of oxygen grown GaAs crystals after heat treatment, showing profiles due to silicon contamination 11 p1848 A67-24740

Chemical impurities and native defects observed in GaAs using photoluminescence at 20 degrees K, noting role of optical activation energy 11 p1848 A67-24742

Anodic behavior of GaAs single crystals at increased current densities in alkaline and acidic solutions, discussing etch tunnels 11 p1848 A67-24743

Heat resistance of GaAs laser diodes from 77 to 300 degrees K, showing relationship to thermal conductivity 11 p1802 A67-24744

GaAs laser diode noting peak optical power, spectra and role of individual diodes in stack operation 11 p1802 A67-24745

Epitaxial vapor growth of GaAs noting reduction of electron concentration and increase in electron mobility 11 p1848 A67-24746

Anomalous IR attenuation in fast neutron irradiated GaAs and CdTe arises through scattering and absorption by highly conducting spike zones 11 p1850 A67-24910

Room temperature laser threshold reduction and stimulated emission delay in GaAs diffused junction diodes 11 p1803 A67-24911

Short circuit current measuring technique and results of electron diffusion lengths in diffused p type and holes in uniformly doped n type GaAs 11 p1850 A67-24912

Microwave amplification and negative conductance for GaAs, InP and CdTe 11 p1850 A67-24916

Optically excited electrons of X minima in gallium arsenide 11 p1803 A67-24998

I-V characteristic of GaAs diode with Fabry-Perot resonator, noting variations during amplification to generation transition 12 p1951 A67-25156

Temperature dependence of current carrier mobility in GaAs crystals irradiated with fast electrons 12 p1979 A67-25163

Nonsinusoidal periodic oscillations observed in high resistivity n-type silicon compensated by zinc and phosphorus 12 p1979 A67-25165

Temperature and impurity ion concentration effect on minority carrier mobility in degenerate gallium arsenide 12 p1979 A67-25166

InAs epitaxial layers grown on GaAs substrate investigated via sandwich method and electron diffraction 12 p1980 A67-25201

UHF oscillations in GaAs thin epitaxial layers deposited on isolating substrates of same material 12 p1981 A67-25279

Trap density is lower in epitaxially grown GaAs crystals than in crystals grown by either horizontal Bridgman /HB/ or floating zone /FZ/ technique 12 p1983 A67-25457

Electric conductivity, Hall effect and photoconductivity of epitaxial single crystal GaAs films obtained by gas transport method 12 p1984 A67-25521

Absorption spectra and luminescence of p-type copper diffusion doped Ga-As crystals, noting appearance of temperature dependent narrow spectral lines 12 p1984 A67-25522

Microwave methods for electric resistivity measurements of semiconductor materials, noting application to GaAs 12 p1916 A67-25999

Explanation of anomalies of experimental static current-voltage characteristics of GaAs tunnel diode oscillators 12 p1917 A67-26098

GaAs gas bombarded by fast electrons investigated for recombination radiation spectra, noting shift of edge emission maximum toward longer wavelengths 13 p2173 A67-26359

Conductivity of cleaved surfaces of GaAs in liquid nitrogen 13 p2174 A67-26371

Time-integrated and time-resolved spectra of GaAs laser diode, noting temperature effect on spectral emission 13 p2125 A67-26427

Time dependence of coherent emission wavelength shift of GaAs-P laser diodes during flat-topped current pulsation 13 p2125 A67-26513

High pressure, uniaxial stress and temperature effects on GaAs electrical resistivity 13 p2180 A67-27159

Interference effects in far field patterns of semiconductor diode lasers 13 p2128 A67-27288

Operation and electrical characteristics of bulk negative resistance semiconductor devices 13 p2183 A67-27562

Metal-semiconductor electric contacts for GaAs bulk effect device noting uniformity, linearity, usefulness, adaptability, etc 13 p2183 A67-27567

Measurements of heterojunctions alloyed with bismuth/indium arsenide/manganese alloy on to GaAs substrate 13 p2184 A67-27575

Electrical and energy performance of high efficiency GaAs solar cells compared to silicon photocells, discussing temperature effect and p-n junction depth 13 p2056 A67-27623

Temperature and carrier concentration effect on threshold electric field of current saturation and saturation drift velocity in gallium arsenide 14 p2364 A67-27826

Transient phenomena in capacitance and reverse current for n-type GaAs Schottky barrier diodes at different carrier concentrations 14 p2364 A67-27827

P-type GaAs laser excited by Q-switched ruby laser at liquid nitrogen temperature, noting spectral shift due to Burstein effect 14 p2329 A67-27831

Etching and X-ray spectrometric techniques to investigate distribution and density of dislocations in deformed and annealed Ga-As and InSb crystal 14 p2365 A67-28260

Negative-resistance Gunn effect in gallium arsenide and indium phosphide due to field excited electron transfer 14 p2366 A67-28474

Emission from p-n junctions in crystals of InP-GaAs solid solution 14 p2366 A67-28486

Misfit dislocations at diamond-sphalerite interface of thin epitaxial Ge layer deposited on GaAs substrate 14 p2366 A67-28497

Delta coefficient of secondary emission of monocrystal of GaAs with various doping 14 p2367 A67-28516

Gas laser radiation applied to light transmittance measurement of heavily doped gallium arsenide in absorption region by free carriers 14 p2368 A67-28528

Nonlinear volt-ampere characteristic of photosensitive GaAs plus copper atoms in

strong electric field 14 p2368 A67-28532
 Volume electroluminescence observation during HF excitation of GaAs using neutral /indium/ contacts and unipolar voltage pulses 14 p2368 A67-28538
 Differential negative conductivity in n-type GaAs, using microwave electron heating 14 p2369 A67-28595
 Large microwave field and small parallel DC field applied across GaAs sample altering conductivity related to carrier velocity-field characteristic 14 p2369 A67-28601
 Pulse modulated data channel operation over parallel optical paths, noting advantages inherent in simple processing and control circuitry 14 p2272 A67-28699
 Temperature stability of several types of modulated radiation sources employing GaAs diodes, examining current change with temperature change 14 p2288 A67-28780
 Current instabilities in GaAs for applied electric field along piezoelectric direction attributed to electron-phonon coupling, determining additional parameters from experimental data 14 p2374 A67-28983
 Thermal lattice conductivity at high temperatures in compound semiconductors, linking dilatation coefficient of molecular theory to ionic nature of interatomic bonds 14 p2374 A67-28984
 Pulsed power output for microwave GaAs oscillator biased into avalanche, with diodes grown by liquid phase 15 p2442 A67-29172
 Volt-ampere characteristics of gallium arsenide tunnel diode 15 p2443 A67-29285
 Epitaxial deposition of p-GaAs on n-GaAs noting dislocations, packing defect concentrations and V-I characteristics 15 p2533 A67-29317
 Electrically active centers distribution in Zn and Te implantations into GaAs 15 p2538 A67-29495
 Solar energy conversion into electric power by GaAs and Si cells analyzed, using photovoltaic cell theory 15 p2538 A67-29503
 Semiconductor laser generating oscillations in external cavity, finding Brewster window effective in suppressing modes within crystal 15 p2498 A67-29511
 Volt-ampere characteristics of epitaxial GaP-GaAs heterojunctions 15 p2538 A67-29785
 Optical ranging system with high power chemical laser noting performance characteristics 15 p2500 A67-29913
 Current carrier distribution in GaAs-Ge heterojunctions measured for energy band diagram 15 p2542 A67-30241
 Transverse magnetic field effect on induced emission of GaAs diodes 15 p2543 A67-30251
 GaAs epitaxial layer in transistors with silicon nitride insulator surpasses silicon MOS device in power gain, frequency response and temperature range 15 p2455 A67-30391
 Electron recombination and capture processes at deep centers in n-type GaAs 16 p2724 A67-30604
 Current saturation and oscillation in photosensitive GaAs explained by high electric fields 16 p2725 A67-30611
 Temperature dependence of properties of acceptor center in iron doped gallium arsenide, noting delocalization of cluster electron density 16 p2726 A67-30814
 Properties of uniformly propagating stable domains in gallium arsenide calculated on basis of velocity-field and diffusion-field characteristics 16 p2727 A67-30851
 Irradiation of gallium arsenide and gallium antimonide monocrystals by electrons, fast neutrons and relativistic protons, discussing Hall coefficient variation 16 p2727 A67-30869
 Pulsed resistivity and Hall effect measurements of n-type GaAs in high electric fields at room temperature below microwave oscillation threshold 16 p2731 A67-31449
 GaAs injection lamp efficiency correlated with presence of trapping levels, noting experimental technique and results 17 p2911 A67-32192
 Interface alloy technique for heterojunctions between GaAs and InSb single-crystal heterojunctions shown by X-ray analysis 17 p2911 A67-32196
 Microwave attenuation change and harmonic generation by n-type GaAs in strong microwave electric fields,

determining current density relation to field strength 17 p2913 A67-32310
 Delay time between current pulse and light emission of GaAs laser diodes, noting nonlinearity between current and delay time 17 p2824 A67-32316
 GaAs single crystals excited to stable longitudinal vibrations by supersonic absorption, determining resonance 17 p2914 A67-32401
 GaAs laser reflectance measurements of tactical landing terrain samples 17 p2858 A67-32483
 Fabrication and properties of p-n junction diodes, noting cut-off frequencies, junction characteristics, etc 17 p2826 A67-32620
 Quantum efficiency in electroluminescent GaAs diodes, considering carrier concentration effect, electron injection ratio, photon absorption and radiative recombination 17 p2914 A67-32654
 GaAs diodes measured for capacitance at 77 degrees K, noting change due to traps photoexcited in space charge layer 17 p2914 A67-32655
 Third order moduli of GaAs by measurement of ultrasonic wave velocities as function of applied stress 17 p2922 A67-33057
 Damage regions in Si, GaAs and InSb irradiated with monoenergetic neutrons determined, using electron microscopy 17 p2922 A67-33060
 Twin orientation in epitaxial gallium arsenide, noting relation to stellite feature 17 p2922 A67-33065
 IR absorption measurements of Li localized vibrational modes in Li and Te doped GaAs 17 p2922 A67-33066
 Gallium arsenide laser pumped by Stokes component of induced Raman scattering in liquid nitrogen of Q-modulated ruby laser light 17 p2870 A67-33310
 Injection luminescence and photoluminescence spectra of epitaxial heterojunctions in GaP-GaAs system 17 p2923 A67-33312
 Hydrostatic pressure and temperature effect on current-voltage characteristics of tunnel p-n junctions in gallium arsenide 17 p2923 A67-33314
 Steady state field distribution of semiconductor laser with nonuniform excitation pumped by electron 17 p2870 A67-33329
 Temperature dependence of electrical properties of compensated GaAs 17 p2923 A67-33336
 Temperature dependence of Hall coefficient of tellurium doped GaAs ternary compound, noting activation energy parameter 17 p2923 A67-33337
 Dynamic theory of hybrid ionic-covalent /homopolar/ bonds applied to physical behavior of GaAs type crystals 18 p3094 A67-33436
 Variation of forbidden bandwidth and linear-expansion coefficient of indium phosphide-gallium arsenide alloys as function of composition 18 p3095 A67-33447
 Impact ionization in gallium arsenide through fast pulse experiment, noting conflict between theoretical and measured current-voltage characteristics 18 p3097 A67-33517
 Ohmic contacts prepared by chemical deposition of metal films on gallium arsenide 18 p3100 A67-33775
 Gallium arsenide single crystal lattice dielectric constant measured noting broad resonance 18 p3101 A67-34010
 Distribution coefficients for impurities in gallium and indium arsenides as periodic function of atomic weight decreasing with increasing atomic number 18 p3102 A67-34289
 Electric conductivity, Hall effect and photoconductivity of epitaxial single crystal GaAs films obtained by gas transport method 18 p3103 A67-34452
 Absorption spectra and luminescence of p-type copper diffusion doped GaAs crystals, noting appearance of temperature dependent narrow spectral lines 18 p3103 A67-34453
 Gunn effect semiconductor oscillator for generating microwave power using GaAs 18 p3013 A67-34525
 Hall effect measurements on Te-doped GaAs crystals diffused with Cu₆₄, studying vacancy-donor interactions, hole concentrations and energy levels 18 p3105 A67-34634
 Surface hillock-like features in epitaxially

grown gallium arsenide studied by X-ray diffraction topography 18 p3106 A67-34636
 Single gallium arsenide crystals sputtered by normally incident low energy argon ions in mass spectrometer 18 p3106 A67-34639
 Localized vibrational modes of lithium in lithium diffused p-type GaAs doped with Mn, Cd or Zn 18 p3106 A67-34644
 Effect of dislocations in GaAs single crystals on diffused p-n junctions structure and recombination radiation parameters 19 p3300 A67-34768
 Electrical characteristics of GaAs p-n diffusion junctions used as solar cells 19 p3300 A67-34769
 Temperature dependence of electric conductivity and Hall effect in epitaxial layers of undoped and Fe-doped n-type GaAs samples 19 p3300 A67-34770
 Photon generation threshold energy temperature dependence for gallium-arsenic epitaxial injection lasers 19 p3238 A67-34773
 Threshold current density dependency on photon energy in diffused and epitaxial p-n junction GaAs injection lasers 19 p3238 A67-34774
 Epitaxial gallium arsenide FET electrical characteristics, noting structural details and feasibility for use at microwave frequencies 19 p3196 A67-35629
 Electron fluctuations variance and correlation coefficients computed for sensitized GaAs, comparing noisiness of deep recombination levels 19 p3306 A67-35732
 Noise spectral density measured at low temperature in sensitized GaAs, studying relaxation time, temperature effect, etc 19 p3307 A67-35733
 Simultaneous diffusion of gallium and arsenic in silicon from gallium arsenide source, obtaining profiles at various temperatures 19 p3308 A67-36035
 Models explaining long time delay between current-pulse application and generation of coherent oscillations in gallium arsenide junction lasers near room temperature 19 p3241 A67-36036
 Voltage breakdown in undoped and chromium doped semiconducting GaAs 19 p3308 A67-36040
 Temperature dependence of diffusion coefficient of zinc in gallium arsenide 20 p3504 A67-36162
 Current saturation in evaporated gallium arsenide films observed noting temperature effect, X-ray measurements, etc 20 p3505 A67-36177
 IR emission in n-type gallium arsenide samples exhibiting current oscillations due to electron-phonon coupling 20 p3508 A67-36423
 Potential field distribution in n-GaAs devices before and after switching indicate carrier generation in narrow region near anode 20 p3510 A67-36853
 Energy band pinch effect in laser-heated GaAs, studying temperature effect on radiative recombination rate 20 p3460 A67-37106
 Majority and minority carrier lifetimes in n-type GaAs single crystals, measuring injection level dependence 20 p3512 A67-37436
 Density and recombination coefficients of nonequilibrium carriers in Ge and GaAs as function of laser excitation intensity 20 p3513 A67-37437
 Impurity conduction causing negative magnetoresistance in Cu doped n-type GaAs crystals at low temperature 20 p3513 A67-37440
 Zn doped polycrystalline GaAs film electrical properties temperature variation 20 p3514 A67-37602
 Current carrier recombination processes in pure, preheated and Cu-doped GaAs, studying temperature and concentration dependence of intrinsic and impurity photoconductivity 21 p3676 A67-37863
 Surface potential of semiconducting gallium arsenide through temperature dependence measurements of transverse conductivity of clamped contact 21 p3676 A67-37869
 Volt-ampere characteristics of n-type GaAs at high fields above Gunn threshold, showing saturation, space charge effect and current controlled negative resistance 21 p3679 A67-38260
 Delay time of quenching response and

recovery in gallium arsenide injection laser 21 p3640 A67-38261
GaAs gas bombarded by fast electrons investigated for recombination radiation spectra, noting shift of edge emission maximum toward longer wavelengths 21 p3680 A67-38316
Conductivity of cleaved surfaces of GaAs in liquid nitrogen 21 p3680 A67-38326
Energy band nonparabolicity effect on GaAs drift velocity vs field curve, especially near Gunn threshold 21 p3680 A67-38348
Gunn effect applied to GaAs crystals for use as diodes, discussing current-voltage characteristics 21 p3684 A67-38444
Solution grown GaAs laser diodes with Fabry-Perot cavity, measuring threshold current density variation with reciprocal laser diode length 21 p3641 A67-38457
Point defect concentration in GaAs determined from lattice constant 21 p3685 A67-38970
Gallium arsenide substrate treatment methods effects on autoepitaxial layer perfection 21 p3685 A67-38972
Arsenic evaporation from gallium arsenide experiment used to study volatile solid evaporation suppression 21 p3686 A67-39134
GaAs pulsed injection laser diode noting characteristics for room temperature operation 22 p3813 A67-39253
Coherent amplification properties of antireflective coated GaAs diodes considered for application to phased array 22 p3813 A67-39254
Photoconductivity measurements for chromium doped seminsulating gallium arsenide, discussing response peak and possible mechanisms 22 p3855 A67-39348
Electric domains in high resistance GaAs single crystals, measuring electric field intensity with Pockels electro-optic effect noting surface state role 22 p3857 A67-39459
Hot electron Hall mobility in n-type GaAs in negative differential mobility region 22 p3858 A67-39518
Solar probe mission planning, evaluating high temperature electronics capability and high flux GaAs solar cell efficiency 22 p3903 A67-39956
Schottky tunneling measurements in GaAs with Au noting fine structure 22 p3861 A67-39996
Gunn effect, describing electron transfer, domain propagation and space charge instabilities in GaAs 22 p3841 A67-40073
Light polarization and intensity for Raman scattering from plasmons and phonons in GaAs 23 p4038 A67-40795
Oscillator diode in limited space charge accumulation oscillation mode, obtaining maximum DC to RF conversion efficiency for sine wave excitation for n-GaAs 23 p3979 A67-40875
Gas laser radiation applied to light transmittance measurement of heavily doped gallium arsenide in absorption region by free carriers 23 p4039 A67-40935
Nonlinear volt-ampere characteristic of photosensitive GaAs plus copper atoms in strong electric field 23 p4039 A67-40939
Volume electroluminescence observation during HF excitation of GaAs using neutral /indium/ contacts and unipolar voltage pulses 23 p4040 A67-40945
Optical system models based on gallium-arsenide laser techniques for SNR measurements 23 p4014 A67-41026
IR absorption spectrum of n-GaAs noting free carrier contribution due to phonons and ionized impurities 23 p4042 A67-41293
Two-terminal GaAs laser diode communication system noting laser driver component selection, system performance, construction, design and ranging and tracking applications 23 p3975 A67-41379
Vapor growth of single crystal heterojunctions of GaAs on Ge or InAs on GaAs using iodine process in closed tube system 23 p4043 A67-41432
Gallium oxide desorption rate and activation energy after O adsorption on GaAs /111/ surface 23 p4045 A67-41464
Lifetime measurements of GaAs diodes determined from p-n junction impedance 23 p3982 A67-41468
High resistance GaAs residual IR absorption measured to determine incident light intensity fraction, showing low

absorption suitable for high power laser modulation 23 p4045 A67-41471
Thin film GaAs solar cell fabrication and operating characteristics, describing two-cell types 23 p4046 A67-41493
Faraday rotation and ellipticity measurements in germanium and gallium arsenide at room temperature in weak magnetic fields 24 p4202 A67-41984
Pressure sintered GaSb-GaAs alloys investigated for densification and thermoelectric properties 24 p4204 A67-42346
GALLIUM COMPOUND
Band structures of gallium selenide and gallium sulfide derived by tight band approach 06 p1058 A67-18905
Fluorescence of n-and p-type gallium arsenic phosphide under optical excitation 07 p1232 A67-19635
Band-to-band radiative recombination in compounds of gallium and indium with phosphorus, arsenic and antimony 12 p1979 A67-25177
Volt-ampere characteristics of diffused p-n junctions in epitaxial GaAsP film obtained by gas transport technique 12 p1984 A67-25519
Chemical etching examination of dislocations and stacking-fault structure of epitaxial gallium arsenic phosphide, considering doping level, growth rate and composition effects 14 p2366 A67-28421
Electric conductivity of p-Ga-Te polycrystals and single crystals in strong electric fields 14 p2375 A67-29085
Optical reflection spectra of GaS, GaSe, and GaTe single crystal semiconductors in electron volt band energy range 16 p2730 A67-31159
Superconducting transitions of three metastable states of Ga 17 p2915 A67-32707
Volt-ampere characteristics of diffused p-n junctions in epitaxial GaAsP film obtained by gas transport technique 18 p3103 A67-34450
Electroluminescent diodes emission efficiency factor for application to lasers 21 p3591 A67-38153
GALLIUM PHOSPHIDE
Band structure of spectra of gallium phosphide, gallium arsenide and solid solutions determined by optical reflection techniques 01 p0086 A67-10067
Solution grown epitaxial red light emitting p-n junctions in GaP preparation, electrical and optical properties, examining I-V characteristics 02 p0297 A67-11876
Electron beam scanning technique measurement of diffusion lengths in Si and GaP p-n junctions and recombination rate of dislocations in n-type Si 02 p0298 A67-11887
Optical and electrical properties of barrier layers in Cu doped GaP, discussing intensity region of superlinearity dependence on temperature and IR light 03 p0491 A67-13202
Lattice vibration spectra and energies of two-phonon summation bands and reststrahlen bands in gallium arsenide phosphide single crystals 03 p0495 A67-13514
Room temperature reflectance spectra of GaAs, GaP and typical alloys in energy range 2.5 to 20 eV and 2.5 and 6 eV at liquid nitrogen temperature 03 p0501 A67-14355
Electronic Raman scattering by neutral Zn and Mg acceptors in GaP, energy level transitions and accompanying phonon wing 04 p0673 A67-14477
GaP electroluminescent junctions, considering feasibility of electroluminescence applications where human eye is detector 04 p0581 A67-15077
Auger effect radiative recombination of excitons bound to neutral donors of GaP and Si and generation of luminescent spectrum C line 04 p0682 A67-15463
Sum and difference frequency mixing of visible and IR gas laser light in GaP at near reststrahl frequencies and relationship to spontaneous Raman scattering 04 p0682 A67-15464
Electron diffraction patterns for GaP semiconducting thin films deposited on indium oxide substrates, determining structure as function of film thickness 04 p0686 A67-15970
Solid state diode matrix display using gallium phosphide light sources to investigate use as data recording device 05 p0771 A67-16313
Volt-ampere characteristics of epitaxial GaP-GaAs heterojunctions 05 p0867 A67-17054

Effect of local states in forbidden band on electron processes in n-GaP crystals, diagramming absorption and photoluminescence excitation spectra 05 p0868 A67-17063
Two-electron transitions in luminescence of excitons bound to neutral donors in gallium phosphide 06 p1051 A67-18210
Silicon-gallium phosphide heterojunction fabricated by epitaxial deposition, presenting V-I characteristics and energy band diagrams 06 p1051 A67-18223
Band structure of GaAs, GaP, InP and AlSb obtained by k.p method 06 p1058 A67-18904
Hall effect, electrical resistivity and optical transmission data and Co impurities in GaP studied via crystal field theory 06 p1061 A67-18926
Optical transitions at isoelectronic traps in GaP and ZnTe, presenting fluorescent spectra 06 p1062 A67-18929
Emission spectrum of GaP diodes analyzed as function of current and temperature 06 p1062 A67-18931
Band structure of spectra of gallium phosphide, gallium arsenide and solid solutions determined by optical reflection techniques 08 p1339 A67-21450
Injection luminescence and photoluminescence spectra of epitaxial heterojunctions in GaP-GaAs system 09 p1554 A67-21975
Steady state field distribution of semiconductor laser with nonuniform excitation pumped by electron 10 p1866 A67-23648
Rapid vapor phase growth of high resistivity GaP for electro-optic modulators, noting high electron mobility 11 p1848 A67-24747
Impurity effect on electroluminescence of gallium phosphide diodes, noting dependence of spectrum on current density through p-n junction 12 p1914 A67-25438
Injection electroluminescence of p-n junctions in GaP doped with tellurium, zinc, ZnO, etc 14 p2368 A67-28531
Double injection and oscillations of current-voltage dependence of alloyed diodes prepared on basis of p-type gallium phosphide 14 p2286 A67-28594
Volt-ampere characteristics of epitaxial GaP-GaAs heterojunctions 15 p2538 A67-29785
Effect of local states in forbidden band on electron processes in n-GaP crystals, diagramming absorption and photoluminescence excitation spectra 15 p2538 A67-29794
Vacuum deposited amorphous and semicrystalline gallium phosphide film properties analyzed by electron diffraction 16 p2729 A67-31065
Impurity diffusion and segregation effects in p-n junctions in compensated solution grown GaP 17 p2921 A67-33053
Injection luminescence and photoluminescence spectra of epitaxial heterojunctions in GaP-GaAs system 17 p2923 A67-33312
Steady state field distribution of semiconductor laser with nonuniform excitation pumped by electron 17 p2870 A67-33329
Gallium phosphide diode-based laser generator of nanosecond light pulse sequence, noting simulation of scintillation counter photoelectric amplifiers, Cerenkov counters, etc 19 p3228 A67-34987
Injection electroluminescence of p-n junctions in GaP doped with tellurium, zinc, ZnO, etc 23 p4039 A67-40938
Light emission spots one to one correspondence with microplasmas in GaP p-n junctions 23 p4043 A67-41437
Internal quantum efficiency of red emitting GaP diodes noting low values due to nonradiative recombination 23 p4045 A67-41460
GALLIUM SELENIDE
Electrical properties of GaSe-layer-semiconductor single crystals used to determine scattering mechanisms of charge carriers, depth of impurity centers, effective mass and forbidden gap 03 p0488 A67-12816
Electrical conductivity of p-GaSe single crystals in strong electric fields 04 p0676 A67-14929
Current voltage characteristics of Cd-GaSe-Bi diode structure, rectification coefficient, activation energy and photocurrent spectral

distribution 04 p0676 A67-14930
Transmission spectra of GaS, GaSe, InSe and TiSe single crystals obtained at 300 degrees K by means of IR spectrometer 04 p0676 A67-14932
Band structures of gallium selenide and gallium sulfide derived by tight band approach 06 p1058 A67-18905
Oscillatory magnetoabsorption of direct transition in layer compound gallium selenide near absolute 06 p1060 A67-18918
Thermal conductivity of laminated GaSe monocrystals studied in two crystallographic directions between 90 and 600 degrees K and effect of unilateral compression 07 p1233 A67-19649
Thermal capacity of gallium and thallium selenides 13 p2174 A67-26367
Thermal capacity of gallium and thallium selenides 21 p3680 A67-38323
Second optical harmonic generation of pulsed ruby laser emission in GaSe crystal suggesting only surface layer contribution to generation 24 p4167 A67-42074

GALVANIC CELL
Physicochemical processes in thin evaporated films studied in terms of emf of galvanic cell with film acting as electrode 02 p0290 A67-11735

GALVANIC SKIN RESPONSE
S ELECTRODERMAL RESPONSE

GALVANOMAGNETISM
Fermi-Dirac statistics, transverse magnetoresistance and galvanomagnetic properties of hexagonal-close-packed Mg and Zn 03 p0495 A67-13511
Galvanomagnetic effect in ferromagnetic metals, developing theory of planar Hall effect in terms of spin-orbit interaction of electrons 03 p0501 A67-14368
Longitudinal magnetoresistance anisotropy and Hall coefficient anisotropy in p-type indium antimonide, noting similarities with galvanomagnetic anisotropy of p-type germanium 04 p0674 A67-14609
Hall effect, voltage generation across current-carrying conductor perpendicular to magnetic field and galvanomagnetic effects based on Lorentz force 04 p0657 A67-15081
Galvanomagnetic effect of anisotropic electron energy spectrum on acoustical branch perturbation spectrum of system of electrons and ions in homogeneous magnetic field 04 p0680 A67-15289
Displacement effects in n-and p-type silicon when exposed to energetic radiation, using electron spin resonance and galvanomagnetic techniques 04 p0684 A67-15689
Temperature dependence of electrical and galvanomagnetic properties of single crystal InSb dendrites 05 p0869 A67-17092
Hall effect and magnetoresistance effect measured on p-and n-CdSb single crystals above 77 degrees K and magnetic fields up to 7500 gauss 06 p1054 A67-18624
Corbino magnetoresistance experiments for n-type surface layers on p-type indium arsenide crystals as function of surface electric field 06 p1064 A67-18941
Nonlinear galvanomagnetic effects due to hot electrons in n-type InSb in quantum limit 06 p1065 A67-18953
Effects of gases flowing in magnetic field analogous to galvanomagnetic Hall effect in conductors analyzed using oxygen 07 p1230 A67-20144
Infinite plate consisting of monopolar semiconductor of given thickness under effect of electric field results in change in galvanomagnetic, piezoresistance and optical properties 08 p1387 A67-20416
Nonlinear dependence of current in electric field in thin semiconductor film in quantizing magnetic field 10 p1694 A67-23591
Galvano- and thermomagnetic phenomena in semiconductors analyzed using transient method, noting extraneous EMF influence on Hall effect 11 p1792 A67-24814
Current carrier concentration gradient in InSb, investigating effect on transverse reluctance coefficient and Hall effect dependence on magnetic field 13 p2173 A67-26360
Galvanomagnetic properties of single crystal antimony as function of temperature, deriving carrier mobilities and densities, detailing nature of Fermi surface 14 p2364 A67-28105
Galvano and thermomagnetic effects in semiconductors determined by using Hall

effect, resistance variations in magnetic field and Nernst-Ettingshausen transverse effect 14 p2385 A67-28314
Low temperature transport effects in n-type gallium antimonide at high magnetic fields, observing oscillatory behavior of Hall coefficient and transverse magnetoresistance 15 p2534 A67-29327
Double-walled cryostat with copper holder for probe measurements of temperature dependence of semiconductor galvanomagnetic effects 16 p2730 A67-31158
Hot carrier galvanomagnetic characteristics of n-type germanium of intermediate carrier concentration, noting Maxwellian distribution 16 p2731 A67-31172
Book on thermodynamics of irreversible phenomenon in liquid metals including Onsager symmetry relations, phenomenological theory, nuclear magnetic resonance, galvano- and thermomagnetic phenomenon, etc 17 p2968 A67-32233
Thermoelectric and galvanomagnetic measurements on p-type bismuth compound, explaining anomalous rise in Hall coefficient with temperature and effective mass ratios change 18 p3105 A67-34632
Semiconductor galvanothermomagnetic characteristics analyzed using all-metal device 19 p3228 A67-34969
Current carrier concentration gradient in InSb, investigating effect on transverse reluctance coefficient and Hall effect dependence on magnetic field 21 p3680 A67-38317

GALVANOMETER
S ELECTROMETER

GAME THEORY
SA ARTIFICIAL INTELLIGENCE
SA WAR GAME
Game theory of economic incentive payment reliability demonstration and prediction 01 p0171 A67-11374
Optimal parameter problem of controlled dynamic systems, considering antagonism between designer and nature, applying results to space flight mechanics 06 p1088 A67-18616
Simulation of pursuit-evasion differential game using variational method, comparing performance of human pilot to optimal pursuer 07 p1136 A67-20170
Design problems for hydraulic loading circuit with random variation of loading with time 09 p1451 A67-22472
Differential games, particularly pursuit of one controlled object by another terminating in shortest time 10 p1620 A67-23421
Indeterminate recognition / game type/ and prediction systems 13 p2088 A67-27022
Two-person zero sum games with differential equation rules, noting location of optimal trajectories, separation properties, etc 15 p2509 A67-29404
Formulation and analysis of class of optimization problems based on contraction mappings in theory underlying dynamic programming 15 p2511 A67-29891
Stochastic differential game with missile and radar, using linear theory in finding optimal strategies 18 p3075 A67-33495
Book on optimal adaptive control systems, detailing material on game theory for use in control system design 21 p3603 A67-38266
Linear differential games associated with vector differential equation in arbitrary dimensional space noting square matrix and convex sets 22 p3826 A67-39214
Interception satellite thrust and steering optimization for pursuing maneuverable satellite, analyzing both evader and pursuer sides with differential game concept 24 p4182 A67-42908

GAMMA FUNCTION
Gamma function concept for varying difference interval and complex argument 11 p1812 A67-23966
Maintainability risk analysis using analytical model with gamma distribution 18 p3021 A67-34685

GAMMA RADIATION
SA BREMSSTRAHLUNG
SA CERENKOV RADIATION
SA NUCLEAR RADIATION
SA SPACE RADIATION
Gamma radiation and fast neutron effects on dark resistance, photoconductivity, majority carrier mobility, recombination kinetics, etc, in CdS single crystal 01 p0128 A67-10086
Hartree-Fock-Slater calculation of internal

conversion coefficients for magnetic multipoles for yttrium-87 with 0.05 or 0.15 mc-square gamma energy 01 p0116 A67-10203
Time resolving capabilities of RCA C-70045, 56 AVP and XP 1020 01 p0087 A67-10659
Photomultipliers 01 p0087 A67-10659
Lunar gamma radiation intensity and spectral composition from Luna X data, deducing cosmic ray and radioactive decay origins 01 p0150 A67-10905
Hybrid propellant burning rate determination using external gamma emission source 01 p0112 A67-11420
Directional correlation of first forbidden beta group and gamma ray in decay of antimony at four beta energies 02 p0269 A67-11863
Gamma, bremsstrahlung and X-ray radiation limitations in aerospace application 02 p0266 A67-12217
Gamma and X-radiographic radioactive sources for nondestructive testing of hydrogenous materials such as rubber, adhesives and explosives in steel or other metal assemblies 02 p0249 A67-12220
Stratospheric measurements of electrons and gamma radiation in cosmic rays, using plastic scintillator and lead sheet supplemented Geiger counters 02 p0310 A67-12584
Nucleon interaction generating high energy gamma rays, discussing photon and energy spectra of electron photon cascade, pion generation and gamma quantum detection in atmospheric nuclear interactions 02 p0316 A67-12763
Internal conversion coefficients for M4 transition in Te, noting gamma energy magnitude, nuclear size effects and eigenvalue results 03 p0472 A67-13335
X-ray and gamma ray navigation systems for helicopter formation flying, examining accuracy and scanning requirements 04 p0653 A67-14605
Primary cosmic ray spectrum at high energies and spectra of gamma rays and muons in atmosphere 04 p0692 A67-14857
Detection of X-ray point sources from rocket and satellite experiments applied to astronomy 04 p0698 A67-14886
Antimatter in meteors from interpretation of mean gamma radiation intensity measurements 04 p0698 A67-14940
Balloon observation of upper limits of solar gamma rays for spectral ranges 20-200 kev and 1-10 mev 04 p0683 A67-14974
Gamma irradiation from Co 60 effect on indium antimonide, determining defect formation on dose and limiting position of Fermi level for n-and p-type material 04 p0680 A67-15283
Isotope effects in gamma radiolysis at 77 degrees K of mixed water and deuterium oxide ice systems 04 p0658 A67-15508
Anomalous permanent changes in transistor gain after low exposure dosage of electron and/or gamma radiation related to recombination current-component buildup 04 p0588 A67-15705
Transient gamma ray effect on thin film insulated gate FETs compared with FETs fabricated on silicon substrate 04 p0589 A67-15717
Gamma radiation effect on SCR correlated with electron radiation encountered by spacecraft 04 p0590 A67-15725
Lunar gamma radiation measured by spectrometer on Luna X orbiter noting lunar rock radiation level, effect of cosmic rays, etc 05 p0887 A67-16055
High energy primary gamma quanta flux outside atmosphere estimated with aid of Proton I satellite 05 p0877 A67-16088
Vertical intensity measurement of rigid gamma quanta at various atmospheric depths 05 p0879 A67-16098
Gamma ray backscatter principles for measurement of atmospheric density, using test results from altitude chambers in balloon and sounding rocket payloads 05 p0840 A67-16527
In-flight instrumentation for prompt miss distance measurement using gamma ray techniques 05 p0841 A67-16533
Lunar and planetary surface elemental analysis technique by analysis of gamma rays resulting from inelastic scattering of neutrons 05 p0843 A67-16545
Cosmic radiation directional intensity during solar activity minimum, noting

- altitude dependence of charged particle photon flux 05 p0883 A67-16878
- Upper limits to high energy gamma flux from quasars 3C 147, 3C 196 and 3C 273 from Crab Nebula and from 53 Cam magnetic variable star 05 p0900 A67-17079
- High altitude balloon flights with gamma ray spark chamber for search of cosmic gamma ray source in Cygnus 06 p1078 A67-18212
- Mathematical model for potential heating from gamma radiation source, determining transient temperature distribution for materials used in nuclear rockets 06 p1116 A67-18363
- Physical pattern of high altitude fission cloud and motion of gamma and beta fission fragments captured by geomagnetic field and observed by Cosmos satellite 07 p1242 A67-19102
- Vertical flux and energy spectra of secondary gamma rays and electrons in upper atmosphere 07 p1242 A67-19621
- Enzyme-isoenzyme changes in rhesus monkeys under gamma irradiation 07 p1134 A67-19860
- Soviet lunar probe measurements of gamma spectrometry, magnetic and gravitational fields, corpuscular radiation intensity, etc 08 p1411 A67-20999
- Production rate of secondary cosmic ray photons in upper atmosphere derived by cascade theory from stratospheric measurements of integral and differential energy spectra 09 p1561 A67-21882
- Directional telescope for measuring intensity and spectral composition of gamma rays in primary cosmic radiation 09 p1497 A67-21899
- Probability of effervescence of superheated liquids as function of temperature and pressure, analyzing N-pentane and hexane under isobaric heating and reduced pressure 09 p1580 A67-21907
- Ruby laser efficiency increase, using gamma irradiation 09 p1515 A67-22430
- Flux and energy spectra of primary cosmic X and gamma rays between 20 kev and 1 mev from balloon-rocket measurements 10 p1701 A67-23231
- Background noise produced by high energy radiation incident on photomultiplier tube, stressing differences between tubes in number of small pulses produced 10 p1618 A67-23809
- Graded dose gamma radiation effect on monkeys, noting change in number of white blood cells and occurrence of gastrointestinal disturbances 10 p1599 A67-23816
- Gamma decay of Se 73 and Se 81 isomeric pairs with half-lives, energies and decay schemes 11 p1822 A67-23980
- Type I supernova exponential decrease in light output due to spontaneous nuclear gamma ray fission of Cf 254, including detection techniques using satellite or balloon-borne telescopes 12 p1995 A67-25765
- Airglow and enhanced penetrating electromagnetic radiation in southern radiation anomaly observed with scintillation crystal during aircraft flight 12 p1996 A67-25775
- Digitized spark chamber for gamma ray and charged particle experiments on balloons and satellites noting construction, performance characteristics and results 12 p1944 A67-25854
- Lithium drifted germanium detector with cylindrical annular shape permitting standardization of gamma spectroscopy techniques 12 p1945 A67-25861
- Gamma flaw detectors for radiographic inspection 13 p2122 A67-26254
- Riometric data on ionospheric absorption applied to determination of dissociative recombination coefficient, noting atmospheric ionization by fragment gamma-radiation 14 p2306 A67-27858
- Solar gamma-ray flux in high energy region analyzed using OSO-I satellite 14 p2381 A67-28057
- Conversion process and ESR in gamma-irradiated dihydrothymine noting reaction rate 14 p2259 A67-28300
- Electron-photon cascade process in intergalactic space, noting role of microwave radiation in gamma ray astronomy 15 p2550 A67-29750
- Isochronous and isothermal annealing of indium antimonide irradiated by X-rays and gamma rays, studying changes in current-carrier concentration 15 p2542 A67-30247
- Cobalt 60 gamma radiation effect on set of B-doped p-type silicon samples, giving radiation-induced defects. 16 p2724 A67-30472
- Primary cosmic ray investigation by Proton I scientific space station concerning energy spectrum, chemical composition, galactic gamma ray and solar radiation hazard 16 p2737 A67-30647
- Gamma ray schemes of resonances in silicon 29-phosphorus 30 reaction for resonant and bound levels of phosphorus 30 properties 16 p2705 A67-31922
- Relationship between oxygen tension and radiosensitivity in complex biological system 17 p2806 A67-31962
- Gamma ray radiation effects on laser glasses, noting ionization and atom displacements in lattice 17 p2867 A67-32374
- Plane structure silicon transistors subjected to Co gamma radiation, considering electrical properties degradation to predict component survival probability 17 p2917 A67-32843
- Radiation effects on silicon transistor parameter behavior characteristics 17 p2917 A67-32843
- Neutron and Co gamma rays radiation effect on lithium drifted p-l-n silicon detectors 17 p2917 A67-32846
- EPR spectra of radicals formed during gamma irradiation of polytetrafluoroethylene 17 p2810 A67-33260
- Possibility of determining content of natural radioactive uranium, thorium and potassium in lunar rocks and of estimating chemical composition of rocks from cosmic ray induced radioactivity 18 p3122 A67-34142
- Emission recombination in n-type Si single crystals irradiated with fast neutrons or gamma quanta 19 p3301 A67-34775
- Lunar rocks composition and radioactivity through satellite gamma-ray measurements indicating basaltic and ultrabasic composition 19 p3319 A67-35258
- Factors influencing secondary electron emission produced by high energy molecular beam impact on metal surface 20 p3488 A67-36438
- Cobalt 60 gamma radiation effect on MOS diodes fabricated on silicon substrates, noting surface state and oxide charge densities 20 p3510 A67-36961
- Mathematical model for potential heating from gamma radiation source, determining transient temperature distribution for materials used in nuclear rockets 21 p3730 A67-37793
- Lunar gamma radiation measured by spectrometer on Luna X orbiter noting lunar rock radiation level, effect of cosmic rays, etc 21 p3701 A67-37842
- Nature of defects in InSb induced by gamma and X-ray irradiation, discussing recovery process 21 p3887 A67-39143
- Gamma radiation energy direct conversion into electrical energy by electrochemical recombination of radiolysis products, proposing new sealed battery 22 p3748 A67-40199
- Nucleon interaction generating high energy gamma rays, discussing photon and energy spectra of electron photon cascade, pion generation and gamma quantum detection in atmospheric nuclear interactions 22 p3876 A67-40265
- Gamma irradiation effect on spinal cord timed differently, considering time factor in reactions of nervous system in guinea pigs 23 p3943 A67-40767
- Guinea pigs exposed to vibrations alternating with intermittent gamma radiation studied for effects on spinal cord activity, noting reflex response depression and parabolic stimulations 23 p3943 A67-40768
- Precentrifugation effect on radiation reactions of vestibular analyzer in guinea pigs, establishing substantial spontaneous electric activity stimulation in hind legs extensor muscles 23 p3944 A67-40773
- Room temperature density-dose behavior of neutron and gamma irradiated polytetrafluoroethylene /PTFE/ noting crystallinity variations 23 p4021 A67-40781
- Ge/Li/ drifted gamma detector for 1/2 to 10 Mev range, measuring response deviation from linearity 23 p3998 A67-40819
- Sulphydrylamine drugs effect for protection in rats exposed to high, low, sublethal, lethal and supralethal dose of X and gamma radiation 23 p3958 A67-41648
- High energy primary gamma quanta flux outside atmosphere estimated with aid of Proton I satellite 24 p4212 A67-42764
- Vertical intensity measurement of rigid gamma quanta at various atmospheric depths 24 p4213 A67-42774
- High energy gamma quanta from high energy cosmic particle interaction with carbon and air nuclei, noting three superhigh energy electron/photon cascades recorded 24 p4218 A67-42835
- High energy nucleon interactions with X-ray films and nuclear emulsions aboard aircraft, with diagram of gamma quanta energy spectra 24 p4218 A67-42836
- GAMMA RAY BEAM**
- Upper limits on cosmic gamma ray flux obtained using OSO-I and sodium iodide scintillation counters 12 p1995 A67-25763
- Energy loss spectrum in CsI at small atmospheric depths, discussing time variation of 0.5-mev gamma-ray flux 16 p2739 A67-31406
- GANTRY CRANE**
- Gantry white rooms at Cape Kennedy 07 p1167 A67-20284
- GAP**
- SA SPARK GAP**
- Gap size effect on pressure and aerodynamic heating over flap of blunt delta wing in hypersonic flow [AIAA PAPER 66-408] 05 p0749 A67-17220
- GARNET**
- SA YTTRIUM-ALUMINUM GARNET /YAG/ CRYSTAL**
- SA YTTRIUM-IRON GARNET /YIG/ CRYSTAL**
- Laser excited electronic Raman spectrum of trivalent Eu ion doped YGa garnet 01 p0091 A67-11084
- Transient growth of magnetostatic modes in yttrium garnet subject to pulsed longitudinal pumping 16 p2732 A67-31704
- IR lattice spectra of rare earth iron garnets noting absorption in low frequency bands and molecular weights 16 p2733 A67-31880
- Lanthanide distribution between omphacite and Garnet, noting abundance ratios to whole rock of Japanese eclogite 24 p4151 A67-42449
- GAS**
- S AIR**
- S ATMOSPHERE**
- S ATOMIC GAS**
- S COSMIC GAS**
- S DIATOMIC GAS**
- S ELECTRON GAS**
- S EXHAUST GAS**
- S EXPLOSIVE GAS**
- S GRAY GAS**
- S HIGH TEMPERATURE GAS**
- S HOT GAS**
- S IDEAL GAS**
- S INTERPLANETARY GAS**
- S INTERSTELLAR GAS**
- S IONIZED GAS**
- S LIGHT GAS PROJECTOR**
- S LIQUID GAS**
- S LORENTZ GAS**
- S MOLECULAR GAS**
- S MONATOMIC GAS**
- S NONCONDENSIBLE GAS**
- S PERFECT GAS**
- S POLAR GAS**
- S POLYATOMIC GAS**
- S RARE GAS**
- S RAREFIED GAS**
- S REAL GAS**
- S RESIDUAL GAS**
- S VAPOR**
- GAS ANALYZER**
- Miniaturized magnetic-type mass spectrometer for multigas analysis in high performance aircraft 01 p0068 A67-10957
- Kryptonate /radioactive source with Kr 85/ for temperature profiles of turbine blades, missile gas analysis, corrosion, oxidation, etc 02 p0265 A67-12214
- Ozone determination by electrochemical and colorimetric methods compared for effects of sensor cell aging 03 p0413 A67-13931
- Helium leak detector characteristics and reception specifications 05 p0804 A67-16302
- Specific degassing of high polymers placed in simulated space environment studied by residual gas analyzer 05 p0832 A67-16304
- Radioactive clathrate technique to detect

- reactive gaseous contaminants in atmosphere in parts per million range 05 p0843 A67-16550
- Surface ionization detector of hydrogen in presence of air at one atm 08 p1330 A67-20376
- Analytical methods using mass spectrometry and gas chromatography for contaminants affecting component reliability in gases enclosed within electronic components 10 p1611 A67-23310
- Plane layer type apparatus for measuring thermal conductivities and accommodation coefficients of gases over wide pressure 10 p1658 A67-23783
- Polarographic and mass gas flowmeter sensors incorporated into bench model for on-line continuous determination of oxygen consumption in human subjects 18 p2995 A67-34711
- Cold cathode ion source /CCIS/ quadrupole mass spectrometer for ultrahigh residue gas analysis 23 p4000 A67-41217
- ### GAS BEARING
- Elastic orifice compensator in externally pressurized gas bearings for flow control, noting increased bearing stiffness 01 p0077 A67-10123
- Gas bearing torques acting on sphere gyroscopically precessing within rotating housing, examining effect of tilt angle 01 p0077 A67-10124
- Gas lubricated bearings used in Brayton cycle closed loop system turbomachinery in design of two-shaft power plant [ASME PAPER 66-GT/CLC-9] 01 p0080 A67-10871
- Closed Brayton cycle power conversion system development, discussing rotating components and single phase operating fluid [AIAA PAPER 66-889] 02 p0183 A67-12268
- Two stabilizing methods for externally pressurized thrust gas bearings using fluid restriction and fluid storage [ASME PAPER 66-LUB-5] 03 p0432 A67-13763
- Stability experiments on partially grooved gas journal bearing, comparing data with previous theoretical analysis [ASME PAPER 66-LUB-6] 03 p0432 A67-13764
- Externally pressurized gas bearing, noting construction applications and performance characteristics of hydrodynamic foil 05 p0812 A67-17106
- Externally pressurized gas journal bearings, evaluating various design parameters for operating at high temperatures and high speeds [ASME PAPER 66-AM 4B2] 08 p1336 A67-21040
- Self-aligning radial clearance seals, discussing design parameters, balance leakage and power loss as function of geometry 10 p1659 A67-22707
- Reynolds equation analysis for pressure distribution in gas bearing clearances by asymptotic solution 10 p1660 A67-23046
- Friction and wear properties of various alumina bearings for use in gas lubricated gyros 10 p1673 A67-23747
- Quasi-static analysis of nonsynchronous response effect of gas bearing pivoted pad design variables and application to operating machinery [ASME PAPER 67-VIBR-15] 11 p1796 A67-24175
- Multistage gas-bearing helium compressor development 13 p2057 A67-27681
- Hydrodynamic gas spin bearing gyroscope design for long duration space missions 14 p2322 A67-29084
- Gas bearing stability determination by step-jump response using observation of growth or decay of motion amplitude [ASME PAPER 67-LUBS-5] 16 p2682 A67-31383
- Galerkin method modifications to obtain static solution of indefinitely long partial-arc self-acting gas bearing 19 p3237 A67-35866
- Free-rotor gyros active damping evaluated through experimental studies 19 p3233 A67-35986
- Dynamic and static gas bearings uses and properties compared with fluid bearings, considering advantages for space applications 20 p3453 A67-36410
- Computers role in fluid film lubrication, computing parameters for bearings lubricated by compressible and incompressible lubricants via iterative finite difference schemes 21 p3632 A67-38135
- Rotor bearing stability, describing incompressible and compressible fluid film bearings, calculating thresholds of instability 21 p3632 A67-38136
- Design and applications of gas-lubricated journal and thrust bearings of self-acting and externally pressurized types 21 p3632 A67-38137
- Motion simulator with spherical self-regulating gas bearing for testing attitude control, analyzing turbine and tilting momentum 22 p3778 A67-39165
- Externally pressurized gas bearings examined for mechanism of series restrictors on pressure distribution, flow quantity and load 23 p4010 A67-41064
- Gas bearings with wide pockets investigated theoretically and experimentally for pressure distribution, flow quantity and load capacity 23 p4010 A67-41065
- Gas bearing Brayton cycle turboalternator rotor system stability and dynamic response to electromagnetic forces 24 p4102 A67-42487
- Flexible membrane hydrostatic air bearing, determining membrane shape, pressure distribution and air gap by Navier-Stokes and membrane analogy equations 24 p4162 A67-42668
- Bounded variation method for optimum load capacity hydrodynamic one-dimensional gas slider bearing, discussing film thickness [ASME PAPER 67-LUB-6] 24 p4162 A67-42670
- ### GAS CELL
- Atomic frequency standards based on rubidium gas cell approach, noting atomic clock types and applications 15 p2487 A67-29582
- Atomic frequency standards, noting cesium and thallium atomic beam devices, H maser, rubidium gas cells, optical pumping, etc 17 p2860 A67-32601
- Modified hot-wire thermal conductivity cell for measuring effects of finite length, pressure and temperature on heat transfer from wire in rare gases 17 p2863 A67-33557
- ### GAS CHROMATOGRAPHY
- Gas-off products from space cabin materials determined by continuous recording instruments, gas chromatography and IR analysis 02 p0189 A67-12388
- High resolution mass spectra obtained from fast magnetic scans of gas chromatographic effluents 03 p0367 A67-13336
- Gas chromatographic and mass spectrometric analysis of chlamydozooids of Ustilago maydis, U. nuda and Sphacelotheca reiliana for hydrocarbon content 03 p0363 A67-13594
- Oils and shales from 3 million to 2.7 billion years old analyzed for hydrocarbon content, using gas chromatography and mass spectrometry 05 p0797 A67-16580
- Unsaturated polyester styrene, showing via gas chromatography and IR spectroscopy effect of reticulation on pyrolytic decomposition 05 p0759 A67-16768
- Physiologically inert gas continuous labelling of pulmonary circulation in one lung compartment and measurement of partial pressure of gas in arterial blood by gas chromatography 07 p1133 A67-19477
- Temperature variation of thermoconductivity of helium-hydrogen gas mixtures and correlation of thermoconductivity curves with gas chromatograms 08 p1426 A67-20805
- System, incorporating Teflon membrane, to selectively remove carrier gas from column effluent prior to entry into mass spectrometer 10 p1602 A67-22946
- High resolution gas chromatography combined with mass spectrometry applied to analysis of pyrolysis products of isoprene from 300 to 1000 degrees C 10 p1602 A67-22947
- Analytical methods using mass spectrometry and gas chromatography for contaminants affecting component reliability in gases enclosed within electronic components 10 p1611 A67-23310
- Aliphatic hydrocarbons in meteorites, examining distribution of isoprenoid and other compounds via gas chromatography and mass spectrometry 10 p1709 A67-23489
- Contaminant control in oxygen for breathing in aviation solved by gas chromatography 12 p1902 A67-25173
- Complex organic compounds analysis by fast-electrical-scanning high resolution mass spectrometry and gas chromatography 14 p2259 A67-28425
- Contaminant concentration in liquid breathing oxygen of aircraft converter determined by gas chromatography 16 p2619 A67-31475
- Design and construction of equipment for oxygen, nitrogen and hydrogen determination in aerospace materials [ONERA-TP-466] 18 p2998 A67-34461
- Ionization mechanism of argon-permanent gas mixture in radioionization detector used for gas chromatography 19 p3228 A67-34797
- Pyrolysis gas chromatography method for life detection and chemical identification of microorganisms 20 p3378 A67-37500
- Paraffinic hydrocarbons composition in Orqueil, Murray, Mokola and other meteorites identified by gas chromatography 21 p3703 A67-38501
- Impurity sources in hermetic electronic packaging investigated using mass spectrometry and gas chromatography, comparing packaging techniques 21 p3636 A67-38632
- Gas chromatography parameters of fluoro derivatives of amino acids compared for use in packed columns or sensitivity evaluation 21 p3578 A67-38764
- Gas chromatography and IR spectrophotometry used to examine monomethyl hydrazine air oxidation, showing evidence of surface catalyzed reaction 21 p3578 A67-38841
- Photolysis of gaseous and liquid benzene, analyzing gaseous products by gas chromatography and mass spectrometry 22 p3757 A67-39443
- Contamination detection by analytical instrumentation considering sampling, IR, atomic absorption spectrophotometer, gas chromatography, colorimetry and polarography 23 p3998 A67-40844
- Physicochemical techniques for gas separation emphasizing pulsed gas chromatography for carbon dioxide removal in spacecraft 23 p3964 A67-41555
- Aliphatic hydrocarbons isolated from Trinidad Lake asphalt by gas chromatography and mass spectrometry appear to be unlike hydrocarbons 24 p4149 A67-42100
- Aromatic compounds in benzene eluate fractions from carbonaceous chondrites by high resolution capillary gas-liquid chromatography 24 p4236 A67-42640
- ### GAS COMPOSITION
- Mass spectrometry of plasma ionic constituents, identifying monatomic and polyatomic ionic species in gaseous plasma by isotopic techniques 05 p0851 A67-16381
- Meteorite age and related problems of cosmic chemistry 12 p1903 A67-25429
- Spectroscopic measurement of combustion gas composition in supersonic flow [AIAA PAPER 65-580] 12 p1990 A67-25899
- Mass spectrometry of background gases composition during sputtering of tantalum films in argon glow discharges 13 p2178 A67-27078
- Particle density and material functions of gases of random composition, calculating values without regard to reaction dissociation 15 p2543 A67-29090
- Cellular flame under constant volume bomb conditions, demonstrating vibratory combustion over range of gas compositions and characteristic initial pressures 17 p2974 A67-33143
- Electrostatic getter-ion pump performance, giving pumping speeds, pressure and starting characteristics, residual gas composition and operating life 21 p3624 A67-37822
- Asymptotic method for solving differential equations, giving equilibrium composition of gaseous combustion products 24 p4178 A67-42390
- Monograph on absorption and laser radiation covering absorption coefficients, high altitude gas concentration, low extinction coefficient measurements, molecular resonance absorption, etc 24 p4168 A67-42412
- ### GAS COOLED REACTOR /GCR/
- Generator parameters and thermal efficiencies optimization for gas-cooled MGD reactor system, studying temperature and partial-pressure relation to power density 16 p2604 A67-30571

Instability of gas-cooled nuclear reactor passages in steady laminar flow studied by time-dependent analysis 19 p3260 A67-35743

AS COOLING SYSTEM

Thermodynamic flow analysis of feasibility of coolant gas addition to nozzle flow for improved particle formation efficiency in mixed flow colloid thruster 06 p0941 A67-18500

[AIAA PAPER 67-85]

Optimal parameters of refrigerators with radiative regenerative gas cycle 10 p1596 A67-23022

Mass transfer cooling of carbon dioxide-nitrogen binary system in laminar boundary layer, stressing dissociation effect [ASME PAPER 67-HT-70] 20 p3550 A67-36750

Condensation history of cooling gas of cosmic composition, stressing chondrite fractionation patterns 20 p3526 A67-37172

AS DENSITY

Rotational temperatures measured in static low density air with electron beam probe 01 p0071 A67-11105

Radioisotope and radiation techniques for terrestrial and planetary gas and solid measurements 02 p0245 A67-12223

Hypersonic wind tunnel for small gas densities noting vacuum pumps, diffuser, cooler, etc 05 p0786 A67-16591

Density dependence of refractive index of air and phase and group refractive index as function of pressure, temperature and composition 05 p0838 A67-16783

Molecular fluxes in lunar atmosphere relationship to gas source distribution, surface temperature and gas emission laws 05 p0904 A67-17404

Upper atmospheric neutral gas density determination from simultaneous satellite position measurements 07 p1172 A67-19626

Verbal communication intelligibility in man-rated altitude simulator with nitrogen or helium added to oxygen 08 p1287 A67-20484

Vacuum ionization gauge reading dependence on localized gas densities caused by chamber temperature nonuniformity 09 p1498 A67-22108

Mean droplet size for cross stream water injection into Mach 8 air flow determined by scattered light angular variation measurement 11 p1779 A67-24366

Local density and temperature measurement in wind tunnels determined by 50-kev electron scattering, using air as test gas 11 p1790 A67-24446

Possible thermal histories of intergalactic gas 11 p1860 A67-24485

Transport coefficients for dense gases via Bogoliubov theory of two-particle nonequilibrium distribution function 11 p1823 A67-24538

Physical foundations of modern kinetic theory, showing interpretation of particular form of Liouville equation in terms of time scales appropriate to system 11 p1823 A67-24545

Approximate expression derivation for calculating propagation rate of strong shock wave in inhomogeneous cosmic medium 15 p2552 A67-29146

Experimental determination of hydrogen atom beam density after focusing by hexapolar magnet 15 p2520 A67-29720

Electromagnetic probing by laser, determining number densities of water, carbon dioxide and oxygen constituents of atmosphere 15 p2500 A67-29911

Local gas density measurements, using large angle scattering from electron beam passing through rarefied gas flow 15 p2490 A67-30152

Scaling-law equation of state for gases in critical region 16 p2778 A67-31061

Collection of papers on aerophysical studies of supersonic flows covering shock tube experiments, gas density, interferometer and photographic measurements, etc 16 p2672 A67-31101

Rarefied gas flow density measurement by determining changes in electron beam-electron concentration while crossing flow 16 p2673 A67-31107

Concentration profile of normal and excited mercury atoms in shock wave front and wake, noting gas density and electron concentration profiles 16 p2673 A67-31108

Density and pressure in real gas behind plane shock wave upon reflection from solid surface 17 p2836 A67-32072

Thermal conductivity relation to density

and temperature for normal hydrogen in dense gaseous and liquid states 17 p2969 A67-32446

Integral curves of two-dimensional shock and detonation waves in gas with varying density 18 p3028 A67-34273

Photodissociation of hydrogen molecules in H I regions of interstellar medium, evaluating lifetime and density 19 p3331 A67-36085

Rayleigh scattered laser light technique for point measurements of time averaged neutral gas density in turbulent wake behind hypersonic velocity body 21 p3565 A67-38876

Thermodynamic properties of low temperature gaseous and liquid mixtures, discussing quantum effects in mixtures containing hydrogen isotopes and high density mixtures 22 p3921 A67-40553

Self-gravitating isothermal nonrotating gas layer stability, discussing amplitude density distributions in space 24 p4225 A67-41826

Kinetic behavior of electrons in air plasmas containing electrophilic gasses studied with microwaves behind reflected shock waves 24 p4196 A67-42196

Interferometer crossed with spectrograph used for electron concentration investigation in ionized argon behind shock waves propagating at high Mach numbers 24 p4197 A67-42358

Gas-solid interactions and buoyancy relation, discussing fluid density effect on Archimedes principle 24 p4119 A67-42695

Approximate expression derivation for calculating propagation rate of strong shock wave in inhomogeneous cosmic medium 24 p4239 A67-43069

GAS DISCHARGE

SA ELECTRIC DISCHARGE

SA GLOW DISCHARGE

Elementary processes in DC gas discharge plasma in helium, comparing measurements of population levels of excited states of atoms with calculated values 01 p0123 A67-10363

Three new visible CW laser lines in discharge in singly-ionized Cl 01 p0089 A67-10373

Resonances in low pressure mercury vapor discharge due to natural resonance modes of cylindrical plasmas 02 p0273 A67-12097

Forward and backward wave striations in constricted positive column of high pressure argon discharge 02 p0273 A67-12188

Current distribution in eddy configuration of atmospheric gas discharge, noting flow surface deformation rate and measurement techniques 02 p0180 A67-12441

Mean electron concentration in SHF helium discharge determined as function of discharge power and pressure 02 p0277 A67-12616

Introductory text on electrical discharges in gases, emphasizing physical behavior of electrons and ions in ionized state 02 p0279 A67-12720

Diagnostic studies of gas discharge and contact ion sources including test equipment, instrumentation, design and characteristics of propulsion concept 03 p0504 A67-13494

Book on microwave breakdown in gases covering electron collisions, Boltzmann equation for ionized gas, breakdown in atmosphere, etc 03 p0369 A67-13559

Low density electron bombardment ion engine, particularly mercury engine and Cs gas discharge ion engine, for electrostatic propulsion 04 p0689 A67-15020

Electric breakdown in gas discharges in nitrogen and hydrogen at high pressure 04 p0661 A67-15652

Argon discharge characteristics used in continuous action ion laser for analysis of inversion production mechanism 05 p0823 A67-16680

Cosmic ray intensity variations using gas discharge counters onboard Soviet satellites, noting Forbush effects 05 p0884 A67-17025

Disturbance current created by acoustic wave propagating in partially ionized gas 05 p0855 A67-17050

Double probe and microwave resonance measurements of gas additives effect on radial variation of electron temperature and density with partial pressures in carbon dioxide-nitrogen-helium gas laser 05 p0826 A67-17274

Elementary processes in DC gas discharge

plasma in helium, comparing measurements of population levels of excited states of atoms with calculated values 06 p1038 A67-17621

Double-chamber plasmatron for low temperature gas discharge plasma investigations 06 p1038 A67-17745

Calibration of low pressure Penning gas discharge gauge and stability of discharge modes 06 p0950 A67-17748

Pumping medium power lasers using artificial meteors to produce intense gas glow in compression wave 06 p1009 A67-17757

Optical maser oscillation lines in HF discharge in mixture of Ar and Br 06 p1011 A67-18545

Retardation energy distribution of ions and electrons in hydrogen discharge 06 p1037 A67-18762

Laser studies at RCA Victor Research Laboratories, Montreal, discussing spectroscopic, interferometric and plasma diagnostic research 07 p1194 A67-19082

Oscillations in stationary gas discharge, describing device for calculation of correlation function for electrical signals 07 p1227 A67-19120

Rate equations for gas discharge modulation of He-Ne laser 07 p1195 A67-19492

LF resonance oscillations in cylindrical plasma column, considering ionization mechanism of Phillips Ionization Gauge /PIG/ discharge 07 p1229 A67-19674

Center frequency shifts of 6328 angstrom neon transition in Zeeman discharge cell measured in terms of discharge current and gas pressure 07 p1197 A67-20100

Equations for ionized positive plasma column of gas discharge between infinite dielectric planes under oblique magnetic field with component in direction of external electric field 08 p1358 A67-20849

Radial current density distribution in homopolar, noting deviation of magnetic field and nature of current distribution around anode 08 p1358 A67-20850

Frequency spectrum during UHF plasma oscillation excitation by monoenergetic primary electrons introduced into low pressure Hg discharge 08 p1358 A67-20869

Gas desorption following Q-switched laser beam bombardment of tungsten target in vacuum 08 p1338 A67-21310

Continuous transition from moving striation to helical oscillation in helium discharge plasma due to increase of applied magnetic field 09 p1536 A67-21570

Current voltage characteristic of gas discharge for one-dimensional stationary case with fixed temperatures at conductor end, noting voltage saturation 09 p1544 A67-21863

Spectral analysis of laser discharge in pure and impure He, obtaining spectra of spark at various pressures, determining electron concentration 09 p1512 A67-22010

High voltage pulsed electrodeless discharge in rare gas as light source for ruby and Nd glass laser excitation and observation of output characteristics 10 p1666 A67-23565

Plasma equilibrium from gas discharge, role of electron concentration and contributions of excited atom transitions and quenching collisions 12 p1977 A67-26132

Intermediate and HF noise of probes immersed in gas discharges explained by space charge sheath and bulk plasma noises 12 p1948 A67-26226

Gas discharge effects on materials employed in thermonuclear research 13 p2132 A67-26692

Mean electron concentration in SHF helium discharge determined as function of discharge power and pressure 13 p2170 A67-27372

Laser gas-discharge tube /without resonator/ amplification relations, considering stimulating radiation, noting application as oscillator 14 p2328 A67-27771

Discharge characteristics of sharp and round edged orifices in transition regime noting variation of pressure ratio, magnitude of Knudsen and Reynolds numbers, etc 14 p2300 A67-28180

Lasing on Si II and Cl II lines in pulsed gaseous discharge, noting possible mechanisms for achieving population inversion 15 p2496 A67-29178

Gas stream discharge studied by using electromagnetic plasma gun to direct

plasmoids toward beam 15 p2472 A67-29726
 Short wave limit for plasma radiation emission of neon gas discharge analyzed by Kirchhoff-Planck relation 15 p2530 A67-29747
 Time varying high density laser induced plasmas formed in high pressure gases studied using Mach-Zehnder interferometer 15 p2488 A67-29903
 Critical field dependence on pressure, tube radius and ion mass derived from ion-acoustic instability growth in low pressure RF discharge 15 p2531 A67-29904
 Atmospheric pressure discharges in inert gases seeded with alkali metal vapor, noting transition to low voltage high current discharge 16 p2709 A67-30513
 Electron number density and number density of electronic states calculated from rate equations for noble gas seeded with alkali metal 16 p2710 A67-30518
 Cleavage method to study pulsed pressure /energy content/ in dense gas-discharge hot plasma 16 p2714 A67-31037
 Collection of papers on charged particles interaction with plasma, including gas discharge and plasma acceleration 16 p2716 A67-31175
 Electron heating by direct discharge during plasmoid interaction involving polarization 16 p2717 A67-31182
 High pressure characteristics of helium and hydrogen pulsed arcs, noting formation of dense, completely ionized plasma 16 p2717 A67-31183
 Approximate solutions of spatial distributions of charged particles as gas discharge plasma obtained by two-point Jacobi expansion method 16 p2720 A67-31241
 Numerical calculations of parameters of steady state HF high pressure vortical discharge of argon in air 16 p2723 A67-31769
 Geometry of steady state annular electrodeless discharge in argon and xenon as function of discharge power, type of gas, gas pressure, etc 16 p2723 A67-31770
 Electrodeless annular discharges in argon and air 17 p2897 A67-32174
 Two peaks in emission from low pressure helium or neon discharge simulating plasma slab with second peak corresponding to plasma cut-off frequency 17 p2901 A67-32369
 Voltage breakdown measurement in various gases at low pressures during simultaneous excitation by RF in superimposed DC field 17 p2902 A67-32672
 Time dependent self-compressed pinch-discharge radiation characteristics in various gases analyzed photographically for luminescence distribution, spectral composition, etc 17 p2904 A67-32918
 Mechanism of positive low pressure column in plasma of low electron density, studying steady state conditions of nonstratified inert gas discharges 17 p2907 A67-33103
 Metastable atomic oxygen state observed in microwave discharge of molecular oxygen, noting g factor of 2 in strong resonance 18 p3082 A67-34029
 Selective enhancement of molecular spectra of HD and diatomic deuterium in argon and krypton 18 p3083 A67-34518
 Plasma sources of refractory ions classified according to methods of producing gas discharge 19 p3228 A67-34981
 Current growth rate instabilities in high current mercury vapor discharges, giving image converter photographs 19 p3265 A67-35091
 Positive column contraction in inert gas discharge, studying electron density and radiation intensity radial distribution and wall current 19 p3272 A67-35092
 Plasma regime creation through boundary perturbations in low-pressure gas discharge, developing moving striations 19 p3273 A67-35096
 Positive column and striations of low pressure discharge of noble gas 19 p3273 A67-35097
 Negative ion accumulation in HF resonant discharges at low pressure and plasmoid formation 19 p3275 A67-35112
 Weakly ionized plasma and gyromagnetic resonances in helium low pressure HF electrodeless discharge in magnetic field 19 p3276 A67-35113
 Structure of ion and electron currents axial emission from cathode measured as function of magnetic field

intensity 19 p3277 A67-35121
 Slepian discharge /steady state DC crossed field discharge/, obtaining solutions for plasma velocity and potential to determine current-voltage characteristics 19 p3277 A67-35122
 Pulsed-discharge-current interruption in constricting aperture by pinch effect, loss of ions, gas heating and oscillation generation 19 p3278 A67-35127
 Excitation and ionization mechanisms in positive DC discharge columns in krypton and xenon 19 p3285 A67-35131
 Thermodynamic model for laser induced gas discharges accounting for transmitted light attenuation, plasma heating, etc 19 p3239 A67-35163
 Diocotron effect in cylindrical charge layers analyzed, noting instability when layer thickness is less than critical, experimenting with plasma discharges 19 p3292 A67-35392
 Unsteady discharge of compressed viscous gas from duct analyzed by finite-difference method 19 p3172 A67-35780
 Damping effect of HF field on instabilities occurring in form of moving striations within plasma of gas laser 19 p3241 A67-35814
 Nonlinear coupling between fast and slow waves of cold homogeneous plasma slab partially filling parallel plate waveguide 20 p3492 A67-36126
 Second derivative of two-probe current measurement method for determining electron energy distribution in gas discharge, noting low sensitivity to noise 20 p3498 A67-36687
 Fast scanning 180 degree magnetic mass spectrometer for monitoring fast changes in residual gas compositions 20 p3448 A67-36875
 Electron-cyclotron harmonic resonances interactions in RFF excited electrodeless helium discharges, discussing magnetic field position measurement and plasma simulation 21 p3662 A67-37757
 Oscillations in stationary gas discharge, describing device for calculation of correlation function for electrical signals 21 p3664 A67-38165
 35 GHz second harmonic generation power and conversion efficiency in low pressure gas discharge, noting pressure and gas species variations 22 p3854 A67-40316
 Laser lines observation in Freon-He mixtures in CW gas discharge 22 p3817 A67-40489
 Threshold properties of CW laser oscillation at 7525.5 angstroms in DC-excited KrII discharge 22 p3818 A67-40490
 Laser gyro development and application noting advantages in cooling, power, starting time and acceleration 23 p3999 A67-40916
 Flash blindness effects on pilot performance simulating inadvertent exposure to nuclear bursts of light by xenon gas discharge tube 23 p3965 A67-41569
 He-Ne gas mixture DC discharge electron temperature and concentration dependence on tube diameter, pressure and composition, using two-probe method 24 p4198 A67-42242
 Ar II population inversion of 4s and 4p states in stationary arc discharge, measuring ionic and atomic spectral line shift, widths and intensities and emission power 24 p4198 A67-42245

GAS DISCHARGE COUNTER

Cosmic radiation data obtained by two gas-discharge counters installed in Luna X artificial satellite 01 p0145 A67-10906
 Luna X shielded gas-discharge counter data on soft corpuscular radiation, noting solar contribution to magnetospheric tail 01 p0145 A67-10907
 High energy cosmic ray interactions analyzed at 3340 m above sea level, using Wilson cloud chambers, gas discharge counters, ionization calorimeter, etc 02 p0248 A67-12746
 Preliminary measurements of variations in cosmic ray intensity using device consisting of gas discharge counters, telescope and ionization chamber mounted on Kosmos XXV satellite 05 p0878 A67-16092
 Cosmos 53 satellite radiation data using on board gas discharge counter 05 p0879 A67-16107
 Penetrating radiation measurement on moon surface obtained by Luna IX spacecraft 08 p1385 A67-20841
 Penetrating radiation intensity on lunar

surface and in space, evaluating counting rate, lunar surface radioactivity and radiation belts absence 18 p3122 A67-34143
 High energy cosmic ray interactions analyzed at 3340 m above sea level, using Wilson cloud chambers, gas discharge counters, ionization calorimeter, etc 22 p3801 A67-40248
 Cosmic ray measurements during low geomagnetic activity using scintillation, gas discharge and semiconductor proton counters mounted on Cosmos satellite 23 p4055 A67-41099
 Preliminary measurements of variations in cosmic ray intensity using device consisting of gas discharge counters, telescope and ionization chamber mounted on Kosmos XXV satellite 24 p4213 A67-42768
 Cosmos 53 satellite radiation data using onboard gas discharge counter 24 p4213 A67-42783

GAS DISSOCIATION

Two sound-absorption maxima in liquid nitrogen tetroxide resulting from relaxation of dissociation equilibrium 01 p0019 A67-10841
 Dissociation pressures of mixed gas hydrates predicted from data for hydrates of methane, propane and nitrogen with water 02 p0190 A67-12234
 Laser induced breakdown of complex organic molecules in vapor state, noting emission accompanied by formation of partially dissociated hot gas 02 p0252 A67-12451
 Current carrier concentration and dynamic coefficients for nondegenerated and highly degenerated Fermi gases subject to nonparabolic isotropic laws of dispersion 02 p0300 A67-12475
 Laminar boundary layer with longitudinal pressure gradient in high velocity flow of uniformly dissociated gas for arbitrary external velocity 03 p0401 A67-12875
 Rate equation for dissociation and recombination of diatomic molecules 03 p0473 A67-13521
 Convective heat transfer measurements for partially dissociated carbon monoxide and hydrogen with high Lewis number [ASME PAPER 65-WA/HT-27] 03 p0537 A67-14012
 Dissociative recombination coefficient of nitrosyl ion with electrons 04 p0567 A67-15765
 Heat transfer to end wall of shock tube behind reflected shock wave in oxygen dissociated to varying degrees and at high temperatures 04 p0729 A67-15813
 Krypton and xenon effect on dissociation rate of fluorine in presence of argon behind shock wave 04 p0567 A67-15951
 Matched asymptotic expansions method for perturbation problem of nearly equilibrium dissociating boundary layer flow 05 p0792 A67-16818
 Electron recombination kinetics in diatomic and polyatomic gases expanding into emptiness 05 p0927 A67-16992
 Hypersonic laminar boundary layer on blunt cones, considering external flow vorticity caused by curved shock wave, calculating gas-enthalpy profile 06 p0936 A67-17734
 Enthalpy of formation and dissociation of explosion of mixtures of hydrogen and excess nitrogen 06 p0955 A67-17985
 Dipole-dipole molecular interaction contribution to thermodynamics and state equation of excited molecular gas, noting dissociation possibility 06 p0991 A67-18802
 Dissociational rate constants and vibrational relaxation times modifications, considering coupling of vibrational and dissociational nonequilibrium of expanding gas in nozzle [AIAA PAPER 66-520] 06 p0992 A67-18851
 Structure of radiation resisted hypersonic shock in simple dissociating gas examined via quasi-equilibrium field for radiation field 06 p0993 A67-18893
 Turbulent boundary layer of gas mixture with dissociation flowing at inlet section of tube 11 p1782 A67-24961
 Stirling cycle using dissociating gas 13 p2221 A67-26390
 Steady state approach in competitive-consecutive gas reactions, establishing criterion for approach time

- estimation 14 p2407 A67-28548
- Compression shocks in one-dimensional steady flow of Lighthill ideal dissociating gas studied, using semiempirical relation for relaxation equation 15 p2471 A67-29578
- Equations to investigate effect of simultaneous oscillation and dissociation relaxation on gas dynamic parameters of supersonic flow past blunt bodies 16 p2592 A67-31114
- Depopulation of vibrational energy levels in fast chemical dissociation 18 p2996 A67-33780
- Turbulent boundary layer on plane catalytic plate in nonequilibrium dissociating gas calculated by successive approximation technique 18 p3027 A67-34204
- Dipole-dipole molecular interaction contribution to thermodynamics and state equation of excited molecular gas, noting dissociation possibility 18 p3029 A67-34421
- Nonequilibrium-transition patterns of quasi-one-dimensional dissociating-gas flow through diverging supersonic nozzle 19 p3211 A67-35759
- Equations of one-dimensional aerothermodynamic flow of dissociating gas 20 p3420 A67-36599
- Mass transfer cooling of carbon dioxide-nitrogen binary system in laminar boundary layer, stressing dissociation effect [ASME PAPER 67-HT-70] 20 p3550 A67-36750
- Gas separation effects in Ranque-Hilsch vortex tube explained by dynamic model of axial flow 22 p3917 A67-39512
- ### GAS DYNAMICS
- #### SA AERODYNAMICS
- #### SA FLUID MECHANICS
- #### SA MAGNETOGASDYNAMICS
- #### SA MAGNETOHYDRODYNAMICS
- #### SA RAREFIED GAS DYNAMICS
- Existence of divergence in density expansion of viscosity and thermal conductivity coefficient of two-dimensional gas of rigid disks 02 p0234 A67-12545
- Soviet book on gas dynamics of combustion including detonation, deflagration, accelerating flames, combustion chambers, etc 02 p0343 A67-12879
- Chemical reaction kinetics and gas dynamics combined to analyze processes occurring in combustion chambers and nozzles of jet and rocket engines [DVL-602] 03 p0366 A67-12999
- Oscillations in burnt gas coupling to gas dynamical interactions occurring at detonation wave front 03 p0402 A67-13465
- Transformation of unknown functions and independent variables entering into differential equations for motion of nonviscous nonheat-conducting gas 03 p0403 A67-13628
- Vorticity jump across discontinuity surface which is not contact surface obtained on kinematical basis, recovering Hayes formula for gas dynamic discontinuity 04 p0600 A67-14456
- Book on kinetic equations of gases and plasmas, with emphasis on theories which start from Liouville equation 04 p0660 A67-14581
- Exact general integral for class of compressible fluids used in boundary value problems for nonlinear equations of gas dynamics 04 p0606 A67-15194
- Kinetic theory of gases through certain correlation functions known as product densities used to explain transitions from gaseous to liquid state 04 p0608 A67-15466
- Mean value definition in one-dimensional gas dynamics applied to nonuniform flow 04 p0609 A67-15747
- Thermodynamic properties of real air, deriving expressions for expansion in isothermal-isentropic mode from subcritical temperatures to 1500 degrees K 04 p0738 A67-15914
- Book on aerogasdynamics in relation to rocket and aviation technology including shock waves, rarefaction flow, heat transfer, skin friction, etc 05 p0747 A67-16173
- One-dimensional self-similar motion of relaxing gas, noting ODEs of process and gas dynamic parameters of flow field 05 p0791 A67-16376
- Gas dynamic equations for determination of heating, vaporization and expansion of substance due to Q-switched laser radiated collimates onto surface of solids 05 p0819 A67-16652
- Laser radiation effect on heating process and gas dynamic motion of finite transparent gas and motionless cold gas at vacuum interface 05 p0927 A67-17008
- Generalization of kinetic theory of gases, deriving Boltzmann kinetic equation for use in singly-partial distribution function 05 p0849 A67-17021
- Equivalent circuit of piezoelectric quartz pressure transducer used with measuring circuit with small input resistance for solving gasdynamic problems 05 p0808 A67-17111
- Second and third virial coefficient of quantum gas expressed in terms of two-particle scattering amplitude, starting from cluster expansion of partition function 05 p0849 A67-17316
- Velocity and temperature profiles of optically thick planar Couette flow, obtaining heat transfer rates for Rosseland mean absorption coefficient variation with temperature 05 p0793 A67-17343
- Gas dynamics and geometry in mixing zone of Freon 12, air and helium jets in wake air flow, determining effect of jet velocity, gas density, etc 06 p0982 A67-17743
- Self-similar solution generalization for Euler-Poisson wave equations, noting application to transonic gas dynamics 06 p1023 A67-17862
- Quantum mechanical calculation of transport coefficients of gas of loaded spheres, obtaining scattering amplitudes and cross sections 06 p1038 A67-19046
- Quadrupole effects on gas diffusion, viscosity and thermal diffusion factors, computing collision integrals 06 p1038 A67-19046
- Thermal insulation for flight vehicles under various conditions of gas-kinetic heating 07 p1266 A67-19146
- Theoretical aspects and technological development of parametric optimization of centripetal turbine stage, including study of turbine nozzle and wheel profiling 07 p1239 A67-19298
- Internal ballistic considerations in hybrid rocket design, noting throttling and regimes of operation involving effects of surface-or gas-phase reaction kinetics [AIAA PAPER 66-628] 07 p1240 A67-19377
- Nonlinear nonsteady wave propagation in plane flow analyzed by introducing perturbations of potential into equation of gas dynamics and equation of characteristics 07 p1169 A67-19731
- Monograph on shock tubes, weak and strong shock waves and rarefaction waves 07 p1169 A67-20205
- Gas dynamics of nonisentropic two-dimensional MHD flow of ideal inviscid perfectly conducting compressible fluid 08 p1357 A67-20593
- Free charged particles interaction with each other and neutral atoms in highly excited states effect on thermodynamic and gas dynamic parameters of shock wave propagating in cesium vapor, taking into account energy losses due to radiation 09 p1540 A67-21791
- Electron temperature higher than gas temperature in dense argon plasma in presence of electric field 09 p1547 A67-22325
- Modified differential approximation for external radiation sources in radiation gas dynamics 10 p1733 A67-23113
- Optimum thrust nozzle contours for chemically reacting gas flows, obtaining set of partial differential equations for gas dynamic properties [AIAA PAPER 66-638] 10 p1592 A67-23118
- Variation problem solution in hypersonic gas dynamics, noting intake portion construction for body with minimum resistance for limited length and flat end 11 p1777 A67-24153
- Stellar dynamics and galactic spiral structure analyzed using gas and plasma dynamics 11 p1863 A67-24534
- Chemical kinetic processes in gasdynamic shock wave interactions, especially vibration in four-center transition states 11 p1773 A67-24535
- Momentum and energy transfer effects on gas kinetic equations of nonequilibrium flows, analyzing diffusion problem 11 p1780 A67-24536
- Macroscopic neutral and ionized gas motions in ionospheric D and E layer interpreted from wind and radio wave scattering measurements 11 p1787 A67-24595
- Gas state equation determination from trajectory analysis of piston in hypersonic wind tunnel 11 p1782 A67-24759
- Dynamic behavior model for gas shock wake motion and reflection in semilinear volume laterally bounded 11 p1782 A67-24954
- Dynamical irreversible evolution of gas with short range repulsive forces, using n-particle distribution function with many-body interactions 11 p1824 A67-25077
- Heat transfer in conducting and radiating gas analyzed, using governing equations reformulated as Lagrangian equations through introduction of potential 12 p2035 A67-25926
- Singularities causing numerical instabilities used in steady gas dynamic Cauchy problem solution, exemplifying with supersonic blunt body 12 p1893 A67-25932
- Formation of Maxwell and non-Maxwell distribution in gases, noting reduction of time reversible to time irreversible equations 12 p1988 A67-26114
- Parameters of gas behind incident and reflected shock waves calculated, using gas dynamic and chemical equilibrium equations for one-dimensional problem 12 p1930 A67-26134
- Discrete ordinate method for evaluating function described by particular integral applied to boundary value problems in gas kinetics 12 p1962 A67-26192
- Interstellar gas dynamics suggests that energy density of galactic cosmic rays places firm upper limit on undetermined constant of solar modulation 13 p2189 A67-26265
- Handbook of engineering sciences, Volume 1, Basic sciences 13 p2155 A67-26266
- Stability of discontinuous solutions of gas dynamic equations noting doubtful case with imaginary eigenvalues 13 p2093 A67-26379
- Invariant transformation of MGD equations where plane flow is situated in transverse magnetic field 13 p2168 A67-26895
- Discrete ordinate method for boundary value problems in gas dynamics using differential equations yields solutions to Couette flow 13 p2101 A67-26962
- Boltzmann equation and statistical properties for two-dimensional gas, analyzing integral iteration for shock wave flow 13 p2103 A67-26975
- Dynamics of weakly ionized gases analyzed using Liouville equation 13 p2167 A67-27003
- Hartmann oscillator problem studied using hydraulic analogy between supersonic compressible gas dynamics and incompressible flows with free surface 14 p2295 A67-27903
- Gas dynamic functions for supersonic gas flow past axisymmetric bodies of various configurations 14 p2239 A67-27991
- Supersonic three-dimensional flows past smooth bodies, calculating flow parameters by characteristic method with analytical approximation of gas-dynamic functions 14 p2240 A67-27992
- Three-dimensional gas flow in region of incidence of shock wave on cylinder situated in high supersonic flow 14 p2297 A67-27995
- Large-dimensional inverse pinch discharge study of impulsive plasma acceleration, gas dynamics and stability of unrestrained current sheet [AIAA PAPER 66-482] 14 p2356 A67-28123
- Partition functions applicability at high temperatures 14 p2405 A67-28131
- Generalization of kinetic theory of gases, deriving Boltzmann kinetic equation for use in singly-partial distribution function 14 p2351 A67-28482
- Calculation of diffusive gas flame in turbulent wake, reducing problem to differential equations of motion 14 p2407 A67-28649
- Aerodynamic flow deflection over convex curved surface noting occurrence of hysteresis 14 p2305 A67-28978
- Vaporization under laser radiation in terms of gas-dynamics, formulating boundary conditions 14 p2334 A67-29074
- Mechanical friction occurring during oscillating motion of gas which absorbs or reflects electromagnetic radiation 14 p2349 A67-29075
- Empirical correlation formulas for density and viscosity of equilibrium air, noting pressure variation at high enthalpies 15 p2579 A67-29436
- Nozzle type similarity solution to axisymmetric viscous transonic equation,

describing shock wave development at nozzle throat 15 p2417 A67-29654

Interaction of supersonic gas stream with inclined surface, calculating parameters and boundary of fluid spreading 15 p2472 A67-29776

Motion of single-component electrically charged gas in elliptical cylindrical cavity analyzed for relative deformation when applying magnetic field 16 p2658 A67-30456

Equations to investigate effect of simultaneous oscillation and dissociation relaxation on gas dynamic parameters of supersonic flow past blunt bodies 16 p2592 A67-31114

Design and construction principles of radio telemetry recording systems for gasdynamic observations in ballistic testing 16 p2624 A67-31124

Von Karman gas dynamics counterflow facility for simulating model high velocities and altitudes of reentry conditions 16 p2655 A67-31261

Unsteady convective heat transfer and hydrodynamic behavior of gas flows in channels 17 p2967 A67-32131

Equilibrium thermodynamic and gas dynamic parameter calculation for low temperature plasma, using electromagnetic and diaphragm-type shock tubes 17 p2894 A67-32148

Steady state plasma accelerators different from gas dynamic accelerators with Laval nozzles due to variety of waves, electric/magnetic fields, etc 17 p2898 A67-32185

Thin airfoils in radiation gas dynamics, formulating linearized theory for plane steady motion via Fourier transform and obtaining solution for absorption coefficient 17 p2791 A67-32556

MHD flow, deriving equation system and boundary conditions for gas dynamic process 17 p2903 A67-32682

Generalization of linearized equation of stationary waves in equilibrium gas dynamics applied to flow along two-dimensional sinusoidal wall 17 p2839 A67-32715

Short duration shock tube molecular beam in helium and oxygen, giving test arrangement and data 17 p2835 A67-33361

Condensation during heterogeneous combustion, discussing kinetics, radiation and gasdynamic heat release 18 p3149 A67-33798

Metallized and nonmetallized composite solid propellant burning rates, analyzing effects of acceleration, noting agglomeration and nonnormal conditions [AIAA PAPER 67-470] 18 p3157 A67-33940

Radiation peak formation mechanism in spectral lines of nonequilibrium gas following passage of shock wave 18 p3083 A67-34060

Laser radiation effect on heating process and gas dynamic motion of finite transparent gas and motionless cold gas at vacuum interface 18 p3160 A67-34270

Closed-cycle generator using gasdynamic forces to transport charged particles against opposing electric field, noting enthalpy role 19 p3175 A67-34801

Turbulent boundary layer flow in conical supersonic nozzle, discussing convective heat transfer and adverse pressure gradient effect 19 p3169 A67-34814

Collapsing shocks and detonation waves gasdynamic problem, evaluating perturbations due to counterpressure and to heat release 19 p3209 A67-35411

Adiabatic pulsations of inhomogeneous gaseous mass consisting of convective core and radiative envelope 19 p3261 A67-35502

Wave propagation in real gases, considering one-dimensional time-dependent disturbances semiinfinite in extent, emphasizing matched asymptotic expansion and coordinate stretching methods 19 p3212 A67-35798

Spherical gas bubble pulsations under pressure waves analyzed in compressible and incompressible fluids 20 p3422 A67-37065

Book on thin wing and aerodynamic characteristics in subsonic gas flow 20 p3359 A67-37206

Soviet monograph on high speed measuring methods in gasdynamics and plasma physics, discussing high temperature plasma and shock wave production 21 p3625 A67-37964

Nonlinearity of unsteady gasdynamic processes in internal combustion engine exhaust systems, using unsteady sources and sinks 21 p3689 A67-38044

Solution methods for Cauchy problem and ideal unstable gas motion in cylindrical and spherical symmetry, discussing shock wave occurrence 21 p3565 A67-38562

Hot shot nitrogen gas source for pulsed MHD accelerator to provide lunar reentry 21 p3608 A67-38863

Exhaust manifold design for two-cycle diesel engine with turbosupercharger using physical simulation, discussing simulation criteria for gasdynamic processes 21 p3696 A67-38908

Three-dimensional heat source influence on solar plasma flow contradicts Parker solar wind theory, based on gasdynamic acceleration 21 p3699 A67-39012

Shock structure in kinetic theory of gases, solving Krook model of Boltzmann equation with small perturbation technique 22 p3782 A67-39196

Continuous phase medium gas representation used to derive variational principles for Liouville, coupled Bogolubov and kinetic equations 22 p3835 A67-39218

Motion and thermodynamic conditions of free piston ballistic compressor test gas taking into account gas leakage, viscous friction and heat losses 22 p3778 A67-39351

Gas dynamic self-regulation of supersonic nozzle consisting of cylindrical channel with central body, measuring nozzle inlet and static pressures 22 p3868 A67-39544

Flame stabilization mechanism of homogeneous combustible fluid flow using air jets through peripheral slits to join main flow producing gasdynamic screens 22 p3921 A67-40455

One-dimensional unstable cloud hydrodynamics analyzed numerically, noting collapse primarily in center and little density growth in outer region 22 p3895 A67-40515

High temperature turbulent jet gasdynamic behavior, discussing high temperature plasma jet experiments 23 p3989 A67-40728

Kinetics of flames propagating in hydrogen-nitrous oxide mixtures diluted with inert gases 23 p4082 A67-41142

Light gas escape flux from atmosphere velocity and angular distributions near critical level using Monte Carlo analysis 24 p4224 A67-41823

Turbojet engine gasdynamic parameters dependence on reduced rotational velocity for in-flight characteristics determination, assuming variable compression and critical pressure ratio 24 p4207 A67-41916

Interferometer employing diffraction grating investigated for applicability to quantitative study of gas dynamics 24 p4158 A67-42723

Colloidal electrogasdynamic energy converters analyzed on basis of power plant specific mass 24 p4109 A67-42888

GAS EVACUATION

Heat transfer in compressed gas evacuated from container, using numerical integration of state equation 07 p1287 A67-19324

Space evacuation of NRC-2 insulation for liquid hydrogen tankage, noting vacuum test apparatus and cold plate test 10 p1734 A67-23727

High vacuum enclosure problems solved by use of magnetic seal for joints of large valves and degassing by direct heating of wall surfaces 17 p2802 A67-32300

GAS EVOLUTION

Transient temperature and mass evolution from solid propellants during pressure decays 04 p0687 A67-14835

High speed photography of laser radiation damage to transparent materials and analysis of destruction mechanisms involved 09 p1516 A67-22660

GAS EXCHANGE

SA OXYGEN PRODUCTION

Low pressure environmental chamber for estimation of gas exchange ratio during exposure of animals under controlled conditions [ASME PAPER 66-WA/HT-52] 04 p0599 A67-15438

Biological life support system for regenerating closed atmosphere by photosynthesis, using gas exchange between man and microalgae 19 p3180 A67-35236

Permeation of neon, nitrogen and sulfur hexafluoride through living tissue in rats, using subcutaneous gas pockets as decompression sickness bubbles model 21 p3574 A67-38079

Theoretical lung with equal ventilation-perfusion ratio used to study determinants in inert gas elimination 21 p3575 A67-38515

Ventilation-perfusion inequality effects studied in inert gas elimination from lungs 21 p3575 A67-38516

Biological regeneration of enclosed atmosphere with algae photosynthesis noting effect of diet change 24 p4114 A67-41845

GAS EXPANSION

Optimum nozzle contours for expansion of Lighthill idealized dissociating gas in one-dimensional flow determined by methods of variational calculus 02 p0305 A67-12353

Nonequilibrium expansion of high temperature diatomic gas through hypersonic convergent-divergent nozzle 02 p0180 A67-12547

Plasma production by conical electrode plasma gun studied by systematically changing gas loading 03 p0476 A67-13353

Kinetic relaxation equation with initial values for uniformly expanding or contracting gas and Maxwellian molecule problem 04 p0604 A67-14792

Charged gas expansion with particle production, noting parameters and applicability to cosmological model of Hoyle 04 p0606 A67-15185

Electron recombination kinetics in diatomic and polyatomic gases expanding into emptiness 05 p0927 A67-16992

Unsteady radial expansion of polytropic gaseous sphere in own gravitational field, using hydrodynamical equations and model limited by shock wave 06 p1083 A67-18064

Free molecular expansion into vacuum of pulsed and steady gas flow from circular orifice 06 p0985 A67-18190

Laval nozzle configuration for sharply bounded carbon dioxide jet in vacuum 06 p0943 A67-18781

Approximate solutions for uniform gas cloud expansion into vacuum with attention to inaccuracies 06 p0993 A67-18890

Unsteady energy transfer in gray radiating gas during expansion at atmospheric pressure for arbitrary optical radius 08 p1323 A67-21391

Model for gas particle exhaust flow from under expanded nozzles 10 p1592 A67-23154

Expandable gas bag for stowable omnidirectional multiple impact landing system 10 p1714 A67-23755

Gas jet expansion near crossed axisymmetric channel, reducing problem to solution of Laplace equation for second-kind boundary conditions 11 p1779 A67-24321

Rarefied gas motion instability, constructing general solution for effect of various force fields 11 p1782 A67-24688

Distribution function and temperatures in monatomic gas under steady expansion into vacuum determined by integrating Bhatnagar-Gross-Krook /BGK/ model equation and moment equations respectively 13 p2104 A67-26982

Nonequilibrium effects in spherical free jet expansions of polyatomic gases and gas mixtures, obtaining moment equations for flow field development 13 p2104 A67-26983

Spherical supersonic source expansion of neutral disparate molecular weight binary gas mixture studied asymptotically as source Knudsen number tends to zero 13 p2104 A67-26984

Laminar motion equation for conducting gas jet expansion along plane wall in presence of transverse magnetic field solved in series form 13 p2168 A67-27304

Effect of wide angle screened diffuser on turbulent velocity fluctuations [ASME PAPER 67-FE-23] 14 p2243 A67-28368

Driver chamber for very high temperatures obtained with ceramic liner for arc driven shock tube, reducing contamination and cooling of driver gas 14 p2293 A67-28749

Boundary form of freely expanding plasma cloud in magnetic field determined, assuming plasma pressure equal to external magnetic field pressure 16 p2706 A67-30457

Heat addition in channels of variable cross section area discussed for one-dimensional, inviscid flow of ideal gases with constant specific heat ratio 16 p2591 A67-30944

Initial phase of expansion of two-component plasma into vacuum analyzed, using extension of Sedov homogeneous relative deformation 18 p3084 A67-33423

Laval nozzle configuration for sharply bounded carbon dioxide jet in vacuum 18 p2982 A67-33723

Free jet plume expanding into vacuum investigated experimentally, comparing with ideal gas characteristics method 18 p3152 A67-33818

Nonlinear effect of gravitational instability in expanding universe, calculating second-order density perturbations by iteration method 19 p3317 A67-34891

Dynamics of channel formation in nonisothermal pulsed discharge and nonequilibrium ionization in inert gas-cesium mixtures 19 p3278 A67-35132

Solution to moment equations for near-equilibrium spherically-symmetric expanding flows by using Bernstein-Greene-Kruskal theory for Boltzmann 19 p3212 A67-35764

Axial electron density profile in weakly ionized seeded argon plasma expanding through supersonic nozzle determined experimentally using microwave interferometer [AIAA PAPER 67-704] 21 p3672 A67-38731

Expandable gas bag for stowable omnidirectional multiple impact landing system 22 p3904 A67-40097

Extragalactic radio sources interpreted as consistent evolutionary sequence, suggesting particle injection, relativistic gas expansion and intergalactic gas pressure equilibrium 23 p4069 A67-41361

GAS EXPLOSION

SA EXPLOSIVE GAS

Text describing physical phenomena and experimental apparatus for observing and measuring shock waves and detonations in gases 02 p0235 A67-12680

Divergence of fragments of force-free gas-filled vessel exploded in vacuum 04 p0708 A67-14793

Hydrogen oxidation noting explosive property as function of temperature, pressure, composition, etc 04 p0565 A67-15091

Carbon disulphide oxidation noting self-ignition temperature, explosion limits, reaction products, cool flame propagation, etc 04 p0566 A67-15093

Plane explosion in conducting gas with initial magnetic field having intensity vector directed at angle to plane 05 p0855 A67-17022

Plane, cylindrical and spherical shock propagation from point source explosion in gas with counterpressure 05 p0793 A67-17099

Similarity in propagation of detonation waves in gaseous and liquid explosives with respect to homogeneity explained in terms of single detonation reaction 06 p1112 A67-17960

Shock and detonation waves in strong localized explosion in combustible gas mixture solved approximately 10 p1733 A67-23040

Energy release effects on unsteady gas flow in explosion [AIAA PAPER 66-517] 13 p2106 A67-27582

Plane explosion in conducting gas with initial magnetic field having intensity vector directed at angle to plane 14 p2359 A67-28484

Motion of two parts formed by rupture of gas-filled vessel in vacuo 16 p2761 A67-30745

GAS FLOW

SA AIRFLOW

SA CHEMICAL RELAXATION

SA KNUDSEN FLOW

SA MAGNETOHYDRODYNAMIC FLOW

SA PLASMA FLOW

Braking of conducting gas by transverse magnetic field in rectangular channel, deriving one-dimensional channel flows 01 p0119 A67-10173

Azimuthal current effect on electrical efficiency of MHD vortex generator 01 p0120 A67-10174

Linear formulation of electromagnetic field effect on supersonic gas flow 01 p0125 A67-10980

Potential flow of ideal gas with acoustic surface coinciding with characteristic 01 p0053 A67-10999

Nonsteady state gas flows with small entropy gradients corresponding to supersonic flight conditions 02 p0178 A67-11629

Transonic plane gas flow equations with algebraic self-similar solutions used for analysis of flow in various nozzles 02 p0178 A67-11951

Diffusion flame in transition region of gas flow 02 p0343 A67-12536

Flow induced by infinite flat oscillating plate in incompressible dusty gas 02 p0234 A67-12548

Fluctuations of potential isentropic supersonic gas flow in finite channel with oscillating walls 02 p0180 A67-12669

Exhaust processes of gases at high initial pressure from tubes, when flow is initiated by acceleration of solid body 02 p0235 A67-12788

Book on supersonic gas flow past blunt bodies under various conditions 03 p0349 A67-12851

Supersonic flow past sphere by hot gas mixture with detonation wave in cases when wave does not split and when splitting occurs 03 p0349 A67-12864

Gas flow of two-phase medium in Laval nozzle in presence of small particle lags in velocity and temperature in one-dimensional formulation 03 p0349 A67-12865

Convective heat transfer in radiating gas, examining boundary layer equations and boundary conditions involving luminescence 03 p0532 A67-12866

Laminar boundary layer with longitudinal pressure gradient in high velocity flow of uniformly dissociated gas for arbitrary external velocity distribution 03 p0401 A67-12875

Two-dimensional nonvortical shock-wave gas flow through Laval nozzle 03 p0350 A67-12886

Aeromagnetic flutter of walls of plane infinite channel with ionized gas flow 03 p0524 A67-13503

Coolant injection in turbulent boundary layer for protection of surfaces from effects of high temperature and high energy gas flows 03 p0536 A67-13526

Electrical current passage across neutral or ionized argon flow in presence of accelerating or decelerating magnetic field 03 p0478 A67-13605

Plane transonic gas flow past symmetrical convex profile at zero angle of attack along axis of channel with parallel walls 03 p0352 A67-13620

Three-dimensional unsteady flow in uniformly expanding layer and dispersion of gas in vacuum 03 p0402 A67-13627

Interference between plane surfaces in supersonic gas flow between two rectangular parallelepipeds 03 p0403 A67-13630

Asymptotic representation of solutions for boundary layers near weak shock waves in conical flows 03 p0352 A67-13631

Gas squeeze film stiffness and damping torques on circular disk oscillating about diameter [ASME PAPER 66-LUB-4] 03 p0432 A67-13762

Gas flow calibration systems noting accuracy degree and factors contributing to errors 03 p0422 A67-13772

Time resolution dependence on ambient gas around rotating mirror in streak camera 03 p0424 A67-13915

Drag measurements of isolated lamellae and cylinders in rarefied gases with low velocity 03 p0404 A67-13972

Equivalency coefficient dependence on angle of attack, Mach number and angle of incidence for subsonic and supersonic gas flow past plate grid 03 p0353 A67-14082

Stability of transverse oscillation of thin finned elastic beam of revolution in gas flow acted upon by tracking force 03 p0520 A67-14172

One-dimensional steady state gas compression flow undergoing thermodynamic relaxation processes 03 p0405 A67-14258

Penetration of flows into stable layer below solar hydrogen convection zone based on detailed model of sun 04 p0894 A67-14470

Transverse and longitudinal Knudsen forces account for experimentally observed thermomolecular flow forces by extension of theory in intermediate pressure range 04 p0803 A67-14731

Hypersonic helium flow past blunt cones compared with flow past sharp cones 04 p0546 A67-14781

Gas flow with accelerated contact surface and attenuated shock wave as example of

gas flow not explainable by ideal one-dimensional theory 04 p0604 A67-14782

Heat transfer and equilibrium temperature of plate in supersonic flow of rarefied gas 04 p0546 A67-14783

V-I characteristics of stagnation point electrodes in lightly ionized atmospheric pressure plasma, calculating electric resistance from conductivity measurements 04 p0664 A67-14821

Continuous spatially varied open channel liquid flow analogy for gas flow, with heat addition and extraction over finite distance 04 p0604 A67-14838

Stability and steadiness of gas flow of argon plasma jet analyzed, using dual grating spectrograph 04 p0664 A67-14848

Aerodynamic coefficients of symmetrical wing profiles and fuselages in rarefied gas calculated for free molecular flow 04 p0547 A67-14992

Nonstationary flow of gas in transverse magnetic field, noting electric conductivity dependence on compressibility and temperature 04 p0665 A67-15178

Linearized Couette flow problem in rarefied gas solved, using one-dimensional radiative heat transfer analogy 04 p0606 A67-15183

Low density gas flow through short tubes at densities varying from continuum to free-molecule regime, noting nitrogen flow [ASME PAPER 66-WA/PID-8] 04 p0606 A67-15331

Temperatures in cylindrical receiver resulting from rapid filling with compressible fluid compared with classical bottle-filling case [ASME PAPER 66-WA/PID-2] 04 p0555 A67-15380

Errors in calculating losses in diffuser elements 04 p0548 A67-15600

Methods of calculating flow velocity losses in diffusers 04 p0548 A67-15601

Hydraulic resistance determination for plane and axisymmetric channels with attached and separated flow, noting terminology 04 p0549 A67-15602

Velocity profile and friction in plane-parallel channel with developed turbulent compressible gas flow 04 p0609 A67-15684

Erosion destruction mechanism in polycrystalline graphite, noting effect of gas flow over surfaces, flow pulsation frequency and generated aerodynamic loads 04 p0642 A67-15761

Gas flow, convective heat transfer, enthalpy rise and surface mass transfer for bodies in cross flow, with application to circular cylinder 04 p0733 A67-15841

Unsteady heat transfer in tubes resulting from changes in heat flow, gas mass flow rate and acoustic balance 04 p0733 A67-15844

Uniform flow of very high temperature radiating gas over semiminfinite flat plate 04 p0737 A67-15863

Radiation transfer effect on equilibrium temperature for laminar boundary layer flow of absorbing-emitting gas over flat plate [ASME PAPER 66-WA/HT-48] 04 p0739 A67-15940

Knudsen limiting law in free molecular gaseous flow in various capillaries with temperature gradient 04 p0739 A67-15948

Group classification by Cartan method of equations of one-dimensional plane wave gas flow 04 p0611 A67-15982

Turbulent subsonic gas jets, importance of Reynolds number and geometrical configuration of nozzle in determination of flow parameter 05 p0790 A67-16033

Difference approximation with second order accuracy of numerical solution for parabolic type equations 05 p0834 A67-16372

Numerical algorithm for supersonic gas flow past blunt bodies with shock wave separation, using Dorodnitsyn method of integral correlation 05 p0791 A67-16374

Friction stress and flow rate for rarefied constant density gas flow past semiminfinite plate treated by approximate diffusion model 05 p0792 A67-16995

Two-dimensional self-similar hot conducting gas outflow into vacuum, for power law variation of gas-vacuum interface temperature 05 p0793 A67-17007

Lagrange variational equation application to dynamic stability problems of plates in gas flow 05 p0923 A67-17188

Two-phase flow of gas over harmonically oscillating flat plate expressed in laminar

boundary layer terms, presenting liquid film thickness, heat transfer rate, skin friction, etc 05 p0793 A67-17338

Plane flow of radiating gas over semiminfinite flat plate, considering upstream effect when energy equation becomes elliptical 05 p0928 A67-17358

Self-similar problems concerning supersonic flows of gaseous fuel mixtures with detonation waves and slow combustion fronts past wedges and cones 06 p0935 A67-17725

Reacting gas flow in nozzle in one-dimensional formulation taking into account nonequilibrium course of chemical reactions 06 p0935 A67-17726

Difference scheme for calculating one-dimensional steady and unsteady Navier-Stokes equations for compressible gas flows 06 p0982 A67-17727

Oscillations of staggered plate cascade in plane subsonic gas flow, showing fluid compressibility effect on aerodynamic characteristics 06 p0935 A67-17729

Hypersonic flow past sphere by relaxing gas with internal degrees of freedom in nonequilibrium 06 p0935 A67-17731

Low rate gas flow meter noting sealing and controlling of piston, differential pressure meter and DC servoamplifier 06 p1000 A67-17753

Mathematical analysis of gas flow equations and shock wave structure in rarefied gas dynamics 06 p0983 A67-17784

Differential equations and mathematical models for gas flows with chemical activity and radiative effects, particularly effects of reentry and propulsion 06 p0983 A67-17785

Navier-Stokes equations for two-dimensional sonic flow of viscous heat-conducting gas assuming particle velocity close to sound speed, studying asymptotic pattern 06 p0937 A67-18031

Discontinuous solutions in supersonic reacting gas flows under nonequilibrium conditions 06 p0984 A67-18112

Perfect gases reacting mixture flows formulated for system of differential equations 06 p0955 A67-18114

Characteristics solution breakdown near leading frozen characteristic for piston induced flow and relaxing gas flow 06 p0984 A67-18128

Solid propellant burning rate, combustion gas influx, tube geometry and propellant and tube thermophysical properties [AIAA PAPER 67-102] 06 p1074 A67-18282

Weakly ionized gas flows about electrically biased bodies under effects of compressibility and electron energy [AIAA PAPER 67-100] 06 p1042 A67-18471

Heat transfer to catalytic and noncatalytic surfaces on sharp flat plate in shock tube gas flow for checking various laminar boundary layer theories [AIAA PAPER 67-163] 06 p0989 A67-18481

Stability of circular cylindrical shell in supersonic nonviscous conducting gas flow with unperturbed velocity and under magnetic field 06 p1106 A67-18622

Gas flow erosion effect on rough surfaces, noting pulsating pattern 06 p0991 A67-18815

Friction coefficient of compressive gas flow growth when negative pressure gradients in channel reach very high levels 06 p0991 A67-18816

Rational approximation method for calculating supersonic axisymmetric flow of perfect gas around given blunt body 06 p0943 A67-18846

Transverse oscillation stability in quasi-one-dimensional flow of conducting gas in magnetic field 07 p1227 A67-19119

Ranque effect, based on model of two-dimensional vortex flow of viscous thermoconductive gas, explains radial temperature distribution 07 p1268 A67-19352

Fluid mechanical model of electric arc balanced magnetically in gas flow, based on photographs showing arc must simulate solid body [AIAA PAPER 67-96] 07 p1240 A67-19437

Numerical solution for heat transfer to reversibly reacting gas in turbulent boundary on surface of rotating cylinder 07 p1268 A67-19575

Gas lens focusing of light beams, using highly transparent gas with weakly varying refractive index to guide coherent transmission with small losses 07 p1188 A67-19789

Potential double waves at interface between two-dimensional nonsteady barotropic gas flow and region of undisturbed gas 07 p1169 A67-20034

Effects of gases flowing in magnetic field analogous to galvanomagnetic Hall effect in conductors analyzed using oxygen 07 p1230 A67-20144

Simple method for determining deviation of supersonic or hypersonic plane parallel flow of inviscid gas caused by auxiliary jet in form of thin layer 07 p1127 A67-20208

Bibliography and subject index to two-phase gas-liquid flow literature 07 p1269 A67-20300

Hypersonic rarefied gas flow past plate with sharp leading edge, determining rarefaction effect on induced pressure distribution and value 08 p1278 A67-20924

Shocked gas flow duration in small diameter shock tubes at low initial pressures 08 p1321 A67-21119

Nuclear energy deposition effect on pressure pulse generation in flssioning gas flow through semiminfinite cylindrical tube analyzed by method of characteristics 08 p1322 A67-21121

Rayleigh problem of compressible viscous heat-conducting radiating gray gas flow near flat plate set impulsively in motion in own plane 08 p1324 A67-21392

Hydraulic analogy applied to axisymmetric nonideal compressible gas systems, considering water table simulation of axisymmetric rocket nozzle 08 p1324 A67-21519

Boundary layer at electrode and center of flow of plane MHD generator calculated numerically by one-dimensional theory for subsonic and supersonic velocities 09 p1443 A67-21808

Direct current electrical discharge investigated in gas flow in magnetic field perpendicular to flow 09 p1542 A67-21816

Electric arc behavior in argon gas flowing through magnetic field, measuring flow velocity, electron temperature, spatial distribution, etc 09 p1543 A67-21824

Unsteady flow of rarefied gas under finite pressure gradient when starting from rest, varying gradient in time until steady flow is obtained 09 p1487 A67-21847

Rarefied gas flow dynamic behavior during reaction with gas measuring device mounted on moving plant 09 p1487 A67-21896

Structural equations with variable coefficients for nonstationary one-dimensional gas flows, using Cartan method 09 p1487 A67-21912

Nonlinear flutter of simply supported rectangular plate under thermal compression in supersonic gas flow 09 p1574 A67-21915

Imaging properties of gas lens, discussing ray trajectory, ray matrix lens formula, optical transfer function, etc 09 p1498 A67-22083

Monte Carlo computer program for calculating molecular gas flow with axisymmetric vacuum structures, showing applications on pumping speed test domes and measuring apparatus for sticking coefficients 09 p1488 A67-22105

Density and direction of gas molecular flow through tube and aperture measured by ionization detector 09 p1489 A67-22107

Rarefied gas flow past sphere studied by multibeam interferometry of density profile and shock structures 09 p1438 A67-22216

Electric arc model in longitudinal gas flow through annular gap between rod cathode and cylindrical anode 09 p1546 A67-22314

Progress in aeronautical sciences, Volume 8 10 p1589 A67-22870

Aerodynamic problems of low density high speed flow of rarefied gases past submerged body 10 p1623 A67-22874

Rarefied gas flow analyzed through transport equation in gas kinetics using bimodal two-stream distribution functions, with application to Couette flow 10 p1624 A67-22914

Equation of relaxation hydrodynamics for diatomic perfect gas when rotational and translational degrees of freedom are in equilibrium and dissipation has not set in 10 p1590 A67-23024

Nozzle thrust increase through gas flow rotation noting dependence on nozzle length 10 p1590 A67-23027

Stability of radial motion of spherical gas

bubble in incompressible inviscid fluid under external pressure 10 p1624 A67-23028

Flow of ideal gas behind shock wave of finite amplitude analyzed, based on equation for one-dimensional adiabatic motion 10 p1624 A67-23033

Concentration field of components in turbulent gas jet determined from temperature field of mixture 10 p1624 A67-23038

Asymptotic properties of solutions to kinetic coefficient equation system, noting mass velocity dependence on time 10 p1625 A67-23042

Multiple wave interferometer application to determine parameters of rarefied gas flow past circular cylinder 10 p1625 A67-23043

Large scale expansion nozzle control by heterogeneous nucleation and mercury vapor and drop growth processes in nitrogen flow [AIAA PAPER 66-85] 10 p1733 A67-23125

Gas flow and shock wave velocity distribution in diaphragmed shock tube photographed analyzed at various opening rates 10 p1626 A67-23407

Stability of flow of ideal compressible gas at low magnetic Reynolds numbers in presence of longitudinal perturbations produced by crossed electromagnetic fields 11 p1832 A67-24026

Approximate iterative calculation of non-Newtonian supersonic gas flow past highly blunt bodies 11 p1741 A67-24156

Wind tunnel test program for simulation of gas-particle rocket exhaust plume, separated flow around nozzle and base recirculation [AIAA PAPER 66-767] 11 p1773 A67-24351

Calculation of weight flow and velocity for real gas, obtaining correction factor 11 p1779 A67-24355

Electrostatic probe and VHF microwave reflectometry study of nitrogen flow around models in hotshot wind tunnels, determining plasma sheath physical characteristics 11 p1839 A67-24445

Dissipation of magnetic fields at neutral lines in two-dimensional field with two intersecting shocks 11 p1862 A67-24498

Plane viscous problem of gas motion through weak straight line discontinuity of acceleration, noting formation of boundary layer 11 p1742 A67-24687

Space charge and eddy currents in ionized gas flow in MHD channel determined, showing effect of cold electrode boundary layer on electrical performance 11 p1746 A67-24874

Conducting gas flow in jet in front of electromagnetic accelerator nozzle exit region analyzed, giving jet shape and parameter distribution 11 p1842 A67-24951

Dynamic behavior model for gas shock wake motion and reflection in semiminfinite volume laterally bounded 11 p1782 A67-24954

Unsteady transonic flow of moving compressible gas filling half-space created by sudden rupture of membrane separating gas from vacuum 11 p1743 A67-24962

Electric arc combustion stability in gas flow, noting relation to weakly ionized plasma conductivity 12 p2033 A67-25314

Two-dimensional temperature field analyzed for laminar gas flow in interspace between parallel thermally thin plates 12 p2033 A67-25319

Equations in hodograph plane obtained for two-dimensional polytropic gas flow in presence of shock waves 12 p1892 A67-25443

Oscillations and stability of cylindrical shell in conducting gas flow in presence of magnetic field 12 p2021 A67-25581

Vortical interaction between free jet boundary layer and outer flow in separation area of hypersonic gas flow past body 12 p1892 A67-25671

Shock wave diffraction and reflection problems on faces of angle situated in nonstationary gas flow 12 p1928 A67-25672

Approximate method for calculating stagnation point laminar boundary layer equations taking into account chemical reactions in gas phase and surface of body 12 p1928 A67-25673

Combined multishaker and gas flow tests as part of reliability test program for Saturn V, S-1C pneumatic systems 12 p1923 A67-25706

Axially flowing gas through arc discharge, examining effect on I-V characteristic and

A-623

small angle of attack in subsonic gas flow and developing harmonic random vibrations studied for aerodynamic interference 17 p2792 A67-32903

Arc oscillation in argon in cross flow facility noting parameter ranges, electrode spacing effects, etc 17 p2906 A67-33037

Stabilized arc discharge characteristics using Elenbaas-Heller equation as basis for calculations 17 p2906 A67-33088

Hydrogen and helium lateral flow in collisionless exosphere calculated on model for various sinusoidal temperature and concentration variations over exobase surface 17 p2852 A67-33235

Fluid flow around magnetosphere boundary analyzed, noting geomagnetic field effect on hot plasma 17 p2853 A67-33252

Transonic plane gas flow equations with algebraic self-similar solutions used for analysis of flow in various nozzles 17 p2841 A67-33268

Radial mass flow effect on electric arcs, obtaining higher axis temperature and enthalpy densities 17 p2910 A67-33366

Ionization effect on external pressure determination for high velocity gas flows past plates and shells with flutter 18 p2981 A67-33424

Approximation solution of three-dimensional problems associated with slender wing motion in transonic gas flow with perturbations 18 p2981 A67-33535

Motion of small solid particles suspended in steady isotropic and locally uniform turbulent gas flow 18 p3025 A67-33626

Rarefied gas flow past sphere studied by multibeam interferometry of density profile and shock structures 18 p2982 A67-33755

Kinetics of coupled atomic recombination and vibrational de-excitation in continuously expanding gas flow 18 p3081 A67-33781

Exhaust gas recirculation for VTOL aircraft 18 p2985 A67-33916

[AIAA PAPER 67-439] 18 p2985 A67-33916

Perfect frictionless supersonic MHD gas flow model for shock wave control, noting nozzle geometry 18 p3088 A67-34123

Parameters of viscous supersonic compressible gas flow past corner, giving smooth coupling conditions for Navier-Stokes and boundary layer solutions 18 p3027 A67-34205

Channel flow transition to jet flow, discussing turbulence determination in flow boundary layer as Reynolds number function 18 p3028 A67-34218

Two-dimensional self-similar hot conducting gas outflow into vacuum, for power law variation of gas-vacuum interface temperature 18 p3028 A67-34269

Exhaust gases effect on satellites optical equipment calculated by determining propane attitude-control jet gas flow parameters 18 p3137 A67-34359

Energy dissipation in turbulent steady isotropic homogeneous gas flow with suspended solid particles 18 p3028 A67-34385

Electrical current passage across neutral or ionized argon flow in presence of accelerating or decelerating magnetic field 18 p3091 A67-34470

Rarefied gas cylindrical Couette flow noting Knudsen number, Bhatnagar-Gross-Krook model for Boltzmann equation, transport integrodifferential equation, etc 18 p3029 A67-34738

Energy flux in steady inhomogeneous turbulent gas flow with arbitrary mean velocity field, deriving velocity spectra and pressure-velocity correlation tensors 18 p3030 A67-34741

Glow-discharge siliocizing of refractory metals by unilow gas method in silicon tetrachloride vapor and hydrogen atmosphere 19 p3242 A67-34917

Energy balance of electric arcs in argon without and with superimposed gas flow investigated at various pressures [DVL-626] 19 p3280 A67-35146

Oscillations of electric arcs with superimposed gas flow in cylindrical nozzle and rectangular channel, determining critical Reynolds number 19 p3280 A67-35147

Ionized gas flow past cylinder and sphere, determining ionization and dissociation effect on displaced shock wave form 19 p3170 A67-35449

Heat transfer to catalytic and noncatalytic surfaces on sharp flat plate in shock tube

gas flow for checking various laminar boundary layer theories 19 p3211 A67-35739

Flow of steady compressible gas expressed in intrinsic relations to derive equations of rotational motions in Euclidean space 19 p3212 A67-35883

Gas flow around wing in presence of moving shock wave with variable gas parameters noting wave equation, velocity potential, etc 20 p3355 A67-36191

Approximate solution for subsonic gas flow, deriving approximation for Chaplygin function for use in boundary value problems 20 p3356 A67-36442

Electron beam probe for determination of local gas parameters in reentry simulation 20 p3445 A67-36588

Equations of one-dimensional aerothermodynamic flow of dissociating gas 20 p3420 A67-36599

Supersonic viscous gas flow around body of revolution involving perturbation damping, analyzing Navier-Stokes and heat transfer equations for flow chart 20 p3357 A67-36810

Correlation method for local and average friction coefficients of laminar and turbulent gas flow through smooth tubes 20 p3422 A67-36941

Theory of supersonic gas ejector with cylindrical mixing chamber, discussing low and high pressure gas flow 20 p3358 A67-37085

Surface pressure distribution on tubelattice cluster with transverse gas flow to determine aerodynamic characteristics 20 p3359 A67-37306

Unbounded laminar plate oscillations in bilateral potential ideal gas flow with uniform physical and mechanical parameters 20 p3542 A67-37539

Mach-Zehnder-Rozhdestvenskii interferometer design for training studies of supersonic and subsonic gas flows and anomalous dispersion 20 p3452 A67-37556

Three-dimensional boundary layer for gas flow past generatrix of cylinder of arbitrary transverse cross section 20 p3360 A67-37658

Stagnation-point flow of rarified gas, using linearized BGK model of Boltzmann equation with small Mach number 20 p3425 A67-37673

Langmuir probe current in weakly ionized gas flow, studying correlation between hydrodynamical turbulence and pressure fluctuations 20 p3503 A67-37674

One-dimensional nonstationary compressible gas flow studied with variational calculus, obtaining approximate analytical periodical solutions 20 p3360 A67-37678

Electrodeless slip-type MHD steady state acceleration of subsonic and supersonic high density gas flows for simulating reentry speeds and altitudes 21 p3607 A67-37778

Molecular gas flow through cylindrical tube, using wall pressure distribution to measure pump speed 21 p3610 A67-37823

Radiative flux and flux divergence for hot gas, considering spectral frequency, gas volume and spectral variation 21 p3730 A67-37825

Turbulent gas flow viscosity, thermoconductivity and friction coefficients in tube 21 p3611 A67-37912

Transverse oscillation stability in quasi-one-dimensional flow of conducting gas in magnetic field 21 p3664 A67-38184

Boundary layer of chemically reacting unstable gas flow along generatrix of body of revolution 21 p3584 A67-38423

Characteristics method to determine radiative energy losses of supersonic gas flows past blunt cones 21 p3564 A67-38424

Transient gas motions for various waves, analyzing motion equations and classifying integral curve fields 21 p3565 A67-38556

DC electric arc in superimposed gas flow behavior in arc tunnel, discussing electrode geometry [AIAA PAPER 67-675] 21 p3671 A67-38708

Panel flutter analysis of hinged closed circular cylindrical shell in supersonic gas flow, considering axial compression and structural damping 21 p3725 A67-38788

Equations in hodograph plane obtained for two-dimensional polytropic gas flow in presence of shock waves 21 p3613 A67-38816

Optimization analysis for axisymmetric rocket motor nozzle design based on assumptions for gas particle flow [AIAA PAPER 66-538] 21 p3565 A67-38875

Instantaneous heat transfer of thin tungsten wires in unsteady transverse airflow 21 p3733 A67-38913

Measurement of rapidly varying temperatures of gas flows with resistance thermometers taking into account heat transfer between heat probe and holders 21 p3630 A67-38914

Unsteady spherically symmetric gas flows with gas particle radial velocity proportional to distance from symmetry center 22 p3739 A67-39216

Steady state solutions for system of partial differential equations with two independent variables describing small perturbations of transonic gas flow near transition point 22 p3844 A67-39391

Ideal gas flow in spherically symmetric gravity field, considering radiant heat transfer and radiation pressure 22 p3880 A67-39407

Erodibility of solid propellants subjected to rapid flow of gas past burning surface 22 p3887 A67-39538

Kramers problem for rarefied gas flow, calculating slip coefficient for various collision frequency models, noting only slight model dependence 22 p3841 A67-39718

Ring laser use for measuring gas flow on ground and fuel and oxidizer flow in rockets 22 p3800 A67-39892

Radiating hydrogen two-dimensional equilibrium flow with variable absorption coefficient in axisymmetric nozzle analyzed in presence of gray radiation, examining transfer equation in diffusive approximation 22 p3785 A67-40013

Procedure for expanding parameter in asymptotic power series of any order to investigate viscous compressible supersonic gas flow past blunt body 22 p3740 A67-40014

Navier-Stokes equations asymptotic solutions used for gas flow laminar boundary layer calculation near corner of body where supersonic gas flow passes through low pressure region 22 p3785 A67-40018

Base pressure behind circular projection in Laval nozzles, measuring dependence on specific heat ratio at different Mach numbers by varying gas 22 p3741 A67-40021

Polytropic exponent along axis shown to approach adiabatic exponent at throat of convergent-divergent nozzle 22 p3742 A67-40112

Analytical prediction of cryogenic propellant venting effects on orbital vehicle dynamic behavior, emphasizing vent thrusting and gas impingement 22 p3906 A67-40165

Gas flow interaction with blunt body in transition flow regime between continuum and free molecule flow calculated using first collision model 22 p3743 A67-40175

Flame stabilization mechanism of homogeneous combustible fluid flow using air jets through peripheral slits to join main flow producing gasdynamic screens 22 p3921 A67-40455

Chromel-alumel thermocouple for high enthalpy gas flow temperature measurement, discussing design and measurement accuracy 23 p4081 A67-40569

Approximate solution for turbulent jet expansion in opposite gas flow, discussing hydraulic drag coefficient formula derivation 23 p3989 A67-40731

Carbon disulfide P-branch transitions with J equals 28 to 46 for 001-100 vibrational transition identified as laser lines in N-carbon disulfide gas system 23 p4011 A67-40789

Linear MHD flow characteristics variation with electric conductivity and gas flow rate changes, noting transverse magnetic flow variation with magnetic Reynolds number 23 p4033 A67-41284

Book on vacuum engineering covering space vacuum simulation, pressure measurement, gas flow and load, vacuum systems and technology 23 p4028 A67-41353

Solid propellant burning rate, combustion gas influx, tube geometry and propellant and tube thermophysical properties 23 p4084 A67-41723

Heat transfer between gas flows and solid /carbon/ surfaces, considering chemical reactions 24 p4252 A67-41935

Ionization gauge calibration by volume expansion, flow rate and multiple orifice techniques 24 p4153 A67-42048

First approximation analysis of rarefied

- hypersonic gas flow asymptotic properties
near surface and front edge of thin plate,
determining
macroparameters 24 p4142 A67-42272
Heat and mass transfer processes in
reacting laminar boundary layer flow with
steady high speed gas
flow 24 p4143 A67-42284
Design of gasdynamic shock tube
described with measuring apparatus
developed for studying ionized gas flows in
magnetic field 24 p4139 A67-42357
Erosion processes and outflow phenomena
in ZnS rocket fuel, noting aluminum
addition and gas leaks
effects 24 p4206 A67-42579
Hypervelocity gas flows at high
temperatures and pressures, discussing
generation of dense plasmas at extreme
temperature by implosion
waves 24 p4092 A67-42753
- AS-GAS INTERACTION**
Limited mutual solubility of gases above
critical point of least volatile
component 06 p1116 A67-18381
Collision broadening cross sections and
effect of resonant interactions on gas-laser
transitions 12 p1953 A67-26196
Potential model for helium-hydrogen
interaction in thermal
diffusion 13 p2161 A67-27729
Shock tube tests with cold argon and
heated helium to determine heated driver
gas effect on effect on shock tube
performance 14 p2294 A67-29053
Boundary condition problem at interface
between immiscible fluids investigated for
nonequilibrium
thermodynamics 21 p3733 A67-39065
- AS GENERATOR**
Rapid gas compression technique to
produce simultaneous values of pressure and
temperature much higher than conventional
techniques 04 p0611 A67-15946
Hybrid rocket operation as gas generator,
surveying advantages and disadvantages for
fuel or oxidizer
pressurization 08 p1410 A67-20802
Similarity parameters for gas generators
obtained from equations governing gas-
stream ejection 15 p2423 A67-30080
Open-cycle gas generator as power supply
source for MHD generators, noting reduction
of wall effects 17 p2802 A67-32179
ADAM II /air deflection and modulation/
propulsion system and application to long
tube vertical propulsive wing aircraft
configurations 17 p2929 A67-32993
SAE PAPER 670353]
M-1 engine system technology items noting
thrust chamber assembly, gas generator, fuel
turbopump, etc
AIAA PAPER 67-520] 18 p3115 A67-33983
Solid propellant gas generator power
systems for normal and emergency space
operations 20 p3533 A67-36601
Cylindrical solid state oxygen generators,
discussing manual and remote electrical
activation 23 p3968 A67-41621
Compact portable high purity H generator
using liquid ammonia for indirect method H-
O fuel cell 24 p4106 A67-42524
- AS GENERATOR ENGINE**
Computer-simulated mathematical model of
thermal environmental effects on expulsion
system design parameters for liquid-
propellant gas-generator rocket engine
[AIAA PAPER 66-686] 02 p0303 A67-11944
High density moisture-proof noncrystalline
family of gas generator propellants,
surveying burning rates, physical properties
and application 15 p2544 A67-29980
Cool burning smokeless propellants for gas
generator applications and low signature
missiles evaluated against
criteria 15 p2544 A67-29981
Control rockets covering very low thrust
operation, gas generation problems, gas
expansion, etc 20 p3516 A67-36881
High density moisture-proof noncrystalline
family of gas generator propellants,
surveying burning rates, physical properties
and application 24 p4207 A67-42921
- AS GUN**
Implosive collapse of liners containing gas
to transfer chemical energy of explosive to
kinetic and internal energy of gas
[AIAA PAPER 67-178] 06 p1118 A67-18485
Design for light-gas gun with light piston
by successive parameter computation of
various parts 16 p2655 A67-31125
- Light gas gun model launching technique
with advantages of aerodynamic and
mechanical methods of sabot
stripping 23 p3988 A67-41751
- GAS HEATING**
Heat transfer to laminar flow of radiation
absorbing-emitting fluid across isothermal
plate 04 p0737 A67-15868
Laser radiation effect on heating process
and gas dynamic motion of finite
transparent gas and motionless cold gas at
vacuum interface 05 p0927 A67-17008
Mass spectrometric observation of ions
formed during shock wave heating of
gaseous krypton and xenon at 3600 to 7800
degrees K 05 p0795 A67-17440
Photometric measurements on deviations
from equilibrium state in burnt gases of
laminar premixed shielded flames at
atmospheric pressure
[AIAA PAPER 67-9] 06 p1072 A67-18345
Possible thermal histories of intergalactic
gas 11 p1860 A67-24485
Thermal electrode boundary layer for
shock wave ionized air ohmic heating in
discharge chamber, noting Joule heat
consumption effect 12 p1975 A67-25894
Thermal propagation in gases studied
through heat transfer equation resulting
from Fourier law 17 p2968 A67-32221
Arc-image furnace for direct gas heating
at high temperature by concentrated
radiation studies and efficient cavity-type
receiver development 17 p2834 A67-32696
Laser radiation effect on heating process
and gas dynamic motion of finite
transparent gas and motionless cold gas at
vacuum interface 18 p3160 A67-34270
Pulsed-discharge-current interruption in
constricting aperture by pinch effect, loss of
ions, gas heating and oscillation
generation 19 p3278 A67-35127
- GAS INJECTION**
Performance and characteristics of valve
for pulsed gas injection into working volume
of coaxial plasma
accelerator 01 p0119 A67-10136
Penetration of gaseous jets injected into
supersonic stream treated by solid body
drag model, noting application to hypersonic
ramjet combustion 02 p0232 A67-11935
Wind tunnel experiments extending range
of data published in 1964 on flow field
associated with sonic injection of
gas 04 p0604 A67-14831
Hydrogen and helium injection effect on
local heat transfer to porous surface from
dissociated turbulent boundary layer
[ASME PAPER 66-WA/HT-24] 04 p0725 A67-15444
Asymptotic flow theory laws of friction
and heat transfer in turbulent boundary
layer 04 p0610 A67-15838
Surface property effects on effectiveness
of mass transfer cooling in laminar boundary
layers with hydrogen injected into free
stream of nitrogen or carbon
dioxide 04 p0733 A67-15840
Turbulent heat transfer at semipermeable
surface during foreign gas injection, solving
energy equation 05 p0927 A67-17000
Current carrier behavior during field and
diffusion injection of electron hole plasma
into semiconductor 06 p1049 A67-17865
Flow field associated with tangential slot
gas injection in supersonic flow, presenting
turbulent mixing zone and stability and
spark shadowgraphs 06 p0987 A67-18300
Skin friction under mass injection on
porous flat plate in supersonic turbulent
flow 06 p0987 A67-18341
Variable laminar boundary layer equations
for air flows over flat plate with injection
of foreign gases through solid
surface 06 p1116 A67-18380
Fuel injection parameters effects on
mixing of gaseous hydrogen fuel with
supersonic air stream for hypersonic ramjet,
determining turbulent diffusion
coefficient 06 p1117 A67-18387
Hydrogen or nitrogen gas injection at
various Mach numbers from nozzle in flat
plate into Mach 2.72 free air stream
[AIAA PAPER 67-225] 06 p0940 A67-18444
Two-dimensional adiabatic laminar
separated regions in supersonic flow,
examining effects of blowing and suction at
wall
- [AIAA PAPER 67-192] 06 p0988 A67-18459
Surface mass addition into turbulent
boundary layer for attaining equilibrium
velocity profiles, determining development
from start of injection 12 p1930 A67-25929
Laminar Couette flow analyzed for gas
injection effects on heat transfer to surface,
temperature profile and convection
interaction with radiation 15 p2578 A67-29129
Coaxial plasma gun for plasmoids showing
higher mean energy when gas admission is
closer to plasma source
end 15 p2525 A67-29252
Stagnation region foreign gas injection in
low Reynolds number hypersonic shock layer
flow 16 p2591 A67-30936
Lateral convex curvature and helium
surface injection effect on turbulent wall
boundary layer characteristics and skin
friction 16 p2659 A67-30952
Time lag effect on dynamic stability
determined, using wind tunnel tests with 10
degree cone as test body simulating ablation
process by gas injection into boundary layer
[AIAA PAPER 66-757] 17 p2792 A67-33004
Ion source using Penning discharge used
to inject hydrogen ions into magnetic
field 19 p3195 A67-35599
Binary laminar boundary layer equations
with second order transverse curvature for
hypersonic flow with mass injection of
foreign gases into air 19 p3211 A67-35737
Theory of supersonic gas ejector with
cylindrical mixing chamber, discussing low
and high pressure gas
flow 20 p3358 A67-37085
Hydrogen or nitrogen gas injection at
various Mach numbers from nozzle in flat
plate into Mach 2.72 free air
stream 21 p3610 A67-37800
Laminar boundary layer gas flows over
slender bodies with massive blowing,
discussing integral method solution and
theoretical model including pressure
effect 22 p3739 A67-39935
Two-dimensional adiabatic laminar
separated regions in supersonic flow,
examining effects of blowing and suction at
wall
[AIAA PAPER 67-192] 22 p3786 A67-40096
Optimum blowing angle of gas into
supersonic nozzle determined by supersonic
wind tunnel investigation of flow
interaction 22 p3743 A67-40452
Absorption times for gases injected into
mammalian eye anterior
chamber 23 p3950 A67-41536
Skin friction under mass injection on
porous flat plate in supersonic turbulent
flow
[AIAA PAPER 67-194] 23 p3991 A67-41713
Integral solution for massive blowing on
slender hypersonic wedges and cones in
laminar flow, assuming homogeneous
nonreacting perfect gas
mixtures 23 p3932 A67-41743
High speed internal flow past cone with
large wall injection velocities, calculating
pressure of outer flow using contact surface
initial slope as parameter 24 p4092 A67-42398
Nonairbreathing internal combustion
engines injector configurations, noting power
supply and lunar surface vehicle
applications 24 p4107 A67-42533
- GAS JET**
Mass transfer and hydrodynamics of gas
jet injection into liquid surface, deriving
empirical equations for hollow truncated
point formed around injection
point 04 p0727 A67-15754
Deflection angle of supersonic gas flow
with oblique shock wave and heat input in
wake, choosing minimum entropy variation
as measure of system
optimality 04 p0550 A67-15898
Free molecular expansion into vacuum of
pulsed and steady gas flow from circular
orifice 06 p0985 A67-18190
Hydrogen or nitrogen gas injection at
various Mach numbers from nozzle in flat
plate into Mach 2.72 free air stream
[AIAA PAPER 67-225] 06 p0940 A67-18444
Switching of supersonic gas jets in
convergent-divergent duct by atmospheric
venting, using phenomena of boundary layer
separation 08 p1279 A67-20436
Stabilized Skylark rocket using N-gas jet
system, solar sensors and magnetometer to
obtain three-axis control 08 p1408 A67-20537
Electric conductivity of high temperature
nitrogen jet as affected by impurity

particles of potassium, metals and metal oxides 09 p1547 A67-22321

Supersonic flow of ideal thermodynamically perfect gas from nozzle into medium at rest 10 p1591 A67-23037

Model for gas particle exhaust flow from under expanded nozzles 10 p1592 A67-23154

Gas jet expansion near crossed axisymmetric channel, reducing problem to solution of Laplace equation for second-kind boundary conditions 11 p1779 A67-24321

Integral relation technique for approximate solution of dynamic and thermal expansion of laminar radial slot gas jets along plane wall 11 p1779 A67-24322

Tailpipe length effect on flame stability in high velocity propane-air stream with bluff body or reverse jet flame holders [ASME PAPER 67-GT-4] 11 p1853 A67-24792

Jet flame stabilization and audible noise reduction using ultrasonic acoustic energy 11 p1883 A67-24842

Conducting gas flow in jet in front of electromagnetic accelerator nozzle exit region analyzed, giving jet shape and parameter distribution 11 p1842 A67-24951

Boundary layer of principal region of turbulent nonisothermal plane-parallel jet of real gas 13 p2095 A67-26885

Laminar motion equation for conducting gas jet expansion along plane wall in presence of transverse magnetic field solved in series form 13 p2168 A67-27304

Axial and radial velocity distributions in axisymmetric free jets of pure gases and binary gas mixtures, noting molecular beam production 14 p2301 A67-28183

Three-dimensional detached flow patterns forming near secondary jet injected into supersonic flow 18 p3027 A67-34207

MHD jet converter research, reviewing basic equations, AC/DC generators and thermodynamic/ electric problems 19 p3268 A67-35062

Argon arc plasma generator with film cooled anode for producing stable high temperature gas jet [ASME PAPER 67-HT-72] 20 p3498 A67-36752

Hydrogen or nitrogen gas injection at various Mach numbers from nozzle in flat plate into Mach 2.72 free air stream 21 p3610 A67-37800

Soviet papers on turbulent jets of air, plasma and real gas 23 p3988 A67-40727

Real gas jet equations of motion, energy and continuity derived, transformed and solved for mixing region, discussing approximate state equation construction 23 p3989 A67-40729

Strong traveling transverse acoustic modes generated by rotating gas jet in cylindrical cavity 23 p3993 A67-41763

Irrational gas jet impinging on and depressing infinite liquid surface, discussing streamlines and rippling 24 p4144 A67-42585

GAS LASER

High current discharge effect on magnetically confined argon laser 01 p0086 A67-10012

Optical surface roughness measurement using coherent radiation produced by helium-neon laser sigma-polarized at 6328 angstroms 01 p0020 A67-10020

Nonlinear attenuation or gain characteristics of Doppler-broadened atomic resonance involving levels with small splittings, noting mode coupling of gas laser 01 p0087 A67-10152

Frequency stability of double beam ammonia laser with thermostatic quartz resonators on 3-2 line 01 p0088 A67-10247

Microwave modulation of helium-neon laser intensity studied as function of temperature and electron density 01 p0088 A67-10260

Decay cross section of pumped metastable He atoms in HeNe laser 01 p0090 A67-10511

Ne-He laser output dependence on pressure and nonexcited atom concentration 01 p0090 A67-10512

Radiation from high energy level transitions excited in He-Ne laser during optical pumping with He lamp 01 p0090 A67-10513

Electron temperature in electric discharge applied to argon ion laser 01 p0090 A67-10550

Inexpensive carbon dioxide molecular gas laser using plano-concave eyeglass lenses 01 p0090 A67-10827

Extensometer for measuring small changes of specimen on tensile testing vacuum

furnace at high temperatures, using CW gas laser as light source 01 p0070 A67-11036

Electron temperature in electric discharge applied to argon ion laser 01 p0091 A67-11058

Laser excited electronic Raman spectrum of trivalent Eu ion doped YGa garnet 01 p0091 A67-11084

Magnetically compressed plasma as high intensity source of near UV and visible radiation experimentally studied in dynamic pinch 02 p0272 A67-11880

Radiative transition probabilities between laser vibrational levels of carbon dioxide, noting relaxation time and dipole moment 02 p0252 A67-11891

Self-locking modes in argon ion laser, observing subnanosecond pulsation of laser output with wideband photomultiplier 02 p0253 A67-12503

Nitric oxide molecular laser obtained by dissociation of NO-Cl in pulsed electrical discharge 02 p0253 A67-12510

Hologram copying method using gas laser as light source 02 p0246 A67-12513

Continuously variable optical delay line using acoustic waves to diffract and frequency shift portion of argon ion laser beam 02 p0253 A67-12517

Optical nonlinearities due to conduction band electrons in InAs, InSb, GaAs and PbTe studied, using Q-switched carbon dioxide laser radiation 02 p0254 A67-12524

Optical mixing due to conduction band electrons in semiconductor 02 p0254 A67-12525

Regenerative radiation from neon line in He-Ne laser, using spherical reflectors in resonator 03 p0434 A67-13096

Continuous helium-neon laser used to obtain short intense light pulses and to study kinetics of autophotocatalytic emission of high resistivity silicon 03 p0436 A67-13142

Oscillation types for gas-laser semiconcentric resonator 03 p0437 A67-13286

Population inversion of upper laser level of carbon dioxide molecules, noting electron-molecule collision and effect of neon addition 03 p0437 A67-13297

Parametric amplification of far IR in Te crystal pumped by carbon dioxide laser 03 p0437 A67-13572

Coupling of pulse powers in TEM of up to 80 mw from He-Ne laser at 6328 angstroms 03 p0437 A67-13678

High power visible CW gas laser beam generation, modulation and deflection for application to visual display technology [SMPE PREPRINT 100-6] 03 p0438 A67-13801

CW He-Ne laser compared with mercury arc source, obtaining Raman spectra of carbon tetrachloride by three methods of excitation 03 p0438 A67-13912

Performance characteristics for pulse type Ar laser with external interferential system of quasi-confocal spherical mirrors 03 p0438 A67-14188

Characteristics of pulsed laser action in He-Ne and He-Ar mixtures at pressures above 200 mm Hg 03 p0438 A67-14189

Radiative power amplification of He-Ne laser with nearly confocal resonators 03 p0438 A67-14190

Effect of Doppler and impact line broadening of spectral characteristics of gas laser, noting standing monochromatic wave saturation 03 p0439 A67-14197

Traveling waves interaction in gas laser, explaining forcing-of-oscillations and traveling wave suppression effect 03 p0439 A67-14371

Self-modulation characteristics of carbon dioxide laser and use in measuring detector response and atmospheric propagation characteristics 03 p0439 A67-14399

Population inversion of upper laser level of carbon dioxide molecules, noting electron-molecule collision and effect of neon addition 04 p0631 A67-14722

Construction methods of DC operated He/Ne laser tubes using optical contact bonds 04 p0631 A67-14763

Oblique modes and energy of gas laser beam 04 p0632 A67-14913

Emission from tellurium single crystal pumped by two waves from carbon dioxide laser 04 p0632 A67-14914

Phase and amplitude fluctuation of gas and solid state lasers, accounting for noise caused by pumping, incoherent decay, lattice

vibrations and atomic collisions 04 p0632 A67-14949

Laser action delay due to plasma-tube-surface decomposition resulting from bombardment by neon ions 04 p0633 A67-15110

Single mode output power modulation analysis of saturation and gain of gas lasers and effects of excitation density modulation and resonator Q modulation 04 p0633 A67-15111

Magneto-optical modulation of IR emission of He-Ne gas laser 04 p0633 A67-15139

Gas laser spectroscopic analysis of hyperfine structure, paramagnetic properties, radiative lifetimes and Doppler broadened transition saturation behavior of excited states of Xe 129 04 p0661 A67-15462

Sum and difference frequency mixing of visible and IR gas laser light in GaP at near reststrahl frequencies and relationship to spontaneous Raman scattering 04 p0682 A67-15464

Vaporization of thin metallic films with focused laser beam, comparing theoretical and experimental results prepared by using pulsed high pressure helium-neon laser 04 p0630 A67-15478

Polarization of light scattered from He-Ne laser beam, applying quantum theory to formula for depolarization ratio 04 p0634 A67-15624

Inertial sensors, discussing magnetic resonance and superconductor gyroscopes, ring lasers, fluid dynamical devices, electrostatic gyroscopes, etc 05 p0806 A67-16517

Fission or radioisotopic nuclear radiation applied to laser pumping, discussing forms, sources, power, solid state and molecular gas lasers, energy transfer, optical fluorescence and cut-off phenomenon 05 p0814 A67-16547

Electron collision rate and density calculations for He-Ne laser plasma 05 p0815 A67-16598

Tube diameter influence on output power and efficiency of gas laser 05 p0816 A67-16629

Transient and steady state IR emission from low-lying vibrational levels of carbon dioxide in laser systems, using DC discharge 05 p0816 A67-16630

Excitation and relaxation mechanisms for closed molecular gas laser 05 p0816 A67-16631

Gas laser pumped microwave emission for producing controlled excited state population for RF spectroscopy of neon 05 p0817 A67-16638

Doppler and impact broadening of spectral lines and pressure effects on power output of gas laser 05 p0818 A67-16643

Lamb self-consistent theory and rate equation approximation study of magnetic depolarization of vapor and polarization of monomode gas laser in magnetic field 05 p0818 A67-16644

Double resonance effects extended to case of stimulated emission in excited states of neon, using gas laser in transverse DC magnetic field 05 p0818 A67-16645

Intracavity time-varying perturbation of losses in gas laser using diamagnetic Faraday effect in glasses analyzed in connection with output intensity 05 p0818 A67-16646

Pulsed gas discharge lasers noting required energy level for maximum efficiency, experimental techniques and results 05 p0819 A67-16650

Argon discharge characteristics used in continuous action ion laser for analysis of inversion production mechanism 05 p0823 A67-16680

Tunable Raman laser obtained by electron mobility subjected to magnetic field, noting threshold pump power 05 p0823 A67-16684

Single mode 6328 angstrom units He-Ne laser having single frequency power output of 50 mwatt stabilized by feedback system whose output is neither amplitude nor frequency modulated 05 p0823 A67-16685

Single mode output power modulation study of saturation and gain of gas laser 05 p0823 A67-16686

Enhanced lasing of high pressure He-Ne laser, commenting on delay time of light pulse emitting through walls of discharge tube from start of exciting pulse 05 p0823 A67-16687

Stimulated emission in triplet system of nitrogen molecule produced by pulsed laser

- discharge, identifying lines and interpreting intensity distribution in rotational band spectrum 05 p0824 A67-16785
- Onset of oscillation in He-Ne laser analyzed using Lamb theory, obtaining time constant value for population of lower laser level 05 p0824 A67-16821
- Internal modulation of IR gas laser using cadmium sulfide or selenide single crystals 05 p0824 A67-16914
- Amplitude of LF oscillations in He-Ne laser 05 p0825 A67-16948
- Gaseous laser output expressed in single or two-line oscillations as function of pumping rates and transition probabilities, considering concept of equivalent network 05 p0825 A67-16979
- Transient behavior of He-Ne lasers under pulsed HF excitation, discussing rate equations representing atomic population density and photon 05 p0825 A67-16980
- Spatially resolved He-Ne laser heterodyne measurements of electron number densities in weakly ionized Ar pulsed discharges 05 p0856 A67-17272
- Double probe and microwave resonance measurements of gas additives effect on radial variation of electron temperature and density with partial pressures in carbon dioxide-nitrogen-hellum gas laser 05 p0826 A67-17274
- Suppression of undesirable axial modes in gas laser oscillating at several frequencies obtained by filling with active gas mixture each of two coupled Fabry-Perot type resonators 05 p0826 A67-17326
- Flizeau fringes produced in laser illuminated Fabry-Perot interferometer to obtain concentration profiles in turbulent and laminar jets 05 p0794 A67-17371
- Inelastic scattering of carbon dioxide laser radiation by mobile Landau-level electrons in n-InSb 06 p1009 A67-17723
- Nonlinear medium anisotropy and saturation effects on orientation of polarization ellipse of gas laser mode 06 p1010 A67-17823
- Electro-optic intra-cavity color switching in krypton ion Fabry-Perot laser 06 p1010 A67-17888
- High power carbon dioxide laser heterodyne detection of beats and linewidth measurements 06 p1010 A67-17891
- He-Ne laser frequency stabilization using four automatic frequency control /AFC/ systems 06 p1010 A67-17965
- Radio electronics, discussing quantum electronics, lasers, microwave devices and technology, plasma physics, etc 06 p0968 A67-18072
- Gas laser behavior in magnetic field, analyzing data on magnetic effect, Zeeman effect and microwave pumping 06 p1011 A67-18168
- Spherical coupler for fastening mirrors and plane-parallel plates at Brewster angle in gas laser 06 p1011 A67-18394
- Polarization characteristics of ionized argon laser in magnetic field 06 p1011 A67-18542
- Optical maser oscillation lines in HF discharge in mixture of Ar and Br 06 p1011 A67-18545
- Resonator Q-modulation technique observation of central dip tuning in modulated power output of gas laser with moving mirror 06 p1011 A67-18758
- Pressure dependence of output power of He-Ne laser on amplitude of periodic high voltage excitation pulses 06 p1012 A67-18784
- Laser line-scanning photographic system, discussing possible extraterrestrial applications 06 p1006 A67-19011
- Lasers and RCA 07 p1193 A67-19080
- Charged particles for lasing, discussing manufacture of argon laser 07 p1194 A67-19083
- Gas laser as source of illumination, with attention to origin of aventurine spots on screen 07 p1195 A67-19142
- Rate equations for gas discharge modulation of He-Ne laser 07 p1195 A67-19492
- Tuning of gas laser resonator 07 p1195 A67-19505
- Relative intensities and cascade transition ratio in CW Ar II laser near 4103.9 angstroms 07 p1195 A67-19560
- Axial magnetic field effect on Ne-He laser power output operating in regime of simultaneous generation of 3.39 and 0.6328 micron lines 07 p1196 A67-19601
- Traveling wave excitation of high power nitrogen and neon lasers with velocity matching that of stimulated emission 07 p1196 A67-20093
- Time behavior of pulsed water vapor laser, noting spiking from far IR emission lines 07 p1197 A67-20095
- Photon counting distributions and intensity fluctuations of modulated laser beams 07 p1197 A67-20125
- Optical range gated filter for detecting moving targets in clutter background, using laser beam for application to MTI radar 08 p1293 A67-20687
- Longitudinal mode oscillations of gas laser when resonator length changes with time, noting polarization and amplitude change related to growth of new oscillation 08 p1338 A67-21314
- Excitation cross section of states of Ne 2, Ar 2 and Kr 2 by electron collision 08 p1339 A67-21376
- Frequency stability of He-Ne lasers analyzed by heterodyning two laser resonators 09 p1509 A67-21558
- Spectral resolution improvement by photoelectric Raman spectrometer with He-Ne laser excitation, noting results for carbon disulfide, carbon tetrachloride and azobenzene 09 p1492 A67-21561
- Hellum-neon CW laser oscillation at 1.523 microns observed in high velocity gas flow system, using rapid mixing of metastable helium atoms with initially unexcited neon 09 p1510 A67-21568
- Scattering of coherent and incoherent light compared, using CW He-Ne gas laser sources 09 p1510 A67-21600
- Q-switched carbon dioxide laser with internal concave rotating mirror, discussing detection with pyroelectric thermal detector 09 p1511 A67-21769
- Hologram fixation by Gabor single beam method, using gas laser as light source 09 p1511 A67-21919
- Zeeman effect in He-Ne gas laser operating in longitudinal magnetic field, noting dependence of frequency difference on field strength 09 p1512 A67-21920
- Gas laser measurement of electron density in xenon pulse discharge 09 p1512 A67-21922
- Population inversion of neon levels in He-Ne microwave discharge as affected by pressure and power scattered by unit discharge volume 09 p1512 A67-21924
- Stimulated emission in negative luminescence region of He-Ne glow discharge, noting effect of pressure and volt current 09 p1512 A67-21925
- Adjustment of compound gas laser resonator provides increase of stimulated emission output without lengthening resonator 09 p1512 A67-21985
- Fluctuation measurements in amplitude of oscillation of ammonia beam maser 09 p1513 A67-22043
- Wave synchronization in gas laser with ring resonator cavity 09 p1513 A67-22063
- Atomic collisions, excitation transfer processes and energy level transition probabilities in plasma of gas lasers 09 p1513 A67-22067
- Gas laser frequency and emitted power dependence on resonator tuning 09 p1513 A67-22070
- Small size CW He-Ne laser pumped by resonant cavity, examining current-voltage characteristics and current dependence of output power 09 p1513 A67-22170
- Internally modulated gas laser at 100 and 4000 MHz, describing electromagnetic field in Fabry-Perot resonator in terms of natural oscillation modes and coupling 09 p1514 A67-22269
- Gas laser dynamic behavior, discussing internal modulation, mode locking, noise and perturbation modes 09 p1515 A67-22431
- Self-locking of He-Ne lasers at various mirror separations by controlling oscillation frequency with intracavity modulator 09 p1516 A67-22432
- Light emission by gas under action of intense laser radiation studied by high speed high sensitivity photomultiplier 09 p1516 A67-22583
- Multiple holographic recording of alphanumeric characters on small area of photographic plate 10 p1652 A67-22700
- Hologram recording and reconstruction through two and three primary colors derived from gas laser 10 p1653 A67-22749
- Rate equation solution for density of excited atoms in He-Ne discharge for steady state 10 p1663 A67-22893
- Single frequency light from argon FM laser with external lithium niobate modulator, discussing overall conversion efficiency and distortion reduction 10 p1664 A67-22906
- Relaxation rate influence on power generation of gas laser and on magnitude of inverse population 10 p1664 A67-23335
- Excitation cross section of upper laser levels in ionized argon by electron collision with ground state neutral atoms measured, using incoherent light technique 10 p1665 A67-23382
- Near field power density incident on eyes due to reflection from CW laser reduced by optical lens and shutter rearrangement 10 p1665 A67-23415
- Holography /recording light in three dimensions/, noting virtual and real images and color production 10 p1657 A67-23623
- Pulsed ruby laser source for holography compared to He-Ne gas laser 10 p1657 A67-23625
- Thermal plasma device /Q machine/ design objectives and proposed features, noting association with normal mode oscillations in gas laser 11 p1830 A67-24006
- Argon laser design for long life noting ion sputtering and gas clean-up 11 p1800 A67-24242
- Light velocity measurement using hollow cathode discharge in Ne-H laser 11 p1818 A67-24479
- Frequency stabilization of gas laser by discriminant, using discharge tube with gain profile split by AC magnetic field 11 p1801 A67-24664
- Optical transient nutation effect in carbon dioxide laser 11 p1802 A67-24829
- Absolute frequency measurement and spectroscopy of gas laser transitions in far IR, analyzing Zeeman effect 11 p1802 A67-24830
- Detection and measurement of mm wave difference frequency between two near laser lines, using optical heterodyne 11 p1803 A67-24832
- Ion radial drift velocity in argon ion laser discharge tube 11 p1803 A67-24931
- Single mode He-Ne laser, noting discontinuities in power output and inhomogeneous nature of gain curve 12 p1951 A67-25147
- Magneto-optical modulation of IR emission of He-Ne gas laser 12 p1951 A67-25162
- Procedure and auxiliary equipment used to focus optical elements of gas laser 12 p1952 A67-25364
- Periodic variations of oscillation modes in He-Ne laser as result of resonator length increase 12 p1952 A67-25437
- Hypersound propagation velocity in toluene cyclohexane, acetic acid, water, etc, determined at 6328 angstrom from He-Ne laser analysis of structure of Rayleigh scattering 12 p1953 A67-25446
- Gaseous laser oscillations in Fabry-Perot resonator with corner-cube prism noting alignment characteristics 12 p1953 A67-25454
- Ionized multiwatt argon lasers, discussing relation between output power and discharge current, gas pressure, magnetic field and tube bore size 12 p1953 A67-26159
- Collision broadening cross sections and effect of resonant interactions on gas-laser transitions 12 p1953 A67-26196
- Polarization phenomena in gas laser in presence of magnetic field 12 p1954 A67-26236
- Negative-ion gas laser with thermal excitation 13 p2125 A67-26386
- Powerful gas lasers using carbon dioxide noting oscillation level lifetime, inversion mechanism, temperature effect, etc 13 p2125 A67-26388
- Carbon dioxide laser history, development stages, performance and applications 13 p2125 A67-26389
- Coupling of laser optical modes by intracavity time varying perturbation 13 p2125 A67-26407
- Pulsed UV laser using nitrogen noting synchronization characteristics, stability, peak power, etc 13 p2126 A67-26700
- Combination tones generation by interaction of orthogonal gas laser

oscillations, showing dependence on polarization states and primary oscillations 13 p2126 A67-27015

Transients in He-Ne plasma laser operating at 0.6328 13 p2128 A67-27088

micrometers 13 p2128 A67-27088

Pulsed neon laser at 5401 13 p2128 A67-27089

angstroms 13 p2128 A67-27089

Heterodyne signal amplitude dependence on optical path length difference for oscillating axial modes in multimode gas laser 13 p2128 A67-27346

Spatially modulated laser recording parameters, emphasizing beam intensity ratio to signal beam, offset angle film transfer characteristic and recording wavelength 13 p2129 A67-27351

Gas laser properties, noting usefulness in physics, chemistry and optics 13 p2129 A67-27364

Gain narrowing and saturation broadening of Doppler broadened neon line in Zeeman scanned laser amplifier 13 p2129 A67-27485

Direct modulation of He-Ne laser with RF excitation, noting kinetic equations of transition processes 14 p2329 A67-27772

Book on gas laser origin, development, properties and construction 14 p2329 A67-27799

Electromagnetic radiation equilibrium in gas lasers, studying effect of cavity length variations on linewidth 14 p2329 A67-27952

Semiconductor integrated circuit slices interconnection processes, using gas laser for thermal micromachining 14 p2281 A67-28023

Hologram fixation by Gabor single beam method, using gas laser as light source 14 p2329 A67-28248

Zeeman effect in Ne-He gas laser operating in longitudinal magnetic field, noting dependence of frequency difference on field strength 14 p2330 A67-28249

Gas laser measurement of electron density in xenon pulse discharge 14 p2330 A67-28251

Population inversion of neon levels in He-Ne microwave discharge as affected by pressure and power scattered by unit discharge volume 14 p2330 A67-28253

Nomogram to predict SNR for certain laser setups 14 p2330 A67-28289

Mode-locked laser traveling pulses proved experimentally to be 180 degree pulses 14 p2330 A67-28292

Laser measurements and standards of energy, power, attenuation and frequency stability, using pulsed ruby and gas lasers as radiation source 14 p2319 A67-28392

CW solid state lasers, considering principal laser crystals 14 p2330 A67-28470

Mechanisms operating in lasers employing optical transitions of molecules in fluids 14 p2331 A67-28471

Gas laser radiation applied to light transmittance measurement of heavily doped gallium arsenide in absorption region by free carriers 14 p2368 A67-28528

Effect of Doppler and impact line broadening of spectral characteristics of gas laser, noting standing monochromatic wave saturation 14 p2331 A67-28542

Optical reconstruction from sampled holograms made with sound waves 14 p2320 A67-28602

Power spectrum and difference frequency spectrum for energy exchange oscillations between three modes of He-Ne laser 14 p2331 A67-28603

Laser applications to satellite tracking, orbit calculation and atmospheric studies 14 p2331 A67-28608

Gas laser mode interaction in Zeeman laser, investigating transition in axial magnetic field 14 p2331 A67-28715

Gas laser quantum theory, deriving motion equation for radiation-density matrix 14 p2332 A67-28716

Function of symmetrical gas-laser resonator analyzed to determine angle of divergence of laser beams generated by various transverse electromagnetic wave modes 14 p2332 A67-28854

Interaction between oppositely moving traveling waves in helium-neon laser with annular resonator 14 p2332 A67-28856

Single frequency, far IR and high power gas laser design and manufacturing 14 p2333 A67-28970

Optimum energy coupling of multimode gas laser determined experimentally 14 p2333 A67-28971

800 mm and 1265 mm optical resonator He-Ne lasers, obtaining maximum output power and application as Raman spectroscopy light source 14 p2333 A67-28972

Gain of flowing carbon dioxide laser systems, noting extent of diameter dependence of gain, population variations, etc 15 p2497 A67-29390

Continuous second harmonic generation of 2572 angstrom argon II laser, noting optimum phase matching, power dependence on crystal temperature, etc 15 p2497 A67-29392

Carbon dioxide laser output observation by high resolution thermographic screen 15 p2497 A67-29393

Precautions required when using continuous gas flow in high current ion lasers 15 p2497 A67-29394

Nonlinear oscillation theory for parametric resonance effect in gas lasers placed in stationary and variable magnetic field 15 p2498 A67-29468

Measurements of short term frequency or phase fluctuations of gas lasers, noting random Gaussian perturbation 15 p2499 A67-29730

Shape of extremely short pulses generated by helium-neon laser with mutual synchronization of intermodal beats achieved by Fabry-perot interferometer 15 p2500 A67-29760

Laser output reduced by rare gas impurities in molecular neutral CO and nitrogen gas lasers 15 p2500 A67-29910

Spectroscopic study of gas discharge parameters in argon ion lasers to determine level inversion mechanism in continuous or pulsed regime of generation 15 p2501 A67-30003

General relations for amplification and oscillation development in optically pumped alkali vapor maser derived and applied to rubidium 85 15 p2501 A67-30095

TV signal transmission over gas laser light beam with ADP crystal at 7GHz modulating frequency 16 p2684 A67-30610

Double exposure holographic formation of contour map over diffusely reflecting surface, using immersion method with liquids of different refractive indexes 16 p2670 A67-30612

Frequency measurement of gas laser transitions in heavy water and acetylene discharges 16 p2685 A67-30824

Internal modulation of IR gas laser using cadmium sulfide or selenide single crystals 16 p2685 A67-30891

Saturated neon absorption inside helium laser, noting output power peak caused by Lamb dip effect 16 p2685 A67-31033

Nonaxial oscillation modes in He-Ne laser interaction with spherical mirror resonator confocal cavity 16 p2685 A67-31038

Magnetohydrodynamic energy converters based on nonequilibrium plasmas for laser construction 16 p2686 A67-31576

Output power of gas laser with numerous axial-oscillation modes calculated as function of resonator length and pumping power 17 p2866 A67-31926

Gas laser applications in construction, mechanics, communications, biology and medicine for control, measurement and experimental work 17 p2867 A67-32366

Line width vs optical thickness in pulsed argon-ion laser used to determine level population in plasma 17 p2867 A67-32452

Frequency and wavelength stabilization of gas lasers, noting wavelength shifts due to gas pressure and gain variations 17 p2815 A67-32611

Helium-neon laser generating simultaneously on two lines, showing pressure dependence and output radiation variation with discharge current 17 p2868 A67-32662

Laser research and development in France and applications to holography, metrology and gyros 17 p2868 A67-32745

Spark produced in cell containing argon when concentrating laser beam in small volume, calculating temperature distribution 17 p2869 A67-32804

Gas laser as source of illumination, with attention to origin of aventurine spots on screen 17 p2869 A67-33220

Polarization properties of single mode operating gas laser in small axial magnetic field with initial cavity anisotropy 17 p2870 A67-33368

Three-space optical resonator model, deriving properties responsible for undesired natural frequencies suppression, noting selection characteristics 18 p3058 A67-33528

Noise analysis in He-Ne laser during RF and DC excitation, noting relation between critical frequency and lifetime of metastable atom 18 p3058 A67-33648

Short stable gas laser construction and properties 18 p3058 A67-33658

Speed of light in vacuum determined by helium-neon gas laser, using Edlen dispersion equation 18 p3059 A67-33671

Pressure dependence of output power of He-Ne laser on amplitude of periodic high voltage excitation pulses 18 p3059 A67-33726

Spectroscopic study of gas discharge parameters in argon ion lasers to determine level inversion mechanism in continuous or pulsed regime of generation 18 p3059 A67-33760

Active medium radial variation in density of neon atoms metastable level as explanation of anomalous laser oscillation 18 p3060 A67-34013

Michelson type carbon dioxide laser for AC discharge analysis, noting apparatus design and performance results 18 p3060 A67-34014

Radiation power of He-Ne laser at 0.63, 1.15 and 3.39 microns, effect on electron concentration 18 p3060 A67-34038

Longitudinal magnetic field effect on radiation intensity of He-Ne laser operating in pulsed regime 18 p3061 A67-34043

Fabry-Perot interferometric observation of spectral line to investigate ionization rate of electrical discharge used for argon ion laser 18 p3061 A67-34044

Design, operation, characteristics and applications of carbon dioxide lasers with DC excitation and fixed mirrors 18 p3061 A67-34350

High resolution holograms using Fresnel biprism to reduce noise 18 p3053 A67-34620

Counter traveling wave regime stability in ring gas laser, studying effects of atomic collisions, isotopic state and wave coupling 19 p3239 A67-34898

Raman effect in solutions of potassium, sodium and ammonium dichromate and potassium dichromate single crystal 19 p3240 A67-35421

Harmonic mixing and heterodyne detection of laser radiation 19 p3240 A67-35623

Thermoplastic-resin film with UV sensitive dispersed compound for carbon-dioxide laser-radiation photography 19 p3240 A67-35694

Tabulation of accidental coincidences between fundamental frequency of one laser and harmonic or subharmonic frequencies of another, as necessary condition for frequency translation between lasers 19 p3240 A67-35700

Damping effect of HF field on instabilities occurring in form of moving striations within plasma of gas laser 19 p3241 A67-35814

Function of symmetrical gas-laser resonator analyzed to determine angle of divergence of laser beams generated by various transverse electromagnetic wave modes 19 p3242 A67-36106

Interaction between oppositely moving traveling waves in helium-neon laser with annular resonator 19 p3242 A67-36107

Calculation of vibration level populations of polyatomic molecules in electronic ground state 20 p3457 A67-36216

Relaxation of carbon dioxide pulsed laser levels by collisions with hydrogen, showing gain dependence on hydrogen pressure 20 p3457 A67-36384

Quasi-CW oscillation at 4880 angstrom of wide-bore AR II ion laser by plasma inductive excitation 20 p3458 A67-36387

Far IR CN laser action shown due to HCN molecule, explaining intense spectral lines around 337 microns 20 p3458 A67-36391

Laser frequency control system using two optical discriminators for long and short term stability 20 p3459 A67-36519

Book on lasers and application to long distance terrestrial or space communications system 20 p3459 A67-36639

Angular divergence of gas-laser radiation as function of output power, analyzing interaction of angular modes 20 p3459 A67-36689

Passive Q-switching of carbon dioxide laser with cavity containing saturable absorber, noting peak power and pulse rate 20 p3460 A67-36854

Gas laser IR radiation hazards to eyes tested on rabbits indicates irreversible changes in cornea leading to impaired vision 20 p3375 A67-37276

He-Ne laser light intensity distribution cumulants for nonlinear oscillation threshold operation 20 p3461 A67-37289

Simultaneous oscillation in UV and IR and interaction of 1st and 2nd plus ve system of bands in molecular nitrogen 20 p3461 A67-37292

Axial magnetic field effect on He-Ne laser power output operating in regime of simultaneous generation of 3.39 and 0.6328 micron lines 20 p3462 A67-37340

Gas laser behavior in magnetic field, analyzing data on magnetic effect, Zeeman effect and microwave 20 p3462 A67-37591

Atmospheric absorption of gas laser radiation at two wavelengths noting dependence on gas pressure and amount of methane 20 p3463 A67-37668

Multipath cell with White mirror system using carbon dioxide and molecular nitrogen gas mixture for gas laser amplifier and oscillator operation 21 p3625 A67-37854

Single crystals of lithium-meta-niobate evaluated for nonlinear optical quality, using gas laser and interferometer 21 p3677 A67-38010

Optical pumping of sodium vapor with deuterium light, discussing optical transparency in excited state mixing cross sections 21 p3639 A67-38018

Molecular and atomic, neutral and ion gas laser advances, noting high power CW carbon dioxide laser 21 p3639 A67-38062

Circular polarization in j equals 1 to j equals zero transition in gas laser shown due to different atomic relaxation processes 21 p3640 A67-38353

Rapid scan spectrometer for carbon dioxide laser studies noting time dependent effects 21 p3641 A67-38460

Nonlinear oscillation theory for parametric resonance effect in gas lasers placed in stationary and variable magnetic field 21 p3641 A67-38549

Hypersound propagation velocity in toluene cyclohexane, acetic acid, water, etc, determined at 6328 angstrom from He-Ne laser analysis of structure of Rayleigh scattering 21 p3642 A67-38820

Negative-ion gas laser with thermal excitation 21 p3642 A67-38823

Operating and performance characteristics of helium-neon pulsed gas laser, discussing application to integrated microcircuits fabrication 22 p3813 A67-39333

Relaxation times of carbon dioxide vibrational levels and afterglow pulsed gain for nonflowing gas laser 22 p3814 A67-39354

Electron density relation to output power in He-Ne laser and magnetic field effect, using microwave resonator 22 p3814 A67-39428

Anomalous nonlinear preference for circular polarization in He-Ne laser noting variation with gas pressure 22 p3815 A67-39522

Gas laser simulation technique to facilitate teaching of laser physics 22 p3816 A67-39923

Lasers as light source in optical telemetry, discussing laser radiation, solid state and gas lasers and critical parameters 22 p3800 A67-39981

Active medium gain required in gas laser output power calculation obtained for intermediate case 22 p3816 A67-40128

Atmospheric absorption of carbon dioxide laser radiation calculation from laboratory absorption coefficient measurements, discussing effects on power transmission and communications 22 p3816 A67-40237

Moving striation modes observed in periodic sidelight intensity oscillations of He-Ne laser 22 p3816 A67-40312

Planetary surface pressure and temperature of lower atmosphere determined from orbiting spacecraft with carbon dioxide laser 22 p3805 A67-40357

Low pressure argon ion laser cold emission cathode, considering electron production by cathode sputtering owing to self-sustained arc

discharge 22 p3817 A67-40413

Power supply system consisting of two-piece coaxial cable and pulse transformer found to possess all characteristics for gas laser operation 22 p3817 A67-40414

Recovery time of carbon dioxide laser excited by electric pulse discharge noting heat conduction toward walls 23 p4011 A67-40692

Laser beam cross section variation during free space propagation and through optical systems, discussing He-Ne laser radiation 23 p4011 A67-40724

Platinum wire heating in sealed carbon dioxide laser results in catalyzing effect permitting high carbon dioxide concentration 23 p4011 A67-40784

Optical mixing of two low level signals in atomic states of He-Ne laser noting amplitude modulation of visible laser output 23 p4012 A67-40891

Laser mode synchronization by electro-optical crystal dielectric constant modulation mounted inside resonator 23 p4013 A67-40903

Gas laser radiation applied to light transmittance measurement of heavily doped gallium arsenide in absorption region by free carriers 23 p4039 A67-40935

Coupled linearized equations for laser-induced optical radiation instabilities in liquids and gases, obtaining differential operator and Green function 23 p4027 A67-41024

Emission wavelength selection in multicolor-emission noble gas laser using linear polarization control device 23 p4014 A67-41025

Pulse regenerative amplification in Q-switched argon-ion laser during buildup time to saturation 23 p4014 A67-41030

Helium-neon laser device for mirror spacing changes by optical heterodyning, discussing application to piezoelectricity 23 p4014 A67-41031

Faraday rotation in YIG studied from measurements at He-Ne laser wavelengths for applications to materials design 23 p4041 A67-41184

Second harmonic generation in Se and Te-Se using carbon dioxide laser, measuring nonlinear coefficients and synchronism direction 23 p4016 A67-41192

Hollow cathode mercury laser providing improved performance, stability and reproducibility 23 p4016 A67-41226

Spectrum line observation of decay transition of structure of gas laser 23 p4016 A67-41324

High resistance GaAs residual IR absorption measured to determine incident light intensity fraction, showing low absorption suitable for high power laser modulation 23 p4045 A67-41471

IR lasers using vibrational rotational transitions of carbon dioxide 24 p4166 A67-41799

Absolute frequency measurements on continuous wave hydrogen cyanide submillimeter laser lines 24 p4166 A67-41861

Optical Raman scattering from atmospheric oxygen and nitrogen via pulsed nitrogen UV laser light source, discussing spectral analysis of air scattering 24 p4147 A67-41883

Thermal development method used for observing and recording laser oscillations from output of nitrogen-carbon dioxide systems 24 p4166 A67-41908

Spatial coherence of radiation field across multimode He-Ne laser beam 24 p4167 A67-42091

He-Ne laser pulse delay when excited in optical resonator noting dependence on gas pressures 24 p4167 A67-42207

Two-photon absorption in alkali halide crystal via gas laser noting F center formation 24 p4167 A67-42361

Plasma discharge instability effect on gas laser operation, discussing moving layers self-excitation and laser beam modulation 24 p4168 A67-42561

Divergence angles of helium-neon laser radiation, discussing resonator with spherical mirrors with unequal curvature radii 24 p4169 A67-42891

Separate studies of power and collision broadening of gas laser transition showing proportional DC laser power to square of gain 24 p4169 A67-43103

GAS LIQUEFACTION
S LIQUEFACTION

GAS-LIQUID INTERACTION

Equilibrium concentrations for air water plasma at various temperatures tabulated for three densities, noting effect on electron concentration 05 p0850 A67-16131

Bibliography and subject index to two-phase gas-liquid flow literature 07 p1269 A67-20300

End-wall pressure distributions in confined vortex [JPLTR-32-1099] 10 p1626 A67-23150

Critterion expressions for Nusselt numbers of mass transfer in two-phase film system at high Prandtl numbers which describe physical properties of both phases 14 p2405 A67-28303

Gas-liquid droplet behavior in geometric nozzle for constant difference between phase velocities, determining appropriate nozzle profile 15 p2472 A67-29777

Two-phase gas-liquid flow photography equipment and techniques, with applications to droplet mass transfer, flow pattern determination, etc 16 p2671 A67-30840

Equilibrium state of two-dimensional lattice liquid-gas system using cluster variation method for nucleation and thin film growth studies 23 p4040 A67-40967

Cluster variation method based on W-shaped cluster in triangular lattice for lattice-gas liquid, phase-separating binary alloy and Ising model 23 p3971 A67-40969

GAS LUBRICANT

Ball bearing lubrication with vapor from volatile organic compounds for wide temperature range and long-term operation 01 p0077 A67-10120

Gas film MGD lubrication in transverse and tangential electromagnetic fields 05 p0810 A67-16273

MGD lubrication, obtaining motion equation of gas in electric or magnetic fields, velocity distributions, pressure differential equations, etc 07 p1192 A67-20210

Leakage and optimum film thickness of gas lubricated high-pressure mainshaft seals for jet engine compressors 10 p1658 A67-22705

Test procedure and apparatus for evaluating oxidation-corrosion characteristics of aircraft gas turbine engine lubricants at high temperature 14 p2326 A67-28794

Galerkin method modifications to obtain static solution of indefinitely long partial-arc self-acting gas bearing 19 p3237 A67-35866

Semimplicit numerical methods for time transient gas-lubrication Reynolds equation stressing numerical stability [ASME PAPER 67-LUB-18] 24 p4163 A67-42677

GAS LUBRICATED BEARING

HF gaseous squeeze film bearing asymptotically analyzed by considering internal and edge regions separately [ASME PAPER 66-LUB-11] 03 p0431 A67-13760

Thermal distortion due to viscous heating in fluid film effects on load capacity of spiral-grooved gas-lubricated thrust bearing [ASME PAPER 66-LUB-10] 03 p0432 A67-13765

Vibrational damping of externally pressurized orifice journal bearings undergoing free vibrations with and without shaft rotation 04 p0627 A67-14432

Literature in 1965 on lubrication and bearings covering friction and wear, boundary, metal working, gear and spline lubrication, rolling element bearings, etc [ASME PAPER 66-WA/LUB-8] 04 p0629 A67-15349

Geometry variation effects on hydrodynamic bearing performance, noting locational dependence relative to pressure producing region 08 p1336 A67-21041

Simplified resonance-amplitude analysis of unbalance vibration superimposed upon steady state eccentricity in aerodynamic bearings 09 p1509 A67-22613

Static characteristics of radial gas dynamic bearing, using differential equation for pressure distribution calculation 13 p2122 A67-26351

Boundary conditions of journal gas bearings lubrication, studying slots effects 20 p3453 A67-36273

Static reaction of radial gas dynamic bearing to journal axis angular displacement determined by splicing asymptotic solutions for low and high pressure levels 22 p3810 A67-39232

Equilibrium stability of rigid rotor in aerodynamic bearings, determining lubricant effect on journal 22 p3811 A67-39316

Boundary layer theory in gas bearing lubrication problems, obtaining pressure asymptotic expansions for infinitely long slider squeeze-film bearing [ASME PAPER 67-LUB-7] 24 p4162 A67-42671

Frequency Response and direct numerical integration of governing differential equations, considering gas-lubricated tilting-pad journal bearing stability [ASME PAPER 67-LUB-8] 24 p4162 A67-42672

GAS MASER

Amplitude and frequency characteristics of hydrogen-atom beam maser 02 p0251 A67-11574

Magnetically tunable IR masers of helium-xenon, considering experimental problem in applying tunable IR maser to IR spectroscopy 04 p0632 A67-14764

Magnetic field gradient relaxation mechanism by random excitation of transitions in F equals 1 level of ground state of hydrogen atoms in maser 05 p0817 A67-16635

Oscillation amplitude modulation in ammonia beam maser oscillator with single cavity followed by two cavities in cascade 05 p0817 A67-16636

Q parameter of hydrogen maser measurement by method of no clock structure modification and by inhomogeneous magnetic field method 11 p1802 A67-24754

Three-level maser detector for far IR using double-quantum pumping 16 p2684 A67-30606

Spin-exchange frequency pulling of ground state hyperfine transition in atomic hydrogen analyzed for self-excited oscillation in hydrogen maser 17 p2889 A67-33225

Midband saturation characteristics of ammonia maser amplifier and variation of maser bandwidth with gain 20 p3458 A67-36431

GAS-METAL INTERACTION

Oxygen adsorption on tungsten crystal face studied by back-reflection low energy electron diffraction 03 p0447 A67-13647

Gas saturation effect on titanium alloys undergoing heat treatment, discussing microhardness and surface crack formation 07 p1205 A67-19277

Gas saturated layer effects on VT5 titanium alloy mechanical properties variation with temperature 10 p1670 A67-23642

Spatial distribution of deuterium and hydrogen molecules and helium scatterer from /111/ plane of epitaxially grown silver 13 p2099 A67-26948

Noble gas molecular beam quasi-specular scattering from metal surfaces noting effects of beam incidence angle, molecular weight and gas temperature 13 p2099 A67-26949

Rates of surface chemical reactions in well-defined flow systems theoretically investigated by data reduction techniques and quantitative predictions 18 p2997 A67-33795

Interaction of oxygen with tungsten surface at room temperature 19 p3244 A67-34940

Analytical procedures for oxygen, nitrogen and hydrogen determination in high melting metals 20 p3467 A67-37120

GAS METER

Equation for laminar gas meter applied to flow coefficient derived from Hagen-Poiseuille relationship, noting effect of heat transfer, compressibility, etc., on meter performance 03 p0404 A67-13778

GAS MIXTURE

SA DETONABLE GAS MIXTURE

Velocity propagation of stable detonations in gas mixtures determined, using Doppler effect obtained by electromagnetic wave reflection 01 p0166 A67-10229

Silicon carbide generation by pyrolysis of gas mixtures on tungsten wires, using X-ray diffraction to analyze structure 01 p0103 A67-10688

Stability of solutions to general equations of steady state one-dimensional relaxed flow of perfect gas mixtures [ONERA-TP-360] 01 p0054 A67-11089

Warren momentum integral method for predicting compressible free mixing of two

dissimilar gases [AIAA PAPER 65-822] 01 p0055 A67-11170

Model of nonequilibrium properties of high temperature carbon dioxide and other gas mixtures in connection with studies for vehicles entering Martian atmosphere 01 p0008 A67-11436

Mixing gaseous propellant injector, injection velocity and momentum flux ratio, combustion pressure and propellant combination effects on HF combustion pressure oscillations in rocket motor 02 p0302 A67-11940

Air velocity and temperature, stabilizer size and blockage effects on fresh mixture entrainment in recirculation zone of bluff body stabilized flames 02 p0342 A67-12029

Diffusive separation of helium-argon mixtures in underexpanded free jets and normal shock waves studied by electron beam 02 p0234 A67-12543

Role of amplification due to impacts of second kind in emission of nitrogen and CO molecular bands in mixture of nitrogen-argon and CO-Ar in glow discharge 02 p0270 A67-12674

Gaseous composition of unknown planetary atmosphere determined, using acoustic experiment combined with pressure and temperature data 03 p0509 A67-13215

Thermodynamic parameters of combustible mixture and ignition system characteristics effect on energy of spark ignition of homogeneous gaseous mixture 03 p0535 A67-13396

Sublimation and gaseous equilibria involving neodymium fluorides and barium fluorides 03 p0367 A67-13519

Characteristics of pulsed laser action in He-Ne and He-Ar mixtures at pressures above 200 mm Hg 03 p0438 A67-14189

Pressure induced monochromatic translational absorption coefficients for homopolar and nonpolar gases and gas mixtures, with application to molecular hydrogen 03 p0515 A67-14323

Mixing at constant section of two flows of different enthalpies, demonstrating phenomenon with arc type reheater 04 p0602 A67-14569

Compatibility of artificial gas mixtures dependent on carbon dioxide and oxygen partial pressures 04 p0562 A67-14573

Chemical reaction effect on heat transfer in thermally decomposing ozone system 05 p0925 A67-16270

Transient exact solutions to integral and differential operators of kinetic equations of gas mixture 05 p0849 A67-17113

Perfect gases reacting mixture flows formulated for system of differential equations 06 p0955 A67-18114

Fuel injection parameters effects on mixing of gaseous hydrogen fuel with supersonic air stream for hypersonic ramjet, determining turbulent diffusion coefficient 06 p1117 A67-18387

Gaseous mixture theory in calculating transport coefficients of combustion product plasma of oxygen and acetylene 06 p1119 A67-18723

Flammability limits of hydrogen-oxygen-nitrogen mixtures at low pressures 07 p1239 A67-19077

Electron components for electrical, thermal conductivity and viscosity coefficients of gas mixtures calculated via molecular kinetic theory 07 p1225 A67-19116

Existence of maximum conductivity of ionized gas mixture as function of thermodynamic parameters 07 p1225 A67-19117

Variable thermal capacity of gas mixture taken into account in calculation of heat regeneration in gas turbine cycles, using working bodies 07 p1266 A67-19181

Exothermal reaction zone in one-dimensional shock wave in argon diluted oxygen-hydrogen and methane-oxygen mixtures 07 p1267 A67-19309

Jet engine thrust augmentation by controlled mixing of exhaust gases with ambient air 07 p1242 A67-20119

Carburization of niobium and tantalum-base alloys through exposure to gaseous mixture of benzene-hydrogen, noting results of creep rupture tests 08 p1341 A67-20765

Temperature variation of thermoconductivity of helium-hydrogen gas mixtures and correlation of thermoconductivity curves with gas

chromatograms 08 p1426 A67-20805

Transverse separation of rare gas-metal vapor mixture components in positive nonisothermal plasma column in plain-symmetric glow discharge 09 p1545 A67-21998

Temperature characteristics, electric conductivity, electrode drop and heat loss of acetylene combustion gas mixed with seed material and nitrogen used as MHD fluid 09 p1580 A67-22151

Collision induced far IR absorption in rare gas mixtures with emission spectrum calculation 09 p1535 A67-22382

Polycyclic aromatic hydrocarbons in soot of premixed acetylene-oxygen flames, discussing graphs of flame height vs mixture composition 10 p1602 A67-22960

Ionosphere as binary two-temperature gas and transfer coefficients for elastic collisions based on Boltzmann equation 10 p1640 A67-23220

Nonlinear system of partial differential equations describing one-dimensional combustion process of gas mixture 11 p1882 A67-24158

Strong small perturbation solutions for steady supersonic flows of inert or reacting gas mixtures around plane corner 11 p1778 A67-24230

Human lung gas mixing efficiency estimated, using residual lung nitrogen content curve 11 p1747 A67-24628

Turbulent boundary layer of gas mixture with dissociation, flowing at inlet section of tube 11 p1782 A67-24961

Thermal conductivity of binary gas mixtures, estimating conductivity at high temperatures 12 p2033 A67-25217

Third Chapman-Enskog approximation to tensor electrical conductivity of partially ionized gas applied to two conductivity mixture rules for atmospheric cesium seeded argon 12 p1975 A67-25893

Gas dynamic stability of plane detonation wave propagating in ideal gas mixture, in terms of small perturbations that may result in surface bending and changes in thickness 12 p1930 A67-25965

Martian entry condition analyzed as nonequilibrium flow field phenomenon noting chemical kinetics and radiation behind shock wave in gas mixtures [AIAA PAPER 67-322] 12 p1930 A67-26037

Concentration limits of ignition of methanol and formaldehyde mixtures at atmospheric pressure and from 20 to 280 degrees C 12 p2039 A67-26118

Ignition delays calculation in hydrogen-air system, using Momtchiloff assumptions 13 p2185 A67-26259

Orthogonal polynomial method to determine distribution function for equilibrium of single species two-temperature gas mixture 13 p2102 A67-26972

Collisional parameters in kinetic model equations for binary gas mixtures, treating shock structure in weakly ionized argon 13 p2103 A67-26977

Nonequilibrium effects in spherical free jet expansions of polyatomic gases and gas mixtures, obtaining moment equations for flow field development 13 p2104 A67-26983

Spherical supersonic source expansion of neutral disparate molecular weight binary gas mixture studied asymptotically as source Knudsen number tends to zero 13 p2104 A67-26984

Laser output pulse time dependence in acetone and nitrogen mixture, using indium antimonide detector 13 p2127 A67-27017

Ethylene oxide and methyl bromide mixture for spacecraft sterilization, discussing penetrating power, effect on components and packing and toxicity 15 p2430 A67-29101

Thermomechanical theory of diffusing and chemically reacting mixture and application to elastic materials mixture subject to diffusion and heat conduction 15 p2517 A67-29463

Changes in structure of gas detonation wave with changes in initial pressure 16 p2656 A67-30452

Magnetically induced ionization in nonseeded helium and argon gas mixtures used to determine nonseeding operation of MHD generator in nonequilibrium ionization mode 16 p2711 A67-30542

Multicomponent reacting laminar boundary layer in chemical equilibrium solved using Stefan-Maxwell relations 16 p2658 A67-30937

Heat loss from wires in nitrogen, helium and mixtures measured at low Reynolds numbers, finding agreement with theory of Kassoy 16 p2779 A67-31217

Temperature dependence of thermal diffusion factors in ternary system He-Ne-Kr by two-bulb method 16 p2661 A67-31223

Ionization levels and thermodynamic functions of theoretical gas mixtures composed of various highly ionized atom types 16 p2720 A67-31387

Slow oxidation of n-octane vapor /oxygen/ nitrogen mixtures at reduced pressures and temperatures 16 p2779 A67-31518

Experiments on oxidation kinetics of refractory metals in oxidized and partly dissociated oxygen-chlorine mixtures 17 p2971 A67-33021

Small perturbations effect on internal gas dynamic structure of flame zone for slow combustion stability 17 p2974 A67-33144

Rate of vibration-vibration energy exchange in gas mixtures 18 p3081 A67-33783

Shock wave investigation of recombination in near-stoichiometric hydrogen-oxygen-argon mixtures at high temperatures 18 p2996 A67-33789

Density induction times for shock wave induced exothermic reaction in lean mixtures of deuterium, hydrogen, ethylene and ethane with oxygen 18 p3081 A67-33792

Atomic nitrogen-oxygen mixtures ion concentration enhancement in hydrocarbons presence, discussing atom recombination rate, etc 18 p3107 A67-33805

Velocity and temperature measurements in turbulent swirling burning free jets of butane-propane-air 18 p3151 A67-33815

Cylindrical expanding detonation waves in gas mixtures, studying detonability limits, propagation velocity and instability and vibratory phenomena 18 p3153 A67-33822

Transverse wave structure in detonations investigated using smoked-foil technique in gas mixtures, showing dependence on tube geometry and heat capacity 18 p3153 A67-33828

Mixing patterns and flow configurations in model for determining combustion performance in well-stirred reactor 18 p3154 A67-33833

Physical and chemical wall effects on mechanism of combustion reaction in gases studied by introducing solids and measuring ignition pressure 18 p3155 A67-33847

Thermodynamic characteristics of equilibrium combustion products of methane-oxygen-nitrogen mixtures over wide range of parameters and compositions, using computer 18 p3159 A67-34051

Linear algebra describing equilibrium chemical systems and complex chemical mixtures, discussing hydrogen-fluorine coupling reaction at elevated temperatures 18 p2997 A67-34124

Transition of supersonic flow of combustible gas mixture to Chapman-Jouguet regime 18 p3028 A67-34214

Ignition temperature and ignition delay of oxyhydrogen gas as function of pressure examined in shock wave tube, using Schlieren photography 18 p3160 A67-34261

Viscosity of neon-nitrogen, helium-carbon dioxide and nitrogen-argon mixtures 18 p3161 A67-34522

Ionization mechanism of argon-permanent gas mixture in radiolionization detector used for gas chromatography 19 p3226 A67-34797

Flame spreading over igniting solid propellant surface in high pressure oxygen-inert environment 19 p3344 A67-34999

Reaction mechanism between oxygen difluoride and diborane based on visual observation, gas composition and pressure-temperature relationships [CI PAPER 67-10] 19 p3309 A67-35005

Reaction rate constants for gaseous chemical species at high temperatures [CI PAPER 67-11] 19 p3345 A67-35006

Mercury-argon low pressure discharge initiation stressing positive column establishment, examining breakdown effects by spectrographic techniques 19 p3272 A67-35088

Dynamics of channel formation in nonisothermal pulsed discharge and nonequilibrium ionization in inert gas-cesium mixtures 19 p3278 A67-35132

Dynamic equations for adiabatic changes

of state for mixtures of partially ionized gases with chemical reactions 19 p3286 A67-35348

Spectral transmittance of mixture of carbon monoxide and nitrous oxide for overlapping absorption bands 19 p3266 A67-35696

Shock tube experiments conducted on mixtures of fine solid particles and gases 20 p3414 A67-36516

Alpha aminonitriles formation by electric discharge through anhydrous methane and ammonia mixture, showing hydrolysis to amino acid as possible bearing on chemical evolution 20 p3369 A67-36764

Solution drops motion in diffusing binary gas mixture, analyzing velocity 20 p3421 A67-36812

Bow shock and combustion zone studies of spheres fired through H₂-O₂ mixtures show ignition zone separation 20 p3359 A67-37128

Molecular flow mass spectrometer analysis of porous metal membranes for gases of different molecular weights 20 p3378 A67-37499

Electron components for electrical, thermal conductivity and viscosity coefficients of gas mixtures calculated via molecular kinetic theory 21 p3659 A67-38161

Existence of maximum conductivity of ionized gas mixture as function of thermodynamic parameters 21 p3659 A67-38162

Oxygen-hydrogen mixtures burning characteristics in shock wave tube, studying ignition processes with schlieren photographs 21 p3731 A67-38366

High temperature gas transport property estimation with chemically reacting gas mixture conduction 21 p3613 A67-38391

Binary gas mixtures transport coefficients calculation, comparing experimental and theoretical values of viscosity and thermoconductivity dependent upon interaction between unlike molecules 21 p3733 A67-39064

Linear equation solving for gaseous mixture quantitative determination, based on combined cognitive system use of computing and programming devices 21 p3631 A67-39116

Helium argon mixture shock wave density profile measurements, discussing shock wave production in flow field at supersonic nozzle exit 22 p3783 A67-39709

Thermodynamic properties of low temperature gaseous and liquid mixtures, discussing quantum effects in mixtures containing hydrogen isotopes and high density mixtures 22 p3921 A67-40553

Inert gas effect on oxygen consumption in living tissue studied by polarographic and Warburg techniques 23 p3960 A67-41706

Absolute measurement of Ar II transition probabilities using tungsten ribbon lamp as calibration standard 24 p4194 A67-41888

Rarefied gas mixtures viscosity and heat conduction temperature dependence calculated, analyzing empirical relations 24 p4142 A67-42220

Chemical reaction effect on viscous boundary layer of hypersonic flow of reacting gas mixture past blunt body 24 p4091 A67-42270

Solubility of niobium carbide in gamma iron determined from experiments using Fe-Nb alloy in equilibrium with hydrogen-methane mixtures 24 p4173 A67-42348

Adsorption equilibrium data obtained at high pressure for methane and propane on silica gel using radioactive tracer pulsing 24 p4118 A67-42584

Heat and mass transfer in chemically reacting gas mixture compressible boundary layer, determining temperature in reaction zone and on porous plate surface 24 p4256 A67-42734

High temperature polyatomic gas and gas mixture transport properties, discussing thermoconductivity, multiple intermolecular potentials and plasmas 24 p4256 A67-42742

Isothermal equilibrium of constant volume gas mixture under external mass forces field deriving from time independent potential 24 p4257 A67-43113

GAS PHASE

Gas phase pyrolysis kinetics of tetranitromethane, noting pressure effect and rate equation of thermal decomposition 01 p0019 A67-10765

Chemiluminescent gas phase reactions involving electronically excited oxygen

molecules trimethylaluminum and diborane near 3 millitorr 01 p0019 A67-11007

Free radicals in gas phase oxidation and spontaneous ignition reactions 02 p0341 A67-11502

Continuous gas deposition of triniobium-tin alloy on moving refractory wire without reaction chamber contamination by by-products 03 p0500 A67-14065

Electron spin resonance application to kinetic studies of free atoms and radicals in gases, particularly OH radical 04 p0566 A67-15173

Liquid and gas viscosity correlation at 1 atm with reduced density for parahydrogen 05 p0873 A67-17224

Combustion reactions during spacecraft reentry, noting degradation of heat shields composed of hydro-and fluorocarbon compounds 05 p0928 A67-17334

Spectrum of glow during gas phase reaction of germanium tetrahydride with atomic oxygen, observing new bands of D-X system 06 p0955 A67-17655

Continuous absorber effect on spectral line reversal gas phase temperature measurement [AIAA PAPER 67-108] 06 p1004 A67-18503

Free energy of spatially homogeneous phase in approximation of self-consistent field for application to fluids and gases 07 p1168 A67-19186

Low pressure low-temperature ignition of hypergolic propellants, particularly hydrazine-nitrogen tetroxide systems, in space environment simulator and conclusions on gas phase reactions 07 p1163 A67-19385

Laser action in zinc selenide crystals at 4600 angstroms prepared under high pressure in closed container by gas phase reaction and following crystallization 07 p1197 A67-20183

Semiconductor diffusion by entrainment of impurity in gas phase 13 p2176 A67-26657

True air life support system, describing concept for deriving fixed percentage binary gas from two steady state cryogenic liquids 13 p2064 A67-27638

Continuous gas deposition of triniobium-tin alloy on moving refractory wire without reaction chamber contamination by by-products 13 p2185 A67-27721

Surface coupled heat release effect on oscillatory amplitude of pressure coupled response in solid propellant 15 p2544 A67-29983

Combustion stability in solid propellant rockets, reviewing Soviet T-sub s and Q models 15 p2581 A67-29986

Magnetohydrodynamic generator functioning by emulsion consisting of gas or vapor in liquid metal 16 p2606 A67-30588

Gas phase reactions of hydrazine with nitrogen dioxide, nitric oxide and oxygen, determining reaction rates, activation energy and order 18 p3109 A67-33837

Rate constant for gas phase recombination of atomic and molecular oxygen into ozone, discussing M effect 18 p3082 A67-34030

Interphase exchange coefficient for gas phase moving through fluidized bed analyzed by tracer gas technique 18 p3160 A67-34290

Temperature effect on gas saturation in alpha and beta titanium alloys 18 p3065 A67-34292

Diffusion saturation methods of alloy surfaces by metals and metalloids classified by physicochemical characteristics of active phase of diffusing element 19 p3242 A67-34916

IR spectra of gaseous, solid and matrix-isolated HNCS and DNCS, studying frequency shift, bending modes, fundamental vibrations, gas phase, etc 19 p3181 A67-35016

Decompression sickness studied by investigating cavitation at liquid-liquid interface 21 p3573 A67-38076

Lattice type gas heat capacity discontinuity near critical point 22 p3790 A67-39509

Solution for coupled system of parabolic partial differential equations describing reactants diffusion and heat conduction in gas phase 23 p4048 A67-41764

GAS POCKET

Permeation of neon, nitrogen and sulfur hexafluoride through living tissue in rats, using subcutaneous gas pockets as decompression sickness bubbles model 21 p3574 A67-38079

GAS PRESSURE

Configurations of HF discharge plasma and dependence on gas pressure and annular electrode potential 01 p0122 A67-10348

Forced convection effects on VHF CW and X-band antenna voltage breakdowns in wind tunnel experiments, using cold nonconducting gas 02 p0213 A67-11647

Dissociation pressures of mixed gas hydrates predicted from data for hydrates of methane, propane and nitrogen with water 02 p0190 A67-12234

Exhaust processes of gases at high initial pressure from tubes, when flow is initiated by acceleration of solid body 02 p0235 A67-12788

Electron motion in gases in pressure range where electron mean free path is comparable to or less than chamber length, showing effect on ion currents 04 p0662 A67-15769

Arc formation at metal surface in hydrogen plasma analyzed at various gas pressures, using Penning discharge, noting heat treatment effect on hydrogen 05 p0850 A67-16066

Vibratory energy dissipation of plates with riveted beams as induced by gas-pumping in structural joints 05 p0924 A67-17285

Manometer for measuring gas pressure from current required to heat platinum wire to certain temperature 06 p1003 A67-18192

Energy balance of stationary discharges in quartz containers filled with gas at various pressures, determining relation of heat and light loss of discharge to gas pressure and discharge power 09 p1544 A67-21854

Pressure dependence of thermoelectricity of gases measured using thermoelectric power of semiconductor 09 p1499 A67-22424

Anomalous losses in plasma confined in magnetic field, correlating loss process with tube dimensions, electron temperature, gas pressure and magnetic field 11 p1829 A67-24002

Gas pressure effect on electrical breakdown and field emission, discussing ion bombardment and whisker formation 11 p1820 A67-24921

Configurations of HF discharge plasma and dependence on gas pressure and annular electrode potential 11 p1844 A67-25021

Blowdown wind tunnel for He-K MHD generator, considering magnetically induced ionization, conductivity, gas temperature, etc 12 p1898 A67-25389

Ionized multiwatt argon lasers, discussing relation between output power and discharge current, gas pressure, magnetic field and tube bore size 12 p1953 A67-26159

Gas pressure bonding for hot isostatic pressing of beryllium powder into complex shapes 13 p2123 A67-27131

Electron density and HF spectrum of beam generated plasma as function of gas pressure and injection parameter 14 p2352 A67-27749

Slotted-sphere antenna immersed in plasma measured for RF admittance 14 p2283 A67-28377

Laminar flame speeds and composition flammability limits at low pressure for ternary mixtures of hydrogen and oxygen with ammonia and nitrous oxide 14 p2406 A67-28547

Sensitized ignitions of methane and oxygen mixtures, with nitrogen oxides and inert gases added, and suggested reaction mechanisms 14 p2407 A67-28549

Driver chamber for very high temperatures obtained with ceramic liner for arc driven shock tube, reducing contamination and cooling of driver gas 14 p2293 A67-28749

Shock tube tests with cold argon and heated helium to determine heated driver gas effect on effect on shock tube performance 14 p2294 A67-29053

Current damping, thermal expansion, radial oscillation, kinetic pressure and other dissipative processes effects on magnetic properties of plasmoids 15 p2524 A67-29244

Fast hydrogen ion generation in coaxial plasma source to determine point in gun chamber where fast particles arise 15 p2525 A67-29251

Gas kinetic pressure measurement in high current rectilinear hydrogen-plasma discharge during electron heating 16 p2718 A67-31188

Gas pressure dependence of attachment and recombination coefficients for thermalized electrons in air and oxygen 17 p2893 A67-32139

Boundary layer effect on primary wave propagation and gas states behind reflected wave in shock tube with nozzle 17 p2837 A67-32346

Pressure measuring apparatus for direct gas pressure measurements in millitorr ranges 17 p2855 A67-32351

Motion of shocks through chromosphere under guidance of magnetic fields 17 p2944 A67-32642

Fluid flow around magnetosphere boundary analyzed, noting geomagnetic field effect on hot plasma 17 p2853 A67-33252

Very low pressure pyrolysis applied to combustion kinetics 18 p3149 A67-33787

Gas temperature increase effect on thin walled container during prepressurization of high pressure blowdown systems [AIAA PAPER 67-443] 18 p3137 A67-33920

Plasma produced by shock wave in low pressure gas measured for phase angle by microwave reflection probes 18 p3088 A67-34076

Electron density decay curves in helium afterglows at high electron densities and gas pressure found controlled by recombination loss process 19 p3270 A67-35071

Sinusoidal frequency oscillations in DC magnetron plasmas discharge, determining magnetic field, anode current and voltage and gas pressure dependence 19 p3277 A67-35124

Radial and axial temperature profiles of free-burning argon arc at various pressures, measuring continuum intensities [DVL-625] 19 p3278 A67-35135

Partition function of partially ionized hydrogen two-component plasma 19 p3285 A67-35346

Instrument for processing and storing gas pressure data noting digital integrator, core storage unit and printer 19 p3230 A67-35565

Axisymmetrical vibrations of cylindrical shell during HF internal pressure pulsations of gas flow containing uniformly distributed burning fuel droplets 20 p3536 A67-36445

Glow-broadening rate dependence on initial pressure and discharge voltage in shock tube containing hydrogen plasma, studying charge distribution variations 20 p3501 A67-37145

Airflow velocity measurement device in cylindrical or rectangular tubes at low gas pressures 20 p3451 A67-37300

Atmospheric absorption of gas laser radiation at two wavelengths noting dependence on gas pressure and amount of methane 20 p3463 A67-37668

Electrical and spectral investigation of pulsed high pressure arc produced by capacitor bank discharge in helium and hydrogen 22 p3845 A67-39426

Apparatus for digital determination and storage of gas pressure variations, showing pressure curve diagram and numerical representation 22 p3804 A67-40328

He-Ne laser pulse delay when excited in optical resonator noting dependence on gas pressures 24 p4187 A67-42207

Pressurized propellant tank system for rocket engine, discussing weight factors, propellant combinations and expellant gas pressure relations 24 p4241 A67-42754

GAS PROPELLANT

Propane gas system for satellite attitude control noting Skylark rocket 01 p0157 A67-11446

Turbulent gas combustion, showing burning rate as function of combustion temperature, pressure and chemical reaction rate in flame 21 p3732 A67-38527

Utilization of lunar geothermal emissions for rocket propellants and life support [AIAA PAPER 67-903] 24 p4165 A67-43011

GAS REACTOR

Steady flow adiabatic stirred reactor to study combustion mechanism of hydrogen-oxygen mixtures, determining reaction-kinetic constants 18 p3154 A67-33834

Gas core reactor, discussing application of fissionable gas to heat hydrogen propellant in nuclear rocket reactor [AIAA PAPER 67-499] 18 p3076 A67-33963

GAS-SOLID INTERFACE

Chemical aspects of evolution of terrestrial atmosphere, noting role of photolysis in oxygen

production 03 p0414 A67-14089

Nozzle type molecular beam measuring distribution of speeds after scattering incident beam from solid surface 05 p0849 A67-17276

Nonequilibrium ionization of gas-solid suspension expanding supersonically in nozzle as function of charge distribution 07 p1227 A67-20258

Conductivity of working fluid in MHD generator using thermionic emission from suspended lanthanum conductivity of working fluid in MHD generator using thermionic emission from suspended lanthanum hexaboride powder 09 p1543 A67-21822

Electric conductivity of high temperature nitrogen jet as affected by impurity particles of potassium, metals and metal oxides 09 p1547 A67-22321

Density profiles in gas-solid suspension flow in round duct 10 p1826 A67-23149

Formula for thermal accommodation coefficient as basis for accommodation coefficient of monatomic gas-solid system calculation 12 p2040 A67-26229

Gas-surface interactions, energy exchange and scattering between particles and surface 13 p2097 A67-26935

Three-dimensional hard spheres theory of gas atom scattering from solid surface noting velocity distribution, energy and momentum accommodation coefficients, etc 13 p2097 A67-26936

Gas atom scattering from solid surface, analyses and comparisons 13 p2097 A67-26937

Interactions of homonuclear diatomic gas molecules with fcc solid surfaces calculated by digital computer 13 p2098 A67-26938

Gas-solid energy exchange model, studying harmonic oscillator and free particle 13 p2098 A67-26939

Unified theory of gas-solid energy transfer in perturbation approximation, examining physical principles 13 p2223 A67-26940

Detection of vibrational structure of gases adsorbed on tungsten by low energy electron scattering 13 p2180 A67-27075

Kinetics of gas-solid reactions at high temperatures, noting mass transfer coefficients attainable, temperature discontinuities, stagnation lines, etc 15 p2582 A67-30022

Numerical calculations of interactions of monatomic gas particles with ideal and contaminated crystal surfaces at epithermal energies 15 p2434 A67-30197

Energy and momentum exchange model for interaction of gas particle with solid body surface 16 p2619 A67-30458

Flame propagation along interface between gas and reacting medium, studying fuel heating ahead of flame, noting radiation and convection role 18 p3151 A67-33816

Interaction of three-dimensional model of gas with solid surface, discussing atomic velocity distribution from surface reflection, energy and momentum accommodation coefficients, etc 19 p3264 A67-34936

Plasma-metal interface electric field intensity, deriving dimensionless formula from nonlinear second order differential equation 19 p3277 A67-35125

Radiative transfer in heterogeneous scattering medium with Fresnel reflection at slab boundary interface, computing transmittance, reflectance and absorbance [ASME PAPER 67-HT-19] 20 p3545 A67-36714

Electron emission models for evaluation of charge distribution and total energy of metal-gas interface, noting role of quantum mechanical corrections 24 p4202 A67-42087

Gas-solid interactions and buoyancy relation, discussing fluid density effect on Archimedes principle 24 p4119 A67-42695

GAS SPECTROSCOPY

Emission microwave spectroscopy of OCS, observing coherent ringing, coherent radiation modulation and pulse echoes 06 p1032 A67-18208

Dielectric relaxation of gases and sharp rise in microwave absorption coefficient in Cytherean atmosphere 08 p1401 A67-21372

Continuous spectra of atomic gases and low temperature plasma, analyzing photoionization cross section and electron transitions in neutral atom field 10 p1882 A67-23067

Stationary high density high temperature plasma production spectroscopic measurements, deducing arc radial

temperature and density profiles from line and continuum intensities and line profiles 19 p3274 A67-35103

Radial and axial temperature profiles of free-burning argon arc at various pressures, measuring continuum intensities [DVL-625] 19 p3278 A67-35135

Mean absorption coefficients for IR radiation of gases expressed as functions of gas spectroscopic and thermodynamic properties [ASME PAPER 67-HT-10] 20 p3545 A67-36708

Accurate determination of atmospheric gases spectral lines positions required for estimating atmospheric absorption coefficient of monochromatic laser radiation 20 p3462 A67-37559

Ion bombardment excitation used to extend excited state range for level crossing spectroscopy studies, giving Zeeman energy level diagram 22 p3835 A67-39239

GAS STREAM

Electric discharges in condensed hydrogen beams in high vacuum 03 p0475 A67-12922

Ignition of explosive powder by hot gas stream, with particular attention to heat transfer between substance and surrounding medium 06 p1112 A67-17956

Evaporation process of particles in high temperature gas stream under nonadiabatic conditions 08 p1428 A67-21424

Laminar diffusion flame in Oseen flow, identifying limiting case with stoichiometric Burke-Schumann flame and frozen flow 09 p1579 A67-21548

Airbrasion technique to improve Gunn oscillator performance using epitaxial GaAs, considering diode shape and contact structure 10 p1616 A67-23536

Nonstationary gas jet stream formation following shock wave outflowing from nozzle, obtaining calculation method 12 p1929 A67-25674

Oscillation of rod in gas stream investigated for nonlinear factor effect on oscillations 14 p2243 A67-28639

Gas stream discharge studied by using electromagnetic plasma gun to direct plasmods toward beam 15 p2472 A67-29726

Interaction of supersonic gas stream with inclined surface, calculating parameters and boundary of fluid spreading 15 p2472 A67-29776

Similarity parameters for gas generators obtained from equations governing gas-stream ejection 15 p2423 A67-30080

Uniform flow ionization in MHD generators produced by electric arc investigated for preionized gas stream 16 p2712 A67-30547

Determination of electron density and temperature, gas temperature, atomic composition and flow velocity of high temperature gas stream 17 p2900 A67-32339

Disintegrating liquid jet penetrating high speed gas stream 17 p2839 A67-33009

Electrode and insulator behavior in experimental MHD generator electrically producing temperature modulation of gas stream 18 p2988 A67-33708

Disintegrating liquid jet penetrating high speed gas stream investigated for amplification of capillary and acceleration waves [AIAA PAPER 67-495] 18 p3026 A67-33959

Conditions of stable burning of electric arc stabilized by gas stream in DC plasma arc torch, determining threshold current 19 p3281 A67-35150

Electric arcs in cross flow with variable magnetic field across electrode space 19 p3281 A67-35154

Two-dimensional turbulent mixing of supersonic reacting and nonreacting gases studied with square shock tube 21 p3606 A67-37772

GAS TRANSPORT

Phase-space collision domains corresponding to hard-sphere N-body problem in gas transport theory 01 p0112 A67-10144

Flame ignition from hot gas pocket, minimum size of gas bubble for flame propagation, dependence on chemical kinetic parameters and transport properties 02 p0342 A67-12030

Analogous studies of simultaneous conductive and radiative heat transfer across transparent laminar gas space, showing position of radiation shield between bounding surfaces 03 p0535 A67-13484

Gas transport cross sections, angular distribution of elastic scattering of colliding gas particles and transport equation degeneration 07 p1225 A67-19129

Monograph on theory of decompression sickness and application to diving tables, including calculation of critical size of localized bubbles formed from dissolved nonrespiration-involved gases in tissues [DVL-623] 11 p1748 A67-25036

Volt-ampere characteristics of diffused p-n junctions in epitaxial GaAsP film obtained by gas transport technique 12 p1984 A67-25519

Electric conductivity, Hall effect and photoconductivity of epitaxial single crystal GaAs films obtained by gas transport method 12 p1984 A67-25521

Gas mixture component concentration in fluid film flowing down wall, determining quantity of gas component transported by fluid per unit time 13 p2094 A67-26638

Volt-ampere characteristics of diffused p-n junctions in epitaxial GaAsP film obtained by gas transport technique 18 p3103 A67-34450

Electric conductivity, Hall effect and photoconductivity of epitaxial single crystal GaAs films obtained by gas transport method 18 p3103 A67-34452

Confined electric arc developed for gas-transport properties determination, noting measurement of flow pressure drop, radiative heat transfer, spectral temperature distribution, etc 18 p3091 A67-34731

Transport phenomena in electronic plasma as initial value problem noting distribution function relaxation 19 p3287 A67-35355

Heat transfer of gas between parallel plates including radiation and rarefaction effects treated, using kinetic theory 20 p3553 A67-36935

Gas transport cross sections, angular distribution of elastic scattering of colliding gas particles and transport equation degeneration 21 p3659 A67-38172

Integrated transport cross sections obtained for nitrogen as function of temperature using gaskinetic formulas 22 p3841 A67-40050

High temperature polyatomic gas and gas mixture transport properties, discussing thermoconductivity, multiple intermolecular potentials and plasmas 24 p4256 A67-42742

GAS TUBE

Neon tube staircase generator performing functions of frequency and voltage division 05 p0769 A67-16023

Hot gas tunnel for determination of material behavior under convective heat transfer conditions similar to that existing in rocket combustion chambers [AIAA PAPER 67-106] 06 p0981 A67-18473

Luminous front in electric shock tube having coaxial gun without current crowbaring measured by phototransistors 14 p2355 A67-27823

Performance of low energy-density electric shock tube in helium driver 14 p2293 A67-28752

Shock tube tests with cold argon and heated helium to determine heated driver gas effect on effect on shock tube performance 14 p2294 A67-29053

High temperature high power gas diodes and thyatrons for large nuclear electrical space power systems, noting parameters of design and performance 15 p2448 A67-29755

GAS TURBINE

SA AIRCRAFT ENGINE

SA TURBINE ENGINE

Nonlinearities such as limitation of linear characteristics, dead band, hysteresis, etc, in aircraft gas turbine control system 01 p0011 A67-10167

Centrifugal pump with vapor core principle combined with spill nozzle for application to aero engine fuel and reheat systems 01 p0014 A67-11267

Stress amplitude of gas turbine blades vibrating in resonance 02 p0336 A67-11466

Compressor cascades with different irregularities in forward flow, noting special case of low aspect ratio blades 02 p0179 A67-12439

BMW model 6012 gas turbine for helicopter application weighs 50 kg but develops 100 hp 03 p0502 A67-13007

Thermal stresses generation in nozzle blades of gas turbines tested in near operating conditions 03 p0429 A67-13332

General and mechanical property requirements for metal matrix composite materials used for aircraft gas turbine compressor blades 03 p0443 A67-13418

Transient air flow rates into gas turbine metered, using two critical flow circular arc venturi 03 p0421 A67-13770

Plastic strains in gas-turbine components under nonuniform cyclic heating, obtaining stress-strain relations 03 p0527 A67-14072

Strains in twisted blades with rectilinear axes, examining general relations and parameters in postulated new theory 03 p0528 A67-14080

Temperature and heat transfer conditions determination on rotating turbine wheel in jet power plant, using electric analogy 04 p0688 A67-14571

Gas turbines, regenerators, Wankel engine and Stirling engines, examining problem areas [AICE PREPRINT 45A] 04 p0691 A67-15944

Entropy and available energy in operation of gas turbine, considering thermodynamic efficiency, heat balance and available energy balance 05 p0873 A67-16742

Enthalpy to work conversion in gas turbines using pulsating combustion chamber 05 p0873 A67-16743

Materials evolution with high resistance to creep, mechanical and thermal fatigue, corrosion and impact, for gas turbine blades 05 p0829 A67-16744

Thermodynamic analysis of flow in gas turbines, for two- and three-dimensional boundary layers and wakes 05 p0748 A67-16745

Cooling gas turbine blades by heat pipe effect for stationary blades and thermosyphon effect for moving blades 05 p0874 A67-16747

Heat resistant nickel-based alloys for gas turbine blades and disks 06 p1018 A67-18232

Variable aerodynamic forces in turbine grid during passage of nonstationary gas flow 07 p1125 A67-19135

Variable thermal capacity of gas mixture taken into account in calculation of heat regeneration in gas turbine cycles, using working bodies 07 p1266 A67-19181

Jet propellant purity, safeguarding gas turbine fuel during production, transportation, storage and use 07 p1239 A67-19210

Thermodynamic cycle for solar power systems using hexafluorobenzene as working fluid, discussing efficiency and radiator area 07 p1131 A67-19366

Book on theory of flow machines covering pumps, turbines, windmills, fluid dynamics, viscous flow fields, cascade flow, etc 08 p1321 A67-20758

Load, vibration, temperature, surface oxides, etc, effect on wear resistance of materials for aircraft gas turbine engines 09 p1506 A67-22194

Hypothetical turbine driven power shaft bearing arrangement for logical analysis and practical approach to selection of optimum rolling bearings [SAE PAPER 670060] 09 p1508 A67-22534

Circumferential seal application and place in seal spectrum relative to gas turbines [SAE PAPER 670062] 09 p1508 A67-22536

Precision rolling for fabrication of small gas turbine compressor blades for use in aircraft and stationary engines [SAE PAPER 670095] 09 p1508 A67-22538

Aircraft gas turbine and fuel control design to meet engine requirement in broad environmental challenges [SAE PAPER 670140] 09 p1560 A67-22541

Gas flow velocity and static pressure profiles experimentally measured in combustion zone of gas turbine combustion chamber model under atmospheric conditions [SAE PAPER 670201] 09 p1561 A67-22545

High strength alloys for gas turbines in Soviet Union, noting wrought and cast nickel-base alloys for turbine blades and vanes 10 p1668 A67-23012

Book on propulsion systems covering gas-turbine engine, ramjet engine, chemical and electrical rockets, components, etc 10 p1698 A67-23689

Hot corrosion of aircraft gas turbine alloys operating in marine environment reproduced in laboratory test, analyzing nature of attack 11 p1804 A67-23918

Irregularly spaced nozzle vanes effect

upon blade vibration in radial flow gas turbine
[ASME PAPER 67-VIBR-42]

11 p1797 A67-24195
Evaluation of wire lacing designs for damping of vibratory stresses on gas turbine blades
[ASME PAPER 67-VIBR-47]

11 p1797 A67-24197
Soviet book on production of gas turbine engines covering manufacturing methods, automation of operations, tooling,
etc 11 p1798 A67-24516

Book on helicopter gas turbine engines 11 p1852 A67-24524

Heat regeneration and high gas temperatures for fuel economy in helicopter gas turbine engines 11 p1852 A67-24525

Annular vaporizing combustion chamber for small-size gas turbine engines, noting fuel-air flow 11 p1853 A67-24526

Control methods for parameters of helicopter gas turbine engines 11 p1853 A67-24527

Peculiarities of helicopter turbine engine with direct rotor drive 11 p1853 A67-24528

Helicopter exhaust-gas expansion and contamination of intake air under unfavorable wind conditions 11 p1853 A67-24529

High strength nickel base alloy with improved oxidation resistance up to 2200 degrees F for applicability to gas turbine engine components

[ASME PAPER 67-GT-1] 11 p1808 A67-24789

Lubrication system design and component arrangements for several oil and gas lubricated closed looped gas turbine machines

[ASME PAPER 67-GT-3] 11 p1799 A67-24791

Gas turbine design, considering thermodynamic and physical properties of various Rankine-cycle working fluids

[ASME PAPER 67-GT-6] 11 p1745 A67-24794

Pneumatic starting systems for gas turbine engines including energy sources, system components and arrangements

[ASME PAPER 67-GT-15] 11 p1854 A67-24800

Dependence of creep, corrosion and thermal fatigue of gas turbine vanes and blades upon inlet temperature and rate of change

[ASME PAPER 67-GT-17] 11 p1808 A67-24801

Vibratory type pressure oscillations in combustor with dual orifice fuel injection analyzed in gas turbine for possible elimination

[ASME PAPER 67-GT-23] 11 p1804 A67-24804

V/STOL aircraft gas turbine systems, discussing propulsion system configurations applied to fighter, fighter attack and transport cargo aircraft

[ASME PAPER 67-GT-48] 11 p1744 A67-24809

Gas turbine bucket alloy improvement via heat treatment, noting performance evaluation results from creep rupture tests

[ASME PAPER 67-GT-55] 11 p1808 A67-24811

Radial gas turbine losses, obtaining rotor loss coefficients, discussing flow pattern for performance prediction 12 p1891 A67-25347

Allison T63 engine sand and dust tolerance development and field experience

[SAE PAPER 670334] 12 p1990 A67-25875

High temperature long life turbine design, noting role of air cooling of critical parts

[SAE PAPER 670345] 12 p1990 A67-25880

Emulsified fuel mixture /JP-4 and water/ tested in model Allison T63 turbine engine

[SAE PAPER 670368] 12 p1987 A67-25883

Emulsified fuel effect on gas turbine combustors, noting good operation in low altitude flight but inhibited combustion at start and at high altitudes

[SAE PAPER 670366] 12 p1987 A67-25884

Gas turbine blade erosion from dust, discussing momentum separators and erosion-resistant coating 12 p1990 A67-25947

Traveling waves onset in gas turbine bladed disks, considering resonant vibrations 12 p2033 A67-26231

Stress-strain state and corrosion and erosion produced by aggressive gas flows in surface layers of gas turbine nozzle blades of ZhS6-K alloy 13 p2187 A67-26451

Self-ignition and fuel combustion at blade cascade taking place at velocities and temperatures comparable to those of gas turbines 13 p2187 A67-26746

Be use in aerospace structure, gas turbines and aircraft brake disks 13 p2138 A67-27118

Energy losses due to bleeding air from compressor for cooling systems of gas turbines 14 p2377 A67-28648

Optimum pressure drop in compressed air driven turbine as function of initial pressure in air cylinder and turbine parameters 14 p2252 A67-28652

Creep behavior of materials in nuclear reactors, gas turbines and electric power plants, noting aluminum alloy and high temperature material 15 p2502 A67-29506

High temperature superalloys for gas turbine applications noting alloys based on cobalt, iron, nickel and dispersion hardening 16 p2686 A67-30487

Requirements for operating characteristics of single and twin gas turbine engines for military helicopters noting system response, deceleration, fuel control, etc 16 p2736 A67-30929

Gas turbine auxiliary power unit design to provide boost to helicopter engine in powered and autorotational flight modes [AHS PAPER 116] 16 p2598 A67-31832

Computer program for design and routing of external plumbing of aircraft gas turbine engines 17 p2928 A67-32006

Film cooling theory applied to aircraft gas turbine chambers shows slot geometry effect as negligible 17 p2967 A67-32126

Book on design and structural strength of aircraft gas turbine engines covering inlet and exhaust systems, compressors, combustion chambers, rotors, etc 17 p2928 A67-32564

Burst strength in high speed rotor in axial blower/gas turbine, noting effect of ductility and centrifugal force 17 p2961 A67-32688

Design criteria and configuration for long-life aircraft gas turbines [SAE PAPER 670344] 17 p2929 A67-32988

Data selection, collecting and processing for automatic performance recording and monitoring of aircraft gas turbine engine, considering hardware and software [SAE PAPER 670360] 17 p2835 A67-32999

Temperature fields in cross section of gas turbine blade with internal coolant during variation of local heat-transfer coefficient 17 p2973 A67-33076

Heat-transfer coefficients for heat transfer from gas to blade surface in gas turbine under operating conditions 17 p2973 A67-33077

Hydrazine as single component fuel for gas generators and rocket engines, noting advantages and performance characteristics 18 p3106 A67-33459

Gas turbine environmental testing, measuring emulsified fuel flow, direct burning effects of JP-4 fuel on extended engine operation, etc 18 p3111 A67-33567

Soviet book on combustion chambers of gas turbine engines covering fuels, working processes, heating, etc 18 p3111 A67-33675

Ignition energy, quenching distance, flame stability and gas turbine burner performance of ammonia-air mixture 18 p3109 A67-33843

Temperature measurement for aircraft gas-turbine engine development 18 p3157 A67-33898

Variable turbine geometry in gas turbine engines, discussing part power fuel consumption, acceleration characteristics, etc [AIAA PAPER 67-417] 18 p3111 A67-33904

Electrostream process for drilling very small diameter holes in superalloys for gas turbine and nozzle vane fabrication [ASTME PAPER MR67-141] 18 p3054 A67-34175

Gas turbine theory based on Coanda effect and turbine efficiency from fluid flow analysis of depressive blade-fitted turbines 20 p3515 A67-36274

Fan jet engine performance and operation as affected by humidity 20 p3515 A67-36448

Air conditioning system of P-3 aircraft, noting redesign to include auxiliary power unit for functioning during ground operation 20 p3363 A67-36512

Gas turbine cooling, discussing high temperature problems, solutions and benefits of air cooled blades and vanes 20 p3517 A67-37168

Cooling losses in cooled gas turbines, correlating Cooling Loss Factor /CLF/ and Cooling Number /CN/ 20 p3517 A67-37484

Distribution of gas flow departure angle from annular turbine cascades 21 p3564 A67-37914

Quantitative method for determining sodium in gas turbine fuels by direct spectral analysis of unashed fuel samples 21 p3688 A67-38016

Heat treatment effects on mechanical properties of steel-forged gas turbine rotor shafts, including microcracks formation and growth and structural strength 22 p3819 A67-39323

Physicochemical combustion of turbulent air-fuel mixture in straight flow combustion chambers, noting effects of various factors and intensification methods 22 p3921 A67-40448

Fuel burnout processes in inlet flow of secondary air stream to turbine combustion chamber determined by working mechanism in inlet section of chamber 22 p3869 A67-40453

Optimum relative angular velocity selected for cooled high temperature gas turbine stages, discussing blade mean cooling depth and cooling heat 22 p3870 A67-40456

Coaxial rotors natural vibrations analysis by computer showing occurrence at rpms above first critical speed 23 p4009 A67-40685

Coated columbium alloy potential as turbine vanes in gas turbine power plants, discussing stress rupture strength, oxidation erosion and thermal fatigue lives [ASM PAPER C6-1.4] 23 p4020 A67-41402

Protective coatings of Ni and Co base superalloys for gas turbine engines, discussing microstructure, chemistry and phase composition [ASM PAPER C6-4.2] 23 p4020 A67-41405

Soviet studies of Ni-and Fe-based heat resistant aging alloys and aircraft gas turbine technology 24 p4169 A67-41919

Fastener applications for gas turbine engines noting materials selection and design 24 p4160 A67-42079

Glass fiber reinforced gas turbine engine compressor blade thermal stability for short cycle heat stress damage 24 p4249 A67-42103

Surface temperature oscillations of externally cooled working blades of gas turbine with air-liquid mixtures 24 p4254 A67-42255

GAS VALVE

Temperature, valve and insulation criteria for designing low thrust subliming solid reaction systems 15 p2544 A67-29979

Pulse-length modulated pressure waves having zero quiescent pulse width, actuating floating flappper disk switching valves of pneumatic servomechanism 16 p2609 A67-31665

GAS VISCOSITY

Molecular quadrupole moments and shape parameters derived from viscosities and second virial coefficients 06 p1038 A67-19047

Electron components for electrical, thermal conductivity and viscosity coefficients of gas mixtures calculated via molecular kinetic theory 07 p1225 A67-19116

Viscosity and thermoconductivity values of partially ionized argon plasmas derived by investigating temperature decay and stream velocity distribution in argon plasma jet 15 p2531 A67-30203

Viscosity of neon-nitrogen, helium-carbon dioxide and nitrogen-argon mixtures 18 p3161 A67-34522

Turbulent gas flow viscosity, thermoconductivity and friction coefficients in tube 21 p3611 A67-37912

Electron components for electrical, thermal conductivity and viscosity coefficients of gas mixtures calculated via molecular kinetic theory 21 p3659 A67-38161

GAS WELDING

SA TUNGSTEN INERT GAS /TIG/ WELDING

Plasma arc welding for fabricating 120-inch-diam D6AC steel rocket motor cases, comparing gas tungsten arc welds 01 p0080 A67-10944

Fabrication of columbium alloy liquid metal loop to study boiling and condensing characteristics of Na and K up to 1000 degrees F with gas tungsten arc welding in helium atmosphere 01 p0080 A67-10945

Transverse oscillated electron beam welding procedures of D6AC steel and mechanical properties evaluation show comparable results to corresponding gas tungsten arc welds 01 p0080 A67-10946

Mississippi Test Facility gas metal-arc welding of T-1 steel critical high pressure

- piping systems for Saturn V launch vehicle 03 p0430 A67-13691
 Crack propagation in heat-affected zone during HF AC current gas-tungsten arc welding of Al alloy test 03 p0430 A67-13693
 Gas-shielded stud welding of magnesium 12 p1950 A67-25739
- GAZEOUS CAVITATION**
 Collapse of isolated spherical vapor-air cavitation pocket moving toward solid surface in incompressible fluid medium 12 p1927 A67-25320
- GAZEOUS DIFFUSION**
 Hydrogen diffusion in tantalum at temperature interval of 0 to 100 degrees C 01 p0102 A67-10941
 HF gaseous squeeze film bearing asymptotically analyzed by considering internal and edge regions separately [ASME PAPER 66-LUB-11] 03 p0431 A67-13760
 Radiation diffusion in gas analyzed by solving transport equation for homogeneous absorbing isotropically scattering spherical shell with point source in center 04 p0695 A67-14656
 Effect of diffusion-pump fluid contamination and degradation on explosion hazard of operating diffusion pumped system 06 p0979 A67-17632
 Thermomechanical theory of diffusing and chemically reacting mixture and application to elastic materials mixture subject to diffusion and heat conduction 15 p2517 A67-29463
 Ion mobility in gases determined, based on kinetic equation for ion velocity distribution function with particular reference to Chapman-Enskog method 16 p2704 A67-31250
 Solution drops motion in diffusing binary gas mixture, analyzing velocity 20 p3421 A67-36812
 Gaseous ternary diffusion instabilities observed by ammonium chloride smoke technique, studying pressure and composition effects 22 p3917 A67-39713
 Concentration distribution time for heavy gas diffusing in light gas steady flow field 22 p3917 A67-39714
 Hydrogen diffusion in tantalum at temperature interval of zero to 100 degrees C 22 p3820 A67-39794
 Two-dimensional diffusion model for gas propagation in lunar atmosphere, discussing contamination by lunar module exhaust gases and solar wind loss mechanism 22 p3883 A67-39817
 Differential equation system for reacting laminar boundary layer heat and mass transfer solved analytically, noting compressible gas and porous foil filter 23 p4081 A67-40744
 Helium RF discharge radiation temperature as magnetic field function measured, discussing enhanced diffusion role in radiation temperature determination 23 p4032 A67-40897
 Space distribution function of Knudsen gas in closed volume investigated using gas model noting dependence of time 24 p4190 A67-41902
 Oxygen diffusion through lubricant to metal surface examined for influence in corrosive wear [ASLE PAPER 67-LC-4] 24 p4164 A67-42743
- GAZEOUS FISSION REACTOR**
 Change in critical mass of large reflector moderated gaseous-fueled cavity reactor due to presence of hot hydrogen gas in cavity 12 p1965 A67-25908
- GAZEOUS IONIZATION**
SA PENNING DISCHARGE
 MHD power generation, presenting electrical conduction in gases, seeding and ionization, equations, conversion efficiency, electrical losses, compressible flow theory and application to various cycles 01 p0013 A67-10556
 Size distribution of electron avalanches in methane gas under electric field no longer satisfy Furry distribution due to first Townsend ionization coefficient 03 p0473 A67-13463
 Plasma formation by dissociation of diatomic hydrogen ions by Lorentz force 04 p0671 A67-15645
 Mass spectrometric observation of ions formed during shock wave heating of gaseous krypton and xenon at 3600 to 7800 degrees K 05 p0795 A67-17440
 Gas ionizing shocks for plane flows with magnetic field lying in flow plane 08 p1358 A67-20895
 Large disk MHD generator studied for plasma properties and fluid mechanics, noting seed ionization effect on performance 12 p1972 A67-25388
 Thermal electrode boundary layer for shock wave ionized air ohmic heating in discharge chamber, noting Joule heat consumption effect 12 p1975 A67-25894
 Ionization structure of elements H, He, C, N, O, Ne in planetary nebulae computed for theoretically determined electron temperature and electron density variation 14 p2382 A67-27847
 Gas-ionizing shock wave with zero electrical conductivity of gas in front of shock wave and infinite conductivity behind 15 p2470 A67-29310
 Decrease in degree of ionization of shock-heated argon resulting from radiative emission 15 p2527 A67-29563
 Ionizing detonation wave model with electrical conductivity jumping from zero to infinity characterized by exothermal energy release and magnetoacoustic speed propagation 15 p2528 A67-29567
 Magnetically induced ionization in nonseeded helium and argon gas mixtures used to determine nonseeding operation of MHD generator in nonequilibrium ionization mode 16 p2711 A67-30542
 Physical/chemical characteristics of thermionic plasma noting equipment and technology involved 16 p2722 A67-31564
 Ionization processes in hot products of combustion processes / flame gases/ as weak plasma media noting flame properties, mass spectroscopy, electron concentration, etc 17 p2967 A67-32140
 Ionization of low temperature supersonic plasma jets, noting kinetics of elementary processes, gas dynamic parameters and effects of combustion and alkali metal admixtures 17 p2896 A67-32170
 Propagation of strong ionizing front at arbitrary oblique angle relative to magnetic field, determining limits to value of electric field ahead of shock 17 p2908 A67-33114
 Energy distributions of hydrogen and deuterium ions from dissociative ionization of hydrogen and deuterium 17 p2889 A67-33226
 Fabry-Perot interferometric observation of spectral line to investigate ionization rate of electrical discharge used for argon ion laser 18 p3061 A67-34044
 Ionization mechanism of argon-permanent gas mixture in radiolionization detector used for gas chromatography 19 p3226 A67-34797
 Ionization decay in cesium vapor explained in terms of dissociative recombination and diffusion, showing strong dependence on vapor pressure 19 p3271 A67-35072
 Ionization rate at higher electron densities in DC fields measured in toroidal discharge tube 19 p3272 A67-35078
 Photon transmission delaying processes and secondary ionization growth time dependence on overvoltage in neon 19 p3264 A67-35086
 Gas ionization and plasma heating by high power microwaves using X-band and S-band frequency magnetrons 19 p3276 A67-35115
 Argon plasma ionization by oscillator supplying power near electron cyclotron resonance, measuring density variation 19 p3276 A67-35116
 Space-charge and potential distributions calculated for region between two plane electrodes of single collision model 19 p3265 A67-35129
 Excitation and ionization mechanisms in positive DC discharge columns in krypton and xenon 19 p3265 A67-35131
 Dynamics of channel formation in nonisothermal pulsed discharge and nonequilibrium ionization in inert gas-cesium mixtures 19 p3278 A67-35132
 Argon, deuterium and air ionization at atmospheric pressure and lower by focused ruby laser radiation, analyzing plasma spectrum 19 p3239 A67-35166
 Partition function of partially ionized hydrogen two-component plasma 19 p3285 A67-35346
 Plane ionization wave propagation in uniform magnetic field compared with flame front expansion during slow burning 19 p3286 A67-35347
 Initial ionization processes in shock heated argon consisting of atom-atom collisions followed by electron-atom processes 19 p3293 A67-35397
 Energy dissipation of strong magnetosonic waves in rarefied plasma, discussing electrons ionizing collisions at wave front 19 p3293 A67-35402
 Ionizational relaxation and excitation behind shock waves, proposing solution for kinetic equation system 19 p3293 A67-35403
 Plasma production by optical irradiation of gases and by solids, considering interaction of laser radiation with surfaces and irradiation of particles of solid material in vacuum [AIAA PAPER 66-174] 21 p3642 A67-38851
 Electric power generation with closed cycle MHD conversion fluid having gases with high equilibrium conductivity, discussing ionization and electrothermal instability 24 p4099 A67-42416
- GASKET**
 Seals, Reference Issue, Machine Design magazine, March 9, 1967 09 p1509 A67-22610
 Potential hazards of Teflon gaskets in liquid fluorine systems 13 p2187 A67-27689
- GASOLINE**
S PETROLEUM
GASTROINTESTINAL SYSTEM
SA DIGESTIVE SYSTEM
SA INTESTINE
 Postulates on microbial hazards of astronauts in prolonged isolation based on studies with animals with locked flora 05 p0755 A67-16281
 Gastrointestinal symptoms and drug use as possible contributing causes of fatal crash of race pilot 09 p1456 A67-21734
 Gastroenterology in space medicine and physiological basis of cosmonaut nutrition 13 p2058 A67-26752
 Physiological regeneration on cornea epithelium and intestines exposed to fractional irradiation with fission neutrons, studying mitotic index and chromosome aberrations content 16 p2613 A67-30909
 Exposure to acceleration and prolonged confinement in bed studied for effects on functional state of human stomach 16 p2613 A67-30915
 Gastroesophageal reflux in fliers measured in evaluation of hiatal hernia and possible esophageal origin of chest pain 21 p3574 A67-38084
 Microbic shock in human organism during prolonged space flight due to intestinal tract flora variation from food consumption lacking variety 22 p3750 A67-39334
 Gastroesophageal reflux measurements in evaluation of hiatus hernia and chest pain in fliers 23 p3954 A67-41599
 Nervous and humoral mechanisms of extralabyrinthine effects on vegetative disturbances during space flight factors 24 p4111 A67-41843
- GAUGE**
SA FUEL GAUGE
SA ION GAUGE
SA IONIZATION GAUGE
SA MCLEOD GAUGE
SA PENNING GAUGE
SA PIRANI GAUGE
SA PRESSURE GAUGE
SA STRAIN GAUGE
SA THERMOCONDUCTIVITY GAUGE
SA THERMOCOUPLE GAUGE
SA VACUUM GAUGE
 Aircraft fuel gauging systems noting float type and reliability defects [SAE PAPER 670263] 11 p1789 A67-23986
- GAUSS FUNCTION**
 Asymptotic rate of convergence of Gauss-Seidel type iterative processes for nonlinear difference equations 03 p0460 A67-13881
 Gauss theorems for tensor with valence other than unity extended to include arbitrary orthogonal coordinates 14 p2349 A67-28738
 Numerical characteristics of random functions applied to aircraft load evaluation 16 p2596 A67-31152
 Linear algebraic equations arising from least squares estimation problem, noting Gaussian elimination process on matrices 16 p2847 A67-31651
 Book on computer solution of linear matrix algebraic systems and errors involved, discussing Gaussian elimination, FORTRAN, ALGOL and PL/1 programs,

etc 17 p2821 A67-32825
 Optical determination accuracy of satellite orbits, investigating orbit elements by Gaussian averaging calculation assuming elliptical orbit 22 p3830 A67-39161
 Interaction of two H atoms in ground states using Hirschfelder-Linnet wave function and Gaussian type function 22 p3756 A67-39385
 Geometrical self-shadowing of random rough surface described by Gaussian statistics in wave backscattering phenomena 23 p3972 A67-40832

GAUSS-MARKOV THEOREM
 Optimal filtration of nonlinear functional of Gaussian signal, obtaining expressions for kernels of optimal filter 05 p0782 A67-16317
 Optimal filtration of nonlinear functional of Gaussian signal, obtaining expressions for kernels of optimal filter 18 p3016 A67-33868

GAUSSIAN DISTRIBUTION
 Stability analysis of nonlinear stochastic systems in presence of random and Gaussian perturbations, determining validity of law of large numbers and amplified law of large numbers 02 p0267 A67-11958
 Adaptive technique determination of optimum operations for pure prediction of discrete time series with respect to mean square error cost function 02 p0207 A67-12138
 Computer program for digital exact representation of spectral frequency-and intensity-distribution by superposition of Gaussian components, applying least squares method, linearizing normal equations and analyzing observational errors 06 p0965 A67-18069
 Generalized Gaussian distribution functional for weak plasma turbulence neglecting three-point correlation function 08 p1366 A67-21415
 Density of Gaussian distributions and Wiener-Hopf integral equation 11 p1812 A67-24100
 Optical configuration for long distance laser beam transmission determined from truncated Gaussian aperture distribution radiation patterns 11 p1754 A67-24724
 Dispersion of number of positive zeros as function of time for realization of quasi-harmonic random signal 11 p1754 A67-24985
 Statistical estimates for Gaussian random processes shown to be asymptotically normal and efficient 12 p1960 A67-25312
 Two uncorrelated Gaussian dependent random variables with non-Gaussian joint distribution may have any maximal correlation coefficient 12 p1960 A67-25313
 Asymptotic methods of obtaining refined solutions for zero moment equations of concentrated loads applied to shells with Gaussian curvature 12 p2028 A67-25630
 Higher order time correlations, skewness, flatness and non-Gaussian probability density distribution in turbulent field 13 p2092 A67-26278
 Collective scattering cross section and collective spectral extinction of Mie scattering with logarithmic Gaussian distributions 13 p2150 A67-26432
 Steady state one-dimensional carrier distribution in depth for electron beam excitation of semiconductors computed, including diffusion and surface recombination 15 p2442 A67-29180
 Gaussian and Lorentzian components separation in analyzing EPR spectrum in ruby, using variance techniques 15 p2536 A67-29499
 Measurements of short term frequency or phase fluctuations of gas lasers, noting random Gaussian perturbation 15 p2499 A67-29730
 Recursive procedures for determining relationships between random parameter of linear system and resulting output random variable 16 p2652 A67-31691
 Stability analysis of nonlinear stochastic systems in presence of random and Gaussian perturbations, determining validity of law of large numbers and amplified law of large numbers 17 p2886 A67-33275
 Feedback-signal lag and channel discreteness effect on rate of information transmission over Gaussian channel with feedback during symbolized coding 18 p2999 A67-33531
 Random processes from physical viewpoint, discussing random function, random noise properties, Gaussian

distribution, digital analysis, Shannon sampling theorem, etc 20 p3483 A67-36459
 Interstellar extinction wavelength dependence, assuming ice particle radii distribution function obeys decreasing power law and graphite particles have Gaussian distribution function 22 p3889 A67-40304
 Molecular band spectra of CN emission assuming Gaussian rotational line profile 23 p4030 A67-41695

GAUSSIAN NOISE
 Comparison of variances evaluated by Kolmogorov and Volterra techniques for phase locked loop subjected to white Gaussian input 01 p0044 A67-10480
 Optimal control system for linear plant with modulus limited control actions 01 p0044 A67-10491
 Book on noise and effect on communication covering random processes, fundamentals and spectra, nonlinear transformations /demodulation/, statistical theory of detection and information theory 01 p0024 A67-10725
 Phase cancellation of sinusoidal signals in presence of Gaussian noise for comparison and threshold decision schemes 01 p0025 A67-10860
 Dynamic programming recursive estimation of modal trajectory for nonlinear non-Gaussian noise and comparison with Bayesian estimation and case of Gaussian white noise 01 p0047 A67-11214
 Gaussian noise model of shadowing effect on wave backscatter from one-dimensional random rough surface 02 p0192 A67-11602
 Digital generation of continuous filtered Gaussian noise 02 p0194 A67-11809
 Passive detection of sonar target in presence of Gaussian noise background with unknown spectral quantities 02 p0217 A67-12087
 Effect of feedback capacity addition to M-ary PAM communication system perturbed by white Gaussian noise 02 p0204 A67-12170
 Time limited receiver signals design for minimizing error probability under energy and frequency constraints 02 p0204 A67-12171
 Equivalent gain and error response of hysteretic system to Gaussian inputs 04 p0593 A67-15637
 Approximate minimax detection of vector signal in Gaussian noise 05 p0834 A67-16493
 Optimum quadratic detection of sample vector from signal random process imbedded in Gaussian noise 05 p0765 A67-17041
 Statistical properties of amplitude and phase of output signal of electron beam quadrupole amplifier with superposition of regular signal plus Gaussian noise at input 05 p0765 A67-17182
 Energy dissipation effect on vibrations of elastic element with one degree of freedom excited by steady state random Gaussian disturbance 05 p0923 A67-17182
 Distribution function for probability density of random process at output of multiplier acted upon by envelopes consisting of Gaussian noise and pulse signal 05 p0767 A67-17397
 Digital computer simulation of nonstationary Gaussian processes using Gaussian white noise, with application to simulation of structural response, ground acceleration, velocity and displacement of earthquake 06 p1109 A67-18839
 Reliability of phase manipulated signal transmission with transient processes in channels and additive white noise 09 p1463 A67-21962
 Optimal control system for linear plant with modulus limited control actions 10 p1621 A67-23613
 Number of intersections of level by Gaussian stochastic process 11 p1812 A67-24099
 Threshold region of FM signals having carrier modulated by Gaussian baseband signal 11 p1752 A67-24124
 Optimum reception problem of two zero mean Gaussian signals solved through comparison of quadratic form in observable waveform with predetermined threshold 11 p1760 A67-24235
 Output characteristic function for two-channel analog cross correlator with each channel input consisting of deterministic signal combined with stationary Gaussian noise 12 p1916 A67-26080
 Output correlation function for N-step symmetric amplitude quantizer with summed

sine wave and Gaussian noise input, noting approximations for low SNR 12 p1908 A67-26084
 Lower bounds on error probability for communication in presence of white Gaussian noise with no bandwidth constraint 12 p1908 A67-26086
 Nonlinear Bayes detector synthesized for Gaussian signal and noise fields using Wiener filters 12 p1919 A67-26087
 Use of limiters for estimating signal to noise ratio 12 p1908 A67-26094
 Energy detection of unknown deterministic signal in white Gaussian noise by energy measuring device 13 p2067 A67-26510
 Set of curves relating statistical properties of envelope detector output to SNR of CW signal in narrow band Gaussian noise at input 13 p2070 A67-27154
 Convolutional encoder for orthogonal tree codes in presence of white Gaussian noise [JPL-TR-32-1120] 14 p2273 A67-28710
 Discriminator threshold and SNR above threshold response when demodulating FM signal undergoing selective fading 14 p2273 A67-28711
 Two-dimensional characteristic function and probability-distribution density of random process which is phase modulated by normal noise 15 p2435 A67-29348
 Permutation modulation systems comparison based on proved-best criterion of alphabet size and minimum distance between signal vectors 15 p2439 A67-30384
 Error probabilities of matched filter receiver operating in additive combination of impulsive and Gaussian noise 17 p2812 A67-32120
 Probability density function of ratio of two nonzero mean Gaussian random variables derived and applied to calibrated signal using noisy calibration levels 17 p2816 A67-32624
 Repeating incoherent pulsed signal detection problem in Gaussian noise studied by binary integration method assuming ideal control criteria 18 p2999 A67-33505
 Random characteristics of second order phase locked loop with Gaussian noise input, using digital simulation 18 p3017 A67-34104
 Optimal multidimensional systems for discriminating and detecting signals dependent on finite number of random parameters and combined with noise 19 p3185 A67-36097
 Linear optimal stationary control system with state dependent white noise disturbances described by differential equation 20 p3408 A67-37077
 Reliability of phase manipulated signal transmission with transient processes in channels and additive white noise 20 p3383 A67-37192
 Asymptotic relative efficiency of mixed statistical threshold tests with Gaussian samples 20 p3412 A67-37495
 Binary symmetrical channel noise effect on PCM picture quality compared with white Gaussian noise effect in PAM system 20 p3386 A67-37496
 Optimal nonlinear filtering, deriving differential equations for probability density or state vector for noise corrupted system 21 p3603 A67-38442
 Orthogonal signaling in sequential decision feedback on communication over additive white Gaussian noise channel, obtaining expression for error probability 22 p3775 A67-39295
 Fredholm equation solution and minimax theory for p-dimensional vector signal detection against p-dimensional Gaussian noise background 22 p3762 A67-39876
 Error correcting codes for white Gaussian channel at low signal to noise ratio, discussing properties and performance criteria 23 p3984 A67-40752
 Random Gaussian signal with unknown mean value reception using adaptive systems 24 p4120 A67-42224
 Error probability for binary signaling through multipath channel with receiver waveform comprising white Gaussian noise and time delayed frequency-shifted signal 24 p4121 A67-42341
 Axis crossing intervals of sine wave plus noise 24 p4122 A67-42343
 Optimal reception of binary signals on background non-Gaussian noise determined

- by logarithm expansion for probability
coefficient into Taylor
series 24 p4122 A67-42377
- GCR**
GAS COOLED REACTOR /GCR/
GEAR
- SA LANDING GEAR**
Gear combination systemization providing
ultraprecise ratios 04 p0627 A67-14706
Torsional vibration and steady state
response of geared system, noting computer
programming
[ASME PAPER 67-VIBR-63] 11 p1797 A67-24205
- Small size cylindrical gear reduction
system design for servomotors of synchro
systems in electronic
equipment 11 p1745 A67-24553
- Gears evaluation testing under vacuum
chamber space simulation
[ASME PAPER 66AM-7A4] 13 p2123 A67-27099
- Transmission noise control to achieve
helicopter cabin noise levels comparable to
fixed wing jet aircraft, discussing system
phasing of planetary gears
[ASME PAPER 67-DE-58] 14 p2328 A67-28883
- Axial gear differential /AGD/ design and
selection for constant speed AC generator
drive for aircraft engines 17 p2800 A67-31976
- Worm gear lubrication with bonded solid
film lubricants, discussing efficiency and
wear life test apparatus
[ASME PAPER 67-LC-18] 24 p4165 A67-42751
- GEAR TOOTH**
Gear lubrication fundamentals and
principles of oil film formation on mating
gear tooth surfaces 02 p0250 A67-12499
- Gear materials and lubrication methods to
satisfy high speed and temperature
requirements in aerospace
applications 14 p2334 A67-27791
- Bending strength of spur gear teeth
calculating methods to optimize design for
high speed, lightweight aircraft gearing
[AHS PAPER 118] 16 p2884 A67-31834
- Surface-temperature conditions in disks
and gears stressing heat transfer coefficient
and lubricated contact
temperature 19 p3237 A67-35840
- Lubricants, metal high temperature and
atmospheric environments effects on gear
load-carrying capacity
[ASME PAPER 67-LUB-27] 24 p4164 A67-42685
- GEIGENSCHEIN**
Lunar and cislunar observation of
interplanetary medium including lunar
magnetic field, solar wind, existence of
collisionless shock wave, gegenschein,
zodiacal light and recovery of interplanetary
particles 04 p0700 A67-15072
- Observational consequences of geocentric
dust cloud whose particles are concentrated
toward plane of ecliptic and which
contribute to zodiacal
light 19 p3222 A67-35460
- GEIGER COUNTER**
SA NEUTRON COUNTER
Flux intensity and energy spectra of
galactic X-ray sources, Tau X-1 and other
celestial bodies studies, using three sensitive
Geiger counters 01 p0144 A67-10562
- Azimuthal asymmetry in distribution of
shower particles around shower axis, using
Geiger-Muller counter
telescopes 01 p0145 A67-11230
- Solar X-ray emission measurements with
Geiger photon counters carried by Elektron
II and IV satellites 02 p0240 A67-11544
- Physical characteristics affecting detection
efficiency of Geiger counters, proportional
counters and ion chambers used in space
measurements of
particles 02 p0244 A67-12209
- Primary cosmic rays of superhigh energy
using extensive air shower data, noting
Geiger-Muller counters, scintillation counters
and muon detector 02 p0311 A67-12589
- Cosmic radiation intensity measurement
using automatic interplanetary stations with
on board Geiger counters 05 p0879 A67-16106
- Cosmic radiation directional intensity
during solar activity minimum, noting
altitude dependence of charged particle
photon flux 05 p0883 A67-16878
- Apparatus used to study exoelectronic
emission from metallic surfaces, detailing
Geiger counter, high voltage rectifier,
scaling device and counting rate
meter 07 p1201 A67-19256
- Energy spectra of Tau X-1 and isotropic
component of galactic X-rays, using
rocketborne scintillation and GM
counters 10 p1701 A67-23229
- Satellite-borne detection of decay protons
as test of solar neutron
observation 17 p2937 A67-32544
- Cosmic radiation intensity measurement
using automatic interplanetary stations with
onboard Geiger counters 24 p4213 A67-42782
- GEL**
Gel permeation chromatography for
analytical fractionation of propellant binder
prepolymers and separating and purifying
labile binder ingredients 04 p0686 A67-14472
- Chemistry and rheology of gelled fuels,
noting structure, thickeners,
etc 10 p1696 A67-22911
- GELATIN**
Automatic rigidizing of expandable fabric
impregnated space structures, detailing
gelatin system 08 p1345 A67-20433
- GEMINI 4 MISSION**
Radiation levels on Gemini IV flight
including Van Allen belt and South Atlantic
Anomaly 15 p2425 A67-29105
- GEMINI 5 MISSION**
Oxygen A band near 7600 angstroms used
by Gemini V astronauts to measure cloud
top altitude, showing method of computing
correction factor 06 p1026 A67-18563
- Cloud measurements from Gemini 5 from
reflected solar radiation spectra of oxygen A
band region 22 p3807 A67-40369
- GEMINI PROJECT**
SA MERCURY PROJECT
Structural safety of Mercury and Gemini
vehicles, noting fail-safe and fracture
tolerant design
[SAE PAPER 660681] 01 p0154 A67-10585
- Vibrating-piston electrostatic field sensor
for Gemini program, examining design
improvements including unity-feedback
preamplifier, noise reduction devices,
etc 01 p0074 A67-11127
- Reliability overstress testing of Gemini
inertial measuring unit system electronics
package, discussing vibration and
temperature/altitude environment
results 01 p0111 A67-11363
- Weather and cloud photography during
Gemini space flights and effect on
interpretation of satellite weather
pictures 01 p0109 A67-11393
- Transmittance measurements and
consequent cloud top determination by
Gemini V hand-held spectrographic
camera 01 p0061 A67-11396
- Manned extravehicular activities and
equipment used in Gemini space flight
program 01 p0018 A67-11414
- Scheduling manned space flight
missions 04 p0704 A67-14902
- Gemini program evaluation, discussing
information gained from experiments
performed during flights
[AIAA PAPER 66-1027] 04 p0704 A67-14979
- Structural dynamics of Gemini program,
discussing environmental prediction,
component testing, docking system, stability,
etc 05 p0924 A67-17212
- Missions of Gemini VI through XI
covering rendezvous, docking, thermal
overloading, translation maneuver,
etc 06 p1094 A67-18198
- Gemini rendezvous results, discussing
equipment, maneuvers, docking,
stationkeeping, orbital calculation,
etc 06 p1098 A67-18649
- Hypergolic propellant ignition experience
during Project Sure Fire of Gemini program
[AIAA PAPER 67-259] 07 p1241 A67-20046
- Mechanized hybrid real time simulation
for Gemini crew to use in rendezvous
procedures
[AIAA PAPER 67-250] 07 p1166 A67-20068
- Gemini rendezvous experience, describing
flight test cycles, type of maneuvers needed,
ground and onboard support systems, etc
[AIAA PAPER 67-272] 07 p1280 A67-20081
- Planned interdependency incentive method
/PIIM/ for Gemini program at lowest cost
and best performance
[AAS PAPER 66-157] 08 p1430 A67-20974
- Management aspects of design and
development of Gemini spacecraft noting
program organization, management
techniques and personnel motivation
[AAS PAPER 66-158] 08 p1430 A67-20975
- Gemini ground support system extension
to cover Apollo program, stressing launch
- complex, deep space tracking, S-band
linkage, communications satellite,
etc 08 p1317 A67-21281
- Visual observations of earth, sea and sky
made by astronauts and cosmonauts during
space flights 09 p1569 A67-22604
- Prism and grating spectra obtained during
Gemini XI mission providing UV energy
distribution data and Balmer
discontinuity 10 p1706 A67-23060
- Gemini experiments program, examining
crew integration, mission planning and
prelaunch operations 10 p1713 A67-23243
- Manned planetary exploration, Mercury
and Gemini flight programs and projected
goals of Apollo Applications
Program 12 p2002 A67-25233
- NASA earth orbital photographic
experiments planned for 1967-1969 as
supplement to Mercury and Gemini
efforts 12 p1940 A67-25433
- EEG data from Astronaut Borman on
Gemini flight GT-7 13 p2062 A67-26919
- Gemini inflight experiments on space
perception via measurements of ocular
counterrolling as test of otolith
function 13 p2062 A67-26920
- Planned interdependency incentive method
/PIIM/ for Gemini program at lowest cost
and best performance
[AAS PAPER 66-157] 13 p2233 A67-27558
- Management aspects of design and
development of Gemini spacecraft noting
program organization, management
techniques and personnel motivation
[AAS PAPER 66-158] 13 p2233 A67-27559
- Gemini-Apollo capability, Apollo
application and proposed earth-orbital
experiments, describing typical missions
with illustrative experimental
payloads 16 p2756 A67-30627
- Gemini guidance and control, discussing
design, ground monitoring, launch and flight
guidance, spacecraft instrumentation,
maneuvering, etc 16 p2700 A67-30659
- Cryogenic fluid storage subsystems for
Gemini program, noting more advanced
designs for Apollo, Lunar Module,
Biosatellite, Manned Orbiting Laboratory,
etc 17 p2954 A67-32013
- Micrometeoroid collection experiments
flown on Gemini IX and Gemini XII
analyzed, using optical and electron
microscopy and mass
spectrometry 19 p3339 A67-35196
- Gemini program study to provide safe and
biologically sound method of man qualifying
for space exploration 19 p3177 A67-35208
- Terrestrial microorganism survival in
space aboard Gemini satellite, discussing
lethal effects of solar
radiation 19 p3178 A67-35223
- Retrofit accountability system
requirements, environment, purpose and
future applications 20 p3556 A67-36545
- Spacecraft optical environment,
considering sky luminance, spacecraft
corona, spacecraft scattered light and glare
sources 21 p3713 A67-38568
- Gemini program engineering aspects
compared to Gemini/Mercury, discussing
basic design rules adopted and Apollo
Applications Project
objectives 22 p3904 A67-40064
- Biomedical results for various human
medical systems during weightlessness
experiments of Gemini program, noting
vestibular function and
EVA 22 p3752 A67-40534
- GEMINI SPACECRAFT**
Design, construction and operation of
vacuum chamber space simulator for testing
Gemini space capsule 01 p0049 A67-10303
- Nautical chart information extracted from
hyperaltitude color photographs obtained on
Gemini orbital flights IV, V and
VII 01 p0059 A67-10322
- Fuel cell construction principles, oxidation
potentials of prospective fuels and Gemini
GT-5 space capsule fuel
cell 01 p0014 A67-10639
- Night sky phenomena and atmospheric
attenuation of light from Beta Canis Majoris
photographed from Gemini
IX 01 p0151 A67-10965
- Data and mission analysis in man-rating of
Gemini launch vehicle 01 p0155 A67-11347
- First orbit rendezvous mission planning
with no ground support after spacecraft
liftoff, considering propellant costs,
procedural timing, terminal approach,

etc 02 p0333 A67-12343
 Reliability considerations in spherical solid
 retrorockets for Gemini spacecraft
 system 02 p0305 A67-12351
 Gemini manned space flight
 program 02 p0327 A67-12363
 Gemini carbon dioxide sensor for
 monitoring in closed loop breathing system
 useful for many gas
 measurements 05 p0806 A67-16549
 Reentry trim angle of attack and lift-drag
 ratios from Gemini flights compared to wind
 tunnel data for aerodynamic studies
 [AIAA PAPER 67-166] 06 p0939 A67-18295
 Gemini VII star sightings analyzed, using
 handheld space sextant in Gemini VI,
 discussing effect of bias, timing angle
 measurement and trajectory
 errors 13 p2154 A67-26817
 Axial vibration /pogo stick effect/ of
 Titan II, as Gemini launch vehicle, studied
 by analog computer simulation for instability
 influences 14 p2394 A67-28086
 Gemini window contamination due to
 outgassing of silicones 15 p2507 A67-29555
 Medicophysiological aspects of NASA
 program stressing cardiovascular, muscular
 and osseous problems 16 p2614 A67-31538
 Reentry trim angle of attack and lift-drag
 ratios from Gemini flights compared to wind
 tunnel data for aerodynamic studies
 [AIAA PAPER 67-166] 17 p2789 A67-32061
 Vacuum system pressure measuring and
 monitoring by remote control methods as
 used in Gemini spacecraft test
 program 17 p2859 A67-32593
 Rescue teams for manned testing in
 environmental chamber for Gemini
 spacecraft noting personnel, chamber and
 personal equipment, test operations and
 rescue function and drill 17 p2807 A67-32598
 Gemini spacecraft antennas performance
 during reentry into ionized medium,
 discussing electron concentration profiles,
 nonearth atmosphere extrapolation and
 antenna breakdown effect 21 p3591 A67-38210

GENERAL DYNAMICS MILITARY
AIRCRAFT
 S F-111 AIRCRAFT
GENERATION
 S HARMONIC GENERATION
 S HEAT GENERATION
 S PLASMA GENERATION
 S REGENERATION
 S VORTEX GENERATION
GENERATOR
 SA ACOUSTIC GENERATOR
 SA ALTERNATING CURRENT
 GENERATOR
 SA ARC GENERATOR
 SA COLLOIDAL GENERATOR
 SA COMMUTATOR
 SA ELECTROSTATIC GENERATOR
 SA FUNCTION GENERATOR
 SA GAS GENERATOR
 SA HALL GENERATOR
 SA HARMONIC GENERATOR
 SA IMPULSE GENERATOR
 SA INDUCTOR
 SA MAGNETOHYDRODYNAMIC
 GENERATOR
 SA OPTICAL GENERATOR
 SA PLASMA GENERATOR
 SA POWER GENERATOR
 SA PULSED GENERATOR
 SA QUANTUM GENERATOR
 SA QUANTUM MECHANICAL
 GENERATOR
 SA SHOCK WAVE GENERATOR
 SA SIGNAL GENERATOR
 SA SOLAR GENERATOR
 SA STATOR
 SA STEAM GENERATOR
 SA TURBOGENERATOR
 SA VOLTAGE GENERATOR
 SA VORTEX GENERATOR
 Optimal regime conditions in engineering
 calculation of generating device with self-
 parametric frequency multiplication, using
 nonlinear inductance in ultrasonic frequency
 range 06 p0970 A67-18171
 Electronic generation of stochastic step
 processes defined by stationary Markov
 chains 07 p1182 A67-20195
 Topological properties of networks
 containing resistors, capacitors, self-
 inductors and controlled current
 generators 07 p1162 A67-20200
 Operation modes of electron beam
 generators with resonant oscillating systems
 and bipolar regenerative amplifiers

developed from them 08 p1305 A67-21272
 Network analysis of frequency stability of
 quartz generators, showing possible
 reduction through additional HF cascades
 introduction into feedback
 loop 11 p1768 A67-24982
 Smoke generator control and performance
 for flow visualization applications
 [JPL-TR-32-1117] 14 p2293 A67-28751
 Design and performance of explosive
 driven magnetic generators, giving line
 drawings and current
 oscillograms 18 p2987 A67-33628
 Light pulse generator circuit using
 hydrogen corona-discharge tube and
 thyratron generator of nanosecond light
 pulses 19 p3228 A67-34988

GENETICS
 SA CHROMOSOME
 SA MUTATION
 Genetic studies in space, discussing free
 balloon, rocket and satellite experiments
 with microorganisms, plants and
 animals 09 p1453 A67-21901
 Genetic transcription as affected by
 ionizing radiation and hydrogen
 peroxide 11 p1747 A67-24786
 Space genetics, discussing space
 environment exposure of experimental
 animals as cause of mutations, hereditary
 damage, etc 24 p4113 A67-42053

GEOCENTRIC COORDINATE
 Geocentric initial conditions for motion of
 bodies leaving moon surface after initial
 instantaneous thrust 01 p0148 A67-10387
 Satellite three-dimensional triangulation
 accuracy, discussing orientation of camera
 axes and plate coordinates of satellite
 images as error sources 06 p0994 A67-17717
 Geodetic program of simultaneous
 measurement of equatorial topocentric
 coordinates of artificial
 satellites 07 p1177 A67-19775
 Calculation of geocentric position errors of
 satellite obtained by nonsimultaneous
 observations 07 p1177 A67-19779
 Vehicle position determination using
 relationship between geographic and inertial
 coordinates, noting distinction between
 geodetic and geocentric latitudes and
 geocentric declination 11 p1786 A67-24353
 Geocentric orbital elements determined
 from quasi-simultaneous direction
 observations to satellites 13 p2199 A67-26852
 Improvement of satellite elliptical orbits
 with small eccentricities using differential
 formulas 16 p2743 A67-30727
 Lunar surface particles geocentric
 trajectories, giving perigee distance and
 velocity curves 18 p3120 A67-33866
 Inclination of quasi-geocentric coordinate
 system from satellite
 observations 20 p3434 A67-37548

GEOCHEMISTRY
 SA GEOPHYSICS
 Oils and shales from 3 million to 2.7
 billion years old analyzed for hydrocarbon
 content, using gas chromatography and mass
 spectrometry 05 p0797 A67-16580
 Geochemical differentiation in terrestrial
 environments, noting vertical planetary
 differentiation 06 p0999 A67-19015
 Geochemical cycle of chemical species
 movement within and into earth crust and
 relaxation time needed to reach
 equilibrium 08 p1325 A67-21212
 Geochemical studies of Wyoming
 Precambrian graywackes concerning
 composition of early and ancient North
 American crust 08 p1326 A67-21267
 Baddeleyite inclusion in Marthas Vineyard
 tektite identified by electron
 microscopy 11 p1858 A67-24065
 German book on space chemistry covering
 age and origin of earth, meteorites, tektites
 and impactites 12 p1903 A67-25427
 Geochronology for earth and components
 using radiometric and thermoluminescence
 methods 12 p1903 A67-25428
 Stable isotope distribution in
 carbonates 14 p2310 A67-27970
 Chemical analysis of meteorite impact
 glass from separated areas across Henbury
 strewnfield 16 p2667 A67-31452

GEODESY
 SA TOPOGRAPHY
 Standard earth geodetic coordinate system
 and Baker-Nunn camera station
 positions 01 p0056 A67-10038
 Critical analysis of Stokes gravity formula
 derivations, noting truncation error

effect 05 p0796 A67-16153
 Density and temperature of upper
 atmosphere, satellite tracking, geodetic
 applications and long distance
 measurements, using laser
 output 06 p1008 A67-17591
 Satellite camera of Potsdam Geodetic
 Institute 07 p1187 A67-19763
 Simultaneously circles used in space geodesy;
 to obtain synchronous observation of trials
 of satellites and determination of absolute
 directions in space of lines joining tracking
 stations 07 p1177 A67-19778
 Equatorial radius of earth and zero-order
 undulation of geoid obtained from data of
 equatorial gravity, earth flattening and
 product of gravity constant and
 mass 08 p1325 A67-20933
 Satellite geodesy program at Smithsonian
 Astrophysical Observatory, with emphasis on
 twelve Baker-Nunn tracking
 stations 10 p1636 A67-23177
 Attainable sets and generalized geodesic
 spheres, noting set properties and meaning
 of conjugate points 13 p2088 A67-27096
 Doppler effect application to solution of
 tracking problems with aid of artificial earth
 satellites 14 p2347 A67-28991
 Flattening of ellipsoid of revolution
 considered as mathematical surface for
 solution of geodetic
 problems 15 p2477 A67-29744
 Artificial satellite radius vector
 determination examined for degree of
 accuracy, discussing geodetic
 applications 15 p2477 A67-29746
 Geophysical instrumentation for
 environmental studies, elucidating
 atmospheric and near-space mechanisms,
 geodesy, gravimetry, etc 17 p2860 A67-32692
 Congruences of geodesic rays of Einstein
 vacuum spaces 18 p3078 A67-33690
 Integrability 18 p3078 A67-33690
 Polish space research noting satellite
 position observations, geodetic computations,
 meteorology, cosmic physics, magnetosphere,
 medicine and biology 19 p3321 A67-35296
 Rigorously geodetic inertial motion of
 extended object in Einstein gravitational
 field, using relativistic
 hydrodynamics 23 p4027 A67-41148

GEODETTIC POSITION
 Satellite three-dimensional triangulation
 accuracy, discussing orientation of camera
 axes and plate coordinates of satellite
 images as error sources 06 p0994 A67-17717
 Geodetic error effect on time dependence
 of satellite tracking data received by ground
 station 06 p1080 A67-17769
 ANNA satellite geodesy experiments
 emphasizing operation of strobe
 light 07 p1176 A67-19766
 Doppler frequency measurements in
 satellite transmissions and use for geometric
 geodesy 07 p1144 A67-19771
 Smithsonian observatory tracking network
 and geodetic results 07 p1177 A67-19774
 Geodetic program of simultaneous
 measurement of equatorial topocentric
 coordinates of artificial
 satellites 07 p1177 A67-19775
 Vehicle position determination using
 relationship between geographic and inertial
 coordinates, noting distinction between
 geodetic and geocentric latitudes and
 geocentric declination 11 p1786 A67-24353
 Astronomic data error effect on position
 of reference surface trigonometric net with
 regard to earth axis of
 rotation 11 p1787 A67-24593
 Geocentric orbital elements determined
 from quasi-simultaneous direction
 observations to satellites 13 p2199 A67-26852
 Satellite geodesy star catalog
 requirements, discussing accuracy of
 coordinates triangulation solution, criteria
 for homogeneity and extent of coverage,
 etc 18 p3043 A67-34586
 Systematic and random error effects on
 geodetic accuracy of results obtained by 3-
 station laser telemetry 19 p3182 A67-35240
 Accurate geodetic altitude and sublatitude
 of low altitude space
 vehicle 22 p3879 A67-39312

GEODETTIC SATELLITE
 NASA-sponsored satellite geodesy program
 using Baker-Nunn camera, noting station
 positions and gravitational potential
 determination 01 p0056 A67-10040
 Geodetic satellites determination of
 positions of earth surface points, earth

- shape, gravitational field parameters, direct mapping and navigation 01 p0154 A67-10852
- Construction of three-dimensional polygon intended as geodetic base for intercontinental geodetic connections, using radio rangefinder measurements and synchronous observations of artificial satellites 01 p0060 A67-10853
- Book of physics and mathematics as foundation for application of satellites to geodesy including spherical harmonics, matrices, orbital geometry, statistical implications and data analysis 04 p0611 A67-14466
- Computational methods employed with Doppler observations and derivation of geodetic results 05 p0894 A67-16571
- Satellite surveying of earth size and shape, discussing ANNA, GEOS A and TAGEOS 05 p0797 A67-16776
- Geometrical methods for solving higher order geodetic problems from satellite observations including direction, position, coordinate, etc 05 p0800 A67-17031
- Earth size, shape and mass determination using satellites 05 p0800 A67-17049
- Maneuverable geodetic satellite for better determination of resonant harmonics in geopotential field [AIAA PAPER 67-122] 06 p1096 A67-18340
- European geodetic network by satellite observation - Conference, Paris, December 1964 07 p1175 A67-17956
- NASA geodetic satellite program noting Beacon Explorer, Geos I and Pageos 07 p1176 A67-17957
- Organization of U.S. geodetic satellite program, discussing responsibilities for various phases of operation 07 p1269 A67-17958
- Geos A space vehicle, discussing orbital motion, instrumentation and operation 07 p1259 A67-17959
- U.S. Passive Geodetic Satellite, describing fabrication, structural integrity, flight preparation, launch, etc 07 p1259 A67-17960
- Cooperative European geodetic observation of luminous objects at high altitude using Echo type satellite 07 p1176 A67-17962
- Geodetic linking of France and North Africa by synchronous photographs of Echo satellite 07 p1176 A67-17967
- Geodetic electronic ranging system of satellites with Sequential Collation of Range SECOR/ transponder 07 p1177 A67-17972
- Triangulation by photogrammetric use of geodetic satellites and data reduction methods 07 p1177 A67-17977
- Lasers for tracking and geometric geodesy as used in Explorer and Geos satellite missions 10 p1664 A67-23071
- Geodetic satellites determination of positions of earth surface points, earth shape, gravitational field parameters, direct mapping and navigation 14 p2394 A67-28241
- Construction of three-dimensional polygon intended as geodetic base for intercontinental geodetic connections, using radio rangefinder measurements and synchronous observations of artificial satellites 14 p2311 A67-28242
- Schmidt satellite cameras to record trail from bearing and elevation fixed in relation to earth, detailing optical system of Royal Radar Establishment /RRE/ camera 18 p3048 A67-34237
- U.S. Navy Doppler geodetic Tranet system configuration and operation, discussing tropospheric and ionospheric refraction, timing and frequency errors 18 p3003 A67-34241
- Satellite geodesy star catalog requirements, discussing accuracy of coordinates triangulation solution, criteria for homogeneity and extent of coverage, etc 18 p3043 A67-34586
- Azimuth and zenith distance determined from simultaneous observations of topocentric coordinates of artificial satellite transformed into astronomical and geodetic quantities 20 p3428 A67-36483
- Optical data acquisition by NASA for National Geodetic Satellite Program flash photography 20 p3382 A67-36888
- Electronic satellite position and motion measurement for satellite geodesy, with rapid data reduction, day-night capability and optical accuracy 20 p3383 A67-36889
- Geometric satellite triangulation for position of fourth satellite, with position equations solved by least squares method and applied to geodetic satellites 20 p3429 A67-36890
- Reduction of dynamic data from geodetic satellites noting satellite tracking station position, gravitational potential, gravity coefficients, synchronous satellites, etc 20 p3429 A67-36891
- Satellite geodesy results compared to other determinations, noting topography-gravity correlation confirmation, gravity field, etc 20 p3429 A67-36892
- Geometrical methods for solving higher order geodetic problems from satellite observations including direction, position, coordinate, etc 21 p3618 A67-38263
- Satellite methods to determine absolute coordinates for geodetic points and to bridge continents 21 p3620 A67-38520
- Terrestrial and satellite geodesy, discussing construction methods of geodetic system by triangulation, astrogeodetic leveling or satellite observation on stellar background 21 p3620 A67-38521
- GEODEIC SURVEYING**
- Radar imagery compilation of vegetation maps, noting extent of capabilities and results obtained 01 p0059 A67-10329
- Construction of three-dimensional polygon intended as geodetic base for intercontinental geodetic connections, using radio rangefinder measurements and synchronous observations of artificial satellites 01 p0060 A67-10853
- Limitations of method of least squares in terms of quality of estimates it provides in geodetic measurements 06 p1022 A67-17715
- U.S. Coast and Geodetic Survey satellite triangulation program based on optical tracking of passive satellites simultaneously from two or more mobile camera stations 07 p1176 A67-17964
- Maryland-Minnesota-Mississippi Echo I satellite observation triangle, discussing principles of triangulation method, camera systems and office data reduction techniques 07 p1176 A67-17965
- Calculation method for energetic photoelectric photometry system for tracing behind radiative source or for distance measurement 08 p1331 A67-21055
- Manned orbiting laboratories for surveying natural resources using advanced remote sensing techniques 08 p1325 A67-21072
- IR spectral techniques for satellite geodetic surveying, discussing spectral matching techniques for discriminating between different types of rocks [AIAA PAPER 67-284] 12 p1938 A67-26001
- Construction of three-dimensional polygon intended as geodetic base for intercontinental geodetic connections, using radio rangefinder measurements and synchronous observations of artificial satellites 14 p2311 A67-28242
- Aerial electronic photomapping and geodetic surveying system describing track-keeping navigation and verticality measuring 16 p2679 A67-31801
- Systematic and random error effects on geodetic accuracy of results obtained by 3-station laser telemetry 19 p3182 A67-35240
- Space research in West Germany noting ionospheric physics, magnetosphere and solar and cosmic radiation 19 p3321 A67-35293
- Optical technique with laser source for range measurements noting use of dispersion between two different light wavelengths 22 p3800 A67-40139
- Three geodetic measurement bases synchronized to within 100 microseconds by transporting atomic clock 23 p3997 A67-40573
- Satellites and balloons for earth surface observation surveyed by types noting operations concerning geodesy, weather, oceanography, vegetation and wildlife 24 p4150 A67-42201
- GEOELECTRICITY**
- SA GEOPOTENTIAL
- SA TELLURIC CURRENT
- Spread in values of vertical magnetic field component during sudden commencements of magnetic storms attributed to local geoelectric conditions 07 p1174 A67-19712
- Earth electrical conductivity, determined from data concerning northern and vertical components of cyclic geomagnetic variations, suggests increases with depth 07 p1174 A67-19714
- Relation between electron and proton distributions and existence of electric fields in magnetosphere 12 p1936 A67-25808
- Instantaneous distribution patterns for aurora on polar region, discussing geoelectric field role in internal structure of magnetosphere 20 p3430 A67-36906
- Earth finite conductivity effect on directivity patterns of vertical antennas taking into account attenuation factor 21 p3590 A67-38119
- GEOGRAPHY**
- SA AFRICA
- SA ANTARCTICA
- SA ARCTIC
- SA EUROPE
- SA NORTH AMERICA
- Remote sensing techniques and data evaluation and processing in geography 01 p0058 A67-10308
- Geographical location and optical path length effects upon fade margin required for desired propagation reliability of microwave signals 13 p2066 A67-26406
- GEOID**
- Formulas for extraterrestrial potential, anomalous gravity force gradient on earth topographic surface, deflections of vertical, etc 04 p0617 A67-15565
- Earth gravitational potential on geoid expressed by vertical and horizontal gradients for gravitational anomalies useful in earth figure determination 21 p3618 A67-38199
- Theory on earth shape, considering surface of geoid assumed as equipotential surface at sea level, obtaining relations between zonal and tesseral harmonics coefficients 22 p3792 A67-39933
- GEOLOGY**
- SA GEOCHEMISTRY
- SA GEOPHYSICS
- SA GLACIOLOGY
- SA LITHOLOGY
- SA LUNAR GEOLOGY
- SA MINERAL
- SA OROGRAPHY
- SA PALEONTOLOGY
- SA PETROGRAPHY
- Local geologic interpretation from intensity of radar return energy modified by illumination, surface roughness and object shape 01 p0058 A67-10310
- IR spectral signatures of rocks and soils in identifying bulk composition by comparison to standard spectral curves 01 p0058 A67-10311
- Solar activity and polar migrations role in origin and evolution of terrestrial life during Eocambrian and subsequent geological epochs 01 p0149 A67-10756
- Space applications research and development 01 p0152 A67-11430
- Geomagnetic anomalies over Pacific-Antarctic ridge and distribution of causal bodies with reference to field reversal 04 p0611 A67-14493
- Geological and astronomical research - Lunar International Laboratory Symposium, Athens, September 1965 04 p0596 A67-15062
- Statistical problems in use of EM data for remote sensing of geological attributes of lithosphere-atmosphere interface 05 p0803 A67-17387
- Low resolution side-looking radar application for geological studies, noting advantage over small scale aerial photography 06 p0994 A67-17833
- Energy, time and physical morphology of atmosphere, hydrosphere and lithosphere surfaces 06 p1091 A67-18994
- Photographs taken by astronauts as part of Synoptic Terrain Photography Experiment including geological features such as Sonora Desert, Agua Blanca and Gulf of Aden 06 p0999 A67-19002
- Cosmological principles of interzonal couplings, noting cyclic and secular change, planetary evolution, terrestrial magnetism, etc 06 p0999 A67-19006
- Earth science advances - Conference, MIT, Cambridge, September-October 1964 07 p1170 A67-19330
- Virial theorem for continuous systems used to seek information about equilibrium of insulated self-gravitating system 07 p1183 A67-20175
- Astrobleme in Australia analyzed for origin of eruptive gas 10 p1706 A67-22958
- Surveying earth resources from high flying aircraft and earth orbiting satellites 10 p1735 A67-23688
- German book on space chemistry covering age and origin of earth, meteorites, tektites

and impactites 12 p1903 A67-25427
 Geochronology for earth and components using radiometric and thermoluminescence methods 12 p1903 A67-25428
 Living relative of Precambrian microfossil Kakabekia isolated from soil specimens collected in UK 15 p2429 A67-29648
 Research into geological history of planetary bodies without atmosphere, discussing techniques for determining time of formation of layered ejecta units 16 p2747 A67-30988
 Internal and surface Martian geology synthesis, investigating parameters favoring organic growth and sites for exploration 19 p3323 A67-35334
 Detection of mineral resources by orbiting satellite photography, using remote sensor techniques 19 p3225 A67-35655
 Geomagnetic field secular variation, with time explained by strength changes of BFD and nondipole field and drift 21 p3620 A67-38980
 Lunar missions evaluated for scientific effectiveness via use of earth analogs assuming hypothetical terrestrial objectives parallel to lunar program 22 p3887 A67-40142
 Earth core surface fluid velocity patterns and magnetic field secular change at earth surface for various epochs 23 p3996 A67-40815
 Earth science and resource studies with orbiting imaging radars onboard space vehicles [AIAA PAPER 87-767] 24 p4258 A67-42936

GEOMAGNETIC ANOMALY
 Integral intensity of charged particles diffusing through drift shells in earth magnetosphere with specific example for protons 02 p0306 A67-11550
 Geomagnetic field disturbance due to earth passage through tail of Halley comet, 1910 II 02 p0236 A67-11654
 Transverse magnetic disturbances at high altitudes in auroral region observed with magnetically oriented satellite 03 p0409 A67-12944
 Geomagnetic anomalies over Pacific-Antarctic ridge and distribution of causal bodies with reference to field reversal 04 p0611 A67-14493
 Captured proton intensity measurement in inner radiation belt in Brazilian anomaly, using satellites Proton I and II 05 p0878 A67-16089
 Depth and form of bodies causing magnetic anomalies determined by two methods 05 p0802 A67-17150
 Latitudinal and vertical current components effects included in longitudinal current system supporting steady state distribution in geomagnetic anomaly 06 p0998 A67-18703
 Coulomb interaction influence upon electron distribution in radiation belts at low altitudes in magnetic anomaly region 10 p1702 A67-23299
 Geomagnetic field anomalies in Southern Hemisphere and effects on cosmic rays, geomagnetically trapped radiation and ionosphere 12 p1933 A67-25770
 South Atlantic proton radiation anomaly measurements using rocket flown spectrometer, examining variation of counting rates with altitude 12 p1995 A67-25771
 Brazil geomagnetic anomaly and artificial radiation belt observations from Cosmos series satellites 12 p1996 A67-25773
 Polar orbiting satellite measurements correlating ionospheric irregularities with trapped and precipitated energetic particles in South American anomaly region 12 p1996 A67-25776
 Geomagnetic field measurements in Brazilian magnetic anomaly, using Alouette topside sounder satellite 12 p1933 A67-25777
 Ionization transport from equator along magnetic lines of force may contribute to formation of diurnal ionization anomaly of F region in intermediate zone 13 p2117 A67-27708
 Geomagnetic ring current observations using Elektron II satellite, noting location, orientation and structural features 14 p2308 A67-27928
 Geomagnetic anomaly studied from equatorial ionosphere vertical probe observations in East Asian zone of Pacific ocean 14 p2308 A67-27937
 Stationary property of random process

approximating anomalous magnetic field, noting optimum filtering 14 p2309 A67-27946
 Dayside distortion of geomagnetic field by solar wind beyond 3.5 earth radii measured and compared with three magnetosphere models 15 p2475 A67-29612
 Vertical incidence ionospheric absorption measurements from ground station criteria for recognizing winter anomaly 15 p2476 A67-29623
 Field-aligned irregularities as effect of increased electron temperature in F-2 layer, analyzing heat production and loss mechanism [AGARDOGRAPH 95] 15 p2484 A67-30305
 Daily geomagnetic variations superpositional nature studied by factorizing frequency functions describing day-to-day variability 16 p2864 A67-30971
 Geomagnetic field disturbance due to earth passage through tail of Halley comet, 1910, II 16 p2865 A67-31069
 Integral intensity of charged particles diffusing through drift shells in earth magnetosphere with specific example for protons 16 p2740 A67-31616
 Geomagnetic field secular variation forecasting method suggesting inclusion of anomalies 17 p2847 A67-32947
 Winter anomaly in ionospheric E-layer 19 p3225 A67-35617
 Ionospheric F-2 region equatorial anomaly dependence on geomagnetic field 20 p3426 A67-36289
 Depth and form of bodies causing magnetic anomalies determined by two methods 21 p3619 A67-38492
 Separation of geomagnetic field into anomalous and normal components, analyzing spectral relation 21 p3622 A67-39024
 Annual and diurnal variations of geomagnetic anomaly in Australasian Zone during sunspot minimum, stressing role in transequatorial propagation of VHF radio signals 22 p3759 A67-39473
 Equatorial anomaly in F-2 layer of ionosphere, examining solar activity, seasonal variation relation to magnetic activity, lunar phase and heights 23 p3996 A67-41082
 VLF transmissions during SIDs for compatibility with general form of theory of waveguide mode 24 p4149 A67-42067
 Geomagnetic field aligned irregularities, explaining ionospheric E-region scattered wave propagation 24 p4120 A67-42150
 E layer critical frequency calculation for 80 selected diurnal variations, considering forenoon anomaly effect 24 p4151 A67-42704
 Captured proton intensity measurement in inner radiation belt in Brazilian anomaly, using satellites Proton I and II 24 p4212 A67-42765

GEOMAGNETIC CROCHET
SA IONOSPHERIC CURRENT
 Geomagnetic crotchets of solar flares based on materials analysis recorded at Hurlerovo, discussing time factors and characteristics 23 p4049 A67-40670
 Characteristics of geomagnetic crotchets associated with proton flares, determining recombination coefficients and electron densities 23 p4050 A67-40671

GEOMAGNETIC EFFECT
 Coaxial cylindrical plasma sheet motion and geomagnetic field/solar wind interaction 01 p0143 A67-10116
 Horizontal drift and anisotropy in F-1 region during geomagnetically active and quiet conditions 01 p0057 A67-10117
 Relation of sporadic E layer to magnetic fluxes based on observations of diurnal variations 02 p0237 A67-11675
 Magnetic activity effect on sporadic E region drifts, comparing plot of K index vs drift velocities 03 p0413 A67-13684
 Total electron content distribution over Europe in terms of geomagnetic activity, noting occurrence of scintillations [RASSA PAPER 1-10-125] 03 p0416 A67-14236
 Autocorrelation function in statistical analysis of geomagnetic activity 04 p0613 A67-14897
 Solar cycle effect on geomagnetic activity and temperature of near-earth tropospheric layer 04 p0616 A67-15227
 Amplitude of 27-day cosmic ray modulation in relation to solar and geomagnetic activities 05 p0881 A67-16122
 Geomagnetic cut-off rigidity effect on

cosmic ray intensity and coupled coefficients 05 p0882 A67-16127
 Comparison of VLF emissions of two conjugate stations, noting statistical results for diurnal variation, magnetic activity, hiss, etc 06 p0997 A67-18698
 Auroral zone position changes as function of magnetic activity and time of day 07 p1178 A67-19816
 Criteria for determination of statistical aurora during IQSY, noting relation to magnetic activity 07 p1180 A67-19932
 Orthogonal functions of time, describing daily perturbations in 100 mb circulation over eastern U.S. 09 p1562 A67-22688
 Characteristic effects of deformed geomagnetic field on trajectories and asymptotic directions of arrival of medium energy cosmic rays 12 p1998 A67-25819
 Coastal effects in magnetic and telluric current variations near complex land, shelving seawater boundary 13 p2108 A67-26317
 Solar activity relationship to terrestrial magnetic and associated auroral, ionospheric and cosmic ray effects 13 p2109 A67-26418
 Equatorial measurement of intensity of protons with energies greater than 400 kev and electrons with energies greater than 2 mev in outer radiation belt center in 1964 13 p2191 A67-26544
 Dependence of seasonal occurrence probability of F-zero layer on level of geomagnetic activity and ionospheric activity observed above Ashkhabad 13 p2110 A67-26549
 Polar aurora of September 13, 1957 and geomagnetic activity attributed to extraordinary solar flares 13 p2115 A67-27393
 Polar auroras statistically analyzed for relation between frequency of redness, solar activity and geomagnetic conditions 13 p2116 A67-27394
 Interplanetary electromagnetic field effects on cosmic ray intensity noting geomagnetism, modulation mechanisms and solar flare particle propagation 14 p2380 A67-27965
 Frequency spread in ionospheric radio propagation 14 p2273 A67-28712
 Solitary waves, discussing electron and ion acceleration and transfer mechanism of solar wind ion kinetic energy to electrons 15 p2475 A67-29613
 Traveling ionospheric disturbance heat conduction waves excited in neutral gas of thermosphere by hydromagnetic waves from magnetopause 15 p2475 A67-29617
 Relation of sporadic E layer to magnetic fluxes based on observations of diurnal variations 16 p2665 A67-31090
 Propagation rate distribution as function of geomagnetic latitude provides evidence for geomagnetic effects on vertical ionization drifts in F region of ionization 16 p2668 A67-31894
 Statistical analysis of solar-diurnal and semidiurnal variations of cosmic ray neutron component with respect to geomagnetic field perturbations 17 p2932 A67-32008
 Geomagnetic activity effect correlation with sporadic E occurrence in African zone, showing longitude dependence 17 p2844 A67-32546
 Artificial satellites lifetime in low altitude orbits, discussing atmospheric, geomagnetic, solar and lunar factors 18 p3136 A67-33550
 Magnetic activity effect on position and characteristics of proton precipitation zone in aurora observed from Canada, noting temperatures and measurement method used 18 p3037 A67-33612
 Amplitude and polarization of radio pulse from extensive cosmic ray air shower indicating geomagnetic deflection mechanism of emission 18 p3116 A67-34196
 Intense negative bays occurring in auroral zone in early evening hours explained by westward extension of polar electrojet 20 p3426 A67-36285
 Geomagnetic activity around conjunction and opposition of planets, noting decrease in years of low solar activity 21 p3711 A67-39004
 Cosmic rays interaction with solar and terrestrial magnetic fields, noting interplanetary plasma flows and solar activity 21 p3699 A67-39006
 Geomagnetic aperiodic variation effect on earth electric conductivity in electromagnetic induction theory for flat earth model 21 p3622 A67-39027

- Outer Van Allen radiation zone intensity maximum position dependence on electron energy and magnetic activity, noting relation to diffusion theory 22 p3870 A67-39620
- Pioneer VII plasma probe data indicating geomagnetic wake at 1000 earth radii downstream from earth 22 p3791 A67-39819
- Amplitude of 27-day cosmic ray modulation in relation to solar and geomagnetic activities 24 p4214 A67-42798
- Geomagnetic cut-off rigidity effect on cosmic ray intensity and coupled coefficients 24 p4215 A67-42803
- ### GEOMAGNETIC EQUATOR
- Incoherent scattering measurements of ionospheric power spectrum and autocorrelation function at geomagnetic equator to determine electron and ion temperatures, ion composition and ion density 03 p0408 A67-12834
- Frequency spectrum of micropulsations analysis from records taken at station near geomagnetic equator 03 p0410 A67-12954
- Electron energy spectrum measured near equator by satellite mounted scintillator 04 p0614 A67-14950
- Continuity equation for electrons in F-2 layer obtained for region near geomagnetic equator at noon including photoionization, recombination, drift, etc 04 p0614 A67-14954
- Primary cosmic ray proton and deuteron flux near geomagnetic equator determined by nuclear emulsion 10 p1703 A67-23543
- Rapid magnetic variations near magnetic equator, determining principal characteristics 12 p1931 A67-25117
- Ionospheric ion and electron densities and temperatures from rocket probes near geomagnetic equator 19 p3219 A67-35232
- Ionospheric F-2 region equatorial anomaly dependence on geomagnetic field 20 p3426 A67-36289
- Latitude variation of critical frequency of F-2 layer in equatorial region during geomagnetic disturbance, discussing ionization density 21 p3622 A67-39036
- Electron content of topside ionosphere studied for equatorial anomaly during diurnal variations 24 p4148 A67-42063
- ### GEOMAGNETIC FIELD
- #### SA MAGNETOSPHERE
- Dynamo theory interpretation of magnetospheric-ionospheric electric current system associated with N-S asymmetry of magnetic daily variation at time of equinox 01 p0057 A67-10113
- Geomagnetic stabilization of satellite initially torque-stabilized, deriving motion equation 01 p0153 A67-10210
- Radio wave scattering propagation caused by geomagnetic field aligned irregularities 01 p0021 A67-10334
- Wide angle counter telescope measurement of cosmic ray equator position near zero meridian 01 p0149 A67-10738
- Geodetic satellites determination of positions of earth surface points, earth shape, gravitational field parameters, direct mapping and navigation 01 p0154 A67-10852
- Magnetic field intensity near moon measured by Luna X magnetometer, noting correlation with earth surface intensity 01 p0150 A67-10909
- Magnetospheric plasma motion in terms of hydromagnetic wave theory, noting effect of variations of geomagnetic field and ionospheric plasma density [AFCLR-66-803] 01 p0145 A67-11263
- Interaction of solar wind and frozen-in magnetic field with geomagnetic field inside and outside magnetosphere, comparing theory with satellite measurements 02 p0320 A67-11461
- Geomagnetic field intensity measurement, based on observation that ferromagnetic minerals cooled in weak magnetic field from above Curie temperature acquire thermoremanent magnetization 02 p0236 A67-11477
- Radial extension of corpuscular flux from chromospheric flares and duration of earth immersion in flux 02 p0306 A67-11653
- Geomagnetic field effect on radio signal in oblique reflection sounding, noting differences between daylight and night measurements 02 p0193 A67-11662
- Magnetic field of M-element interaction with geomagnetic field as second possible cause of irregular fluctuations in velocity of earth diurnal rotation 02 p0237 A67-11678
- Temporal variations in velocity of westward drift of nondipole geomagnetic field and negative correlation with solar activity 02 p0237 A67-11679
- Origin of geomagnetic field, attributing paleomagnetic inversions to electromagnetism induction effects produced by solar corpuscular eruptions 02 p0326 A67-12063
- Solar eclipse effects on geomagnetic field, suggesting geomagnetic observations at low latitudes 03 p0408 A67-12839
- Red shift of magnetic zenith hydrogen line profiles and role of injection pitch-angle distribution of auroral protons 03 p0409 A67-12943
- Interchange of field lines between closed region of magnetosphere and open tail, explaining features of auroral breakup and geomagnetic bays 03 p0410 A67-12955
- ULF emission at two conjugate points signaling onset of negative ionospheric storms 03 p0411 A67-13347
- Secular variation of earth magnetic field 03 p0414 A67-13944
- Soviet papers on geophysics and astronomy 04 p0650 A67-15218
- Relation between E-2 and F-0 ionospheric layer formation and geomagnetic phenomena 04 p0616 A67-15221
- Seasonal and diurnal variations of geomagnetic field in equatorial regions 04 p0616 A67-15224
- Magnitude and direction for shifts in position of mean pole of earth [ASME PAPER 66-WA/APM-7] 04 p0616 A67-15225
- Phenomena accompanying geomagnetic field reversal, using measurements performed on samples of core Papagayo 3G 04 p0617 A67-15543
- Whistler recordings on thermal plasma motions and ionization density near magnetospheric knee, noting whistler attenuation VLF noise, ion effects, electron temperature, etc 05 p0795 A67-16011
- Elektron I and II satellite measurements on outer radiation belt, noting geomagnetic field distortion and boundary dependence on magnetic perturbations 05 p0880 A67-16110
- Asymptotic directions of cosmic rays for Soviet cosmic ray stations 05 p0880 A67-16114
- Transient variation of ionospheric dynamo current systems obtained from sounding rocket measurements of geomagnetic field activities 05 p0797 A67-16582
- Communications satellite orientation with respect to earth, using structure mounted electromagnetic actuator 05 p0905 A67-16831
- Magnetic field observations by rockets and satellites 05 p0798 A67-16870
- Relation between terrestrial gravitational and magnetic field variations and time-dependent changes in shape, density and magnetization of disturbing bodies 05 p0799 A67-17027
- External sources of geomagnetic field at F-2 layer altitude and effects on recurring-orbit satellites 05 p0800 A67-17119
- Solar wind plasma penetration into geomagnetic field under effects of drift in crossed electric-geomagnetic fields 05 p0884 A67-17120
- Geomagnetic activity effect on electron concentration at heights of 100 and 110 km 05 p0801 A67-17143
- Z component of geomagnetic field, determining parameters of sloping dipoles 05 p0802 A67-17149
- Standing transverse hydromagnetic waves effect on longitudinal invariant of particle motion trapped along geomagnetic field 06 p0997 A67-18700
- Matrix techniques for finding geomagnetic field strength in solar ecliptic coordinate system 07 p1170 A67-19111
- Recombination rate increase in F region following magnetic activity due to passage of atmospheric wave 07 p1171 A67-19418
- Tangential magnetic field on earth surface excited by LF plane electromagnetic wave 07 p1142 A67-19449
- Radio pulse coincidence with extensive air showers, noting consistency with Cerenkov radiation and charge separation in terrestrial magnetic field 07 p1242 A67-19619
- Auroral radio blackout correlation with magnetic dip pole motion 07 p1173 A67-19669
- Scatter propagation due to geomagnetic field-aligned irregularities and calculation of scattering cross section 07 p1143 A67-19675
- Effect of higher harmonics of geomagnetic field on cosmic ray trajectories, noting reception cones of Soviet stations 07 p1243 A67-19685
- Diurnal and seasonable altitude variations of E and F layers analyzed for geomagnetic activity from rocket measurement of electron concentration 07 p1173 A67-19686
- Structure of main geomagnetic field over Eurasia, noting difference in spectra over oceans and continents 07 p1173 A67-19697
- Relation between magnetic activity and ionospheric disturbances in F-2 layer studied on basis of 30-year data 07 p1173 A67-19702
- Ionization structure of polar auroras from spatial distribution of radar-reflecting zones, taking into account magnetic field variations 07 p1174 A67-19710
- Earth electrical conductivity, determined from data concerning northern and vertical components of cyclic geomagnetic variations, suggests increases with depth 07 p1174 A67-19714
- Geomagnetic activity and solar corpuscular fluxes forecasting by Bednarova-Novakova method 07 p1175 A67-19719
- Solar wind magnetic field as medium for plasma-magnetosphere interaction 07 p1243 A67-19803
- Electrical conductivity of earth interior from data concerning annual geomagnetic variations for all years of solar cycle 07 p1178 A67-19826
- Solar corpuscular stream magnetic field effect on change in orientation of geomagnetic field related to change in stream geoeffectiveness 07 p1243 A67-19827
- Correlation of time variations of proton and electron intensity of outer radiation belt and dependence on geomagnetic environment 07 p1243 A67-19828
- Interplanetary magnetic field and plasma effect on geomagnetic activity during quiet sun conditions 07 p1251 A67-19912
- IMP-I satellite measurements of neutral sheet in geomagnetic tail noting dimensions, motion and parameters of sheet 07 p1244 A67-19922
- Depression of low energy cosmic ray cut-offs relation to permanent geomagnetic tail using model calculation, explaining PCA midday recovery 07 p1245 A67-19927
- Magnetosheath field, geomagnetic activity index, magnetopause stability and interplanetary magnetic field influence on magnetospheric phenomena 07 p1182 A67-19953
- Growth rate along whistler path for waves propagating at angle to geomagnetic field 08 p1328 A67-21463
- Explorer XXXIII satellite magnetometric measurements of geomagnetic tail at distances beyond lunar orbit 08 p1402 A67-21468
- Frozen field estimation of surface flow of earth core and effects of secular change resulting from flow pattern nonuniformity 08 p1329 A67-21485
- Geomagnetic disturbance and correlation with PCA in auroral zone on February 10, 1958 08 p1329 A67-21539
- Auroral oval properties from magnetic data, role in connecting visible auroras and related ionospheric disturbances to geophysical phenomena at high altitudes 09 p1492 A67-22060
- Energy spectrum of primary cosmic ray alpha particles measured by nuclear photographic emulsion, estimating geomagnetic cut-off energies 09 p1562 A67-22418
- Boundary variations of auroral oval zones, noting dependence on magnetic perturbation intensity 10 p1630 A67-22785
- Limit energy of monopole in field of earth magnetic dipole 10 p1631 A67-22800
- Cartographic representation of diurnal magnetic variations, noting longitudinal asymmetry in amplitude distribution 10 p1631 A67-22808
- Cosmos XLIX measurements of magnetic field intensity compared with calculation from spherical harmonic coefficients 10 p1632 A67-22812
- Ionospheric diffusion spectra, obtaining information on neutral atmospheric winds and ionosphere dynamics 10 p1632 A67-22858
- Energetic solar particle effect on ionosphere, discussing signal phase, amplitude propagation and attenuation 10 p1637 A67-23192

Geomagnetic field values obtained from OGO-2 satellite-mounted rubidium vapor magnetometer 10 p1641 A67-23244

High incidence and erraticism of sporadic E occurrence in temperate zones where horizontal component of geomagnetic field is greatest attributed to horizontal wind shear 10 p1644 A67-23255

FR-1 satellite data on VLF propagation in lower magnetosphere 10 p1649 A67-23301

Geomagnetic and solar control of ionization at 1000 km determined from electron density data obtained from Alouette satellite 10 p1650 A67-23339

Radio emission from cosmic ray showers analyzed at Jodrell Bank, determining effects of geomagnetic field and charge separation 10 p1703 A67-23490

Equivalent dipole moment of geomagnetic field in terms of earth radius deduced from spherical harmonic analyses 10 p1652 A67-23492

Potential buildup on electron emitting ionospheric satellite, noting limitation on current emission by geomagnetic field 11 p1869 A67-23941

Variation of radio brightness of synchrotron radiation from Van Allen belts as function of direction and frequency, using satellite receiver 11 p1855 A67-23944

Long period fading of VLF atmospherics, attributing origin to ionospheric propagation characteristics induced by geomagnetic activity 11 p1785 A67-23947

Pioneer I observations of geomagnetic field, discussing amplitude and polarization of oblique pulses, existence of collisionless oblique magnetic shock waves, soft electron acceleration, etc 11 p1786 A67-24078

Metrological characteristics of three-component magnetometers with ferromagnetic probes installed in Elektron II space station 11 p1789 A67-24079

Absolute speed determination from measurement of induced EMF resulting from movement in geomagnetic field 11 p1791 A67-24455

Satellite measurement of magnetic fields in cislunar space and earth proximity, noting formation of confined geomagnetic field by continuous plasma flow from sun 11 p1863 A67-24549

Igneous rock suitability for determination of ancient geomagnetic field intensity, discussing theory, application and results 11 p1788 A67-24697

Natural remanent magnetization with normal polarity of lower lava flow in Olduvai Gorge, showing stability via thermal demagnetization 11 p1788 A67-24698

Confirmation of reality of Gilsa geomagnetic polarity event, discussing experimental techniques and results 11 p1788 A67-24700

Geomagnetic thruster, noting superiority over electric or chemical propulsion for thrust durations of more than few weeks 11 p1855 A67-25009

Collective effects and centrifugal instability from charged solar wind particle injected into earth magnetosphere near neutral point 12 p1991 A67-25109

Weak cosmic ray burst relation to austral axis pole geomagnetic activity characteristics and propagation in interplanetary space of energetic solar cosmic rays 12 p1992 A67-25116

High velocity particles and slower corpuscles penetration into lower ionosphere occurring after solar flare explained by Sweet mechanism 12 p1993 A67-25134

Multipole parameters for series of spherical analysis of geomagnetic field from 1829 to 1958 12 p1932 A67-25538

Secular variations of geomagnetic field before our era studied by method using archaeological objects 12 p1933 A67-25554

Device for visible recording of H component of geomagnetic field 12 p1941 A67-25556

Geomagnetic field anomalies in Southern Hemisphere and effects on cosmic rays, geomagnetically trapped radiation and ionosphere 12 p1933 A67-25770

Vertical cut-off rigidities in South Atlantic analyzed via sixth degree simulation of geomagnetic field, obtaining results from trajectory analysis of cosmic rays [AFRL-67-0082] 12 p1996 A67-25774

Geomagnetic field measurements in Brazilian magnetic anomaly, using Alouette

topside sounder satellite 12 p1933 A67-25777

Rocketborne magnetometer measurements of midlatitude Sq ionospheric currents 12 p1935 A67-25794

IMP-I earth satellite magnetic field measurement experimental results including solar wind flow effects 12 p1936 A67-25802

Earth magnetosphere at distances 7 to 11.7 earth radii obtained by Elektron satellites, noting differences between measured and calculated field vector 12 p1936 A67-25803

Elektron I and III earth satellite electron and proton energy distribution correlation with geomagnetic phenomena 12 p1996 A67-25804

Inflation of magnetosphere near 8 earth radii in Southern Hemisphere using Explorer XIV satellite 12 p1936 A67-25805

IMP-II and OGO-I measurements on plasma characteristics in transition region between solar wind and geomagnetic field 12 p1997 A67-25806

Magnetic field variations in magnetosphere at distances of 3 to 6 earth radii attributed to distribution of trapped radiation 12 p1997 A67-25814

Ionospheric electric current measurement, determining vertical current density distribution and electron number density for geomagnetic field study 13 p2107 A67-26308

Magnetic field of ring current on earth surface according to observations during IGY 13 p2111 A67-26557

Diurnal variation in principal direction of E and H vectors of Petropavlosk-Kamchatka K index of geomagnetic field in horizon and planetary relation 13 p2111 A67-26558

Identification with tektites of microscopic glassy objects deposited in Australasian area during and after last geomagnetic field polarity reversal 13 p2198 A67-26792

Rocket measurements of equatorial electrojet current 13 p2114 A67-26793

Ponderomotive forces and geomagnetic westward drift in regard to MHD theory and earth core flows 13 p2114 A67-26855

Geomagnetic field influence on cosmic rays simulated by electron beam and terrella situated in vacuum tank 13 p2192 A67-27243

Cosmic ray particle trajectories for various cut-off rigidity values in different points on earth surface, noting integration of motion equations of charged particle 13 p2192 A67-27244

Measurement of atmospheric cosmic ray fluxes over large portions of globe as comparison evaluation for different cut-off rigidity models 13 p2192 A67-27245

Multiaircraft measurements of cosmic ray spectrum and geomagnetic cut-off rigidity 13 p2193 A67-27246

Cyclotron instability range in earth radiation belt analyzed taking into account wave absorption in atmosphere, using measurements of perturbation effects 14 p2378 A67-27916

Magnetosphere rotation problem in presence of solar wind analyzed for auroral particle acceleration, noting perturbing field of induced electric current 14 p2307 A67-27917

Geomagnetic field analytical representation based on Cosmos 49 observational data 14 p2307 A67-27919

Nondipole region of geomagnetic field at magnetosphere boundary and effect on boundary position on daylight side 14 p2308 A67-27931

High altitude dipole equivalence of geomagnetic field properties verified by satellite-detected electron belt investigation 14 p2308 A67-27932

Lunar periodic variation of geomagnetic field on Kheis Island in Franz Joseph Land 14 p2309 A67-27938

Magnetic activity at low latitudes during IGY 14 p2309 A67-27940

Seasonal and latitudinal magnetic activity variations in Northern Hemisphere, investigating time-space characteristics of K index 14 p2309 A67-27943

Errors arising when dividing geomagnetic field into primary and anomalous fields by simple averaging techniques 14 p2309 A67-27947

Geomagnetic field analytical representation, giving equations for moments and distribution of equivalent set of dipoles 14 p2309 A67-27948

Equilibrium of magnetic field confined by impact pressure of beam of ions for general

direction of incidence of beam 14 p2310 A67-28046

Earth bow shock observations with Explorer XII satellite 14 p2383 A67-28047

Auroral zone electron precipitation occurring in strong transient magnetic disturbances observed by bremsstrahlung 14 p2310 A67-28056

Geodetic satellites determination of positions of earth surface points, earth shape, gravitational field parameters, direct mapping and navigation 14 p2394 A67-28241

Magnetosphere, turbulent transition region and shock wave characteristics and dimensions examined with regard to possible active or passive interaction with moon 14 p2388 A67-28619

Electrodynamic forces and torques on charged bodies moving through rarefied and partially ionized earth magnetosphere and upper atmosphere 14 p2362 A67-29039

Large scale structure of chromosphere examined using birefringent filter, comparing filtergrams with spectroheliograms of perturbed and active regions of solar disk 15 p2552 A67-29143

Spatial distribution of electrons and protons trapped by geomagnetic field and charged particle fluxes in interplanetary space 15 p2550 A67-29536

Statistics relating plasmopause position to three magnetic indices to clarify relationship between equatorial geocentric distance to plasmopause and worldwide magnetic activity level 15 p2477 A67-29627

Earth magnetic field effect on ultralong radio wave propagation, considering directional effects from planetary inhomogeneities and reciprocity principle impairment 15 p2479 A67-30168

Partial correlation coefficients between ionospheric, solar and geomagnetic parameters and spread-F occurrence probability 15 p2481 A67-30283

[AGARDOGRAPH 95] 15 p2481 A67-30283

Statistical analysis of spread-F and scintillation data in middle latitude noting diurnal and seasonal variations [AGARDOGRAPH 95] 15 p2481 A67-30284

Intense fluctuations observed above Arecibo during geomagnetically disturbed conditions, using ionospheric backscatter technique 15 p2483 A67-30299

Ionospheric irregularities in F region during night hours /1958-1960/ [AGARDOGRAPH 95] 15 p2483 A67-30300

Radial extension of corpuscular flux from chromospheric flares and duration of earth immersion in flux 16 p2738 A67-31068

Geomagnetic field effect on radio signal in oblique reflection sounding, noting differences between daylight and night measurements 16 p2624 A67-31077

Magnetic field of M-element interaction with geomagnetic field as second possible cause of irregular fluctuations in velocity of earth diurnal rotation 16 p2665 A67-31093

Temporal variations in velocity of westward drift of nondipole geomagnetic field and negative correlation with solar activity 16 p2665 A67-31094

Systematic clockwise rotation of asymmetry axis of main phase decrease during geomagnetic storm 16 p2666 A67-31412

Earth electromagnetic field stable micropulsations /pearls/ properties stressing apparent pearl polarization and polarization behavior 16 p2667 A67-31485

Slow oscillations of fluid in rotating cavity under magnetic field to evaluate Hide theory for nondipole drift of geomagnetic field 16 p2667 A67-31554

Tektites presence in Australian sea sediments, suggesting relation between geomagnetic reversals and fossil plankton changes to cosmic bodies terrestrial intrusions 16 p2754 A67-31864

Relationship between variations of critical frequencies of sporadic E layer and solar activity cycle 16 p2669 A67-31903

Current function of three eccentric dipoles representing main geomagnetic field 16 p2670 A67-31911

Soviet book on cosmic rays including solar-diurnal, 11-year and 27-day variations, temperature effect, geomagnetic field effect, etc 17 p2930 A67-32077

27-day cycle variation in various noncosmic ray electromagnetic complex

- phenomena 17 p2932 A67-32084
Latitude variation of effective geomagnetic cut-off rigidity of cosmic rays in presence of penumbra and constant geomagnetic field 17 p2934 A67-32094
Flight trajectories having apogees unaffected by geomagnetic field, giving numerical solution, discussing radial propagation laws 17 p2941 A67-32239
McIlwain coordinates correlated with vertical cut-off rigidities, estimating cosmic ray rigidities 17 p2936 A67-32537
World maps indicating geomagnetically conjugate locations and L parameters 17 p2844 A67-32547
Magnetosphere and auroral phenomena including Van Allen radiation zones, satellite telemetry, solar wind fluctuations and cyclotron resonance 17 p2844 A67-32664
Nonlocal heating of electrons of daytime ionosphere taking account of displacement along geomagnetic field lines, comparing Dalgarno and Thomson 17 p2844 A67-32708
Luminosity variations of comet 1963 III related to solar and geomagnetic disturbances caused by corpuscular solar particles 17 p2946 A67-32730
MHD of terrestrial liquid core noting geomagnetic field variation, earth mantle movements, etc 17 p2845 A67-32773
Soviet book on geomagnetic field studies 17 p2845 A67-32934
Polar cap anomalous absorption effects from ionosphere and geomagnetic field studies, noting correlation with magnetic storms 17 p2846 A67-32936
Geomagnetic field secular variation forecasting method suggesting inclusion of anomalies 17 p2847 A67-32947
Winter and summer equivalent current systems of polar solar-diurnal variations studied from observations obtained during IGY 17 p2847 A67-32949
Space time distribution of magnetic activity during IGY, noting elliptical region about magnetic pole characterized by increased activity 17 p2848 A67-32950
Polarization of periodic pearl-type oscillations of geomagnetic field at magnetically conjugate points 17 p2850 A67-32974
Curves in polar plot representing auroral arcs over polar region organized in geomagnetic coordinate system and corrected by spherical harmonic terms 17 p2850 A67-33189
Nature of trapping regions, using spherical harmonic expansion for magnetic field created by currents on geomagnetic cavity surface 17 p2938 A67-33207
Resonant interactions between energetic trapped particles and transverse electromagnetic wave, suggesting geophysical applications and examining resonances suppression conditions 17 p2939 A67-33210
Fluid flow around magnetosphere boundary analyzed, noting geomagnetic field effect on hot plasma 17 p2853 A67-33252
Interpretation of multiple structure of auroral arc 18 p3035 A67-33598
Electron precipitation data examined to determine whether electron behavior can be understood on basis of binary collisions with atmospheric constituents and guidance by geomagnetic field 18 p3035 A67-33599
Trajectories of auroral charged particles accelerated in geomagnetic tail computed, using fields of magnetosphere reconnection model 18 p3038 A67-33614
Auroral and polar magnetic substorms related to magnetic field lines reconnection in magnetosphere tail 18 p3117 A67-33615
Geomagnetic eccentric dipole shown equivalent to multipoles superposition, giving geometric parameters and procedure for determining true magnetic poles 18 p3042 A67-34351
Resonances of thin shell model of earth-ionosphere cavity with dipolar magnetic field 18 p3042 A67-34427
Nonrelativistic charged particle transport in geomagnetic dipole field under effect of electromagnetic pulses obtained, using Fokker-Planck equation 19 p3313 A67-35212
Developments in upper atmosphere research noting atmospheric density, temperature, diurnal variations, solar and geomagnetic activity effects, etc 19 p3218 A67-35225
Interaction of plasma stream with three-dimensional magnetic dipole field, discussing current distribution in cavity 19 p3221 A67-35368
Equatorial electrojet parameters in India 19 p3221 A67-35431
Geomagnetic field boundary observations by Explorer XII 19 p3222 A67-35453
Solar wind velocity and interplanetary magnetic field components obtained by IMP II related to geomagnetic field variation 19 p3222 A67-35473
Guidance of audio-frequency electromagnetic waves along earth magnetic field investigated in absence of field-aligned irregularities of ionization 19 p3225 A67-35608
Aurora events of July 1958 attributed to solar flare from study of solar and geomagnetic data 19 p3225 A67-35618
Stability of continuous baroclinic flow in zonal magnetic field examined for zonal-flow profile of hyperbolic tangent form 19 p3253 A67-35918
Ionospheric F-2 region equatorial anomaly dependence on geomagnetic field 20 p3426 A67-36289
IGY data from magnetic observatories analyzed for luni-solar daily variations of geomagnetic field 20 p3525 A67-36869
Daily magnetic variations over England, noting difference between values obtained for summer IQD and other days of year 20 p3429 A67-36870
Main geomagnetic field data, discussing data conversion to computer-readable form 20 p3430 A67-36901
Magnetospheric features, describing magnetic field distribution, electron and proton density, plasma instabilities, bow shock and solar wind 20 p3430 A67-36903
Geomagnetic tail at 1000 earth radii, noting possibility of magnetic force lines connected to earth and tail 20 p3433 A67-37402
Particle trajectories for two model configurations of electric and magnetic fields in geomagnetic tail, noting application to auroral acceleration 20 p3433 A67-37415
Plasma diagnostic measurement simulation, considering electromotive effect from satellite motion through geomagnetic field 20 p3418 A67-37428
Proton mechanism of escape from earth magnetic field, analyzing charged particle in Alfvén wave field 20 p3520 A67-37667
Satellite stabilization in geomagnetic field by applying magnet to satellite axis and using damping elements of soft magnetic materials 21 p3713 A67-38375
External sources of geomagnetic field at F-2 layer altitude and effects on recurring-orbit satellites 21 p3618 A67-38462
Solar wind plasma penetration into geomagnetic field under effects of drift in crossed electric-geomagnetic fields 21 p3698 A67-38463
Geomagnetic activity effect on electron concentration at heights of 100 and 110 km 21 p3619 A67-38485
Z component of geomagnetic field, determining parameters of sloping dipoles 21 p3619 A67-38491
Satellite stabilization with respect to geomagnetic field obtained by applying moments of magnetic forces 21 p3713 A67-38589
Geomagnetic and gravitational field combined effects on magnetized satellite oscillations in plane of circular and elliptical polar orbits 21 p3713 A67-38590
Geomagnetic field configuration and time change using dipole vector, noting variation role 21 p3620 A67-38979
Geomagnetic field secular variation, with time explained by strength changes of BFD and nondipole field and drift 21 p3620 A67-38980
Geomagnetic field intensity influence on atmospheric C-14 production, using two-reservoir model 21 p3620 A67-38981
Geomagnetic field polarity inversion, discussing reverse magnetization of volcanic rocks 21 p3621 A67-38982
Statistical evidence of planetary and lunar modulation of geomagnetic activity 21 p3711 A67-39005
Separation of geomagnetic field into anomalous and normal components, analyzing spectral relation 21 p3622 A67-39024
Deep subterranean electric conductivity using 30-year cyclic geomagnetic field variation data 21 p3622 A67-39025
Western and equatorial components of geomagnetic field drift, noting noncoincidence of rotation axis with earth rotation axis 21 p3622 A67-39026
Solar disturbance variations of geomagnetic field dependence on solar activity indicates interplanetary magnetic field activity 21 p3623 A67-39041
Schuster method calculation of constant geomagnetic field spherical harmonics coefficients 21 p3623 A67-39045
Master matrix containing initial values of geomagnetic inclination and gyrofrequencies for storage in computer memory to calculate ionospheric vertical profiles 21 p3623 A67-39046
Separation of magnetic noise caused by ferromagnetic bodies in geomagnetic field 22 p3795 A67-39227
Ionospheric irregularities field alignment responsible for radio signal fading analyzed, showing no evidence for relation to geomagnetic field 22 p3788 A67-39468
Interplanetary space properties from satellite observations, discussing solar wind, geomagnetic field, comet tail effects, coronal plasma kinetic properties, etc 22 p3883 A67-39668
Quiet condition solar wind geomagnetic field interaction measurements, discussing solar plasma and bow shock wave generation 22 p3870 A67-39670
Mariner IV flight magnetometer data, determining interplanetary field and geomagnetic variability 22 p3790 A67-39800
Electron flux and energy spectrum measurements near polar cap investigated for diurnal intensity variations 22 p3872 A67-39802
Numerical program integrating motion equation of charged particles from realistic geomagnetic field model, with trajectory calculations for solar cosmic rays 22 p3872 A67-39810
Cosmic ray trajectories in geomagnetic field, discussing asymptotic directions, rigidities, crossed telescope measurements and focusing effect 23 p4050 A67-40693
Giant and continuous pulsations and pulsation trains in geomagnetic field studied from six giant pulsation events in 1963, discussing Wilson model 23 p3994 A67-40694
Storm time increase and anomalous type of daily variation during cosmic ray storms caused by lowered threshold rigidities and excess cosmic ray streaming respectively 23 p4050 A67-40695
Nuclear magnetometers for magnetospheric measurements from rockets 23 p3998 A67-40697
Geomagnetic field structure determination by method used to divide geomagnetic field observed along limited magnetic profile derived from mathematical apparatus of correlation analysis 23 p3994 A67-40715
Secular changes in surface flow motion in earth core noting dynamo theories of earth main field 23 p3996 A67-40816
Fourth order multipole parameters derived from spherical harmonic function coefficients for geomagnetic field potential 24 p4146 A67-41784
Boundary variations of auroral oval zones, noting dependence on magnetic perturbation intensity 24 p4149 A67-42121
Limit energy of monopole in field of earth magnetic dipole 24 p4150 A67-42137
Cartographic representation of diurnal magnetic variations, noting longitudinal asymmetry in amplitude distribution 24 p4150 A67-42145
Cosmos XLIX measurements of magnetic field intensity compared with calculations from spherical harmonic coefficients 24 p4150 A67-42149
Geomagnetic field aligned irregularities, explaining ionospheric E-region scattered wave propagation 24 p4120 A67-42150
Elektron I and II satellite measurements on outer radiation belt, noting geomagnetic field distortion and boundary dependence on magnetic perturbations 24 p4214 A67-42786
Asymptotic directions of cosmic rays for Soviet cosmic ray stations 24 p4214 A67-42790
Large scale structure of chromosphere examined using birefringent filter, comparing filtergrams with spectroheliograms of perturbed and active

regions of solar disk 24 p4239 A67-43066

GEOMAGNETIC LATITUDE

VHF backscatter observations of radio auroral radar echo occurrence at sunspot maximum associated with spirals in geomagnetic latitude and time, magnetic disturbance levels and season 03 p0513 A67-14113

Stormer height measurements of aurora, analyzing height distribution at various geomagnetic latitudes, noting relation to solar activity 06 p0997 A67-18694

Latitude distribution curves of two quasi-circular zones of maximum magnetic activity along 12 consecutive meridians of local geomagnetic time 07 p1178 A67-19825

Satellite topside sounder investigation of spread echoes at mid and high latitudes in Northern Hemisphere [AGARDOGRAPH 95] 15 p2480 A67-30276

Diurnal, annual, latitudinal and sunspot cycle-influenced variations of spread-F intensity at very high latitudes [AGARDOGRAPH 95] 15 p2481 A67-30281

Geophysical model of radio star and satellite ionosphere amplitude scintillations at nonequatorial latitudes [AGARDOGRAPH 95] 15 p2482 A67-30286

Measurements on scintillation observed on radio signals from Discoverer satellite, noting intensity increase with latitude and data on diurnal variation [AGARDOGRAPH 95] 15 p2483 A67-30293

Whistler investigation below ionospheric layers at high magnetic latitudes in Sweden 17 p2845 A67-32793

Polar cap absorption on July 1966, discussing solar flare, radio outburst, proton intensity, geomagnetic latitude, etc 19 p3313 A67-35214

Penumbra influence on cosmic ray effective cut-off rigidity calculated, noting case of primary variations and constant magnetic field 21 p3699 A67-39017

Latitude variation in neutron component of cosmic ray intensity within cut-off rigidity at atmospheric depths from 260 to 315 mb 23 p4057 A67-41119

Intensity of ionizing and neutron components measured in stratosphere as function of geomagnetic rigidity, obtaining coupling coefficients for cosmic ray variations 23 p4059 A67-41136

GEOMAGNETIC MICROPULSATION

SA TELLURIC-CURRENT MICROPULSATION

Polarization of type Pcl hydromagnetic oscillations observed at two conjugate geomagnetic stations analyzed by magnetic tape recorder 03 p0406 A67-12818

Geomagnetic micropulsation excitation by solar wind flow around magnetosphere, noting surface wave propagation 10 p1699 A67-22797

Hydromagnetic gradient waves theory extended to weakly ionized medium-density magnetized plasma of type expected in ionospheric E layer 11 p1783 A67-23923

Correlated study of auroral luminosity at different wavelengths, auroral X-rays, geomagnetic micropulsation and ionosphere 12 p1937 A67-25834

Geomagnetic micropulsations and electron bremsstrahlung in northern auroral zone 13 p2108 A67-26321

Frequency spectrum of Pi 2 micropulsation activity and relation to planetary magnetic activity 13 p2109 A67-26327

Ionospheric structure and micropulsations of geomagnetic field correlated, studying magnetodynamic wave damping and solar activity effects 13 p2114 A67-26856

Micropulsations of earth electromagnetic field relation to disturbed diurnal solar variation 14 p2308 A67-27925

Satellite drag analysis of atmospheric temperatures noting effects of UV, solar radiation and geomagnetic fluctuations 14 p2314 A67-29027

Sonagrams for micropulsations, computer simulated, using equations for cyclotron instability and quasi-linear diffusion of protons in bounded plasma 15 p2476 A67-29618

Pc-1 micropulsations, noting harmonic curve for diurnal variations and effect of magnetic and solar activity 15 p2476 A67-29619

Polarization of complex wave form geomagnetic micropulsations of natural and

artificial origin, using physical optics 15 p2476 A67-29620

Earth electromagnetic field stable micropulsations /pearls/ properties stressing apparent pearl polarization and polarization behavior 16 p2667 A67-31485

Diurnal characteristics of geomagnetic micropulsations noting period, amplitude, continuity, time of occurrence, etc, proving existence of hydromagnetic waves generated at magnetosphere 17 p2841 A67-32212

Interplanetary magnetic field data by Mariner II compared to ground-based standard magnetograms and micropulsation recordings for October 7, 1962 geomagnetic storm 17 p2844 A67-32540

Earth magnetic field micropulsation polarization properties at middle latitudes from three-component fluxmeter recordings 17 p2847 A67-32941

Pc 1 micropulsation signals classified as hydromagnetic whistlers and periodic hydromagnetic emissions, suggesting cyclotron instability process as generation mechanism of latter 17 p2853 A67-33253

Geomagnetic micropulsation properties variation over last solar cycle and causes 19 p3325 A67-35486

Pi micropulsation subtypes, one related to charged particles impulsive bursts from magnetospheric tail and another related to auroral electrojet 20 p3433 A67-37414

Diurnal variation of earth-ionosphere cavity resonances and properties and propagation of ELF, ULF and MHD waves 20 p3390 A67-37727

Dispersion characteristics of geomagnetic micropulsation pearls, obtaining magnetospheric proton densities 21 p3617 A67-38127

Micropulsation spectra /sonagrams/ indicating magnetosphere plasma resonances with recognizable modal pattern 21 p3619 A67-38513

Micropulsation pattern changes during magnetospheric transition from quiet to excited state, discussing influence of earth and long period and pearl-type pulsations 22 p3883 A67-39674

Polarizations of Pc 1 micropulsations intermittently recorded in Alaska with analysis of data for presence of right and left hand waves 22 p3793 A67-40078

Geomagnetic micropulsation excitation by solar wind flow around magnetosphere, noting surface wave propagation 24 p4209 A67-42133

GEOMAGNETIC PULSATION

ULF recording of geohydromagnetic micropulsations /whistlers/ 01 p0060 A67-10892

Origin of fluctuations in equatorial electrojet, discussing new type of geomagnetic variation of polar origin 03 p0408 A67-12840

Equatorial geomagnetic field fluctuations in frequency range of 4.0 to 0.003 c/s 03 p0408 A67-12842

Rapid geomagnetic micropulsation activity in low latitude conjugate stations show definitive results on current system 03 p0408 A67-12843

Rapid geomagnetic variations in vicinity of equator 03 p0409 A67-12844

Frequency spectrum of micropulsations analysis from records taken at station near geomagnetic equator 03 p0410 A67-12954

Lunar eclipse brightness variation relation to geomagnetic planetary index, showing that luminescence is in accord with rate of increase of plasma energy 03 p0509 A67-13165

Energetic electron precipitation and 5 to 40 second geomagnetic micropulsations relation to auroral substorms 04 p0615 A67-14968

Micropulsations of terrestrial electromagnetic field, noting statistical correlation between Pc-1 and Pc-2 type oscillations 04 p0616 A67-15219

Geomagnetic pulsations accompanying storm sudden commencements and sudden impulses 05 p0795 A67-16026

Alfven velocity distribution in magnetosphere to understand nature of geomagnetic micropulsation 05 p0795 A67-16062

Diurnal atmospheric oscillations and wind systems producing geomagnetic variations 05 p0798 A67-16859

Specific type of geomagnetic pulsations corresponding to solar corpuscular radiation,

noting flux geometry and intensity variations 05 p0884 A67-17134

Micropulsation dynamic spectra showing nosed tones instead of usual tones explained by helium ion content increase in outer magnetosphere 05 p0803 A67-17408

Long-period pulsations of H and D components of geomagnetic field 06 p0993 A67-17596

Distance compression field /DCF/ of geomagnetic storm, considering micropulsation activity and ionospheric effect 06 p0994 A67-17639

Visual frequency analysis of geomagnetic micropulsation records with computed power spectra for four separate samples of data 07 p1171 A67-19421

Time variation of preferential-polarization vector of pearl type oscillations during course of observations at Lovozero station, U.S.S.R. 07 p1174 A67-19711

Space-time variations in frequency and amplitude of Pcl oscillations observed during April 1964 07 p1179 A67-19837

Geomagnetic field variations in temperate zone sporadic E layer according to wind-shear theory 07 p1179 A67-19849

Mariner IV magnetometer data in earth magnetosheath analyzed to determine character of fluctuations in magnetic field 07 p1179 A67-19911

Spatial and temporal characteristics of bremsstrahlung X-ray due to energetic electron precipitation in auroral zone, noting measurement techniques 07 p1180 A67-19929

Ionosphere-exosphere system response to bomb-like hydromagnetic source and resultant ground level magnetic fluctuations 07 p1181 A67-19940

Correlation between pearl pulsations and interplanetary magnetic field sector boundaries 07 p1182 A67-19946

Evening micropulsation events with rising midfrequency characteristics, discussing possible source mechanisms 07 p1182 A67-19947

X-ray microburst correlation with impulsive microburst 07 p1246 A67-19949

Mathematical reliability of model for vibrating field lines used to explain micropulsation observations 07 p1182 A67-19950

Field aligned currents in magnetosphere as explanation of geomagnetic fluctuation localization to region smaller than applicable hydromagnetic wavelength 08 p1402 A67-21478

Equatorial enhancement of micropulsation pi-2 obtained from magnetograms during IGY, noting diurnal variation and latitudinal dependency similarity to other disturbances 08 p1329 A67-21540

Resonance in plasma magnetized by radial magnetic field solved, obtaining MHD wave equation, noting relation to micropulsations 09 p1545 A67-22196

Strong geomagnetic disturbances distribution in space and time analyzed for correlation of magnetic activity with auroral brightness 10 p1632 A67-22809

Auroral brightness variations related to magnetic field fluctuations, especially to pearl type fluctuations 10 p1632 A67-22811

Background noise curve of geomagnetic variations, attributing minimum spectral energy on ground to existence of permanent static solar wind component 10 p1632 A67-22856

Laminar composition structure and periodicity of variations with time in outer radiation belt investigated by solar radiation satellites 10 p1701 A67-23298

Auroral X radiation, measured by balloon-installed X-ray spectrometer incorporating scintillation counter with high speed analyzer, correlated with ionospheric radioelectric absorption and solar magnetic field variations 10 p1702 A67-23304

Negative ions in night ionosphere, discussing sub-ELF emission and excitation of ion acoustic oscillations in plasma by electron drifts 11 p1784 A67-23933

Partial coherence functions to investigate contribution of solar radiation and gravitational tide in causing geomagnetic variations /ionospheric tides/ 11 p1785 A67-23938

Frequency analysis of continuous and irregular geomagnetic pulsations measured by induction magnetometer 11 p1786 A67-24332

Balloon observations of large scale coherent pulsating electron precipitation events in auroral zone accompanied by geomagnetic continuous pulsations [AFOSR-67-1314] 12 p1931 A67-25112

High energy particle precipitation into upper atmosphere at medium latitude after magnetic storms, dependence on season and latitude and correlation with geomagnetic pulsation enhancement 12 p1991 A67-25113

Charged particle motion in magnetosphere under sudden magnetic pulse, compiling Fokker-Planck equation for particle distribution function 12 p1992 A67-25118

Spectral analysis of geomagnetic pulsations from 0.5 to 100 sec in period for quiet sun condition 12 p1932 A67-25189

Fast variations of electromagnetic field measured by satellites electron I and II used as indication of state of radiation belts and magnetosphere of earth fast variations of electromagnetic field measured 12 p1994 A67-25537

Short pearl type bursts as specific class of geomagnetic pulsation 13 p2110 A67-26454

Generalization of differential equation of dynamo theory of geomagnetic variations to include unsteady dynamo effect in ionosphere 13 p2110 A67-26548

Doppler frequency changes of ionospheric propagating radio waves and relationship to geomagnetic variation 13 p2068 A67-26992

Photometric auroral observations and geomagnetic field fluctuation magnetograms compared, noting relation between geomagnetic and auroral pulsations 14 p2309 A67-27944

Magnetospheric ion density measurement possibility from association of pulsating radio auroral echoes with sudden geomagnetic field fluctuations 14 p2313 A67-28574

Geomagnetic pulsations and auroral activity, using magnetosphere simplified model 15 p2474 A67-29505

Recording and analysis of geomagnetic pulsations of auroral zone and comparison with bremsstrahlung measurement, using two-magnetometer arrangement 15 p2474 A67-29524

ULF radio emission associated with magnetic field disturbances, geomagnetic pulsations, auroras and exospheric particle acceleration 17 p2846 A67-32939

Polar magnetic disturbances accompanied by short period pulsations investigated with magnetogram for negative magnetic bay characteristics 17 p2847 A67-32943

Pearl type oscillations studied by recording ground currents, discussing 24-hr and seasonal variations 17 p2847 A67-32944

Nature of Pcl oscillations in solar cycle, discussing frequency spectra of data obtained 17 p2847 A67-32945

Pearl period shift explained by model showing proton effect and limited spectrum MHD noise 17 p2847 A67-32946

Morphological behavior of damped type geomagnetic pulsations associated with storm sudden commencements and sudden impulses 17 p2851 A67-33211

Cosmic ray intensity short-period variations investigated by high-counting rate detector indicating fluctuations related to geomagnetic cutoff rigidity periodic changes 19 p3315 A67-35537

Ionospheric winds required to produce lunar daily geomagnetic variations deduced from atmospheric dynamo theory, estimating electric conductivity 20 p3425 A67-36281

Geomagnetic variations discussing attempts to explain 27-day recurrence tendency and to relate solar wind and magnetic indices 20 p3430 A67-36902

Correlation of north-south component of telluric currents and brightness fluctuations in quiet form auroras 20 p3431 A67-36994

Irregular pulsations of diminishing periods /IPDP/, discussing cause and low energy electron flux variations 20 p3431 A67-37097

Magnetosheath observations by Vela 3 at 18 earth radii, discussing substructure, shock crossings and pulsations 20 p3433 A67-37410

Dynamic spectrum of long-period geomagnetic pulsations noting Pc range characteristics 20 p3433 A67-37413

Alfven velocity distributions in magnetosphere used to understand nature of geomagnetic micropulsation 21 p3616 A67-37849

Specific type of geomagnetic pulsations

corresponding to solar corpuscular radiation, noting flux geometry and intensity variations 21 p3698 A67-38477

Alfven standing wave formation due to interaction of magnetosphere with geomagnetic pulsation 21 p3621 A67-39023

Irregular pulsations of decreasing period /IPDP/ events detected in magnetosphere, discussing strong correlation with magnetic index 22 p3789 A67-39497

Long period hydromagnetic propagation in theta model geomagnetic tail, deriving TM and TE modes equations 22 p3791 A67-39815

Geomagnetic perturbation data from high altitude nuclear weapon detonations, deriving theoretical model based upon MHD resonance, noting Alfven wave behavior 22 p3792 A67-39932

Giant and continuous pulsations and pulsation trains in geomagnetic field studied from six giant pulsation events in 1963, discussing Wilson model 23 p3994 A67-40694

Strong geomagnetic disturbances distribution and time analyzed for correlation of magnetic activity with auroral brightness 24 p4150 A67-42146

Auroral brightness variations related to magnetic field fluctuations, especially to pearl type fluctuations 24 p4150 A67-42148

GEOMAGNETIC STORM
SA IONOSPHERIC STORM
SA SUDDEN IONOSPHERIC DISTURBANCE /SID/

Solar causes of occurrence of selected geomagnetic storms and geomagnetic quiet, using data of coronal structure at central solar meridian 01 p0060 A67-10789

Recurrent cosmic-ray modulation phenomena with Forbush decrease characteristics correlated with M-region magnetic storms, concluding that each series results from shock wave solar initiated 01 p0145 A67-10919

Neutron component diurnal variation in cosmic radiation during period of coil type magnetic disturbances in tail of geomagnetic storm 02 p0306 A67-11656

Changes in solar cosmic ray and geomagnetic field intensities during magnetic storms accompanied by decrease in galactic cosmic ray intensity, using moving averages method 02 p0311 A67-12593

Magnetic storm accompanied by cosmic ray intensity increase analyzed, considering Forbush effect and determining all peaks 02 p0312 A67-12601

Magnetic storm enhancement of 5577 angstrom airglow emission intensity [AFCL-66-866] 03 p0505 A67-12836

Equatorial ionospheric storms, analyzing sub-peak and total columnar electron content 03 p0408 A67-12841

Satellite measurement of behavior of high latitude energetic electron trapping boundary, noting geomagnetic storm effects 03 p0410 A67-12951

Statistical analysis of auroral radar echoes reveals changes in shape of diurnal variation curve with level of magnetic disturbance and seasonal variation with peaks at equinoxes 03 p0513 A67-14112

Equatorial spread-F and tropical disturbances, supplying data on typhoon, geomagnetic activity and atmospheric pressure waves 04 p0612 A67-14653

Temporal variations of intensities of electrons of various energy ranges trapped in outer radiation zone measured by research satellite Injun 04 p0693 A67-14962

Diurnal variation of sporadic E at high latitude as function of geomagnetic activity 04 p0615 A67-14972

Geomagnetic and auroral storms provide information on interaction of solar plasma flows and magnetosphere 04 p0618 A67-15668

Corpuscular stream parameters based on data from Mariner II concerning cosmic ray variations on earth surface during geomagnetic storms 05 p0881 A67-18121

Magnitude of principal phase DR field of magnetic storm assuming plasma pressure remains constant or varies proportionally with magnetic pressure 05 p0884 A67-17132

Magnetic and kinetic energy calculated for geomagnetic storm as function of velocity distributions 05 p0801 A67-17133

Emf as cause of vertical downward and upward ionization drift in F region of ionosphere during magnetic storm 05 p0801 A67-17141

Ionospheric flux system of initial phase of geomagnetic storm of September 4, 1957 over polar cap 05 p0802 A67-17148

Geophysical and heliophysical characteristics for enhanced cosmic radiation intensity during magnetic storm in February 1959 05 p0885 A67-17498

Distance compression field /DCF/ of geomagnetic storm, considering micropulsation activity and ionospheric effect 06 p0994 A67-17639

F region effects following two severe magnetic storms, noting changes in electron density profile 06 p0995 A67-17972

Aurora and ring current theory confirming role of hydromagnetic plasma flow and frozen-in field lines in geomagnetic storms 06 p0995 A67-17973

Quasi-stationary gas emission from active solar regions and relation to recurrent geomagnetic disturbances 06 p1077 A67-18152

Satellite observation of radiation belt and absorption of cosmic noise in polar aurora during magnetic storms of February 1964 07 p1243 A67-19683

Statistical distribution of monthly median noon critical frequency of F2 layer from ionospheric stations at mid-latitudes, auroral regions and at polar cap 07 p1174 A67-19703

Ionospheric effect of sudden magnetic storm eruption, noting propagation of disturbance above terrestrial surface 07 p1174 A67-19705

Spread in values of vertical magnetic field component during sudden commencements of magnetic storms attributed to local geoelectric conditions 07 p1174 A67-19712

Corpuscular intrusions into earth magnetosphere involving entire auroral zone and occurring only on night side 07 p1174 A67-19713

Solar causes of geomagnetic storm with sudden or gradual commencement 07 p1175 A67-19720

Electron density variation, solar activity and geomagnetic storm effects on ionospheric F-region 07 p1177 A67-19785

Solar wind parameter variation, magnetosphere flux interaction and dependence of geomagnetic storm on magnetospheric conditions and geomagnetic field increase 07 p1243 A67-19804

Auroral occurrence rate at zenith as function of latitude for magnetically quiet and magnetically disturbed periods 07 p1178 A67-19817

Magnetospheric distortion during geomagnetic storm on September 30, 1961, examining Explorer XII satellite evidence on ring currents 07 p1180 A67-19924

Ionospheric heating by Joule dissipation of main-phase ring current associated with asymmetry 07 p1181 A67-19934

Main phase of geomagnetic storms and magnetic and auroral substorms development by analyzing individual geomagnetic storms 07 p1183 A67-20016

Geomagnetic, auroral, ionospheric and cosmic ray perturbations interdependence and relationship with solar activity 07 p1183 A67-20174

Geomagnetic storms due to solar flares statistically analyzed to obtain configuration of solar plasma flow generated by solar flares 08 p1377 A67-21360

Normality of SD variation at dip-equatorial stations suggests origin beyond F layer 08 p1327 A67-21373

Field buildup during sudden commencement of magnetic storms in magnetosphere determined from MHD wave and solar wind pressure measurements 10 p1630 A67-22777

Cosmic ray neutron component intensity during magnetic perturbations, considering effect of magnetospheric deformation 10 p1699 A67-22781

Time delay between geomagnetic storm and corresponding maximum in atmospheric density obtained from satellite drag data 10 p1639 A67-23209

High resolution density data from radar observations of low altitude polar orbiting satellites reveal longitudinal and geomagnetic variation, noting regression analysis 10 p1640 A67-23216

Satellite measurement of upper atmospheric density variations due to geomagnetic disturbances, correlating time delay with geographic

- latitude 11 p1783 A67-23922
Polar magnetic substorms noting flux tube flow, proposing structure for substorm current system 11 p1784 A67-23928 [JPL-TR-32-1094]
Atmospheric density determination from drag of eleven low altitude satellites, discussing correlation with geomagnetic activity and daily periodicity 11 p1784 A67-23937
Geomagnetic disturbances dependence on interplanetary magnetic field sector structure and incident solar ion current at and near minimum of solar cycle 11 p1786 A67-24331
Emission of particles, causing geomagnetic storms, without accompanying radio effects 11 p1787 A67-24594
Visual presentation of geomagnetic displays using normal ionospheric current system with line separation inversely proportional to field perturbation intensity 11 p1788 A67-24699
Forecasting geomagnetic storms and disturbances from solar observations 12 p1931 A67-25110
Detection of solar flare effect during severe geomagnetic disturbances from ionospheric flare effects 12 p1993 A67-25363
Radial displacement of particles excited by solar-wind-induced current at boundary of and ring current within magnetosphere 12 p1994 A67-25531
Cosmic radio wave absorption dependence on frequency and number of electron-ion collisions during atmospheric magnetic storms 12 p1933 A67-25548
Long period hydromagnetic waves in magnetosphere and coupling to solar wind studied by Explorer XIV 12 p1937 A67-25812
Interplanetary solar wind measurements during April 1965 geomagnetic storm using electrostatic analyzers on Vela satellite 13 p2189 A67-26303
Dependence of diurnal cosmic ray variations on angle which is proportional to shortest distance from earth to axis of corpuscular stream 13 p2191 A67-26546
Magnetic field of ring current on earth surface according to observations during IGY 13 p2111 A67-26557
Geomagnetic activity and earth heliolatitude effect on diurnal variation of cosmic radiation, based on IGY neutron component observations 13 p2191 A67-26564
Duration of initial stage of geomagnetic storm based on observations from 1957 through 1959 14 p2308 A67-27929
Synoptic charting of high latitude geomagnetic field distribution during magnetic storm, discussing ring current behavior 14 p2309 A67-27942
Electric current associated with polar magnetic substorms 14 p2313 A67-28573
Early appearance of active aurora during geomagnetic storm caused by westward traveling surges along expanded oval 14 p2313 A67-28575
Quasi-stationary gas emission from active solar regions and relation to recurrent geomagnetic disturbances 16 p2737 A67-30496
Neutron component diurnal variation in cosmic radiation during period of coil type magnetic disturbances in tail of geomagnetic storm 16 p2738 A67-31071
Systematic clockwise rotation of asymmetry axis of main phase decrease during geomagnetic storm 16 p2666 A67-31412
Three-dimensional structure of solar plasma flow generated by solar flares, noting geometric factors in geomagnetic storm intensity decrease 16 p2739 A67-31415
Solar cosmic radiation, discussing effect on geomagnetic storm 16 p2740 A67-31899
Shock wave propagation in solar wind caused by tangential discontinuities and geomagnetic sudden storm commencement 17 p2936 A67-32530
Interplanetary magnetic field data by Mariner II compared to ground-based standard magnetograms and micropulsation recordings for October 7, 1962 geomagnetic storm 17 p2844 A67-32540
Relationship between geomagnetic storms with sudden commencements and perturbations of southern and northern components of meson distribution in Northern Hemisphere 17 p2938 A67-32796
Interplanetary structure revealed through study of cosmic ray storm effects in February 1962 17 p2845 A67-32797
Auroral belt dynamics including edge displacement rate, width, asymmetry of sides and relation to polar geomagnetic disturbances 17 p2850 A67-33184
Geomagnetic time and latitude distribution of magnetic disturbances at auroral and polar cap latitudes 18 p3032 A67-33583
Polar cap auroras frequency patterns relationship to worldwide storms 18 p3037 A67-33611
Geomagnetic activity effect derived from Explorer IX drag data, with atmospheric temperature as geomagnetic storm intensity function and atmospheric density increase 18 p3042 A67-34255
Changes in topside ionosphere during large magnetic storm, studying electron density, slab thickness, scale height, etc 20 p3427 A67-36305
Auroral substorms, examining energy spectrum and flux of precipitating particles and morphology 20 p3431 A67-37100
Charged particles of extraterrestrial ring current during geomagnetic storms, with Ogo 3 measurements of proton and electron differential energy 20 p3432 A67-37401
Reversible betatron acceleration mechanism during geomagnetic storm 20 p3434 A67-37425
Soviet book on ionospheric geomagnetic disturbance prediction and short term radio propagation forecasting 21 p3616 A67-37933
Evening sector polar magnetic substorm disturbance field morphology in transition region 21 p3616 A67-37998
Magnitude of principal phase DR field of magnetic storm assuming plasma pressure remains constant or varies proportionally with magnetic pressure 21 p3698 A67-38475
Magnetic and kinetic energy calculated for geomagnetic storm as function of velocity distributions 21 p3619 A67-38476
EMF as cause of vertical downward and upward ionization drift in F region of ionosphere during magnetic storm 21 p3619 A67-38483
Ionospheric flux system of initial phase of geomagnetic storm of September 4, 1957 over polar cap 21 p3619 A67-38490
Intense negative bays occurring inside evening and midnight sectors of auroral zone during polar magnetic substorms 22 p3789 A67-39477
Solar wind geomagnetic field interactions during disturbed conditions, discussing solar particle emissions, solar plasma activity, ring and ionospheric currents 22 p3870 A67-39672
Transverse field growth studied for generation of magnetic field in boundary layer by currents along magnetopause produced by tangential solar wind 22 p3871 A67-39801
Growth and decay of geomagnetic storms of April 17-18, 1965 studied using data from 88 ground stations, Explorer XXVI and Vela satellites 23 p3995 A67-40814
Field buildup during sudden commencement of magnetic storms in magnetosphere determined from MHD wave and solar wind pressure measurements 24 p4149 A67-42113
Cosmic ray neutron component intensity during magnetic perturbations, considering effect of magnetospheric deformation 24 p4209 A67-42117
Corpuscular stream parameters based on data from Mariner II concerning cosmic ray variations on earth surface during geomagnetic storms 24 p4214 A67-42797
- GEOMAGNETICALLY TRAPPED PARTICLE**
SA PROTON BELT
Superposed electric field effect on longitudinal drift rate of geomagnetically trapped electron 01 p0056 A67-10109
Earth radiation belt, particle motion and magnetic cavity 01 p0143 A67-10254
Rocket measurements of 1/2 to 4 mev trapped protons in near-equatorial magnetosphere [AFRL-66-865] 03 p0505 A67-12835
Trapped particle acceleration by magnetic fluctuation produced by ionospheric currents derived from observations of sharp energy groups of high energy electrons 03 p0409 A67-12942
Optical damage of spacecraft thermal control coatings in simulated space radiation environment of geomagnetically trapped particles 03 p0448 A67-13051
[AIAA PAPER 65-646]
High energy electron intensity measurement beyond atmosphere with aid of proton I and II satellites, showing capture by geomagnetic field 05 p0878 A67-16091
Solar plasma intrusion into model magnetosphere 05 p0859 A67-17441
Physical pattern of high altitude fission cloud and motion of gamma and beta fission fragments captured by geomagnetic field and observed by Cosmos satellite 07 p1242 A67-19102
Pitch-angle distribution and differential energy spectrum of polar aurora protons penetrating earth 07 p1173 A67-19700
Formation mechanism of ionospheric narrow sporadic E layers by high energy electron fluxes captured by geomagnetic field 07 p1179 A67-19835
Radiation belts, energetic charged particle flux and trapped radiation in geomagnetic field as result of neutron albedo decay and plasma-magnetic field interactions 07 p1246 A67-20297
Quasi-trapped whistler mode propagation and generation by trapped electrons in magnetosphere, noting refraction index and wave reflection 08 p1327 A67-21462
Adiabatic invariant analysis of charged particle motion in model magnetosphere 08 p1378 A67-21474
Physics of aurora as magnetospheric and cosmic phenomena 10 p1633 A67-22986
Low altitude electron trapping boundary collapse during magnetic storm due to field line extension into geomagnetic tail 11 p1785 A67-23943
Transfer coefficients of charged particles trapped in magnetic field of earth, examining concept of sudden pulses as basic mechanism 12 p1994 A67-25541
Geomagnetic field anomalies in Southern Hemisphere and effects on cosmic rays, geomagnetically trapped radiation and ionosphere 12 p1933 A67-25770
Fokker-Planck equation for geomagnetically trapped electron distribution as function of longitude, time, energy and mirror-point field intensity 12 p1995 A67-25772
Low energy proton and electron outer radiation belt satellite Cosmos 41 indicate capture and acceleration mechanism 12 p1997 A67-25810
Time variations of intensity in outer belt and near boundary deduced from Elektron I and II data, noting comparison with magnetic field variations 12 p1997 A67-25815
Long term measurement of trapped-electron environment in narrow region of space at lower edge of inner radiation belt 14 p2380 A67-28051
Nature of trapping regions, using spherical harmonic expansion for magnetic field created by currents on geomagnetic cavity surface 17 p2938 A67-33207
Inner Van Allen belt proton dose rate and spectral charged particle environment profiles correlated, noting agreement with theoretical values 19 p3313 A67-35189
Alpha particle proton ratio of geomagnetic field from data from charged-particle telescope on OGO 1 20 p3519 A67-37412
Magnetospheric energetic charged particles interrelations, discussing electron and proton energy spectra, particle population domains, trapped radiation and solar wind kinetic energy 22 p3870 A67-39673
Dynamic equilibrium of Van Allen belts studied for self-consistency through saturation of trapped plasma 22 p3871 A67-39799
Fokker-Planck equation describing distribution of geomagnetically trapped electrons as function of longitude, time, energy and mirror-point field intensity 22 p3791 A67-39808
High energy electron intensity measurement beyond atmosphere with aid of proton I and II satellites, showing capture by geomagnetic field 24 p4213 A67-42767
- GEOMAGNETISM**
SA M-REGION
SA SPHERICAL HARMONICS
Geomagnetic induction arrow direction determined from quiet solar activity variations 13 p2116 A67-27396
IQSY South African participation,

reviewing meteorology, geomagnetism, aurora, airglow, ionosphere, cosmic rays, etc 19 p3315 A67-35477
National IQSY research programs /1964-1965/ 19 p3325 A67-35497
Argentina 1964-1965 IQSY program emphasizing aerology, solar radiation, ozone concentration, geomagnetism, etc 19 p3224 A67-35499
U.S. research program for IQSY 1964-1965 covering solar synoptic observations, zodiacal light, comet tails, atmosphere, etc 19 p3224 A67-35501
Cosmic rays interaction with solar and terrestrial magnetic fields, noting interplanetary plasma flows and solar activity 21 p3699 A67-39006
Magnetospheric open split tail topology noting stability of geometry in all solar wind and interplanetary medium conditions 22 p3792 A67-39820
Energetic outer radiation belt electron spectra spatial and time variations 22 p3873 A67-39822
Earth core surface fluid velocity patterns and magnetic field secular change at earth surface for various epochs 23 p3996 A67-40815
Geomagnetic dynamo laboratory model self-excitation conditions determined from solutions of electrodynamic equations, diagramming magnetic field and current distribution 24 p4231 A67-42353
GEOMETRIC FACTOR
Point discharge from multiple points in irregular configuration, space-charge theory and plant discharge applications 01 p0107 A67-10114
Orbits, altitudes, viewing geometry, coverage and resolution pertinent to satellite observations of earth and atmosphere 01 p0147 A67-10325
Numerical analysis showing dependence of vacuum plasma accelerator geometrical and electrical parameters on plasma acceleration kinematics 01 p0122 A67-10347
Small-perturbation hover dynamics motion equations, characteristic modes, stability derivatives and dimensional analysis [SAE PAPER 660576] 01 p0010 A67-10570
Geometrical factor and radiation pattern for single crystalline detectors and coaxial telescope 02 p0240 A67-11542
Large monolithic radome antenna fabrication 02 p0215 A67-11980
Ohm law deviation in island-structure thin metallic films and current dependence on field strength 03 p0490 A67-13159
Metallurgical and geometrical factors affecting high temperature tensile properties of discontinuous tungsten fiber reinforced composites 03 p0441 A67-13272
Effect of locking dovetail joint geometry on static strength 03 p0528 A67-14077
Turbulent subsonic gas jets, importance of Reynolds number and geometrical configuration of nozzle in determination of flow parameter 05 p0790 A67-16033
Oblique probe data applied to determination of minimum group path of signal for parabolic model of ionosphere 05 p0801 A67-17130
Optimum wedges and semicones in hypersonic viscous flow, examining effect of thickness ratio on lift-drag ratio 05 p0750 A67-17367
Peaking circle graphical method for solving 3-DB points in second order systems 06 p0971 A67-18244
Electrode geometry effect on current and potential distributions in MPD arcs 06 p1074 A67-18335
Invariants of triangular shell element stiffness matrices associated with polyhedral deflection distribution, discussing effect of geometry [AIAA PAPER 67-114] 06 p1103 A67-18356
Initial geometric and boundary condition imperfection effect on stability of shallow spherical shells under uniform pressure [AIAA PAPER 67-111] 06 p1104 A67-18453
Self-preserving turbulent jet ejector, solving equations of motion to determine system geometry corresponding to flow conditions [AIAA PAPER 67-127] 06 p0988 A67-18456
Curvilinear annular turbine outlet diffusers, discussing effects of geometric parameters on diffuser effectiveness 06 p0942 A67-18553
Diurnal variation of Schumann resonances

explained by geometrical factors relating position of sources and observational point, noting propagation difference between EW and NS 06 p0998 A67-18707
Formulas for stress determination on surface of elastic right cylinder, sphere and circular cone taking into account geometrical nonlinearity 07 p1261 A67-19218
Materials and fin tube geometry effects on ultimate size and mass of space radiator 07 p1223 A67-19461
Optimal design of elliptical pumping chambers from numerical calculations containing all geometric sizes of pumping lamps and laser rods and reflectivity of walls 07 p1195 A67-19490
Orbital change problems using Busemann configuration space combined with geometrical properties inherent to Keplerian orbits [AAS PAPER 66-122] 07 p1254 A67-19981
Fiber reinforced plastics, determining composite elastic constants in terms of elastic moduli and geometric parameters of constituents 08 p1346 A67-20910
Stress distribution in unidirectional multifiber composite under external and residual shrinkage loads expressed via displacement potentials 08 p1420 A67-20912
Geometry variation effects on hydrodynamic bearing performance, noting locational dependence relative to pressure producing region 08 p1336 A67-21041
Isomerization rate of iminocarbonates, discussing electronegative hetero-atom bonded to imino carbon 09 p1459 A67-22363
Shear strength of various joint designs measured, using steel adherends and rubbery adhesives to isolate factors affecting shear stress 09 p1577 A67-22503
Self-aligning radial clearance seals, discussing design parameters, balance leakage and power loss as function of geometry 10 p1659 A67-22707
Condon loci geometry of molecular spectrum determined by plotting intensities on Deslandres diagram 10 p1681 A67-22959
Geometrically nonlinear effects of stress concentrations at holes in thin plate with large deformations 11 p1878 A67-24878
Numerical analysis showing dependence of vacuum plasma accelerator geometrical and electrical parameters on plasma acceleration kinematics 11 p1844 A67-25020
Negative-mass instability of cylindrical layer of relativistic electrons in geometrical configuration approximating Astron machine 12 p1970 A67-25254
Voltage breakdown in selectively diffused p-n junction, analyzing dependence on radius of junction curvature 12 p1982 A67-25453
Nonlinear equations in gas dynamics for turbulent nonpotential flows, emphasizing geometry of characteristic surfaces and numerical calculation 12 p1931 A67-26199
Aerodynamic damping and frequency drift of turbomachine blades, discussing wind tunnel testing results for various geometric configurations 13 p2051 A67-27205
Fuel cell research noting gas porous electrodes, effect of geometry on performance and electrocatalysis 14 p2252 A67-29019
Plastic behavior of material continua in terms of Riemannian and non-Riemannian differential geometry 16 p2767 A67-31276
Conducting loop resonant size determination and geometrical shape effect on resonant size in anechoic chamber experiment 16 p2639 A67-31356
Three-dimensional structure of solar plasma flow generated by solar flares, noting geometric factors in geomagnetic storm intensity decrease 16 p2739 A67-31415
Geometrical factor and radiation pattern for single crystalline detectors and coaxial telescope 16 p2677 A67-31608
Geometric dimensional, plasma temperature and pressure effects on capillary discharge with evaporating wall /CDEW/ 17 p2897 A67-32177
Velocity potential near disturbance boundary for steady supersonic flow past body-and-wing model 17 p2790 A67-32403
Thin superconducting films behavior in perpendicular magnetic fields, studying sample geometry effect on reversible magnetization curve 19 p3303 A67-35041
Shape of minimum drag cruciform wing of symmetrical thickness in supersonic flow 20 p3355 A67-36192

Optimal geometry of certain isolated heat-conducting circular fins cooled by radiation 20 p3554 A67-37067
Geometric parameters effect on aerodynamic characteristics of plane compressor cascade with high subsonic flow 20 p3358 A67-37080
Electron content measured using satellite motion and position effects on Faraday rotation 20 p3431 A67-37102
Aircraft structural form optimized through changes in geometry 20 p3542 A67-37531
Oblique probe data applied to determination of minimum group path of signal for parabolic model of ionosphere 21 p3618 A67-38473
Critical strain parameter concept for adhesive bond joints noting strength dependence on geometry and material elastic properties [SAE PAPER 670856] 24 p4160 A67-42003
Conformal representation of ring on complex doubly connected symmetrical region bounded externally by circumference and internally by star shape curve 24 p4249 A67-42106
Design of approximately optimal feedback controllers for systems with bounded states 24 p4134 A67-42178
Electrofluiddynamic /EFD/ power generator unipolar charge generation using corona discharge, noting pressure and geometry effects on ion currents and attractor voltage 24 p4107 A67-42528
Electrofluiddynamic /EFD/ power generator channel performance dependence on charge spreading for various geometries, noting stage efficiency and electric pressure 24 p4107 A67-42529
Measurement of time varying spectra of argon plasma in coaxial gun for two different gun geometries 24 p4198 A67-42730
Hydrodynamic journal bearings in liquid sodium, discussing stability characteristics of different geometries and wear at high temperatures [ASLE PAPER 67-LC-7] 24 p4164 A67-42746
GEOMETRICAL OPTICS
Tropospheric and ionospheric models and parameter variations affecting satellite signal propagation, discussing refractive corrections 01 p0028 A67-11431
Gaussian noise model of shadowing effect on wave backscatter from one-dimensional random rough surface 02 p0192 A67-11602
Geometrical optics method modified for asymptotic solution to scalar wave equation for wave penetrating caustic surface 02 p0192 A67-11637
Emission of point oscillator located in medium having permittivity varying according to traveling wave law 02 p0192 A67-11643
Spherical diffraction solution obtained by reducing it to solution of diffraction problem for circular cylinder via coordinate transformation 02 p0205 A67-12529
Asymptotic evaluation for k approaching infinity of antenna field emerging from currents induced on surface of reflector with incident spherical wave 02 p0223 A67-12796
Field intensity of ultrashort radio waves in superrefraction 03 p0368 A67-13280
Spherical concentric geometry for designing absorber materials for application to curved surfaces determined by specular radar cross section 03 p0371 A67-13863
Room temperature measurements determining mean slope and peak-to-valley height influences on bidirectional spectral reflectance of V-grooved surfaces 03 p0426 A67-14398
Asymptotic characteristic of eigenfunctions of two-dimensional scalar wave equation with boundary conditions at equidistant curves 04 p0570 A67-14743
Sample orientation and electron beam incidence angle variation effects on X-ray spectrometer performance 04 p0621 A67-15114
Change of polarization state of ray due to multiple internal reflections within many-sided reflectors 04 p0657 A67-15307
Approximation method of geometric optics in theory of electromagnetic waves in gyrotropic medium 05 p0762 A67-16347
Self-focusing and self-trapping of intense light beams in nonlinear medium examined, using approximations of geometrical optics and accounting for diffraction

effects 06 p1031 A67-17880
Geometrical light rays in lens-like media and derivation of differential equation 06 p1033 A67-18534
Geometric-optics curvilinear coordinate system computation of scattered field of smooth bodies with sharp edge in terms of phase structure 07 p1143 A67-19588
Pulse distortion in ionospheric plasma, discussing reflection from layer via geometrical optics and quadratic approximation 07 p1143 A67-19594
Radio wave propagation in artificial ionized cloud in upper atmosphere determined, using geometrical optics 07 p1143 A67-19691
Pencil-beam radio telescope adjustment via methods of control of surface of optical telescopes 07 p1189 A67-20244
Imaging properties of gas lens, discussing ray trajectory, ray matrix lens formula, optical transfer function, etc 09 p1498 A67-22083
Control of laser action, noting feedback theory conception and geometrical optics of laser modulation 09 p1513 A67-22146
Signal intensity along short wave path calculated by method based on dead zone existence and geometrical optics 10 p1603 A67-22793
Optical configuration for long distance laser beam transmission determined from truncated Gaussian aperture distribution radiation patterns 11 p1754 A67-24724
Geometrical optics approximation of plane electromagnetic wave reflection from ideally electrically conducting triaxial ellipsoid 11 p1754 A67-24986
Electromagnetic wave diffraction on plasma cylinders calculated using wave equation and geometrical optics approximation 12 p1969 A67-25246
Lambert diffuse reflection from general quadric surfaces 13 p2158 A67-26877
Spherical diffraction solution obtained by reducing it to solution of diffraction problem for circular cylinder via coordinate transformation 14 p2261 A67-28006
Panoramic photograph processing theory 14 p2318 A67-28372
Source free solutions in ionized regions, discussing geometrical optics application to MGD with infinite conductivity 14 p2359 A67-28462
Electromagnetic sensing of absolute rotation with self-oscillating laser version of Sagnac interferometer 14 p2349 A67-28812
Transition functions occurring in diffraction theory of plane stratified medium with increasing refractive index 14 p2349 A67-29063
Diffraction coefficients in Keller theory extended to near-field and shadow-boundary regions of edge, introducing two correction factors 16 p2627 A67-31365
Plasma concentration diagnostics by hydromagnetic probing method, determining concentration profile from latitude dependence of torsional vibrations 16 p2668 A67-31890
Slipping instability of plasma flows, noting instability criteria for long and short wavelength oscillatory 17 p2905 A67-32925
Emulsion shrinkage effect on hologram image space 17 p2863 A67-33303
Four types of holographic imaging systems, discussing optical properties and divergence and convergence 18 p3046 A67-33879
Mean-square value and autocorrelation function for fluctuations of geometrical optical paths 18 p3000 A67-34025
Soviet book on lasers and nonlinear optics covering theory, physical processes and phenomena caused by strong electromagnetic laser radiation 19 p3238 A67-34800
Soviet book on wave propagation in turbulent atmosphere covering geometric optics of electromagnetic and acoustic wave scattering and propagation, etc 19 p3182 A67-35206
Wave propagation and geometrical optics in random media, considering applications to solar corona heating by energy transfer, stellar scintillation and cosmic ray acceleration 19 p3261 A67-35507
Principal polarization radar cross sections as function of azimuth aspect angle for rectangular cylinder 19 p3183 A67-35518
Electromagnetic wave propagation in

absorbing gyrotropic medium in terms of geometrical optics, considering applicability to radiowave propagation in upper atmosphere 19 p3185 A67-36015
Short wave skip distance variation with reflection angles in multilayered ionosphere calculated from improved formula 20 p3382 A67-36763
Geometric-optics curvilinear coordinate system computation of scattered field of smooth bodies with sharp edge in terms of phase structure 20 p3384 A67-37325
Pulse distortion in ionospheric plasma, discussing reflection from layer via geometrical optics and quadratic approximation 20 p3384 A67-37334
Fields with boundaries radiated by electric or magnetic current phased-line distributions, interpreting field constituents as geometric-optical and diffracted contributions 20 p3388 A67-37702
Geometrical-optics approximation method for electromagnetic wave propagation in parametric medium 21 p3580 A67-38113
Radio wave propagation in three-dimensional inhomogeneous magnetoactive ionosphere studied by geometrical optics method 21 p3582 A67-38592
Wave propagation in wave optics transition to geometrical optics in general relativity theory using series expansion 23 p4027 A67-41146
Absorptivity of medium, obtaining results for spectral quantities referred to given radiation frequency 23 p4083 A67-41288
Light beam self-focusing, discussing electromagnetic interaction in nonlinear medium, refractive index dependence on wave intensity and geometrical optics 24 p4187 A67-41770
Signal intensity along short wave path calculated by method based on dead zone existence and geometrical optics 24 p4120 A67-42129
GEOMETRODYNAMICS
Models of spherically symmetric nonstatic processes, including relativistic collapse to Schwarzschild sphere, constructed by space-time metrics [JPL-TR-32-1136] 15 p2564 A67-30438
Three-body problem reduced to two-body problem in general relativity 16 p2745 A67-30747
Alternative approaches to particle solutions obeying Einstein gravitation theory 18 p3077 A67-33553
GEOMETRY
SA ANALYTIC GEOMETRY
SA BOSE GEOMETRY
SA DIFFERENTIAL GEOMETRY
SA FLOW GEOMETRY
SA HYPERGEOMETRIC FUNCTION
SA NONEUCLIDEAN GEOMETRY
SA NOZZLE GEOMETRY
SA PROJECTIVE-DIFFERENTIAL GEOMETRY
SA SURFACE GEOMETRY
SA TANK GEOMETRY
SA TOPOLOGY
SA VARIABLE GEOMETRY STRUCTURE
Geometrical method for endurance theory using stress space, stress-strain relation and surface tensor 02 p0339 A67-12239
Geometrical methods for solving higher order geodetic problems from satellite observations including direction, position, coordinate, etc 05 p0800 A67-17031
Book on geometric programming detailing theory of mathematical method for optimizing engineering design 09 p1469 A67-22435
Geometric interpretation of product form of inverse applied to sparse matrices in linear programming, using graph theory 10 p1673 A67-22833
Geometrical methods for solving higher order geodetic problems from satellite observations including direction, position, coordinate, etc 21 p3618 A67-38263
GEOGRAPHICAL OBSERVATORY
SA OGO
Planetary distribution and interpretation of abrupt increases in cosmic ray intensity observed during periods of maximum solar activity but not related to visible solar phenomena 02 p0312 A67-12602
Rapid geomagnetic micropulsation activity in low latitude conjugate stations show definitive results on current system 03 p0408 A67-12843

Rocket sounding of unpredictable geophysical disturbances, preparations, countdown procedure and difficulties encountered 05 p0904 A67-16295
Geophysical instrumentation for environmental studies, elucidating atmospheric and near-space mechanisms, geodesy, gravimetry, etc 17 p2860 A67-32692
Measuring methods for pole displacements and latitude variations, determining Universal Time from instantaneous pole coordinates, plotting polhody diagram 23 p3997 A67-41349
GEOGRAPHICAL SATELLITE
Supersatellite technology and advantages of larger automaton craft including superweather, superremote sensor, superutility, supersurveillance and superscientific satellite systems 04 p0703 A67-14601
Geophysical rocket determination of aerosol scattering coefficient variation from brightness values at 70-450 km heights 10 p1641 A67-23240
Evaluation of satellite radar altimetry for geophysical and oceanographic measurement 16 p2742 A67-30688
Geophysical instrumentation for environmental studies, elucidating atmospheric and near-space mechanisms, geodesy, gravimetry, etc 17 p2860 A67-32692
Anomalous LF plasma oscillation by particles trapped in potential well behind satellite applied to ionospheric measurements 18 p3117 A67-33512
Schmidt satellite cameras to record trail from bearing and elevation fixed in relation to earth, detailing optical system of Royal Radar Establishment /RRE/ camera 18 p3048 A67-34237
GEOPHYSICS
SA GEOCHEMISTRY
SA INTERNATIONAL GEOPHYSICAL YEAR /IGY/
SA PETROGRAPHY
Manned geophysical observations from satellites as training ground for planetary research, especially Venus atmosphere 01 p0155 A67-11395
Internal structure models for earth, Venus and Mars, discussing earth density distribution and seismic results 02 p0329 A67-12497
Cosmic ray physics - All-Union Conference, Moscow, November 1965 05 p0875 A67-16081
Extrasolar X-ray observation regarded as astronomy in contrast to cosmic ray observation which is considered as local geophysical phenomena 05 p0884 A67-16881
Geophysical and heliophysical characteristics for enhanced cosmic radiation intensity during magnetic storm in February 1959 05 p0885 A67-17498
Long-period pulsations of H and D components of geomagnetic field 06 p0993 A67-17596
Auroral oval properties from magnetic data, role in connecting visible auroras and related ionospheric disturbances to geophysical phenomena at high altitudes 09 p1492 A67-22060
Space research - COSPAR International Symposium, Vienna, May 1968, Volume 1 10 p1641 A67-23246
Internal structure models for earth, Venus and Mars, discussing earth density distribution and seismic results 10 p1709 A67-23365
Theory of statistical analysis of data distributed over sphere 10 p1652 A67-23547
Coastal effects in magnetic and telluric current variations near complex land, shelving seawater boundary 13 p2108 A67-26317
Lunar scientific exploration requirements in post-Apollo period, discussing lunar and earth geophysics 13 p2199 A67-27212
Radioactive isotopes from cosmic ray action in atmosphere and nonatmospheric sources, discussing geophysical mixing and dispersion 14 p2380 A67-27967
Heat flow values correlated with major geological features by analysis of 2000 terrestrial heat flow observations 15 p2477 A67-29763
ULF radio emission properties determination and relation to other geophysical phenomena, noting experimental equipment and correlation with auroral activity 17 p2846 A67-32938

- Advances in geophysics, Volume 12, covering problems of earth crust and mantle, atmosphere interaction with sea surface, etc 18 p3040 A67-34092
- Earth rotation measurement by radio interferometry, discussing rate changes in slowdown, Love number, etc 18 p3043 A67-34529
- IQSY geophysical work in Greece, examining geomagnetism, aurora, ionosphere, airglow, solar activity, etc 19 p3223 A67-35478
- IQSY research activity in Japan, experiments and progress 19 p3223 A67-35481
- Evening auroral activity characterized by westward traveling surges occurring not within auroral zone 20 p3426 A67-36291
- Geophysical theory and computers - Conference, Cambridge, England, June-July 1966 20 p3432 A67-37204
- Solar-terrestrial physics and magnetosphere - Conference, Belgrade, August-September 1966 22 p3882 A67-39667
- Friction in solid parts of earth and moon considered as sink for tidal energy and as geophysical thermal energy source 24 p4229 A67-42316
- GEOPOTENTIAL**
- Gaposchkin satellite gravity results compared with surface gravimetry data 01 p0056 A67-10041
- Radiant heat influx to free atmospheric layers, atmospheric macrocirculation and time-corresponding geopotential field charts 03 p0463 A67-14226
- Nonzonal harmonics of earth gravitational field determined by satellites 05 p0797 A67-16572
- Estimation problems in determining even zonal harmonics of external geopotential from secular satellite motion, examining least squares method 05 p0797 A67-16573
- Earth gravitational field parameters from near-surface satellite observations influenced by zonal and tesseral harmonics 05 p0800 A67-17080
- Orbit perturbation induced by omitting certain harmonics in expansion of earth gravity potential, evaluating covariance integrals [AIAA PAPER 67-93] 06 p1084 A67-18278
- Maneuverable geodetic satellite for better determination of resonant harmonics in geopotential field [AIAA PAPER 67-122] 06 p1096 A67-18340
- Satellite motion for all inclinations around oblate planet with potential including second and fourth zonal harmonics 08 p1382 A67-20398
- Tesseral harmonics of coordinates using Baker-Nunn data and geopotential and dynamical procedures, noting iterative cycle for correction 10 p1636 A67-23178
- Radiant heat influx to free atmospheric layers, atmospheric macrocirculation and time-corresponding geopotential field charts 12 p1963 A67-25482
- Geopotential and wind field calculations for Northern Hemisphere using statistical models 14 p2346 A67-28764
- Effective geopotential at synchronous height determined using observations of Syncom satellites during free drift periods, noting longitude dependence 18 p3041 A67-34251
- Geostationary satellite stability in presence of geopotential field zonal harmonics, using Liapunov theory 19 p3333 A67-35569
- Von Zeipel method and Hamiltonian perturbation mechanics used for orbits at resonance with tesseral harmonics of geopotential 19 p3328 A67-35959
- Baroclinic quasi-geostrophic prediction of geopotential field using two-parameter model 20 p3481 A67-37236
- Perturbation scheme deriving geomagnetic Euler potentials applied to magnetospheric model with solar wind effect 20 p3434 A67-37423
- Orbit perturbation induced by omitting certain harmonics in expansion of earth gravity potential, evaluating covariance integrals 21 p3700 A67-37785
- GEOPOTENTIAL HEIGHT**
- Derivation of accurate solution of equation for geopotential field prognosis using only simple invariant-group solutions and meteorological terminology 05 p0837 A67-16489
- Time dependent geopotential variations analyzed, using straight line techniques 06 p0994 A67-17863
- GEOSTROPHIC WIND**
- Numerical integration of quasi-geostrophic atmospheric model with asymmetric zonal current 06 p0999 A67-18739
- Large scale motions of atmosphere, noting hydrostatic and geostrophic equilibrium 07 p1170 A67-19334
- Geostrophic wind angular momentum transport at 500 mb in Northern Hemisphere, using zonal harmonic analysis, noting quasi-biennial cycle 15 p2512 A67-29201
- Nonlinear features of geostrophic adjustment in one-dimensional barotropic atmosphere number 19 p3253 A67-35917
- Baroclinic quasi-geostrophic prediction of geopotential field using two-parameter model 20 p3481 A67-37236
- Objective criteria for irrotational flow in geostrophic, isalobaric and thermal wind flow 24 p4180 A67-41788
- GEOTROPISM**
- Wheat seedlings grown so that coleoptile and early roots developed in moist air, noting organ orientation in relation to gravity 04 p0560 A67-14407
- GERDIEN CONDENSER**
- Ion concentration in D region, describing wind tunnel experiments to determine electrode configuration for Gerdien condenser rocket probe 03 p0412 A67-13367
- Mechanical construction of two types of Gerdien condenser rocket probes, noting instrumentation racks and inflatable parachutes for descent 03 p0518 A67-13368
- GERMANIUM**
- Electric conductivity on clean cleaved surface of degenerate germanium 01 p0131 A67-10340
- Double crystal spectrometer measurement of X-ray Compton and thermal scattering accompanying Bragg reflection from Si and Ge single crystals 01 p0132 A67-10456
- Calculation of energy band structure of gallium arsenide, using experimental Fourier coefficients for germanium in pseudopotential method 01 p0136 A67-11054
- Voltage induced by electron beam in n-and p-type germanium bars having inhomogeneous resistivity distribution, obtaining equations from one-dimensional model 01 p0137 A67-11059
- Surface color explained using backscattering angle and diffraction properties of germanium films vacuum deposited onto heated substrate 01 p0138 A67-11076
- Thermodynamics of epitaxial growth of GaAs-Ge heterojunctions in closed tube process 02 p0296 A67-11767
- External electron emission measurement from polished n-germanium and n-silicon surfaces 02 p0296 A67-11830
- Current instability of plasma injected into germanium, noting effect of strong electric field in presence of temperature gradient 02 p0297 A67-11833
- Negative photoconductivity in germanium, noting breakdown and negative conductivity in In region, volt-ampere characteristics, etc 02 p0297 A67-11835
- Semiconductor heterojunction properties of epitaxial single crystal layer of GaAs grown on Ge substrate 02 p0299 A67-11895
- Electric characteristics of nGe-pGaAs heterojunctions in multistep recombination-tunneling model 02 p0299 A67-12189
- Potential distribution, I-V characteristics and pulse shape of n-type Ge with sealed-in Sn, In-Sb, Sn-Sb and Pb-Sb contacts in strong electrical field 02 p0300 A67-12480
- Energy and wave functions of singly charged donor impurity centers in silicon and germanium 03 p0488 A67-12857
- Diffusion of antimony and indium in germanium in range from 700 to 855 degrees C, taking into account effect of internal electric field 03 p0489 A67-13149
- Equation of surface diffusion of indium in germanium solved by taking into account effect of external electric field 03 p0489 A67-13150
- Local diffusion of Ga into Sb-doped Ge samples from Ga-doped silicon dioxide films prepared in specially designed vacuum ampoule 03 p0491 A67-13175
- Laser beam-induced recrystallization of amorphous Ge semiconductor thin films prepared by thermal deposition on glass 03 p0498 A67-13839
- Instability of Sb and Au-doped n-type germanium during carrier injection, examining current-voltage and frequency characteristics and illumination effects 03 p0499 A67-13955
- Secondary breakdown relaxation oscillations and I-V characteristics of point contact n-type Ge diode 03 p0386 A67-13964
- Specific radioactivity of Sb-124 and effect on diffusion of antimony in Sb-doped n-type Ge single crystals and Ga-doped p-type Ge single crystals 03 p0500 A67-14067
- Emissive power of germanium and silicon with various surface finishes in temperature range from 700 to 1200 degrees K 04 p0674 A67-14719
- Electrical pinch in elastically deformed germanium, examining redistribution of carriers across sample and current-voltage characteristics 04 p0675 A67-14922
- Crystal dislocation effect on electric properties of germanium 2, noting elastic carrier scattering 04 p0677 A67-14938
- Model of metastable defects in germanium, noting Frenkel defects 04 p0677 A67-14939
- Maximum concentrations estimation for solidus of germanium and silicon solid solutions in retrograde melting 04 p0677 A67-14943
- Temperature dependence of current-carrier concentration and electrical conductivity of p-type germanium containing beryllium and phosphorus 04 p0679 A67-15144
- Photomechanical effect in germanium, noting dependence of mechanical properties on quantity of impurity concentration 04 p0680 A67-15285
- Localized breakdown in Ge mesa diodes due to inclusions 04 p0584 A67-15486
- Functional device based on interaction of two unijunction transistors to perform flip-flop circuit function, noting V-I characteristics and binary counter operation 04 p0593 A67-15489
- Minority carrier lifetime dependence on injection level, obtaining recombination center parameters for neutron irradiated germanium, using photoconductivity 04 p0684 A67-15692
- Sputtered film deposition processes, investigating low pressure sputtered germanium films 04 p0631 A67-15995
- Relation between electrical properties and structural features of gold- and antimony-doped germanium single crystals, noting abrupt decrease in mobility 05 p0861 A67-16398
- Temperature variation of electric conductivity and carrier mobility in diffused germanium resistors doped with antimony for thermometry 05 p0773 A67-16464
- Optical constants of Ge in XUV verified using Kronig-Kramers dispersion relation, optical oscillator strength sum rule, correlation methods and electron energy loss distribution 05 p0864 A67-16784
- Effect of copper on excess and tunneling current of As-doped Ge tunnel junctions 05 p0866 A67-16986
- Capture cross section of photons by zinc and mercury atoms in germanium determined from integral voltaic photosensitivity, using black body as radiation source 05 p0868 A67-17066
- Antimony diffusion into germanium using vacuum furnace, giving graphs with variation of antimony concentration and depth of diffused p-n junction 05 p0869 A67-17089
- Piezoresistive elements of germanium thin films 05 p0871 A67-17481
- Change in temperature conditions during growth of epitaxial germanium films from molecular beam in vacuum 06 p1046 A67-17551
- Disordered regions and energy level position in germanium produced by electron irradiation 06 p1048 A67-17832
- Annealing of fast neutron damage in impurity conducting n-type Ge, noting small activation energy in resistivity below 10 degrees K 06 p1050 A67-18146
- Excess noise and oscillations in gold-doped germanium photodiodes attributed to generation-recombination fluctuations of large bulk resistance 06 p0971 A67-18220
- Photoexcited electron lifetimes measured in extrinsic germanium photoconductors

using Doppler shift and rotating mirror square light pulse method 06 p1005 A67-18715

Electron scattering by neutralized acceptors investigated in Ge and Si through cyclotron resonance 06 p1063 A67-18939

Relaxation time of electrons in pure germanium and silicon measured from line width of cyclotron resonance at liquid helium temperatures taking into account quantum limit 06 p1064 A67-18945

Avalanche multiplication in Ge and GaAs p-n junctions, comparing experimental and theoretical ionization rates, predicting voltage breakdown 06 p1065 A67-18954

Piezoresistance measurement in p-type Ge as function of pressure and impurity concentration at 77 and 300 degrees K 07 p1233 A67-19644

Optical spectrum of normal excitons in deformed and nondeformed n-type Ge single crystal layers for four orientations 08 p1367 A67-20409

Concentration of Ni, Ga and Ge in series of Odessa and Canyon Diablo meteorite specimens 08 p1385 A67-20936

Hall effect on hot carriers in p-type Ge semiconductor in microwave field as function of field strength 08 p1369 A67-20993

Ge and Ga concentration in selected Fe meteorites used to determine quantization in terms of multiple parent body hypothesis and planetary fractionation processes 09 p1564 A67-21738

Built-in voltage decrease in bulk germanium and Ge tunnel diodes under irradiation, noting Fermi level 09 p1471 A67-21764

Performance and stability of germanium tunnel-diode autodyne frequency converter 09 p1472 A67-21957

Planar technique for germanium, outlining manufacture of planar transistor based on amplifier 09 p1555 A67-22037

Band-to-band radiative recombination in semiconductor groups IV, VI and III-V, presenting data on diamond, Si, Ge, Se and Te 09 p1558 A67-22601

Diffusion of antimony and indium in germanium in range from 700 to 855 degrees C, taking into account effect of internal electric field 10 p1690 A67-23098

Equation of surface diffusion of indium in germanium solved by taking into account effect of external electric field 10 p1690 A67-23099

Inertialess polarization energy of charge interaction between neighboring lattice points in Ge crystal, using M-20 computer 10 p1695 A67-23657

Anomalous Hall effect in microcrystalline germanium at SHF 11 p1846 A67-24471

Noise spectral distribution and instability in germanium and silicon photodiodes 11 p1765 A67-24473

LF noise fluctuation anomalies in narrow doped germanium p-n junctions at low temperatures 11 p1765 A67-24476

Thermal conductivity of low temperature silicon and germanium irradiated by fast neutrons noting differences, additive thermal resistivity and possible scattering mechanisms 11 p1849 A67-24899

Temperature dependence of current-carrier concentration and electrical conductivity of p-type germanium containing beryllium and phosphorus 12 p1979 A67-25167

Reduction or elimination of secondary asymmetry voltage in germanium Hall generators noting effect of surface recombination, temperature distribution stabilization, etc 12 p1939 A67-25278

Influence of deep level impurities on uniaxial stress effect of Ge p-n junction 12 p1983 A67-25456

Breakdown voltage characteristics of Ge bonded diode in relation to microwave oscillation, noting avalanche breakdown 12 p1914 A67-25458

Lithium drifted germanium detector with cylindrical annular shape permitting standardization of gamma spectroscopy techniques 12 p1945 A67-25861

Field effect kinetics on pure germanium surface, measuring surface conductivity relaxation time by compensation-bridge techniques 13 p2174 A67-26403

Electric field distribution in p region, space charge layer and n region of p-n abrupt junction germanium diode at room temperature 13 p2078 A67-26788

Recrystallization of Ge and Si thin films

and structural changes due to electron bombardment and thermal annealing 13 p2177 A67-27071

Piezotransmission measurements of phonon-assisted transitions in semiconductors 13 p2179 A67-27157

Current-voltage characteristics of germanium-silicon isotype heterojunctions with regard to capacitance and photoelectric measurements 13 p2183 A67-27569

Design and fabrication of germanium Esaki diodes emphasizing development of planar process, using conventional oxide masking techniques 13 p2083 A67-27572

Laser beam-induced recrystallization of amorphous Ge semiconductor thin films prepared by thermal deposition on glass 13 p2185 A67-27720

Stress effect on minority carrier mobility and concentration in germanium and silicon p-n junctions under uniaxial compression 14 p2364 A67-27825

Resistivity and Hall effect oscillations in antimony doped n-type germanium crystals in metallic impurity conduction state 14 p2365 A67-28231

Misfit dislocations at diamond-sphalerite interface of thin epitaxial Ge layer deposited on GaAs 14 p2366 A67-28497

Measurement of variable Hall electromotive force component created by illumination of thin low resistance germanium samples by modulated 14 p2368 A67-28529

N-type germanium doped with antimony and arsenic investigated for radiation recombination, noting energy spectrum and forbidden band changes 14 p2368 A67-28533

Dislocation-free Ge structural and electrical characteristics after cooling, considering quenching defects 14 p2372 A67-28761

EPR applied to investigation of various semiconductors containing iron, and Mn at liquid nitrogen temperature 14 p2373 A67-28968

Magnetic field influence on AC surface field effect in germanium resulting from change in sample conductance and not from change in surface barrier height 15 p2533 A67-29263

Unique determination for parameters of surface recombination centers in n-type germanium semiconductors 15 p2534 A67-29326

Effect of single-axis compression on radiative impurity recombination in arsenic- and gadolinium-doped germanium 15 p2537 A67-29705

Capture cross section of photons by zinc and mercury atoms in germanium determined from integral voltaic photosensitivity, using black body as radiation source 15 p2538 A67-29797

Diffused base transistor impurity concentration measured nondestructively to determine structure 15 p2448 A67-29801

DC and AC parameters of germanium tunnel diodes in 3 to 5 millamp range measured by ammeter dC and AC parameters of germanium tunnel diodes in 3 to 5 millamp range measured by ammeter 15 p2449 A67-29807

Charge curves for germanium and silicon surface obtained by field effect measurements, noting nature and mechanism of effect 15 p2542 A67-30249

Noise and HF input conductance measurement of double-injection germanium space-charge-limited diode, noting transit-time effect 16 p2637 A67-31034

Hot carrier galvanomagnetic characteristics of n-type germanium of intermediate carrier concentration, noting Maxwellian distribution 16 p2731 A67-31172

Specific resistance, EMF, Hall effect, and minority-carrier lifetime measurement of germanium whiskers bombarded by high energy electrons from linear accelerator 16 p2732 A67-31479

X-ray K-absorption spectra of titanium, vanadium germanium in germanides 16 p2691 A67-31594

Hyperfrequency amplification using electric field effect for conduction modulation of single crystal germanium sheet 16 p2732 A67-31705

Zeeman effect of germanium I and II, discussing configuration-interaction, deriving intermediate-coupling wave

functions 16 p2733 A67-31876

Subthreshold electron irradiation effects on surface recombination properties of n-and p-type germanium and silicon crystals 17 p2916 A67-32834

Irradiated germanium observed for carrier concentration variations, using Hall coefficient measurements 17 p2918 A67-32853

Low temperature thermal conductivity measurement of fast-neutron-irradiated silicon and germanium, showing difference between bombardment induced scattering in two materials 17 p2919 A67-32855

N-type germanium photoconductivity spectrum studied after bombardment with electrons at very low temperatures 17 p2919 A67-32860

Annealing kinetics of n-type germanium exposed to electron bombardment at cryogenic temperature 17 p2919 A67-32861

Accelerated antimony diffusion in germanium due to excess vacancies from proton irradiation, determining migration energy and diffusion length of vacancies 17 p2919 A67-32862

Inertialess polarization energy of charge interaction between neighboring lattice points in Ge crystal, using M-20 computer 17 p2924 A67-33338

Germanium pulse switching triode with fused p-n-p junction 18 p3009 A67-33477

Electrical characteristics of degenerate n-type germanium diode with gold or indium as metallic element 18 p3105 A67-34635

Water adsorption on oxide covered surface of germanium, studying chemisorption dependence on p-type doping 19 p3301 A67-34935

Germanium films crystallization when deposited by evaporation on silicon single crystals studied by optical microscopy and electron diffraction 20 p3509 A67-36473

Germanium and cadmium telluride edge absorption, noting lattice imperfections causing absorption coefficient increase in indirect transition region 20 p3511 A67-37143

Anisotropy of piezothermal EMF in Si and Ge under uniaxial stress 20 p3511 A67-37147

Performance and stability of germanium tunnel-diode autodyne frequency converter 20 p3400 A67-37187

Density and recombination coefficients of nonequilibrium carriers in Ge and GaAs as function of laser excitation intensity 20 p3513 A67-37437

Germanium conductivity dependence on surface and space charges in transverse magnetic field 21 p3676 A67-37862

Electron energy band structure of semiconductor films determined by analysis of structural symmetry of germanium and silicon samples 22 p3861 A67-39919

Germanium distribution in metallic phases of various iron meteorites by electron probe microanalysis 22 p3885 A67-39976

Irradiation damage in germanium monitored by electric conductivity measurements, noting carrier population depletion by introducing acceptor levels into forbidden gap 22 p3862 A67-39997

Ge/Li/ drifted gamma detector for 1/2 to 10 Mev range, measuring response deviation from linearity 23 p3998 A67-40819

Measurement of variable Hall electromotive force component created by illumination of thin low resistance germanium samples by modulated light 23 p4039 A67-40936

N-type germanium doped with antimony and arsenic investigated for radiation recombination, noting energy spectrum and forbidden band changes 23 p4040 A67-40940

Effect of single-axis compression on radiative impurity recombination in arsenic- and gadolinium-doped germanium 24 p4199 A67-41775

Static characteristics of 2N1304 germanium junction transistor exhibited by two surfaces in three-dimensional space 24 p4128 A67-41925

Faraday rotation and ellipticity measurements in germanium and gallium arsenide at room temperature in weak magnetic fields 24 p4202 A67-41984

GERMANIUM ALLOY

Hall effect in semiconductors containing two species of current carriers, p-type PbTe and GeTe, taking into account temperature dependence of energy gap 03 p0489 A67-13148

Lanthanum for germanium partial

substitution effect on thermoelectric properties of single phase and homogeneous samples of GeTe 03 p0500 A67-14231

I-V characteristics of alloyed contacts of germanium with Sn, Pb and In in wide range of resistivities and ambient temperatures, establishing correlation with work function 05 p0864 A67-16909

Tunnel diode capacitance relation to displacement interpreted in terms of impurity drift in nonuniform field of p-n junction in highly doped germanium diodes 05 p0865 A67-16959

Temperature dependence of thermal emf, electrical conductivity, current carrier mobility and thermal conductivity of GeTe-GeSe solid solution 07 p1231 A67-19164

Second breakdown and degradation in Ge alloy junctions, noting failure mechanism and preventive surface treatment 07 p1157 A67-19905

Thermoelectric generator modules with Si-Ge alloys, discussing material preparation and generator fabrication 09 p1445 A67-22180

Hall effect in semiconductors containing two species of current carriers, p-type PbTe and GeTe, taking into account temperature dependence of energy 10 p1689 A67-23097

Photomechanical effect in metals, discussing influence of impurities and heat treatment 13 p2174 A67-26400

I-V characteristics of alloyed contacts of germanium with Sn, Pb and In in wide range of resistivities and ambient temperatures, establishing correlation with work function 16 p2727 A67-30886

Metallography, roentgenography and differential thermal analysis of composition temperature ranges of chromium-germanium phases 16 p2691 A67-31592

GERMANIUM CHLORIDE

Germanium tetrachloride purification process by radiochemical analysis and radioactive tracers investigated to determine possible simplification 18 p3104 A67-34600

GERMANIUM COMPOUND

Current-carrier scattering in germanium telluride 01 p0129 A67-10097

Atomic planes and positions in bulk thinned specimens of crystalline Ge determined, using electron microscopy 03 p0501 A67-14345

Stress-strain time relation in gallium doped p-type germanium, noting crystal dislocation and creep parameter temperature dependence 04 p0677 A67-15121

Spectrum of glow during gas phase reaction of germanium tetrahydride with atomic oxygen, observing new bands of D-X system 06 p0955 A67-17655

Time lag in thermal coefficient of resistivity of Ge whisker explained in terms of point defect diffusion 06 p1050 A67-18144

Temperature dependence of electroconductivity of As-Su-Ge system in vitreous state 06 p1052 A67-18610

Electric conductivity of AsSeGe-AsSGe glasses 06 p1052 A67-18611

Annealing of neutron irradiation induced changes in impurity conduction in Sb-doped Ge 06 p1068 A67-18969

Superconductivity in germanium telluride, noting critical magnetic field 06 p1069 A67-18981

Impurity photoconductivity spectra of p-type germanium at low temperatures, noting parameters of relative depth of equidistant minima oscillations 10 p1693 A67-23583

Systems producing germanide phases noting phase diagrams of germanides of s-elements, ds-elements, fds-elements and sp-elements 13 p2175 A67-26469

GeTe solid solutions reviewed considering thermal EMF, temperature dependence and current carrier mobility 16 p2730 A67-31164

Temperature effect on gold diffusion in crystalline and glassy cadmium germanium arsenide samples 19 p3301 A67-34776

Electrical conductivity variation of low and high resistance germanium due to X-ray radiation absorption 20 p3508 A67-36405

Change patterns in melting point and forbidden bandwidth for anion and cation substituted compounds of AlIBV group 21 p3676 A67-37932

Radiative recombination processes involving neutral donors and acceptors in silicon and germanium, describing extrinsic luminescence bands 22 p3862 A67-39998

GERMANIUM OXIDE

Temperature dependence of elastic wave losses for bismuth germanium oxide, noting possible application for information storage VHF and microwave frequencies 02 p0300 A67-12507

GERMANIUM RECTIFIER

Cryogenic liquid level sensor consisting of diode heated by resistor 01 p0062 A67-10194

Switching and dynamic characteristics of germanium peak diodes used as AM devices 02 p0210 A67-11531

Point-contact germanium diode static characteristics with self-heating and image forces 14 p2289 A67-28825

Structure of wafer type point-contact diodes 18 p3011 A67-34021

Germanium photovoltaic cells as solar conversion devices [ONERA-TP-478] 18 p2990 A67-34464

GERMANY
SA WEST GERMANY

International factors in German air transport, noting progress due to limiting differences between domestic and foreign air carriers 12 p2040 A67-25490

German participation in solar eclipse campaign of ESRO, describing rockets and radar used 15 p2466 A67-29572

German firm participation in designing and constructing third stage of ELDO launch vehicle EUROPA I 16 p2763 A67-31789

German SIAT 223 Flamingo sports, trainer and cross-country aircraft, noting design, components and tabulated technical data 18 p2985 A67-33641

East germany space research in satellite tracking, coupling processes, upper atmosphere, high energy particles, etc 19 p3321 A67-35294

German capability of competing in space travel with other nations 22 p3922 A67-39532

German Gyroscope Testing Laboratory noting revolving platform for simulating rotational velocities, signal testing and signal simulation 23 p4003 A67-41327

GERONTOLOGY

S AGING

GETTER

Saturation effects studied by pumping speed measurements of diode and triode type getter ion pumps for He, molecular hydrogen and nitrogen at low pressures as function of time 08 p1333 A67-21494

Flashed getters for production of ultrahigh vacuum, tantalum most promising based on residual gas analysis 08 p1354 A67-21496

Titanium for sublimation, using combination sublimation-getter ion pump 09 p1503 A67-22101

Design analysis for vacuum systems using diffusion pumps and getter ion pump, comparing parallel and series pumping 09 p1503 A67-22113

Electrostatic getter-ion pump, giving quantitative theory for maximizing ionizing efficiency and design features to attain low pressures and high pumping speed 21 p3624 A67-37821

Electrostatic getter-ion pump performance, giving pumping speeds, pressure and starting characteristics, residual gas composition and operating life 21 p3624 A67-37822

Ti thin films use as getter in electron microscopy of Mo particles at high temperature with minimum oxidation 24 p4172 A67-41978

GIANT STAR

IR stars as supergiants of very late type and not objects in state of gravitational contraction as sustained by Penston theory 03 p0512 A67-13888

Massive star behavior during final catastrophic evolution stages, stressing effect of electron type neutrino interactions, using numerical hydrodynamics coupled with energy transfer methods 03 p0516 A67-14340

Evolution of low mass Population I stars from main sequence to red giant branch in Hertzsprung-Russell diagram, through energy generation phases of p-p chain reactions /dominating over C-N cycle reactions/ and hydrogen burning 09 p1566 A67-22225

Evolution of 2.25 M star from main sequence to helium burning phase noting lifetimes, nuclear burning of core, stellar mass fraction and stellar model algorithm 09 p1566 A67-22226

Solar corona and occurrence of solar wind

and influence on evolution of red giant star 11 p1858 A67-24095

Book on red giants and white dwarfs covering stellar evolution, planets and life, solar system origin, etc 18 p3117 A67-33430

Effective temperature for late type stars with or without water vapor opacity calculated for several masses, determining convective energy transport efficiency 24 p4224 A67-41818

GIBBS EQUATION

Thermomechanical theory of diffusing and chemically reacting mixture and application to elastic materials mixture subject to diffusion and heat conduction 15 p2517 A67-29463

GIBBS PHENOMENON

S FOURIER SERIES

GIMBAL

Single-rotor gyrocompass motion during rocking, determining equilibrium point displacement 12 p1941 A67-25662

Integration of abbreviated motion equations for gyroscopes, obtaining expressions for gimbal errors 12 p1945 A67-25967

Suspension axes defects effect on gyro motion under base angular vibration analyzed, noting large gyro drift 14 p2320 A67-28741

Rotor bearing clearance effects on whirling of gimbal-mounted gyroscope 14 p2328 A67-29004

Free gyroscopes with feedbacks on each gimbal, determining feedbacks and improving operating indices 18 p3047 A67-33993

Two-axis gimbal system for solar simulation spacecraft testing, demonstrating intermediate axis internal drive system and outer axis drive input 24 p4153 A67-42044

GIMBALLED CONTROL

Strap-down inertial navigation system compared with gimbaled system, noting methods of attitude reference and angular readout 01 p0110 A67-10489

Gimbaled jet engine development, noting application to V/STOL aircraft and design of plenum chamber burning engine 03 p0503 A67-13008

Confidence limits for pointing error of gimbaled sensor relative to off-gimbal reference, detailing sources of error and statistical properties 04 p0620 A67-14872

Gimbaled platform thermal control system and design constraints on inertial system housing 04 p0626 A67-15791

Integrated circuit adoption for optimal mixture with remaining discrete devices, particularly gimbal loops 05 p0770 A67-16236

Structural compliance induced cross axis coupling effect on gimballing system stability of rocket engine two-axis attitude TVC system 06 p1097 A67-18448

[AIAA PAPER 67-42] Thrust vector control by supersonic splitline gimbaled nozzle, considering linear aerodynamics to understand magnitude of spring rate torque component 07 p1126 A67-19378

Gimbaled unitized stellar reference inertial platform for space missions, noting optical lobing technique 08 p1331 A67-20699

Gyroscopic drift from centrifugal inertial moment of gimbals in statically balanced systems, noting dynamic imbalance moment expression 11 p1794 A67-25046

Superconducting gyroscope for gimbaled platform application 13 p2122 A67-27683

Calibration of star tracker bias errors on OAO 17 p2955 A67-32479

Construction and operational possibilities of gimbal mounted servo-controlled aircraft model for optical simulation of flight mechanical motions 18 p3019 A67-33458

Strapdown and gimbaled inertial navigation systems history, engineering progress and current developments 19 p3256 A67-35859

Controller design for booster gust alleviation, considering stochastic minimization problem solved by iteration yielding linear finite time controller with time-varying gains 22 p3897 A67-39162

Matrix method for analyzing systems of gimbaled mirrors, prisms and ray projectors 23 p4003 A67-41323

Star tracker error signal processor for onboard current satellite attitude control over wide range of gimbal angles 24 p4154 A67-42175

Structural compliance induced cross axis coupling effect on gimbaling system stability of rocket engine two-axis attitude TVC system [AIAA PAPER 67-42] 24 p4242 A67-42909

GIMBALLLESS INERTIAL REFERENCE SYSTEM

General mechanization in vehicular coordinates of gimballless inertial system for space navigation, obtaining equations for position errors and error damping method 08 p1351 A67-20698

GLACIOLOGY

Solar activity and polar migrations role in origin and evolution of terrestrial life during Eocambrian and subsequent geological epochs 01 p0149 A67-10756

GLAND

SA ADRENAL GLAND
SA ENDOCRINE SYSTEM
SA PITUITARY GLAND
SA THYROID

Gland design variation effects in gaseous helium seal performance from O-ring permeation measurements at pressures up to 1000 psi 17 p2801 A67-31992

GLARE

Visibility of point sources approaching or receding from high luminance source in apparent frontal plane 08 p1351 A67-21103

GLASS

SA SILICA GLASS

Time evolution of laser induced fractures in glass, noting crack propagation accompanied by sparking 02 p0253 A67-12508

Glass in refractive space optics, discussing UV solarization and athermalization [SMPT PREPRINT 100-34] 03 p0469 A67-13808

S-, Se- or Te-based nonoxide chalcogenide glassy systems for airborne IR optical equipment materials 03 p0456 A67-14390

Trivalent neodymium doped glass laser with internal imperfections due to optical pumping examined via optical metallography, transmission electron microscopy and electron diffraction techniques 04 p0632 A67-14927

Laser emission at 1.06 microns from ytterbium-neodymium glass, noting linearity of energy transfer with Yb concentration 05 p0820 A67-16664

Terminal level lifetime and fluorescence line of neodymium doped glass influence on dynamics and efficiency of Q-spooled laser 05 p0822 A67-16675

Saturated absorption of color centers in glass self-Q-switched pulses, as in glass codoped with uranyl oxide and Nd ions 05 p0822 A67-16678

Damage in glass induced by linear absorption of laser radiation non-Q-spooled 05 p0824 A67-16794

Neodymium doped optical glasses for laser technology 05 p0824 A67-16855

Glass encapsulation for various miniature diodes 06 p0968 A67-18096

Electric conductivity of AsSeGe-AsSGe glasses 06 p1052 A67-18611

Micro-and macrocrack formation in organic glass by focusing of laser beam 06 p1021 A67-18808

Space environment effect on refractive optical systems, particularly solar radiation effect on optical properties of glass 08 p1330 A67-20644

Interferoscope used in testing large glass panels for aircraft camera windows 10 p1652 A67-22701

Composite structure of glass with crystalline aluminum oxide and zirconium oxide inclusions tested for strength and elastic properties 11 p1811 A67-24642

Nature of glassy state, reviewing nucleation, crystallization, chemical, physical, and electrical properties and transformation of glasses 13 p2143 A67-26696

Absorption and fluorescence characteristics of Nd-doped phosphate glasses used as laser material 13 p2128 A67-27229

Glass reinforced structural design fundamentals, discussing basic properties of filament materials, matrix material and composite materials [ASME PAPER 67-DE-16] 14 p2402 A67-28871

Transparent plastic materials for aircraft application, noting glass developments and thermal stress conditions 16 p2694 A67-30980

Glass semiconductor threshold switches

application in memory-addressing circuits, decoding matrices and current dividers 18 p3012 A67-34489

Structure and properties of glass-ceramics noting applications to space and oceanographic exploration 20 p3473 A67-36596

Light generation by relative motion of mercury and helium contained in UV transmitting glass, noting intensity decrease with prolonged rotation 22 p3837 A67-39993

Stress distributions within materials sealed across planar interfaces compared with values measured in composite pairs of glass 24 p4175 A67-42374

GLASS COATING

High strength glass damage, discussing protective polymer coating 20 p3473 A67-36159

Radioactively labeled coupling agents adsorption on E-glass surfaces, noting continuous film formation with covalent bonding occurring at interface 20 p3474 A67-37269

Solar cell integral covers, discussing solar simulation, vacuum and thermal tests, performance characteristics, etc 23 p3937 A67-41491

GLASS FIBER

Anisotropy test examining failure behavior of aluminoborosilicate glass fibers under tensile and torsional loading [ACS PAPER 1-G-65F] 01 p0103 A67-10263

Cryogenic strain gauge application to circumferential loads of Centaur hydrogen tank insulation while in launch configuration 01 p0069 A67-11016

Engineering estimates of transverse properties of unidirectional composites compared with conventional glass-reinforced plastics 03 p0522 A67-13443

Thermophysical properties of glass-fiber reinforced plastics for selecting optimum structural patterns when under axisymmetrical load 04 p0708 A67-14787

Local buckling strength of high strength axially compressed maraging steel cylinders circumferentially prestressed with high strength epoxy-protected fiberglass filament windings 05 p0923 A67-17211

Glass fiber reinforced plastics experience for preparing high precision models of complex shape, noting wind tunnel application 06 p1007 A67-18019

Roving machine for impregnating glass fibers with synthetic resins 06 p1007 A67-18023

Molded aircraft wheels of epoxy resin reinforced with noncontinuous glass filaments 06 p1007 A67-18026

Anisotropic elastic constants and strength characteristics of fiberglass reinforced plastics during shear 06 p1020 A67-18099

Effects of 450 and 600 degrees F exposures on mechanical properties of glass-fiber polyimide resin sandwich panels to be used on large skin areas of SST aircraft [AIAA PAPER 67-174] 06 p1021 A67-18484

Material orthotropy effect on directions of principal stresses and strains in fiberglass and boron composites 06 p1108 A67-18654

Glass fiber reinforced parts for Boeing 737 noting fabrication, properties and applications 07 p1193 A67-20252

Refractory glass fibers composition, fiber forming characteristics, construction and operation 07 p1212 A67-20261

Light aircraft design using fiberglass reinforced plastic primary structure for fibrous composite airframe 08 p1414 A67-20429

Polar properties of fiberglass fabric laminates effect on strength for aerospace applications 08 p1345 A67-20431

Literature review on effect of static fatigue on filament wound fiberglass internal pressure vessels, noting program to test and expand data 08 p1415 A67-20432

Stimulated radiation from trivalent Nd ion doped barium crown glass fiber laser without resonator 08 p1337 A67-21203

Combining two or more nonmetallic substances noting applications of fiber reinforced, particulate filled and laminated composites 10 p1871 A67-23013

Glass-fabric reinforced plastic shells fabrication and full scale structural evaluation 10 p1727 A67-23732

Test conditions effects on glass fiber strength data 11 p1811 A67-24587

High temperature polyimide unidirectionally reinforced with silica fiber,

noting precuring process to avoid porosity and strength degradation 11 p1811 A67-24641

Fiber reinforced metal coating by passing silica through molten aluminum, discussing freezing by radial conduction of heat into fiber 12 p1954 A67-25292

Tensometry method to study stress concentration around circular hole in orthotropic glass-fiber reinforced cylindrical shell 12 p2021 A67-25579

Deflection function of glass fiber reinforced circular cylindrical shells under axial supercritical compressive loading 12 p2023 A67-25590

Glass fiber reinforced composite materials for aircraft engine, discussing construction of bearing and compressor casings [SAE PAPER 670333] 12 p1958 A67-25874

Lower and upper critical loads measured in process of axial compression of cylindrical shells of glass fiber reinforced resin 12 p2031 A67-25959

Vacuum chamber for plasma studies consisting of thin stainless steel shell strengthened by glass fiber reinforced plastic with epoxy compound as adhesive 16 p2876 A67-31397

Creep properties of glass fiber reinforced plastics for long-term bearing structures, noting elastic strain, creep rate, etc 16 p2694 A67-31486

Fiberglass-reinforced thermoplastic production processes, discussing strength, rigidity, dimensional stability, etc 17 p2875 A67-31931

High strength high modulus glass fibers, discussing mechanical properties and design 21 p3648 A67-37879

Anisotropy due to molecular structure orientation in vitreous inorganic glass fibers, noting phase equilibrium relation 21 p3648 A67-37880

Hooke law type anisotropic fiberglass reinforced plastic, discussing elastic deformation and brittle fracture, using revised Mises ellipse equation 21 p3649 A67-37907

Loading rate effect on unidirectional fiberglass reinforced plastics under tension, examining mechanical characteristics and determining tensile strength and elastic modulus 21 p3649 A67-37908

Prestressing effects on stress-strain diagram of monodirectional transversely isotropic glass fiber reinforced plastic 21 p3650 A67-37911

Glass fiber reinforced plastics stress and strain, considering applications in structural design 21 p3650 A67-38519

Reinforced plastics, evaluating epoxy resin with glass fiber reinforcements for laminates, measuring tensile, compressive and flexural strengths [ASM PAPER C6-21.1] 23 p4022 A67-41403

Glass fiber reinforced gas turbine engine compressor blade thermal stability for short cycle heat stress damage 24 p4249 A67-42103

Adhesive system for structural bonding of fiberglass reinforced polyester to itself and to metal 24 p4175 A67-42421

GLIDE LANDING

Reusable low weight hypersonic glider /space rotor/ for space vehicle reentry and recovery 15 p2568 A67-29845

GLIDE PATH

Controlled recovery of payloads from high altitudes and at large glide distances, using Para-Foil 08 p1409 A67-20545

Closed form solution for gliding lateral turn at constant height over flat earth of unpowered vehicle, using linearized aerodynamic coefficients 09 p1441 A67-22488

GLIDE SLOPE

Antenna systems and equipment providing ICAO Category I-III performance for ILS, analyzing configurations for localizer, markers, etc, calculating glide slope course bends 08 p1351 A67-20696

Slope derivation from lunar orbiter photography using photometric model and computer program 19 p3230 A67-35322

Airport glide slope visual range determination with single-ended transmissometer by measuring transmission between photosensitive detector and laser light source 23 p3999 A67-41027

GLIDER

SA HYPERSONIC GLIDER
SA PARAGLIDER
SA REENTRY GLIDER
SA SPACE GLIDER

Design principles for sailplane with glide ratio of 100 03 p0358 A67-12976

Medical research in glider plane noting airborne electrocardiograph 04 p0563 A67-14630

Longitudinal stability of rigid glider in towed flight, calculating lift coefficients for various rope-plane configurations 09 p1441 A67-22607

Turbulent atmosphere load effect on gliders noting influence of piloting techniques 13 p2052 A67-26484

Longitudinal static stability margin of glider for small lift coefficients showing effect of torsional deformation 16 p2596 A67-31001

Static structural strengths, aeroelasticity and flutter problems for glider performance 16 p2776 A67-31466

Interaction between gliding contour and ideal fluid flow inhomogeneities 18 p3022 A67-33413

Wing twist distortion effect on glider static longitudinal stability with stick fixed 18 p2986 A67-34373

Semimonocoque aluminum alloy glider design features, recommending integral construction with metal bonding or combination metal bonding and riveting 18 p3054 A67-34374

Glders examined from construction standpoint including damage tolerance, airworthiness, radiation, operational loads and reparability 20 p3360 A67-36454

Polyt IV glider wing noting bonded aluminum sheet/honeycomb sandwich shell 22 p3811 A67-39302

Structural elastic deformations effect on aerodynamic steering loads of glider, examining lift changes caused by wing geometry variations 23 p3933 A67-40640

Dynamic longitudinal stability of rigid glider towed by rigid aircraft with elastic cable subjected to aerodynamic loads, deriving motion differential equations 23 p3935 A67-41418

Elastic wing twisting effect on longitudinal stability and controllability of glider, considering wing rigidity 24 p4094 A67-42021

GLOW DISCHARGE

SA ELECTRIC DISCHARGE

Role of amplification due to impacts of second kind in emission of nitrogen and CO molecular bands in mixture of nitrogen-argon and CO-Ar in glow discharge 02 p0270 A67-12674

Optical properties of evaporated barium films investigated at various wavelengths, using ultrahigh vacuum reflectometer 03 p0499 A67-13909

Interpretations of microwave emission from Venus through experiments in which anomalous signals have been observed in X-band from glow discharges 04 p0699 A67-14952

Annular hollow cathode discharge emitting electron beam to heat cylindrical workpiece located along axis 04 p0628 A67-15311

Tantalum thin film integrated circuits noting fabrication techniques, applications, cost and advantages 05 p0770 A67-16239

Formulas relating detector current to average UHF power obtained for positive plasma column and dark Faraday region of glow discharge 05 p0856 A67-17235

Glowing high voltage discharge produced with hollow anode in discharge gap of various configurations 06 p0968 A67-18093

Energy distribution function in cathode drop space of glow discharges in hydrogen derived by numerical integration of simplified Boltzmann equations 07 p1229 A67-19516

Mercury emission intensity ratios in negative glow of Hg-hydrogen DC abnormal glow discharge 08 p1356 A67-21296

Stimulated emission in negative luminescence region of He-Ne glow discharge, noting effect of pressure and volt current 09 p1512 A67-21925

Transverse separation of rare gas-metal vapor mixture components in plasma nonisothermal plasma column in plain-symmetric glow discharge 09 p1545 A67-21998

Molecular metastables produced in positive column of helium discharge by electron excitation 09 p1548 A67-22368

Prevention system of short circuit in vacuum chambers due to glow discharges 10 p1622 A67-23316

Vapor deposition of thin films by

decomposition of metallic alcoholates in luminescent discharge 10 p1696 A67-23692

Auroral green lambda 5577 of oxygen atom analyzed from glow discharge emission, proposing excitation mechanism on basis of intensity variations 11 p1824 A67-24934

Electronegative plasma kc oscillations during glow discharge, measuring variations of frequency and longitudinal and radial intensity 12 p1970 A67-25261

Steady MHD electric power generation, flow velocity effect on single controlled glow discharge in cesium-seeded argon 12 p1974 A67-25402

Mass spectrometry of background gases composition during sputtering of tantalum films in argon glow discharges 13 p2178 A67-27078

Bennett type RF spectrometer analysis of low pressure plasma discharge, noting effusion current determination 14 p2314 A67-27753

Computer method analysis of electron temperature and density behavior on basis of glow discharge for plasma electron balance equation solution 14 p2353 A67-27755

Phase shift between electron temperature, luminous intensity and electron density in stratified positive column of glow discharge 14 p2353 A67-27757

Propagation rate of LF acoustic waves in low pressure glow discharge in nitrogen 14 p2354 A67-27759

Cathode sputtering, evaporation and anodic oxidation for thin film deposition in integrated circuit technology 15 p2453 A67-30066

Azimuthal motion of glow discharge plasma in space between two coaxial dielectric cylinders in crossed radial magnetic and axial electric fields 16 p2723 A67-31580

Negative glow diffusion model evaluated via generation function determined by discharge voltage and dependence of reduced length of cathode fall 18 p3085 A67-33668

Decomposition of polytetrafluoroethylene in glow discharge studied using helium, helium plus oxygen or oxygen as carrier gas 18 p2998 A67-34369

Soviet book on diffusion cladding of metals covering alloy surfaces diffusion saturation, glow discharge siliconizing of metals, vacuum siliconizing of refractory metals, etc 19 p3235 A67-34915

Glow-discharge siliconizing of refractory metals by unilow gas method in silicon tetrachloride vapor and hydrogen atmosphere 19 p3242 A67-34917

Ring circuit using glow-discharge thyratrons to combine functions of pulse indicator and pulse counter with decimal readings 19 p3228 A67-34990

Glow discharge positive column response to external perturbations, obtaining moving striations profile, structure and backward wave nature 19 p3273 A67-35094

Energy distribution functions for nearly normal glow discharge using two models and statistics 19 p3273 A67-35098

Flow of positive ions from negative glow plasma into cathode dark space determined, discussing ion current density results 19 p3273 A67-35099

One-dimensional models for constricted anomalous glow discharge investigated for various applications 19 p3274 A67-35100

Diode with anode glow type discharge analyzed for relationship between discharge quenching current and structural elements of discharge gap 19 p3282 A67-35160

Hollow anode glow discharge noting motion of ions and electrons in beam configuration 19 p3195 A67-35598

Glow-broadening rate dependence on initial pressure and discharge voltage in shock tube containing hydrogen plasma, studying charge distribution variations 20 p3501 A67-37145

Flow velocity and magnetic field effects on characteristics of single controlled glow discharge in cesium seeded argon 21 p3674 A67-38888

Structures of glow discharge and evaporated silicon oxide films determined by measuring intensity of electron wave scattering at large angles, describing measurement method 21 p3687 A67-39139

Hydrocarbons transformation mechanism

and kinetics at low pressures in glow discharge noting three-way decomposition 22 p3757 A67-39585

Safety control requirements in thermal-vacuum testing involving protection against electric equipment operation in pressure range for glow discharge 22 p3782 A67-40404

Laser detector using glow discharge tube current changes to measure radiation intensity 23 p4012 A67-40894

GLUCOSE

Influence of different stresses on sugar content changes of blood and stabilization at another level as adaptation result of organism 14 p2255 A67-28221

Glucose loading effects on electrocardiogram of pilot applicants evaluated for injection before and after diabetes test 21 p3573 A67-38068

Polydipsia elicited by synergistic action of saccharin and glucose solution 24 p4113 A67-42099

GLUCOSIDE

Effects of anthocyanin glucosides on night vision of airport approach controllers 04 p0561 A67-14633

GLUTAMATE

Radio carbon dioxide fixation, glutamate labeling and Krebs cycle in ribose-grown Hydrogenomonas facilis 20 p3370 A67-36796

GLYCINE

Carbonyl compounds reaction with N-salicylidene-glycinatoaquocopper (II) syntheses of beta-hydroxy alpha-amino acid from glycine 20 p3376 A67-36877

GLYCOGEN

Glycogen accumulation in monkey and cat brain exposed to proton irradiation, discussing astrocytes function in carbohydrate metabolism 04 p0560 A67-14489

Roentgen radiation effect on glycogen metabolism of rat brain 07 p1133 A67-19468

GODDARD RANGE AND RATE SYSTEM

NASA observations for orbit determination from Goddard Range and Range Rate system compared to OGO-B observations 19 p3319 A67-35216

GOLD

Resistivity and Hall coefficient measurement of n-and p-type gold-diffused silicon over wide temperature range 01 p0134 A67-10754

Photoelectric efficiency of thin gold films illuminated from free surface side and support side 02 p0289 A67-11730

Electric resistance of discontinuous thin gold films as function of time and temperature 02 p0292 A67-11747

Thermoelectric power of series of gold films, noting thickness effect on electron diffusion and phonon drag 02 p0293 A67-11749

Photoelectron emission from aluminum-aluminum oxide-gold film system with electric field in dielectric 03 p0492 A67-13295

Photoelectron emission from aluminum-aluminum oxide-gold film system with electric field in dielectric 04 p0674 A67-14720

Temperature dependence of migration of double positioning boundaries during growth of gold films inside electron microscope 04 p0675 A67-14924

K-shell ionization cross sections of silver, tin and gold from electron bombardment 04 p0661 A67-15762

Photoconductivity of silicon alloyed with gold and zinc at various temperatures 05 p0871 A67-17492

Anisotropic resistivity of dislocations produced by deformation measured in high purity Au, Ag and Cu single crystals 07 p1209 A67-19638

Single crystal film structure of fcc metals evaporated in ultrahigh vacuum onto alkali halide surfaces cleaved in air and in situ 09 p1552 A67-21671

Equality conditions for gold and silver electrode zero charge and transient peak potentials by pH and anion effects, using scraped electrodes 10 p1602 A67-23158

198 Au isotope diffusion in n-type indium arsenide at different temperatures 14 p2368 A67-28537

Gold resistance thermometers for measuring surface temperature of semitransparent materials 18 p3051 A67-34505

Temperature effect on gold diffusion in crystalline and glassy cadmium germanium arsenide samples 19 p3301 A67-34776

198 Au isotope diffusion in n-type indium arsenide at different

- temperatures 23 p4040 A67-40944
Velocity distribution of evaporated Au and incident velocity on nucleation of Au on rock salt studied by velocity selector 23 p4009 A67-41015
- GOLD ALLOY**
Amorphous whiskers from cobalt-gold alloy by quenching molten material through electron-beam heating and anvil-cooling device 01 p0135 A67-10895
Superlattice formation and lattice spacing changes in copper-gold alloys annealed for various periods 05 p0862 A67-16506
States density in vicinity of Fermi surface obtained from values of paramagnetic susceptibility for gold-palladium alloys 13 p2133 A67-27006
Recovery of deformed copper-palladium and gold-palladium alloys by isothermal and isochronal annealing, noting vacancy and interstitial migration 13 p2133 A67-27007
Epitaxial silicon layers grown by electron microscopy with small quantities of gold, discussing possible growth mechanisms 23 p4036 A67-40656
- GOLD PLATE**
Absorption, reflection and emission spectra of gold chloride at low temperatures 18 p3101 A67-34187
Sliding friction between spherical steel rider and gold-plated steel flat measured for varied loading, steel combinations and gold film thicknesses 19 p3237 A67-35837
Lubricating action of electroplated gold on stainless steel examined under load by single rub block loaded against rotating disk [ASLE PAPER 67-LC-16] 24 p4165 A67-42750
- GONIOMETER**
HF flight attitude indicator and forward and backward counting radio interferometer operating without rotating goniometer and phase locked oscillators 04 p0619 A67-14533
Reflectometer based on goniometer design employing beam reversal and beam splitter for measuring exit beam intensity 20 p3448 A67-36955
- GONIOMETRY**
Angular sizes of quasi-stellar radio sources in extended interferometric survey 05 p0898 A67-16925
Goniometric measurement accuracy of aerial camera photogrammetric distortion 11 p1793 A67-24864
Goniometric measurements of two angles defining direction of incoming 30 MHz wave reflected by meteor streams, using radio link 14 p2390 A67-28900
- GOSS**
S GROUND OPERATIONAL SUPPORT SYSTEM /GOSS/
- GOTHIC WING**
Quasi-conical motions applied to theory of wings with curved leading edges 07 p1128 A67-20235
- GOURSAT PROBLEM**
Goursat problem for partial differential equation shown not to possess classical solution even under suitable hypothesis 09 p1525 A67-22624
- GRAD EQUATION**
Thirteen-moment equations solved obtaining theory of thermal force acting on spherical particle for entire range of Knudsen numbers 16 p2661 A67-31221
- GRADIENT**
SA POTENTIAL GRADIENT
SA PRESSURE GRADIENT
SA TEMPERATURE GRADIENT
Algorithm encountered while solving trajectory optimization problems, discussing variational concepts, indirect, gradient, second variation and generalized Newton-Raphson methods 06 p1082 A67-17932
Convergence rate of method of gradients relationship to singularity of second variation operator in optimal programming problems 06 p0975 A67-17935
Accelerated gradient method for numerical solution of parameter optimization with nonlinear constraints [AAS PAPER 66-118] 07 p1217 A67-19977
Drag forces on body with nonuniform velocity distribution, considering gradient flow effects on drag coefficients 22 p3740 A67-39941
- GRAIN**
SA PROPELLANT GRAIN
Wheat seedlings grown so that coleoptile and early roots developed in moist air, noting organ orientation in relation to gravity 04 p0560 A67-14407
- Granular superconductor with thin insulating layer at boundary of each homogeneous superconductor grain, using isospin formulation of microscopic theory 10 p1887 A67-22763
Monograph on electron microprobe X-ray analyzer and application in mineralogy 10 p1603 A67-23632
Beryllium brittleness, discussing effect of grain refinement and randomization on properties below 200 degrees C 13 p2138 A67-27120
Carbon and iron grain production in argon arc discharge studied for implications of light scattering in interstellar absorption 22 p3896 A67-40531
- GRAIN BOUNDARY**
Microprobe study of impurities in hot-pressed polycrystalline MgO compact and existence of significant grain boundary volume [JPL-TR-32-1015] 01 p0131 A67-10262
Sintering mechanisms in powdered compacts of carbides, oxides and metals, examining grain growth, pore decrease and diffusion coefficients 01 p0096 A67-10694
Titanium diboride densification at high pressure and high temperature, noting grain growth 01 p0098 A67-10704
Temperature dependence of grain size in nonstoichiometric NbC between 1600 and 3300 degrees K in vacuum and Ar 01 p0102 A67-11245
Electron microscopy study using replica technique of cross section of films of Al and Si vacuum deposited on glass substrates reveal columnar growth of polycrystalline film 02 p0256 A67-12706
Light and electron microscopy used with X-ray diffraction and X-ray fluorescence analysis to study effects of temperatures and stress on As-cast nickel-base superalloy 02 p0256 A67-12706
Creep deformation of hot-rolled Zn-Tl alloys, noting secondary flow originating from strain induced grain growth 03 p0440 A67-13251
Forging and solution treating nickel-chromium alloy 718 to investigate notch ductility and uniform grain size 04 p0640 A67-15459
Molybdenum grain boundary relaxation and embrittling effect of interstitial impurity additions 05 p0829 A67-16505
Grain boundary relaxation in high purity fcc metal using LF torsion pendulum, noting tests for internal friction and creep at constant stress 06 p1016 A67-17899
Kinetics of growth of beta grain in titanium alloy 07 p1200 A67-19245
Etching methods to visualize lattice dislocations and grain boundaries in Czochralski grown calcium tungstate crystals doped with neodymium for laser application 07 p1196 A67-19565
Aging kinetics and lattice defects in Al-Zn and Al-Zn-Mg alloys 11 p1809 A67-24947
Reversed speed effect and grain boundary diffusion as explanations of discrepancy of activation energy values for strain aging under fatigue or simple stress conditions 12 p2013 A67-25284
Pore formation, lifetime and microstructure of thin electrolytic metal films under load and high temperature at grain boundaries 12 p1955 A67-25448
Structure effect on magnetization and critical current density in transverse magnetic field of superconducting V and Nb foils with different grain boundary orientations 12 p1986 A67-26067
Brittle fracture at grain boundaries in samples of electron-beam molybdenum prepared by forging in air after extrusion 13 p2130 A67-26447
Mechanical properties of beryllium with emphasis on influence of anisotropy in forming and grain size in powder metallurgy 13 p2140 A67-27134
Reverse magnetization spike domains analyzed for nucleation and growth 13 p2179 A67-27141
Internal friction in nickel chromium alloys heated to annealing temperature, noting 530 and 800 degree peaks and origin of latter 14 p2338 A67-28675
Premelting of predetermined sites in sodium-potassium alloys studied by transmission UV microscopy 14 p2339 A67-29032
Liquidus curves of various metals with mercury at high temperatures, obtaining corrosion rates and data on grain boundaries penetration 15 p2502 A67-29261
Fracture surface markings and topography for transgranular and intergranular paths studied with electron microscope 16 p2772 A67-31300
Compaction pressure and sintering temperature effect on initiation and propagation of cracks during bend testing of Ni and Mo specimens 16 p2691 A67-31586
Temperature dependence of grain size in nonstoichiometric NbC between 1600 and 3300 degrees K in vacuum and Ar 17 p2875 A67-33168
Strength of single crystals, amorphous materials and other brittle materials lacking grain boundaries, noting loading rate dependence 18 p3069 A67-33491
Crack nucleation in high strength low alloy steel, comparing fatigue processes in quenched and tempered martensite with those in pure metals 18 p3064 A67-34082
Surface, volume and grain-boundary diffusion role in metal sintering process, discussing theoretical equations 19 p3247 A67-35836
Conductance and capacitance measurements on grain boundaries in p-type indium antimonide 20 p3504 A67-36173
Grain boundary diffusion coefficients in tungsten at high temperatures, obtaining activation energy 20 p3470 A67-37388
Pore formation, lifetime and microstructure of thin electrolytic metal films under load and high temperature at grain boundaries 21 p3646 A67-38827
Microsegregation and grain boundary liquation in heat affected zone of 18-Ni maraging steel welds 22 p3812 A67-39448
Two-stage heat treatment effect on strength of high temperature Nimonic 80 alloy noting high brittleness, grain size and boundaries and fracture propagation 23 p4019 A67-41076
- GRAPH**
SA CHART
SA FLOW GRAPH
SA NOMOGRAPH
SA OSCILLOGRAPH
SA SPECTROGRAPH
Graphical estimation of reliability of test results 01 p0104 A67-10157
Graphical techniques in determining circuit-board resistance to shock and vibration 01 p0034 A67-10159
Plotting oriented graph of two-stage electronic circuit with cathode coupling 02 p0224 A67-11915
Separation constants for finite gyrotropic axially-magnetized cold collisionless plasma graphically represented near boundary of complex region 03 p0371 A67-13867
Graphical analysis of step-by-step extremal control system adapted to process with second order inertia before static characteristic 03 p0393 A67-13884
Comparison of temperature differences for similar liquids boiling on various surfaces, with graph correlating heat flux/temperature difference data 04 p0721 A67-14645
Graphical methods for solutions to orbital mechanics problems involving equations derived from Newton and Kepler laws 05 p0901 A67-17206
Peaking circle graphical method for solving 3-DB points in second order systems 06 p0971 A67-18244
Graphical method for converting geocentric satellite coordinates into topocentric, determining azimuth, elevation angle, etc 06 p0964 A67-18577
Graphical method predicting orbital lifetime of satellite, considering oblate earth effects and long period fluctuations in atmospheric density [AAS PAPER 66-96] 07 p1252 A67-19960
Graphical method for ascertaining acceptance number and size of sample in destructive and expensive testing 09 p1506 A67-22197
Network analysis and synthesis using centrally located tree to generate connected linear graph trees 10 p1618 A67-22704
Matrix methods applied to graphs, giving proof for matrix tree theorem 10 p1673 A67-22832
Geometric interpretation of product form of inverse applied to sparse matrices in linear programming, using graph

- theory 10 p1673 A67-22833
 Graphs for frequency plot of closed loop automatic control system from phase amplitude of open loop and frequency relations between open and closed 10 p1621 A67-23852
 Computer programming or software techniques in relation to hardware elements of computer graphics system [ASTME PAPER WES-7-02] 11 p1756 A67-24253
 Computer analysis of curve for total emission from group of separate localized emission points on surface of high vacuum metallic cathode 11 p1820 A67-24922
 Critical alternating-magnetization curves of permalloy films, clarifying theoretical experimental problems and effect of anisotropy field dispersion magnitude on curves 12 p1981 A67-25245
 Phaseplot, on-line graphical output parametric display technique, noting hardware realizations and software requirements 13 p2073 A67-27063
 Graph analytical calculation of MHD generator channel 13 p2169 A67-27308
 Graphical method predicting orbital lifetime of satellite, considering oblate earth effects and long period fluctuations in atmospheric density [AAS PAPER 66-96] 13 p2208 A67-27520
 Radio stars as signal sources for accurate measurement of radar antennas vertical polar diagrams, describing solar noise technique disadvantages 15 p2436 A67-29645
 Peak altitude of multistage sounding rocket vertical trajectory in vacuum determined by dimensionless graphs 16 p2762 A67-31247
 Network-diagram methods theory, discussing CPM, PERT, MPM, noting applications to technology and sociology 16 p2783 A67-31631
 Computer graphics for surface generation, stressing Coons surfaces and parametric representation 17 p2820 A67-32783
 Graphical integration method for calculating optical characteristics of materials used in solar radiation spectral measurements 18 p2990 A67-34492
 Graphic representation of Mises formula for stability analysis of cylindrical shell, discussing critical pressure and time and labor saving 19 p3338 A67-34875
 Graphical method predicting latitudes where satellites in circular orbit are visible, in both Northern and Southern Hemispheres 19 p3182 A67-35268
 Conditions for optimal planar intermediate-thrust /singular/ trajectory in inverse-square-law field analyzed graphically 19 p3333 A67-35749
 Graphical display technique for complex curve display, discussing system components, experimental results and relevant software 19 p3188 A67-36059
 Bridge circuits with nonlinear resistances, calculating statistical characteristics by graphical method for functional transformer 20 p3451 A67-37151
 Fourier integral in terms of maximum harmonic amplitudes 20 p3406 A67-37650
 Basic equation derived for I-V characteristics of p-n-p-n device with graphical solution for related p-n junctions 22 p3766 A67-39251
 Dissipation loss equation solved by graphic form for ripple values of Chebyshev band pass filters 22 p3774 A67-40344
 Visual criteria for stellar spectral classification of Cordoba Observatory Atlas 24 p4227 A67-41967
- GRAPHIC ARTS**
 Digital-graphic computer terminals effect on data processing equipment design, noting CRT use 01 p0029 A67-10669
 Digitally-driven display system for graphic man-computer communication in aerospace industry. 01 p0029 A67-10671
 Design Language I, prototype computer-aided design system that blends graphic techniques with console written language 02 p0207 A67-11813
 Data processing activities and ancillary equipment used in advanced techniques of computer generated graphics for weather observing and forecasting system [AIAA PAPER 66-854] 03 p0376 A67-14128
 Three-dimensional variation diagrams for control of calculations in optimum design [ASME PAPER 66-WA/MD-9] 04 p0629 A67-15345
- Man-computer graphics for computer aided design 05 p0768 A67-17514
 Computer graphic display for dynamic response of nonuniform beam treated by lumped mass-spring representation of structure 10 p1608 A67-23739
 Computer graphic aids with applications of graph plotters, trace analyzers, cathode ray tubes, light pens, etc 13 p2073 A67-27188
 Multidimensional data stereoscopic graphic display principles, viewing and use in engineering design 24 p4157 A67-42434
 Graphics system for space vehicle design and flight plan via light pen, trajectory computation and performance curve display on scope [AIAA PAPER 67-897] 24 p4126 A67-43006
- GRAPHITE**
SA PYROLYTIC GRAPHITE
 Equilibrium carbon monoxide pressures measured by torsion effusion studies of reaction of graphite with hafnium and uranium dioxides at high temperatures 01 p0018 A67-10763
 Ceylon and artificial graphite behavior under very high pressure, examining problem of metallic phase of carbon 01 p0104 A67-10833
 Far UV extinction curve and wavelength dependence of interstellar polarization by graphite grains 01 p0150 A67-10890
 Ultrahigh temperature thermocouple using pure and boron-doped pyrolytic graphite or tungsten and rhenium for operation in vibration and oxidation environment 01 p0076 A67-11139
 Sliding contact wear under very dry high altitude or space conditions due to lack of contact film prevented by using chemical compounds like graphite or lithium carbonate 02 p0221 A67-12435
 Pulsed laser techniques for measuring thermal diffusivity of graphites and chars between 500 and 5000 degrees F [AIAA PAPER 65-644] 03 p0449 A67-13062
 Graphite fiber reinforced epoxy resin matrix composites, determining mechanical properties 03 p0452 A67-13402
 Refractory ceramic and graphite fibers properties and strength in high temperature reinforcements 03 p0452 A67-13406
 Mechanical properties of continuous filament-graphite matrix composite in 0.50 inch diameter rod form, discussing limitation of binder phase and interface 03 p0453 A67-13412
 Behavior and fatigue strength of graphite during testing, plotting curves in semilogarithmic coordinates 04 p0641 A67-14599
 Observed interstellar polarization cannot be explained in terms of graphite-crystal color since polarization must increase monotonically from IR to UV 04 p0699 A67-14982
 Rate controlling mechanism in graphite creep, noting basal slip systems causing general deformation 05 p0833 A67-16892
 Increase in low temperature specific heat and change in electronic density of states of boronated graphite 05 p0833 A67-17197
 Radiation cooled reentry heat shield of graphitic surface over graphite felt insulation with receding surface [AIAA PAPER 67-153] 06 p1115 A67-18320
 Mechanical properties of continuous carbon filament/graphite binder composite including tensile, compressure, flexure, fatigue and shear properties [AIAA PAPER 67-173] 06 p1021 A67-18509
 Carrier-carrier scattering influence on Hall effect and on minority-majority carrier mobility in graphite 06 p1063 A67-18938
 Brazed graphite-stainless steel composites for tube-to-armor joints of high temperature graphite space radiators 07 p1223 A67-19462
 Dimensionality of superconductivity in alkali-metal-graphite lamellar compounds 07 p1236 A67-20138
 Graphite thermochemical response tested in simulated environment for use as thermal shield for hypersonic reentry vehicles [AIAA PAPER 65-643] 08 p1426 A67-20561
 Integral method to study surface chemistry interaction due to combustion and attendant mass transfer on isothermal graphite cone in nonsimilar boundary layer flow 08 p1320 A67-20570
 Ni-graphite antifriction composites capable of high temperature operation with good lubrication properties and oxidation resistance under dry friction conditions 08 p1341 A67-20599
 Elastic interaction between dislocation loops and straight dislocations in orthotropic anisotropic materials analyzed for various graphite configurations 08 p1346 A67-20797
 Graphite fibers as internal electrical resistance heat source for curing structural adhesives demonstrated in lap shears, larger area and sandwich construction 09 p1507 A67-22516
 High modulus high strength reinforcements incorporated in epoxy matrix plastic composites for aerospace structural use 10 p1671 A67-23704
 Microstructural study of adhesive behavior of powdered bakelite in intergrain pores of carbon-graphite compacts in terms of capillary attraction forces 11 p1810 A67-23900
 Solid solubility of boron in graphite as function of temperature and nature of solution from density and lattice constants 12 p1960 A67-26189
 Low pressure diffusion of carbon to nucleation sites and graphite growth in cubic morphology suggested as origin of cliftonite in meteorites 14 p2384 A67-28144
 High temperature testing and evaluation of graphite helical-screw expanders and compressors for use with inert gas Brayton cycle 15 p2492 A67-29427
 Heats of combustion in fluorine of Teflon and graphite and heats of formation of carbon tetrafluoride and carbon hexafluoride 15 p2433 A67-29765
 Isotopic composition and abundance of xenon and krypton in graphite of iron meteorite from Canyon Diablo examined for anomaly pattern 16 p2750 A67-31438
 Melting point and microhardness of carbon-saturated TIC-VC solid solutions, noting temperature of eutectic of TIC-VC with graphite 16 p2691 A67-31588
 Optical behavior of graphite as interstellar matter, discussing appearance as metal or dielectric particle, extinction and optical conductivity 18 p3117 A67-33513
 Graphite material strength prediction by nondestructive test techniques consisting of bulk density and eddy current measurements [ASTM PAPER 54] 18 p3070 A67-34584
 Cesium vapor treatment effect on work function of high melting Ta and Zr carbides, evaporation products and graphite 19 p3176 A67-35080
 Surface ionization of atoms and molecules on nonmetals, determining work functions and activation energies for dissociation 19 p3264 A67-35083
 Impurity effect on optical properties of interstellar graphite particles, examining wavelength dependence of absorption coefficient and refractive index of coals 19 p3323 A67-35423
 Cermet sealing material dry-friction characteristics over wide sliding-speed range, discussing graphite and boron nitride lubricants 19 p3247 A67-35850
 Refractory properties and mechanical characteristics of graphites and carbons, discussing maximum compatibility temperature of graphite 20 p3472 A67-36110
 Plasma arc deposition and gas pressure bonding technique for producing defect-free uniform iridium protective coatings for graphite reentry structures 20 p3465 A67-36607
 Densified carbon and graphite production methods /carbon, metal and resin and carbon with carbon impregnation/ for glass-to-metal sealing jigs 24 p4174 A67-41913
 Benzene and related molecules adsorption on uniform graphite surfaces investigated for lateral interaction and localization of lattice sites 24 p4118 A67-42195
 Microstructure of SGBF graphite under tensile and compressive stresses noting crack generation in layer planes [ACS PAPER 6-N-66F] 24 p4175 A67-42372
 Boron and graphite filament-resin composites tensile and interlaminar shear strengths and Al foil liner cyclic life in cryogenic pressure vessel tests 24 p4176 A67-42470
- GRAPHOF NUMBER**
 Two-dimensional unsteady Navier-Stokes equations for compressible viscous gas in closed region, examining convective flow and heat transfer 14 p2296 A67-27987

GRATING

- SA DIFFRACTION GRATING
SA INTERFERENCE GRATING
Scattering of plane wave by grating of identical cylinder specialized for case in which individual elements of grating scatter isotropically 03 p0374 A67-14353
Piezoelectric grating /PEG/ dispersive device using ultrasonic propagation in prismatic quartz block 04 p0574 A67-15056
Pneumatic grating for complete measuring system, considering fluidic techniques 08 p1330 A67-20439
Design, principles and applications of optical stellar interferometer, gratings, aperture synthesis and pencil beam telescopes 14 p2284 A67-28429
Spectral purity of Ebert type far IR grating spectrometer determined, noting experimental technique 17 p2863 A67-33300
SIMAC spectrography, discussing brightness, speed, etc. of electronic camera and photographic plate recording 20 p3439 A67-36350
Bilateral metal grating effect on E and H polarized radiation from plane parallel layer noting intensity, energy density and reflection at interface with medium 21 p3638 A67-37865

GRAVIMETER

- Closed loop LaCoste and Romberg gravimeter servo system operating at sensitivity approach thermal fluctuation limits 05 p0809 A67-17392
Gravity meter based on levitated superconducting ball over persistent current magnet 22 p3809 A67-40432

GRAVIMETRY

SA THERMOGRAVIMETRY

- Gaposhkin satellite gravity results compared with surface gravimetry data 01 p0056 A67-10041
Six solutions for tesseral harmonic coefficients of geopotential from satellite determinations compared with gravimetry 03 p0414 A67-13933
Critical analysis of Stokes gravity formula derivations, noting truncation error effect 05 p0796 A67-16153
Calorimetric, titrimetric and gravimetric methods for determination of hexogen-octogen mixtures 05 p0872 A67-17153
Equatorial radius of earth and zero-order undulation of geoid obtained from data on equatorial gravity, earth flattening and product of gravity constant and mass 08 p1325 A67-20933
Possible gravimetric study of lunar gravity, tide and free oscillation modes [AAS PAPER 66-191] 08 p1387 A67-20964
Gravitational radiation measurements by HF gravitational wave detector 10 p1652 A67-23545
Molodensky integral equation solvability 13 p2114 A67-26853
Gravitational acceleration determination noting reversible pendulum, free fall and symmetrical free motion methods 15 p2517 A67-29507
Solution of incorrect magnetometric and gravimetric problems represented by integral equations of convolution type with unstable solutions 16 p2863 A67-30866
Gravimetry, discussing absolute determinations, navigation, NBS measurements, etc 20 p3448 A67-36894
Ambient temperature variation effect on gravitational acceleration variations as measured by gravimeter, discussing possible measurement errors 20 p3450 A67-37030
Inertial guidance technology for atmospheric motion measurements, discussing system limitations in accuracy and resolution 23 p4026 A67-41444

GRAVITATION THEORY

- Time-space quantization of gravitational field by formalisms in general relativity theory 01 p0114 A67-10746
Unsteady adiabatic centrally symmetric radial flow of ideal fluid in general theory of relativity 01 p0114 A67-10987
Existence of two points near any planet where third body, given appropriate initial conditions, would remain in libration gravitational equilibrium 02 p0324 A67-11814
Cosmology in last 150 years reviewed, discussing Hubble expansion of universe, Einstein theories on gravity and present concepts 05 p0897 A67-16775
Einsteinian gravitation equations stated in terms of three-dimensional tensor analysis as

- applied in conformal space 08 p1354 A67-20843
General theory of relativity, emphasizing works discussed at London and Tbilisi conferences on gravitation theory 08 p1354 A67-20859
Energy and momentum localization of gravitational field by direct field measurements 09 p1531 A67-21559
Antisymmetric tensor theory of gravitation in flat space-time with energy and momentum conserved 09 p1532 A67-21979
Singularities of cosmological solutions of gravitational equations for space filled with matter 10 p1710 A67-23588
Gravitational instability from reformulation of Lifshitz relativistic theory for galaxy formation in expanding universe and comparison with Bonnor approach 11 p1859 A67-24121
Brans-Dicke theory of gravitational scalar field effect on structure of neutron cold spherical stellar model analyzed and compared with relativity theory 11 p1864 A67-24596
Post-Galilean transformation to which Einstein-Infeld-Hoffmann motion equation is invariant, considering transformation to center of mass system 12 p1965 A67-25125
Time-space quantization of gravitational field by formalisms in general relativity theory 13 p2158 A67-26775
Energy of system of particles defined as related to active gravitational mass, or to inertial mass and passive gravitational mass respectively, in expanding universe 13 p2199 A67-27004
Shear-free flows of gravitating gas investigated on basis of Newtonian mechanics 14 p2348 A67-28580
Three-body problem reduced to two-body problem in general relativity theory 16 p2745 A67-30747
Gravitation equations different from Einstein derived from Lagrangian in general form corresponding to general relativity theory 16 p2702 A67-31045
Gravitation and antigravitation, with relativity review, noting gravitational energy field 16 p2703 A67-31764
Nature of gravity, discussing universal radiation of gravitation quanta, gravity velocity determination, effects on earth formation, etc 18 p3077 A67-33549
Alternative approaches to particle solutions obeying Einstein gravitation theory 18 p3077 A67-33553
Einstein gravitation theory relation to general and special relativity, space time, unified four-dimensional continuum metric and chronogeometric theories 18 p3079 A67-34133
Gravitational instability of homogeneous anisotropic cosmological models 18 p3133 A67-34432
General quantum relativity theory in real universe with large radius and elementary particle structure 18 p3080 A67-34728
Nonlinear effect of gravitational instability in expanding universe, calculating second-order density perturbations by iteration method 19 p3317 A67-34891
Bulgarian research in spectroscopy, solar system, ionosphere, gravitation equations, astrophysics, etc 19 p3320 A67-35283
Quadrant mechanical hypothesis /QMh/ on gravitation, gravitational chemistry and zero gravity effects in various chemical processes 20 p3484 A67-36546
Gravitational theory with all curvilinear coordinate systems and space-time avoided illustrated by applying method to Dirac field case 20 p3484 A67-36836
Einstein vacuum equation solution interpretation for gravitation, space and time concepts, using vector fields oriented in time and Riemann tensorial equations 20 p3487 A67-37684
More general form of metric for explicitly solving field equations of Hoyle-Narlikar conformal theory of gravitation 21 p3657 A67-37924
Gravitation theory, general theory of relativity, field theory and gravitational interactions with elementary particles 22 p3879 A67-39294
Spectral line changes caused by Rydberg constant shift detectable by observing very distant galaxies, discussing gravitational and cosmological theory 22 p3882 A67-39616

- Gravitational instability and star and galaxy formation and structure - Conference, Liege, Belgium, June 1966 22 p3890 A67-40491
Radial motion of spherical self-gravitating mass undergoing gravitational collapse or expansion using Einstein general relativity theory 22 p3892 A67-40495
Unified theory for galaxy spiral formation and radio galaxy and quasar evolutionary dynamics, discussing galactic dipole magnetic field generation 22 p3893 A67-40504
Principles developed for founding of unified field theory of gravitation and electromagnetism, with space-time geodesics as charged particle motion equation 23 p4026 A67-40659
Mach principle manifestation in Jordan extended gravitation theory, calculating rotation of local inertial frame induced by rotating shell of mass 23 p4027 A67-41147
Time dependent gravitational constant theory, studying earth rotation secular acceleration 24 p4229 A67-42321

GRAVITATIONAL COLLAPSE

- Milky Way galaxy mechanism and evolution, examining correlation between period of pulsation of intrinsic variable and galactic velocity 03 p0516 A67-14334
Massive star behavior during final cataclysmic evolution stages, stressing effect of electron type neutrino interactions, using numerical hydrodynamics coupled with energy transfer methods 03 p0516 A67-14340
Partial fragmentation of pregalaxy in early phase of contraction with large internal velocity difference 04 p0697 A67-14806
Local model of quasi-stellar objects based on ejection by gravitational collapse 04 p0700 A67-15199
Pulsating gravitational collapse from point of view of external observer, noting oscillation period and distortion of contraction expansion symmetry 05 p0896 A67-16692
Star collapse observation by detection of high energy neutrino fluxes produced by cataclysmic star contraction 09 p1561 A67-21630
Cold star relativistic collapse kinematics, noting equilibrium and collapse of point masses system interacting by gravitation only 11 p1858 A67-24013
Neutron star structure and evolution from presupernovae stars including gravitational collapse and neutrino emission processes 12 p2007 A67-25768
Primordial element formation, primordial magnetic fields and universe isotropy, showing correctness of big-bang relativistic theory, early anisotropy of universe, etc 12 p2010 A67-26240
Hydrodynamics of gravitating stellar system numerically calculated for nonrotating spherically symmetric case 14 p2393 A67-28997
Mass dependence of behavior of stellar core undergoing gravitational collapse examined, using improved equation of state and mean free path for energy transfer 15 p2553 A67-29183
Pulsating gravitational collapse from point of view of external observer, noting oscillation period and distortion of contraction expansion symmetry 15 p2556 A67-29863
Models of spherically symmetric nonstatic processes, including relativistic collapse to Schwarzschild sphere, constructed by space-time metrics [JPL-TR-32-1136] 15 p2564 A67-30438
Adiabatic gravitational collapse of spherically symmetrical distribution of matter, investigating nonvanishing internal pressure gradient, using Einstein field equation 16 p2746 A67-30865
Supernova explosion and collapse theory using relativistic hydrodynamics 16 p2752 A67-31541
Core of two solar masses of gravitationally collapsing star, analyzing hydrodynamics, heating, helium 4 formation, neutron decay, nucleosynthesis, light output and mass ejection 22 p3882 A67-39622
Gravitational collapse model with pressure gradient and no energy flow, discussing spectral shift and mass radius relation 22 p3884 A67-39833
Radial motion of spherical self-gravitating mass undergoing gravitational collapse or expansion using Einstein general relativity theory 22 p3892 A67-40495

Rotation and pressure gradient effects on gravitational instability of collapsing gas clouds, discussing subsequent fragmentation 22 p3893 A67-40501

Two-body relaxation term in N-body self-gravitating gases of one and three dimensions and validity of Vlasov equation 22 p3894 A67-40508

Globular star cluster, initial gravitational collapse and dynamical mixing, discussing numerical analyses for homogeneous spherical cluster with Maxwell velocity distribution 22 p3894 A67-40509

Interstellar gas cloud gravitational collapse for models initially in gravitational equilibrium without mass motions, analyzing cooling and density distribution effects numerically 22 p3895 A67-40514

One-dimensional unstable cloud hydrodynamics analyzed numerically, noting collapse primarily in center and little density growth in outer region 22 p3895 A67-40515

Collapsing gas cloud noting instability for density fluctuations, rise of turbulence and fragmentation phenomena 22 p3895 A67-40516

Equilibrium configuration for nonspherical cold gas cloud permeated by magnetic field in gravitationally collapsed state 22 p3895 A67-40518

Small stellar systems evolution, double star formation and bound subgroup occurrence after condensation from collapsed cloud calculated numerically 22 p3896 A67-40521

IR nebula in Orion as protocluster with massive stars imbedded in opaque dust cloud, discussing collapse and lifetime 24 p4225 A67-41829

Relativistic gravitational collapse, considering asymmetric nonrotating star collapse 24 p4226 A67-41885

Gravitational collapse considering space time diagrams and curvature of space, suggesting crushing body less than critical size 24 p4228 A67-42309

Einstein field equations derived for thin spherical shell of charged dust falling on spherically symmetric field of massive charged body, considering bounce 24 p4189 A67-42599

GRAVITATIONAL CONSTANT

Structure of universe and role of gravitation in determining dynamic behavior, indicating that universe will stop expanding at certain critical maximum size 03 p0516 A67-14339

Estimated GM values of earth and moon, tracking station locations and lunar radii at impact points, from DSIF radio tracking data of Ranger Block III lunar flights [AAS PAPER 66-105] 07 p1253 A67-19965

Possible annual variation of gravitational constant shown to eliminate systematic errors noted in redeterminations of gravitational constant 09 p1492 A67-22616

Satellite orbit analysis and computer program for earth zonal harmonics determination, considering orbit elements and gravitational constants [AAS PAPER 66-91] 13 p2116 A67-27516

Estimated GM values of earth and moon, tracking station locations and lunar radii at impact points, from DSIF radio tracking data of Ranger Block III lunar flights [AAS PAPER 66-105] 13 p2208 A67-27523

Pulsating gravitation, noting geological evidence such as ocean transgressions, regressions, climate variations, etc 17 p2841 A67-32211

Lunar gravitational field obtained from Lunar Orbiter tracking data, with gravity potential as spherical harmonics series and lunar gravitational constant determined 19 p3318 A67-35190

Selenodesy, determining gravitational constant-lunar mass product, lunar gravitational field variation, physical librations, inertial moments, lunar tides, lunar radius, etc 20 p3525 A67-36893

Solar neutrino astrophysics, universal neutrino sea, high energy neutrinos, neutrino detectors, stellar energy production, solar thermometry and gravitational constant time variation 23 p4056 A67-41111

Self-gravitating isothermal nonrotating gas layer stability, discussing amplitude density distributions in space 24 p4225 A67-41826

GRAVITATIONAL EFFECT

SA LUNAR GRAVITATIONAL EFFECT

SA SOLAR GRAVITATIONAL EFFECT

SA WEIGHTLESSNESS

Earth oblateness effect on torque experienced in nonuniform geogravitational field by satellite with unequal principal moments of inertia 01 p0154 A67-11194

Time variance of earth-moon distance, discussing meteoroidal accretion mechanism effect on capture 02 p0319 A67-11453

Fluid motion in weightlessness, examining effects of weak forces normally suppressed by terrestrial gravitational field 02 p0233 A67-12322

Weight factor effects on optimal motion parameters of variable mass system with limited velocity jet propulsion in gravitational field 02 p0327 A67-12333

Existence and stability of equilibrium orientations of rigid body with gyrostat in nonuniform gravitational field 02 p0268 A67-12385

Combined effect of gravitational and vibrational forces on formation of convection studied by method of averaging with respect to small vibrations 03 p0401 A67-12870

Fluid equilibrium shape under gravity force and surface tension analyzed via variational method 03 p0401 A67-12881

Light propagation through Schwarzschild singular sphere, solving problem of visual image of emitting surface of gravitating sphere as seen by observer 03 p0467 A67-12932

Instability of gravitating slipstreams or mixed streams and cloud fragmentation of interstellar gas 03 p0511 A67-13877

IR stars as supergiants of very late type and not objects in state of gravitational contraction as sustained by Penston theory 03 p0512 A67-13888

Wheat seedlings grown so that coleoptile and early roots developed in moist air, noting organ orientation in relation to gravity 04 p0560 A67-14407

Combined effect of aerodynamic and gravity torques on stability of motion of passive satellites investigated by Liapunov direct method 04 p0704 A67-14827

Cupular function of man under acceleration, noting electroencephalographic results on caloric nystagmus under 1.2, 3 and 4 g and postrotational nystagmus 05 p0756 A67-16324

Generalized Lagrangian for system of gravitating elastic bodies derived from Fokker Lagrangian 05 p0847 A67-17495

Restricted problem of three bodies, two of which are assumed to be point masses, determining motion of third body 06 p1081 A67-17779

Qualitative methods in n-body problem concerned with masses motion in inertial space under gravity, solving motion equation 06 p1081 A67-17781

Simulation of deployment dynamics of spinning spacecraft, discussing test methods emphasizing gravity compensating techniques [AIAA PAPER 67-207] 06 p0980 A67-18325

Computer program for gravity and magnetic profiles across two-dimensional bodies of arbitrary shape 06 p0998 A67-18736

Gravitational red shifts in quasi-stellar objects 07 p1250 A67-19664

Coefficient of major axis of symmetry of spherical harmonic in satellite oscillations 08 p1383 A67-20587

Motion of lunar satellite, noting principal perturbations due to nonspherical lunar gravity and earth attraction, considering moon libration and solar small forces 08 p1397 A67-21184

Statistical analysis of errors in angular measurement of distant objects due to gravitational scattering along light path 08 p1398 A67-21232

Effect of gravitational changes on aerosol deposition in lungs of man, noting particle size and alveolar region 09 p1452 A67-21724

Distribution theory application to derive formula for deflections of vertical from Stokes formula 09 p1492 A67-22681

Semianalytical solution of motion of satellite in lunar orbit, considering perturbations due to lunar and earth gravity and solar attraction 10 p1706 A67-23185

Time and distance measurement of freely falling body to determine acceleration due to gravity 10 p1857 A67-23317

Free and forced liquid sloshing motions in tank of arbitrary shape at low gravity

environments analyzed, using Satterlee-Reynolds method 10 p1629 A67-23832

Gravitational instability due to small irregularities and implications for early universe and galaxy formation 11 p1860 A67-24483

Evolution in close binary star system through mass exchange leading to white dwarf with relatively unevolved companion 11 p1864 A67-24581

Brans-Dicke theory of gravitational scalar field effect on structure of neutron cold spherical stellar model analyzed and compared with relativity 11 p1864 A67-24596

Dynamic effects on satellite motion of mechanical deformations in stabilizing system, deriving equations for rotational motion about center of inertia 11 p1870 A67-24674

Electromechanical system for study of plant or organism growth and development in compensated gravitational fields 11 p1793 A67-24822

Absolute gravitational acceleration determined by timing symmetrical free motion of body moving under attraction of gravity 12 p1965 A67-25126

Light deflection by solar activity 12 p2002 A67-25540

Zero gravity effects on boiling from flat horizontal surface for various subcoolings, fluid properties and heat transfer rates 12 p2034 A67-25720

Saturn IVB flight data evaluation, discussing heat transfer effect on fluid system as function of gravity changes 12 p2034 A67-25721

Steady state model of solar wind flow in equatorial plane solved for radial and azimuthal motions, taking into account pressure gradient, magnetic field and gravitational effects 12 p2010 A67-26241

Diffusion phenomena of increasing mean free path with altitude in rarefied gas analyzed, incorporating gravitational field effect in Boltzmann equations 13 p2099 A67-26952

Earth gravitational field eccentricity effect on deviation of satellites from Kepler ellipse orbits 13 p2200 A67-27322

Plants in low gravity environment simulated by 2 rpm clinostat with horizontal axis, studying growth direction and respiratory metabolism 15 p2426 A67-29114

Urinary output patterns relationship to arterial pressure, pulse rate and parameters of hemoconcentration in study of homeostatic circulation regulation during prolonged gravitational stress 15 p2428 A67-29273

Prolonged recording from single vestibular units in frog during plane and space flight, significance and technique 15 p2430 A67-29281

Nonrotating, hydrostatic models of geochemically likely planets calculated using solar elemental abundances and equations of state for cold materials 16 p2754 A67-31748

Thermal problems peculiar to cryogenics stored in reduced gravity environment 17 p2966 A67-32010

Motion of dynamically symmetric satellite under action of gravitational moments, discussing stability and nonlinear oscillations 17 p2955 A67-32243

Stability analysis of deformable space vehicle in torque free state noting gravitational effect, stability of spin motion, characteristic motion equations, etc 17 p2956 A67-32779

Immersion technique measurement of gravitational stresses using two- and three-dimensional photoelasticity [ASME PAPER 67-APM-11] 17 p2964 A67-33146

Liquid sloshing at simulated low gravity in rigid cylindrical tank, noting analytical model and experimental results [ASME PAPER 67-APM-14] 17 p2840 A67-33147

Balloon satellite orbital elements predicted in advance by computation of solar radiation, gravitational perturbations, etc 18 p3126 A67-34246

Gravitational instability of homogeneous anisotropic cosmological models 18 p3133 A67-34432

Solar system bodies gravitational fields, discussing possibility of holding satellite in orbit 19 p3323 A67-35337

Radiative effects in pair of spherical particles in radiation field produced by omnidirectional gravitational quanta 19 p3325 A67-35556

Restricted three-body problem with two masses under Newtonian gravitation and third obeying semi-Newtonian laws 19 p3327 A67-35664

Gravitational waves, calculating velocity of propagation using perturbation method 19 p3262 A67-35708

Gravitational and magnetic torque effects on rotational motion of asymmetric Pegasus satellite in circular orbit [AIAA PAPER 67-567] 19 p3335 A67-35963

Ascent and descent gravity turn trajectories of rocket in constant gravitational field, considering drag forces in motion equation [AIAA PAPER 67-596] 19 p3336 A67-35992

Iterative guidance mode /IGM/ applied to effective gravity vector prediction, acceleration measurement of noise sensitivity and energy limitations [AIAA PAPER 67-620] 19 p3260 A67-36009

Animal study for motor reflexes under simulated weightlessness and during gravitational pulses 20 p3367 A67-36258

Quadrant mechanical hypothesis /QMH/ on gravitation, gravitational chemistry and zero gravity effects in various chemical processes 20 p3484 A67-36546

Gravitational effect on thermal instabilities, discussing optimization techniques to calculate effects of surface stresses [ASME PAPER 67-HT-22] 20 p3546 A67-36717

Gravity and buoyancy effects on slip ratio, void fraction, flow model and boiling heat transfer [ASME PAPER 67-HT-63] 20 p3549 A67-36745

Nonconstant gravity field effect on free convective heat transfer to or from isothermal flat plate [AICHE PAPER 2] 20 p3552 A67-36825

Gravitational effect upon nucleate boiling analyzed by experimentation on all levels up to maximum attainable by apparatus available [AICHE PAPER 4] 20 p3552 A67-36826

Gravitational effects and cosmic phenomena reconciliation with Einstein relativity scalar-tensor theories 20 p3524 A67-36834

Gravity effect on liver regeneration in rats measured by mitotic count 20 p3372 A67-36963

Weightlessness state in atmosphere and vacuum applied to satellites and space probes, noting effects on passengers and equipment 20 p3418 A67-37260

Effect of electromagnetic field interaction with gravitational field calculated from satellite data, determining difference between frequencies 20 p3386 A67-37523

Quasi-stellar red shift assuming gravitational origin, deriving mass, radius and distance as function of flow density, linewidth and apparent diameter 20 p3531 A67-37683

Motion of rotating plasma cylinder under gravity force assuming temperature time dependency 21 p3663 A67-37931

Satellite with symmetry axis perpendicular to orbit analyzed for rotational motion, determining instability for eccentric orbit, noting gravitational effect 21 p3713 A67-38588

Geomagnetic and gravitational field combined effects on magnetized satellite oscillations in plane of circular and elliptical polar orbits 21 p3713 A67-38590

Satellite-gyroscope asymptotic equilibrium positions obtained by general motion equation, calculating gravitational and aerodynamic moment effects 22 p3898 A67-39187

Tensor calculation of origin of local concentration of matter in universe model, considering effect of gravitational perturbations 22 p3880 A67-39314

Lunar semidiurnal air tide distribution and small lunar gravitational excitation noting lunar diurnal tide detectable only with wind data 22 p3882 A67-39557

Gravitational instability in anisotropic plasma including rotation effect 22 p3848 A67-39694

Similarity parameters of gravity and pressure driven liquid discharge from propellant tanks obtained by dimensional analysis 22 p3785 A67-39969

Nonlinear differential equations describing extensional motion of dumbbell satellite solved on digital computer 22 p3886 A67-40086

Atmosphere of Mars studied using three models generated to show high, mean and low density compositions to account for gravitational and magnetic fields 22 p3887 A67-40140

Clustering process, examining self-gravitating system separation from expanding cosmic distribution 22 p3891 A67-40494

Interstellar gas cloud collision, heating, possible gravitational instability and subsequent cooling 22 p3894 A67-40513

Oscillations of polytropic and compressible cylinders investigated by small perturbation method noting separate mode of gravitational instability 22 p3896 A67-40526

Nongravitational effects in Halley comet motion and arbitrarily rotating comet nucleus model, noting push-effect hypothesis 23 p4062 A67-40672

Nongravitational and splitting effects in comet motion and rotating comet nucleus model, using push-effect hypothesis for post-explosion analysis nongravitational and splitting effects in comet motion and rotating comet nucleus model, using 23 p4062 A67-40673

Brain tissue respiratory processes of rabbits subjected to hypergravity and acute hypoxia noting no significant difference between experimental and control animals 23 p3943 A67-40770

Transverse accelerations remote aftereffect on conditioned alimentary reflexes of rats, discussing prolonged depression of higher nervous activity 23 p3943 A67-40771

Magnetogravitational instability of uniformly rotating compressible medium due to variable amplitude perturbations, stressing Jeans theory 23 p4033 A67-41019

Human circulatory response to sinusoidal gravitational stimulus via Rotational Flight Simulator /RFS/, discussing heart rate variation 23 p3951 A67-41561

Zero gravity perturbation mechanisms affecting electrochemical systems noting transport processes and Curie theorem 23 p3972 A67-41607

Gravitational torque mechanism for radial outward angular momentum transport in solar nebula 24 p4223 A67-41790

Terrestrial gravity anomalies influence on satellite orbits treated by analytical numerical integration 24 p4237 A67-42686

Gravitational effect on free falling electrons in vacuum, showing gravitational induction of electric field outside metal surface 24 p4189 A67-42740

GRAVITATIONAL FIELD

Standard earth geodetic coordinate system and Baker-Nunn camera station positions 01 p0056 A67-10038

Rendezvous maneuver between vehicle and target in free orbital flight in central gravitational field, deriving low acceleration program for elliptical target orbit 01 p0152 A67-10208

Behavior of magnet and ball in gravitational field in five-dimensional continuum 01 p0060 A67-10366

Levi-Civita regularized equations of elliptic motion of particle influenced by massive primary and perturbed by smaller primary, Part I, Trigonometric series solution 01 p0147 A67-10379

Levi-Civita regularized equation of elliptic motion of particle influenced by massive primary and perturbed by smaller primary, Part II, Applications to circular and collision orbits 01 p0147 A67-10380

Certain solutions to problem of motion of solid body with clamped point in homogeneous gravitational field 01 p0114 A67-10990

Rational mechanics principles of inertial navigation and relation to gravitational field structure in vicinity of maneuvering vehicle [ONERA-TP-352] 01 p0110 A67-11088

Variational problem of optimal motion in gravitational field, for limited-power propulsion system in combination with energy accumulator and engine with limited jet velocity 02 p0327 A67-12332

Collision paths of free particle in Newtonian gravitational field examined, using analogy of circular restricted three-

body problem 02 p0328 A67-12403

Anomalous gravitational field representation without using integral equation for density of auxiliary surface layer 03 p0411 A67-13345

Virial theorem for electron plasma obtained by defining potential tensor and superpotential of electric field 03 p0482 A67-13746

Data interpretation for sun grazing family of comets deriving formulas for compressive and tensile stress in spherical bodies for tidal, rotational and self-gravitating fields 03 p0512 A67-13923

Energy impulse vectors and kinetic moment tensor associated with body in gravitational field analyzed, using Brouwer theorem 04 p0658 A67-15494

Formulas for extraterrestrial potential, anomalous gravity force gradient on earth topographic surface, deflections of vertical, etc 04 p0617 A67-15565

Ionospheric irregularities explained by gravitational field and positive electron density gradient joint effect on ionospheric region below electron distribution peak 05 p0760 A67-16002

Variational problem of rocket dynamics in homogeneous gravitational field in empty space reduced to differential equation system 05 p0904 A67-16049

Noncentral nature of lunar gravitational field determined from motion of Luna X lunar orbiter 05 p0886 A67-16050

Derivation of accurate solution of equation for geopotential field prognosis using only simple invariant-group solutions and meteorological terminology 05 p0837 A67-16489

Fine structure of gravitational field in neighborhood of earth orbiting vehicle, analyzing contributions to field from earth, moon, sun, etc 05 p0796 A67-16518

Reconnaissance missions to outer solar system using energy derived from midcourse planetary encounter 05 p0893 A67-16520

Subcritical convective instability, discussing effects of internal heat generation and spatial variation of gravity field on onset of thermal convection 05 p0926 A67-16817

Relativistic trajectory and orbital precession of spinning satellite under nonspherically symmetric gravitational field 05 p0906 A67-16849

Relation between terrestrial gravitational and magnetic field variations and time-dependent changes in shape, density and magnetization of disturbing bodies 05 p0799 A67-17027

Earth gravitational field parameters from near-surface satellite observations influenced by zonal and tesseral harmonics 05 p0800 A67-17080

Matrix solution to free motion of point in randomly perturbed resisting medium in rotating aspherical geopotential field 05 p0901 A67-17110

Altitude of gravitational division level, discussing wind currents above it 05 p0800 A67-17124

Unsteady radial expansion of polytropic gaseous sphere in own gravitational field, using hydrodynamical equations and model limited by shock wave 06 p1083 A67-18064

Simplified gravity force model effect in computing state transition matrices along two-body orbits [AIAA PAPER 67-123] 06 p1087 A67-18455

Gravitational field signatures yield information about interior structure of planets 06 p1092 A67-19008

Zonal harmonics determination through satellite observations processed using computer program, noting necessity for increased number of satellites [AAS PAPER 66-91] 07 p1183 A67-19956

Gravitational field of any primary determined using observations of satellites in orbit about primary, noting numerical integration technique and special perturbation methods [AAS PAPER 66-109] 07 p1253 A67-19969

Lunar external gravitational field, topographic surface and moments of inertia [AAS PAPER 66-189] 08 p1387 A67-20962

Resonant oscillations of artificial earth satellite with nearly repetitive path relative to rotating primary with longitudinally varying gravitational field 08 p1401 A67-21362

Orbital disturbances of satellite produced

by zonal harmonics of gravitational field 09 p1564 A67-21884
 Martian radius determined by measuring gravity field at known surface points [JPL-TR-32-1091] 09 p1569 A67-22682
 Vertical profile of concentration of atmospheric electron-ion gas flux under action of gravitational field 10 p1631 A67-22804
 Covariant decomposition of tensor and gravitational Cauchy problem in Riemann space 10 p1679 A67-22841
 Proposal for computation of unknown parts of gravitation field of earth from successive satellite passages 10 p1636 A67-23180
 Stokes problem solution for intensity of regularized gravity field around earth and at surface in form of rapidly converging series 11 p1812 A67-24162
 Cosmological distortion effect incorporating incident magnetic type gravitational field parameter upper limits measured from galactic cluster photographs 11 p1860 A67-24484
 Parametrization of reduced problem of stationary axially symmetric gravity fields 11 p1819 A67-24597
 Dynamic Newtonian gravitational force gradient fields generator to calibrate response of dynamic gravitational gradient sensor 11 p1794 A67-24903
 Magnetosphere phenomena investigated via atmosphere model to explain planetary nebulas and eruptive solar prominences 12 p1992 A67-25119
 Optimum three-dimensional ascent trajectories in model gravitational field using maximum principle 12 p2000 A67-25211
 Vibrational mode behavior of rotating gravitational mass sensors and sensor design to minimize nonideal effect of manufacturing and external disturbances 12 p1945 A67-25919
 Space flight to Mars, discussing medical problems originating from changing gravitational fields, meteorite dangers, radiation and psychological considerations 13 p2061 A67-26338
 Integration of Einstein gravitational equations implies that corpuses be rigidly connected with particular Fermi space-time system of reference 13 p2158 A67-27298
 Multistage rocket motion optimization in uniform gravitational field formulated as coupled variational problem 13 p2213 A67-27321
 Earth gravitational potential field determined by satellite measurements, showing field in spherical harmonics form 13 p2116 A67-27395
 Earth-moon and moon-earth trajectory parameters related to lunar orbit conditions for synthesizing lunar orbit trajectory 13 p2210 A67-27616
 Optimum trajectories between material points moving along same orbit in gravitational field of spherically symmetric central body, obtaining numerical solutions for circular initial orbit 14 p2382 A67-27852
 Line element describing gravitational field of charged particle embedded in expanding universe 14 p2336 A67-27892
 Method of averaging applied to solution of canonical equation system describing particle motion at high altitude in gravitational field of nonspherical planet 14 p2388 A67-28637
 Gravitational acceleration determination noting reversible pendulum, free fall and symmetrical free motion methods 15 p2517 A67-29507
 Gravitational fields for observation of soft cosmic neutrino and neutretto background predicted by different cosmological theories 15 p2555 A67-29641
 Elliptical motion of material point in terrestrial gravitational field, noting expression for eccentricity under effect of small tangential force 15 p2556 A67-29659
 Momentum and energy of gravitational waves in terms of relativity theory 15 p2518 A67-30005
 Asymptotic calculation of satellite orbit evolution in noncentral gravitational field of earth 16 p2743 A67-30724
 Gravitational stabilization of satellites with respect to orbital system of coordinates 16 p2760 A67-30740
 Non-Markovian evolution equation for velocities distribution in homogeneous gravitational system 16 p2748 A67-31139

Secular increase of stellar noncircular velocities in disk portions of galactic systems, noting gravitational disturbances [AROD-2160-19] 16 p2753 A67-31699
 Gravitation and antigravitation, with relativity review, noting gravitational energy field 16 p2703 A67-31764
 Book on celestial mechanics presenting solution of artificial satellite motion in earth gravitational field, using Lagrange equations 17 p2950 A67-33166
 Scalar gravitational fields in pulsating stars, calculating scalar wave radiation rate and star relaxation time 17 p2952 A67-33319
 Momentum and energy of gravitational waves in terms of relativity theory 18 p3079 A67-33763
 Satellite orbit perturbations in theories determining earth gravitational field, observing relation to departures from Keplerian ellipse 18 p3041 A67-34249
 Periodic trajectories in n stationary attracting centers field, using arbitrary gravitational law 18 p3127 A67-34271
 Schwarzschild criterion validity, reducing initial value problem for hydrodynamic perturbation equation to time independent problem 18 p3029 A67-34737
 Eccentricity change for satellite in librational resonance shown periodic due to gravity dependence on longitude 19 p3220 A67-35254
 Solar system bodies gravitational fields, discussing possibility of holding satellite in orbit 19 p3323 A67-35337
 Navy Navigation Satellite System, discussing naval and civilian application and improved gravitational field model 19 p3255 A67-35638
 Crater forming processes on moon from Ranger VIII impact, ascertaining gravity scaling existence, noting relation to terrestrial soils 19 p3327 A67-35894
 Space probe rendezvous with Halley comet, considering use of planetary gravity field to modify trajectory [AIAA PAPER 67-614] 19 p3329 A67-36003
 Theoretical assumptions determining static long range force sign between particles in general relativity and other theories 20 p3483 A67-36184
 Payload and trajectories determination for consumption optimization for missiles moving in constant gravitational field, using Pontryagin maximum principle 20 p3531 A67-36409
 Extremal space trajectories problems of one-impulse flights and two-impulse orbital transfers in central gravitational field 20 p3522 A67-36617
 Satellite geodesy results compared to other determinations, noting topography-gravity correlation confirmation, gravity field, etc 20 p3429 A67-36892
 Gravimetry, discussing absolute determinations, navigation, NBS measurements, etc 20 p3448 A67-36894
 Ambient temperature variation effect on gravitational acceleration variations as measured by gravimeter, discussing possible measurement errors 20 p3450 A67-37030
 Artificial satellite motion determination of external earth gravity field compared with surface measurements, orbit theory, etc 20 p3432 A67-37205
 Soviet book on electromagnetic and gravitational fields theory based on relativity theories 20 p3486 A67-37207
 Toroidal plasma instabilities analyzed, justifying use of two-dimensional slab models with varying gravitational field simulating magnetic lines curvature effect 21 p3661 A67-37747
 Variational problem of rocket dynamics in homogeneous gravitational field in empty space reduced to differential equation system 21 p3701 A67-37836
 Noncentral nature of lunar gravitational field determined from motion of Luna X lunar orbiter 21 p3701 A67-37837
 Dispersion equation of radioactive compressible nonviscous plasma with finite electric conductivity under gravitational and axial magnetic fields 21 p3663 A67-37918
 Altitude of gravitational division level, discussing wind currents above it 21 p3618 A67-38467
 Ideal gas flow in spherically symmetric gravity field, considering radiant heat

transfer and radiation 22 p3880 A67-39407
 pressure 22 p3880 A67-39407
 Closed form solution for two-dimensional reentry trajectories by transforming motion equations into Bernoulli with two arbitrary functions of inclination, considering constant gravitational field 22 p3881 A67-39526
 Soviet book on motion of artificial satellites in earth gravitational field covering perturbation theory, force field, algorithms for calculations, etc 23 p4063 A67-40734
 Rigorously geodetic inertial motion of extended object in Einstein gravitational field, using relativistic hydrodynamics 23 p4027 A67-41148
 Axisymmetric stationary gravitational field Einstein field equations in rigid uniformly rotating ideal fluid 23 p4028 A67-41149
 Generalized Lorentz transformation for inhomogeneous region in general relativity obtained by transformation leading to nearly straight system of reference 23 p4028 A67-41187
 Higher dimensional spaces and symmetries arising on gravitational fields 23 p4028 A67-41188
 Vertical profile of concentration of atmospheric electron-ion gas flux under action of gravitational field 24 p4150 A67-42141
 Pursuit trajectory plotting in central field of gravity for pursuer and fugitive assuming motion can be predicted successively at small time intervals 24 p4228 A67-42273
 Motion equations for mean orbital and osculating elements of particle rotating in gravitational field of aspherical planet 24 p4228 A67-42274
 Velocity and path of vertical motion of constant thrust rocket in homogeneous gravitational field, giving hyperbolic acceleration expression as time function 24 p4241 A67-42578
GRAVITATIONAL POTENTIAL
 Corrections to Smithsonian astrophysical observing station coordinates and nonzonal harmonics from combination of dynamical and geometrical method 01 p0056 A67-10039
 NASA-sponsored satellite geodesy program using Baker-Nunn camera, noting station positions and gravitational potential determination 01 p0056 A67-10040
 Odd zonal harmonics in terrestrial gravitational potential determined from 14 well distributed satellite orbits 02 p0235 A67-11475
 General inequalities for regular relativistic fluid spheres, noting gravitational potential energy limit 02 p0266 A67-11696
 Gravitational and magnetogravitational stability of rotating fluid layers of uniform thickness under Coriolis force and magnetic field 03 p0482 A67-13744
 Six solutions for tesseral harmonic coefficients of geopotential from satellite determinations compared with gravimetry 03 p0414 A67-13933
 Formulas for extraterrestrial potential, anomalous gravity force gradient on earth topographic surface, deflections of vertical, etc 04 p0617 A67-15565
 Orbital elements determination from reduced Baker-Nunn observations of satellites, noting disturbance by resonance effects of earth gravitational potential sectorial and tesseral harmonics 05 p0763 A67-16562
 Earth potential in ellipsoidal coordinates developed using Lamé function 05 p0796 A67-16564
 Drag free motion of satellite of oblate planet determined by differential equation expressing planet gravitational potential as spherical harmonics 06 p1081 A67-17777
 Relative gravitational potentials through certain regions in Galaxy obtained through rotation curve in plane of Galaxy 08 p1380 A67-20384
 Orbit perturbations due to tesseral harmonics contained in series expansion of gravitational potential determined using computer program 09 p1467 A67-21885
 Corrections to station coordinates and nonzonal coefficients of geogravitational potential from Baker-Nunn observations by combined dynamical and geometrical method 10 p1636 A67-23179
 Newton inverse square force for planets from invariant velocity components of

Keplerian planetary motion by graphical model 10 p1711 A67-23791

Earth figure determination from relation between gravitational potential and vertical gradient anomalies and surface and sea level potential 11 p1783 A67-23899

Stellar dynamics and galactic spiral structure analyzed using gas and plasma dynamics 11 p1863 A67-24534

Molodensky integral equation solvability 13 p2114 A67-26853

Motion of point of variable mass in Newtonian central gravitational field 13 p2199 A67-26894

Nonrelativistic theory of rotating configurations in terms of gravitational potential, center mass density and variable angular velocity 14 p2382 A67-27833

Spheroidal coordinate method for obtaining gravitational potential of oblate planet 15 p2560 A67-30042

Spinor algebra application to Fourier series transformation of spherical harmonics expansion representing earth gravitational potential at space location 15 p2561 A67-30055

Asymptotic calculation of satellite orbit evolution in noncentral gravitational field of earth 16 p2743 A67-30724

Time of flight expressed in terms of perturbed true anomaly in case of large eccentricities 16 p2743 A67-30726

Coefficients of odd zonal harmonics in terrestrial gravitation evaluated from orbital eccentricity analysis of artificial satellites 17 p2853 A67-33249

Lunar gravitational field obtained from Lunar Orbiter tracking data, with gravity potential as spherical harmonics series and lunar gravitational constant 19 p3318 A67-35190

Theoretical assumptions determining static long range force sign between particles in general relativity and other theories 20 p3483 A67-36184

Reduction of dynamic data from geodetic satellites noting satellite tracking station position, gravitational potential, gravity coefficients, synchronous satellites, etc 20 p3429 A67-36891

Earth gravitational potential on geoid expressed by vertical and horizontal gradients for gravitational anomalies useful in earth figure determination 21 p3618 A67-38199

Perturbing gravitational potential of earth expanded with Taylor series along earth relief levels 23 p3996 A67-40859

Gravity gradiometer digital computer program for simulated rotating gravitational mass sensor and gradient contour mapping 23 p4000 A67-41218

GRAVITATIONAL RADIATION

Sign and value of plane gravitational wave energy as function of reference point and wave structure 02 p0268 A67-12417

Nonzonal harmonics of earth gravitational field determined by satellites 05 p0797 A67-16572

Existence of gravitational waves, analyzing feasibility of experimental verification 09 p1531 A67-21653

Calculation of gravitational radiation from pulsating and rotating objects according to weak field limit formula of general relativity and applied to neutron star data 09 p1562 A67-22227

Gravitational radiation measurements by HF gravitational wave detector 10 p1652 A67-23545

Energy variation of two-body system due to gravitational radiation studied within framework of Minkowski theory 12 p1966 A67-25145

Maximum gravitational radiation detection range for binary stellar system analyzed by mechanically resonant antennas 15 p2563 A67-30162

Exact solutions for pure total radiation state, constructing singular electromagnetic fields 17 p2884 A67-32703

LF gravitational waves radiated by electromagnetic field of moving bodies, discussing measurement problems 18 p3117 A67-33527

Nature of gravity, discussing universal radiation of gravitation quanta, gravity velocity determination, effects on earth formation, etc 18 p3077 A67-33549

Gravitation wave radiation rate from binary stars, using Brans-Dicke general

relativity theory 21 p3706 A67-38842

GRAVITY

S ANTIGRAVITY

S ARTIFICIAL GRAVITY

S HIGH GRAVITY ENVIRONMENT

S LUNAR GRAVITATION

S PLANETARY GRAVITATION

S SUBGRAVITY

GRAVITY CENTER

Lapunov stability of gyroscope motion, with Cardan suspension center moving over earth surface 03 p0424 A67-14179

Measurement of dimensions and inertial properties of 50th percentile anthropometric dummy 08 p1289 A67-20611

Lunar rotation about center of gravity, optical libration and physical libration in selenocentric coordinates 08 p1395 A67-21157

Pitching effect on aircraft gravity center during passage through gust, noting autopilot effect on tail assembly 09 p1440 A67-22473

Center of gravity in aircraft design and effects on performance 09 p1441 A67-22670

Location of center of gravity of sensitive element of pendulum effect on stable equilibrium positions of gyrocompass in geographically oriented coordinate system 13 p2118 A67-26349

Closed loop simulation of movement of center of gravity and optimum guidance laws for space vehicles by analog computer techniques 16 p2700 A67-30662

Gravitational stabilization of satellites with respect to orbital system of coordinates 16 p2760 A67-30740

Theodolite device for measuring coordinates of center of gravity of photographed missile in flight 16 p2674 A67-31120

Disk structural characteristics influence on rotors critical angular velocity 19 p3235 A67-34881

Solar magnetic fields studied by measuring Fraunhofer line shifts with circular-polarization analyzer, showing relationship to gravity center 19 p3325 A67-35505

Unsteady spherically symmetric gas flows with gas particle radial velocity proportional to distance from symmetry center 22 p3739 A67-39216

GRAVITY GRADIENT SATELLITE

SA DODGE SATELLITE

Gaposhkin satellite gravity results compared with surface gravimetry data 01 p0056 A67-10041

Flywheel-augmented gravity gradient stabilization /FLAGGS/ 02 p0333 A67-12312

Flight experience of earth-orbiting gravity gradient stabilization systems 02 p0334 A67-12362

Stability of planar librations of dumbbell gravity gradient satellite in elliptic orbit 05 p0901 A67-17104

Requirements for gravity gradient stabilization of medium and synchronous altitude communication satellite systems using zero gain antennas, noting stabilization accuracy, stationkeeping effects, etc 06 p1094 A67-17680

Structural and librational dynamics of satellite deploying flexible booms or antennas [AIAA PAPER 67-43] 06 p1095 A67-18264

Canonical transformation to investigate rotational motion of uniaxial orbiting rigid body influenced by gravity gradient torque [AIAA PAPER 67-125] 06 p1084 A67-18288

Passive attitude control using gravity torques, solar torques and spin stabilization 08 p1410 A67-20622

Motion and stability of spinning spring-mass system in orbital plane with equation linearization 10 p1710 A67-23752

Vertical vee gyro damping system for gravity gradient satellite, considering scaling, inertia, time and torque factors and viscosity change effects 12 p1920 A67-25122

Gravity-gradient oriented satellite stabilization by means of solar pressure torques on adjustable slats 14 p2395 A67-29051

Earth-pointing satellite attitude control system using gravity gradient stabilization, deriving motion equations 15 p2564 A67-29329

Gravity gradient stabilization systems for orientation of spacecraft and for damping of associated librations 16 p2758 A67-30663

Nonlinear resonance effect on attitude librations of undamped rigid gravity gradient

stabilized satellite in circular Earth orbit 16 p2745 A67-30741

Material elasticity effects on planar librational motion of rigid satellite under action of gravity 16 p2761 A67-30743

Active damping concept for gravity gradient satellite attitude control to reduce oscillation time constant, initial capture time and oscillation magnitude 17 p2954 A67-32073

DODGE TV system for evaluating attitude control system in gravity gradient stabilization at synchronous altitude 20 p3452 A67-37571

Gravity gradient stabilization experiments using DODGE satellite at synchronous orbit 21 p3714 A67-39149

Gravity oriented satellite coupled librational motion in circular orbit analyzed for motion stability by numerical methods 24 p4231 A67-42384

Attitude errors of inertially coupled gravity gradient satellite with solar radiation pressure as dominant disturbance, noting slot problems in stabilized package accommodating damper motion 24 p4241 A67-42904

GRAVITY WAVE

Internal gravity-shear waves in troposphere for two- and three-layer model of air density and horizontal velocity, noting phase velocities 02 p0238 A67-12190

Amplitude of perturbations about each interface in internal gravity-shear waves in troposphere according to three-layer model 02 p0239 A67-12191

Perturbation of vertical smoke trails and smoke puffs in lower troposphere explained by internal gravity-shear waves 02 p0239 A67-12192

Solitary waves in compressible atmosphere with arbitrary wind and density profiles, obtaining solution for critical speed by perturbation scheme 03 p0463 A67-14032

Power spectrum of horizontal components of clear air turbulence in upper troposphere, examining influence of degenerating gravity waves on nature of turbulence spectra 05 p0837 A67-16486

Radiation and scattering of transient gravity waves by thin vertical plates in deep ocean 06 p0985 A67-18188

Electron concentration inhomogeneities during traveling gravity wave propagation through F layer 07 p1178 A67-19809

Rocket measurements of small scale structure of ionization profile and wind speed fluctuations, propagation of gravity shock waves and stratification in upper atmosphere 08 p1325 A67-20986

Linearized perturbation equations integrated for cosmological model, giving energy density fluctuations, rotational perturbations, gravity waves and estimated anisotropy of microwave radiation 08 p1398 A67-21233

LF gravitational-acoustic and internal gravity mode wave propagation in temperature-stratified photosphere-low chromosphere region and solar atmospheric resonant responses 08 p1399 A67-21236

Removal of incident wave spectrum by background wind shears during atmospheric gravity waves propagation to ionosphere from lower regions 08 p1328 A67-21477

Generation of oscillations in solar atmosphere by separate granules modeled by bottom zone of isothermal gravitating photospheric layer overlaid by hot corona 10 p1704 A67-22721

Ionospheric thermal conductivity effect on gravitational wave propagation 10 p1631 A67-22803

Atmospheric tides, shorter period gravity waves and shear waves 10 p1643 A67-23249

F layer critical frequency perturbations due to low altitude nuclear explosion 13 p2107 A67-26309

Power spectrum of horizontal components of clear air turbulence in upper troposphere, examining influence of degenerating gravity waves on nature of turbulence spectra 13 p2150 A67-26342

Gravitational wave propagation from upper to lower atmospheric layers analyzed taking into account reflection and refraction 13 p2112 A67-26673

Model thermospheres, studying ducted traveling acoustic gravity waves originating in ionosphere 14 p2310 A67-28054

Ionospheric E region dynamical processes,

- discussing energy phenomena of planetary waves, tidal oscillations and gravity waves 14 p2311 A67-28408
- Sensor and calibration techniques for measurement of infrasonic and gravity waves noting error control and possible applications 16 p2677 A67-31430
- Turbulence in upper atmosphere possibly due to density fluctuations accompanying internal gravity waves 17 p2843 A67-32538
- LF gravitational waves radiated by electromagnetic field of moving bodies, discussing measurement problems 18 p3117 A67-33527
- Gravitational waves, calculating velocity of propagation using perturbation method 19 p3262 A67-35708
- Traveling-ionospheric disturbances observed at midlatitudes by backscattering technique, noting auroral zone and gravity waves role 20 p3425 A67-36280
- Upper atmospheric dynamics, considering day-night density and pressure variation, wind structure, gravity waves, etc 20 p3429 A67-36896
- Gravitational radio wave frequency shift from satellite measurements, noting satellite-ground radio communication system 20 p3386 A67-37524
- Propagation rate of electromagnetic and gravity wave front in synchronous reference system in Riemann space 20 p3486 A67-37554
- Ducted acoustic gravity wave propagation in isothermal atmosphere, obtaining dispersion relations ducted modes and surface wave in incompressible medium 21 p3623 A67-39057
- Long period surface gravity waves in atmosphere 22 p3792 A67-39974
- Rapid temperature increase due to lower photosphere turbulence generation of mechanical waves, discussing gravity wave generation and acoustic noise 23 p4068 A67-41280
- Ionospheric thermal conductivity effect on gravitational wave propagation 24 p4150 A67-42140
- RAY GAS**
- SA NONGRAY ATMOSPHERE**
- Entropy defect and source function in ray atmosphere thermodynamics 03 p0537 A67-14314
- Inviscid hypersonic flow of radiating gray gas over sphere analyzed, noting temperature role in process 08 p1276 A67-20567
- Unsteady energy transfer in gray radiating gas during expansion at atmospheric pressure for arbitrary optical radius 08 p1323 A67-21391
- Rayleigh problem of compressible viscous heat-conducting radiating gray gas flow near flat plate set impulsively in motion in own plane 08 p1324 A67-21392
- Asymptotic analysis of radiative Rayleigh problem in flow of compressible viscous heat-conducting radiating gray gas extended to high plate Mach numbers 11 p1774 A67-23855
- Radiative energy transfer through nongray medium bounded by two flat surfaces, obtaining temperature distribution and heat flux values 15 p2578 A67-29130
- Structure of strong shock wave studied for simple models of nongray radiative transfer 16 p2658 A67-30938
- Interaction of convection and radiation heat transfer in axisymmetric two-dimensional stagnation point low-speed flow of gray absorbing and emitting gas 16 p2591 A67-30939
- Role of Rosseland approximation in convection-radiation interaction, considering flow of gray gas in laminar boundary layer [ASME PAPER 87-HT-9] 20 p3545 A67-36707
- Gas local thermodynamic equilibrium effect on calculated thermal radiation emission [ASME PAPER 87-HT-51] 20 p3548 A67-36733
- Viscous dissipation effect on heat transfer rates for laminar boundary layer flow of gray gas across flat plate 21 p3732 A67-38878
- Radiative heat loss effect on steady axisymmetric hypersonic flow past blunt body using gray gas approximation, with numerical solution for stagnation region 22 p3739 A67-39530
- Laminar free convection of absorbing emitting gas analyzed in region of stagnation point of horizontal cylinder 22 p3920 A67-40418
- Radiative heat transfer in radiating and conducting media, calculating heat flux and temperature distribution for semisotropic model 23 p4083 A67-41718
- Integral equation derived from Boltzmann equation for one-dimensional radiative heat transfer in plane layers of gray media 24 p4252 A67-41934
- Zonal method of determining radiative heat transfer between gray particle cloud and surrounding gray walls of enclosing system 24 p4253 A67-42252
- GREASE**
- Grease lubricants for aerospace application, determining physical properties and testing them at 400 degrees F and under high vacuum [ASLE PAPER 86AM 3C2] 09 p1506 A67-22421
- Wear lifetimes for three greases thickened with submicron boron nitride powder [ASLE PREPRINT 87AM 2C-2] 14 p2325 A67-28785
- Soap and nonsoap base greases physical and chemical nature, composition, characteristics and additives 20 p3455 A67-37265
- GREAT BRITAIN**
- Aeronautical research in U.K. by government establishments, industry and universities 03 p0362 A67-14381
- UK space projects detailing Skylark, Blue Streak, Black Knight and Black Arrow rockets 05 p0905 A67-16727
- Flight simulator acceptance and role in pilot training and checking in UK 13 p2064 A67-27272
- Cambridge /England/ one-mile radiotelescope for study of extragalactic radio sources, discussing two-dimensional antenna synthesis method 15 p2467 A67-30027
- British air transportation, discussing 1946 Bermuda Pact, government control and role of private enterprise 17 p2974 A67-32124
- United Kingdom space research activities since May 1966, noting facilities, ground-based studies and rocket and satellite tracking experiments 19 p3322 A67-35306
- Structure and decomposition of Goose Lake meteorite and fragments 19 p3323 A67-35424
- UK contribution to IQSY in meteorology, geomagnetism, airglow observations, etc 19 p3223 A67-35476
- Daily magnetic variations over England, noting difference between values obtained for summer IQD and other days of year 20 p3429 A67-36870
- Cost comparisons between UK aircraft industry and competing industries elsewhere 22 p3922 A67-40065
- GREB 5 SATELLITE**
- Solar X-ray events observed by 1964-1-D satellite launched by U.S. Naval Research Laboratory in 1964 12 p1999 A67-25836
- GREEN FUNCTION**
- Green function method applied to calculating resonance absorption of electromagnetic radiation for interlevel transitions in thin film 01 p0127 A67-10072
- Maxwell-Green tensor relating forces to displacements in structural elastic beam, showing role of Maxwell influence coefficient 02 p0336 A67-11482
- Shallow impurity states in semiconductor described by Green function method, considering effective-mass equation corrections 02 p0281 A67-11491
- Random phase approximation for plasma, establishing perturbed electron distribution in oscillating electric field 02 p0276 A67-12557
- Existence of Green function and invariability of sign in some boundary value problems for equation y super n equals $g/t/y$ 02 p0260 A67-12739
- Subcritical and nonoscillation intervals for Chaplygin theorem evaluated, using Green and Cauchy functions 03 p0456 A67-13112
- Existence conditions for Green function of boundary value problem, determining and estimating subcritical intervals 03 p0457 A67-13114
- Green function derived for heat conduction along straight line with boundaries in steady motion 04 p0726 A67-15595
- Optimum processes in systems with distributed parameters described by partial differential equations 04 p0647 A67-15874
- Estimates of Green function in first boundary value problem of thermoconductivity equation for cylinder 05 p0927 A67-17002
- Magnetic field effect on static shielding of point charge calculated, using Green function of inverse dielectric function of electron gas plasma 06 p1071 A67-18989
- Coupled Green function equations for Helsenberg ferromagnet approximated via differential equations 07 p1237 A67-20141
- Energy factors of infinite straight dislocations and stresses of piecewise straight dislocation configurations expressed through Green functions of elasticity 08 p1418 A67-20798
- Series solution for average wave field in medium with random inhomogeneities by using Green function for wave equation 08 p1294 A67-20814
- Time dependent Green function for electromagnetic radiation in moving simple media 08 p1296 A67-21430
- Solutions for field aligned flow past magnetic source using Green function, estimating energy dissipation rate 09 p1549 A67-22399
- Stokes flow for sphere in arbitrary external flow pattern solved using Green function, showing uniqueness solution 10 p1629 A67-23831
- Isolated force solution as Green function for formulation of plane problems for cracks along interface of two bonded half-spaces 10 p1731 A67-23848
- Ray solution for point source in medium with varying propagation constant determined, using Green function for scalar wave equation 11 p1751 A67-23969
- Existence and preservation of algebraic sign in Green function for two-point boundary value problem 11 p1813 A67-24519
- Green integrals extended to movement of incompressible viscous conductive fluid in which magnetic field is generated 11 p1840 A67-24620
- Green matrix estimates for homogeneous parabolic boundary value problems, showing proof of integral operator 11 p1813 A67-24850
- Green function theory of nonlinear transport coefficients 12 p1967 A67-25846
- Classical representation of Green-Lebesgue type integral harmonic function in case of unit sphere 12 p1962 A67-26101
- Steady state wave propagation in homogeneous anisotropic media studied from near field behavior of Green matrix 13 p2158 A67-27179
- Radiation field of monopole antenna hinged on spherical conducting support calculated with Green function technique 13 p2081 A67-27200
- Electrodynamic equations for pure and doped two-band superconductors, studying upper critical magnetic field 13 p2184 A67-27630
- Electromagnetic properties of impure anisotropic strong-coupling superconductors, using Green function to obtain response, current density and Josephson tunneling current 14 p2371 A67-28724
- Density of states of pure type II superconductors in high magnetic fields, deriving approximate expression for Green function 15 p2533 A67-29089
- Nonrelativistic approximation for electromagnetic radiation in conducting medium moving with uniform velocity with respect to source 15 p2521 A67-29194
- Time-dependent Green function for moving isotropic nondispersive medium 15 p2509 A67-29199
- Boundary value problems of continuous dislocation theory reduced to elasticity theory, deriving Green formula for internal stresses 15 p2572 A67-29235
- Localized defects in semiconductors, using solid state scattering theory to calculate energies of bound states 15 p2534 A67-29325
- Quasi-isomorphic response of perturbed systems for slow coefficient variation of matrix system differential equation 15 p2512 A67-30050
- Arc operation under nonsteady electrical inputs noting initial conditions, energy equation solution, temperature profiles, application of Green function for moving boundary problem, etc [AIAA PAPER 86-480] 15 p2531 A67-30204
- Second order conductivity tensor of isotropic electron gas theory, using thermodynamic Green

functions 16 p2713 A67-30803
 I-V curve related to state densities on both sides of n-p junction of tunneling system 16 p2725 A67-30808
 Fabry-Perot resonator excitation using integral equations corresponding to boundary value functions 17 p2868 A67-32667
 Hydrodynamic approximation of Green function for superfluid Bose system 18 p3029 A67-34386
 Plane elastic strip with stress-free edges concept studied, noting mechanical coherence for elasticity and bending, expressing results by meromorphic function 19 p3340 A67-35450
 Inhomogeneous elastic medium with nonlocal interaction, considering case of point defects and obtaining Green tensor 20 p3540 A67-37056
 Green function for SH-line source in wedge-shaped medium with apex removed by circular cylinder, determining reflected and refracted fields 21 p3579 A67-37925
 Superconducting critical temperature below Kondo temperature for metal solutions with magnetic impurities calculated, using Green function 21 p3680 A67-38350
 Displacements and temperature accompanying deformation in unbounded thermoelastic medium determined for concentrated force and heat source, using Green functions 21 p3723 A67-38559
 Electrodynamics equations for pure and doped two-band superconductors, studying upper critical magnetic field 21 p3685 A67-38826
 Static Green function for elastic electron scattering by hydrogen atoms, using integrodifferential equations to determine resonance energies 22 p3839 A67-39204
 Anderson model Hamiltonian exchange character application to conduction electron Green function determination 22 p3861 A67-39994
 Mathematical model for vibrating characteristics of structures in statistical mechanics framework, noting closeness to Green function rather than to mode concept [ONERA-TP-467] 22 p3915 A67-40385
 Quantum damping theory formulated in coherent state representation, giving Green function solution to damped harmonic oscillator Fokker-Planck equation, noting density operator 22 p3617 A67-40486
 Coupled linearized equations for laser-induced optical radiation instabilities in liquids and gases, obtaining differential operator and Green function 23 p4027 A67-41024
 Cross correlated photons of laser used to determine correlation functions by applying thermodynamic Green function 24 p4168 A67-42594

GREEN THEOREM
 Optimality of totally singular vector controls governing dynamical systems and extension of Green theory approach to higher dimensions to evaluate optimality of such controls 04 p0594 A67-15875
 Boundary value problem for potentials in volume conductor based on Green theorem 08 p1288 A67-20601
 Quasi-static potential distribution in inhomogeneous volume conductor analyzed using Green theorem 11 p1746 A67-23991
 Two-dimensional flow through bends with turning vanes, using Green theorem to obtain surface pressure distributions [ASME PAPER 67-FE-13] 14 p2304 A67-28362

GREENHOUSE EFFECT
 Nongray model atmospheres of Jovian planets constructed for different relative concentrations of helium and diatomic hydrogen and various likely effective temperatures as chief sources of thermal opacity 09 p1567 A67-22237
 Greenhouse effect in semiminfinite scattering atmospheres, describing steady state distribution of thermal radiation 09 p1567 A67-22238
 Radiant energy transfer below cloud cover in Venus atmosphere, noting greenhouse effect caused by atmosphere containing components capable of IR absorption 14 p2383 A67-27859
 Venus surface temperature and microwave emission, discussing ionospheric model, greenhouse effect, microdischarge model, radio aurora, etc 18 p3135 A67-34543

GREENWICH MEAN TIME S UNIVERSAL TIME

GRENADE
 Atmospheric temperature and wind velocity in mesosphere measured by rocket grenade method 05 p0798 A67-16857

GRID
 SA GRATING
 SA MATRIX
 SA WIRE GRID LENS
 Equivalency coefficient dependence on angle of attack, Mach number and angle of incidence for subsonic and supersonic gas flow past plate grid 03 p0353 A67-14082
 Optimum gridline spacing for photovoltaic cells operating at high solar fluxes, noting maximum power point efficiency dependence on cell and geometric parameters and solar flux level [ASME PAPER 66-WA/SOL-1] 04 p0555 A67-15381
 Penetration factor along grid of plane triode calculated from nomograms 05 p0774 A67-16937
 Multielement antenna scanning grid-phasing method having random function distribution at aperture 05 p0776 A67-17159
 Relation between effective porosity and differential pressure of rigid steel and elastic nylon ribbon grids of various forms and porosities 06 p0944 A67-17630
 Distribution function of modulus of directivity characteristic of antenna grid shown as modified Rayleigh distribution 07 p1143 A67-19596
 Fibrous model of shell shaped grid noting discrete network, properties of cross section surface and stress 10 p1715 A67-22920
 Travel-time effects on quasi-steady state operation characteristics occurring from electron optical characteristics of two-grid-controlled photomultiplier 14 p2277 A67-27769
 Chondritic meteorites two-dimensional classification grid based on chemical and petrologic subdivisions 14 p2391 A67-28949
 Computer program for solution of large deflection nonlinear problems of elastic flat plates using grid analogy 14 p2403 A67-29015
 Grid probe analysis of alkaline plasma, determining density, potential and energy distribution function 15 p2527 A67-29476
 Optimum grid line spacing for photovoltaic cells operating at high solar fluxes, noting maximum power point efficiency dependence on cell and geometric parameters and solar flux level [ASME PAPER 66-WA/SOL-1] 18 p2989 A67-34129
 Grid geometry effect on longitudinal and lateral turbulence intensities, determining decay rate dependence 18 p3030 A67-34740
 Distribution function of modulus of directivity characteristic of antenna grid shown as modified Rayleigh distribution 20 p3384 A67-37335
 Conventional and composite grid designs tested with low voltage Kaufman thruster [AIAA PAPER 67-680] 21 p3692 A67-38711
 TV camera reseau for engineering information on planetary missions and reducing geometric distortion [SMPT PAPER 102-39] 22 p3808 A67-40377

GRIFFITH FRACTURE THEORY
 Griffith energy criterion and stress-strain environmental criterion for fractures in brittle cracked metallic plate 03 p0523 A67-13467
 Three-dimensional stress distribution around elliptical crack under arbitrary shear loading, discussing Griffith-Irwin fracture theory [ASME PAPER 66-APM-N] 04 p0718 A67-15926
 Axisymmetric crack formation problem in elastoplastic material including energy dissipation and face displacement calculations, noting agreement with Griffith theory 10 p1716 A67-22939
 Agreement of crack extension criteria of Griffith and Barenblatt, considering cohesive forces 15 p2504 A67-30093
 Fracture mechanics energy balance analysis using Griffith type fracture criterion 16 p2770 A67-31289
 Griffith initiation criterion extended to fracture initiation and growth in viscoelastic materials using energy formulation 16 p2773 A67-31311
 Crack propagation in solid undergoing cyclic loading using Griffith model, stressing work hardening effect 22 p3911 A67-39680

GRINDING

Integrodifferential equations for product surface area changes and grinding process development obtained by assuming proportionality between fracturing probability and particle size 19 p3236 A67-35725
 Beryllium part fabrication by metal removal, discussing machining and surface treatment methods [SAE PAPER 670803] 24 p4159 A67-41990

GRINDING MACHINE
 Adhesive qualities of lunar soil simulated by rock comminuted in ultrahigh vacuum 24 p4227 A67-42034

GROOVE
 Thermal emittance and reflectance of diffuse-bottomed specular-walled groove in solar radiant-flux environment [AIAA PAPER 66-459] 02 p0342 A67-11939
 Room temperature measurements determining mean slope and peak-to-valley height influences on bidirectional spectral reflectance of V-grooved surfaces 03 p0426 A67-14398
 Groove geometry effect on performance viscoelastic with sealed water in laminar and turbulent conditions [ASME PAPER 66-WA/FE-28] 04 p0630 A67-15356
 Side grooving effect on measurements of plane strain fracture toughness 05 p0922 A67-17086
 Book on spiral groove thrust bearings calculation, use and transmitting force in direction of axis of rotation 06 p1007 A67-17893
 Emissivity and absorptivity of infinite length isothermal trapezoidal grooves with radiating gray walls 18 p3159 A67-34055
 Groove geometry effect on performance viscoelastic with sealed water in laminar and turbulent conditions [ASME PAPER 66-WA/FE-28] 24 p4161 A67-42466

GROUND
 S EARTH

GROUND-AIR-GROUND COMMUNICATION
 Satellite relay techniques providing paths for aircraft-ground communication over ocean used in ATC, noting repeater electronics 01 p0021 A67-10207
 Ground-Air-Ground /G/A/G/ communication channels analyzed in air traffic control 02 p0263 A67-12125
 Transoceanic aircraft control and communication via satellite 09 p1466 A67-22641
 Satellite relay to provide communication paths for aircraft-ground communication over ocean, considering system design for ATC using reflex repeater 16 p2629 A67-31530
 Statistical analysis of observed relationship between independent air traffic and resultant communication channel loading parameters 17 p2810 A67-32110
 Continuous wave laser ground-space-ground experiment in conjunction with Explorer XXII satellite tracking 21 p3578 A67-37858
 Design studies for reliable long range ground-to-air communication, noting line of sight propagation and HF propagation not involving ionospheric reflections 23 p3972 A67-40742

GROUND CONTROL
 Ground-based steerable paraboloid spherical reflector and multiplate type antennas, noting cost per unit area for unit wind speed of 30 mph and frequency of 1400 mc, performance, restrictions, etc [AIAA PAPER 66-324] 06 p0967 A67-17685
 All-digital real time display system for ground monitoring of manned space flight including computers, software, output devices, etc 09 p1483 A67-21677
 Laser radar selenodesy for ground control selection of Apollo landing sites 16 p2623 A67-30982
 Jindivik Mk 103A jet propelled target drone ground and flight control systems stressing climb, cruise, approach and descent commands 21 p3570 A67-39131

GROUND CREW
 Aircraft technician training levels, methods and equipment analysis indicating need for specialty training equipment development 13 p2091 A67-27266
 SST ground and flight personnel training program for system operation, discussing

- expected role of piloted flight simulator 13 p2091 A67-27270
- GROUND EFFECT**
- SA DOWNWASH
- SA LIFT
- SA WAKE
- Induced drag for idealized ground effect wing for optimum lift distribution 01 p0006 A67-10809
- Ground surface erosion due to rocket breaking, calculating flow-induced force parameters 01 p0156 A67-11434
- Flight test method for evaluating ground effect on fixed-wing aircraft in which pilot flies at constant angle of attack and power setting during landing approach [AIAA PAPER 66-468] 02 p0180 A67-11513
- Oscillatory ground wind response of Atlas/Agema examined, using statistical theory of extreme values 06 p1104 A67-18492
- Wind tunnel investigation of effect of ground level on static aerodynamic characteristics of sideslip for rectangular and delta wing with rudder assembly 07 p1126 A67-19886
- Test platform isolated from random long period ground tilts used in calibration of gyroscopes, accelerometers, etc 08 p1314 A67-20580
- Isolated compressor blade within framework of lifting line theory, expressing drag produced by tip-gap in terms of flow rate and wing loading 09 p1437 A67-21739
- Flight test method for evaluating ground effect on fixed-wing aircraft in which pilot flies at constant angle of attack and power setting during landing approach [AIAA PAPER 66-468] 09 p1441 A67-22486
- Ground effect of static circular peripheral jet, comparing derived relations between jet flow, base pressure and hover height with experimental model results 15 p2415 A67-29262
- Flow pattern of thin jet-flapped wing with small deflection angle in proximity to ground 15 p2415 A67-29308
- Thrust augmentation ratio for hovercraft, lift ratio obtained by annular jets of same mass flow and total energy in ground effect and free flight conditions 15 p2419 A67-29674
- Aerodynamic suckdown results obtained in investigation of VTOL ground-proximity effects 17 p2791 A67-32588
- Radiation pattern of linear antenna erected over tapered ground screen, noting system surface impedance variation 22 p3760 A67-39628
- Hatfield V/STOL tunnel design problems and tunnel model test results 22 p3780 A67-40063
- Ground proximity effect on aerodynamic characteristics of slender wings by extension of slender body theory, solving potential function equation 23 p3930 A67-41310
- GROUND EFFECT MACHINE**
- SA AIR CUSHION VEHICLE
- SA FLYING PLATFORM
- Wind tunnel testing of ground effect machine, examining geometric dependence of aerodynamic characteristics, lift due to interference and peripheral jet, pressure increases, etc 02 p0180 A67-11534
- Air cushion vehicle design, calculating annular nozzle, air channel optimum parameters, power capacity, aerodynamic characteristics, etc 02 p0179 A67-12437
- Bertin type air cushion vehicles, examining power supply and refinements required for over-water application 03 p0358 A67-12977
- Lift augmentation parameters in peripheral jets in proximity of ground, namely jet thickness, height from ground and jet curtain inclination [ASME PAPER 66-APM-R] 04 p0550 A67-15910
- Noise and loading actions on helicopters, V/STOL aircraft and ground effect machines - Symposium, University of Southampton, August-September 1965 06 p0945 A67-17905
- Hovercraft noise problem compared with surface transport, noting siting of terminals and noise reduction 06 p0946 A67-17915
- Hovercraft and rotorcraft, discussing design, construction, operation and future 06 p0949 A67-18744
- Peripheral jet behavior in hovercraft described via modified mixing theory 06 p0991 A67-18752
- Air cushion vehicles propulsion noting various methods including air or water jets, air propellers, ducted air propellers, etc 07 p1128 A67-19535
- Two-dimensional jet plane problem, considering rheological solution for applications to ground effect machines 11 p1781 A67-24571
- Ground effect machine development, with table of models and specifications and photographs and drawings of configurations 11 p1744 A67-24705
- SR-N4 hovercraft, optimum size for coastal waters, structural features, performance, control, etc 12 p1895 A67-26168
- Propulsion systems for air cushion craft SKIP-I in marine environment [AIAA PAPER 66-731A] 13 p2054 A67-27593
- Captured air bubble /CAB/ vehicle [AIAA PAPER 67-348] 14 p2246 A67-28730
- Design principles for air-cushion vehicles, noting possible application to aircraft landing gear [ASME PAPER 67-DE-61] 14 p2246 A67-28884
- Thrust augmentation ratio for hovercraft, lift ratio obtained by annular jets of same mass flow and total energy in ground effect and free flight conditions 15 p2419 A67-29674
- Amplification factor of air-cushion vehicles and its physical significance for bell-and peripheral-jet concepts 16 p2596 A67-31444
- Circular planform peripheral jet ground effect machine heaving motion analyzed using motion equations 19 p3172 A67-34867
- Hovercraft principle application noting development, sea-keeping problems, predicted capability and costs 22 p3745 A67-39663
- Peripheral jet air cushion vehicle circular platform design, discussing dimensionless design parameter determination from operating height, translational speed and weight 22 p3745 A67-39726
- Peripheral jet GEM pitching characteristics analysis by longitudinal static stability and dynamic pitching motion 22 p3745 A67-39837
- Steady tunnel operation effects on tracked hovercraft air cushion performance, discussing tunnel entrance problems 22 p3746 A67-40067
- Hovercraft research noting internal and external aerodynamics, test techniques and instrumentation requirements 23 p3934 A67-41167
- Aerodynamic requirements for hovercraft and radial flow fans by adapting blade loading criteria for axial compressors 23 p3931 A67-41331
- GROUND HANDLING**
- Transportation and handling of large solid rocket motors, considering program management aspects [SAE PAPER 660707] 01 p0169 A67-10623
- Air cargo transport from 1960 to 1970, discussing new methods of traffic promotion [AIAA PAPER 66-1018] 03 p0361 A67-14024
- Hydraulic design of Japan YS-11 twin turboprop transport aircraft, noting component accessibility and ground service simplification 19 p3175 A67-34787
- Fokker F-28 aircraft features for minimum turnaround time, noting self-sufficiency provided by auxiliary power unit 19 p3173 A67-35558
- Ground requirements for instrument landing systems noting approach lighting, runway marking, taxi guidance and blind navigation [AIAA PAPER 67-756] 23 p3933 A67-40989
- GROUND HANDLING FACILITY**
- Facilities, ground handling and transport equipment for Titan III ITL system [SAE PAPER 660706] 01 p0050 A67-10599
- Voice communications and control facilities at mission control center in Houston for support of manned space program conducted by NASA 02 p0229 A67-12120
- Communications systems at Kennedy Space Center /KSC/ and future prospects 02 p0230 A67-12121
- UK-3 satellite electrical design and ground checkout equipment 09 p1484 A67-21828
- Airport requirements for Boeing model 747, including description of necessary modification of terminal facilities and ground equipment [AIAA PAPER 67-384] 15 p2468 A67-30353
- Aircraft flotation requirements, emphasizing surface strength 17 p2832 A67-31986
- Boeing SST maintenance requirements considered in terms of aircraft characteristics, economics, facilities, operations, etc [SAE PAPER 670373] 17 p2798 A67-33003
- Large scale liquefaction, storage, transport and ground handling of liquid helium for applications in space operations 22 p3781 A67-40393
- Clean room justification guidelines including contracts, proposals, work loads, environmental requirements, equipment and personnel selection 23 p3987 A67-40855
- GROUND OPERATIONAL SUPPORT SYSTEM /GOSS/**
- Voice communications and control facilities at mission control center in Houston for support of manned space program conducted by NASA 02 p0229 A67-12120
- GROUND RESONANCE**
- Ground resonance of helicopters with zero transverse flexibility analyzed 03 p0360 A67-13393
- GROUND SPEED**
- S AIR SPEED
- S VELOCITY
- GROUND STATE**
- Einstein A coefficient for lambda doublet transitions of ground state of OH 01 p0114 A67-10898
- Absolute direct excitation cross section from neutral ground state for upper levels of transition in argon laser 02 p0253 A67-12520
- Adiabatic harmonic unitary transformations and relation between electron trapping energy and normal lattice modes associated with F center ground state 03 p0495 A67-13515
- Different-orbitals-for-different-spins wave function for singlet S ground state of He expressed in Shull and Loewdin basis orbitals 03 p0473 A67-13522
- Spin relaxation times of ground state of atomic cesium in aromatic gases measured using optical pumping, noting dependency on temperature 04 p0660 A67-14611
- Molecular nitrogen and oxygen properties, calculating Hartree-Fock value for energy in ground state 04 p0660 A67-14693
- Magnetic field gradient relaxation mechanism by random excitation of transitions in F equals 1 level of ground state of hydrogen atoms in maser 05 p0817 A67-16635
- Ground state energies of P, As and Sb donors in Si taking account of dielectric screening of donor potential 06 p1061 A67-18925
- Gamma decay of Se 73 and Se 81 isomeric pairs with half-lives, energies and decay schemes 11 p1822 A67-23980
- Radio astronomical investigations of 18 cm ground state lambda doublet transition of OH suggest maser amplification of radiation takes place in interstellar medium 13 p2198 A67-26715
- Electronic absorption spectrum observed during cyanogen azide flash photolysis 13 p2177 A67-26988
- Electron spin resonance measurement of ground state population in ruby rod during optical pumping 15 p2497 A67-29389
- He-He ground state and first excited state potentials obtained from differential scattering cross sections 17 p2889 A67-33257
- Short range intermolecular interaction of two ground state hydrogen molecules, using rigorous valence bond approach and population analysis 17 p2890 A67-33262
- Ground-state splitting in semiconductor double acceptors 18 p3099 A67-33699
- Spectrum of bound and quasi-bound states of hydrogen-hydrogen scattering and resonance, using Schroedinger equation 18 p3084 A67-34523
- Hyperfine structure of ground state of helium 3 microwave transition radiation from galactic H II regions 19 p3330 A67-36074
- Absorption lines in quasi-stellar source analysis to obtain estimates of either particle density in absorbing region or distance between continuum source and absorber 19 p3330 A67-36082
- Calculation of vibration level populations of polyatomic molecules in electronic ground state 20 p3457 A67-36216
- Ground state hyperfine splitting of singly charged helium calculations by Zwanziger and Sternheim evaluated by examining error

- corrections by Fortson et al 20 p3488 A67-36694
- Intermolecular hydrogen bonds energies estimated for organic semiconductors in ground and first excited states 20 p3512 A67-37301
- Variational approximation for ground state of perturbed Schroedinger equation with single variable wave function 20 p3479 A67-37600
- Ground state and four lowest optically excited states of shallow donor in Si calculated using isotropic effective mass 22 p3854 A67-39245
- Liquid He 4 ground state studied by variation method, deriving radial distribution function 22 p3835 A67-39301
- Interaction of two H atoms in ground states using Hirschfelder-Linnet wave function and Gaussian type 22 p3756 A67-39385
- Conduction electron ground state and anomalous magnetic moment in antiferromagnetic semiconductor, considering magnetic polaron 22 p3857 A67-39462
- Divalent Eu ion ground state splitting in C3h symmetry sites and associated color centers in EPR spectrum study of Eu ion doped lanthanum trichloride 22 p3863 A67-40003
- Empirical formula for representation of cross sections for single ionization of atoms and ions from ground state by electron impact 24 p4194 A67-41890
- ### GROUND STATION
- #### SA TRACKING STATION
- Ground signal station tasks and problems, examining Early Bird satellite and Raisting station in Germany 01 p0023 A67-10453
- Ground station receiver for satellite communication which utilizes liquid-helium-cooled parametric amplifier at top producing extremely low noise temperature 01 p0023 A67-10469
- Digital computer controlled telemetry ground station, examining six subsystems 02 p0229 A67-12002
- Data quality assurance program for telemetry ground station operations, noting frequency division and time division formats 02 p0198 A67-12023
- Hyperbolic space localization system measuring three distance differences from four ground stations 02 p0264 A67-12354
- Meteorological satellites ESSA II and Nimbus II and British ground facilities for receiving cloud cover pictures 03 p0424 A67-13913
- Ground station for space communications and radar and radio physics, noting use of Cassegrain antenna computer guided pointing control, plug-in equipment box, etc 04 p0596 A67-15047
- Satellite ground terminal design considerations using adaptive digital communications techniques, noting analog to digital conversion 06 p0960 A67-17675
- Minimum cost ground receiving station for synchronous satellite system [AIAA PAPER 66-311] 06 p0979 A67-17691
- VHF and UHF communications between transoceanic commercial aircraft and ground stations by means of aeronautical communication satellites 06 p0961 A67-17701
- Geodetic error effect on time dependence of satellite tracking data received by ground station 06 p1080 A67-17769
- DFL mobile telemetry ground station participation in solar eclipse expedition of ESRO in Greece 06 p0980 A67-18020
- Effect of higher harmonics of geomagnetic field on cosmic ray trajectories, noting reception cones of Soviet stations 07 p1243 A67-19685
- Effects of technical parameters of station on results of observations of sporadic E layer, noting that frequencies depend weakly on receiver and transmitter 07 p1173 A67-19689
- Geodetic electronic ranging system of satellites with Sequential Collation of Range /SECOR/ transponder 07 p1177 A67-19772
- Sea station and satellite for long range communication with aircraft 08 p1294 A67-20778
- Ground observations of Martian relief during 1967 optimum period 09 p1565 A67-22014
- Multicavity klystrons and traveling wave tubes and use in ground stations 09 p1478 A67-22257
- Transmission characteristics of high power traveling wave tubes for satellite ground stations 09 p1478 A67-22258
- Ground station antenna steering system for satellite communication, noting design 11 p1758 A67-24061
- Low noise amplifiers at Fucino for reception from Early Bird satellite 12 p1913 A67-25301
- Ionospheric electron content measured using passage of transit IVA radio beacon satellite across view field of observing station 12 p1935 A67-25797
- Mechanization effect on man-machine relationships in flight test engineering analysis 13 p2052 A67-26423
- Satellite Telecommunications with Automatic Routing /STAR/ system composition and operation, detailing signal relaying procedure 13 p2067 A67-26717
- Earth-based navigation for two-spacecraft missions using analytical techniques for POLYDOP tracking data 13 p2155 A67-27526
- Liquid helium traveling wave maser amplifier for low noise ground station satellite communication 14 p2329 A67-27777
- Two-stage parametric amplifier system cooled to 20 degrees K, as low noise amplifier in receiving equipment for satellite communication 14 p2278 A67-27780
- Two-stage fixed-tuned parametric amplifier for satellite communications earth stations, considering circulator development and varactor 14 p2278 A67-27781
- Low noise receivers in transportable satellite communication ground terminals, discussing interrelationships between antenna, receiver and cryogenics 14 p2260 A67-27782
- Low temperature parametric amplifiers, discussing varactors, circulators and demands on cooling systems 14 p2278 A67-27783
- Airborne radio telemetry equipment transmitting in-flight data to ground station for monitoring and analysis, using frequency- and time-division multiplexing 14 p2261 A67-28038
- RF design of communication satellite earth stations, discussing receiving, sensitivity parameters, etc 14 p2273 A67-28798
- Mobile telemetry ground station and maximum reliability procedures for rocket telemetry transmission system used in solar eclipse 15 p2467 A67-29575
- Worldwide network of Doppler observation stations, discussing frequency and time monitoring for enhanced measurement accuracy 15 p2436 A67-29592
- Vertical incidence ionospheric absorption measurements from ground station criteria for recognizing winter anomaly 15 p2476 A67-29623
- Display/control system of Mission Control Center, Houston, operation and performance 15 p2467 A67-29736
- Low noise amplifier specifications for communication satellite earth station 16 p2635 A67-30473
- Satellite communication, noting satellite and ground terminal design performance criteria 16 p2622 A67-30689
- Early Bird project ground stations and launch-synchronizing operations, considering time delay on transmission performance 16 p2780 A67-30692
- Automatic satellite navigation and communication system for aircraft and ships using cooperating ground stations 16 p2700 A67-30695
- Design and electrical properties of 25-meter Cassegrainian antenna installed at Raisting ground station for radio communications via satellites 16 p2622 A67-30699
- Atmospheric trajectories of faint telescopic meteors observed by separate stations simultaneously and probability of plotting 16 p2751 A67-31461
- Large aperture, low noise, steerable antennas for ground station commercial satellite communication networks 16 p2641 A67-31532
- Satellite tracking and data acquisition network of receiving stations /TRANET/ that acquires and processes Doppler frequency shift data 16 p2630 A67-31740
- Spherical analysis of geomagnetic maps to determine asymptotic directions of cosmic rays for Soviet station network 17 p2933 A67-32091
- Multiple laser communication design, considering links between ground stations and earth-synchronous satellite with single telescope and laser 17 p2813 A67-32495
- aboard Early Bird and Intelsat commercial satellite communications system and associated ground stations noting design, power supply, control system, etc 18 p3136 A67-33545
- Central station construction for German ground-station system for research satellites 18 p3021 A67-34607
- High altitude research rocket HF telemetering remote control signal receivers, antennas and earth station, discussing design and circuity of transmitter antenna 19 p3193 A67-35061
- Ground station for satellite communications in Italy covering TV transmission 19 p3207 A67-35568
- Ground-based radio aids to navigation as represented by existing major systems 19 p3255 A67-35857
- High data rate storage system for Nimbus B tested by simulation 20 p3445 A67-36547
- Operational and cost-influencing characteristics of low orbit space operations compared from manned orbital base and earth base [AIAA PAPER 67-654] 20 p3530 A67-37631
- FR-1 satellite-borne oxide cathode used to return to ground polarization current from ambient plasma 21 p3599 A67-38649
- TIROS satellite program accomplishments since 1960, describing operational system, TOS ground-station network and ESSA satellites 22 p3899 A67-39608
- Tracking ground station on Ascension Island to relay communication with Apollo spacecraft via INTELSAT II 23 p3986 A67-40706
- Helicopter landing systems requirements, considering manual instrument approaches with guidance information from ground station including landing environment 23 p4026 A67-41500
- Reception of ground based Loran transmissions by fixed-frequency topside sounder satellite 24 p4119 A67-42061
- ### GROUND SUPPORT EQUIPMENT
- Aerospace ground equipment management problems solved by program ensuring proper recognition by contractor and customer management [SAE PAPER 660686] 01 p0169 A67-10590
- Total systems management technique applied to ground equipment management in development and production of weapons system [SAE PAPER 660687] 01 p0169 A67-10591
- Aerospace ground equipment requirement determination prior to aircraft flight test and operational use [SAE PAPER 660700] 01 p0049 A67-10594
- Space and weapon system support facilities acquisition and management systemization by government and industry [SAE PAPER 660692] 01 p0050 A67-10621
- Full-life product warranty approach in reducing military avionics support costs by tying supplier profits to reliability attainment 01 p0171 A67-11351
- Ground testing, development of engines, stages and ground support equipment of Saturn V launch vehicle [AIAA PAPER 66-840] 02 p0331 A67-12256
- SST servicing and maintenance characteristics and suitability of existing and planned airports 03 p0360 A67-13919
- Mobile launch concept for Apollo/Saturn V lunar landing mission, discussing structural composition, functions and performance of launcher [AIAA PAPER 67-247] 07 p1165 A67-20065
- Umbilical carriers and quick-disconnect facilities of Saturn V ground support equipment noting location, ejecting methods, etc 09 p1484 A67-22038
- Implementation of NASA NPC 250-1 /Reliability Program Provisions for Space Systems Contractors/ as applied to Saturn V Mechanical Ground Support Equipment Program 09 p1582 A67-22292
- Vibration qualification of fly-away umbilical by induced acoustic excitation testing method in Apollo project 12 p1924 A67-25714
- Launch operations requirements for future

space programs
[AAS PAPER 67-37] 15 p2467 A67-30109
Boeing 727 QC aircraft development,
manufacture, design objectives, cargo pallet
system, seat pallet system, etc
[AIAA PAPER 67-395] 15 p2421 A67-30362
Reliability prediction relationship to
system support costs, computing factors for
undersupport and oversupport of tactical
missile system 16 p2782 A67-31256
Spacecraft and ground equipment of Lunar
Orbiter telecommunications 17 p2811 A67-32119
Fuel ground thermal conditioning for
performance gains
[AIAA PAPER 67-442] 18 p3019 A67-33919
Built-in test features in Minuteman II
intercontinental ballistic missile weapons
system electronics, discussing ground
equipment including self-test features and
status display techniques 20 p3417 A67-36973
PCM telemetry system for ELDO program,
discussing data acquisition and
processing 20 p3392 A67-37162
Improved filtration techniques for aircraft
hydraulic systems, noting high pressure
filter unit using paper-based element for
ground service 20 p3418 A67-37169
Purification systems, filters and porous
materials applications to liquids and gas
systems associated with spacecraft, boosters
and ground support 21 p3570 A67-38103
Onboard and ground radio-engineering
system for stratospheric transport balloon
noting telemetering, remote control and
localization functions integrated in
system 21 p3581 A67-38213
GROUND SUPPORT SYSTEM
SA SATELLITE GROUND SUPPORT
NETWORK
Combination ground support and self-
sufficiency concept in Boeing SST aircraft,
discussing engine removal, accessory drive,
wing pivot bearing, inlet control, inertial
navigation and back-up support
[SAE PAPER 660702] 01 p0049 A67-10596
Saturn V ground support instrumentation
systems, emphasizing launcher umbilical
tower /LUT/ 01 p0051 A67-11117
Communications systems at Kennedy
Space Center /KSC/ and future
prospects 02 p0230 A67-12121
Integrated air-ground problem of flight
data acquisition 03 p0374 A67-13379
Telemetry systems, discussing
PAM/FM system, airborne equipment
parts, ground support system and electronic
testing procedures 04 p0577 A67-15728
Space vehicle vs ground systems reliability
[SAE PAPER 660691] 04 p0740 A67-15790
F-111 type hydraulic power supply system
design for supersonic aircraft using ground
support equipment and military
materials 05 p0752 A67-16159
Lincoln Experimental Terminal /LET/
system, ground antenna, RF and signal
processing equipment for communications
via several satellites 06 p0959 A67-17669
Satellite communications system noting
instrumentation, design criteria, frequency
range, propagation aspects and suitable
trajectories 07 p1141 A67-19344
Organization of U.S. geodetic satellite
program, discussing responsibilities for
various phases of
operation 07 p1269 A67-19758
Launch vehicle ground system constraints
including launch window, launch-on-time
influence, turnaround time after scrub,
backup vehicle operations, earth-launch
emergency requirements
[AIAA PAPER 67-285] 07 p1256 A67-20053
Systems analysis applied to identification
of Saturn V launch vehicle support system
requirements and establishment of baseline
logic for vehicle prelaunch processing
simulation and systems optimization
[AIAA PAPER 67-248] 07 p1185 A67-20066
Gemini ground support system extension
to cover Apollo program, stressing launch
complex, deep space tracking, S-band
linkage, communications satellite,
etc 08 p1317 A67-21281
Support requirements for future manned
space programs
[AAS PAPER 67-56] 15 p2562 A67-30120
Trace /tape controlled recording automatic
checkout equipment/ system design to
accommodate aircraft ground support
task 16 p2635 A67-30834

Airline terminal building concept to
provide practical approach to terminal
complex design
[SAE PAPER 670320] 17 p2835 A67-32981
Ground instrumentation system for
Mariner IV occultation experiment, using
Doppler frequency perturbation method for
Mars atmospheric parameters
determination 18 p3049 A67-34498
Central station construction for German
ground-station system for research
satellites 18 p3021 A67-34607
Ground system design approach
integrating reliability and maintainability
with performance requirements, using
Saturn V simulation as
example 18 p3139 A67-34694
High chamber-pressure propulsion systems
and components captive testing, describing
ground support system analysis, design and
mechanisms 20 p3414 A67-36534
Apollo-Saturn program automatic checkout
systems, discussing ground support
equipment facility automation, computer
software and checkout technique
applications to nuclear electronic
systems 20 p3533 A67-36977
Modernizing air traffic control,
governmental procedures, airports and
support facilities to accommodate Boeing 747
and supersonic transports 20 p3418 A67-37442
Systems analysis applied to identification
of Saturn V launch vehicle support system
requirements and establishment of baseline
logic for vehicle prelaunch processing
simulation and systems optimization
[AIAA PAPER 67-248] 21 p3607 A67-37806
High performance automatic
checkout system for boosters, noting rate
improvement and error
reduction 21 p3608 A67-38203
GROUND TEST
Ground testing, development of engines,
stages and ground support equipment of
Saturn V launch vehicle
[AIAA PAPER 66-840] 02 p0331 A67-12256
Instrumentation and control /I and C/
system for ground test of Nerva propulsion
system 03 p0395 A67-13384
Ground tests of 2.3-m-diam models of
foldable foam-reinforced plastic paraboloidal
mirrors for satellite energy supply system
and optimization of optical
characteristics 04 p0558 A67-15957
Arnold Center advanced ground test
facilities for rocket and space vehicle
environmental testing 05 p0788 A67-16617
Imperfect excitation effect on vibration
test results such as admittance, phase curve,
damping coefficient, etc 05 p0920 A67-16769
VTOL test bed for ground effects test,
noting environmental characteristics,
configuration dependence of lift and hot gas
ingestion 06 p0980 A67-18297
Static firing ground testing of Saturn
launch vehicle 07 p1165 A67-20057
Electrical systems except data acquisition
and instrumentation for ground testing of
large booster 07 p1167 A67-20079
Ground test facilities for aircraft air
breathing propulsion system 08 p1315 A67-21063
Evaluation of requirements for ground
testing of electric propulsion devices in
vacuum, noting effects of sputtering
phenomena 09 p1559 A67-22120
Solar simulation, comparing techniques for
reproducing space thermal radiation
environment with sun 16 p2654 A67-30674
Ground installations for development,
qualification and checkout testing of Apollo
space vehicle 16 p2854 A67-30676
Cesium contact ion engine ground and
flight tested for ability to operate under
environments of ground handling, missile
launch and space
ambients 16 p2736 A67-30711
Parametric data on gas ingestion and
ground proximity jet effects experienced by
jet-powered VTOL configurations
[AIAA PAPER 67-440] 18 p2985 A67-33917
Automatic test equipment /ATE/ to
ensure aircraft availability noting operation,
circuitry, computer methods,
etc 21 p3609 A67-39132
Writing and use of ground checkout
procedures in Apollo program using

computer-assisted editing, publishing and
information retrieval 23 p3976 A67-41055
Small scale Rankine cycle power
conversion system using potassium working
fluid under environmental, RF interference
and ground performance
tests 24 p4102 A67-42491
Sub-, super-and hypersonic air breathing
engines, examining developments on ground
test and simulation facilities
[AIAA PAPER 67-779] 24 p4208 A67-42946
GROUND-TO-AIR
TALAR ground-to-aircraft microwave
transmission landing approach system for
use in conjunction with instrument landing
system /ILS/ crosspointer
indicator 06 p1028 A67-17721
Flight trial determination of range and
reliability of LF ground-to-air data link for
air traffic control 09 p1529 A67-22642
Digital simulation role in advanced
avionics system development such as air to
air/air to ground weapon delivery, noting
advantages, performance,
etc 17 p2833 A67-32492
GROUND TRACK
Synchronous satellite orbits exploration,
ground track plots show effects of varying
orbit eccentricity and
inclination 04 p0694 A67-14503
Ground track of earth-period synchronous
/24-hr/ satellites, discussing equatorial,
circular and elliptical
orbits 04 p0704 A67-14826
Ground monitoring system for ILS
localizer signals reflected from landing
aircraft 06 p0957 A67-17578
Ground track location on contour map for
given terrain elevation profile, using digital
computer 19 p3232 A67-35926
GROUND WAVE
Scheme reducing decoding failures due to
atmospheric noise in coherent-phase-shift-
keyed data transmissions by ground
wave 05 p0767 A67-17523
Two digital computer filing programs for
determining ordinates of propagation curves
of ground waves in visible
region 13 p2070 A67-27202
Steady state vertical displacements at
surface of elastic half-space due to Rayleigh
waves from sonic boom, obtaining shock
amplification factors 23 p4074 A67-40632
GROUP BEHAVIOR
Psychosociological problems of small
isolated groups working under extreme
conditions in lunar
laboratory 02 p0185 A67-12374
Model for social system for extended-
duration spaceship crews subject to
isolation, confinement and/or
stress 03 p0366 A67-14293
Group dynamics approach to resistance or
counterpart of planning, conversion and
management of automatic data processing
systems design
[ASME PAPER 66-WA/MBT-10] 04 p0740 A67-15334
Research astronaut
selection 13 p2062 A67-26763
GROUP THEORY
Symmetry groups of motion equation
determined, using generators of Lie spatial
groups 02 p0288 A67-12424
Duality principle for automorphic forms on
semisimple Lie groups extended to include
arbitrary topological unimodular
groups 03 p0458 A67-13387
Lebesgue space in measure theory on
Borel sets and Banach algebra over compact
semigroups 07 p1214 A67-19211
Partially solvable finite groups, discussing
dependence of p-length on Sylow
subgroup 07 p1217 A67-20153
Finite groups with single value generation
of normal divisors, examining conditions for
representation as KM
group 07 p1217 A67-20154
Lapunov theorem extension to onto
mappings in compact sets 10 p1673 A67-22850
Explicit invariant forms of sector
equations for factorization of secular
equations by group 10 p1674 A67-23377
Homogeneous solutions of Einstein-
Lichnerowicz equations for electrically
charged fluid with infinite conductivity
universes 12 p1962 A67-26178
Analysis of steady flows of viscoelastic
materials by introduction of two
dimensionless groups 13 p2096 A67-26931

Similarity solutions for two-dimensional unsteady compressible boundary layer equations using group theoretic methods 14 p2297 A67-28135

Transformation of class of boundary value to initial value problems in terms of one-or two-parameter group of transformations for ordinary differential equations 15 p2511 A67-29892

Flat plate, simultaneous heat and mass transfer for Newtonian fluids in free convection analyzed, using group theory 15 p2582 A67-30217

Proof of continuity of Haar measurable almost periodic functions 17 p2876 A67-32385

Martin boundary for invariant Markov processes investigated on group of affine transformations of straight line 17 p2878 A67-32736

Motion equations of classical point particles determined by known Euclidean symmetry of space 19 p3262 A67-35709

Group properties of differential equations describing axisymmetric thin layer jet flow of ideal fluid propagating along surface of revolution 20 p3422 A67-37063

Similarity analysis of partial differential equations, discussing free parameter analysis, variables separation method, group theory approach and dimensional analysis 24 p4180 A67-43082

GROUP VELOCITY

Oblique probe data applied to determination of minimum group path of signal for parabolic model of ionosphere 05 p0801 A67-17130

Tabulation and plotting of VLF radio wave diurnal phase changes as function of frequency and path 07 p1142 A67-19450

Analytical expression for steady state rate of electric domain movement in semiconductors in terms of electric field distribution at domain center 11 p1846 A67-24482

Speed of light in vacuum determined by helium-neon gas laser, using Edlen dispersion equation 18 p3059 A67-33671

Oblique probe data applied to determination of minimum group path of signal for parabolic model of ionosphere 21 p3618 A67-38473

Electromagnetic wave propagation in moving media filled waveguides noting nondispersive dielectric and cold plasma cases 22 p3759 A67-39361

GROWTH

SA CRYSTAL GROWTH

Courant-Hilbert ray theory and Thomas singular surfaces theory of wave propagation in anisotropic homogeneous linearly elastic medium, based on growth equation 04 p0657 A67-15083

Growth rate along whistler path for waves propagating at angle to geomagnetic field 08 p1328 A67-21463

Weinstein results for pointwise monotone growth and convexity extended in norm to certain Cauchy problems of second order differential equations 12 p1961 A67-26063

Plants in low gravity environment simulated by 2 rpm clinostat with horizontal axis, studying growth direction and respiratory metabolism 15 p2426 A67-29114

Parametric coupling between ion and electron waves noting coefficients, growth rate amplification, etc 17 p2906 A67-33061

Growth rate of oxide and other dielectric contact films on metal crystals computed for ionic diffusion and electron tunneling 18 p3103 A67-34590

Line broadening by collision damping, explaining solar and stellar curves of growth 21 p3700 A67-37731

GRUMMAN MILITARY AIRCRAFT

S F-111 AIRCRAFT

GRUNEISEN CONSTANT

Thermal expansion coefficient of ferromagnetic thin films compared with bulky samples by electronographic technique 12 p1939 A67-25242

GUANINE

Adenine and guanine amounts in DNA determined spectrophotometrically by dialysis of DNA 04 p0564 A67-14406

GUIDANCE

S AIRCRAFT GUIDANCE

S HOMING

S INERTIAL GUIDANCE

S MIDCOURSE GUIDANCE

S NAVIGATION AND GUIDANCE

S REENTRY GUIDANCE

S SATELLITE GUIDANCE

S SPACECRAFT GUIDANCE

S TERMINAL GUIDANCE

GUIDANCE AND CONTROL

Interactions and relationships between man and machine in flight guidance 02 p0185 A67-11551

Mayer technique in calculus of variation for constrained error coefficient criterion function for missile trajectory optimization in aerospace guidance and control 02 p0265 A67-12389

ELDO guidance station in Australia for control of third stage and orbit placement of payload, noting interferometric complex 04 p0654 A67-15625

ELDO guidance station noting master antenna for automatic tracking of third stage 04 p0576 A67-15827

Analog computer design noting operation principles, application to guidance problems and testing and troubleshooting methods 04 p0579 A67-15737

Optimum guidance law simulation by analog computer using logic controlled analog, spatial analog and trajectory riding techniques 06 p1028 A67-17614

Advances in control systems, Volume 3, covering reentry and aerospace vehicle guidance and control, BVP techniques, optimal control, Kalman filtering techniques and state space methods for navigation problems 06 p0973 A67-17921

Onboard digital computer navigation, guidance and control of reentry and aerospace vehicles 06 p1028 A67-17922

Optimal guidance equations for ascent trajectories into circular orbits, developing feedback guidance loop for real onboard control system [AIAA PAPER 67-56] 06 p1029 A67-18495

Explicit guidance law for minimum fuel horizontal translation with bounded control 06 p1090 A67-18867

Balloon-borne telescope guidance by offset sun tracking 07 p1184 A67-19392

Optimization of Saturn vehicle, considering interaction of guidance, control and propellant utilization systems [AAS PAPER 66-117] 07 p1222 A67-19975

Hybrid simulation for design of Apollo guidance navigation and control system [AIAA PAPER 67-233] 07 p1222 A67-20042

Apollo engineering simulation activity, particularly analog-digital real time hybrid simulation for guidance and control [AIAA PAPER 67-230] 07 p1164 A67-20055

Astronaut performance evaluation in Lunar Module hover and landing, separation and docking simulation [AIAA PAPER 67-249] 07 p1165 A67-20067

Controlled recovery of payloads from high altitudes and at large glide distances, using Para-Foil 08 p1409 A67-20545

Airborne guidance computations using prescribed-H-method, representing two-body motion in inertial space, presenting equations for target hitting, circular orbit, etc 08 p1352 A67-21532

Multifunction airborne radar instruments, discussing air to air, air to ground, shared aperture and combined systems, spoiled beam technique for ground mapping, etc 11 p1754 A67-25007

SR-N4 hovercraft, optimum size for coastal waters, structural features, performance, control, etc 12 p1895 A67-26168

Optimal control theory in design of aerodynamic shapes, flight paths, guidance and control logic, data processing logic, etc 13 p2072 A67-26814

Optimization of Saturn vehicle, considering interaction of guidance, control and propellant utilization systems [AAS PAPER 66-117] 13 p2155 A67-27532

Modulation of L/D and bank angle to achieved heading, range and trajectory stabilization, using closed form equations 14 p2347 A67-28114

Multiple format telemetry programmer design using control signals 14 p2275 A67-28689

Guidance and control, International Astronautical Congress, Athens, September 1965, Volume 2 guidance and control - IAF Conference, Athens, September 1965, Volume 2 16 p2699 A67-30649

Guidance and control technology examining inertial guidance systems, Apollo space system, gyros, accelerometers and

computers 16 p2699 A67-30650

Fuel optimum guidance law to achieve required velocity 16 p2700 A67-30655

Guidance station for ELDO third stage, describing equipment and function 16 p2700 A67-30657

Gemini guidance and control, discussing design, ground monitoring, launch and flight guidance, spacecraft instrumentation, maneuvering, etc 16 p2700 A67-30659

Synthesis of optimal linear control system coupled with vehicle configuration design technique for guidance parameters and temperature accumulation along optimum entry trajectories 16 p2758 A67-30660

Control engineering in systems management applied to missile control and guidance 18 p3162 A67-33636

Research areas in future NASA program covering materials, energy conversion, guidance, instrumentation, etc 19 p3349 A67-35645

Design of time-shared multifunction display medium to improve guidance and control displays in manned spacecraft [AIAA PAPER 67-552] 19 p3257 A67-35949

Application of redundancy in Saturn V guidance and control system to achieve desired reliability [AIAA PAPER 67-553] 19 p3257 A67-35950

Effective guidance and control redundancy for spacecraft configurations and mission outcomes, discussing computer systems [AIAA PAPER 67-555] 19 p3257 A67-35952

Apollo gyro reliability covering Guidance, Navigation and Control systems, stressing failure mode prediction 19 p3259 A67-35984

Iterative guidance mode /IGM/ applied to effective gravity vector prediction, acceleration measurement of noise sensitivity and energy limitations [AIAA PAPER 67-620] 19 p3260 A67-36009

Onboard computer equations for rocket vehicle guidance to elliptical orbit, discussing iteration absence from computations and digital simulation results [AIAA PAPER 67-621] 19 p3260 A67-36010

Lunar landing module Doppler radar system in guidance navigation and control system, studying mathematical model performance 19 p3260 A67-36011

Iterative guidance mode, deriving alternate expressions for thrust direction control angle for time savings on Saturn launches 22 p3831 A67-39957

Suboptimal feedback solution to guidance and control in minimum time and fuel for low thrust orbital transfer 22 p3832 A67-40146

Mathematical model of linear guidance law to dynamical system, noting reduction of two-point boundary value class error 23 p4026 A67-41732

GUIDANCE SENSOR

SA IMAGE DISSECTOR TUBE

Spinning-image coded X-ray star camera, based on image coding, permitting reconstruction of two-dimensional image [AIAA PAPER 66-850] 03 p0424 A67-14016

Automatic star trackers for long range aircraft navigation, discussing instrumentation methods and use of pulse code modulation for sensor design 04 p0655 A67-15661

Control signal generator and output characteristics of angular position and velocity sensors used in single-axis sun-oriented system of Vostok spacecraft 12 p1964 A67-25642

Spinning-image coded X-ray star camera, based on image coding, permitting reconstruction of two-dimensional image [AIAA PAPER 66-850] 15 p2486 A67-29440

Canopus star sensor used for roll control of Mariner IV spacecraft 16 p2699 A67-30654

GUIDANCE STABILITY

Guided propulsive solution to Mars atmosphere-decelerated soft landing vehicle trajectory [AIAA PAPER 67-170] 06 p1029 A67-18508

Vehicle systems interaction effect on guidance system stability 22 p3907 A67-40194

GUIDANCE SYSTEM

SA HOMING DEVICE

SA MIDCOURSE GUIDANCE

SA RENDEZVOUS GUIDANCE SYSTEM

Graphical estimation of reliability of test results 01 p0104 A67-10157

Closed loop control system for space vehicle guidance, formulating efficient steering algorithm 01 p0154 A67-11156

- Singularity in motion equations of closed loop optimal guidance 01 p0111 A67-11224
- Systems reliability evaluation and identification of inadequate subsystems, with application to two missile-borne guidance systems 01 p0111 A67-11371
- Temperature control and complex heat path designs inertial components, platforms and strap-down guidance systems, considering floated gyros and accelerometers 02 p0241 A67-11789
- Fluctuation of stellar images and analysis of systematic errors in guidance of telescope as result of atmospheric refraction and flexure of telescope 02 p0241 A67-11993
- Thermal model for transient heat transfer analysis of missile guidance systems for prediction of operating temperature 02 p0263 A67-12104
- Path adaptive guidance modes for Saturn space vehicle, particularly iterative Guidance Mode 02 p0264 A67-12318
- Synthesis of multichannel transponder for radio guidance and tracking station and associated parameters 02 p0264 A67-12355
- Guidance equations for multistage boosters to target change on launch pad and in flight 02 p0265 A67-12718
- Strap-down guidance systems using conventional inertial hardware, discussing computer function, computer selection and system errors 03 p0465 A67-13364
- Onboard guidance scheme as backup to earth-based orbit determination techniques and for approach navigation and orbit correction in planetary capture maneuver 04 p0654 A67-15234
- Nuclear radiation characteristics pertinent to propagation of signals for measurement of range and bearing 05 p0839 A67-16532
- Range control system for lifting body reentry vehicles, using closed form prediction equations for longitudinal and lateral range control [AIAA PAPER 67-136] 06 p1095 A67-18316
- LM guidance and control systems performance verification [AIAA PAPER 67-244] 07 p1165 A67-20064
- Open and closed loop tools and techniques for guidance program validation and postvalidation operations 08 p1350 A67-20629
- Automatic checkout system /ACS/ and digital guidance programs for titan III and Apollo automatic checkout system /ACS/ and digital guidance programs for Titan III and Apollo 08 p1297 A67-20632
- Percentile specifications of orthogonal components and of additive errors of guidance systems 08 p1350 A67-20674
- Self-contained midcourse guidance system with space velocity meter /SVM/ used in returning probe to earth vicinity for data retrieval and orbit control 08 p1331 A67-21101
- Motion of gyro vertical under starting conditions during turn 09 p1498 A67-22035
- Integrated circuit general purpose computer for use in aerospace guidance 09 p1469 A67-22174
- Short range radar with 1 m resolution for FM-CW technique for vehicle guidance in fog, describing equipment 09 p1528 A67-22630
- Closed form solution to three-dimensional rocket trajectory problem, considering flight velocity and acceleration laws for guidance design applications 10 p1709 A67-23484
- Vector equation for determining missile maximum roll rate for effective navigation ratio and time constant for guidance systems 11 p1818 A67-24215
- Soviet book on IR and optical devices for vehicle guidance and homing covering light propagation, radiation from targets, airborne missile homing systems, etc 11 p1791 A67-24514
- Pontryagin maximum principle application to solution of one-dimensional minimum time rendezvous problem for thrust limited rocket with initial and final mass specified 12 p2012 A67-25922
- Control systems functions and programming approaches, Volume B, covering electronic data processing, factory automation and computer center administration 13 p2153 A67-26664
- High accuracy radio guidance and tracking station, discussing relation between basic station parameters, error sources and associated error components 14 p2260 A67-27972
- General purpose digital computer for airborne and spaceborne guidance and navigation systems 14 p2275 A67-28684
- Multiple format telemetry programmer design using control signals 14 p2275 A67-28689
- Confidence limits for percentile analysis of guidance system errors 15 p2515 A67-29740
- Space vehicle automatic control considering order execution from guidance system and vehicle stabilization around its center of gravity 16 p2700 A67-30798
- Inertial guidance system for ground-to-ground ballistic missiles or space vehicle launchers 16 p2700 A67-30799
- Saphir g space vehicle guidance systems consisting of inertial center and computer 16 p2701 A67-30800
- In-flight transfer, fine and maneuver alignment of air to surface missile guidance system 17 p2881 A67-32487
- Main characteristics of Saphir measurement system, definition of parameters to be measured and design problems 17 p2861 A67-33131
- Structural and systems design characteristics of British launch vehicle noting control and guidance system, flight development and test programs 19 p3333 A67-35841
- Deep space navigation and guidance technology, emphasizing simplification of onboard navigation procedures 19 p3255 A67-35856
- Inertial guidance and navigation systems and components testing facility 1100 feet underground [AIAA PAPER 67-538] 19 p3208 A67-35940
- Manual optimal guidance scheme using predictive display applied to launch vehicles during boost for continuous generation of predicted fuel-optimal trajectory 19 p3259 A67-35989
- Guidance system requirements for unmanned Martian propulsive landing capsule [AIAA PAPER 67-619] 19 p3260 A67-36008
- Mathematical models of multichannel radio equipment in presence of noise, including guidance and coordinate measurement systems 19 p3185 A67-36095
- Manual steering problem and function of lunar module /LM/ manual hybrid guidance system, with automatic guidance system produced trajectory 22 p3898 A67-39176
- Nonstationary second order linear differential equation for near time optimal space vehicle guidance system design solved by linear transform 22 p3832 A67-39966
- Speedy generation of space flight guidance command signals and comparative analysis of operational schemes for generating guidance signals 22 p3832 A67-40145
- Guidance and navigation sensors and systems, discussing spacecraft facilitated by microelectronics, computer technology, optimal filtering and gyroscopic sensor design 22 p3834 A67-40335
- V/STOL all-weather guidance system developments and flight experimentation, discussing enroute navigation compatibility and terminal area operations [AIAA PAPER 67-796] 24 p1483 A67-42957
- GUIDE VANE**
- Parametric analysis of supersonic compressors, determining relative efficiencies of various leading and trailing guide vane configurations 03 p0352 A67-13010
- Cascade flow through compressor guide vanes and flow separation at top of vane profiles 05 p0750 A67-17323
- Heat-resistant casting alloy KhH65VMTiU for gas turbine guide vanes, noting structural stability and oxide film 09 p1519 A67-22376
- Flow through blade cascade studied by averaging flow parameters behind cascade for testing internal combustion turbine guide vanes 16 p2736 A67-31005
- Plane compressor and guide vane cascades design, deriving relations for angle of attack, angle of lag, etc 20 p3358 A67-37081
- Boundary layer separation onset and propagation in axial flow compressor stages, discussing guide vane results 21 p3566 A67-38911
- Spiral flow in cylindrical annular chamber behind guide vanes /stators/ noting flow instability in outer region due to vortex generation 23 p3929 A67-41253
- GUIDED MISSILE**
- Altitude control system with optimized guidance device which reduces flight altitude of guided low trajectory missiles over sea surface 04 p0652 A67-14562
- Dither and sinusoidal incidence variations effect on control wing hinge moments of transonic-supersonic rolling maneuvering guided missile [AIAA PAPER 66-755] 17 p2789 A67-32062
- Analytical and simulation procedure for determining environment induced errors in missile guidance 20 p3481 A67-36605
- Electronic equipment components unreliability in guided weapon systems, discussing packaging, environmental conditions and customer-manufacturer relations 24 p4161 A67-42479
- GUINEA PIG**
- Precentrifugation effect on radiation reactions of vestibular analyzer in guinea pigs, establishing substantial spontaneous electric activity stimulation in hind legs extensor muscles 23 p3944 A67-40773
- GULLIVER PROGRAM**
- Gulliver radiolabelled biochemical probe to detect extraterrestrial life 05 p0806 A67-16548
- Unmanned probes designed to land on planetary surfaces to obtain temperature, atmospheric measurement and ground samples chemical analysis 22 p3900 A67-39613
- GUMBEL THEORY**
- S EXTREMUM VALUE**
- GUN**
- S ELECTRON GUN**
- S GAS GUN**
- S HYPERVELOCITY GUN**
- S PLASMA GUN**
- GUN LAUNCHING DEVICE**
- High speed photographic equipment, analyzing gun launching of vehicles in upper atmosphere and design of protection system against space vehicle failure due to meteorites 01 p0068 A67-10968
- HARP program**
- objectives 06 p1098 A67-19021
- Gun-launched rockets for high performance sounding missions 08 p1409 A67-20550
- Meteorological telemetry system for gun launched probes for high altitude research 08 p1292 A67-20664
- Neutral wind structure and time variation over height in lower troposphere observed using gun-launched trails, noting relation to sporadic E layer 10 p1644 A67-23257
- Telemetry systems for gun launched upper atmosphere probes 15 p2436 A67-29412
- Project High Altitude Research Program /HARP/ directed toward use of guns for scientific probing of upper atmosphere [AIAA PAPER 67-38] 15 p2467 A67-30110
- Gun launched scramjet performance using various fuels, comparing weight and volume limitations effects 19 p3311 A67-34822
- Metal projectiles plastic deformation impacting on rigid targets defined, obtaining computer code through direct analysis 22 p3914 A67-40182
- GUNN EFFECT**
- Noise spectra measurements performed on two Read diode and two Gunn oscillators by reflection cavity microwave discriminator technique 01 p0033 A67-10017
- Epitaxial gallium arsenide Gunn effect oscillators in generating continuous wave oscillation 01 p0033 A67-10026
- Gunn effect noting negative bulk conductivity, creation of external negative conductance and zones with different field intensities in semiconductor crystals 01 p0130 A67-10253
- Gunn effect domain traveling wave parametric amplifier pumped by periodic impedance variations in boundary conductor of microstrip transmission line 01 p0040 A67-11309
- Bulk GaAs Gunn effect oscillators and amplifiers and electron transfer between high mobility and low mobility conduction bands 02 p0218 A67-12099
- Gunn effect semiconductors and contact preparation techniques, noting excitation of oscillations and amplification characteristics in GHz range 02 p0220 A67-12198
- Stable domain propagation in gallium arsenide for nonzero constant diffusion coefficient, based on analytic approximation to velocity field

characteristic 03 p0493 A67-13461
 Electric current oscillation mode beyond
 Gunn effect threshold in n-type
 GaAs 03 p0496 A67-13669
 Phase locking of pulsed Gunn oscillators
 with 0.3 to 1 microsecond pulse widths in S-
 band 03 p0382 A67-13672
 Potential distribution and field
 dependence of electron velocity in bulk
 GaAs measured with point contact
 probe 03 p0499 A67-13985
 V-I characteristics and bias field/carrier
 concentration-sample length diagram of
 Gunn effect phenomena 03 p0500 A67-13993
 X-band Gunn oscillator with dielectric
 tuning system 05 p0775 A67-16951
 Band structure and conduction phenomena
 in semiconductors of groups III-V,
 particularly in GaAs, noting signal
 instabilities and Gunn
 effect 05 p0871 A67-17325
 Frequency modes of Gunn effect
 oscillator 05 p0872 A67-17531
 Gunn effect in GaAs caused by field
 induced transfer of electrons from high to
 low conduction band valleys 06 p1067 A67-18961
 Nonlinear PDEs of two-valley model of
 Gunn effect materials, noting microscopic
 transport configurations 06 p1067 A67-18962
 Boltzmann equation for GaAs, noting
 coupling constant scattering between low
 and high mass valleys 06 p1067 A67-18963
 Plasma instabilities in solids noting
 developments in moving domains, nonlinear
 effects, Gunn effect, turbulence,
 etc 06 p1070 A67-18986
 Vapor phase epitaxial deposition of n-type
 GaAs contact layers for Gunn effect X-band
 oscillators 07 p1153 A67-19609
 Gunn diode efficiency for mixed resonant
 transit time and suppressed modes, using
 dynamic drift velocity field strength
 characteristic 09 p1474 A67-22039
 FM noise source in cavity controlled Gunn
 effect oscillator 09 p1474 A67-22040
 Gunn effect devices including lab results,
 design, materials, frequency variation,
 etc 09 p1556 A67-22173
 Noise generation in Gunn diodes suggests
 dependence on avalanching of charges in
 bulk material, making bulk oscillations
 irregular 09 p1556 A67-22263
 Upper frequency limit prediction method
 for Gunn oscillations 09 p1556 A67-22264
 Gunn diode self-pumped parametric
 oscillator, showing power derived from
 variation of domain capacity at second
 harmonic of oscillation frequency 09 p1479 A67-22267
 Circuit load effects on microwave
 properties of Gunn diodes, discussing
 equivalent circuit and graphical analysis of
 quenched and inhibited modes of
 operation 09 p1479 A67-22268
 Pulsed oscillations of microwave Gunn
 effect oscillator in n-type single crystal
 GaAs 10 p1609 A67-22838
 Computer simulation of GaAs Gunn diode
 in resonant circuit noting frequency,
 efficiency and load characteristics 10 p1612 A67-23370
 Gunn effect oscillators constructed from
 epitaxially grown n-type GaAs on n-plus
 substrate to obtain CW oscillations with
 frequencies from 3 to 35 gc 10 p1615 A67-23530
 Epitaxial advantages over melt grown
 GaAs in construction of continuous wave
 and pulsed Gunn effect
 oscillators 10 p1616 A67-23531
 Statistical survey of CW transferred
 electron oscillators /Gunn diode/ made from
 epitaxial gallium arsenide 10 p1616 A67-23532
 Epitaxial GaAs Gunn effect oscillators,
 showing importance in high efficiency of
 preparation and method of contacting
 material and resonant cavity
 design 10 p1616 A67-23533
 Assessment of epitaxial gallium arsenide
 for use in Gunn effect devices from check
 slices on seminsulating
 substrates 10 p1616 A67-23534
 Gunn effect devices high efficiency
 achievement, considering circuit and
 material from theoretical and experimental
 viewpoint 10 p1616 A67-23535
 Phase locking experimental data on
 injection locked X-band Gunn effect
 microwave oscillators 11 p1759 A67-24128
 Relationship between domain transit

frequency and cavity controlled frequency of
 thin Gunn devices 11 p1759 A67-24130
 High power pulsed microwave generation
 in gallium arsenide diode when operated at
 X-band frequencies 11 p1767 A67-24721
 Epitaxial vapor growth of GaAs noting
 reduction of electron concentration and
 increase in electron
 mobility 11 p1848 A67-24746
 Microwave amplification and negative
 conductance for GaAs, InP and
 CdTe 11 p1850 A67-24916
 UHF oscillations in GaAs thin epitaxial
 layers deposited on isolating substrates of
 same material 12 p1981 A67-25279
 Negative-resistance Gunn effect in gallium
 arsenide and indium phosphide due to field
 excited electron transfer 14 p2366 A67-28474
 Gunn diodes using Sn-Ag and In-Au
 contacts studied for electrical properties and
 failure mechanisms 14 p2290 A67-28927
 Gunn effect as only solid state effect
 capable of producing high output power in
 microwave range in pulsed and continuous
 operation, noting physical
 nature 15 p2536 A67-29530
 Microwave power generating
 semiconductor oscillators noting negative
 resistance effect, construction of Gunn
 oscillator diode, etc 15 p2445 A67-29583
 Properties of uniformly propagating stable
 domains in gallium arsenide calculated on
 basis of velocity-field and diffusion-field
 characteristics 16 p2727 A67-30851
 Gunn effect semiconductor oscillator for
 generating microwave power using
 GaAs 18 p3013 A67-34525
 Cooling and illumination effect on Gunn
 oscillators resulting in abrupt shift from
 transit-time frequency mode to higher
 frequency 19 p3305 A67-35628
 Current runaway effects in n-cadmium
 telluride suggest current-density controlled
 resistivity caused by hole-electron pairs
 avalanche 21 p3877 A67-38006
 Volt-ampere characteristics of n-type GaAs
 at high fields above Gunn threshold,
 showing saturation, space charge effect and
 current controlled negative
 resistance 21 p3679 A67-38260
 Energy band nonparabolicity effect on
 GaAs drift velocity vs field curve, especially
 near Gunn threshold 21 p3680 A67-38348
 Gunn effect applied to GaAs crystals for
 use as diodes, discussing current-voltage
 characteristics 21 p3684 A67-38444
 Gunn effect, describing electron transfer,
 domain propagation and space charge
 instabilities in GaAs 22 p3841 A67-40073
 Dynamic behavior of accumulation layer
 and efficiency of Gunn effect
 semiconductors in limited space charge
 mode of operation 22 p3864 A67-40314
 Frequency limitation of Gunn effect
 associated with relaxation time for
 intervalley electron scattering in small signal
 approximation 24 p4205 A67-42811

GUST

SA STORM

SA TURBULENCE

SA WIND

Cartwright-Longuet-Higgins-Rice theory on
 instantaneous maxima of stationary random
 variable for deriving instantaneous maximum
 gust ratio to mean wind
 speed 05 p0837 A67-16426
 Inertial navigation equipment applied to
 meteorological research, using aircraft for
 vertical gust
 measurement 06 p1002 A67-18025
 Upper air turbulence gusts, describing
 vertical component test method using F
 type radiosonde 10 p1678 A67-23085
 Vertical component of gusts in upper
 atmosphere estimated from rotation rate of
 ascending radioprobe fan 12 p1964 A67-26165
 Vertical gust components in altocumulus
 clouds measured by airborne
 instruments 13 p2152 A67-26741

GUST ALLEVIATOR

Design of gust alleviation controls for
 boost phase flight of missiles incorporating
 random winds, time-varying missile
 dynamics, control problem, etc
 [AIAA PAPER 66-969] 02 p0332 A67-12292
 Gust Alleviation and Structural Dynamic
 Stability Augmentation System /GASDSAS/
 design analysis [AIAA PAPER 66-999] 02 p0183 A67-12303
 Optimal control for aircraft gust
 alleviation using frequency domain theory

and short period mode
 approximation 17 p2795 A67-32036
 Ride quality improvement on flexible
 aircraft by means of elastic structural
 bending mode suppression design technique
 [AIAA PAPER 67-571] 19 p3174 A67-35967
 Flight mechanics of gust absorber for high
 speed aircraft, discussing transient effects
 and short response time 21 p3568 A67-38376
 Controller design for booster gust
 alleviation, considering stochastic
 minimization problem solved by iteration
 yielding linear finite time controller with
 time-varying gains 22 p3897 A67-39162
 Circulation control by blowing for gust
 insensitivity in stopped rotor aircraft
 application [AIAA PAPER 67-747] 23 p3933 A67-40981

GUST LOAD

Low level turbulence effects on structure
 of large logistic aircraft
 [SAE PAPER 660670] 01 p0160 A67-10577
 Gust reduction equations governing
 numerical procedure for transforming to
 inertial frame continuous records of air
 turbulence velocity via matrix methods
 [AIAA PAPER 66-967] 02 p0246 A67-12290
 Wind tunnel technique for measuring
 frequency response of flexible airplane to
 vertical sinusoidal gusts [AIAA PAPER 65-787] 03 p0354 A67-12906
 Load factor estimation for flights in
 turbulent conditions by replacing exact
 transfer function with equivalent statistical
 model 03 p0351 A67-12997
 Closed loop gust response control system
 considering airframe loading, local
 accelerations, turbulence, structural mode
 damping, etc [AIAA PAPER 66-997] 03 p0362 A67-14146
 Design techniques for advanced flight
 structures providing statistical assessment of
 environmental loads, forecasts of high
 performance material response and higher
 reliability design criteria 04 p0707 A67-14423
 Pitching effect on aircraft gravity center
 during passage through gust, noting
 autopilot effect on tail
 assembly 09 p1440 A67-22473
 Flexible sailplane designs allowing for
 towing cable analyzed with analog computer
 for gust loading 10 p1593 A67-23011
 Transient buffet loads on wings due to
 gust or maneuver 13 p2215 A67-26533
 Initial VGH data on small turbojet
 operations in commercial transport service
 relating to accelerations, airspeed operating
 practices and unusual events [AIAA PAPER 67-408] 15 p2421 A67-30375
 Structural design for gust loads on USAF
 aircraft based on continuous turbulence and
 failure probabilities 18 p2986 A67-34655
 Generator installation for supersonic gust
 simulation to measure wing forces,
 discussing calibration
 problem 21 p3609 A67-38881

GUTENBERG MODEL

Torsional disturbance propagation in
 Gutenberg-Bullen earth model through
 spectral seismograms, discussing travel times
 and S wave amplitude [SR-16] 20 p3435 A67-37675

GYRATION

SA ROTATION

Spatial-turn simulator using rocking device
 rotating under effect of internal
 forces 10 p1655 A67-22840

GYRATOR

Gyrator-RC filter synthesis procedure
 noting open circuit voltage of network
 configuration 01 p0032 A67-10006
 Integratable gyrator using metal oxide
 semiconductor and bipolar transistors whose
 circuit enables high Q factor inductances to
 be derived from low loss
 capacitors 01 p0041 A67-11322
 Inductorless band pass filter to prove
 validity of hypothesis that all inductors in
 LC filter can be replaced by gyrator
 capacitor equivalents 07 p1154 A67-19611
 Definition, realizability and design of
 active gyrator, using two controlled current
 sources to obtain ideal impedance inverting
 characteristics 11 p1789 A67-24121
 Theoretical realizability, design and
 stability of ideal gyrator with two
 operational amplifiers and resistance
 network 11 p1760 A67-24223
 Grounding of capacitors in integrated
 circuits noting insertion of
 gyrators 13 p2078 A67-26781

- Lossless gyrotransistor realization using parallel connected positive and negative amplifiers in reverse direction 13 p2078 A67-26789
- Gyrotor type circuit which requires only three amplifiers and which, when terminated with capacitor, can replace ungrounded inductor 15 p2456 A67-29240
- Active filter design employing impedance converters, amplifiers and gyrators, providing equations for component values 17 p2824 A67-32394
- GYRO**
- GYROSCOPE**
- GYRO HORIZON**
- Correctable gyrohorizon compass design possible by applying torques around appropriate axes 01 p0068 A67-10988
- GYRO-STABILIZED**
- Closed loop system with reference to different gyro stabilization loops present in modern space vehicle inertial measuring unit, using Prony exponential series curve fitting method as analytical tool 03 p0400 A67-14218
- Permanent axes of rotation for gyrostabilizer under influence of forces depending only on position of gyrostabilizer 06 p1002 A67-18041
- Stabilization of gyrostabilizer using motion equations as given by 06 p1002 A67-18043
- Triaxial gyrostabilized platform drift determination, given oscillations of gyro units relative to platform 06 p1003 A67-18176
- Optimum control of motion stability of solid body with fixed point, using gyrostabilizer rotors 06 p1034 A67-18617
- Lapunov function for motion stability of solid body on earth surface having fixed point and internal gyro 06 p1004 A67-18619
- Optimum stability of body with fixed point, using stabilizing gyros 07 p1224 A67-20028
- Control moment gyros for semipassive damping of satellite librational motion 08 p1330 A67-20586
- Equations for systematic drifts of gyrostabilizer with linear viscous-friction moments on precession axes when perturbations are slow 12 p1942 A67-25663
- Location of center of gravity of sensitive element of pendulum effect on stable equilibrium positions of gyrocompass in geographically oriented coordinate system 13 p2118 A67-26349
- Configuration study for ELDO-PAS test satellite based on communications requirements 17 p2955 A67-32396
- Rod configuration determined optimum for gyro torquer controlled spinning space station subject to impulse disturbance 17 p2955 A67-32477
- Gyromotor electromechanical moment effect on drift of triaxial gyrostabilizer exposed to platform vibrations, formulating rotor motion equations 18 p3047 A67-33992
- Exchange invariance in dissipationless fluid systems, deriving conservation law and stability conditions and application to gyro-stabilized magnetoplasma 20 p3419 A67-36151
- Expressions for determining directional gyroscope drift, considering random perturbations of base 22 p3809 A67-40481
- Gyro power stabilizer in unsteady equilibrium state becoming stable under dry friction defined for controllability in phase space 24 p4155 A67-42299
- GYROCOMPASS**
- Acceleration perturbations, gravity gradient torques and nutational motions effects on pendulums and gyrocompasses used as vertical indicating devices 01 p0064 A67-10644
- Correctable gyrohorizon compass design possible by applying torques around appropriate axes 01 p0068 A67-10988
- Stability of motion of gyro suspension, noting gyrohorizon compass operation for constant suspension point and angular velocities 03 p0424 A67-14158
- Oscillating field of vessel effect on accuracy of readings of gyrocompass with negative fluid/pendulum 03 p0425 A67-14283
- Low weather minima flight control system consisting of autopilot, flight system and gyromagnetic compass 03 p0466 A67-14385
- Equilibrium position of Sperry MK19 gyrocompass axis and effects of earth rotation and motion of body on which gyroscope is mounted 06 p1003 A67-18178
- Time optimum control of alignment process for gyrocompasses 07 p1186 A67-19629
- System error limit in determining equilibrium position of sensing element of ground gyrocompass 09 p1498 A67-22036
- Reading errors of oscillating plant mounted gyrocompass assuming gyromoment compensation and no friction, determining motion through differential equation 11 p1794 A67-25045
- Single-rotor gyrocompass motion during rocking, determining equilibrium point displacement 12 p1941 A67-25662
- Location of center of gravity of sensitive element of pendulum effect on stable equilibrium positions of gyrocompass in geographically oriented coordinate system 13 p2118 A67-26349
- Sensor stability conditions for two rotor gyrocompass on sea-going ship turning in circle 13 p2118 A67-26373
- Mark 19 Sperry gyrocompass with SGN 4 inertial platform 14 p2322 A67-28989
- Mark 27 gyrocompass, discussing suspension by flotation 14 p2322 A67-29083
- Maneuvering stability analysis of single rotor correctable gyrocompass with fluid torsional suspension of sensitive element 15 p2490 A67-30170
- New navigation system/ADVANCE/consisting of two-degrees-of-freedom gyro and accelerometer noting UTM grid-zone distribution system 16 p2701 A67-30928
- Free gyroscopes with feedbacks on each gimbal, determining feedbacks and improving operating indices 18 p3047 A67-33993
- Satellite orientation sensing and orbital gyrocompassing heading reference, examining effect of horizon sensor noise [AIAA PAPER 67-587] 19 p3258 A67-35983
- Gyrocompassing method used for alignment of inertial platform allows gyro-torquer calibration and gyro drift trimming during procedure 22 p3830 A67-39158
- Orbital attitude reference system working model using strapped down principles and digital computer 22 p3907 A67-40187
- Cross coupling effects in strapped down orbital gyrocompass to determine attitude of vehicle with respect to planet-centered coordinate system 22 p3801 A67-40188
- GYROINTERACTION**
- Kinematic analysis of deviation from aircraft-missile line for designing electronic missile firing simulator, with manual telecontrol comprising controlled precession gyroscope for last integration 09 p1486 A67-22419
- Second order gyroviscous stress in collisionless plasma for LF propagation quasi-perpendicular to magnetic field calculated by utilizing higher moments of Vlasov equation 10 p1685 A67-23331
- GYROMAGNETISM**
- Extension of stripline circulator operation calculation by Davies and Cohen to include wider range of stripline geometries 13 p2076 A67-26482
- Weakly ionized plasma and gyromagnetic resonances in helium low pressure HF electrodeless discharge in magnetic field 19 p3276 A67-35113
- Proton gyrofrequency effect on antenna resonance at electron plasma frequency using Alouette II satellite 24 p4125 A67-43111
- GYROSCOPE**
- SA ATTITUDE GYRO**
- SA AUTOGYRO**
- SA CRYOGENIC GYROSCOPE**
- SA ELECTROSTATIC GYROSCOPE**
- SA FLUID ROTOR GYROSCOPE**
- SA NUCLEAR GYROSCOPE**
- SA ROTOR GYROSCOPE**
- SA SYNCHRONOUS GYROSCOPE**
- Gas bearing torques acting on sphere gyroscopically precessing within rotating housing, examining effect of tilt angle 01 p0077 A67-10124
- Rodrigues-Hamilton and Cayley-Klein parameters used in applied theory of gyroscopes 01 p0068 A67-10989
- Apollo Guidance and Navigation System positioning by electrically torquing gyros, discussing error sources 01 p0073 A67-11115
- Dynamics of spherical gyroscope considered as automatic control system operating in presence of random perturbation 06 p1006 A67-18791
- Gyrostat transfer motion from initial stage to predicted orientation maneuver with minimum consumption, using Pontryagin method 07 p1184 A67-19149
- Kinematics of free gyro with gimbal suspension on rotating earth 07 p1186 A67-19627
- Aircraft position determined, using angle indications provided by vertical and directional gyro 07 p1189 A67-20151
- Motion of gyro vertical under starting conditions during turn 09 p1498 A67-22035
- Friction and wear properties of various alumina bearings for use in gas lubricated gyros 10 p1673 A67-23747
- Soviet book on theory of inertial navigation, autonomous systems 11 p1817 A67-24513
- Cardan errors in angle of rotation measurement of gyro-controlled plant 11 p1794 A67-25043
- Astatic gyroscope accuracy dependence on random fluctuations of dry friction moment when under oscillatory motion of bearings, giving correlation function of error dispersion 11 p1794 A67-25044
- Integration of abbreviated motion equations for gyroscopes, obtaining expressions for gimbal errors 12 p1945 A67-25967
- Rate measuring strapdown inertial navigation systems, describing gas bearing gyros and three-axis ring laser 14 p2348 A67-29080
- Fluid sphere gyroscope designed for extreme shock, vibration, temperature and overrate, examining signal processing, design parameters, etc 14 p2322 A67-29081
- Hydrodynamic gas spin bearing gyroscope design for long duration space missions 14 p2322 A67-29084
- Discrete control gyroscopic servosystem for tracing two-dimensional input signal subjected to random noise distortion 15 p2490 A67-30172
- Selection of angular rigidity of shock absorbing system of gyroscopic device 15 p2490 A67-30173
- Selection of gyroscopic reference for commercial aircraft [AIAA PAPER 67-405] 15 p2491 A67-30372
- Precession theory of compensating gyroazimuth, discussing random disturbances reduction by introducing electric mismatch of both sensitive elements 16 p2670 A67-30467
- Guidance and control technology examining inertial guidance systems, Apollo space system, gyros, accelerometers and computers 16 p2699 A67-30650
- Natural oscillations of inertial vertical with nonlinear correction, determining oscillation frequencies and damping rates 16 p2675 A67-31146
- Laser gyroscopes as aid to navigation and guidance, discussing principle, advantages, etc 17 p2868 A67-32726
- Free gyroscopes with feedbacks on each gimbal, determining feedbacks and improving operating indices 18 p3047 A67-33993
- Dynamics of spherical gyroscope considered as automatic control system operating in presence of random perturbation 18 p3049 A67-34456
- Strapdown and gimballed inertial navigation systems history, engineering progress and current developments 19 p3256 A67-35859
- Analog simulation of differential equation system for Cardan-suspended gyro, considering dry friction, support and aircraft motion 20 p3454 A67-36954
- Magnetoresonant gyroscopes simulation by converting motion equations to rotating coordinates system 20 p3451 A67-37154
- Gyrotachometer errors in measuring object angular velocity and acceleration relative to one axis, deriving differential equations of motion 20 p3451 A67-37155
- Motion equations of astatic gyroscope mounted on rocking base and with friction in Cardan suspension axes 21 p3626 A67-38042
- High sensitivity inductive transducer using ferrite rings for measuring nutational oscillations of gyroscopic instruments 21 p3630 A67-38917
- Motion equation derivation permitting analysis of gyrosystems mounted on fixed or moving plants, determining instrumental errors 22 p3795 A67-39230

Error of three degrees of freedom astatic gyro motion owing to viscous friction moments in suspension in case of irregular rocking of base 22 p3810 A67-40484

Laser gyro development and application noting advantages in cooling, power, starting time and acceleration 23 p3999 A67-40916

German Gyroscope Testing Laboratory noting revolving platform for simulating rotational velocities, signal testing and signal simulation 23 p4003 A67-41327

GYROSCOPE FLotation

Temperature control and complex heat path designs inertial components, platforms and strap-down guidance systems, considering floated gyros and accelerometers 02 p0241 A67-11789

Mathematical analysis of problems posed by electrostatic gyroscope with regard to suspension, starting, braking and effect of magnetic induction field on rotor 02 p0242 A67-12039

Thermal diffusion separation of damping fluids in floated gyroscopes 07 p1168 A67-19381

Viscous-and Coulomb-friction forces effect on precessional motion of gyroscope mounted on stationary base 09 p1498 A67-22034

Apollo gyro reliability covering Guidance, Navigation and Control systems, stressing failure mode prediction 19 p3259 A67-35984

GYROSCOPIC COUPLING

Jet engine gyroscopic moments effect on coupling of longitudinal and transverse motions of aircraft 06 p0944 A67-17624

Gyroscopic moment effect on critical speeds of shaft-disk system mounted in short end bearings, obtaining frequency equations [ASME PAPER 67-VIBR-9] 11 p1795 A67-24169

Cross coupling effects in strapdown orbital gyrocompass to determine attitude of vehicle with respect to planet-centered coordinate system 22 p3801 A67-40188

GYROSCOPIC DRIFT

Gyro as force sensor in instrumentation systems, discussing types, testing and calibration procedures 04 p0626 A67-15732

Triaxial gyro-stabilized platform drift determination, given oscillations of gyro units relative to platform 06 p1003 A67-18176

Supersonic transport navigation system accuracy, reliability, directional measurement, inertial speed, etc 07 p1221 A67-19068

Gyroscopic drift from centrifugal inertial moment of gimbals in statically balanced systems, noting dynamic imbalance moment expression 11 p1794 A67-25046

Equations for systematic drifts of gyro-stabilizer with linear viscous-friction moments on precession axes when perturbations are slow 12 p1942 A67-25663

Drift effects of rate gyro under random vibrations, noting doubled eigenfrequency 13 p2153 A67-26624

Suspension axes defects effect on gyro motion under base angular vibration analyzed, noting large gyro drift 14 p2320 A67-28741

Behavior of perfect sphere rotating around axis and under no external force 16 p2677 A67-31715

Long term gyro drift rate evaluation involving time series detrending and autoregression, periodogram, autocorrelation, spectral density and mathematical model analysis 17 p2858 A67-32486

Gyromotor electromechanical moment effect on drift of triaxial gyro-stabilizer exposed to platform vibrations, formulating rotor motion equations 18 p3047 A67-33992

Gyro-stabilized inertial navigation platform system upgraded by applying sampled model reference system, estimating gyro drift rates by stochastic approximation method 18 p3075 A67-34106

Gyrocompassing method used for alignment of inertial platform allows gyro-torquer calibration and gyro drift trimming during procedure 22 p3830 A67-39158

Magnetized gyroscope magnetic moment effect on performance calculated, discussing drift from axis equilibrium state 22 p3796 A67-39231

Expressions for determining directional gyroscope drift, considering random perturbations of base 22 p3809 A67-40481

Gyroscopic large drift angles effect on aperiodic transition condition of four-gyro vertical, deriving precession equations for system 22 p3810 A67-40482

Indirectly corrected gyro vertical used to determine vertical on power plant, considering random plant motion and gyroscopic drift 24 p4155 A67-42298

GYROSCOPIC PENDULUM

HF electromagnetic angular displacement signal generator for use in gyro guidance systems 02 p0220 A67-12224

Oscillatory motion of pendulum-gyroscope system near given position of relative stability 06 p1002 A67-18042

Construction and operational characteristics of device for photographic recording of gyroscopic pendulum trajectory 06 p1003 A67-18177

Location of center of gravity of sensitive element of pendulum effect on stable equilibrium positions of gyrocompass in geographically oriented coordinate system 13 p2118 A67-26349

Analog computer simulation of motions of gyroscopic pendulum, showing imbalance tolerance relationship to error 13 p2118 A67-26350

Gyroscopic large drift angles effect on aperiodic transition condition of four-gyro vertical, deriving precession equations for system 22 p3810 A67-40482

GYROSCOPIC STABILITY

Rotating gyroscope with conical cup on ball support, deriving expressions for moments of forces imposed by support 01 p0064 A67-10419

Precessional motion of corrected gyroscope as affected by viscous friction 01 p0064 A67-10421

Motion equations of gyrostat around fixed point reduced to two-equation system 01 p0067 A67-10821

Inertial system using gyros and accelerometers, determining autonomously plant curvilinear coordinates and plant space orientation parameter 03 p0465 A67-13617

Stability of motion of gyro suspension, noting gyrohorizon compass operation for constant suspension point and angular velocities 03 p0424 A67-14158

Order reduction of equations for gyroscopic systems, using results of Tikhonov study on differential equations with small parameter in front of highest derivative 03 p0424 A67-14159

Lapunov stability of gyroscope motion, with Cardan suspension center moving over earth surface 03 p0424 A67-14179

Cardan error of directional gyro on rocking base, with application to aircraft 03 p0425 A67-14281

Constant component of Cardan error of directional gyro subject to regular rocking 03 p0425 A67-14282

Motion stability of unbalanced gyroscope in Cardan suspension mounted on rotating platform 04 p0620 A67-14790

Gyro-stabilized platform operating mode and stabilization, for use in aircraft as onboard position reference 04 p0624 A67-15537

Inertial guidance platform as position sensor, discussing stabilizing gyro, pitch programmer and alignment sensor 04 p0578 A67-15733

Asymptotic solution for oscillations of quasi-linear gyroscopic systems taking into account internal resonance 07 p1261 A67-19189

Dual quaternions in describing motions of offset unsymmetrical gyroscope [ASME PAPER 66-MECH-6] 08 p1332 A67-21316

Coulomb friction in gyroscopic system analyzed, solving motion 09 p1498 A67-22033

Differential equations of motion for permanent rotation heavy gyro with fixed point 10 p1657 A67-23668

Gyroscopic stabilization of relative equilibrium of satellite 11 p1869 A67-24067

Dissipative gyroscopic force effects on mechanical system, noting necessary and sufficient conditions for stability and controllability 11 p1818 A67-24146

Angular precession and critical speed of two-bearing machines with overhung weight determined, considering shear deformation, gyroscopic moment and rotatory inertia [ASME PAPER 67-VIBR-19] 11 p1796 A67-24176

Motion of arbitrary gyro-stabilizer in central Newtonian force field, applying Lapunov stability conditions for regular precession 11 p1791 A67-24683

Viscous friction in axes of gyroscope suspension further dampens of nutational oscillations and increases precession oscillations of inertial vertical 11 p1794 A67-25051

Vertical vee gyro damping system for gravity gradient satellite, considering scaling, inertia, time and torque factors and viscosity change effects 12 p1920 A67-25122

Single-rotor gyrocompass motion during rocking, determining equilibrium point displacement 12 p1941 A67-25663

Equations for systematic drifts of gyro-stabilizer with linear viscous-friction moments on precession axes when perturbations are slow 12 p1942 A67-25663

Freely precessible gyroscope viscous fluid nutation damping response to translational and vibration accelerations near critical frequencies 12 p1942 A67-25679

Sensor stability conditions for two rotor gyrocompass on sea-going ship turning in circle 13 p2118 A67-26373

Tilt angles for photographs of physically and geographically diverse terrains taken with different types of gyro-stabilized aerial cameras 13 p2118 A67-26463

Rotor bearing clearance effects on whirling of gimbal-mounted gyroscope 14 p2328 A67-29004

Conservative systems motion stability, generalizing precession and nutation of gyroscope with respect to noncyclic coordinate 15 p2518 A67-29685

Attitude stabilization and control system for rotationally symmetric gyroscopic body with two degrees of freedom 15 p2490 A67-30156

Maneuvering stability analysis of single rotor correctable gyrocompass with fluid torsional suspension of sensitive element 15 p2490 A67-30170

Motion equations of astatic gyroscope with vertical rotor axis, with allowance for aircraft motion over pitch, roll and yaw angles 16 p2670 A67-30465

Attitude control for orbiting astronomical observatories, noting system design and performance characteristics 16 p2763 A67-31689

Gyro-controlled rigid rotor system performance, noting steady state and transient response to various excitations [AHS PAPER 131] 16 p2599 A67-31845

Stabilization gyros used for monitoring and detecting performance of avionics inertial navigation system, considering failure modes and effects 17 p2881 A67-32488

Stability of motion of symmetrical rotor gyrostat about fixed point on rotating earth surface 18 p3078 A67-33555

Stability of rotation about symmetry axis of unsteady mechanical system consisting of gyrostat with fixed point and flywheel, deriving motion equations 18 p3078 A67-33556

Gyromotor vibration level variation causes and ball rotation regimes permitting stabilization 18 p3047 A67-33994

Gyroscope circuit model and oscillation behavior analyzed through nonlinear differential equation derived from Euler equation 19 p3227 A67-34843

Dynamic and static gas bearings uses and properties compared with fluid bearings, considering advantages for space applications 20 p3453 A67-36410

Inertia of two-phase asynchronous motor effect on operation of intergimbal correction system of three degree-of-freedom gyroscope 20 p3451 A67-37156

Differential equations of motion for permanent rotation heavy gyro with fixed point 21 p3627 A67-38263

Triaxial attitude control stabilization for second-generation /TIROS/ meteorological satellite 22 p3897 A67-39158

Satellite-gyroscope asymptotic equilibrium positions obtained by general motion equation, calculating gravitational and aerodynamic moment effects 22 p3898 A67-39187

Electrostatic gyro characteristics, design implications, numerical analysis of parameters and corresponding drift rates 22 p3800 A67-40185

Gyro-stabilizer feedback circuit transfer

function with two-phase asynchronous motor equivalent to unit having time constant as function of transmission band of amplifier 22 p3810 A67-40483
Parasitic torques of squeeze-film cylindrical journal bearings in output axis of high performance gyroscopes, discussing tolerance errors [ASME PAPER 67-LUB-5] 24 p4162 A67-42669

GYROTROPIC MEDIUM

Electromagnetic beam propagation in unbounded gyrotropic media taking spatial dispersion into account 02 p0192 A67-11641
Separation constants for finite gyrotropic axially-magnetized cold collisionless plasma graphically represented near boundary of complex region 03 p0371 A67-13867
Magnetic field finiteness effect on effectiveness of gyrotropic plasma waveguide excitation by coaxial line of force 04 p0665 A67-15165
Electromagnetic wave propagation in gyrotropic medium, writing linear equations for alternating field 05 p0761 A67-16207
Approximation method of geometric optics in theory of electromagnetic waves in gyrotropic medium 05 p0762 A67-16347
Approximate technique using perturbation theory in analyzing microwave interaction with gyrotropic media 12 p1908 A67-26183
Magnetic field finiteness effect on effectiveness of gyrotropic plasma waveguide excitation by coaxial line of force 15 p2526 A67-29352
Magnetic field finiteness effect on coordination between gyrotropic plasma waveguide and coaxial line 16 p2718 A67-31190
Electron beam interaction with plasma analyzed using nonquasi-static plasma model 17 p2895 A67-32159
Electron density measurement in ionosphere-magnetosphere transition region using rocketborne gyroplasma swept frequency probe, discussing electron density profile and plasma medium 19 p3229 A67-35201
Electromagnetic wave propagation in absorbing gyrotropic medium in terms of geometrical optics, considering applicability to radiowave propagation in upper atmosphere 19 p3185 A67-36015
Wave propagation in nonuniform slightly gyrotropic medium with parameter less than one solved by differential equations 20 p3389 A67-37708

H

H-51 HELICOPTER S XH-51 HELICOPTER H-ALPHA LINE

Limb intensity profiles at center of hydrogen alpha calculated for several simple models of absorption coefficient at line center, showing abrupt changes in gradient 02 p0323 A67-11693
Line emission of hydrogen alpha limb spectra beyond continuum limb analyzed to yield data about height of formation in solar chromosphere [AFRL-66-834] 02 p0323 A67-11694
H-alpha line profiles and motions of spicules in solar chromosphere studied by spectral photographs taken with noneclipse coronagraph 02 p0328 A67-12483
Spectrophotometric results for H-alpha and K line contours of August 21, 1959 chromospheric flare 05 p0892 A67-16496
Contribution of quasi-static electrons to broadening of hydrogen 2 line profile 10 p1704 A67-22884
H-alpha line profiles and motions of spicules in solar chromosphere studied by spectral photographs taken with noneclipse coronagraph, 10 p1708 A67-23351
Motions of chromospheric fine structure in weak plage analyzed, using time resolved H-alpha spectra for estimating line-of-sight velocities of objects 12 p2001 A67-25222
Hydrogen distribution in upper atmosphere and geocorona, relating H-alpha emission increase to solar activity decrease 17 p2849 A67-32861
H-alpha diurnal and seasonal intensity variations in geocorona indicating hydrogen content build-up during night 17 p2851 A67-33202

Brightening observed near D-2 line of sodium I on July 28, 1966 17 p2939 A67-33396
Hydrogen emission lines photoelectric measures in Ton 1542 indicates radiative recombination in upper levels and sharp intensity increase in red ascribed to nonthermal sources 18 p3120 A67-33997
Mean intensity photospheric H-alpha radiation profile for prominences in solar corona, noting profile dependence on height, velocity and direction 24 p4209 A67-41965
Decrement of Balmer line widths and H-alpha profiles when distributing fine components as function of radial velocity in optical prominences 24 p4232 A67-42595

H-BETA LINE

Asymmetric broadening of H-beta Balmer line in hydrogen doped argon plasma arc 09 p1536 A67-21562
Hydrogen line profiles in model atmospheres using quasi-static approximation for electrons and ions 10 p1704 A67-22883
Energy spectrum and pitch-angle distribution of protons in auroras based on H-beta line profiles 17 p2938 A67-32962
Rapid scan spectrometer used to measure Stark broadened H lines in plasma column, determining electron density 23 p4032 A67-40957

H-WAVE

Slot filters for H waves in circular waveguide 03 p0386 A67-13960
Field distribution at bends in circular zero-normal H and cylindrical surface waveguides 04 p0586 A67-15635
Electromagnetic field emission of infinite package of impedance half-planes produced by cophasal linear sources 05 p0762 A67-16352
Auroral hydrogen emission measurements and indications of proton or electron excitations 05 p0797 A67-16851
Coefficient of reflection of H-11 mode shock wave emitted from aperture of circular waveguide with infinite flange 08 p1302 A67-20825
Intensity and shape of spectral lines of excited hydrogen in radio range 08 p1356 A67-21345
Standing wave solution of homogeneous waveguide field distribution for H-10 wave after conformal mapping and effect of capacitive and inductive irises 10 p1607 A67-23571
Interaction of incident H-wave with infinite conducting cylinder coated with inhomogeneous and anisotropic plasma sheath, noting far field pattern of scattered field 16 p2626 A67-31350
Intensity and shape of spectral lines of excited hydrogen in radio range 17 p2887 A67-31941
Propagation coefficients of leaky waveguide modes improved by corrections to radial line susceptance arising from uniform slot in wall of circular waveguide 17 p2812 A67-32317
Plasma acceleration by SHF waves, worldwide research and results 17 p2904 A67-32915
Electron temperature of H II region related to high temperature main sequence stars determined as function of electron density and radiation dilution factor 19 p3325 A67-35503
H-01 waveguide irregularities causing transfer function fluctuation, calculating rms and relative distortion power from PCM signal 19 p3183 A67-35561

HABITABILITY

Spacecraft habitability, discussing chemical and bacteriological changes, air contamination and biological compatibility for crew selection 13 p2061 A67-26754

HABITUATION

Visual arousal interaction and specificity of nystagmic habituation 17 p2805 A67-31958
Micrometazoa as model systems for studying physiology of memory at cellular level, examining habituation and maze behavior 20 p3369 A67-36657
Habituation transference in Coriolis stimulation for change from passive lateral chair tilts to various active head tilts during rotation 23 p3953 A67-41585

HAFNIUM

Plasma mode work function measurement for studying thermionic emission from Hf, Th and Ti in Cs vapor at reservoir temperature of 414 degrees

K 09 p1450 A67-22353
Depressing effect of hafnium and zirconium on work function of tungsten, tantalum, niobium and rhenium 10 p1668 A67-23091
Fourier analysis of line profiles of X-ray-studied deformation faulting in titanium, zirconium and hafnium 14 p2340 A67-29033

HAFNIUM CARBIDE

Titanium, zirconium and hafnium effect on recrystallization temperature and strength of alloys of molybdenum with carbon 05 p0832 A67-17508
Reaction kinetics of liquid titanium and hafnium with carbon using layer-growth method 16 p2690 A67-31373
Titanium, zirconium and hafnium effect on recrystallization temperature and strength of alloys of molybdenum with carbon 21 p3644 A67-38036

HAFNIUM COMPOUND

Hafnium-tantalum coated refractory metals investigated for use in high temperature rocket motors 22 p3821 A67-39891

HAFNIUM OXIDE

Equilibrium carbon monoxide pressures measured by torsion effusion studies of reaction of graphite with hafnium and uranium dioxides at high temperatures 01 p0018 A67-10763
Hafnium oxidation between 300 and 1200 C, noting occurrence of faster stages in process 13 p2132 A67-26999
Transconductance and voltage gain of MOS/FET using hafnium dioxide 15 p2442 A67-29171
Lattice parameter of bcc Nb-Hf alloy with interstitial solid solution of oxygen 22 p3823 A67-40210

HAILSTONE

Raindrop and melting hailstone absorption, scattering and backscatter cross sections of millimeter waves in satellite communications and weather radars 04 p0577 A67-15685

HALF-PLANE

Stressed state of anisotropic half-plane weakened by finite number of elliptical holes with centers on straight line perpendicular to boundary of half-plane 05 p0907 A67-16018
Electromagnetic field emission of infinite package of impedance half-planes produced by cophasal linear sources 05 p0762 A67-16352
Characteristic for kernels of certain integral equations on semiaxis for determining solvability and number of possible solutions 14 p2344 A67-28809
Wave equation solution for potential of cylindrical Dirac pulse incident on reflecting half-plane 17 p2817 A67-33139
Unsteady dynamic field excited by source moving along elastic half-plane boundary 21 p3716 A67-37967
Impedance strip directional properties when excited through slot in metallic half-plane, noting case of reflector antenna with decreasing impedance 22 p3770 A67-39763

HALF-SPACE

Boundary value problem solution for sound generated at oscillating wall, propagating into half-space, for linear Boltzmann equation with general cut-off molecular potential 01 p0114 A67-10736
Parabolic convolution type equations in bounded cylindrical and noncylindrical regions, discussing smooth operators in half-space 02 p0259 A67-11871
Electromagnetic fields of oscillating electric dipole located over half-space with anisotropic conductivity and dielectric constant 02 p0204 A67-12194
Diffracted field structure of plane wave incident obliquely from air onto sinusoidally modulated half-space at Rayleigh and Bragg wavelengths 02 p0204 A67-12196
Fields of horizontal dipole over stratified anisotropic half-space 03 p0370 A67-13858
Time harmonic Rayleigh wave attenuation in elastic half-space by surface impedance 03 p0371 A67-13945
Book on systematic and unified treatment of electromagnetic radiation from elementary Hertzian dipole in presence of dissipative half-space 03 p0373 A67-14273
Current distribution on half-wave dipole antenna embedded in conducting half-space, noting case where dissipative medium has average earth constants 05 p0769 A67-16006
Classical elasticity-theory determination of stress distribution on boundary plane of

- elastic half-space due to internal body force distribution 05 p0908 A67-16040
- Acoustic field of random pressure pulsations into half-space behind infinite plate with arbitrary number of layers 05 p0846 A67-16708
- Aerodynamic forces on flexible plate embedded in right half-space undergoing arbitrary temporal and spatial motion 08 p1424 A67-21433
- Isolated force solution as Green function for formulation of plane problems for cracks along interface of two bonded half-spaces 10 p1731 A67-23848
- Acoustic field of random pressure pulsations into half-space behind infinite plate with arbitrary number of layers 11 p1820 A67-24930
- Reflection coefficients for electromagnetic waves obliquely incident on sinusoidally stratified half-space 13 p2066 A67-26481
- Theory of Rayleigh waves at surface of elastic half-space, determining ratio of horizontal to vertical component of motion 13 p2156 A67-26602
- Torsion of finite elastic cylindrical rod welded to elastic half-space [ASME PAPER 67-APM-30] 17 p2965 A67-33156
- Circumferentially symmetrical stressed state of half-space determined using Polozhnyi formulas in axisymmetric elasticity theory and p-analytic functions 20 p3538 A67-36918
- Wave propagation in inhomogeneous half-space with refractive index depending on two coordinates analyzed, using parabolic equation method 21 p3580 A67-38114
- Asymptotic solution for electromagnetic field of electric dipole above stratified half-space 22 p3763 A67-40311
- Electromagnetic pulse distortion during total internal reflection in stratified troposphere, discussing reflecting medium inhomogeneity effects on reflection coefficients 23 p3973 A67-40837
- HALIDE**
- SA ALKALI HALIDE
- SA CHLORIDE
- SA FLUORIDE
- SA IODIDE
- SA METAL HALIDE
- High voltage photo-emf in epitaxial zinc telluride films grown on halide substrates 05 p0868 A67-17061
- Molecular laser action on vibrational-rotational transitions between low lying vibrational levels on hydrogen and deuterium halides 13 p2127 A67-27018
- High voltage photo-EMF in epitaxial zinc telluride films grown on halide substrates 15 p2538 A67-29792
- IR vibrational and Raman spectra of thiophosphoryl trichloride, thiophosphoryl dichlorofluoride, thiophosphoryl chlorodifluoride and thiophosphoryl trifluoride 23 p4041 A67-41242
- HALL ACCELERATOR**
- Performance capabilities of Hall current accelerators determined from parameters influencing anode power loss [AIAA PAPER 66-184] 01 p0125 A67-11160
- Theoretical possibilities of using electromagnetic forces for acceleration of plasmas /self-magnetic and Hall acceleration/ in case of axisymmetric electrode arrangement 04 p0687 A67-14559
- Diagnostic measurements in alkali plasma Hall accelerator /alpha/ including azimuth and axial velocity components, energy flux, total beam power, etc [AIAA PAPER 67-46] 06 p1042 A67-18493
- Theoretical possibilities of using electromagnetic forces for acceleration of plasmas /self-magnetic and Hall acceleration/ in case of axisymmetric electrode arrangement 07 p1240 A67-19569
- Langmuir probe velocity and acceleration measurements for coaxial Hall accelerators [AIAA PAPER 66-196] 08 p1375 A67-20575
- Electrode feed system for segmented electrode MHD wind tunnel 12 p1920 A67-25406
- Performance capabilities of Hall current accelerators determined from parameters influencing anode power loss [AIAA PAPER 66-201] 12 p1975 A67-25892
- Screw instability in linear Hall accelerator 15 p2522 A67-29207
- Physical aspects of plasma accelerator using closed Hall currents, discussing equilibrium of forces and potential distribution 21 p3863 A67-37938
- MPD Hall accelerator construction and operation using argon or helium propellants, measuring azimuthal velocities in plume [AIAA PAPER 67-672] 21 p3891 A67-38705
- Alkali plasma Hall accelerator /ALPHA/ thruster performance, discussing acceleration mechanisms and correlating data [AIAA PAPER 67-687] 21 p3892 A67-38718
- HALL EFFECT**
- Photo-Hall effect and photoconductivity on compensated p-InSb at low temperatures, examining temperature dependence of carrier mobility 01 p0128 A67-10093
- Peculiarities of Hall curves of n-type alpha silicon carbide, noting concentration of conduction electrons related to temperature 01 p0129 A67-10102
- Energy levels in forbidden band of gallium arsenide alloyed with silver or gold, determining impurity levels from temperature dependence of electric conductivity and Hall constant 01 p0129 A67-10104
- Hall effect in low temperature plasma consisting of combustion products with admixture of KOH under variable sign magnetic field, demonstrating potential gradient existence 01 p0120 A67-10175
- Hall coefficient tensor in single crystals of titanium measured at room temperature as function of crystallographic orientation in magnetic field 01 p0132 A67-10375
- Anisotropy of Hall effect dependence on field and temperature in dysprosium crystal 01 p0133 A67-10743
- Resistivity and Hall coefficient measurement of n-and p-type gold-diffused silicon over wide temperature range 01 p0134 A67-10754
- Indium arsenide thin films for field effect transistors prepared by coevaporation, obtaining high Hall mobilities and good saturation 01 p0039 A67-10876
- Hall effect and fine structure of X-ray fluorescence and absorption K spectrum of vanadium in silicides 01 p0101 A67-10935
- Hall coefficient variation with substrate temperature of thin films of tellurium, lead telluride and antimony 01 p0138 A67-11231
- Pure selenium conductivity, thermal emf and Hall effect 01 p0138 A67-11297
- Hall coefficient dependency on thickness of semiconducting thin metal films 02 p0294 A67-11757
- Conductivity, Hall coefficient and magnetoresistance of monophase InSb films as function of film thickness 02 p0295 A67-11765
- Electron-hole conductivity effect on temperature variations of Hall coefficient and Nernst-Ettingshausen effect in semiconductor 02 p0296 A67-11829
- Anisotropy of electric resistivity, Seebeck and Hall coefficients and magnetoresistance of n-type single crystal ferric oxide /hematite/ containing tetravalent tin ion as impurity 02 p0299 A67-12085
- Resistivity, temperature coefficient of resistivity and Hall coefficient as function of bismuth film thickness, showing that size quantization of films leads to semiconductor metals 02 p0300 A67-12509
- Anisotropy of magnetoresistance and Hall effect in n-GaAs, discussing conduction band structure in vicinity of edge 03 p0487 A67-12806
- Differential method measurement of Hall effect in presence of large constant magnetic field 03 p0487 A67-12808
- Electrical properties of GaSe-layer-semiconductor single crystals used to determine scattering mechanisms of charge carriers, depth of impurity centers, effective mass and forbidden gap 03 p0488 A67-12816
- Hall effect in semiconductors containing two species of current carriers, p-type PbTe and GeTe, taking into account temperature dependence of energy gap 03 p0489 A67-13148
- Hall mobility and Nernst-Ettingshausen effect in Zn and Cd-doped p-type GaAs at temperatures from 90 to 800 degrees K 03 p0491 A67-13174
- Electrical conductivity and Hall coefficient temperature dependence in pure and alloyed Te 03 p0492 A67-13344
- MHD stability of dense plasma jets flowing into transverse magnetic field, discussing effect of conductivity and Hall factor 03 p0477 A67-13462
- Electrical conductivity, Hall coefficient and absolute thermoelectric power of liquid antimonides and tellurides 03 p0495 A67-13533
- Current density distribution in two-electrode MHD channel operating in amplification and generation mode 03 p0479 A67-13686
- Small amplitude wave propagation in ionized high temperature gas embedded in uniform magnetic field with Hall current 03 p0482 A67-13742
- Temperature-composition relationship for Hall coefficient inversion point in Ti-doped Te single crystals 03 p0500 A67-14232
- Anomalous high temperature Hall data for GaSb explained as effect of electrons in /100/ conduction band minima 03 p0501 A67-14346
- Transverse magnetoresistance and Hall effect measurements on n-type GaSb at various magnetic fields and temperatures, obtaining electron concentration and mobility 03 p0501 A67-14347
- Galvanomagnetic effect in ferromagnetic metals, developing theory of planar Hall effect in terms of spin-orbit interaction of electrons 03 p0501 A67-14368
- Longitudinal magnetoresistance anisotropy and Hall coefficient anisotropy in p-type indium antimonide, noting similarities with galvanomagnetic anisotropy of p-type germanium 04 p0674 A67-14609
- Hall effect and transport properties of single crystals of iodine measured by alternating current technique, using field effect transistors 04 p0675 A67-14757
- Analog carrier frequency multiplier using Hall effect in multiplier element 04 p0581 A67-14892
- Hall effect, voltage generation across current-carrying conductor perpendicular to magnetic field and galvanomagnetic effects based on Lorentz force 04 p0657 A67-15081
- Quantum oscillation of transverse and longitudinal magnetothermal emf in n-type indium antimonide compared with oscillations of transverse and longitudinal magnetoresistance and Hall coefficient 04 p0680 A67-15288
- Phenomenological theory of longitudinal Hall effect in cubic crystals, assuming anisotropic dispersion law and tensorial relaxation time 04 p0681 A67-15291
- Inverse Hall effect of noble metals alloyed with B-group metals as affected by residual resistivity and phonon scattering 04 p0682 A67-15465
- Conical MHD flow of ideal conducting gas with Hall effect in magnetic field, deriving electrodynamic and energy characteristics 04 p0669 A67-15515
- MHD wave propagation emphasizing viscosity, heat and electrical conductivity, Hall current, nonequilibrium phenomena and effect of medium inhomogeneity 05 p0851 A67-16364
- Quantum oscillations of Hall effect and longitudinal and transverse reluctance in n-indium antimonide, noting spin splitting and temperature and electron concentration effect on oscillation maximum 05 p0861 A67-16394
- Composite valence band in p-PbTe obtained from measurement of Hall effect, thermoelectric and optical effects 05 p0868 A67-17062
- Optimum MHD generators using anisotropic plasma, discussing conducting-gas MHD flow, Hall effect, ion slip effect, etc 06 p0950 A67-18089
- Electrode geometry effect on current and potential distributions in MPD arcs 06 p1074 A67-18335
- Quasi-one-dimensional MGD channel flow calculation methods, considering Hall effect, heat transfer, friction and potential drop near sectioned electrode 06 p1043 A67-18675
- Alternating method of measuring Hall constant by modulation of voltage amplitude on arbitrarily shaped plates 06 p1005 A67-18727
- Hall effect and magnetoresistance effect measured on p-and n-CdSb single crystals above 77 degrees K and magnetic fields up to 7500 gauss 06 p1054 A67-18824
- Carrier-carrier scattering influence on Hall effect and on minority-majority carrier mobility in graphite 06 p1063 A67-18938

Conduction band structure and anisotropy of electron scattering in n-GaAs, analyzing magnetoresistance and Hall effect 06 p1064 A67-18943

Hall coefficient and transverse magnetoresistance behavior in n-GaSb at 4.2 degrees K, using DC high magnetic fields 06 p1064 A67-18946

Hall effect in hopping region of Si and Ge attributed to residual thermal and impact ionization 06 p1067 A67-18966

Resistivity, magnetoresistance, Hall effect and thermal conductivity in n-type In-Sb at liquid He temperatures 06 p1068 A67-18968

Contact effects in degenerate semiconductors at low temperature based on Hall study of tunnel junctions 06 p1069 A67-18976

Oscillatory magnetoresistance and Hall effect in single crystals of Sn-doped Bi to decrease Fermi energy 06 p1070 A67-18984

Effects of gases flowing in magnetic field analogous to galvanomagnetic Hall effect in conductors analyzed using oxygen 07 p1230 A67-20144

Current density distribution in MPD arc jet exhaust measured, using Hall effect sensors [AIAA PAPER 66-116] 08 p1375 A67-20573

Combined Rayleigh-Taylor and Kelvin-Helmholtz instability for incompressible plasmas carrying uniform magnetic field including Hall current 08 p1359 A67-20902

Hall effect on hot carriers in p-type Ge semiconductor in microwave field as function of field strength 08 p1369 A67-20993

Electron scattering mechanism in SiC polytypes, noting mobility limiting mechanism from 300 to 800 degrees K 08 p1370 A67-21293

Temperature dependent variations in Hall coefficient of indium and indium-rich alloys with Pb, Cd, Ti and Hg 08 p1371 A67-21438

Thickness dependence of Hall constant, electrical conductivity and Hall mobility in polycrystalline thin layers of InSb 09 p1551 A67-21565

Hall effect in low temperature plasma in nonhomogeneous magnetic field, describing measuring device 09 p1541 A67-21803

Eddy current test systems using magnetic reaction analyzer with Hall element for detector, noting applications to welding, thickness measurement, stress monitoring, etc 09 p1502 A67-21869

Unusual electrode configuration for Hall effect measurements on thin films and field effect devices 09 p1472 A67-21955

Resistivity, Hall effect and thermoelectric power of mercury selenide from 77 to 500 degrees K 09 p1557 A67-22556

High field Hall effect of semiconducting CdS crystals with different mobilities, noting electron density and multiplication 10 p1689 A67-22908

Chemisorbed oxygen effect on Hall mobility and conduction electron concentration of spray deposited CdS thin films 10 p1689 A67-22910

Hall effect in semiconductors containing two species of current carriers, p-type PbTe and GeTe, taking into account temperature dependence of energy gap 10 p1689 A67-23097

Measuring Hall effect in high specific resistance materials by using alternating magnetic field and DC current 10 p1691 A67-23502

Gallium arsenide epitaxial technology noting deposition rate and impurity profile, Hall mobility and morphology of deposits 10 p1692 A67-23511

Gallium arsenide characteristics and preparation noting epitaxial deposition and liquid phase, mobility, impurity and Hall effect data 10 p1692 A67-23512

Temperature dependence of Hall constant and photoconductivity kinetics of gallium antimonide with different tellurium content 10 p1694 A67-23651

Temperature dependence of electrical properties of compensated GaAs 10 p1694 A67-23655

Temperature dependence of Hall coefficient of tellurium doped GaAs ternary compound, noting activation energy parameter 10 p1694 A67-23656

Magnetic resistance and Hall effect dependence on external electric field in semiconductors, noting difference for parabolic and nonparabolic law of carrier

dispersion 10 p1695 A67-23661

Hall effect and electrical resistance of ZrC-NbC and TaC-HfC alloys at room temperature 11 p1804 A67-23904

Structure, conductivity and Hall effect of electron bombardment evaporated silicon films on sapphire substrates, noting deposition temperature source doping effectiveness 11 p1845 A67-24141

One-dimensional flow through nozzle and stability of weakly ionized plasma with induced Hall current 11 p1832 A67-24155

Plasma conductivity measurement based on Hall current and Hall voltage relation to electrical resistance 11 p1839 A67-24424

Anomalous Hall effect in microcrystalline germanium at SHF 11 p1846 A67-24471

Galvano- and thermomagnetic phenomena in semiconductors analyzed using transient method, noting extraneous EMF influence on Hall effect 11 p1792 A67-24814

Current distribution of magnetic field in plasma coaxial injector indicating dominant role of Hall effect in plasma acceleration 11 p1841 A67-24854

Large disk MHD generator studied for plasma properties and fluid mechanics, noting seed ionization effect on performance 12 p1972 A67-25386

Hall voltage reduction in linear MHD generators noting Lorentz force effect 12 p1898 A67-25387

Diagnostic techniques for atmospheric pressure arc plasmas, noting that integrated current density measurements are consistent with measured total arc current 12 p1973 A67-25393

Hall effect and thermoelectric power in doped, conductive titanium oxide ceramics, noting dependence on doping concentration 12 p1982 A67-25452

Forbidden band structure of PbTe and electrical conductivity and Hall effect measurements at high temperatures 12 p1983 A67-25513

Hall coefficient dependence on magnetic field intensity for n-type InSb single crystals at 77 degrees K 12 p1984 A67-25518

Hall EMF measurement in base of negative resistance silicon diode 12 p1917 A67-26097

Stability of self-gravitating two-fluid infinite plasma cylinder model in axial magnetic field 13 p2163 A67-26285

Current carrier concentration gradient in InSb, investigating effect on transverse reluctance coefficient and Hall effect dependence on magnetic field intensity 13 p2173 A67-26360

Electromagnetic effect in n-type InSb samples, measuring magnetic resistance, Hall effect and magnetic EMF 13 p2174 A67-26368

Hall and electric field effects in cadmium sulfide single crystals in terms of current carrier mobility 13 p2174 A67-26369

MHD generator two-dimensional incompressible flow, obtaining expressions for power output, velocity, electrical efficiency, etc 13 p2055 A67-26417

Electromagnetic wave propagation in type II superconductors, noting Hall angles influence 13 p2175 A67-26428

Conductivity, temperature dependence, thermal EMF Hall constant, thermal conductivity and resistivity of aluminides of transition metals 13 p2131 A67-26471

Influence of Hall effect and viscosity on flow relations and power output of MHD generator 13 p2165 A67-26842

Anisotropy of Hall effect dependence on field and temperature in dysprosium crystal 13 p2176 A67-26772

Rocket measurements of equatorial electrojet current 13 p2114 A67-26793

Plastic deformation effect on resistivity and Hall effect of copper-palladium and gold-palladium alloys 13 p2133 A67-27005

Two-dimensional unsteady plasma flows in coaxial channel formed by two profile electrodes calculated in case of finite conductivity in presence of Hall effect 13 p2168 A67-27301

Electrical conductivity and Hall coefficient temperature dependence in pure and alloyed Te 13 p2184 A67-27718

Temperature dependence of electrical conductivity and Hall effect of barium-titanate crystals reduced by hydrogen, observing electron spin resonance and optical absorptions 14 p2363 A67-27824

Resistivity and Hall effect oscillations in

antimony doped n-type germanium crystals in metallic impurity conduction state 14 p2365 A67-28231

Electromagnetic wave propagation characteristics in solid plasmas without magnetic induction, showing dynamic Hall effect 14 p2366 A67-28473

Hall coefficient, electrical resistivity and Seebeck coefficient of p-type lead telluride measured, using two-valence band model 14 p2367 A67-28520

Temperature dependence of Hall mobility of photoelectrons and electrons produced by X radiation in cadmium sulfide single crystals 14 p2387 A67-28525

Measurement of variable Hall electromotive force component created by illumination of thin low resistance germanium samples by modulated 14 p2368 A67-28529

Schubnikow-De Haas oscillation analysis in n-type bismuth telluride indicates multivalley conduction band structure 14 p2369 A67-28596

CdSb single crystals doped with Au at liquid helium temperature studied for temperature dependence and Hall effect 14 p2372 A67-28757

CdSb polycrystals of different structural patterns investigated for dependence of electrical conductivity, Hall mobility and thermal EMF 14 p2372 A67-28758

Lorentzian scalar electrical conductivity as basis of mixture rules proposed for partially ionized gases in magnetic field to calculate tensor conductivity 15 p2523 A67-29218

Low temperature transport effects in n-type gallium antimonide at high magnetic fields, observing oscillatory behavior of Hall coefficient and transverse magnetoresistance 15 p2534 A67-29327

Temperature dependence of electrical conductivity, Hall effect and resistance in transverse magnetic field for tin-doped InSb 15 p2534 A67-29385

Linear signal multiplier using thermally stable InSb, InAs or GaAs sensors with Hall effect voltage linearly dependent on control current 15 p2444 A67-29386

Electrodeless MGD power generation during entry, using torque on magnet taken as rotating member of generator 15 p2422 A67-29443

Lanthanum chromite activation energy determination from electrical resistivity and Hall coefficient variation as function of temperature and IR absorption spectrum 15 p2535 A67-29478

Temperature dependence of lifetime and Hall coefficient in InSb, measuring lifetime by phase shift method, concluding that recombination centers are lattice defects 15 p2535 A67-29483

Parameters for model of two valence bands of SnTe according to Hall effect measurements at high temperatures 15 p2537 A67-29709

Plasma azimuthal inhomogeneity in homopolar system, noting Hall current and stationary plasma acceleration 15 p2529 A67-29723

Composite valence band in p-PbTe obtained from measurement of Hall effect, thermoelectric and optical effects 15 p2538 A67-29793

MHD generator with uniform rectangular duct, considering ion slip and Hall effect in case of two-dimensional flow 15 p2422 A67-29906

Electric and thermoelectric effects in single crystals of zinc-cadmium-antimony solid solution, measuring electrical conductivity, Hall constant and thermoelectric power 15 p2540 A67-30029

Hall coefficient and reluctance dependence on magnetic field inductance in p-type cadmium tin arsenide samples from 250 to 411.7 degrees K 15 p2543 A67-30253

Hall effect in semiconducting electrode MHD generators, noting Joule heating losses, nonlinear electrical conductivity, etc 16 p2600 A67-30533

Ionization saturation and duct shape effects on losses near walls, including large Hall effects, regular current distribution, and plasma conductivity regularization 16 p2711 A67-30536

Hall effect measurement in single crystal of arsenic at liquid helium temperatures in magnetic fields noting quantum oscillations 16 p2727 A67-30820

Irradiation of gallium arsenide and gallium antimonide monocrystals by electrons, fast neutrons and relativistic protons, discussing Hall coefficient variation 16 p2727 A67-30869

Conductivity, Hall effect and Seebeck coefficient measurements on single domain crystals of barium titanate 16 p2729 A67-31060

Electric and thermal conductivity and Hall effect in solid solution of complex semiconductors noting temperature dependence 16 p2729 A67-31155

Temperature dependence of transverse and longitudinal Nernst-Ettingshausen effect and composition effects on Hall electron concentration in InSb-InTe solid solution 16 p2730 A67-31157

Double-walled cryostat with copper holder for probe measurements of temperature dependence of semiconductor galvanomagnetic effects 16 p2730 A67-31158

Pulsed resistivity and Hall effect measurements of n-type GaAs in high electric fields at room temperature below microwave oscillation threshold 16 p2731 A67-31449

Specific resistance, EMF, Hall effect, and minority-carrier lifetime measurement of germanium whiskers bombarded by high energy electrons from linear accelerator 16 p2732 A67-31479

Electrical conductivity and Hall effect of indium arsenide solid solutions, noting temperature dependence and hole mobility 16 p2732 A67-31480

Field effect behavior of thin InSb films noting semiconductor surface properties, mobility decrease with temperature and increase of impurity concentrations 16 p2732 A67-31527

Hall parameter instability and conductivity analysis applied to performance characteristics of subsonic flow generator 17 p2898 A67-32181

Hall field intensity and asymptotic electron temperature of ionized argon-cesium mixture flow in transverse magnetic field with subsonic velocity 17 p2900 A67-32338

Irradiated germanium observed for carrier concentration variations, using Hall coefficient measurements 17 p2918 A67-32853

Minority carrier trapping analyzed from transient decay of photoconductivity in n-type polycrystalline films of InAs 17 p2922 A67-33064

MHD behavior of inviscid fluid in limit of infinite electrical conductivity and mobility exhibiting Hall effect 17 p2908 A67-33109

Temperature dependence of Hall constant and photoconductivity kinetics of gallium antimonide with different tellurium content 17 p2923 A67-33332

Temperature dependence of electrical properties of compensated GaAs 17 p2923 A67-33336

Temperature dependence of Hall coefficient of tellurium doped GaAs ternary compound, noting activation energy parameter 17 p2923 A67-33337

Magnetic resistance and Hall effect dependence on external electric field in semiconductors, noting difference for parabolic and nonparabolic law of carrier dispersion 17 p2924 A67-33342

Hall angle of various superconducting niobium-tantalum alloys in mixed state, noting dependence on current and temperature 18 p3098 A67-33519

Magnetic field effect on Hall coefficient of p-type Ge-Si single crystal alloys 18 p3098 A67-33574

Mobility measurement of electron capture in hydrocarbon flames using Hall effect, noting variation when injecting chlorine 18 p3146 A67-33691

Current distribution in segmented electrode MHD duct and sufficient condition for preventing current leakage between adjacent segments of generator 18 p2987 A67-33703

Speed deficits of oxyacetylene detonation waves passing through MHD channel in electromagnetic field explained by Hall effects altering boundary layer 18 p3086 A67-33825

Stagnation pressure lower than atmospheric pressure in supersonic subatmospheric flow in magnetoaerodynamic generation nozzle, discussing Hall effects for energy conversion

process 18 p3020 A67-34122

Measuring IR Faraday rotation and Hall effect in 6H and 15R polytypes of silicon carbide 18 p3102 A67-34278

Forbidden band structure of PbTe and electrical conductivity and Hall effect measurements at high temperatures 18 p3103 A67-34444

Hall coefficient dependence on magnetic field intensity for n-type InSb single crystals at 77 degrees K 18 p3103 A67-34449

Electric field of AC solenoid of finite length in Hall conducting medium 18 p2990 A67-34500

Hall effect measurements on Te-doped GaAs crystals diffused with Cu₆₄, studying vacancy-donor interactions, hole concentrations and energy levels 18 p3105 A67-34634

Lorentz number, Hall coefficient, magnetoresistance and Hall mobility variations in n-type degenerate semiconductors 18 p3106 A67-34729

Band structure and current carrier scattering in hole-type SnTe, studying temperature dependence of electric conductivity, thermal EMF, Hall effect, etc 19 p3300 A67-34786

Temperature dependence of electric conductivity and Hall effect in epitaxial layers of undoped and Fe-doped n-type GaAs samples 19 p3300 A67-34770

Fast neutron irradiation effect on electrical conductivity and Hall effect in Zn doped n-type indium arsenide single crystals 19 p3301 A67-34771

Resistance and Hall effect measurements on PbTe thin films prepared by vacuum evaporation on amorphous or oriented substrates 19 p3307 A67-35795

Determining resistivity and Hall coefficient using four point contacts placed on Hall plate isotropic uniformly thick two-dimensional sheet with perpendicular magnetic field 19 p3308 A67-36041

Adsorption effect of various metals on electrical conductivity and Hall effect of thin nickel films 20 p3504 A67-36166

Transport phenomena in semiconducting thin films studied using transport equation, obtaining relaxation time relationship to semiconductor 20 p3506 A67-36217

Hall constant of semiconductors noting dependence on specimen size, film and current electrode parameters 20 p3508 A67-36406

Layer removal techniques with Hall effect and sheet resistivity measurements indicate carrier concentrations exceeding thermal equilibrium solubility for antimony implants into silicon 20 p3510 A67-36856

Current distribution in MHD channel with strong magnetic field solved by reduction to Riemann type boundary value problem 20 p3500 A67-37047

Distributed RC parameters influence on Hall voltage magnitude in high resistivity semiconductors, explaining voltage decrease 20 p3513 A67-37452

Current distribution of magnetic field in plasma coaxial injector indicating dominant role of Hall effect in plasma acceleration 20 p3502 A67-37537

Electron drift velocity and mobility in InSb calculated from conductivity and Hall effect measurements, noting microwave emission occurrence 20 p3514 A67-37544

Impurities compensated p-type cadmium antimonide single crystals, determining Hall effect temperature dependence and specific resistance 21 p3678 A67-37868

Displacement detector operating on Hall effect basis with differential magnetic circuit, including displacement transmitters with unified output 21 p3626 A67-38159

Energy indicators calculated for MHD channel flow with finite sectional electrodes and wide Hall parameter variations 21 p3665 A67-38242

Current carrier concentration gradient in InSb, investigating effect on transverse reluctance coefficient and Hall effect dependence on magnetic field intensity 21 p3680 A67-38317

Electromagnetic effect in n-type InSb samples, measuring magnetic resistance, Hall effect and magnetic EMF 21 p3680 A67-38324

Hall and electric field effects in cadmium sulfide single crystals in terms of current carrier mobility 21 p3680 A67-38325

Resonance and noise microwave emission thresholds for InSb electron hole plasma subject to crossed electric and magnetic fields, noting Hall effect 21 p3683 A67-38400

N-type InSb hot electron and nonohmic effects, noting low temperature and magnetic and electric field dependence of Hall coefficient and resistivity 21 p3683 A67-38400

Relation between electric conductivity and Hall coefficient in solid solutions, determining sample composition and temperature for forbidden band width concentration dependence 21 p3684 A67-38440

Hall effect measurements on heat treated and quenched p-type silicon crystals, noting donor centers appearance due to vacancy cluster 21 p3687 A67-39136

Electrical conductivity, Hall coefficient and thermo-EMF measurements in Zn and Te doped gallium antimonide crystals for minority carrier role in impurity conduction 21 p3687 A67-39141

Hall coefficient and mobility measured for annealed polycrystalline and epitaxially grown gold, silver and copper films; discussing size effect 22 p3855 A67-39355

Carrier concentration dependence of thermoelectric power and Hall mobility of undoped and doped lead telluride explained by two-valence model 22 p3857 A67-39490

Current carrier mobility, Hall effect and magnetoresistance in semiconductors with nonuniform ion distribution 22 p3858 A67-39507

Hot electron Hall mobility in n-type GaAs in negative differential mobility region 22 p3858 A67-39518

N-type Hall effect in high temperature Li doped ceramic sample of MnO, measuring electric transport properties 22 p3858 A67-39521

X-ray diffusion from thermal agitation oscillations coupled with plasma waves in indium antimonide, discussing phonon-plasmon interactions and Hall effect measurements 22 p3859 A67-39652

Niobium and tantalum nitrides physical properties including microhardness, electric and thermal conductivities, Hall coefficient and thermal EMF 22 p3861 A67-39917

MHD stability in two-fluid model examined for condition where resistivity and electron inertia are neglected 22 p3851 A67-39984

Conductivity and Hall coefficient measurements for electron mobilities in strontium titanate, discussing electron-phonon coupling and cryogenic experiments 22 p3863 A67-40002

Curves for Hall effect logarithms, current carrier mobility and electric conductivity vs high pressure and temperature effects in InSb 22 p3864 A67-40323

Temperature dependence of Hall mobility of photoelectrons and electrons produced by X radiation in cadmium sulfide single crystals 23 p4039 A67-40932

Measurement of variable Hall electromotive force component created by illumination of thin low resistance germanium samples by modulated light 23 p4039 A67-40936

Parameters for model of two valence bands of SnTe according to Hall effect measurements at high temperatures 24 p4200 A67-41779

Oscillating magnetic field influence on Hall effect and resistance of superconducting niobium 24 p4201 A67-41870

Strong electric field effects on parabolic energy band semiconductor magnetoresistance and Hall coefficients, discussing scattering mechanisms 24 p4202 A67-41982

Space charge layers on surfaces of lead sulfide photoconducting film noting Hall coefficients 24 p4204 A67-42363

Hall potential difference for thin film in magnetic leakage field of domain interface between ferro-and ferrimagnetic 24 p4204 A67-42457

Hall effect, resistivity, spin resonance and thermoelectric properties of poly(N-vinyl carbazole-iodine complex, demonstrating charge transfer state existence in system [JPL-TR-32-1074] 24 p4205 A67-42602

HALL GENERATOR

Primary-secondary voltage imbalance effect on multiplication and thermal properties of Hall generator 05 p0774 A67-16704

- Quasi-one-dimensional plasma motion in linear and radial Hall type MHD generator ducts 09 p1541 A67-21798
- Magnetic field inhomogeneity effect on electrically conducting fluid flow in Hall type generator duct 09 p1443 A67-21806
- Reduction or elimination of secondary asymmetry voltage in germanium Hall generators noting effect of surface recombination, temperature distribution stabilization, etc 12 p1939 A67-25278
- Performance characteristics of Faraday and Hall MHD generators using strong magnetic fields and considering ion slip and finite electrode segmentation effects 16 p2599 A67-30527
- MHD power generation experiments with potassium seeded argon plasmas to study performance at Faraday and Hall parameters 16 p2601 A67-30554
- Large nonequilibrium MHD generator design and preliminary performance, emphasizing electrode-wall shorting phenomenon in channel 16 p2602 A67-30556
- Maximum power density, maximum efficiency of diagonal wall generator, Faraday generators and Hall current generators compared 16 p2608 A67-30597
- Analytical plasma flow model for acceleration process in Hall current device, noting final velocity derivation, temperature, critical velocity, etc 16 p2719 A67-31237
- Operation of Hall generator with variable thickness active layer 20 p3401 A67-37220
- MPD energy conversion duct using heated inert gas working fluid, discussing Hall parameter operation and efficiency factors 24 p4109 A67-42898
- HALLUCINATION**
- Clinicopsychopathological method applied to analysis of hallucination, depersonalization and similar effects resulting from exposure to extremal factors from standpoint of space psychology 24 p4112 A67-41856
- HALOGEN**
- SA BROMINE
- SA CHLORINE
- SA FLUORINE
- SA IODINE
- Rate constants and activation energy in bimolecular transfer reactions for halogen atoms 18 p3154 A67-33835
- Cl, Br and I abundances in carbonaceous chondrites analyzed by neutron activation in estimating primordial halogen abundance ratios 24 p4234 A67-42628
- HALOGEN COMPOUND**
- SA HALIDE
- Magnetically induced circular dichroism and birefringence in ICl electronic spectrum, noting frequency dependence and molecular rotation effect 22 p3758 A67-39638
- Poly-N-vinyl carbazole-iodine charge transfer photovoltaic effect spectral and intensity dependence, noting possible radiation detection and energy conversion applications [JPL-TR-32-1138] 24 p4201 A67-41899
- HAMBURGER HFB 320 AIRCRAFT**
- Design and market research aspects of Hamburger HFB 320 jet executive aircraft 03 p0357 A67-12970
- Executive jet aircraft Hamburger Flugzeugbau HFB 320 Hansa development, testing and production 07 p1129 A67-19670
- HAMILTON-JACOBI EQUATION**
- Suboptimal solutions for class of linear regulator problems with soft saturation constraints, noting Hamilton-Jacobi equation 02 p0226 A67-12150
- Exact solutions in theory of orbits using Hamilton-Jacobi and Laplace equations 05 p0903 A67-17294
- Dynamical system specified by set of generalized coordinates, considering Jacobi and Kepler elements and Poisson and other methods 06 p1031 A67-17774
- Caratheodory unified approach to Hamilton-Jacobi theory in variational calculus problems of optimal control 07 p1162 A67-20275
- Hamilton-Jacobi solutions for Vlasov equation leading to nonsecular perturbation theory for macroscopic quantities 10 p1686 A67-23469
- Stochastic optimal control with noisy observations, obtaining Hamilton-Jacobi stochastic equation in function space [ASME PAPER 66-WA/FE-6] 11 p1770 A67-24276
- Saltykov method applied to second type partial differential dynamics equations of first class 15 p2510 A67-29518
- Orbits and trajectories for plane motion of material point in conservative field of force 16 p2748 A67-31138
- Integration of regularizing canonical and corresponding Hamilton-Jacobi equation applied to two-body problem for construction of perturbation theory 19 p3249 A67-34795
- Set of states reachable in given time in control problem determined by heuristic and rigorous methods 21 p3603 A67-38441
- HAMILTONIAN**
- Effective mass Hamiltonian for conduction band g factor anisotropy of indium antimonide in magnetic field 01 p0134 A67-10785
- Hamilton-Ostrogradskii integral variational principle for holonomic systems with linear constraints 01 p0114 A67-10991
- Perturbation theory in molecular quantum physics using variational principles 02 p0270 A67-12722
- Zero order Hamiltonian in perturbation theory for eigenvalue problems of atom in magnetic field 02 p0271 A67-12723
- Variational perturbation equations and time-independent Schroedinger equation for two-, three- and four-electron atoms 02 p0271 A67-12724
- Von Zelpel transformation solution small divisor problem arising from natural frequencies of orbital resonance motion of 24-hr artificial satellite 03 p0457 A67-13162
- Formal integral construction of Hamiltonian system of n degrees of freedom near equilibrium point 03 p0457 A67-13163
- Resonance phenomena associated with small divisor in third integral of orbital motion 03 p0457 A67-13164
- Asymptotic form of correlation functions facilitated by use of Hamiltonian 03 p0458 A67-13342
- Three-wave interaction Hamiltonians describing nonlinear couplings of plasma oscillation with electromagnetic field derived by Bohm-Pines method 04 p0662 A67-14613
- Two-particle ring term for kinetic equation with Darwin interaction relationship to relativistic Landau equation 04 p0672 A67-15772
- Rigorous error bounds on position and velocity of satellite derived from Hamiltonian theory and von Zelpel method [AAS PAPER 66-94] 07 p1252 A67-19958
- Constructing formal integrals, in form of power series, of time independent Hamiltonian system near equilibrium point [AAS PAPER 66-102] 07 p1216 A67-19964
- Canonical transformation in two-dimensional three-body problem giving power series Hamiltonian 08 p1380 A67-20387
- Hamiltonian function of particle in static magnetic field determined with cyclicity in two degrees of freedom 10 p1684 A67-22900
- Action-angle coordinates for particle motion in magnetic mirror systems 10 p1684 A67-22901
- Exchange model of zero bias tunnelling anomalies, discussing Hamiltonian, interference magnetic scattering and metal junctions 10 p1691 A67-23400
- Quantumstatistical thermodynamics with several temperatures for indivisible observation level 10 p1733 A67-23477
- Diagonalization procedure for Hamiltonian of ferromagnetic thin film, applying canonical transformation in direction of film thickness 11 p1845 A67-23992
- Extension of Pontryagin maximum principle to variable control region, using Hamilton equation 11 p1812 A67-24208
- Hamiltonian for free particle of arbitrary spin and mass formulated in terms of spin matrix polynomials, noting independence of expansion coefficients 11 p1824 A67-25074
- Noether theorems describing continuum mechanics material applied to Hamiltonian principle for motion of piezotropic fluid or ideal gas undergoing polytropic process 13 p2105 A67-27397
- Rigorous error bounds on position and velocity of satellite derived from Hamiltonian theory and von Zelpel method [AAS PAPER 66-94] 13 p2207 A67-27518
- Asymptotic form of correlation functions facilitated by use of Hamiltonian 13 p2149 A67-27713
- Analytic properties of finite-band models in solids as generalization of Kohn procedure 15 p2534 A67-29324
- Free rotation of solid body analyzed using homogeneous canonical transformation 15 p2519 A67-30225
- Birkhoff normalization of Hamiltonian function in neighborhood of stable equilibrium position in connection with Trojan orbits in three-body problem 16 p2747 A67-30985
- Hamiltonian formalism for collisionless electron plasma nonlinear kinetics using quantum statistical perturbational treatment 17 p2902 A67-32670
- Frequency spectrum of annihilation operator for system of harmonic oscillators using motion equation obtained through Hamiltonian 17 p2870 A67-33316
- Dynamic theory of hybrid ionic-covalent /homopolar/ bonds applied to physical behavior of GaAs type crystals 18 p3094 A67-33436
- Hamiltonian equations and Fourier transformations applied to free electron and gap motions in doped semiconductor 18 p3002 A67-34231
- Hamiltonian description of irreversible steady state phenomena and elements of turbulence theory, noting entropy production 19 p3210 A67-35539
- Von Zelpel method and Hamiltonian perturbation mechanics used for orbits at resonance with tesseral harmonics of geopotential 19 p3328 A67-35959
- Hyperfine splitting of spin interaction energy of two hydrogen atoms, determining eigenfunctions for effective Hamiltonian 21 p3658 A67-37814
- Von Zelpel method to eliminate short period terms in first order general planetary theory noting system transformation into canonical equations 22 p3881 A67-39514
- Anderson model Hamiltonian exchange character application to conduction electron Green function determination 22 p3861 A67-39994
- Electronic transport in graded band gap semiconductor heterojunctions without space charges, using method based on intraband transitions between complete Hamiltonian eigenstates 22 p3864 A67-40381
- Compound state resonances in atom/molecule collisions below first excitation threshold 23 p4029 A67-40959
- Book on Hamilton principle and physical systems covering planetary motion, rotating bodies, electromagnetic radiation, quantum theory, etc 24 p4189 A67-42406
- HAND**
- Inertia and muscle tone level effects on intermittence sampling frequency in hand movement control system 17 p2808 A67-33180
- HANDBOOK**
- Computer dictionary and handbook 04 p0579 A67-15947
- Printed circuits handbook covering fabrication, design, assembly, soldering, testing, etc 08 p1334 A67-20739
- Handbook of Physics, Volume 46/2, Cosmic radiation 14 p2379 A67-27960
- Handbook of telemetry and remote control considering position measuring, missile guidance, flight control, data processing, feedback information, communications etc 16 p2633 A67-31916
- HANDLEY PAGE H.P. 137 AIRCRAFT**
- Handley Page Jetstream turboprop aircraft basic design requirements, emphasizing aerodynamic design 22 p3746 A67-40129
- philosophy 22 p3746 A67-40129
- Handley Page Jetstream load carrying structural design, materials employed and structural test program 22 p3746 A67-40130
- Handley Page Jetstream power plant, propeller design, turboprop engine operation and control 22 p3868 A67-40131
- Handley Page Jetstream aircraft major systems, auxiliary equipment and instrumentation 22 p3748 A67-40132
- HANDLING**
- S AIR CARGO HANDLING
- S DATA HANDLING SYSTEM
- S GROUND HANDLING
- S LOW SPEED HANDLING
- HANDLING EQUIPMENT**
- SA STORAGE
- SA TRANSPORTATION
- Operation and control of satellite equipment, discussing automatic, semiautomatic, human and telefactor /man-extension system/ methods

- [AIAA PAPER 66-918] 02 p0204 A67-12250
Optimized equipment systems design studies for handling and transportation of large solid fuel rocket motors
[AIAA PAPER 67-266] 07 p1164 A67-20047
Manipulators for astronauts using anthropomorphic mechanical hands and arms controlled by bilateral servo system in exoskeletal master 11 p1749 A67-25011
Continuous mechanical ladder for troop/cargo lowering and retrieval from CH-47 helicopter 17 p2804 A67-32518
Airport terminal planning for Tampa eliminating long walk, using circular multistory structure with handling equipment for passengers and baggage [SAE PAPER 670319] 17 p2835 A67-32980
Problems of handling people on future giant aircraft noting reservations, ticketing, boarding procedures and baggage-handling functions 22 p3780 A67-39382
Large scale liquefaction, storage, transport and ground handling of liquid helium for applications in space operations 22 p3781 A67-40393

HANDLING QUALITY

- Airborne V/STOL simulators used for handling qualities research at National Aeronautical Establishment, Ottawa [AIAA PAPER 65-705] 03 p0394 A67-12915
Design recommendations to offset greater momenta and sensitivity to gust winds of jointless helicopter rotor 03 p0359 A67-12986
Handling quality evaluation of seven general aviation aircraft of type operated under instrument flight conditions 06 p0947 A67-18200
Handling and operation of XB-70A aircraft at Mach 3 speed noting folding wing tips, variable-geometry air inlet duct, etc 07 p1129 A67-19910
Handling criteria for basic stability and control characteristics of slender wing and V/STOL aircraft 13 p2053 A67-27192
Aircraft handling qualities research with variable static stability aircraft used as in-flight simulator [SAE PAPER 670261] 13 p2054 A67-27296
C-5A flight control system, examining subsystems, handling qualities, hydraulic power distribution and mechanical failures 17 p2794 A67-31997
Flight evaluation of various longitudinal handling qualities involving parameters and region of pilot acceptance [AIAA PAPER 65-780] 17 p2797 A67-32584
Navy variable stability studies of longitudinal handling qualities in simulated carrier approach [AIAA PAPER 67-576] 19 p3174 A67-35971
Lateral-directional flying qualities for power landing approach simulated, studying roll effects and damping [AIAA PAPER 67-577] 19 p3175 A67-35972
Manual altitude and attitude control effects on short-period handling quality requirements 19 p3175 A67-35974
Flight control system for future large aircraft, obtaining structural fatigue reduction, better handling and smoother ride 21 p3570 A67-39133

HANDS

- S HIGH ALTITUDE NUCLEAR DETECTION STUDIES /HANDS/

HANGAR

- Economical hangaring of commercial aircraft as implemented by Spanish airfleet 06 p0947 A67-18028

HANKEL FUNCTION

- Exact solution /by Hankel and Laplace transforms/ of unsteady motion of viscous MHD fluid in cylindrical vessel in axisymmetric constant strength magnetic field 05 p0850 A67-16134
Dynamic surface loads, transient displacement and stresses in elastic cylindrical shell under radial and torsional vibration and elastic spherical shell under radial symmetric vibration, using finite Hankel transformation 05 p0908 A67-16138
Boundary value solutions for current density and radiation patterns in spiral excited sheath antennas in terms of Hankel function 09 p1482 A67-22696
Thermal stresses in isotropic plate analyzed using Hankel transform, obtaining surface temperature for various cases 14 p2402 A67-28813
Synthesis of nonuniformly spaced antenna arrays using lambda functions to reduce space factor and prescribed radiation

- pattern 21 p3602 A67-39071
HANSEN LUNAR THEORY
Differential correction vectors for non-Keplerian reference orbits, reexamining rotating ellipses in Hansen type intermediaries 21 p3705 A67-38612

HARDENING

- SA AGE HARDENING
SA COLD HARDENING
SA DISPERSION HARDENING
SA PRECIPITATION HARDENING
SA STRAIN HARDENING
SA WORK HARDENING
Hardening during plastic deformation of steel samples under compression, deriving stress-strain state in cutting process 03 p0427 A67-13193
Thermoplasticity theory of hardening plastic material under nonuniform heating applied to various trajectories 05 p0911 A67-16175
Structure and certain properties of niobium-tantalum alloys containing tungsten and molybdenum show these alloying elements form continuous series of hard solutions 05 p0831 A67-17503
Hardening and softening of nickel-alumina alloys 12 p1955 A67-25365
Various factors affecting hardening of KhN35VTiU /E1787/ alloy 12 p1955 A67-25367
Laser beam effect on hardening of steel 12 p1955 A67-25372
Concentration ratios of cosmic ray-produced isotopes of helium, neon and argon measured and effective irradiation hardening parameter calculated 17 p2942 A67-32358
Polymer fracture mechanism hypothesized as competition between localized hardening by molecular orientation and localized softening during deformation 18 p3068 A67-33488
Effectiveness of butt-welded joints and optimum heat treatment conditions for thin sheets of maraging steel containing 18 percent nickel 18 p3054 A67-34259
Surface hardening of titanium alloys by carbon and nitrogen, using high-frequency induction heating 19 p3242 A67-34919
Hardening technique for circuits using electrical shielding to withstand radiation effects of nuclear war 20 p3399 A67-36883
Hardening function form in flow theory, showing dependence on cosine of stress velocity vector angle with normal to yield surface 20 p3539 A67-36921
Hardening during deformation in stoichiometric nickel manganite alloy noting temperature effect, surface characteristics and electric resistance 20 p3467 A67-37118
Zirconium addition effect on dynamic strengthening temperature range of niobium alloys, discussing process mechanism 20 p3468 A67-37123
Structure and certain properties of niobium-tantalum alloys containing tungsten and molybdenum show these alloying elements form continuous series of hard solutions 21 p3644 A67-38030

HARDNESS

- SA BRITTLENESS
Microhardness of n-type InSb single crystals and crack formation near indentation area 03 p0489 A67-13093
Hardness of polyesters copolymerized with styrene, determining reticulation and temperature effects 05 p0759 A67-16767
Particle microhardness and microbrittleness measured in powdered refractory compounds, noting relation to electron configuration 06 p1015 A67-17846
Hardness of heat resistant steels at elevated temperatures as function of alloying and heat treatment 07 p1199 A67-19240
Ce and Pr effect on structure, hardness and mechanical properties of cast steel at 800 degrees C 07 p1199 A67-19242
Hardness variation of alloys of system Al-Cu-Cd-Mn-Li as function of composition and aging conditions 07 p1201 A67-19252
Gas saturation effect on titanium alloys undergoing heat treatment, discussing microhardness and surface crack formation 07 p1205 A67-19277
Material combination and hardness effect in rolling contact fatigue life of high speed tool steel, stainless steel and wear resistant materials 09 p1505 A67-22191
Theoretical strength with iron-nickel maraging steels 12 p1957 A67-26125
Knoop hardness anisotropy in unalloyed

- titanium and iodide titanium sheets discussing orientation, hardness variations rolling, cross section planes and indentation [ASTM PAPER 53] 18 p3068 A67-34583
Apparatus for measuring metal/alloy hot hardness using indenter static impressor and unilateral flattening 19 p3227 A67-34930
Temperature dependence of oxide hardness relative to other materials, comparing oxide hardness data to carbide data 20 p3472 A67-36113
Particle microhardness and microbrittleness measured in powdered refractory compounds, noting relation to electron configuration 20 p3471 A67-37588
High temperature microhardness of semiconductors determined by method measuring indentation diagonals of cooled single crystal specimens 22 p3804 A67-40302

HARDWARE

- Apollo manned lunar landings, system hardware, operational problems and development of lunar surface experiments package /ALSEP/ [AIAA PAPER 67-116] 07 p1163 A67-19438
Hardware characteristics of control moment gyro /CMG/, determining nonlinearity effects on performance by simulation 17 p2853 A67-31995
Data selection, collecting and processing for automatic performance recording and monitoring of aircraft gas turbine engine, considering hardware and software [SAE PAPER 670360] 17 p2835 A67-32999
Automatic IC mask artwork generating system for large scale integration environment, describing hardware, software and performance 18 p3055 A67-34558
Variable geometry in SST aircraft, discussing hardware, lift control system, compression inlet and full scale wing pivot [SAE PAPER 670878] 24 p4094 A67-42012

HARKE HELICOPTER**S MIL MI-10 HELICOPTER****HARMONIC ANALYSIS**

- Output power of frequency multiplier using varactor diode for given output voltage and terminal resistances at various harmonics 01 p0039 A67-10857
Oscillation formation by violation of sufficient conditions of asymptotic stability in linear system 01 p0047 A67-11215
Lunar shape from Orbiter measurements of gravitational field determined via harmonic analysis 02 p0320 A67-11474
Harmonic analysis of perturbed satellite motion from exact solution for point motion about two fixed centers [ONERA-TP-420] 02 p0320 A67-11494
Nonlinear servo devices examined, using simplified form of harmonic-equivalent method obtained from multilinear characteristics 02 p0224 A67-11529
Atomic and molecular time-dependent quantum-mechanical perturbation theory with differential equation formulation within Hartree-Fock approximation 02 p0268 A67-12725
Harmonic approximation of infinite crystal dynamics problem, noting collisional case and action of external force on atoms 03 p0520 A67-12930
Drift of small scale E and F layer inhomogeneities in Black Sea coastal region 04 p0616 A67-15222
Fourier transformation related to real half of straight line set of positive harmonic measure 04 p0646 A67-15492
Solar diurnal variation of cosmic ray neutron component in Antarctic during minimum activity period, using harmonic analysis 05 p0881 A67-16119
General elastic problem for some boundary conditions, determining coefficients via harmonic functions 05 p0916 A67-16227
Harmonic analysis of accuracy of reproduction in digital form of operators selecting period of time quantization, duration of analog-to-digital conversion, etc 05 p0781 A67-16258
Harmonic components of current of HF transistor under sinusoidal excitation, using piecewise parabolic approximation 05 p0772 A67-16456
Quasi-spiral nature of change in 27-day cosmic ray variation with solar activity shown by harmonic analysis 05 p0884 A67-17137
Depth and form of bodies causing magnetic anomalies determined by two

methods 05 p0802 A67-17150
Earth topography in spherical harmonic analysis of land, ocean and ice 08 p1325 A67-20937
Linear hyperbolic equations describing one-dimensional wave propagation, with stability conditions by harmonic analysis and second Liapunov method 09 p1533 A67-22400
Equivalent dipole moment of geomagnetic field in terms of earth radius deduced from spherical harmonic 10 p1652 A67-23492
Discrete mass technique for vibration analysis of thin shells [ASME PAPER 67-VIBR-23] 11 p1872 A67-24182
System with two nonlinearities separated by high pass filter, obtaining joint describing function 11 p1760 A67-24275
Radiating slot on dielectric clad cylinder, solving wave equations and finding field expressions via harmonic series representation 11 p1761 A67-24280
One-dimensional weak plasma turbulence, noting structure of spectra for various oscillation frequencies 11 p1837 A67-24393
Sputnik III data application to plotting of total magnetic field intensity chart above U.S.S.R., using spherical harmonic analysis 12 p1933 A67-25652
Statistical and instrumental fluctuations effect on distribution of first-harmonic amplitude and phase in harmonic analysis of cosmic radiation variation 13 p2191 A67-26565
Harmonic and impulse techniques for flight vibration testing to reduce data processing time 14 p2395 A67-27899
[ONERA-TP-477] Harmonic analysis to improve accuracy and reduce computation of coefficients in Chebyshev expansion 14 p2342 A67-27976
Possible directional pattern forms obtainable for single-ring circular arrays, using Fourier harmonic analysis technique 15 p2454 A67-30138
Drift data harmonic analysis correlation between solar quiet diurnal variation and ionospheric drift 16 p2669 A67-31908
Proof of continuity of Haar measurable almost periodic functions 17 p2876 A67-32385
Harmonic spectrum of variations in earth rotation, noting seasonal variation and effects of lunar tides 17 p2843 A67-32444
Harmonic analysis of lunar shape and gravitational field, discussing control systems used 18 p3130 A67-34318
Periodic solutions for quasi-harmonic time-lag system, proposing calculation for periodic regimes in form of integral series 18 p3079 A67-34371
Quasi-biennial oscillation in ozone in northern Hemisphere harmonically analyzed 19 p3225 A67-35921
Book on stationary random processes, discussing prediction theory, interpolation, extrapolation, filtering, linear forecasting, etc 20 p3475 A67-36140
Stability of periodic solution of nonlinear systems with coefficients dependent on amplitude and frequency 20 p3408 A67-37043
Fourier integral in terms of maximum harmonic amplitudes 20 p3406 A67-37650
Response in fundamental mode of simple single span beam with tuned viscoelastic dampers attached at discrete locations, assuming harmonic loading 21 p3719 A67-38147
Quasi-spiral nature of change in 27-day cosmic ray variation with solar activity shown by harmonic analysis 21 p3698 A67-38480
Depth and form of bodies causing magnetic anomalies determined by two methods 21 p3619 A67-38492
Magnus version of first harmonic approximation method for nonlinear systems engineering, using analog computer simulation for accuracy examination 22 p3776 A67-39327
Book on continuous and scanning control systems optimization and random processes theory including numerical techniques, harmonic analysis and Gaussian transformation 22 p3777 A67-40070
Harmonic analysis of half-wave dipole and director parallel to reflecting plane 24 p4132 A67-42715
Solar diurnal variation of cosmic ray neutron component in Antarctic during minimum activity period, using harmonic analysis 24 p4214 A67-42795

HARMONIC EXCITATION

Excitation of phosphor suspensions in solid dielectric by mechanical energy analyzed via impact theory 01 p0113 A67-10354
Ideal incompressible liquid motion in rectangular container due to rectangular double and sinusoidal pulse excitation 03 p0404 A67-13784
Harmonic response due to compressibility in traveling wave plasma devices, discussing magnetoacoustic resonances for case of cylindrical symmetry 03 p0485 A67-14051
Forced parametric oscillations in linear system, obtaining solutions for case where excitation frequency is twice natural frequency 05 p0918 A67-16243
Stability and inverse receptance of multidegree systems under harmonic excitation 08 p1415 A67-20479
Excitation of phosphor suspensions in solid dielectric by mechanical energy analyzed via impact theory 11 p1851 A67-25027
Radiation patterns of annular slots on conducting conical surface subjected to harmonic excitation 13 p2080 A67-27026
Stability and nonlinear vibrations of mechanical systems under harmonic excitation 14 p2397 A67-28087
Cyclotron harmonic wave propagation in warm magnetoplasmas predicted theoretically for perpendicular and oblique damping 19 p3288 A67-35371
Radio wave propagation excitation of second harmonic in nonlinear periodically inhomogeneous communication line 19 p3185 A67-36020
Analytic model for output voltage of fluxgate magnetometer, demonstrating excitation function and core squareness effects 22 p3800 A67-39911
Translational excitation mechanical model applied to space vehicle longitudinal excitation, examining sloshing phenomena 22 p3786 A67-40104
Permanent states of Van der Pol equation in forced sinusoidal state using first harmonic theory which relies on amplitudes of response 23 p4026 A67-40688
Transient processes and initial conditions of excitation of lower harmonic oscillations in resistance-capacitance nonlinear inductance circuit, noting graphical integration 24 p4189 A67-42418
HARMONIC FUNCTION
SA AIRYS STRESS FUNCTION
SA BIHARMONIC EQUATION
Integral representation providing one-to-one correspondence between functions of n complex variables and complex-valued harmonic functions of n plus 1 real variables 02 p0259 A67-11918
Book on main linear boundary value problems for second order linear partial differential equations and systems of such equations satisfying ellipticity 04 p0645 A67-15006
Harmonic series of coordinates of moon in three-body problem of sun-earth-moon treated by numerical method 08 p1382 A67-20395
Nonlinear automatic system with logical device analyzed in presence of external action, obtaining harmonic linearization coefficients 09 p1482 A67-22080
Extensions of Nevanlinna 2-constant theorem for harmonic function on disk and Hadamard 3-circle theorem 10 p1673 A67-22965
Legendre polynomial form of slender body motion in spherical coordinate systems generalized for axially symmetric harmonic functions in three dimensions with validity for Helmholtz equation 11 p1812 A67-24310
Forced oscillations of generalized Lienard equation, examining harmonic solutions in x, y plane with confined trajectories 11 p1812 A67-24311
Harmonic power at TWT taking into account effect of space charge on electron beam bunching 11 p1765 A67-24478
Dispersion of number of positive zeros as function of time for realization of quasi-harmonic random signal 11 p1754 A67-24985
Classical representation of Green-Lebesgue type integral harmonic function in case of unit sphere 12 p1962 A67-26101
Index formula of boundary value problem for system of two harmonic functions 16 p2696 A67-31143

Radio wave propagation excitation of second harmonic in nonlinear periodically inhomogeneous communication line 19 p3185 A67-36020
Zero moment elliptical paraboloid translational shell under uniformly distributed load, reducing solution to Dirichlet problem 20 p3539 A67-36924
Harmonic linearization, estimating quality of oscillatory transients in nonsearching self-adjusting systems described by high order differential equations 20 p3408 A67-37045
Power series expansion of electron velocity distribution function, computing harmonic electric current densities in plasma 21 p3661 A67-37745
Lemmas and theorems for support functions of plurisubharmonic functions proved, discussing complex variables and linear maps 22 p3828 A67-40555
Spatial filtering for altering relative harmonic coefficients in two-dimensional Fourier integral representation of astronomical photographs eliminates ringing effects 23 p3997 A67-40625
Analytic and harmonic transformations applied to Faber series summation, harmonic function approximation and logarithmic potential approximation 23 p4023 A67-40923
Fourth order multipole parameters derived from spherical harmonic function coefficients for geomagnetic field potential 24 p4146 A67-41784
Pump frequency reduction in Adler tubes, examining spatial harmonics of quadrupole structure field and suggesting use of cophas connection 24 p4130 A67-42240
HARMONIC GENERATION
Varactor diodes and frequency multiplier surveyed for application in harmonic generation at microwave frequencies 01 p0034 A67-10165
Anisotropies and harmonics of homogeneous Lorentz plasma under electric field, using approximation method 01 p0121 A67-10230
Optical harmonic generation and first order sum and difference frequencies in plane parallel crystal plate within framework of phenomenological theory 01 p0089 A67-10361
Intense pulse generation at 5300 angstroms by frequency doubling in Q-switched and glass laser and possibility of generating particular harmonics 01 p0090 A67-10759
Statistical effects during generation of second harmonic in optically transparent crystals, noting coefficient of correlation between harmonic and fundamental radiation power of solid state laser 03 p0467 A67-12928
Nonlinear distortions in parallel and series tunnel diode voltage amplifiers 03 p0377 A67-13235
Instabilities in drifting semiconductor plasma, noting dispersion curve and collision ionization for longitudinal oscillations 03 p0496 A67-13674
Coherent interaction of two radio waves in plasma, generation of mutually-harmonic frequency wave and application to radio transmission in ionospheric F layer 03 p0372 A67-14091
Harmonic generation in Taylor vortices between rotating cylinders, measuring amplitude of each harmonic, noting agreement with Davey theory 04 p0601 A67-14462
Gas discharge in argon maintained within waveguide by microwave signal at cyclotron resonance, observing second harmonic radiation 05 p0850 A67-16046
Doubling of frequency of light in nonlinear medium with random nonuniformities 05 p0762 A67-16348
Optical harmonic generation and first order sum and difference frequencies in plane parallel crystal plate within framework of phenomenological theory 06 p1009 A67-17619
Electron plasma oscillations excited by two-beam instability and nonlinear coupling between them 06 p1046 A67-18828
Generation of longitudinal plasma oscillation harmonics near electron cyclotron frequencies 06 p1046 A67-18831
Picosecond laser pulse widths measurement by method using special symmetry properties of second harmonic generation at GaAs crystal surface 07 p1234 A67-20097
Elastic nonlinearity due to acoustic wave-

charge carrier interaction in CdS, noting waveform distortion for zero acoustic dissipation 08 p1353 A67-20485

Microwave third harmonic generation in homogeneous semiconductors at low temperatures, noting ionized impurity scattering effect 08 p1368 A67-20701

Point contact electrically formed semiconductor junction diodes, discussing harmonic generation by various material combinations 09 p1474 A67-22086

Nonlinear harmonic generation in magnetoplasma using Boltzmann equation, noting sharp resonance peaks 14 p2358 A67-28236

Microwave harmonic generation from Josephson junction noting radiation waveguide coupling, bias point, input power level and Josephson equations 15 p2535 A67-29492

Frequency tripling of electromagnetic waves passing through hot electron gas in semiconductors, deriving third harmonic amplitude for helical wave 16 p2628 A67-31500

Microwave attenuation change and harmonic generation by n-type GaAs in strong microwave electric fields, determining current density relation to field strength 17 p2913 A67-32310

Beat frequency generation and multiplication and subsequent harmonic amplification in plasma-beam system, particularly case of plane waves 18 p3087 A67-34037

Tellurium nonlinear optical properties including absorption and refraction indices, discussing second harmonic radiation generation 20 p3507 A67-36324

Optical third-harmonic generation in rare gases, comparing coefficients with Kerr effect coefficients 21 p3639 A67-37962

Nonresonant third order dielectric susceptibility coefficients of gases measured in four-wave mixing experiment to calculate harmonic radiation in laser beam 21 p3639 A67-38008

Single crystals of lithium-meta-niobate evaluated for nonlinear optical quality, using gas laser and interferometer 21 p3677 A67-38010

Solid state laser with mode selection within active medium ensures beam collimation in one plane, noting use in second-harmonic generation and parametric frequency conversion systems 22 p3814 A67-39458

Harmonic generation and turbulence-like spectrum from pulsed HF beam-plasma interaction, tabulating harmonic wave properties 22 p3847 A67-39615

Cyclotron harmonic resonances in plasma frequency conversion output due to harmonic interactions with incident waves 22 p3851 A67-39724

Crossed field cascade tubes as frequency oscillators and microwave generators, discussing improved performance and interaction efficiency of devices 22 p3775 A67-40559

Free carrier effect on higher harmonic generation in semiconductors from nonlinear Boltzmann equation 24 p4202 A67-41985

HARMONIC GENERATOR

Inductive and capacitive tunable tunnel diode harmonic generator in waveguide 01 p0035 A67-10437

Microwave harmonic power generator using varactor diode, noting effect of reverse bias on harmonic output 01 p0041 A67-11319

Step recovery diode utility extension, obtaining high efficiency from harmonic generators in millimeter wavelengths 05 p0780 A67-17529

Electronically swept coherent frequency synthesizer for various bands 17 p2827 A67-32799

Nonlinear impedances used for frequency multiplication 19 p3182 A67-35033

HARMONIC MOTION

Maneuverable geodetic satellite for better determination of resonant harmonics in geopotential field [AIAA PAPER 87-122] 06 p1096 A67-18340

HARMONIC OSCILLATION

Microwave radiation measurements from internal plasma resonance of positive column near electron cyclotron harmonic frequencies 03 p0476 A67-13355

Dynamic reciprocal theorem for sinusoidal

oscillation of elastic medium treated as extension of static reciprocal theorem of Betti and Rayleigh, using continuum mechanics [ASME PAPER 85-WA/MD-21]

Aerodynamics of slender wings executing simple harmonic oscillations and having leading edge separation 03 p0352 A67-13894

Steady state oscillation regime of one-dimensional oscillator determined by replacing arbitrarily shaped hysteresis loop with ellipse of equivalent area, noting higher harmonics effect 03 p0530 A67-14176

Oscillating field of vessel effect on accuracy of readings of gyrocompass with negative fluid pendulum 03 p0425 A67-14283

Ritz averaging method to determine free and forced vibratory response of beams and plates undergoing large amplitude steady state harmonic oscillations 04 p0715 A67-15659

Higher harmonics computation of nonlinear steady oscillation in arbitrary system 05 p0846 A67-16438

Two-phase flow of gas over harmonically oscillating flat plate expressed in laminar boundary layer terms, presenting liquid film thickness, heat transfer rate, skin friction, etc 05 p0793 A67-17338

Coupled system of thin elastic shells, giving response to static or harmonically oscillating loads or to unloaded natural frequencies and mode shapes, using Green matrix [AIAA PAPER 87-45] 06 p1103 A67-18351

Convective heat transfer in tube with gaseous heat carrier pulsating at frequency corresponding to second resonance harmonic 07 p1266 A67-19182

Dependence of first harmonic averaged parameters of transistor on oscillation amplitude in common-emitter circuit in absence of bias current in base circuit 07 p1149 A67-19187

Oscillations induced by two forces in system with nonlinear elastic force and nonlinear damping 07 p1224 A67-20211

Thermoelasticity theorems for harmonic vibrations of continuum, examining spherical wave propagation 07 p1264 A67-20222

Unsteady supersonic flow about conical wing fuselage system with LF harmonic oscillatory motion 07 p1127 A67-20224

Harmonic response and jump phenomena in closed loop systems with dynamic range type nonlinearity under sudden sinusoidal excitation 08 p1312 A67-20721

Summation of convergent series for cyclotron harmonic wave dispersion for numerical and analytic work 11 p1827 A67-23886

Forced steady state response of linear harmonic oscillator with impact absorber attached, developing stability criterion [ASME PAPER 87-VIBR-10] 11 p1795 A67-24170

Subharmonic oscillations in tunnel diode circuits analyzed, including solutions to forced pumping oscillations and frequency characteristic equations 11 p1768 A67-24858

Nonlinear oscillations of elastic plates under simultaneous effect of harmonic and random load 12 p2024 A67-25597

Linear effects of oscillations of liquids in right circular cylinder, determining stability of forced oscillations 14 p2296 A67-27984

Bubble stabilization in pure viscous liquid contained in sinusoidal vibrated tank [ASME PAPER 87-FE-3] 14 p2304 A67-28356

Coupled systems stability constraints and oscillatory behavior, discussing feedback path nonlinearities using differential equations 19 p3200 A67-34849

Finite-amplitude oscillations of Maclaurin spheroids preserving ellipsoidal nature of surface and generating internal motions of uniform vorticity 19 p3263 A67-36078

Vibrating elastic bar motion equation reduced to integral equations system for solutions to boundary value problems 20 p3476 A67-36667

Aerodynamic forces of harmonically oscillating cylindrical duct with supersonic internal flow within framework of potential flow theory 20 p3357 A67-37003

Asymptotic approximations for analysis of nonlinear resonant circuits through differential equations, assuming oscillation processes similar to harmonic system processes 20 p3409 A67-37113

Triode system of reflex klystron, stressing creation of modulated SHF oscillation device 20 p3451 A67-37141

Harmonic oscillations and bending of elastic isotropic shells with variable curvature solved using Fourier transform 21 p3721 A67-38338

Subharmonic and summed and differentiated harmonic oscillations in multiple-degree-of-freedom system with asymmetric nonlinear spring characteristics, studying stability 22 p3910 A67-39400

Swell generation by means of flat paddle board in translational motion 22 p3783 A67-39641

Energy equation solution procedure for heat transfer across two-dimensional oscillating laminar boundary layer 23 p4082 A67-41241

Resonance in unbounded traveling and standing harmonic oscillations/ waves demonstrating equivalence of resonance states using wave equations 23 p4079 A67-41410

Transient processes and initial conditions of excitation of lower harmonic oscillation in resistance-capacitance nonlinear inductance circuit, noting graphical integration 24 p4189 A67-42418

HARMONIC OSCILLATOR

Errors in thermodynamic functions of ideal gases determined from molecular data 03 p0536 A67-13607

Motion stability concepts of synthesis of control devices, with example for harmonic oscillator 06 p1032 A67-18241

Oscillatory process stability in n-circuit transistorized LC oscillators with inductive feedback 06 p0972 A67-18894

Gunn diode self-pumped parametric oscillator, showing power derived from variation of domain capacity at second harmonic of oscillation frequency 09 p1479 A67-22267

Temperature dependence of total intensity in difference band systems, difference transitions between nondegenerate vibrations compared with carbon dioxide band 11 p1821 A67-23967

Gas-solid energy exchange model, studying harmonic oscillator and free particle 13 p2098 A67-26939

Fast warmup crystal oscillator, noting advantages and applications in equipment requiring low power consumption and frequency stability 15 p2445 A67-29584

Thermal, mechanical and electrical design of stable quartz crystal oscillator used for Geos satellite to generate RF carriers and Doppler system timing signals 15 p2445 A67-29585

Frequency spectrum of annihilation operator for system of harmonic oscillators using motion equation obtained through Hamiltonian 17 p2870 A67-33316

Errors in thermodynamic functions of ideal gases determined from molecular data 18 p3161 A67-34472

Crystal frequency stabilization in relaxation-oscillator circuit, showing similar use in astable multivibrator instead of LC circuit 20 p3384 A67-37215

Quantum damping theory formulated in coherent state representation, giving Green function solution to damped harmonic oscillator Fokker-Planck equation, noting density operator 22 p3817 A67-40486

Fundamental statistical oscillation characteristics expressions for quasi-harmonic self-excited oscillators with low noise and many degrees of freedom 24 p4129 A67-42225

HARMONIC RADIATION

Tabulation of accidental coincidences between fundamental frequency of one laser and harmonic or subharmonic frequencies of another, as necessary condition for frequency translation between lasers 19 p3240 A67-35700

HARMONICS

SA SPHERICAL HARMONICS

SA TESSERAL HARMONICS

SA ZONAL HARMONICS

Higher harmonics of anomalous cyclotron emission from partially ionized plasma ascribed to negative absorption 03 p0476 A67-13358

Temporal distribution of first and second harmonic of solar diurnal variation of cosmic rays after radio bursts of fourth type 05 p0881 A67-16116

- Second and third harmonics produced by
p-i-n diode in microwave switching
application 13 p2075 A67-26478
- Higher harmonic components of twecks as
evidence of adequacy of waveguide mode
theory of VLF propagation between earth
and ionosphere 14 p2307 A67-27888
- Temporal distribution of first and second
harmonics of solar diurnal variation of
cosmic rays after radio bursts of fourth
type 24 p4214 A67-42792
- HARP PROJECT**
HARP program
Objectives 06 p1098 A67-19021
- HARTMANN FLOW**
Surface roughness effect on laminar MHD
flow through rectangular duct, deriving
relation between transition friction factor
and Reynolds and Hartmann
numbers 01 p0120 A67-10186
- Analogy between turbulent MHD channel
flow at high Reynolds numbers and
moderate Hartmann numbers and turbulent
boundary layer flow with
magnetization 02 p0277 A67-12569
- Effect of sudden change in magnetic field
and/or pressure gradient on Hartmann flow,
assuming stationary and nonconducting
plates 03 p0482 A67-13745
- MHD analysis of composite slider bearing
using electroconductive lubricant such as
liquid metal, in magnetic field perpendicular
to bearing surface, for large and small
Hartmann numbers
[ASME PAPER 66-LUB-B] 05 p0811 A67-16275
- Solution for parallel plates in steady state
Hartmann flow extended to coaxial flow
between concentric cylinders, noting role of
magnetic field 05 p0856 A67-17356
- Steady flow of viscous conducting fluid in
pipe under magnetic field analyzed for
relations among Hartmann number, Reynolds
number, skin friction, wall conductivity,
etc 10 p1687 A67-23833
- Voltage-current characteristics measured
by Fahleson alternate explanation, based on
properties of Hartmann boundary layer in
continuum type plasma 12 p1972 A67-25384
- Hartmann oscillator problem studied using
hydraulic analogy between supersonic
compressible gas dynamics and
incompressible flows with free
surface 14 p2295 A67-27903
- Pressure driven flow at high Hartmann
number along annular channel between
nonconducting circular
cylinders 14 p2355 A67-27907
- One-dimensional laminar MHD flow at
hydrodynamic stabilization, discussing heat
transfer, Hartmann flow, magnetic field,
Prandtl number and Joule
heating 14 p2358 A67-28283
- Parallel conducting flow along insulating
pipe under applied magnetic field,
elucidating singularities of Hartmann
boundary layers 21 p3668 A67-38495
- HARTREE-FOCK CALCULATION**
Hartree-Fock-Slater calculation of internal
conversion coefficients for magnetic
multipoles for yttrium-87 with 0.05 or 0.15
me-square gamma energy
values 01 p0116 A67-10203
- Absolute direct excitation cross section
from neutral ground state for upper levels
of transition in argon 02 p0253 A67-12520
- Atomic and molecular time-dependent
quantum-mechanical perturbation theory
with differential equation formulation within
Hartree-Fock approximation 02 p0268 A67-12725
- Uniform electric field quadrupole
polarizabilities and shielding factors for S-
state atoms and ions, demonstrating
independence of factors from existence of
field gradient 03 p0472 A67-13321
- Electron excitation cross section of
transitions between spin multiplets of
ground state of neutral oxygen atom
calculated, using continuous state Hartree-
Fock formulation 03 p0472 A67-13322
- Electron conduction band structure of NaI
crystals, using Hartree-Fock-Slater modified
equation 03 p0495 A67-13513
- Molecular nitrogen and oxygen properties,
calculating Hartree-Fock value for energy in
ground state 04 p0660 A67-14693
- Hartree, Hartree and Swirls calculations
for oxygen repeated with superposition of
configurations in determining wave functions
and energy 06 p1034 A67-17647
- Unrestricted projected Hartree-Fock
solutions for two-electron systems, with
application to special configuration
superposition 09 p1535 A67-22380
- Numerical calculations of blast waves by
standard and Hartree techniques compared
with analytical results and application of
Richardson extrapolation method 10 p1625 A67-23110
- Molecular orbital electron charge density
pictures, noting representation close to
Hartree-Fock calculation method 10 p1682 A67-23379
- Spatial correlation and molecular
properties in extended Hartree-Fock
calculations, deriving first and second order
density matrices for ground state of H, Li
and F 11 p1824 A67-24993
- Spin-projected unrestricted self-consistent
field /SCF/ methods for spin density
calculations used to determine hyperfine
coupling constants 13 p2160 A67-26540
- Thermoelectric power increase in low
temperature metals not explained by
residual resistivity in simple model
calculation 15 p2540 A67-30096
- Total energy of beryllium hydride
molecule analyzed, using difference between
SCF energies and single determinant wave
function 20 p3377 A67-37139
- Scaled Unsöld approximation for Hartree-
Fock function in perturbation
expansion 23 p4030 A67-40977
- HASP**
S HIGH ALTITUDE SOUNDING
PROJECTILE /HASP/
- HASTELLOY**
Creep ductility, stress rupture and high
temperature irradiation embrittlement of
neutron-irradiated Hastelloy
N 08 p1343 A67-21195
- Microstructural dislocation tangling and
related changes in tensile properties of
Hastelloy X-280 following thermomechanical
treatments 10 p1668 A67-23174
- High temperature corrosion and
evaporation of Haynes 25 and Hastelloy X-
280 in atmospheres of oxygen, carbon
monoxide, carbon dioxide, water vapor and
methane 14 p2336 A67-28148
- Multipass welded Hastelloy joint age
embrittlement from exposure in inert
atmosphere at high temperature, stressing
ductility, tensile and hardness
tests 17 p2866 A67-33199
- HAWKER HUNTER AIRCRAFT**
S HUNTER F-2 AIRCRAFT
- HAWKER SIDDELEY AIRCRAFT**
S AVRO WHITWORTH HS-748
AIRCRAFT
- HAYSTACK PROJECT**
Structural and mechanical concept, design
and testing of fully steerable radome-
enclosed parabolic Haystack
antenna 03 p0396 A67-13750
- Haystack antenna used for satellite
communications and celestial observation,
noting digital computer for control system
and data processing 05 p0790 A67-17517
- HAZARD**
SA AIRCRAFT HAZARD
SA FLIGHT HAZARD
SA METEOROID HAZARD
SA NOISE HAZARD
SA OPERATIONAL HAZARD
SA RADIATION HAZARD
SA SAFETY
SA SAFETY HAZARD
SA TOXICITY AND SAFETY HAZARD
- Intrinsically safe and nonincendive
electrical installations for hazardous
environments 12 p1900 A67-25677
- HAZE**
S FOG
S VISIBILITY
- HC-1 HELICOPTER**
S CH-47 HELICOPTER
- HEAD MOVEMENT**
Involuntary vestibularly driven head
movements in man during rotational
simulation 23 p3959 A67-41659
- HEALTH**
SA HYGIENE
SA SANITATION
- Disease vector transport by aircraft as
international health hazard 15 p2429 A67-29284
- Prolonged space flight effects on crew
members health concerning crew selection
test methods 16 p2613 A67-30911
- HEARING LOSS**
Hearing discrimination in hyperbaric air
explained by fact that increased ambient
pressure causes disturbances of sound
conduction 09 p1453 A67-21729
- Barotrauma, circulatory constriction and
other in-flight auditory troubles of civil
aeronautical navigation personnel over 40
years old 14 p2257 A67-28214
- Human acoustic analyzer functional state
studied for hypokinesia effects 20 p3368 A67-36267
- Speech audiometry for hearing loss
examinations of middle aged
pilots 22 p3753 A67-40545
- Aerospace and Harvard PB word lists for
speech discrimination testing of aircrew
members while screening against possibility
of Meniere disease and
vertigo 23 p3963 A67-41542
- HEART**
S CARDIOGRAPHY
S CARDIOVASCULAR SYSTEM
- HEART DISEASE**
Cardiovascular response of 37 patients
with heart disease to prolonged passive
upright tilt compared with normal
subjects 07 p1135 A67-19866
- Glucose loading effects on
electrocardiogram of pilot applicants
evaluated for injection before and after
diabetes test 21 p3573 A67-38068
- Cardiovascular integrity restoration in post
myocardially infarcted aviation
personnel 23 p3957 A67-41637
- Restoration of cardiovascular integrity in
post myocardially infarcted aviation
personnel 23 p3971 A67-41709
- HEART FUNCTION**
SA MUSCULAR FUNCTION
- Carotidogram recording of left ventricular
ejection, noting application as diagnostic tool
in heart physiology and in
pathology 04 p0561 A67-14626
- Impedance cardiac output values
simultaneously compared with dye dilution
techniques under rest and exercise
conditions 05 p0755 A67-16278
- High magnetic fields effect on cardiac
activity in spontaneously excited isolated
turtle heart by simultaneous and separate
electrical and mechanical
measurement 05 p0755 A67-16282
- ECG measurement results on ascent in
depressurized chamber, observing diaphragm
of electrical axis of heart due to diaphragm
lift 08 p1287 A67-20643
- Vibrophonocardiographic techniques for
monitoring cardiac dynamics in flight
environment 17 p2806 A67-31954
- Cardiorespiratory functioning in flight
monitored on carrier pilots in
combat 17 p2805 A67-31956
- Thorax radiological changes associated
with physiological and posture changes,
discussing chest dynamics 23 p3956 A67-41625
- HEART RATE**
SA PULSE RATE /BIOL/
- Bed recumbency effect on ventilatory,
metabolic and cardiac response to bicycle
ergometer test, noting possible preventive
effect of muscular exercises and venous
occlusion 01 p0016 A67-10949
- Objective statistical approach to tilt table
data analysis using computer to define
characteristics of cardiovascular
deconditioning resulting from bed rest,
water immersion and space
flight 05 p0754 A67-16276
- Correlation between heart rate, landing
error and field of view for binocular and
monocular sphere of vision of jet
pilots 09 p1455 A67-21717
- Statistical analysis of heart rates of Navy
carrier pilots during bombing attacks
compared with those for launch and
landing 09 p1455 A67-21718
- Effects of inhaled air ions on speed of
response and attention level, heart and
respiration rate and transepithelial DC
potential of men 09 p1452 A67-21720
- Daily physiological rhythm changes
associated with light intensity and color,
noting body temperature oscillations vs light
intensity, heart rate changes,
etc 15 p2426 A67-29109
- Cardiovascular changes at onset of whole
body, X-axis sinusoidal vibration in
anesthetized mongrel dogs and unsedated
humans 15 p2428 A67-29272
- Rate measurements determination and

- evaluation in analysis of space medical data 15 p2431 A67-29293
- Long term biomedical monitoring of human heart rate through lithium chloride impregnated balsa electrodes, noting space flight application 15 p2431 A67-29918
- Electrocardiogram amplifier-transmitter designed for long term heart rate monitoring on unrestrained subjects in orbiting laboratories 15 p2431 A67-29919
- Special preprocessing circuit for cardiac beat recognition discriminates against noise artifacts in electrocardiogram 15 p2432 A67-29920
- Physical exercise effect on oxygen consumption at decreased pressure 17 p2806 A67-31963
- Circadian oscillations of deep body temperature and heart rate in ambulatory primate in controlled environment 23 p3951 A67-41554
- Human circulatory response to sinusoidal gravitational stimulus via Rotational Flight Simulator /RFS/, discussing heart rate variation 23 p3951 A67-41561
- Human cardiac output estimated using impedance plethysmography, discussing simultaneous indicator dilution curves /Dye/ and impedance records /Imp/ 23 p3951 A67-41563
- Lithium chloride impregnated balsa wood and surgically implanted electrodes for continuous heart rate recording over long periods of time 23 p3965 A67-41571
- Oxygen role in cardiac rate in squirrel monkeys during acceleration stress on centrifuge 23 p3956 A67-41635
- Centrifuge tests with squirrel monkeys for pharmacologically denervated primate heart response to acceleration stresses 23 p3957 A67-41636
- Telemetry system for measuring body temperature and heart rate for physiological evaluation of space suits 23 p3969 A67-41651
- Physiological measurements in obtaining energy expenditure and workloads during simulated lunar surface mission 23 p3959 A67-41657
- HEAT**
- S CALORIMETER
- S COMBUSTION HEAT
- S DRY HEAT
- S ENTHALPY
- S ENTROPY
- S FORMATION HEAT
- S NERNST HEAT THEOREM
- S NUCLEAR HEAT
- S SOLAR HEAT
- S SOLUTION HEAT
- S SPECIFIC HEAT
- S SUBLIMATION HEAT
- S THERMAL FATIGUE
- S THERMAL NOISE
- S VAPORIZATION HEAT
- HEAT ACCLIMATIZATION**
- SA THERMAL COMFORT
- Cellular biochemical thermoregulation and organic mass changes in cold and heat-acclimatized monkeys 04 p0560 A67-14582
- HEAT BALANCE**
- Prolonged autonomous existence of humans in space suits, discussing maintenance of heat balance by physiological perspiration 02 p0187 A67-12324
- Steady state heat balance on opaque inner wall of enclosure 02 p0343 A67-12413
- Entropy and available energy in operation of gas turbine, considering thermodynamic efficiency, heat balance and available energy balance 05 p0873 A67-16742
- Heat balance and ventilation of human body in pressure suit 09 p1455 A67-21731
- Aerospace clothing hygiene, discussing climate influence on protective garment selection and physiological responses of living organisms to obtain heat balance 12 p1902 A67-25176
- Heat balance in rocketsonde semiconductor thermometers, noting dissipation constant dependence on altitude and solar radiation 13 p2117 A67-27608
- Uniqueness theorems for Adler fourth and fifth boundary value problems for heat conduction differential equation 14 p2409 A67-28936
- Surface heat balance shown to be useful thermal boundary condition at sea-air-land interface for earth surface mean temperature and macroclimate models 15 p2513 A67-30060
- Heat addition in channels of variable cross section area discussed for one-dimensional, inviscid flow of ideal gases with constant specific heat ratio 16 p2591 A67-30944
- Nonequilibrium flow relation to flow in thermal balance, describing irreversible processes in terms of entropy source field and relaxation resistance 16 p2862 A67-31467
- Lumped parameter model for monopropellant hydrazine reaction chamber developed, using mass and energy balance and reaction and diffusion rate coefficients 17 p2927 A67-31974
- Physical parameter determination for monatomic gas flow based on energy balance, taking into account heating and ionization in thermal nonequilibrium 17 p2837 A67-32337
- Hydrazine effect, alone and with nicotinic acid, on oxygen consumption, respiratory quotient, carbohydrate pool and heat losses in rats studied using gradient calorimeter 18 p2992 A67-34714
- Transpiration cooled porous surface in high temperature forced convection environment, applying transient energy balance with heat-transfer coefficient measurement [ASME PAPER 67-HT-27] 20 p3546 A67-36720
- Jupiter and Saturn models, giving planet constitution, heat balance and atmospheric composition 21 p3710 A67-39001
- Thermographic method for investigation of kinetics of heat evolution 22 p3917 A67-39586
- Monomethylhydrazine effects on metabolism and heat balance using various calorimetric methods 23 p3954 A67-41601
- Absorption of black body radiation by horizontal atmospheric layer, deriving expression of integral coefficient of atmospheric transparency 24 p4255 A67-42590
- HEAT BUDGET**
- SA ATMOSPHERIC HEAT BUDGET
- Radioisotope heating for ionizer temperature of contact ionization thrusters for satellite attitude control and stationkeeping, studying power source mass saving [AIAA PAPER 67-735] 21 p3695 A67-38758
- HEAT CAPACITY**
- Classical meteoric ablation theory generalized to include thermal radiation, conduction and meteoroid heat capacity in causing fragmentation 01 p0147 A67-10357
- Ruby laser as energy source for measuring thermophysical properties of materials via flash technique 04 p0623 A67-15305
- Heat capacity and Debye temperature of NdS, LaSe and LaTe 05 p0867 A67-17056
- Si and Ge heat capacities in terms of equivalent Debye temperature, obtaining coefficient of leading anharmonic contribution to free energy 05 p0870 A67-17199
- Variable thermal capacity of gas mixture taken into account in calculation of heat regeneration in gas turbine cycles, using working bodies 07 p1266 A67-19181
- Heat capacity evaluation between 150 and minus 180 degrees C, using evaporated gold-black coating as primary standard [AIAA PAPER 67-303] 12 p1958 A67-26018
- Thermal capacity of gallium and thallium selenides 13 p2174 A67-26367
- Heat capacity and Debye temperature of NdS, LaSe and LaTe 15 p2538 A67-29787
- Variable heat capacity of gas effects on supersonic flow past blunt body analyzed using dimensionless system of equations 16 p2592 A67-31113
- Shape dependence of detached shock wave in supersonic gas flow of blunt-nosed models on Mach number, heat capacity and bluntness ratio 16 p2593 A67-31131
- Experimental assembly for measuring true heat capacity of heat resistant insulating materials during natural cooling at temperatures from 1200 to 2400 degrees K 16 p2678 A67-31784
- Transverse wave structure in detonations investigated using smoked-foil technique in gas mixtures, showing dependence on tube geometry and heat capacity 18 p3153 A67-33828
- Superconductors with overlapping bands, discussing copper pairing, heat capacity, critical field and ultrasonic attenuation 20 p3512 A67-37435
- Thermal capacity of gallium and thallium selenides 21 p3680 A67-38323
- Lattice type gas heat capacity discontinuity near critical point 22 p3790 A67-39509
- Lattice heat capacities, Debye temperatures, heat capacity, free formation energy and thermodynamic functions of groups II-IV semiconductors 23 p4047 A67-41533
- Niobium carbide enthalpy, heat content and heat capacity variation in homogeneity domain from 1300 to 2500 degrees K 24 p4171 A67-41958
- Semiconducting mixed titanate superconducting transition observed at 0.5 degrees K ascribed to change in valley numbers in conduction band 24 p4205 A67-43098
- HEAT CONTENT**
- Enthalpy and position in heated tube where liquid boiling begins, finding heat content in turbulent liquid flow 14 p2406 A67-28311
- Niobium carbide enthalpy, heat content and heat capacity variation in homogeneity domain from 1300 to 2500 degrees K 24 p4171 A67-41958
- HEAT DISSIPATION**
- Heat dissipation rate in straight bar of constant cross section generating heat internally, using Laplace transforms 01 p0166 A67-10551
- Fluctuation-dissipative ratio between correlation functions of fluctuating parameters and dissipative properties in thermodynamic-nonequilibrium systems with spatial dispersion 04 p0673 A67-15968
- Heat emission from compression shock layer about meteors in thermodynamic equilibrium 05 p0903 A67-17313
- Dissipative effects in converging cylindrical symmetric shock wave, considering ion and electron heat conductivity, ion viscosity and energy exchange 06 p0984 A67-18029
- Liquid cooling of integrated circuit systems to remove increased heat dissipation, noting heat transfer rates 12 p1915 A67-25888
- Heat loss and recovery temperature of fine wires in transonic transitional flow regime, noting experimental and computational results 14 p2405 A67-28177
- Spacecraft package temperature control by interior louver panel system, calculating net heat transfer [ASME PAPER 67-HT-64] 20 p3549 A67-36746
- Supersonic viscous gas flow around body of revolution involving perturbation damping, analyzing Navier-Stokes and heat transfer equations for flow chart 20 p3357 A67-36810
- Thermodynamics of nonlinear materials with internal state variables, analyzing evolution equation, dynamic stability, dissipation, etc 20 p3555 A67-37563
- Plasma sprayed alumina and beryllia dielectric coatings for heat sinks in electronic packaging, emphasizing heat dissipation from heat/generating components 21 p3650 A67-38849
- Motion and thermodynamic conditions of free piston ballistic compressor test gas taking into account gas leakage, viscous friction and heat losses 22 p3778 A67-39351
- Reflex klystron for 1.5 mm wavelength noting high current density cathodes, RF section simplification and better heat dissipation 22 p3768 A67-39493
- Ice single crystal growth rate in supercooled water explained on basis of combined heat dissipation mechanism and molecular growth kinetics 23 p4024 A67-40973
- Thermal protection methods for structures subject to aerodynamic heating, discussing heat dissipation methods and thermophysical materials 23 p4082 A67-41042
- Rocketsonde thermistor mount noting thin film configuration and long lead mount for heat dissipation 23 p4025 A67-41446
- Conductive cooling method for pressure applications in body heat loss promotion at high exercise rate 23 p3964 A67-41558
- HEAT EFFECT**
- SA ABLATION
- SA PELTIER EFFECT
- SA THERMAL DEGRADATION
- Test stand simulating high intensity heating processes which occur in combustion chambers of rocket and jet engines 02 p0231 A67-12440
- High temperature thermomechanical treatment effects on VT10 titanium alloy fine structure

- characteristics 10 p1670 A67-23641
Gas saturated layer effects on VT5
titanium alloy mechanical properties
variation with 10 p1670 A67-23642
temperature
Cesium seeded argon plasma at
atmospheric pressure, noting electron
heating effect on conductivity curve and
applicability to MHD 12 p1970 A67-25253
conversion
Absorption of laser radiation in
semiconductors and mechanisms of
breakdown in process 15 p2537 A67-29704
Heat treating effects on titanium alloy
properties, discussing ductility and strength
annealing, etc 16 p2681 A67-30486
Ultrasonic energy, used for removing
microorganisms from various surfaces for
enumeration, noting texture, pretreatment
and heat effects on recovery
efficiency 19 p3179 A67-34911
Braking and heating effects of atmosphere
on meteors in zodiacal dust to 1-meter size,
discussing interaction at air cap, entry,
etc 20 p3525 A67-36949
Friction heat effect on explosion threshold
noting pressure drop role in reacting system
explosion 20 p3554 A67-37055
Microcracking susceptibility studies of
Inconel 718 weld heat affected zones, noting
hot ductibility, weld circle patch and
flawless fusion welding
tests 22 p3818 A67-39222
Microsegregation and grain boundary
liquidation in heat affected zone of 18-Ni
maraging steel welds 22 p3812 A67-39448
Absorption of laser radiation in
semiconductors and mechanisms of
breakdown in process 24 p4199 A67-41774
CdS single crystal film trap energy
spectrum studied with thermo-stimulated
currents /TSC/ noting effect of SiO
layer 24 p4203 A67-42246
Cryogenic mechanical properties of
poly(ethylene terephthalate) film studied for
effects of stretch and heat set temperature
and time 24 p4176 A67-42469
HEAT ENGINE
SA CARNOT ENGINE
SA ELECTROTHERMAL ENGINE
SA GAS GENERATOR ENGINE
SA INTERNAL COMBUSTION ENGINE
SA POWER PLANT
SA TURBINE
Constant total pressure evaporation with
heat reuse by built-in 14 p2407 A67-28623
Entropy applied to theory of fuel cells,
noting effect of operating 14 p2252 A67-29018
temperature
MHD open circuit solution, operating by
means of ionized gases, may lead to very
high temperature internal combustion heat
machines, discussing heat 18 p3115 A67-34120
cycles
Book on energy conversion covering heat
engines, power sources, solar energy, SNAP
generators, etc 19 p3177 A67-35892
HEAT EQUATION
Additional conditions for boundary value
problem with directional derivative in heat
conduction 02 p0259 A67-11920
Single layer potential solution to boundary
value problems for heat equation in half-
plane with one or two points of
discontinuity in boundary 03 p0459 A67-13590
conditions
Radial heat equation and Laplace
transforms, discussing representations
alternative to two 03 p0460 A67-13819
solutions
First boundary value problem for thermal
conductivity equation involving region with
two angular points on 04 p0721 A67-14661
boundary
Nonstationary heat conductivity solution
for hollow sphere with varying inner surface
and various outer surface 04 p0726 A67-15594
conditions
Green function derived for heat
conduction along straight line with
boundaries in steady 04 p0726 A67-15595
motion
Approximate solution of
thermoconductivity equation for multilayer
cylinder in constant-temperature
medium 04 p0738 A67-15891
Estimates of Green function in first
boundary value problem of
thermoconductivity equation for
cylinder 05 p0927 A67-17002
Boundary value problem for heat equation,
discussing Laplace transform solution and
uniqueness theorem 06 p1111 A67-17645
Thermal conductivity coefficients of
refractory materials at high temperatures
determined by measuring one-dimensional
stationary thermal flux at single
point 07 p1265 A67-19124
Analytic solutions of heat equation for
case when both temperature and heat flow
rate are prescribed at single fixed boundary
applied to phase change 08 p1428 A67-21432
problems
General solutions of heat equation in
stationary homogeneous isotropic finite
region with constant thermal
properties 08 p1429 A67-21436
Alternation direction methods /particular
class of iterative methods/ applied to heat
conduction problems 09 p1468 A67-22051
Steady state Leveque problem generalized to
include time dependence, obtaining eight
solutions for surface 10 p1732 A67-22727
temperature
Heat transfer equations for rocketborne
stratospheric temperature sensor in form of
spherical bead thermistor and experimental
analysis of physical, thermodynamic and
electrical characteristics of rocketsonde
[AIAA PAPER 66-385] 10 p1632 A67-22819
Asymptotic behavior of laminar boundary
layer, reducing system to heat equation,
noting viscosity effects and uniqueness of
homogeneous solution 10 p1623 A67-22878
[ONERA-TP-458]
Reduction of PDE system of heat transfer,
using Hermitian approximating polynomials
to obtain solution to initial
system 10 p1608 A67-23323
Moment stresses in thermoelasticity for
medium described in terms of displacement
and rotational vectors 10 p1720 A67-23599
Rodrigues type formula for generalized
Laguerre polynomials based upon semigroup
property for solutions of heat equation and
generating function related to source
solution 10 p1675 A67-23630
Inverse problem of unsteady heat
conduction equation for unbounded hollow
cylinder, determining specific
heat 11 p1882 A67-24031
Heat equation of thin closed cylindrical
shell exact solution analyzed using least
squares method 12 p2034 A67-25606
Thermal and ablative lag induced by
periodic heat input to oscillating flat plate
in high velocity flow, showing crossover
from dynamically stabilizing to destabilizing
condition as oscillation frequency increases
[AIAA PAPER 67-336] 12 p2039 A67-26050
Structures of solutions and expansion of
radial heat equation with pole type data
function 13 p2145 A67-26492
Heat conduction equation for
inhomogeneous body, obtaining integrable
solutions applicable to boundary value
problems 13 p2224 A67-27055
Maclaurin series expansion representation
of generalized heat 13 p2147 A67-27454
equation
Plated-tube heat exchanger design for
minimizing axial heat conduction losses and
controlling heat transfer surfaces and core
weight 13 p2229 A67-27665
Heat equation for free boundary problem
with prescribed flux at fixed and melting
interface of semiinfinite
slab 14 p2405 A67-28255
Linearization of equation of thermal
explosion and stability of solutions for
boundary conditions of third
kind 14 p2406 A67-28310
Variational integration principles used to
integrate wave and Fourier
thermoconductivity equations, noting
solution by Ritz method 14 p2408 A67-28803
Solution of uniform heat conduction
equation with movable boundaries applied to
problem of electric 16 p2779 A67-31207
contacts
Limiting value calculation for temperature
field criteria, analyzing heat-conduction
equation solution and boundary value
problems 17 p2972 A67-33068
Differential transport equation system in
n-dimensional anisotropic space solved using
matrices, discussing heat conduction
equations 17 p2972 A67-33070
Unsteady heat transfer between solid body
and surrounding fluid flow, using convective
fluid heat transfer and body
thermoconductivity 17 p2972 A67-33071
equations
Static /time-discrete/ electrical model for
mathematical analogy of heat transfer
processes and application to solution of
nonlinear heat conduction
equations 17 p2821 A67-33079
Combined electrical modeling technique
for solution of two-and three-dimensional
problems of unsteady heat
conduction 17 p2973 A67-33081
Inhomogeneous temperature field arising
during laser welding of different materials
with imperfect contact, deriving and solving
heat conduction equations 18 p3053 A67-33630
Turbulent heat-transfer coefficients and
eddy diffusivity profiles for momentum and
heat in Newtonian and non-Newtonian fluids,
giving equation for data
correlation 19 p3344 A67-34869
Critical supersaturations for homogeneous
nucleation of ethanol, hexane, etc,
investigated using thermal diffusion cloud
chamber 20 p3555 A67-37562
Thermal conductivity coefficients of
refractory materials at high temperatures
determined by measuring one-dimensional
stationary thermal flux at single
point 21 p3731 A67-38168
Junction temperature current dependence
in CW operated gallium arsenide laser
diodes 21 p3639 A67-38256
Cooling of cylinder moving through fluid
assuming fluid properties permit boundary
layer approximations 22 p3918 A67-39782
Deriving stability and asymptotic stability
properties of temperature fields governed
by quasi-linear heat 23 p4081 A67-40745
equations
Cauchy problem for heat equation noting
error analysis for numerical procedure and
Stefan problem solution 23 p4081 A67-40860
Analysis of system described by heat
equation where disturbance propagates with
infinite speed as function of
time 23 p4024 A67-41086
HEAT EXCHANGER
SA REGENERATOR
SA TUBE HEAT EXCHANGER
Mathematical model selected for unstable
heat exchange process with single-phase
incompressible heat 03 p0535 A67-13119
conductor
Mass flow from gas-vapor mixture to wall
of recuperative heat-exchanger
condenser 03 p0536 A67-13688
Performance of thermal regenerators in
which rapid flow cycling is accompanied by
large pressure variations with time
[ASME PAPER 66-WA/PID-1] 04 p0724 A67-15379
Fin efficiencies in n-core stack heat
exchanger
[ASME PAPER 66-WA/HT-47] 04 p0724 A67-15432
Low pressure environmental chamber for
estimation of gas exchange ratio during
exposure of animals under controlled
conditions
[ASME PAPER 66-WA/HT-52] 04 p0599 A67-15438
Laminar heat exchange in inlet section of
rectangular channel with incompressible
fluid and temperature 04 p0726 A67-15590
field
System induced instabilities of forced
convection flows with subcooled boiling
restricted to case of water flow in small
circular channels, high L/D ratios, moderate
temperature and pressure 04 p0736 A67-15858
Boundary layer theory of heat exchange in
vortex region of separated flow past
cylinder 06 p1119 A67-18821
Diffusion mass exchange model for
thermal and hydrodynamic
processes 07 p1267 A67-19328
Flame heated thermionic converter noting
electrical, material and combustion problems
of design of 100 watt
device 09 p1448 A67-22341
Fluid and solid temperature determination
in regenerative heat exchangers at any time
and location 10 p1731 A67-22726
Optimal parameters of refrigerators with
radiative regenerative gas
cycle 10 p1596 A67-23022
Liquid metal heat transfer in various
structural configurations 10 p1734 A67-23631
Vacuum or low pressure contamination
removal from space simulation chamber,
using bakeout with externally and internally

supplied heat 11 p1773 A67-24976
Heat pipes and vapor chambers for thermal control of spacecraft, noting design and application [AIAA PAPER 67-310] 12 p2036 A67-26025
Low gravity liquid hydrogen tank venting, considering systems with heat exchange for space missions 13 p2057 A67-27640
Liquid hydrogen heat exchanger for servicing Saturn V S-II 17 p2954 A67-32011
Thermodynamic system for zero g venting, storage and transfer of cryogenic propellants, discussing heat exchanger 17 p2954 A67-32074
Existence of entropy as consequence of asymptotic stability 18 p3160 A67-34285
Hybrid computer for co-current laminar-flow heat exchanger Sturm-Liouville problem 19 p3190 A67-36069
Major difficulties encountered in open and closed cycle MHD, particularly temperature resistance of heat exchanger 20 p3362 A67-36366
Heat exchanger transfer functions obtained from linearization of partial differential equations [ASME PAPER 67-HT-5] 20 p3544 A67-36704
Size and longitudinal conduction influence on wall temperature field and effectiveness of heat exchangers determined by differential equations [ASME PAPER 67-HT-80] 20 p3551 A67-36758
Design, fabrication and performance of 10-millipound resistojet operating on hydrogen or ammonia, describing heat exchanger and nozzle geometry [AIAA PAPER 67-664] 21 p3690 A67-38699
Boiler inlet impedance frequency response in single tube heat exchanger when pumped with oscillating flow 22 p3916 A67-39390
Hydrogen peroxide oxygen-water supply system as backup for long space flights noting storage tanks, catalytic reactor and heat exchanger 22 p3747 A67-39893
Heat exchanger cooling system for controlling aircraft high temperature and thermal inorganic salt for protection against cold for flying personnel 23 p3967 A67-41612

HEAT FLOW
SA SOLAR HEAT FLOW
Temperature dependence of heat-pulse propagation in sapphire at low temperature intervals, noting phonon mean free path 01 p0131 A67-10341
Integral transform associated with boundary conditions containing eigenvalue parameter applied to initial boundary value problem arising in diffusion theory and heat flow 03 p0460 A67-13825
Nucleate boiling mechanism in superheated binary mixtures obtained from extension of theories of van Wijk, Vos and van Stralen by Scriven and Bruijn 04 p0720 A67-14637
Heat flow meter with short response time, measuring influence of acoustic field on forced convection 05 p0790 A67-16034
Digital computer programs for transient and steady state thermal analysis 05 p0929 A67-17452
General solutions to heat conduction equations for three-dimensional unsteady heating of finite solid circular cylinder 06 p1113 A67-18124
Boundary conditions for two-dimensional steady heat flow in rectangular region with temperature discontinuity at corners 06 p1119 A67-18650
Perpendicular magnetic field induced change in electron temperature of current carrying semiconducting plates 06 p1054 A67-18805
Steady state heat flow in dielectric cylinders in boundary scattering limit, considering liquid helium 08 p1426 A67-20716
Analytic solutions of heat equation for case when both temperature and heat flow rate are prescribed at single fixed boundary applied to phase change problems 08 p1428 A67-21432
Plane thermal stress at insulated hole under uniform heat flow in orthotropic medium 10 p1730 A67-23838
Heat flow through Langmuir sheath in presence of electron emission and application to limitation of energy loss rate by thermal conduction 11 p1828 A67-23894
Heat flow mechanisms and thermodynamics of supercritical cryogenic storage problems solved by digital computer

simulation, using finite difference approximation 12 p1925 A67-25722
One-dimensional heat flow to confined ideal gas solved on digital computer, discussing energy equations, thermal gradient induced fluid motion, etc [AIAA PAPER 67-337] 12 p2039 A67-26051
General heat flow problem with convolution integrals eliminated and unsteady temperature distribution expressed as sum of quasi-steady and transient fields, noting region geometry 12 p2040 A67-26185
Solution of one-dimensional diffusion equation of heat flow normal to surfaces, prescribing potential and flow rate along moving parametric curve 14 p2405 A67-28254
Space-time region division method for reducing nonlinear heat conduction to subordinate linear multilayer system problems, assuming stationary time characteristics and coordinates 14 p2408 A67-28804
Steady state heat conduction approximation solution based on effective boundary conditions 14 p2408 A67-28805
Heat flow values correlated with major geological features by analysis of 2000 terrestrial heat flow observations 15 p2477 A67-29763
Approximate iteration procedure for determining temperature field in plate for simultaneously radiative and convective heat transfer 15 p2580 A67-29779
Steady state heat flow and temperature fields in flat rectangular configurations with mixed boundary conditions 16 p2779 A67-31206
Lunar internal heat flow measured by infrared mapping of polar regions from orbiting satellites 16 p2754 A67-31750
Perpendicular magnetic field inducer change in electron temperature of current carrying semiconducting plates 18 p3102 A67-34424
Calibration and recording method for transmission coefficients of thermal wall heat flows, using ONERA wind tunnel [ONERA-TP-470] 18 p3020 A67-34463
Equations for transient temperature distribution and thermal stresses in heated idealized wing structure solved using heat flow analysis method 20 p3541 A67-37489
Thermal-stress deformed condition on heated elastic bodies boundary containing inclusions of spherical thin film with homogeneous infinite heat flow 21 p3720 A67-38295
Magnetic film memory written and read by focused light studied using thermal cycle time and read bandwidth calculations 22 p3765 A67-39910
Radiative transfer in lunar surface diurnal heat flow, studying geometric model of porous medium 22 p3885 A67-39980
Heat flow meter apparatus for rapidly measuring thermal conductivity of flat insulation specimens under cryogenic temperatures 22 p3802 A67-40293
Cryogenic thermoconductivity heat flow meter apparatus for felt, powder and block materials at atmospheric pressure 22 p3803 A67-40298
Thermal stress fracture of brittle ceramics studied for effect of relaxation by creep at high temperature under conditions of quasi-static heat flow 22 p3915 A67-40386
Net convective and radiative heat flow to electrodes of coaxial plasma generator may exceed heat flow from moving arc spot within arc burning region 24 p4098 A67-42250
Heat pipe performance in zero gravity field, discussing isothermal operation of water heat pipe in earth orbit 24 p4256 A67-42926

HEAT FLUX
Radiation calibration of heat flux sensors, comparing resistively heated filament and solar energy device 01 p0069 A67-11019
Heat flux sensor using piezoresistive thermometer for sensing small temperature differentials, discussing design, analysis and test 01 p0069 A67-11020
Heat flux measurement with narrow view angle radiometers, discussing equipment design, performance characteristics and results 01 p0069 A67-11021
Heat flux to SNAP reactor system models in hypersonic continuum flow measured in shock and hyperthermal wind tunnels, using thin film resistance

thermometer 01 p0112 A67-11022
Null point or transient copper calorimeter using single temperature response measurement to determine heat flux, correlating experimental with theoretical data 01 p0070 A67-11035
Heat flux measurement in very short flows in short arc wind tunnels and shock tubes 01 p0168 A67-11091
Calorimeter for measuring heat flux to ablating surface, noting theory of device 01 p0071 A67-11106
Pressure and density measurements of heat flux convected on sharp pointed cone placed in incidence in hypersonic flow 02 p0177 A67-11499
Temperature control and complex heat path designs inertial components, platforms and strap-down guidance systems, considering floated gyros and accelerometers 02 p0241 A67-11789
Turbulent energy dissipation rates, eddy fluxes of sensible heat, momentum and kinetic energy measured above nonhomogeneous surface 02 p0238 A67-12076
Stabilizing effect of wall and thermal flux temperature variations over channel length on heat transfer coefficient of liquid flow 03 p0536 A67-13610
Heat transfer and friction drag for supercritical laminar flow of carbon dioxide through tube at constant thermal flux density at wall 03 p0536 A67-13612
Radiant heat influx to free atmospheric layers, atmospheric macrocirculation and time-corresponding geopotential field charts 03 p0463 A67-14226
Comparison of temperature differences for similar liquids boiling on various surfaces, with graph correlating heat flux/temperature difference data 04 p0721 A67-14645
Viscous friction and heat flux for partially ionized medium flowing in plane channel with anisotropic transport coefficients 04 p0666 A67-15189
Temperature and heat flux distribution in linear liquid-metal MHD device with direct cooling of winding 04 p0556 A67-15528
Simultaneous conductive-convective heat-transfer coefficient and heat flux temperature relation at solid moving liquid interface 04 p0730 A67-15817
Axial temperature and velocity measurements made in water at various aspect ratios, Grashof number and bottom-to-side heat flux ratios for turbulent free convection in closed container 04 p0731 A67-15827
Deflection angle of supersonic gas flow with oblique shock wave and heat input in wake, choosing minimum entropy variation as measure of system optimality 04 p0550 A67-15898
Rayleigh-Ritz method for turbulent heat transfer in curvilinear channel and heat flux magnitudinal and directional effects on stability of isothermal flow in laminar boundary layer 04 p0610 A67-15900
Thrust chamber life estimation from calculable local heat flux and tube temperatures, using assumptions of elastic strain invariance and isotropic material properties 05 p0874 A67-17226
Laminar boundary layer on ellipsoids of revolution situated at zero angle of attack in supersonic flow of perfect gas 06 p0936 A67-17740
Thermal fluxes in plasma jets produced by HF plasmatron in air 06 p1045 A67-18813
Assessment of available methods for direct measurement of radiative heat influx in free atmosphere 07 p1172 A67-19458
Curvature effect on heat transfer for turbulent flow in curved pipes under constant heat flux, considering boundary layer existence along wall 08 p1426 A67-20926
Energy problems in laser welding, examining maximum instantaneous heat flux metals can withstand 09 p1504 A67-22138
Local heat transfer in water flow in horizontal annular tube, estimating local longitudinal and circumferential variations in Nusselt number at tube wall as function of Reynolds and Rayleigh numbers 11 p1881 A67-24025
Heat flux in rarefied gas calculated via transport equations, noting validity of boundary temperature discontinuities 11 p1881 A67-24028
Exponential point method measurement of heat fluxes and surface temperature in

unsteady regime 11 p1882 A67-24030
 Moisture transfer and thermal influx
 equations solutions for atmospheric
 boundary conditions of preinversion
 intramass strata evolution
 scheme 11 p1816 A67-24522
 New thermal radiative flux gauge utilizing
 thin film resistance thermometer and short
 duration test techniques 11 p1792 A67-24821
 Radiant heat influx to free atmospheric
 layers, atmospheric macrocirculation and
 time-corresponding geopotential field
 charts 12 p1963 A67-25482
 Cryogenic fluid storage on moon surface,
 considering Lambert reflection law, thermal
 insulation performance, incident heat flux
 and boil-off rates 12 p1926 A67-26011
 [AIAA PAPER 67-296]
 General heat flow problem with
 convolution integrals eliminated and
 unsteady temperature distribution expressed
 as sum of quasi-steady and transient fields,
 noting region geometry 12 p2040 A67-26185
 Model for vertical eddy heat flux in stable
 atmosphere 13 p2149 A67-26275
 Orographic factors effect on stratospheric
 pressure field, obtaining ascending vortical
 fluxes and heat input equations, discussing
 refractive index for atmospheric
 perturbations 13 p2112 A67-26672
 Meridional and vertical wind components
 analyzed for angular momentum, balance,
 heat influx and internal
 friction 13 p2113 A67-26678
 Thermodynamic possibility of thermal
 convection in earth
 mantle 13 p2117 A67-27577
 Heat leak and pressure decay for single
 phase cryogenic storage in nonequilibrium
 calculated for spherical tanks, using
 simplifying assumptions 13 p2227 A67-27641
 Very low heat background calorimeter
 design for heat-short experiments and
 checking analytical predictions for propellant
 tank insulation 13 p2228 A67-27658
 Absolute emissivity calorimeter design for
 low temperature measurements above 60
 degrees K using liquid helium as cryogenic
 fluid 13 p2122 A67-27661
 Cooldown of shrouded spherical vessels in
 liquid nitrogen, determining smallest tank-
 shield gap compatibility with rapid
 cooldown 13 p2229 A67-27666
 Method to describe finite amplitude
 convection time
 dependence 14 p2295 A67-27901
 Two-dimensional thermal conductivity
 problems for hollow cylinder heated at
 constant rate, estimating axial heat flux
 effect 14 p2406 A67-28306
 Heat flux requirements for cutting low-
 plasticity metal sheets on lathe, noting
 thermal effect 14 p2325 A67-28654
 Lateral heating and sublimation of
 arbitrary thick two-layer plate using thermal
 flux time-dependent on plate
 surface 14 p2408 A67-28802
 Dimensional analysis of heat transfer
 correlations for nucleate boiling in free
 convection, including critical heat flux
 conditions 14 p2408 A67-28932
 Radiative energy transfer through nongray
 medium bounded by two flat surfaces,
 obtaining temperature distribution and heat
 flux values 15 p2578 A67-29130
 Ignition response of solid propellants
 described with model including surface
 regression with verification of igniter flux
 and pressure effects 15 p2581 A67-29988
 Aerodynamic heat flux measurements in
 frozen boundary layer flows taken in
 hyperthermal wind tunnel, considering
 surface catalytic effects 15 p2468 A67-30154
 Integration of laminar boundary layer
 equations in compressible gas by asymptotic
 method, calculating friction and heat
 flux 16 p2660 A67-31135
 Thermal stress concentration in physically
 nonlinear elastic plate with hole in presence
 of uniform heat flux 16 p2768 A67-31148
 Pressure distribution and convective heat
 flux at slender bodies of revolution surface,
 considering sphericity influence of free
 hypersonic flow 16 p2594 A67-31468
 Heat transfer in cryogenic range, noting
 heat flux measurements, use of
 semiconductors, etc 16 p2780 A67-31533
 Unsteady heat transfer in tube during
 heat-flux fluctuations 17 p2967 A67-32130
 Heat transfer by dropwise condensation,
 evaluating average heat

flux 17 p2969 A67-32447
 Critical heat-flux density dependence on
 dominant parameters in bilateral heating in
 annular channels 17 p2969 A67-32459
 Critical heat flux value nonlinearly
 dependent on liquid bulk underheating to
 saturation temperature, deriving empirical
 formula 17 p2970 A67-32460
 Affine solutions for temperature/flux
 distribution on heated horizontal
 plate 17 p2838 A67-32701
 Small scale magnetic fields observed in
 photosphere explained by sunspots made
 invisible by lateral heat
 influx 17 p2953 A67-33404
 A priori bound on difference between free
 boundary positions in two Stefan problems
 derived in terms of initial conditions and
 heat influxes 18 p3071 A67-33664
 Symmetry removal from linear relations
 between forces and fluxes, concluding that
 fading memory in viscoelastic materials
 results from irreversible
 entropy 18 p3159 A67-34005
 Heat transfer process for film boiling
 taking into account growth of prominences
 up to bubble departure and Taylor
 instability 18 p3160 A67-34162
 Vapor volumetric fraction during forced
 convection, calculating true local vapor
 weight, volumetric fraction, location of
 bubble departure, etc 18 p3160 A67-34163
 Wall heat flux in turbulent air flow using
 inner law correlations for velocity and
 temperature 18 p3160 A67-34165
 High intensity heat flux formation during
 heat transfer on steel cylinder in region of
 incident shock wave in supersonic
 flow 18 p3027 A67-34206
 Stabilizing effect of wall and thermal flux
 temperature variations over channel length
 on heat transfer coefficient of liquid
 flow 18 p3161 A67-34475
 Heat transfer and friction drag for
 supercritical laminar flow of carbon dioxide
 through tube at constant thermal flux
 density at wall 18 p3161 A67-34477
 Steady state technique for measuring high
 temperature thermal conductivity of
 nonmetallic materials requiring heat flux
 and temperature gradient
 calculation 18 p3051 A67-34508
 Heat flux measurements in fluid systems
 using joule heating accomplished with single
 calibration and without flow rate
 measurements 18 p3052 A67-34513
 Protonosphere heating by photoelectrons
 escaping from F region, estimating
 protonosphere opacity and daytime escape
 flux 19 p3221 A67-35280
 Temperature field distribution and heat
 flux in thin narrow semiinfinite composite
 plate with moving point
 source 19 p3347 A67-36051
 Radiative heat flux for free burning
 methanol and acetone flames of arbitrary
 size and geometry predicted, using transport
 equation
 [ASME PAPER 67-HT-47] 20 p3547 A67-36729
 Sinusoidal surface vibration effect on
 nucleate pool boiling reveals lowered surface
 temperature for low heat flux, LF and high
 acceleration
 [ASME PAPER 67-HT-49] 20 p3548 A67-36731
 Free convection effect on forced laminar
 flow of water in horizontal tube with
 uniform heat flux and velocity profile fully
 developed
 [ASME PAPER 67-HT-52] 20 p3548 A67-36734
 Incipient boiling prediction extended from
 forced flow water to other fluids and
 natural flow conditions
 [ASME PAPER 67-HT-61] 20 p3549 A67-36743
 Film boiling of potassium on horizontal
 plate, discussing heat fluxes relationship to
 Berenson equation and heat transfer
 [AIChE PAPER 28] 20 p3552 A67-36832
 Heating rate and type effects on
 stationary fluids stability, noting dependence
 on critical Rayleigh
 number 20 p3553 A67-36848
 Transient temperature distribution for
 spherical region subjected to variable heat
 flux at boundary represented by terms of
 known functions and
 quadratures 20 p3555 A67-37610
 Relation between entropy flux and heat
 flux using entropy inequality and natural
 invariance principle for materials with
 fading memory 22 p3918 A67-39742
 Heat transfer experiments with flat plate

heated under constant heat flux, discussing
 wall temperature distribution, Prandtl
 number and Spalding
 function 22 p3918 A67-40041
 Copper oxide and selenium semiconductor
 rectifiers as heat flux sensors, describing
 operation and thermal
 EMF 22 p3801 A67-40217
 Model for straight fin nucleate boiling
 onset criterion, discussing boiling section
 length expression, heat flux and
 temperature profile
 distribution 22 p3919 A67-40387
 Noise occurrence during heat transfer
 from solid to liquid He 2 flux at high
 temperature difference, discussing heat
 flux 22 p3838 A67-40389
 Thin foil heat flux sensor for radiative
 and convective heating rates over wide
 range and dynamic response, noting error
 mechanisms, calibration and
 accuracy 23 p4006 A67-41374
 Radiative and convective heat flux
 measuring instruments calibration for
 aerospace industry 23 p4006 A67-41375
 Fast response thin skinned calorimeters
 for high heat flux profiles of arc jet
 flows 23 p4006 A67-41381
 Radiative heat transfer in radiating and
 conducting media, calculating heat flux and
 temperature distribution for semisotropic
 model 23 p4083 A67-41718
 Calorimeter for measuring heat flux to
 ablating surface, noting theory of
 device 24 p4155 A67-42289
 Incidence angle effects on wall heat flux
 in symmetry plane of cone of revolution in
 hypersonic regime, discussing wall pressure
 measurements 24 p4092 A67-42660
HEAT GAIN
 Atmospheric warming over Central Europe
 related to low solar and magnetic
 activity 14 p2313 A67-28621
 Vacuum jacketed cryogenic globe valve
 design providing tight sealing, low heat leak,
 low cool-down mass and high
 flow 23 p3936 A67-41426
HEAT GENERATION
 Heat metabolism in working men while
 isolated from environment by water-cooled
 suit and environmental chamber
 [ASME PAPER 66-WA/HT-45] 04 p0564 A67-15431
 Subcritical convective instability,
 discussing effects of internal heat
 generation and spatial variation of gravity
 field on onset of thermal
 convection 05 p0926 A67-16817
 Heat regeneration and high gas
 temperatures for fuel economy in helicopter
 gas turbine engines 11 p1852 A67-24525
 Field-aligned irregularities as effect of
 increased electron temperature in F-2 layer,
 analyzing heat production and loss
 mechanism
 [AGARDGRAPH 95] 15 p2484 A67-30305
 Boundary value problems containing
 positive linear differential operators and
 monotone functions of dependent variable
 analyzed via nonlinear heat
 generation 17 p2967 A67-32040
 Forced convection of laminar flow in
 tubes of various cross sections, assuming
 constant temperature gradient and internal
 heat generation 20 p3420 A67-36317
 Arbitrary internal heat generation terms
 in energy equation effect upon limiting
 Nusselt number for heat transfer to pipeline
 flow of non-Newtonian fluids
 [AIChE PAPER 12] 20 p3552 A67-36828
 Superconducting niobium wire magnetic
 moment and heat development during
 external magnetic field variation, discussing
 irreversible behavior 20 p3511 A67-37240
 Resistance spot welding process, using
 heating, cooling and stress development data
 to compute internal
 behavior 20 p3456 A67-37697
 Temperature distributions and heat
 generation in viscoelastic isotropic solid
 resulting from mechanical deformations
 determined by energy
 equation 21 p3715 A67-37894
 Trimming methods for Ti alloy materials
 including plasma arc cutting, band sawing,
 shearing, milling, nibbling and
 blanking 22 p3811 A67-39308
 Self-similar solutions to motion equations
 are possible for internal heat generation in
 confined supersonic flow, assuming constant
 transport properties 22 p3784 A67-39781

HEAT PUMP

Pulse tube refrigeration heat pumping rates 13 p2229 A67-27680
Improved expressions for efficiency of infinite stage thermoelectric heat pump and generator 15 p2422 A67-29639
Compact black body source utilizing thermoelectric heat pumping for uniform and stable temperature control 17 p2862 A67-33288

HEAT REGULATION

Static accuracy of temperature stabilization in thermostat increase by using temperature dependences of heat regulators and active resistance of output transformer 01 p0064 A67-10424
Shock wave formation due to heat addition to one-dimensional flow of ideal inviscid conducting monatomic compressible fluid under transverse magnetic field 08 p1359 A67-20980
MHD generator working fluid temperature reduction 12 p1973 A67-25395
Linear temperature measuring system and automatic regulating system accuracy, investigating heat transfer with random input for recipients of various forms 17 p2973 A67-33074
Three-component heat transfer system for regulating system of three heat conductors, analyzing temperature regime 17 p2973 A67-33078

HEAT REJECTION DEVICE

SA RADIATOR
Analytical solution for determining inlet and outlet temperature for space radiator with heat rejection rate for steady state conditions and zero irradiation environment 08 p1429 A67-21511
Spacecraft package temperature control by interior louver panel system, calculating net heat transfer [ASME PAPER 67-HT-64] 20 p3549 A67-36746
Moebius strip self-irradiation coefficient calculated as function of relative width or area of strip 23 p4083 A67-41287

HEAT RESISTANCE

Transient junction temperature rise, transient thermal resistance and failure energy in transistors by forward-potential sampling method 01 p0040 A67-11235
Heat transfer between metallic surfaces in contact [AIAA PAPER 65-661] 03 p0534 A67-13067
Destruction of heat resistant alloys by repeated heating and cooling, deriving formulas which are applied to thermocyclic loads under conditions of stressed state 03 p0447 A67-14192
Cryogenic temperature resistant plastics in space program, discussing insulation, adhesives, seals, gaskets and expulsion of cryogenic propellant in zero gravity environment [SAE PAPER 66-038] 04 p0642 A67-15788
Titanium surface alloying in aluminum melts at temperatures from 700 to 1000 degrees C 05 p0828 A67-16328
High temperature hardening and creation of highly heat resistant alloys of refractory metals 05 p0831 A67-17501
Endurance and creep of chromium steels with extended thermal treatment 06 p1018 A67-18228
Heat resistant nickel-based alloys for gas turbine blades and disks 06 p1018 A67-18232
Hardness of heat resistant steels at elevated temperatures as function of alloying and heat treatment 07 p1199 A67-19240
Ni, Si and Nb effect on oxidation of binary alloys of titanium in air at high temperature, discussing heat resistance 07 p1205 A67-19275
Oxygen effect on mechanical property and heat resistance of alloys AT3 and AT8 07 p1205 A67-19276
Heat resistance and fatigue strength of Ti alloys examined, using bending techniques 07 p1207 A67-19288
Mechanical properties and heat resistance of titanium alloyed with low and high proportions of Al and Sn 07 p1207 A67-19289
Power output variation of solar Brayton space power plant with heat storage due to solid layer thermal resistance effects 09 p1442 A67-21698
Test method for metal resistance to thermal fatigue under active creep conditions 09 p1519 A67-22168
Heat-resistant casting alloy KhH65VMTi

for gas turbine guide vanes, noting structural stability and oxide film 09 p1519 A67-22376
Titanium and aluminum additions to cobalt-base alloys improve tensile and stress rupture properties and heat resistance 11 p1807 A67-24703
Heat resistance of GaAs laser diodes from 77 to 300 degrees K, showing relationship to thermal conductivity 11 p1802 A67-24744
Differential thermocouple device design for temperature measurements from 300 to 450 degrees K 11 p1793 A67-24866
Heat resistance, bending and tensile creep of multicomponent Ti alloys 12 p1955 A67-25366
Structural changes effect on creep resistance of heat resistant alloys 12 p1955 A67-25371
Heat resistance in air of dispersion hardened nickel alloys containing certain oxides prepared by powder metallurgy methods 14 p2336 A67-27867
Convective self-propulsion of continents 14 p2313 A67-28620
Titanium alloys research and development for aeronautics industry 14 p2338 A67-28627
Polyimide bonded solid lubricants development [ASLE PREPRINT 67AM 7A-1] 14 p2326 A67-28789
Thermal, mechanical stress and moisture resistance reliability tests of plastic encapsulated transistors 15 p2444 A67-29457
Alloyed Ni-Be alloys properties, discussing influence of Mo, W, B, V and Co on heat resistance without impairing physical properties 15 p2504 A67-29974
Heat resistance of Ti alloys, emphasizing significance of chemical interactions, polymorphic transformations and phase diagrams for high temperature performance 15 p2504 A67-30007
Emitter-base voltage vs collector-current characteristic used to study stability of parallel pairs of HF high power transistors 15 p2453 A67-30017
N-type InSb electron thermoconductivity temperature dependence, lattice thermoconductivity and thermal resistance 16 p2730 A67-31163
Heat resistance of Ni alloys with oxides noting experimental procedure, and effect of various additives 16 p2690 A67-31433
Alloying principles for refractory metals based on softening mechanism, examining increased heat resistance of rhenium softened by recrystallization 16 p2691 A67-31589
Experimental assembly for measuring true heat capacity of heat resistant insulating materials during natural cooling at temperatures from 1200 to 2400 degrees K 16 p2678 A67-31784
Adhesives for aircrafts and spacecrafts considering high temperature resistivity, waterproofing and brittleness 16 p2683 A67-31788
Polyimide bonded solid lubricants development 19 p3233 A67-34790
Composition law of thermal resistance in contact between parallel bands 19 p3347 A67-35790
Tungsten-molybdenum alloy heat-resistant properties noting vacuum testing and subsection to plastic deformation, with results related to molybdenum content and temperature 20 p3487 A67-36968
Scaling resistance of nickel and cobalt binary alloys investigated to determine heat resistance as function of composition 20 p3467 A67-37115
Temperature resistant aromatic ordered copolyamide fibers, obtaining tensile properties and radiation resistance 21 p3647 A67-37871
Metal composite materials for higher temperature resistance utilizing filaments, fibers and whiskers, discussing machinability and testing 21 p3643 A67-37954
High temperature hardening and creation of highly heat resistant alloys of refractory metals 21 p3643 A67-38028
Steady state temperature field and stresses determined for infinite body with linear slit having definite heat resistance 21 p3729 A67-39007
Heat resistant stainless steels evaluated experimentally for fatigue properties, corrosion resistance, creep limit and tensile strength 21 p3646 A67-39010

Molybdenum heat resistance improvement after structural polygonization by deformation and annealing, describing durability dependence on treatment conditions 22 p3819 A67-39324
Hot-cracking and microstructure characteristics in weld heat resistant Ni alloys evaluated by synthetic specimen technique 22 p3819 A67-39449
Performance of wide variety of exceptional metals studied for corrosion and temperature resistance characteristics in atomic power application 23 p4018 A67-40899
Si semiconductor strain gauge thermal coefficient of resistance /TCR/ reduction by high energy electron irradiation 23 p4008 A67-41391
Plastics in aircraft and rocket parts construction noting silicon oils and solid polysiloxanes, discussing temperature resistance and rubber-elastic properties 23 p4021 A67-41400
Aging effect on structure and properties of complex alloyed heat resistant steel 24 p4173 A67-42190

HEAT SHIELD
SA RADIATION SHIELDING
SA SPACECRAFT SHIELDING
SA THERMAL PROTECTION
Weight and cost comparative analysis of ablative and combined ablative/radiative heat shields for SV-5 and SV-32 lifting reentry vehicles [AIAA PAPER 66-990] 02 p0333 A67-12301
Maximum temperature profile in phenolic resin-siliceous fiber heat shields on ICBM and Mercury spacecraft [AIAA PAPER 65-638] 03 p0533 A67-13058
Reinforced pyrolyzed plastic composites for aerospace applications, noting high temperature stability and ease of utilization 03 p0443 A67-13415
Heat flux measurements of liquid-nitrogen superinsulation systems, noting effects of material types and assembly techniques 04 p0720 A67-14531
Radiative type heat shields using backface cooling in analysis, including thermal effects and structural heat short effects [AIAA PAPER 66-507] 04 p0711 A67-15252
Noncontour transpiration cooled heat shield for possible application to hypersonic atmospheric flight 04 p0725 A67-15435
Feasibility of making continuous measurements of ablation of spacecraft heat shield by use of radioisotopes embedded in heat shield 05 p0841 A67-16529
Combustion reactions during spacecraft reentry, noting degradation of heat shields composed of hydro- and fluorocarbon compounds 05 p0928 A67-17334
Convective heating in shoulder regions of flat-faced cylinder with large favorable pressure gradient [AIAA PAPER 67-162] 06 p1114 A67-18293
Radiation cooled reentry heat shield of graphitic surface over graphite felt insulation with receding surface [AIAA PAPER 67-153] 06 p1115 A67-18320
Tubular support heat shield effects on insulated noncooled thermal protection, noting Dyna-Flex thermoconductivity discrepancy [AIAA PAPER 67-215] 06 p1117 A67-18443
Ultrasonic techniques for nondestructive testing for Saturn honeycomb heat shields 07 p1928 A67-20166
Testing machine for evaluating high temperature fabrics under dynamic loading and heating conditions 07 p1212 A67-20262
Airframe heat protection for high performance sounding rockets, using plasma jet testing for leading edge design selection 08 p1425 A67-20528
Ablative properties of nylon-phenolic materials used in fabrication of composite heat shield with low residual stresses 09 p1523 A67-22506
Reentry vehicle heatshield materials including graphite, ablative reinforced plastics, etc 10 p1672 A67-23721
Material properties effect on design of reentry vehicle heat shield 10 p1734 A67-23726
Refractory and ablating polymeric reentry heat shield materials evaluated under high radiant fluxes, measuring surface temperature, recession rate, flux emittance, etc refractory and ablating polymeric reentry heat 11 p1811 A67-24054
Transient heat conduction problems

involving time varying radiation boundary condition at surface solved by Goodman integral method 11 p1883 A67-24575

Wind tunnel studies of heat shield over plane surface with film cooling during injection through two tangential slots 11 p1884 A67-25055

Interplanetary transit and atmospheric entry of unmanned vehicle landing on Mars surface, with reference to heat shield technology 12 p2034 A67-25715

[JPL-TR-32-1145] 12 p2034 A67-25715

Convective and radiative heat transfer to entry vehicles protected by ablation heat shield, obtaining absorption coefficients [AIAA PAPER 67-327] 12 p2038 A67-26041

Heat flux measurements of liquid-nitrogen superinsulation systems, noting effects of material types and assembly techniques 13 p2222 A67-26580

Cartridge-actuated thruster system design for jettisoning Apollo spacecraft heat shield for recovery system deployment [ASME PAPER 67-DE-34] 14 p2394 A67-28875

Weight and cost comparative analysis of ablative and combined ablative/radiative heat shields for SV-5 and SV-32 lifting reentry vehicles [AIAA PAPER 66-990] 15 p2564 A67-29421

Optimum entry vehicle design using aerobreaking for manned earth entry at hypersonic speeds, examining blunted conic, biconic and tetrahedral configurations [AIAA PAPER 66-489] 15 p2564 A67-29422

Reflectance of pyrolytic graphite and phenolic nylon chars for radiant heat rejection from nonablating heat shield 15 p2579 A67-29434

Hypersonic trim angle of attack of lifting entry vehicles, correlating stagnation point values obtained from heat shield ablation and pressure distribution measurements 15 p2417 A67-29447

Coated refractory metals thermal emittance measured at high temperatures for design of reentry vehicle under time-temperature-pressure profile 15 p2503 A67-29546

Photographic spectra of ablating plastics in thermodynamic environments related to species and temperatures in boundary layers [AIAA PAPER 66-132] 15 p2582 A67-30206

Ablation heat protection system materials performance in hypersonic regime, discussing potential solutions to shielding during atmospheric entry 16 p2778 A67-30722

Reentry vehicle heat shield materials thermal diffusivity measurements by flush method, using pulsed laser and xenon flash lamp 18 p3051 A67-34506

Aerodynamic, thermodynamic, heat shield and structural design aspects of ballistic vehicle entering planetary atmosphere 19 p3332 A67-35315

Variable geometry entry spacecraft making secondary use of extendable wings in space as antenna and as radiators 20 p3532 A67-36560

Ablative material application to Apollo txcraft for heat shielding using air injection guns 20 p3454 A67-36590

Reentry vehicles heat protection design emphasizing composite material selection/development for coating within acceptable weight limitations 22 p3902 A67-39938

Event recorder for in-flight measurements of missile heat-shield ablation 23 p4006 A67-41377

Convective heating in shoulder regions of flat-faced cylinder with large favorable pressure gradient [AIAA PAPER 67-162] 23 p3932 A67-41714

High temperature thermal insulation consisting of thin refractory metal foils separated by thin refractory oxide layers 24 p4103 A67-42501

Airframe heat protection for high performance sounding rockets, using plasma jet testing for, leading edge design selection 24 p4256 A67-42914

HEAT SINK

Thermal analysis of thin wafer heat flux transducer backed by finite heat sink subjected to reentry and rocket-nozzle heat transfer environments 01 p0071 A67-11095

Heat removal from high density packaged electronics by bonded metallic heat sink [ASME PAPER 67-DE-47] 14 p2408 A67-28880

Endothermic hydrocarbon fuels for supersonic aircraft, noting heat sink capacity effect in overcoming thermal thickening

usability as engine fuel 15 p2543 A67-29305

Vertical energy transfer from stationary disturbances induced by topography and diabatic heat sources and sinks, using primitive motion equations 20 p3480 A67-36504

Electrode with central heat sink used for joining flat-pack leads and copper tracks on printed circuit boards 21 p3835 A67-38624

Plasma sprayed alumina and beryllia dielectric coatings for heat sinks in electronic packaging, emphasizing heat dissipation from heat/generating components 21 p3850 A67-38849

HEAT SOURCE

Temperature field of thin plate with circular region containing pulsed heat source 01 p0166 A67-10365

Low thrust reaction control system utilizing solid propellant which sublimates into low molecular weight vapor, noting heat sources 01 p0142 A67-11407

Transient temperature distributions in simple bodies with internal cycled heat sources [AIAA PAPER 65-660] 03 p0534 A67-13065

Volume density of heat sources in ruby laser rod by numerical integration of pumping and absorption spectra 03 p0434 A67-13117

Approximate solution of problem of radiation cooling and unstable temperature field in solid bodies with internal heat source 03 p0535 A67-13118

Propagation of vertical turbulent hot gas stream in fog from point source of heat 03 p0463 A67-14225

Quasi-static equilibrium of thin plate heated by stationary circular source, obtaining expression for elastoplastic region at heating center, using continuous function 05 p0912 A67-16179

Diathermy, derivation of equation relating monochromatic/integral radiation energy ratio of solid material of fluid heat emitter to temperature 07 p1211 A67-19130

Graphite fibers as internal electrical resistance heat source for curing structural adhesives demonstrated in lap shears, larger area and sandwich construction 09 p1507 A67-22516

Behavior of metals, graphites and reinforced plastics for reentry nose cones tested, using rocket engine exhaust flame as heat source 10 p1698 A67-23460

Localized instantaneous plane heat sources position and strength determined using inert thermometers and time integrals of observed temperature 11 p1883 A67-24901

Propagation of vertical turbulent hot gas stream in fog from point source of heat 12 p1963 A67-25481

Thermoconductivity and diffusivity of amorphous solids determined simultaneously by refined line source technique [AIAA PAPER 67-314] 12 p2037 A67-26029

Fundamental solution of thermoconductivity equations for thin walled shallow shells and infinite plates with various instantaneous interval heat sources 13 p2221 A67-26374

Temperature determination in stratosphere via hydrodynamic equations taking into account energy inputs and atmospheric motion, suggesting existence of integral heat sources 13 p2113 A67-26676

Biennial variations of zonal atmospheric circulation at equatorial latitudes analyzed using hydrothermodynamics 13 p2150 A67-26680

Temperature field in plates and shallow shells with internal heat sources noting solutions for various boundary conditions 13 p2224 A67-27056

Polytropic heat sources effect on ejection of stationary symmetrical plasma from sun 14 p2378 A67-27915

Supersonic gas-particle flow with chemical reactions 15 p2469 A67-29225

Simulation of nonlinear radiant heat transfer for constant emitting heat source by circuit, using semiconductor and pentode 15 p2579 A67-29323

Graphite cloth and felt as resistance heating elements for calibration and simulation facilities, achieving fast changes in heat flux level without sacrificing power efficiency 15 p2490 A67-30153

Model for radial and axial structure of geophysical vortices involving Boussinesq

boundary-layer equations similarity solution in point heat source 16 p2778 A67-30949

Integral equation derived for steady state temperature field in seminfinitesimal body with internal cylindrical heat source 16 p2779 A67-31204

Thermionic space power systems, examining solar, radioisotope and nuclear reactors as heat sources, discussing power density and electrode affinity 17 p2802 A67-32050

Steady state temperature field of uniform body containing heat sources, examining nonlinear boundary value problems of unsteady thermal radiation 17 p2971 A67-32870

Inert thermometers, discussing heat capacity and contact resistance as sources and effect and applications 18 p3050 A67-34502

Use of controlled flow of electrons for analyzing and processing integrated circuits and focused electron beam as heat source for microwelding 19 p3192 A67-35023

Thermal-stress distributions in circular disk due to instantaneous heat source on radius midpoint, assuming no temperature variation over thickness 20 p3536 A67-36418

Vertical energy transfer from stationary disturbances induced by topography and diabatic heat sources and sinks, using primitive motion equations 20 p3480 A67-36504

Theoretical prediction of temperature profiles within heated cylinder and on surface to determine thermal conductivities at high temperature [AICHE PAPER 16] 20 p3552 A67-36829

Convective heat flow nonlinear equations for fluid sphere having heat sources expressed in Boussinesq approximation as perturbation of steady state conduction solution 21 p3731 A67-37926

Three-dimensional heat source influence on solar plasma flow contradicts Parker solar wind theory, based on gasdynamic acceleration 21 p3699 A67-39012

Ground based atmospheric and ionospheric particle temperature measurements, examining methods and thermosphere heat sources 22 p3870 A67-39676

Thin plate temperature distribution from solving conduction equation, considering boundary convection losses and moving discrete heat source 22 p3920 A67-40424

Criterion for minimum weight Carnot limited space power systems 24 p4103 A67-42496

High temperature Pu 238 heat source fuel capsule operable in space environment is applicable to thermoelectricity and Brayton cycle, discussing design and test program 24 p4185 A67-42536

Shield/radiator weight tradeoffs to optimize K Rankine cycle space power plant heat source operating temperature, noting burnup 24 p4185 A67-42537

Stirling, Brayton and Rankine dynamic cycles compatibility with isotope heat sources, emphasizing power system applications to long-duration earth orbital missions 24 p4185 A67-42542

Random intact reentry and earth burial for radioisotope thermoelectric generators disposal without atmospheric contamination, evaluating design concepts for SNAP systems 24 p4241 A67-42559

HEAT TEST

Prolonged high temperature creep and endurance testing of refractory materials in vacuum or inert media 01 p0051 A67-11247

Augmented strain concept and Vrestraint test for hot-cracking sensitivity and weldability of filler metals 03 p0430 A67-13694

Ablative material performance under high shear reentry condition, noting hyperthermal test of cones and wedges for heat shield design 10 p1734 A67-23722

Prolonged high temperature creep and endurance testing of refractory materials in vacuum or inert media 17 p2835 A67-33170

HEAT TOLERANCE

Heat stress effect on human renal function, measuring glomerular filtration rate, renal plasma flow, free water clearance and electrolyte excretion 10 p1599 A67-23811

Temporal characteristics of body temperature during high thermal stress, determining correlation between effective and rectal temperature 10 p1600 A67-23822

Maximum heating temperature of smallest particles of polydisperse material in two-phase flow by approximation
method 17 p2970 A67-32462

Heat stress, skin and rectal temperatures, heat gain and water losses in Army pilots flying combat missions in Mohawk OV-1 aircraft in Vietnam 22 p3750 A67-39595

Liquid transport cooling system for aircrew evaluated by collecting in-flight sweat rate on fighter aircraft flying combat and training in tropics 23 p3966 A67-41581

Heat exchanger cooling system for controlling aircraft high temperature and thermal inorganic salt for protection against cold for flying personnel 23 p3967 A67-41612

Ventilated wet suit /VWS/ for varying flight cockpit environment and emergency condition thermal protection, assessing physiological responses 23 p3967 A67-41614

HEAT TRANSFER

SA AERODYNAMIC HEAT TRANSFER

SA CONVECTIVE HEAT TRANSFER

SA HYPERSONIC HEAT TRANSFER

SA LAMINAR HEAT TRANSFER

SA NUCLEATE BOILING

SA RADIATIVE HEAT TRANSFER

SA STEFAN-BOLTZMANN LAW

SA SUPERSONIC HEAT TRANSFER

SA THERMAL DIFFUSION

SA THERMAL EXPANSION

SA THERMAL RADIATION

SA THERMODYNAMICS

SA TRANSPORT PROPERTY

SA TURBULENT HEAT TRANSFER

Steady state flows without external forces becoming parallel in thermodynamic equilibrium at distance from body, noting relations between drag, shear, heat transfer, entropy, etc 01 p0005 A67-10281

Laminar flow of elastico-viscous fluid between parallel plates obeying Noll constitutive equation, considering heat transfer 01 p0053 A67-10802

Energy transfer to anode, cathode and surroundings in high current argon arc 01 p0125 A67-10976

Heat transfer and equilibrium temperature of heat conducting sharp cones in supersonic rarefied gas flow at zero angle of attack 01 p0007 A67-10977

Bibliography of books and periodicals concerning heat transfer and related topics including applications, boundary layer, phase change, separated flow, etc 01 p0167 A67-10978

Bibliography of Russian works on heat transfer and related topics including heat conduction, thermodynamics, transfer processes involving phase and chemical conversion, etc 01 p0187 A67-10979

Thermal analysis of thin wafer heat flux transducer backed by finite heat sink subjected to reentry and rocket-nozzle heat transfer environments 01 p0071 A67-11095

Thermal model for transient heat transfer analysis of missile guidance systems for prediction of operating temperature 02 p0263 A67-12104

Pressure losses and improved heat transfer in incompressible fluid flow through tubes containing twisted tapes 02 p0233 A67-12200

Fluid motion in weightlessness, examining effects of weak forces normally suppressed by terrestrial gravitational field 02 p0233 A67-12322

Shear layer and internal flow arising from turbulent boundary layer separation and heat transfer over cavity 02 p0179 A67-12344

Steady state heat balance on opaque inner wall of enclosure 02 p0343 A67-12413

Reentry simulation, discussing aerodynamic and thermodynamic parameters, heat transfer and simulation accuracy 02 p0335 A67-12415

Heat transfer and centrifugal force effects on hypersonic inlet boundary layer and pressure recovery [AIAA PAPER 65-605] 03 p0350 A67-12910

Heat transfer and distribution of velocity, temperature and concentration in laminar supersonic boundary layers with blowing of light gas with desired pressure and heat distribution 03 p0532 A67-12990

Pulsed laser techniques for measuring thermal diffusivity of graphites and chars between 500 and 5000 degrees F [AIAA PAPER 65-644] 03 p0449 A67-13062

Book on conductive heat transfer covering lumped, integral and differential

formulations, two-and three-dimensional periodic functions, unsteady problems, Laplace transforms, etc 03 p0535 A67-13075

Coolant injection in turbulent boundary layer for protection of surfaces from effects of high temperature and high energy gas flows 03 p0536 A67-13526

Heat transfer in viscous fluid flow in gap between permeable isothermal surface and rotating disk, solving energy equation 03 p0536 A67-13611

Heat transfer and friction drag for supercritical laminar flow of carbon dioxide through tube at constant thermal flux density at wall 03 p0536 A67-13612

Equation for laminar gas meter applied to flow coefficient derived from Hagen-Poiseuille relationship, noting effect of heat transfer, compressibility, etc, on meter performance 03 p0404 A67-13778

Shock tube flow nonuniformity analyzed where shock and contact surface have maximum separation, applying results to turbulent and laminar boundary layer for heat transfer studies 03 p0397 A67-14027

Passive heat transfer system for metabolic heat removal in extravehicular activity suit 03 p0364 A67-14295

Transitional immersed cylinder heat transfer measurements used in conjunction with theory of boundary layer transition to determine free-stream turbulence intensity 04 p0601 A67-14508

Temperature and heat transfer conditions determination on rotating turbine wheel in jet power plant, using electric analogy 04 p0688 A67-14571

Heat and mass transfer processes in rotationally symmetrical tank partially filled with liquid and subjected to external heating and acceleration in direction of longitudinal axis 04 p0720 A67-14577

Heat transfer in supersonic separated flow over two-dimensional backward-facing step found in entry enlargement region of supersonic parallel diffuser 04 p0546 A67-14640

Soviet papers on laminar boundary layer flow and heat and mass transfer 04 p0721 A67-14708

Composite heat transfer in moving gray medium, obtaining solution based on boundary layer equations 04 p0722 A67-14712

Composite heat transfer and viscous friction of moving gray medium with large optical density, using laminar boundary layer equation, noting hydrodynamic state role 04 p0722 A67-14713

Heat transfer and equilibrium temperature of plate in supersonic flow of rarefied gas 04 p0546 A67-14783

Heat transfer and skin friction rates increase in gas-liquid droplet suspension system flowing over circular cylinder formulated by laminar boundary layer theory 04 p0725 A67-15439

Hydrogen and helium injection effect on local heat transfer to porous surface from dissociated turbulent boundary layer [ASME PAPER 66-WA/HT-24] 04 p0725 A67-15444

Free stream turbulence and pressure gradient effects on flat plate boundary layer velocity profiles and heat transfer [ASME PAPER 66-WA/HT-4] 04 p0608 A67-15448

Heat transfer in plane conducting fluid jet spreading over flat wall in transverse magnetic field, noting solution for temperature distribution for small MHD interaction parameters 04 p0670 A67-15520

Heat transfer - AICE International Conference, Chicago, August 1966, Volume 1, Single phase forced convection 04 p0727 A67-15800

Monte Carlo method analysis of rarefied gas heat transfer between parallel plates in terms of temperature, density and Knudsen number 04 p0728 A67-15807

Laminar tube flow and heat transfer for He gas using Navier-Stokes, energy and continuity equations in finite difference form 04 p0729 A67-15809

Heat transfer in laminar source flow between stationary and rotating disk 04 p0729 A67-15812

Heat transfer to end wall of shock tube behind reflected shock wave in oxygen dissociated to varying degrees and at high temperatures 04 p0729 A67-15813

Heat transfer - AICE International

Conference, Chicago, August 1966, Volume 2, Single phase forced convection and natural convection 04 p0729 A67-15815

Wall shearing stress and heat transfer measurements through turbulent boundary layer on heated flat plate in accelerating and decelerating airflow 04 p0731 A67-15819

Uniform property turbulent boundary layer heat transfer calculation, using solution of integral momentum and kinetic energy equations 04 p0731 A67-15821

Pressure, heat transfer and Pitot pressure profiles measured on wedges and cones at high Mach and Reynolds numbers in hypersonic tunnel 04 p0600 A67-15822

Tip bluntness, surface roughness and angle of attack effects on laminar boundary layer for 10 degree cone, measuring heat transfer and detecting transition 04 p0549 A67-15823

Heat transfer tests of blunt nosed cone containing cylindrical protuberances tested in AEDC tunnel, including effects of local Mach number, Reynolds number and sweepback angle 04 p0549 A67-15832

Heat transfer and pressure in laminar shock wave/boundary layer interaction corner flow at Mach 8 and 10 04 p0610 A67-15834

Heat transfer - AICE International Conference, Chicago, August 1966, Volume 3, Single phase, mass transfer and vibrations 04 p0732 A67-15837

Asymptotic flow theory laws of friction and heat transfer in turbulent boundary layer 04 p0610 A67-15838

Oscillation effect on instantaneous local heat transfer in forced convection from cylinder measured by optical method and theoretically calculated by power series expansion method 04 p0733 A67-15843

Unsteady heat transfer in tubes resulting from changes in heat flow, gas mass flow rate and acoustic balance 04 p0733 A67-15844

Local details of influence of vertical sound field on heat transfer from circular cylinder determined, using schlieren system 04 p0733 A67-15845

Heat transfer - AICE International Conference, Chicago, August 1966, volume 4 04 p0734 A67-15846

Interference conductance between two plates during transient heat transfer 04 p0735 A67-15853

Heat transfer through metal to metal joints, determining influence of number of real contact points and compressive load 04 p0735 A67-15854

Heat transfer - AICE International Conference, Chicago, August 1966, Volume 5, Flow boiling and radiation 04 p0736 A67-15859

Heat transfer in plasma jet generators, considering electric arc types and thermal regime of electrodes 04 p0672 A67-15871

MHD heat transfer in finite duct for fully developed flow conditions with arbitrary oriented applied magnetic field and variable heat flux boundary conditions 04 p0673 A67-15872

Turbulent boundary layer calculation, considering compressible and incompressible flows with pressure gradients and heat transfer 04 p0610 A67-15908

Radiation effects on heat transfer and friction characteristics in natural and forced convection film boiling in boundary layer flows [ASME PAPER 66-WA/HT-6] 04 p0739 A67-15939

Book on aerogas dynamics in relation to rocket and aviation technology including shock waves, rarefaction flow, heat transfer, skin friction, etc 05 p0747 A67-16173

Quasi-static problem of generalized plane stressed state of thin plate, considering heat transfer on lateral surfaces and interaction between strain fields and temperature 05 p0913 A67-16186

Generalized thermally stressed state of thin plate in presence of interaction between strain field and temperature, considering heat exchange with surrounding medium 05 p0913 A67-16187

Heat and mass transfer research - AICE Symposium, Detroit, December 1966, Part 2 05 p0925 A67-16269

Numerical solution of motion and energy equations for non-Newtonian fluid flow in tubes of circular cross section with heat transfer to or from fluid 05 p0925 A67-16271

Transverse curvature effect on

axisymmetric compressible laminar boundary layer flow, obtaining asymptotic solutions for skin friction and heat transfer 05 p0791 A67-16509

Heat transfer processes during ignition of solid propellant rockets, considering radiative and convective components [AIAA PAPER 66-66] 05 p0873 A67-17217

Thermal contact resistance between smooth rigid isothermal planes separated by elastically deformed smooth spheres [AIAA PAPER 66-461] 05 p0928 A67-17223

Book on methods of determining boundary conditions for unsteady state heat transfer 06 p1111 A67-17661

Ignition of explosive powder by hot gas stream, with particular attention to heat transfer between substance and surrounding medium 06 p1112 A67-17956

Difference equations for heat transfer from liquid to solid and conductivity for solid applied to calculation of local temperatures within multilayer walls 06 p1113 A67-17990

Heat transfer in short circuit generalized MHD Couette flow for velocity field and temperature distribution, when walls are at equal and unequal temperatures in transverse magnetic field 06 p1039 A67-18070

Heat transfer for wall adjacent to region of turbulent separated flow 06 p0985 A67-18131

Two-dimensional multiple wave distortions effect on heat transfer to wall in hypersonic flow [AIAA PAPER 67-164] 06 p1115 A67-18294

Tests at Mach 8 on cone, analyzing effect of roughness elements and variable entropy on transition and heat transfer distribution [AIAA PAPER 67-132] 06 p0940 A67-18357

Static temperature-velocity distribution for zero pressure flat plate compressible turbulent boundary layer with heat transfer [AIAA PAPER 67-195] 06 p1116 A67-18362

Variable laminar boundary layer equations for air flows over flat plate with injection of foreign gases through solid surface 06 p1116 A67-18380

Correlation of local heat transfer and friction coefficients for subsonic turbulent flow of air through high temperature annulus 06 p1117 A67-18386

Transient linear transfer problem solution via integral equations for corresponding boundary value problems 06 p1117 A67-18390

Tubular support heat shield effects on insulated noncooled thermal protection, noting Dyna-Flex thermoconductivity discrepancy [AIAA PAPER 67-215] 06 p1117 A67-18443

Two-dimensional adiabatic laminar separated regions in supersonic flow, examining effects of blowing and suction at wall [AIAA PAPER 67-192] 06 p0988 A67-18459

Heat transfer to catalytic and noncatalytic surfaces on sharp flat plate in shock tube gas flow for checking various laminar boundary layer theories 06 p0989 A67-18481

Turbulent boundary layer properties for strong adverse pressure gradients, obtaining layer and displacement thickness, skin friction, heat transfer, etc [AIAA PAPER 67-196] 06 p0989 A67-18489

Pressure pulse and wall-to-jet heat transfer in discrete vortex zone of restrained gas jet in circular channel 06 p1118 A67-18550

Quasi-one-dimensional MGD channel flow calculation methods, considering Hall effect, heat transfer, friction and potential drop near sectioned electrode 06 p1043 A67-18675

Artificial heat conduction mechanism, introducing viscosity term into momentum and energy equations to account for shock discontinuities in flow problems 06 p0992 A67-18830

Shock tunnel heat transfer measurement and hypersonic viscous flow over pointed cones, particularly viscous-layer regime at low Reynolds numbers 06 p0943 A67-18845

Correlation number for calculation of skin friction and heat transfer for laminar compressible boundary layer flow with arbitrary pressure gradient, using von Karman momentum integral 06 p0992 A67-18862

Erosive burning of ammonium perchlorate solid propellants for combustion in turbulent boundary layer determined, using flat plate

heat transfer correlation 07 p1238 A67-19069

Heat transfer in compressed gas evacuated from container, using numerical integration of state equation 07 p1267 A67-19324

Electroanalog analysis of convective and conductive heat transfer and transient temperature field in solid propellant rocket nozzle head 07 p1268 A67-19568

Book on physical processes of heat and mass transfer including thermal conductivity and potential and various integral procedures 07 p1268 A67-20039

Combustion and heat transfer laws for hydrocarbon flames with predetermined visual radiation 08 p1425 A67-20303

Black Brant III sounding rocket analyzed via mathematical model to predict temperature distribution in ablation material 08 p1425 A67-20531

Simultaneous effects of heat and mass transfer on properties of stagnation point flows analyzed over full range of velocity gradients 08 p1276 A67-20568

Initial solid propellant temperature effect on constant pressure burning rate based on granular diffusion flame model /GDFM/ 08 p1375 A67-20581

Dynamical effects of heat absorption or rejection on flow of electrically charged fluid considered within special relativity framework 08 p1426 A67-20923

Heat transfer in constant property turbulent boundary layer with arbitrary distributions of wall temperature and stream velocity 08 p1426 A67-20927

Steady state temperature distribution in disk with radial flow of electric current derived with and without heat transfer conditions 08 p1427 A67-20929

Book on quantitative relationships for non-Newtonian systems, considering classification and fluid behavior of materials with anomalous flow properties 08 p1322 A67-21268

Electric analog simulation of periodic nonuniform heat transfer mechanism in film boiling from coated plate 08 p1427 A67-21321

Heat transfer effect in converging-diverging nozzle flow, considering polytropic process 08 p1278 A67-21526

Vertical transport of latent and sensible heat of IR cooling and short wave heating 09 p1490 A67-21550

Characteristics of atmospheric convection, obtained by vertical and horizontal heat transport processes and represented by difference equation, used to derive analytical solution 09 p1491 A67-21553

Numerical solutions for range of operating conditions in segmented linear MPD generators, using He-Cs working fluids 09 p1443 A67-21811

Airflow characteristics and heat transfer in right angle water-jacketed bend, measuring boundary layer profile at midbend 09 p1487 A67-21831

Dynamic characteristics of thermionic converter noting influence of emitter heat transfer 09 p1447 A67-22335

Optimization of thermionic diode, with electrical conduction and heat transport represented by differential equations 09 p1448 A67-22336

Calorimetric measurements of thermionic converter/ heat pipe system, discussing electron cooling of emitter, thermal emissivity and thermal balance 09 p1448 A67-22342

Stress field near surface of elastic solid during short time interval when heat flow occurs analyzed through strain theory for fracture location and probability 09 p1576 A67-22422

Viscosity variation effect on heat transfer and friction coefficient at wall during Couette flow 09 p1490 A67-22547

Heat losses in conductive and convective transfer through rarefied fluids investigated for dependence on temperature differences, static pressures, test geometries and fluids 10 p1731 A67-22725

Fluid and solid temperature determination in regenerative heat exchangers at any time and location 10 p1731 A67-22726

Heat transfer data obtained from film boiling for four liquid compositions, using flat plate geometry 10 p1732 A67-22729

Method Normalization technique for analysis of heat transfer, considering thermal entrance length, ablation and tektite

problems 10 p1732 A67-22931

Effect of underheating on development of boiling crisis in two-phase nonequilibrium flows 10 p1732 A67-23018

Characteristics of single circuit space power installation with thermoelectric converter noting capacity, temperature and heat transfer 10 p1596 A67-23019

Friction and heat transfer across boundary layer in external flow with transverse inhomogeneity calculated by mean-mass values method 10 p1625 A67-23041

Approximate solution of heat transfer problems with phase change for time dependent surface temperatures 10 p1733 A67-23119

Similar calculation of hypersonic laminar boundary layer characteristics in presence of pressure gradient, specifically heat transfer, skin friction and boundary layer thickness 10 p1592 A67-23141

Ionosphere as binary two-temperature gas and transfer coefficients for elastic collisions based on Boltzmann equation 10 p1640 A67-23220

Approximate heat transfer theory based on parabolic velocity distribution for channel flows 10 p1734 A67-23575

Liquid metal heat transfer in various structural configurations 10 p1734 A67-23631

Material properties effect on design of reentry vehicle heat shield 10 p1734 A67-23726

Space evacuation of NRC-2 insulation for liquid hydrogen tankage, noting vacuum test apparatus and cold plate test 10 p1734 A67-23727

Optimization of base thermal protection system for advanced Saturn II boosters employing strap-on solid propellant motors 10 p1735 A67-23729

Quick change high vacuum window and heat transfer gauge installation for shock tubes 10 p1658 A67-23789

Thermoconductivity of heat resistant materials during cooling at room temperature, using photopyrometer to record temperature gradients 11 p1789 A67-24021

Heat transfer of electrolyte solutions, noting effect of magnetic field on turbulent flow and empirical relation to calculate Nusselt number 11 p1831 A67-24024

Local heat transfer in water flow in horizontal annular tube, estimating local longitudinal and circumferential variations in Nusselt number at tube wall as function of Reynolds and Rayleigh numbers 11 p1881 A67-24025

Exponential point method measurement of heat fluxes and surface temperature in unsteady regime 11 p1882 A67-24030

Heat transfer from isothermal sphere to low Prandtl number fluid in steady and nonsteady potential flow compared with Stokes flow 11 p1882 A67-24119

Heat transfer of pulsating liquid jet impinging on perpendicular flat surface and spreading laminarily 11 p1882 A67-24229

Finite difference network model method with error tolerance for spacecraft heat transfer calculation 11 p1883 A67-24356

Pyroelectric heat-transfer sensor performance compared with thin skin thermocouple heat sensors, noting discrepancy in measurement results in severe environment 11 p1790 A67-24453

Ionized fluid flow analyzed by multifluid theory to evaluate energy transfer mechanisms, noting temperature and compositional nonequilibrium effects 11 p1780 A67-24537

Random motion transport relation to heat propagation noting tensor characteristics, entropy effects and path dependence 11 p1819 A67-24757

Temperature profile of single stage axial flow turbine disk and blades determined by approximation method using impingement cooling [ASME PAPER 67-GT-14] 11 p1854 A67-24799

Heat transfer of fully developed laminar flow of Bingham material between parallel plates and linearly varying wall temperature noting equations of state, velocity and temperature distribution 11 p1883 A67-24944

Electrothermal analogies for heat transfer simulation by equivalent electrical circuits 11 p1884 A67-25047

Arc rotation heat transfer effects in self-induced magnetic field plasma arc heaters

- used for aerodynamic tests 12 p2034 A67-25346
- Zero gravity effects on boiling from flat horizontal surface for various subcoolings, fluid properties and heat transfer rates 12 p2034 A67-25720
- Saturn IVB flight data evaluation, discussing heat transfer effect on fluid system as function of gravity changes 12 p2034 A67-25721
- Liquid cooling of integrated circuit systems to remove increased heat dissipation, noting heat transfer rates 12 p1915 A67-25888
- Heat transfer in conducting and radiating gas analyzed, using governing equations reformulated as Lagrangian equations through introduction of potential 12 p2035 A67-25926
- Acoustic measurement method for following motion of solid-liquid interface, obtaining solution for transient heat conduction problem 12 p1946 A67-25985
- Heat pipes and vapor chambers for thermal control of spacecraft, noting design and application [AIAA PAPER 67-310] 12 p2036 A67-26025
- Effective gap thickness and gap number relation determined from correlation of parameters of thermal contact conductance [AIAA PAPER 67-317] 12 p2037 A67-26032
- Convective and radiative heat transfer to entry vehicles protected by ablation heat shield, obtaining absorption coefficients [AIAA PAPER 67-327] 12 p2038 A67-26041
- Thermal explosion equations for first order catalytic reaction, discussing nonstationary effects superposed on quasi-stationary combustion pattern 12 p2039 A67-26111
- Optimum multiscade photocell constructing procedure from half-cells of arbitrary number, size and shape 13 p2174 A67-26370
- Stirling cycle using dissociating gas 13 p2221 A67-26390
- Ablation study scheme enabling determination, for given environment and material, of ablation starting time and temperature distribution within mass of material 13 p2222 A67-26596
- Surface temperature of one-dimensional homogeneous thermally isotropic body impervious to radiation 13 p2222 A67-26610
- Thermal design of molten carbonate fuel cells using transpiration heating for reducing heat loss and control of temperature 13 p2055 A67-26842
- Short duration technique providing simulation of thermodynamic properties and composition of exhaust products of liquid and solid propellant rocket engines [AIAA PAPER 66-760] 13 p2090 A67-26843
- Condenser parameter effect on maximum heat transport in heat pipes for nonradiative and radiative cases 13 p2222 A67-26844
- Heat transfer and temperature distribution turbulence measurements with inclined hot wires 13 p2222 A67-26913
- Generalized spatially uniform distribution functions for monatomic rarefied gas describing one-dimensional heat transfer in nonuniform flow 13 p2100 A67-26958
- Heat transfer for gas with internal degrees of freedom between parallel plates, noting temperature profiles and jumps 13 p2100 A67-26959
- Nonlinear heat transfer between parallel plates, using ellipsoidal statistical model of Boltzmann equation 13 p2223 A67-26960
- Couette flow and heat transfer of rarefied gas between parallel plates analyzed by Monte Carlo method 13 p2223 A67-26961
- Variational method for linearized problems of rarefied gas dynamics applied to cylindrical Poiseuille flow and heat transfer from sphere, using BGK 13 p2101 A67-26966
- Monte Carlo approach to transition and free molecular flow problems having mass as well as thermal motion of molecules 13 p2101 A67-26967
- Flow and heat transfer in viscous fluid layer expanding over rotating disk, calculating energy and motion equations 13 p2224 A67-27050
- Coupled nonlinear equations integration in boundary layer theory with specific reference to heat transfer near stagnation point in three-dimensional flow 13 p2224 A67-27463
- Saturn S-IB stage fuel system, studying LOX density fluctuations, heat transfer and boiling under various weather conditions 13 p2186 A67-27637
- Semiempirical description of stratification in wall heated containers of cryogenic fluids, noting decrease due to bottom heating 13 p2227 A67-27644
- Cooling system for maintaining uniform low temperature environment under low gravity conditions 13 p2227 A67-27645
- Plated-tube heat exchanger design for minimizing axial heat conduction losses and controlling heat transfer surfaces and core weight 13 p2229 A67-27665
- Book on heat transfer covering basic treatment of heat conduction, convection and radiation 14 p2404 A67-27792
- Asymptotic short wave flow equations simplified for various viscous heat conducting gas flows 14 p2295 A67-27838
- Gas flow at high speed out of solid or liquid surface accompanied by heat transfer investigated for boundary shock wave occurrence 14 p2296 A67-27906
- Thermal conductivities of unidirectional composite materials parallel and normal to filaments, using analogy to shear loading response 14 p2404 A67-28099
- Heat transfer and skin friction increase for gas stream with liquid-droplet suspension flowing over blunt-nosed body near stagnation point 14 p2405 A67-28126
- High Mach number low Reynolds number flow over two-dimensional circular cylinder, obtaining surface pressure and heat transfer distributions 14 p2242 A67-28174
- Wind tunnel heat transfer measurements from circular cylinders to transverse air flow, noting recovery factor as function of Knudsen number 14 p2405 A67-28178
- Molecular speed ratio in low density flows determined via stagnation point heat transfer and flat plate heat transfer measurements 14 p2301 A67-28182
- One-dimensional laminar MHD flow at hydrodynamic stabilization, discussing heat transfer, Hartmann flow, magnetic field, Prandtl number and Joule heating 14 p2358 A67-28283
- Two-dimensional mixed boundary value problem of heat and mass transfer with characteristic equation containing multiple roots 14 p2406 A67-28312
- Inertial criterion relation for determining effect of mass transfer, phase transformation, and Kossovich number on heat and mass transfer 14 p2406 A67-28313
- Constant total pressure evaporation with heat reuse by built-in engine 14 p2407 A67-28623
- Air stream turbulence effect on local and macroscopic transport from cylinder, measuring thermal transfer and pressure coefficients at various Reynolds numbers 14 p2407 A67-28624
- Solid film sublimation cooling effect in Couette gas flow simulating real rarefied gas flow heat transfer, for jet engine application 14 p2408 A67-28800
- Lateral heating and sublimation of arbitrary thick two-layer plate using thermal flux time-dependent on plate surface 14 p2408 A67-28802
- Variational integration principles used to integrate wave and Fourier thermoconductivity equations, noting solution by Ritz method 14 p2408 A67-28803
- Heat removal from high density packaged electronics by bonded metallic heat sink [ASME PAPER 67-DE-47] 14 p2408 A67-28880
- Dimensional analysis of heat transfer correlations for nucleate boiling in free convection, including critical heat flux conditions 14 p2408 A67-28932
- Flight test skin temperatures of supersonic aircraft compared with theoretical results, explaining measurement discrepancies 14 p2243 A67-28977
- Time dependent heat conduction and diffusion equations for fuel-rich H-O flame solved by finite difference method 14 p2409 A67-29064
- Laminar Couette flow analyzed for gas injection effects on heat transfer to surface, temperature profile and convection interaction with radiation 15 p2578 A67-29129
- Hypersonic stagnation point flow between strong shock wave and body involving radiation, conduction and dissociation 15 p2415 A67-29309
- Free stream turbulence and pressure gradient effects on flat plate boundary layer velocity profiles and heat transfer [ASME PAPER 66-WA/HT-4] 15 p2470 A67-29321
- Heat transfer and skin friction rates increase in gas-liquid droplet suspension system flowing over circular cylinder formulated by laminar boundary layer theory [ASME PAPER 66-WA/HT-33] 15 p2579 A67-29322
- Aerodynamic heating through turbulent boundary layer of flat plate determined using Ferrari formula 15 p2415 A67-29328
- High accuracy alternating direction implicit difference schemes for biharmonic, heat conduction and Laplace equations 15 p2510 A67-29520
- Mean diameter/wall thickness optimum ratio and corresponding maximum shear stress for thin walled cylinder under uniform pressure and radial heat transfer 15 p2574 A67-29528
- Heat transfer through rarefied gas between concentric circular cylinders and spheres, using Krook kinetic equation 15 p2579 A67-29570
- Nonaxisymmetric temperature fields for orthotropic hollow cylinder and sphere solved using Bessel functions, noting heat transfer between external and internal surfaces 15 p2579 A67-29697
- Approximate iteration procedure for determining temperature field in plate for simultaneously radiative and convective heat transfer 15 p2580 A67-29779
- References on heat and mass transfer 15 p2580 A67-29780
- Prediction of large rocket nozzle material performance using semiempirical technique, noting mathematical models for internal and external heat and mass transfer 15 p2547 A67-29993
- Aerodynamic heating about vehicle entering atmosphere for corridor and guidance requirements analyzed on basis of Newton two-body problem 15 p2417 A67-30046
- Sensible heat transfer influence on dynamic stability of harmonic perturbations superimposed on zonal current, using Lorentz two-level model 15 p2512 A67-30057
- Flat plate, simultaneous heat and mass transfer for Newtonian fluids in free convection analyzed, using group theory 15 p2582 A67-30217
- Estimation of mean overheating of casing and heated space inside air cooled electronic device 16 p2778 A67-30470
- Heat transfer and fluid mechanics - Conference, La Jolla, Calif., June 1967 16 p2590 A67-30934
- Heat transfer in stagnation-point laminar boundary layer with mass injection and absorption of incident radiation 16 p2658 A67-30941
- Thermal turbulent boundary layer on flat plate with thermally insulated section, determining temperature distribution in presence of heat transfer 16 p2594 A67-31201
- Boundary layer theory applied to solution of problems of combined heat and mass transfer, using approximate single-parameter integral method 16 p2594 A67-31202
- Low Reynolds number flow past heated cylinder studied for fluid properties variation and thermal and velocity slip presence at wall 16 p2779 A67-31216
- Heat loss from wires in nitrogen, helium and mixtures measured at low Reynolds numbers, finding agreement with theory of Kassoy 16 p2779 A67-31217
- Time-dependent mean-mass temperature of argon jet produced by arc plasmatron with powdered metal carbides injected into jet calculated using heat transfer equations 16 p2721 A67-31393
- Heat transfer in cryogenic range, noting heat flux measurements, use of semiconductors, etc 16 p2780 A67-31533
- Transverse curvature effect on axisymmetric compressible laminar boundary layer flow, obtaining asymptotic solutions for skin friction and heat transfer 16 p2662 A67-31600
- Heat transfer, thermal conductivity and thermal diffusivity of loose fibrous materials under vacuum 16 p2780 A67-31772
- Heat transfer in turbulent carbon dioxide pipeflow at supercritical region 16 p2780 A67-31777
- Nucleate boiling heat transfer correlations

graphically estimated for design purposes to compute heat flux and wall superheat 17 p2966 A67-32033

Quartz sand particles descending motion and heat transfer in gas vertical tube, determining temperature profile 17 p2967 A67-32132

Thermal propagation in gases studied through heat transfer equation resulting from Fourier law 17 p2968 A67-32221

Thermal conductivity model for planetary igneous differentiation, discussing melting behavior as function of pressure and temperature 17 p2942 A67-32387

Heat transfer by dropwise condensation, evaluating average heat flux 17 p2969 A67-32447

Separated and reattaching flows emphasizing heat transfer considerations in calculations, especially in supersonic designs 17 p2970 A67-32448

Heat transfer bibliography covering boundary layer, phase change, two-phase flow, channel flow, conduction, liquid metal, MHD, etc 17 p2969 A67-32450

Soviet book on heat transfer and hydrodynamics in two-phase media 17 p2969 A67-32457

Boiling process of binary mixtures examined by heat transfer mechanism at atmospheric pressure 17 p2969 A67-32458

Heat transfer analysis for cavitation and boiling, noting vapor bubble formation 17 p2970 A67-32463

Book on similarity theory applications to heat and mass transfer in moving medium 17 p2970 A67-32464

Transport property difference effect on flow prediction of blunt body stagnation region heat transfer, noting laminar flow and compressible boundary layer equations 17 p2793 A67-33025

Soviet book on heat and mass transfer, Volume 6 17 p2971 A67-33067

Variational technique for temperature field determination in plane system with given heat distribution sources, based on Galerkin-Ritz method 17 p2972 A67-33069

Unsteady heat transfer between solid body and surrounding fluid flow, using convective fluid heat transfer and body thermoconductivity equations 17 p2972 A67-33071

Three-component heat transfer system for regulating system of three heat conductors, analyzing temperature regime 17 p2973 A67-33078

Diurnal variations of ionospheric ion/electron temperatures predicted assuming solar UV radiation heating, collisional cooling and heat transport by conduction 17 p2850 A67-33192

Heat exchange and friction drag coefficients for laminar flow of equilibrium dissociable hydrogen with constant heat flow density at tube wall 17 p2974 A67-33326

Modified hot-wire thermal conductivity cell for measuring effects of finite length, pressure and temperature on heat transfer from wire in rare gases 17 p2863 A67-33357

Heat transfer due to flow of electrically conducting incompressible viscous fluid from rotating insulated disk under influence of axially oriented magnetic field 18 p3084 A67-33667

Rayleigh number effect on importance of convective heat transfer in self-heating gaseous reactions checked against thermal ignition theory 18 p3156 A67-33852

Propellant injection through porous media, advantages, fluid flow nature, heat transfer, characteristics and uses 18 p3026 A67-33934

[AIAA PAPER 67-463] 18 p3026 A67-33934

Semiconductor surface thermocouples, determining heat-transfer rates associated with wind tunnel testing 18 p3048 A67-34103

Heat transfer process for film boiling taking into account growth of prominences up to bubble departure and Taylor instability 18 p3160 A67-34162

S-shaped boiling curves analyzed in terms of nucleation characteristics of heat transfer surface, correlating temperature driving force and density of centers 18 p3160 A67-34164

Wall heat flux in turbulent air flow using inner law correlations for velocity and temperature 18 p3160 A67-34165

Soviet heat transfer bibliography covering heat conduction, convective and radiative heat transfer, mass transfer, drying

processes, high temperature, etc 18 p3160 A67-34166

High intensity heat flux formation during heat transfer on steel cylinder in region of incident shock wave in supersonic flow 18 p3027 A67-34206

Heat transfer in steady axisymmetric MHD flow near stagnation point, with series solutions for velocity, magnetic field and temperature 18 p3161 A67-34381

Heat transfer in viscous fluid flow in gap between permeable isothermal surface and rotating disk, solving energy equation 18 p3161 A67-34476

Heat transfer and friction drag for supercritical laminar flow of carbon dioxide through tube at constant thermal flux density at wall 18 p3161 A67-34477

Heat transfer in steady flow of non-Newtonian fluid between two walls with periodic deformation considered, using perturbation method 18 p3161 A67-34616

Heat transfer intensifying process experimented in wind tunnel by applying longitudinal/transverse pressure gradients through controlled flow pressure field 19 p3346 A67-35633

Heat transfer to catalytic and noncatalytic surfaces on sharp flat plate in shock tube gas flow for checking various laminar boundary layer theories 19 p3211 A67-35739

Finite difference heat conduction method for surface subliming processes in space vehicles 19 p3346 A67-35755

Composition law of thermal resistance in contact between parallel bands 19 p3347 A67-35790

Test data for heat transfer in vortex flows in tubes with band type swirl generator, determining effect of mass inertial forces 20 p3544 A67-36449

Computer program for heat transfer calculation by temperature distribution along wall surface, using Fourier-Bessel series to determine distribution coefficients 20 p3544 A67-36450

Resonance frequency shift analysis of autostabilized light modulator at microwave frequencies noting heat transfer, transition temperature, etc 20 p3459 A67-36503

Cellular cumulus convection confined to cylindrical column in conditionally unstable atmosphere 20 p3480 A67-36505

50 degree semivertex angle sphere-cone Voyager configuration wind tunnel tested in dry nitrogen for aerodynamic characteristics, pressure and heat transfer distribution 20 p3356 A67-36562

Ultrasonic field effects on nucleating fluid in flash boiling system and heat transfer dependence on bubble density parameters [ASME PAPER 67-HT-11] 20 p3545 A67-36709

Heat transfer in region of separated flow over two-dimensional rectangular cavity facing oncoming turbulent boundary layer [ASME PAPER 67-HT-14] 20 p3545 A67-36711

Natural convection in finite nonzero length vertical channels, using integral technique to derive results for two wall conditions [ASME PAPER 67-HT-16] 20 p3545 A67-36712

Friction and heat transfer characteristics of turbulent swirl flow under large transverse temperature gradients [ASME PAPER 67-HT-24] 20 p3546 A67-36718

Laminar boundary layer flow of water over flat plates, noting heat transfer effects on velocity profile stability [ASME PAPER 67-HT-41] 20 p3547 A67-36725

Energy equation for laminar convective heat transfer in combined hydrodynamic and thermal entrance region bound by parallel flat plates [ASME PAPER 67-HT-48] 20 p3548 A67-36730

Transient heat transfer through monatomic collisionless ideal gas enclosed between parallel walls analyzed for step change in one wall temperature [ASME PAPER 67-HT-53] 20 p3548 A67-36735

Coolant passage axial curvature effect on heat transfer to endothermically dissociating supercritical nitrogen tetroxide [ASME PAPER 67-HT-59] 20 p3549 A67-36741

Thermal scaling for test models in heat transfer studies of bodies enveloped in large luminous flames [ASME PAPER 67-HT-60] 20 p3549 A67-36742

Incipient boiling prediction extended from forced flow water to other fluids and natural flow conditions [ASME PAPER 67-HT-61] 20 p3549 A67-36743

Gravity and buoyancy effects on slip ratio, void fraction, flow model and boiling heat transfer [ASME PAPER 67-HT-63] 20 p3549 A67-36745

Heat transfer for one-and two-dimensional pulsating incompressible laminar flow in circular tube with two thermal boundary conditions [ASME PAPER 67-HT-65] 20 p3550 A67-36747

Laminar boundary layer with heat transfer in liquids with variable fluid properties, including velocity and temperature profiles [ASME PAPER 67-HT-69] 20 p3550 A67-36749

Heat and mass transfer conditions in ablation of shear thinning and thickening fluids investigated at stagnation point [ASME PAPER 67-HT-78] 20 p3551 A67-36756

Effect of deviation of inlet fluid temperature change from step change on maximum slopes of transient response curves [ASME PAPER 67-HT-79] 20 p3551 A67-36757

Temperature dependent viscosity effects on heat transfer and drag on wedge-shaped body, calculating boundary layers on surface 20 p3421 A67-36824

Gas-side heat transfer at high temperature combustor sonic points, discussing Reynolds number effect, boundary layer transitions, turbulence intensity, etc [AICHE PAPER 27] 20 p3552 A67-36831

Film boiling of potassium on horizontal plate, discussing heat fluxes relationship to Berenson equation and heat transfer [AICHE PAPER 28] 20 p3552 A67-36832

Approximation integral method for solution of coupled equations of heat and mass transfer in porous medium, discussing nonlinear and linear problems 20 p3553 A67-36938

Fuel cell performance under operating conditions of local nonuniformity in temperature, concentration, potential or current simulated with computer program 20 p3363 A67-37014

Heat transfer in fuel cell battery held in isothermal bath, giving charts for maximum temperatures at different Peclet numbers 20 p3364 A67-37016

Unsteady transverse diffusion of passive impurity and mass and heat transfer in granular layer described by cell type models 20 p3554 A67-37054

Vibrational frequency and amplitude effects on heat transfer intensity from vibrating cylinder into circular channel at low Reynolds numbers 20 p3554 A67-37303

Heat transfer - Conference, Chicago, August 1966, Volume 6 20 p3555 A67-37460

Soviet book on boundary layer of non-Newtonian fluids covering hydrodynamics, heat transfer and mass transfer 20 p3424 A67-37546

Book on fluid dynamics of multiphase systems covering momentum, heat and mass transfers and chemical reactions 20 p3425 A67-37728

Heat transfer analysis using Mach-Zehnder interferometer with laser light source for applications to spacecraft electronics 21 p3731 A67-37959

Lubrication and wear in high vacuum, considering inability to maintain oxide films, evaporation of lubricants, heat transfer and sliding friction 21 p3633 A67-38142

Calibration for pyrometer with different surface heat transfer coefficients of black and gold strip 21 p3627 A67-38446

Pressure dependence of heat transfer by evaporation, obtaining parameters from dimensional analysis 21 p3732 A67-38499

Anode heat transfer in MPD arc, discussing configurations and thrusters [AIAA PAPER 67-673] 21 p3691 A67-38706

Two-dimensional multiple wave distortions effect on heat transfer to wall in hypersonic flow [AIAA PAPER 67-164] 21 p3732 A67-38855

Surface temperatures of two rubbing bodies and heat partition between them determined numerically, using Fredholm integral equation solution 21 p3638 A67-39091

Three-dimensional compressible laminar boundary layer with heat transfer in curvilinear coordinate system linked to streamlines of external flow, assuming transverse flow 21 p3615 A67-39127

Ideal gas flow in spherically symmetric gravity field, considering radiant heat transfer and radiation pressure 22 p3880 A67-39407

Partial differential equations solution in heat transfer between incompressible fluid and porous medium 22 p3917 A67-39640

Infinite horizontal fluid layer heated from below /classical Rayleigh thermal stability problem/ extended to fluid in rigid sphere heated nonuniformly 22 p3918 A67-39715

Similarity solutions for compressible laminar boundary layer, showing pressure and heat and mass transfer effects on wall temperature and shear 22 p3918 A67-39715

Stress 22 p3918 A67-39716

Two-dimensional adiabatic laminar separated regions in supersonic flow, examining effects of blowing and suction at wall [AIAA PAPER 67-192] 22 p3786 A67-40096

Polytropic exponent along axis shown to approach adiabatic exponent at throat of convergent-divergent nozzle 22 p3742 A67-40112

Noise occurrence during heat transfer from solid to liquid He 2 flux at high temperature difference, discussing heat flux 22 p3838 A67-40389

Boiling heat transfer to liquid helium, discussing heat flux as temperature difference function and surface finish effect 22 p3920 A67-40390

Efficient thermal design of steerable antennas, considering space-environmental requirements 22 p3750 A67-40409

Differential equation system for reacting laminar boundary layer heat and mass transfer solved analytically, noting compressible gas and porous foil filter 23 p4081 A67-40744

Heat transfer equations with combined conduction and radiation noting application to spacecraft problems 23 p4082 A67-40997

Energy equation solution procedure for heat transfer across two-dimensional oscillating laminar boundary layer 23 p4082 A67-41243

Heat transfer, skin friction and shearing stress from similar solutions to compressible laminar boundary layer equations for flow over flat plate 23 p4082 A67-41246

Turbulent boundary layer energy and motion equations, heat transfer through layers, energy exchange and phenomenological relations 23 p3991 A67-41249

Three-dimensional heat conduction, heat and mass transfer and thermoelasticity problems solved by approximate method using functional parameters 23 p4083 A67-41290

Turbulent skin friction in incompressible flow with heat transfer, determining Preston surface pitot tube applicability 23 p4004 A67-41341

Radiative and convective heat flux measuring instruments calibration for aerospace industry 23 p4006 A67-41375

Asymptotic solutions of eigenvalue problem with two transition points applied to Graetz problem involving heat transfer in fluid 23 p4083 A67-41668

Friction and heat transfer effects on nonsteady flow behind Chapman-Joulet detonation to analyze transition to steady flow 23 p3993 A67-41744

Approximate methods for solving heat transfer problems with phase change, considering applicability to Stefan problem 23 p4084 A67-41749

Transverse curvature parameter in hypersonic flow regime for modifying effects on velocity profile slope, skin friction and heat transfer rate 23 p3993 A67-41755

Electron neutral heat transfer in plasmas, obtaining data on electron thermal diffusivity from pulsed heat flow experiments in helium afterglow 24 p4194 A67-41872

Heat transfer between gas flows and solid /carbon/ surfaces, considering chemical reactions 24 p4252 A67-41935

Generalized dynamical thermoelasticity theory formulated via heat transfer equation, considering temperature/strain rate coupling effect 24 p4252 A67-41955

Liquid coolant space radiator system for manned spacecraft thermal control, investigating design and transient performance [SAE PAPER 670838] 24 p4252 A67-41994

Heat transfer from plate located on dielectric base to liquid helium in pulsed

regime influencing kinetics of superconductivity in thin films 24 p4254 A67-42258

Temperature distribution of fluid in laminar boundary layer of flat plate and heat flow from fluid to plate wall 24 p4143 A67-42281

Heat and mass transfer processes in reacting laminar boundary layer flow with steady high speed gas flow 24 p4143 A67-42284

Plasma energy and heat transfer to surface with and without electric current, discussing various energy transfer models 24 p4197 A67-42331

High temperature thermal insulation consisting of thin refractory metal foils separated by thin refractory oxide layers 24 p4103 A67-42501

Pu 239 fueled fast spectrum nuclear reactor spacecraft power supply design for 1 kwe noting cost, control, heat transfer and optimization 24 p4185 A67-42538

Optimization of capillary pumping of microgrooved heat pipes, discussing transport equation 24 p4255 A67-42552

Parametric analysis of heat pipes, design, operation principles and performance capabilities 24 p4255 A67-42553

Momentum and heat transfer in axisymmetric turbulent free jets exhausting into quiescent air, using finite difference technique 24 p4092 A67-42608

Heat and mass transfer in chemically reacting gas mixture compressible boundary layer, determining temperature in reaction zone and on porous plate surface 24 p4256 A67-42734

Optimization of base thermal protection system for advanced Saturn II boosters employing strap-on solid propellant motors 24 p4256 A67-42915

Heat transfer to end wall of shock tube after shock wave reflection through steep temperature gradient analyzed using variational method 24 p4257 A67-43092

HEAT-TRANSFER COEFFICIENT

Heat exchange and friction drag coefficients for laminar flow of equilibrium dissociable hydrogen with constant heat flow density at tube wall 01 p0165 A67-10048

Row of parallel circular cylinders in hypersonic flow show determinant factor in boundary layer and heat transfer characteristics 01 p0006 A67-10559

Transient forced convection laminar film condensation on horizontal plate, noting film thickness changes and heat-transfer coefficient variations 01 p0168 A67-11229

Local convection coefficient along windward line of axisymmetric obstacle in hypersonic flow with laminar boundary layer 02 p0178 A67-12061

Potassium metal Rankine cycle power system, testing turbines, bearings and seals, potassium boiler and steam topping cycle analysis obtaining high heat-transfer coefficients [AIAA PAPER 66-1009] 02 p0184 A67-12307

Relation between skin temperature and environmental air supply temperatures in fixed air-ventilated clothing assembly 02 p0188 A67-12346

Approximate distribution of pressure friction and heat-transfer coefficients in laminar boundary layer separation during interaction with supersonic flow 03 p0401 A67-12877

Steady state thermal conductance coefficient at interface formed by nominally-flat rough contacting surface placed in vacuum environment [AIAA PAPER 66-42] 03 p0534 A67-13070

Stabilizing effect of wall and thermal flux temperature variations over channel length on heat transfer coefficient of liquid flow 03 p0536 A67-13610

Helium 2 film free convection heat transfer, discussing mathematical analysis for vertical flat plate and horizontal circular cylinder [ASME PAPER 65-WA/HT-10] 03 p0536 A67-14007

Heat transfer and velocity characteristics of thermal and hydrodynamic laminar flow in ducts of arbitrary cross section, considering boundary conditions at wall [ASME PAPER 65-WA/HT-13] 03 p0537 A67-14008

Heat-transfer coefficient of tube in transverse flow calculated from tube surface

temperature distribution 04 p0726 A67-15598

Heat-transfer coefficient measurements in separated flow regions in heated duct with circumferential grooves, ribs and enlargements, by visual flow techniques 04 p0729 A67-15810

Simultaneous conductive-convective heat-transfer coefficient and heat flux temperature relation at solid moving liquid interface 04 p0730 A67-15817

Mach number and temperature ratio effects on convective heat-transfer coefficient to flat plate through turbulent boundary layer in air and Stanton number calculation in terms of drag coefficient 04 p0731 A67-15820

Mass and heat transfer data from sweptback circular cylinders in Mach 2 wind tunnel with Reynolds number 100,000 04 p0549 A67-15824

Heat transfer and circulation data for rotating mixed convection thermosyphon geometry for application to cooling certain rotating components 04 p0731 A67-15828

Tests for measuring heat-transfer coefficients in horizontal annulus filled with gas and visualization of flow 04 p0732 A67-15829

Unsteady incompressible laminar forced convection around stagnation point due to arbitrary time-wise-variant free stream velocity, considering skin friction and heat transfer 04 p0610 A67-15830

Local heat-transfer coefficients between isothermal flat plate and two-dimensional wall jet 04 p0732 A67-15835

Heat transfer by array of two-dimensional jets directed normal to surfaces including effects of superposed wall-parallel flow 04 p0732 A67-15836

Heat-transfer coefficients and shearing stress in turbulent boundary layer along porous flat plate with uniform fluid injection 04 p0733 A67-15842

Pool film boiling based on cellular model, postulating time-averaged cell configuration to adjust itself to maximize rate of heat transfer 04 p0734 A67-15849

Pebble-bed heater for hypersonic wind tunnel, evaluating heat-transfer coefficients from transient temperature distribution of bed 05 p0926 A67-16429

Two-phase flow of gas over harmonically oscillating flat plate expressed in laminar boundary layer terms, presenting liquid film thickness, heat transfer rate, skin friction, etc 05 p0793 A67-17338

Conductive heat transfer coefficient measurement from sphere to rarified gas mixtures over range of Knudsen numbers 06 p1117 A67-18388

Quasi-stationary heat transfer equations and maximum possible heat-transfer coefficient for solid surface moving in very fluid rotating boiling medium 06 p1118 A67-18549

Leak current, friction and heat-transfer coefficients of compressible laminar boundary layer on insulator wall of MHD channel with anisotropic conductivity 06 p1043 A67-18673

Plasma flow in plane MHD channel in absence of longitudinal thermal flux, considering temperature dependence of heat transfer and viscous energy dissipation coefficients 06 p1045 A67-18811

Temperature variation in wall of square channel due to heat transfer to turbulent flow of water and Hg 07 p1265 A67-19126

Nonstationary heat transfer coefficient and effect of nonstationary hydrodynamic conditions on heat transfer in channels 07 p1266 A67-19183

Phase effect during rectangular pulsations of heat transfer coefficient 07 p1267 A67-19325

Surface pressure, heat transfer coefficient, wave structure and shock disturbances of inviscid supersonic flow field along corner of intersecting wedges [AIAA PAPER 66-128] 08 p1276 A67-20564

Heat-transfer coefficients during dropwise condensation on randomly distributed nucleation sites analyzed through computer simulated model 08 p1426 A67-20925

Rectangular and inverted wedge recompression step effect on recovery factor, heat-transfer coefficient, velocity profile and pressure distribution in open cavity flow [ASME PAPER 65-WA/HT-37]

- 08 p1278 A67-21320
Stagnation temperatures from stagnation point heat transfer rates measured in hypersonic gun tunnel at Mach 9.8
- 09 p1486 A67-22414
Laminar and turbulent flow and heat transfer in boundary layer on continuous moving surface
- 10 p1732 A67-22728
Asymptotic calorimetry, developing general relationship between temperature and unperturbed heat transfer coefficient for steady state nonisothermal heating
- 10 p1656 A67-23139
Heat and mass transfer during stationary adiabatic vaporization of water ethanol and carbon tetrachloride
- 11 p1882 A67-24319
Heat transfer from laminar Newtonian flow through cooled elliptic tubes with variable cross sections
- 12 p2033 A67-25215
Heat transfer and friction coefficients measured for turbulent flow of non-Newtonian fluids in rectangular and circular channels
- 12 p2033 A67-25315
Heat receiver with correcting device for instantaneous temperature measurements in unsteady gas flow, discussing matching of time constants and heat-transfer coefficients
- 13 p2118 A67-26352
Thermal boundary layer equation reduced to ordinary differential equation for flat plate with given heat conductivity
- 13 p2224 A67-27048
Inverse heat transfer problem in air flow past cylinder, calculating heat transfer coefficient and scaling functions
- 13 p2224 A67-27053
Heat conduction equation for inhomogeneous body, obtaining integrable solutions applicable to boundary value problems
- 13 p2224 A67-27055
Heat transfer calculation to turbine blading in cascade in presence of secondary flow, considering flow velocity estimation, blade boundary layer and related heat transfer properties
- 13 p2225 A67-27465
Boundary layer equations reduced to ordinary differential equations without using self-similarity assumptions, noting friction-drag and heat-transfer coefficient along MHD channel
- 14 p2356 A67-27978
Two-way radiative heat transfer between surfaces and volumes of two bodies
- 14 p2406 A67-28309
Steady heat transfer through rib-reinforced wall of material with variable coefficient
- 14 p2407 A67-28646
Infinite plate temperature field determined by approximate method when heat transfer coefficient is time dependent
- 14 p2407 A67-28647
Thermal field of solid rod of uniform cross section and arbitrary profile with time dependent heat transfer
- 14 p2408 A67-28658
Temperature distribution for asymmetric heat transfer in turbulent flow between parallel plates
- 15 p2469 A67-29133
Turbulent boundary layer with large acceleration parameter studied for flow and heat transfer coefficient
- [JPL-TR-32-1119] 16 p2659 A67-30953
Potassium metal Rankine cycle power system, testing turbines, bearings and seals [AIAA PAPER 66-10009]
- 17 p2802 A67-32052
Film cooling theory applied to aircraft gas turbine chambers shows slot geometry effect as negligible
- 17 p2967 A67-32126
Unsteady heat transfer in tube in presence of variable gas flow rate
- 17 p2967 A67-32129
Unsteady heat transfer in tube during heat-flux fluctuations
- 17 p2967 A67-32130
Nusselt results concerning heat transfer extended to include surface tension effect on heat transfer coefficient
- 17 p2970 A67-32461
Field spectrum developed from monochromatic temperature oscillations in bodies due to time variation of heat transfer coefficients caused by unsteady flow velocity
- 17 p2972 A67-33073
Temperature fields in cross section of gas turbine blade with internal coolant during variation of local heat-transfer coefficient
- 17 p2973 A67-33076
Heat-transfer coefficients for heat transfer from gas to blade surface in gas turbine under operating conditions
- 17 p2973 A67-33077
Unsteady heat conduction and transfers by electrical simulation methods, determining temperature field in canonical metal bodies
- 17 p2973 A67-33082
Heat exchange and friction drag coefficients for laminar flow of equilibrium dissociable hydrogen with constant heat flow density at tube wall
- 17 p2974 A67-33326
Laminar boundary layer theory applied to heat transfer in low thrust rocket nozzles, checking with experimental wall temperature data
- [AIAA PAPER 67-447] 18 p3112 A67-33923
Stabilizing effect of wall and thermal flux temperature variations over channel length on heat transfer coefficient of liquid flow
- 18 p3181 A67-34475
Turbulent heat-transfer coefficients and eddy diffusivity profiles for momentum and heat in Newtonian and non-Newtonian fluids, giving equation for data correlation
- 19 p3344 A67-34869
Heat-transfer coefficient effect on final magnitude of stresses in elastoplastic spherical body subjected to cooling process
- 19 p3340 A67-35510
Rocket launching pad exhaust deflector investigated for uncooled efflux deflectors design data, calculating heat transfer coefficient and stagnation temperature
- 19 p3207 A67-35520
Surface-temperature conditions in disks and gears stressing heat transfer coefficient and lubricated contact temperature
- 19 p3237 A67-35840
Mean heat transfer coefficient at flat plate with turbulent boundary layer at zero incidence Mach numbers mean heat-transfer coefficient at flat plate with turbulent boundary layer at zero incidence
- 20 p3543 A67-36275
Local heat-transfer coefficients of turbine blades, evaluating local Nusselt number distribution, Reynolds numbers, and turbulent flow effects
- 20 p3515 A67-36451
Heat transfer characteristics of several aliphatic hydrocarbons in nucleate and film boiling during forced flow in heated tubes [ASME PAPER 67-HT-7]
- 20 p3544 A67-36705
Local heat transfer coefficients, mean temperature and velocity distributions in turbulent natural convection boundary layer on vertical plane surface
- [ASME PAPER 67-HT-17] 20 p3545 A67-36713
Transpiration cooled porous surface in high temperature forced convection environment, applying transient energy balance with heat-transfer coefficient measurement
- [ASME PAPER 67-HT-27] 20 p3546 A67-36720
Turbulent boundary layer and heat-transfer coefficients for air in conical nozzles, noting uncooled inlet length and convergence angle effects
- [ASME PAPER 67-HT-28] 20 p3357 A67-36721
Electric field effects on condensation heat transfer, discussing heat-transfer coefficient dependence on electric field and instability appearance at liquid film interface
- [ASME PAPER 67-HT-39] 20 p3547 A67-36724
Transient mean wall temperature of flat plate with time dependent heat source and cooled by incompressible turbulent flow, discussing heat-transfer coefficient
- [ASME PAPER 67-HT-45] 20 p3547 A67-36727
Approximate solution to heat transfer coefficient on flat plate in linear shearing flow
- [ASME PAPER 67-HT-46] 20 p3547 A67-36728
Sinusoidal surface vibration effect on nucleate pool boiling reveals lowered surface temperature for low heat flux, LF and high acceleration
- [ASME PAPER 67-HT-49] 20 p3548 A67-36731
Surface vibration effect on nucleate pool boiling, measuring heat-transfer coefficient and proposing mechanism
- [ASME PAPER 67-HT-58] 20 p3549 A67-36740
Laminar film boiling on thin wire, determining heat-transfer coefficient and vapor dome spacing and diameter
- [ASME PAPER 67-HT-62] 20 p3549 A67-36744
Heat transfer coefficients from supersonic wind tunnel airflow through grid with rectangular bars
- [ASME PAPER 67-HT-74] 20 p3550 A67-36754
Centripetal radial blowing effect on flow and heat transfer in gap between rotating disk and wall, specifically effect of Reynolds number and dimensionless flow
- 20 p3357 A67-36794
Fin surface geometry optimization with respect to gross heat-transfer coefficient [AICHE PAPER 6]
- 20 p3552 A67-36827
Relative velocity effect on vaporization times and heat-transfer coefficients of water drops in Leidenfrost film boiling on heated rotating wheel
- [AICHE PAPER 32] 20 p3552 A67-36833
Heat transfer in circular channel containing revolving cylinder, considering turbulent flow with microvortices
- 20 p3359 A67-37343
Heat-transfer coefficients for laminar and transitional liquid metal flow in tube with constant wall heat flux
- 20 p3555 A67-37608
Heat transfer dependence in cavity of closed evaporative thermosyphon on device inclination angle and coolant filled fraction of cavity
- 21 p3625 A67-37913
Temperature variation in wall of square channel due to heat transfer to turbulent flow of water and Hg
- 21 p3731 A67-38170
MHD channel wall boundary layer equations for low temperature plasma, determining friction and heat transfer coefficients and leakage current
- 21 p3665 A67-38241
Insulator boundary layers in supersonic MGD channel noting heat transfer rate, current density, stagnation, pressure distribution and skin friction
- [AIAA PAPER 67-717] 21 p3673 A67-38743
Instantaneous heat transfer of thin tungsten wires in unsteady transverse airflow
- 21 p3733 A67-38913
Measurement of rapidly varying temperatures of gas flows with resistance thermometers taking into account heat transfer between heat probe and holders
- 21 p3630 A67-38914
Thermographic method for investigation of kinetics of heat evolution
- 22 p3917 A67-39586
Local coefficient of heat exchange by natural convection on isothermal vertical flat plate in turbulent regime
- 22 p3917 A67-39648
Heat transfer experiments with flat plate heated under constant heat flux, discussing wall temperature distribution, Prandtl number and Spalding function
- 22 p3918 A67-40041
Calorimeter for evacuated multilayer insulation materials to evaluate performance and measure heat transfer rate and thermoconductivity
- 22 p3803 A67-40297
Heat transfer of fluid flow in annular channel with rotating shafts, deriving surface heat transfer estimation without axial flow
- 22 p3921 A67-40457
Temperature field and critical thermal loads for fuel elements with varying convective heat transfer coefficient and ambient temperature
- 23 p4082 A67-41286
Atomic Cs vapor experimental values for heat-transfer coefficient used to determine Cs atoms and molecules interaction potentials
- 24 p4253 A67-42211
Turbulent fluid flow velocity and temperature fields in annular and plane gaps calculated by integral approximation for turbulent viscosity and heat conduction coefficients
- 24 p4142 A67-42213
Heat absorber temperature distribution, considering medium temperature and heat transfer coefficient arbitrary functions of time
- 24 p4154 A67-42215
Surface temperature oscillations of externally cooled working blades of gas turbine with air-liquid mixtures
- 24 p4254 A67-42255
Friction-drag and heat-transfer coefficients of plate in turbulent gas flow, estimating effect of turbulent Prandtl number
- 24 p4143 A67-42283
Rotating boiler for high performance Rankine cycle power generator using water as test fluid, obtaining heat-transfer coefficients
- 24 p4184 A67-42498
Temperature field in solids with time-varying heat-transfer coefficient, giving numerical results for plate, cylinder and sphere
- 24 p4256 A67-42591
HEAT TRANSMISSION
Cooling gas turbine blades by heat pipe effect for stationary blades and thermosyphon effect for moving blades
- 05 p0874 A67-16747
Heat pipe, device with thermoconductivity greater than solid conductors, based on surface tension and latent heat of working fluid
- 08 p1427 A67-21051
HEAT TREATMENT
SA HARDENING
SA QUENCHING
High strength magnesium casting alloys

for aerospace applications, based on heat treatment involving internal precipitation of hydride
[SAE PAPER 660656] 01 p0094 A67-10615

Metal and alloy heat treatment intensification with ultrasonic techniques improve steel recrystallization, etc 01 p0095 A67-10640

Mechanical property and structural changes in titanium alloys subjected to high temperature thermomechanical treatment 01 p0095 A67-10641

Effects of aluminum electrode and hydrogen atom on MOS structure during annealing 01 p0137 A67-11069

Vacuum evaporation of HgTe thin film, examining thermal treatment, electric properties as function of thickness, etc 02 p0280 A67-11463

Neutron bombardment effect on titanium and chromium carbides before and after heat treatment, giving results of X-ray and micrographical analyses, electric resistance, brittleness and microhardness measurements 03 p0447 A67-13639

Oxygen content effect on mechanical properties and phase transformations of VT 16 titanium alloy during thermal treatment 04 p0637 A67-14942

Annealing effect on texture of titanium alloys with electrodeposited chromium and nickel 04 p0637 A67-14944

Metal addition effect on grain growth of matrix oxides, noting inhibitive results in most cases 04 p0642 A67-15086

Maraging steel properties, discussing composition, strengthening mechanism, tensile and impact toughness, mechanical and fatigue properties, etc 04 p0640 A67-15458

Forging and solution treating nickel-chromium alloy 718 to investigate notch ductility and uniform grain size 04 p0640 A67-15459

Arc formation at metal surface in hydrogen plasma analyzed at various gas pressures, using Penning discharge, noting heat treatment effect on hydrogen 05 p0850 A67-16066

Heat treatment conversion of large grain n-type indium antimonide single crystals and twin crystals into p-type samples 05 p0862 A67-16507

Rotating beam S-N fatigue curves for 18 percent Ni maraging steel bars subjected to heat treatments 06 p1014 A67-17800

Heat treatment and microstructural observations in wrought Ni-base superalloy Udmet 700 in static creep, determining fracture and deformation properties 06 p1015 A67-17809

Hydrostatic pressure effect on dispersion of gamma prime phase in precipitation heat treatment of nickel-base superalloy 06 p1016 A67-17902

Optical scattering dependence on heat treatment of monocrystalline silicon containing nitrogen 06 p1050 A67-18183

Heat treatment effect on structure, hardness, microhardness and corrosion resistance of VT1 titanium and OT4 titanium manganese-aluminum alloy sheets 06 p1018 A67-18236

Optical properties of zinc oxide analyzed by exposing samples to mechanical and thermal treatments and UV radiation [AIAA PAPER 67-214] 06 p1052 A67-18514

Thermostability of refractory materials and effects of high brittleness on thermal stress resistance of structural elements under single and multiple heat treatment and loads 07 p1198 A67-19128

Hardness of heat resistant steels at elevated temperatures as function of alloying and heat treatment 07 p1199 A67-19240

Structural changes in titanium alloys during heat treatment 07 p1205 A67-19271

Heat treatment effect on mechanical properties and structure of Ti alloys, noting phase state variation as function of quenching temperature 07 p1206 A67-19282

Heat treatment effect on yield point, impact toughness and plasticity characteristics of Ti alloys 07 p1207 A67-19286

AT13 Ti alloy preparation noting physical and mechanical properties and heat treatment induced phase transformation 07 p1207 A67-19287

VT15 titanium alloy weld properties as

affected by machining and postwelding heat treatment 07 p1208 A67-19294

Obtaining high strength titanium welds without hardening by heat treatment 07 p1190 A67-19295

Beadling in thin walled pipes with localized heating, noting stress deformation state 07 p1192 A67-19752

Blank heating processes in production by pressworking of seamless adapters for detachable tube joints 07 p1192 A67-19754

Spectral distribution of photoconductance and conductance glow curves of CdS single crystals after vacuum heat treatment 07 p1237 A67-20179

Heat treatment optimization for precipitation hardening superalloys, devising mathematical model for test sequence 07 p1192 A67-20249

Fabrication, properties, deformation and fracture of silica fiber reinforced aluminum, noting effect of heat treatment and stress rupture 07 p1211 A67-20260

Oxygen precipitation consisting of point defects as explanation of structural changes of silicon single crystals during thermal treatment 08 p1370 A67-21205

Effects of cold work by rolling and by shock waves on precipitation hardening in Al-6 percent Cu alloy 08 p1343 A67-21544

Thermal etching study of rod shaped formations caused by structural dislocations during heating and cooling of Ti-Mo-Fe-Al system 09 p1518 A67-21967

Carbon fibers of high strength and high breaking strain noting heat treatment, structure and mechanical properties 09 p1520 A67-21988

X-ray structural study of phase transformations during heat treatment of VT3-1 titanium alloy 09 p1518 A67-22030

Temperature dependence of magnetization and resistivity in SHF magnesium-aluminum ferrite 10 p1688 A67-22830

Phase transformations in heat treated nickel-rich Ni-Co-Cr-Al-Ti-C cast alloys noting sigma formation 10 p1668 A67-23173

Microstructural dislocation tangling and related changes in tensile properties of Hastelloy X-280 following thermomechanical treatments 10 p1668 A67-23174

High temperature thermomechanical treatment effects on VT10 titanium alloy fine structure characteristics 10 p1670 A67-23641

Thermal mechanical treatments influence on strength, toughness and environmental failure resistance of low alloy high strength martensitic steel 11 p1806 A67-24363

Soviet book on production of gas turbine engines covering manufacturing methods, automation of operations, tooling, etc 11 p1798 A67-24516

Electron distribution of oxygen grown GaAs crystals after heat treatment, showing profiles due to silicon contamination 11 p1848 A67-24740

Microstructural variations of Ti-Mo-Al alloys due to stress corrosion cracking, noting increased resistance through heat treatment [ASME PAPER 67-GT-5] 11 p1808 A67-24793

Gas turbine bucket alloy improvement via heat treatment, noting performance evaluation results from creep rupture tests [ASME PAPER 67-GT-55] 11 p1808 A67-24811

Martensitically hardened high strength stainless steel, physical properties, heat treatment effects, etc 11 p1810 A67-25103

Width of ferromagnetic resonance curve in nickel and permalloy thin films as function of preparation and thermal treatment techniques 12 p1981 A67-25244

Push-pull low endurance fatigue of En 25 and En 32B steels at 20 and 450 degrees C 12 p2015 A67-25422

Heat sterilization in microelectronic assemblies 12 p1914 A67-25683

Alloy 718 composition, microstructure and heat treatment behavior correlated with mechanical properties, noting strengthening and oxidation resistance [ASME PAPER 67-MET-5] 12 p1956 A67-25949

Photomechanical effect in metals, discussing influence of impurities and heat treatment 13 p2174 A67-26400

Crystallization of boric anhydride obtained only through maintaining high water content in reactive agent during thermal treatment 13 p2143 A67-26812

Maraging steels retaining toughness at cryogenic temperatures by suitable heat treatment 13 p2142 A67-27677

Elastic properties of Ti alloys of ternary system Ti-Zr-Cr, showing sensitivity to heat treatment 13 p2143 A67-27710

Microstructure of aluminum alloys analyzed for composition, fabrication and thermal treatment, using electron microscopy 14 p2334 A67-27803

Thermal processing of precipitation-hardenable aluminum alloys, noting changes in structural and mechanical properties 14 p2335 A67-27804

Commercial aluminum wrought alloys properties, describing temper designation and heat and nonheat treatment classification 14 A67-27808

Cadmium sulfide crystal photoconductivity peaks near band edge, noting heat treatment, temperature and defects 14 p2364 A67-28229

Methods for transformation of titanium alloys by forging or die stamping to meet particular requirements 14 p2324 A67-28630

Biological and engineering problems in spacecraft sterilization, noting heat treatment 15 p2430 A67-29099

Hydrogen treatment effects on molybdenum ductility, noting grain-size and heat treatment contribution to strain-to-fracture difference at various deformation pressures 15 p2503 A67-29562

Machinability of high strength steels, titanium alloys and refractory alloys, examining cutting and RF current induction for heat treatment 15 p2505 A67-30126

Heat treating effects on titanium alloy properties, discussing ductility and strength annealing, etc 16 p2681 A67-30486

Niobium alloys under annealing and aging analyzed, noting formation of oxide, nitride and carbide phases followed by coagulation and brittleness 16 p2687 A67-30844

Alloy steels response to dynamic strain aging in quenched, tempered and ausformed conditions, plotting strength and toughness against straining and tempering temperatures 16 p2688 A67-31306

Inclusion type, forging ratio and heat treatment effect on properties of longitudinal and transverse steel specimens 16 p2689 A67-31310

Electron microscopy of titanium alloys noting preparation, heat treatment of samples, crystallographic structure, etc 17 p2872 A67-32722

X-ray absorption in chromium in chromium silicon after thermal processing at high temperatures 17 p2921 A67-32893

Heat treatment of nickel superalloys for high temperature applications, showing solution-temperature effect on mechanical properties 17 p2865 A67-33045

Thermal nitridation of maraging steels, noting effects on mechanical properties 17 p2875 A67-33046

Maraging stainless steel for high temperature applications, discussing properties, heat treatment and solution temperature effect 17 p2875 A67-33049

Flow stress of fresh dislocations in titanium and vanadium doped MgO single crystals, measuring dependence on heat treatment and test temperature 18 p3097 A67-33492

Paramagnetic and electrical properties of organic polyvinyl-acetate-based semiconductor films irradiated with electrons before and after heating 18 p3099 A67-33694

Fatigue characteristics of chromium-molybdenum steels subjected to various heat treatments, comparing tension-compression and torsion 18 p3065 A67-34258

Effectiveness of butt-welded joints and optimum heat treatment conditions for thin sheets of maraging steel containing 18 percent nickel 18 p3054 A67-34259

Structures from two-step aging of aluminum-magnesium-silicon alloy, discussing effect on needle precipitation 18 p3065 A67-34362

Metal and alloy heat treatment intensification with ultrasonic techniques improve steel properties, recrystallization, etc 18 p3066 A67-34404

Mechanical property and structural changes in titanium alloys subjected to high temperature thermomechanical treatment 18 p3066 A67-34405

Au and P doped n-type Si, noting formation of p-type surface layer of increasing thickness when heat treated 19 p3299 A67-34761

Surface hardening of titanium alloys by carbon and nitrogen, using high-frequency induction heating 19 p3242 A67-34919

Analytical model for microbial population survival times during heat sterilization studied for spacecraft applications, considering environment and exposure time 19 p3180 A67-35264

Indium-antimony alloy thin film preparation by vacuum evaporation, noting effect of heating and annealing on electrical resistivity 19 p3305 A67-35609

Thermal and thermomechanical treatments effect on structure and mechanical properties of Fe-Ni-base alloy with Al and Ti additions 19 p3247 A67-35834

Mechanothermal treatment for high temperature strength increase in metals, noting effects on creep strength, stress relaxation, etc 19 p3247 A67-35852

Heat treatment of indium antimonide crystals with various dislocation densities noting change in conductivity 20 p3506 A67-36227

Heat treating effects on molybdenum properties and structural characteristics 20 p3466 A67-36967

TiNi-TiFe system equilibrium diagram, studying melting points and heat treatment effects on microstructure 20 p3468 A67-37179

Tektite glasses crystallizing tendency studied by subjecting them to heat treatments above strain point and CN slow cooling from melting 20 p3527 A67-37274

Characteristics of niobium annealed at 2000 C, describing texture development and crystal perfection variation with annealing time 20 p3470 A67-37391

Dependence of electric resistance of thin Permalloy films on substrate temperature during evaporation and vacuum heat treatment 20 p3514 A67-37555

Temperature /K-state/ effect on dislocation blocking stresses in nickel alloy studied by mechanical hysteresis method 20 p3471 A67-37558

Electron beam welded D6AC steel plates evaluated after heat treated condition /stress relief/ for mechanical properties 20 p3456 A67-37695

Thermostable fibers from ordered heterocycle amide copolymers tested for tensile and high temperature properties 21 p3647 A67-37872

Niobium and niobium alloy structural changes during heating after pressing and rolling deformation 21 p3644 A67-38031

Heat treatment practices for precipitation hardening steels noting use in missile and aerospace applications 21 p3634 A67-38178

Heat treatment effect on microstructure and notch-bar rupture life of INCONEL alloys 21 p3646 A67-38776

Tensile strength of charred ablation material under rapid heating conditions tested using plasma arc flow and miniaturized specimen 21 p3650 A67-38874

Hall effect measurements on heat treated and quenched p-type silicon crystals, noting donor centers appearance due to vacancy cluster 21 p3687 A67-39138

Astrolay /Ni base superalloy/ disks for jet engine application, discussing chemical composition, basic ingot structure, forging and heat treatment 22 p3818 A67-39226

Qualitative and quantitative variation in alloy phase composition with temperature and age hardening length, studying structural diagram 22 p3818 A67-39321

Heat treatment effects on mechanical properties of steel-forged gas turbine rotor shafts, including microcracks formation and growth and structural strength 22 p3819 A67-39323

Molybdenum heat resistance improvement after structural polygonization by deformation and annealing, describing durability dependence on treatment conditions 22 p3819 A67-39324

Heating and quenching of aluminum and gallium substituted YIG changes magnetization of material due to cations redistribution process 22 p3860 A67-39913

Heat treatment effect in various gaseous media on electrical properties of CdTe films with abnormally high photovoltage, noting structural stabilization 22 p3861 A67-39924

Clean MOS structure bias and temperature /BT/ treatment at high electric fields causing electrochemical reaction affecting surface charge density 22 p3774 A67-40461

Precipitation processes in Ta-Cr solid solutions investigated for temperature dependence and change in alloy properties resulting from precipitation 23 p4018 A67-40712

Two-stage heat treatment effect on strength of high temperature Nimonic 80 alloy noting high brittleness, grain size and boundaries and fracture propagation 23 p4019 A67-41076

Polished glass substrates for thin film microcircuits, analyzing surface resistivity and optical transmittance changes due to heat treatment 23 p4043 A67-41366

Shear spun 300-grade maraging steel evaluated for pressure vessel applications, discussing fracture toughness [ASM PAPER C6-2.4] 23 p4020 A67-41412

Isochronal annealing effects on photovoltaic properties of n-on-p Si solar cells irradiated by energetic proton 23 p3940 A67-41518

Sealed heat sterilizable high impact resistant battery for space missions, grafting acrylic acid and polyethylene by irradiation for separator 24 p4106 A67-42521

Thermal treatment at melting temperature inducing acceptors of electric conductivity in indium antimonide crystals 24 p4204 A67-42577

HEATER

SA FURNACE

Pebble-bed heater for hypersonic wind tunnel, evaluating heat-transfer coefficients from transient temperature distribution of bed 05 p0926 A67-16429

HEATING

SA AERODYNAMIC HEATING

SA ARC HEATING

SA ATMOSPHERIC HEATING

SA AUTOCLAVE PROCESS

SA BASE HEATING

SA GAS HEATING

SA INDUCTION HEATING

SA IONOSPHERIC HEATING

SA JOULE HEATING

SA KINETIC HEATING

SA MAGNETOHYDRODYNAMIC SHEAR HEATING

SA PLASMA HEATING

SA PULSE HEATING

SA RADIANT HEATING

SA RADIO FREQUENCY HEATING

SA RESISTANCE HEATING

SA SHOCK HEATING

SA STRUCTURAL HEATING

SA SUPERHEATING

SA TRANSIENT HEATING

Modulation phase lag in causing overheating of semiconductor diodes as frequency of rectified voltage increases 02 p0209 A67-11508

Heating rate influence on transformations in 18 percent nickel maraging steel 06 p1018 A67-18378

Pressure oscillations induced by forced convection heating of dense hydrogen 13 p2107 A67-27670

Modulation phase lag in causing overheating of semiconductor diodes as frequency of rectified voltage increases 14 p2283 A67-28072

Estimation of mean overheating of casing and heated space inside air cooled electronic device 16 p2778 A67-30470

Critical heat-flux density dependence on dominant parameters in bilateral heating in annular channels 17 p2969 A67-32459

Critical heat flux value nonlinearly dependent on liquid bulk underheating to saturation temperature, deriving empirical formula 17 p2970 A67-32460

Transient heating and cooling of current carriers in semiconductors and highly ionized plasma analyzed, using effective temperature method 20 p3513 A67-37438

HEATING EQUIPMENT

SA FILAMENT

SA FURNACE

Heating unit of device for testing small samples of sintered materials for thermal fatigue 03 p0420 A67-13545

Thick film integrated circuits drying and firing processes describing driers and furnaces for ambient air and synthesized atmospheres 16 p2641 A67-31619

Electric internal heater for heating helium

driver gas to high temperature and pressure for shock tunnel experiments 21 p3606 A67-37770

Thermo-protective systems for ejected aircraft personnel noting cream product producing heat when dissolved in water [AIAA PAPER 67-987] 24 p4117 A67-43045

HEAVING MOTION

Circular planform peripheral jet ground effect machine heaving motion analyzed using motion equations 19 p3172 A67-34867

HEAVY COSMIC RAY PRIMARY

Gas proportional counter and scintillation telescope to search for quarks with unit and fraction charges in cosmic radiation at 3200 m altitude 02 p0316 A67-12767

Tracks of primary cosmic rays with atomic number greater than or equal to 20 in meteorites, discussing relationship between track length and particle mass 07 p1245 A67-19942

Charge spectrum of heavy cosmic ions of iron group in ionographic emulsions exposed in satellite 12 p1999 A67-25829

Heavy cosmic ions recorded on ionographic emulsions exposed on polar satellite 12 p1999 A67-25830

Fragmentation parameters of multicharge component of heavy cosmic ray nuclei on emulsion hydrogen 17 p2936 A67-32251

Gas proportional counter and scintillation telescope to search for quarks with unit and fraction charges in cosmic radiation at 3200 m altitude 22 p3877 A67-40269

Balloon-borne electronic system for heavy primary cosmic ray particle charge identification noting compactness, low power consumption and circuit design 23 p4009 A67-41479

Origin of heavy nuclei abundance in low energy primary cosmic ray flux, discussing association with quasi-stellar objects 24 p4209 A67-41874

HEAVY ELEMENT

Absolute age of earth, heavy elements and meteorites determined by radioactive decay measurements, comparing present and initial ratios of uranium 235 and 238 02 p0329 A67-12496

Heavy metal derivative solid lubricants, properties and application [ASLE PAPER 66AM 2B3] 04 p0627 A67-14707

Tritium production in atmosphere by galactic cosmic rays, by solar flare accelerated particles and accretion from sun 04 p0613 A67-14855

Absolute age of earth, heavy elements and meteorites determined by radioactive decay measurements, comparing present and initial ratios of uranium 235 and 238 10 p1709 A67-23364

Information on early history of solar system material obtained for neutron buildup processes of heavy element synthesis in stars 15 p2519 A67-29156

Helium origin in universe and heavy element creation 17 p2942 A67-32405

Origin and abundance distribution of heavy elements in stars, discussing theories 17 p2946 A67-32694

S-process theory of heavy element formation in solar system confirmed by measuring neutron capture cross sections 24 p4224 A67-41817

HEAVY ION

Charged colloidal heavy particle propulsion and production of heavy particles 04 p0689 A67-15016

Killing and mutagenic efficiencies of heavy ionizing particles in Arabidopsis thaliana 06 p0953 A67-18379

Mutagenic effects of primary cosmic radiation on bacteria 14 p2254 A67-28213

Ionizing and charge transfer processes following heavy particle collisions in ionized gas analyzed using spectroscopic technique 19 p3264 A67-35069

Radiobiological risk of SST flights from heavy ions of cosmic radiation, discussing methods of radiation detection 23 p3945 A67-41074

HEAVY NUCLEUS

Biological effect of heavy particles, noting role of linear energy transfer and irreversible direct type effect 04 p0562 A67-14634

Energy spectrum of cosmic ray heavy nuclei, using stack of nuclear emulsions exposed during Quiet Sun on balloon flight 04 p0692 A67-14960

Low energy heavy nuclei analyzed by slicing emulsion in connection with solar activity studies 06 p1076 A67-17634

Track densities and production rates with increase of heavy cosmic nuclei inside meteorite 09 p1570 A67-22690

Primary cosmic radiation abundance measurements on iron and heavier nuclei, using Cerenkov counter on balloon flights 11 p1856 A67-24504

Preferential acceleration of heavy nuclei on sun compared with ionizing power of primary particles 13 p2195 A67-27341

Ionization loss effect on energy spectra of cosmic ray nuclei undergoing Fermi acceleration 17 p2930 A67-32041

Energy spectrum and composition of primary cosmic rays in high and superhigh energy range of Proton I and II satellites 17 p2935 A67-32246

Unexpected excess of primary cosmic ray helium nuclei flux value in nuclear photographic emulsions 17 p2939 A67-33237

Steady state propagation of cosmic ray nuclei, discussing energy spectrum and path lengths 19 p3317 A67-36099

Cosmic ultrahigh-energy heavy nuclei and fragmentation products producing multiple mesons 20 p3518 A67-37092

Heavy nuclei intensity in primary cosmic rays, long term solar cycle modulation and time lag in various phases 20 p3519 A67-37405

Proton, neutron and alpha particle emission rates for heavy nuclei in elevated temperatures calculated and tabulated 20 p3490 A67-37553

Solar atmosphere absorption of light nuclei generated on sun indicated by satellite observation of heavy nuclei cosmic ray flux and X-ray electron bremsstrahlung 21 p3698 A67-38595

Charge spectrum of very heavy cosmic ray primaries studied from balloon observations in photographic emulsion detector for Texas atmosphere 23 p4050 A67-40676

Heavy and superheavy nuclei energy spectra studied from measurements by Cerenkov counter onboard space stations 23 p4054 A67-41094

Cosmic ray regional variations in intensity and ionization magnitude and duration indicating heavy nucleus and low energy particle influx accompanying solar flares 23 p4055 A67-41100

Heavy nuclei intensity during solar cosmic ray intensity increase accompanying chromospheric flares, proposing magnetic field dynamic dissipation acceleration mechanism for charged particles 23 p4056 A67-41113

Galactic radiation hazard for long term space missions, discussing life shortening effect 23 p3953 A67-41583

Origin of heavy nuclei abundance in low energy primary cosmic ray flux, discussing association with quasi-stellar objects 24 p4209 A67-41874

Energy fraction transfer to neutral pions during interactions with heavy nuclei measured for several energy levels, using ionization calorimeter 24 p4218 A67-42833

HEAVY WATER
S DEUTERIUM OXIDE

HEF
S HIGH ENERGY FUEL /HEF/

HEIGHT
S GEOPOTENTIAL HEIGHT
S PULSE HEIGHT
S SCALE HEIGHT

HEISENBERG THEORY
Coupled Green function equations for Heisenberg ferromagnet approximated via differential equations 07 p1237 A67-20141

Compatibility of some spectral functions with Heisenberg theory in axisymmetric turbulence and in equilibrium range [ONERA-TP-461] 15 p2470 A67-29381

HELICAL ANTENNA
Radiation coupling of helical antenna, noting impedance measurement methods 07 p1158 A67-20294

Balanced helical wire antenna excited by delta function generator, obtaining integral equation for current distribution 09 p1481 A67-22445

Attenuation constant of model helix waveguide determined using approximate method, considering electromagnetic leakage due to wall irregularity 10 p1606 A67-23064

Sheath helix antenna with conducting

core, noting variation of operation characteristics with core size and pitch angle 11 p1760 A67-24277

Axial mode helical antenna radiation and impedance improvement by using tapered feeds and terminations 13 p2076 A67-26514

Helix-conical circularly polarized antenna performance analyzed, noting increased gain and lower sidelobe level 13 p2076 A67-26515

Bifilar complementary loaded helical antenna, determining radiation patterns, near field amplitudes and phase velocities 23 p3979 A67-40834

Equilateral triangular stepped helical aerial observed characteristics including impedance variation, radiation patterns, axial ratio and velocity factor 24 p4128 A67-41970

HELICAL FLOW
Helical flow of conducting fluid between porous cylinders and disk electrodes in radial magnetic field, calculating electric power and efficiency 01 p0120 A67-10183

Magnetic surfaces of straight helical magnetic field in presence of axial current 01 p0122 A67-10344

Reducible helical MHD flows, considering intrinsic formulations of equation for cases where vector products of fluid velocity and magnetic field equal zero 04 p0609 A67-15604

Stabilization of current driven helical waves in weakly ionized plasmas by magnetic wells of finite but small depth 11 p1827 A67-23885

Azimuthal modes of Kadomtsev plasma instability, describing subthreshold response spectra 11 p1829 A67-24001

Physical stabilization mechanism of helical instability of positive column in longitudinal magnetic field due to quasi-linear effects 11 p1831 A67-24012

Magnetic surfaces of straight helical magnetic field in presence of axial current 11 p1843 A67-25017

Nonuniform absorption of gyro-resonant microwave energy by electron gas used to produce helical configuration in magnetoplasmas 13 p2163 A67-26289

High temperature testing and evaluation of graphite helical-screw expanders and compressors for use with inert gas Brayton cycle 15 p2492 A67-29427

Helically symmetric MHD flow of compressible fluid in circular plasma cylinder, considering waves and stability 20 p3492 A67-36132

Radial electron density profile and critical longitudinal magnetic field for helical current convective instability in hollow plasma column via Langmuir probe measurements 22 p3853 A67-40234

Velocity profiles of non-Newtonian fluid /polyisobutylene solution/ in helical flow by flow visualization technique, discussing Poiseuille and viscometric flows 24 p4145 A67-42708

HELICAL INDUCER
Toroidal screw pinch equilibrium and stability in rapidly rising helical magnetic field, discussing experimental setup and results 11 p1827 A67-23888

Helix spurious mode effects on TW amplifier performance analyzed for methods of elimination 22 p3775 A67-40462

HELICAL WINDING
Performance characteristics of helical electromagnetic induction pumps calculated taking into account effect of duct wall and liquid metal layer 16 p2609 A67-31584

HELICOPTER
SA BOLKOW BO-105 HELICOPTER
SA CH-47 HELICOPTER
SA CH-53 HELICOPTER
SA CRANE HELICOPTER
SA MIL MI-10 HELICOPTER
SA MILITARY HELICOPTER
SA RIGID ROTOR HELICOPTER
SA ROTARY WING AIRCRAFT
SA ROTORCRAFT HELICOPTER
SA TANDEM-ROTOR HELICOPTER
SA XH-51 HELICOPTER

Helicopter and VTOL vehicle low air speed measuring techniques and devices including pitot-static tube, hot-wire anemometer, sphere sensor and exotic techniques 01 p0073 A67-11122

Light passenger helicopter similar to Fayre Rotodyne craft and combining principles of autogyro and rotor helicopter 03 p0359 A67-12985

X-ray and gamma ray navigation systems for helicopter formation flying, examining

accuracy and scanning requirements 04 p0653 A67-14605

Helicopter capabilities in solving interurban mass transport problems, particularly cost and time considerations [SAE PAPER 660336] 04 p0552 A67-156112

Proposed system for maintaining helicopters in close-order formation during inclement weather and/or night operations 05 p0839 A67-16531

Noise and loading actions on helicopters, V/STOL aircraft and ground effect machines - Symposium, University of Southampton, August-September 1965 06 p0945 A67-17905

Periodic aerodynamic loading prediction for helicopters and VTOL aircraft 06 p0945 A67-17908

Winged helicopter performance, stability and control with or without auxiliary propulsion 06 p0946 A67-17913

Medium temperature curing general purpose structural adhesive system for use on helicopter 09 p1523 A67-22515

Dust content of air flow created by piston engine Mi-1 and Mi-4 helicopters in landing and takeoff 11 p1744 A67-24530

Rotorcraft technology developments and possible improvements by mid-1970s 11 p1744 A67-24589

Dynamic measurements of heavy landings on experimental helicopter platform and of response to heavy vehicle loads on steel-and-concrete deck flyover 11 p1880 A67-25056

Indications and contraindications for transportation of wounded by helicopter and ambulance 12 p1902 A67-25174

Optimal methods of escape from helicopter, examining rotor avoidance during ejection 14 p2256 A67-27745

Fuel emulsions for helicopters to minimize hazards associated with liquid fuel, discussing composition, stability, corrosion and flow properties 17 p2927 A67-33001

Simplified fire control system for helicopters, noting helmet sight, error source corrections and sighting and tracking convenience 22 p3755 A67-39849

Combat helicopters with reference to Huey/Cobra noting stub wings, armor protection, rotor and weapon systems 23 p3932 A67-40619

VTOL aircraft configurations features and characteristics including helicopter, compound, composite, tilt-wing, lift-fan, lift/cruise and lift engine [SAE PAPER 670686] 24 p4093 A67-41987

Commercial VTOL airline system development through advanced helicopter application noting need for government sponsorship [AIAA PAPER 67-772] 24 p4095 A67-42940

HELICOPTER CONTROL
Flapping motions of helicopters in control axes system 06 p0935 A67-17629

Dynamic analysis of rotor motion of rigid system in hovering state using complex variables 13 p2054 A67-27588

Hover augmentation system /HAS/ design for analog computer helicopter simulation and flight control 17 p2797 A67-32574

Compact air-to-ground laser rangefinder onboard helicopter nose section 23 p3999 A67-41028

HELICOPTER DESIGN
CH-53A military transport helicopter, discussing design constraints, drag, weight and vibration control, power plant selection, reliability, handling qualities, etc 01 p0011 A67-11266

Mi-10 Soviet flying crane, very high four-wheeled landing gear enables it to drive over load and clamp it by hydraulically operated grips 02 p0181 A67-12201

Heligyro configuration in autogyro, helicopter and VTOL aircraft design 03 p0359 A67-12987

Helicopters, Design and Engineering, Book 1, Aerodynamics 04 p0551 A67-15266

Hovercraft and rotorcraft, discussing design, construction, operation and future 06 p0949 A67-18744

Flights tests of XH-51A compound helicopter, discussing rigid rotor concept and results of compound flight research program [AIAA PAPER 67-262] 07 p1130 A67-20075

Mathematical models for use in hybrid computer simulation for design of Integrated Helicopter Avionics System /IHAS/, analyzing operational modes of automatic

- flight control system 08 p1350 A67-20658
/AFCS/
Helicopter design noting speed, maneuverability, handling, carrying capacity and disk loading 11 p1743 A67-23993
Supercritical speed helicopter power transmission shaft for rotor synchronizing, noting viscous damper for controlling shaft vibrations
[ASME PAPER 67-VIBR-20] 11 p1796 A67-24179
Propulsion-lift system interrelationship in compound helicopter and design parameters affects performance vs speed such as disk loading, solidity and tip speed schedule [ASME PAPER 67-GT-18] 11 p1854 A67-24802
Vertebral fractures in pilots from helicopter accidents in dorso-lumbar junction of spinal column 12 p1902 A67-25170
Tip vortex method for helicopter rotor design during vertical descent 14 p2243 A67-28641
Transmission noise control to achieve helicopter cabin noise levels comparable to fixed wing jet aircraft, discussing system phasing of planetary gears [ASME PAPER 67-DE-58] 14 p2328 A67-28883
Book on aircraft design covering turboprop, subsonic turbojet, supersonic and water-based aircraft, missiles, helicopters, etc 15 p2419 A67-29417
Book on design and development of helicopters, Vol. 2 - Vibrations and dynamic stability 16 p2597 A67-31812
Helicopter rotor at high Mach numbers, noting thin blade tips and compressibility effects and tests in wind tunnel [AHS PAPER 102] 16 p2595 A67-31819
Avionics equipment development for Cayuse helicopter, discussing design with respect to weight, size, maintainability and other logistical considerations [AHS PAPER 105] 16 p2680 A67-31822
Electrostatic discharging systems for helicopters, discussing earth field effect and fail-safe concept [AHS PAPER 107] 16 p2610 A67-31824
Empty-weight control in helicopters, with cost estimation of excess weight on helicopters sold to government [AHS PAPER 112] 16 p2783 A67-31828
Hueycobra helicopter design and configuration noting maneuverability range, endurance, crew protection, weapons system, etc [AHS PAPER 113] 16 p2598 A67-31829
Helicopter cargo restraint system program meeting prescribed operational and safety requirements [AHS PAPER 124] 16 p2598 A67-31839
Dynamic stability of low disk loading propeller-rotors as function of various dimensionless parameters characterizing design [AHS PAPER 132] 16 p2777 A67-31846
Shaft power from conventional two-spool turbofan engines for composite aircraft applications [SAE PAPER 670352] 17 p2929 A67-32992
BO 105 light helicopter design and characteristics noting plastic rotor blades, fuselage semimonocoque construction, etc 18 p2985 A67-33642
Rotary wing role in short haul intercity transportation, comparing V/STOL and STOL advantages over fixed wing aircraft, noting need for compound helicopter 21 p3734 A67-38013
Gyrocontrolled rigid rotor system for helicopter high speed performance 21 p3587 A67-38015
AH-56A Cheyenne compound aircraft weapon system and major subsystems, discussing fire control, navigation system and performance characteristics 21 p3588 A67-38133
High speed helicopters and large transport capacity aircraft, discussing combination of rotors with wings and propeller drive, retractable blades and folding rotors 22 p3745 A67-39753
Helicopter landing systems requirements, considering manual instrument approaches with guidance information from ground station including landing environment 23 p4028 A67-41500
HELICOPTER ENGINE
BMW model 6012 gas turbine for helicopter application weighs 50 kg but develops 100 hp 03 p0502 A67-13007
Book on helicopter gas turbine engines 11 p1852 A67-24524
Heat regeneration and high gas temperatures for fuel economy in helicopter gas turbine engines 11 p1852 A67-24525
Control methods for parameters of helicopter gas turbine engines 11 p1853 A67-24527
Peculiarities of helicopter turbine engine with direct rotor drive 11 p1853 A67-24528
Helicopter exhaust-gas expansion and contamination of intake air under unfavorable wind conditions 11 p1853 A67-24529
Requirements for operating characteristics of single and twin gas turbine engines for military helicopters noting system response, deceleration, fuel control, etc 16 p2736 A67-30929
Gas turbine auxiliary power unit design to provide boost to helicopter engine in powered and autorotational flight modes [AHS PAPER 116] 16 p2598 A67-31832
Parametric comparative study of helicopters powered with current-technology engines and advanced non-regenerative and regenerative twin-engine installations [AHS PAPER 119] 16 p2598 A67-31835
HELICOPTER PERFORMANCE
Linear optimal control techniques used as synthesis tool in designing control system for Short Range Station Keeping /SRSK/ task of assault helicopter, noting closed loop dynamics 01 p0111 A67-11201
Dead weight/service load ratio effect on propulsive efficiency and fuel consumption of large helicopters with mechanical, gearless or jet-propulsion drives 03 p0358 A67-12984
Ground resonance of helicopters with zero transverse flexibility analyzed 03 p0360 A67-13393
Helicopter armaments, discussing efficiency and performance of high fire-power chin-mounted turrets 07 p1131 A67-19481
Small helicopter flight test report, discussing testing procedures on 14 models of one-man rotorcraft [AIAA PAPER 67-264] 07 p1129 A67-20041
Steady and dynamic loads on tandem rotor, controls and airframe flight tested with Army helicopter, using automatic data processing 13 p2054 A67-27596
VTOL aircraft with rotor or propeller lift systems for commercial transportation, discussing helicopter role in system development [AIAA PAPER 67-411] 15 p2422 A67-30378
Evaluating, reporting and improving on quality performance of suppliers and subcontractors of helicopter construction firm 15 p2584 A67-30404
Instrument-landing displays evaluated in IFR landing approaches with helicopter, noting flight performance and pilot evaluation of display concepts [AHS PAPER 106] 16 p2680 A67-31823
Composite aircraft performance potential, with helicopter comparison with compound-type aircraft, noting range, speed, weight, productivity, etc 16 p2597 A67-31826
Compound aircraft flying quality improvement methods, noting VTOL characteristic and high speed as compared to pure helicopters [AHS PAPER 111] 16 p2598 A67-31827
Helicopter structural elements safe life through variable-amplitude fatigue tests [AHS PAPER 122] 16 p2777 A67-31837
23 world helicopter records established by YOH-6A helicopter during 10 flights, noting details [AHS PAPER 125] 16 p2598 A67-31840
Optimum use of contingency power rating for increasing permissible operating gross weight in twin-turbine helicopters performing long continuous flights [AHS PAPER 128] 16 p2599 A67-31842
Hydraulic power systems for V/STOL noting self-sufficiency on start-up and auxiliary power source 20 p3366 A67-37552
Gyrocontrolled rigid rotor system for helicopter high speed performance 21 p3587 A67-38015
Helicopter maximum speed increase by generating supplementary forward thrust or additional wings 22 p3744 A67-39540
Lift reduction and increase of helicopter maximum speed by controlling optimum angle of attack of rotor blades over surface of revolution 22 p3744 A67-39548
Helicopter maximum speed increase using rotor with controlled blade oscillation motion, studying flow velocity, distribution and asymmetry elimination 23 p3933 A67-40639
HELICOPTER PROPELLER DRIVE
High speed helicopters and large transport capacity aircraft, discussing combination of rotors with wings and propeller drive, retractable blades and folding rotors 22 p3745 A67-39753
HELICOPTER ROTOR
Design recommendations to offset greater momenta and sensitivity to gust winds of jointless helicopter rotor 03 p0359 A67-12986
Helicopter main rotor blade used as scanning radar antenna 04 p0579 A67-14491
Vortex-rotor disk interaction effect on helicopter rotor performance in forward flight 06 p0945 A67-17907
Lifting rotor-propeller noise prediction for military helicopters and V/STOL aircraft in forward flight 06 p0945 A67-17909
Helicopter blade slap noise as induced by blade passing through tip vortex shed by another blade 06 p0946 A67-17910
Hingeless-rotor structural loads and dynamics research 06 p1099 A67-17911
Periodic aerodynamic loading of helicopter rotor blades approximated by principles of potential flow aerodynamics 06 p0937 A67-17914
Amplitude of limit cycle torsional motion of helicopter blades as function of pitch angle and reduced frequency 06 p0946 A67-17916
Filamentary composite of boron and epoxy applied in design optimization of helicopter blade structure, considering filament orientation and stiffness [AIAA PAPER 67-176] 06 p1102 A67-18322
Helicopter rotor noise prediction and investigation using three-bladed Wessex rotor mounted on whirl tower 08 p1278 A67-20478
Tensile residual stress measurement in area of failure origin in helicopter rotor blade, using laboratory tests and X-ray analysis [SAE PAPER 670154] 09 p1502 A67-21772
Helicopter/rotor blade service life substantiation through tests with rotor excitation panels inducing blade bending moments 10 p1822 A67-23431
Supercritical speed helicopter power transmission shaft for rotor synchronizing, noting viscous damper for controlling shaft vibrations [ASME PAPER 67-VIBR-20] 11 p1796 A67-24179
XH-51A compound research flight test program, discussing adaptation of rigid rotor concept 13 p2052 A67-26421
Rotor downwash angle and tunnel geometry effect on maximum size rotor that can be tested in closed throat wind tunnel 13 p2091 A67-27595
Tip vortex method for helicopter rotor design during vertical descent 14 p2243 A67-28641
Book on aerodynamics of V/STOL aircraft emphasizing use of momentum and finite wing theories, considering deflection of trailing vortex system 14 p2243 A67-28678
Helicopter rotor and pylon stability investigated through motion equation 14 p2246 A67-29048
Vibrations of helicopter rotor in Cardan suspension, dividing problem into three boundary value setups with special conditions at hub 15 p2576 A67-30175
Powered flight rotor instabilities using analysis of second-order flap-lag coupling effects of torsionally rigid blades 16 p2595 A67-30927
Numerical solution for angle-of-attack distribution, downwash and motion of high-speed helicopter rotor 16 p2590 A67-30930
Rotor blade compressibility effects on helicopter performance, describing flight test techniques and data analyses and comparing prediction and test results [AHS PAPER 103] 16 p2595 A67-31820
Aerodynamic loads and aeroelastic divergence characteristics on stopped rotor blades in flight 16 p2595 A67-31821
[AHS PAPER 104]
Radiation pattern changes for helicopter antenna located in rotor blade as result of

flight dynamics
[AHS PAPER 109] 16 p2597 A67-31825
Suppression of oscillatory vertical force transmission from helicopter rotor to driving shaft using higher harmonic pitch angle inputs
[AHS PAPER 129] 16 p2777 A67-31843
Stall flutter instability of helicopter rotor blades analysis based on unsteady aerodynamic data
[AHS PAPER 130] 16 p2777 A67-31844
Dynamic stability of low disk loading propeller-rotors as function of various dimensionless parameters characterizing design
[AHS PAPER 132] 16 p2777 A67-31846
Effect of rotor control feedback loads of two-bladed rotor system on helicopter fuselage vibrations
[AHS PAPER 133] 16 p2777 A67-31847
Circulation control rotor blades of circular or elliptical cross section for helicopters, VTOL and STOL and possible application to aircraft
18 p2987 A67-34707
High lift coefficient production on helicopter rotor blades and application of circulation control by blowing
19 p3170 A67-35519
Aerodynamic characteristics of helicopter main rotor during steep descent, using ring vortices method
20 p3356 A67-36443
Rotor blade airload and dynamic response of large tandem rotor helicopter measured, using computer programs
20 p3536 A67-36462
Nondestructive inspection of composite structures in helicopter rotor blades, discussing structure, loading and quality control capability
22 p3812 A67-39857
Boundary layer control by suction at trailing edge to reduce profile drag of helicopter rotor blades
22 p3742 A67-40133
Large diameter helicopter rotors and V/STOL propellers/axis tilting in vertical plane/ testing system of wind tunnel and aerodynamic torque measuring apparatus
23 p3986 A67-40575
Blade airfoil sections two-dimensional aerodynamic characteristics studied in wind tunnel for aerodynamic optimization calculation of helicopter rotors
23 p3927 A67-40576

HELICOPTER WAKE

Rotor-hovering performance-prediction with test data showing discrepancy increase with wake contraction, blade loading, tip Mach number and blades number
[AHS PAPER 100] 16 p2594 A67-31817

HELICOPTER WING

Helicopter maximum speed increase by generating supplementary forward thrust or additional wings
22 p3744 A67-39540
Combat helicopters with reference to HueyCobra noting stub wings, armor protection, rotor and weapon systems
23 p3932 A67-40619

HELIOCENTRIC ORBIT

Heliocentric earth orbit precursor satellite, noting position outside earth and moon gravitational fields, orbital stability for solar phenomena evaluation,
etc
02 p0335 A67-12410
Feasibility and design study of unguided solar orbital launch vehicle
08 p1404 A67-20493
Tunguska meteorite transfer from heliocentric to geocentric orbit proved impossible by computer calculation
11 p1868 A67-24847
Heliocentric orbits of former Jupiter satellites, relating direct or retrograde satellite to heliocentric semimajor axis as asteroid
17 p2946 A67-32754
Differential coefficients of asteroids Gerda, Flora and Juno in heliocentric coordinate system including Jupiter and Saturn perturbations
20 p3523 A67-36627

HELIOCENTRICITY

Solar wind measurements and small scale structure of interplanetary medium using scintillation technique
13 p2190 A67-26318
Solar particle event of February 1965 observation with Mariner IV and Injun IV showing 70 degrees heliocentric longitudinal distribution in interplanetary space
22 p3872 A67-39811

HELIOGRAPHY

SA SPECTROHELIOGRAPH
Photospheric bridges over sunspots studied by meniscus photoheliograph at Tashkent Astronomical

Observatory 04 p0701 A67-15552
Spoerer and Gleissberg laws for Babcock and Tuominen models of solar activity concerning migration in heliographic latitude of sunspot area and role of solar magnetic field
05 p0897 A67-16809
Rocket photography of sun and spectrum in EUV and soft X-ray
10 p1707 A67-23225
H-alpha and white light cinematograms of September 1963 flare/sunspot group and radio, ionospheric and magnetic field data
10 p1703 A67-23799
Rocket photography of sun and spectrum in EUV and soft X-ray
13 p2200 A67-27334
Solar flare observation with monochromatic heliograph at Mitaka
14 p2384 A67-28095

HELIOMETER

Lunar physical libration constants determined, based on heliometric observations /1877-1915/, including coordinates of crater Mosting
18 p3128 A67-34302
Moon physical libration constants and figure determined, including crater Mosting A coordinates, via heliometric observations with Bessel method
18 p3128 A67-34305
Heliometer replaced by long focus photographic refractor used for moon rotation constant determination
18 p3129 A67-34308
Lunar physical libration constants derived on basis of four series of heliometric observations, studying ellipticity, inertia, mean radius elimination,
etc
18 p3134 A67-34534

HELIOS

S SUN

HELIPORT

Dynamic measurements of heavy landings on experimental helicopter platform and of response to heavy vehicle loads on steel-and-concrete deck flyover
11 p1880 A67-25056
Close coordination of aviation with other transportation facilities, considering airport/heliport planning within city planning, high speed train competition, highways congestion, etc
19 p3347 A67-34969
Elevated vertiport and stolport configurations and design, investigating flight operations, supporting services and legal aspects
[AIAA PAPER 67-891] 24 p4140 A67-43003

HELITRON

S BACKWARD WAVE OSCILLATOR

HELIUM

SA LIQUID HELIUM
Modified adiabatic scattering function applied to positron annihilation in helium
01 p0116 A67-10141
Microwave modulation of helium-neon laser intensity studied as function of temperature and electron density
01 p0088 A67-10260
Differential cross section for excitation of helium electronic states by helium ions
01 p0116 A67-10337
Surveyor throttleable liquid propellant rocket engine for operation on propellants saturated with dissolved liquid gas [AIAA PAPER 66-949] 02 p0304 A67-12283
He I excitation as result of ionization and recombination at chromospheric spicule temperature
02 p0328 A67-12484
Absolute excitation cross sections of helium levels colliding with low energy electrons
02 p0270 A67-12487
Diffusive separation of helium-argon mixtures in underexpanded free jets and normal shock waves studied by electron beam
02 p0234 A67-12543
Intensity and energy distribution of solar plasma determined by mass spectrometers which can separate hydrogen and helium components of plasma stream
02 p0247 A67-12692
Low energy total and momentum-transfer scattering cross sections for electrons on He and Ar compared, using modified effective range formulas
03 p0471 A67-13319
Different-orbitals-for-different-spins wave function for singlet S ground state of He expressed in Shull and Loewdin basis orbitals
03 p0473 A67-13522
Coupling of pulse powers in TEM of up to 80 mw from He-Ne laser at 6328 angstroms
03 p0437 A67-13678
Primordial He 3 and 4 and deuterium abundances in early stages of universal

expansion show dependence on time scale
03 p0515 A67-14322
Construction methods of DC operated He/Ne laser tubes using optical contact bonds
04 p0631 A67-14763
Magnetically tunable IR masers of helium-xenon, considering experimental problem in applying tunable IR maser to IR spectroscopy
04 p0632 A67-14764
Hypersonic behavior of helium flow past highly blunt bodies, noting drag and shape of shock wave
04 p0546 A67-14778
Hypersonic helium flow past blunt cones compared with flow past sharp cones
04 p0546 A67-14781
Laminar tube flow and heat transfer for He gas using Navier-Stokes, energy and continuity equations in finite difference form
04 p0729 A67-15809
Helium isotope formation in cosmic rays during light nuclei fragmentation due to high energy proton interaction
05 p0878 A67-16093
Helium leak detector characteristics and reception specifications
05 p0804 A67-16302
Micropulsation dynamic spectra showing nosed tones instead of usual tones explained by helium ion content increase in outer magnetosphere
05 p0803 A67-17406
Aerodynamic performance characteristics of three entry vehicles designed for maximum L/D ratio of three and two at Mach 19 and Reynolds number 3,200,000 tested in 22-inch Langley helium tunnel [AIAA PAPER 67-138] 06 p0940 A67-18439
Atmospheric composition data from Explorer XVII satellite, obtaining expression for thermal diffusion factor of He
07 p1181 A67-19937
Verbal communication intelligibility in man-rated altitude simulator with nitrogen or helium added to oxygen atmosphere
08 p1287 A67-20484
Temperature variation of thermoconductivity of helium-hydrogen gas mixtures and correlation of thermoconductivity curves with gas chromatograms
08 p1426 A67-20805
Emission occurring when mixing molecular nitrogen with helium ion following charge transfer analyzed spectroscopically
08 p1326 A67-21358
Population inversion of neon levels in He-Ne microwave discharge as affected by pressure and power scattered by unit discharge volume
09 p1512 A67-21924
Stimulated emission in negative luminescence region of He-Ne glow discharge, noting effect of pressure and volt current
09 p1512 A67-21925
Ozone formation in photolysis of oxygen and oxygen-helium mixture as function of pressure and temperature
09 p1457 A67-22025
Evolution of 2.25 M star from main sequence to helium burning phase noting lifetimes, nuclear burning of core, stellar mass fraction and stellar model algorithm
09 p1566 A67-22226
Molecular metastables produced in positive column of helium discharge by electron excitation
09 p1548 A67-22368
Charge exchange cross sections measurements for ion-molecule pairs of hydrogen, argon, krypton, helium and xenon
09 p1535 A67-22381
Abnormal low helium abundance in atmospheres of old halo B star based on weak absorption lines in helium spectra
09 p1568 A67-22438
Effective excitation cross sections of helium singlet levels under proton impacts
10 p1699 A67-22845
He I excitation as result of ionization and recombination at chromospheric spicule temperature
10 p1708 A67-23352
Absolute excitation cross sections of helium levels colliding with low energy electrons
10 p1682 A67-23355
Age and helium content correlations from recent mass determinations of two low mass binary star systems used in stellar evolution theory
11 p1858 A67-23996
Helium ion effects in micropulsation spectrograms of outer magnetosphere
13 p2108 A67-26326
Energy dependence of effective total cross sections of elastic scattering involving H and He atoms and H molecules
13 p2159 A67-26384
Surveyor throttleable liquid propellant rocket engine for operation on propellants

saturated with dissolved liquid gas [AIAA PAPER 66-949] 13 p2188 A67-26834
Comparison of effect of various diluent gases in evoking flyer bends in simulated orbital flights 13 p2062 A67-26916
Thermal accommodation coefficient of nitrogen and helium on nitrogen covered tungsten above room temperature 13 p2223 A67-26944
Emission intensity and spatial distribution of fluorescence measured for transitions in He, noting resonance radiation absorption effect on 5016 angstrom light spread 14 p2317 A67-28196
Population inversion of neon levels in He-Ne microwave discharge as affected by pressure and power scattered by unit discharge volume 14 p2330 A67-28253
Atmosphere model for pure helium star including only helium I and II transitions and electron scattering in calculating opacity 14 p2387 A67-28578
Solar wind modulation of low energy galactic cosmic radiation, estimating primary source spectra, proton and helium fluxes 15 p2550 A67-29614
Temperature and transport properties of helium and argon at high temperatures from ultrasonic determination of sound velocity and sound absorption 15 p2580 A67-29882
Lateral convex curvature and helium surface injection effect on turbulent wall boundary layer characteristics and skin friction 16 p2659 A67-30952
Gland design variation effects in gaseous helium seal performance from O-ring permeation measurements at pressures up to 1000 psi 17 p2801 A67-31992
Helium and neon content and isotopic composition in iron meteorites, noting He 3 deficiency in hexahedrites due to tritium loss 17 p2942 A67-32359
Helium origin in universe and heavy element creation 17 p2942 A67-32405
He abundance in sun suggests He stellar nucleosynthesis was responsible for increase in He abundance in interstellar gas between formation of sun and present time 17 p2947 A67-32763
Surface helium abundance in blue horizontal branch and halo B stars, considering depletion mechanism 17 p2947 A67-32764
Diurnal variations in He twilight emission intensity determined using photoelectric spectrometer 17 p2849 A67-32958
Photographic high atmosphere observations of hydroxyl and helium emission bands, determining solar UV radiation and electron flux 17 p2849 A67-32960
Cross sections for electron capture by protons measured for various energies in nitrogen, argon and helium 17 p2889 A67-33227
He-He ground state and first excited state potentials obtained from differential scattering cross sections 17 p2889 A67-33257
Active medium radial variation in density of neon atoms metastable level as explanation of anomalous laser oscillation 18 p3060 A67-34013
Decomposition of polytetrafluoroethylene in glow discharge studied using helium, helium plus oxygen or oxygen as carrier gas 18 p2998 A67-34369
Diurnal atmospheric density bulge shifts observed by Explorer, showing latitudinal-seasonal variation in helium concentration 19 p3218 A67-35226
Ground state hyperfine splitting of singly charged helium calculations by Zwanziger and Sternheim evaluated by examining error corrections by Fortson et al 20 p3488 A67-36694
Semiempirical electron impact cross sections for He from oscillator strengths, using Born approximation 20 p3489 A67-37416
Electron impact cross sections used to determine helium collision cross sections sets 20 p3489 A67-37417
Relative photon scattering cross sections for He and Ne at Lyman alpha, describing measurement technique 20 p3489 A67-37431
Electric internal heater for heating helium driver gas to high temperature and pressure for shock tunnel experiments 21 p3606 A67-37770
Energy dependence of effective total cross sections of elastic scattering involving H and He atoms and H

molecules 21 p3660 A67-38822
Electron mobility in He, using irreversible quantum statistics theory to obtain momentum dependent relaxation time 22 p3840 A67-39210
Electron affinity of helium measured by analyzing energy of electrons photodetached from negative helium ions beam passing through laser electromagnetic field 22 p3815 A67-39614
German lighter than air technical and economic travel problems of medium speed dirigibles using helium and nuclear power drives 22 p3745 A67-39751
Matrix method to calculate energy eigenvalues and orbital wave functions for various singlet states of helium isoelectronic sequence 22 p3841 A67-40202
Near IR laser transitions in pure helium studied with scanning Fabry-Perot interferometer, determining fine structure components in upper laser levels 22 p3817 A67-40488
Metabolic depression in animals exposed to air after living in helium-oxygen environment, suggesting denitrogenation period effect 23 p3944 A67-40823
Helium isotope formation in cosmic rays during light nuclei fragmentation due to high energy proton interaction 24 p4213 A67-42769
Fast He nuclei from photoemulsion nuclear splitting induced by proton and antiproton bombardment 24 p4193 A67-42860
HELIUM AFTERGLOW
Ion distributions in helium negative glow assuming diffusion from cathode, conversion to molecular ions and recombination 03 p0473 A67-13523
Helium mono and divalent ion electron recombination coefficient determined as function of electron density and temperature 04 p0672 A67-15774
Microwave and optical measurements of decay of neutral metastable and charged species in flowing He afterglow 08 p1356 A67-21300
Decay kinetics of He plasma, examining pair collision, metastable atom diffusion coefficient and afterglow mechanism via spectroscopy 09 p1544 A67-21918
Electron and ion emissions from hydrogen and helium UV glows in nighttime ionosphere 10 p1633 A67-23049
Cyclotron echo formation in rare gas and nitrogen afterglow plasma in presence of inhomogeneous magnetic field, stressing velocity-dependent collision frequency case 14 p2356 A67-28150
Decay kinetics of He plasma, examining pair collision, metastable atom diffusion coefficient and afterglow mechanism via spectroscopy 14 p2358 A67-28247
Helium afterglow observation at high latitudes, determining He line intensity on IR spectrograph and giving time-dependent seasonal variations 17 p2849 A67-32959
Electron density decay curves in helium afterglows at high electron densities and gas pressure found controlled by recombination loss process 19 p3270 A67-35071
Electron temperature spatial variation in late He afterglow due to standing wave microwave heating 22 p3844 A67-39353
Langmuir probes investigated by comparing measurements in ionized He afterglow by cylindrical double probes and by gated microwave radiometer and resonant cavity 24 p4197 A67-42261
HELIUM ATOM
Energy dependence of isotopic composition of primary helium nuclei, considering ionization loss, fragmentation and solar modulation 03 p0505 A67-12956
Nonrelativistic energies of several states of two-electron atoms by Rayleigh-Ritz expansions in independent variables chosen as natural coordinates 04 p0661 A67-15512
Asymmetrical angular elastic scattering distribution of electrons on helium atoms, using Monte Carlo method 06 p1034 A67-17648
Angular correlation in helium atom with electron-electron interaction 13 p2161 A67-27182
Failure of conventional adiabatic criterion in case of excitation of helium atoms by helium ions 15 p2519 A67-29330
Analytic power series solution of nonrelativistic Schroedinger equation for two-electron atom, assuming fixed nucleus

and singlet and triplet S states 15 p2520 A67-30158
Rapidly converging analytic solution by integral series of nonrelativistic Schroedinger equation for He atom 15 p2520 A67-30159
Close-coupling calculations of positions and widths of lowest-lying autoionizing D states in helium 16 p2704 A67-31167
Photoelectron energy measurement and Franck-Condon factors for vibrational transitions of molecular ions when ejected by He resonance line 17 p2888 A67-32356
Metastable helium atom altitude distribution and 10830 angstrom radiation emission rate, discussing possible explanation of helium loss from atmosphere 20 p3427 A67-36310
HELIUM FILM
Film cooling by helium secondary flow injection into incompressible low speed airflow in turbulent boundary layer above flat plate 06 p1116 A67-18385
Energy dissipation and motion equations of superfluid helium flow through pores, describing technique to detect critical velocity in wide channels 22 p3839 A67-40550
HELIUM PLASMA
Elementary processes in DC gas discharge plasma in helium, comparing measurements of population levels of excited states of atoms with calculated values 01 p0123 A67-10363
Oscillations observed from acoustical helium plasma wave in cylindrical hollow cathode attributed to radial shock wave initiated by energy pulse 02 p0273 A67-11899
Rippling mode instabilities in positive helium discharge column at critical longitudinal magnetic field intensity 02 p0277 A67-12615
Mean electron concentration in SHF helium discharge determined as function of discharge power and pressure 02 p0277 A67-12616
Energy relaxation as explanation of changes in electron density and temperature of helium plasma in upper hybrid resonant heating 03 p0477 A67-13360
High resolution echelle monochromator and use in measuring ion temperature of He plasma 04 p0663 A67-14767
Recombination coefficient measurement for He plasma during decay at high pressure in presence of K vapor admixture 04 p0667 A67-15215
Elementary processes in DC gas discharge plasma in helium, comparing measurements of population levels of excited states of atoms with calculated values 06 p1038 A67-17621
Helium plasma density effect on results of spectroscopic electron temperature determination 07 p1228 A67-19514
Argon, helium and nitrogen high temperature plasma compositions used to calculate radial temperature distribution 07 p1229 A67-19566
Continuous transition from moving stration to helical oscillation in helium discharge plasma due to increase of applied magnetic field 09 p1536 A67-21570
Electrical conductivity measurement of He 3 plasma induced by neutron irradiation 09 p1542 A67-21813
Bohn ionization equation applied to helium plasma to include effect of He 2 energy levels 09 p1544 A67-21883
Recombination processes determined from data of time dependence of spectral line intensities and number density in decay plasmas produced in neon and helium-neon mixtures 09 p1548 A67-22360
Recombination processes in decaying helium plasmas as indicated by time dependence of spectral line intensities and ion number density 09 p1548 A67-22361
Dynamic pressures in helium and argon plasma jets in ambient atmosphere measured with sensitive probes 09 p1549 A67-22554
Pressure rise in ionized He plasma cylinder due to Nernst effect 10 p1686 A67-23777
Rate equations for nonequilibrium excitation of neutral helium in plasmas of moderate density solved and compared with population densities 11 p1844 A67-25075
Ionization rate in helium, argon and xenon plasmas determined by microwave technique 12 p1970 A67-25291
Transients in He-Ne plasma laser

operating at 0.6328
micrometers 13 p2128 A67-27088

Rippling mode instabilities in positive helium discharge column at critical longitudinal magnetic field intensity 13 p2170 A67-27371

Mean electron concentration in SHF helium discharge determined as function of discharge power and pressure 13 p2170 A67-27372

Diffusion by microwave breakdown of weakly ionized helium plasma in metal chamber immersed in magnetic field 14 p2358 A67-28293

Coaxial helium-plasma source with superimposed azimuthal magnetic field, noting plasmoid density increase with magnetic field, plasmoid velocity and experimental setup 15 p2526 A67-29254

Recombination coefficient measurement for He plasma during decay at high pressure in presence of K vapor admixture 15 p2532 A67-30263

Wall radiation, temperature, pressure and electric field strength effects on electric conductivity, electron density and ionization time of nonequilibrium He-Ce plasma 16 p2709 A67-30515

Physical properties of binary pulsed discharge plasma in helium and argon seeded with Cs and K vapor 16 p2711 A67-30525

High temperature loop technology of closed cycle MPD generator, noting transport and reaction mechanisms within high temperature regions 16 p2801 A67-30551

Nonequilibrium plasma properties and generator performance due to magnetically induced ionization in closed loop facility using cesium seeded helium 16 p2802 A67-30557

Optimum Mach number for nonequilibrium helium-cesium plasma flow in MHD generator, explaining effect of deceleration temperature and internal efficiency level on optimum pressure 16 p2804 A67-30570

Quasi-equilibrium number density of excited atoms and electronic transition rate in decaying optically-thick helium and hydrogen plasmas, considering Penning ionization 16 p2715 A67-31168

Two peaks in emission from low pressure helium or neon discharge simulating plasma slab with second peak corresponding to plasma cut-off frequency 17 p2901 A67-32369

Electrode heating of arc burning in moving plasma in vacuum, giving setup, heat emission diagrams, etc 17 p2907 A67-33091

Charge recombination coefficient of decaying He and Ar plasmas with Cs vapor additions at increased pressures 19 p3271 A67-35073

Modified duoplasmatron in cusp fields to produce highly ionized and high density quiescent plasma, using DC discharge, noting helium plasma generation 19 p3274 A67-35104

Weakly ionized plasma and gyromagnetic resonances in helium low pressure HF electrodeless discharge in magnetic field 19 p3276 A67-35113

High pressure helium arc plasma behavior in cylindrical duct explained by theoretical model with different electron and heavy particle temperatures 19 p3280 A67-35145

Faraday effect in microwave region used for electron density determination in argon and helium low pressure plasmas and comparison with cyclotron radiation data 19 p3297 A67-35592

Reflection of incident right and left hand circularly polarized plane electromagnetic waves from anisotropic helium afterglow plasma 20 p3389 A67-37707

Electron temperature and density distributions for helium plasma produced in coaxial accelerator measured spectroscopically, checking thermal equilibrium assumption 21 p3661 A67-37752

Electron-cyclotron harmonic resonances interactions in RFF excited electrodeless helium discharges, discussing magnetic field position measurement and plasma simulation 21 p3662 A67-37757

Electrical and spectral investigation of pulsed high pressure arc produced by capacitor bank discharge in helium and hydrogen 22 p3845 A67-39426

Impedance of dipole antennas in isotropic He plasma measured at X band 23 p3979 A67-40833

Helium RF discharge radiation

temperature as magnetic field function measured, discussing enhanced diffusion role in radiation temperature determination 23 p4032 A67-40897

HELIUM 2

Helium 2 film free convection heat transfer, discussing mathematical analysis for vertical flat plate and horizontal circular cylinder [ASME PAPER 65-WA/HT-10] 03 p0536 A67-14007

Singly ionized He measured for radiative lifetimes of various states using high energy atomic beam 13 p2160 A67-28880

Temperature dependence of sound velocity in liquid helium at saturation vapor pressure and cryogenic temperatures 17 p2886 A67-33231

Foil excitation technique used to measure 2p and 3p levels mean lifetime in He 2 cascading and agreement with theoretical value 22 p3840 A67-39206

He ions beam passing through electric field and inducing light intensity fluctuations when emitted from fine structure levels observed via Stark interference 23 p4029 A67-40956

HELIUM 3

Recoll ranges of products from reactions of Cu-65 with 11-35-mev He-3 ions 03 p0473 A67-13926

Control of water moderated nuclear reactor using neutron absorbing helium 3 gas control elements 04 p0656 A67-15989

Energy spectrum of inelastically scattered alpha particles from alpha particle helium 3 reaction 07 p1226 A67-19563

Helium 3 anomaly in octahedrites and low spallogenic tritium content in freshly fallen iron meteorites caused by tritium loss due to solar heating in space 11 p1886 A67-24694

He 3 nuclei in low energy primary cosmic radiation determined, using stack of nuclear emulsions 12 p1993 A67-25479

Cross section of Helium 3 reaction calculated for possible solar neutrino source 16 p2741 A67-31921

Hyperfine structure of ground state of helium 3 microwave transition radiation from galactic H II regions 19 p3330 A67-36074

He 3 ratio to He nuclei in cosmic rays, determining He nuclei path length in space, considering kinetic energy power spectrum 20 p3518 A67-37088

Very long nuclear spin relaxation times in gaseous He by suppressing He surface interactions measured in highly spin polarized samples 24 p4191 A67-42247

HELIUM 4

Liquid He 4 ground state studied by variation method, deriving radial distribution function 22 p3835 A67-39301

HELLMANN-FEYNMAN THEOREM

Hellmann-Feynman theorem in curvilinear coordinates for exact and for floating variational wave functions 07 p1138 A67-20189

Long range interaction of two H atoms calculated with electrostatic Hellmann-Feynman theorem, determining part of second order molecular wave function 22 p3840 A67-39387

Intermolecular forces theory, considering hydrogen atom interaction through Born-Oppenheimer approximation and variational calculations [WIS-TCI-249] 24 p4191 A67-42666

HELMET

Escape equipment, emphasizing Robertshaw helmet design to provide facial protection and retention of high Q conditions 14 p2256 A67-27744

Crash and ballistic protection flight helmet with greater impact energy dissipating characteristics, noting laminated nylon fabric shell and polystyrene liner 21 p3577 A67-38075

Simplified fire control system for helicopters, noting helmet sight, error source corrections and sighting and tracking convenience 22 p3755 A67-39849

HELMHOLTZ EQUATION

SA WAVE EQUATION

Nonhomogeneous Helmholtz equation for optical gratings with perfectly conducting boundaries solved, using distribution theory 08 p1353 A67-20349

Helmholtz velocity profile instability in atmosphere with unstable density gradient /negative Richardson number/ 08 p1323 A67-21388

Legendre polynomial form of slender body

motion in spherical coordinate systems generalized for axially symmetric harmonic functions in three dimensions with validity for Helmholtz equation 11 p1812 A67-24310

Infinite systems of equations for multiply connected finite regions in shells obtained by extending solutions for stressed state in infinite multiply connected regions 12 p2024 A67-25600

Lie series solution of equations resulting from separation of Helmholtz equation in special coordinate systems 15 p2509 A67-29266

Microscopic interpretation of generalized Helmholtz equation, considering particle in charged gas in adiabatic flow as rotating cylinder model 16 p2720 A67-31245

Book on electromagnetic radiation discontinuities presenting solution of Helmholtz and harmonic Maxwell equations and derivation of discontinuities formulas by generalized functions 16 p2829 A67-31628

Two-dimensional steady flows of viscous fluid in external infinite region on basis of fourth order nonlinear Helmholtz equation in vortex terms 18 p2981 A67-33420

Electromagnetic and pressure fields produced by current distributions in compressible magnetoplasmas determined using perturbation theory 20 p3496 A67-36312

Stress concentration near hole in large radius sphere, solved by approximation method for Helmholtz equations in coordinated system 21 p3716 A67-37906

HELMHOLTZ-KELVIN TIME SCALE

Possible excitation of Kelvin-Helmholtz instability in rotating plasmas 08 p1362 A67-21145

HELMHOLTZ S THEOREM

Energy relation for acoustic propagation modes in hot electron plasma considered in application of Helmholtz theorem 01 p0123 A67-10441

Thermoelasticity theorems for harmonic vibrations of continuum, examining spherical wave propagation 07 p1264 A67-20222

Combined Rayleigh-Taylor and Kelvin-Helmholtz instability for incompressible plasmas carrying uniform magnetic field including Hall current 08 p1359 A67-20902

HEMATITE

Anisotropy of electric resistivity, Seebeck and Hall coefficients and magnetoresistance of n-type single crystal ferric oxide /hematite/ containing tetravalent tin ion as impurity 02 p0299 A67-12085

HEMATOCRIT RATIO

Hematocrit ratio in affecting survival and acclimatization of dogs at high altitude 07 p1135 A67-19862

HEMATOLOGY

SA BLOOD

In-vivo inactivation of factor VII by hydrazine in ether anesthetized rats 07 p1134 A67-19858

Graded dose gamma radiation effect on monkeys, noting change in number of white blood cells and occurrence of gastrointestinal disturbances 10 p1599 A67-23816

Dog experiments, determining microwave radiation effects on physiological response 10 p1600 A67-23824

Hemodynamic modifications produced by orthostatism noting changes in cardiac frequency, arterial pressure and central blood volume produced 16 p2616 A67-30754

Hematologic effects of increased oxygen tension, discussing mechanisms of erythrocyte-oxygen interactions 18 p2991 A67-34710

Distribution of red blood corpuscles studied for complications arising from continued stays at high altitude 23 p3945 A67-41073

High performance aircraft flight effect on blood glucose in fasting subjects noting no hypoglycemia tendency 23 p3950 A67-41550

Hematological criteria of chronic acceleration stress and adaptation 23 p3953 A67-41587

Particle electrophoresis technique for rapid clinical microorganism identification in blood elements, noting applications in serum protein analysis and antigen antibody reaction quantitation 23 p3956 A67-41628

HEMATOPOIETIC SYSTEM

S BLOOD GROUP

HEMATURIA

S URINE

HEMISPHERE

S NORTHERN HEMISPHERE
S SOUTHERN HEMISPHERE
HEMISPHERE CYLINDER BODY

Electromagnetic backscatter from edge scattering centers found on cylinders and flat-backed cones, discussing hemispheric scattering 23 p3973 A67-40839

HEMISPHERICAL SHELL

Vibration tests of hemispherical shell with free edge and constant thickness, exploring dynamic behavior through analytical methods 04 p0714 A67-15425

Torsional problem of hemisphere in spherical coordinates based on Fredholm integral equation of second kind 05 p0919 A67-16584

Multicycling metallic bladders for positive expulsion of cryogenic fluids stored in tanks [AIAA PAPER 67-444] 18 p3054 A67-33921

Hemispherical reflectance of metal surfaces investigated for relation of wavelength and surface roughness 22 p3920 A67-40420

HEMODYNAMIC RESPONSE

Space flight acceleration, vibration and ionizing radiation effects on body functions, oxidizing metabolism of central nervous system and fission processes of hemopoietic tissues 01 p0015 A67-10336

Cumulative effects of venesection and lower body negative pressure on circulation 10 p1599 A67-23813

Nervous reflex mechanisms of hemodynamic shift control during rapidly and slowly increasing acceleration 13 p2058 A67-26757

Prophylaxis for negative effect of hypokinesia on human cardiovascular system 13 p2059 A67-26764

Dynamics of pulse waves of intracranial pressure for transverse overloading accelerations 15 p2430 A67-30229

Human brain hemodynamics during prolonged hypokinesia including orthostatic and bed-rest tests, using rheoencephalographic technique 20 p3368 A67-36266

Human acoustic analyzer functional state studied for hypokinesia effects 20 p3368 A67-36267

Hemodynamic responses of conscious dogs exposed to various centrifugation levels and back angles to determine optimum angle for positioning astronauts 22 p3750 A67-39593

Pulmonary isotopic scanning technique in dog to assess embolism before and after lethal decompression 22 p3751 A67-39602

Radioactive isotopes for aviation and space medicine, treating hemodynamic phenomena, metabolism, cytophysiological investigations and fluids distribution in organism 22 p3756 A67-40547

General and cerebral hemodynamics and functions of central nervous system during positive and negative accelerations 23 p3943 A67-40766

Hypoxia stimulated pulmonary arterial pressure increase in dog and baboon noting hemodynamic effects 23 p3953 A67-41588

HEMOGLOBIN

Monomethylhydrazine effect on methemoglobin production in vitro and in vivo 10 p1599 A67-23812

Toxic metabolic effects of MMH, discussing methemoglobinemia as indicator of exposure dosage in animal study 23 p3955 A67-41802

HEMORRHAGE

Hepatic hemorrhagic lesions produced by 32 and 55 Mev proton radiation in rhesus monkeys 23 p3944 A67-41017

Tissue oxygenation during hemorrhage in dogs at 1 and 3 atm oxygen, noting oxygen at high pressure /OHP/ does not prevent stagnant hypoxia [SAM-TR-66-258] 24 p4111 A67-41802

HERMETIC SEAL

Elastomer application in spacecraft launching, flight and reentry such as binder, sealant, base for adhesives, heat shielding, etc [ONERA-TP-407] 05 p0833 A67-16479

Dynamic instability in undamped bellows face seals operating in cryogenic environment with torsional oscillation and diametrical rocking as primary motion [ASLE PAPER 66AM 2C2] 08 p1336 A67-21039

Self-aligning radial clearance seals, discussing design parameters, balance

leakage and power loss as function of geometry 10 p1659 A67-22707

Hermetically sealed semiconductor device tested for leaks with xenon 133 gas, determining radiation safety measures for personnel 14 p2324 A67-28280

Hermetically sealed ballistic facility design and operating principles, for testing at various Mach and Reynolds numbers to calculate aerodynamic coefficients and flow geometry 16 p2855 A67-31115

Terminology associated with hermetically sealed devices in terms of specification inconsistencies, backfill gas requirements and leak rate considerations 16 p2683 A67-31728

Techniques for achieving contaminant-free sealed package of solid state active devices 19 p3236 A67-35024

Book on vacuum sealing techniques covering permanent seals, demountable seals, current transmission, design, materials, etc 19 p3238 A67-35925

Ceramic-to-metal sealing method based on use of ductile nickel-titanium intermetallic compound as braze 20 p3454 A67-36518

Production process of hermetically sealed electronic package for aerospace use 21 p3595 A67-38340

Thick film design considerations covering material and micropart selection, circuit cost, reliability, substrate size and delivery schedule 21 p3596 A67-38346

Electronic flat-pack processes covering sealing methods, material combinations, leakage determination, etc 21 p3634 A67-38621

Impurity sources in hermetic electronic packaging investigated using mass spectrography and gas chromatography, comparing packaging techniques 21 p3636 A67-38632

HERMITIAN POLYNOMIAL

Stability region of complex linear self-conjugate systems of differential equations containing skew-Hermitian matrix 04 p0647 A67-15980

Order of approximation of continuous functions through Hermite-Feller polynomial along entire axis 07 p1213 A67-19161

Beam equation for elastically supported clamped-clamped beam solved for conditions of initial, boundary and distributed load, using Hermitian operator 08 p1415 A67-20488

Reduction of PDE system of heat transfer, using Hermitian approximating polynomials to obtain solution to initial system 10 p1608 A67-23323

Rodriguez type formula for generalized Laguerre polynomials based upon semigroup property for solutions of heat equation and generating function related to source solution 10 p1675 A67-23630

Dynamic properties of elastic one- and two-dimensional continua using matrix method on digital computer and Hermitian polynomials 13 p2216 A67-26621

Ljapunov direct method applied to Hermite theorem on number of positive real part zeros of complex polynomial and stability theory of linear motions 15 p2458 A67-29899

Function of symmetrical gas-laser resonator analyzed to determine angle of divergence of laser beams generated by various transverse electromagnetic wave modes 19 p3242 A67-36106

Stability criterion derivation involving Markov determinants using second method of Ljapunov 23 p4022 A67-40648

HERTZSPRUNG-RUSSELL DIAGRAM

Plasma neutrino process as accelerating mechanism for evolution in UV dwarfs 08 p1396 A67-21180

Evolution of low mass Population I stars from main sequence to red giant branch in Hertzsprung-Russell diagram, through energy generation phases of p-p chain reactions /dominating over C-N cycle reactions/ and hydrogen burning 09 p1566 A67-22225

Evolution in close binary star system through mass exchange leading to white dwarf with relatively unevolved companion 11 p1864 A67-24581

Nonlinear partial differential equations of stellar evolution theory solved under assumption of spherical symmetry of star 14 p2392 A67-28995

Photometry and spectrophotometry of short-period variable stars 19 p3330 A67-36076

HETERODYNE

SA AUTODYNE
SA OPTICAL HETERODYNE
SA SUPERHETERODYNE RECEIVER

Internal modulation and heterodyning in construction of highly linear large-deviation VHF solid state FM oscillator /FMO/ 03 p0381 A67-13636

Two spatial distributions transformed simultaneously with single lens heterodyning Fourier transform of spatial spectra 03 p0423 A67-13904

Large base phase meter design 07 p1186 A67-19587

Frequency stability of He-Ne lasers analyzed by heterodyning two laser resonators 09 p1509 A67-21558

Local oscillators with standardized frequencies in conjunction with central mixer used as wideband noise receiver for increased sensitivity 09 p1481 A67-22480

Doppler frequency-measuring tracking system in which tracking filter or retuned heterodyne is used for definition of signal with unknown frequency 10 p1607 A67-23452

Large base phase meter design 20 p3452 A67-37324

Array antenna directive pattern scanning utilizing difference in phase lead between heterodyne and converted signals at feeder 24 p4130 A67-42234

HETEROGENEITY

Elastic wave propagation in heterogeneous plates, discussing various plate theories, frequency equations, transverse shear deformations, etc 01 p0160 A67-10407

Elastic modulus, Youngs modulus and Poisson ratio for solids containing foreign inclusions imbedded in matrix 03 p0524 A67-13785

Turbulent boundary layer-flat surface interfacial Stefan-Nusselt flow effects on apparent kinetics of heterogeneous chemical reactions in forced convective systems 04 p0567 A67-15681

Macroscopic brittle fracture theory for structural microheterogeneities effect on maximum macrostresses in plates with hyperbolic notches under tensile loads 06 p1100 A67-17950

Propellant characteristics under impaired combustion conditions, noting sufficiency of Chuiko-Margolin stability criteria 12 p2039 A67-26112

Heterogeneous reaction in metal combustion for vapor-phase burning noting collision efficiency 18 p3149 A67-33797

Detonation properties in heterogeneous systems involving mixture of fuel with gaseous oxidant 20 p3551 A67-36815

HEXABORIDE

X-ray study of lanthanum borides to verify existence of homogeneous compounds within large range of variations in composition 11 p1810 A67-23905

HEXAFLUOROBENZENE

Thermodynamic cycle for solar power systems using hexafluorobenzene as working fluid, discussing efficiency and radiator area 07 p1131 A67-19366

HEXAGONAL CELL

Crystallographic structure of hexagonal ferrites of BaO-MeO-ferric oxide system and applications in UHF and microwave regions 02 p0301 A67-12787

Optical energy gap of cubic CdS measured on evaporated mixed cubic-hexagonal layers 06 p1048 A67-17820

Hexagonal diamond content of Canyon Diablo and Goalpara meteorites 08 p1400 A67-21264

Nonlinear analysis of cellular convection induced by surface tension in finite amplitude heated liquid layer, discussing prediction of hexagonal flow pattern 24 p4255 A67-42569

HEXANE

S CYCLOHEXANE
HFB 320 AIRCRAFT
S HAMBURGER HFB 320 AIRCRAFT

HHX HELICOPTER
S CH-53 HELICOPTER

HIGH ALTITUDE

Radioisotope for measurement of electric potential gradient in atmosphere at high altitudes 01 p0088 A67-10870

Eppley-JPL solar constant measurement experiment, noting 12-channel radiometer, filter wavelength limits and high altitude measurements 02 p0328 A67-12396

High altitude high voltage breakdown in

- electric propulsion flight test system 04 p0774 A67-14997
- Recoverable high altitude rocket space probe with paraglider 07 p1259 A67-19573
- Clear air turbulence at high altitudes, showing occurrence where sharp kink in temperature profile exists near core of jet stream 13 p2150 A67-26331
- Earth aerospace thermodynamic properties from 100 to 100,000 km alt predicted, considering diurnal and extreme solar activity variations for engineering applications 13 p2114 A67-26821
- High altitude dipole equivalence of geomagnetic field properties verified by satellite-detected electron belt investigation 14 p2308 A67-27932
- Enzyme activity in erythrocytes when MICORENE is used to prevent death from high altitude hypoxia 14 p2254 A67-28212
- Computational method for high altitude atmosphere density, orbital elements, drag coefficients and potentials from satellite displacement and velocity measurements 15 p2562 A67-30069
- Simultaneous ejection of two vapor trails of different atomic mass, examining turbopause phenomena of atmospheric turbulence 17 p2853 A67-33254
- 70 to 450 km altitude atmospheric brightness at 5300 angstrom measured by rocket noting importance of aerosol component 21 p3623 A67-39043
- ### HIGH ALTITUDE BALLOON PROGRAM
- High altitude balloon-borne polarization measurements relevance in research program of radiation emerging from earth atmosphere 07 p1170 A67-19393
- High altitude balloon top collections of cosmic dust shows evidence of absence of crystal structure in 10 p1708 A67-23239
- Trajectory analysis of EOLE meteorological balloons flights in troposphere over Southern Hemisphere 19 p3332 A67-35276
- ### HIGH ALTITUDE BREATHING
- Cardiac output during rest and work determined via carbon dioxide method at 3800 m altitude 10 p1598 A67-23392
- High altitude effect on work capacity, discussing bicycle ergometer test results on physiological response of human subjects 10 p1598 A67-23393
- ### HIGH ALTITUDE ENVIRONMENT
- Metabolic cerebellum changes under nonlethal hypoxia, noting system compensation during symptomatic stages and destruction of Purkinje cells at critical stages 04 p0561 A67-14629
- Atmospheric mixing time and lifetime of atomic and molecular oxygen at high altitude, noting agreement with barometric distribution law, concentration pattern, etc 07 p1178 A67-19813
- Yellow-green luminosity accompanying injection of triethylborane into upper atmosphere 12 p1932 A67-25208
- Spectrometers, utilizing interference filter wedges, for field use, especially in hostile environments 15 p2491 A67-30430
- High altitude plasma-concentration diagnostics from magnetospheric oscillation spectra 17 p2846 A67-32940
- Environmental Measurements Experiment /EME/ package for applications technology satellites 19 p3226 A67-34788
- Monograph on absorption and laser radiation covering absorption coefficients, high altitude gas concentration, low extinction coefficient measurements, molecular resonance absorption, etc 24 p4168 A67-42412
- Blower compressors for high altitude pressure and climate regulation in commercial aircraft 24 p4109 A67-42709
- ### HIGH ALTITUDE FLYING
- High altitude balloon soundings, noting balloon construction parameters 01 p0010 A67-10934
- Cryogenic pumping capability of liquid helium cooled plate in supersonic flow field at simulated high altitude 04 p0606 A67-14999
- Decompression sickness in high altitude flying, discussing degrees of bends pain among squadron members during five year period [SAM-TR-66-305] 10 p1600 A67-23826
- Airborne camera system for high altitude photography of rocket and spacecraft vehicle launchings describing 16 p2679 A67-31800
- Aerial electronic photomapping and geodetic surveying system describing track-keeping navigation and verticality measuring 16 p2679 A67-31801
- High altitude hypersonic viscous flow degradation of L/D effects on entry vehicle lateral range capability 22 p3742 A67-40114
- ### HIGH ALTITUDE NUCLEAR DETECTION
- #### STUDIES /HANDS/
- Geomagnetic perturbation data from high altitude nuclear weapon detonations, deriving theoretical model based upon MHD resonance, noting Alfvén wave behavior 22 p3792 A67-39932
- ### HIGH ALTITUDE PRESSURE
- Atmospheric density, temperature and pressure profiles obtained in Florida and New Mexico using rockets 12 p1937 A67-25837
- ### HIGH ALTITUDE SOUNDING PROJECTILE /HASP/
- Project High Altitude Research Program /HARP/ directed toward use of guns for scientific probing of upper atmosphere [AIAA PAPER 67-38] 15 p2467 A67-30110
- ### HIGH ALTITUDE TESTING
- Metering and pumping equipment for test channel for high altitude permeability tests of parachute cloth, noting permeability of MIL-C-7350 B, type I 02 p0182 A67-12789
- Dynamic pulmonary work of human males during muscular exertion at 2000 m and different barometric pressures 04 p0561 A67-14631
- Simulated high altitude hypersonic cold wall testing of lifting bodies, measuring lift, drag and static pitching moment 06 p0943 A67-18847
- Radioactivity of Cosmos III satellite after U.S. thermonuclear explosion over Johnston Island 07 p1242 A67-19112
- Instrument testing for 625 A1 research satellite with Nike-Apache BRD-A1 high altitude research rocket 13 p2119 A67-26581
- High altitude parachute systems test techniques for analysis of inflation, stability variations porosity, effects at low dynamic pressure, etc 15 p2419 A67-29433
- Auroral position, motion and brightness measurements from high altitude nuclear tests in 1962 18 p3036 A67-33603
- Optical IR characteristics of long-time afterglow from high altitude nuclear detonations 18 p3036 A67-33605
- Integrated data processing for turbojet and turboprop engines high altitude test facility 20 p3413 A67-36464
- Space and high altitude simulation requirements for testing various rocket engine and propulsion systems 20 p3415 A67-36544
- Distribution of red blood corpuscles studied for complications arising from continued stays at high altitude 23 p3945 A67-41073
- ### HIGH ENERGY ELECTRON
- Time varying energy distribution of high energy electrons producing solar microwave impulsive bursts and X-ray bursts by emission of gyrosynchrotron radiation 01 p0145 A67-11145
- Steady state of earth external radiation belt, considering high energy electrons, kinetic instability, anisotropy, etc 02 p0306 A67-11655
- High energy electron intensity measurement beyond atmosphere with aid of proton I and II satellites, showing capture by geomagnetic field 05 p0878 A67-16091
- Formation mechanism of ionospheric narrow sporadic E layers by high energy electron fluxes captured by geomagnetic field 07 p1179 A67-19835
- Variations in position of mirror points of high energy electrons determined from Cosmos V satellite data 10 p1647 A67-23281
- Cooperative effect among electrons in presence of radial density gradient in cyclotron echo phenomena 11 p1836 A67-24391
- Rare earth metal superconductive shielded magnetic lens for focusing high energy electrons 11 p1802 A67-24765
- High energy particle and electromagnetic space radiation effects on thermal control coating, noting spectral absorptance for various conditions [AIAA PAPER 67-339] 12 p1959 A67-26053
- Electron cascade showers, examining elementary processes, general behavior, three-dimensional theories and large angle single scattering 14 p2379 A67-27961
- Spectrum, intensity, and charge composition of primary cosmic radiation and relevance to origin and propagation of galactic radiation 14 p2379 A67-27963
- Superthermal electron production by quasi-cyclotron acceleration when interacting with monochromatic large amplitude electrostatic plasma wave 15 p2528 A67-29569
- Steady state of earth external radiation belt, considering high energy electrons, kinetic instability, anisotropy, etc 16 p2738 A67-31070
- Specific resistance, EMF, Hall effect, and minority-carrier lifetime measurement of germanium whiskers bombarded by high energy electrons from linear accelerator 16 p2732 A67-31479
- East germany space research in satellite tracking, coupling processes, upper atmosphere, high energy particles, etc 19 p3321 A67-35294
- Silicon transistors transient defect annealing from pulsed particle irradiation, stressing time factors 19 p3305 A67-35667
- High energy electron ionization cross section for hydrogen, noting high quantum number correspondence to classical expression 19 p3266 A67-36090
- High energy proton and electron damage on silicon junctions measured and compared with Van Allen belt radiation damage 20 p3507 A67-36237
- Thermal EMF in semiconductors with electric fields caused by hot carriers, showing energy relaxation of high energy electrons 20 p3513 A67-37451
- Fast electrons formation mechanism during flares ascribed to fast proton deceleration in flare region rather than high energy particle ionization 21 p3699 A67-39013
- Energetic outer radiation belt electron spectra spatial and time variations 22 p3873 A67-39822
- Synchrotron X-ray radiation by high energy electrons in magnetic field with enhancement due to outward propagating hydromagnetic waves proposed as Crab Nebula emission mechanism 23 p4051 A67-40914
- Characteristics of high energy electron radiation and temperature and effect on N/P silicon solar cells 24 p4105 A67-42513
- High energy electron intensity measurement beyond atmosphere with aid of proton I and II satellites, showing capture by geomagnetic field 24 p4213 A67-42767
- ### HIGH ENERGY FUEL /HEF/
- Production, handling and shipping of elemental fluorine, noting materials, health and safety precautions, aerospace applications and toxicity effects 16 p2734 A67-31811
- Book on production of boranes and related research for high energy fuels for air breathing engines 23 p4047 A67-41443
- ### HIGH ENERGY INTERACTION
- High energy interaction of nucleons with complex nuclei described by model of cascade-type nucleon and pion multiplication within nucleus 02 p0312 A67-12604
- High energy cosmic ray interactions analyzed at 3340 m above sea level, using Wilson cloud chambers, gas discharge counters, ionization calorimeter, etc 02 p0248 A67-12746
- Pion energy transmission during inelastic interaction of cosmic particles with Pb nuclei 02 p0315 A67-12756
- Proton-I satellite measurement effective cross section of inelastic interaction of protons with carbon nuclei at extremely high energies 02 p0315 A67-12757
- Ionization calorimeter photoemulsion measurements at mountain altitudes, determining formation mechanism of high energy pions in primary cosmic radiation 02 p0315 A67-12760
- Nucleon interaction generating high energy gamma rays, discussing photon and energy spectra of electron photon cascade, pion generation and gamma quantum detection in atmospheric nuclear interactions 02 p0316 A67-12763
- High energy cosmic ray muons studied, using ionization calorimeter and hodoscope counters 02 p0317 A67-12770
- Interactions of superhigh energy muons in cosmic ray nonelectromagnetic cascade

showers 02 p0317 A67-12771
Positive-to-negative charge ratio of high energy cosmic ray muons 03 p0506 A67-13516
High energy solar cosmic ray spectrum during solar flare of February 23, 1956 07 p1243 A67-19805
Electroexplosive devices, considering safety improvement for exploding and thermal bridgewire initiators 08 p1372 A67-20526
Elastic interaction between dislocation loops and straight dislocations in orthotropic anisotropic materials analyzed for various graphite configurations 08 p1346 A67-20797
Device for studying high energy nuclear active particles of cosmic rays interaction and determination of energy spectrum 12 p1547 A67-26095
Velocity dependence of total scattering cross sections for atom-atom collisions measured in high energy range 13 p2161 A67-27361
Symmetry principles at high energy - Conference, University of Miami, January 1966 14 p2350 A67-27798
Thermodynamical, dynamical, and possible third mechanisms responsible for features in high energy cosmic ray interactions and multiple production of shower secondaries 14 p2379 A67-27962
Nucleon-nucleon collisions, analyzing pair production, electromagnetic cascade, secondary interactions, etc 16 p2703 A67-30965
Proton I and II satellite measurement of effective cross sections of inelastic interactions between billion and trillion ev protons and carbon nuclei 17 p2935 A67-32247
Ionization fluctuations due to interaction between shower particles and absorbing component of ionization calorimeter and effect on accuracy of energy measurement 17 p2855 A67-32250
Cosmic ray nuclei fragmentation without particle production, noting nuclear emulsions and high energy 17 p2936 A67-32363
Cloud-ion chamber stack to measure properties of interactions in light materials of high energy cosmic ray protons and pions 17 p2863 A67-33355
Cosmic ray physics - Conference, Moscow, November 1965 22 p3874 A67-40246
High energy cosmic ray interactions analyzed at 3340 m above sea level, using Wilson cloud chambers, gas discharge counters, ionization calorimeter, etc 22 p3801 A67-40248
Pion energy transmission during inelastic interaction of cosmic particles with Pb nuclei 22 p3876 A67-40258
Proton I satellite measurements of effective cross section of inelastic interaction of protons with carbon nuclei at extremely high energies 22 p3876 A67-40259
Ionization calorimeter photoemulsion measurements at mountain altitudes, determining formation mechanism of high energy pions in primary cosmic radiation 22 p3876 A67-40262
Nucleon interaction generating high energy gamma rays, discussing photon and energy spectra of electron photon cascade, pion generation and gamma quantum detection in atmospheric nuclear interactions 22 p3876 A67-40265
High energy cosmic ray muons investigated, using ionization calorimeter and hodoscope counters 22 p3877 A67-40272
Interactions of superhigh energy muons in cosmic ray nonelectromagnetic cascade showers 22 p3877 A67-40273
Solar neutrino observation, considering inverse nuclear beta decay and elastic scattering by orbital electrons 24 p4210 A67-42583
Photoemulsion data analysis of high energy nuclear interactions in nuclear emulsions exposed to air showers during flights 24 p4192 A67-42827
Shower particles angular distribution investigated using Wilson cloud chamber, obtaining agreement with results by kinematic methods 24 p4217 A67-42828
High energy gamma quanta from high energy cosmic particle interaction with carbon and air nuclei, noting three superhigh energy electron/photon cascades recorded 24 p4218 A67-42835
High energy nucleon interactions with X-ray films and nuclear emulsions aboard aircraft, with diagram of gamma quanta

energy spectra 24 p4218 A67-42836
Characteristic of high energy nucleon-nucleon interaction, analyzing changes due to structural buildup 24 p4192 A67-42839
Isobar decay mechanism for high energy pion generation in cosmic rays propagating through atmosphere 24 p4218 A67-42841
Effective cross section of inelastic interaction between high energy protons and carbon nuclei monitored by Proton I and II 24 p4219 A67-42843
Cross section of inelastic interactions and free path between nuclear active cosmic particles and lead nuclei at high energies 24 p4219 A67-42844
Cosmic particle recording facility at Tskhra-Tskaro, giving data on free path of nuclear active particles in carbon with high energies 24 p4219 A67-42845
Cross section of inelastic interaction between cosmic ray neutrons and carbon nuclei at energies of 100 Gev 24 p4219 A67-42848
High energy nucleon and pi-and K-mesons inelastic interaction cross sections from quasi-linear approximation of optical model 24 p4192 A67-42852
Air shower nuclear active component spectra noting need for mechanism of energy transfer from nucleons into electron-photon avalanches 24 p4220 A67-42862
Extensive air showers accompanying high energy nuclear active particles, discussing nuclear interaction processes and energy transformation 24 p4220 A67-42864
HIGH ENERGY OXIDIZER
S PROPELLANT OXIDIZER
HIGH ENERGY PROPELLANT
Propellant combinations evaluation for minimum weight of high energy propellant reaction control systems [AIAA PAPER 66-947] 02 p0304 A67-12281
Radioisotope heated hydrogen thrusters for propelling high energy upper stage, discussing performance, payload advantages and high energy kick stage [AIAA PAPER 67-509] 18 p3113 A67-33973
Post-Saturn launch vehicle, discussing multipurpose, variable payload boosters, usability, noise levels, etc 20 p3533 A67-36613
Aircraft and missile electric/hydraulic power supplies, describing turboalternator performance, design and applications 24 p4107 A67-42532
Nonairbreathing internal combustion engines injector configurations, noting power supply and lunar surface vehicle applications 24 p4107 A67-42533
HIGH EXPLOSIVE
Emf and electric conductivity in ionized gas produced by detonation of Sakura dynamite to estimate explosion rate 02 p0268 A67-12500
Rapid micro dry combustion determination of carbon, hydrogen and nitrogen in high explosives 05 p0759 A67-17154
HIGH FIELD MAGNET FACILITY
High field type II superconductors, analyzing flux jumps 14 p2373 A67-28916
HIGH FREQUENCY
Man-made HF radio noise level measurement and prediction, discussing spectral and spatial distributions, soil/saltwater conductivity and receiver elevation effects, instrumentation and antennas 01 p0024 A67-10499
HF conducted and radiated RF interference suppression by dielectric and magnetic absorption, pseudoresonant or interfacial loss and artificial skin effect 01 p0024 A67-10500
Resonant cavity field containment of plasma 02 p0273 A67-12178
HF design of DC-DC converters with low weight and high performance for spacecraft power systems 02 p0183 A67-12181
HF conductivity, dispersion and temperature modulation of carrier waves and acoustic amplification in drifted semiconductor plasmas 03 p0496 A67-13558
Crack propagation in heat-affected zone during HF AC current gas-tungsten arc welding of Al alloy test plate 03 p0430 A67-13693
Spectral analysis of HF oscillations with phase modulated fluctuation as functions of phase dispersion and spectral form of modulating fluctuations 03 p0393 A67-13950
Mean energy and energy dissipation of hydrogen ions ejected from HF source 03 p0424 A67-14261

Electrical noises of plasma of steady state HF discharge in magnetic field discussed from standpoint of universal plasma instability 04 p0671 A67-15640
Spectrum broadening of long-duration HF pulses by FM 04 p0577 A67-15675
Radio Aurora and formation mechanism of ionospheric D and F regions, examining HF and VLF propagation via computer ray tracing, ionospheric storms and equatorial sporadic E layers 05 p0795 A67-16010
Harmonic components of current of HF transistor under sinusoidal excitation, using piecewise parabolic approximation 05 p0772 A67-16456
Electron beam excitation as possible explanation of relation between enhanced diffusion and HF oscillation in plasma 05 p0854 A67-16896
HF measurements of thin film CdSe transistors, discussing equivalent circuit, stability factor and power gain 05 p0776 A67-17091
Circuits consisting of HF oscillator, kenotron heater, rectifier, etc, for low power HF voltage generator 05 p0780 A67-17499
Lightweight vertical multiwire antennas for HF range, describing construction and performance 06 p0973 A67-19050
Antennas for HF radio communications integrated with shipboard structures 08 p1301 A67-20772
HF plasma devices structural design, electrical parameters and power characteristics 09 p1547 A67-22322
Semiconductor conductivity in strong SHF electric fields, measuring dielectric constant and Fourier component 10 p1657 A67-23567
Short term and averaged characteristics of nonreciprocal HF ionospheric single and multihop propagation paths 11 p1762 A67-24286
Optimization of injection location in HF plasma accelerators 13 p2165 A67-26586
Electron density and HF spectrum of beam generated plasma as function of gas pressure and injection parameter 14 p2352 A67-27749
Increase in mean electron energy shown to be factor leading to plasma stratification 14 p2353 A67-27756
Radio measurements and standards for power, conductance, impedance and attenuation in upper frequency range 14 p2263 A67-28390
Variable data rate modem for digital signal transmission on HF radio circuits 14 p2272 A67-28705
Mean energy and energy dissipation of hydrogen ions ejected from HF source 14 p2321 A67-28773
F scatter, flutter fading and maximum usable frequency phenomenology from HF radio propagation studies near equator 15 p2438 A67-30297
Nonlinear effects in collisionless plasma during interaction with strong HF field 17 p2905 A67-32920
Energy loss factors for slow electrons in hot gases determined by measuring electron temperature variation with HF electric field power 17 p2890 A67-33367
Mean flow refraction and temperature differences between mixing layer and outside fluid effect on HF component of jet noise 19 p3173 A67-34962
Electrical communications techniques, Part 2, HF techniques 21 p3597 A67-38532
HF fatigue tests in high vacuum environment on recrystallized molybdenum base alloy TZC for elevated temperature fatigue 22 p3822 A67-40058
Modulator-demodulator device using phase shifts between signals in successive time intervals to speed handling of data in HF band 22 p3764 A67-40557
Field scattering by convex cylinders solved by asymptotes expressing reduced wave equations 23 p3972 A67-40751
Dispersion equations for rectangular helix in presence of plasma 24 p4121 A67-42235
Plasma dynamics with HF theta pinch discharges confined in magnetic field 24 p4198 A67-42575
HIGH GRAVITY ENVIRONMENT
Space environment factors effects on living organism including changing gravity, high vacuums and solar radiation 16 p2614 A67-31000

Traumatic sickness in dogs due to high gravity impact noting enzymatic activity changes and immunizing reaction 21 p3575 A67-38509

HIGH LIFT DEVICE

High lift rotor design for jet propulsion VTOL aircraft 03 p0360 A67-13891

Flight experiments to assess stalling behavior and handling problems arising in design, maintenance and operation of suction wing for high lift [AIAA PAPER 65-750] 09 p1441 A67-22483

High lift characteristics of various aircraft configurations in wind tunnel model using different leading and trailing edge lift augmentation devices 23 p3934 A67-41309

Augmentor-Wing research program for developing high lift devices to reduce takeoff/landing speeds of jet aircraft [AIAA PAPER 67-741] 24 p4094 A67-42804

HIGH PASS FILTER

All-pass RC filter network design for constant signal delay in LF systems, noting cascade phase characteristics 01 p0045 A67-11197

System with two nonlinearities separated by high pass filter, obtaining joint describing function 11 p1760 A67-24275

Design for active filters via eight-pin miniature component 14 p2283 A67-28288

LF and HF single stage RC filters with steep frequency characteristic slope in transition region 14 p2289 A67-28863

Ideal SSB modulation theory, discussing DSB Laplace transform formalism, noting Butterworth filters for channel contaminants reduction 19 p3181 A67-34848

HIGH POWER PROJECT

Single frequency, far IR and high power gas laser design and manufacturing 14 p2333 A67-28970

HIGH PRESSURE OXYGEN

Altitude dysbarism treatment with high pressure oxygen, reporting three cases 05 p0756 A67-16291

Mice inoculated with tetanus exposed to high pressure oxygen /OHP/ under immediate and delayed administration 09 p1453 A67-21727

Effects of long term repeated short treatments of mice with hyperbaric oxygen on organ and body weights and hematologic and histologic development 13 p2060 A67-26928

Blood pressure changes and pulmonary edema in rat associated with hyperbaric oxygen 15 p2428 A67-29275

Hematologic effects of increased oxygen tension, discussing mechanisms of erythrocyte-oxygen interactions 18 p2991 A67-34710

Trace contaminant experiment for studying effect of hyperoxic environment at high total pressure on human blood constituents 23 p3960 A67-41703

Tissue oxygenation during hemorrhage in dogs at 1 and 3 atm oxygen, noting oxygen at high pressure /OHP/ does not prevent stagnant hypoxia [SAM-TR-66-258] 24 p4111 A67-41802

HIGH RESOLUTION COVERAGE ANTENNA TECHNIQUE

East-west parabolic reflector array for design of high resolution multielement interferometer for solar noise observations 17 p2864 A67-33402

HIGH SPEED CAMERA

High speed cameras with image converter tubes noting electrical circuits 01 p0067 A67-10774

Optimum frame frequency and virtual exposure coefficient determination for high- and superhigh-speed cameras 01 p0067 A67-10831

Laser light source controlled by Kerr cell coupled with Z-type schlieren optical system to produce multiple flash photographs of detonation wave development 02 p0245 A67-12227

Framing cameras of rotating mirror type, discussing optical principles used in American, British and Russian high speed cameras developed since original NACA camera 03 p0419 A67-13229

Framing cameras of rotating mirror type, discussing optical principles used in American, British and Russian high speed cameras developed since original NACA camera 05 p0806 A67-16699

Frame camera for high speed aerial photography, discussing interlacing with

advances in other areas 05 p0806 A67-16700

Film transport methods and other factors relating to high speed frame cinematography 14 p2315 A67-27871

Sensors and sensor control devices for use in high speed low altitude reconnaissance aircraft 15 p2485 A67-29162

Transposition into holography of optical visualization methods by linking ultrahigh speed camera and solid state laser 15 p2487 A67-29481

High speed spark photography with electronic equipment, describing generating and control units and optical techniques for shock wave observation 16 p2674 A67-31127

Rotating mirror streak cameras, noting development history and future needs 16 p2875 A67-31249

Airborne camera system for high altitude photography of rocket and spacecraft vehicle launchings describing development 16 p2679 A67-31800

Color schlieren and high speed photography technique for transient flows in wind tunnels 20 p3445 A67-36537

Cavitation erosion noting high speed motion picture photographic analysis of kinematic structure of cavitation zone 20 p3420 A67-36631

Flow patterns of two-phase mixtures in cylindrical tubes, using high speed photography 20 p3423 A67-37161

Plasma component velocity distribution and multiple plasmoid production indicated in spectrograms from high speed photography of coaxial injector discharge 21 p3664 A67-37939

Rapid deformation in tubular blank during expansion by pulsed loading studied by high speed motion picture photography 21 p3631 A67-38055

Spray coating particle flow rate dependence on plasma jet flow velocity, specific weight and particle size measured by high speed filming 24 p4159 A67-41961

HIGH SPEED FLYING

Statistical analysis of high speed aircraft piloting, including wing and tail surface effects and pilot work load and performance 04 p0653 A67-14894

Flights tests of XH-51A compound helicopter, discussing rigid rotor concept and results of compound flight research program [AIAA PAPER 67-262] 07 p1130 A67-20075

Long duration random vibration effects on human response in simulated low altitude high speed flights 14 p2257 A67-28660

Flight mechanics of gust absorber for high speed aircraft, discussing transient effects and short response time 21 p3568 A67-38378

High speed helicopters and large transport capacity aircraft, discussing combination of rotors with wings and propeller drive, retractable blades and folding rotors 22 p3745 A67-39753

Advanced high Mach number aircraft secondary power system requirements, discussing high pressure hydraulic systems and complex pneumatic positioning control systems 22 p3749 A67-40341

Civil high speed intercity VTOL aircraft using fan lift engines, discussing noise, installation, aerodynamics and thrust deflection [AIAA PAPER 67-745] 23 p4048 A67-40979

Pilot capability in low level high speed flying analyzed for influence of roughness fatigue, control improvements, vibration and visual problems 23 p3963 A67-41068

HIGH STRENGTH ALLOY

High strength magnesium casting alloys for aerospace applications, based on heat treatment involving internal precipitation of hydride [SAE PAPER 660656] 01 p0094 A67-10615

Strengthening mechanisms in metals and ceramics - Conference, Raquette Lake, N.Y., August 1965 03 p0441 A67-13302

Plastic behavior of simple solids in terms of atomistic processes, emphasizing high strength and ductility 03 p0442 A67-13303

Columbium additions to stainless steel for steam turbine blading 03 p0446 A67-13543

Niobium alloy for elevated temperature strength, considering weldability, liquid metal corrosion resistance and fabricability to form mill products by using zirconium and carbon 09 p1519 A67-22397

High strength alloys for gas turbines in Soviet Union, noting wrought and cast

nickel-base alloys for turbine blades and vanes 10 p1668 A67-23012

Titanium carbide dispersion-strengthened nickel by internal carburization, with fair ductility and stress rupture properties at high temperatures 11 p1806 A67-24361

Titanium-chromium-vanadium system isohardness and isothermal diagrams and characteristic micrographs 11 p1806 A67-24362

High strength nickel base alloy with improved oxidation resistance up to 2200 degrees F for applicability to gas turbine engine components [ASME PAPER 67-GT-1] 11 p1808 A67-24789

Heat resistance in air of dispersion hardened nickel alloys containing certain oxides prepared by powder metallurgy methods 14 p2336 A67-27867

Formation and degradation mechanisms of aluminide coatings on Ni-base superalloys, discussing experimental procedures 16 p2693 A67-31871

Resistance of ideal crystal studied for plastic yielding and brittle cracking, noting composite materials devised to resist both failures 20 p3469 A67-37248

Heavy section forgings of Ti and high tensile strength Ti alloys with thicknesses up to 10 inches 22 p3822 A67-40197

Long term strength limit and fracture propagation of AKN22-16/13 CrNi steel welds and AKN22-16/13 CrNi steel composites welds 23 p4019 A67-41079

Crack propagation related to stress wave emission number and amplitude for high strength steel, Al and Ti alloys 23 p4078 A67-41163

High strength aluminum alloy panel resistance to fatigue crack propagation, discussing axial load fatigue machine 24 p4170 A67-41949

HIGH STRENGTH STEEL

Shape of limiting-state curve for high strength steel predeformed to yield point by repeatedly applying internal load 02 p0255 A67-12667

Moisture effect on slow crack propagation in thin sheets of SAE 4340 steel under static and cyclic loading [ASME PAPER 66-WA/MET-6] 04 p0639 A67-15340

Low cycle fatigue crack propagation characteristics of high strength steels, noting technique for life estimation of structure by numerical integration [ASME PAPER 66-MET-3] 05 p0827 A67-16213

New steels for aerospace tooling, properties and applications 10 p1668 A67-23011

Thermal mechanical treatments influence on strength, toughness and environmental failure resistance of low alloy high strength martensitic steel 11 p1806 A67-24363

Pressure vessel design with ultrahigh strength steels, material strength variations, fracture toughness, minimum defect size and materials melting and fabrication practice [ASME PAPER 67-MET-18] 12 p2031 A67-25954

Theoretical strength with iron-nickel maraging steels 12 p1957 A67-26125

Alloy steels response to dynamic strain aging in quenched, tempered and ausformed conditions, plotting strength and toughness against straining and tempering temperatures 16 p2688 A67-31306

Strength corrosion cracking of high strength steels and titanium alloys in flowing sea water using cantilever loaded test specimen 16 p2690 A67-31385

Effect of thermomechanical treatments on tensile properties of metastable austenitic steels 16 p2693 A67-31872

Crack nucleation in high strength low alloy steel, comparing fatigue processes in quenched and tempered martensite with those in pure metals 18 p3064 A67-34082

Carbide inclusions and distribution effect on fatigue behavior of open hearth and electric-arc furnace steels 20 p3464 A67-36478

Endurance fatigue characteristics of weldable martensitic stainless steel, giving data for butt and spot welds 22 p3811 A67-39447

Gaseous environment influence on fatigue fracture mode in quenched and tempered ultrahigh strength steel investigated by fractographic analysis 22 p3821 A67-40051

Fracture behavior of laminar steel composites studied to determine effect of

interfacial properties on crack propagation 22 p3822 A67-40056
Environmentally induced delayed failure process incubation period of precracked steel from film formation 22 p3822 A67-40060
Co effect on precipitation hardening in high strength stainless steels 23 p4018 A67-40871
Crack propagation related to stress wave emission number and amplitude for high strength steel, Al and Ti alloys 23 p4078 A67-41163
Fatigue crack propagation in ultrahigh strength steels, noting rate sensitivity to moisture and plane strain fracture toughness 24 p4171 A67-41953

HIGH TEMPERATURE AIR

Fluid dynamic sources of radiation during atmospheric entry, considering equilibrium and nonequilibrium radiation, thermal radiation and relaxation processes in hypersonic flow 04 p0703 A67-14703
Atmospheric electrical conductivity of air at high temperatures 04 p0664 A67-14777
High resolution equilibrium radiation spectra for shock layer of blunt bodies at reentry velocities and radiative recombination of N and O ions [AIAA PAPER 66-104] 04 p0546 A67-14816
Thermodynamic properties of real air, deriving expressions for expansion in isothermal-isentropic mode from subcritical temperatures to 1500 degrees K 04 p0738 A67-15914

Impact approximation of spectral line broadening by resonance and Van der Waals forces in air molecule electronic-vibrational systems 05 p0759 A67-16790
Experimental data compared to theory for expansion of high temperature air in equilibrium and nonequilibrium flow through Mach number 10 contoured nozzle [AIAA PAPER 66-2] 05 p0750 A67-17340

Brightness temperature of shock waves dependence on wave amplitude in xenon and air at high temperature 05 p0795 A67-17544
Diffusion and transport equation for turbulent atmosphere with variously heated air masses 06 p0999 A67-18740
Bibliographical research of properties of air at high temperature, noting chemical kinetics and contrasting microscopic and macroscopic approaches 07 p1268 A67-20114

Equilibrium air total radiation mechanism, vacuum UV radiation and relation to hypervelocity entry studied, using shock tube blunt model test flow [AIAA PAPER 66-103] 08 p1426 A67-20569
Radiation from equilibrium air over large temperature and density range 08 p1426 A67-20583

High temperature air plasma total radiant intensity measurements in shock tube [AIAA PAPER 67-311] 12 p2036 A67-26026
Region of air with slight variation in refractive index from surrounding air recorded by holographic technique 15 p2488 A67-29725
Equilibrium radiative transport properties of high temperature air coupled with aerodynamic flow field generated by planetary reentry vehicles 16 p2589 A67-30721

Solid self-lubricating materials mechanically strong and resisting oxidation for high temperature air applications, examining friction-wear characteristics 16 p2683 A67-31752
Black body radiation, pressure and temperature dependences of equilibrium composition, enthalpy, specific heat and electron density of air-carbon plasmas 17 p2894 A67-32147

Nitric oxide production reaction rate measured in shock-heated air at high temperatures, with nitric oxide concentration determined by IR emission 18 p2997 A67-33791

High temperature kinetics of bulk beryllium metal combustion in hydrogen-oxygen-water vapor system, studying flame environments, thermal balance, etc 18 p3151 A67-33809

Absorption coefficient of radiative transfer equation and high temperature air opacity 20 p3485 A67-36930

Nitrogen role in oxidation of titanium in air at elevated temperatures studied by spectrographic analysis 21 p3643 A67-37828

HIGH TEMPERATURE ALLOY

SA REFRACTORY ALLOY

Powder metallurgy - International Conference, New York, June 1965, Volume 2,

Applications 01 p0097 A67-10696
Thermogravimetric analysis and electron microscopy of agglomeration and chemical instability of submicron refractory dispersoids in tungsten 01 p0097 A67-10699
Columbium additions to stainless steel for steam turbine blading 03 p0446 A67-13543
Elevated-temperature tensile testing of thin Rene 41, Hastelloy X and TD Nickel sheet 03 p0446 A67-13553
X-ray and thermal analyses and phase diagram of titanium chromide-tantalum chromide-niobium chromide solid solution at high temperatures 03 p0447 A67-13640
Stress-strain concentration in plates of bilateral cut EI-437B heat resistant alloy and EI-481 austenitic steel under rapid tensile loading at high temperature 03 p0529 A67-14084

Monograph on formation of Ti-based solid solutions and behavior at high temperature under tension 04 p0638 A67-15008
Oxide dispersion hardening of intermetallic NiAl and FeAl compounds for improved high temperature strength 06 p1014 A67-17803

High temperature steady state creep rate analysis of pure Ag and internally ionized Ag-Mg alloys 06 p1014 A67-17805
Newer titanium alloys compared with present production alloys from closed die forgings in typical airframe and engine configuration 06 p1017 A67-17999
Molybdenum and molybdenum alloy stress-rupture characteristics at 2200 degrees C for arc-cast and wrought sintered material 06 p1019 A67-18854

Hardness of heat resistant steels at elevated temperatures as function of alloying and heat treatment 07 p1199 A67-19240

Ce and Pr effect on structure, hardness and mechanical properties of cast steel at 800 degrees C 07 p1199 A67-19242

Ni, Si and Nb effect on oxidation of binary alloys of titanium in air at high temperature, discussing heat resistance 07 p1205 A67-19275

Electrical resistance of manganin coil to 7 kbar and 200 degrees C, use as pressure indicator at elevated temperatures provided correction due to shift of resistance at different temperatures is made 08 p1353 A67-20373

Alloying element selection for heat resistant titanium alloys, obtaining characteristic temperatures and mean quadratic displacement 09 p1518 A67-21968

Heat-resistant casting alloy KhH65VMTi for gas turbine guide vanes, noting structural stability and oxide film 09 p1519 A67-22376

Niobium alloy for elevated temperature strength, considering weldability, liquid metal corrosion resistance and fabricability to form mill products by using zirconium and carbon 09 p1519 A67-22397

High strength alloys for gas turbines in Soviet Union, noting wrought and cast nickel-base alloys for turbine blades and vanes 10 p1668 A67-23012

High strength nickel base alloy with improved oxidation resistance up to 2200 degrees F for applicability to gas turbine engine components [ASME PAPER 67-GT-1] 11 p1808 A67-24789

Nickel-base superalloy technology, stressing structural stability and hot corrosion resistance 12 p1958 A67-26128

Gear materials and lubrication methods to satisfy high speed and temperature requirements in aerospace applications 14 p2334 A67-27791

Tensile creep behavior of thick walled aluminum titanium alloy cylinders under internal pressure at high temperature 14 p2339 A67-29001

Strain hardening of high temperature titanium multiphase solid solution by deformation and subsequent rapid cooling 15 p2504 A67-29971

Heat resistance of Ti alloys, emphasizing significance of chemical interactions, polymorphic transformations and phase diagrams for high temperature performance 15 p2504 A67-30007

High temperature superalloys for gas turbine applications noting alloys based on cobalt, iron, nickel and dispersion hardening 16 p2686 A67-30487

Heat treatment of nickel superalloys for

high temperature applications, showing solution-temperature effect on mechanical properties 17 p2865 A67-33045

Maraging stainless steel for high temperature applications, discussing properties, heat treatment and solution temperature effect 17 p2875 A67-33049

X-ray and thermal analyses and phase diagram of titanium chromide-tantalum chromide-niobium chromide solid solution at high temperatures 17 p2875 A67-33173

Mechanicochemical treatment for high temperature strength increase in metals, noting effects on creep strength, stress relaxation, etc 19 p3247 A67-35852

Brazing alloys and high remelt and conventional techniques developed and evaluated for use in tantalum honeycomb structures 20 p3456 A67-37696

High temperature alloy applications, outlining chemical composition and influencing factors in selection and economic utilization 21 p3650 A67-38533

Physicochemical interactions between components of refractory metals solid solutions, determining metal alloying effects on system structure and high temperature durability 22 p3818 A67-39319

Kinetics of structural changes and failure formation and growth in high temperature alloys undergoing creep 22 p3818 A67-39320

Oxidation process and mechanical properties of austenitic steels and alloys under prolonged loading at high temperatures, giving stress-durability diagrams 22 p3819 A67-39322

Two-stage heat treatment effect on strength of high temperature Nimonic 80 alloy noting high brittleness, grain size and boundaries and fracture propagation 23 p4019 A67-41076

HIGH TEMPERATURE ENVIRONMENT

SA THERMAL ENVIRONMENT

High temperature electrical material evaluation for Rankine cycle [SAE PAPER 660662] 01 p0094 A67-10571

Oxidation resistant thermal protection materials for 4000 degrees F high velocity air environment [SAE PAPER 660659] 01 p0094 A67-10617

Pulsed laser techniques for measuring thermal diffusivity of graphites and chars between 500 and 5000 degrees F [AIAA PAPER 65-644] 03 p0449 A67-13062

Metallurgical and geometrical factors affecting high temperature tensile properties of discontinuous tungsten fiber reinforced composites 03 p0441 A67-13272

High temperature reaction between refractory whiskers of silicon nitride and Al and Ni, observing results by electron microscopy 03 p0445 A67-13528

Emissive capacity of argon in direct current arc at high pressure and temperature, noting experimental setup and results 03 p0478 A67-13602

Long term tensile stress-rupture strength of alloys calculated from static tensile strength tests at elevated temperatures [ASME PAPER 65-MET-12] 05 p0827 A67-16212

Fiber reinforced metal manufacture, discussing possible fiber-matrix combinations and high temperature applications 06 p1047 A67-17713

High temperature condensed phase equilibria in Ti-W-O system examined, using sealed capsule technique 06 p1018 A67-18371

Integral hemispherical and monochromatic radiative capacity of carbon compounds at high temperatures 09 p1497 A67-21877

Relaxation resistance of metals determined from creep test results, comparing calculated and experimental results 11 p1877 A67-24816

Push-pull low endurance fatigue of En 25 and En 32B steels at 20 and 450 degrees C 12 p2015 A67-25422

Element production in early stages of homogeneous expanding universe and within stars, noting nature of background microwave radiation 12 p2010 A67-26239

Empirical correlation formulas for density and viscosity of equilibrium air, noting pressure variation at high enthalpies 15 p2579 A67-29436

References on heat and mass transfer 15 p2580 A67-29780

Kinetics of gas-solid reactions at high temperatures, noting mass transfer coefficients attainable, temperature

discontinuities, stagnation lines, etc 15 p2582 A67-30022

High temperature loop technology of closed cycle MPD generator, noting transport and reaction mechanisms within high temperature regions 16 p2601 A67-30551

X-ray structural and diffraction analysis of Mo-Ni-Bo system at high temperatures noting isothermal sections of phase diagram 16 p2691 A67-31595

Tungsten-carbon phase relations from DTA, X-ray and electron diffraction measurements noting disordered, ordered hexagonal and orthorhombic modifications 16 p2692 A67-31599

SST Concorde hydraulic system noting design and hydraulic fluid selection resulting from high ambient temperatures, weight and space limitations, etc 17 p2800 A67-31971

Errors in high temperature electric-resistance strain gauge measurements 18 p3142 A67-33892

MHD open circuit solution, operating by means of ionized gases, may lead to very high temperature internal combustion heat machines, discussing heat cycles 18 p3115 A67-34120

High temperature operation of air-cooled turbine blades and vanes 18 p3115 A67-34377

Emissive capacity of argon in direct current arc at high pressure and temperature, noting experimental setup and results 18 p3090 A67-34467

Reports on progress in physics, Volume 29, Part I, covering creep in metals and plasma spectroscopy 19 p3263 A67-35853

Proton, neutron and alpha particle emission rates for heavy nuclei in elevated temperatures calculated and tabulated 20 p3490 A67-37553

HIGH TEMPERATURE FLUID

Hydraulic fluid properties and capabilities for high altitude high temperature vehicles [SAE PAPER 660661] 01 p0103 A67-10619

Liquid mercury equation of state and electrical resistivity at high temperatures and pressures 21 p3686 A67-39104

HIGH TEMPERATURE GAS

Uniform flow of very high temperature radiating gas over seminfinit flat plate 04 p0737 A67-15863

Rapid gas compression technique to produce simultaneous values of pressure and temperature much higher than conventional techniques 04 p0611 A67-15946

Plane flow of radiating gas over seminfinit flat plate, considering upstream effect when energy equation becomes elliptical 05 p0928 A67-17358

Mass spectrometric observation of ions formed during shock wave heating of gaseous krypton and xenon at 3600 to 7800 degrees K 05 p0795 A67-17440

First two terms of high temperature equation of state for argon 08 p1355 A67-21255

Evaporation process of particles in high temperature gas stream under nonadiabatic conditions 08 p1428 A67-21424

Microexplosion by optical breakdown of air in focus of laser beam, analyzing volume of concentrated plasma by measuring external magnetic field perturbation 12 p1952 A67-25336

Nozzle thermocouple for low flow rate measurement of high temperature gases, discussing calibration curves and taking into account Reynolds number effect 13 p2121 A67-27464

Temperature and transport properties of helium and argon at high temperatures from ultrasonic determination of sound velocity and sound absorption 15 p2580 A67-29882

Vacuum UV radiation measurement from high temperature nitrogen, detecting radiation from shock layer of ballistic model 16 p2675 A67-31287

Ionization levels and thermodynamic functions of theoretical gas mixtures composed of various highly ionized atom types 16 p2720 A67-31387

Shock wave investigation of recombination in near-stoichiometric hydrogen-oxygen-argon mixtures at high temperatures 18 p2996 A67-33789

Confined electric arc developed for gas-transport properties determination, noting measurement of flow pressure drop, radiative heat transfer, spectral temperature distribution, etc 18 p3091 A67-34731

Pressure transducers for use in high

temperature and pressure gaseous detonation wave phenomena, discussing performance and application 20 p3443 A67-36514

High temperature gas transport property estimation with chemically reacting gas mixture conduction 21 p3613 A67-38391

Chemical bond calculations with high temperature chemistry, discussing hydride molecular energy, dissociation energies and diatomic molecules 21 p3578 A67-38394

Arsenic evaporation from gallium arsenide experiment used to study volatile solid evaporation suppression 21 p3686 A67-39134

Optimum relative angular velocity selected for cooled high temperature gas turbine stages, discussing blade mean cooling depth and cooling heat 22 p3870 A67-40456

High temperature polyatomic gas and gas mixture transport properties, discussing thermoconductivity, multiple intermolecular potentials and plasmas 24 p4256 A67-42742

HIGH TEMPERATURE LUBRICANT

Machinery wear, galling and scuffing reduction by using graphite and molybdenum disulfide as dry film lubricants 14 p2324 A67-27999

Polyimide bonded solid lubricants development 14 p2326 A67-28789

Temperature stable lubrication of supersonic aircraft [ASLE PREPRINT 67AM 7A-1] 14 p2326 A67-28793

Test procedure and apparatus for evaluating oxidation-corrosion characteristics of aircraft gas turbine engine lubricants at high temperature 14 p2326 A67-28794

Polyimide bonded solid lubricants development 19 p3233 A67-34790

Temperature effect on thermostability of high temperature synthetic lubricants for turbojets 24 p4162 A67-42484

High temperature lubricants for ball bearing applications, discussing bearing endurance and rolling-contact fatigue tests on synthetic paraffinic oil [ASME PAPER 67-LUB-21] 24 p4163 A67-42679

HIGH TEMPERATURE MATERIAL

Ultrahigh temperature thermocouple using pure and boron-doped pyrolytic graphite or tungsten and rhenium for operation in vibration and oxidation environment 01 p0076 A67-11139

Dielectric behavior and point imperfections of high temperature KCl in microwave frequency range 02 p0299 A67-11896

Structural design problems of hypersonic air vehicles with air breathing propulsion, discussing relation to future hypersonic commercial air transport 03 p0362 A67-14383

Activation energy of high temperature internal friction for Cu, Al, Fe, Mo, W, Pb, Cd, Ni and Zn 04 p0640 A67-15978

High temperature cobalt iron alloy for square loop and power transformer applications 05 p0864 A67-16833

Hydrogen effect on high temperature plasticity failure and mechanical properties of titanium shown to be similar to that caused by strain hardening 07 p1200 A67-19248

Adhesive systems for substructure bonding to solid ablators and to honeycomb operating in extreme environments 09 p1578 A67-22524

Stabilization of high temperature beryllium allotropes through transition element addition, noting appearance of superconductivity 10 p1688 A67-22890

High temperature thermal expansion of Ti, Zr, Hf, Nb and Ta diborides 10 p1697 A67-23380

Material properties effect on design of reentry vehicle heat shield 10 p1734 A67-23726

High temperature polyimide unidirectionally reinforced with silica fiber, noting precuring process to avoid porosity and strength degradation 11 p1811 A67-24641

High temperature behavior and testing techniques for refractory materials of different groups 12 p1939 A67-25321

Pore formation, lifetime and microstructure of thin electrolytic metal films under load and high temperature at grain boundaries 12 p1955 A67-25448

Wideband-gap high atomic number

semiconductor materials for high temperature counting radiation detectors 12 p1985 A67-25862

Beryllium joints and structures tested for static and repeated loading fatigue at room and high temperatures 13 p2123 A67-27132

Thermophysical properties of high temperature solid materials, Volume 3, Ferrous alloys 13 p2141 A67-27152

Alloys, cermets and ceramics used in bearing applications at 600 to 2000 degrees F, noting significance of oxides 14 p2324 A67-28001

Temperature resistant elements and compounds for use above 3000 degrees F considering melting points, atomic radii and densities 14 p2340 A67-28380

High temperature strength of thermomechanical nickel dependent upon previous thermal and mechanical history, measuring elastic strain energy in matrix 14 p2337 A67-28418

Creep behavior of materials in nuclear reactors, gas turbines and electric power plants, noting aluminum alloy and high temperature material fatigue 15 p2502 A67-29506

Electrical and thermal conductivity and integral degree of blackness of tantalum at temperatures above 1000 degrees C 16 p2692 A67-31771

High temperature oxidation of titanium at reduced oxygen pressures governed by dissolution of oxygen in metal 17 p2873 A67-32812

Silicon and phosphorus role in crack formation in manually welded high temperature resistant steel plate 18 p3063 A67-33673

Filament-metal matrix composites for high temperature range, discussing kinetic phenomena [ASTM PAPER 1] 18 p3066 A67-34567

Maximum entropy principle to derive reliability functions for creep failure modes of engineering materials at high temperatures, noting stress analysis, probability distribution, etc 18 p3145 A67-34675

Soviet book on high temperature nonmetallic thermocouples and sheaths covering thermal control automation of metallurgical processes, thermoelectric and refractory properties, electrodes, electromotive force, etc 19 p3227 A67-34922

Book on coatings of high temperature materials covering properties and characteristics and coated refractory metals 19 p3244 A67-34956

Methods of producing coatings based on metal-like high temperature materials 19 p3244 A67-34957

Ceramic material requirements for MHD generator electrodes and duct walls, discussing tests in alkali-seeded plasma 20 p3472 A67-36114

Tungsten-rhenium thermocouple systems evaluated for high temperature measurement 20 p3443 A67-36515

Plasma arc deposition and gas pressure bonding technique for producing defect-free uniform iridium protective coatings for graphite reentry structures 20 p3465 A67-36607

Gas turbine cooling, discussing high temperature problems, solutions and benefits of air cooled blades and vanes 20 p3517 A67-37168

High temperature resistance fibers - ACS conference, Phoenix, January 1966 21 p3647 A67-37870

Fibers of ordered aromatic copolyamides, performance characteristics and resistance to degradation at high temperature 21 p3647 A67-37873

High temperature properties of aromatic polyimide fibers, noting thermal and dimensional stability 21 p3648 A67-37874

Poly(phenylene/hydrazide) fibers mechanical properties, thermal stability and potential application 21 p3648 A67-37876

Soviet book on high temperature materials for vacuum or inert gas industrial processes 21 p3645 A67-38600

Pore formation, lifetime and microstructure of thin electrolytic metal films under load and high temperature at grain boundaries 21 p3646 A67-38827

Design, performance and development of aircraft wiring cables noting need for high temperature operation 21 p3572 A67-39073

- Aircraft skin friction balance components for hostile environments noting system design 22 p3794 A67-39188
- FAA certification standards for SST engines and components, emphasizing thermal environment testing and high temperature materials 22 p3867 A67-39224
- Book on inspection, construction, operation, maintenance and repair of aircraft and aerospace vehicles including metal, steel frames, wood structures and high temperature structural material 22 p3811 A67-39441
- Electron beam welding of high temperature metals in vacuum 22 p3812 A67-39541
- Bainite beta to alpha transformation in titanium-oxygen system, using high temperature metallography techniques 22 p3821 A67-39825
- High temperature resins and elastomers with high strength covalent bonded backbone for aerospace applications 22 p3825 A67-39852
- High temperature polyimide laminates for radomes and other supersonic aircraft components, discussing index flexural strength, dielectric constant and dissipation factor 22 p3825 A67-39853
- Fiber reinforced plastic components for structural materials noting high temperature polymers 22 p3825 A67-39854
- High performance engineering thermoplastic /Polymer 360/ mechanical and electrical properties and environmental factors effects 22 p3825 A67-39858
- Solar probe mission planning, evaluating high temperature electronics capability and high flux GaAs solar cell efficiency 22 p3903 A67-39956
- Multiple reflective metal foil structure with separating matrix transient thermal response, determining number of radiation shields for given thermal protection 22 p3919 A67-40115
- High temperature materials assessed for properties needed for aerospace applications including metals, alloys, refractory fasteners, aluminide coats, ablative insulation and ceramic compositions 22 p3824 A67-40333
- Slide wire strain gauge to measure static strains and stresses at high temperatures 22 p3809 A67-40476
- Performance of wide variety of exceptional metals studied for corrosion and temperature resistance characteristics in atomic power application 23 p4018 A67-40899
- Barrier system for oxidation resistant protective coating for high temperature protection of refractory coatings 23 p4018 A67-40900
- Thermal protection methods for structures subject to aerodynamic heating, discussing heat dissipation methods and thermophysical materials 23 p4082 A67-41042
- Polymeric materials for extreme temperature emphasizing thermal stability 23 p4021 A67-41228
- Reinforced plastics, evaluating epoxy resin with glass fiber reinforcements for laminates, measuring tensile, compressive and flexural strengths [ASM PAPER C6-21.1] 23 p4022 A67-41403
- Titanium-magnesium and titanium-beryllium oxides physical properties under electron bombardment in vacuum indicate usability for SHF oscillation energy absorbers 24 p4202 A67-42069
- High temperature low cycle creep range strain fatigue behavior estimation from tensile and stress rupture properties 24 p4251 A67-42483
- High temperature Pu 238 heat source fuel capsule operable in space environment is applicable to thermoelectricity and Brayton cycle, discussing design and test program 24 p4185 A67-42536
- Dewrinkling and diffusion mass transport mechanisms in high temperature tensile and shear plastic deformation of pyrolytic carbons [JPL-TR-32-1137] 24 p4177 A67-42711
- HIGH TEMPERATURE PLASMA**
- Free energy of electron gas in compensating field at high temperatures determined from displacements in collective variables, using equation of statistical sum of steady state plasma 01 p0119 A67-10133
- High temperature single solid particle plasma generation by focused giant pulse Q-spoiled ruby laser beam irradiation of LiH suspended in vacuum electric fields 03 p0485 A67-14047
- Argon, helium and nitrogen high temperature plasma compositions used to calculate radial temperature distribution 07 p1229 A67-19566
- Plasma jet applications, emphasizing generation of high temperatures for refractory coatings in form of intermetallic compounds and cermets 09 p1545 A67-22172
- Electron recombination in argon plasma at atmospheric pressure in vicinity of 10,000 degrees K 09 p1550 A67-22584
- Dielectronic recombination effect in hot dilute plasmas extended to energetically overlapping metastable levels involving matrix inversion in formal description 10 p1681 A67-22722
- Spectroscopic methods for measuring plasma temperatures from 1000 to 10,000 degrees K, distinguishing optically thick and thin media 12 p1938 A67-25188
- Velocity space diffusion coefficient of electrons in thermal radiation field, using Hamilton-Jacobi theory 12 p1969 A67-25192
- Relativistic velocity shock wave propagation in stellar high temperature high density plasmas with pair production, thermonuclear reactions and neutrino emissions 14 p2355 A67-27953
- Drift of theta pinch plasma due to asymmetry of magnetic field analyzed, using high speed photography 14 p2357 A67-28233
- Yield variation of excited hydrogen atoms formed by charge exchange with gas target thickness described by analytical model 16 p2714 A67-30874
- Physical/chemical characteristics of thermionic plasma noting equipment and technology involved 16 p2722 A67-31564
- Quantum statistics of high temperature plasma in thermodynamical balance, introducing effective potentials for partition function evaluation and calculating free energy 18 p3089 A67-34300
- Stationary high density high temperature plasma production spectroscopic measurements, deducing arc radial temperature and density profiles from line and continuum intensities and line profiles 19 p3274 A67-35103
- Radial instreaming mass flow effect on cylindrically-symmetric arc with transpiration cooling, noting heat flux reduction 19 p3280 A67-35148
- High temperature plasma generation from dense plasma with moving metallic walls, evaluating electrical conductivity and energy breakdown periods 19 p3282 A67-35159
- Production and behavior of magnetically stabilized high density high temperature plasma, describing experiment 19 p3282 A67-35167
- Thermal conductivity ionization coefficient of cesium plasma at high temperature and low pressure 19 p3287 A67-35359
- Hot plasma corpuscular diagnostics methods, noting particle beam determination of hot plasma density, electron temperature and plasma electric fields 19 p3296 A67-35586
- Monochromator for measuring spectral distribution of laser light scattered by high temperature plasmas 19 p3230 A67-35593
- Density and temperature measurements of high temperature nitrogen plasma jet using schlieren photographic method 19 p3231 A67-35595
- Plasma furnace for treating refractory products at high temperature to determine various oxides solidification temperature 19 p3299 A67-35900
- Dispersion equations and solution for transverse magnetic waves in parallel-plate waveguide partially filled with plasma slab, discussing existing modes 20 p3492 A67-36127
- Plasma microinstability theory, predicting dangerous instability above critical density, discussing applications to very high temperature plasma 20 p3495 A67-36153
- Argon arc plasma generator with film cooled anode for producing stable high temperature gas jet [ASME PAPER 67-HT-72] 20 p3498 A67-36752
- Quantum corrections to Maxwell plasma free energy in compensating electromagnetic field by method of displacements and collective variables for high temperatures 21 p3663 A67-37861
- Soviet monograph on high speed measuring methods in gasdynamics and plasma physics, discussing high temperature plasma and shock wave production 21 p3625 A67-37964
- Laser application to high temperature research, discussing high temperature production using lasers, high temperature plasma and laser-irradiated surface particle emission 21 p3640 A67-38392
- Tenuous high temperature plasma electromagnetic wave scattering, with relativistic corrections for scattered radiation spatial and spectral distribution 22 p3849 A67-39699
- Second virial coefficient contribution to high temperature plasma free energy calculated by means of derived pseudopotential 22 p3851 A67-39785
- High temperature turbulent jet gasdynamic behavior, discussing high temperature plasma jet experiments 23 p3989 A67-40728
- Ar plasma refractive index measured at very high temperatures using gas laser 23 p4032 A67-40961
- HIGH TEMPERATURE RESEARCH**
- Enthalpy measurement for self-binding silicon carbide at high temperatures 03 p0446 A67-13609
- Molecular beam technique for mass spectrometric sampling of high temperature systems at high atmospheric pressure [AIAA PAPER 67-37] 06 p0956 A67-18305
- Tubular support heat shield effects on insulated noncooled thermal protection, noting Dyna-Flex thermoconductivity discrepancy [AIAA PAPER 67-215] 06 p1117 A67-18443
- Spectral emissivity measurements of carbon dioxide band made at high temperatures identifying hot transitions through Q-branches 06 p1118 A67-18539
- Soviet book on high temperature strength of materials noting test stands, stresses, loads, applications to jet and rocket technologies, etc 07 p1208 A67-19299
- Thermal diffusivity and specific heat of molybdenum at high temperatures measured, using variable heating in induction furnace 09 p1517 A67-21866
- High temperature spectral directional hemispherical reflectance of refractory metals and ceramics measured with integrating sphere and He-Ne CW laser source [AIAA PAPER 67-300] 12 p2035 A67-26015
- Polycrystalline beryllium creep at high temperature 13 p2139 A67-27122
- Self-sustaining high temperature and electrically conducting gas layer formation observed in nonsteady interaction of compressible electrically conducting medium with magnetic field 14 p2355 A67-27839
- Partition functions applicability at high temperatures 14 p2405 A67-28131
- Liquidus curves of various metals with mercury at high temperatures, obtaining corrosion rates and data on grain boundaries penetration 15 p2502 A67-29261
- Refractory carbides for high temperature applications, stressing use of metal-impregnated tantalum carbide [ONERA-TP-453] 15 p2502 A67-29378
- High temperature testing and evaluation of graphite helical-screw expanders and compressors for use with inert gas Brayton cycle 15 p2492 A67-29427
- Arc-image furnace for direct gas heating at high temperature by concentrated radiation studies and efficient cavity-type receiver development 17 p2834 A67-32696
- Combustion processes studied by shock tubes, discussing experimental techniques of combustion science, high temperature measurement by spectrum line reversal method, etc 18 p3019 A67-33779
- Atomic oxygen effect on vibrational relaxation of oxygen in shock waves at high temperatures, using laser schlieren technique 18 p3081 A67-33784
- Carbon monoxide and atomic oxygen recombination in expansion wave of single-pulse shock tube at high temperatures 18 p2997 A67-33790
- Enthalpy measurement for self-binding silicon carbide at high temperatures 18 p3066 A67-34474
- Vapor pressure of natural tektite melts at high temperatures determined by boiling point technique, applied to aerodynamic analysis 18 p3134 A67-34495

Steady state technique for measuring high temperature thermal conductivity of nonmetallic materials requiring heat flux and temperature gradient
 calculation 18 p3051 A67-34508
 Ultrasonic thermometry in solids and gases at elevated temperatures 18 p3051 A67-34509
 Short time tensile and long time creep-rupture properties of HF and HH iron-chromium-nickel alloys at high temperatures [ASTM PAPER 52] 18 p3068 A67-34582
 Logarithmic, diffusion and high temperature creep in metals 19 p3248 A67-35854
 Physicochemical and mechanical properties of refractory materials at high temperature - Conference, Paris, June-July 1965 20 p3471 A67-36109
 Temperature effect on mechanical properties of solids with high melting point, with quasi-static hardness as strength measure at high temperatures 20 p3463 A67-36111
 Traction test apparatus for vacuum and high temperature testing of refractory metals, with modifications for rupture and brittleness tests 20 p3463 A67-36112
 Temperature dependence of oxide hardness relative to other materials, comparing oxide hardness data to carbide data 20 p3472 A67-36113
 Refractory metals and compounds vaporization study, using Knudsen effusion method and mass spectrometry for vapor tension and vaporization energy 20 p3463 A67-36116
 Temperature measurement problem in high temperature chemistry and International Practical Temperature Scale 20 p3435 A67-36117
 NERVA engine development, discussing NRX tests and Phoebus reactor tests for high temperature and power operation 20 p3482 A67-36571
 Progress in high temperature physics and chemistry, Volume 1, covering air opacity and state equation 20 p3485 A67-36928
 Equations of state of matter at high pressures and temperatures, discussing temperature density regions, theoretical calculations, etc 20 p3485 A67-36929
 Lifetime of structural sections subjected to creep deformation at high temperatures, showing relation to energy dissipation forces 20 p3540 A67-37058
 Analytical procedures for oxygen, nitrogen and hydrogen determination in high melting metals 20 p3487 A67-37120
 Mass spectrometry of titanium subfluorides at high temperatures, determining sublimation pressures and heat and dissociation energy 20 p3377 A67-37135
 High temperature fuel cells with molten carbonate mixtures as electrolyte analyzed at high temperature 20 p3386 A67-37545
 Electric internal heater for heating helium driver gas to high temperature and pressure for shock tunnel experiments 21 p3606 A67-37770
 High temperature technology - Conference, Pacific Grove, California, September 1967 21 p3578 A67-38390
 Laser application to high temperature research, discussing high temperature production using lasers, high temperature plasma and laser-irradiated surface particle emission 21 p3640 A67-38392
 Chemical bond calculations with high temperature chemistry, discussing hydride molecular energy, dissociation energies and diatomic molecules 21 p3578 A67-38394
 UV absorption of ammonia at high temperatures behind shock waves, discussing NH radical formation from shock tube ammonia decomposition 22 p3756 A67-39442
 HF fatigue tests in high vacuum environment on recrystallized molybdenum base alloy TZC for elevated temperature fatigue 22 p3822 A67-40058
 Niobium carbide enthalpy, heat content and heat capacity variation in homogeneity domain from 1300 to 2500 degrees K 24 p4171 A67-41958

HIGH VACUUM

Spacecraft environmental effects covering outgassing in high vacuum, deterioration of materials by evaporation, lubrication and changes in mechanical and electrical properties of plastics 04 p0704 A67-14995
 High vacuum welding of cermet seals with

titanium 04 p0630 A67-15632
 International Vacuum Congress, Stuttgart, June-July 1965, Volume 2, Part III 09 p1484 A67-22116
 Cathode sputtering thin film preparation at low pressure, describing duoplasmatron and sputron ion sources 10 p1661 A67-23693
 High vacuum enclosure problems solved by use of magnetic seal for joints of large valves and degassing by direct heating of wall surfaces 17 p2802 A67-32300
 Materials of high vacuum technology, Volume 1, Metals and metalloids 20 p3463 A67-36134
 Lubrication and wear in high vacuum, considering inability to maintain oxide films, evaporation of lubricants, heat transfer and sliding friction 21 p3633 A67-38142
 HF fatigue tests in high vacuum environment on recrystallized molybdenum base alloy TZC for elevated temperature fatigue 22 p3822 A67-40058
 Device for metering variety of metals for high vacuum evaporation designed for thin film metal-insulator-metal diodes fabrication 23 p4001 A67-41223
 High vacuum environment and vacuum outgassing time effects on magnesium alloys fatigue properties under constant load and reversed bending 24 p4172 A67-42037
HIGH VACUUM ORBITAL SIMULATOR /HIVOS/
 Vacuum or low pressure contamination removal from space simulation chamber, using bakeout with externally and internally supplied heat 11 p1773 A67-24976
HILBERT SPACE
 Existence and uniqueness theorem of Riccati equation arising in solution of optimal linear regulator problems in Hilbert space 01 p0047 A67-11213
 Approximate solutions for integral equations with Hilbert kernel and degenerate nucleus 02 p0258 A67-11625
 Stationary methods in continuous spectra perturbation theory of nonrelativistic quantum-mechanical scattering in Hilbert space 02 p0288 A67-12726
 Book on numerical realization of variational methods, discussing Hilbert space elements, Ritz and Bubnov-Galerkin stability processes, spectral and nonlinear problems, etc 04 p0645 A67-15009
 First-kind operator equation solution by reduction to dual extremum problem, proving existence and convergence 05 p0834 A67-16375
 Lower bound procedure in quantum mechanical energy equation eigenvalue problem by partitioning and bracketing Hilbert space 05 p0848 A67-16836
 Minimum energy problems in Hilbert function space for continuous and discrete linear systems, noting operator transformation into linear differential equations 07 p1216 A67-19908
 Computational methods for determining lower bounds for eigenvalues of operators in Hilbert space 07 p1217 A67-20018
 Stresses and strains in nonlinear viscous elasticity, examining tensors in abstract form 12 p2018 A67-25444
 Regularity properties in temporal variable of solutions of n-dimensional Navier-Stokes system, using various interpolation methods 13 p2145 A67-26604
 Hilbert space methods in elliptic partial differential equations 14 p2341 A67-27849
 Reproductive property of Navier-Stokes equations, generalizing notion of periodicity 15 p2510 A67-29462
 Fractional powers of operators applied to boundary value problems of quasi-linear elliptic equations 15 p2510 A67-29661
 Hilbert boundary problem extension for flexural problems of cracks in mixed media, noting Cauchy integrals, Plemelj formulae, etc 16 p2770 A67-31292
 Bogoliubov existence theorem for one-dimensional integral manifold and two-dimensional local integral manifold extended to Hilbert space 17 p2879 A67-32879
 German book on differential operators of mathematical physics covering Hilbert space h, Schroedinger spectral theory, etc 20 p3475 A67-36434
 Stresses and strains in nonlinear viscous elasticity, examining tensors in abstract form 21 p3726 A67-38829
 Nonlinear equation solution existence in real Hilbert space with linear and nonlinear

operator 24 p4178 A67-42721
HILBERT TRANSFORM
 Tension of homogeneous anisotropic elastic seminfinite plate with rigid stiffener attached on segment of straight boundary 05 p0910 A67-16150
 Integral operators associated with Poisson transforms and operator H sub alpha 05 p0835 A67-16733
 Soviet book on boundary value problems for analytic functions as applied to integral equations with Cauchy and Hilbert kernels 08 p1347 A67-20760
 Phase objects observation method using spatial filtering and Hilbert transform 20 p3458 A67-36388
 Solution of linear system of equations with singularity and stable with respect to small changes in matrix elements 23 p4023 A67-41048
HILL EQUATION
 Natural families of periodic orbits, using generalized Hill equation 13 p2205 A67-27476
 Equations of Hill plane lunar problem for two rectangular coordinates in rotating system reduced to one differential equation for radius vector 15 p2560 A67-30039
HILL LUNAR THEORY
 Reduction of differential equations of Hill lunar problem using Jacobi integral 08 p1382 A67-20396
 Equations of Hill plane lunar problem for two rectangular coordinates in rotating system reduced to one differential equation for radius vector 15 p2560 A67-30039
 Book on celestial mechanics covering Laplace-Newcombe method, Hill planet and lunar methods and periodic orbits methods using differential equations 23 p4069 A67-41429
HINGE
SA FLAPPING HINGE
 Resonance transition of hinged ponderable rod with nonlinear supports 06 p1109 A67-18666
HINGE MOMENT
 Dither and sinusoidal incidence variations effect on control wing hinge moments of transonic-supersonic rolling maneuvering guided missile [AIAA PAPER 66-755] 17 p2789 A67-32062
 Flapped finite-span wing lift, center-of-pressure and hinge moment moving near solid wall determined as functions of flap length, rotation angle, etc 17 p2792 A67-32902
HINGED ROTOR BLADE
 VTOL and STOL aircraft comparison, discussing advantages and disadvantages of hinged and folding rotors, hinged wings, jet thrust and fan-in-wing principle 17 p2798 A67-32833
HISTOGRAM
 Prefix coding of histograms for minimal storage 14 p2272 A67-28703
HISTOLOGY
 Vestibular section of labyrinth contribution to postrotational changes in level of adrenalin and noradrenalin content in some tissues of white rats 03 p0365 A67-14330
 Acute hyperbaric oxygenation histological effects on pulmonary circulation of rabbits 16 p2614 A67-31473
 Lung changes resulting from prolonged exposure to 100 percent oxygen at 550 mm Hg suggest media erosion and evidence of hypertrophy and hyperplasia 22 p3751 A67-39601
 Histochemical investigation of effect of hypothermia and hypobiosis on activity of oxidizing tissue enzymes of carbohydrate, amino acid, nucleotide and aliphatic metabolism of rats 24 p4112 A67-41853
HISTORY
SA CASE HISTORY
 Techniques for determining cosmic ray age and stable and radioactive nuclide production rates in meteorites 14 p2380 A67-27968
HIVOS
S HIGH VACUUM ORBITAL SIMULATOR /HIVOS/
HL-10 REENTRY VEHICLE
 Joint NASA-USAF lifting body flight test program and M2/F2, HL-10 and SV-5P research vehicles 06 p0947 A67-18197
HO-6 HELICOPTER
S OH-6 HELICOPTER
HODOGRAPH
 Perfect fluid model for observed phenomena of plane transonic flow past

given profile with attached shock wave, starting with lemma on possible hodograph configuration 07 p1128 A67-20282

Newton inverse square force for planets from invariant velocity components of Keplerian planetary motion by graphical model 10 p1711 A67-23791

Graphs for frequency plot of closed loop automatic control system from phase amplitude of open loop and frequency relations between open and closed 10 p1621 A67-23852

Relativistic magnetic hydrodynamics profile streamlining and hodograph transformation 21 p3664 A67-38237

HODOGRAPH METHOD

MGD flows in channels analyzed, using transformation of hodograph for vortical velocity distribution 01 p0119 A67-10172

Tunnel diode circuit stability, equivalent circuit and conductivity 03 p0386 A67-13965

Subsonic drag rise for airfoil determined by limit line analysis in hodograph plane [AIAA PAPER 67-4] 06 p0938 A67-18248

Astrodynamical perturbation theory in which perturbed space-vehicle motion is described in terms of osculating hodograph applied to lunar landing [AIAA PAPER 67-25] 06 p1085 A67-18304

Manual guidance for interplanetary flight by graphical methods, nomographs and relevant general equations 08 p1352 A67-21104

Plane constant pressure contours determined by hodograph mapping used to design lift engine intakes 12 p1891 A67-25213

Hyperbolic region solutions of equation approximating Chaplygin equation near supersonic flow vacuum line in hodograph plane 12 p1962 A67-26181

Hodograph transformation in two-dimensional problems of MHD of viscous flow 13 p2170 A67-27318

Subsonic drag rise for airfoil determined by limit line analysis in hodograph plane [AIAA PAPER 67-4] 13 p2051 A67-27599

Plotting inverse of transfer function, deriving equations for hodograph and for gain values which yield greater or equal damping ratios 15 p2457 A67-29372

Transonic blade cascades determined by mixed analog-numerical method starting from velocity distribution law and hodograph method 16 p2594 A67-31710

Soviet book on high velocity hydrodynamics including airfoil motion at distances from screen, hodograph method in MGD, drag coefficient determination, etc 18 p3021 A67-33409

Strong and weak magnetic field effects on qualitative characteristics of compressible media analyzed using Chaplygin-Sedov hodograph method 18 p3084 A67-33421

Stability range of feedback networks determined with respect to independent circuit parameter using root hodographs 19 p3201 A67-34910

Optimum two-impulse orbital transfer for arbitrary terminal conditions, discussing analytic characteristics 19 p3329 A67-35979

Two-dimensional incompressible fluid jet penetration analyzed kinematically via free streamline theory and notched hodograph 20 p3422 A67-36845

Turbine blade profile calculation by hybrid method 23 p3928 A67-41244

HODOGRAPH THEORY

Hodographic theory of Newtonian mechanics for trajectory hodograph analysis, noting powered trajectories and multiple body problems 08 p1384 A67-20618

HOHMANN ORBITAL TRANSFER

Hohmann-type orbital transfer between two coplanar concentric circular orbits by short duration powered flight with finite constant thrust 16 p2744 A67-30736

Suboptimal Hohmann orbital transfer extension to nonaligned two-impulse elliptical transfer 20 p3526 A67-37253

Economical Hohmann type orbital transfer between coplanar circular orbits with fixed duration and limited thrust 20 p3527 A67-37258

HOHMANN TRAJECTORY

Interplanetary trajectory design, considering energy and duration of mission, arrival velocity at target and earth, use of Hohmann transfer orbit, trajectory maps, etc 08 p1401 A67-21282

HOLDER

SA FLAME HOLDER

Photodiode holder design for ITT FW-114A high speed planar photodiode for monitoring glant pulse laser output 20 p3397 A67-36528

Measurement of rapidly varying temperatures of gas flows with resistance thermometers taking into account heat transfer between heat probe and holders 21 p3630 A67-38914

HOLE DISTRIBUTION

Stressed state in isotropic medium weakened by row of curvilinear holes, considering approximate effect of adjacent holes on concentration of stresses around each hole as loaded 01 p0158 A67-10217

Concentration of stresses around curvilinear holes in thin shells solved with nonlinear law of elasticity, reducing problem by boundary shape perturbation 01 p0158 A67-10218

Steady state elastic oscillations in case of plane deformation for infinite plane weakened by round arbitrarily arranged holes 01 p0159 A67-10224

Electron-hole pair energy in CdS and CdSe single crystals 03 p0490 A67-13155

Electron-hole pair separation energy in CdS single crystal during 5 to 50 kev electron bombardment 03 p0490 A67-13160

Hole-drilling method of measuring residual stresses in elastic materials determined by empirically derived relation between magnitudes of principle stresses and strain relaxation about hole 03 p0531 A67-14360

Stressed state of anisotropic half-plane weakened by finite number of elliptical holes with centers on straight line perpendicular to boundary of half-plane 05 p0907 A67-16018

Classical elasticity theory determination of computational error of fibrous body treated as simply connected multiple hole disks 05 p0907 A67-16037

Current and hole distribution calculated for p-n junction acted upon by sinusoidal voltage of arbitrary amplitude-small injection level 05 p0865 A67-16910

Hole-weakened spherical body represented by deformation of two spherical shells with reinforcing rings under uniform internal load beyond elastic limit 05 p0923 A67-17187

Current-controlled NDR, electron-hole generation and switching to higher current lower voltage state in GaAs 05 p0870 A67-17275

Infinite plate consisting of monopolar semiconductor of given thickness under effect of electric field results in change in galvanomagnetic, piezoresistance and optical properties 08 p1367 A67-20416

Hall effect on hot carriers in p-type Ge semiconductor in microwave field as function of field strength 08 p1369 A67-20993

Electron-hole pair energy in CdS and CdSe single crystals 10 p1690 A67-23103

Electron-hole pair separation energy in CdS single crystal during 5 to 50 kev electron bombardment 10 p1690 A67-23107

Short circuit current measuring technique and results of electron diffusion lengths in diffused p type and holes in uniformly doped n type GaAs 11 p1850 A67-24912

Stressed and strained state of orthotropic cylindrical shell weakened by circular hole 12 p2021 A67-25578

Tensometry method to study stress concentration around circular hole in orthotropic glass-fiber reinforced cylindrical shell 12 p2021 A67-25579

Stress concentration calculated at holes in shallow shells subjected to finite deformation via iteration method 12 p2023 A67-25594

Asymptotic elastoplastic condition of spherical shell weakened by circular hole and sustaining residual deflections 12 p2028 A67-25631

Hole effective masses in p-type CdSb determined by measuring magnetoresistance effect and magnetic susceptibility 12 p1987 A67-26225

Exciton molecule formation in semiconductors in case of large radius exciton, determining dissociation energy and temperature 13 p2173 A67-26363

Carrier distribution function in degenerate p-type germanium in presence of hole scattering on acoustic phonons, considering heating in arbitrary electric and magnetic

fields 13 p2181 A67-27281

Difference leveling between electron and hole concentrations near junction by compensating charges of donors and acceptors with semiconductor space charges 15 p2542 A67-30242

Current and hole distribution calculated for p-n junction acted upon by sinusoidal voltage of arbitrary amplitude-small injection level 16 p2727 A67-30887

Tensile stress of infinite plane weakened by hole or Zhukovskii profile with rounded edges 16 p2765 A67-31053

Stress-strain state determination of nonlinear plate with circular holes, deriving boundary conditions and basic equations 16 p2766 A67-31147

Excitement of slow and fast recombination waves in semiconductors with mutually independent current-carrier concentrations and lifetime 18 p3099 A67-33696

Ground-state splitting in semiconductor double acceptors 18 p3099 A67-33699

Cauchy type integral applied to second boundary value problem for elastic plane with doubly periodic system of identical holes 18 p3145 A67-34601

Hall effect measurements on Te-doped GaAs crystals diffused with Cu₆₄, studying vacancy-donor interactions, hole concentrations and energy levels 18 p3105 A67-34634

Mechanisms involved in damage in metal-insulator-semiconductor /MIS/ devices through exposure to nuclear radiation 19 p3306 A67-35676

Nonequilibrium current carrier lifetime in p-type InSb samples alloyed with Cu and Ge, noting hole concentration and temperature effects 20 p3510 A67-36761

Dynamic response of nondegenerate electron hole plasma in semiconductor, obtaining frequency spectrum and Landau damping rate of plasma oscillation 20 p3499 A67-36945

Stress analysis in theory of circular cylindrical shell weakened by doubly periodic system of identical circular holes 20 p3542 A67-37664

Indium antimonide hole surfaces approximated within second order perturbation theory, discussing energy contours, Baguley cyclotron resonance data and maximum energy value 21 p3679 A67-38255

Exciton molecule formation in semiconductors in case of large radius exciton, determining dissociation energy and temperature 21 p3680 A67-38320

P-n junction devices static behavior assuming Van Roosbroeck differential equations in bulk and transition regions 21 p3598 A67-38571

Stress distribution on boundaries of two unequal circular holes in infinite plate determined by mapping region conformally onto annulus 21 p3730 A67-39086

Anisotropic plate with two elliptical holes studied for stresses under edge load by solving linear algebraic equations infinite system 22 p3910 A67-39452

Frozen stress photoelastic technique used to determine hoop and radial stresses at hole boundaries for different flat disk configurations 23 p4077 A67-41154

HOLE MOBILITY

Electron-hole conductivity effect on temperature variations of Hall coefficient and Nernst-Ettingshausen effect in semiconductor 02 p0296 A67-11829

Optical transitions and k conservation in crystalline solids explained in terms of localization of hole produced by excitation 04 p0674 A67-14526

Hole electron product of p-n junctions, plotting numerical results for electrostatic potential, quasi-Fermi levels and carrier concentration of n-p junction 09 p1553 A67-21946

Diffusion effect on hole mobility in base of semiconductor device with p-n-p-n structure 11 p1765 A67-24480

Photoconductivity kinetics and regeneration recombination noise spectrum of p-InSb crystals, showing association with hole capture, lifetime and alloying impurity 12 p1983 A67-25512

Lifetime for nonequilibrium current carriers in n-type indium antimonide crystals from generation-recombination noise measurements at various

temperatures 12 p1984 A67-25523
Silicon avalanche diode behavior for short duration surge current in reverse direction 13 p2084 A67-27576
Galvanomagnetic properties of single crystal antimony as function of temperature, deriving carrier mobilities and densities, detailing nature of Fermi surface 14 p2364 A67-28105
Ionization threshold energy of electrons and holes in silicon 14 p2368 A67-28535
Hole mobility produced by single pulses of electrons in films of polyvinyl acetate semiconductors with sputtered gold electrodes, determining relation between film conductivity and mobility 15 p2537 A67-29703
Microwave emission from magnetic-field-free electron hole plasma in p-type InSb at 77 degrees K 15 p2539 A67-29820
IR modulator utilizing field-induced free carrier absorption, with expressions for modulation index in terms of geometrical and physical properties of materials 15 p2491 A67-30428
Diffusion, solubility and electrical behavior of lithium in gallium antimonide 16 p2726 A67-30811
Thermal conductivity of group of molten and solid chalcogenides at various temperatures, estimating heat transfer mechanism role 16 p2731 A67-31388
Electrical conductivity and Hall effect of indium arsenide solid solutions, noting temperature dependence and hole mobility 16 p2732 A67-31480
Photoconductivity kinetics and regeneration recombination noise spectrum of p-InSb crystals, showing association with hole capture, lifetime and alloying impurity 18 p3103 A67-34443
Lifetime for nonequilibrium current carriers in n-type indium antimonide crystals from generation-recombination noise measurements at various temperatures 18 p3103 A67-34454
Transverse Nernst-Ettingshausen thermomagnetic effect in intrinsic conductivity region in InSb single crystals subjected to magnetic field 19 p3300 A67-34763
Photomagnetic effect and kinetic photoconductivity in cadmium sulfide single crystals, determining lifetime and mobility of nonequilibrium holes 20 p3504 A67-36158
Superconductor resistive behavior as hole motion in flux lattice under peak effect influence 20 p3505 A67-36209
Carrier concentration dependence of thermoelectric power and Hall mobility of undoped and doped lead telluride explained by two-valence model 22 p3857 A67-39490
Space charge limited (SCL) hole current in Si noting mobility, capacitance, current density, I-V characteristics and double injection 23 p4038 A67-40878
Ionization threshold energy of electrons and holes in silicon 23 p4040 A67-40942
Size effects in platelets of multivalley bipolar semiconductors with long scattering and electron-hole recombination times, studying electric pinch effect 23 p4042 A67-41292
G factor of holes in Ge and Si semiconductors computed in quasi-classical region noting dependence on hole moves relative to magnetic field 23 p4042 A67-41297
Hole mobility produced by single pulses of electrons in films of polyvinyl acetate semiconductors with sputtered gold electrodes, determining relation between film conductivity and mobility 24 p4199 A67-41773

HOLMIUM

Hyperfine structure and modified Zeeman effect in trivalent holmium in hexagonal lanthanum trichloride 12 p1987 A67-26237

HOLOGRAPHY

Holographic techniques for recording and reconstructing three-dimensional objects 01 p0062 A67-10192
Wave front scattering and refraction by laser spark studied by holograms of air plasma formed by giant ruby laser pulse 01 p0087 A67-10234
Holographic resolution as affected by materials, installation vibration, hologram dimension and light source 01 p0063 A67-10355
Noise limitations in obtaining three-dimensional images by holographic

techniques, considering graininess of photographic emulsion 01 p0067 A67-10834
Holography theory and applications, discussing Fresnel and Fourier holographies, interferential information processing, incoherent objects and associative memory 01 p0068 A67-11005
Stroke and Restrict method used in Fourier transform application to spectroscopy and astronomy and in obtaining holograms 01 p0069 A67-11008
Fourier transform holography for diffusion of coherent laser light beam, examining distortion term in reconstructed image 01 p0070 A67-11063
Hologram process for object reflecting or diffusing quasi-monochromatic light, including effects of partial spatial coherence 01 p0070 A67-11079
Holograms with incoherent illumination, noting patterns produced and resolution parameters 01 p0070 A67-11081
Space bandwidth theorem for Fresnel and Fraunhofer holograms, taking into account effects of photographic film 01 p0071 A67-11083
Holographic interference pattern magnification and observation by looking through objective end of microscope 02 p0242 A67-12027
Hologram copying method using gas laser as light source 02 p0246 A67-12513
Interferometric holography in diffused light, obtaining interferogram of phase shifting object 03 p0420 A67-13451
Holograms of objects immersed in water and illuminated by 7-mc sound waves and reconstruction of optical images from sound holograms using laser 03 p0420 A67-13570
Focused image holography with extended sources for real image in proximity of hologram plate 03 p0420 A67-13574
Negative lens property responsible for reconstruction of original scene in full three-dimensional reality 03 p0420 A67-13676
Zone plate free from chromatic aberration and application to three-color holography 03 p0420 A67-13681
Diffraction of plane wave at sinusoidally stratified dielectric grating, using hologram analysis 03 p0423 A67-13905
Tracing rays through hologram treated as generalized case of tracing rays through diffraction grating, determining local diffracting power by geometry and wavelength of beams 03 p0423 A67-13906
Wavefront reconstruction with light of finite coherence length 03 p0424 A67-13911
Hologram copying by laser techniques using original hologram as object for second hologram 03 p0426 A67-14397
Holography using bright field microscopy and examination a posteriori in reconstruction by dark field, phase contrast or interference 04 p0618 A67-14496
Holography, discussing color reproduction, character recognition and vision by sound or ultrasound 04 p0623 A67-15301
Holographic laboratory experiments, discussing Lippman method and imagery through diffusing media contour line implantation 04 p0623 A67-15302
Sonoholograms, techniques and information content 04 p0625 A67-15678
Object-image relationships in scattered laser light 05 p0824 A67-16792
Wavefront reconstruction imaging technique and amplitude and phase recording techniques in hologram preparation 05 p0807 A67-16800
Holography with scatter plate as beam splitter and pulsed ruby laser as light source 05 p0807 A67-16931
White light display of holograms 05 p0808 A67-17320
Holographic study of second harmonic wave emitted by ruby laser, examining influence of defects of spatial coherence of wave 05 p0808 A67-17322
Image formation in holograms 05 p0809 A67-17530
Optical information transformation using incoherent and coherent light 06 p0999 A67-17570
Bibliography on lasers covering modes, scattering mechanisms, quantum electrodynamics, matter-radiation interaction, plasma, holography and optics 06 p1010 A67-17890

Fresnel-Kirchhoff diffraction theory interpretation of plane and three-dimensional hologram 06 p1003 A67-18105
Model predicting effects of finite hologram emulsion resolving power on field range recorded in hologram and resolution in reconstructed image 06 p1004 A67-18543
Laser spark holography with time resolution 06 p1006 A67-18786
Laser holography, discussing various methods of wave front reconstruction 07 p1183 A67-19092
Optical systems and holography in reconstruction of SHF antenna radiation patterns from field measurements in Fresnel zone 07 p1183 A67-19143
Image distances and relative intensities for zone plates determined from holographic theory 07 p1185 A67-19401
Holographic evaluation of spatial frequency response of photographic emulsions 07 p1186 A67-19493
Image reconstruction of nonexistent three-dimensional equilateral tetrahedron using theoretically calculated automatically plotted photo-reduced hologram 07 p1186 A67-19558
Wave front reconstruction imaging technique for hologram production of aerial image of lens 07 p1188 A67-19787
Holographic technique for restoration of third-dimension information in recording of conventionally focused photographs 07 p1188 A67-19788
Holographic synthesis of computer generated holograms 07 p1188 A67-19796
Simple physical argument to explain effect of pseudoscopic inversion of holograms 07 p1188 A67-19799
3-D imagery and holograms of objects illuminated in white light photographed through fly eye lens 07 p1189 A67-20098
Image restoration via phase holograms, noting applications to deteriorated photographic negatives and positives 08 p1331 A67-20842
Prisms for dispersion compensation and single plane diffraction grating as correcting element for achromatizing white light reconstruction of two-beam surface hologram 09 p1492 A67-21567
Low spatial frequency white light hologram production on Diazo materials 09 p1493 A67-21572
Fraunhofer hologram process when illumination is partially coherent quasi-monochromatic radiation 09 p1493 A67-21589
Holographic techniques for interferometric measurements of small translations and rotations undergone by general three-dimensional object 09 p1494 A67-21614
Nonparaxial imaging, magnification and aberration properties in holography, examining point source object 09 p1496 A67-21707
Reconstructions of visible images from reduced scale replicas of polarized microwave holograms 09 p1496 A67-21709
Color image reproduction by conventional hologram techniques 09 p1496 A67-21710
High intensity reciprocity failure in Kodak 649-F spectroscopic plates revealed by holograms obtained with Q-switched ruby laser 09 p1496 A67-21711
Hologram of cold mercury arc spectrum obtained by triangle path interferometer 09 p1497 A67-21766
Spectral differentiation and hologram filtering in reducing optical signal comparison to signal correlation 09 p1497 A67-21826
Hologram fixation by Gabor single beam method, using gas laser as light source 09 p1511 A67-21919
Holographic applications, examining character identification, imaging technique and interferometric techniques 09 p1501 A67-22555
Multiple holographic recording of alphanumeric characters on small area of photographic plate 10 p1652 A67-22700
Multiple wavelength and source holography with constant depth contours superimposed used in cross section tracing or contour mapping 10 p1652 A67-22710
Apparent rotation of spectral lines as viewed through holograms, obtaining equations for angular change of image position 10 p1653 A67-22717
Holography for particle size analysis noting wave formation and reconstruction, hologram camera, etc 10 p1653 A67-22748

Hologram recording and reconstruction through two and three primary colors derived from gas laser 10 p1653 A67-22749

Hologram copies by recording interference pattern between undiffracted and diffracted waves 10 p1654 A67-22754

Three-dimensional photography based on laser derived hologram, examining split-beam technique 10 p1655 A67-23072

Holography /recording light in three dimensions/, noting virtual and real images and color production 10 p1657 A67-23623

Pulsed ruby laser source for holography compared to He-Ne gas laser 10 p1657 A67-23625

Interferometer producing focusing hologram diffraction grating, noting photograph of spectrum 10 p1658 A67-23788

Microwave optical field distribution patterns visualized using IR thermosensitive transducer method 11 p1792 A67-24714

Three-dimensional film plane hologram recording of object without external source reference beams 11 p1793 A67-24828

Visible three-dimensional ultrasonic imaging of interior and exterior of optically opaque objects, using synthetic holographic technique 11 p1793 A67-24831

Holography applications including vibration analysis, flow visualization, etc 11 p1793 A67-24837

Laser holography combined with schlieren techniques to measure ray deviations in optically inhomogeneous field of transient phenomenon 11 p1794 A67-24927

Holographic resolution as affected by materials, installation vibration, hologram dimension and light source 11 p1794 A67-25028

Wave front reconstruction from magnetization distribution on magnetic tape, discussing possibilities based on magneto-optical Kerr effect, hypersonic wave generation and powder patterns 12 p1939 A67-25237

Pulsed ruby laser to obtain Fourier holograms in light reflected from diffusely scattering objects, discussing relaxation of resolving power of photographic emulsions 12 p1939 A67-25335

Holographic imaging methods for improving luminosity, detection and resolution of spectroscopic and astronomical instruments 12 p1948 A67-26238

System using holography for character recognition according to Gabor proposals 13 p2118 A67-26258

Holography applied to radio frequencies, noting recording technique with locally produced reference wave 13 p2119 A67-26518

Reconstruction method for image with good definition via partially coherent source 13 p2119 A67-26587

Holography preserving correspondency of polarization components in reconstructed image and in object 13 p2120 A67-26881

Image transmission through optical fiber, discussing reconstruction of refracted image via holography 13 p2120 A67-27209

Spatially modulated laser recording parameters, emphasizing beam intensity ratio to signal beam, offset angle film transfer characteristic and recording wavelength 13 p2129 A67-27351

Hologram temporal filtering properties applicability to Doppler mapping of moving objects and wavefront reconstruction process on noncoherent object images 13 p2121 A67-27352

Gas laser properties, noting usefulness in physics, chemistry and optics 13 p2129 A67-27364

Holography developments and applications, with emphasis on recording and transmitting pictorial information 13 p2121 A67-27565

Hologram fixation by Gabor single beam method, using gas laser as light source 14 p2329 A67-28248

Coherent and noncoherent holography, noting relationship to corresponding case using lenses 14 p2319 A67-28472

Nonlinear imaging phenomena discussed in connection with holography, describing holoscopes permitting three-dimensional magnification in real time 14 p2319 A67-28495

Optical reconstruction from sampled holograms made with sound waves 14 p2320 A67-28602

Spherical wave Fourier holography modifications using different scheme for incidence of reference beam and

illumination of object 15 p2486 A67-29237

Transposition into holography of optical visualization methods by linking ultrahigh speed camera and solid state laser 15 p2487 A67-29481

Images reconstructed from multiple-exposure hologram separated by selecting appropriate-reconstructed pupil 15 p2487 A67-29500

Region of air with slight variation in refractive index from surrounding air recorded by holographic technique 15 p2488 A67-29725

Selective polarization filtering during hologram construction enhancing reconstructed image resolution and tonal range by eliminating specular reflection recording 15 p2488 A67-29818

Optical image reconstruction from sampled hologram using wavefront reconstruction technique 15 p2488 A67-29819

Electrodynamics applied to two-dimensional problem of determining resolution of images reproduced from ideally plane infinitely thin holograms 15 p2489 A67-30006

Holograms of three-dimensional objects, discussing experimental setup and results 15 p2489 A67-30077

Holography applications in quality assurance including checking jigs, fixtures, molds, vibration analysis, etc 15 p2491 A67-30405

Multicolor image reconstruction from holograms behaving as planar diffraction gratings, excluding crosstalk images formation 15 p2491 A67-30431

Feedback control system for hologram interference fringe stabilization, noting phase disturbances due to different effects 15 p2491 A67-30432

Holography theory and applications, discussing Fresnel and Fourier holographies, interferential information processing, incoherent objects and associative memory 16 p2670 A67-30489

Double exposure holographic formation of contour map over diffusely reflecting surface, using immersion method with liquids of different refractive indexes 16 p2670 A67-30612

Temperature distribution field of flame studied by applying holographic techniques in obtaining interferogram of inhomogeneity created by flame 16 p2672 A67-31066

Source size effect on resolution in Fourier transform holography comparing theoretical and experimental results 16 p2681 A67-31883

Autonomous landmark tracking by holography for space navigation 17 p2881 A67-32436

Lens arrays use in holograms 17 p2860 A67-32619

Acoustic hologram formation retaining holographic properties of Leith-Upatneiks holograms 17 p2860 A67-32625

Laser research and development in France and applications to holography, metrology and gyros 17 p2868 A67-32745

Optical systems and holography in reconstruction of SHF antenna radiation patterns from field measurements in Fresnel zone 17 p2861 A67-33222

Experimental techniques in making multicolor white light reconstructed holograms, discussing signal to noise ratio, coherent light and photographic emulsion 17 p2862 A67-33299

Holographic testing of large optical surfaces, using laser sources and interferometer guidance 17 p2863 A67-33301

Emulsion shrinkage effect on hologram image space 17 p2863 A67-33303

Laser beam slitting hologram production technique using polarization controller and birefringent prism 17 p2864 A67-33359

Interferometric comparison between two nearly identical shapes by superimposing hologram reconstruction of one onto real surface of second 17 p2864 A67-33388

Holography characteristics and possible future uses noting properties, resolution limits and depth of field of high resolution holographic microscopy 18 p3043 A67-33546

Laser spark holography with time resolution 18 p3044 A67-33728

Electrodynamics applied to two-dimensional problem of determining resolution of images reproduced from ideally plane infinitely thin holograms 18 p3046 A67-33767

Four types of holographic imaging systems, discussing optical properties and divergence and convergence 18 p3046 A67-33879

Limitations arising during reconstruction of plane-grating hologram with characteristic X radiation to operate at optical wavelengths 18 p3047 A67-33884

Holographic exposure times controlled by direct viewing of reconstructed image during exposure 18 p3048 A67-34012

Point holograms, reconstituting wavefronts from high quality lenses and mirrors and use as optical elements for replacing lenses in optical systems 18 p3048 A67-34194

Processing and obtaining phase holograms of elementary particle tracks in gelatin bubble and emulsion chambers 18 p3049 A67-34387

High resolution holograms using Fresnel biprism to reduce noise 18 p3053 A67-34620

Holographic image magnification by recording wave interference and illuminating object by coherent beam 18 p3053 A67-34622

Holographic devices and principles, discussing application to plasma studies 19 p3228 A67-34949

Holographic interferometry in fractional-fringe density plasmas, discussing sensitivity and advantages of combined method 19 p3232 A67-35691

Application of double-exposure holographic interferometry technique by using tri-X Pan film for hologram recording 19 p3232 A67-35693

Holographic moire patterns as white light viewing technique for aerodynamic flow visualization 19 p3232 A67-35699

Holographic interferometry by superimposed holograms before or after photographic development 19 p3232 A67-35890

Image reconstruction of diffusely reflecting objects using pulsed hologram technique 19 p3233 A67-36102

Image reconstruction from coarsely sampled acoustical hologram made from ordinary microphone waves 19 p3233 A67-36104

Holography by amplitude division, eliminating destructive interference by using optical prism 20 p3435 A67-36200

Focused image holograms, amplitude-or phase-recorded, reconstructing sharp images by reflection from incoherent illumination 20 p3435 A67-36201

Formulas describing hologram properties, considering emulsion thickness effect on recording and reconstruction 20 p3435 A67-36202

Corrective image deconvolution of smearing caused by extended instrument functions in optical imaging possible by holographic Fourier transform division 20 p3435 A67-36204

Coherent light applications in holography and spatial filtering including Fourier transform holography and pattern recognition 20 p3457 A67-36333

White light reflection holography, discussing recording, reconstruction and color images 20 p3438 A67-36349

Digital image formation from electronically detected holograms noting advantage in imagery of weak objects 20 p3448 A67-36852

High quality holography of back-lighted objects using achromatic-fringe interferometry 20 p3450 A67-37022

Hologram reconstruction of objects in fog-like medium 20 p3450 A67-37027

Holographic interferometry in electrochemical studies, examining advantages in less critical alignment and preparation and observation of changes 20 p3450 A67-37137

Three-dimensional hologram reconstruction and image speckle, considering three-dimensional boundary value problem 20 p3451 A67-37309

Reconstructed image scanning by hologram rotation 21 p3624 A67-37852

Hologram-moire interferometry for transparent objects of moderate optical quality 21 p3624 A67-37853

Holographic measurement of surface strains noting fringe pattern for displacements 21 p3625 A67-37944

Microwave and acoustic frequency holography and possible application to target shape recognition and inverse scattering in radar 21 p3626 A67-38063

Moving point trajectory recorded by

hologram 21 p3627 A67-38347
 Rayleigh-Sommerfeld diffraction formula to obtain imaging behavior of Gabor type holograms of transparencies for reconstructed wave forms with large diffraction angles 22 p3835 A67-39241
 Film resolution limitation on hologram size, Rayleigh resolution and interference pattern recording 22 p3796 A67-39259
 Bandwidth reduction for holographic data transmission systems noting application to TV 22 p3796 A67-39260
 Book on theory and applications of holography, mathematical analysis of process as imaging technique, limitations and partial coherence 22 p3798 A67-39633
 Nonpseudoscopic real image production from arbitrary hologram using different geometries for reference and reconstructed waves 23 p3998 A67-40701
 Holography /phase-recording of diffracted wavelets/ for phase contrast and stroboscopy, interferometry in polarized light and 3-D photoelasticity 23 p3999 A67-41179
 Three-beam holographic interferometry using only one exposure of photographic emulsion 23 p4001 A67-41259
 Computer generated binary Fraunhofer holograms for mathematically known objects, discussing diffraction theory, computational and plotting procedures 23 p4002 A67-41267
 Hologram copying by Gabor holography of transparencies 23 p4002 A67-41268
 Photographic film nonlinearities effect in holographic recording of coherent wavefront using two-beam interferometry, describing phenomenological model 23 p4002 A67-41269
 Dynamical theory of X-ray diffraction for optical holography noting anomalous light transmission at Bragg angle 23 p4009 A67-41462
 Hologram duplication noting stability factors and process for producing coherent copy 24 p4153 A67-41910
 Hologram technique using reference beam totally reflected from air-emulsion boundary of hologram plate permits close spacing 24 p4156 A67-42362
 Image processing by computer generated binary filters 24 p4156 A67-42432
 Digital image formation and reconstruction from photographic and direct electronically detected holograms 24 p4157 A67-42437
 Character recognition via holography using Gabor principle of two coherent waves falling simultaneously on photographic plate 24 p4157 A67-42456
 Moire patterns generated on computer printout when superimposing sampling grid over two-dimensional function to be plotted 24 p4158 A67-42809
 Local reference beam principle for laser long distance hologram construction 24 p4158 A67-42819
 Spatial filters for code translation and image sharpening produced by holograph in reasonably good approximation 24 p4159 A67-43097

HOMEOSTASIS
 Urinary output patterns relationship to arterial pressure, pulse rate and parameters of hemoconcentration in study of homeostatic circulation regulation during prolonged gravitational stress 15 p2428 A67-29273

HOMING
 Minimum tracking data in guidance technique functioning comparable to proportional navigation homing system, noting tests in computer simulations and in laboratory model 02 p0263 A67-12158
 Target homing of tracking systems receiving signal packages only in absence of fading 04 p0591 A67-14659

HOMING DEVICE
SA GUIDANCE SYSTEM
 Servo control system selection for air-launched missile with homing guidance system, reviewing four major designs of torque-proportional hardware 02 p0182 A67-11842
 Final value homing missile guidance 07 p1221 A67-19383
 Divergence from and oscillation about nominal path in proportional navigation homing system 11 p1817 A67-24226
 Soviet book on IR and optical devices for vehicle guidance and homing covering light propagation, radiation from targets, airborne missile homing systems, etc 11 p1791 A67-24514

HOMODYNE

Coherent homodyne detection at 10.6 micrometers with aluminum-doped silicon photoconductor, presenting noise spectra and voltage 03 p0438 A67-13989
 Line width of CW Ga-As lasers measured using homodyne detection and autocorrelation 05 p0821 A67-16670

HOMOGENEITY

Qualitative study of first order homogeneous equation, by introducing auxiliary variables, plane curve is associated with differential equation 03 p0459 A67-13587
 Homogeneity of solar prominences studied photographically in monochromatic light 14 p2382 A67-28941

HOMOGENEOUS TURBULENCE

Inertia and pressure effects on energy potential of homogeneous and isotropic turbulence in weakly compressible medium 02 p0235 A67-12643
 Large scale structure of homogeneous turbulence generated at initial instant by distribution of random impulsive forces, noting statistical properties 09 p1490 A67-22417
 Model ionosphere with homogeneous isotropic turbulence investigated for values of kinematic viscosity and dissipation rate of turbulent energy determined from rocket measurements 10 p1646 A67-23273
 Mutual coherence factor for plane electromagnetic wave propagating in stochastic locally homogeneous and isotropic medium of dielectric turbulence 11 p1818 A67-24415
 Maintenance of electromagnetic field by dynamo effect in homogeneous isotropic turbulence without mirror symmetry 17 p2883 A67-32355
 Homogeneous MHD turbulence on large scale structure, finding asymptotic forms of velocity and magnetic field correlations 19 p3295 A67-35540
 Experimental duct for plane deformation of homogeneous turbulence, measuring mean velocities in axis and symmetry plane 20 p3420 A67-36393

HONEYCOMB

SA CERAMIC HONEYCOMB
SA MULTILAYER STRUCTURE
 Compact rocket engine concept utilizing very small thrust units confined between and joined to plates, resulting in honeycomb structure [AIAA PAPER 66-924] 02 p0303 A67-12276
 Adhesive bonded honeycomb horizontal stabilizers, considering strength, aerodynamics, cost, endurance and serviceability 09 p1577 A67-22508
 Adhesive-honeycomb relationship including filletting effect on honeycomb properties, compression properties, stresses at fillet, etc 09 p1577 A67-22509
 Wing-fuselage section panels of hypersonic aircraft built by brazing welded refractory honeycomb 10 p1660 A67-23171
 Energy absorption characteristics of honeycomb structures under static and impact loading 10 p1727 A67-23745
 Compact rocket engine concept utilizing very small thrust units confined between and joined to plates, resulting in honeycomb structure [AIAA PAPER 66-924] 15 p2545 A67-29435

HONEYCOMB CORE

Insert size, shape and core undercut diameter and depth effect on insert tensile strength of honeycomb sandwich fasteners 02 p0248 A67-11943
 Synthetic spherulites in plastic foam and synthetic tube segments in honeycomb form as fillers in sandwich construction 03 p0521 A67-13022
 Fiber reinforced composites with high strength high temperature resistance, using powder metallurgy and honeycomb structures 03 p0429 A67-13437
 Thermal conductance determinations on L-605 cobalt-base alloy panels of variable geometry made to around 2000 degrees F in high vacuum and air 04 p0735 A67-15852
 Ultrasonic techniques for nondestructive testing for Saturn honeycomb heat shields 07 p1192 A67-20166
 Single stage bonding of tapered aluminum honeycomb panels employing wrap-around skins and nonperforated core 09 p1507 A67-22507
 Vibrational experiments with honeycomb type core sandwich beams on lowest natural

frequency, node locations and damping, noting core shear flexibility [ASME PAPER 67-VIBR-11]

11 p1872 A67-24171
 Heat resistant stainless steel honeycomb cores for cylindrical applications, measuring energy absorption characteristics [ASME PAPER 67-DE-14] 14 p2402 A67-28870
 Brazing alloys and high remelt and conventional techniques developed and evaluated for use in tantalum honeycomb structures 20 p3456 A67-37696
 Poly IV gilder wing noting bonded aluminum sheet/honeycomb sandwich shell 22 p3811 A67-39302
 Structural analysis of welded joints in composite welded panels using beam column concepts 22 p3813 A67-40181
 Honeycomb sandwich structures for aircraft and missile construction, discussing panel configurations 23 p4077 A67-41047

HOOKE LAW

Stress-strain and Hooke law in orthotropic elasticity presented through matrix algebra and tensor coordinates 06 p1108 A67-18656
 Angular correlation in helium atom with electron-electron interaction 13 p2161 A67-27182

HOPE SPACECRAFT

S HYDROGEN OXYGEN /HOPE/ SPACECRAFT

HORIZON

S GYRO HORIZON
S INFRARED HORIZON
S RADIO HORIZON

HORIZON SCANNER

Miniature optically immersed thermistor bolometer arrays employed for earth atmospheric horizon scanning from orbiting vehicles 19 p3231 A67-35684

HORIZON SENSING

SA ATTITUDE CONTROL
 Self-contained orbital navigation system using earth-horizon measurements in 14-16 mu carbon dioxide absorption band, using Kalman linear filter theory 02 p0263 A67-11925
 IR horizon sensor systems for spacecraft attitude determination, detailing field switched edge tracker 04 p0625 A67-15664
 Horizon sensor data processing with compensation for statistical properties of errors, noting application of optimal filtering theory 11 p1817 A67-24336
 Kalman filter divergence control, noting analytical and empirical modification methods 14 p2347 A67-28116
 Luminance profiles of earth sunlit limb through visible spectrum for navigation and research 19 p3213 A67-34804
 Satellite orientation sensing and orbital gyrocompassing heading reference, examining effect of horizon sensor noise [AIAA PAPER 67-587] 19 p3258 A67-35983
 Orbital attitude reference system working model using strapped down principles and digital computer 22 p3907 A67-40187
 Cross coupling effects in strapdown orbital gyrocompass to determine attitude of vehicle with respect to planet-centered coordinate system 22 p3801 A67-40188
 Optimal filtering theory for horizon sensor data processing for orbital navigation, examining statistical characteristics 22 p3834 A67-40196

HORIZONTAL TAIL SURFACE
 Horizontal tail two-stage hydraulic servoactuator for F-111 horizontal stabilizer control 05 p0752 A67-16160

HORMONE

SA ADRENOCORTICOTROPIN /ACTH/
SA HYDROCORTISONE
 Vasopressin-aldoosterone interrelation in diuretics and antidiuretics to explain body fluid weight loss in astronauts during space travel 21 p3574 A67-38082

HORN ANTENNA

Choke slots or corrugated structure in walls of horn antenna for reducing sidelobe and backlobe level by controlling illumination of E-plane edge 02 p0211 A67-11601
 Linearly polarized horn antenna with same power pattern in all planes through axis made from synthetic material for which boundary conditions on E and H planes are same 02 p0213 A67-11616
 Correction for gain computations based on pattern integration during translational motion of antenna 11 p1763 A67-24297
 Reflection coefficient of parabolic

- reflector antenna illuminated by horn radiator with sector shaped radiation pattern 11 p1767 A67-24716
- Nancay radiotelescope energy collection, illumination choice and development 12 p1914 A67-25310
- Helix-conical circularly polarized antenna performance analyzed, noting increased gain and lower sidelobe level 13 p2076 A67-26515
- Japanese weather radar facility featuring network relay equipment functioning in PPI/RHI mode, noting parabolic horn antenna 14 p2250 A67-28698
- Mutual coupling between sectoral horns side-by-side formulated in terms of rays, modes and mode caustics excited in each horn 16 p2839 A67-31355
- Diffraction coefficients in Keller theory extended to near-field and shadow-boundary regions of edge, introducing two correction factors 16 p2827 A67-31365
- Antenna field strength measurement above 1 GHz, discussing formulas for high accuracy gain determination, multipath interference and antenna separation 17 p2815 A67-32609
- Transit drift-scan observations of radio sources using cornucopia horn reflector antenna 19 p3330 A67-38073
- Higher order mode excitation by multipath propagation in deep fading of receiving horn-reflector antenna 20 p3385 A67-37355
- Sidelobe reduction by stepping E-plane field distribution on rectangular horn antenna aperture, finding values of geometrical parameters 22 p3767 A67-39273
- Launcher for trapped surface waves over ice-covered sea by ferrite loaded horn device 22 p3783 A67-40306
- RF interference reduction by using choke balun on feed horns of reflector type antennas 24 p4132 A67-42717
- HOT CATHODE**
- Cathode phenomena in plasma thrusters with self-magnetic acceleration low mass-flow rates "DVL-631" 19 p3297 A67-35900
- HOT CYCLE PROPULSION SYSTEM**
- Hot cycle rotor wing aircraft for high speed city-center transportation, estimating cost and performance [AIAA PAPER 67-770] 24 p4095 A67-42938
- HOT ELECTRON**
- Electric conductivity due to tunnel effect in aluminum-alumina-silver sandwich structures, determining potential barrier in alumina and absorption coefficient of hot electrons 02 p0295 A67-11762
- Implantation of Cs and Na ions into p-type silicon, effect on hot electron emission from p-n junction 02 p0299 A67-11897
- Field and charge density distributions in semiconductor with hot electrons, showing domain movement type oscillations due to stationary wave propagation 04 p0680 A67-15286
- Thermalization of cathodic electron flux by Langmuir oscillations in cesium arc plasma 04 p0678 A67-15971
- Properties of dense plasma with preheated electrons in ion cyclotron resonance region, using magnetic mirror trap 05 p0853 A67-18755
- Anisotropic semiconductor in hot electron theory, deriving volt-ampere characteristics 05 p0887 A67-17053
- Hot electron emission from polar semiconductors with nonparabolic dispersion law, specifically qualitative effect of nonparabolicity and field on electron emission 06 p1052 A67-18423
- Nonlinear galvanomagnetic effects due to hot electrons in n-type InSb in quantum limit 06 p1065 A67-18953
- Field and charge distribution in hot electron semiconductor, discussing drift and recombination nonlinearity 06 p1068 A67-18960
- MHD of flows with hot electrons in MHD ducts at low magnetic Reynolds numbers, emphasizing boundary layer and shock wave theory 09 p1541 A67-21797
- High field mobility degradation effect on characteristics of insulated gate FET, considering drift velocity proportional to field square root and constant drift velocity 09 p1471 A67-21944
- Domain originated functional integrated circuits with possible solid-state bulk effect extension from microwave systems to whole of electronics 14 p2281 A67-28022
- Differential negative conductivity in n-type GaAs, using microwave electron heating 14 p2398 A67-28895
- Anisotropic semiconductor in hot electron theory, deriving volt-ampere characteristics 15 p2582 A67-29784
- Passage of hot electrons through metal film in semiconductor-metal-semiconductor system 15 p2541 A67-30289
- Book on effects of hot electrons associated with carrier concentration in semiconductors at very low temperatures 17 p2614 A67-32378
- Hydrogen plasma discharge with hot electrons, investigating plasma decay and electron and plasma density 21 p3686 A67-32368
- N-type InSb hot electron and nonohmic effects, noting low temperature and magnetic and electric field dependence of Hall coefficient and resistivity 21 p3683 A67-38465
- Hard X-ray emission by hot electron plasma trapped in discharge tube due to magnetic field rise 21 p3687 A67-38413
- Hot electron Hall mobility in n-type GaAs in negative differential mobility region 22 p3858 A67-39518
- Hot electron plasma confinement in magnetic mirror fields with compensating curvature, discussing experimental observations and hybrid configuration formation 22 p3849 A67-39698
- Spectral dependence of enhanced quantum efficiency and overlap integrals in InSb semiconductors, calculating impact ionization and hot electrons thermalization 23 p4040 A67-41061
- HOT GAS**
- Flame ignition from hot gas pocket, minimum size of gas bubble for flame propagation, dependence on chemical kinetic parameters and transport properties 02 p0342 A67-12030
- Radiant heating by inhomogeneous hot gases, determining spectral transmittances of inhomogeneous optical paths using Curtis-Godson approximation 02 p0342 A67-12050
- Autolization effects in UV absorption spectra of hot atomic gases 03 p0471 A67-13222
- Propagation of vertical turbulent hot gas stream in fog from point source of heat 03 p0463 A67-14225
- VTOL test bed for ground effects test, noting environmental characteristics, configuration dependence of lift and hot gas ingestion [AIAA PAPER 67-181] 06 p0980 A67-18297
- Electron temperature vs plasma cell power input measured, determining electron energy loss factor for hot diatomic gases in electric field 12 p1973 A67-25398
- Book on spectroscopic gas temperature measurement covering principles, radiometric and spectroscopic methods, instruments, applications to pyrometry, etc 12 p1940 A67-25431
- Propagation of vertical turbulent hot gas stream in fog from point source of heat 12 p1963 A67-25481
- Region of air with slight variation in refractive index from surrounding air recorded by holographic technique 15 p2488 A67-29725
- Prediction of solid propellant hot-gas ignition based on preignition transient convective heat transfer model [AIAA PAPER 65-67] 15 p2562 A67-30196
- Hot flame gases ionization by electron reactions at atmospheric pressure 17 p2968 A67-32149
- Thermal and synchrotron cosmic X-ray sources 17 p2937 A67-32639
- Energy loss factors for slow electrons in hot gases determined by measuring electron temperature variation with HF electric field power 17 p2890 A67-33367
- Flat pack interconnection technique using hot gas soldering, discussing inspection and control requirements 21 p3635 A67-38626
- HOT GAS SYSTEM**
- Ignition of explosive powder by hot gas stream, with particular attention to heat transfer between substance and surrounding medium 06 p1112 A67-17956
- Flame ignition from spherical hot gas pocket, finding minimum size of bubble for flame propagation and dependence on kinetic parameters 06 p1114 A67-18189
- Hot gas tunnel for determination of material behavior under convective heat transfer conditions similar to that existing in rocket combustion chambers [AIAA PAPER 67-106] 06 p0961 A67-18473
- Indigenous lunar power from geothermal deposits of hot water-rich gases and brines 06 p1317 A67-21065
- High pressure hot gas solid propellant cartridge starter for aircraft turbine engine [ASME PAPER 67-GT-21] 11 p1354 A67-24303
- Plasma azimuthal inhomogeneity in homopolar system, noting Hall current and stationary plasma acceleration 15 p2526 A67-29723
- HOT JET EXHAUST**
- Model testing for design evaluation of major components and configurations of static test and launch facilities, noting hot jet model [AIAA PAPER 67-237] 07 p1165 A67-20060
- HOT PRESSING**
- Titanium diboride densification at high pressure and high temperature noting grain growth 01 p0096 A67-10704
- Hot pressing of electrolytic grade CR beryllium, noting powder manufacturing process and quality control procedure 01 p0099 A67-10707
- Compacting effect of additive oxides of Ti, Zr, Si, Fe, Zn and Al on hot pressing of MgO 01 p0102 A67-11243
- Compatibility and interaction characteristics of SiC and B fibers with metal matrices in composites prepared from powder metallurgy by hot pressing 03 p0444 A67-13430
- Hot pressing technique for aluminum sheet and stainless steel wire to produce composite high tensile strength plate 12 p1954 A67-25289
- Statistical analysis of beryllium cross-rolled sheet, hot pressed block and ring rolled forgings 13 p2140 A67-27135
- Densification and wear resistance of hot pressed pure and binary systems of diboride established with TaC and other refractory additives 17 p2875 A67-33407
- HOT SPOT**
- Electromagnetic irradiation of pyroelectric hot spots and regional variation of response 02 p0299 A67-11893
- Design technique predicting hot spot temperature and location in thin film circuit, determining power rating 02 p0215 A67-11972
- Second breakdown and hot spot formation in simplified HF silicon power transistor with interdigitated comb emitter structure 02 p0222 A67-12649
- Numerical calculation of critical hot spot thermal explosion conditions for plane slab, cylindrical and spherical symmetry 07 p1264 A67-19071
- Surface geometry demonstrated to be insignificant in production of lunar hot spots during eclipse 18 p3135 A67-34545
- HOT WIRE**
- Radiation heat transfer by flames to wire temperature sensor corrected by technique combining radiative input and catalytic activity 21 p3733 A67-38683
- Instantaneous heat transfer of thin tungsten wires in unsteady transverse airflow 21 p3733 A67-38913
- HOT-WIRE ANEMOMETER**
- Vortex strength in wake of circular cylinders and comparison of vortex velocity distribution with that of Hoffman and Joubert, using hot-wire anemometers at various Reynolds numbers 01 p0005 A67-10256
- Helicopter and VTOL vehicle low air speed measuring techniques and devices including pitot-static tube, hot-wire anemometer, sphere sensor and exotic techniques 01 p0073 A67-11122
- Meteorological instrumentation for measuring physical characteristics of atmosphere 04 p0649 A67-14886
- Heat flow meter with short response time, measuring influence of acoustic field on forced convection 05 p0790 A67-16034
- Schlieren and hot-wire anemometric observation of supersonic wakes in wind tunnel turbulent flows [ONERA-TP-417] 05 p0748 A67-18482
- Projectile wake turbulence measurements using hot-wire anemometer 05 p0750 A67-17346
- Hot-wire anemometer for instantaneous measurements of rapidly time-varying wind flows 06 p1000 A67-17533
- Wind tunnel study of boundary layer

transition structure on ogive nose cylinders aligned parallel to flow
 [AIAA PAPER 87-129] 06 p0939 A67-18314
 Turbulent boundary layer characteristics of compliant surfaces, using hot-wire anemometer to measure velocity profiles, Reynolds stresses and skin friction
 [AIAA PAPER 87-128] 06 p0987 A67-18336
 Self-preserving turbulent jet ejector, solving equations of motion to determine system geometry corresponding to flow conditions
 [AIAA PAPER 87-127] 06 p0988 A67-18456
 Constant temperature difference hot thermocouple anemometer, discussing operation principle and performance 10 p1654 A67-22822
 Short method measurement of Reynolds stresses in turbulent flow, using constant current hot-wire anemometer 10 p1629 A67-23845
 Turbulent boundary layer on smooth flat wall, measuring skin friction, turbulence intensity, shearing stress, transverse integral scale, etc 11 p1776 A67-24045
 Signal to noise ratios of transistorized constant current and constant temperature hot-wire anemometers 12 p1947 A67-26121
 Hot-wire anemometry, discussing constant current and constant temperature measurement systems 13 p2120 A67-27020
 Stability of multiple rows of vortices created behind tripping cylinders at low Reynolds number 14 p2294 A67-27795
 Constant temperature hot-wire anemometer circuit using solid state amplifiers, obtaining frequency response expression 14 p2315 A67-28159
 Flow field measurement near sharp leading edge of cooled flat plate parallel to low density hypersonic stream 14 p2241 A67-28165
 Feedback control theory for constant temperature hot-wire anemometers using differential equation applied to frequency response optimization 14 p2320 A67-28750
 Obstacle effect on turbulence intensity in boundary layer, discussing results of hot-wire anemometer measurements 15 p2471 A67-29651
 Instabilities of Ekman layer measured using hot-wire anemometers 15 p2471 A67-29655
 Velocity measurement in turbulent flow near smooth wall by hot-wire anemometer 18 p3027 A67-34184
 Hot-wire anemometer response in turbulent flow studied requires correction leading to constant results when applied to flat plate bluff body wakes normal to stream 19 p3230 A67-35523
 Heated thin film anemometer used to measure fluctuating velocity in airflow, noting relation of dynamic sensitivity to static calibration 20 p3447 A67-36846
 Correlation measurement in turbulent flow with hot wire anemometer downstream from grid, considering velocity effects 22 p3783 A67-39704

HOT-WIRE MEASUREMENT

Hot-wire probe measurement of friction temperature and convection coefficient of low pressure flows and wake of cylinder 01 p0006 A67-10757
 Hot-wire anemometer measurements of transition in incompressible wake of cone at low Reynolds number 05 p0751 A67-17439
 Thermoconductivity of nitrosyl bromide at 290-900 degrees K and 200-600 torr measured by hot filament techniques 11 p1881 A67-24022
 First collision effects in rarefied high speed flows in low density wind tunnel, noting measurement techniques and apparatus used 14 p2317 A67-28197
 Heat conductivity coefficient of cesium vapor at temperatures from 1000 to 1600 degrees K and 1 to 5 torr measured by hot tungsten filament method 17 p2895 A67-32156
 Modified hot-wire thermal conductivity cell for measuring effects of finite length, pressure and temperature on heat transfer from wire in rare gases 17 p2863 A67-33357
 Laminar-turbulent boundary layer transition over aircraft components measured by method using negative-temperature-coefficient resistors compared to hot wire measurements 19 p3230 A67-35573
 Transition region of hypersonic boundary layer on flat plate surveyed with hot wires,

giving analysis for limited wire calibration 19 p3212 A67-35765
HOT-WIRE TURBULENCE MEASURING APPARATUS
 Hot wire measurement of tangential velocity and Reynolds stresses in spiral laminar-turbulent flow 01 p0054 A67-11163
 Pressure variational law effect along boundary layer of flat plate on formation of turbulent spots measured via hot-wire technique 04 p0802 A67-14598
 Hot-wire probe measurements of time average velocity, flow directions, turbulence intensities and growth of skewed three-dimensional turbulent boundary layers in low speed flow
 [ASME PAPER 86-WA/FE-2] 04 p0608 A67-15386
 Heat transfer and temperature distribution turbulence measurements with inclined hot wires 13 p2222 A67-26913
 Hot wire response equations including tangential velocity effects and nonlinearities caused by high intensity turbulence 13 p2095 A67-26914
 Enhancement of signal to noise ratio of turbulence measurements by cross correlation and heat transfer transducer 18 p3050 A67-34499
 Self-aligning hot-wire probe for direction, velocity and turbulence measurements in two-dimensional flow 22 p3800 A67-40069
 Longitudinal turbulence intensities, autocorrelations, energy spectra and peak energy dissipation frequencies for organic solvents flowing in smooth round tubes 24 p4141 A67-41927
HOTSHOT TUNNEL
 Hypersonic testing methods at ONERA, discussing wind tunnel apparatus [ONERA-TP-371] 05 p0748 A67-16475
 Electrostatic probe and VHF microwave reflectometry study of nitrogen flow around models in hotshot wind tunnels, determining plasma sheath physical characteristics 11 p1839 A67-24445
 Hot shot tunnel F operation as combustion test facility using air, discussing oxygen depletion, particle contamination and reservoir decay 21 p3606 A67-37775
 Hypersonic reentry plasma electron density measurement in free stream wake and shock layer using hotshot wind tunnel simulation 23 p3986 A67-40574
HOVERING
 Small-perturbation hover dynamics motion equations, characteristic modes, stability derivatives and dimensional analysis [SAE PAPER 860576] 01 p0010 A67-10570
 Simulation system and hovering vehicle prototype design for use in development of VTOL aircraft 04 p0600 A67-15540
 Aircraft sizing methodology and hover control comparative analysis on V/STOL fighter-bomber using lift plus lift cruise propulsion [AIAA PAPER 87-133] 06 p0948 A67-18358
 V/STOL transport testing and operational requirement, discussing hover rig, pedestal and simulator 14 p2245 A67-27746
 Hover augmentation system reducing VTOL pilot task in maintaining position by providing damping signals for automatic flight modes with accurate path control 14 p2246 A67-29082
 Rotor-hovering performance-prediction with test data showing discrepancy increase with wake contraction, blade loading, tip Mach number and blades number [AHS PAPER 100] 16 p2594 A67-31817
 Jet VTOL aircraft problems, considering vertical thrust/aircraft weight, thrust application to aircraft gravity center, stability in hovering, thrust exertion, etc 17 p2796 A67-32392
 Hover augmentation system /HAS/ design for analog computer helicopter simulation and flight control 17 p2797 A67-32574
HOVERING STABILITY
 Altitude control for VTOL aircraft facilitates control of hovering flight, noting construction, operation principles and performance 03 p0383 A67-12981
 Hovering stability of crane helicopter with hanging load, noting effects of supporting point of wire and length, using root locus method 05 p0751 A67-16439
 Divergent vertical helicopter oscillations resulting from physical presence of pilot in collective control loop 11 p1744 A67-24591

HP-137 AIRCRAFT
 S HANDLEY PAGE H.P. 137 AIRCRAFT
HS-748 AIRCRAFT
 S AVRO WHITWORTH HS-748 AIRCRAFT
HUB-TIP RATIO
 Three-dimensional flow in axial fan, consisting of rotor only, having finite number of blades, by method of isolated airfoil of finite span 19 p3171 A67-35712
HUECKEL THEORY
 Characteristic optical density and equilibrium of alkyl-sodium and aromatic hydrocarbons as function of temperature and wavelengths, correlating electron affinity with enthalpy values 09 p1458 A67-22214
HUGHES MILITARY AIRCRAFT
 S OH-8 HELICOPTER
HUGONIOT EQUATION OF STATE
 SA PLASTICITY
 Hugoniot equation of state of alkali metals, using technique based on isentropic sound speed measurement at room temperature 06 p1032 A67-18141
HUMAN BEHAVIOR
 SA PERSONALITY
 Informal automaton simulating certain processes of information processing by human brain controlled by servosystems 03 p0365 A67-13084
 Troubleshooting problems in oscillator circuit solved via Bayesian computer program simulating critical behavior 09 p1456 A67-22369
 Second order personality factor analysis applied to air traffic control specialists 13 p2063 A67-26929
 Aircraft accident prevention dynamics and data recording role noting repetitive causal factors, limitations and information loss 17 p2796 A67-32218
 Anatomical locus of behavior reinforcement, discussing survival mechanism development in animals and humans 20 p3373 A67-37432
 Adaptive processes of human operator during control tasks involving sudden change of controlled plant dynamics 21 p3576 A67-37948
 Performance characteristics in zero potential energy manual task, discussing work output 21 p3577 A67-38074
HUMAN BODY
 SA LIMB
 Moments of inertia calculated for human body as whole and of certain parts in unsupported positions of weightlessness 02 p0187 A67-12325
 Combined linear and vibratory accelerations effects on human body dynamics and pilot performance capabilities 02 p0189 A67-12409
 Human body as source of power for implanted electronic devices [AIAA PAPER 86-930] 03 p0366 A67-14137
 Urine composition in twelve dehydrated subjects in periods of activity, water immersion and reclining in deck chair [SAM-TR-86-305] 09 p1453 A67-21730
 Heat balance and ventilation of human body in pressure suit 09 p1455 A67-21731
 Weightlessness effect on human body noting brain hemodynamics, cardiovascular system, calcium metabolism, task performance, etc 20 p3369 A67-36668
 Reduction of microbial shedding from humans, comparing and evaluating clothing and surgical mask use 20 p3374 A67-36802
 Microorganism shedding by human beings studied by isolation of specific sources and washing or sanitizing of arms 20 p3374 A67-36803
 Acceleration problems in astronautics noting axis determination and effect on human body 20 p3371 A67-36822
 Anatomical locus of behavior reinforcement, discussing survival mechanism development in animals and humans 20 p3373 A67-37432
 Soviet monograph on problem of acceleration in aviation medicine 20 p3375 A67-37466
 Isolation of *Acinetobacter anitratus* from subject and room area during spacecraft environmental tests 21 p3573 A67-38072
 Gastroesophageal reflux in fliers measured in evaluation of hiatal hernia and possible esophageal origin of chest pain 21 p3574 A67-38084
 Medical problems in aircraft flight

accidents and traumatic mechanisms 21 p3575 A67-38508

Ground based simulation program for EVA evaluation including center of mass and inertia products of model astronaut 22 p3780 A67-40153

Determination of energy, water and protein requirements of man under simulated aerospace conditions 23 p3952 A67-41573

Field Effect Monitor for biomonitoring cardiovascular variables and LF physiological electromagnetic phenomena 23 p3966 A67-41582

Long term space mission sanitation, personal hygiene and body cleansing to control microbe populations on body surface and teeth 23 p3967 A67-41611

Indigenous microflora as determined in men undergoing simulated space conditions, considering microbic shock postulated on long term missions 23 p3958 A67-41656

HUMAN CENTRIFUGE

Biochemical measures made as part of habituation experiment in which four subjects were exposed to rotation for 6 days 05 p0754 A67-16277

Urinary output patterns relationship to arterial pressure, pulse rate and parameters of hemoconcentration in study of homeostatic circulation regulation during prolonged gravitational stress 15 p2428 A67-29273

Simulated acceleration and dynamic pressure environments generated by space vehicle flight ranging from weightlessness to impact from ground landing [AIAA PAPER 67-279] 15 p2465 A67-29425

Physiological reactions of man to effect of overload during space flight compared to results of laboratory /centrifuge/ tests 16 p2610 A67-30752

Feasibility of short radius centrifuge incorporation in space station, testing radius effects on operator performance of tasks 23 p3965 A67-41567

Physiological response and acceleration tolerance in dynamic simulation via human centrifuge, noting symptoms occurrence frequency 23 p3953 A67-41590

Color photographic study of blackout during radial acceleration on human centrifuge, presenting evidence confirming central retinal arterial collapse 23 p3957 A67-41638

Fluorescence angiography technique to study human centrifugal acceleration effects on retinal circulation during blackout 23 p3957 A67-41639

Human response to low intensity long duration transverse acceleration, discussing increase in splanchnic blood flow during centrifugation and orthostatic intolerance 23 p3958 A67-41652

Peripheral venous renin levels changes used to evaluate angiotensin system response to acceleration 23 p3960 A67-41700

HUMAN ENGINEERING

SA ANTHROPOMETRY

SA CYBERNETICS

SA MAN-MACHINE SYSTEM

Optimum passenger handling in long haul air transportation for various airport facilities [AIAA PAPER 66-843] 02 p0181 A67-12257

Human engineering aspects of design of future military high performance aircraft, noting automatic control and display system requirements 04 p0562 A67-14535

Human body motions during load handling tasks for application in designing manipulators, walking machine and powered exoskeletons [ASME PAPER 66-WA/BHF-2] 04 p0563 A67-15398

Mockup of manned hardware systems in industrial design, describing application to LRV and LEM development, crew compartment design for undersea craft /DSRV/, etc 05 p0757 A67-17378

SAE Stapp Car Crash Conference, Holloman AFB, New Mexico, November 1966 08 p1288 A67-20609

Integrated cockpit research in man-machine relationship in aircraft 08 p1350 A67-20666

Psychology and space flight 09 p1454 A67-22056

Shortcomings in complex reentry system design caused by human factors 09 p1456 A67-22290

Roll-angle indicators used for avoiding spatial disorientation during instrument flight 13 p2063 A67-26927

Optimization of man-machine environmental interface problems in framework of large-scale and long-term space operations [AAS PAPER 67-80] 15 p2432 A67-29947

Rigid articulated pressure suits, discussing design, construction and operation for low external pressure, mobility requirements, etc 16 p2618 A67-30779

Airport terminal planning for Tampa eliminating long walk, using circular multistory structure with handling equipment for passengers and baggage [SAE PAPER 670319] 17 p2835 A67-32980

Human engineering research to aid system designers to optimize mans role as control element in space systems 18 p2995 A67-34687

Human engineering performance data for equipment design for manned space systems, discussing zero gravity maintenance and repair [AIAA PAPER 67-653] 20 p3375 A67-37630

HUMAN FACTOR

Environment, mission requirements and subsystem interfaces effect on space vehicle structure [SAE PAPER 660673] 01 p0153 A67-10580

Prolonged autonomous existence of humans in space suits, discussing maintenance of heat balance by physiological perspiration 02 p0187 A67-12324

Human performance correlation with changes in incentive conditions and weld lengths, using simulated welding tasks 05 p0756 A67-16072

Probabilistic displays and decision making effectiveness in situation with uncertain or fallible information 05 p0757 A67-16308

Electro-optical imaging systems used in military aerial TV display, emphasizing variables involved in viewing related to visual interpretation 05 p0757 A67-16309

Large space environmental simulation chamber design problems arising due to man-rated feature 05 p0788 A67-16618

Medical, design and operational aspects of quality requirements for reliability of man-rated space environment simulation chambers 05 p0788 A67-16621

Dynamic characteristics of human operator in tracking system under spaceflight conditions onboard Voskhod II spacecraft dynamic characteristics of human operator in tracking system under space flight conditions 07 p1135 A67-19106

Man-machine interaction in visual displays of computer output 07 p1148 A67-19658

Inclusive classified bibliography pertaining to modeling human operator as element in automatic control system 07 p1137 A67-20173

Heat stress effect on human renal function, measuring glomerular filtration rate, renal plasma flow, free water clearance and electrolyte excretion 10 p1599 A67-23811

Computer techniques for data problems encountered by task analysts 13 p2063 A67-27260

Medical/human factors affecting pilots during atmospheric turbulence 13 p2064 A67-27262

Human factors in air traffic control displays 13 p2064 A67-27563

Human factors information utilization by designers, noting test results on conceptual drawing of equipment configuration according to design 15 p2431 A67-29897

Revision of military terminology for weapon systems considering human factors, safety and maintainability and reliability relations 16 p2780 A67-30440

Operational efficiency of astronauts evaluated on basis of Voskhod I and II flights, discussing manual operation, EVA memory efficiency, etc 16 p2618 A67-30780

Prediction and measurement of metabolic energy cost for space suit system operation, noting procedure and test results 16 p2618 A67-30781

Subjective/objective measurement types required for systematic aircraft noise regulation around airports, based on maximum permissible noise exposure criterion 17 p2795 A67-32121

Variability in human estimation of total cloud cover data by satellite-photograph interpretation, noting use of Nimbus I photographs 17 p2880 A67-32555

Human factors and anthropotechnology in development of weapon systems 18 p2993 A67-33643

Operational system for handling and processing aerospace-system human-factors task data in government/contractor environment 18 p2994 A67-34343

Quantification for effective human performance implementation into system designs during conceptual, design and acquisition phases 18 p2994 A67-34655

Anthropotechnical reliability establishing methods considering ability of man to assimilate amount of information in unit of time 22 p3754 A67-39280

Simplified fire control system for helicopters, noting helmet sight, error source corrections and sighting and tracking convenience 22 p3755 A67-39849

Evaluation and analysis of critical human performance for rating man-machine interface 22 p3755 A67-40154

Resolution, contrast and time factors in visual target acquisition 22 p3755 A67-40410

Microbial interaction factors determined between men and environment in closed systems 23 p3962 A67-40858

Air Force undershoot and overshoot experience examined to establish relative frequency, historical trend, associated variables and human factors 23 p3970 A67-41701

Human factors in fatal and nonfatal general aviation accidents, discussing cause of death and relationship of experience, occupation and alcohol 23 p3971 A67-41708

Hazard studies and safety analyses qualitative method using checklist of possible mishaps and human errors [AIAA PAPER 67-935] 24 p2480 A67-43025

Implementation of safety provisions in manned systems [AIAA PAPER 67-937] 24 p4096 A67-43027

HUMAN PATHOLOGY

Vertebral fractures in pilots from helicopter accidents in dorso-lumbar junction of spinal column 12 p1902 A67-25170

Carbon dioxide breathing effects on forearm blood vessels, discussing vascular resistance and carbon dioxide role in blood flow regulation 20 p3373 A67-37584

Gastroesophageal reflux measurements in evaluation of hiatus hernia and chest pain in fliers 23 p3954 A67-41599

HUMAN PERFORMANCE

SA ASTRONAUT PERFORMANCE

SA OPERATOR PERFORMANCE

SA PILOT ERROR

Crew performance evaluation via behavioral and psychophysiological tests in Lunex II simulated lunar mobile laboratory 01 p0017 A67-11392

Human capability to perform support functions in space 01 p0018 A67-11405

Operator reorientation of attitude of simulated remote maneuvering unit /RMU/ using on-off acceleration command control system 02 p0186 A67-12230

Problem solving under sequential and batch display conditions, noting effects of data density 02 p0186 A67-12231

Pharmacology in prolonged space flight noting increasing resistance of organism to extremal flight factors, use of pharmaceuticals during flight, etc 02 p0185 A67-12320

Effect on human performance of whole-body vibration at various frequencies, determining minimum G level producing significant decrement 02 p0189 A67-12632

Optimization of display configurations for group viewing 03 p0385 A67-13299

Compatibility of artificial gas mixtures dependent on carbon dioxide and oxygen partial pressures 04 p0562 A67-14573

Dynamic pulmonary work of human males during muscular exertion at 2000 m and different barometric pressures 04 p0561 A67-14631

Effects of anthocyanin glucosides on night vision of airport approach controllers 04 p0561 A67-14633

Reduced gravity, pressure suit and load effect on human self-locomotion on lunar surface [ASME PAPER 66-WA/BHF-6] 04 p0564 A67-15400

Heat metabolism in working men while isolated from environment by water-cooled suit and environmental chamber [ASME PAPER 66-WA/HT-45]

Phase shifts of human circadian system and performance deficit during periods of transition in north-south flight 04 p0564 A67-15431

Cupular function of man under acceleration, noting electroencephalographic results on caloric nystagmus under 1.2, 3 and 4 g and postrotational nystagmus 05 p0756 A67-16289

Biological significance of space effort including colonization and adaptation of man to extraterrestrial habitats 06 p0954 A67-19040

Adaptive functions of man in vehicle control systems 07 p1221 A67-18194

Muscle system participation in bending and straightening of elbow joint muscle system participation in bending and straightening of elbow joint 07 p1133 A67-19346

Cardiovascular health of air traffic controllers age-matched with noncontrollers 07 p1134 A67-19859

Manual control dynamics for single loop systems facilitating man-machine system design 07 p1162 A67-19907

Static firing ground testing of Saturn launch vehicle [AIAA PAPER 67-234] 07 p1165 A67-20057

Effect on human performance of variations from true values in simulation of extraterrestrial visual environment [AIAA PAPER 67-251] 07 p1166 A67-20069

Critical tracking task for man-machine research related to operator effective delay time 07 p1136 A67-20171

Human error causes, accidents and effects of fatigue, microsleep and flicker fusion frequency 07 p1137 A67-20229

Human performance on earth and in space noting depth perception, visual acuity, walking ability, reaction time, etc 08 p1289 A67-21068

Experimental program for orbiting biomedical/behavioral laboratory, discussing functions 08 p1287 A67-21069

Manned orbital laboratory for biological research, discussing experimental possibilities and requirements on spacecraft 08 p1287 A67-21070

Verbal-analytical model of human operator performance in compensatory tracking 10 p1618 A67-22733

Cardiac output during rest and work determined via carbon dioxide method at 3800 m altitude 10 p1598 A67-23392

High altitude effect on work capacity, discussing bicycle ergometer test results on physiological response of human subjects 10 p1598 A67-23393

Standard prolonged work test for evaluation of fatigue and stress in man 10 p1600 A67-23817

Human lung gas mixing efficiency estimated, using residual lung nitrogen content curve 11 p1747 A67-24626

Immobilization effects on electrical activity of brain and intellectual and perceptual motor processes 11 p1748 A67-25064

First order factors affecting driver ability to safely control typical lunar vehicle through simulated mission profile over representative terrain [SMPTE PAPER 101-54] 12 p1920 A67-25469

Airline operation, reliability, personnel and training techniques [SAE PAPER 670343] 12 p2041 A67-25879

Signal duration effect on detection in presence of masking noise by human auditory system, using electric analogy for testing purposes 12 p1903 A67-26126

Secondary task interference in tracking 13 p2061 A67-26490

Secondary verbal task effect on tracking performance 13 p2061 A67-26491

Analytic measure for difficulty of human control as constrained by capability, training and stress 13 p2061 A67-26709

Human transfer function problem and compensatory tracking, analyzing variance and determining average rate of stick motion as underlying variable 13 p2063 A67-26923

Barotrauma, circulatory constriction and other in-flight auditory troubles of civil aeronautical navigation personnel over 40 years old 14 p2257 A67-28214

Long duration random vibration effects on human response in simulated low altitude

high speed flights 14 p2257 A67-28660

Task load and type of underwater exposure effects on response time to signal light in visual periphery of novice divers 14 p2258 A67-28662

Peripheral vision displays for dynamic tracking information during difficult flight control tasks improve operator performance 14 p2258 A67-28663

Auditory vigilance task, assessing effects on performance of signal detection value, miss or false detection cost and set size from which signals were drawn 14 p2258 A67-28664

Independent effects of error magnification and field of view on compensatory tracking performance, analyzing display and optical magnification 14 p2258 A67-28667

Miniature multichannel pulse-duration-modulated multiplex telemetry unit for medical monitoring of human subjects pulse, temperature, airflow, etc, under stress 14 p2259 A67-28688

Human circadian rhythms in activity, body temperature and other physiological functions, discussing oscillator multiplicity, internal desynchronization and entrainment 15 p2426 A67-29110

Advanced vision research for extended space flight 15 p2430 A67-29274

Recognition thresholds for lunar crater sizes, noting elliptical image measurements and generation of appropriate computer program 15 p2431 A67-29894

Simultaneous primary and secondary voice message monitoring, discussing methods and experimental setup 15 p2431 A67-29895

Physiological testing under simulated reduced gravity conditions with subject suspended and performing exercises on inclined treadmill 16 p2616 A67-30756

Two 15-day experiments of three subjects performing work-rest cycles in isolation chamber studying psychological functions, cardiovascular system, etc 16 p2613 A67-30912

Prolonged confinement in small chambers effect on biodynamic processes of walking and other movements in special positions 16 p2613 A67-30914

Reduced gravity, pressure suit and load effect on human self-locomotion on lunar surface [ASME PAPER 66-WA/BHF-6] 17 p2807 A67-32814

Human operator performance in continuous pursuit tracking with advanced and delayed visual display 18 p2994 A67-34339

Human controller as adaptive low pass filter to track signal contaminated with noise 18 p2994 A67-34340

Human performance relation research relationship with aerospace mission oriented simulation studies, discussing methodological resolution and limitation 18 p2994 A67-34341

Interactionist models of human performance in complex system or formal work organization, discussing multidimensional models 18 p2994 A67-34654

Man capability to operate in cislunar space and lunar surface through Apollo program, discussing practical applications 19 p3326 A67-35644

Human sensor-motor coordination testing in simulated weightlessness 20 p3368 A67-36263

Tracking activity of human operator under effect of certain space flight factors, establishing relationship between control habits and level of hypoxia and hypercapnia 20 p3368 A67-36265

Human experiments to study somnolent and precollapoid/collapoid states when falling asleep and during prolonged standing tests 20 p3368 A67-36268

Color normals differences, discussing classification and correlation methods 20 p3372 A67-37026

Heat and exercise induced hypohydration effects upon physical performance of women, showing some deterioration in cardiovascular system 20 p3372 A67-37033

Data on crew workload in C-141 aircraft used for extended mission living and working schedules, showing major disruptions in regular patterns 21 p3576 A67-38073

Antimotion sickness drugs and placebos effect on altering motion sickness susceptibility in Skyraider aircraft aerobatics and Slow Rotation Room dial test 21 p3574 A67-38083

Central factor influence in pure tone induced auditory fatigue while performing threshold tracking or other mental activity 21 p3576 A67-39060

Short term memory of paired associates studied using continuous technique, noting recall as function of number of interpolated pairs 22 p3750 A67-39318

Air Force accident history noting importance of maintenance/material area 22 p3754 A67-39598

Evaluation and analysis of critical human performance for rating man-machine interface 22 p3755 A67-40154

Feedback changes effects on reaction time in stopping chronometer 22 p3756 A67-40536

Cockpit environment thermal stress effect on psychological test performance and biomedical parameters 22 p3753 A67-40539

Mathematical technique to determine probabilities associated with critical system performance capability measured under varying human and environmental conditions 23 p3964 A67-41547

Human respiratory system impedance simulator for dynamic testing of aircraft breathing equipment to detect possible instabilities 24 p4114 A67-41782

Human Error Research and Analysis Program /HERAP/ for man-machine system, investigating pilot error and performance and aircraft accident prevention [AIAA PAPER 67-848] 24 p4117 A67-42984

Scaling laws and hydrodynamic model design techniques for high fidelity underwater simulation of zero and partial-g environments for manned space activities [AIAA PAPER 67-925] 24 p4140 A67-43021

HUMAN REACTION

Bed recumbency effect on ventilatory, metabolic and cardiac response to bicycle ergometer test, noting possible preventive effect of muscular exercises and venous occlusion 01 p0016 A67-10949

Statistical evaluation of changes in serum potassium, sodium and chlorides for aerospace flights 01 p0015 A67-10952

Biomedical assessments of human circadian system, noting increase in subjective fatigue and psychological and physiological performance 01 p0018 A67-10955

Variations in friction and inertia characteristics of rotary control determined, noting preference ratings of control characteristics 02 p0186 A67-12229

Reaction of human organism to time shifts experienced during flights of modern aircraft [DVL-611] 02 p0185 A67-12428

Heat, noise, vibration and acceleration simulation to determine beneficial effects of boost and reentry stresses on humans 03 p0366 A67-14389

Human reactions and attention shifts during flight tracking tasks 04 p0582 A67-14544

Human body response to acceleration according to various models [ASME PAPER 66-WA/BHF-13] 04 p0564 A67-15402

Human body response to stationary and nonstationary vibration [ASME PAPER 66-WA/BHF-15] 04 p0564 A67-15937

Terminal connections of spinothalamic and distribution in human thalamus, noting pain relay question 06 p0953 A67-18775

Cardiovascular changes due to orthostasis, evaluating influence of intravascular instrumentation on orthostatic tolerance of normal men 06 p0953 A67-18776

In-flight measurement of human response transfer characteristics of pilot [AIAA PAPER 67-240] 07 p1136 A67-20061

Relation between human mechanical impedance and coupling of human center of mass to environment, noting transfer function 09 p1456 A67-22370

Helmet mounted sight as operational element in quick reaction boresighting system, using static and moving targets, obtaining field test data 09 p1456 A67-22371

Backward, forward and transverse acceleration effects on cardiopulmonary systems of men and dogs 10 p1599 A67-23810

Complex measuring instrumentation effect upon tilt table response 10 p1602 A67-23823

Mechanism and pattern of human cerebrovascular regulation after rapid changes in blood carbon dioxide tension 11 p1746 A67-23889

Orientation and navigation in space-time 11 p1820 A67-24936
Physiological effects of high altitude flights on human organism 12 p1903 A67-26164
Gastroenterology in space medicine and physiological basis of cosmonaut nutrition 13 p2058 A67-26752
Flight simulator motion enhancement and potential for flight crew training, examining human vestibular system 13 p2064 A67-27268
Graphical demonstration of human reaction to shock or vibration input in horizontal plane to study physiological functions of equilibration 13 p2064 A67-27274
Skilled response organization, discussing stimulus coherence, tracking task, spatial and temporal coherence, secondary task, sequence length and task coding 14 p2254 A67-28034
Factors affecting human spatial orientation system functioning during flights 14 p2254 A67-28211
Radiobiological aspects of radiation safety in cosmic flights 14 p2255 A67-28222
Control-display association preferences for concentric controls 14 p2258 A67-28665
Lowering of psychic tone, absentmindedness and vigilance decline during astronaut weightlessness on long space flights 15 p2425 A67-29103
Extraterrestrial vestibular research in orientation of humans in space, noting possible disorders due to radiation and lack of protection 15 p2425 A67-29106
Phase shifts in human circadian system noting individual differences, performance deficit, physiological changes and dissociation from time zone displacements 15 p2425 A67-29108
Probability and payoff as factors influencing two-choice reaction time 15 p2427 A67-29134
Stimulus thresholds for perception of angular acceleration in man 15 p2427 A67-29267
Plasma 17 hydroxycorticosteroids in healthy subjects after water immersion of 12 hr duration shows no stressful effect 15 p2427 A67-29270
Plasma volume and tilt table response of humans to water immersion deconditioning experiments, using extremity cuffs to study protective effect 15 p2428 A67-29271
Cardiovascular changes at onset of whole body, X-axis sinusoidal vibration in anesthetized mongrel dogs and unsedated humans 15 p2428 A67-29272
Human response model identification in manual control system applied to study of stability and performance of man-machine system 15 p2432 A67-30315
Prolonged acceleration effect on human organism tested using retinal blood circulation observations 16 p2610 A67-30755
Physiological limits of adaptation of eye with respect to body noting increase of pressure in ophthalmic artery under different conditions of hypoxia 16 p2611 A67-30757
Mutation of human tissue by cosmic radiation, discussing results of cell studies from male and female subjects 16 p2611 A67-30766
Weightlessness effect on human cardiovascular system noting mechanical forces, amount of work done to overcome hydrostatic pressure, etc 16 p2612 A67-30773
Physiological reaction of human body to applied stimuli, developing method evaluating metabolism 16 p2612 A67-30907
Manrating of space environment simulators, emphasizing integration of physical facility requirements and operation procedure to provide safety 17 p2807 A67-31960
Aortic insufficiency in flying personnel, discussing case histories and cardiovascular system 17 p2806 A67-31965
Human reaction to intermittent photic stimulation in environmental chamber under IFR conditions 17 p2807 A67-31966
Radiation and weightlessness effect on human organism in space flights, discussing galactic cosmic, solar and Van Allen belt radiation 18 p3116 A67-33700
Control display linkages tested with human subjects for response time 18 p2993 A67-34338
Subjective evaluation of relative annoyance of sonic booms, explosions and

jet aircraft noise 18 p2986 A67-34393
Evoked potential display procedures yielding photographic superposition of large number of average responses 19 p3179 A67-34955
Vibration effect on task performance evaluated from test series, using vibration simulator 19 p3181 A67-35557
Continuous /24 hr/ wide band noise effect on human body, discussing subjective/objective fatigue 20 p3369 A67-36670
Weightlessness state in atmosphere and vacuum applied to satellites and space probes, noting effects on passengers and equipment 20 p3418 A67-37260
Anatomical locus of behavior reinforcement, discussing survival mechanism development in animals and humans 20 p3373 A67-37432
EEG and rhythmical tremor in outstretched upper extremities in man analyzed by autocorrelation and cross correlation 20 p3373 A67-37525
Retinal discrimination and visual acuity at different degrees of hypoxia by reading symbol E individually and combined, using oxygen-poor mixtures 21 p3575 A67-38507
Perceptual motor-skills forgetting in simple printing task, attributing decrements to retroactive interferences 21 p3576 A67-39099
Reinforcement intervals /RI/ effect in paired-associate learning using within-subjects, noting error dependence on RI 21 p3576 A67-39100
Sonic boom and subsonic aircraft noise test results 21 p3569 A67-39118
Biomedical results for various human medical systems during weightlessness experiments of Gemini program, noting vestibular function and EVA 22 p3752 A67-40534
Sudden strong stimulus effects on pilot simple visual reaction time and fatigued muscle strength 22 p3756 A67-40537
Laboratory psychophysiological efficiency in flying personnel of various ages covering pursuit reaction tests, serial motor activity and optico-acoustic signal analysis 22 p3753 A67-40544
Speech audiometry for hearing loss examinations of middle aged pilots 22 p3753 A67-40545
Intermittency hypothesis suggesting temporal integration of data processing of human central nervous system achieved through control of clock generating time points 23 p3944 A67-41020
Manned space flight predicted exposure effects vs actual medical findings 23 p3945 A67-41067
Cerebral blood flow and metabolism during combined hypoxia and hypercapnia, noting cerebral vasodilatation effect 23 p3945 A67-41080
Absorption times for gases injected into mammalian eye anterior chamber 23 p3950 A67-41536
High performance aircraft flight effect on blood glucose in fasting subjects noting no hypoglycemia tendency 23 p3950 A67-41550
Cineradiographic analysis of human visceral responses to short duration acceleration impact 23 p3951 A67-41553
Inactivity and water immersion effects on fluid balance and tilt-table performance in dehydrated subjects, assessing vasopressin and positive pressure breathing effects 23 p3951 A67-41557
Conductive cooling method for pressure applications in body heat loss promotion at high exercise rate 23 p3964 A67-41558
Continuous EKG recording during free fall parachuting, discussing tachycardia as normal response 23 p3964 A67-41560
Human circulatory response to sinusoidal gravitational stimulus via Rotational Flight Simulator /RFS/, discussing heart rate variation 23 p3951 A67-41561
Acetazolamide effects in aiding altitude accommodation, examining action on blood and cerebrospinal fluid 23 p3951 A67-41566
Physiological response and acceleration tolerance in dynamic simulation via human centrifuge, noting symptoms occurrence frequency 23 p3953 A67-41590
Physiological responses to cold in men during extended period of sleep loss 23 p3955 A67-41615
Renin secretion measurement for human

adaptation to circulatory stress from G acceleration, discussing high plasma renin levels during acceleration 23 p3956 A67-41634
Involuntary vestibularly driven head movements in man during rotational simulation 23 p3959 A67-41659
Subjective effects of fatigue on aircrew expressed in work cycle terms from data of continuing daily activity log 23 p3959 A67-41663
Isolation effects in constant environment on cycles of physiological functions and performance levels of man 23 p3959 A67-41697
Human blood circulation times during weightlessness produced by parabolic flight 23 p3959 A67-41698
Autogeneous and exogenous suggestion applied to changing of psychophysiological state of human organism after exposure to prolonged bed rest 24 p4112 A67-41855
Electric stimulus effect on vestibular apparatus responses to acceleration increasing or decreasing reactions depending on applied voltage polarity 24 p4112 A67-41859
Manned chamber testing of lunar module environmental control subsystem, describing equipment and support systems 24 p4139 A67-42050
HUMAN TOLERANCE
Spacecraft shielding combinations for astronaut protection, comparing magnetic, electrostatic and passive methods on basis of dosage and mission duration 01 p0153 A67-10425
Command and control display system requirements noting dependence on human visual mechanism 03 p0365 A67-13300
Physiological responses of subjects in prolonged immersion to neck level, measuring losses of heat, fluid and electrolytes 03 p0364 A67-14294
Human dynamic force response to impact examined, using spring-mass-damper system with refined parameter values 04 p0564 A67-15401
Tilt table responses of human subjects improved by application of lower body negative pressure 05 p0755 A67-16286
Sensitivity of manned planetary spacecraft design to shield weight, onboard radiation and uncertainties in space environment radiation 07 p1258 A67-19376
Human perception of airflow resistance and perception thresholds under various conditions 07 p1133 A67-19478
Biological effects of supersonic flight, discussing radiation at high altitudes and preventive measures 07 p1134 A67-19532
Jet engine noise sources, discussing noise radiation patterns, penalties for improved specific fuel consumption, etc 09 p1559 A67-21701
Temporal characteristics of body temperature during high thermal stress, determining correlation between effective and rectal temperature 10 p1600 A67-23822
Human tolerance to changes in aircraft cabin pressurization 10 p1602 A67-23825
Decompression sickness in high altitude flying, discussing degrees of bends pain among squadron members during five year period [SAM-TR-66-305] 10 p1600 A67-23826
Weightlessness and manned space flight medical data to date 12 p1902 A67-25727
Space physiology acceleration problems including engineering aspects of impact absorption 13 p2059 A67-26760
Human body resistance limit for ejection through aircraft canopy 14 p2257 A67-28215
Maximal intensity inflight stress effects on human tolerance investigated, noting deceleration experiments 14 p2257 A67-28218
Long duration random vibration effects on human response in simulated low altitude high speed flights 14 p2257 A67-28660
Possible decompression effects in supersonic transport cabin in terms of biomedical considerations for passenger safety 14 p2258 A67-28666
Depressurization behavior of human organism, noting endurance as flight duration and altitude function, and von Beckh chimpanzee absolute-vacuum experiments 16 p2615 A67-31766
Antixposure assemblies evaluation in low temperature water, recording body heat loss and tolerance time for application to helicopter crews 17 p2807 A67-31959

Polarographic and mass gas flowmeter sensors incorporated into bench model for on-line continuous determination of oxygen consumption in human subjects 18 p2995 A67-34711

Gemini program study to provide safe and biologically sound method of man qualifying for space exploration 19 p3177 A67-35208

Human brain hemodynamics during prolonged hypokinesia including orthostatic and bed-rest tests, using rheoencephalographic technique 20 p3368 A67-36266

Human acoustic analyzer functional state studied for hypokinesia effects 20 p3368 A67-36267

Human natural immunity with respect to substitution of Chlorella proteins for animal proteins, studying lysozyme activity in saliva and blood serum 20 p3368 A67-36269

Fatal injuries resulting from extreme water impact studied from necropsy data on persons jumping from Golden Gate Bridge 21 p3573 A67-38069

Extreme flight factor effects on human organism determined by simulation, noting physiological function level increase before stress increases resistance 22 p3752 A67-40533

Manned space flight predicted exposure effects vs actual medical findings 23 p3945 A67-41067

Human visceral response to short duration impact analyzed by cineradiography 23 p3960 A67-41704

HUMAN WASTE

SA URINE

Mineralization of human solid and liquid wastes by methods of thermal and thermocatalytic oxidation for autotrophic and heterotrophic organism use 02 p0187 A67-12326

Effects of various diets and simulated space conditions on human waste and water consumption applied to life support system development 02 p0188 A67-12339

Waste management and physiological response to substandard hygiene under controlled environmental conditions 03 p0366 A67-14289

Metabolism of dihydroxyphenylalanine in human subjects 09 p1454 A67-21982

Contaminant concentration due to human habitation of space cabin simulator at 258 mm Hg and oxygen atmosphere environment 23 p3964 A67-41559

Indigenous biological flora of human male subjects in closed environment and effects of diet on fecal flora 23 p3957 A67-41642

Fecal waste management unit for life support simulator or aerospace flights [SAE PAPER 670852] 24 p4115 A67-42001

Continuous culture system for Hydrogenomonas bacteria in waste management of life support system [SAE PAPER 670854] 24 p4115 A67-42002

HUMIDITY

SA WATER VAPOR

Airborne double bolometer technique for deriving atmospheric water vapor profiles by solving radiative transfer equations 01 p0108 A67-10315

Doppler-displaced lines of water vapor originating in atmosphere of Venus observed on three Coude spectrograms 02 p0324 A67-11774

Atmospheric water vapor distribution estimated from satellite measurements, using Planck radiance and assuming temperature distribution to be given 02 p0239 A67-12364

Maritime precipitation analyzed using radar data and satellite photographs of cloud cover 02 p0262 A67-12404

Physical aspects of stratocumulus including temperature, liquid water content, drop size, wind effect, shape, etc 03 p0462 A67-13499

Humidity and simulated space environment effect on various cadmium-sulfide thin film solar cells, noting degradation rates 10 p1596 A67-23163

Radiation data measured by Tiros IV satellite for determination of global distribution of atmospheric water vapor 10 p1677 A67-23195

Moisture transfer and thermal influx equations solutions for atmospheric boundary conditions of preinversion intramass strata evolution scheme 11 p1816 A67-24522

Temperature and humidity fields vertical

structure determined under conditions of stratified cloudiness 14 p2348 A67-28765

Influence of surface roughness and humidity on endurance of rubbed films of various lamellar solids on steel 16 p2681 A67-30853

Tropospheric water vapor analysis via Tiros IV satellite, determining spatial and temporal temperature, humidity and mass variations 17 p2880 A67-32550

Formulas for potential temperatures derived from thermodynamic principles, considering four stages of reversible adiabatic transformation of humid air 17 p2844 A67-32566

Atmospheric heating due to radiative heat transfer of direct and earth-reflected solar rays calculated as function of moisture content 19 p3251 A67-34851

Fan jet engine performance and operation as affected by humidity 20 p3515 A67-36448

Cellular cumulus convection confined to cylindrical column in conditionally unstable atmosphere 20 p3480 A67-36505

Atmospheric humidity effect on lower atmospheric layer turbulence above oceans, discussing velocity, temperature and humidity profile calculation formulas 22 p3828 A67-39220

HUMIDITY MEASUREMENT

SA HYGROMETER

Michelson type interferometer for Nimbus meteorological satellite to obtain vertical temperature, humidity and ozone profile 02 p0246 A67-12365

Aluminum oxide hygrometer performance obtained from balloon flight tests 05 p0808 A67-17307

Absorption and brightness temperature variations of atmosphere on basis of statistical characteristics of vertical temperature and humidity structures 11 p1785 A67-23956

Satellite radiation data application to synoptic weather analysis including cloud pattern mapping, tropospheric relative humidity and vertical cloud structure inference 13 p2149 A67-26274

Geographical distribution of surface temperature of ground and/or clouds and mean relative humidity of upper troposphere 15 p2513 A67-30059

Earth atmosphere humidity profiles and cloud densities interpreted from 1 cm microwave absorption measurement, water vapor resonance and radiosonde measurement 22 p3806 A67-40359

HUMMINGBIRD AIRCRAFT

S XV-4 AIRCRAFT

HUNGARY

Cosmic space research activities in Hungary, discussing data recording, satellite tracking, etc 19 p3320 A67-35291

HUNTER F-2 AIRCRAFT

Joint NASA-USAF lifting body flight test program and M2/F2, HL-10 and SV-5P research vehicles 06 p0947 A67-18197

HURRICANE

Main processes pertinent to convective storm development, with emphasis on structure and mechanics of storms already formed 18 p3074 A67-34094

HUYGENS PRINCIPLE

Characteristics of dielectric rod excited with dominant propagating mode 18 p3011 A67-34020

Fast and slow magnetosonic wave propagation in plasma analyzed by Huygens principle 21 p3670 A67-38687

Laser beam expansion in turbulent medium using Huygens-Kirchhoff principle and Fresnel diffraction approximation 22 p3761 A67-39739

HYBRID COMBUSTION

Visualization of combustion through transparent chamber walls, noting problems concerning hybrid rockets, ignition lags and hybrid combustion instabilities [ONERA-TP-474] 14 p2377 A67-27895

HYBRID COMPUTER

Hybrid CDC 3200 digital computer acquisition of response data from acoustic and high force vibration tests 01 p0029 A67-11025

Digital computers for navigation and guidance solving design problem by combining general purpose/GP/ and digital differential analyzer/DDA/ approaches to produce hybrid computer 01 p0111 A67-11258

Hybrid computer simulation of reentry guidance for lifting vehicle, noting

compatibility of temperature rate flight control system with other vehicle controls 01 p0051 A67-11438

Three and six degrees of freedom missile subsystem design analysis using flight simulation by hybrid computer 05 p0789 A67-17515

Analogue/hybrid computer design, noting inclusion of solid state and integrated circuits for reliability cost reduction and speed 05 p0769 A67-17519

Apollo engineering simulation activity, particularly analogue-digital real time hybrid simulation for guidance and control [AIAA PAPER 67-230] 07 p1164 A67-20055

Lunar Module evaluation and test using analog and hybrid computer simulation with LM guidance and control hardware [AIAA PAPER 67-232] 07 p1164 A67-20056

Apollo spacecraft hybrid real time flight simulation ensuring 40 msec sampling interval [AIAA PAPER 67-255] 07 p1166 A67-20071

Three-dimensional chaff simulator to provide video inputs to operational radar equipment for exposing operators to jamming 08 p1314 A67-20656

Mathematical models for use in hybrid computer simulation for design of integrated Helicopter Avionics System/THAS/, analyzing operational modes of automatic flight control system /AFCS/ 08 p1350 A67-20658

Full mission engineering simulator/FMES/ design for integrating hardware into lunar module system as hardware is made available by subcontractors 08 p1319 A67-21546

Fourier series and integrals in analog, digital and hybrid computation 09 p1470 A67-22667

Solution of optimal control problems using hybrid computers 11 p1770 A67-24426

Digital and hybrid pulse analyzer designs for automatic measuring pulse characteristics digital and hybrid pulse analyzer designs for automatically measuring pulse characteristics 13 p2075 A67-26411

Hybrid computer calculation of instantaneous and peak amplitude probability distribution of random signal 15 p2440 A67-29774

Process identification by cyclic parameter adjustment with automatic iteration, using analog and hybrid computers 15 p2465 A67-30342

Hybrid simulators used for aerospace and military programs consisting of analog computers, digital computers and interface units for handling data flow 18 p3019 A67-33635

Quantization error bounds for hybrid control systems by time varying function 19 p3202 A67-35625

Design of time-shared multiformat display medium to improve guidance and control displays in manned spacecraft [AIAA PAPER 67-552] 19 p3257 A67-35949

Hybrid computer Monte Carlo techniques for solving partial differential equations of continuous Markov processes 19 p3188 A67-36057

Parameter optimization by modified sequential random perturbation technique using hybrid computer, considering initial conditions and analog computer errors effect, for dynamic systems 19 p3188 A67-36058

Hybrid simulation for analysis and design of nuclear reactors feedback control systems 19 p3189 A67-36068

Hybrid computer for co-current laminar-flow heat exchanger Sturm-Liouville problem 19 p3190 A67-36069

Errors in state vector from amplitude quantization in feedback control loop, noting finite word length in hybrid computer simulation 24 p4134 A67-42023

HYBRID PROPELLANT

Hybrid fuel regression rate, discussing oxidizer flow rate and burner pressure interdependence [AIAA PAPER 66-113] 05 p0873 A67-17347

Pressure dependence of nonmetalized hybrid fuel regression rates in demonstrating major heat release reactions as heterogeneous or homogeneous 10 p1697 A67-23133

Propulsion systems for booster rockets and space vehicles 14 p2377 A67-27875

HYBRID PROPULSION

Ignition methods for strongly and weakly hypergolic hybrid propulsion systems, examining steady state combustion problems and combustion instability
01 p0139 A67-11416
Solid and hybrid propulsion relationship to sounding rocket vehicle design and mission analysis, particularly application to synoptic meteorology
08 p1374 A67-20492
Propulsion by solid/liquid or hybrid rocket motor
17 p2929 A67-32727

HYBRID ROCKET

Solid propellant regression rate in hybrid rocket motor examined via combustion process model, assuming homogeneous flow in central channel
05 p0874 A67-16766
Internal ballistic considerations in hybrid rocket design, noting throttling and regimes of operation involving effects of surface-or gas-phase reaction kinetics
[AIAA PAPER 66-628]
07 p1240 A67-19377
Hybrid rocket operation as gas generator, surveying advantages and disadvantages for fuel or oxidizer
08 p1410 A67-20802
Ablation rate of hybrid rocket solid propellants in two-dimensional engine simulated chamber
08 p1373 A67-20804
Propulsion by liquid-solid or hybrid rocket engines, performance and design
13 p2188 A67-27292
Visualization of combustion through transparent chamber walls, noting problems concerning hybrid rockets, ignition lags and hybrid combustion instabilities
[ONERA-TP-474]
14 p2377 A67-27895
Boundary layer combustion in hybrid rockets from simplified model comprising convective transport and chemical kinetic factors, analyzing fuel regression rate
[AIAA PAPER 67-471]
18 p3157 A67-33941
Hybrid rocket design combining flexibility of liquid fuel with simplicity and reliability of solid propellant
20 p3516 A67-36487

HYDRATE

Dissociation pressures of mixed gas hydrates predicted from data for hydrates of methane, propane and nitrogen with water
02 p0190 A67-12234
X-ray analysis of hydrate of diethylamine three-dimensional crystal structure, determining bond distances and angles
22 p3757 A67-39634

HYDRATION

SA DEHYDRATION

Observations with birefringent interferometer and photoelectric spectrophotometer of Martian surface materials composition, noting strong band at 3.1 micron suggesting hydrated minerals
11 p1865 A67-24603
Water deficit effects on thermal sweating, noting extraneous effects due to higher body temperature and wet skin
24 p4110 A67-41781

HYDRAULIC ACTUATOR

Cavitation effect on braking throttle actuating mechanism loaded with inertial mass
01 p0012 A67-10496
F-111 wing sweep actuator with irreversible Acme-thread jackscrew driven by hydraulic servomotor
05 p0752 A67-16157
Horizontal tail two-stage hydraulic servoactuator for F-111 horizontal stabilizer control
05 p0752 A67-16160
F-111 aircraft wing spoilers controlled by hydraulic servoactuators
05 p0753 A67-16162
Multiplex electrohydraulic actuators development, noting fault detection and feedback signals to prevent output drift
05 p0754 A67-16752
Main parameters of two-stage hydraulic amplifier-actuator system determined with aid of pressure and flow-rate amplification factors
10 p1597 A67-23321
Cavitation effect on braking throttle actuating mechanism loaded with inertial mass
10 p1597 A67-23618
Local loss coefficients for multistage hydraulic actuators with various working fluid temperatures
16 p2608 A67-31007
Linearized differential equations for invariant servodrive with hydraulic actuator controlled by throttle slide
16 p2809 A67-31378
SST flight control system electronic and hydraulic systems, discussing system design, components, reliability and test programs
[AIAA PAPER 67-570]
19 p3174 A67-35966

HYDRAULIC ANALOGY

Continuous spatially varied open channel liquid flow analogy for gas flow, with heat addition and extraction over finite distance
04 p0604 A67-14838
Hydraulic analogy applied to axisymmetric nonideal compressible gas systems, considering water table simulation of axisymmetric rocket nozzle
08 p1324 A67-21519
Hydraulic approximation for calculating MHD flows in ducts
09 p1541 A67-21804
Perturbation technique based on hydraulic analogy for estimating optimum efficiency and performance of axial flow compressor from description of geometry and aerodynamic environment
09 p1560 A67-22491
Hydraulic analog for qualitative analysis of flow field of expansion-deflection nozzle
14 p2297 A67-28136

HYDRAULIC CONTROL

SA ELECTROHYDRAULIC CONTROL
Altitude control for VTOL aircraft facilitates control of hovering flight, noting construction, operation principles and performance
03 p0363 A67-12981
Synchronization errors in parallel jacks system with closed loop control by hydraulic relays, using nonlinear differential equations
[ASME PAPER 66-WA-AUT-5]
04 p0555 A67-15389
Dual circuit hydraulic powered brake control system for effective short landing of F-111 aircraft
05 p0753 A67-16164
Feasibility of pure-fluid missile control system demonstrated by systems analyses, preflight tests and flight tests
07 p1257 A67-19360
Classification of working fluids including applications in hydraulic control technology
07 p1212 A67-19733
Static and dynamic sealing concepts and materials for propellant feed systems and pneumatic and hydraulic control systems of liquid propellant rocket engines
17 p2864 A67-31990
Hydraulic line models for fluid control system analysis, discussing frequency and transient response calculation
20 p3366 A67-37365
Fluid control system design by third order linear differential equation with transient response, showing relationship to frequency response
20 p3366 A67-37370
Testing machine operated by hydraulic pressure for mechanical properties of materials at medium rates of strain
23 p4079 A67-41332

HYDRAULIC EQUIPMENT

Coefficient of hydraulic resistance derived for plane flow of electrically conducting fluid in traveling magnetic field
04 p0670 A67-15534
Hydraulic research data concerning control valve sizing and arrangement, noting liquid and gas control-valve formulas with limitations, Reynolds number effect, etc
15 p2423 A67-30400
Cavitation in spool control valve orifices, showing effect on flow discharge coefficient over range of conditions
20 p3366 A67-37371
Hydraulic servodrive with supply source, control valve, actuator and feedback components analyzed for stability, deriving motion equations
21 p3570 A67-38048
Handley Page Jetstream aircraft major systems, auxiliary equipment and instrumentation
22 p3748 A67-40132
Hydraulic angular acceleration sensor motion equation obtained by kinetostatic method
22 p3809 A67-40477

HYDRAULIC FLUID

SA OIL
Pump loop testing and operational evaluation of SST hydraulic fluids
[SAE PAPER 660664]
01 p0103 A67-10572
Hydraulic fluid properties and capabilities for high altitude high temperature vehicles
[SAE PAPER 660661]
01 p0103 A67-10619
Variable sweep wing F-111 aircraft cooling systems for temperature control of hydraulic fluid of type II system
05 p0752 A67-16161
Fire resistance of hydraulic fluids - ASTM and SAE Symposium, New Orleans, January 1966
09 p1520 A67-22244
Closed compartment fire-resistance test for hydraulic fluids leaking near heated aircraft skin with or without electric arcing
09 p1521 A67-22245
Fire resistance of aircraft fluids, analyzing likelihood of spontaneous ignition by

flashpoint and isothermal enclosure methods
09 p1521 A67-22247
Ignition of flammable fluids by hot surfaces tested on static hot plate rig and on wind tunnel rig, noting data on kerosene, lubricating oil and hydraulic fluid
09 p1580 A67-22248
Spontaneous ignition temperature of flammable fluid in facsimile high speed aircraft hydraulic system
09 p1521 A67-22249
Resistance of aviation hydraulic fluids, mineral, snuffer, phosphate ester, siloxane and chlorosilicone to wheel brake fires, evaluating lab test techniques and simulation testing
09 p1521 A67-22250
Thermal stability and degradation of n-hexadecane, mineral oils, and oligomers measured as function of time and temperature
16 p2695 A67-31754

HYDRAULIC PUMP

Cost and power requirements influence on aircraft hydraulic pump design
05 p0753 A67-16751
Forces acting in electromagnetic pump channel on gas inclusions in liquid metal, assessing increase in hydraulic resistance
13 p2169 A67-27316
Hydraulic power units for supersonic aircraft noting trends in component power, speed, flow, pressure, design, etc
17 p2800 A67-31969

HYDRAULIC SHOCK

Stationary free-surface mercury flow in channels under magnetic field, analyzing hydraulic jump and influence of field on location
01 p0120 A67-10179

HYDRAULIC SYSTEM

SA AIRCRAFT HYDRAULIC SYSTEM
Hydraulic gimbalng system with closed loop design for orienting Saturn S-IVB engine
03 p0363 A67-13535
Externally pressurized bearings treated as hydraulic closed loop servomechanism analyzed, using transfer functions
[ASME PAPER 66-LUB-7]
03 p0431 A67-13759

Computer simulation of hydraulic system using time delay elements independently of boundary conditions
[ASME PAPER 66-WA-AUT-18]
04 p0555 A67-15413

Transfer function and input impedance of pressurized fluid piping system, using distributed parameters and block diagram feedback methods
[ASME PAPER 66-WA-AUT-13]
04 p0555 A67-15416

Directed graphs application to calculation of forced pressure oscillations in hydraulic systems of flight vehicles and engines
04 p0557 A67-15886

Hydraulic power distribution system for flight control of F-111 aircraft
05 p0752 A67-16158

F-111 type hydraulic power supply system design for supersonic aircraft using ground support equipment and military materials
05 p0752 A67-16159

Component design advances with fatigue tests on hydraulic tubes and outline of seal development
05 p0753 A67-16749

Design problems for hydraulic loading circuit with random variation of loading with time
09 p1451 A67-22472

Book on hydraulic control systems covering fluid flow theory, hydraulic pumps, motors, valves, power elements, etc
12 p1899 A67-25558

Hydraulic properties of duct of constant rectangular cross section functioning in closed circuit used to measure MHD flow velocity
13 p2165 A67-26593

Stability analysis of computer controlled linear hydraulic antenna control system
13 p2088 A67-26996

Fluid bulk modulus and density effect on typical hydraulic servomechanism
[ASME PAPER 67-FE-19]
14 p2252 A67-28366

Hydraulic systems reliability and maintenance, designing corrective measures to eliminate fluid leakage
[AIAA PAPER 67-403]
15 p2423 A67-30370

Hydraulic power units for supersonic aircraft noting trends in component power, speed, flow, pressure, design, etc
17 p2800 A67-31969

Flight control power distribution systems for hypersonic aircraft, considering cooled and pulsating flow hydraulic, liquid metal, pneumatic and mechanical systems
17 p2800 A67-31970

SST Concorde hydraulic system noting design and hydraulic fluid selection resulting from high ambient temperatures, weight and space limitations, etc 17 p2800 A67-31971

Pneumatic power for attitude control of long-life orbiting satellite, considering parameters, mission objectives, etc 17 p2801 A67-31983

Growth of dendriform crystal contaminant in hydrocarbon fuel or hydraulic system during stagnant storage, discussing possible effects and corrections 17 p2801 A67-31991

Boeing SST maintenance requirements considered in terms of aircraft characteristics, economics, facilities, operations, etc [SAE PAPER 670373] 17 p2798 A67-33003

Calculation of frequency characteristics of hydraulic main line sections with parameters varying continuously along length 20 p3363 A67-36444

Contamination control in hydraulic system of Saturn S-IVB stage, noting five-fold approach to anticontamination procedure 20 p3363 A67-36801

Contamination control of hydraulic system achieved when contamination level of fluid is within contamination tolerance level of system components 20 p3365 A67-37363

Hydraulic component material properties relationship to particulate material removed due to cavitation, showing particle size distribution definition 20 p3469 A67-37366

Nonlinear fluid mechanical systems design using numerical least squares method in fitting second order differential equation to straight line approximation of state variable 20 p3366 A67-37368

Approximate solutions for nonlinear differential equations to study periodic motions for analysis of pressure relief system 20 p3366 A67-37369

Hydraulic power systems for V-STOL noting self-sufficiency on start-up and auxiliary power source function 20 p3366 A67-37552

Hydraulic support system for free flight simulation with Saturn V-Apollo vehicle, discussing stability requirements, upper bounds of system design, conversion from nonlinear to linear model, etc 21 p3607 A67-37796

Blue Streak launch vehicle control system, discussing destabilizing resonance effects, hydraulic system, propellant movement in tanks and testing 21 p3570 A67-38102

Advanced high Mach number aircraft secondary power system requirements, discussing high pressure hydraulic systems and complex pneumatic positioning control systems 22 p3749 A67-40341

Procedures, facilities and equipment used in contamination control of Saturn S-IVB stage hydraulic system 23 p3935 A67-40848

Part and component cleanliness maintenance for hydraulic systems, liquid propellants and spacecraft interiors, noting protective methods [SAE PAPER 670825] 24 p4159 A67-41989

Hydraulic failure detection system in Titan booster servo injector module featuring anticipation and correction of servomodule failure 24 p4099 A67-42426

Chemical dynamic hydraulic power unit /HPU/ performance, weight and volume efficiencies, noting applications to solid and liquid propellants 24 p4107 A67-42531

Aircraft and missile electric/hydraulic power supplies, describing turboalternator performance, design and applications 24 p4107 A67-42532

HYDRAULIC VALVE

Binding in hydraulic servo control valves as affected by heat transfer from valve housing to spool and to surroundings [ASME PAPER 66-WA/AUT-15] 04 p0555 A67-15391

Cavitation erosion in Hawker Siddeley Trident hydraulic system and steps to find solution 05 p0753 A67-18748

Piezoelectric transducer electromechanical properties compared to electromagnetic actuator, noting fluid applications 14 p2248 A67-28267

HYDRAULICS

SA FLUID MECHANICS

Hydraulics and fluid mechanics - Australasian Conference, University of Auckland, December 1965 hydraulics and fluid mechanics - Australasian Conference, University of Auckland,

December 10 p1626 A67-23553
Hydraulic resistance coefficient of rotating tubes, taking into account centrifugal mass forces effect on flow inside tube 20 p3421 A67-36793

HYDRAZINE

SA METHYL HYDRAZINE

Metallic material compatibility with medium energy hypergolic propellant components hydrazine/UDMH and nitrogen tetroxide, used in ELDO rocket 01 p0139 A67-10211

Monograph on organic chemistry of hydrazine 05 p0758 A67-18073
Chemiluminescence from oxygen atom-hydrazine flames suggesting excited NO formed by energy transfer 06 p1072 A67-17987

Atomization, mixing and reaction characteristics of hydrazine and nitrogen tetroxide injected from quadlet element [AIAA PAPER 67-107] 06 p1072 A67-18308

In-vivo inactivation of factor VII by hydrazine in ether anesthetized rats 07 p1134 A67-19856

Photolysis of hydrazine vapor in vacuum UV, examining emission as function of pressure and photolysis time 07 p1138 A67-20190

Hydrazine synthesis from ammonia in concentric barrier discharge reactor 10 p1603 A67-23498

Hydrazine as single component fuel for gas generators and rocket engines, noting advantages and performance characteristics 18 p3106 A67-33459

Gas phase reactions of hydrazine with nitrogen dioxide, nitric oxide and oxygen, determining reaction rates, activation energy and order 18 p3109 A67-33837

Reaction zones of ammonia-oxygen and hydrazine decomposition flames, measuring temperature and concentration profiles 18 p3155 A67-33838

Effect of additives on hydrazine nitrogen trioxide droplet flame structure and burning rate [AIAA PAPER 67-482] 18 p3158 A67-33951

Hydrazine effect, alone and with nicotinic acid, on oxygen consumption, respiratory quotient, carbohydrate pool and heat losses in rats studied using gradient calorimeter 18 p2992 A67-34714

Hydrazine effect on carbohydrate metabolism in vivo and in vitro, studying hyperlactatemia, hypoglycemia, oxygen consumption inhibition, etc 18 p2992 A67-34720

Additives effect on ignition delay and pressure of hypergolic hydrazine-nitrogen tetroxide propellant 19 p3310 A67-35012

Flame structure of hydrazine burning in oxidizing atmosphere determined by measuring temperature and specific contractions at 90 degrees from stagnation point 19 p3310 A67-35014

Atomization, mixing and reaction characteristics of hydrazine and nitrogen tetroxide injected from quadlet element [AIAA PAPER 67-107] 19 p3310 A67-35766

Combustion characteristics of hydrazine type propellants and resultant reactions in low thrust engines prior to ignition 21 p3687 A67-37798

Fine structure of nitrogen 14 resonance in hydrazine analyzed for Zeeman effect 21 p3688 A67-38418

Far IR spectra and space group of crystalline hydrazine and hydrazine-d4 noting coupling of translational and librational motions 23 p4048 A67-41532

Hydrazine effects on free amino acid concentrations of plasma and urine in dogs 23 p3952 A67-41570

HYDRAZINE ENGINE /NIMPHE/

Mariner IV midcourse 50-lb thrust pressure-controlled monopropellant hydrazine propellant system, predicting impulse and velocity error as function of burn time [AIAA PAPER 66-948] 02 p0304 A67-12282

Lumped parameter model for monopropellant hydrazine reaction chamber developed, using mass and energy balance and reaction and diffusion rate coefficients 17 p2927 A67-31974

Mariner IV midcourse 50-lb thrust pressure-controlled monopropellant hydrazine propellant system, predicting impulse and velocity error as function of

burn time 21 p3712 A67-37797

HYDRAZINE NITRATE

Preignition phenomena in small Aerozine-50/nitrogen tetroxide pulsed rocket engines shown partly due to hydrazine nitrate accumulation 18 p3114 A67-33979

HYDRAZINE PERCHLORATE

T-burner tests for combustion stability evaluation of hydrazine diperchlorate [AIAA PAPER 66-599] 04 p0723 A67-15246

Self-deflagration process of hydrazine diperchlorate studied for three suggested pressure regimes 14 p2376 A67-28551

HYDRIDE

S ANHYDRIDE

S BERYLLIUM HYDRIDE

S BORON HYDRIDE

S LITHIUM HYDRIDE

HYDROACOUSTICS

Hydrodynamic pressure on elastic cylindrical shell from acoustic shock wave, using higher order asymptotic approximations 21 p3717 A67-37973

HYDROCARBON

SA CYCLIC HYDROCARBON

Ball bearing lubrication with vapor from volatile organic compounds for wide temperature range and long-term operation 01 p0077 A67-10120

Electron affinity data for various pentacyclic aromatic hydrocarbons, predicting ionization potentials 01 p0019 A67-10882

Oils and shales from 3 million to 2.7 billion years old analyzed for hydrocarbon content, using gas chromatography and mass spectrometry 05 p0797 A67-16580

Characteristic optical density and equilibrium of alkyl-sodium and aromatic hydrocarbons as function of temperature and wavelengths, correlating electron affinity with enthalpy values 09 p1458 A67-22214

High resolution gas chromatography combined with mass spectrometry applied to analysis of pyrolysis products of isoprene from 300 to 1000 degrees C 10 p1602 A67-22947

CH molecule solar spectral observations interpreted using several upper photosphere models and assuming local thermodynamic equilibrium 11 p1861 A67-24495

Reactions between alkane and cycloalkane molecular ions analyzed, using conventional and tandem mass spectrometry 12 p1903 A67-25969

Thermal stability and degradation of n-hexadecane, mineral oils, and oligomers measured as function of time and temperature 16 p2695 A67-31754

Growth of dendriform crystal contaminant in hydrocarbon fuel or hydraulic system during stagnant storage, discussing possible effects and corrections 17 p2801 A67-31991

Ion-molecule chemistry of Jupiter upper atmosphere, studying equilibrium and nonequilibrium abundances of hydrocarbon products due to UV radiation reaction 18 p3135 A67-34540

Heat transfer characteristics of several aliphatic hydrocarbons in nucleate and film boiling during forced flow in heated tubes [ASME PAPER 67-HT-7] 20 p3544 A67-36705

Amine-tin antioxidant systems for aliphatic hydrocarbons and related alkyl substituted fluids 20 p3474 A67-37594

Paraffinic hydrocarbons composition in Orgueil, Murray, Mokoia and other meteorites identified by gas chromatography 21 p3703 A67-38501

Hydrocarbons transformation mechanism and kinetics at low pressures in glow discharge noting three-way decomposition 22 p3757 A67-39585

Aliphatic hydrocarbons isolated from Trinidad Lake asphalt by gas chromatography and mass spectrometry appear to be unlike 24 p4149 A67-42100

HYDROCARBON COMBUSTION

Hydrocarbon flame ionization, discussing second process occurring in flames with acetylene and related unsaturated compounds 04 p0719 A67-14488

Combustion reactions during spacecraft reentry, noting degradation of heat shields composed of hydro- and fluorocarbon compounds 05 p0928 A67-17334

Experimental equipment for chemical reaction analysis in fluid systems based on

study of partial oxidation of methane at high pressures 05 p0759 A67-17540
 Combustion and heat transfer laws for hydrocarbon flames with predetermined visual radiation 08 p1425 A67-20303
 Electron-ion recombination behind shock waves in argon containing dilute lean mixtures of hydrocarbons and oxygen 09 p1457 A67-22024
 Polycyclic aromatic hydrocarbons in soot of premixed acetylene-oxygen flames, discussing graphs of flame height vs mixture composition 10 p1602 A67-22960
 Plasma behavior in laminar and turbulent hydrocarbon-air flames, discussing flame ionization, electron concentration and recombination, detonation wave ionization data, ignition, etc 17 p2968 A67-32168
 Mobility measurement of electron capture in hydrocarbon flames using Hall effect, noting variation when injecting chlorine 18 p3146 A67-33691
 Hydrocarbon pyrolysis and H/D substitution reaction rates, using single-pulse shock tube as chemical reactor 18 p2996 A67-33788
 Role of electronically excited CH in formation of C₃H₃ ion and contribution to overall chemionization process 18 p3150 A67-33802
 Atomic nitrogen-oxygen mixtures ion concentration enhancement in hydrocarbons presence, discussing atom recombination rate, etc 18 p3107 A67-33805
 Carbon formation in oxygen premixed acetylene and benzene flames 18 p3151 A67-33808
 Spectrophotometric study of multiple reaction zones of premixed trimethylaluminum-oxygen flames, emphasizing microstructure 18 p3109 A67-33840
 Chemical structure of premixed flames of methane and perchloric acid vapor diluted with argon obtained in terms of composition, temperature and velocity profiles 18 p3109 A67-33841
 Spectral brightness of metal chelate liquid fuel-air flames [CI PAPER 87-2] 19 p3309 A67-34997
HYDROCARBON FUEL
 Flame study of turbulence effects induced by sonic or ultrasonic vibration on combustion of liquid hydrocarbon jet 01 p0167 A67-10942
 Anodic oxidation and molecular structure influence on performance of normal saturated hydrocarbons in fuel cells 10 p1595 A67-22927
 Instrumentation and fuel systems for turbocharged and/or pressurized aircraft, discussing vapor lock problem, hydrocarbon fuels and vapor pressure equipment [SAE PAPER 870262] 12 p1899 A67-25510
 Liquid hydrogen for SST fuel compared with hydrocarbons, considering range, payload, weight, drag, engine design, storage and safety 13 p2186 A67-27635
 Lead, copper and cobalt oxides effects upon ignition kinetics of paraffinic and aromatic fuels 14 p2407 A67-28550
 Mobile hydrogen generators for alkaline electrolyte cells and medium temperature fuel cells for autonomous hydrocarbon electricity units 14 p2253 A67-29021
 Endothermic hydrocarbon fuels for supersonic aircraft, noting heat sink capacity effect in overcoming thermal thicket and usability as engine fuel 15 p2543 A67-29305
 Book on motor fuels, performance and testing, including fuel source and nature, gasoline combustion, diesel, turbine fuels, etc 16 p2734 A67-30998
 Secondary ion generation in flames by electron impact noting application of mass-spectrometry and hydrocarbon fuels analysis 16 p2780 A67-31520
 Intensity of light scattered from soot particles in diffusion flame of hydrocarbons burning in air 18 p3149 A67-33799
 Gun launched scramjet performance using various fuels, comparing weight and volume limitations effects 19 p3311 A67-34822
 Detonation properties in heterogeneous systems involving mixture of fuel with gaseous oxidant 20 p3551 A67-38815
 SST aircraft influence on fuel quality requirements, considering use of liquefied gaseous hydrocarbon fuels 21 p3688 A67-38192
 Thermodynamic and electrical properties

of MHD conversion fluid /K-seeded combustion products/ obtained by hydrocarbon fuel combustion, discussing electrical conductivity calculations 24 p4099 A67-42415
HYDROCHLORIC ACID
 Upper limits on liquid water content in Venus atmosphere 17 p2945 A67-32652
HYDROCORTISONE
 9-alpha-fluorohydrocortisone and venous occlusive cuffs effects on plasma volume and orthostatic tolerance following 28 to 78 days of bed rest 01 p0016 A67-10960
HYDRODYNAMIC EQUATION
 Hydrodynamic thermal explosion of stationary axisymmetric non-Newtonian fluid in infinitely long cylindrical tube 01 p0052 A67-10681
 Asymptotic form of correlation functions facilitated by use of Hamiltonian 03 p0458 A67-13342
 Solar rotation, coronal self-gravitational attraction and interplanetary magnetic fields effect on solar wind, presenting linearized hydrodynamic equations 03 p0508 A67-14313
 Wave excitation in compressible partially ionized plasma by electromagnetic and acoustic /or mechanical/ sources, describing set of linearized hydrodynamic and Maxwell equations 05 p0859 A67-17436
 Dissipative effects in converging cylindrical symmetric shock wave, considering ion and electron heat conductivity, ion viscosity and energy exchange 06 p0984 A67-18029
 Unsteady radial expansion of polytropic gaseous sphere in own gravitational field, using hydrodynamical equations and model limited by shock wave 06 p1083 A67-18064
 Radiation effect on hydrodynamic shock wave parameter distribution for bodies entering dense atmospheric layers at supersonic velocities 07 p1125 A67-19110
 Numerical solution of hydrodynamic equations adaptable to finite difference methods 07 p1187 A67-19157
 Hydrodynamic equations describing motion of electrons in weakly ionized plasma in external electric field derived from Boltzmann equation, using Chapman-Enskog method 07 p1228 A67-19503
 MHD approximation of solar plasma fluxes observed by Mariner II as free rotating jets 07 p1243 A67-19802
 Shock wave propagation in plasma across magnetic field, solving problem via two-component hydrodynamic equation 08 p1358 A67-20858
 Deformed figures of Maclaurin spheroids from solving post-Newtonian hydrodynamic equations for uniformly rotating axisymmetric bodies 08 p1354 A67-21245
 Nonsymmetric oscillations in plasma in magnetic field arising from electron beam passage through plasma, deriving dispersion equation 09 p1545 A67-22003
 Four-plasmon hydrodynamic equations describing weak turbulence spectrum in universal equilibrium region of plasma without magnetic field 10 p1686 A67-23597
 Modified Chapman-Enskog method for obtaining transport properties of nonequilibrium partially ionized gas, giving hydrodynamic equations 11 p1775 A67-23866
 Turbulence tensor within framework of hydrodynamic relativity, noting generalization of Weber equation 11 p1782 A67-24760
 Hydrodynamic thermal explosion of stationary axisymmetric non-Newtonian fluid in infinitely long cylindrical tube 11 p1783 A67-25068
 Dispersion equations obtained for numerical forecasting of meteorological fields from basic hydrothermodynamic equations, using Reynolds stresses 13 p2149 A67-26272
 Lagrange and Euler representations of particle shapes and vortex theorems in hydrodynamic flow 13 p2094 A67-26644
 Diurnal variations in structural parameters of upper atmosphere determined via differential equations of hydrodynamics 13 p2112 A67-26669
 Upper atmosphere hydrodynamic equation additional terms account for hydrodynamic effects of dissociative recombination and ion molecule reactions 13 p2112 A67-26670
 Transfer of large scale tropospheric perturbations into stratosphere analyzed using hydrodynamic model, noting role of

atmospheric stratification, refractive index, etc 13 p2112 A67-26674
 Temperature determination in stratosphere via hydrodynamic equations taking into account energy inputs and atmospheric motion, suggesting existence of integral heat sources 13 p2113 A67-26676
 Asymptotic form of correlation functions facilitated by use of Hamiltonian 13 p2149 A67-27713
 Hydrodynamic equations for electric field in steady collision-dominated three-component plasma 14 p2358 A67-28240
 Certain integral equations of first kind reduced to Abel equation and equation of second kind when solving elasticity and hydrodynamic problems 14 p2344 A67-28742
 Geopotential and wind field calculations for Northern Hemisphere using statistical models 14 p2346 A67-28764
 Book on experimental superfluidity covering He properties, low temperature production, temperature measurement, two-fluid model and macroscopic quantization, generalized hydrodynamic equations, etc 15 p2517 A67-29265
 Motion equation for nonideal relativistic electron gas, reviewing hydrodynamics obtained from Landau equation 15 p2527 A67-29517
 Two-fluid hydrodynamic equations for London superconductors obtained in inviscid approximation 15 p2540 A67-30004
 Counterpart of Stokes hydrodynamical paradox for linearized viscous fluid flow obtained from application of singular perturbation to Oseen equations 16 p2857 A67-30827
 Hydrodynamic stability problems solutions by numerical methods of Orr-Sommerfeld equations 16 p2861 A67-31419
 Supernova explosion and collapse theory using relativistic hydrodynamics 16 p2752 A67-31541
 Hydrodynamic field of falling sphere in viscous liquid within cylindrical container noting streamlines, velocity variations, etc 17 p2837 A67-32288
 Critical heat flux value nonlinearly dependent on liquid bulk underheating to saturation temperature, deriving empirical formula 17 p2970 A67-32460
 Hydrodynamic equations for automatic control of speed and coordinates of craft with underwater foils moving on disturbed body of water 18 p3074 A67-33416
 Supercavitating engines noting design principles, performances of existing models and connection between parameters 18 p3023 A67-33417
 Supercavitating engines, defining optimum curvature and thickness distribution, performance optimization, etc 18 p3023 A67-33418
 Numerical solutions of multidimensional singular integral equations in problems of hydrodynamics 18 p3024 A67-33537
 Lift and drag coefficients of wing profile with elliptical pressure distribution calculated by approximate linearized theory 18 p3024 A67-33541
 Wave propagation velocity in relativistic fluids determined using new hydrodynamic equations 18 p3025 A67-33683
 Two-fluid hydrodynamic equations for London superconductors obtained in inviscid approximation 18 p3100 A67-33782
 Classical hydrodynamics equations accounting for dissipative processes 18 p3027 A67-34089
 Structure of shock waves in collision-free plasma at angle to external magnetic field studied by hydrodynamic equations 19 p3288 A67-35372
 Regularity of generalized solutions of general nonlinear and nonstationary Navier-Stokes equations, improving differential properties by data smoothness 19 p3209 A67-35445
 Chapman-Enskog expansion applied to Fokker-Planck equation for plasma allows transport coefficients calculation without further approximation in presence/absence of magnetic field 22 p3843 A67-39266
 Nonlinear hydrodynamic equation term effects on rotational fluid motion in galactic plane, discussing velocity perturbations and discontinuities 22 p3893 A67-40502
 Second order accurate approximation to advection terms in hydrodynamics equations noting aliasing effects, amplitude and phase

- errors and stability criterion 23 p4024 A67-40994
- Rigorously geodetic inertial motion of extended object in Einstein gravitational field, using relativistic hydrodynamics 23 p4027 A67-41148
- Hydrodynamic solution for shock wave parameters of monatomic gases assuming exponential molecular interaction potentials and absence of mass forces 24 p4142 A67-42271
- Bounded variation method for optimum load capacity hydrodynamic one-dimensional gas slider bearing, discussing film thickness [ASME PAPER 67-LUB-6] 24 p4162 A67-42670
- Characteristic of high energy nucleon-nucleus interaction, analyzing changes due to structural buildup 24 p4192 A67-42839
- High order accurate difference methods in hydrodynamics 24 p4146 A67-43095
- ### HYDRODYNAMIC STABILITY
- Loss in hydrodynamic thermostability of viscoplastic material with stress tensor deviator related to strain rate tensor deviator 01 p0052 A67-10682
- Hydrodynamic stability Cauchy problem for continuous spectrum of two-dimensional parallel flow of nonviscous incompressible fluid 03 p0402 A67-13172
- Hydrodynamic drift-dissipation instability of plasma with nonuniform temperature 03 p0476 A67-13296
- Stability analysis of adiabatic flow of incompressible fluid without equation linearization and by constructing functional from hydrodynamic fields 03 p0402 A67-13619
- Hydrodynamic drift-dissipation instability of plasma with nonuniform temperature 04 p0663 A67-14721
- Volterra method used for two-dimensional problems of pressure penetration and penetration of small wedge into layer of incompressible liquid 04 p0604 A67-14778
- Energy methods of subcritical convective instability theory and critical Rayleigh number dependence on Nusselt number 05 p0926 A67-16816
- Stability of rotating liquid mass /e.g. earth/, following Jeans treatment of Jacobi ellipsoidal equilibrium configurations 06 p1080 A67-17768
- Large scale motions of atmosphere, noting hydrostatic and geostrophic equilibrium 07 p1170 A67-18334
- Advances in applied mechanics, Volume 9, covering hydrodynamic stability, free oscillations, nonlinear vibrations and viscoplasticity 08 p1352 A67-20308
- Initial value problem for hydrodynamic instability of parallel flow of inviscid fluid 08 p1319 A67-20309
- Nonlinear hydrodynamic stability theory of one-dimensional detonations based on perturbation techniques, detailing cases of ideal gas unimolecular reactions 11 p1774 A67-23857
- Rotor supported in fluid film journal bearings, eliminating self-excited vibrations through motion equation [ASME PAPER 67-VIBR-28] 11 p1797 A67-24186
- Hydrodynamic stability problems solved through approximate and numerical methods involving eigenvalue spectrum and Orr-Sommerfeld equation for parallel flow 11 p1781 A67-24552
- Hydrodynamic and overheating instability of nonisothermal plasma flux in crossed electric and magnetic fields in flat dielectric walled channel 11 p1842 A67-24950
- Loss in hydrodynamic thermostability of viscoplastic material with stress tensor deviator related to strain rate tensor deviator 11 p1783 A67-25070
- Lower bounds for periodic solutions of steady state hydrodynamic boundary value problem 13 p2093 A67-26617
- Stability of arbitrary one-dimensional hydrodynamical flow in quasi-isothermal case 13 p2105 A67-27413
- Rayleigh problem in hydrodynamic stability for two-dimensional parallel flow of nonviscous incompressible fluid 13 p2106 A67-27456
- Large-dimensional inverse pinch discharge study of impulsive plasma acceleration, gas dynamics and stability of unrestrained current sheet [AIAA PAPER 66-482] 14 p2356 A67-28123
- One-dimensional laminar MHD flow at hydrodynamic stabilization, discussing heat transfer, Hartmann flow, magnetic field, Prandtl number and Joule heating 14 p2358 A67-28283
- Hydrodynamics of gravitating stellar system numerically calculated for nonrotating spherically symmetric case 14 p2393 A67-28997
- Hydrodynamic stabilization of plane Poiseuille flow by modulating pressure gradient 15 p2470 A67-29332
- Hydrodynamic stability of plane incompressible viscous wall jet subjected to small disturbances, determining critical Reynolds number, eigenvalues and eigenfunctions 16 p2680 A67-31213
- Hydrodynamic stability problems solutions by numerical methods of Orr-Sommerfeld equations 16 p2681 A67-31419
- Plane wave disturbances in infinite rotating collisionless system for wave vector normal to axis of rotation [AD-653420] 16 p2753 A67-31700
- Slipping instability of plasma flows, noting instability criteria for long and short wavelength oscillatory instability 17 p2905 A67-32925
- Hydrodynamic structure of exothermic reaction zone behind one-dimensional shock fronts in gaseous detonation studied by optical method 18 p3153 A67-33827
- Conditions of time-symmetry for four classes of flows, discussing instabilities 18 p3079 A67-34004
- Hydrodynamic stability of flame front propagation in tube 20 p3543 A67-36396
- Tanh η form laminar mixing layer and nonlinear inviscid equation two-dimensional solutions with linearized stability theory perturbations 22 p3782 A67-39528
- Hydrodynamic stability of rotating flow with cylindrical free surface requiring Rayleigh criterion 24 p4144 A67-42568
- ### HYDRODYNAMIC TUNNEL
- Hydrodynamic tunnel wall effect on minimum cavitation number in axisymmetric cavitation flow around solids 02 p0232 A67-11631
- Current voltage characteristics of argon cesium plasma in inductive hydrodynamic shock tube 14 p2354 A67-27761
- Flow and cavitation erosion tests in closed circuit hydrodynamic tunnel 14 p2295 A67-27869
- Cavitation correlation with sound pressure and vibration acceleration in closed circuit hydrodynamic tunnel, showing cavitation noise spectrum 14 p2295 A67-27870
- Fully developed velocity profile for prediction of hydrodynamic entrance lengths for ducts of arbitrary cross section [ASME PAPER 67-FE-4] 14 p2304 A67-28357
- ### HYDRODYNAMICS
- SA ELASTOHYDRODYNAMICS
- SA ELECTROHYDRODYNAMICS
- SA FLOW THEORY
- SA FLUID MECHANICS
- SA HYDRAULICS
- SA KROOK EQUATION
- SA MAGNETOHYDRODYNAMICS
- Inverse optimization for calculating refractive index and electrical resistivity of plasma in reentry and surface tension coefficient in ephedrohydrodynamics 02 p0333 A67-12347
- Massive star behavior during final catastrophic evolution stages, stressing effect of electron type neutrino interactions, using numerical hydrodynamics coupled with energy transfer methods 03 p0516 A67-14340
- Composite heat transfer and viscous friction of moving gray medium with large optical density, using laminar boundary layer equation, noting hydrodynamic state role 04 p0722 A67-14713
- Research and facility of Institute of Fluid-Flow Machinery at Gdansk, Poland 06 p0981 A67-18823
- Nonstationary heat transfer coefficient and effect of nonstationary hydrodynamic conditions on heat transfer in channels 07 p1266 A67-19183
- Soviet papers on hydroaeromechanics including turbulent flow of conducting fluid, heat transfer, temperature stress in plates, etc 07 p1125 A67-19320
- Diffusion mass exchange model for thermal and hydrodynamic processes 07 p1267 A67-19328
- Equation of relaxation hydrodynamics for diatomic perfect gas when rotational and translational degrees of freedom are in equilibrium and dissipation has not set in 10 p1590 A67-23024
- Hydrodynamic coefficients of equations of perturbed motion for body with cavity in form of circular cylinder with flat bottom 10 p1624 A67-23032
- Interplanetary magnetic field effect on hydrodynamic supersonic expansion of solar corona noting solar wind velocity, nonradial flow, wave motion, etc 10 p1709 A67-23546
- Hydrodynamic drawing together problem for aerosol particles oscillating in sonic field at small Reynolds numbers, showing optimal field frequency-approach velocity correspondence 10 p1627 A67-23643
- Physical and hydrodynamic processes induced in vaporizable solids by pulsed light radiation from sources using explosives 11 p1782 A67-24955
- Biennial variations of zonal atmospheric circulation at equatorial latitudes analyzed using hydrothermodynamics 13 p2150 A67-26680
- Soviet papers on quantum field theory and hydrodynamics 13 p2105 A67-27410
- Turbulent mixing at interface of two different density media under influence of pressure gradient, considering diffusion 13 p2105 A67-27411
- UF-XS Japanese STOL seaplane used to investigate slow speed flying quality and hydrodynamic characteristics of PX-S aircraft 14 p2245 A67-27743
- Hydrodynamics of liquid-gaseous metal mixture flowing through nozzles, discussing heat exchange rate and condensation effects 16 p2656 A67-30574
- Hydrodynamic detonation theory, noting equations of state, nonsteady detonation, further problem areas, etc 16 p2778 A67-30837
- Approximate calculation of coefficients in equation for perturbed motion of rigid body containing liquid 16 p2765 A67-31051
- Prigogine-Glandsdorf local potential calculated for usual transport effects case using variational principle 16 p2661 A67-31440
- Book on nonlinear programming covering various methods and use in control 17 p2818 A67-32424
- Incipient cavitation calculation in hydrodynamics as example for applying quadratic programming to mechanical system subject to one-sided constraints 17 p2838 A67-32429
- Soviet book on heat transfer and hydrodynamics in two-phase media 17 p2969 A67-32457
- Hydroaerodynamics of carrying surfaces - Conference, Kiev, October 1965 17 p2792 A67-32901
- Steady state relaxation hydrodynamic theory with generalized Prandtl-Meyer flows in nonequilibrium hydrodynamics [AFOSR-67-1992] 17 p2840 A67-33137
- Potential equations for hydrodynamic and thermoelastodynamic linear wave motions applied to linear wave motion of isotropic thermally conducting elastic solids and viscous fluids [ASME PAPER 67-APM-32] 17 p2886 A67-33159
- Soviet book on high velocity hydrodynamics including airflow motion at distances from screen, hodograph method in MGD, drag coefficient determination, etc 18 p3021 A67-33409
- Airfoil unsteady motion problem near screen in incompressible fluid with given horizontal/ vertical velocity 18 p2981 A67-33410
- Relativistic generalization of Bernoulli equation from three-dimensional vector analysis of acoustic and entropy waves 18 p3084 A67-33422
- Soviet book on high velocity hydrodynamics 18 p3023 A67-33534
- Integral equation solution of hydrodynamic problem through computer program 18 p3024 A67-33543
- Solar physics and hydrodynamics - Conference, Tatranska Lomnica, Czechoslovakia, October 1964 18 p3118 A67-33749
- Hydrodynamic drawing together problem for aerosol particles oscillating in sonic field at small Reynolds numbers, showing optimal field frequency-approach velocity correspondence 18 p3029 A67-34412

- Linear theory for steady motions in rotating stratified fluid 19 p3209 A67-35410
- Soviet book on boundary layer of non-Newtonian fluids covering hydrodynamics, heat transfer and mass transfer 20 p3424 A67-37546
- One-dimensional unstable cloud hydrodynamics analyzed numerically, noting collapse primarily in center and little density growth in outer region 22 p3895 A67-40515
- HYDROFLUORIC ACID**
- HF acid vapor technique for room temperature etching of photolithographic stage of planar silicon dioxide device 04 p0682 A67-15488
- HYDROFOIL**
- SA AIRFOIL**
- Theory for incompressible two-dimensional flow of inviscid liquid past array of similar hydrofoils, behind each of which extends cavity of finite length 01 p0053 A67-10851
- Foil hydrodynamic design of Convairst subcavitating hydrofoil /HYSTAD/, discussing cavitation-free operation, foil selection and sections [AIAA PAPER 65-449] 03 p0402 A67-12919
- Force measurements and visual observations made in water tunnel on fully wetted and ventilated flows past family of conical ring wing hydrofoils having flat plate section geometry [ASME PAPER 66-WA/UNT-4] 04 p0608 A67-15383
- Two supercavitating flat plate hydrofoils near free surface with ensuing boundary value problem converted to mixed boundary value problem 06 p0984 A67-18126
- Inviscid steady partially cavitating flow through cascade of flat plate hydrofoils 18 p2682 A67-31550
- Elliptic planform vertical submerged hydrofoils, determining circulation distribution over foil span at arbitrary Froude numbers 18 p3022 A67-33414
- Steady motion of craft with aerial lifting surfaces over rough water, defining conditions for safe operation 18 p3022 A67-33415
- HYDROFOIL BOAT**
- Adhesives for bonding overlay materials to substrates for high speed hydrofoils, describing water tunnel and rotating arm tests 21 p3632 A67-38131
- HYDROFOIL OSCILLATION**
- Unsteady incompressible flow of two-dimensional supercavitating hydrofoils with finite cavity length, considering wake nature [ASME PAPER 67-FE-15] 14 p2304 A67-28363
- Functional sensitivity to cavitation of hydrofoil cascade, solving Fredholm type integral equations 20 p3419 A67-36188
- HYDROGEN**
- SA DEUTERIUM**
- SA LIQUID HYDROGEN**
- SA LOX-HYDROGEN ENGINE**
- SA PARA HYDROGEN**
- SA TRITIUM**
- Heat exchange and friction drag coefficients for laminar flow of equilibrium dissociable hydrogen with constant heat flow density at tube wall 01 p0165 A67-10048
- Hydrogen diffusion in tantalum at temperature interval of 0 to 100 degrees C 01 p0102 A67-10941
- Mach interactions and propagation mode of spinning detonation wave front in stoichiometric oxyhydrogen 02 p0232 A67-11564
- Radiation absorption by ionized hydrogen in plane of galaxy to explain brightness profiles for declination minus 37 degrees 02 p0307 A67-11688
- Spectrophotometric study of hydrogen alpha, beta, gamma, epsilon and hydrogen and K spectral lines of chromospheric flare of August 21, 1959 02 p0308 A67-11850
- Profile difference of two IR hydrogen lines in facula and in photosphere 02 p0308 A67-12488
- Intensity and energy distribution of solar plasma determined by mass spectrometers which can separate hydrogen and helium components of plasma stream 02 p0247 A67-12692
- Electric discharges in condensed hydrogen beams in high vacuum 03 p0475 A67-12922
- Red shift of magnetic zenith hydrogen line profiles and role of injection pitch-angle distribution of auroral protons 03 p0409 A67-12943
- Heats of adsorption of hydrogen and oxygen on semiconductors of zinc blende type calculated, using Clausius-Clapeyron and Bering-Serpinski equations 03 p0496 A67-13646
- Lower bound electronic energy calculations for positive H, using methods of truncated Hamiltonians and of Temple and Kato 03 p0469 A67-13943
- Pressure induced monochromatic translational absorption coefficients for homopolar and nonpolar gases and gas mixtures, with application to molecular hydrogen 03 p0515 A67-14323
- Exact vibrational matrix elements for molecular hydrogen and intensity of quadrupole rotation-vibration spectrum 03 p0515 A67-14324
- Upper limit to neutral atomic hydrogen density in halo regions of spiral galaxies 04 p0694 A67-14480
- Hydrogen diffusion in earth upper atmosphere near critical level 04 p0612 A67-14654
- Identification of diatomic H bands in large sunspot spectrum 04 p0698 A67-14916
- Hydrogen oxidation noting explosive property as function of temperature, pressure, composition, etc 04 p0565 A67-15091
- Transient heat transfer and thermal stresses for nuclear rocket due to sudden hydrogen coolant flow increase [ASME PAPER 66-WA/NE-4] 04 p0656 A67-15373
- Hydrogen line profile in Paschen series of solar spectrum, taking into account Stark effect and line broadening 04 p0702 A67-15567
- Electric breakdown in gas discharges in nitrogen and hydrogen at high pressure 04 p0661 A67-15652
- Hydrogen molecule excitation by electron impact extended to D excited state, noting values for oscillator strength 04 p0662 A67-15767
- Resonances in proton hydrogen and positron hydrogen scattering predicted at energies just below excitation thresholds 04 p0662 A67-15768
- Hugoniot-Rankine conditions, dissociation and ionization of hydrogen and nitrogen gas behind high speed shock wave and radiation effects 05 p0790 A67-16036
- Arc formation at metal surface in hydrogen plasma analyzed at various gas pressures, using Penning discharge, noting heat treatment effect on hydrogen 05 p0850 A67-16066
- Nucleonic quality gauging system for two-phase hydrogen pipeflow 05 p0842 A67-16539
- Auroral hydrogen emission measurements and indications of proton or electron excitations 05 p0797 A67-16851
- Solar hydrogen convection zone interaction with photosphere restricted to relation of convection theory to granulation and supergranulation 05 p0899 A67-17070
- Rapid micro dry combustion determination of carbon, hydrogen and nitrogen in high explosives 05 p0759 A67-17154
- Hydrogen arcjet plume spectroscopy, examining exhaust at various H mass flow rates 05 p0874 A67-17357
- Auroral hydrogen line emission quenching by collisional ionization 05 p0804 A67-17413
- Electron microscopy analysis of dissolved hydrogen induced fracture in room temperature cantilever bend fatigue testing of dispersion strengthened aluminum-aluminum oxide alloy 06 p1013 A67-17796
- Diurnal variation of hydrogen exosphere treated by simulation technique involving critical circle and magnetopause circle 06 p0897 A67-18701
- Hydrogen distribution between phases in alpha and beta/ titanium alloys at various temperatures 07 p1200 A67-19246
- Hydrogen effect on processes occurring in alloy VT3-1 during aging shown to increase beta phase 07 p1200 A67-19247
- Hydrogen effect on high temperature plasticity failure and mechanical properties of titanium shown to be similar to that caused by strain hardening 07 p1200 A67-19248
- Exothermal reaction zone in one-dimensional shock wave in argon diluted oxygen-hydrogen and methane-oxygen mixtures 07 p1287 A67-19309
- Spatial growth of ionization in molecular hydrogen, using thin film cathode 07 p1226 A67-19853
- Effect of thermal escape on neutral hydrogen density above 120 km 07 p1181 A67-19936
- Surface ionization detector of hydrogen in presence of air at one atm 08 p1330 A67-20376
- Temperature variation of thermoconductivity of helium-hydrogen gas mixtures and correlation of thermoconductivity curves with gas chromatograms 08 p1426 A67-20805
- Intensity and shape of spectral lines of excited hydrogen in radio range 08 p1356 A67-21345
- Charge exchange cross sections measurements for ion-molecule pairs of hydrogen, argon, krypton, helium and xenon 09 p1535 A67-22381
- Electron and ion emissions from hydrogen and helium UV glows in nighttime ionosphere 10 p1633 A67-23049
- Performance capability of transpiration cooled constricted arc heater, treating hydrogen 10 p1698 A67-23122
- Average distribution and time variation of ozone in stratosphere and mesosphere in study of contribution of photochemical reactions involving hydrogen 10 p1645 A67-23263
- Profile difference of two IR hydrogen lines in facula and in photosphere 10 p1702 A67-23356
- Spiral and irregular galaxies total mass to neutral hydrogen mass ratio derived from mass-luminosity relations 11 p1858 A67-23995
- Nb embrittlement by H at ambient temperatures under work hardening effect, noting correlation between elastic limit and deformability in H 11 p1806 A67-24427
- Q parameter of hydrogen maser measurement by method of no clock structure modification and by inhomogeneous magnetic field method 11 p1802 A67-24754
- Change in critical mass of large reflector moderated gaseous-fueled cavity reactor due to presence of hot hydrogen gas in cavity 12 p1965 A67-25908
- Detectability of ion recombination free-free emission from H II regions 12 p2011 A67-26252
- Energy dependence of effective total cross sections of elastic scattering involving H and He atoms and H molecules 13 p2159 A67-26384
- Injection coefficients of hydrogen and oxygen during buildup of discharge in homogeneous electric field 13 p2160 A67-26813
- Hydrogen and nitrogen effect on ductility of beryllium purified by zone refining 13 p2136 A67-27103
- Carbon dioxide purge and thermal protection system for liquid hydrogen tanks of hypersonic aircraft, comparing with helium purge system 13 p2227 A67-27647
- Hydrogen vent flare stack performance in adverse weather conditions 13 p2188 A67-27651
- Burn-pond concept of test facility for disposing of hydrogen at high flow rates 13 p2092 A67-27652
- Pressure oscillations induced by forced convection heating of dense hydrogen 13 p2107 A67-27670
- Hydrogen influence on fracture propagation of titanium alloy during tension tests 14 p2337 A67-28286
- Stark broadening of hydrogen lines of large principal quantum number for RF transitions by electron and ion impact approximation 14 p2389 A67-28839
- Nitrogen, oxygen and hydrogen determined by spark-source mass spectrography, noting reduction of instrument blank levels 15 p2433 A67-29403
- Dispersion relations of moving striations in rare gases, noting wave nature and dependence on discharge current 15 p2472 A67-29733
- Dissociation cross section of hydrogen molecule exchange excited by electron impact from ground to triplet state, using one-center wave functions 15 p2521 A67-30379
- High pressure hydrogen environment effects on mechanical properties of steels at high temperatures 16 p2689 A67-31327
- Solid solutions of titanium, tungsten, chromium prepared by carbidization of mixtures in hydrogen medium and obtained

as fine-grained carbide powders 16 p2691 A67-31587

State equation for interpolation and computations including parahydrogen thermodynamic properties using one set of 24 coefficients for all fluid states 16 p2780 A67-31763

Intensity and shape of spectral lines of excited hydrogen in radio range 17 p2887 A67-31941

No appreciable systematic differential motion between nearby neutral hydrogen and stars determined from measurement of relative velocity of former with respect to sun 17 p2943 A67-32443

Thermal conductivity relation to density and temperature for normal hydrogen in dense gaseous and liquid states 17 p2969 A67-32446

Upper limit on concentration of molecular hydrogen in interstellar space by comparison of Lyman bands in absorption spectra of early type stars and laboratory source 17 p2945 A67-32651

Hydrogen distribution in upper atmosphere and geocorona, relating H-alpha emission increase to solar activity decrease 17 p2849 A67-32961

Rotational velocity of neutral hydrogen subsystem in outer regions of Galaxy outside galactic plane 17 p2950 A67-33163

Short range intermolecular interaction of two ground state hydrogen molecules, using rigorous valence bond approach and population analysis 17 p2890 A67-33262

Heat exchange and friction drag coefficients for laminar flow of equilibrium dissociable hydrogen with constant heat flow density at tube wall 17 p2974 A67-33326

Upper limit in flux density of intergalactic gas UV radiation measured from interplanetary satellite, showing temperature effect 18 p3116 A67-33524

IR chemiluminescence in hydrogen-diatomic bromine and hydrogen-hydrogen bromide IR chemiluminescence in hydrogen-diatomic bromine and hydrogen-hydrogen bromide 18 p2996 A67-33786

Hydrogen-air reaction kinetics analyzed using standing wave normal shock, noting wall effects, ignition delay and recombination [AIAA PAPER 87-479] 18 p3157 A67-33948

Hydrogen effect on stability of beta phase in alloy VT15 18 p3065 A67-34291

Hydrogen coverage at metal surface during dissolution in corrosion process 18 p3066 A67-34368

Ion-molecule reactions of diatomic deuterium cation with diatomic deuterium and diatomic hydrogen 18 p3083 A67-34521

Glow-discharge silicizing of refractory metals by unilow gas method in silicon tetrachloride vapor and hydrogen atmosphere 19 p3242 A67-34917

Lean hydrogen-oxygen mixture combustion, studying induction period kinetics and spikes in OH profile 19 p3345 A67-35004

Absolute intensities of Lyman hydrogen alpha and beta lines used for interpretation of electron temperatures and density of emitting layers 19 p3325 A67-35464

Hydrogen and hydroxyl emissions in nightglow 19 p3223 A67-35483

Operation of ion source with cylindrical symmetry of crossed electric and magnetic fields 19 p3297 A67-35596

Photodissociation of hydrogen molecules in H I regions of interstellar medium, evaluating lifetime and density 19 p3331 A67-36085

High energy electron ionization cross section for hydrogen, noting high quantum number correspondence to classical expression 19 p3286 A67-36090

Beta-Ti alloy mechanical properties variation with hydrogen content for various temperatures and hydrogen embrittlement mechanism 20 p3468 A67-37176

Atmospheric pressure at cloud top and hydrogen abundance in Jupiter atmosphere determined by analyzing methane spectral line widths 20 p3529 A67-37479

Low energy electron scattering from hydrogen molecules in ground electronic and vibrational states, calculating rotational excitation cross section 20 p3491 A67-37687

Hydrogen emission by sun offers no unique interpretation for Lyman alpha profile 21 p3700 A67-37733

Performance of hydrogen driven shock tube investigated for usefulness, considering shock wave attenuation and helium driver performance 21 p3605 A67-37769

Energy dependence of effective total cross sections of elastic scattering involving H and He atoms and H molecules 21 p3660 A67-38822

Hydrogen integrator in pulsed mode of operation used to determine current pulse integrals 22 p3795 A67-39228

Shock wave thickness in hydrogen gas as function of shock speed and postshock plasma mean free path 22 p3783 A67-39723

Hydrogen diffusion in tantalum at temperature interval of zero to 100 degrees C 22 p3820 A67-39794

Radiating hydrogen two-dimensional equilibrium flow with variable absorption coefficient in axisymmetric nozzle analyzed in presence of gray radiation, examining transfer equation in diffusive approximation 22 p3785 A67-40013

Auroral proton precipitation and hydrogen emissions 23 p3993 A67-40564

Kinetics of flames propagating in hydrogen-nitrous oxide mixtures diluted with inert gases 23 p4082 A67-41142

Compact portable high purity H generator using liquid ammonia for indirect method H-O fuel cell 24 p4106 A67-42524

HYDROGEN ATOM

Electron impact induced transitions between principal quantum number levels in atomic hydrogen estimated via impact parameter method 01 p0124 A67-10780

Effects of aluminum electrode and hydrogen atom on MOS structure during annealing 01 p0137 A67-11069

Amplitude and frequency characteristics of hydrogen-atom beam maser 02 p0251 A67-11574

Numerical integration of averaged cross section for electron induced resonance charge exchange and ionization of accelerated beam of hydrogen atoms 02 p0278 A67-12629

Intergalactic atomic neutral hydrogen detection in emission in clusters of galaxy and in noncluster field 03 p0514 A67-14318

Spin temperature of intergalactic atomic hydrogen calculated as function of electron density and kinetic temperature 03 p0515 A67-14319

Angular dependence of elastic scattering resonance structure in atomic hydrogen 04 p0660 A67-14946

Cross sections for electron collisions with hydrogen atoms and hydrogen-like ions for excitation of ground and other levels 04 p0671 A67-15642

Magnetic field gradient relaxation mechanism by random excitation of transitions in F equals 1 level of ground state of hydrogen atoms in maser 05 p0817 A67-16635

Hydrogen atom excitation by Lyman alpha radiation absorption in electric field 05 p0848 A67-16795

Angular distribution of fast hydrogen atoms from exothermic reaction measured for various proton energies and scattering angles 07 p1225 A67-19495

Variational bound method applied to calculation of lower bounds on S-wave phase shifts for scattering of electrons by hydrogen atoms 07 p1226 A67-19499

Electron capture cross section by protons in hydrogen atom obtained, using perturbed wave functions due to electric field 07 p1226 A67-19501

Charge exchange of protons in alkali metal vapors with formation of highly excited hydrogen atoms, noting cross section, reaction mechanism, etc 08 p1358 A67-20855

Intercomparison of hydrogen and cesium frequency standard 09 p1494 A67-21616

Calculation of effective excitation cross sections of hydrogen atoms for collisions with nitrogen molecules and hydrogen atoms 09 p1534 A67-21850

Reaction rate kinetics of combination of H atoms with NO plus third body /M/ compared with H and O atoms plus M relative to argon 11 p1749 A67-24238

Automatic cavity tuning of hydrogen masers to achieve frequency source of absolute accuracy over unlimited time periods 13 p2125 A67-26512

Free radical formation in amino acids exposed to thermal hydrogen

atoms 13 p2065 A67-26869

Numerical integration of averaged cross section for electron induced resonance charge exchange and ionization of accelerated beam of hydrogen atoms 13 p2171 A67-27387

Temperature dependence of electrical conductivity and Hall effect of barium-titanate crystals reduced by hydrogen, observing electron spin resonance and optical absorptions 14 p2363 A67-27824

Experimental determination of hydrogen atom beam density after focusing by hexapolar magnet 15 p2520 A67-29720

Yield variation of excited hydrogen atoms formed by charge exchange with gas target thickness described by analytical model 16 p2714 A67-30874

Spin-exchange frequency pulling of ground state hyperfine transition in atomic hydrogen analyzed for self-excited oscillation in hydrogen maser 17 p2889 A67-33225

Accidental degeneracy of hydrogen atom levels using Schroedinger equation, deriving eigenfunctions 18 p3083 A67-34072

Long range first order interaction between two excited hydrogen atoms yielding perturbation energy matrix, discussing diagonalization process 18 p3083 A67-34517

Excitation cross sections for protons incident on atomic hydrogen calculated by nonadiabatic method 20 p3491 A67-37686

Hyperfine splitting of spin interaction energy of two hydrogen atoms, determining eigenfunctions for effective Hamiltonian 21 p3658 A67-37814

Nonlinear variational trial function for atomic hydrogen dynamic polarizability, discussing first order perturbed wave function and perturbation-variation method 21 p3659 A67-38004

Static Green function for elastic electron scattering by hydrogen atoms, using integrodifferential equations to determine resonance energies 22 p3839 A67-39204

Interaction of two H atoms in ground states using Hirschfelder-Linnet wave function and Gaussian type function 22 p3756 A67-39385

Long range interaction of two H atoms calculated with electrostatic Hellmann-Feynman theorem, determining part of second order molecular wave function 22 p3840 A67-39387

Degree of ionization effect on yield of excited atoms from gas target 22 p3852 A67-39987

Satellite and ground based measurements of incident proton neutral hydrogen flux and Balmer alpha optical emission in auroral hydrogen arc 23 p3995 A67-40803

Empirical formula for representation of cross sections for single ionization of atoms and ions from ground state by electron impact 24 p4194 A67-41890

Intermolecular forces theory, considering hydrogen atom interaction through Born-Oppenheimer approximation and variational calculations [WIS-TCI-249] 24 p4191 A67-42666

HYDROGEN BOND

Hydrogen bonding of derivatives of guanosine and cytidine soluble in chloroform studied in IR, confirming geometrical specificity in two-stranded nucleic acids 02 p0190 A67-11585

Spectrum of bound and quasi-bound states of hydrogen-hydrogen scattering and resonance, using Schroedinger equation 18 p3084 A67-34523

Intermolecular hydrogen bonds energies estimated for organic semiconductors in ground and first excited states 20 p3512 A67-37301

HYDROGEN CHLORIDE

Venus atmosphere spectra obtained by Michelson interferometer, finding HCl lines consistent with 2-mm Amagat of gas [JPL-TR-32-1106] 11 p1863 A67-24510

High resolution far IR lamellar grating interferometer with double beam differencing 20 p3438 A67-36347

HYDROGEN COMPOUND

LCAO MO calculation of charge carrier mobility in hydrogen phthalocyanine 03 p0495 A67-13525

Hydrogen atom-molecule exchange reaction effect on transfer coefficients of dissociating mixture, noting anisotropy and collision integrals 03 p0473 A67-13606

Decomposition rates of hydrogen halides

- examined behind incident shock waves between 2800 to 4600 degrees K, using IR techniques 11 p1750 A67-24995
- Hydrogen atom-molecule exchange reaction effect on transfer coefficients of dissociating mixture, noting anisotropy and collision integrals 18 p3083 A67-34471
- HYDROGEN CYANIDE**
- Amino acid formation by formamide thermal decomposition, noting support for hydrogen cyanide oligomerization hypothesis 20 p3376 A67-36700
- Streaming thermal plasma /STP/ devices, discussing plasma jet synthesis of HCN from cold methane and thermal nitrogen plasma 21 p3578 A67-38393
- Absolute frequency measurements on continuous wave hydrogen cyanide submillimeter laser lines 24 p4166 A67-41861
- HYDROGEN DEUTERIUM OXIDE**
- Hyperfine structure in rotational spectrum of HDO and deuterium oxide analyzed by beam maser spectroscopy, evaluating coupling constants 20 p3461 A67-37287
- HYDROGEN FLUORIDE**
- IR spectroscopy of absorption and emission in hydrogen-fluorine flames for more data on high temperature spectral properties of HF 10 p1697 A67-23134
- Heats of combustion in fluorine of Teflon and graphite and heats of formation of carbon tetrafluoride and carbon hexafluoride 15 p2433 A67-29765
- Relationship between absorption of hydrogen fluoride by lined filter papers and exposure dosages investigated under controlled conditions of various factors 16 p2675 A67-31211
- Hydrofluoric acid for chemical vibration-rotation laser emission 20 p3462 A67-37564
- HYDROGEN FUEL**
- Resistojet design and fabrication, using hydrogen propellant and having 3-kw power input [AIAA PAPER 66-224] 02 p0302 A67-11937
- Mechanism of hydrogen combustion near lower ignition limit studied, using electron paramagnetic resonance /EPR/ measurements 03 p0536 A67-13842
- Fuel injection parameters effects on mixing of gaseous hydrogen fuel with supersonic air stream for hypersonic ramjet, determining turbulent diffusion coefficient 06 p1117 A67-18387
- Hydrogen fuel battery, discussing construction, operation and performance characteristics 09 p1445 A67-22184
- Ignition of hydrogen-oxygen propellant combination by chlorine trifluoride 10 p1697 A67-23132
- Ignition delays calculation in hydrogen-air system, using Momtchiloff assumptions 13 p2185 A67-26259
- Annex circuits for regulating electrolyte grade, cell temperature, reactant supply, fluid circulation and generated electricity of unit cells grouped in batteries 14 p2253 A67-29024
- Supersonic combustion simulation facility and duplicable static parameters for hydrogen fuel [AIAA PAPER 66-743] 15 p2465 A67-29437
- Test program assessing propulsion performance of cryogenic and ambient temperature gaseous parahydrogen expanded through conical thrust nozzles 16 p2734 A67-30705
- Subcooled liquid and slush hydrogen fuels effects on space vehicle design and performance, discussing propulsion, insulation, pressurization, venting, management, etc [AIAA PAPER 67-467] 18 p3137 A67-33937
- Gas core reactor, discussing application of fissionable gas to heat hydrogen propellant in nuclear rocket reactor [AIAA PAPER 67-499] 18 p3076 A67-33963
- Radioisotope heated hydrogen thrusters for propelling high energy upper stage, discussing performance, payload advantages and high energy kick stage [AIAA PAPER 67-509] 18 p3113 A67-33973
- Hypervelocity vehicle volume decreasing method by applying dual-fuel concept [AIAA PAPER 67-559] 19 p3174 A67-35958
- Hydrogen fire visualization detection techniques including application of photography, TV and image converter in IR and UV regions 20 p3445 A67-36540
- Variable thickness insulation system for transport of hydrogen propellant into earth orbit for docking transfer to lunar and interplanetary mission vehicles [ASME PAPER 67-HT-50] 20 p3548 A67-36732
- 30 cell 1 kw hydrogen fuel battery for room temperature operation, noting construction and performance 22 p3749 A67-40231
- HYDROGEN ION**
- Limiting behavior of absorption cross sections of negative hydrogen ion 01 p0116 A67-10359
- Electron resonances of hydrogen ion calculated and illustrated by waves, using variational principle incorporating outgoing-wave boundary conditions 01 p0117 A67-10781
- Mean energy and energy dissipation of hydrogen ions ejected from HF source 03 p0424 A67-14261
- Perturbation treatment of diatomic hydrogen ion, improving polarized hydrogen-atom treatment by using zero-order wave function 03 p0474 A67-14333
- Approximate molecular orbitals, Part I 03 p0474 A67-14351
- Approximate molecular orbitals, Part II 03 p0474 A67-14352
- Equilibrium constants and internal energies of hydrogen molecular ion calculated as function of temperature and pressure, using partition function 04 p0697 A67-14807
- Cross sections for electron collisions with hydrogen atoms and hydrogen-like ions for excitation of ground and other levels 04 p0671 A67-15642
- Plasma formation by dissociation of diatomic hydrogen ions by Lorentz force 04 p0671 A67-15645
- Very intense source of negative ions, based on formation and destruction mechanism of negative hydrogen ions in reflex arc 05 p0851 A67-16597
- Cross section of proton production for molecular ion beams of hydrogen passing through lithium plasma 05 p0852 A67-16600
- Surface blistering of metals due to low energy hydrogen ion bombardment, determining solar absorptance change in gold-plated specimens 08 p1343 A67-21520
- Absolute cross section for dissociation of hydrogen ion by electron impact measured, using cross beam technique 09 p1535 A67-22377
- Hydrogen-molecule ion dissociation by electron collision, noting various transition states 09 p1535 A67-22378
- Mean energy and energy dissipation of hydrogen ions ejected from HF source 14 p2321 A67-28773
- Fast hydrogen ion generation in coaxial plasma source to determine point in gun chamber where fast particles arise 15 p2525 A67-29251
- Ion-molecular reactions of hydrogen with inert gases caused by low energy electrons in low temperature plasmas, considering energy level populations, reaction cross sections, etc 17 p2808 A67-32141
- Solution of linearized Boltzmann collision equation for ion motion through gas in inhomogeneous electric field, describing energy distribution functions for hydrogen ions 17 p2907 A67-33102
- Energy distributions of hydrogen and deuterium ions from dissociative ionization of hydrogen and deuterium 17 p2889 A67-33226
- Trapping of hydrogen ions in molybdenum, titanium, tantalum and zirconium measured by mass spectrometric technique 17 p2810 A67-33384
- Ion source using Penning discharge used to inject hydrogen ions into magnetic field 19 p3195 A67-35589
- Electron scattering from diatomic molecules in fixed nucleus approximation using polarized single-center orbitals method applied to positively ionized hydrogen 20 p3491 A67-37689
- Intermediate range intermolecular forces with overlapping wave functions and exchange effects calculated for ionized H molecule using perturbation theory 23 p4029 A67-40971
- HYDROGEN OXYGEN /HOPE/**
- SPACECRAFT**
- Effect of several injector face baffle configurations on screech in 20,000-lb thrust hydrogen-oxygen rocket 04 p0691 A67-15987
- HYDROGEN PEROXIDE**
- Early Bird hydrogen peroxide control system maneuvers to place satellite into final stationary position 06 p1093 A67-17663
- Thermodynamic properties of hydrogen peroxide between 273 and 2000 K, deriving equations of state 07 p1265 A67-19123
- Sulfur compound in carbonaceous chondrites explained by oxidation of troilite by oxygen and HOOH 07 p1249 A67-19539
- Genetic transcription as affected by ionizing radiation and hydrogen peroxide 11 p1747 A67-24786
- Ionizing radiation effect on bacterial cells noting inhibition due to generated hydrogen peroxide 13 p2059 A67-26867
- Thermodynamic properties of hydrogen peroxide between 273 and 2000 K, deriving equations of state 21 p3731 A67-38167
- Hydrogen peroxide and disulphane molecules force constant and vibrational spectra investigation indicates little change in elastic properties 22 p3757 A67-39583
- Hydrogen peroxide oxygen-water supply system as backup for long space flights noting storage tanks, catalytic reactor and heat exchanger 22 p3747 A67-39693
- HYDROGEN PLASMA**
- Spectrographic method for measurement of temperature in plasma jets at atmospheric pressure, using amplification of beta line of hydrogen 01 p0124 A67-10773
- Plasma components transmission from occluded-hydrogen titanium-washer source into mirror machine along curved field lines of magnetic cusp 03 p0485 A67-14048
- Electron recombination in rapid cooling of magnetized plasma jet expanding into vacuum 03 p0486 A67-14195
- Vertical hydrogen beam oscillator serving as atomic clock, noting design principle and operation 04 p0632 A67-14898
- Electron recombination in laser produced hydrogen discharge, noting temperature decay due to radiation, expansion cooling and electron loss 04 p0665 A67-15109
- Luminous density distribution of decaying hydrogen plasma recorded by photoelectronic method 04 p0672 A67-15653
- Self-absorption of radiation in high temperature plasma jet of hydrogen, argon and nitrogen 05 p0851 A67-16522
- Time resolved spectroscopic measurements of intensity and Stark width during decay of hydrogen plasma produced by ruby laser, determining electron density and temperature decay 05 p0852 A67-16653
- Short hydrogen plasmoid production by electromagnetic waves in decimeter range 05 p0855 A67-16997
- Nonlinear constant profile plane waves in cold Vlasov hydrogen plasma under influence of external magnetic field 08 p1359 A67-20896
- Normal ionizing shocks propagating through hydrogen in sub-Alfvénic and trans-Alfvénic regimes in coaxial electromagnetic shock tube 08 p1363 A67-21381
- Time resolution spectroscopy applied to electron recombination in H plasma due to azimuthal pinch 11 p1841 A67-24769
- Hydrogen plasma produced by coaxial gun located in magnetic mirror 13 p2163 A67-26291
- Electron recombination in rapid cooling of magnetized plasma jet expanding into vacuum 14 p2380 A67-28540
- Active corpuscular plasma diagnostics method applied to hydrogen plasma study 15 p2526 A67-29257
- Digital computer methods for calculating impulsive relaxation in unbalanced hydrogen plasma 15 p2529 A67-29713
- Interaction between SHF field and created plasma in electron-cyclotron resonance state 15 p2529 A67-29715
- Reflection coefficient for electromagnetic wave in circular cylindrical shock tube incident on moving plasma calculated numerically 15 p2531 A67-29905
- Automatic recording and computer analysis of double probe measurements in plasma research, calculating electron temperature and plasma density 15 p2489 A67-30092
- Quasi-equilibrium number density of excited atoms and electronic transition rate in decaying optically-thick helium and hydrogen plasmas, considering Penning ionization 16 p2715 A67-31168
- Gas kinetic pressure measurement in high current rectilinear hydrogen-plasma discharge during electron

- heating 16 p2718 A67-31188
 HF electrostatic instability in low density plasma stream guided by magnetic field, discussing cause and anomalous loss of diamagnetism 17 p2907 A67-33106
 Instability and related anomalous diffusion of magnetized weakly ionized hydrogen plasma of RF discharge in cylindrical geometry 17 p2908 A67-33113
 Pulsed high current arc in hydrogen showing initial instability, discharge stability, impurity content, pinch effect, decay, etc 18 p3087 A67-34047
 Stationary high density high temperature plasma production spectroscopic measurements, deducing arc radial temperature and density profiles from line and continuum intensities and line profiles 19 p3274 A67-35103
 Plasma column in magnetic field created by diffusion from low pressure pulsed discharge in hydrogen, with plasma density dependent on gas pumping 19 p3275 A67-35108
 Radial pressure distribution in hydrogen arc located in axial magnetic field using Saha equation, determining temperatures and electron densities 19 p3279 A67-35139
 Temperature distribution in vortex cooled hydrogen arc obtained by emission and absorption coefficients in plasma source 19 p3279 A67-35142
 Partition function of partially ionized hydrogen two-component plasma 19 p3285 A67-35346
 Transport coefficients of fully ionized hydrogen plasma in magnetic field calculated from Fokker-Planck equation 19 p3286 A67-35350
 Chapman-Ferraro problem analyzed by impinging high speed hydrogen plasma stream against three-dimensional magnetic dipole, discussing boundary shape 19 p3288 A67-35366
 Torsional Alfvén waves attenuation in decaying hydrogenous plasma 19 p3290 A67-35377
 Hydrogen thermal ionization rate behind strong shock wave, considering nonadiabatic collisions and various relaxation mode interactions in shock speed range 19 p3292 A67-35394
 Glow-broadening rate dependence on initial pressure and discharge voltage in shock tube containing hydrogen plasma, studying charge distribution variations 20 p3501 A67-37145
 Hydrogen plasma discharge with hot electrons, investigating plasma decay and electron and plasma density 21 p3666 A67-38368
 Dielectric susceptibility and ion density measurement for polarized hydrogen plasma moving through transverse magnetic field 22 p3845 A67-39424
 Electrical and spectral investigation of pulsed high pressure arc produced by capacitor bank discharge in helium and hydrogen 22 p3845 A67-39426
 Cold Cu electrode interaction with H plasma, measuring electrode I-V characteristics, interelectrode charge concentration, electron temperature, etc 22 p3846 A67-39505
 Double probe method for determining electron temperature and density variations in HF hydrogen plasma during second harmonic cyclotron resonance 22 p3848 A67-39650
 Neutral and charged particle trapping using waves, discussing wave attenuation from particle interaction, plasma waveguide and laser beam trapping 23 p4017 A67-41681
 Dense hydrogen plasma ohmic heating in quasi-stationary discharge without external magnetic field, obtaining stable impurity-free plasma column 24 p4195 A67-41939
- HYDROGEN RECOMBINATION**
 Isotope effect in hydrogen molecule dissociative attachment at low energy, noting short negative-ion formation lifetime and long separation time 17 p2889 A67-33223
 Carbon monoxide and hydrogen flames ionization and electron temperatures with methane premixing 18 p3151 A67-33807
 Post-induction kinetics in shock initiated hydrogen-oxygen reactions investigated by computer methods 18 p3153 A67-33823
- HYDROGEN SULFIDE**
 Hydrogen sulfide oxidation, role of temperature and pressure, determining explosion levels 04 p0566 A67-15094
 Chemiluminescent reactions of atomic oxygen with carbonyl sulfide and hydrogen sulfide in flow system as function of reaction time and reactant concentrations 14 p2260 A67-28781
- HYDROGENATION**
 Hydrogen treatment effects on molybdenum ductility, noting grain-size and heat treatment contribution to strain-to-fracture difference at various deformation pressures 15 p2503 A67-29562
 Hydrogen solubility in eutectic sodium-potassium mixture, noting usefulness as nuclear reactor coolants, and dependence on pressure and temperature variations 16 p2619 A67-30620
 Sterically controlled synthesis of optically active alpha-amino acids from alpha-keto acids by reductive amination 20 p3376 A67-36874
 Optically active alpha amino acids synthesized from alpha keto acids by hydrogenolytic asymmetric transamination 24 p4119 A67-42703
- HYDROGENOLYSIS**
 Sterically controlled synthesis of optically active alpha-amino acids from alpha-keto acids by reductive amination 20 p3376 A67-36874
- HYDROGENOMONAS**
 Electrolysis-Hydrogenomonas bacterial bioregenerative life support system for manned space flight of long duration 16 p2617 A67-30774
 Radio carbon dioxide fixation, glutamate labeling and Krebs cycle in ribose-grown Hydrogenomonas facilis 20 p3370 A67-36796
 Autotrophic and heterotrophic carbon dioxide fixation regulation in Hydrogenomonas, discussing two Calvin cycle enzymes 20 p3370 A67-36797
 Continuous culture system for Hydrogenomonas bacteria in waste management of life support system [SAE PAPER 670854] 24 p4115 A67-42002
- HYDROLOGY**
S METEOROLOGY
HYDROLYSIS
 SA EXTRACTION
 SA HYDRATION
 Hydrolysis of phthalimide ring with carboxylate group linked through alkyl group as anionic intramolecular catalyst 10 p1602 A67-23159
 Inactivation of thermal catalytically active polyanhydro-alpha-amino acids by heating in buffered solution, noting hydrolysis of cyclic imide bonds 13 p2065 A67-26733
- HYDROMAGNETIC FLOW**
S MAGNETOHYDRODYNAMIC FLOW
HYDROMAGNETIC STABILITY
S MAGNETOHYDRODYNAMIC STABILITY
HYDROMAGNETIC WAVE
S MAGNETOHYDRODYNAMIC WAVE
HYDROMAGNETISM
 SA MAGNETOHYDRODYNAMICS
 SA MAGNETOHYDROSTATICS
 SA PLASMA
 Hydromagnetic wave propagation and energy transfer in stratified isothermal plasma embedded in parallel uniform gravity and magnetic fields 11 p1868 A67-25083
 Long-duration monochromatic emission with worldwide character in frequency spectrum of magnetic storm 18 p3041 A67-34193
 Long period hydromagnetic propagation in theta model geomagnetic tail, deriving TM and TE modes equations 22 p3791 A67-39815
- HYDROMETALLURGY**
 Nickel-thoria powder produced by pressure hydrometallurgy techniques and dispersion-strengthened by compaction and rolling, noting tensile stress-rupture properties revealed by optical and electron microscopy 01 p0097 A67-10697
- HYDROMETEOROLOGY**
 Papers from Scientific Research Institute of Hydrometeorological Instrument Design covering radiosonde, sensing elements, etc 07 p1187 A67-19736
 Bimetallic sensing elements calculation method employed by Russian Scientific Research Institute of Hydrometeorological Instrument Design 07 p1187 A67-19738
 Microwave reflection from region with nonuniform hydrometeor for case where dimensions vary greatly and relation to wavelength is arbitrary 11 p1754 A67-24981
- Summit areas of severe storms, measuring stratospheric-tropospheric interchange, air flow and hydrometeors 19 p3252 A67-35057
- HYDROPLANE**
 Tire hydroplaning, noting lift force on planing surface and pressure distribution 09 p1441 A67-22492
- HYDROSPHERE**
 Energy, time and physical morphology of atmosphere, hydrosphere and lithosphere surfaces 06 p1091 A67-18994
 Discrete equilibrium temperatures of hypothetical planet with atmosphere and hydrosphere of one-component two-phase system under constant solar radiation 13 p2116 A67-27462
- HYDROSTATIC PRESSURE**
 Plastic deformation including instability of circular membrane subject to hydrostatic pressure, obtaining stress-strain curve 01 p0161 A67-10776
 Machine design, capillary control selection, hydraulic circuitry and oil selection of two two-surface angular hydrostatic bearings used for azimuth turntable of radar antenna pedestals 03 p0431 A67-13749
 Elastoplastic deformation of circular cylindrical shells of ideally plastic incompressible material under uniform supercritical hydrostatic pressure 05 p0922 A67-17176
 Hydrostatic pressure effect on dispersion of gamma prime phase in precipitation heat treatment of nickel-base superalloy 06 p1016 A67-17902
 Hydrostatic pressure effect on energy gap, carrier concentration and electron and hole mobilities of indium antimonide 07 p1231 A67-19061
 Gross hydrostatic pressure effect as related to foil and wire strain gauges 07 p1185 A67-19412
 Gap anisotropy increase in superconducting thallium transition temperature dependence on lattice defect density due to hydrostatic deformation 07 p1235 A67-20128
 Imperfection sensitivity of eccentrically axial and ring stiffened cylindrical shells under axial compression and hydrostatic pressure 08 p1417 A67-20552
 Environmentally induced stresses in encapsulated electronic modules measured using hydrostatically pressure-sensitive transducer, noting internal stress changes 08 p1306 A67-21418
 Hydrostatic pressure and temperature effect on current-voltage characteristics of tunnel p-n junctions in gallium arsenide 09 p1554 A67-21977
 Hydrostatic pressure measurement by direct loading of semiconductor strain gauges 09 p1498 A67-22031
 Asymptotic solution of typical bay in hydrostatically loaded ring-reinforced noncircular cylinder of finite length 10 p1729 A67-23766
 Hydrostatic pressure effect on surface microstructure, dislocation substructure and stress-strain behavior of beryllium 11 p1805 A67-24110
 Conical shell stability under hydrostatic pressure for various in-plane boundary conditions, stressing axial restraint effect 11 p1873 A67-24214
 Plastic zone about circular hole in infinite plate under uniform hydrostatic tension 11 p1879 A67-24887
 Shallow conical shell stability acted upon by external hydrostatic pressure 12 p2028 A67-25635
 Metal working methods, discussing high hydrostatic pressure, pressurized liquid, extrusion and high rate 13 p2123 A67-26699
 Beryllium deformation under hydrostatic pressure 13 p2139 A67-27124
 Metal-to-semiconductor transition measurements of hydrostatic pressure shift and uniaxial stress of temperature 13 p2180 A67-27164
 Model with hydrostatic gas pressure distribution to interpret equivalent widths of atomic and ionic lines in spectra of umbrae 13 p2203 A67-27426
 Similarity criteria for plastic behavior of polymers under combined effect of nonuniform temperature field and hydrostatic pressure 15 p2573 A67-29466
 Hydrostatic pressure effects on brittleness in Cr and yielding in center annealed iron specimen studying brittle-ductile transition

- of former 16 p2689 A67-31328
High hydrostatic pressure effects on load cell using foil strain gauges and calibration for small uniaxial loads 17 p2855 A67-32393
Orthotropic circular cylindrical shell of elastic material instability under combined torsion and hydrostatic pressure investigated for simply supported and clamped ends 17 p2963 A67-33016
Rayleigh-Ritz method used to predict elastic buckling of prolate spheroidal shells under hydrostatic pressure 17 p2963 A67-33017
Hydrostatic pressure and temperature effect on current-voltage characteristics of tunnel p-n junctions in gallium arsenide 17 p2923 A67-33314
Monography on plastic axisymmetric collapse of ring stiffened cylindrical shells under external hydrostatic pressure 18 p3140 A67-33432
Compression tests with superimposed hydrostatic pressure to study rheological behavior of elastomer filled with granular potassium chloride 19 p3340 A67-35465
[SESA PAPER 1224] 18 p3142 A67-33891
Compression tests with superimposed hydrostatic pressure to study rheological behavior of elastomer filled with granular potassium chloride 19 p3340 A67-35465
Piezoresistance effect measurement in PbTe single crystals, obtaining coefficients for principal valence band through hydrostatic and uniaxial stresses in several crystallographic directions 21 p3683 A67-38389
Eccentrically stiffened cylinders instability under axial compression, lateral or hydrostatic pressure and torsion 21 p3722 A67-38545
Load carrying capacity of hydrostatic bearing having communicating chambers and operating with laminar flow of incompressible fluid, showing shaft vibration elimination 21 p3636 A67-38837
Hydrostatic and uniaxial compressional stress effects on strontium titanate superconductive transition temperature 22 p3863 A67-40244
Pressure effects on fatigue reported for Fe, Al and Ni wires subjected to oscillating strains, discussing several fatigue models 23 p4075 A67-40666
Thin elastic shell neutral equilibrium under axial compression and hydrostatic pressure, obtaining parametric terms for expressions by using quadratic functional 24 p4249 A67-42303
Torsion creep theory for circular and noncircular tubes using Bredt equation, measuring anisotropy in tubes, calculating torsion stresses 24 p4250 A67-42381
Flexible membrane hydrostatic air bearing, determining membrane shape, pressure distribution and air gap by Navier-Stokes and membrane analogy equations [ASME PAPER 67-LUB-1] 24 p4162 A67-42668
Electron tunneling into superconductors to investigate pressure induced energy shifts in Pb phonon spectrum 24 p4206 A67-43100
HYDROSTATICS
SA MAGNETOHYDROSTATICS
Equilibrium shape of earth, discussing space science discoveries and hydrostatic flattening mechanism 06 p0994 A67-17767
Schwarzschild criterion for convective instability in general relativity extended to Einstein hydrostatics to formulate buoyancy principle with aid of initial value problem 18 p3133 A67-34375
HYDROTHERMAL CRYSTAL GROWTH
Research and development for better manufacturing emphasizing hydrothermal growth of ruby crystal 09 p1505 A67-22143
HYDROX ENGINE
Cryogenic hydrogen-oxygen ignition with hydrogen-gas entrained Raney nickel as catalyst 09 p1579 A67-21706
Detonation wave interaction with hydrogen-oxygen flow fields in clarifying rocket combustion instability and supersonic combustion 12 p1929 A67-25898
Flame propagation in hydrogen-oxygen mixtures at temperatures and pressures corresponding to ignition peninsula 22 p3919 A67-40223
HYDROXYL
Einstein A coefficient for lambda doublet transitions of ground state of OH 01 p0114 A67-10898
Proton induced hydroxyl formation on lunar surface simulated by bombarding glass, chemically similar to silicate minerals, with high energy protons 02 p0324 A67-11857
[AFRL-66-795]
Forces holding hydroxyl ions to surfaces of MgO particles 04 p0642 A67-15087
Electron spin resonance application to kinetic studies of free atoms and radicals in gases, particularly OH radical 04 p0566 A67-15173
Vibrational and rotational temperature at altitudes between 50 to 250 km determined from analysis of airglow in OH bands, using Fastie-Ebert spectrometer 07 p1172 A67-19562
Hydroxyl catalyzed chain decomposition of ozone, proposing new reaction mechanism [JPL-TR-32-1063] 07 p1138 A67-20192
Correction of calculations of Einstein A coefficient for transition of OH 09 p1532 A67-21989
Angular size of OH emission measured using high resolution interferometer 10 p1709 A67-23491
Polarization of cosmic OH 18-cm radiation 11 p1864 A67-24565
OH emission regions investigated using Millstone and Haystack antennas with interferometer, noting radio sources for base-line calibration and instrumental phase monitoring 12 p2009 A67-25972
Radio astronomical investigations of 18 cm ground state lambda doublet transition of OH suggest maser amplification of radiation takes place in interstellar medium 13 p2198 A67-26715
Anomalous polarization of four cosmic OH lines predicted from states of polarization in OH maser amplifier 13 p2161 A67-27289
OH emission in H II region W3, using improved equipment 14 p2389 A67-28845
Space-time properties of hydroxyl emission observed by spectrophotometry, giving diagrams of periodic variations and measurement errors 17 p2848 A67-32954
Hydroxyl emission at high latitudes during winter months of 1960 through 1963 measured with spectroscopy 17 p2848 A67-32955
Periodic variations in rotational temperatures of OH emission bands determined by spectroscopic measurements 17 p2849 A67-32956
IQSY electrophotometric and spectrometric measurements of annual and nighttime variations in rotational temperatures and integral intensity of hydroxyl emission bands 17 p2849 A67-32957
Photographic high atmosphere observations of hydroxyl and helium emission bands, determining solar UV radiation and electron flux 17 p2849 A67-32960
Hydroxyl radical formed by radiolysis of ice at 77 degrees K identified as center producing EPR lines 17 p2890 A67-33258
Excitation and radiation of OH molecules and alkali metals in low pressure flames and rocket exhausts 18 p3152 A67-33819
Measurements of induction period, ammonia consumption rate after induction and radiation from electronically excited OH radicals in ammonia-oxygen reaction 18 p3155 A67-33836
Lean hydrogen-oxygen mixture combustion, studying induction period kinetics and spikes in OH profile 19 p3345 A67-35004
Hydrogen and hydroxyl emissions in nightglow 19 p3223 A67-35483
Upper limit of arc for hydroxyl /OH/ emission region associated with radio source W3, using Michelson interferometer consisting of two spaced radio telescope stations 20 p3523 A67-36648
Radio source W49 and anomalous OH emission at radio wavelengths explained as OH formation in electronically excited state by two-body process 21 p3701 A67-37896
Circular and linear polarization of OH line radiation from NGC 6334 nebulae region using Parkes radio telescope 24 p4230 A67-42333
HYGIENE
SA HEALTH
SA SANITATION
Waste management and physiological response to substandard hygiene under controlled environmental conditions 03 p0366 A67-14289
Clothing hygiene with particular reference to aerospace problems 06 p0954 A67-17998
Aerospace clothing hygiene, discussing climate influence on protective garment selection and physiological responses of living organisms to obtain heat balance 12 p1902 A67-25176
Hygiene of aerospace protective clothing, studying garments characteristics, disinfection and related skin diseases 16 p2619 A67-31476
Human microbial shedding using sterile stainless steel shedding chamber, discussing clean room clothing reducing shed rate 23 p3962 A67-40857
Microbial interaction factors determined between men and environment in closed systems 23 p3962 A67-40858
Long term space mission sanitation, personal hygiene and body cleansing to control microbe populations on body surface and teeth 23 p3967 A67-41611
Indigenous microflora as determined in men undergoing simulated space conditions, considering microbial shock postulated on long term missions 23 p3958 A67-41656
HYGROMETER
Aluminium oxide hygrometer performance obtained from balloon flight tests 05 p0808 A67-17307
Barium fluoride film electric hygrometer element aging and possible causes of calibration drift with time in storage 24 p4156 A67-42380
HYPERBOLIC EQUATION
Equations for nonlinear wave propagation in incompressible heat-conducting elastic material, noting propagation of shocks in isotropic material 01 p0162 A67-10846
Limit lines of generalized Cauchy problem for homogeneous differential equations with two independent variables analyzed, using concept of regular variables and formal solution of Meyer 02 p0260 A67-12433
Exact difference replacement for hyperbolic equation system where $n \times n$ symmetric matrices become coefficients of vectors in two-dimensional space 03 p0460 A67-13880
Goursat problem of first order nonlinear hyperbolic equations, introducing characteristic parameters with reduction to standard form 03 p0462 A67-14109
Boundary value problem of hyperbolic equation with discontinuous boundary conditions 05 p0834 A67-16371
Uniqueness and existence theorems for mixed problem of second order degenerate hyperbolic equation with discontinuous coefficients 05 p0834 A67-16494
Periodic solutions of hyperbolic equations containing small parameter by extending Cesari method for differential equations 07 p1218 A67-20213
Space-time diffraction for asymptotic solution of Klein-Gordon dispersive hyperbolic equation in bounded domain 07 p1218 A67-20270
Linear hyperbolic equations describing one-dimensional wave propagation, with stability conditions by harmonic analysis and second Liapunov method 09 p1533 A67-22400
Goursat problem for partial differential equation shown not to possess classical solution even under suitable hypothesis 09 p1525 A67-22624
Inviscid conical flow around pointed cone at angle of attack transformed into hyperbolic flow 10 p1592 A67-23136
Existence, uniqueness and stability investigation of periodical solutions for nonlinear hyperbolic partial differential equations 10 p1674 A67-23387
Linearization of hyperbolic equation for data analysis of stability of elastic column and plate structures, determining critical load 11 p1874 A67-24224
Optimal solutions to mixed initial boundary value problems for control processes described by semilinear hyperbolic partial differential equations in two independent variables 11 p1770 A67-24423
Cauchy problem and mixed boundary value problem of linear and quasi-linear degenerate hyperbolic second order equations applied to cylinder 11 p1814 A67-24851
Problem of Vallee-Poussin type for linear hyperbolic equations with spatial variable coefficients 11 p1814 A67-25049
Mixed problem for linear hyperbolic partial differential equation asymptotically

represented and reduced to boundary value problem and Cauchy problem 13 p2144 A67-26377

Characteristic initial value problem for linear second order hyperbolic partial differential equation 13 p2147 A67-27180

Hyperbolic difference equations, reviewing Courant-Friedrichs-Lewy paper in light of recent developments 14 p2342 A67-28154

Difference methods for parabolic equations and alternating direction implicit methods for elliptic equations 14 p2342 A67-28155

Riemann matrix in linear symmetric-hyperbolic systems of partial differential equations with constant coefficients in two-space and one-time variables 17 p2876 A67-32031

Steady state wave propagation in homogeneous anisotropic media governed by symmetric hyperbolic partial differential equations 18 p3077 A67-33429

Nonlinear hyperbolic equation solution formulation based on Riemann invariants 18 p3072 A67-34288

Boundary value wave problem in elastoviscoplastic medium solved by approximate method using Courant concept 19 p3340 A67-35444

Perturbation method using stream function for investigating anisotropic wave propagation describable by hyperbolic differential equations 21 p3611 A67-37891

Tanh η form laminar mixing layer and nonlinear inviscid equation two-dimensional solutions with linearized stability theory perturbations 22 p3782 A67-39528

Nonlinear hyperbolic equations of compressible duct flow solved using centered difference method, compared with method of characteristics 22 p3784 A67-39945

Elastic wave problems involving one space variable solved by hyperbolic partial differential equations 23 p4072 A67-40610

Complex Fourier transform technique in variable coefficient partial differential equations applied to Cauchy-Kowalewski and Petrowski-Leray theorems 24 p4178 A67-42202

Velocity and path of vertical motion of constant thrust rocket in homogeneous gravitational field, giving hyperbolic acceleration expression as time function 24 p4241 A67-42578

Hyperbolic noninvariance in partial differential equations, discussing existence theorems for nonhyperbolic initial value problem systems 24 p4178 A67-42727

HYPERBOLIC ORBIT

Optimal transfer between hyperbolic orbits in Newtonian field of attraction of heavy sphere of nonzero radius 01 p0152 A67-11411

Orbital transfer by hyperbolic encounter maneuver in perturbed gravity fields 04 p0695 A67-14541

Onboard guidance scheme as backup to earth-based orbit determination techniques and for approach navigation and orbit correction in planetary capture maneuver 04 p0654 A67-15234

Optimum energy transfer from hyperbolic orbit in Newtonian central force field in absence of transfer time limitations 07 p1247 A67-19094

Hyperbolic revised orbital data of comet Cunningham /1941 I/ hyperbolic revised orbital data of Comet Cunningham /1941 I/ 07 p1247 A67-19168

Single-impulse transition in Newtonian central force field from hyperbolic to elliptical orbit in case of radial impulse 12 p2002 A67-25638

Computer iteration scheme for calculating arbitrary hyperbolic transfer orbit in field of attracting center, based on Gaussian equations 12 p2002 A67-25640

Meteor hyperbolic motion and geocentric trajectory determination 13 p2196 A67-26497

HYPERBOLIC POSITION LINE

Configurations of hyperbolic position-fixing systems using synchronous satellites, showing Loran-like networks on earth resulting from these configurations 09 p1526 A67-22393

Hyperbolic region solutions of equation approximating Chaplygin equation near supersonic flow vacuum line in hodograph plane 12 p1962 A67-26181

HYPERBOLIC REENTRY

Optimum entry vehicle design using aerobreaking for manned earth entry at

hyperbolic speeds, examining blunted conic, biconic and tetrahedral configurations [AIAA PAPER 66-489] 15 p2564 A67-29422

HYPERBOLIC SPACE

Invariant properties of partially polarized electromagnetic waves analyzed in Poincare and Cayley-Klein models of hyperbolic space, using geometric constructions 09 p1460 A67-21588

HYPERBOLIC SYSTEM

Hyperbolic space localization system measuring three distance differences from four ground stations 02 p0264 A67-12354

Numerical solution of two-dimensional quasi-linear hyperbolic systems using characteristic method, obtaining approximate equations 05 p0834 A67-16436

Representation of characteristic surfaces of unsteady axisymmetric flow and steady three-dimensional supersonic flow by hyperbolic system of quasilinear differential equations 22 p3785 A67-40010

HYPERCAPNIA

Carbon dioxide breathing effects on forearm blood vessels, discussing vascular resistance and carbon dioxide role in blood flow regulation 20 p3373 A67-37584

Cerebral blood flow and metabolism during combined hypoxia and hypercapnia, noting cerebral vasodilatation effect 23 p3945 A67-41080

Chronic hypercapnia effects on pH level, Ca and P metabolism and electrolyte metabolism in normal sedentary man 23 p3955 A67-41605

Rats resistance and reactivity in hypothermal state to very low atmospheric pressure by hypercapnia-hypoxia exposure 24 p4111 A67-41849

HYPERFINE STRUCTURE

Gas laser spectroscopic analysis of hyperfine structure, paramagnetic properties, radiative lifetimes and Doppler-broadened transition saturation behavior of excited states of Xe 129 04 p0661 A67-15482

Fabry-Perot interferometers with electronic determination of Doppler line widths, discussing effect of hyperfine and isotopic structure 07 p1185 A67-19399

Correction of calculations of Einstein A coefficient for transition of OH 09 p1532 A67-21989

Molecular beam electric resonance /MBER/ spectrometer for hyperfine structure of rubidium fluoride 11 p1821 A67-23961

Spin-projected unrestricted self-consistent field /SCF/ methods for spin density calculations used to determine hyperfine coupling constants 13 p2160 A67-26540

Absolute oscillator strengths of three titanium resonance lines from absorption measurements in atomic beam 14 p2351 A67-28581

Hyperfine structure of ground state of helium 3 microwave transition radiation from galactic H II regions 19 p3330 A67-36074

Magnetic field induced hyperfine structure in mono- and divalent iron ions in magnesium and calcium oxide, showing evidence of paramagnetic resonance 20 p3506 A67-36211

Very high resolution Fourier transform spectrometer, discussing path difference variation 20 p3438 A67-36346

Computer method for evaluating hyperfine structure recordings obtained by photoelectric Fabry-Perot interferometer 20 p3440 A67-36357

Ground state hyperfine splitting of singly charged helium calculations by Zwanigler and Sternheim evaluated by examining error corrections by Fortson et al 20 p3488 A67-36694

Hyperfine structure in rotational spectrum of HDO and deuterium oxide analyzed by beam maser spectroscopy, evaluating coupling constants 20 p3461 A67-37287

Ammonia inversion transition hyperfine structure for nitrogen 14 and 15 nuclear masses measured with two-cavity maser spectrometer 20 p3462 A67-37585

Hyperfine splitting of spin interaction energy of two hydrogen atoms, determining eigenfunctions for effective Hamiltonian 21 p3658 A67-37814

Hyperfine interaction between unpaired trapped electron and adjacent titanium 47 and 49 nuclei in F center ESR line in barium titanate 21 p3684 A67-38417

Electromagnetic interactions in hyperfine structure of vibrational and rotational states

in rubidium and potassium /isotopes/ fluorides, using electric resonance method 22 p3839 A67-3920

Filter with hyperfine doublet splitting using Paschen-Back effect for optics pumping 22 p3816 A67-4032

Hyperfine coupling constants of lithium energy levels, using Weiss 45-configuration wave functions 24 p4190 A67-4209

Mossbauer spectra of FeMo alloys for closed space compositions show overlap of disturbed surroundings of impurity iron atoms and magnetic moment 24 p4203 A67-4210

HYPERGEOMETRIC FUNCTION

Continued fraction in theory of electro energy for ground state of one-electron diatomic molecule near united atom 01 p0118 A67-1088

General Fuchs type theorem for partial differential equations applicable to hypergeometric functions with two variables 09 p1525 A67-2257

Undetermined coefficient method compared with confluent hypergeometric functions for solving first order perturbation equation for refractive index of He 11 p1813 A67-2478

Transverse vibrations of tapered cantilever beam solved in terms of generalized hypergeometric function by Frobenius method [ASME PAPER 67-APM-25] 17 p2964 A67-3315

Nonuniform RC lines with hypergeometric and spheroidal wave functions solutions calculating driving point impedance 19 p3190 A67-3484

Hypergeometric functions studied for solution of problems on elastic equilibrium of circular plates and shells of revolution 22 p3909 A67-3939

HYPERGOLIC PROPELLANT

Metallic material compatibility with medium energy hypergolic propellant components hydrazine/UDMH and nitrogen tetroxide, used in ELDO rocket 01 p0139 A67-1021

Ignition methods for strongly and weakly hypergolic hybrid propulsion systems examining steady state combustion problems and combustion instability causes 01 p0139 A67-1141

Kinetically based mathematical model of hypergolic ignition in space ambient engine for predicting delay time and conditions from which pressure spikes result [AIAA PAPER 66-950] 02 p0302 A67-1228

Flame spreading velocity over surface of igniting solid rocket propellants as function of atmospheric pressure and chemistry and specimen surface condition 06 p1073 A67-1885

Low pressure low-temperature ignition of hypergolic propellants, particularly hydrazine-nitrogen tetroxide systems, in space environment simulator and conclusions on gas phase reactions 07 p1163 A67-1938

Hypergolic propellant ignition experience during Project Sure Fire of Gemini program [AIAA PAPER 67-259] 07 p1241 A67-2000

Ignition of hydrogen-oxygen propellant combination by chlorine trifluoride 10 p1697 A67-2313

Factors influencing rocket ignition pressures and conditions leading to large ignition overpressures, estimating residual propellant in rocket combustor [AIAA PAPER 67-515] 18 p3114 A67-3397

Pregnition phenomena in small Aerozine 50/nitrogen tetroxide pulsed rocket engine shown partly due to hydrazine nitrate accumulation [AIAA PAPER 67-516] 18 p3114 A67-3397

Additives effect on ignition delay and pressure of hypergolic hydrazine-nitrogen tetroxide propellant systems 19 p3310 A67-3501

Kinetically based mathematical model of hypergolic ignition in space ambient engine for predicting delay time and conditions from which pressure spikes result 19 p3311 A67-3574

Vapor phase decontamination for removing residual hypergolic propellants in Apollo propulsion system 20 p3516 A67-3657

HYPERON

Weak electromagnetic decays of hyperon in broken SU(3) model 20 p3489 A67-3709

HYPEROXIA

Fundus oculi observation of retinal vessels

caliber alteration during changes in arterial gas tensions 17 p2805 A67-31961
Oxygen role in cardiac rate in squirrel monkeys during acceleration stress on centrifuge 23 p3956 A67-41635
Trace contaminant experiment for studying effect of hyperoxic environment at high total pressure on human blood constituents 23 p3960 A67-41703
Rats exposed to different hyperoxic atmospheres for 20 days studied for toxic lipids formation 24 p4112 A67-41854

HYPERPLANE

Algorithm based on penalty functions to determine hyperplane used as iterative resolution for separating convex sets 01 p0028 A67-10495
Partitions of n-space by hyperplanes, examining applications in switching theory 01 p0106 A67-10733
Algorithm based on penalty functions to determine hyperplane used as iterative resolution for separating convex sets 10 p1608 A67-23617

HYPERPNEA

Experiments for relief of astronauts from cardiovascular and respiratory distress during EVA 23 p3953 A67-41586

HYPERSONIC AIRCRAFT

Boundary layer effect on lift and drag characteristics of hypersonic lifting bodies 03 p0351 A67-12991
Aerodynamic problems due to air intake and exhaust nozzles effect on propulsion of hypersonic aircraft [ONERA-TP-416] 05 p0748 A67-16481
Heating and effectiveness of control surfaces on lifting reentry vehicle or hypersonic aircraft [ONERA-TP-365] 05 p0750 A67-17403
Thrust deflection in hypersonic air breathing vehicles, noting increased cruise range and effects of gross thrust/ram drag ratio 09 p1441 A67-22497

Wing-fuselage section panels of hypersonic aircraft built by brazing welded refractory honeycomb 10 p1660 A67-23171
Hypersonic transport design, considering payload vs range and weight and power plant, aerodynamic, structural and flight profile problems 11 p1744 A67-24579
High performance aerodynamic vehicle design noting configuration variables, optimum performance parameters, vehicle force characteristics, optimization of hypersonic aircraft performance, etc [AIAA PAPER 66-486] 13 p2054 A67-27584

Carbon dioxide purge and thermal protection system for liquid hydrogen tanks of hypersonic aircraft, comparing with helium purge system 13 p2227 A67-27647
Future supersonic and hypersonic aircraft horizontal liquid hydrogen fuel tank requirements, discussing insulation optimization using variable thickness 13 p2054 A67-27657

Endothermic hydrocarbon fuels for supersonic aircraft, noting heat sink capacity effect in overcoming thermal thicket and usability as engine fuel 15 p2543 A67-29305
Flight control power distribution systems for hypersonic aircraft, considering cooled and pulsating flow hydraulic, liquid metal, pneumatic and mechanical systems 17 p2800 A67-31970

Integration of propulsion system into airframe of hypersonic cruise aircraft, discussing configurations, cooling and supersonic combustion 17 p2796 A67-32475
Parametric analysis on hydrogen-fueled hypersonic aircraft for long range passenger transport missions and launch vehicle missions, noting propulsion system-airframe interactions [AIAA PAPER 67-493] 18 p2985 A67-33957

Hypersonic wave rider flow and aerodynamic problems, discussing shaping, leading edge cooling and supersonic combustion propulsion 23 p3929 A67-41251

HYPERSONIC BOUNDARY LAYER

Rarefaction parameter for planar bodies with sharp leading edge and tip defining hypersonic boundary of strong interaction regime 01 p0007 A67-11182
Controlled three-dimensional roughness effect on hypersonic laminar boundary layer transition [AIAA PAPER 66-26] 04 p0547 A67-14819
Complex flow interactions within laminar hypersonic boundary layers 04 p0604 A67-14846

Reynolds number effect on surface pressure distributions and boundary layer velocity profiles on three-quarter power law bodies of revolution in hypersonic flow 05 p0747 A67-16431
Hypersonic laminar boundary layer on blunt cones, considering external flow vorticity caused by curved shock wave, calculating gas-enthalpy profile 06 p0936 A67-17734

Hypersonic boundary layer behavior in adverse pressure gradients used in designing high Mach number intake diffuser system 06 p0942 A67-18750

Monograph on hypersonic heat transfer calculation methods for boundary layers in presence of surface catalyzed reactions 09 p1489 A67-22198

Hypersonic turbulent boundary layers transformation to incompressible form 14 p2297 A67-28137

Laminar boundary layer transition in hypersonic shock tunnel of cone, noting effect of high Mach numbers and tip surface roughness, using surface heat transfer gauges [AIAA PAPER 66-494] 15 p2418 A67-30191

Hypersonic weak and strong interaction theory for case of uniform flow past flat plate, discussing boundary layer characteristics 15 p2473 A67-30220

Shock tunnel experiments with hypersonic turbulent boundary layer flow over flat plates with blunt and sharp leading edges and wall of expansion nozzle 16 p2659 A67-30954

Transition region of hypersonic boundary layer on flat plate surveyed with hot wires, giving analysis for limited wire calibration 19 p3212 A67-35765

Hypersonic weak-interaction similarity solutions for viscous heat-conducting compressible flow past flat plate, using Navier-Stokes equations 20 p3357 A67-36849

Hypersonic aerodynamics, discussing tunnel testing, inviscid flows, airfoil shapes, real gas effect, shock wave theory and boundary layers 23 p3930 A67-41307

Flared afterbody aerodynamic characteristic predictions for aircraft stability at high Mach numbers, discussing turbulent separation 24 p4093 A67-42924

HYPERSONIC COMBUSTION

Penetration of gaseous jets injected into supersonic stream treated by solid body drag model, noting application to hypersonic ramjet combustion 02 p0232 A67-11935

Impact-induced combustion in hypersonic ramjet engines, determining hypersonic fuel-air mixing from hydrogen concentration at Laval nozzle outlet [DVL-601] 03 p0503 A67-13014

HYPERSONIC FLIGHT

Ablative materials for thermal protection and minimum mass transfer of aircraft flying at hypersonic speeds [DVL-603] 03 p0532 A67-13026

Noncontour transpiration cooled heat shield for possible application to hypersonic atmospheric flight 04 p0725 A67-15435

Simulated high altitude hypersonic cold wall testing of lifting bodies, measuring lift, drag and static pitching moment 06 p0943 A67-18847

Flow fields of inlets for real or perfect gases determined through four methods for application to supersonic and hypersonic flight regimes [AIAA PAPER 66-605] 13 p2050 A67-26831

Paracone emergency escape system for rescuing space crews from orbits at hypersonic velocities 17 p2794 A67-32001

Potential advantages of hypersonic vehicles compatible with missions combining more than one cruise-flight regime, discussing gas dynamic heating for propulsion [SAE PAPER 670354] 17 p2798 A67-32994

Supersonic combustion characteristics of hypersonic ramjet predicted by analytical method using constant-mass tube technique, discussing flow field properties [AIAA PAPER 67-494] 18 p2983 A67-33958

Supersonic combustion simulation for hypersonic flight in relation to scramjet operation, discussing auto-ignition limits [CI PAPER 67-6] 19 p3344 A67-35001

Limits of application of binary scaling for hypersonic flight 19 p3212 A67-35769

Hypersonic flight programs, considering

Air Force, Navy and NASA research programs on scramjets 20 p3517 A67-37447
Langley Hypersonic Nitrogen Facility flow evaluation covering pitot pressure survey of nozzle wall boundary layer, centerline and Mach number 21 p3607 A67-37777

HYPERSONIC FLOW

Row of parallel circular cylinders in hypersonic flow show determinant factor in boundary layer and heat transfer characteristics 01 p0006 A67-10559

Three-dimensional boundary layer and inviscid hypersonic flow interaction on infinitely thin triangular wing 01 p0007 A67-10982

Interaction between boundary layer and external inviscid flow, noting unsteady motion of gas around infinite plate and steady flow around semiminfinite plate 01 p0053 A67-10983

Mass effect on blast wave equations of shock generation by secondary injection of fluid into hypersonic flow 01 p0141 A67-11179

Hypersonic flow over blunt flat plate with surface mass transfer 01 p0007 A67-11180

Model of nonequilibrium properties of high temperature carbon dioxide and other gas mixtures in connection with studies for vehicles entering Martian atmosphere 01 p0008 A67-11436

Pressure and density measurements of heat flux convected on sharp pointed cone placed in incidence in hypersonic flow 02 p0177 A67-11499

Low altitude hypersonic flow simulation by means of supersonic compressor, considering capability of providing true temperature sea-level flight duplication at Mach 9 02 p0229 A67-11933

Approximate determination of sonic line and pressure distribution on surface of blunt body in supersonic and hypersonic flows 02 p0178 A67-12042

Local convection coefficient along windward line of axisymmetric obstacle in hypersonic flow with laminar boundary layer 02 p0178 A67-12061

Hypersonic flow past lower surface of slender delta wing for wide-range of angle of attack, determining velocity component, pressure and density distribution 03 p0350 A67-12874

Hypersonic flow separation over simple geometries and aerodynamic controls, noting pressure gradients and heating-rate distributions [AIAA PAPER 65-753] 03 p0350 A67-12911

Hypersonic flow of air past circular cylinder with nonequilibrium oxygen dissociation, including dissociation of free stream 03 p0351 A67-13000

Separation points occurring in Newtonian theory of hypersonic flow locally treated by modifying shock layer equations, thus verifying free layer theory 04 p0545 A67-14463

Vibration temperature of relaxing hypersonic gas flow measured by electron beam technique 04 p0545 A67-14542

Fluid dynamic sources of radiation during atmospheric entry, considering equilibrium and nonequilibrium radiation, thermal radiation and relaxation processes in hypersonic flow 04 p0703 A67-14703

Hypersonic behavior of helium flow past highly blunt bodies, noting drag and shape of shock wave 04 p0546 A67-14779

Hypersonic helium flow past blunt cones compared with flow past sharp cones 04 p0546 A67-14781

Optimum shaped-bodies of maximum lift-to-drag ratio in hypersonic flow for modified Newtonian pressure distribution and constant skin friction 04 p0546 A67-14817

Variation of transition Reynolds number with wall to recovery temperature ratio at hypersonic speeds, comparing transition measurements with and without Pitot tube 04 p0604 A67-14836

Laminar convective heat transfer to cavities in hypersonic low density flow 04 p0732 A67-15833

Aircraft skin panel fatigue failure under hypersonic conditions, noting effect of natural vibration frequency and axisymmetric oscillations 05 p0916 A67-16229

One-dimensional self-similar motion of relaxing gas, noting ODEs of process and gas dynamic parameters of flow 05 p0791 A67-16376

Transport of vorticity and enthalpy in

flow field in nose region of blunt body in viscous hypersonic flow 05 p0749 A67-16820

Gap size effect on pressure and aerodynamic heating over flap of blunt delta wing in hypersonic flow [AIAA PAPER 66-408] 05 p0749 A67-17220

Atmospheric argon effect on hypersonic stagnation point convective heat transfer, using arc-heated shock tube simulating flight velocities up to 34,000 fps [AIAA PAPER 66-29] 05 p0928 A67-17337

Velocity and temperature profiles of optically thick planar Couette flow, obtaining heat transfer rates for Rosseland mean absorption coefficient variation with temperature 05 p0793 A67-17343

Hydromagnetic compressible boundary layer flow past flat plate analyzed via von Karman integral method 05 p0794 A67-17361

Optimum wedges and semicones in hypersonic viscous flow, examining effect of thickness ratio on lift-drag ratio 05 p0750 A67-17367

Mass transfer perturbations about reversed flow profiles of Stewartson, noting computation of solutions to Falkner-Skan equation 05 p0794 A67-17369

Hypersonic flow past sphere by relaxing gas with internal degrees of freedom in nonequilibrium 06 p0935 A67-17731

Explosion analogy in flows past slender blunt bodies, noting accuracy improvement by placing explosion center ahead of origin 06 p0936 A67-17732

Hypersonic flow in compressed layer between tapered blunt leading edge of wing and internal shock wave forming in front when nonuniform flow moves past, considering expansion plane 06 p0936 A67-17733

Three-dimensional flows with Mach interaction between shock waves, drawing conclusions on possible types of interference between wing and wall 06 p0936 A67-17736

Two-dimensional multiple wave distortions effect on heat transfer to wall in hypersonic flow [AIAA PAPER 67-164] 06 p1115 A67-18294

Shock tunnel data on surface pressure resulting from hypersonic stream interaction with two transverse jets [AIAA PAPER 67-190] 06 p0939 A67-18299

Laminar, transitional and turbulent boundary layer flows with adverse pressure gradient on axisymmetric blunted conical flared body at Mach 10 06 p0943 A67-18844

Shock tunnel heat transfer measurement and hypersonic viscous flow over pointed cones, particularly viscous-layer regime at low Reynolds numbers 06 p0943 A67-18845

Three-dimensional boundary layer flow over windward side of flat delta wing in hypersonic flow at moderate angle of attack, examining viscous-inviscid interaction [AIAA PAPER 66-492] 06 p0943 A67-18848

Laminar boundary layer separation length data in hypersonic flow show strong Mach number dependence 06 p0992 A67-18878

Book on inviscid hypersonic flow theory including nonequilibrium effects, flows on blunted bodies, shock layer, conical flows, etc 07 p1127 A67-20204

Simple method for determining deviation of supersonic or hypersonic plane parallel flow of inviscid gas caused by auxiliary jet in form of thin layer 07 p1127 A67-20208

Inviscid hypersonic flow of radiating gray gas over sphere analyzed, noting temperature role in process 08 p1276 A67-20567

Flow field in turbulent far wake at high Mach and Reynolds numbers, obtaining solution of boundary layer equations 08 p1277 A67-20577

Boundary layer transition measurements of contoured nozzle flow at hypersonic Mach numbers 08 p1320 A67-20584

Inviscid hypersonic flow over plane power law bodies where blast theory applies as first approximation, determining shape and pressure distribution 08 p1277 A67-20708

Hypersonic rarefied gas flow past plate with sharp leading edge, determining rarefaction effect on induced pressure distribution and value 08 p1278 A67-20924

Wall temperature effect on behavior of hypersonic stagnation region shock layer in incipient merged layer flow, obtaining enthalpy function profile 08 p1278 A67-20928

Optimum hypersonic shapes for outer flow

region, using Newtonian approximative model 10 p1589 A67-22734

Aerodynamic problems of low density high speed flow of rarefied gases past submerged body 10 p1623 A67-22874

Thin shock layer stagnation region analysis in hypersonic flow, emphasizing lateral asymmetry for planar and perturbed axisymmetrical cases 10 p1624 A67-22936

Mach number effect on hypersonic flow past delta wing with blunt edges at zero angle of attack 10 p1590 A67-23036

Symmetrical equilibrium flow past blunt body at superorbital reentry conditions calculated by integrating motion equations across shock layer 10 p1591 A67-23109

Similar calculation of hypersonic laminar boundary layer characteristics in presence of pressure gradient, specifically heat transfer, skin friction and boundary layer thickness 10 p1592 A67-23141

Flight control magnetic source interaction with ionized gas induced by bow shock ahead of blunt body in hypersonic flow 10 p1592 A67-23143

Steady hypersonic inviscid flow, including detached shock, around blunt body, using finite difference computations 10 p1593 A67-23633

Flutter of panels mounted on wedges in hypersonic flow of perfect gas, neglecting acoustic waves 10 p1593 A67-23735

Fluid dynamic fields from hypersonic flow around slender bodies, using extension of Vallander tangent cone method for zero angle of attack 11 p1741 A67-24091

Variation problem solution in hypersonic gas dynamics, noting intake portion construction for body with minimum resistance for limited length and flat end 11 p1777 A67-24153

Conditions at head shock wave in viscous hypersonic flow past blunt body for study of boundary layer separation 11 p1741 A67-24157

Aerodynamic characteristics of wedge wings determined for hypersonic viscous flow 11 p1742 A67-24347

Mean droplet size for cross stream water injection into Mach 8 air flow determined by scattered light angular variation measurement 11 p1779 A67-24366

Behavior of high current arcs driven by strong external magnetic fields with respect to hypersonic flow generation by MHD forces 12 p1974 A67-25399

Vortical interaction between free jet boundary layer and outer flow in separation area of hypersonic gas flow past body 12 p1892 A67-25671

Parameterization of minimum-drag slender pointed cone situated in viscous hypersonic gas flow 13 p2050 A67-26882

Hypersonic flow near stagnation point of blunt body taking radiation into account, noting large enthalpy and density gradients 13 p2050 A67-26897

Skin friction drag coefficient at supersonic-hypersonic speeds as function of transition on delta wing 13 p2051 A67-27597

Free stream variables from continuum effect followed experimentally into transition flow regime to investigate impact probe in rarefied hypersonic flows of diatomic gases 14 p2294 A67-27794

Asymptotic and numerical solutions of Goulard integrodifferential equation describing hypersonic flow near stagnation point past blunt bodies, allowing for radiative transfer effects 14 p2296 A67-27981

Effect of Reynolds number on hypersonic flow of rarefied gas past sphere obtained from pressure distribution at surface 14 p2240 A67-27996

Transitional rarefied flow regime noting drag on simple bodies, flows at sharp edges, lifting bodies, etc 14 p2299 A67-28161

Viscous hypersonic flow past leading edge of sharp flat plate analyzed, using Navier-Stokes equation and velocity slip and temperature jump wall boundary conditions 14 p2299 A67-28162

Continuum flow analysis for leading edge region of flat plate, using model based on hypersonic thin layer type of approximation 14 p2240 A67-28163

Pressure on sharp-edged insulated flat plate in low density hypersonic flow, noting results and possible sources of error 14 p2241 A67-28164

Flow field measurement near sharp leading edge of cooled flat plate parallel to

low density hypersonic stream 14 p2241 A67-28165

Electron beam density survey in low density hypersonic flow field over sharp flat plate, noting results in outer and inner part of shock layer 14 p2241 A67-28167

Flow field experiments for shock wave and boundary layer development on two-dimensional and axisymmetric bodies 14 p2241 A67-28168

Local flow field measurements of static temperature, density and local impact pressure of hypersonic rarefied flow over 10 degree cone 14 p2241 A67-28169

Hypersonic low density flow analysis with shock tunnel and electron beam densitometer, noting density profiles at various Mach and Knudsen numbers 14 p2300 A67-28176

Collimation of low density hypersonic jet from shock tube for atomic beam production, noting relation between beam intensity and velocity distribution 14 p2301 A67-28188

Flow rate and pressure coefficients approximate determination for surface of symmetrical hypersonic flow past circular cone 14 p2243 A67-28656

Axisymmetric blunt bodies shock standoff distances in hypersonic flow determined by numerical and analytic methods 14 p2244 A67-29056

Hypersonic stagnation point flow between strong shock wave and body involving radiation, conduction and dissociation 15 p2415 A67-29309

Testing conditions for near-wake study of solids of revolution in supersonic and hypersonic flow, using streamlined supports in magnetic suspension [ONERA-TP-454] 15 p2416 A67-29379

Hotshot wind tunnel for ionized wakes of models in nitrogen hypersonic flow, determining electron temperature and density [ONERA-TP-455] 15 p2416 A67-29380

Interval size effect on minimum drag coefficients and optimum shapes of bodies of revolution determined from Newtonian impact theory 15 p2416 A67-29407

Minimum drag for slender body in hypersonic flow, assuming pressure coefficient is modified Newtonian and surface-averaged skin friction coefficient is constant 15 p2416 A67-29408

Shock wave shapes around spherical and cylindrical-nosed bodies, assuming hyperbolic profile asymptotic to freestream Mach angle or attached shock angle 15 p2417 A67-29448

Formula for pressure vs flow deflection at hypersonic speeds, useful in studies involving pressure on inclined surfaces 15 p2472 A67-29675

Far wake behavior of hypersonic spheres analyzed using schlieren techniques 15 p2417 A67-30190

Stagnation region foreign gas injection in low Reynolds number hypersonic shock layer flow 16 p2591 A67-30936

Three-dimensional slender wings of maximum lift/drag ratio in hypersonic flow studied by variational calculus under several lift and volume conditions 16 p2592 A67-30964

Pressure distribution and convective heat flux at slender bodies of revolution surface, considering sphericity influence of free hypersonic flow 16 p2594 A67-31468

Hypersonic magnetohydrodynamic flow over blunt bodies for small magnetic Reynolds number hypersonic magnetohydrodynamic flow over blunt bodies for small magnetic Reynolds number hypersonic magnetohydrodynamic flow over blunt 16 p2594 A67-31579

Hypersonic gas flow past slender body, obtaining pressure coefficient and shock wave curvature by linearizing differential equations involving stream function 17 p2791 A67-32868

Approximate solution for hypersonic flow past unyawed cone by small disturbance stream function equation 17 p2793 A67-33024

Lobb empirical relation applied to method for computing flow past blunt body when predicting sphere shock standoff distance 17 p2793 A67-33026

Ionization effect on external pressure determination for high velocity gas flows past plates and shells with flutter 18 p2981 A67-33424

- Shock and boundary layers about blunted two-dimensional slender bodies in hypersonic flow
[AIAA PAPER 67-451] 18 p2982 A67-33925
- Three-dimensional hypersonic flow past blunt cones calculated by modified method of characteristics, taking into account physicochemical equilibrium conversions 18 p2984 A67-34213
- Numerical solutions of hypersonic sharp leading edge flows, with full time-dependent Navier-Stokes equations solved 18 p2984 A67-34739
- Vibrational and/or chemical relaxation effects behind various shock waves in hypersonic air streams determined for equilibrium and nonequilibrium conditions 19 p3169 A67-34813
- Magnetospheric boundary and standing shock wave for earth scaled down to apply to Mars 19 p3324 A67-35442
- Inviscid hypersonic flow in stagnation region of circular cylinder with detached shock wave, considering real-gas effects 19 p3171 A67-35713
- Inviscid hypersonic axisymmetric flow over cylinder and sphere near stagnation point, including dissociation and detached shock wave 19 p3171 A67-35722
- Hypersonic rarefied flow past sharp leading edge of flat plate noting incomplete compression phenomenon 19 p3171 A67-35735
- Binary laminar boundary layer equations with second order transverse curvature for hypersonic flow with mass injection of foreign gases into air 19 p3211 A67-35737
- Shock tunnel data on surface pressure resulting from hypersonic stream interaction with two transverse jets 21 p3610 A67-37799
- Two-dimensional multiple wave distortions effect on heat transfer to wall in hypersonic flow
[AIAA PAPER 67-164] 21 p3732 A67-38855
- Nose bluntness and cone angle effects on base pressure and heating in laminar hypersonic flow regime, using free flight telemetry technique 21 p3565 A67-38882
- Drag measurements of cones in rarefied flow regime extended to higher and lower cone semivertex angles 21 p3565 A67-38884
- Second order weak interaction expansion for hypersonic flow past adiabatic flat plate, obtaining expressions for static pressure, displacement thickness and skin friction 21 p3566 A67-38892
- Transitional and turbulent boundary layers on cold flat plate in hypersonic flow noting bluntness, Reynolds and Mach numbers effects 21 p3615 A67-39080
- Inviscid hypersonic flow field between barrel shock and free boundary for source flow representing high altitude jet exhaust 22 p3739 A67-39410
- Radiative heat loss effect on steady axisymmetric hypersonic flow past blunt body using gray gas approximation, with numerical solution for stagnation region 22 p3739 A67-39530
- V-shaped wings with plane sides and sharp edges investigated for aerodynamic properties, deriving equations for flow parameters at Mach 6 22 p3741 A67-40016
- Hypersonic boundary layer of sharp cone, considering boundary layer interaction with outer viscous flow 22 p3741 A67-40027
- Dynamic destabilization for hypersonic flow around slender cone with severely blunt nose analyzed by blast wave analogy 22 p3742 A67-40109
- Viscous degradation of hypersonic lift-drag ratio in manned spacecraft, noting free stream Mach and Reynolds numbers 22 p3742 A67-40113
- High altitude hypersonic viscous flow degradation of L/D effects on entry vehicle lateral range capability 22 p3742 A67-40114
- Wind tunnel hypersonic flow visualizations under low flow density conditions, comparing schlieren and phase-contrast methods 23 p3985 A67-40568
- Second order boundary layer equations for hypersonic flow, noting interaction between pressure gradients 23 p3991 A67-41252
- Asymptotic perturbation of hypersonic flow over blunt slender cones and wedges showing oscillatory nature 23 p3931 A67-41665
- Integral solution for massive blowing on slender hypersonic wedges and cones in laminar flow, assuming homogeneous nonreacting perfect gas mixtures 23 p3932 A67-41743
- Transverse curvature parameter in hypersonic flow regime for modifying effects on velocity profile slope, skin friction and heat transfer rate 23 p3993 A67-41755
- Shock waves and boundary layer structure near tip of slender cone in rarefied hypersonic flow, discussing surface pressure peaks 23 p3932 A67-41762
- Chemical reaction effect on viscous boundary layer of hypersonic flow of reacting gas mixture past blunt body 24 p4091 A67-42270
- First approximation analysis of rarefied hypersonic gas flow asymptotic properties near surface and front edge of thin plate, determining macroparameters 24 p4142 A67-42272
- Incidence angle effects on wall heat flux in symmetry plane of cone of revolution in hypersonic regime, discussing wall pressure measurements 24 p4092 A67-42660
- HYPERSONIC GLIDER**
- Critical heating conditions in hypersonic glider reentry 06 p1113 A67-17981
- Hypersonic reentry heating problems for glider of composite structure with critical temperature condition, buckling, etc 11 p1869 A67-24092
- Reusable low weight hypersonic glider /space rotor/ for space vehicle reentry and recovery 15 p2568 A67-29845
- Range of hypersonic gliders for various flight and reentry conditions, assuming small flight path angle and constant bank angle 16 p2595 A67-30963
- HYPERSONIC HEAT TRANSFER**
- Hypersonic aerodynamics and heating of blunt body at high and low Reynolds numbers 06 p0937 A67-17982
- Reynolds number scaling theory for hypersonic ablation, deriving heat and mass transfer relationship
[AIAA PAPER 67-155] 06 p1117 A67-18478
- Monograph on hypersonic heat transfer calculation methods for boundary layers in presence of surface catalyzed reactions 09 p1489 A67-22198
- High speed photography of laser radiation damage to transparent materials and analysis of destruction mechanisms involved 09 p1516 A67-22660
- HYPERSONIC INLET**
- Heat transfer and centrifugal force effects on hypersonic inlet boundary layer and pressure recovery
[AIAA PAPER 65-605] 03 p0350 A67-12910
- HYPERSONIC NOZZLE**
- Pressure and density of heat flux at surface of pointed or blunt nosed obstacle in divergent truncated cone of hypersonic nozzle 01 p0005 A67-10258
- Nonequilibrium expansion of high temperature diatomic gas through hypersonic convergent-divergent nozzle 02 p0180 A67-12547
- HYPERSONIC REENTRY**
- Heat flux to SNAP reactor system models in hypersonic continuum flow measured in shock and hyperthermal wind tunnels, using thin film resistance thermometer 01 p0112 A67-11022
- Winged lifting reentry hypersonic vehicles, discussing design, analysis, fabrication and testing of hot and cooled structures and materials
[AIAA PAPER 65-367] 02 p0331 A67-11929
- Angle of attack measurements of hypersonic reentry vehicle derived from flight test pressure data 02 p0178 A67-11942
- Integral relations method applied to separation of laminar boundary layer on cooled hypersonic reentry body 02 p0179 A67-12348
- Wind tunnel tests of lifting reentry body at Mach numbers up to 16.5 and at angles of attack up to 50 degrees 04 p0546 A67-14567
- Viscous and bluntness induced pressures for flat plates, wedges, cylinders and cones at Mach 41
[AIAA PAPER 65-399] 04 p0546 A67-14815
- Optimum trajectory control for minimum heating paths during manned vehicle reentry at hyperbolic speeds
[AIAA PAPER 67-59] 06 p1095 A67-18268
- Graphite thermochemical response tested in simulated environment for use as thermal shield for hypersonic reentry vehicles
[AIAA PAPER 65-643] 08 p1426 A67-20561
- Hypersonic reentry heating problems for glider of composite structure with critical temperature condition, buckling, etc 11 p1869 A67-24092
- Nose bluntness effect on hypersonic unsteady aerodynamics of ablating flared or conical slender reentry vehicles 15 p2416 A67-29442
- Hypersonic reentry, inertial guidance tests and construction of two-stage Diamant satellite launcher 15 p2571 A67-30089
- Hypersonic reentries with thermal and structural integrity problems studied by Saphir rocket firings 17 p2955 A67-32376
- Hypersonic reentry heating problems due to kinetic energy of space vehicle at reentry at orbital and escape velocity 17 p2970 A67-32828
- Optimum trajectory control for minimum heating paths during manned vehicle reentry at hyperbolic speeds
[AIAA PAPER 67-59] 19 p3331 A67-34815
- Stagnation ablation of blunt body hypersonic reentry with nonreacting gas, deriving laminar flow equations 20 p3356 A67-36509
- Electrodeless slip-type MHD steady state acceleration of subsonic and supersonic high density gas flows for simulating reentry speeds and altitudes 21 p3607 A67-37778
- Hypersonic reentry plasma electron density measurement in free stream wake and shock layer using hotshot wind tunnel simulation 23 p3986 A67-40574
- Aerodynamic power and moment coefficients of space-transport configurations for hypersonic reentry and trajectory calculations 23 p3931 A67-41399
- HYPERSONIC SAIL**
- Stretched sail behavior in sonic, supersonic and hypersonic flows, discussing profile dependence on angle of attack and free-stream Mach number 21 p3563 A67-37889
- HYPERSONIC SHOCK**
- Structure of radiation resisted hypersonic shock in simple dissociating gas examined via quasi-equilibrium field for radiation field 06 p0993 A67-18893
- Steady hypersonic inviscid flow, including detached shock, around blunt body, using finite difference computations 10 p1593 A67-23633
- Shock wave structure in air at supersonic and hypersonic velocities studied by electron-beam density method 14 p2297 A67-27997
- Equilibrium radiant heat transfer to bodies at hypersonic velocities in carbon dioxide atmosphere noting shock layer, shock standoff distance, shock velocity, etc 15 p2582 A67-30216
- Microwave experimental technique for continuous velocity measurement of shock and contact discontinuities bounding air plasma generated in cylindrical hypersonic shock tube 18 p3020 A67-34105
- Integral relations method for nonequilibrium hypersonic planetary entry, emphasizing flow fields and thermal environment determinations for blunt body vehicle configuration 22 p3740 A67-39936
- Surface mass transfer effects on viscous hypersonic shock layer of blunt body including suction and injection of air into air 22 p3743 A67-40417
- HYPERSONIC SPEED**
- Hypersonic aerodynamic coefficients for bodies of revolution in yaw 02 p0179 A67-12314
- Mach-Zehnder interferometer used with axisymmetric free flight models at hypersonic speeds, noting isopycnals and light gas gun 05 p0789 A67-17355
- Transition from laminar to turbulent boundary layer flow at hypersonic Mach numbers, noting measurement techniques
[AIAA PAPER 67-130] 06 p0989 A67-18474
- Equilibrium air study extended to reentry speeds up to 70,000 fps, using transport and thermodynamic properties to examine stagnation point convective heat transfer including blowing rates 06 p0943 A67-18843
- Control surface instabilities of lifting body configurations at very high speeds and with separated flows analyzed by wind tunnel tests for unsteady control surface load problems
[AIAA PAPER 67-15] 07 p1258 A67-19430
- Hypersonic air breathing engine, specifically scramjet, noting vehicle design, combustion system, nozzle, friction, etc 10 p1697 A67-22873
- Thermal behavior of vehicle entering

earth atmosphere at velocities approaching 15 km/sec 13 p2224 A67-27325

Hypersonic decelerator deployment investigated for interactions between decelerator, connecting cable and wake of forebody it tails 14 p2244 A67-29055

Slender two-dimensional wing lift-drag ratio at hypersonic speed maximized, assuming modified pressure coefficient 15 p2416 A67-29409

Hypersonic trim angle of attack of lifting entry vehicles, correlating stagnation point values obtained from heat shield ablation and pressure distribution measurements 15 p2417 A67-29447

Ablation heat protection system materials performance in hypersonic regime, discussing potential solutions to shielding during atmospheric entry 16 p2778 A67-30722

Separation shock near base of conical bodies at hypersonic speeds noting inflections in bow shock shape 17 p2793 A67-33044

Slender wing maximum lift-drag ratio at hypersonic speeds obtained assuming modified Newtonian pressure distribution and skin-friction drag 20 p3357 A67-36953

Lift-drag ratio attainable by slender flat-top body at supersonic speeds, considering Newtonian pressure distribution and constant skin friction 20 p3359 A67-37124

Wing shape and size selection for hypersonic velocities formulated as extremum problem of drag, aerodynamic property, temperature and coolant consumption for given wing volume 22 p3741 A67-40015

HYPERSONIC TEST APPARATUS

Hypersonic testing methods at ONERA, discussing wind tunnel apparatus [ONERA-TP-371] 05 p0748 A67-16475

Hypersonic aerodynamics, discussing tunnel testing, inviscid flows, airfoil shapes, real gas effect, shock wave theory and boundary layers 23 p3930 A67-41307

HYPERSONIC VEHICLE

Hypersonic velocity effects on errors in vertical channel of inertial navigation system, particularly aboard artificial earth satellite 01 p0110 A67-10420

Structural design of hypersonic vehicle flight tank for liquid hydrogen fuel, discussing loading, material, support system, stress analysis, testing and analytical problems [SAE PAPER 660679] 01 p0161 A67-10583

Manned hypersonic vehicle /MHV/ design, considering performance, shape, size, propulsion, etc 03 p0360 A67-13792

Material selection and structural design problems for hypersonic vehicles 03 p0525 A67-13793

Wind tunnel testing of hypersonic vehicles with complete simulation of entire hypersonic environment is not yet possible 03 p0396 A67-13794

Prediction of subsonic base drag of hypersonic reentry vehicles [AIAA PAPER 66-991] 03 p0353 A67-14144

Structural design problems of hypersonic air vehicles with air breathing propulsion, discussing relation to future hypersonic commercial air transport 03 p0362 A67-14383

Nozzle requirements for hypersonic vehicle at transonic conditions, noting results of tests in high velocity wind tunnel 04 p0545 A67-14536

Supersonic combustion air breathing engines as propulsion systems for hypersonic vehicles [AIAA PAPER 66-826] 04 p0688 A67-14624

Hypersonic thermal structural concepts to satisfy design requirements including insulated, insulated and cooled and hot load carrying approaches [SAE PAPER 660678] 04 p0716 A67-15789

Fuel injection parameters effects on mixing of gaseous hydrogen fuel with supersonic air stream for hypersonic ramjet, determining turbulent diffusion coefficient 06 p1117 A67-18387

Aerodynamic performance characteristics of three entry vehicles designed for maximum L/D ratio of three and two at Mach 19 and Reynolds number 3,200,000 tested in 22-inch Langley helium tunnel [AIAA PAPER 67-138] 06 p0940 A67-18439

Specific impulse and thrust coefficient performance as function of flight Mach number and altitude for air augmented solid propellant propulsion vehicle using

supersonic combustion

[AIAA PAPER 67-226] 06 p1097 A67-18517

Flexible wings for hypersonic vehicles allowing for safe controllable landings, stressing leading edge parawing concept, flow visualization, lift-drag ratio, etc [AIAA PAPER 67-200] 07 p1258 A67-19440

Convective laminar heat transfer to hypersonic vehicle, deriving similarity relations between stagnation temperature profile and mass fractions of chemical species 09 p1579 A67-21699

Refractory materials for hypersonic vehicle leading edges 10 p1670 A67-23723

Drag coefficients of hypersonic optimum bodies at nonoptimum Mach numbers 12 p1892 A67-25744

Liquid hydrogen fuel tankage thermal protection in manned hypersonic vehicles, discussing results of tests in steady state conditions [AIAA PAPER 67-297] 12 p2035 A67-26012

Thermal performance of liquid hydrogen in horizontal hypersonic vehicle fuel tank 13 p2186 A67-27646

Potential advantages of hypersonic vehicles compatible with missions combining more than one cruise-flight regime, discussing gas dynamic heating for propulsion [SAE PAPER 670354] 17 p2798 A67-32994

Hypervelocity vehicle volume decreasing method by applying dual-fuel concept [AIAA PAPER 67-559] 19 p3174 A67-35956

Precursor IR resonance radiation from hypervelocity ablating vehicles observed and related to photon absorption and water vapor presence in air 22 p3917 A67-39712

HYPERSONIC WAKE

Mach-Zehnder Interferometer study of fluctuations in turbulent wakes of slender cones and spheres in ballistic flight [AIAA PAPER 65-809] 01 p0007 A67-11166

Spatial distributions of free electrons in near wakes of spheres in hypersonic flight [AIAA PAPER 66-55] 04 p0547 A67-14820

Aerothermochemical eddy diffusion model for predicting rapid wake ionization decay behind hypersonic slender clean cone obtained in free flight ballistic range [AIAA PAPER 67-21] 06 p0938 A67-18257

Schlieren techniques used in free flight range study of far wake of hypersonic cones [AIAA PAPER 67-31] 06 p0938 A67-18261

Base pressure behind supersonic vehicle, calculating existence conditions for wake solutions and location of stable and unstable singularities [AIAA PAPER 67-60] 06 p0986 A67-18269

Laminar boundary layer separation and near wake flow for smooth blunt body at supersonic and hypersonic speeds [AIAA PAPER 67-62] 06 p0986 A67-18270

Decay of mean, variance and gradient variance of temperature and velocity measured in initially heated wake of sphere in water tunnel [AIAA PAPER 67-20] 06 p0987 A67-18347

Flow field and stability of far wake of circular cylinders at hypersonic speeds, noting Reynolds number role [AIAA PAPER 67-32] 06 p0939 A67-18348

Flow field model for laminar hypersonic near-wake in inviscid expansion, viscous sublayer and recirculating flow [AIAA PAPER 67-63] 06 p0940 A67-18353

Statistical mechanics predictions of turbulent fluctuations in hypersonic wake from ballistic range experiments and theoretical stochastic model of gas particle motion [AIAA PAPER 67-22] 07 p1168 A67-19431

Laboratory hypersonic wake fluid mechanics transition data over range of Reynolds number structured into three laws of far and near wake and interpolation regime [AIAA PAPER 67-33] 08 p1275 A67-20379

Transient ionization levels of hypersonic velocity projectile wakes measured by open microwave resonators phase shift 11 p1790 A67-24452

Transition sticking in wake of slender hypersonic cone as Reynolds number increases 12 p1893 A67-25927

Shape effects on hypersonic slender body wake geometry and transition distance 13 p2050 A67-26832

Laminar boundary layer separation and near wake flow for smooth blunt body at supersonic and hypersonic speeds

[AIAA PAPER 67-62] 14 p2240 A67-28112

Far wake behavior of hypersonic spheres analyzed using schlieren techniques 15 p2417 A67-30190

Schlieren techniques used in free flight range study of far wake of hypersonic cones [AIAA PAPER 67-31] 17 p2793 A67-33006

Aerodynamic characteristics of wakes behind hypervelocity bodies [AIAA PAPER 66-53] 19 p3171 A67-35741

Wake turbulence regimes for flows behind typical hypersonic bodies 22 p3743 A67-40222

Reynolds number effect on base pressure behind wedge in supersonic and hypersonic flow based on Chapman wake flow recompression model 23 p3930 A67-41306

Chemiluminescent radiation from far wake of hypersonic spheres launched from light gas gun measured with filtered photomultiplier 23 p3931 A67-41712

HYPERSONIC WIND TUNNEL

Internal wall pressure of obstacles in hypersonic wind tunnels with reflected shock waves measured by piezoelectric gauge system 01 p0005 A67-10259

Pressure and stagnation temperature distribution in test chamber of blowdown hypersonic wind tunnel 01 p0049 A67-10558

Wind tunnel testing of hypersonic vehicles with complete simulation of entire hypersonic environment is not yet possible 03 p0396 A67-13794

Hypersonic low density wind tunnel for high Mach numbers and stagnation temperatures, analyzing measurements made, noting heater, nozzle, diffuser, etc 04 p0595 A67-14561

Total pressure losses in hypersonic wind tunnel with Eiffel chamber, calculating coefficient of pressure recovery 04 p0546 A67-14780

Battery power supply for split-ring plasma arcs operating as P hypersonic propulsion tunnel heaters 04 p0556 A67-15638

Pressure, heat transfer and Pitot pressure profiles measured on wedges and cones at high Mach and Reynolds numbers in hypersonic tunnel 04 p0600 A67-15822

Laminar convective heat transfer to cavities in hypersonic low density flow 04 p0732 A67-15833

Pebble-bed heater for hypersonic wind tunnel, evaluating heat-transfer coefficients from transient temperature distribution of bed 05 p0926 A67-16429

Piston motion effect on flow uniformity in hypersonic gun tunnel, using perforated plate technique to prevent piston fluctuation 05 p0791 A67-16430

Hypersonic wind tunnel for small gas densities noting vacuum pumps, diffuser, cooler, etc 05 p0786 A67-16591

Diffuser use in low density hypersonic wind tunnel and method of evaluating global performance for diffusers with conical inlet followed by cylindrical mixing section 05 p0748 A67-16763

Forced oscillation method measurement of aerodynamic coefficient of hypersonic blowdown wind tunnel 05 p0788 A67-16764

Scramjet testing with wave superheater hypersonic tunnel [AIAA PAPER 67-182] 06 p0980 A67-18343

Error determination for transient heat transfer experiments using least squares method 06 p1024 A67-18389

Flow properties in laminar and turbulent near wake of cones and wedges using hypersonic shock tunnels, obtaining wake centerline and stagnation temperature profile [AIAA PAPER 67-30] 07 p1126 A67-19432

Temperature measurement in hypersonic gun tunnel, using modified line reversal two-beam optical pyrometer with measurements in shock layer at front of cylinder 09 p1486 A67-22413

Stagnation temperatures from stagnation point heat transfer rates measured in hypersonic gun tunnel at Mach 9.8 09 p1486 A67-22414

Free flight hypersonic wind tunnel testing technique noting pneumatic launcher, data acquisition and processing 10 p1622 A67-23390

Forward facing jets effect on blunt configurations aerodynamic characteristics from wind tunnel tests at Mach 6, emphasizing drag increase 11 p1742 A67-24354

Pyroelectric heat-transfer sensor performance compared with thin skin thermocouple heat sensors, noting

- discrepancy in measurement results in severe environment 11 p1790 A67-24453
- Gas state equation determination from trajectory analysis of piston in hypersonic wind tunnel 11 p1782 A67-24759
- Simulated high speed aerodynamic testing methods, factors complicating prediction of actual aerodynamics and various tunnels used 11 p1774 A67-25012
- Hypersonic gun tunnel design and performance up to 1000 atm 12 p1926 A67-26129
- Low density hypersonic wind tunnel, noting surface pressure and flow field measurements 14 p2293 A67-28166
- Sphere drag coefficients measured using ultralightweight models launched from two-stage light-gas gun 14 p2242 A67-28172
- Air condensation in hypersonic wind tunnel strongly related to flow expansion rate 16 p2657 A67-30708
- Scramjet testing with wave superheater hypersonic tunnel 19 p3208 A67-35767
- [AIAA PAPER 67-182] 19 p3208 A67-35767
- High pressure hypersonic gun tunnel calibration with performance estimation method compared with tests, discussing high altitude Mach 10 flight simulation 21 p3607 A67-37779
- Hot shot nitrogen gas source for pulsed MHD accelerator to provide lunar reentry 21 p3608 A67-38863
- HYPERTENSION**
- S BLOOD PRESSURE**
- HYPERVELOCITY**
- USA HYPERSONIC SPEED**
- Hypersonic velocity effects on errors in inertial channel of navigation system, particularly aboard artificial earth satellite 01 p0110 A67-10420
- Soviet book on physical optics 12 p1967 A67-26131
- Computer program for synthesizing and analyzing performance of preliminary designs of hypervelocity cruise vehicles 17 p2819 A67-32474
- Hypervelocity techniques - Conference, University of Denver, March 1967, Volume 1, Advanced experimental techniques for study of hypervelocity flight 21 p3605 A67-37767
- HYPERVELOCITY ACCELERATOR**
- MHD accelerators for hypervelocity test facilities, showing Faraday accelerator is best suited to operation at high flow densities required 14 p2294 A67-29042
- HYPERVELOCITY CRATERING**
- Hypervelocity impact and crater formation based on earlier work describing similarity solution for impact on compressible fluid 01 p0165 A67-11444
- Hypervelocity crater size and target strength, relating force per unit area of crater surface to tensile strength of material 02 p0338 A67-12034
- Meteoritic bombardment damage to lunar surface with reference to terrestrial craters and hypervelocity impact 08 p1389 A67-21018
- Penetration depth of hypervelocity impact craters photographed by Luna and Ranger vehicles indicate granular lunar surface 23 p4065 A67-41003
- Cratering produced by high velocity impact of stainless steel threaded rod on cold-rolled steel target 23 p4080 A67-41467
- HYPERVELOCITY FLOW**
- Reentry simulation, discussing aerodynamic and thermodynamic parameters, heat transfer and simulation 02 p0335 A67-12415
- ONERA hot-shot wind tunnel flow stability and homogeneity and measurement of plasma electromagnetic field, skin friction, etc [ONERA-TP-447] 15 p2465 A67-29377
- Time-resolved spectra for hypervelocity spheres and cones in free-flight ballistic range obtained by large aperture spectrograph and image converter camera 17 p2862 A67-33290
- Aerodynamic characteristics of wakes behind hypervelocity bodies [AIAA PAPER 66-53] 19 p3171 A67-35741
- Spark discharge generated blast wave application to shock on shock simulation, free-stream sound speed determination and hypervelocity flow measurements [AIAA PAPER 66-763] 19 p3208 A67-35753
- JPL free piston shock tube design, calibration and performance 21 p3606 A67-37773
- Langley Hypersonic Nitrogen Facility flow evaluation covering pitot pressure survey of nozzle wall boundary layer, centerline and Mach number 21 p3607 A67-37777
- Gas flow interaction with blunt body in transition flow regime between continuum and free molecule flow calculated using first collision model 22 p3743 A67-40175
- Hypervelocity gas flows at high temperatures and pressures, discussing generation of dense plasmas at extreme temperature by implosion waves 24 p4092 A67-42753
- HYPERVELOCITY GUN**
- High pressure hypersonic gun tunnel calibration with performance estimation method compared with tests, discussing high altitude Mach 10 flight simulation 21 p3607 A67-37779
- Chemiluminescent radiation from far wake of hypersonic spheres launched from light gas gun measured with filtered photomultiplier 23 p3931 A67-41712
- Constant acceleration flows applied to high speed fixed geometry guns using H propellant in constant projectile acceleration problem 23 p3992 A67-41716
- HYPERVELOCITY IMPACT**
- Effectiveness of meteoroid shielding from hypervelocity impact penetration and cratering 01 p0155 A67-11406
- Hypervelocity impact and crater formation based on earlier work describing similarity solution for impact on compressible fluid 01 p0165 A67-11444
- Impact physics and meteoroid population, with particular reference to space flight problems and research in high velocity impact 04 p0705 A67-15000
- Impact resistance of spacecraft structures indicate performance criterion effect on final structural configuration and importance of hypervelocity of realistic hypervelocity test specimens 04 p0705 A67-15001
- Impact of cylindrical or spherical projectiles of dural and polyethylene at high velocities in seminfinit targets, analyzing crater shape and relation to kinetic energy 04 p0710 A67-15002
- Hypervelocity impact of polythene projectiles on seminfinit aluminum targets at various obliquity angles, using RARDE gas launcher 04 p0710 A67-15003
- Solid-solid impact at hypervelocities using flow equations, noting variations of impact velocity, projectile shape and density and state equation 04 p0710 A67-15004
- Momentum transfer during impact, penetration depth, crater form and mass loss at various velocities, using spherical aluminum projectiles and aluminum targets 04 p0710 A67-15005
- Stress waves reflection and transmission in composite laminates and parameters affecting ability to resist fracture by hypervelocity impact [AIAA PAPER 67-140] 06 p1102 A67-18289
- Correlation of meteoroid environments in solar system, analyzing meteor mass measurement results, hypervelocity impact and solar electromagnetic radiation effects [AIAA PAPER 67-151] 06 p1085 A67-18319
- Surveyor study of lunar ejecta fragments expelled from lunar surface during hypervelocity impact 08 p1411 A67-20948
- Meteoritic matter investigation with Venus II and Zond III probes, discussing impact rate and distribution along flight path 10 p1708 A67-23241
- Thin plate targets response to hypervelocity impact to determine effectiveness of meteoroid bumpers composed of two layers of distinct materials 10 p1725 A67-23716
- Expandable gas bag for stowable omnidirectional multiple impact landing system 10 p1714 A67-23755
- Peculiarities of dispersion of matter resulting from meteorite impact on lunar surface as explanation of concentric nature of structure of crater 12 p2002 A67-25646
- Obstacles at variable angles attached to pendulum with two degrees of freedom used to study high speed impact of solid particles 12 p1926 A67-25956
- Australasian tektite origin criticized regarding magnitude of atmosphere removal 14 p2390 A67-28889
- Model for hemispherical cratering of structural metals by hypervelocity impact, determining elastic-plastic threshold stress by true tensile strength
- measurement 17 p2958 A67-32217
- Sensors used in cosmic dust experiments studied for response to microparticle hypervelocity impacts, noting relationship to velocity 19 p3229 A67-35210
- Solid interplanetary matter in moon vicinity through piezoelectric sensors, giving impact rate, trajectory projections and increased matter density
- hypothesis 19 p3319 A67-35275
- Cosmic ultrahigh-energy heavy nuclei and fragmentation products producing multiple mesons 20 p3518 A67-37092
- Body porosity effect on hypervelocity impact, computing pressure, velocity, density and specific internal energy profiles 22 p3912 A67-39748
- Vacuum type lensless spectrograph in intermediate and far UV for evaluating shock compressed metals resulting from hypervelocity impact 22 p3799 A67-39749
- Expandable gas bag for stowable omnidirectional multiple impact landing system 22 p3904 A67-40097
- Cratering produced by high velocity impact of stainless steel threaded rod on cold-rolled steel target 23 p4080 A67-41467
- Correlation of meteoroid environments in solar system, analyzing meteor mass measurement results, hypervelocity impact and solar electromagnetic radiation effects [AIAA PAPER 67-151] 23 p4070 A67-41719
- Preatmospheric hypervelocity impact black glass in Cachari eucrite studied by optical microscopy, electron microprobe and X-ray diffraction 24 p4233 A67-42623
- HYPERVELOCITY PROJECTILE**
- Equilibrium air total radiation mechanism, vacuum UV radiation and relation to hypervelocity entry studied, using shock tube blunt model test flow [AIAA PAPER 66-103] 08 p1426 A67-20569
- Radiometer system with photomultiplier tube for measuring absolute radiation from hypervelocity projectile flow fields 11 p1790 A67-24447
- Mass of shaped charge accelerator generated fragments determined via high speed flash X-ray photography of projectiles in flight 11 p1790 A67-24448
- Double Langmuir probe measurement of turbulent structure and ionization intensity of hypervelocity projectile and spectral characteristics of probe signal fluctuation 11 p1790 A67-24449
- Transient ionization levels of hypersonic velocity projectile wakes measured by open microwave resonators phase shift 11 p1790 A67-24452
- Vacuum UV radiation measurement from high temperature nitrogen, detecting radiation from shock layer of ballistic model 16 p2675 A67-31267
- Wake plasma turbulence of projectiles studied using electrostatic probe array 17 p2861 A67-33023
- Dynamic flight stability characteristics of 5 inch projectile with nonlinear magnus moment, noting Mach number, wind tunnel data, etc 21 p3563 A67-37805
- HYPERVELOCITY WIND TUNNEL**
- Plasma wind tunnel facility for producing steady flow high conductivity collisionless plasma simulating solar wind interaction with magnetosphere 14 p2294 A67-29036
- Hotshot wind tunnel for ionized wakes of models in nitrogen hypersonic flow, determining electron temperature and density [ONERA-TP-455] 15 p2416 A67-29380
- 50 degree semivertex angle sphere-cone Voyager configuration wind tunnel tested in dry nitrogen for aerodynamic characteristics, pressure and heat transfer distribution 20 p3356 A67-36562
- Hot shot tunnel F operation as combustion test facility using air, discussing oxygen depletion, particle contamination and reservoir decay 21 p3606 A67-37775
- HYPERVENTILATION**
- Reaction time during voluntarily controlled alveolar hyperventilation used to study effects on psychomotor performance of aircrew 09 p1453 A67-21728
- HYPOELASTICITY**
- Generalized hypoelasticity theory includes theory of anisotropic elasticity as special case and thermal effects 12 p2032 A67-26169
- HYPOGLYCEMIA**
- Functional or reactive hypoglycemia as potential cause of flight accidents, showing

alimentary behavior of pilot brings about apparition of hypoglycemic phases 14 p2254 A67-28216
Hydrazine effect on carbohydrate metabolism in vivo and in vitro, studying hyperlactatemia, hypoglycemia, oxygen consumption inhibition, etc 18 p2992 A67-34720

HYPOTENSION S BLOOD PRESSURE

HYPOTHALAMUS

Blockage of electrically evoked pupillodilation in cat by irradiating hypothalamus with cyclotron-accelerated alpha particles 10 p1598 A67-23394

HYPOTHERMIA

Improved response acquisition in deep hypothermia adapted rats 20 p3373 A67-37433
Ability of hypothermia-adapted rats to learn and perform at low body temperature 20 p3373 A67-37669
Death and survival during water immersion in plane crashes near Cape Cod and Hamilton Bay 23 p3970 A67-41707
Rats resistance and reactivity in hypothermal state to very low atmospheric pressure by hypercapnia-hypoxia exposure 24 p4111 A67-41849
Histochemical investigation of effect of hypothermia and hypobiosis on activity of oxidizing tissue enzymes of carbohydrate, amino acid, nucleotide and aliphatic metabolism of rats 24 p4112 A67-41853

HYPOTHESIS

S INTERMITTENCY HYPOTHESIS
S NULL HYPOTHESIS
S SIMILARITY HYPOTHESIS
S VORTICITY TRANSPORT HYPOTHESIS

HYPOXIA

SA ANOXIA
Effect of hypoxia on psychomotor behavior at simulated cabin altitudes of 5000 and 8000 ft 01 p0017 A67-10953
Prolonged centrifugal acceleration effect on gas exchange and resistance to hypoxia in rats 01 p0016 A67-11425
Metabolic cerebellum changes under nonlethal hypoxia, noting system compensation during symptomatic stages and destruction of Purkinje cells at critical stages 04 p0561 A67-14629
Individual phospholipids in hemispheres of rat brains and rate of turnover of phosphate groups during oxygen deprivation 04 p0562 A67-15548
Tonometric and tonographic investigations of intraocular tension in hypoxia 06 p0953 A67-17995
Cardiac changes under hypoxia, experimental morphological study 13 p2058 A67-26756
Enzyme activity in erythrocytes when MICORENE is used to prevent death from high altitude hypoxia 14 p2254 A67-28212
Physiological limits of adaptation of eye with respect to body noting increase of pressure in ophthalmic artery under different conditions of hypoxia 16 p2611 A67-30757
Hypoxia effect on cellular and humoral immunity of mice to bacterial infection 16 p2612 A67-30906
Aminazine injection and electrolysis effects on formatio reticularis of animals after exposure to hypoxia 20 p3367 A67-36255
Pilot performance in simulator training during acute hypoxia noting effect on altitude, engine power and directional control 20 p3374 A67-36264
Retinal discrimination and visual acuity at different degrees of hypoxia by reading symbol E individually and combined, using oxygen-poor mixtures 21 p3575 A67-38507
Cerebral blood flow and metabolism during combined hypoxia and hypercapnia, noting cerebral vasodilatation effect 23 p3945 A67-41080
Hypoxia stimulated pulmonary arterial pressure increase in dog and baboon noting hemodynamic effects 23 p3953 A67-41588
Treatment of hypoxia by determining primary site of oxygen tension attenuation in transfer from respiratory environment to cellular level 23 p3953 A67-41591
Hypoxia warning systems, discussing spurious warning avoidance and mask mounted sensor 23 p3968 A67-41629
Brightness thresholds and reading ability tests evaluated for male subjects under varied simulated conditions of altitude and

oxygen breathing 23 p3959 A67-41694
Tissue oxygenation during hemorrhage in dogs at 1 and 3 atm oxygen, noting oxygen at high pressure /OHP/ does not prevent stagnant hypoxia [SAM-TR-66-258] 24 p4111 A67-41802
Rats resistance and reactivity in hypothermal state to very low atmospheric pressure by hypercapnia-hypoxia exposure 24 p4111 A67-41849
Space cabin atmosphere relation to environmental and operational variables, discussing effect of hypoxia and hypercapnia on spacemen and mission safety [AIAA PAPER 67-855] 24 p4117 A67-42999

HYSTERESIS

SA ANTIFERROMAGNETISM

SA DAMPING

Polarization and domain structure of barium titanate single crystals with double hysteresis loop 03 p0497 A67-13700
Steady state oscillation regime of one-dimensional oscillator determined by replacing arbitrarily shaped hysteresis loop with ellipse of equivalent area, noting higher harmonics effect 03 p0530 A67-14176
Airflow instability with square edge circular orifice, discussing hysteresis effect on discharge coefficient 04 p0601 A67-14487
Stator whirl with rotors in bearing clearance noting jump and hysteresis phenomena [ASME PAPER 66-WA/MD-8] 04 p0629 A67-15346

Hysteresis losses in nonideal superconductors calculated, using phenomenological equations of flux motion 06 p1048 A67-17819
Hysteresis effects in steady laminar two-dimensional MHD flow of gas between moving planes and coaxial cylinders in TM field 06 p1043 A67-18671
Hysteresis effect on cosmic ray intensity of solar cycle variations 07 p1242 A67-19620
Dislocation density and magnetic hysteresis in superconducting state of 110-oriented Nb single crystals as function of angle of torsion 07 p1209 A67-19646
Experimental tests of critical state model of hysteresis in type II superconductors, considering critical currents in field and transport currents in zero 07 p1233 A67-19842
Hysteresis effects in one-dimensional conducting gas flow through rectangular MHD converter channel with constant magnetic gap and variable electron spacing 09 p1444 A67-21859
One-dimensional steady solutions for shock wave propagation in class of nonlinear viscoelastic materials deduced from stated balance laws and representation theorem for compressive and expansive motions 09 p1576 A67-22410
Force-deflection relationship under arbitrary loading for structure exhibiting hysteresis behavior 10 p1727 A67-23751
Two-cycle shift register calculated, using magnetic element with rectangular hysteresis loop without shunting diode 11 p1769 A67-25042
Uniaxial anisotropy and rotational hysteresis in thin gadolinium films 13 p2179 A67-27144
Aerodynamic flow deflection over convex curved surface noting occurrence of hysteresis 14 p2305 A67-28978
Hysteretic superconductor, analyzing critical state and constrained reversibility relations in diamagnetic and temperature paths 17 p2912 A67-32269
High-elongation foil strain gauges evaluation for measuring cyclic plastic strains, determining Poisson ratio 18 p3142 A67-33890
Silicon doped YIG containing iron ions, studying loss mechanism, low temperature anisotropy, annealing and rotational hysteresis 18 p3105 A67-34629
Hysteretic superconductor, showing trapped flux or remnant magnetic moment linear relationship with average internal field in low but not in high k superconductors 19 p3302 A67-35036
Multilayer cantilever beam subjected to varying load, studying cases where slip region propagates from edge to interior 19 p3341 A67-35579
Thermal fatigue hysteresis loop shape variations for Coffin-type test samples, stressing temperature-cycle effect 19 p3343 A67-35820

Temperature /K-state/ effect on dislocation blocking stresses in nickel alloy studied by mechanical hysteresis method 20 p3471 A67-37551
Time variation of magnetic flux distribution in type II superconductor under sinusoidal magnetic field, obtaining flux penetration rate, pinning forces and hysteresis loop 21 p3685 A67-39071
Fe rods in Fe-Sb matrix eutectic system measuring rod diameter and Fe volume fraction effects on magnetic properties 23 p4039 A67-40881

I-BEAM

Strain amplitude and flange width-to-thickness ratio effects on dynamic buckling in modified I-beams subjected to pure reverse bending 17 p2958 A67-32031
I-beam ratio of depth to flange width for minimum weight obtained via modulus of rupture 21 p3722 A67-38541

IBM 7040 COMPUTER

Open-shop remote computing terminal system using direct coupled system of IBM 7094 and 7040 computers for core-to-core transmission, discussing experience gained from using and managing it 02 p0206 A67-11801
Digital analog simulation program for IBM 7040 based on signal flow diagram, noting use of Runge-Kutta integration method 17 p2821 A67-32801

IBM 7090 COMPUTER

Optimal temperature control design using IBM 7094 digital computer program for thermal environment simulation of stabilized multisurfaced earth-orbiting spacecraft structure [ASME PAPER 66-WA/HT-44] 04 p0724 A67-15430

Saturn computer design and fault simulation on IBM 7090 computer 21 p3588 A67-38181

IBM 7094 COMPUTER

Open-shop remote computing terminal system using direct coupled system of IBM 7094 and 7040 computers for core-to-core transmission, discussing experience gained from using and managing it 02 p0206 A67-11801

ICE

Isotope effects in gamma radiolysis at 77 degrees K of mixed water and deuterium oxide ice systems 04 p0658 A67-15501
Cleavage and separation of dye-doped ice and paraffin instantaneously heated by laser pulse, measuring mechanical pulse at energy concentrations below vaporization heat 06 p1119 A67-18801
Proton mobility in ice when limited by lattice scattering calculated, using Boltzmann transport equation 13 p2160 A67-28991
Hydroxyl radical formed by radiolysis of ice at 77 degrees K identified as center producing EPR lines 17 p2890 A67-33251
Evaporation of Saturn ice rings by UV and solar wind sputtering or by photosputtering in IR and proton bombardment 21 p3705 A67-38591

ICE FORMATION

SA DEICING SYSTEM

Photometry of integrated light of Venus inferring presence of ice in atmosphere from halo effect of brightness dispersion 05 p0892 A67-16407
Frost phenomena on Mars examined on basis of Martian wave of darkening, noting necessity of deliquescent salts to attract and retain water on surface 06 p1089 A67-18641
Ice single crystal growth rate in supercooled water explained on basis of combined heat dissipation mechanism and molecular growth kinetics 23 p4024 A67-40971
Thunderstorms endanger air traffic and travel, considering turbulence, ice formation hail and lightning 23 p4025 A67-41301
Noctilucent cloud fine structure wave form due to visibility through ice condensed on dust particles in wave-like pattern 24 p4146 A67-41791
Ice nucleating properties of meteoritic material 24 p4231 A67-42371

ICE NUCLEUS

Continuous automatic and portable instrument for ice nuclei detection and counting 10 p1654 A67-22818

- Meteor stream relation to natural ice
nuclei and precipitation 13 p2205 A67-27461
- Interstellar extinction wavelength
dependence, assuming ice particle radii
distribution function obeys decreasing power
law and graphite particles have Gaussian
distribution function 22 p3889 A67-40304
- Ice nucleating properties of meteoritic
material 24 p4231 A67-42371
- ICE PREVENTION**
- Ice removal from solid nonmetallic aircraft
propeller blade by nonsteady-state
heating 14 p2405 A67-28305
- ICING**
- S DEICING SYSTEM**
- IDEAL FLUID**
- Perturbation estimation theorems and
stability of plane steady curvilinear flows of
ideal fluid 03 p0402 A67-12883
- Matter tensor of generally relativistic
perfect fluid derived from invariant integral
by Marx variational principle 03 p0468 A67-13392
- Ideal incompressible liquid motion in
rectangular container due to rectangular
double and sinusoidal pulse
excitation 03 p0404 A67-13784
- Forced small axisymmetric oscillations of
elastic right circular cylinder with end
plates in form of shallow spherical shell
filled with heavy ideal fluid 03 p0530 A67-14174
- Existence and stability of uniform rotation
of heavy blunt profile immersed in perfect
incompressible irrotational fluid 05 p0792 A67-16595
- Book on principles of ideal fluid
aerodynamics covering vector algebra and
calculus, Euler equations, steady and
unsteady acyclic motion, complex variable,
lift, etc 05 p0793 A67-17151
- Gas dynamics of nonisentropic two-
dimensional MHD flow of ideal inviscid
perfectly conducting compressible
fluid 08 p1357 A67-20593
- Subsonic jet flow past solids, examining
two classes of exact solutions in ideal fluid
for plane nonvortical steady state
flow 08 p1321 A67-20836
- Stability of rotational motion of body with
cavity containing ideal fluid, considering
fluid motion as potential flow, determining
velocity potential and inertia moments 10 p1679 A67-23031
- Invariant transformation for pulse and
continuity equations of one-dimensional
unstabilized motions of ideal compressible
fluid 10 p1628 A67-23678
- Rigid disk impact against ideal fluid
surface in cylinder, deriving formula for
impulse pressure at disk 12 p1928 A67-25669
- Fluid vibratory behavior in rigid
containers, noting surface wave behavior
governed by linearized boundary value
solution 12 p1931 A67-26182
- Three-dimensional flow of ideal fluid past
body enveloped by air cavern, deriving
normal velocity components 14 p2239 A67-27985
- Averaged axisymmetric vortex flow of
ideal incompressible fluid in turbine
engine 14 p2296 A67-27986
- Motion of gyroscope with conical cavity
filled with ideal incompressible fluid
describing rotating motion 15 p2518 A67-30171
- Lagrange equations of perfect fluid flow
linked to datum point and geometric surface
arbitrarily moved within 16 p2863 A67-31709
- Interaction between gliding contour and
ideal fluid flow 18 p3022 A67-33413
- Inhomogeneities 18 p3022 A67-33413
- Ideal fluid energy-momentum tensor
derivation of Crocco-Vazsonyi equation for
ideal fluid relativistic hydrodynamics,
discussing continuity equation for specific
entropy 19 p3210 A67-35707
- Three-dimensional flow through rotor of
single stage axial fan with prescribed
spanwise variable circulation 19 p3171 A67-35714
- Perfect fluid theory analyzed from
resistance viewpoint and compared with flow
past material body when viscous, discussing
potential flow 20 p3419 A67-36189
- Free vibrations frequency of ideal fluid in
elastic bottom cylinder in form of spherical
shell 20 p3420 A67-36441
- Group properties of differential equations
describing axisymmetric thin layer jet flow
of ideal fluid propagating along surface of
revolution 20 p3422 A67-37063
- Motion equations for elastically deforming
body containing cavity partly filled with
ideal fluid 20 p3481 A67-37380
- Potential linear theory applied to
oscillatory profiles moving at uniform
velocity inside ideal fluid 20 p3424 A67-37593
- Single parameter Ball cylinders
representation of multiply connected surface
vortical motion axes congruence 21 p3611 A67-37902
- Congruence of screw axes attached to
body with multiply connected surface in
vortical motion in ideal fluid 21 p3611 A67-37905
- Invariant transformation for pulse and
continuity equations of one-dimensional
unstabilized motions of ideal compressible
fluid 21 p3612 A67-38279
- Dynamic instability of longitudinal
oscillations of cylindrical shell charged with
ideal fluid established by approximate
reduction of nonlinear equations 21 p3720 A67-38297
- Steady state problem solution in linear
formulation concerning movable load
influence on thin elastic plate on ideal
compressible fluid 21 p3720 A67-38300
- Oscillation stability of rotating cylindrical
shell filled with ideal incompressible
weightless fluid, determining instability
region distribution 21 p3721 A67-38302
- Ideal incompressible fluid axisymmetrical
oscillations in elastic cylindrical shell,
determining normal modes and natural
frequencies of shell and fluid 21 p3613 A67-38789
- Plane motion of container formed by two
concentric cylinders and radial partitions
partly filled with small vibrating ideal
fluid 22 p3786 A67-40029
- Axisymmetric stationary gravitational field
Einstein field equations in rigid uniformly
rotating ideal fluid interior 23 p4028 A67-41149
- IDEAL GAS**
- SA PERFECT GAS**
- Potential flow of ideal gas with acoustic
surface coinciding with characteristic 01 p0053 A67-10999
- Stability of solutions to general equations
of steady state one-dimensional relaxed flow
of perfect gas mixtures [ONERA-TP-360] 01 p0054 A67-11089
- Shock wave in half-space filled with ideal
gas in linear approximation 02 p0233 A67-11969
- Plane adiabatic flow of ideal gas behind
separated shock wave for uniform
supersonic symmetrical flow past smooth
profile 03 p0349 A67-12873
- Errors in thermodynamic functions of
ideal gases determined from molecular
data 03 p0536 A67-13607
- Book on propagation, reflection and
superposition of shock waves in ideal gases
based on theory of hyperbolic nonlinear
PDEs 04 p0601 A67-14487
- Conical MHD flow of ideal conducting gas
with Hall effect in magnetic field, deriving
electrodynamic and energy characteristics 04 p0669 A67-15515
- Simultaneous free and parametric
oscillations of elastic cylindrical shell of
infinite length and subsonic flow of ideal
gas in shell 04 p0717 A67-15888
- Single parameter MHD flow of ideal
incompressible infinitely electroconductive
gas 05 p0855 A67-17114
- Low magnetic Reynolds number two-
dimensional and axisymmetric MHD flow of
conducting ideal gas through supersonic
nozzle 06 p1043 A67-18669
- Compressible ideal gas flow through
elliptic pipe 08 p1322 A67-21169
- Flow of ideal gas behind shock wave of
finite amplitude analyzed, based on equation
for one-dimensional adiabatic
motion 10 p1624 A67-23033
- Analytic solution to blunt body problem in
supersonic flow of ideal gas approximated,
using power series [NOR REPORT 65-239] 10 p1593 A67-23454
- Nonlinear hydrodynamic stability theory of
one-dimensional detonations based on
perturbation techniques, detailing cases of
ideal gas unimolecular reactions 11 p1774 A67-23857
- Stability of flow of ideal compressible gas
at low magnetic Reynolds numbers in
presence of longitudinal perturbations
produced by crossed electromagnetic
fields 11 p1832 A67-24026
- Polytropic process of variations in state of
system composed of gas and solid
particles 12 p2033 A67-25317
- Gas dynamic stability of plane detonation
wave propagating in ideal gas mixture, in
terms of small perturbations that may result
in surface bending and changes in
thickness 12 p1930 A67-25965
- One-dimensional heat flow to confined
ideal gas solved on digital computer,
discussing energy equations, thermal
gradient induced fluid motion, etc
[AIAA PAPER 67-337] 12 p2039 A67-26051
- Interaction of shock-induced flow in ideal
gas and transverse magnetic field analyzed
for steady state and transient one-
dimensional effects 13 p2162 A67-26280
- Unsteady ideal gas flow along moving wall
treated by method of characteristics 13 p2093 A67-26635
- Noether theorems describing continuum
mechanics material applied to Hamiltonian
principle for motion of piezotropic fluid or
ideal gas undergoing polytropic
process 13 p2105 A67-27397
- Plane shock wave in ideal gas
characterized by infinitesimally thin
discontinuity, determining width and
distribution function 13 p2105 A67-27412
- Two-dimensional self-similar problem for
uniform penetration of plate into half-plane
of perfect gas flow, determining flow
pattern 14 p2239 A67-27982
- Compression shocks in one-dimensional
steady flow of Lighthill ideal dissociating
gas studied, using semiempirical relation for
relaxation equation 15 p2471 A67-29578
- Unbounded laminar plate oscillations in
bilateral potential ideal gas flow with
uniform physical and mechanical
parameters 15 p2575 A67-30009
- Heat addition in channels of variable cross
section area discussed for one-dimensional,
inviscid flow of ideal gases with constant
specific heat ratio 16 p2591 A67-30944
- Shock wave in half-space filled with ideal
gas in linear approximation 17 p2841 A67-33286
- Free jet plume expanding into vacuum
investigated experimentally, comparing with
ideal gas characteristics method
results 18 p3152 A67-33818
- Supersonic flow past smooth body with
internal duct incident at angle of
attack 18 p2984 A67-34212
- Errors in thermodynamic functions of
ideal gases determined from molecular
data 18 p3161 A67-34472
- Transient heat transfer through monatomic
collisionless ideal gas enclosed between
parallel walls analyzed for step change in
one wall temperature 20 p3548 A67-36735
- [ASME PAPER 67-HT-53] 20 p3548 A67-36735
- Unbounded laminar plate oscillations in
bilateral potential ideal gas flow with
uniform physical and mechanical
parameters 20 p3542 A67-37539
- Solution methods for Cauchy problem and
ideal unstable gas motion in cylindrical and
spherical symmetry, discussing shock wave
occurrence 21 p3565 A67-38562
- Relaxation toward Maxwell distribution
function of classical gas with initial
nonequilibrium distribution function as
velocity modulus function 22 p3782 A67-39406
- Ideal gas flow in spherically symmetric
gravity field, considering radiant heat
transfer and radiation pressure 22 p3880 A67-39407
- Equations for arc length derived for two-
dimensional isentropic compression surface
for ideal gas 22 p3742 A67-40102
- Adiabatic constant formula which holds
for ideal and real gas derived, noting
application of thermodynamics and gas
dynamics formulas to real
gas 24 p4256 A67-42592
- IDENTIFICATION**
- Sampling plans for identification of
inadequate subsystems 01 p0084 A67-11370
- System reliability evaluation and
identification of inadequate subsystems, with
application to two missile-borne guidance
systems 01 p0111 A67-11371
- Dynamic systems identification by digital
computer modeling in state space

formulation of ordinary differential equation [ASME PAPER 66-WA/AUT-10]

Transfer function parameters of stationary controlled plants in identification problem estimated, using Laplace transform and least squares method 05 p0782 A67-16319

Identification in automatic control systems - Conference, Prague, June 1967, Part 2 15 p2462 A67-30329

Predictive identification and fast moving target recognition technique for adaptive control and tracking 15 p2463 A67-30330

Random noise and measurement errors limitation upon system identification in time domain 15 p2463 A67-30332

Process identification with use of search controlled adaptive model 15 p2464 A67-30334

Experimental identification of systems by adapting parallel model 15 p2464 A67-30336

Similarities between model-reference adaptive control systems and parameter identification by adjustable 15 p2464 A67-30337

Parameter estimation representing differential equation coefficient of controlled system for quick-response adaptive identification 15 p2464 A67-30338

Rate variation of aerodynamic parameters of pitching equation for aircraft, identifying them with linear plant model for simulation studies 15 p2420 A67-30340

Process identification by cyclic parameter adjustment with automatic iteration, using analog and hybrid 15 p2465 A67-30342

Identification techniques with stochastic computers for advanced automatic control systems in form of learning machines 15 p2441 A67-30344

Transfer function parameters of stationary controlled plants in identification problem estimated, using Laplace transform and least squares method 18 p3017 A67-33870

Identification problem solution by gradient and Newtonian methods, using algorithm simplified by sensitivity function 19 p3205 A67-35914

Gradient method of parametric identification of processes through mathematical model 19 p3206 A67-35915

Dynamic identification of loop system consisting of square-law operator, with behavior function of input signal and initial conditions 19 p3206 A67-35916

Cross-spectral method application problems in feedback system analysis, identification and linear time invariant system 20 p3407 A67-36785

IDEP

S INTERSERVICE DATA EXCHANGE PROGRAM /IDEP/

IE-A

S EXPLORER XX SATELLITE

IFR

S INSTRUMENT FLIGHT RULE /IFR/

IGNITER

Elimination of rocket motor ignition by electrostatic initiation through development of electrically insensitive igniter and nonelectric stimulus transfer system 08 p1372 A67-20525

Ignitor-contributed noise deleterious effect on low noise radar receivers, noting influence of TR device inserted in front of receiver 10 p1611 A67-23329

Starter cartridges for jet engines, discussing operational problems and mechanical design, igniter and propellant development, etc 15 p2423 A67-29982

Igniter performance in solid propellant rocket motors, examining mass discharge rate effect on chamber pressure transients [AIAA PAPER 66-680] 19 p3310 A67-34811

S and X band igniter design eliminating spike leakage variations in tracking radar tubes 24 p4131 A67-42350

IGNITION

SA COMBUSTION

SA SOLID PROPELLANT IGNITION

SA SPARK IGNITION

Kinetically based mathematical model of hypergolic ignition in space ambient engines for predicting delay time and conditions from which pressure spikes result [AIAA PAPER 66-950] 02 p0302 A67-12284

Ignition of seminfinitesimal reacting space in ideal contact with hot medium having different thermophysical properties 05 p0927 A67-16990

Ignition of explosive powder by hot gas stream, with particular attention to heat transfer between substance and surrounding medium 06 p1112 A67-17956

Condensed explosive ignition by conductive heat inflow from low thermoconductivity media 07 p1267 A67-19314

Cryogenic hydrogen-oxygen ignition with hydrogen-gas entrained Raney nickel as catalyst 09 p1579 A67-21706

Sensitized ignitions of methane and oxygen mixtures, with nitrogen oxides and inert gases added, and suggested reaction mechanisms 14 p2407 A67-28549

Lead, copper and cobalt oxides effects upon ignition kinetics of paraffinic and aromatic fuels 14 p2407 A67-28550

Ignition and combustion characteristics of single aluminum and beryllium particles burning in gaseous environment, discussing oxides role 18 p3149 A67-33796

Cadmium compounds catalytic effect on ammonium perchlorate decomposition rate and ignition temperature 18 p3107 A67-33810

Detonative ignition induced by shock merging ahead of accelerating flame in hydrogen-oxygen mixture analyzed by stroboscopic laser-schlieren photography 18 p3153 A67-33826

Ignition energy, quenching distance, flame stability and gas turbine burner performance of ammonia-air mixture 18 p3109 A67-33843

Rayleigh number effect on importance of convective heat transfer in self-heating gaseous reactions checked against thermal ignition theory 18 p3156 A67-33852

Vacuum-ignition phenomena in Apollo rocket engine when oriented in upward-firing attitude 18 p3114 A67-33977

Kinetically based mathematical model of hypergolic ignition in space ambient engines for predicting delay time and conditions from which pressure spikes result 19 p3311 A67-35744

Hazards of rocket launching noting propellant toxicity, airborne fragmentation, inadvertent ignition and nuclear radiation 22 p3900 A67-39884

IGNITION LIMIT

Thermodynamic parameters of combustible mixture and ignition system characteristics effect on energy of spark ignition of homogeneous gaseous mixture 03 p0535 A67-13396

Mechanism of hydrogen combustion near lower ignition limit studied, using electron paramagnetic resonance /EPR/ measurements 03 p0536 A67-13842

Carbon disulphide oxidation noting self-ignition temperature, explosion limits, reaction products, cool flame propagation, etc 04 p0566 A67-15093

Hydrogen sulfide oxidation, role of temperature and pressure, determining explosion levels 04 p0566 A67-15094

Oxidation by nitrous oxide, nitric oxide, nitrogen dioxide and ozone, considering various reactions 04 p0566 A67-15095

Flame ignition from spherical hot gas pocket, finding minimum size of bubble for flame propagation and dependence on kinetic parameters 06 p1114 A67-18189

Concentration limits of ignition of methanol and formaldehyde mixtures at atmospheric pressure and from 20 to 280 degrees C 12 p2039 A67-26118

Hydrogen vent flare stack performance in adverse weather conditions 13 p2186 A67-27651

Physical and chemical wall effects on mechanism of combustion reaction in gases studied by introducing solids and measuring ignition pressure 18 p3155 A67-33847

Critical reaction rate for ignition, temperature rise and induction period for various geometries calculated for conductive theory, including reactant consumption 18 p3156 A67-33850

SA CHOKER

SA IGNITER

SA STARTER

Low pressure low-temperature ignition of hypergolic propellants, particularly hydrazine-nitrogen tetroxide systems, in space environment simulator and conclusions on gas phase reactions 07 p1163 A67-19385

Ignition systems for turbine engines, discussing low and high energy, semiconductor spark plugs, effects of

electric constants on performance, etc 09 p1559 A67-21691

Ignition of hydrogen-oxygen propellant combination by chlorine trifluoride 10 p1697 A67-23132

Solid propellant highly restartable electric trigger microthruster, noting triggering electrode and feed system 11 p1746 A67-25013

Ignition delays calculation in hydrogen-air system, using Momtchiloff assumptions 13 p2185 A67-26259

Pyrotechnic actuation, discussing parameters, equipment and performance of explosive devices 15 p2543 A67-29304

Causes of ignition failure in solid-fuel rocket motors, obtaining simultaneous pressure and temperature data 15 p2543 A67-29773

Space pressure and temperature environment simulation facility for liquid rocket space-ignition reliability testing [AIAA PAPER 67-428] 18 p3112 A67-33912

Fluid dynamics and chemical phenomena near injector exit of idealized supersonic combustion burner, noting parameters of ignition delay length 18 p3158 A67-33960

Flame spreading over igniting solid propellant surface in high pressure oxygen-inert environment 19 p3344 A67-34999

IGNITION TEMPERATURE

S COMBUSTION TEMPERATURE

S SPONTANEOUS IGNITION

TEMPERATURE

IGNITRON

Combination flash photolysis-flash pyrolysis system with timing circuit, using Tektronix pulse generators and Ignitron circuit for firing spectroscopic lamp 02 p0247 A67-12689

Inductive energy storage and control system using Ignitron switching 24 p4197 A67-42249

IGY

S INTERNATIONAL GEOPHYSICAL

YEAR /IGY/

ILLUMINANCE

Bezold-Brucke hue shift measurements in color naming situation using optical system 22 p3835 A67-39238

Luminance of lunar surface site predicted by direct solar and earth reflected illumination together with local albedo variations 22 p3887 A67-40143

ILLUMINATION

SA FLARE

Choke slots or corrugated structure in walls of horn antenna for reducing sidelobe and backlobe level by controlling illumination of E-plane edge 02 p0211 A67-11801

Transmittance increase of silicon film when illuminated by silicon dioxide layer in long wave IR spectrum 03 p0488 A67-12891

Transmittance increase of silicon film when illuminated by silicon dioxide layer in long wave IR spectrum 06 p1054 A67-18769

Gas laser as source of illumination, with attention to origin of aventurine spots on screen 07 p1195 A67-19142

Thermally stimulated current peak distribution changes with illumination time and intensity for semi-insulating gallium arsenide 07 p1234 A67-20102

Operational and circuit features of laboratory device built to simulate dynamic electrical output characteristics of programmable solar array in orbital flight 08 p1315 A67-20660

Stroboscopic distortion during rotation of uniformly accelerated disk illuminated by light pulses 11 p1757 A67-23917

Optimum illumination for maximum power transfer between two opposed rotationally symmetric antennas 11 p1762 A67-24291

Reflection coefficient of parabolic reflector antenna illuminated by horn radiator with sector shaped radiation pattern 11 p1767 A67-24716

Primary illumination laws for parabolic reflector for maximum quality factor determined, considering multimode sources for cold antennas 12 p1913 A67-25307

Resonance properties of semiconductor with moving electrical domains, showing periodic variation with illumination intensity 12 p1983 A67-25517

Optical reconstruction from sampled holograms made with sound waves 14 p2320 A67-28602

Shutter speed and illumination data for cinematographic documentation of total solar eclipse 15 p2555 A67-29576

Solar radiation increase using orbiting reflector satellite, discussing illumination capability [AAS PAPER 67-118] 15 p2570 A67-29964

Illumination impinging on geocentric satellite during eclipse by earth 16 p2761 A67-30958

Gas laser as source of illumination, with attention to origin of auroral spots on screen 17 p2869 A67-33220

Resonance properties of semiconductor with moving electrical domains, showing periodic variation with illumination intensity 18 p3103 A67-34448

Gravitational model for chromosphere flarelike brightenings following disparities brusques, examining prominence and chromospheric characteristics 19 p3324 A67-35437

Semiconductor thermoconductivity increase due to illumination on one face by radiated energy 19 p3304 A67-35461

Cooling and illumination effect on Gunn oscillators resulting in abrupt shift from transit-time frequency mode to higher frequency 19 p3305 A67-35628

Stroboscopic distortion during rotation of uniformly accelerated disk illuminated by light pulses 21 p3601 A67-38945

Solar cell array model constrained at four points, with computer simulating V-I characteristics for environmental temperature and illumination intensity effects 23 p3940 A67-41515

ILLUSION

S MOON ILLUSION

ILYUSHIN IL-18 AIRCRAFT

Parameters to be calculated in checking airport possibilities for accommodating IL-18 aircraft, considering maximum takeoff weight 03 p0360 A67-13780

IMAGE

SA OPTICAL IMAGE

SA RETINAL IMAGE

Image transmission by two-dimensional contour coding using edge point coordinates studied by computer simulation 11 p1791 A67-24713

Neighbor model for computer simulation of field ion images in fcc point lattice 17 p2887 A67-32205

Holographic exposure times controlled by direct viewing of reconstructed image during exposure 18 p3048 A67-34012

IMAGE CONTRAST

Holographic resolution as affected by materials, installation vibration, hologram dimension and light source 01 p0063 A67-10355

Aerial photograph physics in correct and faulty colors, discussing recognition of relation between landscape and photographic density 05 p0804 A67-16064

Electro-optical imaging systems used in military aerial TV display, emphasizing variables involved in viewing related to visual interpretation 05 p0757 A67-16309

Brightness angular velocity and geometry of moving object relationship to camera parameter to determine exposure and focal length and contrast for optimum recording 05 p0808 A67-17032

Diffraction based criteria use for image quality in automatic optical design, reviewing aberration tolerance theory 06 p1030 A67-17573

Luminance amplifier as intensifying tubes for faint or rapidly changing images 07 p1189 A67-20156

Restoration of digitized turbulence-degraded images by corrective processing of harmonic representation according to measured optical transfer function 11 p1789 A67-24414

Picture quality in PCM transmission of low resolution monochrome still pictures as affected by system parameter changes 11 p1791 A67-24712

Enlarged internal laser beam projecting high contrast images generated on photochromic plate within laser cavity 11 p1801 A67-24717

Holographic resolution as affected by materials, installation vibration, hologram dimension and light source 11 p1794 A67-25028

Corrective image deconvolution of smearing caused by extended instrument

functions in optical imaging possible by holographic Fourier transform 20 p3435 A67-36204

Image degradation comparison between photographic and image orthicon systems, discussing image orthicon receptor advantages when used for space applications 20 p3446 A67-36606

Brightness angular velocity and geometry of moving object relationship to camera parameter to determine exposure and focal length and contrast for optimum recording 21 p3627 A67-38264

Two-dimensional optical image analysis program for image prediction and enhancement, discussing transfer function 24 p4157 A67-42433

Image shear analysis utilizing conventional coordinate and projective transformations performed on computer 24 p4157 A67-42603

IMAGE CONVERTER

High speed cameras with image converter tubes noting electrical circuits 01 p0067 A67-10774

Spinning-image coded X-ray star camera, based on image coding, permitting reconstruction of two-dimensional image [AIAA PAPER 66-850] 03 p0424 A67-14016

Plasma vortex filaments produced in pairs as shown by image converter photographs of interfaces between magnetic field and accelerated plasma 03 p0486 A67-14054

Image converter observation of radial striated light filaments during gas breakdown and current sheath buildup in dense plasma focus coaxial discharge 03 p0486 A67-14055

Synthesis of capacitive converters of angular displacements into digital code 06 p1003 A67-18175

Power source for image converter tubes /ITC/ with regulated output voltage 06 p1004 A67-18393

Image scanning systems applied to filmed data processing 07 p1148 A67-19745

Mosaic of photosensors for solid state imaging, discussing electro-optical conversion, structure and characteristics 09 p1476 A67-22209

Photographing satellites, using optical system and image converter for determining coordinates 10 p1606 A67-23184

Performance characteristics of photosensors and limitation by statistical fluctuation in absorption rate of light quanta in primary photoprocess 11 p1768 A67-24627

Lunar Orbiter photographic system readout for image conversion to video signals [SMPT PAPER 101-45] 12 p1940 A67-25463

Scan converter for Apollo TV performing time base conversion with destructive readout storage element and flicker correction with magnetic disk [SMPT PAPER 101-53] 12 p1904 A67-25468

X-ray sensitive TV system with image enlargement for nondestructive testing [SAE PAPER 670362] 12 p1950 A67-25882

Spinning-image coded X-ray star camera, based on image coding, permitting reconstruction of two-dimensional image [AIAA PAPER 66-850] 15 p2486 A67-29440

Time-resolved spectra for hypervelocity spheres and cones in free-flight ballistic range obtained by large aperture spectrograph and image converter camera 17 p2862 A67-33290

Electron image manipulation and charge-image storage perform equivalent of incoherent optical-image transformation 18 p3047 A67-33881

Current growth rate instabilities in high current mercury vapor discharges, giving image converter photographs 19 p3265 A67-35091

IMAGE CORRELATION

Algorithm based on affine transformation of plane figures used to compare images of written letters of alphabet 01 p0028 A67-10541

Correlation function of stellar image fluctuations and pulsations due to earth atmospheric influences for two stars separated by small angular distances 02 p0325 A67-11964

Atmospheric turbulence effect on quality of star images based on telescopic observations of stars shows pronounced correlation 02 p0261 A67-11989

Multiple scan correlator construction stressing flashing lamp system and rapid

film processor 20 p3452 A67-37312

IMAGE DISSECTOR TUBE

All-electronic, ultra-fast scanning spectrometer utilizing image dissector for power spectral density function measurements of rapidly time varying optical emission 16 p2680 A67-31803

Image dissector camera providing high resolving power, photometric fidelity and long life for use in meteorological satellite 20 p3445 A67-36541

IMAGE FILTER

Linear least squares filtering of distorted images, stressing turbulent atmosphere effect 18 p3047 A67-33882

IMAGE FURNACE

Arc image ignition of solid propellants compared to conductive ignition, outlining corrective steps and deriving ignition time delay 15 p2581 A67-29987

Arc-image furnace for direct gas heating at high temperature by concentrated radiation studies and efficient cavity-type receiver development 17 p2834 A67-32696

IMAGE INTENSIFIER

SA LASER

Image restoration via phase holograms, noting applications to deteriorated photographic negatives and positives 08 p1331 A67-20842

High resolution holograms using Fresnel biprism to reduce noise 18 p3053 A67-34620

High resolution spectra of Venus and Jupiter using image intensifier and solar spectrograph, measuring abundances in planetary atmospheres 20 p3521 A67-36309

Displacement effects analyzed for one beam of laser streak interferometer relative to another on image intensity distribution 22 p3795 A67-39199

Sensitivity of film with and without image intensifier compared, using emulsion densities as function of number of incident quanta 22 p3796 A67-39278

Image tube properties in astronomical data acquisition, discussing photographic plate failure and various image intensifier applications 22 p3799 A67-39774

IMAGE ORTHICON TUBE

Automatic electrostatic image orthicon camera with small weight, volume and input power, having full low-light level sensitivity capability 17 p2858 A67-32481

Low light level TV as aid to nighttime air rescue, describing ionoscope and image orthicon of camera system 17 p2859 A67-32506

Cinematographic observations of fast auroral variations 18 p3033 A67-33587

Simultaneous recording of rocket trajectory and rapid auroral variations using high sensitivity image orthicon TV system 18 p3034 A67-33594

S-10 and S-20 image orthicon tubes evaluated for radiometric measurements against reentry vehicles, considering radiometric response, resolution and calibration stability 20 p3452 A67-37311

IMAGE TRANSDUCER

Reconstructed image scanning by hologram rotation 21 p3624 A67-37852

IMAGE TUBE

Electron bombardment induced electroconductivity, with application to image tubes 03 p0387 A67-14092

Linearized model of readout process in image tubes incorporating progressive erasure of stored image, noting increased effects of erasure with increasing beam modulation 03 p0426 A67-14396

Luminance amplifier as intensifying tubes for faint or rapidly changing images 07 p1189 A67-20156

Image storage tubes /cathode ray tubes with memory device to store visual information/ 07 p1189 A67-20157

Image analyzer tube for IR TV based on phenomenon of accumulation at semiconductor junctions 07 p1189 A67-20158

Electronic zoom by varying vidicon raster size 14 p2321 A67-28920

Flood beams incidence angle and current density distribution effects on half-tone reproduction of visual storage tube with cathode collimator 19 p3194 A67-35543

Potential fields representation for electrostatic image tubes with curved cathodes, using analytic functions 19 p3194 A67-35544

Cathode study using electron images of recording storage tube

cathodes 19 p3197 A67-35813
 Vidicon type image tube sensitive in near UV developed for space applications 21 p3599 A67-38654
 Image tube properties in astronomical data acquisition, discussing photographic plate failure and various image intensifier applications 22 p3799 A67-39774
 SNR performance of SEC vidicon image storage tube at optimum and reduced readout rates 22 p3773 A67-39961
 Image tubes to obtain signal and noise solutions, determining Noise Equivalent Power /NEP/, Detectivity Star and Detective Quantum Efficiency 22 p3805 A67-40352

IMAGE VELOCITY SENSOR
SA SPATIAL FILTERING
 Control signal generator and output characteristics of angular position and velocity sensors used in single-axis sun-oriented system of Vostok spacecraft 12 p1964 A67-25642
 Hologram temporal filtering properties applicability to Doppler mapping of moving objects and wavefront reconstruction process on noncoherent object images 13 p2121 A67-27352
 Fluid flow measurement through optical radiation detection, determining local velocities and image-space motion 15 p2488 A67-29766
 Image velocity sensing technique applying moving reticle scanners, with time-dependent correlation function analyzed by frequency discriminator 19 p3231 A67-35689

IMAGERY
 TV system resolution improvement without bandwidth increase, discussing accuracy of random alphabetic characters 23 p3975 A67-41282

IMAGING TECHNIQUE
 Optimum frame frequency and virtual exposure coefficient determination for high- and superhigh-speed cameras 01 p0067 A67-10831
 Noise limitations in obtaining three-dimensional images by holographic techniques, considering graininess of photographic emulsion 01 p0067 A67-10834
 Holography theory and applications, discussing Fresnel and Fourier holographies, interferential information processing, incoherent objects and associative memory 01 p0068 A67-11005
 Hologram process for object reflecting or diffusing quasi-monochromatic light, including effects of partial spatial coherence 01 p0070 A67-11079
 Ultimate sensitivity of space camera imaging devices with particular reference to slow scan vidicon 02 p0245 A67-12245
 Focused image holography with extended sources for real image in proximity of hologram plate 03 p0420 A67-13574
 Pattern recognition, property filtering and lunar feature data experiments coupled with Tiros cloud photographs demonstrate preprocessing for systems design [SMPT PREPRINT 100-13] 03 p0376 A67-13805
 IR and visible images of eclipsed moon made from scan data and magnetically recorded analog signals from observation of total lunar eclipse on December 19, 1964 04 p0697 A67-14741
 Single pulsed electron beam used in machining and imaging modes for creating machine scan device 04 p0623 A67-15316
 Programmable display synthesizing system for man-machine communications research based on electronic animation technique 05 p0786 A67-16314
 Photographic technique for photometric comet observations, noting automatic polarograph and high transmission meniscus telescope 05 p0890 A67-16333
 Wavefront reconstruction imaging technique and amplitude and phase recording techniques in hologram preparation 05 p0807 A67-16800
 White light display of holograms 05 p0808 A67-17320
 Fog penetrating imaging device using germanium panel, horn and waveguide 05 p0809 A67-17512
 Image formation in holograms 05 p0809 A67-17530
 Image orthicon TV system and application to auroral observations, noting data acquisition mechanism 06 p0993 A67-17563
 Model predicting effects of finite

hologram emulsion resolving power on field range recorded in hologram and resolution in reconstructed image 06 p1004 A67-18543
 Image reconstruction of nonexistent three-dimensional equilateral tetrahedron using theoretically calculated automatically plotted photo-reduced hologram 07 p1186 A67-19558
 Wave front reconstruction imaging technique for hologram production of aerial image of lens 07 p1188 A67-19787
 Holographic technique for restoration of third-dimension information in recording of conventionally focused photographs 07 p1188 A67-19788
 Holographic synthesis of computer generated holograms 07 p1188 A67-19796
 3-D imagery and holograms of objects illuminated in white light photographed through fly eye lens 07 p1189 A67-20098
 Selective imaging of objects in range using pulsed laser illuminator synchronized with Kerr cell camera, obtaining elimination of film exposure due to backscatter in turbid atmosphere 08 p1337 A67-20683
 Print-etch and negative-pattern image transfer techniques for fabrication 08 p1334 A67-20743
 Electromagnetic wavefront perturbations from plane wave propagation resolved into random tilt and residual phase perturbation 09 p1461 A67-21596
 Nonparaxial imaging, magnification and aberration properties in holography, examining point source object 09 p1496 A67-21707
 Holographic applications, examining character identification, imaging technique and interferometric techniques 09 p1501 A67-22555
 Hologram copies by recording interference pattern between undiffracted and diffracted waves 10 p1654 A67-22754
 X-ray image transformation, transmission and amplification directly into video signals for inspection of missile case walls and weldments 10 p1622 A67-22929
 Three-dimensional photography based on laser derived hologram, examining split-beam technique 10 p1655 A67-23072
 Optical resolution, light intensity and true perspective effect on imaging characteristics and parallax and image brightness influence on display realism of visual simulation 11 p1749 A67-24629
 Visible three-dimensional ultrasonic imaging of interior and exterior of optically opaque objects, using synthetic holographic technique 11 p1793 A67-24831
 Photographic technique for obtaining solar image in rays of Lyman alpha line spectrum, using quartz crystal 11 p1793 A67-24862
 Pulsed ruby laser to obtain Fourier holograms in light reflected from diffusely scattering objects, discussing relaxation of resolving power of photographic emulsions 12 p1939 A67-25335
 IR imagery from remote sensing, use in agriculture and forestry [AIAA PAPER 67-281] 12 p1967 A67-26000
 Reconstruction method for image with good definition via partially coherent source 13 p2119 A67-26587
 Optical interference method of two-dimensional Fourier transform with spatially incoherent illumination to derive relations for transforms of images 13 p2121 A67-27290
 Image and other techniques to measure and reduce stray and scattered light in sunspot photometry, emphasizing possibility of using partial solar eclipse 13 p2203 A67-27424
 Light sensitive arrays based on photodiodes combined with MOS devices analyzed for use of image, pattern detection and other applications 14 p2282 A67-28026
 Earth atmosphere effect on propagation of radio waves from space, image formation, phase stability, technical problems and multiperture instruments 14 p2285 A67-28437
 Coherent and noncoherent holography, noting relationship to corresponding case using lenses 14 p2319 A67-28472
 Nonlinear imaging phenomena discussed in connection with holography, describing holoscopes permitting three-dimensional magnification in real time 14 p2319 A67-28495
 Optical reconstruction from sampled holograms made with sound waves 14 p2320 A67-28602
 Optical system consisting of circular sweep camera for recording useful streak

images on Polaroid film 14 p2320 A67-28748
 Electronic zoom by varying vidicon raster size 14 p2321 A67-28920
 View function to images of surface in nonplanar specular reflector determined by general mathematical expressions [JPL-TR-32-939] 15 p2516 A67-29131
 Optical image recording, storage and reproduction using Gudden-Pohl effect 15 p2487 A67-29470
 Optical image producing method of complex ultrasonic field using light diffraction of laser beam 15 p2487 A67-29498
 Images reconstructed from multiple-exposure hologram separated by selecting appropriate-reconstructed pupil 15 p2487 A67-29500
 Optical image reconstruction from sampled hologram using wavefront reconstruction technique 15 p2488 A67-29819
 Electrodynamics applied to two-dimensional problem of determining resolution of images reproduced from ideally plane infinitely thin holograms 15 p2489 A67-30006
 Holograms of three-dimensional objects, discussing experimental setup and results 15 p2489 A67-30077
 Holography applications in quality assurance including checking jigs, fixtures, molds, vibration analysis, etc 15 p2491 A67-30405
 Multicolor image reconstruction from holograms behaving as planar diffraction gratings, excluding crosstalk images formation 15 p2491 A67-30431
 Holography theory and applications, discussing Fresnel and Fourier holographies, interferential information processing, incoherent objects and associative memory 16 p2670 A67-30489
 Image analysis by Fourier transformation into incoherent illumination, applied to point source of light /star/ 16 p2671 A67-30863
 Millimeter wave resonant interferometer capable of measuring spatial distribution of electrons in low density transient plasma column subject to perturbation 16 p2675 A67-31263
 Coordinatograph and electro-optical data visualization unit for digital computers noting details 16 p2634 A67-31633
 Optical detectors for images and selected radiation signals using Bendix Channeltron multiplier, describing types, properties and applications 17 p2858 A67-32480
 Raster scan parameters influencing target identification in image recognition experiments using video display 17 p2859 A67-32508
 Airborne imagery screening using automatic target recognition device 17 p2859 A67-32509
 Parallel electro-optical technique for implementing linear threshold adaptive networks 17 p2860 A67-32616
 Fiber optic window fitted to stainless steel field ion microscope permitting use of direct contact photography for image recording 17 p2863 A67-33354
 Electrodynamics applied to two-dimensional problem of determining resolution of images reproduced from ideally plane infinitely thin holograms 18 p3046 A67-33767
 Four types of holographic imaging systems, discussing optical properties and divergence and convergence 18 p3046 A67-33879
 Electron image manipulation and charge-image storage perform equivalent of incoherent optical-image transformation 18 p3047 A67-33881
 Optical system devised to alter relative harmonic coefficients and eliminating ringing effects for photographs represented in two-dimensional Fourier series applied to lunar photography 18 p3047 A67-33998
 Lunar topography from ground-based photographs taken under oblique illumination, discussing exposure times, resolution, etc 18 p3132 A67-34330
 IR imaging system with multiple target capability for measuring IR radiation emitted by missiles during launch, boost and reentry 18 p3052 A67-34532
 Holographic image magnification by recording wave interference and illuminating object by coherent beam 18 p3053 A67-34622
 Vegetation mapping from K-band radar imagery using image discrimination

- enhancement, combination and sampling
system 19 p3227 A67-34798
- Photomask application to microelectronics
equipment and die fabrication, discussing systems
for step-and-repeat operation elimination in
image array making 19 p3236 A67-35021
- Image reconstruction of diffusely
reflecting objects using pulsed hologram
technique 19 p3233 A67-36102
- Image reconstruction from coarsely
sampled acoustical hologram made from
ordinary microphone 19 p3233 A67-36104
- Focused image holograms, amplitude-or
phase-recorded, reconstructing sharp images
by reflection from incoherent
illumination 20 p3435 A67-36201
- Spaceborne fiber optics TV system
emphasizing image enhanced flexible front
end optical assembly 20 p3445 A67-36554
- Image degradation comparison between
photographic and image orthicon systems,
discussing image orthicon receptor
advantages when used for space
applications 20 p3446 A67-36606
- Digital image formation from electronically
detected holograms noting advantage in
imaging of weak objects 20 p3448 A67-36852
- High quality holography of back-lighted
objects using achromatic-fringe
interferometry 20 p3450 A67-37022
- Hologram reconstruction of objects in fog-
like medium 20 p3450 A67-37027
- Three-dimensional hologram reconstruction
and image speckle, considering three-
dimensional boundary value
problem 20 p3451 A67-37309
- Imaging systems of ground-viewing
satellite, discussing TV, lasers, radar,
etc. 20 p3452 A67-37310
- Multiple scan correlator construction
stressing flashing lamp system and rapid
film processor 20 p3452 A67-37312
- Reconstructed image scanning by hologram
rotation 21 p3624 A67-37852
- Field ion images from single crystals of
titanium carbide, noting development of two
crystallographic regions 21 p3645 A67-38093
- Moving point trajectory recorded by
hologram 21 p3627 A67-38347
- Maximum likelihood method used as
criterion in processing optical images
propagated through turbulent
atmosphere 21 p3586 A67-38954
- Visual image description with aid of
spectral power redistribution functions,
discussing input arrangement in TV
recognition system 21 p3605 A67-39114
- Rayleigh-Sommerfeld diffraction formula
to obtain imaging behavior of Gabor type
holograms of transparencies for
reconstructed wave forms with large
diffraction angles 22 p3835 A67-39241
- Bandwidth reduction for holographic data
transmission systems noting application to
TV 22 p3796 A67-39260
- Book on theory and applications of
holography, mathematical analysis of process
as imaging technique, limitations and partial
coherence 22 p3798 A67-39633
- Nomograph construction for earth pointing
cameras, evaluating imaging system
effectiveness as ground resolution and scale
factor, plotting system performance
characteristics 22 p3800 A67-40106
- Microwave multiband spectral
reconnaissance of earth and space vehicles
using imaging radar on
spacecraft 22 p3806 A67-40362
- Spatial filtering for altering relative
harmonic coefficients in two-dimensional
Fourier integral representation of
astronomical photographs eliminates ringing
effects 23 p3997 A67-40625
- Nonpseudoscopic real image production
from arbitrary hologram using different
geometries for reference and reconstructed
waves 23 p3998 A67-40701
- Computer generated binary Fraunhofer
holograms for mathematically known objects,
discussing diffraction theory, computational
and plotting procedures 23 p4002 A67-41267
- Hologram duplication noting stability
factors and process for producing coherent
copy 24 p4153 A67-41910
- Linear defects imaging in single crystals
by interpreting anomalous behavior of
propagating X-rays ascribed to structural
defects 24 p4202 A67-42072
- Computerized imaging techniques -
Conference, Washington, D.C., June
1967 24 p4156 A67-42428
- Digital imaging techniques used in
sinusoidal frequency response modification
with or without computer control and
display on operator console 24 p4125 A67-42429
- Three-dimensional surface projection
method by computer plotting program
applicable to surfaces with large amount of
detail 24 p4125 A67-42430
- Brightness distortions quantitative
determinations in digitized Tiros/ESSA
satellite vidicon data to normalize scene to
uniformly illuminated image 24 p4156 A67-42431
- Image processing by computer generated
binary filters 24 p4156 A67-42432
- Two-dimensional optical image analysis
program for image prediction and
enhancement, discussing transfer
function 24 p4157 A67-42433
- Multidimensional data stereoscopic graphic
display principles, viewing and use in
engineering design 24 p4157 A67-42434
- Multichannel image data handling and
processing system using multispectral
analysis for remote agricultural sensing and
surveying from aerospace
platforms 24 p4157 A67-42435
- Digital computer restoration of
atmospherically degraded images, studying
techniques and limitations of former and
mechanisms of latter 24 p4157 A67-42436
- Digital image formation and reconstruction
from photographic and direct electronically
detected holograms 24 p4157 A67-42437
- Digital computer and coherent optical
image processing techniques compared,
reviewing data transfer schemes and
available hardware 24 p4125 A67-42438
- Character recognition via holography using
Gabor principle of two coherent waves
falling simultaneously on photographic
plate 24 p4157 A67-42456
- Image shear analysis utilizing conventional
coordinate and projective transformations
performed on computer 24 p4157 A67-42603
- Spatial filters for code translation and
image sharpening produced by holograph in
reasonably good approximation 24 p4159 A67-43097
- IMBEDDING**
S INVARIANT IMBEDDING
IMIDAZOLE
Copolymers containing imidazopyrrolone
and imide groups tested for thin film tensile
properties, degradation by strong acids and
bases and thermal stability 22 p3824 A67-39851
- IMIDE**
SA PYRIMIDINE
Hydrolysis of phthalimide ring with
carboxylate group linked through alkyl
group as anionic intramolecular
catalyst 10 p1602 A67-23159
- High temperature polyimide
unidirectionally reinforced with silica fiber,
noting precuring process to avoid porosity
and strength degradation 11 p1811 A67-24641
- Inactivation of thermal catalytically active
polyanhydro-alpha-amino acids by heating in
buffered solution, noting hydrolysis of cyclic
imide bonds 13 p2065 A67-26733
- Polyimide bonded solid lubricants
development
[ASLE PREPRINT 67AM 7A-1] 14 p3236 A67-28789
- Polyimide bonded solid lubricants
development 19 p3233 A67-34790
- High temperature properties of aromatic
polyimide fibers, noting thermal and
dimensional stability 21 p3848 A67-37874
- Copolymers containing imidazopyrrolone
and imide groups tested for thin film tensile
properties, degradation by strong acids and
bases and thermal stability 22 p3824 A67-39851
- IMINE**
Shock tube measurement of dissociation
energy of NH radical in reflected shocks
through nitrogen-hydrogen-krypton and
ammonia-krypton mixtures 01 p0117 A67-10787
- Imines reacting with difluoramine produce
diazirines and other products having
potential as missile propellant components 01 p0020 A67-11147
- Isomerization rate of iminocarbonates,
discussing electronegative hetero-atom
bonded to imino carbon 09 p1459 A67-22363
- IMMERSION**
Water-immersion weightlessness simulation
to determine astronaut EVA capabilities and
man-machine interfaces [AIAA PAPER 66-903] 02 p0187 A67-12270
- Physiological responses of subjects in
prolonged immersion to neck level,
measuring losses of heat, fluid and
electrolytes 03 p0364 A67-14294
- Urine composition in twelve dehydrated
subjects in periods of activity, water
immersion and reclining in deck chair
[SAM-TR-66-305] 09 p1453 A67-21730
- Weightlessness simulation by bed rest and
water immersion, evaluating validity of
protective measures, recovery time and tilt
response 15 p2424 A67-29102
- Plasma 17 hydroxycorticosteroids in
healthy subjects after water immersion of 12
hr duration shows no stressful
effect 15 p2427 A67-29270
- Plasma volume and tilt table response of
humans to water immersion deconditioning
experiments, using extremity cuffs to study
protective effect 15 p2428 A67-29271
- Water-immersion weightlessness simulation
to determine astronaut EVA capabilities and
man-machine interfaces [AIAA PAPER 66-903] 15 p2431 A67-29439
- Effect upon cardiovascular system of
weightlessness simulated by immersion in
brine 17 p2805 A67-31952
- Tilt table response and plasma volume
changes in experimental subjects evaluated
before and after short term periods of
deconditioning 17 p2805 A67-31953
- Immersion technique measurement of
gravitational stresses using two-and three-
dimensional photoelasticity [ASME PAPER 67-APM-11] 17 p2964 A67-33146
- Positive pressure breathing effects on
inhibition of diuresis during water
immersion 18 p2992 A67-34721
- Immersion effect on concentrating and
increasing pump flux of laser incident on
absorbing core, considering rod and
sphere 21 p3638 A67-37857
- Intrapulmonary pressures chosen during
immersion in thermally neutral water,
comparing transpharyngeal and transthoracic
pressure gradients for various breathing
devices 22 p3751 A67-39604
- IMMUNITY**
Traumatic sickness in dogs due to high
gravity impact noting enzymatic activity
changes and immunizing reaction 21 p3575 A67-38509
- IMP**
Energetic particle monitoring satellites,
discussing design and development of four
IMP generations 01 p0156 A67-11415
- Decontamination techniques and
sterilization environment, discussing
compatibility with components and hardware
of lunar orbiting spacecraft 02 p0249 A67-12386
- Satellite measurement of behavior of high
latitude energetic electron trapping
boundary, noting geomagnetic storm
effects 03 p0410 A67-12951
- Radial temperature profile of
magnetospheric plasma near equatorial plane
observed by IMP satellites 06 p0996 A67-18432
- Interplanetary magnetic field and plasma
effect on geomagnetic activity during quiet
sun conditions 07 p1251 A67-19912
- IMP-II and OGO-I measurements on
plasma characteristics in transition region
between solar wind and geomagnetic
field 12 p1997 A67-25806
- Interplanetary sector structure observed
by IMP-I satellite compared with
photospheric magnetic field and plage
structure observations 17 p2953 A67-33400
- IMP-A**
S EXPLORER XVIII SATELLITE
IMP-D
S EXPLORER XXXIII SATELLITE
IMPACT
SA ELECTRON IMPACT
SA HYPERVELOCITY IMPACT
SA ION IMPACT
SA PENETRATION
SA PROTON IMPACT
Impact expansions and interference
patterns in atomic scattering theory for
cases of forward scattering, backscatter,
inversion problem and screened Coulomb
potential approximation 01 p0112 A67-10143

Quantum mechanical theory of microwave nonresonant absorption and dielectric and magnetic relaxation in
gases 01 p0116 A67-10145

Computational method for determination corridors of launch vehicle trajectory and impact dispersions
[AIAA PAPER 66-483] 02 p0325 A67-11941

Doppler and impact broadening of spectral lines and pressure effects on power output of gas laser 05 p0818 A67-16643

Initiation of explosion by impact of plate against charge surface 06 p1112 A67-17955

Impact problem of passage of longitudinal and transverse waves arising in elastic infinite thread over sequence of absolutely smooth nonrotating
pulleys 07 p1261 A67-19163

Schroeter rule and modification of lunar crater impact morphology 13 p2210 A67-27602

Metal projectiles plastic deformation impacting on rigid targets defined, obtaining computer code through direct analysis 22 p3914 A67-40182

IMPACT ACCELERATION

Forced oscillations of two-mass dynamic system with impact
reaction 02 p0248 A67-11964

Stability of two-impacts-per-cycle motion of impact damper 04 p0631 A67-15911

Electric analog and mechanical model used to investigate single particle impact dampers 07 p1262 A67-19410

Forced steady state response of linear harmonic oscillator with impact absorber attached, developing stability criterion [ASME PAPER 67-VIBR-10] 11 p1795 A67-24170

Short duration shock
machine 12 p1923 A67-25707

Cumulative effect of impact acceleration on physiological functions of rats, studying particularly lung lesions 16 p2612 A67-30904

Forced oscillations of two-mass dynamic system with impact
reaction 17 p2866 A67-33281

Short range FM transmitter-receiver system for shock measurements required to optimize shock absorber
design 21 p3581 A67-38395

Calibration of shock accelerometers, discussing velocity change and impact force methods with specific examples of systems in use 23 p4003 A67-41335

Cineradiographic analysis of human visceral responses to short duration acceleration impact 23 p3951 A67-41553

Energy transfer effects on
pathophysiological responses of guinea pigs and bradycardia response in monkeys under minus G impact
acceleration 23 p3955 A67-41610

Human visceral response to short duration impact analyzed by
cineradiography 23 p3960 A67-41704

IMPACT DAMAGE

SA METEOR HAZARD

Bird impact hazard to aircraft simulated with hens propelled against windshields and metal targets 01 p0049 A67-10539

Sedimentologic process which comminutes, transports and deposits material by impact on planetary surfaces 02 p0235 A67-11451

Mechanical impact attenuation system for Apollo spacecraft provides stable land landing platform, noting deployed heat shields, extended legs, pneumatic bags, etc [AIAA PAPER 66-989] 02 p0333 A67-12300

Impact of cylindrical or spherical projectiles of dural and polyethylene at high velocities in seminfinite targets, analyzing crater shape and relation to kinetic energy 04 p0710 A67-15002

Cavitation pitting and flow regime in cavitating venturi using water and mercury indicate microjet impingement is most important damaging mechanism [ASME PAPER 66-WA/FE-39] 04 p0608 A67-15447

Nonlinear equations for supercritical axisymmetric elastic deformation of circular cylindrical shell under longitudinal impact from rigid body 05 p0907 A67-16015

Sounding rocket disintegration studies to avoid falling mass hazards, noting design of pyrotechnic core in sandwich construction 08 p1407 A67-20520

Estimated reliability impairment of space equipment due to shortings from particle impact 09 p1481 A67-22312

Strong plane shock attenuation from

impact studied with numerical method of characteristics for one-dimensional unsteady flow, showing late-stage
equivalence 11 p1820 A67-24905

Effect of axisymmetric impact against water on shallow clamped aluminum spherical shell-type caps 12 p0230 A67-25937

Experimental apparatus for study of impact ionization and associated recombination radiation in
semiconductors 13 p2168 A67-27228

Mechanical impact attenuation system for Apollo spacecraft provides stable land landing platform, noting deployed heat shields, extended legs, pneumatic bags, etc [AIAA PAPER 66-989] 15 p2564 A67-29423

Aircraft front windshields, discussing thermal stability, clear vision maintenance, bird impact, atmospheric pressure effect, cabin pressure changes and tensile strength 18 p2986 A67-34099

Fatal injuries resulting from extreme water impact studied from necropsy data on persons jumping from Golden Gate Bridge 21 p3573 A67-38069

Small particle bombardment of stone and iron meteorites, obtaining comparative erosion rates 21 p3704 A67-38504

Penetration depth of hypervelocity impact craters photographed by Luna and Ranger vehicles indicate granular lunar surface 23 p4065 A67-41003

Ll interactions with complex damage clusters produced by neutrons in Si solar cells, discussing annealing, radiation hardening and energy
dependence 23 p3940 A67-41520

Human spinal column stiffness under deflection rate /axial compression/ produced by impact 23 p3954 A67-41592

Animal study of irreversible trauma in lateral impact when restrained only by aircraft lap seat belt 23 p3954 A67-41595

Bird strikes on high speed transport jet aircraft stabilizers 24 p4094 A67-42278

Docking mechanisms for spacecraft systems noting hard vs soft and in-line vs off-set systems
[AIAA PAPER 67-908] 24 p4244 A67-43015

IMPACT DECELERATION

Properties of crushable impact attenuation materials used to absorb and dissipate kinetic energy of impacting
body 04 p0711 A67-15238

Dynamic analysis and development of response histories and tradeoff study charts for spherical impact limiters for protecting hard landing planetary
payloads 10 p1727 A67-23738

Energy absorption characteristics of honeycomb structures under static and impact loading 10 p1727 A67-23745

Simulated acceleration and dynamic pressure environments generated by space vehicle flight ranging from weightlessness to impact from ground landing
[AIAA PAPER 67-279] 15 p2485 A67-29425

Unmanned rough-landing survival capsules design considerations for potential planetary payloads 19 p3332 A67-35335

Energy dissipation criteria for object falling on viscoelastic foundation or vehicle impacting without mass separation from support structure 23 p4072 A67-40609

Canine cardiac displacement and cardiovascular dynamic response during abrupt deceleration impact, discussing traumatic ruptures and pressure
effects 23 p3951 A67-41552

IMPACT LOAD

Unstabilized rod buckling from impact load with longitudinal compression wave reflection 01 p0165 A67-11303

Dynamic elastic response of ring loaded transiently on both edges 04 p0718 A67-15921

Orthogonal function energy method calculation of stress concentration in ring under impact loads distributed along inner and outer edges 05 p0918 A67-16420

Finite elastic deformation theory applied to transverse nonlinear oscillation of cables in rubber-like materials 06 p1111 A67-18863

Fusion welding of nickel maraging steel to lower strength steels to produce leaf spring subjected to tensile impact
loading 07 p1198 A67-19213

Compressed air gun for impulsively loading structures, measuring response by high speed photographic
technique 08 p1414 A67-20374

Physicochemistry of substances under

impact compression, considering thermodynamic parameters, phase transformation and compressibility
curves 11 p1749 A67-24322

Flexible plate elastic stability under effect of suddenly applied and short term forces 12 p2024 A67-25599

Impact bending and tension processes using drop hammer technique evaluated with improved method using oscillography for high quality load-time
measurements 13 p2215 A67-26399

Stress concentration of hollow sphere under uniformly distributed impact loads along inner and outer
surfaces 13 p2215 A67-26520

Vibrational stress of clamped free rectangular rods of constant cross section under effect of instantaneous impulse 13 p2220 A67-27277

Book on safety of
structures 14 p2395 A67-28030

Dynamic buckling under step loading studied on basis of general nonlinear theory of elastic stability 14 p2397 A67-28085

Cylindrical shell stability under longitudinal impact, examining buckling processes with high speed motion picture camera 14 p2401 A67-28736

Cross sectional strain and stress distributions in cylindrical elastic bars subjected to pressure-step and velocity impact loading
[ASME PAPER 67-APM-33] 17 p2965 A67-33158

Tensile testing equipment using impact load facilitates rupture stress measurements by conventional strain
gauges 18 p3141 A67-33719

Flexible filament under transverse impact from sphere, considering friction forces 19 p3341 A67-35704

Plastic wave propagation in seminfinite bar subjected to axially applied impact stress 20 p3536 A67-36416

Elastic and dynamic response of viscoelastic plate with finite thickness to rigid body impact 20 p3539 A67-36920

Dynamic stability of spherical segments subjected to impact loading, discussing buckling in relation to rise in center and time dependence 22 p3910 A67-39456

Bird strike data on piston engine transport horizontal stabilizers summarized by bird weight, impact velocity, target-station distance and simulated and test load 22 p3746 A67-39845

Change in brittle fracture work during combined impact and tensile load of polymer noting variation according to maximum law 23 p4072 A67-40595

Strain rate sensitivity and bending extension interaction in one degree of freedom deformation of clamped beam considering vibration and load duration 23 p4072 A67-40607

Permanent deformation of clamped plastic beam with central mass concentration subject to impulse
loading 23 p4072 A67-40606

IMPACT PREDICTION

Simple impact position model for predicting subsonic mass flow for opposing axisymmetric jet 14 p2303 A67-28331

Space-time wind variability for forecasting from near ground surface sampling for unguided rocket impact
prediction 17 p2880 A67-32551

Mission flight profile, considering thrust failure prior to attaining orbital speed, analyzing instantaneous impact point /IIP/ 22 p3831 A67-39610

IMPACT PRESSURE

Rigid disk impact against ideal fluid surface in cylinder, deriving formula for impulse pressure at disk
surface 12 p1928 A67-25665

Free stream variables from continuum effect followed experimentally into transition flow regime to investigate impact probe in rarefied hypersonic flows of diatomic gases 14 p2294 A67-27794

Equilibrium of magnetic field confined by impact pressure of beam of ions for general direction of incidence of
beam 14 p2310 A67-28040

Local flow field measurements of static temperature, density and local impact pressure of hypersonic rarefied flow over degree cone 14 p2241 A67-28161

Wakes behind circular cylinders in free

molecule flow, noting inaccuracy in off-axis impact pressure 14 p2300 A67-28175

Local mass flux and local impact pressure measurement in arc jet exhaust flow fields 17 p2861 A67-33029

Short duration shock tube molecular beam in helium and oxygen, giving test arrangement and data 17 p2835 A67-33361

comparisons 17 p2835 A67-33361

Impact characterization and length, determining contact energy with Hertz equation and integrating nonlinear differential equation for system motion 20 p3483 A67-36195

Shock processes pertinent to lunar terrain fragmentation and lithification noting Surveyor and Lunar Orbiter pictures 23 p4064 A67-40948

Liquid drop impact on liquid, calculating velocity potential, initial pressure and time dependence of cavity depth and wall velocity 23 p3991 A67-41459

Microscopic and X-ray diffraction study of octahedrite shock history 24 p4234 A67-42631

IMPACT SENSITIVITY

Impact excitation of oscillation with oscillating circuit in anode and cathode 07 p1150 A67-19236

Cold brittleness, impact toughness and crack resistance of titanium alloys at low temperatures 09 p1518 A67-21966

Cratering produced by high velocity impact of stainless steel threaded rod on cold-rolled steel target 23 p4080 A67-41467

Human visceral response to short duration impact analyzed by cineradiography 23 p3960 A67-41704

IMPACT TEST

Excitation of phosphor suspensions in solid dielectric by mechanical energy analyzed via impact theory 01 p0113 A67-10354

Impact resistance of spacecraft structures indicate performance criterion effect on final structural configuration and importance of hypervelocity of realistic hypervelocity test specimens 04 p0705 A67-15001

Model tests for determination of structural response of Apollo Command Module to water impact 07 p1257 A67-19368

Impact tests on animals at velocity changes suggestive of automobile crash conditions, confirming effect of isovolumetric containment of torso on increased survival limits 08 p1289 A67-20612

Charpy impact specimens cooling rates in low temperature quenching baths evaluated including specimen size, notch geometry and material chemistry 11 p1874 A67-24265

Excitation of phosphor suspensions in solid dielectric by mechanical energy analyzed via impact theory 11 p1851 A67-25027

Thermal phenomena arising upon projectile impact on metal surface 13 p2220 A67-27383

Effect of drilled holes on notch toughness of iron alloys, noting impact and slow bending testing, notch toughness improvement, etc 16 p2888 A67-31304

Impact ionization in gallium arsenide through fast pulse experiment, noting conflict between theoretical and measured current-voltage characteristics 18 p3097 A67-33517

Titanium plasticity and durability under large temperature range as affected by Re, Ta, Pd and La alloying elements 20 p3468 A67-37175

IMPACT TESTING MACHINE

Human dynamic force response to impact examined, using spring-mass-damper system with refined parameter values 04 p0564 A67-15401

High speed information generation by projectile impact machine, explosive forming and capacitor-discharge energy with very high strain rates, presenting failure modes related to forming velocity 23 p4078 A67-40737

IMPACT TOLERANCE

Nickel effect on tensile strength, impact toughness and cold shortness threshold of low carbon steel 04 p0636 A67-14750

GUT, GPT, MDH, LDH, SDH and aldolase serum enzyme activity in dogs subjected to moderate impact 06 p0953 A67-17997

Yielding phenomena in beryllium wire plastic composites, discussing static strength

and moduli, failure modes and impact resistance 08 p1341 A67-20428

Air Force biodynamic research on injury due to impact during air crash or ejection 08 p1289 A67-20615

Evaluation of plasticity, durability and impact ductility of nonbrittle austenitic steel during high and low temperatures 17 p2873 A67-32767

Nickel effect on tensile strength, impact toughness and cold shortness threshold of low carbon steel 18 p3066 A67-34408

Crash and ballistic protection flight helmet with greater impact energy dissipating characteristics, noting laminated nylon fabric shell and polystyrene liner 21 p3577 A67-38075

Traumatic sickness in dogs due to high gravity impact noting enzymatic activity changes and immunizing reaction 21 p3575 A67-38509

Trauma in lateral impact at high entrance velocity compared with rearward and forward facing body orientations of baboons when restrained by lap belt only 22 p3750 A67-39594

IMPEDANCE

SA ACOUSTIC IMPEDANCE

SA ELECTRIC IMPEDANCE

SA MECHANICAL IMPEDANCE

SA RESPIRATORY IMPEDANCE

Effect of couplings and losses on frequency stability in self-oscillatory system with three circuits 02 p0221 A67-12418

Scattering matrix equations for waveguide structure of varying surface impedance boundaries 11 p1751 A67-23968

Induced impedance dependence on scanning angle and array parameters calculated, analyzing edge effects 14 p2279 A67-28005

Experimental evaluation of fluidic transmission line theory, studying frequency response and sending impedance 14 p2251 A67-28349

Restriction elimination in interchanges of reference impedances of scattering matrices 16 p2630 A67-31719

Slowly decaying broad maximum of parallel conductance explained by tunneling for surface states near Si-silicon oxide interface 18 p3101 A67-34018

Nonlinear impedances used for frequency multiplication 19 p3182 A67-35033

Human respiratory system impedance simulator for dynamic testing of aircraft breathing equipment to detect possible instabilities 24 p4114 A67-41782

IMPEDANCE MATCHING

SA ANTENNA COUPLER

Impedance matching of infinite phased array by dielectric sheets, noting radiation pattern dependence on beam scan angle 01 p0040 A67-11312

Ring trapped mode resonator for use in microwave filters, developing expressions for unloaded Q and resonant frequency in transverse electric mode 02 p0217 A67-12091

Voltage generator consisting of quadrupole injectors where output voltage is complex function of previously chosen input voltages 03 p0392 A67-13450

Impedance matching conditions, gain nonlinearity and bistable mode instability in solid state parametric frequency converters 03 p0381 A67-13637

Passband narrowing due to coupling between passive oscillating system and active substance contained in resonator cavity represented by RLC circuit 05 p0780 A67-17474

Pulse width modulated series switch with input and output filtering for automatic impedance matching in DC circuits regardless of load or source characteristics 08 p1311 A67-20650

Measuring techniques and limitations as related to small reflections in precision coaxial transmission line 09 p1495 A67-21824

Isolation bandwidth characteristics of Y circulator junction modified by external tuning elements 09 p1474 A67-22087

Thermionic low voltage converter-regulator systems, discussing relation between thermionic source, electron cooling and impedance-matching characteristics 09 p1449 A67-22346

Phased array antenna impedance matched for all scan angles assuming connecting circuits are lossless 11 p1758 A67-23975

Criterion of accuracy for given

approximate current distribution based on difference between variationally computed stationary and nonstationary antenna impedances 11 p1759 A67-24131

Measurement and theory of two modes in antenna apertures of magnitudes one to two wavelengths, obtaining field distribution 11 p1763 A67-24295

Triode version of active LF directional coupler compared to passive coupler 13 p2081 A67-27198

IMPEDANCE MEASUREMENT

Reflection measurements with broadband FM using long transmission lines 02 p0193 A67-11783

Theory of influence of surface states on impedance of semiconductor-insulator interface, determining relaxation times which directly affect cut-off frequency of device 03 p0487 A67-12810

Transfer function and input impedance of pressurized fluid piping system, using distributed parameters and block diagram feedback methods [ASME PAPER 66-WA/AUT-13] 04 p0555 A67-15416

Fields of two parallel wires immersed in plasma derived, obtaining formula for driving point impedance of probe 05 p0849 A67-16004

Input admittance of slot antenna after RF voltage breakdown 05 p0775 A67-16947

Varactor diode impedance behavior in parametric amplifiers under low temperature conditions 07 p1152 A67-19551

Impedance test performed with plane dielectric antenna of various configurations 07 p1158 A67-20295

Dispersion and interaction impedance of slow wave structures from cold tests measured, using resonance methods 09 p1476 A67-22212

Attenuation and coupling impedance of backward dipole surface wave on cylindrical plasma column with reference to oscillator design 09 p1546 A67-22281

Plasma electron density determined from mutual impedance measurements obtained as function of frequency 09 p1501 A67-22561

Impedance and admittance measurements of periodically time-varying dipole and application to microwave varactor diode 10 p1610 A67-22925

Impedance measurement of 39.5 meter tip-to-tip dipole antenna made during ionospheric rocket flight 10 p1611 A67-23292

Simulator measurements of active impedance of phased array antenna element at two different scan angles by single element in waveguide 11 p1763 A67-24299

Impedance of strip antenna embedded in dielectric layer overlain by cold plasma, considering reflection coefficient and static magnetic field effect 11 p1783 A67-24305

Antenna impedance dependence on excitation of acoustic waves by biconical dipoles encased in dielectric sphere immersed in warm plasma 11 p1769 A67-25030

High input impedance obtained with junction transistors, discussing circuit design for different frequency modulators, FET properties and applications 13 p2077 A67-26661

Radio measurements and standards for power, conductance, impedance and attenuation in upper frequency range 14 p2263 A67-28390

Input impedance of short dipole antennas on Nike-Apache rocket 15 p2444 A67-29504

Surface impedance of cylindrically stratified anisotropic ionosphere in presence of static magnetic field, calculating propagation parameters 16 p2631 A67-31853

Impedance measurements in coaxial waveguide systems propagating TEM wave, using precision coaxial line standards and connectors 17 p2815 A67-32605

Impedance and reflection coefficient measurement in uniconductor waveguide noting experimental techniques, coefficient standards, etc 17 p2815 A67-32606

Spherical dipole for Italian satellite, calculating radiation impedance and pattern, input admittance, efficiency, radiated field and antenna Q factor 17 p2826 A67-32780

Miniaturized cavity resonator, giving criterion for evaluation of resonant frequencies of corrugated resonators 17 p2827 A67-32786

Impedance wall validity range for microwave structure, discussing tunable

filter 17 p2816 A87-32787
Impedance measurements of RF discharge in single turn coil with superimposed static magnetic field, noting dependences and two resonances 19 p3276 A87-35119
Mutual admittance of slot antennas measured for free space and ionized environment by different techniques 19 p3194 A87-35516
Discontinuity problem solution between unloaded rectangular waveguide and same waveguide completely loaded with transversely magnetized ferrite 20 p3380 A87-36381
Current distribution coefficients determination and antenna 20 p3400 A87-37219
Standing wave ratio and impedance measurement method for rectangular waveguides at microwave frequencies 22 p3767 A87-39371
Active impedance and current distribution in infinite, planar and collinear arrays of cylindrical antennas, deriving Fourier series for antenna current 22 p3769 A87-39629
Radiation pattern, absorption and impedance measurements of conical antenna plasma sheath about dielectric coated metal cone excited by axial radiating slot 23 p3973 A87-40840
Lifetime measurements of GaAs diodes determined from p-n junction impedance 23 p3982 A87-41468

IMPEDANCE PROBE
SA RADIO FREQUENCY IMPEDANCE PROBE
Ionospheric electron density measurement by gyro plasma impedance probe 01 p0064 A87-10566
Upper atmospheric plasma measurements with impedance probe, determining gyro and hybrid resonance frequencies 05 p0798 A87-16861
Ionospheric electron density profiles determined by impedance probe and Doppler effect probe aboard rockets 06 p0993 A87-17595
Fredholm integral equation system for magnetic currents induced on wedge under impedance boundary condition 08 p1295 A87-21273
Quasi-static theory of cylindrical impedance probe for magnetoplasma extended to include vacuum sheath effects 09 p1549 A87-22451
Ionospheric thin layer stratifications and valley region analyzed by integrating propagation method and by impedance probe 10 p1648 A87-23290
Transmission line approach for determining input admittance of slotted antenna array covered by dielectric sheet 11 p1762 A87-24293
Frequency characteristics of planar and spherical plasma resonance probes and RF impedance probe in magnetic field, considering equivalent electric circuit 20 p3503 A87-37670
Ionospheric plasma electron density profile and plasma resonance effects at base of magnetosphere measured by rocketborne gyro-plasma probe 22 p3793 A87-40043

IMPELLER
SA PUMP IMPELLER
SA ROTOR BLADE
SA STATOR
SA TURBINE WHEEL
Strain gauge method for determining stress concentration in radial flow impellers 04 p0708 A87-14537

IMPELLER BLADE
Stresses calculated in centrifugal impeller with cover disk by two-dimensional stress analysis and digital computer program [ASME PAPER 65-WA/FE-17] 01 p0080 A87-10873
Secondary vorticity for compressible flow in centrifugal impeller, noting parameter effects on motion 03 p0402 A87-13337
Energy transfer by circulatory and Coriolis forces in centrifugal and axicentrifugal compressors 04 p0690 A87-15897
Strain gauge measurement data on rotating impeller blades of aircraft turbines, discussing errors in determination of stress amplitude 09 p1576 A87-22458
Singularity carrier auxiliary curves for design of straight cascades of slightly curved blades 20 p3360 A87-37596
Gruber method for radial flow impellers

of greatly cambered forward curved blading, analyzing parameter variation effect on velocity distribution curves 21 p3614 A87-39053
Slip factors for centrifugal impellers, presenting empirical expression and correction for range and number of blade angles [ASME PAPER 66-WA/FE-18] 24 p4143 A87-42463

IMPINGEMENT
SA JET IMPINGEMENT
Centrifugal force field with rotation or static impingement separation for water handling in absence of gravity 01 p0017 A87-10958
Temperature profile of single stage axial flow turbine disk and blades determined by approximation method using impingement cooling [ASME PAPER 67-GT-14] 11 p1854 A87-24799
Viscoelastic lubricant in squeeze film configuration for sphere impinging on lubricant covered plane, noting pressure peak sensitivity to viscoelastic constants [ASME PAPER 67-LUB-24] 24 p4164 A87-42682

IMPLANTATION
Ion implantation technique for production of n-on-p silicon solar cells applied to dendritic material 10 p1596 A87-23162
Electrically active centers distribution in Zn and Te implantations into GaAs 15 p2536 A87-29495
Mass analysis of ion beams from low voltage spark ion source for ion-implantation doping of semiconductors 15 p2536 A87-29496
Conductivity profiles investigated as function of ion energy, total flux and annealing schedule, when implanting boron into silicon 19 p3307 A87-35812
Implantation process for thin silicon solar cell fabrication, discussing leakage losses and efficiency 23 p4046 A87-41488

IMPLOSION
Radial implosion of deuterium in theta pinch in which initial level of ionization was controlled, relating diamagnetism of plasma to mass of gas in motion 04 p0671 A87-15646
Implosive collapse of liners containing gas to transfer chemical energy of explosive to kinetic and internal energy of gas [AIAA PAPER 67-178] 06 p1118 A87-18485
Imploding shocks and detonations propagation investigated by similarity solution extended to early imploding processes, using Oshima quasi-similar approximation 23 p3992 A87-41722

IMPREGNATED MATERIAL
Roving machine for impregnating glass fibers with synthetic resins 06 p1007 A87-18023
Automatic rigidizing of expandable fabric impregnated space structures, detailing gelatin system 08 p1345 A87-20433
Operating lifetime of porous bearings, discussing dependence on quality of impregnating lubricant 10 p1859 A87-22831
Refractory carbides for high temperature applications, stressing use of metal-impregnated tantalum carbide [ONERA-TP-453] 15 p2502 A87-29378
Densified carbon and graphite production methods /carbon, metal and resin and carbon with carbon impregnation/ for glass-to-metal sealing jigs 24 p4174 A87-41913

IMPREGNATION
S DOPING
S FINISH
IMPULSE
SA ELECTRIC IMPULSE
SA SPECIFIC IMPULSE
Impulse measurements of temperature conduction in n-type semiconductors 02 p0297 A87-11848
Impulse measurements of small electric engines by vacuum microbalance technique, also suitable for average thrust measurements in millipound and micropound ranges 04 p0620 A87-14734
Relative motion of body about satellite in orbit, determining impulses which cause body to remain in satellite vicinity 04 p0706 A87-15249
Impulse response of dynamic systems using cross correlation techniques 13 p2081 A87-27220

IMPULSE GENERATOR
Short triple electric and light pulse generation noting equipment design and performance 03 p0388 A87-14270

Avalanche transistors circuit generating high current fast risetime pulses suitable for driving injection lasers 09 p1510 A87-21644
Construction method for pulse generators in digital magnetic devices and current generators in magnetic deflecting system 10 p1613 A87-23444
Laser-diode impulse generator constructed by four-layer diodes and thyristors supplying high current intensity short impulses to low resistance load 21 p3639 A87-37944

IMPULSE NOISE
SA CONTINUOUS NOISE
Combined use of time-domain waveform detection probability and false alarm probability for selection of optimum sampling period and quantization interval for detection of impulse waveforms 09 p1459 A87-21588
Error probabilities of matched filter receiver operating in additive combination of impulsive and Gaussian noise 17 p2812 A87-32122
Evaluation technique for correlational functions and power spectrum of randomly shaped pulse train using stationary process 21 p3604 A87-38994

IMPULSE ORBITAL TRANSFER
Optimal one- and two-impulse orbital transfer maneuvers, considering shallow intersecting coplanar orbits 01 p0148 A87-10422
First order solution of economical impulse transfer between near-circular, coplanar or noncoplanar, close orbits by linearization of circular nominal orbit 01 p0152 A87-11404
Optimal rocket trajectories, discussing role and significance of intermediate thrust arc of rocket extremals in vacuum 02 p0335 A87-12335
Gravity loss in motion of body propelled from vicinity of planet into space trajectory 04 p0695 A87-14511
Finite thrust explicit guidance law for nearly circular orbital rendezvous 05 p0906 A87-17202
Fixed time rendezvous by two-impulse transfer maneuver in statistical optimization [AIAA PAPER 67-57] 06 p1029 A87-18262
Primer vector of fixed-time impulse thrust trajectories [AIAA PAPER 67-54] 06 p1086 A87-18335
Minimum fuel vehicle transfers between coaxial orbits of coplanar and noncoplanar types, using impulses [AAS PAPER 66-119] 07 p1253 A87-19971
Optimum deorbit positioning on planetocentric elliptic orbit for single impulse reentry treated by two coupled quartic polynomials [AAS PAPER 66-123] 07 p1254 A87-19986
Three-impulse orbital transfer from lunar orbits and earth reentry trajectory applications [AAS PAPER 66-134] 07 p1255 A87-19995
Quasi-linearization determination of optimum finite thrust and impulsive orbital transfers 10 p1706 A87-23131
Single-impulse transition in Newtonian central force field from hyperbolic to elliptical orbit in case of radial impulse 12 p2002 A87-25631
Minimum fuel vehicle transfers between coaxial orbits of coplanar and noncoplanar types, using impulses [AAS PAPER 66-119] 13 p2209 A87-27551
Optimum deorbit positioning on planetocentric elliptic orbit for single impulse reentry treated by two coupled quartic polynomials [AAS PAPER 66-123] 13 p2209 A87-27551
Three-impulse orbital transfer from lunar orbits and earth reentry trajectory applications [AAS PAPER 66-134] 13 p2210 A87-27552
Analytic solution obtained for minimum impulse transfer between two neighboring low eccentricity orbits 15 p2554 A87-29404
Optimal interorbital transfers between near-circular noncoplanar closely spaced orbits described in terms of linearized theory 15 p2563 A87-30303
Optimum two-impulse orbital transfer for arbitrary terminal conditions, discussing analytic characteristics 19 p3329 A87-35979
Extremal space trajectories problems one-impulse flights and two-impulse orbital transfers in central gravitational field 20 p3522 A87-38661
Minimum velocity increment for bielliptic transfer between noncoplanar circular

- orbits 20 p3526 A67-37126
- Suboptimal Hohmann orbital transfer extension to nonaligned two-impulse elliptical transfer 20 p3526 A67-37253
- Probability distribution errors effect in linear and planar impulse orbital transfers, considering angular orientation and impulsive velocity 20 p3527 A67-37259
- Minimum total impulse for optimum two impulse transfer trajectory between coplanar circular close orbits 22 p3884 A67-39958
- Three-impulse interplanetary rendezvous trajectory as solution of time fixed multimimpulse space problem 22 p3887 A67-40137
- IMPURITY
- SA ATMOSPHERIC IMPURITY
- SA PURITY
- Charged and neutral impurities effect on heat conductivity of bismuth telluride crystal lattice 01 p0127 A67-10073
- Microprobe study of impurities in hot-pressed polycrystalline MgO compact and existence of significant grain boundary volume [JPL-TR-32-1015] 01 p0131 A67-10262
- Impurity and lattice vacancy effects on compensation in doped binary semiconductors 01 p0132 A67-10455
- Problems in fuel systems associated with chemical impurities such as sulfur and chlorine compounds, examining effects of particulate matter and free water [SAE PAPER 660714] 01 p0140 A67-10603
- Exciton and impurity states in optical absorption spectra of nonmetallic crystals in pseudopotential theory 02 p0281 A67-11489
- Exciton and impurity states in Kr and Xe crystals and in rare-gas solids containing Xe impurity calculated by pseudopotential theory 02 p0281 A67-11490
- Shallow impurity states in semiconductor described by Green function method, considering effective-mass equation corrections 02 p0281 A67-11491
- Impurity concentration and electric field distribution determined in drift region of silicon p-n detectors from capacity as function of reverse voltage 02 p0296 A67-11823
- Isospin impurity mixing in distorted deuteron reaction 02 p0270 A67-12526
- Energy and wave functions of singly charged donor impurity centers in silicon and germanium 03 p0488 A67-12857
- Frequency dependent two-photon absorption radiation-matter interaction and secondary harmonic generation in n-and p-type impurity semiconductors 03 p0435 A67-13126
- Laser type regime of semiconductor having radiation induced by impurity band transitions of current carriers 03 p0436 A67-13137
- Diffusion of antimony and indium in germanium in range from 700 to 855 degrees C, taking into account effect of internal electric field 03 p0489 A67-13149
- Emitter sidewall junction capacitance in double diffused transistors, using linearly graded junction equation and two-dimensional impurity distribution 03 p0382 A67-13679
- Diffusion coefficient for electroactive impurity in semiconductor based on current carrier concentration variations during successive removal of surface layers 03 p0498 A67-13841
- Kinetic phenomena in impure ionic semiconductors of cubic symmetry, finding region for dominant scattering mechanism 04 p0675 A67-14923
- Ionized impurities effect on current output from shock-loaded piezoelectric quartz disk 04 p0678 A67-15122
- Light absorption and photolocalization of shallow impurity levels in semiconductors during acoustic phonon scattering 04 p0678 A67-15135
- Temperature and impurity ion concentration effect on minority carrier mobility in degenerate gallium arsenide 04 p0679 A67-15143
- Recombination radiation from Ga-Sb p-n junctions, noting spectral composition as function of current density and impurity concentration 04 p0681 A67-15297
- Impurity atom behavior in diatomic InSb and GaSb crystal lattices analyzed, using nuclear gamma resonance, measuring absolute values of f, chemical displacements and line widths 05 p0861 A67-16392
- Relation between electrical properties and structural features of gold-and antimony-doped germanium single crystals, noting abrupt decrease in mobility 05 p0861 A67-16398
- Electrical properties of indium antimonide single crystals with noncompensated impurity concentration, determining position of deep-seated levels in forbidden band 05 p0861 A67-16399
- Silicon electrical properties at low temperatures and various carrier concentrations, noting impurity 05 p0861 A67-16502
- Impurity states theory for semiconductors with In-Sb type band structure, calculating ionization potential and numerical values for energy levels 05 p0863 A67-16694
- Tunnel diode capacitance relation to displacement interpreted in terms of impurity drift in nonuniform field of p-n junction in highly doped germanium diodes 05 p0865 A67-16959
- Impurity concentration profiles in silicon epitaxial wafer determined, using MOS capacitors 05 p0866 A67-16985
- Impurity distribution in epitaxial films at film/ substrate interface after oxidation under different oxidation conditions for silicon planar devices 05 p0869 A67-17095
- Impurity effect /primarily O/ in reactions between liquid alloys and solid metals undergoing deformation 06 p1017 A67-17951
- Injected carrier flow in semiconductor containing deep impurity density gradient 06 p1051 A67-18221
- Hall effect and resistivity in n-GaAs with Si as shallow donor, obtaining ionization energy and impurity band conduction values 06 p1052 A67-18570
- Impurity effects on electroconductivity of vitreous AsSe 06 p1053 A67-18612
- Changes in ultrasonic attenuation of superconducting niobium at low magnetic fields, considering effects of low critical field impurity phases 06 p1053 A67-18757
- Local mode absorption bands for Al impurities in InSb and for P impurities in GaAs at various temperatures, using grating spectroscopy 06 p1059 A67-18910
- Electron spin resonance of impurities in semiconductors, with attention to shallow centers 06 p1061 A67-18922
- Impurity band tails in degenerate semiconductors, showing relation between decay in density of states and screening density 06 p1061 A67-18923
- Impurity centers arising from sulfur in silicon identified, using IR absorption technique and uniaxial stress effect 06 p1061 A67-18924
- Hall effect, electrical resistivity and optical transmission data and Co impurities in GaP studied via crystal field theory 06 p1061 A67-18928
- Highly spin polarized carriers for studying neutral impurity scattering in P doped silicon 06 p1063 A67-18937
- Annealing of neutron irradiation induced changes in impurity conduction in Sb-doped Ge 06 p1068 A67-18969
- Electron spin resonance in P-doped Si at liquid He temperature, noting effects of P concentration, impurity scattering, etc 06 p1068 A67-18973
- Impurity energy levels in semiconductors described by equivalent Schrodinger equation containing short range as well as conventional terms for long range Coulomb potential 07 p1230 A67-19060
- Piezoresistance measurement in p-type Ge as function of pressure and impurity concentration at 77 and 300 degrees K 07 p1233 A67-19644
- Concentration effect on light absorption and dispersion by impurity centers in case of weak electron-phonon coupling 07 p1233 A67-19648
- Effect of spin exchange scattering by magnetic impurities on electronic properties of superconductor 07 p1235 A67-20129
- Constants of superconducting alloys for arbitrary temperatures and impurity concentrations, calculating free energy density by using Gorkov equation 07 p1236 A67-20140
- Electrical resistance and weight increase measurements in aluminum and Al-Mg alloys, noting relation between oxidation rate and Mg content during annealing 08 p1341 A67-20796
- IR absorption in high purity boron films, showing absence of absorption peaks at 2-15 microns 09 p1533 A67-22132
- Optimum design method for variable capacitance diodes with m-th power characteristic for wide voltage range, emphasizing impurity distribution 09 p1476 A67-22213
- Impurity free CsF effect on work function of tungsten surface, discussing amount of impurities, type and control 09 p1450 A67-22354
- Induced absorption in far IR by impurities and defects of single crystal of potassium bromide 09 p1557 A67-22571
- Monte Carlo calculations of impurity band states in degenerate semiconductor 09 p1558 A67-22618
- Cryogenic thermoconductivity of impure tin in superconducting and normal state, noting anisotropy and superconducting energy gap independence from impurity type 10 p1687 A67-22761
- Correlation of anisotropic energy gap with thermal conductivity in pure and impure superconducting tin 10 p1687 A67-22762
- Diffusion of antimony and indium in germanium in range from 700 to 855 degrees C, taking into account effect of internal electric field 10 p1690 A67-23098
- Relaxation rate influence on power generation of gas laser and on magnitude of inverse population 10 p1664 A67-23335
- Impurity photoconductivity spectra of p-type germanium at low temperatures, noting parameters of relative depth of equidistant minima oscillations 10 p1693 A67-23583
- Static Jahn-Teller effect on impurity centers in semiconductors, discussing nature and magnitude of splitting of ground state 10 p1694 A67-23593
- Channel transistor characteristics for impurity distribution taking into account space charge penetration into gate 11 p1765 A67-24481
- Association energy of vacancy-impurity dipole obtained from electrical conductivity of magnesium fluoride-doped lithium fluoride at ambient temperature 12 p1978 A67-25149
- Light absorption and photolocalization of shallow impurity levels in semiconductors during acoustic phonon scattering 12 p1978 A67-25159
- Temperature and impurity ion concentration effect on minority carrier mobility in degenerate gallium arsenide 12 p1979 A67-25166
- Impurity effect on electroluminescence of gallium phosphide diodes, noting dependence of spectrum on current density through p-n junction 12 p1914 A67-25438
- Influence of deep level impurities on uniaxial stress effect of Ge p-n junction 12 p1983 A67-25456
- Impurities effect on electrical and thermomagnetic properties of cadmium tin arsenide 13 p2184 A67-27707
- Alloying elements and impurities effects on aluminum-alloy systems properties including neutron absorption, temperature changes, electric conductivity, etc 14 p2335 A67-27805
- Resistivity and Hall effect oscillations in antimony doped n-type germanium crystals in metallic impurity conduction state 14 p2365 A67-28231
- Resistivity and magnetoresistance for metallic impurity conduction in phosphorus doped silicon at low temperature with various donor concentrations 14 p2365 A67-28232
- Apparatus for determining impurity distribution in semiconductor structure 14 p2317 A67-28281
- Gas laser radiation applied to light transmittance measurement of heavily doped gallium arsenide in absorption region by free carriers 14 p2368 A67-28528
- Two-zone superconductor with nonmagnetic impurity, noting correspondence of thermodynamic values to single-zone pure state except for density 14 p2369 A67-28672
- HF localized and LF resonant impurity modes valence effect on energy gap and transition temperature in isotropic superconductors 14 p2370 A67-28720
- Transitional impurity effects on superconducting critical temperature of

normal metals, stressing localized states with no magnetic moments 14 p2371 A67-28727

Diffusion due to ion-ion collisions between different ion species, stressing impurities diffusion in rotating plasmas 14 p2363 A67-29066

Precautions required when using continuous gas flow in high current ion lasers 15 p2497 A67-29394

Diffused base transistor impurity concentration measured nondestructively to determine structure 15 p2448 A67-29801

Impurity states theory for semiconductors with In-Sb type band structure, calculating ionization potential and numerical values for energy levels 15 p2539 A67-29865

Polyatomic gaseous impurity effect on electric conductivity of alkaline plasma from axial field and electron temperature measurements 16 p2710 A67-30520

Impurity concentration and temperature dependence of reverse current in indium antimonide diodes, determining components 16 p2637 A67-31162

Cesium impurities analyzed for behavior in thermionic converters, investigating equilibrium state as function of pressure and temperature 16 p2609 A67-31399

Phonon drag part of thermoelectric power in metals formula, by assuming electron scattering description by relaxation time 16 p2731 A67-31445

Niobium-iron binary alloys structural added, noting phase instabilities for various added impurities 17 p2871 A67-32042

Impurity atoms and defects distributions in Si and Ge bombarded by different ions of medial energies calculated by Monte Carlo method 17 p2916 A67-32839

Impurity effect on annealing behavior of irradiated silicon studied via isothermal annealing of minority carrier lifetime 17 p2921 A67-33051

Impurity diffusion and segregation effects in p-n junctions in compensated solution grown GaP 17 p2921 A67-33053

Solubility of impurities in semiconductors and mechanism for deviation from stoichiometry 18 p3096 A67-33449

Impurity diffusion role in silicon device technology, discussing error function distribution 18 p3096 A67-33455

Probability of tunneling across impurity level of p-n junction 18 p3099 A67-33695

Pulsed high current arc in hydrogen showing initial instability, discharge stability, impurity content, pinch effect, decay, etc 18 p3087 A67-34047

Distribution coefficients for impurities in gallium and indium arsenides as periodic function of atomic weight decreasing with increasing atomic number 18 p3102 A67-34289

Lorentz number, Hall coefficient, magnetoresistance and Hall mobility variations in n-type degenerate semiconductors 18 p3106 A67-34729

Detection properties of n-type InSb in microwave and IR ranges, studying impurity and magnetic field effects 19 p3300 A67-34762

Impurity photoconductivity in cadmium sulfide energy levels at red luminescence centers depth 19 p3300 A67-34765

Impurities in high-purity niobium determined chemically and spectroscopically 19 p3243 A67-34927

Specific heat of superconductors containing paramagnetic impurities calculated, noting effect of ordering impurity spins 19 p3303 A67-35045

Deuterium plasma heating by multiply charged hot impurity ions 19 p3287 A67-35357

Deuterium plasmod structure, impurity distribution, passage through pulsed magnetic barrier and capture by longitudinal magnetic field with mirror geometry 19 p3288 A67-35364

Impurity effect on optical properties of interstellar graphite particles, examining wavelength dependence of absorption coefficient and refractive index of coals 19 p3323 A67-35423

Active impurities concentration in p-type semiconductors by measuring temperature at zero thermoelectric potential 19 p3308 A67-35875

Base impurity distribution design consideration for figure of merit of HF transistors, considering accelerating, decelerating and neutral electric field 20 p3398 A67-36770

Si optical and electrical properties and energy levels with Mg as donor impurity 20 p3510 A67-36916

Unsteady transverse diffusion of passive impurity and mass and heat transfer in granular layer described by cell type models 20 p3554 A67-37054

Impurity conduction causing negative magnetoresistance in Cu doped n-type GaAs crystals at low temperature 20 p3513 A67-37440

Impurities compensated p-type cadmium antimonide single crystals, determining Hall effect temperature dependence and specific resistance 21 p3676 A67-37688

Superconducting critical temperature below Kondo temperature for metal solutions with magnetic impurities calculated, using Green function 21 p3680 A67-38350

Temperature effect on diffusion coefficient of radioactive phosphorus in epitaxial Si layer 21 p3681 A67-38361

Impurity effect on solubility of another impurity in p-n silicon tunnel diodes studied by measuring current-voltage characteristics 21 p3682 A67-38364

Quantum transport theories for calculating multiple scattering in doped semiconductors 21 p3682 A67-38366

Base region thickness, minority carrier lifetime and impurity concentration effects on conduction characteristics of silicon diodes and thyristors 21 p3597 A67-38523

Impurity sources in hermetic electronic packaging investigated using mass spectroscopy and gas chromatography, comparing packaging techniques 21 p3636 A67-38632

Electrical conductivity, Hall coefficient and thermo-EMF measurements in Zn and Te doped gallium antimonide crystals for minority carrier role in impurity conduction 21 p3687 A67-39141

Concentric ring junction to prevent surface breakdown in planar p-n junctions 22 p3766 A67-39252

Frequency limitations of field effect transistor as amplifier in connection with impurity profile, discussing figure of merit 22 p3767 A67-39275

Photoconductivity measurements for chromium doped seminsulating gallium arsenide, discussing response peak and possible mechanisms 22 p3855 A67-39348

Al impurity redistribution near Si semiconductor surface subjected to high temperature oxidation 22 p3857 A67-39502

Magnetic element impurity effects on semiconductor resistivity, calculating spin dependent scattering of free carriers 22 p3859 A67-39625

Heterodiffusion of metallic impurities in body-centered phases of doped zirconium and titanium, determining diffusion coefficients via radioactive isotopes 22 p3820 A67-39823

Clean MOS structure bias and temperature /BT/ treatment at high electric fields causing electrochemical reaction affecting surface charge density 22 p3774 A67-40461

Gas laser radiation applied to light transmittance measurement of heavily doped gallium arsenide in absorption region by free carriers 23 p4039 A67-40935

EPR spectrum of divalent Mn ion impurity in CdTe single crystals noting concentration dependence, ion distribution and interaction nature 23 p4042 A67-41294

Tunneling of electrons from normal metal to superconductor containing paramagnetic impurity atoms, discussing current voltage characteristics 23 p4043 A67-41300

Magnetic impurities in tunnel junction barriers investigated for effect on junction resistance 24 p4200 A67-41865

Mossbauer spectra of FeMo alloys for closed space compositions show overlap of disturbed surroundings of impurity iron atoms and magnetic moment 24 p4203 A67-42108

Thermodynamic property of superconductors with nonmagnetic impurity analyzed using overlapping energy bands near Fermi energy 24 p4203 A67-42162

Maximum Corbino magnetoresistivity in indium antimonide single crystals, investigating impurity concentration and layer distribution 24 p4203 A67-42208

Apollo spacecraft H-O chemical to electric

energy converting fuel cell performance degradation resulting from O electrochemical contamination due to inert diluent impurities in O supply 24 p4106 A67-42522

IN-FLIGHT MONITORING

Flight test method for evaluating ground effect on fixed-wing aircraft in which pilot flies at constant angle of attack and power setting during landing approach [AIAA PAPER 66-468] 02 p0180 A67-1151

Space radiation monitoring system aboard manned spacecraft to provide solutions to medical problems and safety of flight guidelines for mission control 02 p0188 A67-12338

Guidance equations for multistage booster offer target change on launch pad and in flight 02 p0265 A67-1271

In-flight measurement of human response transfer characteristics of pilot [AIAA PAPER 67-240] 07 p1136 A67-2006

Telemetry applications to in-flight physiological measurements 09 p1457 A67-2246

Flight test method for evaluating ground effect on fixed-wing aircraft in which pilot flies at constant angle of attack and power setting during landing approach [AIAA PAPER 66-468] 09 p1441 A67-2248

Field testing of self-powered recorder for vibration data in environmental studies 12 p1942 A67-2568

Portable self-powered magnetic tape recorder for gathering data on vibration temperature and shock on ground and in flight aircraft 12 p1942 A67-2568

Aircraft detection and in-flight tracking by real time computers, assessing role in missile and satellite tracking 13 p2153 A67-2666

In-flight transfer, fine and maneuver alignment of air to surface missile guidance system 17 p2881 A67-3248

Body temperature monitoring in external auditory meatus in pre-in-flight testing showing correlation between sublingual and aural temperatures 18 p2995 A67-3470

Test signal techniques for measurement and video monitoring used in ORT network 22 p3796 A67-3923

Preliminary spacecraft concept for real time operational space environment monitoring system 22 p3901 A67-3992

Differential piezoelectric accelerometer charge system for monitoring in-flight jet engine vibrations 23 p4007 A67-4138

In-flight aeromedical monitoring of cardiorespiratory response of naval pilot during aircraft carrier combat operations discussing physiological effects determination 23 p3963 A67-4154

Field Effect Monitor for biomonitoring cardiovascular variables and LF physiological phenomena 23 p3966 A67-4158

Ultrasonic monitoring technique for fatigue damage and crack formation and propagation in aircraft structures [AIAA PAPER 67-793] 24 p4251 A67-4295

Data analysis methods for integrated data processing system for onboard in-flight checkout for launch vehicle evaluation [AIAA PAPER 67-911] 24 p4127 A67-4301

INCASCENCE

S FILAMENT

INCIDENCE

SA WAVE INCIDENCE CONTROL

Relativistic solution to normal incidence on semifinite longitudinally drifting homogeneous temperate magnetoplasma obtaining reflected and transmitted waves 11 p1832 A67-2430

Viscous flow around flat plate at various angles of incidences at high Mach number to evaluate shock wave intensity variation and wall pressure distribution 11 p1742 A67-2476

Integral correlation technique used for first approximation solution in polar coordinate system to determine plane supersonic jet incidence on plane at arbitrary angle 22 p3786 A67-4002

INCIDENT RAY

Total and spectral reflectance of carbon dioxide cryodeposits on test vehicles and space simulator walls as function of deposit thickness, rate of formation, angle of incidence of light, etc 09 p1533 A67-2212

Selective polarization filtering during hologram construction enhancing reconstructed image resolution and tonal range by eliminating specular reflection

- recording 15 p2488 A67-29818
Flood beams incidence angle and current density distribution effects on half-tone reproduction of visual storage tube with cathode collimator 19 p3194 A67-35543
Absorbance and emittance of metal surfaces determined via cyclic incident radiation, noting error computation and method accuracy 19 p3346 A67-35742
parameters 19 p3346 A67-35742
Oblique incidence millimeter wave technique using ray theory for measuring collisionless plasma electron density profile 20 p3496 A67-36311
Hemispherical reflectance of metal surfaces investigated for relation of wavelength and surface roughness 22 p3920 A67-40420
Field scattering by convex cylinders solved by asymptotes expressing reduced wave equations 23 p3972 A67-40751
[NYU-EM-217]
Satellite and ground based measurements of incident proton neutral hydrogen flux and Balmer alpha optical emission in auroral hydrogen arc 23 p3995 A67-40803
Maximum permissible energy density incident on retina determined for eye safety in viewing laser beam 23 p3962 A67-41052
High resistance GaAs residual IR absorption measured to determine incident light intensity fraction, showing low absorption suitable for high power laser modulation 23 p4045 A67-41471
Cascade particles interaction functions with substance determined by inverse problem method 24 p4221 A67-42875
INCINERATOR
S BURNER
S FURNACE
INCLINATION
Radio observation of Cosmos satellites with flight path inclination angle of 65 and 51 degrees, discussing signal audibility, atmospheric density and ionospheric effects 03 p0518 A67-13540
Heat transfer dependence in cavity of closed evaporative thermosyphon on device inclination angle and coolant filled fraction of cavity 21 p3625 A67-37913
INCOHERENT SCATTERING
SA NEUTRON SCATTERING
SA NUCLEAR SCATTERING
Incoherent scattering measurements of ionospheric power spectrum and autocorrelation function at geomagnetic equator to determine electron and ion temperatures, ion composition and ion density 03 p0408 A67-12834
Electron number density profile measurements of moderate and heavy sporadic E over Arecibo by incoherent backscatter technique 03 p0409 A67-12946
Method for recording Fresnel transformations of two- and three-dimensional scenes illuminated by spatially incoherent light 03 p0423 A67-13907
Dual beam wind measurement by incoherent radar 04 p0648 A67-14675
Statistical properties of superposition of coherent and incoherent electromagnetic fields studied in terms of coherent state formalism 10 p1667 A67-23778
Electron and ionic temperatures from incoherent diffusion spectra, noting dependence on height and permanent thermodynamic equilibrium below 130 km 12 p1931 A67-25108
Spectral characteristics of small scale refractive index fluctuations in troposphere using radar echoes 13 p2068 A67-26790
Optical interference method of two-dimensional Fourier transform with spatially incoherent illumination to derive relations for transforms of images 13 p2121 A67-27290
F region and magnetosphere observation by incoherent backscatter radar technique 14 p2265 A67-28410
Strength of radio signals incoherently scattered from ionosphere and distribution of ionospheric electron concentration 16 p2632 A67-31901
Nonlinear incoherent light scattering from two frequency-differing coherent beams of electromagnetic radiation propagating in homogeneous plasma without magnetic field 17 p2901 A67-32354
F region and magnetosphere data obtained by incoherent-backscatter radar technique, studying ion and electron temperatures relationship to height, electron density profiles, etc 17 p2843 A67-32369
Ionospheric electron temperature measurements confirming predawn enhancement of 6300 angstroms airglow 18 p3039 A67-33624
Diffuse reflected and transmitted spectral line profile calculations for uniform noncoherently scattering media 19 p3183 A67-35555
Laser and nonlaser light transmission through atmosphere, noting no difference in propagation 19 p3240 A67-35695
Autocorrelation function of signal scattered incoherently from ionosphere, observing resonance at multiples of proton gyroperiod 21 p3578 A67-37758
Neutral atmospheric temperatures calculated from data provided by incoherent scatter soundings of ionosphere 22 p3794 A67-40474
Integral equation derived to relate source function for spectral line formed by noncoherent resonance scattering to thermodynamics of radiating medium 22 p3896 A67-40529
Diffraction and image formation in coherent and noncoherent light with relation to Fourier transform 23 p3972 A67-40708
INCOMPRESSIBLE FLOW
Incompressible plane jet turbulent mixing into external parallel flow 01 p0052 A67-10646
Theory for incompressible two-dimensional flow of inviscid liquid past array of similar hydrofoils, behind each of which extends cavity of finite length 01 p0053 A67-10851
Boundary layer equations for nonstationary plane flow of viscous incompressible fluid 02 p0232 A67-11921
Viscous incompressible flow past finite flat plate obtained under Oseen approximation for large and moderate Reynolds numbers, using Wiener-Hopf technique 02 p0234 A67-12546
Flow induced by infinite flat oscillating plate in incompressible dusty gas 02 p0234 A67-12548
Approximate method of treating three-dimensional laminar incompressible boundary layer equations when cross flow is small [ASME PAPER 66-WA/FE-34] 04 p0607 A67-15365
Mixing length flow theory of turbulent incompressible flow integral diffusion model extended for boundary layer, channel and Couette flows 04 p0609 A67-15811
Turbulent boundary layer calculation, considering compressible and incompressible flows with pressure gradients and heat transfer 04 p0610 A67-15908
Hot-wire anemometer measurements of transition in incompressible wake of cone at low Reynolds number 05 p0751 A67-17439
Film cooling by helium secondary flow injection into incompressible low speed airflow in turbulent boundary layer above flat plate 06 p1116 A67-18385
Numerical analysis of free boundary problem inviscid incompressible flow field of impinging jet and two-dimensional Joukowski airfoil in sheared wind tunnel flow [AIAA PAPER 67-217] 06 p0988 A67-18460
Viscous incompressible slow flow over circular arc wall projections or depressions with shear flow far from projection 06 p0992 A67-18887
Nonlinear singularities method for calculating velocity distribution over thick wing of finite aspect ratio situated at zero angle of attack in incompressible frictionless potential flow 07 p1127 A67-19887
Turbulence effects on laminar skin friction and heat transfer from plates and circular cylinders in incompressible flow, using two low turbulence wind tunnels 08 p1427 A67-21118
Two-dimensional incompressible potential flow theory for airfoil design with prescribed velocity distribution over surface 09 p1437 A67-21740
Unsteady incompressible flow of viscous electrically conducting fluid near stagnation point, determining skin friction and heat transfer at wall 09 p1544 A67-21934
Lamellar homogeneous jet layer deformation under aerodynamic forces acting in incompressible flow 09 p1439 A67-22578
Disturbance diffusion in incompressible zero pressure gradient flow 10 p1626 A67-23144
Solid body translational movement in viscous incompressible conductive flow in magnetic field solved for case of zero magnetic Reynolds number 11 p1832 A67-24055
Three-dimensional flow in single stage axial flow fan rotor with prescribed and variable circulation along span 12 p1893 A67-25971
Navier-Stokes asymptotic solutions for large Reynolds number flows, emphasizing incompressible axial flow past semilinear circular cylinders 12 p1930 A67-26179
Radial flow of two-dimensional viscous conducting fluid in wedge shaped channel under magnetic field, reducing flow equation to differential equation 12 p1977 A67-26180
Wire screen roughnesses effect on turbulent boundary layer along flat plate without pressure gradient 13 p2093 A67-26529
Existence of three-dimensional solution of boundary layer equations of viscous incompressible flow in neighborhood of stagnation point 13 p2050 A67-26912
Hartmann oscillator problem studied using hydraulic analogy between supersonic compressible gas dynamics and incompressible flows with free surface 14 p2295 A67-27903
Hypersonic turbulent boundary layers transformation to incompressible form 14 p2297 A67-28137
Static and dynamic characteristics of interaction region for fluid jet and receiver-load system, examining stability conditions 14 p2248 A67-28270
Static operating characteristics of vented single-stage momentum exchange proportional amplifiers, noting applicability for compressible and incompressible flow regimes 14 p2250 A67-28329
Reattachment of two-dimensional jet to adjacent plate assuming new hypothesis on path of dividing streamline 14 p2303 A67-28338
Planar incompressible free turbulent mixing with arbitrary velocity ratio and axial pressure gradient 14 p2304 A67-28359
[ASME PAPER 67-FE-9]
Unsteady incompressible flow of two-dimensional supercavitating hydrofoils with finite cavity length, considering wake nature [ASME PAPER 67-FE-15] 14 p2304 A67-28363
Boundary layer equations similar solutions obtained for incompressible flow with external velocity and suction 16 p2657 A67-30613
Circular vortex ring motion and decay in incompressible flow field considered for Navier-Stokes equations solution by boundary layer technique 16 p2660 A67-31212
Relation between drag and dissipation in incompressible flows 17 p2839 A67-32710
Wind tunnel measurement of turbulent transport terms for unstable curved mixing layer of incompressible flow 18 p3030 A67-34751
Concentrated vortex model for Karman street in two-dimensional viscous incompressible laminar flow past bluff body 19 p3210 A67-35446
Laminar incompressible boundary layer on isothermal flat plate with strong blowing, comparing different solutions 19 p3211 A67-35754
Heat transfer for one- and two-dimensional pulsating incompressible laminar flow in circular tube with two thermal boundary conditions [ASME PAPER 67-HT-65] 20 p3550 A67-36747
Rear stagnation point solution for viscous incompressible electrically conducting MHD flow 20 p3499 A67-36850
Three-dimensional incompressible flow with colinear magnetic field, studying stability by numerical method 20 p3423 A67-37242
Exact solutions of incompressible Navier-Stokes equation for irrotational Beltrami nonconvective two-dimensional swirl and axially symmetric cross flows 21 p3609 A67-37737
Approximate solutions of Prandtl boundary layer problem for incompressible laminar flow derived, using Nagumo-Westphal theorem on parabolic differential operators 21 p3563 A67-37888
Inviscid incompressible flow of normal and slightly oblique static round jet impinging on ground, noting velocity distribution 21 p3565 A67-38544
Incompressible two-dimensional turbulent

channel flow, calculating velocity profile and obtaining resistance

formula 22 p3782 A67-39409
Incompressible laminar boundary layer flow on semiminfinite flat plate with impulsive motion solved using Meksyn steady pressure gradient boundary layer method 22 p3786 A67-40039

Electromagnetic forces effects on steady rotating motions of conducting viscous incompressible fluids via adjustable local boundary layer first order approximation 23 p4031 A67-40604

Incompressible potential flow about thick wing profiles and cascades for blade profiles with angular and round tapered trailing edges 23 p3929 A67-41254

Turbulent skin friction in incompressible flow with heat transfer, determining Preston surface pitot tube applicability 23 p4004 A67-41341

Delta wing with leading edge vortices, calculating inviscid incompressible flow field near center of rolled up vortex sheet assuming conical velocity field 24 p4092 A67-42570

INCOMPRESSIBLE FLUID

Stokes creeping flow equations and steady flow of incompressible viscous fluid past liquid drop 01 p0051 A67-10458

Approximate solution of stationary boundary layer problems involving flow of viscous incompressible conducting fluid around flat plate in presence of magnetic field 01 p0123 A67-10540

Unsteady laminar flow of incompressible fluid in gap between parallel disks with gap width varying with time, obtaining solutions for Navier-Stokes and thermal energy equations 02 p0231 A67-11469

Solution to boundary layer equations for unsteady flow of viscous incompressible fluid under injection or suction 02 p0233 A67-11948

Eigenvalues and eigenfunctions of free oscillations of viscous incompressible fluid in arbitrarily shaped vessel under gravitational field, asymptotically expressed 02 p0233 A67-11950

Center of pressure stabilization for thin wing profile with downward deflected trailing edge, when placed in steady state flow of ideal incompressible fluid 02 p0179 A67-12438

Algorithm for numerical calculation of three-dimensional boundary layer of incompressible fluid 03 p0401 A67-12876

Hydrodynamic stability Cauchy problem for continuous spectrum of two-dimensional parallel flow of nonviscous incompressible fluid 03 p0402 A67-13172

Stability analysis of adiabatic flow of incompressible fluid without equation linearization and by constructing functional from hydrodynamic fields 03 p0402 A67-13619

MHD flow past bodies in electroconductive viscous incompressible flow 03 p0482 A67-13743

Series coefficients of flow stream functions for plane laminar flows of viscous incompressible fluids in channels and near corners at small Reynolds numbers 03 p0405 A67-14259

Statistical electrointegrator for numerical solution of boundary layer theory problems for incompressible fluid and compressible gas 04 p0603 A67-14642

Volterra method used for two-dimensional problems of pressure penetration and penetration of small wedge into layer of incompressible liquid 04 p0604 A67-14778

Laboratory experiments on atmospheric simulation, mainly rapidly rotating fluids, with limitation to incompressible fluids 04 p0613 A67-14802

Solvability of parallel-wall cavitation flow problem of perfect incompressible fluid past symmetric smooth arc 04 p0606 A67-15195

Unsteady laminar flow of viscous incompressible fluid between two infinite parallel rotating disks with angular velocities varying with time 04 p0609 A67-15605

Preston tube measurements of skin friction and velocity profiles in incompressible turbulent boundary layer, considering pressure gradient effects 04 p0609 A67-15818

Small oscillations of viscous incompressible fluid in container with free surface under action of potential force field 05 p0791 A67-16373

Existence and stability of uniform rotation of heavy blunt profile immersed in perfect incompressible irrotational fluid 05 p0792 A67-16595

MHD steady laminar flow of viscous incompressible electrically conducting liquid in rectangular pipe between conducting plates 05 p0853 A67-18723

Lie series formalism applied to solution of Bessel equation describing behavior of laminary oscillating MHD fluid 05 p0854 A67-18989

Single parameter MHD flow of ideal incompressible infinitely electroconductive gas 05 p0855 A67-17114

Sixth order polynomial calculation of axisymmetric laminar boundary layer of incompressible fluid removed by suction and arbitrary velocity distribution 05 p0749 A67-17184

Attenuation law of turbulent pulsations in viscous sublayer of turbulent boundary layer of incompressible fluid 06 p0982 A67-17741

Inertia effects of internal liquid column on vibration of thin walled pressurized elastic cylindrical bellows type container [AIAA PAPER 67-38] 06 p0986 A67-18262

Turbulent MHD boundary layer flow of constant-electroconductivity incompressible fluid past dielectric plate in TM field, for small magnetic Reynolds numbers 06 p1043 A67-18672

Incompressible fluid flow in symmetric flat channel, for case of constant electric conductivity and low Reynolds number 06 p1043 A67-18676

Motion about fixed point of solid body with cavity filled with viscous incompressible fluid 06 p0991 A67-18810

Transverse magnetic field effect on laminar radial flow of incompressible fluid between closely spaced parallel plates, presenting graphs of pressure distribution 06 p1046 A67-18829

Three-dimensional boundary layer flow of incompressible second order viscous fluid near spinning cone 06 p0992 A67-18868

Asymptotic properties of fluid temperature field and Nu numbers in nonstationary heat transfer during passage of laminar flow of viscous incompressible fluid through rectilinear channel 07 p1265 A67-19125

Approximate solution of integral equations with aid of least squares for steady motions of viscous incompressible fluid in rotating cylinder 07 p1168 A67-19217

Time dependent stress behavior of incompressible elastic fluid for various homogeneous deformation histories 07 p1169 A67-19728

Navier-Stokes equation for viscous incompressible fluid flow between stationary and uniformly moving parallel plates with uniform suction along stationary plate 08 p1322 A67-21179

Approximate solution of some nonstationary boundary layer problems with allowance for magnetic field, discussing nonsteady flow of viscous incompressible electrically conducting fluid past flat plate 08 p1362 A67-21202

Two-dimensional laminar jet of incompressible fluid issuing into uniform stream in direction of main flow, considering two coordinate type expansions 09 p1489 A67-22412

Forced and free oscillation characteristics of ideal incompressible fluid contained in cavity shaped as rectangular parallelepiped with free surface under deformations 10 p1679 A67-23030

Finite difference scheme for solving set of Prandtl equations for nonstationary flow of viscous incompressible fluid 10 p1628 A67-23672

Transverse fluid flow stability between permeable boundaries for case with exact solution of perturbation spectrum 10 p1628 A67-23675

Numerical technique for time dependent calculation of two incompressible fluids interaction to study viscid and inviscid Rayleigh-Taylor instability 11 p1774 A67-23859

Constant Reynolds number applied to data evaluation for turbulent jet flow in converging-diverging axisymmetric tube using free turbulent jet 11 p1742 A67-24272

Incompressible Newtonian fluid applied to dynamic reversibility of flows, analyzing motion equation and possible integration of

Navier-Stokes equation 11 p1778 A67-24273

Stability of incompressible fluid in Couette flow between coaxial circular cylinders, using Galerkin method to obtain critical Taylor number 11 p1781 A67-24570

Laminar turbulent transition of nonisothermal incompressible forced flows in pipes measured for several working fluids and temperatures, using Reynolds number as criterion 11 p1781 A67-24574

Green integrals extended to movement of incompressible viscous conductive fluid in which magnetic field is generated 11 p1840 A67-24620

Behavior of solution of system of equations for unsteady boundary layer of two-dimensional liquid as time approaches infinity 11 p1782 A67-24669

Current distribution in incompressible fluid flow in magnetic field at low Reynolds number, estimating Lorentz force effect 11 p1842 A67-24952

Collapse of isolated spherical vapor-air cavitation pocket moving toward solid surface in incompressible fluid medium 12 p1927 A67-25320

Oscillation and stability of system of thin elastic shells in potential inviscid and incompressible fluid flow 12 p2023 A67-25589

Variational methods for calculating small axisymmetrical oscillations of conical shell of revolution partially filled with ideal incompressible fluid 12 p2028 A67-25633

Asymptotic solutions for free and forced oscillations of solid having cavity filled with viscous fluid, considering several degrees of freedom and arbitrary cavity shapes 12 p2029 A67-25657

Incremental pressure drop in incompressible fluid laminar flow at entrance of rectilinear duct, using conformal mapping technique 12 p1930 A67-26166

Vibration of cylindrical shell containing flowing incompressible perfect fluid 13 p2215 A67-26528

Dissipative energy effect on laminar heat transfer from disk rotating in uniform forced stream 13 p2221 A67-26531

Alfven wave propagation in viscous incompressible infinitely conductive fluid under effect of gradually varying magnetic field 13 p2170 A67-27363

Rayleigh problem in hydrodynamic stability for two-dimensional parallel flow of nonviscous incompressible fluid 13 p2106 A67-27456

Averaged axisymmetric vortex flow of ideal incompressible fluid in turbine engine 14 p2296 A67-27986

Upstream velocity profile effect on free mixing of jets with ambient fluid 14 p2240 A67-28107

Incompressible fluid flow in convergent nozzle with finite aspect ratio, predicting offset on nozzle flow and jet reattachment 14 p2303 A67-28334

Time dependent problems of heat transfer in laminar flow of viscous incompressible fluid in cylinder and cylindrical annulus 14 p2408 A67-28892

Flow pattern of thin jet-flapped wing with small deflection angle in proximity to ground 15 p2415 A67-29308

Small parameter method to study steady state flow of viscous incompressible fluid in journal bearing 15 p2493 A67-29692

Motion of gyroscope with conical cavity filled with ideal incompressible fluid describing rotating motion 15 p2518 A67-30171

Velocity profile of vortex region formed downstream of step-shaped wall calculated, assuming flow is turbulent, using similarity hypothesis 16 p2662 A67-31469

Reduction of steady viscous magnetohydrodynamic flows having orthogonal magnetic and velocity field distributions to associated flows having zero magnetic field 16 p2721 A67-31552

Second order incompressible fluid equation of motion, compatibility equation and dissipation function 16 p2663 A67-31703

Electromagnetic field effect on heat transfer during laminar flow of electrically conducting incompressible fluid in flat channel 16 p2723 A67-31774

Approximation method for steady laminar flows of incompressible viscous fluid in curved pipes, obtaining flow rate 17 p2836 A67-32038

MHD boundary layer theory principles,

demonstrating similarity solutions existing in incompressible fluid 17 p2901 A67-32348
Incompressible fluid drag force on sphere moving at constant speed in closed-end tube [ASME PAPER 67-APM-18] 17 p2840 A67-33149
Solution to boundary layer equations for unsteady flow of viscous incompressible fluid under injection or suction 17 p2840 A67-33265
Eigenvalues and eigenfunctions of free oscillations of viscous incompressible fluid in arbitrarily shaped vessel under gravitational field asymptotically expressed 17 p2841 A67-33267
Airfoil unsteady motion problem near screen in incompressible fluid with given horizontal/vertical velocity 18 p2981 A67-33410
Wing profile effect on thin wing aerodynamic characteristics approaching screen in incompressible fluid potential flow 18 p2981 A67-33412
Incompressible fluid flow past semiinfinite flat plate during ejection of another fluid from plane surface into main flow solved using motion equations 18 p3025 A67-33571
Characteristics of cross flow fan determined as function of blade angle, diameter ratio of impeller and vortex position 18 p3025 A67-33650
Heat transfer due to flow of electrically conducting incompressible viscous fluid from rotating insulated disk under influence of axially oriented magnetic field 18 p3084 A67-33667
Electrical analogy calculation of incompressible and rotational axisymmetric flow around variable-circulation streamlined propeller 18 p3025 A67-33681
Existence and stability of rectilinear translation motions of blunt body submerged in potential flow of incompressible fluid at rest at infinity 18 p3027 A67-34183
Existence and uniqueness theorem for axisymmetric problem with initial data for Euler equation in case of incompressible fluid 18 p3027 A67-34201
Potential flow stability of weightless incompressible fluid for specific flow geometries 18 p3028 A67-34219
Pressure fluctuations beneath incompressible turbulent boundary layer with mass addition 18 p3030 A67-34742
Diffusion of free isothermal turbulent jet of incompressible fluid flowing from nozzle into coaxial surrounding uniform stream 19 p3209 A67-35443
Flow of incompressible viscous fluid past plane body, when flow boundary layer detaches from body producing aerodynamic wake 19 p3171 A67-35632
Three-dimensional vortex flow inverse problem through axial fan solved using isolated airfoil method 19 p3171 A67-35723
Plane incompressible wall jet ejected from slot into boundary layer in case of stationary and nonstationary external flow with and without pressure 20 p3420 A67-36277
Stream function of plane flow of incompressible viscous fluid around parabolic profile, using successive approximations method 20 p3420 A67-36394
Convective secondary flow in channel flow of quasi-incompressible fluid noting temperature gradient role [ASME PAPER 67-HT-26] 20 p3546 A67-36719
Modifying effect of base bleed investigated photographically for incompressible wake behind two-dimensional bluff body, estimating base pressure 20 p3421 A67-36844
Two-dimensional incompressible fluid jet penetration analyzed kinematically via free streamline theory and notched hodograph 20 p3422 A67-36845
Spherical gas bubble pulsations under pressure waves analyzed in compressible and incompressible fluids 20 p3422 A67-37065
Velocity and pressure fields in viscous incompressible fluid flow in inlet of flat channel 20 p3423 A67-37066
Motion equations of incompressible nonisothermal fluid jet studied by closed similarity solutions, obtaining temperature distributions 20 p3423 A67-37209
Three-dimensional boundary layer for gas flow past generatrix of cylinder of arbitrary transverse cross section 20 p3360 A67-37658
Incompressible cylindrical jet interaction

with incompressible unbounded homogeneous stream, determining contact surface 20 p3360 A67-37661
Asymptotic properties of fluid temperature field and Nu numbers in nonstationary heat transfer during passage of laminar flow of viscous incompressible fluid through rectilinear channel 21 p3731 A67-38169
Finite difference scheme for solving set of Prandtl equations for nonstationary flow of viscous incompressible fluid 21 p3612 A67-38273
Transverse fluid flow stability between permeable boundaries for case with exact solution of perturbation spectrum 21 p3612 A67-38276
Rigid cylinder two-dimensional motion in rotating incompressible fluid compared to motion in isotropic incompressible conducting medium under magnetic field 21 p3668 A67-38552
Load carrying capacity of hydrostatic bearing having communicating chambers and operating with laminar flow of incompressible fluid, showing shaft vibration elimination 21 p3636 A67-38837
Incompressible hydromagnetic fluid oscillation in rotating spherical shell pervaded by strong toroidal and weak poloidal magnetic field for geomagnetic secular variation 21 p3621 A67-38983
Curve approximation method applied to incompressible laminar boundary layer, comparing Head approximation method and exact solutions 21 p3615 A67-39081
Partial differential equations solution in heat transfer between incompressible fluid and porous medium 22 p3917 A67-39640
Navier-Stokes differential equations for unsteady incompressible viscous fluid motion solution method, considering quadratic inertial terms 22 p3783 A67-39682
Prandtl equation system for two-dimensional incompressible flows expanded to construct solutions for three-dimensional unsteady flows by straight lines method 24 p4177 A67-42200
Incompressible viscous fluid rotary turbulent flow microstructure between rotating cylinders, analyzing centrifugal force effects on turbulent heat transfer processes 24 p4142 A67-42214
Transverse magnetic field effect on two-dimensional jet of incompressible fluid 24 p4198 A67-42565
Steady flow extremum principles for incompressible viscous fluid generalized to liquid flow containing suspended solid bodies and drops of another liquid 24 p4144 A67-42567
Integration of motion equations of second order incompressible fluid 24 p4146 A67-43106
INCONEL
Heat treatment effect on microstructure and notch-bar rupture life of INCONEL alloys 21 p3646 A67-38776
Microcracking susceptibility studies of Inconel 718 weld heat affected zones, noting hot ductility, weld circle patch and fillerless fusion welding tests 22 p3818 A67-39222
INDENTATION
SA KNOOP INDENTATION
Buckling phenomena involving formation of indentation in thin circular cylindrical shells under axial compression 05 p0907 A67-16021
Apparatus for measuring metal/alloy hot hardness using indenter static impression and unilateral flattening 19 p3227 A67-34930
Adsorbed ions and organic molecules effect on mobility of half-loops dislocation introduced by indenter into MgO surfaces 23 p4035 A67-40655
INDEPENDENT VARIABLE
Cauchy and boundary value problems for homogeneous differential equations with two independent variables analyzed, establishing generalized solution existing on uniqueness maximal domain 02 p0260 A67-12432
Transformation of unknown functions and independent variables entering into differential equations for motion of nonviscous nonheat-conducting gas 03 p0403 A67-13628
Synthesis of optimal Liapunov-Bellman function, noting sequential solution method for independent variables and method using

first order partial differential equation 09 p1525 A67-22077
Iteration process by difference scheme for numerical solution to Dirichlet problem of two-dimensional Poisson equation 13 p2148 A67-27613
Mutually adjoint boundary value problems for linear systems of first order equations of composite type with two independent variables 14 p2344 A67-28670
New integral in restricted three-body problem expressed in terms of Delaunay variables 15 p2557 A67-29877
First variation theory in extremal problems, noting generalization of classical variational problems and optimal control problems for functions with single independent variable 17 p2876 A67-32043
Soviet book on new methods for solving elliptic equations including equations in many-dimensional space, index problem in functional equation theory, etc 17 p2878 A67-32686
Geometrical and equilibrium equations derived for circular plates, introducing Lagrange type coordinate as independent variable 17 p2961 A67-32807
Approximation method for plotting function of three independent variables 17 p2821 A67-32866
Neumann boundary value problem for second order elliptic equation system with many independent variables 18 p3071 A67-34169
Numerical differentiation and smoothing of equally and nonequally spaced experimental data in independent variable 19 p3250 A67-35615
Thermodynamics of nonlinear materials with internal state variables, analyzing evolution equation, dynamic stability, dissipation, etc 20 p3555 A67-37563
Initial boundary value problem for Chaplygin equation using Cauchy and Dirichlet data 20 p3478 A67-37574
Integral integer-valued functions of several complex variables, proving Gelfond-Straus results by using modification of Schneider method 21 p3651 A67-37921
Independent variable changes in dynamical systems and applications to systems regularization, giving canonical and Lagrangian motion equations with tensor notation 23 p4027 A67-41006
Boundary value problem theory for ordinary differential equations, discussing compact and noncompact intervals of independent variables 23 p4023 A67-41018
High order accurate difference methods in hydrodynamics 24 p4146 A67-43095
INDEX
S ABSORPTIVE INDEX
S ENVIRONMENTAL INDEX
S MORPHOLOGICAL INDEX
S PSYCHOLOGICAL INDEX
S REFRACTIVE INDEX
INDIA
Nuclear emulsion measurements of primary cosmic ray alpha particle flux over Hyderabad during high solar activity in 11-year cycle 03 p0506 A67-13720
Aeronautical research in India, precision instrumentation design and production development, facilities, rocket launching station, etc 11 p1885 A67-24653
Rocket and balloon studies of solar radiation, wind characteristics, equatorial electrojet and lower ionosphere electron density 19 p3223 A67-35474
INDICATOR
SA ANALYZER
SA ATTITUDE INDICATOR
SA DETECTOR
SA ENGINE FAILURE INDICATOR
SA FLOW DIRECTION INDICATOR
SA FORCE DISPLACEMENT INDICATOR
SA POSITION INDICATOR
SA RADIATION INDICATOR
SA RANGE INDICATOR
SA TEMPERATURE INDICATOR
SA VOLTAGE VARIATION INDICATOR
Flaw detection methods using penetrating fluids, emphasizing fluorescent materials and pigments 13 p2122 A67-26255
CRT display provided by integrated circuit indicator packing circuitry in single plug-in module, noting timing, sweep, generation, etc 14 p2288 A67-28769
Airborne analyzer and digital recording system to assess, diagnose and predict turbojet engine health on immediate and

long term basis
[SAE PAPER 670359] 17 p2861 A67-32998
High speed methods of frame scanning in
character output element with character
point shaping on CRT
screen 17 p2822 A67-33100

INDIUM

Fermi surface curvature of indium single
crystals measured from RF size effect at
reference point 01 p0133 A67-10742
Diffusion of antimony and indium in
germanium in range from 700 to 855 degrees
C, taking into account effect of internal
electric field 03 p0489 A67-13149
Equation of surface diffusion of indium in
germanium solved by taking into account
effect of external electric
field 03 p0489 A67-13150
Time dependence of current in In-CdS-In
sandwich plate system at various voltages,
using X-and Z-cut monocrystal
CdS 03 p0490 A67-13157
Optical properties of thin indium films of
varying thicknesses 05 p0862 A67-16599
Photoionization cross section of negatively
charged In atoms in n-type silicon from
comparison of intrinsic photoconductivity
with impurity 08 p1367 A67-20410
Diffusion of antimony and indium in
germanium in range from 700 to 855 degrees
C, taking into account effect of internal
electric field 10 p1690 A67-23098
Equation of surface diffusion of indium in
germanium solved by taking into account
effect of external electric
field 10 p1690 A67-23099
Time dependence of current in In-CdS-In
sandwich plate system at various voltages,
using X-and Z-cut monocrystal
CdS 10 p1690 A67-23105
Fermi surface curvature of indium single
crystals measured from RF size effect at
reference point 13 p2176 A67-26771
Indium concentrations determined by
neutron activation in petrological suite of L-
group chondrites 23 p4069 A67-41474

INDIUM ALLOY

Plastic deformation of indium and indium-
thallium alloys, noting change of pure
indium lattice to fcc with increase of
thallium content 02 p0255 A67-18669
Pressure composition diagrams of thallium
rich portion of thallium-indium system at
high
pressure-temperature 04 p0635 A67-14511
Magnetic properties of second kind
superconductivity of indium-lead alloys as
function of temperature down to 0.38
degrees K 05 p0864 A67-16893
Temperature dependent variations in Hall
coefficient of indium and indium-rich alloys
with Pb, Cd, Tl and Hg 08 p1371 A67-21438
Pinning fluxoids by spatial
inhomogeneities of Tl-Pb and Pb-In alloys,
noting I-H characteristics and type II
superconductor resistance 09 p1556 A67-22135
Superconducting indium-bismuth alloy
films immersed in strong magnetic fields
parallel and perpendicular to surface,
studying film thickness effect by tunneling
technique 14 p2371 A67-28723
Phonon scattering at point defects theory
found to disagree with experimental results
on InSb-InTe 16 p2730 A67-31156

INDIUM ANTIMONIDE

Indium arsenic antimonide single crystals
in p-n junction laser 01 p0097 A67-10087
Spontaneous and induced coherent
radiation from indium antimonide electron-
hole plasma 01 p0087 A67-10088
Photo-Hall effect and photoconductivity on
compensated p-InSb at low temperatures,
examining temperature dependence of
carrier mobility 01 p0128 A67-10093
Optical reflection, transparency and
Faraday effect for indium antimonide,
calculating effective electron mass, relation
between energy and wave number,
etc 01 p0128 A67-10095
Electron mobility in p-type indium
antimonide, noting entrainment of minority
carriers by majority 01 p0129 A67-10098
Coherent microwave power at K-band
frequencies from indium antimonide
structures, presenting theory of two-stream
interaction in transverse magnetic
field 01 p0131 A67-10371
InSb submillimeter detector as mixer in
superheterodyne receiver shows performance

two orders less than ideal
receiver 01 p0036 A67-10440
Geometrical /current distribution/
influence on magnetoresistance effect in
indium antimonide and indium arsenide at
34 gc/s 01 p0132 A67-10467
Effective mass Hamiltonian for conduction
band g factor anisotropy of indium
antimonide in magnetic
field 01 p0134 A67-10785
Ionized impurity scattering mechanisms
causing energy and momentum losses in n-
type InSb below 77 degrees
K 01 p0134 A67-10806
Temperature dependence of diffusion
coefficient of Li in InSb prepared in wafer
form 01 p0137 A67-11067
Oscillatory low temperature
photoconductive spectral response of p-type
indium antimonide as function of electric
field strength and
temperature 02 p0280 A67-11487
Conductivity, Hall coefficient and
magnetoresistance of monophase InSb films
as function of film
thickness 02 p0295 A67-11765
Photoconductivity resonances and
recombination radiation in PbTe and InSb
due to multiple photon interband transitions
between Landau levels in high intensity
magnetic fields 02 p0254 A67-12522
Differential method measurement of Hall
effect in presence of large constant
magnetic field 03 p0487 A67-12808
Microhardness of n-type InSb single
crystals and crack formation near
indentation area 03 p0489 A67-13093
Instabilities in drifting semiconductor
plasma, noting dispersion curve and collision
ionization for longitudinal
oscillations 03 p0496 A67-13674
Room temperature recombination radiation
induced by Lorentz field in InSb and
ternary alloy of mercury, cadmium and
tellurium under cross field
conditions 03 p0496 A67-13675
Indium antimonide specimens plastically
bent to introduce excess of dislocations,
examining dependence of lower yield stress
for bending on direction of
bend 03 p0498 A67-13870
Longitudinal magnetoresistance anisotropy
and Hall coefficient anisotropy in p-type
indium antimonide, noting similarities with
galvanomagnetic anisotropy of p-type
germanium 04 p0674 A67-14609
Comparison of experimentally obtained
electron effective masses for high electron
concentration in InSb and
InAs 04 p0677 A67-14935
V-I characteristics of p-n junctions on In-
Sb base, noting effects of surface etching,
temperature and impurity
concentration 04 p0680 A67-15157
Gamma irradiation from Co 60 effect on
indium antimonide, determining defect
formation on dose and limiting position of
Fermi level for n-and p-type
material 04 p0680 A67-15283
Quantum oscillation of transverse and
longitudinal magnetothermal emf in n-type
indium antimonide compared with
oscillations of transverse and longitudinal
magnetoresistance and Hall
coefficient 04 p0680 A67-15288
Synthesis and growth of dendritic InSb
films by electron beam microzone melting of
vacuum deposited composite indium and
antimony films, noting electrical
properties 04 p0682 A67-15319
Anomalous high photoconductivity of
indium antimonide thin films due to
negative charge transfer to oxide surface
layer during illumination 04 p0683 A67-15650
Annealing production of acceptor defect
centers in indium antimonide single
crystal 04 p0683 A67-15651
Impurity atom behavior in diatomic InSb
and GaSb crystal lattices analyzed, using
nuclear gamma resonance, measuring
absolute values of f, chemical displacements
and line widths 05 p0861 A67-16392
Quantum oscillations of Hall effect and
longitudinal and transverse reluctance in n-
indium antimonide, noting spin splitting and
temperature and electron concentration
effect on oscillation
maximum 05 p0861 A67-16394
Electrical properties of indium antimonide
single crystals with noncompensated
impurity concentration, determining position

of deep-seated levels in forbidden
band 05 p0861 A67-16394
Heat treatment conversion of large grain
n-type indium antimonide single crystals and
twin crystals into p-type
samples 05 p0862 A67-16500
Large signal AC field effect measurement
on A and B real surfaces of InSb exposed to
different ambients 05 p0862 A67-16600
Semiconductor lasers and fast II
detectors, discussing InAs, InSb and three
types of mercury cadmium telluride
detectors 05 p0821 A67-16666
Impurity states theory for semiconductor
with In-Sb type band structure, calculating
ionization potential and numerical values for
energy levels 05 p0863 A67-16669
Etching and X-ray spectrometric
techniques to investigate distribution and
density of dislocations in deformed and
annealed GaAs and InSb
crystal 05 p0865 A67-16922
Temperature dependence of electrical and
galvanomagnetic properties of single crystal
InSb dendrites 05 p0869 A67-17099
Orientation dependence of surface charge
on anodized indium antimonide from MO
capacitance measurements 05 p0869 A67-17099
Landau level structure and transition
matrix elements of InSb near Brillouin zone
center during valence band cyclotron
resonance 05 p0870 A67-17118
Temperature dependence of three-phonon
processes in solids noting application to Si,
Ge, GaAs and InSb 05 p0870 A67-17119
Inelastic scattering of carbon dioxide laser
radiation by mobile Landau-level electrons
in n-InSb 06 p1009 A67-17722
Singularities of Faraday effect in n-type
InSb in millimeter band at 77.8 degrees K as
function of sample thickness and magnetic
field intensity 06 p1047 A67-17755
Pinch effect in InSb degenerate plasma
discussing electric conductivity and
recombination emission
spectra 06 p1049 A67-17877
Far IR lattice bands in n-type indium
antimonide single crystal 06 p1059 A67-18900
Deformation potential of valence band of
indium antimonide, using piezoelectric
technique of shifting intrinsic recombination
under uniaxial stress 06 p1062 A67-18939
Nonlinear galvanomagnetic effects due to
hot electrons in n-type InSb in quantum
limit 06 p1065 A67-18950
Time dependence of V-I curves in n-type
In-Sb at low temperatures, determining
electron-hole pair generation
rate 06 p1066 A67-18955
Interband magnetoabsorption of InSb
noting anomalies caused by enhanced
polaron self-energy
effects 06 p1066 A67-18955
Negative magnetoresistance in
semiconductors caused by magnetic system
in random lattice of impurity
atoms 06 p1067 A67-18966
Resistivity, magnetoresistance, Hall effect
and thermal conductivity in n-type In-Sb at
liquid He temperatures 06 p1068 A67-18966
Hydrostatic pressure effect on energy gap
carrier concentration and electron and hole
mobilities of indium
antimonide 07 p1231 A67-19066
Transport coefficients for minority carrier
scattering in InSb 07 p1209 A67-19655
Hall mobility and thermal emf in indium
antimonide with mixed electron scattering
mechanism 07 p1237 A67-20181
Nonequilibrium charge carrier lifetime in
indium antimonide single crystals with Ge
and Au impurities 08 p1367 A67-20411
Coherent radiation generation in electron
hole indium antimonide plasma, discussing
emission spectrum 08 p1367 A67-20411
Thickness dependence of Hall constant
electrical conductivity and Hall mobility in
polycrystalline thin layers of
InSb 09 p1551 A67-21566
IR photovoltaic response, quantum
efficiency and V-I characteristics of InSb
MOS structures 09 p1551 A67-21577
Electron temperature variation in polar
indium antimonide with dominant optical
scattering 09 p1552 A67-21677
Thin films of indium antimonide for active
devices grown by various methods including
atomic mixing, flash evaporation,
etc 09 p1474 A67-22111
Conduction electrons interaction with
deformation potential and piezoelectric

phonons to explain hot electron results in n-type InSb, taking into account screening of scattering potential 09 p1558 A67-22619

Electron-hole plasma pinch instability in InSb on application of longitudinal magnetic fields shows change to helical rotating plasma 10 p1683 A67-22760

Surface treatment effect in field effect anomaly of cleaved and etched n-type indium antimonide at high magnetic fields 10 p1688 A67-22903

Generation-recombination and modulation noise power spectrum of high purity p-type InSb at 77 degrees K 10 p1693 A67-23566

Strong electrical field effect on Faraday effect in n-type InSb 10 p1695 A67-23663

Temperature dependence of thermal conductivity and phonon and electron components in solid and liquid n-and p-type semiconductors 11 p1851 A67-24975

Photoconductivity kinetics and regeneration recombination noise spectrum of p-InSb crystals, showing association with hole capture, lifetime and alloying impurity 12 p1983 A67-25512

Hall coefficient dependence on magnetic field intensity for n-type InSb single crystals at 77 degrees K 12 p1984 A67-25518

Lifetime for nonequilibrium current carriers in n-type indium antimonide crystals from generation-recombination noise measurements at various temperatures 12 p1984 A67-25523

Microwave power coupling from waveguide to helicon mode in doped indium antimonide by placing aluminium oxide cones on semiconductor surface 12 p1986 A67-26160

Current carrier concentration gradient in InSb, investigating effect on transverse reluctance coefficient and Hall effect dependence on magnetic field intensity 13 p2173 A67-26360

Electromagnetic effect in n-type InSb samples, measuring magnetic resistance, Hall effect and magnetic EMF 13 p2174 A67-26368

Microwave field distribution in waveguide partially filled with solid state plasma for application to isolator 13 p2076 A67-26521

Combined resonance transition in indium antimonide induced by single photon absorption 13 p2178 A67-27083

Quantum limit galvanomagnetic phenomena in n-InSb 13 p2184 A67-27690

Etching and X-ray spectrometric techniques to investigate distribution and density of dislocations in deformed and annealed Ga-As and InSb crystal 14 p2365 A67-28260

V-I characteristics of p-n junctions on InSb base, noting effects of surface etching, temperature and impurity concentration 15 p2534 A67-29344

Current-voltage characteristic determination for n-InSb Corbino disk, noting capacitance and internal resistance current source at cryogenic temperature 15 p2534 A67-29359

Temperature dependence of electrical conductivity, Hall effect and resistance in transverse magnetic field for tin-doped InSb 15 p2534 A67-29385

Temperature dependence of lifetime and Hall coefficient in InSb, measuring lifetime by phase shift method, concluding that recombination centers are lattice defects 15 p2535 A67-29483

Microwave emission from magnetic-field-free electron hole plasma in p-type InSb at 77 degrees K 15 p2539 A67-29820

Impurity states theory for semiconductors with In-Sb type band structure, calculating ionization potential and numerical values for energy levels 15 p2539 A67-29865

Relaxation oscillations in n-type indium antimonide crystal under magnetic field effect and responsivity measurements in far IR 15 p2540 A67-29931

Crystal dislocation in InSb by fast neutron bombardment assuming displacement wedges with electron type conductivity 15 p2541 A67-30234

Temperature dependent noise spectra of InSb single crystals, noting deep energy level and impurity energy 15 p2541 A67-30235

Isochronous and isothermal annealing of indium antimonide irradiated by X-rays and gamma rays, studying changes in current-carrier concentration 15 p2542 A67-30247

Surface etching effects on positively sloped current-voltage characteristics of p-n

junctions in fused indium antimonide 16 p2730 A67-31161

Impurity concentration and temperature dependence of reverse current in indium antimonide diodes, determining components 16 p2637 A67-31162

N-type InSb electron thermoelectricity temperature dependence, lattice thermoelectricity and thermal resistance 16 p2730 A67-31163

Field effect behavior of thin InSb films noting semiconductor surface properties, mobility decrease with temperature and increase of impurity concentrations 16 p2732 A67-31527

Interface alloy technique for heterojunctions between GaAs and InSb single-crystal heterojunctions shown by X-ray analysis 17 p2911 A67-32196

Microwave emission phenomena from n and p type indium antimonide, noting no essential difference 17 p2914 A67-32375

Shubnikov-de Haas and Gurevich-Firson oscillations of photomagnetic effect in n-InSb magnetic field 17 p2914 A67-32451

Microwave emission intensity from InSb, examining dependence on angle between DC electric and magnetic fields 17 p2914 A67-32615

Two-stream instability in semiconductor InSb plasmas, noting collision conditions, surface space charge, wave growth, etc 17 p2921 A67-33052

Damage regions in Si, GaAs and InSb irradiated with monoenergetic neutrons determined, using electron microscopy 17 p2922 A67-33060

Laminar slow wave coupler applied to waveguide to detect very low power slow waves in indium antimonide subjected to combined effects of applied electric and magnetic fields 17 p2922 A67-33087

Strong electrical field effect on Faraday effect in n-type InSb 17 p2924 A67-33344

Mean internal potential for InSb lattice calculated, comparing empirical results with those obtained from Hartree and Thomas-Fermi-Dirac methods 18 p3095 A67-33442

Nonexistence of critical current for pinching in electron-hole plasmas 18 p3098 A67-33523

Ground-state splitting in semiconductor double acceptors 18 p3099 A67-33699

Temperature and magnetic field intensity dependence of microwave emission from n-type indium antimonide 18 p3101 A67-34016

Collision induced instability in semiconductor plasmas, noting system consisting of electrons and holes with transverse relative drift to static magnetic field 18 p3102 A67-34348

Photoconductivity kinetics and regeneration recombination noise spectrum of p-InSb crystals, showing association with hole capture, lifetime and alloying impurity 18 p3103 A67-34443

Hall coefficient dependence on magnetic field intensity for n-type InSb single crystals at 77 degrees K 18 p3103 A67-34449

Lifetime for nonequilibrium current carriers in n-type indium antimonide crystals from generation-recombination noise measurements at various temperatures 18 p3103 A67-34454

Detection properties of n-type InSb in microwave and IR ranges, studying impurity and magnetic field effects 19 p3300 A67-34762

Transverse Nernst-Ettingshausen thermomagnetic effect in intrinsic conductivity region in InSb single crystals subjected to magnetic field 19 p3300 A67-34763

Contact potential difference between crystal surfaces of indium antimonide cleaved in ultrahigh vacuum measured by Kelvin method 19 p3302 A67-34939

Indium-antimony alloy thin film preparation by vacuum evaporation, noting effect of heating and annealing on electrical resistivity 19 p3305 A67-35609

X-ray diffusion intensity by transverse polarization phonons in indium antimonide at various temperature ranges 19 p3307 A67-35793

Active impurities concentration in p-type semiconductors by measuring temperature at zero thermoelectric potential 19 p3308 A67-35875

Conductance and capacitance measurements on grain boundaries in p-type

indium antimonide 20 p3504 A67-36173

Heat treatment of indium antimonide crystals with various dislocation densities noting change in conductivity 20 p3506 A67-36227

Magnetometer with Gauss sensor describing n-type InSb pickup bridge instrument sensitivity 20 p3447 A67-36760

Nonequilibrium current carrier lifetime in p-type InSb samples alloyed with Cu and Ge, noting hole concentration and temperature effects 20 p3510 A67-36761

Electron drift velocity and mobility in InSb calculated from conductivity and Hall effect measurements, noting microwave emission occurrence 20 p3514 A67-37544

Indium antimonide hole surfaces approximated within second order perturbation theory, discussing energy contours, Baggeley cyclotron resonance data and maximum energy value 21 p3679 A67-38255

Current carrier concentration gradient in InSb, investigating effect on transverse reluctance coefficient and Hall effect dependence on magnetic field intensity 21 p3680 A67-38317

Electromagnetic effect in n-type InSb samples, measuring magnetic resistance, Hall effect and magnetic EMF 21 p3680 A67-38324

Pinch effect in degenerate indium antimonide plasma in longitudinal and transverse electromagnetic fields 21 p3666 A67-38369

Resonance and noise microwave emission thresholds for InSb electron hole plasma subject to crossed electric and magnetic fields, noting Hall effect 21 p3683 A67-38403

Moving high field domain and current saturation in optically excited n-InSb 21 p3683 A67-38404

N-type InSb hot electron and nonohmic effects, noting low temperature and magnetic and electric field dependence of Hall coefficient and resistivity 21 p3683 A67-38405

Indium antimonide-indium arsenide solid solution carrier mobility related to sample composition and temperature, measuring Hall coefficient and electrical conductivity 21 p3684 A67-38452

Nature of defects in InSb induced by gamma and X-ray irradiation, discussing recovery process 21 p3687 A67-39143

IR technology and electromagnetism spectrum, discussing manufacture of circulators and isolators using Faraday rotation in InSb 22 p3835 A67-39213

X-ray diffusion from thermal agitation oscillations coupled with plasma waves in indium antimonide, discussing phonon-plasmon interactions and Hall effect measurements 22 p3859 A67-39652

Curves for Hall effect logarithms, current carrier mobility and electric conductivity vs high pressure and temperature effects in InSb 22 p3864 A67-40323

N-type InSb microwave noise emission at low temperatures in low electric field regime, measuring magnetic field threshold and background continuum 22 p3864 A67-40345

Spectral dependence of enhanced quantum efficiency and overlap integrals in InSb semiconductors, calculating impact ionization and hot electrons thermalization 23 p4040 A67-41061

Frequency dependence of attenuation coefficient for longitudinal ultrasonic waves in InSb over range 50 to 210 MHz for temperatures between 200 and 600 degrees K 24 p4202 A67-41980

Maximum Corbino magnetoresistivity in indium antimonide single crystals, investigating impurity concentration and layer distribution 24 p4203 A67-42208

Impact ionization avalanche plasma production and instabilities in InSb at low temperatures, measuring current variation with electric field strength 24 p4204 A67-42344

Thermal treatment at melting temperature inducing acceptors of electric conductivity in indium antimonide crystals 24 p4204 A67-42577

INDIUM ARSENIDE

Diffusion and electrical transfer of zinc in indium arsenide as affected by temperature 01 p0127 A67-10068

Diffusion parameters and solubility of Cd in InAs measured with aid of radioactive

isotopes compared with diffusion coefficient measurement by p-n junction method 01 p0128 A67-10082

Coherent emission of indium arsenide phosphide p-n junction 01 p0087 A67-10101

Geometrical /current distribution/ influence on magnetoresistance effect in indium antimonide and indium arsenide at 34 gc/s 01 p0132 A67-10467

Spin-magnetophononic and magnetophononic oscillations of magnetic resistance in n-InAs 01 p0133 A67-10547

Spin-magnetophononic and magnetophononic oscillations of magnetic resistance in n-InAs 01 p0137 A67-11055

Negative magnetoresistance of n-type InAs in longitudinal magnetic fields 03 p0490 A67-13156

Comparison of experimentally obtained electron effective masses for high electron concentration in InSb and InAs 04 p0677 A67-14935

Transverse magnetoresistance of n-type InAs, noting temperature effect and correlation with quantum theory 04 p0681 A67-15293

Semiconductor lasers and fast IR detectors, discussing InAs, InSb and three types of mercury cadmium telluride detectors 05 p0821 A67-16668

Indium arsenide diode laser fabrication using liquid phase epitaxy, noting quantum efficiency 05 p0825 A67-17096

Corbino magnetoresistance experiments for n-type surface layers on p-type indium arsenide crystals as function of surface electric field 06 p1064 A67-18941

Magnetic effect on photoresponse of illuminated InAs p-n junctions 07 p1237 A67-20181

Diffusion and electrical transfer of zinc in indium arsenide as affected by temperature 08 p1371 A67-21451

Diffusion parameters and solubility of Cd in InAs measured with aid of radioactive isotopes compared with diffusion coefficient measurement by p-n junction method 08 p1371 A67-21459

Narrowband optical heterodyne detection, describing InAs photodiode arrangement 10 p1654 A67-22752

Negative magnetoresistance of n-type InAs in longitudinal magnetic fields 10 p1690 A67-23104

Avalanche multiplication of current carriers at low temperatures in p-n junctions of InAs, determining carrier ionization coefficient and dependence on electrical field 10 p1695 A67-23660

InAs epitaxial layers grown on GaAs substrate investigated via sandwich method and electron diffraction 12 p1980 A67-25201

Recombination radiation spectra of InAs with different current carrier concentrations in initial material and different current densities 12 p1914 A67-25516

Current voltage characteristics of alloyed p-n junctions in n-type InAs, discussing contribution of tunnel current 12 p1986 A67-26099

HF photoconductive phase responses in single crystal n-type indium arsenide, deriving carrier lifetimes 14 p2364 A67-28104

198 Au isotope diffusion in n-type indium arsenide at different temperatures 14 p2368 A67-28537

Quantum oscillations of Nernst-Ettingshausen effect in indium arsenide 14 p2376 A67-29087

Electrical conductivity and Hall effect of indium arsenide solid solutions, noting temperature dependence and hole mobility 16 p2732 A67-31480

Preparation of doped and undoped epitaxial InAs with open tube vapor-phase transport system noting properties, temperature effects, electron mobilities, etc 17 p2911 A67-32194

Electric field effect on magnetoresistance of p-type indium arsenide surface in high magnetic fields at low temperatures 17 p2911 A67-32206

Minority carrier trapping analyzed from transient decay of photoconductivity in n-type polycrystalline films of InAs 17 p2922 A67-33064

Avalanche multiplication of current carriers at low temperatures in p-n junctions of InAs, determining carrier ionization coefficient and dependence on electrical field 17 p2924 A67-33341

Time constants of fast photodetectors measured, using mercury wetted relay and epitaxial indium arsenide diode laser 18 p3046 A67-33746

Distribution coefficients for impurities in gallium and indium arsenides as periodic function of atomic weight decreasing with increasing atomic number 18 p3102 A67-34289

Recombination radiation spectra of InAs with different current carrier concentrations in initial material and different current densities 18 p3012 A67-34447

Time and temperature dependent diffusion of vaporized Zn and Cd in n-type InAs 19 p3299 A67-34760

Fast neutron irradiation effect on electrical conductivity and Hall effect in Zn doped n-type indium arsenide single crystals 19 p3301 A67-34771

IR reflection spectra of tellurium and zinc doped indium arsenide single crystals, discussing reflection minima and spectral curves given 19 p3306 A67-35705

Low temperature dependence of relative efficiency of forward biased InAs diode emitter 19 p3198 A67-36046

Indium arsenide-tellurium ternary compounds chemical bond, microhardness and structure 20 p3506 A67-36226

Odd and even photomagnetic effect oscillations in InSb, measuring EMF at low temperatures and strong fields 21 p3677 A67-38095

Indium antimonide-indium arsenide solid solution carrier mobility related to sample composition and temperature, measuring Hall coefficient and electrical conductivity 21 p3684 A67-38452

Interband and free carrier Faraday rotation in n-type InAs at room and low temperature, determining conduction band parameters 22 p3863 A67-40204

198 Au isotope diffusion in n-type indium arsenide at different temperatures 23 p4040 A67-40944

Vapor growth of single crystal heterojunctions of GaAs on Ge or InAs on GaAs using iodine process in closed tube system 23 p4043 A67-41432

INDIUM COMPOUND

Crystal structure of alpha- and beta-indium selenide semiconductor 03 p0493 A67-13361

Temperature dependence of electrical properties of alpha-indium selenide n-type semiconductor single crystals 03 p0493 A67-13362

Transmission spectra of GaS, GaSe, InSe and TlSe single crystals obtained at 300 degrees K by means of IR spectrometer 04 p0676 A67-14932

Band-to-band radiative recombination in compounds of gallium and indium with phosphorus, arsenic and antimony 12 p1979 A67-25177

Temperature dependence of transverse and longitudinal Nernst-Ettingshausen effect and composition effects on Hall electron concentration in InSb-InTe solid solution 16 p2730 A67-31157

InSb-InAs solid solution thin films absorption spectra, noting band structure, temperature change and Hall EMF reduction 18 p3096 A67-33450

InBi single crystal electrophysical properties, giving temperature dependences 20 p3514 A67-37605

INDIUM PHOSPHIDE

Indium phosphide based semiconductor laser amplification, loss factor and radiation pattern 01 p0086 A67-10065

Emission spectra and I-V characteristics of diffusion p-n junctions in InP and spontaneous radiative recombination in presence of small current 04 p0679 A67-15138

Open circuit voltage and short circuit current capability of solar energy converter photoelement made of single crystal n-type indium phosphide 04 p0679 A67-15141

Emission from p-n junctions in crystals of InP-GaAs solid solution 05 p0885 A67-16941

Band structure of GaAs, GaP, InP and AlSb obtained by k.p method 06 p1058 A67-18904

Indium phosphide based semiconductor laser amplification, loss factor and radiation pattern 08 p1339 A67-21448

Eutectic alloys of heavy metal phases with InP compound analyzed, noting phase orientation parallel to solidification direction 09 p1552 A67-21880

Emission spectra and I-V characteristics of

diffusion p-n junctions in InP and spontaneous radiative recombination in presence of small current 12 p1979 A67-25161

Open circuit voltage and short circuit current capability of solar energy converter photoelement made of single crystal n-type indium phosphide 12 p1979 A67-25164

Emission from p-n junctions in crystals of InP-GaAs solid solution 14 p2366 A67-28486

Radiative recombination mechanisms in photoluminescence of n-type InP, discussing emission bands 16 p2732 A67-31450

Variation of forbidden bandwidth and linear-expansion coefficient of indium phosphide-gallium arsenide alloys as function of composition 18 p3095 A67-33444

Spectral and recombination radiation intensity changes from indium phosphide diode under different uniaxial compressions 18 p3100 A67-33718

Coherent emission observation in indium phosphide excited by injection laser at 77 degrees K 22 p3814 A67-39461

INDIUM SULFIDE

Intrinsic and impurity photoconductivity kinetics over wide temperature and illumination range of p-type indium sulfide single crystals obtained by zone melting 21 p3676 A67-37859

INDIUM TELLURIDE

Thermal power and electrical conductivity of SnTe-InTe crystals, discussing temperature effect 04 p0683 A67-15581

Phase state of thin layers of vapor deposited InTe with Te 50-60 percent 08 p1369 A67-20994

Solubility of impurities in semiconductors and mechanism for deviation from stoichiometry 18 p3096 A67-33449

INDOCHINITE

Chemical composition of indochinities, determining nonuniform distribution of elements via electron microprobe counts 11 p1866 A67-24695

Tektite origin, composition, identification, strewn fields and configurations 12 p2009 A67-26232

INDUCED FLUID FLOW

Steady motion of electrically conducting viscous fluid due to slow rotation of thin dielectric disk inside housing immersed in magnetic field 21 p3665 A67-38247

INDUCER

SA HELICAL INDUCER

Single-phase and two-phase cavitating flow regime performance of liquid propellant rocket engine turbopump inducers [ASME PAPER 66-WA/FE-23] 04 p0554 A67-15353

Single-phase and two-phase cavitating flow regime performance of liquid propellant rocket engine turbopump inducers [ASME PAPER 66-WA/FE-23] 24 p4143 A67-42464

INDUCTANCE

Inductance coefficient dependence on geometric air gap of ferrite cup cores, showing use for design of stable resonance circuits 02 p0280 A67-11464

Transistor circuit realization of inductance with three transistors and one power supply 05 p0785 A67-17536

Inductive correction effect on single stage tunnel diode RC amplifier, noting increase of upper frequency limit and shortening of wave front buildup time 06 p0970 A67-18213

Standing wave solution of homogeneous waveguide field distribution for H-10 wave after conformal mapping and effect of capacitive and inductive irises 10 p1607 A67-23571

Microminiaturizable transistorized circuit for generating wide frequency range high Q inductances from semiconductor devices for integrated selective circuits 13 p2081 A67-27201

Active and reactive resistance components of p-n diodes with minimum distribution of steady state carrier concentration in base 13 p2182 A67-27282

Inductive correction effect on single stage tunnel diode RC amplifier, noting increase of upper frequency limit and shortening of wave front buildup time 16 p2635 A67-30479

INDUCTION

SA MAGNETIC INDUCTION

SA RLC CIRCUIT

Negative differential resistances and inductive effects in alpha-modified SiC p-n junction diodes 04 p0679 A67-15136

Differential inductive sensor with

correcting windings for monitoring and measuring various nonelectric quantities and processes 06 p1003 A67-18173

Shock induced supersonic combustion of fuel-air mixtures used to obtain induction time, evaluating kinetic data and effect of small contamination levels [AIAA PAPER 67-105] 06 p1114 A67-18284

Geomagnetic induction arrow direction determined from quiet solar activity variations 13 p2116 A67-27396

Material limitations in MHD induction generator, discussing effect of conducting channel walls and thermal insulation on performance 16 p2605 A67-30582

Inductive characteristics of junction transistors, showing Q-factor increase achieved by using negative impedance produced by avalanche multiplication 18 p3009 A67-33479

Measurements of induction period, ammonia consumption rate after induction and radiation from electronically excited OH radicals in ammonia-oxygen reaction 18 p3155 A67-33836

Critical reaction rate for ignition, temperature rise and induction period for various geometries calculated for conductive theory, including reactant consumption 18 p3156 A67-33850

Shock induced supersonic combustion of fuel-air mixtures used to obtain induction time, evaluating kinetic data and effect of small contamination levels [AIAA PAPER 67-162] 21 p3732 A67-38858

INDUCTION HEATING

Induction heating contributions to solid state technology including zone refining and zone leveling, growth of metallic and nonmetallic single crystals, thin film production and epitaxial growth 01 p0080 A67-10972

Induced argon discharge shown to have shape of plasma filament, noting detachment from chamber walls 17 p2897 A67-32176

Surface hardening of titanium alloys by carbon and nitrogen, using high-frequency induction heating 19 p3242 A67-34919

Chromizing of steel by HF induction heating in vacuum using low-carbon ferrochrome and electrolytic chromium mixture 19 p3236 A67-34920

RF induction heating and production of low pressure plasmas, discussing plasma electron density function [AIAA PAPER 67-732] 21 p3674 A67-38756

INDUCTION SYSTEM

Solid state inductive element with magnetoresistance used for increase of Q 01 p0032 A67-10006

Traveling field and coil symmetrization of induction machine with open magnetic loop 01 p0012 A67-10187

Symmetric inductor with multipole magnetic field for stable plasma confinement, calculating input parameters 01 p0012 A67-10188

Conical induction plasma gun construction in strongly preionized regime and results of electrostatic probe measurements made with discharge camera 04 p0668 A67-15280

Inductive sensor development for measurement of pressure, airspeed, altitude and acceleration during aircraft testing 09 p1501 A67-22465

Self-excited liquid metal MHD induction generator 12 p1897 A67-25378

Mathematical model of MHD induction generator, deriving electrical diagram 15 p2527 A67-29472

High bypass ratio turbofan engine installation noting induction system, exhaust system, thrust reverser configuration requirements, accessories, etc [AIAA PAPER 67-390] 15 p2548 A67-30358

Liquid metal energy converters using magnetohydrodynamic induction noting electrodynamic aspects 16 p2606 A67-30586

Electromechanical servosystem in conjunction with inductive pickup circuit for thrust measurements in jet engine bed tests 22 p3797 A67-39536

Steady state matching of inlets, engines and exhaust nozzle for SST [AIAA PAPER 67-754] 23 p3928 A67-40988

Varactor inductance effects on design varactor tuned circuits above 50 MHz 23 p3982 A67-41504

Comparison of flat channel linear MHD induction generator analysis stressing gross power output in constant current and

voltage modes 23 p3942 A67-41737

Inductive energy storage and control system using ignitron switching 24 p4197 A67-42249

INDUCTOR

SA MAGNETIC COIL

Cylindrical inductor with inhomogeneous field, analyzing case of strong field inhomogeneity when inductor radius is much greater than pole pitch 04 p0556 A67-15522

Magnetic field structure in working space of linear multiphase inductive MHD generator 04 p0556 A67-15523

One-dimensional linear approximation of effects of magnetic and electric shunting of linear inductor edges on constant velocity MHD channel flow 04 p0556 A67-15524

X and Z components of ponderomotive forces acting on conductive strip of finite width in EM field produced by unidirectional inductor 04 p0556 A67-15525

AC power generation by linear channel liquid metal MHD inductive generator 05 p0754 A67-17348

Inductorless band pass filter to prove validity of hypothesis that all inductors in LC filter can be replaced by gyrator-capacitor equivalents 07 p1154 A67-19615

Gyrator type circuit which requires only three amplifiers and which, when terminated with capacitor, can replace ungrounded inductor 15 p2456 A67-29240

Striated layer flow of working fluid in duct of synchronous induction MGD generator studying stability by approximation 16 p2807 A67-30594

Thin film circuits for narrow band radar receivers, discussing manufacture of inductors, capacitors and LC resonant circuits 21 p3589 A67-37917

Radiation resistance and reactance of thin film inductor in microwave integrated circuit determined using Fourier transform 24 p4128 A67-41924

INDUSTRIAL SAFETY

Production, handling and shipping of elemental fluorine, noting materials, health and safety precautions, aerospace applications and toxicity 16 p2734 A67-31811

Incident/accident information exchange system for hazard information flow to safety teams 18 p3163 A67-34692

Beryllium component machine tool installations and operation, discussing contamination protective systems for toxic dust 23 p4009 A67-40687

INDUSTRY

SA AIRCRAFT INDUSTRY

SA DEFENSE INDUSTRY

NASA quality assurance program and NASA industry quality relationships, particularly for large space systems procurement 05 p0930 A67-17242

Mockup of manned hardware systems in industrial design, describing application to LRV and LEM development, crew compartment design for undersea craft /DSRV/, etc 05 p0757 A67-17378

Future industrial automation prediction based on present knowledge 13 p2231 A67-27514

Management aspects of technological capability within large hardware systems business 14 p2409 A67-28697

Trends in digital flight simulation for training 17 p2833 A67-32489

Book on Japanese activities in space exploration including 1966-1967 programs 17 p3136 A67-34618

Soviet book on high temperature materials for vacuum or inert gas industrial processes 21 p3845 A67-38600

Developments in optics and applications in industry - Conference, Sussex, April 1967 22 p3836 A67-39328

INELASTIC BODY

Plane strain equations for elastoviscoplastic compressible bodies without strain hardening 05 p0908 A67-16039

Reciprocal theorem applied to linear and angular displacements due to creep or plastic strains in inelastic bodies 14 p2398 A67-28097

Boundary value wave problem in elastoviscoplastic medium solved by approximate method using Courant concept 19 p3340 A67-35444

Book on inelastic shell theory and research covering field equations, viscous and plastic response, viscoelasticity,

elastoplastic deformation, limit analysis, steady creep, etc 21 p3722 A67-38531

INELASTIC COLLISION

Inelastic collisions of electrons with diatomic molecules, noting effect on speed of energy exchange in nonhomogeneous plasma 01 p0118 A67-10044

Pion energy transmission during inelastic interaction of cosmic particles with Pb nuclei 02 p0315 A67-12756

Proton-I satellite measurement effective cross section of inelastic interaction of protons with carbon nuclei at extremely high energies 02 p0315 A67-12757

Ionization calorimeter determination of effective cross section of high energy primary cosmic ray proton inelastic interaction with atmospheric atomic particles 02 p0315 A67-12759

Inelastic collisions by drifting ions studied by series of experiment in which mass analyzed ion beam is injected into drift tube containing gas 04 p0661 A67-15509

Ochkur and Rudge approximation for exchange in electron-atom collisions adapted for atom-atom collisions 06 p1034 A67-17649

Vainshtein method calculation of inelastic collision of electrons with atoms 07 p1225 A67-19207

Excess tunnel current due to inelastic electron molecule interactions near metal insulator interface 10 p1689 A67-23074

Kinetic model equation for polyatomic gas with internal structure based on Wang Chang-Uhlenbeck 11 p1775 A67-23864

Electron velocities distribution in plasma, studying boltzmann equation inelastic and superelastic collision operator, considering eigenfunctions and eigenvalues for electronic excitations and deexcitations 13 p2165 A67-26437

Physics of plasmas, Volume 2, Weakly ionized gas, covering inelastic collision, free electron scattering, intermediary plasmas, etc 13 p2168 A67-27221

Inelastic collisions of proton beam with carbon monoxide target molecules, determining ionization cross section and charge transfer 14 p2390 A67-28943

Calculating characteristics of cesium plasma in stationary state under electric field, considering excitation and ionization by inelastic electron collisions 16 p2713 A67-30868

Kinetic equation for electron, ion and atom concentrations for Coulomb plasma taking into account inelastic processes 16 p2715 A67-31040

Electron velocity distribution function in nonequilibrium plasma having spatial distribution governed by electron-electron and inelastic collisions 16 p2723 A67-31768

Proton I and II satellite measurement of effective cross sections of inelastic interactions between billion and trillion ev protons and carbon nuclei 17 p2935 A67-32247

Local electronic energy balance formulation, including radiative transport effect in nonuniform seeded plasma, described by two-temperature model 17 p2906 A67-33010

Inelastic collisions of electrons with diatomic molecules, noting effect on speed of energy exchange in nonhomogeneous plasma 17 p2890 A67-33322

Ion-molecule reactions of diatomic deuterium cation with diatomic deuterium and diatomic hydrogen 18 p3083 A67-34521

High energy electron ionization cross section for hydrogen, noting high quantum number correspondence to classical expression 19 p3266 A67-36090

Energy spectrum and production rates for secondary antiprotons from inelastic collisions of high energy galactic cosmic radiation with interstellar gas nuclei 19 p3316 A67-36098

Inelastic electron impact cross sections for ionization and vibrational excitation of atmospheric molecular oxygen 20 p3489 A67-37419

Pion energy transmission during inelastic interaction of cosmic particles with Pb nuclei 22 p3876 A67-40258

Proton I satellite measurements of effective cross section of inelastic interaction of protons with carbon nuclei at extremely high energies 22 p3876 A67-40259

Ionization calorimeter determination of effective cross section of high energy

primary cosmic ray proton inelastic interaction with atmospheric atomic particles 22 p3876 A67-40261

Effective cross section of inelastic interaction between high energy protons and carbon nuclei monitored by Proton I and II 24 p4219 A67-42843

Cross section of inelastic interactions and free path between nuclear active cosmic particles and lead nuclei at high energies 24 p4219 A67-42844

Cross section of inelastic interaction between cosmic ray neutrons and carbon nuclei at energies of 100 GeV 24 p4219 A67-42848

High energy nucleon and pi-and K-mesons inelastic interaction cross sections from quasi-linear approximation of optical model 24 p4192 A67-42852

Pion nucleon inelastic collisions at 17 GeV/c momentum, discussing proton pulse spectra and ionization losses 24 p4192 A67-42853

Secondary particle pulse spectra and mean inelasticity coefficient dependence on particle multiplicity and primary proton energy in 20 GeV/c proton-proton interactions 24 p4193 A67-42854

INELASTIC SCATTERING

SA ELASTIC SCATTERING

SA NEUTRON SCATTERING

SA NUCLEAR SCATTERING

Differential cross section for excitation of helium electronic states by helium ions 01 p0116 A67-10337

Lunar and planetary surface elemental analysis technique by analysis of gamma rays resulting from inelastic scattering of neutrons 05 p0843 A67-16545

Inelastic scattering of carbon dioxide laser radiation by mobile Landau-level electrons in n-InSb 06 p1009 A67-17723

Energy spectrum of inelastically scattered alpha particles from alpha particle helium 3 reaction 07 p1226 A67-19563

Scattering mechanisms and role of interelectron collisions in n-Pb-Te and certain other semimetals analyzed by concentration dependence of mobility and thermal EMF 12 p1983 A67-25514

Generalized potentials for medium energy inelastic nuclear scattering derived with projection operator method 14 p2350 A67-27789

Inelastic differential scattering cross sections and angular distribution of Ni first-excited-state protons determined by distorted wave calculation 17 p2888 A67-32733

Scattering mechanisms and role of interelectron collisions in n-Pb-Te and certain other semimetals analyzed by concentration dependence of mobility and thermal EMF 18 p3103 A67-34445

Differential cross sections for inelastic large angle alpha particle scattering from unnatural parity states in Mg showing diffraction pattern 20 p3488 A67-36931

Peak energy dependence on atomic number in inelastic alpha particle scattering at 24.8 MeV by Ni 58, Cu, Ag, Ta and Au 21 p3659 A67-38401

Excited nuclei electromagnetic de-excitation rate by inelastic scattering in stellar particles calculated as function of temperature, density, transition energy and multipole functions 21 p3660 A67-38846

Nuclear active cosmic ray particles and Fe atom nuclei inelastic interaction cross section 24 p4219 A67-42849

INEQUALITY /MATH/

Determination of maximum number of nonzero elements in nonnegative matrix and first power for which maximum density is assumed 01 p0105 A67-10731

Clausius-Duhem inequality in general formulation of second law of thermodynamics 01 p0167 A67-10798

Optimal nonlinear feedback control derived from quartic and higher order performance criteria 01 p0046 A67-11206

Two proofs for Cauchy inequality between arithmetical and geometrical means of set of nonnegative numbers 04 p0643 A67-14728

Nonequilibrium thermodynamics of irreversible processes in approach based on fundamental inequality derived from second law of thermodynamics 04 p0718 A67-15925

Inequalities for difference and pseudodifferential operators, providing sharp form of Garding inequality 06 p1025 A67-18642

Algebraic theory of finite systems of linear inequalities based on Minkowski theorem and boundary solution principle 07 p1216 A67-19582

Five-variable extreme copositive quadratic forms, presenting previously unknown forms for application to inequality theory and block design analysis 08 p1348 A67-21154

Optimum design of curve generating four-bar linkages with inequality constraint [ASME PAPER 66-MECH-20] 08 p1336 A67-21317

Coercivity inequalities for second order elliptical operators with increasing coefficients 11 p1814 A67-24978

Inequality to derive error estimation of performance of automatic pulse servosystem inside interval of discreteness 11 p1772 A67-25039

Integral inequalities for two functions 12 p1960 A67-25258

Estimations for majorizing functions for solutions of Dirichlet problem for second order elliptic equations or inequalities 12 p1961 A67-25670

Hypothesis of convexity of economic function for generalizing problem of inequalities in nonlinear stochastic programming 17 p2819 A67-32428

First order generalized planetary theory from Poisson form, deriving trigonometric expansion of disturbing functions, periodic inequalities, etc 18 p3120 A67-33865

Uniqueness theorem for Cauchy problem, elliptic equations with double characteristics derived by imposing smoothness condition 20 p3475 A67-36456

Testing procedures for null hypothesis sensitive to ordered alternatives where at least one inequality is strict 21 p3650 A67-37780

Pointwise bounds for perturbed parabolic and elliptic equations using known bounds for corresponding strictly differential problems, noting Rayleigh-Ritz procedure 21 p3652 A67-38174

Inequality for pointwise bounds of second initial boundary value problem for second order semilinear parabolic equation, noting Rayleigh-Ritz method 21 p3652 A67-38176

Axiomatic foundation for continuum thermodynamics theory, discussing first law and second law inequality 22 p3918 A67-39742

Relation between entropy flux and heat flux using entropy inequality and natural invariance principle for materials with fading memory 22 p3918 A67-39742

Popov method extension for absolute stability of nonlinear feedback systems containing distributed elements 23 p3984 A67-40870

Penalty function approach for inequality constrained optimal control problems 24 p4135 A67-42180

INERT ATMOSPHERE

Mineral additive effect on thermal stability of phenolic resins in inert and oxidative atmospheres at atmospheric pressure [ONERA-TP-324] 09 p1520 A67-22155

Inert gas effect on oxygen consumption in living tissue studied by polarographic and Warburg techniques 23 p3960 A67-41706

INERT GAS

S RARE GAS

INERTIA

Inertia and pressure effects on energy potential of homogeneous and isotropic turbulence in weakly compressible medium 02 p0235 A67-12643

Upper and lower bounds of transverse vibrational frequencies of variable cross section cantilever bars, considering transverse shear and rotary inertia effects 05 p0910 A67-16151

Inertia effects of internal liquid column on vibration of thin walled pressurized elastic cylindrical bellows type container [AIAA PAPER 67-38] 06 p0986 A67-18262

Motion of solid body with rotating flywheels rotating at constant velocities relative to inertial space and body 15 p2493 A67-29686

Inertia and muscle tone level effects on intermittence sampling frequency in hand movement control system 17 p2808 A67-33180

Inert thermometers, discussing heat capacity and contact resistance as sources and effect and applications 18 p3050 A67-34502

INERTIA MOMENT

SA ANGULAR MOMENTUM

Moments of inertia calculated for human body as whole and of certain parts in unsupported positions of weightlessness 02 p0187 A67-12325

Inertia constants of rigid bodies determined, using ground vibration tests [ONERA-TP-386] 05 p0786 A67-16476

Measurement of dimensions and inertial properties of 50th percentile anthropometric dummy 08 p1289 A67-20611

Lunar external gravitational field, topographic surface and moments of inertia [AAS PAPER 66-189] 08 p1387 A67-20986

Earth density and elasticity variation reexamined by applying data on earth oscillations and considering earth inertial moment 08 p1325 A67-20985

Differences in lunar moments of inertia determined from libration constants obtained from heliometric observations 08 p1388 A67-21010

Lunar shape in relation to internal structure and moments of inertia found by harmonic analysis 08 p1388 A67-21011

Lunar core and convection in analysis of lunar principal moments of inertia and surface ellipticity 08 p1389 A67-21013

Stability of rotational motion of body with cavity containing ideal fluid, considering fluid motion as potential flow, determining velocity potential and inertia moments 10 p1679 A67-23031

Natural frequency and mode shape for nonuniform simply supported beam, using Fourier series to approximate deflection, mass and inertia moment 11 p1874 A67-24429

Gyroscopic drift from centrifugal inertial moment of gimbal in statically balanced systems, noting dynamic imbalance moment expression 11 p1794 A67-25046

Lunar structure from lunar moments of inertia, noting thick layer denser than lead near surface 17 p2947 A67-32757

Physical libration of moon determined from heliometric observations, obtaining value as function of inertia moment 17 p2950 A67-33125

Minimax fuel requirement of aircraft angular stabilization for undetermined inertial moment probability distribution 19 p3202 A67-35887

Selenodesy, determining gravitational constant-lunar mass product, lunar gravitational field variation, physical librations, inertial moments, lunar tides, lunar radius, etc 20 p3525 A67-36893

Inertia of two-phase asynchronous motor effect on operation of intergimbal correction system of three degree-of-freedom gyroscope 20 p3451 A67-37156

Euler motion generalization of solid body, discussing inertial and kinetic moments 22 p3836 A67-39403

Ground based simulation program for EVA evaluation including center of mass and inertia products of model astronaut 22 p3780 A67-40153

Moon moment of inertia calculated for model with homogeneous core and homogeneous mantle, varying mantle density, core density and core radius 23 p4066 A67-41011

Earth core growth rate by convection used to calculate earth inertia moment changes, hypothesizing day length variation with age 24 p4151 A67-42319

Total principal constraints on I curves in two-dimensional photoelastic medium 24 p4251 A67-42658

INERTIA PRINCIPLE

SA MACH INERTIA PRINCIPLE

Graphical analysis of step-by-step extremal control system adapted to process with second order inertia before static characteristic 03 p0393 A67-13884

General lateral stability and control equations for steep gradient aircraft in terms of equivalent aircraft in level flight without inertial cross coupling 06 p0949 A67-18597

INERTIAL ACCELEROMETER

Soviet book on theory of inertial navigation, autonomous systems 11 p1817 A67-24513

Inertial acceleration indicators which operate on magnetic-restraint principle, employing one or more permanent magnets to create magnetic field 15 p2489 A67-30087

INERTIAL COORDINATE SYSTEM

Inertial system using gyros and accelerometers, determining autonomously plant curvilinear coordinates and plant space orientation parameter 03 p0465 A67-13617

Error equations for Schuler vertical, estimating discrepancy between solutions for various changes in coefficients 03 p0465 A67-14160

Vehicle position determination using relationship between geographic and inertial coordinates, noting distinction between geodetic and geocentric latitudes and geocentric declination 11 p1786 A67-24353

INERTIAL FORCE

SA FROUDE NUMBER

Cavitation effect on braking throttle actuating mechanism loaded with inertial mass 01 p0012 A67-10496

Variations in friction and inertia characteristics of rotary control determined, noting preference ratings of control characteristics 02 p0186 A67-12229

Characteristics of transverse vibrations of p-i-n jointed trusses obtained by use of rational method of lumping inertia forces 03 p0529 A67-14103

Bubnov-Galerkin and energy method solutions of stability and oscillatory motion equations for conical shell under inertial loading 04 p0717 A67-15890

Inertial force effect on stress distribution around blade roots of turbine disk analyzed, using low Young modulus material and stroboscopy 05 p0811 A67-16602

Inertial force effect on propagation of plastic deformation in specimen under dynamic load 05 p0921 A67-16936

Inaccuracies arising from measuring mean value of parameter calculated, using inertial instrument 07 p1187 A67-19739

Temperature distribution, stress distribution and displacement components for circular disk when temperature distribution at disk rim is step function of time, considering inertial terms in thermoelasticity equations 08 p1418 A67-20723

Inertial forces on straight light appendage used as antenna on artificial satellite 08 p1410 A67-20786

Pressure feedback in electrohydraulic servomechanisms for high inertia loads to increase stability, using dynamic analysis and differential equations 09 p1442 A67-21687

Cavitation effect on braking throttle actuating mechanism loaded with inertial mass 10 p1597 A67-23618

Viscous friction in axes of gyroscope suspension further damps of nutational oscillations and increases precession oscillations of inertial vertical 11 p1794 A67-25051

Flexible plate elastic stability under effect of suddenly applied and short term forces 12 p2024 A67-25599

Large deformations of zero moment orthotropic shells of revolution under action of inertial loads caused by centrifugal acceleration of shells 12 p2028 A67-25629

Spectral distribution of turbulent energy, noting space-time correlations, instantaneous motion of fluid, existence of nonlinear inertial forces, etc 17 p2837 A67-32289

Inertial motion of solid body in space of constant curvature, obtaining solution to differential equation 18 p3079 A67-34372

Apparent forces of analytical mechanics for several cases of motion 19 p3261 A67-35049

Test data for heat transfer in vortex flows in tubes with band type swirl generator, determining effect of mass inertial forces 20 p3544 A67-36449

Inertial effects of rotor on synchronous motion of simply supported and cantilever arrangements of rotor shaft systems 20 p3453 A67-36500

Inertial instrument testing with precision centrifuges 22 p3781 A67-40384

Flexural vibration of stiffened circular plates with respect to rotatory inertia, obtaining differential equation 23 p4073 A67-40613

Definition, terminology and classification of experimental accelerations 23 p3961 A67-40765

Autopropulsion of gas bubble by rocket effect noting equivalent particle concept and applications to boiling, flow and cavitation erosion 24 p4141 A67-41904

INERTIAL GUIDANCE

Hypersonic velocity effects on errors in vertical channel of inertial navigation system, particularly aboard artificial earth satellite 01 p0110 A67-10420

Strap-down inertial navigation system compared with gimbaled system, noting methods of attitude reference and angular readout 01 p0110 A67-10489

Rational mechanics principles of inertial navigation and relation to gravitational field structure in vicinity of maneuvering vehicle [ONERA-TP-352] 01 p0110 A67-11088

Space inertial sensors for long-term orbiting satellites and interplanetary missions will require capability of measuring very low-level acceleration inputs 01 p0074 A67-11125

KC-70 low cost inertial navigation system noting use of inertial sensors and digital computers 01 p0076 A67-11256

Inertia stabilized attitude control system for space vehicle, noting selection of compensating network parameters 02 p0331 A67-12160

HF electromagnetic angular displacement signal generator for use in gyro guidance systems 02 p0220 A67-12224

Hughes-USAFA VATE /Versatile Automatic Test Equipment/ system for fault detection and isolation and acceptance testing of inertial guidance equipment 03 p0399 A67-14208

Inertial guidance platform as position sensor, discussing stabilizing gyro, pitch programmer and alignment 04 p0578 A67-15733

Inertial sensors, discussing magnetic resonance and superconductor gyroscopes, ring lasers, fluid dynamical devices, electrostatic gyroscopes, etc 05 p0806 A67-16517

Inertial guidance system accuracy and error sources, determining offset circular-or spherical-target error probabilities by approximate chi-square distribution 06 p1028 A67-17222

Inertial sensors requirements for unmanned planetary missions 09 p1499 A67-22396

Performance errors analysis of navigation using inertial guidance and radar tracking 11 p1817 A67-24334

Hypersonic reentry, inertial guidance tests and construction of two-stage Diamant satellite launcher 15 p2571 A67-30089

Guidance and control technology examining inertial guidance systems, Apollo space system, gyros, accelerometers and computers 16 p2699 A67-30650

Inertial guidance system for ground-to-ground ballistic missiles or space vehicle launchers 16 p2700 A67-30799

Saphir g space vehicle guidance systems consisting of inertial center and computer 16 p2701 A67-30800

Vehicle angular velocity determined, using configurations with only linear accelerometers and no gyroscopes for inertial navigation systems 16 p2675 A67-31266

Error damping procedures for gimbaled inertial navigational systems 16 p2701 A67-31268

Iterative guidance mode with application to three-dimensional upper stage vacuum flight 17 p2881 A67-32058

Lateral-directional stability equations for aircraft with nonzero product of inertial flying along steep flight path gradient 17 p2796 A67-32219

Linear/Monte Carlo method performance evaluation of intercept/rendezvous guidance and navigation for advanced space missions 17 p2882 A67-32493

Strapdown and gimbaled inertial navigation systems history, engineering progress and current developments 19 p3256 A67-35859

Inertial guidance system in ELDO-A satellite launch vehicle performance assessed using onboard computer 20 p3481 A67-37187

Thomson motion equation derivation for variable mass system extended for flight simulation equations for variable mass inertially guided system 22 p3832 A67-40099

Laser gyro development and application noting advantages in cooling, power, starting time and acceleration influence 23 p3999 A67-40916

Inertial guidance technology for

atmospheric motion measurements, discussing system limitations in accuracy and resolution 23 p4026 A67-41444

INERTIAL MEASURING UNIT

Reliability overstress testing of Gemini inertial measuring unit system electronics package, discussing vibration and temperature/altitude environment results 01 p0111 A67-11383

Closed loop system with reference to different gyro stabilization loops present in modern space vehicle inertial measuring unit, using Prony exponential series curve fitting method as analytical tool 03 p0400 A67-14218

Updated inertial navigation of continuously powered space vehicle during lunar landing mission, utilizing altimeter and Doppler radar 22 p3833 A67-40195

INERTIAL NAVIGATION

Ring laser inertial sensor for aerospace systems obtaining high accuracy angular resolution and mechanical simplicity 04 p0625 A67-15665

Time-invariant system of linear perturbation equations for error analyses of rocket boost inertial navigation systems 05 p0839 A67-17353

Design technique for inertial navigation instruments makes it possible to package within instrument electronics necessary to control and operate each of its facilities 05 p0779 A67-17464

Cruise error analysis for strapdown inertial navigation system with pulse torqued instruments in presence of small amplitude oscillations 06 p0947 A67-18007

Inertial navigation equipment applied to meteorological research, using aircraft for vertical gust measurement 06 p1002 A67-18025

AVNI low cost IC airborne digital inertial navigation system with analog input and display, using MOS LSI techniques 08 p1297 A67-20633

General mechanization in vehicular coordinates of gimbaled inertial system for space navigation, obtaining equations for position errors and error damping method 08 p1351 A67-20698

Aircraft inertial navigator performance estimation techniques 09 p1526 A67-22392

Soviet book on theory of inertial navigation, autonomous systems 11 p1817 A67-24513

Inertial navigation system including aircraft interfaces, system modes of operation and performance [SAE PAPER 670329] 12 p1964 A67-25871

Inertial navigation system with damping of oscillations for enhancement of stability of stationary platform 13 p2118 A67-26375

Gravitational satellite stabilization, star tracking, targets and sensors for orientation and inertial navigational instrumentation 14 p2347 A67-27878

Gyroscope for stabilizing inertial navigation platform 14 p2322 A67-29010

Rate measuring strapdown inertial navigation systems, describing gas bearing gyros and three-axis ring laser 14 p2348 A67-29080

Commercial automatic inertial navigator for subsonic and supersonic aircraft provides global navigation and guidance within ATC limits without dependence on external aids 15 p2514 A67-29739

Inertial navigation system and onboard navigation course computer evaluated, noting performance data and circular error 15 p2515 A67-29742

Inertial systems application to airline operation, discussing data insertion, power supply integrity, alignment display, dynamic testing, etc [AIAA PAPER 67-396] 15 p2515 A67-30363

Operational accuracy of inertial navigation system as function of accelerometer and integrator error 16 p2699 A67-30468

New navigation system/ADVANCE/ consisting of two-degrees-of-freedom gyro and accelerometer noting UTM grid-zone distribution system 16 p2701 A67-30928

Inertial navigation horizontal position errors for medium L/D lifting body reentry vehicle using reference altitude for vertical channel stabilization 17 p2881 A67-32476

Stabilization gyros used for monitoring and detecting performance of avionics inertial navigation system, considering failure modes and effects 17 p2881 A67-32488

Gyro-stabilized inertial navigation platform system upgraded by applying sampled model reference system, estimating gyro drift rates by stochastic approximation method 18 p3075 A67-34106

Navigation system for concorde aircraft, considering inertial navigation 19 p3255 A67-35805

Strapdown and gimbaled inertial navigation systems history, engineering progress and current developments 19 p3256 A67-35859

Inertial guidance and navigation systems and components testing facility 1100 feet underground [AIAA PAPER 67-538] 19 p3208 A67-35940

Strapped-down inertial navigation computational problems solved by Euler parameter algorithms require less computer time 21 p3656 A67-38951

Digital temperature compensation and statistical filtering procedures for fast reaction alignment of inertial navigators 22 p3831 A67-39886

Discrete methods for control network implementation using integrated circuitry to reduce inertial navigation systems complexity 22 p3800 A67-40184

Strapdown system application studies related to surface to surface missile, considering angular vibration environment and constant rates about output and spin axes of gyro 22 p3833 A67-40186

Updated inertial navigation of continuously powered space vehicle during lunar landing mission, utilizing altimeter and Doppler radar 22 p3833 A67-40195

Efficient inertial navigation system with He 2 superfluid persistent current gyro element having small drift rate 22 p3808 A67-40395

Book on inertial navigation covering laws of rational mechanics, gyroscopes, accelerometers, platform stabilization and control panels 23 p4025 A67-40633

Satellite navigation systems requirements including Loran, inertial navigation and Navy systems 23 p4025 A67-41363

Kalman-Bucy filter for optimum radio inertial navigation, discussing a priori estimation 24 p4182 A67-42184

Inertial navigation system operation errors on moving power plant due to inaccurate initial data feeding into computer 24 p4182 A67-42300

INERTIAL PLATFORM

SA NAVIGATION INSTRUMENT

Temperature control and complex heat path designs inertial components, platforms and strap-down guidance systems, considering floated gyros and accelerometers 02 p0241 A67-11789

Gimbaled platform thermal control system and design constraints on inertial system housing 04 p0626 A67-15791

Angular acceleration sensor for control system stabilization using MHD principles, obtaining transfer function 08 p1331 A67-20697

Gimbaled unitized stellar reference inertial platform for space missions, noting optical lobing technique 08 p1331 A67-20699

Mark 19 Sperry gyrocompass with SGN 4 inertial platform 14 p2322 A67-28989

Gyroscope for stabilizing inertial navigation platform 14 p2322 A67-29010

Natural oscillations of inertial vertical with nonlinear correction, determining oscillation frequencies and damping rates 16 p2675 A67-31146

Optimum mixer-filter for aircraft navigation systems consisting of inertial platform aided by Doppler and/or Loran designed, using Kalman filtering 17 p2825 A67-32525

Gyrocompassing method used for alignment of inertial platform allows gyro-torquer calibration and gyro drift trimming during procedure 22 p3830 A67-39158

INERTIAL REFERENCE SYSTEM

SA GIMBALESS INERTIAL REFERENCE SYSTEM

Strap-down guidance systems using conventional inertial hardware, discussing computer function, computer selection and system errors 03 p0465 A67-13364

Lorentz invariance of special relativistic thermodynamics equations in inertial frame of observer 04 p0658 A67-15610

Inertial frame of reference for measuring accelerations, considering external galaxies,

stellar system in our galaxy and planetary system 07 p1250 A67-19678

Gimbaled unitized stellar reference inertial platform for space missions, noting optical lobing technique 08 p1331 A67-20699

Selection of gyroscopic reference for commercial aircraft [AIAA PAPER 67-405] 15 p2491 A67-30372

Inertial tracker position error evolution, discussing equations and applicability to vehicle on ground or in circular orbit 17 p2882 A67-32725

Gyro-stabilized inertial navigation platform system upgraded by applying sampled model reference system, estimating gyro drift rates by stochastic approximation method 18 p3075 A67-34106

Strapdown inertial reference and navigation system initial alignment utilizing coordinate-transformation matrix computer [AIAA PAPER 67-556] 19 p3257 A67-35953

Strapdown system application studies related to surface to surface missile, considering angular vibration environment and constant rates about output and spin axes of gyro 22 p3833 A67-40186

Orbital attitude reference system working model using strapped down principles and digital computer 22 p3907 A67-40187

Mach principle manifestation in Jordan extended gravitation theory, calculating rotation of local inertial frame induced by rotating shell of mass 23 p4027 A67-41147

INFECTION

S AIRBORNE INFECTION

INFINITE SOLID

Cosine series analysis of nonuniform internal pressure effect on crack extension in infinite body 04 p0716 A67-15797

Internal fracture of solids analyzing initiation by converging tensile pulses in prolate spheroid and crack propagation in infinite solid 16 p2773 A67-31315

Emissivity and absorptivity of infinite length isothermal trapezoidal grooves with radiating gray walls 18 p3159 A67-34055

Uniformly moving crack in infinite body, in antiplane strain, driven by loads in simultaneous travel 20 p3536 A67-36415

Steady state temperature field and stresses determined for infinite body with linear slit having definite heat resistance 21 p3729 A67-39007

INFLATABLE DEVICE

Expandable gas bag for stowable omnidirectional multiple impact landing system 10 p1714 A67-23755

Expandable gas bag for stowable omnidirectional multiple impact landing system 22 p3904 A67-40097

INFLATABLE STRUCTURE

SA BALLOON

Expandable and modular structures for support on manned space missions, reviewing inflatable, chemically rigidizable, unfurlable and elastic recovery structures 02 p0333 A67-12342

Mechanical construction of two types of Gerdien condenser rocket probes, noting instrumentation racks and inflatable parachutes for descent 03 p0518 A67-13368

Inflatable parachute system developed for deceleration of ionospheric probe instrumentation descending after expulsion from rocket 03 p0359 A67-13369

Nonlinear membrane theory for thin elastic inflatable shells during pressurization phase 11 p1875 A67-24432

Perturbation solutions for finite inflation, under internal pressure, of elastic toroidal membrane of circular cross section 11 p1879 A67-25002

INFLATION

Finite inflation of isotropic elastic toroidal membrane possessing strain-energy function by uniform internal pressure 17 p2956 A67-31932

INFLUENCE COEFFICIENT

Nonlinear influence coefficient obtained by extension of Reissner nonlinear analysis to include uniform pressure loading over surface of spherical shell 01 p0164 A67-11178

Maxwell-Green tensor relating forces to displacements in structural elastic beam, showing role of Maxwell influence coefficient 02 p0336 A67-11482

Vibrational characteristics of inflatable wing model, determining resonant frequencies and mode shapes by using influence coefficients 06 p1100 A67-18002

Transient response of beams using lumped

parameter models calculated by Euler method to eliminate influence coefficient normally required 06 p1111 A67-18889

Computer calculation of induced circulations and influence coefficients for turbine blades with arbitrary profiles and oscillation shift 10 p1591 A67-23044

Individual section dampers relation to modal damping of series mass spring in lumped parameter systems 10 p1729 A67-23770

Natural and forced lateral vibration analysis of free-free beam by integration and finite difference methods, considering influence coefficients [ASME PAPER 67-VIBR-54] 11 p1873 A67-24202

Influence coefficients for stresses at circular holes in shallow cylindrical shells with both flat and curved reinforcements [AIAA PAPER 67-365] 14 p2401 A67-28733

INFORMATION

Two electronic displays for aircraft using basic elements necessary for flight path control in problem of easy assimilation of information by pilot 10 p1601 A67-22905

INFORMATION PROCESSING

Counting errors and amplitude spectra distortion in detectors for statistical characteristics of information contained in signals 01 p0066 A67-10653

Error probabilities for partially coherent diversity reception, noting linearized receiver performance during random noise output 01 p0026 A67-10863

Holography theory and applications, discussing Fresnel and Fourier holographies, interferential information processing, incoherent objects and associative memory 01 p0068 A67-11005

Informal automaton simulating certain processes of information processing by human brain controlled by servosystems 03 p0365 A67-13084

Aerospace technology information transfer to biology and medicine [AIAA PAPER 66-952] 03 p0366 A67-14023

Advanced feedback system simulation technique for strategic planning in business, noting manpower allocation 04 p0739 A67-14498

Probability aspects of information transmission, deriving optimum coding and decoding algorithms 04 p0592 A67-14884

Probabilistic displays and decision making effectiveness in situation with uncertain or fallible information 05 p0757 A67-16308

Information criteria for threshold setting in simple binary hypothesis tests 06 p0962 A67-17948

Radio waves and information transmission, discussing antennas, waveguides, diffraction and scattering modulation theory, etc 06 p0962 A67-18071

Stability analysis of parametric phase-locked subharmonic tunnel diode oscillator circuits capable of bistable phase operation 07 p1153 A67-19610

Magnetic recording process in dynamic magnetic storage method with bias magnetization, using Preisach magnetic particle model for case of static transparency in information carrier 07 p1147 A67-19633

Asynchronous control of information transmission in networks consisting of independent sequential circuits 07 p1161 A67-19884

Data processing and reduction on board spacecraft and on ground using generalized information system 12 p1909 A67-25865

Management control system for technical, production, financial and contractual management of large scale or technical industry programs [AAS PAPER 67-153] 15 p2583 A67-29969

Systems approach for product and test equipment failure information reporting, including cause and corrective and preventive measures 15 p2584 A67-30410

Holography theory and applications, discussing Fresnel and Fourier holographies, interferential information processing, incoherent objects and associative memory 16 p2870 A67-30489

Graphic information acquisition, processing and analysis noting requirements, application of computer, etc 16 p2781 A67-30636

Satellite onboard multichannel systems for information processing, discussing construction, quick response memory and

- block diagrams 16 p2633 A67-30673
 Programming system design for
 incremental data assimilation in open ended
 man-computer information systems 19 p3187 A67-35680
 Sonic film memory for digital information
 storage, discussing block-oriented random
 access memory /BORAM/ 19 p3189 A67-36067
 DODGE satellite vidicon cameras and
 information processing system electronics
 design and performance 20 p3452 A67-37572
 Coded information transmission with
 reduced band emphasizing pulse prediction
 through redundancy, information quantity
 and delta signal 21 p3585 A67-38763
 High sensitivity information storage filter
 for spectrum analysis 21 p3601 A67-39067
 Reactive optical information processing
 maximum efficiency from phase object in
 laser cavity, discussing modulation depth
 and power gain 23 p4002 A67-41270
 Statistical significance of mathematical and
 logical foundations of information processing
 method applied to meteor stream 23 p4070 A67-41690
 Double signal modulation used to increase
 authenticity of information transmission in
 binary systems having resolving feedback 24 p4122 A67-42378
 Computer and information sciences -
 Conference, Columbus, Ohio, August
 1966 24 p4136 A67-42696
 AIDS data processing and analysis system
 for automated fault diagnosis and equipment
 trend prediction, describing methods applied
 to aircraft [AIAA PAPER 67-792] 24 p4126 A67-42953
- INFORMATION RETRIEVAL**
SA DATA RETRIEVAL
 Extremely wideband information storage
 and retrieval systems employing laser or
 electron beam on silver halide or electron
 beam on thermoplastic film 01 p0077 A67-11437
 Cryogenic associative memory system for
 information retrieval 02 p0208 A67-12163
 Microdensitometry in retrieval of data
 recorded on photographic film 06 p1001 A67-17791
 IBM System/360 Model 91 storage system
 design concepts 11 p1755 A67-23952
 Photographically recorded information
 retrieval by isodensitometry [SMPT PAPER 101-89] 12 p1941 A67-25473
 Environmental operations analysis
 function, discussing data accumulation,
 storage and retrieval 12 p1921 A67-25678
 DIALOG /computer implemented retrieval
 system/ capabilities, design, philosophy and
 performance 17 p2819 A67-32468
 Computer memory systems for handling
 Air Force information, discussing types of
 memory, storage techniques and device
 technologies 17 p2819 A67-32473
 Centralized parts and materials reliability
 information center /PRINCE/APIC/
 explaining data storage and retrieval 18 p3007 A67-34659
 Rapid Availability of Information and Data
 for Safety /RAIDS/ system as tool of system
 safety engineering 18 p3007 A67-34703
 Time-shared computer system design and
 application, noting memory, remote
 terminals, program debugging, etc 19 p3186 A67-35678
 Electronic system for measuring operator
 information retrieval in bisensory
 configuration, using video-record radar set
 and playback 20 p3419 A67-37639
 Devices for information exchange between
 man and machine, emphasizing video display
 equipment 21 p3577 A67-38158
 Information Service, computerized storage
 and retrieval system for Apollo spacecraft
 parts, materials and processes 22 p3765 A67-39951
 Writing and use of ground checkout
 procedures in Apollo program using
 computer-assisted editing, publishing and
 information retrieval 23 p3976 A67-41055
 Real time systems and applications 23 p3976 A67-41056
 Radar information automatic extraction by
 digital techniques, outlining information
 quantization, target detection and coordinate
 measurement principles 24 p4122 A67-42407
 Proactive inhibition, recency and limited
 channel capacity under acoustic stress 24 p4116 A67-42701
- INFORMATION THEORY**
SA COMMUNICATION THEORY
 Optimum /in Shannon sense/ truncated
 probability of signal for case of constant
 power and other conditions 02 p0194 A67-11908
 Shannon expression of information entropy
 measure and average uncertainty 02 p0203 A67-12168
 Information model for manual control of
 astronaut motion and space orientation in
 free space 02 p0188 A67-12330
 Dispersion method of spontaneous
 subdivision of image space into compact sets
 /images/ 03 p0374 A67-13081
 Quantum effects in noise-free
 communication channels with infinite and
 limited pass bands in channels with noise, in
 quantum counters and coherent
 amplifiers 03 p0368 A67-13140
 Synthesis of phase synchronization system
 providing maximum level filtering of
 external fluctuation noise, using generalized
 integral criterion 03 p0393 A67-13949
 Optimization via information flow in
 system without memory, discussing ideal
 correction minimal and maximal
 error 04 p0592 A67-14904
 Learning and self-learning in automatic
 control, noting quantitative aspects of
 information theory, solution algorithms and
 convergence criteria 04 p0592 A67-14905
 Shannon model for band-limited time-
 continuous channel to provide more realistic
 model of communication system 04 p0574 A67-15075
 Information theory assessment of
 optimizing criteria and approximation for
 steady state gain of optimum filter, based
 on Wiener type 04 p0586 A67-15639
 Converse of channel coding theorem,
 relating average probability of error to
 distortion measure of source sink pair 06 p0965 A67-17946
 Optimal threshold level resulting in
 minimum residual probability of distortion
 in transmission of pulse coded signals in
 systems with information feedback 06 p0975 A67-18218
 Space communications, present and
 future 06 p0965 A67-19028
 Redundancy reduction methods for data
 compression, noting application to
 photographs of Tiros, Gemini and
 Ranger 09 p1470 A67-22676
 Measurement interpreted as information
 process in terms of exactly defined basic
 concepts of information theory 10 p1654 A67-22756
 Law of propagation of covariance in
 matrix form obtained from least squares
 adjustment 10 p1674 A67-23004
 Information theoretic derivation of limit
 theorem for Markov chain with countable
 number of states and constant transition
 probabilities 11 p1770 A67-24421
 Effects of placing restrictions on
 derivations of unrestricted rewriting
 systems 12 p1962 A67-26120
 Computer-implemented minimization
 techniques used to determine realizability of
 N-variable switching function with single
 threshold-element device 13 p2073 A67-27065
 Information theory research
 development 14 p2269 A67-28456
 Entropy of sequence Y obtained from
 coded sequence of random variables
 X 14 p2292 A67-28935
 Optimal threshold level resulting in
 minimum residual probability of distortion
 in transmission of pulse coded signals in
 systems with information feedback 16 p2642 A67-30484
 Error correction block encoding for high
 speed HF digital data transmission
 system 17 p2811 A67-32112
 Algorithm for converting binary code into
 uniform binary code with maximum
 predetermined number of zero symbols in
 any code combination 18 p2999 A67-33532
 Number of feasible information networks
 with single channel redundancy for remote
 control of telemechanical system 18 p3016 A67-33572
 Indices optimal diagnostic value using
 mathematical evaluation of information
 theory 19 p3186 A67-34889
 Book on probability in communication
 engineering covering probability theory,
 information and reliability theory, random
 processes and noise and random phasor
 sums 20 p3378 A67-36137
 Reliable efficient communication channel
 utilization by use of sequential
 decoding 20 p3384 A67-37348
 Binary pulse compression codes generation
 with low periodic autocorrelation 20 p3386 A67-37493
 Sequential decoding algorithm with
 memoryless channel, obtaining lower bound
 to distribution of computation and limiting
 factor [JPL-TR-32-1121] 20 p3412 A67-37494
 Soviet book on information theory and
 application to problems in automatic
 monitoring and control 20 p3413 A67-37633
- INFRARED ASTRONOMY**
 IR colorimetry of Martian bright and dark
 areas indicates correlations with limonite
 terrestrial rocks and volcanic
 ash 02 p0319 A67-11456
 Liquid nitrogen cooled rocketborne
 telescope, measuring IR signals from diffuse
 and discrete astronomical
 sources 02 p0243 A67-12047
 IR observations of R Monocerotis
 preplanetary system, reporting on flux
 density and circumstellar
 dust 03 p0510 A67-13506
 IR stars as supergiants of very late type
 and not objects in state of gravitational
 contraction as sustained by Penston
 theory 03 p0512 A67-13888
 Ray craters and hot spot on lunar surface
 during solar eclipse [AAS PAPER 66-184] 08 p1387 A67-20959
 Lunar surface optical properties and IR
 emission [AAS PAPER 66-185] 08 p1387 A67-20960
 Carbon dioxide study in Mercury
 atmosphere yields negative results from
 observations made with IR spectrometer and
 61 inch reflector 09 p1565 A67-22016
 IR star in Orion nebula noting
 photometric result, comparing IR flux with
 energy distribution of black body as
 function of wavelength 09 p1567 A67-22239
 Solution of angular distribution of
 outgoing thermal radiation from planetary
 atmosphere, using Chandrasekhar diffuse
 scattering and transmission
 functions 09 p1567 A67-22240
 Wavelength dependence of polarization of
 IR star in Cygnus measured by far IR lead
 sulfide photopolarimeter 11 p1863 A67-24509
 Scanning IR radiometer equipment to
 produce pictorial maps of lunar radiance
 patterns or of possible variations in lunar
 surface composition 15 p2492 A67-30434
 Optical search of sky near X-ray positions
 of Cyg X-1 and Cyg X-2 for identification
 purposes 17 p2937 A67-32649
 Far IR surveys of sky for thermal
 radiation from interstellar grains and other
 sources of far IR radiation, using balloon
 sounding 17 p2952 A67-33362
 Matter density and other physical
 properties of Martian surface estimated
 from radio and IR
 observations 18 p3119 A67-33860
 Lunar surface roughness and brightness
 temperature anomalies from IR image
 study 18 p3134 A67-34537
 Physical parameters of IR nebula
 discovered in Orion 19 p3330 A67-36080
 Intrinsic optical polarization of Taurus IR
 source 19 p3330 A67-36081
 Search for IR stars at various temperature
 ranges reveals dense interstellar clouds, cool
 Mira Stars and circumstellar
 clouds 20 p3523 A67-36647
 IR nebula in Orion as protocluster with
 massive stars imbedded in opaque dust
 cloud, discussing collapse and
 lifetime 24 p4225 A67-41829
 IR line intensity of planetary nebula NGC
 7027, noting presence of measurable
 continuum flux of stellar
 radiation 24 p4225 A67-41830
- INFRARED DETECTOR**
 IR spectral signatures of rocks and soils
 in identifying bulk composition by
 comparison to standard spectral
 curves 01 p0058 A67-10311
 Environmental corrections for airborne IR
 radiation thermometer 01 p0063 A67-10313
 Photovoltaic effect in p-n junctions of
 lead tin telluride diodes indicate potential
 for IR detection throughout 8-14 microns
 atmospheric window 02 p0221 A67-12514
 Coherent homodyne detection at 10.6
 micrometers with aluminum-doped silicon
 photoconductor, presenting noise spectra
 and voltage 03 p0438 A67-13989

Semiconductor lasers and fast IR detectors, discussing InAs, InSb and three types of mercury cadmium telluride detectors 05 p0821 A67-16668

Cooling requirements for intrinsic photoconductive IR detector, comparing theory and experiment 06 p1005 A67-18713

Supersensitive laser light detector for wideband receivers to approach theoretical SNR limit set by noise in signal 07 p1194 A67-19085

IR photovoltaic response, quantum efficiency and V-I characteristics of InSb MOS structures 09 p1551 A67-21577

Background limit to sensitivity of point to point optical communication obtained through signal to noise ratio of optical point detectors under BLIP condition 09 p1462 A67-21641

Microwave optical field distribution patterns visualized using IR thermosensitive transducer method 11 p1792 A67-24714

IR radiation detection by doped semiconductor with induced reflectivity variation 13 p2181 A67-27231

Dynamic components thermal characteristics determination by IR optic techniques, studying metal fatigue, wear and friction phenomena [ASME PAPER 67-DE-24] 14 p2328 A67-28873

Radar, IR and laser sensors production trends for airborne reconnaissance 15 p2485 A67-29163

Detection properties of n-type InSb in microwave and IR ranges, studying impurity and magnetic field effects 19 p3300 A67-34762

IR technology influence on military aircraft design 19 p3173 A67-35932

Minimum detectable signal and frequency response of mercury-doped germanium detector, measuring response time and SNR through optical heterodyne techniques 21 p3590 A67-38009

IR for electronic circuit component diagnosis, discussing design criteria, quality control and acceptance testing 22 p3769 A67-39631

Optical and IR wideband communication between earth and interplanetary spacecraft, discussing tracking, detectors, pointing and beam formation 22 p3762 A67-39960

Josephson junctions as high speed far IR detectors, describing point contact junctions used in experiment 22 p3838 A67-40434

IR detectors analyzed for dependences of detectivities on temperature, noting noise role 24 p4201 A67-41907

Generation-recombination noise voltage in IR detector materials, discussing impurity and intrinsic photoconductors 24 p4201 A67-41909

INFRARED FILTER

Far IR Fabry-Perot interference filters consisting of parallel close-spaced metal meshes 19 p3262 A67-35686

INFRARED HORIZON

Errors of IR-horizon of pickups due to satellite determination of vertical 02 p0240 A67-11541

IR horizon sensor systems for spacecraft attitude determination, detailing field switched edge tracker 04 p0625 A67-15664

Errors of IR-horizon pickups due to satellite determination of vertical 16 p2877 A67-31607

Miniature optically immersed thermistor bolometer arrays employed for earth atmospheric horizon scanning from orbiting vehicles 19 p3231 A67-35684

INFRARED INSPECTION

Indirect techniques such as IR and temperature sensing to overcome limitations of hard-wired test points but still monitor complete ensemble of components in built-in test equipment 03 p0388 A67-14216

Thermal IR inspection technique for bond flaw inspection in simulated solid propellant rocket engines 09 p1508 A67-22528

IR techniques for reliability enhancement of microelectronics 10 p1610 A67-22977

Decomposition rates of hydrogen halides examined behind incident shock waves between 2800 to 4600 degrees K, using IR techniques 11 p1750 A67-24995

Optical IR characteristics of long-time afterglow from high altitude nuclear detonations 18 p3036 A67-33605

Design and development of IR signature analysis technique for nondestructive testing of electronic and electromechanical

assemblies 18 p3052 A67-34512

Microcircuit nondestructive IR inspection and equipment used for mask alignments 19 p3192 A67-35025

IR monitoring technique to improve accuracy of welding inspection using voltage feedback to regulate output 21 p3634 A67-38620

INFRARED INSTRUMENT

Solar chromospheric structure noting network pattern of absorption in He 10830 angstrom region 03 p0514 A67-14312

S-, Se- or Te-based nonoxide chalcogenide glassy systems for airborne IR optical equipment materials 03 p0456 A67-14390

Nimbus II AVCS, APT, HRIR and MRIR sensory data analysis 04 p0613 A67-14801

Three-channel IR-UV rocket radiometer for onboard measurement of exhaust plumes under severe high altitude environmental conditions 06 p1005 A67-18714

Structural stress measurements in terms of induced temperature increments, using IR radiometer 11 p1877 A67-24827

Microwave thermography used to measure microwave optical field patterns, using Czerny IR thermosensitive transducer process 12 p1939 A67-25196

Temperature measurements of grassland, desert and water surfaces using IR radiometer found to compare favorably with miniature thermistors 13 p2117 A67-27606

Performance characteristics of nonstoichiometrically doped p-n junctions in Cd-Hg-Te alloy operated as IR photovoltaic detector 14 p2366 A67-28496

Crystals for UV and IR optics, discussing solubility, hardness, melting, expansion coefficients and design factors 18 p3078 A67-33565

IR imaging system with multiple target capability for measuring IR radiation emitted by missiles during launch, boost and reentry 18 p3052 A67-34532

IR technology and electromagnetic spectrum, discussing manufacture of circulators and isolators using Faraday rotation in InSb 22 p3835 A67-39213

IR Q-switched neodymium glass laser rangefinder performance and advantages 23 p3999 A67-41029

Ground and water surface temperature measurements using IR radiometers onboard aircraft 24 p4181 A67-41789

IR lasers using vibrational rotational transitions of carbon dioxide 24 p4166 A67-41799

INFRARED MASER

Magnetically tunable IR masers of helium-xenon, considering experimental problem in applying tunable IR maser to IR spectroscopy 04 p0632 A67-14764

High resolution spectroscopy using Zeeman-tuned IR maser oscillating at transitions between 3 and 9 microns 05 p0816 A67-16633

Isotope substitution effect on natural frequencies of vibrational-rotational transitions in diatomic and triatomic molecules and generation of new IR maser frequencies 05 p0816 A67-16634

Internal modulation of IR gas laser using cadmium sulfide or selenide single crystals 05 p0824 A67-16914

Visual display of output patterns of IR lasers using heat sensitive phosphors 09 p1500 A67-22433

IR modulator utilizing field-induced free carrier absorption, with expressions for modulation index in terms of geometrical and physical properties of materials 15 p2491 A67-30428

Internal modulation of IR gas laser using cadmium sulfide or selenide single crystals 16 p2685 A67-30891

Continuous IR chemical maser action in carbon dioxide, using chemi-optical resonant pumping 17 p2866 A67-32275

Simultaneous oscillation in UV and IR and interaction of 1st and 2nd plus ve system of bands in molecular nitrogen laser 20 p3461 A67-37292

INFRARED PHOTOGRAPHY

IR imagery and concurrent aerial photography in depicting Arctic terrain features and conditions during daylight 01 p0058 A67-10312

IR imagery application in locating anomalously hot earth in Yellowstone National Park 01 p0059 A67-10332

IR images of lunar crater Tycho during lunar night provide evidence that thermal anomaly is produced by solar rather than internal heat 09 p1565 A67-22013

IR imagery from remote sensing, use in agriculture and forestry [AIAA PAPER 67-281] 12 p1967 A67-26000

Sensors and sensor control devices for use in high speed low altitude reconnaissance-aircraft 15 p2485 A67-29162

Carbon dioxide laser output observation by high resolution thermographic screen 15 p2497 A67-29393

Lunar internal heat flow measured by infrared mapping of polar regions from orbiting satellites 16 p2754 A67-31750

Hydrogen fire visualization detection techniques including application of photography, TV and image converter in IR and UV regions 20 p3445 A67-36540

Problems encountered in preparation of final meteorological radiation tapes, using Tiros IR radiation data 01 p0108 A67-10320

Total emissivity and upper limit of hot water vapor determined from IR spectral emissivity 01 p0167 A67-10973

Absorption spectra models analyzed for use in IR radiation propagation in atmosphere 01 p0109 A67-11043

Profile difference of two IR hydrogen lines in facula and in photosphere 02 p0308 A67-12488

Spontaneous-emission probability and absolute intensity for IR absorption band of nitrous oxide 03 p0467 A67-12854

Electric-field-induced IR absorption in diamond type crystals with Raman-active vibration modes 03 p0492 A67-13260

Air ionization rate behind high speed shock waves, determining electron density from IR emission 03 p0405 A67-14028

Correlation between free IR and acoustic signals produced during optical measuring of heat 04 p0619 A67-14545

Donor electron IR absorption coefficients in semiconductors in 3-10 micron range used to study wavelength dependence 04 p0674 A67-14608

Sum and difference frequency mixing of visible and IR gas laser light in GaP at near reststrahl frequencies and relationship to spontaneous Raman scattering 04 p0682 A67-15464

Lunar IR emission and solar radiation reflected by moon in visible region measured by Luna X orbiter 05 p0886 A67-16052

Transient and steady state IR emission from low-lying vibrational levels of carbon dioxide in laser systems, using DC discharge 05 p0816 A67-16630

Annealing behavior and uniaxial stress response of radiation induced defects in Si causing 1.8, 3.3 and 3.9 micron IR absorption bands examined via EPR studies 05 p0870 A67-17194

Bias and random radiometer errors in estimation of atmospheric downward, upward, net and equivalent IR irradiance 05 p0803 A67-17385

Mechanism regulating total amount of earth and Mars atmosphere transparent to visible and IR radiation 06 p0995 A67-18952

Extreme IR atmospheric absorption calculation shown in graphs and compared with available results in submillimeter and millimeter range 06 p0998 A67-18717

Electric field induced IR absorption in GaAs p-n junction diodes 07 p1231 A67-19553

Elastic wave and IR light interactions with moving high field domain in piezoelectric semiconductor, noting acoustic impedance 07 p1232 A67-19556

IR observations in one to seven micron region using astronomical telescope on Aerobee rocket above atmosphere 08 p1397 A67-21185

Quantum mechanical theory for IR absorption by excitons due to photoionization and intraband lattice scattering 09 p1552 A67-21670

IR transition zone between earth and space studied by gyro-stabilized satellite 10 p1637 A67-23196

Profile difference of two IR hydrogen lines in facula and in photosphere 10 p1702 A67-23356

IR emission measurement of lunar-like materials during simulated eclipse, noting dependence on time [AIAA PAPER 67-290] 12 p2009 A67-26007

Thermal coordinate analysis of lunar IR scan data for directional effects caused by surface geometry, illumination and sensor angle
[AIAA PAPER 67-291] 12 p2009 A67-26008
Detectability of ion recombination free-free emission from H II regions 12 p2011 A67-26252
IR flux for water vapor and flux divergence in atmosphere computed for rate of radiative cooling of atmosphere at coastal and continental stations 13 p2150 A67-26419
Sensor beam, scan mode and perinadir nadir angle determination for Tiros IR data using simplified graph
method 13 p2117 A67-27612
Radiant energy transfer below cloud cover in Venus atmosphere, noting greenhouse effect caused by atmosphere containing components capable of IR absorption 14 p2383 A67-27859
IR radiation measurements by spectrometers flown on board stratospheric balloons, considering sky brightness, vertical distribution and thermal atmospheric emissions 14 p2313 A67-28768
Detectability of massive star from opaque dust cocoon through IR radiation 14 p2388 A67-28833
Coherent resonant absorption and emission in IR and visible spectrum, discussing Lorentz oscillator and Dicke spin model of radiating molecule 15 p2519 A67-29190
Electronic equipment used for IR radiation measurement during space experiment, describing thermal effect detectors [ONERA-TP-465] 15 p2486 A67-29382
Relaxation oscillations in n-type indium antimonide crystal under magnetic field effect and resistivity measurements in far IR 15 p2540 A67-29931
Experimental results on CN laser operated with pulsed or DC discharges 16 p2684 A67-30605
Nitric oxide production reaction rate measured in shock-heated air at high temperatures, with nitric oxide concentration determined by IR emission 18 p2997 A67-33791
IR thermal emission from lunar nighttime surface, noting anomalies location and observational procedure 18 p3134 A67-34497
IR imaging system with multiple target capability for measuring IR radiation emitted by missiles during launch, boost and reentry 18 p3052 A67-34532
Lunar thermal anomalies exhibiting slower cooling rates during eclipse, discussing IR observations 18 p3135 A67-34546
Enhanced radiation energy for visible and near IR during electron emission calculated by energy balance 19 p3176 A67-35081
Spectral composition of earth IR radiation measured from satellites, giving radiation intensity and temperature distributions 19 p3219 A67-35253
Ground based solar electromagnetic radiation environment studies in visible and radio windows 19 p3323 A67-35332
Balloon-borne diffusing system designed to measure absorption of minor atmospheric constituents, as sun set and passed below horizon 19 p3232 A67-35697
IR emission in n-type gallium arsenide samples exhibiting current oscillations due to electron-phonon coupling 20 p3508 A67-36423
Pure capacitance type IR radiation detector concept, comparing various materials as to pyroelectric effect [ACS PAPER 27E-66F] 20 p3459 A67-36644
Mean absorption coefficients for IR radiation of gases expressed as functions of gas spectroscopic and thermodynamic properties [ASME PAPER 67-HT-10] 20 p3545 A67-36708
IR absorption in alkali-halide crystals containing molecular ion impurities caused by intralonic vibrations 20 p3511 A67-37140
Lunar IR emission and solar radiation reflected by moon in visible region measured by Luna X orbiter 21 p3701 A67-37839
Model for lunar surface roughness effect on emission of thermal IR radiation and casting of shadows in sunlight 21 p3702 A67-38188
Limb darkening of earth deduced from statistical analysis of IR radiance data from measurements by Tiros

satellites 21 p3655 A67-38579
Electrical circuits for earth IR radiation emission measurements, describing apparatus and incorporated miniaturized pneumatic receiver 21 p3629 A67-38661
Precursor IR resonance radiation from hypervelocity ablating vehicles observed and related to photon absorption and water vapor presence in air 22 p3917 A67-39712
IR laser rangefinder using neodymium doped rods, noting noise peak value and advantages over ruby laser 22 p3799 A67-39780
Terrestrial surface spectral IR emissivities determined in situ interferometrically, noting igneous and sedimentary rock composition and texture 22 p3805 A67-40354
Planetary atmosphere radiation spectral distribution sounded with 4.3 micron carbon dioxide band to determine temperature profile 22 p3805 A67-40355
IR absorption and Raman scattering spectra of diagonal cubic crystal structures 23 p4037 A67-40758
IR absorption spectrum of n-GaAs noting free carrier contribution due to phonons and ionized impurities 23 p4042 A67-41293
High resistance GaAs residual IR absorption measured to determine incident light intensity fraction, showing low absorption suitable for high power laser modulation 23 p4045 A67-41471
Radiometer using black plate with radiation toward night sky balanced by IR radiation transfer in vacuum 24 p4152 A67-41787
Planetary nebulae IR emission intensities, discussing radiative recombination, ionization equilibrium and fine structure level population 24 p4223 A67-41811
IR C atom multiplet in solar spectrum at 10,700 angstroms, noting C abundance dependence on convective velocities and deviations from black body function and local thermodynamic equilibrium 24 p4237 A67-42655
INFRARED REFLECTION
Paint film thickness of spacecraft coatings, effect on spectral directional reflectance and binormal transmittance in far IR [AIAA PAPER 65-653] 03 p0447 A67-13033
Diffuse spectral reflectance of optically thick cloud and powder layers composed of particles with strong IR resonance, noting effect of particle size [AIAA PAPER 65-667] 03 p0467 A67-13047
Far IR reflectivity of potassium tantalate analyzed as function of temperature, noting soft mode as temperature lowers towards Curie temperature far IR reflectivity of potassium tantalate 10 p1688 A67-22786
Infrared reflectance and optical constants of tektites for origin mode, noting constituent dependence on geographic location 16 p2753 A67-31897
IR reflection spectra of tellurium and zinc doped indium arsenide single crystals, discussing reflection minima and spectral curves given 19 p3306 A67-35705
INFRARED SCANNER
IR and visible images of eclipsed moon made from scan data and magnetically recorded analog signals from observation of total lunar eclipse on December 19, 1964 04 p0697 A67-14741
IR scanning of lunar disk during total eclipse of December 1964, noting hot spots identified with craters or white areas 08 p1392 A67-21086
Synchronized high speed scanning IR spectrometer 13 p2121 A67-27353
Sensor beam, scan mode and perinadir nadir angle determination for Tiros IR data using simplified graph 13 p2117 A67-27612
Spectrometers, utilizing interference filter wedges, for field use, especially in hostile environments 15 p2491 A67-30430
Scanning IR radiometer equipment to produce pictorial maps of lunar radiance patterns or of possible variations in lunar surface composition 15 p2492 A67-30434
Design of receiver circuitry for IR surveillance system having high signal detectability 17 p2882 A67-33289
IR scanning nondestructive testing program for microwelds to evaluate quality 20 p3454 A67-36666
INFRARED SPECTROMETER
Balloon-borne Czerny-Turner grating

spectrometer used to measure atmospheric transmittance in spectral regions between 2 and 14 mu 07 p1184 A67-19389
Synchronized high speed scanning IR spectrometer 13 p2121 A67-27353
Inconsistency in Martian surface pressure as calculated by Gray explained, using Leighton and Murray observations 14 p2389 A67-28842
Spectrometers, utilizing interference filter wedges, for field use, especially in hostile environments 15 p2491 A67-30430
Spectra of noble gases in 4-micron region, using IR spectrometer equipped with cooled lead sulphide detector 18 p3082 A67-33876
Near IR grating spectrometer converted to multiplex instrument by adding encoding disk in spectrum plane 20 p3437 A67-36339
Scintillation and dynamic range problems mitigated for Fourier spectrometry by rapid scanning 20 p3438 A67-36342
INFRARED SPECTROPHOTOMETER
IR spectral emittance measurements of optical materials by comparison with black body radiation at same temperature 03 p0470 A67-14392
Nitrogen presence in solar material, using measurements of high resolution spectrophotometric record of Fraunhofer spectrum [AFRL-67-0479] 15 p2554 A67-29516
IR spectrophotometer developed for airborne study of spectral energy distribution in atmospheric self-radiation 19 p3227 A67-34859
Gas chromatography and IR spectrophotometry used to examine monomethyl hydrazine air oxidation, showing evidence of surface catalyzed reaction 21 p3578 A67-38841
Carbon influence on copper precipitation in dislocation free silicon single crystals with low oxygen, discussing growth mechanism and edge dislocation 21 p3686 A67-39136
Contamination detection by analytical instrumentation considering sampling, IR, atomic absorption spectrophotometer, gas chromatography, colorimetry and polarography 23 p3998 A67-40844
INFRARED SPECTROSCOPY
SA RAMAN SPECTROSCOPY
Carbon dioxide abundance at 200 degrees K determined from high dispersion IR spectrograms of Mars 03 p0514 A67-14309
Magnetically tunable IR masers of helium-xenon, considering experimental problem in applying tunable IR maser to IR spectroscopy 04 p0632 A67-14764
High resolution spectroscopy using Zeeman-tuned IR maser oscillating at transitions between 3 and 9 microns 05 p0816 A67-16633
Unsaturated polyester styrene, showing via gas chromatography and IR spectroscopy effect of reticulation on pyrolytic decomposition 05 p0759 A67-16768
IR spectroscopy using Michelson interferometer coupled with computer and wave analyzer 07 p1190 A67-20272
Book on IR spectroscopy covering molecular spectroscopy, lattice vibrations, semiconductor electronic effects, IR detectors, far IR, etc book on IR spectroscopy covering molecular spectroscopy, lattice vibrations, semiconductor 08 p1353 A67-20762
Photometric, polarimetric and IR study of lunar surface including polarization of moonlight, thermal measurements, lunar radar echo signals, etc 08 p1395 A67-21160
IR absorption in high purity boron films, showing absence of absorption peaks at 2-15 microns 09 p1533 A67-22132
IR spectroscopy of absorption and emission in hydrogen-fluorine flames for more data on high temperature spectral properties of HF 10 p1697 A67-23134
Absolute frequency measurement and spectroscopy of gas laser transitions in far IR, analyzing Zeeman effect 11 p1802 A67-24830
Radar, radio astronomic and IR spectroscopic observations of Venus surface and atmosphere, examining general and surface data, chemical composition and atmospheric model 11 p1867 A67-24843
Photoelectric observation of Fraunhofer line profiles by high dispersion solar spectrograph 13 p2198 A67-26706

Refractive index dispersion of CdSe and CdTe crystals in visible and infrared spectral range at room temperature 16 p2732 A67-31481

Vaporization by dissociation of amine-type perchlorates revealed by infrared spectroscopy, proving role of proton transfer reaction in perchlorates thermal decomposition 16 p2619 A67-31536

Spectral purity of Ebert type far IR grating spectrometer determined, noting experimental technique 17 p2863 A67-33300

Spectral composition of earth IR radiation measured from satellites, giving radiation intensity and temperature distributions 19 p3219 A67-35253

IR reflection spectra of tellurium and zinc doped indium arsenide single crystals, discussing reflection minima and spectral curves given 19 p3306 A67-35705

Asymmetric interferogram for spectral transmittance measurements in magnitude and phase obtained by far IR Michelson interferometer 20 p3437 A67-36335

Fourier spectroscopy in far IR for routine investigation through Michelson and lamellar grating interferometers 20 p3437 A67-36340

IR spectroscopy by variable wavelength semiconductor lasers 20 p3439 A67-36354

INFRARED SPECTRUM

SA NEAR INFRARED

IR spectral signatures of rocks and soils in identifying bulk composition by comparison to standard spectral curves 01 p0058 A67-10311

Spectral polarimetry signature of terrestrial and planetary materials through remote sensing 01 p0059 A67-10331

Flashlight/incoherent/pumping of visible and IR, InSb and CdS-CdSe lasers 01 p0089 A67-10447

Optical transmittance of fused silica at elevated temperatures, showing shift in UV to IR absorption with increasing temperature 01 p0138 A67-11074

Spectral scans of Mars and region of moon in IR range obtained with 82-inch telescope reduced, using scans of moon and sun, to spectral reflectivity curve 02 p0319 A67-11454

IR brightness temperature of Uranus used to establish current lower limit at which brightness temperature of celestial object can be measured 02 p0324 A67-11773

Calibration procedures for earth albedo experimental package of Orbiting Solar Observatory 02 p0246 A67-12401

Lunar disk color index derivation by applying method of photographic photometry in UV and IR spectral regions 02 p0329 A67-12493

Transmittance increase of silicon film when illuminated by silicon dioxide layer in long wave IR spectrum 03 p0488 A67-12891

Far IR reflection spectra of silicate mineral at room and liquid nitrogen temperatures [AIAA PAPER 65-668] 03 p0508 A67-13048

Optical or inertial electron mass dependence on N-concentration in IR spectrum of n-type GaAs monocrystal with S, Se and Te impurities 03 p0490 A67-13161

Paraformaldehyde hypothesis of IR spectrum of Saturn ring 03 p0509 A67-13167

Panoramic facsimile camera for unmanned space operation providing 360 degrees IR and visible spectrum imagery [SMPTE PREPRINT 100-40] 03 p0423 A67-13806

Transmission spectra of GaS, GaSe, InSe and TlSe single crystals obtained at 300 degrees K by means of IR spectrometer 04 p0676 A67-14932

Vapor phase IR spectrum of planar structure of trimethylenecyclopropane 04 p0566 A67-15511

Stark and Zeeman splitting in far IR spectra of erbium, dysprosium and samarium ethyl sulphate 04 p0686 A67-15778

Frequency shift and absorption bands in IR spectra of some alpha,omega-dinitroxy alkanes 05 p0758 A67-16367

IR optical properties of vanadium dioxide above and below transition temperature 05 p0680 A67-16380

IR spectra of Mars bright areas compared with terrestrial rock, drawing conclusions regarding Mars mineralogy and detrital cover 05 p0896 A67-16717

Carbon dioxide solid matrix study of carbon trioxide production, IR spectrum and molecular structure 05 p0759 A67-16838

Impurity IR photoconductivity of silicon surface doped with gold 05 p0871 A67-17491

Spectral transmission of far IR Michelson interferometer with dielectric film beam-dividers 06 p1005 A67-18716

Transmittance increase of silicon film when illuminated by silicon dioxide layer in long wave IR spectrum 06 p1054 A67-18769

Two-phonon IR absorption and Raman scattering spectra to provide information about phonon spectra of crystals and phonon-electron interaction in filled valence bands 06 p1059 A67-18907

Lattice IR reflection and transmission spectra and Raman spectrum of monocrystalline and hot pressed pellets of ZnSe 06 p1059 A67-18909

IR spectra of undoped and Li doped ZnSe and CdS 06 p1059 A67-18911

Anomalous temperature dependence of IR absorption in p-type germanium attributed to phonon induced effects 06 p1060 A67-18913

Impurity centers arising from sulfur in silicon identified, using IR absorption technique and uniaxial stress effect 06 p1061 A67-18924

Interband magnetoabsorption of InSb, noting anomalies caused by enhanced polaron self-energy 06 p1066 A67-18956

Optical problems when making IR astrophysical observations with balloon-borne telescope noting data documentation, focusing, image slicer, spectrometer, aberration correction, etc 07 p1184 A67-19388

Image analyzer tube for IR TV based on phenomenon of accumulation at semiconductor junctions 07 p1189 A67-20158

Rapid remote sensing of lunar surface by IR spectrum matching technique using simple matching device or scanning instrument 08 p1385 A67-20935

IR observations for presence of ethane in atmospheres of Jupiter and Saturn reanalyzed and found consistent with previous results 08 p1398 A67-21218

IR laser emission at cryogenic temperatures and various wavelengths obtained from diodes of lead tin selenide and lead tin telluride 09 p1551 A67-21571

Transmission of artificial quartz at room temperature, obtaining optical constants in far IR region 09 p1553 A67-21917

Molecular vibrational rotational parameters measured with IR heterodyning technique 09 p1535 A67-22136

IR spectra of low temperature stars of type M, N/R/ and S, as well as NML objects in Cygnus and Taurus, noting atmospheric differences 09 p1566 A67-22224

Faraday effect optical isolator for IR region using lead glass rod in magnetic field as nonreciprocal element 09 p1500 A67-22425

Optical or inertial electron mass dependence on N-concentration in IR spectrum of n-type GaAs monocrystal with S, Se and Te impurities 10 p1690 A67-23108

Lunar disk color index derivation by applying method of photographic photometry in UV and IR spectral regions 10 p1708 A67-23361

Black body radiation deduced by analyzing spectrum of lightning in near IR at very high temperatures 11 p1816 A67-24755

IR spectral techniques for satellite geodetic surveying, discussing spectral matching techniques for discriminating between different types of rocks [AIAA PAPER 67-284] 12 p1938 A67-26001

Thermal properties of moon by comparing IR and microwave measurements of spectrum with theoretical calculation of upper layer temperature distribution [AIAA PAPER 67-289] 12 p2009 A67-26006

Visible and near IR spectral reflectance and emittance at high temperature of ablation chars, carbon and graphite [AIAA PAPER 67-326] 12 p2037 A67-26040

Fe IR line excitation in solar corona, noting abundance of iron relative to H and linear polarization of IR lines in coronal streamer 12 p2010 A67-26242

Identification of forbidden nitrogen IR multiplet in Fraunhofer spectrum 14 p2382 A67-27848

Transmission of artificial quartz at room temperature, obtaining optical constants in far IR region 14 p2365 A67-28246

IR spectrum evaluation procedures and optical measurement as applied to

atmosphere physics 14 p2311 A67-28401

Trifluoramine oxide IR spectrum measured, determining structure, symmetry and rotational, vibrational and thermodynamic properties 15 p2433 A67-29880

Infrared lattice vibration spectra of II-VI compounds analyzed by Drude dispersion, obtaining transverse-optical-mode frequency 16 p2724 A67-30603

Mid-IR spectral emittance measuring apparatus, discussing range of performance, systems response, etc 16 p2677 A67-31429

IR lattice spectra of rare earth iron garnets noting absorption in low frequency bands and molecular weights 16 p2733 A67-31880

Refractive index of amorphous boron films determined from interference of transmission curves 16 p2734 A67-31884

Forbidden nitrogen I lines in IR solar spectrum, computing oscillation frequencies, nitrogen abundance and equivalent widths, comparing predictions to observational results 17 p2948 A67-32819

IR absorption measurements of Li localized vibrational modes in Li and Te doped GaAs 17 p2922 A67-33066

Spectral brightness, reflectivity and polarization characteristics of clouds in IR band, measuring angular structure of underlying radiation field 18 p3073 A67-33563

Design problems in IR optical systems including materials limitation, reflection losses, environmental requirements, etc 18 p3078 A67-33566

IR chemiluminescence in hydrogen-diatom bromine and hydrogen-hydrogen bromide IR chemiluminescence in hydrogen-diatom bromine and hydrogen-hydrogen bromide 18 p2996 A67-33786

Lunar surface absorption coefficient in IR range, discussing limb-darkening, reflectivity, subsolar point temperature, radiation, spectral properties, etc 18 p3122 A67-34139

IR spectra of gaseous, solid and matrix-isolated HNCS and DNCS, studying frequency shift, bending modes, fundamental vibrations, gas phase, etc 19 p3181 A67-35016

Balloon-borne Michelson interferometer for far IR solar spectrometry 20 p3438 A67-36344

Isotope shifts measurement in IR with variable length laser cavity 20 p3439 A67-36355

Transitions in neutral spectra observed in near IR wavelength region in noble gases 20 p3460 A67-36859

Optical glass selection for design of double-lens objective for IR region of spectrum, considering aberrations 20 p3451 A67-37157

Stimulated Raman scattering in IR active nontotally symmetric vibration of alpha quartz crystal, noting parametric oscillation 21 p3641 A67-38459

Conductivity and IR absorption spectra of organic semiconductors in polycrystalline, melt and liquid states 22 p3861 A67-39922

Airborne multiple scan interferometry for low temperature IR emission spectral distribution of minerals 22 p3807 A67-40368

Symmetry of phonons and rules of corresponding selection for IR absorption and Raman diffusion for two phonons 23 p4026 A67-40689

UV light photolyzing ozone dispersed in solid carbon dioxide matrix causes formation of new substance showing IR absorption 23 p3971 A67-40970

IR vibrational and Raman spectra of thiophosphoryl trichloride, thiophosphoryl dichlorofluoride, thiophosphoryl chlorodifluoride and thiophosphoryl trifluoride 23 p4041 A67-41242

Far IR spectra and space group of crystalline hydrazine and hydrazine-d4 noting coupling of translational and librational motions 23 p4048 A67-41532

Wavelengths and intensities of IR coronal lines of silicon and magnesium ions from airborne total solar eclipse observations 24 p4224 A67-41822

INFRASONIC FREQUENCY

Virtual reflection-height oscillations and infrasonic waves in ionospheric F layer 06 p0995 A67-17974

Infrasonic and hydromagnetic wave propagation in atmosphere and ionosphere measured by array of underwater and acoustic sensors 13 p2122 A67-27701

Atmospheric wind effects on guided

- propagation of VLF infrasonic waves over long distances, including variable wind and temperature profiles 13 p2117 A67-27702
- Rocket engine noise study in infrasonic range from launching pad ignition phase through flight phase, including ignition signals from upper stages 14 p2393 A67-28053
- Sensor and calibration techniques for measurement of infrasonic and gravity waves moting error control and possible applications 16 p2677 A67-31430
- Infrasonic waves from auroral and magnetic activity, origin in superionic movement of large scale auroral forms 17 p2841 A67-32209
- Viscoelastic properties of capron under torsion at infrasonic frequencies and polymer resin complex shear modulus temperature dependence 21 p3647 A67-37866
- Oscillating mass flow characteristics in modified Moore variometer configuration for step, triangular and infrasonic functions 23 p4000 A67-41221
- Infrasonic wave anisotropic radiation from moving auroras analyzed using shock wave model, discussing sound propagation and ray tracing 24 p4147 A67-41882
- INGESTION**
- Pressure patterns, gas ingestion and sealing capacity of viscoelastic investigated using oil, water and liquid sodium as sealed fluids 03 p0428 A67-13226
- Parametric data on gas ingestion and ground proximity jet effects experienced by jet-powered VTOL configurations [AIAA PAPER 67-440] 18 p2985 A67-33917
- INHALATION**
- Muller maneuver/forced inhalation with closed glottis/ improves tolerance to negative G 12 p1901 A67-25172
- INHIBITION**
- Enzymatic activity and inhibition, thermal stability and electrophoretic properties of induced and constitutive acid phosphatases of *Escherichia coli* 10 p1598 A67-23397
- INHIBITOR**
- Quenching diameter of premixed fuel-oxidizer flames by volatile inhibitors, noting nature of oxidizers, particularly oxygen 02 p0342 A67-12031
- Aircraft exfoliation corrosion, discussing methods for prevention in fastener holes 07 p1210 A67-20087
- Protein synthesis reduced and turnover stimulated by valine in *P. saccharophila* in nonaerobic inducing conditions 13 p2058 A67-26584
- Kinetic mechanisms in combustion peninsula of three-limit explosion reactions with trace inhibitors, studying quadratic chain-breaking processes by static method 18 p3156 A67-33848
- INHOMOGENEITY**
- Inhomogeneity parameter for excited atom distributions and line width variations for dispersion contour of spectral line, noting dependency on frequency 01 p0125 A67-11045
- Inhomogeneity parameter over cross section of spectral line contour for case of Doppler distribution 01 p0125 A67-11046
- Electron microscopy analysis of microinhomogeneities in commercial Si used in preparation of p-n junction devices 02 p0257 A67-12434
- Successive approximations for determining direct and backward wave in inhomogeneous medium and consequently reflection coefficient and total field 03 p0467 A67-12893
- Successive approximations for determining direct and backward wave in inhomogeneous medium and consequently reflection coefficient and total field 06 p1034 A67-18771
- Graphical and analytical solutions to wave propagation in inhomogeneous media in conditions of wave number variations oscillating along coordinate 06 p1034 A67-18814
- Electron concentration inhomogeneities during traveling gravity wave propagation through F layer 07 p1178 A67-19809
- Stochastic waveguides containing media with constitutive parameters having random variations not necessarily small or statistically homogeneous [SR-2] 09 p1460 A67-21593
- Effect of weak random inhomogeneities on long distance wave propagation, calculating first two statistical moments 09 p1461 A67-21595
- Effect of ligation inhomogeneity on superconducting properties of ternary alloy, noting enhancement of critical current density in wire prepared from this alloy 10 p1689 A67-23089
- Laser holography combined with schlieren techniques to measure ray deviations in optically inhomogeneous field of transient phenomenon 11 p1794 A67-24927
- Ionospheric inhomogeneity winter drifts during periods of high and low solar activity 14 p2308 A67-27936
- Motion and dispersion of inhomogeneity in unbounded plasma in magnetic and electric fields 14 p2359 A67-28504
- Plasma azimuthal inhomogeneity in homopolar system, noting Hall current and stationary plasma 15 p2529 A67-29723
- Ionospheric electron density profiles obtained by dispersive Doppler from beacons on research rockets, noting inhomogeneities [AGARDOGRAPH 95] 15 p2483 A67-30296
- Drift azimuths, sizes and displacements of spatial inhomogeneities in oxygen atom emission at 5577 angstroms during night airglow 17 p2848 A67-32952
- Inhomogeneous temperature field arising during laser welding of different materials with imperfect contact, deriving and solving heat conduction equations 18 p3053 A67-33630
- Excess carrier distribution in inhomogeneous semiconducting rectangular plate under two illumination conditions 19 p3308 A67-36026
- Inhomogeneous plasma oscillations, studying drift and flute instabilities and dielectric constant 20 p3492 A67-36130
- Reflected wave amplitude dependence on degree of inhomogeneity of medium 21 p3580 A67-38112
- Spicules and inhomogeneities in corona and interplanetary plasma compared assuming mutual relationship spicules and inhomogeneities in corona and interplanetary plasma compared assuming mutual 21 p3711 A67-39028
- Inhomogeneity formation probability in initially homogeneous Friedmann universe inhomogeneity formation probability in initially homogeneous Friedmann universe 22 p3891 A67-40493
- Exact equation for potential oscillations of inhomogeneous plasma cylinder via Fourier transformations, discussing drift, cyclotron oscillations and flute instability 23 p4034 A67-41679
- Duhamel principle for internal radiation field in inhomogeneous finite atmosphere based on existence and uniqueness theorem for Milne integral 24 p4189 A67-42598
- Complex wave propagation and coupling in inhomogeneous media, discussing WKB type amplitude coefficients and electromagnetic and space charge waves 24 p4123 A67-42657
- INITIAL VALUE PROBLEM**
- Geocentric initial conditions for motion of bodies leaving moon surface after initial instantaneous thrust 01 p0148 A67-10387
- Continuous automatic interval computation for numerical integration of initial value problem 01 p0105 A67-10515
- Slow decay of solution of initial boundary value problem for wave equation in exterior of three-dimensional smooth star-shaped body 01 p0052 A67-10519
- Extension of Waltman theorems regarding oscillation and asymptotic behavior of solutions of nonlinear differential equation, proving solution existence for initial value problem 01 p0105 A67-10730
- Normal burning velocity theory, considering Cauchy problem for initial equations 01 p0167 A67-10998
- Disturbance theory linearized initial value problems for free trajectories passively moving above smooth earth surface 02 p0320 A67-11465
- Kantorovich theorem, Goodman-Lance method and two-point boundary value problems, noting numerical results obtained on IBM 7094 computer 02 p0259 A67-11836
- Cauchy problem for Euler-Poisson-Darboux equation solved for all values of time and specified values of parameter 02 p0260 A67-12431
- Pointwise bounds for solutions of first initial boundary value problem for second order semilinear parabolic equation 03 p0460 A67-13821
- Integral transform associated with boundary conditions containing eigenvalue parameter applied to initial boundary value problem arising in diffusion theory and heat flow 03 p0460 A67-13825
- Exact difference replacement for hyperbolic equation system where $n \times n$ symmetric matrices become coefficients of vectors in two-dimensional space 03 p0460 A67-13880
- Initial value formulation of Chandrasekhar problem for diffuse reflection of radiation from planetary atmosphere 03 p0462 A67-13903
- Parabolic conditions for general second order PDE, discussing bicharacteristic condition, initial boundary value problem, Monge-Ampere equations and quasi-linear equation systems 03 p0461 A67-14105
- Successive approximation solution of initial value problem, noting convergence of sequence 04 p0642 A67-14481
- Implicit difference methods for initial boundary value problems based on Wiener-Hopf factorization 04 p0645 A67-15085
- Uniqueness and existence theorems for mixed problem of second order degenerate hyperbolic equation with discontinuous coefficients 05 p0834 A67-16494
- Pointwise bounds for linear and nonlinear second initial boundary value problem of parabolic type 05 p0836 A67-17046
- Optimum thrust programming for sounding rocket extended by reducing state to single variable to obtain sufficient conditions for specific extremal solution 05 p0906 A67-17225
- Statistical initial value problem for Burger model equation of turbulence, examining velocity correlation functions, energy spectra and other statistical properties 05 p0794 A67-17419
- Boundary value problem for heat equation, discussing Laplace transform solution and uniqueness theorem 06 p1111 A67-17645
- Asymptotic kinetic equation for inhomogeneous plasma compared to results for initial value problem and Bogolubov method 06 p1042 A67-18572
- Constant pressure turbulent jet mixing between two compressible nonisoenergetic streams of identical composition with finite initial boundary layer effects 06 p0992 A67-18880
- Truncated elliptic systems of partial differential equations for reducing two-point boundary value problems in vector space to initial value problems by projection 08 p1348 A67-21192
- Initial and boundary value problems in compressible fluid flow with moving boundaries governed by Navier-Stokes equation 08 p1322 A67-21384
- Difference assessment between secular and long period perturbations generated by similar initial conditions for celestial mechanics problems 09 p1563 A67-21637
- D'Alembert initial value problem for cylindrical waves, obtaining linearized potential equation for plane and symmetrically spherical case 09 p1488 A67-21932
- Stability of stepwise solution methods of initial value problems for second order differential equations 09 p1524 A67-21935
- Stability of Pehlberg method when applied to solution of initial value problems for second order differential equations 09 p1524 A67-21936
- Numerical solution of class of nonlinear high order differential equations with two-point asymptotic boundary conditions for thermal boundary layers in laminar and turbulent flow 10 p1627 A67-23560
- Digital computer analysis of inviscid two-dimensional parallel flow stability, using finite difference method to solve resulting initial value problem 11 p1778 A67-24220
- Independent cometary orbit correction permitting checkout of initial coordinate and velocity components 11 p1868 A67-25084
- Weinstein results for pointwise monotone growth and convexity extended in norm to certain Cauchy problems of second order differential equations 12 p1961 A67-26063
- Structures of solutions and expansion of radial heat equation with pole type data function 13 p2145 A67-26492
- Numerical solution of initial and boundary value Rayleigh problems for nonlinear Krook equation at large wall velocities 13 p2102 A67-26968
- Characteristic initial value problem for

linear second order hyperbolic partial differential equation 13 p2147 A67-27180
 Stability of solutions of Navier-Stokes equations for boundary value problem and convergence to steady state 13 p2106 A67-27455
 Dielectrophoretic methods for positioning cryogenic liquids in zero gravity environment, solving one-dimensional nonlinear problem for time history 13 p2106 A67-27642
 Existence theorem for initial value problems in differential equation leading to Volterra integral equation in several variables 13 p2149 A67-27736
 Small one-dimensional deviations of plasma parameters from equilibrium state, obtaining exact solution in form of inverse Laplace integral 14 p2353 A67-27754
 Constant and variable coefficient initial and boundary value problems for second order differential equations 14 p2343 A67-28626
 Continuous solutions of Cauchy problem for linear first order PDEs with discontinuous coefficients, noting conditions imposed 14 p2344 A67-28905
 Numerical analysis of PDEs with singular coefficients, noting equivalence of stability and convergence 15 p2510 A67-29519
 Order and asymptotic form of error of numerical methods for solving initial value problem for differential equations 15 p2471 A67-29632
 Family of periodic orbits around triangular libration points in restricted three-body problem 15 p2557 A67-29876
 Transformation of class of boundary value to initial value problems in terms of one or two-parameter group of transformations for ordinary differential equations 15 p2511 A67-29892
 All Markov transition functions in denumerable state space satisfying prescribed initial condition with given matrix 17 p2878 A67-32734
 Vlasov equation for anisotropic electron plasma in external magnetic field solved by Laplace transform of density perturbation in initial value problem 17 p2907 A67-33104
 Separation and stall of impulsively started elliptic cylinder including interactions between boundary layer and outer flow [ASME PAPER 67-APM-31] 17 p2840 A67-33157
 Constructing solution of Cauchy initial value problem when Riemann function is unknown for one-dimensional linear viscoelasticity 18 p3139 A67-33428
 Schwarzschild criterion for convective instability in general relativity extended to Einstein hydrostatics to formulate buoyancy principle with aid of initial value problem 18 p3133 A67-34375
 Schwarzschild criterion validity, reducing initial value problem for hydrodynamic perturbation equation to time independent problem 18 p3029 A67-34737
 Collisionless electron plasma dynamics in one dimension, investigating nonlinear Vlasov equation for Landau damping and instability 18 p3092 A67-34747
 Glow discharge positive column response to external perturbations, obtaining moving striations profile, structure and backward wave nature 19 p3273 A67-35094
 Charge, current, and self-consistent field transport properties of collisionless plasma derived using initial value solutions to Vlasov equation 19 p3285 A67-35343
 Transport phenomena in electronic plasma as initial value problem noting distribution function relaxation 19 p3287 A67-35355
 Linearized system of water waves initial value problem, obtaining eigenvalue with parameter in boundary condition 19 p3210 A67-35703
 Initial conditions effect on transient states of linear systems 19 p3205 A67-35909
 Operators spectrum properties and corresponding singular eigenfunctions encountered in plasma problems, showing application to initial and boundary value problems 20 p3494 A67-36148
 Longitudinal oscillations and Landau damping of electron plasma with fixed ion background, discussing initial and boundary value problems 20 p3494 A67-36150
 Existence and uniqueness of classical solutions of nonstationary boundary and initial value problem in

MHD 20 p3497 A67-36430
 Finite difference scheme based on Douglas-Rachford implicit alternating direction method for nonstationary Navier-Stokes equation initial value problems 20 p3423 A67-37213
 Formulating Cauchy problem and mixed problem for second order self-adjoint equation, establishing initial data and boundary value dependence 20 p3479 A67-37657
 Inequality for pointwise bounds of second initial boundary value problem for second order semilinear parabolic equation, noting Rayleigh-Ritz method 21 p3652 A67-38176
 Trajectory optimization initial value problem, considering various conditions, methods of solution and reentry heating minimization 21 p3703 A67-38440
 Flat plate bending and two-dimensional, axisymmetric and boundary value problems in elasticity theory investigated using Vlasov initial function method 21 p3725 A67-38792
 Master matrix containing initial values of geomagnetic inclination and gyrofrequencies for storage in computer memory to calculate ionospheric vertical profiles 21 p3623 A67-39046
 Perturbation theory for solving initial and boundary value problem in unsteady MHD flow past thin symmetrical bodies with inwardly diffusing magnetic field 22 p3850 A67-39707
 Initial value problem with vanishing energy density at infinity investigated for interstellar gas oscillations 24 p4224 A67-41815
 Prandtl limit behavior near zero skin friction, with perturbation methods generalizing Poiseuille and Couette flows 24 p4142 A67-42170
 Three-dimensional disturbance after perturbation of supercritical Poiseuille flow between parallel planes treated by initial value method 24 p4144 A67-42562
 Hyperbolic noninvariance in partial differential equations, discussing existence theorems for nonhyperbolic initial value problem systems 24 p4178 A67-42727
 Integral equations for nonlinear problems in partial differential equations, including Volterra, boundary value and initial value problems 24 p4180 A67-43088
 Difference methods for soft solutions to partial differential equations, discussing initial value problem 24 p4180 A67-43090

INITIATION

S INDUCTION

INJECTION

SA BLOWING
 SA CARRIER INJECTION
 SA FLUID INJECTION
 SA FUEL INJECTION
 SA GAS INJECTION
 SA ION INJECTION
 SA LIQUID INJECTION
 SA SECONDARY INJECTION

Injection electroluminescence of p-n junctions in GaP doped with tellurium, zinc, ZnO, etc 14 p2368 A67-28531
 Injection electroluminescence of p-n junctions in GaP doped with tellurium, zinc, ZnO, etc 23 p4039 A67-40938

INJECTION LASER

S CHEMICAL LASER

INJECTOR

SA PUMP

Thermodynamics of injector of magnetohydrodynamic power unit using two-phase vapor-liquid metallic working fluid 16 p2607 A67-30591
 M-1 injector baffles, ablative chamber and start system design and development, using subscale testing [AIAA PAPER 67-461] 18 p2988 A67-33932
 Hydrogen plasmoids produced by pulsed two-cascade injectors, using electron guns for plasma ionization and acceleration 19 p3297 A67-35597

INJUN III SATELLITE

Frequency spectra of VLF hiss near auroral zone analyzed by Injun III satellite 04 p0614 A67-14958
 Temporal variations of intensities of electrons of various energy ranges trapped in outer radiation zone measured by research satellite Injun III 04 p0693 A67-14962
 Injun III rocket orbital parameters determined by optical and radar observations to provide inclination values

for studying upper atmosphere rotational speed 17 p2952 A67-33251

INJURY

S BACK INJURY
 S BRAIN INJURY
 S BURN INJURY
 S CRASH INJURY
 S EJECTION INJURY

INLET

SA AIR INLET
 SA CONICAL INLET
 SA DUCT
 SA HYPERSONIC INLET
 SA SUPERSONIC INLET
 Finite length inductive MHD generator, solving inlet and outlet effects on boundary value problem 13 p2165 A67-26613
 Subsonic diffuser with vortex generator as integral design feature for supersonic transport aircraft inlet [AIAA PAPER 67-464] 18 p2983 A67-33935
 Fan-in-wing aerodynamics evaluated for datum inlet with circular arc lips with and without vanes [AIAA PAPER 67-746] 23 p3928 A67-40980

INLET FLOW

Circumferential asymmetry in axial flow compressors 01 p0008 A67-11272
 Uniform wall suction effect on inlet flow of porous cylindrical tube, noting laminar to turbulent transition 03 p0404 A67-13973
 Finite difference solution of parabolic equation for laminar heat transfer in inlet of rectangular duct as function of wall temperature and Nusselt number for different aspect ratios 04 p0728 A67-15805
 Circumferential inlet velocity distortion effect on normal force response and stall characteristics of rotating blade in axial flow turbomachine 06 p0938 A67-18255
 Three-dimensional internal flows in intakes and exhaust nozzles computed by combined characteristics and finite difference method [AIAA PAPER 67-224] 06 p0942 A67-18518
 Inlet/door performance characteristic of VTOL lift engines studied in full scale wind tunnel tests [AIAA PAPER 66-655] 09 p1438 A67-22490
 Turbulent boundary layer of gas mixture with dissociation flowing at inlet section of tube 11 p1782 A67-24961
 Boeing SST inlet, control and power system development, discussing test program, design objectives and cost [SAE PAPER 670318] 12 p1990 A67-25886
 Flow fields of inlets for real or perfect gases determined through four methods for application to supersonic and hypersonic flight regimes [AIAA PAPER 66-605] 13 p2050 A67-26831

Motion equation of non-Newtonian fluids in initial section of cylindrical tube 18 p3024 A67-33539
 Attenuation of circumferential inlet distortion in multistage axial compressors, predicting flow field and pressure distortion via zero axial clearance approximation [AIAA PAPER 67-415] 18 p2982 A67-33902
 Velocity and pressure fields in viscous incompressible fluid flow in inlet of flat channel 20 p3423 A67-37066
 Axial compressor inlet stator tests determining pressure loss relationship to geometric parameters 20 p3516 A67-37082
 Circumferential inlet velocity distortion effect on normal force response and stall characteristics of rotating blade in axial flow turbomachine 21 p3565 A67-38536
 Fuel burnout processes in inlet flow of secondary air stream to turbine combustion chamber determined by working mechanism in inlet section of chamber 22 p3869 A67-40453

INLET PRESSURE

Nacelle design for high inlet pressure recovery and low external cowl drag, for high by-pass fan engine subsonic aircraft [SAE PAPER 660733] 01 p0140 A67-10633
 Subsonic-transonic drag of supersonic, two-dimensional and axisymmetric plug inlets 13 p2051 A67-27592
 Boiler inlet impedance frequency response in single tube heat exchanger when pumped with oscillating flow 22 p3916 A67-39396
 Gas dynamic self-regulation of supersonic nozzle consisting of cylindrical channel with central body, measuring nozzle inlet and static pressures 22 p3868 A67-39544

INNER RADIATION BELT

SA ARTIFICIAL RADIATION BELT

SA OUTER RADIATION BELT
SA VAN ALLEN BELT
Captured proton intensity measurement in inner radiation belt in Brazilian anomaly, using satellites Proton I and
05 p0878 A67-16089
Explorer XII observations of charged particles in inner radiation zone after solar activity maximum and before Star Flsh explosion
08 p1378 A67-21471
Satellite measurements of electron flux and electron energy spectra in inner radiation belt
13 p2191 A67-26324
Long term measurement of trapped electron environment in narrow region of space at lower edge of inner radiation belt
14 p2380 A67-28051
Inner Van Allen belt proton dose rate and spectral charged particle environment profiles correlated, noting agreement with theoretical values
19 p3313 A67-35189
Inner zone electron intensity distribution model for solar activity
19 p3219 A67-35238
Energetic proton flux measurements in magnetosphere using sounding rocket, discussing radial diffusion
20 p3518 A67-36998
Low energy, positive ion flux from inner radiation zone, noting losses due to charge exchange, night sky emissions and lifetimes
21 p3697 A67-37996
Captured proton intensity measurement in inner radiation belt in Brazilian anomaly, using satellites Proton I and
24 p4212 A67-42765

INORGANIC COATING
Wing-fuselage section panels of hypersonic aircraft built by brazing welded refractory honeycomb
10 p1660 A67-23171
High endurance thermionic cathodes for Kaufman thrusters, discussing emissive coatings and emissive layer starvation
[AIAA PAPER 67-678] 21 p3696 A67-38929
High emittance coatings radiation characteristics investigated for space applications, considering thickness effect on high temperature emittance and space environment effect at moderate temperatures
[ASM PAPER C6-4.3] 23 p4020 A67-41404

INORGANIC COMPOUND
Anisotropy due to molecular structure orientation in vitreous inorganic glass fibers, noting phase equilibrium
21 p3648 A67-37880

INPUT
Resonance methods for measuring input admittance of low power electronic tubes of type used in telemetry, radar and TV over frequency range from 50 to 1000 MHz
02 p0279 A67-11462
Stability and asymptotic stability of control systems with multiple nonlinearities and inputs, using frequency criterion in connection with transfer function
06 p0973 A67-17601
High resolution flying-spot scanner as input device for computer simulation of optical character-recognition systems
18 p3006 A67-34403
Optimum output-input characteristic of memoryless nonlinear system determined from solution of integral
20 p3407 A67-36382

INSECT
SA DROSOPHILA
Radar observation of insects in free flight, noting backscatter and velocity measurement results
[AFCRRL-67-0127] 03 p0371 A67-13916
Tracks of dot angels, insects and birds obtained by ultrasensitive multiwavelength radars
04 p0569 A67-14680

INSERT
Insert size, shape and core undercut diameter and depth effect on insert tensile strength of honeycomb sandwich fasteners
02 p0248 A67-11943

INSERTION
Microwave swept frequency measurements on RF transmission line systems and development of VSWR and insertion loss test set
01 p0039 A67-11038
Cost-and labor-saving advantages of automatic and semiautomatic insertion of components in circuit
08 p1335 A67-20748
Superconducting microwave filters, discussing minimum insertion loss, loss dependence on various factors and effect of peak fields on maximum

power
14 p2289 A67-28915
Microwave direct-coupled cavity filter design using single insertion loss formula for case of Chebyshev equal-ripple characteristic
17 p2828 A67-33084

INSOLATION
Space environment effect on refractive optical systems, particularly solar radiation effect on optical properties of glass
08 p1330 A67-20644
Thermal performance of insulated current carrying leads for cryogenic apparatus
13 p2229 A67-27663

INSPECTION
SA INFRARED INSPECTION
SA QUALITY CONTROL
SA X-RAY INSPECTION
Inspector role in prelaunch checkout of space system hardware
05 p0930 A67-17241
Ultrasonic immersion inspection apparatus for structural defects detection in turbine blades
06 p1007 A67-18103
Ultrasonic nondestructive inspection of adhesively bonded components, discussing pulse echo reflection, pulsed through transmission and sweep frequency coupling methods and scanning equipment
09 p1507 A67-22526
Estimating maintenance man-hours per flight hour for business turbojet airplanes
[SAE PAPER 670228] 13 p2053 A67-27294
Quality program planning criteria for NASA contracts involving NPC
20 p3556 A67-36602
Maintenance schedule for small commercial aircraft fleet, periodic inspection check principles and engine reliability program
24 p4094 A67-42277
Fail-safe design, nondestructive testing and inspection facilities at design stage for aircraft structures
24 p4250 A67-42442

INSTABILITY
SA COMBUSTION INSTABILITY
SA MAGNETOSPHERIC INSTABILITY
SA PLASMA INSTABILITY
SA SPUTTERING
SA TAYLOR INSTABILITY
SA THERMAL INSTABILITY
SA WHIRL INSTABILITY
Two-cell solution to vorticity equations in unstably stratified atmosphere
06 p1026 A67-18565
Stability-instability transition of equilibrium configuration of linear elastic system under nonconservative follower forces
06 p1105 A67-18589
Three diagonal conducting wall MHD generators, discussing time averaged behavior, instabilities and working fluid conductivity
12 p1898 A67-25381
Frequency domain instability criteria generated from stability criteria for time varying and nonlinear feedback problems
15 p2455 A67-29167

INSTALLATION
French installations for space research, describing laboratory work and industrial investments for satellite launching
14 p2320 A67-28606
High bypass ratio turbofan engine installation noting induction system, exhaust system, thrust reverser configuration requirements, accessories, etc
[AIAA PAPER 67-390] 15 p2548 A67-30358

INSTALLATION MANUAL
AFSCM 375-5 as methodology for system engineering, discussing management, documentation, applications, development, operation, design, etc
18 p3161 A67-33494

INSTRUCTION
Cost effectiveness criterion for instruction repertoire selection for aerospace computer
17 p2820 A67-32502
Instructional broadcast satellites programming methods to reduce educational cost of students time without adding to technological cost
[AIAA PAPER 67-787] 24 p4258 A67-42950

INSTRUMENT
SA APPROACH AND LANDING
INSTRUMENT
SA ELECTROMAGNETIC INSTRUMENT
SA ELECTROSTATIC INSTRUMENT
SA FLIGHT INSTRUMENT
SA INFRARED INSTRUMENT
SA MAGNETIC INSTRUMENT
SA OPTICAL INSTRUMENT
SA RECORDING INSTRUMENT
SA SOLAR INSTRUMENT
Mechanical suspensions for instrument components
06 p1007 A67-18061

INSTRUMENT APPROACH
Houston intercontinental airport planning and development for supersonic jet, superjet and SST aircraft
22 p3779 A67-39374

INSTRUMENT ERROR
Accuracy of real-time tracking of space vehicles using radar or L-shaped interferometer
01 p0110 A67-10266
Environmental corrections for airborne IR radiation thermometer
01 p0063 A67-10313
Error theory for counter frequency meter
01 p0063 A67-10415
Statistical correlation theory of accuracy and error relationships of sensing element during parametric excitations caused by random vibrations
01 p0064 A67-10417
Bias and variability errors in analog data reduction equipment
[SAE PAPER 660716] 01 p0028 A67-10605
Digital computer compensation of strain gauge data to extend measuring bandwidth to transient or HF phenomena
01 p0030 A67-11098
Thermocouple errors resulting from heat conduction along thermocouple wire embedded in low conductivity ablative material indicate helicoil wire for optimum design
01 p0071 A67-11104
Transducers role in problems associated with accurate and precise measurements during static firing tests of solid propellant motors
01 p0073 A67-11111
Technique to monitor system noise and automatic digital system qualification using data obtained by shunt calibration and proper analysis
01 p0073 A67-11112
Apollo Guidance and Navigation System positioning by electrically torquing gyros, discussing error sources
01 p0073 A67-11115
Octantal error of frequency band over which Adcock direction finder operates, noting observed and true bearing relation of arriving signal
01 p0027 A67-11327
Errors of IR-horizon pickups due to satellite determination of vertical
02 p0240 A67-11541
Boresight error in radar caused by effect of radome material and means to avoid it
02 p0215 A67-11973
Angular section errors effect on directive gain coefficient of parabolic antenna with automatic phasing
02 p0215 A67-11975
Fluctuation of stellar images and analysis of systematic errors in guidance of telescope as result of atmospheric refraction and flexure of telescope
02 p0241 A67-11993
On-line estimation of states and parameters for noisy discrete nonlinear dynamic system
02 p0226 A67-12153
Error probability of binary receivers for digital transmission over radio channels characterized by specular and selective fading components
02 p0203 A67-12166
Contact resistance variation effect on strength tests, noting strain gauge reading error magnitudes
02 p0340 A67-12444
Accuracy testing of Zeiss stereocomparator
03 p0419 A67-13263
Reversible dekatron counter pulse-to-voltage converter, noting maximum conversion error
03 p0425 A67-14265
Cardan error of directional gyro on rocking base, with application to aircraft
03 p0425 A67-14281
Constant component of Cardan error of directional gyro subject to regular rocking
03 p0425 A67-14282
Oscillating field of vessel effect on accuracy of readings of gyrocompass with negative fluid/pendulum
03 p0425 A67-14283
Different rotation bearings as method of reducing bearing friction and directional gyro errors from random disturbances
03 p0425 A67-14285
Optimum continuous electrical correction of dynamic characteristics of inertial pickups
03 p0426 A67-14286
Radiation losses effects on temperature measurements with transparent sheathed thermometers
03 p0426 A67-14344
Error in R-meter measurement of velocity spread of meteorological targets resulting from radar frequency instabilities
04 p0648 A67-14673
Confidence limits for pointing error of gimbaled sensor relative to off-gimbaled reference, detailing sources of error and statistical properties
04 p0620 A67-14872
Algorithms in ZAM-2 computer program to calculate recording error parameters of

linear scale measuring device 04 p0621 A67-14918

Fourier transform used in correction of instrument contour error when observing solar spectral line profile 04 p0624 A67-15564

Time-invariant system of linear perturbation equations for error analyses of rocket boost inertial navigation systems 05 p0839 A67-17353

Bias and random radiometersonde temperature errors effects in estimation of atmospheric downward, upward, net and equivalent IR irradiance 05 p0803 A67-17385

Inertial guidance system accuracy and error sources, determining offset circular-or spherical-target error probabilities by approximate chi-square distribution 06 p1028 A67-17722

Doppler frequency measurements in satellite transmissions and use for geometric geodesy 07 p1144 A67-19771

Percentile specifications of orthogonal components and of additive errors of guidance systems 08 p1350 A67-20674

Micrometer U-tube manometers for medium vacuum measurements 08 p1332 A67-21493

Measurement accuracy of deflection data for industrial specimens 08 p1333 A67-21534

Design and operation of reference temperature compensator in thermoelectric temperature gauge 09 p1496 A67-21690

System error limit in determining equilibrium position of sensing element of ground gyrocompass 09 p1498 A67-22036

Vacuum gauge calibration error with conductance-determined pressure divider 09 p1498 A67-22109

VHF ILS equipment achieves necessary instrumental accuracy for automatic landing operation 09 p1529 A67-22643

Dead time instability effect on neutron monitor performance 10 p1699 A67-22799

Transducers, transmission systems and display and implementation systems of radio telemetry and effect upon measurement 10 p1605 A67-22997

Error of measurement of mean square value of fluctuation signals due to voltmeter calibration 10 p1607 A67-23451

Potential sensitivity of energy radiation detectors, examining measurement error causes for radiation power of natural and artificial sources 10 p1607 A67-23569

Structural design of large orbiting radio telescope employing structural flexibility rather than rigidity for dimensional accuracy 10 p1723 A67-23698

Performance errors analysis of navigation using inertial guidance and radar tracking 11 p1817 A67-24334

Trajectory measurement errors for powered spacecraft using matrix analysis [AIAA PAPER 64-650] 11 p1817 A67-24335

Reading errors of oscillating plant mounted gyrocompass assuming gyromoment compensation and no friction, determining motion through differential equation 11 p1794 A67-25045

Mean declinations correction for Talcott pairs of 191 stars from zenith telescope observations 11 p1868 A67-25088

Kinematic coupling effect in stabilization axes of flight vehicle as result of errors in gyrocompass gimbals and coordinate system 11 p1870 A67-25101

Recovery factor associated with moving fluid temperature measurement is dependent on thermodynamic and transport properties of fluid, noting probe errors 12 p1928 A67-25353

Integration of abbreviated motion equations for gyroscopes, obtaining expressions for gimbal errors 12 p1945 A67-25967

Systematic local errors in radio leveling of aircraft for different scales and tracks, using aerial camera 13 p2118 A67-26462

Errors, due to inaccurate tentative aerial observations, in determination of identification points for vertical aerial photography 13 p2118 A67-26464

Gemini VII star sightings analyzed, using handheld space sextant in Gemini VI, discussing effect of bias, timing angle measurement and trajectory errors 13 p2154 A67-26817

Heat balance in rocketsonde semiconductor thermometers, noting dissipation constant dependence on altitude and solar radiation 13 p2117 A67-27608

Linearized manual space navigation incorporating redundant measurements to compensate for instrumentation inaccuracies 14 p2347 A67-28128

Reversible dekatron counter pulse-to-voltage converter, noting maximum conversion error 14 p2321 A67-28777

Error possibility in temperature measurements of 30-60 km region, noting solar irradiation effects on thermistor bead 15 p2474 A67-29202

Measurement errors of arrival direction of radio whistler caused by propagation in earth-ionosphere waveguide 15 p2436 A67-29480

Confidence limits for percentile analysis of guidance system errors 15 p2515 A67-29740

Selection of angular rigidity of shock absorbing system of gyroscopic device 15 p2490 A67-30173

Laser interferometers for metrology applications, considering sources of error 15 p2501 A67-30411

Operational accuracy of inertial navigation system as function of accelerometer and integrator error 16 p2699 A67-30468

Photoelectric method measuring separation of head shock wave from supersonically-moving body, detailing equipment design and operation 16 p2674 A67-31128

Dollar consequence functions for producer and consumer risks due to product faults noting optimization 16 p2782 A67-31257

Errors of IR-horizon pickups due to satellite determination of vertical 16 p2877 A67-31607

Calibration system for PRESS optical aircraft program utilizing portable collimators 16 p2679 A67-31796

Modes of boresight shift in conical-scan and sequential-lobing types of amplitude sensitive angle-tracking antennas 17 p2814 A67-32523

Systematic boresight and off-boresight tracking errors in planar monopulse phased rectangular arrays produced by analog phase shifters with nonlinear transfer characteristics 17 p2825 A67-32617

Inertial tracker position error evolution, discussing equations and applicability to vehicle on ground or in circular orbit 17 p2882 A67-32725

Unidentified landmark navigation from orbiting vehicle by computer simulation, noting instrumentation accuracies 17 p2882 A67-33018

Errors in high temperature electric-resistance strain gauge measurements 18 p3142 A67-33892

Grid electrostatic probe for ionospheric measurement of electron density and temperature, examining measurement errors due to environmental disturbances 18 p3048 A67-34225

U.S. Navy Doppler geodetic Tranelet system configuration and operation, discussing tropospheric and ionospheric refraction, timing and frequency errors 18 p3003 A67-34241

Lunar Planetary Laboratory selenodetic measurement precision and comparison with contemporary selenodetic triangulations 18 p3131 A67-34323

Various boundary layer parameters and transducer shape effect on Measurement error of random pressure field by finite size transducer 19 p3228 A67-34964

Transient Stark and Zeeman spectral line shifts in plasma emission measured with multiple beam Flzeau interferometer, discussing instrument errors 20 p3439 A67-36351

Instrument errors in HF radio rangefinder 20 p3446 A67-36632

Blockage effects of centrally located sample on reflectance measurement by modified integrating sphere [ASME PAPER 67-HT-54] 20 p3447 A67-36736

Thermocouple surface temperature measurement errors in space simulation chambers due to heat conduction and radiation of wires [ASME PAPER 67-HT-57] 20 p3447 A67-36739

Ambient temperature variation effect on gravitational acceleration variations as measured by gravimeter, discussing possible measurement errors 20 p3450 A67-37030

Gyrotachcelerometer errors in measuring object angular velocity and acceleration relative to one axis, deriving differential equations of motion 20 p3451 A67-37155

Doppler frequency measurement error due to short fading relative to time constant of automatic phase control loop 21 p3584 A67-38674

Motion equation derivation permitting analysis of gyrosystems mounted on fixed or moving plants, determining instrument errors 22 p3795 A67-39230

Carrier frequency measurement accuracy using panoramic radio receiver, discussing statistical estimate of errors using two different reading methods 22 p3772 A67-39871

Lunar rendezvous spacecraft guidance system performance for various initial conditions and instrument errors simulated by Monte Carlo computer program 22 p3832 A67-39961

Error of three degrees of freedom static gyro motion owing to viscous friction moments in suspension in case of irregular rocking of base 22 p3810 A67-40484

Equivalent temperature of cosmic microwave background radiation at 3.2 cm wavelength, discussing Dicke type radiometer and error sources 23 p4063 A67-40922

Differentiation between true variation, amplitude and statistical instrument error, deriving diurnal variation amplitude and phase distribution expressions 23 p4059 A67-41131

Temperature effect on zero shift of piezoelectric crystal accelerometers under shock loading using Hopkinson bar technique 23 p4006 A67-41376

Dead time instability effect on neutron monitor performance 24 p4209 A67-42135

Digital computer compensation of strain gauge data to extend measuring bandwidth to transient or HF phenomena 24 p4155 A67-42290

Inertial navigation system operation errors, on moving power plant due to inaccurate initial data feeding into computer 24 p4182 A67-42300

INSTRUMENT FLIGHT RULE /IFR/

Handling quality evaluation of seven general aviation aircraft of type operated under instrument flight conditions 06 p0947 A67-18200

Sensory input overload effects on performance of civil aviation pilots during simulated instrument flights in Link AN 2550-1 trainer 09 p1455 A67-21726

Human reaction to intermittent photic stimulation in environmental chamber under IFR conditions 17 p2807 A67-31966

Computer simulated flights of manual control for VTOL IFR operations indicate display and control subsystem deficiencies 17 p2808 A67-33183

INSTRUMENT LANDING SYSTEM

Method for plotting aircraft along prescribed paths, particularly for manually controlled complete instrument landings 04 p0550 A67-14548

Aircraft radio guidance system combining ILS and precision approach radar 04 p0653 A67-15042

Low clouds effect on ILS jet landing at Bombay airport during monsoon season, noting airfield climatology data 05 p0838 A67-16711

Centering accuracy, off-course sensitivity, mean modulation depth and relative tone phase of ILS signal measurement improved by phase locked detection technique 06 p0957 A67-17577

Ground monitoring system for ILS localizer signals reflected from landing aircraft 06 p0957 A67-17578

TALAR ground-to-aircraft microwave transmission landing approach system for use in conjunction with instrument landing system /ILS/ crosspointer indicator 08 p1028 A67-17721

Far field localizer and glide path monitoring for ILS installations, noting spaced antennas system and receiver for detection of radio interference 07 p1222 A67-19653

Instrument landing system transmitter monitors for automatic blind landing, noting near field monitors and internal monitors 07 p1222 A67-19654

ILS equipment for category III all-weather landing 07 p1222 A67-19671

Antenna systems and equipment providing ICAO Category I-III performance for ILS, analyzing configurations for localizer, markers, etc, calculating glide slope course

- ends 08 p1351 A67-20696
- En-route guidance system using ILS 08 p1351 A67-20696
- calization techniques for both en-route 08 p1351 A67-20696
- navigation and landing 09 p1528 A67-22634
- High integrity guidance for approach and 09 p1528 A67-22634
- landing, noting VHF ILS system and 09 p1528 A67-22634
- downwind antenna system 09 p1529 A67-22638
- VHF ILS equipment achieves necessary 09 p1529 A67-22638
- instrumental accuracy for automatic landing 09 p1529 A67-22638
- operation 09 p1529 A67-22643
- Ground integrity monitor for category III 09 p1529 A67-22643
- ILS for use with automatically landing 09 p1529 A67-22643
- aircraft 09 p1529 A67-22644
- STAN 37-38-39, designed to meet 09 p1529 A67-22644
- operational requirements of category III all- 09 p1529 A67-22644
- weather landings and providing ground 09 p1529 A67-22644
- beacon requirements of ILS 09 p1529 A67-22644
- systems 09 p1529 A67-22645
- Audiofrequency ILS /phase II/ used with 09 p1529 A67-22645
- PAF generator to check ILS 09 p1529 A67-22645
- instruments 11 p1745 A67-24554
- Electronics package for category II 11 p1745 A67-24554
- qualified jet business aircraft and function 11 p1745 A67-24554
- of system components 11 p1745 A67-24554
- [SAE PAPER 670254] 12 p1941 A67-25504
- ILS as guidance component of all-weather 12 p1941 A67-25504
- automatic landing system, discussing 12 p1941 A67-25504
- operational need and specific 12 p1941 A67-25504
- vulnerabilities 13 p2154 A67-26985
- Radio propagation influence on 13 p2154 A67-26985
- performance of azimuth channel of ILS 13 p2154 A67-26985
- defining characteristics of ILS signals 13 p2154 A67-26985
- relevant to monitor 13 p2154 A67-26985
- design 13 p2154 A67-26986
- Instrumentation development making it 13 p2154 A67-26986
- possible to land safely under poor visibility 13 p2154 A67-26986
- conditions, goal being zero-zero 13 p2154 A67-26986
- landing 14 p2347 A67-28990
- Soviet book on aircraft navigation covering 14 p2347 A67-28990
- theory, earth shape, map use, coordinate 14 p2347 A67-28990
- systems, instrumentation and aeronautical 14 p2347 A67-28990
- astronomy 19 p3254 A67-34894
- Instrument-landing system including 19 p3254 A67-34894
- microwave apparatus 19 p3255 A67-35807
- Ground requirements for instrument 19 p3255 A67-35807
- landing systems noting approach lighting, 19 p3255 A67-35807
- runway marking, taxi guidance and blind 19 p3255 A67-35807
- navigation 19 p3255 A67-35807
- [AIAA PAPER 67-756] 23 p3933 A67-40989
- INSTRUMENT ORIENTATION 23 p3933 A67-40989
- Gaseous laser oscillations in Fabry-Perot 23 p3933 A67-40989
- resonator with corner-cube prism noting 23 p3933 A67-40989
- alignment characteristics 12 p1953 A67-25454
- INSTRUMENT PACKAGE 12 p1953 A67-25454
- Scientific lunar payload communications 12 p1953 A67-25454
- system 02 p0196 A67-11999
- Instrumenting techniques for models 02 p0196 A67-11999
- under aerodynamic transient 02 p0196 A67-11999
- heating 11 p1793 A67-24826
- Electronics package for category II 11 p1793 A67-24826
- qualified jet business aircraft and function 11 p1793 A67-24826
- of system components 11 p1793 A67-24826
- [SAE PAPER 670254] 12 p1941 A67-25504
- Book on reusable protective packaging of 12 p1941 A67-25504
- military, electronic and aerospace 12 p1941 A67-25504
- instruments and systems 22 p3771 A67-39832
- INSTRUMENTATION 22 p3771 A67-39832
- SA AIRCRAFT INSTRUMENTATION 22 p3771 A67-39832
- SA BIOINSTRUMENTATION 22 p3771 A67-39832
- SA MICROINSTRUMENTATION 22 p3771 A67-39832
- SA RADAR INSTRUMENTATION 22 p3771 A67-39832
- SA ROCKET INSTRUMENTATION 22 p3771 A67-39832
- SA SATELLITE INSTRUMENTATION 22 p3771 A67-39832
- SA SPACECRAFT INSTRUMENTATION 22 p3771 A67-39832
- Instrumentation and control for magnetic 22 p3771 A67-39832
- pulse metal forming including pulse 22 p3771 A67-39832
- generation, energy transfer, electrical 22 p3771 A67-39832
- operations, etc 22 p3771 A67-39832
- [SAE PAPER 660066] 01 p0078 A67-10569
- Long-term biomedical instrumentation in 01 p0078 A67-10569
- Air Force space program 01 p0017 A67-11029
- Air monitoring instruments used in 01 p0017 A67-11029
- detection and control of air 01 p0017 A67-11029
- pollution 01 p0050 A67-11037
- Fixed voltage, fixed energy and variable 01 p0050 A67-11037
- voltage variable energy pulsed neutron 01 p0050 A67-11037
- devices and applications in nuclear 01 p0050 A67-11037
- propulsion, radiation dosimetry, velocity 01 p0050 A67-11037
- measurements, etc 02 p0266 A67-12216
- Instrument methods determining function 02 p0266 A67-12216
- and density of length distribution of random 02 p0266 A67-12216
- radio emissions 03 p0369 A67-13586
- Range instrumentation developments for 03 p0369 A67-13586
- trajectory measurements including 03 p0369 A67-13586
- cinetheodolites and tracking radars, noting 03 p0369 A67-13586
- error sources, weapons systems problems, 03 p0369 A67-13586
- etc 04 p0568 A67-14436
- Papers from Scientific Research Institute 04 p0568 A67-14436
- of Hydrometeorological Instrument Design 04 p0568 A67-14436
- covering radiosonde, sensing elements, 04 p0568 A67-14436
- etc 07 p1187 A67-19736
- Bimetallic sensing elements calculation 07 p1187 A67-19736
- method employed by Russian Scientific 07 p1187 A67-19736
- Research Institute of Hydrometeorological 07 p1187 A67-19736
- Instrument Design 07 p1187 A67-19736
- Inaccuracies arising from measuring mean 07 p1187 A67-19736
- value of parameter calculated, using inertial 07 p1187 A67-19736
- instrument 07 p1187 A67-19739
- Queueing model of many-instrument visual 07 p1187 A67-19739
- sampling 07 p1136 A67-20172
- Test platform isolated from random long 07 p1136 A67-20172
- period ground tilts used in calibration of 07 p1136 A67-20172
- gyroscopes, accelerometers, 07 p1136 A67-20172
- etc 08 p1314 A67-20580
- Book on modern analytical design of 08 p1314 A67-20580
- instrument servomechanism noting computer 08 p1314 A67-20580
- programming, optimization, amplifier 08 p1314 A67-20580
- saturation, gear stiffness, 08 p1314 A67-20580
- etc 08 p1332 A67-21171
- Book on range instrumentation covering 08 p1332 A67-21171
- optical, radar, support systems, 08 p1332 A67-21171
- etc 10 p1604 A67-22992
- Instrumentation for ballistic pendulum 10 p1604 A67-22992
- shock accelerometer calibrator provides 10 p1604 A67-22992
- readout and display of peak 10 p1604 A67-22992
- amplitudes 12 p1943 A67-25708
- Instrumentation in space and laboratory - 12 p1943 A67-25708
- Conference, Boston, October 12 p1943 A67-25708
- 1966 12 p1943 A67-25850
- Apparatus for particulate smokes 12 p1943 A67-25850
- generation, control and sampling, noting 12 p1943 A67-25850
- combination with angular scanning 12 p1943 A67-25850
- spectropolarimeter 12 p1946 A67-25982
- Stability analysis of minimum variance 12 p1946 A67-25982
- estimations used to self-calibrate missile 12 p1946 A67-25982
- tracking instrumentation 12 p1946 A67-25982
- complex 13 p2120 A67-26815
- Instrumentation development making it 13 p2120 A67-26815
- possible to land safely under poor visibility 13 p2120 A67-26815
- conditions, goal being zero-zero 13 p2120 A67-26815
- landing 14 p2347 A67-28990
- Range instrumentation ships electronic 14 p2347 A67-28990
- capabilities, operation, electronic systems 14 p2347 A67-28990
- function, accuracy and future role 14 p2347 A67-28990
- [AAS PAPER 67-52] 15 p2468 A67-30117
- Handbook of electronic instruments and 15 p2468 A67-30117
- measurement techniques covering tools and 15 p2468 A67-30117
- instruments, components and equipment 15 p2468 A67-30117
- testing 15 p2490 A67-30232
- Airborne photo-optical instrumentation - 15 p2490 A67-30232
- Conference, Cocoa Beach, Florida, February 15 p2490 A67-30232
- 1967 16 p2678 A67-31791
- Instrumentation for space vacuum 16 p2678 A67-31791
- simulation used in testing operations, 16 p2678 A67-31791
- discussing pressure measurement 16 p2678 A67-31791
- requirements 17 p2860 A67-32594
- Geophysical instrumentation for 17 p2860 A67-32594
- environmental studies, elucidating 17 p2860 A67-32594
- atmospheric and near-space mechanisms, 17 p2860 A67-32594
- geodesy, gravimetry, etc 17 p2860 A67-32594
- Lunar exploration by nuclear experiment, 17 p2860 A67-32594
- discussing instrument specifications for 17 p2860 A67-32594
- neutron gamma 17 p2860 A67-32594
- measurements 19 p3229 A67-35318
- New methods of instrumental spectroscopy 19 p3229 A67-35318
- Conference, Paris University, April 19 p3229 A67-35318
- 1966 20 p3436 A67-36334
- Aerospace instrumentation - Conference, 20 p3436 A67-36334
- Cranfield, Beds., England, March 1966, 20 p3436 A67-36334
- Volume 4 20 p3441 A67-36457
- Computer principles-equipment and 20 p3441 A67-36457
- programming for instrumentation systems, 20 p3441 A67-36457
- comparing digital computers with analog 20 p3441 A67-36457
- computers 20 p3390 A67-36463
- Aircraft performance, stability and control 20 p3390 A67-36463
- characteristics in nonsteady flight with high 20 p3390 A67-36463
- accuracy instrumentation 20 p3390 A67-36463
- system 20 p3442 A67-36466
- Instrumentation grounding at Cape 20 p3442 A67-36466
- Kennedy, noting characteristics of ground 20 p3442 A67-36466
- system used for safety and clean space 20 p3442 A67-36466
- signals 20 p3398 A67-36837
- Hovercraft research noting internal and 20 p3398 A67-36837
- external aerodynamics, test techniques and 20 p3398 A67-36837
- instrumentation 20 p3398 A67-36837
- requirements 23 p3934 A67-41167
- ISA Conference, Chicago, September 1967, 23 p3934 A67-41167
- Volume 22, Part I, Measurement standards 23 p3934 A67-41167
- instrumentation 23 p4003 A67-41334
- ISA Conference, Chicago, September 1967, 23 p4003 A67-41334
- Volume 22, Part II, Physical and mechanical 23 p4003 A67-41334
- measurement 23 p4004 A67-41367
- instrumentation 23 p4004 A67-41367
- ISA Conference, Chicago, September 1967, 23 p4004 A67-41367
- Volume 22, Part III, Advances in 23 p4004 A67-41367
- instrumentation including data handling and 23 p4004 A67-41367
- computation 23 p4008 A67-41419
- instrumentation 23 p4008 A67-41419
- Basic displacement transducers, 23 p4008 A67-41419
- electromagnetic transducer theory and 23 p4008 A67-41419
- design 23 p4008 A67-41422
- ISA Conference, Chicago, September 1967, 23 p4008 A67-41422
- Volume 22, Part IV, Applications in industry 23 p4008 A67-41422
- and science 23 p4008 A67-41423
- Coriolis force effect on gross reach 23 p4008 A67-41423
- movements for instrument control 23 p4008 A67-41423
- consoles 23 p3956 A67-41630
- INSTRUMENTATION PROGRAM 23 p3956 A67-41630
- White Sands Missile Range 23 p3956 A67-41630
- Instrumentation modernization program, 23 p3956 A67-41630
- discussing advanced range testing, reporting 23 p3956 A67-41630
- and control /ARTRAC/ system, telemetry 23 p3956 A67-41630
- and electronic and optical 23 p3956 A67-41630
- sensors 02 p0229 A67-12003
- Development of kinetheodolites for 02 p0229 A67-12003
- satellite tracking 18 p3048 A67-34238
- Rubidium vapor magnetometer used for 18 p3048 A67-34238
- near earth orbiting spacecraft, 18 p3048 A67-34238
- instrumentation and in-flight 18 p3048 A67-34238
- performance 20 p3443 A67-36513
- INSULATED STRUCTURE 20 p3443 A67-36513
- Insulated gate FET tetrode with high 20 p3443 A67-36513
- drain breakdown 20 p3443 A67-36513
- potential 01 p0033 A67-10025
- Composite metallic and dielectric 01 p0033 A67-10025
- insulators for high current arc 01 p0033 A67-10025
- electrodes 02 p0250 A67-12697
- Multilayer insulation system materials and 02 p0250 A67-12697
- design data for use on spacecraft in 02 p0250 A67-12697
- temperature range from 300 to 800 degrees 02 p0250 A67-12697
- K 08 p1302 A67-20918
- Integrated semiconductor circuits and thin 08 p1302 A67-20918
- film hybrid circuits on insulating substrate 08 p1302 A67-20918
- developed in Europe for linear 08 p1302 A67-20918
- circuits 08 p1302 A67-20919
- Bonding of rigid insulation to case of solid 08 p1302 A67-20919
- propellant rocket motor, considering 08 p1302 A67-20919
- fabrication, operation and storage 08 p1302 A67-20919
- requirements 09 p1578 A67-22512
- Plane thermal stress at insulated hole 09 p1578 A67-22512
- under uniform heat flow in orthotropic 09 p1578 A67-22512
- medium 10 p1730 A67-23838
- Cryogenic fluid storage on moon surface, 10 p1730 A67-23838
- considering Lambert reflection law, thermal 10 p1730 A67-23838
- insulation performance, incident heat flux 10 p1730 A67-23838
- and boil-off rates 10 p1730 A67-23838
- [AIAA PAPER 67-296] 12 p1926 A67-26011
- Future supersonic and hypersonic aircraft 12 p1926 A67-26011
- horizontal liquid hydrogen fuel tank 12 p1926 A67-26011
- requirements, discussing insulation 12 p1926 A67-26011
- optimization using variable 12 p1926 A67-26011
- thickness 13 p2054 A67-27657
- Very low heat background calorimeter 13 p2054 A67-27657
- design for heat-short experiments and 13 p2054 A67-27657
- checking analytical predictions for propellant 13 p2054 A67-27657
- tank insulation 13 p2228 A67-27658
- Radiation effects in metal-insulator- 13 p2228 A67-27658
- semiconductor /MIS/ devices, noting shift 13 p2228 A67-27658
- and shape change in characteristic 13 p2228 A67-27658
- curve 18 p3012 A67-34345
- Polymeric materials used for selected 18 p3012 A67-34345
- subsystems of Mariner IV space probe 18 p3012 A67-34345
- [JPL-TR-32-1031] 19 p3334 A67-35889
- Voyager thermal insulation requirements 19 p3334 A67-35889
- noting tests of vapor deposited Au on Mylar 19 p3334 A67-35889
- and Kapton 19 p3334 A67-35889
- [AIAA PAPER 67-777] 24 p4257 A67-42945
- INSULATION 24 p4257 A67-42945
- SA ELECTRIC INSULATION 24 p4257 A67-42945
- SA PROTECTION 24 p4257 A67-42945
- SA TEMPERATURE CONTROL 24 p4257 A67-42945
- SA THERMAL INSULATION 24 p4257 A67-42945
- SA WATERPROOFING 24 p4257 A67-42945
- Wall conductance of insulating gaps 24 p4257 A67-42945
- between electrode segments shown as cause 24 p4257 A67-42945
- of inferior performance of MHD 24 p4257 A67-42945
- generators 16 p2599 A67-30526
- Tungsten-rhenium thermocouple systems 16 p2599 A67-30526
- evaluated for high temperature 16 p2599 A67-30526
- measurement 20 p3443 A67-36515
- Variable thickness insulation system for 20 p3443 A67-36515
- transport of hydrogen propellant into earth 20 p3443 A67-36515
- orbit for docking transfer to lunar and 20 p3443 A67-36515
- interplanetary mission vehicles 20 p3443 A67-36515
- [ASME PAPER 67-HT-50] 20 p3548 A67-36732
- INSULATOR 20 p3548 A67-36732
- SA EXCITON 20 p3548 A67-36732
- Cryogenic temperature resistant plastics in 20 p3548 A67-36732
- space program, discussing insulation, 20 p3548 A67-36732
- adhesives, seals, gaskets and expulsion of 20 p3548 A67-36732
- cryogenic propellant in zero gravity 20 p3548 A67-36732
- environment 20 p3548 A67-36732
- [SAE PAPER 660638] 04 p0642 A67-15788
- Hypersonic thermal structural concepts to 04 p0642 A67-15788
- satisfy design requirements including 04 p0642 A67-15788
- insulated, insulated and cooled and hot load 04 p0642 A67-15788
- carrying approaches 04 p0642 A67-15788
- [SAE PAPER 660678] 04 p0716 A67-15789

Thermal conductivity measurement of fibrous insulations up to 2500 degrees F, determining relative contributions from gaseous conduction, solid conduction and radiation 04 p0735 A67-15855

RF sputtering of insulators noting deposition rate, film properties, etc 04 p0631 A67-15993

Current-voltage-temperature dependence of symmetric tunnel junctions, noting role of insulator thickness 07 p1237 A67-20184

Space charge varactor compared to p-n junction varactor, noting applications 15 p2449 A67-29804

Experimental assembly for measuring true heat capacity of heat resistant insulating materials during natural cooling at temperatures from 1200 to 2400 degrees K 16 p2678 A67-31784

Mechanisms of atomic recombination at surfaces analyzed, considering behavior of insulators and semiconductor oxides 18 p2997 A67-33794

E/k/-relation for complex insulator band structure, explaining polarity effect on tunneling through asymmetric barrier 20 p3508 A67-36425

Time-dependent current flow equations solved for insulator with traps if injected space charge produces negligible perturbation on external electric field 20 p3509 A67-36506

150-180 watts at 1000 MHz tetrode, examining mechanical durability and temperature stability of metallic electrodes and ceramic insulators 22 p3772 A67-39873

INTAKE

SA WATER INTAKE

Plane constant pressure contours determined by hodograph mapping used to design lift engine intakes 12 p1891 A67-25213

Intake aerodynamics of upper wing surface studied with two-dimensional potential flow models and suction models, considering inlet problems 14 p2243 A67-28702

Response of bare wire thermocouple to temperature variation in jet engine intake, noting temperature pickup selection for desired response 17 p2859 A67-32589

Boundary layer effect on mass flow parameter and ram efficiency of submerged intakes 20 p3360 A67-37490

INTEGER

Bombieri theorem on primes in arithmetic progression applied to proof of Hardy-Littlewood statement on representation of integers 06 p1025 A67-18733

Solving general integer programs, investigating cutting methods, rounding algorithm, branch and bound method and partition method 17 p2819 A67-32427

INTEGRAL

SA CAUCHY INTEGRAL

SA ELLIPTIC INTEGRAL

SA FRESNEL INTEGRAL

SA JACOBI INTEGRAL

SA LEBESGUE THEOREM

SA PHASE-SPACE INTEGRAL

SA RIEMANN INTEGRAL

SA TRANSFORM INTEGRAL

Contour integral method applied to solution of three-dimensional mixed problem for second order parabolic equation under mixed type boundary conditions containing time differentiation 03 p0457 A67-13115

Formal integral construction of Hamiltonian system of n degrees of freedom near equilibrium point 03 p0457 A67-13163

Resonance phenomena associated with small divisor in third integral of orbital motion 03 p0457 A67-13164

Ergodic theory of measurable partitions in Lebesgue space, extending Rokhlin-Sinai theory of increasing to flows generated by automorphism 04 p0644 A67-14756

Invariants in inhomogeneous turbulent flow related to Loitsianskii integral 05 p0794 A67-17418

Nonlinear DC circuits analyzed by digital computer for application to path integrals and stability problems 08 p1346 A67-20333

Rosen restricted variational principle used to obtain surface integral applicable to solution of kinetic theory boundary value problems 08 p1324 A67-21408

New integral in restricted three-body problem expressed in terms of Delaunay variables 15 p2557 A67-29877

INTEGRAL EQUATION

SA FREDHOLM INTEGRAL EQUATION

SA SINGULAR INTEGRAL EQUATION

SA TRANSPORT THEORY

SA VOLTERRA EQUATION

Stress concentration in annular rotor with notch /or crack/ on inner surface, using integral equation 01 p0159 A67-10276

Langmuir probe method, obtaining exact results for small amplitude plasma oscillations 01 p0123 A67-10461

Motion equations of gyrostat around fixed point reduced to two-equation system 01 p0067 A67-10821

Statistical-dynamical model for total chemical reaction cross sections using activated complex concept and integral equation 01 p0019 A67-10884

Three-dimensional supersonic gas flow with shock waves around flat wing analyzed, using integral relations 01 p0007 A67-10981

Shell theory results compared with results obtained by asymptotic integration of three-dimensional equations of elasticity theory and error correction 01 p0163 A67-10986

Functional integration analysis of exponential behavior of nonlinear feedback control systems 01 p0047 A67-11211

Differential equation solution by separation of multiplicative derivative, by perturbation method, by reduction to Volterra equation and by integral series 01 p0107 A67-11250

Solution of boundary value problems describing two-dimensional flow in plastic regions 01 p0165 A67-11304

Existence of periodic solutions for infinite system of integro-differential equation 02 p0260 A67-12537

Stationary phase technique synthesis of continuous linear antenna and integral equation for determining radiation pattern 03 p0378 A67-13284

Arbitrary profile disk design, taking into account temperature gradient, based on simultaneous solution of integral equations 03 p0429 A67-13331

Self-sustained periodic solution in nonlinear difference differential equation proved under appropriate assumptions for various parameters 03 p0459 A67-13655

Iteration method applied to integral equations arising in structural mechanics problems 03 p0461 A67-14079

Torsion of infinite hollow cylinder with axially symmetric load, discussing deformations in terms of integral equations 03 p0529 A67-14164

Generalized mixing length argument in turbulent diffusion, obtaining integral equation for continuous case 04 p0603 A67-14648

Exact general integral for class of compressible fluids used in boundary value problems for nonlinear equations of gas dynamics 04 p0606 A67-15194

First transcendent integrals of motion equations of heavy solid about fixed point 04 p0659 A67-15756

Uniform property turbulent boundary layer heat transfer calculation, using solution of integral momentum and kinetic energy equations 04 p0731 A67-15821

Josephson current in alternating field between two superconductors separated by dielectric barrier 05 p0853 A67-16697

Spence integrodifferential equation for flow around slender slightly curved profile with jet at trailing edge 05 p0749 A67-16842

Solution concept definition for integral equation with discontinuous operator 05 p0835 A67-16938

Integral motion equations of rigid body with cavity partly filled with viscous incompressible fluid with free surface 05 p0921 A67-17005

Reduction of problems of diffraction of scalar and vector waves at open curvilinear screen to integral equations of second kind 05 p0785 A67-17157

Hydromagnetic compressible boundary layer flow past flat plate analyzed via von Karman integral method 05 p0794 A67-17361

Nekrasov method application to construction of algorithm for small solutions to nonlinear integral equations, using recursion techniques 05 p0836 A67-17488

Error bounds for asymptotic solutions of differential equations, using Volterra equations for actual and formal solution vectors 06 p1021 A67-17565

Possio integral equation kernel derived in analytical form for wing flow 06 p0935 A67-17623

Time-independent radiative transfer through circular cylindrical medium, using numerical methods 06 p1111 A67-18774

Wave propagation in random medium, examining stochastic PDEs, solutions and method of regularization 06 p1032 A67-18101

Mathematical analysis of jet flap with high lift coefficient, solving numerically integral equation obtained from boundary value problem [AIAA PAPER 67-2] 06 p0938 A67-18247

Transient linear transfer problem solution via integral equations for corresponding boundary value problems 06 p1117 A67-18394

Existence or nonexistence of continuous shockless transonic flow around symmetric wing profile, using Oswatitsch integral equation 06 p0942 A67-18586

Fundamental frequency of natural oscillations of plate, using integrodifferential equations derived from elasticity theory in form of power series 06 p1108 A67-18662

Differential descent in solution of multidimensional variation problem as applied to nonlinear system 07 p1212 A67-19136

Expansion of solutions of integrodifferential equation not having holomorphic solutions vanishing with x in vicinity of x equals zero 07 p1213 A67-19173

Existence of solutions to differential and integrodifferential equations possessing asymptotic parabolas 07 p1214 A67-19174

Approximate solutions for differential and integral equations in form of second order asymptotic polynomials 07 p1214 A67-19216

Approximate solution of integral equations with aid of least squares for steady motions of viscous incompressible fluid in rotating cylinder 07 p1168 A67-19217

Mikusinski operator solution of partial integrodifferential equations 07 p1215 A67-19471

Constructing formal integrals, in form of power series, of time independent Hamiltonian system near equilibrium point [AAS PAPER 66-102] 07 p1216 A67-19961

Simplified equations for equilibrium problem in large deflection theory for thin annular plates 08 p1414 A67-20348

Oseen flow past semilinear plate and vertical force formulated by integral equations solved for drag and lifting singularities distribution, using Wiener-Hopf technique 08 p1319 A67-20350

Two methods of numerical construction of derivatives involved in inversion of Laplace transform 08 p1347 A67-20370

Soviet book on boundary value problems for analytic functions as applied to integral equations with Cauchy and Hilbert kernels 08 p1347 A67-20760

Monograph on integral equations covering Fredholm and Volterra equations, applications to theory of differential equations, properties of Cauchy type integrals, etc 08 p1348 A67-20761

Asymptotic solution of Cauchy problem for integrodifferential equation with small parameter associated with derivative 08 p1348 A67-21152

Interpretation of class of divergent integrals in terms of limit sums, using generalized function theory 08 p1349 A67-21193

Numerical solution of integrodifferential equations 08 p1349 A67-21261

Integral equation for propagation of second order correlation function assuming statistical independence of wave function and refractive index fluctuations 09 p1460 A67-21594

Existence theorems of algebraic integral equations /AIR/ with nonlinear functionals 09 p1524 A67-21649

Relativistic rotation of perigee of satellite determined from first integral of motion equation 09 p1563 A67-21658

Isotropic scattering of radiation in finite two-dimensional atmosphere using integral equation, solved by power series 09 p1532 A67-21662

General purpose quadrature method for numerical evaluation of specific definite integrals 09 p1524 A67-21834

Integral equation solution with Mellin inversion formulas for light scattering problems 09 p1524 A67-21872

- Generalization of Gaussian arbitrary constant sign curvature to shallow shells by introducing corrections in Lauricella-Sherman potentials 09 p1575 A67-21927
- Distribution theory application to derive formula for deflections of vertical from Stokes formula 09 p1492 A67-22681
- Incompressible potential flow about arbitrary body shapes calculated, using singularity distribution over body surface computed as solution of integral equation 10 p1589 A67-22871
- Plane problem of rigid die penetration into elastic medium solved, using divergent series form 10 p1721 A67-23671
- Absolute extrema of certain integrals from method for finding corresponding functions with prescribed endpoints 11 p1812 A67-24087
- Expansion of arbitrary function of Mehler-Fok integral form in terms of spherical functions 11 p1812 A67-24149
- Dual integral equation and dual series analysis and application to mixed boundary value problems in elasticity, hydrodynamics and electrostatics 11 p1812 A67-24150
- Dual integral equations in elasticity theory, noting Mehler-Fok transformation of spherical functions, Fredholm equation and application to mixed boundary value problems 11 p1812 A67-24151
- Boundary between applicability ranges of network and steepest descent methods in equation integration of Timoshenko theory in analysis of plate deformation 11 p1871 A67-24159
- Singular integral equations with constant coefficients solved by Jacobi polynomials and applied to problems in fluid dynamics, crack propagation, plane elastic theory, etc 11 p1813 A67-24678
- Integral equations of second boundary value problem of equilibrium of elastic body of revolution, treating cylinder under pressure 11 p1878 A67-24877
- Modified collocation method for linear boundary value problem for integrodifferential equation, giving approximate solutions which converge to exact solution 11 p1814 A67-25048
- Integral energy equation for three-dimensional laminar boundary layer element on porous surface in presence of suction 11 p1783 A67-25052
- Boundary value problem for region with arbitrary smooth boundary solved, using second order degenerate elliptical equations 12 p1961 A67-25441
- Matrix integral equations to calculate vertical stresses and natural frequencies of oscillation of thin walled isotropic shells of revolution 12 p2022 A67-25585
- Asymptotic integration technique for small axisymmetrical oscillations of thin walled elastic shell of revolution for case of double reversal point 12 p2029 A67-25675
- Auxiliary singularity-carrier-curve theorems derived for blade profile design calculations 12 p1893 A67-25970
- Integral equations for radiative heat transfer inside solid whose solution leads to temperature-distance profile integral equations solution for radiative heat transfer inside solid leads to temperature- [AIAA PAPER 67-287] 12 p2035 A67-26004
- Classical representation of Green-Lebesgue type integral harmonic function in case of unit sphere 12 p1962 A67-26101
- Inversion of spectroscopic integral equation which relates emission coefficient to integrated intensity distribution for optically thin and asymmetrical light source 12 p1968 A67-26175
- Ion temperature gradients causing plasma instabilities when magnetic shear is present, deriving governing integral equation 13 p2162 A67-26284
- Maxwell dispersion of particles of molecular gas flow at wall of circular channel described by integral equation, determining particles experiencing mirror intercollisions 13 p2158 A67-26671
- Existence of continuous transonic flow and model representing velocity distribution by Oswatitsch integral equation 13 p2050 A67-26808
- Molodensky integral equation solvability 13 p2114 A67-26853
- Axially symmetric potential flow about slender body, noting source strength distribution and solution via integral equations 13 p2095 A67-26911
- Distribution function and temperatures in monatomic gas under steady expansion into vacuum determined by integrating Bhatnagar-Gross-Krook /BGK/ model equation and moment equations respectively 13 p2104 A67-26982
- Pointwise bounds extended for Cauchy problem solution by establishing Cauchy problem maximum property for any second order linear hyperbolic operator 13 p2146 A67-27097
- Three-dimensional elastostatic problems for infinite solid with geometric discontinuities solved using potential functions 13 p2221 A67-27735
- Numerical solution of linear differential equation and Volterra linear integral equation of second kind based on Lobatto four-point quadrature formula 14 p2342 A67-27977
- Asymptotic and numerical solutions of Goulard integrodifferential equation describing hypersonic flow near stagnation point past blunt bodies, allowing for radiative transfer effects 14 p2296 A67-27981
- Integral expression derived for current distribution on infinite antenna aligned with magnetic field immersed in plasma, using generalized eigenfunctions 14 p2284 A67-28378
- Functional-analytic techniques providing understanding of some nonlinear circuits action on input to output signal production 14 p2291 A67-28453
- Theory of singular integrodifferential operators on compact manifolds, discussing basic principles, concept of uniformly nonelliptic systems, etc 14 p2343 A67-28503
- Integral equations in automatic control theory, deriving theorem which leads to Popov frequency domain stability criterion 14 p2292 A67-28635
- Theorems derived from approximate methods of analysis applied to collocation, moment and Galerkin methods for solving linear integral and differential equations 14 p2344 A67-28671
- Certain integral equations of first kind reduced to Abel equation and equation of second kind when solving elasticity and hydrodynamic problems 14 p2344 A67-28742
- Characteristic for kernels of certain integral equations on semiaxis for determining solvability and number of possible solutions 14 p2344 A67-28809
- Collocation method applied to approximation solution of loaded integral equations 14 p2344 A67-28895
- Numerical solution of Cauchy problem class of nonlinear integrodifferential equations 14 p2344 A67-28896
- Formulation of upper and lower bounds on Knudsen flow rate of gas through channel of arbitrary geometry by reciprocal variational principles 15 p2469 A67-29195
- Linear integrodifferential equations describing oscillatory processes, with asymptotic solutions in terms of parameter μ through WBK method 15 p2509 A67-29232
- Josephson current in alternating field between two superconductors separated by dielectric barrier 15 p2530 A67-29868
- Extension of Vainberg method for studying nonlinear integral equations with aid of Hart theorem to cover Urysohn type equations 15 p2511 A67-29888
- Arc operation under nonsteady electrical inputs noting initial conditions, energy equation solution, temperature profiles, application of Green function for moving boundary problem, etc [AIAA PAPER 66-480] 15 p2531 A67-30204
- Turbulent boundary layer flow properties predicting velocity profiles in region of velocity maximum decay 16 p2657 A67-30614
- Pressure distributions and shock wave shapes on conical wings calculated by numerical solution of integral equations 16 p2589 A67-30619
- Nontrivial real or complex solutions of nonlinear integral equations of Hammerstein type bifurcating from identically vanishing solution 16 p2695 A67-30858
- Existence theorems for systems of nonlinear integral equations of Hammerstein type with positive definite kernels 16 p2687 A67-30859
- Solution of incorrect magnetometric and gravimetric problems represented by integral equations of convolution type with unstable solutions 16 p2663 A67-30866
- Integration of laminar boundary layer equations in compressible gas by asymptotic method, calculating friction and heat flux 16 p2680 A67-31135
- Numerical solution of nonlinear integral equations with variable upper limit, applicable to Cauchy and boundary value problems 16 p2696 A67-31142
- Book on variational calculus and integral equations, examining extremum conditions, Fredholm and Volterra integral equations, Pontryagin maximum principle, etc 16 p2696 A67-31200
- Integral equation derived for steady state temperature field in semilinear body with internal cylindrical heat source 16 p2779 A67-31204
- Abel integral inverter discussing design, construction and performance of analog computer for solution of Abel integral equation 16 p2634 A67-31428
- Real trajectories of n-body problem calculated by convergent integral iterations on basis of differential equations for motion of centers of gravity 16 p2750 A67-31441
- Convolution type integral equation solution via reduction to Riemann problem in class of generalized functions 16 p2698 A67-31735
- Incorrect problems of mathematical physics examined and illustrated by classical Cauchy problem for Laplace equation 16 p2698 A67-31736
- Solvability and methods of solution of boundary value problems noting uniqueness, potential theory application in solving polyharmonic equations and second-order equation 16 p2698 A67-31737
- Plasma concentration diagnostics by hydromagnetic probing method, determining concentration profile from latitude dependence of torsional vibrations 16 p2668 A67-31890
- Rolling friction with axial thrust analyzed for elastic cylinder, assuming Coulomb friction law and using integral equation 17 p2865 A67-32263
- Wiener-Hopf technique for class of nonhomogeneous difference-differential integral equations 17 p2877 A67-32560
- Coupled integral equations for transverse and axial currents for asymmetrically cylindrical antenna driven by EMF 17 p2826 A67-32618
- Fabry-Perot resonator excitation using integral equations corresponding to boundary value functions 17 p2868 A67-32667
- Iterative solution through boundary value problem and integral equations for axisymmetric deformation of body remote from symmetry axis 17 p2962 A67-32874
- Electromagnetic wave diffraction by convex spherical surface considered in terms of mutual impedance between two radial electric dipoles, using integral equation 17 p2817 A67-32930
- Ion radial distribution functions for primitive model of electrolyte solution using Percus-Yevick and convolution-hypernetted-chain integral equations 17 p2810 A67-33256
- Integral motion equations of rigid body with cavity partly filled with viscous incompressible fluid with free surface 18 p3028 A67-34267
- Periodic solutions for quasi-harmonic time-lag system, proposing calculation for periodic regimes in form of integral series 18 p3079 A67-34371
- Rarefied gas cylindrical Couette flow noting Knudsen number, Bhatnagar-Gross-Krook model for Boltzmann equation, transport integrodifferential equation, etc 18 p3029 A67-34738
- Current-voltage characteristics of low pressure discharge in magnetron, giving integral equations and current stability 19 p3277 A67-35120
- Buckling of aging linearly viscoelastic beam columns with time variable mechanical properties, deriving integrodifferential equations and stability conditions 19 p3343 A67-35781
- Approximate method of solving integral equations of local radiation characteristics applied to numerical solution of specific problems of radiative heat transfer 19 p3347 A67-35898
- Collocation method convergence in problems other than general linear problem of ordinary integral equations and those

with homogeneous kernel 19 p3250 A67-36047
 Prognostic equation asymptotic solution for atmospheric pressure forecast 20 p3479 A67-36125
 Forced convection of laminar flow in tubes of various cross sections, assuming constant temperature gradient and internal heat generation 20 p3420 A67-36317
 Optimum output-input characteristic of memoryless nonlinear system determined from solution of integral equation 20 p3407 A67-36382
 Two-point boundary value problem approximate solution using Monte Carlo path integral calculation 20 p3475 A67-36481
 Boundary value problem and singular integral equation applied to automatic control theory 20 p3475 A67-36652
 Vibrating elastic bar motion equation reduced to integral equations system for solutions to boundary value problems 20 p3476 A67-36667
 Integral equations for weight function of optimum filter and correlation function of random absolute error 20 p3408 A67-37040
 Iterative technique applied to solution of problems in elasticity involving minimization of double integral subjected to certain boundary conditions 20 p3541 A67-37487
 Galerkin method applicability to boundary value problems and eigenfunctions and eigenvalues for integrodifferential equations with deviating arguments 20 p3478 A67-37580
 Boundary value problem for region with arbitrary smooth boundary solved, using second order degenerate elliptical equations 20 p3479 A67-37724
 Poiseuille flow of rarefied gases through cylindrical tube, solving integral equation, noting variational calculation of hydrodynamic velocity 21 p3609 A67-37738
 Plane problem of rigid die penetration into elastic medium solved, using divergent series form 21 p3719 A67-38272
 Elastic spherical shell stability under thermal stresses from abrupt temperature change at shell equator solved, using Fredholm integral equation 21 p3721 A67-38308
 Spherical symmetric problems in general relativity 21 p3707 A67-38962
 Static Green function for elastic electron scattering by hydrogen atoms, using integrodifferential equations to determine resonance energies 22 p3839 A67-39204
 Integral equation for asymptotic expansions of plane electromagnetic and acoustic fields diffracted by convex surfaces of variable curvature 22 p3836 A67-39389
 Asymptotic solution for class of integral equations of first kind with application to contact problem of infinite elastic cylinder 22 p3909 A67-39400
 Radiation pattern of dielectric antenna using integral equations, noting differences between real antenna and idealized linear traveling wave antenna 22 p3770 A67-39656
 Cracked cylindrical shell stress-strain state under symmetric load, discussing shell curvature effect and integral equation solution 22 p3911 A67-39684
 Approximate integrodifferential equations determining ensemble mean and covariance of particle distribution function of Vlasov plasma, discussing incompressible Navier-Stokes turbulence 22 p3850 A67-39703
 HF plane waves diffraction on plane circular diaphragm solved by functional theoretic methods for integral equation for Fourier transform of screen covering 22 p3912 A67-39783
 Integral equation with transfer function density restrictions defining characteristic function of Markov process functional, deriving several limit theorems 22 p3827 A67-39878
 Laminar boundary layer gas flows over slender bodies with massive blowing, discussing integral method solution and theoretical model including pressure effect 22 p3739 A67-39935
 Integral equation for discontinuous flows and free streamline solutions for axisymmetric bodies at zero and small angles of attack 22 p3743 A67-40166
 Compressible laminar boundary layer in pressure gradient, analyzing suction on basis of momentum and thermal integral equations 22 p3788 A67-40421
 Integral equations with integral operators and excitation frequencies for forced

oscillation, solving friction via orthogonal iteration approximation 22 p3916 A67-40454
 Integral equation derived to relate source function for spectral line formed by noncoherent resonance scattering to thermodynamics of radiating medium 22 p3896 A67-40529
 Corrections for three results in asymptotic solution of nonideal Bose-Einstein particle system nonlinear integral equations 23 p4026 A67-40718
 Soviet book on approximate methods for boundary value problem solutions of ordinary and partial differential equations and certain integral equations 23 p4022 A67-40841
 Methods of increasing rate of convergence in convergence processes for improper integral of first kind 23 p4022 A67-40861
 Maxwell-Euler equations reformulated into equivalent matrix integral equation, obtaining dispersion relation from integral equation kernel for compressible electron plasma 23 p3974 A67-41204
 Electrically thick monopole transmitting antenna integral equation for current distributions and admittance 23 p3981 A67-41207
 Integral equation derived from Boltzmann equation for one-dimensional radiative heat transfer in plane layers of gray media 24 p4252 A67-41934
 Escape probability of photon from homogeneous plane parallel medium, discussing coherent scattering process and integral equation 24 p4191 A67-42596
 Electrical conductivity of ionized plasma taking into account particle impenetrability, using Boltzmann and collision at distance integrals 24 p4198 A67-42662
 Integral equations for nonlinear problems in partial differential equations, including Volterra, boundary value and initial value problems 24 p4180 A67-43088

INTEGRAL FUNCTION

Energy functionals and universal integrals of motion for force field symmetric about axis of rotation 01 p0113 A67-10680
 Interaction between atoms of solid surface and gas phase, obtaining closed-form solution of motion equations 01 p0118 A67-11295
 Integral transform associated with boundary conditions containing eigenvalue parameter applied to initial boundary value problem arising in diffusion theory and heat flow 03 p0460 A67-13825
 Interpolation sets satisfying several conditions considered for application to integral functions with gap power series 03 p0461 A67-13941
 Growth of integral functions of many complex variables 05 p0833 A67-16315
 Numerical algorithm for supersonic gas flow past blunt bodies with shock wave separation, using Dorodnitsyn method of integral correlation 05 p0791 A67-16374
 Integral representation for transonic flow about thick airfoils obtained from equations for two-dimensional inviscid flow and locally surface-orthogonal shock waves [AIAA PAPER 67-3] 06 p0939 A67-18331
 Relations among various definitions of order of growth of integral functions with many complex variables 06 p1024 A67-18554
 Topology of three-dimensional integral surface projection of section of energy integral by third integral 08 p1380 A67-20382
 Integral relations for separating flow 10 p1826 A67-23142
 Dirichlet problem of toroidal segment, noting integral transformation of spherical function 10 p1675 A67-23669
 Generalized integro-exponential weighting functions allow accurate computations of Fraunhofer lines in solar intensity and stellar flux/spectra 11 p1859 A67-24113
 Increasing modulus maximum of integral function relation to moduli of coefficients of power series 11 p1813 A67-24520
 Time discretization method applied to determination of peak duration distribution of normal noise envelope 11 p1754 A67-24987
 Energy functionals and universal integrals of motion for force field symmetric about axis of rotation 11 p1821 A67-25069
 Integral inequalities for two functions 12 p1960 A67-25258
 Index and solvability of general linear boundary value problem for composite type

system of equations 13 p2144 A67-26380
 Singular point topological classification and analytical criteria relating singular points to generalized Liapunov-Krasovskii functions 14 p2342 A67-28338
 Rapidly converging analytic solution by integral series of nonrelativistic Schroedinger equation for He atom 15 p2520 A67-30151
 Light field distribution in optical resonator of Fabry-Perot type interferometer with nonparallel mirrors using Airy function for localizing field concentration planes 17 p2853 A67-31921
 Method of finite integral transforms a format for employment of incomplete eigenfunctions, discussing application of equilateral transform 17 p2876 A67-32422
 Invariant integral from use of Noether's theorem of calculus of variations applied to optimal control problem 19 p3204 A67-35900
 Steady flow equations with symmetry of revolution, obtaining first integrals for perfect fluid 20 p3420 A67-36398
 Index and solvability of general linear boundary value problem for composite type system of equations 20 p3479 A67-37722
 Integral integer-valued functions of several complex variables, proving Gelfond-Straus results by using modification of Schneider method 21 p3651 A67-37922
 Dirichlet problem of toroidal segment noting integral transformation of spherical function 21 p3652 A67-38270
 Boundary value problems of wave propagation in plane, investigating coverage source distribution and velocity perturbations 21 p3615 A67-39093
 Weierstrass canonical product analog for integral functions of many complex variables, discussing existence problems and canonical function construction 22 p3827 A67-39215
 Integrals properties with respect to paraboloid and asymptotics of Born approximations in scattering theory for Schroedinger equation applied to parabola 22 p3835 A67-39307
 Spiral field rotation with motion integrals as distribution function arguments, discussing potential, density and spiral arm stability 22 p3893 A67-40507
 Relations among various definitions of order of growth of integral functions with many complex variables 23 p4022 A67-40820
 Spectral dependence of enhanced quantum efficiency and overlap integrals in InSb semiconductors, calculating impact ionization and hot electrons thermalization 23 p4040 A67-41061
 Integral solution for massive blowing on slender hypersonic wedges and cones in laminar flow, assuming homogeneous nonreacting perfect gas mixtures 23 p3932 A67-41743
 Sampling interval criteria with nonlinear integrands in discrete-continuous feedback control systems, obtaining performance surfaces in object function-parameter space 24 p4134 A67-42024
 Integral pulse FM effect on feedback control, obtaining stability of equivalent nonlinear discrete system 24 p4135 A67-42182

INTEGRAL OPERATOR

Energy dissipation and heating due to oscillation of polymers whose rheological properties are described by elastic heredity theory, considering homogeneous and reinforced plastics 01 p0102 A67-10220
 Integral operators associated with Poisson transforms and operator H sub alpha 05 p0835 A67-16733
 Asymptotic representation of integral operator used in describing time-varying load function in quasi-static and dynamic elastic heredity problems of creep materials 06 p1107 A67-18638
 Analytic properties of solutions to generalized axisymmetric Schroedinger equation 08 p1346 A67-20355
 Spectral theory of Wiener-Hopf type integral operators on generalized Sobolev spaces 10 p1674 A67-22968
 Nonlinear automatic control with random parameters, noting change of system operator as function of disturbances on system 11 p1770 A67-24211
 Green matrix estimates for homogeneous parabolic boundary value problems, showing proof of integral operator 11 p1813 A67-24850
 Algorithms for operator partitioning

- method in reducing shell equations solution
to calculation of solid intersecting rod
systems 12 p2026 A67-25617
- Relaxation of velocity distribution to
equilibrium in electron plasma, showing
linearized collision operator covers
continuous spectrum of
eigenvalues 12 p1977 A67-26176
- Electron velocities distribution in plasma,
studying boltzmann equation inelastic and
superelastic collision operator, considering
eigenfunctions and eigenvalues for electronic
excitations and
deexcitations 13 p2165 A67-26437
- Asymptotic form of uniform approximation
of abstract functions by single family of
linear integral operators occurring in Banach
space topology 14 p2341 A67-27834
- Integrodifferential equation solvability by
investigation of adjoint Cauchy
problem 15 p2511 A67-29890
- Book on analytical methods in vibrations
covering general mathematical formulations
for common features of various vibrating
systems 16 p2765 A67-30999
- Integral equations with integral operators
and excitation frequencies for forced
oscillation, solving friction via orthogonal
iteration approximation 22 p3916 A67-40454
- Compact integral operator base problem
for Hilbert-Schmidt integral operators
existence, discussing Schmidt classical
operator approximations and
eigenvalues 22 p3828 A67-40554
- Elastohereditary /viscoelastic/ media
mechanics, analyzing linear and nonlinear
equilibrium equations, uniqueness and
existence theorems and solution
methods 23 p4077 A67-40750
- Nonlinear equation solution existence in
real Hilbert space with linear and nonlinear
operator 24 p4178 A67-42721
- ### INTEGRATED CIRCUIT
- #### SA PRINTED CIRCUIT
- Epitaxial diffused integrated circuit
structure containing p-n-p and n-p-n
transistors 01 p0033 A67-10021
- Integrated circuit application engineering
and resultant advantages 01 p0034 A67-10271
- Integrated digital logic circuits including
resistor transistor, diode transistor, emitter
coupled and transistor-transistor
logic 01 p0038 A67-10760
- Diffusion processes for fabricating
integrated circuits, examining open and
sealed tube techniques 01 p0080 A67-10971
- Flowgraph teaching techniques, discussing
problem formulation, construction
procedures and symbolic and numerical
evaluation in network
analysis 01 p0030 A67-11042
- High resolution optical shaft angle encoder
with gallium arsenide diodes as light sources
and compatible with integrated circuit
techniques 01 p0073 A67-11113
- Packaging, manufacturing and design
techniques used in total-system-in-box
concept for integrated
circuits 01 p0039 A67-11116
- Semiconductor integrated circuit negative
feedback amplifier design with high
response characteristics for carrier terminal
equipment application 01 p0040 A67-11241
- Electronic Circuit Analysis Program
/ECAP/, integrated system of digital
computer programs producing DC, AC or
transient network analyses from circuit
topology, excitation, etc 01 p0031 A67-11336
- Integrated circuit reliability survey
showing relationship of failure rate and
temperature 01 p0042 A67-11365
- Failure rate and failure mechanism schools
test philosophies combined to know and
improve integrated circuits
reliability 01 p0042 A67-11366
- Physical and management aspects of
reliability of integrated circuits for
Minuteman II 01 p0042 A67-11367
- Integrated ceramic printed and thin film
circuitry in microelectronic
technology 01 p0043 A67-11385
- Integrated circuit reliability and
nondestructive testing, noting component
failure analysis, self-maintenance, network
parameter determination,
etc 02 p0224 A67-11526
- Integrated circuit eliminating pilot tones
in digital data by simultaneously phase
modulating binary data and bit-timing signals
on carrier 02 p0194 A67-11797
- National Electronics Conference, Chicago,
October 1966 02 p0199 A67-12086
- Integrated circuit design of CLEM
functional electronic block /FEB/
breadboards 02 p0219 A67-12109
- Simple gates, multilevel arrays and
interconnection in integrated circuits for
computers 02 p0219 A67-12110
- Digital integrated circuits and methods of
testing for AC, DC and ground noise
margins, dynamic impedance, capacitance
and inductance factors 02 p0207 A67-12112
- Cryogenic associative memory system for
information retrieval 02 p0208 A67-12163
- Integrated circuit development noting role
of NASA and industry
[AIAA PAPER 66-835] 02 p0220 A67-12254
- Isolation-diffusion of phosphorus in silicon
with low surface concentration, with
applicability to preparation of integrated
solid state circuits 02 p0223 A67-12736
- Cr-SiO cermet material used in precision
thin film resistors for monolithic integrated
circuits 03 p0381 A67-13663
- Digital range tracking system using
integrated circuits at SPANDAR radar
site 03 p0370 A67-13831
- Stability criterion for PWM feedback
systems containing one integrating
element 03 p0393 A67-13984
- Integrated circuits with evaporated thin
film conductors, resistors and
capacitors 03 p0387 A67-13999
- Integrated circuit fabrication on silicon
single crystals 03 p0387 A67-14000
- Transistor and integrated circuits
applications including high input impedance
amplifier using MOSFET transistor, pulse
forming circuit, stable sawtooth generator,
etc 04 p0579 A67-14402
- Solid state circuits - IEEE Conference,
Philadelphia, February 1966, Part
1 04 p0580 A67-14594
- Temperature sensor controller in form of
linear monolithic integrated silicon
device 04 p0619 A67-14595
- Interconnection patterns for slice-level
subsystems of integrated
circuits 04 p0585 A67-15490
- Damage mechanism in semiconductor
from space radiation and effects on various
microcircuits 04 p0588 A67-15702
- Transient response of MOS transistors and
integrated circuits to ionizing
radiation 04 p0589 A67-15719
- Transient radiation response and
permanent radiation damage in monolithic
silicon-junction-transistorized integrated
circuit 04 p0589 A67-15720
- Hardening monolithic integrated circuits
to transient ionizing radiation by controlling
photocurrent and by evaluating fabrication
processes 04 p0590 A67-15722
- Integrated circuit adoption for optimal
mixture with remaining discrete devices,
particularly gimbal loops 05 p0770 A67-16236
- Beam lead sealed junction technology for
planar processes, noting preparation and
application 05 p0770 A67-16238
- Tantalum thin film integrated circuits
noting fabrication techniques, applications,
cost and advantages 05 p0770 A67-16239
- Planar integrated circuit technology and
beam lead sealed junctions, noting
fabrication techniques, performance and
applications 05 p0770 A67-16240
- Microwave integrated circuits combining
tantalum thin film technology and beam lead
devices, noting fabrication, advantages and
performance 05 p0770 A67-16241
- Silicon integrated circuit data encoder for
Isis A satellite particle counting experiment,
noting design and
construction 05 p0770 A67-16292
- Circuit element types and technology for
design engineers 05 p0776 A67-17036
- Trends in microelectronics and related
technology 05 p0776 A67-17040
- Analog/hybrid computer design, noting
inclusion of solid state and integrated
circuits for reliability cost reduction and
speed 05 p0769 A67-17519
- PCM telemetry system for satellite test
vehicle of ELDO program using
transistorized printed circuit
technology 06 p0957 A67-17613
- Synthesis of potentially bistable oscillator
configurations serving as prototypes for
integrated nearly sinusoidal
applications 06 p0967 A67-17812
- Family of custom linear integrated circuits
- using general purpose functional
block 06 p0967 A67-17813
- Monolithic IC design of diodes and X-band
microswitch transmission line fabricated on
Si substrate 06 p0968 A67-18053
- Postmortem flaw detection methods and
equipment for IC failure
analysis 06 p0968 A67-18054
- Pulsed power technique and capacitive
coupling between digital integrated circuits
provide micropower redundant circuits with
automatic error
correction 07 p1155 A67-19844
- Read-only memory composed of MOS-FETs
on single silicon chip 07 p1155 A67-19845
- Book on introduction to microelectronics
including integrated circuits, thin film
devices, etc 07 p1158 A67-20280
- Pole-zero sensitivity minimization with
respect to active and passive elements in
active RC circuit design 08 p1308 A67-20322
- Design procedure and manufacturing
techniques for multielement fluidic plate
using wall attachment devices, discussing
integrated arrays 08 p1281 A67-20452
- AVNI low cost IC airborne digital inertial
navigation system with analog input and
display, using MOS LSI
techniques 08 p1297 A67-20633
- Fabrication concepts for large scale
integration /LSI/ circuits 08 p1300 A67-20634
- LSI effect on aerospace computer design,
considering cost, size and power
consumption of logical
elements 08 p1297 A67-20635
- LSI application to computer design using
functional partition of control and data path
structures 08 p1298 A67-20636
- Computer logic cost effectiveness
modeling applied to integrated circuits,
discussing comparisons between existing
equipment, Conalag and
redesigns 08 p1311 A67-20657
- Adaptable large scale integrated military
and space systems, discussing
microelectronic circuit, logistics and dynamic
redundancy 08 p1311 A67-20665
- Semiconductor integrated circuits,
discussing fabrication processes, component
characteristics and electrical isolation
methods 08 p1301 A67-20788
- Thin film and semiconductor integrated
circuits, discussing functional flexibility,
fabrication by microengraving, isolation and
computer fabrication 08 p1301 A67-20791
- Logical design and fabrication of Si
integrated circuit 08 p1301 A67-20792
- Planar and sandwich resistor structures in
Si thin film integrated
circuits 08 p1302 A67-20793
- Comparison of integrated microcircuits
deposited on semiconductor and insulating
substrates, noting vacuum deposition
techniques 08 p1302 A67-20918
- Integrated semiconductor circuits and thin
film hybrid circuits on insulating substrate
developed in Europe for linear
circuits 08 p1302 A67-20919
- Operational amplifier using monolithic
integrated circuit noting calculation, layout
and topological
integration 08 p1302 A67-20920
- Relays, ICs and hybrid /two-chip/ driver
circuit for Motorola Digital Test Command
System /DTCS/ 08 p1303 A67-21028
- Integrated circuit in optimal design of
aerospace systems, discussing potential low
cost and use in computer analyses of
circuits 08 p1303 A67-21060
- High density microelectronic circuitry,
discussing interconnection through use of
advanced materials and
techniques 08 p1303 A67-21189
- Probability of signal acquisition by phase
locked oscillator system operating in
frequency search mode, determining
maximum admissible search rate without
noise 08 p1295 A67-21275
- Computer logic device development,
discussing interdependence of various
components and packaging
methods 09 p1466 A67-21683
- Computer packaging technology, discussing
form lead joining, interconnection,
maintainability, handling,
etc 09 p1467 A67-21684
- Integrated circuit general purpose
computer for use in aerospace
guidance 09 p1469 A67-22174
- TV camera to be used by Apollo
astronauts noting integrated circuits, optical

system, light intensifier, etc 09 p1499 A67-22175

Failure reporting, analysis and correction on satellite programs, discussing system reliability 09 p1480 A67-22289

High reliability integrated circuit selection and specification by using effective screening test and analyzing failure mechanism 09 p1480 A67-22299

Screening to improve reliability of silicon integrated circuit, noting failure mode and mechanism 09 p1480 A67-22300

Cost improvement for Minuteman II integrated circuits from failure rate reduction, using failure mode model and measurement system 09 p1480 A67-22305

Dielectric isolation techniques for elements of integrated circuit 10 p1610 A67-22971

Processing techniques for integrated microwave circuits using silicon-on-sapphire /SOS/ transistors for high frequency power outputs 10 p1610 A67-22972

Integrated circuit technology for microwave equipment including guidelines and system design 10 p1610 A67-22973

Functional properties of semiconductor devices and integrated circuits, considering network design 10 p1610 A67-22976

GaAs Schottky diodes for integrated circuits, discussing fabrication, parameters and performance 10 p1615 A67-23527

Aviation avionics microelectronic devices stressing reliability, maintenance, circuitry, etc [SAE PAPER 670253] 11 p1758 A67-23985

Axial lead package and stack design of batch fabricated matrices to speed integrated circuit assembly 11 p1760 A67-24260

Video mapping technique making possible radar moving target indication for permanent echoes only 12 p1909 A67-25128

Packaging method for integrated microwave transistor amplifier constructed on ceramic substrates 12 p1910 A67-25265

Testing instrument for determination of lead wire mechanical properties and bond strengths within semiconductor devices 12 p1911 A67-25270

Packaging integrated circuit airborne tape control unit 12 p1911 A67-25273

High density power converter using integrated circuits and thyristors, noting packaging 12 p1911 A67-25274

Liquid cooling of integrated circuit systems to remove increased heat dissipation, noting heat transfer rates 12 p1915 A67-25888

Mass production lines for monolithic integrated circuits 12 p1916 A67-25995

Semiconductor substrate photochemical processing and coating photoresistant techniques 12 p1916 A67-25996

Dielectric isolation of integrated circuit via ceramic medium, discussing technique, testing and results 12 p1916 A67-25997

Computer-aided design of linear integrated circuits 12 p1919 A67-26156

Microelectronics technique, particularly integrated circuits, basic theory and research 12 p1917 A67-26202

Semiconductor integrated circuits, discussing hybrid, multichip and beam-lead methods in digital and linear circuit applications 12 p1917 A67-26203

Thin film integrated circuit technology, discussing reliability, production, packaging, components, etc 12 p1917 A67-26204

Reliability and cost analysis of semiconductor integrated circuit and vapor deposited thin film IC, discussing failures and defects 12 p1918 A67-26207

Photoengraving and use as precision processing technique 12 p1951 A67-26213

Bonding and packaging techniques in production of semiconductor integrated circuits, discussing chip, lead and thermopressure bonding 12 p1951 A67-26214

Standardization techniques for integrated circuit production, particularly logic circuits 12 p1918 A67-26215

Microminiature circuits in space electronics 12 p1918 A67-26216

Preferential epitaxial growth method for electrical element isolations in IC, noting no lattice defect effect on electrical characteristics of element 12 p1918 A67-26217

MOS transistor digital switch integrating methods, presenting operating conditions

and design factors for IC inverter 12 p1918 A67-26218

Thin film integrated circuit, discussing development of large value resistors and capacitors 12 p1918 A67-26219

Encoding and decoding techniques using integrated circuits and applicable to binary digitizing of electrical analog information 13 p2072 A67-26412

Plastic molded transistors for hybrid integrated circuits, production and reliability 13 p2077 A67-26651

Large scale monolithic integration of subassemblies combined with upside-down assembly technique for more complex low cost high performance microcircuits 13 p2077 A67-26658

Grounding of capacitors in integrated circuits noting insertion of gyrators 13 p2078 A67-26783

Resonant gate transistor permitting high-Q frequency selection to be incorporated into silicon integrated circuits 13 p2079 A67-26870

Book on MOSFET covering device theory, characteristics and usage in discrete and integrated circuit form and application to practical circuit design 13 p2079 A67-26997

Passive reactive circuit conversion into circuit that shapes radio pulse with rectangular envelope 13 p2069 A67-27042

Microminiaturizable transistorized circuit for generating wide frequency range high Q inductances from semiconductor devices for integrated selective circuits 13 p2081 A67-27201

Reliability of integrated circuit amplifier improved by using nonlinear variable capacitances at LF 13 p2081 A67-27293

Digital circuits in resistor-transistor, diode-transistor and transistor-transistor logic 13 p2082 A67-27388

Photolithographic and metal aperture masks for integrated and thin film circuit manufacturing 13 p2124 A67-27390

Military electronics equipment packaging, discussing integrated circuits, module board design, interconnectors, nuclear radiation effect, heat dissipation, power supply design and cooling 13 p2083 A67-27447

Multiple internal communications system concept using single coaxial cable handling information transfer by integrated circuits 13 p2083 A67-27448

Microcellular techniques for fabricating integrated circuit arrays 13 p2074 A67-27495

Sawtooth voltage oscillation of triangular shape for pulse width modulation pulse shapers 13 p2089 A67-27704

Integrated circuits - Conference, Eastbourne, Sussex, England, May 1967 14 p2279 A67-28011

Flip-flop type current mode switching circuits, discussing features incorporated and performance 14 p2280 A67-28012

Design concept for microwave integrated circuits, noting realization and performance evaluation 14 p2280 A67-28013

Integrated memory arrays, discussing packaging methods and comparing monolithic and hybrid large scale integration 14 p2280 A67-28014

Tantalum thin film resistors for integrated circuits, noting manufacture and applications 14 p2280 A67-28015

Thin film technique interconnecting integrated circuits by ultrasonic welding and multilayer thin film conductor networks 14 p2280 A67-28016

Microelectronic technique application to active filter design, noting monolithic realization of operational amplifier 14 p2280 A67-28017

Metal oxide silicon transistors as high performance analog switching elements, noting design and performance 14 p2281 A67-28018

Gate capacitance storage property of p-channel enhancement MOSTs used in achieving low power consumption values 14 p2281 A67-28020

MOSTSIM 2 computer program for design of integrated circuits 14 p2281 A67-28021

Domain originated functional integrated circuits with possible solid-state bulk effect extension from microwave systems to whole of electronics 14 p2281 A67-28022

Semiconductor integrated circuit slices interconnection processes, using gas laser for thermal micromachining 14 p2281 A67-28023

Integrated circuit interconnection system

design exemplified by 920 M digital computer 14 p2274 A67-28025

Monolithic circuits for RF communications systems 14 p2282 A67-28027

High Noise Immunity Logic Family /HNIL/ digital switching microcircuits for long distance signal transmission operating at high voltage 14 p2282 A67-28028

PSIN /P region, Seminsulating region, N region/ diode array fabrication, performance characteristics and applications 14 p2282 A67-28029

Design for active filters via eight-pin miniature component 14 p2283 A67-28288

Tester to check altimeter of Apollo lunar module 14 p2318 A67-28282

Diaphragm element for digital logic requirements of data processing equipment, discussing functions and integrated circuit employed 14 p2274 A67-28346

Advances in microelectronics, emphasizing role of MOS transistors 14 p2285 A67-28458

Progress in linear circuit theory, discussing scattering matrices, broadband matching and distributed and mixed lumped networks 14 p2291 A67-28460

Thin film passive elements for monolithic integrated circuits, using cermet and dielectrics 14 p2286 A67-28610

Thin film resistive and capacitive circuit design 14 p2287 A67-28611

Chemical deposition of dielectrics for thin film circuits and components 14 p2369 A67-28612

CRT display provided by integrated circuit indicator packing circuitry in single plug-in module, noting timing, sweep, generation, etc 14 p2288 A67-28765

Military radar intercept calculator, discussing small size, low power supply, high performance and MOS memory 15 p2439 A67-29161

Discretionary wiring method and polycell approach to large scale integration 15 p2444 A67-29456

High speed automatic testing of semiconductor devices, discussing wafers and integrated circuits 15 p2449 A67-29812

Microwave modules using integrated circuits 15 p2451 A67-29926

Balanced broadband microwave transistor amplifiers using tantalum integrated circuitry 15 p2452 A67-29927

Magnetic devices for microwave integrated circuits, discussing ferrite substrate use as medium for microstrip transmission lines 15 p2452 A67-29928

Hybrid microwave integrated circuits, discussing use of planar and passivated chip devices 15 p2452 A67-29929

Large scale integration of arithmetic functions utilizing picosecond circuits, noting ease of fabrication, flexibility and module multipliers 15 p2452 A67-29936

Metal oxide semiconductor field effect transistor /MOSFET/ inverter transient response determination, noting mobility dependency on gate voltage 15 p2452 A67-29940

Cathode sputtering, evaporation and anodic oxidation for thin film deposition in integrated circuit technology 15 p2453 A67-30066

MOS and bipolar integrated circuits compared, noting MOS IC advantages 16 p2637 A67-31194

Book on microelectronics in U.S. covering semiconductor and thin film integrated circuits, hybrid circuits, fabrication, applications, etc 16 p2637 A67-31255

Compatible integrated circuits using thin films on silicon for application in space telemetry systems 16 p2641 A67-31555

Thick film integrated circuits drying and firing processes describing driers and furnaces for ambient air and synthesized atmospheres 16 p2641 A67-31611

Assembly of thick film microcircuit production facility detailing equipment materials, marketing, etc 16 p2641 A67-31621

Electronic components - IEEE and EIA Conference, Washington, May 1967 16 p2641 A67-31722

Fluorine and electronic integrated circuits compared, presenting state of art in packaging 16 p2610 A67-31723

Resonant gate transistor used in integrated circuits as frequency selector element for tuning problems 16 p2642 A67-31724

Twenty-eight volt monolithic integrated

- logic circuit suitable for aircraft applications 16 p2642 A67-31725
- Operation and design principles of 200 MHz counter/shift register, noting integrated circuit fabrication 17 p2824 A67-32306
- Active filter design employing impedance converters, amplifiers and gyrators, providing equations for component values 17 p2824 A67-32394
- Narrow beam microwave integrated circuit phased array system design for tactical communications satellite requirements 17 p2956 A67-32497
- Aircraft electric power systems and future use of solid state high power devices, integrated microcircuits and solid rotor generator 17 p2804 A67-32512
- Electrical design, mechanical fabrication and performance data of integrated broadband balanced transistor amplifier 17 p2825 A67-32599
- Book on integrated and active network analysis and synthesis including integrated device operation, basic characteristics and network techniques 17 p2830 A67-32732
- Variable-ratio frequency divider using integrated circuits of resistor-transistor-micrologic type 17 p2827 A67-32798
- Semiconductor device and transient ionizing radiation effects on monolithic integrated circuits 17 p2828 A67-32836
- Electron bombardment effect on insulated-gate and junction-gate FETs and MOS IC indicates FET resistance to ionizing radiation 17 p2918 A67-32850
- Monolithic operational amplifiers with simplified frequency-compensated network using minimum stages and integrated circuit components 17 p2828 A67-32899
- Integrated electronic display for V/STOL flight evaluated, considering vehicle dynamics, handling qualities, etc., and representing performance 17 p2861 A67-33182
- Fundamentals of silicon integrated device technology, Volume 1, Oxidation, diffusion and epitaxy 18 p3096 A67-33453
- Identification, coding and enumeration of distinguishable subnetwork configurations employing combinatorial analysis 18 p3016 A67-33496
- Digital filters with ICs boost Q without inductors 18 p3012 A67-34490
- Thin film resistor used to improve performance of picosecond silicon integrated digital circuit with p-n junction isolation 18 p3014 A67-34551
- Monolithic or thin film microcircuits design and performance limitations resolved by combining characteristics of thick and thin films 18 p3014 A67-34552
- Large scale integration of circuits studied for high yield, using concept of redundancy adjustment of probability 18 p3014 A67-34553
- MOSFET approach to small scale integration of large scale circuits 18 p3014 A67-34555
- High density cryotron array production in associative memory application, using lock-out design feature 18 p3014 A67-34556
- Automatic IC mask artwork generating system for large scale integration environment, describing hardware, software and performance 18 p3055 A67-34558
- Microelectronics technology extended to microwave frequencies, considering development of solid state devices and ICs 18 p3015 A67-34562
- Optimum short term screen tests developed for integrated circuits 18 p3018 A67-34649
- Circuit for integral majority-voting logic elements intended for satellite design, analyzing reliability and performance 18 p3007 A67-34664
- Detection of contaminating processes in integrated circuits, describing characteristics associated with incipient failure in operational equipment 18 p3057 A67-34665
- Development and maintenance of equipment containing integrated circuits, discussing processing, fault isolation and human error 18 p3016 A67-34670
- Synthesis of potentially bistable oscillator configurations serving as prototypes for integrated nearly sinusoidal applications [AIAA PAPER 65-363] 19 p3227 A67-34821
- Scattering and transmission parameter methods for semiconductor device measurement, discussing linear integrated circuit test requirement 19 p3191 A67-34944
- Collection of papers on integrated circuit technology covering instrumentation and techniques for measurement, process and failure analysis 19 p3192 A67-35018
- Diffusion and epitaxial equipment controlling doping level in semiconductor integrated circuits, discussing fabrication materials and techniques 19 p3236 A67-35019
- Use of controlled flow of electrons for analyzing and processing integrated circuits and focused electron beam as heat source for microwelding 19 p3192 A67-35023
- Microcircuit nondestructive IR inspection and equipment used for mask alignments 19 p3192 A67-35025
- Stencil screening methods for printing integrated circuit patterns for resistors, capacitors, etc., discussing automation possibilities 19 p3192 A67-35026
- Automatic high speed IC test equipment and procedure 19 p3192 A67-35027
- Instrumentation and microelectronic measuring methods based on nondestructive IR and UV techniques used in operation of superconductive cryogenic memory 19 p3193 A67-35028
- Space environment effects on integrated circuits, discussing FET-MOS type 19 p3196 A67-35675
- Materials technology expansion in electronics industry, discussing complete equipment components processed on semiconductor slices and large scale integrated electronics 19 p3198 A67-36054
- System/semiconductor interface with complex integrated circuits, examining different designs 19 p3199 A67-36055
- Computer program utilizing graphic data processing system for mask artwork design of hybrid integrated circuits 19 p3188 A67-36061
- Automated logic design techniques for integrated circuitry technology, with wafer design and logic arrays described for different logic functions 19 p3189 A67-36062
- Rotationally switched rod memory system with 100 nsec cycle time, discussing cost and performance factors 19 p3189 A67-36064
- Integrated circuit memory with 64 eight-bit words and compatible with high speed current-mode gates for high speed computers 19 p3189 A67-36066
- MOS transistor advantages in integrated circuits 20 p3395 A67-36320
- Silicon semiconductor strain-gauge techniques applied to transducer design noting small light units, high sensitivity, silicon integrated circuits, reliability, etc 20 p3442 A67-36458
- Reliability evaluation of MOS large scale integration devices, using simplified circuit to test individual small elements 20 p3398 A67-36800
- Generation of arbitrary binary sequence with integrated circuits, describing logic circuit by means of circuit algebra 21 p3590 A67-37946
- Integrated MOS-FET analog gate for pointing and logic of space telemetry switch 21 p3592 A67-38227
- Electronic control system for triaxial control of geocentric satellite and second stage of CORALIE booster 21 p3656 A67-38231
- Packaging of IC core memory for aerospace use, discussing design and production of boards 21 p3595 A67-38338
- Thin film integrated circuits, considering vacuum deposition and cathode sputtering 21 p3597 A67-38496
- Book on analysis and design of digital and linear integrated circuits covering transistor models, system parameters, etc 21 p3597 A67-38500
- Propagation behavior analyzed for fundamental mode of parallel plate waveguide 21 p3597 A67-38566
- Modular packaging technique using dual in-line integrated circuits, discussing advantages, interconnection matrix and conversion from logic diagram to graphic format 21 p3634 A67-38619
- Pure magnetic integrated logic circuit for space research, noting improvement on speed factor 21 p3588 A67-38675
- Soviet book on microminiaturized aerospace digital computers noting production problems, reliability, electronics, storage units and foreign computers 21 p3588 A67-38765
- Operating and performance characteristics of helium-neon pulsed gas laser, discussing application to integrated microcircuits fabrication 22 p3813 A67-39333
- Chromate conversion process applicable to IC interconnecting aluminization reveals defective areas under normal quality control procedures 22 p3771 A67-39835
- LF solid state equipment improves mission reliability through use of integrated molecular circuit and modular redundancy 22 p3771 A67-39840
- Distributed power generation for radar and communications covering cost comparisons, antenna subsystems and reliability of solid state devices 22 p3761 A67-39861
- Radiation effects on bipolar transistors field effect devices and integrated circuits noting damage in degraded current gain, increased saturation voltages and leakage 22 p3772 A67-39863
- Temperature stable ferrite materials for laminated memory arrays compatible with integrated semiconductor drive circuit 22 p3861 A67-39914
- Discrete methods for control network implementation using integrated circuitry to reduce inertial navigation systems complexity 22 p3800 A67-40184
- Spacecraft flight control and computerized systems, discussing redundant systems, integrated circuits and simulation for man-machine interaction and lack of response 22 p3908 A67-40336
- Scanning electron microscope signal processing and application to electronic devices failures, processes variations, integrated circuits and thin film circuit continuity 22 p3774 A67-40411
- MOSFET integrated circuits for use in analog computers noting simplicity and switching qualities for control of hybrid devices 22 p3775 A67-40465
- Logic gate with coupled integrated circuit transmitters 23 p3977 A67-40662
- High level transistor/transistor logic 16-bit memory element function, characteristics and applications 23 p3975 A67-40698
- Integrated circuit for TV camera including photosensitive array and self-scanned solid state image sensor 23 p3998 A67-40868
- IC emitter follower line driver with input filtering for PWM signal conditioning, solving onboard high impedance problems in drop tests with piezoelectric accelerometer 23 p4005 A67-41372
- Flexible integrated deployable solar cell array design, environmental testing and performance prediction 23 p3939 A67-41511
- Laser applications in welding and machining thin film and semiconductor integrated circuits 23 p3983 A67-41765
- Radiation resistance and reactance of thin film inductor in microwave integrated circuit determined using Fourier transform 24 p4128 A67-41924
- Power amplifiers using IC, calculating average and peak power dissipation by final transistors of push-pull circuit with resistive and reactive load 24 p4131 A67-42411
- Monolithic integrated circuit design, considering thin film circuits, hybrid techniques and MOS devices 24 p4132 A67-42687
- Repetitive circuit arrays combined with multilayer interconnections using discretionary wiring to improve array yield 24 p4132 A67-42688
- Nuclear radiation damage to circuits noting Compton effect, ionization current effects, resistance drops, electron-hole pair formation, etc 24 p4132 A67-42702
- Microelectronic integrated checkout equipment interfacing subsystems under test with test subsystem [AIAA PAPER 67-952] 24 p4133 A67-43036

INTEGRATION

SA BINARY INTEGRATION

SA FUNCTIONAL INTEGRATION

SA NUMERICAL INTEGRATION

SA RUNGE-KUTTA INTEGRATION

Maxwell equations for time-dependent fields integrated directly by using scalar-vector analog of Green theorem and Dirac delta function 03 p0469 A67-13716

Integration of nonhomogeneous equations for axisymmetric bending of spherical shells by variation of parameters 04 p0717 A67-15887

Spherical harmonics integration of low

- order spectral form of primitive meteorological equations 06 p1025 A67-18051
- Multistep generalization of Runge-Kutta methods with four or five stages 07 p1218 A67-20198
- Single and double integration in method of variation of parameters for mean longitude or anomaly analyzed for influence on set not including such function 08 p1347 A67-20397
- Asymptotic integration of elasticity theory equations and analysis of stressed state of anisotropic shell 11 p1871 A67-24160
- Normalization of mixture of pulse signal and noise by postdetector integration 13 p2069 A67-27044
- Saltykov method applied to second type partial differential dynamics equations of first class 15 p2510 A67-29518
- Real-valued function integration with respect to additive set function with real Banach space 17 p2879 A67-32810
- Congruences of geodesic rays of Einstein vacuum spaces integrability 18 p3078 A67-33690
- Integration scheme for variational r sub ij wave functions containing unlinked four-electron correlated terms for atoms up to neon 18 p3082 A67-34026
- Solid body of variable mass with cavities filled with ideal incompressible fluid, analyzing differential equations of motion 18 p3080 A67-34604
- Integration of regularizing canonical and corresponding Hamilton-Jacobi equation applied to two-body problem for construction of perturbation theory 19 p3249 A67-34795
- Relativistic Boltzmann collisionless equation solution in presence of certain external fields 19 p3286 A67-35710
- Supersonic blunt body problem noting sonic point singularity for reformulated integral relations 21 p3614 A67-38879
- Partial differential equations with more equations than unknowns investigated for solution by reducing integrable systems to ordinary differential equations 21 p3654 A67-39095
- Payload integration process for space experimentation 22 p3922 A67-39962
- INTEGRATOR**
- SA DIGITAL INTEGRATOR
- Solar radiation integrator, discussing design, composition and performance characteristics 05 p0808 A67-17310
- Describing functions for nonlinearity consisting of bang-bang with dead zone characteristic followed by linear integrator with constrained integration range 16 p2652 A67-31690
- Electric vortex-field integrator using aluminum foil sheet and external field to simulate circular flow about wing profile at various angles of attack 17 p2834 A67-32905
- Static τ /time-discrete/ electrical integrators for solution of boundary layer equations 17 p2821 A67-33080
- Fourier analysis of amplifier commutated capacitor type integrator output signal 18 p3011 A67-34107
- Integrating pyranometer operating on silicon photovoltaic solar cell for use by climatological stations and mesoscale networks 21 p3628 A67-38580
- Hydrogen integrator in pulsed mode of operation used to determine current pulse integrals 22 p3795 A67-39228
- INTELLIGENCE**
- SA ARTIFICIAL INTELLIGENCE
- Immobilization effects on electrical activity of brain and intellectual and perceptual motor processes 11 p1748 A67-25064
- INTELSAT SATELLITE**
- International Consortium for Telecommunications by Satellites /Intelsat/, noting Comsat connections 06 p0956 A67-17556
- International Telecommunications Satellite /INTELSAT/ Consortium and COMSAT participation in program [AIAA PAPER 66-332] 06 p1120 A67-17707
- Intelsat and communications satellites economic, political and social consequences, UN General Assembly Resolutions and use of satellite facilities for distribution of TV transmissions to broadcasting stations 18 p3162 A67-34354
- Space utilization by joint venture approach, discussing communications, ocean studies, etc 19 p3350 A67-35651
- Tracking ground station on Ascension Island to relay communication with Apollo spacecraft via INTELSAT II 23 p3986 A67-40706
- INTELSAT I communications satellite, discussing communications gear design and U.S. domestic satellite program 23 p4086 A67-41430
- INTENSIFIER TUBE**
- S IMAGE INTENSIFIER
- INTENSITY**
- SA ELECTRON INTENSITY
- SA LIGHT INTENSITY
- SA LUMINESCENT INTENSITY
- SA LUMINOUS INTENSITY
- SA MAGNETIC FIELD INTENSITY
- SA NOISE INTENSITY
- SA PARTICLE INTENSITY
- SA RADIATION INTENSITY
- Electrostatic, induction and radiation field effects of lightning discharge on intensity spectrum of atmospheric source signals 14 p2346 A67-27880
- INTERACTION**
- S ELECTROMAGNETIC INTERACTION
- S ELECTRON INTERACTION
- S ELECTRON-PHONON INTERACTION
- S FLAME INTERACTION
- S GAS-GAS INTERACTION
- S GAS-LIQUID INTERACTION
- S GAS-METAL INTERACTION
- S GYROINTERACTION
- S HIGH ENERGY INTERACTION
- S ION-ATOM INTERACTION
- S MOLECULAR INTERACTION
- S NUCLEAR INTERACTION
- S SPIN-ORBIT INTERACTION
- S SURFACE INTERACTION
- S WAVE INTERACTION
- INTERCEPTION**
- Microelectronic radar intercept calculator /RIC/ for ground-controlled intercept capability when used with air search radar feeding information to PPI display 08 p1293 A67-20690
- Probability of overlapping intercept by system of random intercepts and application to detection of flying objects in cloudy skies 20 p3477 A67-37036
- Interception satellite thrust and steering optimization for pursuing maneuverable satellite, analyzing both evader and pursuer sides with differential game concept 24 p4182 A67-42908
- INTERCEPTOR**
- SA SATELLITE INTERCEPTOR
- Next generation interceptor aircraft to follow F-106A, including YF-12A and evolving F-111B, would serve largely as missile launching platforms 04 p0550 A67-14422
- Military radar intercept calculator, discussing small size, low power supply, high performance and MOS memory 15 p2439 A67-29161
- INTERCONTINENTAL BALLISTIC MISSILE /ICBM/**
- S MINUTEMAN ICBM
- S TITAN I ICBM
- S TITAN II ICBM
- INTERCRANIAL CIRCULATION**
- Dynamics of pulse waves of intercranial pressure for transverse overloading accelerations 15 p2430 A67-30229
- INTERFACE**
- SA GAS-SOLID INTERFACE
- SA LIQUID-LIQUID INTERFACE
- SA LIQUID-SOLID INTERFACE
- SA LIQUID-VAPOR INTERFACE
- Interfaces in composite materials, discussing matrix-fiber interfaces, interfacial chemical interactions, microstructure and thermodynamic instability 03 p0454 A67-13426
- Analysis of existing support systems and guide for planning of new systems presenting example of manual test system and automatic test system 03 p0424 A67-14214
- Refraction of plane shock wave by interface between different gases, reducing motion equation to polynomial of degree 12 04 p0601 A67-14465
- Power source disturbance method for linear theory of flow past bodies 05 p0749 A67-17006
- Interface management of aerospace systems noting associated disciplines, documentation, contractor interrelationships and procuring agencies [AAS PAPER 66-159] 08 p1430 A67-20976
- Bibliography on thin dielectric films, interfaces and surfaces 08 p1370 A67-21188
- Shear modulus effect on stress distribution of planar array of screw dislocations near bimetallic welded half-planes interface 11 p1804 A67-24107
- Reflection and transmission of electromagnetic waves at interface between stationary isotropic medium and moving anisotropic medium 11 p1820 A67-24919
- Interface management of aerospace systems noting associated disciplines, documentation, contractor interrelationships and procuring agencies [AAS PAPER 66-159] 13 p2233 A67-27556
- Evaluation method for deposited thin film interfacial interconnections 14 p2369 A67-28613
- Polyhedral boundary precipitations of complex heat resistant nickel alloy in carbide phase caused by boron and cerium 14 p2338 A67-28674
- Strength and durability in friction tests of soft, vacuum deposited, thin-metal gold film lubricants, noting dependence on film-substrate interface 16 p2684 A67-31816
- Power source disturbance method for linear theory of flow past bodies 18 p2984 A67-34268
- Bicrystals use in optical receivers based on bicrystal interface anomalies 20 p3457 A67-36238
- INTERFACE STABILITY**
- Perturbations of gas-dynamic parameters behind shock wave front propagating from rarefied into dense gas with boundary between interfaces 01 p0053 A67-10984
- Thermal conductance at interface of two materials in contact, investigating surface and lubrication effects [AIAA PAPER 65-662] 03 p0534 A67-13068
- Surface treatment and interface stability of boron filaments reinforcing plastic composite materials 03 p0455 A67-13428
- Fluid interface instability suppression via feedback, noting stability criteria and parameters 03 p0483 A67-14036
- Liquid equilibrium configurations and disturbances of vehicle motion due to liquid sloshing in space 04 p0605 A67-14989
- Adhesive bonding of solid propellants in rocket motors, emphasizing propellant liner interface and bonding at interface 09 p1578 A67-22514
- Stability of motion of plane boundary interface between two different density coupled fluid jets analyzed to determine role of viscosity in drop formation 11 p1782 A67-24959
- Turbulent mixing at interface of two different density media under influence of pressure gradient, considering diffusion 13 p2105 A67-27411
- Transmission electron microscopy of interfacial areas in metal-matrix composites 14 p2336 A67-28096
- Steady two-dimensional magnetic bottle in which moving, compressible and electrically conducting plasma is confined by horizontally aligned magnetic field 15 p2528 A67-29568
- Supersonic unsteady flow of cylindrical body past diaphragm model at interface between density-differing gases, studying flow patterns 16 p2593 A67-31133
- MOS instabilities from ion drift, temperature dependent deep trapping and fast interface states from temperature stress, noting instabilities elimination techniques 17 p2823 A67-32195
- Parameters governing high resistance of reinforced resins, stressing elastomechanical equilibrium at interface [ONERA-TP-468] 18 p3069 A67-34462
- Electric field effects on condensation heat transfer, discussing heat-transfer coefficient dependence on electric field and instability appearance at liquid film interface [ASME PAPER 67-HT-39] 20 p3547 A67-36724
- INTERFACIAL ENERGY**
- SA SURFACE ENERGY
- Energy distribution of surface states at steam-grown silicon-silicon dioxide interfaces determined by LF differential capacitance measurements of MOS structures 04 p0683 A67-15622
- INTERFACIAL STRAIN**
- Condensation heat transfer in presence of noncondensables, interfacial resistance, superheating, variable properties and

- diffusion 04 p0720 A67-14644
Isolated force solution as Green function for formulation of plane problems for cracks along interface of two bonded half-spaces 10 p1731 A67-23848
Glass filament wound interlaminar shear specimen design and instrumentation 11 p1875 A67-24614
Misfit dislocations at diamond-sphalerite interface of thin epitaxial Ge layer deposited on GaAs 14 p2366 A67-28497
Alloy effects in low pressure diffusion bonding of superalloys, presenting time, pressure, bond strength and temperature curves 17 p2866 A67-33200
Stress distributions within materials sealed across planar interfaces compared with values measured in composite pairs of glass 24 p4175 A67-42374
- INTERFERENCE**
SA ELECTROMAGNETIC COMPATIBILITY
SA RADIO INTERFERENCE
SA WAVE DIFFRACTION
Impact expansions and interference patterns in atomic scattering theory for cases of forward scattering, backscatter, inversion problem and screened Coulomb potential approximation 01 p0112 A67-10143
Interferences between waves diffracted by circular screens or thin wires and coherent background provided by laser, producing rings or rectilinear fringes 01 p0087 A67-10231
Interferential method of testing high resolution photographic laser as light source 01 p0091 A67-10832
Interference induced elongation of light scattering indicatrix of particle conglomeration 02 p0263 A67-12671
Spectrum signature data applied to interference analysis, noting data truncation 05 p0781 A67-17538
Optical paths and variable-contrast interference at Michelson interferometer which adds two groups of two laser coherent waves 06 p1009 A67-17636
Electron number density determined using interference pattern recorded by satellite ionograms at high latitudes 06 p0996 A67-18568
Translucent and opaque photocathodes analysis 07 p1185 A67-19408
Incidence of missed reply and garbled pulse trains and fruit interference effect determined in extraction of secondary radar plots 09 p1530 A67-22653
Quantum mechanical theory of interference between independent nonmonochromatic light beams using nonmonochromatic modes of radiation field 10 p1863 A67-22866
Interference effects in far field patterns of semiconductor diode lasers 13 p2128 A67-27288
Feedback control system for hologram interference fringe stabilization, noting phase disturbances due to different effects 15 p2491 A67-30432
Laser beam study by interferometric technique using diverging spherical comparison wave noting interference patterns 16 p2685 A67-31032
High frequency asymptotic behavior of wave field in two-dimensional diffraction problem on inhomogeneous cylinder of arbitrary cross section 18 p2628 A67-31505
Intermodulation interference effect on PCM/FM error rates studied using power series as mathematical model 20 p3380 A67-36563
Wave interference and radiation tunneling phenomena influences on thermal radiation energy transfer between two separated solid dielectrics, noting spacing effect [ASME PAPER 67-HT-21] 20 p3546 A67-36716
Electron-interference experiment using laser light, discussing electron wave function phase change and electron interference pattern displacement 20 p3460 A67-36999
HF skywave propagation computer model for interference 20 p3387 A67-37646
Transient interference studied for emission from pulsed ruby laser 23 p4012 A67-40883
- INTERFERENCE DRAG**
Engine nacelle location, size and shape effects on drag due to wing thickness and drag due to lift
- [AIAA PAPER 66-665] 17 p2791 A67-32567
- INTERFERENCE FACTOR TABLE**
Interference ratios in space telecasting, considering methods of control for cochannel broadcasting 06 p0960 A67-17692
Solar supercorona observations using three-base interferometer with correlation radiometer, discussing concentration ellipses, supercoronal inhomogeneities and interference fringe modulation 20 p3529 A67-37515
- INTERFERENCE GRATING**
Holographic interference pattern magnification and observation by looking through objective end of microscope 02 p0242 A67-12027
Image distances and relative intensities for zone plates determined from holographic theory 07 p1185 A67-19401
Moire fringes as parametric curves 09 p1574 A67-21837
Interference filter of Fabry-Perot interferometer type for studying millimeter and submillimeter plasma radiation 09 p1545 A67-22000
Film resolution limitation on hologram size, Rayleigh resolution and interference pattern recording 22 p3796 A67-39259
- INTERFERENCE LIFT**
Semiempirical method for predicting aerodynamic interference of circular jet exhausting at right angles from wing, showing effect on lift loss 11 p1742 A67-24659
Aerodynamic interference effect with jet lift V/STOL aircraft under static and forward-speed conditions, stressing adverse flow 20 p3357 A67-36952
- INTERFERENCE MONOCHROMATIZATION**
Degree of coherence of two points illuminated by plane quasi-monochromatic source 06 p1000 A67-17574
- INTERFEROMETER**
SA FABRY-PEROT INTERFEROMETER
SA MACH-ZEHNDER INTERFEROMETER
SA MICHELSON INTERFEROMETER
SA MICROWAVE INTERFEROMETER
SA PHASE-SWITCHING INTERFEROMETER
SA RADIO INTERFEROMETER
SA RING LASER
Three-mirror laser interferometer measuring electron densities in repetitively pulsed plasmas 02 p0241 A67-11875
Twyman-Green arrangement of interferometer with narrow laser beam and twin photomultipliers, examining strong shocks in argon in 15.2 cm shock tube 02 p0247 A67-12688
Construction methods of DC operated He/Ne laser tubes using optical contact bonds 04 p0631 A67-14763
Interferometer with compensated phase fluctuation applicable over entire wavelength range used in radio astronomy 04 p0621 A67-15166
Interferometer design for use with laser light in fluid mechanics 04 p0624 A67-15455
Coherence and fluctuations of light including stellar correlation interferometry, photon bunching, etc 06 p1008 A67-17569
Low accuracy of interferometric measurement of coefficient of ultrasound absorption in gas 06 p1004 A67-18395
Performance of wideband interferometers using interferometer ambiguity function for radar application 08 p1300 A67-20680
Transversal mode excitation in electrostrictively operated scanning interferometer and optical matching to laser cavity 09 p1492 A67-21563
Hologram of cold mercury arc spectrum obtained by triangle path interferometer 09 p1497 A67-21766
Laser for length measurement, checking absolute wavelength stability by Fabry-Perot spectrometer 09 p1499 A67-22148
Laser interferometer for precise measurement of long distances, noting function and industrial use 09 p1499 A67-22149
Two-beam Mach-Zehnder and Michelson interferometers using coherence properties of lasers, construction and applications 10 p1652 A67-22709
Interferometer producing focusing hologram diffraction grating, noting photograph of spectrum 10 p1658 A67-23788
OH emission regions investigated using Millstone and Haystack antennas with interferometer, noting radio sources for base-line calibration and instrumental phase monitoring 12 p2009 A67-25972
Four-plate compensators of Jamin and Lowe type for interferometers, emphasizing linear dependence of phase difference on dispersion and rotation angle 14 p2315 A67-28074
Jupiter decametric radiation analyzed with interferometer for manifestations of solar wind effects 14 p2385 A67-28404
Electromagnetic sensing of absolute rotation with self-oscillating laser version of Sagnac interferometer 14 p2349 A67-28812
Radio sources in declination ranges of minus 07 to 20 degrees and 40 to 80 degrees using Cambridge interferometer at 178 mc 15 p2551 A67-29095
Interferometer with compensated phase fluctuation applicable over entire wavelength range used in radio astronomy 15 p2436 A67-29353
Stimulated emission from pulsed electrical discharge through helium with wavelength measured and transition identified with interferometer 15 p2497 A67-29395
Laser interferometers for metrology applications, considering sources of error 15 p2501 A67-30411
French interferometer for satellite tracking featuring antennas with single radiating element covering all useful space 16 p2621 A67-30681
Millimeter wave resonant interferometer capable of measuring spatial distribution of electrons in low density transient plasma column subject to perturbation 16 p2675 A67-31263
Faint radio sources investigated for isotropy applying Scheuer statistical method rendering quasars local origin theory improbable 16 p2752 A67-31623
Spherical interferometers used in measuring time-resolved spectra of ruby laser relaxation oscillations 19 p3241 A67-35804
High resolution far IR lamellar grating interferometer with double beam differencing 20 p3438 A67-36347
Transient Stark and Zeeman spectral line shifts in plasma emission measured with multiple beam Fizeau interferometer, discussing instrument errors 20 p3439 A67-36351
Solar supercorona observations using three-base interferometer with correlation radiometer, discussing concentration ellipses, supercoronal inhomogeneities and interference fringe modulation index 20 p3529 A67-37515
Interference method for measuring polarization of linearly polarized radiation 20 p3403 A67-37518
Interferometer standing on L-shaped base for velocity and distance measurements, noting tests on aircraft and rockets and solar reflections effect 21 p3599 A67-38643
Displacement effects analyzed for one beam of laser streak interferometer relative to another on image intensity distribution 22 p3795 A67-39199
Interferometer employing diffraction grating investigated for applicability to quantitative study of gas dynamics 24 p4158 A67-42723
- INTERFEROMETER SYSTEM**
Stellar interferometer at Narrabri, Australia, to determine angular diameters of approximately 50 bright stars 01 p0062 A67-10283
Correlation measurement of stellar interferometer at Narrabri, Australia 01 p0063 A67-10284
Large-base radio interferometer system without radio relaying that independently records intermediate-frequency signals on each antenna and subsequently combines them 02 p0213 A67-11635
Interferometric holography in diffused light, obtaining interferogram of phase shifting object 03 p0420 A67-13451
Radio interferometric observations of decimeter emissions from planet Jupiter 05 p0892 A67-16408
Interferometer for small optical path difference measurements, noting high sensitivity and environmental stability 05 p0807 A67-16789
Laser studies at RCA Victor Research Laboratories, Montreal, discussing spectroscopic, interferometric and plasma diagnostic research 07 p1194 A67-19082

Balloon-borne high resolution Fourier interference spectrometers analyzed in terms of IR Michelson interferometer and near IR cats-eye interferometer [JPL-TR-32-1071] 07 p1184 A67-19391

Phase compensation technique for signals received at widely spaced antennas and processed at central location 07 p1155 A67-19876

Coherent analog of compound intensity interferometer for measuring arbitrary distributions of incoherent radio sources, discussing simple and compound systems 09 p1493 A67-21609

Type III solar radioburst characteristics determined using sweep frequency interferometer 10 p1699 A67-22886

Multiple wave interferometer application to determine parameters of rarefied gas flow past circular cylinder 10 p1625 A67-23043

Angular size of OH emission measured using high resolution interferometer 10 p1709 A67-23491

Grating interferometer observation of slowly varying components of solar radio emission 10 p1711 A67-23802

Mixed single and double sideband interferometer receiving system having phase processing and delay simplicity and multiple RF return cable 11 p1764 A67-24308

Quantitative schlieren interferometry, measuring thermal distributions near heated vertical plate and horizontal cylinder 11 p1791 A67-24668

Laser interferometer for accurate determination of vibration amplitude, noting basic characteristics 12 p1943 A67-25696

Reflectance, transmittance and absorptance of muscovite type mica as function of thickness measured, using prism and grating spectrophotometers [AIAA PAPER 67-288] 12 p1958 A67-26005

Design, principles and applications of optical stellar interferometer, gratings, aperture synthesis and pencil beam telescopes 14 p2284 A67-28429

Electronic technique producing quadrature signal from laser feedback interferometer 15 p2502 A67-30436

Quasar observations using interferometer baselines, noting regular fringes and small phase scintillation in Gaussian source model 17 p2947 A67-32760

Holographic testing of large optical surfaces, using laser sources and interferometer guidance 17 p2863 A67-33301

Interferometer operated with independent oscillators and without wide bandwidth communication link between elements, making operation possible at very long base lines 17 p2864 A67-33363

East-west parabolic reflector array for design of high resolution multiple element interferometer for solar noise observations 17 p2864 A67-33402

Interference and spectroscopic devices improving photographic detection of astronomical telescopes on ground and in space 18 p3048 A67-34189

Radio astronomy sensitivity and resolution, discussing aperture synthesis and interferometric techniques for accurate position determinations 18 p3135 A67-34585

Fourier spectroscopy in far IR for routine investigation through Michelson and lamellar grating interferometers 20 p3437 A67-36340

Hologram-moire interferometry for transparent objects of moderate optical quality 21 p3624 A67-37853

Laser interferometric measurements of electron density in plasma arc discharge at atmospheric pressure 21 p3664 A67-38017

Optical interferometer for refractive plasma diagnosis, noting Q-switched ruby laser and pulsed arc lamp 21 p3630 A67-38768

Velocity of sound in liquids measurement using ultrasonic interferometry and laser diffraction spectra 21 p3630 A67-38772

High resolution interferometer data from radio source 3C 273 recorded at NASA deep space stations in Australia 21 p3712 A67-39122

Lloyd mirror experiment applied to testing flatness of large surfaces, using moire technique for visualizing and measuring fringe deviation 23 p4002 A67-41263

Hakenmethode theory and experimental technique, presenting basic arrangement for hook formation in crossed interferometer-

spectrometer system 23 p4002 A67-41264

Photographic film nonlinearities effect in holographic recording of coherent wavefront using two-beam interferometry, describing phenomenological model 23 p4002 A67-41269

Interferometer crossed with spectrograph used for electron concentration investigation in ionized argon behind shock waves propagating at high Mach numbers 24 p4197 A67-42358

Submillimeter wave laser resonator mode calculation using laser-resonator interferometry 24 p4169 A67-43105

INTERFEROMETRY

SA DIFFERENTIAL INTERFEROMETRY

Degenerate parametric amplifiers in interferometry, discussing noise temperature and pump locking 02 p0240 A67-11622

Film thickness determination by balance/oscillating crystal and multiple beam interferometry methods and steam-jet thickness methods 02 p0288 A67-11720

Interferometric technique for measuring thickness and optical constant of thin antimony trisulfide films 02 p0288 A67-11721

Optical methods and equipment used in checking surface finish and volume and surface inhomogeneities of active media and interferometric mirrors of lasers 03 p0436 A67-13143

Lasers used to extend RF plasma diagnostic procedures to optical frequencies by interferometric and Thomson diffusion methods 03 p0477 A67-13474

Heat and mass transfer from vertical plates boundary layer in convection at low Reynolds number by interferometry [ASME PAPER 65-WA/HT-39] 03 p0404 A67-14011

Elliptically polarized wave reception by antenna, itself elliptically polarized, for use in interferometry problems, noting relation to complex vector 04 p0658 A67-15626

Coherence properties of light from optical fibers noting applications to interferometry 05 p0825 A67-16978

Laser interferometric measurement of power spectral density of integrated particle density fluctuations in turbulent exhaust of sonic jet 08 p1337 A67-21142

Holographic techniques for interferometric measurements of small translations and rotations undergone by general three-dimensional object 09 p1494 A67-21614

Lattice constant of thin silicon specimens determined using electron diffraction techniques 09 p1553 A67-21881

Laser interferometry application to detection of rotation in system by splitting light from source into two coherent beams 09 p1499 A67-22150

Holographic applications, examining character identification, imaging technique and interferometric techniques 09 p1501 A67-22555

Interferometry analysis of stresses in plate due to pin 10 p1718 A67-23245

Fringe visibility dependence on path length difference in laser illuminated two-beam interferometer 11 p1790 A67-24420

Ruby laser generation spectrum width analyzed interferometrically as function of mirror spacing and pumping 12 p1952 A67-25325

Interferometry of resonator modes in submillimeter wave laser 13 p2129 A67-27347

Shadowgraphic and interferometric investigation of transversely impinging two-dimensional jet flows 14 p2303 A67-28325

Interferometric system of Diane satellite tracking stations permits high altitude tracking and measurements with larger solid angle 16 p2621 A67-30680

Interferometric comparison between two nearly identical shapes by superimposing hologram reconstruction of one onto real surface of second 17 p2864 A67-33388

Shadow photometer conversion to various interferometer types for studying inhomogeneous three-dimensional fluid flows in transparent media 19 p3228 A67-34985

Holographic interferometry in fractional-fringe density plasmas, discussing sensitivity and advantages of combined method 19 p3232 A67-35691

Application of double-exposure holographic interferometry technique by using tri-X Pan film for hologram recording 19 p3232 A67-35693

Holographic interferometry by superimposed holograms before or after

photographic development 19 p3232 A67-35890

White light reflection holography, discussing recording, reconstruction and color images 20 p3438 A67-36349

High quality holography of back-lighted objects using achromatic-fringe interferometry 20 p3450 A67-37022

Holographic interferometry in electrochemical studies, examining advantages in less critical alignment and preparation and observation of changes 20 p3450 A67-37137

Shock waves and related phenomena in shock tube investigated by streak interferometry and electrostatic probes measuring plasma density and temperature 21 p3611 A67-37961

Book on optical interferometry from coherence theory viewpoint, considering wave front and amplitude division, interference spectroscopy, multiple and laser interference, etc 21 p3658 A67-39066

Terrestrial surface spectral IR emissivities determined in situ interferometrically, noting igneous and sedimentary rock composition and texture 22 p3805 A67-40354

Electron density between shock front and discharge plasma in electromagnetic shock tube determined by interferometric technique, using guided waves 22 p3810 A67-40523

Laser application as research tool and for ranging and metrology noting laser availability and performance 23 p4015 A67-41050

Holography /phase-recording of diffracted wavelets/ for phase contrast and stroboscopy, interferometry in polarized light and 3-D photoelasticity 23 p3999 A67-41179

Interferometer phase and amplitude measurements for coherence ratio and wavefront correlation, discussing scattered flux 23 p3974 A67-41197

Three-beam holographic interferometry using only one exposure of photographic emulsion 23 p4001 A67-41259

INTERGALACTIC MEDIUM

Intergalactic atomic neutral hydrogen detection in emission in clusters of galaxy and in noncluster field 03 p0514 A67-14318

Spin temperature of intergalactic atomic hydrogen calculated as function of electron density and kinetic temperature 03 p0515 A67-14319

Anisotropic uniform model of universe with uniform intergalactic field 07 p1248 A67-19482

Possible thermal histories of intergalactic gas 11 p1860 A67-24485

High energy photons, cosmic X-rays and hard radiation production mechanisms in interstellar gas, galactic halo and intergalactic medium 14 p2380 A67-27964

Approximate expression derivation for calculating propagation rate of strong shock wave in inhomogeneous cosmic medium 15 p2552 A67-29146

Luminous and intergalactic matter, background radiation, radio sources, quasars, cosmic rays and other observational data relevant to cosmological models 19 p3327 A67-35870

UV and X-ray background measurements by Venus 3 may lead to mean density estimation of matter in universe through determination of intergalactic medium density and thermal history 21 p3705 A67-38591

Extended radio sources confinement through suggested dynamic process permitting intergalactic medium density deduction possibility 24 p4226 A67-41881

Approximate expression derivation for calculating propagation rate of strong shock wave in inhomogeneous cosmic medium 24 p4239 A67-43069

INTERIOR BALLISTICS

System requirements effect on ballistic and hardware design of cast double-base solid propellant rocket motors 15 p2548 A67-30000

Calorimetric investigation of role of ballistic modifier in nitrocellulose propellants combustion [CI PAPER 67-1] 19 p3309 A67-34996

INTERMEDIATE FREQUENCY AMPLIFIER

Intermediate frequency logarithmic amplifier using twin-gain stages and transistors and avoiding successive detection principle and video delay line 01 p0025 A67-10814

Book on transistor IF amplifier design for radio, television and radar 05 p0769 A67-16071

Wideband solid state intermediate frequency repeater for communications satellites, using waveguide-cavity diode down converter transistor amplifier and varactor upconverter 06 p0960 A67-17682

IF amplifier circuit diagrams, obtaining logarithmic amplitude characteristic by switching nonlinear elements to plate or cathode circuits 06 p0972 A67-18899

Monolithic circuits for RF communications systems 14 p2282 A67-28027

Solid state pulsed carrier IF-AGC system design for microwave receivers noting input network, video circuit, AGC loop gain, etc 18 p3016 A67-34597

Estimation of fluctuation sensitivity of measuring radio receiver modulated by intermediate frequency amplifier 19 p3198 A67-36016

INTERMETALLICS

SA ALLOY

SA SEMICONDUCTOR

Oxide dispersion hardening of intermetallic NiAl and FeAl compounds for improved high temperature strength 06 p1014 A67-17803

Microstructural and X-ray analysis of intermediate phases of Ti-Ir and Ti-Rh intermetallic compounds, including microhardness and fusion point variations 07 p1204 A67-19263

Chemical and crystal structural analysis of solid solution of titanium chromide and zirconium chromide 07 p1204 A67-19265

Rolling friction studies of intermetallic and zirconium oxide for control surface bearings for space reentry vehicle [ASLE PAPER 66AM 5D4] 08 p1335 A67-21037

Plasma jet applications, emphasizing generation of high temperatures for refractory coatings in form of intermetallic compounds and cermetes 09 p1545 A67-22172

Wideband-gap high atomic number semiconductor materials for high temperature counting radiation detectors 12 p1985 A67-25862

Properties of fabricated ingot beryllium sheet selectively alloyed with copper to obtain improved strength 13 p2139 A67-27125

Activated sintering of beryllium 13 p2140 A67-27129

Zn-Sb intermetallic compounds preparation for single crystals in semiconductor phase 14 p2372 A67-28826

Book on mechanical properties of ordered alloys including formation of superlattices 15 p2504 A67-30028

Book on intermetallic compounds discussing bonding, crystal structure, microstructure, formation, stability, kinetics, transformations and properties 16 p2692 A67-31867

Alloying volatile metals with refractory metals in Nb-Zn system, noting thermal analysis and microhardness determination 19 p3243 A67-34926

Chemical diffusion coefficients and heats of activation in nickel-aluminum intermetallic phases and solid solution calculated from layer growth experiments 21 p3645 A67-38775

Strong coupling superconductivity in intermetallic compounds, possibly due to all electrons having same kinetic energy 24 p4205 A67-42738

INTERMITTENCY HYPOTHESIS

Prandtl shear stress theory applied to similarity models of free turbulence 16 p2657 A67-30857

Inertia and muscle tone level effects on intermittence sampling frequency in hand movement control system 17 p2808 A67-33180

Intermittency hypothesis suggesting temporal integration of data processing of human central nervous system achieved through control of clock generating time points 23 p3944 A67-41020

INTERMODULATION

Interference Prediction Model /IPM/ for RF interference study at satellite tracking stations 01 p0023 A67-10498

Method for intermodulation output spectrum generation in semiconductor diode junction 03 p0381 A67-13664

Graphing spurious intermodulation responses in tunable superheterodyne

receiver to determine susceptibility to RF environment 03 p0383 A67-13789

Small signal suppression and third order intermodulation products of ferrite frequency-selective limiters 05 p0780 A67-17532

Intermodulation rejection in mixers, discussing performance characteristics of various combinations 08 p1304 A67-21223

System characteristics of tunnel diode amplifiers, discussing noise figure, intermodulation, AM-PM conversion, etc 09 p1481 A67-22479

Intermodulation noise calculated for case of distortion variable in any way with frequency 13 p2070 A67-27195

Matching factor for energy exchange in electromagnetic interaction between ionic and electronic gases in amplitude-amplitude ionospheric intermodulation 13 p2070 A67-27196

Intermodulation distortion of phase-locked loop demodulator as influenced by system parameters 14 p2273 A67-28708

Bandpass hard limiter intermodulation with low input signal to noise ratio 20 p3385 A67-37356

Intermodulation due to nonlinearities in transistor amplifiers, discussing design guidelines for optimizing 20 p3404 A67-37634

INTERNAL COMBUSTION ENGINE

SA PISTON ENGINE

Quality control and internal combustion aircraft engine reliability from mechanical engineering viewpoint 05 p0812 A67-17243

Internal combustion engine fuelled with cryogenic hydrogen and oxygen [AIAA PAPER 67-421] 18 p2988 A67-33906

MHD open circuit solution, operating by means of ionized gases, may lead to very high temperature internal combustion heat machines, discussing heat cycles 18 p3115 A67-34120

Nonlinearity of unsteady gasdynamic processes in internal combustion engine exhaust systems, using unsteady sources and sinks 21 p3689 A67-38044

Internal combustion engine vibration signals application to automatic fault diagnosis, discussing engine instrumentation and signal analysis [SAE PAPER 670872] 24 p4207 A67-42009

Nonairbreathing internal combustion engines injector configurations, noting power supply and lunar surface vehicle applications 24 p4107 A67-42533

INTERNAL CONVERSION COEFFICIENT

Hartree-Fock-Slater calculation of internal conversion coefficients for magnetic multipoles for yttrium-87 with 0.05 or 0.15 mc-square gamma energy values 01 p0116 A67-10203

Internal conversion coefficients for M4 transition in Te, noting gamma energy magnitude, nuclear size effects and eigenvalue results 03 p0472 A67-13335

INTERNAL ENERGY

Equilibrium constants and internal energies of hydrogen molecular ion calculated as function of temperature and pressure, using partition function 04 p0697 A67-14807

Implosive collapse of liners containing gas to transfer chemical energy of explosive to kinetic and internal energy of gas [AIAA PAPER 67-178] 06 p1118 A67-18485

Differential reaction cross section and internal excitation function from K and Br molecule crossed beam velocity analysis 11 p1750 A67-24991

Heat transfer for gas with internal degrees of freedom between parallel plates, noting temperature profiles and jumps 13 p2100 A67-26959

Mean internal potential for InSb lattice calculated, comparing empirical results with those obtained from Hartree and Thomas-Fermi-Dirac methods 18 p3095 A67-33442

Thermodynamics of nonlinear materials with internal state variables, analyzing evolution equation, dynamic stability, dissipation, etc 20 p3555 A67-37563

Thermodynamic interpretation for Cauchy elasticity, showing formulation of constitutive equations in continua theories 21 p3733 A67-39085

Pressure, volume, temperature and internal energy data for He using constant volume calorimeter and gas thermometer, discussing He melting 22 p3920 A67-40392

INTERNAL FRICTION

Recording assembly for measurement of flexural and torsional moduli and internal friction at various frequencies and temperatures of small samples, using constant amplitude undamped oscillations 01 p0062 A67-10163

Amplitude-dependent internal friction and defect structures measured in aluminum excited longitudinally by mechanical resonator 01 p0067 A67-10842

Amplitude-dependent internal friction and defect structures in pure aluminum measured by bridge-circuit method for difference temperatures 01 p0100 A67-10843

Amplitude-dependent internal friction and defect structures in pure aluminum from bridge-circuit measurements performed by combined kHz-mHz method 01 p0101 A67-10844

Amplitude-dependent internal friction and defect structures in aluminum, measuring critical alternating shearing stress by bridge-circuit method 01 p0101 A67-10845

High internal damping properties of magnesium alloy with zirconium addition 04 p0638 A67-15175

Dislocation-induced relaxation in silicon single crystals by measuring internal friction and Young's modulus at temperatures from 77 to 300 degrees K 04 p0681 A67-15294

Activation energy of high temperature internal friction for Cu, Al, Fe, Mo, W, Pb, Cd, Ni and Zn 04 p0640 A67-15978

Internal friction in 18 percent Ni maraging steel noting rapid dislocation recovery, independence of temperature and age hardening characteristics 05 p0828 A67-16468

Grain boundary relaxation in high purity fcc metal using LF torsion pendulum, noting tests for internal friction and creep at constant stress 06 p1016 A67-17899

Interrelation between relaxation center in tungsten and molybdenum and high temperature internal friction background of spectrum 07 p1210 A67-20010

Friction stress acting upon moving dislocation derived from microstrain studies 09 p1518 A67-22020

Influence of internal friction on high speed rotor stability using motion equation, noting bearing support flexibility and damping role [ASME PAPER 67-VIBR-14] 11 p1795 A67-24174

Bubble stabilization in pure viscous liquid contained in sinusoidal vibrated tank [ASME PAPER 67-FE-3] 14 p2304 A67-28356

Internal friction in nickel chromium alloys heated to annealing temperature, noting 530 and 800 degree peaks and origin of latter 14 p2338 A67-28675

Space vehicle potentiometer, noting niobium diselenide lubricant and minimum frictional torque 14 p2325 A67-28770

Internal friction of annealed and cold-worked niobium and tantalum wires containing oxygen and nitrogen measured, noting cold-work peaks in addition to Snoek peaks 15 p2503 A67-29748

Iodine refining of vanadium, presenting internal friction and shear modulus curves for estimating interstitial impurity concentrations 19 p3243 A67-34924

Dynamic compliance of two degrees of freedom nonrotating beam undergoing flexural vibrations, taking into account internal friction 21 p3726 A67-38833

Tungsten strain amplitude dependent dislocation damping measured as temperature function, discussing inconsistency with Friedel thermally activated breakaway theory 22 p3819 A67-39352

Low dose reactor irradiation effect on temperature dependence of dynamic modulus and internal friction of as-deposited pyrolytic graphite 23 p4021 A67-41075

INTERNAL PRESSURE

Effect of internal fluid pressure and installation inaccuracies on fatigue resistance of line connections for aircraft hydraulic and gas systems 02 p0184 A67-12448

Fatigue life of thin walled shells with inside pressure and outside support during axial motion [ASME PAPER 66-WA/MET-13] 04 p0712 A67-15377

Conical shell stability during axial compression and internal pressure under conditions of heating, noting reduction of

critical load 05 p0913 A67-16192
Cylindrical shell subjected simultaneously to axial compression and internal pressure 05 p0917 A67-16246
Steady state creep stress in shells under uniform internal pressure derived, using transition theory of Seth 05 p0920 A67-16722
Bending stresses in cylindrical shell with rigid circular inclusion examined under axial tension and internal pressure [AIAA PAPER 66-525] 05 p0924 A67-17351
Load carrying capacity of plane and reinforced cylindrical shells clamped along edges and subjected to uniformly distributed internal pressure 10 p1720 A67-23600
Nonlinear membrane theory for thin elastic inflatable shells during pressurization phase 11 p1875 A67-24432
Torsional buckling stress of orthotropic cylindrical shells with high order terms due to internal pressure rise 11 p1876 A67-24701
Vlasov engineering theory of equilibrium of shells used to study stress-strain state of closed circular cylindrical shell loaded by internal pressure 12 p2028 A67-25632
Anisotropic circular cylindrical shell stability under linear axial stress and internal pressure 14 p2400 A67-28642
Tensile creep behavior of thick walled aluminum titanium alloy cylinders under internal pressure at high temperature 14 p2339 A67-29001
Two-dimensional expansion-deflection nozzle studied for internal pressure distribution and resultant thrust determination 14 p2244 A67-29050
Adiabatic gravitational collapse of spherically symmetrical distribution of matter, investigating nonvanishing internal pressure gradient, using Einstein field equation 16 p2746 A67-30865
Finite inflation of isotropic elastic toroidal membrane possessing strain-energy function by uniform internal pressure 17 p2956 A67-31932
Forced bending oscillations for three-layer cylindrical shell under pulsed internal pressure 19 p3338 A67-34878
Small elastic-plastic deformation /caused by internal pressure/ of thin walled tube clamped at one end to rigid support 19 p3341 A67-35715
Axisymmetrical vibrations of cylindrical shell during HF internal pressure pulsations of gas flow containing uniformly distributed burning fuel droplets 20 p3536 A67-36445
Laterally flattened cylindrical shells under internal pressure representing aircraft sections strength analyzed, deriving formulas for stress-strain 21 p3724 A67-38784
Ten thin walled cylindrical shells under internal load investigated for bending stability, comparing experimental and analytical results 21 p3724 A67-38785
Stress-strain state of tubular blanks expanding under uniform distributed internal load 21 p3637 A67-38925
Koiter theorem generalized for examining unstable temperature field cyclic effects concerning progressive failure in elastoplastic bodies 22 p3910 A67-39453
Extended radio sources confinement through suggested dynamic process permitting intergalactic medium density deduction possibility 24 p4226 A67-41881
Leakage rate due to meteoroid penetration of single and multiple hulled spacecraft, discussing effect on internal pressure 24 p4251 A67-42928
Validity of formula of relativistic heat transformation, discussing pressure concept definition 24 p4257 A67-43107

INTERNAL STRESS
Dynamic stresses in thick walled spherical shell of Voigt material subjected to internal pressure load 01 p0164 A67-11174
Internal stresses of thin metallic and dielectric films, discussing methods for stress measurement, stress models and formulas 02 p0287 A67-11717
Dynamic stress field of cylindrical shell subject to internal stresses 02 p0341 A67-12664
Shape of limiting-state curve for high strength steel predeformed to yield point by repeatedly applying internal load 02 p0255 A67-12667
Bending of plates under moment induced and internal stresses 05 p0907 A67-16016
Internal stress calculation in multilayer

materials 05 p0919 A67-16590
Hole-weakened spherical body represented by deformation of two spherical shells with reinforcing rings under uniform internal load beyond elastic limit 05 p0923 A67-17187
Nuclear magnetic resonance and nuclear quadrupole resonance techniques for nondestructive testing of reinforced plastics for curing and internal stresses 08 p1345 A67-20425
Environmentally induced stresses in encapsulated electronic modules measured using hydrostatically pressure-sensitive transducer, noting internal stress changes 08 p1306 A67-21418
Asymptotic elastoplastic condition of spherical shell weakened by circular hole and sustaining residual deflections 12 p2028 A67-25631
Three-dimensional photoelasticity and determination of axes of birefringents and change in phase by scattering polarized light 13 p2219 A67-27092
Boundary value problems of continuous dislocation theory reduced to elasticity theory, deriving Green formula for internal stresses 15 p2572 A67-29235
Internal fracture of solids analyzing initiation by converging tensile pulses in prolate spheroid and crack propagation in infinite solid 16 p2773 A67-31315
Shells of revolution produced by fiber-wound distributing internal and boundary stresses uniformly over fiber contours 19 p3337 A67-34871
Stability condition for inhomogeneous elastic body subjected to internal stresses 20 p3535 A67-36392
Pulse magnitude and distribution due to energy release in liquid, on walls of shells submerged in liquid, used to calculate loads 21 p3611 A67-38056
Surface active lubricant influence on internal stresses in sign variable slippage case, discussing chemisorption, wear resistance and stress distribution 22 p3810 A67-39219

INTERNATIONAL COOPERATION
International Satellites for Ionospheric Studies /ISIS/ program using radio sounders 01 p0057 A67-10293
International space control agency needed for 1970s 02 p0343 A67-11815
Worldwide meteorological data acquisition capability proposal for improving upper air observations, noting satellite system role 02 p0231 A67-12383
Soviet book on space and problem of world peace 03 p0538 A67-13200
British-French cooperation in aeronautics, discussing Concorde SST, variable geometry aircraft, Olympus 593 turbojet, etc 03 p0362 A67-14379
UN activity concerning agreement in space problem 04 p0740 A67-14549
Coding method for transmitting digital data over IRIG-FM/FM telemetry system applied to German-American high altitude/space flight program 04 p0569 A67-14572
International law and peaceful uses of outer space 04 p0740 A67-15990
International Consortium for Telecommunications by Satellites /Intelsat/, noting Comsat connections 06 p0958 A67-17556
European Conference on Telecommunications by Satellites /CETS/, recommendations and patterns of cooperation 06 p1119 A67-17558
International Telecommunications Satellite /INTELSAT/ Consortium and COMSAT participation in program [AIAA PAPER 66-332] 06 p1120 A67-17707
Electric propulsion research in foreign countries [AIAA PAPER 67-53] 06 p1075 A67-18494
German contribution to space flight and aerospace technology in international community 07 p1269 A67-19587
Cooperative European geodetic observation of luminous objects at high altitude using Echo type satellite 07 p1176 A67-19762
VTOL capability in military and civil aircraft, discussing Italian and German efforts 07 p1130 A67-20122
Solar eclipse study program in Argentina 07 p1280 A67-20226
Mediterranean cooperation on solar energy use - General Spring Session, University of Marseille, May 1966 07 p1132 A67-20285

Experimental Inter-American Meteorological Rocket Network /EXAMETNET/ for Southern Hemisphere research 08 p1350 A67-20549
International factors in German air transport, noting progress due to limiting differences between domestic and foreign air carriers 12 p2040 A67-25490
International planetary organization with jurisdiction over activities on celestial bodies and lunar and planetary launches 12 p2042 A67-26136
Principles and general standards on rights and responsibilities in lunar exploration 12 p2042 A67-26137
Satellite telecommunications system, merits of single global system and legal aspects 12 p2042 A67-26140
International legal principles and cooperation requirements for worldwide radio and TV broadcasting by satellite telecommunications networks 12 p2043 A67-26144
Legal and political aspects of international meteorological data collection and distribution system, including use of satellites 12 p2044 A67-26153
U.S. and U.S.S.R. in space science and technology, noting limited progress in legal management, control, use and equitable division of space 12 p2044 A67-26154
Legal forms of international cooperation of U.S.S.R. in peaceful exploration of outer space, discussing bilateral and multilateral agreements between government and nongovernment organizations 12 p2044 A67-26155
Political ramifications of lunar landings, noting UN resolution concerning national possession of moon 13 p2230 A67-26339
Formal foundation of law of outer space 13 p2230 A67-27098
Bistatic CW radar observations of Venus conducted by U.S.S.R. and Great Britain during 1966 14 p2265 A67-28403
U.S. international telecommunications requirements through 1975 14 p2272 A67-28704
Book on third international operation of longitudes as part of IGY covering history, characteristics, standard hour, etc 14 p2314 A67-28957
European aerospace transporter feasibility and worth 15 p2567 A67-29839
Jaguar, Franco-British military aircraft designed for combat training and tactical support during 1970s 15 p2420 A67-30127
San Marco project, joint effort of NASA and Italian Space Commission to launch satellite for atmospheric and ionospheric measurements 16 p2757 A67-30642
Methodology for numerically defining international magnitude of space rescue requirements 16 p2781 A67-30771
Space law education 16 p2782 A67-30789
German Azur research satellite program design, instrumentation, payload, etc, and NASA role 18 p3162 A67-33640
Contribution of earth-made observations to direct planet exploration 18 p3121 A67-34136
Trajectory analysis of EOLE meteorological balloons flights in troposphere over Southern Hemisphere 19 p3332 A67-35276
Pakistan space research noting facilities, sounding rocket experiments and satellite- and ground-based observations 19 p3321 A67-35297
Mexican space research activities noting studies in meteorology, aeronomy, solar radiation, communications, tracking, astronomy and geomagnetism 19 p3321 A67-35298
International aspects of space applications and political, legal and economic problems involved 19 p3349 A67-35639
International Telecommunications Satellite Consortium /INTELSAT/ organization 19 p3349 A67-35640
Space utilization by joint venture approach, discussing communications, ocean studies, etc 19 p3350 A67-35651
Salvage and removal problems of man-made objects from outer space, stressing need for international procedures and standards 20 p3556 A67-36484
Space activity and research in industry noting European participation, international cooperation /ELDO program/ and research organizations 20 p3556 A67-37164
AZUR project /first German satellite/

cooperation with NASA, testing, signal recording, etc 23 p4071 A67-41326

Transonic and supersonic grid wind tunnel loaned to Germany by NASA for testing blades 23 p3987 A67-41328

Outer Space Treaty by 82 nations evaluated, emphasizing nature of task facing each nation in developing own methods for compliance 24 p4257 A67-42389

ESRO II satellite project objectives, design, testing program and mission requirements 24 p4241 A67-42402

Electric propulsion research in foreign countries

[AIAA PAPER 67-53] 24 p4208 A67-42902

Geopolitical factors connected with navigation satellite operation and control [AIAA PAPER 67-960] 24 p4260 A67-43041

Stationary satellite to provide educational TV to underdeveloped lands noting design, transmission terminals and safeguards against control and propaganda [AIAA PAPER 67-963] 24 p4260 A67-43042

INTERNATIONAL GEOPHYSICAL YEAR

IGY/

Auroral spectrograph data, 1959 02 p0238 A67-12036

IGY and IQSY data on maximum electron density variation in F-2 layer 05 p0800 A67-17126

Geomagnetic disturbance and correlation with PCA in auroral zone on February 10, 1958 08 p1329 A67-21539

IGY and IQSY auroral observations at Murmansk of frequency of occurrence of polar auroras in years of solar activity maxima and minima 10 p1630 A67-22787

Magnetic field variation at high latitude from quiet days in summer of IGY based on calculations for winter 10 p1632 A67-22810

Magnetic field of ring current on earth surface according to observations during IGY 13 p2111 A67-26557

Seasonal and diurnal variation of parameters of vertical electron density distribution 14 p2308 A67-27934

Magnetic activity at low latitudes during IGY 14 p2309 A67-27940

Seasonal and latitudinal magnetic activity variations in Northern Hemisphere, investigating time-space characteristics of K index 14 p2309 A67-27943

Book on third international operation of longitudes as part of IGY covering history, characteristics, standard hour, etc 14 p2314 A67-28957

IQSY and IGY comparison of night airglow OI latitude observations 16 p2667 A67-31517

Space time distribution of magnetic activity during IGY, noting elliptical region about magnetic pole characterized by increased activity 17 p2848 A67-32950

February 11, 1958 aurora observation during IGY, determining specific aurora features by all-sky camera and spectrographic techniques 17 p2849 A67-32964

IGY data from magnetic observatories analyzed for luni-solar daily variations of geomagnetic field 20 p3525 A67-36869

IGY and IQSY data on maximum electron density variation in F-2 layer 21 p3618 A67-38469

Latitude variation and motion of instantaneous pole from astronomical stations during IGY, using differential method for coordinate system 23 p3997 A67-41350

Equatorial electrojet currents studied from IGY data from South American stations 24 p4148 A67-42065

Sq currents in American equatorial zone during IGY 24 p4148 A67-42066

Magnetic field variation at high latitude from quiet days in summer of IGY based on calculations for winter 24 p4150 A67-42147

INTERNATIONAL LAW

Rule on exhaustion of local remedies and liability for damages inflicted by space vehicles 04 p0740 A67-15991

Communications satellites, legal analysis and prognosis 06 p1120 A67-17711

Extraterritorial extent of powers of aircraft commander for maintaining safety and order on board 07 p1269 A67-19519

Admiralty principles extended to occurrences involving aircraft flight over navigable water 12 p2040 A67-25486

International aspects of aviation and attitudes of governments toward IATA 12 p2040 A67-25488

Economic regulatory powers of Civil

Aeronautics Board 12 p2040 A67-25489

International factors in German air transport, noting progress due to limiting differences between domestic and foreign air carriers 12 p2040 A67-25490

International factors in air transport under treaty establishing European Economic Community 12 p2040 A67-25491

[SAE PAPER 670231] 12 p2040 A67-25491

International outer space law - IAF Conference, Madrid, October 1966 12 p2041 A67-26135

International planetary organization with jurisdiction over activities on celestial bodies and lunar and planetary launches 12 p2042 A67-26136

Principles and general standards on rights and responsibilities in lunar exploration 12 p2042 A67-26137

Lawful concept of heavenly bodies 12 p2042 A67-26138

Legal status of heavenly bodies 12 p2042 A67-26139

Communications satellites within framework of space law, noting relation of commercial treaties to communication systems 12 p2042 A67-26141

Legal problems of space research connected with telecommunication and meteorological activity 12 p2042 A67-26142

Resolutions of Institute of International Law and UN give state international responsibility for space activity 12 p2043 A67-26145

Legal status of space objects according to different criteria noting international rights, obligations and jurisdiction 12 p2043 A67-26146

Legal problems of salvage and removal of man-made objects from outer space 12 p2043 A67-26147

Legal status of space vehicles, nationality /unilateral decisions/ vs internationality /multinational operation/ 12 p2043 A67-26148

Peaceful utilization concept in international cosmic law in relation to UN resolutions and ambiguity 12 p2044 A67-26152

U.S. and U.S.S.R. in space science and technology, noting limited progress in legal management, control, use and equitable division of space 12 p2044 A67-26154

Aviation insurance characteristics, types of policy in force and regulations applying under internal law 14 p2409 A67-28933

International aspects of space applications and political, legal and economic problems involved 19 p3349 A67-35639

Salvage and removal problems of man-made objects from outer space, stressing need for international procedures and standards 20 p3556 A67-36484

INTERNATIONAL PRACTICAL

TEMPERATURE SCALE /PTS/ P

Temperature measurement problem in high temperature chemistry and International Practical Temperature Scale 20 p3435 A67-36117

INTERNATIONAL QUIET SUN YEAR

/IQSY/

Lambda and Kappa rocket sounding observations of electron density, electron temperature, thermal electron energy distribution, plasma space electric potential and ion composition 01 p0060 A67-10335

IGY and IQSY data on maximum electron density variation in F-2 layer 05 p0800 A67-17126

Interplanetary gas, solar corpuscular activity and magnetic storms and zodiacal dust cloud from satellite observations during IQSY and use of cometary tail as plasma probe 07 p1248 A67-19333

Ionospheric direct observation by sounding rockets during IQSY 07 p1186 A67-19677

Vertical measurement of ionospheric absorption at continuously varying frequency, showing diurnal variation of absorption 07 p1174 A67-19706

Criteria for determination of statistical aurora during IQSY, noting relation to magnetic activity 07 p1180 A67-19932

IGY and IQSY auroral observations at Murmansk of frequency of occurrence of polar auroras in years of solar activity maxima and minima 10 p1630 A67-22787

Polar based riometric observations of solar cosmic ray events during IQSY 10 p1701 A67-23193

Diurnal variation of telluric currents near magnetic equator during IGY and IQSY suggests equatorial electrojet as main source

for current 10 p1651 A67-23343

Lyman alpha emission from sun near solar minimum 11 p1862 A67-24503

Riometer observations in polar caps of solar cosmic ray events during IQSY 12 p1993 A67-25228

Solar X-ray monitoring during IQSY 12 p1999 A67-25833

Spatial distribution of auroral radio signal reflection centers based on radar observations 13 p2111 A67-26566

Seasonal and diurnal variation of parameters of vertical electron density distribution 14 p2308 A67-27934

Diurnal and annual variations of occurrence frequency and dispersion of whistlers during IGY and IQSY 15 p2478 A67-30068

Measurements at Ibadan of drift velocity of ionospheric irregularities for E and F layers during IQSY 16 p2663 A67-30969

IQSY and IGY comparison of night airglow OI latitude observations 16 p2667 A67-31517

UK contribution to IQSY in meteorology, geomagnetism, airglow observations, etc 19 p3223 A67-35476

IQSY South African participation, reviewing meteorology, geomagnetism, aurora, airglow, ionosphere, cosmic rays, etc 19 p3315 A67-35477

IQSY geophysical work in Greece, examining geomagnetism, aurora, ionosphere, airglow, solar activity, etc 19 p3223 A67-35478

Isolated solar events effects on neutral and charged earth atmosphere studied in West Germany during IQSY 1964-1965 19 p3223 A67-35479

Italian scientific research program during IQSY, with summarization of preliminary results 19 p3223 A67-35480

IQSY research activity in Japan, experiments and progress 19 p3223 A67-35481

IQSY program in U.S.S.R. /1964-1966/ including meteorology, aurora studies, solar activity, etc 19 p3223 A67-35482

National IQSY research programs /1964-1965/ 19 p3325 A67-35497

Canadian program for IQSY including aurora studies, solar observation, space research, etc 19 p3224 A67-35498

Argentina 1964-1965 IQSY program emphasizing aerology, solar radiation, ozone concentration, geomagnetism, etc 19 p3224 A67-35499

U.S. research program for IQSY 1964-1965 covering solar synoptic observations, zodiacal light, comet tails, atmosphere, etc 19 p3224 A67-35501

Night airglow research during IQSY noting correlation of low activity with sunset minimum 20 p3430 A67-36905

IGY and IQSY data on maximum electron density variation in F-2 layer 21 p3618 A67-38469

All-sky camera data used to construct isoauroral diagrams for IQSY period describing incidence of auroral forms and behavior pattern 22 p3791 A67-39806

Azimuths of extended auroral features measured on all-sky photography during IQSY, discussing arc alignments and auroral oval 22 p3791 A67-39807

Photometry of zodiacal light during IQSY, discussing extension to poles 24 p4152 A67-43114

INTERNATIONAL SATELLITE FOR

IONOSPHERIC STUDY

S ISIS SATELLITE

INTERPLANETARY COMMUNICATION

Interplanetary communication problems and available techniques 02 p0205 A67-12540

Attenuation of radio waves from Taurus A in interplanetary space and in space about sun 03 p0368 A67-13278

Half-tone Teletypewriter prints out picture from slow scan digital TV source 05 p0806 A67-16622

Data transmission capabilities of Mars probes and landing capsules [AAS PAPER 66-62] 07 p1146 A67-19998

Electrostatically focused extended interaction S-band klystron amplifier using helical buncher resonators for interplanetary spaceborne communication systems 09 p1477 A67-22252

Communication problems connected with deep space transmissions of interplanetary distances range 14 p2268 A67-28454

Optical and IR wideband communication between earth and interplanetary spacecraft, discussing tracking, detectors, pointing and

beam formation 22 p3762 A67-39960

INTERPLANETARY DUST

SA ZODIACAL DUST CLOUD

Time variance of earth-moon distance, discussing meteoroidal accretion mechanism effect on capture phenomena 02 p0319 A67-11453

Forces acting on small dust particles orbiting near earth and in interplanetary space and existence or nonexistence of terrestrial dust belt 04 p0615 A67-14967

Lunar and cislunar observation of interplanetary medium including lunar magnetic field, solar wind, existence of collisionless shock wave, gegenschein, zodiacal light and recovery of interplanetary particles 04 p0700 A67-15072

Comet disintegration as basic source of interplanetary dust based on zodiacal isophots 04 p0701 A67-15559

Solid interplanetary matter in vicinity of moon observed by Luna X piezoelectric pickups attached to orbiter 05 p0887 A67-16058

Skin

Structure function of interstellar absorption, noting spatial and frequency distribution of dust concentrated in clouds 05 p0897 A67-16774

Near-earth cosmic dust cloud and data obtained from satellite, rocket and ground measurement 06 p1083 A67-18161

Theory and experiment relating to interplanetary bodies larger than molecules but smaller than asteroids 07 p1246 A67-19054

Micrometeorite flux through thin aluminum foil determined using Ariel II satellite 12 p2008 A67-25824

Thermal radiation emission detection from interplanetary dust, showing that zodiacal dust extends to within 4 solar radii of sun and confirming Poynting-Robertson effect 13 p2189 A67-26264

Astronomical and satellite measurements of meteoroid environment of spacecraft in solar system 15 p2555 A67-29535

Near-earth cosmic dust cloud and data obtained from satellite, rocket and ground measurement 16 p2741 A67-30505

Dynamic phenomena in diurnal variation of cosmic rays used to determine width and existence of separate flows in interplanetary medium 16 p2740 A67-31898

Model of dust distribution in interplanetary space accounting for solar effects 17 p2947 A67-32758

Solar wind perturbation of uncharged interplanetary dust particle orbits, calculating particle lifetime 17 p2951 A67-33234

Gravitational capture of cosmic dust by sun and planets and evolution of circumterrestrial cloud 18 p3119 A67-33863

Effective braking height /EBH/ for small interplanetary particles of cosmic velocity entering Martian upper atmosphere 18 p3135 A67-34541

Cosmic ray and interplanetary medium and magnetic field studies in Bolivia 19 p3320 A67-35284

Solid interplanetary matter in vicinity of moon observed by Luna X piezoelectric pickups attached to orbiter 21 p3701 A67-37845

Zodiacal light and interplanetary dust, discussing brightness, polarization, color, spectrum and dust cloud about earth 22 p3794 A67-40426

Motion of small spherical particles entering upper atmosphere of earth with cosmic velocities studied for terminal velocities 22 p3890 A67-40472

Dynamical interaction of interplanetary particles with upper atmosphere studied by simplification of motion equation 22 p3890 A67-40473

INTERPLANETARY EXPLORER

S EXPLORER XVIII SATELLITE

S EXPLORER XXXIII SATELLITE

INTERPLANETARY FLIGHT

Space inertial sensors for long-term orbiting satellites and interplanetary missions will require capability of measuring very low-level acceleration

Inputs 01 p0074 A67-11125

Propulsion systems including chemical, nuclear, etc, for manned interplanetary mission 01 p0142 A67-11402

Linearly-approximated characteristics of maneuvers correcting near-planet positions of spacecraft with pulsed flight velocity

characteristics 02 p0321 A67-11536

Soviet program of planetary exploration with aid of automatic interplanetary stations, examining problems due to trajectory errors and communications 02 p0326 A67-12041

breakdown

Integrated space suit, suit loop and backpack system for intravehicular operation on interplanetary missions 04 p0563 A67-15235

Manned interplanetary flights before Mars landing, using Saturn-Apollo technology 06 p1092 A67-19031

Mission requirements for unmanned exploration of solar system including energy and flight time, noting thrust vs ballistic vehicles 08 p1393 A67-21096

Maximum data recovery from interplanetary reconnaissance probe by returning vehicle to earth vicinity, using space velocity meter as navigation instrument 08 p1332 A67-21102

Manual guidance for interplanetary flight by graphical methods, nomographs and relevant general equations 08 p1352 A67-21104

Approximate formulas for determining speed reduction, maximum deceleration and orbit modifications for ballistic vehicle that grazes atmosphere 08 p1394 A67-21106

Energy dissipation and other problems for alien planetary atmospheric entry at high speeds of interplanetary flight 08 p1394 A67-21155

Interplanetary flight reliability problem treated by availability concept in terms of function, duty cycle and subsequent reliability 11 p1869 A67-24339

Manned interplanetary program planning, suggesting basic parameters for manned trip to Mars and Venus 13 p2210 A67-27546

Velocity requirements for scientific probe vehicles in direct flight and planetary swingby modes of operation throughout solar system 14 p2387 A67-28618

Future planning of interplanetary voyages based on capabilities and economic advantages of classical propulsion, noting high escape velocity 14 p2392 A67-28961

Navigational technique for manned interplanetary missions, noting resemblance to traditional nautical technique 15 p2514 A67-29598

Future interplanetary unmanned space missions, examining velocity requirements and launch vehicle and payload sizes necessary for scientific investigation of solar system [AIAA PAPER 67-29] 15 p2562 A67-30104

Linearly-approximated characteristics of maneuvers correcting near-planet positions of spacecraft with pulsed flight velocity characteristics 16 p2752 A67-31602

Plasma propulsion for interplanetary flight, discussing optimization of specific impulse, weight distribution and flight path 17 p2928 A67-32226

Earth-Mars round-trip flight maximum payload delivery variational problem, determining optimum trajectories and minimum flight time dependence on engine parameters 17 p2941 A67-32240

Mission risk appraisal technique for identification and quantification of high risk areas for unmanned interplanetary missions 18 p3163 A67-34682

Economics related to practical extraction of logistics and water from moon, nearby planets and asteroids 19 p3327 A67-35652

Multipurpose entry vehicle requirements for unmanned landings on bodies in solar system having tenuous atmospheres [AIAA PAPER 67-599] 19 p3336 A67-35995

Multipoint mission for Jupiter, Saturn, Uranus and Neptune, using swingby technique for probe launched in late 1970s [AIAA PAPER 67-613] 19 p3329 A67-36002

Variational method used to obtain extremal flight conditions, considering flights between circular orbits and planets close to each other 21 p3705 A67-38585

Low thrust Jupiter flyby mission analysis for interplanetary vehicles with solar electric propulsion [AIAA PAPER 67-708] 21 p3706 A67-38735

Optimal algorithm for single parameter linear and nonlinear correction of interplanetary flight, noting application to space vehicle approach to designated planet 22 p3830 A67-39193

Three-impulse interplanetary rendezvous

trajectory as solution of time fixed multimpulse space problem 22 p3887 A67-40137

Planning and design of Voyager for future interplanetary flight, discussing RTG and spacecraft system redundancy 23 p4071 A67-40867

INTERPLANETARY GAS

Lunar eclipse brightness variation relation to geomagnetic planetary index, showing that luminescence is in accord with rate of increase of plasma energy 03 p0509 A67-13165

Quasar 3C-48 radio wave scattering by interplanetary plasma 03 p0509 A67-13204

Inhomogeneities

Interplanetary gas, solar corpuscular activity and magnetic storms and zodiacal dust cloud from satellite observations during IQSY and use of cometary tail as plasma probe 07 p1248 A67-19333

Enhanced interplanetary scintillations associated with solar flares from radio sources survey 07 p1243 A67-19667

Shock waves in interplanetary medium caused by sudden expansion of solar corona following flare [AFOSR-66-2638] 07 p1251 A67-19848

Cometary tails relationship to interplanetary gas properties and solar wind velocities deduced from observation of type I ionic cometary tails 08 p1399 A67-21238

Solar corona and interplanetary gas corotation with sun and effects of solar wind, considering poloidal magnetic field of rotating star 08 p1399 A67-21239

Particle effects of interplanetary shock wave, noting discontinuous drop in solar proton intensities 08 p1378 A67-21469

Radio source scintillations caused by electron density fluctuations extended to regime with large phase fluctuations, discussing autocorrelation function for any regime 09 p1565 A67-22222

Torque on sun calculated from solar wind motion, taking rotation and magnetic field effects into consideration 11 p1857 A67-23931

Solar magnetic field in photosphere, discussing evolution through expanding solar wind plasma 11 p1863 A67-24548

Catalog tabulating 1600 comet tail orientation observations 14 p2386 A67-28481

Structure of interplanetary plasma and magnetic field from long-period observations 14 p2362 A67-29047

No appreciable systematic differential motion between nearby neutral hydrogen and stars determined from measurement of relative velocity of former with respect to sun 17 p2943 A67-32443

Radio sources fluctuations due to inhomogeneities of solar supercorona and interplanetary plasma, studying solar wind and brightness distribution 20 p3520 A67-37513

Radio emission point sources fluctuations resulting from interplanetary plasma inhomogeneities observed at meter wavelength 20 p3529 A67-37514

Steady state model of system consisting of solar corona and interplanetary plasma, noting plasma efflux from sun 20 p3529 A67-37520

Wave equation for electromagnetic wave propagation in randomly varying refractive index medium, noting focusing for radio waves in interplanetary plasma 20 p3386 A67-37521

Spicules and inhomogeneities in corona and interplanetary plasma compared assuming mutual relationship spicules and inhomogeneities in corona and interplanetary plasma compared assuming mutual 21 p3711 A67-39028

Interplanetary space properties from satellite observations, discussing solar wind, geomagnetic field, comet tail effects, coronal plasma kinetic properties, etc 22 p3883 A67-39668

Solar system environment, discussing solar magnetic field, flare flux and energy spectrum, interplanetary plasma and radiation, asteroids, meteoroids and comets 22 p3889 A67-40407

Cosmic ray acceleration mechanisms for fast particle generation under outer space conditions 23 p4057 A67-41114

Streaming and spatial gradient equations of cosmic ray particles in interplanetary medium model, discussing Fokker-Planck equation and heliocentric field modulation 24 p4208 A67-41832

INTERPLANETARY MAGNETIC FIELD

Interaction of solar wind and frozen-in magnetic field with geomagnetic field inside and outside magnetosphere, comparing theory with satellite measurements 02 p0320 A67-11461

Temperature effect in neutron component of cosmic rays and seasonal changes in intensity affected by interplanetary magnetic field 02 p0307 A67-11666

Cosmic rays from solar flare and interplanetary space properties, covering particle scattering and magnetic field induced one-dimensional particle diffusion 02 p0310 A67-12575

Survey in satellite era of energetic particle radiations, plasmas and magnetic fields in space including solar wind, solar cosmic rays, etc 03 p0506 A67-13050

Forbush effect relation to location of large solar flares, noting association of magnetic bottles with phenomena 03 p0507 A67-14003

Solar rotation, coronal self-gravitational attraction and interplanetary magnetic fields effect on solar wind, presenting linearized hydrodynamic equations 03 p0508 A67-14313

Charged particle motion in random magnetic field, describing time evolution of particle distribution in pitch angle and position in terms of Fokker-Planck coefficients 03 p0508 A67-14317

Statistical properties of interplanetary magnetic field variations, charged particles propagation in solar system and photospheric processes analyzed, using Mariner II magnetometer 04 p0698 A67-14951

Structurally regular magnetic field in circumlunar space recorded by Luna X orbiter, noting variations in intensity and solar wind effect 05 p0887 A67-16056

Space satellite power converter-regulator design for minimum magnetic disturbance 05 p0754 A67-17462

High energy solar proton propagation in interplanetary magnetic field by Fokker-Planck equation 07 p1243 A67-19806

Interplanetary magnetic field and plasma effect on geomagnetic activity during quiet sun conditions 07 p1251 A67-19912

Correlation between pearl pulsations and interplanetary magnetic field sector boundaries 07 p1182 A67-19946

Magnetosheath field, geomagnetic activity index, magnetopause stability and interplanetary magnetic field influence on magnetospheric phenomena 07 p1182 A67-19953

Anisotropic proton velocity distribution obtained from solar wind measurements on Pioneer VI spacecraft 08 p1378 A67-21475

Large-scale structure of solar magnetic field during declining and minimum phases of solar cycle and effect on interplanetary magnetic field 10 p1700 A67-23055

Model of formation of magnetic bottle as result of interaction of drawn-out magnetic fields of solar origin, noting sunward flow of plasma 10 p1712 A67-23805

Polarity patterns of interplanetary magnetic field observed by Mariner IV during solar rotations 11 p1857 A67-23942

Geomagnetic disturbances dependence on interplanetary magnetic field sector structure and incident solar ion current at and near minimum of solar cycle 11 p1786 A67-24331

Satellite measurement of magnetic fields in cislunar space and earth proximity, noting formation of confined geomagnetic field by continuous plasma flow from sun 11 p1863 A67-24549

Spacecraft rotation effect on measurement of hydromagnetic radiation in solar wind 12 p1934 A67-25782

Solar corpuscular stream magnetic field theoretical model including hydromagnetic stability conditions and undisturbed solar wind 12 p1998 A67-25821

Preliminary results of magnetic field measurements in vicinity of magnetosphere and interplanetary space from Mariner IV 12 p2007 A67-25822

Solar wind interaction with solar dipole magnetic field in coupled hydrodynamic and hydromagnetic equations [AIAA PAPER 66-509] 12 p2008 A67-25920

Interplanetary solar wind measurements during April 1965 geomagnetic storm using electrostatic analyzers on Vela satellite 13 p2189 A67-26303

Solar wind plasma properties, noting relation between positive ion component and interplanetary magnetic field as measured by Mariner II [JPL-TR-32-1107] 13 p2190 A67-26304

Magnetic properties of meteorites, residual thermomagnetic capacity and determination of space magnetic fields 14 p2383 A67-27926

Interplanetary electromagnetic field effects on cosmic ray intensity noting geomagnetism, modulation mechanisms and solar flare particle propagation 14 p2380 A67-27965

IMP II satellite measurements of magnetic fields in interplanetary space by onboard monoaxial fluxgate magnetometers 14 p2310 A67-28052

Launching of space probes and data obtained on radiation particles and magnetic fields in space 14 p2392 A67-28960

Structure of interplanetary plasma and magnetic field from long-period observations 14 p2362 A67-29047

Temperature effect in neutron component of cosmic rays and seasonal changes in intensity affected by interplanetary magnetic field 16 p2738 A67-31081

Anisotropic phase of cosmic ray flares analyzed using kinetic equation in Fokker-Planck approximation 16 p2740 A67-31891

Solar proton diffusion data for model of quiescent interplanetary medium 17 p2937 A67-32539

Interplanetary magnetic field data by Mariner II compared to ground-based standard magnetograms and micropulsation recordings for October 7, 1962 geomagnetic storm 17 p2844 A67-32540

Interplanetary sector structure observed by IMP-I satellite compared with photospheric magnetic field and plage structure observations 17 p2953 A67-33400

Cosmic ray and interplanetary medium and magnetic field studies in Bolivia 19 p3320 A67-35284

Interplanetary magnetic field and plasma velocity variations observed during Mariner II flight 19 p3324 A67-35451

Interplanetary magnetic field variation properties and effects on solar cosmic rays determined through Mariner II recordings employed to develop model 19 p3314 A67-35452

Solar wind velocity and interplanetary magnetic field components obtained by IMP II related to geomagnetic field variation 19 p3222 A67-35473

Particle acceleration in solar flares and relative abundance of various nuclei among energetic solar particles 19 p3315 A67-35492

Interplanetary space magnetic clouds velocity and spatial distribution obtained from cosmic ray modulation data, noting relation to solar activity 19 p3325 A67-35493

Satellite observations made by two or more satellites simultaneously on interplanetary medium 20 p3521 A67-36501

Cosmic ray diffusion in interplanetary magnetic field, examining statistical homogeneity and isotropy 20 p3520 A67-37473

Galactic cosmic ray density distribution anisotropy in solar system, discussing outward convection of cosmic rays by solar wind and inward diffusion model 20 p3520 A67-37474

Structurally regular magnetic field in circumlunar space recorded by Luna X orbiter, noting variations in intensity and solar wind effect 21 p3701 A67-37843

Cosmic rays interaction with solar and terrestrial magnetic fields, noting interplanetary plasma flows and solar activity 21 p3699 A67-39006

Interplanetary magnetic field normal to ecliptic plane influence on interplanetary cosmic ray flux, discussing solar origin of field 21 p3699 A67-39019

Interplanetary magnetic field magnitude determination by considering particle motion along magnetic lines of force and trajectories divergence in earth vicinity during cosmic ray bursts 21 p3700 A67-39030

Solar disturbance variations of geomagnetic field dependence on solar activity indicates interplanetary magnetic field activity 21 p3623 A67-39041

Intense fluxes of charged particles associated with disturbances in interplanetary medium during 1966 22 p3871 A67-39797

Mariner IV flight magnetometer data,

determining interplanetary field and geomagnetic variability 22 p3790 A67-39800

Temporal and spatial low energy solar proton intensity variations indicating interplanetary medium changes effects on magnetospheric configuration 22 p3873 A67-39813

Magnetospheric open split tail topology noting stability of geometry in all solar wind and interplanetary medium conditions 22 p3792 A67-39820

Double sunspot cycle or 22-yr variation in cosmic ray diurnal variation phase, discussing streaming mechanisms 22 p3874 A67-40046

Drift equation supplemented by collision terms for describing interplanetary regular magnetic field and solar wind velocity fluctuation effects on cosmic ray propagation 23 p4056 A67-41105

Cosmic ray intensity variation mechanisms due to motion of solar system and quasi-radial interplanetary magnetic field 23 p4056 A67-41107

INTERPLANETARY MONITORING

PLATFORM /IMP/

S EXPLORER XXXIII SATELLITE

S IMP

INTERPLANETARY NAVIGATION

Self-contained midcourse guidance system with space velocity meter /SVM/ used in returning probe to earth vicinity for data retrieval and orbit control 08 p1331 A67-21101

Orientation and navigation in space-time 11 p1820 A67-24936

INTERPLANETARY PROPULSION

CONFIGURATION

Direct ballistic gravity-assisted ballistic and nuclear electric low thrust flight modes for interplanetary exploration 02 p0327 A67-12366

Megawatt ion-propulsion power conditioning system design for manned interplanetary missions, noting payload-mass ratio problems, advantages, etc [AIAA PAPER 67-52] 06 p1075 A67-18449

Guided propulsive solution to Mars atmosphere-decelerated soft landing vehicle trajectory [AIAA PAPER 67-170] 06 p1029 A67-18508

Optimum performance of propulsion acceleration calculated by approximation method, noting earth-Mars transfer and Jupiter and Saturn missions 16 p2760 A67-30735

Wave propagation and flow past obstacle in fluid magnetodynamics 20 p3503 A67-37676

INTERPLANETARY SPACE

Meteoritic matter obtained by piezoelectric pickups applied to Luna X, noting impact frequency for interplanetary space 01 p0150 A67-10910

Angular dimensions of radio sources from interplanetary flickering in radio emission intensity used to study structure of sun supercorona at large distances 02 p0322 A67-11684

Cosmic ray physics - All-Union Conference, Apatity, U.S.S.R., August 1964 02 p0308 A67-12570

Solar particles zones of incidence during maximum and minimum solar activity 02 p0310 A67-12574

Fluctuation characteristics and spectrum of monochromatic radio waves when propagating in interplanetary medium 04 p0575 A67-15163

Outer ionospheric structure and transition into interplanetary medium 05 p0886 A67-16012

Radio emission intensity measurements in interplanetary space at 20 to 210 kHz by Zond II and III and Venera II stations 05 p0887 A67-16060

Secular modulation of galactic cosmic rays in interplanetary space as function of solar activity 05 p0877 A67-16083

Energy spectrum of secular variations of cosmic ray intensity in interplanetary space, using data from stratospheric measurements 05 p0879 A67-16104

Interplanetary space properties studied from IMP-I satellite data on cosmic ray variations 05 p0880 A67-16115

Cosmic ray nuclei propagation in interstellar space and solar system examined from balloon, rocket and satellite soundings 08 p1378 A67-21473

Solar cosmic ray diffusion coefficient

dependence on cosmic ray energy and distance to sun studied via solar flares 12 p1991 A67-25111

Weak cosmic ray burst relation to austral axis pole geomagnetic activity characteristics and propagation in interplanetary space of energetic solar cosmic rays 12 p1992 A67-25116

Cosmic ray measurements in interplanetary space and on moon noting intensity increase 12 p1992 A67-25123

Magnetic and plasma observations of Explorer X and Mariner II confirmed that interplanetary shock waves give rise to sudden storm commencements magnetic and plasma observations of Explorer X 12 p2008 A67-25823

Interplanetary medium including solar wind, geomagnetosphere and observation instruments 12 p2009 A67-26173

Solar wind measurements and small scale structure of interplanetary medium using scintillation technique 13 p2190 A67-26318

Technical and economical possibilities of fast interplanetary space flight systems 13 p2211 A67-26577

Interplanetary particle diffusion model analysis in terms of energy, position in space, direction and time 13 p2193 A67-27250

Solar flare electron propagation in interplanetary space 13 p2194 A67-27251

Antenna in interplanetary plasma, noting fluctuation noise in exosphere and radiation impedance when exposed to solar wind 14 p2279 A67-27856

Measurement of angular spectrum of radio waves from sources outside solar system 14 p2386 A67-28445

Fluctuation characteristics and spectrum of monochromatic radio waves when propagating in interplanetary medium 15 p2435 A67-29350

Forbush effect causing solar flares not originating from same active solar region, discussing long connection to sun and interlocking 16 p2739 A67-31458

Cosmic ray intensity 11-year variation energy characteristics, discussing spectrum bending due to integral modulation in interplanetary space 17 p2932 A67-32083

Solar cosmic ray observations, discussing emission spectrum, interplanetary particle distribution, diffusion coefficient, magnetic field strength, space-time distribution, etc 17 p2934 A67-32096

Galactic and solar ray behavior equations, with cosmic ray drift velocity and diffusion tensor determined for interstellar space in anisotropic-diffusion approximation 17 p2935 A67-32109

Solar proton diffusion data for model of quiescent interplanetary medium 17 p2937 A67-32539

Model of dust distribution in interplanetary space accounting for solar effects 17 p2947 A67-32758

Interplanetary structure revealed through study of cosmic ray storm effects in February 1962 17 p2845 A67-32797

Zodiacal dust particle flux measurements from OGO 3 and Mariner IV spacecraft in cislunar and interplanetary space 19 p3318 A67-35185

Synoptical and monitoring projects for solar activity, interplanetary space, magnetosphere, ionosphere, aeronomy, etc 19 p3223 A67-35475

Interplanetary space magnetic clouds velocity and spatial distribution obtained from cosmic ray modulation data, noting relation to solar activity 19 p3325 A67-35493

Interplanetary space environment effect on surface thermal radiative properties, noting results of exposure to simulated solar plasma, solar UV, solar wind, etc 19 p3249 A67-35748

Satellite observations made by two or more satellites simultaneously on interplanetary medium 20 p3521 A67-36501

Outer ionospheric structure and transition into interplanetary medium 20 p3530 A67-37589

Radio emission intensity measurements in interplanetary space at 20 to 210 kHz by Zond II and III and Venera II stations 21 p3701 A67-37847

Planetary and interplanetary environments based on experimental data and quantitative information, noting influence of sun in solar system mass 21 p3707 A67-38946

Solar wind general dynamical theory,

discussing interplanetary space condition determined by coronal expansion 22 p3883 A67-39669

Solar particle event of February 1965 observation with Mariner IV and Injun IV showing 70 degrees heliocentric longitudinal distribution in interplanetary space 22 p3872 A67-39811

Interplanetary space cosmic ray intensity variation with time and distance from sun measured by Zond III and Venera II simultaneously 23 p4055 A67-41102

Cosmic ray intensity solar cycle variations in terms of solar wind properties defined by solar activity characteristics parameters 23 p4056 A67-41106

1 to 5 Mev solar proton emissions observed by increased counting rates on Venera II and III and Zond III interplanetary probes 23 p4056 A67-41112

Secular modulation of cosmic ray intensity in interplanetary space using Parker diffusion model 23 p4057 A67-41117

Cosmic ray variations over celestial sphere investigated by matrices applied to distribution model 23 p4059 A67-41134

Secular modulation of galactic cosmic rays in interplanetary space as function of solar activity 24 p4212 A67-42759

Energy spectrum of secular variations of cosmic ray intensity in interplanetary space, using data from stratospheric measurements 24 p4213 A67-42780

Interplanetary space properties studied from IMP-I satellite data on cosmic ray variations 24 p4214 A67-42791

INTERPLANETARY SPACECRAFT

Mathematical technique of midcourse guidance for spin stabilized interplanetary spacecraft, specifically computer simulation for flight to Jupiter 02 p0264 A67-12369

Cosmic radiation intensity measurement using automatic interplanetary stations with on board Geiger counters 05 p0879 A67-16106

Feasibility design study of solar powered ion propulsion system for interplanetary spacecraft [AIAA PAPER 66-214] 07 p1240 A67-19364

Sterilization environment effects on structural systems design for interplanetary spacecraft 10 p1714 A67-23758

Spacecraft orientation during interplanetary flights, using system employing two rigidly connected telescopes, one aimed at sun and other aimed at stars 11 p1751 A67-24084

Parabolic reflectors providing auxiliary solar energy for space stations and spacecraft, manufacturing and testing procedures 13 p2211 A67-26335

Automatic unique acquisition of Canopus for roll control of interplanetary spacecraft, discussing identification, discrimination and calibration [AIAA PAPER 67-585] 19 p3258 A67-35980

High payload electric propulsion spacecraft powered by solar array for multiple interplanetary missions [AIAA PAPER 67-711] 21 p3714 A67-38738

Flight control system for automatic interplanetary stations /AIS/, comparing Venera series orientation and correction system to Mariner 22 p3898 A67-39185

Cosmic radiation intensity measurement using automatic interplanetary stations with onboard Geiger counters 24 p4213 A67-42782

Satellite rise and set time of distant primary and occultation interaction determined for case of Martian satellite 24 p4238 A67-42925

Sterilization effect on functional reliability of interplanetary spacecraft systems and reliability of mission success, considering internally sterile electronic piece parts [AIAA PAPER 67-776] 24 p4116 A67-42944

INTERPLANETARY TRAJECTORY

Accuracy problems for interplanetary trajectory correction system design and development, discussing orientation circuits and standards 02 p0321 A67-11537

Interplanetary trajectory correction via radial heliocentric velocity pulses, noting calculation by linear approximation 02 p0321 A67-11538

Reconnaissance missions to outer solar system using energy derived from midcourse planetary encounter 05 p0893 A67-16520

Asymptotic matching in optimization of minimum fuel power-limited interplanetary trajectory

[AAS PAPER 66-114] 07 p1253 A67-1999

Venus swingby trajectory for manned Mars mission as possibility in 1978-1986 [AAS PAPER 66-125] 07 p1254 A67-1999

Interplanetary trajectories for vehicle using high and low thrust propulsion systems, considering three two-body transfers and role of hyperbolic excess speeds [AAS PAPER 66-128] 07 p1241 A67-1999

Flight trajectories to moon, Venus and Mars 08 p1394 A67-2111

Interplanetary trajectory design, considering energy and duration of mission arrival velocity at target and earth, using Hohmann transfer orbit, trajectory map etc 08 p1401 A67-2121

Space trajectory analysis of nuclear electric propelled vehicle 13 p2199 A67-2711

Asymptotic matching in optimization of minimum fuel power-limited interplanetary trajectory [AAS PAPER 66-114] 13 p2208 A67-2751

Venus swingby trajectory for manned Mars mission as possibility in 1978-1986 [AAS PAPER 66-125] 13 p2209 A67-2751

Interplanetary trajectories for vehicle using high and low thrust propulsion systems, considering three two-body transfers and role of hyperbolic excess speeds [AAS PAPER 66-128] 13 p2214 A67-2751

Matched asymptotic expansions and patched conics used to simplify flyby interplanetary trajectories [AIAA PAPER 65-689] 16 p2743 A67-3077

Accuracy problems for interplanetary trajectory correction system design and development, discussing orientation circuits and standards 16 p2752 A67-3160

Interplanetary trajectory correction via radial heliocentric velocity pulses, noting calculation by linear approximation 16 p2752 A67-3160

Solid interplanetary matter in moon vicinity through piezoelectric sensors, giving impact rate, trajectory projections and increased matter density hypothesis 19 p3319 A67-3521

Interplanetary transfer trajectory simulation, discussing planet ephemeris coordinate systems, low and high power and coasting segments 19 p3322 A67-3533

INTERPLANETARY TRANSFER

Mars stopover mission with Venus swingby technique, discussing velocity requirements, trip times and initial mass in earth orbit [AIAA PAPER 67-27] 06 p1085 A67-1833

Mars stopover mission with Venus swingby technique, discussing velocity requirements, trip times and initial mass in earth orbit [AIAA PAPER 67-27] 17 p2940 A67-3201

Interplanetary transfer trajectory simulation, discussing planet ephemeris coordinate systems, low and high power and coasting segments 19 p3322 A67-3533

INTERPOLATION

SA COMPUTATION

Identity of uniqueness and convergence constants of interpolation problems, discussing Abel-Goncharov function 02 p0258 A67-1161

Erdos and Turan theory of fine and rough convergence of interpolation and quadrature processes 02 p0259 A67-1191

Real function interpolation method for synthesis of electric networks in time domain by sinusoidal exponential series 03 p0458 A67-1351

Quadratic detector with diodes, based on linear interpolation of parabola 04 p0581 A67-1481

Commutativity of two interpolation functions, solving spaces of functions 04 p0644 A67-1491

Smooth surface interpolation applied to finite element displacement analysis rectangular plate 05 p0925 A67-1731

Vertical interpolation of data from constant pressure to constant density surfaces for meteorological purposes 06 p0999 A67-1871

Maximum errors of polynomial approximations defined by interpolation at least squares method 08 p1349 A67-2121

Interpolation between given data points using spline functions 09 p1468 A67-2201

Interpolation errors visualization spectrum of sampled data waveform 10 p1605 A67-2301

Regularity properties in temporal variables

of solutions of n-dimensional Navier-Stokes system, using various interpolation methods 13 p2145 A67-26604

De la Vallée Poussin linear homogeneous differential equation of nth order with continuous functions as coefficients 13 p2147 A67-27467

Variation diminishing spline approximation method of linear interpolation 13 p2147 A67-27468

Mechanical quadrature theory and convergence problems 13 p2148 A67-27469

Novel type of interpolation derived by introducing operator B and Chebyshev spaces 13 p2148 A67-27472

Automatic positioning control and problems in normalizing programming codes used in numerical control 14 p2276 A67-28956

Minimizing nonlinear function of several variables without constraints, solution obtained by combination of interpolation techniques and Levenberg method 17 p2818 A67-32426

Interpolation methods for solving nonlinear algebraic/transcendental equations applied to maximum principle boundary value problems 18 p3071 A67-33879

Lagrange interpolation pattern synthesis technique using moment criterion, for optimum pattern approximation by nonuniform antenna array 18 p3012 A67-34430

Book on stationary random processes, discussing prediction theory, interpolation, extrapolation, filtering, linear forecasting, etc 20 p3475 A67-36140

Interpolation of Poisson equation by method adjusting equations to insure existence of discrete solution 23 p4023 A67-40865

INTERPRETATION

S PHOTOGRAPH INTERPRETATION

INTERSERVICE DATA EXCHANGE PROGRAM /IDEP/

Navy method for integrating all reliability data by Integrated Data Plan, discussing Interagency Data Exchange and Failure Rate Data programs 18 p3007 A67-34660

INTERSTELLAR COMMUNICATION

Plausibility of extra solar intelligence, suggesting electromagnetic or optical means of communication 06 p0954 A67-19039

Hydroxyl radical emission, hypotheses attempting to explain OH emission origin, including possible maser mechanism and interstellar communications 21 p3704 A67-38567

INTERSTELLAR GAS

Irregularity of galactic magnetic field structure in vicinity of sun indicated by starlight polarization, interstellar cloud motion and Milky Way photography 01 p0151 A67-11275

Energy dissipation channels of nuclear and electron components of cosmic rays in Galaxy and Metagalaxy 01 p0145 A67-11276

Polarization measurements of distribution of ionized interstellar gas near galactic plane using two galactic region models 02 p0322 A67-11645

Instability of gravitating sllstreams or mixed streams and cloud fragmentation of interstellar gas 03 p0511 A67-13877

Steady state ionization fronts for H-2 regions with magnetic fields 03 p0514 A67-14316

Interstellar magnetic fields and influence on motion of gaseous matter in galaxies studied by Zeeman splitting and Faraday rotation techniques 03 p0516 A67-14336

Upper limit to neutral atomic hydrogen density in halo regions of spiral galaxies 04 p0694 A67-14480

Possible thermal histories of intergalactic gas 11 p1860 A67-24485

Delta electrons formed in interstellar hydrogen-galactic ray collision 12 p1994 A67-25645

Interstellar gas dynamics suggests that energy density of galactic cosmic rays places firm upper limit on undetermined constant of solar modulation 13 p2189 A67-26265

High energy photons, cosmic X-rays and hard radiation production mechanisms in interstellar gas, galactic halo and intergalactic medium 14 p2380 A67-27964

Stability of interstellar gas to perturbations in gas pressure, magnetic field and cosmic ray pressure from hydromagnetic viewpoint taking rotation into account 14 p2388 A67-28832

Maser effect hypothesized as cause of 21

cm radiation in clouds of interstellar hydrogen in galactic corona 15 p2551 A67-29139

Secular increase of stellar noncircular velocities in disk portions of galactic systems, noting gravitational disturbances [AROD-2160-19] 16 p2753 A67-31699

No appreciable systematic differential motion between nearby neutral hydrogen and stars determined from measurement of relative velocity of former with respect to sun 17 p2943 A67-32443

Upper limit on concentration of molecular hydrogen in interstellar space by comparison of Lyman bands in absorption spectra of early type stars and laboratory source 17 p2945 A67-32651

Photoadsorption of X-rays by interstellar gas using photoionization cross sections, showing neon K edge as distinctive feature of spectrum 17 p2937 A67-32752

Upper limit in flux density of intergalactic gas UV radiation measured from interplanetary satellite, showing temperature effect 18 p3116 A67-33524

Photodissociation of hydrogen molecules in H I regions of interstellar medium, evaluating lifetime and density 19 p3331 A67-36085

Equilibrium state for interstellar gas-magnetic field system as described by model 20 p3528 A67-37472

Antiproton production by primary cosmic ray collisions with atmospheric nuclei compared with interstellar gas 21 p3620 A67-38843

Rotation and pressure gradient effects on gravitational instability of collapsing gas clouds, discussing subsequent fragmentation 22 p3893 A67-40501

Galactic plasma dynamics related to galactic magnetic field generation and topology, discussing agreement with Hoyle-Ireland model and Morris-Berg observations 22 p3854 A67-40503

Interstellar gas properties noting insufficient information for constructing models or drawing conclusions 22 p3894 A67-40512

Interstellar gas cloud collision, heating, possible gravitational instability and subsequent cooling 22 p3894 A67-40513

Interstellar gas cloud gravitational collapse for models initially in gravitational equilibrium without mass motions, analyzing cooling and density distribution effects numerically 22 p3895 A67-40514

Collapsing gas cloud noting instability for density fluctuations, rise of turbulence and fragmentation phenomena 22 p3895 A67-40516

Equilibrium configuration for nonspherical cold gas cloud permeated by magnetic field in gravitationally collapsed state 22 p3895 A67-40518

Nonlinear growth of interstellar gas clouds and forces in three dimensions 24 p4223 A67-41812

Interstellar gas dynamic instability caused by galactic cosmic rays and magnetic field, showing turbulent and fragmentation enhancement of ambipolar diffusion 24 p4223 A67-41813

Interstellar gas and magnetic field periodic system stability noting free-fall time 24 p4224 A67-41814

Initial value problem with vanishing energy density at infinity investigated for interstellar gas oscillations 24 p4224 A67-41815

Low energy cosmic ray proton flux as representative of interstellar medium, discussing electron density in neutral H I regions 24 p4208 A67-41833

Maser effect hypothesized as cause of 21 cm radiation in clouds of interstellar hydrogen in galactic corona 24 p4239 A67-43062

INTERSTELLAR MAGNETIC FIELD

Interstellar magnetic fields and influence on motion of gaseous matter in galaxies studied by Zeeman splitting and Faraday rotation techniques 03 p0516 A67-14336

Interplanetary magnetic field effect on hydrodynamic supersonic expansion of solar corona noting solar wind velocity, nonradial flow, wave motion, etc 10 p1709 A67-23546

Stability of interstellar gas to perturbations in gas pressure, magnetic field and cosmic ray pressure from hydromagnetic viewpoint taking rotation into account 14 p2388 A67-28832

Equilibrium state for interstellar gas-magnetic field system as described by model 20 p3528 A67-37472

Synchrotron X-ray radiation by high energy electrons in magnetic field with enhancement due to outward propagating hydromagnetic waves proposed as Crab Nebula emission mechanism 23 p4051 A67-40914

INTERSTELLAR MATERIAL

SA COSMIC DUST

SA INTERPLANETARY DUST

Einstein A coefficient for lambda doublet transitions of ground state of OH 01 p0114 A67-10898

Interstellar molecule formation as result of chemical exchange reactions between atoms of interstellar gas and atoms chemically bound to interstellar grains 02 p0323 A67-11689

Interstellar and intergalactic gas, dust and magnetic fields 02 p0330 A67-12579

Autoionization mechanism role in formation of astrophysical spectra 03 p0509 A67-13217

Distribution function for temperature of interstellar H-I clouds from exact statistics of cloud collisions and quantitative treatment of cooling mechanisms 04 p0694 A67-14471

Structure function of interstellar absorption, noting spatial and frequency distribution of dust concentrated in clouds 05 p0897 A67-16774

Observational distinction between ice and graphite models of interstellar grains 06 p1082 A67-17978

Optical properties of interstellar grains, noting complex index of refraction as function of wavelength 06 p1087 A67-18410

Interstellar polarization with graphite grains covered with dirty ice mantles matched with entire range of observed interstellar extinction 09 p1569 A67-22439

See X-1 physical characteristics noting ionization, possible stellar wind and pressure equilibrium effects 11 p1862 A67-24506

Wavelength dependence of polarization of IR star in Cygnus measured by far IR lead sulfide photopolarimeter 11 p1863 A67-24509

Optical behavior of graphite as interstellar matter, discussing appearance as metal or dielectric particle, extinction and optical conductivity 18 p3117 A67-33513

Interstellar material, emphasizing chemical characterization of dust by absorption spectroscopy 19 p3323 A67-35331

Impurity effect on optical properties of interstellar graphite particles, examining wavelength dependence of absorption coefficient and refractive index of coals 19 p3323 A67-35423

Search for IR stars at various temperature ranges reveals dense interstellar clouds, cool Mira Stars and circumstellar clouds 20 p3523 A67-36647

Interstellar extinction wavelength dependence, assuming ice particle radii distribution function obeys decreasing power law and graphite particles have Gaussian distribution function 22 p3889 A67-40304

Small stellar systems evolution, double star formation and bound subgroup occurrence after condensation from collapsed cloud calculated numerically 22 p3896 A67-40521

Carbon and iron grain production in argon arc discharge studied for implications of light scattering in interstellar absorption 22 p3896 A67-40531

Microwave background in steady state universe explained by starlight absorption and microwave reemission by interstellar dust, discussing young spiral galaxies 24 p4226 A67-41875

Friedman cosmological models describing spatially homogeneous and isotropic universe 24 p4231 A67-42454

INTERSTELLAR NUCLEOGENESIS

He abundance in sun suggests He stellar nucleosynthesis was responsible for increase in He abundance in interstellar gas between formation of sun and present time 17 p2947 A67-32763

INTERSTELLAR RADIATION

Far UV extinction curve and wavelength dependence of interstellar polarization by graphite grains 01 p0150 A67-10890

Cosmic ray variations methodology, considering solar system geometry, interstellar cosmic ray gradient, phase and

- amplitude modulation, etc 17 p2934 A67-32103
- Far IR surveys of sky for thermal radiation from interstellar grains and other sources of far IR radiation, using balloon sounding 17 p2952 A67-33362
- Far UV interstellar absorption lines evaluated for main-sequence B stars 19 p3330 A67-36075
- Circular and linear polarization of OH line radiation from NGC 6334 nebulae region using Parkes radio telescope 24 p4230 A67-42333
- ### INTERSTELLAR SPACE
- Electron-photon cascade process in intergalactic space, noting role of microwave radiation in gamma ray astronomy 15 p2550 A67-29750
- Launch vehicle, payload size, velocity requirements, etc, for probes exploring solar system and near interstellar space 19 p3323 A67-35330
- He 3 ratio to He nuclei in cosmic rays, determining He nuclei path length in space, considering kinetic energy power spectrum 20 p3518 A67-37088
- Depolarization problem and correlation method for cosmic radio emission polarization measurements in interstellar space 22 p3761 A67-39757
- Total to selective interstellar absorption ratio, with improved values calculated for six-star group, considering spectral energy distribution and color excesses 22 p3883 A67-39767
- ### INTERSTELLAR TRAVEL
- Fusion propulsion for interstellar missions, examining requirements for detection of extra solar life 06 p1076 A67-19027
- Interstellar flight justification by science fiction writer 06 p1120 A67-19041
- Marx model for interstellar travel in vehicle propelled by terrestrial laser beam 08 p1376 A67-20989
- Visual aspects of transstellar space flight 12 p2009 A67-26233
- Interstellar space travel evaluation 13 p2206 A67-27509
- Propulsion sources for one-way unmanned subrelativistic interstellar probes, discussing interaction with deep space environment for vehicle control 19 p3322 A67-35316
- Biostasis /suspended animation/ by frozen storage investigated for application to interstellar voyages, noting possible damage prevention during space trips 19 p3181 A67-35325
- ### INTERSTICE
- Interstices in multiplate antennas, determining gap and shadowing losses, receiving cross section variations and radiation pattern 02 p0210 A67-11593
- ### INTERSTITIAL ATOM
- Rate controlling mechanism during yielding and flow of alpha-titanium below 0.4 times melting point 03 p0441 A67-13258
- Force constants and local mode frequencies for vibrations of interstitial lithium positive ion in Si crystal, using covalent orbital bond model 04 p0683 A67-15609
- Molybdenum grain boundary relaxation and embrittling effect of interstitial impurity additions 05 p0629 A67-18505
- Yield point and strain aging in tantalum, identifying interstitial atom in electron-beam melted tantalum after incremental plastic deformation 06 p1015 A67-17896
- Niobium and tantalum purification from interstitial impurities by high vacuum annealing, noting effect on electric resistivity 07 p1210 A67-20112
- Temperature effect, including liquid helium temperature, on yield stress of commercial purity alpha titanium 11 p1805 A67-24111
- Model for concentrated interstitial solid solutions applied to carbon solution in gamma iron 13 p2131 A67-26574
- Triangular flux line lattices observation by electron microscope in type II superconductors 14 p2369 A67-28599
- Oxygen caused bright spots in field ion microscope patterns of tungsten, noting oxygen variation effects 16 p2893 A67-31873
- Recovery Stage III in neutron irradiated Al-Cu alloy, discussing vacancies and interstitials 17 p2873 A67-32743
- Iodine refining of vanadium, presenting internal friction and shear modulus curves for estimating interstitial impurity concentrations 19 p3243 A67-34924
- Electronic structure of irradiation defects in ionic solids vacancies, interstitials and dislocations, explaining electronic relaxation 19 p3306 A67-35673
- Interstitial oxygen solubility in niobium using X-ray diffraction, micrographic and thermal techniques, discussing lattice structure 22 p3823 A67-40209
- Lattice parameter of bcc Nb-Hf alloy with interstitial solid solution of oxygen 22 p3823 A67-40210
- Oxygen interstitial solid solubility in niobium, noting decrease with addition of tungsten and molybdenum 22 p3823 A67-40211
- Interstitial solid solubility of N in Nb and Nb binary alloys containing Hf, Mo and W as function of pressure and temperature 24 p4172 A67-41976
- Hf, Mo and W influence on maximum interstitial solid solubility of N in Nb rich ternary systems 24 p4172 A67-41977
- ### INTESTINE
- ### SA ABDOMEN
- ### SA DIGESTIVE SYSTEM
- ### SA GASTROINTESTINAL SYSTEM
- Postulates on microbial hazards of astronauts in prolonged isolation based on studies with animals with locked flora 05 p0755 A67-16281
- ### INTRACRANIAL PRESSURE
- Intracranial pressure measurements and electroplethysmographic examination of blood content in dog cranial cavity for transverse acceleration up to 40 g 13 p2057 A67-26456
- Intracranial pressure in Macaca speciosa monkeys during controlled abrupt linear deceleration 23 p3954 A67-41596
- ### INVARIANCE
- Formulated conditions for proving existence of invariant surfaces of system not circumscribed by ordinary perturbation theory 03 p0456 A67-13110
- Invariance and sensitivity theories applied to automatic control system design 03 p0391 A67-13186
- Invariant control device synthesis in multidimensional nonlinear automatic control systems 03 p0391 A67-13187
- Necessary and sufficient conditions of invariance and autonomy of multidimensional nonlinear automatic control systems with right-hand discontinuities in describing differential equations 03 p0391 A67-13188
- Invariance theory for automatically controlled underwater wings ensuring ship motion stability in perturbed medium 03 p0359 A67-13189
- Invariants in inhomogeneous turbulent flow related to Loitsianskii integral 05 p0794 A67-17418
- Unitary and orthogonal invariants of square matrices 07 p1217 A67-20024
- Invariance principle applied to motions of material particle that do not depend on particle mass 07 p1224 A67-20026
- Invariant stress and deformation functions for doubly curved shells, noting reduction of equilibrium equations and surface strain-displacement relations into compatibility equation 10 p1730 A67-23834
- Invariant operating regime of optimum threshold receiver during binary signal reception 16 p2624 A67-31029
- Applicability to elastic flight vehicle control system of two variants for realization of invariance conditions 17 p2862 A67-33097
- Exchange invariance in dissipationless fluid systems, deriving conservation law and stability conditions and application to gyro-stabilized magnetoplasma 20 p3419 A67-36151
- Optimality and invariance conditions for linear free-time problem 20 p3412 A67-37582
- Invariance principle proposed for controller analytical design for nonlinear invariant systems by reducing problem to quasi-linear problem 21 p3604 A67-39111
- Sign of energy gain and direction of energy flow shown invariant under Lorentz transformation for two relatively moving systems possessing equal proper temperature 21 p3733 A67-39124
- Parameter invariance problem for linear systems solved by obtaining necessary and sufficient conditions for invariance in optimal control systems 23 p3984 A67-41159
- Caratheodory method in variational calculus and partial differential equations, discussing coordinate-free invariance usage

- and extremal theory 24 p4178 A67-42203
- Extended dynamical systems in Banach space and use of invariance principle for stability theory of partial differential equations 24 p4178 A67-42652
- Hyperbolic noninvariance in partial differential equations, discussing existence theorems for nonhyperbolic initial value problem systems 24 p4178 A67-42727
- ### INVARIANT IMBEDDING
- Invariant imbedding and numerical integration of boundary value problem for unstable linear systems of ordinary differential equations 07 p1218 A67-20214
- Invariant imbedding and time dependent scattering processes including applications to particles moving in rod, radiative transfer in slab, photon diffusion and homogeneous diffusion processes 07 p1224 A67-20274
- Dynamic programming for control system synthesis, noting invariant imbedding and optimality principle use in optimum design problems 08 p1312 A67-20752
- Book on electromagnetic wave propagation and turbulent media covering invariant imbedding method, turbulence generation, statistical methods of analysis, etc 08 p1295 A67-20984
- Numerical solution methods of invariant imbedding equation for reflection function of spherical shell with absorption and isotropic multiple scattering 10 p1680 A67-23634
- Line profiles and equivalent widths from diffuse reflection of sunlight from model planetary atmosphere calculations, using invariant imbedding 10 p1710 A67-23635
- Invariant imbedding method applied to energy dependent neutron radiation penetration problems in thick and heterogeneous shields 11 p1817 A67-25063
- Numerical techniques for process identification in automatic control systems, discussing methods such as autocorrelation, spectral density, differential approximation, etc 15 p2460 A67-30310
- Neutron transport and radiative transfer analysis via generating function technique, confining analysis to one energy model 17 p2876 A67-32557
- Functional equations in internal radiation field in finite inhomogeneous isotropically scattering atmosphere, using invariant imbedding and Duhamel principle 24 p4189 A67-42597
- ### INVENTORY CONTROL
- National space inventory of launch vehicles, spacecraft, space station studies, facilities and projected modifications evaluated for USAF low earth orbital logistics 03 p0519 A67-14017
- [AIAA PAPER 66-866] Static and dynamic inventory control models for logistics planning and operational readiness with cost constraints 18 p3162 A67-34680
- ### INVERSION
- ### SA POPULATION INVERSION
- Book on numerical inversion of Laplace transform for computers 06 p1023 A67-17942
- Stress-strain relations of linear theory of shells extended to corresponding inversion with more complex results 06 p1100 A67-18117
- Geometric interpretation of product form of inverse applied to sparse matrices in linear programming, using graph theory 10 p1673 A67-22833
- Inversion of symmetrical matrices by computer, noting storage space advantages 17 p2820 A67-32800
- Inversion formulas for parabolic functions: solution to vibration equation in diffraction at paraboloid of revolution 21 p3652 A67-38111
- ### INVERTER
- Transistor behavior in phase inverter as LF as function of type /p-n-p or n-p-n/ and value of internal capacity 01 p0038 A67-10777
- Design and performance characteristics of two-bridge controlled autonomous compensation inverter for DC to AC conversion 07 p1150 A67-1931
- MOS transistor digital switch integrating methods, presenting operating conditions and design factors for IC inverter 12 p1918 A67-2621
- ### INVISID FLOW
- ### SA VISCOUS FLOW
- Three-dimensional boundary layer and invisid hypersonic flow interaction and

- infinitely thin triangular wing 01 p0007 A67-10982
- Interaction between boundary layer and external inviscid flow, noting unsteady motion of gas around infinite plate and steady flow around semiminfinite plate 01 p0053 A67-10983
- Shock wave formation due to nonlinear vibrations in tube containing fluid subjected to transverse magnetic field with plane heater at midsection and externally supplied energy 02 p0273 A67-12058
- Hypersonic flow of air past circular cylinder with nonequilibrium oxygen dissociation, including dissociation of free stream 03 p0351 A67-13000
- Reflection and refraction of plane MHD waves at plane interface discontinuity of two semiminfinite homogeneous conducting fluids of different densities 03 p0480 A67-13727
- Inviscid stability of incompressible half-jet under aligned magnetic field, determining neutrally stable eigenvalues 03 p0483 A67-14034
- Simple waves for nonlinear system of partial differential equations applied to multidimensional compressible inviscid flows 05 p0790 A67-16045
- Inviscid flow method predicting nonlinear supersonic and hypersonic lift component of highly swept wings with low aspect ratio 06 p0937 A67-18013
- Inviscid linearized perturbations of supersonic entropy layers analyzed, using approximating partial differential equations by simultaneous ordinary differential equations [AIAA PAPER 67-6] 06 p0938 A67-18249
- Supersonic flow over axisymmetric bodies with continuous or discontinuous slope solved via parametric differentiation [AIAA PAPER 67-5] 06 p0939 A67-18303
- Flow field model for laminar hypersonic near-wake in inviscid expansion, viscous sublayer and recirculating flow [AIAA PAPER 67-63] 06 p0940 A67-18353
- Linearized long wave diffraction theory of supersonic inviscid flow past slender circular cylindrical bodies and thin wings 06 p0942 A67-18729
- Hypersonic boundary layer behavior in adverse pressure gradients used in designing high Mach number intake diffuser system 06 p0942 A67-18750
- Book on inviscid hypersonic flow theory including nonequilibrium effects, flows on blunt bodies, shock layer, conical flows, etc 07 p1127 A67-20204
- Initial value problem for hydrodynamic instability of parallel flow of inviscid fluid 08 p1319 A67-20309
- Surface pressure, heat transfer coefficient, wave structure and shock disturbances of inviscid supersonic flow field along corner of intersecting wedges [AIAA PAPER 66-128] 08 p1276 A67-20564
- Inviscid hypersonic flow of radiating gray gas over sphere analyzed, noting temperature role in process 08 p1276 A67-20567
- Gas dynamics of nonisentropic two-dimensional MHD flow of ideal inviscid perfectly conducting compressible fluid 08 p1357 A67-20593
- Inviscid hypersonic flow over plane power law bodies where blast theory applies as first approximation, determining shape and pressure distribution 08 p1277 A67-20708
- Stability of radial motion of spherical gas bubble in incompressible inviscid fluid under external pressure 10 p1624 A67-23028
- Inviscid flow characterized by annular elliptical region between shock wave and ducted body calculated by integral relation method, noting contraction coefficient values 10 p1591 A67-23045
- Behavior of inviscid supersonic conical flow fields near crossflow stagnation points studied by constructing coordinate expansions of exact conical flow equations [AIAA PAPER 66-491] 10 p1591 A67-23112
- Inviscid conical flow around pointed cone at angle of attack transformed into hyperbolic flow 10 p1592 A67-23136
- Inviscid axisymmetric radiating flow over blunt body, analyzing paraboloidal shock wave thermal radiation effects on temperature, density, velocity, etc 10 p1592 A67-23453
- Inviscid two-dimensional flow using extension of Hele-Shaw analogy, noting axisymmetric, compressible and MHD cases 10 p1627 A67-23554
- Lateral efflux from flow along wall into suction slot computed by conformal mapping contraction coefficient 10 p1627 A67-23559
- Steady hypersonic inviscid flow, including detached shock, around blunt body, using finite difference computations 10 p1593 A67-23633
- Deformation of velocity profile in inhomogeneous magnetic field, noting anisotropic conductivity of flow 10 p1686 A67-23670
- Inviscid flow theory in internal aerodynamics, discussing irrotational, secondary and flow past thin airfoils and slender bodies 11 p1776 A67-24049
- Digital computer analysis of inviscid two-dimensional parallel flow stability, using finite difference method to solve resulting initial value problem 11 p1778 A67-24220
- Oscillation and stability of system of thin elastic shells in potential inviscid and incompressible fluid flow 12 p2023 A67-25589
- Partial differential equations for three-dimensional inviscid flow solved for flow field over blunt body shapes at various angles of attack, for application to Apollo spacecraft [AIAA PAPER 66-413] 14 p2240 A67-28110
- Nonlinear inviscid transonic flow in throat of two-dimensional curved nozzle, using approximate method [ASME PAPER 67-FE-11] 14 p2242 A67-28360
- Far wake behavior of hypersonic spheres analyzed using schlieren techniques 15 p2417 A67-30190
- Unsteady flow of inviscid, electrically conducting but thermally nonconducting gas at small magnetic reynolds numbers in MHD generator channel unsteady flow of inviscid electrically conducting but thermally nonconducting gas at small magnetic 16 p2706 A67-30451
- Multidimensional unsteady flow field of inviscid fluid calculated with application of method of characteristics and digital computer 16 p2662 A67-31535
- Inviscid steady partially cavitating flow through cascade of flat plate hydrofoils 16 p2662 A67-31550
- Two-dimensional inviscid flow pattern of gas behind shock front in neighborhood of stagnation point of cylindrical body acting as magnetic field source 16 p2723 A67-31581
- MHD behavior of inviscid fluid in limit of infinite electrical conductivity and mobility exhibiting Hall effect 17 p2908 A67-33109
- Dynamic phenomena in two identical cylindrical shells placed side by side in inviscid supersonic flow of compressible fluid 18 p3024 A67-33540
- Conditions of time-symmetry for four classes of flows, discussing instabilities 18 p3079 A67-34004
- Inviscid hypersonic flow in stagnation region of circular cylinder with detached shock wave, considering real-gas effects 19 p3171 A67-35713
- Inviscid hypersonic axisymmetric flow over cylinder and sphere near stagnation point, including dissociation and detached shock wave 19 p3171 A67-35722
- Steady flow of perfectly conducting inviscid liquid past thin symmetrical airfoil of finite conductivity in aligned magnetic field 20 p3494 A67-36146
- Compressible inviscid fluid MHD motion, stressing quasi-aligned field flows 20 p3496 A67-36272
- Compressible boundary layer-inviscid flow interactions in entrance region of internal flows, including shock tube boundary layer and effects of mass injection or suction [ASME PAPER 67-HT-2] 20 p3421 A67-36701
- Burning in unmixed reactants for high enthalpy inviscid flow of opposed streams studied for one-step reaction model and Lewis-Semenov number 20 p3554 A67-37132
- Single parameter Ball cylindroids representation of multiply connected surface vortical motion axes 21 p3611 A67-37902
- Deformation of velocity profile in inhomogeneous magnetic field, noting anisotropic conductivity of flow 21 p3666 A67-38271
- Inviscid incompressible flow of normal and slightly oblique static round jet impinging on ground, noting velocity distribution 21 p3565 A67-38544
- Inviscid hypersonic flow field between barrel shock and free boundary for source flow representing high altitude jet exhaust 22 p3739 A67-39410
- Tanh y form laminar mixing layer and nonlinear inviscid equation two-dimensional solutions with linearized stability theory perturbations 22 p3782 A67-39528
- Vorticity component change rate expressions for arbitrary configuration inviscid flow, discussing local instabilities 23 p3990 A67-41166
- Inviscid instability of cylindrical two-dimensional free boundary layer vortex flow, using approximation by axisymmetrical vortex model 23 p3990 A67-41169
- Two-dimensional incompressible flow near airfoil trailing edge treated by inviscid flow model, with constant vorticity inducing velocity field causing flow retardation 23 p3928 A67-41245
- Oscillating infinitely thin wing profile in inviscid subsonic compressible flow, deriving perturbation pressure 23 p3929 A67-41250
- Liquid mercury conductor flow in annular gap electromagnetically accelerated by Lorentz force, showing restricted nonexistence proof for inviscid problem 23 p3992 A67-41742
- Inviscid steady axisymmetric flow inside closed annulus solution derived with extremal principle [ARL-66-0173] 24 p4140 A67-41807
- Delta wing with leading edge vortices, calculating inviscid incompressible flow field near center of rolled up vortex sheet assuming conical velocity field 24 p4092 A67-42570
- IODIDE**
- SA CESIUM IODIDE
- SA METHYL HALIDE
- SA POTASSIUM IODIDE
- SA SILVER IODIDE
- SA SODIUM IODIDE
- Optical method observations of phase transition of ferroelectric monocrystal SbSI 06 p1047 A67-17758
- Crossed molecular beam kinetics of reactive asymmetry of oriented methyl iodide polar molecules reacting with rubidium 06 p0955 A67-17831
- Iodide refining of vanadium, presenting internal friction and shear modulus curves for estimating interstitial impurity concentrations 19 p3243 A67-34924
- IODINE**
- Hall effect and transport properties of single crystals of iodine measured by alternating current technique, using field effect transistors 04 p0675 A67-14757
- Photodetachment probability for Cs and negative I due to simultaneous absorption of two ruby quanta 05 p0815 A67-16627
- Crab Nebula X-ray spectrum from balloon observations, noting importance of correction for escaped iodine K component 07 p1251 A67-19944
- Laser oscillation on hyperfine transitions in ionized iodine, noting Fabry-Perot fringes 10 p1662 A67-22699
- Xenon-iodine dating, sharp isochronism in chondrites 12 p2002 A67-25525
- Vapor growth of single crystal heterojunctions of GaAs on Ge or InAs on GaAs using iodine process in closed tube system 23 p4043 A67-41432
- Poly-N-vinyl carbazole-iodine charge transfer photovoltaic effect spectral and intensity dependence, noting possible radiation detection and energy conversion applications [JPL-TR-32-1138] 24 p4201 A67-41899
- Iodine isotope mass-yield distributions from spontaneous plutonium 242 fission, discussing heavy xenon isotopes from extinct plutonium 244 in meteorites 24 p4191 A67-42450
- IODINE 125**
- Rats exposed to simulated altitude studied for acute changes in iodine metabolism, noting dichotomy between thyroidal iodine uptake and secretion rates 15 p2428 A67-29279
- ION**
- SA CESIUM ION
- SA FREE RADICAL
- SA HEAVY ION
- SA HYDROGEN ION
- SA METAL ION

SA NITROGEN ION

- Methods for calculating interaction potentials of atoms, molecules and ions 03 p0473 A67-13613
- Methods for calculating interaction potentials of atoms, molecules and ions 18 p3083 A67-34478

ION-ATOM INTERACTION

- F-2 layer ion-atom interchange coefficients, ion-neutral diffusion coefficient and flux of solar ionizing radiation, comparing ionospheric data 01 p0056 A67-10108
- Impact expansions and interference patterns in atomic scattering theory for cases of forward scattering, backscatter, inversion problem and screened Coulomb potential approximation 01 p0112 A67-10143
- Effective cooling of free electrons in plasma due to ambipolar diffusion and elastic collision with ions and neutrals 01 p0122 A67-10346
- Tandem mass spectrometers for study of ion-molecule reactions, noting ion gun, deceleration lens and collision chamber 02 p0247 A67-12690
- Photoionization mass spectrometer for ion-molecule reaction studies, determining ion residence times, drift velocities, diffusion coefficients and ion temperatures 07 p1137 A67-20187
- Photoionization mass spectrometer for charge transfer reaction analysis 07 p1137 A67-20188
- Cross sections for excitation of upper and lower ion states by electron impact with ground state neutral argon atoms found by measuring coherent and incoherent light of laser beam 09 p1514 A67-22272
- Charge exchange cross sections measurements for ion-molecule pairs of hydrogen, argon, krypton, helium and xenon 09 p1535 A67-22381
- Mass spectrometric investigations of interaction of atmospheric ions with molecules of rocket gas release 10 p1640 A67-23215
- Properties of partially ionized Ar computed via Chapman-Enskog-Burnett expressions noting ambipolar diffusion coefficient, electron-atom momentum, electrical and thermal conductivity, etc 11 p1775 A67-23865
- Reliability of laboratory thermal rate coefficients for positive ion/neutral reactions in ionosphere 11 p1785 A67-23945
- Measuring atomic radiation and collision cross section coefficients of plasmas 11 p1839 A67-24551
- Effective cooling of free electrons in plasma due to ambipolar diffusion and elastic collision with ions and neutrals 11 p1843 A67-25019
- Atomic collisions with negative ions, deriving transition matrices for resonance reactions and scatterings to analyze rearrangement process of associative electron detachment 14 p2350 A67-28149
- Rate constant of atomic oxygen ions reaction with vibrationally excited nitrogen molecules 17 p2889 A67-33201
- Ion mobility and reactions in argon measured using Townsend and Tyndall techniques with mass analysis 20 p3492 A67-37690
- Measurement of cesium and mercury ion-atom resonance charge exchange cross section [AIAA PAPER 67-682] 21 p3660 A67-38713
- Laboratory measurements of ionospheric ion-molecule reaction rates noting unmeasured reactions in D region 23 p3993 A67-40565
- ION BEAM**
- Cesium ion beam generation by accelerating cesium in space charge sheath located between ionizer and plasma filled region [AIAA PAPER 66-927] 02 p0303 A67-12251
- Ripples in acceleration potential affect ion beam of electrostatic propulsion system by superimposing AC potential of 50 cps of variable amplitude on constant acceleration potential 02 p0306 A67-12790
- Quasi-linear theory of plasma cyclotron instability for one-dimensional oscillation spectrum, noting energy of interaction with electromagnetic field, ion velocities, etc 03 p0475 A67-12933
- Ion beam generation for drilling thin metallic coatings deposited on glass-ceramic

- substrates 03 p0432 A67-14269
- Microthrust ion engine system with thrust vector control, using ion beam deflection [AIAA PAPER 66-204] 04 p0706 A67-15241
- Cross sections for charge transfer between alkali-metal ions and cesium atoms determined as function of primary ion beam energy, noting structure consisting of oscillations 04 p0661 A67-15766
- Hydrogen density in coaxial plasma injector prior to application of high voltage to electrodes, noting experimental setup and results 06 p1040 A67-18086
- Radioactive tracer technique for measurement of yield and angular distribution of molybdenum sputtered by cesium ion beam 06 p1036 A67-18139
- Tungsten films with fcc structure obtained by ion beam sputtering in vacuum onto substrates of glass, rock salt and mica at various temperatures 07 p1232 A67-19557
- Quasi-linear theory of ion beam instabilities of LF waves in plasma 07 p1230 A67-20145
- Ion beam excitation of drift waves in alkali plasma, discussing sinusoidal signal propagation characteristics, variations with beam velocity and with modulation frequency 08 p1361 A67-21135
- Self-consistent field approximation to ion-beam-plasma boundary interaction noting effect on ion beam structure, boundary conditions and resulting current density 08 p1363 A67-21307
- Synthesized plasma ion beams by electron injection from hot filament noting electrostatic instabilities and growth rates corresponding to nonlinear regime 11 p1838 A67-24403
- Ion beam interaction with beam produced plasma, showing excitation of waves at electron plasma frequency 11 p1840 A67-24562
- Electron bombardment ion thrusters with two accelerator-grid systems for producing ion beams in directions 180 or 90 degrees apart [AIAA PAPER 66-284] 12 p1990 A67-25891
- Equilibrium of magnetic field confined by impact pressure of beam of ions for general direction of incidence of beam 14 p2310 A67-28046
- Ion beam generation for drilling thin metallic coatings deposited on glass-ceramic substrates 14 p2325 A67-28779
- Mass analysis of ion beams from low voltage spark ion source for ion-implantation doping of semiconductors 15 p2536 A67-29496
- Ion beam generation and applications, discussing duoplasmatron, RF source, contact ionization source and Penning discharge 15 p2488 A67-29756
- Yield and angular distribution of cesium ion-sputtered copper, noting dependence on angle of incidence, target temperature and energy 16 p2728 A67-31056
- Nonlinear instability, demonstrated for electron plasma waves driven toward instability by small ion beam but linearly stabilized by electron Landau damping 16 p2719 A67-31228
- Unsteady Vlasov equation for class of beam-like initial distributions associated with ion engines 17 p2928 A67-32158
- Density contour determination for magnetically confined plasma by energetic molecular ion beam probe of plasma and atomic ion measurement from collisional dissociation 17 p2910 A67-33356
- Exact expression for line profile of stigmatic spectrograph without vignetting, noting results with foil-excited ions as light source 18 p3082 A67-33877
- Hollow anode glow discharge noting motion of ions and electrons in beam configuration 19 p3195 A67-35598
- Ion source using Penning discharge used to inject hydrogen ions into magnetic field 19 p3195 A67-35599
- Cross section measurement for charge transfer reactions, using crossed ion and neutral beam configuration and product ion mass analysis in nitrogen dioxide production 20 p3377 A67-37404
- Counterstreaming ion electrostatic instability at cyclotron frequency to enhance trapping of injected ion beam 21 p3661 A67-37748
- Gaseous mercury discharges through orifice as ion beam neutralizer for electrostatic thrusters

- [AIAA PAPER 67-669] 21 p3691 A67-38703
- Sputtering yields and energy-transfer efficiency measurements by ion beam sputtering of liquid metals indicate no justification for incorporation into low thruster [AIAA PAPER 67-683] 21 p3692 A67-38714
- Foil excitation technique used to measure 2p and 3p levels mean lifetime in He 2 cascading and agreement with theoretical value 22 p3840 A67-39206
- Flow equations for electron emitter placed in ion stream and transparent to ions, showing previous results due to incorrect choice of boundary conditions 22 p3843 A67-39262
- Excited levels mean life in multiply ionized oxygen and neon measured by beam-foil technique 23 p4029 A67-40955
- He ions beam passing through electric field and inducing light intensity fluctuations when emitted from fine structure levels observed via Stark interference 23 p4029 A67-40956
- Ion optical system for extraction of dense ion beams from plasma discharges, studying beam forming characteristics via automatic trajectory tracer model 23 p4034 A67-41463
- Quasi-neutral ion beam focusing by axisymmetric electromagnetic field with closed electron drift, noting ion velocity distribution effects for longitudinal and azimuthal components 23 p4035 A67-41682
- Cesium ion beam generation by accelerating cesium in space charge sheath located between ionizer and plasma filled region [AIAA PAPER 66-927] 23 p4049 A67-41736
- ION BOMBARDMENT**
- Change in resistance of titanium films deposited in high vacuum from argon ion bombardment, noting dependence on energy value 01 p0129 A67-10099
- High specific impulse thrust by sputter ejection of atoms from single crystals following ion bombardment, useful in space propulsion 02 p0306 A67-12716
- Low energy electron diffraction techniques for niobium /110/ surface, noting argon ion bombardment 02 p0257 A67-12729
- Laser action delay due to plasma-tube-surface decomposition resulting from bombardment by neon ions 04 p0633 A67-15110
- Fabrication technique and characteristics of photovoltaic energy converters produced by bombarding p-type Si with phosphorus ions 04 p0680 A67-15284
- Thrust generation from neutral particle sputtering from solid target, noting advantages such as storage, operating life, etc 05 p0873 A67-16515
- Mass spectrometric investigation of composition of negative ion sputtering products of solid metal surfaces under cesium ion bombardment 06 p1036 A67-18425
- Surface blistering of metals due to low energy hydrogen ion bombardment, determining solar absorptance change in gold-plated specimens 08 p1343 A67-21520
- Ion implantation technique for production of n-on-p silicon solar cells applied to dendritic material 10 p1596 A67-23162
- Argon laser design for long life noting ion sputtering and gas clean-up 11 p1800 A67-24242
- Gas pressure effect on electrical breakdown and field emission, discussing ion bombardment and whisker formation 11 p1820 A67-24921
- Solar wind trapping in solids using ion bombardment of aluminum foils at various energies and temperatures 11 p1825 A67-25079
- Radiation-induced electroconductivity and secondary emission in alkali halide single crystals under positive ion bombardment 13 p2177 A67-27073
- Energy distribution of electrons emitted from alkali halide films on Mo substrates during positive helium and argon ion bombardment 13 p2177 A67-27074
- Mono- and polycrystalline samples of Al and Cu bombardment by argon ions in presence of oxygen and by oxygen and nitrogen ions under vacuum 14 p2351 A67-28513
- Silicon surface purified by argon ion bombardment and annealing, studying field effect kinetics 14 p2372 A67-28755
- Failure of conventional adiabatic criterion

in case of excitation of helium atoms by
helium ions 15 p2519 A67-29330

Optical properties of moon quantitatively
compared with powder samples, bombarded
with ions from hydrogen discharge
plasma 16 p2753 A67-31744

Electron microprobe analysis of quartz and
aluminum darkening upon solar wind ion
bombardment, noting existence of iron,
tungsten and carbon in 16 p2753 A67-31745

Surface leakage current and reverse
current flow in silicon p-n junction diode
affected by positive ion bombardment and
oxygen adsorption 17 p2911 A67-32202

Impurity atoms and defects distributions
in Si and Ge bombarded by different ions of
medium energies calculated by Monte Carlo
method 17 p2916 A67-32839

Single gallium arsenide crystals sputtered
by normally incident low energy argon ions
in mass spectrometer source 18 p3106 A67-34639

Surface bombardment damage on
molybdenum and tungsten crystals by inert
gas ions 19 p3246 A67-35784

Conductivity profiles investigated as
function of ion energy, total flux and
annealing schedule, when implanting boron
into silicon 19 p3307 A67-35812

Thin cadmium telluride bombardment with
medium ions, finding doping efficiency
dependence on ion energy and
temperature 20 p3504 A67-36160

Ion bombardment excitation used to
extend excited state range for level crossing
spectroscopy studies, giving Zeeman energy
level diagram 22 p3835 A67-39239

ION CHAMBER

Physical characteristics affecting detection
efficiency of Geiger counters, proportional
counters and ion chambers used in space
measurements of particles 02 p0244 A67-12209

Lyman alpha emission from sun near solar
minimum 11 p1862 A67-24503

Cloud-ion chamber stack to measure
properties of interactions in light materials
of high energy cosmic ray protons and
neutrons 17 p2863 A67-33355

Solar x-ray spectral intensity distribution
using atmospheric extinction of solar
radiation as measured by
satellites 19 p3314 A67-35441

ION CHARGE

Equality conditions for gold and silver
electrode zero charge and transient peak
potentials by pH and anion effects, using
scrapped electrodes 10 p1602 A67-23158

Conductivity of almost intrinsic infinite p-
n junction semiconductor, noting volume
charge effect on behavior of
junction 10 p1695 A67-23662

Charge spectrum of heavy cosmic ions of
iron group in ionographic emulsions exposed
in satellite 12 p1999 A67-25829

Negative oxygen ion reaction rate
constants for ion loss processes in
ionospheric D region obtained by laboratory
measurement 17 p2851 A67-33195

Conductivity of almost intrinsic infinite p-
n junction semiconductor, noting volume
charge effect on behavior of
junction 17 p2924 A67-33343

Elastic moduli, bond parameters and
effective ion charges for wurtzite and
sphalerite binary crystal lattices 18 p3094 A67-33437

Deuterium plasma heating by multiply
charged hot impurity ions 19 p3287 A67-35357

ION CURRENT

Ion transport on and through thin oxide
layers of MOS structure investigated by
charge comparison method 02 p0293 A67-11750

Ion extraction and plasma sheath
formation in nitrogen discharge studied by
quadrupole mass-spectrometric sampling
probe, noting ion current ratio dependence
on probe potential 02 p0272 A67-11889

Acceleration mechanism in plasma current
layer forming when strong magnetic field
moves at high speed into initially stationary
field-free plasma 02 p0274 A67-12341

Positive ion current characteristics of
cylindrical probe in low density plasma
stream, determining sheath thickness and
speed ratio 04 p0663 A67-14766

Electron motion in gases in pressure range
where electron mean free path is
comparable to or less than chamber length,

showing effect on ion
currents 04 p0662 A67-15769

Response of trigger
noting ion current
component 06 p0950 A67-17750

V-I characteristics in flame by double
probe method at atmospheric
pressure 08 p1428 A67-21426

Dominant ionic species in cesium plasma
diode determined as atomic cesium ion
rather than molecular cesium
ion 09 p1448 A67-22337

Ion current from duoplasmatron ion
source with expansion cuvette increased by
superimposing weak magnetic induction in
expansion zone and insulating cuvette
walls 09 p1550 A67-22598

Measurements of positive ion composition
of mesosphere and ionospheric D layer from
rocket experiments 10 p1645 A67-23264

Dependence of ion current from RF ion
source on plasma density at boundary and
longitudinal magnetic field
intensity 10 p1687 A67-23794

Geomagnetic disturbances dependence on
interplanetary magnetic field sector
structure and incident solar ion current at
and near minimum of solar
cycle 11 p1786 A67-24331

Argon plasma accelerator producing
diamagnetic discharge measured along axis
for plasma properties 14 p2362 A67-29046

Space-charge limited ionic currents in
MOS structure oxide film, noting
relationship between interface ion trapping
rate and SCL currents 15 p2539 A67-29825

Positive column contraction in inert gas
discharge, studying electron density and
radiation intensity radial distribution and
wall current 19 p3272 A67-35092

Flow of positive ions from negative glow
plasma into cathode dark space determined,
discussing ion current density
results 19 p3273 A67-35099

Pulsed-discharge-current interruption in
constricting aperture by pinch effect, loss of
ions, gas heating and oscillation
generation 19 p3278 A67-35127

Discharge length influence on reflex
discharge characteristics, considering
conditions for charged particles extraction
from discharge 20 p3498 A67-36686

Tangential drag measurements at
electrodes of arc in plasma accelerator, ion
current partitioning at cathode and
electrode damage 21 p3670 A67-38693

Thermionic energy converter operation
showing anomalous electron and ion currents
in plasma mode, discussing heating power
and emitter temperature 24 p4103 A67-42502

Electrofluidynamic (EFD) power
generator unipolar charge generation using
corona discharge, noting pressure and
geometry effects on ion currents and
attractor voltage 24 p4107 A67-42528

ION CYCLOTRON

Collisionless electron heating by ion
cyclotron wave attributed to Landau
damping, discussing current
generation 02 p0275 A67-12556

Spatial waveform of azimuthal electric
field of Faraday shielded Stix coils for ion
cyclotron resonance heating of plasma to
thermonuclear temperatures 02 p0279 A67-12685

Small amplitude electromagnetic wave
propagation in cold homogeneous ionospheric
plasma including negative ions and immersed
in static magnetic field 04 p0614 A67-14957

Properties of dense plasma with preheated
electrons in ion cyclotron resonance region,
using magnetic mirror
trap 05 p0853 A67-16755

Cyclotron resonance instability of ion
cyclotron and magnetosonic waves
propagating at angle to magnetic field in
infinite uniform plasma 08 p1359 A67-20898

Harmonic ion cyclotron wave propagation
and attenuation investigated
experimentally 13 p2163 A67-26287

Ion cyclotron resonance heating limitation
in shallow magnetic beach explained by
wave reflection 15 p2523 A67-29212

Stabilization of ion cyclotron plasma in
mirror machines by energy spreading and
application of high frequency electric
field 16 p2714 A67-30873

Pc 1 micropulsation signals classified as
hydromagnetic whistlers and periodic
hydromagnetic emissions, suggesting
cyclotron instability process as generation

mechanism of latter 17 p2853 A67-33253

Ion cyclotron frequency wave generation
in plasma confined in magnetic well for
maximal density 19 p3295 A67-35419

Noncollisional ion heating from
accelerations in microfields of turbulent
plasma waves 20 p3497 A67-36531

Electrostatic ion cyclotron waves
excitation in plasma and ion heating due to
cyclotron damping 21 p3667 A67-38407

Ion-molecule collision cross section
determined from pressure broadening of ion
cyclotron resonance lines at high electric
field/pressure ratio 22 p3840 A67-39365

Ion cyclotron instability potential and
adiabatic compression of plasma in mirror
machine, measuring plasma decay rate and
potential 22 p3846 A67-39487

Cyclotron instability examined for plasma
in magnetic mirror machines with
anisotropic nonmonotonic ion distribution in
velocity space 22 p3852 A67-39988

Stability of collisionless plasma with ions
moving relative to electrons under electric
field of ion cyclotron
wave 22 p3852 A67-39989

ION DENSITY

SA IONOSPHERIC ION DENSITY

SA MAGNETOSPHERIC ION DENSITY

Diagnostic measurement techniques for
statistical properties of ionized particles of
equilibrium turbulent plasma, using
electrostatic probe and high resolution
microwave probe 02 p0275 A67-12550

Interactions in low density plasma beams
of electrostatic thrust engine exhaust,
discussing neutralization, instabilities, plasma
wind tunnel, etc 04 p0690 A67-15022

Dissociative recombination coefficient of
nitrosyl ion with
electrons 04 p0567 A67-15765

Mass spectrometry of plasma ionic
constituents, identifying monatomic and
polyatomic ionic species in gaseous plasma
by isotopic techniques 05 p0851 A67-16381

Chromium ion concentration and
temperature effects on spin-lattice
relaxation times in ruby at liquid He
temperatures in zero magnetic
field 05 p0817 A67-16637

Ion density profiles in boundary layers
associated with supersonic flow of shock
heated air over flat plate measured by
cylindrical and flush-mounted electrostatic
probes [AIAA PAPER 66-159] 05 p0856 A67-17345

Ion density profiles and ionization rate in
air behind high speed shock waves
[AIAA PAPER 67-94] 06 p1037 A67-18502

Perturbations caused by cylindrical body
in plasma, obtaining electric field and
electron and ion concentration dependences
on distance 07 p1250 A67-19811

Electron and ion densities and
temperatures measured by rockets in active
auroras and correlated with directly
measured ionizing flux 10 p1650 A67-23307

Higher fast ion density achieved by fast
neutral particle injection into closed-line
magnetic trap 10 p1686 A67-23466

Effect of varying magnetic field, vacuum
and ion density at 27 MHz on properties of
cylindrical argon plasma column, using
capacitive and inductive
coupling 10 p1686 A67-23504

Distribution curves of ion density and
condensation particle concentration in layers
of atmosphere near sea level, noting criteria
for instruments 10 p1657 A67-23695

Peak density in single ended Q machine
described in agreement with equilibrium
theory 11 p1833 A67-24368

Connection between sub-ELF ionospheric
emissions at night and high negative ion
concentration, noting ion-acoustic wave
excitation 11 p1787 A67-24399

Local magnetic field, ion density flow and
electric field in plasma measured
downstream of theta-pinch accelerator in
presence of uniform guide field
[AIAA PAPER 66-155] 12 p1975 A67-25895

Molecular ion concentration around dawn-
dusk auroral zone satellite
orbit 13 p2108 A67-26315

Solar wind ion concentration and velocity
measurements from Venus III and Pioneer
IV 13 p2195 A67-27343

Ion density concentration in magnetic-
field-aligned rotating plasma columns
/plasma eddies/ 13 p2171 A67-27433

Day and night ion concentration as height

function 17 p2842 A67-32258
 Motion of artificial high density ionization cloud released in ionosphere 17 p2844 A67-32545
 Atomic nitrogen-oxygen mixtures ion concentration enhancement in hydrocarbons presence, discussing atom recombination rate, etc 18 p3107 A67-33805
 Carbon monoxide and hydrogen flames ionization and electron temperatures with methane premixing 18 p3151 A67-33807
 Charge transfer role in formation and maintenance of molecular and metal-ion layer in E region of ionosphere 19 p3217 A67-35204
 Molecular and atomic ion concentration in earth upper atmosphere observed from low altitude satellite, discussing diurnal variation and solar effect 19 p3220 A67-35262
 Rotational velocity and ion density profiles of plasma vortices by measuring radial electric field 19 p3288 A67-35361
 D-region positive ion density during solar eclipse of May, 1966 observed by cylindrical Langmuir probe onboard rocket 19 p3222 A67-35454
 Ion-density data modifications due to temperature variations, discussing normalization and electron density relationship 19 p3224 A67-35491
 Theory of Langmuir probes in plasmas with negative ions, considering different ion concentrations and electron temperatures 19 p3296 A67-35587
 Influence of Langmuir probe losses on ion-density measurements in thermal cesium plasma with homogeneous magnetic field 19 p3296 A67-35589
 Flat plate continuum Langmuir probe ion density measurements, analyzing boundary layer and sheath of supersonic flow behind shock wave 19 p3296 A67-35590
 Guidance of audio-frequency electromagnetic waves along earth magnetic field investigated in absence of field-aligned irregularities of ionization density 19 p3225 A67-35608
 Far UV interstellar absorption lines evaluated for main-sequence B stars 19 p3330 A67-36075
 Dielectric susceptibility and ion density measurement for polarized hydrogen plasma moving through transverse magnetic field 22 p3845 A67-39424

ION DISTRIBUTION

Electron current and positive ion current in flames measured by improved single-probe technique using grid and ring electrode 01 p0070 A67-11068
 Unstable transverse waves in anisotropic multicomponent plasma, establishing stability criteria, noting role of electron distribution 02 p0276 A67-12562
 Ion mobility in gas formed by ions, defining gas temperature, obtaining solution of kinetic equation for ion distribution function 02 p0270 A67-12625
 Instability of nonlinear stationary oscillations of potential in electron-ion flows useful in distribution functions of ions and electrons 03 p0470 A67-12935
 Ion distributions in helium negative glow assuming diffusion from cathode, conversion to molecular ions and recombination 03 p0473 A67-13523
 Mass spectrometric study of energy distribution of ions of accelerated plasma produced by coaxial source 04 p0668 A67-15216
 Reaction rates controlling densities of ions and electrons in F region determined so that calculated ion and electron distribution may agree with rocket observations 06 p0996 A67-18430
 Ionic composition measurements of topside ionosphere from mass spectrometer flown on Explorer XXXI satellite 06 p0996 A67-18646
 Retardation energy distribution of ions and electrons in hydrogen 06 p1037 A67-18762
 Chemical and photochemical reactions controlling ion composition of atmosphere between 150 and 300 km 07 p1170 A67-19100
 Quasi-linear theory of loss cone instability of plasma confined in mirror type trap 08 p1359 A67-20899
 Magnetized plasma oscillations for arbitrary initial distributions of electrons and ions, obtaining dispersion equation in fifth degree 09 p1550 A67-22617
 Vertical profile of concentration of

atmospheric electron-ion gas flux under action of gravitational field 10 p1631 A67-22804
 Measurements of positive ion composition of mesosphere and ionospheric D layer from rocket experiments 10 p1645 A67-23264
 Ion mobility in gas formed by ions, defining gas temperature, obtaining solution of kinetic equation for ion distribution function 13 p2161 A67-27381
 Modified Thomson mass spectroscopy for visual observation of energy spectra of ion component of plasmoid 15 p2486 A67-29260
 Mass spectrometric study of energy distribution of ions of accelerated plasma produced by coaxial source 15 p2532 A67-30264
 Heating of ions in current carrying nonisothermal plasma deriving noise spectral density and electron and ion distribution functions 16 p2715 A67-31047
 Boundary value problem for electrical potential and ion distribution function obeying Poisson-Vlasov equations when applied to rarefied plasma disturbance by supersonic body 17 p2909 A67-33205
 Ion radial distribution functions for primitive model of electrolyte solution using Percus-Yevick and convolution-hypernetted-chain integral equations 17 p2810 A67-33256
 Pump radiation induced optical distortion in Nd-doped glass laser rods measured and compared to theory 18 p3062 A67-34625
 NO role in sunrise E region compared to Barth NO distribution, determining density profiles, relative ion ratios, etc 19 p3216 A67-35191
 Radiation effects on MOS devices, analyzing electrical characteristics degradation mode and conduction threshold voltage variation 20 p3396 A67-36321
 Instability of plasma with anisotropic ion velocity distribution, deriving equations for temperature variations and magnetic field energy changes 21 p3669 A67-36680
 Diagnostic probe for low density plasma beam ion velocity distribution measurement in steady state and pulsed plasma exhausts [AIAA PAPER 67-706] 21 p3872 A67-38733
 Current carrier mobility, Hall effect and magnetoresistance in semiconductors with nonuniform ion distribution 22 p3858 A67-39507
 Heating and quenching of aluminum and gallium substituted YIG changes magnetization of material due to cations redistribution process 22 p3860 A67-39913
 Cyclotron instability examined for plasma in magnetic mirror machines with anisotropic nonmonotonic ion distribution in velocity space 22 p3852 A67-39988
 Vertical profile of concentration of atmospheric electron-ion gas flux under action of gravitational field 24 p4150 A67-42141

ION EMISSION
 Full temperature range electron and ion emission from polycrystalline surfaces of Nb, Mo, Ta, W, Re, Os and Ir in cesium vapor 02 p0269 A67-11878
 Electron and ion emission from iridium in lithium vapor, noting surface ionization, work functions and experimental setup 04 p0660 A67-15108
 Positive ion emission from tungsten surfaces laser irradiated studied, using time-of-flight spectrometer 05 p0819 A67-16651
 Molecular nitrogen ion emission in twilight, discussing intensities, rotational distribution, charge transfer zenith measurement and ion-atom interchange reaction 05 p0803 A67-17409
 Resonance emission of H and K lines of ionized calcium during twilight spectrographically observed, suggesting meteoritic origin 06 p0998 A67-18704
 Electron and ion emissions from hydrogen and helium UV glows in nighttime ionosphere 10 p1633 A67-23049
 Correlation between diurnal meteor activity and twilight emission of ionized calcium H and K lines confirmed by Quadrantides swarm 11 p1857 A67-24756
 Stark-broadened isolated ion line agreement between theory and experiment obtained by Griem theory or by impact approximation of GBKO 15 p2520 A67-29678
 Expulsion of ions from comets toward sun examined for source, dissociation and

ionization of parent particles, velocity, etc 16 p2746 A67-30979
 Thermionic and electrical sorption properties of tungsten in alkali iodide vapors at high pressure 17 p2887 A67-32201
 Thermionic work functions and electron emission S curves for contaminated copper surface in oxygen and cesium vapors, separate and mixed 17 p2887 A67-32203
 Cesium ion emission patterns from rear-faced porous refractory metals studied by thermal emission microscope 17 p2888 A67-33059
 Structure of ion and electron currents axial emission from cathode measured as function of magnetic field intensity 19 p3277 A67-35121
 Line profiles and Stark widths of singly ionized carbon and calcium atoms measured using plasma source 19 p3299 A67-36092
 Recombination and bremsstrahlung continuum radiation measurements of atomic and ionic oxygen in plasma 19 p3299 A67-36093
 Nonthermal plasma electron density calculated from ratio of spectral line intensities of given ion 20 p3501 A67-37294
 Duo-emitter cesium thermionic converter, discussing electron and cesium ion emission to increase transport efficiency 21 p3571 A67-38610
 Temperature of metal surface irradiated by giant pulse laser beam by measuring energy of emitted thermal ions 23 p4015 A67-41035

ION ENGINE
SA PLASMA ENGINE
 Porous high efficiency predictable-pore-density tungsten ionizers for cesium ion engine 01 p0140 A67-10703
 Computer program providing ion thruster design criteria and power and weight requirements for specific satellite control mission [AIAA PAPER 66-498] 02 p0302 A67-11515
 Weight, efficiency and control requirements of subsystems of electric propulsion applied to Mars missions, selecting power-conditioning modules for ion propulsion engines [AIAA PAPER 66-501] 02 p0302 A67-11516
 Steady state charge distribution on surface of spaceship and in plasma beam emanating from ion engine under conditions of slight decomposition 02 p0302 A67-11549
 Ion engine arcing frequency from micrometeoroid impact [AIAA PAPER 66-205] 02 p0302 A67-11936
 Mercury ion rocket propulsion system compared to cesium ion system 02 p0305 A67-12338
 Ripples in acceleration potential affect ion beam of electrostatic propulsion system by superimposing AC potential of 50 cps of variable amplitude on constant acceleration potential 02 p0306 A67-12790
 Theoretical possibilities of using electromagnetic forces for acceleration of plasmas/self-magnetic and Hall acceleration/ in case of axisymmetric electrode arrangement 04 p0687 A67-14555
 Comparison of performance of atom-ion and colloidal thruster systems for orbital transfers, noting influence of various parameters on mission capabilities 04 p0688 A67-14560
 Metallurgical viewpoint of current status of porous refractory materials technology related to cesium contact ionizers 04 p0638 A67-15014
 CS contact ion engine technological status engine life and performance characteristics 04 p0689 A67-15015
 Low density electron bombardment ion engine, particularly mercury engine and Cs gas discharge ion engine, for electrostatic propulsion 04 p0689 A67-15020
 Ionic propulsion research performed on Kaufman type source 04 p0689 A67-15021
 Ion thrust motors used to overcome solar lunar attraction, earth triaxiality, solar pressure and other forces tending to perturb satellite orbit or modify orientation 04 p0705 A67-15027
 Comparison of various electrostatic thrusters and proposed low pressure colloidal power converter for high payload lunar and planetary missions [AIAA PAPER 66-211] 05 p0874 A67-17216
 Sputtering yields of aluminum, copper and titanium measured as function of cesium ion

energies for use as electrodes on cesium ion engines
 [AIAA PAPER 66-203] 05 p0871 A67-17349
 Design, operational characteristics and testing of ion engine for spacecraft propulsion, considering mission analysis, orbit parameters and spacecraft orientation
 [AIAA PAPER 67-87] 06 p1074 A67-18342
 Electric propulsion research in foreign countries
 [AIAA PAPER 67-53] 06 p1075 A67-18494
 Feasibility design study of solar powered ion propulsion system for interplanetary spacecraft
 [AIAA PAPER 66-214] 07 p1240 A67-19364
 Electric propulsion for satellite applications, noting cesium contact microthruster ion engine system
 [AIAA PAPER 67-80] 07 p1240 A67-19435
 Permanent magnet low thrust engines performance and tests, starting from cesium electron bombardment ion microthruster
 [AIAA PAPER 67-81] 07 p1240 A67-19436
 Theoretical possibilities of using electromagnetic forces for acceleration of plasmas /self-magnetic and Hall acceleration/ in case of axisymmetric electrode arrangement
 [AIAA PAPER 67-81] 07 p1240 A67-19569
 Porous structures for ion engine application, discussing ionizer materials preparation, based on powder metallurgy and two-phase tungsten base alloy
 [AIAA PAPER 66-221] 08 p1341 A67-20576
 Evaluation of requirements for ground testing of electric propulsion devices in vacuum, noting effects of sputtering phenomena
 [AIAA PAPER 67-81] 09 p1559 A67-22120
 Ion thruster, including mercury feed system and shielded neutralizer, designed and tested for spacecraft station keeping and attitude control
 [AIAA PAPER 66-247] 10 p1698 A67-23120
 Plasma measurements in cesium electron bombardment ion engine indicate that reversed cathode-anode configuration improves radial ion distribution
 [AIAA PAPER 66-246] 10 p1698 A67-23121
 Electron bombardment ion thrusters with two accelerator-grid systems for producing ion beams in directions 180 or 90 degrees apart
 [AIAA PAPER 66-284] 12 p1990 A67-25891
 Electron bombardment thrusters using diode mercury cathodes noting lifetime, propellant and power efficiency, feed system, temperature limits, etc.
 [AIAA PAPER 66-216] 13 p2188 A67-26822
 Lightweight flight prototype mercury ion engine system development and testing
 [AIAA PAPER 66-216] 13 p2188 A67-26823
 Low thrust divergent flow cesium-on-tungsten contact ionization electrostatic thruster for satellite attitude control and station-keeping missions
 [AIAA PAPER 66-569] 13 p2188 A67-26824
 Computer program providing ion thruster design criteria and power and weight requirements for specific satellite control mission
 [AIAA PAPER 66-498] 13 p2188 A67-26825
 Steady state charge distribution on surface of spaceship and in plasma beam emanating from ion engine under conditions of slight decomposition
 [AIAA PAPER 66-569] 16 p2736 A67-31615
 Unsteady Vlasov equation for class of beam-like initial distributions associated with ion engines
 [AIAA PAPER 66-569] 17 p2928 A67-32158
 Electrostatic ion engine timetable, noting contact ion and electron bombardment engines and application to NASA Applications Technology Satellite series
 [AIAA PAPER 66-569] 17 p2928 A67-32435
 Comparison of performance of atom-ion and colloidal thruster systems for orbital transfers, noting influence of various parameters on mission capabilities
 [AIAA PAPER 66-569] 20 p3515 A67-36407
 Permanent magnet low thrust engines performance and tests, starting from cesium electron bombardment ion microthruster
 [AIAA PAPER 67-666] 21 p3690 A67-37790
 Cesium bombardment ion engine performance, giving starting circuit and automatic discharge power control system
 [AIAA PAPER 67-666] 21 p3690 A67-38700
 Optimum discharge chamber configuration of permanent magnet mercury-bombardment thruster for SERT II mission
 [AIAA PAPER 67-668] 21 p3691 A67-38702
 Mercury fed plasma bridge neutralizers for in-flight operation of SERT II electron

bombardment ion thruster
 [AIAA PAPER 67-670] 21 p3691 A67-38704
 Conventional and composite grid designs tested with low voltage Kaufman thruster
 [AIAA PAPER 67-680] 21 p3692 A67-38711
 Cesium propellant systems utilizing surface tension to position and transfer liquid propellant in zero-g environment studied with high voltage electrical isolation methods
 [AIAA PAPER 67-681] 21 p3692 A67-38712
 Clustered mercury electron bombardment ion engine system experiments showing feasibility, discussing components
 [AIAA PAPER 67-698] 21 p3693 A67-38727
 Electric propulsion applied to satellite station-keeping and attitude control, noting ion engine resistor combination providing complete redundancy
 [AIAA PAPER 67-722] 21 p3697 A67-38961
 Electric propulsion ion engine systems using solar power source for Mars and Jupiter exploratory unmanned spacecraft is adaptable to existing launch vehicles
 [AIAA PAPER 67-713] 22 p3868 A67-39844
 Electric propulsion research in foreign countries
 [AIAA PAPER 67-53] 24 p4208 A67-42902
 Kaufman mercury-ion thruster grid design, discussing radial slot configuration
 [AIAA PAPER 67-53] 24 p4208 A67-42929
ION EXCHANGE
 Classification of ions capable of replacing Ti in barium titanate
 [AIAA PAPER 67-53] 03 p0497 A67-13703
 Energy transfer from single chromium ions to closely coupled pairs of chromium ions in ruby
 [AIAA PAPER 67-53] 05 p0862 A67-18659
 Fuel cells such as KOH, high temperature and ion exchanger diaphragm noting applications and performance characteristics
 [AIAA PAPER 67-53] 14 p2253 A67-29025
 Magnetostriction of trivalent Yb and Ce ions in YIG, measuring temperature dependence, noting exchange and interaction of crystal field splitting for Yb
 [AIAA PAPER 67-53] 22 p3855 A67-39363
ION EXTRACTION
 Ion extractor system for electrostatic thrusters designed, using salient features of digital computer and electrolytic tank analog methods
 [AIAA PAPER 67-53] 06 p1075 A67-18877
 Plasma Separator Thruster, advanced ion thruster design based on independent operation and optimization of plasma source and plasma extraction system
 [AIAA PAPER 66-598] 22 p3868 A67-40084
 Discharge model for relative abundances of different ions extracted from Ar duoplasmatron from Langmuir probe measurements
 [AIAA PAPER 66-598] 23 p4033 A67-41190
 Ion optical system for extraction of dense ion beams from plasma discharges, studying beam forming characteristics via automatic trajectory tracer model
 [AIAA PAPER 66-598] 23 p4034 A67-41463
ION GAUGE
 Reduced X-ray photoelectric current in modified Bayard-Alpert ion gauge for vacuum pressure measurements below 10 to minus tenth torr
 [AIAA PAPER 66-598] 05 p0805 A67-18462
 Low density air flow measured by anemometer with pulsed ion generation in air stream
 [AIAA PAPER 66-598] 10 p1658 A67-23787
ION IMPACT
 Intensity distribution in rotational structure of molecular spectra bands upon excitation by ion impacts
 [AIAA PAPER 66-598] 06 p1035 A67-17877
 Momentum transfer accompanying ionizing impact of electrons against atoms of inert gases
 [AIAA PAPER 66-598] 06 p1037 A67-18426
 Stark broadening of hydrogen lines of large principal quantum number for RF transitions by electron and ion impact approximation
 [AIAA PAPER 66-598] 14 p2389 A67-28839
 Electron correlations influence on plasma-broadened Lyman alpha line
 [AIAA PAPER 66-598] 15 p2520 A67-29679
 Velocity limitations of accelerated plasma by momentum loss due to electrode impact of accelerated ions, proposing modified snowplow model
 [AIAA PAPER 66-598] 15 p2531 A67-30030
 Long-lived impact excitation states of particles measured from cross section of nonelastic collision with second particle
 [AIAA PAPER 66-598] 17 p2809 A67-32142
 Impact ionization in gallium arsenide through fast pulse experiment, noting conflict between theoretical and measured current-voltage characteristics
 [AIAA PAPER 66-598] 18 p3097 A67-33517
 Spectral dependence of enhanced quantum efficiency and overlap integrals in InSb

semiconductors, calculating impact ionization and hot electrons thermalization
 [AIAA PAPER 66-598] 23 p4040 A67-41061
ION INJECTION
 Plasma formation by dissociation of diatomic hydrogen ions by Lorentz force
 [AIAA PAPER 66-598] 04 p0671 A67-15645
 Increased electric conductivity of gas in MHD generator obtained, using small auxiliary electrodes
 [AIAA PAPER 66-598] 09 p1443 A67-21810
 Energetic molecular hydrogen ions injected into resonant nonadiabatic magnetic mirror trap, studying particle mean lifetime, noting cold plasma stabilizing effect
 [AIAA PAPER 66-598] 12 p1969 A67-25248
 Optimization of injection location in HF plasma accelerators
 [AIAA PAPER 66-598] 13 p2185 A67-26586
 Injection coefficients of hydrogen and oxygen during buildup of discharge in homogeneous electric field
 [AIAA PAPER 66-598] 13 p2160 A67-26813
 Asymmetric proton injection into magnetosphere using Vlasov equation, with solution in terms of electric potential
 [AIAA PAPER 66-598] 16 p2666 A67-31403
 Plasma injection into closed magnetic trap, studying effects of helical magnetic field on containment time, density and cross section distribution
 [AIAA PAPER 66-598] 17 p2903 A67-32910
 Toroidal stellarator magnetic trap with time-varying double coil magnetic field and external plasma injection
 [AIAA PAPER 66-598] 17 p2904 A67-32911
 Magnetron cut-off characteristics modification via altering electron cloud resonant properties by injecting positive ions in interaction space
 [AIAA PAPER 66-598] 20 p3489 A67-37105
 Thermally activated inert gas ion injection into tungsten and gold to correlate energies associated with peaks in desorption spectrum
 [AIAA PAPER 66-598] 23 p4030 A67-41357
ION MICROSCOPE
 Scanning microscope for studying Si p-n junctions by electron or ion bombardment
 [AIAA PAPER 66-598] 13 p2120 A67-27069
 Field ion microscope design and operation, noting construction and experimental results
 [AIAA PAPER 66-598] 14 p2314 A67-27770
 Oxygen caused bright spots in field ion microscope patterns of tungsten, noting oxygen variation effects
 [AIAA PAPER 66-598] 16 p2693 A67-31873
 Fiber optic window fitted to stainless steel field ion microscope permitting use of direct contact photography for image recording
 [AIAA PAPER 66-598] 17 p2863 A67-33354
 Field ion microscopy of Ni-Mo alloys
 [AIAA PAPER 66-598] 18 p3065 A67-34364
 Threshold voltage for onset of image-spot blurring of field-ion microscope screen and function of tip temperature
 [AIAA PAPER 66-598] 23 p3998 A67-40896
 Field-ion micrograph indexing noting equivalence of pseudostereographic projection to Brandon proposals for pole identification
 [AIAA PAPER 66-598] 24 p4154 A67-42173
ION MOBILITY
 Ion mobility in gas formed by ions, defining gas temperature, obtaining solution of kinetic equation for ion distribution function
 [AIAA PAPER 66-598] 02 p0270 A67-12625
 Ion radial drift velocity in argon ion laser discharge tube
 [AIAA PAPER 66-598] 11 p1803 A67-24931
 Proton mobility in ice when limited by lattice scattering calculated, using Boltzmann transport equation
 [AIAA PAPER 66-598] 13 p2160 A67-26991
 Ion mobility in gas formed by ions, defining gas temperature, obtaining solution of kinetic equation for ion distribution function
 [AIAA PAPER 66-598] 13 p2161 A67-27381
 Ion mobility in gases determined, based on kinetic equation for ion velocity distribution function with particular reference to Chapman-Enskog method
 [AIAA PAPER 66-598] 16 p2704 A67-31250
 Mobility and diffusion of neon positive ions in neon, deriving ion energy and collisional cross section
 [AIAA PAPER 66-598] 19 p3271 A67-35074
 Nitrogen ion drift velocities in plasma jet flowing into vacuum chamber noting ion mobilities in parent and foreign gas
 [AIAA PAPER 66-598] 19 p3271 A67-35075
 Ion mobility and reactions in argon measured using Townsend and Tyndall techniques with mass analysis
 [AIAA PAPER 66-598] 20 p3492 A67-37690
 Distributions of current, potential, electron density and pressure and ion velocity vector orientation in MPD arc, verifying electromagnetic effects presence
 [AIAA PAPER 67-676] 21 p3671 A67-38709
 Corona discharge propulsion system with space charge limited emission of negative

- ions, noting ion mobility performance and efficiency 21 p3696 A67-38856
- D-region mobility and constituents abundance spectrometer device based on continuum concepts 22 p3799 A67-39816
- Atmospheric ion mobility spectrograms measured with aspiration 22 p3810 A67-40524
- ### ION MOTION
- #### SA PENNING DISCHARGE
- Measurement of ion velocity distribution in plasma stream of pulsed coaxial accelerator agreeing with computation from momentum transfer and mass flow measurements 02 p0276 A67-12568
- Finite ion Larmor radius in stabilizing rippling mode of Furth-Killen-Rosenbluth dissipative instabilities in plasma with finite resistance gradient 02 p0277 A67-12613
- Ion velocity in rotating plasma treated by conservation equations of plasma constituents 03 p0485 A67-14053
- Kinetic energies of ions produced by giant laser pulses, noting dependence of mean square ion velocity on pulse peak intensity 04 p0633 A67-15099
- Arc diffusion measurements of electron temperature and density profile across magnetic field 05 p0858 A67-17433
- Motion equations for ionized irregularity of finite length applied to barium ion cloud, deriving expression for ionospheric electric field 08 p1326 A67-21357
- Wind shear theory of formation of temperate zone blanketing sporadic E layers, noting motion equation for ions in ionospheric E region 10 p1844 A67-23258
- Ion motion under influence of electric field and density gradient with charge transfer collision between ions and neutral gas background 13 p2162 A67-26269
- Transfer of electrons from emitter or space charge region to collector in thermionic energy converter by negative ions 13 p2056 A67-27002
- Finite ion Larmor radius in stabilizing rippling mode of Furth-Killen-Rosenbluth dissipative instabilities in plasma with finite resistance gradient 13 p2170 A67-27369
- Collision plasma instability analysis based on MHD equations and ion motion along magnetic field 16 p2715 A67-31041
- MOS instabilities from ion drift, temperature dependent deep trapping and fast interface states from temperature stress, noting instabilities elimination techniques 17 p2823 A67-32195
- Solution of linearized Boltzmann collision equation for ion motion through gas in inhomogeneous electric field, describing energy distribution functions for hydrogen ions 17 p2907 A67-33102
- Stable motion of rarefied plasma ions and electrons in crossed electric and magnetic fields 22 p3853 A67-40024
- ### ION OSCILLATION
- Plasma electron and ion oscillations excitation by low voltage electron beams provide examples of turbulence 01 p0126 A67-11311
- Decaying plasma density determined from high mode oscillations produced in magnetic trap with metallic chamber at 2000 to 6000 oe 02 p0274 A67-12464
- Ion acoustic oscillations in collisionless region of fully ionized plasma excited by electric current 02 p0277 A67-12612
- Ion resonance in uniform plasma, analyzing behavior of RF resonance probe by comparing ion resonance with electron resonance 04 p0663 A67-14616
- Force constants and local mode frequencies for vibrations of interstitial lithium positive ion in Si crystal, using covalent orbital bond model 04 p0683 A67-15609
- Instability due to nonlinear coupling of electron plasma oscillation and ion acoustic oscillation to driving transverse field extended to longitudinal driving field 04 p0672 A67-15771
- Energy transfer from single chromium ions to closely coupled pairs of chromium ions in ruby 07 p1234 A67-20124
- Ion acoustic oscillations in collisionless region of fully ionized plasma excited by electric current 13 p2170 A67-27368
- Ion oscillations excitation by beam-plasma interaction near ion-plasma frequency, studying instability as function of magnetic field, plasma density and other

- parameters 14 p2360 A67-28553
- Influence of strong HF electrical fields on plasma instability originated in buildup of potential field oscillations 15 p2530 A67-29728
- Spectroscopic observation of ion wings produced by plasma ion oscillations in laser produced plasma 17 p2901 A67-32368
- Interaction between ion and electron waves in plasma 18 p3089 A67-34186
- ### ION PROBE
- Probe measurements of intermediate and high pressure plasmas in cases where mean free path of particles is greater than probe dimension 09 p1539 A67-21783
- Grid probe analysis of alkaline plasma, determining density, potential and energy distribution function 15 p2527 A67-29476
- Wind-driven plasma turbulence structure resolved by continuum ion probes at high Reynolds numbers, determining plasma density fluctuation from argon gas flow 18 p3030 A67-34743
- Ion resonance probe for plasma density measurement using direct display method with frequency swept signal generator 21 p3627 A67-38258
- ### ION PRODUCTION
- Twilight effects of solar ionizing radiation absorption, discussing ion production rates and fluorescence 05 p0885 A67-17410
- Estimation of ion formation rate at various altitudes in ionosphere and zenith angles during low and high solar activity periods 07 p1178 A67-19830
- Meteoritic ion pair production probability by total ablation of micron-size Fe particles in air and Ar as function of particle velocity 08 p1399 A67-21241
- Positive ion layers in E region explained by wind shear theory, obtaining steady state solutions for simple model 08 p1326 A67-21359
- Seasonal and annual variations of electron density in ionospheric F layer interpreted as changes in production rate and ionization loss caused by atmospheric composition variations from neutral atmosphere 10 p1647 A67-23274
- Dependence of ion energy on irradiated laser power, discussing production of ions of two discrete energies 10 p1667 A67-23793
- Positive ion production during illumination of cesium vapor-filled thermionic cell with laser beam 12 p1973 A67-25396
- Secondary ion generation in flames by electron impact noting application of mass-spectrometry and hydrocarbon fuels analysis 16 p2780 A67-31520
- H, C, N, O, Cl, Ca and Al negative ion formation in plasma, noting role of continuous radiation, formation temperature and metastable and stable states 17 p2893 A67-32136
- Photoionization study of diatomic ion formation in argon, krypton and xenon by collision process 17 p2888 A67-32631
- Production mechanism of atomic nitrogen ions in upper atmosphere, showing predominance of nitrogen molecule dissociative photoionization 17 p2851 A67-33204
- Isotope effect in hydrogen molecule dissociative attachment at low energy, noting short negative-ion formation lifetime and long separation time 17 p2889 A67-33223
- Role of electronically excited CH in formation of C3H3 ion and contribution to overall chemionization process 18 p3150 A67-33802
- Plasma sources of refractory ions classified according to methods of producing gas discharge 19 p3228 A67-34981
- Low-energy electron collisions and interactions with atoms and molecules, discussing vibrational excitation, ion formation, ionization cross section, etc 19 p3264 A67-35068
- Ion formation rate in F-2 layer under nocturnal ionospheric conditions, determining electron densities 21 p3623 A67-39037
- Plasma and sheath characteristics computation for alkali plasma devices involving contact ionization for ion production [AIAA PAPER 67-691] 22 p3868 A67-39843
- Mass species abundance ratio of hydrogen ion beam from Oak Ridge type duoplasmatron ion source, discussing pressure dependent

- characteristics 23 p4034 A67-41434
- Na-acenaphthene reaction temperature dependence, studying optical density, precipitation, ion pair formation, coupling constants and hyperfine structure [JPL-TR-32-1144] 24 p4118 A67-42322
- ### ION PUMP
- Ultrahigh vacuum installation using ion getter pumps for analysis of adhesion between plastics and metals in space environment 02 p0228 A67-11555
- Vacuum deposition of thin films, noting importance of low pressure environment with attention to diffusion and ion pumps 04 p0631 A67-15599
- Emission of electrically charged and film producing particles from sputter ion pumps describing experimental facility and two methods for examination 07 p1190 A67-20288
- Saturation effects studied by pumping speed measurements of diode and triode type getter ion pumps for He, molecular hydrogen and nitrogen at low pressures a function of time 08 p1333 A67-21499
- Titanium for sublimation, using combination sublimation-getter ion pump 09 p1503 A67-22101
- Design analysis for vacuum systems using diffusion pumps and getter ion pump comparing parallel and series pumping 09 p1503 A67-22111
- Modulated molecular beam apparatus with chopper used in conjunction with field emission microscope for studies of atomic interactions with surfaces 09 p1499 A67-22111
- High vacuum pump selection requirements, discussing contamination problems 17 p2884 A67-32599
- Electrostatic getter-ion pump, giving quantitative theory for maximizing ionizing efficiency and design features to attain low pressures and high pumping speed 21 p3624 A67-37822
- Electrostatic getter-ion pump performance giving pumping speeds, pressure and starting characteristics, residual gas composition and operating life 21 p3624 A67-37822
- ### ION RECOMBINATION
- #### SA ELECTRON-ION RECOMBINATION
- Thermally ionized cesium plasma confinement investigated in magnetic mirror geometry, in terms of collisional diffusion and end plate ion recombination 02 p0276 A67-12568
- Doppler profiles of nocturnal green line /5577 angstroms/ nonthermal emission resulting from molecular oxygen ion dissociative recombination [AFRL-67-0443] 05 p0803 A67-17411
- Ion-ion recombination coefficient corrections required because of nonuniform ion density and diffusion losses 08 p1355 A67-20711
- Molecular metastables produced in positive column of helium discharge by electron excitation 09 p1548 A67-22361
- Diatomic molecular ion composition and variation of effective recombination coefficient in ionosphere in terms of altitude, time of day, solar activity, temperature, etc 10 p1630 A67-22788
- Detectability of ion recombination free free emission from H II regions 12 p2011 A67-26255
- Upper atmosphere hydrodynamic equation additional terms account for hydrodynamic effects of dissociative recombination and ion molecule reactions 13 p2112 A67-26677
- Nocturnal recombination processes in ionospheric F region for nitrogen and oxygen based on 5200 and 6300 angstrom lines 18 p3040 A67-33669
- Diatomic molecular ion composition and variation of effective recombination coefficient in ionosphere in terms of altitude, time of day, solar activity, temperature, etc 24 p4149 A67-42122
- ### ION SCATTERING
- Ionized impurity scattering mechanism causing energy and momentum losses in n type InSb below 77 degrees K 01 p0134 A67-10800
- Sensitivity increase in leak detector by using grid to eliminate residual gas from scattered ions 04 p0625 A67-15633
- Collision induced dissociation of deuterium by argon and nitrogen examined with angular ion scattering apparatus, determining kinetic energy and angular distribution 05 p0648 A67-16833

Alkali ion scattering coefficient from tungsten single crystals surface and dependence on incidence angle 06 p1036 A67-18424

Exponential sintering temperature dependence of conduction electrons density and attendant decrease of mobility due to ionized impurity scattering in cadmium oxide 10 p1691 A67-23503

Conduction band structure and scattering processes of cadmium mercury telluride mixed crystal determined from thermoelectric power, effective mass and electron mobility 12 p1979 A67-25178

Electron transfer to multiply charged ions of various gases, noting scattering characteristics 13 p2167 A67-26989

Mass spectrometric method for measuring double charge exchange cross sections of low energy positive ions, investigating current distribution 22 p3797 A67-39427

ION SOURCE

Tandem mass spectrometers for study of ion-molecule reactions, noting ion gun, deceleration lens and collision chamber 02 p0247 A67-12690

High current duoplasmatron ion source with ferrite permanent magnets and extraction lens system 02 p0279 A67-12694

Diagnostic studies of gas discharge and contact ion sources including test equipment, instrumentation, design and characteristics of propulsion 03 p0504 A67-13494

Nanosecond pulse ion source for electrostatic accelerator 03 p0425 A67-14262

Pressure dependence of mean electron energy of plasma emerging from anode aperture of duoplasmatron ion source 04 p0663 A67-14768

Plasma ion gun with Pierce electrode 04 p0663 A67-14771

Cesium ionization and transport phenomena for developing porous-surface ion sources 04 p0689 A67-15013

Physical mechanisms and operational principles of electron bombardment ion sources with reference to Lewis geometry and duoplasmatron configuration 04 p0664 A67-15017

Kaufman type electron bombardment ion source with 2.5 cm diameter for satellite low thrust attitude control system 04 p0554 A67-15018

Very intense source of negative ions, based on formation and destruction mechanism of negative hydrogen ions in reflex arc 05 p0851 A67-16597

Ion current from duoplasmatron ion source with expansion cuvette increased by superimposing weak magnetic induction in expansion zone and insulating cuvette walls 09 p1550 A67-22598

Cathode sputtering thin film preparation at low pressure, describing duoplasmatron and sputron ion sources 10 p1681 A67-23693

Dependence of ion current from RF ion source on plasma density at boundary and longitudinal magnetic field intensity 10 p1687 A67-23794

Porous W-Ta emitters as ion source for production of quiescent alkali plasmas of improved symmetry, reproducibility and uniformity 11 p1838 A67-24411

Pressure gradient in duoplasmatron ion source as function of parameters of discharge 14 p2359 A67-28512

Nanosecond pulse ion source for electrostatic accelerator 14 p2321 A67-28774

Coaxial helium-plasma source with superimposed azimuthal magnetic field, noting plasmoid density increase with magnetic field, plasmoid velocity and experimental setup 15 p2526 A67-29254

Mass analysis of ion beams from low voltage spark ion source for ion-implantation doping of semiconductors 15 p2536 A67-29496

Duoplasmatron ion source study with Langmuir probe, finding that pressure dependent discharge characteristics relate to magnetic field radial components 17 p2902 A67-32659

HF magnetic fields for plasma sheath with perpendicularly superimposed static magnetic field and resonance excitation of electron cyclotron waves 19 p3276 A67-35117

Operation of ion source with cylindrical symmetry of crossed electric and magnetic fields 19 p3297 A67-35596

Spectroscopic properties of ionic beam source, discussing particle densities, source

purity, etc 19 p3231 A67-35682

Ion source using electron bombardment without magnetic source field, studying focusing and optimal operating conditions of electron accelerating system 22 p3847 A67-39641

Cold cathode ion source /CCIS/ quadrupole mass spectrometer for ultrahigh residual gas analysis 23 p4000 A67-41217

Mass species abundance ratio of hydrogen ion beam from Oak Ridge type duoplasmatron ion source, discussing pressure dependent characteristics 23 p4034 A67-41436

Pulsed ion flow energy and mass spectra analyzer suitable for 1 to 3 msec duration and time variation over 10 msec 24 p4158 A67-42741

ION TEMPERATURE

High resolution echelle monochromator and use in measuring ion temperature of He plasma 04 p0663 A67-14767

Plasma electron density as function of radius compared with ion cyclotron heating theory and stability criteria [AIAA PAPER 66-158] 04 p0664 A67-14823

Steady oblique nonlinear waves in warm collision-free plasma 05 p0857 A67-17425

Production and diagnostic measurement of deuterium, helium and neon plasmas, stressing electron and ion heating and cooling and attendant equilibration 06 p1041 A67-18147

Energy balance equations including effects of heating by electron gas, cooling and energy coupling obtained for various ion species, assuming each ion gas has Maxwellian velocity distribution 08 p1326 A67-21363

Electron and ion temperature changes in sporadic E layer based on wind shear theory, using energy equation 08 p1327 A67-21366

Ion temperatures in topside ionosphere from spectroradiometry 08 p1327 A67-21371

Ion temperature profiles obtained from satellite measurements of dawn-dusk auroral zone orbits 08 p1329 A67-21482

Laser interferometry and photon scattering in high temperature plasma diagnostics 09 p1536 A67-21602

Plasma potential and particle energies in cesium plasma measured by simultaneous observation of ion and electron energy spectra 09 p1548 A67-22338

Electron and ion densities and temperatures measured by rockets in active auroras and correlated with directly measured ionizing flux 10 p1650 A67-23307

Effects related to ion cooling in Q device 11 p1833 A67-24371

Electron and ionic temperatures from incoherent diffusion spectra, noting dependence on height and permanent thermodynamic equilibrium below 130 km 12 p1931 A67-25108

Rocket and satellite measurements of electron and ion thermal structure of ionospheric F region 12 p1935 A67-25796

Ion temperature gradients causing plasma instabilities when magnetic shear is present, deriving governing integral equation 13 p2162 A67-26284

Modulated electron beam interaction with plasma formed by beam causes ion heating to energies of hundreds of volts in magnetic mirror field 13 p2164 A67-26299

Ionospheric ion temperature determination from variations in collector current of ion trap mounted on rotating satellite 13 p2115 A67-27330

Energetic plasma confined in magnetic mirrors shown to have little interaction with main plasma body 15 p2523 A67-29213

Numbers, flow velocities and temperatures of positive ions emitted by He and Ar plasmas pulsed into evacuated region by plasma gun determined by time-of-flight analysis 15 p2523 A67-29214

Ion temperature, cell temperature, cell voltage and current in electrolytic technique for reproducible growth of molybdenum /IV/ oxide crystals 15 p2533 A67-29295

Electron drift mobility and electron and ion temperatures difference in two-component plasma obtained from momentum and energy balance equations 16 p2706 A67-30450

Mean absorption coefficient for optically thin plasma derived taking into account radiative losses, noting electron and ion

temperature ratios 16 p2706 A67-30459

Boundary layer equations for two-temperature plasma, showing distinction between electron and ion thermal boundary layer thickness 16 p2712 A67-30544

Interferometrically-measured ion temperatures compared to electron temperatures in pure barium and barium-cesium plasmas produced by contact ionization 16 p2720 A67-31243

Ionization, ion temperature and density dependence of cesium plasma on pressure of added rare gas 16 p2720 A67-31244

Ion temperature measurements in upper atmosphere to determine diurnal variation 16 p2666 A67-31416

Electron heating in diurnal ionosphere noting electron and ion temperatures as function of altitude 17 p2842 A67-32295

F region and magnetosphere data obtained by incoherent-backscatter radar technique, studying ion and electron temperatures relationship to height, electron density profiles, etc 17 p2843 A67-32389

Electron temperature/ion temperature ratio and oxygen atom ratio to sum of oxygen molecule and nitric oxide in F-1 layer obtained by radar 17 p2843 A67-32529

Upper atmosphere ion temperature profile transitional behavior analyzed by fractional separation in terms of energy budget, including multiple ion effects 17 p2843 A67-32531

Diurnal variations of ionospheric ion/electron temperatures predicted assuming solar UV radiation heating, collisional cooling and heat transport by conduction 17 p2850 A67-33192

Measurement of Doppler-broadened emission line width by Fabry-Perot interferometer to study ion temperature of pulsed plasma 17 p2862 A67-33292

Ionospheric ion and electron densities and temperatures from rocket probes near geomagnetic equator 19 p3219 A67-35232

Infinitesimal driven plane wave characteristics in uniform plasma with finite electron drift velocity found, using Navier-Stokes and Poisson equations, energy conservation continuity and perfect gas law 19 p3290 A67-35376

Thin cadmium telluride bombardment with indium ions, finding doping efficiency dependence on ion energy and temperature 20 p3504 A67-36160

Ionosphere information via rocket and satellite measurements covering ion temperatures and concentration, electron content variation, etc 20 p3430 A67-36907

Ionospheric electron and ion temperatures during 10.7 cm-solar radio flux activity, giving scatter diagrams 21 p3616 A67-38000

Thermonuclear origin of neutron emission in theta pinch plasma, determining ion temperature from scattering of ruby laser beam 22 p3843 A67-39244

F-2 layer contribution to vertical radio wave absorption, using information about structure, electron and ion temperatures 22 p3789 A67-39472

Plasma electron and positive ion temperatures measurement using orbit magnetic analyzer probes 22 p3798 A67-39626

Ionospheric and magnetospheric temperature measurements using rockets and satellites including neutral particle, ion and electrons 22 p3871 A67-39677

Neutral atmospheric temperatures calculated from data provided by incoherent scatter soundings of ionosphere 22 p3794 A67-40474

ION TRAP

Satellite orientation with respect to velocity vector determined using attached planar ion traps 09 p1571 A67-21890

Ionospheric ion temperature determination from variations in collector current of ion trap mounted on rotating satellite 13 p2115 A67-27330

Turbulent plasma state from unstable, current driven drift waves, noting ion damping effect on amplitude of spectrum, density gradient, etc 16 p2719 A67-31231

IONIC COLLISION

Plasma behavior in magnetic trap with opposite fields, noting Coulomb ion-ion collisions and proton charge reversal 04 p0667 A67-15211

Inelastic collisions by drifting ions studied by series of experiment in which mass analyzed ion beam is injected into drift tube

containing gas 04 p0661 A67-15509
 Gas kinetic theory of negative ion collisional detachment, using elastic sphere model 05 p0844 A67-16003
 Auroral hydrogen line emission quenching by collisional ionization 05 p0804 A67-17413
 Plasma-neutral coupling in ionospheric motions having short durations compared with time between neutral particle collisions with ions 08 p1325 A67-21151
 Electrostatic probe theory in moderately ionized gas taking into account effect of electron-ion collisions 08 p1324 A67-21393
 Electron transport phenomena in thermionic converter plasmas, emphasizing electron-ion collisions to electron momentum transfer collision frequency 09 p1450 A67-22351
 Effect of ion collisions and other terms on resistive-g instability in plasmas 11 p1826 A67-23873
 Ion-ion collision and shear stabilizing effect on resistive drift mode, applying dispersion relation with BGK collision operator 11 p1834 A67-24374
 Diffusion due to ion-ion collisions between different ion species, stressing impurities diffusion in rotating plasmas 14 p2363 A67-29066
 Plasma behavior in magnetic trap with opposite fields, noting Coulomb ion-ion collisions and proton charge reversal 15 p2532 A67-30259
 Molecular nitrogen and oxygen ions colliding with atomic sodium examined in crossed-beam experiment for resonance charge transfers 16 p2705 A67-31758
 Lyman-alpha radiation emission from ion-target-gas collision measured for various projectile energies 17 p2889 A67-33224
 Energy dissipation of strong magnetosonic waves in rarefied plasma, discussing electrons ionizing collisions at wave front 19 p3293 A67-35402
 Photoelectric contribution to magnetospheric electron density on basis of pitch redistribution of collision component 20 p3425 A67-36283
 Stabilizing effect of ion-ion collisions on collisional types of interchange instability, giving numerical solution of relevant normal mode equations 22 p3845 A67-39484

IONIC CONDUCTION
 Electric conductivity variation with temperature for solid ammonium perchlorate, determining energy barrier and enthalpy of lattice defect formation and migration 20 p3377 A67-37134

IONIC CRYSTAL
 Kinetic phenomena in impure ionic semiconductors of cubic symmetry, finding region for dominant scattering mechanism 04 p0675 A67-14923
 Impact ionization in ionic semiconductors for arbitrary temperatures and electric field intensities 09 p1554 A67-21971
 Crystal lattice defects as centers promoting dislocations during plastic deformation of ionic crystals 13 p2175 A67-26448
 Optical constants of ionic crystals at low temperatures determined from reflection spectra, noting correlation between absorption coefficient, magnitude and phonon difference processes 14 p2374 A67-28986
 Second order phase transitions in ionic crystals caused by vibronic interaction analogous to Jahn-Teller effect in ideal crystals 16 p2726 A67-30813
 Impact ionization in ionic semiconductors for arbitrary temperatures and electric field intensities 17 p2923 A67-33308
 Shear stress distribution and dislocation processes at moving crack tips in ionic crystals 18 p3097 A67-33483
 Electronic structure of irradiation defects in ionic solids vacancies, interstitials and dislocations, explaining electronic relaxation 19 p3306 A67-35673
 Electron paramagnetic resonance of trivalent rare earth-monovalent alkaline earth ion pairs in calcium fluoride 21 p3676 A67-37815
 Nonlocal elasticity theory for materials with long range cohesive forces derived from lattice theory by writing strain energy in integral form 22 p3908 A67-39288

IONIC DIFFUSION
 F-2 layer ion-atom interchange coefficients, ion-neutral diffusion coefficient

and flux of solar ionizing radiation, comparing ionospheric data 01 p0056 A67-10108
 Diffusion and lifetime of plasma charged particles in magnetic field covering instability, contraction, decay, recombination, etc 01 p0123 A67-10389
 Two oxidation mechanisms for Ti-Al alloys based on increased diffusion rate and decreased oxidation rate 05 p0829 A67-16492
 Temperature dependence of residual resistivity of diffusing ions for electromigration of silver in copper and gold and self-diffusion of copper in aluminum 07 p1209 A67-19647
 Volt-ampere characteristics of grooved collector thermionic diode indicate ions generated in cavities diffuse to cavity free region and neutralize electron space charge 09 p1448 A67-22340
 Electrical migration of Li and Cu in GaAs, noting ionic charge decrease due to drag by electrons 09 p1558 A67-22603
 Growth rate of oxide and other dielectric contact films on metal crystals computed for ionic diffusion and electron tunneling 18 p3103 A67-34590
 Mobility and diffusion of neon positive ions in neon, deriving ion energy and collisional cross section 19 p3271 A67-35074
 Zinc penetration through regenerated cellulose membrane separators shown to be growth mechanism in silver-zinc cell 22 p3758 A67-40227

IONIC PROPULSION
 Colloid particle electrostatic thrusters for lunar ferry missions in specific impulse range 1000-3000 sec 03 p0503 A67-13492
 Electrical propulsion of space vehicles using solar energy, electrostatic drive, drifting field plasma accelerator, etc 03 p0503 A67-13493
 Ion propulsion systems development for near term mission, noting solar cell weight reduction [AIAA PAPER 66-1026] 03 p0504 A67-14275
 Physics and technology of ion motors - AGARD Conference, Athens, July 1963 04 p0688 A67-15012
 Charged colloidal heavy particle propulsion and production of heavy particles 04 p0689 A67-15016
 Ionic propulsion research performed on Kaufman type source 04 p0689 A67-15021
 Electrostatic propulsion using positive and negative ions, considering neutralization effects, thrust/surface and thrust/power ratios, etc 04 p0690 A67-15023
 Ion thrust motors used to overcome solar-lunar attraction, earth triaxiality, solar pressure and other forces tending to perturb satellite orbit or modify orientation 04 p0705 A67-15027
 Energy and angular distributions of neutral atoms and charge-exchange ions from mercury electron bombardment thruster, determining particle effluxes [AIAA PAPER 67-82] 06 p1075 A67-18498
 German rocket prototype with mercury vapor plasma or xenon plasma engine, discussing design and performance 08 p1410 A67-20641
 Space trajectory analysis of nuclear-electric propelled vehicle 13 p2199 A67-27169
 Cesium contact ion engine ground and flight tested for ability to operate under environments of ground handling, missile launch and space ambients 16 p2736 A67-30711
 Thermionic work functions and electron emission S curves for contaminated copper surface in oxygen and cesium vapors, separate and mixed 17 p2887 A67-32203
 Gaseous mercury discharges through orifice as ion beam neutralizer for electrostatic thrusters [AIAA PAPER 67-669] 21 p3691 A67-38703
 Mercury electron bombardment thruster system performance as function of mass utilization and specific impulse, noting magnetic field shape and ion optical system design effects [AIAA PAPER 67-697] 21 p3693 A67-38726
 Thrust, power and performance requirements for synchronous satellite simulated for evaluating ion propulsion feasibility [AIAA PAPER 67-720] 21 p3694 A67-38746
 Electrostatic ion propulsion and KEMAN MPD thruster research in Germany [AIAA PAPER 67-724] 21 p3694 A67-38749

Radioisotope heating to provide ionizer temperatures in contact ion thrusters [AIAA PAPER 67-734] 21 p3695 A67-38757
 Radioisotope heating for ionizer temperature of contact ionization thrusters for satellite attitude control and stationkeeping, studying power source mass saving [AIAA PAPER 67-735] 21 p3695 A67-38758
 Corona discharge propulsion system with space charge limited emission of negative ions, noting ion mobility performance and efficiency 21 p3696 A67-38856
 Plasma Separator Thruster, advanced ion thruster design based on independent operation and optimization of plasma source and plasma extraction system [AIAA PAPER 66-598] 22 p3868 A67-40084

IONIC REACTION
 Competing alternative pathways for formation of particular ion in mass spectra of substituted benzophenones 01 p0018 A67-10105
 Four-linked rare earth chelate with sodium ion obtained with benzoylacetone and europium, analyzing molecular and ionic transitions by absorption and emission spectra 02 p0251 A67-11518
 Nonrelativistic energies and mass polarization shifts of excited S states of lithium cation 03 p0472 A67-13323
 Energetic and angular studies of argon deuteride and nitrogen deuteride positive ion formation using angular ion scattering apparatus 05 p0848 A67-16835
 Substituent effects on unimolecular ion decomposition reactions, noting role of Hammett equation and electron energies 06 p0954 A67-17568
 Equilibrium temperatures of Fe and Mg ions in chondritic meteorites 08 p1400 A67-21266
 Flowing afterglow reaction device for measuring ionospheric ion-molecule reactions 10 p1644 A67-23259
 Upper atmosphere hydrodynamic equation additional terms account for hydrodynamic effects of dissociative recombination and ion molecule reactions 13 p2112 A67-26670
 Electrode-to-plasma conduction process effect on MHD generator performance, noting current saturation conditions and results 16 p2601 A67-30550
 Ion-molecular reactions of hydrogen with inert gases caused by low energy electrons in low temperature plasmas, considering energy level populations, reaction cross sections, etc 17 p2808 A67-32141
 Rate constant of atomic oxygen ions reaction with vibrationally excited nitrogen molecules 17 p2889 A67-33201
 Ion-molecule reactions in propane studied using mass and energy resolved ion beams in tandem mass spectrometer 17 p2810 A67-33264
 Ion and neutral particle interaction effects on F region winds, considering plasma forces 22 p3789 A67-39479

IONIC WAVE
SA IONOSPHERIC CONDUCTIVITY
 Dielectric constant of homogeneous fully ionized two-temperature plasma for determining conditions under which ion waves can be found 02 p0275 A67-12555
 Ion wave excitation due to Hall current compared with current parallel to static magnetic field in weakly ionized plasma on basis of two-fluid model 03 p0476 A67-13354
 Transverse electromagnetic wave transformation into ion-acoustic plasma oscillations with formation of intermediate Langmuir electron wave 04 p0668 A67-15275
 Solar radiation drift flares in decimeter range produced by ionic sound interaction with plasma fluctuations 06 p1077 A67-18155
 Supersonic Langmuir probe application of propagation and dispersion of ionic waves 08 p1357 A67-20801
 Ion wave amplification in two-component plasma due to isothermal electron gas 08 p1365 A67-21414
 Spectrum of ionic waves in plasma located in electrical field and interacting with charged particle beam, obtaining dispersion equation 09 p1544 A67-21846
 Excitation of ion-acoustic waves in potassium-cesium plasma when passing current through it, finding natural frequencies of system when plasma is drifting along axis 09 p1544 A67-21853
 Current instability in inhomogeneous

plasma formed by drift and ion-acoustic waves with oscillation frequencies 10 p1685 A67-23461

Potassium plasma current instability, turbulence and diffusion across magnetic field for large amplitudes of oscillations treated as ionic sound waves 11 p1834 A67-24377

Electron temperature variation induced effects and Landau damping of ion acoustic waves studied in quiescent discharge tube plasma 11 p1837 A67-24395

Ion-acoustic wave excitation by vertical density gradients, noting effect of resulting instability on ionospheric fine structure 11 p1786 A67-24398

Ionic waves in plasma in electric field interacting with beam of charged particles at relaxation time, using dispersion equation 11 p1841 A67-24869

Turbulent electrostatic shock in plasmas, discussing determination of structure by ion wave instabilities [SR-1] 13 p2162 A67-26281

Ionospheric fine structure, considering excitation of ion-acoustic waves by vertical gradients of density 13 p2109 A67-26329

Increase in mean electron energy shown to be factor leading to plasma stratification 14 p2353 A67-27756

Ion cyclotron resonance heating limitation in shallow magnetic beach explained by wave reflection 15 p2523 A67-29212

Solar radiation drift flares in decimeter range produced by ionic sound interaction with plasma fluctuations 16 p2741 A67-30499

Ion-acoustic interaction in weakly turbulent plasma deriving time variation of plasmon number 16 p2715 A67-31046

Parametric coupling between ion and electron waves noting coefficients, growth rate amplification, etc 17 p2906 A67-33061

Ionizing wave in plasma gun with crossed electric-magnetic fields, obtaining burning voltage of discharge and bias magnetic field ratios 19 p3277 A67-35123

Plane ionization wave propagation in uniform magnetic field compared with flame front expansion during slow burning 19 p3286 A67-35347

Homogeneous, fully ionized plasma HF conductivity computed using kinetic equation, showing application to two-temperature plasma 19 p3286 A67-35353

Phase velocity and attenuation of ionic plasma waves in weakly ionized gases measured in absence and presence of external magnetic fields 19 p3290 A67-35378

Spectroscopic properties of ionic beam source, discussing particle densities, source purity, etc 19 p3231 A67-35682

Acoustic wave generation in weakly ionized plasma by fusion and damping of two ion-sound waves 20 p3501 A67-37291

Classical nonisothermal two-component plasma correlation functions and pressure contribution from Coulomb interaction 20 p3502 A67-37603

Ion cyclotron wave propagation in plasma, considering Larmor radius effects, quasi-static dispersion relation, phase velocity and cyclotron resonance 21 p3661 A67-37750

Drift and ion acoustic waves and coupled waves in highly ionized dense plasma of finite ion temperature 21 p3667 A67-38412

Acoustic ion waves phase velocity and attenuation constant measurements verify predicted dependence on ion mass, with attenuation due to ion-neutral collisions 21 p3675 A67-39054

Ion wave dispersion relation in mercury vapor plasma, explaining cut-off frequency dependence on electron drift velocity 22 p3842 A67-39207

Ion wave velocities and damping measurements in quiescent plasma used for diagnosis of temperatures and drift velocities 22 p3846 A67-39488

Electrostatic energy per degree of freedom of two-temperature plasma examined for validity of resonant approximations in ion wave region 22 p3852 A67-39986

Ion wave propagation in weakly ionized gases 23 p4032 A67-40960

IONIZATION

SA ATMOSPHERIC IONIZATION
SA AURORAL IONIZATION
SA DEIONIZATION
SA ELECTRON IONIZATION
SA EXCITATION

SA FLAME IONIZATION
SA GASEOUS IONIZATION
SA METEORITIC IONIZATION
SA NONEQUILIBRIUM IONIZATION
SA PHOTODISSOCIATION
SA PHOTOIONIZATION
SA SURFACE IONIZATION

Competing alternative pathways for formation of particular ion in mass spectra of substituted benzophenones 01 p0018 A67-10105

Analog computer ionization recombination parameters and balance equation of charged particles in F-2 layer 02 p0236 A67-11659

Nondiffusive radiation transfer and ionization equilibrium of impurity in plasma 03 p0483 A67-13837

Steady state ionization fronts for H-2 regions with magnetic fields 03 p0514 A67-14316

Ionization probability of bound state of atoms in variable electric field 03 p0474 A67-14375

Ionization recombination mechanisms and density-time profiles for electric propulsion unit efflux 04 p0690 A67-15024

Structure of MHD shock wave taking into account ionization process 04 p0669 A67-15517

Small signal negative resistance and avalanche region of impact ionization avalanche transit time /IMPATT/ diodes, particularly Read diodes 05 p0777 A67-17319

Aerothermochemical eddy diffusion model for predicting rapid wake ionization decay behind hypersonic slender clean cone obtained in free flight ballistic range [AIAA PAPER 67-21] 06 p0938 A67-18257

Upper atmospheric formation of electron cloud produced by chemionization reactions of chemical release agents [AIAA PAPER 67-148] 06 p0995 A67-18360

Vainshtein method calculation of inelastic collision of electrons with atoms 07 p1225 A67-19207

Radio wave propagation in artificial ionized cloud in upper atmosphere determined, using geometrical optics 07 p1143 A67-19691

Equilibrium particle ionization effect on electron density of gas particle plasma 08 p1360 A67-21124

Ionization and temperature measurement in MHD experiment, noting microwave interferometer response as electron density function and line reversal measurement 09 p1538 A67-21777

Electrostatic probes for collision dominated weakly ionized plasma noting mathematical formulation, density and V-A characteristics 09 p1539 A67-21782

Shock tube studies of magnetically induced nonequilibrium ionization in potassium-seeded argon plasma, noting electrical conductivity, current density, wall potential, Soule dissipation and radiation loss 09 p1540 A67-21788

Measurements of conductivity, electron density and ionization rate of cesium in argon on alkali shock tube, describing MHD generator wind tunnel experiment 09 p1540 A67-21789

Relaxation process and magnitude of nonthermal ionization in MHD generator, describing experimental equipment and results in xenon and in argon 09 p1540 A67-21790

Impact ionization in ionic semiconductors for arbitrary temperatures and electric field intensities 09 p1554 A67-21971

Effects related to ion cooling in Q device 11 p1833 A67-24371

Experimental apparatus for study of impact ionization and associated recombination radiation in semiconductors 13 p2168 A67-27228

Nondiffusive radiation transfer and ionization equilibrium of impurity in plasma 13 p2172 A67-27716

Porous cesium ionizer with improved lifetime obtained by adding secondary tantalum to tungsten powder [AIAA PAPER 66-219] 14 p2376 A67-28124

Kinetic energy distribution of ions produced by dissociative attachment dependence on ion thermal energy and electron affinity of oxygen 14 p2350 A67-28151

UV spectra of Mg III and Mg IV investigated by sliding spark in vacuum, noting various ionization charges in vacuum 14 p2351 A67-28944

Analog computer ionization recombination parameters and balance equation of charged particles in F-2 layer 16 p2665 A67-31074

Close-coupling calculations of positions and widths of lowest-lying autoionizing D states in helium 16 p2704 A67-31167

Ionization, ion temperature and density dependence of cesium plasma on pressure of added rare gas 16 p2720 A67-31244

Solar UV spectrum interpretation taking into account dielectronic recombination processes in ionization equilibrium computation, obtaining spectral lines intensities, abundances and atmospheric structure indications 17 p2941 A67-32235

Impact ionization in ionic semiconductors for arbitrary temperatures and electric field intensities 17 p2923 A67-33308

Fractional excitation and ionization for argon beam extracted from arc-heated supersonic free jet, noting molecular ions and neutralization 18 p3082 A67-34028

Detection and measurement of precursor ionization in electromagnetic shock tube 18 p3091 A67-34727

Ionizing and charge transfer processes following heavy particle collisions in ionized gas analyzed using spectroscopic technique 19 p3264 A67-35069

Air ionization behind shock wave front, estimating free electron concentration, ionization time and collision frequency 19 p3293 A67-35401

High energy electron ionization cross section for hydrogen, noting high quantum number correspondence to classical expression 19 p3266 A67-36090

IONIZATION CHAMBER

Porous high efficiency predictable-pore-density tungsten ionizers for cesium ion engine 01 p0140 A67-10703

Ionizing accompaniment of near 170 bev nucleons at 2000 m altitude recorded by spark chamber /Geiger counter/ ionization chamber apparatus 02 p0312 A67-12609

Calorimetric measurement of ionization burst at 3200 m above sea level 02 p0315 A67-12758

Ionization calorimeter determination of effective cross section of high energy primary cosmic ray proton inelastic interaction with atmospheric atomic particles 02 p0315 A67-12759

Ionization calorimeter photoemulsion measurements at mountain altitudes, determining formation mechanism of high energy pions in primary cosmic radiation 02 p0315 A67-12760

Ionization calorimeter measurements of energy transmission by photons in cosmic nuclear-active pion and nucleon interactions with various nuclei 02 p0316 A67-12761

Transport and ionization properties of molecular gases in transverse magnetic field, using ionization chamber 03 p0474 A67-14358

Preliminary measurements of variations in cosmic ray intensity using device consisting of gas discharge counters, telescope and ionization chamber mounted on Kosmos XXV satellite 05 p0878 A67-16092

Rocket measurement of altitude dependence of flux intensity of solar vacuum UV radiation, using ionization chambers 05 p0799 A67-16874

Quiescent cesium plasma production in thermal ionization chamber at high temperatures and low ionization level 11 p1838 A67-24412

Preferential acceleration of heavy nuclei on sun compared with ionizing power of primary particles 13 p2195 A67-27341

Thermodynamical, dynamical, and possible third mechanisms responsible for features in high energy cosmic ray interactions and multiple production of shower secondaries 14 p2379 A67-27962

Ionization fluctuations due to interaction between shower particles and absorbing component of ionization calorimeter and effect on accuracy of energy measurement 17 p2855 A67-32250

Electrostatic getter-ion pump, giving quantitative theory for maximizing ionizing efficiency and design features to attain low pressures and high pumping speed 21 p3624 A67-37821

Calorimetric measurement of ionization burst at 3200 m above sea level 22 p3876 A67-40260

Ionization calorimeter determination of effective cross section of high energy

primary cosmic ray proton inelastic interaction with atmospheric atomic particles 22 p3876 A67-40261

Ionization calorimeter photoemulsion measurements at mountain altitudes, determining formation mechanism of high energy pions in primary cosmic radiation 22 p3876 A67-40262

Ionization calorimeter measurements of energy transmission by photons in cosmic nuclear-active pion and nucleon interactions with various nuclei 22 p3876 A67-40263

Cosmic ray regional variations in intensity and ionization magnitude and duration indicating heavy nucleus and low energy particle influx accompanying solar flares 23 p4055 A67-41100

Low inductance three-electrode spark source for vacuum UV generating high degree ionization spectra 23 p4000 A67-41214

Solar flare energetic X-ray events detected by onboard satellite ionization chambers, studying relationship to radio burst and space particle emission 23 p4060 A67-41232

Preliminary measurements of variations in cosmic ray intensity using device consisting of gas discharge counters, telescope and ionization chamber mounted on Kosmos XXV satellite 24 p4213 A67-42768

Relativistic particles producing ionization bursts studied for energy spectrum recorded during operation of stack of ionization chambers alternating with lead and graphite layers 24 p4218 A67-42834

IONIZATION COEFFICIENT

Effective hot carrier ionization rate in epitaxial gallium arsenide p-n junction determined from photomultiplier measurements 02 p0299 A67-12186

Size distribution of electron avalanches in methane gas under electric field no longer satisfy Furry distribution due to first Townsend ionization coefficient 03 p0473 A67-13463

Air ionization rate behind high speed shock waves, determining electron density from IR emission 03 p0405 A67-14028

Temperature effect on impact ionization coefficient in SiC semiconductor p-n junctions with reversed current in strong electric field 05 p0865 A67-16916

Silicon p-n junction avalanche breakdown voltages obtained from formula for ionization coefficient 05 p0869 A67-17090

Multiphoton ionization of krypton atom by ruby laser radiation 06 p1037 A67-18796

Current and voltage measuring methods for impact ionization analysis including lag and avalanche time, peak fields, etc, noting instability 06 p1070 A67-18987

Ionization coefficient in selenium p-n step junction of rectifier cell 09 p1551 A67-21656

Ionization coefficients in helium over pressure range near to atmospheric show destruction of metastable states in gas accounts for dependence on electric field 10 p1681 A67-22962

Avalanche multiplication of current carriers at low temperatures in p-n junctions of InAs, determining carrier ionization coefficient and dependence on electrical field 10 p1695 A67-23660

Reliability of laboratory thermal rate coefficients for positive ion/neutral reactions in ionosphere 11 p1785 A67-23945

Ionization rate in helium, argon and xenon plasmas determined by microwave technique 12 p1970 A67-25291

Ionization and diffusion cross sections of Ca, Fe, Si and Mg atoms of disintegrated meteors 12 p2002 A67-25551

Arbitrary ionization ratio plasma conductivity in presence of constant and uniform magnetic field 14 p2355 A67-27955

Temperature effect on impact ionization coefficient in SiC semiconductor p-n junctions with reversed current in strong electric field 16 p2727 A67-30893

Avalanche multiplication of current carriers at low temperatures in p-n junctions of InAs, determining carrier ionization coefficient and dependence on electrical field 17 p2924 A67-33341

Ionizer with three-electrode electron gun, noting potential distribution between electrodes and ionization efficiency 18 p3080 A67-33722

Multiphoton ionization of krypton atom by ruby laser radiation 18 p3083 A67-34415

Time dependence of avalanche in silicon

junctions including effects of different ionization rates and velocities of charge carriers 18 p3105 A67-34628

Secondary ionization processes in mercury vapor, calculating relative populations of excited and metastable atoms per ion pair 19 p3265 A67-35090

Thermal conductivity ionization coefficient of cesium plasma at high temperature and low pressure 19 p3287 A67-35359

Ionization and recombination effects on MHD wave propagation through three-component magnetoplasma, deriving nonlinear motion equations 21 p3660 A67-37743

Electron impact ionization cross sections and rate coefficients for atoms and ions of Hg, rare gas and alkali metal groups 21 p3660 A67-39098

Intensity of ionizing and neutron components measured in stratosphere as function of geomagnetic rigidity, obtaining coupling coefficients for cosmic ray variations 23 p4059 A67-41136

IONIZATION COUNTER

Nuclear cascade process in iron absorber of ionization calorimeter, comparing empirical and experimental values 02 p0248 A67-12747

Electron-photon shower measurement using ionization calorimeter type device 02 p0271 A67-12755

High energy cosmic ray muons studied, using ionization calorimeter and hodoscope counters 02 p0317 A67-12770

Ionization calorimeter performance simulation using Monte Carlo 09 p1497 A67-21900

Density and direction of gas molecular flow through tube and aperture measured by ionization detector 09 p1489 A67-22107

Vacuum ionization gauge reading dependence on localized gas densities caused by chamber temperature nonuniformity 09 p1498 A67-22108

Nuclear cascade process in iron absorber of ionization calorimeter, comparing empirical and experimental values 22 p3801 A67-40249

Electron-photon shower measurement using ionization calorimeter type device 22 p3842 A67-40257

High energy cosmic ray muons investigated, using ionization calorimeter and hodoscope counters 22 p3877 A67-40272

Hard component penetration of cosmic rays investigated by ionization calorimeter and hodoscope counters 24 p4222 A67-42878

IONIZATION CROSS SECTION

Electron collisions in nitrogen studied by mass spectrometer, measuring dissociative ionization cross section of nitrogen 01 p0117 A67-10779

Electrode losses in MHD generators with nonequilibrium and equilibrium ionization compared, attributing differences to coupling between conductivity and local dissipation 01 p0014 A67-11159

Ionization cross sections of neutral atoms caused by electron impact with Maxwellian velocity distribution 02 p0269 A67-12486

Ionization efficiency and cross section of meteor trails during collision between particles of meteoric vapor and air molecules 02 p0329 A67-12494

Absolute direct excitation cross section from neutral ground state for upper levels of transition in argon laser 02 p0253 A67-12520

Numerical integration of averaged cross section for electron induced resonance charge exchange and ionization of accelerated beam of hydrogen atoms 02 p0278 A67-12629

Autoionization mechanism role in formation of astrophysical spectra 03 p0509 A67-13217

Solar corona temperature measurements, noting discrepancy between results from observations of forbidden emission lines and ionization balance calculations 03 p0470 A67-13218

Electron collision cross section resonance mechanism analyzed via matrix methods, noting threshold effect application to electron scattering 03 p0470 A67-13219

Autoionization calculation describing scattering aspect of phenomenon 03 p0471 A67-13220

Neutron collision cross section and calculation of energy loss of displaced Si

atoms to ionization 03 p0494 A67-13481

Cross section estimates for symmetric resonant charge exchange between ions differing by one electronic charge, noting effect on heat conduction in plasmas 03 p0484 A67-14038

Absorption spectra of Te, Sn, Pb, PbTe and SnTe at various energy ranges, noting role of wave functions involved in absorption by d-electrons 04 p0681 A67-15295

Cross sections for electron collisions with hydrogen atoms and hydrogen-like ions for excitation of ground and other levels 04 p0671 A67-15642

Radial distribution of plasma formed in simple mirror machines by quantum effect field ionization of fast neutral atoms 04 p0671 A67-15644

K-shell ionization cross sections of silver, tin and gold from electron bombardment 04 p0661 A67-15762

Cross sections for charge transfer between alkali-metal ions and cesium atoms determined as function of primary ion beam energy, noting structure consisting of oscillations 04 p0661 A67-15766

Role of solar photon and corpuscular radiation in dissociation and ionization of water molecules in cometary atmospheres 05 p0888 A67-16203

Oblique probe data applied to determination of minimum group path of signal for parabolic model of ionosphere 05 p0801 A67-17130

Temporal variations in values of variability characteristic of parameters of ionosphere cross sections below principal maximum 05 p0801 A67-17142

Negative resistance regions in Si Zener diodes explained in terms of impact ionization and junction breakdown combination 06 p0968 A67-17814

Nitrogen and oxygen excitation by proton shocks, measuring emission cross sections of radiation and analyzing vibrational structure 06 p1037 A67-18706

Multichannel photoionization of atomic systems obtained with dipole approximation assuming LS coupling, using wave functions 07 p1226 A67-19498

Limiting daytime flux of ionization into protonosphere, obtaining expression for maximum upward flux supported by diffusion 07 p1180 A67-19918

Photoionization cross section of negatively charged In atoms in n-type silicon from comparison of intrinsic photoconductivity with impurity photoconductivity 08 p1367 A67-20410

Excitation cross section of states of Ne 2, Ar 2 and Kr 2 by electron collision 08 p1339 A67-21376

Cross sections for excitation of upper and lower ion states by electron impact with ground state neutral argon atoms found by measuring coherent and incoherent light of laser beam 09 p1514 A67-22272

High field Hall effect of semiconducting CdS crystals with different mobilities, noting electron density and multiplication 10 p1689 A67-22908

Continuous spectra of atomic gases and low temperature plasma, analyzing photoionization cross section and electron transitions in neutral atom field 10 p1682 A67-23067

Solar X-ray spectrum of Tousey analyzed using criteria of abundance of elements of Pottasch 10 p1707 A67-23227

Ionization cross sections of neutral atoms caused by electron impact with Maxwellian velocity distribution 10 p1682 A67-23354

Ionization efficiency and cross section of meteor trails during collision between particles of meteoric vapor and air molecules 10 p1709 A67-23362

Excitation cross section of upper laser levels in ionized argon by electron collision with ground state neutral atoms measured, using incoherent light technique 10 p1665 A67-23382

Properties of partially ionized Ar computed via Chapman-Enskog-Burnett expressions noting ambipolar diffusion coefficient, electron-atom momentum, electrical and thermal conductivity, etc 11 p1775 A67-23865

Direct ionization and secondary excitation in proton auroras, noting magnitude of contribution by various processes 11 p1784 A67-23927

Behavior of nighttime equatorial F-2 layer under ambipolar diffusion and electrodynamic drift 11 p1784 A67-23935
 Blowdown wind tunnel for He-K MHD generator, considering magnetically induced ionization, conductivity, gas temperature, etc 12 p1898 A67-25389
 Neutral silicon photoionization cross sections for continuous UV absorption measured near ionization limits by shock tube technique 12 p1968 A67-26248
 Numerical integration of averaged cross section for electron induced resonance charge exchange and ionization of accelerated beam of hydrogen atoms 13 p2171 A67-27387
 Collision frequencies in D region and stratospheric-mesospheric relations, noting oxygen as error source and electron-density height profile 14 p2311 A67-28407
 Inelastic collisions of proton beam with carbon monoxide target molecules, determining ionization cross section and charge transfer 14 p2390 A67-28943
 Turbulent state and diffusion of plasma during drift instability, noting increase with oscillation amplitude 14 p2363 A67-29068
 Ionization probability of hydrogen atom by electron impact in terms of three-body problem of classical mechanics 14 p2351 A67-29072
 Charge transfer prediction by classical binary-encounter theory approximation and quantum mechanical approximation 15 p2519 A67-29331
 Potentials occurring in excitation of highly ionized ions by electron impacts 15 p2520 A67-29527
 Momentum transfer collision frequency for electrons in cesium plasmas from electrical conductivity and plasma properties measurement in cesium arc column 16 p2719 A67-31236
 Ionization of low temperature supersonic plasma jets, noting kinetics of elementary processes, gas dynamic parameters and effects of combustion and alkali metal admixtures 17 p2896 A67-32170
 Trapped plasma build-up in magnetic field by ionization of injected atomic beam, noting ionization cross section parameters 17 p2908 A67-33115
 Lyman-alpha radiation emission from ion-atom-gas collision measured for various projectile energies 17 p2889 A67-33224
 Low-energy electron collisions and interactions with atoms and molecules, discussing vibrational excitation, ion formation, ionization cross section, etc 19 p3264 A67-35068
 Mobility and diffusion of neon positive ions in neon, deriving ion energy and collisional cross section 19 p3271 A67-35074
 Semiempirical electron impact cross sections for He from oscillator strengths, using Born approximation 20 p3489 A67-37416
 Electron impact cross sections used to determine helium collision cross sections sets 20 p3489 A67-37417
 Electron impact excitation and ionization cross sections data of molecular nitrogen synthesized using modified Born approximation 20 p3489 A67-37418
 Inelastic electron impact cross sections for ionization and vibrational excitation of atmospheric molecular oxygen 20 p3489 A67-37419
 Excitation cross sections for protons incident on atomic hydrogen calculated by nonadiabatic method 20 p3491 A67-37686
 Oblique probe data applied to determination of minimum group path of signal for parabolic model of ionosphere 21 p3618 A67-38473
 Temporal variations in values of variability characteristic of parameters of ionosphere cross sections below principal maximum 21 p3619 A67-38484
 Measurement of cesium and mercury ion-atom resonance charge exchange cross section [AIAA PAPER 67-682] 21 p3660 A67-38713
 Electron impact ionization cross sections and rate coefficients for atoms and ions of Hg, rare gas and alkali metal groups 21 p3660 A67-39098
 Cesium plasma ionization in low voltage arc discharge, measuring electron ionization capacity, electron temperature and cesium ionization and excitation cross sections 22 p3847 A67-39510

Capture, ionization and ionization capture in collisions of protons with argon atoms 23 p4030 A67-41687
 Empirical formula for representation of cross sections for single ionization of atoms and ions from ground state by electron impact 24 p4194 A67-41890
 High energy cosmic ray nuclear interaction cross section dependence on interacting material atomic weight determined by ionization calorimeter and Geiger counters 24 p4219 A67-42847
 Ionization cross section in slow atom collisions calculated by modified Franck-Condon principle 24 p4194 A67-42889
IONIZATION FREQUENCY
 Critical ionization frequencies in F-2 layer in near-polar region observed at Northern Hemisphere high latitude stations 07 p1179 A67-19832
 Energy absorption profile and ionization rates for electron beam dependence on beam energy, altitude and atmospheric layer thickness and mass 14 p2379 A67-27921
 Ionization frequency distribution in HF discharge produced by long single turn coil 19 p3276 A67-35118
 Hydrogen thermal ionization rate behind strong shock wave, considering nonadiabatic collisions and various relaxation mode interactions in shock speed range 19 p3292 A67-35394
 Spread ionization in topside of ionosphere from satellite observations 24 p4148 A67-42060
IONIZATION GAUGE
SA PENNING GAUGE
 Trigger discharge gauge compared with ionization gauge and partial pressure analyzer 06 p0950 A67-17749
 Surface ionization detector of hydrogen in presence of air at one atm 08 p1330 A67-20376
 Electron bombardment type ionization gauge with logarithmic differential circuit 10 p1610 A67-22950
 Ionization mechanism of argon-permanent gas mixture in radioionization detector used for gas chromatography 19 p3226 A67-34797
 Penning ionization gauge discharge nonlinear response to VHF signals, discussing resonance behavior 19 p3275 A67-35110
 Ionization gauge circuit for studies of solid explosives initiation by gaseous detonation waves and reflected wave trajectories in shock tunnels 21 p3630 A67-38770
 Explorer 32 satellite atmospheric density experiment gas calibrations, comparing operation and pressure response of various ionization gauges 23 p4004 A67-41356
 Ionization gauge calibration by volume expansion, flow rate and multiple orifice techniques 24 p4153 A67-42048
 Electromagnetic showers in lead recorded with ionization calorimeter, discussing cascade curve 24 p4221 A67-42870
IONIZATION POTENTIAL
 Electron affinity data for various pentacyclic aromatic hydrocarbons, predicting ionization potentials 01 p0019 A67-10882
 Energy dependence of isotopic composition of primary helium nuclei, considering ionization loss, fragmentation and solar modulation 03 p0505 A67-12956
 Shallow donor potential in silicon 03 p0493 A67-13363
 Methods for calculating interaction potentials of atoms, molecules and ions 03 p0473 A67-13613
 Relaxation process leading to thermal equilibrium behind ionizing shock waves in argon analyzed, using optical techniques 04 p0601 A67-14458
 Interactions in low density plasma beams of electrostatic thrust engine exhaust, discussing neutralization, instabilities, plasma wind tunnel, etc 04 p0690 A67-15022
 Neutron energy deposition in silicon in ionization and elastic interactions calculated, noting effects of atomic recoils 04 p0684 A67-15688
 Impurity states theory for semiconductors with In-Sb type band structure, calculating ionization potential and numerical values for energy levels 05 p0863 A67-16694
 Hall effect and resistivity in n-GaAs with Si as shallow donor, obtaining ionization energy and impurity band conduction

values 06 p1052 A67-18570
 Diurnal and seasonal altitude variations of E and F layers analyzed for geomagnetic activity from rocket measurement of electron concentration 07 p1173 A67-19686
 Red shift relationship with ionization potential for absorption lines in quasi-stellar object 3C 191 08 p1400 A67-21251
 Ionization capability of cosmic rays in low ionosphere, considering relativistic energies and high energy 09 p1561 A67-21841
 Bohn ionization equation applied to helium plasma to include effect of He 2 energy levels 09 p1544 A67-21883
 Equality conditions for gold and silver electrode zero charge and transient peak potentials by pH and anion effects, using scraped electrodes 10 p1602 A67-23158
 Geomagnetic and solar control of ionization at 1000 km determined from electron density data obtained from Alouette satellite 10 p1650 A67-23339
 Pulsed RF slot antenna breakdown controlled by preionization and diffusion 11 p1758 A67-24126
 Nonequilibrium MHD generator for closed and open cycles, noting K seed ionization by energy transfer from excited N molecules 12 p1898 A67-25388
 Ionization dependence of Na, K, Ca, Mg, Al, Fe and Si on arc temperature, noting correlations between temperature and electron concentration independent of plasma composition 12 p1977 A67-26108
 Multiple ionization of rare gases analyzed in mass spectrometer with trapped ion source, noting energies of metastable levels 15 p2519 A67-29189
 Impurity states theory for semiconductors with In-Sb type band structure, calculating ionization potential and numerical values for energy levels 15 p2539 A67-29865
 Conductivity and Hall effect in analysis of temperature dependence of current carrier concentration and mobility in silicon, explaining ionization energy 15 p2541 A67-30240
 Interferometrically-measured ion temperatures compared to electron temperatures in pure barium and barium-cesium plasmas produced by contact ionization 16 p2720 A67-31243
 Ionization levels and thermodynamic functions of theoretical gas mixtures composed of various highly ionized atom types 16 p2720 A67-31387
 Time and space distribution of anomalous ionization in ionospheric F-2 layer above Southern Hemisphere, noting maximums of ionization distribution 16 p2668 A67-31893
 Ionization loss effect on energy spectra of cosmic ray nuclei undergoing Fermi acceleration 17 p2930 A67-32041
 Chemical processes in low temperature plasmas, stressing nonequilibrium characteristics, temperature and collision factors, ionization and particle excitation 17 p2809 A67-32188
 Ionization in E region due to influx of micrometeorites 17 p2943 A67-32542
 Pauling empirical equation relating thermal effect of reaction to negative ionization potential of solid substances 18 p3094 A67-33438
 Electron concentration in turbulent boundary layer of weakly ionized plasma when injecting electrons through pores in wall 18 p3087 A67-34053
 Methods for calculating interaction potentials of atoms, molecules and ions 18 p3083 A67-34478
 Microwave transmission through quiescent cesium plasma studied, noting apparatus for thermal ionization studies 19 p3288 A67-35370
 Cesium vapor ionization on porous tungsten substrate creates gradients in surface atom concentrations diminishing ionization efficiency 20 p3487 A67-36170
 Highly ionized S, Cl, Ar and K resonance lines recorded, noting application for coronal Ca ions 20 p3528 A67-37478
 Energy level behavior of metastable alkali atoms against autoionization and radiative decay 20 p3492 A67-37691
 Ionization potentials of clustered sodium atoms measured, describing experiment involving mass spectrometry 21 p3660 A67-39109
 Resonance lines originating from autoionization energy levels far above ionization potential observed for highly

ionized atoms of Na I isoelectronic sequence 22 p3840 A67-39237

Field-aligned irregularity instabilities in ionization vertical gradient, showing unstable E region for irregularities of scale size 20 m-6 km 22 p3789 A67-39475

East-west asymmetry effect in cosmic rays obtained together with ionizing and hard components, using crossed telescope 23 p4060 A67-41137

Planetary nebulae IR emission intensities, discussing radiative recombination, ionization equilibrium and fine structure level population 24 p4223 A67-41811

Lithium content of T Tauri stars shown to exceed ionization of Li in solar atmosphere 24 p4227 A67-42161

Photoexcited electroluminescence spectra of rare earth ions in cadmium fluoride semiconductor single crystal 24 p4205 A67-42893

IONIZED GAS

SA PLASMA

Three new visible CW laser lines in discharge in singly-ionized Cl 01 p0089 A67-10373

Radiation absorption by ionized hydrogen in plane of galaxy to explain brightness profiles for declination minus 37 degrees 02 p0307 A67-11688

Induction velocimetry measurement of average velocity of free jet of ionized gas influenced by transverse uniform magnetic field 02 p0272 A67-11881

Resonance absorption of electromagnetic power by weakly ionized gas produced in cylindrical discharge tube 02 p0273 A67-12184

Emf and electric conductivity in ionized gas produced by detonation of Sakura dynamite to estimate explosion rate 02 p0268 A67-12500

Diffusion of fully ionized plasma across magnetic field in computer model consisting of one thousand charged rods in two-dimensional motion 02 p0276 A67-12558

Ion acoustic oscillations in collisionless region of fully ionized plasma excited by electric current 02 p0277 A67-12612

Ion mobility in gas formed by ions, defining gas temperature, obtaining solution of kinetic equation for ion distribution function 02 p0270 A67-12625

Herman and Gibbons conclusions on radiation energy concentration in ionized gas shown to be erroneous 03 p0411 A67-12961

Aeromagnetic flutter of walls of plane infinite channel with ionized gas flow 03 p0524 A67-13503

Ionized gas electric conductivity measurement based on magnetic flux changes and deflection of lines of forces during gas-magnetic field interaction 03 p0478 A67-13604

Small amplitude wave propagation in ionized high temperature gas embedded in uniform magnetic field with Hall current 03 p0482 A67-13742

Kinetic model for three-component plasmas with ionization resulting from electron-neutral collisions 03 p0484 A67-14037

Relaxation process leading to thermal equilibrium behind ionizing shock waves in argon analyzed, using optical techniques 04 p0601 A67-14458

Partially ionized two-temperature plasma, deriving distribution function of first approximation associated with viscosity 04 p0666 A67-15186

Viscous friction and heat flux for partially ionized medium flowing in plane channel with anisotropic transport coefficients 04 p0666 A67-15189

Conductance theory for electrolytes and weakly ionized plasmas using pair distribution function in space in presence of short range forces 04 p0670 A67-15578

Hugoniot-Rankine conditions, dissociation and ionization of hydrogen and nitrogen gas behind high speed shock wave and radiation effects 05 p0790 A67-16036

Shanlavsikil multiply ionized gas model for theoretical calculation of thermodynamic equilibrium parameters of shock tube 05 p0790 A67-16249

Nonlinear instability of optical frequencies in partially ionized plasma, noting nonlinear frequency buildup for strong plasma waves 05 p0852 A67-16691

Anomalous emission at electron cyclotron frequency in partially ionized plasmas 05 p0854 A67-16895

Stimulated emission of electromagnetic wave in decaying ionized plasma 05 p0855 A67-16998

Disturbance current created by acoustic wave propagating in partially ionized gas 05 p0855 A67-17050

Spatially resolved He-Ne laser heterodyne measurements of electron number densities in weakly ionized Ar pulsed discharges 05 p0856 A67-17272

Frequency effects in radar return from turbulent weakly ionized missile wakes, obtaining relationship between radar cross section and electron density distribution [AIAA PAPER 67-23] 06 p0963 A67-18258

Weakly ionized gas flows about electrically biased bodies under effects of compressibility and electron energy [AIAA PAPER 67-100] 06 p1042 A67-18471

Polarization characteristics of ionized argon laser in magnetic field 06 p1011 A67-18542

Electron-neutral particle collision and electron thermal conductivity effect on upper atmospheric electron and ion temperatures 06 p0998 A67-18702

Instability of inhomogeneous weakly ionized plasma in crossed electric and magnetic fields in quasi-approximation 07 p1228 A67-19508

Velocity distribution function relaxation and runaway of electrons in weakly ionized plasmas 07 p1228 A67-19510

LF resonance oscillations in cylindrical plasma column, considering ionization mechanism of Phillips Ionization Gauge /PIG/ discharge 07 p1229 A67-19674

Energy balance equations including effects of heating by electron gas, cooling and energy coupling obtained for various ion species, assuming each ion gas has Maxwellian velocity 08 p1326 A67-21363

Precursor wave velocity, electron density and current content in electromagnetically driven shock tube, using hydrogen and argon 08 p1363 A67-21380

Normal ionizing shocks propagating through hydrogen in sub-Alfvénic and trans-Alfvénic regimes in coaxial electromagnetic shock tube 08 p1363 A67-21381

Transverse electromagnetic waves with constant phase velocity in fully ionized Vlasov plasmas 08 p1364 A67-21401

Anomalous bremsstrahlung and cyclotron emission in partially ionized plasmas 08 p1366 A67-21441

Amplification of RF wave in partially ionized gases with large Ramsauer effect in absence of magnetic field, due to negative absorption of stimulated bremsstrahlung 08 p1366 A67-21442

Gas ionization by fast electron beam directed along waveguide leading to longitudinal distribution of secondary electron concentration 09 p1545 A67-22002

Excitation and damping of drift waves in stable regime of ionized plasma radially confined by axial magnetic field 09 p1550 A67-22679

Oxygen IV transition multiplet relative intensities for measuring decay rates, using triply ionized emitters 10 p1678 A67-22718

Motion of structures in coma and tail of Morehouse comet compared with hydrodynamic model interaction between solar wind and cometary plasma 10 p1704 A67-22720

Sound propagation in partially ionized plasma, noting kinetic quadrature calculation results 10 p1683 A67-22783

Flight control magnetic source interaction with ionized gas induced by bow shock ahead of blunt body in hypersonic flow 10 p1592 A67-23143

Ambipolar diffusion of plasma cloud imbedded in ionized gas with homogeneous magnetic field, assuming electric current is not vanishing 10 p1648 A67-23293

Modified Chapman-Enskog method for obtaining transport properties of nonequilibrium partially ionized gas, giving hydrodynamic equations 11 p1775 A67-23866

Electromagnetic wave propagation in partially ionized paramagnetic gas in static magnetic field 11 p1751 A67-23970

Free electron density and effective collision frequency of ionized argon in wake of shock wave measured, using microwave probe methods 11 p1775 A67-24017

Ionized shock-nitrogen conductivity measured by four-electrode device 11 p1832 A67-24057

Peak density in single ended Q machine described in agreement with equilibrium theory 11 p1833 A67-24368

Density measurements in Q-device by resonance fluorescence scattering, Langmuir probe and microwave methods compared, examining causes of discrepancy 11 p1838 A67-24405

Ionized fluid flow analyzed by multifluid theory to evaluate energy transfer mechanisms, noting temperature and compositional nonequilibrium effects 11 p1780 A67-24533

Boundary layer behavior in fully ionized two-temperature plasma 11 p1840 A67-24675

Ion acceleration region demonstrated by coupling two HF magnetic field gradient accelerators 11 p1841 A67-24767

Gross behavior and properties of laboratory plasma generation with combined transverse and longitudinal ionizing currents parallel to magnetic field 11 p1845 A67-25098

Electrical field in solar atmosphere caused by pressure gradient in case of partially ionized gas 12 p2000 A67-25133

Hydrodynamic axial-symmetric model of plasma flow on sunward side of comet assuming cometary gas is ionized by solar UV radiation only 12 p1993 A67-25227

Ionized gas flow rate behind detonation wave used with Chapman-Jouguet condition to determine speed of sound in reaction products 12 p1929 A67-25752

Channel profiles for producing vortex flows in weakly ionized gases in transverse magnetic fields 12 p1977 A67-26076

Stabilization of clusters of galaxies by ionized gas studied for recombination radiation 12 p2011 A67-26250

Kinetic equation for completely ionized plasma generalized for several particle species case 13 p2165 A67-26585

Electric potential distribution in flame for electronegative gas layer present between two electrodes 13 p2165 A67-26597

Singly ionized He measured for radiative lifetimes of various states using high energy atomic beam 13 p2160 A67-26888

Dynamics of weakly ionized gases analyzed using Liouville equation 13 p2167 A67-27003

Matching factor for energy exchange in electromagnetic interaction between ionic and electronic gases in amplitude-amplitude ionospheric intermodulation 13 p2070 A67-27196

Ionized gas flow past oscillating interface in presence of magnetic field, based on MHD boundary layer model with constant velocity profile 13 p2168 A67-27302

Laminar motion equation for conducting gas jet expansion along plane wall in presence of transverse magnetic field solved in series form 13 p2168 A67-27304

Velocity dependence of total scattering cross sections for atom-atom collisions measured in high energy range 13 p2161 A67-27361

Ion acoustic oscillations in collisionless region of fully ionized plasma excited by electric current 13 p2170 A67-27368

Ion mobility in gas formed by ions, defining gas temperature, obtaining solution of kinetic equation for ion distribution function 13 p2161 A67-27381

Propagation rate of LF acoustic waves in low pressure glow discharge in nitrogen 14 p2354 A67-27759

Ionospheric satellite trail, noting relation between length scales of medium properties and scales determined by body dimensions 14 p2302 A67-28207

Source free solutions in ionized regions, discussing geometrical optics application to MGD with infinite conductivity 14 p2359 A67-28462

Coefficient for electron ion recombination during triple particle collision, using Boltzmann kinetic equations 14 p2363 A67-29077

Magnetic field strength effects on pulse and CW operation of large diameter ionized gas lasers 15 p2496 A67-29173

Steady state velocity distribution in fully ionized plasma in DC electric field obtained through Bhatnagar-Gross-Krook equation 15 p2522 A67-29206

Screw instability in linear Hall accelerator 15 p2522 A67-29207

Diffusive separation due to electrical

coupling of ions and hot electrons and effect on shock wave structure in plasmas 15 p2470 A67-29227
Hotshot wind tunnel for ionized wakes of models in nitrogen hypersonic flow, determining electron temperature and density [ONERA-TP-455] 15 p2416 A67-29380
Microwave transmission measurements of electrical properties of shock ionized air noting dielectric constant, electron density, conductivity, attenuation, etc 15 p2470 A67-29490
Gas stream discharge studied by using electromagnetic plasma gun to direct plasmoids toward beam 15 p2472 A67-29728
Nonlinear instability of optical frequencies in partially ionized plasma, noting nonlinear frequency buildup for strong plasma waves 15 p2530 A67-29862
Potential distribution and volt-ampere characteristics of ionized gas flows in ducts 16 p2713 A67-30598
Electron velocity distribution function obtained for partially ionized gas in weak, steady electric field by solving Boltzmann-Fokker-Planck equation 16 p2704 A67-31235
Ionization levels and thermodynamic functions of theoretical gas mixtures composed of various highly ionized atom types 16 p2720 A67-31387
Hot flame gases ionization by electron reactions at atmospheric pressure 17 p2968 A67-32149
Unsteady Vlasov equation for class of beam-like initial distributions associated with ion engines 17 p2928 A67-32158
Magneto-Fanno flow shock tube experiments to determine one-dimensional MGD interactions between partially ionized gas flow and external magnetic field 17 p2898 A67-32183
Voltage induced by magnetic field using shock tube with high velocity ionized argon flow 17 p2898 A67-32184
Partially ionized gases application to industry, stressing power units incorporating plasma converters, plasma electrolytic fuel elements and MHD generators 17 p2899 A67-32187
Linear theory of collision-induced instability of partially ionized gases for waves propagating along external magnetic field 17 p2902 A67-32669
Wave equations for disturbances in partly ionized gas due to current sources determined, using three-fluid model 17 p2906 A67-33056
Excited state and steady state populations in high pressure plasma with heavy particle collisional ionization and electron-ion recombination 17 p2909 A67-33228
Acoustic wave mode in weakly ionized gas analyzed, noting charge separation and electroacoustic effects 17 p2909 A67-33230
Ionization effect on external pressure determination for high velocity gas flows past plates and shells with flutter 18 p2981 A67-33424
Anomalous LF plasma oscillation by particles trapped in potential well behind satellite applied to ionospheric measurements 18 p3117 A67-33512
Highly ionized two-fluid plasma confined magnetically analyzed for stability 18 p3086 A67-33986
Nonlinear and second order thermal diffusion of electrons in ionized gas, using kinetic theory 18 p3083 A67-34401
Ionized gas electric conductivity measurement based on magnetic flux changes and deflection of lines of forces during gas-magnetic field interaction 18 p3090 A67-34469
Phenomena in ionized gases - Conference, Belgrade, August 1965, Volume 1, electronic and ionic collision phenomena, surface phenomena, electrical discharges 19 p3288 A67-35067
Ionizing and charge transfer processes following heavy particle collisions in ionized gas analyzed using spectroscopic technique 19 p3284 A67-35069
Atomic collision processes in ionized gases, studying ambipolar diffusion, electron attachment, electron-ion recombination and Penning ionization by afterglow technique 19 p3284 A67-35070
Weakly ionized plasma and gyromagnetic resonances in helium low pressure HF electrodeless discharge in magnetic

field 19 p3276 A67-35113
Plasma-density distribution produced in gas by tubular electron beam 19 p3278 A67-35128
Shock waves and spectrographic properties of emitted light during high energy linear discharge in ionized gaseous filament 19 p3176 A67-35133
Electric conductance exponential decay in column of wall stabilized nitrogen arc after current interruption 19 p3282 A67-35157
Diode with anode glow type discharge analyzed for relationship between discharge quenching current and structural elements of discharge gap 19 p3282 A67-35160
Ionized gas produced by exploded lithium wires, presenting physical measurements, finding self-consistent solution of temperature and electron concentration 19 p3261 A67-35162
Phenomena in ionized gases - Conference, Belgrade, Yugoslavia, August 1965, Volume 2, Plasma physics 19 p3282 A67-35338
Significance of far field portion of plasma microfield 19 p3285 A67-35344
Dynamic equations for adiabatic changes of state for mixtures of partially ionized gases with chemical reactions 19 p3286 A67-35348
Transport coefficients of fully ionized hydrogen plasma in magnetic field calculated from Fokker-Planck equation 19 p3286 A67-35350
Homogeneous, fully ionized plasma HF conductivity computed using kinetic equation, showing application to two-temperature plasma 19 p3286 A67-35353
Transport phenomena in electronic plasma as initial value problem noting distribution function relaxation 19 p3287 A67-35355
Ohm law extended to electrical conduction of partially ionized plasmas and nonneutral ionized gases 19 p3287 A67-35356
Plasma-magnetic shock wave propagation in high pressure, partially ionized argon plasma 19 p3293 A67-35400
Ionized gas flow past cylinder and sphere, determining ionization and dissociation effect on displaced shock wave form 19 p3170 A67-35449
Mutual admittance of slot antennas measured for free space and ionized environment by different techniques 19 p3194 A67-35518
Phenomena in ionized gases - Conference, Belgrade, Yugoslavia, August 1965, Volume II 19 p3295 A67-35585
Trigatron spark gap using low voltage plasma jet as switch analyzed for properties, time lag and mechanisms 19 p3298 A67-35602
Alfvén waves in ionized plasma of finite electrical conductivity, giving equations for semiphenomenological model 20 p3496 A67-36271
Ionized gas properties for use in various microwave components to obtain amplification through electron beam plasma interaction 20 p3497 A67-36489
Langmuir probe current in weakly ionized gas flow, studying correlation between hydrodynamical turbulence and pressure fluctuations 20 p3503 A67-37674
Mach number effect on electron temperature structure of partially ionized monatomic and diatomic gas shocks 21 p3610 A67-37760
Magnetic field effect on flow field and drag of blunt body in partially ionized argon plasma, obtaining electron density and temperature [AIAA PAPER 67-729] 21 p3673 A67-38753
Formation mechanism of luminous gas sphere/ionized vortex configuration/ due to atmospheric electrical discharge 21 p3655 A67-38902
Pinch-discharge source of ionizing plasmoids for aerophysical investigations at high pressures, emphasizing stabilization and passage of AC current through vortex 21 p3675 A67-38912
Chapman-Enskog expansion applied to Fokker-Planck equation for plasma allows transport coefficients calculation without further approximation in presence/absence of magnetic field 22 p3843 A67-39266
Plasma continuity equations, deriving oscillation frequency equations for LF oscillations in partially ionized gases 22 p3844 A67-39383
Chapman-Enskog transport collision integrals calculated for repulsive and

attractive screened Coulomb potentials in ionized gases 22 p3850 A67-39717
Momentum, heat and magnetic field diffusion in viscous, thermal and magnetic boundary layers of different thicknesses in MHD fluid 22 p3850 A67-39721
Ionized plasma electric conductivity calculation using Druyvesteyn and Maxwellian distribution for electrons and ions respectively 22 p3851 A67-39725
Degree of ionization effect on yield of excited atoms from gas target 22 p3852 A67-39987
Antenna immersed in plasma problem solved using electromagnetic radiation in ionized medium principles 23 p3978 A67-40707
HF conductivity of partially ionized plasma in long wavelength limit, treating particle interactions by BBGKY and Boltzmann collision integral methods 23 p4031 A67-40888
Ion wave propagation in weakly ionized gases 23 p4032 A67-40980
Accuracy of scalar electrical conductivity calculations of partially ionized plasma using third Chapman-Enskog approximation method 23 p4035 A67-41753
Sound propagation in partially ionized plasma, noting kinetic coefficients and quadrature calculation 24 p4195 A67-42119
Stellar and planetary magnetic field formation theory based on concept of existing ionized turbulent mass flow on these celestial bodies 24 p4230 A67-42352
Design of gasdynamic shock tube described with measuring apparatus developed for studying ionized gas flows in magnetic field 24 p4139 A67-42357
Interferometer crossed with spectrograph used for electron concentration investigation in ionized argon behind shock waves propagating at high Mach numbers 24 p4197 A67-42358
Electrical conductivity of ionized plasma taking into account particle impenetrability, using Boltzmann and collision at distance integrals 24 p4198 A67-42662
IONIZING RADIATION
SA PENNING DISCHARGE
Space flight acceleration, vibration and ionizing radiation effects on body functions, oxidizing metabolism of central nervous system and fission processes of hemopoietic tissues 01 p0015 A67-10336
Model describing effect of ionizing radiation on metal-oxide-silicon surfaces, showing relation to study of defect structure of silica 01 p0036 A67-10475
Ionization calorimeter measurement of contribution of ionizing particles of star radiation to electron induced ionization of cosmic ray shower 02 p0271 A67-12754
Ionization calorimeter measurement of absorption of energy flux of primary cosmic radiation nuclear active component in iron 02 p0318 A67-12762
Polya distribution describing photon correlations in ionizing laser beams enables differentiation between various multiphoton ionization processes 03 p0438 A67-13982
Glycogen accumulation in monkey and cat brain exposed to proton irradiation, discussing astrocytes function in carbohydrate metabolism 04 p0560 A67-14489
Transient response of transistor exposed to ionizing radiation environment determined, using lumped model technique 04 p0588 A67-15697
Pulsed high energy ionizing radiation effects on behavior and output frequency of electronic quartz oscillator crystals 04 p0685 A67-15700
Transient radiation effects on microcircuits 04 p0588 A67-15701
Ionizing radiation effects on silicon planar bipolar transistors determine degradation mechanisms 04 p0588 A67-15707
Instability effect in n-channel silicon MOS transistors bombarded with ionizing radiation 04 p0589 A67-15716
Intensity of ionizing and neutron component of cosmic rays, noting correlation for sporadic cyclic variations and solar activity cycles 05 p0879 A67-16103
Twilight effects of solar ionizing radiation absorption, discussing ion production rates and fluorescence 05 p0885 A67-17410
Killing and mutagenic efficiencies of heavy ionizing particles in Arabidopsis thaliana 06 p0953 A67-18379
Surface generation-recombination and

channel effects on p-n junctions and transistors exposed to ionizing radiation 06 p1054 A67-18822

Pair production in irradiated semiconductors within framework of plasmon decay, considering variation of radiation ionization energies with band gap energy 06 p1063 A67-18935

Ionograms of chromospheric eruptions with eruptive filament of December 1965, obtaining morphological data and determining radiation frequency range 09 p1561 A67-21842

Blockage of electrically evoked pupillodilation in cat by irradiating hypothalamus with cyclotron-accelerated alpha particles 10 p1598 A67-23394

DNA-agar annealing of residual DNA after degradation by ionizing radiation 11 p1746 A67-23919

Ionizing radiation in space, discussing detection techniques, devices, etc 11 p1791 A67-24619

Genetic transcription as affected by ionizing radiation and hydrogen peroxide 11 p1747 A67-24786

Sudden cosmic noise absorption correlated with solar microwave flux to establish daily mean value 13 p2190 A67-26311

Variations of ionizing radiation of E layer, eliminating aeronomic effects by considering seasonal variations of ionization index 13 p2191 A67-26767

Ionizing radiation effect on bacterial cells noting inhibition due to generated hydrogen peroxide 13 p2059 A67-26867

Fourth-week syndrome in addition to normal medullary syndrome in DBA/2J mouse strain response to acute ionizing lethal irradiation 13 p2059 A67-26868

Model for shifts in gate turn-on voltage of insulated-gate field effect devices induced by ionizing radiation 13 p2079 A67-26871

Ionizing radiation dosimetry for space pilots on short-and long-term space flights 16 p2617 A67-30764

Mouse, rat and dog organism reaction to ionizing radiation, vibration and acceleration 16 p2611 A67-30765

Semiconductor device and transient ionizing radiation effects on monolithic integrated circuits 17 p2828 A67-32836

Ionizing radiation effect on polymers used in electronics, producing temporary effects also found in mineral insulators like anodic tantalum oxide 17 p2917 A67-32841

Paramagnetic and electrical properties of organic polyvinyl-acetate-based semiconductor films irradiated with electrons before and after heating 18 p3099 A67-33694

Ionizing radiation received by biological tissue during space flights measured by nuclear-emulsion technique 20 p3368 A67-36260

Primitive-earth atmosphere models irradiated with UV light and ionizing radiation for primordial organic synthesis 20 p3369 A67-36656

Junction field effect transistors for onboard satellite equipment, noting resistance to ionizing radiation 21 p3600 A67-38659

Back collection of charge due to ionizing alpha or beta particles by silicon p-n junction detector with space charge width less than range 22 p3797 A67-39345

Ionization calorimeter measurement of contribution of ionizing particles of star radiation to electron induced ionization of cosmic ray shower 22 p3842 A67-40256

Ionization calorimeter measurement of absorption of energy flux of primary cosmic radiation nuclear active component in iron 22 p3842 A67-40264

Bibliography dealing with vibration, acceleration and ionizing radiation on vestibular apparatus, noting lack of information 23 p3943 A67-40764

Combined effect of acceleration and ionizing radiations on conditioned reflexes of rats noting alleviation on radiation leukopenia 23 p3943 A67-40772

Satellite and probe data analysis on ionizing component, primary cosmic rays and albedo particle flux intensity near atmospheric outer boundary 23 p4055 A67-41098

Ionizing radiation effects on dark current and noise pulse spectrum of photomultiplier tubes used in balloon and satellite X-ray

observations 23 p4000 A67-41216

Increased oxygen tension causing increased free radical flux in rat kidney tissue akin to ionizing radiation exposure 23 p3958 A67-41654

Ionization fronts stability, finding no instabilities for strong D type fronts 24 p4224 A67-41816

Protective effect of substrates against ionizing radiation on enolase and lactic dehydrogenase [SAM-TR-66-264] 24 p4111 A67-41841

Preirradiated organism reaction to space flight acceleration studied in determination of admissible ionizing radiation dose 24 p4113 A67-42393

Intensity of ionizing and neutron component of cosmic rays, noting correlation for sporadic cyclic variations and solar activity cycles 24 p4213 A67-42779

IONOSONDE

Seasonal and yearly variations of atmospheric ozone sounded by electrochemical ionosonde 03 p0405 A67-12804

Electron number density profile measurements of moderate and heavy sporadic E over Areibo by incoherent backscatter technique 03 p0409 A67-12946

Vertical incidence ionospheric absorption measurements from ground station criteria for recognizing winter anomaly 15 p2476 A67-29623

Observation methods, mechanisms, geomorphology, time variations and associated effects of equatorial type spread-F [AGARDOGRAPH 95] 15 p2480 A67-30274

Topside ionosphere irregularity studied by Alouette I ionograms and ground based ionosonde records, noting spread-f occurrence topside ionosphere irregularity studied by Alouette I ionograms and ground based ionosonde 16 p2667 A67-31515

IONOSPHERE

SA C LAYER

SA D LAYER

SA E LAYER

SA F LAYER

SA ISIS SATELLITE

SA LOWER IONOSPHERE

SA LUNAR IONOSPHERE

SA NIGHT IONOSPHERE

SA UPPER ATMOSPHERE

SA UPPER IONOSPHERE

Diurnal and seasonal variations of ionospheric turbidity 02 p0236 A67-11670

Ionospheric properties and wave-electron interaction 03 p0405 A67-12801

Error estimation in numerical prediction of ionospheric index 06 p0995 A67-18049

MHD wave theory for slow processes in ionosphere and magnetosphere 07 p1181 A67-19933

Ionosphere-stratosphere coupling and effect of atmospheric seasonal variations on plasma behavior 10 p1645 A67-23266

Model ionosphere with homogeneous isotropic turbulence investigated for values of kinematic viscosity and dissipation rate of turbulent energy determined from rocket measurements 10 p1646 A67-23273

Correlated study of auroral luminosity at different wavelengths, auroral X-rays, geomagnetic micropulsation and ionosphere 12 p1937 A67-25834

Ionospheric structure and micropulsations of geomagnetic field correlated, studying magnetodynamic wave damping and solar activity effects 13 p2114 A67-26856

Matching factor for energy exchange in electromagnetic interaction between ionic and electronic gases in amplitude-amplitude ionospheric intermodulation 13 p2070 A67-27196

Corpuscular emission role in formation of lower ionosphere 13 p2194 A67-27329

Absorption intensity in ionospheric sporadic E layer 14 p2308 A67-27935

Correlation of measurements of precipitated electrons with ionospheric effects of winter anomaly in midlatitude D layer 14 p2310 A67-28043

Spatial HF radio focusing caused by electron distribution between ionospheric layers, even in absence of horizontal density gradients 14 p2261 A67-28048

Automatic measurement of diurnal resonance frequency variations of earth/ionosphere cavity 15 p2489 A67-30071

Diurnal and seasonal variation of ionospheric turbidity 16 p2665 A67-31085

Book on ionospheric chemistry, noting chemical and photochemical reactions above 60 km, and ionization processes 16 p2619 A67-31252

Heating of upper atmosphere electron gas by indirect Joule dissipation of reverse current in ambient electrons demonstrated for high fluxes 16 p2739 A67-31405

Computer method using coefficient linearity along diagonal of matrices to calculate N/h/ profiles of ionosphere 16 p2669 A67-31897

Upper atmosphere ion temperature profile transitional behavior analyzed by fractional separation in terms of energy budget including multiple ion effects 17 p2843 A67-32531

Electromagnetic fluctuation structure associated with resonance properties of earth-ionosphere bounded cavity 17 p2847 A67-32942

Bulgarian research in spectroscopy, solar system, ionosphere, gravitation equations, astrophysics, etc 19 p3320 A67-35283

Space research in West Germany noting ionospheric physics, magnetosphere and solar and cosmic radiation 19 p3321 A67-35293

Synoptical and monitoring projects for solar activity, interplanetary space, magnetosphere, ionosphere, aeronomy, etc 19 p3223 A67-35475

Kinetic theory of ionospheric satellite trail, discussing neutral and charged components from BGK model equation [AIAA PAPER 66-477] 21 p3706 A67-38862

IONOSPHERE ELECTRON DENSITY

Ionospheric observations using Elektron I and III satellites, discussing state of ionosphere, electron concentration variation, etc 22 p3760 A67-39734

IONOSPHERE EXPLORER-A

S EXPLORER XX SATELLITE

IONOSPHERIC ABSORPTION

D region equilibrium solution using absorption measurements, considering region as nonsteady plasma under special conditions 01 p0061 A67-11288

Systematic measurement of ionospheric absorption at vertical incidence made by pulse reflection method at frequencies in range 2-3 mc at Colombo, Ceylon 03 p0406 A67-12822

Continuous flux of solar protons entering earth atmosphere important in energy balance of ionosphere and sun [RASSA PAPER 1-10-140] 03 p0417 A67-14248

Seasonal and solar-cyclic variations of nondeviate absorption in ionospheric D region 04 p0617 A67-15570

Ionospheric absorption variation with solar zenith angle measured with continuous wave recording 04 p0576 A67-15634

Recombination coefficient in D region determined by comparing electron density profile with ionization rate profile 06 p0995 A67-18073

Winter radio absorption anomaly at middle latitudes theory in terms of temperature and nitric oxide distributions in D region 07 p1171 A67-19415

Radio wave absorption at high latitudes dependent on frequency, noting AZA and PCA are inversely proportional to powers of frequency 07 p1144 A67-19693

Vertical measurement of ionospheric absorption at continuously varying frequency, showing diurnal variation of absorption 07 p1174 A67-19706

Sidereal time recorder used with riometer for detection of radio noise absorption in ionosphere 08 p1329 A67-21489

Low ionosphere with suitable selected track for absorption observation as indicator of galactic cosmic rays modulation by solar wind 09 p1561 A67-21844

Ionospheric absorption as indicator of particle flux below point of long radio wave reflection, noting relation to solar cosmic rays 09 p1561 A67-21844

Deflection absorption of radio waves in ionosphere 09 p1491 A67-21845

Seasonal observations of nocturnal ionospheric absorption, noting connection with structural state of sporadic E layer 09 p1491 A67-21930

Virtual heights and absorption of radio waves in ionosphere, discussing methods of computation 09 p1464 A67-22441

Ionization density as decisive factor in integral radio wave absorption increase accompanying increase in critical sporadic E

layer frequency 10 p1631 A67-22807
 Height distributions of enhanced lower ionospheric ionization estimated from cosmic radio noise absorption 10 p1634 A67-23059
 Winter anomaly of nondeviative ionospheric absorption of radio waves and relation to diurnal, seasonal, local and solar cycle variations 10 p1646 A67-23267
 Vertical drift of charged particles effect on electron density profile as cause of seasonal variations in ionospheric absorption 10 p1646 A67-23269
 Ionospheric absorption effects in D and E layers, noting refraction role and effective collision frequency 10 p1646 A67-23270
 Galactic radio noise intensity decrease correlated with decline in solar activity, calculating D and F region 11 p1784 A67-23934
 Ionospheric absorption determination by measuring amplitudes of wave components of satellite transmission 11 p1786 A67-24059
 Ionospheric absorption relationship with frequency, extending lower limiting frequency to 2 MHz 11 p1753 A67-24302
 Solar constant and sunspot relationship interpreted by solar radio flux effect on lower ionosphere density 12 p1932 A67-25342
 Ionospheric radio wave absorption, noting inverse correlation between solar activity with stability of reflections from sporadic E layer 12 p1933 A67-25544
 Position of anomalous radio absorption in ionosphere during various phases of solar activity cycle 12 p1933 A67-25550
 ULF electromagnetic radiations related to magnetic bays and ionospheric phenomena at high latitudes 13 p2110 A67-26455
 Diurnal and annual variation of absorption of short waves in ionosphere 13 p2066 A67-26486
 Solar cosmic ray interaction with earth ionosphere and resultant cosmic radio noise absorption 13 p2194 A67-27254
 Cosmic noise intensity at 25 MHz noting nighttime variation dependence on solar activity 13 p2201 A67-27392
 Riometric data on ionospheric absorption applied to determination of dissociative recombination coefficient, noting atmospheric ionization by fragment gamma-radiation 14 p2306 A67-27858
 Ionospheric structural studies via absorption measurements 14 p2378 A67-27911
 Cyclotron instability range in earth radiation belt analyzed taking into account wave absorption in atmosphere, using measurements of perturbation effects 14 p2378 A67-27916
 Seasonal variations and attenuation of ionospheric absorption, using A3 method 14 p2312 A67-28570
 Vertical incidence ionospheric absorption measurements from ground station criteria for recognizing winter anomaly 15 p2476 A67-29623
 Scattering and absorption of ultrashort coherent radiation pulses passing through electron gas applied to ionosphere 17 p2812 A67-32312
 Properties of slowly varying ionospheric absorption events in auroral zone analyzed using balloon soundings 17 p2845 A67-32794
 Radio wave absorption associated with auroras 18 p3038 A67-33619
 Ionospheric radio-wave absorption measurement by multiple and single echo techniques, applying vertical probing at fixed frequencies 20 p3378 A67-36124
 Ionogram data used to identify high absorption periods, analyzing diurnal variations of critical frequency F-2 layer showing no echo 20 p3432 A67-37275
 Ionospheric pulse absorption study of measurements taken in Bulgaria during solar eclipse of May 1966 21 p3616 A67-37995
 Winter anomaly of ionospheric adsorption studied by field strength recordings 21 p3617 A67-38001
 Absorption of VHF waves in whistler mode at low latitudes calculated for various ionospheric conditions during sunspot activity 21 p3617 A67-38065
 Ionospheric discontinuity dimensions determined from satellite signal findings at 20 and 40 mc correlating amplitudes 21 p3621 A67-39021
 Block diagram and basic circuit for measuring ionospheric radio wave absorption 21 p3586 A67-39044

F-2 layer contribution to vertical radio wave absorption, using information about structure, electron and ion temperatures 22 p3789 A67-39472
 Ionospheric absorption from unabsorbed cosmic radio noise intensity, discussing electron density and collision frequency profiles 23 p3994 A67-40778
 Ionization density as decisive factor in integral radio wave absorption increase accompanying increase in critical sporadic E layer frequency 24 p4150 A67-42144
IONOSPHERIC COMPOSITION
 Ionospheric D-region concentration of neutral NO estimated, based on dissimilarity of sunspot cycle variation 01 p0056 A67-10111
 Incoherent scattering measurements of ionospheric power spectrum and autocorrelation function at geomagnetic equator to determine electron and ion temperatures, ion composition and ion density 03 p0408 A67-12834
 Energy dependence of isotopic composition of primary helium nuclei, considering ionization loss, fragmentation and solar modulation 03 p0505 A67-12956
 Herman and Gibbons conclusions on radiation energy concentration in ionized gas shown to be erroneous 03 p0411 A67-12961
 Anomalous variation in composition of lower ionospheric ion recombination coefficient as function of height, zenith angle and level of solar activity 03 p0411 A67-13346
 Soviet papers on geophysics and astronomy 04 p0650 A67-15218
 Relation between E-2 and F-0 ionospheric layer formation and geomagnetic phenomena 04 p0618 A67-15221
 Book on mass spectrometry principles and application to ion and neutral atom composition of upper atmosphere 04 p0624 A67-15587
 F region effects following two severe magnetic storms, noting changes in electron density profile 06 p0995 A67-17972
 Ionic composition measurements of topside ionosphere from mass spectrometer flown on Explorer XXXI satellite 06 p0996 A67-18646
 Field aligned electron concentration profiles of equatorial anomaly, using parametric description for theoretical results 06 p0997 A67-18697
 Mean ionospheric height measurement from analysis of radio signals from beacon satellite 08 p1328 A67-21479
 Diatomic molecular ion composition and variation of effective recombination coefficient in ionosphere in terms of altitude, time of day, solar activity, temperature, etc 10 p1630 A67-27288
 Hydrogen and He UV glow in night sky as ion and electron source, estimating intensities and ionization rate 10 p1633 A67-22949
 Neutral particle densities of nitrogen, molecular and atomic oxygen and argon in upper atmosphere, noting density profile irregularities, diffusive separation altitude, etc 10 p1639 A67-23213
 Ionosphere as binary two-temperature gas and transfer coefficients for elastic collisions based on Boltzmann equation 10 p1640 A67-23220
 Flowing afterglow reaction device for measuring ionospheric ion-molecule reactions 10 p1644 A67-23259
 Subsonic parachute-borne blunt probes for charged particle measurement in ionosphere 10 p1645 A67-23260
 Electron-ion recombination coefficients for atmospheric ions determined in laboratory and compared with ionospheric analysis 10 p1682 A67-23261
 Measurements of positive ion composition of mesosphere and ionospheric D layer from rocket experiments 10 p1645 A67-23264
 Role of corpuscular radiation in lower ionosphere formation noting charged particle flux, energy spectra, etc 10 p1647 A67-23283
 Neutral wind structure effects on ionospheric sporadic E layer variations, noting daytime evolution, nighttime characteristics and electron density profiles 11 p1783 A67-23924
 Outer ionosphere and transition into interplanetary space noting altitude and structure characteristics 11 p1786 A67-24261
 Ion-acoustic wave excitation by vertical density gradients, noting effect of resulting instability on ionospheric fine

structure 11 p1786 A67-24398
 Soft electrons and ions study by traps on Cosmos V satellite 12 p1994 A67-25529
 Electron and ion concentrations as function of solar radiation intensity and variation of ionospheric conditions, noting nitrous oxide/oxygen ion 12 p1933 A67-25649
 Nighttime topside ionosphere composition, measuring concentrations of H, He and O by mass spectrometry 13 p2108 A67-26310
 Rocket soundings of electron angular distributions during auroral substorms, noting effects of anisotropy, intensity variations, etc 15 p2473 A67-29187
 Surface impedance of cylindrically stratified anisotropic ionosphere in presence of static magnetic field, calculating propagation parameters 16 p2631 A67-31853
 Electron heating in diurnal ionosphere noting electron and ion temperatures as function of altitude 17 p2842 A67-32295
 Nonlocal heating of electrons of daytime ionosphere taking account of displacement along geomagnetic field lines, comparing Dalgarno and Thomson probes 17 p2844 A67-32708
 Continuity equation for electron density in F-2 layer, noting solution for given diffusion, loss, time dependence, etc 17 p2853 A67-33245
 Auroras and airglows in relation to ionospheric phenomena 18 p3033 A67-33584
 Twilight observations for 80-100 km region, noting orthohelium measurements for solar radiation and dust and alkali-metal concentrations for D-region ionic constitution 18 p3035 A67-33601
 Near earth and outer ionosphere plasma waves and oscillations in VLF and ELF bands 19 p3317 A67-34932
 Master matrix containing initial values of geomagnetic inclination and gyrofrequencies for storage in computer memory to calculate ionospheric vertical profiles 21 p3623 A67-39046
 Ionospheric ion-neutral reactions studied by photolionization mass spectrometer, noting temperature independent reactions 22 p3793 A67-40077
 Laboratory measurements of ionospheric ion-molecule reaction rates noting unmeasured reactions in D region 23 p3993 A67-40565
 Diatomic molecular ion composition and variation of effective recombination coefficient in ionosphere in terms of altitude, time of day, solar activity, temperature, etc 24 p4149 A67-42124
IONOSPHERIC CONDUCTIVITY
SA IONIC WAVE
 Changeability laws in quiet solar diurnal magnetic variations in 1964 and relation to state of ionosphere resulting from dynamo effect 05 p0802 A67-17147
 Correction of Fatkullin expressions for LF conductivities of homogeneous plasma in presence of electron-ion collisions in ionosphere 07 p1179 A67-19834
 Charge separation mechanism of auroral electrojets, noting enhanced ionospheric conductivity by electron bombardment 07 p1245 A67-19931
 LF ionospheric measurement of admittances of three orthogonal shock dipoles, noting impedance variation with respect to frequency attitude and voltage 10 p1648 A67-23286
 Height distribution of Sq current intensity in midlatitude ionosphere as function of electrostatic field 11 p1786 A67-24333
 Rocket measurements of equatorial electrojet current 13 p2114 A67-26793
 Ionospheric micropulsations induced by enhanced conductivity of current due to meteors, noting end effect from finite ion trail length 14 p2383 A67-28044
 Ionospheric conductivities, electric currents and field height variations in equatorial electrojet region calculated from model, including solar activity 21 p3617 A67-38066
 Changeability laws in quiet solar diurnal magnetic variations in 1964 and relation to state of ionosphere resulting from dynamo effect 21 p3619 A67-38489
IONOSPHERIC CROSS MODULATION
 Changes in electron concentration in lower ionosphere with temperature dependent effective recombination coefficient during

transmission of pulse radio signals 10 p1630 A67-22791
Solar wind modulation of far daytime field of extra-long radio waves in ionospheric C layer 12 p1933 A67-25549
Changes in electron concentration in lower ionosphere with temperature dependent effective recombination coefficient during transmission of pulse radio signals 24 p4149 A67-42127

IONOSPHERIC CURRENT

SA GEOMAGNETIC CROCHET

Dynamo theory interpretation of magnetospheric-ionospheric electric current system associated with N-S asymmetry of magnetic daily variation at time of equinox 01 p0057 A67-10113
Radar observations of equatorial electrojet irregularities indicate reversal during nighttime of daylight westward traveling electrons stream 03 p0408 A67-12837
Equatorial geomagnetic field fluctuations in frequency range of 4.0 to 0.003 c/s 03 p0408 A67-12842
Trapped particle acceleration by magnetic fluctuation produced by ionospheric currents derived from observations of sharp energy groups of high energy electrons 03 p0409 A67-12942
Vertical profiles of horizontal wind in lower ionosphere treated by spectral energy density estimates 04 p0615 A67-14970
[AFCR-67-0054] Transient variation of ionospheric dynamo current systems obtained from sounding rocket measurements of geomagnetic field activities 05 p0797 A67-16582
Magnetic field observations by rockets and satellites 05 p0798 A67-16870
Kappa rocket sounding of ionospheric Sq-currents, using rubidium vapor magnetometer 05 p0799 A67-16871
Height profile of Sq current in ionosphere, showing dependence on electric field direction 05 p0799 A67-16872
Latitudinal and vertical current components effects included in longitudinal current system supporting steady state distribution in geomagnetic anomaly 06 p0998 A67-18703
Equatorial electrojet relationship with worldwide Sq currents 07 p1171 A67-19417
Magnetic disturbances at midlatitudes, noting origin from locally generated currents 07 p1174 A67-19709
Ionospheric stabilization of interchange mode calculation applied to electron debris of Star Fish event, noting role of ionospheric current 07 p1182 A67-19948
East-West ionospheric wind component measured by CW meteor radar 10 p1644 A67-23253
Potential buildup on electron emitting ionospheric satellite, noting limitation on current emission by geomagnetic field 11 p1869 A67-23941
Height distribution of Sq current intensity in midlatitude ionosphere as function of electrostatic field direction 11 p1786 A67-24333
Visual presentation of geomagnetic displays using normal ionospheric current system with line separation inversely proportional to field perturbation intensity 11 p1788 A67-24699
Rocketborne magnetometer measurements of midlatitude Sq ionospheric currents 12 p1935 A67-25794
Latitudinal cross section of ionospheric current density profile of equatorial electrojet from rocketborne magnetometers 13 p2107 A67-26307
Ionospheric electric current measurement, determining vertical current density distribution and electron number density for geomagnetic field study 13 p2107 A67-26306
Generalization of differential equation of dynamo theory of geomagnetic variations to include unsteady dynamo effect in ionosphere 13 p2110 A67-26548
Rocket measurements of equatorial electrojet current 13 p2114 A67-26793
Observed micropulsation activity during meteor shower compared with predicted magnetic agitation value determined from equation by Chapman and Ashour 14 p2383 A67-28045
Equatorial electrojet width and intensity analyzed with ground level magnetic field measurements from Peru and Nigeria 14 p2312 A67-28572

Electric current associated with polar magnetic substorms 14 p2313 A67-28573
Early appearance of active aurora during geomagnetic storm caused by westward traveling surges along expanded oval 14 p2313 A67-28575
Seasonal variations in position and intensity of equatorial electrojet and correlation of latter with sunspot number 15 p2478 A67-30061
Magnetic variation measurements at Addis Ababa indicate intermittent existence of inverse direction equatorial electrojet 15 p2478 A67-30070
Auroral arc orientations determination and attempt to verify ionospheric currents flow along auroral arc during display 16 p2667 A67-31511
Distribution of auroras during magnetically quiet and disturbed periods related to magnetosphere shape 17 p2849 A67-32965
Static electric fields produced in magnetosphere and effects such as motion of visual and radio aurora and currents in ionosphere 18 p3035 A67-33600
Stratosphere and mesosphere, discussing energetics, energy transfer, ionospheric currents, magnetic fields, atmospheric trace components, solar UV radiation measurements, etc 20 p3430 A67-36897
Diurnal variation investigated by rocket, discussing ionospheric electric currents and magnetosphere-ionosphere electric field 20 p3431 A67-36908
Sudden commencement and initial phase of magnetic storm explained in terms of currents induced in ionosphere 20 p3434 A67-37422
Solar wind geomagnetic field interactions during disturbed conditions, discussing solar particle emissions, solar plasma activity, ring and ionospheric currents 22 p3870 A67-39672
IONOSPHERIC DRIFT
Horizontal drift and anisotropy in F-1 region during geomagnetically active and quiet conditions 01 p0057 A67-10117
Drift velocities change in F layer as function of time explained by movement of reflection point over ionospheric surface 01 p0061 A67-11262
Mitra three-receiver method improvement for measuring winds and diffraction of radioelectric waves in ionosphere 03 p0406 A67-12819
Horizontal drift measurements in E and F regions of ionosphere over magnetic equator in India 03 p0407 A67-12829
Model for ionospheric drift measurements made by spaced receiver method when scattered wave has frequency above plasma frequency of scattering region 03 p0407 A67-12831
Lunar tidal variations in ionosphere in power spectrum analysis from geomagnetic data obtained during IGY 03 p0508 A67-12849
Drift of small scale E and F layer inhomogeneities in Black Sea coastal region 04 p0816 A67-15222
Objection to Martin ionospheric drift theory based on dynamo electric field, atmospheric tidal wind field and F-2 layer drift motion 05 p0796 A67-16063
Diurnal atmospheric oscillations and wind systems producing geomagnetic variations 05 p0798 A67-16859
Emf as cause of vertical downward and upward ionization drift in F region of ionosphere during magnetic storm 05 p0801 A67-17141
Velocity of vertical motion of lower ionosphere determined, using radio spectral analysis 05 p0801 A67-17144
Vertical drift velocity of small scale ionization inhomogeneities in ionosphere, noting seasonal variation 05 p0802 A67-17146
Upper atmospheric rotation speed reevaluated from satellite orbital inclination changes 05 p0803 A67-17412
Ionospheric F layer rise during magnetically quiet night as caused by charge carrier drift induced by electric field 06 p0993 A67-17561
Ten years ionospheric drift measurements in LF range 07 p1171 A67-19420
Ambipolar diffusion theory for describing diffusion of nonuniformities in ionosphere including F region 07 p1230 A67-19717
Plasma-neutral coupling in ionospheric motions having short durations compared with time between neutral particle collisions with ions 08 p1325 A67-21151

Ionospheric drift velocities observed by spaced receiver method compared with neutral winds from luminous rocket trails 10 p1643 A67-23252
Ionospheric inhomogeneity winter drifts during periods of high and low solar activity 14 p2308 A67-27936
Ionospheric aerodynamics, discussing flow field properties, satellite motion, flight characteristics, etc 14 p2242 A67-28200
Ionospheric movement detection using frequency swept sounder and rhombic antenna 15 p2484 A67-30301
[AGARDOGRAPH 95] Magnetoplasma diffusion equation of F-2 layer allowing electric currents and temperature variations, noting transverse drift of field 16 p2666 A67-31402
Frequency shifts on whistler mode signals from stabilized VLF transmitter from ionosphere and magnetosphere effects, noting electron density 16 p2631 A67-31856
Propagation rate distribution as function of geomagnetic latitude provides evidence for geomagnetic effects on vertical ionization drifts in F region of ionization 16 p2668 A67-31894
Drift data harmonic analysis correlation between solar quiet diurnal variation and ionospheric drift 16 p2669 A67-31908
Stream instabilities in magnetolonic plasmas in presence of DC magnetic field, noting possibilities of growing waves 19 p3292 A67-35389
Rate of transequatorial plasma diffusion along geomagnetic field lines in topside ionosphere, considering electron distribution asymmetries in equatorial F-2 layer 20 p3431 A67-37098
EMF as cause of vertical downward and upward ionization drift in F region of ionosphere during magnetic storm 21 p3619 A67-38483
Velocity of vertical motion of lower ionosphere determined, using radio spectral analysis 21 p3619 A67-38486
Vertical drift velocity of small scale ionization inhomogeneities in ionosphere, noting seasonal variation 21 p3619 A67-38488
Lower ionospheric drift studied from signal recordings from distant medium wave broadcasting stations 22 p3788 A67-39467
IONOSPHERIC ELECTRON DENSITY
International Satellites for Ionospheric Studies /ISIS/ program using radio sounders 01 p0057 A67-10293
Ionospheric electron density measurement by gyro plasma impedance probe 01 p0064 A67-10566
Radio wave reflection from ionosphere with perturbed electron density profile 02 p0192 A67-11618
Radio wave scattering and resonance scattering in wake of body moving in lower ionosphere plasma due to disturbance of electron concentration 02 p0192 A67-11657
External ionosphere electron concentration measurement from data on Doppler shift variations in frequency of coherent radio signals from Cosmos and Elektron satellite 02 p0192 A67-11658
Lunar tide effects on ionospheric characteristics near magnetic equator, noting fluctuations in electron concentration 02 p0237 A67-11673
Beacon satellite measurement of Faraday rotation and diurnal and seasonal variations of total electron content of ionosphere near Nairobi 03 p0406 A67-12825
Equatorial ionospheric storms, analyzing sub-peak and total columnar electron content 03 p0408 A67-12841
Oblique echo presence during winter nights on auroral and subauroral latitudes ionograms, analyzing electron number density of nighttime F region in midlatitude trough vicinity 03 p0409 A67-12947
Ionospheric electron density profile determined by local measurements of VLF fields radiated by ground emitter 03 p0413 A67-13531
Automatic recording equipment measuring polarization angle of Syncom III 137 mc/s radio signal and determination of ionospheric total electron content 03 p0415 A67-14110
Noon electron density variation of F-2 layer at low latitudes and associated transport processes, using modified least squares method 03 p0415 A67-14111
Electron density profiles of Nike-Apache

rocket observations of nitric oxide ionization by Lyman alpha radiation in E region at sunrise 03 p0415 A67-14114

Explorer XXII satellite measurement of total electron content from Faraday rotation recordings, noting correlation with solar activity above 80 solar flux units [RASSA PAPER 1-10-124] 03 p0416 A67-14235

Total electron content distribution over Europe in terms of geomagnetic activity, noting occurrence of scintillations [RASSA PAPER 1-10-125] 03 p0416 A67-14236

Latitudinal and diurnal variation of ionospheric electron content in auroral zone proximity [RASSA PAPER 1-10-126] 03 p0416 A67-14237

Explorer XXII satellite measurement of total electron content from observations of Faraday effect [RASSA PAPER 1-10-128] 03 p0372 A67-14239

Syncom III satellite measurement of time variation of total ionospheric electron content [RASSA PAPER 1-10-129] 03 p0417 A67-14240

Early Bird satellite measurement of ionospheric electron content by determining polarization twist of VHF radio signals [RASSA PAPER 1-10-130] 03 p0417 A67-14241

Early Bird satellite measurement of ionospheric electron content obtained from Faraday rotation data [RASSA PAPER 1-10-131] 03 p0417 A67-14242

Topside ionosphere over American continents, noting electron density and scale height distribution [RASSA PAPER 1-10-132] 03 p0417 A67-14243

Electron cloud-like distribution in ionosphere shown from phase measurements of 162 and 324 mc emissions of Transit and Anna satellites [RASSA PAPER 1-10-135] 03 p0417 A67-14246

Power spectrum of electromagnetic wave incoherently diffused by ionospheric electrons 04 p0571 A67-14896

Charged particle redistribution due to rockets and satellites flying in ionosphere influence on electromagnetic propagation in region of body and interpretation of Langmuir probe 04 p0664 A67-14990

E-2 and F-0 intermediate ionospheric layer morphology, occurrence, electron density and signal reflection 04 p0616 A67-15220

Ionospheric stratification and electron density distribution in F-1 layer by Serafimov method 04 p0618 A67-15572

Sunrise effect on atmospheric radio noise intensity, directional variations and formation of D region 04 p0618 A67-15575

Ionospheric irregularities explained by gravitational field and positive electron density gradient joint effect on ionospheric region below electron distribution peak 05 p0760 A67-16002

High altitude vertical photoelectron distribution from electron concentration measurements by Cosmos V and IMP I and II 05 p0795 A67-16061

Differential Doppler measurements of satellite radio emissions for obtaining ionospheric electron content 05 p0764 A67-16930

IGY and IQSY data on maximum electron density variation in F-2 layer 05 p0800 A67-17126

Daytime profile of electron density in C and D layers of ionosphere from measurements of surface ultralong wave fields and atmospheric pressure 05 p0801 A67-17131

Geomagnetic activity effect on electron concentration at heights of 100 and 110 km 05 p0801 A67-17143

Ionospheric electron density profiles determined by impedance probe and Doppler effect probe aboard 06 p0993 A67-17595

Loss coefficient and vertical transport velocity for nighttime F region during solar activity 06 p0995 A67-17971

Recombination coefficient in D region determined by comparing electron density profile with ionization rate 06 p0995 A67-18073

Meteoritic dust particle effect on steady state distribution of electrons and ions in lower ionosphere, deriving expression for recombination coefficient from auroral radio absorption data 06 p0995 A67-18074

Field aligned electron concentration profiles of equatorial anomaly, using

parametric description for theoretical results 06 p0997 A67-18697

Conjugate ducting observation via fixed frequency topside-sounder satellite, estimating electron concentration difference 06 p0997 A67-18699

Diurnal and seasonal altitude variations of E and F layers analyzed for geomagnetic activity from rocket measurement of electron concentration 07 p1173 A67-19688

Electron density variation, solar activity and geomagnetic storm effects on ionospheric F-region theory 07 p1177 A67-19785

Cyclic variations in maximum electron concentration of F-2 layer with solar activity explained by upper atmosphere temperature variations 07 p1178 A67-19818

Dependence of electron concentration in F-1 layer on zenith angle of sun 07 p1178 A67-19820

Electron-concentration distribution in ionospheric F-2 layer with vertical distribution of electron-ion gas 07 p1178 A67-19821

Relation between solar radiation and electron concentration up to F layer analyzed in winter and summer 07 p1179 A67-19831

Formation mechanism of ionospheric narrow sporadic E layers by high energy electron fluxes captured by geomagnetic field 07 p1179 A67-19835

Electron temperature and concentration at 1000 km altitude, obtaining resolution of two full diurnal cycles of ionospheric behavior 07 p1181 A67-19935

High latitude increase in ionization of F layer correlating in space and time with auroral precipitation as shown by ionospheric electron number density data 08 p1328 A67-21481

Rocket measurement of quiet D-region electron number density profiles near sunrise 08 p1379 A67-21488

Electron concentration in ionosphere by coherent frequency method, examining Cosmos XI and Elektron I satellite measurement errors 09 p1491 A67-21893

Corpuscular streams and photodetachment of electrons reaction effect on formation of D layer of ionosphere 09 p1491 A67-21894

Changes in electron concentration in lower ionosphere with temperature dependent effective recombination coefficient during transmission of pulse radio signals 10 p1630 A67-22791

Hydrogen and He UV glow in night sky as ion and electron source, estimating intensities and ionization rate 10 p1633 A67-22949

Total electron content calculated by measurement of Faraday and Doppler effects of satellites 10 p1604 A67-22987

Ionospheric electron content calculated from beacon satellite data on Faraday rotation 10 p1641 A67-23235

Satellite measurement of ionospheric electron density, determining Faraday null times 10 p1641 A67-23236

Ionospheric electron density perturbation with horizontal movement studied by satellite and rocket 10 p1643 A67-23251

Wind shears and ionospheric electron densities measured by vapor trail method and rocketborne Langmuir probe respectively during twilight and night 10 p1644 A67-23256

Possible major effect of minor neutral constituents of mesosphere on free electron density in D layer 10 p1645 A67-23265

Seasonal and annual variations of electron density in ionospheric F layer interpreted as changes in production rate and ionization loss caused by atmospheric composition variations from neutral atmosphere 10 p1647 A67-23274

Ionospheric probes for measuring electron density in E region through detection of plasma resonances 10 p1658 A67-23285

Upper ionospheric electron density measurement by signals propagated between two parts of high altitude rocket 10 p1648 A67-23287

Ionospheric thin layer stratifications and valley region analyzed by integrating propagation method and by impedance probe 10 p1648 A67-23290

Ionospheric electron density measurement by gyroplasma probe, using sweep frequency impedance technique 10 p1648 A67-23291

Approximate method for diurnal variation of peak electron density in F-2 layer, estimating effect of time varying drifts 10 p1650 A67-23336

Geomagnetic and solar control of ionization at 1000 km determined from electron density data obtained from Alouette satellite 10 p1650 A67-23339

F layer changes during solar eclipse observed at equatorial station, obtaining values for effective electron loss coefficients 10 p1651 A67-23340

Diurnal and seasonal variation of total columnar ionospheric electron content at magnetic equator analyzed, using Faraday rotation technique 10 p1651 A67-23341

Electron density variation from photochemical rates in equatorial F layer during October 1959 solar eclipse 10 p1651 A67-23342

Seasonal variations in ionospheric total electron content measured by observing Faraday rotation of linearly polarized wave from geostationary satellite Syncom III 10 p1651 A67-23346

Ionospheric electron density profile measurement via radio wave interaction technique, noting superiority of partial reflection method 11 p1785 A67-23946

Ionospheric electron density distribution investigated by ground reception of satellite signals from Elektron I 11 p1788 A67-24073

Computer method study of reflection and transmission coefficients in VLF range, noting effect of ionospheric D region electron density profiles 11 p1752 A67-24219

Ionosphere rocket sounding for positive ion density, electron density and electron temperature, noting sunspot effect 11 p1787 A67-24643

Lunar influence on total electron content of winter ionosphere at minimum solar activity 11 p1788 A67-24771

Local electron concentration determination by dispersion method and satellite proved unreliable because of horizontal ionization gradient and ionospheric instability 12 p1932 A67-25539

Seasonal variations of total electron content of ionosphere during sunspot minimum 12 p1935 A67-25795

Ionospheric electron content measured using passage of transit IVA radio beacon satellite across view field of observing station 12 p1935 A67-25797

Rocket observations of lowest ionosphere at sunrise and sunset 12 p1935 A67-25798

Altitude-time distribution of electron concentration of outer ionosphere measured by coherent signals from Elektron I satellite 12 p1936 A67-25799

Inhomogeneous formations and disturbances of electron concentrations in outer ionosphere indicated by Doppler shift differences measured by Elektron I satellite 12 p1936 A67-25800

Nighttime ionosphere maintained by downward flux of electrons from protonosphere as shown by columnar electron contents measurements, noting decay rate 13 p2107 A67-26305

Temperature of F region deduced from electron number density profiles 13 p2108 A67-26322

Ionospheric fine structure, considering excitation of ion-acoustic waves by vertical gradients of density 13 p2109 A67-26329

Doppler frequency shift for radio waves radiating coherently from satellite in ionosphere, considering electron concentration and angles of refraction 13 p2067 A67-26568

Chemical recombination parameters in F layer of day ionosphere determined from electron density profiles 13 p2115 A67-27211

Measurement of total number of electrons in ionosphere, horizontal gradients, equivalent height and vertical profile from recorded Elektron satellite signals 14 p2307 A67-27922

Model thermospheres, studying ducted traveling acoustic gravity waves originating in ionosphere 14 p2310 A67-28054

Collision frequencies in D region and stratospheric-mesospheric relations, noting oxygen as error source and electron-density height profile 14 p2311 A67-28407

F region phenomena, discussing charged particles dynamics, equatorial and seasonal anomalies and nighttime F layer maintenance, using Alouette I

data 14 p2312 A67-28409
Total electron content calculation by measuring Faraday and Doppler effects of satellites on reception 14 p2270 A67-28607
Electron density perturbations caused by descending rocket in ionosphere studied by radio pulse signals 14 p2313 A67-28622
Omicron I satellite measurements of total ionospheric electron content, comparing values at Houghton, Michigan, with others for different latitudes 15 p2474 A67-29193
Night F layer behavior, considering height and electron density, noting computer program for nonsteady state continuity equation with neutral gas movement 15 p2474 A67-29523
Global response of topside ionosphere to magnetic disturbances at solar minimum studied from electron concentration measurements at 640 km 15 p2475 A67-29610
Ionospheric electron content variation across sunrise and sunset lines deduced from radio-beacon satellite transmissions 15 p2476 A67-29624
Mean variations of total electron density with latitude and local time during winter obtained from dispersive Doppler investigations 15 p2477 A67-29666
Ionospheric electron content obtained as function of longitude and latitude, using satellite measurements of Faraday rotation 15 p2478 A67-29923
Nuclear explosion effects on atmospheric pressure, electron density, and F-2 layer height, noting dependence on time, season, etc 15 p2478 A67-30067
Range of undistorted propagation of traveling disturbances, noting shape of altitude-frequency characteristics of ionosphere with parabolic electron density distribution 15 p2479 A67-30074
Equipment used in rocketborne LF propagation experiment to measure electron distribution in D region of ionosphere 15 p2489 A67-30136
Observation methods, mechanisms, geomorphology, time variations and associated effects of equatorial type spread-F [AGARDOGRAPH 95] 15 p2480 A67-30274
Time and space study of onset and early development of single occurrence of spread-F in equatorial region [AGARDOGRAPH 95] 15 p2480 A67-30275
Large-scale structure of F layer studied by observing Faraday rotation of satellite signals, noting irregularities in total electron content 15 p2483 A67-30295
Ionospheric electron density profiles obtained by dispersive Doppler from beacons on research rockets, noting inhomogeneities [AGARDOGRAPH 95] 15 p2483 A67-30296
Intense fluctuations observed above Arecibo during geomagnetically disturbed conditions, using ionospheric backscatter technique 15 p2483 A67-30299
Diurnal temperature change effect on F-2 layer, noting maximum electron density height dependence on neutral-gas temperature variations 16 p2663 A67-30967
Radio wave scattering and resonance scattering in wake of body moving in lower ionosphere plasma due to disturbance of electron concentration 16 p2624 A67-31072
External ionosphere electron concentration measurement from data on Doppler shift variations in frequency of coherent radio signals from Cosmos and Elektron satellite 16 p2624 A67-31073
Lunar tide effects on ionospheric characteristics near magnetic equator, noting fluctuations in electron concentration 16 p2665 A67-31088
Ionospheric electron content as function of longitude and latitude calculated from Faraday fading of radio waves 16 p2627 A67-31362
Differential Doppler effect on earth satellite radio signal and application to ionospheric electron density studies 16 p2627 A67-31463
F-region electron-density perturbations transmitted to magnetically conjugate region, noting electrostatic coupling mechanism 16 p2667 A67-31509
Frequency shifts on whistler mode signals from stabilized VLF transmitter from ionosphere and magnetosphere effects, noting electron density 16 p2631 A67-31856
Strength of radio signals incoherently

scattered from ionosphere and distribution of ionospheric electron concentration 16 p2632 A67-31901
Photochemical analysis of diurnal variations of electron concentration and temperature of upper ionosphere 16 p2669 A67-31902
Altitude of lower boundary of ionosphere determined by electron density profile, considering absorption coefficient and magnetoionic signal 16 p2669 A67-31906
Solar flare effect on electron production and electron density in lower ionosphere 17 p2936 A67-32382
Seasonal variations in afternoon and evening maxima of F-2 layer and dependence of temperature and frequency on minimum zenith angle of sun 17 p2842 A67-32384
F region and magnetosphere data obtained by incoherent-backscatter radar technique, studying ion and electron temperatures relationship to height, electron density profiles, etc 17 p2843 A67-32389
Diurnal and seasonal variation of electron content and diurnal variation of slab thickness investigated, emphasizing relation between electron content and scintillation occurrence 17 p2850 A67-33190
Continuity equation for electron density in F-2 layer, noting solution for given diffusion, loss, time dependence, etc 17 p2853 A67-33245
Grid electrostatic probe for ionospheric measurement of electron density and temperature, examining measurement errors due to environmental disturbances 18 p3048 A67-34225
Ionosphere collision frequencies and densities studied by rocket measurements of magnetic field of VLF wave radiated from ground 18 p3041 A67-34233
Polar ionosphere by satellite-borne electron traps, measuring electron density, temperature, quasi-energetic electron flux, etc 19 p3215 A67-35174
Rocket observation of ionospheric electron density using VLF doppler shift formula, determining wave polarization 19 p3215 A67-35180
Electron density measurement in ionosphere-magnetosphere transition region using rocketborne gyroplasma swept frequency probe, discussing electron density profile and plasma medium 19 p3229 A67-35201
Ionospheric electron density profile microstructure studied by rocketborne gyroplasma probe discovering electron density irregularities 19 p3217 A67-35202
Electron density and temperature, solar UV radiation and upper atmosphere neutral components measured using rockets 19 p3218 A67-35215
Upper ionospheric electron density profile variation with sunspot number controlled by temperature and ion composition as shown from rocket data 19 p3218 A67-35222
Day-and nighttime electron density profiles in ionospheric D layer 19 p3218 A67-35227
Ionospheric ion and electron densities and temperatures from rocket probes near geomagnetic equator 19 p3219 A67-35232
Lower ionosphere electron density distribution estimated through impact ionization and photoionization 19 p3221 A67-35433
Rocket and balloon studies of solar radiation, wind characteristics, equatorial electrojet and lower ionosphere electron density 19 p3223 A67-35474
Changes in topside ionosphere during large magnetic storm, studying electron density, slab thickness, scale height, etc 20 p3427 A67-36305
E and F region electron density and temperature measurements, using electrostatic probe and MOS electrometer 20 p3441 A67-36383
Langmuir probe for electron density and temperature measurements in lower ionosphere 20 p3444 A67-36526
Rate of transequatorial plasma diffusion along geomagnetic field lines in topside ionosphere, considering electron distribution asymmetries in equatorial F-2 layer 20 p3431 A67-37098
Electron content measured using satellite motion and position effects on Faraday

rotation 20 p3431 A67-37102
Scattered radio signals received during solar eclipse examined for indication of electron clouds masked by daytime high electron density 20 p3432 A67-37208
High altitude vertical photoelectron distribution from electron concentration measurements by Cosmos V and IMP I and II 21 p3615 A67-37848
Ionosphere thermal nonequilibrium during sunspot minimum noting electron density and temperature measurements and daily variations 21 p3616 A67-37999
Ionospheric ion and electron densities by Langmuir probes, stressing solid state logarithmic amplifier for spatial electrometry 21 p3592 A67-38223
IGY and IQSY data on maximum electron density variation in F-2 layer 21 p3618 A67-38469
Daytime profile of electron density in C and D layers of ionosphere from measurements of surface ultralong wave fields and atmospheric pressure profile 21 p3619 A67-38474
Geomagnetic activity effect on electron concentration at heights of 100 and 110 km 21 p3619 A67-38485
Seasonal and diurnal variations of trough and ionospheric electron content and slab thickness, using S-66 satellite observation 21 p3789 A67-39471
Nighttime E region electron concentration profile valley structure variations for quiet and disturbed geomagnetic activity 22 p3791 A67-39814
Ionospheric plasma electron density profile and plasma resonance effects at base of magnetosphere measured by rocketborne gyro-plasma probe 22 p3793 A67-40043
Radar-derived results for midlatitude F-region densities and temperatures at sunspot minimum noting seasonal anomalies 22 p3793 A67-40080
Star Fish high altitude nuclear explosion effect on electron loss rate in F-2 region 22 p3793 A67-40082
Explorer XXII coherent frequency phase difference data for polar ionospheric integral electron density, discussing diurnal and seasonal variation 22 p3794 A67-40121
Characteristics of geomagnetic crotches associated with proton flares, determining recombination coefficients and electron densities 23 p4050 A67-40671
Diurnal, latitudinal and seasonal variations of midlatitude topside ionosphere electron density profiles and plasma scale heights calculated from Alouette I ionograms 23 p3994 A67-40775
Explorer XXII amplitude recordings, analyzing duration, strength and frequency of ionospheric electron density horizontal gradients 23 p3974 A67-41177
Rocket measurements with HF impedance probe for ionospheric electron density, discussing plasma gyro resonance frequency factors 23 p4003 A67-41321
Ionospheric electron temperature and electron and ion density profiles from Japanese sounding rocket 23 p3997 A67-41478
Ionospheric electron distribution observed and computed values discrepancy analyzed, noting diurnal variation role 24 p4146 A67-41785
Ionospheric electron content and OI nightglow in Hawaii, discussing ionization density increases throughout bottomside F layer 24 p4147 A67-41878
Electron scale heights from topside ionograms studied for radiation effects during quiet and disturbed conditions, noting relation to ionospheric plasma temperature 24 p4147 A67-42055
Electron concentration from topside ionograms for heights below satellite 24 p4147 A67-42056
Ionospheric composition and temperature for South Atlantic latitudes from scale height values obtained by Alouette I satellite 24 p4147 A67-42057
Storm behavior of topside ionosphere studied from electron concentration satellite data, discussing height and latitude effects 24 p4148 A67-42058
Solar eclipse effects on topside ionosphere electron concentration, noting decrease for magnetic quiet conditions 24 p4148 A67-42059
Electron-resonance spikes on Alouette I ionograms observed for proton gyro-effects in topside ionosphere 24 p4148 A67-42062

- Electron content of topside ionosphere studied for equatorial anomaly during diurnal variations 24 p4148 A67-42063
- Diurnal variations of electron concentration in topside ionosphere studied at low and middle latitudes using satellite data, noting secondary nighttime maximum 24 p4148 A67-42064
- Changes in electron concentration in lower ionosphere with temperature dependent effective recombination coefficient during transmission of pulse radio signals 24 p4149 A67-42127
- Ionospheric observation using Japanese sounding rocket, discussing electron density profile, ion density and electron temperature measurements 24 p4150 A67-42151
- E layer critical frequency calculation for 30 selected diurnal variations, considering forenoon anomaly effect 24 p4151 A67-42704
- IONOSPHERIC F-SCATTER**
- Experimental aperture-to-medium coupling loss between one and two large antennas 02 p0213 A67-11620
- Fluctuations in diurnal variations of ionization of F-2 layer interfering with radio wave propagation determined by series expansion 07 p1173 A67-19687
- Geophysical rocket determination of aerosol scattering coefficient variation from brightness values at 70-450 km heights 10 p1641 A67-23240
- Radar/backscatter/ cross section of wakes of vehicles in ionosphere, showing creation of mild electron depletion under broadside incidence conditions 14 p2261 A67-28125
- F region and magnetosphere observation by incoherent backscatter radar technique 14 p2265 A67-28410
- Observation methods, mechanisms, geomorphology, time variations and associated effects of equatorial type spread-F [AGARDOGRAPH 95] 15 p2480 A67-30274
- Field-aligned irregularities caused by low energy charged particles penetrating to F layer heights [AGARDOGRAPH 95] 15 p2484 A67-30304
- Autocorrelation function of signal scattered incoherently from ionosphere, observing resonance at multiples of proton gyroperiod 21 p3578 A67-37758
- IONOSPHERIC HEATING**
- Ionospheric heating by Joule dissipation of main-phase ring current associated with asymmetry 07 p1181 A67-19934
- Electron temperature and density in F region analyzed for nighttime heating, using Langmuir probe measurements 08 p1327 A67-21364
- Protonosphere heating by photoelectrons escaping from F region, estimating protonosphere opacity and daytime escape flux 19 p3221 A67-35280
- Electric field heating of D-region electrons shown to be inadequate to raise temperature above gas temperature [AFCRL-67-0121] 24 p4148 A67-41808
- IONOSPHERIC ION DENSITY**
- Magnetospheric plasma motion in terms of hydromagnetic wave theory, noting effect of variations of geomagnetic field and ionospheric plasma density [AFCRL-66-803] 01 p0145 A67-11263
- Monograph on rocket experiments for studies of D region ion concentration and emission from released chemicals in twilight and aurora 03 p0412 A67-13366
- Ion concentration in D region, describing wind tunnel experiments to determine electrode configuration for Gerdien condenser rocket probe 03 p0412 A67-13367
- Diurnal variations of ionospheric ion composition over Arecibo at various altitudes for solar minimum winter and summer conditions 04 p0614 A67-14955
- Moving and stationary fluid type facilities to simulate aerodynamics of charged particles in ionosphere 04 p0595 A67-14991
- Outer ionospheric structure and transition into interplanetary medium 05 p0886 A67-16012
- Ionospheric charged particle density measurements during IQSY by sounding rocket 05 p0798 A67-16860
- Critical frequencies of F-2 and E layers in ionosphere relation to total daily influx of solar wave radiation into earth atmosphere 05 p0800 A67-17128
- Temporal variations in values of variability characteristic of parameters of ionosphere cross sections below principal maximum 05 p0801 A67-17142
- Positive ion layers in E region explained by wind shear theory, obtaining steady state solutions for simple model 08 p1326 A67-21359
- Energy balance equations including effects of heating by electron gas, cooling and energy coupling obtained for various ion species, assuming each ion gas has Maxwellian velocity distribution 08 p1326 A67-21363
- Ion temperatures in topside ionosphere from spectroradiometry 08 p1327 A67-21371
- Ionospheric rocket sounding, measuring ion density and electron temperature between E and F layers 10 p1633 A67-22948
- High incidence and erraticism of sporadic E occurrence in temperate zones where horizontal component of geomagnetic field is greatest attributed to horizontal wind shear 10 p1644 A67-23255
- Ion composition and effective recombination coefficient variation of ionosphere in study of X and UV radiation ionization of E layer 10 p1647 A67-23280
- Nike-Cajun rocket investigation of equatorial D and E region parameters and effect on electrojet 10 p1648 A67-23288
- Atomic ions of meteoric origin indicated as source of midlatitude E region in IQSY rocket measurement 10 p1648 A67-23289
- Aerobee rocket sounding of ionospheric sporadic E layer, noting abundance of metallic ions in layer and NO above and below 11 p1784 A67-23926
- Negative ions in night ionosphere, discussing sub-ELF emission and excitation of ion acoustic oscillations in plasma by electron drifts 11 p1784 A67-23933
- Diurnally oscillating component of thermospheric east-west pressure acceleration at equator, noting balancing effect of viscous diffusion, ion distribution, etc 11 p1785 A67-23939
- Ionosphere rocket sounding for positive ion density, electron density and electron temperature, noting sunspot effect 11 p1787 A67-24643
- Electron and ion concentrations as function of solar radiation intensity and variation of ionospheric conditions, noting nitrous oxide/oxygen ion ratio 12 p1933 A67-25649
- Unstable diurnal and seasonal variation of ionization of F region of ionosphere during years of minimum solar activity over Ashkhabad 12 p1938 A67-26100
- Minimum effective heights of ionospheric layers in continuous recording for study of ionization and disturbance 13 p2119 A67-26562
- Ionization transport from equator along magnetic lines of force may contribute to formation of diurnal ionization anomaly of F region in intermediate zone 13 p2117 A67-27708
- Lower E-region positive ion concentrations measured at time of declining solar activity by rocket installed mass spectrometer 14 p2310 A67-28049
- Nuclear explosion effects on radio propagation, noting new ionization in ionosphere and radio signals generation 14 p2266 A67-28417
- Negative ion density and composition in lower ionosphere 16 p2665 A67-31019
- Nighttime profiles calculated with allowance for ionization beyond lower bound of frequency range of ionospheric station 16 p2689 A67-31896
- Day-and nighttime electron and ion density profiles in lower ionosphere deduced from blunt probe theory and measurements 19 p3218 A67-35213
- Ionospheric ion and electron densities and temperatures from rocket probes near geomagnetic equator 19 p3219 A67-35232
- Ion layer formation in E region, assuming sinusoidal vertical motions and ion-electron recombination following attachment law 19 p3222 A67-35456
- Thermal diffusion in topside ionosphere, stressing effect on ion density profiles 20 p3427 A67-36304
- Ionosphere information via rocket and satellite measurements covering ion temperatures and concentration, electron content variation, etc 20 p3430 A67-36907
- Outer ionospheric structure and transition into interplanetary medium 20 p3530 A67-37589
- Ionospheric ion and electron densities by Langmuir probes, stressing solid state logarithmic amplifier for spatial electrometry 21 p3592 A67-38223
- Critical frequencies of F-2 and E layers in ionosphere relation to total daily influx of solar wave radiation into earth atmosphere 21 p3618 A67-38471
- Temporal variations in values of variability characteristic of parameters of ionosphere cross sections below principal maximum 21 p3619 A67-38484
- Ionospheric positive ion density as function of altitude measured by Langmuir probe 21 p3629 A67-38662
- Latitude variation of critical frequency of F-2 layer in equatorial region during geomagnetic disturbance, discussing ionization density 21 p3622 A67-39036
- Ion formation rate in F-2 layer under nocturnal ionospheric conditions, determining electron densities 21 p3623 A67-39037
- Particle and energy continuity equations derived and solved by computer method ion composition and plasma temperature measured by Explorer XXII particle and energy continuity equations derived and solved by computer method for ion composition 22 p3790 A67-39804
- D-region mobility and constituents abundance spectrometer device based on continuum concepts 22 p3799 A67-39816
- Charged particle/ion/ collection rates using supersonic atmospheric sounding rocket with electrode at stagnation point, noting electric field effect 22 p3791 A67-39818
- Sporadic E blanketing frequencies during November 1965 as indicator of wind structure in lower ionosphere and meteor influx 23 p3995 A67-40806
- Ionospheric electron temperature and electron and ion density profiles from Japanese sounding rocket 23 p3997 A67-41478
- Ionospheric composition and temperature for South Atlantic latitudes from scale height values obtained by Alouette I satellite 24 p4147 A67-42057
- Ionospheric observation using Japanese sounding rocket, discussing electron density profile, ion density and electron temperature measurements 24 p4150 A67-42151
- IONOSPHERIC IRREGULARITY**
- SA SUDDEN IONOSPHERIC DISTURBANCE /SID/**
- Auroral region disturbances generating atmospheric waves in F layer that produce atmospheric mixing 01 p0056 A67-10112
- Radio communications disruptions during magnetolonic disturbances in ionosphere at high latitudes during decreasing solar activity 02 p0193 A67-11660
- Ionospheric F-2 layer inhomogeneities attributed to plasma flute instability, using kinetic drift equations to describe plasma oscillations 02 p0236 A67-11669
- Contribution of regular and irregular components to ionospheric instability 02 p0237 A67-11671
- Properties of equatorial sporadic E layer irregularities studied by HF observation, including scattering spectrum and diffraction pattern formed by reflection from ground 03 p0406 A67-12823
- F region ionization equatorial anomaly during two periods of minimum sunspot activity in 1965 03 p0407 A67-12827
- Nighttime F layer irregularities at equator responsible for scintillation of signals from radio sources and satellites 03 p0407 A67-12828
- Ionospheric studies using tracking beacon on Early Bird synchronous satellite, noting scintillations due to irregularities 03 p0407 A67-12832
- Spaced antenna technique for determining drift and anisotropy of equatorial E and F region irregularities 03 p0407 A67-12833
- Anomalous variation in composition of lower ionospheric ion recombination coefficient as function of height, zenith angle and level of solar activity 03 p0411 A67-13346
- Statistical analysis of auroral radar echoes reveals changes in shape of diurnal variation curve with level of magnetic disturbance and seasonal variation with peaks at equinoxes 03 p0513 A67-14112

Radio star and satellite scintillations, discussing wave propagation through random media, interplanetary scintillations and ionospheric irregularities [RASSA PAPER 1-10-133] 03 p0372 A67-14244

Jovian decametric pulses compared with satellite and radio star scintillations in terrestrial ionosphere [RASSA PAPER 1-10-134] 03 p0373 A67-14245

Transhorizon propagation modes from signals transmitted by orbiting radio beacon ionospheric satellite /ORBIT/, showing paths sustained by ionospheric ducts or usual hop modes [RASSA PAPER 1-10-146] 03 p0373 A67-14253

Sunset peak in occurrence of F layer field-aligned echoes explained by Martyn amplification mechanism, estimating ionization vertical velocities from electron number density 04 p0615 A67-14959

Drift of small scale E and F layer inhomogeneities in Black Sea coastal region 04 p0616 A67-15222

Ionospheric irregularities explained by gravitational field and positive electron density gradient joint effect on ionospheric region below electron distribution peak 05 p0760 A67-16002

Fast regular scintillation of VHF signals received from earth satellites distinguished from scintillation associated with irregular ionospheric diffracting phase screen, showing correlation with sporadic E layer 07 p1141 A67-19416

Recombination rate increase in F region following magnetic activity due to passage of atmospheric wave 07 p1171 A67-19418

Relation between magnetic activity and ionospheric disturbances in F-2 layer studied on basis of 30-year data 07 p1173 A67-19702

Statistical distribution of monthly median noon critical frequency of F-2 layer from ionospheric stations at mid-latitudes, auroral regions and at polar cap 07 p1174 A67-19703

Electron concentration inhomogeneities during traveling gravity wave propagation through F layer 07 p1178 A67-19809

Electron precipitation from outer radiation belt as cause of ionospheric disturbances, noting relation to time 07 p1245 A67-19928

Ionospheric disturbances from high altitude nuclear detonations observed as changes in F-2 layer critical frequency 07 p1181 A67-19939

Vertical incidence CW Doppler phase path sounder spectral analysis of ionospheric motions and irregularities due to atmospheric wave propagation into ionosphere from below 07 p1182 A67-19952

Calculation of time behavior of forenoon anomaly in diurnal variations of critical frequency of normal E layer 07 p1183 A67-20118

Irregular refraction of radio waves caused by large scale electronic inhomogeneities in ionosphere 08 p1326 A67-21352

Motion equations for ionized irregularity of finite length applied to barium ion cloud, deriving expression for ionospheric electric field 08 p1326 A67-21357

Normality of SD variation at dip-equatorial stations suggests origin beyond F layer 08 p1327 A67-21373

Spectrum of echoes from irregularities in equatorial electrojet at oblique incidence 08 p1328 A67-21465

Auroral oval properties from magnetic data, role in connecting visible auroras and related ionospheric disturbances to geophysical phenomena at high altitudes 09 p1492 A67-22060

Auroral zone irregularity correlated with perturbations in outer radiation belt, noting simultaneous displacement of boundary zone of perturbations 10 p1699 A67-22784

Maximum usable frequency for single discontinuity radio line calculated taking horizontal ionization gradients into account 10 p1604 A67-22794

Bispectral analysis of electromagnetic wave diffraction by ionosphere, obtaining information on altitude and scale of irregularities 10 p1604 A67-22888

Intense diurnal activity in sporadic E layer interpreted as effect of Omicron-Cetid meteoric stream 10 p1633 A67-22896

Latitudinal variations of ionospheric irregularities studied via synchronous and 1000 km satellites, noting Early Bird data, scintillation index graphs, radio star signals, etc 10 p1640 A67-23234

Ionospheric electron density perturbation with horizontal movement studied by satellite and rocket 10 p1643 A67-23251

Anisotropy of coarse ionospheric inhomogeneities determined from measurements of irregular radioastronomic refraction 11 p1787 A67-24464

Irregular refraction of radio waves by large ionospheric inhomogeneities elongated close to meridional direction 11 p1787 A67-24477

Nature of middle latitude ionospheric perturbations 12 p1932 A67-25543

Solar activity dependence of sporadic E layer, noting cyclic variation in characteristics from 1957 to 1964 12 p1933 A67-25545

Polar orbiting satellite measurements correlating ionospheric irregularities with trapped and precipitated energetic particles in South American anomaly region 12 p1996 A67-25776

Inhomogeneous formations and disturbances of electron concentrations in outer ionosphere indicated by Doppler shift differences measured by Elektron I satellite 12 p1936 A67-25800

Automatic multichannel system for data recording and processing obtained in studies of ionospheric structural inhomogeneities containing magnetic-tape memory and device for digital computer input 13 p2119 A67-26561

Data processing of signal reception from Soviet satellites indicates radio signals scintillation caused by diffraction of waves from ionospheric nonuniformities 14 p2260 A67-27857

Geomagnetic anomaly studied from equatorial ionosphere vertical probe observations in East Asian zone of Pacific ocean 14 p2308 A67-27937

Ionospheric E region dynamical processes, discussing energy phenomena of planetary waves, tidal oscillations and gravity waves 14 p2311 A67-28408

Magnetosphere-ionosphere coupling mechanisms at middle and low latitudes 14 p2312 A67-28411

ELF and micropulsations phenomena divided into earth-ionosphere cavity resonances and regular and irregular pulsations 14 p2266 A67-28415

Electrostatic waves in LF noise bands as cause of diffuse traces observed by Louette satellite ionospheric probe electrostatic waves in LF noise bands as cause of diffuse traces observed by Alouette satellite 14 p2312 A67-28518

Electron density perturbations caused by descending rocket in ionosphere studied by radio pulse signals 14 p2313 A67-28622

Diurnal and seasonal variations in occurrence probability of screening and semitransparent types of sporadic E layer 15 p2474 A67-29387

Characteristic enhancement of forbidden doublet in nitrogen excitation observed in night airglow during traveling ionospheric F region perturbation 15 p2474 A67-29479

Ionospheric electron content variation across sunrise and sunset lines deduced from radio-beacon satellite transmissions 15 p2476 A67-29624

Ionospheric discontinuity motion in E layer at 100 km, using long distance ultrashort-wave propagation data obtained by diversity-reception method 15 p2479 A67-30148

Observation methods, mechanisms, geomorphology, time variations and associated effects of equatorial type spread-F [AGARDOGRAPH 95] 15 p2480 A67-30274

Satellite topside sounder investigation of spread echoes at mid and high latitudes in Northern Hemisphere [AGARDOGRAPH 95] 15 p2480 A67-30276

F region irregularities studied by scintillation of radio signals from earth satellites [AGARDOGRAPH 95] 15 p2481 A67-30285

Geophysical model of radio star and satellite ionosphere amplitude scintillations at nonequatorial latitudes [AGARDOGRAPH 95] 15 p2482 A67-30286

Nature of nighttime F-layer irregularities responsible for scintillation of VHF signals received from radio stars and earth satellites [AGARDOGRAPH 95] 15 p2482 A67-30290

Diffraction of HF radio waves by ionospheric layer containing field-aligned inhomogeneities [AGARDOGRAPH 95] 15 p2482 A67-30291

VHF radar reflections from artificial earth satellites used to analyze amplitude scintillations in ionosphere [AGARDOGRAPH 95] 15 p2482 A67-30292

Large-scale structure of F layer studied by observing Faraday rotation of satellite signals, noting irregularities in total electron content 15 p2483 A67-30295

Ionospheric electron density profiles obtained by dispersive Doppler from beacons on research rockets, noting inhomogeneities [AGARDOGRAPH 95] 15 p2483 A67-30296

Intense fluctuations observed above Arecibo during geomagnetically disturbed conditions, using ionospheric backscatter technique 15 p2483 A67-30299

Ionospheric irregularities in F region during night hours /1958-1960/ [AGARDOGRAPH 95] 15 p2483 A67-30300

Ionospheric irregularity observation near F layer maximum, determining traveling velocities [AGARDOGRAPH 95] 15 p2484 A67-30302

Properties of irregularities responsible for spread-F, discussing hydromagnetic waves [AGARDOGRAPH 95] 15 p2484 A67-30303

Field-aligned irregularities caused by low energy charged particles penetrating to F layer heights [AGARDOGRAPH 95] 15 p2484 A67-30304

Strong ionospheric effects observed on ionograms after high altitude detonation including changes in F layer critical frequency, height and spread [AGARDOGRAPH 95] 15 p2484 A67-30306

Spread-F occurrence studied using hourly soundings near magnetic equator [AGARDOGRAPH 95] 15 p2484 A67-30307

Measurements at Ibadan of drift velocity of ionospheric irregularities for E and F layers during IQSY 16 p2663 A67-30969

Magnetic storm effects on F-2 layer near equatorial zone boundary causing variations in critical frequency of layer 16 p2663 A67-30970

Radio communications disruptions during magnetotonic disturbances in ionosphere at high latitudes during decreasing solar activity 16 p2624 A67-31075

Ionospheric F-2 layer inhomogeneities attributed to plasma flute instability, using kinetic drift equations to describe plasma oscillations 16 p2665 A67-31084

Contribution of regular and irregular components to ionospheric instability 16 p2665 A67-31086

F-region electron-density perturbations transmitted to magnetically conjugate region, noting electrostatic coupling mechanism 16 p2667 A67-31509

Topside ionosphere irregularity studied by Alouette I ionograms and ground based ionosonde records, noting spread-F occurrence topside ionosphere irregularity studied by Alouette I ionograms and ground based ionosonde 16 p2667 A67-31515

Calculation of Doppler shift of radio waves propagating through changing ionosphere by Fermat principle 16 p2829 A67-31516

Correlation reception of wideband signals from ionospheric inhomogeneities, considering effectiveness for signal distortion discrimination 16 p2632 A67-31909

Irregular refraction of radio waves caused by large scale electronic inhomogeneities in ionosphere 17 p2841 A67-31948

Motion of artificial high density ionization cloud released in ionosphere 17 p2844 A67-32545

Polar cap anomalous absorption effects from ionosphere and geomagnetic field studies, noting correlation with magnetic storms 17 p2846 A67-32936

Interpretation of multiple structure of auroral arc 18 p3035 A67-33598

Enhanced VLF emissions near and south of auroral zone, discussing properties, geomagnetic disturbances, riometer absorption, time interval, polarity, etc 18 p3039 A67-33622

Traveling ionospheric disturbances effect on and measurement of direction of movement of downcoming F-2 region perturbation 18 p3043 A67-34526

Ionospheric irregularity effect on lateral deviation of reflected radio waves from ionosphere, noting variation with solar

activity 18 p3004 A67-34617
 Ionospheric irregularities following solar proton flare of July 1966 observed with Alouette topside sounders 19 p3312 A67-35176
 Standard scintillation index method for describing ionospheric effects, discussing power calibration, scaling, deviations, etc 19 p3220 A67-35256
 Greek space research noting satellite optical tracking, solar photosphere and chromosphere, atmospheric electricity and solar eclipse measurements 19 p3320 A67-35292
 Winter anomaly in ionospheric E-layer 19 p3225 A67-35617
 Traveling-ionospheric disturbances observed at midlatitudes by backscattering technique, noting auroral zone and gravity waves role 20 p3425 A67-36280
 Changes in topside ionosphere during large magnetic storm, studying electron density, slab thickness, scale height, etc 20 p3427 A67-36305
 Soviet book on ionospheric geomagnetic disturbance prediction and short term radio propagation forecasting 21 p3616 A67-37933
 Latitude, altitude and local time variation of forces controlling 100 to 700 km atmospheric winds, noting effects on ionospheric phenomena 21 p3654 A67-37994
 Winter anomaly of ionospheric adsorption studied by field strength recordings 21 p3617 A67-38001
 Ionospheric irregularities field alignment responsible for radio signal fading analyzed, showing no evidence for relation to geomagnetic field 22 p3788 A67-39468
 F layer irregularities transverse scale measurements by two-frequency scintillation-ratio technique yielding 600-700 m scales in auroral zone 22 p3789 A67-39470
 Seasonal and diurnal variations of trough and ionospheric electron content and slab thickness, using S-66 satellite observation 22 p3789 A67-39471
 Field-aligned irregularity instabilities in ionization vertical gradient, showing unstable E region for irregularities of scale size 20 m-6 km 22 p3789 A67-39475
 Isolated irregularities in auroral ionosphere studied by analyzing radio signals from rockets and Beacon satellite 22 p3760 A67-39627
 Ionospheric refractive irregularities and traveling disturbances from Alouette I satellite data, calculating electron density profiles using lamination method 23 p3994 A67-40780
 Equatorial anomaly in F-2 layer of ionosphere, examining solar activity, seasonal variation relation to magnetic activity, lunar phase and heights 23 p3996 A67-41082
 Electron scale heights from topside ionograms studied for radiation effects during quiet and disturbed conditions, noting relation to ionospheric plasma temperature 24 p4147 A67-42055
 Auroral zone irregularity correlated with perturbations in outer radiation belt, noting simultaneous displacement of boundary zone of perturbations 24 p4209 A67-42120
 Maximum usable frequency for single discontinuity radio line calculated taking horizontal ionization gradients into account 24 p4120 A67-42130
IONOSPHERIC NOISE
 Galactic emissions and LF and MF radio noises in ionosphere 05 p0898 A67-16867
 Japanese sounding rocket measurements of intensity and frequency time variations in ionosphere to determine VLF radio noise 05 p0763 A67-16868
 Natural ELF electromagnetic noise properties during solar flare of July 7, 1966, considering radiation compression effects on earth-ionosphere cavity 10 p1700 A67-23057
 VLF radio noise during auroral display studied by ground and rocketborne receivers, suggesting emissions triggered by high energy electron fluxes 20 p3428 A67-36374
IONOSPHERIC PROPAGATION
 SA RADIO PROPAGATION
 SA SCATTER PROPAGATION
 SA WAVE PROPAGATION
 Simulation of curvature in straight model earth-ionosphere waveguide, using planar structure loaded by inhomogeneous dielectric 01 p0040 A67-11310

Tropospheric and ionospheric models and parameter variations affecting satellite signal propagation, discussing refractive corrections 01 p0028 A67-11431
 Wave seepage through caustic surface in parabolic plasma layer 02 p0191 A67-11582
 Elevation angle of arrival of ionospherically propagated HF radio signals determined with circular antenna arrays 02 p0217 A67-12088
 Faraday fading rate of satellite signal as calculated from Appleton-Hartree formula for refraction index /without collision/ near transverse propagation 03 p0372 A67-14238
 [RASSA PAPER 1-10-127]
 ORBIS satellite experimental results, noting long range propagation at night and during sunrise 03 p0373 A67-14254
 [RASSA PAPER 1-10-147]
 Satellite to satellite communications experiment simulation via digital computer, proving existence of whispering gallery propagation in lower ionosphere 03 p0373 A67-14255
 [RASSA PAPER 1-10-148]
 Radio propagation in microwave terrestrial model waveguide of variable surface impedance, using reciprocity theorem 04 p0570 A67-14865
 Oblique z-mode echoes in topside ionosphere between plasma and upper hybrid frequencies 04 p0614 A67-14956
 Small amplitude electromagnetic wave propagation in cold homogeneous ionospheric plasma including negative ions and immersed in static magnetic field 04 p0614 A67-14957
 Ionospheric sporadic E layer propagation characteristics and signal strength calculation, noting decrease in antenna gain when using highly directional antennas 04 p0576 A67-15503
 Transmission loss for ionospheric propagation over 4000 km path measured at several frequencies in HF 05 p0760 A67-16005
 Radio Aurora and formation mechanism of ionospheric D and F regions, examining HF and VLF propagation via computer ray tracing, ionospheric storms and equatorial sporadic E layers 05 p0795 A67-16010
 Radio propagation and ion effects in ionosphere and exosphere observed by spacecraft 05 p0763 A67-16866
 Longitudinal propagation of SLF electromagnetic waves through plane-laminar magnetoactive ionospheric plasma 05 p0765 A67-16955
 Oblique probe data applied to determination of minimum group path of signal for parabolic model of ionosphere 05 p0801 A67-17130
 ELF and VLF wave propagation in earth-ionosphere waveguide at wide frequency range, giving amplitude spectra and mean phase velocity for day and night 06 p0994 A67-17970
 Spread-F effects on WWV transequatorial propagation of HF radio waves 06 p0964 A67-18575
 Diurnal variation of Schumann resonances explained by geometrical factors relating position of sources and observational point, noting propagation difference between EW and NS 06 p0998 A67-18707
 Ionospheric propagation index for short term prediction of short wave propagation 07 p1248 A67-19409
 VLF atmospheric noise level fluctuations, discussing daily variations as function of solar zenithal angles, sunrise and sunset and confusion of ionospheric propagation 07 p1171 A67-19422
 HF limits for radio transmission calculated from oblique and vertical sweep frequency records over 2000 km north-south subauroral path 07 p1142 A67-19446
 Amplitude and phase velocity of electromagnetic waves in 1-30 kc range near earth surface for plane and spherical earth-ionosphere waveguide 07 p1144 A67-19695
 Ionospheric effect of sudden magnetic storm eruption, noting propagation of disturbance above terrestrial surface 07 p1174 A67-19705
 Long distance propagation of ultrashort radio waves by ionospheric scattering in subpolar region, noting graphs of signal level changes 07 p1144 A67-19707
 Electron concentration inhomogeneities during traveling gravity wave propagation through F layer 07 p1178 A67-19809
 Frequency correlation of ionospheric radio

waves in inhomogeneous thin layer medium and effect of irregular horizontal ionization gradients 07 p1144 A67-19836
 Plasma ringing phenomena stimulated by Alouette I and other ionospheric probes at upper hybrid frequency and cyclotron frequency harmonics in near zero group velocity regions 07 p1179 A67-19916
 Dispersion equation for whistler mode for velocity distribution with loss cone, discussing critical stability 08 p1324 A67-20894
 Geometric analysis of refractive index, absorption index and polarization characteristics of ionospheric radio waves 08 p1295 A67-21168
 Quasi-trapped whistler mode propagation and generation by trapped electrons in magnetosphere, noting refraction index and wave reflection 08 p1327 A67-21462
 Decimeter wave propagation over large distance indicates signal propagation does not follow great circle 09 p1492 A67-22593
 Ionospheric thermal conductivity effect on gravitational wave 10 p1631 A67-22803
 Energetic solar particle effect on ionosphere, discussing signal phase, amplitude propagation and attenuation 10 p1637 A67-23192
 Long period fading of VLF atmospheric, attributing origin to ionospheric propagation characteristics induced by geomagnetic activity 11 p1785 A67-23947
 Satellite emitted radio wave propagation mechanism based on radio wave paths in horizontally inhomogeneous spherically stratified ionosphere with variable electron density 11 p1751 A67-24070
 Short term and averaged characteristics of nonreciprocal HF ionospheric single and multipath propagation 11 p1762 A67-24286
 Nonreciprocal characteristics of long distance HF ionospheric propagation path interpreted as interaction of waves with transmitting and receiving antennas 11 p1754 A67-24718
 Wave propagation in earth-ionosphere waveguide, obtaining modal solutions 12 p1904 A67-25216
 Contribution of propagation factors in terrestrial atmosphere to noise received by antenna at hyperfrequencies 12 p1904 A67-25308
 Relation between ionospheric no-echo conditions and absorption of cosmic radio noise measured using riometer, plotting diurnal variation values 13 p2114 A67-26794
 Scintillation characteristics of radio waves after passing through ionosphere 13 p2115 A67-26857
 Doppler frequency changes of ionospheric propagating radio waves and relationship to geomagnetic variation 13 p2068 A67-26992
 Ionospheric dispersion of AM-FM artificial satellite signals noting distortion effects, synchronization and interference difficulties 13 p2070 A67-27197
 Ionospheric waveguide channels for long distance radio links below maximum of F-2 layer 13 p2071 A67-27328
 Radio whistlers occurrence relationship to solar and magnetic activities at various latitudes 14 p2265 A67-28413
 Error rate expression for canonic binary receivers, evaluating performance of incoherent detection 14 p2272 A67-28706
 Frequency spread in ionospheric radio propagation 14 p2273 A67-28712
 Simulation of magnetospheric effects for possible application to ionospheric probes 14 p2294 A67-29035
 Measurement errors of arrival direction of radio whistler caused by propagation in earth-ionosphere waveguide 15 p2436 A67-29480
 Frequency dependence of radio star scintillations 15 p2555 A67-29621
 Vertical incidence ionospheric absorption measurements from ground station criteria for recognizing winter anomaly 15 p2476 A67-29623
 Troposphere and ionosphere effects on different frequency radio wave propagation for space communication 15 p2437 A67-29953
 [AAS PAPER 67-93]
 Data analysis from oblique incidence soundings during spread-F conditions [AGAROGRAPH 95] 15 p2481 A67-30280
 F scatter, flutter fading and maximum

usable frequency phenomenology from HF radio propagation studies near equator 15 p2438 A67-30297

Oblique sounding of transequatorial path [AGARDOGRAPH 95] 15 p2438 A67-30298

Digital technique for recording of step-frequency ionospheric soundings, obtaining maximum and lowest observed frequencies 16 p2625 A67-31340

Solar flares, analyzing X-ray emission, radio emission and superposition of ionospheric effect 16 p2739 A67-31459

Radio ray divergence in ionosphere using computer techniques, noting ionospheric models and limitations 16 p2629 A67-31512

Attenuation rates at vlf from aircraft measurements presented as curves of dominant waveguide mode vs. geomagnetic bearing of propagation path 16 p2631 A67-31854

Numerical analysis of ionospheric radio wave propagation, examining, attenuation polarization and power flow as function of electron density profiles 16 p2631 A67-31857

Changes of phase and signal amplitude of VLF radio waves during solar flares noting waveguide mode characteristics 16 p2632 A67-31859

Attenuation of natural hydromagnetic waves /Pcl/ in ionosphere, noting amplitude reduction and particle distribution in magnetosphere 17 p2843 A67-32536

Whistler investigation below ionospheric layers at high magnetic latitudes in Sweden 17 p2845 A67-32793

High latitude disturbances influence on VLF propagation, showing high correlation with auroral absorption 18 p3004 A67-34426

Satellite system with solid state transmitters with different frequencies in HF band for ionospheric guided propagation research 20 p3394 A67-36246

Propagation characteristics of ELF electromagnetic waves investigated below anisotropic ionosphere, considering magnetic field 20 p3379 A67-36282

CW transmission measured for carrier and modulation phase, examining carrier phase perturbations due to mode interference CW transmission measured for carrier and modulation phase, examining carrier phase 20 p3379 A67-36292

Resonance for VLF waves by ionospheric propagation using Haselgrove whistler ray tracing method, interpreting path shape as function of gradients 20 p3427 A67-36372

Excitation of earth-ionosphere waveguide by VLF source for case of azimuth dependent properties of source and ionosphere 20 p3428 A67-36373

Short wave skip distance variation with reflection angles in multilayered ionosphere calculated from improved formula 20 p3382 A67-36763

Time delay of remote-resonance trace of polarized electromagnetic pulse propagating through topside ionosphere 20 p3527 A67-37403

VLF radio wave tracking stations for ionospheric propagation investigation using atomic clock 20 p3386 A67-37481

HF skywave propagation computer model for interference prediction 20 p3387 A67-37646

Full wave solutions for coupled modes corresponding to ionospheric propagation in vacuum, stressing numerical swamping problem 20 p3389 A67-37710

Schumann Resonance frequencies, Q-factor and waveguide propagation constant derived at ELF for ionospheric profiles 21 p3579 A67-37993

Oblique probe data applied to determination of minimum group path of signal for parabolic model of ionosphere 21 p3618 A67-38473

Radio wave propagation in three-dimensional inhomogeneous magnetoactive ionosphere studied by geometrical optics method 21 p3582 A67-38592

Compact ionospheric station for six fixed frequencies, compared with automatic station 21 p3586 A67-39047

Dispersion relation for wave propagation in electro-magneto-ionic medium under electric and magnetic fields obtained using Maxwell-Boltzmann-Vlasov equations, discussing cut-off frequency 22 p3788 A67-39469

Propagation anomalies of atmospheric acoustic signals of nuclear explosions due to

nonlinearities and refraction effects 22 p3790 A67-39645

Wave propagation in random plasma medium with inhomogeneous parabolic electron density profile background for ionospheric propagation applications 23 p3974 A67-41199

Ionospheric thermal conductivity effect on gravitational wave propagation 24 p4150 A67-42140

Medium range radio communication system using artificial ionosphere consisting of ion-electron cloud created by Cs-Al mixture explosion [AIAA PAPER 67-789] 24 p4152 A67-42952

IONOSPHERIC REFLECTION

Direct backscatter recordings from polar cap F-layer reflections used to predict communications 01 p0020 A67-10007

Oscillations of vertical component of ionospheric refraction measured, using cliff radio interferometer and signals from satellites 01 p0022 A67-10390

Radio wave reflection from ionosphere with perturbed electron density profile 02 p0192 A67-11618

Spectral analysis of pulsed signal reflected from ionospheric F-2 layer 02 p0193 A67-11672

Existence of anomalously close radio reflections from sporadic ionization zone linked with polar aurora 02 p0193 A67-11674

Radio wave propagation in multimode waveguides of arbitrary height, assuming ionosphere boundary to be perfectly reflecting 02 p0198 A67-12070

Fading characteristics of radio waves reflected from sporadic E layer of ionosphere over magnetic equator 03 p0406 A67-12824

Spaced receiver method for measuring ground diffraction pattern of vertically reflected radio waves 03 p0407 A67-12830

Ray tracing study of HF ducting propagation with satellites [RASSA PAPER 1-10-145] 03 p0373 A67-14252

E-2 and F-0 intermediate ionospheric layer morphology, occurrence, electron density and signal reflection variations 04 p0616 A67-15220

Sporadic E layer stratification and morphology of M and N reflections produced by transparent and semitransparent E layer 05 p0799 A67-17029

Calculation method for distortion of envelope of pulses during reflection from inhomogeneous ionospheric plasma during topside sounding 05 p0765 A67-17125

Diffusion reflections during cycle of solar activity, showing frequency changes according to increase in solar activity 05 p0800 A67-17127

Number of reverse signals reflected from F-2 layer during oblique reflection sounding 05 p0802 A67-17145

Virtual reflection-height oscillations and infrasonic waves in ionospheric F layer 06 p0995 A67-17974

Antenna orientation effect on polarization components of radio waves reflected from ionosphere, noting occurrence and properties of magnetoionic component of polarization 07 p1173 A67-19690

Ionospheric plasma density determined by phase difference of incident waves on and reflected from plasma 07 p1173 A67-19701

Parametric analysis of stability of reflection from sporadic E layer during 11-year solar cycle 07 p1174 A67-19704

Fast phase fluctuations of signal reflected from F-2 layer 07 p1144 A67-19819

Virtual heights and absorption of radio waves in ionosphere, discussing methods of computation 09 p1464 A67-22441

Ionospheric movement measurement with LF radio waves, using triangulation coupled with cross spectrum analysis of signal fading 11 p1784 A67-23936

Satellite-emitted short radio wave field intensity and ionospheric parameters 11 p1751 A67-24071

MF and HF portions of radio spectrum relationship to communication systems, presenting amplitude and phase variation in conjunction with effects of fading, time and frequency spread and atmospheric noise [IEEE PAPER 19-CP-65-482] 11 p1755 A67-25080

Angular scattering of reflected radio waves from ionosphere, giving results of 300 cases 12 p1933 A67-25547

Design of broadband steerable Wullenweber antenna arrays allowing HF element rings to be within LF rings 13 p2074 A67-26257

Statistical properties of phase and amplitude fluctuations during total reflection of waves from ionospheric layer 13 p2067 A67-26551

Reception of signals reflected from ionosphere in vertical radar probing, examining frequency-difference combinations 13 p2067 A67-26569

Ionospheric index of solar activity obtained together with quadratic equation regression coefficients by minimizing standard error of F-2 layer critical frequency 14 p2311 A67-28375

Influence of spread-F upon apparent reflection coefficients of F region for HF radio waves [AGARDOGRAPH 95] 15 p2481 A67-30279

Data analysis from oblique incidence soundings during spread-F conditions [AGARDOGRAPH 95] 15 p2481 A67-30280

Spectral analysis of pulsed signal reflected from ionospheric F-2 layer 16 p2624 A67-31087

Existence of anomalously close radio reflections from sporadic ionization zone linked with polar aurora 16 p2624 A67-31089

Oblique incidence ionospheric reflections, from phase and amplitude variations of Loran-C pulse signals, noting lower ionosphere two-layer formation 16 p2632 A67-31862

Reflection coefficients of sharply bounded ionosphere for plane waves incident from arbitrary direction at magnetic equator 16 p2632 A67-31863

Coefficient characterizing stability of continuous radio signal reflections declining occurrence probability from sporadic ionospheric layer 16 p2669 A67-31907

Vertical electron density profile method for determining altitude of lower boundary of ionosphere 17 p2842 A67-32383

Radio signals reflection by free radicals in ionosphere, observing predicted intensity and particle detection 17 p2817 A67-33233

Rocket observations of energy spectra of auroral electrons 18 p3034 A67-33591

Ionospheric irregularity effect on lateral deviation of reflected radio waves from ionosphere, noting variation with solar activity 18 p3004 A67-34617

Autocorrelation functions for amplitude of multiple echoes of fading radio signals reflected from ionosphere 20 p3379 A67-36293

Screening frequency dependence on reflection cut-off frequency in sporadic E layer 20 p3428 A67-36762

Ionospheric radio wave theory using coupled vacuum modes with set of coupled wave equations 20 p3389 A67-37709

Calculation method for distortion of envelope of pulses during reflection from inhomogeneous ionospheric plasma 21 p3582 A67-38468

Diffusion reflections during cycle of solar activity showing frequency changes according to increase in solar activity 21 p3618 A67-38470

Number of reverse signals reflected from F-2 layer during oblique reflection sounding 21 p3619 A67-38487

Seasonal and long term variations in duration of continuous radio signal reflections from sporadic E layer 21 p3623 A67-39038

Fading rate relation to ionospheric drift speed of radio waves, estimating size of irregularities 23 p3996 A67-41083

IONOSPHERIC SOUNDING

International Satellites for Ionospheric Studies /ISIS/ program using radio sounders 01 p0057 A67-10293

Lambda and Kappa rocket sounding observations of electron density, electron temperature, thermal electron energy distribution, plasma space electric potential and ion composition 01 p0060 A67-10335

One-trap probe measurement of ionospheric electron density, electron temperature, plasma space potential relative to vehicle potential of sounding rocket, mean ion mass, composition and temperature 01 p0064 A67-10565

Inflatable parachute system developed for deceleration of ionospheric probe instrumentation descending after expulsion from rocket 03 p0359 A67-13369

PCA events during 1938-1955 detected from vertical incidence ionospheric soundings at high latitude, identifying some with proton flares 03 p0507 A67-13813

E layer stratification, fine structure and boundary accuracy in frequency measurements based on seasonal variations in solar activity 04 p0618 A67-15574

Calculation method for distortion of envelope of pulses during reflection from inhomogeneous ionospheric plasma during topside sounding 05 p0765 A67-17125

Order of recombination coefficient in E layer determined, using ionospheric data 06 p0999 A67-18737

Ionospheric direct observation by sounding rockets during IQSY 07 p1186 A67-19677

Ionospheric sounding data obtained principally by ground-based ionosondes, topside sounders and incoherent backscatter systems 10 p1630 A67-22775

Vertically moving perturbations in nighttime ionosphere studied from vertical ionospheric sounding data, discussing type A4 which develops in F layer near maximum ionization 10 p1631 A67-22805

Ionospheric electron content calculated from beacon satellite data on Faraday rotation 10 p1641 A67-23235

Ionospheric probes for measuring electron density in E region through detection of plasma resonances 10 p1656 A67-23285

Impedance measurement of 39.5 meter tip-to-tip dipole antenna made during ionospheric rocket flight 10 p1611 A67-23292

Early results from topside sounder experiments in Alouette II satellite, presenting ionograms, plasma spike, electron number density and scale height 10 p1649 A67-23302

Ionosphere rocket sounding for positive ion density, electron density and electron temperature, noting sunspot effect 11 p1787 A67-24643

Design of rocketborne ionospheric plasma probe considering probe shape, location, payload, etc 12 p1937 A67-25838

Relation between diurnal, seasonal and cyclic variations of stratifications in E layer and fine structure of sporadic E layer and E-2 layer 13 p2110 A67-26550

Infrasonic and hydromagnetic wave propagation in atmosphere and ionosphere measured by array of underwater and acoustic sensors 13 p2122 A67-27701

Radio noise spectrum on VLF bands in ionosphere observed by sounding rocket K-9M-19 14 p2307 A67-27886

Circuit for multifrequency ionospheric probing, with basic frequency scanning unit containing sawtooth pulse oscillator 14 p2315 A67-27949

Time and space study of onset and early development of single occurrence of spread-F in equatorial region 15 p2480 A67-30275

[AGARDOGRAPH 95] Satellite topside sounder investigation of spread echoes at mid and high latitudes in Northern Hemisphere 15 p2480 A67-30276

[AGARDOGRAPH 95] Field aligned structure of ionization associated with boundaries of spread-F at middle latitudes studied by combining topside and fast-sweeping ground-based ionograms 15 p2480 A67-30277

Data analysis from oblique incidence soundings during spread-F conditions [AGARDOGRAPH 95] 15 p2481 A67-30280

French satellite FR-1 to be launched in late 1965 by NASA for ionospheric studies, noting instrumentation, data transmission, etc 16 p2757 A67-30641

Morning effect on F region, noting seasonal variation of corresponding solar zenith angle and worldwide distribution of predawn minimum 16 p2664 A67-30976

Nighttime profiles calculated with allowance for ionization beyond lower bound of frequency range of ionospheric station 16 p2669 A67-31896

Hydroxyl emission at high latitudes during winter months of 1960 through 1963 measured with spectroscopy 17 p2848 A67-32955

Anomalous LF plasma oscillation by particles trapped in potential well behind satellite applied to ionospheric measurements 18 p3117 A67-33512

Ionospheric observations of thick layer structure accompanying auroral activity,

emphasizing ionization profiles, electric fields, aurora generation and global distribution 18 p3039 A67-33620

Ionospheric irregularities following solar proton flare of July 1966 observed with Alouette topside sounders 19 p3312 A67-35176

IQSY South African participation, reviewing meteorology, geomagnetism, aurora, airglow, ionosphere, cosmic rays, etc 19 p3315 A67-35477

IQSY geophysical work in Greece, examining geomagnetism, aurora, ionosphere, airglow, solar activity, etc 19 p3223 A67-35478

Iranian ionospheric observations, giving monthly median values of vertical-incidence data and critical frequency 19 p3224 A67-35489

Plasma scale height errors from Alouette I topside sounder ionogram analysis 20 p3433 A67-37409

Onboard and ground radio-engineering system for stratospheric transport balloon noting telemetering, remote control and localization functions integrated in system 21 p3581 A67-38213

Noisy signal improvement through compact instrument, giving circuit and operational aspects and applications in ionospheric research 21 p3582 A67-38396

Calculation method for distortion of envelope of pulses during reflection from inhomogeneous ionospheric plasma 21 p3582 A67-38468

Topside ionospheric swept-frequency pulsed sounder onboard Alouette 2 satellite, discussing transmitter power, large range receiver and antenna array 21 p3583 A67-38636

Magnetic deviation ion mass spectrometer for ionospheric rocket probes, noting onboard application 21 p3628 A67-38657

Ionospheric observations using Elektron I and III satellites, discussing state of ionosphere, electron concentration variation, etc 22 p3760 A67-39734

Neutral atmospheric temperatures calculated from data provided by incoherent scatter soundings of ionosphere 22 p3794 A67-40474

Electron concentration from topside ionograms for heights below satellite 24 p4147 A67-42056

Vertically moving perturbations in nighttime ionosphere studied from vertical ionospheric sounding data, discussing type A4 which develops in F layer near maximum ionization 24 p4150 A67-42142

IONOSPHERIC STORM

SA SUDDEN IONOSPHERIC DISTURBANCE /SID/

Frequency dependence of enhanced absorption of cosmic radio emission during abrupt ionospheric disturbance 02 p0307 A67-11676

Equatorial ionospheric storms, analyzing sub-peak and total columnar electron content 03 p0408 A67-12841

ULF emission at two conjugate points signaling onset of negative ionospheric storms 03 p0411 A67-13347

Continuous flux of solar protons entering earth atmosphere important in energy balance of ionosphere and sun [RASSA PAPER 1-10-140] 03 p0417 A67-14248

Ionospheric flux system of initial phase of geomagnetic storm of September 4, 1957 over polar cap 05 p0802 A67-17148

Distance compression field /DCF/ of geomagnetic storm, considering micropulsation activity and ionospheric effect 06 p0994 A67-17639

Propagation of magnetodynamic disturbance through loss ionosphere and entry into earth surface 07 p1174 A67-19718

Geomagnetic, auroral, ionospheric and cosmic ray perturbations interdependence and relationship with solar activity 07 p1183 A67-20174

Vertical ionospheric perturbations observed from January 1963 through May 1965 10 p1630 A67-22789

Ionospheric measurements at Antarctic station in south radiation anomaly region showing precipitated electron flux associated with ionospheric disturbances 12 p1934 A67-25778

Dependence of seasonal occurrence probability of F-zero layer on level of geomagnetic activity and ionospheric activity observed above Ashkhabad 13 p2110 A67-26549

Radio waves effect on ionospheric F layer, showing decrease in critical frequency and disturbance of stationary electron and ion concentration 14 p2307 A67-27923

Global response of topside ionosphere to magnetic disturbances at solar minimum studied from electron concentration measurements at 640 km 15 p2475 A67-29610

Traveling ionospheric disturbance heat conduction waves excited in neutral gas of thermosphere by hydromagnetic waves from magnetopause 15 p2475 A67-29617

Frequency dependence of enhanced absorption of cosmic radio emission during abrupt ionospheric disturbance 16 p2738 A67-31091

High latitude disturbances influence on VLF propagation, showing high correlation with auroral absorption 18 p3004 A67-34426

Storm-time change and average electron density profile of polar topside ionosphere at sunspot minimum 19 p3218 A67-35230

Similarities between Jupiter decametric radiation and satellite induced ionospheric disturbances 20 p3521 A67-36308

Ionospheric flux system of initial phase of geomagnetic storm of September 4, 1957 over polar cap 21 p3619 A67-38490

Storm behavior of topside ionosphere studied from electron concentration satellite data, discussing height and latitude effects 24 p4148 A67-42058

Vertical ionospheric perturbations observed from January 1963 through May 1965 24 p4149 A67-42125

IONOSPHERIC TEMPERATURE

Incoherent scattering measurements of ionospheric power spectrum and autocorrelation function at geomagnetic equator to determine electron and ion temperatures, ion composition and ion density 03 p0408 A67-12834

Seasonal variation in temperature in nighttime F region through analysis of emission intensity of oxygen red line and upper atmosphere structure 06 p0996 A67-18431

Electron and ion temperature changes in sporadic E layer based on wind shear theory, using energy equation 08 p1327 A67-21366

Rocket and satellite measurements of electron and ion thermal structure of ionospheric F region 12 p1935 A67-25796

Temperature of F region deduced from electron number density profiles 13 p2108 A67-26322

Ionospheric ion temperature determination from variations in collector current of ion trap mounted on rotating satellite 13 p2115 A67-27330

Upper atmosphere densities and temperatures at 105-165 km from diffusion and spectral intensity of aluminum oxide trails 14 p2310 A67-28050

Photochemical analysis of diurnal variations of electron concentration and temperature of upper ionosphere 16 p2669 A67-31902

Diurnal variations of ionospheric ion/electron temperatures predicted assuming solar UV radiation heating, collisional cooling and heat transport by conduction 17 p2850 A67-33192

Ionospheric electron temperature incoherent backscatter measurements confirming predawn enhancement of 6300 angstroms airglow 18 p3039 A67-33624

Ionospheric and magnetospheric neutral and charged particles temperature vertical distribution, noting effects producing variations 18 p3040 A67-34033

Grid electrostatic probe for ionospheric measurement of electron density and temperature, examining measurement errors due to environmental disturbances 18 p3048 A67-34225

Ion-density data modifications due to temperature variations, discussing normalization and electron density relationship 19 p3224 A67-35491

Ground based atmospheric and ionospheric particle temperature measurements, examining methods and thermosphere heat sources 22 p3870 A67-39676

Ionospheric and magnetospheric temperature measurements using rockets and satellites including neutral particle, ion and electrons 22 p3871 A67-39677

Radar-derived results for midlatitude F-region densities and temperatures at sunspot

minimum noting seasonal anomalies 22 p3793 A67-40080

IPTS
S INTERNATIONAL PRACTICAL TEMPERATURE SCALE /IPTS/

IQSY
S INTERNATIONAL QUIET SUN YEAR /IQSY/

IRAN
Iranian ionospheric observations, giving monthly median values of vertical-incidence data and critical frequency graphs 19 p3224 A67-35489

IRIDIUM
Microstructural and X-ray analysis of intermediate phases of Ti-Ir and Ti-Rh intermetallic compounds, including microhardness and fusion point variations 07 p1204 A67-19263
Intermediate phases in alloys of Ti with Ir, Rh and Qs indicate possibility of polymorphism 13 p2131 A67-26472
Reflectance and optical constants of evaporated iridium films measured in vacuum ultraviolet 16 p2733 A67-31878
Plasma arc deposition and gas pressure bonding technique for producing defect-free uniform iridium protective coatings for graphite reentry structures 20 p3465 A67-36607

IRON
Ionization calorimeter measurement of absorption of energy flux of primary cosmic radiation nuclear active component in iron 02 p0316 A67-12762
Propulsion through drag interaction between magnetically-accelerated iron particle suspension and air [AIAA PAPER 66-926] 03 p0504 A67-14136
Flow characteristics of Fe single crystals and behavior of 04 p0640 A67-15793
O-to-Fe ratio determined in active solar corona from intensity ratio of O-8 to Fe-17 lines and in quiet corona from O-7 to Fe-14 ratio 06 p1083 A67-18068
Meteoritic iron pair production probability by total ablation of micron-size Fe particles in air and Ar as function of particle velocity 08 p1399 A67-21241
Equilibrium temperatures of Fe and Mg ions in chondritic meteorites 08 p1400 A67-21266
Isotope analysis of iron migration in Ni-Cd cells with pocket electrodes 09 p1458 A67-22178
Iron doped gallium arsenide transistor with better frequency performance and higher operating temperatures 10 p1617 A67-23538
Fast neutron activation cross sections of Se and Fe measured, noting subshell closure effect and isomer ratio 11 p1822 A67-23979
Primary cosmic radiation abundance measurements on iron and heavier nuclei, using Cerenkov counter on balloon flights 11 p1856 A67-24504
Failure mode at tip of crack predicted using cleavage strength and shear strength of perfect crystals, noting tungsten and iron 11 p1880 A67-25090
Neel temperature in NiO and MnO with divalent Fe measured using Mossbauer effect 12 p1985 A67-25844
Fe IR line excitation in solar corona, noting abundance of iron relative to H and linear polarization of IR lines in coronal streamer 12 p2010 A67-26242
Model for concentrated interstitial solid solutions applied to carbon solution in gamma iron 13 p2131 A67-26574
Visible continuous spectrum of comets rules out hypothesis of iron particles major role in scattering solar light 15 p2554 A67-29515
Temperature homogenization effect on structure of industrial aluminum, determining mechanical properties dependency on Fe/Si ratio 15 p2504 A67-29975
Temperature dependence of properties of acceptor center in iron doped gallium arsenide, noting delocalization of cluster electron density 16 p2726 A67-30814
Hydrostatic pressure effects on brittleness in Cr and yielding in center annealed iron specimen studying brittle-ductile transition of former 16 p2889 A67-31328
Differential depressions of iron I levels and red shifts of spectral lines under pressure, demonstrating error in assumed air

refractive indices 17 p2886 A67-33162
Hydrogen coverage at metal surface during dissolution in corrosion process 18 p3066 A67-34368
Epitaxial growth of iron on tungsten field-emission points studied by field-emission microscopy 19 p3302 A67-34938
Magnetic field induced hyperfine structure in mono- and divalent iron ions in magnesium and calcium oxide, showing evidence of paramagnetic resonance 20 p3506 A67-36211
Solar X-ray emission line spectrum from 1.3 to 20 angstroms in solar flares identified as Fe XXVI through Fe XX transitions 20 p3519 A67-37396
Ionization calorimeter measurement of absorption of energy flux of primary cosmic radiation nuclear active component in iron 22 p3842 A67-40264
Fe rods in Fe-Sb matrix eutectic system, measuring rod diameter and Fe volume fraction effects on magnetic properties 23 p4039 A67-40884
Chemical history of Fe traced in nebular material assuming preplanetary particles were similar to those presently discarded by sun 23 p4068 A67-41360
Nuclear active cosmic ray particles and Fe atom nuclei inelastic interaction cross section 24 p4219 A67-42849
Nuclear cascade avalanche absorption in Fe analyzed by ionization calorimeter 24 p4219 A67-42850
Iron radiation length unit from electromagnetic cascades produced by bremsstrahlung of horizontal cosmic ray muons 24 p4221 A67-42869

IRON ALLOY
SA PERMALLOY
SA STEEL
Atom distribution in double matrix cell of ordered solid solution in alnico-titanium alloy 02 p0254 A67-11864
Strain-hardening and temperature dependence of mechanical properties of ternary ordered alloys on nickel-iron base 02 p0255 A67-12675
Activity of oxygen in liquid Fe-Pt alloy system, determining temperature and composition effect on equilibrium constant 02 p0256 A67-12708
Decay of K-state in Ni-Cr, Ni-Cr-Mo and Fe-Ni-Cr-Mo alloys studied in terms of electric conductivity during plastic deformation 04 p0635 A67-14429
Phase work hardening of austenitic Fe-Ni alloys in phase transformation process 04 p0635 A67-14430
Stability of austenite in some Fe-Cr-Ni alloys under low temperature strain 04 p0636 A67-14753
Annealing temperatures effect on Young modulus, temperature coefficient and crystallographic texture of Fe-Ni-Ti alloys after deformation 05 p0831 A67-17485
Structural change effects on plasticity and fracture characteristics on iron alloys with annealing 06 p1017 A67-18227
Solubility limit of Fe in close-packed hexagonal alpha-Ti noting temperature dependence and superconductivity 06 p1051 A67-18370
Alloying effect on aluminum K and iron L X-ray emission spectra in Al-Fe binary system 08 p1343 A67-21304
Low noise SiFe sheet development and application, considering effects on magnetic properties 13 p2178 A67-27139
Thermophysical properties of high temperature solid materials, Volume 3, Ferrous alloys 13 p2141 A67-27152
Effect of drilled holes on notch toughness of iron alloys, noting impact and slow bending testing, notch toughness improvement, etc 16 p2688 A67-31304
Slip step role in early stages of stress corrosion cracking in face centered iron-nickel-chromium alloy thin foils 16 p2690 A67-31384
Niobium-iron binary alloys structural study, noting phase instabilities for various added impurities 17 p2871 A67-32042
Temperature and composition effect on ductility transitions, yield stress and dislocation pinning strength in iron base alloys due to change in slip 18 p3063 A67-33485
Iron-chromium-bauxite cermets preparation and properties 18 p3065 A67-34260
Stability of austenite in some Fe-Cr-Ni alloys under low temperature

strain 18 p3066 A67-34411
Structural transformations in alnico alloy with titanium studied by X-ray 19 p3245 A67-35467
Thermal and thermomechanical treatments effect on structure and mechanical properties of Fe-Ni-base alloy with Al and Ti additions 19 p3247 A67-35834
Phase and chemical compositions of structural components forming in iron-nickel-chromium alloys with aluminum and titanium content 22 p3820 A67-39788
Mossbauer spectra of FeMo alloys for closed space compositions show overlap of disturbed surroundings of impurity iron atoms and magnetic moment 24 p4203 A67-42108
Solubility of niobium carbide in gamma iron determined from experiments using Fe-Nb alloy in equilibrium with hydrogen-methane mixtures 24 p4173 A67-42348

IRON COMPOUND
SA FERRITE
Fe spectrum energy levels for various subshell configurations, calculating oscillator strengths and transition probabilities 03 p0511 A67-13649
Iron hydroxide formation in producing surface color of Mars 06 p1083 A67-18160
Structure of X-ray K absorption edge of iron in Fe compounds, noting nature of chemical bond and structure of electron energy spectrum 12 p1957 A67-28109
Iron hydroxide formation in producing surface color of Mars 16 p2741 A67-30504
Stoichiometric composition effect on semiconducting properties of gamma iron telluride at high temperature phase 17 p2911 A67-32220
Linear melting curve of fayalite up to 40 kb determined, using piston cylinder and thermocouples 21 p3617 A67-38190

IRON METEORITE
Age determination of iron meteorites by comparing isotopic abundance of primordial potassium in inclusions with terrestrial standards 02 p0326 A67-12044
Neutron activation analysis applied to determination of Ar 40 and K 41 content of iron meteorites 02 p0326 A67-12045
Spallation produced Ar 40 in iron meteorites for determining cosmic ray exposure ages from radiogenic Ar 40 content 02 p0326 A67-12308
Kamacite and taenite superstructures and metastable tetragonal phase in iron meteorite 03 p0510 A67-13334
Emissivity, absorptivity and thermal inertia effects on calculation of iron meteoroid temperatures at earth distance from sun 04 p0699 A67-14965
Radioactive isotopes in iron meteorite used to determine cosmic ray origin and to study nuclear processes in early history of solar system 05 p0877 A67-18084
Kamacite-taenite interface relationship in iron meteorite, discussing shock wave transformation 06 p1087 A67-18377
Mundrabilla meteorite, describing iron meteorites found in Australia 07 p1247 A67-19058
Iron-rich silicates significance in Mezo-Madaras chondrite [AFCL-67-0012] 07 p1256 A67-20013
Concentration of Ni, Ga and Ge in series of Odessa and Canyon Diablo meteorite specimens 08 p1385 A67-20936
Potassium-argon age of metal phase of Weekeroo Station iron meteorite 08 p1400 A67-21265
Ge and Ga concentration in selected Fe meteorites used to determine quantization in terms of multiple parent body hypothesis and planetary fractionation processes 09 p1564 A67-21738
Trace element concentration in iron meteorites determined using lithium drifted Ge semiconductor detector 09 p1569 A67-22686
Cosmogenic tritium content in Sikhote Aln iron meteorite irradiated with reactor neutrons 09 p1569 A67-22688
X-ray diffraction and metallographic investigation show iron meteorites shock at pressures of at least 130 kbar 10 p1705 A67-22954
Electron microprobe analysis for examining oxidation reduction mechanism in iron meteorites 11 p1885 A67-24606
Helium 3 anomaly in octahedrites and low spallogenic tritium content in freshly fallen

- iron meteorites caused by tritium loss due to solar heating in space 11 p1866 A67-24694
- Iron and stony meteorite cooling rates determined by measuring kamacite bandwidth, bulk nickel content and composition 11 p1868 A67-24872
- Amphibole richterite found in graphite nodules of iron meteorite, using electron microprobe and X-ray powder diffraction 11 p1868 A67-24873
- Revision of Levin average value of accommodation coefficient K for iron meteorite bodies 13 p2198 A67-26572
- Cohenite grains from iron meteorites studied by X-ray diffraction for establishing pressure scale, using solid state recrystallization 13 p2200 A67-27235
- Magnetic properties of meteorites, residual thermomagnetic capacity and determination of space magnetic fields 14 p2383 A67-27926
- Techniques for determining cosmic ray age and stable and radioactive nuclide production rates in meteorites 14 p2380 A67-27968
- Neutron activation analysis to determine trace elements in iron meteorites 14 p2391 A67-28947
- Lamellar troilite occurrence and origin in iron meteorites 14 p2391 A67-28948
- Isotope fractionation processes and reproducibility of age of iron meteorites studied from cosmic ray exposure ages 15 p2556 A67-29664
- Age determination of iron meteorite by Rb-Sr isotopic analyses of silicate inclusions, proving formation of younger solid objects in solar system 16 p2749 A67-31434
- Isotopic composition and abundance of xenon and krypton in graphite of iron meteorite from Canyon Diablo examined for anomaly pattern 16 p2750 A67-31438
- Iron and iron-stony meteorites cooling rates in relation to Ni content and Widmanstätten structure suggest development in different thermal environments 16 p2750 A67-31453
- Chemical analyses of stony meteorite and iron meteorite with silicate inclusions 16 p2751 A67-31456
- Tritium diffusion from iron meteorite shortly after fall established by artificial proton irradiation 17 p2942 A67-32357
- Concentration ratios of cosmic ray-produced isotopes of helium, neon and argon measured and effective irradiation hardening parameter calculated 17 p2942 A67-32358
- Helium and neon content and isotopic composition in iron meteorites, noting He 3 deficiency in hexahedrites due to tritium loss 17 p2942 A67-32359
- Abundance of stable isotopes of neon, argon, krypton and xenon in Costilla Peak iron meteorite, observing spallation components 21 p3702 A67-38124
- Ferrous ion order-disorder in meteoritic pyroxenes, using Moosbauer iron 57 absorption, noting metamorphic history of chondrites 21 p3702 A67-38128
- Strontium and rubidium 87 measurements on iron meteorite silicate inclusions, with age determination at 4.4 to 4.8 billion years 22 p3881 A67-39495
- Germanium distribution in metallic phases of various iron meteorites by electron probe microanalysis 22 p3885 A67-39976
- Spectroscopic analysis of iron meteoroid radiation by emission growth curve method covering temperature factors and atom and electron concentrations 23 p4062 A67-40674
- Anoka, Minnesota, iron meteorite noting composition, chemistry, structure and cooling rate 23 p4069 A67-41449
- Hot working effects in octahedrite parent gamma phase, discussing spinel twinning and polycrystal assembly of gamma phase before kamacite precipitation 24 p4232 A67-42609
- Chlorine abundance and distribution in iron meteorites from neutron activation analysis and metallographic examination, discussing terrestrial contamination effects 24 p4232 A67-42610
- Iron meteorite with partially preserved fusion crust from atmospheric flight noting martensitic structures due to rapid cooling 24 p4232 A67-42611
- Coexisting sphalerite, troilite and daubreelite in Odessa meteorite and sphalerite inclusions in kamacite in Odessa and Canon Diablo analyzed for chemical composition 24 p4233 A67-42620
- Cooling rates for Widmanstätten pattern formation in iron meteorites used to obtain data on parent meteorite bodies 24 p4234 A67-42627
- Iron meteorite chemical classification, measuring Ni, Ga, Ge and Ir concentrations for Fe groups and pallasites 24 p4237 A67-42650
- Radioactive isotopes in iron meteorite used to determine cosmic ray origin and to study nuclear processes in early history of solar system 24 p4212 A67-42760
- IRON OXIDE**
- Anisotropy of electric resistivity, Seebeck and Hall coefficients and magnetoresistance of n-type single crystal ferric oxide/hematite/containing tetraivalent tin ion as impurity 02 p0299 A67-12085
- Observations with birefringent interferometer and photoelectric spectrophotometer of Martian surface materials composition, noting strong band at 3.1 micron suggesting hydrated minerals 11 p1865 A67-24603
- Chondrites metamorphosis and equilibrium, studying iron oxide and rare gas content, petrological factors and material formation 18 p3134 A67-34494
- Iron titanium oxides and oxygen fugacity in volcanic rocks noting temperature effect 22 p3792 A67-39975
- IRON 57**
- Measurement of half-life of 14.4 kev level of 57 Fe with scintillation detectors and digital timer 03 p0471 A67-13225
- Ferrous ion order-disorder in meteoritic pyroxenes, using Moosbauer iron 57 absorption, noting metamorphic history of chondrites 21 p3702 A67-38128
- IRRADIATION**
- SA DEUTERON IRRADIATION**
- SA PROTON IRRADIATION**
- SA X-RAY IRRADIATION**
- Power spectrum of irradiance for precessing cylinder computed as function of time for given value of phase angle 10 p1652 A67-22714
- Silicon solar cell with drift fields of various widths and magnitudes, considering performance changes before and after radiation 10 p1596 A67-23161
- Dependence of ion energy on irradiated laser power, discussing production of ions of two discrete energies 10 p1687 A67-23793
- Irradiation of gallium arsenide and gallium antimonide monocrystals by electrons, fast neutrons and relativistic protons, discussing Hall coefficient variation 16 p2727 A67-30869
- Relationship between oxygen tension and radiosensitivity in complex biological system 17 p2806 A67-31962
- Concentration ratios of cosmic ray-produced isotopes of helium, neon and argon measured and effective irradiation hardening parameter calculated 17 p2942 A67-32358
- Irradiation effect on minority carrier lifetime for p-n junction devices in epitaxial film and single crystal 19 p3308 A67-35670
- Rocketborne UV radiometers for solar spectral intensity distribution, calculating irradiance and earth reflectivity 22 p3794 A67-40363
- Moebius strip self-irradiation coefficient calculated as function of relative width or area of strip 23 p4083 A67-41287
- IRREVERSIBLE PROCESS**
- Thermomolecular pressure differential in wide capillaries at low Knudsen numbers calculated, using irreversible thermodynamics 02 p0343 A67-12678
- Radiation from flames and chemical perturbations of atmosphere, examining flame structure, irreversible processes, photoemissive events, etc 04 p0721 A67-14701
- Nonequilibrium thermodynamics of irreversible processes in approach based on fundamental inequality derived from second law of thermodynamics 04 p0718 A67-15925
- Constitutive equations derived based on thermodynamics of irreversible processes and coupled thermoelasticity, formulating variational and reciprocity theorems 05 p0910 A67-16165
- Solution to chain of kinetic gas equations, showing effect of fast reversible and slow irreversible processes on particle distribution function 05 p0847 A67-17541
- Validity of Onsager-Casimir reciprocal relations with theoretical framework of macroscopic nonequilibrium thermodynamics 07 p1268 A67-19574
- Moment stresses in thermoelasticity for medium described in terms of displacement and rotational vectors 10 p1720 A67-23599
- Matched asymptotic expansions method for developing higher order approximations to structure of laminar detonation wave supported by irreversible unimolecular chemical reaction 11 p1749 A67-23858
- Dynamical irreversible evolution of gas with short range repulsive forces, using n-particle distribution function with many-body interactions 11 p1824 A67-25077
- Thermo- and viscothermoelasticity foundations and problems 13 p2216 A67-26608
- Onsager formalism of irreversible thermodynamics applied to steady state laminar hydromagnetic energy conversion, analyzing nature of coupling 13 p2055 A67-27001
- Book on thermodynamics of irreversible phenomenon in liquid metals including Onsager symmetry relations, phenomenological theory, nuclear magnetic resonance, galvano- and thermomagnetic phenomenon, etc 17 p2968 A67-32233
- Hamiltonian description of irreversible steady state phenomena and elements of turbulence theory, noting entropy production 19 p3210 A67-35539
- Type II superconductors properties, studying Ginzburg-Landau equations, vortex lines, reversible magnetic behavior and irreversible phenomena in mixed state 19 p3307 A67-35868
- Superconducting niobium wire magnetic moment and heat development during external magnetic field variation, discussing irreversible behavior 20 p3511 A67-37240
- Time symmetry in oscillating cosmologies with locally irreversible processes, obtaining formalism for statistical processes and boundary conditions 21 p3706 A67-38844
- Nonequilibrium thermodynamics canonical equations determination on basis of variational principle for transport equations governing irreversible processes 22 p3918 A67-39786
- Book on thermoelasticity associating elasticity and heat conduction theories for thermodynamics of irreversible processes and differential equation problems 24 p4246 A67-41891
- IRROTATIONAL FLOW**
- Existence and stability of uniform rotation of heavy blunt profile immersed in perfect incompressible irrotational fluid flow 05 p0792 A67-16595
- Book on principles of ideal fluid aerodynamics covering vector algebra and calculus, Euler equations, steady and unsteady acyclic motion, complex variable, lift, etc 05 p0793 A67-17151
- Irrotational fluctuations near turbulent boundary layer in Phillips theory and relation between one- and two-dimensional wave number spectra 08 p1320 A67-20705
- Impossibility of three confluent shocks in two-dimensional irrotational flow proved independently of state equation form 08 p1322 A67-21383
- Swirl effect on nozzle flow applied to solid propellant nozzles assuming irrotational flow so that tangential velocity field has free vortex characteristics 19 p3311 A67-34826
- Exact solutions of incompressible Navier-Stokes equation for irrotational Beltrami nonconvective two-dimensional swirl and axially symmetric cross flows 21 p3609 A67-37737
- Integral equation for discontinuous flows and free streamline solutions for axisymmetric bodies at zero and small angles of attack 22 p3743 A67-40166
- Objective criteria for irrotational flow in geostrophic, isobaric and thermal wind flow 24 p4180 A67-41788
- Irrotational gas jet impinging on and depressing infinite liquid surface, discussing streamlines and rippling 24 p4144 A67-42585
- ISCHEMIA**
- Cannulation of renal capsular lymphatics in anesthetized dogs, testing if lymph fluid can serve to assess tissue oxidation 06 p0952 A67-17853
- ISENTROPIC PROCESS**
- Wave solutions for plane waves propagating in isotropic elastic solid using isentropic approximation 01 p0162 A67-10847
- Hugoniot equation of state of alkali metals, using technique based on isentropic

sound speed measurement at room temperature 06 p1032 A67-18141
Hypersonic boundary layer behavior in adverse pressure gradients used in designing high Mach number intake diffuser system 06 p0942 A67-18750
Isentropic compression due to motion of heavy piston in gun tunnel noting nozzle throat effect on motion and stagnation pressure 11 p1773 A67-24577
Equations for arc length derived for two-dimensional isentropic compression surface for ideal gas 22 p3742 A67-40102

ISIS-A

LF modulation technique used aboard Canadian ionospheric research satellite ISIS-A for tape recording of signals with VLF components 08 p1298 A67-20662

ISIS SATELLITE

International Satellites for Ionospheric Studies /ISIS/ program using radio sounders 01 p0057 A67-10293
Thermal design of Isis A spacecraft, noting possibility of passive thermal control and computer programmed multinode heat balance analysis 05 p0904 A67-16294

ISOBAR

Experimental study of turbulent transfer phenomena in isobaric mixing layer of supersonic flow containing preexisting boundary layer [ONERA-TP-327] 01 p0054 A67-11003

Four-momentum transfer, inelasticity and mass of target isobars in cosmic ray jets 07 p1246 A67-20278

Analytic representation of absolute topography of isobaric surfaces by linear combination of arbitrary surfaces represented by Chebyshev polynomials 21 p3654 A67-38087

ISOBUTYLENE

S POLYISOBUTYLENE

ISOCYANATE

Klegocell G-300 mechanical and thermal properties tested for thermal insulation for cryogenic stage for liquid hydrogen on space vehicle 13 p2228 A67-27659

ISOLATION

SA SOCIAL ISOLATION

Two 15-day experiments of three subjects performing work-rest cycles in isolation chamber studying psychological functions, cardiovascular system, etc 16 p2813 A67-30912
Degree of isolation between radar tracking data and motion of ship determined, using frequency domain 20 p3415 A67-36555

ISOLATOR

Magnetic delay line vibration isolation system as heart of airborne special purpose computer in USN E-2A early warning aircraft 05 p0779 A67-17458
Buckling isolator system for carrier aircraft landing and catapult shock environment allowing use of available clearance for dynamic deflection 05 p0814 A67-17459

Faraday effect optical isolator for IR region using lead glass rod in magnetic field as nonreciprocal element 09 p1500 A67-22425

Microwave field distribution in waveguide partially filled with solid state plasma for application to isolator 13 p2076 A67-26521

Optimization for linear vibration isolators considering vibration clearance tradeoff for random base motion 16 p2703 A67-31642

IR technology and electromagnetic spectrum, discussing manufacture of circulators and isolators using Faraday rotation in InSb 22 p3835 A67-39213

Damping constant of electromagnetic wave in plane parallel waveguide with ferrite resonant isolator, using perturbation theory, considering dielectric and magnetic losses 22 p3770 A67-39659

Nonreciprocal waveguide device consisting of ferrite loaded coaxial branch and crystal diode useful as isolator, modulator and filter 22 p3774 A67-40459

ISOMER

Free radical addition of perfluoroacetonitrile to vinyl fluoride, noting formation of one isomeric compound 09 p1459 A67-22365

Gamma decay of Se 73 and Se 81 isomeric pairs with half-lives, energies and decay schemes 11 p1822 A67-23980

Absolute cross sections and isomeric yield ratios for d,p reactions up to 15 mev in various metals 14 p2350 A67-27790

ISOMERIZATION

Isomerization rate of iminocarbonates,

discussing electronegative hetero-atom bonded to imino carbon 09 p1459 A67-22363

ISOPERICMETRIC PROBLEM

Estimation of lower bounds to minimum Rayleigh number inducing state of convective motion in quasi-incompressible fluid with temperature gradient in body force direction 17 p2968 A67-32410

ISOPHOTE

Comet disintegration as basic source of interplanetary dust based on zodiacal isophots 04 p0701 A67-15559

Isophotes of extended light sources in night sky, Stokes parameters, brightness and degree of polarization for Rayleigh-scattered light in earth atmosphere 08 p1326 A67-21243

Comet Burnham C2 coma photometry, discussing error sources in isophotes and photometric scale and tabulating oval isophote size against axes mean ratio 17 p2943 A67-32442

Lunar charting for selenocentric coordinates from densitometric analysis and altitude measurements, using photometric methods and Isodensitracer 18 p3049 A67-34333

Moon elevation profiles and lunar slopes determined by photometry and isodensitometric measurements of Ranger IX photographs 18 p3133 A67-34335

ISOSTATIC PRESSURE

Gas pressure bonding for hot isostatic pressing of beryllium powder into complex shapes 13 p2123 A67-27131

ISOTHERMAL FLOW

Nonisothermal steady state flow of fluid with constant density and kinematic viscosity coefficient past thin plate 04 p0603 A67-14710

Approximate relations for solution to equations of nonisothermal laminar boundary layer 04 p0722 A67-14711

Stability of arbitrary one-dimensional hydrodynamical flow in quasi-isothermal case 13 p2105 A67-27413

Steady state fluid flow in thin passage analyzed using energy model and including compressibility effects 14 p2302 A67-28264

Frictional pressure drop for isothermal incompressible flow in isosceles triangular duct, with correlations for laminar and turbulent flow [ASME PAPER 67-FE-18] 14 p2243 A67-28365

Steady state laminar and turbulent mixing in unsteady isothermal flow in wake behind body with incident shock wave 18 p2984 A67-34203

Diffusion of free isothermal turbulent jet of incompressible fluid flowing from nozzle into coaxial surrounding uniform stream 19 p3209 A67-35443

Thermally induced boundary layer flows in isothermal rigid body rotation 20 p3421 A67-36843

Stabilization conditions of isothermal plasma drift in magnetic trap for comparable electron and ion temperatures 21 p3663 A67-37996

Constant acceleration flows applied to high speed fixed geometry guns using H propellant in constant projectile acceleration problem 23 p3992 A67-41716

ISOTHERMAL LAYER

Turbulent velocity fluctuation field in isothermal boundary layer with homogeneous injection and combustion [AIAA PAPER 65-820] 01 p0054 A67-11169

Heat transfer in viscous fluid flow in gap between permeable isothermal surface and rotating disk, solving energy equation 03 p0536 A67-13611

Photogrammetric refraction in high altitude surveying for isothermal atmosphere and for atmospheric polytropic through altitude of 11 km 05 p0808 A67-17033

Generation of oscillations in solar atmosphere by separate granules modeled by bottom zone of isothermal gravitating photospheric layer overlaid by hot corona 10 p1704 A67-22721

Moisture transfer and thermal influx equations solutions for atmospheric boundary conditions of preinversion intramass strata evolution scheme 11 p1816 A67-24522

Emissivity and absorptivity of infinite length isothermal trapezoidal grooves with radiating gray walls 18 p3159 A67-34055

Heat transfer in viscous fluid flow in gap between permeable isothermal surface and rotating disk, solving energy

equation 18 p3161 A67-34476

Thermal boundary layer theory for steady cellular convection in viscous rotating flow 20 p3553 A67-36937

Photogrammetric refraction in high altitude surveying for isothermal atmosphere and for atmospheric polytropic through altitude of 11 km 21 p3627 A67-38265

Ducted acoustic gravity wave propagation in isothermal atmosphere, obtaining dispersion relations ducted modes and surface wave in incompressible medium 21 p3623 A67-39057

Local coefficient of heat exchange by natural convection on isothermal vertical flat plate in turbulent regime 22 p3917 A67-39648

Coronal line spectra of 1952 total solar eclipse, noting emitted energies and isothermic coronal region 22 p3889 A67-40206

Self-gravitating isothermal nonrotating gas layer stability, discussing amplitude density distributions in space 24 p4225 A67-41826

Benzene and related molecules adsorption on uniform graphite surfaces investigated for lateral interaction and localization of lattice sites 24 p4118 A67-42195

ISOTHERMAL PROCESS

Isothermal steady state process of fluid with constant density and kinematic viscosity coefficient flowing past thin plate 04 p0603 A67-14709

Carbide forming elements effect on kinetics of isothermal transformation of austenite and mechanical properties of manganese-molybdenum steel 07 p1199 A67-19239

Isothermal transformation diagrams for titanium-molybdenum alloys 07 p1199 A67-19243

Isothermal transformations in hypo- and hypereutectoid titanium-chromium alloys 07 p1200 A67-19244

Hydrogen effect on stability of beta phase in alloy VT15 18 p3065 A67-34291

Accumulated plastic deformation during sequence of isothermal and nonisothermal loading 19 p3242 A67-34887

Radiant heat transfer computations from gray isothermal dispersions with isotropic scattering, using approximation methods and integrodifferential equation [ASME PAPER 67-HT-8] 20 p3544 A67-36706

ISOTOPE

SA DEUTERIUM

SA RADIOACTIVE ISOTOPE

SA TRITIUM

Age determination of iron meteorites by comparing isotopic abundance of primordial potassium in inclusions with terrestrial standards 02 p0326 A67-12044

Isotope effects in gamma radiolysis at 77 degrees K of mixed water and deuterium oxide ice systems 04 p0658 A67-15508

Helium isotope formation in cosmic rays during light nuclei fragmentation due to high energy proton interaction 05 p0878 A67-16093

Fabry-Perot interferometers with electronic determination of Doppler line widths, discussing effect of hyperfine and isotopic structure 07 p1185 A67-19399

Diffusive fractionation and two-component models for trapped meteoritic neon and isotopic composition of neon in carbonaceous chondrites 07 p1249 A67-19536

Origin of fissionogenic Xe isotopes in Pasamonte achondrite 08 p1386 A67-20938

Solar spectrum reexamination determining lower limit for C12/C13 isotopic abundance ratio in photosphere [AFCRL-67-0480] 09 p1566 A67-22231

Stable isotope distribution in carbonates 14 p2310 A67-27970

Age determination of iron meteorite by Rb-Sr isotopic analyses of silicate inclusions, proving formation of younger solid objects in solar system 16 p2749 A67-31434

Isotopic composition and abundance of xenon and krypton in graphite of iron meteorite from Canyon Diablo examined for anomaly pattern 16 p2750 A67-31438

Helium and neon content and isotopic composition in iron meteorites, noting He 3 deficiency in hexahedrites due to tritium loss 17 p2942 A67-32359

Abundance of stable isotopes of neon, argon, krypton and xenon in Costilla Peak iron meteorite, observing spallation components 21 p3702 A67-38124

Krypton isotope composition in three unequilibrated and two gas rich chondrites,

with correction for cosmic ray spallation 22 p3881 A67-39494
Rare gas isotopic analysis using ruby pulsed laser and mass spectrometer 22 p3816 A67-40241
Li isotopic composition and abundance in chondrites and iron meteorites measured, noting implications for earth and meteoritic parent body formation 24 p4235 A67-42632
Helium isotope formation in cosmic rays during light nuclei fragmentation due to high energy proton interaction 24 p4213 A67-42769

ISOTOPE SHIFT
Rotational intensity distribution of vacuum UV absorption spectrum bands of carbon monoxide arising through mixing of D state with neighboring states 02 p0269 A67-12450
Isotope substitution effect on natural frequencies of vibrational-rotational transitions in diatomic and triatomic molecules and generation of new IR maser frequencies 05 p0816 A67-16634
Large deuterium isotope effect on fluorescence emission spectra and quantum yields observed in number of chromospheres that contain proton donor groups 05 p0758 A67-16701
Line-narrowing effect induced by laser radiation applied to measurements of isotope shifts for two optical transitions in neon 13 p2127 A67-27080
Isotope shifts measurement in IR with variable length laser cavity 20 p3439 A67-36355
Ammonia inversion transition hyperfine structure for nitrogen 14 and 15 nuclear masses measured with two-cavity maser spectrometer 20 p3462 A67-37565

ISOTOPIC SPIN
Isospin impurity mixing in distorted deuteron reaction 02 p0270 A67-12526
Granular superconductor with thin insulating layer at boundary of each homogeneous superconductor grain, using isospin formulation of microscopic theory 10 p1687 A67-22763

ISOTROPIC MEDIUM
Local three-dimensional static and dynamic contact reactions between elastic isotropic bodies 01 p0158 A67-10216
Stressed state in isotropic medium weakened by row of curvilinear holes, considering approximate effect of adjacent holes on concentration of stresses around each hole as loaded 01 p0158 A67-10217
Stability and free oscillations of three-layer plates of symmetrical structure with isotropic outer layers and light transversal isotropic filler and weakened by central rectangular cut-outs 01 p0158 A67-10219
Reinforcing round hole in isotropic plate by elastic gasket or thin multicomponent ring consisting of set of homogeneous component rings sweated together 01 p0158 A67-10222
Second-order effects in propagation of elastic waves through homogeneous isotropic media 01 p0113 A67-10405
Universal relations for static deformations in isotropic compressible elastic bodies determined by method that may be applied to isotropic incompressible elastic bodies 01 p0162 A67-10799
Equations for nonlinear wave propagation in incompressible heat-conducting elastic material, noting propagation of shocks in isotropic material 01 p0162 A67-10846
Wave solutions for plane waves propagating in isotropic elastic solid using isotropic approximation 01 p0162 A67-10847
Elastic equilibrium of isotropic plane weakened by bi-periodic series of identical circular holes with sealed-in elastic rings of different material 02 p0340 A67-12659
Boundary value and contact problem solution using elasticity theory for transversely isotropic layer 03 p0529 A67-14165
Scattering of plane wave by grating of identical cylinder specialized for case in which individual elements of grating scatter isotropically 03 p0374 A67-14353
Displacement and stress fields in isotropic elastic solids determined by integrating displacements for point nuclei of strain 04 p0711 A67-15102
Radiative heat transfer and intensity distribution in one-dimensional absorbing isotropic scattering medium 04 p0737 A67-15862

Relations between mean stresses and strains of elastic body consisting of soldered isotropic layers, noting thermal effect 05 p0912 A67-16184
Transverse elastic impact of isotropic sphere against thin rectangular anisotropic plate 05 p0922 A67-17174
Temperature distribution in isotropic solid with variable specific heat and thermoconductivity treated by Kantorovich method 05 p0929 A67-17373
Boundary value analysis of static problems of transversely isotropic solid and hollow elastic cylinders 06 p1099 A67-17864
Radiation transport theory and spatial radiative heat transfer in absorbing and isotropically scattering medium 06 p1118 A67-18552
Penny shaped crack embedded in isotropic material treated by linear elasticity, noting stress singularities 06 p1109 A67-18732
Iterative solution for spherically symmetric mutual coherence function representing radiation propagating through statistically homogeneous and isotropic random medium 09 p1460 A67-21592
Isotropic scattering of radiation in finite two-dimensional atmosphere using integral equation, solved by power series 09 p1532 A67-21662
EH solutions of Maxwell equations describing guided electromagnetic waves in homogeneous isotropic medium at velocity of light 09 p1465 A67-22550
Fibrous model of shell shaped grid noting discrete network, properties of cross section surface and stress 10 p1715 A67-22920
Thermal stress distribution around crack in elastic solid of transversely isotropic material 10 p1716 A67-22934
Elastic deformation of unbounded transversely isotropic body with internal plane circular slot under slot surface load 11 p1876 A67-24681
Bending under transverse load of isotropic plate with elastic base, using Ambartsumian theory of anisotropic plates 11 p1878 A67-24857
Thermal stresses in isotropic plate analyzed using Hankel transform, obtaining surface temperature for various cases 14 p2402 A67-28813
Coherent scattering of solar radiation in uniform isotropic medium containing point source surrounded by cavity 15 p2549 A67-29144
Time-dependent Green function for moving isotropic nondispersive medium 15 p2509 A67-29199
Numerical calculation of self-focusing of axisymmetric electromagnetic-wave packets in nonabsorbing cubic isotropic media based on parabolic equation 16 p2628 A67-31504
Thermodynamic aspects of energy studied in forms of localized and isotropic magnitude and motion in single direction 16 p2780 A67-31557
Modal interference of VLF radio waves investigation from field strength data, noting isotropic case 16 p2631 A67-31850
Fields generated by infinitesimal, arbitrarily oriented, electric-dipole source located in isotropic medium bounded by parallel plane-stratified, anisotropic media 16 p2632 A67-31858
Singularities due to concentrated couples in infinite linear elastic isotropic Cosserat continuum, noting dissimilar singular solutions 17 p2964 A67-33141
Dispersion of longitudinal or extensional waves in isotropic linear elastic bars with rectangular cross section [ASME PAPER 67-APM-17] 17 p2964 A67-33148
Primary diffuse X-ray flux and spectrum found isotropic by balloon measurements made in three particular directions 19 p3313 A67-35244
Progressing wave method for linear partial differential equation systems, including Maxwell equations, applied to electromagnetic waves from moving sources 19 p3184 A67-35665
Media with cold homogeneous isotropic lossless plasma dispersion characteristics exhibiting no electromagnetic drag 19 p3298 A67-35828
Iterative solution for directional emissivities of two-dimensional semiinfinite slab of absorbing-scattering medium with gray isothermal dispersion

[ASME PAPER 67-HT-12] 20 p3545 A67-36710
Antenna array radiation pattern in isotropic linear medium by radiation pattern synthesis in moving medium 21 p3598 A67-38607
Numerical data for plane thermal stresses in isotropic elastic square plate bounded by edge stiffeners and under symmetric temperature distributions 23 p4073 A67-40611
Impedance of dipole antennas in isotropic He plasma measured at X band 23 p3979 A67-40833
Three-dimensional heat conduction, heat and mass transfer and thermoelasticity problems solved by approximate method using functional parameters 23 p4083 A67-41290
Composite, reinforced and porous elastic body isotropic deformation, deriving macroscopic moduli, mean stress and strain values and dispersion 24 p4249 A67-42102
Coherent scattering of solar radiation in uniform isotropic medium containing point source surrounded by cavity 24 p4222 A67-43067

ISOTROPIC TURBULENCE
Decay of dynamically passive reactant in stationary isotropic turbulent velocity field investigated, using direct interaction and modified quasi-normal closures 02 p0234 A67-12549
Inertia and pressure effects on energy potential of homogeneous and isotropic turbulence in weakly compressible medium 02 p0235 A67-12643
Cosmic ray isotropy mechanism, examining plasma beam instability and cosmic ray scattering at plasma turbulent pulsations 04 p0693 A67-15554
Approximate calculation of local characteristics of sound waves into liquid and gaseous media 05 p0846 A67-16707
Stratospheric free air turbulence detection from slant-range FPS-16 radar tracked Jimsphere balloons 10 p1676 A67-22815
Model ionosphere with homogeneous isotropic turbulence investigated for values of kinematic viscosity and dissipation rate of turbulent energy determined from rocket measurements 10 p1646 A67-23273
Four-plasmon hydrodynamic equations describing weak turbulence spectrum in universal equilibrium region of plasma without magnetic field 10 p1686 A67-23597
Mutual coherence factor for plane electromagnetic wave propagating in stochastic locally homogeneous and isotropic medium of dielectric turbulence 11 p1818 A67-24415
Approximate calculation of local characteristics of turbulence developing during intense injection of sound waves into liquid and gaseous media 11 p1820 A67-24929
Weak random initial magnetic field evolution in highly conducting isotropically turbulent fluid, noting exact initial growth expression of magnetic energy spectrum 15 p2469 A67-29223
Initially isotropic turbulence, characterized by three dimensionless numbers, suppressed by applying uniform magnetic field 15 p2471 A67-29656
Wall-turbulence interaction for infinite flat plate inserted into homogeneous isotropic turbulence, measuring growth of inhomogeneity layer 17 p2837 A67-32286
Maintenance of electromagnetic field by dynamo effect in homogeneous isotropic turbulence without mirror symmetry 17 p2883 A67-32355
Grid geometry effect on longitudinal and lateral turbulence intensities, determining decay rate dependence 18 p3030 A67-34740
Viscoelastic theory solving Lighthill paradox by accounting for acoustic energy damping in fine grained isotropic turbulence 21 p3610 A67-37759
Viscoelastic fluid isotropic turbulence decay approximating non-Newtonian effects by perturbation method 22 p3787 A67-40221
Turbulence onset from small eddies in shear flow analyzed by nonlinear approach 23 p3990 A67-41173

ISOTROPISM
SA ANISOTROPY
SA SPATIAL ISOTROPY
Isotropic mass loss effect on binary star system orbital elements and period eccentricity relationship 08 p1380 A67-20385
Sandwich plate problem involving subjection to concentrated force of plate

having filler flexural rigidity only, giving solution in form similar to that of thin isotropic plate 10 p1716 A67-22937

Faint radio sources investigated for isotropy applying Scheuer statistical method rendering quasars local origin theory improbable 16 p2752 A67-31623

Series solution for end effect in semilinear transversely isotropic cylinders, noting elastic analysis 17 p2962 A67-33014

Radiant heat transfer computations from gray isothermal dispersions with isotropic scattering, using approximation methods and integrodifferential equation [ASME PAPER 67-HT-8] 20 p3544 A67-36706

ITALIAN SATELLITE

S SAN MARCO SATELLITE

ITALY

Genoa airport construction problems on land reclaimed from sea 05 p0789 A67-17100

Air transport effect on Italian balance of payments 08 p1429 A67-20767

Plaggio-Douglas PD-808, Italian executive jet emphasizing safety [AGARDOGRAPH 95] 15 p2422 A67-30399

Italian scientific research program during IQSY, with summarization of preliminary results 19 p3223 A67-35480

ITERATION

Linear fractional programming application to Markov renewal programming, determining stationary optimal policy for cost/time minimization 07 p1218 A67-20269

Iterative algorithm for increasing stability of adaptive control systems 08 p1308 A67-20319

Rational iteration function with high order convergence for solving equations compared with other methods 08 p1349 A67-21258

Schroeder fixed point theorem for convergence rate of iteration series extended to concave operators which need not remain constant 14 p2345 A67-28937

ITERATIVE NETWORK

Iterative realization of pattern recognition networks consisting of multilayer of linear threshold elements 02 p0208 A67-12174

ITERATIVE SOLUTION

Successive approximations to determine vector in theory of optimal control 01 p0043 A67-10236

Algorithm based on penalty functions to determine hyperplane used as iterative solution for separating convex sets 01 p0028 A67-10495

Simultaneous effect of transverse curvature and fluid injection on boundary layer flow over parabola of revolution, obtaining iterative solution to differential equation 01 p0055 A67-11175

Receptance and support receptance methods in iterative solution of torsional vibration problems 01 p0164 A67-11271

Slide rule for calculating liftless free-flight trajectories in resisting media by iteration technique 02 p0240 A67-11553

Block successive overrelaxation method /BSOR/ compared with direct method for solving fourth order partial differential equation 02 p0258 A67-11800

Iterative procedure for computing fixed-time fuel-optimal controls for problem of hitting hypersphere centered at origin at state space 02 p0303 A67-12149

Iterative procedure for changing constraint minimization problem to mathematical programming formulation in solving discrete terminal control problem 02 p0226 A67-12152

Exact and approximate solutions to Cauchy problem for nonlinear wave equation in affine connection field theory 03 p0457 A67-13171

Dynamic system with unknown parameters identified through iterative and least squares methods suitable for computer programming 03 p0392 A67-13658

Asymptotic rate of convergence of Gauss-Seidel type iterative processes for nonlinear difference equations 03 p0460 A67-13881

Iteration method applied to integral equations arising in structural mechanics problems 03 p0461 A67-14079

Triangular iteration method of vector-matrix equation, noting role of continuous function 03 p0462 A67-14328

Iterative solution for large deflection analysis of rotationally symmetric nonlinear membranes 04 p0715 A67-15658

Approximate method for measuring distance between head wave and tip of body

in supersonic flow past blunt tip body 04 p0550 A67-15894

Temperature induced in medium due to suddenly applied pressure inside spherical cavity investigated, using iteration method 05 p0910 A67-16148

Iteration method of general linear programming on digital computer using penalty functions compared to equilibrium problem of mechanical system 05 p0781 A67-16259

Function approximation from finite number of arbitrary points, using iteration methods 05 p0833 A67-16260

Matrix method formulation of vibration and stability problems yielding upper bounds for natural frequencies 05 p0917 A67-16301

Iterative method determination of output signal, impulse response and transfer function of variable parameter linear sampled data system 05 p0784 A67-16705

Computer program for digital exact representation of spectral frequency and intensity-distribution by superposition of Gaussian components, applying least squares method, linearizing normal equations and analyzing observational errors 06 p0965 A67-18069

Generalized Stodola iteration method for computer analysis of axisymmetric buckling of ring-stiffened orthotropic shells of revolution [AIAA PAPER 67-109] 06 p1103 A67-18339

Fixed time fuel-optimal controls computed by iterative procedure developed by Pontryagin principle 06 p1097 A67-18522

Acceleration of iteration process convergence when dividing polynomial by quadratic trinomial, approximating curves for remainder coefficients by straight lines 06 p1025 A67-18557

Convergence of solution of nonlinear functional equations, noting iteration processes applications 07 p1215 A67-19329

Combination into unified setting of various results for approximate solution of fixed point equation, using iterative process 07 p1218 A67-20212

Identification of unknown transfer function in nonlinear sampled data systems, using iterative method 08 p1310 A67-20336

Iterative method for two-dimensional problem of incompressible viscous MHD free jet flow from thin slot in plane wall 08 p1361 A67-21143

Recurrence relation for determining asymptotic error constant of rational function iterative methods for solving equations 08 p1349 A67-21263

Optimum design of curve generating four-bar linkages with inequality constraint [ASME PAPER 66-MECH-20] 08 p1336 A67-21317

Boundary value problem for Poisson-Vlasov equations resulting from interaction of conducting body and supersonic flow of rarefied plasma solved, using iterative method 08 p1363 A67-21368

Iterative solution for spherically symmetric mutual coherence function representing radiation propagating through statistically homogeneous and isotropic random medium 09 p1460 A67-21592

Solution properties and stability for system of nonlinear difference equations 09 p1524 A67-21926

Approximation of zero of transcendental equation by iterative methods 09 p1468 A67-22049

Alternation direction methods /particular class of iterative methods/ applied to heat conduction problems 09 p1488 A67-22051

Electrode ends effect on flow of fluid in MHD generator, using iterative solution 09 p1549 A67-22563

Tesseral harmonics of coordinates using Baker-Nunn data and geopotential and dynamical procedures, noting iterative cycle for correction 10 p1636 A67-23178

Algorithm based on penalty functions to determine hyperplane used as iterative solution for separating convex sets 10 p1608 A67-23617

Controllability of quasi-linear systems proved by Picard classical method of successive approximation 10 p1681 A67-23682

Thirteen moment equation solved for problem of plane Couette flow by iteration scheme, showing functional dependence on Mach and Knudsen

numbers 11 p1774 A67-23863

Approximate iterative calculation of non-Newtonian supersonic gas flow past highly blunt bodies 11 p1741 A67-24156

Waveguide discontinuity problems solved through matrix iterative analysis 11 p1760 A67-24237

Flight time estimation methods for iterative solutions of optimum trajectories by numerical integration 11 p1859 A67-24436

Convex polyhedron theorem in determining whole set of optimal solutions in linear programming 11 p1814 A67-24979

Vibration characteristics of cantilever type pretwisted turbine blading, considering effects of taper, calculating frequencies and mode shapes 12 p2014 A67-25414

Stress concentration calculated at holes in shallow shells subjected to finite deformation via iteration method 12 p2023 A67-25594

Computer iteration scheme for calculating arbitrary hyperbolic transfer orbit in field of attracting center, based on Gaussian equations 12 p2002 A67-25640

Iteration solution for system of equations for nonlinear deflection and stability of anisotropic plates 13 p2217 A67-26632

Flat plate loading effects for large displacements, determining solution to plates of arbitrary shape under general loading by iterative matrix technique 13 p2217 A67-26704

Frequencies of turbine blade vibrations calculated by iteration method, considering coupling between bending and torsion 13 p2217 A67-26744

Correlation method for generating sensitivity coefficients of dynamic system on high speed iterative analog computer 13 p2073 A67-27061

Iterative methods for solving nonlinear least squares problems by choosing linear nonsingular transformations of finite-dimensional Euclidean space 13 p2147 A67-27171

Iterative numerical method for solving equations of single variable by using several approximations applied to parallel processing environment 13 p2148 A67-27487

Iteration process by difference scheme for numerical solution to Dirichlet problem of two-dimensional Poisson equation 13 p2148 A67-27613

Convergence of methods of tangential parabolas and hyperbolas used in nonlinear equation solution with nondifferentiable operators convergence of methods of tangential parabolas and hyperbolas used in nonlinear equation solution 13 p2149 A67-27619

Magnification problems facing aircraft designers analyzed by computerized iterative procedures 14 p2245 A67-28062

Qualitative analysis of nonlinear systems described by ordinary or partial differential equations or by functional equations 14 p2291 A67-28452

Stellar pulsational instability phenomena calculated numerically for infinitesimal amplitude of central core motion 14 p2392 A67-28996

Iterative procedures for elastic, plastic and creep deformation of beams 14 p2339 A67-29003

Optimal control applications of Fletcher-Reeves conjugate gradient minimization method and comparison with second variational technique 15 p2456 A67-29362

High accuracy alternating direction implicit difference schemes for biharmonic, heat conduction and Laplace equations 15 p2510 A67-29520

Unique iterative solution to degenerate quasi-linear elliptic equations and systems 15 p2511 A67-30001

Limitations of observability and controllability of dynamic system determined, using approximation of performance matrix and iterative procedure 15 p2461 A67-30316

Control system identification for noise corrupted input/output data, using algorithmic approach and iteration procedure 15 p2461 A67-30320

Process identification by cyclic parameter adjustment with automatic iteration, using analog and hybrid computers 15 p2465 A67-30342

Successive overrelaxation iterative method for solving elliptic partial differential

equations 16 p2695 A67-30830
 Optimal nonlinear filter construction for steady-state random process correction using iterative method 16 p2636 A67-30925
 Monotone iterations for nonlinear elliptic differential equations in boundary-value problems applied to Gauss-Seidel methods 16 p2697 A67-31331
 Iterative technique for calculating electromagnetic propagating structures with nonuniform gross perturbations obtaining convergence improvement 16 p2626 A67-31346
 Iterative solution methods for minimizing convex, differentiable function in Euclidean space 16 p2697 A67-31424
 Coaxial and magnetohydrodynamic waveguide matching obtaining reflection coefficient of former and wave amplitude of latter 16 p2722 A67-31575
 Iterative guidance mode with application to three-dimensional upper stage vacuum flight 17 p2881 A67-32058
 Iterative procedure for solving linear differential equations with given boundary conditions on analog computer 17 p2818 A67-32296
 Iterative on-line reliability calculation of automatically repaired space computer, noting reliability and performance 17 p2820 A67-32501
 Iterative method for design of bullet-like fairing, giving subsonic subcritical flow with desired velocities at junction of two wings 17 p2791 A67-32586
 Linear boundary value problem solution using iterative method 17 p2877 A67-32678
 Iterative solution of boundary value problem for optimal trajectory, applying smoothing procedure 17 p2830 A67-32869
 Iterative solution through boundary value problem and integral equations for axisymmetric deformation of body remote from symmetry axis 17 p2962 A67-32874
 Noise removal and deconvolution techniques applied to resolution of beam collision experiments 17 p2886 A67-33261
 Iterative methods for integration of linear partial differential equations, determining relaxation factor 18 p3071 A67-33753
 Lunar forced physical librations calculation improved by using digital computer programmed to generate iterative solutions 18 p3129 A67-34307
 Nonlinear effect of gravitational instability in expanding universe, calculating second-order density perturbations by iteration method 19 p3317 A67-34891
 Spacecraft performance, operation and design optimization solved by variational analysis [AIAA PAPER 67-557] 19 p3174 A67-35954
 Inference of vehicle and atmosphere parameters from free flight motion measurements using iterative calculations of parameter values 19 p3337 A67-35996
 Iterative guidance mode /IGM/ applied to effective gravity vector prediction, acceleration measurement of noise sensitivity and energy limitations [AIAA PAPER 67-620] 19 p3260 A67-36009
 Second order nonlinear parabolic type partial differential equations with divergence structure, noting role of maximum principle 20 p3475 A67-36502
 Intersection points for satellite orbit and earth shadow /shadow equation/ solved for small eccentricities by iteration 20 p3523 A67-36624
 Iterative solution for directional emissivities of two-dimensional semiinfinite slab of absorbing-scattering medium with gray isothermal dispersion [ASME PAPER 67-HT-12] 20 p3545 A67-36710
 Stochastic models for forecasting seasonal and nonseasonal time series using iterative method 20 p3477 A67-36790
 Iterative technique applied to solution of problems in elasticity involving minimization of double integral subjected to certain boundary conditions 20 p3541 A67-37487
 Wave propagation in nonuniform slightly gyrotropic medium with parameter less than one solved by differential equations 20 p3389 A67-37708
 Controllability of quasi-linear systems proved by Picard classical method of successive approximation 21 p3653 A67-38283
 Controller design for booster gust alleviation, considering stochastic minimization problem solved by iteration yielding linear finite time controller with

time-varying gains 22 p3897 A67-39162
 Reflection coefficient for arbitrary lossy waveguide with large number of identical periodically positioned inhomogeneities determined by iteration 22 p3770 A67-39661
 Iterative guidance mode, deriving alternate expressions for thrust direction control angle for time savings on Saturn launches 22 p3831 A67-39957
 Integral equations with integral operators and excitation frequencies for forced oscillation, solving friction via orthogonal iteration approximation 22 p3916 A67-40454
IVUNA METEORITE
 Magnetite crystals of asymmetrical shape observed in Alals, Ivuna and Orgeu carbonaceous meteorites noting particle corrosion 22 p3881 A67-39496

J

JACKING EQUIPMENT

Synchronization errors in parallel jacks system with closed loop control by hydraulic relays, using nonlinear differential equations [ASME PAPER 66-WA/AUT-5] 04 p0555 A67-15389

JACOBI INTEGRAL

Reduction of differential equations of Hill lunar problem using Jacobi integral 08 p1382 A67-20396
 Two-dimensional isothermal liquid flow electrically conducting in channel under electromagnetic fields, finding self-modeling solutions using Jacobi functions 09 p1544 A67-21861
 Doubly symmetric orbits about collinear Lagrangian points, computing jacobians eigenvalues 13 p2205 A67-27482
 Mathematical investigation of satellite motion in vicinity of critical inclination, analyzing singularity 14 p2384 A67-28077
 Restricted three-body problem in post-Newtonian approximation, obtaining equations of motion 17 p2943 A67-32441
 Bounded isoenergetic displacement of periodic orbits in restricted circular three-body problem 18 p3135 A67-34542
 Integrals of motion in plane elliptic restricted three-body problems for orbits with small eccentricity near primaries 18 p3136 A67-34588
 Conformal representation using Jacobi and Welterstrass elliptic function applied to extremal problems, noting electric modeling solutions 23 p4023 A67-40924

JACOBI MATRIX METHOD

Spectral properties of two possible generalizations of Jacobi matrices for use in difference methods for numerical solutions of differential equations 03 p0460 A67-13820
 Stability theorem for damped dynamic systems based on commutativity of class of mathematical models 06 p1099 A67-17644

JACOBI POLYNOMIAL

Contact problem of half-plane inelasticity theory using Jacobi polynomials and taking into account thermal stresses and presence of adhesion and friction in contact area 11 p1876 A67-24677
 Singular integral equations with constant coefficients solved by Jacobi polynomials and applied to problems in fluid dynamics, crack propagation, plane elastic theory, etc 11 p1813 A67-24678
 Mechanical quadrature theory and convergence problems 13 p2148 A67-27469
 Approximate solutions of spatial distributions of charged particles as gas discharge plasma obtained by two-point Jacobi expansion method 16 p2720 A67-31241

JAHN-TELLER EFFECT

Static Jahn-Teller effect on impurity centers in semiconductors, discussing nature and magnitude of splitting of ground state 10 p1694 A67-23593
 Far IR absorption spectra of chromium and titanium ions in aluminum oxide crystal, indicating Jahn-Teller effect reduction of trigonal field and spin-orbit coupling 14 p2370 A67-28714
 Second order phase transitions in ionic crystals caused by vibronic interaction analogous to Jahn-Teller effect in ideal crystals 16 p2726 A67-30813

JAMMING

Selection of optimum ranging signal for

jam resistant satellite communications system 06 p0959 A67-17671
 Three-dimensional chaff simulator to provide video inputs to operational radar equipment for exposing operators to jamming 08 p1314 A67-20656
JAPAN
 Quality control around twin turboprop utility plane MU-2 at experimental stage 05 p0812 A67-17245
 Book on Japans activities in space exploration including 1966-1967 programs 17 p3136 A67-34618
 Japanese national report on space research to COSPAR 19 p3321 A67-35300
 IQSY research activity in Japan, experiments and progress 19 p3223 A67-35481
JAVELIN ROCKET
 Rigid body ejection dynamics of split-fairing system for four-stage Javelin sounding rocket under various parameter changes 08 p1408 A67-20536
JEANS THEORY
 Stability of rotating liquid mass /e.g. earth/, following Jeans treatment of Jacobi ellipsoidal equilibrium configurations 06 p1080 A67-17768
 Effect of thermal escape on neutral hydrogen density above 120 km 07 p1181 A67-19938
 Plane wave disturbances in infinite rotating collisionless system for wave vector normal to axis of rotation [AD-653420] 16 p2753 A67-31700
 Galactic rotation effects on gaseous spiral arm stability for magnetic critical wavelength less than Jeans critical wavelength case 22 p3893 A67-40506
 Magnetogravitational instability of uniformly rotating compressible medium due to variable amplitude perturbations, stressing Jeans theory 23 p4033 A67-41019
JENSEN THEORY
 Sunspot appearance and stars with pulsating magnetic field from Jensen theory of magnetic tubes 12 p2000 A67-25135
JET
 S AIR JET
 S ANNULAR JET
 S ARC JET
 S EXHAUST JET
 S FLUID JET
 S FREE JET
 S GAS JET
 S LAMINAR JET
 S PERIPHERAL JET
 S PLASMA JET
 S REACTION JET
 S SUPERSONIC JET
 S TURBULENT JET
 S TWIN JET
 S TWO-DIMENSIONAL JET
 S VAPOR JET
 S WALL JET
JET AIRCRAFT
 Jet aircraft noise alleviation problems near national airports noting noise limits fixations, engine noise reduction, steeper takeoff and landings, etc [AIAA PAPER 66-909] 02 p0181 A67-12274
 Design and market research aspects of Hamburger HFB 320 jet executive aircraft 03 p0357 A67-12970
 Stalling in swept wing jet aircraft with reference to satisfying airworthiness regulations and aerodynamic problems 03 p0362 A67-14300
 Airline viewpoint on air traveler handling and airport problems and effects of new jet aircraft [AIAA PAPER 66-845] 04 p0595 A67-14978
 Executive jet aircraft Hamburger Flugzeugbau HFB 320 Hansa development, testing and production 07 p1129 A67-19670
 British aircraft one-eleven 500 series, detailing stretched version, flight tests to begin in August 1967 with aerodynamic prototype 11 p1743 A67-24039
 Three STOL commercial transports performance and cost compared with conventional transports 12 p1894 A67-25492
 Thrust reversers for business jet aircraft noting limitations, performance gains, technical aspects of analysis and testing, etc [SAE PAPER 670235] 12 p1989 A67-25493
 Aerodynamic development of configuration and control system of Gulfstream II business jet, discussing wing optimization, engine characteristics, etc 12 p1894 A67-25497
 Estimating maintenance man-hours per flight hour for business turbojet airplanes

- [SAE PAPER 670228] 13 p2053 A67-27294
Yak 40, Soviet three-engine jet airliner, for operation off short natural-surface airfields 14 p2245 A67-27893
Planning integration of Boeing 747 jet aircraft into commercial airline [AIAA PAPER 67-394] 15 p2421 A67-30361
Flight control hydraulic systems for Boeing 2707 SST noting absence of radical changes in operating procedures 17 p2793 A67-31968
Jet VTOL aircraft problems, considering vertical thrust/aircraft weight, thrust application to aircraft gravity center, stability in hovering, thrust exertion, etc 17 p2796 A67-32392
Parametric data on gas ingestion and ground proximity jet effects experienced by jet-powered VTOL configurations [AIAA PAPER 67-440] 18 p2985 A67-33917
Microbiological organisms in jet aircraft wing fuel tanks as major corrosion sources, with fuel additives tested to inhibit microbial growth 20 p3515 A67-36485
Three STOL commercial transports performance and cost compared with conventional transports 20 p3362 A67-37530
Cost effectiveness of VTOL short range jet airlines, discussing significance of block time [AIAA PAPER 67-797] 21 p3568 A67-38543
Master plan for Philadelphia International Airport to accommodate increased air travel, cargo and jet aircraft 21 p3608 A67-38806
Smaller airports to support small jet feeder line service noting need for expansion and integration of airports with urban centers 22 p3744 A67-39378
Microbial contamination of jet aircraft fuel systems [SAE PAPER 670869] 24 p4206 A67-42007
Bird strikes on high speed transport jet aircraft stabilizers 24 p4094 A67-42278
Augmentor-Wing research program for developing high lift devices to reduce takeoff/landing speeds of jet aircraft [AIAA PAPER 67-741] 24 p4094 A67-42804
System-safety mathematical model for commercial jet airplanes using fault-tree modeling technique [AIAA PAPER 67-910] 24 p4096 A67-43017
V/STOL and STOL concepts as applied to short haul transportation [AIAA PAPER 67-941] 24 p4097 A67-43031
- JET AIRSTREAM**
Position of tropopause in middle latitude jet flow 02 p0240 A67-12642
Lamellar homogeneous jet layer deformation under aerodynamic forces acting in incompressible flow 09 p1439 A67-22578
- JET AMPLIFIER**
SA FLUID JET AMPLIFIER
Behavior of momentum effect jet interaction proportional amplifier using flow visualization on water table and large scale pneumatic model 08 p1282 A67-20460
- JET AUGMENTED WING FLAP**
Flow pattern of thin jet-flapped wing with small deflection angle in proximity to ground 15 p2415 A67-29308
- JET BOUNDARY**
Numerical analysis of free boundary problem inviscid incompressible flow field of impinging jet and two-dimensional Joukowski airfoil in sheared wind tunnel flow [AIAA PAPER 67-217] 06 p0988 A67-18460
Attachment time of thin turbulent jet to adjacent parallel flat plate calculated using quasi-steady analysis and correlated empirically 08 p1280 A67-20440
Flow equations for convective heating associated with recirculating flow in clustered engine boosters for free viscous shear layer along exhaust jet boundary 16 p2591 A67-30942
Underexpanded jet boundary streamline calculations by exact and approximate methods 19 p3171 A67-35768
- JET CONDENSER**
Liquid metal magnetohydrodynamic power generation systems using condensing ejector or two-phase jet pump 16 p2606 A67-30589
- JET CONTROL**
Jet direction variation via secondary fluid injection resulting in booster trajectory control, increased payload and reliability 01 p0142 A67-11409
Jet attitude control system analysis when subjected to external disturbing torques [AIAA PAPER 67-537] 19 p3174 A67-35939
Sun pointing attitude control acquisition by space vehicle with jet control system 24 p4182 A67-41974
- JET DAMPING**
Motion equations of spin-stabilized rocket under thrust with jet damping, variable mass and momentum effects and all angular disturbances 19 p3334 A67-35938
- JET ENGINE**
SA PULSE JET ENGINE
SA RESISTOJET ENGINE
Estimated structural response to aeroacoustic pressure loading due to jet and rocket engines and boundary layer turbulence [SAE PAPER 660721] 01 p0010 A67-10625
High by-pass fan engine installation in subsonic transport in terms of configuration, environmental severity, structures and systems [SAE PAPER 660737] 01 p0140 A67-10636
Pressures and temperatures occurring in jet engine exhaust nozzles during speed changes on basis of compression and detonation wave theory 01 p0141 A67-11150
Jet-engine problem areas in relation to SST 01 p0141 A67-11200
Transport jet engine inspection with radioactive isotopes, noting techniques and results 02 p0303 A67-12219
Test stand simulating high intensity heating processes which occur in combustion chambers of rocket and jet engines 02 p0231 A67-12440
Gimballed jet engine development, noting application to V/STOL aircraft and design of plenum chamber burning engine 03 p0503 A67-13008
Effect of bleeding air behind compressor for VTOL stabilization on dynamic behavior of jet engine 03 p0503 A67-13009
Directional solidification and single-crystal casting for jet engine turbine blades 03 p0429 A67-13541
Design and construction of mobile test plant for jet engines to avoid engine removal during control and checkout procedure 04 p0594 A67-14413
V/STOL aircraft design evolution, discussing propeller and jet engine configuration, control surfaces and jets for attitude control 05 p0751 A67-16382
Optimization of single-shaft jet and two-shaft dual-flow engines for given flight conditions 06 p1073 A67-17606
Fluid amplifiers and sensors for jet-engine control systems 06 p0949 A67-17611
Jet engine gyroscopic moments effect on coupling of longitudinal and transverse motions of aircraft 06 p0944 A67-17624
Supersonic transport engine requirements in light of past jet transport operation [SAE PAPER 660296] 07 p1129 A67-19624
Jet engine thrust augmentation by controlled mixing of exhaust gases with ambient air 07 p1242 A67-20119
Ignition systems for turbine engines, discussing low and high energy, semiconductor spark plugs, effects of electric constants on performance, etc 09 p1559 A67-21691
Jet engine noise sources, discussing noise radiation patterns, penalties for improved specific fuel consumption, etc 09 p1559 A67-21701
Control of multishaft jet engines, discussing compressor geometry, afterburner and engine fuel flow, nozzle area effects, etc [SAE PAPER 670139] 09 p1559 A67-21770
Leakage and optimum film thickness of gas lubricated high-pressure mainshaft seals for jet engine compressors 10 p1658 A67-22705
Business jet aircraft engine design for increased service life, detailing turbine nozzles, bearings, rotors, etc [SAE PAPER 670234] 11 p1851 A67-23981
Trapped fluid effect on high speed rotor vibration, discussing asynchronous and synchronous whirl for fully and partially wetted cavities [ASME PAPER 67-VIBR-29] 11 p1797 A67-24187
Erratic vibration peaks, recognized as variable acoustic resonance, during tests of jet engine compressors [ASME PAPER 67-VIBR-57] 11 p1852 A67-24204
JR 100 H lift jet engine height control studies by NAL 11 p1852 A67-24287
Soviet book on production of gas turbine engines covering manufacturing methods, automation of operations, tooling, etc 11 p1798 A67-24516
- Cartridge-pneumatic dual mode jet engine starter design and function, discussing energy conversion and handling of high pressure gas produced by starter cartridge [ASME PAPER 67-GT-49] 11 p1855 A67-24810
Engine design to reduce overall cost and improve power plant component for flight schedule reliability [SAE PAPER 670330] 12 p1990 A67-25872
Digital computer used for on-line control of jet engine 13 p2074 A67-27190
Soviet book on pilotless aircraft and missiles covering jet engine design, automatic control, radio engineering and aircraft aerodynamics 15 p2564 A67-29242
Reinforced plastics composites for jet lift engines 15 p2508 A67-29671
Starter cartridges for jet engines, discussing operational problems and mechanical design, igniter and propellant development, etc 15 p2423 A67-29982
Aircraft radiography for turbojet engine integrity and serviceability determination [AIAA PAPER 67-380] 15 p2494 A67-30350
Concorde jet engine silencer concept and characteristics [AIAA PAPER 67-391] 15 p2549 A67-30359
Oil Mist Deposits Test for differentiating deposit forming tendencies of jet engine lubricants, discussing mechanism and threshold temperature 16 p2683 A67-31755
Vectoring and nonvectoring nozzles of different geometries for lift and lift/cruise engines 17 p2928 A67-32569
Response of bare wire thermocouple to temperature variation in jet engine intake, noting temperature pickup selection for desired response 17 p2859 A67-32589
Fluidic jet engine controls for closed loop control, noting overtemperature prevention, reliability, etc 18 p2989 A67-34097
Fan jet engine performance and operation as affected by humidity 20 p3515 A67-36448
Soviet papers on aerodynamic characteristics of blade compressors and jet engines 20 p3358 A67-37078
Axial compressor inlet stator tests determining pressure loss relationship to geometric parameters 20 p3516 A67-37082
Pressure fluctuation onset conditions in jet engine combustion chambers with supersonic nozzles, discussing design factors effect on combustion process stability 21 p3696 A67-38909
Astrolol /Ni base superalloy/ disks for jet engine application, discussing chemical composition, basic ingot structure, forging and heat treatment 22 p3818 A67-39226
Electromechanical servosystem in conjunction with inductive pickup circuit for thrust measurements in jet engine bed tests 22 p3797 A67-39536
Supersonic aircraft evolution emphasizing Dassault series, Northrop T-38 and F-5 and Swedish Draken and Viggen 22 p3746 A67-39883
Engine test facilities on Concorde examined for effect on supersonic Olympus engine development [AIAA PAPER 67-753] 23 p4049 A67-40987
Differential piezoelectric accelerometer charge system for monitoring in-flight jet engine vibrations 23 p4007 A67-41384
Diagnostic system for jet engine malfunctions detection using digital computer sonic vibration analysis [SAE PAPER 670871] 24 p4207 A67-42008
Sub-, super- and hypersonic air breathing engines, examining developments on ground test and simulation facilities [AIAA PAPER 67-779] 24 p4208 A67-42946
- JET EXHAUST**
SA HOT JET EXHAUST
Flow field about subsonic jet exhausting into quiescent and low velocity air stream [AIAA PAPER 65-704] 01 p0055 A67-11254
Pressure distribution on rectangular wing with jet exhausting normally from lifting surface into uniform air stream [AIAA PAPER 67-1] 06 p0941 A67-18463
Local turbulent properties of supersonic jet exhaust measured optically by crossed beam correlation technique 16 p2591 A67-30943
Strong forward flow of engine exhaust gas in blast deflection flow field of twin jet F-111B 17 p2797 A67-32568
Local mass flux and local impact pressure measurement in arc jet exhaust flow

- fields 17 p2861 A67-33029
Probe for total enthalpy measurements in
arc jet exhausts 17 p2971 A67-33030
Inviscid hypersonic flow field between
barrel shock and free boundary for source
flow representing high altitude jet
exhaust 22 p3739 A67-39410
Fuel additives investigated for jet engine
exhaust smoke elimination
[SAE PAPER 670866] 24 p4206 A67-42006
- JET FLAME**
Velocity and temperature measurements in
turbulent swirling butane-propane air flames
in high exit velocity
range 11 p1882 A67-24217
Jet flame stabilization and audible noise
production using ultrasonic acoustic
energy 11 p1883 A67-24842
Velocity and temperature measurements in
turbulent swirling burning free jets of
butane-propane-air
mixture 18 p3151 A67-33815
- JET FLAP**
Damping in yaw on jet-flap blowing model
measured by decaying oscillation
technique 06 p0979 A67-17919
Mathematical analysis of jet flap with high
lift coefficient, solving numerically integral
equation obtained from boundary value
problem
[AIAA PAPER 67-2] 06 p0938 A67-18247
Aerodynamic balance for wind tunnel
measurement of forces and moments on jet
flap 07 p1163 A67-19350
Simple method for determining deviation
of supersonic or hypersonic plane parallel
flow of inviscid gas caused by auxiliary jet
in form of thin layer 07 p1127 A67-20208
Profile velocity distribution and shape
determinations for flow around thin profile
with jet flap 19 p3172 A67-35819
- JET FLIGHT**
Biomedical assessments of human circadian
system, noting increase in subjective fatigue
and psychological and physiological
performance 01 p0016 A67-10955
Optimum thrust direction for horizontal
jet flight of maximum duration determined,
using variational calculus 18 p3136 A67-33557
- JET FLOW**
Swirling axisymmetric radial jet flow of
conducting fluid in presence of axial
magnetic field, citing conditions for
singularity in two-dimensional
case 01 p0124 A67-10800
Turbulence in free shear layer in mixing
region of circular jet, comparing statistical
characteristics of mathematical and physical
models
[AIAA PAPER 65-805] 01 p0054 A67-11164
Turbulent mixing of axisymmetric jet of
partially dissociated nitrogen with ambient
air, establishing mixing and decay
characteristics 01 p0055 A67-11171
Steady flow of jet from orifice at nose of
body and opposing supersonic free
stream 02 p0178 A67-11565
Corresponding compressible and
incompressible jets and wakes in boundary
layer equations of turbulent and laminar
cases 03 p0350 A67-12988
Boundary layer type theory for
compressible half-jet with aligned magnetic
field 03 p0483 A67-14033
Inviscid stability of incompressible half-jet
under aligned magnetic field, determining
neutrally stable
eigenvalues 03 p0483 A67-14034
Velocity field in MHD jet flow discharging
into immersed bounded
space 04 p0669 A67-15518
Heat transfer in plane conducting fluid jet
spreading over flat wall in transverse
magnetic field, noting solution for
temperature distribution for small MHD
interaction parameters 04 p0670 A67-15520
Disruption of water jet into large drops
studied by photography 04 p0609 A67-15591
Spence integrodifferential equation for
flow around slender slightly curved profile
with jet at trailing edge 05 p0749 A67-16842
Fizeau fringes produced in laser
illuminated Fabry-Perot interferometer to
obtain concentration profiles in turbulent
and laminar jets 05 p0794 A67-17371
Shock tunnel data on surface pressure
resulting from hypersonic stream interaction
with two transverse jets
[AIAA PAPER 67-190] 06 p0939 A67-18299
Laval nozzle configuration for sharply
bounded carbon dioxide jet in
vacuum 06 p0943 A67-18781
Jet deviation by curved convex wall and
Reynolds number explained as effect of
boundary layer separation 08 p1320 A67-20450
Aerodynamics of sounding rockets,
discussing stabilization by fins, conical
flares, etc
[ONERA-TP-441] 08 p1275 A67-20498
Subsonic jet flow past solids, examining
two classes of exact solutions in ideal fluid
for plane nonvortical steady state
flow 08 p1321 A67-20836
MHD flow of viscous conducting fluid jets
and MHD flows with nonlinear temperature
dependent conductivity 09 p1541 A67-21807
Device for analyzing propagation of
nonrotating jet in rotating ambient flow,
noting graphs for longitudinal and tangential
velocity distributions 09 p1490 A67-22594
Two-dimensional jet plane problem,
considering rheological solution for
applications to ground effect
machines 11 p1781 A67-24571
Semilempirical method for predicting
aerodynamic interference of circular jet
exhausting at right angles from wing,
showing effect on lift
loss 11 p1742 A67-24659
Bulk properties of three-dimensional
turbulent incompressible jets regarding axis
velocity decays, half-width boundaries,
etc 12 p1892 A67-25901
Fluid flow processes for secondary sonic
jet injection into Mach 6 free stream, noting
upstream flow into separated flow
regions 12 p1893 A67-25934
Boundary layer of principal region of
turbulent nonisothermal plane-parallel jet of
real gas 13 p2095 A67-26885
Turbulent mixing in plane nonisothermal
jets, deriving solutions for velocity,
temperature and pressure
distribution 13 p2105 A67-27052
Anisotropic velocity distribution function
measurements in jet flows using electron
beam fluorescence
technique 14 p2300 A67-28181
Collimation of low density hypersonic jet
from shock tube for atomic beam
production, noting relation between beam
intensity and velocity
distribution 14 p2301 A67-28188
Expansion of plane jet of conducting
liquid in magnetic field 14 p2302 A67-28304
Shadowgraphic and interferometric
investigation of transversely impinging two-
dimensional jet flows 14 p2303 A67-28325
Transverse secondary flow effects on
laminar turbulent transition of free
axisymmetric jet 14 p2303 A67-28328
Impact stage of impacting jet amplifiers
studied by interposing disk between two
opposing coaxial jets, obtaining pressure
gain 14 p2250 A67-28332
Control flow effect on power jet
reattachment location and pressure in
separation bubble enclosed by power jet for
fluidic devices 14 p2250 A67-28336
Ground effect of static circular peripheral
jet, comparing derived relations between jet
flow, base pressure and hover height with
experimental model
results 15 p2415 A67-29262
High altitude jet structure for two-
dimensional and axisymmetric cases with
very large exit/ambient pressure
ratio 15 p2418 A67-30208
Turbulent jet spread issuing into parallel
moving airstreams 16 p2657 A67-30615
Laminar jet flow of electrically conducting
fluid over plane solid surface in transverse
magnetic field solved using motion and
continuity equations 16 p2722 A67-31571
Transverse magnetic field effect on
turbulent MHD jet flow in bounded space,
noting channel wall
conductivity 17 p2901 A67-32565
Transonic jet flow study with electric
analogy methods, solving Frankl and Tricomi
problems for mixed type
PDE 18 p2982 A67-33684
Laval nozzle configuration for sharply
bounded carbon dioxide jet in
vacuum 18 p2982 A67-33723
Channel flow transition to jet flow,
discussing turbulence determination in flow
boundary layer as Reynolds number
function 18 p3028 A67-34218
Jet flow turbulence energy balance,
measuring point-pressure/velocity
correlations and spatial mean gradients,
giving energy equation 19 p3170 A67-35412
Diffusion of free isothermal turbulent jet,
of incompressible fluid flowing from nozzle
into coaxial surrounding uniform
stream 19 p3209 A67-35443
Two-dimensional problem of penetration of
subsonic compressible fluid jet into channel
solved by modified Chaplygin
method 20 p3357 A67-37052
Group properties of differential equations
describing axisymmetric thin layer jet flow
of ideal fluid propagating along surface of
revolution 20 p3422 A67-37063
Short tube orifices, confined turbulent
jets, jet-wall and jet-receiver interactions
and characteristics of diffusion process for
design of fluid amplifiers 20 p3365 A67-37361
Incompressible cylindrical jet interaction
with incompressible unbounded
homogeneous stream, determining contact
surface 20 p3360 A67-37661
Shock tunnel data on surface pressure
resulting from hypersonic stream interaction
with two transverse jets 21 p3610 A67-37799
Inviscid compressible relativistic half-jet
plasma flow stability, discussing disturbance
equations and eigenvalues 22 p3850 A67-39705
Force defect coefficient method applied to
calculation of compressible jet flow
discharge for asymmetric two-dimensional
orifice 23 p3936 A67-41330
Mixed flow of five plane turbulent air jets
discharged into atmosphere through slotted
nozzles 24 p4143 A67-42285
- JET FUEL**
SA JP-4 JET FUEL
Jet fuel lubricity noting poor performance
due to polar compounds, improving lubricity
by surface active
additives 01 p0139 A67-10602
Flame study of turbulence effects induced
by sonic or ultrasonic vibration on
combustion of liquid hydrocarbon
jet 01 p0167 A67-10942
Jet propellant purity, safeguarding gas
turbine fuel during
production, storage and
transportation, use 07 p1239 A67-19210
Scramjet performance analysis stressing
construction problems and importance of
fuel choice 11 p1853 A67-24748
Emulsified jet engine fuel noting lower
volatility and flammability and resistivity to
corrosion and acceleration
[SAE PAPER 670385] 12 p1988 A67-25885
Jet fuel lubricity noting poor performance
due to polar compounds, improving lubricity
by surface active additives
[SAE PAPER 680712] 12 p1988 A67-26163
Jet fuels in U.S. and Great Britain,
chemical composition, technical
specifications, thermal stability and
corrosion effect 13 p2185 A67-27068
Liquified natural gas application to SST,
noting improvement in engine performance
with use of methane 13 p2185 A67-27439
Book on motor fuels, performance and
testing, including fuel source and nature,
gasoline combustion, diesel, turbine fuels,
etc 16 p2734 A67-30998
Quantitative method for determining
sodium in gas turbine fuels by direct
spectral analysis of unashed fuel
samples 21 p3688 A67-38016
- JET IMPINGEMENT**
Impingement of supersonic jet on flat
plate studied for variety of jet Mach
numbers, plate incidence angles and plate
locations downstream of nozzle
outlet 01 p0006 A67-10792
Ground surface erosion due to rocket
breaking, calculating flow-induced force
parameters 01 p0156 A67-11434
Thermal and pressure effects of rocket
exhaust impinging on flat plate surface at
high vacuum
[AIAA PAPER 66-46] 02 p0341 A67-11934
Working equations for dimensions and
orientation of impinging propellant sheets in
liquid rocket engine
injectors 02 p0182 A67-11946
Supersonic underexpanded jet interacting
with obstacle in numerical solution using
integral relations and
characteristics 03 p0350 A67-12879
Cavitation pitting and flow regime in
cavitating venturi using water and mercury
indicate microjet impingement is most
important damaging mechanism
[ASME PAPER 66-WA/FE-39]

Heat transfer by array of two-dimensional jets directed normal to surfaces including effects of superposed wall-parallel flow 04 p0732 A67-15836

Interaction of two cylindrical jets of uniform flow as far downstream as possible impinging at included angle of 60 degrees 06 p0944 A67-18888

Heat transfer of pulsating liquid jet impinging on perpendicular flat surface and spreading laminarily 11 p1882 A67-24229

Lunar surface erosion by rockets simulated in laboratory to study hazards of retrorocket landing on airless planetary bodies 12 p1922 A67-25701

Shadowgraphic and interferometric investigation of transversely impinging two-dimensional jet flows 14 p2303 A67-28325

Criteria for optimum liquid mixing for impinging jet injector elements, noting parameters for maximum efficiency 15 p2545 A67-29445

Two-dimensional incompressible fluid jet penetration analyzed kinematically via free streamline theory and notched hodograph 20 p3422 A67-36845

Inviscid incompressible flow of normal and slightly oblique static round jet impinging on ground, noting velocity distribution 21 p3565 A67-38544

Peripheral jet air cushion vehicle circular platform design, discussing dimensionless design parameter determination from operating height, translational speed and weight 22 p3745 A67-39726

Analytical prediction of cryogenic propellant venting effects on orbital vehicle dynamic behavior, emphasizing vent thrusting and gas impingement 22 p3906 A67-40165

JET LIFT

Hoverbug VTOL twin-jet flying simulator operational experience and management and construction techniques [AIAA PAPER 66-799] 01 p0009 A67-10537

VTOL power plant design noting jet deflection, lift fans, RB-162 engine, etc 04 p0687 A67-14435

Inlet/door performance characteristic of VTOL lift engines studied in full scale wind tunnel tests [AIAA PAPER 66-655] 09 p1438 A67-22490

Design aspects of power plants for V/STOL aircraft, examining lift jets, thrust vectoring and lift fans [ASME PAPER 67-GT-7] 11 p1744 A67-24795

Aerodynamic interference effect with jet lift V/STOL aircraft under static and forward-speed conditions, stressing adverse flow 20 p3357 A67-36952

JET MIXING

Incompressible plane jet turbulent mixing into external parallel flow 01 p0052 A67-10646

Warren momentum integral method for predicting compressible free mixing of two dissimilar gases [AIAA PAPER 65-822] 01 p0055 A67-11170

Intersecting turbulent jet mixing studied for velocity fields, pressure and temperature 04 p0609 A67-15592

Constant pressure turbulent jet mixing between two compressible nonisoenergetic streams of identical composition with finite initial boundary layer effects 06 p0992 A67-18880

Supersonic stream interaction with two-dimensional secondary jet from rectangular planform wedge 10 p1592 A67-23116

Internal structure of highly underexpanded transverse jets in supersonic cross stream 12 p1892 A67-25900

Axissymmetric supersonic jet injection from conical nozzle into supersonic wake flow or medium at rest 13 p2050 A67-26896

Upstream velocity profile effect on free mixing of jets with ambient fluid 14 p2240 A67-28107

Criteria for optimum liquid mixing for impinging jet injector elements, noting parameters for maximum efficiency 15 p2545 A67-29445

Liquid metal magnetohydrodynamic power generation systems using condensing ejector or two-phase jet pump 16 p2606 A67-30589

Turbulent base pressure in supersonic axisymmetric flow behind blunt body [AIAA PAPER 67-446] 18 p3026 A67-33922

Monograph on turbulent mixing of rotating jets in circular confined

duct 21 p3615 A67-39128

Real gas jet equations of motion, energy and continuity derived, transformed and solved for mixing region, discussing approximate state equation 23 p3989 A67-40729

Isobaric mixing chamber configuration determination method for maintaining constant static pressure along flow during turbulent jet mixing 23 p3927 A67-40730

Mixing effect in dual flow turbojet engines analyzed to obtain better conversion of combustion into kinetic energy 23 p3931 A67-41317

Model for compressible free jet with moving environment in core and developed region of exhaust plume 23 p3992 A67-41731

JET NOISE

FAA study of jet takeoff and landing noise effect on population around airport, establishing numerical value of noisiness 03 p0358 A67-12979

Interactions among technical, economic and political aspects of aircraft noise problem, examining relation between thrust and jet engine noise 03 p0539 A67-14384

Noise and pressure measurement in difficult conditions of vibrations and temperature for use in pressure-transducer design of jet and rocket systems 09 p1497 A67-21939

Human response to comparative sounds from aircraft and objective measurement of reference sound, determining acceptable noise levels 09 p1456 A67-21940

Extended plug nozzles in suppression of jet noise in small turbojet engines [SAE PAPER 670157] 09 p1561 A67-22544

Similarity laws for jet noise and shear flow instability as suggested by experiments 10 p1628 A67-23830

Acoustic characteristics of jet determined, using Lighthill equation for free turbulent jet when components of flow fluctuation rate, turbulent vortex volume and turbulent fluctuation frequency are known 14 p2302 A67-28301

JT9D engine design from viewpoint of incorporated noise reduction features [SAE PAPER 670331] 17 p2929 A67-32984

Subjective evaluation of relative annoyance of sonic booms, explosions and jet aircraft noise 18 p2986 A67-34393

Mean flow refraction and temperature differences between mixing layer and outside fluid effect on HF component of jet noise 19 p3173 A67-34962

JET NOZZLE

Chemical reaction kinetics and gas dynamics combined to analyze processes occurring in combustion chambers and nozzles of jet and rocket engines [DVL-602] 03 p0366 A67-12999

Supersonic flow of ideal thermodynamically perfect gas from nozzle into medium at rest 10 p1591 A67-23037

Flow processes and static and dynamic performance characteristics of axisymmetric fluid jet modulator and single receiver-diffuser studied experimentally 14 p2248 A67-28269

Apparent mass of supersonic jet stream under off-design flow conditions 14 p2242 A67-28302

Jet reattachment for inclined walls at low Reynolds numbers and moderate nozzle aspect ratios [ASME PAPER 67-FE-25] 14 p2305 A67-28369

JET PILOT

Naval jet replacement pilot training failures examined for significant data 23 p3966 A67-41579

JET PLUME

Hydrogen arcjet plume spectroscopy, examining exhaust at various H mass flow rates 05 p0874 A67-17357

Three-channel IR-UV rocket radiometer for onboard measurement of exhaust plumes under severe high altitude environmental conditions 06 p1005 A67-18714

Wind tunnel test program for simulation of gas-particle rocket exhaust plume, separated flow around nozzle and base recirculation [AIAA PAPER 66-787] 11 p1773 A67-24351

X-band attenuation by rocket exhaust plume measured with AM/PM noise for various propellant systems 15 p2436 A67-29429

Free jet plume expanding into vacuum investigated experimentally, comparing with

ideal gas characteristics method results 18 p3152 A67-3381

Measurement within rocket exhaust plumes 18 p3051 A67-3450

Rocket exhaust jet plume effects on radi signal, calculating degradation by electromagnetic diffraction propagation 20 p3381 A67-3657

Approximating method for predicting multiengine exhaust geometry and thermodynamic properties with single reference engine 22 p3902 A67-3994

JET PROPULSION

Weight factor effects on optimal motion parameters of variable mass system with limited velocity jet propulsion in gravitational field 02 p0327 A67-1233

Dead weight/service load ratio effect of propulsive efficiency and fuel consumption of large helicopters with mechanical gearless or jet-propulsion drives 03 p0358 A67-1298

High lift rotor design for jet propulsion VTOL aircraft 03 p0360 A67-1389

Aerodynamic characteristics of pneumatic elements with jet propulsion and Coanda effect 05 p0791 A67-1637

Status and possibilities of VTOL propulsion, noting weight/payload ratio role 13 p2189 A67-2749

Air breathing reusable rocket launcher for European development, comparing ramrocket and turboramjet propulsion 15 p2568 A67-2984

Engine development and manufacture in Sweden 17 p2928 A67-3212

Jindivik Mk 103A jet propelled target, drone ground and flight control systems stressing climb, cruise, approach and descent commands 21 p3570 A67-3913

Peripheral jet GEM pitching characteristics analysis by longitudinal static stability and dynamic pitching motion 22 p3745 A67-39837

Spacecraft motion with limited power jet engine, applying simulation technique to determine operation modes for engine and control system 24 p4240 A67-42296

JET PUMP

Self-preserving turbulent jet ejector, solving equations of motion to determine system geometry corresponding to flow conditions [AIAA PAPER 67-127] 06 p0988 A67-18456

Jet compressors for closed Brayton cycle MPD to study momentum transfer of two high velocity gas or vapor streams of very different molecular weight 18 p2604 A67-30566

JET STREAM

Satellite photographs received from APT facility used in analysis of old occluded depression structure, deducing jet stream position and sea-ice presence 04 p0650 A67-14866

Atmospheric jet streams in tropical latitudes, discussing velocities, seasonal variations, etc 04 p0652 A67-15474

Mean monthly winds at low level calculated for equatorial station in East Africa, noting monsoon patterns and jet streams 06 p1025 A67-18024

Constant pressure turbulent jet mixing between two compressible nonisoenergetic streams of identical composition with finite initial boundary layer effects 06 p0992 A67-18880

Clear air turbulence connection with jet stream, wind speed, convection clouds, flight hazard, etc 07 p1220 A67-19533

Nonstationary gas jet stream formation following shock wave outflowing from nozzle, obtaining calculation method 12 p1929 A67-25674

Monodisperse sprays production technique using Rayleigh criterion for breakup of capillary jets by mechanically vibrating uniform size capillary needles arranged in parallel 12 p1946 A67-2598

Clear air turbulence power spectra in free atmosphere near jet stream level, discussing CAT generation 15 p2513 A67-30058

Time-dependent mean-mass temperature of argon jet produced by arc plasmatron with powdered metal carbides injected into jet calculated using heat transfer equations 16 p2721 A67-3139

Tangentially injected plane jet spreading in slipstream at various Reynolds numbers at jet inlet slot studied in wind tunnel for dynamic behavior 17 p2839 A67-32900

Soviet book on aeronautical meteorology covering wind and cloud effects on takeoff, landing and supersonic flying in storms and jet stream layers 18 p3074 A67-33676
Reflection coefficient determined for plane monochromatic electromagnetic wave incident on idealized laminar plane stratified jet stream, deriving Riccati type differential equation 23 p3974 A67-41201
JET THRUST
Method for matching jet engine intake and ejector pumping characteristics to evaluate static and in-flight performance of air-augmented nozzles, considering external aerodynamics influence 03 p0350 A67-12903
Suppressor applications of nozzles in reduction of sound power level generated in exhaust jet wake and ground surface deterioration from VTOL lift 03 p0350 A67-12916
Generalized MGD equation for thrust in jet engine, with application to rocket engine and pulsed jet 03 p0503 A67-13086
Critical mass flow rate existence for maximum thrust from MPD arc 06 p1075 A67-18866
Forward facing jets effect on blunt configurations aerodynamic characteristics from wind tunnel tests at Mach 6, emphasizing drag increase 11 p1742 A67-24354
Aerodynamic suckdown results obtained in investigation of VTOL ground-proximity effects 17 p2791 A67-32588
VTOL and STOL aircraft comparison, discussing advantages and disadvantages of hinged and folding rotors, hinged wings, jet thrust and fan-in-wing 17 p2798 A67-32833
Performance of radioisotope heated ammonia thruster for spacecraft application [AIAA PAPER 67-425] 18 p3075 A67-33909
JET TRANSPORT
BOEING 737 AIRCRAFT
BOEING 747 AIRCRAFT
Flight safety improvement in design and maintenance procedure brought about by jet transport accident investigation data [AIAA PAPER 66-809] 01 p0008 A67-10035
Production program and MAC operational experience of C-141A jet cargo transport [AIAA PAPER 66-791] 01 p0009 A67-10534
Optimum passenger handling in long haul jet transportation for various airport facilities [AIAA PAPER 66-843] 02 p0181 A67-12257
Computer simulation for turbulence/upset studies on jet transports, emphasizing time dependency and nonlinear aerodynamics [AIAA PAPER 66-1002] 02 p0181 A67-12304
V/STOL transport aircraft design and application, noting performance with varying number of propulsion 03 p0357 A67-12972
Ozone concentration in commercial jet aircraft measured for possible seasonal and meteorological correlation 06 p0947 A67-18008
Leakages in hydraulic system of Hawker Siddeley Trident jet transport due to cavitation erosion 07 p1132 A67-20149
Flight safety improvement in design and maintenance procedure brought about by jet transport accident investigation data [AIAA PAPER 66-809] 10 p1595 A67-23550
JT9D turbofan engine for Boeing 747 commercial transport aircraft, analyzing design and performance potentials [AIAA PAPER 67-374] 15 p2548 A67-30346
JET VANE
GUIDE VANE
STREAM AIRCRAFT
HANDLEY PAGE H.P. 137 AIRCRAFT
JETTISON SYSTEM
Load carrying capability of thin walled pressurized tanks under compression and bending with postwrinkling included, improved by addition of jettisonable shell [SAE PAPER 660683] 01 p0161 A67-10586
Scaling equations for wind tunnel simulation of trajectory of jettisoned stores from aircraft 06 p0979 A67-18006
Cartridge-actuated thruster system design for jettisoning Apollo spacecraft heat shield for recovery system deployment [ASME PAPER 67-DE-34] 14 p2394 A67-28875
INDIVIK TARGET AIRCRAFT
Indivik Mk 103A jet propelled target drone ground and flight control systems stressing climb, cruise, approach and descent

commands 21 p3570 A67-39131
JOINT
SA BONDING
SA FASTENER
SA LAP JOINT
SA METAL JOINT
SA RIVETED JOINT
SA SOLDERED JOINT
SA WELDED JOINT
Attachment concepts and problems in fibrous composite aerospace structures 03 p0523 A67-13444
Vibratory energy dissipation of plates with riveted beams as induced by gas-pumping in structural joints 05 p0924 A67-17285
Wear effects in polymer-metal joints under frictional loads 07 p1211 A67-19170
Exothermically brazed tubing joints for XB-70 hydraulic system 07 p1190 A67-19212
Strength of threaded joints compared under static and dynamic conditions 07 p1190 A67-19353
Brazed graphite-stainless steel composites for tube-to-armor joints of high temperature graphite space radiators 07 p1223 A67-19462
Criterion characterizing adhesive joints in structural bonding of military materiel 09 p1522 A67-22500
Shear strength of various joint designs measured, using steel adherends and rubbery adhesives to isolate factors affecting shear stress 09 p1577 A67-22503
Adhesive bonding techniques for aluminum, advantages, drawbacks, joint design and surface treatment before bonding 14 p2323 A67-27820
Reference issue on fastening and joining 16 p2682 A67-31563
Tangential and normal tearing stresses distribution in adhesive joint under various loads and bending 21 p3716 A67-37909
Electrode with central heat sink used for joining flat-pack leads and copper tracks on printed circuit boards 21 p3635 A67-38624
JOINT /BIOL/
S BONE
JORDAN FORM
Nonsingular linear transformation of time-invariant linear dynamic system into canonical /phase-variable/ form 01 p0048 A67-11223
Jordan form matrix algorithm of Wasow for reducing systems of first order ordinary differential equations with turning point 05 p0835 A67-16779
Controllability and observability of parallel and tandem connections of two linear time invariant differential systems of Jordan canonical form 24 p4135 A67-42181
JOSEPHSON CURRENT
Josephson current in alternating field between two superconductors separated by dielectric barrier 05 p0853 A67-16697
Weak superconductivity electrodynamics and EM wave propagation in Josephson tunnel junction in presence of vortices 06 p1054 A67-18806
Josephson and ordinary tunneling currents for two-band model superconductor, treating niobium-tin junction 09 p1551 A67-21667
Kinetic tunneling theory in superconductors clarifies conditions for onset of Josephson 09 p1555 A67-22071
Microwaves parametric amplification experiments in superconducting Josephson tunnel junctions, showing signal amplification as function of temperature, absorption dip of rutile resonator, etc 12 p1915 A67-25745
Electromagnetic properties of impure anisotropic strong-coupling superconductors, using Green function to obtain response, current density and Josephson tunneling current 14 p2371 A67-28724
Microwave frequency superconductor materials, applying bulk and thin film properties to filter, amplifier, oscillator, junction and Josephson effect 14 p2289 A67-28917
Microwave harmonic generation from Josephson junction noting radiation waveguide coupling, bias point, input power level and Josephson equations 15 p2535 A67-29492
Josephson current in alternating field between two superconductors separated by dielectric barrier 15 p2530 A67-29868
Broadening of lines emitted by tunnel

superconductor, noting unfeasibility of simultaneous amplitude-frequency prescription of Josephson current 16 p2728 A67-31044
Josephson junction as ideal zero impedance voltage source with discrete voltage for simultaneous application of microwave and magnetic fields 17 p2915 A67-32657
Electromagnetic properties associated with presence of overlapping bands in pure superconductors, discussing temperature dependence 17 p2915 A67-32718
Temperature dependence of Josephson critical current in superconductor model having anisotropic energy gap 17 p2915 A67-32719
Weak superconductivity electrodynamics and EM wave propagation in Josephson tunnel junction in presence of vortices 18 p3102 A67-34425
Image-force effects in normal state tunneling through lead-oxide-lead junctions exhibiting Josephson effect [JPL-TR-32-1154] 18 p3106 A67-34647
Lossless small-area Josephson junction analyzed from viewpoint of quantum dynamics, considering system of two superconducting plates 20 p3505 A67-36207
Properties of steps appearing on voltage-current characteristic of Josephson current in superconducting tunneling, noting nonlinear resonance effects 20 p3509 A67-36690
Alternating Josephson current and electromagnetic field interaction in generation of Pb-dielectric-Pb tunnel junction, noting steps in IV characteristics 21 p3877 A67-38096
Direct Josephson current dependence on magnetic field in tunnel junctions noting temperature dependence of oscillation periods 22 p3857 A67-39504
Current fluctuations in Josephson superconducting tunnel junctions 22 p3865 A67-40433
Josephson junctions as high speed IR detectors, describing point contact junctions used in experiment 22 p3838 A67-40434
Millidegree noise thermometry based on linewidth of Josephson radiation 22 p3865 A67-40436
Josephson junction as switching device or logic element, discussing tunneling states and transition characteristics 22 p3865 A67-40437
Microwave mixing with weakly coupled Josephson superconducting diodes, discussing Fourier components 22 p3865 A67-40439
Book on low temperature physics covering Josephson effect, superfluid He flow, superconductivity, etc 22 p3866 A67-40548
Josephson effect and quantum coherence measurements in superconductors and superfluids, discussing perturbation theory and tunnel junctions interference effects 22 p3866 A67-40549
Voltage-biased superconducting point contact Josephson radiation line width investigation for thermal noise contributions useful for low temperature thermometer 23 p4038 A67-40790
Constant voltage steps of AC Josephson effect observed in drop-form junctions exposed to radiation 24 p4200 A67-41864
JOULE HEATING
Distribution of electromagnetic fields, density of forces and Joule losses with higher spatial harmonics in asymmetric type of MHD induction generator allowing for conducting walls 03 p0475 A67-13178
Ionospheric heating by Joule dissipation of main-phase ring current associated with asymmetry 07 p1181 A67-19934
Energy transfer spectra and Joule effect dissipation in decline of homogeneous turbulence in presence of uniform magnetic field with small Reynolds number 09 p1549 A67-22565
Thermal electrode boundary layer for shock wave ionized air ohmic heating in discharge chamber, noting Joule heat consumption effect 12 p1975 A67-25894
One-dimensional laminar MHD flow at hydrodynamic stabilization, discussing heat transfer, Hartmann flow, magnetic field, Prandtl number and Joule heating 14 p2358 A67-28283
Hall effect in semiconducting electrode MHD generators, noting Joule heating losses,

nonlinear electrical conductivity, etc 16 p2600 A67-30533

Heating of upper atmosphere electron gas by indirect Joule dissipation of reverse current in ambient electrons demonstrated for high fluxes 16 p2739 A67-31405

Heat flux measurements in fluid systems using joule heating accomplished with single calibration and without flow rate measurements 18 p3052 A67-34513

Fringing effects on electric efficiency variation with slip for cylindrical induction MHD device operable as accelerator, generator or Joule heater [AIAA PAPER 67-714] 21 p3673 A67-38740

JOURNAL BEARING

Stability, wear and seizure characteristics of hydrodynamic journal bearings of various materials and designs in sodium at temperatures to 800 degrees F 03 p0428 A67-13227

Steady state and dynamic characteristics of tilting pad journal bearing in laminar and turbulent flow regime [ASME PAPER 66-LUB-19] 03 p0431 A67-13756

Stability regions for compressible fluid squeeze-film journal bearing of infinite length, considering motion along axis [ASME PAPER 66-LUB-15] 03 p0431 A67-13758

Stability experiments on partially grooved gas journal bearing, comparing data with previous theoretical analysis [ASME PAPER 66-LUB-6] 03 p0432 A67-13764

Vibrational damping of externally pressurized orifice journal bearings undergoing free vibrations with and without shaft rotation 04 p0627 A67-14432

Hydrodynamic journal bearing tests in molten lithium at 600 to 800 degrees F to support compact canned rotor liquid metal pump [ASME PAPER 66-WA/LUB-6] 04 p0629 A67-15338

Wear and compatibility of liquid metal bearing materials, including surface coatings and cemented refractory carbides, analyzed for Rankine cycle power plants [ASME PAPER 66-WA/LUB-3] 04 p0630 A67-15350

Velocity profiles for infinite cylindrical journal bearing, using small eccentricity perturbation calculation and modified Reynolds number as parameter [ASME PAPER 66-WA/APM-17] 04 p0630 A67-15408

Infinite length journal bearing performance of non-Newtonian fluids with shear dependent viscosity in analytical investigation at constant temperature 05 p0810 A67-16274

Load and friction torque of Rayleigh step film scheme applied to journal bearing, using Reynolds equation [ASME PAPER 65-WA/LUB-2] 08 p1335 A67-20917

Externally pressurized gas journal bearings, evaluating various design parameters for operating at high temperatures and high speeds [ASLE PAPER 66AM 4B2] 08 p1336 A67-21040

Rotor supported in fluid film journal bearings, eliminating self-excited vibrations through motion equation [ASME PAPER 67-VIBR-28] 11 p1797 A67-24186

AC and DC magnetic bearings efficient load support and development potentials [ASLE PREPRINT 67AM 6D-4] 14 p2325 A67-28788

Small parameter method to study steady state flow of viscous incompressible fluid in journal bearing 15 p2493 A67-29692

Gas bearing stability determination by step-jump response using observation of growth or decay of motion amplitude [ASME PAPER 67-LUBS-5] 16 p2682 A67-31383

Boundary conditions of journal gas bearings lubrication, studying slots effects 20 p3453 A67-36273

Design and applications of gas-lubricated journal and thrust bearings of self-acting and externally pressurized types 21 p3632 A67-38137

Static reaction of radial gas dynamic bearing to journal axis angular displacement determined by splicing asymptotic solutions

for low and high pressure levels 22 p3810 A67-39232

Equilibrium stability of rigid rotor in aerodynamic bearings, determining lubricant effect on journal 22 p3811 A67-39316

AC and DC magnetic bearings efficient load support and development potentials [ASLE PREPRINT 67AM 6D-4] 22 p3813 A67-40219

Partial differential equation in lubricant pressure based on mixing-length theory, presenting full journal bearings in turbulent and laminar regimes 23 p4010 A67-41342

Parasitic torques of squeeze-film cylindrical journal bearings in output axis of high performance gyroscopes, discussing tolerance errors [ASME PAPER 67-LUB-5] 24 p4162 A67-42669

Frequency Response and direct numerical integration of governing differential equations, considering gas-lubricated tilting-pad journal bearing stability [ASME PAPER 67-LUB-8] 24 p4162 A67-42672

Steady state and dynamic properties of cylindrical floating ring journal bearing with pressurized lubricant supply, considering turbulent flow and whirl instability [ASME PAPER 67-LUB-13] 24 p4162 A67-42674

Squeeze film journal bearing load support capability, noting axial pressure distribution in finite case is considerably greater than infinite case [ASME PAPER 67-LUB-14] 24 p4163 A67-42675

Analysis divided into step and ridge regions used to obtain linearized PH solution to Reynolds equation, neglecting side leakage [ASME PAPER 67-LUB-17] 24 p4163 A67-42676

Hydrodynamic journal bearings in liquid sodium, discussing stability characteristics of different geometries and wear at high temperatures [ASLE PAPER 67-LC-7] 24 p4164 A67-42746

JP-4 JET FUEL

GE T64 engine operation on emulsified fuel /JD1/, noting corrosion effects on fuel system components due to water additive [SAE PAPER 670369] 17 p2927 A67-33002

Gas turbine environmental testing, measuring emulsified fuel flow, direct burning effects of JP-4 fuel on extended engine operation, etc [SAE PAPER 670367] 18 p3111 A67-33567

JUMP

Sharp cut-off nonlinear filter design with jump effect for rapid gain increase with small frequency increment 03 p0386 A67-13981

Stator whirl with rotors in bearing clearance noting jump and hysteresis phenomena [ASME PAPER 66-WA/MD-8] 04 p0629 A67-15346

Boundary curves for jump resonance criteria of nonlinear control systems and conditions in second order servo system with idealized saturation 06 p0977 A67-18528

Finite discontinuity jump conditions for plasma in strong magnetic field determined by approximation and Maxwell equation, noting possible application to satellite data 22 p3843 A67-39269

JUNCTION

SA BARRIER LAYER

SA N-P JUNCTION

SA N-P-N JUNCTION

SA P-N JUNCTION

SA P-N-P JUNCTION

SA P-N-P-N JUNCTION

SA SILICON JUNCTION

Thermodynamics of epitaxial growth of GaAs-Ge heterojunctions in closed tube process 02 p0296 A67-11767

Semiconductor heterojunction properties of epitaxial single crystal layer of GaAs grown on Ge substrate 02 p0299 A67-11895

Six-port circulator with common pair of ferrite disks serving multiple junctions, used in frequency separation networks and tunnel diode amplifiers 02 p0217 A67-12094

Metal-semiconductor surface barrier and prediction using concepts of covalent and ionic crystals 03 p0494 A67-13475

Majority carrier current flow in metal-semiconductor barriers according to theory incorporating Schottky diffusion theory and

Bethe thermionic emission theory 03 p0494 A67-13476

Scattering matrix coefficients and relation between transmission and reflection coefficients of three-port circulator 05 p0770 A67-16170

Change in basic barrier relation for heterojunction compared to homojunction of wide gap emitter injection laser 05 p0825 A67-17097

Semiconductor heterojunctions noting preparation, properties, measurement and results 06 p1053 A67-18756

Copper telluride-cadmium telluride thin film heterojunction fabrication and characteristics for solar cell applications 08 p1285 A67-20730

Forward bias V-I characteristics for heterojunction in which tunneling dominates, noting temperature effect 09 p1551 A67-21686

Josephson and ordinary tunneling currents for two-band model superconductor, treating niobium-tin junction 09 p1551 A67-21687

Injection luminescence and photoluminescence spectra of epitaxial heterojunctions in GaP-GaAs system 09 p1554 A67-21975

Surface conditions effects on silicon planar transistor current gain 11 p1759 A67-24139

Exact calculation of electrical performance of rectangular waveguide T-junction having arbitrary cross section used to find equivalent circuit 11 p1767 A67-24732

Triple-tuned broadband UHF junction circulator using lumped element technique 13 p2076 A67-26483

Current-voltage characteristics of germanium-silicon isotype heterojunctions with regard to capacitance and photoelectric measurements 13 p2183 A67-27569

Measurements of heterojunctions alloyed with bismuth/indium arsenide/manganese alloy on to GaAs substrate 13 p2184 A67-27575

Microwave frequency superconductor materials, applying bulk and thin film properties to filter, amplifier, oscillator, junction and Josephson effect devices 14 p2289 A67-28917

Equivalent circuit model for solid state junction devices with single energy level defect centers including transient properties 15 p2456 A67-29170

Secondary electron detector for electronic microcircuits bombarded by electron beam used to observe potential distribution in junction breakdown 15 p2453 A67-30065

Interface alloy technique for heterojunctions between GaAs and InSb single-crystal heterojunctions shown by X-ray analysis 17 p2911 A67-32196

Injection luminescence and photoluminescence spectra of epitaxial heterojunctions in GaP-GaAs system 17 p2923 A67-33312

Relation between current, voltage and magnetic field of weakly connected double-contact junctions in superconductors 17 p2926 A67-33406

Resonance methods for microwave measurement of scattering matrix of two-port reciprocal junction 18 p3002 A67-34223

Image-force effects in normal state tunneling through lead-oxide-lead junctions exhibiting Josephson effect [JPL-TR-32-1154] 18 p3106 A67-34647

Monograph on waveguide junctions theory and microwave network analysis, stressing model characteristic definition and impedance 20 p3399 A67-36950

High efficiency tunable ferrite frequency doubler consisting of yttrium-iron-garnet disk at waveguide junction 21 p3598 A67-38572

Current fluctuations in Josephson superconducting tunnel junctions 22 p3865 A67-40433

Josephson junctions as high speed far IR detectors, describing point contact junctions used in experiment 22 p3838 A67-40434

Josephson junction as switching device or logic element, discussing tunneling states and transition characteristics 22 p3865 A67-40437

Population noise in semiconductor laser junctions calculated by quantum mechanical Langevin method 24 p4166 A67-41887

JUNCTION DIODE

Semiconductor laser array structure with common n-type substrate and individual

contacts to p-layer for higher optical power output 01 p0086 A67-10023

Surface effect on temperature, I-V and watt-ampere characteristics of p-n junction semiconductor injection laser diode as coherent light source 01 p0087 A67-10077

Minimum spectral line width, threshold current density, radiation-peak displacement and possible recombination mechanism for GaSb laser diode p-n junctions in coherent radiation 01 p0087 A67-10085

Origin of polarization of radiation from GaAs diodes, noting intensity dependence on current density and effect of anisotropic electron velocity distribution 01 p0034 A67-10090

Cryogenic liquid level sensor consisting of diode heated by resistor 01 p0062 A67-10194

Efficient electroluminescence at 300 degrees K from GaAs diode amphoteric dopant Si as dominant impurity on both sides of p-n junction 01 p0131 A67-10368

Locked oscillation of silicon p-n junction avalanche diodes in 50 to 140 GHz range 01 p0035 A67-10436

Continuous coherent radiation of GaAs semiconductor laser with epitaxial p-n junction at ambient temperature of 77 degrees K 01 p0090 A67-10548

Nuclear radiation intensity effect on switching time of fast diodes, examining produced stability changes 01 p0066 A67-10655

X-ray radiation effect on p-n junctions of germanium diodes, noting changes in V-I characteristics 01 p0136 A67-11047

Continuous coherent radiation of GaAs semiconductor laser with epitaxial p-n junction at ambient temperature of 77 degrees K 01 p0091 A67-11056

Electron tunneling through space charge region of uniformly doped metal-semiconductor barriers calculated in effective-mass approximation 02 p0280 A67-11483

Switching and dynamic characteristics of germanium peak diodes used as AM devices 02 p0210 A67-11531

Strong injection in nondegenerated p-n junction producing electron-hole plasma in n region near junction 02 p0296 A67-11827

Microelectronic applications of silicon-on-sapphire /SOS/ and MOS-FET large scale arrays /LSA/ 02 p0219 A67-12108

Photovoltaic effect in p-n junctions of lead tin telluride diodes indicate potential for IR detection throughout 8-14 microns atmospheric window 02 p0221 A67-12514

Second breakdown in junction transistors examined, using scanning electron microscope 02 p0222 A67-12653

Time dependent light emission due to voltage breakdown in mesoplasma region in Si on Si diode surfaces 02 p0301 A67-12658

Equivalent noise current equations and spontaneous fluctuations of leakage current due to carrier generation in depletion layer of reverse-biased junction diode 03 p0379 A67-13479

Method for intermodulation output spectrum generation in semiconductor diode junction 03 p0381 A67-13664

Potential distribution and field dependence of electron velocity in bulk GaAs measured with point contact probe 03 p0499 A67-13985

Temperature stability of several types of modulated radiation sources employing GaAs diodes, examining current change with temperature change 03 p0388 A67-14271

Negative differential resistances and inductive effects in alpha-modified SiC p-n junction diodes 04 p0679 A67-15136

Avalanching transit time diode, noting dynamic resistance mechanism of formation and linear and nonlinear diode behavior 04 p0583 A67-15154

Scanning electron microscope used in emissive mode to quantitatively measure depletion layer widening in silicon mesa diode 04 p0584 A67-15484

Book on semiconductor devices including thermal processes and microwave frequency conversion in semiconductor diodes 05 p0771 A67-16447

Thermal properties of semiconductor diode under steady and pulsed operation 05 p0772 A67-16448

Matrix analysis of small signal microwave frequency conversion based on linear operation of semiconductor

diode 05 p0772 A67-16449

Tunneling through junctions with nonuniform electric field, calculating probabilities and currents by WKB method 05 p0866 A67-16973

Step recovery diode utility extension, obtaining high efficiency from harmonic generators in millimeter wavelengths 05 p0780 A67-17529

Negative resistance regions in Si Zener diodes explained in terms of impact ionization and junction breakdown combination 06 p0968 A67-17814

Electron beam spatial scanning of coherent emission of GaAs junction laser at low temperatures, making current distribution nonuniform 06 p0101 A67-18150

Emission spectrum of GaP diodes analyzed as function of current and temperature 06 p1062 A67-18931

Soviet book on junction processes in pulse type semiconductor diodes 07 p1150 A67-19302

Electric field induced IR absorption in GaAs p-n junction diodes 07 p1231 A67-19553

Avalanche characteristics and failure mechanisms in junction diodes, showing negative resistance regions due to space charge effect of carriers 07 p1156 A67-19899

Capacitance voltage and V-I characteristics of four-layer p-n-nu-n semiconductor diode structures 08 p1303 A67-21054

Optical and electrical properties of epitaxial and diffused GaAs injection lasers noting spectral characteristics, optical gain, current distribution, etc 08 p1338 A67-21289

GaAs p-n-i-n diode as light activated switch, noting electrical and optical properties 08 p1306 A67-21295

Surface effect on temperature, I-V and watt-ampere characteristics of p-n junction semiconductor injection laser diode as coherent light source 08 p1339 A67-21455

Transient phenomena in reverse current and capacitance in gallium arsenide Schottky barrier diode in monochromatic light 09 p1471 A67-21762

Thermal noise in space-charge-limited solid state diodes, showing equivalence of noise resistance 09 p1472 A67-21951

Short aging test results on GaAs diodes, noting surface changes and dependence on nonradiative excess current component on device perimeter 09 p1472 A67-21952

High injection theories of p-n junction, commenting on corrections made in connection with junction voltage 09 p1472 A67-21953

Point contact electrically formed semiconductor junction diodes, discussing harmonic generation by various material combinations 09 p1474 A67-22086

Far field radiation patterns with Hermite-Gaussian symmetry in junction plane of GaAs lasers 09 p1513 A67-22133

Optimum design method for variable capacitance diodes with m-th power characteristic for wide voltage range, emphasizing impurity distribution 09 p1476 A67-22213

Microwave frequency oscillations obtained from p-n junction diodes reversed-biased into avalanche region, noting dependence on temperature and impedance of microwave circuit 09 p1479 A67-22265

Crystal orientation effect on epitaxial growth gallium arsenide crystals for smooth laser junction 09 p1515 A67-22275

Output and emission spectra of p-n junction diodes analyzed in connection with laser effect in GaSb 09 p1516 A67-22600

Varactor junction diode frequency multipliers emphasizing maximum conversion power and efficiency 10 p1609 A67-22836

Excess tunnel current due to inelastic electron molecule interactions near metal insulator interface 10 p1689 A67-23074

Space charge conductance and electron drift velocity measurements for avalanching p-n-n diode 10 p1611 A67-23169

Field dependent mobility effects in excess noise of junction gate FETs 10 p1612 A67-23376

Solution regrowth technology of electroluminescent devices noting reduced threshold current densities, external quantum efficiency and adaptation to planar technology 10 p1665 A67-23518

GaAs laser diodes in pulse operation at liquid nitrogen temperature, comparing

reflection and diffraction losses with absorption losses 10 p1666 A67-23521

Radiative recombination processes in GaAs p-n junctions, noting correlation between temperature behavior and carrier transport mechanism 10 p1693 A67-23523

Quantum efficiency of optimized GaAs diodes with Zn diffused in skin layer, noting dependence on junction depth 10 p1614 A67-23524

Systematic degradation of GaAs light emitter quantum efficiency, noting relation to current density 10 p1615 A67-23525

Factors of degradation of GaAs electroluminescent diodes, discussing surface leakage and change in spectral characteristics as major causes 10 p1615 A67-23526

GaAs Schottky diodes for integrated circuits, discussing fabrication, parameters and performance 10 p1615 A67-23527

Metal GaAs diodes as frequency changers, discussing fabrication, performance characteristics and parameters 10 p1615 A67-23528

Diffused GaAs varactor diodes, showing planar processes applied to production of diode based on metal-GaAs junction 10 p1615 A67-23529

P-n junction capacitance in transition region currents obtained by integral of holes or electron concentration 11 p1759 A67-24136

Traveling wave IR and sub-mm light modulator design using free carrier absorption in reverse biased p-n junction diodes 11 p1759 A67-24137

GaAs laser diode noting peak optical power, spectra and role of individual diodes in stack operation 11 p1802 A67-24745

P-type Au compensated Si diode with negative resistance, determining reversed conductivity recovery time 11 p1768 A67-24861

Room temperature laser threshold reduction and stimulated emission delay in GaAs diffused junction diodes 11 p1803 A67-24911

Low bias non-Esaki current in tunneling p-n junction diodes with large excess currents 11 p1768 A67-24926

Electrical and photovoltaic properties of PbS-Si heterodiodes 12 p1980 A67-25180

High resistance region effect in neighborhood of linear junction on series resistance analyzed for microwave varactor design 12 p1912 A67-25280

Impurity effect on electroluminescence of gallium phosphide diodes, noting dependence of spectrum on current density through p-n junction 12 p1914 A67-25438

Hall EMF measurement in base of negative resistance silicon diode 12 p1917 A67-26097

P-i-n diode switches, discussing driving techniques for series and parallel biased switches, pulse leakage and RF turn-off delay minimization 12 p1917 A67-26194

Electric field distribution in p region, space charge layer and n region of p-n abrupt junction germanium diode at room temperature 13 p2078 A67-26788

Active and reactive resistance components of p-n-n diodes with minimum distribution of steady state carrier concentration in base 13 p2182 A67-27282

Transient phenomena in capacitance and reverse current for n-type GaAs Schottky barrier diodes at different carrier concentrations 14 p2364 A67-27827

Doping distribution optimum for minimizing minority carrier transit time through base to improve overall HF performance of diodes and transistors 14 p2287 A67-28676

Temperature stability of several types of modulated radiation sources employing GaAs diodes, examining current change with temperature change 14 p2288 A67-28780

Pulsed power output for microwave GaAs oscillator biased into avalanche, with diodes grown by liquid phase epitaxy 15 p2442 A67-29172

Avalanching transit time diode, noting dynamic resistance mechanism of formation and linear and nonlinear diode behavior 15 p2443 A67-29341

Effect of capture levels on current-voltage characteristic of semiconductor p-n diode with ohmic back contact 16 p2635 A67-30471

Silicon negative-resistance junction diodes, studying n-p-n structure and diode

- characteristics dependence on light, temperature, voltage and frequency 16 p2636 A67-30898
- Localized uniaxial force effect on voltage-current relationship of gold-potassium tantalate Schottky barrier diodes, noting reversible changes 16 p2637 A67-31036
- IMPATT diode operation based on combination of avalanche-current multiplication and transit-time delay to produce negative resistance 17 p2824 A67-32332
- Fabrication and properties of p-n junction diodes, noting cut-off frequencies, junction characteristics, etc 17 p2826 A67-32620
- Superconducting tunnel junction, discussing effect of exceeding critical current in one film 17 p2922 A67-33058
- Schottky approximate formula adaptation for abrupt junctions with asymmetric doping ratios 18 p3106 A67-34646
- Flowgraph models describing relationships between thermal and electrical parameters of devices and associated circuits 19 p3206 A67-36034
- Polarity reversal with DC bias in hot-carrier microwave diode 19 p3198 A67-36038
- P-n junction diode frequency doubler operating in charge-storage/step-recovery mode efficiency and power 20 p3395 A67-36315
- Effect of irradiation of silicon by fast neutrons on switching time of alloy diode synthesized on silicon base 20 p3508 A67-36402
- Controlled differential negative resistance silicon junction diodes with cadmium alloyed base 20 p3397 A67-36696
- Junction temperature current dependence in CW operated gallium arsenide laser diodes 21 p3639 A67-38256
- GaAs pulsed injection laser diode noting characteristics for room temperature operation 22 p3813 A67-39253
- Coherent amplification properties of antireflective coated GaAs diodes considered for application to phased array 22 p3813 A67-39254
- Junction potential measurement in irradiated tunnel diode showing no oscillation in any bias voltage 22 p3767 A67-39369
- Microminiaturization problems associated with design and preparation of solid state Si microdiode matrices 22 p3769 A67-39580
- Semiconductor device noise theory emphasizing junction diodes, bipolar transistors and field effect transistors 22 p3770 A67-39773
- Microwave mixing with weakly coupled Josephson superconducting diodes, discussing Fourier components 22 p3865 A67-40439
- Field induced photoelectron emission /FPE/ from Si surface barrier diodes, discussing FPE measurement using xenon arc lamp and grating monochromator 23 p3980 A67-40890
- Noise in polarized Si semiconductor avalanche junctions at RF and microwave frequencies noting determination of impact ionization parameters 23 p3980 A67-41189
- Lifetime measurements of GaAs diodes determined from p-n junction impedance 23 p3982 A67-41468
- Constant voltage steps of AC Josephson effect observed in drop-form junctions exposed to radiation 24 p4200 A67-41864
- Magnetic impurities in tunnel junction barriers investigated for effect on junction resistance 24 p4200 A67-41865
- Radiation resistant silicon diode fast neutron monitors, discussing fission spectra and leakage currents in damaged diodes 24 p4183 A67-42473
- Logarithmic nature of I-V characteristics of silicon junction diodes for design of analog multiplier with differential operational amplifier 24 p4131 A67-42478
- Silicon avalanche oscillators under continuous operation at millimeter wavelengths, discussing efficiency and power densities 24 p4133 A67-42815
- JUNCTION TRANSISTOR**
- Epitaxial diffused integrated circuit structure containing p-n-p and n-p-n transistors 01 p0033 A67-10021
- Gunn effect noting negative bulk conductivity, creation of external negative conductance and zones with different field intensities in semiconductor crystals 01 p0130 A67-10253
- Silicon power transistor use in power supply, line operated audio output, video amplifier and TV horizontal deflection high voltage circuits 01 p0038 A67-10761
- Current transmission through semiconductors with impurities, calculating V-I characteristics at high temperatures during acceptor level creation 01 p0135 A67-10925
- Transient junction temperature rise, transient thermal resistance and failure energy in transistors by forward-potential sampling method 01 p0040 A67-11235
- Junction type field effect transistors and metal oxide semiconductor devices for switching functions in digital circuitry 02 p0215 A67-11971
- Initial saturation voltage effects in alloy-type transistors at high injection levels 02 p0215 A67-11977
- Second breakdown protection of Si power transistors by applying emitter resistances 02 p0222 A67-12654
- Secondary breakdown characterization technique in Ge p-n-p alloyed junction transistors with open base condition 02 p0223 A67-12655
- NGe-pGaAs heterojunctions, diffusion or emission theories of current transport do not explain electrical characteristics but validate Anderson model, considering tunneling as transport mechanism 03 p0494 A67-13478
- Emitter sidewall junction capacitance in double diffused transistors, using linearly graded junction equation and two-dimensional impurity distribution 03 p0382 A67-13679
- Cut-off frequency of diffusion transistor calculated, using series expansion for current transport factor 03 p0382 A67-13685
- Transient response of junction transistors in case of inductive load, deriving switching-on time, switching-off voltage maximum value, etc 03 p0386 A67-13978
- Activity criterion determination of boundary between active region and saturation region in transistor, using Ebers and Moll large signal equations 03 p0386 A67-13980
- Base spreading resistance and junction temperature of uniform base junction transistors 04 p0582 A67-15098
- Compressive stress effect on band gap widening and diffusion current in GaAs junctions 04 p0677 A67-15107
- Photoconductivity and negative resistance caused by carrier lifetime change in response to change in injection level in SiC p-n junctions 04 p0680 A67-15156
- V-I characteristics of p-n junctions on In-Sb base, noting effects of surface etching, temperature and impurity concentration 04 p0680 A67-15157
- Noise spectra of double base diode for case of uniform field in base and comparison with experimental noise measurements 04 p0585 A67-15619
- Beam lead sealed junction technology for planar processes, noting preparation and application 05 p0770 A67-16238
- Planar integrated circuit technology and beam lead sealed junctions, noting fabrication techniques, performance and applications 05 p0770 A67-16240
- Microwave integrated circuits combining tantalum thin film technology and beam lead devices, noting fabrication, advantages and performance 05 p0770 A67-16241
- Radiative interband recombination in strong electric field of p-n junction, calculating radiation intensity as function of quantum energy and applied voltage 05 p0863 A67-16689
- Reactive properties of p-n-n semiconductor structures at high injection levels for monomolecular electron-hole recombination 06 p1049 A67-17866
- Current and frequency dependent differential resistance and diffusion capacity of junctions of p-n-n structures at high current densities 06 p1049 A67-17868
- Parametric action in back biased p-n junctions carrying injected currents, discussing photoparametric frequency converters, transistor amplifiers and frequency doublers 06 p0969 A67-18106
- Second breakdown in transistors examined by thermal concept, noting transient junction temperature rise 07 p1156 A67-19900
- Second breakdown and degradation in Ge alloy junctions, noting failure mechanism and preventive surface treatment 07 p1157 A67-19905
- Incremental stress effects in transistors at emitter-base junction due to piezoresistive and piezoelectric effects 09 p1472 A67-21950
- Large signal transient response of junction transistor in switching and pulse operation treated by charge control analysis 10 p1603 A67-22772
- Chemical etching of dislocation and stacking fault structure of epitaxial GaAs, noting possible effect on electroluminescence 10 p1692 A67-23514
- Double diffused n-p-n gallium arsenide transistor, discussing ways oxygen modifies p-n junctions to increase voltage breakdown 10 p1617 A67-23537
- Field effect transistor transition from pentode-to triode-like characteristics with increasing drain bias 11 p1759 A67-24138
- Cut-off frequency of drift transistor, discussing function of drift field parameter 11 p1759 A67-24143
- Bulk reverse current in diffused Si power rectifiers, interpreting reverse characteristics in terms of thermal pair production 11 p1760 A67-24144
- Gallium arsenide electron photon transistor electrical properties at cryogenic and room temperature, determining total internal quantum yield of photons 11 p1765 A67-24475
- Diffusion effect on hole mobility in base of semiconductor device with p-n-p structure 11 p1765 A67-24480
- Photovoltage measurement across lifetime junction produced by electron irradiation and by changing surface recombination velocity 11 p1850 A67-24917
- Piezotransistor static characteristics approximated by exponential function of two variables 12 p1939 A67-25281
- High input impedance obtained with junction transistors, discussing circuit design for different frequency modulators, FET properties and applications 13 p2077 A67-26661
- Fabrication of small geometry planar bipolar transistors by using electron beam 13 p2084 A67-27574
- Doping distribution optimum for minimizing minority carrier transit time through base to improve overall HF performance of diodes and transistors 14 p2287 A67-28676
- Critical frequency dependence of p-l type semiconductor triodes on emitter current or injection level 14 p2289 A67-28824
- Superconducting storage device with Josephson tunneling junction replacing cryotron 14 p2289 A67-28921
- Interband states in vicinity of metallurgical junction, deriving formula for depletion layer capacitance of abrupt junctions with interface states 14 p2373 A67-28929
- Photoconductivity and negative resistance caused by carrier lifetime change in response to change in injection level in SiC p-n junctions 15 p2534 A67-29343
- V-I characteristics of p-n junctions on InSb base, noting effects of surface etching, temperature and impurity concentration 15 p2534 A67-29344
- Temperature distribution from local regions of microscopically thin film junctions of metal structures, noting effect on average temperature 15 p2444 A67-29415
- Characteristics and mathematical model of junction field effect devices with small length-to-width ratios 15 p2446 A67-29636
- GaSb properties and perspective applications, noting junction formation, production processes, etc 15 p2536 A67-29700
- Radiative interband recombination in strong electric field of p-n junction, calculating radiation intensity as function of quantum energy and applied voltage 15 p2539 A67-29859
- Emitter-base voltage vs collector-current characteristic used to study stability of parallel pairs of HF high power transistors 15 p2453 A67-30017
- Nonuniform base width effects on h-parameters of junction transistor 16 p2635 A67-30795
- Analog-to-code converter using negative resistance of unijunction transistor, noting construction and results 16 p2636 A67-30900

Surface potential contrast induced by electron beam of scanning microscope on unbiased planar transistors, investigating beam voltage effect on contrast information 17 p2823 A67-32197

Computer-aided transistor design, characterization and optimization 17 p2823 A67-32198

Josephson junction as ideal zero impedance voltage source with discrete voltage for simultaneous application of microwave and magnetic fields 17 p2915 A67-32657

Germanium pulse switching triode with fused p-n-p junction 18 p3009 A67-33477

Thermal stabilization of inverse current of p-n junction by additional gate for minority carriers extraction 18 p3009 A67-33478

Inductive characteristics of junction transistors, showing Q-factor increase achieved by using negative impedance produced by avalanche multiplication 18 p3009 A67-33479

Conduction mechanism in GaSb tunnel p-n junctions from 77 to 380 degrees K, noting temperature dependence of basic parameters, V-I characteristics, etc 18 p3098 A67-33573

Lattice and junction imperfection effect on behavior of reverse biased p-n junctions, noting voltage breakdown parameters, origin of microplasma behavior, etc 18 p3102 A67-34344

Saturation current measurement in diffusion transistors by method yielding current amplification factors and voltage dependence of emitter current 19 p3197 A67-35726

Indirect measurement of differential switching parameters examined for admittance matrix of common emitter coupling for field effect and junction transistors 20 p3396 A67-36379

Time dependent variations in parameters of junction semiconductors investigated for stability 20 p3401 A67-37450

Electro-optic phase modulation of visible and IR light by p-n, p-i-n and metal semiconductor junctions and heterojunctions, noting propagation modes 21 p3684 A67-38453

HF noise spectrum of drain and gate currents of junction FET computed from current series expansion 21 p3597 A67-38569

Junction field effect transistors for onboard satellite equipment, noting resistance to ionizing radiation 21 p3600 A67-38659

Switching behavior equations derived for FET with solutions applied to MOS and junction gate FET circuits 21 p3602 A67-39069

Direct Josephson current dependence on magnetic field in tunnel junctions noting temperature dependence of oscillation periods 22 p3857 A67-39504

n-m/ junction structures transient characteristics, forward and back bias cases show inductive and capacitive element behavior respectively 22 p3858 A67-39574

Measuring method for minority carriers recombination rate at base surfaces of n-m/ contact without passing DC through contact 22 p3858 A67-39575

HF and switching characteristics of junction transistors analyzed using power series expansions 24 p4201 A67-41900

Static characteristics of 2N1304 germanium junction transistor exhibited by two surfaces in three-dimensional space 24 p4128 A67-41925

JUPITER /PLANET/

Rotation period of Jupiter determined by radio observations explaining cyclic drift 01 p0146 A67-10294

Observations of 24 comets, 11 minor planets and Jupiter VIII, using computer 01 p0148 A67-10386

1414 mc/sec observations of Jupiter using radio telescope and crystal mixer receiver with linearly polarized rotating feed horn 03 p0411 A67-13166

Jovian decametric pulses compared with satellite and radio star scintillations in terrestrial ionosphere [RASSA PAPER 1-10-134] 03 p0373 A67-14245

Computer investigation of approach of Comet 1759 III to Jupiter before perihelion passage, considering possibility of capture by Jupiter 04 p0701 A67-15450

Radio interferometric observations of decimeter emissions from planet

Jupiter 05 p0892 A67-16408

Spectral types of decametric radiation bursts from Jupiter, noting classification based on duration or high resolution dynamic spectra 05 p0898 A67-16927

Planet rotation and orbiting of satellite Io modulations effect on maximum RF of storms 05 p0904 A67-17408

Short duration pulses association with subsidiary B and C sources of Jovian decametric radiation 06 p1086 A67-18375

Unmanned Jupiter space flights, discussing requirements for flyby, Orbiter and low thrust missions 07 p1249 A67-19570

Integrodifferential motion equations for Jupiter satellites 07 p1250 A67-19724

Solution within planetary theory with no secular terms in metric elements applied to problem of first order theory of Vesta disturbed by Jupiter 07 p1250 A67-19725

Elliptic restricted problem of periodic Trojan orbit and nonperiodic libration frequency and angular motion of Jupiter 08 p1381 A67-20388

Faraday rotation effects in spectral records of Jupiter decametric radiation 09 p1588 A67-22401

Oscillating libration orbits with period rigorously commensurable in rational fraction to basic long period 11 p1866 A67-24775

Meridian observation of Jupiter for planet position determination, analyzing discrepancies between ephemerides and observations, noting random error 11 p1868 A67-25087

Satellites Europa, Ganymede, Callisto and Amalthea show no effect on probability or spectral character of decametric radio emission of Jupiter 12 p2010 A67-26243

Horseshoe-shaped orbits in Jupiter-sun restricted problem, comparing Runge-Kutta and Steffensen integration methods 13 p2205 A67-27475

Jupiter decametric radiation analyzed with interferometer for manifestations of solar wind effects 14 p2385 A67-28404

High time-resolution polarimeter observations of Jupiter decametric radio bursts 14 p2388 A67-28836

Mean flux density and polarization degree of radio emission from Jupiter in centimeter spectral range 14 p2389 A67-28837

Decametric radio noise data from Jupiter apparitions /1960-1964/ 14 p2389 A67-28838

Cometary orbit evolution of Jupiter family, considering influence of Jupiter 15 p2553 A67-29155

Jupiter observations /1965-1966/, noting activity of NEB and long duration spots in NTB 15 p2558 A67-30025

Interaction between red spot and white oval spots on Jupiter, explaining dimensional variations of WOS during conjunction 15 p2558 A67-30026

Jovian decametric emission of millisecond pulse variety analysis from observations of four apparitions 15 p2558 A67-30032

Commensurability cases of asteroid and Jupiter within framework of secular perturbation theory 15 p2559 A67-30038

L-pulses of Jupiter radiation, attributing 1-sec component of time structure on decametric emission to diffraction by solar wind inhomogeneities 17 p2944 A67-32643

Three-body problem of Jupiter satellites orbits under solar influence, computing initial elements, determining orbital stability and solving satellite motion equations 17 p2946 A67-32753

Heliocentric orbits of former Jupiter satellites, relating direct or retrograde satellite to heliocentric semimajor axis as asteroid 17 p2946 A67-32754

General theory of planets in connection with progress in space research 18 p3124 A67-34157

Similarities between Jupiter decametric radiation and satellite induced ionospheric disturbances 20 p3521 A67-36308

Motion theory of comet Wolf I during 1918-1925 revolution which included close approach to Jupiter in 1922 20 p3524 A67-36659

Jupiter internal structure and energy emission 20 p3525 A67-36867

Jupiter Great Red Spot and three white ovals show correlation between oval rotational velocity and longitudinal distance from Red Spot 20 p3527 A67-37400

Jupiter atmosphere, interior and surface

properties, speculating on possibility of life in spite of presence of noxious gases 21 p3703 A67-38191

Trajectory optimization, performance and other factors in analysis of low thrust solar electric propulsion Jupiter flyby mission [AIAA PAPER 67-710] 21 p3706 A67-38737

Soviet book on planetary physics covering Martian, Venusian and Mercurian atmospheres, Venusian surface temperature and Jovian radio emission 21 p3707 A67-38933

21.2 cm spectra of Jupiter, Venus, Mars and Saturn noting mean effective brightness temperatures 21 p3709 A67-38993

9.4 cm radiation from Jupiter and Saturn and 21.2 cm radiation from Saturn 21 p3709 A67-38994

Microwave radiations of Jupiter, deriving equivalent black body temperature, magnetic field data, radiation belts data and electron energy 21 p3710 A67-38995

Decimeter radiation from Jupiter originating in synchrotron radiation of ultrarelativistic energy electrons in 1 gauss field 21 p3710 A67-38996

Morphology of Jupiter decametric radio sources 21 p3710 A67-38997

Magnetic field rotation, satellite Io and interplanetary propagation effects accounting for time variation of Jupiter magnetic flux and polarization 21 p3710 A67-38998

Jupiter and Saturn models, giving planet constitution, heat balance and atmospheric composition 21 p3710 A67-39001

Jupiter rotation variability used to understand internal physical processes, stressing variation of radio and Great Red Spot periods 21 p3710 A67-39002

Jupiter internal structure investigated by observing visible surface and radio emission, discussing magnetic field origin and hydrodynamics of fluid regions 21 p3710 A67-39003

Apparent Jupiter rotation rate change from decameter emission probability histograms shown to differ from dynamic radiation spectra 23 p4065 A67-41002

Dependence of decametric radio emission from Jupiter on positions of Galilean satellites with respect to sun, earth and Jovian magnetic plane 23 p4069 A67-41362

Thermophysical research requirements for Venus Lander, Jupiter Entry Probe and Mercury Orbiter planetary exploration missions 24 p4227 A67-42041

Millisecond bursts in radio emission from Jupiter not imposed by interplanetary scintillation but by amplitude or frequency variation in source 24 p4231 A67-42452

Cometary orbit evolution of Jupiter family, considering influence of Jupiter 24 p4240 A67-43078

JUPITER ATMOSPHERE

Spectral study of Jupiter, Saturn and rings of Saturn, determining methane concentration in cloud layers 04 p0701 A67-15557

Science subsystems for Jupiter flyby missions, discussing equipment selection, mission planning, spacecraft design and trajectory and constraints on vehicle configuration [AIAA PAPER 67-120] 06 p1084 A67-18287

Jovian atmosphere simulation with energy from corona discharge, producing simple organic molecules 07 p1246 A67-19057

Relationship between terrestrial and Jovian atmospheric circulations due to solar activity 08 p1398 A67-21215

IR observations for presence of ethane in atmospheres of Jupiter and Saturn reanalyzed and found consistent with previous results 08 p1398 A67-21218

Stimulation of Jupiter radio emission by Io 12 p2000 A67-25204

Magnetospheric model of Jupiter from numerical calculation of maximum number density of plasma 12 p2000 A67-25206

Structure and composition of Jupiter atmosphere, noting laboratory and observational data supporting hypothesis of consistency with solar elements abundance 16 p2746 A67-30932

Model for distribution of thermal plasma in magnetosphere of Jupiter under assumption of corotation with planet 17 p2951 A67-33196

Atomic and molecular processes in Cytherean, Martian and Jovian upper atmospheres 18 p3124 A67-34158

Ion-molecule chemistry of Jupiter upper

atmosphere, studying equilibrium and nonequilibrium abundances of hydrocarbon products due to UV radiation reaction 18 p3135 A67-34540

Nonthermal radio emission from Jupiter atmosphere, studying Io modulation effect 19 p3317 A67-34933

High resolution spectra of Venus and Jupiter using image intensifier and solar spectrograph, measuring abundances in planetary atmospheres 20 p3521 A67-36309

Jupiter Great Red Spot and three white ovals show correlation between oval rotational velocity and longitudinal distance from Red Spot 20 p3527 A67-37400

Atmospheric pressure at cloud top and hydrogen abundance in Jupiter atmosphere determined by analyzing methane spectral line widths 20 p3529 A67-37479

Taylor columns occurrence criterion in Jupiter atmosphere investigated experimentally, giving flow patterns 21 p3614 A67-38999

Experimental method for studying Taylor columns over hills and holes in Jupiter atmosphere 21 p3614 A67-39000

Planet Jupiter research, noting unresolved questions of cosmology, interior structure and Great Red Spot 21 p3711 A67-39092

Photometric observation data on Jupiter atmospheric activity /1964-1965/ noting three-month periodic change 22 p3879 A67-39299

Jupiter environment, effects of huge mass, high rotation rate, temperature and dominant H and He atmosphere 22 p3887 A67-40141

JUPITER PROJECT

Mathematical technique of midcourse guidance for spin stabilized interplanetary spacecraft, specifically computer simulation for flight to Jupiter 02 p0264 A67-12369

Automated spacecraft flights and cost /1965 to September 1966/, discussing Voyager, Jupiter probe, technology satellite, synchronous meteorological satellite and voice/TV broadcast 05 p0904 A67-16384

Saturn V launch vehicle and Apollo spacecraft hardware systems applied to unmanned exploration of Jupiter 22 p3887 A67-40138

K

K-BAND

Coherent microwave power at K-band frequencies from indium antimonide structures, presenting theory of two-stream interaction in transverse magnetic field 01 p0131 A67-10371

K spectrum to obtain structure and regularities of occupation of external energy bands in transition from Sc to Cr 04 p0640 A67-15975

Spectrophotometric results for H-alpha and K line contours of August 21, 1959 chromospheric flare 05 p0892 A67-16496

K-absorption spectrum of Ni as function of concentration of alloying elements and arrangement of atoms of alloying elements into Ni crystal lattice 06 p1017 A67-17952

K beta 5 emission band and fundamental K-edge absorption of vanadium analyzed and results compared with vanadium spectra from other series 08 p1342 A67-20808

Alloying effect on aluminum K and iron L X-ray emission spectra in Al-Fe binary system 08 p1343 A67-21304

Emission and absorption bands in K spectral region of titanium, using single setup 10 p1668 A67-23093

Solar K-line intensity and emission area at various phases of sunspot cycle 11 p1861 A67-24493

Photoadsorption of X-rays by interstellar gas using photolionization cross sections, showing neon K edge as distinctive feature of spectrum 17 p2937 A67-32752

X-ray K spectra of phosphorus absorption and emission in indium, gallium and boron phosphide semiconductors and red phosphorus 18 p3095 A67-33440

Superheterodyne receiver operating in K-band having solid state low noise characteristics 18 p3011 A67-34068

Vegetation mapping from K-band radar imagery using image discrimination, enhancement, combination and sampling

system 19 p3227 A67-34798

Spectral analysis of K alpha type X-ray transitions in solar atmosphere and laboratory plasma 19 p3331 A67-36086

K-MESON

S KAON

K-SHELL

Relativistic photoelectric cross section for two electrons of K-shell computed, using numerical program 04 p0661 A67-15763

Covalent bonds found more prevalent than ionic bonds in X-ray spectral study of Al and Sb in A-III B-V type semiconductor compounds 18 p3095 A67-33443

Relation between changes in ferrite lattice parameter at magnetic conversion temperature and changes in ferrite metal ion charges due to electron exchange 18 p3095 A67-33444

KALMAN-SCHMIDT FILTER

Self-contained orbital navigation system using earth-horizon measurements in 14-16 mu carbon dioxide absorption band, using Kalman linear filter 02 p0263 A67-11925

Kalman filter estimation of covariance parameters of linear system subjected to Gaussian driving functions 02 p0227 A67-12157

Observability and controllability in providing heuristic understanding of control problems, noting Kalman filter theory 02 p0227 A67-12159

Linear filtering equations and Kalman filtering techniques for linear, quasi-linear, nonlinear and optimum mixer filter problems, orbit determination, space vehicle ballistic coefficient estimation, etc 06 p1028 A67-17720

Kalman filter, modern version of Gaussian least squares method linear estimation of orbital elements of celestial body 06 p0974 A67-17926

Kalman filter alternate form extended to include multiple simultaneous correlated measurements, testing with ballistic model and using square root formulation for trajectory determination 06 p1023 A67-18277

[AIAA PAPER 67-90]

Dynamic filtering fundamentals, considering mathematical modeling 13 p2086 A67-26414

Kalman filter divergence control, noting analytical and empirical modification methods 14 p2347 A67-28116

Orbiting navigation with compensation for periodic errors, using modified Kalman filtering technique 15 p2513 A67-29595

Kalman filter alternate form extended to include multiple simultaneous correlated measurements, testing with ballistic model and using square root formulation for trajectory determination 15 p2563 A67-30202

Precomputed approximation to weighting matrix in extended Kalman filter for ballistic reentry vehicle trajectories estimation 16 p2651 A67-31682

Optimum filtering and control of randomly-sampled linear and nonlinear systems with Gaussian or non-Gaussian statistics, synthesizing generalized Kalman filter 16 p2651 A67-31683

Optimum mixer-filter for aircraft navigation systems consisting of inertial platform aided by Doppler and/or Loran designed, using Kalman filtering 17 p2825 A67-32525

Error effect in continuous Kalman filters used in orbit determination problems, deriving error bounds 19 p3199 A67-34779

Lunar terrain uncertainties effect on trajectory optimization using Kalman filter during lunar landing powered descent [AIAA PAPER 67-543] 19 p3256 A67-35942

Initial-convergence examination of Kalman filter for various autonomous navigation modes [AIAA PAPER 67-623] 19 p3260 A67-36012

Error divergence elimination in recursive minimum variance estimation of space vehicle trajectories 21 p3587 A67-39148

Minimum variance simulation for satellite attitude determination reliability using magnetic and solar measurements 21 p3715 A67-39150

KAMACITE

Kamacite and taenite superstructures and metastable tetragonal phase in iron meteorite 03 p0510 A67-13334

Kamacite-thenite interface relationship in

iron meteorite, discussing shock wave transformation 06 p1087 A67-18377

Iron and stony meteorite cooling rates determined by measuring kamacite bandwidth, bulk nickel content and composition 11 p1868 A67-24872

Coexisting sphalerite, troilite and daubreelite in Odessa meteorite and sphalerite inclusions in kamacite in Odessa and Canon Diablo analyzed for chemical composition 24 p4233 A67-42620

Concentration and distribution of phosphorus in kamacite and taenite in Mount Edith medium octahedrite determined by electron probe microanalysis 24 p4236 A67-42643

KAON

Proton-proton and pion and kaon elastic scattering from protons at high energy, deriving approximate formula for differential cross section, noting nucleon structure 24 p4193 A67-42855

KAPPA ROCKET

Lambda and Kappa rocket sounding observations of electron density, electron temperature, thermal electron energy distribution, plasma space electric potential and ion composition 01 p0060 A67-10335

Kappa rocket sounding of ionospheric Sq-currents, using rubidium vapor magnetometer 05 p0799 A67-16871

KARMAN VORTEX STREET

Free streamline theory of two-dimensional separated potential flow past bluff body and formation of periodic vortex turbulent wake 02 p0178 A67-12233

Flow induced vibration and noise in tube bank heat exchangers due to Karman vortex streets analyzed, noting shedding frequency, lift, etc [ASME PAPER 67-VIBR-48] 11 p1777 A67-24198

Karman vortices in heat exchanger, noting no vortex shedding in supercritical Reynolds number range and wake turbulence 11 p1782 A67-24657

Concentrated vortex model for Karman street in two-dimensional viscous incompressible laminar flow past bluff body 19 p3210 A67-35446

KEPLER LAW

Levi-Civita regularized equation of elliptic motion of particle influenced by massive primary and perturbed by smaller primary, Part II, Applications to circular and collision orbits 01 p0147 A67-10380

Graphic solution of Lambert time of flight equation for spacecraft correctional maneuvers with respect to initial velocity 01 p0152 A67-11399

Interplanetary trajectory correction via radial heliocentric velocity pulses, noting calculation by linear approximation 02 p0321 A67-11538

Near circular orbit of satellite in terrestrial gravitational field analyzed, using approximate solution of perturbed Kepler motion 02 p0327 A67-12373

Von Zeipel transformation solution small divisor problem arising from natural frequencies of orbital resonance motion of 24-hr artificial satellite 03 p0457 A67-13162

Functional relation between mass, radius and angular velocity of earth, solar mass and corresponding lunar quantities shown via reciprocity principle 04 p0702 A67-15582

Graphical methods for solutions to orbital mechanics problems involving equations derived from Newton and Kepler laws 05 p0901 A67-17206

Reference orbit for integration through boundaries of activity spheres, replacing six osculating Keplerian reference orbits 08 p1383 A67-20590

Newton inverse square force for planets from invariant velocity components of Keplerian planetary motion by graphical model 10 p1711 A67-23791

Earth gravitational field eccentricity effect on deviation of satellites from Kepler ellipse orbits 13 p2200 A67-27322

Elliptical motion of material point in terrestrial gravitational field, noting expression for eccentricity under effect of small tangential force 15 p2556 A67-29659

Spinor representation of energetic identities of Kepler motion, showing identity of Lambert theorem for position triangle and Stumpf theorem for velocity triangle 15 p2561 A67-30054

Orbits of artificial satellites for suitable

- variables, noting oblate shape of earth and air resistance 16 p2743 A67-30725
- Interplanetary trajectory correction via radial heliocentric velocity pulses, noting calculation by linear 16 p2752 A67-31604
- Economical transfers between Keplerian orbits in time-free case, considering hyperbolas, exterior ellipses and launching orbits (ONERA-TP-482) 18 p3133 A67-34465
- Differential correction vectors for non-Keplerian reference orbits, reexamining rotating ellipses in Hansen type intermediaries 21 p3705 A67-38612
- KERNEL FUNCTION
- Improved numerical procedure for harmonically deforming lifting surfaces from supersonic kernel function method (AIAA PAPER 66-78) 01 p0007 A67-11162
- Approximate solutions for integral equations with Hilbert kernel and degenerate nucleus 02 p0258 A67-11625
- Extreme value problem of constant type and extremal approximating operators with positive kernels 03 p0461 A67-14106
- Finite groups with single value generation of normal divisors, examining conditions for representation as KM 07 p1217 A67-20154
- Integral equation solution with Mellin inversion formulas for light scattering problems 09 p1524 A67-21872
- Characteristic for kernels of certain integral equations on semiaxis for determining solvability and number of possible solutions 14 p2344 A67-28809
- Extension of Vainberg method for studying nonlinear integral equations with aid of Hart theorem to cover Urysohn type equations 15 p2511 A67-29888
- KEROGEN
- Hydrogen peroxide oxidation and ozonolysis of polymer type material in coal, kerosene and Orgueil meteorite 08 p1289 A67-21174
- KEROSENE
- SA FUEL
- SA PETROLEUM
- Ignition of flammable fluids by hot surfaces tested on static hot plate rig and on wind tunnel rig, noting data on kerosene, lubricating oil and hydraulic fluid 09 p1580 A67-22248
- Effect of metals and alloys on thermal stability of Avtur 50 aviation kerosene from ASTM-CRC and high temperature coker tests 13 p2185 A67-26703
- Thermal stability aspects of commercial kerosene for supersonic transport (AIAA PAPER 66-670) 17 p2926 A67-32570
- KERR CELL
- Output characteristics of half-wave mode Kerr cell ruby oscillator used as optical radar for clear air turbulence /CAT/ detection 02 p0198 A67-12053
- Degenerate stimulated four-photon interaction and four-wave parametric amplification observed in ruby laser and liquid cell arrangements 05 p0844 A67-16379
- Kerr cell properties noting four-electrode cell giving frequency shift of 60 mc for laser beam 07 p1142 A67-19552
- Selective imaging of objects in range using pulsed laser illuminator synchronized with Kerr cell camera, obtaining elimination of film exposure due to backscatter in turbid atmosphere 08 p1337 A67-20683
- KERR EFFECT
- SHF modulation techniques for laser radiation, covering Faraday, Kerr and Pockel effects, circular dichroism, etc 03 p0436 A67-13138
- Equations for longitudinal Faraday and Kerr effects in gyroelectric thin films bounded by nonmagnetic medium, considering multiple inner reflections 05 p0865 A67-16971
- Longitudinal Kerr and Faraday effects in Ni and permalloy films using photoelectric polarization spectrometer, choosing various refractive indices and gyroelectric constants 05 p0865 A67-16972
- Self-focusing of elliptically polarized light resulting in formation of channels with linear polarization 08 p1340 A67-21503
- Free carrier electro-magneto-optical phenomenon in semiconductors, noting conductivity tensor, Faraday effect, Derr effect and Voigt effect 09 p1558 A67-22602
- Microwave reflection analysis of plasma surface phenomena, noting dependence on electron density and collision frequency 11 p1844 A67-25097
- Wave front reconstruction from magnetization distribution on magnetic tape, discussing possibilities based on magneto-optical Kerr effect, hypersonic wave generation and powder patterns 12 p1939 A67-25237
- Surface density gradient and collision frequency effects on polarization of microwaves reflected from plasma surface 13 p2164 A67-26300
- Kerr metric as Einstein field equations solution, considering Synge g method as possible Kerr metric 20 p3486 A67-37089
- Optical third-harmonic generation in rare gases, comparing coefficients with Kerr effect coefficients 21 p3639 A67-37962
- Worm motion of domain walls in Permalloy films using Kerr magneto-optic apparatus under pulse drive with nanosecond rise time 22 p3860 A67-39901
- Electronic ellipsometer for measurement of very small changes in elliptically polarized light, discussing refractive index, Kerr effect and calibration 24 p4152 A67-41901
- KETONE
- Mass spectra of amino ketones and amino alcohols and related substances 09 p1458 A67-22057
- Classification of 2-oxazolidones, examining preparation, physical chemistry, properties and polymerized derivatives 23 p3971 A67-41041
- 1, 3-diones and beta-ketoesters with cobalt for room temperature curing of unsaturated polyester resins by organic peroxide 24 p4175 A67-42420
- KEYING
- S FREQUENCY-SHIFT KEYING
- S PHASE-SHIFT KEYING
- KIDNEY
- SA RENAL FUNCTION
- SA URINE
- Cannulation of renal capsular lymphatics in anesthetized dogs, testing if lymph fluid can serve to assess tissue oxidation 06 p0952 A67-17853
- Cardiovascular and renal 24 hr synchronized and desynchronized circadian rhythm 11 p1747 A67-24785
- KINEMATIC EQUATION
- Vorticity jump across discontinuity surface which is not contact surface obtained on kinematical basis, recovering Hayes formula for gas dynamic discontinuity 04 p0600 A67-14456
- Kinematic nonlinearities effect on existence, properties and stability of vibrations in unison of particle with two degrees of freedom 11 p1818 A67-24085
- Computer model of aircraft accident investigator, discussing generation and testing of kinematic hypotheses on basis of programmed empirical data 15 p2420 A67-29896
- Generalized streamline hypothesis for turbulent boundary layer flow with spatial variation of viscosity 15 p2473 A67-30210
- Moment-kinematic and moment-energetic characteristics of servomotors applied to point and functional problems of servomechanisms in space 24 p4098 A67-42094
- KINEMATICS
- SA BODY KINEMATICS
- SA MICROWAVE REFLECTOMETRY
- Optimum design of curve generating four-bar linkages with inequality constraint (ASME PAPER 66-MECH-20) 08 p1336 A67-21317
- Damped least squares method for kinematic synthesis of plane curves described by paired coordinates for four-bar linkage mechanism (ASME PAPER 66-MECH-13) 08 p1336 A67-21318
- Book on applied kinematics covering synthesis techniques for link-and-cam motion other than uniform rotation in high speed high performance automatic machines 11 p1795 A67-23921
- Cardan errors in angle of rotation measurement of gyro-controlled plant 11 p1794 A67-25043
- Kinematic coupling effect in stabilization axes of flight vehicle as result of errors in gyrocompass gimbals and coordinate system 11 p1870 A67-25101
- Kinematic, spectroscopic and photometric data for pygmy stars /blue ultradwarfs/ 17 p2945 A67-32645
- Book on continuum mechanics including kinematics, principles and linear theories of continuum mechanics, elasticity and viscoelasticity 17 p2963 A67-33092
- Line element not precluding peculiar motions or assuming isotropy and homogeneity of mass distribution of universe, considering kinematical consequences 18 p3117 A67-33427
- Cavitation erosion noting high speed motion picture photographic analysis of kinematic structure of cavitation zone 20 p3420 A67-36631
- Book on functional mechanisms for engineering design, presenting kinematic characteristics of output motion, planar linkage and spatial cycloidal crank and flexural mechanisms 20 p3454 A67-36766
- Plane-strain problem of plasticity theory with two yield conditions applied to stress and velocity fields defined by differential equilibrium equations 20 p3541 A67-37299
- Negative pion-and proton-nucleon reactions at 17 and 24 GeV/c, using Lobachevskii-Einstein velocity space images method to obtain kinematics 24 p4193 A67-42858
- KINESTHESIS
- Properties of favorable coding schemes, applying results to text transmission through auditory and tactile senses 12 p1907 A67-26081
- KINETIC ENERGY
- SA FROUDE NUMBER
- One-dimensional compressible gas-channel flow under thermal and mechanical effects analyzed within generalized energy coordinates 01 p0119 A67-10170
- Excitation of phosphor suspensions in solid dielectric by mechanical energy analyzed via impact theory 01 p0113 A67-10354
- Kinetics of stored energy buildup in alkali halide crystals after proton irradiation, noting dependence on lattice energy of crystal 01 p0136 A67-11050
- Turbulent energy dissipation rates, eddy fluxes of sensible heat, momentum and kinetic energy measured above nonhomogeneous surface 02 p0238 A67-12076
- Steady flow possessing extremal kinetic energy compared to equivortex flow for stability analysis 03 p0402 A67-13618
- Impact of cylindrical or spherical projectiles of dural and polyethylene at high velocities in semilinear targets, analyzing crater shape and relation to kinetic energy 04 p0710 A67-15002
- Kinetic energies of ions produced by giant laser pulses, noting dependence of mean square ion velocity on pulse peak intensity 04 p0633 A67-15099
- Properties of crushable impact attenuation materials used to absorb and dissipate kinetic energy of impacting body 04 p0711 A67-15238
- Prediction of turbulent boundary layer development in conical diffusers, using kinetic energy deficit equation 04 p0549 A67-15750
- Uniform property turbulent boundary layer heat transfer calculation, using solution of integral momentum and kinetic energy equations 04 p0731 A67-15821
- Plasma stream translational energy transformation into random motion in connection with collisionless shock wave propagation along magnetic field 05 p0853 A67-16756
- Collision induced dissociation of deuterium by argon and nitrogen examined with angular ion scattering apparatus, determining kinetic energy and angular distribution 05 p0848 A67-16834
- Magnetic and kinetic energy calculated for geomagnetic storm as function of velocity distributions 05 p0801 A67-17133
- Deriving Lagrangian for system of extended rotating bodies, noting contribution of relativistic corrections for kinetic energy of rotation 05 p0847 A67-17496
- Implosive collapse of liners containing gas to transfer chemical energy of explosive to kinetic and internal energy of gas (AIAA PAPER 67-178) 06 p1118 A67-18485
- Interdiurnal pressure variability as measure of kinetic energy of air masses 06 p1027 A67-18606
- Nonlinear instability of nonisothermal

plasma in external electric field, determining ion-acoustic noise spectrum and time dependent variations in kinetic energy of plasma electrons and ions 06 p1045 A67-18801

Pair production in irradiated semiconductors within framework of plasmon decay, considering variation of radiation ionization energies with band gap energy 06 p1063 A67-18935

Frangible sounding rocket vehicle and explosive fragmentation system, determination of impact kinetic energy of fragments and flight tests 08 p1407 A67-20521

Electric conductivity and kinetic energy in seeded and unseeded airflow MHD experiments in hypersonic shock tunnels for aerospace applications 09 p1542 A67-21809

Statistical energy analysis for multimodal random vibration of complex system, discussing power flow, modal responses, kinetic energies, etc [ASME PAPER 67-VIBR-8] 11 p1872 A67-24168

Excitation of phosphor suspensions in solid dielectric by mechanical energy analyzed via impact theory 11 p1851 A67-25027

Solar cosmic ray diffusion coefficient dependence on cosmic ray energy and distance to sun studied via solar flares 12 p1991 A67-25111

Magnetospheric model of Jupiter from numerical calculation of maximum number density of plasma 12 p2000 A67-25206

He 3 nuclei in low energy primary cosmic radiation determined, using stack of nuclear emulsions 12 p1993 A67-25479

Equations for elastic system free oscillations with parallelogram shaped hysteresis loop derived from kinetic energy changes, describing system time dependent dynamic behavior 12 p1967 A67-25660

Meteor distribution estimation attempted through radar observation, measuring kinetic energy level, velocity and electron distribution in meteor trails 13 p2197 A67-26507

Characteristic scales of thermal convection in unstable atmosphere, discussing time evolution of total kinetic energy and lifetime for dry air case 13 p2116 A67-27460

Kinetic energy distribution of ions produced by dissociative attachment dependence on ion thermal energy and electron affinity of oxygen 14 p2350 A67-28151

Effect of wide angle screened diffuser on turbulent velocity fluctuations [ASME PAPER 67-FE-23] 14 p2243 A67-28368

Frangible sounding rocket vehicle and explosive fragmentation system, determination of impact kinetic energy of fragments and flight tests 15 p2565 A67-29449

Relativistic effects in HF plasma accelerators, noting decrease in transverse kinetic energy and axial velocity 15 p2527 A67-29475

Solitary waves, discussing electron and ion acceleration and transfer mechanism of solar wind ion kinetic energy to electrons 15 p2475 A67-29613

Gradient stabilization of cryogenic liquids in pendulum and sloshing motions, noting response to kinetic energy input, oscillation frequency period and stability criteria 17 p2836 A67-32053

Eigenvalue method prediction of two-phase fluid critical flow rates via energy model, comparing empirical and theoretical results 17 p2838 A67-32689

Hypersonic reentry heating problems due to kinetic energy of space vehicle at reentry at orbital and escape velocity 17 p2970 A67-32828

Kinetic energy transport outwards in transition region between chromosphere and corona discussed qualitatively, postulating connection with spicules 17 p2952 A67-33393

High kinetic energy electrons associated with solar flares, noting prompt and delayed types 17 p2940 A67-33401

Nonlinear instability of nonisothermal plasma in external electric field, determining ion-acoustic noise spectrum and time dependent variations in kinetic energy of plasma electrons and ions 18 p3090 A67-34420

Ion-molecule reactions of diatomic

deuterium cation with diatomic deuterium and diatomic hydrogen 18 p3083 A67-34521

Stratospheric mean adiabatic vertical motion and temporal correlations with temperature, isobaric height, zonal/meridional wind and horizontal kinetic energy computed based on seasonal averages 19 p3224 A67-35529

Mixing-length velocity profile in boundary layers with transpiration, discussing Tennekes theory and turbulent kinetic energy change rate 19 p3211 A67-35752

Secondary dose equivalent model for calculating secondary proton and neutron doses determined, using random sampling techniques 20 p3482 A67-37551

Properties of kinetic energy and squared vorticity in two-dimensional inviscid turbulent flow, using Navier-Stokes equation and conservation laws 21 p3609 A67-37735

Magnetic and kinetic energy calculated for geomagnetic storm as function of velocity distributions 21 p3619 A67-38476

Primary cosmic ray energy and jet CMS velocity estimations by three methods corrected by analyzing known energy interactions 23 p4051 A67-40913

Ion energies in expanding plasma stream generated by intense giant pulse laser light in focus on solid LiD and LiH targets 23 p4033 A67-41152

Mixing effect in dual flow turbojet engines analyzed to obtain better conversion of combustion into kinetic energy 23 p3931 A67-41317

Error in calculating rate coefficients from cross section data in limited energy range, noting m-point Laguerre integration formula 23 p4030 A67-41530

Autopropulsion of gas bubble by rocket effect noting equivalent particle concept and applications to boiling, flow and cavitation erosion 24 p4141 A67-41904

Kinetic behavior of electrons in air plasmas containing electrophilic gasses studied with microwaves behind reflected shock waves 24 p4196 A67-42196

Ar atomic beam produced by plasma burner measured for kinetic energy and Mach number 24 p4198 A67-42576

Strong coupling superconductivity in intermetallic compounds, possibly due to all electrons having same kinetic energy 24 p4205 A67-42738

KINETIC EQUATION

Kinetic equation describing microphysical random condensation of cloud droplets 01 p0109 A67-10684

Gas phase pyrolysis kinetics of tetranitromethane, noting pressure effect and rate equation of thermal decomposition 01 p0019 A67-10765

Ionospheric F-2 layer inhomogeneities attributed to plasma flute instability, using kinetic drift equations to describe plasma oscillations 02 p0236 A67-11669

Power energy spectrum of cosmic rays as solution of general covariant kinetic equation 02 p0308 A67-12491

Ion mobility in gas formed by ions, defining gas temperature, obtaining solution of kinetic equation for ion distribution function 02 p0270 A67-12625

Exact solutions to kinetic moment equations of monatomic gas in absence of external forces to case of mixture of monatomic Maxwellian gases with external forces 03 p0401 A67-12869

Parametric resonance in plasma situated in magnetic field noting oscillation, frequency stability, kinetic equations, electric field effect, etc 03 p0475 A67-12931

Kinetic equation derivation from density matrix for case of quantum generation of secondary optical harmonic in laser cavity under various optical pumping conditions 03 p0435 A67-13127

Kinetic equations derived for plasma with particle interactions 03 p0481 A67-13735

Kinetic plasma equations in form of Boltzmann equation or Fokker-Planck or Vlasov type of equations applied to astrophysics 03 p0481 A67-13736

Electron velocity distribution equation extended to small wave numbers for electron-ion plasma 03 p0483 A67-13914

Light absorption by free current carriers role in kinetic equations of semiconductor laser/radiation system 03 p0439 A67-14376

Book on kinetic equations of gases and plasmas, with emphasis on theories which

start from Liouville 04 p0660 A67-14581

Energy impulse vectors and kinetic moment tensor associated with body in gravitational field analyzed, using Brouwer theorem 04 p0658 A67-15494

Chapman-Enskog method applied to kinetic equation describing evolution of singlet distribution function in dense gas of perfectly rough spheres 04 p0658 A67-15507

Kinetic theory of quantum electron gas coupled to radiation field under uniform external magnetic field 04 p0672 A67-15770

Two-particle ring term for kinetic equation with Darwin interaction relationship to relativistic Landau equation 04 p0672 A67-15772

Transient exact solutions to integral and differential operators of kinetic equations of gas mixture 05 p0849 A67-17113

Asymptotic kinetic equation for inhomogeneous plasma compared to results for initial value problem and Bogoliubov method 06 p1042 A67-18572

Kinetic equation for homogeneous nongyrotropic magnetoplasma, discussing collective effects and errors in Sundaresan analysis 06 p1042 A67-18574

Charged particles motion in magnetic field with regular and random components, deriving kinetic equation for distribution function and then diffusion equation 06 p1037 A67-18800

Scaling of binary titanium alloys in carbon dioxide at high temperatures using kinetic, metallographic and electron probe microanalysis [AAS PAPER 66-190] 08 p1341 A67-20763

Kinetic equation for unstable homogeneous plasma in uniform magnetic field when subjected to sudden uniform electric field 08 p1360 A67-21127

Models for collision processes and changes of degree of freedom in kinetic equation for polyatomic gases 08 p1323 A67-21386

Kinetic equations for homogeneous electron gas derived to all orders in plasma parameter λ_{De} /reciprocal number of electrons per Debye sphere/ 08 p1363 A67-21394

Kinetic equation for inhomogeneous electron plasma derived from Liouville equation by Prigogine-Balescu diagram technique 08 p1366 A67-21431

Excitation-recombination statistics in semiconductors with donor and center interacting with both bands for given thermal disequilibrium, treating silicon 09 p1551 A67-21669

Asymptotic properties of solutions to kinetic coefficient equation system, noting mass velocity dependence on time 10 p1625 A67-23042

Power energy spectrum of cosmic rays as solution of general covariant kinetic equation 10 p1703 A67-23359

Kinetic model equation for polyatomic gas with internal structure based on Wang Chang-Uhlenbeck 11 p1775 A67-23864

Local potential variational method to study runaway stability of electrons in two-component plasma 11 p1826 A67-23872

Analytical expression for steady state rate of electric domain movement in semiconductors in terms of electric field distribution at domain center 11 p1846 A67-24482

Inhomogeneous gas of weakly coupled relativistic electrons, deriving kinetic equation for particle electromagnetic field system 11 p1782 A67-24781

Kinetic equation for electron gas in classical limit derived from quantum mechanical transport equation, using equilibrium analogy 11 p1844 A67-25076

Nonequilibrium process in one dimension in presence of constant and oscillating electric field, using distribution function 11 p1824 A67-25078

Kinetic approximation of penetration of electric field into plasma layer situated in stationary magnetic field, determining plasma field 13 p2164 A67-26396

Kinetic equation for completely ionized plasma generalized for several particle species case 13 p2165 A67-26585

Small parameter method for rarefied gas dynamics problems using Boltzmann equation hierarchy and kinetic equations 13 p2099 A67-26953

- Monte carlo evaluation of Boltzmann collision integral for translational relaxation and plane steady shock problems 13 p2103 A67-26974
- Collisional parameters in kinetic model equations for binary gas mixtures, treating shock structure in weakly ionized argon 13 p2103 A67-26977
- Solar corona broadening mechanism studied using microscopic model including kinetic equations, determining proton escape velocity from sun 13 p2194 A67-27340
- Ion mobility in gas formed by ions, defining gas temperature, obtaining solution of kinetic equation for ion distribution function 13 p2161 A67-27381
- Direct modulation of He-Ne laser with RF excitation, noting kinetic equations of transition processes 14 p2329 A67-27772
- Coulomb interaction effect on time dependent variations of electron distributions in Van Allen belt, using kinetic equation 14 p2378 A67-27918
- Linearized Fokker-Planck kinetic equation, describing approach to equilibrium of test electrons injected into electron plasma in thermal equilibrium 14 p2356 A67-28203
- Ionospheric satellite trail, noting relation between length scales of medium properties and scales determined by body dimensions 14 p2302 A67-28207
- Equation describing electron transfer between semiconductor surface bands and space bands, applying Fermi concept 14 p2371 A67-28754
- Boltzmann kinetic equation solution for completely ionized plasma in magnetic field 14 p2363 A67-29071
- Coefficient for electron ion recombination during triple particle collision, using Boltzmann kinetic equations 14 p2363 A67-29077
- Kinetic equation for plasma with electromagnetic interactions, using shielding approximation 15 p2519 A67-29209
- Lenard-Balescu kinetic equation solved by Chapman-Enskog method for transport coefficients of plasmas noting diminishing value 15 p2522 A67-29210
- Heat transfer through rarefied gas between concentric circular cylinders and spheres, using Krook kinetic equation 15 p2579 A67-29570
- Kinetics of gas-solid reactions at high temperatures, noting mass transfer coefficients attainable, temperature discontinuities, stagnation lines, etc 15 p2582 A67-30022
- Kinetic equation for electron, ion and atom concentrations for Coulomb plasma taking into account inelastic processes 16 p2715 A67-31040
- Ionospheric F-2 layer inhomogeneities attributed to plasma flute instability, using kinetic drift equations to describe plasma oscillations 16 p2665 A67-31084
- Monograph on upper atmosphere kinetics noting Boltzmann equations, MHD processes, thermal diffusion, etc 16 p2686 A67-31166
- Ion mobility in gases determined, based on kinetic equation for ion velocity distribution function with particular reference to Chapman-Enskog method 16 p2704 A67-31250
- Anisotropic phase of cosmic ray flares analyzed using kinetic equation in Fokker-Planck approximation 16 p2740 A67-31891
- Exact stability criteria for kinetics equations of coupled-core nuclear reactors, using Pontryagin theorem and models for time-distribution of coupling neutrons [ASME PAPER 66-WA/AUT-16] 17 p2882 A67-32015
- Kinetic equation for chemical and electron processes in low temperature plasma flows 17 p2896 A67-32169
- Kinetic equation derivation for one particle species fluid using closure hypothesis 17 p2883 A67-32290
- Hamiltonian formalism for collisionless electron plasma nonlinear kinetics using quantum statistical perturbational treatment 17 p2902 A67-32670
- Book on plasma physics covering plasma clouds in electromagnetic force field, kinetic equations, Boltzmann equation, etc 18 p3089 A67-34370
- Charged particles motion in magnetic field with regular and random components, deriving kinetic equation for distribution function and then diffusion equation 18 p3083 A67-34419
- Kinetic equation for inhomogeneous plasma in uniform external magnetic field, for application in studies of transport and high frequency wave phenomena 19 p3285 A67-35342
- Convergence of solutions for AC and DC electric conductivity of plasma with collisions 19 p3286 A67-35352
- Homogeneous, fully ionized plasma HF conductivity computed using kinetic equation, showing application to two-temperature plasma 19 p3286 A67-35353
- Ionizational relaxation and excitation behind shock waves, proposing solution for kinetic equation system 19 p3293 A67-35403
- Statistics and kinetic equations of plasma in opacity region taking into account relativistic effects 20 p3502 A67-37662
- Plasma model kinetic equation, discussing collision operator approximating momentum and energy transfer rates 22 p3843 A67-39265
- Elastodynamic problems using kinetic-stress functions 22 p3909 A67-39399
- Thermographic method for investigation of kinetics of heat evolution 22 p3917 A67-39586
- Kinetic equation for spatially uniform unstable plasma with collision term containing wave effect / plasmons/ in system and Lenard-Balescu equation 22 p3848 A67-39690
- Kinetic equations for electrons and photons in homogeneous plasma in strong magnetic field derived from Maxwell and classical motion equations 22 p3851 A67-39736
- Kinetic equation for steady state electron-ion system with electrons drifting under electric field, calculating HF resistivity drift velocity dependence 23 p4033 A67-40962
- Path-probability method applied to thin film nucleation and growth on substrate by vapor deposition, deriving kinetic equations 23 p4040 A67-40968
- Integral turbulent transfer model using velocity distribution function to develop mixing length flow theory 24 p4141 A67-41933
- KINETIC FRICTION**
- Literature in 1965 on lubrication and bearings covering friction and wear, boundary, metal working, gear and spline lubrication, rolling element bearings, etc [ASME PAPER 66-WA/LUB-8] 04 p0629 A67-15349
- Chandrasekhar dynamical friction theory for star in cluster adapted to Fokker-Planck electron in two-component plasma theory and including multiple encounters 10 p1711 A67-23790
- Mechanical friction occurring during oscillating motion of gas which absorbs or reflects electromagnetic radiation 14 p2349 A67-29075
- KINETIC HEATING**
- Spin temperature of intergalactic atomic hydrogen calculated as function of electron density and kinetic temperature 03 p0515 A67-14319
- Digital computer CPU control of kinetic heating processes in engine of supersonic aircraft under simulated flight conditions 08 p1315 A67-21007
- Monograph on hypersonic heat transfer calculation methods for boundary layers in presence of surface catalyzed reactions 09 p1489 A67-22198
- Approximate formulae for transient temperature prediction due to kinetic heating in aircraft type structures 11 p1883 A67-24661
- Equilibrium deviation occurring in plasma with variable kinetic temperature due to radiation transport within plasma volume and outflow beyond limits of volume 16 p2723 A67-31767
- Direct numerical control by computer of 150 heating circuits for safe kinetic heating test simulation of flying conditions for large supersonic aircraft 17 p2820 A67-32748
- Degree of blackness of normal black body radiation for various metals, studying temperature and kinetic relations and blackness of opaque oxide films 18 p3064 A67-34052
- Calibration and recording method for transmission coefficients of thermal wall heat flows, using ONERA wind tunnel [ONERA-TP-470] 18 p3020 A67-34463
- Tungsten cermet emissivity study using electron heating 20 p3466 A67-36913
- SST aircraft influence on fuel quality requirements, considering use of liquefied gaseous hydrocarbon fuels 21 p3688 A67-38192
- Radio telemetry links perturbations during ballistic missile reentry due to plasma from kinetic heating 21 p3581 A67-38228
- Thermographic method for investigation of kinetics of heat evolution 22 p3917 A67-39586
- Integrated transport cross sections obtained for nitrogen as function of temperature using gaskinetic formulas 22 p3841 A67-40050
- KINETIC THEORY**
- SA BIOKINETIC THEORY**
- SA DIFFUSION**
- Elastic stability theory formation by combining thermodynamic and mechanical stability 01 p0159 A67-10402
- Boltzmann equations in kinetic theory of rarefied gas dynamics [ONERA-TP-379] 01 p0054 A67-11092
- Current carrier concentration and dynamic coefficients for nondegenerated and highly degenerated Fermi gases subject to nonparabolic isotropic laws of dispersion 02 p0300 A67-12475
- Plasma kinetic theory calculation via direct perturbation expansion of singular distribution for single system, comparing Dupree and Dawson-Nakayama version of BBGKY hierarchy 02 p0279 A67-12800
- Kinetic moment in celestial mechanics, noting application to satellite orbit determination in terrestrial gravitational field 03 p0510 A67-13456
- Kinetic phenomena in impure ionic semiconductors of cubic symmetry, finding region for dominant scattering mechanism 04 p0675 A67-14923
- Kinetic theory of electromagnetic propagation in confined magnetoactive plasma 04 p0668 A67-15272
- Metastable dislocation crack transformation into polygonal walls of edge dislocations caused by diffusion over crack surface 04 p0711 A67-15282
- Kinetic theory of gases through certain correlation functions known as product densities used to explain transitions from gaseous to liquid state 04 p0608 A67-15466
- Gas kinetic theory of negative ion collisional detachment, using elastic sphere model 05 p0844 A67-18003
- Steady one-dimensional heat conduction in rarefied gas at rest analyzed from viewpoint of kinetic theory to determine existence or possible departure from Fourier law 05 p0925 A67-16272
- Kinetic theory of electromagnetic wave propagation in layered plasma waveguide in strong magnetic field 05 p0761 A67-16341
- Generalization of kinetic theory of gases, deriving Boltzmann kinetic equation for use in singly-partial distribution function 05 p0849 A67-17021
- Collisionless aspects of strong shock wave structure as approximated by Boltzmann equation examined, using orthogonal polynomial expansion technique in velocity space 05 p0794 A67-17421
- Spherical electrostatic probe in stationary plasma analyzed based on kinetic theory using Krook type model for collision integral formulation 05 p0857 A67-17423
- Solution to chain of kinetic gas equations, showing effect of fast reversible and slow irreversible processes on particle distribution function 05 p0847 A67-17541
- Thermal stability of ammonium perchlorate-lithium perchlorate mixture, noting explosion above 280 degrees C for various compositions 07 p1239 A67-19078
- Electron components for electrical, thermal conductivity and viscosity coefficients of gas mixtures calculated via molecular kinetic theory 07 p1225 A67-19116
- Electrodynamic properties of homogeneous magnetoactive plasmas including wave propagation, excitation, scattering, etc 08 p1358 A67-20863
- Mott-Smith type moment method and restricted variational principle determinations of shock structure 08 p1355 A67-21141
- Kinetic theory-plasma dynamics theory calculations of magnetospheric solar wind proton velocity distribution as function of particle speed 08 p1377 A67-21315
- Rosen restricted variational principle used to obtain surface integral applicable to solution of kinetic theory boundary value problems 08 p1324 A67-21408

Decay kinetics of He plasma, examining pair collision, metastable atom diffusion coefficient and afterglow mechanism via spectroscopy 09 p1544 A67-21918

Sound propagation in partially ionized plasma, noting kinetic quadrature calculation results 10 p1683 A67-22783

Quantum mechanical kinetic theory of gas loaded spheres to obtain limit of transport coefficients and relaxation time 10 p1682 A67-23383

Thin electrostatic sheath adjacent to body immersed in flowing weakly ionized continuum plasma analyzed for arbitrary Debye length mean free path ratios 11 p1825 A67-23868

Physical foundations of modern kinetic theory, showing interpretation of particular form of Liouville equation in terms of time scales appropriate to system 11 p1823 A67-24545

Rarefied gas motion instability, constructing general solution for effect of various force fields 11 p1782 A67-24688

Dynamical irreversible evolution of gas with short range repulsive forces, using n-particle distribution function with many-body interactions 11 p1824 A67-25077

Gas-surface interactions, energy exchange and scattering between particles and surface 13 p2097 A67-26935

Kinetic theory and rarefied gas dynamics, discussing and analyzing Boltzmann equation 13 p2099 A67-26951

Kinetic model with velocity dependent collision frequency applied to forced wave propagation in half-space and other unsteady problems 13 p2100 A67-26956

Heat transfer for gas with internal degrees of freedom between parallel plates, noting temperature profiles and jumps 13 p2100 A67-26959

Discrete ordinate method for boundary value problems in gas dynamics using differential equations yields solutions to Couette flow 13 p2101 A67-26962

Kinetic theory description of flow over right circular cylinder at low speed based on Lees moment method 13 p2102 A67-26969

Monte Carlo calculation of kinetics of chemically reacting multicomponent gas for finite number of particles followed through random collision processes 13 p2102 A67-26971

Decay kinetics of He plasma, examining pair collision, metastable atom diffusion coefficient and afterglow mechanism via spectroscopy 14 p2358 A67-28247

Generalization of kinetic theory of gases, deriving Boltzmann kinetic equation for use in singly-partial distribution function 14 p2351 A67-28482

Thermal accommodation coefficients determination in temperature jump region 15 p2580 A67-29883

Velocity distribution functions in statistical theory of turbulence, deriving moment equations and comparing properties with kinetic theory 16 p2660 A67-31220

Plane wave propagation in kinetic theory, discussing Boltzmann equation use and asymptotic results beyond critical frequency 17 p2905 A67-32927

Plane wave propagation in kinetic theory, noting Boltzmann equation and kinetic model 17 p2885 A67-32928

General equation for explosion limits from unified thermal and chain theory, noting application to hydrogen and oxygen systems 18 p3156 A67-33849

Nonlinear and second order thermal diffusion of electrons in ionized gas, using kinetic theory 18 p3083 A67-34401

Book on electrodynamics of plasmas covering analysis of collective properties of plasma based on classical and quantum-statistical mechanics 19 p3267 A67-34866

Kinetic theory of transport processes in weakly turbulent plasma with and without magnetic field 19 p3286 A67-35351

Plasma oscillations, discussing kinetics, macroscopic and Vlasov equations, Landau damping and beam instabilities [AFOSR-66-2823] 19 p3299 A67-35871

Plasma kinetic theory, discussing BBGKY hierarchy, nonequilibrium processes and unstable plasma kinetic equations 20 p3495 A67-36154

Proton velocity distribution in solar wind flow around magnetosphere 20 p3518 A67-36653

Heat transfer of gas between parallel plates including radiation and rarefaction effects treated, using kinetic theory 20 p3553 A67-36935

Soviet book on rarefied gas dynamics involving methods and approaches for kinetic description of gas behavior, emphasizing Boltzmann equation 20 p3423 A67-37086

Kinetic theory of electromagnetic wave propagation in laminar plasma medium situated in steady HF or LF magnetic field normal to plasma layer interfaces 21 p3663 A67-37860

Electron components for electrical, thermal conductivity and viscosity coefficients of gas mixtures calculated via molecular kinetic theory 21 p3659 A67-38161

Electromagnetic wave propagation in plasma layer bounded by external constant magnetic field, using kinetic theory with Maxwell equations and distribution function 21 p3670 A67-38685

Boundary conditions at wall for low density flow problems treated by kinetic theory, synthesizing relation between distribution functions of incident and reflected particles 21 p3614 A67-38861

Kinetic theory of ionospheric satellite trail, discussing neutral and charged components from BGK model equation [AIAA PAPER 66-477] 21 p3706 A67-38862

Shock structure in kinetic theory of gases, solving Krook model of Boltzmann equation with small perturbation technique 22 p3782 A67-39196

Ion wave dispersion relation in mercury vapor plasma, explaining cut-off frequency dependence on electron drift velocity 22 p3842 A67-39207

Continuous phase medium gas representation used to derive variational principles for Liouville, coupled Bogoliubov and kinetic equations 22 p3835 A67-39218

Kinetic theory of electromagnetic propagation through magnetoactive plasma, determining reflection, transmission and absorption coefficients and plasma field configuration 22 p3761 A67-39758

Negative cyclotron resonance absorption due to electron elastic collisions with noble gas atoms, comparing results with kinetic plasma wave theory predictions 22 p3842 A67-40346

Kinetic approach to fatigue investigation in calculation of cyclic lifetime from static test data 23 p4074 A67-40663

Book on dynamics of rarefied gas, discussing kinetic theory, shock wave structure, Couette flow, gas flow between coaxial cylinders and plasma dynamics 23 p3989 A67-40873

Collection efficiency of plane acting as pump in vacuum system, discussing parameter measurements, partial pressure analyzer and kinetic theory values 23 p4004 A67-41354

Kinetic prediction theory for viscosity, thermal conductivity and diffusivity of binary liquid mixtures composed of molecules interacting with square-well potential 23 p4083 A67-41531

Sound propagation in partially ionized plasma, noting kinetic coefficients and quadrature calculation results 24 p4195 A67-42119

KINETICS

SA CHEMICAL KINETICS

SA ELECTROKINETICS

Continuous helium-neon laser used to obtain short intense light pulses and to study kinetics of autophotocatalytic emission of high resistivity silicon 03 p0436 A67-13142

Carbide forming elements effect on kinetics of isothermal transformation of austenite and mechanical properties of manganese-molybdenum steel 07 p1199 A67-19239

Kinetics of growth of beta grain in titanium alloy 07 p1200 A67-19245

Kinetics of nonuniform generation of longitudinal plasma waves by transverse wave beam with narrow spectrum, noting effect of magnetic field 09 p1545 A67-21995

Temperature dependence of small signal AC field effect kinetics in silicon within 170-300 K, considering majority carriers and one energy level theory 13 p2176 A67-26708

Beryllium aging kinetics when having different purities 13 p2136 A67-27105

Silicon surface purified by argon ion bombardment and annealing, studying field effect kinetics 14 p2372 A67-28755

Semiconductor photoconductivity kinetics as affected by surface recombination, considering bi-and monopolar photoconductivity 14 p2372 A67-28756

Kinetic model of matter for energy momentum tensor of general relativity, noting freedom of divergence 17 p2883 A67-32360

Radiation kinetics of laser with resonator having lens system and low absorption nonlinear medium, showing time shift of kinetic curve 17 p2868 A67-32666

KIRCHHOFF LAW

Displacement formulations of first order linear thin elastic shell equations in terms of stress resultant and middle surface, using modified Kirchhoff hypothesis 08 p1417 A67-20551

Spectral coefficients of blackness in materials with low thermoconductivity determined by measuring radiation intensity and solving equations derived from Planck and Kirchhoff laws 18 p3048 A67-34056

Combined frequency and space correlation of wave fields scattered by rough surfaces where conditions of applicability of Kirchhoff approximation hold true 22 p3760 A67-39660

Dynamic boundary conditions for Kirchhoff constrained shell, obtaining symbolic scalar relationship for shell mechanics 24 p4249 A67-42152

KIWI B REACTOR

Nuclear rocket propulsion development, hot test results, one breadboard engine configuration and flight stage planning [AIAA PAPER 67-981] 24 p4187 A67-43054

KIWI ROCKET REACTOR

Ground technology program for nuclear rocket development, discussing NERVA and KIWI programs 18 p3077 A67-34706

KLEIN-GORDON EQUATION

Space-time diffraction for asymptotic solution of Klein-Gordon dispersive hyperbolic equation in bounded domain 07 p1218 A67-20270

Nonrelativistic approximation for electromagnetic radiation in conducting medium moving with uniform velocity with respect to source 15 p2521 A67-29194

Time-dependent Green function for moving isotropic nondispersive medium 15 p2509 A67-29199

Solution behavior of second order nonlinear differential equation with restriction on one constant 21 p3651 A67-37922

KLYSTRON

Klystron amplifier performance, noting increased efficiency by using double interaction in output circuit 02 p0222 A67-12531

Reflex klystron operation modes such as phase locked amplifier, regenerative amplifier, detector and mixer 03 p0387 A67-14101

Fluctuation spectra of amplitude and frequency of reflex klystron oscillations excited by fluctuation noise /Schottky effect/ 04 p0583 A67-15169

Klystron with broad electron flux and excited traveling and standing electromagnetic waves, analyzing electron grouping 05 p0771 A67-16356

Spectra of unlocked driven semiconductor oscillators observed with millimeter wave reflex klystrons, noting gradual controllable frequency pulling 05 p0780 A67-17522

Klystron with axisymmetric output cavity without conventional coupling loop or iris for obtaining minimum harmonic power output 05 p0780 A67-17534

Bandwidth, phase and amplitude characteristics calculated for reflex klystron divider in case of multiple frequency division 07 p1158 A67-20243

Electrostatically focused extended interaction S-band klystron amplifier using helical buncher resonators for interplanetary spaceborne communication systems 09 p1477 A67-22252

Noise measurements on pulsed four-cavity electrostatically focused S-band klystrons 09 p1477 A67-22253

Small signals of wideband and high gain multicavity klystron amplifier showing similarity to traveling wave tube 09 p1478 A67-22254

Multicavity klystrons and traveling wave tubes and use in ground stations 09 p1478 A67-22257

Electronic conversion efficiency in gridless two-cavity klystrons for cylindrical and sheet beams 10 p1611 A67-23062

Frequency stabilization of power klystron used in spectrometer for relaxation time measurement 11 p1767 A67-24752

Optimum efficiency of high power klystrons for operation in fourth and fifth TV band, noting space charge effect 14 p2277 A67-27773

Medium power millimeter wave klystron w/Laddertron/ construction and characteristics 14 p2278 A67-27800

Klystron amplifier performance, noting increased efficiency by using double interaction in output circuit 14 p2279 A67-28008

Fluctuation spectra of amplitude and frequency of reflex klystron oscillations excited by fluctuation noise /Schottky effect/ 15 p2443 A67-29355

Electron bunching in sweep klystron, deriving electric field equation, motion equations and continuity criteria for arbitrary charge density distribution 18 p3010 A67-33501

Automatic frequency-control system using superconducting resonator and reflex klystron 19 p3192 A67-34984

Discriminator for fine automatic frequency control of reflex-klystron by error signal 19 p3228 A67-34991

Low power pulsed reflex klystron used to produce hyperfrequency-wave trains for short time periods 19 p3193 A67-35416

Input-to-output amplitude and phase modulation characteristics derived for multicavity klystron 19 p3197 A67-35809

Cut-off amplifiers in frequency stabilization klystron designed to cut off only HF wave applied to discriminator 20 p3396 A67-36327

Mutual pulling system between two klystrons, deriving equations for pulling bandwidth and for various system responses 20 p3398 A67-36772

Triode system of reflex klystron, stressing creation of modulated SHF oscillations device 20 p3451 A67-37148

Reflex klystron electron admittance dependence on potential distribution in repeller space, showing electrode structure and space charge effects 21 p3598 A67-38604

Reflex klystron for 1.5 mm wavelength noting high current density cathodes, RF section simplification and better heat dissipation 22 p3768 A67-39493

Extension of nonlinear TWT equations to floating drift relativistic klystron, noting formulas for first harmonic of current in two- and three-cavity klystron 22 p3770 A67-39655

Klystron amplifier stability during double interaction in output circuit determined assuming zero HF potential and electron flow not bunched 24 p4129 A67-42193

KNOOP INDENTATION

Knoop hardness anisotropy in unalloyed titanium and iodide titanium sheets, discussing orientation, hardness variations, rolling, cross section planes and indentation [ASTM PAPER 53] 18 p3068 A67-34583

Knoop hardness yield loci for two Ti alloys 21 p3646 A67-38777

KNUDSEN CELL

Nonisothermal changes in properties and composition during chemical and physical reactions, noting application to Knudsen cell vaporization [AIAA PAPER 67-156] 08 p0956 A67-18321

Absolute manometer of Knudsen for any temperature ratios and arbitrary accommodation coefficient on boundaries 08 p1331 A67-20867

Knudsen cell used in mass spectrometry of thermodynamics of refractory substances vaporization 19 p3242 A67-34864

Chromium activities in binary Cr-Ti solid solutions measured by Knudsen effusion technique, noting deviations from Raoult law and free energy calculation 20 p3469 A67-37384

KNUDSEN FLOW

Knudsen layer in steady shear flow with temperature gradient along infinite flat wall 01 p0052 A67-10460

Transverse and longitudinal Knudsen

forces account for experimentally observed thermomolecular flow forces by extension of theory in intermediate pressure range 04 p0603 A67-14731

Knudsen limiting law in free molecular gaseous flow in various capillaries with temperature gradient 04 p0739 A67-15948

Boltzmann equation applicability to flows satisfying condition of molecular chaos, noting role of Knudsen layer 06 p1022 A67-17724

Exact theory of enclosed molecular radiometer using flow field solution from Wu-revised thermal transpiration theory in two cases 10 p1681 A67-22864

Knudsen low voltage discharge with hot cathode, determining electron distribution, velocity profiles, V-I characteristics, etc 11 p1831 A67-24020

Velocity distribution function of re-emitted molecules effect on slip flow boundary conditions 13 p2102 A67-28970

Formulation of upper and lower bounds on Knudsen flow rate of gas through channel of arbitrary geometry by reciprocal variational principles 15 p2469 A67-29195

Refractory metals and compounds vaporization study, using Knudsen effusion method and mass spectrometry for vapor tension and vaporization energy 20 p3463 A67-36116

Rarefied gas axisymmetric stagnation point flow, clarifying relationship between continuum and Knudsen layer flow 22 p3784 A67-39836

Space distribution function of Knudsen gas in closed volume investigated using gas model noting dependence of time 24 p4190 A67-41902

KNUDSEN NUMBER

BGK intermolecular collision model of sphere drag at high Knudsen numbers and low Mach numbers 08 p1322 A67-21140

Cesium vapor flow from orifices and tubes into vacuum analyzed, noting dependence of angular distribution and center line intensity on Knudsen numbers 08 p1324 A67-21495

Thirteen moment equation solved for problem of plane Couette flow by iteration scheme, showing functional dependence on Mach and Knudsen numbers 11 p1774 A67-23863

Spherical supersonic source expansion of neutral disparate molecular weight binary gas mixture studied asymptotically as source Knudsen number tends to zero 13 p2104 A67-26984

Discharge characteristics of sharp and round edged orifices in transition regime noting variation of pressure ratio, magnitude of Knudsen and Reynolds numbers, etc 14 p2300 A67-28180

Nonequilibrium aspects of fluid mechanics of freely expanding jet analyzed, using aerodynamic molecular beam system 14 p2301 A67-28184

Time of flight distribution measurement of weak molecular beam, noting limitations due to signal to noise ratio 14 p2316 A67-28185

Thirteen-moment equations solved obtaining theory of thermal force acting on spherical particle for entire range of Knudsen numbers 16 p2661 A67-31221

Rarefied gas cylindrical Couette flow noting Knudsen number, Bhatnagar-Gross-Krook model for Boltzmann equation, transport integrodifferential equation, etc 18 p3029 A67-34738

Control rockets covering very low thrust operation, gas generation problems, gas expansion, etc 20 p3516 A67-36881

KOLMOGOROFF THEORY

Comparison of variances evaluated by Kolmogorov and Volterra techniques for phase locked loop subjected to white Gaussian input 01 p0044 A67-10480

Noise effect on ideal relay element with lagging feedback analyzed using Kolmogoroff equations, comparing performance with ideal forcing element connected to linear amplifier 05 p0782 A67-16321

Approximate calculation of local characteristics of sound waves into liquid and gaseous media 05 p0846 A67-16707

Inclusion probability of stochastic dynamical system shown to satisfy Kolmogoroff backward equation 08 p1308 A67-20323

Approximate calculation of local characteristics of turbulence developing

during intense injection of sound waves into liquid and gaseous media 11 p1820 A67-24929

Noise effect on ideal relay element with lagging feedback analyzed using Kolmogoroff equations, comparing performance with ideal forcing element connected to linear amplifier 18 p3017 A67-33873

Tracking interruption probability determination in radars reduced to Kolmogoroff equation in dimensionless form taking dynamic error into account 21 p3585 A67-38815

KROOK EQUATION

Thermal creep in rarefied gas investigated using Boltzmann-Krook equation 03 p0402 A67-13359

Discrete ordinate method for unsteady linearized Boltzmann Bhatnagar-Gross-Krook equation of rarefied gas flow 08 p1324 A67-21409

Numerical solution of initial and boundary value Rayleigh problems for nonlinear Krook equation at large wall velocities 13 p2102 A67-26988

Solution for shock wave of bimodal distribution using Bhatnagar-Gross-Krook models, noting symmetry property destruction and recovery by using modified BGK model 15 p2470 A67-29226

Kinetic theory of ionospheric satellite trail, discussing neutral and charged components from BGK model equation [AIAA PAPER 66-477] 21 p3706 A67-38862

Shock structure in kinetic theory of gases, solving Krook model of Boltzmann equation with small perturbation technique 22 p3782 A67-39196

KRYPTON

Exciton and impurity states in Kr and Xe crystals and in rare-gas solids containing Xe impurity calculated by pseudopotential theory 02 p0281 A67-11490

Kryptonate /radioactive source with Kr 85/ for temperature profiles of turbine blades, missile gas analysis, corrosion, oxidation, etc 02 p0265 A67-12214

Crystal absorption and lamp emission spectra for CW pumping of Nd-doped YAG by water-cooled Kr arcs 03 p0437 A67-13576

Multiphoton ionization of krypton atom by ruby laser radiation 06 p1037 A67-18796

Mass spectrometric detection of cosmic-ray-produced krypton isotope in meteorites and possibility of Kr-Kr dating 07 p1256 A67-20228

Charge exchange cross sections measurements for ion-molecule pairs of hydrogen, argon, krypton, helium and xenon 09 p1535 A67-22381

Isotopic composition of krypton in high and low calcium achondrites, noting measurement results 09 p1569 A67-22685

Radioactive krypton content in stone meteorites determined via mass spectrometry, deriving spill ratios and radiation ages 11 p1866 A67-24692

Isotopic composition and abundance of xenon and krypton in graphite of iron meteorite from Canyon Diablo examined for anomaly pattern 16 p2750 A67-31438

Spallation and fissionogenic xenon and krypton content in Pasamonte achondrite as evidence for extinct radioactivity in meteorites 16 p2754 A67-31747

Multiphoton ionization of krypton atom by ruby laser radiation 18 p3083 A67-34415

Excitation and ionization mechanisms in positive DC discharge columns in krypton and xenon 19 p3265 A67-35131

Krypton isotope composition in three unequilibrated and two gas rich chondrites, with correction for cosmic ray spallation 22 p3881 A67-39494

Threshold properties of CW laser oscillation at 7525.5 angstroms in Dc-excited KrII discharge 22 p3818 A67-40490

Optically pumped Rb in collisions with Kr inducing relaxation, noting two different correlation times due to kinetic collisions and metastable states present 23 p4012 A67-40792

L

L-500 AIRCRAFT
S LOCKHEED L-500 AIRCRAFT
L-BAND

Performance and design characteristics of solid state microwave converters for

converting VLF telemetry receivers to L-and S-bands 02 p0196 A67-12006
 Alloying effect on aluminum K and iron L X-ray emission spectra in Al-Fe binary system 08 p1343 A67-21304
 L-band rattle traveling wave maser, discussing slowing factor and inverted susceptibility 09 p1514 A67-22270
 Microwave oscillation-amplifying L-band platinotron tube to amplify peak power of radar transmitter 10 p1605 A67-23061
 High speed wideband L-band tunnel diode frequency deviator tunable over octave bandwidth by 160 mv change in input voltage [IEEE PAPER 19-TP-67-1175] 23 p3978 A67-40743

LABORATORY

SA ASTRONOMICAL OBSERVATORY
 SA ENGINE TESTING LABORATORY
 SA ENVIRONMENTAL LABORATORY
 SA LUNAR MOBILE LABORATORY /MOLAB/
 SA MANNED ORBITAL LABORATORY /MOL/
 SA MANNED ORBITAL RESEARCH LABORATORY /MORL/
 SA SPACE LABORATORY
 SA TEST FACILITY
 Functions of Lunar Receiving Laboratory including lunar samples distribution to scientists, quarantine, storage, contamination, etc 07 p1164 A67-20021

LABORATORY APPARATUS

Book on laser microemission spectrum analysis covering laser properties, Q-switching technique, controlled negative feedback lasers, applications, etc 15 p2501 A67-30147
 Automated biological laboratory /ABL/, comprehensive integrated system for detection of life on Mars 16 p2762 A67-31488
 Laboratory equipment protection from vibration environment, noting instrumentation and results 17 p2833 A67-32066
 Apparatus for uniform sized liquid drop production by ultrasonic wave action on fluid jet, with drop formation recorded by photography 18 p3052 A67-34610
 Laboratory equipment for R and D on fibrous refractory materials 21 p3649 A67-37883
 German Gyroscope Testing Laboratory noting revolving platform for simulating rotational velocities, signal testing and signal simulation 23 p4003 A67-41327

LABYRINTH

Vestibular section of labyrinth contribution to postrotational changes in level of adrenalin and noradrenalin content in some tissues of white rats 03 p0365 A67-14330
 Nervous and humoral mechanisms of extralabyrinthine effects on vegetative disturbances during space flight factors 24 p4111 A67-41843

LAG

Modulation phase lag in causing overheating of semiconductor diodes as frequency of rectified voltage increases 02 p0209 A67-11508
 Modulation phase lag in causing overheating of semiconductor diodes as frequency of rectified voltage increases 14 p2283 A67-28072

LAGRANGE COORDINATE

Infeld method of introducing Lagrange variables in special relativity as applied to describe fluid system in general relativity 01 p0114 A67-10869
 Exploration of role of Lagrangian points of earth-moon system within solar system exploration program, using libration point satellites 02 p0328 A67-12405
 Governing mechanical and thermal equations in Lagrangian coordinates, reviewing isentropic theory 06 p1099 A67-17643
 Book on linear vibration theory including generalized properties and numerical methods 09 p1576 A67-22423
 Equilateral position stability of equilibrium in planar restricted problem of three bodies for mass ratio values 13 p2205 A67-27477
 Lagrange equations of perfect fluid flow linked to datum point and geometric surface arbitrarily moved within flow 16 p2663 A67-31709
 Lagrangian for interaction of electric

charge with field induced by scalar magnetic charge to determine electrical dipole moment 17 p2883 A67-32100
 Geometrical and equilibrium equations derived for circular plates, introducing Lagrange type coordinate as independent variable 17 p2961 A67-32807
 Three-dimensional periodic motion about collinear Lagrangian equilibrium points, determining motion, variational and orbit equations and numerical integration 22 p3889 A67-40427

LAGRANGE EQUATION

Satellite rendezvous guidance laws applicable to circular, near-circular and elliptical orbits, using Lagrangian formulas for position and velocity in two-body orbit 02 p0264 A67-12315
 Characteristics of one-dimensional cold electron plasma produced by uniform background of ions 02 p0278 A67-12626
 Rayleigh dissipation function and Lagrange equations of nonlinear friction forces 04 p0658 A67-15584
 Lagrange variational equation application to dynamic stability problems of plates in gas flow 05 p0923 A67-17188
 Generalized Lagrangian for system of gravitating elastic bodies derived from Fokker Lagrangian 05 p0847 A67-17495
 Deriving Lagrangian for system of extended rotating bodies, noting contribution of relativistic corrections for kinetic energy of rotation 05 p0847 A67-17496
 Model estimation programming to determine optimum design criteria for rocket propulsion system using estimating function, approximation solved by Lagrange method [AIAA PAPER 67-208] 06 p1024 A67-18330
 Lagrange theorem for series expansion with remainder for weak function whose argument satisfies implicit relation 06 p1025 A67-18731
 Lagrangian dynamical system determined under parametric form of motions applied to two-and three-body problems 07 p1216 A67-19722
 Lagrange equations of motion for solid body with liquid-filled cavities derived, using Hamilton-Ostrogradskii principle of least action 07 p1224 A67-20029
 Charged particle motion in static magnetic fields without axial symmetry derived, employing Lagrange equation in transformed coordinate system and Alfvén motion 11 p1855 A67-23929
 Ordinary waves in viscoelastic mediums analyzed, using Green tensor relation to Kirchhoff tensor 11 p1877 A67-24750
 Heat transfer in conducting and radiating gas analyzed, using governing equations reformulated as Lagrangian equations through introduction of potential 12 p2035 A67-25926
 Lagrange and Euler representations of particle shapes and vortex theorems in hydrodynamic flow 13 p2094 A67-26644
 Characteristics of one-dimensional cold electron plasma produced by uniform background of ions 13 p2171 A67-27382
 Doubly symmetric orbits about collinear Lagrangian points, computing jacobians eigenvalues 13 p2205 A67-27482
 Lighthill uniformization technique applied to singular perturbation problems using Lagrange expansion 14 p2346 A67-29059
 Variational technique involving Lagrange function representation of Grad magnetohydrostatic equation extended to symmetrical solenoid field 15 p2530 A67-29727
 Gravitation equations different from Einstein derived from Lagrangian in general form corresponding to general relativity theory 16 p2702 A67-31045
 Orbits and trajectories for plane motion of material point in conservative field of force 16 p2748 A67-31138
 Book on celestial mechanics presenting solution of artificial satellite motion in earth gravitational field, using Lagrange equations 17 p2950 A67-33166
 Lagrange interpolation pattern synthesis technique using moment criterion for optimum pattern approximation by nonuniform antenna array 18 p3012 A67-34430
 Evaluation of transfer functions using Lagrangian equations, giving dynamic expressions 19 p3206 A67-36033

State space equations formulated for general class of nonlinear networks, deriving block diagram of relationships 20 p3407 A67-36332
 Wave kinetics of free Alfvén oscillations using Lagrange function of collisionless plasma, calculating energy growth rate and relaxation times 21 p3667 A67-38372
 Independent variable changes in dynamical systems and applications to systems regularization, giving canonical and Lagrangian motion equations with tensor notation 23 p4027 A67-41006

LAGRANGE MULTIPLIER

Resource allocation for maximum system reliability, noting weight allocation in spacecraft and Lagrange multiplier approach 01 p0084 A67-11354
 Lagrange multiplier matrix in minimum weight and fully stressed optimum structural design techniques 03 p0525 A67-13966
 General problem of least squares solved using method of Lagrange multipliers 10 p1674 A67-23003
 Optimal interorbital transfers between near-circular noncoplanar closely spaced orbits described in terms of linearized theory 15 p2563 A67-30389
 Point-to-point mapping technique in combination with variational calculus for solving optimum control problems for piecewise linear dynamic systems 22 p3776 A67-39776
 Lagrange multipliers in two-point boundary condition problems for trajectory optimization estimated by direct method 22 p3885 A67-39963

LAGUERRE FUNCTION

Functional integration analysis of exponential behavior of nonlinear feedback control systems 01 p0047 A67-11211
 Rodrigues type formula for generalized Laguerre polynomials based upon semigroup property for solutions of heat equation and generating function related to source solution 10 p1875 A67-23630
 Convergence of solutions for AC and DC electric conductivity of plasma with collisions 19 p3286 A67-35352
 Error in calculating rate coefficients from cross section data in limited energy range, noting m-point Laguerre integration formula 23 p4030 A67-41530

LAMBDA ROCKET

Lambda and Kappa rocket sounding observations of electron density, electron temperature, thermal electron energy distribution, plasma space electric potential and ion composition 01 p0060 A67-10335

LAMBERT SURFACE

Rayleigh scattering and Lambert ground reflection effect on solar energy absorbed by ozone in earth molecular atmosphere evaluated on basis of transfer equation 12 p1932 A67-25341
 Cryogenic fluid storage on moon surface, considering Lambert reflection law, thermal insulation performance, incident heat flux and boil-off rates [AIAA PAPER 67-296] 12 p1926 A67-26011
 Lambert diffuse reflection from general quadric surfaces 13 p2158 A67-26877
 Radiative heat exchange between surfaces of telescoped cylinders, determining angular radiation coefficients 14 p2406 A67-28308
 Lambert theorem used to find required trajectory to effect rendezvous in space 19 p3332 A67-34828
 Model for lunar surface roughness effect on emission of thermal IR radiation and casting of shadows in sunlight 21 p3702 A67-38188

LAME POLYNOMIAL

Earth potential in ellipsoidal coordinates developed using Lame function 05 p0796 A67-16564

LAME WAVE EQUATION

Contour integral representation of eigenvalues of first boundary value problem of elasticity theory 17 p2962 A67-32832
 Vector eigenfunctions solution of three-dimensional elastic theory problems, reviewing literature on bodies of revolution in various coordinates 24 p4248 A67-42101

LAMINA

S LAMINAR BOUNDARY LAYER

SEPARATION

S MONOMOLECULAR LAYER

LAMINAR BOUNDARY LAYER

Laminar boundary layer on flat plate at high Prandtl number, obtaining temperature

- profile, recovery factor and heat transfer 01 p0052 A67-10795
- Cyclic formation of turbulence in wake of profiled obstacle with laminar boundary layer 01 p0053 A67-10943
- Heat transfer and equilibrium temperature of heat conducting sharp cones in supersonic rarefied gas flow at zero angle of attack 01 p0007 A67-10977
- Steady state combustion model of mono- and double-base solid propellant with laminar flow 01 p0143 A67-11450
- Local convection coefficient along windward line of axisymmetric obstacle in hypersonic flow with laminar boundary layer 02 p0178 A67-12061
- Integral relations method applied to separation of laminar boundary layer on cooled hypersonic reentry body 02 p0179 A67-12348
- Reentry simulation, discussing aerodynamic and thermodynamic parameters, heat transfer and simulation accuracy 02 p0335 A67-12415
- Laminar Prandtl boundary layer arising during steady flow past blunt cone at angle of attack studied by finite difference method 03 p0349 A67-12868
- Laminar boundary layer with longitudinal pressure gradient in high velocity flow of uniformly dissociated gas for arbitrary external velocity 03 p0401 A67-12875
- Heat transfer and distribution of velocity, temperature and concentration in laminar hypersonic boundary layers with blowing of light gas with desired pressure and heat distribution 03 p0532 A67-12990
- Geometric body profiles assumed by sphere and initially pointed cone during processes of ablation and shearing analyzed and combined to apply to sphere cones [AIAA PAPER 86-992] 03 p0353 A67-14145
- Velocity, energy and concentration fields in laminar boundary layers with arbitrarily distributed mass transfer at surface 04 p0603 A67-14643
- Soviet papers on laminar boundary layer flow and heat and mass transfer 04 p0721 A67-14708
- Approximate relations for solution to equations of nonisothermal laminar boundary layer 04 p0722 A67-14711
- Composite heat transfer and viscous friction of moving gray medium with large optical density, using laminar boundary layer equation, noting hydrodynamic state role 04 p0722 A67-14713
- Controlled three-dimensional roughness effect on hypersonic laminar boundary layer transition [AIAA PAPER 86-28] 04 p0547 A67-14819
- Complex flow interactions within laminar hypersonic boundary layers 04 p0604 A67-14846
- Approximate analysis of electrostatic probe on reentry vehicle for electron density measurements in laminar boundary layer of continuum plasma 04 p0705 A67-15231
- Approximate method of treating three-dimensional laminar incompressible boundary layer equations when cross flow is small [ASME PAPER 66-WA/FE-34] 04 p0607 A67-15365
- Nongray radiation effects on laminar boundary layer of absorbing gas over flat plate at low Eckert numbers [ASME PAPER 66-WA/HT-35] 04 p0724 A67-15428
- Heat transfer and skin friction rates increase in gas-liquid droplet suspension system flowing over circular cylinder formulated by laminar boundary layer theory 04 p0725 A67-15439
- Heat transfer and pressure in laminar shock wave/boundary layer interaction corner flow at Mach 8 and 10 04 p0610 A67-15834
- Surface property effects on effectiveness of mass transfer cooling in laminar boundary layers with hydrogen injected into free stream of nitrogen or carbon dioxide 04 p0733 A67-15840
- Gas flow, convective heat transfer, enthalpy rise and surface mass transfer for bodies in cross flow, with application to circular cylinder 04 p0733 A67-15841
- Natural convective heat transfer in closed cavity between two disks in central force field for laminar flow in boundary layers 04 p0738 A67-15893
- Rayleigh-Ritz method for turbulent heat transfer in curvilinear channel and heat flux magnitudinal and directional effects on stability of isothermal flow in laminar boundary layer 04 p0610 A67-15900
- Nonsimilar free convection boundary layer from vertical flat plate with step discontinuities in surface temperature [ASME PAPER 66-WA/HT-17] 04 p0739 A67-15930
- Radiation transfer effect on equilibrium temperature for laminar boundary layer flow of absorbing-emitting gas over flat plate [ASME PAPER 66-WA/HT-48] 04 p0739 A67-15940
- Three-dimensional flow separation over structures with various geometric configurations, calculating limiting streamlines for subsonic laminar boundary layer conditions 05 p0747 A67-16293
- Transverse curvature effect on axisymmetric compressible laminar boundary layer flow, obtaining asymptotic solutions for skin friction and heat transfer 05 p0791 A67-16509
- Sixth order polynomial calculation of axisymmetric laminar boundary layer of incompressible fluid removed by suction and arbitrary velocity distribution 05 p0749 A67-17184
- Two-phase flow of gas over harmonically oscillating flat plate expressed in laminar boundary layer terms, presenting liquid film thickness, heat transfer rate, skin friction, etc 05 p0793 A67-17338
- Hypersonic laminar boundary layer on blunt cones, considering external flow vorticity caused by curved shock wave, calculating gas-enthalpy profile 06 p0936 A67-17734
- Laminar boundary layer on ellipsoids of revolution situated at zero angle of attack in supersonic flow of perfect gas 06 p0936 A67-17740
- Aerodynamics of diffuse combustion in laminar boundary layer of two plane-parallel accompanying flows, emphasizing flame structure 06 p1112 A67-17961
- Laminar boundary layer separation and near wake flow for smooth blunt body at supersonic and hypersonic speeds [AIAA PAPER 87-62] 06 p0986 A67-18270
- Supersonic laminar two-dimensional boundary layer separation in compression corner with and without cooling [AIAA PAPER 87-191] 06 p0940 A67-18361
- Nonsimilar solution to complex boundary layer problems, using matrix concept to integral relations via Taylor series expansion of parameters [AIAA PAPER 87-218] 06 p0988 A67-18364
- Variable laminar boundary layer equations for air flows over flat plate with injection of foreign gases through solid surface 06 p1116 A67-18380
- Two-dimensional adiabatic laminar separated regions in supersonic flow, examining effects of blowing and suction at wall [AIAA PAPER 87-192] 06 p0988 A67-18459
- Taylor series expansion of stream function, pressure and temperature about separation or reattachment points used to calculate incompressible closed streamline flows of unknown shape [AIAA PAPER 87-64] 06 p0989 A67-18468
- Transition from laminar to turbulent boundary layer flow at hypersonic Mach numbers, noting measurement techniques [AIAA PAPER 87-130] 06 p0989 A67-18474
- Three-dimensional laminar boundary layer equations solved by finite difference methods for application to boundary layer flow on blunted cone, noting effect on crossflow [AIAA PAPER 87-159] 06 p0989 A67-18480
- Heat transfer to catalytic and noncatalytic surfaces on sharp flat plate in shock tube gas flow for checking various laminar boundary layer theories [AIAA PAPER 87-163] 06 p0989 A67-18481
- Leak current, friction and heat-transfer coefficients of compressible laminar boundary layer on insulator wall of MHD channel with anisotropic conductivity 06 p1043 A67-18673
- Parametric method of calculating laminar boundary layer in MHD 06 p1044 A67-18679
- Laminar, transitional and turbulent boundary layer flows with adverse pressure gradient on axisymmetric blunted conical flared body at Mach 10 [AIAA PAPER 86-493] 06 p0943 A67-18844
- Correlation number for calculation of skin friction and heat transfer for laminar compressible boundary layer flow with arbitrary pressure gradient, using von Karman momentum integral 06 p0992 A67-18862
- Laminar boundary layer separation length data in hypersonic flow show strong Mach number dependence 06 p0992 A67-18878
- Jet deviation by curved convex wall and Reynolds number explained as effect of boundary layer separation 08 p1320 A67-20450
- Laminar boundary layer calculated by approximation of momentum and kinetic integral equation for boundary conditions 09 p1489 A67-22158
- Viscosity variation effect on heat transfer and friction coefficient at wall during Couette flow 09 p1490 A67-22547
- Interaction of transverse distributed surface vibration with adjacent laminar flow, superimposing oscillatory pressure and velocity field developed in boundary layer fluid over idealized steady fluid flow 10 p1623 A67-22861
- Asymptotic behavior of laminar boundary layer, reducing system to heat equation, noting viscosity effects and uniqueness of homogeneous solution [ONERA-TP-458] 10 p1623 A67-22878
- Approximate closed form solutions for supersonic separated and reattaching laminar flow problem with boundary layer/shock wave interaction 10 p1591 A67-23115
- Similar calculation of hypersonic laminar boundary layer characteristics in presence of pressure gradient, specifically heat transfer, skin friction and boundary layer thickness 10 p1592 A67-23141
- Matched asymptotic expansions method for developing higher order approximations to structure of laminar detonation wave supported by irreversible unimolecular chemical reaction 11 p1749 A67-23858
- Asymptotic solution method for frozen dissociated laminar boundary layer flow over flat plate surface with arbitrarily distributed catalytic 11 p1781 A67-24573
- Eckert reference temperature yields approximations for heat transfer, skin friction and recovery temperature in high speed laminar diatomic nitrogen and carbon dioxide boundary layers 11 p1883 A67-24576
- Integral energy equation for three-dimensional laminar boundary layer element on porous surface in presence of suction 11 p1783 A67-25052
- Transverse magnetic field interaction with laminar boundary layer on rotating cone during reentry, assessing effect on spin and controlling torques 12 p1892 A67-25385
- Approximate method for calculating stagnation point laminar boundary layer equations taking into account chemical reactions in gas phase and surface of body 12 p1928 A67-25673
- Similar solution of compressible laminar boundary layer equations for Laval nozzle flow contour 13 p2049 A67-26639
- Unsteady perturbation effect of external velocity on laminar boundary layer 13 p2094 A67-26645
- Stewartson-Crocco equations solved by differential method for compressible laminar boundary layers 13 p2094 A67-26649
- Short duration technique providing simulation of thermodynamic properties and composition of exhaust products of liquid and solid propellant rocket engines [AIAA PAPER 86-760] 13 p2090 A67-26843
- Laminar boundary layer separation and near wake flow for smooth blunt body at supersonic and hypersonic speeds [AIAA PAPER 87-62] 14 p2240 A67-28112
- Continuum flow analysis for leading edge region of flat plate, using model based on hypersonic thin layer type of approximation 14 p2240 A67-28163
- Thick laminar boundary layer effect on aerodynamic behavior of simple shapes in supersonic low density flow 14 p2241 A67-28170
- Similarity solution to laminar boundary layer heat transfer from monatomic gas to cooled wall with no applied electric or magnetic fields [JPL-TR-32-1143] 15 p2523 A67-29219
- Chapman-Enskog method modified for

formulation of multicomponent laminar boundary layer problem for numerical solution 15 p2469 A67-29220

Heat transfer and skin friction rates increase in gas-liquid droplet suspension system flowing over circular cylinder formulated by laminar boundary layer theory [ASME PAPER 66-WA/HT-33] 15 p2579 A67-29322

Laminar boundary layer equations solved in presence of nonuniform velocity and enthalpy profiles in initial cross section or on bodies extending to infinity upstream and downstream 15 p2472 A67-29689

Numerical integration of differential equation describing gas flow in laminar boundary layer for core of conical external flow 16 p2656 A67-30454

Multicomponent reacting laminar boundary layer in chemical equilibrium solved using Stefan-Maxwell relations 16 p2658 A67-30937

Heat transfer in stagnation-point laminar boundary layer with mass injection and absorption of incident radiation 16 p2658 A67-30941

Theory and supporting experimental results on application of small heated film for skin friction measurements in laminar and turbulent boundary layers 16 p2659 A67-30950

Integration of laminar boundary layer equations in compressible gas by asymptotic method, calculating friction and heat flux 16 p2660 A67-31135

Transverse curvature effect on axisymmetric compressible laminar boundary layer flow, obtaining asymptotic solutions for skin friction and heat transfer 16 p2662 A67-31600

Conrad-type probe used to determine, in boundary layer of flattened ellipsoid, mean velocity of flow 16 p2663 A67-31711

Difference method of solving boundary layer equation for laminar suction boundary layer using Crocco form 17 p2790 A67-32260

Stationary laminar boundary layer equations of Ostwald-de Waele power law fluids, flow and temperature boundary layer differential equation solutions 17 p2836 A67-32262

Three-dimensional laminar boundary layer flow, calculating skin friction and velocity profiles 17 p2790 A67-32284

Intensity and specific heat ratio effects for laminar compressible boundary layers arising behind traveling shock waves 17 p2837 A67-32347

Affine solutions for temperature/flux distribution on heated horizontal plate 17 p2838 A67-32701

Wake from bluff bodies interaction with initially laminar boundary layer [AIAA PAPER 66-126] 17 p2793 A67-33005

Mixing function parameter behavior in boundary layer separations by Crocco-Lees method, noting linearized Glick differential equations 17 p2840 A67-33031

Correction for experimental velocity profile in compressible laminar boundary layer flow over flat plate 17 p2840 A67-33165

Computer integration of Faulkner-Skan equation in presence of normal and tangential flow velocity components on surface of body 18 p3024 A67-33538

Existence of affine solutions in natural convection along vertical flat heating plate, deriving expressions for thermal and dynamic boundary layers 18 p3025 A67-33685

Laminar boundary layer theory applied to heat transfer in low thrust rocket nozzles, checking with experimental wall temperature data [AIAA PAPER 67-447] 18 p3112 A67-33923

Shock and boundary layers about blunted two-dimensional slender bodies in hypersonic flow [AIAA PAPER 67-451] 18 p2982 A67-33925

Concentration profiles in fixed laminar boundary layer with catalyst distribution on wall, discussing Schmidt number effect and approximations 18 p3159 A67-34161

Longitudinal surface curvature effects on steady, two-dimensional incompressible laminar boundary layers, noting partial differential equations, computer solution, velocity profile, etc 19 p3209 A67-35415

Laminar-turbulent boundary layer transition over aircraft components measured by method using negative-temperature-coefficient resistors compared to hot wire

measurements 19 p3230 A67-35573

Laminar boundary layer for two-dimensional flow on bodies of revolution, noting suction velocity 19 p3210 A67-35721

Compressible laminar spanwise boundary layer on yawed infinite cylinder with disturbed suction calculated using momentum equation 19 p3342 A67-35724

Heat transfer to catalytic and noncatalytic surfaces on sharp flat plate in shock tube gas flow for checking various laminar boundary layer theories 19 p3211 A67-35739

Laminar incompressible boundary layer on isothermal flat plate with strong blowing, comparing different solutions 19 p3211 A67-35754

Role of Rosseland approximation in convection-radiation interaction, considering flow of gray gas in laminar boundary layer [ASME PAPER 67-HT-9] 20 p3545 A67-36707

Local heat transfer coefficients, mean temperature and velocity distributions in turbulent natural convection boundary layer on vertical plane surface [ASME PAPER 67-HT-17] 20 p3545 A67-36713

Laminar boundary layer flow of water over flat plates, noting heat transfer effects on velocity profile stability [ASME PAPER 67-HT-41] 20 p3547 A67-36725

Laminar boundary layer with heat transfer in liquids with variable fluid properties, including velocity and temperature profiles [ASME PAPER 67-HT-69] 20 p3550 A67-36749

Mass transfer cooling of carbon dioxide-nitrogen binary system in laminar boundary layer, stressing dissociation effect [ASME PAPER 67-HT-70] 20 p3550 A67-36750

Laminar and turbulent free shear layers analysis unifying treatment of mixing layers, assessing Mach number, Prandtl number and temperature ratio effects on constant pressure mixing [ASME PAPER 67-HT-81] 20 p3551 A67-36759

Wind tunnel tests for load and pressure distributions on flat-top cylinders with thick boundary layer 20 p3421 A67-36781

Laminar MHD boundary layer over finite dielectric disk in presence of magnetic field, determining velocity profiles 20 p3501 A67-37305

Rott approximate method applied to steady compressible laminar boundary layer on unyawed semiminfinite solid circular cone with attached shock wave 20 p3360 A67-37595

Physical analysis of convective heat transfer in laminar and turbulent flow through ducts and boundary layers, deriving trailing functions by variational method 21 p3730 A67-37736

Incident and reflected shocks from laminar and turbulent boundary layers measured over various Mach numbers 21 p3610 A67-37771

Growth of laminar compressible boundary layer with stationary origin on uniformly moving flat plate, noting analogy to shock induced flow 21 p3611 A67-37927

Laminar compressible boundary layer induced by plane shock wave passing over flat wall using empirical viscosity-temperature relation for Prandtl number 21 p3611 A67-37928

Stability technique for gas flow past body impeding laminar-turbulent boundary layer transition via crossed electric and magnetic fields 21 p3666 A67-38251

Mass injection effect on compressible three-dimensional laminar boundary layers analyzed for nonreacting gas, using conservation equations for flow velocity profiles 21 p3613 A67-38852

Viscous dissipation effect on heat transfer rates for laminar boundary layer flow of gray gas across flat plate 21 p3732 A67-38878

Curve approximation method applied to incompressible laminar boundary layer, comparing Head approximation method and exact solutions 21 p3615 A67-39081

Three-dimensional compressible laminar boundary layer with heat transfer in curvilinear coordinate system linked to streamlines of external flow, assuming transverse flow 21 p3615 A67-39127

Similarity solutions for compressible laminar boundary layer, showing pressure and heat and mass transfer effects on wall temperature and shear stress 22 p3918 A67-39716

Laminar boundary layer gas flows over slender bodies with massive blowing, discussing integral method solution and

theoretical model including pressure effect 22 p3739 A67-39955

Navier-Stokes equations asymptotic solutions used for gas flow laminar boundary layer calculation near corner of body where supersonic gas flow passes through low pressure region 22 p3785 A67-40018

Friction and heat flow resistances for three-dimensional compressible laminar gas boundary layer over ellipsoid of revolution at angle of attack 22 p3786 A67-40028

Incompressible laminar boundary layer flow on semiminfinite flat plate with impulsive motion solved using Meksym steady pressure gradient boundary layer method 22 p3786 A67-40096

Two-dimensional adiabatic laminar separated regions in supersonic flow, examining effects of blowing and suction at wall [AIAA PAPER 67-192] 22 p3786 A67-40096

Compressible laminar boundary layer in pressure gradient, analyzing suction on basis of momentum and thermal integral equations 22 p3788 A67-40421

Differential equation system for reacting laminar boundary layer heat and mass transfer solved analytically, noting compressible gas and porous foil filter 23 p4081 A67-40744

Laminar boundary layer subject to local three-dimensional disturbance, studying growth, flow field and transition to turbulence 23 p3991 A67-41175

Energy equation solution procedure for heat transfer across two-dimensional oscillating laminar boundary layer 23 p4082 A67-41243

Second order boundary layer equations for hypersonic flow, noting interaction between pressure gradients 23 p3991 A67-41252

Compressible laminar boundary layer on infinite swept cylinder analyzed for effects of suction on spanwise profile 23 p3993 A67-41746

Plane and turbulent fluid jets dynamic and thermal behavior expanding in magnetic field described by differential equations system 24 p4195 A67-41930

Boundary layer electric current temperature, velocity and density profile calculation on nonconducting MGD channel wall assuming smaller magnetic Reynolds number than unity 24 p4196 A67-42212

Temperature distribution of fluid in laminar boundary layer of flat plate and heat flow from fluid to plate wall 24 p4143 A67-42281

Heat and mass transfer processes in reacting laminar boundary layer flow with steady high speed gas flow 24 p4143 A67-42284

Heat and mass transfer in chemically reacting gas mixture compressible boundary layer, determining temperature in reaction zone and on porous plate surface 24 p4256 A67-42734

LAMINAR BOUNDARY LAYER SEPARATION

Approximate distribution of pressure friction and heat-transfer coefficients in laminar boundary layer separation during interaction with supersonic flow 03 p0401 A67-12877

LAMINAR FLAME

Laminar diffusion flame stability analyzed examining transient characteristics to infinitesimal disturbances of steady state solutions 02 p0342 A67-12021

Aerodynamics of diffuse combustion in laminar boundary layer of two plane-parallel accompanying flows, emphasizing flame structure 06 p1112 A67-17961

Photometric measurements on deviations from equilibrium state in burnt gases at laminar premixed shielded flames at atmospheric pressure [AIAA PAPER 67-9] 06 p1072 A67-18341

Flame separation explained in terms of processes taking place in mixing zone of internal cone in laminar burner flame 08 p1425 A67-20306

Laminar diffusion flame in Oseen flow identifying limiting case with stoichiometric Burke-Schumann flame and frozen flow 09 p1579 A67-21544

One-dimensional steady laminar premixed flame characterized by matched asymptotic expansions 10 p1733 A67-23141

Laminar flame speeds and composition flammability limits at low pressure for

- ternary mixtures of hydrogen and oxygen with ammonia and nitrous oxide 14 p2406 A67-28547
- Plasma behavior in laminar and turbulent hydrocarbon-air flames, discussing flame ionization, electron concentration and recombination, detonation wave ionization data, ignition, etc 17 p2968 A67-32168
- Collisional de-excitation rate or quenching of sodium in flat premixed laminar flames 18 p3150 A67-33803
- HF response of local burning rate in laminar diffusion flames subjected to transverse sound waves in free stream 18 p3108 A67-33831
- Parallel porous wall burner for studying premixed and diffusion flames in stagnation flows 19 p3345 A67-35002
- [ASME PAPER 67-7]
- ### LAMINAR FLOW
- Heat exchange and friction drag coefficients for laminar flow of equilibrium dissociable hydrogen with constant heat flow density at tube wall 01 p0165 A67-10048
- Laminar flow of elastico-viscous fluid between parallel plates obeying - Noll constitutive equation, considering heat transfer 01 p0053 A67-10802
- Hot wire measurement of tangential velocity and Reynolds stresses in spiral laminar-turbulent flow 01 p0054 A67-11163
- Heat transfer and friction drag for supercritical laminar flow of carbon dioxide through tube at constant thermal flux density at wall 03 p0536 A67-13612
- Steady state and dynamic characteristics of tilting pad journal bearing in laminar and turbulent flow regime [ASME PAPER 66-LUB-19]
- 03 p0431 A67-13756
- Heat transfer and velocity characteristics of thermal and hydrodynamic laminar flow in ducts of arbitrary cross section, considering boundary conditions at wall [ASME PAPER 65-WA/HT-13]
- 03 p0537 A67-14008
- Series coefficients of flow stream functions for plane laminar flows of viscous incompressible fluids in channels and near corners at small Reynolds numbers 03 p0405 A67-14259
- Book on propagation, reflection and superposition of shock waves in ideal gases based on theory of hyperbolic nonlinear PDEs 04 p0601 A67-14467
- Laminar flow on adiabatic surface measured, using Stanton tube and supersonic wind tunnel 04 p0547 A67-14849
- Laminar electrohydrodynamic flow in plane diffuser, taking into account molecular diffusion of space charge 04 p0668 A67-15277
- Interferometer measurements of laminar forced convection in entrance region between parallel flat plates [ASME PAPER 66-WA/HT-16]
- 04 p0608 A67-15449
- Kinetic theory of gases through certain correlation functions known as product densities used to explain transitions from gaseous to liquid state 04 p0608 A67-15466
- Unsteady laminar flow of viscous incompressible fluid between two infinite parallel rotating disks with angular velocities varying with time 04 p0609 A67-15605
- Temperature-vorticity analogy validity in laminar turbulent flows extended to compressible fluids, noting temperature relation to shear stress 04 p0727 A67-15680
- Laminar tube flow and heat transfer for He gas using Navier-Stokes, energy and continuity equations in finite difference form 04 p0729 A67-15809
- Heat transfer in laminar source flow between stationary and rotating disk 04 p0729 A67-15812
- Numerical solution of motion and energy equations for non-Newtonian fluid flow in tubes of circular cross section with heat transfer to or from fluid 05 p0925 A67-16271
- MHD steady laminar flow of viscous incompressible electrically conducting liquid in rectangular pipe between conducting plates 05 p0853 A67-16723
- Laminar shearing flows breakdown for second order viscoelastic fluids in channels of critical width 05 p0792 A67-16724
- Lie series formalism applied to solution of Bessel equation describing behavior of laminary oscillating MHD fluid 05 p0854 A67-16989
- Mass transfer perturbations about reversed flow profiles of Stewartson, noting computation of solutions to Falkner-Skan equation 05 p0794 A67-17369
- Fixed vertical plane surface effect on velocity of solid sphere in free fall in laminar region of incident viscous flow for various Reynolds numbers 06 p0983 A67-17928
- Hysteresis effects in steady laminar two-dimensional MHD flow of gas between moving planes and coaxial cylinders in TM field 06 p1043 A67-18671
- Transverse magnetic field effect on laminar radial flow of incompressible fluid between closely spaced parallel plates, presenting graphs of pressure distribution 06 p1046 A67-18829
- Turbulence effects on laminar skin friction and heat transfer from plates and circular cylinders in incompressible flow, using two low turbulence wind tunnels 08 p1427 A67-21118
- Book on quantitative relationships for non-Newtonian systems, considering classification and fluid behavior of materials with anomalous flow properties 08 p1322 A67-21268
- Pressure field, Bernoulli sum variation, momentum and energy relations in laminar zone of separation 08 p1323 A67-21389
- Sealing coefficient of visco seal for laminar and turbulent flow, noting Reynolds number effect 10 p1659 A67-22706
- Laminar and turbulent flow and heat transfer in boundary layer on continuous moving surface 10 p1732 A67-22728
- Pressure drop correlation in developed, isothermal, laminar and turbulent flow in rectangular ducts 10 p1627 A67-23555
- Lateral efflux from flow along wall into suction slot computed by conformal mapping contraction coefficient 10 p1627 A67-23559
- Numerical solution of class of nonlinear high order differential equations with two-point asymptotic boundary conditions for thermal boundary layers in laminar and turbulent flow 10 p1627 A67-23560
- Approximate heat transfer theory based on parabolic velocity distribution for channel flows 10 p1734 A67-23575
- Laminar flow between parallel plates for arbitrary initial velocity distribution and time varying pressure gradient 10 p1629 A67-23842
- Numerical finite difference solution of three-dimensional equations of motion for laminar natural convection, noting Navier-Stokes equation transformation 11 p1774 A67-23861
- Hydrodynamic stability problems solved through approximate and numerical methods involving eigenvalue spectrum and Orr-Sommerfeld equation for parallel flow 11 p1781 A67-24552
- Laminar turbulent transition of nonisothermal incompressible forced flows in pipes measured for several working fluids and temperatures, using Reynolds number as criterion 11 p1781 A67-24574
- Heat transfer of fully developed laminar flow of Bingham material between parallel plates and linearly varying wall temperature noting equations of state, velocity and temperature distribution 11 p1883 A67-24944
- Two-dimensional temperature field analyzed for laminar gas flow in interspace between parallel thermally thin plates 12 p2033 A67-25319
- Incremental pressure drop in incompressible fluid laminar flow at entrance of rectilinear duct, using conformal mapping technique 12 p1930 A67-26166
- Energy equation for laminar flow of compressible Newtonian fluid, calculating temperature profiles of fluid 13 p2224 A67-27049
- Laminar flow of incompressible conducting fluid in diffuser in presence of transverse magnetic field 13 p2169 A67-27313
- Laminar boundary flow over dielectric disk with homogeneous magnetic field perpendicular to plane of disk, obtaining liquid velocity and electric field density 14 p2358 A67-28282
- Laminar NOR unit feasibility, operating characteristics and performance 14 p2250 A67-28335
- Frictional pressure drop for isothermal incompressible flow in isosceles triangular duct, with correlations for laminar and turbulent flow [ASME PAPER 67-FE-18]
- 14 p2243 A67-28365
- Viscoseal operation in superlaminar flow regime noting pressure patterns, end effect, gas ingestion and sealing capacity 14 p2327 A67-28797
- Laminar Couette flow analyzed for gas injection effects on heat transfer to surface, temperature profile and convection interaction with radiation 15 p2578 A67-29129
- Nonsimilar boundary layer flow and heat transfer of cone rotating in forced flow [ASME PAPER 65-WA/HT-31]
- 15 p2475 A67-29320
- Unbounded laminar plate oscillations in bilateral potential ideal gas flow with uniform physical and mechanical parameters 15 p2575 A67-30009
- Laminar and turbulent MHD flows of liquid sodium in rectangular duct with conducting walls, determining wall and magnetohydraulic losses 16 p2712 A67-30573
- Laminar flow with forced convection heat transfer in parallel plate channel under influence of intense, longitudinal, resonant acoustic field 16 p2778 A67-30947
- Effect of temperature dependence of plasma conductivity on magnetohydrodynamic channel flows 16 p2721 A67-31392
- Laminar flow through porous annulus with constant suction velocity at walls and swirl, using differential equations 16 p2662 A67-31551
- Laminar jet flow of electrically conducting fluid over plane solid surface in transverse magnetic field solved using motion and continuity equations 16 p2722 A67-31571
- Laminar flow of electrically-conducting fluid suddenly expanding in magnetic field calculated by approximate method 16 p2722 A67-31573
- Approximation method for steady laminar flows of incompressible viscous fluid in curved pipes, obtaining flow rate 17 p2836 A67-32038
- Nusselt results concerning heat transfer extended to include surface tension effect on heat transfer coefficient 17 p2970 A67-32461
- Electrohydrodynamic flow laminarization with tritium ionizer, obtaining Poiseuille flow stability 17 p2839 A67-32907
- Transport property difference effect on flow prediction of blunt body stagnation region heat transfer, noting laminar flow and compressible boundary layer equations 17 p2793 A67-33025
- Cone and disk laminar flows of power-law fluids similarity solution by Navier-Stokes equation 17 p2793 A67-33040
- Measuring laminar flow development in square duct using laser Doppler flow meter [ASME PAPER 67-APM-37]
- 17 p2861 A67-33161
- Correction for experimental velocity profile in compressible laminar boundary layer flow over flat plate 17 p2840 A67-33165
- Heat exchange and friction drag coefficients for laminar flow of equilibrium dissociable hydrogen with constant heat flow density at tube wall 17 p2974 A67-33326
- Counterflow diffusion flame in forward stagnation region of porous cylinder, detailing flame stability and velocity gradient 18 p3155 A67-33842
- Heat transfer and friction drag for supercritical laminar flow of carbon dioxide through tube at constant thermal flux density at wall 18 p3161 A67-34477
- Behavior of finite-amplitude disturbances periodic in motion direction for plane parallel laminar flows studied, using partial differential equations 19 p3208 A67-35051
- Concentrated vortex model for Karman street in two-dimensional viscous incompressible laminar flow past bluff body 19 p3210 A67-35446
- Instability of gas-cooled nuclear reactor passages in steady laminar flow studied by time-dependent analysis 19 p3280 A67-35743
- Hybrid computer for co-current laminar-flow heat exchanger Sturm-Liouville problem 19 p3190 A67-36069
- Forced convection of laminar flow in tubes of various cross sections, assuming constant temperature gradient and internal heat generation 20 p3420 A67-36317
- Test data for heat transfer in vortex flows in tubes with band type swirl generator, determining effect of mass inertial forces 20 p3544 A67-36449
- Stagnation ablation of blunt body

hypersonic reentry with nonreacting gas, deriving laminar flow equations 20 p3356 A67-36509

Approximate solution to heat transfer coefficient on flat plate in linear shearing flow

[ASME PAPER 67-HT-46] 20 p3547 A67-36728

Free convection effect on forced laminar flow of water in horizontal tube with uniform heat flux and velocity profile fully developed

[ASME PAPER 67-HT-52] 20 p3548 A67-36734

Heat transfer for one- and two-dimensional pulsating incompressible laminar flow in circular tube with two thermal boundary conditions

[ASME PAPER 67-HT-65] 20 p3550 A67-36747

Hydraulic resistance coefficient of rotating tubes, taking into account centrifugal mass forces effect on flow inside tube 20 p3421 A67-36793

Correlation method for local and average friction coefficients of laminar and turbulent gas flow through smooth tubes 20 p3422 A67-36941

Bluntness influence on nose cone heating in laminar flow in supersonic flight investigated to determine optimum design of rocket or space vehicle nose 20 p3359 A67-37165

Boundary layer theory applied to laminar flow with chemical reaction, considering coolant blown through porous wall and wall reaction with laminar boundary layer 20 p3424 A67-37345

Unbounded laminar plate oscillations in bilateral potential ideal gas flow with uniform physical and mechanical parameters 20 p3542 A67-37539

Heat-transfer coefficients for laminar and transitional liquid metal flow in tube with constant wall heat flux 20 p3555 A67-37608

Approximate solutions of Prandtl boundary layer problem for incompressible laminar flow derived, using Nagumo-Westphal theorem on parabolic differential operators 21 p3563 A67-37888

Rotor bearing stability, describing incompressible and compressible fluid film bearings, calculating thresholds of instability 21 p3632 A67-38136

Book on parallel laminar flow stability covering channel and pipe flows, jets, wakes, free shear and boundary layers 22 p3783 A67-39632

Laminar nonrelativistic finite amplitude hydromagnetic wave propagation in low temperature ionized plasma, using two-fluid model 22 p3852 A67-39990

Laminar free convection of absorbing emitting gas analyzed in region of stagnation point of horizontal cylinder 22 p3920 A67-40418

Velocity and pressure distributions and flow field for laminar incompressible source flow between two coaxial parallel disks rotating at different speeds 23 p3988 A67-40602

Laminar flow field between rotating turbine disks solved for low Reynolds number and partial admission flow 23 p3988 A67-40614

Partial differential equation in lubricant pressure based on mixing-length theory, presenting full journal bearings in turbulent and laminar regimes 23 p4010 A67-41342

Jet interaction low power-consumption fluid amplifier, NOR logic element switched from laminar to accelerated expansion flow mode by control signal 23 p3936 A67-41420

Integral solution for massive blowing on slender hypersonic wedges and cones in laminar flow, assuming homogeneous nonreacting perfect gas 23 p3932 A67-41743

Three-dimensional disturbance after perturbation of supercritical Poiseuille flow between parallel plates treated by initial value method 24 p4144 A67-42562

Irrational gas jet impinging on and depressing infinite liquid surface, discussing streamlines and rippling 24 p4144 A67-42585

Two- and three-dimensional laminar viscous boundary layer flow nonlinear partial differential equations solved analytically, studying difference equation substitution 24 p4145 A67-43087

LAMINAR HEAT TRANSFER
Blunt cone laminar friction drag evaluated, using Reynolds analogy 01 p0007 A67-11181

Analogous studies of simultaneous

conductive and radiative heat transfer across transparent laminar gas space, showing position of radiation shield between bounding surfaces 03 p0535 A67-13464

Numerical solutions of equations of motion and energy for heating of non-Newtonian fluids in rectilinear axisymmetric laminar flow in circular tubes extended to case of cooling at constant tube-wall temperature 04 p0720 A67-14510

Condensation heat transfer in presence of noncondensables, interfacial resistance, superheating, variable properties and diffusion 04 p0720 A67-14644

Wall temperature prediction for internal laminar heat transfer based on Graetz number 04 p0721 A67-14646

Numerical solution for laminar flow heat transfer in circular tubes with axial conduction and developing thermal and velocity fields

[ASME PAPER 66-WA/HT-7] 04 p0726 A67-15446

Laminar heat exchange in inlet section of rectangular channel with incompressible fluid and temperature 04 p0726 A67-15590

Variational analysis of Graetz problem of forced-convective laminar heat transfer in duct, for various cross sections and given wall temperature and temperature gradient 04 p0728 A67-15802

Finite difference solution of parabolic equation for laminar heat transfer in inlet of rectangular duct as function of wall temperature and Nusselt number for different aspect ratios 04 p0728 A67-15805

Von Karman-Pohlhausen boundary layer analysis of temperature and velocity profiles in inlet region between two parallel planes with relative motion and pressure gradient 04 p0729 A67-15808

Laminar convective heat transfer to cavities in hypersonic low density flow 04 p0732 A67-15833

Laminar heat transfer in thermal viscous MHD flow past semilinear flat plate 05 p0857 A67-17416

Mars atmospheric composition and laminar convective heating and ablation studied to predict performance of heat protection systems during entry 06 p1119 A67-18849

Asymptotic properties of fluid temperature field and Nu numbers in nonstationary heat transfer during passage of laminar flow of viscous incompressible fluid through rectilinear channel 07 p1265 A67-19125

Turbulence effects on laminar skin friction and heat transfer from plates and circular cylinders in incompressible flow, using two low turbulence wind tunnels 08 p1427 A67-21118

Convective laminar heat transfer to hypersonic vehicle, deriving similarity relations between stagnation temperature profile and mass fractions of chemical species 09 p1579 A67-21699

Laminar heat transfer rate to two-dimensional blunt base in supersonic flow evaluated for varying Reynolds, flow and shock Mach numbers 11 p1882 A67-24222

Dissipative energy effect on laminar heat transfer from disk rotating in uniform forced stream 13 p2221 A67-26531

Differential equations for heat and mass transfer in laminar boundary layer of binary gas mixture flow past porous wet flat plate 14 p2242 A67-28307

Time dependent problems of heat transfer in laminar flow of viscous incompressible fluid in cylinder and cylindrical annulus 14 p2408 A67-28892

Similarity solution to laminar boundary layer heat transfer from monatomic gas to cooled wall with no applied electric or magnetic fields 15 p2523 A67-29219

Nonsimilar boundary layer flow and heat transfer of cone rotating in forced flow [ASME PAPER 65-WA/HT-31] 15 p2415 A67-29320

Laminar natural convection heat transfer between vertical plate and power-law fluid with high Prandtl number 16 p2780 A67-31553

Electromagnetic field effect on heat transfer during laminar flow of electrically conducting incompressible fluid in flat channel 16 p2723 A67-31774

Simultaneous heat and mass transfer in laminar free convection boundary layer at

vertical surface with moving interface 19 p3346 A67-35611

Laminar film boiling on thin wire determining heat-transfer coefficient and vapor dome spacing and diameter [ASME PAPER 67-HT-62] 20 p3549 A67-36747

Heat transfer in fully developed laminar flow through rectangular and isosceles triangular ducts, determining Nusselt numbers 20 p3553 A67-36941

Asymptotic properties of fluid temperature field and Nu numbers in nonstationary heat transfer during passage of laminar flow of viscous incompressible fluid through rectilinear channel 21 p3731 A67-38181

Laminar heat transfer computing method for spherically blunted cone at angle of attack requiring small numerical calculations 22 p3740 A67-39932

LAMINAR JET
Fizeau fringes produced in laser illuminated Fabry-Perot interferometer to obtain concentration profiles in turbulent and laminar jets 05 p0794 A67-17373

Two-dimensional laminar jet of incompressible fluid issuing into uniform stream in direction of main flow considering two coordinate type expansions 09 p1489 A67-22411

Integral relation technique for approximate solution of dynamic and thermal expansion of laminar radial slot gas jets along plane wall 11 p1779 A67-24322

Temperature effect on seeding atom emission in argon plasma laminar jet 20 p3497 A67-36332

LAMINAR MIXING
Finite difference solution to nonsimilar laminar mixing of streams undergoing nonequilibrium chemical reactions 04 p0609 A67-15811

Steady state laminar and turbulent mixing in unsteady isothermal flow in wake behind body with incident shock wave 18 p2984 A67-34220

Tanh γ form laminar mixing layer on nonlinear inviscid equation two-dimensional solutions with linearized stability theory perturbations 22 p3782 A67-39522

LAMINAR WAKE
Hot-wire anemometer measurements of transition in incompressible wake of cone at low Reynolds number 05 p0751 A67-17433

Flow field model for laminar hypersonic near-wake in inviscid expansion, viscous sublayer and recirculating flow [AIAA PAPER 67-63] 06 p0940 A67-18355

Viscous interaction theory for laminar supersonic near wake applied to calculation of recirculation region for range of flow conditions [AIAA PAPER 67-61] 06 p0941 A67-18446

Taylor series expansion of stream function, pressure and temperature about separation or reattachment points used to calculate incompressible closed streamlines flows of unknown shape [AIAA PAPER 67-64] 06 p0989 A67-18446

Laminar viscous wake interaction with supersonic external inviscid flow downstream treated by implicit finite difference method [AIAA PAPER 66-454] 15 p2417 A67-30181

Wake from bluff bodies interaction with initially laminar boundary layer [AIAA PAPER 66-126] 17 p2793 A67-33000

Aerodynamic characteristics of wake behind hypervelocity bodies [AIAA PAPER 66-53] 19 p3171 A67-35744

LAMINATE
SA MULTILAYER STRUCTURE
Machining techniques for paper-base and glass-base laminates of various grades for printed circuit boards 08 p1334 A67-20744

Multilayer laminating process in printed circuit wiring board design and production 08 p1335 A67-20744

Matched pulses for two-layer laminates discussing complete energy transfer to base and uniform momentum transfer 10 p1724 A67-23700

LAMINATED MATERIAL
Strain gauges applied to epoxy laminate in liquid hydrogen insulation systems 01 p0072 A67-11100

Statistical theory for strength of laminar composites used to optimize biaxial and multidirectional tensile strength properties of laminated materials 03 p0522 A67-13444

Anisotropy effect of continuous filaments

composites on material strength, noting dependency on test specimen configuration in evaluation of mechanical properties 03 p0523 A67-13446

Finite element method structural analysis of laminated orthotropic shell of revolution 03 p0524 A67-13787

Relations between mean stresses and strains of elastic body consisting of soldered orthotropic layers, noting thermal effect 05 p0912 A67-16184

Stress waves reflection and transmission in composite laminates and parameters affecting ability to resist fracture by hypervelocity impact [AIAA PAPER 67-140] 06 p1102 A67-18289

Thermal conductivity of laminated GaSe monocrystals studied in two crystallographic directions between 90 and 600 degrees K and effect of unilateral compression 07 p1233 A67-19649

Mechanical property correlation between high performance composites and cast epoxy resin data 08 p1344 A67-20423

Polar properties of fiberglass fabric laminates effect on strength for aerospace applications 08 p1345 A67-20431

Copper clad phenolic paper, epoxy paper and epoxy glass laminates used as printed circuit base materials 08 p1334 A67-20741

UVFD-1 ultrasonic velocimetric flaw detector for inspection of nonmetallic laminated structures and products 09 p1502 A67-22096

Combining two or more nonmetallic substances noting applications of fiber reinforced, particulate filled and laminated composites 10 p1671 A67-23013

Dynamic effective stiffness theory of layered and unidirectionally fiber reinforced composites, detailing field equations for laminated composite 10 p1724 A67-23708

Fiber spacing and array geometry effect on modulus of composites of laminate configurations used in aerospace structures 10 p1729 A67-23768

Tension and compression, dynamic and static flexural loading and vibration tests of laminate filament wound composite [AIAA PAPER 1219] 18 p3141 A67-33889

Correlation and analysis of ultrasonic test results in evaluating reinforced resin laminates 19 p3249 A67-35554

Crash and ballistic protection flight helmet with greater impact energy dissipating characteristics, noting laminated nylon fabric shell and polystyrene liner 21 p3577 A67-38075

Orthotropic laminated layer with heat emission investigated for thermoconductivity and temperature stress distribution 21 p3731 A67-38299

High temperature polyimide laminates for radomes and other supersonic aircraft components, discussing index flexural strength, dielectric constant and dissipation factor 22 p3825 A67-39853

Performance reliability of reinforced plastics for structural load-bearing components using nondestructive testing, defining material-energy interactions 22 p3826 A67-39860

Temperature stable ferrite materials for laminated memory arrays compatible with integrated semiconductor drive circuit 22 p3861 A67-39914

Fracture behavior of laminar steel composites studied to determine effect of interfacial properties on crack propagation 22 p3822 A67-40056

Viscoelastic behavior of laminated orthotropic plates, discussing single layer or homogeneous orthotropic viscoelastic plate problem 22 p3914 A67-40108

Shear modulus measurements in fiber-reinforced composites by plate-twisting test and torsion tube in terms of classical laminated plate and shell theory 23 p4021 A67-40738

Reinforced plastics, evaluating epoxy resin with glass fiber reinforcements for laminates, measuring tensile, compressive and flexural strengths [ASM PAPER C6-21.1] 23 p4022 A67-41403

LAMP

S ARC LAMP

S ELECTROLUMINESCENT LAMP

LAND

S EARTH

LANDAU DAMPING

Landau damping in weakly inhomogeneous

plasma related to Cerenkov radiation of accelerated electrons moving in external static field causing inhomogeneity 02 p0272 A67-11636

Collisionless electron heating by ion cyclotron wave attributed to Landau damping, discussing current generation 02 p0275 A67-12556

Landau damping in anisotropic electron plasma treated by kinetic dispersion equation 03 p0474 A67-12920

Electron velocity distribution equation extended to small wave numbers for electron-ion plasma 03 p0483 A67-13914

Electron thermal conductivity of fully ionized Lorentz gas, determining energy transfer from Landau damping of plasma waves and collision parameters 03 p0484 A67-14039

Landau damping and growth applied to electron plasma waves for Maxwellian velocity distribution in slab and cylindrical geometries 08 p1365 A67-21403

Electron temperature variation induced effects and Landau damping of ion acoustic waves studied in quiescent discharge tube plasma 11 p1837 A67-24395

Damping of plane sinusoidal wave in cold collisionless plasma, studying supercritical amplitude oscillatory process 13 p2171 A67-27615

Fourier-Hermite solutions of Vlasov equations for electron motion against positive neutralizing background examined in linearized limit, noting Landau damping recovery 15 p2509 A67-29205

LF plasma instabilities indicated by Landau electron attenuation computation for short wavelengths 15 p2528 A67-29710

Collision integral for Landau plasma in strong magnetic field to obtain time evolution of one-particle distribution function 15 p2532 A67-30382

Nonlinear instability, demonstrated for electron plasma waves driven toward instability by small ion beam but linearly stabilized by electron Landau damping 16 p2719 A67-31228

Collisionless electron plasma dynamics in one dimension, investigating nonlinear Vlasov equation for Landau damping and instability 18 p3092 A67-34747

Fokker-Planck damping introduced into Fourier-Hermite representation of Vlasov equation produces Landau and Van Kampen treatments 18 p3030 A67-34754

Particle trajectories analysis for drift instability mechanism, considering resonant and nonresonant particles 19 p3267 A67-34890

Cyclotron harmonic wave propagation in warm magnetoplasmas predicted theoretically for perpendicular and oblique damping 19 p3288 A67-35371

Damping of high frequency waves in homogeneous fully ionized plasma with relative electron-ion drift calculated, using fokker-planck kinetic equation 19 p3292 A67-35391

Longitudinal wave echo in collisionless electron plasma with Landau damping 19 p3295 A67-35534

Plasma oscillations, discussing kinetics, macroscopic and Vlasov equations, Landau damping and beam instabilities [AFOSR-66-2823] 19 p3299 A67-35871

Longitudinal oscillations and Landau damping of electron plasma with fixed ion background, discussing initial and boundary value problems 20 p3494 A67-36150

Dynamic response of nondegenerate electron hole plasma in semiconductor, obtaining frequency spectrum and Landau damping rate of plasma oscillation 20 p3499 A67-36945

Ion wave dispersion relation in mercury vapor plasma, explaining cut-off frequency dependence on electron drift 22 p3842 A67-39207

Energy dissipation due to spatial dispersion proven identical to dissipation due to Landau damping for large waves 22 p3847 A67-39649

Steady state nonlinear Landau damping of electron plasma wave obtained from random phase approximation by balancing nonlinear and collision effects 22 p3848 A67-39691

Electrostatic relaxation wave dispersion in isotropic Lorentz gas, considering Landau damping and balancing of elastic electron-atom collisions 22 p3848 A67-39692

Vlasov equation solved by taking

continuous spectrum of infinite matrix belonging to moment equations into account, obtaining Landau damping results 22 p3852 A67-39992

Collisionless small and large amplitude electron plasma wave damping compared, showing small amplitude waves damp exponentially and large amplitude waves exhibit amplitude oscillations collisionless small and large amplitude electron 22 p3853 A67-40242

LANDING

S AIRCRAFT LANDING

S APPROACH AND LANDING

S GLIDE LANDING

S LUNAR LANDING

S PLANETARY LANDING

S SKID LANDING

S SOFT LANDING

S TAKEOFF AND LANDING

S WATER LANDING

LANDING AID

SA AIR TRAFFIC CONTROL

SA AIRPORT

SA APPROACH AND LANDING

INSTRUMENT

SA RUNWAY

Digital computer driven display system of electronic data and semiautomatic film plotters for rapid evaluation of aircraft carrier landing parameters 07 p1164 A67-19623

Landing task and pilot acceptance of displays for landing in reduced weather minimums [AIAA PAPER 65-722] 09 p1457 A67-22493

GaAs laser reflectance measurements of tactical landing terrain samples 17 p2858 A67-32483

LANDING DEVICE

Onboard equipment designed for transport aircraft landings with visibilities less than 200 ft and runways less than 2600 ft, having all devices duplicated 03 p0464 A67-13001

STAN 37-38-39, designed to meet operational requirements of category III all-weather landings and providing ground beacon requirements of ILS systems 09 p1529 A67-22645

Entry/Lander vehicle for Mars mission discussed in terms of gross payload, basic vehicle and preentry system 16 p2756 A67-30629

LANDING GEAR

SA AIRCRAFT TIRE

SA AIRFRAME

SA FAIRING

MI-10 Soviet flying crane, very high four-wheeled landing gear enables it to drive over load and clamp it by hydraulically operated grips 02 p0181 A67-12201

C-5A aircraft design load criteria for landing gear of large aircraft that must operate from semlimproved airfields [AIAA PAPER 65-711] 03 p0360 A67-13781

Main landing gear door and aerodynamic speed brake combination in F-111 aircraft, considering weight minimization and control of landing gears 05 p0753 A67-16163

OV-10A aircraft testing in landing and takeoff from fields, jungle clearings and primitive roadways 10 p1594 A67-23391

Measurement of torsional fatigue loads on aircraft undercarriage under service conditions 11 p1880 A67-25057

Design principles for air-cushion vehicles, noting possible application to aircraft landing gear [ASME PAPER 67-DE-61] 14 p2246 A67-28884

Aircraft wheel and brake designs especially for 63 Series of DC-8 noting materials, properties, construction, etc [AIAA PAPER 67-404] 15 p2421 A67-30371

Jet aircraft tire testing machine simulating taxiing, takeoff and landing loads 16 p2656 A67-31914

C-5A landing gear, discussing design and evolution of requirements such as kneeling, steering, weight and flotation 17 p2794 A67-31988

Landing gear for operating off rough terrain and unprepared airstrips in OV-10A Bronco aircraft for counter insurgency 17 p2794 A67-31989

Wheel acceleration influence on landing gear operation at touchdown, noting effect on shock absorption system and elastic deformation of supporting legs 21 p3566 A67-37949

Air-oil separator for aircraft hydraulic system stops nose wheel shimmying, based

on lowering pressure principle and using filter screen barrier 24 p4099 A67-42427

LANDING LOAD

Dynamic measurements of heavy landings on experimental helicopter platform and of response to heavy vehicle loads on steel-and-concrete deck flyover 11 p1880 A67-25056

LANDING MODULE

SA LUNAR LANDING MODULE

SA MARS EXCURSION MODULE /MEM/

Fabrication procedure for biologically clean planetary landing module for later sterilization 02 p0188 A67-12380

Guided propulsive solution to Mars atmosphere-decelerated soft landing vehicle trajectory

[AIAA PAPER 67-170] 06 p1029 A67-18508

Model tests for determination of structural response of Apollo Command Module to water impact 07 p1257 A67-19368

Instrument integration for landing capsule payloads of planetary missions, considering functional operation, environmental constraints and interface definition

[AIAA PAPER 66-59] 07 p1188 A67-19996

LANDING SIMULATION

Ground and flight tests to evaluate lunar landing research vehicle fly-by-wire control system

[AIAA PAPER 67-273] 07 p1129 A67-20048

Lunar Module evaluation and test using analog and hybrid computer simulation with LM guidance and control hardware

[AIAA PAPER 67-232] 07 p1164 A67-20056

Lunar surface mechanical properties at Surveyor landing site according to telemetry data and photographs 08 p1386 A67-20942

Optical resolution, light intensity and true perspective effect on imaging characteristics and parallax and image brightness influence on display realism of visual simulation 11 p1749 A67-24629

Lunar surface erosion by rockets simulated in laboratory to study hazards of retrorocket landing on airless planetary bodies 12 p1922 A67-25701

Landing characteristics of SV-5P lifting body vehicle analyzed using six degree of freedom piloted simulation, noting gust effect

[AIAA PAPER 67-574] 20 p3533 A67-37133

LANDING SITE

SA LUNAR LANDING SITE

Lifting body reentry vehicle for return from orbit to continental U.S. 04 p0706 A67-15253

Surveyor touchdown-dynamics experimental study of spacecraft motion and landing site surface 08 p1411 A67-20949

Extended stay lunar exploration mission in terms of lunar landing site with relaxation of certain Apollo constraints and ground rules 08 p1394 A67-21109

Roughness data and statistical analysis of off-runway landing areas in Canada, using aerial photography for profile measurement 10 p1622 A67-23388

Aircraft noise and siting of major airport 13 p2089 A67-26536

Surveyor I spacecraft location and identification on moon surface by photographs taken by Orbiter III 20 p3524 A67-36649

Floating airports proposed as solution to short haul air traffic problems in New York 20 p3418 A67-37445

Recovery site location importance in determining entry vehicle future requirements 21 p3607 A67-37804

Noise reduction in residential areas near landing strips using Tu-124 aircraft studied with suggested takeoff and landing piloting techniques 21 p3569 A67-38928

Helicopter landing systems requirements, considering manual instrument approaches with guidance information from ground station including landing environment 23 p4026 A67-41500

STOL and VTOL takeoff and landing areas, discussing urban and suburban air transportation and operational weather requirements

[AIAA PAPER 67-795] 24 p4258 A67-42956

LANDING SPEED

Criteria for determination of minimum usable approach speed for landing of carrier based aircraft

[AIAA PAPER 67-578] 19 p3175 A67-35973

LANDING SYSTEM

SA AUTOMATIC LANDING SYSTEM

SA INSTRUMENT LANDING SYSTEM

Mechanical impact attenuation system for Apollo spacecraft provides stable land landing platform, noting deployed heat shields, extended legs, pneumatic bags, etc [AIAA PAPER 66-989] 02 p0333 A67-12300

Properties of crushable impact attenuation materials used to absorb and dissipate kinetic energy of impacting body 04 p0711 A67-15238

Rotor entry vehicle systems /REVS/ concept based on lifting bodies L/D after entry with rotor needed only for improved landing

[AIAA PAPER 67-203] 06 p0949 A67-18490

Airport lighting for category II landings with aid of all-weather landing systems by following ICAO guidelines, noting threshold markings, runway lights, etc 07 p1167 A67-20150

Base-mounted landing rocket system for Apollo type vehicle evaluated for heat-shield water pressure, ground effect, vehicle dynamics, etc 08 p1413 A67-21515

Expandable gas bag for stowable omnidirectional multiple impact landing system 10 p1714 A67-23755

Mechanical impact attenuation system for Apollo spacecraft provides stable land landing platform, noting deployed heat shields, extended legs, pneumatic bags, etc [AIAA PAPER 66-989] 15 p2564 A67-29423

Rotor entry vehicle system /REVS/ concept based on lifting bodies L/D after entry with rotor needed only for improved landing

[AIAA PAPER 67-203] 15 p2419 A67-29444

Spacecraft landing systems technology, materials and hardware, model impact testing and para-sail landing rocket program 15 p2570 A67-29856

Long and short range air navigation trends, discussing digital computer application, collision prevention and landing systems 19 p3256 A67-35864

Expandable gas bag for stowable omnidirectional multiple impact landing system 22 p3904 A67-40097

Helicopter landing systems requirements, considering manual instrument approaches with guidance information from ground station including landing environment 23 p4026 A67-41500

LANGMUIR PROBE

Effective electron scattering cross section in helium and argon plasma with cesium vapor admixture measured by Langmuir probe theory 01 p0119 A67-10134

Langmuir probe method, obtaining exact results for small amplitude plasma oscillations 01 p0123 A67-10461

Scattering of electromagnetic waves in plasma, noting effect of eddy current fluctuations 03 p0367 A67-12938

Charged particle redistribution due to rockets and satellites flying in ionosphere influence on electromagnetic propagation in region of body and interpretation of Langmuir probe 04 p0664 A67-14990

Rotating Langmuir probes for flow velocity distribution measurements in highly ionized supersonic low density MPD arc 05 p0851 A67-16466

Quasi-linear relaxation in unsteady states of noncollision plasma, noting electron beam distribution function and Langmuir plasma oscillations 05 p0852 A67-16896

Langmuir probe analysis when immersed in slightly ionized collision-dominated plasma, computing current-voltage characteristics and Poisson and diffusion equations 05 p0856 A67-17341

Problems in using Langmuir probes in ionized medium for measuring electron and ion energy density, temperature and distribution 06 p1000 A67-17590

Propellant injection through electrodes effect on potential distribution in MPD arc [AIAA PAPER 67-49] 06 p1074 A67-18435

Langmuir calorimetric probe to determine average energy per ion in tenuous plasma beam 06 p1076 A67-18879

Langmuir probe velocity and acceleration measurements for coaxial Hall accelerators [AIAA PAPER 66-196] 08 p1375 A67-20575

Supersonic Langmuir probe application of propagation and dispersion of ionic waves 08 p1357 A67-20801

Langmuir probe experiments on electric and magnetic field, density and temperature profiles, I-V characteristic, etc, for rotating plasma in B-3 stellarator 08 p1361 A67-21137

Electron temperature and density in F region analyzed for nighttime heating, using Langmuir probe

measurements 08 p1327 A67-21364

Electrostatic probes for collision dominated weakly ionized plasma noting mathematical formulation, density and V-A characteristics 09 p1539 A67-21782

Langmuir probe and spectrometric electron temperature measurements in negative glow plasma compared, finding probe temperatures significantly higher 11 p1788 A67-23963

Plasma turbulence and diffusion across magnetic field investigated by plasma instabilities in case of large amplitudes of oscillation measured by Langmuir probes 11 p1834 A67-24376

Density measurements in Q-device by resonance fluorescence scattering, Langmuir probe and microwave methods compared, examining causes of discrepancy 11 p1838 A67-24405

Barium Q plasma device for optical diagnosis of oscillatory microinstabilities compared with Langmuir probe 11 p1838 A67-24406

Double Langmuir probe measurement of turbulent structure and ionization intensity of hypervelocity projectile and spectral characteristics of probe signal fluctuation 11 p1790 A67-24449

Electron number densities measured behind shock wave in pressure-driven shock tube by microwave resonant cavity technique and by electrostatic quasi-Langmuir probe 11 p1790 A67-24451

Langmuir probe and microwave transmission methods compared for plasma density measurement 12 p1939 A67-25256

Oscilloscope plotting of Langmuir probe and double probe characteristics corresponding to time varying plasma properties 12 p1947 A67-26122

Cylindrical Langmuir probes examined in high density plasma flow 13 p2166 A67-26650

Plasma in diffusion regime situated in nonhomogeneous RF field with rotation symmetry 14 p2354 A67-27765

Magnetic field, pressure and discharge current effects on saturation electron current of electrostatic probe used to measure magnetoplasma electron density 14 p2358 A67-28237

Quasi-linear relaxation in unsteady states of noncollision plasma, noting electron beam distribution function and Langmuir plasma oscillations 15 p2530 A67-29867

Shock tube performance of Langmuir probe suitable for ballistic range applications, noting low pressure turbulent wakes 15 p2490 A67-30212

Effect of decomposition of Langmuir waves on interaction of electron beam with nonisothermal plasma 16 p2705 A67-30448

Duoplasmatron ion source study with Langmuir probe, finding that pressure dependent discharge characteristics relate to magnetic field radial components 17 p2902 A67-32659

Nonlinear effects in collisionless plasma during interaction with strong HF field 17 p2905 A67-32920

Acceleration mechanisms of isolated plasma particles under effect of weak or strong field with frequency of order of Langmuir frequency of electron 17 p2905 A67-32922

Wake plasma turbulence of projectiles studied using electrostatic probe array 17 p2861 A67-33023

Wing slope techniques for analysis of Langmuir probe characteristics in low density plasma, using I-V characteristics and spherical and cylindrical geometries 17 p2906 A67-33054

Periodic spatial variations of parameters of positive column plasma in magnetic field along obstacle shadow due to electron wakes 19 p3273 A67-35093

Electron temperature, concentration and potential distribution, measurement in moving striations by Langmuir probe method 19 p3273 A67-35095

Electron energy distribution and thermalization measurement in Langmuir mode discharge in plasmas, using electron energy spectrometer 19 p3274 A67-35105

Electron temperature observation in E region with Langmuir probes on Nike Apache rockets, discussing solar radiation

effect 19 p3216 A67-35193
 D-region positive ion density during solar
 eclipse of May, 1966 observed by cylindrical
 Langmuir probe onboard 19 p3222 A67-35454
 Electron density and temperature
 measurements using RF capacitance probe
 and double Langmuir probe in auroral
 zone 19 p3222 A67-35455
 Theory of Langmuir probes in plasmas
 with negative ions, considering different ion
 concentrations and electron
 temperatures 19 p3296 A67-35587
 Cesium plasma created in diode equipped
 with Langmuir probe 19 p3296 A67-35588
 Influence of Langmuir probe losses on
 ion-density measurements in thermal cesium
 plasma with homogeneous magnetic
 field 19 p3296 A67-35589
 Flat plate continuum Langmuir probe ion
 density measurements, analyzing boundary
 layer and sheath of supersonic flow behind
 shock wave 19 p3296 A67-35590
 Langmuir probe collection of ions in low
 density plasma flows, with electron density
 agreeing with microwave
 data 19 p3297 A67-35591
 Langmuir probe for electron density and
 temperature measurements in lower
 atmosphere 20 p3444 A67-36526
 Langmuir probe current in weakly ionized
 gas flow, studying correlation between
 hydrodynamical turbulence and pressure
 fluctuations 20 p3503 A67-37674
 Ion resonance effect in Langmuir probe
 exhibiting ion plasma
 frequency 21 p3663 A67-37765
 Circular planar satellite electrostatic probe
 theory based on reversible particle
 trajectories, showing relation between
 boundary curve in velocity space and
 current-voltage
 characteristics 21 p3625 A67-37899
 Ionospheric ion and electron densities by
 Langmuir probes, stressing solid state
 logarithmic amplifier for spatial
 electrometry 21 p3592 A67-38223
 Ionospheric positive ion density as
 function of altitude measured by Langmuir
 probe 21 p3629 A67-38662
 Density, electric field and volt-ampere
 characteristics for spherical electrostatic
 Langmuir probe in collision plasma with
 weak ionization and recombination, using
 asymptotic method
 [AIAA PAPER 67-705] 21 p3672 A67-38732
 Spectral and probe methods of plasma
 temperature measurement, discussing
 current-voltage
 characteristics 22 p3853 A67-40216
 Radial electron density profile and critical
 longitudinal magnetic field for helical
 current convective instability in hollow
 plasma column via Langmuir probe
 measurements 22 p3853 A67-40234
 Discharge model for relative abundances
 of different ions extracted from Ar
 plasmation from Langmuir probe
 measurements 23 p4033 A67-41190
 Plasma column and plasma-electron beam
 interaction properties by Langmuir and SHF
 probes noting resonance, coupling and
 microwave surface waves 24 p4194 A67-41911
 Hot Langmuir probe in Cs plasma studied
 for method of controlling current voltage
 characteristics 24 p4154 A67-42210
 Langmuir probes investigated by
 comparing measurements in ionized He
 afterglow by cylindrical double probes and
 by gated microwave radiometer and resonant
 cavity 24 p4197 A67-42261
LANGUAGE
ASA MACHINE LANGUAGE
ASA SPEECH
 Naming sequentially presented letters and
 words 06 p0954 A67-18533
 Interspecies communication involving
 human and mammalian brain as computer
 with programs and metaprograms
 [AAS PAPER 66-77] 07 p1135 A67-20000
LANGUAGE PROGRAMMING
 Language and system design of numerical
 analysis problem solving system
 /NAPSS/ 02 p0206 A67-11803
 Unsolvability of recognition of linear
 context-free language, searching for
 algorithm and generalizing to metalinear
 languages 03 p0375 A67-13562
 Digital simulation of boundary value
 problems of trajectory optimization, using
 variational and functional analysis and IBM-

FORMAC language
 [AAS PAPER 66-116] 07 p1149 A67-19976
 Heuristic computer programming for
 solution of complex
 problems 08 p1299 A67-21199
 Digital simulation of boundary value
 problems of trajectory optimization, using
 variational and functional analysis and IBM-
 FORMAC language
 [AAS PAPER 66-116] 13 p2074 A67-27531
 Problem oriented language for mechanical
 problems programming applied to steady
 state vibrations, static problems and stress-
 strain relation 14 p2276 A67-29000
 Spaceborne programming language for
 Surveyor guidance, discussing impact on
 flight software
 development 15 p2439 A67-29600
 Computerized method for on-line data
 analysis, elucidating SLIP language, request,
 processing, interpretation, time sharing,
 background activity, etc 17 p2821 A67-32865
 K-multiple automata for language
 recognition or generation, discussing
 generalization from simple to multiple
 automata 19 p3202 A67-35607
 Heuristic computer programming for
 solution of complex
 problems 22 p3764 A67-39866
LANSRAUX SERIES
S BESSEL FUNCTION
S HANKEL FUNCTION
LANTHANIDE
 Lanthanide abundance variation and
 coordination number, comparing abundances
 in terrestrial and meteoritic materials with
 average chondrite 03 p0413 A67-13507
 Lanthanide partition coefficient for
 crystallization under calcium effect, noting
 inflectional pattern for inverse ionic radius
 variation 21 p3617 A67-38123
 Lanthanide distribution between
 omphacite and Garnet, noting abundance
 ratios to whole rock of Japanese
 eclogite 24 p4151 A67-42449
LANTHANUM
 Temperature dependence of La-139 nuclear
 quadrupole resonance in lanthanum
 fluoride 01 p0129 A67-10149
 Electron-tunneling measurements of
 energy gap in lanthanum explaining
 differences between various
 measurements 01 p0135 A67-10918
 Thermal conductivity of lanthanum and
 monochalcogenides, noting role and
 temperature dependence of crystal-lattice
 conductivity 04 p0680 A67-15287
 Titanium alloy weld properties as affected
 by boron, beryllium and lanthanum
 additions 07 p1207 A67-19291
 Superconducting energy gap of cubic and
 hexagonal LA obtained by point contact
 tunneling to bulk samples, noting V-I
 characteristics and temperature
 dependency 11 p1846 A67-24585
LANTHANUM CHLORIDE
 Hyperfine structure and modified Zeeman
 effect in trivalent holmium in hexagonal
 lanthanum trichloride 12 p1987 A67-26237
 Multiphonon relaxation in neodymium
 doped lanthanum chloride, determining
 transition rates between stark levels with
 lifetime and quantum efficiency
 measurements 16 p2728 A67-31057
 Multiphonon orbit-lattice relaxation of
 lower lying excited states of Dy doped
 lanthanum chloride investigated, using IR
 fluorescence and quantum counter
 techniques 19 p3302 A67-35035
 Divalent Eu ion ground state splitting in
 C3h symmetry sites and associated color
 centers in EPR spectrum study of Eu ion
 doped lanthanum
 trichloride 22 p3863 A67-40003
 Lanthanide salts replacing lithium salts in
 Leclanche cell electrolyte, noting good
 capacity over widened temperature
 range 22 p3748 A67-40228
LANTHANUM COMPOUND
 Formation conditions for yttrium boride-
 lanthanum boride solid solution by reduction
 of Y and La oxides in
 vacuum 01 p0138 A67-11244
 Heat capacity and Debye temperature of
 NdS, LaSe and LaTe 05 p0867 A67-17056
 Conductivity of working fluid in MHD
 generator using thermionic emission from
 suspended lanthanum conductivity of
 working fluid in MHD generator using
 thermionic emission from suspended
 lanthanum hexaboride

powder 09 p1543 A67-21820
 X-ray study of lanthanum borides to verify
 existence of homogeneous compounds within
 large range of variations in
 composition 11 p1810 A67-23905
 X-ray and metallographic examination of
 tungsten alloys, noting decrease of work
 function during thermal emission upon
 addition of lanthanum
 hexaboride 13 p2131 A67-26468
 Lanthanum germanide synthesis using arc
 furnace, noting chemical
 properties 13 p2131 A67-26470
 Lanthanum chromite activation energy
 determination from electrical resistivity and
 Hall coefficient variation as function of
 temperature and IR absorption
 spectrum 15 p2535 A67-29478
 Heat capacity and Debye temperature of
 NdS, LaSe and LaTe 15 p2538 A67-29787
 Spectroscopic properties of mixed
 complexes with two different ligand groups
 surrounding lanthanide ion, discussing
 energy transfer and
 absorption 23 p3971 A67-40747
 Stimulated emission and spectroscopic
 investigations of double lanthanum-sodium
 molybdate single crystals with neodymium
 impurities, considering applicability in
 lasers 23 p4039 A67-40901
LANTHANUM FLUORIDE
 Temperature dependence of La-139 nuclear
 quadrupole resonance in lanthanum
 fluoride 01 p0129 A67-10149
 Near UV optical constants of lanthanum
 fluoride 03 p0470 A67-14400
 Two photon stepwise absorption of low
 power He-Ne laser light in erbium doped
 yttrium oxide and lanthanum fluoride
 crystals 13 p2177 A67-27013
LANTHANUM TELLURIDE
 Lanthanum for germanium partial
 substitution effect on thermoelectric
 properties of single phase and homogeneous
 samples of GeTe 03 p0500 A67-14231
 Heat capacity and Debye temperature of
 NdS, LaSe and LaTe 05 p0867 A67-17056
 Heat capacity and Debye temperature of
 NdS, LaSe and LaTe 15 p2538 A67-29787
LAP JOINT
 Stresses in ordinary lap joint compared to
 variable adhesive joint 09 p1577 A67-22504
 Durability of adhesive lap-shear joints
 with sustained stress, describing portable
 jig 09 p1578 A67-22522
LAPLACE EQUATION
 Neumann problems of Laplace equation
 with nonhomogeneous boundary conditions
 in theory of probe measurements of
 parameters of semiconductor
 films 01 p0136 A67-10997
 Characteristic impedance of TEM mode
 transmission lines, extracting upper and
 lower bounds on finite difference solution of
 Laplace equation 02 p0194 A67-11784
 Nonuniform network procedure for solving
 Dirichlet problem for Laplace equation in
 finite and infinite regions with canonical
 points 04 p0643 A67-14670
 Exact solutions in theory of orbits using
 Hamilton-Jacobi and Laplace
 equations 05 p0903 A67-17294
 Legendre polynomial form of slender body
 motion in spherical coordinate systems
 generalized for axially symmetric harmonic
 functions in three dimensions with validity
 for Helmholtz equation 11 p1812 A67-24310
 Gas jet expansion near crossed
 axisymmetric channel, reducing problem to
 solution of Laplace equation for second-kind
 boundary conditions 11 p1779 A67-24321
 Infinite systems of equations for multiply
 connected finite regions in shells obtained
 by extending solutions for stressed state in
 infinite multiply connected
 regions 12 p2024 A67-25600
 Eigenvalues of Laplace equation for
 diurnal and semidiurnal tidal oscillations
 solved using Galerkin
 method 13 p2112 A67-26668
 Small one-dimensional deviations of plasma
 parameters from equilibrium state, obtaining
 exact solution in form of inverse Laplace
 integral 14 p2353 A67-27754
 Incorrect problems of mathematical
 physics examined and illustrated by classical
 Cauchy problem for Laplace
 equation 16 p2698 A67-31736
 Voltage gradient determination throughout
 two-dimensional electric field by electro-
 optic analog, noting applicability to boundary

value problems satisfying Laplace equation 17 p2818 A67-32418
Limiting value calculation for temperature field criteria, analyzing heat-conduction equation solution and boundary value problems 17 p2972 A67-33068

Linearized system of water waves initial value problem, obtaining eigenvalue with parameter in boundary condition 19 p3210 A67-35703

Flow velocity calculation by analog computer, discussing Laplace equation role 20 p3424 A67-37302

9-point difference formula accuracy in Laplace equation compared to 5-point formula, discussing convergence rate and Dirichlet boundary value problem 22 p3826 A67-39195

Finite difference solution accuracy for potential gradient along conductor boundary near reentrant corner of thin plate 24 p4131 A67-42447

Electromagnetic wave diffraction in magnetoactive plasma by conducting wedge using Laplace integral in rotating reference frame 24 p4123 A67-42706

LAPLACE TRANSFORM

Exact solution, using Laplace transform, for problem of transient characteristic of semiconductor diode, challenging Novos view 01 p0035 A67-10398

Network analysis by digital computer covering methods and programs for ladder networks, nodal, electronic circuit and state variable analysis, etc 01 p0028 A67-10462

Partial fraction expansion in derivation of inverse Laplace transform of rational function with complex and/or repeated poles 01 p0104 A67-10479

Heat dissipation rate in straight bar of constant cross section generating heat internally, using Laplace transforms 01 p0166 A67-10551

Evaluation of residue integral for finite number of poles in behavior function of control circuit 01 p0045 A67-10796

Interaction between atoms of solid surface and gas phase, obtaining closed-form solution of motion 01 p0118 A67-11295

Book on conductive heat transfer covering lumped, integral and differential formulations, two- and three-dimensional periodic functions, unsteady problems, Laplace transforms, etc 03 p0535 A67-13075

Radial heat equation and Laplace transforms, discussing representations alternative to two solutions 03 p0460 A67-13819

Diffuse reflection of radiation from nonstationary plane-parallel layer solved on basis of Ambartsumian invariance principle 04 p0695 A67-14657

Stability analysis of multiloop multirate sampled systems using identities expressing Laplace transforms of sampled signals in terms of shifted transforms of same signals sampled with smaller periods 04 p0591 A67-14825

New matrix formula for obtaining inverse Laplace transformation [ASME PAPER 66-WA/AUT-3] 04 p0646 A67-15420

Exact solution /by Hankel and Laplace transforms/ of unsteady motion of viscous MHD fluid in cylindrical vessel in axisymmetric constant strength magnetic field 05 p0850 A67-16134

Transfer function parameters of stationary controlled plants in identification problem estimated, using Laplace transform and least squares method 05 p0782 A67-16319

Boundary value problem for heat equation, discussing Laplace transform solution and uniqueness theorem 06 p1111 A67-17645

Book on numerical inversion of Laplace transform for computers 06 p1023 A67-17942

Matrix method determination of time response of time invariant linear systems to range of deterministic functions 06 p0976 A67-18402

Electromagnetic wave diffraction problems solved by two-dimensional Laplace transforms 07 p1147 A67-20298

Two methods of numerical construction of derivatives involved in inversion of Laplace transform 08 p1347 A67-20370

Transient processes in linear automatic control systems dependent on parameters which appear when differential equations of analyzing system are transformed by

Laplace-Karson method 08 p1313 A67-21324
Criterion for spatial amplification or nontransmittance using double Laplace transforms in light of complex values of wave vector 09 p1463 A67-21992

Fresnel formulas for transformation of transverse electromagnetic wave into longitudinal plasma wave at dielectric-plasma interface, using Laplace transforms 09 p1464 A67-21993

Time variable linear transmission systems with arbitrary initial state in case of abruptly varying periodic or nonperiodic system parameters and input signal analyzed, using Laplace transform 10 p1608 A67-23638

Synthesis of time functions with finite number of discontinuities by constructing functional scheme of system from Laplace transform of output 11 p1769 A67-24122

Stability of cylindrical shell of oval cross section compressed along generatrix and under external pressure analyzed, using Laplace transforms 12 p0205 A67-25612

Finite length inductive MHD generator, solving inlet and outlet effects on boundary value problem 13 p2165 A67-26613

Maintenance replication rate and spares provisioning measurement using Laplace transform 16 p2634 A67-30444

Effect of magnetic field gradients at inlet and outlet on linear two-dimensional induction MHD generator calculated by bilateral Laplace transform 16 p2605 A67-30579

Transient plane wave magnetic field attenuation through semiinfinite plate using simplified Laplace transfer function, noting infinite product form for LPTF 16 p2626 A67-31349

Oscillation mode in open-ended circular cylindrical microwave cavity resonant frequency computed by Laplace transform and Wiener-Hopf techniques 17 p2828 A67-33083

Vlasov equation for anisotropic electron plasma in external magnetic field solved by Laplace transform of density perturbation in initial value problem 17 p2907 A67-33104

Uniqueness theorem for general linear anisotropic time-variable viscoelastic body under boundary conditions, using Laplace transformation 17 p2964 A67-33135

Transfer function parameters of stationary controlled plants in identification problem estimated, using Laplace transform and least squares method 18 p3017 A67-33870

Ideal SSB modulation theory, discussing DSB Laplace transform formalism, noting Butterworth filters for channel contaminants reduction 19 p3181 A67-34848

X-transform for open/closed loop sampled data system with zero-order hold device 19 p3263 A67-35927

Variational formulation of Laplace transformed heat diffusion problem [ASME PAPER 87-HT-77] 20 p3551 A67-38755

Vibrating annular membrane problem, including load per unit area and asymmetry of load and vibration, using finite transform derivation 20 p3539 A67-37006

Laplace transformation of solution of linear differential equations with variable coefficients and time lags, analyzing motion stability 20 p3478 A67-37579

Axial shear wave radial propagation in nonhomogeneous elastic medium under axisymmetric loading solved by Laplace transform and characteristics method 21 p3719 A67-38146

Discrete Laplace transform for analyzing pulsed automatic systems with variable parameters, noting special type of complex variable 21 p3605 A67-39112

Numerical solution methods for partial differential equations, discussing dynamic programming, Laplace transform and quadrature technique 24 p4180 A67-43084

LARA AIRCRAFT S OV-10 AIRCRAFT

LARMOR ORBIT

Finite ion Larmor radius in stabilizing rippling mode of Furth-Killen-Rosenbluth dissipative instabilities in plasma with finite resistance gradient 02 p0277 A67-12613

Wave propagation in rarefied two-component plasma situated in uniform constant magnetic field with finite Larmor radius 03 p0483 A67-13875

Finite plasma pressure effect on interchange mode in finite Larmor radius

weakly unstable regime 05 p0858 A67-17430
Combined Rayleigh-Taylor and Kelvin-Helmholtz instability for incompressible plasmas carrying uniform magnetic field including Hall current 08 p1359 A67-20902

Two-fluid theory for plasma stability, obtaining equation on velocity field perturbation by considering Ohm law, stress tensor with Larmor radius and viscosity from collisions 10 p1685 A67-23465

Cesium plasma measurements to determine steady state parameters and LF oscillation characteristics 11 p1834 A67-24379

Finite ion Larmor radius effect on superposed fluid stability investigated for general perturbation direction, noting magnetically stabilized configurations become overstable 13 p2167 A67-26993

Finite ion Larmor radius in stabilizing rippling mode of Furth-Killen-Rosenbluth dissipative instabilities in plasma with finite resistance gradient 13 p2170 A67-27369

Finite-ion Larmor radius effect on wave propagation in rarefied rotating plasma, noting solar corona application 15 p2533 A67-30396

Ion cyclotron wave propagation in plasma, considering Larmor radius effects, quasi-static dispersion relation, phase velocity and cyclotron resonance 21 p3661 A67-37750

Flute instability of maximally inhomogeneous rarefied plasma cylinder with thick transition layer amounting to two Larmor radii 21 p3667 A67-38371

LASER

SA CHEMICAL LASER

SA FABRY-PEROT LASER

SA GAS LASER

SA LIQUID LASER

SA MASER

SA ORGANIC LASER

SA PULSED LASER

SA RING LASER

SA RUBY LASER

SA SEMICONDUCTOR LASER

SA SOLID STATE LASER

SA TRANSIENT OSCILLATION

Optical modulator using electro-optic effect in lithium tantalate for PCM transmission systems operating at 224 megacycle bit rate 01 p0033 A67-10013

Masers and lasers from Einstein discovery of stimulated emission to present 01 p0089 A67-10503

Signal excitation in negatively charged antenna rod in effect of unfocused laser beam 01 p0091 A67-10835

Nonlinear optical materials properties discussed on basis of Soviet and foreign studies involving lasers 01 p0115 A67-11011

Extremely wideband information storage and retrieval systems employing laser or electron beam on silver halide or electron beam on thermoplastic film 01 p0077 A67-11437

Laser, electron and plasma energy beam types and application to manufacturing technology 02 p0249 A67-12179

Particle emission from surface interacting with laser beam 02 p0252 A67-12180

Laser light source controlled by Kerr cell coupled with Z-type schlieren optical system to produce multiple flash photographs of detonation wave development 02 p0245 A67-12227

Lasers applied to photo-optical instrumentation problems, detailing schlieren systems, interferometry, high speed streak photography and transmissometer 02 p0245 A67-12243

Self-excitation of nonsteady processes in two-photon laser 02 p0252 A67-12421

Powerful laser employing induced two-quanta luminescence 03 p0433 A67-12856

Soviet papers on quantum electronics 03 p0434 A67-13124

Kinetic equation derivation from density matrix for case of quantum generation of secondary optical harmonic in laser cavity under various optical pumping conditions 03 p0435 A67-13127

Optical methods and equipment used in checking surface finish and volume and surface inhomogeneities of active media and interferometric mirrors of lasers 03 p0436 A67-13143

Electron temperature and concentration in DC plasma arc determined from Thomson scattering of laser radiation 03 p0437 A67-13209

Lasers used to extend RF plasma

- diagnostic procedures to optical frequencies
by interferometric and Thomson diffusion
methods 03 p0477 A67-13474
- Heating and scattering of plasma produced
by giant laser pulse focused on solid
target 03 p0486 A67-14194
- Stimulated emission by electron beam
bombardment of laser
materials 03 p0439 A67-14394
- Sensitivity of optical system used in
schlieren setup in determining quality of
recorded information 04 p0619 A67-14806
- Laser backscatter signatures and
transmissivity over horizontal and slant
paths with respect to measuring extinction
coefficients of scattering
media 04 p0649 A67-14877
- Two-level resonator type laser using
neutron-irradiated quartz single crystal with
high recurrent inversion
frequency 04 p0633 A67-15158
- Annual Electron and Laser Beam
Symposium, University of Michigan, Ann
Arbor, April 1966 04 p0622 A67-15300
- Interferometer design for use with laser
light in fluid mechanics 04 p0624 A67-15455
- Ring laser inertial sensor for aerospace
systems obtaining high accuracy angular
resolution and mechanical
simplicity 04 p0625 A67-15665
- Parametric amplifiers and
lasers 05 p0814 A67-16361
- Thermal high resolution recording using
moving laser spot on metallic and organic
thin films 05 p0815 A67-16586
- Laser as source of optical Fourier analysis
of atomic structure of
crystals 05 p0824 A67-16921
- Calcium fluoride-cerium fluoride with
neodymium additions as active medium for
lasers, discussing absorption and
luminescence spectra and induced
radiation 05 p0825 A67-16922
- Kinetics of formation and healing of
damage caused by laser pulse in lithium
fluoride single crystals 05 p0867 A67-17057
- Laser applicability to line-of-sight
atmospheric turbulence
parameters 05 p0839 A67-17383
- Temperature distribution in two-layer
plate during welding by laser light
flux 05 p0814 A67-17548
- Pumping medium power lasers using
artificial meteors to produce intense gas
glow in compression wave 06 p1009 A67-17757
- Viewing system for laser operating in
production shop 06 p1009 A67-17792
- Bibliography on lasers covering modes,
scattering mechanisms, quantum
electrodynamics, matter-radiation interaction,
plasma, holography and
optics 06 p1010 A67-17890
- Laser holography, discussing various
methods of wave front
reconstruction 07 p1183 A67-19092
- Lead azide and pentaerythrite tetranitrate
explosion triggered by laser
radiation 07 p1195 A67-19315
- Multilayer interference filter having
various transmission characteristics,
emphasizing filters with narrow stop bands
used to eliminate laser beam
hazard 07 p1224 A67-19400
- Book on lasers, light amplifiers and
oscillators noting optical resonators, optical
pumping, pulsed lasers,
etc 07 p1195 A67-19469
- Optimal design of elliptical pumping
chambers from numerical calculations
containing all geometric sizes of pumping
lamps and laser rods and reflectivity of
walls 07 p1195 A67-19490
- Impulse discharge tubes for laser
employing industrial glass 07 p1195 A67-19506
- Etching methods to visualize lattice
dislocations and grain boundaries in
Czochralski grown calcium tungstate crystals
doped with neodymium for laser
application 07 p1196 A67-19585
- Effects of gain saturation by strong
traveling fields in dilute laser media, noting
atomic motion and line
broadening 07 p1197 A67-20126
- Laser interferometric measurement of
power spectral density of integrated particle
density fluctuations in turbulent exhaust of
sonic jet 08 p1337 A67-21142
- Electronics methods used in laser
technology and vice versa, emphasizing
microwave photoelectronic devices, self-
consistent gas discharges at optical
frequencies, etc 08 p1338 A67-21269
- Laser technology development, ruby, gas
and semiconductor lasers, applications and
comparisons with other technologies for
communications, fire control, ground radar,
etc 08 p1295 A67-21283
- Laser transition in B 2, Br 2 and Sn in
pulsed discharges of boron chloride,
hydrogen bromide and stannic chloride
respectively 08 p1339 A67-21379
- Bibliography on lasers and laser
applications 09 p1511 A67-21713
- Atmospheric turbulence determined from
coherence deterioration of laser
beam 09 p1511 A67-21825
- Laser welding and machining - Seminar,
Pennsylvania State University, June-July
1965 09 p1504 A67-22137
- Energy problems in laser welding,
examining maximum instantaneous heat flux
metals can withstand 09 p1504 A67-22138
- Laser as drilling and welding tool, noting
industrial guidelines, pulse control
techniques, micromachining,
etc 09 p1504 A67-22140
- Laser equipment for fusion welding of
aerospace structural materials, examining
ruby laser properties, flash tube and overall
system 09 p1504 A67-22141
- Laser as drilling tool 09 p1504 A67-22142
- Laser radiation effect on solids, noting
laser properties, temperature rise, melting,
vaporization and particle emission of
materials 09 p1513 A67-22144
- Industrial laser application, giving
background information on laser
theory 09 p1505 A67-22145
- Laser for length measurement, checking
absolute wavelength stability by Fabry-Perot
spectrometer 09 p1499 A67-22148
- Laser interferometer for precise
measurement of long distances, noting
function and industrial
use 09 p1499 A67-22149
- Microwave and optical generation and
amplification - International Conference,
Cambridge, England, September
1966 09 p1476 A67-22251
- Coupled laser quenching and transient
buildup in rate equation analysis, noting
spike suppression 09 p1514 A67-22274
- Self-focusing laser beam in inhomogeneous
plasma 09 p1515 A67-22276
- High speed photography of laser radiation
damage to transparent materials and analysis
of destruction mechanisms
involved 09 p1516 A67-22660
- Laser oscillation on hyperfine transitions
in ionized iodine, noting Fabry-Perot
fringes 10 p1662 A67-22699
- Two-beam Mach-Zehnder and Michelson
interferometers using coherence properties
of lasers, construction and
applications 10 p1652 A67-22709
- Quantum mechanical theory of
interference between independent
nonmonochromatic light beams using
nonmonochromatic modes of radiation
field 10 p1663 A67-22866
- Laser applications in military technology
including precision measurement, secure
communication, target location,
etc 10 p1664 A67-23070
- Lasers for tracking and geometric geodesy
as used in Explorer and Geos satellite
missions 10 p1664 A67-23071
- Satellite range measurements using laser
in conjunction with photoelectric receiver
and Baker-Nunn camera 10 p1606 A67-23182
- Luminescence of CdS at low temperature
excited by very high intensity laser
light 10 p1667 A67-23779
- Quantum noise theory for lasers, obtaining
rate equations and noise sources with
moments appropriate to shot noise and
amplitude spectrum 11 p1799 A67-24239
- Nonlinear optical materials properties
discussed on basis of Soviet and foreign
studies involving lasers 12 p1986 A67-25361
- Automatic laser tracker system for close-
up photographic coverage of rocket test
[SMPTTE PAPER 101-90] 12 p1905 A67-25474
- Raman laser physics covering gain
formula, stimulated and spontaneous
scattering and cavities 12 p1953 A67-26124
- Absorption and fluorescence
characteristics of Nd-doped phosphate
glasses used as laser
material 13 p2128 A67-27229
- Laser as source of optical Fourier
transforms in analysis of atomic structure of
crystals 14 p2330 A67-28261
- Calcium fluoride-cerium fluoride with
neodymium additions as active medium for
lasers, discussing absorption and
luminescence spectra and induced
radiation 14 p2330 A67-28282
- Heating and scattering of plasma produced
by giant laser pulse focused on solid
target 14 p2360 A67-28539
- Rate measuring strapdown inertial
navigation systems, describing gas bearing
gyros and three-axis ring
laser 14 p2348 A67-29080
- Radar, IR and laser sensors production
trends for airborne
reconnaissance 15 p2485 A67-29163
- Two-level resonator type laser using
neutron-irradiated quartz single crystal with
high recurrent inversion
frequency 15 p2496 A67-29345
- Kinetics of formation and healing of
damage caused by laser pulse in lithium
fluoride single crystals 15 p2538 A67-29788
- 1967 SWIEECO record - IEEE
Conference, Dallas, April
1967 15 p2450 A67-29901
- Laser interferometers for metrology
applications, considering sources of
error 15 p2501 A67-30411
- Electron beam and laser beam line scan
recorders requirements, limits, applications
and techniques 17 p2857 A67-32470
- Rastering nanosecond laser sensitizer
for materials responsive to short duration
signals, discussing recording, sensitizer
and measuring subsystem 17 p2858 A67-32482
- Laser applications utilizing power density
for studying reflectance, Raman spectra,
photography, holography,
etc 17 p2868 A67-32691
- Laser gyroscopes as aid to navigation and
guidance, discussing principle, advantages,
etc 17 p2868 A67-32726
- Pump induced optical distortion in
isotropic laser materials analyzed using
Fermat principle, predicting ray refraction,
beam divergence, etc 18 p3062 A67-34624
- Soviet book on radio physics quantum
amplifiers covering lasers, maser,
paramagnetic resonance,
etc 19 p3238 A67-34799
- Soviet book on lasers and nonlinear optics
covering theory, physical processes and
phenomena caused by strong electromagnetic
laser radiation 19 p3238 A67-34800
- Quantum theory of laser having only
single-mode oscillation and ignoring atomic
motion and spatial variations in cavity
mode 19 p3239 A67-35034
- Laser bibliography V /July-december 1966/
covering giant-pulse techniques, Raman and
Brillouin scattering, interaction effects,
propagation, holography, etc laser
bibliography V /July-December
1966/ 21 p3641 A67-38455
- Laser applications - Conference, Paris,
July 1967 23 p4013 A67-41021
- Laser applications - Conference, Paris,
July 1967 23 p4014 A67-41034

LASER COMMUNICATION

- Photoelectronic components and electronic
measurement techniques in reception and
demodulation of HF modulated laser
beams 01 p0088 A67-10300
- Voice communications system using GaAs
room-temperature injection laser and TV
communications system using GaAs crystals
as modulators for laser
beams 02 p0194 A67-11786
- Laser application to radar signal
processing and communications
equipment 04 p0576 A67-15303
- System design analysis of laser methods of
deep space communication, examining local
heterodyne system /LHS/, direct detection
system /DDS/ and transmitted reference
system 06 p0957 A67-17835
- GaAs room temperature laser diode
application to communication and radar
systems 07 p1194 A67-19086
- High data rate laser communication
system, discussing integration of laser and
wideband modulator and experimental
results under field
conditions 08 p1292 A67-20672
- Laser application to laser telephone
circuits, noting experimental data and
effects of fog 08 p1337 A67-20769
- Marx model for interstellar travel in
vehicle propelled by terrestrial laser
beam 08 p1376 A67-20989

Elements of laser communication system including transmission media, terminals, generators, modulators, etc 09 p1462 A67-21875

Diademe satellites design including laser beam range determination reflectors for spatial geodesy, laser telemetry, etc 10 p1712 A67-22860

Laser development, deep space communication system studies and designs 10 p1606 A67-23069

Laser application to deep space communication noting advantages of optical frequencies for high rate transmission of data 11 p1752 A67-24252

Parameters of multiple-scattered optical radiation applied to laser communication system design 12 p1906 A67-25988

Optical computing principles, techniques and configurations for communication problems noting Fourier transform, coding, etc 12 p1907 A67-25990

SNR and transmission error probability in pulse modulated optical communication 13 p2067 A67-26663

Laser communication system for black and white tv signal transmission noting focusing, noise level and light modulation laser communication system for black and white TV signal transmission noting focusing, noise 13 p2068 A67-26724

Behavior in atmosphere of laser beam modulated for black and white TV signal transmission 13 p2068 A67-26725

Laser applications to telemetry, radar, navigation, telecommunications, medicine, boring and welding 14 p2333 A67-28974

TV signal transmission over gas laser light beam with ADP crystal at 7GHz modulating frequency 16 p2684 A67-30610

Equivalent resistance of traveling wave phototube for large modulation index 16 p2636 A67-30897

Lasers for short-distance communication and space, ranging, and detection applications 16 p2685 A67-31195

System for information transmission over optical path using microwave subcarrier, noting satisfactory SNR 17 p2812 A67-32237

Gas laser applications in construction, mechanics, communications, biology and medicine for control, measurement and experimental work 17 p2867 A67-32366

Multiple laser communication design, considering links between ground stations and earth-synchronous satellite with single telescope and laser 17 p2813 A67-32495

Optical communication experiments to compare coherent and noncoherent optical detection fading characteristics in different weather conditions, using laser transmitter and optical superheterodyne receiver 19 p3184 A67-35685

Optical subcarrier communications, noting use space-oriented missions and RF techniques optical subcarrier communications, noting use in space-oriented missions and RF techniques 20 p3378 A67-36183

Lasers for wideband planetary communication, describing heterodyne receiver and transmitter designs 20 p3381 A67-36566

Book on lasers and application to long distance terrestrial or space communications system 20 p3459 A67-36639

Optical and IR wideband communication between earth and interplanetary spacecraft, discussing tracking, detectors, pointing and beam formation 22 p3762 A67-39960

Atmospheric absorption of carbon dioxide laser radiation calculation from laboratory absorption coefficient measurements, discussing effects on power transmission and communications 22 p3816 A67-40237

Deep-space communication capability spectral dependence analysis indicates optical transmissions would be several orders of magnitude poorer than RF technology 22 p3764 A67-40558

Mobile laser transceiver for atmospheric targets detection, discussing real time technique for determining atmospheric function 23 p4014 A67-41022

Broad bandwidth digital laser communication system utilizing pulse coded polarization modulation and binary detection including optical communication link and performance data 23 p3973 A67-41039

Atmospheric scintillation effects on optical

data channel for application to laser radar noting SNR role 23 p3975 A67-41266

Two-terminal GaAs laser diode communication system noting laser driver component selection, system performance, construction, design and ranging and tracking applications 23 p3975 A67-41379

R and D deep space communication system planning methodology for comparing laser, IR and mm wave possibilities, analyzing tradeoff and optimizations [AIAA PAPER 67-973] 24 p4280 A67-43050

LASER MODE

Generating mode number in solid state lasers using traveling wave and standing wave 01 p0086 A67-10069

Competition of two types of oscillations in traveling wave laser 01 p0089 A67-10362

Single self-mode-locked pulse selection from bleachable dye Q-switched Nd-doped glass laser 01 p0091 A67-10875

Optical pumping with diode laser into Fabry-Perot resonator face of thin highly-absorbing semiconductor, noting variable mode spacing including single mode output 01 p0091 A67-10879

Spontaneous emission spectra and ratio of number of photons in various oscillation modes of laser with nonlinear filter type lock 02 p0251 A67-11573

Optical frequency translation of pulses from mode locked laser, noting Doppler shifts of large magnitude 02 p0253 A67-12506

First and second order correlation functions for field obtained by superposition of two laser modes through Youngs experiment, used to determine coherence and statistical properties 02 p0254 A67-12634

Laser emission in pure cadmium sulfide crystals bombarded by electron beams 03 p0433 A67-12812

Possible oscillation modes in cylindrical solid state laser and dependence of pumping threshold, output power and divergence angle on resonator length 03 p0435 A67-13129

Effect of diffusion of excitation on conditions of multimode generation in laser radiation 03 p0437 A67-13207

Mode characteristics of solid state lasers from analytical solution of conservative equation 03 p0437 A67-13208

Steady state regime and stability of two-photon laser, noting field dependence of intensity and duration of frequency pulse and resonance excitation curves 04 p0631 A67-14745

Oblique modes and energy of gas laser beam 04 p0632 A67-14913

Amplitude and frequency characteristics of traveling wave ring laser 04 p0635 A67-15777

Inertial sensors, discussing magnetic resonance and superconductor gyroscopes, ring lasers, fluid dynamical devices, electrostatic gyroscopes, etc 05 p0806 A67-16517

Excess photon noise in detected photocurrent of multimode laser for uncoupled and phase locked modes 05 p0815 A67-16623

Accuracy and limit analysis of statistical distribution of EM radiation field by photoelectron counting distributions from photodetector for single mode laser near threshold 05 p0815 A67-16624

Internally scanned laser beam having high deflection rate produced by pulsed optical delay line 05 p0818 A67-16647

Laser brightness gain and single transverse mode operation by compensation for thermal distortion with external gas laser 05 p0819 A67-16656

Multiphoton absorption processes, coherence of radiation fields and statistical properties of laser light absorption 05 p0823 A67-16681

Hypersonic excitations due to Brillouin scattering for case with Stokes feedback, deriving quantum equation of motion for creation of laser and Stokes modes and coupled acoustic mode 05 p0823 A67-16683

Suppression of undesirable axial modes in gas laser oscillating at several frequencies obtained by filling with active gas mixture each of two coupled Fabry-Perot type resonators 05 p0826 A67-17326

Competition of two types of oscillations in travelling wave laser 06 p1009 A67-17620

Nonlinear medium anisotropy and saturation effects on orientation of polarization ellipse of gas laser

mode 06 p1010 A67-17820

Optical maser oscillation lines in H discharge in mixture of Ar and Br 06 p1011 A67-18540

Laser line-scanning photographic system discussing possible extraterrestrial applications 06 p1006 A67-19000

Laser studies at RCA Victor Research Laboratories, Montreal, discussing spectroscopic, interferometric and plasma diagnostic research 07 p1194 A67-19060

Laser application to meteorology, discussing Rayleigh, aerosol and Raman scattering, system configuration and measurement problems 07 p1194 A67-19000

Wave interaction in saturable absorber noting hole burning in dye switched rub laser 07 p1234 A67-20050

Ruby laser mode locking and mode competition using RG-8 filter as passive modulator 07 p1197 A67-20140

Frequency and phase locking of laser oscillators by externally injected signal 08 p1338 A67-21300

Longitudinal mode oscillations of gas laser when resonator length changes with time noting polarization and amplitude change related to growth of new oscillation 08 p1338 A67-21310

Gain saturation effect on oscillating mode of optical masers 08 p1339 A67-21370

Generating mode number in solid state lasers using traveling wave and standing wave 08 p1339 A67-21450

Phase locking of longitudinal modes of gas laser by cavity mirror translation at constant velocity 09 p1510 A67-21570

Modulation linearity improvement using separate analyzer assembly with each electro-optic crystal 09 p1511 A67-21640

Laser mode combination tones detected by coupled high resolution optical amplifier corresponding to simultaneously oscillating frequencies 09 p1511 A67-21740

Laser mode-locking during resonator Q factor modulation 09 p1513 A67-22006

Far field radiation patterns with Hermite Gaussian symmetry in junction plane of Ga As lasers 09 p1513 A67-22130

Internally modulated gas laser at 100 and 4000 MHz, describing electromagnetic field in Fabry-Perot resonator in terms of natural oscillation modes and coupling 09 p1514 A67-22260

Gain curves in multifrequency optical oscillators, measuring vanishing frequencies as function of losses in resonator, noting attenuation in laser discharge tube 09 p1514 A67-22270

Self-locking of He-Ne lasers at various mirror separations by controlling oscillation frequency with intracavity modulator 09 p1516 A67-22430

Wave equation solution yielding steady absorption coefficient for laser diode 09 p1516 A67-22660

Laser mode selection by internal reflection prisms 10 p1662 A67-22740

Multiple pass effects in laser pumping cavities, noting mercury lamp performance 10 p1662 A67-22740

Mode discrimination of laser cavity exploiting transmission characteristics of Fabry-Perot 10 p1663 A67-22830

Longitudinal modes of carbon dioxide laser cavity by varying optical length of cavity 10 p1663 A67-22840

Thermal plasma device /Q machine/ design objectives and proposed features, noting association with normal mode oscillations in gas laser 11 p1830 A67-24006

Fringe visibility dependence on path length difference in laser illuminated two-beam interferometer 11 p1790 A67-24420

Toroidal laser resonator, analyzing modal properties of inner field and optical stability of beam 12 p1951 A67-25197

Emission spectrum of single and multicomponent ruby laser, observing decrease in number of modes during transition from solid to multielement instrument 12 p1952 A67-25436

Periodic variations of oscillation modes in He-Ne laser as result of resonator length increase 12 p1952 A67-25437

Laser interferometer for accurate determination of vibration amplitude, noting basic characteristics 12 p1943 A67-25696

Oscillation characteristics and special features of doubly segmented laser, noting

maximum suppression of unwanted modes 12 p1953 A67-26221
 HF properties of laser cavities with anisotropic dielectric filling, calculating Q-factor and shunt resistance 13 p2075 A67-28399
 Coupling of laser optical modes by intracavity time varying perturbation 13 p2125 A67-26407
 Self-locking of modes in passive Q-switched laser 13 p2126 A67-26727
 High speed correlation technique to measure time development of width of ultrashort pulses generated by mode locked Nd trivalent ion glass laser 13 p2126 A67-27014
 Phase distribution in laser aperture based on analysis of radiation in Fresnel zone 13 p2127 A67-27029
 Nonlinear theory of internally loss modulated laser including effect of arbitrary atomic line shape, saturation and mode pulling 13 p2127 A67-27084
 Deformed laser resonator mode, studying diffraction losses, amplitude and phase distribution during pumping pulse 13 p2127 A67-27087
 Heterodyne signal amplitude dependence on optical path length difference for oscillating axial modes in multimode gas laser 13 p2128 A67-27346
 Interferometry of resonator modes in submillimeter wave laser 13 p2129 A67-27347
 Amplitude, phase distribution and output beam characteristics in transverse modes of unstable optical cavities analyzed using pulsed gas laser 13 p2129 A67-27350
 Mode-locked laser traveling pulses proved experimentally to be 180 degree pulses 14 p2330 A67-28292
 High power laser emitting monochromatic radiation at single frequency applicable in spectroscopy, telemetry and telecommunication 14 p2330 A67-28469
 Mechanisms operating in lasers employing optical transitions of molecules in fluids 14 p2331 A67-28471
 Power spectrum and difference frequency spectrum for energy exchange oscillations between three modes of He-Ne laser 14 p2331 A67-28603
 Gas laser mode interaction in Zeeman laser, investigating transition in axial magnetic field 14 p2331 A67-28715
 Function of symmetrical gas-laser resonator analyzed to determine angle of divergence of laser beams generated by various transverse electromagnetic wave modes 14 p2332 A67-28854
 Optimum energy coupling of multimode gas laser determined experimentally 14 p2333 A67-28971
 Normal modes for solid state laser noting linear and elliptic polarization, resonant frequency and reflection loss 15 p2497 A67-29388
 Modes in unstable optical resonators and lens waveguides, noting spherical wave characteristics of geometrical eigenmodes 15 p2497 A67-29391
 Double sapphire plate resonator to control multiple modes of commercial laser /Korad K-1Q/ without use of saturable dye 15 p2498 A67-29497
 Threshold temperature variation, output power and emission spectrum of short ruby crystals operated in quasi-continuous mode 15 p2498 A67-29665
 Material processing in microelectronics with laser beam noting solid state lasers, power density, pulse frequency, etc 15 p2493 A67-29682
 Internal and coupling modulation and mode locking of continuous ruby laser 15 p2499 A67-29729
 Short term stability of beat frequency of two stable single-frequency carbon dioxide-nitrogen-helium lasers 15 p2499 A67-29732
 Angular distribution of laser radiation and variation in beam direction of stimulated radiation as function of misadjustment angle of resonator mirrors 15 p2500 A67-29759
 Shape of extremely short pulses generated by helium-neon laser with mutual synchronization of intermodal beats achieved by Fabry-perot interferometer 15 p2500 A67-29760
 Ultrasonic devices for coherent optical systems, discussing CdS transducers, laser scanners and microwave signal processing 15 p2500 A67-29912

Master equation for statistical operator of laser mode leads to photon number distribution for arbitrary pumping 15 p2501 A67-30124
 Book on laser microemission spectrum analysis covering laser properties, Q-switching technique, controlled negative feedback lasers, applications, etc 15 p2501 A67-30147
 Small scale trapping of laser beam and frequency shift in Raman radiations observed under various polarization conditions 16 p2684 A67-30607
 Nonaxial oscillation modes in He-Ne laser interaction with spherical mirror resonator confocal cavity 16 p2685 A67-31038
 Nonlinear laser theory to calculate amplitudes, frequencies and beat frequencies of circularly polarized modes in laser with axial magnetic field 16 p2686 A67-31562
 Mode-locked laser described in traveling light pulse terms, with saturable absorber, noting pulse width under steady state 16 p2686 A67-31808
 Output power of gas laser with numerous axial-oscillation modes calculated as function of resonator length and pumping power 17 p2866 A67-31926
 Periodic relaxation pulses caused by thermal resonance drift, studying diffraction loss and other effects on transverse modes in crystal lasers 17 p2867 A67-32362
 Confocal ruby laser mode structure analyzed for relation between mode number and spiking regularity, noting frequency hopping 17 p2867 A67-32402
 Radiation from two optically coupled cavities of compound laser identical in time and spectral composition without tuning one cavity to other 17 p2868 A67-32661
 Fabry-Perot interferometer for discriminating gas laser modulation at frequencies less than Doppler bandwidth 17 p2869 A67-33294
 Polarization properties of single mode operating gas laser in small axial magnetic field with initial cavity anisotropy 17 p2870 A67-33368
 Short stable gas laser construction and properties 18 p3058 A67-33658
 Temperature gradient in steady state thermally operated solid state lasers, calculating end face curvatures and light paths for resonator mode correction 18 p3059 A67-33714
 Vacuum UV and X-ray lasers from electron ejection from inner shells of atoms through photoionization 18 p3060 A67-34015
 Spectrum of continuous action laser with confocal resonator, showing mode degeneration association with phase distortions of wave front caused by mirror defects 18 p3060 A67-34039
 Laser frequency variation and emission kinetics during generation process, investigating spectra at scanning rate and pumping energy ranges 18 p3061 A67-34619
 Phase relationships between self-locked modes in lasers and agreement with predictions based on maximum emission principle 18 p3062 A67-34640
 Neodymium glass laser radiation investigation, using moving active body method, for spatial inhomogeneity of mode field in spectrum random structure 19 p3238 A67-34895
 Spectral characteristics of solid state laser with large angular divergence of light, showing contribution from degenerate modes 19 p3239 A67-34903
 Plasma electron density measurement method using beat frequencies between two dual frequency lasers 19 p3231 A67-35594
 Tabulation of accidental coincidences between fundamental frequency of one laser and harmonic or subharmonic frequencies of another, as necessary condition for frequency translation between lasers 19 p3240 A67-35700
 Spherical interferometers used in measuring time-resolved spectra of ruby laser relaxation oscillations 19 p3241 A67-35804
 Scheme for obtaining zero beats using broad range of phase frequency modulations for direct determination of laser frequencies 19 p3241 A67-36024
 Function of symmetrical gas-laser resonator analyzed to determine angle of divergence of laser beams generated by various transverse electromagnetic wave

modes 19 p3242 A67-36106
 Phase-locking effects between longitudinal modes in lasers, treating several-mode oscillations 20 p3456 A67-36171
 Transverse-mode distribution of emission intensity of solid state laser with plane mirrors 20 p3459 A67-36688
 Laser induced gas electrical breakdown theories, predicting high threshold field strengths invalidated by single mode, phase-locked and laser measurements 20 p3459 A67-36851
 Passive Q-switching of carbon dioxide laser with cavity containing saturable absorber, noting peak power and pulse rate 20 p3460 A67-36854
 Modes and eigenvalues of symmetric cylindrical Fabry-Perot laser resonator with circular output-coupling apertures 20 p3460 A67-37024
 He-Ne laser light intensity distribution cumulants for nonlinear oscillation threshold operation 20 p3461 A67-37289
 Laser population inversion using Fabrikant method, analyzing electron energy distribution in hollow cathode discharge 21 p3638 A67-37940
 Two-mode laser beam electromagnetic field statistical properties tend to Bose-Einstein form 21 p3642 A67-39117
 Book on laser systems covering quantum electronics, coherent radiation, modulation and spectral, distance, velocity and communication applications 22 p3814 A67-39445
 Solid state laser with mode selection within active medium ensures beam collimation in one plane, noting use in second-harmonic generation and parametric frequency conversion systems 22 p3814 A67-39458
 Lande factors of neon atoms subjected to magnetic field and multimode laser irradiation measured by observing resonant saturations in fluorescent light emitted 22 p3815 A67-39651
 Radiation fluctuation of single mode continuously operating laser, deriving fluctuation spectral density and emission line intrinsic width 22 p3815 A67-39738
 Moving striation modes observed in periodic sidelight intensity oscillations of He-Ne laser 22 p3816 A67-40312
 Filter with hyperfine doublet splitting using Paschen-Back effect for optical pumping 22 p3816 A67-40321
 Laser interferometric velocity measurements of moving objects, discussing accuracy improvements by recorder resolution power increase and atmospheric and seismic disturbance elimination 23 p3997 A67-40571
 Intrinsic modes of spherical mirror resonators, noting parameters identifying beams generated by such resonators 23 p3998 A67-40709
 Laser light production and properties based on quantum mechanical equations, describing nonlinear interaction between radiation and matter 23 p4011 A67-40761
 Laser emission mode splitting of CN laser, discussing wavelength to resonance length and Fabry-Perot interferometer permitting line splitting observation 23 p4012 A67-40893
 Laser mode synchronization by electro-optical crystal dielectric constant modulation mounted inside resonator 23 p4013 A67-40903
 Self-synchronization of axial modes of LF oscillations of laser giant pulse intensity with saturable filters 23 p4013 A67-40908
 Pulse regenerative amplification in Q-switched argon-ion laser during buildup time to saturation 23 p4014 A67-41030
 Neutral and charged particle trapping using waves, discussing wave attenuation from particle interaction, plasma waveguide and laser beam trapping 23 p4017 A67-41681
 Spatial coherence of radiation field across multimode He-Ne laser beam 24 p4167 A67-42091
 Cross correlated photons of laser used to determine correlation functions by applying thermodynamic Green function 24 p4168 A67-42594
 Functional half-adder using optical coupling in injection laser noting design criteria and mode propagation delay 24 p4169 A67-42822
 Longitudinal mode generation in ruby laser emission operating in single pulse regime with resonant mirror

- reflector 24 p4169 A67-42894
Separate studies of power and collision broadening of gas laser transition showing proportional DC laser power to square of gain 24 p4169 A67-43103
Submillimeter wave laser resonator mode calculation using laser-resonator interferometry 24 p4169 A67-43105
- ### LASER OUTPUT
- High current discharge effect on magnetically confined argon laser 01 p0086 A67-10012
Optical surface roughness measurement using coherent radiation produced by helium-neon laser sigma-polarized at 6328 angstroms 01 p0020 A67-10020
Semiconductor laser array structure with common n-type substrate and individual contacts to p-layer for higher optical power output 01 p0086 A67-10023
LiF single crystal destruction as function of laser beam energy, examining dislocation pattern arising from crack propagation 01 p0086 A67-10071
Polymethylmethacrylate and polystyrene exposure to ruby and neodymium-glass laser radiation, noting appearance of EPR 01 p0086 A67-10075
Current injection effect on time delay of GaAs laser radiation 01 p0087 A67-10083
Laser producing two or three light pulses in sequence with interval between pulses mechanically controlled by optical wedge inserted into resonator 01 p0087 A67-10161
Adjustment procedure for laser with polygonal resonator, noting spatial mirror adjustment in addition to angular adjustment 01 p0087 A67-10162
Nickel-copper cone calorimeter design and fabrication for laser energy measurements 01 p0062 A67-10193
Interferences between waves diffracted by circular screens or thin wires and coherent background provided by laser, producing rings or rectilinear fringes 01 p0087 A67-10231
CW laser using 3-inch ruby crystals with 15 percent mirror transmission, pumping power of double threshold value and 1.6 watt power output 01 p0088 A67-10244
Laser action in optically pumped CN, discussing vibrational-rotational transitions 01 p0089 A67-10370
Three new visible CW laser lines in discharge in singly-ionized Cl 01 p0089 A67-10373
Diffusely transmitting integrating sphere with solid state photodiode used in laser output measurement 01 p0089 A67-10445
Ne-He laser output dependence on pressure and nonexcited atom concentration 01 p0090 A67-10512
Laser lines of pulsed discharge in iodine vapor 01 p0090 A67-10549
Interferential method of testing high resolution photographic laser as light source 01 p0091 A67-10832
Radiation of giant pulses of superluminescence by highly excited active medium of Nd glass with rapid cut-in of amplification 01 p0091 A67-10837
Thermalization rate of highly ionized plasma with initially hot ions and cold electrons, using laser scattering to observe time variation of electron temperature 01 p0125 A67-10912
Narrow beam divergent Q-switched laser pulse generation, noting output characteristics and applications 01 p0091 A67-11024
Laser lines of pulsed discharge in iodine vapor 01 p0091 A67-11057
Spatial coherence of laser light beam after extreme wavefront distortions on diffusion explained on basis of Fraunhofer and Fresnel diffraction 01 p0115 A67-11062
Fourier transform holography for diffusion of coherent laser light beam, examining distortion term in reconstructed image 01 p0070 A67-11063
Laser excited electronic Raman spectrum of trivalent Eu ion doped YGa garnet 01 p0091 A67-11084
Temperature dependence of threshold for stimulated emission of Nd trivalent ion in several host lattices estimated from intensity variation of laser active fluorescence component 01 p0091 A67-11085
Dynamical optical element characterized by variable-geometry fluid prism that deflects beam of light or electromagnetic energy 01 p0075 A67-11132
Audio frequency proportional to rotation rate of reentrant laser cavity system derived from single output beam 01 p0091 A67-11322
Laser characteristics of narrow band type I solar radio burst and magnetic dipole transitions in split Zeeman sublevels of hydrogen atoms of solar corona in ground level 02 p0322 A67-11652
Three-mirror laser interferometer measuring electron densities in repetitively pulsed plasmas 02 p0241 A67-11875
Second harmonic generations and mixings of Raman lines produced in cyclohexane, acetone, benzene and carbon disulfide, photographing first order Stokes radiation 02 p0252 A67-12052
Velocity aberration and atmospheric refraction pertaining to laser satellite communication experiments, obtaining equations for estimation of effects 02 p0198 A67-12054
Self-focusing of laser beam in plasma, solving wave equation for slab and cylindrical beam configurations 02 p0252 A67-12089
Self-focusing of ruby laser beam in NaCl crystals 02 p0252 A67-12481
Self-locking modes in argon ion laser, observing subnanosecond pulsation of laser output with wideband photomultiplier 02 p0253 A67-12503
Time evolution of laser induced fractures in glass, noting crack propagation accompanied by sparking 02 p0253 A67-12508
Hologram copying method using gas laser as light source 02 p0246 A67-12513
Pumping of organic dyes in organic solvents, using pulsed ruby laser 02 p0253 A67-12515
H-2 Stokes Raman oscillator operating at 9755 angstroms, finding performance as expected of laser oscillators with beam instability not developed 02 p0253 A67-12516
Absolute direct excitation cross section from neutral ground state for upper levels of transition in argon laser 02 p0253 A67-12520
Twyman-Green arrangement of interferometer with narrow laser beam and twin photomultipliers, examining strong shocks in argon in 15.2 cm shock tube 02 p0247 A67-12688
Ruby laser pumping threshold energy, divergence angle and output power as affected by resonator length 03 p0433 A67-12855
Statistical effects during generation of second harmonic in optically transparent crystals, noting coefficient of correlation between harmonic and fundamental radiation power of solid state laser 03 p0467 A67-12928
Giant coherent light pulse generation by Q-factor modulated laser 03 p0433 A67-12941
Ruby laser frequency conversion technique by laser beam scattering and mixing of combined frequencies 03 p0433 A67-13094
Tunable dispersion resonator and broadening of laser emission spectral range to obtain operating frequency other than fundamental 03 p0435 A67-13131
Uncoupled intensity peaks in laser emission 03 p0435 A67-13132
Emission losses in solid state laser resonator calculated for Nd glass laser 03 p0435 A67-13133
Steady state laser radiation during relaxation, discussing time-dependent spectral composition, oscillation modes and polarization characteristics 03 p0435 A67-13134
SHF modulation techniques for laser radiation, covering Faraday, Kerr and Pockel effects, circular dichroism, etc 03 p0436 A67-13138
Fluorescent emission of neodymium laser triggered by Pockels effect as function of population inversion 03 p0436 A67-13201
Performance of two-photon laser operating in continuous wave mode, deriving formula for pulse frequency 03 p0437 A67-13292
Calorimeter using enameled copper wire with variable resistance for measuring laser energy and output power 03 p0437 A67-13536
Laser beam-induced recrystallization of amorphous Ge semiconductor thin films prepared by thermal deposition on glass 03 p0498 A67-13839
Computer calculations permitting investigation of time characteristics of radiation in investigation of laser with passive cell 03 p0438 A67-13962
Polya distribution describing photon correlations in ionizing laser beams enables differentiation between various multiphoton ionization processes 03 p0438 A67-13982
Statistical distribution of AM laser signal envelope upon passage through turbulent atmosphere 03 p0438 A67-13988
Ring laser rotation sensing system, evaluating accuracy limit for minimized inaccuracy of known sources of error 03 p0438 A67-13992
Estimated greatest permissible mirror misalignment, active medium inhomogeneity, and extra-axial beam losses for artificial realization of very narrow radiation pattern in real laser 03 p0438 A67-14185
Characteristics of pulsed laser action in He-Ne and He-Ar mixtures at pressures above 200 mm Hg 03 p0438 A67-14189
Radiative power amplification of He-Ne laser with nearly confocal resonators 03 p0438 A67-14190
Temporal-spatial variation of cross sectional flux distribution of stimulated emission from Nd glass pulsed laser 03 p0439 A67-14280
Interferences between coherent light background and light diffracted by small aperture in case of strongly astigmatic beam 04 p0631 A67-14416
Optical system consisting of polarized laser beams for monitoring missile attitude during early launch phase 04 p0619 A67-14505
Trivalent neodymium doped glass laser with internal imperfections due to optical pumping examined via optical metallography, transmission electron microscopy and electron diffraction techniques 04 p0632 A67-14927
Phase locked laser loop for amplitude and phase measuring device for coherent optical wave fronts 04 p0632 A67-15076
Kinetic energies of ions produced by giant laser pulses, noting dependence of mean square ion velocity on pulse peak intensity 04 p0633 A67-15099
Neodymium-glass laser using spontaneous amplified emission in nonresonant system to obtain high brightness output pulse 04 p0633 A67-15100
Electron recombination in laser produced hydrogen discharge, noting temperature decay due to radiation, expansion cooling and electron loss 04 p0665 A67-15109
Single mode output power modulation analysis of saturation and gain of gas lasers and effects of excitation density modulation and resonator Q modulation 04 p0633 A67-15111
Pulsed lasers as machine tools for material removal, noting tests on titanium, aluminum oxide, steel, etc 04 p0628 A67-15308
Laser system for diamond piercing in wire-drawing dies and closed circuit TV viewing system for monitoring operation 04 p0628 A67-15309
Modular liquid-cooled cylindrical ruby laser microwelder design and construction 04 p0628 A67-15310
Data record and readout systems dependence on precise spot and line scan methods, using diffraction limited spots of laser generated light 04 p0623 A67-15321
Diffraction limited performance achieved for flying spot recording and readout, using concentric optical system, applied to laser scanner 04 p0658 A67-15322
Multigigawatt oscillator-amplifier ruby laser system for high temperature plasma research [ASME PAPER 66-WA/ENER-2] 04 p0634 A67-15371
Laser microprobe used to study small inclusions in metals 04 p0634 A67-15461
Population inversion variation during laser emission as shown by measurements of fluorescence intensity 04 p0634 A67-15497
Fraction of luminous energy captured by optical pumping lasers in given geometrical configuration, obtaining functioning threshold depending only on crystal 04 p0634 A67-15498
Laser guidance system for rendezvous and docking providing data acquisition for guidance computer 04 p0655 A67-15663
Performance of GaAs semiconductor laser with resonator, noting dependence of forbidden zone width and absorption coefficient on free carrier concentration and incident photon energy 04 p0634 A67-15759

Interchannel generation transfer and multichannel generation in laser with four unsplit levels, noting radiation density, temperature effect and variations in coefficients of losses 04 p0634 A67-15760

Steady state intensity fluctuations and statistics of laser operating above threshold 04 p0635 A67-15776

Nature of excited state resulting from two-quantum absorption associated with fluorescence in anthracene produced by ruby laser 05 p0814 A67-16130

Visual acuity decrement from laser lesion in fovea of stump tail macaque monkeys 05 p0756 A67-16287

Fission or radioisotopic nuclear radiation applied to laser pumping, discussing forms, sources, power, solid state and molecular gas lasers, energy transfer, optical fluorescence and cut-off phenomenon 05 p0814 A67-16547

Frequency fluctuations of laser field determined by measuring cross correlation function at two points 05 p0815 A67-16625

Semiclassical and rate equations compared for determination of output power of steady state ruby laser 05 p0815 A67-16628

Tube diameter influence on output power and efficiency of gas laser 05 p0816 A67-16629

Transient and steady state IR emission from low-lying vibrational levels of carbon dioxide in laser systems, using DC discharge 05 p0816 A67-16630

Excitation and relaxation mechanisms for closed molecular gas laser 05 p0816 A67-16631

Molecular gas laser Q-switching techniques, determining rotational collision sections for carbon dioxide and cross sections for vibrational relaxation 05 p0816 A67-16632

High resolution spectroscopy using Zeeman-tuned IR maser oscillating at transitions between 3 and 9 microns 05 p0816 A67-16633

Gas laser pumped microwave emission for producing controlled excited state population for RF spectroscopy of neon 05 p0817 A67-16638

Second harmonic generation of light by focused laser beams in nonlinear crystals at exit surface 05 p0817 A67-16640

Doppler and impact broadening of spectral lines and pressure effects on power output of gas laser 05 p0818 A67-16643

Intracavity time-varying perturbation of losses in gas laser using diamagnetic Faraday effect in glasses analyzed in connection with output intensity 05 p0818 A67-16646

Properties of self-trapped light filaments noting stimulated Raman emission and creation, containment and termination mechanisms 05 p0818 A67-16648

Self-focusing due to intensity dependent anomalous dispersion effect on electromagnetic radiation, emphasizing laser radiation in saturated amplifying medium 05 p0819 A67-16649

Positive ion emission from tungsten surfaces laser irradiated studied, using time-of-flight spectrometer 05 p0819 A67-16651

Gas dynamic equations for determination of heating, vaporization and expansion of substance due to Q-switched laser radiated collimates onto surface of solids 05 p0819 A67-16652

Output spectra of Nd doped YAG and ruby lasers, determining mechanisms responsible for observed overall linewidths 05 p0820 A67-16660

Divalence samarium ion doped calcium fluoride laser action at low temperatures obtained with giant pulse ruby laser excitation 05 p0820 A67-16661

Equation for dynamical behavior of laser, solving case of deep modulation of output, noting pulsation problems 05 p0820 A67-16662

Electron densities in helium plasma measured by laser amplifier with maximum gain and minimum bandwidth at point nearest threshold 05 p0820 A67-16663

Laser emission at 1.06 microns from ytterbium-neodymium glass, noting linearity of energy transfer with Yb concentration 05 p0820 A67-16664

CW argon ion laser scattering in argon plasma, noting resonance and correlation between data and plasma properties 05 p0820 A67-16665

Passive core fiber laser does not remove completely need for optical quality in

cladding material 05 p0821 A67-16666

Oscillation in CdS crystal by ruby laser induced two-photon excitation, noting proportionality of absorption coefficient to light beam intensity 05 p0821 A67-16667

Line width of CW Ga-As lasers measured using homodyne detection and autocorrelation 05 p0821 A67-16670

Terminal level lifetime and fluorescence line of neodymium doped glass influence on dynamics and efficiency of Q-spooled laser 05 p0822 A67-16675

Q-switched laser operation observed using liquid selenium mirror as reflector in ruby laser measuring reflectivity changes 05 p0822 A67-16679

Tunable Raman laser obtained by electron mobility subjected to magnetic field, noting threshold pump power 05 p0823 A67-16684

Single mode 6328 angstrom units He-Ne laser having single frequency power output of 50 mwatt stabilized by feedback system whose output is neither amplitude nor frequency modulated 05 p0823 A67-16685

Single mode output power modulation study of saturation and gain of gas laser 05 p0823 A67-16686

Spectrochemical analysis of solid specimen from vapor formed by laser beam and excited by spark 05 p0824 A67-16786

Object-image relationships in scattered laser light 05 p0824 A67-16792

Wavelength dependence of spectrum of laser beams traversing atmosphere 05 p0763 A67-16793

Damage in glass induced by linear absorption of laser radiation non-Q-spooled 05 p0824 A67-16794

Onset of oscillation in He-Ne laser analyzed using Lamb theory, obtaining time constant value for population of lower laser level 05 p0824 A67-16821

Threshold of parametric oscillator system with idler modes in same frequency spacing as laser pump source 05 p0824 A67-16823

Amplitude of LF oscillations in He-Ne laser 05 p0825 A67-16948

Ruby crystals grown by Czochralski technique using induction heated iridium crucible, noting laser oscillations in pulled crystals 05 p0866 A67-16975

Gaseous laser output expressed in single or two-line oscillations as function of pumping rates and transition probabilities, considering concept of equivalent network 05 p0825 A67-16979

Transient behavior of He-Ne lasers under pulsed HF excitation, discussing rate equations representing atomic population density and photon 05 p0825 A67-16980

Laser radiation effect on heating process and gas dynamic motion of finite transparent gas and motionless cold gas at vacuum interface 05 p0927 A67-17008

Laser beam effect on benzene and other organic compounds, noting formation of dark readily coagulating deposit 05 p0759 A67-17028

Submillimeter wavelength electronic devices, examining development of lasers and reflected wave tubes with overlapping effective wave range 05 p0825 A67-17168

Laser mirror design in lens form for decoupling diffraction limited parallel beam, based on theorems concerning Gaussian beam imaging and behavior 05 p0826 A67-17327

Faraday rotation measurement of trapped magnetic fields in theta pinch plasma, using gas laser beam 05 p0859 A67-17447

Operation of synchronized neodymium laser time variable reflection /TVR/ oscillator, using single pockels cell to obtain Q-switching and cavity dumping 05 p0826 A67-17525

Density and temperature of upper atmosphere, satellite tracking, geodetic applications and long distance measurements, using laser output 06 p1008 A67-17591

Time structure and amplitude self-modulation of emission from GaAs injection laser observed, using electron-optical converter 06 p1009 A67-17756

Luminescence spectrum of CuCl at low temperatures excited by double photon absorption from high intensity laser beam 06 p1010 A67-17822

Giant pulse formation theory, measuring

shape and duration of neodymium glass laser pulses for various values of inverse population 06 p1010 A67-17876

Laser displays application, performance and status of existing devices 06 p1001 A67-17887

Electro-optic intra-cavity color switching in krypton ion Fabry-Perot laser 06 p1010 A67-17888

He-Ne laser frequency stabilization using four automatic frequency control /AFC/ systems 06 p1010 A67-17965

Extension of paper on saturable absorber giant pulse lasers to include effects of finite absorber lifetime on pulse parameters, noting pump role 06 p1011 A67-18148

Plasma formed by laser pulse on tungsten target, measuring radius, temperature and radiative properties, developing model 06 p1041 A67-18149

Electron beam spatial scanning of coherent emission of GaAs junction laser at low temperatures, making current distribution nonuniform 06 p1011 A67-18150

Gas laser behavior in magnetic field, analyzing data on magnetic effect, Zeeman effect and microwave pumping 06 p1011 A67-18168

Treatment of steel with laser beam, obtaining precision holes without affecting microhardness of metal 06 p1008 A67-18234

Laser velocimeter measurement of point velocities in turbulent liquid flow in pipe, using statistical analysis to verify results [AIAA PAPER 67-179] 06 p0990 A67-18511

UV radiation generation from output of Nd glass laser by frequency doubling in ammonium dihydrogen phosphate crystals 06 p1011 A67-18712

Resonator Q-modulation technique observation of central dip tuning in modulated power output of gas laser with moving mirror 06 p1011 A67-18758

High power laser beam polarization direction effects on electron emission from Ag surface 06 p1012 A67-18759

Laser extensometer measuring small dimensional changes of specimen in tensile testing furnace at high temperatures 06 p1012 A67-18778

Pressure dependence of output power of He-Ne laser on amplitude of periodic high voltage excitation pulses 06 p1012 A67-18784

Charged particle motion in magnetic field under action of laser emission 06 p1012 A67-18787

Multiphoton ionization of krypton atom by ruby laser radiation 06 p1037 A67-18796

Dynamics of narrowing effect of surface and spatial dispersing agents on radiation line of ruby laser with nonresonance feedback 06 p1012 A67-18797

Cleavage and separation of dye-doped ice and paraffin instantaneously heated by laser pulse, measuring mechanical pulse at energy concentrations below vaporization heat 06 p1119 A67-18807

Micro- and macrocrack formation in organic glass by focusing of laser beam 06 p1021 A67-18808

RCA papers on laser research and engineering 07 p1193 A67-19079

Laser spectroscopy, discussing advantages, precision attainable, line shape and position measurements 07 p1194 A67-19087

Laser digital devices, discussing use as switching circuit in digital computer 07 p1194 A67-19088

Safety program for laser hazards, discussing eye and body protection 07 p1194 A67-19089

Microscopic hole drilling into metals by laser beams, noting energy and power correlation with hole magnitude 07 p1190 A67-19090

Changes in giant molecule structure of polypropylene films under action of laser pulses analyzed by optical microscopy 07 p1211 A67-19169

Translucent and opaque photocathodes analysis 07 p1185 A67-19408

High altitude atmospheric scattering of intense light from ruby laser beam interpreted principally in terms of Rayleigh scattering from atmospheric molecules 07 p1171 A67-19419

Kerr cell properties noting four-electrode cell giving frequency shift of 60 mc for laser beam 07 p1142 A67-19552

Spectral properties of Nd doped yttrium vanadate grown from melt, noting reduced

Stark splitting leading to laser action 07 p1195 A67-19559

Relative intensities and cascade transition ratio in CW Ar II laser near 4103.9 angstroms 07 p1195 A67-19560

Particle number fluctuation in single cell of Kastler photon set, discussing statistical properties of laser emission in multimode excitation regime 07 p1196 A67-19599

Axial magnetic field effect on Ne-He laser power output operating in regime of simultaneous generation of 3.39 and 0.6328 micron lines 07 p1196 A67-19601

Error due to multiple propagation in distance measurement by comparison of modulation phases on transmitted and reflected laser beam 07 p1186 A67-19606

Gallium arsenide laser output increase due to aluminum evaporated coating on silicon dioxide used as reflective coating 07 p1196 A67-19794

Far field pattern of sheet-like laser beam from electron bombarded CdS and ZnO single crystals 07 p1196 A67-19798

Traveling wave excitation of high power nitrogen and neon lasers with velocity matching that of stimulated emission 07 p1196 A67-20093

Time behavior of pulsed water vapor laser, noting spiking from far IR emission lines 07 p1197 A67-20095

Picosecond laser pulse widths measurement by method using special symmetry properties of second harmonic generation at GaAs crystal surface 07 p1234 A67-20097

Laser action in zinc selenide crystals at 4600 angstroms prepared under high pressure in closed container by gas phase reaction and following crystallization 07 p1197 A67-20183

Crystal deformation by electrostriction produced by laser beam 08 p1336 A67-20315

Frequency doubling of light in ruby laser due to laser light interaction with corundum lattice, anti-Stokes-Raman scattering of laser light, etc 08 p1336 A67-20316

Pulse generator for high power injection lasers at room temperature noting small size, cheapness, simplicity, and capability of switching several thousand amperes 08 p1337 A67-20372

Laser photography, discussing equipment used and shadowgraphs obtained in free flight range 08 p1330 A67-20595

Induced radiation at high photon densities, noting applicability of perturbation theory to multiphoton resonance radiation of lasers 08 p1337 A67-20823

Laser beam effect on hydrodynamic bearings, discussing microcracks and critical energy, explaining breakdowns 08 p1337 A67-20840

Laser radiation effect on metals, noting disintegration mechanism, indentation formation and vapor formation 08 p1337 A67-20856

Frequency broadening of natural oscillations of optical resonator upon interaction with two-level atom in electromagnetic field 08 p1337 A67-20868

Stimulated radiation from trivalent Nd ion doped barium crown glass fiber laser without resonator 08 p1337 A67-21203

Ruby laser irradiation by similar laser situated at right angle to first results in radiation intensity reduction of irradiated laser 08 p1338 A67-21204

Effect of load mismatch on laser output, determining nonlinear dependence of equivalent negative conductance as function of oscillation amplitude in laser resonator cavity 08 p1338 A67-21270

Laser effect on electron gas and excited state populations in xenon discharges 08 p1338 A67-21306

Stokes light generated in off-axis resonator for quantitative measurements of stimulated Raman effect in self-focusing materials 08 p1339 A67-21375

Error signal generation method to control laser frequency of laser oscillator 08 p1339 A67-21378

Wave propagation in random medium analyzed by solving stochastic wave equation with random function for refractive index coefficient and applied to laser beam 08 p1296 A67-21434

LIF single crystal destruction as function of laser beam energy, examining dislocation pattern arising from crack

propagation 08 p1339 A67-21454

Current injection effect on time delay of GaAs laser radiation 08 p1340 A67-21460

Frequency stability of He-Ne lasers analyzed by heterodyning two laser resonators 09 p1509 A67-21558

Helium-neon CW laser oscillation at 1.1523 microns observed in high velocity gas flow system, using rapid mixing of metastable helium atoms with initially unexcited neon 09 p1510 A67-21568

Laser emission from electron beam excitation of CdS crystals due to crystal uniformity and radiative transitions resulting from CD-rich growth conditions 09 p1510 A67-21569

IR laser emission at cryogenic temperatures and various wavelengths obtained from diodes of lead tin selenide and lead tin telluride 09 p1551 A67-21571

Laser interferometry and photon scattering in high temperature plasma diagnostics 09 p1536 A67-21602

Fringe counting in laser interferometers and phase quadrature signals for bidirectional counting at good efficiency without mechanical or optical complications 09 p1493 A67-21613

Calorimetric measurement of pulsed ruby laser output energy 09 p1510 A67-21615

Stimulated Brillouin scattering in liquids used for passive Q-switch applicable to visible and IR lasers 09 p1511 A67-21749

Cylindrical optics in converting laser emission into second harmonic in ADP and KDP crystals, obtaining high conversion efficiency 09 p1511 A67-21916

Polarization of waves generated by annular laser resonators of triangular shape, obtaining directions of electric field vectors 09 p1512 A67-21923

Adjustment of compound gas laser resonator provides increase of stimulated emission output without lengthening resonator 09 p1512 A67-21985

Spectral analysis of laser discharge in pure and impure He, obtaining spectra of spark at various pressures, determining electron concentration 09 p1512 A67-22010

Internal mirror reflections elimination in laser beam output intensity distribution by filtering device 09 p1512 A67-22042

Gas laser frequency and emitted power dependence on resonator tuning 09 p1513 A67-22070

Frequency stabilization of Zeeman laser, using intensity crossover region with cavity tuning between oscillations on two orthogonally circularly polarized axial modes 09 p1513 A67-22134

Laser interferometry application to detection of rotation in system by splitting light from source into two coherent beams 09 p1499 A67-22150

Small size CW He-Ne laser pumped by resonant cavity, examining current-voltage characteristics and current dependence of output power 09 p1513 A67-22170

Cross sections for excitation of upper and lower ion states by electron impact with ground state neutral argon atoms found by measuring coherent and incoherent light of laser beam 09 p1514 A67-22272

Laser sources emphasizing TV display output power needs 09 p1515 A67-22362

Apparent size and hue variations of single spot of 6328 angstrom laser light, analyzing physical correlates 09 p1515 A67-22373

Ruby laser efficiency increase, using gamma irradiation 09 p1515 A67-22430

Visual display of output patterns of IR lasers using heat sensitive phosphors 09 p1500 A67-22433

Light emission by gas under action of intense laser radiation studied by high speed high sensitivity photomultiplier 09 p1516 A67-22583

Absolutely calibrated radiometer for CW laser radiation in visible and near IR bands which relies on heat flow through standard thermal impedance 09 p1502 A67-22615

Duration and waveform of short single pulse emitted by injection semiconductor laser 09 p1516 A67-22659

Variance of log amplitude of laser beam evaluated for horizontal propagation path through atmosphere by following Schmelzter results 10 p1603 A67-22713

Triangular low filament laser diodes, considering alteration of internal reflection to achieve phase shift

phenomena 10 p1662 A67-22716

Hologram recording and reconstruction through two and three primary colors derived from gas laser 10 p1653 A67-22749

Laser variable output coupler, construction, performance and applications 10 p1662 A67-22753

Phonon lifetime variation effect on stimulated Brillouin and Raman scattering in gases by temperature, pressure and laser power variation and comparison with Stokes gain theories 10 p1662 A67-22758

Spectrum of second order Raman lines in coupling of radiation and matter, using Green function 10 p1663 A67-22855

Single frequency light from argon FM laser with external lithium niobate modulator, discussing overall conversion efficiency and distortion reduction 10 p1664 A67-22906

Laser and electron beam welding techniques, noting weld joint characteristics and tungsten inert gas arc welding 10 p1660 A67-23008

Laser generation through rare earth chelate solutions, requirements for working solutions and apparatus 10 p1664 A67-23068

Three-dimensional photography based on laser derived hologram, examining split-beam technique 10 p1655 A67-23072

Hazards of laser radiation, mechanisms, control and management 10 p1601 A67-23328

Self-focusing processes of laser pulses in dissipative medium, analyzing temporal nonlinear aberrations connected with thermal effects 10 p1664 A67-23332

Currents caused by light pressure on metal surface and in flare plasma when laser beam hits surface 10 p1664 A67-23333

Relaxation rate influence on power generation of gas laser and on magnitude of inverse population 10 p1664 A67-23335

Near field power density incident on eyes due to reflection from CW laser reduced by optical lens and shutter rearrangement 10 p1665 A67-23415

High voltage pulsed electrodeless discharge in rare gas as light source for ruby and Nd glass laser excitation and observation of output characteristics 10 p1666 A67-23565

Giant pulse generation range in transverse direction after Q-switching in ruby laser, examining resonator properties 10 p1666 A67-23584

Laser radiation generation at indirect band transitions with free carrier participation in pure semiconductor 10 p1667 A67-23654

Beam wavelength and laser intensity effect on attenuation in carbon disulfide induced by ruby laser indicate two-photon absorption 10 p1667 A67-23776

Dependence of ion energy on irradiated laser power, discussing production of ions of two discrete energies 10 p1667 A67-23793

Laser beam modulation by atmospheric turbulence as function of receiving aperture size, range and atmospheric conditions 11 p1799 A67-24236

Ruby laser output energy losses when passing from normal to passive Q-switched operation 11 p1800 A67-24241

Optical power gain characteristics of continuous wave carbon dioxide laser studied parametrically with single-pass amplifier 11 p1800 A67-24244

Compact nonresonant five-pass carbon dioxide laser amplifier structure giving small signal gains 11 p1800 A67-24245

Detectability of coherent optical signals against incoherent Gaussian background noise radiation in heterodyne receiver with laser local oscillator 11 p1800 A67-24419

Laser for remote vibration measurement and detection without mechanical contact with structure under test 11 p1798 A67-24433

Laser-produced dielectric breakdown at particle sites in liquids with resulting absorption of secondary light beam 11 p1801 A67-24560

Plasma production by ruby laser pulse irradiation of LID investigated, results suggest collisionless electrostatic shock propagation at expanding plasma ball edge 11 p1840 A67-24561

Transient emission characteristics of pulsed argon ion laser, noting capillary discharge due to radiation trapping effect 11 p1801 A67-24649

Atmosphere effects on laser beam propagation noting diameter, intensity

- amplitude and power dependence on transmitter and receiver aperture dimensions 11 p1801 A67-24665
- Transient behavior of three-level paramagnetic maser, discussing rate equations, spin-lattice relaxation, time measurement, etc 11 p1801 A67-24667
- Peak and average output power of cyanide laser in far IR measured, indicating usefulness of available oversize waveguide instrumentation at HF 11 p1801 A67-24715
- Enlarged internal laser beam projecting high contrast images generated on photochromic plate within laser cavity 11 p1801 A67-24717
- Optical configuration for long distance laser beam transmission determined from truncated Gaussian aperture distribution radiation patterns 11 p1754 A67-24724
- Power output at 119 micron in water vapor laser, noting inhibition of laser action during discharge current 11 p1801 A67-24728
- Multiply reflective laser detector diode design, showing internal reflection effect for trapping light in silicon due to large refractive index 11 p1802 A67-24737
- Optical and laser properties of trivalent Yb and Eu ion doped yttrium orthovanadate 11 p1847 A67-24739
- Detection and measurement of mm wave difference frequency between two near laser lines, using optical heterodyne 11 p1803 A67-24832
- Laser activity from terbium trifluoroacetylacetonate in p-dioxane and acetonitrile at room temperature 11 p1803 A67-24833
- Laser emission temperature dependence resulting from variation in radiationless transfer of excitation in trivalent erbium and thulium 11 p1803 A67-24836
- Superradiant transition in high gain pulsed laser 11 p1803 A67-24841
- Room temperature laser threshold reduction and stimulated emission delay in GaAs diffused junction diodes 11 p1803 A67-24911
- Laser holography combined with schlieren techniques to measure ray deviations in optically inhomogeneous field of transient phenomenon 11 p1794 A67-24927
- Central tuning dip in power output of continuous wave submillimeter molecular laser to measure radiative lifetime and collision line broadening 11 p1803 A67-24932
- Single mode He-Ne laser, noting discontinuities in power output and inhomogeneous nature of gain curve 12 p1951 A67-25147
- Fracture line formation in glass specimen as result of laser beam focusing, noting refractive index variation 12 p1951 A67-25148
- Laser beam acceleration of inhomogeneous plasma by imparting high energies to ionizing ions 12 p1969 A67-25198
- Heterodyne detector of submillimeter radiation using CN maser as continuous wave source of coherent radiation 12 p1951 A67-25209
- Atmospheric absorption problem solution, using cavity maser operating at 4 mm wavelength 12 p1952 A67-25297
- Ruby laser generation spectrum width analyzed interferometrically as function of mirror spacing and pumping power 12 p1952 A67-25325
- Water cooled mercury arc discharge lamp for room temperature optimum optical pumping of CW lasers 12 p1952 A67-25331
- Automatic photographic recording of laser output energy vs excitation energy obtained from fluorescence of ruby used to integrate laser light 12 p1952 A67-25333
- Microexplosion by optical breakdown of air in focus of laser beam, analyzing volume of concentrated plasma by measuring external magnetic field perturbation 12 p1952 A67-25336
- Laser beam effect on hardening of steel 12 p1955 A67-25372
- Positive ion production during illumination of cesium vapor-filled thermionic cell with laser beam 12 p1973 A67-25396
- Premature generation breakdown in ruby laser, noting effect of additional media on pumping level/generation time ratio 12 p1953 A67-25445
- Hypersound propagation velocity in toluene cyclohexane, acetic acid, water, etc, determined at 6328 angstrom from He-Ne laser analysis of structure of Rayleigh scattering 12 p1953 A67-25448
- Fluorescein family organic dyes exhibiting laser action when excited by ruby and neodymium second harmonics 12 p1953 A67-25748
- Spin wave interaction in YIG with acoustic, magnetoplastic and relaxation oscillations excited by laser and microwave 12 p1953 A67-25749
- Simple giant pulse ruby laser of high spectral brightness 12 p1953 A67-25984
- High temperature spectral directional hemispherical reflectance of refractory metals and ceramics measured with integrating sphere and He-Ne CW laser source [AIAA PAPER 67-300] 12 p2035 A67-28015
- Plasmoid generated by Q-switched neodymium-glass laser radiation focused on solid target, estimating plasma electron temperature 12 p1986 A67-28065
- Ionized multiwatt argon lasers, discussing relation between output power and discharge current, gas pressure, magnetic field and tube bore size 12 p1953 A67-28159
- Powerful gas lasers using carbon dioxide noting oscillation level lifetime, inversion mechanism, temperature effect, etc 13 p2125 A67-28388
- Carbon dioxide laser history, development stages, performance and applications 13 p2125 A67-28389
- Oscillation effect on power and time characteristics of ruby laser output with variable threshold ratios of axial and inner radiation modes 13 p2125 A67-28398
- Automatic cavity tuning of hydrogen masers to achieve frequency source of absolute accuracy over unlimited time periods 13 p2125 A67-28512
- Effect of multiple zinc diffusions on threshold and CW output power of semiconductor laser 13 p2125 A67-28522
- Pulsed UV laser using nitrogen noting synchronization characteristics, stability, peak power, etc 13 p2126 A67-28700
- Radio astronomical investigations of 18 cm ground state lambda doublet transition of OH suggest maser amplification of radiation takes place in interstellar medium 13 p2198 A67-28715
- Giant pulse operation of many-element laser with composite Q-switch consisting of spinning prism and saturable glass plate 13 p2126 A67-28729
- Discharge formation and propagation in He-Ne laser excited with pulsed RF voltage 13 p2126 A67-28730
- X-ray laser resonator proposal involving three-dimensional puckered ring arrangement of crystals at Bragg angle, discussing polarization losses 13 p2126 A67-27012
- Two photon stepwise absorption of low power He-Ne laser light in erbium doped yttrium oxide and lanthanum fluoride crystals 13 p2127 A67-27013
- High speed correlation technique to measure time development of width of ultrashort pulses generated by mode locked Nd trivalent ion glass laser 13 p2126 A67-27014
- Laser output pulse time dependence in acetone and nitrogen mixture, using indium antimonide detector 13 p2127 A67-27017
- Molecular laser action on vibrational-rotational transitions between low lying vibrational levels on hydrogen and deuterium halides 13 p2127 A67-27018
- Line-narrowing effect induced by laser radiation applied to measurements of isotope shifts for two optical transitions in neon 13 p2127 A67-27080
- Fabrication and operation of divalent dysprosium doped calcium fluoride laser, discussing magnetic field effects, Q-switching, cooling, etc 13 p2127 A67-27086
- Pulsed neon laser at 5401 angstroms 13 p2128 A67-27089
- Laser light deflecting methods, detailing scanlaser, laser resonator combining features of laser and cathode ray tube 13 p2128 A67-27237
- Small optical rotations in near IR measured by ring laser, discussing dynamic behavior of polarization state 13 p2128 A67-27345
- Beckmann theory on scattering applied to laser mirrors, predicting wavelength dependence of scattering profiles 13 p2129 A67-27348
- Pumping efficiency of optically pumped laser, considering electric energy conversion, absorption, etc 13 p2129 A67-27349
- Gain narrowing and saturation broadening of Doppler broadened neon line in Zeeman scanned laser amplifier 13 p2129 A67-27485
- Backscattered light intensity from laser beam for measuring atmospheric density variations, discussing optimization of sensitivity 13 p2072 A67-27609
- Long spark formation in air under weakly focused laser radiation, deriving formula for mean propagation rate of spark beyond focal field 13 p2129 A67-27628
- Diffraction losses in resonator cavity decreased by thermal deformation of neodymium-glass crystal due to pumping with periodic pulses 13 p2130 A67-27629
- Laser beam-induced recrystallization of amorphous Ge semiconductor thin films prepared by thermal deposition on glass 13 p2185 A67-27720
- Laser gas-discharge tube /without resonator/ amplification relations, considering stimulating radiation, noting application as oscillator 14 p2328 A67-27771
- P-type GaAs laser excited by Q-switched ruby laser at liquid nitrogen temperature, noting spectral shift due to Burstein effect 14 p2329 A67-27831
- Cylindrical optics in converting laser emission into second harmonic in ADP and KDP crystals, obtaining high conversion efficiency 14 p2329 A67-28245
- Polarization of waves generated by annular laser resonators of triangular shape, obtaining directions of electric field vectors 14 p2330 A67-28252
- Nomogram to predict SNR for certain laser setups 14 p2330 A67-28289
- Laser measurements and standards of energy, power, attenuation and frequency stability, using pulsed ruby and gas lasers as radiation source 14 p2319 A67-28392
- High power laser emitting monochromatic radiation at single frequency applicable in spectroscopy, telemetry and telecommunication 14 p2330 A67-28469
- Spontaneous visible light emission due to laser action in carbon dioxide laser plasma, examining plasma current change with phase-lock technique 14 p2331 A67-28494
- Competitive and cascade coupling between transitions in CW water vapor laser 14 p2331 A67-28498
- Generation mechanism of laser emission in cadmium sulfide-cadmium selenide crystals in presence of two-photon excitation at various temperatures 14 p2331 A67-28534
- Solid state lasers and pulsed ruby lasers for continuous and quasi-continuous operation, noting applications in micromachining 14 p2331 A67-28559
- Laser transition absorption cross section at room temperature for neodymium ion in yttrium-aluminum garnet determined by two methods 14 p2331 A67-28713
- Blind current density induction of double-frequency laser beam from superconducting metal 14 p2371 A67-28722
- Ruby laser with Fabry-Perot interferometer selector studied for wavelength and thermal stability control 14 p2332 A67-28759
- Microwaves and laser links for spacecraft-earth communications noting limitations by external noise effects, atmospheric turbulence, fabrication tolerances, etc 14 p2273 A67-28799
- Electromagnetic sensing of absolute rotation with self-oscillating laser version of Sagnac interferometer 14 p2349 A67-28812
- Laser technology noting applications to range finding, target illumination, tracking, welding, etc 14 p2332 A67-28818
- Effect of semiconductor glass shield temperature on absorption coefficient, output energy, pulse duration and energy and peak power of ruby laser 14 p2332 A67-28857
- 800 mm and 1265 mm optical resonator He-Ne lasers, obtaining maximum output power and application as Raman spectroscopy light source 14 p2333 A67-28972
- Stimulated inverse Raman effect, noting experimental laser setup and theory based on optical phonon emission 14 p2333 A67-28985
- Vaporization under laser radiation in terms of gas-dynamics, formulating boundary

conditions 14 p2334 A67-29074
 Electron-electron scattering in field of monochromatic laser beam, noting resonances in effective Moller scattering cross section 14 p2334 A67-29078
 Influence of higher order contributions to correlation function of intensity fluctuation in laser near threshold determined using Fokker-Planck equation 15 p2496 A67-29091
 Power output of pulse laser measured in terms of ultrasonic vibration intensity induced in piezocrystals by radiation 15 p2485 A67-29125
 Magnetic field strength effects on pulse and CW operation of large diameter ionized gas lasers 15 p2496 A67-29173
 Lasing on Si II and Cl II lines in pulsed gaseous discharge, noting possible mechanisms for achieving population inversion 15 p2496 A67-29178
 Semiconductor laser output power varied by decreasing inverse population through heating electron-hole gas by intense optical radiation 15 p2496 A67-29236
 Large screen displays for group interaction simulation noting cost factors, techniques and performance characteristics 15 p2486 A67-29302
 Neodymium activated alpha-gagarinite crystal laser, noting ternary fluoride systems characterized by optical centers 15 p2496 A67-29360
 Continuous second harmonic generation of 2572 angstrom argon II laser, noting optimum phase matching, power dependence on crystal temperature, etc 15 p2497 A67-29392
 Carbon dioxide laser output observation by high resolution thermographic screen 15 p2497 A67-29393
 Precautions required when using continuous gas flow in high current ion lasers 15 p2497 A67-29394
 Michelson interferometer with laser source analyzed for beam frequency and wavelength, refraction coefficient, etc 15 p2486 A67-29467
 Laser emission under external signal, analyzing competition between amplification mode and parasitic generation arising at resonant frequency, noting signal role 15 p2498 A67-29469
 Development of plasmoid density due to laser ionization measured using Fabry-Perot interferometer 15 p2527 A67-29474
 Giant pulse time evolution influenced by pump-induced material inhomogeneities studied by analyzing laser rate equations 15 p2498 A67-29484
 Double sapphire plate resonator to control multiple modes of commercial laser /Korad K-1Q/ without use of saturable dye 15 p2498 A67-29497
 Optical image producing method of complex ultrasonic field using light diffraction of laser beam 15 p2487 A67-29498
 HeNe laser output measured as function of axial magnetic field strength 15 p2498 A67-29512
 Laser light photon counting statistics using probability density for laser light intensity 15 p2498 A67-29513
 Generation of large pulses of extremely short duration in ruby laser by rotating mirror technique at lower frequencies 15 p2498 A67-29642
 Radiation polarization in ruby laser with resonator shaped like rectangular parallelepiped 15 p2498 A67-29701
 Absorption of laser radiation in semiconductors and mechanisms of breakdown in process 15 p2537 A67-29704
 Laser radiation control techniques using saturation filter or negative feedback circuit with resonator Q-factor depending on radiation field power 15 p2499 A67-29722
 Measurements of short term frequency or phase fluctuations of gas lasers, noting random Gaussian perturbation 15 p2499 A67-29730
 ZnS two-photon absorption spectrum to establish two-photon pumping capabilities of semiconducting crystals 15 p2500 A67-29816
 Spectral narrowing and tunability over wide spectral range demonstrated in solid/liquid dye lasers using diffraction gratings as cavity reflectors 15 p2500 A67-29817
 CW operation of ultrathin CdSe platelet laser excited optically by HeNe laser 15 p2500 A67-29821

Electronic, vibrational and rotational temperatures in laser-produced flames measured spectroscopically 15 p2433 A67-29879
 Electron density and temperature in plasma measured, using self-focused laser beams 15 p2488 A67-29902
 Laser output reduced by rare gas impurities in molecular neutral CO and nitrogen gas lasers 15 p2500 A67-29910
 Electromagnetic probing by laser, determining number densities of water, carbon dioxide and oxygen constituents of atmosphere 15 p2500 A67-29911
 Color TV laser display using Ne-He and argon-ion laser in modulation and scanning system 15 p2489 A67-29914
 Nuclear reactor use in space environment as energy source for chemical synthesis and laser action [AAS PAPER 67-115] 15 p2558 A67-29962
 Book on laser microemission spectrum analysis covering laser properties, Q-switching technique, controlled negative feedback lasers, applications, etc 15 p2501 A67-30147
 Measurement of laser frequency control characteristics of piezoelectric transducers, noting effect of mechanical structure supporting transducer on frequency control characteristics 15 p2502 A67-30426
 Output energy for ruby laser with parallel mirrors for varying excitation energies, pulse lengths, mirror reflectivities and losses due to absorption, scattering and reflection 15 p2502 A67-30427
 Electronic technique producing quadrature signal from laser feedback interferometer 15 p2502 A67-30436
 Direct lasing of conventional ruby rods requiring 200-joule xenon pump deriving energy from chemical reaction 15 p2502 A67-30437
 Laser action of ruby and neodymium glass rods in case of axicon pumping 16 p2684 A67-30460
 Rectangular light guides transfer energy from injection type semiconductor laser to laser with logic element 16 p2684 A67-30461
 Experimental results on CN laser operated with pulsed or DC discharges 16 p2684 A67-30605
 Three-level maser detector for far IR using double-quantum pumping 16 p2684 A67-30606
 Double exposure holographic formation of contour map over diffusely reflecting surface, using immersion method with liquids of different refractive indexes 16 p2670 A67-30612
 Mixed crystals with fluoride base, investigating spectrum and time behavior of laser emission for operation below room temperature 16 p2725 A67-30809
 Absorption, fluorescence and laser emission spectra of triply ionized neodymium yttrium in compound below room temperature 16 p2726 A67-30810
 Changes in length measured by tandem laser device investigating mirror separation modulation by piezoelectric materials 16 p2671 A67-30823
 Frequency measurement of gas laser transitions in heavy water and acetylene discharges 16 p2685 A67-30824
 High power argon ion laser with wall stabilized arc discharge determining laser output 16 p2685 A67-30825
 Laser radar selenodesy for ground control selection of Apollo landing sites 16 p2623 A67-30982
 Laser beam study by interferometric technique using diverging spherical comparison wave noting interference patterns 16 p2685 A67-31032
 Saturated neon absorption inside helium laser, noting output power peak caused by Lamb dip effect 16 p2685 A67-31033
 Laser characteristics of narrow band type I solar radio burst and magnetic dipole transitions in split Zeeman sublevels of hydrogen atoms of solar corona in ground level 16 p2747 A67-31067
 Photographic recording of fast moving plasma clouds during pulsed discharges in rarefied gas using Topler apparatus 16 p2721 A67-31396
 Quasi-continuous divalent dysprosium ion doped calcium fluoride laser with pyrotechnic excitation 16 p2686 A67-31484
 Ultrashort light pulses, discussing laser

modes, Q-switching pulse duration measurements, etc 16 p2686 A67-31741
 Atmosphere effect on laser beam scintillation measurements after propagating over 8 km path near ground for various collector sizes and environmental conditions 16 p2686 A67-31879
 Laser scattering from gas particles and diffuse surfaces, noting difference in intensity of speckle patterns formed 16 p2686 A67-31882
 Output power of gas laser with numerous axial-oscillation modes calculated as function of resonator length and pumping power 17 p2866 A67-31926
 French Diademe satellites power supply systems and planned laser experiments 17 p2941 A67-32232
 Interference from laser light beam superposition at single photon level, noting existence of fringes 17 p2866 A67-32277
 Effective cross section of stimulated emission, noting fluorescence band profile during laser emission 17 p2866 A67-32293
 Propagation loss dependence in laser ranging systems on meteorological visibility and target-receiver range, noting inverse-square law confirmation 17 p2812 A67-32305
 Gamma ray radiation effects on laser glasses, noting ionization and atom displacements in lattice 17 p2867 A67-32374
 Laser-energized explosive device /LEED/ for pyrotechnic device actuation noting power source, ruby laser, metallic fiber-optic conductor, missile design, etc 17 p2803 A67-32437
 Laser energy and power measurement, discussing radiation attenuation devices, measurement standards, etc 17 p2867 A67-32612
 Helium-neon laser generating simultaneously on two lines, showing pressure dependence and output radiation variation with discharge current 17 p2868 A67-32662
 Radiation kinetics of laser with resonator having lens system and low absorption nonlinear medium, showing time shift of kinetic curve 17 p2868 A67-32663
 Gaseous chemical reaction dynamics analyzed with monochromatic laser light-induced photocatalysis 17 p2868 A67-32772
 Spark produced in cell containing argon when concentrating laser beam in small volume, calculating temperature distribution 17 p2869 A67-32804
 Ionization of media, sterile plasma production, dense plasma heating and plasma trap falling, by laser emission 17 p2904 A67-32917
 Saturable organic dye absorber giant pulse lasers in limit of large absorber cross section, normalized initial inversion and relaxation time 17 p2869 A67-33055
 Carbon dioxide laser emission, discussing extension of wavelength range with carbon isotopes 17 p2869 A67-33062
 Single laser pulse generation noting high peak power, subnanosecond time duration, optical cavity length, etc 17 p2869 A67-33063
 Measuring laminar flow development in square duct using laser Doppler flow meter [ASME PAPER 67-APM-37] 17 p2861 A67-33161
 Fabry-Perot interferometer for discriminating gas laser modulation at frequencies less than Doppler bandwidth 17 p2869 A67-33294
 Potassium dihydrogen phosphate inside laser cavity to achieve HF modulation 17 p2869 A67-33297
 Many-element lasers spiking emission for Fabry-Perot and confocal geometry, including time resolved spectroscopy and far and near field patterns 17 p2870 A67-33298
 Experimental techniques in making multicolor white light reconstructed holograms, discussing signal to noise ratio, coherent light and photographic emulsion 17 p2862 A67-33299
 Ruby laser radiation transmission by Crofon plastic fiber optics 17 p2870 A67-33302
 Laser radiation generation at indirect band transitions with free carrier participation in pure semiconductor 17 p2870 A67-33335
 Laser beam slitting hologram production technique using polarization controller and birefringent prism 17 p2864 A67-33359
 Measurement of ensemble distribution of intensity fluctuations of laser radiation at

- threshold 18 p3098 A67-33522
- Inhomogeneous temperature field arising during laser welding of different materials with imperfect contact, deriving and solving heat conduction equations 18 p3053 A67-33630
- Laser oscillation cessation with strong pumping, interpreting effect as consequence of line broadening due to pumping strokes 18 p3059 A67-33726
- Pressure dependence of output power of He-Ne laser on amplitude of periodic high voltage excitation pulses 18 p3059 A67-33726
- Charged particle motion in magnetic field under action of laser emission 18 p3059 A67-33729
- Time constants of fast photodetectors measured, using mercury wetted relay and epitaxial indium arsenide diode laser 18 p3046 A67-33746
- Laser energy output measured using formed calibrated hollow sphere of thin insulated copper wire as calorimeter 18 p3046 A67-33747
- Detonative ignition induced by shock merging ahead of accelerating flame in hydrogen-oxygen mixture analyzed by stroboscopic laser-schlieren photography 18 p3153 A67-33826
- Evaporation of thin films of high melting point materials by focused laser beam and reflectance and relative transmittance in vacuum UV 18 p3059 A67-33885
- Active medium radial variation in density of neon atoms metastable level as explanation of anomalous laser oscillation 18 p3060 A67-34013
- Numerical solution of electromagnetic wave equations for semiconductor junction laser using McWhorter model 18 p3060 A67-34019
- Laser excited vibrational fluorescence measurements in carbon dioxide noting energy transfer rates, system kinetics, radiative coupling, etc 18 p3060 A67-34027
- Radiation power of He-Ne laser at 0.63, 1.15 and 3.39 microns, effect on electron concentration 18 p3060 A67-34038
- Laser heating of plasma situated in strong longitudinal magnetic field 18 p3060 A67-34041
- External corrective system significantly decreased angular radiation divergence of single pulse laser, determining effect on focal spacing of corrective lens 18 p3061 A67-34042
- Longitudinal magnetic field effect on radiation intensity of He-Ne laser operating in pulsed regime 18 p3061 A67-34043
- Relationship between axial magnetic field necessary to extinguish oscillation from Brewster-angled laser and spontaneous intensity 18 p3061 A67-34200
- Laser radiation effect on heating process and gas dynamic motion of finite transparent gas and motionless cold gas at vacuum interface 18 p3160 A67-34270
- Earth to lunar ground points measurement by lasers, describing experimental set-up, transmitting and receiving apparatus, etc 18 p3130 A67-34316
- Laser ranging using reflectors proposed for investigating lunar motion and various lunar parameters 18 p3130 A67-34317
- Design, operation, characteristics and applications of carbon dioxide lasers with DC excitation and fixed mirrors 18 p3061 A67-34350
- Multiphoton ionization of krypton atom by ruby laser radiation 18 p3083 A67-34415
- Dynamics of narrowing effect of surface and spatial dispersing agents on radiation line of ruby laser with nonresonance feedback 18 p3061 A67-34416
- Spatial amplitude of field of ideally parallel laser beam focused by optical systems with spherical aberration 18 p3061 A67-34439
- Emission statistics of nonresonant feedback laser produced by radiation scattering, showing fluctuations intensity, distribution function, etc 18 p3062 A67-34621
- Frame-camera interferogram data for Nd-doped glass rod during laser pumping analyzed through optical path length changes 18 p3062 A67-34623
- Pump radiation induced optical distortion in Nd-doped glass laser rods measured and compared to theory 18 p3062 A67-34625
- Laser driven plasma detonation waves in gases observed with Schlieren system, discussing shock wave growth 18 p3092 A67-34734
- Probability function for turbulent velocity in duct flow determined from Doppler shift of scattered laser radiation 18 p3030 A67-34752
- Photon generation threshold energy temperature dependence for gallium-arsenic epitaxial injection lasers 19 p3238 A67-34773
- Neodymium glass laser radiation investigation, using moving active body method, for spatial inhomogeneity of mode field in spectrum random structure 19 p3238 A67-34895
- Laser pulse duration effect on photonuclear processes, as affected by matter-radiation interactions, observing ionization in gases and surface photoeffects 19 p3238 A67-34897
- Two-channel single-pulse neodymium glass laser with 180 joule pulse, performance and optical features 19 p3239 A67-34986
- Gallium phosphide diode-based laser generator of nanosecond light pulse sequence, noting simulation of scintillation counter photoelectric amplifiers, Cerenkov counters, etc 19 p3228 A67-34987
- Deflected laser beam use in TV, machining, photo etching, space navigation and data storage 19 p3239 A67-35060
- Thermodynamic model for laser induced gas discharges accounting for transmitted light attenuation, plasma heating, etc 19 p3239 A67-35163
- Spark perturbation of magnetic and electromagnet fields, studying plasma-magnetic interaction and spark plasma characteristics 19 p3239 A67-35165
- Argon, deuterium and air ionization at atmospheric pressure and lower by focused ruby laser radiation, analyzing plasma spectrum 19 p3239 A67-35166
- French laser telemetry network, noting Q-switched ruby laser, Doppler effect measurement and local spatial geodesy program 19 p3182 A67-35239
- Systematic and random error effects on geodetic accuracy of results obtained by 3-station laser telemetry 19 p3182 A67-35240
- Nonlinear effects of laser radiation interaction with turbulent dense plasma, discussing wave propagation, plasma diagnostics, etc 19 p3291 A67-35385
- Transmission decrease of various aqueous solutions under ruby laser irradiation 19 p3240 A67-35420
- On-the-ground optical determination method of stratospheric aerosol particle numbers and sizes from ruby laser radiation measurement scattering 19 p3225 A67-35531
- Photoelectric recording of Raman spectra excited by ruby laser 19 p3240 A67-35546
- Monochromator for measuring spectral distribution of laser light scattered by high temperature plasmas 19 p3230 A67-35593
- FM laser frequency stabilization employing stabilization discriminant derived from residual phase variation and laser beat note 19 p3240 A67-35622
- High photon energy densities generation and concept of exponential amplifier for use as laser probes 19 p3240 A67-35692
- Thermoplastic-resin film with UV sensitive dispersed compound for carbon-dioxide laser-radiation photography 19 p3240 A67-35694
- Laser and nonlaser light transmission through atmosphere, noting no difference in propagation 19 p3240 A67-35695
- Laser mirror transmissivity optimization in high power optical cavities noting reflection coefficient selection 19 p3241 A67-35701
- Microsphere ablation in free-flight range observed by laser photography, giving shadowgraphs with density contour map 19 p3346 A67-35757
- Multiquantum photoionization applied to laser-induced breakdown thresholds in cesium and rubidium vapors 19 p3241 A67-35810
- Damping effect of HF field on instabilities occurring in form of moving striations within plasma of gas laser 19 p3241 A67-35814
- Pulsed injection laser radar for rendezvous and docking operations, giving results of test performance [AIAA PAPER 67-606] 19 p3259 A67-35997
- Spectral-line narrowing in ruby laser during standing wave field displacement with respect to active center of ruby crystal 19 p3241 A67-36023
- Laser emission from HF molecules rotational transition initiated by pulsed electrical discharge, listing wavelengths 19 p3241 A67-36103
- Effect of semiconductor glass shield temperature on absorption coefficient, output energy, pulse duration and energy and peak power of ruby laser 19 p3242 A67-36108
- Statistical probability of fractures in polymethylmethacrylate by laser radiation 20 p3473 A67-36161
- Two-photon photoconductivity in pulsed ruby laser excited cadmium sulfide, determining carrier density and density dependence on light intensity 20 p3456 A67-36164
- Pulse width of ultrashort light pulses measured by Michelson type arrangement of nonlinear optics 20 p3456 A67-36172
- Rose bengal saturable filter for production of high peak power neodymium laser pulses by regeneration switching 20 p3457 A67-36175
- Plasma production by ruby laser beam irradiation of lithium hydride particle, measuring electron temperatures 20 p3496 A67-36212
- Absorption spectra, spectral dependence of luminescence quantum output, glow curves and radiation spectra of color centers in ruby crystal 20 p3506 A67-36223
- Absorption of optical photons in molecular crystals, noting results of laser output on naphthalene 20 p3457 A67-36326
- IR spectroscopy by variable wavelength semiconductor lasers 20 p3439 A67-36354
- Isotope shifts measurement in IR with variable length laser cavity 20 p3439 A67-36355
- Multiple stimulated Brillouin scattering from liquid within Q-switched ruby laser cavity, noting changes in pulse shape, output power and spectral characteristics 20 p3457 A67-36385
- Microwave sound generation by transient heating of material surface with laser pulses 20 p3457 A67-36386
- Quasi-CW oscillation at 4880 angstrom of wide-bore AR II ion laser by plasma inductive excitation 20 p3458 A67-36387
- Sum generation of tunable two-frequency pulse output of gain-switched ruby laser 20 p3458 A67-36389
- Measurement of variation of formation time of Q-switched ruby laser as function of loop gain 20 p3458 A67-36432
- Neodymium doped calcium tungstate single crystals synthesized, obtaining continuous laser action 20 p3458 A67-36494
- Semipermanent optical memory design using laser light source, acoustic light deflector and hologram array as information storage elements for address selection 20 p3390 A67-36511
- Laser frequency control system using two optical discriminators for long and short term stability 20 p3459 A67-36519
- Photodiode holder design for ITT FW-114A high speed planar photodiode for monitoring giant pulse laser output 20 p3397 A67-36528
- Pulsar circuit for studying large signal transient response in plasma lasers 20 p3445 A67-36530
- Angular divergence of gas-laser radiation as function of output power, analyzing interaction of angular modes 20 p3459 A67-36689
- Equivalent electrical circuit model, corresponding to laser energy-level model, used to describe laser action in terms of circuit theory 20 p3459 A67-36768
- Meteorology, goals and methods, prospects for effective utilization of satellites and new techniques 20 p3480 A67-36823
- Passive Q-switching of carbon dioxide laser with cavity containing saturable absorber, noting peak power and pulse rate 20 p3460 A67-36854
- Organic dyes as broadband pulsed light amplifiers, noting input frequency relation to laser oscillation 20 p3460 A67-36855
- Quenching Superradiant high gain pulsed lasers measured for single pass gain by comparing single pass and double pass radiation intensities 20 p3460 A67-36858
- Direct excitation in argon gas from metastable state to upper laser state compared with two-step excitation 20 p3460 A67-36860

Electron-interference experiment using laser light, discussing electron wave function phase change and electron interference pattern displacement 20 p3460 A67-36999

Scintillation of ground-to-space laser beam through atmospheric turbulence 20 p3383 A67-37023

Energy band pinch effect in laser-heated GaAs, studying temperature effect on radiative recombination rate 20 p3460 A67-37106

Spectral variations resulting from thermal processes in crystals subjected to focused ruby laser beam 20 p3460 A67-37146

Device for automatic recording of laser emission and of energy of pumping pulse 20 p3460 A67-37149

Fokker-Planck equation for distribution function over laser observable values derived from quantum-mechanical laser master equation by expanding statistical operator 20 p3461 A67-37182

Laser Fokker-Planck equation transient solution in threshold region investigated for laser distribution function, mean intensity and mean squared deviation 20 p3461 A67-37183

Semiconductor laser light field amplitude equation of van der Pol oscillator derived and shown valid for optical band-to-band transitions 20 p3461 A67-37184

Electron beam deflection by standing light wave of laser shows momentum transfer resulting in Bragg relationship for reflection angle 20 p3461 A67-37185

Gas laser IR radiation hazards to eyes tested on rabbits indicates irreversible changes in cornea leading to impaired vision 20 p3375 A67-37276

High efficiency optical pumping system for crystal laser rods with application to CW output 20 p3461 A67-37290

Simultaneous oscillation in UV and IR and interaction of 1st and 2nd plus v system of bands in molecular nitrogen 20 p3461 A67-37292

Emission intensity dependence in CdS on laser excitation intensity for free and phonon-assisted exciton recombination at cryogenic temperature 20 p3461 A67-37295

Particle number fluctuation in single cell of Kastler photon set, discussing statistical properties of laser emission in multimode excitation regime 20 p3462 A67-37338

Axial magnetic field effect on Ne-He laser power output operating in regime of simultaneous generation of 3.39 and 0.6328 micron lines 20 p3462 A67-37340

Solid state laser theory and technology, describing media, pumping sources, illuminators, component elements, etc 20 p3462 A67-37547

Accurate determination of atmospheric gases spectral lines positions required for estimating atmospheric absorption coefficient of monochromatic laser radiation 20 p3462 A67-37559

Hydrofluoric acid for chemical vibration-rotation laser emission 20 p3462 A67-37564

Gas laser behavior in magnetic field, analyzing data on magnetic effect, Zeeman effect and microwave pumping 20 p3462 A67-37591

Laboratory investigation of laser emission line absorption by atmospheric gases in vacuum multiple-pass cell, obtaining data free of aerosol scattering 20 p3386 A67-37606

Multipath cell with White mirror system using carbon dioxide and molecular nitrogen gas mixture for gas laser amplifier and oscillator operation 21 p3625 A67-37854

Vibrational energy levels leading to laser oscillation in UV, noting process using Lyman discharge 21 p3638 A67-37855

Immersion effect on concentrating and increasing pump flux of laser incident on absorbing core, considering rod and sphere 21 p3638 A67-37857

Continuous wave laser ground-space-ground experiment in conjunction with Explorer XXII satellite tracking 21 p3578 A67-37858

Diffraction coefficient of open laser resonators coupled in series, discussing boundary conditions 21 p3638 A67-37864

Induced three-photon combination scattering kinetics applied to laser pumping 21 p3638 A67-37867

Rapid adiabatic cooling of gas systems for population inversion states 21 p3638 A67-37942

Injection lasers threshold current densities, emission spectra, emission polarization and power characteristics 21 p3639 A67-37943

Laser-diode impulse generator construction by four-layer diodes and thyristors supplying high current intensity short impulses to low resistance load 21 p3639 A67-37945

Nonresonant third order dielectric susceptibility coefficients of gases measured in four-wave mixing experiment to calculate harmonic radiation in laser beam 21 p3639 A67-38008

Laser interferometric measurements of electron density in plasma arc discharge at atmospheric pressure 21 p3664 A67-38017

Molecular and atomic, neutral and ion gas laser advances, noting high power CW carbon dioxide laser 21 p3639 A67-38062

Self-focusing of laser light pulses in ruby and leucosapphire crystals, noting different damage forms for fundamental and second harmonics 21 p3639 A67-38094

Far IR maser oscillators with water and deuterium oxide, presenting construction and operating characteristics 21 p3639 A67-38253

Junction temperature current dependence in CW operated gallium arsenide laser diodes 21 p3639 A67-38256

Plasma production by pulsed laser irradiation of aluminum in space chamber vacuum 21 p3666 A67-38259

Temperature effect on Ni thermal diffusivity measured using ruby laser pulse 21 p3640 A67-38262

Circular polarization in j equals i to j equals zero transition in gas laser shown due to different atomic relaxation processes rates 21 p3640 A67-38353

Spectral analysis of intensity fluctuations of laser at threshold noting confirmation of time resolution in terms of weighted sum of exponential 21 p3640 A67-38355

Angular divergence of solid state laser radiation for case of variable resonator and pump parameters 21 p3640 A67-38367

Spectroscopic investigations of emission under free generation and Q-switching conditions of mixed-fluoride crystal lasers 21 p3682 A67-38370

Laser application to high temperature research, discussing high temperature production using lasers, high temperature plasma and laser-irradiated surface particle emission 21 p3640 A67-38392

Ruby laser radiation frequency temperature dependence, observing narrow spectral width with Fabry-Perot interferometer 21 p3640 A67-38451

Solid state CW optically pumped microwave masers using divalent Tm in calcium fluoride and strontium fluoride hosts 21 p3640 A67-38454

Zinc telluride laser generation by electron-beam excitation noting high threshold values 21 p3641 A67-38458

Frequency stabilization of laser oscillator against reference laser amplifier, noting residual AM effects 21 p3641 A67-38461

Michelson interferometer with laser source analyzed for beam frequency and wavelength, refraction coefficient, etc 21 p3628 A67-38548

Laser emission under external signal, analyzing competition between amplification mode and parasitic generation arising at resonant frequency, noting signal role 21 p3641 A67-38550

Frequency stability of molecular beam laser in space environment during prolonged continuous and repeatedly interrupted operation 21 p3582 A67-38594

Strong blast waves and laser generated plasma dynamics in high pressure gas investigated using Mach-Zehnder interferometer and pressure probe measurements [AIAA PAPER 67-696] 21 p3672 A67-38725

Plasma diagnostics using self-focused laser beams, determining electron density and temperature 21 p3673 A67-38734

Velocity of sound in liquids measurement using ultrasonic interferometry and laser diffraction spectra 21 p3630 A67-38772

Premature generation breakdown in ruby laser, noting effect of additional media on pumping level/generation time ratio 21 p3642 A67-38819

Hypersound propagation velocity in toluene cyclohexane, acetic acid, water, etc,

determined at 6328 angstrom from He-Ne laser analysis of structure of Rayleigh scattering 21 p3642 A67-38820

Long spark formation in air under weakly focused laser radiation, deriving formula for mean propagation rate of spark beyond focal field 21 p3642 A67-38824

Diffraction losses in resonator cavity decreased by thermal deformation of neodymium-glass crystal due to pumping with periodic pulses 21 p3642 A67-38825

Plasma production by optical irradiation of gases and by solids, considering interaction of laser radiation with surfaces and irradiation of particles of solid material in vacuum [AIAA PAPER 66-174] 21 p3642 A67-38855

Rayleigh scattered laser light technique for point measurements of time averaged neutral gas density in turbulent wake behind hypersonic velocity body 21 p3565 A67-38876

Crystal block structure and slip plane influence on laser radiation, discussing radiation energy distribution in space and divergence determination 21 p3642 A67-38968

Laser thermal and radiation effect on metals, discussing mechanical damage 21 p3646 A67-39011

Book on optical interferometry from coherence theory viewpoint, considering wave front and amplitude division, interference spectroscopy, multiple and laser interference, etc 21 p3658 A67-39066

Displacement effects analyzed for one beam of laser streak interferometer relative to another on image intensity distribution 22 p3795 A67-39199

Thermonuclear origin of neutron emission in theta pinch plasma, determining ion temperature from scattering of ruby laser beam 22 p3843 A67-39244

Neodymium doped YAG Q-spoiled laser system for switching high voltage spark gap at 50 pps with nanosecond jitter 22 p3813 A67-39258

Operating and performance characteristics of helium-neon pulsed gas laser, discussing application to integrated microcircuits fabrication 22 p3813 A67-39333

Neodymium-glass laser amplifier gain saturation investigation using laser driving signal, discussing Schulz-DuBois steady state theory and inversion density 22 p3813 A67-39349

Relaxation times of carbon dioxide vibrational levels and afterglow pulsed gain for nonflowing gas laser amplifiers 22 p3814 A67-39354

Electron density relation to output power in He-Ne laser and magnetic field effect, using microwave resonator technique 22 p3814 A67-39428

Coherent emission observation in indium phosphide excited by injection laser at 77 degrees K 22 p3814 A67-39461

Q-switched laser use as light source for photographing droplets in spray containing fluorescent dye excited by second harmonic of ruby light 22 p3797 A67-39492

Photoconductivity in cadmium sulfide crystals induced by light from ruby laser with Q-factor modulation, showing photocurrent dependence on laser power 22 p3814 A67-39511

Anomalous nonlinear preference for circular polarization in He-Ne laser noting variation with gas pressure 22 p3815 A67-39522

Electron affinity of helium measured by analyzing energy of electrons photodetached from negative helium ions beam passing through laser electromagnetic field 22 p3815 A67-39614

Book on theory and applications of holography, mathematical analysis of process as imaging technique, limitations and partial coherence 22 p3798 A67-39633

Landé factors of neon atoms subjected to magnetic field and multimode laser irradiation measured by observing resonant saturations in fluorescent light emitted 22 p3815 A67-39651

Radiation fluctuation of single mode continuously operating laser, deriving fluctuation spectral density and emission line intrinsic width 22 p3815 A67-39738

Laser beam expansion in turbulent medium using Huygens-Kirchhoff principle and Fresnel diffraction approximation 22 p3761 A67-39739

Steady laser oscillation by Maxwell equations, with allowance for diffusion effects, shows no qualitative changes in field distribution pattern 22 p3815 A67-39759

Three-photon combination process used to increase laser emission frequency, determining laser field strength 22 p3815 A67-39760

Ruby and neodymium-glass lasers light emission mixing, noting created wave frequency is sum of two initial wave frequencies 22 p3815 A67-39765

IR laser rangefinder using neodymium doped rods, noting noise peak value and advantages over ruby laser 22 p3799 A67-39780

Laser radiation photon number and amplitude fluctuations quantum mechanical calculation by deriving two coupled equations 22 p3815 A67-39784

Attenuation of continuous and pulsed laser emission studied for various thicknesses of artificial water fog 22 p3816 A67-39921

Lasers as light source in optical telemetry, discussing laser radiation, solid state and gas lasers and critical parameters 22 p3800 A67-39981

Active medium gain required in gas laser output power calculation obtained for intermediate case 22 p3816 A67-40128

Optical technique with laser source for range measurements noting use of dispersion between two different light wavelengths 22 p3800 A67-40139

Coherent optics technology, presenting effective black body temperature of six radiation sources and output and pulse duration of four laser sources 22 p3817 A67-40351

Atmospheric density, temperature and composition altitude variation measured by satellite observation of laser backscatter Raman component 22 p3806 A67-40366

Laser output power determination technique by rotating plane parallel wafer in resonant cavity to vary value of total losses 22 p3817 A67-40412

Q-switched laser single pulse visual recording by oscillograph with storage tube/photodiode combination 22 p3817 A67-40415

Fabry-Perot etalon resonator studied for incidence angles for use as filter, test instrument and control device for laser output 22 p3809 A67-40469

Ruby rods in concentric spherical cavities observing spiking, mode structure and output energy distribution 22 p3817 A67-40485

Electronic transitions optical saturations in polyatomic organic molecules with high intensity laser radiation, discussing relation to bleaching of dyes 22 p3817 A67-40487

Near IR laser transitions in pure helium studied with scanning Fabry-Perot interferometer, determining fine structure components in upper laser levels 22 p3817 A67-40488

Laser lines observation in Freon-He mixtures in CW gas discharge 22 p3817 A67-40489

Threshold properties of CW laser oscillation at 7525.5 angstroms in DC-excited KrII discharge 22 p3818 A67-40490

Laser beam cross section variation during free space propagation and through optical systems, discussing He-Ne laser radiation 23 p4011 A67-40724

Laser light production and properties based on quantum mechanical equations, describing nonlinear interaction between radiation and matter 23 p4011 A67-40761

Laser and maser noise quantum theory emphasizing equations of motion and fluctuation problem, deriving density matrix equation 23 p4011 A67-40762

Pulsed water vapor laser single wavelength operation using three diffraction gratings to make resonator frequency-selective 23 p4011 A67-40783

Platinum wire heating in sealed carbon dioxide laser results in catalyzing effect permitting high carbon dioxide concentration 23 p4011 A67-40784

Multiple stimulated Brillouin scattering used for nanosecond high intensity pulse generation combining ruby laser with liquid cell and Fabry-Perot etalon 23 p4011 A67-40786

Carbon disulfide P-branch transitions with J equals 28 to 46 for 001-100 vibrational

transition identified as laser lines in N-carbon disulfide gas system 23 p4011 A67-40789

Laser induced damage reduction in lithium tantalate and niobate crystals, proposing mechanism to explain observed reduction 23 p4012 A67-40876

Directional characteristics in optical heterodyne detection processes including finite sources, bandwidth, random phase sources and rough surfaces 23 p4012 A67-40877

Transient interference studied for emission from pulsed ruby laser 23 p4012 A67-40883

Optical mixing of two low level signals in atomic states of He-Ne laser noting amplitude modulation of visible laser output 23 p4012 A67-40891

Laser detector using glow discharge tube current changes to measure radiation intensity 23 p4012 A67-40894

Index of refraction measurements near damage spots in KTN due to laser beam and electric field simultaneous presence 23 p4013 A67-40895

Michelson interferometer used as tunable mirror in laser resonators, obtaining internal modulation of initial intensity 23 p4013 A67-40902

Analysis of laser with selective resonator indicating stimulated emission basic characteristics determined by active medium band shape and Q-factor 23 p4013 A67-40907

Laser gyro development and application noting advantages in cooling, power, starting time and acceleration influence 23 p3999 A67-40916

Generation mechanism of laser emission in cadmium sulfide-cadmium selenide crystals in presence of two-photon excitation at various temperatures 23 p4040 A67-40941

Two-photon absorption theory extension to include vibronic mixing between different electronic states using two-photon laser excitation of polycyclic atomic molecules 23 p4013 A67-40964

Laser radiation in calibration of spectrometer scanning function by duplicating spatial coherence characteristics of radiation 23 p4014 A67-41023

Coupled linearized equations for laser-induced optical radiation instabilities in liquids and gases, obtaining differential operator and Green function 23 p4027 A67-41024

Emission wavelength selection in multicolor-emission noble gas laser using linear polarization control device 23 p4014 A67-41025

Optical system models based on gallium-arsenide laser techniques for SNR measurements 23 p4014 A67-41026

Airport glide slope visual range determination with single-ended transmissometer by measuring transmission between photosensitive detector and laser light source 23 p3999 A67-41027

Compact air-to-ground laser rangefinder onboard helicopter nose section 23 p3999 A67-41028

IR Q-switched neodymium glass laser rangefinder performance and advantages 23 p3999 A67-41029

Temperature of metal surface irradiated by giant pulse laser beam by measuring energy of emitted thermal ions 23 p4015 A67-41035

Moon-earth distance and moon-earth system astrometric parameters by laser ranging, describing artificial light reflector design 23 p4066 A67-41037

Giant pulse ruby laser having tunable two-frequency output noting spectral measurements made with Fabry-Perot interferometer 23 p4015 A67-41038

Broad bandwidth digital laser communication system utilizing pulse coded polarization modulation and binary detection including optical communication link and performance data 23 p3973 A67-41039

Laser safety - Conference, London, November 1966 23 p4015 A67-41049

Laser application as research tool and for ranging and metrology noting laser availability and performance 23 p4015 A67-41050

Lasers in ophthalmology, discussing surgery and hazards 23 p3962 A67-41051

Maximum permissible energy density

incident on retina determined for eye safety in viewing laser beam 23 p3962 A67-41052

Safety of personnel from laser hazards covering installation containment, operator screening and eye protection 23 p4015 A67-41053

Laser experiment safety procedures for protection of personnel and persons not involved in laser work 23 p4015 A67-41054

50 Hz ruby pulse laser emission, discussing power output, electromagnetic spectrum and transverse mode interaction 23 p4016 A67-41153

Second harmonic generation in Se and Te-Se using carbon dioxide laser, measuring nonlinear coefficients and synchronism direction 23 p4016 A67-41192

Emission of GaSb injection lasers in pulse regime, demonstrating existence of two staggered laser lines originating in diode regions 23 p4016 A67-41193

Hollow cathode mercury laser providing improved performance, stability and reproducibility 23 p4016 A67-41226

Energy detection of multipulse returns from optically rough target using Q-switched laser 23 p4016 A67-41265

Reactive optical information processing maximum efficiency from phase object in laser cavity, discussing modulation depth and power gain 23 p4002 A67-41270

Optically concentrated laser radiation beam properties using plane and spherical faced ruby resonators 23 p4016 A67-41322

Spectrum line observation of decay transition of structure of gas laser 23 p4016 A67-41324

Scanning laser device using modified electro-optic display tube and potassium phosphate crystal mode selector 23 p4017 A67-41393

Optical mixing process for study of polarized light in wedge shaped cells of Raman active medium 23 p4017 A67-41433

Numerically computed power outputs and efficiency of continuous room temperature ruby lasers in good agreement with theoretical model 23 p4017 A67-41465

Laser irradiation effect on semiconductor crystals surfaces using pulsed ruby laser 23 p4045 A67-41470

Laser applications in welding and machining thin film and semiconductor integrated circuits 23 p3983 A67-41765

Radiation polarization in ruby laser with resonator shaped like rectangular parallelepiped 24 p4166 A67-41771

Absorption of laser radiation in semiconductors and mechanisms of breakdown in process 24 p4199 A67-41774

IR lasers using vibrational rotational transitions of carbon dioxide 24 p4166 A67-41799

Optical Raman scattering from atmospheric oxygen and nitrogen via pulsed nitrogen UV laser light source, discussing spectral analysis of air scattering 24 p4147 A67-41883

Laser radiation model of superimposed coherent and incoherent radiation, determining statistics of photons 24 p4166 A67-41903

Thermal development method used for observing and recording laser oscillations from output of nitrogen-carbon dioxide systems 24 p4166 A67-41908

Fluoride crystals for laser applications, discussing crystal absorption spectrum 24 p4166 A67-41983

Multiphoton absorption in monatomic gases causing ionization of atom applied to plasma production by intense radiation from lasers 24 p4190 A67-42098

Electrification of single crystals of semiconductor compounds of AlIBVI and AlIIBV type after exposure to ruby laser pulses 24 p4167 A67-42164

Thick walled carbon cone calorimeter in pulsed lasers used for calibration purposes, discussing error sources 24 p4154 A67-42174

ADP electro-optic crystal in laser emission control tested in beam deflection device and Michelson interferometer modulator, noting refractive index changes 24 p4167 A67-42239

Absorption characteristics for laser power stabilization using Rayleigh active material 24 p4167 A67-42360

Second harmonic power generation associated with simultaneous application of DC fields and gas laser beams to narrow band gap semiconductors 24 p4168 A67-42364

Laser pulse compression of RF signals using Bragg scattering produced in transparent solid by ultrasonic waves 24 p4188 A67-42368

Laser emission nonlinear effects for materials with internal induced absorption noting pulse elongation and spatial smoothing 24 p4168 A67-42370

Monograph on absorption and laser radiation covering absorption coefficients, high altitude gas concentration, low extinction coefficient measurements, molecular resonance absorption, etc 24 p4168 A67-42412

Plasma discharge instability effect on gas laser operation, discussing moving layers self-excitation and laser beam modulation 24 p4168 A67-42561

Frequency and intensity of laser light analyzed for reaction of coupled optical resonator 24 p4168 A67-42574

Laser pulses producing local dissociation process in AIIIBV semiconductor compounds 24 p4168 A67-42725

Local reference beam principle for laser long distance hologram construction 24 p4158 A67-42819

Divergence angles of helium-neon laser radiation, discussing resonator with spherical mirrors with unequal curvature radii 24 p4169 A67-42891

Efficiency of optical system of solid state laser with cathode luminescence pumping 24 p4169 A67-42892

Laser-created alumina plasma ion-energy spectrum, measuring plasma characteristics with pentagrid energy analyzer 24 p4199 A67-43102

Separate studies of power and collision broadening of gas laser transition showing proportional DC laser power to square of gain 24 p4169 A67-43103

Laser-irradiated plasma theoretical study indicating absorption enhancement in external magnetic field 24 p4199 A67-43104

LASER RADAR

S LIDAR

LATERAL CONTROL

Natural trajectory optimization for lateral turn at constant height 06 p1098 A67-18865

Motion equations used in determining lateral stability and control derivatives for STOL aircraft 10 p1595 A67-23551

LATERAL OSCILLATION

Closed form solution for gliding lateral turn at constant height over flat earth of unpowered vehicle, using linearized aerodynamic coefficients 09 p1441 A67-22488

Rectangular plate under periodic in-plane edge load investigated for transition mechanisms attendant to parametric vibrations [ASME PAPER 67-VIBR-5] 11 p1871 A67-24165

LATERAL STABILITY

Lateral-directional stability equations for aircraft with nonzero product of inertial flying along steep flight path gradient 17 p2796 A67-32219

Eccentrically stiffened cylinders instability under axial compression, lateral or hydrostatic pressure and torsion 21 p3722 A67-38545

Lateral stability augmentation of supersonic aircraft using linear multichannel state-vector optimal feedback control 22 p3746 A67-40155

LATERAL STABILITY AND CONTROL

Lateral-directional flying qualities for power landing approach simulated, studying roll effects and damping [AIAA PAPER 67-577] 19 p3175 A67-35972

LATEX

SA RUBBER

Centrifugal disk photosedimentometer used for size analysis of latex emulsions 23 p3972 A67-41066

LATITUDE

SA GEOMAGNETIC LATITUDE

Latitudinal effects on satellite beacon scintillations as observed from three stations [AFRL-66-864] 03 p0406 A67-12820

Magnitude and direction for shifts in position of mean pole of earth [ASME PAPER 66-WA/APM-7] 04 p0616 A67-15225

Seasonal-latitudinal variations in lower thermospheric density, temperature and composition 10 p1639 A67-23210

Latitudinal variations of ionospheric irregularities studied via synchronous and

1000 km satellites, noting Early Bird data, scintillation index graphs, radio star signals, etc 10 p1640 A67-23234

Magnetic activity at low latitudes during IGY 14 p2309 A67-27940

Seasonal and latitudinal magnetic activity variations in Northern Hemisphere, investigating time-space characteristics of K index 14 p2309 A67-27943

Quiet sun current system effects on seasonal variations of critical frequency in E region, noting dependence on local time and latitude 14 p2312 A67-28569

Occurrence frequency of midlatitude blanketing sporadic E studied for seasonal, diurnal and latitudinal variations 15 p2476 A67-29622

Statistical correlation of latitude with time of maximum darkening of Mars dark areas, noting consistency of 2 18 p2749 A67-31401

Cosmic ray intensity, discussing modulation due to earth heliolatitude variation 17 p2932 A67-32086

Latitudinal effect on neutron-monitor data taken by Soviet ship in North Pacific, obtaining relation between coupling constant and cut-off rigidity 17 p2933 A67-32092

Coupling coefficient and latitude distribution in intensity of cosmic rays inclined component measured by Soviet ship 17 p2933 A67-32093

Primary cosmic ray spectrum changes from differential response functions and specific yield functions of neutron monitors 17 p2938 A67-32533

Hydroxyl emission at high latitudes during winter months of 1960 through 1963 measured with spectroscopy 17 p2848 A67-32955

Helium afterglow observation at high latitudes, determining He line intensity on IR spectrograph and giving time-dependent seasonal variations 17 p2849 A67-32959

Worldwide auroral morphology, discussing latitude and local time distribution and temporal variations 18 p3032 A67-33581

Geomagnetic time and latitude distribution of magnetic disturbances at auroral and polar cap latitudes 18 p3032 A67-33583

Lower thermosphere composition and mean molecular weight analyzed for diurnal and latitude effects, using mass spectrometric measurements 19 p3220 A67-35265

Graphical method predicting latitudes where satellites in circular orbit are visible, in both Northern and Southern Hemispheres 19 p3182 A67-35268

LATITUDE SENSING

Measuring methods for pole displacements and latitude variations, determining Universal Time from instantaneous pole coordinates, plotting polhody diagram 23 p3997 A67-41349

Latitude variation and motion of instantaneous pole from astronomical stations during IGY, using differential method for coordinate system 23 p3997 A67-41350

LATTICE

S CRYSTAL LATTICE

S MOLECULAR CHAIN

S SPIN-LATTICE RELAXATION

LATTICE IMPERFECTION

SA INTERSTITIAL ATOM

Localized electron states of semiconductor surface due to lattice defects, determining excited state, ground state and bonding energies 01 p0128 A67-10078

Impurity and lattice vacancy effects on compensation in doped binary semiconductors 01 p0132 A67-10455

Dielectric behavior and point imperfections of high temperature KCl in microwave frequency range 02 p0299 A67-11896

Thermal emf in plastic deformation of copper, considering effects of crystal lattice defects and lattice elastic distortions 02 p0301 A67-12740

Annealing production of acceptor defect centers in indium antimonide single crystal 04 p0683 A67-15651

Metal resistivity change due to multiple point imperfections and lattice distortions, noting aggregate effect estimation from scattering power of isolated defects 05 p0830 A67-17190

Electron paramagnetic resonance of photosensitive donors in zinc oxide with

oxygen vacancies 06 p1054 A67-18832

Etching methods to visualize lattice dislocations and grain boundaries in Czochralski grown calcium tungstate crystals doped with neodymium for laser application 07 p1196 A67-19565

Interrelation between relaxation center in tungsten and molybdenum and high temperature internal friction background of spectrum 07 p1210 A67-20010

Gap anisotropy increase in superconducting thallium transition temperature dependence on lattice defect density due to hydrostatic deformation 07 p1235 A67-20121

Temperature effect on equilibrium carrier concentrations and intrinsic lattice defects in semiconductor with self-activated conductivity, considering cuprous oxide 07 p1237 A67-20177

Spectral distribution of photoconductance and conductance glow curves of CdS single crystals after vacuum heat treatment 07 p1237 A67-20179

Elastic and inelastic lattice strain at oxide window edges determined from imperfections of n and p type 08 p1370 A67-21297

Localized electron states of semiconductor surface due to lattice defects, determining excited state, ground state and bonding energies 08 p1371 A67-21456

Occurrence, size and distribution of lattice defects in type III superconductor analyzed using electron microscopy, noting defect influence on critical current density 09 p1557 A67-22437

Aging kinetics and lattice defects in Al-Zn and Al-Zn-Mg alloys 11 p1809 A67-24947

Preferential epitaxial growth method for electrical element isolations in IC, noting no lattice defect effect on electrical characteristics of element 12 p1918 A67-26217

Structure and properties of thin films in terms of deposition conditions, noting conditions for continuity, surface roughness, grain size, lattice defect density, crystalline orientation, purity, etc [AIAA PAPER 66-727] 13 p2054 A67-27591

Triangular flux line lattices observation by electron microscope in type II superconductors 14 p2369 A67-28599

Book on mechanical properties of ordered alloys including formation of superlattices 15 p2504 A67-30028

Energy necessary for fracture shown independent of lattice defects by low cycle fatigue tests at constant true mean stress amplitude 16 p2774 A67-31318

MQST behavior under irradiation studied for defect creation and ionization, charge displacements and preexistent trap ionization 17 p2918 A67-32852

Radiation effects on carrier recombination and mobility and on lifetime of semiconductor devices 17 p2919 A67-32858

Influence of fast proton and electron irradiation on diffusion of substitution impurities in silicon 18 p3100 A67-33750

Defect interaction and diffusion zone of short gold-silver couples 18 p3064 A67-34081

Measuring IR Faraday rotation and Hall effect in 6H and 15R polytypes of silicon carbide 18 p3102 A67-34278

Lattice and junction imperfection effect on behavior of reverse biased p-n junctions, noting voltage breakdown parameters, origin of microplasma behavior, etc 18 p3102 A67-34344

Dissolution of single crystal silicon by aqueous solutions of hydrofluoric acid and chromium oxide studied as function of etchant composition 19 p3301 A67-34934

Electric conductivity variation with temperature for solid ammonium perchlorate, determining energy barrier and enthalpy of lattice defect formation and migration 20 p3377 A67-37134

Germanium and cadmium telluride edge absorption, noting lattice imperfections causing absorption coefficient increase in indirect transition region 20 p3511 A67-37143

Point defect concentration in GaAs determined from lattice constant 21 p3685 A67-38970

Interstitial oxygen solubility in niobium using X-ray diffraction, micrographic and thermal techniques, discussing lattice structure 22 p3823 A67-40209

Surface superconductivity in dilute Ta-Nb alloy ascribed to decrease in mean free path

due to lattice defects 23 p4036 A67-40657

LATTICE POINT
Cluster variation method based on W-shaped cluster in triangular lattice for lattice-gas liquid, phase-separating binary alloy and Ising model 23 p3971 A67-40969

LATTICE VIBRATION
Current-carrier scattering in germanium telluride 01 p0129 A67-10097
Lattice vibration spectra and energies of two-phonon summation bands and reststrahlen bands in gallium arsenide phosphide single crystals 03 p0495 A67-13514
Adiabatic harmonic unitary transformations and relation between electron trapping energy and normal lattice modes associated with F center ground state 03 p0495 A67-13515
Phase and amplitude fluctuation of gas and solid state lasers, accounting for noise caused by pumping, incoherent decay, lattice vibrations and atomic collisions 04 p0632 A67-14949
Neutron diffraction in ordered nickel-manganese alloys with near equilibrium distribution of atoms over lattice points 05 p0863 A67-16758
Ruby laser-induced effect of pulsed pressure on KDP crystal surface and thermal bulk effect on excitation of ultrasonic oscillation in crystal 08 p1337 A67-20417
Book on IR spectroscopy covering molecular spectroscopy, lattice vibrations, semiconductor electronic effects, IR detectors, far IR, etc book on IR spectroscopy covering molecular spectroscopy, lattice vibrations, semiconductor 08 p1353 A67-20762
Electron temperature variation in polar indium antimonide with dominant optical scattering 09 p1552 A67-21672
Excitation of potential LF electromagnetic waves in electron-hole plasma of solid body for negative volt-ampere characteristics of carrier current 15 p2537 A67-29702
Multiphonon relaxation in neodymium doped lanthanum chloride, determining transition rates between stark levels with lifetime and quantum efficiency measurements 16 p2728 A67-31057
Operator for spin-phonon interaction between conduction electrons and polarization-induced longitudinal oscillations of semiconductor lattice 18 p3099 A67-33697
Absorption spectra of rare earth trichlorides with trivalent Pr, observing vibronic transitions noting assignments of phonon branches 22 p3840 A67-39435
Far IR spectra and space group of crystalline hydrazine and hydrazine-d4 noting coupling of translational and librational motions 23 p4048 A67-41532
Excitation of potential LF electromagnetic waves in electron-hole plasma of solid body for negative volt-ampere characteristics of carrier current 24 p4199 A67-41772

LAUE DIFFRACTION
Structural properties of Si anodic oxide layers studied by X-ray analysis, using Laue photograph method 21 p3681 A67-38360

LAUNCH
S AIR LAUNCH
S LUNAR LAUNCH
S ORBITAL LAUNCH
S PRELAUNCH TESTING

LAUNCH COMPLEX
Mobile launch concept for Apollo/Saturn V lunar landing mission, discussing structural composition, functions and performance of launcher [AIAA PAPER 67-247] 07 p1165 A67-20065
Space flight technology developments, particularly for booster rockets and space vehicles 14 p2393 A67-27873
Space center under construction in French Guiana for launching rocket probes and satellites with aid of Diamant booster, discussing optical sites, storage tanks, LOX factory, etc 18 p3019 A67-33652
Indonesian space center, describing radar and optical tracking systems, launch complex telemetry system, etc 19 p3207 A67-35234

LAUNCH SITE
Rocket launching site in Sweden operated by ESRO for studies of polar auroras and polar cap absorption 03 p0395 A67-13498
Minuteman missile site selection and investigation program, considering field reconnaissance, data compilation and formulation 05 p0787 A67-16607

Model testing for design evaluation of major components and configurations of static test and launch facilities, noting hot jet model [AIAA PAPER 67-237] 07 p1165 A67-20060
Wind compensation system at Kagoshima Space Center, University of Tokyo, consists of radar system for obtaining wind data and method for finding launch angle compensation 08 p1314 A67-20542
Aeronautical research in India, precision instrumentation design and production development, facilities, rocket launching station, etc 11 p1885 A67-24653
French space program /1966-1970/ techniques and installations for satellite launching and tracking 14 p2409 A67-28605
Soviet northern cosmodrome location determination from data obtained through radio/visual observation of Cosmos satellites 18 p3004 A67-34358
Space research in Brazil, discussing rocket launching facility, meteorological experiments, X-ray astronomy, satellite observations, etc 19 p3320 A67-35285
Prelaunch checkout in 1970s, discussing vehicle subsystems, prelaunch requirements and operations and launch site technology 20 p3415 A67-36579
U.S. launch operations techniques emphasizing launch site testing prior to launch [AIAA PAPER 67-889] 24 p4140 A67-43002

LAUNCH TIME
Launch-on-time probability, showing dependence on initial countdown reliability and cumulative percentage of failures [AIAA PAPER 67-271] 07 p1260 A67-20080
Launch-on-time capability performance measuring for Surveyor 08 p1413 A67-21528
Launch-on-time probability, showing dependence on initial countdown reliability and cumulative percentage of failures [AIAA PAPER 67-271] 21 p3712 A67-37808
Launch time prediction with mathematical appendix [AIAA PAPER 67-906] 24 p4244 A67-43013

LAUNCH VEHICLE
SA ATLAS AGENA LAUNCH VEHICLE
SA ATLAS CENTAUR LAUNCH VEHICLE
SA ATLAS LAUNCH VEHICLE
SA BOOSTER
SA CENTAUR LAUNCH VEHICLE
SA DIAMANT LAUNCH VEHICLE
SA ELDORADO LAUNCH VEHICLE
SA MISSILE LAUNCHER
SA NATIONAL LAUNCH VEHICLE PROGRAM
SA RECOVERY LAUNCH VEHICLE
SA SATURN I LAUNCH VEHICLE
SA SATURN IB LAUNCH VEHICLE
SA SATURN V LAUNCH VEHICLE
SA SATURN LAUNCH VEHICLE
SA SCOUT LAUNCH VEHICLE
SA THOR LAUNCH VEHICLE
SA TITAN III LAUNCH VEHICLE
SA TITAN LAUNCH VEHICLE
Fixed service tower for flight preparation, buildup and servicing of launch vehicles [SAE PAPER 660705] 01 p0050 A67-10598
Computer display and control system for launch vehicle test operation 01 p0050 A67-10672
Computational method for determination corridors of launch vehicle trajectory and impact dispersions [AIAA PAPER 66-483] 02 p0325 A67-11941
National space inventory of launch vehicles, spacecraft, space station studies, facilities and projected modifications evaluated for USAF low earth orbital logistics [AIAA PAPER 66-866] 03 p0519 A67-14017
Soviet 10 million lb thrust booster in manned lunar flight 03 p0519 A67-14099
Environmental test program for third stage of European launch vehicle 04 p0595 A67-14570
External damper effectiveness in attenuating vibration of launch vehicle near launch umbilical tower 04 p0598 A67-15248
Wind variability effect on impact point of launch vehicle with reference to range safety at Western Test Range [AIAA PAPER 67-187] 06 p0980 A67-18323
Replacement of chemical launching rockets by advanced propulsion system, with particular reference to nuclear rocket 07 p1242 A67-20264

German papers on space research with satellites and space probes, Volume 1, Physical principles and methods of constructing carrier rockets 07 p1260 A67-20265
Spin rate effect on stability and transient response of vehicle treated by root locus technique 08 p1405 A67-20507
Passive separation system for APL spacecraft providing despin, solar blade unfolding, yaw of injection rocket, battery elimination, etc 09 p1571 A67-22061
Launch vehicle development in reusable and airbreathing configurations 09 p1572 A67-22674
Launch vehicle preparation and firing, discussing instrumentation, missile safety and range operations 10 p1622 A67-23001
Solid propellant rocket motor for third stage of satellite launcher, performance requirements and design 10 p1698 A67-23483
Advanced structures and materials in future launch vehicles evaluated by design synthesis technique for component weight reduction, equivalent payload gained and cost ratio 10 p1723 A67-23699
Saturn IB flight test loads, comparing measured and calculated bending moment, noting launch time wind profile 10 p1713 A67-23734
Motion equations for planar simulation of flexible Saturn IB launch vehicles under in-flight winds using Appell equation, noting sloshing mode 10 p1713 A67-23750
Flight Load Survey program, written in Fortran IV, for accurate and rapid sounding of wind-induced loads on aerospace launch vehicle [AIAA PAPER 66-470] 13 p2212 A67-26820
Axial vibration /pogo stick effect/ of Titan II, as Gemini launch vehicle, studied by analog computer simulation for instability influences 14 p2394 A67-28086
French installations for space research, describing laboratory work and industrial investments for satellite launching 14 p2320 A67-28606
Satellite launch vehicle performance analysis based on velocity requirements and gravity and drag losses for applications to booster configurations 14 p2394 A67-28701
Near term reusable rocket launch vehicle concepts 15 p2566 A67-29831
Long term study for prediction of launch vehicle costs, emphasizing estimate accuracy and application of statistical analysis 15 p2568 A67-29847
Land recovery of launch vehicles, applying intersecting pressure vessel theory for shaping of tanks and hinged tail panels 15 p2569 A67-29852
Trends in technology for reusable launch vehicles 15 p2569 A67-29854
Structural technologies applicable to future large launch vehicles 15 p2569 A67-29855
Flight control requirements of reusable launch vehicles 15 p2570 A67-29857
Propulsion and vehicle systems for commercial exploitation of space, emphasizing transportation to and from earth orbit [AIAA PAPER 67-82] 15 p2570 A67-29949
Future interplanetary unmanned space missions, examining velocity requirements and launch vehicle and payload sizes necessary for scientific investigation of solar system [AIAA PAPER 67-29] 15 p2562 A67-30104
Structural dynamic load and instability problems in launch vehicles and spacecraft in lunar exploration emphasizing reliability, crew safety and mission success 16 p2654 A67-30677
Inertial guidance system for ground-to-ground ballistic missiles or space vehicle launchers 16 p2700 A67-30799
Launch vehicle performance and engineering trade-off, considering mass fraction, weight reduction, specific impulse, losses and stage selection 16 p2762 A67-31489
Initial weight prediction of single and multistage launching vehicles by coordinating practical and theoretical aspects 16 p2762 A67-31490
Optimal feedback control calculation for launch vehicle synthesizing optimal controller with sensitivity constraints to reduce trajectory dispersion 16 p2763 A67-31679
Wind variability effect on impact point of

launch vehicle with reference to range safety at Western Test 19 p3207 A67-34834

Range 19 p3207 A67-34834

Launch vehicle, payload size, velocity requirements, etc, for probes exploring solar system and near interstellar space 19 p3323 A67-35330

Vostok launch vehicle design characteristics evaluated including performance, propellant weights, booster phase burning period, etc 19 p3334 A67-35843

Optimal payload lifting and nonlifting trajectories of winged boost-launch vehicle [AIAA PAPER 67-558] 19 p3335 A67-35955

Linear optimal control technique for flexible-booster control system design, showing drift minimum model with matrix transformations for closed-loop dynamics 19 p3336 A67-35988

Manual optimal guidance scheme using predictive display applied to launch vehicles during boost for continuous generation of predicted fuel-optimal trajectory 19 p3259 A67-35989

Post-Saturn launch vehicle, discussing multipurpose, variable payload boosters, usability, noise levels, etc 20 p3533 A67-36613

Wind profile criterion for structural design of launch vehicles, representing wind statistically by bivariate-normal distribution function 21 p3712 A67-37813

Electronic equipment in space booster, considering test methods, environment simulation and electronic packaging 21 p3592 A67-38229

Launch vehicles of post-Saturn class noting requirements for launch facilities at Kennedy Space Center 21 p3608 A67-38808

Two-channel control system for programmed roll of rapidly rotating carrier rocket, analyzing efficiency 22 p3898 A67-39175

Unmanned probe and launch vehicle selection for solar system exploration, considering tradeoffs in terms of reliability, cost, weight, experimental accuracy, etc 22 p3900 A67-39617

Base flow characteristics and thermal environment of launch vehicles with strap-on solid rocket motors 22 p3902 A67-39939

Launch vehicle response in lateral vibration modes to nonstationary random transonic buffeting 22 p3907 A67-40167

Load and response design values determination by statistical method for structural systems such as launch vehicles, considering discrete forcing functions 22 p3907 A67-40178

Solid propellant space propulsion technology covering developments in missiles, launch vehicles, fabrication and range of application 22 p3869 A67-40334

Systems planning for transportation of large launch vehicles and spacecraft noting land transporter and seagoing barge used for Apollo booster 23 p4070 A67-40584

Wind profiles properties application to launch vehicle design and operation, emphasizing wind shears and turbulence effects on vehicle dynamic response 24 p4242 A67-42918

Vehicle flight readiness review, technique for assuring maximum probability of mission success [AIAA PAPER 67-888] 24 p4140 A67-43001

Booster recovery systems development, payload and operational costs evaluated using postulated space program [AIAA PAPER 67-909] 24 p4245 A67-43016

Data analysis methods for integrated data processing system for onboard in-flight checkout for launch vehicle evaluation [AIAA PAPER 67-911] 24 p4127 A67-43018

LAUNCH VEHICLE CONFIGURATION

Saturn V Mobile Launcher configuration, design and testing 02 p0228 A67-11840

Optimal design configuration for third stage of European launching vehicle 02 p0334 A67-12376

ELDO-PAS configuration consisting of fourth-stage addition to three-stage Europa I launcher, with apogee motor integrated in satellite, for telecommunications 06 p1093 A67-17557

Launch vehicle parameter design for optimal support of communications satellites 06 p1093 A67-17678

Aerospacecraft, reusable self-contained man-rated vehicle, noting economy, propulsion system and possible

configurations 06 p1098 A67-19022

Optimal stage sizes and trajectory for multistage launch vehicle determined by various techniques 07 p1259 A67-19972

[AAS PAPER 66-113]

Feasibility and design study of unguided solar orbital launch vehicle 08 p1404 A67-20493

High energy booster and upper stage combinations for space research, discussing mission capabilities, cost factors, reliability, etc 08 p1412 A67-21075

Nonlinear programming model for launch vehicle design and costing 12 p2013 A67-26193

Optimal stage sizes and trajectory for multistage launch vehicle determined by various techniques 13 p2214 A67-27529

[AAS PAPER 66-113]

Effect of payload weight, density and type on performance and design of reusable launch systems 15 p2568 A67-29841

Russian rocket hardware exhibited in Paris noting Vostok launcher 22 p3899 A67-39523

LAUNCH WINDOW

Launch vehicle ground system constraints including launch window, launch-on-time influence, turnaround time after scrub, backup vehicle operations, earth-launch emergency requirements [AIAA PAPER 67-285] 07 p1256 A67-20053

Guidance, navigation and two phases of targeting of Saturn V lunar landing mission, analyzing launch, boost to orbit and iterative guidance 17 p2881 A67-32057

Digital computer simulation of orbital launch window problem for departure-trajectory analyses [AIAA PAPER 67-615] 19 p3329 A67-36004

Computer program for calculating optimal launch windows for orbiting satellites 19 p3190 A67-36071

LAUNCHING

SA CATAPULT

SA SATELLITE LAUNCHING

Dynamical and statistical approach to range safety problems, noting impact-density function of space vehicle destruction at early launch stage [AAS PAPER 67-45] 15 p2572 A67-30113

Launching efficiency of PE-20 and PM-11 modes in dielectric-loaded trough waveguide excited by dielectric-loaded rectangular waveguide 19 p3194 A67-35514

Launch operations optimization for mission planning through analysis of performance data from past programs 20 p3532 A67-36557

Gemini booster launch photographic recording with 50 cameras collecting engineering data and motion pictures of prelaunch, launch and postlaunch 22 p3807 A67-40372

LAUNCHING DEVICE

SA GUN LAUNCHING DEVICE

SA MISSILE LAUNCHER

SA ROCKET LAUNCHING DEVICE

High altitude balloon soundings, noting balloon construction parameters 01 p0010 A67-10934

Free flight hypersonic wind tunnel testing technique noting pneumatic launcher, data acquisition and processing 10 p1822 A67-23390

High speed linear bearing to take launch uploads in aircraft-launching steam catapult 12 p1948 A67-25328

Sailplanes with self-contained launching apparatus noting minimum performance, motor propulsion and auxiliary equipment 22 p3744 A67-39303

Launcher for trapped surface waves over ice-covered sea by ferrite loaded horn device 22 p3763 A67-40306

Light gas gun model launching technique with advantages of aerodynamic and mechanical methods of sabot stripping 23 p3988 A67-41751

LAUNCHING FACILITY

Facilities, ground handling and transport equipment for Titan III ITL system [SAE PAPER 660706] 01 p0050 A67-10599

Saturn V ground support instrumentation systems, emphasizing launcher umbilical tower /LUT/ 01 p0051 A67-11117

Mobile launch concept of Launch Complex 39 in which mobile launcher and crawler transporter are used to transport vehicle from vehicle assembly building to launch site 02 p0228 A67-11837

Space launch facilities, discussing site plan, zoning and development of John F.

Kennedy Space Center at Merritt Island 02 p0228 A67-11838

Dragon rocket probe, launch history and flight modifications 03 p0517 A67-13028

Integration, testing and launching of flight hardware for Apollo/Saturn V space vehicle at Kennedy Space Center [AIAA PAPER 66-837] 03 p0397 A67-14126

Launch operation requirements for manned space flight in 1970s [AIAA PAPER 66-865] 03 p0397 A67-14130

Space age facilities - ASCE Conference, Cocoa Beach, Florida, November 1965 05 p0786 A67-16606

Minuteman missile site selection and investigation program, considering field reconnaissance, data compilation and formulation 05 p0787 A67-16607

Manned lunar launch area site selection and planning, considering safety hazards, spaceport zoning, instrumentation, interference control, community relations, etc 05 p0787 A67-16608

Saturn V mobile launch facility design, discussing vertical assembly of space vehicle on launch platform, transfer to launch pad, automatic checkout and remote control of launch operation 05 p0788 A67-16616

COSPAR manual on establishment of rocket launch facility 06 p0979 A67-17553

Mobile Aerobee Launch Facility /MALF/, noting applications to space science 08 p1314 A67-20544

Umbilical carriers and quick-disconnect facilities of Saturn V ground support equipment noting location, ejecting methods, etc 09 p1484 A67-22038

Launching missiles safely from advanced marine systems 10 p1821 A67-22769

Launch vehicle preparation and firing, discussing instrumentation, missile safety and range operations 10 p1622 A67-23001

Launch operations requirements for future space programs [AAS PAPER 67-37] 15 p2467 A67-30109

Von Karman gas dynamics counterflow facility for simulating model high velocities and altitudes of reentry conditions 16 p2655 A67-31261

Italian space-research activities /1966-1967/, discussing San Marco 2 satellite project 19 p3321 A67-35295

Digital computer test program for automatic checkout of Saturn launch vehicles allowing manual intervention 20 p3391 A67-36574

Launch vehicles of post-Saturn class noting requirements for launch facilities at Kennedy Space Center 21 p3608 A67-38808

European rockets characteristics and launch firing ranges, discussing rocket probes for near-earth and space environments 21 p3714 A67-39049

LAUNCHING PAD

Effect on protective coatings of launch pads of exhaust products, chamber pressure, nozzle diameter, etc, from aluminized solid propellant rocket motors [AIAA PAPER 66-972] 02 p0304 A67-12294

Effect on protective coatings of launch pads of exhaust products, chamber pressure, nozzle diameter, etc, from aluminized solid propellant rocket motors [AIAA PAPER 66-972] 17 p2928 A67-32064

Rocket launching pad exhaust deflector investigated for uncooled efflux deflectors design data, calculating heat transfer coefficient and stagnation temperature 19 p3207 A67-35520

LAVA

SA MAGMA

Similarity between Icelandic lava field photographs and Luna IX lunar surface photographs 23 p4065 A67-40954

LAVAL NUMBER

Gas flow of two-phase medium in Laval nozzle in presence of small particle lags in velocity and temperature in one-dimensional formulation 03 p0349 A67-12865

Compressibility effect on characteristic curve of axial-flow compressor stage, using simplified assumptions and loss-free cascade flow 03 p0353 A67-14307

Similar solution of compressible laminar boundary layer equations for Laval nozzle flow contour 13 p2049 A67-26639

LAW

S CAUCHY LAW

S CLOSURE LAW

S CONSERVATION LAW

S FOURIER LAW

- S HOOKE LAW
S INTERNATIONAL LAW
S KEPLER LAW
S KIRCHHOFF LAW
S NEWTON SECOND LAW
S OHM LAW
S REGULATION
S SCALING LAW
S SIMILITUDE LAW
S SPACE LAW
S STEFAN-BOLTZMANN LAW
S STOKES LAW
S STRESS-OPTIC LAW
S WEBER-FECHNER LAW
- LAYER
S BARRIER LAYER
S BOUNDARY LAYER
S D LAYER
S E LAYER
S EKMAN LAYER
S F LAYER
S FLAT LAYER
S ISOTHERMAL LAYER
S MONOMOLECULAR LAYER
S PLASMA LAYER
S SHEAR LAYER
S SHOCK LAYER
S STRATIFIED LAYER
S SUBSTRATE
S SURFACE LAYER
S TRANSITION LAYER
C CIRCUIT
- Synchronous phase LC oscillator 03 p0378 A67-13290
Transistor hybrid equivalent circuit of large amplitude sinusoidal voltage used in design of LC oscillators, power amplifiers, etc 03 p0387 A67-13998
Transient cut-off processes of transistorized switch with LC load 05 p0773 A67-16460
Combination of approximations method for natural oscillations in circuit containing p-n junction capacitance and nonlinear inductance 05 p0777 A67-17237
Continuous high resolution measurement of solid propellant burning rate using resonant LC circuit [AIAA PAPER 67-69] 06 p1072 A67-18450
Oscillatory process stability in n-circuit transistorized LC oscillators with inductive feedback 06 p0972 A67-18894
Inductorless band pass filter to prove validity of hypothesis that all inductors in LC filter can be replaced by gyrator-capacitor equivalents 07 p1154 A67-19615
Topological properties of networks containing resistors, capacitors, self-inductors and controlled current generators 07 p1162 A67-20200
LC smoothing filter in rectifier for pulse supply source stabilized by pulse width modulation 10 p1611 A67-22980
Cauer polynomials forming procedure suitable for synthesis of LC ladder filters without mutual coupling, giving design procedure of Cauer filter 15 p2452 A67-29935
Plasma conductivity measurement, applying Fishbeck nonperturbing method 17 p2896 A67-32165
Thin film circuits for narrow band radar receivers, discussing manufacture of inductors, capacitors and LC resonant circuits 21 p3589 A67-37917
Continuous high resolution measurement of solid propellant burning rate using resonant LC circuit [AIAA PAPER 67-69] 21 p3688 A67-38857
Transistorized LF LC filter with positive and negative feedback, analyzing circuit to increase Q-factor and narrow passband 22 p3772 A67-39869
- LEAD
SA ELECTRIC LEAD
Amplitude dependent attenuation in normal and superconducting lead for ultrasonic determination of superconducting energy gap 01 p0135 A67-10916
Radial distribution analysis of films of Pb-12 percent Bi and beryllium in metastable phases prepared by low temperature condensation for electron diffraction tests 01 p0137 A67-11061
Pion energy transmission during inelastic interaction of cosmic particles with Pb nuclei 02 p0315 A67-12756
Extreme variations of electronic effective mass with temperature cannot lead to satisfactory explanation of specific heat anomaly in superconducting lead 04 p0676 A67-14934
Absorption spectra of Te, Sn, Pb, PbTe and SnTe at various energy ranges, noting role of wave functions involved in absorption by d-electrons 04 p0681 A67-15295
Anisotropy of energy gap in superconducting Pb analyzed using superconductive tunneling 07 p1236 A67-20137
Critical fields in strong coupling superconductors, using Ginsburg-Landau equations 19 p3303 A67-35042
Temperature and frequency effects on amplitude-independent longitudinal ultrasonic attenuation in superconducting lead 19 p3304 A67-35536
Lead abundance in sun computed from measurement of Pb lines equivalent widths 19 p3331 A67-36087
Flux line lattice and laminar magnetic structure of mixed state in type II superconductors consisting primarily of lead 21 p3681 A67-38351
Lead 206/lead 204 vs lead 207/lead 204 plots for young mantle-derived volcanics support upheaval predicted by lunar capture hypothesis 22 p3881 A67-39554
Pion energy transmission during inelastic interaction of cosmic particles with Pb nuclei 22 p3876 A67-40258
Electromagnetic showers in lead recorded with ionization calorimeter, discussing cascade curve 24 p4221 A67-42870
- LEAD ALLOY
Photovoltaic effect in p-n junctions of lead tin telluride diodes indicate potential for IR detection throughout 8-14 microns atmospheric window 02 p0221 A67-12514
Magnetic properties of second kind superconductivity of indium-lead alloys as function of temperature down to 0.38 degrees K 05 p0864 A67-16893
Response of superconducting sheath state of lead-indium in AC and DC magnetic fields studied, noting transition changes response of superconducting sheath state of lead-indium in AC and DC magnetic fields studied, 12 p1985 A67-25847
Electron-phonon interaction and phonon spectrum observed for electron tunneling measurements in fcc alloys of Pb alloys, noting electron concentration changes 13 p2175 A67-26426
- LEAD COMPOUND
Electron diffraction structural studies of lead bismuth selenide systems 01 p0136 A67-11009
Ferroelectric properties and morphotropic phase boundary in phase diagram of ternary system of compounds of lead, titanium and nickel 03 p0498 A67-13704
Lead azide and pentaerythrite tetranitrate explosion triggered by laser radiation 07 p1195 A67-19315
IR laser emission at cryogenic temperatures and various wavelengths obtained from diodes of lead tin selenide and lead tin telluride 09 p1551 A67-21571
Dielectric and electro-optic properties of lead magnesium niobate, noting second order ferroelectric transition 11 p1803 A67-24834
- LEAD OXIDE
Quenching examination of phase equilibrium in system lead oxide-titanium oxide-zirconium oxide, determining isotherms lines, melting points, etc 12 p1986 A67-26188
- LEAD SELENIDE
Preparation temperature and condensation rate effect on current carrier mobility in lead selenide and telluride films 01 p0128 A67-10089
Thermal and electrical properties and width of forbidden bands of PbTe and PbSe from 90 to 800 degrees K 12 p1986 A67-26094
- LEAD SULFIDE
Sublimation technique applied to high mobility PbS and CdS thin film deposition under ultrahigh vacuum equilibrium conditions 11 p1847 A67-24738
Electrical and photovoltaic properties of PbS-Si heterodides 12 p1980 A67-25180
Space charge layers on surfaces of lead sulfide photoconducting film noting Hall coefficients 24 p4204 A67-42363
- LEAD TELLURIDE
Preparation temperature and condensation rate effect on current carrier mobility in lead selenide and telluride films 01 p0128 A67-10089
Powder metallurgy techniques for thermoelectric materials particularly lead telluride, germanium bismuth telluride and zinc antimonide 01 p0099 A67-10709
Hall coefficient variation with substrate temperature of thin films of tellurium, lead telluride and antimony 01 p0138 A67-11231
Semiconducting properties of lead telluride thin films, analyzing electron transport phenomena 02 p0294 A67-11756
Photoconductivity resonances and recombination radiation in PbTe and InSb due to multiple photon interband transitions between Landau levels in high intensity magnetic fields 02 p0254 A67-12522
Hall effect in semiconductors containing two species of current carriers, p-type PbTe and GeTe, taking into account temperature dependence of energy gap 03 p0489 A67-13148
Cyclotron absorption in n type lead telluride with wide range of carrier concentrations, showing increase in transverse effective mass and decrease in anisotropic mass ratio 03 p0493 A67-13352
Composite valence band in p-PbTe obtained from measurement of Hall effect, thermoelectric and optical effects 05 p0868 A67-17062
Current carrier scattering mechanism in PbTe determined from ratio of electric conductivity and Wiedemann-Franz ratio 05 p0868 A67-17067
Interaction between helicon waves and drift currents in layered lead telluride structure 07 p1232 A67-19555
Solar thermoelectric flat plate generator application to auxiliary power systems for incident solar fluxes from 130 to 1000 watts/square ft 08 p1286 A67-20737
Pinning fluxoids by spatial inhomogeneities of Ti-Pb and Pb-In alloys, noting I-H characteristics and type II superconductor resistance 09 p1558 A67-22135
Double valence band and thermoelectric properties of lead telluride-tin telluride solutions 10 p1688 A67-22848
Hall effect in semiconductors containing two species of current carriers, p-type PbTe and GeTe, taking into account temperature dependence of energy gap 10 p1689 A67-23097
Forbidden band structure of PbTe and electrical conductivity and Hall effect measurements at high temperatures 12 p1983 A67-25513
Scattering mechanisms and role of interelectron collisions in n-Pb-Te and certain other semimetals analyzed by concentration dependence of mobility and thermal EMF 12 p1983 A67-25514
Thermal and electrical properties and width of forbidden bands of PbTe and PbSe from 90 to 800 degrees K 12 p1986 A67-26094
Hall coefficient, electrical resistivity and Seebeck coefficient of p-type lead telluride measured, using two-valence band model 14 p2367 A67-28520
Variable composition samples method for preparation of lead telluride semiconductor films by vacuum deposition 14 p2372 A67-28823
Composite valence band in p-PbTe obtained from measurement of Hall effect, thermoelectric and optical effects 15 p2538 A67-29793
Current carrier scattering mechanism in PbTe determined from ratio of electric conductivity and Wiedemann-Franz ratio 15 p2539 A67-29798
Forbidden band structure of PbTe and electrical conductivity and Hall effect measurements at high temperatures 18 p3103 A67-34444
Scattering mechanisms and role of interelectron collisions in n-Pb-Te and certain other semimetals analyzed by concentration dependence of mobility and thermal EMF 18 p3103 A67-34445
PbTe thin films vacuum-vaporized onto amorphous or oriented substrates studied for crystallographic properties as function of deposition temperature, film thickness, etc 19 p3304 A67-35422
Resistance and Hall effect measurements on PbTe thin films prepared by vacuum evaporation on amorphous or oriented substrates 19 p3307 A67-35795
Piezoresistance effect measurement in PbTe single crystals, obtaining coefficients for principal valence band through hydrostatic and uniaxial stresses in several

crystallographic directions 21 p3683 A67-38389
Carrier concentration dependence of thermoelectric power and Hall mobility of undoped and doped lead telluride explained by two-valence model 22 p3857 A67-39490

LEAD TITANATE

Ultrasonic flow meter for directly measuring average stream velocity using sing-around velocimeter with piezoelectric ceramics 10 p1656 A67-23079

LEAD TUNGSTATE

Stolzite and scheelite single crystal dielectric constant 20 p3505 A67-36179

LEADING EDGE

SA SHARP LEADING EDGE

Hypersonic flow over blunt flat plate with surface mass transfer 01 p0007 A67-11180
Rarefaction parameter for planar bodies with sharp leading edge and tip defining hypersonic boundary of strong interaction regime 01 p0007 A67-11182
Leading edge blowing effects on pressure distribution of half-cone body with 75 degree sweep angle, obtaining normal and axial forces and pitching moments 02 p0178 A67-12225

Aerodynamics of slender wings executing simple harmonic oscillations and having leading edge separation 03 p0352 A67-13894
Boundary layer measurements of friction losses due to finite thickness of leading edges of turbine blades 03 p0353 A67-14306
Quasi-conical supersonic flow around lifting system with curved leading edge 05 p0749 A67-16843

Hypersonic flow in compressed layer between tapered blunt leading edge of wing and internal shock wave forming in front when nonuniform flow moves past, considering expansion plane 06 p0936 A67-17733

Flexible wings for hypersonic vehicles allowing for safe controllable landings, stressing leading edge parawing concept, flow visualization, lift-drag ratio, etc [AIAA PAPER 67-200] 07 p1258 A67-19440

Quasi-conical motions applied to theory of wings with curved leading edges 07 p1128 A67-20235

Antisymmetrical thin delta wing with flow separation at subsonic leading edge 07 p1128 A67-20236

Hypersonic rarefied gas flow past plate with sharp leading edge, determining rarefaction effect on induced pressure distribution and value 08 p1278 A67-20924

Vortex separated delta wing leading edge in supersonic flow, noting effect on pressure distribution and role of flow equation 09 p1438 A67-22496

Airflow past wing profile with leading edge slot blowing foreign gases, noting schlieren photographs of flow patterns and concentration distribution measurement 10 p1589 A67-22724

Sub-or supersonic wing leading edge in unsteady supersonic flow, presenting discontinuities in vibration modes and calculating wing stress forces 10 p1590 A67-22879

Matched asymptotic expansion for singular pressure loading behavior for oscillating wings or control surface edges 10 p1593 A67-23712

Refractory materials for hypersonic vehicle leading edges 10 p1670 A67-23723

Method of characteristics used in solving nonlinear boundary value problem of thickness of delta wing with transonic leading edge 13 p2049 A67-28646

Lighthill uniformization technique applied to singular perturbation problems using Lagrange expansion 14 p2346 A67-29059

Flow turbulence on leading edge of attachment line of swept wing studied in wind tunnel 16 p2589 A67-30618

Flow around thin delta wing under supersonic conditions, considering flow separation at leading edges 19 p3170 A67-35542

Influence of sweptback wing leading edge geometry on boundary layer instability using supersonic flat plates 23 p3928 A67-41247

Hypersonic wave rider flow and aerodynamic problems, discussing shaping, leading edge cooling and supersonic combustion propulsion 23 p3929 A67-41251

High lift characteristics of various aircraft configurations in wind tunnel model using different leading and trailing edge lift augmentation devices 23 p3934 A67-41309

LEAKAGE

Safety problems during loading and reduction of leakage hazards in management of liquid propellants including cavitation, oscillation and zero-g migration 04 p0703 A67-14604

Leakage measurement, resolution and accuracy of leak detection unit and theoretical and practical minimum leak detectable 04 p0556 A67-15630

Sensitivity increase in leak detector by using grid to eliminate residual gas from scattered ions 04 p0625 A67-15631

Helium leak detector characteristics and reception specifications 05 p0804 A67-16302

Leak current, friction and heat-transfer coefficients of compressible laminar boundary layer on insulator wall of MHD channel with anisotropic conductivity 06 p1043 A67-18673

Satellite sealed subsystems individual leak rates in thermal-vacuum environment measured with mass spectrometer 12 p1921 A67-25690

Propellant leakage degradation of multilayer insulation system of cryogenic storage tank 13 p2186 A67-27654

Hermetically sealed semiconductor device tested for leaks with xenon 133 gas, determining radiation safety measures for personnel 14 p2324 A67-28280

Terminology associated with hermetically sealed devices in terms of specification inconsistencies, backfill gas requirements and leak rate considerations 16 p2683 A67-31728

Magnetic bottles leakage in fusion reactors, describing differences between microinstabilities and MHD theories 16 p2724 A67-31865

Metal-to-metal seal for separable joints /Bobbin seal/ utilizing elastic and plastic responses of seal structure and interface 17 p2864 A67-31993

Testing for leak-proof encapsulation of semiconductor devices by use of krypton 85 as radioactive tracer gas 17 p2823 A67-32297

Leakage current on insulating walls in MHD channel calculations, evaluating variable electrical conductivity in plasma boundary layer plasma boundary layer leakage current on insulating walls in MHD 18 p3088 A67-34061

Optical instrument for measurement and control of tube flares in connections in liquid propulsion systems 18 p3054 A67-34366

Leak detection methods in vacuum devices including compressed air, discharge tube, halogen tracers, radioactive krypton, pressure rebuild, etc 20 p3443 A67-36474

Electromagnetic shielding effectiveness of enclosure determined by measurement of perpendicular magnetic field along conducting wall surface, emphasizing continuity of seams 20 p3404 A67-37640

MOSFET gate breakdown nondestructively determined by measurement of leakage component 21 p3598 A67-38574

Electronic flat-pack processes covering sealing methods, material combinations, leakage determination, etc 21 p3634 A67-38621

Leakage rate due to meteoroid penetration of single and multiple hulled spacecraft, discussing effect on internal pressure 24 p4251 A67-42928

LEARNING

SA CONDITIONED RESPONSE

SA MACHINE LEARNING

SA MEMORY

SA TRAINING

Ability of hypothermia-adapted rats to learn and perform at low body temperature 20 p3373 A67-37669

Reinforcement intervals /RI/ effect in paired-associate learning using within-subjects, noting error dependence on RI 21 p3576 A67-39100

Short term memory of paired associates studied using continuous technique, noting recall as function of number of interpolated pairs 22 p3750 A67-39318

Recall of two messages of equal word number presented with words of one message sequentially alternating with other 22 p3754 A67-39587

LEARNING SYSTEM

Convergence theorems for sequence of expected values or random variables of stochastic learning process with time-dependent probabilities 01 p0104 A67-10280

Learning control system seeking optimum point of bimodal static characteristics by polynomial conjecture 01 p0048 A67-11236

Monograph on system philosophy of automatic learning systems in application to autopilots, discussing man-aircraft system cybernetics, human behavior, environmental effects, etc 02 p0186 A67-12084

Compound statistical decision theory for pattern recognition based on Bayes conditional probability 02 p0208 A67-12164

Automated learning methods used to design fault diagnosis procedures 03 p0400 A67-14217

Learning and self-learning in automatic control, noting quantitative aspects of information theory, solution algorithms and convergence criteria 04 p0592 A67-14905

Learning machines used for classifying measurement data of objects representable as points in n-dimensional space after training by forced learning 10 p1654 A67-22757

DC-9 training program using classroom responder system and programmed-type learning aids 13 p2064 A67-27261

Digital computer application to direct control of system dynamics and implementation of adaptive/ learning loop 15 p2441 A67-30266

Input/output model of system with finite settling time, using error correcting technique employed in pattern recognition 15 p2460 A67-30314

Identification techniques with stochastic computers for advanced automatic control systems in form of learning machines 15 p2441 A67-30344

Learning in unknown stationary environment using stochastic approximation, discussing Bayesian interference, pattern recognition, automatic control and statistical communications 18 p3070 A67-33497

Learning control systems, discussing adaptive time, searching, strategy, teaching, association, principle and behavior 22 p3776 A67-39412

Pattern recognition model as self-learning algorithm noting Nagy and Shelton scheme 24 p4137 A67-42821

LEAST SQUARES METHOD

Least squares gradient method for boundary value and optimization problems found in flight mechanics and astrodynamics 02 p0260 A67-12372

Dynamic system with unknown parameters identified through iterative and least squares methods suitable for computer programming 03 p0392 A67-13658

Transfer function parameters of stationary controlled plants in identification problem estimated, using Laplace transform and least squares method 05 p0782 A67-16319

Estimation problems in determining even zonal harmonics of external geopotential from secular satellite motion, examining least squares method validity 05 p0797 A67-16573

Limitations of method of least squares in terms of quality of estimates it provides in geodetic measurements 06 p1022 A67-17715

Computer program for digital exact representation of spectral frequency-and intensity-distribution by superposition of Gaussian components, applying least squares method, linearizing normal equations and analyzing observational errors 06 p0965 A67-18069

Error determination for transient heat transfer experiments using least squares method 06 p1024 A67-18389

Approximate solution of integral equations with aid of least squares for steady motions of viscous incompressible fluid in rotating cylinder 07 p1168 A67-19217

Data smoothing, signal processing and exact minimum mean square error procedures 07 p1218 A67-20267

Incremental and cumulative methods for analysis of diameter-frequency relation for craters, with special application to moon 08 p1385 A67-20932

Maximum errors of polynomial approximations defined by interpolation and least squares method 08 p1349 A67-21262

Damped least squares method for kinematic synthesis of plane curves described by paired coordinates for four-bar linkage mechanism [ASME PAPER 66-MECH-13]

Least squares methods for calculating stability derivatives of aircraft from unsteady flight data 09 p1438 A67-22474
Instrumental accuracy of missile range instrumentation systems, discussing error sources, detection and correction 10 p1605 A67-23002
General problem of least squares solved using method of Lagrange multipliers 10 p1674 A67-23003
Law of propagation of covariance in matrix form obtained from least squares adjustment 10 p1674 A67-23004
Heat equation of thin closed cylindrical shell exact solution analyzed using least squares method 12 p2034 A67-25606
Book on space-time relations of stellar positions on celestial sphere, detailing long focus astrometry, emphasizing mathematical principles 13 p2199 A67-26933
Nonlinear correction method for determining orbital parameters of space vehicle, using residuals and least squares technique 14 p2384 A67-28127
Parameter estimation in automatic control systems using statistical techniques such as likelihood, Markov and least square estimates 15 p2460 A67-30311
Dynamic model parameter estimation using method of generalized least squares 15 p2462 A67-30326
Linear algebraic equations arising from least squares estimation problem, noting Gaussian elimination process on matrices 16 p2647 A67-31651
Span loading on wing of complete aircraft configuration determined, using segmented wing in wind tunnel test technique and least squares method [AIAA PAPER 66-768] 17 p2834 A67-32576
Least squares method for heat problems and approximate similarity law covering orthogonal expansions and compatibility between contradictory requirements 18 p3071 A67-33752
Transfer function parameters of stationary controlled plants in identification problem estimated, using Laplace transform and least squares method 18 p3017 A67-33870
Linear least squares filtering of distorted images, stressing turbulent atmosphere effect 18 p3047 A67-33882
Lunar physical libration constants derived on basis of four series of heliometric observations, studying ellipticity, inertia, mean radius elimination, etc 18 p3134 A67-34534
Bang-bang control using adaptive-predictive model applied to least-square error trajectory control of settling-time nonlinear systems 19 p3199 A67-34784
Artificial earth satellite orbital element accuracy, describing least squares method of choosing time intervals for reducing errors 20 p3523 A67-36825
Geometric satellite triangulation for position of fourth satellite, with position equations solved by least squares method and applied to geodetic satellites 20 p3429 A67-36890
Nonlinear sequential estimation problem from noisy measurement data using nonstatistical least squares formulation, obtaining approximate solution to two-point boundary value problem 20 p3410 A67-37319
Nonlinear fluid mechanical systems design using numerical least squares method in fitting second order differential equation to straight line approximation of state variable 20 p3366 A67-37368
Optimal wave path parameters determined by experimentally recorded pulsed signals processing, using least squares method 21 p3580 A67-38120
Position fix and range data techniques for preliminary orbit determination for lunar satellites, using least squares method for data smoothing 22 p3879 A67-39310
Atmospheric opacity and extraterrestrial radio source intensity related by improved Taylor series technique using least squares method [JPL-TR-32-1115] 23 p4062 A67-40733
Least squares deconvolution technique for reducing Fabry-Perot spectrometer data to Voigt profiles 23 p4002 A67-41262
Distributed model for photovoltaic cell via nonlinear least square techniques, discussing p-n silicon cells 23 p4046 A67-41487
Mathematical methods for incorporating

thermodynamic data into least squares fit 24 p4177 A67-42083
Isotope ratios of fission and spallation xenon in meteorites from abundance data analysis by least squares method 24 p4238 A67-42886
LEBESGUE THEOREM
Fourier convergence of Lebesgue integrable functions 07 p1215 A67-19473
LECLANCHE BATTERY
Lanthanide salts replacing lithium salts in Leclanche cell electrolyte, noting good capacity over widened temperature range 22 p3748 A67-40228
LEE WAVE
Physical model of turbulence used in developing forecasting scheme of clear air turbulence /CAT/ over mountains [AIAA PAPER 67-184] 06 p1026 A67-18298
Mountain lee waves, comparing wavelengths observed on satellite pictures with calculations assuming wind speed increase with height 21 p3655 A67-38578
LEG
Leg volume changes in response to lower body negative pressure due to blood redistribution 23 p3955 A67-41619
LEGAL LIABILITY
Property damage caused by sonic booms, discussing recovery of damages under Federal Tort Claims Act 05 p0930 A67-16772
International factors in air transport under treaty establishing European Economic Community [SAE PAPER 670231] 12 p2040 A67-25491
Lawful concept of heavenly bodies 12 p2042 A67-26138
Legal problems of space research connected with telecommunication and meteorological activity 12 p2042 A67-26142
Resolutions of Institute of International Law and UN give state international responsibility for space activity 12 p2043 A67-26145
Legal status of space objects according to different criteria noting international rights, obligations and jurisdiction 12 p2043 A67-26146
Legal status of space vehicles, nationality /unilateral decisions/ vs internationality /multinational operation/ 12 p2043 A67-26148
Juridical regime of craft and space installations 12 p2043 A67-26149
Nomenclature applicable to juridical norms regulating outer atmosphere and space activities 12 p2043 A67-26150
Legal and political aspects of international meteorological data collection and distribution system, including use of satellites 12 p2044 A67-28153
Aviation insurance characteristics, types of policy in force and regulations applying under internal law 14 p2409 A67-28933
Legal aspects of use of satellites in exploiting earthbound or near-in natural resources 19 p3349 A67-35641
Legal and financial problems in obtaining airline tickets for third persons 20 p3555 A67-36300
Medicolegal problems in aircraft flight accidents and traumatic mechanisms 21 p3575 A67-38508
Legal problems associated with telecommunications and meteorological satellites and with launching and retrieval of manned spacecraft 24 p4257 A67-42387
LEGENDRE FUNCTION SERIES
Legendre series solution to contact problem of torsion of elongated ellipsoid of revolution under arbitrary torsional loading 03 p0530 A67-14199
LEGENDRE POLYNOMIAL
Legendre polynomial form of slender body motion in spherical coordinate systems generalized for axially symmetric harmonic functions in three dimensions with validity for Helmholtz equation 11 p1812 A67-24310
Nonrelativistic theory of rotating configurations in terms of gravitational potential, center mass density and variable angular velocity 14 p2382 A67-27833
Optimal control problem solving by Legendre polynomial expansions and relating function sequence correspondence approximated by finite nonlinear programming 23 p3983 A67-40647
Expressions for angular distribution function of electrons at various depths in cascade showers with given primary particle energy 24 p4221 A67-42872
Equilibrium angular distribution function

computer calculations for cascade particle numbers in iron and lead reveal dependence on primary particle energy 24 p4221 A67-42873
LEGENDRE TRANSFORM
Induced magnetic moment and surface fields of ideal superconducting torus in uniform magnetic field calculated using Legendre functions 11 p1850 A67-24918
Book on theory of energy transfers and conversions including thermodynamics and Legendre transform 20 p3484 A67-36650
LEIDENFROST PHENOMENON
Theoretical dimensionless correlation for vaporization times of drops in film boiling on flat plate in Leidenfrost state 04 p0734 A67-15850
Antimatter and cosmology 11 p1858 A67-23994
Relative velocity effect on vaporization times and heat-transfer coefficients of water drops in Leidenfrost film boiling on heated rotating wheel [AICHE PAPER 32] 20 p3552 A67-36833
LEM
S LUNAR EXCURSION MODULE /LEM/
LENS
SA CONTACT LENS
SA LUNEBERG LENS
SA VISUAL ACCOMMODATION
SA WIDE ANGLE LENS
SA WIRE GRID LENS
Inexpensive carbon dioxide molecular gas laser using plano-concave eyeglass lenses 01 p0090 A67-10827
Mass spectrometer resolution improved by variable focus at any arbitrary ion current through three-element unipotential lens 02 p0248 A67-12700
Negative lens property responsible for reconstruction of original scene in full three-dimensional reality 03 p0420 A67-13676
Light absorption in transparent materials measured using thermal lens method 03 p0439 A67-14395
Geometrical light rays in lens-like media and derivation of differential equation 06 p1033 A67-18534
Wave front reconstruction imaging technique for hologram production of aerial image of lens 07 p1188 A67-19787
Gas lens focusing of light beams, using highly transparent gas with weakly varying refractive index to guide coherent transmission with small losses 07 p1188 A67-19789
Thinned aperture computed lens /TACOL/ of hard point demonstration array radar /HAPDAR/ phased array radar system 08 p1315 A67-20679
Focal distance of lens controlled digitally using electro-optics 10 p1653 A67-22750
Point holograms, reconstituting wavefronts from high quality lenses and mirrors and use as optical elements for replacing lenses in optical systems 18 p3048 A67-34194
LENS ANTENNA
Waveform coefficient variation F-matrix analysis of electromagnetic wave propagation in light waveguide with gas lens, considering field distribution and impedance analogy 01 p0026 A67-11237
LENS DESIGN
SA OPTICAL CORRECTION PROCEDURE
Laser mirror design in lens form for decoupling diffraction limited parallel beam, based on theorems concerning Gaussian beam imaging and behavior 05 p0826 A67-17327
Imaging properties of gas lens, discussing ray trajectory, ray matrix lens formula, optical transfer function, etc 09 p1498 A67-22083
Light beam waveguide using lens-like media with periodic hyperbolic temperature distribution, discussing construction, optimum design and operating conditions 10 p1606 A67-23066
Rare earth metal superconductive shielded magnetic lens for focusing high energy electrons 11 p1802 A67-24765
Electron lens with hyperbolic field configuration designed to focus or modulate electron lenses, noting hyperbolic application to electron guns 14 p2276 A67-27768
Ultraviolet camera lenses for space flight use discussing techniques for testing and evaluating performance 16 p2680 A67-31805
Lens arrays use in holograms 17 p2860 A67-32619
Radiation kinetics of laser with resonator

having lens system and low absorption nonlinear medium, showing time shift of kinetic curve 17 p2868 A67-32663

Afocal field corrector for astronomical telescopes with paraboloidal mirrors 17 p2862 A67-33296

External corrective system significantly decreased angular radiation divergence of single pulse laser, determining effect on focal spacing of corrective lens 18 p3061 A67-34042

Optical glass selection for design of double-lens objective for IR region of spectrum, considering aberrations 20 p3451 A67-37157

Differential geometry and vector analysis used to design axisymmetric lens of arbitrary shape for observing phenomena in arbitrary flow field of revolution 21 p3610 A67-37810

Surveyor variable and fixed focal length TV camera lenses, discussing zoom lens design criteria, focal plane shutter and color filter wheel 22 p3807 A67-40375

Optics for Queen Elizabeth II telescope noting design, tolerance, quartz mirror and test procedures 23 p4001 A67-41257

LENTICULAR BODY

Martian clouds analysis and topographical relationships, discussing white and yellow classification and frequency of occurrences 18 p3124 A67-34156

LEONHARD STABILITY

Stability criteria of Leonhard-Michailov and Nyquist for polynomial 06 p0973 A67-17626

LEONID METEOR

Micrometeoroid sampling with Luster sounding rocket during Leonid meteor shower, detailing contamination control program 04 p0699 A67-14966

Aerobee rocket measurement in sampling of micrometeoroid debris during peak of Leonid meteor shower 10 p1707 A67-23237

Contamination control program developed for investigation and elimination of contaminant particles from 1965 Leonid Meteor Shower micrometeoroids collected by rocket payload 23 p3986 A67-40850

LEPTON

Lifetime of atomic state against decay induced by lepton coupling, estimating neutrino power radiation and astrophysical implications 11 p1821 A67-23959

LES

S LINCOLN EXPERIMENTAL SATELLITE /LES/

LESA

S LUNAR EXPLORATION SYSTEM FOR APOLLO /LESA/

LEUKOCYTE

SA BLOOD GROUP

Hematological criteria of chronic acceleration stress and adaptation 23 p3953 A67-41587

LEWIS NUMBER

Convective heat transfer measurements for partially dissociated carbon monoxide and hydrogen with high Lewis number [ASME PAPER 65-WA/HT-27] 03 p0537 A67-14012

Diffusion flame stability criteria for one-dimensional model at unity Lewis number 13 p2221 A67-26260

Burning in unmixed reactants for high enthalpy inviscid flow of opposed streams studied for one-step reaction model and Lewis-Semenov number unity 20 p3554 A67-37132

LIAPUNOV FUNCTION

Liapunov second method applied to elastostatic stability, discussing applicability of Dirichlet principle and Galerkin method 01 p0181 A67-10647

Liapunov second method in treating system stability 01 p0107 A67-10967

Steady motion stability of heavy homogeneous body of revolution on absolutely rough horizontal plane 01 p0115 A67-10992

Liapunov method application to adaptive loop redesign, using differential equations for model system errors coupled with squares of parameter differences 01 p0045 A67-11202

Optimal nonlinear feedback control derived from quartic and higher order performance criteria 01 p0046 A67-11206

Low order model to determine approximate time optimal switching function

for given plant in stability analysis of predictive control system 01 p0046 A67-11207

[AFOSR-67-1339]

Asymptotic stability of nonlinear systems, noting application to systems with control and Liapunov function 01 p0048 A67-11318

Quadratic performance criteria for discrete control systems, using Liapunov matrix equation and digital computer program 02 p0225 A67-12074

Stability in the sense of Liapunov, Poincare, Lagrange and others for dynamical systems 02 p0268 A67-12502

Liapunov function of ninth order system represented by differential equation which, in phase variable form, can be represented by matrix equation 03 p0392 A67-13682

Pulse amplitude range estimated for which PWM system is asymptotically stable, using method of Murphy and Wu 03 p0393 A67-13983

Second order autonomous differential equation stability and boundedness obtained, using computing algorithm based on tracking function method 03 p0376 A67-13987

Liapunov stability of gyroscope motion, with Cardan suspension center moving over earth surface 03 p0424 A67-14179

First order differential equations with homogeneous right sides to construct Liapunov function and stability behavior 03 p0462 A67-14257

Suboptimal policies for fuel optimal control and energy optimal control problems for linear time invariant system obtained, using Liapunov functions 04 p0590 A67-14418

Combined effect of aerodynamic and gravity torques on stability of motion of passive satellites investigated by Liapunov direct method 04 p0704 A67-14827

Book on qualitative behavior of trajectories of system of differential equations characterizing rate of growth of solutions by Liapunov indices 04 p0645 A67-15011

Format method for generating Liapunov and scalar functions for autonomous and nonautonomous systems 04 p0593 A67-15415

Liapunov method for estimating statistical averages of randomly perturbed system 04 p0647 A67-15740

Solution to external biharmonic problem for simply connected region bounded by Liapunov curve given in form of Fourier series and applied to elasticity theory 05 p0908 A67-16041

Liapunov matrix equation solved by introducing skew symmetric matrix 05 p0835 A67-16950

Stability of finite connection of linear passive time-variable circuits demonstrated by Liapunov second method 05 p0785 A67-17300

Liapunov theory of stochastic stability, discussing use to obtain information about random trajectories 06 p0974 A67-17931

Permanent axes of rotation for gyrostat under influence of forces depending only on position of gyrostat 06 p1002 A67-18041

Attitude stability of spinning rigid symmetric satellite in elliptic orbit examined for motion about equilibrium position with spin axis normal to orbit plane [AIAA PAPER 67-124] 06 p1095 A67-18312

Liapunov function for motion stability of solid body on earth surface having fixed point and internal gyro 06 p1004 A67-18619

Model reference adaptive systems having linear processes and models of same form and order synthesized by Liapunov second method 07 p1160 A67-19196

Stability of model reference control systems determined by direct Liapunov method 07 p1160 A67-19197

Model reference control systems design using Liapunov synthesis 07 p1162 A67-20203

Topological analysis of local stability and instability of nonlinear periodic RLC network based on Liapunov theorems 08 p1308 A67-20320

Transient response of autonomous nonlinear systems examined using Liapunov function, obtaining time constant 08 p1310 A67-20341

Generalized Zubov formulation from Liapunov function of limit cycle behavior in third order nonlinear systems 08 p1311 A67-20345

General dynamical system in metrical space, extending Liapunov method to analyze stability properties by using single Liapunov functional 09 p1532 A67-21661

Synthesis of optimal Liapunov-Bellman function, noting sequential solution method for independent variables and method using first order partial differential equation 09 p1525 A67-22077

Linear hyperbolic equations describing one-dimensional wave propagation, with stability conditions by harmonic analysis and second Liapunov method 09 p1533 A67-22400

Liapunov theorem extension to onto mappings in compact sets 10 p1673 A67-22850

Liapunov stability theory applied to control system, noting stability of function and stochastic differential equations 10 p1620 A67-23422

Stability of linear integro-differential equations for processes with distributed parameters 10 p1681 A67-23667

Liapunov-Schmidt method combined with topological method show secondary flows formed after stability loss 10 p1734 A67-23673

Singular characteristics of dynamic systems with steady state motion, noting effect of constantly acting small perturbations 11 p1818 A67-24147

Liapunov stability of motion of heavy rigid body with fixed point moving along spherical surface 11 p1818 A67-24163

Dynamic programming and Liapunov function for optimization of systems employing digital controllers 11 p1770 A67-24210

Motion of arbitrary gyrostat in central Newtonian force field, applying Liapunov stability conditions for regular precession 11 p1791 A67-24683

Finite time stability of system trajectory under perturbing forces and within specified regions of state space 11 p1771 A67-24892

Liapunov functions generated by transformation of Companion matrix to Routh or Schwarz canonical forms, for asymptotically stable linear time-invariant multivariable systems 11 p1814 A67-24942

Interpretation of results obtained by Liapunov method, using parallelepiped imbedded in region of asymptotic stability 12 p1919 A67-25912

Alserman problem concerning absolute stability of zero solution to nonlinear third order system of differential equations 13 p2087 A67-26616

Stability and asymptotic behavior of dynamical systems defined by autonomous functional or partial differential equation and conditions for applying Liapunov theorem 14 p2342 A67-28081

Singular point topological classification and analytical criteria relating singular points to generalized Liapunov-Krasovskii functions 14 p2342 A67-28381

Liapunov function analysis applied to derivation of general stability criterion for control system 14 p2292 A67-28898

Frequency domain instability criteria generated from stability criteria for time varying and nonlinear feedback problems 15 p2455 A67-29167

Parameter stability regions with frequency response, noting interpretation for several parameters 15 p2457 A67-29366

Liapunov second method and extensions used in control problems of differential systems 15 p2574 A67-29633

Stochastic Liapunov function existence demonstrated for continuous strong Markov process with certain stochastic stability properties 15 p2458 A67-29898

Liapunov direct method applied to Hermite theorem on number of positive real part zeros of complex polynomial and stability theory of linear motions 15 p2458 A67-29899

Liapunov functional for aeroelastic divergence noting application to partial differential equations 15 p2575 A67-30021

Liapunov functions generating methods applicable to nonlinear and linear autonomous systems 15 p2511 A67-30048

Similarities between model-reference adaptive control systems and parameter identification by adjustable models 15 p2464 A67-30337

Motion stability of earth-orbiting nonsymmetrical satellite with elastically-connected moving parts studied by Liapunov analysis on mathematical

model 16 p2762 A67-30962
 Liapunov function for modeling and bounding solutions of distributed processes defined by interacting subsystems describable by stable differential equation 16 p2646 A67-31638
 Liapunov-derived fixed gain flight control system design to fulfill response requirements over wide range of parametric variations 16 p2763 A67-31644
 Behavior of high-order linear control systems analyzed using Liapunov second method, by finding low-order model with closely approximate response behavior of high order linear control systems analyzed, using Liapunov second method, 16 p2647 A67-31648
 Suboptimal control function sequence generation by combining approximation in control policy space with stability criteria from direct method of 16 p2648 A67-31658
 Synthesis technique applying Liapunov theory for state vector tracking of nonlinear multivariable control systems illustrated by reactor control design 16 p2649 A67-31662
 Tolerance of nonlinearities in input transducer of time-varying optimal control systems, using Liapunov 17 p2829 A67-32307
 Liapunov subcenter manifold, showing that real C-1 Hamiltonian system of ODEs has m distinct two-dimensional invariant manifolds 17 p2877 A67-32558
 Liapunov approach to obtain sufficient conditions for stability of parametrically excited random vibrational system [ASME PAPER 67-APM-9] 17 p2886 A67-33145
 Existence of entropy as consequence of asymptotic stability 18 p3160 A67-34285
 Definition of asymptotic stability conditions and instability of zero solutions of differential equations 18 p3080 A67-34605
 Algebraic method applied for control optimization of nonlinear systems, acquiring asymptotic stability by using Liapunov function 19 p3199 A67-34825
 Liapunov function from quadratic polynomial for n-order nonlinear differential equations 19 p3250 A67-34842
 Stability of equilibrium of holonomic system in critical cases by means of search for Liapunov functions, using power series 19 p3261 A67-35050
 Geostationary satellite stability in presence of geopotential field zonal harmonics, using Liapunov theory 19 p3333 A67-35569
 Attitude stability of spinning rigid symmetric satellite in elliptic orbit examined for motion about equilibrium position with spin axis normal to orbit plane 19 p3333 A67-35747
 Closure and convexity of attainable control sets in finite and infinite dimensions, noting Liapunov theorem 20 p3408 A67-37075
 Equilibrium stability conditions for mechanical system of solid bodies derived using Liapunov function 21 p3626 A67-37991
 Variational approach to error analysis in dynamic system computer simulation, applying maximum principle and Liapunov second method 21 p3588 A67-38180
 Stability of linear integro-differential equations for processes with distributed parameters 21 p3657 A67-38268
 Liapunov-Schmidt method combined with topological method show secondary flows formed after stability loss 21 p3731 A67-38274
 Stability of nonlinear sampled data control systems, investigating pulse frequency modulation using Liapunov function 22 p3777 A67-39829
 Validity of Liapunov first approximation theorems for motion stability when not satisfying power series 22 p3837 A67-39881
 Stability criterion derivation involving Markov determinants using second method of Liapunov 23 p4022 A67-40648
 Multivariable Popov criterion application to stable and to state feedback law linear finite-dimensional systems, noting toleration of nonlinearities 23 p3984 A67-41158
 Parameter variation of optimal linear control systems with quadratic performance index /Liapunov 23 p3985 A67-41161

Algebraic and transcendental equations solutions using analog computer model described by differential equations, noting Liapunov stability theorem and asymptotic equilibrium 23 p3976 A67-41392
 Matrix version of Kalman-Yacubovich lemma for deriving stability conditions for continuous time dynamical systems with m-feedback nonlinearities 23 p3985 A67-41726
 Mathematical model, representing two-dimensional panel fluttering in supersonic flow, to study stability criterion via Liapunov second method 23 p4081 A67-41752
 Bounded-input bounded-output stability on nonlinear time varying discrete control system using Liapunov function extension 24 p4135 A67-42183
 Transient behavior of autonomous nonlinear control system phase space domains, finding relative stability domains for special time dependent Liapunov function 24 p4135 A67-42186
 Extended dynamical systems in Banach space and use of invariance principle for stability theory of partial differential equations 24 p4178 A67-42652
 Vector Liapunov function existence during conditionally or asymptotically stable motion 24 p4189 A67-42690
 Stability boundary of periodic oscillation described by third order differential equations near Liapunov critical case 24 p4137 A67-43108

LIBRATION

Solar perturbation effect on motion near collinear earth-moon libration points [AIAA PAPER 67-24] 06 p1084 A67-18259
 Feedback control system to position satellite in vicinity of unstable collinear libration point with application to lunar communication problem [AAS PAPER 66-132] 07 p1146 A67-19991
 Error analysis shows laser-radar method improves accuracy of astronomical parameters of earth-moon system, taking into account physical libration 13 p2200 A67-27327
 Feedback control system to position satellite in vicinity of unstable collinear libration point applied to lunar communication problem [AAS PAPER 66-132] 13 p2210 A67-27543
 Family of periodic orbits around triangular libration points in restricted three-body problem 15 p2557 A67-29876
 Measure of moon - Conference, Manchester University, England, May-June 1966 18 p3127 A67-34301
 Selenodesy, determining gravitational constant-lunar mass product, lunar gravitational field variation, physical librations, inertial moments, lunar tides, lunar radius, etc 20 p3525 A67-36893

LIBRATIONAL MOTION

Oscillatory motions of orbiting body around center of mass, noting stability of these librations if amplitude is always limited in time 01 p0153 A67-10411
 Dynamics of physical librations of moon, refining standard theory by using reduced estimate of mechanical ellipticity of lunar equator 01 p0149 A67-10803
 Solar-lunar perturbation of 24-hour satellite, independence of librational motion and impossibility of 02 p0321 A67-11498
 Cassini second and third laws of lunar rotation are independent of first one 05 p0889 A67-16296
 Stability of planar librations of dumbbell gravity gradient satellite in elliptic orbit 05 p0901 A67-17104
 Three-body problem of orbital motion, examining periodic librations of planetoid around triangular equilibrium point 06 p1079 A67-17762
 Particle motion in vicinity of triangular libration point in earth-moon system solved in form of analytical expressions with time-dependent coordinates 06 p1079 A67-17763
 Long period features of motion of Trojan planets in vicinity of equilateral triangle configurations 06 p1079 A67-17764
 Long period of nonperiodic librational motion about equilateral points of restricted three-body problem 06 p1080 A67-17765
 Nonperiodic librational motions in restricted three-body problem for relatively elliptic motion of two finite masses 06 p1080 A67-17766
 Structural and librational dynamics of

satellite deploying flexible booms or antennas [AIAA PAPER 67-43] 06 p1095 A67-18264
 Planar librational stability boundaries for flexible satellite under solar heating influence, using phase space concept [AIAA PAPER 67-126] 06 p1095 A67-18313
 Periodic solutions of elliptical and restricted four-body problems about libration points of restricted three-body problem [AAS PAPER 66-101] 07 p1252 A67-19963
 Dust cloud moons of earth, discussing results of photographic measurements 07 p1256 A67-20165
 Lunar satellite motion under terrestrial perturbations and lunar potential 08 p1383 A67-20404
 Control moment gyros for semipassive damping of satellite librational motion 08 p1330 A67-20586
 Differences in lunar moments of inertia determined from libration constants obtained from heliometric observations 08 p1388 A67-21010
 Lunar rotation about center of gravity, optical libration and physical libration in selenocentric coordinates 08 p1395 A67-21157
 Observation methods for determination of moon shape including libration effect, local topography and determination of apparent contour 08 p1395 A67-21159
 Motion of lunar satellite, noting principal perturbations due to nonspherical lunar gravity and earth attraction, considering moon libration and solar small forces 08 p1397 A67-21184
 General method of averaging applied to slightly damped librations problem in perturbed one degree of freedom system 08 p1424 A67-21435
 Stability analysis of long period Trojan librations treated as short period oscillations about long period reference solution 11 p1866 A67-24774
 Oscillating libration orbits with period rigorously commensurable in rational fraction to basic long period 11 p1866 A67-24775
 Periodic motion around triangular libration point in restricted four-body problem of earth-moon-sun system 13 p2205 A67-27478
 Motion analysis near triangular libration point within framework of elliptic restricted three-body problem 15 p2559 A67-30036
 24-hr satellite positions studied for librations, using lunar theory 15 p2560 A67-30043
 Librational and flexural resonances induced in satellite whose center of mass is moving in planar elliptic orbit 15 p2572 A67-30195
 Nonlinear resonance effect on attitude librations of undamped rigid gravity gradient stabilized satellite in circular Earth orbit 16 p2745 A67-30741
 Material elasticity effects on planar librational motion of rigid satellite under action of gravity 16 p2761 A67-30743
 Soviet book on moon figure and motion covering coordinate systems, surface features positions, rotational parameters, etc 17 p2948 A67-33118
 Moon rotational parameters determined by refractometric observations of craters position angles, tabulating selenographic and topocentric coordinates, reference system conversion corrections, etc 17 p2949 A67-33121
 Physical libration of moon determined from heliometric observations, obtaining value as function of inertia moment 17 p2950 A67-33125
 Lunar libration in terms of heliometric observations, giving numerical values for limb coordinates and reference altitude 17 p2950 A67-33126
 Correctness of Watts moon-limb maps, giving numerical values for corrections required 17 p2950 A67-33127
 Book on theory of orbits covering restricted problem of three bodies, two bodies in rotating coordinate system and periodic orbits 18 p3120 A67-34032
 Lunar physical libration constants determined, based on heliometric observations /1877-1915/, including coordinates of crater Mosing A 18 p3128 A67-34302
 Moon mechanical ellipticity determined by

modification of Habibullin method adapted to Schrutka-Rechtenstamm
 article 18 p3128 A67-34304
 Moon physical libration constants and figure determined, including crater Mosing A coordinates, via heliometric observations with Bessel method 18 p3128 A67-34305
 Moon physical libration in longitude 18 p3129 A67-34306
 Lunar forced physical librations calculation improved by using digital computer programmed to generate iterative solutions 18 p3129 A67-34307
 Laser ranging using reflectors proposed for investigating lunar motion and various lunar parameters 18 p3130 A67-34317
 Observational uncertainties affecting lunar control solution, considering distortions of magnitudes greater than desired increment of detection, analyzing displacements in recorded images 18 p3130 A67-34320
 Lunar physical libration constants derived on basis of four series of heliometric observations, studying ellipticity, inertia, mean radius elimination, etc 18 p3134 A67-34534
 Photography from aircraft of cloud-like objects in vicinity of libration points L4 and L5 of earth-moon system 19 p3251 A67-34953
 Eccentricity change for satellite in librational resonance shown periodic due to gravity dependence on longitude 19 p3220 A67-35254
 Nonlinear analysis of earth-moon system motion stability in three dimensions near L4 libration point when perturbed by sun 19 p3228 A67-35962
 Strength of synchronous rotation of moon in terms of upper and lower limits on rotational period, using Runge-Kutta integration 22 p3885 A67-39978
 Satellite motion in libration point vicinity, neglecting lunar eccentricity and solar perturbation, discussing lunar communication system utilizing libration point satellites 22 p3886 A67-40107
 Far IR spectra and space group of crystalline hydrazine and hydrazine-d4 noting coupling of translational and librational motions 23 p4048 A67-41532
 Gravity oriented satellite coupled librational motion in circular orbit analyzed for motion stability by numerical methods 24 p4231 A67-42384
 Stable libration points of degenerate three-body problem with negligible space vehicle mass 24 p4231 A67-42401

LIDAR

Avalanche transistor pulser designed to drive GaAs radar-laser diode 03 p0376 A67-12964
 Radio location by coherent light with quantum structure 03 p0368 A67-13283
 Laser radar returns from lower troposphere compared with vertical ozone distributions indicate inverse relationship 04 p0612 A67-14676
 Clear air turbulence detection with laser radar, noting airborne equipment and results 04 p0650 A67-15304
 Traveling wave ruby laser as radar transmitter noting power gain, coherence, frequency shift and single mode of operation 05 p0819 A67-16657
 Range capability of gallium arsenide injection LIDAR against extended targets and corner reflectors under both negligible and high background radiation conditions 09 p1462 A67-21640
 Laser rangefinder limit for rocket, balloon or satellite trajectory, noting effects of various parameters related to source, receiver, etc 10 p1663 A67-22881
 [ONERA-TP-460]
 Laser applications to satellite tracking, orbit calculation and atmospheric studies 14 p2331 A67-28608
 Laser measurements of long distances using laser interferometers, modulated laser beams and laser radar 17 p2867 A67-32613

LIE GROUP

Lie series formalism applied to solution of Bessel equation describing behavior of laminary oscillating MHD fluid 05 p0854 A67-16989
 Exact solutions of Einstein-Maxwell equation of Petrov class N when propagation vector of gravitational field is hypersurface orthogonal 07 p1218 A67-20281
 Critical volume of cylindrical reactors calculated using n-group diffusion

theory 10 p1675 A67-23396
 Advances in microwaves, Volume 1, covering stanford accelerator design, directional couplers, waveguide singular integral equations, Lie algebras, microwave network application, etc advances in microwaves, Volume 1, covering 12 p1906 A67-25975
 Nonuniform distributed network problems solved by Lie algebras 12 p1919 A67-25979
 Lie series solution of equations resulting from separation of Helmholtz equation in special coordinate systems 15 p2509 A67-29266
 Inhomogeneous second order linear differential equation solution based on Lie formalism, presenting physical applications 19 p3250 A67-35891
 Equation system for conducting perfect gas motion group analyzed leading to possible invariant solutions of system applicable to MHD equations 24 p4197 A67-42354

LIFE

S ABIOTIC GENESIS
 S BIOGENESIS
 S EVOLUTION
 S EXTRATERRESTRIAL LIFE
 S FATIGUE LIFE
 LIFE DETECTOR
 Gulliver radioisotopic biochemical probe to detect extraterrestrial life 05 p0806 A67-16548
 Biotic signatures, discussing detection and epistemology 06 p0954 A67-19017
 Sample acquisition from planetary surface by unmanned probes in life detection experiments 07 p1189 A67-19999
 [AAS PAPER 66-70]
 U.S. and U.S.S.R. search for extraterrestrial civilizations 07 p1255 A67-20001
 [AAS PAPER 66-78]
 Extraterrestrial life detection method based on catalysis of isotopic oxygen exchange between water and oxygen-containing anions 09 p1454 A67-22015
 Detecting planetary life from earth 11 p1747 A67-24063
 Pasteur Probe, assay of asymmetry of D, L amino acids in detection of Martian life 15 p2433 A67-29116
 Exobiology and effect of physical factors on microorganisms 15 p2427 A67-29117
 Detection of microbial life on near planets by measuring physical parameters 16 p2611 A67-30768
 Extraterrestrial life detection methods compared, discussing sampling and method requirements 19 p3180 A67-35250
 Pyrolysis gas chromatography method for life detection and chemical identification of microorganisms 20 p3378 A67-37500

LIFE SCIENCE

Biologic signatures, discussing detection and epistemology 06 p0954 A67-19017
 Life sciences in fiscal year 2001, advanced concepts with emphasis on neurophysiological and behavioral problems 13 p2061 A67-27505
 Life sciences and space research Conference, Vienna, May 1966 15 p2423 A67-29096
 Nucleic acid molecule reproduction discussing probability of life development under favorable environmental circumstances 16 p2611 A67-30767
 Synthesis of single cycle of natural metabolic processes to be used as basis of space-vehicle self-sufficient life support systems 20 p3368 A67-36262
 Origin of life on earth, formation of nucleic acid molecules and metabolic mechanism 24 p4112 A67-42052

LIFE SUPPORT SYSTEM

SA CLOSED ECOLOGICAL SYSTEM
 SA EMERGENCY LIFE SUSTAINING SYSTEM
 SA PRESSURIZED CABIN
 SA PRESSURIZED SUIT
 Manned extravehicular activities and equipment used in Gemini space flight program 01 p0018 A67-11414
 Completely regenerative spacecraft life support systems, discussing loop closure techniques and possible conversion methods for metabolic wastes [AIAA PAPER 66-935] 02 p0187 A67-12278
 Bioengineering parameters influencing life support systems for manned exploration of moon including mission duration and closed regenerable systems 02 p0230 A67-12310

Effects of various diets and simulated space conditions on human waste and water consumption applied to life support system development 02 p0188 A67-12339
 Space radiation monitoring system aboard manned spacecraft to provide solutions to medical problems and safety of flight guidelines for mission control 02 p0188 A67-12387
 LEM optical astronomy package /OAP/ containing astronomical telescope, spectrophotometer, data processing subsystem and other devices, for unmanned landing and life support 02 p0246 A67-12414
 Integrated space suit, suit loop and backpack system for intravehicular operation on interplanetary missions 04 p0563 A67-15235
 Integration of life support system and propulsion system for manned interplanetary space missions 04 p0563 A67-15245
 Low pressure environmental chamber for estimation of gas exchange ratio during exposure of animals under controlled conditions [ASME PAPER 66-WA/HT-52] 04 p0599 A67-15438

Emergency Global Rescue, Escape and Survival System /EGRESS/ to protect space crew in emergencies encountered in earth-orbital operations 05 p0906 A67-17204
 Post Apollo space flight technology, discussing recoverable and reusable booster rockets, spacecraft, life support systems, etc 08 p1391 A67-21065
 Lunar resources for space and planetary exploration, discussing application of solar radiation, extraction of mineral resources from meteorites, etc 09 p1568 A67-22406
 Mixed cultures of *Chlorella pyrenoidosa* TX 71105 and various bacteria and use in closed systems for support of man 10 p1598 A67-23626
 Pressure and thermal protection of man during earth-moon flight and life on moon surface 12 p1901 A67-25175
 Spacecraft life support systems should ensure radiation protection, food, power supply, waste removal, etc 13 p2061 A67-26753
 True air life support system, describing concept for deriving fixed percentage binary gas from two steady state cryogenic liquids 13 p2064 A67-27638
 Hardware and life-support systems on submarines and space vehicles, discussing oxygen supply, temperature-humidity control, etc 14 p2259 A67-28732
 [AIAA PAPER 67-364]
 Lunar surface exploration noting sample collection, instrument planting, long term economic possibilities, etc 15 p2553 A67-29301
 Life in spacecraft, International Astronautical Congress, Athens, Greece, September 1965 life in spacecraft - IAF Conference, Athens, September 1965, Volume 7 - 16 p2615 A67-30751
 Normalization of noise produced by life support systems in spaceship cabins during prolonged flights 16 p2617 A67-30762
 Electrolysis-Hydrogenomonas bacterial bioregenerative life support system for manned space flight of long duration 16 p2617 A67-30774
 Physiological-ecological investigations of *Chlorella* cultures as link in closed ecological system 16 p2617 A67-30775
 Efficiency and stability of complex closed ecological system operating on solar energy and with internal feedbacks evaluated from thermodynamic and kinetic viewpoints 16 p2618 A67-30777
 Biological value of plant proteins for closed life-support system, studying diet effects on rats 16 p2612 A67-30908
 Linear programming algorithm for optimizing life support systems of space vehicles in terms of minimum weight/efficiency ratio 17 p2807 A67-32254
 Biological problems in prolonged space voyages including oxygen replacement, water supply and food regeneration 19 p3179 A67-35209
Chlorella and *Scenedesmus* unicellular algae mixture tested for biological protein value in humans for possible food source 19 p3179 A67-35228
 Biological life support system for regenerating closed atmosphere by photosynthesis, using gas exchange between man and microalgae 19 p3180 A67-35236

Automatic life-support system tried on leeches for space applications 19 p3180 A67-35248

Synthesis of single cycle of natural metabolic processes to be used as basis of space-vehicle self-sufficient life support systems 20 p3368 A67-36262

Space suit support loop for use within manned space cabin simulator 20 p3374 A67-36548

Molecular sieves using regenerable carbon dioxide solid adsorbents for spacecraft life support systems 20 p3374 A67-36611

Potable water quality control and standards for aerospace systems 21 p3576 A67-38071

Food, water and oxygen regeneration and reclamation techniques for long duration space flights, considering carbon dioxide removal, water reclamation from urine and contamination control 22 p3755 A67-40340

Physiological Support Division facility for training crew members of SR-71 aircraft 23 p3968 A67-41616

Chemical, physical, microbiological and radiological standards of aerospace system water potability 23 p3968 A67-41620

Unicellular algae continuous culture as autotrophic component of closed ecological system, discussing stabilization of biomass concentration to provide oxygen requirement 24 p4114 A67-41844

Biological regeneration of enclosed atmosphere with algae photosynthesis noting effect of diet change 24 p4114 A67-41845

Environmental control and life support system design for NASA Biosatellite program, discussing experimental results [SAE PAPER 670839] 24 p4114 A67-41995

Dynamic mass transfer equation for design parameters of regenerable absorption beds for carbon dioxide removal in spacecraft life support system [SAE PAPER 670842] 24 p4115 A67-41996

Oxygen regeneration life support system for multiple mission manned space flights evaluated with subsystem model [SAE PAPER 670849] 24 p4115 A67-42000

Fecal waste management unit for life support simulator or aerospace flights [SAE PAPER 670852] 24 p4115 A67-42001

Continuous culture system for Hydrogenomonas bacteria in waste management of life support system [SAE PAPER 670854] 24 p4115 A67-42002

Utilization of lunar geothermal emissions for rocket propellants and life support [AIAA PAPER 67-903] 24 p4165 A67-43011

Integrated Life Support System program contributions to aerospace technology [AIAA PAPER 67-924] 24 p4117 A67-43020

LIFESPAN

Life cycle cost concept adaptation by DOD affecting logistics engineer, discussing reliability relation, maintainability, etc 23 p4084 A67-40580

Galactic radiation hazard for long term space missions, discussing life shortening effect 23 p3953 A67-41583

LIFETIME

SA PLASMA LIFETIME

SA SATELLITE LIFETIME

Temperature and stress dependence of electron lifetime in p-type Si-B and Ge-Zn between 1.5 and 4.2 degrees K 02 p0301 A67-12523

Bulk minority carrier lifetime measured directly in solar cell by measuring short circuit current decay constant which is dependent on cell thickness and carrier type 04 p0554 A67-15128

Neutron induced degradation of carrier lifetime in n-and p-type silicon containing oxygen and dopant impurities 04 p0684 A67-15691

Minority carrier lifetime dependence on injection level, obtaining recombination center parameters for neutron irradiated germanium, using photoconductivity 04 p0684 A67-15692

Lithium interaction with radium induced damage in silicon solar cells to produce center preserving minority carrier lifetime 04 p0556 A67-15703

Excess carrier lifetime in semiconductors by measuring photoconductive phase shift of spreading resistance under point contact 05 p0861 A67-16501

Nanosecond lifetime measurement for minority carriers in long diodes 05 p0775 A67-17004

Extension of paper on saturable absorber giant pulse lasers to include effects of finite absorber lifetime on pulse parameters, noting pump role 06 p1011 A67-18148

Lifetime and recombination of excess carriers in silicon over seven orders of magnitude of injected carrier density 06 p0971 A67-18226

Photoexcited electron lifetimes measured in extrinsic germanium photoconductors using Doppler shift and rotating mirror square light pulse method 06 p1005 A67-18715

Surface oxide films and lifetime of vacancies in thin crystals analyzed for pure aluminum and dilute aluminum alloys 08 p1369 A67-20794

Environmental and experimental testing of electronic systems component reliability 08 p1302 A67-20906

Electron mobility and lifetime variations effects on drift field in silicon junction devices 10 p1612 A67-23374

Lifetime of atomic state against decay induced by lepton coupling, estimating neutrino power radiation and astrophysical implications 11 p1821 A67-23959

Photovoltage measurement across lifetime junction produced by electron irradiation and by changing surface recombination velocity 11 p1850 A67-24917

Singly ionized He measured for radiative lifetimes of various states using high energy atomic beam 13 p2160 A67-26880

Generalization of Oepik theory of planetary bodies collision to include case where orbits of both colliding bodies are ellipses 14 p2384 A67-28055

Porous cesium ionizer with improved lifetime obtained by adding secondary tantalum to tungsten powder [AIAA PAPER 66-219] 14 p2376 A67-28124

Dislocation-free Ge structural and electrical characteristics after cooling, considering quenching defects 14 p2372 A67-28761

Wear lifetimes for three greases thickened with submicron boron nitride powder [ASLE PREPRINT 67AM 2C-2] 14 p2325 A67-28785

Magnetic trap electron capture lifetime dependence on magnetic field determined by scattering by residual gas, noting adiabaticity parameter critical value 15 p2526 A67-29361

Temperature dependence of lifetime and Hall coefficient in InSb, measuring lifetime by phase shift method, concluding that recombination centers are lattice defects 15 p2535 A67-29483

Minority carrier lifetime in p-silicon, analyzed varying temperature and injection level and studying recombination 16 p2725 A67-30807

Systematic clockwise rotation of asymmetry axis of main phase decrease during geomagnetic storm lifetime 16 p2866 A67-31412

Quasi-particle recombination lifetimes in superconductors measured experimentally shown to differ from calculated lifetimes 17 p2913 A67-32370

Temperature, resistivity and injection level dependence of recombination processes in neutron irradiated silicon explained by two-level recombination model 17 p2916 A67-32837

Isotope effect in hydrogen molecule dissociative attachment at low energy, noting short negative-ion formation lifetime and long separation time 17 p2889 A67-33223

Solar wind perturbation of uncharged interplanetary dust particle orbits, calculating particle lifetime 17 p2951 A67-33234

Lifetime and diffusion coefficient of lowest excited state of molecular nitrogen from intensity decay measurements of Vegard-Kaplan band 17 p2889 A67-33243

Noise analysis in He-Ne laser during RF and DC excitation, noting relation between critical frequency and lifetime of metastable atom 18 p3058 A67-33648

Excitement of slow and fast recombination waves in semiconductors with mutually independent current-carrier concentrations and lifetime 18 p3099 A67-33696

Light absorption of single-band semiconductor calculated from wave function of electron-hole pairs located near charged impurities, obtaining pair lifetime 19 p3300 A67-34767

Irradiation effect on minority carrier lifetime for p-n junction devices in epitaxial film and single crystal forms 19 p3306 A67-35670

Photomagnetic effect and kinetic photoconductivity in cadmium sulfide single crystals, determining lifetime and mobility of nonequilibrium holes 20 p3504 A67-36158

Phase shift method for obtaining radiative lifetimes by electron collisions current 20 p3488 A67-36665

Nonequilibrium current carrier lifetime in p-type InSb samples alloyed with Cu and Ge, noting hole concentration and temperature effects 20 p3510 A67-36781

Lifetime of structural sections subjected to creep deformation at high temperatures, showing relation to energy dissipation forces 20 p3540 A67-37058

Excess carrier lifetime in semiconductors by measuring photoconductive phase shift of spreading resistance under point contact 20 p3512 A67-37317

Majority and minority carrier lifetimes in n-type GaAs single crystals, measuring injection level dependence 20 p3512 A67-37436

Lifetime decrease of metastable state of chromium ion in ruby and emerald due to temperature raise, showing radiative transition 21 p3676 A67-37816

Low energy, positive ion flux from inner radiation zone, noting losses due to charge exchange, night sky emissions and lifetimes 21 p3697 A67-37996

Base region thickness, minority carrier lifetime and impurity concentration effects on conduction characteristics of silicon diodes and thyristors 21 p3597 A67-38523

Foil excitation technique used to measure 2p and 3p levels mean lifetime in He 2 cascading and agreement with theoretical value 22 p3840 A67-39206

Life cycle cost covering accessibility, automated fault isolation, corrosion control, maintenance, etc 23 p4085 A67-40586

Logistics resource development and approaches to life cycle economics in 1970s 23 p4085 A67-40587

Resonance transfer of energy as mechanism for quenching interaction between rare earth ions affecting fluorescent lifetime 23 p3971 A67-40974

Lifetime measurements of GaAs diodes determined from p-n junction impedance 23 p3982 A67-41468

Lifetime gradient and Demer photovoltages in n and p type germanium and silicon semiconductors 23 p4045 A67-41483

Lifetimes of n-type Cd-He-Tc alloy, showing Hall-Shockley-Read type recombination at low temperatures 24 p4205 A67-42664

LIFT

SA DRAG

SA GROUND EFFECT

SA INTERFERENCE LIFT

SA JET LIFT

SA ROTOR LIFT

SA ZERO LIFT

Slender body theory application in obtaining aerodynamic stability derivatives for reentry vehicles via electrical analogy 03 p0354 A67-12918

Wing lift and pitching moment variation due to fin on supersonic aircraft 09 p1437 A67-22163

Minimum of maximum overload in braking of vehicle in atmosphere, examining aerodynamic lift on basis of Pontryagin maximum principle 14 p2393 A67-27855

Airplane automatic-flare system actuating flaps and elevators as lift and moment controllers 15 p2418 A67-29313

Aerodynamic lift in future space vehicle design and implications for testing [AAS PAPER 67-34] 15 p2571 A67-30106

Aerodynamic lift, studying production of cosmic energy level supporting mechanism, explaining electromagnetic Magnus effect for gravity-free device 20 p3484 A67-36821

LIFT AUGMENTATION

SA DOWNWASH

Lift augmentation through drag reduction and variable wing profile in light aircraft 01 p0005 A67-10265

Lift augmentation parameters in peripheral jets in proximity of ground, namely jet thickness, height from ground and jet curtain inclination

[ASME PAPER 66-APM-R]

04 p0550 A67-15910
Flight experiments to assess stalling behavior and handling problems arising in design, maintenance and operation of suction wing for high lift

[AIAA PAPER 65-750] 09 p1441 A67-22483
Boundary layer control for improvement of lift at lower angles of attack by carrier-based supersonic aircraft

[AIAA PAPER 65-751] 09 p1441 A67-22484
Lift gain of flapped wing through use of wing-slot suction of friction layer near knee of flap.

10 p1590 A67-22917
Aerodynamic boundary layer control by blowing, considering problems of lift increase, airfoil properties, etc

11 p1741 A67-24101
Thrust augmentation ratio for hovercraft, lift ratio obtained by annular jets of same mass flow and total energy in ground effect and free flight conditions

15 p2419 A67-29674
Compressed-air control system for lift capacity and maneuverability increment of Buccaneer type aircraft during landing and takeoff

19 p3173 A67-35876
Lift penetration and growth effects on space vehicle response based on slender body theory

19 p3337 A67-35999
Airfoil and profiles theories emphasizing boundary layer theory, lift augmentation and wing aerodynamics

23 p3930 A67-41305
High lift characteristics of various aircraft configurations in wind tunnel model using different leading and trailing edge lift augmentation devices

LIFT COEFFICIENT

Hybrid computer simulation of reentry guidance for lifting vehicle, noting compatibility of temperature rate flight control system with other vehicle controls

01 p0051 A67-11438
Pivot center position effect on aerodynamic characteristics of variable sweepback wings during rotation

03 p0351 A67-12994
Water tunnel investigation of unsteady partial, full and supercavitation in cascade flow, determining force coefficients

[ASME PAPER 66-WA/FE-25] 04 p0607 A67-15355
Boundary layer control system of Buccaneer carrier based combat aircraft for producing high lift coefficient at relatively low speed

04 p0552 A67-15541
Mathematical analysis of jet flap with high lift coefficient, solving numerically integral equation obtained from boundary value problem

[AIAA PAPER 67-2] 06 p0938 A67-18247
Lift curve slope and aerodynamic center for variable sweep wing configurations estimated using semiempirical technique

[AIAA PAPER 67-135] 06 p0939 A67-18315
Tire hydroplaning, noting lift force on planing surface and pressure distribution

09 p1441 A67-22492
Longitudinal stability of rigid glider in towed flight, calculating lift coefficients for various rope-plane configurations

09 p1441 A67-22607
High lift techniques for STOL aircraft compared based on maximum lift coefficient, noting airfoil stall characteristics and flow separation delay devices

[SAE PAPER 670245] 12 p1894 A67-25500
Longitudinal static stability margin of glider for small lift coefficients showing effect of torsional deformation

16 p2596 A67-31001
Dynamic response of sailplanes to longitudinal maneuvers based on steady lift coefficients on wing and tails

16 p2596 A67-31465
Limit of circulatory lift on wings with finite span, deriving lift and drag for flat and rolled up vortex sheets

17 p2789 A67-32035
High lift coefficient production on helicopter rotor blades and application of circulation control by blowing

19 p3170 A67-35519
Lifting line theory for blade cascade in subsonic shear flow, noting compressibility effect dependence on harmonic mean upstream Mach number

LIFT DEVICE

SA HIGH LIFT DEVICE

Inlet/door performance characteristic of VTOL lift engines studied in full scale wind tunnel tests

[AIAA PAPER 66-655] 09 p1438 A67-22490
JR 100 H lift jet engine height control studies by NAL

11 p1852 A67-24267
Plane constant pressure contours determined by hodograph mapping used to design lift engine intakes

12 p1891 A67-25213
VTOL aircraft configurations features and characteristics including helicopter, compound, composite, tilt-wing, lift-fan, lift/cruise and lift engine

[SAE PAPER 670686] 24 p4093 A67-41987
Variable geometry in SST aircraft, discussing hardware, lift control system, compression inlet and full scale wing pivot

[SAE PAPER 670878] 24 p4094 A67-42012

LIFT DISTRIBUTION

Induced drag for idealized ground effect wing for optimum lift distribution

01 p0006 A67-10809
Oscillating variables of flow past cylinder, calculating magnitude and frequency of lift

07 p1168 A67-19258
Linear aerodynamic theory of rotor blades for predicting lift distribution, considering wake vortex sheet

13 p2051 A67-27589
Lift reduction and increase of helicopter maximum speed by controlling optimum angle of attack of rotor blades over surface of revolution

22 p3744 A67-39548
Exponential vertical flow shear effect on induced drag of elliptically loaded lifting line

23 p3932 A67-41735

LIFT-DRAG RATIO

Aerodynamic coefficients of finite wing with built-in lifting fans, noting additional lift and drag due to supercirculation at trailing end

01 p0006 A67-10769
Effects of space station logistic requirements on design of spacecraft configurations with various hypersonic lift/drag ratios, comparing payload, cost, etc

[AIAA PAPER 66-958] 02 p0332 A67-12286
Parametric investigations of supersonic long-haul aircraft, discussing operational profile, optimal lift-drag ratio, takeoff weight, civilian and military aircraft

03 p0358 A67-12975
Lift-drag ratio, specific impulse, aspect ratio and weight of payload and power plant considered for STOL

03 p0358 A67-12980
Boundary layer effect on lift and drag characteristics of hypersonic lifting bodies

03 p0351 A67-12991
Aerodynamic qualities of flexible wings noting performance, lift drag ratio, application to powered aircraft and cargo gliders

03 p0359 A67-12993
Vented profile in free surface flow of finite depth, computing lift and drag

03 p0402 A67-13449
Optimum shaped-bodies of maximum lift-to-drag ratio in hypersonic flow for modified Newtonian pressure distribution and constant skin friction

04 p0546 A67-14817
Book on aeroelastic static phenomena covering aerodynamic load characteristics, elastic deformation, drag effect on lift distribution, etc

05 p0924 A67-17227
Optimum wedges and semicones in hypersonic viscous flow, examining effect of thickness ratio on lift-drag ratio

05 p0750 A67-17367
Reentry trim angle of attack and lift-drag ratios from Gemini flights compared to wind tunnel data for aerodynamic studies

[AIAA PAPER 67-168] 06 p0939 A67-18295
Aerodynamic performance characteristics of three entry vehicles designed for maximum L/D ratio of three and two at Mach 19 and Reynolds number 3,200,000 tested in 22-inch Langley helium tunnel

[AIAA PAPER 67-138] 06 p0940 A67-18439
Heating restraints effect on aeroglide and aerocruise synergetic maneuver performance investigated for high lift-drag ratio vehicle

[AIAA PAPER 67-169] 06 p1097 A67-18483
Rotor entry vehicle systems /REVS/ concept based on lifting bodies L/D after entry with rotor needed only for improved landing

[AIAA PAPER 67-203] 06 p0949 A67-18490
Lift-drag ratio, lift and drag coefficients and angle of attack effects on Gemini and Apollo reentry vehicles measured in shock tunnel under free flight conditions

[AIAA PAPER 67-165] 06 p0941 A67-18507
Simulated high altitude hypersonic cold wall testing of lifting bodies, measuring lift, drag and static pitching

moment 06 p0943 A67-18847

Aerodynamic effect of volume addition to high lift to drag wing-body ratio at Mach 6

07 p1126 A67-19382
Flexible wings for hypersonic vehicles allowing for safe controllable landings, stressing leading edge parawing concept, flow visualization, lift-drag ratio, etc

[AIAA PAPER 67-200] 07 p1258 A67-19440
Maximum lift/drag ratio wing for supersonic environment

07 p1127 A67-20035
VTOL/STOL aircraft evaluation via performance characteristics

07 p1130 A67-20219
Isolated compressor blade within framework of lifting line theory, expressing drag produced by tip-gap in terms of flow rate and wing loading

09 p1437 A67-21739
Thrust deflection in hypersonic air breathing vehicles, noting increased cruise range and effects of gross thrust/ram drag ratio

09 p1441 A67-22497
Optimum hypersonic shapes for outer flow region, using Newtonian approximative model

10 p1589 A67-22734
Lift and drag of trapezoidal wing models in blown flow near free surface studied for sweepback angle effect on aerodynamic characteristics

13 p2093 A67-26595
Optimum shape variations of minimum-drag body with given lifting force and volume solved through Euler equations

14 p2239 A67-27983
Para-Foil models tested in wind tunnel and free flight for flight capability, L/D ratios, deployment, control and maneuverability, etc

14 p2246 A67-29054
Slender two-dimensional wing lift-drag ratio at hypersonic speed maximized, assuming modified pressure coefficient

15 p2416 A67-29409
Rotor entry vehicle system /REVS/ concept based on lifting bodies L/D after entry with rotor needed only for improved landing

[AIAA PAPER 67-203] 15 p2419 A67-29444
Three-dimensional slender wings of maximum lift/drag ratio in hypersonic flow studied by variational calculus under several lift and volume conditions

16 p2592 A67-30964
Reentry trim angle of attack and lift-drag ratios from Gemini flights compared to wind tunnel data for aerodynamic studies

[AIAA PAPER 67-166] 17 p2789 A67-32061
Cross sectional shape and thickness ratio variation effect on maximum high lift/drag ratio examined, using flat-topped conical bodies

17 p2789 A67-32071
Lift and drag coefficients of wing profile with elliptical pressure distribution calculated by approximate linearized theory

18 p3024 A67-33541
Lift-drag ratio, lift and drag coefficients and angle of attack effects on Gemini and Apollo reentry vehicles measured in shock tunnel under free flight conditions

[AIAA PAPER 67-165] 19 p3169 A67-34818
Heating restraints effect on aeroglide and aerocruise synergetic maneuver performance investigated for high lift-drag ratio vehicle

[AIAA PAPER 67-169] 19 p3332 A67-34831
Flare and landing performance of glide vehicles with low lift-drag ratio, noting aerodynamic characteristics effect

[AIAA PAPER 67-575] 19 p3335 A67-35970
Variable geometry entry spacecraft making secondary use of extendable wings in space as antenna and as radiators

20 p3532 A67-36560
Thrust augmented maneuvering /TAM/ for lifting reentry vehicle compared with other glide vehicles using lift/drag ratio

20 p3533 A67-36584
Slender wing maximum lift-drag ratio at hypersonic speeds obtained assuming modified Newtonian pressure distribution and skin-friction drag

20 p3357 A67-36953
Lift-drag ratio attainable by slender flat-top body at supersonic speeds, considering Newtonian pressure distribution and constant skin friction

20 p3359 A67-37124
Landing characteristics of SV-5P lifting body vehicle analyzed using six degree of freedom piloted simulation, noting gust effect

[AIAA PAPER 67-574] 20 p3533 A67-37133
Viscous degradation of hypersonic lift-drag ratio in manned spacecraft, noting free stream Mach and Reynolds numbers

22 p3742 A67-40113

High altitude hypersonic viscous flow degradation of L/D effects on entry vehicle lateral range capability 22 p3742 A67-40114

Blade airfoil sections two-dimensional aerodynamic characteristics studied in wind tunnel for aerodynamic optimization calculation of helicopter rotors 23 p3927 A67-40576

Commercial aircraft noise system solution, considering engines, nacelles, operational procedures and airport options [AIAA PAPER 67-761] 23 p3933 A67-40992

Large plane changes by synergetic maneuver with drag cancelled by thrust, noting reduced efficiency due to high altitude L/D decay 24 p4242 A67-42911

LIFT FAN

VTOL power plant design noting jet deflection, lift fans, RB-162 engine, etc 04 p0687 A67-14435

Design aspects of power plants for STOL aircraft, examining lift jets, thrust vectoring and lift fans [ASME PAPER 67-GT-7] 11 p1744 A67-24795

Turboprop lift fan concept for VTOL propulsion system, noting control capability, future potential, etc [AHS PAPER 115] 16 p2737 A67-31831

Aerial delivery concepts including drag cones, lift platforms, gliding parachutes, ballute parachute, ultrafast-opening parachute, etc 17 p2796 A67-32519

Civil high speed intercity VTOL aircraft using fan lift engines, discussing noise, installation, aerodynamics and thrust deflection [AIAA PAPER 67-745] 23 p4048 A67-40979

LIFT FORCE

Flexible wing analysis based on slender body theory, calculating wing profiles, pressure distribution as function of stress and lift force values 03 p0351 A67-12992

Fuselage interference effect on annular airfoils determined by measuring lift and drag of model aircraft equipped with annular wing for each semispan and empennage 03 p0352 A67-13313

Supersonic nozzle producing lift force without downward deflection analyzed by characteristics method 04 p0545 A67-14440

Lifting capacity of two-layer cylindrical shell made of different elastically hardening materials, considering temperature effect 05 p0912 A67-16180

Inviscid flow method predicting nonlinear supersonic and hypersonic lift component of highly swept wings with low aspect ratio 06 p0937 A67-18013

Inviscid steady partially cavitating flow through cascade of flat plate hydrofoils 16 p2662 A67-31550

LIFTING BODY

SA M-2 LIFTING BODY

Manned lifting entry vehicle capability, minimum weight, variable geometry, retractable landing engines, etc [AIAA PAPER 66-959] 02 p0332 A67-12287

Maneuvering-range constraints effects on lifting-vehicle design parameters as velocity increments, propellant consumption, heating rates and acceleration tolerance [AIAA PAPER 66-961] 02 p0332 A67-12288

Aerodynamic deceleration systems, discussing basic materials and fabrication techniques of BALLUTE program [AIAA PAPER 66-988] 02 p0181 A67-12299

Manned lifting body flight test program, noting NASA M2-F2 and HL-10 and USAF SV-5P [AIAA PAPER 66-838] 03 p0519 A67-14127

Lifting requirements of entry vehicles for near-earth planetary missions [AIAA PAPER 66-956] 03 p0520 A67-14140

Lifting body reentry vehicle for return from orbit to continental U.S. 04 p0706 A67-15253

Quasi-conical supersonic flow around lifting system with curved leading edge 05 p0749 A67-16843

Joint NASA-USAF lifting body flight test program and M2/F2, HL-10 and SV-5P research vehicles 06 p0947 A67-18197

Simulated high altitude hypersonic cold wall testing of lifting bodies, measuring lift, drag and static pitching moment 06 p0943 A67-18847

Control surface instabilities of lifting body configurations at very high speeds and with separated flows analyzed by wind tunnel tests for unsteady control surface load problems

[AIAA PAPER 67-15] 07 p1258 A67-19430

Lifting entry vehicles requirements for near earth and planetary missions, noting four thermal protection systems 09 p1572 A67-22671

Maneuvering-range constraints effects on lifting-vehicle design parameters as velocity increments, propellant consumption, heating rates and acceleration tolerance 13 p2212 A67-26829

Optimum shape variations of minimum-drag body with given lifting force and volume solved through Euler equations 14 p2239 A67-27983

Rigid lifting body movement transfer function derived from translational and angular velocity components transfer functions 14 p2393 A67-28061

Transitional rarefied flow regime noting drag on simple bodies, flows at sharp edges, lifting bodies, etc 14 p2299 A67-28161

Motion of solid body with rotating flywheels rotating at constant velocities relative to inertial space and body 15 p2493 A67-29686

Ballistic vs lifting body and winged recovery techniques for space launch vehicles, noting cost and operational capabilities 15 p2567 A67-29834

Land recovery of launch vehicles, applying intersecting pressure vessel theory for shaping of tanks and hinged tail panels 15 p2569 A67-29852

Inertial navigation horizontal position errors for medium L/D lifting body reentry vehicle using reference altitude for vertical channel stabilization 17 p2881 A67-32476

Pressure distribution in subsonic flow for vertical stabilizer calculated, using orthogonal function 18 p2982 A67-33655

Landing characteristics of SV-5P lifting body vehicle analyzed using six degree of freedom piloted simulation, noting gust effect [AIAA PAPER 67-574] 20 p3533 A67-37133

Recovery site location importance in determining entry vehicle future requirements 21 p3607 A67-37804

Large plane changes by synergetic maneuver with drag cancelled by thrust, noting reduced efficiency due to high altitude L/D decay 24 p4242 A67-42911

LIFTING REENTRY

Winged lifting reentry hypersonic vehicles, discussing design, analysis, fabrication and testing of hot and cooled structures and materials [AIAA PAPER 65-367] 02 p0331 A67-11929

Lifting reentry vehicles for achieving orbital plane changes by synergetic maneuvers [AIAA PAPER 66-960] 03 p0520 A67-14141

Wind tunnel tests of lifting reentry body at Mach numbers up to 16.5 and at angles of attack up to 50 degrees 04 p0546 A67-14567

Lifting body reentry vehicle for return from orbit to continental U.S. 04 p0706 A67-15253

Heating and effectiveness of control surfaces on lifting reentry vehicle or hypersonic aircraft [ONERA-TP-365] 05 p0750 A67-17403

Range control system for lifting body reentry vehicles, using closed form prediction equations for longitudinal and lateral range control [AIAA PAPER 67-136] 06 p1095 A67-18316

Trajectory control scheme effect on performance of lifting entry vehicles [AIAA PAPER 66-407] 07 p1257 A67-19362

Lifting entry vehicles requirements for near earth and planetary missions, noting four thermal protection systems 09 p1572 A67-22671

Lifting reentry vehicles for achieving orbital plane changes by synergetic maneuvers [AIAA PAPER 66-960] 13 p2212 A67-26846

Earth-orbital transport systems noting configurations, cost, capabilities, operational requirements, etc 15 p2567 A67-29835

Aerodynamic lift in future space vehicle design and implications for testing [AAS PAPER 67-34] 15 p2571 A67-30106

Potential requirements imposed upon ranges and networks by future unmanned reentry vehicles [AAS PAPER 67-35] 15 p2571 A67-30107

Simulation evaluation of closed form lifting reentry guidance

[AIAA PAPER 67-597] 19 p3259 A67-35993

Velocity and altitude at bottom of first plunge for reentry-vehicle pitch-plane maneuvers compared with digital simulation 20 p3532 A67-36577

Thrust augmented maneuvering /TAM/ for lifting reentry vehicle compared with other glide vehicles using lift/drag ratio 20 p3533 A67-36584

Manned lifting reentry vehicle optimization using Optimum Compromise between Conflicting Operational Factors /OCCOF/ computer program 22 p3902 A67-39947

LIFTING ROTOR

Rotor entry vehicle systems /REVS/ concept based on lifting bodies L/D after entry with rotor needed only for improved landing [AIAA PAPER 67-203] 06 p0949 A67-18490

Rotor entry vehicle system /REVS/ concept based on lifting bodies L/D after entry with rotor needed only for improved landing [AIAA PAPER 67-203] 15 p2419 A67-29444

LIFTING SURFACE

Improved numerical procedure for harmonically deforming lifting surfaces from supersonic kernel function method [AIAA PAPER 66-78] 01 p0007 A67-11162

Curved flow effect on lift characteristics of blade using Scholz method, noting role of correction coefficient of lift curve slope and zero lift angle 05 p0791 A67-16427

Pressure distribution on rectangular wing with jet exhausting normally from lifting surface into uniform air stream [AIAA PAPER 67-1] 06 p0941 A67-18463

Approximation solution of three-dimensional problems associated with slender wing motion in transonic gas flow with perturbations 18 p2981 A67-33535

Nonlinear theory of lifting wing surface of arbitrary aspect ratio, deriving velocity potential, lift coefficient and induced drag 18 p2981 A67-33536

Motion equation of system of two banked wings near solid surface with optimum circulation distribution 18 p3024 A67-33542

Quasi-conical motion past wing-body lifting system, determining pressure distribution, potential expression and axial disturbance velocity 20 p3356 A67-36278

LIGHT

SA AIRPORT LIGHT

SA COHERENT LIGHT

SA EXTRAGALACTIC LIGHT

SA FLASH

SA GLARE

SA LUMINESCENCE

SA MERCURY LIGHT

SA PHOTON

SA POLARIZED LIGHT

SA RUNWAY LIGHT

SA ULTRAVIOLET LIGHT

SA XENON LIGHT

SA ZODIACAL LIGHT

Growth rate limitations with interactions of light and carbon dioxide investigated for two species of Chlorella 20 p3369 A67-36791

LIGHT, SPEED OF

Short pulse Q-switched laser with variable pulse length 05 p0817 A67-16641

EH solutions of Maxwell equations describing guided electromagnetic waves in homogeneous isotropic medium at velocity of light 09 p1465 A67-22550

Light velocity measurement using hollow cathode discharge in Ne-H laser 11 p1818 A67-24479

Speed of light in vacuum determined by helium-neon gas laser, using Edlen dispersion equation 18 p3059 A67-33671

Faster-than-light particles with spacelike four-momentum within special relativity theory, discussing quantum field theory rejection of objections 20 p3486 A67-37091

LIGHT ABSORPTION

Electroabsorption measurements on rutile in clarifying band structure and dichroic nature at absorption edge 01 p0131 A67-10339

Light modulation at hyperfine frequencies in optically pumped potassium vapor, noting detection techniques, optical absorption and dispersion 02 p0251 A67-11818

Pulsed laser Q-factor modulation using nonlinear resonator functions in absorbing medium 03 p0436 A67-13135

Light absorption by uranium glass in excited state, showing relaxation time relation to luminescence 03 p0436 A67-13141

Electric-field-induced IR absorption in diamond type crystals with Raman-active vibration modes 03 p0492 A67-13260

Light absorption by free current carriers role in kinetic equations of semiconductor laser/radiation system 03 p0439 A67-14376

Light absorption in transparent materials measured using thermal lens method 03 p0439 A67-14395

Light absorption and photoionization of shallow impurity levels in semiconductors during acoustic phonon scattering 04 p0678 A67-15135

Nature of excited state resulting from two-quantum absorption associated with fluorescence in anthracene produced by ruby laser 05 p0814 A67-16130

Photometry of comet Arend-Roland, 1956 h, calculating brightness decrease along tail streams 05 p0888 A67-16201

Luminescence spectrum of CuCl at low temperatures excited by double photon absorption from high intensity laser beam 06 p1010 A67-17822

Burning rate of N powder dependence on light flux density and initial temperature range 06 p1112 A67-17958

Concentration effect on light absorption and dispersion by impurity centers in case of weak electron-phonon coupling 07 p1233 A67-19648

Frequency broadening of natural oscillations of optical resonator upon interaction with two-level atom in electromagnetic field 08 p1337 A67-20868

Ruby laser irradiation by similar laser situated at right angle to first results in radiation intensity reduction of irradiated laser 08 p1338 A67-21204

Absorption coefficient of light in semiconductors in crossed electric and magnetic fields, examining conditions for Franz-Keldysh effect occurring in magnetic field 10 p1693 A67-23590

Laser-produced dielectric breakdown at particle sites in liquids with resulting absorption of secondary light beam 11 p1801 A67-24560

Performance characteristics of photosensors and limitation by statistical fluctuation in absorption rate of light quanta in primary photoprocess 11 p1766 A67-24627

Light absorption and photoionization of shallow impurity levels in semiconductors during acoustic phonon scattering 12 p1978 A67-25159

Fundamental absorption edge of silicon heavily doped with boron, arsenic, phosphorus or antimony 13 p2173 A67-26361

Relation between attenuation coefficients of oriented and diffusive light fluxes in turbid media for arbitrary light scattering levels 13 p2151 A67-26686

Atomic-absorption flame photometric instrumentation and techniques 13 p2120 A67-26811

Light attenuation measurement in chilled silicon noting attenuation increase with incident intensity 16 p2685 A67-30870

Dust content in upper atmosphere of earth from satellite light absorption measurements 17 p2842 A67-32257

Darkness of clouds of upper and middle levels in various spectral intervals and in thermal spectrum range 18 p3073 A67-33560

Light absorption of single-band semiconductor calculated from wave function of electron-hole pairs located near charged impurities, obtaining pair lifetime 19 p3300 A67-34767

Cadmium telluride electrical light absorption oscillations noting comparisons between experiment and theory, electric field, temperature range, etc 19 p3301 A67-34772

Absorption spectra, spectral dependence of luminescence quantum output, glow curves and radiation spectra of color centers in ruby crystal 20 p3506 A67-36223

Radiative transfer in heterogeneous scattering medium with Fresnel reflection at slab boundary interface, computing transmittance, reflectance and absorptance [ASME PAPER 67-HT-19] 20 p3545 A67-36714

Brightness and contrast study of noctilucous clouds in twilight layer indicating preferability of satellite observation 20 p3434 A67-37426

Fundamental absorption edge of silicon heavily doped with boron, arsenic, phosphorus or antimony 21 p3680 A67-38318

UV absorption of ammonia at high temperatures behind shock waves, discussing NH radical formation from shock tube ammonia decomposition 22 p3756 A67-39442

Total to selective interstellar absorption ratio, with improved values calculated for six-star group, considering spectral energy distribution and color excesses 22 p3883 A67-39767

Electronic transitions optical saturations in polyatomic organic molecules with high intensity laser radiation, discussing relation to bleaching of dyes 22 p3817 A67-40487

Carbon and iron grain production in argon arc discharge studied for implications of light scattering in interstellar absorption 22 p3896 A67-40531

Siegman maximum signal theorem for coherent scattering detection, estimating attenuation through scattering medium 23 p3973 A67-40835

High resistance GaAs residual IR absorption measured to determine incident light intensity fraction, showing low absorption suitable for high power laser modulation 23 p4045 A67-41471

Laser emission nonlinear effects for materials with internal induced absorption noting pulse elongation and spatial smoothing 24 p4168 A67-42370

LIGHT ADAPTATION
SA VISUAL ACCOMMODATION
Independent effect of receptor adaptation level and pupil size on production of flashblindness by high intensity short-duration flashes 13 p2060 A67-26925

LIGHT AIRCRAFT
Lift augmentation through drag reduction and variable wing profile in light aircraft 01 p0005 A67-10265

Lift-drag ratio, specific impulse, aspect ratio and weight of payload and power plant considered for STOL aircraft 03 p0358 A67-12980

Supercharging turbojet engine for light aircraft compared to piston and turbojet engines 03 p0502 A67-13006

Light aviation, problems, prospects and performance 04 p0739 A67-14434

Light aircraft design using fiberglass reinforced plastic primary structure for fibrous composite airframe 08 p1414 A67-20429

Aircraft fuel gauging systems noting float type and reliability defects [SAE PAPER 670263] 11 p1789 A67-23986

Arava light twin-turboprop STOL transport aircraft operating from short rough airfield, noting wind tunnel results 11 p1743 A67-24213

Two-stroke cycle light aircraft engine with respect to competitive power plants 12 p1989 A67-25496

Small pressurized cabin design for light commercial aircraft including safe life vs fail-safe approaches, fatigue strength testing, etc [SAE PAPER 670259] 12 p2016 A67-25508

Reinforced plastic materials for light aircraft wing structures, calculating torque strength 22 p3912 A67-39729

Low altitude flight load spectra for light aircraft 24 p4094 A67-42755

LIGHT AMPLIFIER
SA LASER
Soviet and other papers on nuclear emission detectors, using electron-optical light amplifiers 01 p0069 A67-11006

Frequency dependences of amplification index of linear amplifier at 3.39 micron wavelength for various excitation levels 02 p0191 A67-11576

Radiative power amplification of He-Ne laser with nearly confocal resonators 03 p0438 A67-14190

Multigawatt oscillator-amplifier ruby laser system for high temperature plasma research [ASME PAPER 66-WA/ENER-2] 04 p0634 A67-15371

Book on lasers, light amplifiers and oscillators noting optical resonators, optical pumping, pulsed lasers, etc 07 p1195 A67-19469

Luminance amplifier as intensifying tubes for faint or rapidly changing images 07 p1189 A67-20156

Gain curves in multifrequency optical oscillators, measuring vanishing frequencies as function of losses in resonator, noting attenuation in laser discharge

tube 09 p1514 A67-22271

Amplification and detection of high power TW laser pulses, noting superradiance limit 09 p1514 A67-22273

Time-integrated and time-resolved spectra of GaAs laser diode, noting temperature effect on spectral emission 13 p2125 A67-26427

Soviet and other papers on nuclear emission detector, using electron-optical light amplifiers 16 p2670 A67-30494

Electron image manipulation and charge-image storage perform equivalent of incoherent optical-image transformation 18 p3047 A67-33881

High photon energy densities generation and concept of exponential amplifier for use as laser probes 19 p3240 A67-35692

Frequency stabilization of laser oscillator against reference laser amplifier, noting residual AM effects 21 p3641 A67-38461

Coherent amplification properties of antireflective coated GaAs diodes considered for application to phased array 22 p3813 A67-39254

LIGHT ARMED RECONNAISSANCE
AIRCRAFT /LARA/
S OV-10 AIRCRAFT
LIGHT COMMUNICATION DEVICE
Waveform coefficient variation F-matrix analysis of electromagnetic wave propagation in light waveguide with gas lens, considering field distribution and impedance analogy 01 p0026 A67-11237

System design analysis of laser methods of deep space communication, examining local heterodyne system /LHS/, direct detection system /DDS/ and transmitted reference system 06 p0957 A67-17635

Plausibility of extra solar intelligence, suggesting electromagnetic or optical means of communication 06 p0954 A67-19039

Laser technology development, ruby, gas and semiconductor lasers, applications and comparisons with other technologies for communications, fire control, ground radar, etc 08 p1295 A67-21283

Elements of laser communication system including transmission media, terminals, generators, modulators, etc 09 p1462 A67-21675

Transmission of large number of instrumentation channels over parallel pulse-modulated light beams, using electro-optical mosaic sources and detectors 11 p1764 A67-24444

Optical communication system components, discussing cost and potential information capacity factors in picture phone and newspaper transmission facilities 22 p3759 A67-39329

Broad bandwidth digital laser communication system utilizing pulse coded polarization modulation and binary detection including optical communication link and performance data 23 p3973 A67-41039

Optical communications systems capable of microwave bandwidths evaluated experimentally and theoretically 24 p4123 A67-42805

LIGHT EMISSION
Time variation in intensity of light emitted from CW GaAs laser diodes 01 p0088 A67-10243

Efficient electroluminescence at 300 degrees K from GaAs diode amphoteric dopant Si as dominant impurity on both sides of p-n junction 01 p0131 A67-10368

Time resolving capabilities of RCA C-70045, 56 AVP and XP 1020 photomultipliers 01 p0087 A67-10659

Background noise effect on low level light intensity measurement of microsecond transient discharge 02 p0243 A67-12185

Laser induced breakdown of complex organic molecules in vapor state, noting emission accompanied by formation of partially dissociated hot gas 02 p0252 A67-12451

Time dependent light emission due to voltage breakdown in mesoplasma region in Si on Si diode surfaces 02 p0301 A67-12658

Intensity of light emitted by individual microplasmas of silicon p-n junctions increases with voltage to maximum and then decreases 03 p0491 A67-13176

Artificial cloud produced in twilight over Wallops Island by payload containing sodium azide and lithium azide 03 p0412 A67-13371

Light generation from rectangular cross section electron beam interacting with

metallic diffraction grating 03 p0468 A67-13593
 Light emission spectrum changes due to forced transitions during passage through finite volume with negative absorption factor 04 p0709 A67-14812
 Zodiacal-light photometric measurements, analyzing effect of twilight radiation on observable brightness 04 p0617 A67-15558
 Comet photometry for measuring weak fluxes of light produced by heavenly bodies, analyzing photoelectromultipliers 05 p0805 A67-16336
 Optically pumped ruby noting absorption and emission spectrum, transition stages and phonon terminated amplification 05 p0820 A67-16658
 Plasma in Ar positive column DC discharge examined for wavelike perturbations about equilibrium, noting striation dispersion relation, density variations and electron temperature 05 p0857 A67-17427
 Plasma resonance emission of thin Ag foils irradiated by light, noting intensity and direction of polarization 08 p1368 A67-20787
 GaAs p-n-i-n diode as light activated switch, noting electrical and optical properties 08 p1306 A67-21295
 Light emission by gas under action of intense laser radiation studied by high speed high sensitivity photomultiplier 09 p1516 A67-22583
 Duration and waveform of short single pulse emitted by injection semiconductor laser 09 p1516 A67-22659
 Semiconductor lasers for discrete outputs in broad spectral range determined by material characteristics, noting electronic applications 10 p1688 A67-22824
 GaAs laser diodes in pulse operation at liquid nitrogen temperature, comparing reflection and diffraction losses with absorption losses 10 p1666 A67-23521
 Systematic degradation of GaAs light emitter quantum efficiency, noting relation to current density 10 p1615 A67-23525
 Coherent and noncoherent light emission in II-VI compounds, potential for laser applications in spectral region from 3200 to 7772 angstroms 11 p1801 A67-24735
 Physical and hydrodynamic processes induced in vaporizable solids by pulsed light radiation from sources using explosives 11 p1782 A67-24955
 Photoemission study of electronic structure of CdTe, considering two strong reflectivity peaks in optical reflectivity spectrum [AFCLR-67-0405] 12 p1983 A67-25478
 Combustion parameters of powders and explosives as function of density of light flux and transparency of burning substance 12 p2039 A67-26113
 Inversion of spectroscopic integral equation which relates emission coefficient to integrated intensity distribution for optically thin and asymmetrical light source 12 p1988 A67-26175
 Light-emitting semiconductors and solid state lasers using various electron-exciting mechanisms 13 p2176 A67-26810
 Photoemission of semiconductor, theoretical treatment of phenomena, properties and production methods 14 p2363 A67-27748
 Spontaneous visible light emission due to laser action in carbon dioxide laser plasma, examining plasma current change with phase-lock technique 14 p2331 A67-28494
 Electric discharge in vacuum consisting of two successive phases, arc formation characterized by X-ray emission and weak current and arc characterized by light emission 14 p2349 A67-28899
 Processes influencing radiative decay in compound semiconductors 15 p2536 A67-29634
 Ultrashort light pulse generation by forcing oscillation modes, noting role played by dispersion of medium within resonator cavity 16 p2702 A67-31042
 Radiation transport in spectral lines as photon absorptions and emissions, discussing contemporary theories, approximation methods and applications 17 p2893 A67-32143
 Delay time between current pulse and light emission of GaAs laser diodes, noting nonlinearity between current and delay time 17 p2824 A67-32316
 Light interaction with solids, discussing photoconductivity and

phototropy 17 p2913 A67-32373
 Representation of rotating gaseous emission rings in eclipsing binary systems by periodic orbits around more massive component in restricted three-body problem 17 p2944 A67-32640
 Many-element lasers spiking emission for Fabry-Perot and confocal geometry, including time resolved spectroscopy and far and near field patterns 17 p2870 A67-33298
 Weakly ionized plasma and gyromagnetic resonances in helium low pressure HF electrodeless discharge in magnetic field 19 p3276 A67-35113
 Shock waves and spectrographic properties of emitted light during high energy linear discharge in ionized gaseous filament 19 p3176 A67-35133
 Hydrofluoric acid for chemical vibration-rotation laser emission 20 p3462 A67-37564
 Ruby and neodymium-glass lasers light emission mixing, noting created wave frequency is sum of two initial wave frequencies 22 p3815 A67-39765
 Light generation by relative motion of mercury and helium contained in UV transmitting glass, noting intensity decrease with prolonged rotation 22 p3837 A67-39993
 CdTe photoemission absolute energies determined by correlating electron energy distribution structure with structure in optical data 22 p3862 A67-40001
 OH Meinel band, nitrogen dioxide continuum and O 1S to 1D transitions maxima altitudes in midlatitude night airglow emissions from rocket radiometer measurements 23 p3995 A67-40813
 Formation of short ruby laser light pulse and repetition frequency control using mode locking with saturable absorbers 23 p4015 A67-41036
 Black body visible light at 2800 degrees K changed into energy distribution at 5500 degrees K via Fabry-Perot filter for white light standards for colorimetry 23 p3999 A67-41180
 Light emission spots one to one correspondence with microplasmas in GaP p-n junctions 23 p4043 A67-41437
 Internal quantum efficiency of red emitting GaP diodes noting low values due to nonradiative recombination 23 p4045 A67-41460
LIGHT GAS PROJECTOR
 Design for light-gas gun with light piston by successive parameter computation of various parts 16 p2655 A67-31125
LIGHT INTENSITY
SA BRIGHTNESS DISCRIMINATION
SA LUMINESCENT INTENSITY
SA LUMINOUS INTENSITY
 Approximate absolute values of pumping power, threshold power and critical excess population for ruby laser determined from relative flash tube intensity measurements 01 p0088 A67-10245
 Intense pulse generation at 5300 angstroms by frequency doubling in Q-switched and glass laser and possibility of generating particular harmonics 01 p0090 A67-10759
 Strong fluctuations of light intensity during propagation in ground layer of atmosphere approximated by smooth perturbation method 02 p0236 A67-11640
 Uncoupled intensity peaks in laser emission 03 p0435 A67-13132
 Neodymium-glass laser using spontaneous amplified emission in nonresonant system to obtain high brightness output pulse 04 p0633 A67-15100
 Fraction of luminous energy captured by optical pumping lasers in given geometrical configuration, obtaining functioning threshold depending only on crystal 04 p0634 A67-15498
 Steady state intensity fluctuations and statistics of laser operating above threshold 04 p0635 A67-15776
 Solid state diode matrix display using gallium phosphide light sources to investigate use as data recording device 05 p0771 A67-16313
 Diffraction grating technique for measuring dynamic plastic strain exceeding 4 percent deformation at high strain rates in variable intensity light source 05 p0920 A67-16824
 LF photocurrent oscillation in high resistivity n-type GaAs, noting relation between amplitude temperature and light intensity 05 p0866 A67-16987

Coherence and fluctuations of light including stellar correlation interferometry, photon bunching, etc 06 p1008 A67-17569
 Nonlinear optical reflection laws governing direction, polarization and intensity of second harmonic light generated in reflection 06 p1030 A67-17571
 Laser spectroscopy, discussing advantages, precision attainable, line shape and position measurements 07 p1194 A67-19087
 Multiple beam interference in opaque photocathodes, determining intensity function via multiplication of amplitude by complex conjugate 07 p1185 A67-19407
 Internal turbulence scale for convection jets determined, using measurements of light intensity fluctuations 07 p1220 A67-20003
 Electroconductivity variations in CdS and CdSe single crystals with SHF electric field strength, intensity of bias lighting and temperature in minus 70 to plus 70 degrees C interval 08 p1370 A67-20996
 Envelope and phase velocities for laser pulse propagating in nonlinear dielectric with intensity dependent index of refraction 09 p1511 A67-21748
 Silicon oxide film thickness determined from intensity of reflected light 09 p1553 A67-21954
 Variable-duty-cycle spacecraft power switching circuit design giving high efficiency crewman illumination control of reticle within optical alignment sight 10 p1597 A67-23308
 Luminescence of CdS at low temperature excited by very high intensity laser light 10 p1667 A67-23779
 Analytical expressions for multiply scattered light mean intensity and light source function in homogeneous planetary atmosphere derived using mathematical model 13 p2113 A67-26683
 Statistical verification of hypothesis explaining observed scintillations of light curve of quasi-stellar radio sources by explosions of supernovas 13 p2198 A67-26766
 Arc jet exhaust velocity compared with propagation velocity of random light fluctuations 13 p2188 A67-26839
 Backscattered light intensity from laser beam for measuring atmospheric density variations, discussing optimization of sensitivity 13 p2072 A67-27609
 Solar corona temperature from intensity gradients measured during total eclipse of May 30, 1965 14 p2387 A67-28564
 Special lighting equipment for high speed cinematography delivering high intensity light pulses in nanosecond range for use in shock wave and explosion filming 14 p2319 A67-28585
 Daily physiological rhythm changes associated with light intensity and color, noting body temperature oscillations vs light intensity, heart rate changes, etc 15 p2426 A67-29109
 Michelson interferometer with laser source analyzed for beam frequency and wavelength, refraction coefficient, etc 15 p2486 A67-29467
 Laser light photon counting statistics using probability density for laser light intensity 15 p2498 A67-29513
 Power spectrum of pulsating aurora measured at HF, noting relation to modulation mechanism in flux of primary particles 17 p2850 A67-33193
 Intensity of light scattered from soot particles in diffusion flame of hydrocarbons burning in air 18 p3149 A67-33799
 Relationship between axial magnetic field necessary to extinguish oscillation from Brewster-angled laser and spontaneous intensity 18 p3061 A67-34200
 Light intensity fluctuations along inclined inhomogeneous path with variable turbulence characteristics in lower atmospheric layer 18 p3080 A67-34437
 Statistical properties of strong light intensity fluctuations propagating in ground layer of atmosphere investigated to measure frequency spectra 19 p3254 A67-36017
 Two-photon photoconductivity in pulsed ruby laser excited cadmium sulfide, determining carrier density and density dependence on light intensity 20 p3456 A67-36164
 Low intensity photoelectric signal detection by Fabry-Perot spectrometer using SNR enhancing method 20 p3439 A67-36356

He-Ne laser light intensity distribution cumulant for nonlinear oscillation threshold operation 20 p3461 A67-37289

Emission intensity dependence in CdS on laser excitation intensity for free and phonon-assisted exciton recombination at cryogenic temperature 20 p3461 A67-37295

Observational results consisting of meteor trail photographs for determining processes responsible for relative intensity of brightness and trail length 20 p3530 A67-37665

Analytical expressions for multiply scattered light, mean intensity and light source function in homogeneous planetary atmosphere derived using mathematical model 21 p3618 A67-38427

Unstable light scattering in atmospheric models studied in relation to medium optical properties, using phase shift measurement 21 p3627 A67-38448

Michelson interferometer with laser source analyzed for beam frequency and wavelength, refraction coefficient, etc 21 p3628 A67-38548

Maximum current and total light output of triggered lightning strokes at close range upon ship deck, noting photographs of discharge 22 p3793 A67-39979

Light generation by relative motion of mercury and helium contained in UV transmitting glass, noting intensity decrease with prolonged rotation 22 p3837 A67-39993

Light polarization and intensity for Raman scattering from plasmons and phonons in GaAs 23 p4038 A67-40795

He ions beam passing through electric field and inducing light intensity fluctuations when emitted from fine structure levels observed via Stark interference 23 p4029 A67-40956

Ion energies in expanding plasma stream generated by intense giant pulse laser light in focus on solid LiD and LiH targets 23 p4033 A67-41152

Optical mixing process for study of polarized light in wedge shaped cells of Raman active medium 23 p4017 A67-41433

Structure of image of diffused surface in coherent illumination investigated for mean intensity and noise-like obscuring component 24 p4155 A67-42336

LIGHT METAL

Book on light metals 20 p3465 A67-36634

Beryllium corrosion occurrence, causes, effects, prevention and advantages over steel and aluminum 20 p3465 A67-36636

Magnesium and magnesium alloy corrosion, discussing treatments for prevention of various kinds of corrosion 20 p3466 A67-36637

Distribution function of durability in light structural alloys based on mass fatigue tests analyzed for influence of scale factor and stress concentration 22 p3915 A67-40301

LIGHT MODULATOR

SA OPTICAL MASER MODULATOR

SA ULTRASONIC LIGHT MODULATOR /ULM/

Light modulation by large single crystal ZnS with negligible strain birefringence 01 p0138 A67-11330

Propagation characteristics of cylindrical waveguide partially filled with dielectric light modulation material 02 p0193 A67-11780

Optimum processing of photocell output to produce Poisson photoelectron flux 03 p0368 A67-13282

Spin echo and free decay signals in Rubidium optical pumping analyzed, using pulse method and light modulation technique 04 p0632 A67-14770

Low loss phase modulator for optical signals, using piezoelectric effect 04 p0576 A67-15506

Kerr cell properties noting four-electrode cell giving frequency shift of 80 mc for laser beam 07 p1142 A67-19552

Book on reticles in electro-optical devices 08 p1353 A67-20757

Gain curves in multifrequency optical oscillators, measuring vanishing frequencies as function of losses in resonator, noting attenuation in laser discharge tube 09 p1514 A67-22271

Equivalent resistance divided by interaction impedance of CEF photodemodulators for coherent light 09 p1479 A67-22278

Traveling wave IR and sub-mm light modulator design using free carrier

absorption in reverse biased p-n junction diodes 11 p1759 A67-24137

Laser communication system for black and white tv signal transmission noting focusing, noise level and light modulation laser communication system for black and white TV signal transmission noting focusing, noise 13 p2068 A67-26724

Tunable microwave-frequency light modulator consisting of rectangular cross section coaxial cavity with two electro-optical crystals 15 p2501 A67-30141

Light pulse generator circuit using hydrogen corona-discharge tube and thyratron generator of nanosecond light pulses 19 p3228 A67-34988

Resonance frequency shift analysis of autostabilized light modulator at microwave frequencies noting heat transfer, transition temperature, etc 20 p3459 A67-36503

Electro-optic phase modulation of visible and IR light by p-n, p-i-n and metal semiconductor junctions and heterojunctions, noting propagation modes 21 p3684 A67-38453

Optical communication systems modulation, discussing TV link, modulator, optical waveguides and materials availability 22 p3759 A67-39330

Magnetic film memory written and read by focused light studied using thermal cycle time and read bandwidth calculations 22 p3765 A67-39910

LIGHT PRESSURE

Perturbations of satellite orbital elements caused by pressure of solar radiation reflected from earth 05 p0894 A67-16566

Radiation effect on satellite in presence of partly diffuse and partly specular reflecting body 05 p0905 A67-16567

Passive spin propulsion of large flexible spherically shaped satellites by solar radiation field 05 p0905 A67-16568

Malkin theorem for satellite attitude control subjected to light pressure perturbation 11 p1870 A67-24723

Very high satellite air drag acceleration studied by University of London Observatory, discussing solar radiation pressure acceleration 18 p3042 A67-34257

Passive orientation of space vehicle toward sun by black and white coating, analyzing free oscillation about equilibrium 21 p3713 A67-38598

LIGHT PROBE

Interferometric holography in diffused light, obtaining interferogram of phase shifting object 03 p0420 A67-13451

Holographic laboratory experiments, discussing Lippman method and imagery through diffusing media contour line implantation 04 p0623 A67-15302

Interferometer for small optical path difference measurements, noting high sensitivity and environmental stability 05 p0807 A67-16789

Self-focusing and self-trapping of intense light beams in nonlinear medium examined, using approximations of geometrical optics and accounting for diffraction effects 06 p1031 A67-17880

UV sensitivity increase in sodium salicylate photomultiplier combination 07 p1185 A67-19405

Threshold characteristics of photoresistors with noiseless contacts on CdS base 07 p1152 A67-19592

Stress measurement in metal components with photoelastic coatings and thin walled structures, using reflected light technique 09 p1575 A67-22169

Holograms of three-dimensional objects, discussing experimental setup and results 15 p2489 A67-30077

Threshold characteristics of photoresistors with noiseless contacts on CdS base 20 p3401 A67-37331

LIGHT SCATTERING

SA ATMOSPHERIC SCATTERING

Composite surface and composite correlation approaches to frequency dependence and surface roughness problems of lunar surface signal scattering 01 p0020 A67-10019

Band structure of spectra of gallium phosphide, gallium arsenide and solid solutions determined by optical reflection techniques 01 p0086 A67-10067

Approximation method for deriving expressions for small angle polydispersed indicatrix of gamma distribution of particles in light field 01 p0107 A67-10125

Mie scattering and plane wave diffraction theory for small angle light dispersion from sphere 01 p0112 A67-10131

Scattered light spectrum in thiatron plasma, noting onset of ion wave instability 01 p0121 A67-10248

Ruby laser with scattering induced feedback and absence of resonance type oscillations 01 p0090 A67-10740

Thermalization rate of highly ionized plasma with initially hot ions and cold electrons, using laser scattering to observe time variation of electron temperature 01 p0125 A67-10912

Optical scattering cross sections for polydispersions of dielectric spheres, showing dependence on ratio of third to second moment of shape and size distribution function 01 p0115 A67-11077

Particle size measurements based on use of optical mean scattering cross sections 01 p0070 A67-11078

Phasing system using steered beam of coherent light for RF array 01 p0027 A67-11320

Aerosol measurements using light scattering from searchlight probing, noting attenuation coefficient as function of altitude [AFCRL-67-0003] 02 p0238 A67-12048

Scattering of partially coherent radiation by neutral molecules formulated as random process 02 p0201 A67-12096

Spherical diffraction solution obtained by reducing it to solution of diffraction problem for circular cylinder via coordinate transformation 02 p0205 A67-12529

Interference induced elongation of light scattering indicatrix of particle conglomeration 02 p0263 A67-12671

Ruby laser frequency conversion technique by laser beam scattering and mixing of combined frequencies 03 p0433 A67-13094

Electron temperature and concentration in DC plasma arc determined from Thomson scattering of laser radiation 03 p0437 A67-13209

Diffraction of plane wave at sinusoidally stratified dielectric grating, using hologram analysis 03 p0423 A67-13905

Photon scattering in three-dimensional semilinear medium for constant frequency and survival probability 04 p0695 A67-14655

Laser backscatter signatures and transmissivity over horizontal and slant paths with respect to measuring extinction coefficients of scattering media 04 p0649 A67-14677

Data record and readout systems dependence on precise spot and line scan methods, using diffraction limited spots of laser generated light 04 p0623 A67-15321

Diffraction limited performance achieved for flying spot recording and readout, using concentric optical system, applied to laser scanner 04 p0658 A67-15322

Polarization of light scattered from He-Ne laser beam, applying quantum theory to formula for depolarization ratio 04 p0634 A67-15624

Degenerate stimulated four-photon interaction and four-wave parametric amplification observed in ruby laser and liquid cell arrangements 05 p0844 A67-16379

Properties of self-trapped light filaments noting stimulated Raman emission and creation, containment and termination mechanisms 05 p0818 A67-16648

Inelastic scattering of carbon dioxide laser radiation by mobile Landau-level electrons in n-InSb 06 p1009 A67-17723

Statistical determination of correlation functions of plasma scattered coherent light 06 p1039 A67-17824

Diffusion broadening in inelastic light scattering of cyclohexane-polystyrene near critical point for mixing 06 p1035 A67-17829

Bibliography on lasers covering modes, scattering mechanisms, quantum electrodynamics, matter-radiation interaction, plasma, holography and optics 06 p1010 A67-17890

Optical scattering dependence on heat treatment of monocryalline silicon containing nitrogen 06 p1050 A67-18183

Light scattering in research and technology [AIAA PAPER 67-35] 06 p1032 A67-18465

Multiple scattering of light in turbulent atmosphere noting relation to refraction index and power spectra, using Born series

solution to wave equation 06 p1033 A67-18536
 Book on atmospheric absorption, diffusion and polarization of light and radioelectric radiation 06 p0998 A67-18718
 Image distances and relative intensities for zone plates determined from holographic theory 07 p1185 A67-19401
 Diffuse polychromatic light reflection from infinitely deep one-dimensional medium of atoms with three energy levels, with all interlevel transitions 07 p1248 A67-19484
 allowed
 Electric field induced optical refractivity changes /Franz-Keldysh effect/ and nonlinear light scattering, light beam deflection and modulation in neutron-irradiated Si at 95 degrees 07 p1231 A67-19487
 K
 Cometary dust studied by analysis of scattered sunlight in heads and tails of comets 07 p1250 A67-19668
 Light waves traveling backward and forward in very small filaments of optical material result in standing waves producing visible spatial beats, allowing detection of changes in refractive index 07 p1224 A67-19841
 Light scattering influence on effective value of extinction coefficient considered as function of optical parameters of medium and of angular characteristics of source and receiver 07 p1221 A67-20007
 Anisotropic nonconservative scattering in modified Schuster-Schwarzschild approximation and Venus cloud layer 08 p1385 A67-20931
 Statistical analysis of errors in angular measurement of distant objects due to gravitational scattering along light path 08 p1398 A67-21232
 Isophotes of extended light sources in night sky, Stokes parameters, brightness and degree of polarization for Rayleigh-scattered light in earth atmosphere 08 p1326 A67-21243
 Band structure of spectra of gallium phosphide, gallium arsenide and solid solutions determined by optical reflection techniques 08 p1339 A67-21450
 Optical beam deflection method based on polarization change of acoustically deflected light as compared to incident beam 09 p1510 A67-21574
 Scattering of coherent and incoherent light compared, using CW He-Ne gas laser sources 09 p1510 A67-21600
 Daytime sky brightness relationship to atmospheric anisotropic light scattering 09 p1491 A67-21638
 Atmospheric turbulence determined from coherence deterioration of laser beam 09 p1511 A67-21825
 Dual observation method for determining photoelastic parameters in scattered light 09 p1574 A67-21840
 Integral equation solution with Mellin inversion formulas for light scattering problems 09 p1524 A67-21872
 Statistical quantities needed to fix scattering regime obtained from observations of radio scintillations, showing correlation length in electron density fluctuations 09 p1565 A67-22223
 Self-focusing laser beam in inhomogeneous plasma 09 p1515 A67-22276
 Volume scattering of Mie spherical particle polydispersion and irregular particles 10 p1879 A67-22747
 Radiation absorption and scattering by small spherical solid carbon particles in wavelength range 0.2 to 40 μ calculated by classical Mie theory [AIAA PAPER 66-134] 10 p1682 A67-23146
 Numerical solution methods of invariant imbedding equation for reflection function of spherical shell with absorption and isotropic multiple scattering 10 p1680 A67-23634
 Measuring method for beam divergence of Q-switched ruby laser rods 10 p1667 A67-23782
 Wavelength selectivity in solar collector design, noting role of scatter in determining radiative properties of surfaces 11 p1817 A67-24052
 Mean droplet size for cross stream water injection into Mach 8 air flow determined by scattered light angular variation measurement 11 p1779 A67-24366
 Light scattering by flattened ellipsoids at 90 and zero degree of incidence 12 p1965 A67-25136

Parameters of multiple-scattered optical radiation applied to laser communication system design 12 p1906 A67-25988
 Analytical expressions for multiply scattered light mean intensity and light source function in homogeneous planetary atmosphere derived using mathematical model 13 p2113 A67-26683
 General algorithm for solving atmospheric optics problem applicable to short wave radiation transfers of atmospheres with various light scattering, using Monte Carlo method 13 p2151 A67-26684
 Relation between attenuation coefficients of oriented and diffusive light fluxes in turbid media for arbitrary light scattering levels 13 p2151 A67-26686
 Ruby laser with scattering induced feedback and absence of resonance type oscillations 13 p2126 A67-26769
 Lambert diffuse reflection from general quadric surfaces 13 p2158 A67-26877
 Three-dimensional photoelasticity and determination of axes of birefringents and change in phase by scattering polarized light 13 p2219 A67-27092
 Beckmann theory on scattering applied to laser mirrors, predicting wavelength dependence of scattering profiles 13 p2129 A67-27348
 Sunspot observation methods and techniques in white light, considering requirements, diffraction limitations on resolution, site selection and local seeing and telescope choice 13 p2202 A67-27421
 Image and other techniques to measure and reduce stray and scattered light in sunspot photometry, emphasizing possibility of using partial solar eclipse 13 p2203 A67-27424
 Spherical diffraction solution obtained by reducing it to solution of diffraction problem for circular cylinder via coordinate transformation 14 p2261 A67-28006
 Spherically symmetrical planetary atmosphere brightness derivation using transport equation 14 p2313 A67-28766
 Visible continuous spectrum of comets rules out hypothesis of iron particles major role in scattering solar light 15 p2554 A67-29515
 Two-color photoelectric photometry of earthshine, determining earth albedos 15 p2477 A67-29626
 Multiple light scattering in inhomogeneous spherically symmetrical planetary atmosphere with exponentially varying attenuation coefficient 16 p2698 A67-31096
 Laser scattering from gas particles and diffuse surfaces, noting difference in intensity of speckle patterns formed 16 p2686 A67-31882
 Ruby laser light scattering by theta pinch plasma measured with Fabry-Perot spectrometer, noting cooperative density fluctuations superimposed on thermal density fluctuations 17 p2899 A67-32274
 Nonlinear incoherent light scattering from two frequency-differing coherent beams of electromagnetic radiation propagating in homogeneous plasma without magnetic field 17 p2901 A67-32354
 Spectroscopic observation of ion wings produced by plasma ion oscillations in laser produced plasma 17 p2901 A67-32368
 Laser applications utilizing power density for studying reflectance, Raman spectra, photography, holography, etc 17 p2868 A67-32691
 Resonances in wave mechanics and anomalous light dispersion, obtaining value of displacement 17 p2884 A67-32704
 Photomultiplier gate for stimulated spontaneous light scattering discrimination, showing high cut-off efficiency, linearity and absence of spurious effect 17 p2863 A67-33353
 Higher order atmospheric light scattering at zenith of twilight sky, tabulating ratio between higher order scattering and primary twilight intensity 18 p3040 A67-33631
 Thomson scattering of Q-switched ruby laser beam in shock wave plasma, determining electron densities, spectral distribution of scattered light, etc 18 p3084 A67-33649
 Speed of light in vacuum determined by helium-neon gas laser, using Edlen dispersion equation 18 p3059 A67-33871
 Intensity of light scattered from soot particles in diffusion flame of hydrocarbons

burning in air 18 p3149 A67-33799
 Propagation of narrow beam of light in turbid medium with strongly extended scattering 18 p3080 A67-34438
 On-the-ground optical determination method of stratospheric aerosol particle numbers and sizes from ruby laser radiation measurement scattering 19 p3225 A67-35531
 Monochromator for measuring spectral distribution of laser light scattered by high temperature plasmas 19 p3230 A67-35593
 Fluctuating light scattering cross section and Lorentz-Lorenz refractive index formula derived from microscopic equations 20 p3483 A67-36174
 Linear/nonlinear molecule optical properties obtainable from light scattering in gas by strong optical field 20 p3488 A67-36437
 Radiative transfer in heterogeneous scattering medium with Fresnel reflection at slab boundary interface, computing transmittance, reflectance and absorptance [ASME PAPER 67-HT-19] 20 p3545 A67-36714
 Hologram reconstruction of objects in fog-like medium 20 p3450 A67-37027
 Radiance of debris cloud ejected from manned spacecraft, effect on optical environment and astronomical observations 20 p3525 A67-37099
 Relative photon scattering cross sections for He and Ne at Lyman alpha, describing measurement technique 20 p3489 A67-37431
 Bouguer law applicability for describing narrow collimated light beams attenuation in scattering media in terms of optical thickness 20 p3462 A67-37666
 Induced three-photon combination scattering kinetics applied to laser pumping 21 p3638 A67-37867
 Analytical expressions for multiply scattered light, mean intensity and light source function in homogeneous planetary atmosphere derived using mathematical model 21 p3618 A67-38427
 General algorithm for solving atmospheric optics problem applicable to short wave radiation transfers of atmospheres with various light scattering, using Monte Carlo method 21 p3618 A67-38428
 Unstable light scattering in atmospheric models studied in relation to medium optical properties, using phase shift measurement 21 p3627 A67-38448
 Rayleigh scattered laser light technique for point measurements of time averaged neutral gas density in turbulent wake behind hypersonic velocity body 21 p3565 A67-38876
 Cooperative light scattering from density fluctuations in theta pinch plasmas, discussing peaks obtained 22 p3842 A67-39208
 Rayleigh-Sommerfeld diffraction formula to obtain imaging behavior of Gabor type holograms of transparencies for reconstructed wave forms with large diffraction angles 22 p3835 A67-39241
 Thermonuclear origin of neutron emission in theta pinch plasma, determining ion temperature from scattering of ruby laser beam 22 p3843 A67-39244
 Carbon and iron grain production in argon arc discharge studied for implications of light scattering in interstellar absorption 22 p3896 A67-40531
 Intervening galaxy effect on radiation from distant objects, studying Faraday rotation, 21-cm absorption, optical scattering and absorption lines 24 p4223 A67-41810
 Optical Raman scattering from atmospheric oxygen and nitrogen via pulsed nitrogen UV laser light source, discussing spectral analysis of air scattering 24 p4147 A67-41883
 Laser pulse compression of RF signals using Bragg scattering produced in transparent solid by ultrasonic waves 24 p4188 A67-42368
LIGHT SOURCE
 Holograms with incoherent illumination, noting patterns produced and resolution parameters 01 p0070 A67-11081
 Magnetically compressed plasma as high intensity source of near UV and visible radiation experimentally studied in dynamic pinch 02 p0272 A67-11880
 Atmospheric agitation effect on image of extended celestial light sources, showing importance in long-range tropospheric propagation of ultrashort radio wave 02 p0325 A67-11986

Lower atmospheric layer and meteorological conditions effect on oscillations of image of artificial source of light 02 p0238 A67-11987

Reflecting surface geometry calculated by reflection and scattering of light source 02 p0268 A67-12446

Hologram copying method using gas laser as light source 02 p0246 A67-12513

Sensitivity of optical system used in schlieren setup in determining quality of recorded information 04 p0619 A67-14606

Fluctuations of angle of incoming light waves from distributed source in atmosphere with turbulent pulsations of refractive index 05 p0761 A67-16346

Galactic depolarization of 21 cm wavelength radiation of extragalactic sources explained as function of distance traveled by radiation through halo 05 p0895 A67-16601

Bibliography on lasers covering modes, scattering mechanisms, quantum electrodynamics, matter-radiation interaction, plasma, holography and optics 06 p1010 A67-17890

Light source devices for electronic functions, discussing p-n junction 07 p1231 A67-19081

Gas laser as source of illumination, with attention to origin of aventurine spots on screen 07 p1195 A67-19142

High voltage pulsed electrodeless discharge in rare gas as light source for ruby and Nd glass laser excitation and observation of output characteristics 10 p1666 A67-23565

Semiconductor diode light sources, discussing phenomenon of p-n junction luminescence and potential application in optical displays and data transmission 12 p1979 A67-25169

Light sources used for solar simulation testing in terms of operational characteristics and effect of different spectral irradiance characteristics on thermal control coatings 12 p1925 A67-25723

Copper anode lamp for solar simulation facilities, discussing effect on arc brightness and anode loading of magnetic fields, gas mixtures, pressure, etc 12 p1925 A67-25734

Inversion of spectroscopic integral equation which relates emission coefficient to integrated intensity distribution for optically thin and asymmetrical light source 12 p1968 A67-26175

800 mm and 1265 mm optical resonator He-Ne lasers, obtaining maximum output power and application as Raman spectroscopy light source 14 p2333 A67-28972

Images reconstructed from multiple-exposure hologram separated by selecting appropriate-reconstructed pupil 15 p2487 A67-29500

Spectral linewidth and shift of TI I lines produced by neutral argon atoms analyzed using high pressure arc as light source 16 p2703 A67-30665

Gas laser as source of illumination, with attention to origin of aventurine spots on screen 17 p2869 A67-33220

Experimental techniques in making multicolor white light reconstructed holograms, discussing signal to noise ratio, coherent light and photographic emulsion 17 p2862 A67-33299

Semipermanent optical memory design using laser light source, acoustic light deflector and hologram array as information storage elements for address selection 20 p3390 A67-36511

High magnification microscopes for semiconductor research noting advantages of illumination system and light sources 21 p3630 A67-38895

Q-switched laser use as light source for photographing droplets in spray containing fluorescent dye excited by second harmonic of ruby light 22 p3797 A67-39492

Lasers as light source in optical telemetry, discussing laser radiation, solid state and gas lasers and critical parameters 22 p3800 A67-39981

Optimization of high energy neutral particles source /Eollon/ measurements, noting application to atomic collisions problem 24 p4153 A67-41912

LIGHT TRANSMISSION

SA DIFFRACTION
SA FIBER OPTICS
SA ILLUMINATION
SA OPTICAL COUPLING

**SA REFRACTION
SA VISIBILITY**

Electromagnetic theory of wave propagation modes in dielectric cylinders applied to coherent light transmission in optical fibers 02 p0190 A67-11528

Index and thickness of absorbant thin film determined from reflection and transmission coefficients 02 p0289 A67-11727

Clear line-of-sight through atmosphere determined, using probability estimates [AFCRL-66-838] 02 p0262 A67-12080

Light propagation through Schwarzschild singular sphere, solving problem of visual image of emitting surface of gravitating sphere as seen by observer 03 p0467 A67-12932

Quenching of one pulsed ruby laser oscillation by another, noting coupled rate equations for steady state and transient behavior 05 p0823 A67-16862

Wavelength dependence of spectrum of laser beams traversing atmosphere 05 p0763 A67-16793

Parametric fluctuations of spatially restricted light beam in turbulent atmosphere 05 p0786 A67-17229

Light beam deflection with low losses, using thermal gradient effects in gases 07 p1141 A67-19406

Gas lens focusing of light beams, using highly transparent gas with weakly varying refractive index to guide coherent transmission with small losses 07 p1188 A67-19789

Transmission of artificial quartz at room temperature, obtaining optical constants in far IR region 09 p1553 A67-21917

Electronic processes on semiconductor device surfaces analyzed using scanning light beam, for application to Si planar transistors 09 p1472 A67-21949

Variance of log amplitude of laser beam evaluated for horizontal propagation path through atmosphere by following Schmelzer results 10 p1603 A67-22713

Mode discrimination of laser cavity exploiting transmission characteristics of Fabry-Perot interferometer 10 p1663 A67-22835

Light beam waveguide using lens-like media with periodic hyperbolic temperature distribution, discussing construction, optimum design and operating conditions 10 p1606 A67-23066

Plasma resonance absorption measurement in thin potassium foils, observing polarized light transmission at lambda 3270 10 p1691 A67-23478

Optical lossless double pass network synthesis techniques using birefringent crystals extended to complex and real transmittance amplitudes 11 p1818 A67-24418

Solthane 113 urethane rubber composition analyzed via constant strain rate tests, noting birefringent sensitivity and optical transmission properties 11 p1811 A67-24615

Reflection and transmission of electromagnetic waves at interface between stationary isotropic medium and moving anisotropic medium 11 p1820 A67-24919

Light deflection by solar activity 12 p2002 A67-25540

Light diffraction by elastic waves in YIG noting values of photoelastic tensor components 12 p1984 A67-25746

Water-vapor rotational band transmission function calculations by atmospheric inhomogeneity approximate methods 13 p2151 A67-26682

Relation between attenuation coefficients of oriented and diffusive light fluxes in turbid media for arbitrary light scattering levels 13 p2151 A67-26686

Image transmission through optical fiber, discussing reconstruction of refracted image via holography 13 p2120 A67-27209

Laser light deflecting methods, detailing scanlaser, laser resonator combining features of laser and cathode ray tube 13 p2128 A67-27237

Transmission of artificial quartz at room temperature, obtaining optical constants in far IR region 14 p2365 A67-28246

Gas laser radiation applied to light transmittance measurement of heavily doped gallium arsenide in absorption region by free carriers 14 p2368 A67-28528

Optical means for enhancing quantum efficiency of tri-alkali photocathode, discussing standing wave pattern in spaced-

reflective and reflective photocathodes 17 p2861 A67-33287

Skylight polarimeter based on sequential detection of light transmitted by polarizers oriented at various angles 18 p3046 A67-33748

Radiative heating of H and He containing suspension of solid particle absorbers, noting proportionality between gas particle dispersion decrease and energy absorption [AIAA PAPER 67-501] 18 p3158 A67-33965

Directional fluctuations in light waves propagating from edge of solar disk caused by atmospheric turbulence 18 p3080 A67-34436

Thermodynamic model for laser induced gas discharges accounting for transmitted light attenuation, plasma heating, etc 19 p3239 A67-35163

Diffuse reflected and transmitted spectral line profile calculations for uniform noncoherently scattering media 19 p3183 A67-35555

Laser and nonlaser light transmission through atmosphere, noting no difference in propagation 19 p3240 A67-35695

Sensitivity of single-mirror schlieren system, deriving expression relating film density change with angular light deflection 20 p3441 A67-36400

Radiative transfer in heterogeneous scattering medium with Fresnel reflection at slab boundary interface, computing transmittance, reflectance and absorbance [ASME PAPER 67-HT-19] 20 p3545 A67-36714

Light deflection by solar gravity measuring method using radar interferometer 20 p3485 A67-36995

Soviet book on atmospheric visibility noting photometry, range, threshold, runway visual range, atmospheric transmittance and atmospheric boundary layer problems 23 p4024 A67-40600

EM radiation reflection, absorption and transmission through dielectric medium measured, studying other aspects by electric dipole oscillator model 23 p4037 A67-40757

Geometrical self-shadowing of random rough surface described by Gaussian statistics in wave backscattering phenomena 23 p3972 A67-40832

Gas laser radiation applied to light transmittance measurement of heavily doped gallium arsenide in absorption region by free carriers 23 p4039 A67-40935

Airport glide slope visual range determination with single-ended transmissometer by measuring transmission between photosensitive detector and laser light source 23 p3999 A67-41027

Absorption spectra of quasi-stellar objects /QSO/, suggesting origin in galaxies through which light passes on way to earth 23 p4069 A67-41442

Dynamical theory of X-ray diffraction for optical holography noting anomalous light transmission at Bragg angle 23 p4009 A67-41462

Light reflection and transmission by thick optical atmosphere according to phase function 24 p4147 A67-41819

Radiative heat transfer for light reflection and transmission by optically thick scatterers with three-term phase function, obtaining asymptotic formulas 24 p4147 A67-41820

Two-photon absorption in semiconductor laser in relation to upper limit of transmission power 24 p4200 A67-41863

LIGHTHILL METHOD

Acoustic characteristics of jet determined, using Lighthill equation for free turbulent jet when components of flow fluctuation rate, turbulent vortex volume and turbulent fluctuation frequency are known 14 p2302 A67-28301

Lighthill uniformization technique applied to singular perturbation problems using Lagrange expansion 14 p2346 A67-29059

Steady two-dimensional magnetic bottle in which moving, compressible and electrically conducting plasma is confined by horizontally aligned magnetic field 15 p2528 A67-29568

LIGHTHILL MODEL

Compression shocks in one-dimensional steady flow of Lighthill ideal dissociating gas studied, using semiempirical relation for relaxation equation 15 p2471 A67-29578

Viscoelastic theory solving Lighthill paradox by accounting for acoustic energy

damping in fine grained isotropic turbulence 21 p3610 A67-37759

LIGHTING

Radioisotope and phosphor research and increased brightness of self-luminous devices 05 p0842 A67-16543

Lighting and viewing conditions posing visibility problems for lunar landing mission 20 p3521 A67-36598

LIGHTING EQUIPMENT

Special lighting equipment for high speed cinematography delivering high intensity light pulses in nanosecond range for use in shock wave and explosion filming 14 p2319 A67-28585

LIGHTNING

Black body radiation deduced by analyzing spectrum of lightning in near IR at very high temperatures 11 p1816 A67-24755

Lightning strikes on aircraft in flight from 1949 to 1966 12 p1896 A67-26170

Electrostatic, induction and radiation field effects of lightning discharge on intensity spectrum of atmospheric source signals 14 p2346 A67-27880

Atmospherics characteristics at source and propagation 14 p2265 A67-28412

Directional dependency of slow tail ELF atmospheric waveforms, noting generation by cloud to ground type lightning discharges 14 p2312 A67-28571

Lightning theories from Mount San Salvatore /Switzerland/ observations, noting corona currents 18 p3074 A67-33995

Main processes pertinent to convective storm development, with emphasis on structure and mechanics of storms already formed 18 p3074 A67-34094

Frequency amplitude spectra of atmospheric from multiple stroke lightning, showing shift to VLF 20 p3480 A67-36290

Instrumentation grounding at Cape Kennedy, noting characteristics of ground system used for safety and clean space signals 20 p3398 A67-36837

Maximum current and total light output of triggered lightning strokes at close range upon ship deck, noting photographs of discharge 22 p3793 A67-39979

Light effects and aircraft safety studied for lightning strikes, noting temporary blindness and slowing of psychomotor reactions 23 p3945 A67-41069

Shielding factors for electrostatic aerials 24 p4129 A67-41973

LIGHTWEIGHT

Economics and technology of efficient lightweight structural design 06 p1105 A67-18595

LIMB

SA LUNAR LIMB

Darkening of solar limb in UV spectral band observed through rocket sounding 17 p2945 A67-32647

Photospheric mean alpha hydrogen radiation intensity profile computed for various heights above solar surface taking into account limb-darkening effect 17 p2946 A67-32729

Instrumentation for observing limb darkening of solar continuum during annular eclipse of May 1966 20 p3529 A67-37502

Limb darkening of earth deduced from statistical analysis of IR radiance data from measurements by Tiros satellites 21 p3655 A67-38579

Visually controlled placing response tests for kittens reared without sight of limbs 24 p4113 A67-42221

LIMITER

SA POWER LIMITER

Signal suppression in ferrite frequency selective limiters evaluated using parametric subharmonic generator model 02 p0217 A67-12093

Small signal suppression and third order intermodulation products of ferrite frequency-selective limiters 05 p0780 A67-17532

Frequency selective parametric limiting by parallel pumping of subharmonic magnetoelastic waves in YIG 13 p2077 A67-26523

Hard limiter effect on test signal phase angle, considering single and two interfering signals 21 p3586 A67-38955

LIMITER AMPLIFIER

Oscillating limiter effect on message modulation for band pass filter with flat amplitude and linear phase characteristics in input signal frequency

range 01 p0025 A67-10859

Use of limiters for estimating signal to noise ratio 12 p1908 A67-26090

Bandpass hard limiter intermodulation with low input signal to noise ratio 20 p3385 A67-37356

Limiter circuits for NERVA reactor control, discussing design requirements and operation 24 p4183 A67-42472

LINCOLN EXPERIMENTAL SATELLITE /LES/

Lincoln experimental satellite program, discussing communications satellites applications 24 p4242 A67-42906

LINE

S DELAY LINE

S FORCE LINE

S FRAUNHOFER LINE

S H-ALPHA LINE

S H-BETA LINE

S LOOP

S PIPELINE

S SIGHT LINE

S SPECTRAL LINE

S TETHERLINE

S TRANSMISSION LINE

LINE CURRENT

Line source antenna radiation pattern computed from complex voltage patterns measured at various range lengths in near field 11 p1763 A67-24301

Characteristic impedance of waveguides from equivalent voltage and current definitions 22 p3765 A67-39212

LINE SHAPE

Line profile in one-electron approximation compared with impact approximation 02 p0270 A67-12521

Line broadening due to cold working Ta-10 percent Re and W-20 percent Re studied by Fourier analysis, integral breadth measurements and variance analysis 02 p0256 A67-12701

Moire fringes as parametric curves 09 p1574 A67-21837

Central tuning dip in power output of continuous wave submillimeter molecular laser to measure radiative lifetime and collision line broadening 11 p1803 A67-24932

Competitive and cascade coupling between transitions in CW water vapor laser 14 p2331 A67-28498

Plasma spectroscopy, discussing line profiles, local thermal equilibrium, methods of measuring number densities and temperatures 19 p3298 A67-35855

Quasi-stellar red shift assuming gravitational origin, deriving mass, radius and distance as function of flow density, linewidth and apparent diameter 20 p3531 A67-37683

Shape of line of deflection in systems subjected to flexural vibrations of rotating weightless shaft supporting eccentrically distributed mass points or disks 21 p3636 A67-38831

Ion-molecule collision cross section determined from pressure broadening of ion cyclotron resonance lines at high electric field/pressure ratio 22 p3840 A67-39365

LINE SPECTRUM

SA SPECTRAL LINE

Line emission of hydrogen alpha limb spectra beyond continuum limb analyzed to yield data about height of formation in solar chromosphere [AFRL-66-834] 02 p0323 A67-11694

Homogeneous transfer equation in line formation, noting correlation between thermalization length and line source function of two-level atom 02 p0266 A67-11698

Regenerative radiation from neon line in He-Ne laser, using spherical reflectors in resonator 03 p0434 A67-13096

Quark confusion with electric-dipole transition in far UV solar spectrum 04 p0694 A67-14479

Auroral hydrogen line emission quenching by collisional ionization 05 p0804 A67-17413

Sharp line emission spectra due to alkali metal doping in ZnO crystals at low temperatures 06 p1060 A67-18914

Criteria for accuracy of line intensity and mean absorption coefficient measurements 07 p1185 A67-19404

Pressure scanned Fabry-Perot etalon for measuring ruby line widths at room temperature 10 p1862 A67-22741

Stark broadening of hydrogen lines of large principal quantum number for RF

transitions by electron and ion impact approximation 14 p2389 A67-28839

Line contours for Fe-I-6302.5 angstrom across sunspot in west solar limb measured simultaneously with magnetic field strengths and direction and Evershed velocity 15 p2554 A67-29460

Rydberg series in extreme UV observed in absorption spectrum of helium-nitrogen discharges and active nitrogen [AFRL-66-835] 17 p2888 A67-32629

Photoelectric spectrophotometric study of emission line spectrum of quasi-stellar source 17 p2944 A67-32636

Interpretation of UVB measurements of quasi-stellar sources 17 p2944 A67-32637

Stationary high density high temperature plasma production spectroscopic measurements, deducing arc radial temperature and density profiles from line and continuum intensities and line profiles 19 p3274 A67-35103

Micropulsation spectra /sonagrams/ indicating magnetosphere plasma resonances with recognizable modal pattern 21 p3619 A67-38513

Coronal line spectra of 1952 total solar eclipse, noting emitted energies and isothermic coronal region 22 p3889 A67-40206

Equivalent widths of line spectrum analyzed by modification of Milne-Eddington growth procedure curve 22 p3896 A67-40528

Monograph on quasi-stellar objects including identification, line spectra, radio emission, continuum radiation, red shift and models 23 p4069 A67-41438

LINEAR ACCELERATOR

Plasma acceleration across magnetic field in linear accelerator, calculating values from voltages at electrode ends 12 p1977 A67-26075

Vehicle angular velocity determined, using configurations with only linear accelerometers and no gyroscopes for inertial navigation systems 16 p2675 A67-31266

Specific resistance, EMF, Hall effect, and minority-carrier lifetime measurement of germanium whiskers bombarded by high energy electrons from linear accelerator 16 p2732 A67-31479

LINEAR ARRAY

Currents in elements of linear uniformly spaced antenna array when mutual impedance between neighboring elements is taken into account 01 p0041 A67-11326

Imperfectly conducting cylindrical transmitting antenna design, examining contribution by ohmic resistance to distribution of current and impedance 02 p0210 A67-11590

Equivalent linear antenna substitution for antenna with plane aperture in statistical analysis of antennas 03 p0386 A67-13958

Statistical parameters of linear antenna arrays after removal of emitters 04 p0583 A67-15149

Radiation pattern of linear nonequidistant antenna array 05 p0775 A67-16964

Angular resolving power limitations for linear arrays of equispaced elements receiving EM or acoustic waves, in cases of mechanical rotation and electron beam scanning 06 p0966 A67-17576

Transient condition effects on radiation resistance and expansion in linear antennas 08 p1302 A67-20826

Eagle antenna parameters for planar and three-dimensional beam rocking 09 p1472 A67-21956

Asymmetrically fed linear antenna loaded with loading impedance analyzed in terms of two coexistent current distributions 10 p1609 A67-22774

Optimal discrete binary system of electrical control of beam position of phased linear antenna array 10 p1611 A67-22982

Reduction in directivity and increase in main lobe width of linear antenna due to turbulent troposphere 10 p1607 A67-23442

Waveguide dispersion effect on radiation pattern and directivity of series-fed linear arrays 11 p1762 A67-24289

Independent control of angular location of independent zeros of directional pattern for linear array 11 p1762 A67-24290

Frequency scanning array of emitters on convex curve 13 p2069 A67-27031

Statistical performance of wide aperture sampling linear array in HF direction finding 13 p2082 A67-27405

Directivity factor of linear antenna array with Chebyshev radiation pattern 14 p2289 A67-28862
 Statistical parameters of linear antenna arrays after removal of emitters 15 p2443 A67-29336
 Eagle antenna parameters for planar and three-dimensional beam 20 p3400 A67-37186
 rocking 20 p3400 A67-37186
 Solid state photosensitive devices combining p-n diodes and MOS circuitry noting application in electrical readout, image and pattern detection 22 p3796 A67-39332
 Radiation pattern of linear antenna erected over tapered ground screen, noting system surface impedance variation 22 p3760 A67-39628
 Mathematical model for linear memory arrays cross coupling problems, discussing signal distortion due to common mode capacitance effect 22 p3765 A67-39912
 Linear correlation-detection transducer arrays for directional noise field signals, giving N-element coherent detector performance in propagating and turbulent boundary layer 22 p3801 A67-40233
 Antenna linear array design with limited amplitude tapering, showing desirable pattern characteristics in partially uniform array 23 p3978 A67-40827

LINEAR CIRCUIT

Stability of finite connection of linear passive time-variable circuits demonstrated by Liapunov second method 05 p0785 A67-17300
 Family of custom linear integrated circuits using general purpose functional block 06 p0967 A67-17813
 Integrated semiconductor circuits and thin film hybrid circuits on insulating substrate developed in Europe for linear circuits 08 p1302 A67-20919
 Computer-aided design of linear integrated circuits 12 p1919 A67-26156
 Semiconductor integrated circuits, discussing hybrid, multichip and beam-lead methods in digital and linear circuit applications 12 p1917 A67-26203
 Linear microcircuits evaluation and application covering offset voltage and current, noise properties, input impedance, etc 18 p3013 A67-34548
 Scattering and transmission parameter methods for semiconductor device measurement, discussing linear integrated circuit test requirement 19 p3191 A67-34944
 Oscillation conditions of microwave tunnel diode theoretically and experimentally evaluated for mounting at feed point of semicircular loop antenna 19 p3196 A67-35660
 Linear autodyne circuit allowing sensitivity control irrespective of oscillation level useful in NMR lines 19 p3202 A67-35791
 Book on linear active network theory, emphasizing related circuit theory 20 p3407 A67-36119
 Linear operation of diffused planar transistor in common emitter connection studied by mathematical models 20 p3396 A67-36377
 Algorithm for generating normally distributed variables set with given correlation matrix in digital computer simulation of electronic circuit performance 20 p3401 A67-37315
 Book on analysis and design of digital and linear integrated circuits covering transistor models, system parameters, etc 21 p3597 A67-38500
 Charge time determined as circuit constants function in designing linear detectors 24 p4158 A67-42716

LINEAR EQUATION

SA NONLINEAR EQUATION
 SA REYNOLDS EQUATION
 SA SIMULTANEOUS LINEAR EQUATION
 Special functions for solving second-order or higher linear differential equations with variable coefficients in elasticity theory problems 01 p0158 A67-10215
 Series integration of linear differential equations with deviating argument 01 p0104 A67-10289
 Existence, uniqueness and reversion theorems, necessary optimality criteria and nonfixed time case for optimal control problem of n-dimensional linear parabolic equations 01 p0105 A67-10679
 Linear formulation of electromagnetic field effect on supersonic gas

flow 01 p0125 A67-10980
 Accuracy of DC amplifiers solving linear differential equations with constant coefficients, examining effect of drift and grid currents 01 p0031 A67-11264
 Integration of second order linear differential equation with boundary conditions of third kind by graphic method of Drymael 02 p0257 A67-11478
 Convergence theorem for second-order linear three-level difference scheme for class of quasi-linear parabolic differential equation 02 p0258 A67-11556
 Artificial nonlinearization method of solving linear second order equations with variable coefficients, with application to two-dimensional electromagnetic propagation along inhomogeneous dielectric layers 02 p0191 A67-11572
 Generalized solutions to second order linear or quasi-linear uniform parabolic equation 02 p0259 A67-11916
 Integral variational principles in mechanics when initial position and velocity are known 02 p0267 A67-11965
 Stabilizability of class of linear stochastic systems 02 p0259 A67-12064
 Linear equations solving methods on analog computers where system parameters are reproduced, using potentiometers and admittances 02 p0209 A67-12683
 First order linear differential equation describing line-of-sight system of air-to-air missiles in two-dimensional case 02 p0265 A67-12731
 Quasi-linear equations for inhomogeneous plasma in magnetic field applied to pumping of energy of Langmuir oscillations 03 p0475 A67-12936
 Differential moduli of differential spaces on ring or on differential solid with variable coefficients 03 p0458 A67-13460
 Stability analysis of adiabatic flow of incompressible fluid without equation linearization and by constructing functional from hydrodynamic fields 03 p0402 A67-13619
 Emitter sidewall junction capacitance in double diffused transistors, using linearly graded junction equation and two-dimensional impurity distribution 03 p0382 A67-13679
 Solar rotation, coronal self-gravitational attraction and interplanetary magnetic fields effect on solar wind, presenting linearized hydrodynamic equations 03 p0508 A67-14313
 Book on main linear boundary value problems for second order linear partial differential equations and systems of such equations satisfying ellipticity 04 p0645 A67-15006
 Newton-Raphson quasi-linearization applied to orbit determination from angular data, range and range rate, noting linear differential equations controlling orbit 05 p0894 A67-16563
 Error estimation in linear matrix equation systems by rounding-off inaccuracies 05 p0834 A67-16721
 Power source disturbance method for linear theory of flow past bodies 05 p0749 A67-17006
 Error estimate for approximate solution of linear parabolic equation using Kantorovich theorem on functional analysis in normalized space 05 p0836 A67-17108
 Downrange radar and optical data reduction used for evaluation of ejection velocities of ballistic missile penetration aids at deployment [AIAA PAPER 66-405] 05 p0902 A67-17209
 Bending stresses in cylindrical shell with rigid circular inclusion examined under axial tension and internal pressure [AIAA PAPER 66-525] 05 p0924 A67-17351
 Wave excitation in compressible partially ionized plasma by electromagnetic and acoustic /or mechanical/ sources, describing set of linearized hydrodynamic and Maxwell equations 05 p0859 A67-17436
 Reduction of systems of linear differential equations to generalized L-diagonal form 05 p0836 A67-17487
 Poincare method applied to moon motion in vicinity of equilibrium configuration, using equations of linear variation 06 p1031 A67-17775
 Lower estimates of complexity of solution of linear equations systems in summation field of integers modulo 2 06 p1023 A67-17837
 State space method for navigation

problems of nominal trajectories 06 p1028 A67-17927
 Navier-Stokes equations for two-dimensional sonic flow of viscous heat-conducting gas assuming particle velocity close to sound speed, studying asymptotic pattern 06 p0937 A67-18031
 Improving estimates of solutions of linear perturbed-motion equations of mechanical systems with variable coefficients 06 p1023 A67-18038
 Characteristic method analysis of linear system of dynamic cylindrical equation for axisymmetric motion, including rotary inertia and shear correction factor [AIAA PAPER 67-79] 06 p1104 A67-18497
 Certain properties of solutions to ordinary linear differential equations with bounded coefficients 07 p1214 A67-19178
 Modification of functional scheme of Chaplygin method applied to solution of first boundary value problem for class of quasi-linear second order parabolic equation 07 p1215 A67-19220
 Algebraic theory of finite systems of linear inequalities based on Minkowski theorem and boundary solution principle 07 p1216 A67-19582
 Solvability of Cauchy problem for second order linear parabolic equations in classes of exponentially increasing functions 07 p1216 A67-19584
 Solvability of class of linear differential equations with polynomial coefficients 07 p1217 A67-20152
 Error analysis of direct solution of linear equations with computational errors expressed as perturbations on data 07 p1149 A67-20197
 Combination into unified setting of various results for approximate solution of fixed point equation, using iterative process 07 p1218 A67-20212
 Invariant imbedding and numerical integration of boundary value problem for unstable linear systems of ordinary differential equations 07 p1218 A67-20214
 Existence theorem for nth order linear stochastic ordinary differential equations 08 p1347 A67-20356
 Simultaneous approximation of function and derivatives, ensuring uniqueness by imposing linear conditions on coefficients of polynomials 08 p1347 A67-20368
 Error in application of WKB method to linearized postburnout equation of motion of sounding rocket 08 p1406 A67-20510
 Displacement formulations of first order linear thin elastic shell equations in terms of stress resultant and middle surface, using modified Kirchhoff hypothesis 08 p1417 A67-20551
 Van der Monde systems and numerical differentiation based on Neville formula 08 p1349 A67-21194
 Ordinary linear differential equations with variable coefficients solved by phase plane displacements 09 p1524 A67-21648
 Solution of ill-conditioned linear equations when matrix of coefficients is not sparse or otherwise specialized, noting error analyses of elimination methods 09 p1468 A67-22045
 Dynamic simulation of linear differential equations 09 p1469 A67-22620
 Solving quasi-linear autonomous system with n degrees of freedom in cases of incommensurable frequencies by approximation method 10 p1673 A67-22935
 Modified first boundary value problem for linear elliptic nonself-adjoint partial differential equation in two-dimensional plane 10 p1674 A67-23077
 Field method application to linear differential equation for numerical solution of two-point boundary value problems in structural mechanics 10 p1679 A67-23147
 Unified theory for bending and buckling of honeycomb type sandwich shell and linearized governing equations applied to axially compressed circular cylinder shells 10 p1728 A67-23761
 General solutions for linearized three-dimensional equations of elastic stability of medium compressed along one axis 11 p1870 A67-23896
 Automatic technique of root location and determination of nth order polynomial equation using simple linear computing elements 11 p1756 A67-24639
 Contact problem for elastic rectangle solved by reducing problem to solution of

quasi-fully regular infinite set of linear algebraic equations with bounded free terms 11 p1876 A67-24679

Elastic stability theory according to three-dimensional linearized equations, noting necking process under 11 p1878 A67-24876

Multidimensional linear differential equations with almost periodic coefficients analyzed for error of exact solution 11 p1814 A67-24977

Problem of Vallee-Poussin type for linear hyperbolic equations with spatial variable coefficients 11 p1814 A67-25049

Existence, uniqueness and reversion theorems, necessary optimality criteria and nonfixed time case for optimal control problem of n-dimensional linear parabolic equations 11 p1814 A67-25067

Variational principles and reciprocity theorems for dynamic problems of elastic shell theory, particularly motion described by linear equations of Timoshenko type theory 12 p2019 A67-25563

Representation and uniqueness theorems for second order linear parabolic partial differential equations 12 p1961 A67-26061

Relaxation time for spatially homogeneous electron gas calculated by direct numerical integration of linearized Fokker-Planck equation 13 p2164 A67-26297

Zeta transformation applied to numerical integration operator to determine stability of solution to system of linear differential equations on digital differential analyzer 13 p2072 A67-26348

Elasticity problems for bounded connected region consisting of finite number of rectangles solved by relaxation techniques 13 p2215 A67-26372

Stability and asymptotic stability conditions for coefficients of system of linear first order differential equations 13 p2144 A67-26443

Solutions for piecewise linear differential equation obtained by plotting exciter amplitude against exciter frequency in treating pulling-in phenomena 13 p2145 A67-26625

Two-dimensional operator calculus for solving all second order linear partial differential equations of two dimensions 13 p2146 A67-26745

Asymptotic theory for near-continuum gas flows applied to BGKW equation, deriving slip coefficient 13 p2101 A67-26964

Inverse heat transfer problem in air flow past cylinder, calculating heat transfer coefficient and scaling functions 13 p2224 A67-27053

Interval arithmetic methods used for error bounding in matrix calculations of linear equations 13 p2147 A67-27170

Two LMS algorithms related to steepest descent method, obtaining generalized theorems 13 p2147 A67-27173

Elliptic regularization for symmetric positive system of linear first order partial differential equations with irregular boundaries 13 p2147 A67-27178

Characteristic initial value problem for linear second order hyperbolic partial differential equation 13 p2147 A67-27180

De la Vallee Poussin linear homogeneous differential equation of nth order with continuous functions as coefficients 13 p2147 A67-27467

Novel type of interpolation derived by introducing operator B and Chebyshev spaces 13 p2148 A67-27472

Asymptotic form of uniform approximation of abstract functions by single family of linear integral operators occurring in Banach space topology 14 p2341 A67-27834

Navier-Stokes equations governing flow linearized by using weak solution technique 14 p2295 A67-27894

Linearization of equation of thermal explosion and stability of solutions for boundary conditions of third kind 14 p2406 A67-28310

Long wave type solutions for quasi-linear elliptic equations, noting parameter lambda for small nontrivial solutions 14 p2343 A67-28386

Linear lumped component three-terminal transformerless RC circuits analyzed using digital computers 14 p2291 A67-28459

Chapman-Enskog method modified for formulation of multicomponent laminar boundary layer problem for numerical

solution 15 p2469 A67-29220

Linear integrodifferential equations describing oscillatory processes, with asymptotic solutions in terms of parameter mu through WBK method 15 p2509 A67-29232

Lie series solution of equations resulting from separation of Helmholtz equation in special coordinate systems 15 p2509 A67-29266

Stationary functionals construction for linear boundary value problem solution or solution derivatives at specified but arbitrary point 15 p2509 A67-29383

Irreducible systems existence in class of linear differential equations with quasi-periodic coefficients having frequencies represented by algebraic numbers 15 p2510 A67-29629

Unique iterative solution to degenerate quasi-linear elliptic equations and systems 15 p2511 A67-30001

Book on structural matrix analysis for engineers, giving examples of matrix algebra practical application and methods of linear equation investigation 16 p2764 A67-30966

Conditions for stability of solutions of second order linear differential equation with periodic coefficients 16 p2696 A67-31010

Fluctuating function method for approximate solution of boundary value problems for linear differential equations with reduced variational problems 16 p2696 A67-31013

Numerical approximation of evolution equation solution for linear and nonlinear operators by finite difference method 16 p2696 A67-31198

Optimization of numerical solution to linear ordinary differential equation with homogeneous boundary value conditions 16 p2698 A67-31546

Linear algebraic equations arising from least squares estimation problem, noting Gaussian elimination process on matrices 16 p2647 A67-31651

First slip time of phase locked loop of arbitrary order shown as solution of first order linear differential equation 17 p2811 A67-32117

Algorithm for constructing state equations corresponding to linear time varying system of differential equations 17 p2829 A67-32627

Linear boundary value problem solution using iterative method 17 p2877 A67-32678

Simplification of linear equation of first kind with Tikhonov smoothing functionals 17 p2878 A67-32680

Generalization of linearized equation of stationary waves in equilibrium gas dynamics applied to flow along two-dimensional sinusoidal wall 17 p2839 A67-32715

Boundary value problem of linear partial differential equation reduced to linear equation system with block-tridiagonal matrix by difference approximation 17 p2820 A67-32801

Book on computer solution of linear matrix algebraic systems and errors involved, discussing Gaussian elimination, FORTRAN, ALGOL and PL/1 programs, etc 17 p2821 A67-32825

General solution of linear differential equation of first order with quasi-periodic coefficients 17 p2879 A67-32880

Integral variational principles in mechanics when initial position and velocity are known 17 p2887 A67-33282

Integral equation solution of hydrodynamic problem through computer program 18 p3024 A67-33543

Differential equations extremal solutions, introducing infrsolution and Cauchy infrsolution concepts 18 p3070 A67-33548

Power source disturbance method for linear theory of flow past bodies 18 p2984 A67-34268

Existence theorems for defining solubility of certain boundary value problems for ordinary second order linear differential equation 18 p3072 A67-34384

Algorithm for construction of discrete approximations to linear differential expressions in terms of ordinates 18 p3072 A67-34394

Properties of solutions of linear homogeneous differential-difference equations with linear coefficients and real differences 18 p3073 A67-34814

Book on optimal control covering theory and application of linear algebra, vector analysis, Euclidean space, Pontryagin

principle, etc 18 p3018 A67-34758

Single-step numerical integration stability analysis applied to linear differential equations with known root locations 19 p3249 A67-34839

Resolving equations of linear theory of isotropic viscoelastic shells subject to external load and steady temperature field 19 p3340 A67-35508

Inhomogeneous second order linear differential equation solution based on Lie formalism, presenting physical applications 19 p3250 A67-35891

Optimal terminal guidance law for linearized equations of air-to-surface missile 19 p3258 A67-35975

Analog computer solution of linear algebraic equations system modified to eliminate negative coefficients, guaranteeing computational system stability 19 p3187 A67-36032

First boundary value problem for linear elliptic differential equations involving two small parameters 20 p3477 A67-36942

Reciprocal theorem in linearized theory of couple stresses for perfectly elastic nonhomogeneous anisotropic materials 20 p3540 A67-37281

Initial boundary value problem for Chaplygin equation using Cauchy and Dirichlet data 20 p3478 A67-37574

Laplace transformation of solution of linear differential equations with variable coefficients and time lags, analyzing motion stability 20 p3478 A67-37579

Biorthogonality relation derived between eigenfunctions of operator representing linearized anisotropic multilayer warm plasma and eigenfunctions of adjoint operator 20 p3503 A67-37711

Positive linear second order differential equation solutions, with proof of general theorems about qualitative asymptotic behavior 21 p3652 A67-38195

Elastic stability of three-layer cylindrical shell filled with corrugated metallic sheets under combined loads, deriving linear equations 21 p3724 A67-38786

Linear equation solving for gaseous mixture quantitative determination, based on combined cognitive system use of computing and programming devices 21 p3631 A67-39116

Automatic control of Block II Apollo ECS space radiator system, deriving linearized control equations for subsystem 22 p3916 A67-39174

Linear equations of motion of concentrated defect in elastic medium using variational principle 22 p3909 A67-39292

Saint Venant principle in linear and nonlinear plane elasticity in two-dimensional isotropic body 22 p3912 A67-39743

Nonstationary second order linear differential equation for near time optimal space vehicle guidance system design solved by linear transform 22 p3832 A67-39966

Stability of collisionless plasma with ions moving relative to electrons under electric field of ion cyclotron wave 22 p3852 A67-39989

Approximation method for finite element bending analysis of variable structural plates, giving linear equations defining nodal values 23 p4073 A67-40627

Boundary value problem solution convergence conditions applied to linear ordinary differential equations involving two parameters 23 p4022 A67-40746

Linear Boltzmann equation approximation by Fokker-Planck equation leading to logical inconsistency 23 p4029 A67-40963

Coupled linearized equations for laser-induced optical radiation instabilities in liquids and gases, obtaining differential operator and Green function 23 p4027 A67-41024

Shock curvature and flow variable gradients at tip of pointed axisymmetric body in nonequilibrium flow, solving linear differential equations and singularity 23 p3928 A67-41176

Cauchy problem solution for linear partial differential equation with coefficients which are functions of three-dimensional variable, deriving maximal class of uniqueness of solution 23 p4024 A67-41692

Sensitivity analysis of linear differential-difference equations with hereditary influences 24 p4134 A67-42026

Existence theorems for defining solubility

of certain boundary value problems for ordinary second order linear differential equations 24 p4177 A67-42199

Prandtl equation system for two-dimensional incompressible flows expanded to construct solutions for three-dimensional unsteady flows by straight lines method 24 p4177 A67-42200

Coupled micropolar thermoelasticity equations using strict motion invariance conditions, presenting reciprocity and variational theorems 24 p4251 A67-42659

Extrapolated Crank-Nicolson difference scheme for quasi-linear parabolic equations 24 p4180 A67-43091

LINEAR FILTER

SA WIENER FILTER

Recursive space navigation applied to navigating in near orbit of planet by measuring directions to known landmarks 01 p0110 A67-11157

Kalman filtering technique applied to classical Wiener problem, deriving equations for discrete and continuous processes 01 p0048 A67-11257

Self-contained orbital navigation system using earth-horizon measurements in 14-16 μ carbon dioxide absorption band, using Kalman linear filter 02 p0263 A67-11925

Lumped-constant filters whose bandpass depends only on one parameter of transmission coefficient, having lower bandpass for given transient process delay time 03 p0380 A67-13582

Linear nonstationary optimum filter discrimination and prediction in case of arbitrary additive noise 03 p0392 A67-13599

Signal distortion introduced by series-fed array compensated in presence of noise by prefilter and postfilter 04 p0570 A67-14874

Nonstationary problem of linear filtering in presence of additive noise solved by computer simulation 05 p0782 A67-16262

Optimal filtration of nonlinear functional of Gaussian signal, obtaining expressions for kernels of optimal filter 05 p0782 A67-16317

Linear filtering equations and Kalman filtering techniques for linear, quasi-linear, nonlinear and optimum mixer filter problems, orbit determination, space vehicle ballistic coefficient estimation, etc 06 p1028 A67-17720

Optimal signal transmission in detection system characterized by optimal linear filtration of reflected signal 06 p0963 A67-18216

Closed form general complete solution to linear time invariant second-order optimal filter 07 p1161 A67-19791

Optimization techniques for linear matched filters to obtain maximum signal to noise ratio for certain signal waveforms 10 p1621 A67-23573

Horizon sensor data processing with compensation for statistical properties of errors, noting application of optimal filtering theory 11 p1817 A67-24336

Optimal smoothing filter and smoothing error covariance matrix equations for discrete linear systems, using orthogonal projection 11 p1770 A67-24422

Computation of optimal estimators synthesis reduced through partitioning of system state vector 11 p1764 A67-24443

Local and overall stability of nonlinear discrete system with variable modes consisting of linear filter preceded by impulse modulator 11 p1770 A67-24751

Linear nonstationary optimum filter discrimination and prediction in case of arbitrary additive noise 14 p2290 A67-27845

Kalman filter divergence control, noting analytical and empirical modification methods 14 p2347 A67-28116

Simulation experiments to describe effects of measurement function nonlinearity and ambiguities when linear filters are applied in distant planet satellite orbit parameter estimation 14 p2347 A67-28130

Identification of continuous time invariant systems from input-output data, analyzing state determination problem for distributed parameter systems 15 p2460 A67-30312

Optimal signal transmission in detection system characterized by optimal linear filtration of reflected signal 16 p2620 A67-30482

Feedback realization of continuous-time optimal filter, with application in redundant signal mixing 16 p2643 A67-31269

Extrapolation of time series with discrete Laguerre polynomials, deriving general recursion relation for expansion coefficients 16 p2697 A67-31418

Filter and error-covariance equations developed for optimal fixed-point smoothing for continuous linear systems 16 p2648 A67-31652

Optimal filtration of nonlinear functional of Gaussian signal, obtaining expressions for kernels of optimal filter 18 p3016 A67-33868

Computer method for determining time-frequency-domain response specifications of transversal linear wave filters, using thin film RC distributed networks 18 p3015 A67-34560

Multistage linear dynamic systems with sequentially correlated noise, evaluating filtering, prediction and smoothing procedures 19 p3206 A67-35941

Output SNR dependence on difference between input signal and natural frequencies for quasi-optimal linear filters, noting improvement for mismatched input 22 p3761 A67-39867

Asymmetry and peakedness variation from normal distribution of random process at output of linear filter matched with broadband PM and PPM signal 22 p3761 A67-39868

Optimal filtering theory for horizon sensor data processing for orbital navigation, examining statistical characteristics 22 p3834 A67-40196

Kalman-Bucy filter for optimum radio inertial navigation, discussing a priori estimation 24 p4182 A67-42184

LINEAR PREDICTION

Stress-rupture data for refractory metals which yields linear relationship between Larson-Miller parameter and logarithm of applied stress 03 p0441 A67-13253

Anomalous polarization of four cosmic OH lines predicted from states of polarization in OH maser amplifier 13 p2161 A67-27289

Optimum estimation of linear dynamic systems with stochastic transition and output model matrices, independent from one sample point to next, with known mean and covariance 16 p2652 A67-31693

LINEAR PROGRAMMING

SA DUAL CONTROL PROBLEM

SA NONLINEAR PROGRAMMING

Optimized distribution of personnel reduction in naval overhaul and repair activities with minimum reduction in readiness 01 p0016 A67-10932

Continuous linear programming problems with time delays in constraints, noting construction of solutions to dual problem from solution to primal problem 02 p0207 A67-12059

Quadratic programming applied to design of digitally compensated sampled data control system 03 p0393 A67-13902

Iteration method of general linear programming on digital computer using penalty functions compared to equilibrium problem of mechanical system 05 p0781 A67-16259

Weight factor of optimizing functional determined by distribution of roots for analytical design of optimal controls 06 p0977 A67-18547

Solution approximation for nonlinear parabolic PDEs, using linear combination of finite set of selected functions 07 p1213 A67-19159

Class of problems of parametric linear programming of set of convex polyhedron having only target function coefficients dependent on parameter 07 p1219 A67-19167

Linear fractional programming application to Markov renewal programming, determining stationary optimal policy for cost/time minimization 07 p1218 A67-20269

Model for synthesizing and analyzing communication systems, detailing use in converting command and control information transfer into physical and performance specifications 08 p1292 A67-20673

Experiment selection process for specific flights in Apollo applications program /AAP/, using algorithms [AAS PAPER 66-142] 08 p1411 A67-20967

Repetitive analog computer for Monte Carlo method solution of linear stochastic programming problems 08 p1299 A67-21198

Geometric interpretation of product form of inverse applied to sparse matrices in linear programming, using graph

theory 10 p1673 A67-22833

Static and kinematic formulation of plastic analysis of structures and duality in linear programming 11 p1876 A67-24623

Convex polyhedron theorem in determining whole set of optimal solutions in linear programming 11 p1814 A67-24979

Experiment selection process for specific flights in Apollo applications program /AAP/, using algorithms [AAS PAPER 66-142] 13 p2214 A67-27548

Sampled data feedback control system using quadratic programming to determine optimum compensator 16 p2646 A67-31636

Optimal trajectories for linear discrete system with respect to minimax criteria using standard programming code 16 p2650 A67-31670

Linear programming algorithm for optimizing channel assignments in satellite communication systems 17 p2810 A67-32111

Linear programming algorithm for optimizing life support systems of space vehicles in terms of minimum weight/efficiency ratio 17 p2807 A67-32254

Generalized linear programming applied to control theory noting use of differential equations 17 p2829 A67-32430

Design procedure for production of radiation resistant NOR gate logic circuit 21 p3603 A67-38185

Weight factor of optimizing functional determined by distribution of roots for analytical design of optimal controls 22 p3776 A67-39747

Repetitive analog computer for Monte Carlo method solution of linear stochastic programming problems 22 p3784 A67-39865

Fredholm equation solution and minimax theory for p-dimensional vector signal detection against p-dimensional Gaussian noise background 22 p3762 A67-39876

Solution of linear system of equations with singularity and stable with respect to small changes in matrix elements 23 p4023 A67-41048

LINEAR SYSTEM

SA NONLINEAR SYSTEM

Noise factor of linear receiving systems in quantum and classical regions, noting role of dual push-pull amplifier and frequency converter 01 p0022 A67-10393

Elastic stability theory formation by combining thermodynamic and mechanical stability 01 p0159 A67-10402

Optimal control system for linear plant with modulus limited control actions 01 p0044 A67-10491

Invariant and optimal linear systems with periodic parameters analyzed by transfer function calculation 01 p0044 A67-10492

Undetermined coefficients method for obtaining particular solution of linear ordinary system with constant coefficients, solving final matrix equation 01 p0105 A67-10729

Lateral motion of simply supported axially loaded viscoelastic column governed by system of linear ordinary differential equations with periodic coefficients 01 p0106 A67-10732

Limiting theorem for weak convergence of solutions of differential equations with random right hand part to Markov process 01 p0106 A67-10922

Algorithm for reducing linear time-invariant differential systems to state form applied to systems described by transfer functions 01 p0047 A67-11219

Closed loop realization of optimum control law superior to open loop implementation for linear system not asymptotically stable or subject to random disturbances 01 p0048 A67-11225

Minimax rendezvous time of two linear uniform control plants, constructing optimal pursuit 02 p0225 A67-11956

Synthesis of optimum discrete control for eventual state of linear stochastic system, reducing problem to solution of Bellman functional equation 02 p0225 A67-11957

Damping linear system with aftereffect 02 p0225 A67-11962

Computational method for optimization of infinite time control problem for linear systems and quadratic indexes of performance 02 p0226 A67-12148

Suboptimal solutions for class of linear regulator problems with soft saturation constraints, noting Hamilton-Jacobi equation 02 p0226 A67-12150

Kalman filter estimation of covariance parameters of linear system subjected to Gaussian driving 02 p0227 A67-12157

Role of second order internal resonance in problem of stability of equilibrium of system neutral in linear approximation 03 p0467 A67-12860

Necessary conditions for stability of trivial solutions of parabolic systems of partial differential equations 03 p0456 A67-12861

Restrictions placed on transfer function of linear system with input and output coordinates in presence of given plant in control loop 03 p0390 A67-13098

Soviet book on theory of automatic control systems of regular linear, special linear and nonlinear types 03 p0390 A67-13108

Linear optimal systems with time delays 03 p0392 A67-13270

Stability of single-frequency solutions to quasi-linear autonomous systems with two degrees of freedom 03 p0468 A67-13625

Periodic perturbations accumulation in linear system with one degree of freedom 03 p0469 A67-14178

Suboptimal policies for fuel optimal control and energy optimal control problems for linear time invariant system obtained, using Liapunov functions 04 p0590 A67-14418

Minimum norm control for linear time-varying system by fixed point method 04 p0594 A67-15878

Stability region of complex linear self-conjugate systems of differential equations containing skew-Hermitian matrix 04 p0647 A67-15980

Forced parametric oscillations in linear system, obtaining solutions for case where excitation frequency is twice natural frequency 05 p0916 A67-16243

Optimization of linear control systems when placing step limitations on control, using functional analysis 05 p0781 A67-16251

Synthesis problem of optimum dynamic characteristics of multivariate linear control systems with random input signals 05 p0781 A67-16252

Numerical procedure for optimizing stability of linear dynamic system by applying steepest descent method 05 p0845 A67-16437

Synthesis and control strategy of optimal final value linear system under random environment statistically considered, using Bellman dynamic programming 05 p0783 A67-16442

Linear system providing maximum signal to noise ratio for given parameters of correlation function of incoming quasi-harmonic signal mixed with white noise 05 p0787 A67-17396

Book on linear automatic control systems with varying parameters 06 p0973 A67-17714

Optimum control of multidimensional and multilevel systems, discussing linear systems, load distribution, cyclic optimization and aggregated systems 06 p0974 A67-17933

Optimal control of linear stochastic systems with complexity constraints applied to sampled data system 06 p0975 A67-17934

Asymptotic stability of periodic solutions of nonautonomous quasi-linear systems with two degrees of freedom 06 p0975 A67-18037

Matrix method determination of time response of time invariant linear systems to range of deterministic functions 06 p0976 A67-18402

Uniqueness of extremal controls for minimum fuel problems pertaining to single input linear time-invariant systems 06 p1098 A67-18523

Minimum time and fuel problems for PFM systems, deriving optimal control by heuristic argument 06 p0977 A67-18524

Stability-instability transition of equilibrium configuration of linear elastic system under nonconservative follower forces 06 p1105 A67-18589

Sign codes and patterns of state variables for finding all possible responses in linear third order closed loop feedback control system 06 p0978 A67-18721

Approximation method of determining statistical characteristics of phase coordinates of linear automatic control systems 06 p0978 A67-18792

Sommerfeld effect in linear oscillating system with randomly variable natural

frequency 07 p1261 A67-19140

Asymptotic solution for oscillations of quasi-linear gyroscopic systems taking into account internal resonance 07 p1261 A67-19189

Computer generation of error probability distribution for linear system response to random conditions 07 p1217 A67-20117

Optimal control for linear system with respect to performance functional which includes trajectory sensitivity 08 p1309 A67-20327

Transfer function of linear system obtained from discrete values of input-output data 08 p1311 A67-20344

Stability and inverse receptance of multidegree systems under harmonic excitation 08 p1415 A67-20479

Imparting motion to system of two masses coupled by linear elastic shaft in infinite set of piecewise continuous loads, by variational method of influence functions 08 p1354 A67-21047

Optimum transformation of linear system with minimal rms error from given point to fixed delta-environment of another given point 08 p1313 A67-21322

Transient processes in linear automatic control systems dependent on parameters which appear when differential equations of analyzing system are transformed by Laplace-Karson method 08 p1313 A67-21324

Optimal control analysis of system behavior described by linear stochastic differential equations 08 p1313 A67-21325

Dynamic properties of linear system with damping analyzed by matrix technique 09 p1575 A67-22160

Optimum control and prediction in designing self-adjusting controllers for linear systems with correlated disturbances 10 p1618 A67-22732

Stability of linear systems with time delay analyzed by introducing stability indicative function, noting applications to differential-difference equations 10 p1679 A67-22916

Independent linearized solutions closely approximating Mises and Tresca /M-T/ limit loads in linear theory of plasticity for plane strain 10 p1716 A67-22933

Analytical design of controllers for linear autonomous systems of arbitrary order 10 p1619 A67-23320

Waveform independent condition for transmission coefficient in linear time-independent transmission system to provide upper limit to signal distortion 10 p1620 A67-23572

Optimal control system for linear plant with modulus limited control actions 10 p1621 A67-23613

Invariant and optimal linear systems with periodic parameters analyzed by transfer function calculation 10 p1621 A67-23614

Time variable linear transmission systems with arbitrary initial state in case of abruptly varying periodic or nonperiodic system parameters and input signal analyzed, using Laplace transform 10 p1608 A67-23638

Book on modern control systems covering feedback control system, root locus and frequency response method, time-domain analysis, etc 11 p1769 A67-24062

Mean square asymptotic stability of linear system described by nth order equation with random coefficients 11 p1818 A67-24161

Approximate normal mode technique, providing solution to sinusoidal and white noise randomly excited damped linear multidegree of freedom system, for application to mathematical model [ASME PAPER 67-VIBR-2] 11 p1871 A67-24164

Automatic optimization problem for linear Diophantine plant via analysis of discrete extremal problems 11 p1770 A67-24209

Generalization of binary processes, discussing time domain and frequency domain analysis 11 p1813 A67-24312

Penalty function method used for bounded phase coordinate optimal control problem for linear discrete systems with quadratic cost functionals 11 p1771 A67-24891

Gradient acceleration technique for solving optimal systems with unbounded control 11 p1771 A67-24896

Eigenvector scalar product solutions for closed loop time optimal control of linear systems 11 p1771 A67-24897

Equation for linear dynamic systems simplification applicable to all cases

irrespective of nature of eigenvalues and eigenvectors 11 p1772 A67-24898

Liapunov functions generated by transformation of Companion matrix to Routh or Schwarz canonical forms, for asymptotically stable linear time-invariant multivariable systems 11 p1814 A67-24942

Amplitude and phase frequency characteristics of linear system determined from transfer characteristics 11 p1772 A67-24980

General formula for numerical solution of ODE of any order and linear and nonlinear systems 12 p1960 A67-25434

Relation between correlation functions of stationary random input and output for linear discrete systems 13 p2144 A67-26430

Multidegree of freedom linear system analysis by dividing method for relations between system constants and solutions 13 p2156 A67-26527

Time optimum control in n-dimensional linear dynamic system with constant coefficients determined by matrix method 13 p2087 A67-26619

Time optimal control problems of linear systems with state and control vectors 13 p2087 A67-26723

Analog computer application in linear, nonlinear and time-varying systems 13 p2072 A67-26995

Restoration of distorted signals for linear and nonlinear process converters 13 p2088 A67-27021

Dynamic errors in electronic analog computers, noting expressions for shift in characteristic roots of equations under solution 13 p2073 A67-27064

Algorithm for minimal realization of linear finite-dimensional dynamical system displayed by Markov parameters 14 p2291 A67-28066

Energy method extended to stability analysis of linear system under action of nonconservative forces 14 p2398 A67-28094

Deflection limits on plate-twisting test 14 p2399 A67-28102

One-dimensional small signal linear model of fluid transmission line using finite lumped parameter elements and Navier-Stokes equations 14 p2247 A67-28265

Dynamical systems control problem in connection with differential equations with lagging arguments 14 p2291 A67-28384

Characteristic vectors theory and application to study of asymptotic behavior of solutions to differential systems 14 p2342 A67-28385

Mutually adjoint boundary value problems for linear systems of first order equations of composite type with two independent variables 14 p2344 A67-28670

Space-time region division method for reducing nonlinear heat conduction to subordinate linear multilayer system problems, assuming stationary time characteristics and coordinates 14 p2408 A67-28804

Computational worst error algorithm for linear systems and quadratic error criteria, showing flowgraph and computer execution results 15 p2457 A67-29367

Approximate model for simplification of linear dynamic system, neglecting effect of higher order time constants 15 p2457 A67-29370

Plotting inverse of transfer function, deriving equations for hodograph and for gain values which yield greater or equal damping ratios 15 p2457 A67-29372

Computational error caused by finite word length of aerospace computers 15 p2439 A67-29596

Liapunov direct method applied to Hermite theorem on number of positive real part zeros of complex polynomial and stability theory of linear motions 15 p2458 A67-29899

Liapunov functions generating methods applicable to nonlinear and linear autonomous systems 15 p2511 A67-30048

Continuous estimation of frequency response of linear system directly from random input and output data measurements 15 p2465 A67-30345

Minimum realization of linear time-varying nonanticipative system characterized by its impulse response matrix 16 p2697 A67-31426

Behavior of high-order linear control systems analyzed using Liapunov second method, by finding low-order model with

closely approximate response behavior of high order linear control systems analyzed, using Liapunov second method, by 16 p2647 A67-31648

Filter and error-covariance equations developed for optimal fixed-point smoothing for continuous linear systems 16 p2648 A67-31652

Conjugate gradients providing convergent means to solve optimal-control problems for linear systems with quadratic performance index 16 p2651 A67-31678

Continuous control process with random variable stopping time of known probability distribution, presenting optimal feedback control, trajectory and minimum cost 16 p2651 A67-31681

Adjoint simulation technique extended to signals consisting of continuous, sampled and multirate sampled systems with random inputs 16 p2652 A67-31684

Recursive procedures for determining relationships between random parameter of linear system and resulting output random variable 16 p2652 A67-31691

Necessary and sufficient conditions for decoupling time-invariant linear multivariable system by state variable feedback, discussing transfer matrix consequences 16 p2652 A67-31692

Optimum estimation of linear dynamic systems with stochastic transition and output model matrices, independent from one sample point to next, with known mean and covariance 16 p2652 A67-31693

Riemann matrix in linear symmetric-hyperbolic systems of partial differential equations with constant coefficients in two-space and one-time variables 17 p2876 A67-32031

Inaccurate determination effect of input-signal characteristics on filtration quality, deriving equations for estimating upper limit of relative increase of rms filtration error 17 p2829 A67-32223

Boundary value problem of linear partial differential equation reduced to linear equation system with block-tridiagonal matrix by difference approximation 17 p2820 A67-32801

Linear temperature measuring system and automatic regulating system accuracy, investigating heat transfer with random input for recipients of various forms 17 p2973 A67-33074

Liapunov approach to obtain sufficient conditions for stability of parametrically excited random vibrational system [ASME PAPER 67-APM-9] 17 p2886 A67-33145

Sufficient conditions guaranteeing asymptotic stability of class of linear dynamic systems with bounded narrow band parametric excitation [ASME PAPER 67-APM-24] 17 p2830 A67-33152

Sommerfeld effect in linear oscillating system with randomly variable natural frequency 17 p2965 A67-33217

Minimax rendezvous time of two linear uniform control plants, constructing optimal pursuit 17 p2831 A67-33273

Synthesis of optimum discrete control for eventual state of linear stochastic system, reducing problem to solution of Bellman functional equation 17 p2831 A67-33274

Damping linear system with aftereffect 17 p2831 A67-33279

Correlation function for random process energy spectrum at linear system output, obtaining expression of envelope distribution for radio signals 18 p2999 A67-33506

Stability and instability of tridiagonal linear system, noting application to stability analysis of differential equation 18 p3070 A67-33644

Iterative methods for integration of linear partial differential equations, determining relaxation factor 18 p3071 A67-33753

Construction and uniqueness of time optimal control of multidimensional linear system with constraints on control signal amplitudes and rates 18 p3017 A67-34280

Requirements of optimal controller for system with constraints imposed on control magnitude 18 p3018 A67-34283

Linear theory of initially straight elastic rods, discussing wave propagation, thermal effects for extension and flexure and torsion 18 p3144 A67-34287

Response of logarithmic frequency

characteristics of dynamic linear systems to small parameter variations 18 p3018 A67-34441

Approximation method of determining statistical characteristics of phase coordinates of linear automatic control systems 18 p3018 A67-34457

Design of optimal waveforms for optimal estimation or prediction of state of linear dynamical system in presence of Markov and white noise 19 p3201 A67-34965

Progressing wave method for linear partial differential equation systems, including Maxwell equations, applied to electromagnetic waves from moving sources 19 p3184 A67-35665

Virtual work principle shown equivalent to linear coupled thermoelasticity theory 19 p3342 A67-35763

Initial conditions effect on transient states of linear systems 19 p3205 A67-35909

Estimation and filtering in discrete linear systems with reference to Gaussian statistical hypothesis 19 p3250 A67-35910

Collocation method convergence in problems other than general linear problem of ordinary integral equations and those with homogeneous kernel 19 p3250 A67-36047

Book on viscoelasticity covering linear theory as part of applied mechanics, differential equations, hereditary integrals, etc 20 p3535 A67-36138

Cross-spectral method application problems in feedback system analysis, identification and linear time invariant system 20 p3407 A67-36785

Crank-Nicolson technique for first order linear time-invariant differential equation solution, discussing truncation error 20 p3477 A67-36933

Existence theorems for linear optimal control problems with nonlinear cost functionals 20 p3408 A67-37076

Linear optimal stationary control system with state dependent white noise disturbances described by differential equation 20 p3408 A67-37077

Approximating probability characteristics of mismatch for steady mode of operation of astatic servosystem with modulation 20 p3409 A67-37201

Optimal control theory for distributed parameter systems using dynamic programming, showing use in two-point boundary control problems involving partial differential equations 20 p3410 A67-37320

Optimal control theory for linear distributed parameter systems, presenting solution algorithms and computational results for several problems 20 p3411 A67-37321

Numerical methods for linear optimal control problems, noting applicability of algorithms to certain nonlinear problems 20 p3411 A67-37375

Multiple integration method for determining coefficients and differential equation order for linear dynamic systems 20 p3412 A67-37378

Optimality and invariance conditions for linear free-time problem 20 p3412 A67-37582

Potential linear theory applied to oscillatory profiles moving at uniform velocity inside ideal fluid 20 p3424 A67-37593

Synthesis procedure for linear automatic feedback control systems, examining time-domain response 20 p3413 A67-37679

Analytic representation of absolute topography of isobaric surfaces by linear combination of arbitrary surfaces represented by Chebyshev polynomials 21 p3654 A67-38087

Necessary and sufficient conditions for linear system response to input vector with limited amplitude and slope, noting singular case existence 21 p3603 A67-38175

Inequality for pointwise bounds of second initial boundary value problem for second order semilinear parabolic equation, noting Rayleigh-Ritz method 21 p3652 A67-38176

Linear boundary value problem for system of first order partial differential equations having real and imaginary characteristics 21 p3653 A67-38398

Linear oscillator forced motion subjected to harmonic AM perturbations studied for servomechanisms 21 p3658 A67-38554

Atmospheric inhomogeneities effect on large antenna directive gain, noting dependence on length and wave field 21 p3600 A67-38812

Rapid parameter identification system for linear time-invariant plant with only input and output measurable 21 p3604 A67-38867

Perturbation scheme for linear system performance determination based on component performance information 21 p3654 A67-39063

Matrix method proposed for systems of linear differential equations governing satellite attitude control in elliptical orbits, considering integral criteria calculation 22 p3897 A67-39160

Satellite-gyroscope asymptotic equilibrium positions obtained by general motion equation, calculating gravitational and aerodynamic moment effects 22 p3898 A67-39187

Linear differential games associated with vector differential equation in arbitrary dimensional space noting square matrix and convex sets 22 p3826 A67-39214

Optimal control of quasi-linear system perturbed motion, developing approximation method 22 p3776 A67-39305

Point-to-point mapping technique in combination with variational calculus for solving optimum control problems for piecewise linear dynamic systems 22 p3776 A67-39776

Multivariable linear system noninteracting control realized by relays sliding motions 22 p3777 A67-39839

Book on continuous and scanning control systems optimization and random processes theory including numerical techniques, harmonic analysis and Gaussian transformation 22 p3777 A67-40070

Suboptimal linear control laws involving parameter optimization 22 p3777 A67-40156

Terminal guidance problem involving optimal control for deviations in systems with transport lag 22 p3833 A67-40158

Linear servosystem parametric optimization and application to satellite attitude control, discussing selective and gradient methods 23 p4070 A67-40577

Serial/matrix technique extended to give multivariable linear system responses defined in state space terms 23 p3983 A67-40646

Coates flow graph gain formula modification by introducing loop-set and two-loop-set for linear systems analysis 23 p3984 A67-40649

Multivariable Popov criterion application to stable and to state feedback law linear finite-dimensional systems, noting toleration of nonlinearities 23 p3984 A67-41158

Parameter invariance problem for linear systems solved by obtaining necessary and sufficient conditions for invariance in optimal control systems 23 p3984 A67-41159

Parameter variation of optimal linear control systems with quadratic performance index /Liapunov function/ 23 p3985 A67-41161

Comparison of flat channel linear MHD induction generator analysis stressing gross power output in constant current and voltage modes 23 p3942 A67-41737

Invariant form of strain-energy function of linearized elastic potential of isotropic thin shell using three-dimensional theory 24 p4249 A67-42156

Piecewise linear switching functions design for suboptimal regulation of linear plants with relay controller in regard to transient response performance criterion 24 p4135 A67-42179

Controllability and observability of parallel and tandem connections of two linear time invariant differential systems of Jordan canonical form representation 24 p4135 A67-42181

Design procedure for estimating state vector of discrete-time linear stochastic system with constrained memory estimator 24 p4135 A67-42185

Controller design method for linear feedback control systems with transport lag by parameter plane and dominant root methods 24 p4136 A67-42291

Vector space convexity and nonmonotonicity proof, discussing 34-dimensional linear space and l-implicial convexity 24 p4179 A67-42729

Linear optimal control in systems with uncertain parameters, noting application to design of compensating network for flexible booster for uncertain value of first bending mode 24 p4137 A67-42903

LINEAR TRANSFORMATION

Nonsingular linear transformation of time-invariant linear dynamic system into canonical /phase-variable/ form 01 p0048 A67-11223

Signal-space quantization and bandwidth compression examined, using theory of mappings of signal spaces with Riemann matrices 01 p0027 A67-11239

Differential equations describing wave transformation in weakly inhomogeneous plasma 04 p0668 A67-15217

Linear transformation of normalized static capacitance matrix used to describe TEM propagation on array of parallel conductors 08 p1304 A67-21224

Quantumstatistical thermodynamics with several temperatures for indivisible observation level 10 p1733 A67-23477

Bound solutions for elliptical equation in n-dimensional vector space obtained, using linear transformation into Martin boundary 11 p1814 A67-24852

Iterative methods for solving nonlinear least squares problems by choosing linear nonsingular transformations of finite-dimensional Euclidean space 13 p2147 A67-27171

Extension of Zygmund approximation series to two dimensions, noting periodic function role 14 p2345 A67-28938

Transformation of class of boundary value to initial value problems in terms of one-or two-parameter group of transformations for ordinary differential equations 15 p2511 A67-29892

Differential equations describing wave transformation in weakly inhomogeneous plasma 15 p2532 A67-30265

Martin boundary for invariant Markov processes investigated on group of affine transformations of straight line 17 p2878 A67-32736

Lower bounds for eigenvalues of differential linear elliptical operator using Rayleigh-Ritz approximation extension 24 p4177 A67-42154

LINEAR VIBRATION

Book on linear vibration theory including generalized properties and numerical methods 09 p1576 A67-22423

Power series solutions of singular vibration problems converted to quotient of polynomials by transformation into continued fractions, using perturbation technique [ASME PAPER 67-VIBR-7] 11 p1872 A67-24167

Linear effects of oscillations of liquids in right circular cylinder, determining stability of forced oscillations 14 p2296 A67-27984

Optimization for linear vibration isolators considering vibration clearance tradeoff for random base motion 16 p2703 A67-31642

Book on control systems and linear vibrational mechanical systems emphasizing use of analog and digital computers, frequency response, complex plane and root locus plots, FORTRAN method, etc 17 p2822 A67-33133

System parameters of linear time-variant space communication channels from input-output viewpoint, measuring correlation functions and Doppler spread 24 p4123 A67-42476

LINEARITY

SA NONLINEARITY

Linearity of MOS transistor as variable resistor improved by keeping substrate floating and connecting substrate to drain 01 p0036 A67-10439

Internal modulation and heterodyning in construction of highly linear large-deviation VHF solid state FM oscillator /FMO/ 03 p0381 A67-13636

Motion theory of discrete defects in linear elastic continuum 05 p0908 A67-16038

Phase linearity of microwave component and interaction of cascaded devices, giving analysis of two-port device 08 p1303 A67-21029

Computer method using coefficient linearity along diagonal of matrices to calculate N/h/ profiles of ionosphere 16 p2669 A67-31897

Ge/Li/ drifted gamma detector for 1/2 to 10 Mev range, measuring response deviation from linearity 23 p3998 A67-40819

LINEARIZATION

SA BERNOULLI EQUATION

First order solution of economical impulse

transfer between near-circular, coplanar or noncoplanar, close orbits by linearization of circular nominal orbit 01 p0152 A67-11404

Signal stabilization by linearization of time independent nonlinearities using extra signal and nonlinearity, noting role of pulse width modulation [ASME PAPER 66-WA/AUT-21] 04 p0592 A67-15392

Statistical linearization of nonlinear aerodynamic coefficient of angle-of-attack moment of aircraft 04 p0549 A67-15884

Piecewise linear approximation procedure for linearization of readings of nondifferential vibrating and string transducers 06 p1003 A67-18174

Nonlinear equations of thin shell theory, especially equilibrium equations, taking into account displacements, elongations and shear, noting linearization in stability problems 12 p2025 A67-25605

Modified quasi-linearization method for numerically solving trajectory optimization problems with undetermined terminal time 12 p2008 A67-25913

Lagrange and Euler representations of particle shapes and vortex theorems in hydrodynamic flow 13 p2094 A67-26644

Discrete ordinate technique for nonlinear Boltzmann equation for hard sphere molecules, considering pseudoshock relaxation 13 p2102 A67-26973

General dispersion relation for linear waves in multicomponent plasmas 13 p2172 A67-27726

Linear waves in weakly ionized multicomponent plasmas investigated using dispersion relation 13 p2172 A67-27728

Four-plate compensators of Jamin and Lowe type for interferometers, emphasizing linear dependence of phase difference on dispersion and rotation 14 p2315 A67-28074

Nonlinear differential equations of systems describable by state model solved by incremental linearization technique 15 p2458 A67-29908

Optimal interorbital transfers between near-circular noncoplanar closely spaced orbits described in terms of linearized theory 15 p2563 A67-30389

LINER

Acoustic liners to suppress screech in hydrogen-oxygen engines 04 p0691 A67-15988

Driver chamber for very high temperatures obtained with ceramic liner for arc driven shock tube, reducing contamination and cooling of driver gas 14 p2293 A67-28749

Thermal stresses in thin shell in contact with smooth rigid container 14 p2403 A67-29011

Metal lined glass filament-wound pressure vessel performance at cryogenic temperatures, discussing fibers, resins and liners [ASTM PAPER 17] 18 p3067 A67-34578

LING-TEMCO-VOUGHT MILITARY AIRCRAFT

S A-7 AIRCRAFT

LINK

SA CROSS LINKING

SA DATA LINK

Optimum design of curve generating four-bar linkages with inequality constraint [ASME PAPER 66-MECH-20] 08 p1336 A67-21317

Damped least squares method for kinematic synthesis of plane curves described by paired coordinates for four-bar linkage mechanism [ASME PAPER 66-MECH-13] 08 p1336 A67-21318

LILOVILLE EQUATION

Book on kinetic equations of gases and plasmas, with emphasis on theories which start from Liouville equation 04 p0660 A67-14581

Kinetic equation for inhomogeneous electron plasma derived from Liouville equation by Prigogine-Balescu diagram technique 08 p1366 A67-21431

Perturbation theory developed to estimate magnetic surface stability against field irregularities, noting role of field resonances 10 p1686 A67-23468

Physical foundations of modern kinetic theory, showing interpretation of particular form of Liouville equation in terms of time scales appropriate to system 11 p1823 A67-24545

Kinetic equation for completely ionized plasma generalized for several particle species case 13 p2165 A67-26585

Dynamics of weakly ionized gases analyzed using Liouville equation 13 p2167 A67-27003

Radiation field interaction with particles in assemblage of electrons and atoms or ions using perturbation theory and Liouville equation 19 p3284 A67-35339

Continuous phase medium gas representation used to derive variational principles for Liouville, coupled Bogoliubov and kinetic equations 22 p3835 A67-39218

LIPID

SA ADIPOSE TISSUE

SA FATTY ACID

Optical rotation of lipids extracted from soils, sediments and Orgueil carbonaceous meteorite 08 p1289 A67-21173

Thiobarbituric acid reacted substance reaction with ribonuclease may be possible source of age pigment 15 p2433 A67-29296

Enzyme activity of light and heavy crude ribosomal fractions in Saccharomyces cerevisiae indicating subcellular sites of lipid synthesis 21 p3573 A67-37919

LIPID METABOLISM

Individual phospholipids in hemispheres of rat brains and rate of turnover of phosphate groups during oxygen deprivation 04 p0562 A67-15548

Acetylative capacity and lipid metabolic changes and readjustment to normality in rats in oxygen-rich environment 14 p2256 A67-28588

Rats exposed to different hyperoxic atmospheres for 20 days studied for toxic lipids formation 24 p4112 A67-41854

LIPSCHITZ CONDITION

Upper and lower bounds on distance between zeros of components of solutions of second order ordinary nonlinear differential equations 12 p1961 A67-26062

Nonlinear differential equations of systems describable by state model solved by incremental linearization technique 15 p2458 A67-29908

LIQUEFACTION

Crossed electric and magnetic fields effect on quasi-liquefaction process of nonconducting particles by electrolyte 01 p0121 A67-10189

Conservation of cryogenic propellants on long duration space missions by reliquefaction of vapor 13 p2091 A67-27636

Microsegregation and grain boundary liquation in heat affected zone of 18-Ni maraging steel welds 22 p3812 A67-39448

Large scale liquefaction, storage, transport and ground handling of liquid helium for applications in space operations 22 p3781 A67-40393

LIQUID

SA ORGANIC LIQUID

Shear relaxation in liquids, criticizing Knollman, Miles and Hamamoto relaxation time distribution measurement method 05 p0758 A67-16133

Cavitation induced detonation of stoichiometric liquid mixtures 11 p1884 A67-24956

Liquid crystal - Conference, Kent State University, August 1965, Part III 18 p2991 A67-33633

Liquid-zone melting process for preparing alloy bars with variable compositions 18 p3065 A67-34294

Conductivity and IR absorption spectra of organic semiconductors in polycrystalline, melt and liquid states 22 p3861 A67-39922

LIQUID AMMONIA

Compact portable high purity H generator using liquid ammonia for indirect method H-O fuel cell 24 p4106 A67-42524

LIQUID ATOMIZATION

Mean droplet size for cross stream water injection into Mach 8 air flow determined by scattered light angular variation measurement 11 p1779 A67-24366

Disintegrating liquid jet penetrating high speed gas stream 17 p2839 A67-33009

Apparatus for uniform sized liquid drop production by ultrasonic wave action on fluid jet, with drop formation recorded by photography 18 p3052 A67-34610

Injector inlet conditions effects on combustion delay time in liquid bipropellant rocket engine, noting propellant atomization and droplet vaporization 22 p3868 A67-40161

LIQUID COOLED REACTOR

Hydrogen solubility in eutectic sodium-

potassium mixture, noting usefulness as nuclear reactor coolants, and dependence on pressure and temperature variations 16 p2619 A67-30620

LIQUID COOLING

Ground station receiver for satellite communication which utilizes liquid-helium-cooled parametric amplifier at top producing extremely low noise temperature 01 p0023 A67-10469

X-band ruby maser design with liquid hydrogen cooling for high gain at low pumping power 07 p1194 A67-19131

Charpy impact specimens cooling rates in low temperature quenching baths evaluated including specimen size, notch geometry and material chemistry effects 11 p1874 A67-24265

Liquid cooling of integrated circuit systems to remove increased heat dissipation, noting heat transfer rates 12 p1915 A67-25888

Cooldown of shrouded spherical vessels in liquid nitrogen, determining smallest tank-shroud gap compatibility with rapid cooldown 13 p2229 A67-27666

Separation of variables method for cylinder cooling with turbulent fluid flow parallel to axis 17 p2972 A67-33072

Optimum relative angular velocity selected for cooled high temperature gas turbine stages, discussing blade mean cooling depth and cooling heat 22 p3870 A67-40456

Liquid transport cooling system for aircrew evaluated by collecting in-flight sweat rate on fighter aircraft flying combat and training in tropics 23 p3966 A67-41581

Experiments on undercooling and overcooling with liquid cooling garments, noting correct cooling defined by narrow biothermal response band 23 p3970 A67-41655

Liquid coolant space radiator system for manned spacecraft thermal control, investigating design and transient performance [SAE PAPER 670838] 24 p4252 A67-41994

LIQUID DROP

Stokes creeping flow equations and steady flow of incompressible viscous fluid past liquid drop 01 p0051 A67-10458

Polarized light crystallization microanalysis for supercooled water droplets with additives applied to spherical single crystals of ice during droplet freezing 01 p0109 A67-11010

Combustion of gaseous fuel jets in oxidizing atmosphere 04 p0726 A67-15453

Disruption of water jet into large drops studied by photography 04 p0609 A67-15591

Liquid droplet combustion at high pressures revealing effects of vapor source distribution on predicted burning time at supercritical pressures 05 p0929 A67-17359

Stability of motion of plane boundary interface between two different density coupled fluid jets analyzed to determine role of viscosity in drop formation 11 p1782 A67-24959

Combustion of pure liquid monopropellant droplet burning in own combustion products at low Reynolds numbers 14 p2376 A67-28552

Droplets and bubbles in liquids studied using general thermodynamic equilibrium criteria 17 p2971 A67-33043

Effect of additives on hydrazine nitrogen trioxide droplet flame structure and burning rate [AIAA PAPER 67-482] 18 p3158 A67-33951

Ignition and extinction characteristics of liquid fuel droplets burning in oxidizing atmosphere calculated, using finite rate kinetics 19 p3214 A67-35000

Water injection for alleviating reentry plasma sheath-induced communication blackout, analyzing spherical drop evaporation in free molecular flow 19 p3211 A67-35762

Flow pattern caused by low speed splash of liquid drop into pool computer examined, obtaining configuration plots various splash stages 19 p3212 A67-35895

Theoretical collision efficiencies for cloud droplets in steady Stokes flow suggest near unity coalescence probability 23 p4024 A67-40636

Liquid drop impact on liquid, calculating velocity potential, initial pressure and time dependence of cavity depth and wall velocity 23 p3991 A67-41459

LIQUID-FILLED SHELL

Vibrations of elastic shells containing

liquids 01 p0165 A67-11441

Forced small axisymmetric oscillations of elastic right circular cylinder with end plates in form of shallow spherical shell filled with heavy ideal fluid 03 p0530 A67-14174

Temperatures in cylindrical receiver resulting from rapid filling with compressible fluid compared with classical bottle-filling case [ASME PAPER 66-WA/PID-2] 04 p0555 A67-15380

Kollmann theory on critical rpm of hollow shells of revolution containing liquid, explaining unstable oscillations appearance in supercritical region 06 p1100 A67-17992

Inertia effects of internal liquid column on vibration of thin walled pressurized elastic cylindrical bellows type container [AIAA PAPER 67-38] 06 p0986 A67-18262

Linear shell theory for nonlinear transverse coupled vibrations of partially filled circular cylindrical elastic tank [AIAA PAPER 67-74] 06 p1101 A67-18272

Lagrange equations of motion for solid body with liquid-filled cavities derived, using Hamilton-Ostrogradskii principle of least action 07 p1224 A67-20029

Dynamics of booster rockets and spacecraft with cavities partially filled with liquid 08 p1412 A67-21113

Lumped parameter analysis of liquid-filled shells with application to 1/10-scale Saturn V model 10 p1713 A67-23749

Lower modes and frequencies of natural elastic oscillations of vessel formed by liquid-filled shell of revolution taking into account fluid surface wave and shell inertia 12 p2020 A67-25566

Three-layer shell with lightweight filler under creep studied for initial forms of equilibrium 12 p2024 A67-25598

Variational methods for calculating small axisymmetrical oscillations of conical shell of revolution partially filled with ideal incompressible fluid 12 p2028 A67-25633

Vibration of cylindrical shell containing flowing incompressible perfect fluid 13 p2215 A67-26528

Flutter and dynamic stability of closed thin walled elastic cylindrical shell filled with liquid 13 p2219 A67-26903

Time dependent pressure distribution and threshold acceleration for bubble formation in longitudinally vibrating flexible liquid filled cylinder [ASME PAPER 67-FE-1] 14 p2304 A67-28354

Motion of gyroscope with conical cavity filled with ideal incompressible fluid describing rotating motion 15 p2518 A67-30171

Approximate calculation of coefficients in equation for perturbed motion of rigid body containing liquid 16 p2765 A67-31051

Dynamic instability of longitudinal oscillations of cylindrical shell charged with ideal fluid established by approximate reduction of nonlinear equations 21 p3720 A67-38297

Oscillation stability of rotating cylindrical shell filled with ideal incompressible weightless fluid, determining instability region distribution 21 p3721 A67-38302

Nonlinear mechanical model with mathematical pendulums for solid bodies containing nonlinearly oscillating liquid in motion 21 p3612 A67-38307

Linear shell theory for nonlinear transverse coupled vibrations of partially filled circular cylindrical elastic tank [AIAA PAPER 67-74] 21 p3727 A67-38866

Plane motion of container formed by two concentric cylinders and radial partitions partly filled with small vibrating ideal fluid 22 p3786 A67-40029

LIQUID FLOW
SA WATER FLOW

Stability of dry patches forming in thin liquid film flowing over heated surface, noting effects of vapor thrust and thermocapillarity 01 p0167 A67-10975

Heat transfer in viscous fluid flow in gap between permeable isothermal surface and rotating disk, solving energy equation 03 p0536 A67-13611

Ideal incompressible liquid motion in rectangular container due to rectangular double and sinusoidal pulse excitation 03 p0404 A67-13784

Generalized Couette-type flow with variable viscosity in plane and annular

channels, liquid being injected or sucked through porous surfaces 04 p0602 A67-14639

Quantity of separated liquid deposited on wall of rectangular channel from turbulent air-water dispersed annular flow, calculating liquid flow rate 04 p0602 A67-14641

Volterra method used for two-dimensional problems of pressure penetration and penetration of small wedge into layer of incompressible liquid 04 p0604 A67-14778

Continuous spatially varied open channel liquid flow analogy for gas flow, with heat addition and extraction over finite distance 04 p0604 A67-14838

Wave flow of thinly layered fluid on vertical plane, noting fluid-gas interface stress 04 p0609 A67-15597

Frozen layer that forms when warm liquid flows over flat plate cooled below freezing temperature of liquid by coolant flowing along other side of plate 04 p0735 A67-15856

MHD effects in liquid crystals 05 p0846 A67-16736

Supersonic liquid jets produced by ballistic extrusion with velocities of 4.58 km/sec 06 p0982 A67-17603

Laser velocimeter measurement of point velocities in turbulent liquid flow in pipe, using statistical analysis to verify results [AIAA PAPER 67-179] 06 p0990 A67-18511

Free boundary flows of viscous liquid, analyzing Stokes flow at zero Reynolds number 06 p0990 A67-18641

Turbulent flow of electrically conducting fluid in pipe located in longitudinal magnetic field 06 p1044 A67-18689

Flow of thin layer of liquid on surface of rotating body of revolution in moving system of coordinates connected with body 06 p0991 A67-18817

Motion instability of liquid in interspace between two rotating spheres when ratio of radii approaches 2 06 p0992 A67-18820

Convective heat transfer through stabilized turbulent flow of chemically homogeneous liquid in circular pipe under supercritical pressure conditions 07 p1265 A67-19127

Outflow of perfect ponderable fluid from opening in bottom of cylindrical container measured by numerical integration method by finite differences 07 p1169 A67-20207

Bibliography and subject index to two-phase gas-liquid flow literature 07 p1269 A67-20300

Numerical calculation of free oscillations of liquid in static container 08 p1319 A67-20310

Linear theory solution of eigenvalue problem for natural convection in horizontal layers giving characteristic Rayleigh numbers for first ten modes 08 p1427 A67-21139

Cauchy problem for nonstationary linearized Navier-Stokes equations for fixed container partially filled with liquid 09 p1532 A67-21873

Spatial dispersion of viscosity coefficients of liquids near critical point 09 p1487 A67-21904

Motion equations and boundary conditions for viscous liquid, noting operator characteristics of viscosity coefficients near critical point 09 p1487 A67-21909

Forced convection heat transfer to liquid flowing within unsymmetrically heated rectangular ducts 10 p1733 A67-23481

Dynamic response of periodic liquid flow systems as function of structural support motions, noting resonance points and pressure amplitudes 10 p1628 A67-23737

Liquid film flowing instability down inclined plane with respect to Tollmien-Schlichting wave compared with surface wave formation 11 p1774 A67-23860

Book on hydraulic control systems covering fluid flow theory, hydraulic pumps, motors, valves, power elements, etc 12 p1899 A67-25558

Gas mixture component concentration in fluid film flowing down wall, determining quantity of gas component transported by fluid per unit time 13 p2094 A67-26638

Stabilizing or destabilizing effect of electromagnetic force on liquid film flow 13 p2167 A67-26930

Steady state fluid flow in thin passage analyzed using energy model and including compressibility effects 14 p2302 A67-28264

Laminar boundary flow over dielectric disk with homogeneous magnetic field

perpendicular to plane of disk, obtaining liquid velocity and electric field density 14 p2358 A67-28282

Expansion of plane jet of conducting liquid in magnetic field 14 p2302 A67-28304

Enthalpy and position in heated tube where liquid boiling begins, finding heat content in turbulent liquid 14 p2406 A67-28311

Compressible fluid flow in capillary tubes, discussing reduction in variation of pressure difference/mass flow ratio 14 p2303 A67-28350

Liquid discharge from cylindrical container exposed to longitudinal vibration, noting flow retardation 16 p2658 A67-30946

Lagrange equations of perfect fluid flow linked to datum point and geometric surface arbitrarily moved within 16 p2663 A67-31709

Transverse magnetic field effect on barrier wake oscillation in electrically conducting liquid 16 p2723 A67-31714

Stationary flow in viscous fluid film on rotating body of revolution, using differential equations 17 p2836 A67-32261

Unsteady heat transfer between solid body and surrounding fluid flow, using convective fluid heat transfer and body thermoconductivity equations 17 p2972 A67-33071

Separation of variables method for cylinder cooling with turbulent fluid flow parallel to axis 17 p2972 A67-33072

Empirical equations for compressive properties of liquids, noting applicability at high pressures 17 p2841 A67-33386

High speed liquid jet in standing acoustic field with velocity vector transverse to jet axis, testing injector orifice diameter, viscosity, etc [AIAA PAPER 67-473] 18 p3026 A67-33943

Heat transfer in viscous fluid flow in gap between permeable isothermal surface and rotating disk, solving energy equation 18 p3181 A67-34476

Acoustic vibration effect on heterogeneous mass transfer at sphere surface in high Prandtl number liquids 20 p3554 A67-37068

Convective heat transfer through stabilized turbulent flow of chemically homogeneous liquid in circular pipe under supercritical pressure conditions 21 p3731 A67-38171

Similarity parameters of gravity and pressure driven liquid discharge from propellant tanks obtained by dimensional analysis 22 p3785 A67-39969

Propulsion and time requirements for low gravity liquid settling obtained from known Bond number 22 p3869 A67-40171

Forced resonant nonlinear oscillation of liquid in cylindrical tank 22 p3787 A67-40192

Heat transfer of fluid flow in annular channel with rotating shafts, deriving surface heat transfer estimation without axial flow 22 p3921 A67-40457

Liquid drop impact on liquid, calculating velocity potential, initial pressure and time dependence of cavity depth and wall velocity 23 p3991 A67-41459

Liquid mercury conductor flow in annular gap electromagnetically accelerated by Lorentz force, showing restricted nonexistence proof for inviscid problem 23 p3992 A67-41742

Longitudinal turbulence intensities, autocorrelations, energy spectra and peak energy dissipation frequencies for organic solvents flowing in smooth round tubes 24 p4141 A67-41927

LIQUID GAS

Self-diffusion coefficients of simple liquids as predicted by Rice-Allnatt theory, noting friction coefficient and correlation function 06 p1035 A67-17989

WKB approximation of quantum radial distribution function for neon intermolecular pair potential taking into account particle exchange effect 06 p1038 A67-19044

Liquidified natural gas application to SST, noting improvement in engine performance with use of methane 13 p2185 A67-27439

Apparatus for plasma investigation of pulsed arc discharge in high pressure argon 23 p4035 A67-41886

LIQUID-GAS MIXTURE

Dynamic control for two-phase liquid-gas medium under weightlessness solved by surface energy, using computer for boundary value problem involved 02 p0231 A67-11540

Formation of cavities and microjets in liquids and role in initiation and growth of explosion 11 p1883 A67-24631

Vacuum vaporization of saturated liquids on weightlessness, showing that separated bubbles remain in nucleation sites 12 p2034 A67-25726

Pressure drop study of near saturation Freon 11, noting flowing liquid quality condition for estimates 13 p2106 A67-27668

Heat transfer and skin friction increase for gas stream with liquid-droplet suspension flowing over blunt-nosed body near stagnation point 14 p2405 A67-28126

Incompressible two-phase mixed flow through sharp edge orifice including shear force between phases 14 p2305 A67-29012

Criteria for optimum liquid mixing for impinging jet injector elements, noting parameters for maximum efficiency 15 p2545 A67-29445

Dynamic control for two-phase liquid-gas medium under weightlessness solved by surface energy, using computer for boundary value problem involved 16 p2663 A67-31606

Detonation properties in heterogeneous systems involving mixture of fuel with gaseous oxidant 20 p3551 A67-36815

LIQUID HELIUM

Steady state heat flow in dielectric cylinders in boundary scattering limit, considering liquid helium 08 p1426 A67-20716

Large helium refrigerators for very high speed cryopumping techniques required in space simulation facilities 12 p1924 A67-25716

Absolute emissivity calorimeter design for low temperature measurements above 60 degrees K using liquid helium as cryogenic fluid 13 p1212 A67-27661

Size and power requirements of liquid helium temperature refrigerators 13 p2057 A67-27679

Multistage gas-bearing helium compressor development 13 p2057 A67-27681

Light-weight liquid helium dewar for use on Apollo spacecraft 13 p2057 A67-27682

Cooling system for maser amplifier for ground station satellite communication 14 p2277 A67-27778

CdSb single crystals doped with Au at liquid helium temperature studied for temperature dependence and Hall effect 14 p2372 A67-28757

Electric breakdown, dielectric constant and dissipation factors of cryogenic liquid nitrogen, hydrogen and helium 14 p2341 A67-28891

Book on experimental superfluidity covering He properties, low temperature production, temperature measurement, two-fluid model and macroscopic quantization, generalized hydrodynamic equations, etc 15 p2517 A67-29265

Temperature dependence of sound velocity in liquid helium at saturation vapor pressure and cryogenic temperatures 17 p2886 A67-33231

Liquid He 4 ground state studied by variation method, deriving radial distribution function 22 p3835 A67-39301

Liquid helium technology - Conference, Boulder, June 1966 22 p3838 A67-40388

Boiling heat transfer to liquid helium, discussing heat flux as temperature difference function and surface finish effect 22 p3920 A67-40390

Lightweight liquid helium dewar for LEM program, with 670 liter capacity, 10 percent ullage and 1.5 percent boiloff per day 22 p3808 A67-40391

Pressure, volume, temperature and internal energy data for He using constant volume calorimeter and gas thermometer, discussing He melting 22 p3920 A67-40392

Large scale liquefaction, storage, transport and ground handling of liquid helium for applications in space operations 22 p3781 A67-40393

Cryogenically stored helium pressurization system for LEM descent stage propulsion system, discussing weight advantages and liquid helium heat transfers 22 p3749 A67-40394

Liquid helium application in electromagnetic DC, LF and HF AC devices 22 p3838 A67-40397

Thermodynamic properties of low temperature gaseous and liquid mixtures, discussing quantum effects in mixtures containing hydrogen isotopes and high density mixtures 22 p3921 A67-40553

Helium sorption by nitrogen, oxygen and argon cryodeposits, discussing pumping speeds and capture coefficients 24 p4115 A67-42047

Heat transfer from plate located on dielectric base to liquid helium in pulsed regime influencing kinetics of superconductivity in thin films 24 p4254 A67-42258

Collected papers of Kapitza, Volume 3 covering low temperature production, stereoscopic films, liquid He, etc 24 p4188 A67-42294

Pionic and muonic K-series X-rays studied by liquid He scintillation counter, obtaining separation peaks 24 p4192 A67-42735

LIQUID HELIUM 2

Noise occurrence during heat transfer from solid to liquid He 2 flux at high temperature difference, discussing heat flux 22 p3838 A67-40389

Efficient inertial navigation system with He 2 superfluid persistent current gyro element having small drift rate 22 p3808 A67-40395

LIQUID HYDROGEN

Materials for use as rolling-contact bearing lubricants in liquid hydrogen environment 01 p0077 A67-10119

Structural design of hypersonic vehicle flight tank for liquid hydrogen fuel, discussing loading, material, support system, stress analysis, testing and analytical problems [SAE PAPER 660679] 01 p0161 A67-10583

Strain gauges applied to epoxy laminates in liquid hydrogen insulation systems 01 p0072 A67-11107

Calibration of flow meters in liquid hydrogen at high flow rates for establishing limits of extrapolations from lower flow rate data 03 p0422 A67-13771

Mechanical properties of Kh21G7AN5 steel at liquid hydrogen temperature 04 p0636 A67-14751

Nucleonic cryogenic quality meter design and development and fluid monitoring through hydrogen vent line on Saturn S-IVB stage under orbital conditions 05 p0842 A67-16540

Silicon surface barrier detector beta gauge for density measurements in liquid hydrogen 05 p0842 A67-16541

Pure and applied cryogenics, Volume 5, Liquid hydrogen 05 p0927 A67-17010

Critical phenomena in fluids with reference to liquid hydrogen 05 p0928 A67-17011

Physical properties of liquid hydrogen 05 p0928 A67-17012

Liquid hydrogen use in nuclear rocket testing, noting Kiwi reactor, Dewar system, transfer line, etc 05 p0789 A67-17013

Liquid oxygen and liquid hydrogen as propellants for rocket engines noting propulsor chamber, turbopump feed system and U.S. and French designs 05 p0874 A67-17014

Liquid hydrogen production techniques in purification, ortho-para conversion and refrigeration 05 p0789 A67-17017

Liquid hydrogen tank insulation, content gauging and design of transfer lines and valves 05 p0789 A67-17018

Liquid hydrogen pressure, temperature, flow and liquid level measuring techniques 05 p0807 A67-17019

X-band ruby maser design with liquid hydrogen cooling for high gain at low pumping power 07 p1194 A67-19131

Space evacuation of NRC-2 insulation for liquid hydrogen tankage, noting vacuum test apparatus and cold plate test 10 p1734 A67-23727

Liquid hydrogen fuel tankage thermal protection in manned hypersonic vehicles, discussing results of tests in steady state conditions [AIAA PAPER 67-297] 12 p2035 A67-26012

Liquid hydrogen for SST fuel compared with hydrocarbons, considering range, payload, weight, drag, engine design, storage and safety 13 p2186 A67-27635

Conservation of cryogenic propellants on long duration space missions by reliquefaction of vapor 13 p2091 A67-27636

Low gravity liquid hydrogen tank venting, considering systems with heat exchange for space missions 13 p2057 A67-27640

Stratification similitude laws for liquid hydrogen determined and extrapolated to

full size tanks from small tank data 13 p2186 A67-27643

Thermal performance of liquid hydrogen in horizontal hypersonic vehicle fuel tank 13 p2186 A67-27646

Safety practices for high energy physics research equipment filled with liquid hydrogen or deuterium 13 p2092 A67-27649

Project Rover liquid hydrogen safety 13 p2092 A67-27650

Future supersonic and hypersonic aircraft horizontal liquid hydrogen fuel tank requirements, discussing insulation optimization using variable thickness 13 p2054 A67-27657

Klegcell G-300 mechanical and thermal properties tested for thermal insulation for cryogenic stage for liquid hydrogen on space vehicle 13 p2228 A67-27659

Electric breakdown, dielectric constant and dissipation factors of cryogenic liquid nitrogen, hydrogen and helium 14 p2341 A67-28891

Bypass flow reduction in liquid hydrogen and liquid oxygen tank mounted boost pumps on Centaur launch vehicle 17 p2800 A67-31978

Liquid hydrogen heat exchanger for servicing Saturn V S-II stage 17 p2954 A67-32011

Polymeric materials in expulsion bladders for cryogenic liquids, describing fabrication, flexibility, permeability, storage, transfer, control factors, etc [AIAA PAPER 67-457] 18 p3069 A67-33931

Generation and loading of triple point hydrogen for high performance aircraft, boosters and spacecraft [AIAA PAPER 67-468] 18 p3110 A67-33938

Liquid hydrogen pumping for Phoebus reactor, discussing feed systems, nozzles, configurations, design, testing, etc [AIAA PAPER 67-478] 18 p3077 A67-34402

Mechanical properties of Kh21G7AN5 steel at liquid hydrogen temperature 18 p3066 A67-34409

Turbulent boundary layer in liquid hydrogen tank, determining attachment point, velocity and temperature profiles 19 p3310 A67-34810

Variable thickness insulation system for transport of hydrogen propellant into earth orbit for docking transfer to lunar and interplanetary mission vehicles [ASME PAPER 67-HT-50] 20 p3548 A67-36732

Forced convective film boiling heat transfer to H studied from experiments on cooling down Cu test section by liquid H 22 p3918 A67-40092

Improvement of high performance liquid fuel rocket engine by optimization of liquid hydrogen /LOX/ propulsion mixtures 23 p4049 A67-41319

Flight strain gauge system for Centaur /AC-6/ liquid hydrogen fuel tank skin 23 p4008 A67-41390

LIQUID INJECTION

SA FUEL INJECTION

SA WATER INJECTION

Mass transfer and hydrodynamics of gas jet injection into liquid surface, deriving empirical equations for hollow truncated point formed around injection 04 p0727 A67-15754

Yellow-green luminosity accompanying injection of triethylborane into upper atmosphere 12 p1932 A67-25208

Liquid metal MHD cycles with condensation by multistage injection of liquid 12 p1897 A67-25379

Thrust vector controls for solid rockets, discussing liquid secondary injection, jet tabs, direct chamber bleed, omniaxial movable nozzle and lockseal 15 p2545 A67-29136

Energy conversion with liquid metal working fluids in MHD converter, proposing stepwise injection and expansion to reduce impact losses 16 p2604 A67-30572

Liquid metal injection techniques used in magnetohydrodynamic converters 16 p2606 A67-30587

Behavior of high speed, coherent, turbulent liquid jet in planar, standing, transverse acoustic field 16 p2658 A67-30945

Volatile liquid pressurization as expulsion method for storable propellants noting in-flight refueling system design parameters 17 p2953 A67-31973

Disintegrating liquid jet penetrating high speed gas stream investigated for

amplification of capillary and acceleration waves [AIAA PAPER 67-495] 18 p3026 A67-33959

Nonairbreathing internal combustion engines injector configurations, noting power supply and lunar surface vehicle applications 24 p4107 A67-42533

LIQUID LASER

Liquid lasers use of rare earth ions, chelate structures, selenium oxychloride, etc 15 p2501 A67-30086

LIQUID LEVEL

Cryogenic liquid level sensor consisting of diode heated by resistor 01 p0062 A67-10194

Liquid metal level measurements using thermocouple type probes as tank sensors, noting usage of electrical resistance of probe sheath 01 p0070 A67-11027

LIQUID-LIQUID INTERFACE

SA SURFACE TENSION

Numerical determination of axisymmetric equilibrium shapes of interface between two nonmixing liquids uniformly rotating in vessel under weak centrifugal and capillary forces and zero gravity conditions 03 p0402 A67-12882

Droplets and bubbles in liquids studied using general thermodynamic equilibrium criteria 17 p2971 A67-33043

Mass-transfer coefficients through plane surface in liquid-liquid systems, examining interphase turbulence 19 p3345 A67-35566

Geometric prediction method extension to quaternary liquid-liquid equilibria in two-phase systems comprising two type I ternaries 19 p3346 A67-35612

Decompression sickness studied by investigating cavitation at liquid-liquid interface 21 p3573 A67-38076

LIQUID MERCURY

S MERCURY /METAL/

LIQUID METAL

SA MERCURY /METAL/

Oscillation of fluid metal droplet, free or immersed in fluid dielectric, in steady and uniform magnetic field 01 p0120 A67-10181

Small oscillations of viscous liquid-metal droplet under capillary force and in presence of magnetic field 01 p0120 A67-10182

Two-phase flow and material attrition problems for Rankine cycle liquid metal power plants [ASME PAPER 66-GT/CLC-4] 01 p0014 A67-10872

Fabrication of columbium alloy liquid metal loop to study boiling and condensing characteristics of Na and K up to 1000 degrees F with gas tungsten arc welding in helium atmosphere 01 p0080 A67-10945

Liquid metal level measurements using thermocouple type probes as tank sensors, noting usage of electrical resistance of probe sheath 01 p0070 A67-11027

Activity of oxygen in liquid Fe-Pt alloy system, determining temperature and composition effect on equilibrium constant 02 p0256 A67-12708

Electrical conductivity, Hall coefficient and absolute thermoelectric power of liquid antimonides and tellurides 03 p0495 A67-13533

Hydrodynamic journal bearing tests in molten lithium at 600 to 800 degrees F to support compact canned rotor liquid metal pump [ASME PAPER 66-WA/LUB-6] 04 p0629 A67-15338

Wear and compatibility of liquid metal bearing materials, including surface coatings and cemented refractory carbides, analyzed for Rankine cycle power plants [ASME PAPER 66-WA/LUB-3] 04 p0630 A67-15350

Density of liquid alkali metals in generalized equation obtained by method of thermodynamic similarity 04 p0640 A67-15596

Liquid metal MHD converter with multistage thermodynamic drive for use as power source in space vehicles as alternative to thermionic converter 04 p0559 A67-15965

Staustahlrohr experiments in thermodynamic acceleration process for liquid metal of MHD converter for space vehicle propulsion 04 p0580 A67-15966

MHD analysis of composite slider bearing using electroconductive lubricant such as liquid metal, in magnetic field perpendicular to bearing surface, for large and small

Hartmann numbers [ASME PAPER 66-LUB-B]

05 p0811 A67-16275

AC power generation by linear channel liquid metal MHD inductive generator 05 p0754 A67-17348

Electric conductivity of liquid metals as function of electron oscillation frequency 06 p1032 A67-18125

Chemical behavior of metallic elements predicted by periodic table, noting formation of liquid and solid metallic solutions, binary and complex metallides and nature of chemical bond 06 p1018 A67-18233

Longitudinal magnetic field effect on convective heat transfer during turbulent MHD pipeflow of liquid Ga 06 p1044 A67-18682

AC MHD generator with liquid metal working fluid operating under self-excitation conditions 06 p0951 A67-18683

Hydraulics of electromagnetic liquid-metal metering device with constant inlet pressure, noting dose value dependence on parameters and operating conditions 06 p0951 A67-18684

Two-phase liquid metal cycle MHD conversion, discussing thermodynamic aspect, hot gas system and possibility for use in spacecraft and ground power plants 12 p1896 A67-25121

Self-excited liquid metal MHD induction generator 12 p1897 A67-25378

Liquid metal MHD cycles with condensation by multistage injection of liquid 12 p1897 A67-25379

Linear induction MHD generator with cryogenically cooled coil windings for alleviating large gap and short stator problems 12 p1898 A67-25380

MHD power generation using bifluid liquid metal system /such as Li and Cs/ with two-phase generation 12 p1901 A67-25897

Electron bombardment thrusters using liquid mercury cathodes noting lifetime, propellant and power efficiency, feed system, temperature limits, etc 13 p2188 A67-26822

Forces acting in electromagnetic pump channel on gas inclusions in liquid metal, assessing increase in hydraulic resistance 13 p2169 A67-27316

Dynamic-seal technology in applications employing liquid metals, gas and standard organic fluids for ground, aerospace and space turbomachinery [ASME PAPER 67-DE-50] 14 p2328 A67-28881

Energy conversion with liquid metal working fluids in MHD converter, proposing stepwise injection and expansion to reduce impact losses 16 p2604 A67-30572

Hydrodynamics of liquid-gaseous metal mixture flowing through nozzles, discussing heat exchange rate and condensation effects 16 p2656 A67-30574

Magnetohydrodynamic generators operating with two-phase liquid metal flows, describing design and performance 16 p2604 A67-30577

Liquid metal magnetohydrodynamic power generation for space vehicle use 16 p2605 A67-30583

Fluid metal magnetohydrodynamic power conversion program results 16 p2606 A67-30584

Liquid metal energy converters using magnetohydrodynamic induction noting electrodynamic aspects 16 p2606 A67-30586

Liquid metal injection techniques used in magnetohydrodynamic converters 16 p2606 A67-30587

Magnetohydrodynamic generator functioning by emulsion consisting of gas or vapor in liquid metal 16 p2606 A67-30588

Liquid metal magnetohydrodynamic power generation systems using condensing ejector or two-phase jet pump 16 p2606 A67-30589

Magnetohydrodynamic liquid metal power conversion systems investigated using thermodynamic properties 16 p2606 A67-30590

Thermodynamics of injector of magnetohydrodynamic power unit using two-phase vapor-liquid metallic working fluid 16 p2607 A67-30591

Hydrogen solubility in eutectic sodium-potassium mixture, noting usefulness as nuclear reactor coolants, and dependence on pressure and temperature variations 16 p2619 A67-30620

Reaction kinetics of liquid titanium and hafnium with carbon using layer-growth

method 16 p2690 A67-31373

Performance characteristics of helical electromagnetic induction pumps calculated taking into account effect of duct wall and liquid metal layer 16 p2609 A67-31584

Thermodynamics of MHD converter cycles with previously mixed liquid metal used as working body, discussing thermal, electrical and energetic efficiency 16 p2610 A67-31780

Liquid-metal and plasma MHD systems for power generation in space environments, noting Rankine and Brayton cycles [JPL-TR-32-1129] 17 p2802 A67-32049

Book on thermodynamics of irreversible phenomenon in liquid metals including Onsager symmetry relations, phenomenological theory, nuclear magnetic resonance, galvanic and thermomagnetic phenomenon, etc 17 p2968 A67-32233

Two-phase liquid metal MHD generators, appraising friction losses and conductivity limitations 19 p3175 A67-34802

MHD generators using liquid metals examined for advantages/limitations, discussing loop design 19 p3268 A67-35063

Operating characteristics of induction pump with asymmetrical current supply, calculating magnetic induction, currents and forces in liquid metal layer 20 p3365 A67-37307

Heat-transfer coefficients for laminar and transitional liquid metal flow in tube with constant wall heat flux 20 p3555 A67-37608

Oscillation of liquid sodium drop in dielectric medium in presence of constant magnetic field 21 p3665 A67-38245

Dimensional analysis method for determining similarity criteria for MHD processes in liquid metals and alloys 21 p3665 A67-38248

Liquid metal cathode electron bombardment thruster operable at high temperatures, noting stability in neutralizer current range [AIAA PAPER 67-667] 21 p3690 A67-38701

Sputtering yields and energy-transfer efficiency measurements by ion beam sputtering of liquid metals indicate no justification for incorporation into low thruster [AIAA PAPER 67-683] 21 p3692 A67-38714

Cycle and separator efficiencies and specific radiator area compared for liquid alkali metal-lithium MHD power generators 21 p3572 A67-38864

Liquid metal properties - Conference, Upton, N.Y., September 1966, Part 1 21 p3685 A67-39101

Pseudopotential-structure factor relation for small wave vector applied to liquid alkali metal electric resistivities and temperatures 21 p3686 A67-39102

Liquid metal properties - Conference, Upton, New York, September 1966, Part 2 21 p3686 A67-39103

Liquid mercury equation of state and electrical resistivity at high temperatures and pressures 21 p3686 A67-39104

Surrounded atom model for thermodynamic enthalpy and entropy characteristics of mixing in liquid binary alloys 21 p3733 A67-39105

Sodium-potassium alloy thermodynamic properties and ordering, with pairing model for configurational entropy loss 21 p3733 A67-39106

Properties of liquid metals - Conference, Upton, New York, September 1966, Part 3 21 p3686 A67-39107

Electrical conductivity and transport properties of pure liquid metals 21 p3686 A67-39108

Electron-electron interaction effect on Li soft X-ray emission spectrum, liquid metal optical absorption and alkali metal dielectric response 23 p4037 A67-40760

Liquid metal MHD converters with multistage injection condensation, calculating cyclic process efficiency through thermodynamics 24 p4098 A67-42085

Technical feasibility of rocket propellant combinations involving metal combustion and chemical heating of excess H 24 p4206 A67-42403

Electric power generation using two-phase liquid-metal cycles in MHD converter, discussing liquid metal dynamics 24 p4099 A67-42417

SNAP-8, nuclear electric power-conversion system /PCS/ designed for operation in space, using liquid metals as working

fluids 24 p4184 A67-42497

LIQUID METAL COOLED REACTOR /LMCR/

Shield-radiator weight tradeoffs to optimize K Rankine cycle space power plant heat source operating temperature, noting burnup 24 p4185 A67-42537

LIQUID NITROGEN

Heat flux measurements of liquid-nitrogen superinsulation systems, noting effects of material types and assembly techniques 04 p0720 A67-14531

Film boiling of saturated nitrogen flowing upward in vertical heated tube, noting annular-flow regime change to vapor matrix [ASME PAPER 65WA/HT-26] 08 p1427 A67-21319

Cryopumps incorporated into liquid N shrouds for small space simulation chambers 12 p1900 A67-25710

Conductivity of cleaved surfaces of GaAs in liquid nitrogen 13 p2174 A67-26371

Heat flux measurements of liquid-nitrogen superinsulation systems, noting effects of material types and assembly techniques 13 p2222 A67-26580

Man rating requirements of space environment simulation laboratory consisting of two large chambers with floors which can be cooled by liquid nitrogen down to 92 degrees K 13 p2090 A67-26841

Electric breakdown, dielectric constant and dissipation factors of cryogenic liquid nitrogen, hydrogen and helium 14 p2341 A67-28891

Gravity and buoyancy effects on slip ratio, void fraction, flow model and boiling heat transfer [ASME PAPER 67-HT-63] 20 p3549 A67-36745

Conductivity of cleaved surfaces of GaAs in liquid nitrogen 21 p3680 A67-38326

Thermal conductivities of cryogenic insulation systems determined by two methods using calorimetry measurement of boil-off rate of liquid cryogen 22 p3802 A67-40292

LIQUID OXIDIZER

Atlas booster materials compatibility with fluorine oxidizers 13 p2186 A67-27687

LIQUID OXYGEN /LOX/

SA LOX-HYDROGEN ENGINE

Liquid oxygen and liquid hydrogen as propellants for rocket engines noting propulsor chamber, turbopump feed system and U.S. and French designs 05 p0874 A67-17014

Saturn S-IB stage fuel system, studying LOX density fluctuations, heat transfer and boiling under various weather conditions 13 p2186 A67-27637

Contaminant concentration in liquid breathing oxygen of aircraft converter determined by gas chromatography 16 p2619 A67-31475

Bypass flow reduction in liquid hydrogen and liquid oxygen tank mounted boost pumps on Centaur launch vehicle 17 p2800 A67-31978

Improvement of high performance liquid fuel rocket engine by optimization of liquid hydrogen /LOX/ propulsion mixtures 23 p4049 A67-41319

LIQUID PHASE

Thermal emf and electric conductivity in solid and liquid semiconducting copper-antimony-ditelluride 02 p0297 A67-11846

Second harmonic generation in liquid crystals, noting absence of effective center in molecular configuration 09 p1517 A67-22680

LIQUID POTASSIUM

Potassium metal Rankine cycle power system, testing turbines, bearings and seals, potassium boiler and steam topping cycle analysis obtaining high heat-transfer coefficients [AIAA PAPER 66-1009] 02 p0184 A67-12307

Carbon and nitrogen mass transfer rates by liquid potassium in 16 thermal convection loops of type 316 stainless steel with niobium/one-percent-zirconium and stainless steel tabs at 1200 to 1800 degrees F 07 p1223 A67-19465

Electrical conductivity measurement of liquid-vapor potassium mixture flowing in circular steel tube simulating MHD oscillator conditions 16 p2712 A67-30575

Potassium metal Rankine cycle power system, testing turbines, bearings and seals [AIAA PAPER 66-1009] 17 p2802 A67-32052

LIQUID PROPELLANT

Liquid propulsion systems operating in

space and resulting problems of phase transformation, noting plug formation and flow stoppage 01 p0055 A67-11386

Optimization of Saturn vehicle, considering interaction of guidance, control and propellant utilization systems [AAS PAPER 66-117] 07 p1222 A67-19975

Thermodynamic processes influencing choice of rocket engine propellants 07 p1239 A67-20088

Packaged liquid power plants for meteorological rockets, design and performance 08 p1408 A67-20523

Liquid propellant utilization for sounding rockets 08 p1372 A67-20524

Flame propagation on liquid fuel surface, analyzing fuel heating in front of flame until ignition temperature is reached, noting radiation and convection role 09 p1581 A67-22605

Formation of cavities and microjets in liquids and role in initiation and growth of explosion 11 p1883 A67-24631

Small liquid propulsion systems testing in space environment simulator with high vacuum and low pumping capacity 13 p2089 A67-26840

Optimization of Saturn vehicle, considering interaction of guidance, control and propellant utilization systems [AAS PAPER 66-117] 13 p2155 A67-27532

Propulsion systems for booster rockets and space vehicles 14 p2377 A67-27875

Liquid and solid rocket propellants, examining use of metals as fuels 14 p2376 A67-27877

Combustion of liquid fuel droplet in sound field, noting rate dependence on sound parameters 15 p2580 A67-29778

High energy liquid propellant boosters, noting design, performance characteristics and limitations 16 p2760 A67-30703

High pressure liquid propellant rocket engines, noting high thrust, smaller engine dimensions, and combustion chamber cooling 16 p2735 A67-30704

Liquid discharge from cylindrical container exposed to longitudinal vibration, noting flow retardation 16 p2658 A67-30946

Significant-structure theory of liquids applied to rocket fuels, calculating vapor pressure, thermal expansion, dielectric constant, etc 16 p2734 A67-31537

Liquid fluorine closed flow loop and rocket engine test position design, construction and operation 17 p2832 A67-32012

Propulsion by solid/liquid or hybrid rocket motor 17 p2929 A67-32727

Hybrid rocket design combining flexibility of liquid fuel with simplicity and reliability of solid propellant rockets 20 p3516 A67-36487

Liquid fuel polydisperse jet total combustion time curve determined based on droplet of fuel and medium parameters 21 p3732 A67-38528

Similarity parameters of gravity and pressure driven liquid discharge from propellant tanks obtained by dimensional analysis 22 p3785 A67-39969

Propulsion and time requirements for low gravity liquid settling obtained from known Bond number 22 p3869 A67-40171

Sampling bottle with valves and high pressure filter holder for fuel and oxidizer, by weighing bottle before and after sampling amount of fuel passing through filter can be calculated 23 p3998 A67-40849

Part and component cleanliness maintenance for hydraulic systems, liquid propellants and spacecraft interiors, noting protective methods [SAE PAPER 670825] 24 p4159 A67-41989

Sloshing stability of three-stage ELDO A launch vehicle during first stage flight 24 p4241 A67-42396

Chemical dynamic hydraulic power unit /HPU/ performance, weight and volume efficiencies, noting applications to solid and liquid propellants 24 p4107 A67-42531

Reentry vehicle solid propellant and liquid fuel compact turboalternator electric power system operating characteristics and performance 24 p4108 A67-42534

Liquid rocket propellant combustion processes covering liquid phase mixing, vaporization, spray formation, atomization, gas-phase mixing and chemical reaction 24 p4256 A67-42720

LIQUID PROPELLANT ROCKET ENGINE

SA HYDROX ENGINE

Nonlinear combustion instability in liquid propellant rocket engines, describing nonsteady combustion process with aid of Crocco time-lag hypothesis 01 p0142 A67-11412

Computer-simulated mathematical model of thermal environmental effects on expulsion system design parameters for liquid-propellant gas-generator rocket engine [AIAA PAPER 66-686] 02 p0303 A67-11944

Working equations for dimensions and orientation of impinging propellant sheets in liquid rocket engine injectors 02 p0182 A67-11946

Surveyor throttleable liquid propellant rocket engine for operation on propellants saturated with dissolved liquid gas [AIAA PAPER 66-949] 02 p0304 A67-12283

Kinetically based mathematical model of hypergolic ignition in space ambient engines for predicting delay time and conditions from which pressure spikes result [AIAA PAPER 66-950] 02 p0302 A67-12284

Liquid propellant rocket engine development in France, Egypt and Germany 02 p0335 A67-12430

Performance, weight, design, flexibility, engine cycles and reliability of liquid propellant rocket engines used in NASA and USAF vehicles [AIAA PAPER 66-828] 03 p0504 A67-14123

Extension of manual control to liquid rocket engine necessary to enable pilot to save primary mission or to change to planned secondary mission 04 p0703 A67-14426

LF instability of liquid propellant rocket motors, noting combustion time effect on phase relations and oscillation excitation, obtaining transfer function 04 p0723 A67-15193

Single-phase and two-phase cavitating flow regime performance of liquid propellant rocket engine turbopump inducers [ASME PAPER 66-WA/FE-23] 04 p0554 A67-15353

Thrust chamber life estimation from calculable local heat flux and tube temperatures, using assumptions of elastic strain invariance and isotropic material properties 05 p0874 A67-17226

Silicon semiconductor combustion pressure transducer for high temperature HF pressure measurements within liquid rocket motor chambers 11 p1792 A67-24820

Vibration environment of liquid propellant rocket engines 12 p1989 A67-25704

Surveyor throttleable liquid propellant rocket engine for operation on propellants saturated with dissolved liquid gas [AIAA PAPER 66-949] 13 p2188 A67-26834

Linear fluorinated hydrocarbon polymer oils and grease mixtures with low molecular weight polytetrafluoroethylene thickener as lubricant for liquid fueled rocket motors [ASLE PREPRINT 67AM 84-4] 14 p2327 A67-28796

Saphir test vehicle, two-stage guided and controlled rocket 15 p2571 A67-30090

Liquid-bipropellant pressure-fed propulsion systems in lower thrust range and use for spacecraft maneuvering 16 p2736 A67-30707

Static and dynamic sealing concepts and materials for propellant feed systems and pneumatic and hydraulic control systems of liquid propellant rocket engines 17 p2864 A67-31990

Fuel consumption precision measurements for low thrust auxiliary rockets using impeller wheel and photometric devices [AIAA PAPER 67-507] 18 p2989 A67-33971

Statistical method for demonstrating reliability of clustered liquid propellant rocket engines 18 p3116 A67-34662

Kinetically based mathematical model of hypergolic ignition in space ambient engines for predicting delay time and conditions from which pressure spikes result 19 p3311 A67-35744

Liquid rocket propellants use in U.S. space program, particularly Apollo project, discussing future trends 20 p3515 A67-36880

Narrow and wide passband measurements of LRBA liquid propellant motors using test bench automatic measurement equipment 21 p3607 A67-38202

Frequency pattern analysis for liquid rocket pump fluid cavitation characteristics 21 p3613 A67-38437

Cesium propellant systems utilizing surface tension to position and transfer liquid propellant in zero-g environment studied with high voltage electrical isolation methods [AIAA PAPER 67-681] 21 p3692 A67-38712

Injector inlet conditions effects on combustion delay time in liquid bipropellant rocket engine, noting propellant atomization and droplet vaporization 22 p3868 A67-40161

Improvement of high performance liquid fuel rocket engine by optimization of liquid hydrogen /LOX/ propulsion mixtures 23 p4049 A67-41319

Solid propellant motors relative performance as related to intermediate payload missions, considering reusable liquid strap-on stages for post-Saturn payloads [DOUGLAS PAPER-4452] 24 p4240 A67-42388

Single-phase and two-phase cavitating flow regime performance of liquid propellant rocket engine turbopump inducers [ASME PAPER 66-WA/FE-23] 24 p4143 A67-42464

Stability boundaries of double-dead-time model describing chugging in liquid bipropellant rocket engine 24 p4207 A67-42689

Cryogenic liquid propellant rocket engine technology and design [AIAA PAPER 67-978] 24 p4208 A67-43053

LIQUID ROTATION

Velocity and pressure distributions and free shape of conducting liquid in rotating circular cylinder under magnetic and electric fields 21 p3668 A67-38561

LIQUID SLOSHING

Axisymmetric sloshing oscillations of liquid in U-tube type connected cylindrical tanks, obtaining velocity, pressure and wave height 03 p0522 A67-13213

Safety problems during loading and reduction of leakage hazards in management of liquid propellants including cavitation, oscillation and zero-g migration 04 p0703 A67-14604

Liquid equilibrium configurations and disturbances of vehicle motion due to liquid sloshing in space 04 p0605 A67-14989

Nonlinear lateral sloshing in rigid tanks of various geometries, noting frequency-amplitude response 05 p0790 A67-16135

Damping of liquid oscillations in cylindrical tanks, determining rigid and flexible baffle loss coefficients, baffle efficiency and maximum bending stress [AIAA PAPER 66-97] 05 p0793 A67-17210

Dynamic response, sloshing frequencies and stability of free surface of liquid in circular cylindrical elastic tank with flexible bottom [AIAA PAPER 67-76] 06 p0986 A67-18274

Free and forced liquid sloshing motions in tank of arbitrary shape at low gravity environments analyzed, using Satterlee-Reynolds method 10 p1629 A67-23832

Stability of motions of satellite with rotor and cavity with liquid, reducing problem to solution of minimum change in potential energy of system 13 p2213 A67-27319

Damping coefficients for rigid and flexible ring baffles for slosh suppression 15 p2470 A67-29438

Fluid motion in shallow trapezoidal container, noting dimensionless quantity relating frequencies to volume and rim dimensions, sloshing modes, eigenvalues, etc 16 p2661 A67-31421

Gradient stabilization of cryogenic liquids in pendulum and sloshing motions, noting response to kinetic energy input, oscillation frequency period and stability criteria 17 p2836 A67-32053

LEM-CSM analysis, elastic bending and propellant sloshing 17 p2955 A67-32478

Analytical solution for sloshing of liquid in vessel of complex geometry using homogeneous boundary condition 17 p2839 A67-32886

Liquid sloshing at simulated low gravity in rigid cylindrical tank, noting analytical model and experimental results [ASME PAPER 67-APM-14] 17 p2840 A67-33147

Dynamic response, sloshing frequencies and stability of free surface of liquid in circular cylindrical elastic tank with flexible bottom [AIAA PAPER 67-76] 21 p3614 A67-38868

Saturn V S-IVB stage propellant slosh amplification minimization at boost thrust

termination analysis, simulating slosh wave motion by time varying nonlinear spring-mass model 22 p3903 A67-39970

Translational excitation mechanical model applied to space vehicle longitudinal excitation, examining sloshing phenomena 22 p3786 A67-40104

Liquid sloshing cylindrical tank with elastic bottom for investigating surface tension effect at liquid gas interface of partly filled container 22 p3787 A67-40179

Propellant sloshing effect on vehicle dynamics under zero gravity conditions studied by programming motion equation into digital simulation of spacecraft, control and propellant 22 p3907 A67-40180

Mathematical model for studying liquid slosh effects on rendezvous dynamics by incorporating sloshing dynamics into vehicle motion equation 22 p3888 A67-40189

Low gravity slosh simulation parameters and scaling law used to extrapolate data to full scale spacecraft 24 p4141 A67-42032

Sloshing stability of three-stage ELDO A launch vehicle during first stage flight 24 p4241 A67-42396

LIQUID SODIUM

Laminar and turbulent MHD flows of liquid sodium in rectangular duct with conducting walls, determining wall and magnetohydraulic losses 16 p2712 A67-30573

Hydrodynamic journal bearings in liquid sodium, discussing stability characteristics of different geometries and wear at high temperatures [ASLE PAPER 67-LC-7] 24 p4164 A67-42746

LIQUID-SOLID INTERFACE

One-dimensional freezing of semilinear isotropic homogeneous liquid-solid system with temperature-varying thermal properties 01 p0166 A67-10758

Contact angle measurements for epoxy resin on boron filaments, demonstrating surface treatment effects 03 p0429 A67-13427

Ultrasonic reflectivity of liquid-solid interface used as indicator of near surface properties of solid in cold work, grain orientation, etc 04 p0621 A67-15264

Turbulent boundary layer-flat surface interfacial Stefan-Nusselt flow effects on apparent kinetics of heterogeneous chemical reactions in forced convective systems 04 p0567 A67-15681

Simultaneous conductive-convective heat-transfer coefficient and heat flux temperature relation at solid moving liquid interface 04 p0730 A67-15817

Equilibrium diagram of niobium-nickel system determined by thermal analysis, microscopical metallography and X-ray techniques 05 p0828 A67-16387

Impurity effect /primarily O/ in reactions between liquid alloys and solid metals undergoing deformation 06 p1017 A67-17951

Diffusion bonding of Be, Mo and W by interdiffusion of mating surfaces through solid or liquid-state reactions 07 p1192 A67-20248

Liquid metal heat transfer in various structural configurations 10 p1734 A67-23631

Acoustic measurement method for following motion of solid-liquid interface, obtaining solution for transient heat conduction problem 12 p1946 A67-25985

Hydrodynamic lubrication in face seals, discussing mechanism of fluid film, surface roughness, wear, leakage, thickness, temperature, pressure, etc [BHRA PAPER E5] 14 p2324 A67-27889

Rohsenow nucleate pool-boiling data correlation, stressing coefficients dependence on surface preparation and liquid-surface combination [ASME PAPER 67-HT-33] 20 p3547 A67-36723

Approximate method for calculating interaction between flow and soft spherical shell 21 p3717 A67-37976

LIQUID SURFACE

Free surface distortion and subsequent gas ingestion in emptying cylindrical tank, emphasizing maximum height of liquid surface when gas reaches outlet 02 p0233 A67-11945

Surface tension and equilibrium surfaces in weightless liquids, with application to spacecraft systems design 03 p0404 A67-13890

Dynamic response, sloshing frequencies and stability of free surface of liquid in circular cylindrical elastic tank with flexible bottom

[AIAA PAPER 67-76] 06 p0986 A67-18274
Gas flow at high speed out of solid or liquid surface accompanied by heat transfer investigated for boundary shock wave occurrence 14 p2296 A67-27906
Steady motion of craft with aerial lifting surfaces over rough water, defining conditions for safe operation 18 p3022 A67-33415
Dynamic response, sloshing frequencies and stability of free surface of liquid in circular cylindrical elastic tank with flexible bottom [AIAA PAPER 67-76] 21 p3614 A67-38868
Liquid surface tension effect on maximum particle size in two-phase nozzle flow, discussing drag exerted by accelerating gas stream 22 p3787 A67-40225
Nonlinear analysis of cellular convection induced by surface tension in finite amplitude heated liquid layer, discussing prediction of hexagonal flow pattern 24 p4255 A67-42569
Irrotational gas jet impinging on and depressing infinite liquid surface, discussing streamlines and rippling 24 p4144 A67-42585
Liquid-VAPOR EQUILIBRIUM
Density-temperature formulae for coexisting liquid and vapor and for freezing liquid para hydrogen 06 p1118 A67-18521
Thermodynamic investigation of singularity properties of critical point of vapor-liquid equilibrium 13 p2230 A67-27725
Superposition approximation for dense gases and liquids equilibrium theory, using phase-space distribution functions from maximization of information entropy 18 p3078 A67-33669
Liquid-VAPOR INTERFACE
Fluid management techniques for control in space of functions such as liquid expulsion, vapor venting, gauging and center-of-gravity control 04 p0553 A67-14427
Liquid-vapor interface in weightless environment noting dynamic behavior, configuration parameters and dependence on model size 04 p0605 A67-14988
Boundary layer cooling by spattering of ablating liquid films [ASME PAPER 66-WA/HT-5] 04 p0726 A67-15445
Wave flow of thinly layered fluid on vertical plane, noting fluid-gas interface stress 04 p0609 A67-15597
Shape and stability of liquid-gas interface in annular tank in force field determined by numerical integration of boundary value problem and eigenvalue [AIAA PAPER 66-425] 05 p0793 A67-17218
Evaporation kinetics of small droplets is dependent on size, liquid and gas state and gas-liquid interface 11 p1884 A67-24989
Surface film boiling under free convection 13 p2222 A67-26532
Incompressible two-phase mixed flow through sharp edge orifice including shear force between phases 14 p2305 A67-29012
Droplets and bubbles in liquids studied using general thermodynamic equilibrium criteria 17 p2971 A67-33043
Heat transfer process for film boiling taking into account growth of prominences up to bubble departure and Taylor instability 18 p3160 A67-34162
Laminar film boiling on thin wire, determining heat-transfer coefficient and vapor dome spacing and diameter [ASME PAPER 67-HT-62] 20 p3549 A67-38744
Vertical magnetic induction effect on nucleate boiling of mercury on horizontal heating surface [AIChE PAPER 20] 20 p3552 A67-38830
Liquid sloshing cylindrical tank with elastic bottom for investigating surface tension effect at liquid gas interface of partly filled container 22 p3787 A67-40179
LITHIUM
Diffusion coefficient of lithium in p-type silicon determined by method using electrophotographic developing agents 01 p0127 A67-10061
Temperature dependence of diffusion coefficient of Li in InSb prepared in wafer form 01 p0137 A67-11067
Nonrelativistic energies and mass polarization shifts of excited S states of lithium cation 03 p0472 A67-13323
Rocket payload with weight of 9 lb for release of sodium and lithium in aurora for study of D-region ion concentration and

emission 03 p0413 A67-13375
Hydrodynamic journal bearing tests in molten lithium at 600 to 800 degrees F to support compact canned rotor liquid metal pump [ASME PAPER 66-WA/LUB-6] 04 p0629 A67-15338
Force constants and local mode frequencies for vibrations of interstitial lithium positive ion in Si crystal, using covalent orbital bond model 04 p0683 A67-15609
Lithium interaction with radium induced damage in silicon solar cells to produce center preserving minority carrier lifetime 04 p0556 A67-15703
Cross section of proton production for molecular ion beams of hydrogen passing through lithium plasma 05 p0852 A67-16600
Defects in silicon p-n solar cells with Li diffused N region produced by electron irradiation and spontaneously annealed at room temperature interpreted as Li ions 05 p0870 A67-17273
Width of I band of p-i-n nuclear emission detector during Li ion drift through doped Si semiconductor detector 05 p0872 A67-17500
Mass transfer rates of Nb-based alloys in high temperature Li determined in thermal convection loops under dynamic flow conditions 07 p1223 A67-19463
Corrosion tests of W-, Mo-, Rh-based materials for compatibility in lithium at 2500, 2800 and 3000 degrees F 07 p1208 A67-19466
Diffusion coefficient of lithium in p-type silicon determined by method using electrophotographic developing agents 08 p1371 A67-21447
Li film structure on compact tungsten faces by diffraction method, using free electron beams 14 p2372 A67-28760
Diffusion, solubility and electrical behavior of lithium in gallium 16 p2726 A67-30811
Thermodynamic characteristics and plasma parameters of lithium vapor in wide pressure and high temperature range 18 p2721 A67-31389
Lithium plasma source current-voltage characteristics in vacuum, obtaining parameters valid for arcs burning under atmospheric pressure and nonzero magnetic fields 17 p2906 A67-33089
Resonance effect in low energy or low velocity Li-Hg total scattering cross section 18 p3082 A67-34031
Localized vibrational modes of lithium in lithium diffused p-type Ga-As doped with Mn, Cd or Zn 18 p3106 A67-34644
Cycle and separator efficiencies and specific radiator area compared for liquid alkali metal-lithium MHD power generators 21 p3572 A67-38864
Lithium in electrolyte and active metallic nickel formation effects on capacity and plate mechanical strength in alkaline storage batteries 22 p3748 A67-40229
Electron-electron interaction effect on Li soft X-ray emission spectrum, liquid metal optical absorption and alkali metal dielectric response 23 p4037 A67-40760
Li interactions with complex damage clusters produced by neutrons in Si solar cells, discussing annealing, radiation hardening and energy dependence 23 p3940 A67-41520
Li behavior in self-healing radiation resistant Si solar cells 23 p3941 A67-41522
Li containing p-on-n and n-on-p Si cell degradation by bombardment noting carrier removal damage, annealing and radiation damage resistance 23 p3941 A67-41524
Li doped p-plus/n solar cells optimum design and radiation resistance, noting concentration and room temperature annealing conditions 23 p3942 A67-41528
Hyperfine coupling constants of lithium energy levels, using Weiss 4s-configuration wave functions 24 p4190 A67-42097
Lithium content of T Tauri stars shown to exceed ionization of Li in solar atmosphere 24 p4227 A67-42161
Li isotopic composition and abundance in chondrites and iron meteorites measured, noting implications for earth and meteoritic parent body formation 24 p4235 A67-42632
LITHIUM CHLORIDE
Long term biomedical monitoring of human heart rate through lithium chloride impregnated balsa electrodes, noting space

flight application 15 p2431 A67-29918
LITHIUM COMPOUND
Temperature tuning of lithium niobate optical parametric oscillator in visible spectrum, noting generated frequency dependence on pump frequency and longitudinal mode distribution 02 p0253 A67-12511
Polarized radiation measurements of far IR absorption coefficient and refractive indices in lithium niobium oxide 03 p0496 A67-13571
Reaction of lithium diphenyl phosphide with diphenylacetylene producing high yields of stereochemically pure vinyl phosphides in presence of primary or secondary amine 04 p0565 A67-14523
Tunable lithium niobate optical oscillator with external mirrors 09 p1510 A67-21576
Plasma production by ruby laser pulse irradiation of LiD investigated, results suggest collisionless electrostatic shock propagation at expanding plasma ball edge 11 p1840 A67-24561
Alpha particle spectral analysis in various lithium compounds 13 p2159 A67-26435
Single crystals of lithium-meta-niobate evaluated for nonlinear optical quality, using gas laser and interferometer 21 p3677 A67-38010
Self-decoration effect in thermally etched polycrystalline lithium ferrite, discussing geometric symmetry relation to crystallographic surface orientation 22 p3855 A67-39344
Temperature dependence and electro-optic coefficients in lithium niobate single crystal measured, noting relationship in paraelectric perovskites 22 p3863 A67-40235
Laser induced damage reduction in lithium tantalate and niobate crystals, proposing mechanism to explain observed reduction 23 p4012 A67-40876
LITHIUM FLUORIDE
LiF single crystal destruction as function of laser beam energy, examining dislocation pattern arising from crack propagation 01 p0086 A67-10071
Lithium fluoride thermoluminescent responses to neutrons, studying first and second order kinetics of decay and phosphor experiment 04 p0685 A67-15710
Kinetics of formation and healing of damage caused by laser pulse in lithium fluoride single crystals 05 p0867 A67-17057
Vacuum UV resonance lamp design to eliminate difficulty of window seal caused by discharge 08 p1329 A67-20354
LiF single crystal destruction as function of laser beam energy, examining dislocation pattern arising from crack propagation 08 p1339 A67-21454
Association energy of vacancy-impurity dipole obtained from electrical conductivity of magnesium fluoride-doped lithium fluoride at ambient temperature 12 p1978 A67-25149
Kinetics of formation and healing of damage caused by laser pulse in lithium fluoride single crystals 15 p2538 A67-29788
LiF crystals doped with Ti studied for electrical and optical properties, finding atomically dispersed Ti fractions in form of doubly positively charged centers 21 p3687 A67-39137
LiF freshly cleaved crystal reflectance spectrum between UV and 28 ev, computing dielectric response function and measuring gamma exciton band 23 p4038 A67-40774
LITHIUM HYDRIDE
High temperature single solid particle plasma generation by focused giant pulse Q-spoiled ruby laser beam irradiation of LiH suspended in vacuum electric fields 03 p0485 A67-14047
Generation of series limit continua with aid of sliding sparks for absolute measurements in vacuum UV, observing bremsstrahlung 13 p2155 A67-26271
Plasma production by ruby laser beam irradiation of lithium hydride particle, measuring electron temperatures 20 p3496 A67-36212
Post-Saturn launch vehicle, discussing multipurpose, variable payload boosters, usability, noise levels, etc 20 p3533 A67-36613
Ion energies in expanding plasma stream generated by intense giant pulse laser light in focus on solid LiD and LiH targets 23 p4033 A67-41152

LITHIUM OXIDE

Post-Saturn launch vehicle, discussing multipurpose, variable payload boosters, usability, noise levels, etc 20 p3533 A67-36613

LITHOLOGY

Terrestrial surface spectral IR emissivities determined in situ interferometrically, noting igneous and sedimentary rock composition and texture 22 p3805 A67-40354

LITHOSPHERE

S EARTH SURFACE

LIVER

Phagocytic activity and hepatic function following localized proton radiation to liver, discussing results of experiments performed on white rats 10 p1599 A67-23814

Hepatic effects of breathing pure oxygen for eight months upon rats, dogs and monkeys 10 p1600 A67-23818

Rhesus monkeys liver damage after irradiation by penetrating protons 14 p2254 A67-28064

Gravity effect on liver regeneration in rats measured by mitotic count 20 p3372 A67-36963

Hepatic hemorrhagic lesions produced by 32 and 55 Mev proton radiation in rhesus monkeys 23 p3944 A67-41017

LMCR

S LIQUID METAL COOLED REACTOR

/LMCR/

LOAD DISTRIBUTION

Elastic behavior of load cell operating on variable capacitance principle designed to fit spaces restricted in one dimension 01 p0034 A67-10296

Experimental determination of column initial deflection and load eccentricity in aluminum alloy indicate minor magnitude of load eccentricity 01 p0160 A67-10561

Structural design and fatigue life of Chinook helicopter [SAE PAPER 660667] 01 p0010 A67-10575

Nonlinear boundary value problem solution as applied to effect of uniformly distributed pressure and concentrated load on spherical dome 03 p0524 A67-13623

Load concentration effects on stability of rigidly reinforced strictly convex shell, determining upper critical load 03 p0526 A67-14063

Coupled flatwise and edgewise vibrations of beam rotating about one end 04 p0707 A67-14492

Shape of meridian cross section, stressed state and deflection of circular plate of uniform strength loaded symmetrically 04 p0708 A67-14785

Performance characteristics and bearing load-deflection equations of shaft supported by n roller bearings [ASME PAPER 66-WA/LUB-4] 04 p0629 A67-15339

Circular ring subjected to two diametrical, equal and opposite forces with results converted into stress-strain charts 04 p0715 A67-15603

General critical stressed state of strictly convex shell under arbitrary load distributed over edge 04 p0719 A67-15983

Stressed state of viscoelastic cylinder with star shaped cavity caused by steady temperature field and distributed surface load in problem of elasticity 05 p0912 A67-16185

Critical stresses of three-layer wing panel compressed by load distributed along two sides, determining temperature stresses in bearing layers and equilibrium equations 05 p0913 A67-16191

Bending problem of isotropic shallow helical cantilever shell under distributed normal load 05 p0915 A67-16220

Free hinged cylindrical shell problem with radial load on outer edge of cross section solved via linear differential equations 05 p0915 A67-16222

Bending of circular plate with two square holes under uniform load distribution around hole perimeters 05 p0916 A67-16225

Axisymmetric deformation of shallow shells of revolution, noting membrane solutions 05 p0917 A67-16245

Hovering stability of crane helicopter with hanging load, noting effects of supporting point of wire and length, using root locus method 05 p0751 A67-16439

Separation of load eccentricity and initial deviation determined through column compressive tests, using aluminum alloy bars and strain gauges 05 p0919 A67-16588

Initial postbuckling behavior of double curvature shell segments under several loading conditions determined, using Koiter theory 05 p0921 A67-16885

Axisymmetric bending of circular sandwich plates with lightweight compressible filler subject to special transverse or local loads 05 p0922 A67-17175

Optimum control of multidimensional and multilevel systems, discussing linear systems, load distribution, cyclic optimization and aggregated systems 06 p0974 A67-17933

Asymptotic solution to elasticity theory problem for hollow isotropic cylinder of finite dimensions and small thickness under axisymmetric load distributed over entire surface 06 p1100 A67-18033

Stress distribution in thin walled shell during transfer of concentrated load to surface area of mechanical contact 06 p1106 A67-18623

Strength of isotropic plates under bending by transverse loads in plastic range 06 p1108 A67-18660

Book on roller bearings noting construction, operation and performance characteristics 06 p1008 A67-18837

Beam equation for elastically supported clamped-clamped beam solved for conditions of initial, boundary and distributed load, using Hermitian operator 08 p1415 A67-20488

Imparting motion to system of two masses coupled by linear elastic shaft in infinite set of piecewise continuous loads, by variational method of influence functions 08 p1354 A67-21047

Axially loaded cylindrical structures analyzed for optimum weight construction consistent with cost constraint, emphasizing beryllium-aluminum alloys 08 p1424 A67-21521

Hydrostatic pressure measurement by direct loading of semiconductor strain gauges 09 p1498 A67-22031

Structural reliability determined when stress and strength distributions are described by normal statistical distribution 09 p1575 A67-22298

Load carrying capability of adhesive bonded studs, analyzing resin systems and flexible linears 09 p1507 A67-22502

Effect of mass distribution and loading sequence on elastic rod, solving eigenvalue problem by Galerkin method 10 p1715 A67-22912

Action of concentrated loads in plane problem of mechanics of deformable solids 10 p1715 A67-22921

Model ten-member redundant structure under constant-amplitude loads analyzed, determining statistical distribution of consecutive failures for fall safe design applications 10 p1718 A67-23432

Load carrying capacity of plane and reinforced cylindrical shells clamped along edges and subjected to uniformly distributed internal pressure 10 p1720 A67-23600

Exact solution of transverse shear deformation effect on axisymmetric large deflection of circular sandwich plates for different loading states and boundary conditions 10 p1728 A67-23762

Bifurcation phenomena in spherical shells under concentrated and ring loads taking into account finite prebuckling deformation 10 p1728 A67-23764

Shells of revolution having arbitrary stiffness distribution of loads and temperatures 10 p1730 A67-23771

Asymptotic expansion procedure applied to Donnell equations for cylindrical shell, obtaining solution for interaction of infinite cylinder reinforced by radially loaded ring [ASME PAPER 66-WA/APM-27] 10 p1730 A67-23839

Large deflections of beam loaded and supported at two points 11 p1871 A67-24088

Stress intensity analysis for flat plates loaded close to edge crackline, giving intensity dependence on crack length and specimen shape 11 p1875 A67-24588

Elastic deformation of unbounded transversely isotropic body with internal plane circular slot under slot surface load 11 p1876 A67-24681

Bending theory for sandwich plates solved by Galerkin method assuming load distribution over upper and lower faces of plate 11 p1880 A67-25095

Stress-strain state of thin walled zero moment shell under uniformly distributed multiple load assuming various tensile and compression strengths 12 p2020 A67-25569

Locally loaded orthotropic shells of revolution under radial concentrated forces 12 p2021 A67-25575

Approximate theory for stress-strain state of thin cylindrical shell reinforced with elastic ribs having bending rigidity 12 p2022 A67-25584

Stress-strain state of thin cylindrical shell under effect of local forces 12 p2024 A67-25601

Natural oscillation frequency of multilayer shells of revolution with nonsymmetrical structure containing rigid filler and subjected to transverse load 12 p2027 A67-25626

Asymptotic methods of obtaining refined solutions for zero moment equations of concentrated loads applied to shells with Gaussian curvature 12 p2028 A67-25630

Elastoplastic equilibrium of rectangular compressible and incompressible plates under load concentrated near edge determined by elastic solutions and finite difference 12 p2031 A67-25960

Turbulent atmosphere load effect on gliders noting influence of piloting techniques 13 p2052 A67-26484

Spanwise distribution of aerodynamic shear and bending-moment on cantilever tapered wings 13 p2215 A67-26485

Stress concentration of hollow sphere under uniformly distributed impact loads along inner and outer surfaces 13 p2215 A67-26526

Thin elastic plate with uniformly distributed load over area and Navier condition on edge solved for deflection 13 p2217 A67-26631

Flat plate loading effects for large displacements, determining solution to plates of arbitrary shape under general loading by iterative matrix technique 13 p2217 A67-26704

Program attachment to fatigue testing machines intended for two-stage programs 13 p2217 A67-26796

Apparatus for programming thermal cycles in fatigue tests of materials 13 p2218 A67-26797

Load concentration effects on stability of rigidly reinforced strictly convex shell, determining upper critical load 13 p2221 A67-27722

General critical stressed state of strictly convex shell under arbitrary load distributed over edge 14 p2400 A67-28492

Bounds for natural frequency eigenvalues of simply supported uniform beam with constant end load and uniformly distributed axial load 14 p2403 A67-29005

Fatigue failure prevention noting load redistributing, stress concentration reduction, critical section size increases, mean stress reduction, etc 15 p2494 A67-30098

Stresses computation at surface of contact between disk and circular ring under influence of concentrated loads 15 p2577 A67-30186

Transversally isotropic cylindrical shell under periodically spaced axisymmetric band loads, comparing expressions derived for stresses and displacements by elasticity and shell theories 15 p2578 A67-30271

Noncircular cylindrical shell of orthotropic material under distributed load numerically analyzed by shell theory 15 p2578 A67-30272

Westergaard method of crack analysis extended for crack problems within infinite medium with cracks under applied loads at infinity 16 p2765 A67-30995

Double curvature influence on rigidity of shell of revolution analyzed for surface loading and cross sectional linear loading, using Fourier series 16 p2766 A67-31149

Vortex wake and aerodynamic load distribution of slender rectangular wings 17 p2790 A67-32215

Thin elastic circular ring equilibrium stability in rigid cavity subjected to parallel loading, considering small ring separation region at buckling [ASME PAPER 67-APM-19] 17 p2958 A67-32406

Stress distribution in reinforced-material models consisting of isolated fiber embedded in brittle matrix analyzed by photoelastic technique 17 p2966 A67-33387

Stress-strain state of rod with end load

and time variable load on other end, discussing forced and free oscillations 19 p3338 A67-34879

Multilayer cantilever beam subjected to varying load, studying cases where slip region propagates from edge to interior 19 p3341 A67-35579

Circular plate on nonlinearly elastic base with uniform load force at center, tangential force and contour moments for plate deflection 20 p3539 A67-36923

Zero moment elliptical paraboloid translational shell under uniformly distributed load, reducing solution to Dirichlet problem 20 p3539 A67-36924

Vibrating annular membrane problem, including load per unit area and asymmetry of load and vibration, using finite transform derivation 20 p3539 A67-37006

Square-law elasticity theory accounting for second order terms in load parameter of stress-strain relations 21 p3721 A67-38306

Elastic stability of three-layer cylindrical shell filled with corrugated metallic sheets under combined loads, deriving linear equations 21 p3724 A67-38786

Strain energy method for analyzing large deflections of trapezoidal plates with constant thickness and rigidly clamped edges under uniformly distributed load 21 p3725 A67-38794

Minimum mass bar design for axial vibration of beam with load distribution at specified natural frequency 21 p3728 A67-38890

Stress-strain state of tubular blanks expanding under uniform distributed internal load 21 p3637 A67-38925

Netting analysis of reinforced sheets for load envelopes which combine tension and shear, determining optimum fiber arrangements 21 p3729 A67-39082

Displacement and stress distribution in shallow spherical shell under concentrated loads including normal force, tangential force and bending moment 21 p3730 A67-39087

Approximate solution of elastic buckling of radially constrained circular ring under uniformly distributed loading 22 p3908 A67-39287

Stability of elastic structure in rest state based on break-point determinant, discussing bound, conjugated, affine and space and body-fixed load 23 p4078 A67-41196

Currents in load impedance of transmission lines near cylindrical scatterer noting antenna field equations 23 p3981 A67-41209

Bifurcation phenomena in spherical shells under concentrated and ring loads taking into account finite prebuckling deformation 23 p4080 A67-41728

Exponential vertical flow shear effect on induced drag of elliptically loaded lifting line 23 p3932 A67-41735

High vacuum environment and vacuum outgassing time effects on magnesium alloys fatigue properties under constant load and reversed bending 24 p4172 A67-42037

Bounded variation method for optimum load capacity hydrodynamic one-dimensional gas slider bearing, discussing film thickness [ASME PAPER 67-LUB-6] 24 p4162 A67-42670

Film thickness, pressure distribution and load carrying capacity of loaded line contact in presence of viscoelastic lubricant noting high pressure spike [ASME PAPER 67-LUB-23] 24 p4163 A67-42681

Spline friction effect on multiple disk brake and clutch packs, including torque and load variation and pressure distribution equations [ASME PAPER 67-LUB-26] 24 p4164 A67-42684

LOAD FACTOR

SA LANDING LOAD

SA SHOCK LOAD

SA TRANSIENT LOAD

Plastic flow of axially symmetric notched bars pulled in tension, obtaining load factors 01 p0159 A67-10401

Aperture admittance, material loading and higher order modes effect on rectangular cavity slot antenna design 02 p0218 A67-12098

Load factor estimation for flights in turbulent conditions by replacing exact transfer function with equivalent statistical model 03 p0351 A67-12997

Steady state response of viscoelastic cylindrical shells to moving loads, obtaining exact solution with correction for shear deformation and rotatory inertia effects via Fourier transforms 03 p0522 A67-13211

C-5A aircraft design load criteria for landing gear of large aircraft that must operate from semimproved airfields [AIAA PAPER 65-711] 03 p0360 A67-13781

Unsteady viscous fluid flow in MHD channel under action of pressure gradient solved for arbitrary load coefficient 04 p0669 A67-15519

Hypersonic thermal structural concepts to satisfy design requirements including insulated, insulated and cooled and hot load carrying approaches [SAE PAPER 660678] 04 p0716 A67-15789

Soviet monograph on dynamics and durability of machines 05 p0915 A67-16219

Hardness of polyesters copolymerized with styrene, determining reticulation and temperature effects 05 p0759 A67-16767

Plastic deformation of textured Ti alloy sheet examined, using tension testing along different directions and combined stress loading along principal axes of anisotropy 06 p1018 A67-17900

Span loading of swept wing which produces minimum induced drag with constraints on lift and pitching moment 06 p0937 A67-18010

Analytical and empirical results on shell panel flutter boundaries compared, using nonlinear Donnell theory and linear piston theory approximation [AIAA PAPER 67-78] 06 p1104 A67-18452

Complementary energy method for flexural buckling of initially straight elastic bars 06 p1110 A67-18840

Closed form solution for transverse-symmetric and asymmetric loadings on circular fixed beam 06 p1110 A67-18842

Small oscillations and stability of hyperelastic incompressible rectangular strip under uniformly distributed biaxial load 06 p1111 A67-18892

Stability of equilibrium of elastic systems under nonconservative load, discussing criteria of stability, modes of instability, follower force problems, etc 08 p1422 A67-21048

Effect of load mismatch on laser output, determining nonlinear dependence of equivalent negative conductance as function of oscillation amplitude in laser resonator cavity 08 p1338 A67-21270

Mathematical model of microscopically heterogeneous medium undergoing elastoplastic deformation, deriving equations for stress-strain distribution under uniaxial loading 09 p1575 A67-21931

Longitudinal stability of L-29 aircraft, comparing measurement results from independent experiments 09 p1440 A67-22469

Nonlinearities in elastic energy release rate during load-deflection measurements of specimens with varying crack length 10 p1718 A67-23327

Dynamic snap-through of shallow arches under stochastically varying transverse loads 10 p1725 A67-23711

Matched asymptotic expansion for singular pressure loading behavior for oscillating wings or control surface edges 10 p1593 A67-23712

Energy absorption characteristics of honeycomb structures under static and impact loading 10 p1727 A67-23745

Volumetric loading factor expression derived for side burning solid propellant grains by imposing constraint on port channel flow Mach number 11 p1851 A67-24227

Free oscillations of plates, strips, rods and cylinders subjected to arbitrary dynamic edge load 11 p1874 A67-24314

Dynamic vibration in aircraft power plant components, noting responsiveness of parts and fatigue life evaluation [SAE PAPER 670237] 12 p1989 A67-25495

Vlasov variational method application to stressed state of flexible plates and shells, linearizing partial differential equations by successive loadings 12 p2020 A67-25570

Cylindrical shell stability under nonuniform load, noting critical load dependence on subtending angle 12 p2020 A67-25573

Rigidly reinforced conical shell stability under external load investigated for

boundary conditions 12 p2027 A67-25622

effect 12 p2027 A67-25622

Explosively driven MHD generator, obtaining conversion efficiency dependence on magnetic Reynolds number, load-to-channel inductance ratio and magnetic/kinetic energies ratio 12 p1901 A67-25896

Aircraft engine reliability, considering local surface stresses, engine component distortion under load, vibration problems and material variability 13 p2188 A67-27000

Stress-strain problems in design load of commercial aircraft, noting role of frequency distribution curves 14 p2245 A67-28060

Elastic rod, string or torsional member under effect of accelerating axial load, solving differential equation of motion in fixed end condition 14 p2399 A67-28140

Thickness transition configurations for cylindrical pressure vessels with hemispherical heads, noting weight, load effects, etc 15 p2573 A67-29419

Vibrations of helicopter rotor in Cardan suspension, dividing problem into three boundary value setups with special conditions at hub 15 p2576 A67-30175

Plastic yielding near crack tip, noting general solution for deformation and stress distributions for various loads 16 p2769 A67-31288

Dynamic response of sailplanes to elevator control in longitudinal maneuvers, discussing load factors and tail loads as function of aerodynamic and inertial parameters 16 p2597 A67-31786

Structural analysis and design of large area solar array, noting factors such as temperature distribution, dynamics, internal loads, permissible weight, etc 17 p2954 A67-31980

Column shape for maximum Euler buckling load determined using energy method calculations 17 p2960 A67-32421

Conducting plate backscatter minimization method by load adjusting of loop in front of plate, noting experimental verification 17 p2815 A67-32622

Immersion technique measurement of gravitational stresses using two-and three-dimensional photoelasticity [ASME PAPER 67-APM-11] 17 p2964 A67-33146

Tangential and normal tearing stresses distribution in adhesive joint under various loads and bending moment 21 p3716 A67-37909

Bearing selection for designers, considering available working types and load change during variable speed machine operation 21 p3633 A67-38145

Steady state problem solution in linear formulation concerning movable load influence on thin elastic plate on ideal compressible fluid surface 21 p3720 A67-38300

Load carrying capacity of hydrostatic bearing having communicating chambers and operating with laminar flow of incompressible fluid, showing shaft vibration elimination 21 p3636 A67-38837

Variable loading effect on durability of D16T aluminum alloy exposed to continuous action of corrosive medium 21 p3642 A67-39009

Load and response design values determination by statistical method for structural systems such as launch vehicles, considering discrete forcing functions 22 p3907 A67-40178

Fracture in engineering design in terms of fracture mechanics 23 p4076 A67-40696

Bifilar complementary loaded helical antenna, determining radiation patterns, near field amplitudes and phase velocities 23 p3979 A67-40834

Externally pressurized gas bearings examined for mechanism of series restrictors on pressure distribution, flow quantity and load capacity 23 p4010 A67-41064

Gas bearings with wide pockets investigated theoretically and experimentally for pressure distribution, flow quantity and load capacity 23 p4010 A67-41065

Simplified equations for thin circular cylindrical shells under loading investigated for possible elimination of inconsistencies 23 p4080 A67-41664

Stress-strain relation in viscoelastoplastic bodies noting static instability under

conservative load 24 p4246 A67-41932
 Fatigue crack propagation rate in sheet specimens under various loadings simulating rivet forces 24 p4247 A67-41944
 Electro-fluid dynamic power generation, discussing Mach number, charged particle mobility, pressure level and radial space charge field effects on load characteristic and conversion ratio 24 p4107 A67-42527

LOAD TEST

Static and fracture tests with C-160 /Transall/ transport 01 p0048 A67-10212
 Dynamic load analysis of Titan III booster structure using dynamically scaled model in vibration survey [SAE PAPER 660684] 01 p0154 A67-10588

Cryogenic strain gauge application to circumferential loads of Centaur hydrogen tank insulation while in launch configuration 01 p0069 A67-11016
 Strain gauge bridge outputs combined during flight to measure airloads directly and inexpensively in fatigue test program 01 p0030 A67-11103

Aircraft structural design criteria and analysis methods, noting procedures which result in discrepancies between design loadings and actual flight test results [AIAA PAPER 66-881] 02 p0339 A67-12263
 Calculating combined radial and axial loads sustained by ball bearings in aircraft engines, turbine systems, propellers and other units 03 p0432 A67-14083

Load carrying capacity of thin plates of rigid perfectly plastic material with different tensile and compressive yield strength, using method of limit analysis 03 p0531 A67-14366
 Saturn IB flight test loads, comparing measured and calculated bending moment, noting launch time wind profile 10 p1713 A67-23734

Dynamic measurements of heavy landings on experimental helicopter platform and of response to heavy vehicle loads on steel-and-concrete deck flyover 11 p1880 A67-25056
 Measurement of torsional fatigue loads on aircraft undercarriage under service conditions 11 p1880 A67-25057

Impact bending and tension processes using drop hammer technique evaluated with improved method using oscillography for high quality load-time measurements 13 p2215 A67-26391

Testing techniques for electroformed thin shells noting tensile properties determination 13 p2219 A67-27184

Strain gauge bridge outputs combined during flight to measure airloads directly and inexpensively in fatigue test program 14 p2315 A67-28002

Column consisting of flexible and rigid section measured for buckling load, using Southwell method 14 p2404 A67-29057

SnTe samples under uniform load studied for relation between electrical and thermal conductivity, thermal EMF and microhardness 16 p2730 A67-31165

Compaction pressure and sintering temperature effect on initiation and propagation of cracks during bend testing of Ni and Mo specimens 16 p2691 A67-31586

Helicopter structural elements safe life through variable-amplitude fatigue tests [AHS PAPER 122] 16 p2777 A67-31837

Structural reliability of fatigue loaded rotorcraft estimated through S-N and spectrum testing [AHS PAPER 123] 16 p2777 A67-31838

Wind tunnel tests for load and pressure distributions on flat-top cylinders with thick boundary layer 20 p3421 A67-38781

Aircraft structural design criteria and analysis methods, noting procedures which result in discrepancies between design loadings and actual flight test results 21 p3568 A67-38537

Oxidation process and mechanical properties of austenitic steels and alloys under prolonged loading at high temperatures, giving stress-durability diagrams 22 p3819 A67-39322

Crack line loading methods for measuring fracture toughness noting advantages over remote loading test procedures 22 p3820 A67-39630

Potential energy release of stressed elastic body due to material removal and crack extension 22 p3911 A67-39679

Programmer for operational strength tests during aircraft

construction 22 p3912 A67-39755
 Stress-strain curves under variable stress sequences in high stress range 22 p3913 A67-40036

Wear characteristics of polytetrafluoroethylene studied under various loading and sliding speeds in air and vacuum 23 p4009 A67-41062

Fatigue crack propagation in aluminum alloy studied for influence of maximum stress, stress range and sequence of load application 24 p4171 A67-41954

Aerospace vehicle structure loading under structural integrity tests with simulated aerodynamic heating conditions, discussing computer relaxation solution for rod temperature distribution 24 p4172 A67-42036

LOAD TESTING MACHINE

Five-million pound load cell design and compression calibration at NBS 01 p0050 A67-11097

Apparatus for testing thin walled tubular samples under combined torsional and tensile load, using stressed state timer 06 p1107 A67-18639

Testing machine for evaluating high temperature fabrics under dynamic loading and heating conditions 07 p1212 A67-20262

Jet aircraft tire testing machine simulating taxiing, takeoff and landing loads 16 p2656 A67-31914

High hydrostatic pressure effects on load cell using foil strain gauges and calibration for small uniaxial loads 17 p2855 A67-32393

Stability of cylindrical shells under torsion 18 p3144 A67-34171

Testing machine effect on buckling load of electroformed cylindrical shells under axial compression 22 p3909 A67-39291

Lubricants, metal high temperature and atmospheric environments effects on gear load-carrying capacity [ASME PAPER 67-LUB-27] 24 p4164 A67-42685

LOADING

SA AERODYNAMIC LOAD

SA AXIAL LOAD

SA BLAST LOADING

SA COMPRESSION LOADING

SA CRITICAL LOADING

SA CYCLIC LOAD

SA DYNAMIC LOAD

SA EDGE LOADING

SA GUST LOAD

SA HUGONIOT EQUATION OF STATE

SA IMPACT LOAD

SA RANDOM LOAD

SA SPAN LOADING

SA STATIC LOADING

SA STRESS AND LOAD

SA TRANSIENT LOAD

SA VIBRATORY LOADING

SA WING LOADING

Electrical efficiency of MHD generator cycles, determining external load resistance 01 p0012 A67-10178

Load carrying capability of thin walled pressurized tanks under compression and bending with postwrinkling included, improved by addition of jettisonable shell [SAE PAPER 660683] 01 p0161 A67-10586

Stresses in solids moving during loading, using velocity vector and strain rate tensor as variables for instantaneous state of body motion 05 p0914 A67-16194

Transverse normal loading of doubly periodic unidirectional elastic fiber reinforced infinite elastic matrix 14 p2398 A67-28098

Classification of combined loadings in plasticity theory 15 p2578 A67-30146

Moire topography techniques for partial slope and macroscopic curvature measurements of cylindrical and conical shells due to loading 17 p2960 A67-32455

Accumulated plastic deformation during sequence of isothermal and nonisothermal loading 19 p3242 A67-34887

Response of plate to fluid loading, determining fluid pressure induced by plate motion 20 p3539 A67-37009

Aircraft terminal apron design, considering passenger convenience, variations in aircraft configuration and changes in aircraft mix and loading facilities 22 p3779 A67-39379

LOADING APPARATUS

Human body motions during load handling tasks for application in designing manipulators, walking machine and powered exoskeletons [ASME PAPER 66-WA/BHF-2]

Gate arrival terminal design for Kansas City MCI airport noting loading positions, maintenance hangars, service roads, post office, etc 22 p3779 A67-39375

LOADING MOMENT

Two jointed seminfinit plates loaded by concentrated moment or doublet 05 p0914 A67-16217

Thin isotropic circular plate bending under eccentric moment load for clamped and simply supported cases 05 p0918 A67-16419

Deflection and bending moment coefficient for clamped skew plate under uniform pressure obtained, using double series satisfying boundary conditions for differential equation 09 p1575 A67-22165

Creep index determination by tests on stress relaxation with elastic members, noting importance of stress distribution at initial moment of loading 11 p1877 A67-24815

Stability criteria in stress-rupture strength theory, deriving stress and moment influence functions and damage tensor 21 p3717 A67-37969

Shallow spherical shell dynamic stability under variable moment load 22 p3911 A67-39683

LOADING RATE

Loading rate effect on critical behavior of cylindrical shell responses 01 p0164 A67-11187

Variability of conveyor belt velocity during loading and operation, unloading and stopping under load analyzed, using distribution theory 05 p0908 A67-16043

Stress-strain relationships in materials under high rate of torsional loading and torsional plastic wave propagation in long Cu tube 05 p0909 A67-16144

Wear effects in polymer-metal joints under frictional loads 07 p1211 A67-19170

Stress-strain analysis of effects of rapid loading rate of restraint harness webbing, especially during air crash 08 p1289 A67-20613

Load and friction torque of Rayleigh step film scheme applied to journal bearing, using Reynolds equation [ASME PAPER 65-WA/LUB-2] 08 p1335 A67-20917

Axisymmetric plastic buckling of axially compressed cylindrical shells initiated under increasing load 17 p2961 A67-32776

Strength of single crystals, amorphous materials and other brittle materials lacking grain boundaries, noting loading rate dependence 18 p3069 A67-33491

Loading rate effect on unidirectional fiberglass reinforced plastics under tension, examining mechanical characteristics and determining tensile strength and elastic modulus 21 p3649 A67-37908

Loading frequency influence on endurance characteristics of V95 aluminum alloy notched for stress concentration 21 p3644 A67-38051

Fatigue behavior of Cr steel and Ni-Cr alloy examined for influence of direction of first loading stroke of push-pull testing 23 p4019 A67-41155

LOADING WAVE

Flexural wave propagation along beam with arbitrary periodic concentrated load 02 p0340 A67-12501

Book on strength under high transient loads and nonlinear elastic and elastoplastic wave propagation 04 p0715 A67-15617

Metal mechanical properties determination during deformation by uniform ultrasonic loading 21 p3722 A67-38450

Magnetically tunable multisection bandpass filter in ferrite-loaded evanescent waveguide 22 p3772 A67-39907

LOBE

Lobular scattering of 1 ev energy chopped argon beams from silver, mica and brass surfaces, noting distributions and contamination effects 13 p2099 A67-26950

LOCALIZATION

Hyperbolic space localization system measuring three distance differences from four ground stations 02 p0264 A67-12354

LOCKHEED CL-595 HELICOPTER

S XH-51 HELICOPTER

LOCKHEED L-500 AIRCRAFT

SA C-5 AIRCRAFT

Lockheed 500, derivative of USAF C-5A transport, discussing logistic capabilities, economics and representative approaches [AIAA PAPER 66-1019] 03 p0362 A67-14152

LOCKHEED MILITARY AIRCRAFT

S C-5 AIRCRAFT
S C-141 AIRCRAFT
S P-3 AIRCRAFT
S XH-51 HELICOPTER
S XV-4 AIRCRAFT
S YF-12 AIRCRAFT

LOCOMOTION

SA ASTRONAUT LOCOMOTION
First order factors affecting driver ability to safely control typical lunar vehicle through simulated mission profile over representative terrain
[SMPTF PAPER 101-54] 12 p1920 A67-25469
Vestibular organ acceleration while walking at lunar and earth gravity 23 p3953 A67-41584

LOG PERIODIC ANTENNA

Log periodic antennas operating in SHF bands having nonserrated radiation patterns 01 p0036 A67-10444
Broadside log-periodic antenna, noting lab dimensions of models, power patterns and input impedance 01 p0036 A67-10472
Wideband and optimum antennas, using Lepidopter antenna as example 10 p1613 A67-23506
Gain bandwidth relations in H-plane array of log periodic dipole elements 12 p1914 A67-25426
Log periodic antenna theory and applications including HF, VHF, UHF and SHF aerials 15 p2454 A67-30139
Radant, integrated radome antenna system incorporating three trapezoidal-tooth log periodic radiating elements 18 p3016 A67-34598

LOG SPIRAL ANTENNA

Substantial size reduction of conical log-spiral antenna by loading with magnetodielectric material 02 p0212 A67-11612
Radiation pattern and standing wave ratio for antenna system consisting of paraboloidal cylindrical reflector and frequency-independent feed 02 p0213 A67-11644
Vector potential representation of planar logarithmic spiral antenna 03 p0378 A67-13285
Inclined log spiral antenna, noting back radiation reduction and frequency independence 11 p1763 A67-24294

LOGARITHM

Distribution of maintenance manhour intervals for tasks on military aircraft compared with logarithmic normal distribution, presenting histograms and cumulative distributions 01 p0171 A67-11382
Logarithmic particular solutions of nonhomogeneous equation of cyclic deformation of shallow conical shell under nonuniform heating 06 p1109 A67-18664
IF amplifier circuit diagrams, obtaining logarithmic amplitude characteristic by switching nonlinear elements to plate or cathode circuits 06 p0972 A67-18899
Collective scattering cross section and collective spectral extinction of Mie scattering with logarithmic Gaussian distributions 13 p2150 A67-26432

LOGARITHMIC RECEIVER

Transistorized logarithmic amplitude converter for recording pulses of radiation detector, automatic switching of conversion scale permits amplitude measurement 01 p0062 A67-10160
Error equation for accuracy of monopulse radar in search mode applied to monopulse radar systems, using logarithmic normalization 01 p0022 A67-10446
Intermediate frequency logarithmic amplifier using twin-gain stages and transistors and avoiding successive detection principle and video delay line 01 p0025 A67-10814
Selective transistorized logarithmic amplifier design and logarithmic amplitude characteristic computation from cascade output voltages 02 p0215 A67-11978
Logarithmic tunnel diode amplifier design techniques and characteristics 04 p0580 A67-14597
Logarithmic amplifier designs based on follower type circuits 12 p1915 A67-25858
Radio spectrographs for solar observation, broadband and fine structure spectrography techniques and logarithmic amplifiers use in receiver 14 p2386 A67-28443
Measuring assembly containing logarithmic-response electrometric amplifiers for

sounding rockets 21 p3592 A67-38222
Solar radio spectrograph using broadband logarithmic antenna, considering receiver operation and frequency range 21 p3627 A67-38497

LOGIC

SA BOOLEAN ALGEBRA
SA FLUID LOGIC
SA THRESHOLD LOGIC
SA TRANSISTOR LOGIC
Heuristic computer programming for solution of complex logic 08 p1299 A67-21199
Computerized weather forecasting based on informational and probability 13 p2152 A67-27275
Maintainability and reliability cost effectiveness program /MARCEP/ applied to logic and computer limitation 18 p2995 A67-34689
Heuristic computer programming for solution of complex logic 22 p3764 A67-39866

LOGIC CIRCUIT

Harmonic linearization of logic law control systems, deriving complex equivalent transmission coefficient for nonlinear part of circuit with variable structural elements 01 p0044 A67-10241
Bistable logic delay circuit using tunnel diodes in circuit branches, noting fast response time and numerical division capability 01 p0044 A67-10661
Integrated digital logic circuits including resistor transistor, diode transistor, emitter coupled and transistor-transistor logic 01 p0038 A67-10760
Saturated transistor logic circuit using rectifier diodes to provide nonlinear current feedback from collector to base of transistor 01 p0038 A67-10817
Junction type field effect transistors and metal oxide semiconductor devices for switching functions in digital circuitry 02 p0215 A67-11971
Time domain analysis of bridge doubler circuit for varactor multiplier 02 p0218 A67-12100
High speed magnetic logic circuits for operation in nuclear radiation environment 02 p0219 A67-12161
Graphical derivation of switching trajectories of transistor-tunnel diode logic circuits 03 p0389 A67-12803
Synthesis method for generating p-level pseudorandom signals derived from corresponding m-sequences, using standard binary logic elements 03 p0393 A67-13997
Book on digital transistor circuits in semiconductor devices based on Boolean algebra and logical and switching circuit principles 04 p0622 A67-15268
Logic and memory circuits and operational dynamics of system of pulsed elements operating on tunnel diodes 05 p0772 A67-16451
Microelectronics in digital subsystems of logic, memory, input/output and power supply 05 p0784 A67-17037
Modular 100 MHz digital time analyzer using flexible plug-in logic 06 p1001 A67-17852
Fluidic devices operating on digital signals, showing logic 06 p0952 A67-18833
Navigation system test by phase shifter, noting signal generator which simulates omnirange systems 07 p1155 A67-19839
Transfer logic of double dialog high security data transmission system using long loop principle 07 p1146 A67-20159
Control of adaptive systems using sensitivity coefficients and logic 08 p1308 A67-20318
Pneumatic grating for complete measuring system, considering fluidic techniques 08 p1330 A67-20439
Pneumatic digital step optimizing device consisting of logic elements of ZPA system for process control 08 p1280 A67-20441
Fluidic digital rectilinear displacement indicator emphasizing transducer, logic circuitry and readout 08 p1281 A67-20456
Fluid circuits used in drilling sequence control, detailing ring counter, binary counting stage and comparator 08 p1281 A67-20458
Optimal design of pneumatic control jet of fluid amplifier to obtain maximum logic gain 08 p1282 A67-20459
Logic methods using conventional piston

valves applied to general automation 08 p1282 A67-20470
LSI effect on aerospace computer design, considering cost, size and power consumption of logical elements 08 p1297 A67-20635
Fluidic system design including coded tape valves, vibrating reed frequency sensor, flow control, pneumatic switches, etc 08 p1286 A67-21053
Simulator studies of MOL tracking experiments 08 p1317 A67-21105
Defining noise margins on noise immunity in binary electrological systems, discussing static /steady state/, with graphs for exemplary integrated logical units 09 p1469 A67-22097
Logical redundancy technique based on failure-erasure circuitry for masking P-1 failures in P identical elements connected in parallel 09 p1470 A67-22668
Micropower electronics noting effects of input capacitance and container and wiring capacitances on HF characteristics 12 p1917 A67-26206
Standardization techniques for integrated circuit production, particularly logic circuits 12 p1918 A67-26215
Development of pneumatic logical elements and systems 13 p2056 A67-27239
Digital circuits in resistor-transistor, diode-transistor and transistor-transistor logic 13 p2082 A67-27388
PSIN /P region, Seminsulating region, N region/ diode array fabrication, performance, characteristics and applications 14 p2282 A67-28029
Laminar NOR unit feasibility, operating characteristics and performance 14 p2250 A67-28335
Static operating characteristics of diaphragm pneumatic logic device 14 p2275 A67-28347
High speed fluidic logic circuitry for pneumatic stepping motor 14 p2251 A67-28351
Thick film hybrid modules discussed for speed, circuit, power density and versatility 16 p2641 A67-31618
Fluid logic components utilizing Coanda wall effect for control systems 17 p2802 A67-32228
Interconnecting fluid elements and hardware components for construction of complex systems 17 p2802 A67-32229
Battery charger system for aircraft application noting nickel-cadmium battery, logic circuitry, wide environmental operation conditions, etc 17 p2804 A67-32515
Fluidic breadboard version of rocket engine sequence control, describing pneumatic logic package and general limitations
[AIAA PAPER 67-518] 18 p3114 A67-33981
Determination of limits of correct operation of comparison and decision circuits in Akima model band subdivision demodulator 18 p3002 A67-34222
Design of large scale integrated MOS-FET devices for general logic circuit applications 18 p3014 A67-34554
MOSFET approach to small scale integration of large scale circuits 18 p3014 A67-34555
High density cryotron array production in associative memory application, using lock-out design feature 18 p3014 A67-34556
Automatic IC mask artwork generating system for large scale integration environment, describing hardware, software and performance 18 p3055 A67-34558
Circuit for integral majority-voting logic elements intended for satellite design, analyzing reliability and performance 18 p3007 A67-34664
Automated logic design techniques for integrated circuitry technology, with wafer design and logic arrays described for different logic functions 19 p3189 A67-36062
Navigational system accuracy and breakdown detection, discussing efficiency criterion for logic device operation 20 p3399 A67-37069
Generation of arbitrary binary sequence with integrated circuits, describing logic circuit by means of circuit algebra 21 p3590 A67-37946
Design procedure for production of radiation resistant NOR gate logic circuit 21 p3603 A67-38185
Pure magnetic integrated logic circuit for space research, noting improvement on

speed factor 21 p3588 A67-38675
 Logic gate with coupled integrated circuit transmitters 23 p3977 A67-40662
 Limiter circuits for NERVA reactor control, discussing design requirements and operation 24 p4183 A67-42472
 Functional half-adder using optical coupling in injection laser noting design criteria and mode propagation delay 24 p4169 A67-42822
 Gigahertz tunnel diode logic, static and dynamic behavior of circuits under DC worst case tolerance analysis, timing analysis, etc 24 p4133 A67-42825

LOGIC NETWORK

Simple gates, multilevel arrays and interconnection in integrated circuits for computers 02 p0219 A67-12110
 Functional properties of semiconductor devices and integrated circuits, considering network design 10 p1610 A67-22976
 Diaphragm element for digital logic requirements of data processing equipment, discussing functions and integrated circuit employed 14 p2274 A67-28346
 Twenty-eight volt monolithic integrated logic circuit suitable for aircraft applications 16 p2642 A67-31725
 Computer theory and physics field relationship noting signal mechanics, geometry, logical networks, etc 19 p3202 A67-35606
 Associative memory system of persistent current bit-cells using cryotrons in selection and control network 21 p3587 A67-37955
 Jet interaction low power-consumption fluid amplifier, NOR logic element switched from laminar to accelerated expansion flow mode by control signal 23 p3936 A67-41420

LOGICAL DESIGN

Integrated circuit application engineering and resultant advantages 01 p0034 A67-10271
 Inputs and outputs of digital pneumatic jet components design for adaptation to standardized pressure range for use in installations 08 p1281 A67-20448
 Design procedure and manufacturing techniques for multielement fluidic plate using wall attachment devices, discussing integrated arrays 08 p1281 A67-20452
 Integrated circuit interconnection system design exemplified by 920 M digital computer 14 p2274 A67-28025
 Rectangular light guides transfer energy from injection type semiconductor laser to laser with logic element 16 p2684 A67-30461
 Digital sequencing systems containing error-detecting and -correcting properties 16 p2647 A67-31647
 Fluid state trigger logic element and bidirectional counter 16 p2609 A67-31663
 IBM CP-2 militarized digital computer noting design, maintainability and performance 17 p2820 A67-32500
 System/semiconductor interface with complex integrated circuits, examining different designs 19 p3199 A67-36055
 Automated logic design techniques for integrated circuitry technology, with wafer design and logic arrays described for different logic functions 19 p3189 A67-36062
 Saturn computer design and fault simulation on IBM 7090 computer 21 p3588 A67-38181

LOGISTICS

SA LUNAR LOGISTICS
 SA MAINTENANCE
 SA SPACE LOGISTICS
 SA TRANSPORTATION

Requirements of economical and effective orbital logistics support system [AIAA PAPER 66-863] 03 p0519 A67-14129
 Monte Carlo simulation provides realistic analysis of set of stochastic processes involved in flow within maintenance and logistics system 03 p0400 A67-14223
 Adaptable large scale integrated military and space systems, discussing microelectronic circuit, logistics and dynamic redundancy 08 p1311 A67-20665
 Systems analysis with computer techniques to examine future weapons system, discussing logistic simulation, interpretation, maintenance, engineering, management, documentation and reliability 17 p2833 A67-32490
 Locating general drop zone and desired impact point, identifying receiving unit and dropping supplies for aerial delivery systems 17 p2797 A67-32587
 Airport terminal planning for Tampa

eliminating long walk, using circular multistory structure with handling equipment for passengers and baggage [SAE PAPER 670319] 17 p2835 A67-32980
 Air Force programs for development of effectiveness and reliability data analysis systems 18 p3007 A67-34658
 Development and application of Monte Carlo logistic simulation model for measuring system availability dependence on reliability, maintainability and logistic support 18 p3021 A67-34674
 Development of quantitative logistics performance parameters related to time, resources and cost in Concept Formulation Phase and Contractual Definition Phase 18 p3162 A67-34678
 Oxygen concentration system for aviator breathing 18 p2995 A67-34717
 Requirements of economical and effective orbital logistics support system [AIAA PAPER 66-863] 19 p3331 A67-34809
 Minimizing time for deployment of infantry force by airlift analyzed by computer procedures based on loading, effectiveness and productivity 20 p3361 A67-37529
 Utility aircraft costs lower than specialized aircraft in meeting mixed mission requirements in counterinsurgency environment, considering changes, uncertainty and logistics 22 p3745 A67-39618
 Life cycle cost concept adaptation by DOD affecting logistics engineer, discussing reliability relation, maintainability, etc 23 p4084 A67-40580
 Maintainability problems analyzed noting Apollo/Saturn program 23 p4070 A67-40581
 Computerized system for calculating spares quantities and providing overall adequacy within monetary, weight or volume constraint 23 p4085 A67-40583
 Logistics resource development and approaches to life cycle economics in 1970s 23 p4085 A67-40587
 Mississippi Test Facility /MTF/ of NASA noting rocket testing facilities, scientific laboratories and industrial complex 23 p3986 A67-40588
 Logistics simulation modeling for optimizing spares mix needed for maintenance of airborne systems at minimum cost 23 p4085 A67-40590
 Earth orbital integrated logistics system extendable to space and lunar operations, considering technical and economic feasibility 23 p4061 A67-40592
 Short haul military requirements /1970-1980/, considering assault and logistic airlifts supporting ground forces and V/STOL aircraft [SAE PAPER 670827] 24 p4093 A67-41992
 Lunar transportation systems for exploration logistics support after first Apollo flight, feasibility, candidates, selection and evolution [AIAA PAPER 67-873] 24 p4244 A67-42994
 Reusable shuttle transportation system for lunar base logistics, estimating cost and performance [AIAA PAPER 67-874] 24 p4140 A67-42995
 Docking mechanisms for spacecraft systems noting hard vs soft and in-line vs off-set systems [AIAA PAPER 67-908] 24 p4244 A67-43015

LOH HELICOPTER
 S OH-6 HELICOPTER
 LONG PERIOD EFFECT
 Long period vibrometer with small spring constant and minimized solid friction by HF vibration of support 14 p2348 A67-28257
 Expression analytically representing progressive and long-term variations of earth rotation velocity 16 p2667 A67-31442
 Rotational time scale and analytical representation by single formula for earth rotation variation 16 p2750 A67-31443
 Dynamic spectrum of long-period geomagnetic pulsations noting Pc range characteristics 20 p3433 A67-37413
 Discovery position plotting of various long period comets, showing tendency to cluster near sun in morning sky, orbit distribution and estimated probabilities 21 p3705 A67-38614
 Seasonal and long term variations in duration of continuous radio signal reflections from sporadic E layer 21 p3623 A67-39038
 Photoelectric observations of 27 long period variable stars on UVB photometric

system 22 p3880 A67-39415
 Von Zeipel method to eliminate short period terms in first order general planetary theory noting system transformation into canonical equations 22 p3881 A67-39514
 Micropulsation pattern changes during magnetospheric transition from quiet to excited state, discussing influence of earth and long period and pearl-type pulsations 22 p3883 A67-39674
 Long period hydromagnetic propagation in theta model geomagnetic tail, deriving TM and TE modes equations 22 p3791 A67-39815
 Long period surface gravity waves in atmosphere 22 p3792 A67-39974
 Periodicity of sunspot groups covering number and importance characteristics, formation frequency and long term spot period 22 p3890 A67-40428
 Long term changes of earth RD length with respect to AD due to superposition of linear and alternating components 23 p3993 A67-40675
 Trapped radiation levels via API-5 and AE1-3 model environments noting long term effects 23 p4061 A67-41517
 Lithium chloride impregnated balsa wood and surgically implanted electrodes for continuous heart rate recording over long periods of time 23 p3965 A67-41571

LONG RANGE
 ORBIS satellite experimental results, noting long range propagation at night and during sunrise [RASSA PAPER 1-10-147] 03 p0373 A67-14254
 Coulomb long range interaction effect on refractive index dependence on light frequency and on absorption lines shape of dipole active excitons 13 p2173 A67-26365
 High Noise Immunity Logic Family /HNIL/ digital switching microcircuits for long distance signal transmission operating at high voltage 14 p2282 A67-28028
 Hydrodynamic gas spin bearing gyroscopes design for long duration space missions 14 p2322 A67-29084
 Pulsations in electron intensities in postbreakup aurora, noting possibility of distant processes affecting electrons 17 p2844 A67-32765
 Sofar bomb signature identification by separation of desired signal from multipath signals with digital computer 20 p3484 A67-36558
 Long range retarded interaction energies, obtaining energy term coefficient from minimal principle using Karplus and Kolker method 22 p3757 A67-39636

LONG RANGE NAVIGATION

SA LORAN
 SA LORAN C

Automatic star trackers for long range aircraft navigation, discussing instrumentation methods and use of pulse code modulation for sensor design 04 p0655 A67-15661
 Long range navigation aids for use as possible alternative to existing aids in interface between en route and terminal area 09 p1531 A67-22655
 FAA navigation improvement program, discussing approach and landing, short and long distance navigation and performance assurance 15 p2514 A67-29738
 Commercial automatic inertial navigator for subsonic and supersonic aircraft provides global navigation and guidance within ATC limits without dependence on external aids 15 p2514 A67-29739
 Long distance air navigation aids, stressing supersonic flight safety requirements 16 p2701 A67-31248
 Satellite relay to provide communication paths for aircraft-ground communication over ocean, considering system design for ATC using reflex repeater 16 p2629 A67-31530
 Australian ATC radar network describing long range surveillance and control of neighboring airport 17 p2834 A67-32749
 Navigation system for long range transport aircraft providing accurate and reliable fixing, discussing takeoff and landing 19 p3254 A67-35312
 Long and short range air navigation trends, discussing digital computer application, collision prevention and landing systems 19 p3256 A67-35864
 Analog and digital long range automatic radar tracking systems design characteristics and implementation by solid state

- components 20 p3379 A67-36244
- LONG RANGE WEATHER FORECASTING**
 - Long range weather forecasting, discussing synoptic, statistical and physical approaches 06 p1027 A67-18604
 - Long range weather forecasting, discussing necessity of nonadiabatic processes 06 p1027 A67-18605
 - Soviet book on practical utilization of observational data from meteorological satellites covering radiation and cloud cover, emphasizing weather forming systems analysis, aerological and synoptical data comparisons, etc 10 p1676 A67-23017
 - Environmental prediction using orbital sensors [AAS PAPER 67-104] 15 p2478 A67-29959
 - Large scale atmospheric motions control, discussing weather control, long term effect and instability 24 p4182 A67-42756
- LONG WAVE RADIATION**
 - Electromagnetic radiation absorption coefficient of atmospheric water vapor in long-wave portion of submillimeter range 02 p0190 A67-11568
 - Seasonal variation of morning and nighttime absorption of long waves 04 p0617 A67-15571
 - Radiosonde radiometer to measure long wave emission from earth and intervening atmosphere during night ascents 06 p1005 A67-18742
 - IR flux for water vapor and flux divergence in atmosphere computed for rate of radiative cooling of atmosphere at coastal and continental stations 13 p2150 A67-26419
 - Zonal and meridional distributions of 5-day averaged outgoing long wave radiation and relation to Northern Hemisphere circulation 17 p2879 A67-32548
 - Long-wave radiation cooling effect in troposphere/stratosphere calculated based on vertical temperature and moisture profiles from nighttime probe 19 p3213 A67-34852
 - Atmospheric radiation balance studies via daytime balloon measurements, obtaining vertical profile curves for albedos, total and reflected radiation, etc 19 p3214 A67-34853
 - Long radio wave propagation in earth ionosphere waveguide channel, determining eigenvalues of boundary value problem from complex transcendental equation containing Bessel function 21 p3580 A67-38116
- LONGITUDE**
 - SA SOLAR LONGITUDE**
 - Astronomical data regarding longitude differences studied, deriving evening averages, time parameters, coefficients, etc, via Chebyshev approximation 14 p2384 A67-28075
 - Book on third international operation of longitudes as part of IGY covering history, characteristics, standard hour, etc 14 p2314 A67-28957
 - Geomagnetic activity effect correlation with sporadic E occurrence in African zone, showing longitude dependence 17 p2844 A67-32546
 - Effective geopotential at synchronous height determined using observations of Syncom satellites during free drift periods, noting longitude dependence 18 p3041 A67-34251
 - Eccentricity change for satellite in librational resonance shown periodic due to gravity dependence on longitude 19 p3220 A67-35254
 - LONGITUDE SENSING**
 - Fokker-Planck equation describing distribution of geomagnetically trapped electrons as function of longitude, time, energy and mirror-point field intensity 22 p3791 A67-39808
- LONGITUDINAL CONTROL**
 - Airplane longitudinal controllability criteria for range of small deviations from reference conditions of steady straight and level flight 02 p0182 A67-12733
 - Flight evaluation of various longitudinal handling qualities involving parameters and region of pilot acceptance [AIAA PAPER 65-780] 17 p2797 A67-32584
 - Frequency response of longitudinal control transmission of transonic aircraft 19 p3176 A67-35570
 - Heat transfer intensifying process experimented in wind tunnel by applying longitudinal/transverse pressure gradients through controlled flow pressure field 19 p3346 A67-35633
 - Navy variable stability studies of longitudinal handling qualities in simulated carrier approach [AIAA PAPER 67-576] 19 p3174 A67-35971
- LONGITUDINAL STABILITY**
 - Experimental fixed and moving-base flight simulator investigation of generalized aircraft longitudinal pilot induced oscillations [AIAA PAPER 65-793] 03 p0365 A67-12913
 - Linear and nonlinear three-dimensional longitudinal stability coefficients from free flight measurements aboard missiles 04 p0703 A67-14553
 - Air density gradient effect on longitudinal aircraft motion 06 p0944 A67-17625
 - Mathematical analysis of certain problems concerning longitudinal oscillations of compound bars consisting of elastic and elastoviscous sections 07 p1214 A67-19176
 - Longitudinal stability of L-29 aircraft, comparing measurement results from independent experiments 09 p1440 A67-22469
 - Electron-hole plasma pinch instability in InSb on application of longitudinal magnetic fields shows change to helical rotating plasma 10 p1683 A67-22760
 - Torsional stiffness of ribs effect on buckling strength of longitudinally stiffened plates compressed in direction of ribs 10 p1719 A67-23474
 - Physical stabilization mechanism of helical instability of positive column in longitudinal magnetic field due to quasi-linear effects 11 p1831 A67-24012
 - Relativistic solution to normal incidence on semiminfinite longitudinally drifting homogeneous temperate magnetoplasma, obtaining reflected and transmitted waves 11 p1832 A67-24304
 - Wiener-Hopf and Aleksandrov methods solve plane and axisymmetric problems of equilibrium longitudinal cracks in thin plates with edges free of stresses 12 p2019 A67-25565
 - Cylindrical shell stability under longitudinal impact, examining buckling processes with high speed motion picture camera 14 p2401 A67-28736
 - Dynamic response of sailplanes to longitudinal maneuvers based on steady lift coefficients on wing and tails 16 p2596 A67-31465
 - Longitudinal and transverse collective fluctuation modes of order parameter in pure type II superconductor in high critical field region 19 p3302 A67-35039
 - Dynamic instability of longitudinal oscillations of cylindrical shell charged with ideal fluid established by approximate reduction of nonlinear equations 21 p3720 A67-38297
 - Aircraft autopilot system in longitudinal flight stabilization regime, using synthesis method based on time characteristics 22 p3831 A67-39609
 - Radial electron density profile and critical longitudinal magnetic field for helical current convective instability in hollow plasma column via Langmuir probe measurements 22 p3853 A67-40234
 - Longitudinal oscillations with multiple degree of freedom obtained over sections of adopted stress-strain diagram, characterizing elastoplastic properties 23 p4076 A67-40683
 - Dynamic longitudinal stability of rigid glider towed by rigid aircraft with elastic cable subjected to aerodynamic loads, deriving motion differential equations 23 p3935 A67-41418
 - Design and flying qualities of variable geometry aircraft, discussing wing pivot location and longitudinal stability characteristics [SAE PAPER 670879] 24 p4094 A67-42013
- LONGITUDINAL STABILITY AND CONTROL**
 - Cessna tandem twin aerodynamics noting propeller slipstream variation effects, comparing front and rear engine operation [SAE PAPER 670243] 12 p1894 A67-25498
 - Longitudinal static stability margin of glider for small lift coefficients showing effect of torsional deformation 16 p2596 A67-31001
 - Dynamic response of sailplanes to elevator control in longitudinal maneuvers, discussing load factors and tail loads as function of aerodynamic and inertial parameters 16 p2597 A67-31786
 - Longitudinal stability and control wind tunnel results, considering swept and variable geometry wing aircraft during deep stall conditions 23 p3932 A67-40567
- Elastic wing twisting effect on longitudinal stability and controllability of glider, considering wing rigidity 24 p4094 A67-42021
- LONGITUDINAL WAVE**
 - GaAs epitaxial layer ultrasonic wave transducers fabricated from seminsulator material, for generation of longitudinal waves 03 p0426 A67-14302
 - Longitudinal and transverse waves transformation in nonuniform plasma 04 p0668 A67-15276
 - Longitudinal waves in viscoelastic rod caused by sinusoidal stress applied at one end, noting temperature dependency of mechanical properties of rod [ASME PAPER 66-WA/APM-29] 04 p0714 A67-15423
 - Impact problem of passage of longitudinal and transverse waves arising in elastic infinite thread over sequence of absolutely smooth nonrotating pulleys 07 p1261 A67-19163
 - Landau type damping of plasma oscillations and Bernstein mode electrostatic propagation perpendicular to weak magnetic field 08 p1360 A67-21129
 - Excitation and propagation of Bernstein modes in nonuniform plasmas near electron cyclotron harmonics 08 p1361 A67-21130
 - Resonant frequencies of standing wave Bernstein modes propagating in magnetized homogeneous plasma columns and effects of anisotropy of unperturbed electron velocity and ambipolar-diffusional electric field 08 p1361 A67-21131
 - Diffraction of plane longitudinal wave in interior of elastic solid, where wave is harmonic in time and impinging on surface of penny shaped crack 09 p1573 A67-21663
 - Transmission and reflection coefficients in coupling of transverse and longitudinal waves below second electron cyclotron harmonic 09 p1548 A67-22383
 - Monochromatic longitudinal wave amplification by charged particle beam in nonlinear plasma, noting amplitude dependence on coordinate 10 p1686 A67-23587
 - Longitudinal acoustic wave attenuation in superconducting aluminum measured, verifying acoustic attenuation predictions 14 p2373 A67-28858
 - Liquid discharge from cylindrical container exposed to longitudinal vibration, noting flow retardation 16 p2658 A67-30946
 - Laminar flow with forced convection heat transfer in parallel plate channel under influence of intense, longitudinal, resonant acoustic field 16 p2778 A67-30947
 - Attenuation characteristics of longitudinal wave propagating in weakly inhomogeneous plasma, deriving expression for oscillations damping constant 16 p2628 A67-31498
 - Transverse and longitudinal waves in ultrasonic light modulators, noting superiority of transverse waves in polarization rotations 17 p2815 A67-32614
 - Acceleration mechanisms of isolated plasma particles under effect of weak or strong field with frequency of order of Langmuir frequency of electron 17 p2905 A67-32922
 - Dispersion relations for coupled electromagnetic and longitudinal waves propagating along isotropic inhomogeneous cylindrical hot plasma column 17 p2908 A67-33107
 - Dispersion of longitudinal or extensional waves in isotropic linear elastic bars with rectangular cross section [ASME PAPER 67-APM-17] 17 p2964 A67-33148
 - Plastic resonance problem for longitudinal elastoplastic waves in finite bar solved, considering bodies with rigid unloading characteristics 18 p3140 A67-33465
 - Systematic errors limiting velocity measurement accuracy of longitudinal ultrasonic waves when using pulse-delay methods, for application to ultrasonic equipment 18 p3044 A67-33734
 - Time and space development equations for longitudinal and transverse modes in Vlasov plasma 18 p3092 A67-34745
 - Longitudinal wave echo in collisionless electron plasma with Landau damping 19 p3295 A67-35534
 - Longitudinal oscillations and Landau damping of electron plasma with fixed ion background, discussing initial and boundary value problems 20 p3494 A67-36150

Longitudinal ultrasound attenuation in polycrystalline superconducting mercury at 9.3 GHz, studying temperature dependence 20 p3514 A67-37568
Isolated longitudinal wave pulse amplitude and phase velocity dependence on trapped particle density in ion-electron and electron-positron plasmas 21 p3669 A67-38683
Nonlinear theory of longitudinal plasma waves, formulating distribution function and Maxwell equation for electric field 22 p3845 A67-39421
Solitary pulse longitudinal waves existence in electron plasma related to trapped ions presence, studying ion pulse shape and oscillation stability 22 p3845 A67-39423
Electromagnetic propagation in plasma layer in magnetic field, determining absorption coefficient 22 p3762 A67-40123
Branch cut contribution to longitudinal electric field in relativistic Maxwell plasma using non-Laplace transformation procedure 22 p3854 A67-40319
Transverse electric field generated by interaction of various longitudinal plasma waves in ion electron plasmas 23 p4033 A67-41151
Frequency dependence of attenuation coefficient for longitudinal ultrasonic waves in InSb over range 50 to 210 MHz for temperatures between 200 and 600 degrees K 24 p4202 A67-41980

LOOK ANGLE

Tilt angles for photographs of physically and geographically diverse terrains taken with different types of gyrostabilized aerial cameras 13 p2118 A67-26463

LOOP

SA CIRCUIT
SA CLOSED LOOP SYSTEM
SA RING
SA SERVO LOOP
Conducting loop resonant size determination and geometrical shape effect on resonant size in anechoic chamber experiment 16 p2639 A67-31356
First slip time of phase locked loop of arbitrary order shown as solution of first order linear differential equation 17 p2811 A67-32117
Coronal condensation analysis observed photographically during total solar eclipse, finding good correspondence of loop system spatial trajectories to force line configurations 17 p2945 A67-32690
Dynamic energy losses in thin Ni-Fe films during magnetization reversal studied by observation of M-H loop 22 p3860 A67-39902

LOOP ANTENNA

Short wave and very short wave direction finding from aircraft 03 p0465 A67-13394
Horizontal loop antenna for observation of whistler-like ELF radio waves between 3 and 60 c/s 14 p2306 A67-27885
Radiation properties of low-gain ring antenna on ground plane, showing by patterns effect of geometrical parameters and frequency 17 p2827 A67-32781
Oscillation conditions of microwave tunnel diode theoretically and experimentally evaluated for mounting at feed point of semicircular loop antenna 19 p3196 A67-35660
Ground vertical loop radio antenna for army use noting shape, performance, mobility, etc 20 p3399 A67-36884
Field of loop antenna with arbitrary current distribution located inside cylinder with arbitrary dielectric constant studied for effects on radiation pattern 23 p3982 A67-41666

LOR

S LUNAR ORBITAL RENDEZVOUS
/LOR/

LORAN

Configurations of hyperbolic position-fixing systems using synchronous satellites, showing Loran-like networks on earth resulting from these configurations 09 p1526 A67-22393
Satellite navigation systems requirements including Loran, inertial navigation and Navy systems 23 p4025 A67-41363
Reception of ground based Loran transmissions by fixed-frequency topside sounder satellite 24 p4119 A67-42061

LORAN C

Oblique incidence ionospheric reflections, from phase and amplitude variations of Loran-C pulse signals, noting lower ionosphere two-layer formation 16 p2632 A67-31862

LORENTZ

Room temperature recombination radiation induced by Lorentz field in InSb and ternary alloy of mercury, cadmium and tellurium under cross field conditions 03 p0496 A67-13675
Umov-Poynting theorem, Lorentz lemma, complex conjugate lemmas and quadratic relations for EM field intensity in electrodynamics of moving media 05 p0844 A67-16354

LORENTZ FORCE

Hall effect, voltage generation across current-carrying conductor perpendicular to magnetic field and galvanomagnetic effects based on Lorentz force 04 p0657 A67-15081
Plasma formation by dissociation of diatomic hydrogen ions by Lorentz force 04 p0671 A67-15645
Source model for predicting aerodynamic drag on moving arc column in crossflow yields relationship between crossflow velocity and balancing magnetic field 08 p1356 A67-20579

Relaxation process and magnitude of nonthermal ionization in MHD generator, describing experimental equipment and results in xenon and in argon 09 p1540 A67-21790
Decomposition, in orthogonal universal vectors, of electromagnetic universal force created by point charge animated by universal velocity and acceleration 09 p1534 A67-22590
Current distribution in incompressible fluid flow in magnetic field at low Reynolds number, estimating Lorentz force effect 11 p1842 A67-24952
Hall voltage reduction in linear MHD generators noting Lorentz force effect 12 p1898 A67-25387

Stability of self-gravitating two-fluid infinite plasma cylinder model in axial magnetic field 13 p2163 A67-26285
Escalation effect by interaction of conduction and induction currents in niobium alloy wires 15 p2539 A67-29826
Current distribution in segmented electrode MHD duct and sufficient condition for preventing current leakage between adjacent segments of generator 18 p2987 A67-33703

Lorentz number, Hall coefficient, magnetoresistance and Hall mobility variations in n-type degenerate semiconductors 18 p3106 A67-34729
Limited instability and flux jumping variation with magnetic field for flux pinning and Lorentz forces equilibrium in mixed state of type II superconductor 22 p3856 A67-39438
Time reversible difference procedures including Lorentz and continuity equations, relativistic orbits and gyrocenter motion 23 p4027 A67-40996
Liquid mercury conductor flow in annular gap electromagnetically accelerated by Lorentz force, showing restricted nonexistence proof for inviscid problem 23 p3992 A67-41742

LORENTZ GAS

Anisotropies and harmonics of homogeneous Lorentz plasma under electric field, using approximation method 01 p0121 A67-10230
Soviet book on electromagnetic shock waves associated with not-very-high powers, using Maxwell-Lorentz equations 06 p1031 A67-17949
Nonequilibrium line radiation for generalized Lorentz profiles in spherical plasma of large optical thickness 13 p2166 A67-26728
Lorentzian scalar electrical conductivity as basis of mixture rules proposed for partially ionized gases in magnetic field to calculate tensor conductivity 15 p2523 A67-29218
One-dimensional electron plasma model, transport coefficient determination, Lorentz plasma conductivity measurement, decay rate, etc 18 p3092 A67-34748
Physical changes in exploding wires before gas ionization observed by X-ray technique, studying resistivity variation with density 19 p3261 A67-35161
Electron distribution function of homogeneous imperfect Lorentz plasma disturbed by electric field 19 p3295 A67-35418
Electrostatic relaxation wave dispersion in isotropic Lorentz gas, considering Landau

damping and balancing of elastic electron-atom collisions 22 p3848 A67-39692

LORENTZ TRANSFORMATION

Radiation in Lorentzian moving anisotropic plasma 01 p0123 A67-10442
Electromagnetic analysis of rotating fluid systems containing rigid and inhomogeneous parts within fluid by introducing additional relativistic transformation of gravitational constant 01 p0113 A67-10470
Lorentz invariance of special relativistic thermodynamics equations in inertial frame of observer 04 p0658 A67-15610
Equivalent vector method for obtaining Lorentz transformations of special relativity shown to have apparent variants 08 p1347 A67-20366
Lorentz transform applied to solution of problem in interaction of waves within nonlinear medium 09 p1465 A67-22478
Lorentz invariance, momentum energy tensors and formulation of MHD problem 10 p1685 A67-23083
Post-Galilean transformation to which Einstein-Infeld-Hoffmann motion equation is invariant, considering transformation to center of mass system 12 p1965 A67-25125
Matrix inversion formula applied to moving media electrodynamics and scaling operator in Lorentz transformation 15 p2509 A67-29175
Propagation and radiation of waves excited by electric dipole in dispersionless uniaxial moving medium 18 p3002 A67-34199
Sign of energy gain and direction of energy flow shown invariant under Lorentz transformation for two relatively moving systems possessing equal proper temperature 21 p3733 A67-39124

Particle mass not related to velocity with respect to other particles velocity explained in terms of relativistic uniformly accelerated motion 22 p3837 A67-39879
Generalized Lorentz transformation for inhomogeneous region in general relativity obtained by transformation leading to nearly straight system of reference 23 p4028 A67-41187

LOSS
S ENERGY LOSS
S HEARING LOSS
S LEAKAGE
S OHMIC LOSS
S PLASMA LOSS
S TRANSMISSION LOSS
S WATER LOSS

LOUDSPEAKER

Push-pull electrostatic loudspeaker for aircraft cockpit, helmet and ear-insert communication 11 p1767 A67-24702

LOW ALTITUDE

Ejection capability vs decision to eject 22 p3754 A67-39596
Low altitude atmospheric turbulence analysis methods 22 p3828 A67-39665

LOW ASPECT RATIO WING

Low aspect ratio wings at high incidence in wind tunnel study of surface pressure and vortex flow 10 p1593 A67-23549
Stress analysis methods applied to hollow thin walled low-aspect-ratio wings, considering small deflection law 14 p2401 A67-28657
Approximate solutions obtained in closed forms for low aspect wing stressed state under transverse load 21 p3724 A67-38780
Network method to derive differential difference equations for boundary condition of clamped and free edges and point supports of low aspect orthotropic wings network method to derive differential-difference 21 p3724 A67-38782

LOW DENSITY GAS

Low density gas flow through short tubes at densities varying from continuum to free-molecule regime, noting nitrogen flow [ASME PAPER 66-WA/PID-8] 04 p0606 A67-15331
Laminar convective heat transfer to cavities in hypersonic low density flow 04 p0732 A67-15833
Low density air flow measured by anemometer with pulsed ion generation in air stream 10 p1658 A67-23787
Normal and tangential momentum accommodation coefficients in low density facility 13 p2098 A67-26947
Attenuation cross section and refractive index using collision theory, calculating resonance profiles of autoionizing lines based on scattering

theory 14 p2351 A67-28811

LOW DENSITY WIND TUNNEL

Hypersonic low density wind tunnel for high Mach numbers and stagnation temperatures, analyzing measurements made, noting heater, nozzle, diffuser, etc 04 p0595 A67-14561

Turning-arm apparatus operating in rarefied gas chamber and low pressure wind tunnel for drag 04 p0596 A67-14993

Low density wind tunnel, with results of tests on free expanding cold jets 04 p0596 A67-14994

Diffuser use in low density hypersonic wind tunnel and method of evaluating global performance for diffusers with conical inlet followed by cylindrical mixing section 05 p0748 A67-16763

Source flow expansion of partially ionized gas into vacuum for predicting flow properties of low density free jet plasma expansions [AIAA PAPER 67-99] 06 p1041 A67-18281

Low density wind tunnel enabling simulation of aerodynamic flows at high altitudes with rarefied air 17 p2835 A67-33132

Limiting driven conditions corresponding to optimum expansion and low density shock tube flow for overexpanded nozzle 21 p3609 A67-38886

Wind tunnel hypersonic flow visualizations under low flow density conditions, comparing schlieren and phase-contrast methods 23 p3985 A67-40568

LOW FREQUENCY

Radio whistler occurrence in nighttime and daytime during maximum and minimum solar activity 01 p0057 A67-10261

Solid state high power LF and VLF telemetry transmitters, considering power amplifier design, RF output network, cooling systems, etc 02 p0218 A67-12106

Transistor life expectancy and failure predictions from LF noise measurements 03 p0389 A67-14277

Amplitude of LF oscillations in He-Ne laser 05 p0825 A67-16948

Daytime profile of electron density in C and D layers of ionosphere from measurements of surface ultralong wave fields and atmospheric pressure profile 05 p0801 A67-17131

LF high-Q resonances in mixed state of pure outgassed Ne 06 p1048 A67-17818

Ten years ionospheric drift measurements in LF range 07 p1171 A67-19420

Comparative analysis of magnetization modes for magnetic storage of LF signals, using flux-sensitive and inductive reproducing heads in magnetic recorders 07 p1147 A67-19632

Filtering properties of frequency-stability transport circuits of molecular beam generator, noting design considerations for high efficiency 08 p1305 A67-21274

LF test generator producing ramp output for phase shift detection in electronic systems at different input voltages 08 p1307 A67-21537

Defining noise margins on noise immunity in binary electrological systems, discussing static/steady state, with graphs for exemplary integrated logical units 09 p1469 A67-22097

Comparison of electron tubes, transistors and FET noise figures as function of source impedance of generator 10 p1810 A67-22924

LF noise fluctuation anomalies in narrow doped germanium p-n junctions at low temperatures 11 p1765 A67-24478

Characteristic cut-off frequencies of transistors determined from simple LF measurements 13 p2077 A67-26859

Propagation rate of LF acoustic waves in low pressure glow discharge in nitrogen 14 p2354 A67-27759

Total resistance of p-n diode calculated assuming high injection levels in base and moderate frequencies 14 p2286 A67-28530

Directional dependency of slow tail ELF atmospheric waveforms, noting generation by cloud to ground type lightning discharges 14 p2312 A67-28571

LF plasma instabilities indicated by Landau electron attenuation computation for short wavelengths 15 p2528 A67-29710

LF gravitational waves radiated by electromagnetic field of moving bodies, discussing measurement problems 18 p3117 A67-33527

Noise theory for self-sustaining discharge verified for low frequencies, noting temperature dependence, silicon, etc 18 p3106 A67-34638

Solid-propellant combustion instability models describing combustion zone dynamics applied to acoustic and nonacoustic instability in low frequency regime [CI PAPER 67-13] 19 p3311 A67-35007

LF noise in MOS-FET, discussing relationship to drain current and power dissipation 19 p3198 A67-36044

Daytime profile of electron density in C and D layers of ionosphere from measurements of surface ultralong wave fields and atmospheric pressure profile 21 p3619 A67-38474

Total resistance of p-n diode calculated assuming high injection levels in base and moderate frequencies 23 p3980 A67-40937

Lunar crater utilization as LF radio astronomy parabolic reflector, noting electromagnetic characteristics [AIAA PAPER 67-904] 24 p4125 A67-43012

LOW LEVEL TURBULENCE

Incident of severe low level turbulence in clear air 01 p0108 A67-10226

Low level turbulence effects on structure of large logistic aircraft [SAE PAPER 660670] 01 p0160 A67-10577

Low turbulence wind tunnel driven by airfoil centrifugal blower, noting design for best performance 09 p1485 A67-22162

Incident of severe low level turbulence in clear air [AIAA PAPER 65-642] 14 p2297 A67-28108

Atmospheric humidity effect on lower atmospheric layer turbulence above oceans, discussing velocity, temperature and humidity profile calculation 22 p3828 A67-39220

LOW PASS FILTER

All-pass RC filter network design for constant signal delay in LF systems, noting cascade phase characteristics 01 p0045 A67-11197

Digital generation of continuous filtered Gaussian noise 02 p0194 A67-11809

Impulse and step responses of band stop equal element filters with varying degrees of dissipation calculated for transient responses of resonant circuits 02 p0220 A67-12177

Minimum phase shift low pass filters with given departure from constant attenuation and given nonlinearity of phase response in passband 03 p0380 A67-13579

Low pass filters approximating phase and modulus of exponential function near frequency origin 03 p0386 A67-13976

Design for active filters via eight-pin miniature component 14 p2283 A67-28288

LF and HF single stage RC filters with steep frequency characteristic slope in transition region 14 p2289 A67-28863

Microwave direct-coupled cavity filter design using single insertion loss formula for case of Chebyshev equal-ripple characteristic 17 p2828 A67-33084

Human controller as adaptive low pass filter to track signal contaminated with noise 18 p2994 A67-34340

Computer method for determining time-frequency-domain response specifications of transversal linear wave filters, using thin film RC distributed networks 18 p3015 A67-34560

Relationship between switching time, transient suppression and filter complexity for filter-type diode switches 19 p3186 A67-35659

Audioconducted and RF radiated susceptibility thresholds of active low pass filter circuits, determining limitations and meeting specification requirements 20 p3406 A67-37652

Transient performance of delay equalized low pass filters studied for optimal response 21 p3582 A67-38529

Electrically tunable low pass filter using Permalloy films near resonance 22 p3772 A67-39906

Unilateral parametric amplifier using two varactor diode low pass filter with pumping phase difference, noting bandwidth and gain 24 p4128 A67-41969

LOW PRESSURE CHAMBER

Long term effects of oxygen environment on rat colony at 210 mm Hg absolute showed no significant physiological changes and no difficulty in readaptation 05 p0755 A67-16285

Large helium refrigerators for very high speed cryopumping techniques required in space simulation facilities 12 p1924 A67-25716

Lung, liver, kidney and heart pathology of dogs, monkeys, rats and mice exposed for 2 to 13 weeks to pure oxygen atmosphere at reduced pressure 13 p2059 A67-26918

Acetazolamide effects in aiding altitude accommodation, examining action on blood and cerebrospinal fluid 23 p3951 A67-41566

Leg volume changes in response to lower body negative pressure due to blood redistribution 23 p3955 A67-41619

Seven year follow-up X-ray survey for bone changes in low pressure chamber operators to determine long term effects of altitude decompression sickness 23 p3957 A67-41641

LOW SPEED HANDLING

UF-XS Japanese STOL seaplane used to investigate slow speed flying quality and hydrodynamic characteristics of PX-S aircraft 14 p2245 A67-27743

Reliability and safety for STOL aircraft and low airspeed operation, discussing automatic flight control system, air traffic control, etc [AIAA PAPER 67-797] 24 p4095 A67-42958

LOW SPEED STABILITY

Divergent vertical helicopter oscillations resulting from physical presence of pilot in collective control loop 11 p1744 A67-24591

Low speed aerodynamic static stability of winged and wingless reentry configurations 14 p2239 A67-27796

LOW SPEED WIND TUNNEL

Strain gauged sting balance for use in small low speed wind tunnel for measuring lift, drag and pitching moment 01 p0051 A67-11270

Fan system of 14 by 9 ft open circuit wind tunnel structural principles and operation, discussing blade fabrication, hub design, spinner and motor fairing 03 p0397 A67-14104

Low turbulence wind tunnel driven by airfoil centrifugal blower, noting design for best performance 09 p1485 A67-22162

Low speed wind tunnel design, structure, performance and cost 11 p1773 A67-24640

LOW TEMPERATURE ENVIRONMENT

Radial distribution analysis of films of bismuth and gallium prepared by low temperature condensation for electron diffraction tests 01 p0137 A67-11060

Radial distribution analysis of films of Pb-12 percent Bi and beryllium in metastable phases prepared by low temperature condensation for electron diffraction tests 01 p0137 A67-11061

Mechanical properties and chemical composition of industrial niobium VN2 and VN2A at low temperatures 05 p0832 A67-17506

Optical phonon production, showing existence of electric field strength range at low temperature scattering in which phonon emission results in electron stoppage 06 p1010 A67-17884

Low temperature characteristics of Ga-As varactor diode junction properties, calculating spreading resistance 09 p1471 A67-21827

Charpy impact specimens cooling rates in low temperature quenching baths evaluated including specimen size, notch geometry and material chemistry 11 p1874 A67-24265

Multiposition grips for automatic mounting of metal or plastic specimens for low temperature mechanical tests 11 p1877 A67-24819

High energy density Zn/O battery system, noting good low oxygen pressure and low temperature performance characteristics 13 p2055 A67-26836

Man rating requirements of space environment simulation laboratory consisting of two large chambers with floors which can be cooled by liquid nitrogen down to 92 degrees K 13 p2090 A67-26841

Large space simulation chamber for studying low temperature, absolute vacuum and solar radiation effects 15 p2466 A67-29571

Low temperature conductivity of semiconductors in electric and magnetic fields analyzed, noting electron-photon interactions and photon heating effect 15 p2542 A67-30248

Ionization wave velocity in nonisothermal,

low temperature plasma discussed, using generalized Ohm law, law of conservation of electron energy and SAHA equation 16 p2711 A67-30540

Experiments and design of low temperature seeded inert gas MHD power generator operating in nonthermal ionization mode 16 p2801 A67-30548

Clustering in AL-GP zone alloys after low temperature neutron irradiation 17 p2872 A67-32742

Alpha particle irradiation effect at liquid-helium temperature on transition temperature of superconductive tin, indium and thallium foils 17 p2926 A67-33405

AC motor design for operation in He in cryogenic to room temperature range, noting performance parameters and design considerations [AIAA PAPER 67-456] 18 p2988 A67-33930

Open circuit voltage, short circuit current and maximum power for silicon solar cells at low temperatures 18 p2989 A67-34101

Composite material with titanium strength-weight ratio and aluminum safety for aerospace vehicle construction [ASTM PAPER 15] 18 p3067 A67-34576

Noise spectral density measured at low temperature in sensitized GaAs, studying relaxation time, temperature effect, etc 19 p3307 A67-35733

Low temperature dependence of relative efficiency of forward biased InAs diode emitter 19 p3198 A67-36046

Existence of ozone difluoride established by low temperature experiments and correlation with mass spectrometric EPR, IR and NMR 20 p3377 A67-37136

Mechanical properties and chemical composition of industrial niobium and alloys VN2 and VN2A at low temperatures 21 p3644 A67-38034

Low temperature effect on physical and mechanical properties of engineering materials and cryogenic fluids, discussing heat generation and removal at rubbing surfaces 21 p3633 A67-38141

Twinning and low temperature mechanical properties of high purity polycrystalline niobium and molybdenum, discussing grain size effects 22 p3823 A67-40208

Survival of desert algae at extremely low temperatures and diurnal freeze thaw cycles 23 p3945 A67-41346

LOW TEMPERATURE PHYSICS

SA CRYOGENICS

Calibration of pressure transducers in liquid-hydrogen to liquid-helium temperature range, using cryogenic test setup 01 p0069 A67-11018

Calorimetric apparatus for measurement of low temperature emittance of materials as function of temperature [AIAA PAPER 65-703] 03 p0418 A67-13037

Low temperature technology and space flight 04 p0720 A67-14538

Monograph on low temperature oxidation including kinetic mechanism, oxidation of various compounds, knock phenomenon, etc 04 p0565 A67-15089

Silicon electrical properties at low temperatures and various carrier concentrations, noting 05 p0861 A67-16502

Iron and chromium films prepared at 4 degrees K analyzed by radial distribution, showing electron diffraction patterns of amorphous state 05 p0866 A67-16976

Hall coefficient and transverse magnetoresistance behavior in n-GaSb at 4.2 degrees K, using DC high magnetic fields 06 p1064 A67-18946

Localized instantaneous plane heat sources position and strength determined using inert thermometers and time integrals of observed temperature transient 11 p1883 A67-24901

Thermal ionization for low temperature plasma confined in magnetic field, examining magnetic field effect on ionization 12 p1975 A67-25757

Total hemispherical emittance of transparent materials at low temperatures measured using calorimetry 13 p2159 A67-27356

Absolute emissivity calorimeter design for low temperature measurements above 60 degrees K using liquid helium as cryogenic fluid 13 p2122 A67-27661

Thermoelectric power increase in low temperature metals not explained by

residual resistivity in simple model calculation 15 p2540 A67-30096

Low temperature plasma - Conference, Moscow, July 1965 17 p2890 A67-32134

Elementary processes in low temperature plasma 17 p2893 A67-32135

Low temperature plasma production in combustion chamber for use in MHD generators, giving equations for plasma composition 17 p2893 A67-32167

Thermal magnetic noise fluctuations reduction in superconductors below 4.2 degrees K 17 p2913 A67-32272

Absorption, reflection and emission spectra of gold chloride at low temperatures 18 p3101 A67-34187

Cellular injury and resistance in freezing organisms - Conference, Sapporo, Japan, August 1966, Volume 2 20 p3367 A67-36141

Parameter diagnostics of low temperature plasma in cesium diode, comparing probe measurements with transport equation solutions 22 p3845 A67-39425

Book on low temperature physics covering Josephson effect, superfluid He flow, superconductivity, etc 22 p3866 A67-40548

Thermodynamic properties of low temperature gaseous and liquid mixtures, discussing quantum effects in mixtures containing hydrogen isotopes and high density mixtures 22 p3921 A67-40553

Deformable aluminum alloys low temperature mechanical properties 24 p4170 A67-41923

Collected papers of Kapitza, Volume 3 covering low temperature production, stereoscopic films, liquid He, etc 24 p4188 A67-42294

LOW THRUST PROPULSION

Low thrust reaction control system utilizing solid propellant which sublimates into low molecular weight vapor, noting heat sources 01 p0142 A67-11407

Mariner IV midcourse 50-lb thrust pressure-controlled monopropellant hydrazine propellant system, predicting impulse and velocity error as function of burn time [AIAA PAPER 66-948] 02 p0304 A67-12282

Direct ballistic gravity-assisted ballistic and nuclear electric low thrust flight modes for interplanetary exploration 02 p0327 A67-12366

Necessary conditions for optimal fixed-time powered transfers with multiple coasts and thrusts between circular orbits 02 p0328 A67-12402

High specific impulse thrust by sputter ejection of atoms from single crystals following ion bombardment, useful in space propulsion 02 p0306 A67-12716

Approximation for low thrust trajectory without singularity at escape and having correct behavior up to and beyond escape, using motion equation 05 p0903 A67-17363

Low thrust engine spacecraft control during boost phase, independent of velocity vector determination, by stabilizing osculating orbit plane relative to planetocentric coordinate system 11 p1869 A67-24068

Maximum payload for air-scooping low thrust space propulsion system 13 p2212 A67-26893

Variational problem of maximum payload in mechanics of flights with limited propulsion power and energy storage unit 16 p2780 A67-30719

Fuel consumption precision measurements for low thrust auxiliary rockets using impeller wheel and photometric devices [AIAA PAPER 67-507] 18 p2989 A67-33971

Low thrust cold-gas reaction jets in vacuum studied for pulsed propulsive performance for use in spacecraft attitude control 19 p3310 A67-34805

Mariner IV midcourse 50-lb thrust pressure-controlled monopropellant hydrazine propellant system, predicting impulse and velocity error as function of burn time 21 p3712 A67-37797

Combustion characteristics of hydrazine type propellants and resultant reactions in low thrust engines prior to ignition 21 p3687 A67-37798

Single nozzle thermal storage resistojet thruster for low thrust satellite attitude and orbit control applications, noting design and performance [AIAA PAPER 67-662] 21 p3690 A67-38698

Low thrust Jupiter flyby mission analysis

for interplanetary vehicles with solar electric propulsion [AIAA PAPER 67-708] 21 p3706 A67-38735

Trajectory optimization, performance and other factors in analysis of low thrust solar electric propulsion Jupiter flyby mission [AIAA PAPER 67-710] 21 p3706 A67-38737

Optimal parameters of transfer function of low thrust power limited engines by approximate solution of differential equation 22 p3898 A67-39181

LOW VELOCITY

Drag measurements of isolated lamellae and cylinders in rarefied gases with low velocity 03 p0404 A67-13972

LOWER ATMOSPHERE

Microwave spaced-cavity refractometer for measuring small-scale variations of refractive index, wind speed, temperature, etc, in lower atmosphere 01 p0025 A67-10816

Lower atmospheric layer and meteorological conditions effect on oscillations of image of artificial source of light 02 p0238 A67-11987

Laser radar returns from lower troposphere compared with vertical ozone distributions indicate inverse relationship 04 p0612 A67-14676

Optical effects of thermal structure in lower atmosphere 10 p1679 A67-22745

Effect of macrometeorological conditions and local peculiarities on lower atmospheric temperature, humidity and wind distribution 11 p1815 A67-24326

Monograph on problems of cloud physics covering evolution of preinversion stratiforms and vertical velocities determination in lower atmospheric layer 11 p1816 A67-24521

Vertical atmospheric flow mean velocity determination within fixed area from wind probe observations at fixed points 11 p1816 A67-24523

Estimation of parameters of transverse diffusion in lowest atmospheric layer using Lagrange and Euler turbulence characteristics 16 p2698 A67-31095

Lower atmosphere nucleonic component measurement, noting attenuation coefficient dependence on atmospheric depth 17 p2842 A67-32364

Space-time wind variability for forecasting from near ground surface sampling for unguided rocket impact prediction 17 p2880 A67-32551

Auroral oval between outer boundary of trapping region and ionosphere and dynamical and atomic interactions between magnetospheric plasma and neutral atmosphere 18 p3035 A67-33597

Tethered sonde for micrometeorological soundings of lower atmosphere noting pressure transducer, servoswitching system, thermistor, hygistor, data acquisition, etc 21 p3628 A67-38582

Planetary surface pressure and temperature of lower atmosphere determined from orbiting spacecraft with carbon dioxide laser 22 p3805 A67-40357

LOWER IONOSPHERE

SA C LAYER

Altitude dependent electron attachment rates and molecular oxygen concentrations indicating three-body attachment process in lower ionosphere 03 p0410 A67-12960

Daytime profile of electron density in C and D layers of ionosphere from measurements of surface ultralong wave fields and atmospheric pressure profile 05 p0801 A67-17131

Propagation of magnetodynamic disturbance through loss ionosphere and entry into earth surface 07 p1174 A67-19718

Ionization capability of cosmic rays in low ionosphere, considering relativistic energies and high energy 09 p1561 A67-21841

Low ionosphere with suitable selected track for absorption observation as indicator of galactic cosmic rays modulation by solar wind 09 p1561 A67-21843

Ionospheric absorption as indicator of particle flux below point of long radio wave reflection, noting relation to solar cosmic rays 09 p1561 A67-21844

Changes in electron concentration in lower ionosphere with temperature dependent effective recombination coefficient during transmission of pulse radio signals 10 p1630 A67-22791

Vertical drift of charged particles effect on electron density profile as cause of

- seasonal variations in ionospheric absorption 10 p1646 A67-23269
- Macroscopic neutral and ionized gas motions in ionospheric D and E layer interpreted from wind and radio wave scattering measurements 11 p1787 A67-24595
- High velocity particles and slower corpuscles penetration into lower ionosphere occurring after solar flare explained by Sweet mechanism 12 p1993 A67-25134
- Solar constant and sunspot relationship interpreted by solar radio flux effect on lower ionosphere density 12 p1932 A67-25342
- Oblique incidence ionospheric reflections, from phase and amplitude variations of Loran-C pulse signals, noting lower ionosphere two-layer formation 16 p2632 A67-31862
- Altitude of lower boundary of ionosphere determined by electron density profile, considering absorption coefficient and magnetotonic signal 16 p2669 A67-31906
- Solar flare effect on electron production and electron density in lower ionosphere 17 p2936 A67-32382
- Day-and nighttime electron and ion density profiles in lower ionosphere deduced from blunt probe theory and measurements 19 p3218 A67-35213
- Electron temperature and density profiles in lower ionosphere at sunset, describing temperature measurement technique 19 p3229 A67-35246
- Thermal tidal motions in lower ionosphere and differential charge mobility pictured as producing earth atmosphere electrical structure 19 p3220 A67-35255
- Two-ion D region model for polar cap absorption events 20 p3426 A67-36302
- Lower ionospheric drift studied from signal recordings from distant medium wave broadcasting stations 22 p3788 A67-39467
- Changes in electron concentration in lower ionosphere with temperature dependent effective recombination coefficient during transmission of pulse radio signals 24 p4149 A67-42127
- LOX**
- S LIQUID OXYGEN /LOX/**
- LOX-HYDROGEN ENGINE**
- Ignition of hydrogen-oxygen propellant combination by chlorine trifluoride 10 p1697 A67-23132
- Development of liquid hydrogen-oxygen propulsion stage in France, discussing structure, thermal isolation, storage, etc 18 p3111 A67-33653
- Internal combustion engine fuelled with cryogenic hydrogen and oxygen [AIAA PAPER 67-421] 18 p2988 A67-33906
- M-1 injector baffles, ablative chamber and start system design and development, using subscale testing [AIAA PAPER 67-461] 18 p2988 A67-33932
- LRV**
- S LUNAR ROVING VEHICLE /LRV/**
- LUBRICANT**
- SA GAS LUBRICANT
- SA GRAPHITE
- SA GREASE
- SA HIGH TEMPERATURE LUBRICANT
- SA OIL
- SA PETROLEUM
- SA SOLID LUBRICANT
- Materials for use as rolling-contact bearing lubricants in liquid hydrogen environment 01 p0077 A67-10119
- System design and lubricating materials for spacecraft lubrication 02 p0250 A67-12453
- Aerospace requirements for bearings and lubricants in natural environments 02 p0250 A67-12454
- MHD analysis of composite slider bearing using electroconductive lubricant such as liquid metal, in magnetic field perpendicular to bearing surface, for large and small Hartmann numbers [ASME PAPER 66-LUB-B] 05 p0811 A67-16275
- Pressure distribution between lubricated rolling bearings, comparing static and dynamic stresses in cylindrical disks, noting film thickness 08 p1333 A67-20361
- Ni-graphite antifriction composites capable of high temperature operation with good lubrication properties and oxidation resistance under dry friction conditions 08 p1341 A67-20599
- Grease lubricants for aerospace application, determining physical properties and testing them at 400 degrees F and under high vacuum [ASLE PAPER 66AM 3C2] 09 p1506 A67-22421
- Operating lifetime of porous bearings, discussing dependence on quality of impregnating lubricant 10 p1659 A67-22831
- Lubricant selection for lunar missions and manned spacecraft based on compatibility with oxygen-rich environment, propellant, anodic coatings and sliding friction behavior in vacuum [ASLE PAPER 66AM-7A2] 13 p2123 A67-27100
- Conducting Bingham plastic fluids considered as lubricants in rheostatic bearing in presence of constant magnetic field [ASME PAPER 67-LUBS-4] 16 p2682 A67-31382
- Viscous, compressible fluid flow through narrow gap, noting compressibility effect on pressure distribution 16 p2661 A67-31420
- Thermal stability and degradation of n-hexadecane, mineral oils, and oligomers measured as function of time and temperature 16 p2695 A67-31754
- Extreme pressure /EP/ films from lubricants containing borate esters, studying structure and mode of action 16 p2683 A67-31756
- Lubricant requirements for aircraft parts noting high and low temperature, radiation conditions, lubrication capability limits, etc 19 p3248 A67-34993
- Polymeric materials used for selected subsystems of Mariner IV space probe [JPL-TR-32-1031] 19 p3334 A67-35889
- Papers on lubrication and lubricants 20 p3455 A67-37261
- Synthetic lubricants noting chemical and physical properties of nonhydrocarbons, classes of synthetics, etc 20 p3455 A67-37264
- Surface active lubricant influence on internal stresses in sign variable slippage case, discussing chemisorption, wear resistance and stress distribution 22 p3810 A67-39219
- Viscoelastic lubricant in squeeze film configuration for sphere impinging on lubricant covered plane, noting pressure peak sensitivity to viscoelastic constants [ASME PAPER 67-LUB-24] 24 p4164 A67-42682
- LUBRICATING OIL**
- Flight environment effect on lubrication requirements of Pratt-Whitney SST engine [SAE PAPER 660711] 01 p0013 A67-10601
- Jet fuel lubricity noting poor performance due to polar compounds, improving lubricity by surface active additives 01 p0139 A67-10602
- Gear lubrication fundamentals and principles of oil film formation on mating gear tooth surfaces 02 p0250 A67-12499
- Ball bearing life operating in vacuum with molybdenum disulfide and oils as lubricant [ASLE PAPER 66AM 7A3] 08 p1335 A67-21036
- Phenothiazine carboxylic acid esters as improved antioxidants in stable and sludge-free synthetic oils 09 p1520 A67-21705
- Ignition of flammable fluids by hot surfaces tested on static hot plate rig and on wind tunnel rig, noting data on kerosene, lubricating oil and hydraulic fluid 09 p1580 A67-22248
- Jet aircraft lubrication oil application and degradation factors 10 p1597 A67-23411
- Cold starting and service test evaluation of SAE 10W30 aircraft engine oil [SAE PAPER 670249] 11 p1811 A67-23982
- Lubricants for utility aircraft piston engines, cost, availability, compatibility, etc [SAE PAPER 670248] 12 p1989 A67-25502
- Jet fuel lubricity noting poor performance due to polar compounds, improving lubricity by surface active additives [SAE PAPER 660712] 12 p1988 A67-26163
- Linear fluorinated hydrocarbon polymer oils and grease mixtures with low molecular weight polytetrafluoroethylene thickener as lubricant for liquid fueled rocket motors [ASLE PREPRINT 67AM 8A-4] 14 p2327 A67-28796
- Oil Mist Deposits Test for differentiating deposit forming tendencies of jet engine lubricants, discussing mechanism and threshold temperature 16 p2683 A67-31755
- Computers role in fluid film lubrication, computing parameters for bearings lubricated by compressible and incompressible lubricants via iterative finite difference schemes 21 p3632 A67-38135
- Extent of lubricating film for which oil flow is plane, discussing lubricant compressibility, heat release, load capacity and pressure distribution 22 p3811 A67-39317
- High temperature lubricants for ball bearing applications, discussing bearing endurance and rolling-contact fatigue tests on synthetic paraffinic oil [ASME PAPER 67-LUB-21] 24 p4163 A67-42679
- Lubricants, metal high temperature and atmospheric environments effects on gear load-carrying capacity [ASME PAPER 67-LUB-27] 24 p4164 A67-42685
- Oxygen diffusion through lubricant to metal surface examined for influence in corrosive wear [ASLE PAPER 67-LC-4] 24 p4164 A67-42743
- LUBRICATION**
- SA BOUNDARY LUBRICATION
- SA SELF-LUBRICATING MATERIAL
- SA SPACE ENVIRONMENTAL LUBRICATION
- SA SPACECRAFT MECHANISM LUBRICATION
- Liquid solid film lubrication of hydrodynamic bearings, including effects of solid particles in liquid base lubricant 01 p0077 A67-10122
- Gear lubrication fundamentals and principles of oil film formation on mating gear tooth surfaces 02 p0250 A67-12499
- Turbulent annular airflows in turbulent film lubrication of high speed bearings [ASME PAPER 66-LUB-14] 03 p0403 A67-13755
- Turbulent lubrication analysis in fluid film theory and turbulent shear flow, with application to bearings [ASME PAPER 66-LUB-12] 03 p0431 A67-13761
- MHD lubrication flow in externally pressurized thrust bearing analyzed, including fluid inertia effects 04 p0627 A67-14461
- Spacecraft environmental effects covering outgassing in high vacuum, deterioration of materials by evaporation, lubrication and changes in mechanical and electrical properties of plastics 04 p0704 A67-14995
- Friction, lubrication and wear, survey of work done during last decade 05 p0809 A67-16065
- Gas film MGD lubrication in transverse and tangential electromagnetic fields 05 p0810 A67-16273
- Lubrication and wear - IME Convention, Scheveningen, Netherlands, May 1966 09 p1505 A67-22190
- Film thicknesses in elastohydrodynamic lubrication by silicone fluids obtained from oscillatory shear related to continuous shear 09 p1506 A67-22193
- Lubrication and wear - IME Conference, Plymouth, England, May 1967 12 p1948 A67-25327
- Gear materials and lubrication methods to satisfy high speed and temperature requirements in aerospace applications 14 p2334 A67-27791
- Lubrication mechanisms defined via electrodeposited solid film systems, noting porous structure formation 19 p3233 A67-34789
- Papers on lubrication and lubricants 20 p3455 A67-37261
- Lubrication and wear - IME Conference, London, September 1967, Session 2, Fluid film lubrication 21 p3632 A67-38134
- Lubrication and wear - Conference, London, September 1967, Session 4, Lubrication and materials 21 p3632 A67-38138
- Lubrication and wear - IME Conference, London, September 1967, Session 5, Specific environments 21 p3633 A67-38140
- Lubrication and wear in high vacuum, considering inability to maintain oxide films, evaporation of lubricants, heat transfer and sliding friction 21 p3633 A67-38142
- Lubrication and wear - Conference, London, September 1967, Session 6, Synthesis 21 p3633 A67-38144
- Synthetic molybdenum sulfide film examined for lubricating performance under extreme pressure conditions in air and immersed in fluids [ASLE PAPER 67-LC-15] 24 p4165 A67-42749

LUBRICATION SYSTEM

Rolling-element bearings design and material processing for special conditions, noting stress and fatigue 01 p0079 A67-10726

Elastohydrodynamic lubrication in rolling bearings for avoiding oil-film breakdown in contact zone 01 p0079 A67-10728

Literature in 1965 on lubrication and bearings covering friction and wear, boundary, metal working, gear and spline lubrication, rolling element bearings, etc [ASME PAPER 66-WA/LUB-8]

Lubrication system design and component arrangements for several oil and gas lubricated closed looped gas turbine machines 04 p0629 A67-15349

[ASME PAPER 67-GT-3] 11 p1799 A67-24791

Hydrodynamic lubrication in face seals, discussing mechanism of fluid film, surface roughness, wear, leakage, thickness, temperature, pressure, etc [BHRA PAPER E5] 14 p2324 A67-27889

MHD lubrication flow in self-acting step type thrust bearing configuration, showing torque reduction 24 p4162 A67-42566

LUBRICATION TESTING MACHINE

Lubricant testing system optimizing with respect to machine ability and cost 01 p0077 A67-10121

Lubricant testing for supersonic aircraft, examining temperature requirements, viscosity, evaporation characteristics, etc [DVL-606] 03 p0426 A67-13016

Soap and nonsoap base greases physical and chemical nature, composition, characteristics and additives 20 p3455 A67-37265

Life tests of tapered roller bearings in mineral oils and synthetic fluids, demonstrating lubrication effect on contact fatigue crack propagation [ASME PAPER 67-LUB-20] 24 p4163 A67-42678

Optical elastohydrodynamic system for evaluation of lubricants using interference pattern obtained from metal ball rolling against plate glass [ASLE PAPER 67-LC-12] 24 p4164 A67-42747

Lubricating action of electroplated gold on stainless steel examined under load by single rub block loaded against rotating disk [ASLE PAPER 67-LC-16] 24 p4165 A67-42750

Worm gear lubrication with bonded solid film lubricants, discussing efficiency and wear life test apparatus [ASLE PAPER 67-LC-18] 24 p4165 A67-42751

LUMINESCENCE

SA BIOLUMINESCENCE

SA CHEMILUMINESCENCE

SA ELECTROLUMINESCENCE

SA FLUORESCENCE

SA LIGHT

SA LUNAR LUMINESCENCE

SA PHOSPHORESCENCE

SA PHOTOLUMINESCENCE

SA SELF-LUMINOUS BODY

SA THERMOLUMINESCENCE

Radiation of giant pulses of superluminescence by highly excited active medium of Nd glass with rapid cut-in of amplification 01 p0091 A67-10837

High intensity triboluminescence in europium tetrakis /dibenzoylmethide/-triethylammonium crystals under mechanical impact 01 p0019 A67-10897

Meteor luminescence during atmospheric motion, obtaining radiation coefficient as function of cross sections of particle excitation and pulse transfer processes 01 p0151 A67-11287

Ionization luminescence of air and possibilities of using it to record extensive air showers 02 p0318 A67-12781

Temperature dependence of spectral distribution of radiation, excitation and quantum output of green luminescence of cadmium sulfide films 03 p0433 A67-12889

Effect of thermal processing in various atmospheres and of additives of group I and III elements in periodic table on luminescent properties of cadmium sulfide 03 p0433 A67-12890

Luminescence of alcoholic solution of europium chelate at low temperatures, noting changes in intensity of optical excitation at various energy levels 03 p0433 A67-12894

Light absorption by uranium glass in excited state, showing relaxation time relation to luminescence 03 p0436 A67-13141

Luminescence in cadmium sulfide mixed crystals of widely varying composition in presence of excitation by ruby laser emission 03 p0436 A67-13153

Calcium fluoride-cerium fluoride with neodymium additions as active medium for lasers, discussing absorption and luminescence spectra and induced radiation 05 p0825 A67-16922

Two-electron transitions in luminescence of excitons bound to neutral donors in gallium phosphide 06 p1051 A67-18210

Spectrum of meteorite luminescence emission after irradiation with protons and UV radiation, using spectrophotometer 08 p1390 A67-21021

Stimulated emission, absorption spectra and luminescence of neodymium-activated YAG crystals in pulsed laser 09 p1513 A67-22068

Luminescence in cadmium sulfide mixed crystals of widely varying composition in presence of excitation by ruby laser emission 10 p1664 A67-23102

Yellow-green luminosity accompanying injection of triethylborane into upper atmosphere 12 p1932 A67-25208

Calcium fluoride-cerium fluoride with neodymium additions as active medium for lasers, discussing absorption and luminescence spectra and induced radiation 14 p2330 A67-28262

Time dependent self-compressed pinch-discharge radiation characteristics in various gases analyzed photographically for luminescence distribution, spectral composition, etc 17 p2904 A67-32918

Red luminescent band and photoconductivity in cadmium sulfide single crystal, discussing IR quenching of photocurrent 19 p3300 A67-34764

Impurity photoconductivity in cadmium sulfide energy levels at red luminescence centers depth 19 p3300 A67-34765

Luminance profiles of earth sunlit limb through visible spectrum for navigation and research 19 p3213 A67-34804

Luminescence from ruthenium complexes, investigating charge-transfer absorption bands 19 p3181 A67-35880

Luminescence decay kinetics of trivalent Nd ions in antiferromagnetic Rb manganese fluoride, showing mechanism of transfer process of excitation energy of Mn ions 20 p3506 A67-36218

Absorption spectra, spectral dependence of luminescence quantum output, glow curves and radiation spectra of color centers in ruby crystal 20 p3506 A67-36223

Cadmium sulfide edge luminescence energy shift dependence on excitation intensity and free carrier concentration 20 p3512 A67-37288

Ionization luminescence of air and possibilities of using it to record extensive air showers 22 p3878 A67-40283

LUMINESCENT INTENSITY

SA LIGHT INTENSITY

Thermoluminescence of achondrite meteorites on lunar surface based on rate of temperature rise of lunar terminator 01 p0146 A67-10249

Solvent and temperature effects on fluorescent emission of europium beta diketones 01 p0131 A67-10297

Luminescence spectra of terbium complex compounds with pyrazolone derivatives 03 p0433 A67-12888

Luminescent intensity and spectral energy distribution determined for exciton luminescence of anthracene crystals for spontaneous and stimulated emission 03 p0436 A67-13136

Electroluminescence, discussing semiconductor lasers with various excitation sources, luminescent efficiency, etc 06 p1010 A67-17889

Luminescence spectra of terbium complex compounds with pyrazolone derivatives 06 p1012 A67-18768

UV imaging system for lunar missions to detect luminescing minerals on lunar surface 08 p1331 A67-21079

Space correlation of main emission lines for night sky emission spectra and altitude distribution of sodium luminescence 10 p1647 A67-23279

Absolute threshold of cat optic nerves determined by inspection of poststimulus time histograms, computed from responses of identical flashes of white light 10 p1598 A67-23581

Stimulated emission in GaSb injection lasers with steep flat p-n junction, noting dependence of luminescence intensity on current density 10 p1667 A67-23665

Luminescence of CdS at low temperature excited by very high intensity laser light 10 p1667 A67-23779

Orbit, luminescence and spectrum of July 5, 1962 bolide orbit, luminescence and spectrum of July 5, 1962 bolide orbit, luminescence and spectrum of July 5, 1962 13 p2197 A67-26502

Effect of single-axis compression on radiative impurity recombination in arsenic- and gadolinium-doped germanium 15 p2537 A67-29705

Stimulated emission in GaSb injection lasers with steep flat p-n junction, noting dependence of luminescence intensity on current density 17 p2870 A67-33346

Nightglow emission structure and variation at airglow equator, discussing predawn and storm effects, intensity variations with solar cycle, OH bands, etc 18 p3036 A67-33607

Lunar surface luminescence in IR and UR bands, discussing luminescence distribution, luminoform nature and surface irregularities 22 p3879 A67-39298

Effect of single-axis compression on radiative impurity recombination in arsenic- and gadolinium-doped germanium 24 p4199 A67-41775

LUMINOSITY

SA STELLAR LUMINOSITY

Absolute radio luminosity empirical relationship with surface brightness for extragalactic radio sources 03 p0515 A67-14320

Smear camera used to measure detonation front velocity of explosive or propellant 06 p1001 A67-17793

Spiral and irregular galaxies total mass to neutral hydrogen mass ratio derived from mass-luminosity relations 11 p1858 A67-23995

Perseid meteor brightness studied from data of photoelectric observations by use of electronic multiplier 11 p1867 A67-24846

Luminosity variations of comet 1963 III related to solar and geomagnetic disturbances caused by corpuscular solar particles 17 p2946 A67-32730

Perspective and path length effects on determination of spatial distribution of auroral luminosity from optical observations 17 p2851 A67-33206

Plasma time-dependent luminosity from pulsed discharge in vacuum, determining excitation temperature distribution and discharge spectral lines 18 p3087 A67-34049

LUMINOUS INTENSITY

Ultimate sensitivity of space camera imaging devices with particular reference to slow scan vidicon 02 p0245 A67-12245

Photographic measurement of plasma jet velocity using time shift in brightness fluctuation 04 p0666 A67-15188

Observed meteor luminosity and deceleration compared with theoretical values 05 p0889 A67-16209

Luminosity of galactic disk in 12.8 micron radiation, obtaining from volume integral stellar photon flux density and thermal radio emission rate 05 p0892 A67-16412

Stefan-Boltzmann radiation law of fixed stars, calculating stellar temperature, diameter and luminosity 05 p0846 A67-16730

Spectral radiance of low current graphite arc anode determined, using high accuracy spectroradiometer 05 p0846 A67-16787

Threshold characteristics of photoresistors with noiseless contacts on CdS base 07 p1152 A67-19592

Transient lunar brightening, discussing attempted correlation with solar wind activity 07 p1256 A67-20160

Combustion and heat transfer laws for hydrocarbon flames with predetermined visual radiation 08 p1425 A67-20303

Electric field domain motion in Ge samples with Au and Sb impurities, noting temperature and illumination effect on V-I characteristics 08 p1367 A67-20411

Plasma resonance emission of thin Ag foils irradiated by light, noting intensity and direction of polarization 08 p1368 A67-20787

Normal temperatures for optically thin plasma in state of local thermodynamic equilibrium [DVL-644] 09 p1536 A67-21557

Rate equation solution for density of

excited atoms in He-Ne discharge for steady state 10 p1663 A67-22893

Amplitude distributions of solar photospheric fluctuations 10 p1711 A67-23795

Chromospheric background intensity difference between equatorial and polar regions of sun 10 p1711 A67-23800

Silicon photocells at high luminous flux concentrations, noting increase in multiplicity of power with series resistance 13 p2056 A67-27622

Phase shift between electron temperature, luminous intensity and electron density in stratified positive column of glow discharge 14 p2353 A67-27757

Luminous front in electric shock tube having coaxial gun without current crowbarring measured by phototransistors 14 p2355 A67-27823

Electron measurements near weak aurora during rocket flight 18 p3034 A67-33595

Near-earth meteor flux estimate through luminous efficiency and ionizing probability application to data on radio and photographic meteor 19 p3319 A67-35217

Nitrogen and oxygen dayglow emissions observed during total solar eclipse of May 1965, studying emission/continuum intensity ratio 20 p3427 A67-36368

Threshold characteristics of photoresistors with noiseless contacts on CdS base 20 p3401 A67-37331

LUNAR ATMOSPHERE

Molecular fluxes in lunar atmosphere relationship to gas source distribution, surface temperature and gas emission laws 05 p0904 A67-17404

Resonance scattering measurement from solar illuminated lunar atmospheric constituents 06 p1091 A67-18999

Lunar data covering mass, shape, dimensions, earth-moon relations, orbits, selenography, etc 20 p3530 A67-37549

Two-dimensional diffusion model for gas propagation in lunar atmosphere, discussing contamination by lunar module exhaust gases and solar wind loss mechanism 22 p3883 A67-39817

LUNAR BASE

Research and system requirements for two-to-six-man lunar scientific laboratory to investigate lunar habitability 04 p0597 A67-15063

Lunar resources discussing exploitation methods for various forms of resources available 06 p1092 A67-19029

Lunar base concepts and operational modes for long duration lunar surface studies 09 p1485 A67-22402

Lunar bases planning and development, noting parallel with Antarctic exploration missions 09 p1486 A67-22404

Extended manned lunar surface operations in study of lunar origin and history with respect to solar system 09 p1568 A67-22408

Meteorological observations of earth from lunar surface 12 p1920 A67-25648

Future manned earth orbital flights [AAS PAPER 67-26] 15 p2562 A67-30101

Integrated thermoelectric SNAP-8 Rankine power system for manned lunar base missions, studying man-system interactions effect on design criteria 24 p4185 A67-42544

Integrated design requirements of SNAP-8 Rankine power system for manned lunar base mission, discussing mission requirements and reactor shield system 24 p4185 A67-42545

SNAP-8 type reactors and shield subsystems for MORL and manned lunar base plants, discussing Rankine and thermoelectric power conversion systems 24 p4186 A67-42546

Lunar transportation systems for exploration logistics support after first Apollo flight, feasibility, candidates, selection and evolution [AIAA PAPER 67-873] 24 p4244 A67-42994

Reusable shuttle transportation system for lunar base logistics, estimating cost and performance [AIAA PAPER 67-874] 24 p4140 A67-42995

Potential benefits of lunar resources, discussing water deposits location, mining and processing [AIAA PAPER 67-876] 24 p4238 A67-42996

LUNAR COMMUNICATION

Scientific lunar payload communications system 02 p0196 A67-11999

Lunar communication satellites, discussing

satellite relay, librational, random and synchronous satellite design, lunar orbits, etc

[AIAA PAPER 66-315] 06 p0961 A67-17705

Feedback control system to position satellite in vicinity of unstable collinear libration point with application to lunar communication problem

[AAS PAPER 66-132] 07 p1146 A67-19991

Feedback control system to position satellite in vicinity of unstable collinear libration point applied to lunar communication problem

[AAS PAPER 66-132] 13 p2210 A67-27543

Lunar communications using satellites in astrodynamical aspects of lunar orbital stability and effective communications zone 16 p2622 A67-30730

Satellite motion in libration point vicinity, neglecting lunar eccentricity and solar perturbation, discussing lunar communication system utilizing libration point satellites 22 p3886 A67-40107

LUNAR COMPOSITION

Propellant preparation from extraterrestrial materials on moon and planets rather than transportation from earth as economical source of fuel for interplanetary manned traffic 04 p0695 A67-14555

Lunar surface composition, strength and failure modes, determining ability to support LEM 05 p0895 A67-16612

Chemical analysis of lunar surface composition by instruments on board soft landing probes 07 p1186 A67-19571

Photometric investigations of simulated lunar surfaces confirm high porosity and low albedo without postulating necessity for fine dust layer 12 p2003 A67-25740

Probable internal structure of moon in light of thermal history examined searching for explanation of lunar core and crust formation 16 p2747 A67-30992

Unmanned exploration of moon, summarizing results on surface structure, back side and material composition 16 p2748 A67-31199

Lunar core precession and coupling between assumed liquid core and moon mantle 16 p2754 A67-31746

Lunar structure from lunar moments of inertia, noting thick layer denser than lead near surface 17 p2947 A67-32757

Lunar surface absorption coefficient in IR range, discussing limb-darkening, reflectivity, subsolar point temperature, radiation, spectral properties, etc 18 p3122 A67-34139

Lunar surface materials choice narrowing method via albedo, color and polarization property examinations to find possible candidates for lunar surface model 21 p3701 A67-37897

Mineral deposits on moon noting probable magmatic segregation, fumarole products, carbonaceous deposits, etc 21 p3711 A67-39119

Moon moment of inertia calculated for model with homogeneous core and homogeneous mantle, varying mantle density, core density and core radius 23 p4066 A67-41011

LUNAR CRATER

Errors in estimates of lunar crater slope angles and surface roughness in Ranger VII and Ranger VIII pictures due to interpretation of dark areas as shadows [JPL-TR-32-994] 01 p0147 A67-10319

Lunar craters, quadrant IV, designation, diameter, position, central peak information, etc 01 p0152 A67-11331

Lunar crater photographs obtained by Ranger VIII and IX compared with those of laboratory craters overlain with granular material, for depth interpretation [JPL-TR-32-1021] 02 p0320 A67-11459

Interpretations of lunar crater erosion other than used by Jaffe from Ranger VII pictures 02 p0325 A67-11860

Directional absorptivity characteristics of conical cavities and use as thermal model for lunar meteor craters [AIAA PAPER 65-669] 03 p0508 A67-13049

Stochastic model of cratering and survival of craters on moon, discussing approximate diameter distribution of primary and secondary craters 04 p0696 A67-14739

Color events on moon observed through color filters alternately, noting crater Gassendi 05 p0888 A67-16155

Classification of lunar banded craters of

Abineri and Lenham complemented by addition of Kunowsky class characterized by extremely large and dark floors 05 p0895 A67-16578

Ranger VII telescopic observation of crater topography of Mare Cognitum 05 p0901 A67-17084

Wall of large circular formation on moon shown on Orbiter photographs as convex body resembling flow of viscous lava 05 p0901 A67-17202

Size distribution of lunar craters from Ranger pictures show that frequency of crater occurrence is inversely proportional to square of diameter 05 p0903 A67-17293

Fielder analysis on diameter frequency and distribution of centers and number density of lunar craters 05 p0903 A67-17295

Lunar crater diameter-depth relationship from Ranger VII photographs 06 p1087 A67-18376

Martian and lunar craters and volcanic activity 06 p1089 A67-18648

Incremental and cumulative methods for analysis of diameter-frequency relation for craters, with special application to moon 08 p1385 A67-20932

Lunar cratering statistics interpretation in terms of meteoroid impact hypothesis, noting equilibrium distribution function [AAS PAPER 66-183] 08 p1387 A67-20958

Lunar crater distortion implication on past shape of moon, noting earth-moon system evolution 08 p1389 A67-21016

Meteoritic influx and crater formation on moon, noting Apollo type asteroids and cometary nuclei 08 p1389 A67-21017

Meteoritic bombardment damage to lunar surface with reference to terrestrial craters and hypervelocity impact 08 p1389 A67-21018

Relative depths of moon mountain rings and craters in region of Mare Nubium 08 p1390 A67-21027

IR scanning of lunar disk during total eclipse of December 1964, noting hot spots identified with craters or white areas 08 p1392 A67-21086

Lunar crater depth distribution in stochastic model of formation, obliteration, filling and isostatic readjustment of craters 08 p1397 A67-21209

IR images of lunar crater Tycho during lunar night provide evidence that thermal anomaly is produced by solar rather than internal heat 09 p1565 A67-22013

Morphology of lunar craters from Ranger photographs, noting distribution and possible competing processes of crater formation and destruction 11 p1865 A67-24608

Peculiarities of dispersion of matter resulting from meteorite impact on lunar surface as explanation of concentric nature of structure of crater 12 p2002 A67-25646

Schroeter rule and modification of lunar crater impact morphology 13 p2210 A67-27602

Formation of Flamsteed Ring slopes on moon investigated, noting wall consistency with fragmental debris from moon quakes 15 p2553 A67-29160

Interpretation of tests for randomness of lunar craters, noting clustering and alignment 15 p2554 A67-29458

Recognition thresholds for lunar crater sizes, noting elliptical image measurements and generation of appropriate computer program 15 p2431 A67-29894

Lunar crater classification by morphological types discussing ring structures 16 p2747 A67-30984

Moon rotational parameters determined by refractometric observations of craters position angles, tabulating selenographic and topocentric coordinates, reference system conversion corrections, etc 17 p2949 A67-33121

Lunar physical libration constants determined, based on heliometric observations /1877-1915/, including coordinates of crater Mosting A 18 p3128 A67-34302

Moon physical libration constants and figure determined, including crater Mosting A coordinates, via heliometric observations with Bessel method 18 p3128 A67-34305

Lunar physical libration constants derived on basis of four series of heliometric observations, studying ellipticity, inertia, mean radius elimination, etc 18 p3134 A67-34534

Lunar craters and fragments compared with terrestrial low velocity secondary

volcanic impact craters and ejectra on basis of distribution relations 18 p3134 A67-34538

Crater forming processes on moon from Ranger VIII impact, ascertaining gravity scaling existence, noting relation to terrestrial soils 19 p3327 A67-35894

Morphology of Flamsteed Ring hills compared to other craters 20 p3525 A67-36997

Lunar crater Alphonsus emission flare noting C-2 Swan system proposal 20 p3528 A67-37470

Theoretical lunar crater formation data compared to experimental measurements, discussing lunar crater structures and crater fields 22 p3879 A67-39297

Estimated thickness of fragmental surface layer of Oceanus Procellarum from laboratory impact cratering studies 22 p3885 A67-39977

Lunar scar and ghost crater origin theories illustrated with Ranger 3-D slides 23 p4064 A67-40951

Haskell viscous flow equations describing very slow linearly viscous liquid with initially crater shaped surfaces solved and applied to lunar craters 23 p4065 A67-40998

Impact crater size vs incidence analyzed statistically in study of validity of time dependence on saturation for moon and Mars 23 p4066 A67-41007

Lunar Orbiter II lunar surface photographs noting Copernicus H and Copernicus crater interior peak cluster 23 p4066 A67-41012

Lunar geology using probe data to distinguish impact and volcanic surface shaping processes [AIAA PAPER 67-862] 24 p4238 A67-42986

Lunar crater utilization as LF radio astronomy parabolic reflector, noting electromagnetic characteristics [AIAA PAPER 67-904] 24 p4125 A67-43012

LUNAR CRUST

Crustal features of moon and Mars analyzed for mantle convections, noting correspondence to spherical harmonics of various orders 08 p1397 A67-21208

Probable internal structure of moon in light of thermal history examined searching for explanation of lunar core and crust formation 16 p2747 A67-30992

Lunar events analyzed and related to lunar crust disturbance through internal causes 17 p2942 A67-32388

Lunar structure from lunar moments of inertia, noting thick layer denser than lead near surface 17 p2947 A67-32757

Mineral deposits on moon noting probable magmatic segregation, fumarole products, carbonaceous deposits, etc 21 p3711 A67-39119

LUNAR DISK

Dynamics of physical librations of moon, refining standard theory by using reduced estimate of mechanical ellipticity of lunar equator 01 p0149 A67-10803

Dynamic ellipticities of moon as supported by strength of interior 08 p1388 A67-21009

Differences in lunar moments of inertia determined from libration constants obtained from heliometric observations 08 p1388 A67-21010

Lunar shape in relation to internal structure and moments of inertia found by harmonic analysis 08 p1388 A67-21011

Lunar ablateness due to thermal effects associated with decrease of mean surface temperature from equator toward poles 08 p1389 A67-21012

Lunar core and convection in analysis of lunar principal moments of inertia and surface ellipticity 08 p1389 A67-21013

IR scanning of lunar disk during total eclipse of December 1964, noting hot spots identified with craters or white areas 08 p1392 A67-21086

Moon physical libration constants and figure determined, including crater Misting A coordinates, via heliometric observations with Bessel method 18 p3128 A67-34305

Moon physical libration in longitude 18 p3129 A67-34306

Selenodetic measurement methods, considering point coordinates determination on lunar surface near limb or center, including moon profile studies during solar eclipse 18 p3129 A67-34309

Selenodetic evaluation of 11 selected original photographic plates from 1894-1909 Paris Observatory collection of lunar

photographs 18 p3129 A67-34311

Lunar profile deviations from circle determined from annular solar eclipses, discussing measurement techniques 18 p3130 A67-34314

LUNAR DUST

Nature of lunar surface, discussing interpretations of Luna IX photographs by Jaffe and Kuiper 03 p0512 A67-13934

Tektite structure and lunar ash flows, noting theoretical computations of pressure, temperature and voidage 03 p0512 A67-13936

TV pictures of Surveyor I compartment radiators taken on June 11 and July 12, 1966, discussing cause of some changes in dust locations 08 p1386 A67-20944

LUNAR ECHO

Short-pulse radio reflections to determine average scattering behavior of lunar surface at 23 cm wavelength 02 p0325 A67-11858

Radar methods in lunar probing, discussing data obtained from surface soundings [AAS PAPER 66-186] 08 p1387 A67-20961

LUNAR ECLIPSE

Anomalous cooling of moon surface during lunar eclipse explained possibly by lunar surface roughness in form of cracks and declivities at centimeter scale 02 p0320 A67-11460

Lunar eclipse brightness variation relation to geomagnetic planetary index, showing that luminescence is in accord with rate of increase of plasma energy 03 p0509 A67-13165

Red-green-IR three-beam high resolution photoelectric photometry during lunar eclipse for lunar colorimetric studies 04 p0696 A67-14735

IR and visible images of eclipsed moon made from scan data and magnetically recorded analog signals from observation of total lunar eclipse on December 19, 1964 04 p0697 A67-14741

IR scanning of lunar disk during total eclipse of December 1964, noting hot spots identified with craters or white areas 08 p1392 A67-21086

IR emission measurement of lunar-like materials during simulated eclipse, noting dependence on time [AIAA PAPER 67-290] 12 p2009 A67-26007

Radiometric observations of total lunar eclipse of December 19, 1964 at wavelength of 3.3 mm indicate no significant temperature difference [JPL-TR-32-1097] 12 p2011 A67-26245

Surface geometry demonstrated to be insignificant in production of lunar hot spots during eclipse 18 p3135 A67-34545

Lunar thermal anomalies exhibiting slower cooling rates during eclipse, discussing IR observations 18 p3135 A67-34546

Correlating lunar eclipse brightness, solar activity and corona ellipticity data 20 p3528 A67-37462

LUNAR EFFECT

High altitude satellites orbital curves, considering moon effect 15 p2560 A67-30044

Lunar events analyzed and related to lunar crust disturbance through internal causes 17 p2942 A67-32388

Statistical evidence of planetary and lunar modulation of geomagnetic activity 21 p3711 A67-39005

LUNAR ENVIRONMENT

Physics of moon and environment - Conference, London, June 1965 08 p1388 A67-21008

Lunar environment effects on Surveyor I components, particularly white paint degradation as function of time 15 p2579 A67-29451

Lunar environment simulation test bed, noting lunar gravity effect on astronaut performance 17 p2832 A67-32003

TV in lunar environment, discussing development and performance of instrument used during Surveyor I mission 21 p3629 A67-38658

Prediction of lunar surface temperature through digital computer program noting heat transfer equations 22 p3884 A67-39930

Environmental, thermal and foreign particle effects on Surveyor vidicon performance and expected tube life [SMPT PAPER 102-32] 22 p3807 A67-40373

Lunar geothermal deposits, discussing recovery applications and energy tapping [AIAA PAPER 67-901] 24 p4239 A67-43009

LUNAR EVOLUTION

Calculating past states of earth-moon

system based on three time scales for dynamical change 04 p0698 A67-14854

Lunar origin, tidal evolution of earth-moon system, thermal background of lunar interior, figure and composition of moon and radial density profile 04 p0702 A67-15560

Tidal friction theory of lunar origin and dynamic evolution [AAS PAPER 66-192] 08 p1387 A67-20965

Lunar thermal history computed for different radioactive elements distribution 18 p3119 A67-33862

Moon surface origin and present surfaces of moon, Venus and Mars as determined from lunar photographs and data by flyby probes 18 p3121 A67-34135

Lunar surface evolution model implying partial melting due to impacts as only cause of primitive plutonic activity 20 p3525 A67-36948

Morphology of Flamsteed Ring hills compared to other craters 20 p3525 A67-36997

Lead 206/lead 204 vs lead 207/lead 204 plots for young mantle-derived volcanics support upheaval predicted by lunar capture hypothesis 22 p3881 A67-39554

Lunar silicate rock appearance and genesis conditions with emphasis on vesiculation processes 23 p4064 A67-40947

Shock processes pertinent to lunar terrain fragmentation and lithification noting Surveyor and Lunar Orbiter pictures 23 p4064 A67-40948

Lunar scar and ghost crater origin theories illustrated with Ranger 3-D slides 23 p4064 A67-40951

Seleno-geological evidence for lunar surface properties from Surveyor I, discussing weathering products and volcanic genesis 23 p4064 A67-40952

Lunar origin and earth-moon system, discussing dynamical requirements based on secular variation of some parameters 24 p4230 A67-42322

Fission hypothesis of lunar origin, reviewing energy, dynamics, angular momentum, geology and physical properties 24 p4230 A67-42323

Lunar origin related to earth rotational instability due to earth core formation 24 p4230 A67-42324

LUNAR EXCURSION MODULE /LEM/

Environment, mission requirements and subsystem interfaces effect on space vehicle structure [SAE PAPER 660673] 01 p0153 A67-10580

Environmental simulation techniques to supplement facility capabilities for environmental test program of Lunar Excursion Module /LEM/ [SAE PAPER 660682] 01 p0049 A67-10587

U.S. Saturn/Apollo moon program, considering Saturn V booster, Apollo spacecraft and Lunar Excursion Module 01 p0154 A67-11001

Transducer measuring water quantity in water storage tanks of LEM under zero g conditions 01 p0073 A67-11114

LEM data reduction system performing real-time telemetry conversion and data processing 01 p0030 A67-11118

Omnidirectional penetrometer for lunar surface parametric impact testing and certification of safe soft-landing site for Apollo LEM 01 p0074 A67-11123

Methods, schedules and cost of applying computer technology to circuit design, including Apollo and LEM programs 01 p0031 A67-11335

Dynamic analysis of reaction control system /RCS/ propellant feed network on lunar module using digital computers 01 p0142 A67-11435

Multiprogramming system for computer controlled telemetry, data reduction system 02 p0206 A67-11807

Communications subsystem providing S-band link between LEM and earth and VHF link between LEM and Command Module 02 p0205 A67-12273

LEM optical astronomy package /OAP/ containing astronomical telescope, spectrophotometer, data processing subsystem and other devices, for unmanned landing and life support 02 p0246 A67-12414

Local scientific survey module /LSSM/, small lunar vehicle designed to provide two astronauts with transportation and portable scientific lab on lunar surface 03 p0400 A67-14308

Microwave and thermal vacuum testing to demonstrate design maturity of LEM rendezvous radar during simulated mission 04 p0576 A67-15397

Mockup of manned hardware systems in industrial design, describing application to LRV and LEM development, crew compartment design for undersea craft /DSRV/, etc 05 p0757 A67-17378

Testing of three individual propulsion systems of lunar module space vehicle in preparation for man-rated flight service [AIAA PAPER 67-258] 07 p1166 A67-20073

MARCO 4418 binary computer for strapdown guidance system in LEM/AGS 08 p1297 A67-20627

Thermal design of attitude translational control assembly /ACTA/ of lunar excursion module /LEM/ 08 p1303 A67-21062

System concepts, combinations and missions for lunar exploration using LEM 08 p1316 A67-21082

Apollo Extension System for lunar surface missions, discussing extension of mission time by unmanned LEM 08 p1316 A67-21083

LEM Truck concept based on Apollo hardware, delivering payloads for increase of lunar staytime and radius of operations 08 p1316 A67-21084

Apollo mission constraint deviations required to permit landing anywhere on moon and to extend lunar stay time 13 p2199 A67-27215

Light-weight liquid helium dewar for use on Apollo spacecraft 13 p2057 A67-27682

Landing radar system for Apollo lunar module using three-beam Doppler velocity sensor and single-beam altimeter 14 p2318 A67-28290

Tester to check altimeter of Apollo lunar module 14 p2318 A67-28291

Explosive-actuated cutting mechanism for severing electrical service lines connecting Apollo command module to service module and lunar module to spacecraft-LM adapter [ASME PAPER 67-DE-33] 14 p2394 A67-28874

Lunar surface exploration noting sample collection, instrument planting, long term economic possibilities, etc 15 p2553 A67-29301

Future lunar surface missions, defining adequate spacecraft configurations by applying technology and hardware developed on Apollo Lunar Module program [AIAA PAPER 67-27] 15 p2571 A67-30102

LEM-CSM analysis, elastic bending and propellant sloshing 17 p2955 A67-32478

Start characteristics of LM Ascent Engine determined by test series, noting effects of altitude variation, propellant lead time, temperature and valve slow-down [AIAA PAPER 67-522] 18 p3115 A67-33985

Acceptance checkout equipment spacecraft for centralized control and LEM and CSM systems testing 20 p3391 A67-36976

Cordwood packaging concept for electronics thermal control in LEM, obtaining electronic package temperature field from finite difference equations 21 p3594 A67-38329

Electronic circuit packaging in Apollo lunar module signal conditioning equipment 21 p3635 A67-38628

Lightweight liquid helium dewar for LEM program, with 670 liter capacity, 10 percent ullage and 1.5 percent boiloff per day 22 p3808 A67-40391

Cryogenically stored helium pressurization system for LEM descent stage propulsion system, discussing weight advantages and liquid helium heat transfers 22 p3749 A67-40394

Manned chamber testing of lunar module environmental control subsystem, describing equipment and support systems 24 p4139 A67-42050

Structural and mechanical design of Lunar Module Descent Engine, discussing component testing effect on development schedule 24 p4207 A67-42394

LUNAR EXPLORATION

Crew performance evaluation via behavioral and psychophysiological tests in Lunex II simulated lunar mobile laboratory 01 p0017 A67-11392

Bioengineering parameters influencing life support systems for manned exploration of moon including mission duration and closed regenerable systems 02 p0230 A67-12310

Ground and flight spacecraft instrumentation for lunar and planetary

exploration 03 p0420 A67-13378

Lunar International Laboratory /LIL/ exploration and lunar physics 04 p0597 A67-15065

Reduced gravity, pressure suit and load effect on human self-locomotion on lunar surface [ASME PAPER 66-WA/BHF-6] 04 p0564 A67-15400

Navigation functional display requirements associated with early manned lunar exploration vehicles 04 p0655 A67-15662

Unmanned remotely operated lunar surface Emplaced Scientific Station /ESS/ design and objectives as Apollo follow-on lunar missions [AIAA PAPER 67-117] 06 p0980 A67-18286

Planetary transportation model application to space program 06 p1093 A67-19032

Scientific value of manned lunar exploration 06 p1093 A67-19036

Projected ten-year manned exploration of lunar surface 06 p1093 A67-19037

Manned vs unmanned space exploration, discussing increased mechanization of operation 08 p1392 A67-21067

Lunar ground data for interpretation of AES orbital experiments such as electromagnetic radiation monitoring, photographic data evaluation, spectrography, etc 08 p1392 A67-21078

Apollo Extension System for lunar surface missions, discussing extension of mission time by unmanned LEM 08 p1316 A67-21083

Measurements that could be carried out during traverse of moon in Kepler-Encke region to determine subsurface structure, surface density and chemical composition, etc 08 p1316 A67-21085

Mobile Lunar Laboratory system design and mission application 08 p1316 A67-21088

Saturn V with maximum payload lunar-landing stage for extended lunar exploration, noting LESA delivery modes 08 p1412 A67-21089

Scientific objectives for Lunar Exploration Systems for Apollo, noting compatibility with geoscience operation and radiation investigation 08 p1393 A67-21090

Manned lunar exploration systems for Saturn-Apollo 08 p1393 A67-21091

Aerojet Carbothermal Process for oxygen manufacture from lunar resources, discussing experimental results from research operations 08 p1316 A67-21092

Lunar water sources, considering hydrous minerals, cold trapped volatile products of volcanic origin and dispersed hydrates 08 p1317 A67-21093

Indigenous lunar power from geothermal deposits of hot water-rich gases and brines 08 p1317 A67-21095

Lunar base concepts and operational modes for long duration lunar surface studies 09 p1485 A67-22402

Lunar bases planning and development, noting parallel with Antarctic exploration missions 09 p1486 A67-22404

Composition and internal structure of moon and related research tasks of first lunar laboratory 09 p1568 A67-22409

Far field radiation patterns of Advanced Antenna System presented by Surveyor I on lunar surface [JPL-TR-32-1079] 11 p1763 A67-24298

Communications of lunar and planetary laboratory, Volume 5, University of Arizona 11 p1860 A67-24457

Principles and general standards on rights and responsibilities in lunar exploration 12 p2042 A67-26137

Lunar scientific exploration requirements in post-Apollo period, discussing lunar and earth geophysics 13 p2199 A67-27212

Proposed emplaced scientific station for lunar surface studies 15 p2553 A67-29300

Lunar surface exploration noting sample collection, instrument planting, long term economic possibilities, etc 15 p2553 A67-29301

Apollo/Saturn V vehicle launching site, assembly building and lunar flight 15 p2569 A67-29849

Structural dynamic load and instability problems in launch vehicles and spacecraft in lunar exploration emphasizing reliability, crew safety and mission success 16 p2654 A67-30677

Evaluation of relative scientific effectiveness of various lunar exploration

programs through analysis of results from hypothetical missions to selected earth-analog sites 16 p2747 A67-30991

Reduced gravity, pressure suit and load effect on human self-locomotion on lunar surface [ASME PAPER 66-WA/BHF-6] 17 p2807 A67-32814

Experimental determination of orientation elements of FK3 catalog from short series of lunar observations 17 p2950 A67-33128

Astronomical determination of position on moon 18 p3120 A67-33864

MIRA 150A variable thrust rocket engine applied to manned lunar exploration flying systems [AIAA PAPER 67-505] 18 p3113 A67-33969

Lunar exploration by nuclear experiment, discussing instrument specifications for neutron gamma measurements 19 p3229 A67-35318

Prototype model of petrographic microscope for lunar and planetary missions, discussing design and fabrication 19 p3229 A67-35320

Operational capabilities of Saturn-Apollo space vehicle, discussing lunar missions 19 p3333 A67-35643

Collection, processing and return to earth of lunar specimens as part of Apollo program 19 p3328 A67-35929

Spacecraft in lunar exploration by type and properties, emphasizing soft landing and orbiting mooncraft 20 p3526 A67-37249

Lunar mission simulators for Saturn-Apollo project noting optimal computer approach on flexibility, accuracy, cost, etc 20 p3418 A67-37482

Lunar missions evaluated for scientific effectiveness via use of earth analogs assuming hypothetical terrestrial objectives parallel to lunar program 22 p3887 A67-40142

Mission planning for post-Apollo period including selection of lunar landing sites and definition of preferred scientific activity 22 p3888 A67-40144

Environmental, thermal and foreign particle effects on Surveyor vidicon performance and expected tube life [SMPT PAPER 102-32] 22 p3807 A67-40373

Soviet space activity /1933-1967/ noting Sputnik, Venera I, Luna and Zond programs 23 p4086 A67-40919

Oxygen consumption rate during ambulatory lunar surface exploration, describing lunar simulator 23 p3966 A67-41597

Lunar exploration planning methodology for after post-Apollo landing based on equipment evolution [AIAA PAPER 67-865] 24 p4238 A67-42988

Economic exploitation of lunar mineral resources for near earth orbit manufacturing [AIAA PAPER 67-872] 24 p4238 A67-42993

Potential benefits of lunar resources, discussing water deposits location, mining and processing [AIAA PAPER 67-876] 24 p4238 A67-42996

Lunar electric power systems transported by Saturn V noting Brayton cycle, Rankine cycle, solar cells and thermoelectric systems [AIAA PAPER 67-902] 24 p4110 A67-43010

Utilization of lunar geothermal emissions for rocket propellants and life support [AIAA PAPER 67-903] 24 p4165 A67-43011

Lunar applications of spent Saturn V-S-IVB/IU stage concept, discussing payload capabilities [AIAA PAPER 67-986] 24 p4246 A67-43058

LUNAR EXPLORATION SYSTEM FOR APOLLO /LESA/

Apollo lunar module /LM/ rendezvous radar system and tracking device 06 p0962 A67-18056

Extended stay lunar exploration mission in terms of lunar landing site with relaxation of certain Apollo constraints and ground rules 08 p1394 A67-21109

Surface mobility systems for lunar exploration and vehicle characteristics of chosen concepts 09 p1486 A67-22407

Lunar transportation systems for exploration logistics support after first Apollo flight, feasibility, candidates, selection and evolution [AIAA PAPER 67-873] 24 p4244 A67-42994

LUNAR FAR SIDE

Table of names of formations on moon far side identified by Zond III lunar orbiter photographs 02 p0329 A67-12498

Zond III interplanetary probe lunar

surface photographs analyzed, considering asymmetry of moon, far side and relation of moon to solar system 05 p0887 A67-16059

Table of names of formations on moon far side identified by Zond III Lunar Orbiter photographs 10 p1709 A67-23366

Catalog for interpretation of objects in eastern sector of far side of moon 11 p1867 A67-24844

Zond III interplanetary probe lunar surface photographs analyzed, considering asymmetry of moon, far side and relation of moon to solar system 21 p3701 A67-37846

LUNAR FLIGHT

Soviet 10 million lb thrust booster in manned lunar flight 03 p0519 A67-14099

Pressure and thermal protection of man during earth-moon flight and life on moon surface 12 p1901 A67-25175

Future cislunar transportation techniques for exploration and commercial application 13 p2213 A67-27507

LUNAR GEOLOGY

SA SELENOGRAPHY

VHF radar techniques for detecting and mapping subsurface discontinuities such as solid layering, rock interfaces and ore deposits in lunar and planetary surfaces 01 p0021 A67-10324

Lunar shape from Orbiter measurements of gravitational field determined via harmonic analysis 02 p0320 A67-11474

Lunar geological research, discussing thermal and optical properties of lunar soil, morphology of terrestrial formations on lunar surface, etc 04 p0699 A67-15064

Functions of Lunar Receiving Laboratory including lunar samples distribution to scientists, quarantine, storage, contamination, etc 07 p1164 A67-20021

Dynamic ellipticities of moon as supported by strength of interior 08 p1388 A67-21009

Lunar shape in relation to internal structure and moments of inertia found by harmonic analysis 08 p1388 A67-21011

Lunar core and convection in analysis of lunar principal moments of inertia and surface ellipticity 08 p1389 A67-21013

Electric conductivity of lunar interior assuming olivine predominance and analogy to earth mantle 08 p1389 A67-21019

Measurements that could be carried out during traverse of moon in Kepler-Encke region to determine subsurface structure, surface density and chemical composition, etc 08 p1316 A67-21085

Internal lunar structure considered from direct measurements and extrapolation of data on constitution of solar system bodies and meteorites 08 p1395 A67-21161

Composition and internal structure of moon and related research tasks of first lunar laboratory 09 p1568 A67-22409

Moon thermal history investigated using thermal model, comparing results with astrophysical and geological evidence including melting and fluid convection effects 14 p2390 A67-28888

Lunar surface rocks viscosity, volcanic origin, etc, with reference to Flamsteed Ring putative magma 15 p2553 A67-29159

Thermal conductivity model for planetary igneous differentiation, discussing melting behavior as function of pressure and temperature 17 p2942 A67-32387

Lunar events analyzed and related to lunar crust disturbance through internal causes 17 p2942 A67-32388

Possibility of determining content of natural radioactive uranium, thorium and potassium in lunar rocks and of estimating chemical composition of rocks from cosmic ray induced radioactivity 18 p3122 A67-34142

Lunar rocks composition and radioactivity through satellite gamma-ray measurements indicating basaltic and ultrabasic composition 19 p3319 A67-35258

Mineral deposits on moon noting probable magmatic segregation, fumarole products, carbonaceous deposits, etc 21 p3711 A67-39119

Lunar surface geology from results of Ranger, Luna IX and Surveyor I missions for selection of manned lunar landing site 22 p3879 A67-39309

Lunar silicate rock appearance and genesis conditions with emphasis on vesiculation processes 23 p4064 A67-40947

Lunar geology using probe data to distinguish impact and volcanic surface

shaping processes [AIAA PAPER 67-862] 24 p4238 A67-42986

LUNAR GRAVITATION

Lunar shape from Orbiter measurements of gravitational field determined via harmonic analysis 02 p0320 A67-11474

Noncentral nature of lunar gravitational field determined from motion of Luna X lunar orbiter 05 p0886 A67-16050

Possible gravimetric study of lunar gravity, tide and free oscillation modes [AAS PAPER 66-191] 08 p1387 A67-20964

Inclination variation with time of 24-hr low inclination orbits perturbed by solar-lunar gravitation 08 p1402 A67-21508

Metabolic rates during lunar gravity simulation 13 p2062 A67-26922

Lunar studies by laser techniques, considering optics, principles for distinguishing between useful and noise signals, precision of measurements, etc 14 p2386 A67-28468

Variations in lunar gravitational field noting hydrostatic equilibrium state and relation to lunar topography 18 p3127 A67-34252

Harmonic analysis of lunar shape and gravitational field, discussing control systems used 18 p3130 A67-34318

Satellite orbit perturbation analysis for lunar gravitational field determination using von Zeipel transformation 18 p3131 A67-34325

Gravity data from lunar orbiter tracking, discussing Kepler element role 18 p3131 A67-34326

Zonal gravity harmonics of moon from tracking data 18 p3135 A67-34539

Lunar gravitational field obtained from Lunar Orbiter tracking data, with gravity potential as spherical harmonics series and lunar gravitational constant determined 19 p3318 A67-35190

Selenodesy, determining gravitational constant-lunar mass product, lunar gravitational field variation, physical librations, inertial moments, lunar tides, lunar radius, etc 20 p3525 A67-36893

Noncentral nature of lunar gravitational field determined from motion of Luna X lunar orbiter 21 p3701 A67-37837

Moon-earth trajectories, with formulas for given angular ranges of flight, obtaining optimum velocity to depart from lunar gravitational field 21 p3704 A67-38584

Lunar gravitational fields based on Cassini and Euler rotation laws compared with solar, Saturnian and Jovian effects on Saturn and Jupiter satellites 24 p4229 A67-42311

LUNAR GRAVITATIONAL EFFECT

Metabolic work requirement of man wearing pressure suit and associated biomechanical characteristics while locomoting on lunar gravity simulator 02 p0189 A67-12393

Lunar gravitational field determined from orbital motion of Luna X satellite 03 p0510 A67-13341

Tracking geometry and dynamics of lunar satellite, estimating orbital elements and lunar gravitational field parameters through earth based range and range rate observations [AIAA PAPER 66-39] 05 p0902 A67-17207

Lunar landing problem, determining position, velocity and acceleration as functions of time from ignition to shutdown [AAS PAPER 66-121] 07 p1254 A67-19980

Lunar gravitational field and effect on motion of lunar satellite 08 p1395 A67-21163

Perturbation of lunar satellite due to lengthening of one of lunar axis 08 p1396 A67-21184

Ellipticities of moon for radial shift and rotation of unperturbed orbit of close satellite in plane of instantaneous motion 08 p1396 A67-21178

Amplitude variations in earth free and forced polar motion indicate periodic solar activity and moon tidal forces influence 10 p1631 A67-22798

Lunar landing problem, determining position, velocity and acceleration as functions of time from ignition to shutdown [AAS PAPER 66-121] 13 p2239 A67-27535

Lunar gravitational field determined from orbital motion of Luna X satellite 13 p2211 A67-27714

Expression analytically representing progressive and long-term variations of earth rotation velocity 16 p2867 A67-31442

Rotational time scale and analytical

representation by single formula for earth rotation variation 16 p2750 A67-31443

Lunar environment simulation test bed, noting lunar gravity effect on astronaut performance 17 p2832 A67-32003

Deformations of earth crust produced by known forces of luni-solar and surface types 18 p3040 A67-34093

Vestibular organ acceleration while walking at lunar and earth gravity 23 p3953 A67-41584

Amplitude variations in earth free and forced polar motion indicate periodic solar activity and moon tidal forces influence 24 p4149 A67-42134

Lunar gravity, reduced pressure and suit encumbrance effects examined in lunar surface environment simulation test bed, assessing astronaut performance [AIAA PAPER 67-866] 24 p4117 A67-42989

LUNAR IONOSPHERE

Luna X lunar-orbiter satellite observations of charged particles in lunar ionosphere, using magnetic trap 03 p0513 A67-14066

LUNAR LANDING

SA SOFT LANDING

Terminal descent design for unmanned vehicle soft lunar landing in Surveyor project [AIAA PAPER 64-644] 02 p0263 A67-11923

Space station role in manned space flight noting mission goals, earth, moon and planet-oriented applications, etc [AIAA PAPER 66-906] 02 p0332 A67-12272

Lunar landing type of Doppler radar system evaluated by space dynamic simulation testing, using helicopter and various types of terrain 02 p0205 A67-12412

Research and operational results obtained with nonaerodynamic variable stability flying platform for examining problem associated with lunar landing 06 p0948 A67-18202

Astrodynamic perturbation theory in which perturbed space-vehicle motion is described in terms of osculating hodograph applied to lunar landing [AIAA PAPER 67-25] 06 p1085 A67-18304

Apollo manned lunar landings, system hardware, operational problems and development of lunar surface experiments package /ALSEP/ [AIAA PAPER 67-116] 07 p1163 A67-19438

Lunar landing problem, determining position, velocity and acceleration as functions of time from ignition to shutdown [AAS PAPER 66-121] 07 p1254 A67-19980

Propellant requirements for unmanned lunar and interplanetary soft landing vehicles presented with equations that couple injection, midcourse and terminal phases [AAS PAPER 66-129] 07 p1241 A67-19988

Flight attitude control problems of manned lunar landing vehicles emphasizing pitch control [AIAA PAPER 67-239] 07 p1129 A67-20045

Ground and flight tests to evaluate lunar landing research vehicle fly-by-wire control system [AIAA PAPER 67-273] 07 p1129 A67-20048

Vertical component seismograph for use in Surveyor lunar landing missions 08 p1411 A67-20947

Surveyor touchdown-dynamics experimental study of spacecraft motion and landing site surface 08 p1411 A67-20949

Saturn V with maximum payload lunar-landing stage for extended lunar exploration, noting LESA delivery modes 08 p1412 A67-21089

Extended stay lunar exploration mission in terms of lunar landing site with relaxation of certain Apollo constraints and ground rules 08 p1394 A67-21109

Surveyor vernier propulsion system, discussing design of thrust chamber, propellant tank assemblies, functions of VPS, etc [AIAA PAPER 66-593] 08 p1413 A67-21516

Space programs and space politics, possible internal and international political effects of lunar or planetary landing 12 p2040 A67-25235

Apollo mission constraint deviations required to permit landing anywhere on moon and to extend lunar stay time 13 p2199 A67-27215

Lunar landing problem, determining position, velocity and acceleration as functions of time from ignition to shutdown [AAS PAPER 66-121] 13 p2209 A67-27535

Propellant requirements for unmanned lunar and interplanetary soft landing vehicles presented with equations that couple injection, midcourse and terminal phases
[AAS PAPER 66-129] 13 p2214 A67-27540

Landing radar system for Apollo lunar module using three-beam Doppler velocity sensor and single-beam altimeter 14 p2318 A67-28290

Guidance, navigation and two phases of targeting of Saturn V lunar landing mission, analyzing launch, boost to orbit and iterative guidance 17 p2881 A67-32057

Apollo lunar landing mission noting lunar geodetic, cartographic and topographic information deficiencies and correction programs 18 p3132 A67-34329

Prototype model of petrographic microscope for lunar and planetary missions, discussing design and fabrication 19 p3229 A67-35320

Moon probe photographs studied to ascertain moon surface material, structural condition and carrying capacity for future landings on moon 19 p3327 A67-35830

Lunar terrain uncertainties effect on trajectory optimization using Kalman filter during lunar landing powered descent [AIAA PAPER 67-543] 19 p3256 A67-35942

Terminal guidance concept for soft and accurate lunar landing of unmanned spacecraft [AIAA PAPER 67-594] 19 p3259 A67-35990

Unmanned probes designed to land on planetary surfaces to obtain temperature, atmospheric measurement and ground samples chemical analysis 22 p3900 A67-39613

Mass optimal trajectory problems with variable endpoints solved using initial and terminal coasting arcs 22 p3884 A67-39955

Updated inertial navigation of continuously powered space vehicle during lunar landing mission, utilizing altimeter and Doppler radar 22 p3833 A67-40195

U.S. space flight affairs and decisions /1957-1967/ 23 p4086 A67-40918

Apollo historical perspectives, background to U.S. man on moon decision in mid-1961, rocket booster development and space mobility [AIAA PAPER 67-839] 24 p4259 A67-42978

LUNAR LANDING MODULE

Thermal control subsystem for Apollo lunar surface experiments package, noting construction and operation principles 02 p0184 A67-12357

Free flying lunar landing research vehicle tested for more than two years and used in lunar landing simulations supporting Apollo project [AIAA PAPER 67-238] 07 p1129 A67-20044

Lunar Module evaluation and test using analog and hybrid computer simulation with LM guidance and control hardware [AIAA PAPER 67-232] 07 p1164 A67-20056

Lunar landing simulation data, noting pilot performance and manual control modes [AIAA PAPER 67-241] 07 p1165 A67-20062

LM guidance and control systems performance verification [AIAA PAPER 67-244] 07 p1165 A67-20064

Astronaut performance evaluation in Lunar Module hover and landing, separation and docking simulation [AIAA PAPER 67-249] 07 p1165 A67-20067

Construction of lunar landing module with high reliability and low weight 07 p1260 A67-20246

Full mission engineering simulator /FMES/ design for integrating hardware into lunar module system as hardware is made available by subcontractors 08 p1319 A67-21546

Lunar module onboard guidance equipment design, noting operational strategies, control systems, etc 15 p2514 A67-29601

Solderless-wrap lightweight interconnection board for Lunar Module landing radar, noting manufacturing details 16 p2642 A67-31919

Descent engine for lunar module specifications and operational requirements covering throttling, firing duration, crushable nozzle skirt, etc [AIAA PAPER 67-521] 18 p3115 A67-33984

Lunar landing module Doppler radar system in guidance navigation and control system, studying mathematical model performance 19 p3260 A67-36011

Lunar Module rendezvous with Command and Service Modules in lunar orbit, discussing thrusting-maneuver schedule 21 p3714 A67-39145

Apollo lunar landing mission strategy development concerning guidance, control and landing and propulsion systems 22 p3897 A67-39166

Manual steering problem and function of lunar module /LM/ manual hybrid guidance system, with automatic guidance system produced trajectory 22 p3898 A67-39176

Information Service, computerized storage and retrieval system for Apollo spacecraft parts, materials and processes 22 p3765 A67-39951

Lunar landing simulation data, noting pilot performance and manual control modes [AIAA PAPER 67-241] 22 p3780 A67-40100

Biomedical safety monitoring instrumentation for Lunar Module oxygen filled internal environment 23 p3969 A67-41640

White Sands Test Facility /WSTF/ constructed by NASA for hot firing tests of lunar module at simulated altitude 24 p4138 A67-42031

Apollo manned Lunar Module /LM/ earth orbital development missions, reviewing key subsystems and technical problems [AIAA PAPER 67-863] 24 p4244 A67-42987

Lunar transportation systems for exploration logistics support after first Apollo flight, feasibility, candidates, selection and evolution [AIAA PAPER 67-873] 24 p4244 A67-42994

LUNAR LANDING SITE

Lunar landing sites from photographic reconnaissance by Lunar Orbiter II 05 p0888 A67-16154

Lunar surface mechanical properties at Surveyor landing site according to telemetry data and photographs 08 p1386 A67-20942

Lunar surface bearing strength estimate from Orbiter II photograph, noting Sabine D crater measurement as potential landing site for Surveyor and Apollo [JPL-TR-32-1156] 16 p2746 A67-30931

Laser radar selenodesy for ground control selection of Apollo landing sites 16 p2623 A67-30982

Soviet book on first panoramic views of lunar surface covering Lunik IX soft landing, data on morphological and geological characteristics of landing site, etc 17 p2948 A67-32966

Conventional guidance-problem parameters and basic parameters applicable to Surveyor in relation to accuracy of lunar landing 19 p3257 A67-35943

Lighting and viewing conditions posing visibility problems for lunar landing mission 20 p3521 A67-36598

Lunar surface geology from results of Ranger, Luna IX and Surveyor I missions for selection of manned lunar landing site 22 p3879 A67-39309

Mission planning for post-Apollo period including selection of lunar landing sites and definition of preferred scientific activity 22 p3888 A67-40144

Surveyor I landing site soil data covering mechanical, optical, thermal and electrical properties 23 p4064 A67-40950

LUNAR LAUNCH

Manned lunar launch area site selection and planning, considering safety hazards, spacecraft zoning, instrumentation, interference control, community relations, etc 05 p0787 A67-16608

NASA Apollo-Saturn V Moon Project crawlerway construction for lunar launch complex 05 p0788 A67-16615

LUNAR LIMB

Photometric features of eastern and western limb zones of lunar surface compared with data on photometric mean 02 p0329 A67-12492

Preliminary drawings of lunar limb area 05 p0896 A67-16718

Photometric features of eastern and western limb zones of lunar surface compared with data on photometric mean 10 p1708 A67-23360

Reductive determination of refraction-free photographic coordinates of lunar limb profile points and disk 11 p1860 A67-24458

Comparison of lunar limb profiles referred to system of reference points and limb region maps, giving data conversion formulas

and map inaccuracies 17 p2949 A67-33124

Lunar libration in terms of heliometric observations, giving numerical values for limb coordinates and reference altitude 17 p2950 A67-33126

Selenodetic measurement methods, considering point coordinates determination on lunar surface near limb or center, including moon profile studies during solar eclipse 18 p3129 A67-34309

Photographic systems and photoelectric scanner for observation of solar annular eclipse 18 p3049 A67-34312

Photometric determination of moon limb shape during annular solar eclipse, using rotating prisms 18 p3129 A67-34313

Observational uncertainties affecting lunar control solution, considering distortions of magnitudes greater than desired increment of detection, analyzing displacements in recorded images 18 p3130 A67-34320

Moon shape determined from topocentric terminator deviation, using photometry 18 p3132 A67-34334

Luminance profiles of earth sunlit limb through visible spectrum for navigation and research 19 p3213 A67-34804

LUNAR LOGISTICS

Cargo delivery to lunar surface using Apollo hardware and Saturn V 09 p1486 A67-22403

Lunar resources for space and planetary exploration, discussing application of solar radiation, extraction of mineral resources from meteorites, etc 09 p1568 A67-22406

Earth orbital integrated logistics system extendable to space and lunar operations, considering technical and economic feasibility 23 p4061 A67-40592

LUNAR LUMINESCENCE

Thermoluminescence of achondrite meteorites on lunar surface based on rate of temperature rise of lunar terminator 01 p0146 A67-10249

Lunar eclipse brightness variation relation to geomagnetic planetary index, showing that luminescence is in accord with rate of increase of plasma energy 03 p0509 A67-13165

Red-green-IR three-beam high resolution photoelectric photometry during lunar eclipse for lunar colorimetric studies 04 p0696 A67-14735

Spectrometric and colorimetric observations of luminescence on moon surface 08 p1390 A67-21020

Lunar observation in wavelength range one to three mm, noting brightness temperature drop during total eclipse, obtaining dielectric constant 08 p1390 A67-21022

Lunar radio brightness distribution measured at various wavelengths, determining surface temperature decrease and dielectric constant 08 p1390 A67-21023

Lunar events analyzed and related to lunar crust disturbance through internal causes 17 p2942 A67-32388

Lunar surface luminescence in IR and U bands, discussing luminescence distribution, luminoform nature and surface irregularities 22 p3879 A67-39298

Lunar surface luminescence transient enhancement noting photoabsorbing color center formation, increased reflectivity and photoluminescence, photoionization and photoemission 23 p4065 A67-41004

LUNAR MAGNETIC FIELD

Magnetic field intensity near moon measured by Luna X magnetometer, noting correlation with earth surface intensity 01 p0150 A67-10909

Lunar core precession and coupling between assumed liquid core and moon mantle 16 p2754 A67-31746

Magnetic dipole moments of moon, Mars and Venus using space probes, discussing solar wind near-earth planetary field interaction measurements [JPL-TR-32-1059] 21 p3709 A67-38992

LUNAR MAP

SA SELENOGRAPHY

Control system of ACIC augmented by 100 points, constructing corresponding contour map 02 p0319 A67-11457

Radar mapping of lunar surface made with 10 ft beamwidth antenna at Arecibo, Puerto Rico 02 p0324 A67-11856

Radiometric maps of brightness temperature contours on lunar disk from measurements of 3.3 mm wavelength thermal emission

- [JPL-TR-32-1058] 08 p1399 A67-21242
Lunar libration in terms of heliometric observations, giving numerical values for limb coordinates and reference altitude 17 p2950 A67-33126
Correctness of Watts moon-limb maps, giving numerical values for corrections required 17 p2950 A67-33127
Observations of exact shape of moon, discussing catalog and map planning 18 p3130 A67-34319
Control integration for lunar mapping 18 p3131 A67-34321
Absolute lunar coordinate determination methods based on stereoscopic method 18 p3131 A67-34322
Residuals and rms residuals of control measurements made by Manchester Lunar Group members, showing reduced heights not affected by personal errors 18 p3132 A67-34331
Lunar cartography using space vehicles, considering satellite orbits and information transmission 21 p3703 A67-38197
Absolute coordinates of 910 lunar features determined by stereoscopic method 23 p4065 A67-41005
- LUNAR MARE**
Ranger VII records in support of lunar maria being formed by material flow processes 05 p0896 A67-18715
Ranger VII telescopic observation of crater topography of Mare Cognitum 05 p0901 A67-17084
Structural and mechanical properties of lunar maria surface material derived from satellite and earth-based data 11 p1864 A67-24557
Size-frequency distribution of particles and craters and optical, thermal, radio and other properties of lunar surface obtained from Surveyor I landing 19 p3318 A67-35179
- LUNAR MOBILE LABORATORY /MOLAB/**
Mobile Lunar Laboratory system design and mission application 08 p1316 A67-21088
Surface mobility systems for lunar exploration and vehicle characteristics of chosen concepts 09 p1486 A67-22407
- LUNAR OBSERVATORY**
Astronomical observatory construction on moon 03 p0513 A67-14098
Meteorological observatory on moon for observations of earth atmosphere and cloud cover and solar activity 04 p0597 A67-15066
Lunar astronomical observatory, discussing telescopes and optical devices, instrumentation transportation to moon and expectations for astronomical information acquisition 04 p0597 A67-15067
Moon trajectory and rotation effects on lunar astronomical telescope 04 p0597 A67-15068
Instrumentation and research potentialities of lunar radio astronomy observatory 04 p0598 A67-15069
Eclipse observation from moon and cislunar space 04 p0700 A67-15070
Solar corona and chromosphere activity observations at lunar observatory in gamma, X-ray and XUV regions 04 p0598 A67-15071
Lunar and cislunar observation of interplanetary medium including lunar magnetic field, solar wind, existence of collisionless shock wave, gegenschein, zodiacal light and recovery of interplanetary particles 04 p0700 A67-15072
Two-dimensional aperture synthesis in lunar CW radar astronomy, showing measurement possibility for Fourier transform components of sky brightness distribution 14 p2385 A67-28442
Lunar physical libration constants determined, based on heliometric observations /1877-1915/, including coordinates of crater Mosting A 18 p3128 A67-34302
Lunar research at Egyptian observatory at Kottamia 18 p3020 A67-34310
Lunar Planetary Laboratory selenodetic measurement precision and comparison with contemporary selenodetic triangulations 18 p3131 A67-34323
- LUNAR OCCULTATION**
Radio source MSH 21-23 observation during lunar occultation, using parabolic antenna and switched-type gain modulated receiver 03 p0515 A67-14326
Lunar occultation of celestial radio sources noting brightness distribution and spectral resolution 05 p0891 A67-16402
- Interferometer radio observations of two lunar occultations of Crab Nebula 10 p1705 A67-22941
Geometry of lunar eclipse of earth satellite for shadow function as quartic polynomial in cosine of true anomaly 11 p1859 A67-24357
Localization of radio source 3C 17 from moon occultations and identification with near galaxy 12 p2011 A67-26249
Scattering function derivation using lunar limb occultation of solar disk during partial eclipse 14 p2386 A67-28475
Lunar occultations of two radio sources observed at various frequencies, estimating emersion time 14 p2389 A67-28841
Weak radio sources of small angular size studied by lunar occultation technique, using steerable telescope 17 p2943 A67-32634
Very high optical resolution via lunar occultation noting experimental technique 17 p2945 A67-32646
Difference between ephemeris and universal time based on observations of lunar occultations 17 p2950 A67-33129
Annular solar eclipse of May 20, 1966 visible at Bordeaux, noting active center on occultation curve 19 p3325 A67-35506
Diameter and position of radio source 3C 132 determined by lunar occultation, confirming identification with red galaxy 21 p3706 A67-38616
- LUNAR ORBIT**
Poincare method applied to moon motion in vicinity of equilibrium configuration, using equations of linear variation 06 p1031 A67-17775
Approximate method for predicting lunar satellite lifetimes and application to lunar orbit mission analysis 07 p1255 A67-19989
[AAS PAPER 66-130]
Abort velocity requirements for three-burn transfer maneuver out of lunar polar orbit 07 p1255 A67-19992
[AAS PAPER 66-133]
Harmonic series of coordinates of moon in three-body problem of sun-earth-moon treated by numerical method 08 p1382 A67-20395
Dynamical capture of moon by earth 08 p1389 A67-21014
Multispectral photography for AES missions, describing lunar color studies [AFCLR-66-796] 08 p1331 A67-21081
Lunar motion analysis showing slight acceleration to that allowed by celestial mechanics, extrapolating observed motion to past epochs 08 p1395 A67-21162
Lunar orbit evolution caused by tidal friction in earth and moon interiors 09 p1583 A67-21634
Semianalytical solution of motion of satellite in lunar orbit, considering perturbations due to lunar and earth gravity and solar attraction 10 p1706 A67-23185
Approximate method for predicting lunar satellite lifetimes and application to lunar orbit mission analysis 13 p2209 A67-27541
[AAS PAPER 66-130]
Earth-moon and moon-earth trajectory parameters related to lunar orbit conditions for synthesizing lunar orbit trajectory 13 p2210 A67-27618
Physical libration of moon determined from heliometric observations, obtaining value as function of inertia moment 17 p2950 A67-33125
Action variables to take account of essential characteristics of Delaunay lunar theory 18 p3118 A67-33687
Cassini second and third laws are independent of first law 18 p3128 A67-34303
Laser ranging using reflectors proposed for investigating lunar motion and various lunar parameters 18 p3130 A67-34317
Smithsonian Astrophysical Observatory Differential Orbit Improvement program for lunar orbits, with selenocentric reference system 18 p3132 A67-34327
Ephemeris time corrections /1900-1966/ with respect to UT after revision of Brown lunar theory 22 p3881 A67-39518
Strength of synchronous rotation of moon in terms of upper and lower limits on rotational period, using Runge-Kutta integration 22 p3885 A67-39978
Lunar orbit precession due to quadrupole moment of sun arising from solar oblateness 23 p4066 A67-41014
- LUNAR ORBITAL RENDEZVOUS /LOR/**
Lunar surface accessibility study for

- manned lunar orbit rendezvous missions, discussing nonfree return and translunar trajectories 07 p1255 A67-19990
[AAS PAPER 66-131]
Lunar surface accessibility study for manned lunar orbit rendezvous missions, discussing nonfree return and translunar trajectories 13 p2209 A67-27542
[AAS PAPER 66-131]
Lunar Module rendezvous with Command and Service Modules in lunar orbit, discussing thrusting-maneuver schedule 21 p3714 A67-39145
- LUNAR ORBITER**
Lunar shape from Orbiter measurements of gravitational field determined via harmonic analysis 02 p0320 A67-11474
Lunar orbiter command and telemetry data handling system at deep space stations 02 p0194 A67-11808
Flight path control in software system for Lunar Orbiter, discussing optimization program for midcourse aim point and lunar injection point 02 p0265 A67-12382
Decontamination techniques and sterilization environment, discussing compatibility with components and hardware of lunar orbiting spacecraft 02 p0249 A67-12386
Lunar landing sites from photographic reconnaissance by Lunar Orbiter II 05 p0888 A67-16154
Data from Lunar Orbiter spacecraft used to test validity of corrections to lunar ephemeris reveals residual patterns [JPL-TR-32-1087] 05 p0901 A67-17201
Wall of large circular formation on moon shown on Orbiter photographs as convex body resembling flow of viscous lava 05 p0901 A67-17202
FM feedback system for lunar orbit signal demodulation, discussing system composition and performance 06 p0975 A67-18108
Earth-based mission control system of Lunar Orbiter I 07 p1260 A67-20082
[AIAA PAPER 67-276]
Shroud for Lunar Orbiter atop Atlas-Agena launch vehicle, noting structural alloys used 07 p1193 A67-20255
Lunar Orbiter observations of lunar surface as formed possibly by impact, volcanic, tectonic and mass wasting processes 08 p1386 A67-20957
[AAS PAPER 66-180]
Apollo spacecraft, discussing performance of Command and Service Module with typical payloads 08 p1412 A67-21077
Aerospace and electronic systems - Convention, Los Angeles, February 1967 09 p1466 A67-21674
Orbital reconnaissance of Mars in 1971 using modified Lunar Orbiter spacecraft, noting photographic system, trajectory, launch system, etc 09 p1570 A67-21681
Film camera and video transmission system onboard Lunar Orbiter II 10 p1857 A67-23624
Lunar Orbiter photographic system readout for image conversion to video signals [SMPT PAPER 101-45] 12 p1940 A67-25463
Lunar Orbiter photographic system design including film processing, image conversion, relay, reconstitution, performance, characteristics, etc [SMPT PAPER 101-46] 12 p1940 A67-25464
Dual camera for Lunar Orbiter, design, performance and hardware modifications [SMPT PAPER 101-47] 12 p1940 A67-25465
Ground based conversion of Lunar Orbiter II video signals into photographic images, describing reconstruction electronics, signal processor, etc 12 p1940 A67-25466
High quality film processing in Lunar Orbiter spacecraft photo system, noting separate environmental control system [SMPT PAPER 101-49] 12 p1941 A67-25467
Orbiter II lunar photography analysis, noting surface characteristics of Southern Hemisphere of moon 14 p2387 A67-28506
Lunar surface bearing strength estimate from Orbiter II photograph, noting Sabine D crater measurement as potential landing site for Surveyor and Apollo [JPL-TR-32-1156] 16 p2746 A67-30931
Air-bearing facility for Lunar Orbiter attitude control system testing minimizing external disturbances in platform, platform mass deflection and room thermal currents 16 p2655 A67-31260

- Lunar orbiter quality assurance program, emphasizing management, design, procurement, fabrication, quality control, etc 16 p2783 A67-31629
- Spacecraft and ground equipment of Lunar Orbiter telecommunications 17 p2811 A67-32119
- Reflection and scattering from lunar surface of meter radio waves emitted by Lunar orbiter 17 p2948 A67-32976
- Continuous wave signals from Lunar Orbiter I after reflection from lunar surface, noting mapping use 17 p2817 A67-33364
- Lunar orbiter velocity control system design, discussing interface problems between actuator electronics and flight control system 18 p3137 A67-33968
- [AIAA PAPER 67-504] 18 p3137 A67-33968
- Gravity data from lunar orbiter tracking, discussing Kepler element 18 p3131 A67-34326
- Lunar gravitational field obtained from Lunar Orbiter tracking data, with gravity potential as spherical harmonics series and lunar gravitational constant 19 p3318 A67-35190
- Lunar radius facing earth determined from radar measurement data and lunar orbiters 19 p3319 A67-35263
- Lunar orbiter missions goals and design, spacecraft construction and equipment and examination of lunar surface 19 p3319 A67-35266
- Slope derivation from lunar orbiter photography using photometric model and computer program 19 p3230 A67-35322
- Lunar Orbiter Attitude Control System design and space flight performance [AIAA PAPER 67-533] 19 p3334 A67-35935
- Orbit determination for Lunar Orbiter, describing computer program and studying Doppler residuals 19 p3328 A67-35944
- [AIAA PAPER 67-545] 19 p3328 A67-35944
- Lunar Orbiter power subsystem reliability tradeoff, methodology, performance prediction, etc 20 p3363 A67-36594
- Lunar Orbiter flight programmer, electronic design, development, application and performance 21 p3601 A67-39062
- Supercleaning processes for Lunar Orbiter calling for personnel training, clean room garments, chemical cleaners, special packaging and inspection for particulate contamination 23 p3962 A67-40854
- Lunar Orbiter II lunar surface photographs noting Copernicus H and Copernicus crater interior peak cluster 23 p4066 A67-41012
- Lunar Orbiter design, development, testing and space flight 24 p4241 A67-42404
- Lunar geology using probe data to distinguish impact and volcanic surface shaping processes 24 p4238 A67-42986
- [AIAA PAPER 67-862] 24 p4238 A67-42986
- LUNAR PERTURBATION
- Solar-lunar perturbation of 24-hour satellite, independence of librational motion and impossibility of equilibrium 02 p0321 A67-11498
- Cassini second and third laws of lunar rotation are independent of first one 05 p0889 A67-16296
- Lunar-solar gravitational perturbation of satellite with sidereal day period, discussing stability 20 p3523 A67-36626
- LUNAR PHASE
- Transient changes on moon during last three centuries, considering type of event, lunar phase, correlation with solar activity, etc 05 p0895 A67-16594
- Lunar influence on total electron content of winter ionosphere at minimum solar activity 11 p1788 A67-24771
- Two-color photoelectric photometry of earthshine, determining earth albedos 15 p2477 A67-29626
- Attenuation of lunar microwave emission measured by artificial moon method, determining phase dependence of lunar temperature 18 p3119 A67-33861
- LUNAR PHOTOGRAPH
- Zond III interplanetary probe lunar surface photographs analyzed, considering asymmetry of moon, far side and relation of moon to solar system 05 p0887 A67-16059
- Lunar crater diameter-depth relationship from Ranger VII 06 p1087 A67-18376
- TV pictures of Surveyor I compartment radiators taken on June 11 and July 12, 1966, discussing cause of some changes in dust locations 08 p1386 A67-20944
- Depth of loose and loosely bonded material on lunar surface determined using Ranger VII, VIII and IX photographs 08 p1401 A67-21361
- Selenological analysis of Ranger IX photographs, examining origin and age of craters and mountain chains 10 p1705 A67-22898
- Lunar photography by refractor and reflector telescopes at Pic du Midi Observatory 10 p1710 A67-23563
- Lunar soil composition determined to be porous fine-grain moderately cohesive rock powder, from Surveyor I and Luna IX pictures 11 p1865 A67-24607
- Panoramic photograph processing theory 14 p2318 A67-28372
- Scanning and transformation of panoramic lunar surface photographs 14 p2319 A67-28373
- Lunar surface photographs taken by Luna IX and Surveyor I showing linear and circular ground features, rock blocks and dust 17 p2948 A67-33094
- Selenodetic evaluation of 11 selected original photographic plates from 1894-1909 Paris Observatory collection of lunar photographs 18 p3129 A67-34311
- Photometric methods for determination of lunar relief 18 p3132 A67-34328
- Moon shape determined from topocentric terminator deviation, using photometry 18 p3132 A67-34334
- Lunar orbiter missions goals and design, spacecraft construction and equipment and examination of lunar surface photographs 19 p3319 A67-35266
- Zond III interplanetary probe lunar surface photographs analyzed, considering asymmetry of moon, far side and relation of moon to solar system 21 p3701 A67-37846
- LUNAR PHOTOGRAPHY
- Errors in estimates of lunar crater slope angles and surface roughness in Ranger VII and Ranger VIII pictures due to interpretation of dark areas as shadows [JPL-TR-32-994] 01 p0147 A67-10319
- Lunar crater photographs obtained by Ranger VIII and IX compared with those of laboratory craters overlain with granular material, for depth interpretation [JPL-TR-32-1021] 02 p0320 A67-11459
- Surveyor I photographs of lunar surface in support of theories that no mechanism exists on moon for sorting different sized particles into layers 03 p0512 A67-13892
- Lunar landing sites from photographic reconnaissance by Lunar Orbiter II 05 p0888 A67-16154
- Structure of lunar lithosphere using data from ground telescopes and Ranger photographs 06 p1092 A67-19004
- Lunar AIMP photographic data processing system which transforms photographic scans of moon into rectified lunar pictures, particularly ground processor system 08 p1330 A67-20861
- Lunar photography application to creation of selenographic coordinates enveloping near and far sides of moon 08 p1388 A67-21000
- Ranger photographs of lunar surface noting erosion and fragmentation by meteorite bombardment 08 p1390 A67-21026
- Relative depths of moon mountain rings and craters in region of Mare Nubium 08 p1390 A67-21027
- Pictures of moon taken by Ranger, Surveyor and Orbiter spacecraft analyzed for origin, history, libration, temperature and properties 08 p1401 A67-21428
- Boulder size distribution in Luna IX surface photographs 09 p1570 A67-22692
- Communications of lunar and planetary laboratory, Volume 5, University of Arizona 11 p1860 A67-24457
- Reductive determination of refraction-free photographic coordinates of lunar limb profile points and disk 11 p1860 A67-24458
- Scale transfer for lunar photographs, using selenodetic controls with suitable point pattern 11 p1860 A67-24460
- Lunar rotational constants determined from measurements on scaled and oriented photographs, using least squares analysis and rigorous formalism 11 p1860 A67-24462
- Measures and reductions for 1868 points on Yerkes lunar photograph No. 1289, listing uncorrected and refraction-free photographic coordinates 11 p1860 A67-24463
- Morphology of lunar craters from Ranger photographs, noting distribution and possible competing processes of crater formation and destruction 11 p1865 A67-24608
- Lunar optical properties simulated with commercial Portland cement and maroon and black coloring powders, noting blue-green color index discrepancy 11 p1865 A67-24609
- Lunar Orbiter photographic system readout for image conversion to video signals [SMPT PAPER 101-45] 12 p1940 A67-25463
- Lunar Orbiter photographic system design including film processing, image conversion, relay, reconstitution, performance, characteristics, etc [SMPT PAPER 101-46] 12 p1940 A67-25464
- High quality film processing in Lunar Orbiter spacecraft photo system, noting separate environmental control system [SMPT PAPER 101-49] 12 p1941 A67-25467
- Photometric investigations of simulated lunar surfaces confirm high porosity and low albedo without postulating necessity for fine dust layer 12 p2003 A67-25740
- Orbiter II lunar photography analysis, noting surface characteristics of Southern Hemisphere of moon 14 p2387 A67-28506
- Electro-optical rectifier, types of materials generated, operational capability and lunar and aerial photographic application 14 p2321 A67-28828
- Ranger Block III television system for lunar surface photography 16 p2620 A67-30643
- Lunar surface bearing strength estimate from Orbiter II photograph, noting Sabine D crater measurement as potential landing site for Surveyor and Apollo [JPL-TR-32-1156] 16 p2746 A67-30931
- Comparison of lunar surface photography from space probes and ground-based observatories 16 p2871 A67-30990
- Soviet book on first panoramic views of lunar surface covering Lunik IX soft landing, data on morphological and geological characteristics of landing site, etc 17 p2948 A67-32966
- Motion of lunar images in focal plane of horizontal telescope without coelostat arrangement 17 p2950 A67-33130
- Optical system devised to alter relative harmonic coefficients and eliminating ringing effects for photographs represented in two-dimensional Fourier series applied to lunar photography 18 p3047 A67-33998
- Analysis of lunar surface panoramas transmitted by automatic station Lunik IX after soft landing 18 p3122 A67-34138
- Heliometer replaced by long focus photographic refractor used for moon rotation constant determination 18 p3129 A67-34308
- Palomar Schmidt telescope use as moon-star camera proved impractical 18 p3049 A67-34315
- Observational uncertainties affecting lunar control solution, considering distortions of magnitudes greater than desired increment of detection, analyzing displacements in recorded images 18 p3130 A67-34320
- Lunar topography from ground-based photographs taken under oblique illumination, discussing exposure times, resolution, etc 18 p3132 A67-34330
- Resolution improvement of earth-based lunar photography, discussing film speeds, emulsions, etc 18 p3049 A67-34332
- Lunar data covering mass, shape, dimensions, earth-moon relations, orbits, selenography, etc 20 p3530 A67-37549
- Lunar cartography using space vehicles, considering satellite orbits and information transmission 21 p3703 A67-38197
- Earth shine illuminated lunar surface TV picture taking by modifying Surveyor equipment to provide light integration [SMPT PAPER 102-40] 22 p3808 A67-40378
- Shock processes pertinent to lunar terrain fragmentation and lithification noting Surveyor and Lunar Orbiter pictures 23 p4064 A67-40948
- Lunar scar and ghost crater origin theories illustrated with Ranger 3-D slides 23 p4064 A67-40951
- Ranger, Surveyor and Orbiter probe lunar surface photographic data, discussing lunar event distribution, lunar craters and maria distribution 23 p4065 A67-40953
- Similarity between Icelandic lava field photographs and Luna IX lunar surface photographs 23 p4065 A67-40954
- Lunar Orbiter II lunar surface

photographs noting Copernicus H and Copernicus crater interior peak cluster 23 p4066 A67-41012
 Cauchy domes in Mare Tranquillitatis, deriving relief pictures with photometry 23 p4066 A67-41013
 Surveyor V scientific experiment, comparing lunar surface sampling with that in Surveyor III, noting resemblance to granular terrestrial soil 24 p4228 A67-42308

LUNAR PROBE
 SA EXPLORER XXXIII SATELLITE
 SA LUNIK II LUNAR PROBE
 SA LUNIK IX LUNAR PROBE
 SA LUNIK X LUNAR PROBE
 SA PIONEER SPACE PROBE
 SA RANGER VII LUNAR PROBE
 SA RANGER VII LUNAR PROBE
 SA SURVEYOR I SPACECRAFT
 Thermoradioisotope propulsion and integrated power application to cislunar and planetary space missions 01 p0155 A67-11413
 Space flight problems in cislunar space, noting lunar probes, high apogee satellite specifications and orbital stability 05 p0897 A67-16732
 Specification and evaluation of space projects and programs, noting model construction and planning 06 p1093 A67-19033
 Soviet lunar probe measurements of gamma spectrometry, magnetic and gravitational fields, corpuscular radiation intensity, etc 08 p1411 A67-20999
 Lower bounds for lunar surface strength obtained from data of Ranger and Luna spacecraft [JPL-TR-32-1068] 08 p1397 A67-21210
 Lunar figure and orbit parameters measured by optical location method 12 p2002 A67-25647
 Unmanned exploration of moon, summarizing results on surface structure, back side and material composition 16 p2748 A67-31199
 Magnetic field in moon proximity constructed from Lunik x satellite plasma and magnetic measurements 16 p2755 A67-31889
 Penetrating radiation intensity on lunar surface and in space, evaluating counting rate, lunar surface radioactivity and radiation belts absence 18 p3122 A67-34143
 Estimate of dynamical center from four lunar surface impact points determined by tracking Ranger probes from three earth-based stations 18 p3131 A67-34324
 Moon probe photographs studied to ascertain moon surface material, structural condition and carrying capacity for future landings on moon 19 p3327 A67-35830
 Lunar probe data interpretation - AAS Conference, Huntington Beach, California, September 1966 23 p4063 A67-40946

LUNAR PROGRAM
 U.S. Saturn/Apollo moon program, considering Saturn V booster, Apollo spacecraft and Lunar Excursion Module 01 p0154 A67-11001
 Functions of Lunar Receiving Laboratory including lunar samples distribution to scientists, quarantine, storage, contamination, etc 07 p1184 A67-20021
 Evaluation of relative scientific effectiveness of various lunar exploration programs through analysis of results from hypothetical missions to selected earth-analog sites 16 p2747 A67-30991
 Residuals and rms residuals of control measurements made by Manchester Lunar Group members, showing reduced heights not affected by personal errors 18 p3132 A67-34331
 Lunar applications of spent Saturn V/S-IVB/IU stage concept, discussing payload capabilities [AIAA PAPER 67-986] 24 p4246 A67-43058

LUNAR RADIATION
 Lunar X-rays excited by electrons of magnetospheric tail provide information on chemical composition of moon 01 p0144 A67-10563
 Lunar gamma radiation intensity and spectral composition from Luna X data, deducing cosmic ray and radioactive decay origins 01 p0150 A67-10905
 Hazards to man on moon from flare-produced solar particle beams and galactic radiation, noting estimate for life shortening 02 p0189 A67-12394
 Lunar IR emission and solar radiation reflected by moon in visible region

measured by Luna X orbiter 05 p0886 A67-16052
 Lunar gamma radiation measured by spectrometer on Luna X orbiter noting lunar rock radiation level, effect of cosmic rays, etc 05 p0887 A67-16055
 Magnitude of lunar neutron emission due to cosmic rays estimated from atmospheric measurements 05 p0879 A67-16105
 Transient lunar brightening, discussing attempted correlation with solar wind activity 07 p1256 A67-20160
 Degassing or other external causes as possible mechanism for anomalous increases in radiation from moon 08 p1398 A67-21219
 Ozone number densities in 30 to 75 km altitude determined at night by rocket measurements of lunar UV radiation absorption in various bands 10 p1638 A67-23203
 Observational study of lunar visible emission according to study of line depths 13 p2210 A67-27601
 Lunar radio emission in 30 to 60 cm range, showing mean radio temperature of moon as 225 degrees K and independence of wavelength 15 p2552 A67-29148
 Linear polarization of lunar radio emission observed using radio telescope 15 p2552 A67-29149
 Scanning IR radiometer equipment to produce pictorial maps of lunar radiance patterns or of possible variations in lunar surface composition 15 p2492 A67-30434
 Radiation level on lunar surface noting degree of danger to astronaut, solar activity effect, creation of secondary emission, etc 16 p2737 A67-30782
 Moon spectrophotometric measurements from space probe compared with solar spectrum structure, calculating lunar albedo curve 18 p3122 A67-34140
 UV spectra of lunar surface photographed from Zond III automatic space probe 18 p3122 A67-34141
 Penetrating radiation intensity on lunar surface and in space, evaluating counting rate, lunar surface radioactivity and radiation belts absence 18 p3122 A67-34143
 IR thermal emission from lunar nighttime surface, noting anomalies location and observational procedure 18 p3134 A67-34497
 Lunar IR emission and solar radiation reflected by moon in visible region measured by Luna X orbiter 21 p3701 A67-37839
 Lunar gamma radiation measured by spectrometer on Luna X orbiter noting lunar rock radiation level, effect of cosmic rays, etc 21 p3701 A67-37842
 Magnitude of lunar neutron emission due to cosmic rays estimated from atmospheric measurements 24 p4213 A67-42781
 Lunar radio emission in 30 to 60 cm range, showing mean radio temperature of moon as 225 degrees K and independence of wavelength 24 p4239 A67-43071
 Linear polarization of lunar radio emission observed using radio telescope 24 p4239 A67-43072

LUNAR ROVING VEHICLE /LRV/
 Open and closed cabin lunar roving vehicles including unmanned Tumbling Explorer /TEX/ surface vehicle 03 p0396 A67-13889
 Surface mobility systems for lunar exploration and vehicle characteristics of chosen concepts 09 p1486 A67-22407
 Vehicle volume and design criteria for manned lunar roving vehicles investigated by evaluating subjects performance under prolonged simulated lunar environment 23 p3970 A67-41658

LUNAR SATELLITE
 Luna X shielded gas-discharge counter data on soft corpuscular radiation, noting solar contribution to magnetospheric tail 01 p0145 A67-10907
 Noncentral nature of lunar gravitational field determined from motion of Luna X lunar orbiter 05 p0886 A67-16050
 Lunar orbit characteristics and perturbations of Lunar Orbiter and Anchored IMP 05 p0895 A67-16576
 Tracking geometry and dynamics of lunar satellite, estimating orbital elements and lunar gravitational field parameters through earth based range and range rate observations [AIAA PAPER 66-39] 05 p0902 A67-17207
 Lunar communication satellites, discussing

satellite relay, librational, random and synchronous satellite design, lunar orbits, etc [AIAA PAPER 66-315] 06 p0961 A67-17705
 Motion of near lunar satellite in initially circular orbit analyzed by integrating equations for time rates of change of orbit elements [AAS PAPER 66-95] 07 p1252 A67-19956
 Approximate method for predicting lunar satellite lifetimes and application to lunar orbit mission analysis [AAS PAPER 66-130] 07 p1255 A67-19989
 Lunar satellite motion under terrestrial perturbations and lunar potential 08 p1383 A67-20404
 Solution of motion equations for lunar satellites in near equatorial plane using transformation of variables 08 p1383 A67-20582
 Lunar gravitational field and effect on motion of lunar satellite 08 p1395 A67-21163
 Perturbation of lunar satellite due to lengthening of one of lunar axis 08 p1396 A67-21164
 Motion of lunar satellite, noting principal perturbations due to nonspherical lunar gravity and earth attraction, considering moon libration and solar small forces 08 p1397 A67-21184
 Motion of near lunar satellite in initially circular orbit analyzed by integrating equations for time rates of change of orbit elements [AAS PAPER 66-95] 13 p2207 A67-27519
 Approximate method for predicting lunar satellite lifetimes and application to lunar orbit mission analysis [AAS PAPER 66-130] 13 p2209 A67-27541
 Luna IX and Luna X near moon, studying injection phase, orbit and landing phase from transmitted frequency observations 18 p3003 A67-34242
 Noncentral nature of lunar gravitational field determined from motion of Luna X lunar orbiter 21 p3701 A67-37837
 Position fix and range data techniques for preliminary orbit determination for lunar satellites, using least squares method for data smoothing 22 p3879 A67-39310

LUNAR SCATTERING
 Lunar line waveguide parameters calculated for inner conductor displacement and ratio of radii 05 p0775 A67-16958
 Surveyor study of lunar ejecta fragments expelled from lunar surface during hypervelocity impact 08 p1411 A67-20948
 Electronic polarimeter applied to Stokes parameter measurement of lunar surface, determining reflected light ellipticity 15 p2552 A67-29147
 Time average of autocorrelation function measured by CW radar illuminating moon calculated without lunar surface properties knowledge 21 p3703 A67-38189
 Electronic polarimeter applied to Stokes parameter measurement of lunar surface, determining reflected light ellipticity 24 p4239 A67-43070

LUNAR SEISMOGRAPH
 Interior structure of moon and planets studied by geophysical seismic methods 04 p0702 A67-15561
 Seismic experimentation methods to be performed on moon, giving P and S wave travel time curves for models of lunar interior 08 p1387 A67-20963
 Lunar scientific exploration requirements in post-Apollo period, discussing lunar and earth geophysics 13 p2199 A67-27212

LUNAR SHADOW
 November 12, 1966 total eclipse observation from aircraft flying in moon shadow, describing instrumentation and results 06 p1004 A67-18383
 Geometry of lunar eclipse of earth satellite for shadow function as quartic polynomial in cosine of true anomaly 11 p1859 A67-24357
 Model for lunar surface roughness effect on emission of thermal IR radiation and casting of shadows in sunlight 21 p3702 A67-38188

LUNAR SHELTER
 Construction of lunar microcosm, considering recycling based on photosynthesis 02 p0185 A67-12313

LUNAR SOIL
 Photometric, polarimetric and IR study of lunar surface including polarization of moonlight, thermal measurements, lunar

- adar echo signals, etc 08 p1395 A67-21160
- Lunar soil composition determined to be porous fine-grain moderately cohesive rock powder, from Surveyor I and Luna IX pictures 11 p1865 A67-24607
- Lunar soil density problem investigated by sieving clean powders of different materials with different grain sizes and drop heights under ultrahigh vacuum 12 p2000 A67-25207
- Crater forming processes on moon from Ranger VIII impact, ascertaining gravity sealing existence, noting relation to terrestrial soils 19 p3327 A67-35894
- Lunar soil cohesive and disruptive properties from Surveyor I data, discussing micrometeorite impacts, thermal fracturing, metal vapor deposition and atomic adhesion 23 p4064 A67-40949
- Surveyor I landing site soil data covering mechanical, optical, thermal and electrical properties 23 p4064 A67-40950
- Lunar surface layer soil density limits estimated in simulation study of adhesion, composition, grain size and grain shape effects 23 p4066 A67-41008
- Adhesive qualities of lunar soil simulated by rock comminuted in ultrahigh vacuum 24 p4227 A67-42034
- Surveyor V scientific experiment, comparing lunar surface sampling with that in Surveyor III, noting resemblance to granular terrestrial soil 24 p4228 A67-42308
- LUNAR SPACECRAFT
- SA APOLLO SPACECRAFT
- SA SURVEYOR III SPACECRAFT
- SA SURVEYOR SPACECRAFT
- Lunar and planetary terminal point guidance using optical correlator 02 p0264 A67-12317
- Reliability effect on design of lunar soft landing spacecraft (Surveyor), Syncoms I, II and III, Applications Technology Satellites, Early Bird and four Intelsat 09 p1582 A67-22302
- Apollo manned space flight program including mission profile, spacecraft and constituent systems 16 p2756 A67-30626
- Spacecraft in lunar exploration by type and properties, emphasizing soft landing and orbiting mooncraft 20 p3526 A67-37249
- Comparative microbial contamination levels in clean rooms used for assembly and test of lunar spacecraft 23 p3961 A67-40851
- LUNAR SURFACE
- SA SELENOGRAPHY
- Composite surface and composite correlation approaches to frequency dependence and surface roughness problems of lunar surface signal scattering 01 p0020 A67-10019
- Geocentric initial conditions for motion of bodies leaving moon surface after initial instantaneous thrust 01 p0148 A67-10387
- Centimeter-and millimeter scale roughness of lunar surface produced by micrometeorite impact 01 p0150 A67-10893
- Stratified and faceted forms on panoramas obtained from Luna IX space station, noting connection with mineral composition of lunar surface 01 p0150 A67-10904
- Lunar surface structure implied by millimeter-sized features in Luna IX photographs 01 p0151 A67-10964
- Omnidirectional penetrometer for lunar surface parametric impact testing and certification of safe soft-landing site for Apollo LEM 01 p0074 A67-11123
- Thermal behavior of certain lunar areas differing sharply from that of surrounding terrain explained by lack of insulating debris over anomalous areas 02 p0320 A67-11458
- Anomalous cooling of moon surface during lunar eclipse explained possibly by lunar surface roughness in form of cracks and declivities at centimeter scale 02 p0320 A67-11460
- Possible lunar surface vacuum layer structure from effective thermoconductivity coefficient based on radioastronomical data 02 p0322 A67-11567
- Quantitative study of radar cross polarization factor D in order to obtain data on lunar surface roughness and dielectric properties 02 p0192 A67-11603
- Two-layer model of lunar surface analyzed, using criteria of transparency to microwave radiation 02 p0324 A67-11700
- Proton induced hydroxyl formation on lunar surface simulated by bombarding glass, chemically similar to silicate minerals, with high energy protons [AFCRL-66-795] 02 p0324 A67-11857
- Short-pulse radio reflections to determine average scattering behavior of lunar surface at 23 cm wavelength 02 p0325 A67-11858
- Thermal control subsystem for Apollo lunar surface experiments package, noting construction and operation principles 02 p0184 A67-12357
- LEM optical astronomy package /OAP/ containing astronomical telescope, spectrophotometer, data processing subsystem and other devices, for unmanned landing and life support 02 p0246 A67-12414
- Photometric features of eastern and western limb zones of lunar surface compared with data on photometric mean 02 p0329 A67-12492
- Lunar disk color index derivation by applying method of photographic photometry in UV and IR spectral regions 02 p0329 A67-12493
- Surveyor I photographs of lunar surface in support of theories that no mechanism exists on moon for sorting different sized particles into layers 03 p0512 A67-13892
- Apollo lunar surface experiments package /ALSEP/ of scientific instruments and supporting subsystems [AIAA PAPER 66-919] 03 p0397 A67-14133
- Local scientific survey module /LSSM/, small lunar vehicle designed to provide two astronauts with transportation and portable scientific lab on lunar surface 03 p0400 A67-14308
- Temperature dependent thermal property models of lunar surface and radiative energy transport deduced from RF and IR observations 04 p0697 A67-14740
- Micrometric measurement of absolute and relative heights of 163 unobtrusive points on lunar surface, comparing values of Maedler, Schmidt and U.S. Army Map Service 04 p0700 A67-15177
- Intensity of characteristic spectral lines of Si, Al and Mg of lunar surface rock made fluorescent by solar X-rays determined from Luna X measurements 05 p0886 A67-16051
- Primary cosmic radiation in interplanetary space, lunar surface albedo and soft particle fluxes in magnetosphere measured by Luna X orbiter 05 p0875 A67-16053
- Color events on moon observed through color filters alternately, noting crater Gassendi 05 p0888 A67-16155
- Lunar surface chemical analysis using interaction of monoenergetic alpha particles with matter [JPL-TR-32-1065] 05 p0805 A67-16463
- Lunar and planetary surface elemental analysis technique by analysis of gamma rays resulting from inelastic scattering of neutrons 05 p0843 A67-16545
- Neutron activation analysis of Si, Fe, Al, Mg and O content of lunar and planetary surfaces 05 p0843 A67-16546
- Transient changes on moon during last three centuries, considering type of event, lunar phase, correlation with solar activity, etc 05 p0895 A67-16594
- Lunar surface composition, strength and failure modes, determining ability to support LEM 05 p0895 A67-16612
- Ranger VII photographic interpretation and lunar surface structures 05 p0896 A67-16714
- Color study of lunar surface suggesting nonexistence of cosmic dust layer 05 p0901 A67-17083
- Radionuclide production in lunar surface activated by solar proton with reference to radiation shielding and reflection 05 p0885 A67-17386
- Book on moon covering motion of moon and dynamics of earth-moon system, internal constitution, topography, radiation and surface structure 06 p1087 A67-18428
- Continental-oceanic boundaries of earth and relevance to tectonic speculations about moon and planets, noting role of radiogenic heat 06 p1091 A67-19003
- Structure of lunar lithosphere using data from ground telescopes and Ranger photographs 06 p1092 A67-19004
- Projected ten-year manned exploration of lunar surface 06 p1093 A67-19037
- Soft landing of manned spacecraft on lunar surface 07 p1258 A67-19429
- Flamsteed P volcanic rings from Orbiter I and Surveyor I lunar photographs 07 p1249 A67-19659
- Polarization and brightness temperature distributions across lunar disk observed with Parkes radio telescope at various wavelengths 07 p1251 A67-19854
- Lunar surface accessibility study for manned lunar orbit rendezvous missions, discussing nonfree return and translunar trajectories [AAS PAPER 66-131] 07 p1255 A67-19990
- Error model digital computer program applied to lunar surface hybrid navigation concepts, noting accuracy requirements from 1972 to 1985 08 p1351 A67-20675
- Penetrating radiation measurement on moon surface obtained by Luna IX spacecraft 08 p1385 A67-20841
- Middle and far IR spectra of silicate minerals for remote sensing of lunar or planetary surface composition 08 p1385 A67-20934
- Rapid remote sensing of lunar surface by IR spectrum matching technique using simple matching device or scanning instrument 08 p1385 A67-20935
- Surveyor I spacecraft exploration results of lunar surface 08 p1386 A67-20939
- Thermal properties of lunar surface as observed from Surveyor I spacecraft 08 p1386 A67-20940
- Radar characteristics of lunar surface from Surveyor I spacecraft 08 p1386 A67-20941
- Lunar surface mechanical properties at Surveyor landing site according to telemetry data and photographs 08 p1386 A67-20942
- Soil mechanics surface sampler experiment for Surveyor 08 p1410 A67-20945
- Lunar surface chemical composition analysis by Surveyor-borne instrument based on alpha interaction with matter [JPL-TR-32-1090] 08 p1411 A67-20946
- Lunar Orbiter observations of lunar surface as formed possibly by impact, volcanic, tectonic and mass wasting processes [AAS PAPER 66-180] 08 p1386 A67-20957
- Ray craters and hot spot on lunar surface during solar eclipse 08 p1387 A67-20959
- Lunar surface optical properties and IR emission [AAS PAPER 66-185] 08 p1387 A67-20960
- Lunar external gravitational field, topographic surface and moments of inertia [AAS PAPER 66-189] 08 p1387 A67-20962
- Lunar ablateness due to thermal effects associated with decrease of mean surface temperature from equator toward poles 08 p1389 A67-21012
- Lunar crater distortion implication on past shape of moon, noting earth-moon system evolution 08 p1389 A67-21016
- Lunar radio brightness distribution measured at various wavelengths, determining surface temperature decrease and dielectric constant 08 p1390 A67-21023
- Moon and planet surfaces analyzed based on thermal radiation for information on parameters of material of upper layer 08 p1390 A67-21024
- Ranger photographs of lunar surface noting erosion and fragmentation by meteorite bombardment 08 p1390 A67-21026
- UV imaging system for lunar missions to detect luminescing minerals on lunar surface 08 p1331 A67-21079
- Lunar surface analysis via analysis of reflected signals from RF pulses 08 p1295 A67-21080
- Book on moon in space age covering lunar motion around gravity center, nature of lunar soil, lunar satellite perturbations, etc 08 p1395 A67-21156
- Observation methods for determination of moon shape including libration effect, local topography and determination of apparent contour 08 p1395 A67-21159
- Color phenomena on moon 08 p1396 A67-21165
- Crustal features of moon and Mars analyzed for mantle convections, noting correspondence to spherical harmonics of various orders 08 p1397 A67-21208
- Lower bounds for lunar surface strength obtained from data of Ranger and Luna spacecraft [JPL-TR-32-1068] 08 p1397 A67-21210
- Coordinates determining relative altitudes on lunar surface obtained through coordinate measuring instrument 08 p1398 A67-21216
- Depth of loose and loosely bonded

material on lunar surface determined using Ranger VII, VIII and IX
 photographs 08 p1401 A67-21361
 Pictures of moon taken by Ranger, Surveyor and Orbiter spacecraft analyzed for origin, history, libration, temperature and properties 08 p1401 A67-21428
 Lunar surface according to Luna IX and Surveyor I 09 p1568 A67-22405
 Composition and internal structure of moon and related research tasks of first lunar laboratory 09 p1568 A67-22409
 UV reflectance measurements of granitic, gabbroic and serpentine rocks used to identify lunar silicates 09 p1569 A67-22689
 Boulder size distribution in Luna IX surface photographs 09 p1570 A67-22692
 Enhancement of fine detail in presence of large radiance differences, noting radiance profiles and moon 10 p1653 A67-22746
 Photometric features of eastern and western limb zones of lunar surface compared with data on photometric mean 10 p1708 A67-23360
 Lunar disk color index derivation by applying method of photographic photometry in UV and IR spectral regions 10 p1708 A67-23361
 Systematic errors in earthward coordinates of selenodetic points, noting results of triangulation 11 p1860 A67-24461
 Mathematical model of flooded random surface and applications to lunar terrain 11 p1863 A67-24556
 Structural and mechanical properties of lunar maria surface material derived from satellite and earth-based data 11 p1864 A67-24557
 Transient radiative heat exchange on moon surface observed in 8 to 2 micron band during lunar eclipse, using model for quantitative comparisons transient radiative heat exchange on moon surface observed in 8 to 12 micron band during lunar 11 p1865 A67-24604
 Lunar surface erosion by rockets simulated in laboratory to study hazards of retrorocket landing on airless planetary bodies 12 p1922 A67-25701
 Photometric investigations of simulated lunar surfaces confirm high porosity and low albedo without postulating necessity for fine dust layer 12 p2003 A67-25740
 Thermal properties of moon by comparing IR and microwave measurements of spectrum with theoretical calculation of upper layer temperature distribution [AIAA PAPER 67-289] 12 p2009 A67-26006
 Thermal coordinate analysis of lunar IR scan data for directional effects caused by surface geometry, illumination and sensor angle [AIAA PAPER 67-291] 12 p2009 A67-26008
 Cryogenic fluid storage on moon surface, considering Lambert reflection law, thermal insulation performance, incident heat flux and boil-off rates [AIAA PAPER 67-296] 12 p1926 A67-26011
 Lunar surface accessibility study for manned lunar orbit rendezvous missions, discussing nonfree return and translunar trajectories [AAS PAPER 66-131] 13 p2209 A67-27542
 Lunar radar echoes depolarization studied via lunar surface backscattering characteristics at 23 cm wavelength 14 p2261 A67-28374
 Lunar studies by laser techniques, considering optics, principles for distinguishing between useful and noise signals, precision of measurements, etc 14 p2386 A67-28468
 Orbiter II lunar photography analysis, noting surface characteristics of Southern Hemisphere of moon 14 p2387 A67-28506
 Electronic polarimeter applied to Stokes parameter measurement of lunar surface, determining reflected light ellipticity 15 p2552 A67-29147
 Reflection coefficient for electromagnetic waves incident at various angles on plane laminar medium of lunite 15 p2552 A67-29150
 Lunar surface rocks viscosity, volcanic origin, etc, with reference to Flamsteed Ring putative magma 15 p2553 A67-29159
 Formation of Flamsteed Ring slopes on moon investigated, noting wall consistency with fragmental debris from moon quakes 15 p2553 A67-29160
 Proposed emplaced scientific station for

lunar surface studies 15 p2553 A67-29300
 Lunar surface exploration noting sample collection, instrument planting, long term economic possibilities, etc 15 p2553 A67-29301
 Future lunar surface missions, defining adequate spacecraft configurations by applying technology and hardware developed on Apollo Lunar Module program [AIAA PAPER 67-27] 15 p2571 A67-30102
 Scanning IR radiometer equipment to produce pictorial maps of lunar radiance patterns or of possible variations in lunar surface composition 15 p2492 A67-30434
 Radiation level on lunar surface noting degree of danger to astronaut, solar activity effect, creation of secondary emission, etc 16 p2737 A67-30782
 Lunar surface bearing strength estimate from Orbiter II photograph, noting Sabine D crater measurement as potential landing site for Surveyor and Apollo [JPL-TR-32-1156] 16 p2746 A67-30931
 Lunar crater classification by morphological types discussing ring structures 16 p2747 A67-30984
 Comparison of lunar surface photography from space probes and ground-based observatories 16 p2671 A67-30990
 Probable internal structure of moon in light of thermal history examined searching for explanation of lunar core and crust formation 16 p2747 A67-30992
 Rocket fuel production possibilities on moon surface and other planets for planetary explorations 16 p2655 A67-31008
 Unmanned exploration of moon, summarizing results on surface structure, back side and material composition 16 p2748 A67-31199
 Polarization characteristics of radio emission from rough lunar surface, analyzing averaging effects of antenna radiation pattern and surface roughness 16 p2628 A67-31495
 Proton-irradiation darkening of rock powders, noting contamination, temperature effects and applications to solar wind darkening of moon [JPL-TR-32-1130] 16 p2753 A67-31743
 Optical properties of moon quantitatively compared with powder samples, bombarded with ions from hydrogen discharge plasma 16 p2753 A67-31744
 Polarimetric properties of simulated lunar surface, showing polarization effect on particle size 16 p2754 A67-31749
 Soviet book on first panoramic views of lunar surface covering Lunik IX soft landing, data on morphological and geological characteristics of landing site, etc 17 p2948 A67-32966
 Reflection and scattering from lunar surface of meter radio waves emitted by lunar orbiter 17 p2948 A67-32976
 Lunar surface photographs taken by Luna IX and Surveyor I showing linear and circular ground features, rock blocks and dust 17 p2948 A67-33094
 Soviet book on moon figure and motion covering coordinate systems, surface features positions, rotational parameters, etc 17 p2948 A67-33118
 Catalog of selenocentric rectangular coordinates, selenographic longitudes and latitudes and absolute altitudes of lunar surface features 17 p2949 A67-33119
 Coordinate systems for lunar surface detail positions, accuracy and practical value and corrections for system conversion 17 p2949 A67-33120
 Thermal conditions effect on moon figure, reviewing methods for determining lunar geometric form 17 p2949 A67-33122
 Isostatic equilibrium form of moon model having homogeneous semimolten core and homogeneous solid 17 p2949 A67-33123
 Permafrost layer existence beneath lunar surface, noting possible detection techniques 17 p2952 A67-33250
 Continuous wave signals from Lunar Orbiter I after reflection from lunar surface, noting mapping use 17 p2817 A67-33364
 Attenuation of lunar microwave emission measured by artificial moon method, determining phase dependence of lunar temperature 18 p3119 A67-33861
 Lunar surface particles geocentric trajectories, giving perigee distance and velocity curves 18 p3120 A67-33866
 Moon surface origin and present surfaces

of moon, Venus and Mars as determined from lunar photographs and data by flyby probes 18 p3121 A67-34135
 Lunar surface and U.S. Ranger program significance and interpretation 18 p3121 A67-34137
 Analysis of lunar surface panoramas transmitted by automatic station Lunik IX after soft landing 18 p3122 A67-34138
 Lunar surface absorption coefficient in IR range, discussing limb-darkening, reflectivity, subsolar point temperature, radiation, spectral properties, etc 18 p3122 A67-34139
 Moon spectrophotometric measurements from space probe compared with solar spectrum structure, calculating lunar albedo curve 18 p3122 A67-34140
 UV spectra of lunar surface photographed from Zond III automatic space probe 18 p3122 A67-34141
 Penetrating radiation intensity on lunar surface and in space, evaluating counting rate, lunar surface radioactivity and radiation belts absence 18 p3122 A67-34143
 Heliometer replaced by long focus photographic refractor used for moon rotation constant determination 18 p3129 A67-34308
 Observations of exact shape of moon, discussing catalog and map planning 18 p3130 A67-34319
 Absolute lunar coordinate determination methods based on stereoscopic method 18 p3131 A67-34322
 Photometric methods for determination of lunar relief 18 p3132 A67-34328
 Apollo lunar landing mission noting lunar geodetic, cartographic and topographic information deficiencies and correction programs 18 p3132 A67-34329
 IR thermal emission from lunar nighttime surface, noting anomalies location and observational procedure 18 p3134 A67-34497
 Moon Blink project for detecting red or blue temporary color phenomena 18 p3134 A67-34535
 Lunar surface roughness and brightness temperature anomalies from IR image study 18 p3134 A67-34537
 Lunar craters and fragments compared with terrestrial low velocity secondary volcanic impact craters and ejecta on basis of distribution relations 18 p3134 A67-34538
 Surface geometry demonstrated to be insignificant in production of lunar hot spots during eclipse 18 p3135 A67-34545
 Lunar thermal anomalies exhibiting slower cooling rates during eclipse, discussing IR observations 18 p3135 A67-34546
 Size-frequency distribution of particles and craters and optical, thermal, radio and other properties of lunar surface obtained from Surveyor I landing 19 p3318 A67-35179
 Lunar radius facing earth determined from radar measurement data and lunar orbiters 19 p3319 A67-35263
 Solid interplanetary matter in moon vicinity through piezoelectric sensors, giving impact rate, trajectory projections and increased matter density hypothesis 19 p3319 A67-35275
 Soviet national report to COSPAR, summarizing findings in upper atmosphere, on lunar surface and outer space from 1964 to 1966 19 p3322 A67-35308
 Slope derivation from lunar orbiter photography using photometric model and computer program 19 p3230 A67-35322
 Conceptual design of active seismic experiment for lunar surface missions, analyzing communication approaches 19 p3323 A67-35328
 Man capability to operate in cislunar space and lunar surface through Apollo program, discussing practical applications 19 p3326 A67-35644
 Moon probe photographs studied to ascertain moon surface material, structural condition and carrying capacity for future landings on moon 19 p3327 A67-35830
 Lighting and viewing conditions posing visibility problems for lunar landing mission 20 p3521 A67-36598
 Surveyor I spacecraft location and identification on moon surface by photographs taken by Orbiter III 20 p3524 A67-36649
 Lunar surface evolution model implying partial melting due to impacts as only cause of primitive plutonic activity 20 p3525 A67-36948

Morphology of Flamsteed Ring hills compared to other craters 20 p3525 A67-36997

Intensity of characteristic spectral lines of Si, Al and Mg of lunar surface rock made fluorescent by solar X-rays determined from Luna X measurements 21 p3701 A67-37838

Primary cosmic radiation in interplanetary space, lunar surface albedo and soft particle fluxes in magnetosphere measured by Luna X orbiter 21 p3697 A67-37840

Lunar surface materials choice narrowing method via albedo, color and polarization property examinations to find possible candidates for lunar surface model 21 p3701 A67-37897

Model for lunar surface roughness effect on emission of thermal IR radiation and casting of shadows in sunlight 21 p3702 A67-38188

Theoretical lunar crater formation data compared to experimental measurements, discussing lunar crater structures and crater fields 22 p3879 A67-39297

Lunar surface luminescence in IR and UR bands, discussing luminescence distribution, luminoform nature and surface irregularities 22 p3879 A67-39298

Lunar surface geology from results of Ranger, Luna IX and Surveyor I missions for selection of manned lunar landing site 22 p3879 A67-39309

Radiative transfer in lunar surface diurnal heat flow, studying geometric model of porous medium 22 p3885 A67-39980

Luminance of lunar surface site predicted by direct solar and earth reflected illumination together with local albedo variations 22 p3887 A67-40143

Shock processes pertinent to lunar terrain fragmentation and lithification noting Surveyor and Lunar Orbiter pictures 23 p4064 A67-40948

Lunar soil cohesive and disruptive properties from Surveyor I data, discussing micrometeorite impacts, thermal fracturing, metal vapor deposition and atomic adhesion 23 p4064 A67-40949

Seleno-geological evidence for lunar surface properties from Surveyor I, discussing weathering products and volcanic genesis 23 p4064 A67-40952

Ranger, Surveyor and Orbiter probe lunar surface photographic data, discussing lunar event distribution, lunar craters and maria distribution 23 p4065 A67-40953

Similarity between Icelandic lava field photographs and Luna IX lunar surface photographs 23 p4065 A67-40954

Penetration depth of hypervelocity impact craters photographed by Luna and Ranger vehicles indicate granular lunar surface 23 p4065 A67-41003

Impact crater size vs incidence analyzed statistically in study of validity of time dependence on saturation for moon and Mars 23 p4066 A67-41007

Lunar Orbiter II lunar surface photographs noting Copernicus H and Copernicus crater interior peak cluster 23 p4066 A67-41012

Cauchy domes in Mare Tranquillitatis, deriving relief pictures with photometry 23 p4066 A67-41013

Surveyor III lunar surface sampler for picking, digging, scraping and transporting material, noting design and operation 23 p4005 A67-41370

Solar cell array for LEM electric power system during lunar surface operation noting requirements and tradeoffs 23 p3939 A67-41510

Physiological measurements in obtaining energy expenditure and workloads during simulated lunar surface mission 23 p3959 A67-41657

Surveyor V scientific experiment, comparing lunar surface sampling with that in Surveyor III, noting resemblance to granular terrestrial soil 24 p4228 A67-42308

Electronic polarimeter applied to Stokes parameter measurement of lunar surface, determining reflected light ellipticity 24 p4239 A67-43070

Reflection coefficient for electromagnetic waves incident at various angles on plane laminar medium of lunite 24 p4239 A67-43073

LUNAR SURFACE VEHICLE

Navigation functional display requirements associated with early manned lunar exploration vehicles 04 p0655 A67-15662

Dynamic analysis of lunar surface vehicle including power spectral density terrain definition, vehicle velocity limiting criteria and nonlinear analysis of vehicle freedom to pitch, bounce and roll 07 p1163 A67-19369

First order factors affecting driver ability to safely control typical lunar vehicle through simulated mission profile over representative terrain [SMPT PAPER 101-54] 12 p1920 A67-25469

Lunar pogo stick, discussing velocities, horizontal and vertical displacements and weight estimates of man-carrying vehicle 17 p2832 A67-32065

Design and construction of power supply without hookup cables for manned lunar vehicle 21 p3571 A67-38337

Lunar gravity, reduced pressure and suit encumbrance effects examined in lunar surface environment simulation test bed, assessing astronaut performance [AIAA PAPER 67-866] 24 p4117 A67-42969

LUNAR TEMPERATURE

Thermal behavior of certain lunar areas differing sharply from that of surrounding terrain explained by lack of insulating debris over anomalous areas 02 p0320 A67-11458

Thermal radio emission measurements at wavelengths 7.93, 11.0, 14.2 and 20.8 cm, discussing phase dependence 02 p0322 A67-11581

Ray craters and hot spot on lunar surface during solar eclipse [AAS PAPER 66-184] 08 p1387 A67-20959

Lunar surface optical properties and IR emission [AAS PAPER 66-185] 08 p1387 A67-20960

Lunar observation in wavelength range one to three mm, noting brightness temperature drop during total eclipse, obtaining dielectric constant 08 p1390 A67-21022

Dependence of thermal conductivity of lunite on temperature, noting properties of moon surface 09 p1565 A67-21987

Heat transfer through various silicate powders measured for lunar surface temperature studies, comparing theoretical results [AIAA PAPER 67-285] 12 p2035 A67-26002

Thermal properties of moon by comparing IR and microwave measurements of spectrum with theoretical calculation of upper layer temperature distribution [AIAA PAPER 67-289] 12 p2009 A67-26006

Radiometric observations of total lunar eclipse of December 19, 1964 at wavelength of 3.3 mm indicate no significant temperature difference [JPL-TR-32-1097] 12 p2011 A67-26245

Moon thermal history investigated using thermal model, comparing results with astrophysical and geological evidence including melting and fluid convection effects 14 p2390 A67-28888

Lunar radio emission in 30 to 60 cm range, showing mean radio temperature of moon as 225 degrees K and independence of wavelength 15 p2552 A67-29148

Lunar internal heat flow measured by infrared mapping of polar regions from orbiting satellites 16 p2754 A67-31750

Attenuation of lunar microwave emission measured by artificial moon method, determining phase dependence of lunar temperature 18 p3119 A67-33861

Lunar thermal history computed for different radioactive elements distribution 18 p3119 A67-33862

Lunar surface roughness and brightness temperature anomalies from IR image study 18 p3134 A67-34537

Surface geometry demonstrated to be insignificant in production of lunar hot spots during eclipse 18 p3135 A67-34545

Lunar thermal anomalies exhibiting slower cooling rates during eclipse, discussing IR observations 18 p3135 A67-34546

Higher lunar radio temperatures than IR measurements using temperature dependence of radiant energy transfer, considering thermal conductivity of lunar materials 22 p3886 A67-40119

Lunar geothermal deposits, discussing recovery applications and energy tapping [AIAA PAPER 67-901] 24 p4239 A67-43009

Lunar radio emission in 30 to 60 cm range, showing mean radio temperature of moon as 225 degrees K and independence of wavelength 24 p4239 A67-43071

LUNAR TIDE

Weight of moon, considering approaches of tides and force of attraction exerted by moon on element of earth 01 p0148 A67-10506

Phase reversal in lunar variations of critical frequencies of F-2 layer at Waltair, India 01 p0600 A67-11232

Lunar tide effects on ionospheric characteristics near magnetic equator, noting fluctuations in electron concentration 02 p0237 A67-11673

Lunar tidal variations in ionosphere in power spectrum analysis from geomagnetic data obtained during IGY 03 p0508 A67-12849

Possible gravimetric study of lunar gravity, tide and free oscillation modes [AAS PAPER 66-191] 08 p1387 A67-20964

Amplitude variations in earth free and forced polar motion indicate periodic solar activity and moon tidal forces influence 10 p1631 A67-22798

Lunar periodic variation of geomagnetic field on Khels Island in Franz Joseph Land 14 p2309 A67-27938

Lunar tide effects on ionospheric characteristics near magnetic equator, noting fluctuations in electron concentration 16 p2665 A67-31088

Harmonic spectrum of variations in earth rotation, noting seasonal variation and effects of lunar tides 17 p2843 A67-32444

Deformations of earth crust produced by known forces of luni-solar and surface types 18 p3040 A67-34093

Ionospheric winds required to produce lunar daily geomagnetic variations deduced from atmospheric dynamo theory, estimating electric conductivity 20 p3425 A67-36281

Auroral zone diurnal tidal effect studied by high resolution spectrum analysis, noting large diurnal conductivity variation giving rise to lunar auroral electrojet 20 p3521 A67-36298

Selenodesy, determining gravitational constant-lunar mass product, lunar gravitational field variation, physical librations, inertial moments, lunar tides, lunar radius, etc 20 p3525 A67-36893

Lunar tide in E layer, diurnal/semidiurnal components and seasonal variation 21 p3616 A67-37997

Lunar semidiurnal air tide distribution and small lunar gravitational excitation noting lunar diurnal tide detectable only with wind data 22 p3882 A67-39557

Minimum distance and orbit inclination in earth-moon system, considering tidal friction effects 23 p4065 A67-41000

Amplitude variations in earth free and forced polar motion indicate periodic solar activity and moon tidal forces influence 24 p4149 A67-42134

LUNAR TOPOGRAPHY

SA SELENOGRAPHY

Photographic observation of lunar topography and Mars 07 p1247 A67-19332

Lunar surface topography analyzed using Ranger photographs, particularly texture of lunar maria such as ray craters, ridges, collapse depressions, etc 08 p1390 A67-21025

Observation methods for determination of moon shape including libration effect, local topography and determination of apparent contour 08 p1395 A67-21159

Mathematical model of flooded random surface and applications to lunar terrain 11 p1863 A67-24556

Soviet book on moon figure and motion covering coordinate systems, surface features positions, rotational parameters, etc 17 p2948 A67-33118

Catalog of selenocentric rectangular coordinates, selenographic longitudes and latitudes and absolute altitudes of lunar surface features 17 p2949 A67-33119

Coordinate systems for lunar surface detail positions, accuracy and practical value and corrections for system conversion 17 p2949 A67-33120

Moon rotational parameters determined by refractometric observations of craters position angles, tabulating selenographic and topocentric coordinates, reference system conversion corrections, etc 17 p2949 A67-33121

Variations in lunar gravitational field noting hydrostatic equilibrium state and relation to lunar topography 18 p3127 A67-34252

Measure of moon - Conference,

Manchester University, England, May-June 1966 18 p3127 A67-34301
 Harmonic analysis of lunar shape and gravitational field, discussing control systems used 18 p3130 A67-34318
 Observations of exact shape of moon, discussing catalog and map planning 18 p3130 A67-34319
 Observational uncertainties affecting lunar control solution, considering distortions of magnitudes greater than desired increment of detection, analyzing displacements in recorded images 18 p3130 A67-34320
 Lunar Planetary Laboratory selenodetic measurement precision and comparison with contemporary selenodetic triangulations 18 p3131 A67-34323
 Estimate of dynamical center from four lunar surface impact points determined by tracking Ranger probes from three earth-based stations 18 p3131 A67-34324
 Lunar topography from ground-based photographs taken under oblique illumination, discussing exposure times, resolution, etc 18 p3132 A67-34330
 Lunar charting for selenocentric coordinates from densitometric analysis and altitude measurements, using photometric methods and 18 p3049 A67-34333
 Moon elevation profiles and lunar slopes determined by photometry and isodensitometric measurements of Ranger IX photographs 18 p3133 A67-34335
 Zonal gravity harmonics of moon from tracking data 18 p3135 A67-34539
 Lunar radius facing earth determined from radar measurement data and lunar orbiters 19 p3319 A67-35263
 Lunar terrain uncertainties effect on trajectory optimization using Kalman filter during lunar landing powered descent [AIAA PAPER 67-543] 19 p3256 A67-35942
 Cauchy domes in Mare Tranquillitatis, deriving relief pictures, with photometry 23 p4066 A67-41013
 Oxygen consumption rate during ambulatory lunar surface exploration, describing lunar simulator 23 p3966 A67-41597

LUNAR TRACKING
 Estimated GM values of earth and moon, tracking station locations and lunar radii at impact points, from DSIF radio tracking data of Ranger Block III lunar flights [AAS PAPER 66-105] 07 p1253 A67-19965
 Estimated GM values of earth and moon, tracking station locations and lunar radii at impact points, from DSIF radio tracking data of Ranger Block III lunar flights [AAS PAPER 66-105] 13 p2208 A67-27523

LUNAR TRAJECTORY
 SA EARTH-MOON TRAJECTORY
 SA MOON-EARTH TRAJECTORY
 Flight trajectories to moon, Venus and Mars 08 p1394 A67-21115
 Numerical integration of restricted problem of three bodies for finding lunar trajectories, using motion equations and Taylor series 08 p1396 A67-21181

LUNEBERG LENS
 Broadband monopulse three-element tracking feeds for spherical Luneberg lens scanning antenna, discussing radiator design, radiation pattern and cross coupling between error channels 15 p2451 A67-29924

LUNG
 SA ALVEOLAR AIR
 SA PULMONARY CIRCULATION
 SA PULMONARY FUNCTION
 Effect of gravitational changes on aerosol deposition in lungs of man, noting particle size and alveolar region 09 p1452 A67-21724
 Cumulative effect of impact acceleration on physiological functions of rats, studying particularly lung lesions 16 p2612 A67-30904
 Ventilation-perfusion inequality effects studied in inert gas elimination from lungs 21 p3575 A67-38516
 Lung changes resulting from prolonged exposure to 100 percent oxygen at 550 mm Hg suggest media erosion and evidence of hypertrophy and 22 p3751 A67-39601

LUNG MORPHOLOGY
 Absorptional atelectasis breathing oxygen at simulated altitude, discussing prevention by using inert gas 09 p1453 A67-21732
 Bronchial tube diameter makes possible alveolar ventilation with minimum metabolism or entropy production in

musculature 09 p1454 A67-21986
 Periodic prolonged low-intensity acceleration stress provided by short radius centrifuge in baboons 13 p2059 A67-26917
 Lung changes relation to fatal outcome of 100 percent oxygen exposure 23 p3958 A67-41649

LUNIK II LUNAR PROBE
 Interaction of solar wind and frozen-in magnetic field with geomagnetic field inside and outside magnetosphere, comparing theory with satellite measurements 02 p0320 A67-11461

LUNIK IX LUNAR PROBE
 Stratified and faceted forms on panoramas obtained from Luna IX space station, noting connection with mineral composition of lunar surface 01 p0150 A67-10904
 Lunar surface structure implied by millimeter-sized features in Luna IX photographs 01 p0151 A67-10964
 Nature of lunar surface, discussing interpretations of Luna IX photographs by Jaffe and Kuiper 03 p0512 A67-13934
 Lunar surface according to Luna IX and Surveyor I 09 p1568 A67-22405
 Soviet book on first panoramic views of lunar surface covering Lunik IX soft landing, data on morphological and geological characteristics of landing site, etc 17 p2948 A67-32966
 Lunar surface photographs taken by Luna IX and Surveyor I showing linear and circular ground features, rock blocks and dust 17 p2948 A67-33094
 Analysis of lunar surface panoramas transmitted by automatic station Lunik IX after soft landing 18 p3122 A67-34138
 Luna IX and Luna X near moon, studying injection phase, orbit and landing phase from transmitted frequency observations 18 p3003 A67-34242
 Similarity between Icelandic lava field photographs and Luna IX lunar surface photographs 23 p4065 A67-40954

LUNIK X LUNAR PROBE
 Lunar gamma radiation intensity and spectral composition from Luna X data, deducing cosmic ray and radioactive decay origins 01 p0150 A67-10905
 Cosmic radiation data obtained by two gas-discharge counters installed in Luna X artificial satellite 01 p0145 A67-10906
 Luna X shielded gas-discharge counter data on soft corpuscular radiation, noting solar contribution to magnetospheric tail 01 p0145 A67-10907
 Charged particle traps installed in Luna X providing evidence for moon passing through tail of earth magnetosphere, noting effect of solar wind 01 p0145 A67-10908
 Magnetic field intensity near moon measured by Luna X magnetometer, noting correlation with earth surface intensity 01 p0150 A67-10909
 Meteoritic matter obtained by piezoelectric pickups applied to Luna X, noting impact frequency for interplanetary space 01 p0150 A67-10910
 Lunar gravitational field determined from orbital motion of Luna X satellite 03 p0510 A67-13341
 Luna X lunar-orbiter satellite observations of charged particles in lunar ionosphere, using magnetic trap 03 p0513 A67-14066
 Lunar gravitational field determined from orbital motion of Luna X satellite 13 p2211 A67-27714
 Magnetic field measurement with Lunik x near lunar orbit noting magnitude, time behavior and existence of terrestrial magnetic tail 16 p2755 A67-31888
 Magnetic field in moon proximity constructed from Lunik x satellite plasma and magnetic measurements 16 p2755 A67-31889
 Luna IX and Luna X near moon, studying injection phase, orbit and landing phase from transmitted frequency observations 18 p3003 A67-34242

LUTETIUM COMPOUND
 Fluorescence spectrum of activating europium ion in lutetium oxide matrix and appearance in crystalline-field model 19 p3307 A67-35794

LUXEMBOURG EXPERIMENT
 S LANGMUIR PROBE

LUNAR ALPHA RADIATION
 Electron density profiles of Nike-Apache rocket observations of nitric oxide ionization by Lyman alpha radiation in E region at

sunrise 03 p0415 A67-14114
 Hydrogen atom excitation by Lyman alpha radiation absorption in electric field 05 p0848 A67-16795
 Hydrogen and He UV glow in night sky as ion and electron source, estimating intensities and ionization rate 10 p1633 A67-22949
 Scattered Lyman alpha radiation in geocorona analyzed using satellite mounted equipment 10 p1706 A67-23223
 Lyman alpha emission from sun near solar minimum 11 p1862 A67-24503
 Molecular oxygen densities in range 70-90 km determined by rocket measurements of atmospheric absorption of solar UV radiation in Southern Hemisphere 12 p1934 A67-25786
 Intensity and polarization of hydrogen Lyman alpha lines in day airglow as function of altitude for principal far UV emission 14 p2314 A67-28849
 Maser effect hypothesized as cause of 21 cm radiation in clouds of interstellar hydrogen in galactic corona 15 p2551 A67-29139
 Electron correlations influence on plasma-broadened Lyman alpha line 15 p2520 A67-29679
 High resolution UV spectrograph with echelle, noting optical line-up for photographing H-Lyman alpha line at 1216 angstroms 16 p2680 A67-31875
 Lyman-alpha radiation emission from ion-target-gas collision measured for various projectile energies 17 p2889 A67-33224
 Absolute intensities of Lyman hydrogen alpha and beta lines used for interpretation of electron temperatures and density of emitting layers 19 p3325 A67-35464
 Relative photon scattering cross sections for He and Ne at Lyman alpha, describing measurement technique 20 p3489 A67-37431
 Hydrogen emission by sun offers no unique interpretation for Lyman alpha profile 21 p3700 A67-37733
 Profile of night sky hydrogen Lyman alpha emission line determined using data from rocketborne hydrogen-filled filter tube 22 p3790 A67-39805
 Maser effect hypothesized as cause of 21 cm radiation in clouds of interstellar hydrogen in galactic corona 24 p4239 A67-43062

LYMAN BETA RADIATION
 Absolute intensities of Lyman hydrogen alpha and beta lines used for interpretation of electron temperatures and density of emitting layers 19 p3325 A67-35464

LYMAN SPECTRUM
 Degree of coherence for extended source, considering electron transitions, found to depend on electron initial and final state 01 p0091 A67-11227
 Photographic technique for obtaining solar image in rays of Lyman alpha line spectrum, using quartz crystal 11 p1793 A67-24862
 Astronomical satellite for photoelectric spectrometry in UV region to measure stars of galactic clusters 12 p2002 A67-25460
 Generation of series limit continua with aid of sliding sparks for absolute measurements in vacuum UV, observing bremsstrahlung 13 p2155 A67-26271
 Upper limit on concentration of molecular hydrogen in interstellar space by comparison of Lyman bands in absorption spectra of early type stars and laboratory source 17 p2945 A67-32651
 Book on vacuum UV spectroscopy techniques noting Lyman continuum, synchrotron radiation, Bremsstrahlung radiation, UV radiation, resolution, etc 20 p3446 A67-36664

LYMPH
 Cannulation of renal capsular lymphatics in anesthetized dogs, testing if lymph fluid can serve to assess tissue oxidation 06 p0952 A67-17853
 Rapid decompression effect on lymph pressure of dog, discussing immediate and delayed rise phases 22 p3751 A67-39600



U. of ILL. LIBRARY

JAN 3 1968

CHICAGO CIRCLE

AIAA TECHNICAL INFORMATION SERVICE

750 THIRD AVENUE

NEW YORK, N. Y. 10017